1992 Syntex Award Lecture
Model biomembranes: quantitative studies of peroxidation, antioxidant action, partitioning, and oxidative stress[1]

L. R. C. BARCLAY
Chemistry Department, Mount Allison University, Sackville, N.B., Canada E0A 3C0

Received May 27, 1992

This lecture is dedicated to Keith Ingold

Can. J. Chem. Downloaded from www.nrcresearchpress.com by 88.255.202.194 on 09/08/12
For personal use only.

L. R. C. BARCLAY. Can J. Chem. **71**, 1 (1993).

This review outlines a decade of research that employs quantitative kinetic methods of autooxidation to phospholipids aggregated into membranes. The classical rate law for autoxidation:

$$-\frac{d[O_2]}{dt} = \frac{k_p}{(2k_t)^{1/2}}[R{-}H]R_i^{1/2}$$

was found to apply to heterogeneous systems of bilayers and micelles, where k_p and $2k_t$ are the rate constants for chain propagation and termination, respectively, and R_i, the rate of chain initiation, is controlled by thermal initiators. The *oxidizability* of a typical lipid chain, linoleate 18:2, at 30°C was similar (0.02–0.04 $M^{-1/2}$ $s^{-1/2}$) in different media (solution, micelles, bilayers) and for different procedures using water-soluble or lipid-soluble initiators and inhibitors. A reduction in the absolute rate constant for termination, $2k_t$, by a hundredfold in bilayers of dilinoleoylphosphatidyl choline (DLPC) compared to that in *tert*-butyl alcohol solution, and a drop in the k_p by a factor of five are interpreted in terms of diffusion of polarized peroxyl radicals from the hydrophobic bilayer phase to the aqueous surface, where peroxyls are strongly solvated by water. Such phenomena may also account for significant changes as observed by ^{31}P NMR spectra in bilayer lamellar structure accompanying extensive peroxidation. Analysis of the hydroperoxides formed by peroxidation of mixed bilayers of DLPC + DPPC (16:0) initiated by a water-soluble initiator, azobis(2-amidinopropane·HCl) (ABAP), showed a linear trend between the ratio of *cis,trans* to *trans,trans* geometrical isomeric hydroperoxides and [DPLC] consistent with a peroxidation mechanism proposed in homogeneous solution.

The antioxidant activities, k_{inh}, of three classes of antioxidants: (*a*) polyalkyl-6-hydroxychromans (e.g., vitamin E), (*b*) polyalkyl-4-methoxyphenols, and (*c*) trialkylphenols, were measured in DLPC membranes. The results show an overall leveling and depression of k_{inh} values in DLPC membranes in the series (*a*) (by several orders of magnitude), (*b*), and (*c*) compared to known values in solution in chlorobenzene. In aqueous bilayers it is proposed that k_{inh} values are attenuated by hydrogen bonding by water at both the *para* ether oxygen and phenolic groups. Restricted diffusion (e.g., of α-tocopherol) may also reduce antioxidant activities in membranes. A synergistic effect between ascorbic acid and α-tocopherol was discovered under conditions of inhibited peroxidation of linoleate in SDS micelles. The natural peptide glutathione, GSH, however, acts as a *co-antioxidant* with vitamin E by trapping peroxyls in the aqueous phase.

Solid cholesterol was found to partition directly into PC lipsomes by shaking, above or below the phase transition temperature, and membrane-bound cholesterol, unlike the solid, undergoes facile peroxidation. A water-soluble form of α-tocopherol complexed with bovine serum albumin (α-toc:BSA) is an effective antioxidant for autoxidations of linoleate in SDS micelles. In contrast, α-toc:BSA required a long equilibration time (e.g., 12 h) with liposomes (DLPC) before the α-tocopherol was transferred to the liposomes to provide effective antioxidant action.

Carbon radicals from thermolysis under nitrogen of the lipidic azo initiator, 6,6′-azobis(6-cyanododecanoic acid), 6,6′, in unilamellar liposomes were spin-trapped by phenyl *tert*-butyl nitrone (PBN) to give membrane-bound trapped radicals as observed by broad anisotropic ESR spectra. However, under oxygen, 6,6′ in liposomes formed derived peroxyl radicals, which were trapped in the aqueous phase by water-soluble 4-trimethylammonium-PBN.

The Total (peroxyl) Radical Trapping Antioxidant Parameter (TRAP) of a biological fluid, the number of peroxyl radicals trapped per volume of fluid under "oxidative stress" under known conditions of chain initiation (R_i), was determined for blood plasmas of humans. A control group (n = 6) gave an average TRAP of 775 μM peroxyls trapped compared to athletes (n = 5) where the average TRAP of 1226 μM was 45% higher. Vigorous exercise was found to increase the uric acid contribution to TRAP.

L. R. C. BARCLAY. Can. J. Chem. **71**, 1 (1993).

Dans cette revue, on décrit une décade de recherches faisant appel à des méthodes quantitatives d'auto-oxydation appliquées aux phospholipides agrégés dans des membranes. On a trouvé que la loi de vitesse classique des auto-oxydations :

$$-\frac{d[O_2]}{dt} = \frac{k_p}{(2k_t)}[R{-}H]R_i^{1/2}$$

s'applique aux systèmes hétérogènes des bicouches et des micelles, alors que k_p et $2k_t$ sont respectivement les constantes de vitesse de la propagation et de la terminaison de la chaîne et que R_i, la constante de vitesse de l'initiation de la chaîne, est contrôlée par les initiateurs thermiques. L'*oxydabilité* d'une chaîne lipidique typique, le linoléate 18 : 2, à 30°C, est assez constante (0,02–0,04 $M^{-1/2}$ $s^{-1/2}$) dans divers milieux (solution, micelles et bicouches) et diverses

[1]This Syntex Award Lecture was delivered by Dr. Barclay at the Annual Conference of the Canadian Society for Chemistry, Edmonton, Alberta, June 4, 1992.

procédures utilisant des initiateurs et des inhibiteurs solubles dans l'eau ou liposolubles. On attribue une réduction de la constante absolue de la vitesse de terminaison, $2k_t$, qui est plus de cent fois plus lente dans des bicouches de dilinoléylphosphatidyl choline (DLPC) par comparaison avec la même réaction dans une solution d'alcool *tert*-butylique, et une réduction par un facteur de cinq de la valeur de k_p à une diffusion des radicaux peroxyles polarisés de la bicouche hydrophobe vers la surface aqueuse où les radicaux hydroxyles sont fortement solvatés par l'eau. Un tel phénomène peut aussi expliquer les changements significatifs qui accompagnent une peroxydation extensive. L'analyse des hydroperoxydes qui se forment lors de la peroxydation de bicouches mixtes de LDPC + DPPC (16 : 0) initiées par un initiateur hydrosoluble, l'azobis(2-amidinopropane)·HCl) (ABAP), présente une tendance linéaire entre le rapport des isomères géométriques *cis,trans/trans,trans* des hydroperoxydes et [DLPC]; cette observation est en accord avec un mécanisme de peroxydation proposé pour les réactions en milieu homogène.

On a mesuré les activités antioxydantes, k_{inh}, de trois classes d'antioxydantes : (*a*) les polyalkyl-6-hydroxychromanes (comme la vitamine E); (*b*) les polyalkyl-4-méthoxyphénols et (*c*) les trialkylphénols dans des membranes de DLPC. Les résultats présentent un effet global limitant et, par comparaison avec les valeurs connues en solution dans le chlorobenzène, une diminution des valeurs de k_{inh} dans les membranes DLPC des séries (*a*) (plusieurs puissance de 10), (*b*) et (*c*). Dans les bicouches aqueuses, on suggère que les valeurs de k_{inh} sont atténuées par une liaison hydrogène entre l'eau et les oxygènes en *para* ainsi que les groupes phénoliques. Une diffusion restreinte (comme avec l'α-tocophérol) peut aussi réduire les activités anti-oxydantes dans les membranes. Dans des conditions de peroxydation inhibée du linoléate dans des micelles de SDC, on a découvert un effet synergique entre l'acide ascorbique et l'α-tocophérol. Toutefois, le peptide naturel glutathion, GSH, agit comme *co-antioxydant* avec la vitamine E en piégeant les peroxyles dans la phase aqueuse.

On a trouvé que, en l'agitant au-dessus at au-dessous de la température de transition de phase, le cholestérol solide se partitionne directement dans les liposomes PC et que, comparativement au produit solide, le cholestérol lié à la membrane subit une peroxydation facile. Une forme d'α-tocophérol complexée avec de l'albumine de sérum bovin et soluble dans l'eau (α-toc : BSA) est un antioxydant efficace pour les auto-oxydations du linoléate dans le SDS. Par ailleurs, le complexe α-toc : BSA nécessite une longue période d'équilibre (environ 12 h) avec les liposomes (DLPC) avant que l'α-tocophérol soit transféré aux liposomes pour fournir une action antioxydante efficace.

Utilisant de la phényl *tert*-butyl nitrone (PBN), on a piégé les radicaux carbonés provenant de la thermolyse, sous atmosphère d'azote, de l'initiateur azo lipidique, 6,6′-azobis(acide-6-cyanododécanoïque), 6,6′, dans des liposomes unilamellaires; on a ainsi obtenu des radicaux piégés, liés à une membrane, que l'on a observé par leurs spectres RPE anisotropiques. Toutefois, en présence d'oxygène, le 6,6′ dans les liposomes conduit à des radicaux peroxyles dérivés que l'on a piégé en phase aqueuse par le 4-triméthylammonium-PBN soluble dans l'eau.

Le Paramètre de Piégeage Total de Radicaux (peroxyles) d'un Antioxydant d'un fluide biologique est le nombre total de radicaux peroxyles piégés par unité de volume de fluide sous «stress oxydant», dans ces conditions connues d'initiation (R_i) de chaîne; on a déterminé ce paramètre pour des plasmas sanguins humains. Un groupe de contrôle (n 6) conduit à une valeur de ce paramètre qui est égale 775 μm de peroxydes piégés; par comparaison, ce paramètre est égal à 1226 μm (45% plus élevé) pour des plasmas de sang d'athlètes. On a trouvé que l'exercice vigoreux augmente la contribution de l'acide urique à ce paramètre.

[Traduit par la rédaction]

1. Introduction

Free radical peroxidation of unsaturated chains in biomembrane lipids disrupts the important structural and protective function of membranes and is associated with a variety of significant pathological events. Various environmental factors, operating *externally*, that affect us adversely include ultraviolet radiation, pollutants (e.g., smog), and tobacco smoke. Such factors can promote cancer and cataract. Other events that may be promoted *internally* by oxygen-centred radicals include atherosclerosis, inflammation, damage to neuronal tissue leading to stroke, and damage to sensitive tissue during reperfusion. Several *medical* aspects of "oxidative stress" have been included in various books (1–3) and conference proceedings (4–9).

The biomedical aspects of cellular oxidative damage have catalyzed interest in this field of membrane research and resulted in a remarkable increase in activity and publications related to the biological phenomena of membrane damage. On the other hand, *quantitative kinetic* studies at the molecular–chemical level have lagged behind. Over a decade ago the author visited Keith Ingold's laboratory at the National Research Council, Ottawa, where we initiated a study that led to applications of quantitative kinetic methods of autoxidation and inhibition to membranes. This research was continued at Mount Allison University and this paper describes some of the progress made over the last decade. Our research benefitted greatly from the continued encouragement of Keith Ingold and the participation of other collaborators.

Our research has certain basic objectives, which are formulated in terms of fundamental questions:

1. Can free radical reactions propagated by peroxyls, ROO·, be initiated *under controlled conditions* of the rate of chain initiation, R_i, and quantitative measurements be made in membranes?

2. Is the classical rate law for autoxidation applicable to model membrane systems?

3. What is the effect of such microenvironments as bilayers and micelles on the *oxidizability* and *products* from the polyunsaturated fatty acid (PUFA) chain of lipid membranes?

4. What is the activity of phenolic antioxidants in membranes compared to that in homogeneous solution, and do cooperative interactions occur between lipid-soluble antioxidants (vitamin E) and water-soluble ones (vitamin C, Trolox, and thiols)?

5. What role does diffusion or partitioning play in distributing substances such as vitamin E, cholesterol, and PUFA-derived peroxyl radicals in membranes?

This research employed phosphatidylcholine (PC) bilayers, since these mimic the behaviour of natural phospholipid membranes in many respects (10), as multilamellar vesicles (MLV) or unilamellar vesicles (ULV) prepared by

Can. J. Chem. Downloaded from www.nrcresearchpress.com by 88.255.202.194 on 09/08/12
For personal use only.

known methods (11) of extrusion, dialysis, or sonication. The lamellar structures, MLV or ULV, of these vesicles were studied by electron microscopy (e.g., ref. 12) or ^{31}P NMR in our research. Some experiments were also done in sodium dodecylsulfate (SDS) as a model biphasic system of hydrophobic and hydrophilic phases.

2. Kinetics and mechanism: peroxidation and inhibition

Various chemical and physical methods used to measure the extent of lipid peroxidation have been reviewed (13–15) and the GC/MS method improved (16). The well-known thiobarbituric acid (TBA) test, based on a colour reaction of TBA with malondialdehyde formed during peroxidation of certain PUFA, has some disadvantages (17). Our approach for quantitative studies used direct oxygen uptake studies and, where desirable, product analyses.

2.1. The kinetic approach to peroxidation, and the oxidizability of linoleate in different media: solution, micelles, membranes

Quantitative kinetic methods of autoxidation are superior in the study of peroxidation of lipids. These methods are well known for reactions in homogeneous solution (18–20) and were first applied to model membrane systems in Ingold's laboratory in 1981 (21). In this method, the rate of free radical chain initiation, R_i, is controlled by using a thermal azo initiator with a known constant, k_i, and the R_i is measured with an efficient antioxidant. Oxygen uptake is measured with a sensitive pressure transducer system custom-made in our laboratory for reactions in aqueous dispersions (22). When combined with HPLC product analysis for specific oxidation products (23, 24), these procedures provide the best approach for quantitative studies of phospholipid peroxidation.

The known mechanism for free radical chain autoxidation is outlined in eqs. [1]–[4].

[1] Initiation: $\mathrm{R{-}N{=}N{-}R} \xrightarrow{2k_i} 2\mathrm{R}\cdot + \mathrm{N_2}$

Propagations:

[2] $\mathrm{R}\cdot + \mathrm{O_2} \xrightarrow{\text{fast}} \mathrm{R{-}O{-}O}\cdot$ (peroxyl)

[3] $\mathrm{R{-}O{-}O}\cdot + \mathrm{R{-}H(substrate)} \xrightarrow{k_p} \mathrm{ROOH} + \mathrm{R}\cdot$

[4] Termination: $2\mathrm{R{-}O{-}O}\cdot \xrightarrow{2k_t}$ nonradical products + $\mathrm{O_2}$

A simple steady state expression is used for the kinetic equations for oxygen uptake,

$$[5] \quad -\frac{d\mathrm{O_2}}{dt} = k_p[\mathrm{RO_2}\cdot][\mathrm{R{-}H}]$$

At steady state, the rate of initiation = the rate of termination as shown in eq. [6], where e = initiator efficiency. This correction, e, is needed since only those radicals which "escape" the solvent cage in which they are formed can react with oxygen and initiate reaction.

$$[6] \quad 2k_i \times e[\mathrm{RN_2R}] = 2k_t[\mathrm{RO_2}\cdot]^2$$

Substituting for $[RO_2\cdot]$ in eq. [5]:

$$[7] \quad -\frac{d\mathrm{O_2}}{dt} = \frac{k_p}{2k_t^{1/2}}[2k_i \times e(\mathrm{RN_2R})]^{1/2} \times [\mathrm{R{-}H}] = \frac{k_p}{2k_t^{1/2}} \times [\mathrm{R{-}H}] \times R_i^{1/2}$$

The susceptability of a substrate to undergo autoxidation, known as its oxidizability, is given by eq. [8]:

$$[8] \quad \text{Oxidizability} = \frac{k_p}{2k_t^{1/2}} = \frac{-d\mathrm{O_2}/dt}{[\mathrm{R{-}H}] \times R_i^{1/2}}$$

For quantitative determinations the R_i must be measured and this is usually done by adding a phenolic inhibitor, known to trap two peroxyls, and by measuring the induction period during which oxidation is suppressed when eq. [9] applies.

$$[9] \quad R_i = 2 \times [\mathrm{ArOH}]/\tau$$

where τ = inhibition period. The absolute rate constants for chain propagation, k_p, eq. [3], and termination, $2k_t$, eq. [4], were determined by the modified rotating sector method (25).

These quantitative kinetic studies showed that the classical rate law for autoxidation, eq. [7], operates in SDS micelles for the oxidation of linoleic acid photoinitiated by benzophenone (26). Oxygen uptake was shown to be first order in linoleate concentration and half order in light intensity (or R_i). Such excellent quantitative studies in micelles are relatively straightforward. Micelles are optically clear and "solutions" are prepared almost as easily as homogeneous solutions in organic solvents. Micelles are used as models for membranes since they are said to be "a halfway house" between homogeneous solutions and bilayers (27); however, they are *not* really very similar to biomembranes. Micelles are a very *dynamic* species with short half-lives between monomers and aggregates whereas membranes are composed of static aggregates of dual chain phospholipids. If lipids are suddenly removed from the protective bilayer the latter is said to become "*leaky*", with catastrophic results!

Classical quantitative kinetic studies are much more difficult to carry out in membranes than in homogeneous solution or micelles, for several reasons. Thermal azo initiators have a very low initiator efficiency ($e \simeq 9\%$) when solubilized in the bilayer phase because of high cage recombination in this region of high microviscosity (21) and it is not desirable to insert large amounts of initiator into the bilayer. Secondly, *the concentration of oxidizable lipid in a pure PC is a fixed value, independent of the amount used.* Therefore, special procedures are required to check the rate law for autoxidation. A couple of key "breakthroughs" enabled us to solve these kinetic problems:

1. Collaborative research with Keith Ingold and Graham Burton of the National Research Council showed that quantitative kinetic studies of autoxidation in membranes could be carried out by inserting thermal azo initiators into the aqueous phase and measuring the R_i with a water-soluble antioxidant, Trolox (28).

2. We discovered that the kinetic order in membrane oxidizable substrate [RH] can be determined by using a mixed bilayer system containing variable amounts of an unsaturated substrate, dilinoleoylphosphatidylcholine (DLPC), mixed with saturated PC's such as dimyristoylphosphatidylcholine (DMPC) or dipalmitoylphosphatidylcholine (DPPC) (29, 30).

These developments permitted us to measure the kinetic orders in oxidizable substrate and in the R_i as illustrated in Figs. 1 and 2 (29). It was now possible to determine the oxidizability of a typical lipid chain, e.g., linoleate, in solution and in micellar and bilayer phases. More importantly, the absolute rate constants for propagation, k_p, and termi-

Can. J. Chem. Downloaded from www.nrcresearchpress.com by 88.255.202.194 on 09/08/12
For personal use only.

TABLE 1. Oxidizability of linoleate in microenvironments compared to homogeneous solution:

Substrate	Medium	Initiator[a]	Oxidizability $k_p/2k_t^{1/2}$ ($M^{-1/2}$ $s^{-1/2}$)	k_p ($M^{-1}s^{-1}$)	$2k_t$ (M^{-1} s^{-1} × 10^{-6})
Methyl linoleate	C_6H_5Cl	ACHN(l)	0.0194	31	2.7
Methyl linoleate	o-$C_6H_4Cl_2$	DBHN(l)	0.0408		
Linoleic acid	0.50 MSDS micelles	ABAP(w)	0.034	15	0.20
Methyl linoleate	DMPC bilayer (pH = 7.0)	ABAP(w)	0.0179		
Linoleic acid	DMPC bilayer	DBHN(l)	0.0259		
		ABAP(w)	0.0300		
DLPC	*tert*-Butyl alcohol	ACHN(l)	0.029 per linoleate chain	150	6.8
DPLC	Bilayer	ABCP(l)	0.028	16	0.08
ELPC	Bilayer	ABAP(w)	0.024	10	0.16 Photoinitiated, rotating sector

[a]Abbreviations: l, lipid soluble; w, water soluble.

Can. J. Chem. Downloaded from www.nrcresearchpress.com by 88.255.202.194 on 09/08/12
For personal use only.

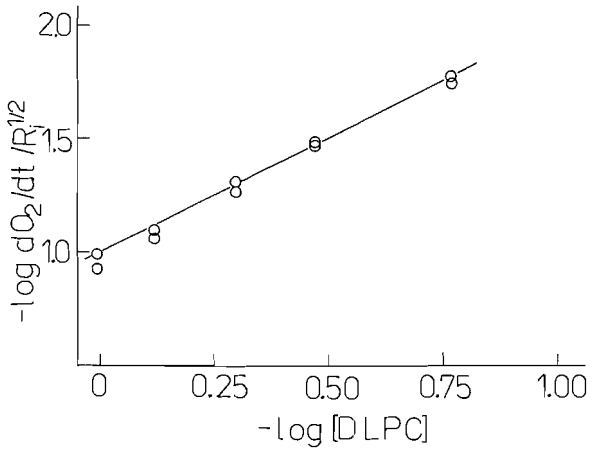

FIG. 1. Kinetic order plot for the autoxidation of mixed bilayers of DLPC + DMPC, initiated by lipid-soluble ADVN.

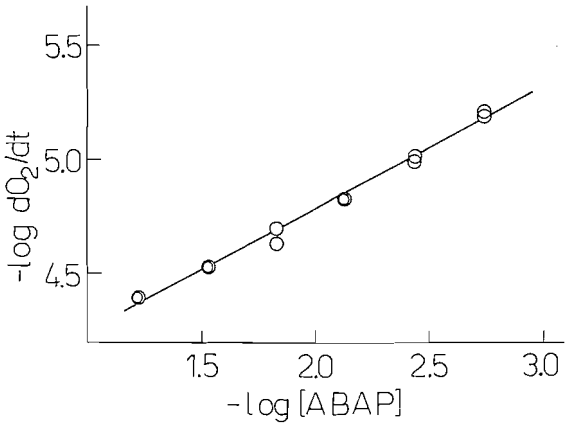

FIG. 2. Kinetic order plot of oxygen consumption with concentration of the water-soluble initiator, ABAP, for autoxidation of mixed bilayers of DLPC + DPPC.

nation $2k_t$, were determined in these different media. Some of the these results are collected in Table 1. The oxidizability of the linoleate lipid chain, a general property of its overall susceptibility to free radical autoxidation, varies within a limited range of 0.02–0.04 $M^{-1/2}$ $s^{-1/2}$ even under a wide variety of conditions and in different media, which were varied from homogeneous solution, SDS micelles, linoleate monomers in saturated DMPC, and finally DLPC bilayers. Also various combinations of lipid-soluble and water-soluble initiators and inhibitors were used in these studies, showing that oxidizability, as expected, is independent of the method of initiation and inhibition. It is of particular significance to find that aggregation of lipid chains into bilayers does not change their oxidizability. We find it remarkable that the charged water- soluble initiator, ABAP, appears to have access to the various layers of the MLV systems and especially that water-soluble Trolox can trap peroxyl radicals in membranes apparently as effectively as lipid-soluble vitamin E! These phenomena will be discussed in more detail (*vide infra*).

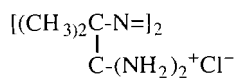

2.2. *Absolute rate constants,* k_p *and* $2k_t$*, in bilayers and the "Floating Peroxyl Radical Hypothesis"*

Absolute rate constants provide important insights into the behaviour of peroxyl radicals in membranes. We discovered a remarkable *decrease* in the termination rate constant, $2k_t$, for autoxidation of the DLPC bilayer compared to that in homogeneous solution, say in *tert*-butyl alcohol (see Table 1). The decrease amounted to as much as a hundredfold. Peroxyl radicals are known to be strongly polarized; the dipole moment of benzylperoxyl was determined to be 2.45 D (31). A collaborative study with Susan Boyd, Mount St. Vincent University, and Russell Boyd, Dalhousie University, showed that various saturated and unsaturated peroxyl radicals have large dipole moments in the 2.3–2.6 D range (32). We speculate that such polar peroxyl radicals would diffuse rapidly away from the nonpolar bilayer phase where they are formed initially towards the more polar aqueous surface. This so-called "Floating Peroxyl Radical Hypothesis" is illustrated schematically in Fig. 3. The consequence of this postulate is that polar peroxyl radicals would

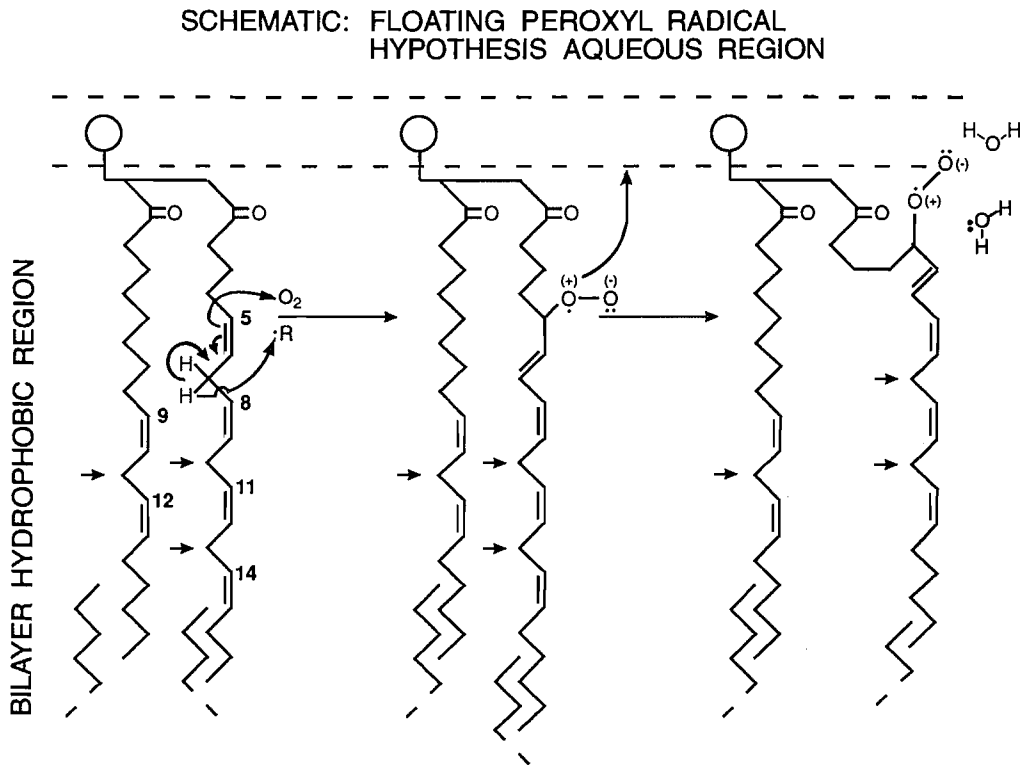

FIG. 3. Schematic for diffusion of polar lipid peroxyl radicals from a hydrophobic region to a polar interface during peroxidation.

terminate in the aqueous-lipid interface. The reduction in $2k_t$ would be due to stabilization of the polar peroxyl radicals by hydrogen bonding with water: The reduction in k_p

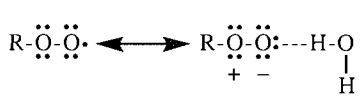

found in bilayers follows because the solvated peroxyls would not readily abstract the labile CH_2 groups that are deeper in the bilayer.[2]

Such diffusion of peroxyls would have very important consequences for bilayer structure and integrity. Some ^{31}P NMR studies give indications of the effect on lamellar structure. Factors affecting the ^{31}P NMR line shapes of membranes include particle tumbling and lateral diffusion of the chains within the particles (33), the former being restricted in larger liposomes and the latter depending on the microviscosity inside the bilayer. These factors are shown in some typical ^{31}P NMR spectra in Fig. 4. Multilamellar liposomes and large unilamellar ones show the effect of restricted tumbling motion whereby the ^{31}P NMR lines are very broad with a chemical shift anisotropy $\Delta\sigma \simeq -40$ ppm (Fig.4*a*). On the other hand, smaller unilamellar liposomes give a single isotropic line shape (Fig.4*c*). Very significant changes occur in the lamellar structure of liposomes during the course of extensive peroxidation as illustrated in Fig. 4 for controlled peroxidation of egg lecithin liposomes (Fig.4*d*). We started with unilamellar vesicles showing a single symmetrical line shape. There was no observable change in ^{31}P spectra up to 10% overall oxidation based on oxygen uptake studies. However, by 30% oxidation the unsymmetrical anisotropic spectrum appeared and it predominated on further oxidation. Such results indicate that the vesicles must fuse together and form larger ones or larger ones may even fracture and encapsulate smaller ones and become multilamellar. Such gross changes in lamellar structure could have been initiated by diffusion of peroxyl radicals during oxidation. The consequences of such structural damage on the protective properties required of biomembranes could be quite catastrophic!

2.3. Products of peroxidation and mechanism

The products of free radical autoxidation of linoleate are known to be the 9- and 13-hydroperoxy-substituted 9-*cis*,11-*trans*; 10-*trans*,12-*cis*; 9-*trans*,11-*trans*; and 10-*trans*,12-*trans* octadecadienoates, which are analyzed by reduction and conversion to the corresponding hydroxymethyl esters (structures are shown in Fig. 5). Outstanding research by Porter and co-workers (summarized in ref. 23) showed that the product ratios of kinetic products to thermodynamic products, the *cis*,*trans* to *trans*,*trans* ratios, are directly related to the hydrogen atom donating ability of the medium; for example, to the linoleate concentration. The Porter mechanism for lipid peroxidation is summarized schematically in Fig. 5. A student and I enjoyed the hospitality of Porter's laboratory at Duke University on several occasions and the technology for HPLC analyses of these oxidation products was transferred to our laboratory. These product analyses were very important to our studies in biphasic systems. The same linear trend of *cis*,*trans* to *trans*,*trans* (*c*,*t*/*t*,*t*) product ratios was observed for peroxidation of lino-

[2]However, recent spectral data for *tert*-butylperoxyl radicals show that, while k_p is much lower in water than in nonpolar solutions, the overall termination is similar in polar and nonpolar solvents (ref. 75).

Can. J. Chem. Downloaded from www.nrcresearchpress.com by 88.255.202.194 on 09/08/12
For personal use only.

Can. J. Chem. Downloaded from www.nrcresearchpress.com by 88.255.202.194 on 09/08/12
For personal use only.

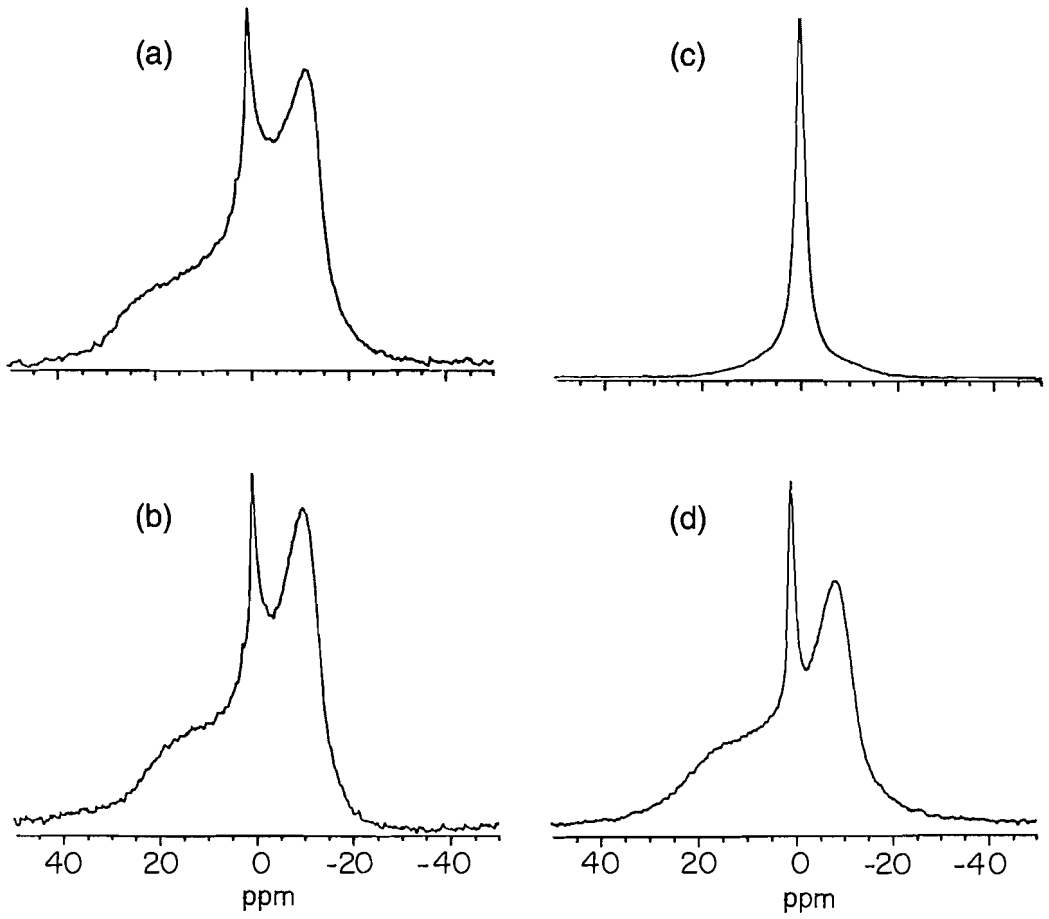

FIG. 4. ^{31}P nmr spectra of phosphatidylcholine liposomes (0.1 mmol) in 2.0 mL of THAM buffer (pH 7.0) at 40°C; (*a*) multilamellar DPLC, purified by HPLC; (*b*) oxidized DLPC, 60% conversion of active methylene groups; (*c*) unilamellar egg lecithin; (*d*) egg lecithin from (*c*) after >30% oxidation.

leate in SDS micelles when the reaction was initiated by lipid-soluble or water-soluble azo initiators and by lipid-soluble or water-soluble photo initiators, implying that the autoxidation mechanism is the same (e.g., Porter) under these different conditions (26).

It was especially important to determine the trend in product analysis with substrate concentration during initiation with a *water-soluble* initiator in membrane autoxidation. The results from such experiments using the initiator ABAP and varying linoleate concentration with mixed bilayers of DLPC + DPPC are illustrated in Fig. 6. The linear trend in *c,t/t,t* ratio with [DLPC] indicates (1) that the general mechanism of Porter applies to mixed bilayer systems and (2) that the water-soluble initiator, ABAP (or ABAP-peroxyls), has access to the hydrophobic region of bilayers to provide effective H-atom abstraction from reactive methylene groups at position 12. Such results complement our kinetic results obtained with water-soluble initiators (28), and they facilitate further quantitative kinetic studies. It is no longer necessary to incorporate the initiator into the bilayer phase during membrane preparation to control the rate of free radical chain initiation.

2.4. *Kinetics of inhibition and antioxidant activities in membranes*

The mechanism of action and activity of protective free radical chain-breaking antioxidants is the major interest of our research. Several recent reviews reflect a continuing outstanding interest and activity in this field (7, 34–37). The mechanism and kinetics of a typical phenolic antioxidant (e.g., vitamin E) are outlined in eqs. [10]–[14] below:

$$[10]\quad \mathrm{ROO\cdot} + \mathrm{ArOH} \xrightarrow{k_{\text{inhibitor}}} \mathrm{ROOH} + \mathrm{ArO\cdot}$$

$$[11]\quad \mathrm{ROO\cdot} + \mathrm{ArO\cdot} \xrightarrow{\text{fast}} \mathrm{ROOArO}$$

During inhibition, the rate of peroxyls formed (initiation) equals the rate of peroxyls trapped, therefore

$$[12]\quad R_i = 2k_i e[\text{Initiator}] = k_{inh} \times 2[\mathrm{ArOH}] \times [\mathrm{ROO\cdot}]$$

$$[13]\quad [\mathrm{ROO\cdot}] = R_i/k_{inh} \times 2[\mathrm{ArOH}]$$

and substituting for [ROO·] into eq. [5] gives the suppressed O_2 uptake during inhibition:

$$[14]\quad \frac{dO_2}{dt} = \frac{k_p}{k_{inh}} \times \frac{[\mathrm{R{-}H}] \times R_i}{2[\mathrm{ArOH}]}$$

To be efficient antioxidants phenols should possess certain general structural features. (1) They should give stabilized phenoxyl radicals in order to promote the rate-limiting hydrogen atom transfer, eq. [10]. (2) The resulting k_{inh} must be several orders of magnitude greater than the rate constant for propagation of the substrate; e.g., the ratio of k_p/k_{inh} needs

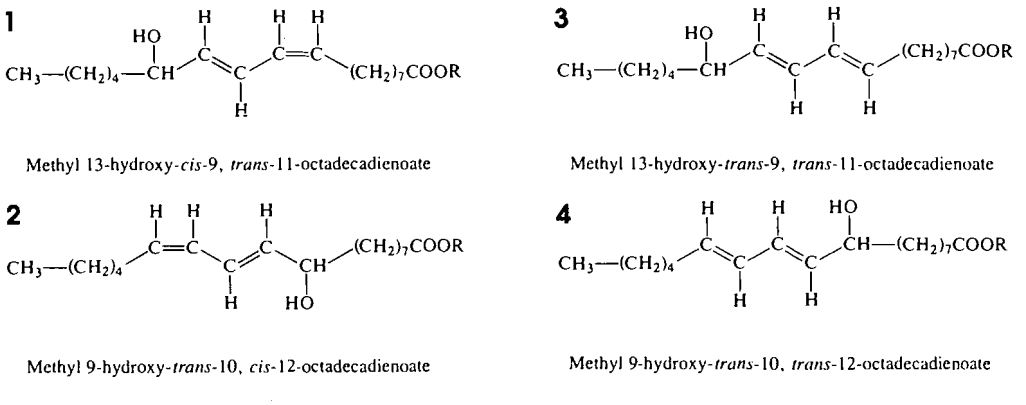

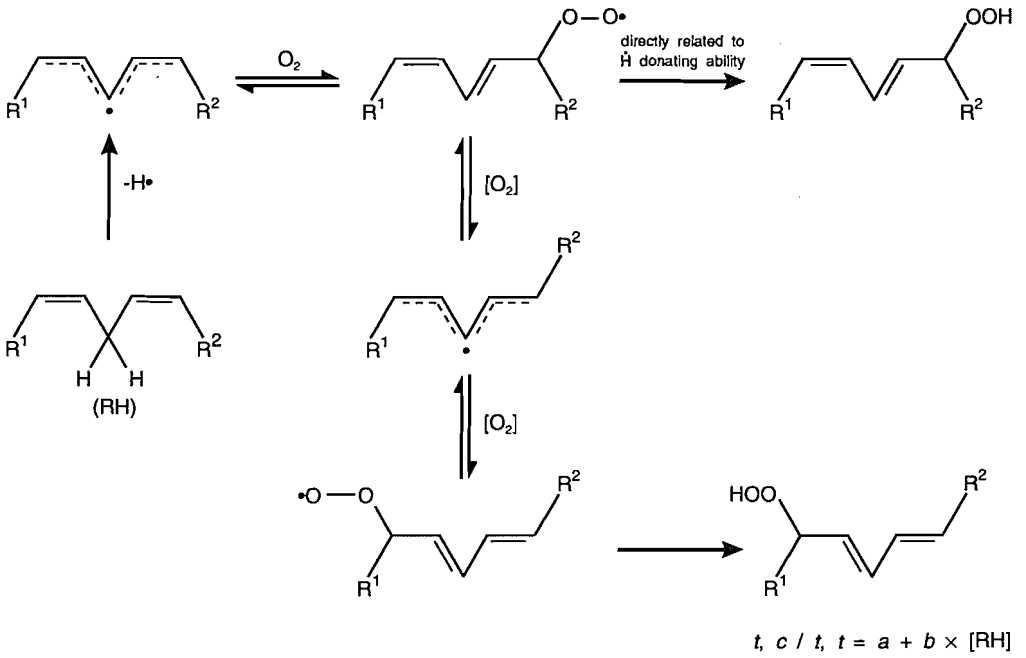

FIG. 5. Mechanistic scheme for peroxidation of unsaturated lipids, and hydroxy esters **1**–**4** prepared from peroxidized membranes for analysis (see Fig. 6).

to be small. (3) The phenoxyl radical ArO· must *not* itself initiate new radical chains by hydrogen abstraction. Hindered phenols, such as the vitamin E class, are known to meet these requirements (35).

The discovery by Ingold's group of the remarkable antioxidant activity of vitamin E (35) and their finding that it is the major lipid-soluble chain-breaking antioxidant in human blood (38) has led to the search for new synthetic models that might be more active than vitamin E itself (39, 40). Such studies were usually carried out in homogeneous solution, the main exceptions being some studies in micelles by our laboratory (26) and by others (41, 42). *The determination of antioxidant activities in* membrane systems *is a more significant but a much more difficult experiment.* Nevertheless, we were able to conduct such measurements in DLPC liposomes for which the required propagation rate constant, $k_p = 36\ M^{-1}\ s^{-1}$, was also determined (43). Melinda Vinqvist of our laboratory conducted very careful oxygen uptake studies during antioxidant–inhibition periods (eq. [14]) on an ultra-sensitive pressure transducer system. The values for k_{inh} were measured by using the integrated expression for the kinetics during inhibition, eq. [15].

$$[15] \quad \Delta[O_2]_t = -k_p/k_{inh} \times [R\text{—}H]\ln(1 - t/\tau)$$

where τ is the inhibition period, and the oxygen uptake, $[O_2]_t$, is measured at various times, t, during this period. The k_{inh}'s are then obtained from the linear plots of $\Delta[O_2]$ versus $\ln(1 - t/\tau)$ and the known k_p for this system ($36\ M^{-1}\ s^{-1}$).

The antioxidant activities of three important classes of phenols were determined during suppressed, thermally initiated, autoxidation of DLPC in MLV liposomes. The three classes of structures shown in Fig. 7 include (*a*) the hydroxychromans of the vitamin E class, (*b*) the polyalkyl 4-methoxyphenols, and (*c*) polyalkylphenols. The actual experimental traces of oxygen uptake under known and controlled rate of free radical chain initiation, R_i, are indicative of the antioxidant efficiencies of these three classes. Quantitative data, the absolute rate constants for inhibition,

Can. J. Chem. Downloaded from www.nrcresearchpress.com by 88.255.202.194 on 09/08/12
For personal use only.

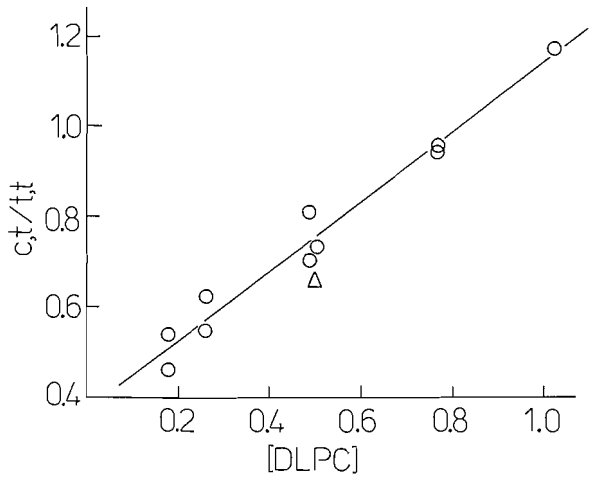

FIG. 6. Concentration dependence of the product ratios (*cis,trans/trans,trans*) of hydroxy linoleate esters derived from the autoxidation of mixtures of DLPC + DPPC. [DLPC] is the substrate concentration in the total (reaction) volume of DLPC + DPPC. The result from palmitoyl linoleoyl PC is shown as Δ.

k_{inh}'s, obtained from the corresponding linear plots of oxygen uptake versus $-\ln(1 - t/\tau)$, are also shown here. Values of k_{inh} in membranes and some results in homogeneous solution are given in Table 2. Very striking differences found for activities of these phenolic antioxidants in membranes compared to homogeneous solution are summarized below.

1. The activities of all three classes a, b, *and* c *are dramatically reduced in bilayers compared to solution.* For example, α-tocopherol (vitamin E) is more than 500 times *less* reactive in membranes than in chlorobenzene. A similar, though less dramatic, trend was discovered for the other antioxidants.

2. The activities of all three classes of inhibitors are quite similar in bilayers; e.g. there appears to be a levelling effect operating. This is in marked contrast to differences observed by Ingold's group for measurements in solution where some hydroxy anisoles (DBHA) and phenols (BHT, our "breakfast cereal antioxidant") showed k_{inh}'s orders of magnitude *less* than those of the vitamin E class, *a*. We now find that "BHT" has close to the same activity as vitamin E in membranes.

These major changes in protective activity of phenols in membranes compared to solution were at first very surprising and certainly disturbing! In homogeneous solution of *non-protic* solvents like chlorobenzene, the main factors controlling antioxidant activities are electronic and steric effects. Thus the different antioxidant activities of phenols such as polyalkylhydroxychromans of the vitamin E class and hydroxy anisoles were explained by Ingold and co-workers in terms of carefully considered electronic and steric effects (39). They concluded that the stabilization of the aryloxyl radical formed in the rate-determining inhibition step, eq. [10] above, depends mainly on the extent of orbital overlap between the 2*p* lone pairs on the *para* ether oxygen and the aromatic π system. The lone pairs in the heterocyclic chroman ring are constrained to be nearly perpendicular to the aromatic ring so there is stabilization of the α-tocopheroxyl radical by a type of through resonance referred to as "stereoelectronic effects" (39). We conclude that the remarkable lowering and levelling of activities in biphasic membrane systems must be due to environmental effects, namely, differential solvation effects and diffusion control in viscous bilayers. These two phenomena are evaluated as follows:

1. *The main environmental factor controlling phenolic antioxidant activities in membranes is the solvation effect of water*

We assume that the hydroxychromans reside near the polar head group of membranes as demonstrated for vitamin E (44) and that the trapping of polar peroxyl radicals occurs in this region. In these circumstances, the activity of these compounds is reduced by hydrogen bonding with water at both the ether oxygen at site A and the phenolic group, site B, as illustrated: The combined effects of solvent inter-

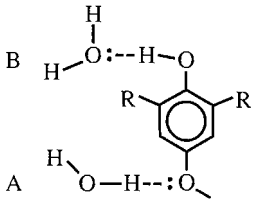

action at A and B level the antioxidant activity of the hydroxychromans toward that of BHT, whereas vitamin E is more than 200 times *more* reactive in chlorobenzene. The *higher* reactivity of **4***b* (DBHA) in bilayers is interesting in view of its diminished reactivity in solution, attributed to steric effects provided by *two* ortho tert-*butyl groups* to the approach of peroxyl radicals (39). In aqueous membranes there is a balance between steric inhibition of hydrogen transfer to peroxyl and steric hindrance to solvation of the phenolic OH by *ortho-tert*-butyl groups, so that the main effect operating to give DBHA higher "residual" activity is steric hindrance to hydrogen bonding at the phenolic hydroxyl. For the same reason the antioxidant activity of the polyalkyl phenols **7***c* and **8***c* switches on changing from chlorobenzene to membranes, so that **8***c* now is much less reactive because *ortho* methyl groups are not so effective at blocking solvation at the phenolic hydroxyl.

Through the generosity of samples provided by Professor K. Mukai of Ehime University, Japan, we were able to determine the antioxidant activities of two new synthetic polyalkyl hydroxy chromans, one bearing two isopropyl groups *ortho* to the hydroxyl (**4***a*) and the other *ortho-tert*-butyl and methyl (**4***b*). The results of this study, shown in Table 3, are very interesting indeed. The activities of **4***a* and **5***b* *in solution* are similar to that of 5,7-dimethyltocol, **6***a* (39), indicating that the reduction in activity here compared to PMHC is due to the absence of the stabilizing electron-donating methyl group at position 8 on the aryloxyl radical; steric hindrance to attack by peroxyl is not significant. *In DLPC membranes* these synthetic model compounds are *significantly more active as antioxidants* than any other compounds of the vitamin E class, being more active by one order of magnitude than α-tocopherol itself and three to four times more active than PMHC. These results demonstrate the importance of hydrogen bonding at the phenolic hydroxyl in controlling antioxidant activity. Steric hindrance to such effects provided by two *ortho*-isopropyl groups in **4***a* and an *ortho-tert*-butyl in **5***a* "free" the phenolic hydroxyl for more facile hydrogen atom transfer in the rate-controlling inhibition step, eq. [10].

Can. J. Chem. Downloaded from www.nrcresearchpress.com by 88.255.202.194 on 09/08/12
For personal use only.

Can. J. Chem. Downloaded from www.nrcresearchpress.com by 88.255.202.194 on 09/08/12
For personal use only.

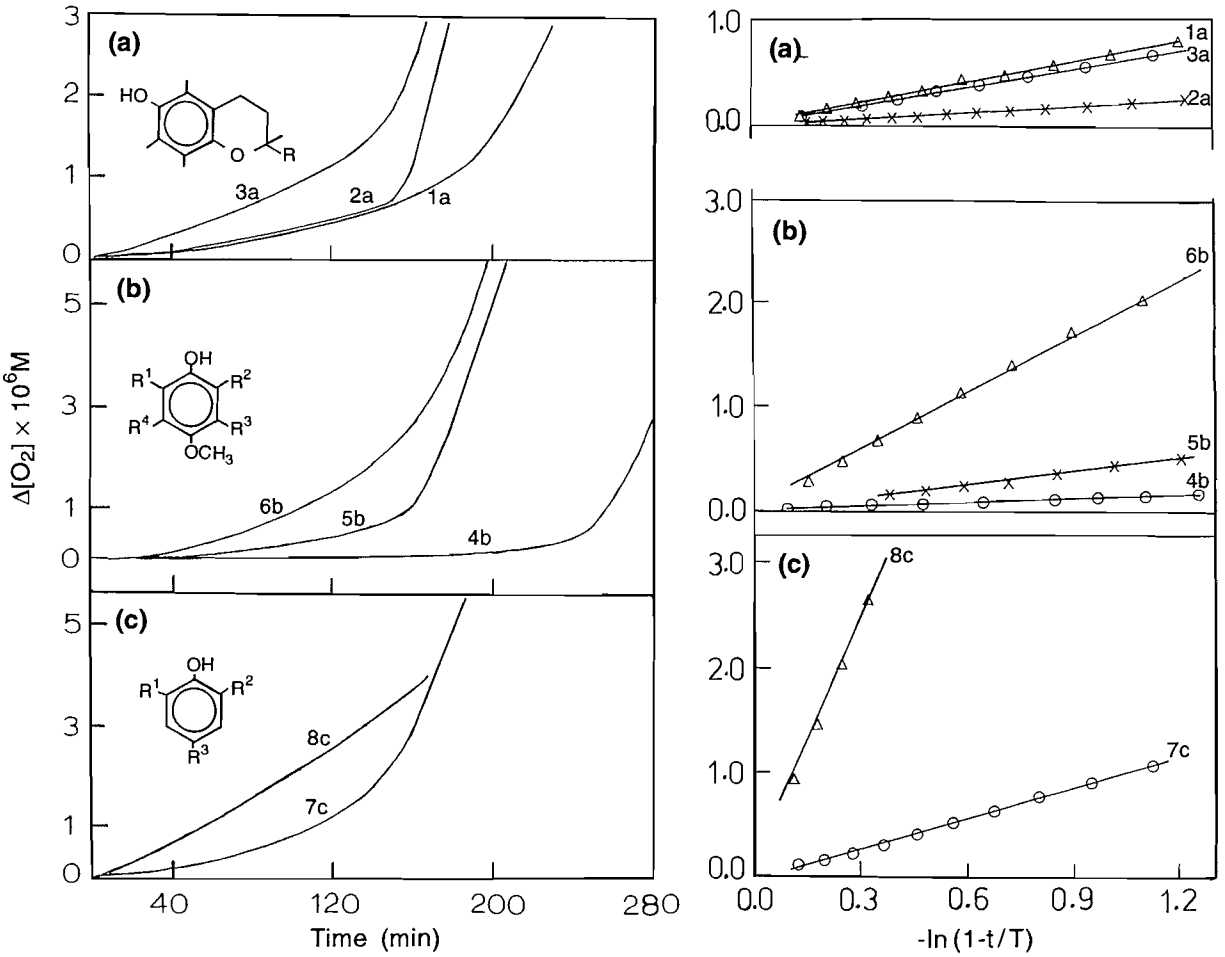

FIG. 7. Effects of antioxidants on peroxidation of DLPC liposomes thermally initiated by azobis-2,4-dimethylvaleronitrile (ADVN) at 37°C, and plots of oxygen uptake during inhibition periods versus $-\ln(1 - t/\tau)$ during peroxidation. **1***a*, α-tocopherol; **2***a*, R = CH_3; **3***a*, R = COOH; **4***b*, $R_1 = R_2 = C(CH_3)_2$, $R_3 = R_4 = H$; **5***b*, $R_1 = R_2 = R_3 = CH_3$, $R_4 = H$; **6***b*, $R_1 - R_4 = CH_3$; **7***c*, $R_1 = R_2 = C(CH_3)$, $R_3 = CH_3$; **8***c*, $R_1 - R_3 = CH_3$ (for amounts used, see ref. 43).

Our results demonstrate clearly the need to measure antioxidant activities of compounds in model membrane systems (as well as in solution) in order to judge their potential protective capacity against peroxyl radical attack in natural biological systems. The results may also be useful in designing new antioxidants that could be more reactive against peroxyl radicals *in membranes*.

2. *Diffusion limiting effects of bilayers on phenolic antioxidants*.

The long phytyl hydrocarbon chain of α-tocopherol may restrict the freedom of motion of this antioxidant in the viscous bilayer region and cause some diffusion control of interaction with peroxyl radicals. As a result, molecules without this chain but possessing the hydroxychroman system (**2***a*,**4***a*,**5***a*) are more active antioxidants than α-tocopherol, and this may in part be due to their greater freedom of motion. Diffusion control between micelles is cited to cause reduced antioxidant activity of lipopholic phenols such as α-tocopherol (41). Also, it is interesting to note that PMHC, **2***a*, is able to transfer between liposomal membranes whereas diffusion of α-tocopherol between membranes is suppressed (45).

A recent proposal of a two-step mechanism of phenolic antioxidant action, electron transfer followed by proton transfer (46), does not change these conclusions on the effects of aqueous membranes on antioxidant activities.

2.5. Cooperative interaction of antioxidants: synergism

Biological systems contain a variety of substances that act as free radical chain breaking antioxidants and these can be classified into a *lipid-soluble group*, which includes tocopherols, β-carotene, ubiquinones, vitamin(s) K, and estrogens, and a *water-soluble group*, which includes ascorbate, uric acid, and thiols such as glutathione. Biomembranes are protected against attack by oxygen-centred radicals through combinations of antioxidants and there is probably a "cascade" of free radical trapping and repair mechanisms involved where some antioxidants may be regenerated at the expense of others. Such an interaction between vitamin E and vitamin C was first suggested many years ago by Golumbic (47). Steven Locke, in our laboratory, was the first to demonstrate the synergistic effect of ascorbic acid and α-tocopherol *under controlled conditions of peroxidation*, using a model system consisting of linoleate in SDS micelles (48). This was followed by independent findings that ascorbate in the aqueous phase of liposomes can interact with vitamin E in the lipid phase to prolong the antioxidant capacity of vi-

TABLE 2. Antioxidant activities: k_{inh} (M^{-1} s^{-1} × 10^{-4})

Compound	No.		C_6H_5Cl, styrene (AIBN)[a]	DLPC membranes (ADVN)[b]
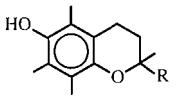	**1***a*	R = $C_{16}H_{33}$ (E)	320	0.58
	2*a*	R = CH_3	380	1.78
	3*a*	R = COOH	110	0.58
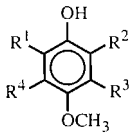	**4***b*	R^1, R^2 = $(CH_3)_3C$	11	2.75
	5*b*	R^1–R^3 = CH_3	130	1.04
	6*b*	R^1–R^4 = CH_3	39	0.21
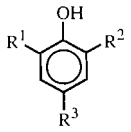	**7***c*	R^1, R^2 = $(CH_3)_3C$ (BHT)	1.4	0.37
	8*c*	R^1, R^2 = CH_3	8.5	0.056

[a]Reference 39.
[b]Reference 43

TABLE 3. Antioxidant activities: k_{inh} (M^{-1} s^{-1} × 10^{-4})

Compound	No.		C_6H_5Cl styrene (AIBN)	DLPC membranes (ADVN)
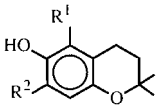	**4***a*	R^1, R^2 = $CH(CH_3)_2$	228	5.5
	5*a*	R^1 = CH_3, R^2 = $C(CH_3)_3$	199	6.1
	6*a*	R^1, R^2 = CH_3	(180)[a]	
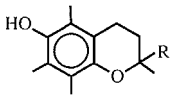	**1***a*	R = $C_{16}H_{33}$ (E)	(320)[a]	0.58
	2*a*	R = CH_3 (PMHC)	360	1.78

[a]Reference 39.

tamin E; e.g., synergistic interactions occurred between them in the different phases (49, 50). For ascorbic acid (A—H) to regenerate α-tocopherol from the α-tocopheroloxyl radical, the reaction [16]

[16] $A—H + \dot{E} \rightarrow E + \dot{A}$

must compete with the "fast" addition reaction of peroxyl radicals with Ė (e.g., eq. [11]) and the latter has been estimated to be at least two orders of magnitude faster than reaction [16] (48). However, concentration factors, especially a relatively high concentration of ascorbate and favourable site-specific interactions, may favour reaction [16].

The tripeptide glutathione, GSH, which occurs intracellularly in relatively high concentrations (e.g., millimolar), is known to have antioxidant properties in biological systems (ref. 51, and references therein) and these properties appear to be "vitamin E dependent." The role of GSH and other thiols is not well understood and remains a matter of continuing interest (6). Model experiments in our laboratory using liposomes showed that GSH does *not* regenerate α-tocopherol from the radical but it does act as a *co-antioxidant* to extend the inhibition of oxidation when reaction is initiated in the aqueous phase (51). It is suggested that GSH may function mainly by trapping radicals in the aqueous phase of membranes. We found very recently that thiols such as GSH and homocysteine are able to prevent the oxidative decay of aqueous solutions of ascorbate and even to regenerate ascorbate from its primary oxidation product, dehydroascorbate. The implication for biological fluids is particularly significant. Sulfhydryl groups (e.g., GSH and plasma proteins) present in relatively high concentrations function to protect or "repair" ascorbate while the latter is able to act synergistically with vitamin E to maintain its concentration in the lipid phase. There is evidence for such combined interactions of antioxidants in human blood plasma (52). Evidence has been given to indicate that ascorbate is the "outstanding antioxidant" in human blood plasma at the expense of the thiol plasma proteins, with the implication that the recommended daily allowance (RDA) of vitamin C should be doubled (53).

2.6. *Free radical peroxidation and neuronal tissue damage. Is there a relationship between antioxidant action and protection against central nervous system damage?*

Lipid peroxidation is implicated in the loss of neuronal tissue following brain or spinal cord injury, stroke, and

Can. J. Chem. Downloaded from www.nrcresearchpress.com by 88.255.202.194 on 09/08/12
For personal use only.

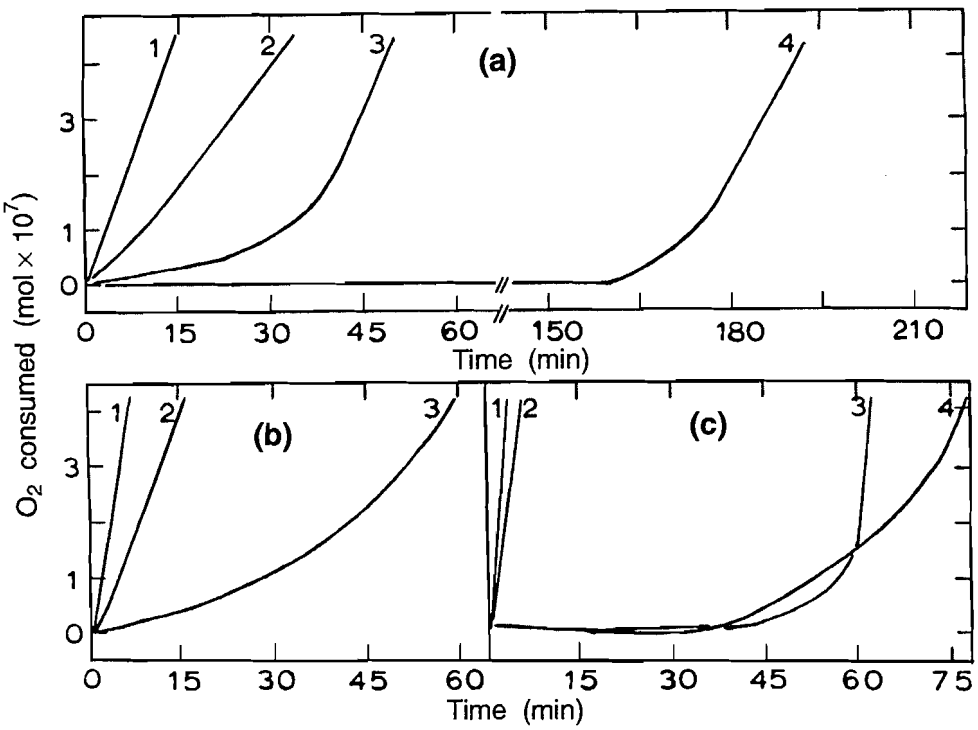

FIG. 8. Autoxidation of DLPC (2.50×10^{-5} mol) in phosphate buffer, pH 7.0. (*a*) Multilamellar DLPC liposomes. Initiated with DBHN (1.23×10^{-5} mol) at 30°C: 1, uninhibited reaction; 2, effect of α-T·BSA (1.76×10^{-8} mol); 3, inhibited by Trolox (0.431×10^{-8} mol); 4, inhibted by α-tocopherol (bilayer, 6.43×10^{-8} mol). (*b*) Large unilamellar DLPC liposomes. Initiated with ABAP (3.66×10^{-5} mol) at 30°C: 1, uninhibited reaction; 2, effect of α-T·BSA (1.24×10^{-8} mol) and immediate initiation with ABAP; 3, effect of α-T·BSA (1.24×10^{-8} mol) with shaking (4 h) *before* initiation with ABAP. (*c*) Small unilamellar DLPC liposomes. Initiated with ABAP (3.66×10^{-5} mol); 1, uninhibited reaction; 2, effect of α-T·BSA (1.24×10^{-8} mol) and immediate initiation with ABAP; 3, inhibited by Trolox (2.49×10^{-8} mol); 4, effect of α-T·BSA (1.24×10^{-8} mol) with shaking (12 h) *before* initiation with ABAP.

neurological disorders (e.g., Parkinson's disease) (54). The Upjohn Company has developed a number of novel "21-aminosteroids" that show promise in the treatment of head and spinal cord injuries (54). The question arises as to the antioxidant activity of such compounds, especially under our conditions of controlled rate of free radical chain initiation. Exploratory results in our laboratory using one such compound (U74500A, ref. 54), incorporated into DLPC liposomes or added in methanol solution, shows that it does act as an effective antioxidant when reaction is initiated either in the aqueous phase with ABAP or in the lipid phase with azobis-2,4-dimethylvaleronitrile (DMVN). In that latter case, the antioxidant activity of the amino steroid ($k_{inh} = 0.60 \times 10^3$ M^{-1} s^{-1}) was somewhat less than that of water-soluble Trolox ($k_{inh} = 1.64 \times 10^3$ M^{-1} s^{-1}) but the former gave a higher stoichiometric factor, $n = 3$ compared to $n = 2$ for Trolox. The mechanism of antioxidant action of these amino steroids is unknown. It may involve electron transfer from tertiary amino groups to peroxyl radicals, followed by hydrogen transfer.

3. Partitioning and diffusion in membranes

3.1. Cholesterol

Cholesterol is a very important constituent of biomembranes. Half of all deaths in the U.S. are attributed to atherosclerosis due to deposits of cholesterol plaque derived from low-density lipoproteins (LDL) that circulate in the blood. The public's attention to "cholesterol levels" became widespread after the 1973 discovery by Brown and Goldstein at the University of Texas of LDL-specific receptors on biomembranes that function to remove cholesterol from LDL and sequester it into the membrane phase, thereby preventing arterial blockage (55). Our recent research on cholesterol led to two very significant results!

1. *We found that solid cholesterol can partition directly from its solid state into phosphatidylcholine bilayers* by shaking the two together at 37°C (56). Both spectroscopic (^{31}P NMR of the membranes and ^2H quadrupole NMR of labelled cholesterol) and analytical data showed that the solid cholesterol partitions up to 21 mol% into the membrane phase. The implication is that cholesterol atherosclerotic plaque may be cleared by transfer to phospholipids directly.

2. *Cholesterol, when transferred into saturated liposomes (DMPC or DPPC), undergoes free radical peroxidation when initiated by either a water-soluble initiator, ABAP, or in the membrane phase with DMVN. The oxidation is inhibited more efficiently by the water-soluble antioxidant, Trolox, than by lipid-soluble α-tocopherol (56).* This latter unexpected result is attributed to diffusion control, in the bilayer region of high microviscosity, of the large molecules, α-tocopherol and cholesterol peroxyl radical, which must meet in the rate-controlling inhibition reaction. In contrast to its susceptibility to peroxidation in bilayers, solid cholesterol does *not* undergo peroxidation under conditions of controlled initiation with a water-soluble or a lipid-soluble initiator.

These fundamental studies on cholesterol partitioning and peroxidation in model membranes have additional biomed-

Can. J. Chem. Downloaded from www.nrcresearchpress.com by 88.255.202.194 on 09/08/12
For personal use only.

Can. J. Chem. Downloaded from www.nrcresearchpress.com by 88.255.202.194 on 09/08/12
For personal use only.

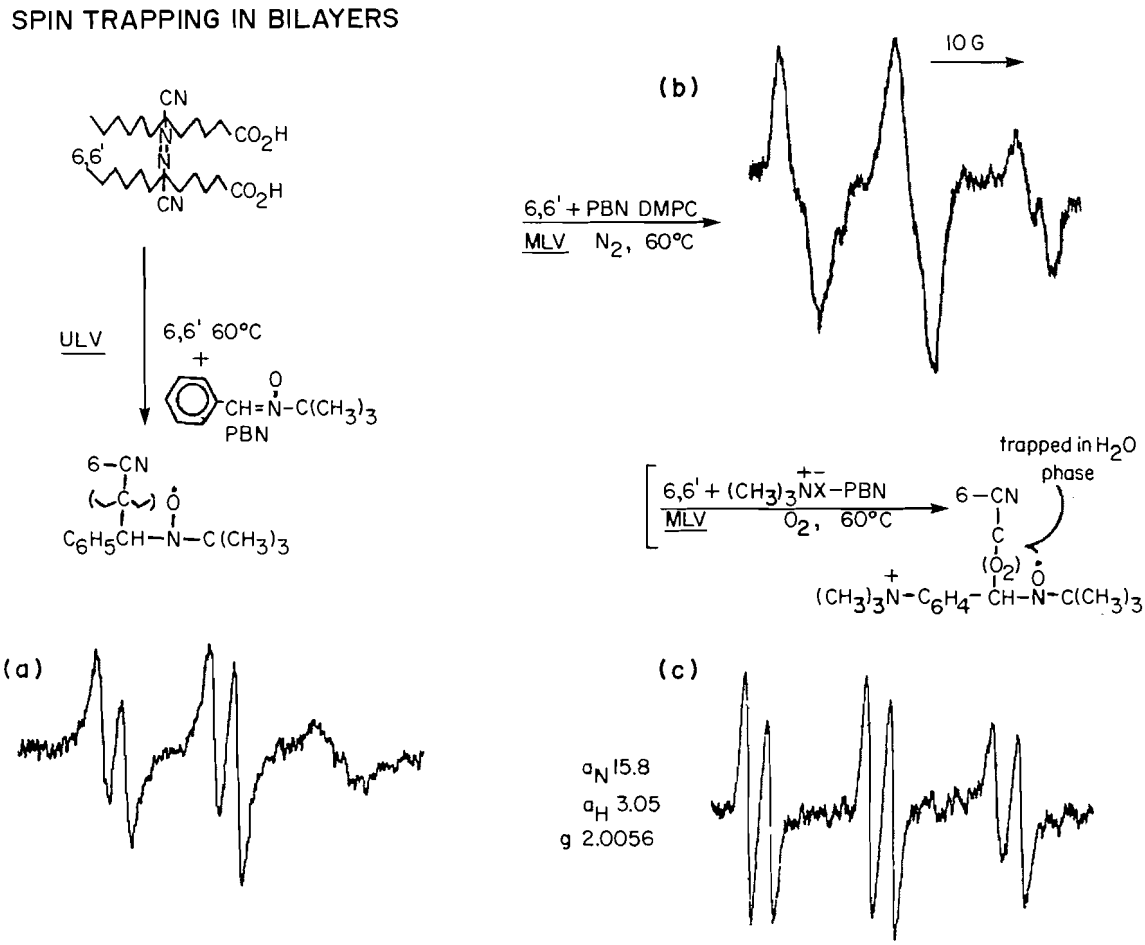

FIG. 9. The esr spectra of radicals formed by thermolysis of 6,6′-azobis(6-cyanododecanoic acids(6,6′) and spin trapped: (*a*) by phenyl-*tert*-butylnitrone(PBN) in unilamellar vesicles(ULV), (*b*) by PBN in multilamellar vesicles(MLV), and (*c*) by *para*-trimethylammonium-PBN after peroxidation.

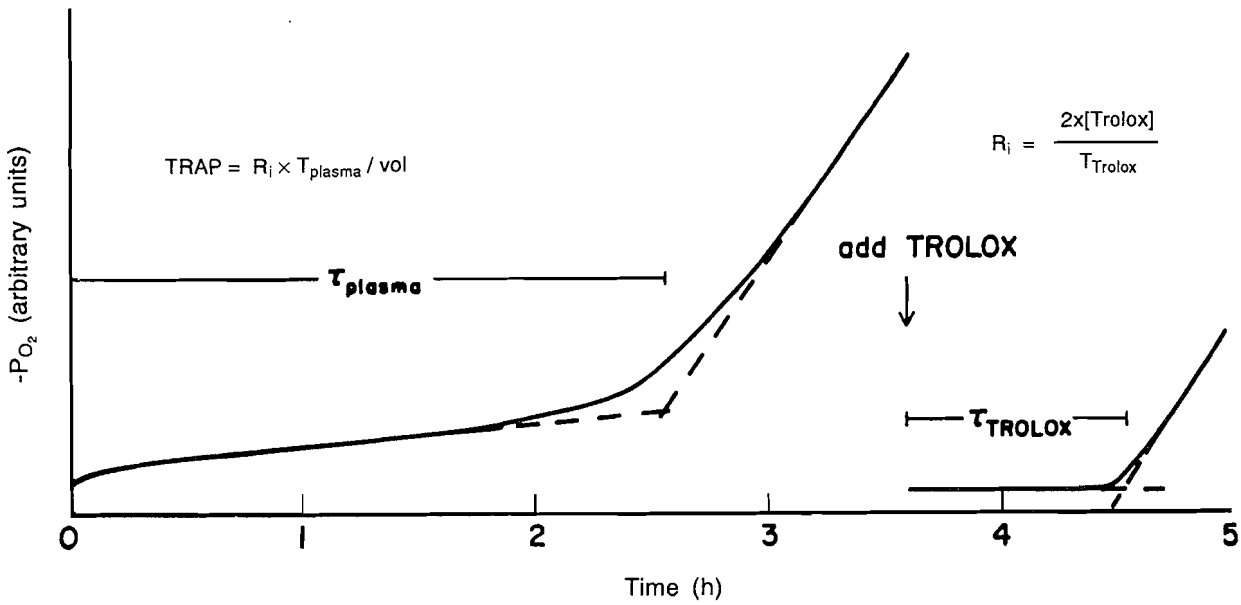

FIG. 10. Schematic for determination of the Total Radical-Trapping Antioxidant Parameter (TRAP) of blood plasma.

TABLE 4. TRAP values of biological fluids

Plasma source	*n*	TRAP, μM	Comment
Students	6	775 ± 72	Control group urate 284 ± 54 μM
Random	10	570–896	
Athletes	5	1126 ± 87	*Before* practice
Cancer patients	6	1037 ± 210	Avg. age 60
Amniotic fluids	10	1176 ± 53	Late gestation urate 540 ± 94 μM
Rats	4	294 ± 88	Urate 28–102 μM

ical implications as a result of research of independent groups in Canada at the University of Manitoba (57) and in Russia (58). Both groups conclude that oxidation of cholesterol in LDL may play an important role in the development of atherosclerosis. Further research in this aspect of LDL will be of considerable interest.

3.2. α-Tocopherol (vitamin E)

The insolubility of α-tocopherol in water prevents its direct transport through an aqueous phase into preformed phospholipid bilayers. Therefore, it is introduced by co-evaporation with the phospholipid from an organic solvent. This limited the application of this otherwise excellent antioxidant to studies on reconstituted membranes. α-Tocopherol is transported in blood within plasma lipoproteins (e.g., LDL and HDL) (7). In experiments designed to mimic the natural transfer of α-tocopherol into membranes, we prepared a *water soluble* form of α-tocopherol (8×10^{-4} M) by complexing it with a readily available protein, bovine serum albumin (BSA). This α-T.BSA proved to be an excellent antioxidant for free radical autoxidations initiated *in SDS micelles* for reactions initiated by either a lipid-soluble initiator (DMVN) or a water-soluble one (ABAP). The α-T.BSA gave well-defined induction periods immediately upon injection into a reaction and the suppression of oxygen uptake was comparable to that provided by Trolox or α-T.SDS.

Remarkably different results were discovered when α-T.BSA was added to autoxidations initiated *in DLPC membranes*. Some typical oxygen uptake traces are shown in Fig. 8. In reactions initiated by di-*tert*-butylhyponitrite (DBHN) in the lipid phase, α-T.BSA did not give any definite induction period, but only a reduction of the rate (Fig. 8*a*, Nos. 1 and 2) whereas both Trolox and membrane-bound α-tocopherol were efficient inhibitors (Nos. 3 and 4). These results demonstrate again the different behaviour of micellar and bilayer systems.

When samples of α-T.BSA were equilibrated under nitrogen with DLPC bilayers for up to 12 h *before initiation* of autoxidation, effective inhibition was observed as shown in Fig. 8*c*, No. 4. Such results indicate rather slow transfer of α-tocopherol from the protein to the bilayer, and only when it is released from the protein does it act as an effective antioxidant.

3.3. Diffusion and spin-trapping of radicals

Spin trapping of carbon- and oxygen-centred radicals in biomembranes and model systems is expected to provide important information on the dynamics of radicals in membranes. Radicals trapped in the lipid phase of micelles (59) or membranes (60) show anisotropic line shapes due to restriction of motion whereas those located in the bulk phase should exhibit isotropic or near-isotropic behaviour. Such behaviour should allow for determination of the position and possibly the site of action of radicals in membranes.

In a test of this idea, Steven Locke from our group and Peter Krygsman in Ed Janzen's laboratory carried out spin-trapping experiments using the water-soluble initiation, ABAP, in membranes. In this study, ABAP was encapsulated in the *inner aqueous core* of unilamellar, saturated PC membranes (DMPC) and a water-soluble spin trap, 4-carboxyphenyl-*tert*-butylnitrone (PBN), was added to the outer bulk phase. After irradiation (1 min, 75 W), isotropic radical signals, assigned to carbon radicals derived from ABAP, appeared; a_N = 15.4 G, a_H^β = 3.84 G. We conclude that charged ABAP or derived radical is able to penetrate the bilayer structure of membranes. This accounts at least in part for the useful properties of this azo initiator in quantitative kinetic and product studies from membrane peroxidation.

Spin-trapping results provide some support for the hypothesis that polar lipid peroxyl radicals diffuse to the aqueous phase. For this research we were able to employ the interesting lipidic azo initiator (6,6′) provided by Ned Porter

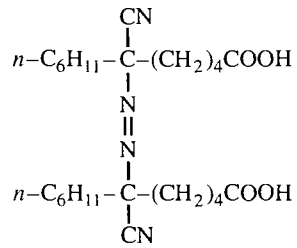

(61). Thermolysis under nitrogen of this 6,6′ diazene in unilamellar vesicles of DMPC containing the spin trap, PBN, gave an ESR spectrum, Fig. 9*a*, with a broadened high absorption typical of radicals with restricted motion in bilayers and to which we assign the structure 6-cyanododecanoic acid (CDDA) spin adduct; a_N = 15.8 G, a_H^β = 3.55 G, τ_c = 1.2 x 10^{-10} s. When this experiment was carried out using multilamellar vesicles (MLV) of DMPC, 6,6′, and PBN the ESR spectrum was completely anisotropic (Fig. 9*b*), an indication of an immobilized spin adduct in the larger, more complex bilayer system. Figure 9*c* shows the effect of oxygenation of the MLV system on the site of spin trapping of radicals derived from the 6,6′ diazene. In this experiment, a water-soluble spin trap 4-trimethylammonium-PBN was used. The isotropic spectrum now observed indicates that radicals are trapped in the bulk, aqueous phase. The structure assigned in this case is a trapped oxygen-centred radical, the CDDA-O-O· peroxyl, a_N = 15.8 G, a_H^β = 3.05 G, g = 2.0056. This kind of experiment supports the hypothesis that polar lipid peroxyl radicals will diffuse out of a bilayer towards the aqueous phase.

4. Exercise and "oxidative stress"

4.1. What is meant by "oxidative stress"?

Oxidative stress has been defined in the biological–biomedical field as "a disturbance in the prooxidant-antioxidant balance in favour of the former" (3). Recent workshops on oxidative stress held in Canada (62) and the United States (63) indicate the increased attention given to this

Can. J. Chem. Downloaded from www.nrcresearchpress.com by 88.255.202.194 on 09/08/12
For personal use only.

TABLE 5. Effect of physical stress on plasma antioxidant capacity TRAP and urate

Source	n	TRAP, μm		Urate, μM	
		Before	After (1.5 h)	Before	After
Athletes	5	1126 ± 87	985 ± 125	316 ± 61	365 ± 54
% Urate share of TRAP[a]		24.6 ± 4.4	35.7 ± 7.7		
Students	6	775 ± 52		284 ± 54	
% Urate share[a]		25.2 ± 6.1			

[a]Urate destroyed and TRAP re-run:

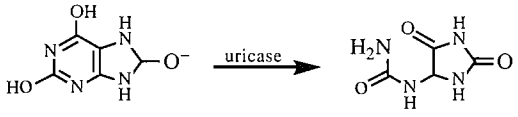

TABLE 6. Effect of physical stress on plasma antioxidant capacity TRAP of an individual

Source	TRAP, μM		Urate, μM	
	Before aerobics	After	Before	After
Researcher	470	589	229	450
Instructor	696	717	459	623

concept as applied to human biological systems. A review (64) in the latter (63) indicates the wide variety of analytical and spectroscopic methods used to measure "Oxidative Stress Status" (OSS) in humans. Oxidative stress in a biological system implies that some oxygen-related damage by reactive oxygen species, such as free radicals, and its effects are implicated in the pathology of several diseases and aging (1–9). As emphasized before (64), it is desirable to establish a routine and reliable method to determine the OSS in humans. As outlined below, we have used a general *kinetic approach* to measure the antioxidant capacity of human blood plasma and now report on a pilot study to determine the effect of physical exercise on OSS.

4.2. The protective antioxidant capacity of human blood plasma (TRAP)

Human blood plasma is a readily available biological fluid that has been used recently as a model for determination of protective antioxidant capacity in humans (52, 53). The principles involved in the kinetics of autoxidation and the antioxidant action of efficient phenolic antioxidants are used to measure the antioxidant capacity of blood plasma and other fluids. For this measurement, we generate peroxyl radicals in the fluid at a constant (and measured) rate and measure the time (τ) during which natural antioxidants in the fluid "trap" peroxyl radicals and thereby suppress oxygen uptake by oxygen-sensitive compounds in plasma, such as lipids and proteins. The rate at which peroxyls are generated is then measured by adding the water-soluble antioxidant, Trolox, known to trap two peroxyl radicals for each molecule of Trolox. The "Total Radical-trapping Antioxidant Parameter" (TRAP), the number of peroxyl radicals trapped per volume of plasma, is defined by eq. [17] (52)

$$[17] \quad \text{TRAP} = R_i \text{ (rate of ROO}\cdot \text{ formation)} \times \tau$$

$$[18] \quad R_i \text{ (measured)} = 2 \times [\text{Trolox}]/\tau_{\text{Trolox}}$$

This method to measure TRAP, developed with Ingold's group (52), involves only two relatively simple measurements: the time a known volume of plasma inhibits peroxidation, and then a measurement of the rate, R_i, at which peroxyls are generated. The procedure is illustrated schematically in Fig. 10.

4.3. "Trap" of bio-fluids and effect of exercise

Lipid peroxidation in humans is enhanced during intense physical exercise (65). Methods used to determine the possible effect of exercise on OSS in humans include the measurement of vitamin E levels (66–68), plasma levels of malondialdehyde (69), and effects on enzyme levels (68, 70–72).

It was anticipated that the kinetic TRAP procedure would be a sensitive and reliable method to determine the OSS in humans and could also be used to determine the effect of exercise on OSS.

Some TRAP values of blood plasma from various sources and of amniotic fluids are given in Table 4. A group of six students, non-smokers and non-drinkers, on a known diet were studied as a "control" group. Their average TRAP values, 775 μM peroxyls trapped, varied only 10–15% over a 4 month period. The higher TRAP values of athletes, and of amniotic fluids, are related to increased levels of uric acid, a known antioxidant. Lower levels of urate in animals, such as rats, and consequently lower TRAP, may be related to evolutionary trends and life span (73).

We carried out a pilot study of the effect of strenuous exercise on athletes with interesting results as shown in Table 5. Before a 1.5 h varsity soccer practice, the athletes had a high TRAP, 1126 μM, or 45% higher than a selected student sample of non-athletes. Immediately after their 1.5 h practice, the athletes experienced a slight decrease of 13% in their TRAP values, but the average TRAP remained high. The urate contribution to their TRAP actually increased by 11%. Thus the urate's share of TRAP actually increased as a result of exercise. This is probably at the expense of vitamin C (which was not monitored), since the amounts of other natural antioxidants did not change significantly: vitamin E from 12.5 to 12.5 μM and thiols from 460 to 464 μM.

These studies used rather selected groups and the conclusions may not apply to any individual. For example, one of our co-workers performed aerobics "to exhaustion" as compared to her instructor with the results shown in Table 6. In

Can. J. Chem. Downloaded from www.nrcresearchpress.com by 88.255.202.194 on 09/08/12
For personal use only.

this case the individual ("researcher") experienced a 25% increase in TRAP during aerobics and her urate increased an amazing 100%! The instructor with already a typical average TRAP experienced very little increase although the urate increased by 35%.

These TRAP measurements on human plasma, although only exploratory in nature, do indicate that they are indicative of physical conditioning and exercise. Blood is *the* common fluid taken for various types of clinical testing. It is postulated that clinical testing for antioxidant capacity of the plasma would be useful, especially for humans exposed chronically to toxic substances such as cigarette smoke.

5. Future directions

1. The mechanisms of action and activity of antioxidants are now well established in homogeneous solution; however, our studies indicate that very significant differences occur in model membranes where future testing should be done. In addition, the interaction between antioxidants in vivo needs to be better understood because important differences may emerge when compared to model systems (74).

2. The biomedical aspects of oxygen-centred radicals continue to be of intense interest and lipid peroxidation is implicated in various degenerative diseases. Nevertheless, direct evidence of the role of peroxidation in real biomembranes (e.g., intact cells) is not yet extensive. NMR imaging of tissue slices or whole vital organs subjected to oxidative stress is expected to provide such evidence.

3. A variety of drugs are "traditionally" prescribed to treat inflammatory diseases such as arthritis and neuronal damage. Drugs with antioxidant properties are potentially useful as anti-inflammatory agents. It is desirable to direct efforts towards scientific drug design in this field and antioxidants should play a role in this research.

Can. J. Chem. Downloaded from www.nrcresearchpress.com by 88.255.202.194 on 09/08/12
For personal use only.

Acknowledgements

I am grateful to Keith Ingold of the National Research Council (NRC) for his scientific leadership and enthusiasm which initiated this research. Graham Burton of the NRC provided practical help especially during the early phases. Professor Ned Porter of Duke University provided the technology for product studies, and Bruce Forrest assisted with NMR studies at the Atlantic Regional Magnetic Resonance Centre. Interest in peroxyl radicals is continuing through collaborative theoretical studies by Russell Boyd and Susan Boyd at Dalhousie University.

This research would not have been completed without the enthusiastic participation of students and other co-workers at Mount Allison University. In addition, Roger Smith and Allister MacDonald provided valuable technical help. Financial support provided by the Natural Sciences and Engineering Research Council of Canada, the Terry Fox Fund for Cancer Research (New Brunswick), and a NATO Grant for International Collaborative Research is gratefully acknowledged.

1. W.A. Pryor (*Editor*). Free radicals in biology. Vols. I–VII, Academic Press, New York. 1976–1980.
2. B. Halliwell and J.M.C. Gutteridge. Free radicals in biology and medicine. Clarendon Press, Oxford. 1985.
3. H. Sies (*Editor*). Oxidative stress. Academic Press, London. 1985.
4. D.C.H. McBrien and T.F. Slater (*Editors*). Protective agents in cancer. Academic Press, London. 1983.
5. W. Bors, M. Saran, and D. Tait (*Editors*). Oxygen radicals in chemistry and biology. Proc. 3rd Int. Conf. Neuherberg, Germany. W. de Gruyter, New York. 1983.
6. Proc. Symp. Biol. Oxid. Syst. San Diego, Calif. Academic Press, New York. 1990.
7. A.T. Diplock, L.J. Machlin, L. Packer, and W.A. Pryor. Ann. N. Y. Acad. Sci. **570**, (1989).
8. F. Minisci. NATO ASI Ser. Ser. C: **260** (1988).
9. M.A.J. Rodgers and E.L. Powers (*Editors*). Oxygen and oxyradicals in chemistry and biology. Academic Press, New York. 1981.
10. J.H. Fendler. Membrane mimetic chemistry. Wiley, New York. 1982.
11. G. Gregoriadis (*Editor*). Liposome technology. CRC Press, Inc., Boca Raton, Fla. 1986; Ann. N. Y. Acad. Sci. **308**, (1978).
12. R.L. Hamilton, J. Goerke, L.S.S. Guo, M.C. Williams, and R.J. Havel. J. Lipid Res. **21**, 981 (1980).
13. C.V. Smith and R. E. Anderson. Free Radical Biol. Med. **3**, 341 (1987).
14. J.M.C. Gutteridge and B. Halliwell. Trends Biochem. Sci. **15**, 129 (1990).
15. J.I. Gray. J. Am. Oil. Chem. Soc. **55**, 539 (1978).
16. D.W. Thomas, F.J.G.M. van Kuijk, E.A. Dratz, and R.J. Stephens. Anal. Biochem. **198**, 104 (1991).
17. O. Hayaishi and T. Shimizu. *In* Lipid peroxides in biology and medicine. Academic Press, New York. 1982. pp. 41–53.
18. K.U. Ingold. Acc. Chem. Res. **2**, 1 (1969).
19. F.R. Mayo. Acc. Chem. Res. **1**, 193 (1968).
20. J.A. Howard. Adv. Free Radical Chem. **4**, 49 (1972).
21. L.R.C. Barclay and K.U. Ingold. J. Am. Chem. Soc. **103**, 6478 (1981).
22. G.W. Burton and D.D.M. Wayner. *In* Handbook of free radicals and antioxidants in biomedicine. Vol. 3. *Edited by* J. Miguel. CRC Press, Boca Raton, Fla. 1988.
23. N.A. Porter. Acc. Chem. Res. **19**, 262 (1986).
24. L.R.C. Barclay, K.A. Baskin, D. Kong, and S.J. Locke. Can. J. Chem. **65**, 2541 (1987).
25. J.A. Howard and K.U. Ingold. Can. J. Chem. **43**, 2729 (1965); **43**, 2737 (1965).
26. L.R.C. Barclay, K.A. Baskin, S.J. Locke, and T.D. Schaefer. Can. J. Chem. **65**, 2529 (1987).
27. W.A. Pryor, M.J. Kaufman, and D.F. Church. J. Org. Chem. **50**, 281 (1985).
28. L.R.C. Barclay, S.J. Locke, J.M. MacNeil, J.S. VanKessel, G.W. Burton, and K.U. Ingold. J. Am. Chem. Soc. **106**, 2479 (1984).
29. L.R.C. Barclay, K.A. Baskin, D. Kong, and S.J. Locke. Can. J. Chem. **65**, 2541 (1987).
30. L.R.C. Barclay, D. Kong, and J.S. VanKessel. Can. J. Chem. **64**, 2103 (1986).
31. R.W. Fessenden, A. Hitachi, and V. Nagarajan. J. Phys. Chem. **88**, 107 (1984).
32. S.L. Boyd, R.J. Boyd, and L.R.C. Barclay. J. Am. Chem. Soc. **112**, 5724 (1990).
33. E.E. Burnell, P.R. Cullis, and B. DeKruijff. Biochim. Biophys. Acta, **603**, 63 (1980).
34. N.I. Krinsky. Ann. N. Y. Acad. Sci. **551**, 17 (1988).
35. G.W. Burton and K.U. Ingold. Acc. Chem. Res. **9**, 194 (1986).
36. E. Niki. Chem. Phys. Lipids, **44**, 227 (1987).
37. A. Bendich, L.J. Machlin, O. Scandurra, G.W. Burton, and D.D.M. Wayner. Adv. Free Radical Biol. Med. **2**, 419 (1986).
38. G.W. Burton, A. Joyce, and K.U. Ingold. Arch. Biochem. Biophys. **221**, 281 (1983).
39. G.W. Burton, T. Doba, E.J. Gabe, L. Hughes, F.L. Lee, L. Prasad, and K.U. Ingold. J. Am. Chem. Soc. **107**, 7053 (1985).
40. (*a*) K. Mukai, Y. Kageyama, T. Ishida, and K. Fukuda. J. Org.

Chem. **54**, 552 (1989); (*b*) K. Mukai, K. Okabe, and H. Hosose. J. Org. Chem. **54**, 557 (1989).
41. L. Castle and M.J. Perkins. J. Am. Chem. Soc. **108**, 6381 (1986).
42. W.A. Pryor, T. Strickland, and D.F. Church. J. Am. Chem. Soc. **110**, 2224 (1988).
43. L.R.C. Barclay, K.A. Baskin, K.A. Dakin, S.J. Locke, and M.R. Vinqvist. Can. J. Chem. **68**, 2258 (1990).
44. I.H. Ekiel, L. Hughes, G.W. Burton, P.A. Jovall, K.U. Ingold, and I.C.P. Smith. Biochemistry, **27**, 1432 (1988).
45. E. Niki, A. Kawakami, M. Saito, Y. Yamamoto, J. Tsuchiya, and Y. Kamiya. J. Biol. Chem. **260**, 2191 (1985).
46. S. Nagaoka, A. Kuranaka, H. Tsuboi, U. Nagashima, and K. Mukai. J. Phys. Chem. **96**, 2754 (1992).
47. C. Golumbic. *In* Biological antioxidants. *Edited by* C.G. MacKenzie. Tosioh Macy, Jr. Foundation, New York. pp. 42–48.
48. L.R.C. Barclay, S.J. Locke, and J.M. MacNeil. Can. J. Chem. **61**, 1288 (1983); **63**, 366 (1985).
49. T. Doba, G.W. Burton, and K.U. Ingold. Biochim. Biophys. Acta, **835**, 298 (1985).
50. E. Niki, A. Kawakami, Y. Yamamoto, and Y. Kamiya. Bull. Chem. Soc. **58**, 1971 (1985).
51. L.R.C. Barclay. J. Biol. Chem. **263**, 16138 (1988).
52. D.D.M. Wayner, G.W. Burton, K.U. Ingold, L.R.C. Barclay, and S.J. Locke. Biochim. Biophys. Acta, **924**, 408 (1987).
53. B. Frei, L. England, and B.N. Ames. Proc. Natl. Acad. Sci. U.S.A. **86**, 6377 (1989).
54. E.J. Jacobsen, J.M. McCall, D.E. Ayer, F.J. VanDoornik, J.R. Palmer, K.L. Belonga, J.M. Braughler, E.D. Hall, D.J. Houser, M.A. Krook, and T.A. Runge. J. Med. Chem. **33**, 1145 (1990).
55. M.S. Brown and J.L. Goldstein. Sci. Am. **251**, 58 (1984).
56. L.R.C. Barclay, R.C. Cameron, B.J. Forrest, S.J. Locke, R. Nigam, and M.R. Vinqvist. Biochim. Biophys. Acta, **1047**, 255 (1990).
57. K. Liu, T.G. Maddaford, B. Ramjiauan, M.J.B. Kutryk, and G.N. Pierce. Mol. Cell. Biochem. **108**, 39 (1991); **108**, 49 (1991).
58. O.M. Panasenko, T.V. Vol'nova, O.A. Azizova, and Y.A. Vladimirov. Free Radical Biol. Med. **10**, 137 (1991).
59. E.G. Janzen and G.A. Coulter. J. Am. Chem. Soc. **106**, 1962 (1984).
60. J.B. Feix and B. Kalyanaraman. Biochim. Biophys. Acta, **992**, 230 (1989).
61. N.A. Porter, R.C. Petter, and W.J. Brittain. J. Am. Chem. Soc. **106**, 813 (1984).
62. E.G. Janzen. Oxidative stress workshop. University of Guelph, Guelph, Ont. Feb. 1991.
63. Free Radical Biol. Med. **10**, 173 ff (1991).
64. W.A. Pryor and S.S. Godber. Free Radical Biol. Med. **10**, 173 (1991).
65. R. Bielinski, Y. Schutz, and E. Jéquier. Am. J. Clin. Nutr. **42**, 69 (1985).
66. L. Packer, A.L. Almada, L.M. Rothfuss, and D.S. Wilson. Ann. N.Y. Acad. Sci. **570**, 311 (1989).
67. K.V. Reddy, T.C. Kumar, M. Prasad, and P. Peddanna. Biochem. Int. **26**, 863 (1992).
68. J.G. Cannon, S.F. Orencole, R-A. Fielding, M. Meydani, S.N. Meydani, M.A. Fiatarone, J.B. Blumberg, and W.J. Evans. Am. J. Physiol. **259**, R1214 (1990).
69. R. Loulin, W. Cottle, I. Pyke, M. Kavanagh, and A.N. Belcastro. Eur. J. Appl. Physiol. **56**, 313 (1987).
70. M.M. Kanter, L.A. Kaminsky, J. Laham-Saeger, G.R. Lesmes, and N.D. Nequin. Ann. Sports Med. **3**, 39 (1986).
71. M.M. Kanter, G.R. Lesmes, L.A. Kaminsky, J. Laham-Saeger, and N.D. Nequin. Eur. J. Appl. Physiol. **57**, 60 (1988).
72. L.L. Ji and R. Fu. J. App. Physiol. **72**, 549 (1992).
73. B.N. Ames, R. Cathcart, E. Schwiers, and P. Hochstein. Proc. Natl. Acad. Sci. U.S.A. **75**, 6858 (1981).
74. G.W. Burton, U. Wronska, L. Stone, D.O. Foster, and K.U. Ingold. Lipids, **25**, 199 (1990).
75. J. E. Bennett. J. Chem. Soc. Faraday Trans. **86**, 3247 (1990).

Can. J. Chem. Downloaded from www.nrcresearchpress.com by 88.255.202.194 on 09/08/12
For personal use only.

An ion-exchange/atomic absorption method for the measurement of ionized calcium and magnesium at micromolar concentrations

AMITHA K. HEWAVITHARANA AND BYRON KRATOCHVIL[1]

Department of Chemistry, University of Alberta, Edmonton, Alta., Canada T6G 2G2

Received January 28, 1992[2]

AMITHA K. HEWAVITHARANA and BYRON KRATOCHVIL. Can. J. Chem. **71**, 17 (1993).

A quantitative ion-exchange/atomic absorption method is described for measuring the concentration of free (hydrated) calcium and magnesium in solution at micromolar levels. Sample solutions are pumped through a micro-column of strong acid-type cation-exchange resin until equilibrium has been achieved between resin and solution. After removal of interstitial solution by first air, then water, the sorbed metal ion is eluted from the resin with nitric acid directly into an atomic absorption spectrophotometer. In a 0.1 M 1:1 electrolyte, here KNO_3, the amount of metal ion sorbed on the resin is directly proportional to the free metal ion concentration in solution over a concentration range of 1.25 to 5×10^{-5} mol/L (12–50 μmol/L). Selectivities for free calcium and magnesium in the presence of complexing ligands such as citrate and phosphate compare well with calculated values.

AMITHA K. HEWAVITHARANA et BYRON KRATOCHVIL. Can. J. Chem. **71**, 17 (1993).

On décrit une méthode quantitative d'échange d'ions/absorption atomique qui permet de mesurer la concentration du calcium et du magnésium libre (hydraté) en solution, à des niveaux micromoléculaires. On pompe des solutions d'échantillons dans une microcolonne d'une résine échangeuse de cations d'un type fortement acide jusqu 'à l'obtention d'un équilibre entre la résine et la solution. Après avoir enlevé la solution interstitielle à l'aide d'air, puis d'eau, on élue l'ion métallique de la résine à l'aide d'acide nitrique directement dans un spectrophotomètre d'absorption atomique. Dans un électrolyte 1 : 1 à 0, 1 M, dans ce cas du KNO_3, la quantité d'ion métallique adsorbée sur la résine est directement proportionnelle à la concentration d'ion métallique en solution, à des concentrations allant de 1,25 à 5×10^{-5} mol/L (12–50 μmol/L). On a comparé les sélectivités pour le calcium et le magnésium libre en présence de ligands complexants comme le citrate et le phosphate avec les valeurs calculées.

[Traduit par la rédaction]

Knowledge of the concentrations of ionic (free, hydrated) calcium and magnesium in the presence of complexed or bound metal ion in solution is frequently of interest because the free form is often the most biologically or environmentally active form. Several methods have been proposed for measuring pCa. These include ion selective electrode potentiometry and spectrophotometry using calcium indicators. Each method has significant drawbacks, however, such as interferences from other metals, pH sensitivity, and inconvenience. For magnesium the problem is even greater, for there are no satisfactory magnesium ion-selective electrodes or spectrophotometric reagents. Therefore a method for measuring pMg could be quite useful.

A recently developed approach to metal ion speciation involves pumping the sample solution through an ion-exchange column until the column has reached equilibration. The technique has been employed to determine free copper ion concentrations in natural waters (1), free nickel in sewage (2), and free calcium at millimolar levels in solutions containing a range of ligands (3). In this paper the technique is shown to give linear calibration curves for free magnesium and calcium ion concentrations at micromolar levels in solutions containing ligands such as citrate or phosphate. The theory behind the method has been outlined in previous studies of nickel (2) and copper (3) systems. The same principles described for these ions apply to both calcium and magnesium.

An ideal system for measuring pM, where M is any metal, introduces little or no perturbation of the system. The column equilibration technique meets this criterion by pumping fresh sample solution past the ion-exchange resin until the resin has come to equilibrium with the solution. In this way the uptake of ions by the resin has not changed the composition of the sample solution with which it is in equilibrium. A necessary requirement of the method is that the sample solution contain sufficient univalent electrolyte, usually a sodium or potassium salt, to allow no more than a percent or so of the total exchange capacity of the resin to be taken up by the metal ion being measured. This level must be matched in the calibration solutions. For some matrices, such as sea water, serum, or blood plasma, the concentration of sodium and potassium may already be at a level sufficient to provide the swamping conditions necessary for many divalent ions.

Experimental

Apparatus

The major components of the instrument consist of a Minipuls model 2 peristaltic multichannel pump and a Perkin Elmer model 4000 atomic absorption spectrophotometer. The flow system is shown in Fig. 1. Construction of the micro-column, which for this study contained about 0.7 mg of 100–200 mesh Dowex 50 strongly acidic cation-exchange resin, is described elsewhere (4). Depending on the position of the 6-port rotary valve (A in Fig. 1), solution, air, or water may be pumped through the column; valve C allows a choice of either water or eluent. By means of valve B the flow from either valve A or C can be directed through the column while the other is diverted to waste.

The calcium ion selective electrode used in this study was based on the neutral carrier ETH 1001 designed by the research group of W. Simon (ETH, Zurich), and was provided by the research group of Dr. D. J. Harrison of this department; it was used with a standard calomel electrode as reference. pH measurements were made with a Fisher glass–calomel electrode pair calibrated with Fisher standard buffers at pH 4 and 7. All pH and voltage readings were made with a Fisher model 520 digital pH/ion meter.

[1]Author to whom correspondence may be addressed.

[2]Revision received September 10, 1992.

Can. J. Chem. Downloaded from www.nrcresearchpress.com by 88.255.202.194 on 09/08/12
For personal use only.

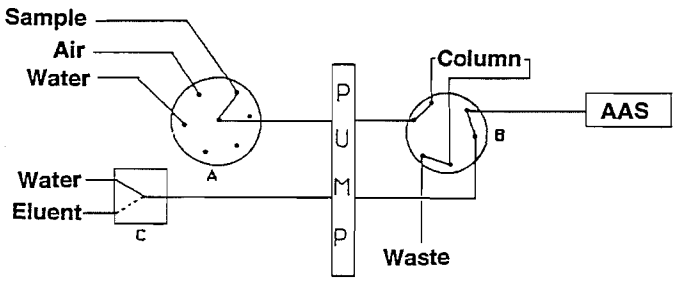

Valve positions when equilibrating column with sample

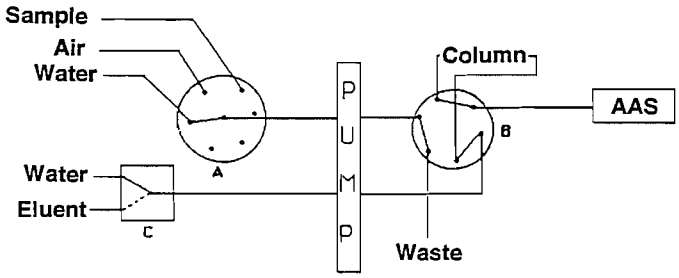

Valve positions when eluting from column into AAS

FIG. 1. Flow system for ion-exchange column equilibration, washing, and elution into atomic absorption spectrophotometer. A, Six-port rotary valve; B, rotary sample injection valve; C, three-way slider valve. Upper diagram: valve positions during column load cycle; lower diagram: valve positions during column wash cycle.

Can. J. Chem. Downloaded from www.nrcresearchpress.com by 88.255.202.194 on 09/08/12
For personal use only.

Reagents

All chemicals used were reagent grade or better. Stock solutions of $Ca(NO_3)_2$ and $Mg(NO_3)_2$ were prepared by dissolving $CaCO_3$ and metallic Mg in HNO_3. Potassium nitrate was used to maintain the desired ionic strength, with the potassium ion concentration held at a level sufficient to ensure the resin exchange sites were primarily in the K^+ form. Analytical grade 100–200 mesh Dowex 50W X8 strong acid-type cation exchanger (J. T. Baker Chemical Co.) was pretreated as described in the literature (5). The ion-exchange capacity of this resin is reported as 5.1 mequiv./g on a dry basis.

Procedure

The flow rate through the column was maintained at 5 mL/min with the peristaltic pump. The flow system and procedure were based on that described in previous work (1–3), with one modification. In the previous system the ion-exchange equilibrium established during the load cycle was found to be perturbed by the wash cycle that immediately followed. Dilution of the sample solution by the initial front of the wash water lowered the swamping electrolyte concentration, resulting in an increase in uptake by the resin of the divalent ion under study. Therefore in this work an air-purge cycle was introduced between the loading and wash cycles to reduce this perturbation. The valve system shown in Fig. 1 was used to perform the following sequence of operations.

The column was first washed by pumping water through it for 1 min. Next the solution of interest was loaded by passing it through the column to waste until complete breakthrough was achieved (upper diagram in Fig. 1). At this stage the composition of the column influent and effluent are the same and the resin is in equilibrium with the test solution. After the loading cycle, air was passed through the column for 1 min to remove interstitial sample, followed by backwash water through valves C and B for 1 min (lower diagram in Fig. 1). This wash cycle was followed by a 30-s elution of the sorbed ions with 2 mol/L HNO_3 directly into the atomic absorption spectrophotometer (AAS). During elution the AAS was set to integrate the peak area. After elution the column was washed with water before introduction of the next test solution.

Results and discussion

Time of equilibration and calibration curves

The time required to achieve complete equilibration of the resin with a sample solution was examined using 2.5×10^{-5} mol/L Ca^{2+} or Mg^{2+} in 0.1 mol/L KNO_3. The column was equilibrated for varying lengths of time, the sorbed calcium or magnesium eluted, and the peak area measured as described earlier. The results show that the time required to achieve complete equilibration was less than 3 min for both metals at this concentration. Therefore, equilibration times of 3 min were used for all Ca^{2+} and Mg^{2+} standards prepared with the same electrolyte concentration.

Calibration plots were linear for concentrations of Ca^{2+} or Mg^{2+} over the range of 1.25 to 5×10^{-5} mol/L, in 0.1 mol/L KNO_3. All solutions were adjusted to pH 5.2 ± 1 using small amounts of KOH or HNO_3 as needed. Calibration plots were linear over this range for both elements.

Selectivity of the method for free over bound calcium and magnesium

The presence of complexing ligands results in the binding of metal ions and thereby lowers free metal ion concentrations in solution. Depending on ligand charge, the metal ligand complexes may be cationic, anionic, or neutral. In the ion-exchange column-equilibration method employed here, it is assumed that only free, hydrated metal ions are sorbed onto the resin. However, sorption of cationic or neutral

Can. J. Chem. Downloaded from www.nrcresearchpress.com by 88.255.202.194 on 09/08/12
For personal use only.

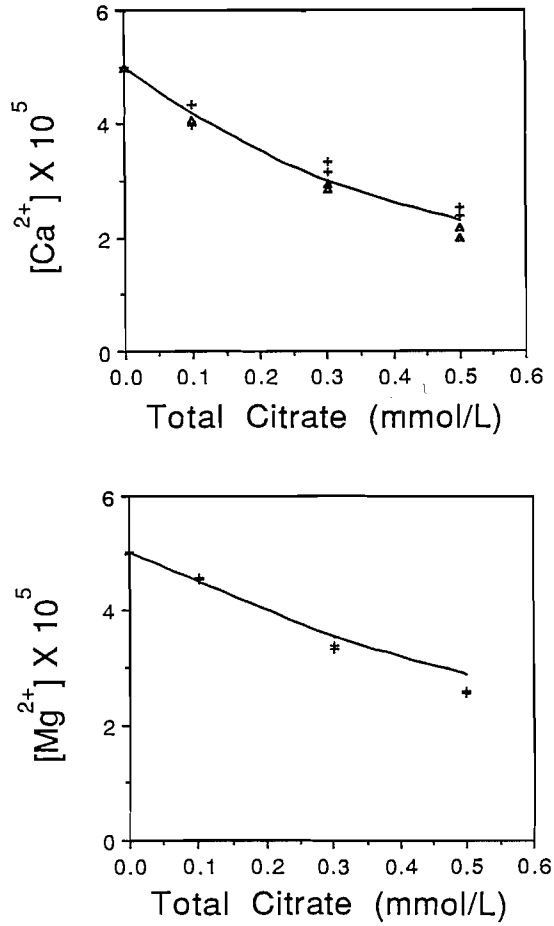

FIG. 2. Variation of free Ca^{2+} (top) and free Mg^{2+} (bottom) concentrations with total citrate, at pH range 6–7, as measured by: +, ion exchange and Δ, ISE potentiometry. Solid lines show the calculated values. Total Ca^{2+} and Mg^{2+} is 5×10^{-5} mol/L throughout.

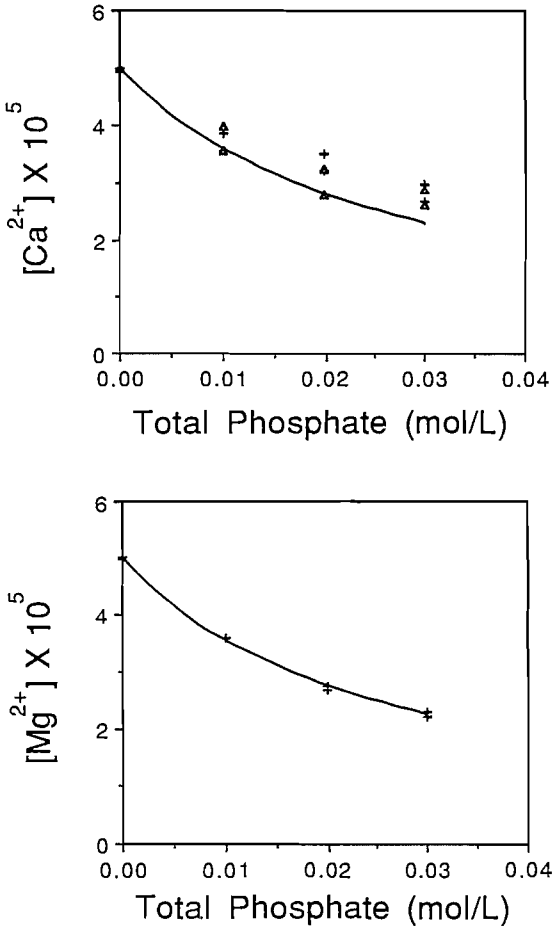

FIG. 3. Variation of free Ca^{2+} (top) and free Mg^{2+} (bottom) concentrations with total phosphate, at pH 7, as measured by: +, ion exchange and Δ, ISE potentiometry. Solid lines show the calculated values. Total Ca^{2+} and Mg^{2+} is 5×10^{-5} mol/L throughout.

complexes would give rise to falsely high free metal values (1). To assess the extent to which this process might occur, the free metal in solutions containing 5×10^{-5} mol/L total calcium or total magnesium and variable concentrations of citrate and phosphate was measured by the ion-exchange method as described above and, for calcium, also by potentionmetry using a calcium ion selective electrode. The pH values of the solutions were adjusted to fall in the range of 6–6.9. The fraction of free metal ion in each solution was also calculated from equilibrium-constant data by computer using the program COMICS (6).

Results obtained for the fraction of free calcium and free magnesium in the presence of varying amounts of total citrate are shown in Fig. 2. Calculated values, shown as solid lines in the figures, are based on complexes of the type $MCit^-$, MHCit, MH_2Cit^+, $KCit^{2-}$ (7), and $KHCit^-$ (8). Here M denotes either Ca^{2+} or Mg^{2+} and Cit denotes the triply charged citrate anion Cit^{3-}. Where values were not available for 0.1 ionic strength (7), they were recalculated from other ionic strengths using the Davies equation. The agreement among calculated and free calcium concentrations measured by ion exchange and potentiometry can be considered satisfactory, especially in light of the low levels and the uncertainities in reported equilibrium constant values. The results indicate that the column selectively sorbs free calcium in the presence of calcium–citrate species. Similar agreement is obtained for magnesium, indicating high selectivity by the method for free magnesium in the presence of citrate.

The variation of free metal fractions in the presence of varying amounts of total phosphate at pH 7 was studied in a similar manner; results are shown in Fig. 3. Calculated values are based on formation of the complexes MPO_4^-, $MHPO_4$, $MH_2PO_4^+$ (9), KPO_4^{2-}, $KHPO_4^-$, and KH_2PO_4 (10). Ionic strength corrections were carried out as for the citrate system. Here, too, agreement between the calculated and measured values was satisfactory for both metal ions. The differences in agreement between calculated and measured values are likely due to a combination of factors, including uncertainties in measured pH and metal ion concentrations, uncertainties in reported stability constants, and ionic strength corrections using the Davies equation. The agreement between calculated and measured values for free magnesium with both citrate and phosphate is especially good. Thus, even though the resin might be expected to sorb cationic or neutral calcium or magnesium–ligand complexes, under the conditions used such sorption processes appear to be negligible. Since there is no reliable ion selective electrode

available for magnesium, a comparison with other than calculated values was not possible.

The advantages of this ion-exchange method over ion selective potentiometry are twofold. One is that the resin is not affected by the presence of small amounts of nonionic solutes in the sample solution except insofar as they alter ionic activities through bulk solvent effects. Another is that use of atomic absorption spectroscopy provides both high sensitivity and selectivity. The major disadvantage is that sample solutions must contain sufficient swamping electrolyte possessing a univalent cation so that at equilibrium the column has fewer than 1% of its exchange sites occupied by calcium or magnesium ions. A concentration of about 0.1 mol/L is ample for this purpose when the concentrations of ions under study are of the order of 10^{-5} mol/L or less.

In summary, this work describes a procedure for the estimation of free calcium and free magnesium at micromolar levels in the presence of ligands such as citrate and phosphate. The method should be applicable over a wide pH range and can be made even more sensitive by increasing the amount of resin in the column. Small resin quantities have the advantage of more rapid equilibration and smaller sample volume requirements, but since preparation of the column is relatively simple, a variety of columns containing differing resin quantities can be prepared beforehand, and interchanged as required to match sample solution properties or available volumes.

Acknowledgments

Financial support by the Natural Sciences and Engineering Research Council of Canada and by the University of Alberta is gratefully acknowledged. The authors appreciate the loan of a calcium ion-selective electrode by Dr. D. J. Harrison and A. Chan of the Department of Chemistry, University of Alberta.

1. J. A. Sweileh, D. Lucyk, B. Kratochvil, and F. F. Cantwell. Anal. Chem. **59**, 586 (1987).
2. F. F. Cantwell, J. S. Nielson, and S. E. Hrudey. Anal. Chem. **54**, 1498 (1982).
3. A. K. Hewavitharana, V. Mutucumarana, and B. Kratochvil. Can. J. Chem. **69**, 1976 (1991).
4. J. Treit, J. S. Nielson, B. Kratochvil, and F. F. Cantwell. Anal. Chem. **55**, 1650 (1983).
5. F. Helfferich. Ion exchange. McGraw–Hill, New York. 1962. p. 230.
6. D. D. Perrin and I. G. Sayce. Talanta, **14**, 833 (1967).
7. A. E. Martell and R. M. Smith. Critical stability constants. Vol. 3. Other organic ligands. Plenum Press, New York. 1977.
8. V. Cucinotta, P. G. Daniele, C. Rigano, and S. Sammartano. Inorg. Chim. Acta, **56**, L45 (1981).
9. A. E. Martell and R. M. Smith. Critical stability constants. Vol. 4. Inorganic complexes. Plenum Press, New York. 1976.
10. P. G. Daniele, M. Grasso, C. Rigano, and S. Sammartano. Ann. Chim. (Rome), **73**, 495 (1983).

Can. J. Chem. Downloaded from www.nrcresearchpress.com by 88.255.202.194 on 09/08/12
For personal use only.

Mechanism of atomization in a Massmann-type graphite furnace using the basic principles of thermodynamics

S. J. CATHUM[1]

Centre for Analytical and Environmental Chemistry, Department of Chemistry, Carleton University, Ottawa, Ont., Canada K1S 5B6

Received January 15, 1992

S. J. CATHUM. Can. J. Chem. **71**, 21 (1993).

A method has been developed to determine the enthalpy of atom formation in a graphite furnace without invoking the order of reaction. The method is based on the equation $\ln (AT) = -\Delta H^0/RT + C$, where A is the peak-height absorbance, T is the absolute temperature, ΔH^0 is the enthalpy of atom formation which, for highly endothermic reactions, is considered to be equal to the activation energy, R and C are the universal gas constant and the constant of integration, respectively. The plot of $\ln (AT)$ vs. $1/T$ is similar to an Arrhenius-type plot and should yield the activation energy. Atomization mechanisms for eight elements, Cu, Co, Ga, Au, Ni, Fe, Ag, and Al, are proposed by correlating the experimental enthalpy with a very limited set of possible primary reactions. One significant result of this work is that the experimentally observed enthalpy of reaction correlates well with the activation energy, this means no excess energy other than the enthalpy of atomization is involved in the reaction.

S. J. CATHUM. Can. J. Chem. **71**, 21 (1993).

On a développé une méthode permettant de déterminer l'enthalpie de formation atomique dans un four graphite, sans impliquer l'ordre de la réaction. La méthode repose sur l'équation $\ln (AT) = -\Delta^0/RT + C$, dans laquelle A est l'absorbance à la hauteur maximale du pic, T est la température absolue et ΔH^0 est l'enthalpie de formation atomique que l'on considère, pour des réactions fortement endothermiques, comme étant égale à l'énergie d'activation alors que R et C sont respectivement la constante universelle des gaz et la constante d'intégration. La courbe de $\ln (AT)$ vs. $1/T$ est semblable à une courbe de type Arrhenius et elle devrait fournir l'énergie d'activation. Utilisant une corrélation de l'enthalpie expérimentale avec un ensemble limité de réactions primaires possibles, on propose des mécanismes d'atomisation pour huit éléments, Cu, Co, Ga, Au, Ni, Fe, Ag et Al. Un résultat important de ce travail établit qu'il existe une bonne corrélation entre l'enthalpie de réaction observée expérimentalement et l'énergie d'activation; ce résultat signifie qu'il n'y a pas d'énergie en excès, à l'exception de l'enthalpie d'atomisation, d'impliquer dans la réaction.

[Traduit par la rédaction]

Introduction

In graphite furnace atomic absorption spectrometry, GF-AAS, researchers are concerned with the laws of analyte reactions during atomization. These laws are mainly divided into two types: thermodynamic and kinetic. In thermodynamics, conclusions are reached on the basis of changes in the Gibb's free energy of the system. From the value of Gibb's free energy it is possible to predict the direction in which a chemical reaction will take place. Thermodynamics cannot, however, give information on the rate of atom formation by which the analyte is converted into atoms. In many situations studied so far, much information can be obtained from both thermodynamic and kinetic measurements. A complete picture of atom formation and loss is incomplete unless both two approaches are considered. Hence, to postulate a mechanism of atom formation it would be helpful to consider all thermodynamic and kinetic data that are available.

To illustrate the relationship between the above two approaches one can assume copper oxide (CuO) is the precursor for gaseous copper atoms. When atomization occurs two steps need to be considered, one step is the reduction of CuO by graphite,

$$CuO_{(s)} + C_{(s)} \rightarrow Cu_{(s)} + CO_{(g)} \quad \text{(reduction)}$$

and the other is the sublimation of the reduced metal,

$$Cu_{(s)} \rightarrow Cu_{(g)} \quad \text{(sublimation)}$$

For the reduction of $CuO_{(s)}$ by $C_{(s)}$ to take place, about 19.2 kJ mol^{-1} of energy must be acquired by collisions between copper oxide and carbon, whereas sublimation of copper requires 337.6 kJ mol^{-1} of energy. The latter is, therefore, likely to be slow compared to the former, and hence is the rate-determining step.

The thermodynamic approach (1–3) has been used in studying the mechanism of atomization in GF-AAS. Campbell and Ottaway (1) concluded from their study of 27 elements that the reduction of the metal oxide by carbon was thermodynamically feasible. Sturgeon *et al.* (4, 5) used a combined thermodynamic and kinetic approach to obtain the activation energy of atom release from the onset of a plot of natural logarithm of the absorbance vs. the reciprocal of the absolute temperature. Frech *et al.* (2) developed a thermodynamic model to study the distribution of solid, liquid, and gaseous analyte species in the graphite furnace as a function of temperature for 16 elements. Chakrabarti *et al.* (3) reported the importance of carbon in determining the partial pressure of CO as well as other gaseous species, such as O and O_2, in a graphite furnace. Fuller used a kinetic approach (6), developed under isothermal conditions, to study the mechanism of atom formation emphasizing the need for considering thermochemical properties of the element and its chemical compounds that may form during atomization.

By applying thermodynamics and assuming that the change in the analyte vapour pressure varies directly as the rate of atom release (7), one can formulate an Arrhenius-type plot to determine the heat of atomization. The necessary assumptions are the ideal gas behaviour of the analyte atomic vapour and equality of the activation energy with the en-

[1]Present address: Center for Land and Biological Resources Research, Central Experimental Farm, Agriculture Canada, Ottawa, Ont. K1A 0C6.

Can. J. Chem. Downloaded from www.nrcresearchpress.com by 88.255.202.194 on 09/08/12
For personal use only.

Can. J. Chem. Downloaded from www.nrcresearchpress.com by 88.255.202.194 on 09/08/12
For personal use only.

thalpy of the reaction. The latter seems to be not unreasonable and has sufficient support from various authors (4, 5, 8, 9). The experimental activation energy, or the enthalpy of atomization, is defined here as the energy required to produce gaseous atoms (4, 10). Several factors play an important role in determining the observed value of the enthalpy of atomization. Among these factors is the energy required, in the rate-determining step, to break existing bonds to release the free atoms. In the category of breaking bonds, one may include desorption and re-deposition of gaseous analyte atoms on the graphite surface.

This work is an attempt to determine the enthalpy of atomization by a method derived from basic principles of thermodynamics. A comparison between the method and those reported in the literature (4, 11) will be made. The mechanisms of atomization of Cu, Co, Ga, Au, Ni, Fe, Ag, and Al will be proposed.

Theory

This method assumes that the release of atoms from the graphite surface is a desorption process (4, 12–14). Once a desorption process is assumed for a system, thermodynamic relationships can be applied to experimental data to yield the heat of desorption (15). A number of authors (16–18) have also reported that thermodynamic equilibrium is established at each stage of atom formation between the solid phase and the gaseous analyte atoms as follows:

$$[1] \quad M_w \leftrightharpoons M_g$$

where M_w is the number of analyte atoms left unatomized on the graphite surface and M_g is the number of atoms in the gas phase. The expression for the equilibrium constant K_p for the above reaction is given by

$$[2] \quad K_p = P = \exp(-\Delta G^0/RT)$$

where P is the atomic vapour pressure of the element in the atomizer at time t, R and T are the gas constant and the absolute temperature, respectively, and ΔG^0 is the standard Gibb's free energy change which is defined by the following general equation:

$$[3] \quad \Delta G^0 = \Delta H^0 - T\Delta S^0$$

where ΔH^0 is the standard enthalpy and ΔS^0 is the standard entropy change. According to eq. [2], K_p, and hence P, increases with temperature. Thus, M_g will also increase as the temperature increases. On substituting eq. [3] into eq. [2] and taking natural logarithm of both sides of the resulting equation, one gets

$$[4] \quad \ln P = -\Delta H^0/RT + C'$$

where C' is a constant and ΔH^0 is the molar enthalpy of vaporization, sublimation, or desorption. From eq. [4], a plot of ln P vs. $1/T$ should be linear with slope $= -\Delta H^0/R$ and intercept $= C'$. The value of P, however, is difficult to measure in the graphite furnace as a function of time during atomization because of the extremely small value of this vapour pressure. For this reason it would be better to relate P to the absorbance, A, i.e. $A = f(P)$. Thus, for ideal gas behaviour one gets

$$PV = nRT$$

where V is the graphite furnace volume approximately equal to the analysis volume and n is the number of moles of absorbing atoms that have gone to the gas phase, $n = M_g/L$, where L is Avogadro's number. In this case, eq. [4] can be rewritten as follows:

$$\ln(M_g RT/LV) = -\Delta H^0/RT + C'$$

The measured absorbance is related to the number of analyte atoms through the general equation, $A = QM_g$, where Q is a constant containing all the necessary physical and geometrical constants. Therefore, the above equation may be expressed as follows:

$$\ln(ART/QLV) = -\Delta H^0/RT + C'$$

which is slightly modified to

$$[5] \quad \ln(AT) = -\Delta H^0/RT + C$$

where

$$C = C' + \ln(QLV/R)$$

The plot of ln (AT) vs. $1/T$ is similar to the Arrhenius plot and can be used to obtain ΔH^0 from the slope. Agreement between their experimentally determined activation, E_a, energy and the enthalpy of sublimation for several elements Sturgeon *et al.* (4, 5, 12) have reported that E_a may be equated to ΔH^0. The Arrhenius plot then becomes in effect a van't Hoff plot (19) and one can conclude that the atomization of the analyte element at the appearance temperature is thermodynamically favourable.

The following energy terms play an important role in proposing a mechanism of atomization (6): The enthalpy of vaporization, ΔH^0(M), of the element (sublimation if there is no liquid phase); the enthalpy of vaporization (or sublimation) of the metal oxide, ΔH^0(MO); the dissociation energy of the metal oxide, D_0(M—O); and the dissociation energy of the metal carbide, D_0(M—C). These energy terms are summarized in Table 1. The release of analyte atoms into the gas phase is determined to a large extent by these terms as well as some other kinetic factors. To evaluate the reduction of $MO_{(s)}$ by $C_{(s)}$ these terms should be considered. Generally, production of gaseous analyte atoms $M_{(g)}$ is given by the following equations:

$$[6] \quad MO_{(s)} + C_{(s)} \rightarrow M_{(s)} + CO_{(g)}$$

$$[7] \quad MO_{(s)} + CO_{(g)} \rightarrow M_{(s)} + CO_{2(g)}$$

$$[8] \quad MO_{(s)} \rightarrow MO_{(g)}$$

$$[9] \quad MO_{(g)} \rightarrow M_{(g)} + (1/2)O_{2(g)}$$

$$[10] \quad M_{(s)} \rightarrow M_{(g)}$$

The reduction of metal oxide by carbon, eq. [6], becomes favourable as the temperature increases. As mentioned above the extent of the reaction in each of the above chemical equations depends on many factors. Of prime importance are the change in the Gibb's free energy and the absolute temperature which have a tremendous effect on the relative magnitude of the equilibrium constant involved in the reaction. The latter helps in predicting which reaction is thermodynamically more favourable at a given temperature. The following three reactions determine the thermo-

TABLE 1. Production of gaseous analyte atoms from the metal oxide

$MO_{(s)}$		
sublimation	reduction	
$MO_{(g)}$	reduction with concurrent sublimation or vaporization	$M_{(s)} + (1/2)O_{2(g)}$
dissociation		sublimation or vaporization
$M_{(g)} + (1/2)O_2$	$M_{(g)} + (1/2)O_{2(g)}$	$M_{(g)}$
atomization in the gas phase	atomization from the surface	atomization from the surface
$\Delta H^0(MO) < D_0(MO)$	$\Delta H^0(M) < D_0(MO)$	$D_0(MO) < \Delta H^0(M)$

dynamic competitiveness of carbon and carbon monoxide as reducing agents in the graphite furnace:

[11] $C_{(s)} + O_{2(g)} \rightarrow 2CO_{(g)}$

[12] $C_{(s)} + O_{2(g)} \rightarrow CO_{2(g)}$

[13] $2CO_{(g)} + O_{2(g)} \rightarrow 2CO_{2(g)}$

Assuming unit activities for all of the above species a quantitative comparison of relative affinities of carbon or carbon monoxide for oxygen may be made as follows: the particular advantage of carbon as a reducing agent over the other two reactions can be understood by reference to the change in the Gibb's free energy, ΔG^0. As T increases ΔG^0 becomes more negative for reaction [11], remains almost the same for reaction [12], and becomes more positive for reaction [13]. Because the change in the entropy, ΔS^0, for reaction [11] is positive, the greater the temperature, the more negative ΔG^0 will be and hence the greater will be the thermodynamic advantage of reaction [11] over reactions [12] and [13]. With the unit activity assumption for all of the species reaction [13] is more effective (as a reducing agent) than reactions [11] and [12] only at temperatures below 973 K. However, the change in the Gibb's free energy is the measure of the actual drive of the reaction towards equilibrium. In the graphite furnace, the activity of carbon is one and the fugacity of carbon monoxide is much less than one (20, 21). The partial pressure of CO in the graphite furnace at a heating rate of 1500 K/s is about 0.001 atm (21). At equilibrium, the decrease in ΔG^0 as the temperature increases means K_p will increase and therefore products will be favoured over reactants to a greater extent. The reduction of the metal oxide by carbon is well documented in the literature (1, 4, 5, 19, 22, 23). And even if the reduction of the metal oxide is not thermodynamically favourable at the appearance temperature formation of free metal atoms may be attributed to the thermal dissociation of the metal oxide (4). Another important factor that has a profound effect on the reduction of the metal oxide is the kinetics of the reaction. The rate of formation of the free metal from the oxide depends on the energy barrier to be surmounted, amounts of species that appear in the rate law of the chemical reaction and the pre-exponential factor of the Arrhenius law. If the reduction of the metal oxide by carbon in eq. [6] is kinetically controlled the rate of disappearance of the metal oxide from the surface may be expressed by a pseudo first-order reaction. This is possible since carbon is present in a large amount which is considered constant, whereas the rate of reduction of the metal oxide by carbon monoxide is expressed by second-order kinetics. In order for the carbon monoxide to reduce the metal oxide the carbon monoxide molecule must become adsorbed onto the condensed phase of the metal oxide. At a low surface coverage of carbon monoxide (where the partial pressure of CO is very low) the reduction of the metal oxide occurs at a lower rate than the reduction by carbon. Moreover, the metal oxide is in intimate contact with the graphite surface during atomization which should kinetically favour reduction by carbon over that by CO. It is therefore reasonable to conclude that reduction by carbon is the most predominant pathway for generating free analyte atoms.

Experimental

Apparatus

Absorbance measurements were made with a Perkin-Elmer atomic absorption spectrophotometer, model 503, equipped with a Deuterium Arc Background Corrector and a Heated Graphite Atomizer (HGA) model 400, operated in the gas-stop mode. Argon gas of purity 99.997% and pyrolytically coated electrographite tubes (The Perkin-Elmer Corporation, part No. B009-1504) were used. Hollow cathode lamps of Al, Ga, Au, Ni, Ag, and Fe (Westinghouse), Co (Varian Techtron), and Cu (Cathodeon) were used.

Standards and reagents

Standards were prepared by using chemicals or elements of the highest purity commercially available. Stock solutions of cobalt, iron, nickel, and gallium were prepared separately by dissolving the appropriate mass of pure metal in nitric acid (ULTREX, Baker Chemical Co.) and making up the solution to 1000 μg mL^{-1} in 1% (v/v) nitric acid. The stock solution of silver was prepared by dissolving an appropriate mass of silver nitrate in ultrapure water and diluting the solution to 1000 μg mL^{-1} with ultrapure water. The stock solution of copper was prepared by dissolving copper metal in 50% (v/v) nitric acid (ULTREX) with heating; the final solution was made to 1000 μg mL^{-1} in 1% (v/v) nitric acid by diluting with ultrapure water. The stock solution of aluminum was

Can. J. Chem. Downloaded from www.nrcresearchpress.com by 88.255.202.194 on 09/08/12
For personal use only.

TABLE 2. Experimental and instrumental parameters

Element	Mass, ng	λ, nm
Al	0.10	309.3
Cu	0.02	240.7
Co	0.01	324.8
Ga	0.01	248.3
Au	0.01	232.0
Ni	0.30	287.4
Fe	0.10	242.8
Ag	0.01	328.1

prepared by dissolving pure aluminum in 20% (v/v) nitric acid with heating and diluting the solution to 1000 μg mL^{-1} with ultrapure water. The stock solution of gold was prepared by dissolving the appropriate mass of the gold metal in aqua regia and diluting the solution with ultrapure water to 1000 μg mL^{-1}. All test solutions were prepared daily by serial dilution of the stock solutions with ultrapure water to contain 1% (v/v) nitric acid. Ultrapure water of resistivity of 18.3 megohm-cm was obtained directly from a milli-Q2 water purification system (Millipore Corporation).

Procedure

The experimental and instrumental conditions used are listed in Table 2. The tube wall temperature was measured by automatic pyrometers series 1100 and 300 (Ircon Inc., Skokie, Ill.) — the former for high temperatures and the latter for low temperatures. The pyrometer was focused through the injection hole on the inner surface of the graphite tube and the temperature of the sample area (a few mm^2) was monitored. It seems most appropriate to use the tube wall temperature as, in fact, if the atomization is determined by solid phase dissociation, the tube wall temperature is in any case the most relevant one. If the atomization is governed by gas phase dissociation this process will be predominant in the hottest zone, the zone at the middle part of the tube where the sample is deposited. Because of the large activation energies to be expected for the dissociation reaction, the number of atoms generated at the cold extreme ends of the graphite tube will be small.

In all cases 10 μL aliquots were deposited manually in the graphite furnace with an Eppendorf micropipet fitted with disposable plastic tips. The signals were stored on floppy discs using a digital oscilloscope, model 4094 (Nicolet Corporation), and recalled later for evaluation.

Results and discussion

Plots of ln (AT) vs. $1/T$ for the eight elements are shown in Fig. 1. Enthalpies of atomization have been calculated from the slopes of the linear segments using data points at the beginning of the absorbance, i.e., immediately after the appearance temperature. The latter is defined as the temperature at which the absorbance is 0.0044 A.U. Table 3 shows the enthalpy of atomization, ΔH^0, measured by this method. Also, shown in this table is a comparison with the activation energy, E_a, measured for this work by the method of Sturgeon *et al.* (4) and the Smets' method (11). Figure 2 shows a typical plot for copper compared with those of Sturgeon *et al.* (4) and Smets (11). To make the comparison possible all of the data points of the three methods are normalized.

The results shown in Fig. 2 and those presented in Table 3 indicate that there is no significant difference among the three methods. This means that, for the elements under investigation, the ΔH^0 and E_a values are about the same. Over the initial part of the leading edge of the absorbance, a

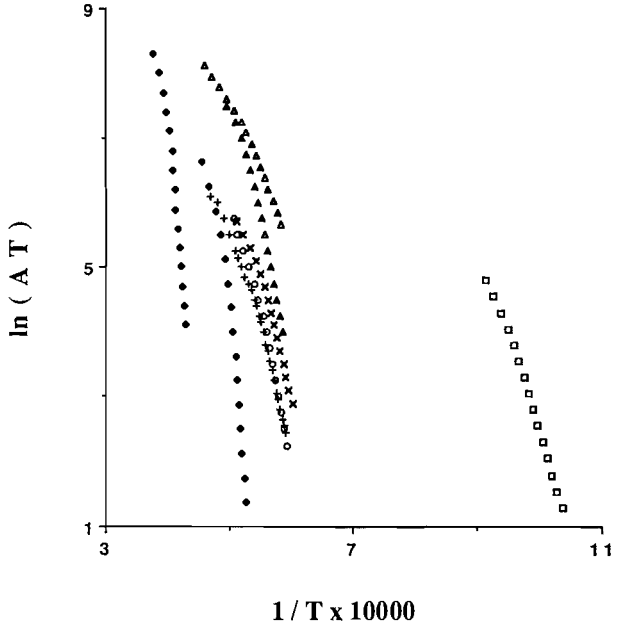

FIG 1. Plots of ln (AT) vs. $1/T$. ◇: Al; △: Ga; ▲: Fe; □: Ag; ◆: Co; ○: Au; ×: Ni; and +: Cu.

TABLE 3. Comparison of the experimental enthalpy, ΔH^0, with the experimental activation energy, E_a

Element	ΔH^0, kJ mol^{-1} this method	E_a, kJ mol^{-1}[a] Smets (11)	E_a, kJ mol^{-1}[a] Sturgeon (4)
Al	1340 ± 50	1350 ± 60	1370 ± 80
Cu	337 ± 10	340 ± 13	339 ± 17
Co	395 ± 17	421 ± 15	443 ± 1
Ga	261 ± 10	249 ± 10	248 ± 15
Au	371 ± 12	364 ± 15	364 ± 15
Ni	428 ± 15	432 ± 17	430 ± 16
Fe	409 ± 18	416 ± 15	416 ± 19
Ag	260 ± 8	284 ± 10	279 ± 12

[a]Graphite furnace was operated in the gas-flow mode.

thermodynamic equilibrium may be established in a thin boundary or diffusion layer above the solid phase wherein multiple release-adsorption processes occur resulting in equilibrium prior to diffusion of the atomic vapour into the analysis volume. In such circumstances equilibrium exists and the Arrhenius plot yields the enthalpy for the overall reaction of atomization (12). Hence, one may conclude that at the very beginning of the absorbance, atom formation can be modelled by either kinetics or thermodynamics (24).

All of the plots of ln (AT) vs. $1/T$ of the elements under investigation show bending towards the abscissa as they approach the absorbance maximum. This bending was also reported by Sturgeon *et al.* (4, 5) and Smets (11). There are several explanations for this curvature (7, 12, 24–27). The explanation put forward by this work is the temperture dependence of the activation energy and the pre-exponential factor in the Arrhenius law which cause this deviation. In derivation of those plots it has been assumed that the pre-exponential factor and the activation energy do not vary with temperature. This assumption is not necessarily true. Ac-

Can. J. Chem. Downloaded from www.nrcresearchpress.com by 88.255.202.194 on 09/08/12
For personal use only.

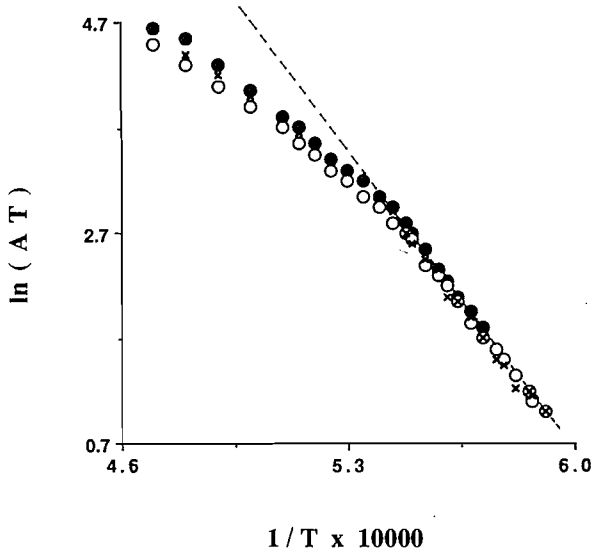

FIG. 2. Plot of ln (AT) vs. $1/T$ for copper compared with the results obtained by the method of Sturgeon *et al.* (4) and the Smets' method (11). ●: This work; ×: Smets; ○: Sturgeon *et al.* The broken line is the theoretical plot, shown for comparison.

cording to the Arrhenius plot, when the pre-exponential factor is temperature dependent, the activation energy is also temperature dependent (26). One may also state that the order of reaction (7) and the non-homogeneity of the atomic vapour inside the graphite furnace (28) may be another cause for this nonlinearity.

The experimental enthalpy of atomization, which is mainly related to breaking bonds in molecular species, can be correlated with the energy associated with the rate-determining step. With the determination of this term it is possible to propose a mechanism for atom formation. One should also consider the heat of formation of the metal carbides and the metal oxides since these are the most likely two chemical compounds that may form during atomization. The heat of formation is useful in explaining the thermal stability of the chemical compound at a given temperature. For example, a chemical compound with a high negative heat of formation is thermally more stable than that having a less negative heat of formation. Table 4 presents the heat of formation of metal oxides and metal carbides of the elements under investigation. The heat of formation in Table 4 equals the heat of atomization, as reported by L'vov (29). It can be seen from these data that all metal oxides are thermally more stable than the carbides. Some of the metal oxides and carbides, such as those of Au and Ag, are unstable at high temperatures. Thus, one may conclude that the oxides are likely to be the precursors to atom formation for this group of metals (taken as nitrates). The main contribution of this work is that the results presented have been obtained by using an equation derived from the basic principles of thermodynamics without invoking the order of the reaction. This is especially useful for atomization reactions that do not proceed by first-order kinetics. The experimentally observed enthalpies are in agreement with those obtained by applying the method of Sturgeon *et al.* (4) and Smets (11). Our results confirm the experimental observation by Sturgeon *et al.* (4) that atom formation involves no energy barrier other than the enthalpy of atomization, and the experimentally measured activation energy is equal to the enthalpy of atomization.

TABLE 4. Heat of formation, ΔH_f, of the metal oxides and carbides

Element	Species	ΔH_f, kJ mol^{-1}	Reference
Al	Al_2O_3	−1673.6	39
	Al_2O_2	−1527.1	32
	AlO	83.7	42
	AL_4C_3	−208.8	39
Cu	CuO	−157.3	39
Co	CoO	−237.9	42
Ga	Ga_2O_3	−998.3	39
	GaO	279.5	42
	Ga_2C_2	560.7	42
Ni	NiO	−238.9	42
	Ni_3C	67.4	39
Fe	FeO	−272.0	39
	Fe_3C	25.1	42
Ag	Ag_2O	−31.0	39
Au	Unstable	—	

TABLE 5. Change in Gibb's free energy ΔG_f of reduction reactions calculated at the appearance temperature[a]

Reaction	ΔG_f, kJ mol^{-1}
$Al_2O_{3(s)} + 3C_{(s)} \rightarrow 2Al_{(s)} + 3CO_{(g)}$	−129.7
$CuO_{(s)} + C_{(s)} \rightarrow Cu_{(s)} + CO_{(g)}$	−288.7
$CoO_{(s)} + C_{(s)} \rightarrow Co_{(s)} + CO_{(g)}$	−172.0
$Ga_2O_3 + 2C_{(s)} \rightarrow 2Ga_{(s)} + 3CO_{(g)}$	−260.2
$NiO_{(s)} + C_{(s)} \rightarrow Ni_{(s)} + CO_{(g)}$	−295.8
$FeO_{(s)} + C_{(s)} \rightarrow Fe_{(s)} + CO_{(g)}$	−130.1

[a]Data were collected from refs. 39 and 42.

The purpose of studying the atomization mechanism is to understand the sequence of atomization reactions. Before postulating a mechanism of atomization one has to consider thermodynamic feasibilities of the proposed elementary reactions and their relative rates. In this context, the enthalpy of reaction is a useful concept and can be used to probe the reaction mechanism (31). An elementary reaction that requires higher energy (expressed as the enthalpy of the reaction) relative to other steps is likely to be slow and hence can be considered the rate-determining step. This approach is useful to generate data for studying the mechanism of atomization and has been reported in the literature (4, 31).

Proposed mechanism of atomization

Aluminum

Upon heating, the aqueous solution of aluminum nitrate is converted into Al_2O_3 (5, 30) before the graphite furnace attains the appearance temperature of 2070 K. The high heat of formation of Al_2O_3 compared to that of the simple carbide Al_4C_3 (Table 5) rules out the formation of any significant amount of the carbide.

The overall reaction for producing free aluminum from Al_2O_3 is

[14] $Al_2O_{3(s)} + 3C_{(s)} \rightarrow 2Al_{(s)} + 3CO_{(g)}$

The Gibb's free energy change for the above reaction (cal-

Can. J. Chem. Downloaded from www.nrcresearchpress.com by 88.255.202.194 on 09/08/12
For personal use only.

culated at the appearance temperature, 2070 K) is −129 kJ mol^{-1} which indicates that the reaction is thermodynamically favourable. In the calculation it has been assumed that the partial pressure of the carbon monoxide equals 0.001 atm (21) and that ΔH^0 and ΔS^0 do not change appreciably with temperature. This is a reasonable assumption. The following atomization mechanism is proposed:

[15] $Al_2O_{3(s)} + C_{(s)} \rightarrow Al_2O_{2(g)} + CO_{(g)}$

[16] $Al_2O_{2(g)} \rightarrow 2Al_{(g)} + O_{2(g)}$

[17] $O_{2(g)} + 2C_{(s)} \rightarrow 2CO_{(g)}$

For reaction [15] to proceed only 38.0 kJ mol^{-1} of energy is required, whereas reaction [16] must acquire 1527.1 kJ mol^{-1}. The latter is likely to be slow and hence is considered the rate-determining step. Comparison of the experimentally determined enthalpy of atomization, 1390 ± 50 kJ mol^{-1}, with the heat of atomization of Al_2O_2, 1527 kJ mol^{-1} (32), suggests that gaseous aluminum atoms mainly come from the dissociation of Al_2O_2. The latter has been observed mass-spectrometrically in the graphite furnace by Styris.[2] Another possible mechanism for the formation of gaseous aluminum atoms is by autocatalytic reduction of aluminum oxide by gaseous carbides, such as Al_4C_3 that may form during atomization (33–37).

[18] $4Al_{(g)} + 3C_{(s)} \rightarrow Al_4C_{3(s)}$

[19] $2Al_4C_{3(s)} \rightarrow 3Al_2C_{2(g)} + 2Al_{(g)}$

[20] $2Al_2O_{3(s)} + 3Al_2C_{2(g)} \rightarrow 10Al_{(g)} + 6CO_{(g)}$

Gallium

Below the appearance temperature of gallium, 1500 K, Ga(III) nitrate or hydroxide in aqueous solutions are converted into Ga_2O_3 (ref. 32, p. 1093). The latter is reduced to metal by carbon at 1500 K. There are no carbides of gallium that are stable at room temperature (32), but formation of volatile carbides at low temperature is possible. The calculated ΔG_{1500} value, −260.2 kJ mol^{-1} (Table 5), suggests that the reduction of Ga_2O_3 by carbon at the appearance temperature is thermodynamically favourable. The overall reduction-reaction is therefore

[21] $Ga_2O_{3(s)} + 3C_{(s)} \rightarrow 2Ga_{(s)} + 3CO_{(g)}$

which, like the aluminum reaction, indicates that it is not an elementary reaction as such a reaction would require the collision of four molecules, the probability of which is very small. The following mechanism is, therefore, proposed:

[22] $Ga_2O_{3(s)} + C_{(s)} \rightarrow 2GaO_{(g)} + CO_{(g)}$

[23] $GaO_{(g)} + C_{(s)} \rightarrow 2Ga_2O_{(s)} + CO_{(g)}$

[24] $Ga_2O_{(s)} + C_{(s)} \rightarrow 2Ga_{(s)} + CO_{(g)}$

[25] $Ga_{(s)} \rightarrow Ga_{(g)}$

The observed value of the enthalpy of atomization, 261 ± 10 kJ mol^{-1}, correlates with the heat of vaporization of gallium, 277.0 kJ mol^{-1}, rather than with the enthalpy of reaction [22], 245.1 kJ mol^{-1}. The formation of the gaseous oxide (GaO) may explain the relatively low atomization efficiency of gallium (38).

[2]D. L. Styris. Seminar at Carleton University, Ottawa, Ont., Canada. October 14, 1990.

TABLE 6. Some properties of the elements

Element	Appearance temperature, K	Melting point, K	Phase at appearance temperature
Al	2070	934	Liquid
Cu	1450	1357	Liquid
Co	1480	1768	Solid
Ga	1500	303	Liquid
Au	1450	1358	Liquid
Ni	1960	1728	Liquid
Fe	1500	1808	Solid
Ag	960	1235	Solid

Copper

Upon heating, an aqueous solution of copper nitrate is converted into copper oxide (CuO) before the furnace attains the appearance temperature of 1450 K (4, 5, 39). Upon further heating, copper oxide is reduced by carbon to free copper, which then sublimes to gaseous atoms. The calculated ΔG_{1450} value is −288.7 kJ mol^{-1} (Table 5). The experimental enthalpy of atomization (337 ± 10 kJ mol^{-1}) correlates with the heat of sublimation of copper (337.6 kJ mol^{-1}). Because the heat of desorption of copper from the graphite surface is approximately equal to the heat of sublimation of copper (24), the correlation between the experimentally observed enthalpy and the heat of sublimation is reasonable. The following atomization mechanism is therefore proposed:

[27] $CuO_{(s)} + C_{(s)} \rightarrow Cu_{(s)} + CO_{(g)}$

[28] $Cu_{(s)} \rightarrow Cu_{(g)}$

Reaction [27] requires only 46.8 kJ mol^{-1} of energy, whereas reaction [28] requires 337.6 kJ mol^{-1} of energy, the latter therefore is the rate-determining step. The fair agreement between the heat of sublimation of copper and the experimentally determined enthalpy of atomization support the above mechanism. Although Cu is in liquid form at the appearance temperature (Table 6), it seems that the atomization of Cu occurs by sublimation. This is explained by thermodynamic calculations. According to these calculations the small amount of copper may vaporize totally at a temperature below the melting point of copper without passing through the liquid phase.

Recently, Wang *et al.* (40) determined an activation energy of 130 ± 8 kJ mol^{-1} for copper under vacuum conditions using the higher temperature region of the Arrhenius plot and reported that the initial part of such a plot is unusable for studying the atomization mechanism. Their mechanism for copper atom formation is $Cu(NO_3)_2 \rightarrow CuO_{(ads)} \rightarrow Cu_{(ads)} \rightarrow Cu_{(g)}$, in which the desorption of copper atoms from the graphite surface at individual active site is the rate-determining step.

Cobalt

Upon heating, an aqueous solution of cobalt (as nitrate or chloride) is converted into CoO below the appearance temperature (4, 30). At higher temperature CoO is reduced by carbon to Co as follows:

$$CoO_{(s)} + C_{(s)} \rightarrow Co_{(s)} + CO_{(g)}$$

The above reaction is thermodynamically favourable with $\Delta G_{1480} = -172.0$ kJ mol^{-1}. The observed enthalpy of

Can. J. Chem. Downloaded from www.nrcresearchpress.com by 88.255.202.194 on 09/08/12
For personal use only.

atomization (395 ± 17 kJ mol^{-1}) correlates with the heat of sublimation of the pure metal (428.4 kJ mol^{-1}). The formation of gaseous cobalt atoms is believed to be as follows:

[29] $CoO_{(s)} + C_{(s)} \rightarrow Co_{(s)} + CO_{(g)}$

[30] $Co_{(s)} \rightarrow Co_{(g)}$

The reduction of CoO by carbon requires 127.4 kJ mol^{-1} of energy, whereas the sublimation of cobalt requires 428.4 kJ mol^{-1}; hence, the latter is considered the rate-determining step. The fair agreement between the experimental enthalpy of atomization and the heat of sublimation of cobalt supports the above atomization mechanism. Based on thermochemical calculations, Ham and McAllister (19) have also reported similar atomization mechanism for Co. They used, for their calculations, small amounts of Co (as nitrate or chloride) normally taken for determination by the graphite furnace.

Nickel

Upon heating, an aqueous solution of nickel nitrate or chloride is thermally decomposed into NiO (4, 5) below the appearance temperature, 1960 K. On further heating, NiO is reduced by carbon to Ni, which then sublimes. The overall reduction-reaction is

$$NiO_{(s)} + C_{(s)} \rightarrow Ni_{(s)} + CO_{(g)}$$

The calculated ΔG_{1960} at the appearance temperature of nickel (1960 K) is −295.8 kJ mol^{-1}. The observed enthalpy of atomization (428 ± 15 kJ mol^{-1}) correlates with the heat of sublimation of Ni (428.4 kJ mol^{-1}). The following atomization mechanism is proposed:

[31] $NiO_{(s)} + C_{(s)} \rightarrow Ni_{(s)} + CO_{(g)}$

[32] $Ni_{(s)} \rightarrow Ni_{(g)}$

For reaction [31] to proceed 129.2 kJ mol^{-1} of energy is required, whereas sublimation of Ni requires 430.1 kJ mol^{-1}. The latter, therefore, is the rate-determining step. The good agreement between the experimentally determined enthalpy of atomization and the enthalpy of sublimation of pure nickel suggests that nickel atoms is formed by sublimation of the reduced metal. Although nickel is liquid at the appearance temperature (Table 6), the observed enthalpy of atomization correlates with the heat of sublimation and not with the heat of vaporization of the pure metal which is 375 kJ mol^{-1}. Probably, the reason for this is similar to that mentioned above for copper.

Iron

Upon heating an aqueous solution of ferric or ferrous nitrate to a temperature higher than 848 K at low oxygen partial pressure (ref. 32, vol. 3, p. 1008) it is converted into FeO, which is reduced by carbon to Fe at the appearance temperature of 1500 K as follows:

$$FeO_{(s)} + C_{(s)} \rightarrow Fe_{(s)} + CO_{(g)}$$

The calculated ΔG_{1500} for the above reaction is −130.1 kJ mol^{-1}. At 1500 K Fe sublimes. The observed enthalpy of atomization (409 ± 18 kJ mol^{-1}) correlates with the heat of sublimation of Fe (415.3 kJ mol^{-1}). The following atomization mechanism is therefore proposed:

[33] $FeO_{(s)} + C_{(s)} \rightarrow Fe_{(s)} + CO_{(g)}$

[34] $Fe_{(s)} \rightarrow Fe_{(g)}$

The enthalpies of reactions [33] and [34] are 161.4 and 415.5 kJ mol^{-1}, respectively. Because of the high energy required reaction [34] is likely to be slow and hence is the rate-determining step. The correlation of the measured enthalpy of atomization with the enthalpy of sublimation of Fe gives support for the above mechanism.

Silver

When an aqueous solution of a soluble Ag salt is heated, Ag_2O is formed at a temperature below 523 K. When the concentration of the oxygen is extremely small (as is the case in a graphite furnace), the Ellingham diagram (41) predicts that, even in the absence of carbon, Ag_2O decomposes into 2 Ag and (1/2) O_2 when heated above 473 K. At the appearance temperature of silver, 960 K, the absorbance is attributed to the sublimation of Ag. The observed enthalpy of atomization (260 ± 8 kJ mol^{-1}) correlates with the heat of sublimation of silver, 283.0 kJ mol^{-1} (39, 42).

Gold

Aqueous solutions of gold chloride, upon heating, produce Au_2O_3 well below 1450 K (the appearance temperature). Upon further heating, Au_2O_3 decomposes to 2Au and (3/2) O_2. Since Au is in liquid state (Table 6) at the appearance temperature, the correlation of the heat of formation with the heat of vaporization of Au is possible. The observed enthalpy of atomization (371 ± 17 kJ mol^{-1}), however, correlates well with the heat of sublimation (368.2 kJ mol^{-1}) and not with the heat of vaporization (343 kJ mol^{-1}), probably for reasons similar to those mentioned above for nickel and copper.

Acknowledgements

The author is grateful to Professor C. L. Chakrabarti and Professor J. P. Byrne for helpful comments.

1. W. C. Campbell and J. M. Ottaway. Talanta, **21**, 837 (1974).
2. W. Frech, E. Lundberg, and A. Cedergren. Prog. Anal. At. Spectrosc. **8**, 257 (1985).
3. C. L. Chakrabarti, S. B. Chang, and S. E. Roy. Spectrochim. Acta, **38B**, 447 (1983).
4. R. E. Sturgeon, C. L. Chakrabarti, and C. H. Langford. Anal. Chem. **48**, 1792 (1976).
5. R. E. Sturgeon and C. L. Chakrabarti. Prog. Anal. At. Spectrosc. **1**, 5 (1978).
6. C. W. Fuller. Electrothermal atomization for atomic absorption spectrometry. The Chemical Society. 1977. pp. 22–40.
7. J. A. Holcombe, G. D. Rayson, and N. Akerlind, Jr. Spectrochim. Acta, **37B**, 319 (1982).
8. S. G. Salmon and J. A. Holcombe. Anal. Chem. **54**, 630 (1982).
9. D. A. Katzakov, I. L. Grinshtein, and L. P. Kruglikova. Zh. Prikl. Spektrosk. **33**, 804 (1980).
10. J. J. Schwab and R. J. Lovett. Spectrochim. Acta, **45B**, 281 (1990).
11. B. Smets. Spectrochim. Acta, **35B**, 33 (1980).
12. R. E. Sturgeon and J. S. Arlow. J. Anal. At. Spectrom. **1**, 359 (1986).
13. J. R. Arthur and A. Y. Cho. Surf. Sci. **36**, 641 (1973).
14. J. McNally and J. A. Holcombe. Anal. Chem. **56**, 1105 (1987).
15. S. W. Benson. The foundation of chemical kinetics. McGraw-Hill Book Co., New York. 1982. p. 26.
16. S. L. Paveri-Fontana, G. Tessari, and G. Torsi. Anal. Chem. **46**, 1032 (1974).
17. A. Guerrieri, L. Lampugnani, and G. Tessari. Spectrochim. Acta, **39B**, 193 (1984).

Can. J. Chem. Downloaded from www.nrcresearchpress.com by 88.255.202.194 on 09/08/12
For personal use only.

18. S. L. Paveri-Fontana, G. Tessari, and G. Torsi. Anal. Chem. **46**, 943 (1974).
19. N. S. Ham and T. McAllister. Spectrochim. Acta, **43B**, 789 (1988).
20. R. E. Sturgeon, K. W. M. Siu, G. J. Gardner, and S. S. Berman. Anal. Chem. **58**, 42 (1986).
21. G. F. R. Gilchrist, C. L. Chakrabarti, and J. P. Byrne. J. Anal. At. Spectrom. **4**, 533 (1989).
22. C. W. Fuller. Analyst, **100**, 229 (1975).
23. C. W. Fuller. Analyst, **99**, 739 (1974).
24. R. E. Sturgeon. Fresenius Z. Anal. Chem. **324**, 807 (1986).
25. Y.-P. Yan, T.-Z. Lin, and Z.-J. Liu. Talanta, **38**, 167 (1990).
26. K. J. Laidler. Chemical kinetics. 3rd ed. Harper & Row, New York. 1987. p. 282.
27. A. Kh. Gilmutdinov and O. M. Shlyakhtina. Spectrochim. Acta, **46B**, 1121 (1991).
28. A. Kh. Gilmutdinov, Yu.A. Zakharov, V. P. Ivanov, and A. V. Voloshin. J. Anal. At. Spectrom. **6**, 505 (1991).
29. B. V. L'Vov and L. A. Pelieva. Zh. Anal. Khim. **33**, 1695 (1978).
30. C. Duval. Inorganic thermogravimetric analysis. 2nd ed. Elsevier, New York. 1963.
31. H. E. Avery. Basic reaction kinetics and mechanisms. The Macmillan Press Ltd., London. 1974. p. 6.
32. A. F. Trotman-Dickerson. Comprehensive inorganic chemistry. Vol. 1. Pergamon Press, Great Britain. 1973. p. 1034.
33. C. Bendico and M. T. C. de Loss-Vollebregt. Spectrochim. Acta, **45B**, 547 (1990).
34. B. V. L'Vov and A. S. Savin. Zh. Anal. Khim. **38**, 1925 (1983).
35. B. V. L'Vov and A. S. Savin. Zh. Anal. Khim. **38**, 1933 (1983).
36. B. V. L'Vov. Zh. Anal. Khim. **38**, 1953 (1984).
37. B. V. L'Vov and A. S. Savin. Zh. Anal. Khim. **37**, 2116 (1982).
38. R. E. Sturgeon and S. S. Berman. Anal. Chem. **55**, 190 (1983).
39. R. C. Weast (*Editor*). Handbook of chemistry and physics. 66th ed. CRC Press, Boca Raton, Fla. 1985–1986.
40. P. Wang, V. Majidi, and J. A. Holcombe. Anal. Chem. **61**, 2652 (1989).
41. P. W. Atkin. Physical chemistry. 3rd ed. W. H. Freeman and Company, New York. 1986. p. 227.
42. R. J. Dean (*Editor*). Lange's handbook of chemistry. 13th ed. McGraw-Hill, Inc., New York. 1985.

Can. J. Chem. Downloaded from www.nrcresearchpress.com by 88.255.202.194 on 09/08/12
For personal use only.

Transition metal complexes of 6-amino 2-thiouracil; crystal structure of bis(6-amino-2-thiouracilato)aquazinc(II) dihydrate

M. Angustias Romero,[1] M. Purificación Sánchez, Miguel Quirós, Francisco Sánchez, Juan Manuel Salas, and Miguel N. Moreno

Departamento de Química Inorgánica. Universidad de Granada, 18071 Granada, Spain

AND

René Faure

Laboratoire de chimie analytique II, Université Claude Bernard, 69622 Villeurbanne, France

Received February 25, 1992[2]

M. Angustias Romero, M. Purificación Sánchez, Miguel Quirós, Francisco Sánchez, Juan Manuel Salas, Miguel N. Moreno, and René Faure. Can. J. Chem. **71**, 29 (1993).

Complexes of 6-amino-2-thiouracil (H_2ATU) with the metal ions Ni(II), Co(II), Zn(II), Cd(II), Cu(I), Ag(I), and Hg(II) have been isolated and characterized by means of elemental analysis, infrared, NMR, and visible spectroscopies, and magnetic measurements. The crystal structure of $[Zn(HATU)_2(H_2O)] \cdot 2H_2O$ has been solved by X-ray diffraction showing that the metal atom is five-coordinated by a water molecule and two ligands that bind through the sulphur and N1 atoms, closing a four-member chelate ring. Diffuse reflectance spectra and magnetic measurements suggest that $[Co(HATU)_2(H_2O)] \cdot 2H_2O$ has a similar structure to that of the zinc complex, and that the nickel complexes $[Ni(HATU)_2]$ and $[Ni(HATU)_2(H_2O)_2]$ have, respectively, a tetrahedral and a D_{4h}-distorted octahedral environment.

M. Angustias Romero, M. Purificación Sánchez, Miguel Quirós, Francisco Sánchez, Juan Manuel Salas, Miguel N. Moreno et René Faure. Can. J. Chem. **71**, 29 (1993).

Les complexes de 6-amino-2-thiouracil (H_2ATU) avec les ions métalliques Ni(II), Co(II), Zn(II), Cd(II), Cu(I), Ag(I) et Hg(II) ont été isolés et caractérisés par analyse élémentaire, spectroscopies infrarouge, RMN et visible et par mesures magnétiques. La structure cristalline de $[Zn(HATU)_2(H_2O)] \cdot 2H_2O$ a été résolue par diffraction des rayons X. Le métal Zn est pentacoordinné par une molécule d'eau et deux ligands dont la liaison de chacun se fait à travers l'atome du soufre et N1, formant ainsi un chelate de quatre membres. Le spectre de réflectance diffuse et les mesures magnétiques montrent que $[Co(HATU)_2(H_2O)] \cdot 2H_2O$ a une structure similaire à celle du complexe de zinc; les deux complexes $[Ni(HATU)_2]$ et $[Ni(HATU)_2(H_2O)_2]$ ont, respectivement, un environnement tétraédrique et octaédrique distordu D_{4h}.

Introduction

This article continues our work on the interaction of metal ions with thiopyrimidine derivatives containing the NH—C=S group, and which display the tautomerism:

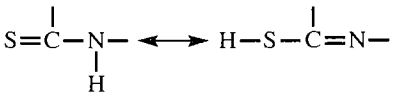

6-Amino-2-thiouracil (H_2ATU) exhibits antiviral and chemotherapeutic activity (1). The X-ray study of this compound showed that the thione form is the one present in solid state (2).

We previously reported the synthesis and characterization of several complexes of 4,6-diamino-2-thiopyrimidine (3), 4-amino-5-nitroso-6-oxo-2-thiopyrimidine (4), and 2-thioisoorotic acid (5) and, following this line, we describe in this paper the synthesis and characterization of eight new compounds formed by the interaction of H_2ATU with Co(II), Ni(II), Zn(II), Cd(II), Hg(II), Cu(I), and Ag(I). The crystal structure of $[Zn(HATU)_2(H_2O)] \cdot 2H_2O$ has been solved by single crystal X-ray diffraction.

Experimental

Preparations

6-Amino-2-thiouracil (H_2ATU) and 6-amino-2-methylthiouracil (HMATU) were prepared using previously described methods (6). The metal complexes $[Ni(HATU)_2]$ (**1**), $[Co(HATU)_2(H_2O)] \cdot 2H_2O$ (**2**), $[Zn(HATU)_2(H_2O)] \cdot 2H_2O$ (**3**), $[Cd(HATU)_2(H_2O)] \cdot H_2O$ (**4**), $Cu(HATU) \cdot H_2O$ (**5**), $Ag(HATU) \cdot 1/2H_2O$ (**6**), and $Hg(HATU)_2$ (**7**) were synthesized by adding 2 mmol of the metal salt (nickel, cobalt, zinc, and cadmium acetate, silver nitrate, copper perchlorate, and mercury chloride) dissolved in the minimum amount of water to an aqueous solution (50 mL) of 2 mmol of H_2ATU (4 mmol for the copper compound since part of the ligand is used in reducing the Cu(II) to Cu(I)). The mixtures were heated at 70–80°C for 1 h with continuous stirring and then allowed to cool to room temperature until the solid compounds appeared, when they were filtered off, washed with water and ethanol, and dried with diethyl ether. A second nickel complex, $[Ni(HATU)_2(H_2O)_2]$ (**8**), was obtained by evaporation of the filtrate of **1**. Elemental analyses of the isolated complexes are shown in Table 1.

Methods

Infrared spectra were recorded as KBr pellets in a Perkin–Elmer 983-G spectrophotometer. ^1H and ^{13}C NMR spectra were recorded on a Bruker AM300 300 MHz spectrometer, using DMSO-d_6 as solvent and TMS as internal standard. Magnetic susceptibilities were measured at room temperature using a Faraday Bruker Magnet B-E15 electrobalance with $HgCo(NCS)_4$ as standard. Diffuse reflectance spectra were recorded in a Schimadzu MPC-3100 spectrophotometer.

X-ray work

A prismatic crystal of **3** was mounted at room temperature on a Nonius CAD-4 diffractometer with graphite-monochromatized MoKα radiation (λ = 0.71069 Å). Twenty-five randomly oriented reflections were used to obtain the lattice parameters and the orientation matrix. The observed extinctions were consistent with the space groups $C2/c$ and Cc, the structure satisfactorily solved in the former. Data were measured in the 2–70° 2θ range with a $\omega:\theta/3$ scan and corrected for Lorentz and polarization factors but not for absorption.

[1]Author to whom correspondence may be addressed.

[2]Revision received September 18, 1992.

Can. J. Chem. Downloaded from www.nrcresearchpress.com by 88.255.202.194 on 09/08/12
For personal use only.

Can. J. Chem. Downloaded from www.nrcresearchpress.com by 88.255.202.194 on 09/08/12
For personal use only.

TABLE 1. Analytical data for the isolated complexes of 6-amino-2-thiouracil[a]

Compound	Colour	C(%)	H(%)	N(%)
1	Yellow-green	27.85	2.36	25.35
		(28.01)	(2.33)	(24.51)
2	Violet	24.28	3.56	22.02
		(24.19)	(3.53)	(21.16)
3	White	24.41	3.55	21.86
		(23.80)	(3.47)	(20.82)
4	White	22.14	2.32	19.27
		(22.18)	(2.77)	(19.41)
5	White	22.04	2.86	19.27
		(21.46)	(2.68)	(18.77)
6	White	18.90	1.71	15.31
		(18.53)	(1.93)	(16.21)
7	White	19.06	1.66	17.13
		(19.79)	(1.64)	(17.32)
8	Green	25.11	3.20	22.61
		(25.35)	(3.20)	(22.16)

[a]Calculated values are in parentheses.

The metal atom was located from a Patterson synthesis and the remaining non-hydrogen atoms from subsequent Fourier syntheses. The structure was refined by full-matrix least squares. The non-coordinated water molecule (O2W) appears in the ΔF map as a very broad peak, indicating intense thermal motion, and it could only be refined isotropically, attempts for disordering it into two positions not yielding satisfactory results. The possibility of a wrong assignment for N6 and O4 due to the pseudo symmetry plane that the ligand has through S, C2, and C5 is clearly ruled out by the location of the amino hydrogens as well as by the values of the C6—N6 and C4—O4 distances. All hydrogen atoms of the organic ligand were located in ΔF maps and refined with fixed B (4.0 Å^2) and no geometric constraints.

Final residues are indicated in Table 2, together with other crystal data. Non-hydrogen coordinates are listed in Table 3. Hydrogen coordinates, thermal parameters, and structure factor tables are included in the supplementary material.[3] Calculations were made by means of the Enraf–Nonius SDP System.

Results and discussion

Spectroscopic studies

H_2ATU is in the thione form in the solid state (2) and, accordingly, its spectrum displays the characteristic thioamide bands (7) at 1546 (thioamide **1**) and 1185 cm^{-1} (thioamide **3**). In the complexes with the ligand in monoanionic form (**1**–**8**), the latter is not observed, and appearing in its place are two intense new bands at 1245 ± 10 and 995 ± 10 cm^{-1}. These spectra exhibit a remarkable similarity to that of 6-amino-2-methylthiouracil (HAMTU) over the whole region below 1500 cm^{-1}. Similar features have been observed in the spectra of complexes of 4,6-diamino-2-thiopyrimidine (3*a*), where the ligand is S,N bidentately coordinated.

Several vibration modes, including mainly ν(C=O), δ(NH_2), and δ(H_2O), converge in a single broad peak with several shoulders centred at 1625 cm^{-1} in the spectra of **2**–**6** and **8**, while two separate peaks at 1605 and 1645 cm^{-1} are visible for **1** and **7**. All spectra exhibit only minor changes

TABLE 2. Crystallographic data for $[Zn(HATU)_2(H_2O)]\cdot 2H_2O$

Formula	$ZnC_8H_{14}N_6O_5S_2$
Crystal aspect	White prisms
Crystal dimensions (mm)	0.25 × 0.25 × 0.25
Crystal system	Monoclinic
Space group	$C2/c$
a (Å)	9.391 (2)
b (Å)	10.497 (2)
c (Å)	15.360 (1)
β (deg.)	101.02 (1)
V (Å^3)	1486.1
Z	4
Calcd. density (g cm^{-3})	1.80
Exptl. density (flotation, g cm^{-3})	1.81
μ (cm^{-1})	20
Independent reflections	3267
Observed reflections ($I > 3\sigma(I)$)	1819
R	0.042
R_w	0.046

TABLE 3. Positional parameters and their esd's

Atom	x	y	z	B(Å^2)
Zn	0	0.1338(1)	0.25	2.37(1)
N1	0.0873(3)	0.1171(3)	0.3955(2)	1.99(5)
C2	0.2110(3)	0.0662(3)	0.3837(2)	2.04(5)
S	0.2279(1)	0.0328(1)	0.2765(1)	2.70(2)
N3	0.3197(3)	0.0393(3)	0.4523(2)	2.13(5)
C4	0.3104(4)	0.0662(3)	0.5398(2)	2.01(5)
O4	0.4206(3)	0.0401(3)	0.5986(2)	2.62(5)
C5	0.1806(4)	0.1190(3)	0.5526(2)	2.18(6)
C6	0.0703(3)	0.1441(3)	0.4800(2)	1.96(5)
N6	−0.0557(3)	0.1966(3)	0.4880(2)	2.91(6)
O1W	0	0.3213(4)	0.25	3.15(8)
O2W[a]	0.3548(5)	0.2372(5)	0.1495(3)	6.7(1)

[a]Atom refined isotropically.

TABLE 4. Nuclear magnetic resonance data (δ, ppm)

	H_2ATU	HAMTU	**3**	**4**	**7**
^1H:					
H_2O	3.45	3.58	3.56	3.39	3.34
C5-H	4.71	4.91	4.75	4.71	4.80
NH_2	6.39	6.48	6.36	6.03	6.18
N-H	11.63	11.5	11.54	11.46	11.60
CH_3	—	2.40	—	—	—
^{13}C:					
C2	174.53	164.13	175.64	174.37	164.03
C4	161.90	163.40	164.07	163.71	163.39
C5	78.22	81.19	79.78	79.81	81.21
C6	154.48	162.31	160.53	161.12	162.70
CH_3	—	12.44	—	—	—

[3]Supplementary material consisting of the following: Table S-1, positional parameters of hydrogen atoms; Table S-2, anisotropic parameters; Table S-3, plane calculations; Table S-4, observed and calculated structure factor amplitudes, may be purchased from: The Depository of Unpublished Data, Document Delivery, CISTI, National Research Council Canada, Ottawa, Canada KIA 0S2.

Table S-1 has also been deposited with the Cambridge Crystallographic Data Centre and can be obtained on request from The Director, Cambridge Crystallographic Data Centre, University Chemical Laboratory, 12 Union Road, Cambridge, CB2 IEZ, U.K.

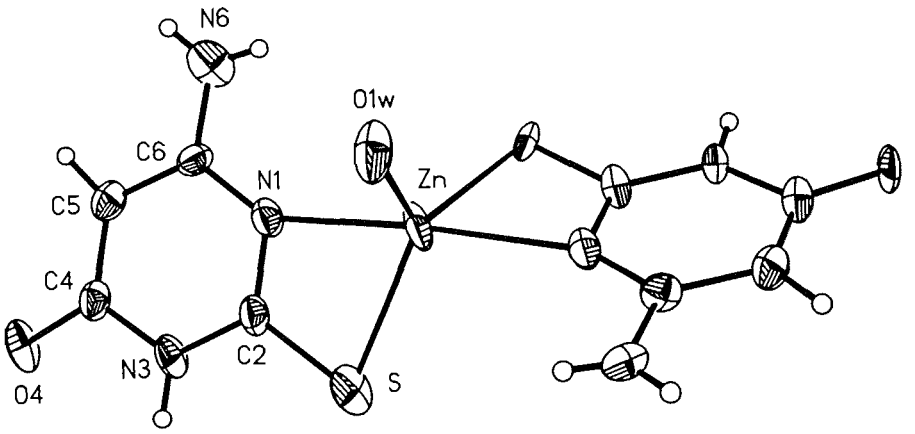

FIG. 1. View of the molecule of $[Zn(HATU)_2(H_2O)]$. 50% probability thermal ellipsoids are shown.

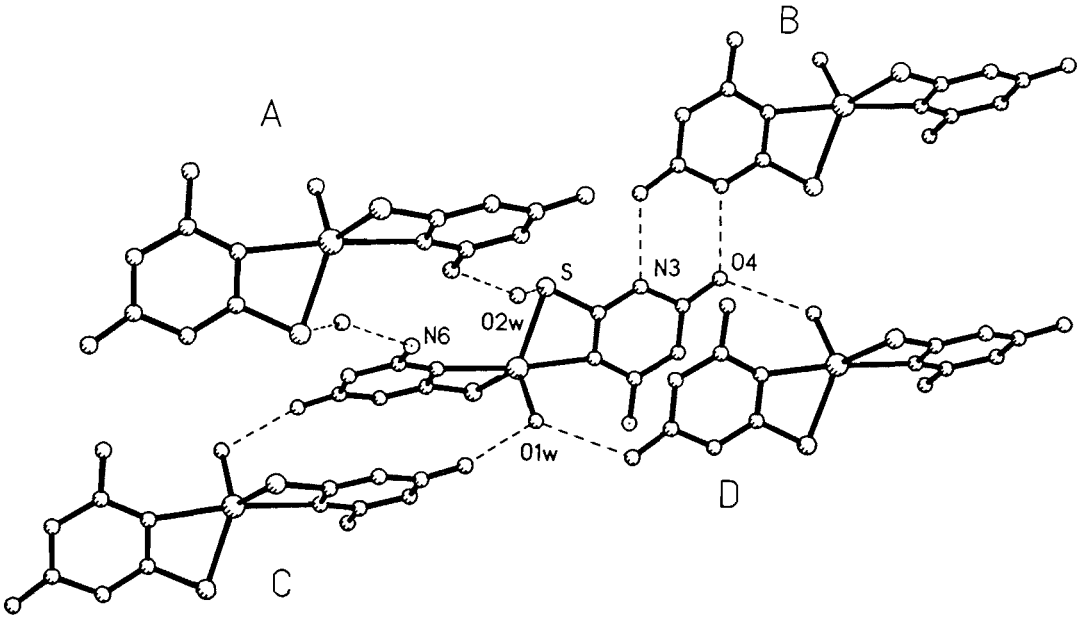

FIG. 2. Hydrogen bonds formed between a molecule of $[Zn(HATU)_2(H_2O)]$ and some of its neighbours. Considering the central molecule as placed at x, y, z, the symmetry codes for the rest are as follows: Molecule A: $1/2 - x, 1/2 - y, -z$. Molecule B: $1 - x, -y, 1 - z$. Molecule C: $-1/2 - x, 1/2 - y, -z$. Molecule D: $1/2 - x, 1/2 - y, 1 - z$.

when the samples are heated at 250°C (anhydrous complexes); the compound **8**, in particular, when heated at this temperature, displays a spectrum appreciably different from that of compound **1**.

The signals of the ^1H and ^{13}C spectra of H_2ATU and its zinc, cadmium, and mercury complexes are listed in Table 4. The spectrum of 6-amino-2-methylthiouracil (HAMTU) has also been included for comparison. Assignments were made comparing the spectra with those of 6-methyl-2-thiouracil (8), 4,6-diamino-2-thiopyrimidine (3*b*), 2-thiouracil (9), and pyrimidine-2-thione (10).

The spectra of zinc and cadmium complexes are virtually identical, the only significant difference with respect to the free ligand being the downfield shift by more than 6 ppm of the C6 resonance. This may be due to N1 deprotonation and coordination, the binding through the amino group being ruled out by the unchanged NH_2 signal in the proton spectra; the sulphur atom seems not to bind in solution as deduced from the unchanged C2 resonance.

Contrarily, the ^{13}C spectrum of the mercury complex exhibits an upfield shift of C2 by more than 10 ppm and a downfield shift of C6 by 8 ppm, this spectrum being almost identical to that of HAMTU. We can explain this fact by supposing that a strong binding of the mercury to the sulphur atom takes place in solution, generating an electronic distribution similar to that of the methyl derivative, with the mercury playing a role similar to that of the methyl group.

The solid state diffuse reflectance spectrum of 8 is typical for Ni(II) in a tetragonally distorted octahedral environment (D_{4h} symmetry) (11), with bands at 7860, 9760, 12 440, 14 700, and 25 150 cm^{-1}, assignable to the transitions from the ground state $^3B_{1g}$ to, respectively, ^3E_g (T_2), $^3B_{2g}$, $^3A_{2g}$, ^3E_g (T_1), $^3A_{2g}$, and ^3E_g (P) (the two latter are overlapped), the transitions to the ^3E_g levels being more intense, as expected.

The other nickel(II) complex (**1**) displays a spectrum assignable to a tetrahedral environment, with bands at 15 850 ($^3T_1 \rightarrow {}^3T_1$ (P), band with a shoulder) and 7600 cm^{-1} ($^3T_1 \rightarrow$

Can. J. Chem. Downloaded from www.nrcresearchpress.com by 88.255.202.194 on 09/08/12
For personal use only.

TABLE 5. Bond distances and angles

Distances (Å)		Angles (deg)	
Zn—N1	2.235(2)	N1—Zn—S	69.16(7)
Zn—S	2.353(1)	N1—Zn—O1W	94.50(8)
Zn—O1W	1.968(4)	S—Zn—O1W	116.78(3)
N1—C2	1.322(4)	N1—Zn—N1[a]	171.0(1)
N1—C6	1.367(4)	N1—Zn—S[a]	106.6(1)
C2—S	1.721(3)	S—Zn—S[a]	126.4(1)
C2—N3	1.350(4)	Zn—N1—C2	93.4(2)
N3—C4	1.392(4)	Zn—N1—C6	147.8(2)
C4—O4	1.266(4)	C2—N1—C6	118.6(2)
C4—C5	1.387(5)	N1—C2—S	117.2(2)
C5—C6	1.394(4)	N1—C2—N3	122.1(3)
C6—N6	1.332(5)	S—C2—N3	120.7(3)
		Zn—S—C2	80.0(1)
		C2—N3—C4	122.2(3)
		N3—C4—O4	116.8(3)
		N3—C4—C5	115.9(3)
		O4—C4—C5	127.3(3)
		C4—C5—C6	120.0(3)
		N1—C6—C5	121.1(3)
		N1—C6—N6	116.1(3)
		C5—C6—N6	122.7(3)
Distances (Å) in hydrogen bonding:			
O2W—S (x, y, z)		3.274(5)	
N6—O2W ($1/2 - x$, $1/2 - y$, $1/2 + z$)		2.853(7)	
O1W—O4 ($1/2 - x$, $1/2 - y$, $1 - z$)		2.724(5)	
N3—O4 ($1 - x$, $-y$, $1 - z$)		2.825(4)	

[a] $\bar{x}$, y, $1/2 - z$.

$^3A_2$), the transition $^3T_1 \rightarrow {}^3T_2$ not being observed. The forbidden transitions to levels ^1D are observable as weak bands at 10 150 and 10 810 cm^{-1}. The room temperature magnetic moments of the two nickel complexes are 3.20 and 3.44 Bohr magneton (B.M.) respectively, with a higher orbital contribution for the tetrahedral geometry.

On the other hand, the diffuse reflectance spectra of the cobalt complex (**2**, room temperature magnetic moment 4.42 B.M.), with bands at 22 200 (shoulder), 17 750, 12 800, and 5400 cm^{-1}, does not fit for either an octahedral or for a tetrahedral environment (11), but is very similar to the spectrum of $[CoL_2Br]Br$ (L = acetone-4-phenylthiosemicarbazone) (12), in which the geometry around the metal ion is a distorted trigonal bipyramid. The presence of relatively intense bands between 11 500 and 13 000 cm^{-1} is usually taken as diagnostic for five-coordinated Co(II) (13), although it is not easy to distinguish between the trigonal bipyramidal and the square pyramidal environments.

Description of the crystal structure of
$[Zn(HATU)_2(H_2O)] \cdot 2H_2O$

The X-ray diffraction study of **3** shows that the metal atom is placed in a crystallographic twofold axis that relates two 2-thiopyrimidinato ligands that bind the zinc atom through their sulphur and nitrogen-1 atoms. The twofold axis also passes through a coordinated water molecule, which completes a coordination number of five for this complex (Fig. 1).

The geometry is somewhat irregular, but may be described as a trigonal bipyramid in which the N1 atoms of the two ligands occupy the axial apices with the sulphur atoms deviating 0.76 Å from the equatorial plane due to the formation of the four-member chelate ring (the "equatorial plane" is defined as the mediatrix plane of the N1–N1 segment). This also distorts the bond angles around the metal atom.

The distance Zn—O1W (Table 5) is similar to those in other compounds with water (14) coordinated to Zn, whereas the distances Zn—S and Zn—N1 are comparable to those in compounds with five-membered S,N coordinated chelate rings around zinc (15); we have not found any bibliographic reference including a Zn—N—C—S four-member chelate. The chelate ring deviates appreciably from planarity, with C2 placed 0.08 Å out of the plane defined by Zn, S, and N1.

The distances C2—S and C2—N1 are, respectively, significantly longer and shorter than those in the free ligand (*2b*), as could be expected for the deprotonation of N1. Changes in the angles around C2 and N1 (−4.7° for S—C2—N1, +6.5° for N3—C2—N1, −5.3° for C2—N1—C6) are due to the same reason plus the chelation effect. The changes in the remaining distances are below 3σ whereas the changes in the remaining angles are below 2.5°. The pyrimidine moiety is virtually planar with endocyclic atoms deviating less than 0.01 Å from the average plane, with only O4 placed 0.04 Å out of it. The dihedral angle between this plane and the one defined by Zn, S, and N1 is 5.4° and the dihedral angle between the two pyrimidine planes coordinated to the metal atom is 50.5°.

The hydrogen bonding network is represented in Fig. 2, the corresponding distances appearing in Table 5. The O2W · · · S contact has been considered as a weak hydrogen bond because the distance involved is just below the sum of

Can. J. Chem. Downloaded from www.nrcresearchpress.com by 88.255.202.194 on 09/08/12
For personal use only.

the van der Waals radii (16). The loose attachment of O2W to the structure may explain the high thermal motion of this atom.

1. (*a*) V. N. Krishnamurthy, K. V. Naglowara, P. L. Narasumha, and B. Praphulla. Br. J. Pharmacol. Chemother. **31**, 1 (1967); (*b*) R. Truhant and M. Declercq. Rev. Fr. Etud. Clin. Biol. **7**, 298 (1962); (*c*) R. H. Lindsay, H. Nakagawa, and P. P. Cohen. Endocrinology, **76**, 728 (1965).
2. (*a*) S. Swaminathan and K. K. Chacko. Acta Crystallogr. Sect. B: Struct. Crystallogr. Cryst. Chem. **B34**, 3108 (1978); (*b*) E. S. Raper, R. E. Oughtred, and I. W. Nowell. Acta Crystallogr. Sect. C: Cryst. Struct. Commun. **C41**, 758 (1985).
3. (*a*) M. A. Romero, M. D. Gutiérrez, R. López, J. M. Salas, M. I. Arriortúa, and F. J. Zúñiga. Inorg. Chim. Acta, **136**, 87 (1987); (*b*) M. D. Gutiérrez, R. López, M. A. Romero, and J. M. Salas. Can. J. Chem. **66**, 249 (1988); (*c*) M. D. Gutiérrez, M. A. Romero, R. López, and J. M. Salas. Transition Metal Chem. **13**, 451 (1988); (*d*) M. D. Gutiérrez, M. A. Romero, R. López, M. Nogueras, and A. Sánchez. Thermochim. Acta, **168**, 197 (1990); (*e*) M. A. Romero, J. M. Salas, R. López, M. D. Gutiérrez, K. Panneerselvam, K. K. Chacko, K. Aoki, and H. Yamazaki. Inorg. Chim. Acta, **172**, 253 (1990).
4. (*a*) M. P. Sánchez, J. M. Salas, M. A. Romero, E. Colacio, and M. N. Moreno. Thermochim. Acta, **93**, 77 (1985); (*b*) M. P. Sánchez, J. M. Salas, and M. A. Romero. J. Therm. Anal. **31**, 361 (1986); (*c*) M. P. Sánchez, J. M. Salas, and M. A. Romero. Monatsh. Chem. **118**, 883 (1987).
5. F. Hueso, M. N. Moreno, J. M. Salas, and M. A. Romero. Thermochim. Acta, **177**, 119 (1991).
6. (*a*) W. Traube. Justus Liebigs Ann. Chem. **331**, 64 (1904); (*b*) B. R. Baker, J. P. Joseph, and R. E. Schaud. J. Org. Chem. **19**, 631 (1954).
7. E. S. Raper. Coord. Chem. Rev. **61**, 115 (1985).
8. J. R. Lusty, J. Peeling, and M. A. Abdel-Aal. Inorg. Chim. Acta, **56**, 21 (1981).
9. (*a*) G. C. Stocco, A. Tamburello, and M. A. Girasolo. Inorg. Chim. Acta, **78**, 57 (1983); (*b*) Y. Wei-Da and H. Yin-Ping. Polyhedron, **9**, 2747 (1990).
10. (*a*) D. Kovala, P. Kyrkou, and I. Zakharoba. Polyhedron, **10**, 1507 (1991); (*b*) R. Shunmugam and D. N. Sathyanarayana. Indian J. Chem. **23A**, 742 (1984).
11. A. B. P. Lever. Inorganic electronic spectroscopy. Elsevier, Amsterdam. 1984. pp. 479–534.
12. G. Dessy, V. Fares, L. Scaramuza, A. A. G. Tomlinson, and G. De Munno. J. Chem. Soc. Dalton Trans. 1549 (1978).
13. (*a*) I. Bertini, D. Gatteschi, and A. Scozzafava. Inorg. Chem. **14**, 812 (1975); (*b*) C. Bellito, A. A. G. Tomlinson, C. Furlani, and G. De Munno. Inorg. Chim. Acta, **27**, 269 (1978).
14. M. Quirós, J. M. Salas, M. P. Sánchez, J. R. Alabart, and R. Faure. Inorg. Chem. **30**, 2916 (1991).
15. (*a*) V. L. Goedken and G. G. Christoph. Inorg. Chem. **12**, 2316 (1973); (*b*) D. C. Liles, M. McPartlin, and P. A. Tasker. J. Am. Chem. Soc. **99**, 7704 (1977).
16. A. Bondi. J. Phys. Chem. **68**, 441 (1964).

Can. J. Chem. Downloaded from www.nrcresearchpress.com by 88.255.202.194 on 09/08/12
For personal use only.

Estérification de l'acide stéarique catalysée par les titanates greffés

CLAUDINE BLANDY, JEAN-LOUIS PELLEGATTA ET ROBERT CHOUKROUN

Laboratoire de chimie de coordination du Centre national de la recherche scientifique, Unité propre de recherche 8241 liée par conventions à l'Université Paul Sabatier et à l'Institut National Polytechnique, 205 route de Narbonne, 31077 Toulouse CEDEX, *France*

ET

BERNARD GILOT[1] ET ROLAND GUIRAUD

Laboratoire de physicochimie des procédés de l'École nationale supérieure d'ingénieurs de génie chimique, 18 chemin de la Loge, 31078 Toulouse CEDEX, *France*

Reçu le 19 juin 1992

CLAUDINE BLANDY, JEAN-LOUIS PELLEGATTA, ROBERT CHOUKROUN, BERNARD GILOT et ROLAND GUIRAUD. Can. J. Chem. **71**, 34 (1993).

L'estérification de l'acide stéarique a été étudiée en utilisant comme catalyseurs des titanates greffés sur alumine ou silice. La réaction de greffage, obtenue par action de $CH_3Ti(OR)_3$ sur les sites acides du support, a été étudiée avec différents temps de contact et différentes concentrations. L'utilisation du titanate supporté conduit à une efficacité plus grande que celle du titanate employé en milieu homogène. L'activité du catalyseur est fortement augmentée en présence d'un solide broyé. Le catalyseur a pu être réutilisé plusieurs fois. La stabilité de la liaison (M)–$Ti(OR)_3$ (avec M = Al_2O_3 ou SiO_2) a été mise en évidence par des mesures cinétiques et par des réactions d'échanges des groupements alkoxy fixés sur le titane avec un alcool lourd.

CLAUDINE BLANDY, JEAN-LOUIS PELLEGATTA, ROBERT CHOUKROUN, BERNARD GILOT, and ROLAND GUIRAUD. Can. J. Chem. **71**, 34 (1993).

The esterification of stearic acid using titanates fixed on alumina or silica as catalysts has been studied. The anchoring of titanium, obtained by action of $CH_3Ti(OR)_3$ with the acid sites of the support, has been studied using different contact times and different concentrations. The heterogeneized catalyst leads to a better efficacity than the homogeneous system. The activity of the catalyst is strongly increased by using crushed solid instead of balls. The catalyst has been recovered and recycled. The stability of the (M)–$Ti(OR)_3$ bond (with M = Al_2O_3 or SiO_2) has been shown by kinetic measures and exchange reactions of the alcoxy groups fixed on titanium with heavy alcohol.

Introduction

Nous avons étudié l'estérification de l'acide stéarique par l'isopropanol pour laquelle l'utilisation de catalyseurs acides n'est pas assez sélective car elle conduit à haute température à la deshydratation de l'isopropanol et à un ralentissement de la réaction dû à la présence d'eau (1).

L'utilisation des titanates en milieu homogène, largement développée en estérification et transestérification (2), permet, tout en diminuant le temps de réaction, d'obtenir des esters de masse molaire élevée et d'indice d'acide faible. Mais il faut, pour obtenir l'ester pur, les éliminer en fin de réaction par une hydrolyse à la vapeur d'eau suivie d'une filtration.

Nous avons donc cherché à greffer le catalyseur sur un support solide pour éviter ces opérations de finition et permettre une production continue par passage sur le solide catalytique. Les essais préliminaires ont montré que les performances du système homogène étaient maintenues en hétérogène (3). Nous avons donc étudié les conditions d'obtention, la récupération et la réutilisation du titanate greffé.

Resultats et discussion

Greffage sur un solide

La fixation d'un composé du titane sur un support peut se réaliser en faisant réagir une liaison Ti—Cl avec des groupements hydroxyle de la surface du solide (4). Nous avons préféré utiliser la réaction de $CH_3Ti(Oi\text{-}Pr)_3$ avec les sites de Brönsted, même très faibles, d'une alumine ou d'une silice. On peut écrire la réaction de greffage :

$$[1] \quad CH_3Ti(Oi\text{-}Pr)_3 + HO\text{-}[M] \rightarrow CH_4 + [M]OTi(Oi\text{-}Pr)_3$$

avec M = Al, Si.

On peut suivre facilement la réaction [1] par mesure du volume de méthane dégagé et par dosage du titane dans le solide. Les quantités fixées sont fonction de l'état du solide, de la durée du contact et de la concentration de la solution de $CH_3Ti(Oi\text{-}Pr)_3$.

Comme on pouvait s'y attendre, la réaction de fixation est beaucoup plus rapide sur des solides en poudre qu'avec les billes poreuses. Nous avons testé l'influence du temps de contact du titanate avec le support : pour une concentration de 0,07 M de $CH_3Ti(Oi\text{-}Pr)_3$, on obtient 8,6 et 10,1 mg/g de titane fixé sur le support pour des temps respectifs de 12 et 72 h. Pour un temps de contact donné, la quantité de titane greffé augmente avec la concentration de la solution de $CH_3Ti(Oi\text{-}Pr)_3$. La figure 1 montre l'influence de la concentration pour un temps de contact de 12 h. On constate donc que, si les billes sont plus faciles à manipuler, leur greffage est limité par diffusion du réactif à l'intérieur des pores, phénomène déja observé lors de la fixation de $TiCl_4$ sur de la silice (4). Nous verrons que les mêmes limitations vis à vis de la réaction d'estérification diminueront l'activité apparente du catalyseur.

Le spectre d'émission des rayons X (RX) montre une répartition homogène des atomes de titane dans le solide (1,1 atome de titane/nm^2).

Nous avons également cherché à réaliser un greffage de $(N_3)_2Ti(Oi\text{-}Pr)_2$ sur de la silice pour essayer de fixer le ti-

[1]Auteur à qui adresser toute correspondance.

Can. J. Chem. Downloaded from www.nrcresearchpress.com by 88.255.202.194 on 09/08/12
For personal use only.

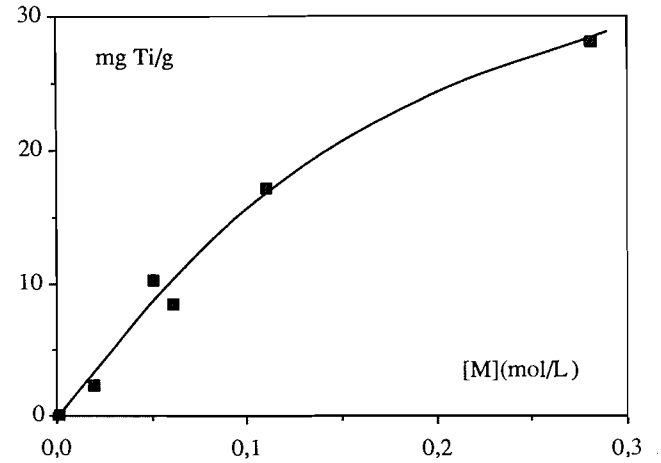

FIG. 1. Greffage sur le support : influence de la concentration en $CH_3Ti(Oi\text{-}Pr)_3$, temps de contact : 12 h, température : 25°C.

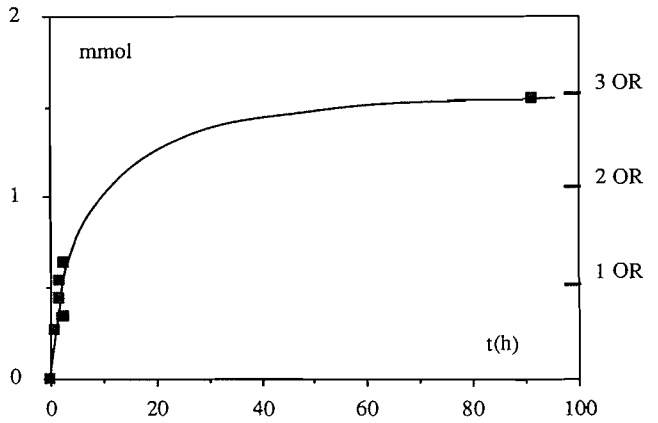

FIG. 2. Réaction du support greffé avec le 1-dodécanol à 50°C : production du 2-propanol (mmol) en fonction du temps (h) (à droite sont indiqués les nombres de groupements alcoxy échangés).

tane sur deux sites acides voisins avec libération de N_3H comme cela a déjà été observé en phase homogène en présence d'alcools (5). Nous avons obtenu la formation d'une seule liaison Si—O—Ti par titane, comme cela a déja été décrit lors du greffage sur silice de Cp_2TiCl_2 et $TiCl_4$ (6).

Caractérisation et irréversibilité du greffage

Pour faire le bilan de la réaction de greffage et vérifier la stabilité des liaisons Si—O—Ti, nous utilisons l'échange des groupements alkoxy par réaction du composé greffé avec un alcool lourd selon la réaction :

$$[Si]\ OTi(Oi\text{-}Pr)_3 + 3C_{12}H_{25}OH \rightarrow 3i\text{-}PrOH + [Si]\ OTi(OC_{12}H_{25})_3$$

La libération de l'isopropanol attendue a été suivie au cours du temps par chromatographie en phase gazeuse. La figure 2 montre que l'échange est relativement lent à 50°C et correspond à la stoechiométrie attendue. Le titane reste donc bien fixé sur le support, les liaisons Si—O—Ti n'étant pas rompues.

Une opération analogue avec le solide greffé par $(N_3)_2Ti(Oi\text{-}Pr)_2$ nous a montré l'existence d'une seule liaison support–titane et donc l'intérêt de cette méthode d'échange pour connaître la nature des solides mis en jeu.

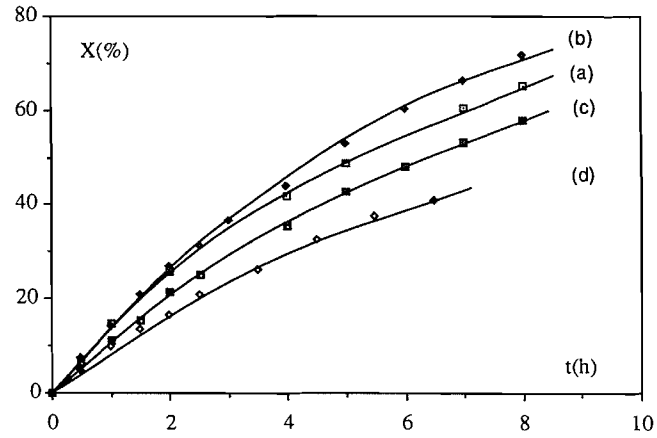

FIG. 3. Catalyse par le titanate greffé : avancement de l'estérification à 180°C en fonction du temps (h) pour (*a*) Al_2O_3, (*b*) Al_2O_3 greffée, (*c*) Al_2O_3 greffée partiellement hydrolysée, (*d*) réaction non catalysée. Indice d'acide de départ $n = 200$.

Le catalyseur hétérogène a également été caractérisé par son spectre de RMN du ^{13}C à l'état solide (voir spectre 1) qui se présente sous la forme de deux singulets (δ = 65,8 et

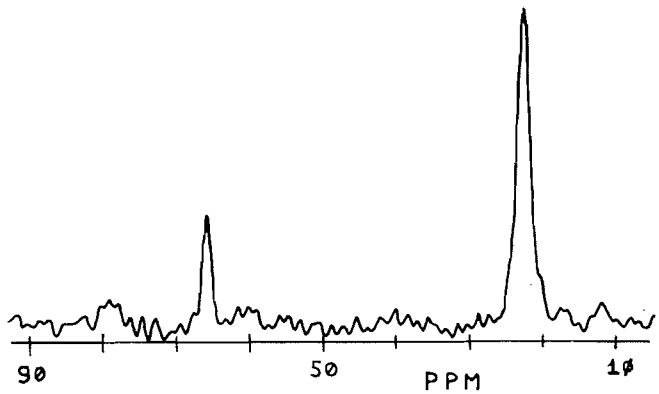

22,3 ppm) attribuables respectivement aux C_α (méthine) et C_β du groupe isopropyle par comparaison avec les déplacements obtenus pour $CH_3Ti(Oi\text{-}Pr)_3$ à l'état pur (δ = 76,3 (C_α) et 25,1 ppm (C_β)) (7).

Utilisation du solide greffé

Comme pour les estérifications de l'acide stéarique en milieu homogène, nous avons utilisé un réacteur semi-continu (8). La réaction étudiée :

$$CH_3(CH_2)_{16}COOH + C_3H_7OH \rightarrow CH_3(CH_2)_{16}COOC_3H_7 + H_2O$$

se produit lentement en absence de catalyseur mais elle est aussi très légèrement accélérée par le support seul qui présente des sites acides.

La figure 3 compare des courbes donnant les taux de conversion en fonction du temps pour différentes conditions de réaction : avec l'alumine greffée la vitesse de réaction est augmentée (courbe (*b*)), les courbes (*a*) et (*d*) correspondent à l'alumine seule et à la réaction non catalysée; on peut paraître surpris de ne pas voir un grand écart entre les courbes (*a*) et (*b*) mais il faut rappeler qu'en début de réaction, lorsque la concentration en acide est grande, la contribution de la réaction non catalysée est importante (3) et masque l'effet du titane. On verra plus loin (figure 7) que ce n'est plus

Can. J. Chem. Downloaded from www.nrcresearchpress.com by 88.255.202.194 on 09/08/12
For personal use only.

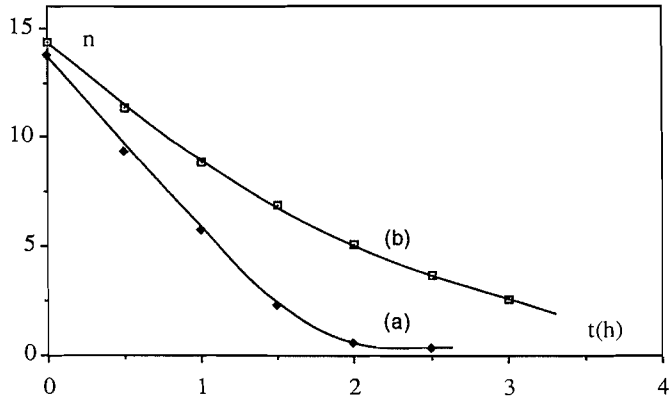

FIG. 4. Comparaison de la catalyse homogène et hétérogène : tracé de l'indice d'acide (n) en fonction du temps (h) à 180°C; (a) catalyseur hétérogène contenant 11 mg Ti/g; (b) catalyseur homogène, soit 8 mmol L^{-1} de Ti(O*i*-Pr)$_4$.

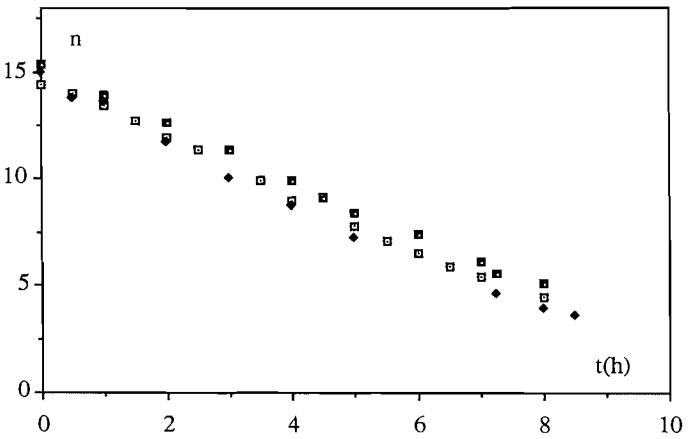

FIG. 5. Réutilisation du titanate supporté : tracé de l'indice d'acide (n) en fonction du temps (h) à 180°C pour 34 g L^{-1} de silice contenant 2,4 mg Ti/g.

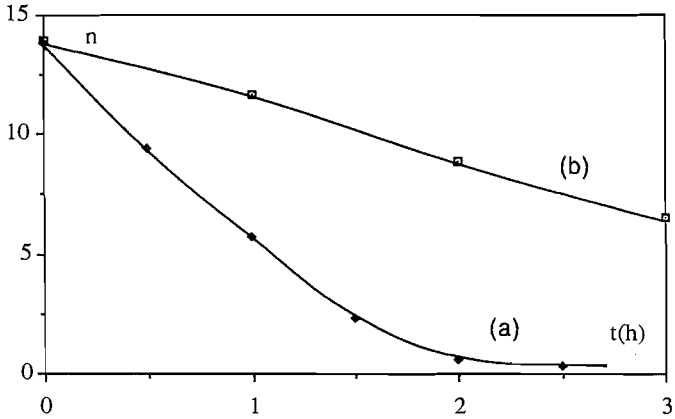

FIG. 6. Limitation diffusionnelle : tracé de l'indice d'acide (n) en fonction du temps (h) à 180°C pour 44 g L^{-1} de catalyseur hétérogène contenant 17 mg Ti/g (a) en poudre, (b) en billes.

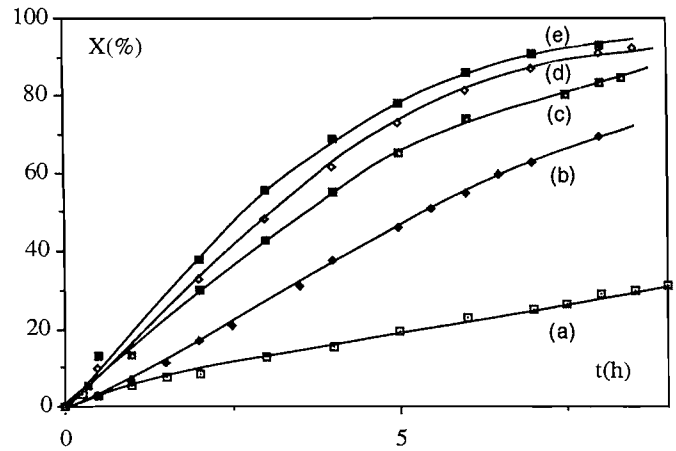

FIG. 7. Influence de la teneur en titane du solide : avancement relatif de la réaction (%) en fonction du temps (h) à 180°C pour 34 g L^{-1} de silice contenant (a) 0, (b) 2,4, (c) 7,6, (d) 17,1 et (e) 28,1 mg Ti/g. Indice d'acide de départ n = 15.

le cas lorsque l'indice d'acide est beaucoup plus faible. La courbe (c) correspond à l'utilisation d'un catalyseur greffé partiellement hydrolysé (réemployé sans précaution). On voit que cette hydrolyse n'a pas libéré les sites acides du support : la liaison Ti—O*i*—Pr semble donc plus sensible à l'hydrolyse que les liaisons Al—O—Ti.

Nous avons ensuite pour une même concentration apparente en titane comparé l'activité du catalyseur hétérogène avec celle de Ti(O*i*-Pr)$_4$ utilisé en milieu homogène. La figure 4 montre que, dans ces conditions (à 180°C), le titane greffé est plus efficace que le titane employé en milieu homogène. Les constantes de vitesse apparentes sont assez différentes : $1,7 \times 10^{-4}$ s^{-1} pour le milieu homogène, $5,2 \times 10^{-4}$ s^{-1} pour l'hétérogène. Ce résultat est facile à interpréter si on considère qu'un composé dimère ne peut se former à la surface du solide et donc que tout le titane fixé est actif.

Stabilité et réutilisation du catalyseur supporté

L'activité catalytique se maintient au cours de la réaction puisque le même modèle cinétique peut représenter l'ensemble des points expérimentaux relatifs à une expérience. On peut, moyennant quelques précautions en fin de réaction (élimination de l'alcool sous vide), réutiliser efficacement le catalyseur. La figure 5 montre trois cycles de réutilisation successifs de 10 h. Les dosages de titane permettent d'affirmer que celui-ci reste solidement accroché au support : on en retrouve 97% après 8 h d'utilisation continue et 90% après les trois cycles, soit après 30 h d'utilisation.

Si le catalyseur ne se transforme pas au cours de la réaction, il est par contre très probable qu'à 180°C les groupements alkoxy fixés sur le titane s'échangent dès le début de la réaction avec un ou plusieurs groupements acyle. Les échanges entre acide stéarique et titanate sont déja connus en milieu homogène (9).

Nous développons une étude analogue par action de divers acides sur le catalyseur supporté.

Limitations diffusionnelles

Nous avons ensuite comparé les activités des billes et d'une poudre obtenue à partir des billes broyées. La figure 6 montre que le broyage cause une très grande augmentation d'activité : pour obtenir 50% d'avancement, il faut 3 h avec les billes et seulement 50 min pour la même quantité de catalyseur broyé. De même, si on greffe sur des billes des teneurs en titane croissantes (concentration en $CH_3Ti(O$*i*$-Pr)_3$ plus importante) on n'obtient pas un accroissement correspondant d'activité (figure 7). En effet, en présence d'une

Can. J. Chem. Downloaded from www.nrcresearchpress.com by 88.255.202.194 on 09/08/12
For personal use only.

TABLEAU 1. Caractérisation des solides

Solides	Composition	Caractéristiques	
		Physiques	Chimiques[a]
Alumine	Al_2O_3 95%	145 $m^2 g^{-1}$	
Condéa	SiO_2 0,035%	Pores 0,45 $cm^3 g^{-1}$	$H_0 > 4,8$
Puralox NWA 150	Na_2O 50 ppm	Particules 100–500 μm	
Silice	$Na_2O < 3000$ pm	277 $m^2 g^{-1}$	
Rhône-Poulenc	$CaO < 1500$ ppm	Billes 5–6 mm	$3,3 < H_0 < 4,8$
SPH 540	$SO_4^- < 400$ ppm	Poudre 90% < 200 μm	

[a] H_0 = fonction d'acidité de Hammet (10).

faible quantité de titane, les sites les plus accessibles sont greffés les premiers et, en augmentant la quantité de titane, on greffe les sites moins accessibles peu utiles à la catalyse.

Conclusion

Le greffage du titane sur un support solide semble une solution intéressante pour la catalyse. Il est préférable d'utiliser un solide en poudre (même grossière). L'absence probable de dimère conduit à-des activités importantes à basse température. Le solide greffé est très stable : on peut envisager des applications pour l'obtention d'esters ou de polyesters exempts de titane sans opération de finissage compliquée.

Nous pensons étudier maintenant l'emploi de ces solides pour des réactions de transestérification à basse température.

Partie expérimentale

Techniques analytiques

Les acidités des supports ont été estimées par la méthode de titrage par une amine en présence de rouge neutre et de *p*-dimethylaminoazobenzène comme indicateurs (10). Les supports sont chauffés sous vide à 160°C pendant 24 h avant utilisation; leurs caractéristiques sont données dans le tableau 1. Les catalyseurs supportés sont obtenus sous atmosphère inerte en utilisant comme solvant du toluène distillé sur sodium et dégazé avant usage. Les composés $CH_3Ti(Oi\text{-}Pr)_3$ et $(N_3)_2Ti(Oi\text{-}Pr)_2$ ont été synthétisés en utilisant les méthodes décrites respectivement selon les références 11 et 5.

Les avancements de réaction sont déterminés par le suivi de l'indice d'acide (*n*) du mélange réactionnel selon la norme AFNOR, T 60-112, 1959. Les dosages de titane ont été déterminés par colorimétrie à 410 nm sur des complexes dans des solutions sulfuriques d'eau oxygénée obtenus par un traitement à reflux de 12 h dans l'acide. Les chromatographies en phase gazeuse ont été effectuées sur Intersmat IGC 121ML équipé d'une colonne de 2 m remplie de 10% Carbowax 20 M sur support Chromosorb PAW 80/100. Les spectres d'émission de RX ont été enregistrés sur Camebax SX50. Le spectre RMN du ^{13}C a été enregistré sur Bruker MSL 300 à 75,47 MHz équipé d'une tête de mesure de type «double bearing», en polarisation croisée (temps de contact 5 ms) et en utilisant le TMS comme référence externe.

Préparation du catalyseur greffé

On ajoute à température ambiante une solution de $CH_3Ti(Oi\text{-}Pr)_3$ (0,11 g; 0,87 mmol) dans le toluène (15 mL) sur une suspension de Al_2O_3 (2 g) dans le toluène (10 mL). On mesure le volume de méthane dégagé à l'aide d'une «Topler pump» (0,9 CH_4/Ti). Le solide est ensuite lavé à l'isopropanol et séché sous vide à 160°C pendant 24 h. La valeur obtenue pour le dosage de titane (13 mg Ti/g) correspond au nombre de sites acides atteints lors du greffage.

Réaction d'estérification

Elle est effectuée dans un réacteur semi-continu sous pression atmosphérique avec une alimentation automatique d'alcool de façon à maintenir sa concentration constante dans le milieu réactionnel (débit de l'ordre de 100 mL/h). L'acide stéarique (200 g; 0,7 mol) est chauffé à 180°C dans le réacteur en présence du catalyseur avec un rapport molaire [catalyseur]/[acide] variant de 0,07 à 0,7%. La distillation en continu de l'isopropanol permet d'éliminer l'eau formée et conduit à une estérification totale.

Réutilisation du catalyseur

Il est nécessaire d'éliminer complètement l'alcool du réacteur par barbotage de gaz inerte avant de séparer le solide catalytique de l'ester car il faut empêcher toute libération d'eau avant séparation.

Remerciements

Nous remercions Mr Autefage (INSA, Toulouse, France) pour les enregistrements d'émission de RX et M. Lefebvre (IRC, Villeurbanne, France) pour la RMN du ^{13}C. La société Rhône-Poulenc nous a fourni la silice. Ce travail a été soutenu financièrement par la région Midi Pyrénées (France).

1. Z. Zaidan, S. Domenech et B. Gilot. Entropie, **129**, 62 (1986).
2. D. Seebach, E. Hugerbuehler, R. Naef, P. Schurrenbeger, B. Weid Man et M. Zueger. Synthesis, **138** (1982).
3. C. Blandy, D. Gervais, J.-L. Pellegatta, B. Gilot et R. Guiraud. J. Mol. Catal. **64**, L1 (1991).
4. (*a*) O. H. Ellestad. J. Mol. Catal. **33**, 289 (1985); (*b*) W. Skupinski, I. Cieslowska-Glinska et A. Wasilewski. J. Mol. Catal. **33**, 129 (1985).
5. R. Choukroun et D. Gervais. J. Chem. Soc. Dalton Trans. 1800 (1980).
6. D. H. Ellestad. J. Mol. Catal. **9**, 423 (1980).
7. C. Blandy, R. Guerreiro et D. Gervais. J. Organomet. Chem. **128**, 415 (1977).
8. E. S. M. Nasr. Thèse Docteur Ingénieur, Toulouse, 22 juin 1983.
9. K. C. Pande et R. C. Mehrotra. Z. Anorg. Allg. Chem. **290**, 87 (1957).
10. K. Tanabe. Solid acid and base catalysts. Academic Press, London. 1969.
11. K. Clauss. Justus Liebigs Ann. Chem. **711**, 19 (1968).

Can. J. Chem. Downloaded from www.nrcresearchpress.com by 88.255.202.194 on 09/08/12
For personal use only.

Vinyl ether hydrolysis XXVIII. The mechanism of reaction of methyl α-(2,6-dimethoxyphenyl)vinyl ether[1]

J. JONES[2] AND A. J. KRESGE[3]

Department of Chemistry, University of Toronto, Toronto, Ont., Canada M5S 1A1

Received May 8, 1992

J. JONES and A. J. KRESGE. Can. J. Chem. **71**, 38 (1993).

The acid-catalyzed hydrolysis of methyl α-(2,6-dimethoxyphenyl)vinyl ether in aqueous solution at 25°C occurs with the hydronium ion catalytic coefficient $k_{H^+} = 2.86\ M^{-1}\ s^{-1}$ and gives the solvent isotope effect $k_{H^+}/k_{D^+} = 3.68$; this indicates that reaction occurs by rate-determining proton transfer from the catalyst to the substrate to generate an alkoxycarbocation intermediate. An oxygen-18 tracer study shows further that, despite the steric hindrance provided by its two *ortho* substituents, this cation then reacts by addition of water to the cationic carbon atom to generate a hemiacetal, and not by nucleophilic attack of water on the methyl group remote from the carbocationic center:

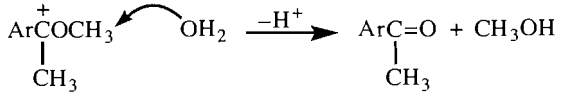

J. JONES et A. J. KRESGE. Can. J. Chem. **71**, 38 (1993).

L'hydrolyse acidocatalysée de l'oxyde de méthyle et de l'α-(2,6-diméthoxyphényl)vinyle, en solution aqueuse, à 25°C, se produit avec un coefficient catalytique de l'ion hydronium, $k_{H^+} = 2{,}86\ M^{-1}\ s^{-1}$, et un effet isotopique du solvant $k_{H^+}/k_{D^+} = 3{,}68$; ces résultats indiquent que l'étape déterminante de la réaction implique un transfert de proton du catalyseur vers le substrat avec la formation d'un intermédiaire alkoxycarbocation. Une étude à l'aide d'un marqueur contenant de l'oxygène-18 montre de plus que ce cation réagit alors par addition d'eau sur l'atome de carbone cationique pour générer un hémiacétal et, non pas, par une attaque nucléophile de l'eau sur le groupe méthyle qui se trouve loin du centre carbocationique :

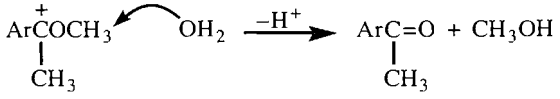

[Traduit par la rédaction]

The generally accepted reaction mechanism for acid-catalyzed hydrolysis of vinyl ethers consists of rate-determining protonation of the vinyl group on the β-carbon, followed by rapid hydration of the alkoxycarbocation thus formed and fast decomposition of the ensuing hemiacetal intermediate, eq. [1].[4] An alternative scheme involving nucleo-

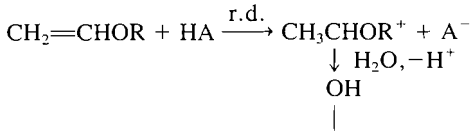

[1]

philic attack of water on the alkyl group of the cation, eq. [2], has been ruled out by an early study using oxygen-18

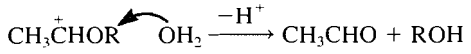

[2]

enriched water as the solvent, which showed that the oxygen atom of the alcohol product was not enriched in the oxygen tracer (2). This alternative mechanism is also inconsistent with the fact that ethyl vinyl ethers are more reactive than methyl vinyl ethers (3), inasmuch as nucleophilic attack on an alkyl group such as that shown in eq. [2] would occur more rapidly on methyl than on ethyl.

It is possible, however, that this alternative mechanism might operate in the hydrolysis of vinyl ethers with substituents that shield the α-carbon atom of its vinyl group, for then addition of water to the carbocationic center needed to form the hemiacetal intermediate in the conventional mechanism of eq. [1] would be impeded. This idea is supported by the fact that 2,4,6-trimethoxyacetophenone could not be converted into its dimethyl ketal by acid-catalyzed addition of methanol,[5] despite the ease with which this reaction can be used to prepare ketals of acetophenones without two *ortho* substituents (4). The synthesis of ketals by this route is similar to the hydrolysis of vinyl ethers by the conventional mechanism in that it requires addition of an oxygen nucleophile to an alkoxy carbocation, and its failure in the case of 2,4,6-trimethoxyacetophenone presumably occurs because approach to the carbocationic center is hindered by the *ortho* methoxyl groups, eq. [3].

We have undertaken to determine whether this structural feature can produce a mechanistic change in vinyl ether hydrolysis. Since only the *ortho* substituents are needed to produce this effect, we have chosen to perform our study with methyl α-(2,6-dimethoxyphenyl)-vinyl ether, **1**.

[1]Part XXVII: See ref. 8.

[2]Permanent address: Institute of Chemistry, Federal University of Rio de Janeiro, Rio de Janiero, Brazil.

[3]Author to whom correspondence may be addressed.

[4]For a brief review of the evidence and references to earlier literature, see ref. 1.

[5]G. M. Loudon, personal communication.

Can. J. Chem. Downloaded from www.nrcresearchpress.com by 88.255.202.194 on 09/08/12
For personal use only.

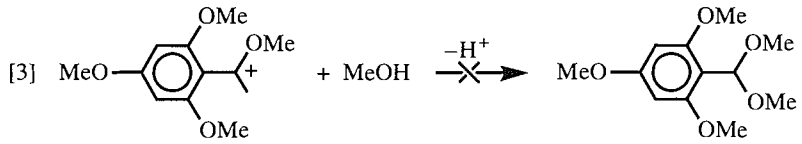

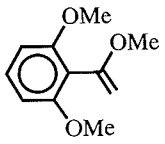

1

Experimental

Materials

Methyl α-(2,6-dimethoxyphenyl)vinyl ether was prepared by *O*-methylation of 2,6-dimethoxyacetophenone. A solution of 2.0 g 2,6-dimethoxyacetophenone (Aldrich), 2.5 g methyl *p*-toluenesulfonate, 1.5 g potassium *tert*-butoxide, and 3,5 g 18-crown-6-ether in 75 mL dimethylformamide was stirred at 100°C for 15 days. The reaction mixture was then cooled to room temperature, 150 mL of water was added, and the resulting solution was extracted with three 100-mL portions of diethyl ether. The combined ether extracts were dried with $MgSO_4$, the ether was removed by evaporation, and the residue was subjected to flash chromatography using 90:10 hexane: ethyl acetate as the eluant. This produced 2.2 g of a colorless solid: mp 48–50°C; ^{1}H NMR ($CDCl_3$), δ: 3.86 (s, 3H), 3.96 (s, 6H), 4.31 (*d*, *J* = 2.1 Hz, 1H), 4.65 (*d*, *J* = 2.1 Hz, 1H), 6.68–6.74 (m, 2H), 7.35–7.44 (m, 1H); MS, *m/e*: 194 (49%), 179 (42%), 163 (100%), 151 (20%), 135 (50%), 105 (28%), 91 (40%); HRMS, *m/e*, calcd.: 194.0943; found: 194.0931.

All other materials were best available commercial grades.

Kinetics

Rates of hydrolysis of methyl α-(2,6-dimethoxyphenyl)vinyl ether were determined by monitoring the increase in absorbance of the 2,6-dimethoxyacetophenone reaction product at λ = 270 nm. Measurements were made with a Cary 2200 spectrometer whose cell compartment was thermostatted at 25.0 ± 0.05°C. Reactions were performed by first allowing 3.0-mL portions of aqueous acids contained in quartz cuvettes to come to temperature equilibrium with the spectrometer cell compartment: 5.0-μL portions of acetonitrile stock solutions of substrate (ca. 10^{-2} M) were then added to the cuvettes, the cuvettes were shaken to effect mixing, and absorption measurements were begun. The data so obtained conformed well to the first-order rate law, and observed first-order rate constants were evaluated by least-squares fitting to an exponential function.

Product analysis

The origin of the carbonyl oxygen atom in the 2,6-dimethoxyacetophenone product of hydrolysis of methyl α-(2,6-dimethoxyphenyl)vinyl ether was determined by conducting the reaction in oxygen-18 enriched water. A solution containing 0.01 M $HClO_4$ was prepared by mixing one part of 1.0 M acid with 10 parts of enriched water (Aldrich, 20 at.% oxygen-18), and 10 μL of an acetonitrile stock solution of vinyl ether substrate (10^{-2} M) was added to 0.50 mL of this acid solution; this mixture was shaken to effect mixing and was then allowed to stand at room temperature. After 15 min (the hydrolysis half-time under these conditions is 20 s), the reaction mixture was extracted with two 0.5-mL portions of diethyl ether, the combined extracts were dried with $MgSO_4$, and the dried solution was subjected to analysis by gas chromatography (HP 5890) – mass spectroscopy (VG 70-250S), using electron impact ionization with an electron energy of 70 eV.

TABLE 1. Rates of hydrolysis of methyl α-(2,6-dimethoxyphenyl)vinyl ether in aqueous perchloric acid solutions at 25°C[a]

[Acid]/10^{-2} M	k/10^{-2} s^{-1}
H_2O:	
0.200	0.572, 0.574
0.400	1.08, 1.17, 1.20
0.600	1.73, 1.68, 1.78
0.800	2.21, 2.29, 2.38
1.50	4.29, 4.34, 4.42
2.00	5.83, 5.74, 5.54
k_{obs}/s^{-1} = (1.13 ± 3.38) × 10^{-4} + (2.86 ± 0.03)[$HClO_4$]	
D_2O:	
1.20	0.901, 0.893, 0.913
3.00	2.44, 2.50, 2.47
4.80	3.70, 3.58, 3.61
8.00	6.35, 6.19, 6.24
k_{obs}/s^{-1} = (0.86 ± 6.06) × 10^{-4} + (7.78 ± 0.12) × 10^{-1}[$DClO_4$]	
k_{H^+}/k_{D^+} = 3.68 ± 0.07	

[a]Ionic strength = 0.10 M ($NaClO_4$).

A control experiment was also performed in which an authentic sample of 2,6-dimethoxyacetophenone was used in place of methyl α-(2,6-dimethoxyphenyl)vinyl ether; the ketone was treated in exactly the same way for the same period of time as the vinyl ether.

Results

Rates of hydrolysis of methyl α-(2,6-dimethoxyphenyl)-vinyl ether were determined in dilute perchloric acid solutions of H_2O and D_2O. The data are summarized in Table 1 and are displayed in Fig. 1. It may be seen that observed first-order rate constants obtained in both solvents are accurately proportional to acid concentration; least-squares analysis gave the catalytic coefficients k_{H^+} = 2.86 M^{-1} s^{-1} and k_{D^+} = 0.778 M^{-1} s^{-1}, which provide the solvent isotope effect k_{H^+}/k_{D^+} = 3.68.

Mass spectral analysis of the product remaining in a spent hydrolysis reaction mixture showed a pattern identical to that obtained from an authentic sample of 2,6-dimethoxyacetophenone, with a parent peak at *m/e* 180, a more-abundant peak corresponding to loss of a methyl group at *m/e* 165, and additional less-abundant peaks produced by further loss of methyls at *m/e* 150 and 135. Each of these peaks was accompanied by weaker signals one mass unit higher, whose intensities were consistent with expectation for ions containing carbon-13 at its natural abundance.

Mass spectral analysis of the product obtained from a hydrolysis reaction conducted in oxygen-18 enriched water gave a pattern with the same features plus additional peaks two

Can. J. Chem. Downloaded from www.nrcresearchpress.com by 88.255.202.194 on 09/08/12
For personal use only.

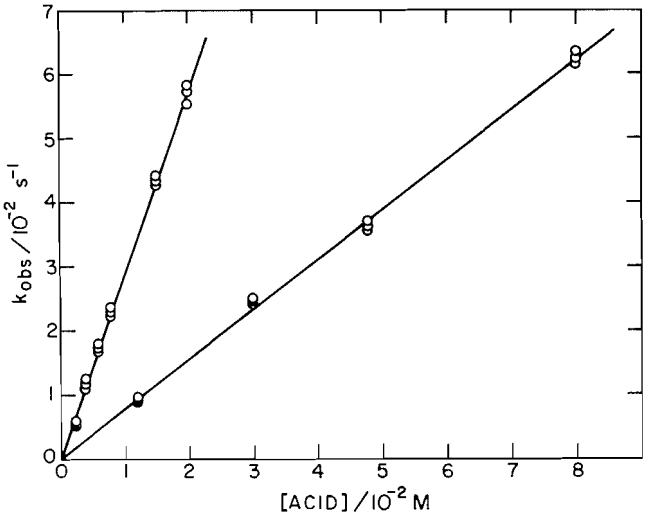

FIG. 1. Relationship between acid concentration and observed first-order rate constants for the hydrolysis of methyl α-(2,6-dimethoxyphenyl)vinyl ether in aqueous solution at 25°C; upper line: H_2O, lower line: D_2O.

mass units higher, i.e., at *m/e* 182, 167, 152, and 137, with carbon-13 satellites one mass unit above each of these. This shows that the 2,6-dimethoxyacetophenone hydrolysis product had become enriched in oxygen-18. The extent of this enrichment could be estimated by comparing the intensities of the signals of the ions in each of the groups at *m/e* 180–183, 165–168, and 159–153 (the signals at *m/e* 137 and 138 were too weak to be useful); the average of these three independent determinations, 22.6 ± 2.4%, agrees with the enrichment of the water used as the solvent, 19.8%.

A control experiment showed that 2,6-dimethoxyacetophenone does not undergo oxygen exchange with solvent water under the conditions of the vinyl ether hydrolysis reaction. This ketone was dissolved in oxygen-18 enriched water (19.8% enrichment) containing 0.01 M $HClO_4$, and, after a period of time corresponding to 40 hydrolysis half-times, was extracted from this solvent and subjected to mass spectral analysis. The spectrum obtained was identical with that given by a sample of 2,6-dimethoxyacetophenone that had not been exposed to enriched water.

Discussion

The solvent isotope effect on hydron transfer from the hydronium ion is generally smaller than that on hydron transfer from other oxygen acids because it contains an inverse ($k_H/k_D < 1$) secondary component in addition to a primary effect in the normal ($k_H/k_D > 1$) direction (5), and the isotope effect observed here for the hydrolysis of methyl α-(2,6-dimethoxyphenyl)vinyl ether, $k_{H^+}/k_{D^+} = 3.7$, is in fact a near-maximum value for this kind of effect (6). This isotope effect thus has an appreciable primary component, and it consequently provides clear indication that the present reaction occurs by rate-determining hydron transfer from the hydronium ion.

This conclusion is consistent with either the conventional reaction mechanism of eq. [1] or the alternative route of eq. [2], and it is therefore not diagnostic. The result of the oxygen-18 tracer experiment performed here, however, is diagnostic. In the conventional mechanism, addition of water to the carbocationic center of the alkoxycarbocation intermediate produces a hemiacetal whose hydroxyl group has the same isotopic composition as the solvent water. Decomposition of the hemiacetal then gives a carbonyl compound whose carbonyl oxygen atom is derived from the hemiacetal hydroxyl group and must therefore also have the same isotopic composition as the solvent water.[6] The hydrolysis of methyl α-(2,6-dimethoxyphenyl)vinyl ether by the conventional mechanism in oxygen-18 enriched water will thus produce 2,6-dimethoxyacetophenone with the same isotopic composition as the solvent, as observed.

In the alternative mechanism, on the other hand, nucleophilic attack on the alkyl group remote from the cationic center displaces a carbonyl compound whose carbonyl oxygen atom is derived from the original vinyl ether. Hydrolysis by this mechanism in oxygen-18 enriched water will therefore not produce an oxygen-18 enriched product, contrary to the present observation.

An oxygen-18 enriched product could also have been formed in the present case if 2,6-dimethoxyacetophenone underwent hydration–dehydration under the conditions of the hydrolysis reaction. The control experiment designed to detect this, however, showed that this did not happen. It is safe to conclude, therefore, that the vinyl ether hydrolysis reaction investigated here occurs by the conventional mechanism.

It is interesting that hydrolysis of the present substrate occurs only 3.8 times more rapidly than that of the parent substance with no α-substituent, methyl vinyl ether, **2**, for which $k_{H^+} = 0.76\ M^{-1}\ s^{-1}$ (6). The present substrate is also

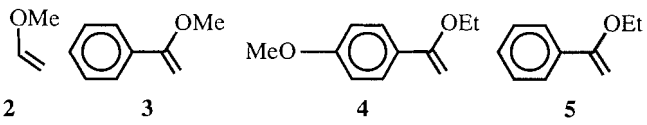

2 **3** **4** **5**

19 times less reactive than methyl α-phenylvinyl ether, **3**, for which $k_{H^+} = 53\ M^{-1}\ s^{-1}$ (6), despite the fact that the addition of methoxy groups to the aromatic ring might have been expected to make the present substrate more reactive: ethyl α-(4-methoxyphenyl)vinyl ether, **4**, for example, undergoes hydrolysis 5.5 times more rapidly than its unsubstituted analog, ethyl α-phenylvinyl ether, **5** (4*b*, 6). These unusual substituent effects imply that the aromatic ring of methyl α-(2,6-dimethoxyphenyl)vinyl ether is not very effective at stabilizing the positive charge of the carbocationic intermediate formed in its hydrolysis reaction, presumably because steric interactions between the cationic side chain and its *ortho* methoxy groups have forced the aromatic ring to rotate out of coplanarity with the cation's σ-bonded framework. This puts the methoxyl groups of the aromatic ring into positions where they can impede approach of a nucleophile to the cationic carbon atom, but apparently that impediment is not sufficient to exclude reaction by this route if the nucleophile is as small as a water molecule.

[6]This argument ignores oxygen kinetic isotope effects, but these will be small (see ref. 7) and can be neglected.

Can. J. Chem. Downloaded from www.nrcresearchpress.com by 88.255.202.194 on 09/08/12
For personal use only.

Acknowledgements

We are grateful to Conselho Nacional de Desenvolvimento Científico e Tecnológico for a fellowship to J.J. and to the Natural Sciences and Engineering Research Council of Canada for additional financial support of this work.

1. A. J. Kresge. Acc. Chem. Res. **20**, 364 (1987).
2. L. A. Kiprianova and A. F. Rekasheva. Dokl. Akad. Nauk S.S.S.R. **142**, 589 (1962).
3. Y. Chiang, W. K. Chwang, A. J. Kresge, and S. Szilagyi. Can. J. Chem. **58**, 124 (1980).
4. (*a*) G. M. Loudon, C. K. Smith, and S. E. Zimmerman. J. Am. Chem. Soc. **96**, 465 (1974); (*b*) Y. Chiang, W. K. Chwang, A. J. Kresge, L. H. Robinson, D. S. Sagatys, and C. I. Young. Can. J. Chem. **56**, 456 (1978).
5. A. J. Kresge and D. P. Onwood. J. Am. Chem. Soc. **86**, 5014 (1964); A. J. Kresge, D. P. Onwood, and S. Slae. J. Am. Chem. Soc. **90**, 6982 (1968); R. A. More O'Ferrall, G. W. Koeppl, and A. J. Kresge. J. Am. Chem. Soc. **93**, 9 (1971).
6. A. J. Kresge, D. S. Sagatys, and H. L. Chen. J. Am. Chem. Soc. **99**, 7228 (1977).
7. L. Melander and W. H. Saunders, Jr. Reaction rates of isotopic molecules. John Wiley, New York. 1980. pp. 273–275.
8. A. J. Kresge and M. Leibovitch. J. Am. Chem. Soc. **114**, 3099 (1992).

Can. J. Chem. Downloaded from www.nrcresearchpress.com by 88.255.202.194 on 09/08/12
For personal use only.

Synthesis and characterization of dimethyl- and dimethoxyphenylbis(*N*,*N*-dialkyldithiocarbamato)tellurium(IV) and chlorodimethyl- and chlorodimethoxyphenyl-(*N*,*N*-dialkyldithiocarbamato)tellurium(IV). Crystal structures of $Me_2Te[S_2CNMe_2]_2$ and $(p\text{-}MeOC_6H_4)_2Te[S_2CNMe_2]_2$

JANE H. E. BAILEY[1] AND JOHN E. DRAKE

Department of Chemistry and Biochemistry, University of Windsor, Windsor, Ont., Canada N9B 3P4

Received June 1, 1992

JANE H. E. BAILEY and JOHN E. DRAKE. Can. J. Chem. **71**, 42 (1993).

The compounds $Me_2Te[S_2CNR_2]_2$, $Me_2TeCl[S_2CNR_2]$, $(p\text{-}MeOC_6H_4)_2Te[S_2CNR_2]_2$, and $(p\text{-}MeOC_6H_4)_2TeCl[S_2CNR_2]$, where R = Me, Et, have been prepared and characterised primarily by vibrational and NMR spectroscopy. Variable temperature NMR spectroscopy and qualitative time studies indicate that in solution the dimethoxyphenyltellurium derivatives undergo the reductive-elimination noted for analogous phenyl derivatives but the reductive-elimination does not occur with the dimethyl tellurium derivatives. The crystal structures of $Me_2Te[S_2CNMe_2]_2$, **1**, and $(p\text{-}MeOC_6H_4)_2Te[S_2CNMe_2]_2$, **5**, were completed. The cell parameters for **1**, which crystallizes as monoclinic in space group $P2_1/n$, are a = 13.550(2), b = 13.034(2), c = 17.854(2) Å, β = 106.61(1)°, V = 3021.6(7) Å^3, Z = 8, R = 0.0368, and R_w = 0.0402 and for **5**, which crystallizes as monoclinic in space group $C2/c$, are a = 35.36(1), b = 11.063(3), c = 12.778(3) Å, β = 96.16(3)°, V = 4963(3) Å^3, Z = 8, R = 0.0627, and R_w = 0.0646.

JANE H. E. BAILEY et JOHN E. DRAKE. Can. J. Chem. **71**, 42 (1993).

On a préparé les composés $Me_2Te[S_2CNR_2]_2$, $Me_2TeCl[S_2CNR_2]$, $(p\text{-}MeOC_6H_4)_2TeCl[S_2CNR_2]_2$ dans lesquels R = Me et Et et on les a caractérisés principalement par spectroscopies vibrationnelle et RMN. La spectroscopie RMN à température variable et des études qualitatives en fonction du temps indiquent que, en solution, les dérivés diméthoxyphényltellure subissent l'élimination réductrice notée avec les dérivés phénylés analogues; toutefois, l'élimination réductrice ne se produit pas avec les dérivés diméthyl tellure. On a déterminé les structures cristallines du $Me_2Te[S_2CNMe_2]_2$, **1**, et du $(p\text{-}MeOC_6H_4)Te[S_2CNMe_2]_2$, **5**. Le composé **1** cristallise dans le groupe d'espace $P2_1/n$ avec a = 13,550(2), b = 13,034(2) et c = 17,854(2) Å, β = 106,61(1)°, V = 3021,6(7) Å^3, Z = 8, R = 0,0368 et R_w = 0,0402 alors que le composé **5** cristallise dans le groupe d'espace $C2/c$ avec a = 35,36(1), b = 11,063(3) et c = 12,778(3) Å, β = 96,16(3)°, V = 4963(3) Å^3, Z = 8, R = 0,0627 et R_w = 0,0646.

[Traduit par la rédaction]

Introduction

In the majority of the extensive studies carried out on dithiocarbamate complexes (1–7), the dithiocarbamate group is observed to act in a bidentate fashion (3–7). This appears to be particularly true for transition metal compounds (8, 9) and the relatively few examples of monodentate ligands appear to occur with mixed ligands as is the case for $Pt[S_2CN(i\text{-}Bu)_2]_2[PMe_2Ph]_2$ (10). Within main group elements, bidentate ligands are still common as with $BuSn[S_2CNEt_2]$ (11) and $Zn[S_2CNR_2]_2$ species (12, 13) but we found only anisobidentate linkages with germanium compounds (14–17). This was also the case in previous reports of diphenyl(*N*,*N*-dialkyldithiocarbamato)tellurium(IV) compounds (18, 19). These compounds underwent extensive reductive-elimination in solution regardless of the nature of the dithiocarbamate ligand. In this study we report on changes that are observed when the phenyl groups are substituted by methyl and paramethoxyphenyl groups.

Experimental

Materials

$TeCl_4$, $(p\text{-}MeOC_6H_4)_4Sn$, Me_3SnH, anisole, toluene, *n*-hexane, diethyl ether, petroleum ether, carbon tetrachloride, and chloroform were obtained from Aldrich. With the exception of chloroform and toluene, which were distilled, all others were used as received. Carbon disulfide, obtained from BDH Chemical, was distilled from P_4O_{10} prior to use. Both NaS_2CNMe_2 and NaS_2CNEt_2, purchased from Aldrich as hydrated salts, were dried in vacuum for 4–5 days prior to use. All deuterated solvents were obtained from Aldrich.

Me_2TeCl_2 and $(p\text{-}MeOC_6H_4)_2TeCl_2$ were prepared by a previously described method (20) by reaction of $TeCl_4$ with Me_3SnH and $(p\text{-}MeOC_6H_4)_4Sn$, respectively.

*Synthesis of dimethylbis(*N,N*-dimethyldithiocarbamato)-tellurium(IV), $Me_2Te[S_2CNMe_2]_2$, **1**, and dimethylbis(*N,N*-diethyldithiocarbamato)tellurium(IV), $Me_2Te[S_2CNEt_2]_2$, **2***

Typically, sodium *N*,*N*-dimethyldithiocarbamate (2 mmol, 0.29 g), which had been previously dried *in vacuo* for 4–5 days, was introduced from a finger tube attached to the side of a flask, into a solution of dimethyltellurium dichloride (1 mmol, 0.23 g) in dried carbon disulfide (15 mL). The contents were refluxed at 45°C for 3 h while nitrogen gas was bubbled through. The solution was filtered to remove sodium chloride and any unreacted materials. A few drops of petroleum ether were added to the solution before it was left in the refrigerator at −6°C. Typically crystals formed after approximately three days. The product $Me_2Te[S_2CNMe_2]_2$ was filtered, washed with *n*-hexane, and dried in vacuum; 0.31 g; 77% yield; yellow crystals; mp 120–122°C. Similarly $Me_2Te[S_2CNEt_2]_2$ was formed; 72% yield; yellow crystals; mp 107–109°C. Anal. calcd. for $C_{12}H_{26}N_2S_4Te$: C 31.73, H 5.77, N 6.17; found: C 29.93, H 6.03, N 6.41.

*Synthesis of chlorodimethyl(*N,N*-dimethyldithiocarbamato)-tellurium(IV), $Me_2TeCl[S_2CNMe_2]$, **3**, and chlorodimethyl-(*N,N*-diethyldithiocarbamato)tellurium(IV), $Me_2TeCl[S_2CNEt_2]$, **4***

Typically, sodium *N*,*N*-dimethyldithiocarbamate (1 mmol, 0.14 g) was slowly added, as described above, to a solution containing an equimolar amount of dimethyltellurium dichloride (1 mmol, 0.23 g) in carbon disulphide (15 mL). A continuous stream of nitrogen gas was maintained throughout the experiment. The mixture was stirred in an ice bath for 15 min before the solution was

[1]Present address: The Pulp and Paper Centre, University of Toronto, Toronto, Ont, Canada M5S 1A4.

Can. J. Chem. Downloaded from www.nrcresearchpress.com by 88.255.202.194 on 09/08/12
For personal use only.

Can. J. Chem. Downloaded from www.nrcresearchpress.com by 88.255.202.194 on 09/08/12
For personal use only.

allowed to warm to ambient and then refluxed for 3.5 h. Sodium chloride and any unreacted material were filtered off and the remaining solution left in the refrigerator to crystallize. The product $Me_2TeCl[S_2CNMe_2]$ was washed with *n*-hexane and recrystallized from chloroform; 0.21 g; 67% yield; yellow crystals; mp 100–102°C. Anal. calcd. for $C_5H_{12}NS_2ClTe$: C 19.17, H 3.86, N 4.47; found C 19.24, H 3.98, N 4.53%. Similarly $Me_2TeCl[S_2CNEt_2]$ was formed; 63% yield; yellow crystals; mp 101–103°C. Anal. calcd. for $C_7H_{16}NS_2ClTe$: C 24.63, H 4.72, N 4.10; found: C 24.71, H 4.83, N 4.28.

*Synthesis of dimethoxyphenylbis(*N,N*-dimethyldithiocarbamato)-tellurium(IV), (*p*-$MeOC_6H_4)_2Te[S_2CNMe_2]_2$, **5**, and dimethoxyphenylbis(*N,N*-diethyldithiocarbamato)-tellurium(IV), (*p*-$MeOC_6H_4)_2Te[S_2CNEt_2]_2$, **6***

Typically, dimethoxyphenyltellurium dichloride (1 mmol, 0.41 g) was dissolved in CS_2 (8 mL) in an ice bath. The salt, NaS_2CNMe_2 (2 mmol, 0.29 g) previously dried *in vacuo* for 3–4 days, was slowly introduced from a side arm. The mixture was stirred for 20 min while a continuous stream of nitrogen gas was maintained. The ice bath was then removed and the solution was refluxed for 3.5 h. The product mixture was then filtered and placed in a refrigerator at −6°C to evaporate the solvent. The resulting solid was washed with *n*-hexane and recrystallized from chloroform; 0.37 g; 63% yield; yellow crystals, mp 112–114°C. Similarly (p-$MeOC_6H_4)_2Te[S_2CNEt_2]_2$ was formed; 70% yield; yellow crystals; mp 68–70°C. Anal. calcd. for $C_{24}H_{34}N_2O_2S_4Te$: C 45.16, H 5.37, N 4.39; found: C 45.59, H 5.57, N 4.28.

*Synthesis of chlorodimethoxyphenyl(*N,N*-dimethyldithiocarbamato)tellurium(IV), (*p*-$MeOC_6H_4)_2TeCl[S_2CNMe_2]$, **7**, and chlorodimethoxyphenyl(*N,N*-diethyldithiocarbamato)-tellurium(IV). (*p*-$MeOC_6H_4)_2TeCl[S_2CNEt_2]$, **8***

Sodium *N,N*-dimethyldithiocarbamate (1 mmol, 0.14 g) was gradually introduced to a solution containing dimethoxyphenyltellurium dichloride (1 mmol, 0.41 g) in CS_2 (10 mL). The solution was kept under a nitrogen gas atmosphere throughout the procedure. After the solution was stirred in an ice bath for 30 min it was allowed to reach ambient temperature. The mixture was then refluxed for 4 h at 45°C. Sodium chloride and any unreacted materials were removed by filtration. After several days of refrigeration the product (p-$MeOC_6H_4)_2TeCl[S_2CNMe_2]$ was formed, washed with *n*-hexane, and recrystallized from chloroform; 0.34 g; 68% yield; mp 91–93°C. Similarly (p-$MeOC_6H_4)_2TeCl[S_2CNEt_2]$ was formed; 61% yield, yellow crystals; mp 81–83°C. Anal. calcd. for $C_{19}H_{23}NO_2S_2ClTe$: C 43.42, H 4.60, N 2.67; found: C 43.94, H 4.69, N 2.85.

Physical measurements

All solvents were dried and distilled prior to use. Elemental analyses were performed by Guelph Laboratories. Density measurements were obtained using the flotation method in carbon tetrachloride and benzene. The infrared spectra were recorded on a Bohmem infrared spectrometer as KBr pellets for the middle range and between polyethylene films for the far infrared spectra. Samples for Raman spectroscopy were sealed in capillary tubes and the spectra recorded on a Ramanor U-1000 spectrometer using the 4880 Å excitation line of an argon ion laser. ^1H and $^{13}C\{H\}$ NMR spectra were recorded on a Bruker AC 300 spectrometer in either CS_2 or $CDCl_3$ using tetramethylsilane as the internal standard for CS_2 solutions. ^{125}Te NMR spectra were recorded on a Bruker AC 200 and referenced to dimethyltellurium. All melting points were determined on a Fisher-Johns apparatus.

X-Ray crystallographic analysis

A crystal of $Me_2Te[S_2CNMe_2]_2$, **1**, was sealed in a thin-walled glass capillary and mounted on a Rigaku four-circle AFC6S diffractometer, with graphite monochromated Mo Kα radiation. The orientation matrix for data collection was refined using 25 high-angle reflections ($34° < 2\theta < 39°$). On the basis of the systematic absences *h*0*l*: $h + l \neq 2n$, 0*k*0: $k \neq 2n$, and the successful solution and refinement of the structure, the space group was determined to be $P2_1/n$ (No. 14).

The data were collected by the ω–2θ scan technique to a maximum 2θ value of 50.0° and at a maximum scan rate of 32.0 deg min^{-1}. The intensities of three representative reflections which were measured after every 150 reflections remained constant throughout data collection indicating crystal and electronic stability (no decay correction was applied). An empirical absorption correction, based on azimuthal scans of several reflections, was applied which resulted in transmission factors ranging from 0.87 to 1.00. The data were corrected for Lorentz and polarization effects. All data processing was performed on a VAX workstation 3520 using the TEXSAN crystallographic package (Version 5.0 obtained from Molecular Structure Corp., The Woodlands, TX) (21).

A crystal of (p-$MeOC_6H_4)_2Te[S_2CNMe_2]_2$, **5**, was sealed in a capillary and mounted along the largest dimension on a Syntex P_21 diffractometer. The X-ray diffraction data were collected by the procedures described in detail elsewhere (15) by the coupled θ(crystal)/2θ(counter) method to a maximum 2θ value of 40° at a variable scan speed of 2.02–4.88 deg min^{-1}. On the basis of the systematic absences *hkl*: $h + k \neq 2n$; *h*0*l*: h, $l \neq 2n$, and the successful solution and refinement of the structure, the space group was determined to be $C2/c$ (No. 15). The least-squares refinement of the setting angles of 15 reflections in the range $15° < 2\theta < 30°$ led to the cell dimensions given in Table 1. During data collection, the intensities of three monitor reflections measured every 100 reflections remained constant and so no decay correction was applied. The data were corrected for Lorentz and polarization effects. Sources of scattering factors and computer programs used have been given elsewhere (15).

The final atomic coordinates and isotropic thermal parameters (Tables 2 and 3) are given respectively for **1** and **5** for the non-hydrogen atoms and important distances and bond angles in Tables 4 and 5. The molecular structures of both compounds are displayed in Figs. 1 and 2. Tables of final thermal parameters of non-hydrogen atoms, final fractional coordinates, and thermal parameters of hydrogen atoms as well as tables of observed and calculated structure factors have been deposited.[2]

Results and discussion

The dimethyltellurium(IV) and dimethoxyphenyltellurium(IV) derivatives were made by the reaction of the appropriate diorganotellurium dichloride with the sodium salts of *N,N*-dimethyl- and *N,N*-diethyldithiocarbamic acids in two-fold excess or equimolar amounts.

$$R_2TeCl_2 + 2NaS_2CNR'_2 \rightarrow R_2Te[S_2CNR'_2]_2 + 2NaCl$$

$$R_2TeCl_2 + NaS_2CNR'_2 \rightarrow R_2TeCl[S_2CNR'_2] + NaCl$$

(R = Me or *p*-$MeOC_6H_4$; R′ = Me or Et)

In earlier papers (18, 19) we noted the difficulty of relying on solution-phase spectra for characterization. Thus every effort was made to prepare X-ray quality crystals but, unfortunately, this was only achieved for two of the products.

*The crystal structures of $Me_2Te[S_2CNMe_2]_2$, **1**, and (p-$MeOC_6H_4)_2Te[S_2CNMe_2]_2$, **5***

In both cases the geometry around tellurium is best described as the saw-horse structure typical of tellurium(IV) compounds in which the lone-pair is apparently stereochemically active and occupying an equatorial position in a distorted trigonal bipyramid. The two organic groups occupy the other two equatorial positions with the axial posi-

[2]A complete set of data may be purchased from: The Depository of Unpublished Data, Document Delivery, CISTI, National Research Council Canada, Ottawa, Canada K1A 0S2.

Can. J. Chem. Downloaded from www.nrcresearchpress.com by 88.255.202.194 on 09/08/12
For personal use only.

TABLE 1. Summary of crystal data, intensity collection, and structural refinement for $Me_2Te[S_2CNMe_2]_2$, **1**, and $(p\text{-}MeOC_6H_4)_2Te[S_2CNMe_2]$, **5**

Parameter	$C_8H_{18}N_2S_4Te$ **1**	$C_{20}H_{26}N_2O_2S_4Te$ **5**
Cell constants		
a (Å)	13.550(2)	35.36(1)
b (Å)	13.034(2)	11.063(3)
c (Å)	17.854(2)	12.778(3)
β (deg)	106.61(1)	96.16(3)
Cell volume (Å^3)	3021.6(7)	4963(3)
Crystal system	Monoclinic	Monoclinic
Space group	$P2_1/n$	$C2/c$
Mol. wt. (g mol^{-1})	398.1	582.3
Z	8	8
$\rho_{obsd.}$, $\rho_{calcd.}$, (g cm^{-3})	1.72, 1.75	1.61, 1.56
Crystal dimensions, mm	0.47 × 0.33 × 0.45	0.52 × 0.73 × 0.47
Absorption coefficient μ (cm^{-1})	24.71	12.68
Temperature °C	23 ± 1	24 ± 1
Radiation	MoKα 0.71069Å	
Monochromator	Highly oriented graphite	
Total reflections measured	5923	7038
Unique data used	3450	2268
No. of parameters (NP)	271	262
$R = (\Sigma\|\|F_o\| - \|F_c\|\|/\Sigma\|F_o\|)$	0.0368	0.0627
$R_w = [\Sigma w(\|F_o\| - \|F_c\|)^2/\Sigma w\|F_o^2\|]^{1/2}$	0.0402	0.0646
Largest Δρ (e Å^{-3}) shift/error max.	0.001	0.006
Largest residual electron density (e Å^{-3})	1.01	1.00
Atom associated with residual density	Te	Te

TABLE 2. Final fractional coordinates and equivalent isotropic thermal parameters (Å^2 × 10^3) for non-hydrogen atoms of $Me_2Te[S_2CNMe_2]_2$, **1**

Atom	x	y	z	U_{eq}	Atom	x	y	z	U_{eq}
Te1	0.60043(4)	0.06211(4)	0.63540(3)	40.4(3)	Te2	0.91083(4)	0.37813(4)	0.49150(3)	39.5(3)
S1	0.4185(1)	0.1145(2)	0.5400(1)	50(1)	S5	0.7852(2)	0.5348(2)	0.4480(1)	61(1)
S2	0.5730(2)	0.2832(2)	0.5577(1)	61(1)	S6	0.8407(2)	0.4512(2)	0.3102(1)	61(1)
S3	0.7585(2)	−0.0246(2)	0.7355(1)	52(1)	S7	1.0181(2)	0.2244(2)	0.5658(1)	50(1)
S4	0.8057(2)	0.1904(2)	0.7005(1)	61(1)	S8	1.0039(2)	0.2172(2)	0.3960(1)	54(1)
N1	0.3839(5)	0.2927(5)	0.4625(4)	49(3)	N3	0.7561(5)	0.6343(5)	0.3162(4)	47(3)
N2	0.9472(5)	0.0522(5)	0.7638(4)	51(3)	N4	1.1091(4)	0.0832(5)	0.5021(4)	47(3)
C1	0.4548(5)	0.2368(6)	0.5158(4)	43(3)	C9	0.7916(5)	0.5467(6)	0.3526(4)	42(7)
C2	0.2818(6)	0.2553(8)	0.4240(5)	67(4)	C10	0.7101(6)	0.7144(6)	0.3521(5)	54(4)
C3	0.4055(7)	0.3954(7)	0.4437(5)	62(4)	C11	0.7653(7)	0.6552(7)	0.2380(5)	70(5)
C4	0.8474(6)	0.0731(6)	0.7351(4)	47(3)	C12	1.0493(5)	0.1669(6)	0.4856(4)	46(3)
C5	0.9850(7)	−0.0508(7)	0.7919(6)	73(5)	C13	1.1341(6)	0.0265(6)	0.4400(5)	61(4)
C6	1.0257(6)	0.1283(8)	0.7705(5)	73(5)	C14	1.1496(6)	0.0384(6)	0.5788(5)	61(4)
C7	0.5642(6)	0.1441(6)	0.7262(4)	56(6)	C15	0.8928(7)	0.4156(6)	0.6037(5)	65(4)
C8	0.5193(6)	−0.0742(7)	0.6527(5)	62(4)	C16	0.7817(6)	0.2808(6)	0.4579(5)	53(4)

tions being occupied by a sulfur atom from each of the dithiocarbamate groups (Figs. 1 and 2). The average Te—C bond length in $Me_2Te[S_2CNMe_2]_2$, **1** is 2.13(1) Å, not significantly shorter than the average distance of 2.145(15) Å for $(p\text{-}MeOC_6H_4)_2Te[S_2CNMe_2]_2$, **5**. The Te—C bond length for the analogous phenyl derivative, $Ph_2Te[S_2CNMe_2]_2$, is also essentially the same at 2.140(5) Å (18). However, the fact that all are so similar may well be significant because, in general, a shorter Te—C bond is expected for bonds involving aromatic as opposed to alkyl linkages to tellurium. Thus in a collation of reported bond lengths involving organic derivatives (22), the mean Te—C(aromatic) bond length is 2.116 Å compared with a value of 2.158 Å for the Te—C(alkyl) bond. On this basis, the Te—C bonds in $(p\text{-}MeOC_6H_4)_2Te[S_2CNMe_2]_2$, $Ph_2Te[S_2CNMe_2]_2$, and other analogous species such as $Ph_2Te[S_2CNEt_2]_2$ (23) and $Ph_2Te[S_2CNBu_2]_2$ (19) are relatively long and the bond in $Me_2Te[S_2CNMe_2]_2$ is relatively short.

In $Me_2Te[S_2CNMe_2]_2$ the Te—S bond distances cover the range 2.605(2) to 2.654(1) Å at an average of 2.63(1) Å, comparable to the average distance in $(p\text{-}MeOC_6H_4)_2Te[S_2CNMe_2]_2$ of 2.62(1) Å. These values are also essentially the same as the value of 2.621(1) Å reported for $Ph_2Te[S_2CNMe_2]_2$ (18) and the related compounds $Ph_2Te[S_2CNEt_2]_2$ (23) and $Ph_2Te[S_2CNBu_2]_2$ (19), where the Te—S bonds range from 2.6179(4) to 2.6303(9) Å for the two forms

TABLE 3. Final fractional coordinates and equivalent isotropic thermal parameters (Å^2 × 10^3) for non-hydrogen atoms of (p-MeOC$_6$H$_4$)$_2$Te[S$_2$CNMe$_2$]$_2$, **5**

Atom	x	y	z	U_{eq}	Atom	x	y	z	U_{eq}
Te	0.60738(2)	0.36694(6)	0.91841(5)	32.3(5)					
S1	0.6313(1)	0.2207(3)	0.7775(2)	40(2)	S3	0.5863(1)	0.5128(3)	1.0617(2)	44(2)
S2	0.5621(1)	0.1156(3)	0.8590(2)	46(2)	S4	0.5647(1)	0.6106(3)	0.8445(3)	53(2)
O1	0.6921(2)	0.0828(8)	1.3030(6)	56(5)	O2	0.7581(3)	0.6611(9)	0.8841(8)	65(6)
N1	0.5817(3)	0.0811(9)	0.6657(8)	43(6)	N2	0.5281(3)	0.6597(8)	1.0098(8)	42(6)
C1	0.5890(3)	0.1319(9)	0.7617(9)	36(6)	C4	0.5560(3)	0.6015(9)	0.9716(8)	35(7)
C2	0.5470(4)	0.002(1)	0.647(1)	63(9)	C5	0.5195(4)	0.647(1)	1.119(1)	55(9)
C3	0.6045(4)	0.098(1)	0.578(1)	63(8)	C6	0.5023(4)	0.735(1)	0.944(1)	68(9)
C7	0.6347(3)	0.2627(9)	1.0483(9)	37(7)	C14	0.6575(3)	0.4696(9)	0.9037(7)	26(6)
C8	0.6170(3)	0.2479(9)	1.1378(9)	36(7)	C15	0.6803(4)	0.511(1)	0.994(1)	55(8)
C9	0.6352(4)	0.188(1)	1.2255(9)	44(7)	C16	0.7127(4)	0.573(1)	0.984(1)	55(9)
C10	0.6707(3)	0.140(1)	1.2211(9)	41(7)	C17	0.7242(3)	0.598(1)	0.885(1)	46(8)
C11	0.6887(4)	0.1494(9)	1.126(1)	46(8)	C18	0.7025(3)	0.560(1)	0.7949(9)	49(8)
C12	0.6695(3)	0.2114(9)	1.0437(9)	40(7)	C19	0.6694(3)	0.495(1)	0.8044(9)	44(7)
C13	0.6772(4)	0.080(1)	1.404(1)	71(8)	C20	0.7705(4)	0.691(1)	0.785(1)	72(9)

TABLE 4. Interatomic distances (Å) in compounds **1** and **5**[a]

Me$_2$Te[S$_2$CNMe$_2$]$_2$, **1**				(p-MeOC$_6$H$_4$)$_2$-Te[S$_2$CNMe$_2$]$_2$, **5**	
Atoms	Distance	Atoms	Distance	Atoms	Distance
Te1—S1	2.654(2)	Te2—S5	2.629(2)	Te—S1	2.628(3)
Te1—S2	3.173(2)	Te2—S6	3.244(2)	Te—S2	3.258(3)
Te1—S3	2.621(2)	Te2—S7	2.605(2)	Te—S3	2.609(3)
Te1—S4	3.167(2)	Te2—S8	3.182(2)	Te—S4	3.183(3)
Te1—C7	2.113(7)	Te2—Cl5	2.143(8)	Te—C7	2.16(1)
Te1—C8	2.158(8)	Te2—Cl6	2.104(8)	Te—Cl4	2.13(1)
S1—C1	1.759(8)	S5—C9	1.738(8)	S1—C1	1.78(1)
S2—C1	1.674(8)	S6—C9	1.689(7)	S2—C1	1.66(1)
S3—C4	1.754(8)	S7—C12	1.771(8)	S3—C4	1.78(1)
S4—C4	1.685(8)	S8—C12	1.674(8)	S4—C4	1.69(1)
N1—C1	1.355(9)	N3—C9	1.334(9)	N1—C1	1.35(1)
N1—C2	1.44(1)	N3—C10	1.456(9)	N1—C2	1.50(1)
N1—C3	1.43(1)	N3—C11	1.46(1)	N1—C3	1.46(1)
N2—C4	1.330(9)	N4—C12	1.341(9)	N2—C4	1.32(1)
N2—C5	1.47(1)	N4—C13	1.45(1)	N2—C5	1.47(2)
N2—C6	1.43(1)	N4—C14	1.45(1)	N2—C6	1.44(1)
				O1—C10	1.38(1)
				O1—C13	1.44(2)
				O2—C17	1.39(1)
				O2—C20	1.45(2)
				Ring C7—C12	
				Mean C—C	1.38(1)
				Ring C14—C19	
				Mean C—C	1.38(1)

[a]The esd's on mean values have been calculated with the use of the scatter formula $\sigma = [\Sigma(d_i - d)^2/N]^{1/2}/(N-1)^{1/2}$, where d_i is the ith and d is the mean of N measurements.

of the ethyl derivative and 2.622(2) Å for the butyl derivative.

The deviation of the S—Te—S angles from 180° increases along the series (p-MeOC$_6$H$_4$)$_2$Te[S$_2$CNMe$_2$]$_2$, 177.8(1)°, Ph$_2$Te[S$_2$CNMe$_2$]$_2$, 172.0(1)°, and Me$_2$Te[S$_2$CNMe$_2$]$_2$, 167.58(7) and 165.39(7)°, which is suggestive of a trend based on the nature of the organo group attached to tellurium. However, more data on alkyl tellurium R$_2$Te[dtc]$_2$ species are needed to ensure that the distortion is indeed larger for such groups. For the C—Te—C bond angles, the values are smallest for (p-MeOC$_6$H$_4$)$_2$Te[S$_2$CNMe$_2$]$_2$ at 92.6(4)° compared to 99.4(1)° for Ph$_2$Te[S$_2$CNMe$_2$]$_2$. The values of 93.9(2)° and 95.5(3)° for Me$_2$Te[S$_2$CNMe$_2$]$_2$ are not only closer to those of the methoxyphenyl derivatives but also to the two forms of Ph$_2$Te[S$_2$CNEt$_2$]$_2$, 94.2(1)° and 94.077(1)° (23) and Ph$_2$Te[S$_2$CNBu$_2$]$_2$, 95.3(2)° (19), so no obvious trend exists. In all three dimethyldithiocarbamate derivatives, the aniso-bonded sulfur atoms are at a similar distance from tellurium ranging from 3.167(2) to 3.244(2) Å in Me$_2$Te[S$_2$CNMe$_2$]$_2$, 3.183(3) to 3.258(3) Å in (p-MeOC$_6$H$_4$)$_2$Te[S$_2$-

Can. J. Chem. Downloaded from www.nrcresearchpress.com by 88.255.202.194 on 09/08/12
For personal use only.

Can. J. Chem. Downloaded from www.nrcresearchpress.com by 88.255.202.194 on 09/08/12
For personal use only.

TABLE 5. Bond angles (deg) in compounds **1** and **5** with standard deviations in parentheses[a]

$Me_2Te[S_2CNMe_2]_2$, **1**				$(p\text{-}MeOC_6H_4)_2Te[S_2CNMe_2]_2$, **5**	
Bonds	Angle	Bonds	Angle	Bonds	Angle
S1—Te1—S3	167.58(7)	S5—Te2—S7	165.39(7)	S1—Te—S3	177.8(1)
S1—Te1—C7	89.2(2)	S5—Te2—C15	82.1(2)	S1—Te—C7	92.7(3)
S1—Te1—C8	83.4(2)	S5—Te2—C16	88.2(2)	S1—Te—C14	86.3(3)
S3—Te1—C7	91.1(2)	S7—Te2—C15	84.0(2)	S3—Te—C7	85.9(3)
S3—Te1—C8	84.2(2)	S7—Te2—C16	88.8(2)	S3—Te—C14	92.0(3)
C7—Te1—C8	93.9(2)	C15—Te2—C16	95.5(3)	C7—Te—C14	92.6(4)
Te1—S1—C1	96.7(3)	Te2—S5—C9	98.6(2)	Te—S1—C1	95.1(4)
Te1—S3—C4	96.5(3)	Te2—S7—C12	98.1(3)	Te—S3—C4	94.8(8)
S1—C1—S2	121.1(4)	S5—C9—S6	120.6(4)	S1—C1—S2	121.2(7)
S1—C1—N1	117.8(6)	S5—C9—N3	116.3(5)	S1—C1—N1	114.2(9)
S2—C1—N1	121.1(6)	S6—C9—N3	123.1(6)	S2—C1—N1	124.6(8)
S3—C4—S4	120.1(4)	S7—C12—S8	120.0(4)	S3—C4—S4	119.8(7)
S3—C4—N2	118.3(6)	S7—C12—N4	115.8(6)	S3—C4—N2	116.9(8)
S4—C4—N2	121.6(6)	S8—C12—N4	124.3(6)	S4—C4—N2	123.3(8)
C1—N1—C2	123.0(7)	C9—N3—C10	122.6(6)	C1—N1—C2	118(1)
C1—N1—C3	121.0(7)	C9—N3—C11	120.5(7)	C1—N1—C3	125(1)
C2—N1—C3	115.9(7)	C10—N3—C11	116.9(7)	C2—N1—C3	117(1)
C4—N2—C5	122.3(7)	C12—N4—C13	120.3(7)	C4—N2—C5	123(1)
C4—N2—C6	122.6(7)	C12—N4—C14	125.4(7)	C4—N2—C6	122(1)
C5—N2—C6	115.2(7)	C13—N4—C14	114.3(6)	C5—N2—C6	115(1)
S1—Te1—S2	61.0(3)	S5—Te2—S6	59.8(3)	C10—01—C13	118(1)
S3—Te1—S4	61.1(3)	S7—Te2—S8	61.1(3)	C17—02—C20	118(1)
				Ring C7—C12 Mean C—C—C	120(1)
				Ring C14—C19 Mean C—C—C	120(1)
				S1—Te—S2	60.1(4)
				S3—Te—S4	61.5(4)

[a]The esd's on mean values have been calculated with the use of the scatter formula $\sigma = [\Sigma(d_i - d)^2/N]^{1/2}/(N - 1)^{1/2}$, where d_i is the ith and d is the mean of N measurements.

$CNMe_2]_2$, and 3.186(2) Å in $Ph_2Te[S_2CNMe_2]_2$ (18), and subtend similar bite angles which average to 60.8(3)° in $Me_2Te[S_2CNMe_2]_2$ and to 60.8(7)° in $(p\text{-}MeOC_6H_4)_2Te[S_2CNMe_2]_2$, comparable to 61.0(1)° in $Ph_2Te[S_2CNMe_2]_2$ (18). Distances close to 3.2 Å and bite-angles close to 61° appear to be characteristic of all dithiocarbamates aniso-bonded to tellurium (18, 19, 23). The sum of the van der Waals radii of tellurium and sulfur is considerably longer at 4.0 Å (24), while the bite-angle in a fully bidentate ligand is over 64° (25). There was no sign of any bridging by the dithiocarbamate group as has been reported for $Ph_3Te[S_2CN(i\text{-}Pr)_2]$ (26); there being no Te---S intermolecular distances below 4.0 Å involving the aniso-sulfur atom and the tellurium atom of an adjacent molecule in either **1** or **5**.

The similarities in the characteristics associated with the Te—S bonding extend to the bonds in the ligands themselves. In both $(p\text{-}MeOC_6H_4)_2Te[S_2CNMe_2]_2$, **5**, and $Me_2Te[S_2CNMe]_2$, **1**, the C—S terminal bond, 1.66(1) and 1.69(1) Å in **5** and ranging from 1.674(8) to 1.689(7) Å in **1**, is considerably shorter than the C—S(Te) bond which is 1.78(1) Å in **5** and ranges from 1.738(8) to 1.771(8) Å in **1**. The C—S bond length in CS_3^{2-} is reported to be 1.71 Å (27), emphasizing that the partial π-bond delocalization clearly extends to the S_2C—N bond which is considerably shorter, 1.32(1) and 1.35(1) Å in **5** and 1.330(9) to 1.355(9) Å in **1**, than the N—CH_3 bonds which range from 1.44(1) to 1.50(1) Å in **5** and 1.43(1) to 1.47(1) Å in **1**.

Infrared and Raman spectra

The assignments of selected features in the infrared and Raman spectra of compounds **1** to **8** are given in Table 6. The assignments are made in conjunction with those made earlier on a variety of analogous diphenyltellurium derivatives (18, 19). The characteristic ν(C—NR_2) stretch, which is observed readily in all eight compounds, ranges from 1480–1508 cm^{-1}, well within and near the mean of the generally accepted range of 1450–1550 cm^{-1}. The average C—NR_2 bond lengths in $Me_2Te[S_2CNMe_2]_2$, **1**, and $(p\text{-}MeOC_6H_4)_2Te[S_2CNMe]_2$, **5**, and the mean of the ν(C—NR_2) vibrational frequencies in the two compounds are much closer to those expected for a C=N double bond (approximately 1.27 Å and 1600 cm^{-1}) than for a C—N single bond (approximately 1.46 Å and 1000 cm^{-1}), reflecting the significant π-character in the bond.

The conventional assignment of the C—S vibration in dithiocarbamates in the 980 cm^{-1} region places it well above the weighted averaged of ν(C—S) in the CS_3^{2-} ion which is closer to 800 cm^{-1} (28). This is consistent with the average C—S bond length of the terminal or aniso-bonded sulfur atom, being 1.681(8) and 1.68(2) Å, respectively, for $Me_2Te[S_2CNMe_2]_2$, **1**, and $(p\text{-}MeOC_6H_4)_2Te[S_2CNMe_2]_2$, **5**, compared with the C—S bond length of 1.71 Å in the CS_3^{2-} ion

Can. J. Chem. Downloaded from www.nrcresearchpress.com by 88.255.202.194 on 09/08/12
For personal use only.

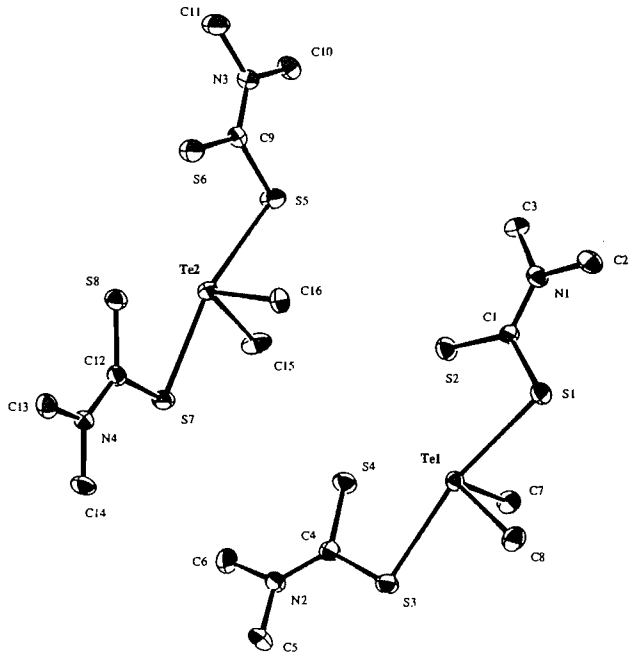

FIG. 1. ORTEP plot of the molecule $Me_2Te[S_2CNMe_2]_2$, **1**, showing the two independent molecules. The atoms are drawn with 20% probability ellipsoids. Hydrogen atoms are omitted for clarity.

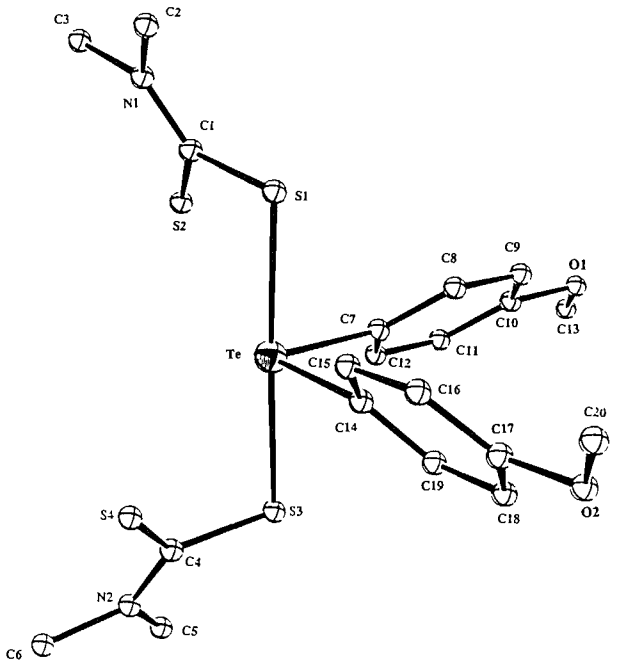

FIG. 2. ORTEP plot of the molecule $(p\text{-}MeOC_6H_4)_2Te[S_2CNMe_2]_2$, **5**. The atoms are drawn with 20% probability ellipsoids. Hydrogen atoms are omitted for clarity.

(27). The symmetrical Te—S stretching vibration shows up clearly in the Raman spectra of all four *bis* species in the range 362–372 cm^{-1} which is 9–15 cm^{-1} to higher wavenumber than the corresponding asymmetric Te—S stretch. A similar phenomenon was noted for the Te—Cl stretches in Me_2TeCl_2 (29). The value of ν(Te—S) is generally higher for the $Me_2TeCl[S_2CNR_2]$ and $(p\text{-}MeOC_6H_4)_2TeCl[S_2CNR_2]$ species which is presumably indicative of a shorter Te—S bond in the halo-derivatives, as was found for $Ph_2TeCl[S_2CNEt_2]$, $Ph_2TeCl[S_2CN(i\text{-}Pr)_2]$ (18), and $Ph_2TeBr[S_2CNEt_2]$ (19). Moreover, as was the case for the $Ph_2TeCl[S_2CNR_2]$ species (18), the characteristic Te—Cl stretching vibration is in the 180–209 cm^{-1} range for **3**, **4**, **7**, and **8**, presumably reflecting a longer Te—Cl bond than that in Me_2TeCl_2 where the Te—Cl vibrations are in the range 241–276 cm^{-1} (29). In Me_2TeCl_2, where the Te—C bond length is 2.09 Å (30) the Te—C stretches were both assigned at 544 cm^{-1} (29). Two distinct peaks are seen in this region for compounds **1** to **4**, particular in the Raman effect, which are assigned to the symmetric and asymmetric Te—C stretching vibrations, respectively. The slightly lower frequencies in the dithiocarbamates are consistent with the Te—C bond length in $Me_2Te[S_2CNMe_2]_2$ being longer than in Me_2TeCl_2, and presumably therefore in the other species **2**, **3** and **4**.

NMR spectroscopy

Previously reported studies (18, 19) on the diphenyltellurium analogues, $Ph_2Te[S_2CNR_2]_2$, indicated that in solution such species undergo rapid exchange, rearrangement, and reductive-elimination regardless of the nature of the alkyl group in the dialkyldithiocarbamate ligand. It was of interest to note if this would also be the case for these dimethyl- and dimethoxyphenyl-tellurium derivatives. The ^1H and ^{13}C NMR spectra reported in Table 7 were recorded immediately after dissolution in $CDCl_3$ solution. In all cases only one set of peaks is observed for the NR_2 groups, as was the case for the diphenyltellurium compounds (18, 19). Studies on related compounds have lead to the conclusion that the exchanges indicated by this equivalence are predominantly metal-centred rearrangements (31, 32).

For all of the dimethyltellurium dithiocarbamate species, **1** to **4**, the peaks remain unchanged even after several days in solution. In the ^1H NMR spectra, the first-order triplet-quartet pattern associated with the $N(CH_2CH_3)_2$ group in **2** and **4** remains sharp over time and with temperature change so that the exchange bringing about equivalence must be fast on the NMR time scale. The chemical shifts of the $N(CH_3)_2$ groups in **1** and **3** and of $N(CH_2CH_3)_2$ groups in **2** and **4** are essentially the same for the *bis* and *mono*-substituted species, as was found for the corresponding diphenyl derivatives (18). The chemical shift of the CH_3-group attached to tellurium is the same for **1** and **2** and also identical for **3** and **4**, so these shifts are apparently dependent on the number of dithiocarbamate groups attached to tellurium. Thus there is an upfield shift of 0.38 ppm on substituting one chlorine atom in Me_2TeCl_2 by a dithiocarbamate group and a shift of a further 0.29 ppm when the second chlorine is replaced. Similar comments are applicable to the changes in the chemical shifts in the ^{13}C NMR spectra as can readily be seen in Table 7.

In contrast to the dimethyltellurium series, the ^1H and ^{13}C NMR spectra of the dimethoxyphenyltellurium species, **5**–**8**, change rapidly with time. Nevertheless, the chemical shifts of the spectra recorded immediately after the solutions were formed show the same sorts of trends for the methyl and ethyl groups in the dithiocarbamate entities as just described for compounds **1**–**4**. The methyl protons in the methoxyphenyl groups appear in the ^1H NMR spectra as sharp singlets at close to 3.8 ppm in all four species and also essentially in the

TABLE 6. Selected features in the vibrational spectra (cm^{-1}) of compounds **1** to **8**[a]

Compound	ν(C—NR$_2$)		ν(C—S)		ν(Te—S)		ν(Te—Cl)	
	IR	Raman	IR	Raman	IR	Raman	IR	Raman
$Me_2Te[S_2CNMe_2]_2$, **1**	1491(ms)	1485(20)	971(m)	973(20)	349(m)	362(100)[b]		
$Me_2Te[S_2CNEt_2]_2$, **2**	1486(ms)	1485(15)	979(ms)	985(20)	361(m)	373(100)[b]		
$Me_2TeCl[S_2CNMe_2]$, **3**	1493(s)	1495(20)	980(m)	969(25)	385(m)	385(100)	189(m)	179(100)
$Me_2TeCl[S_2CNEt_2]$, **4**	1508(m)	1495(20)	970(m)	984(15)	384(m)	382(100)	180(m)	176(30)
$(p\text{-}MeOC_6H_4)_2Te[S_2CNMe_2]_2$, **5**	1494(ms)	1485(20)	969(m)	978(30)	347(m)	363(100)[b]		
$(p\text{-}MeOC_6H_4)_2Te[S_2CNEt_2]_2$, **6**	1485(s)	1480(20)	982(m)	984(20)	358(m)	372(100)[b]		
$(p\text{-}MeOC_6H_4)_2TeCl[S_2CNMe_2]$, **7**	1484(m)	1493(25)	963(m)	965(20)	359(m)	362(100)	200(ms)	198(50)
$(p\text{-}MeOC_6H_4)_2TeCl[S_2CNEt_2]$, **8**	1489(m)	1490(30)	979(ms)	977(25)	361(m)	360(100)	209(ms)	199(40)

[a]Parentheses denote relative intensities in Raman; in the infrared s = strong, m = medium.
[b]For the "bis" species, there are both *sym* and *asym* modes.

TABLE 7. ^1H and ^{13}C chemical shifts in the NMR spectra of compounds **1** to **8**[a]

Compounds	C_6H_5 [C_6H_5]	CH_3 [CH_3]	NCH_n [NCH_n]	$NCCH_n$ [$NCCH_n$]
$Me_2Te[S_2CNMe_2]_2$, **1**		2.46s [16.6]	3.44s [44.1]	
$Me_2Te[S_2CNEt_2]_2$, **2**		2.47s (6H) [16.7]	3.89q (8H) [48.4]	1.25t (12H) [12.2]
$Me_2TeCl[S_2CNMe_2]$, **3**		2.75s (6H) [20.5]	3.43s (6H) [44.0]	
$Me_2TeCl[S_2CNEt_2]$, **4**		2.75s (6H) [20.4]	3.82q (4H) [49.1]	1.26t (6H) [12.1]
$(p\text{-}MeOC_6H_4)_2Te[S_2CNMe_2]_2$, **5**	7.95–7.92, 6.93–6.90 (8H) [161.6, 136.5, 123.8, 115.2]	3.79s (6H) [55.2]	3.39 (12H) [44.0]	
$(p\text{-}MeOC_6H_4)_2Te[S_2CNEt_2]_2$, **6**	7.96–7.93, 6.92–6.90 (8H) [160.9, 136.5, 124.7, 115.1]	3.79s (6H) [55.2]	3.84q (8H) [48.3]	1.20t (6H) [12.2]
$(p\text{-}MeOC_6H_4)_2TeCl[S_2CNMe_2]$, **7**	7.97–7.93, 6.98–6.93 (8H) [161.5, 135.1, 123.7, 115.4]	3.80s (6H) [55.4]	3.39s (6H) [43.9]	
$(p\text{-}MeOC_6H_4)_2TeCl[S_2CNEt_2]$, **8**	7.98–7.93, 6.96–6.93 (8H) [161.5, 136.1, 123.6, 115.4]	3.80s [55.4]	3.81q (4H) [48.9]	1.20t (6H) [12.2]
$(p\text{-}MeOC_6H_4)_2Te$	7.61–7.59, 6.75–6.72 (8H) [159.6, 139.6, 115.3, 104.2]	3.75s (6H) [55.1]		
$(p\text{-}MeOC_6H_4)_2TeCl_2$	7.97–7.94, 7.02–6.98 (8H) [162.0, 135.5, 125.3, 115.6]	3.84s (6H) [55.5]		

[a]^{13}C-NMR chemical shifts given in [ ]; s = singlet, d = doublet, t = triplet, q = quartet.

same position, 55.3 ± 1 ppm, in the ^{13}C NMR spectra. The ^1H NMR chemical shifts of the phenyl rings are also similar regardless of the nature of the attached dithiocarbamate group or whether it is a *bis*- or *mono*-substituted derivative. In all cases the two sets of peaks are seen as expected for the *meta* and *ortho* protons. In the ^{13}C NMR spectrum of $(p\text{-}MeOC_6H_4)_2TeCl_2$, two peaks are predominant in the phenyl region at 115.7 and 135.5 ppm which are attributable to C(3,5) and C(2,6) respectively, where C(1) is the carbon atom attached to tellurium (33). The corresponding peaks in $(p\text{-}MeOC_6H_4)_2Te$ occur at 115.3 and 139.7 ppm. The peak attributable to C(1) is reported at 162.4 and 159.6 ppm, respectively, for $(p\text{-}MeOC_6H_4)_2TeCl_2$ and $(p\text{-}MeOC_6H_4)_2Te$ and that attributable to C(6) at 125.4 and 104.4 ppm (33). In all of the compounds, **5** to **8**, the ^{13}C NMR chemical shifts of the ring carbon atoms bear a much closer resemblance to those of $(p\text{-}MeOC_6H_4)_2TeCl_2$ than $(p\text{-}MeOC_6H_4)_2Te$. This is consistent with electronegativity effects associated with the dithiocarbamate group being fairly similar to a chlorine atom and the environment around tellurium in the solid state being mantained in solution when the compounds are initially dissolved.

The ^1H and ^{13}C NMR spectra recorded one week after compounds **5** and **6** are dissolved in $CDCl_3$ no longer appear as just described but in fact are dominated by peaks attributable to $(p\text{-}MeOC_6H_4)_2Te$ and the diligands, in accord with the reductive-elimination:

$$(p\text{-}MeOC_6H_4)_2Te[S_2CNR_2]_2 \rightarrow (p\text{-}MeOC_6H_4)_2Te + R_2NCS_2S_2CNR_2$$

When spectra were recorded after a few hours, the intensity of peaks associated with $(p\text{-}MeOC_6H_4)_2Te[S_2CNR_2]_2$ had diminished considerably, as much as 90% in 48 h, and those associated with $(p\text{-}MeOC_6H_4)_2Te$ and $R_2NCS_2S_2CNR_2$ had correspondingly increased. The collection time involved in obtaining ^{125}Te NMR spectra (Table 8) was sufficiently long

Can. J. Chem. Downloaded from www.nrcresearchpress.com by 88.255.202.194 on 09/08/12
For personal use only.

TABLE 8. ^{125}Te NMR chemical shifts in solutions of compounds **1** to **8** and selected related examples

Compound	Chemical shift[a]			
	R_2TeCl_2	R_2TeClL	R_2TeL_2	R_2Te
$Me_2Te[S_2CNMe_2]_2$, **1**			475	
$Me_2Te[S_2CNEt_2]_2$, **2**			463	
$Me_2TeCl[S_2CNMe_2]$, **3**		554		
$Me_2TeCl[S_2CNEt_2]$, **4**		545		
$(p\text{-}MeOC_6H_4)_2Te[S_2CNMe_2]_2$, **5**			724	671
$(p\text{-}MeOC_6H_4)_2Te[S_2CNEt_2]_2$, **6**			711	671
$(p\text{-}MeOC_6H_4)_2TeCl[S_2CNMe_2]$, **7**	929	794		671
$(p\text{-}MeOC_6H_4)_2TeCl[S_2CNEt_2]$, **8**	929	788		671
Me_2TeCl_2	728			
$(p\text{-}MeOC_6H_4)_2TeCl_2$	929			
Me_2Te				0
$(p\text{-}MeOC_6H_4)_2Te$				671

[a]L = dithiocarbamate, R = Me, p-$MeOC_6H_4$.

that even the initial spectra often showed evidence of $(p\text{-}MeOC_6H_4)_2Te$ and after a week there was no evidence of any *bis* species still being present.

For the $(p\text{-}MeOC_6H_4)_2TeCl[S_2CNR_2]$ species, **7** and **8**, within a week the ^{1}H, ^{13}C, and ^{125}Te NMR spectra all showed the presence of $(p\text{-}MeOC_6H_4)_2TeCl_2$, $(p\text{-}MeOC_6H_4)_2Te$, and diligand although peaks attributable to the original molecules **7** and **8** were still of equivalent importance. This is consistent with the following mode of decomposition:

$$2(p\text{-}MeOC_6H_4)_2TeCl[S_2CNR_2]$$
$$\rightarrow (p\text{-}MeOC_6H_4)_2Te[S_2CNR_2]_2 + (p\text{-}MeOC_6H_4)_2TeCl_2$$
$$\downarrow$$
$$(p\text{-}MeOC_6H_4)_2Te + R_2CNS_2S_2CNR_2$$

The relative rates of each step are presumably such that the concentration of *bis* species is never high enough to be detected.

The contrast between the ease of reductive-elimination of $(p\text{-}MeOC_6H_4)_2Te[S_2CNR_2]_2$ to give $(p\text{-}MeOC_6H_4)_2Te + [S_2CNR_2]_2$ and the stability of the $Me_2Te[S_2CNR_2]_2$ species is surprising in view of the fact that in both cases the overall reaction involves the breaking of two apparently identical Te—S bonds and the making of one S—S bond. In view of the similarity in the structures of **1** and **5** it is difficult to argue that the difference results from the non-availability of a kinetic pathway in the case of the dimethyl derivative. However, if it is assumed that the reactions are close to being thermally neutral, then the reductive-elimination could be unfavourable if the Te—C bonds in $Me_2Te[S_2CNR_2]_2$ are stronger relative to those in Me_2Te, while the reductive-elimination could become favourable in the case of the dimethoxyphenyl species if the Te—C bonds in $(p\text{-}MeOC_6H_4)_2Te[S_2CNR_2]_2$ are now weaker relative to those in $(p\text{-}MeOC_6H_4)_2Te$. In this regard we return to a point made during the discussions of the structures that suggested that the Te—C bonds in $Me_2Te[S_2CNR_2]_2$ are relatively shorter than is normal for Te—C(alkyl) bonds while the Te—C bonds in $(p\text{-}MeOC_6H_4)_2Te[S_2CNR_2]_2$ and $Ph_2Te[S_2CNR_2]_2$ species are relatively longer than is normal for T—C(aryl) bonds.

Acknowledgements

We thank the Natural Sciences and Engineering Research Council of Canada and the University of Windsor for financial support.

1. C. D. Thorn and R. A. Ludwig. The dithiocarbamates and related compounds. Elsevier, Amsterdam. 1962.
2. D. Coucouvanis. Prog. Inorg. Chem. **11**, 233 (1970).
3. J. Willemse, J. A. Gras, J. J. Steggerda, and C. P. Keijzers. Struct. Bonding (Berlin), **28**, 83 (1976).
4. J. L. Templeton and B. C. Ward. Inorg. Chem. **19**, 1753 (1980).
5. M. G. Kanatzidis, D. Coucouvanis, A. Simopoulos, A. Koshkas, and V. J. Papaefthymiou. J. Am. Chem. Soc. **107**, 4925 (1985).
6. (*a*) M. G. B. Drew, D. A. Rice, and D. M. Williams. J. Chem. Soc. Dalton Trans. 1821 (1985); (*b*) E. J. Peterson, R. B. von Dreele, and T. M. Brown. Inorg. Chem. **17**, 1410 (1978).
7. (*a*) S. J. M. Burgmayer and J. L. Templeton. Inorg. Chem. **24**, 2224 (1985); (*b*) T. C. W. Mak, K. S. Jasim, and C. Chieh. Inorg. Chem. **24**, 1587 (1985); (*c*) C. D. Garner, N. C. Howlader, F. E. Mabbs, A. T. McPhail, R. W. Miller, and K. D. Onan. J. Chem. Soc. Dalton Trans. 1582 (1978).
8. P. R. H. Alderman, P. G. Owston, and J. M. Rowe. J. Chem. Soc. 668 (1962).
9. R. Hesse. Ark. Kemi, **20**, 481 (1963).
10. I. J. B. Lin, H. W. Chen, and J. P. Fackler, Jr. Inorg. Chem. **17**, 394 (1978).
11. J. S. Morris and E. D. Schlemper. J. Cryst. Mol. Struct. **9**, 1 (1979).
12. H. P. Klug. Acta Crystallogr. **21**, 536 (1966).
13. M. Bonamico, G. Mazzone, A. Vaciago, and L. Zambonelli. Acta Crystallogr. **19**, 898 (1965).
14. R. K. Chadha, J. E. Drake, and A. B. Sarkar. Inorg. Chem. **23**, 4769 (1984).
15. R. K. Chadha, J. E. Drake, and A. B. Sarkar. Inorg. Chem. **25**, 2201 (1986).
16. R. K. Chadha, J. E. Drake, and A. B. Sarkar. Inorg. Chimi. Acta, **143**, 31 (1988).
17. R. K. Chadha, J. E. Drake, A. B. Sarkar, and M. Wong. Acta Crystallogr. Sect. C: Cryst. Struct. Commun. **C45**, 37 (1989).
18. J. H. E. Bailey, J. E. Drake, A. B. Sarkar, and M. L. Y. Wong. Can. J. Chem. **67**, 1735 (1989).
19. J. H. E. Bailey, J. E. Drake, and M. L. Y. Wong. Can. J. Chem. **69**, 1948 (1991).

Can. J. Chem. Downloaded from www.nrcresearchpress.com by 88.255.202.194 on 09/08/12
For personal use only.

20. R. C. Paul, K. K. Bhasin, and R. K. Chadha. J. Inorg. Nucl. Chem. **37**, 2337 (1975).
21. Texsan-Texray structure analysis package. Molecular Structure Corp. (1985).
22. F. H. Allen, O. Kennard, D. G. Watson, L. Brammer, A. G. Orpen, and R. Taylor. J. Chem. Soc. Perkin Trans. 2, S1 (1987).
23. D. Dakternieks, R. DiGiacomo, R. W. Gable, and B. F. Hoskins. J. Organomet. Chem. **349**, 305 (1988).
24. A. J. Bondi. J. Phys. Chem. **68**, 441 (1964).
25. D. Dakternieks, R. DiGiacomo, R. W. Gable, and B. F. Hoskins. J. Am. Chem. Soc. **110**, 6753 (1988).
26. J. E. Drake and M. L. Y. Wong. J. Organomet. Chem. **377**, 43 (1988).
27. A. F. Wells. Structural inorganic chemistry. 4th ed. Clarendon Press, Oxford. 1975. p. 733.
28. S. D. Ross. Inorganic IR and Raman spectra. McGraw Hill, London, 1972. p. 160.
29. G. C. Hayward and P. J. Hendra. J. Chem. Soc. A, 1760 (1969).
30. G. D. Christofferson, R. A. Sparks, and J. D. McCullough. Acta Crystallogr. **11**, 782 (1958).
31. A. N. Bhat, F. C. Fay, D. F. Lewis, A. F. Lindmark, and S. H. Strauss. Inorg. Chem. **13**, 887 (1974).
32. M. A. Khadin, V. Kumar, P. H. Bird, B. C. Pant, and L. D. Colebrook. Org. Magn. Reson. **19**, 185 (1982).
33. R. K. Chadha and J. M. Miller. J. Chem. Soc. Dalton Trans. 117 (1982).

Can. J. Chem. Downloaded from www.nrcresearchpress.com by 88.255.202.194 on 09/08/12
For personal use only.

The boron trifluoride – base system: application of the coordination model of reaction mechanisms[1]

XIAOBO OU, ROBERT WALLACE, AND ALEXANDER F. JANZEN[2]
Department of Chemistry, University of Manitoba, Winnipeg, Man., Canada R3T 2N2

Received June 1, 1992

XIAOBO OU, ROBERT WALLACE, and ALEXANDER F. JANZEN. Can. J. Chem. **71**, 51 (1993).

The mechanism of reaction of boron trifluoride with amines, dialkyl ethers, and pyridine has been analyzed on the basis of the coordination model of reaction mechanisms. This model is tested mathematically by carrying out kinetic simulations of pathways P(*X*,*C*), accompanied by the calculation of structures of postulated intermediates by GAUSSIAN86 methods. Analyses of reaction mechanisms, including calculation of concentration vs. time curves, are reported for the following systems: NH_3–BF_3, $MeNH_2$–BF_3, Me_2O–Et_2O–BF_3, Me_2O–Et_2O:BF_3, pyridine–BF_3, pyridine–Me_3N–BF_3, F_3B:N–N:BF_3, and (N–N)BF_2^+.

XIAOBO OU, ROBERT WALLACE et ALEXANDER F. JANZEN. Can. J. Chem. **71**, 51 (1993).

Faisant appel au modèle de coordination des mécanismes réactionnels, on a analysé le mécanisme réactionnel du trifluorure de bore avec les amines, les éthers dialkylès et la pyridine. On a évalué le modèle d'une façon mathématique en effectuant des simulations cinétiques des diverses voies réactionnelles P(*X*,*C*), tout en calculant les structures des intermédiaires présumés par des méthodes gaussiennes-86. On rapporte des analyses des mécanismes réactionnels, y compris des calculs de concentration vs. temps, pour les systèmes suivants : NH_3–BF_3, $MeNH_2$–BF_3, Me_2O–Et_2O–BF_3, Me_2O–Et_2O:BF_3, pyridine–BF_3, pyridine–Me_3N–BF_3, F_3B:N–N:BF_3 et (N–N)BF_2^+.

[Traduit par la rédaction]

The coordination model of reaction mechanisms (1–3) describes in a formal way the discrete changes in coordination number and electron count of individual atoms and represents the connectivity of atoms in multistep pathways in graphical form as pathway P(*X*,*C*).[3] In this paper we wish to describe a mathematical test of the coordination model by comparing calculated results with extensive experimental data that are available for the reactions of boron trifluoride with Lewis bases (4–6). The model assumes that intermolecular steps, +C, are limited by the rate of diffusion and that steps which decrease the coordination number, −C and $-C^c$, are slower and depend on the strength of the bond that is cleaved, but cyclic intramolecular *n*-center steps, $+C^c$, are statistically favoured, particularly in the case of 3-, 4-, 5-, and 6-center steps. Kinetic simulation of pathways P(*X*,*C*) is carried out by associating elementary rate constants with the four coordination number operators +C, −C, $+C^c$, and $-C^c$, while molecular orbital calculations are helpful in estimating relative rate constants for intermediates where experimental data are not available.

Any mechanistic description of the BF_3–base system must accommodate the following experimental facts: (*a*) the formation of base:BF_3 is a bimolecular process with rate constants in the range 10^8–10^{10} M^{-1} s^{-1} (7); (*b*) rates of reaction of base:BF_3 are inversely proportional to the gas phase enthalpies of dissociation (5); (*c*) equilibrium data for BF_3–base systems (8); (*d*) two modes of exchange in BX_3–base systems involving both halogen and base exchange (5, 9); (*e*) excess BF_3 accelerates the rate of fluorine exchange in base:BF_3 (5); (*f*) the boron cation (amine)$_2BF_2^+$ is an elusive species although, once formed, it is stable even in water (4); (*g*) some adducts such as HMPA:BF_3 and tetramethylurea:BF_3 are in equilibrium with the ionic species (base)$_2$-$BF_2^+BF_4^-$ (10); (*h*) the formation of mixed base adducts such as $(Me_3N)(pyridine)BF_2^+$ depends on the order of addition of base (4); and (*i*) formation of chelated boron cations with bidentate ligands (N–N)BF_2^+ occurs in some cases (11), but not in others (12).

Results and discussion

The NH_3–BF_3 and $MeNH_2$–BF_3 systems

The analysis of the NH_3–BF_3 system by the coordination model begins by considering all possible interactions between the atoms of ammonia and boron trifluoride, of which the strongest will most likely involve B—N, H--N, and H--F bonds. The model is tolerant of higher coordination numbers as these reflect interactions between reactants and intermediates, but weakly bound intermediates will decompose rapidly and consequently their effect can be neglected, unless they are a prerequisite for further reaction along a multistep pathway. Pathways P(*X*,*C*) are constructed after choosing a minimum set of coordination numbers for the NH_3–BF_3 system, i.e., B(3) B(4) N(3) N(4) F(1) F(2) H(1) H(2), and this minimum set of coordination numbers is used for all base–BF_3 systems, with the exception of pyridine, where N(2) N(3) is more appropriate, and dialkyl ether, where O(2) O(3) is used. The formation of B—N, H--N, and H--F bonds in the NH_3–BF_3 system is an example of pathway P(3,1), as illustrated in eqs. [1]–[3].

For the testing of the coordination model, each +C and −C must be associated with elementary rate constants and these are selected as follows: intermolecular steps, +C, are

[1]Presented at the 203rd ACS National Meeting, San Francisco, April 5–10, 1992.

[2]Author to whom correspondence may be addressed.

[3]Notation: A graph P(*X*,*C*) consists of a vertex set *X* of reactants, intermediates, and products, and an edge set *C* of coordination number operators +C, −C, $+C^c$, and $-C^c$, which are drawn above the edges for forward steps and below for reverse steps; dashed lines refer to intermolecular steps, +C or −C, and solid lines to cyclic intramolecular steps, $+C^c$ or $-C^c$; $+C_{M(m)N(n)}$ increases the coordination number of elements M and N by 1, from *m* to *m* + 1 and *n* to *n* + 1, and $-C_{M(m)N(n)}$ decreases the coordination numbers by 1 from *m* + 1 to *m* and *n* + 1 to *n*; $+C^{n\text{-center}}_{M(m)N(n)}$ and $-C^{n\text{-center}}_{M(m)N(n)}$ define coordination changes that occur via cyclic *n*-center steps; and pathway P(5,2) contains 5 vertices and 2 edges, as described previously (1).

Can. J. Chem. Downloaded from www.nrcresearchpress.com by 88.255.202.194 on 09/08/12
For personal use only.

Can. J. Chem. Downloaded from www.nrcresearchpress.com by 88.255.202.194 on 09/08/12
For personal use only.

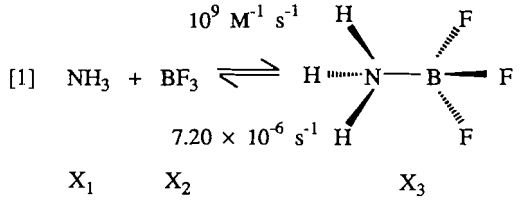

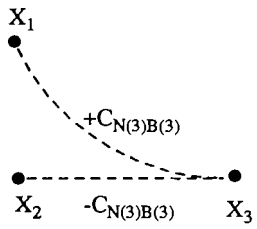

P(3,1)

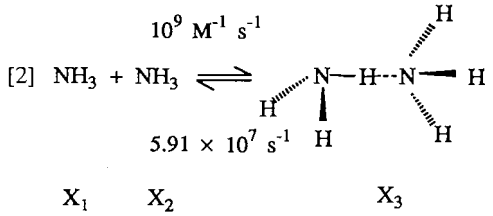

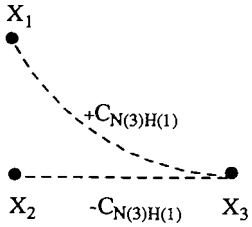

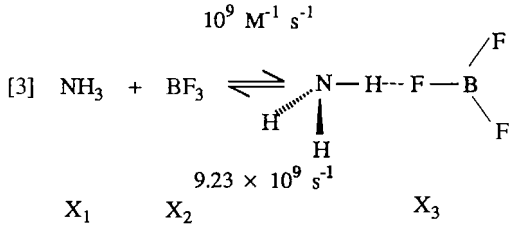

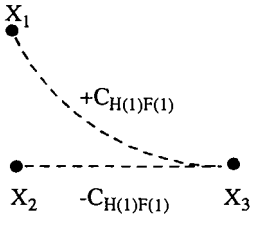

assigned rate constants equal to the diffusion-controlled value of about 10^9 M^{-1} s^{-1}, while rate constants associated with bond cleavage, −C, are calculated with the aid of equation $k = Ae^{-\Delta H/RT}$, where $A = 10^{11}$, $T = 298$ K, and ΔH is the bond enthalpy associated with a specific −C, as listed in Table 1. The rate constants are shown in eqs. [1]–[3], and by selecting rate constants in this way, without any further modification, ΔH becomes the only adjustable parameter of our mechanistic analysis, and a semiquantitative but stringent test of the coordination model is now possible, even for multistep processes.

Kinetic simulations were carried out by means of the Runge–Kutta algorithm (13) on a 386PC using the MathCad 3.1 program (14), and the calculated concentration vs. time curves for the reaction of NH_3 and BF_3 in a 1:1 molar ratio using the rate constants of eqs. [1]–[3] are shown in Fig. 1. Identical pathways P(3,1) are assumed for the reaction of BF_3 with $MeNH_2$ and the kinetic simulation of a 1:1 reaction using the bond enthalpies of Table 1 and the rate constants of eqs. [4]–[6] are displayed in Fig. 2.

$$[4]\quad MeNH_2 + BF_3 \underset{8.36 \times 10^{-9}\ s^{-1}}{\overset{10^9\ M^{-1}\ s^{-1}}{\rightleftharpoons}} MeNH_2{:}BF_3$$

$$[5]\quad MeNH_2 + MeNH_2 \underset{3.20 \times 10^{8}\ s^{-1}}{\overset{10^9\ M^{-1}\ s^{-1}}{\rightleftharpoons}} MeHN\text{-}H\text{--}NH_2Me$$

$$[6]\quad MeNH_2 + BF_3 \underset{9.23 \times 10^{9}\ s^{-1}}{\overset{10^9\ M^{-1}\ s^{-1}}{\rightleftharpoons}} MeHN\text{-}H\text{--}F\text{-}BF_2$$

The experimental rate constants for reaction of boron trifluoride with ammonia and methylamine were determined by Kistiakowsky and Williams (7), $k(NH_3) = 2.7 \times 10^8$ and $k(MeNH_2) = 6.7 \times 10^8$ M^{-1} s^{-1} at 25°C, and the slower reaction with ammonia was attributed to an activation energy ranging from 8 kJ for ammonia to near zero for heavier amines; however, the activation energies could not be confirmed experimentally. The coordination model does not assume an activation energy for +C, and a theoretical CNDO study has concluded that no activation energy is necessary for the formation of $H_3N{:}BF_3$ (15), but the slower reaction of ammonia as compared to methylamine, which is displayed in Fig. 1 as a lower yield of $H_3N{:}BF_3$ (0.72 M) as compared to $MeNH_2$ (0.84 M) after 10^{-8} s, must arise from a weaker B—N and a stronger N--H bond for the ammonia reaction because the rate constants, +C, are fixed at 10^9 M^{-1} s^{-1} and N--F bond enthalpies were estimated to be equal (Table 1). The weaker B—N bond of $H_3N{:}BF_3$ results in a slightly greater dissociation of the ammonia adduct, eq. [1], while greater hydrogen bonding between ammonia molecules increases the concentration of the hydrogen-bonded intermediate, eq. [2], and thereby reduces slightly the overall rate of formation of $H_3N{:}BF_3$, as compared to $MeNH_2{:}BF_3$. Statistical factors (16) related to the number of equivalent pathways by which H--N or H--F bonds can be formed were not included in our calculation, but they would also favour the ammonia intermediates and further reduce the overall rate of formation of the ammonia adduct, as compared to the methylamine adduct, in agreement with experiment.

The Me_2O–Et_2O–BF_3 system

This system was studied by Rutenberg, Palko, and Drury (8), by means of ^{19}F NMR and their reported equilibrium composition of three mixtures of Et_2O, Me_2O, and BF_3 is shown in Table 2. We calculated concentration vs. time curves for the same mixtures using the bond enthalpies of Table 1 and rate constants of eqs. [7] and [8], and Fig. 3 shows the results for an initial mixture of $Et_2O{:}Me_2O{:}BF_3$ = 7.51:2.27:3.06. As seen in Fig. 3, equilibrium is reached rapidly, within about 10^{-9} s, and a comparison of calcu-

TABLE 1. Bond enthalpies required for calculation of rate constants

Species	Bond	$-\Delta H$ (kJ mol^{-1})[a]	Comment (ref.)
$Me_2O:BF_3$	O—B	54.81	Gas phase (5)
$Et_2O:BF_3$	O—B	44.35	Gas phase (26)
$H_3N:BF_3$	N—B	92.05	Gas phase (21)
$MeNH_2:BF_3$	N—B	108.8	Gas phase (21)
$Me_3N:BF_3$	N—B	129.3	Gas phase (27)
$py:BF_3$	N—B	104.6	Solution (27)
$py_2BF_2^+$, $py:BF_2$--F--BF_3	N—B	104.6	Est., same as $py:BF_3$
N–N:BF_3, (N–N)BF_2^+	N—B	129.3	Est., same as $Me_3N:BF_3$
H_2NH--NH_3	N--H	18.4	Gas phase (28)
MeHNH--NH_2Me	N--H	14.2	Gas phase (28)
H_2NH--FBF_2, MeHNH--FBF_2	H--F	5.9	Est. (29)
base:BF_2--F--BF_3	B--F—B	15.0–25.0	Est., see text

[a]Converted from literature values in kcal mol^{-1}.

Can. J. Chem. Downloaded from www.nrcresearchpress.com by 88.255.202.194 on 09/08/12
For personal use only.

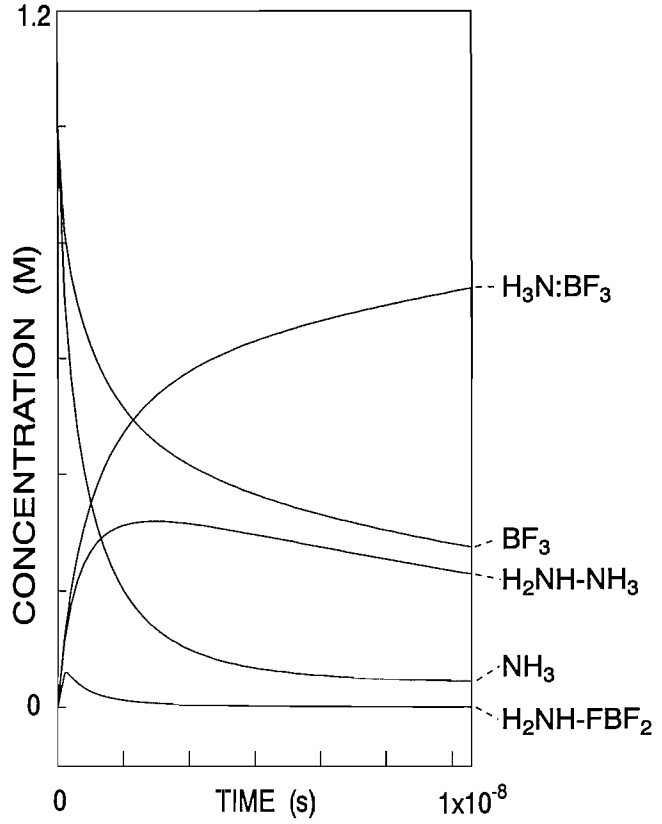

FIG. 1. Calculated concentration vs. time curves for the 1:1 reaction of BF_3 with NH_3. Input rate constants are given in eqs. [1]–[3]. The concentration of $H_3N:BF_3$ after 1×10^{-8} s is 0.72 M.

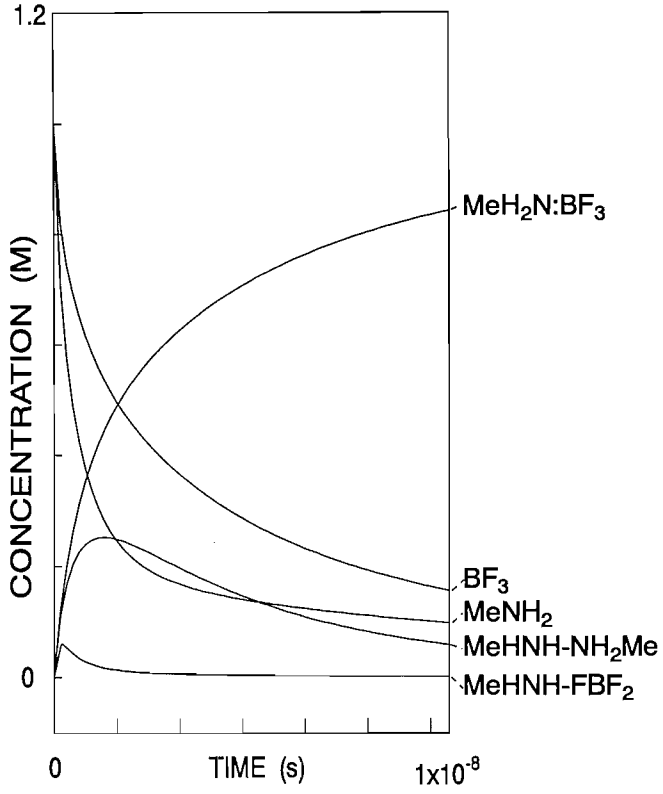

FIG. 2. Calculated concentration vs. time curves for the 1:1 reaction of BF_3 with $MeNH_2$. Input rate constants are given in eqs. [4]–[6]. The concentration of $MeNH_2:BF_3$ after 1×10^{-8} s is 0.84 M.

lated and experimental equilibrium concentrations for all three sets of initial conditions, Table 2, shows moderately good agreement. An exact agreement is not expected because all

$$[7] \quad Me_2O + BF_3 \underset{26.3\ s^{-1}}{\overset{10^9\ M^{-1}\ s^{-1}}{\rightleftharpoons}} Me_2O:BF_3$$

$$[8] \quad Et_2O + BF_3 \underset{1.77 \times 10^3\ s^{-1}}{\overset{10^9\ M^{-1}\ s^{-1}}{\rightleftharpoons}} Et_2O:BF_3$$

the data of Table 2 are based on simplifications: the ^{19}F NMR results of Rutenberg *et al.* neglect the effect of ionic species such as base:BF_2^+ and (base)$_2BF_2^+$ on the chemical shift and linewidth, while our calculations neglect entropy effects and assume a uniform rate constant for the formation, +C, of base:BF_3 adducts.

The Me_2O and $Et_2O:BF_3$ system

If rapid diffusion-controlled steps, +C, have rate constants of about 10^9 M^{-1} s^{-1}, then slow reactions must depend on −C, or on ratios of C's, and the concentration of reactive intermediates in slow reactions must be exceedingly low. A slow reaction may be analyzed by calculating

TABLE 2. Comparison of calculated and experimental equilibrium concentrations for the Me_2O–Et_2O–BF_3 system

Compound	Initial conc. (8) (M)	Equil. conc. at 26°C (8) (M)	Calcd.[a] conc. after 2×10^{-8} s (M)
Experiment 1			
Et_2O	7.51	5.73	5.14
Me_2O	2.27	0.99	1.54
BF_3	3.06	0.0	5.8×10^{-7}
Et_2O:BF_3	0.0	1.78	2.37
Me_2O:BF_3	0.0	1.28	0.71
Experiment 2			
Et_2O	5.77	2.21	2.15
Me_2O	3.98	1.42	1.48
BF_3	6.12	0.0	1.63×10^{-6}
Et_2O:BF_3	0.0	3.56	3.62
Me_2O:BF_3	0.0	2.56	2.50
Experiment 3			
Et_2O	4.59	0	0.024
Me_2O	4.59	0	0.024
BF_3	9.18	0	0.049
Et_2O:BF_3	0.0	4.59	4.57
Me_2O:BF_3	0.0	4.59	4.57

[a]Calculations are based on the initial conditions of column 1 and rate constants of eqs. [7] and [8].

Can. J. Chem. Downloaded from www.nrcresearchpress.com by 88.255.202.194 on 09/08/12
For personal use only.

the outcome of a reaction of Et_2O:BF_3 with Me_2O, in a 4.00:2.76 ratio, using identical rate constants, eqs. [9] and [10], as for the previous Me_2O–Et_2O–BF_3 system which reached equilibrium within about 10^{-9} s. The calculations show that after 6×10^{-6} s the concentration of Et_2O:BF_3

$$[9] \quad Et_2O{:}BF_3 \underset{10^9\ M^{-1}\ s^{-1}}{\overset{1.77 \times 10^3\ s^{-1}}{\rightleftharpoons}} Et_2O + BF_3$$

$$[10] \quad Me_2O + BF_3 \underset{26.3\ s^{-1}}{\overset{10^9\ M^{-1}\ s^{-1}}{\rightleftharpoons}} Me_2O{:}BF_3$$

(3.96 M) and Me_2O (2.72 M) decreased slightly while Me_2O:BF_3 (0.041 M) slowly increased, but the concentration of the reactive intermediate BF_3 was maintained at a low concentration of about 10^{-6} M. Synthetic reactions utilizing R_2O:BF_3 are often carried out in the presence of excess dialkyl ether, and this calculation illustrates a common role of solvent as stabilizer and dispenser of reactive intermediates.

The pyridine–BF_3 system

The behaviour of the base–BF_3 systems discussed above is largely determined by the cleavage of B—N and B—O bonds and all calculations point to a small or negligible concentration of uncomplexed BF_3. However, the existence of two modes of exchange in these systems has been known for a long time and exchange is particularly influenced by an excess of BF_3. The most likely role of excess BF_3 is to form fluorine-bridged intermediates, and we therefore associate the two modes of exchange with the cleavage, −C, of two types of bonds, namely, bridging B--F--B bonds, as well as B—N or B—O bonds, and our proposed mechanism of reaction of pyridine with boron trifluoride is summarized as pathway P(9,4).

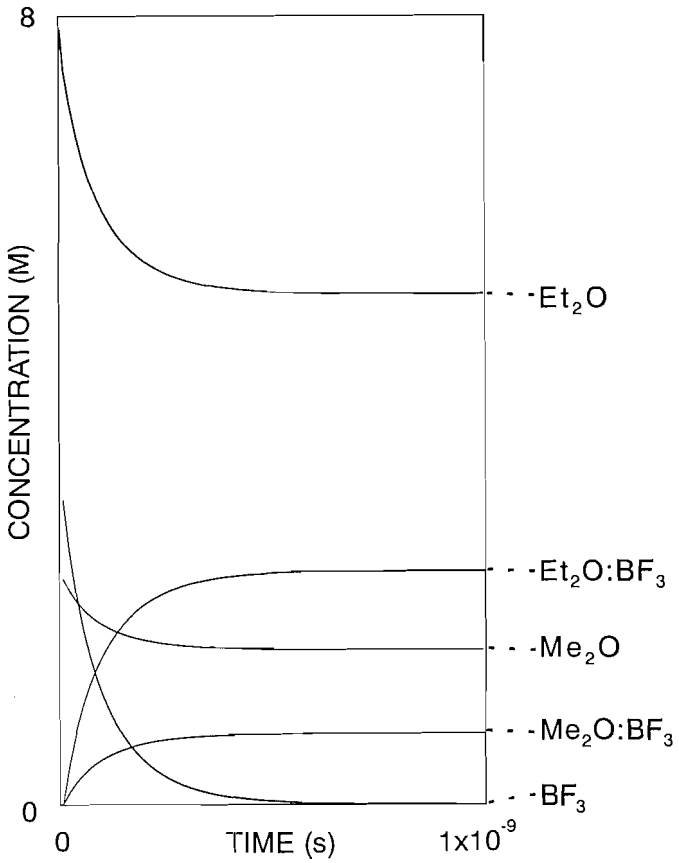

FIG. 3. Calculated concentration vs. time curves for the reaction of BF_3 with Me_2O and Et_2O. Input rate constants are given in eqs. [7] and [8].

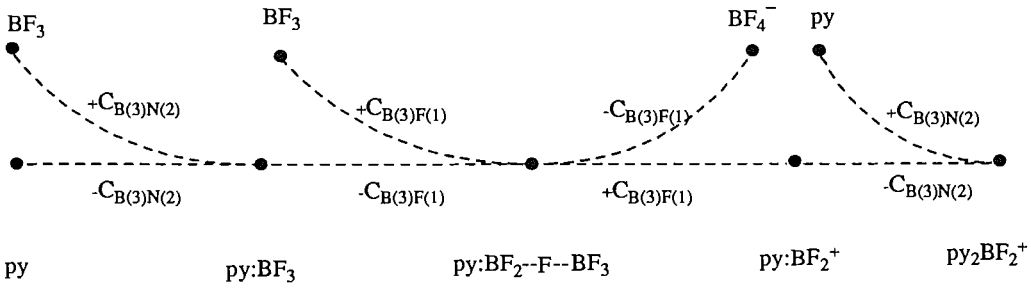

A systematic study of $(base)_2BF_2^+$ cations has been reported recently by Farquharson and Hartman (4) and fluorine-bridged adducts such as $base:BF_2\text{--}F\text{--}BF_3$ have been postulated before (17); furthermore, $F_3B\text{--}F\text{--}BF_3^-$ is stable at low temperature but undergoes rapid bond cleavage at ambient temperature (18). To simplify the analysis of the pyridine–BF_3 system, we considered only one fluorine-bridged intermediate in pathway P(9,4) although it is implicitly assumed that BF_3 can interact with all fluorine-containing species to generate other intermediates such as $py_2BF\text{--}F\text{--}BF_3^+$. Inclusion of the latter cation in a larger pathway would be a straightforward task and would be necessary if the analysis were extended to species such as py_2BF^{2+} or py_3BF^{2+}.

Our calculations require an estimate of the strength of these bridging B--F--B bonds for which experimental data are not available but, since NMR studies of fluorine exchange show "activation energies" in the range of about 15–25 kJ for boron fluorides (19), we assume that bond enthalpies are of about this magnitude. We carried out GAUSSIAN86 calculations of two possible fluorine-bridged intermediates and, as seen in Fig. 4, these show significant differences in relative bond lengths. We therefore assign, somewhat crudely, a bond strength of 25 kJ for the shorter bridging bond and 15 kJ for the longer bridging bond. An experimental B—N bond energy is not available for $py_2BF_2^+$; thus we assume the same value as for $py:BF_3$, and with these approximations it is possible to assign the rate constants of eqs. [11]–[14] and calculate a concentration vs. time curve for a 1 : 1.5 reaction of pyridine and BF_3, as shown in Fig. 5.

$$[11]\quad py + BF_3 \underset{4.53 \times 10^{-8}\ s^{-1}}{\overset{10^9\ M^{-1}\ s^{-1}}{\rightleftharpoons}} py:BF_3$$

$$[12]\quad py:BF_3 + BF_3 \underset{2.34 \times 10^{8}\ s^{-1}}{\overset{10^9\ M^{-1}\ s^{-1}}{\rightleftharpoons}} py:BF_2\text{--}F\text{--}BF_3$$

$$[13]\quad py:BF_2\text{--}F\text{--}BF_3 \underset{10^9\ M^{-1}\ s^{-1}}{\overset{4.13 \times 10^{6}\ s^{-1}}{\rightleftharpoons}} py:BF_2^+ + BF_4^-$$

$$[14]\quad py + py:BF_2^+ \underset{4.53 \times 10^{-8}\ s^{-1}}{\overset{10^9\ M^{-1}\ s^{-1}}{\rightleftharpoons}} py_2BF_2^+$$

Figure 5 reveals that species $py:BF_2\text{--}F\text{--}BF_3$, $py:BF_2^+$, and $py_2BF_2^+$ are present in relatively modest concentration and since the rate constants for cleavage of B--F--B bonds are large it is not surprising that previous attempts to identify individual species in solution by NMR have been met with difficulty. The acceleration of fluorine exchange by excess BF_3 is readily explained by eqs. [12] and [13], and the stability of $(base)_2BF_2^+$, once isolated (4), is consistent with the estimated rate constants of eq. [14], which predict a large and favourable equilibrium constant.

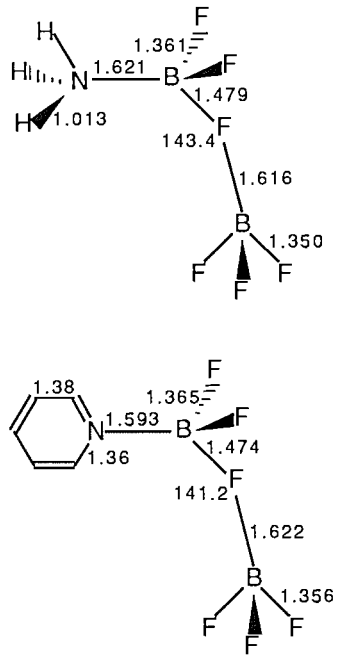

FIG. 4. GAUSSIAN86 calculations of $H_3N:BF_2\text{--}F\text{--}BF_3$ and $py:BF_2\text{--}F\text{--}BF_3$ at the 3-21G* level with full optimization, except for fixed geometry of pyridine.

Pathway P(9,4) is in agreement with previous mechanisms that require dissociation of boron-base bonds or halogen-bridge bonds, but it differs significantly in its suggestion that base exchange occurs via intermediates $(base)_2BF_2^+$ or $(base)(base')BF_2^+$ rather than exchange by collision or S_N2 processes. The latter mechanisms, if correct, would require a change in the minimum set of coordination numbers to include either B(5) or N(5), but pathway P(9,4) makes such proposals unnecessary.

$(R_3N)(py)BF_2^+$ and order of addition of base

Farquharson and Hartman found that $(R_3N)(py)BF_2^+$ is formed more rapidly when R_3N is added to $py:BF_2Br$ than when pyridine is added to $R_3N:BF_2Br$ (4). We considered the order of addition of base by analyzing the addition of trimethylamine to $py:BF_3$, eqs. [15]–[19], as compared to adding pyridine to $Me_3N:BF_3$, eqs. [20]–[24], using the bond enthalpies of Table 1 and the assumption that B—N bond

Can. J. Chem. Downloaded from www.nrcresearchpress.com by 88.255.202.194 on 09/08/12
For personal use only.

Can. J. Chem. Downloaded from www.nrcresearchpress.com by 88.255.202.194 on 09/08/12
For personal use only.

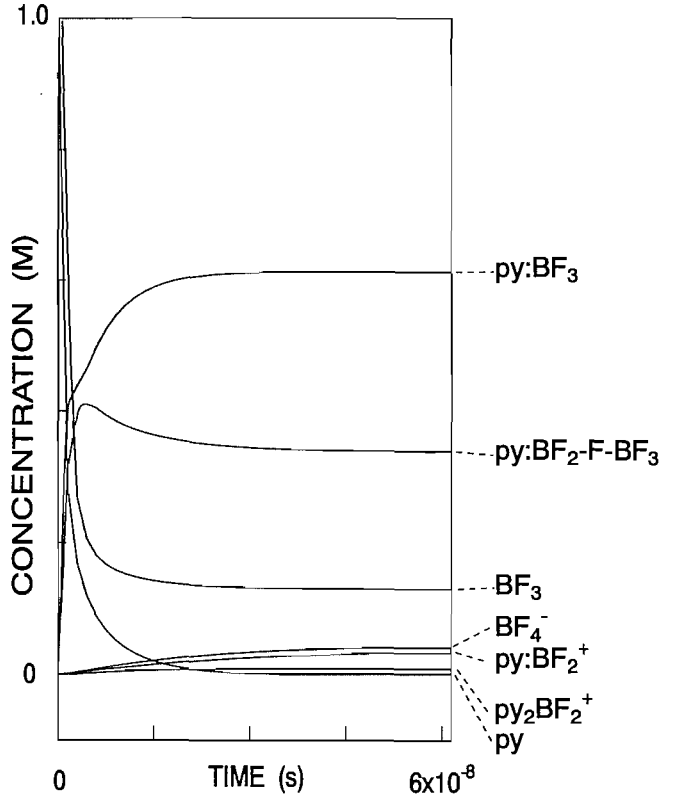

FIG. 5. Calculated concentration vs. time curves for the 1:1.5 reaction of pyridine with BF_3. Input rate constants are given in eqs. [11]–[14]. Concentration of $py_2BF_2^+$ after 6×10^{-8} s is 0.0085 M.

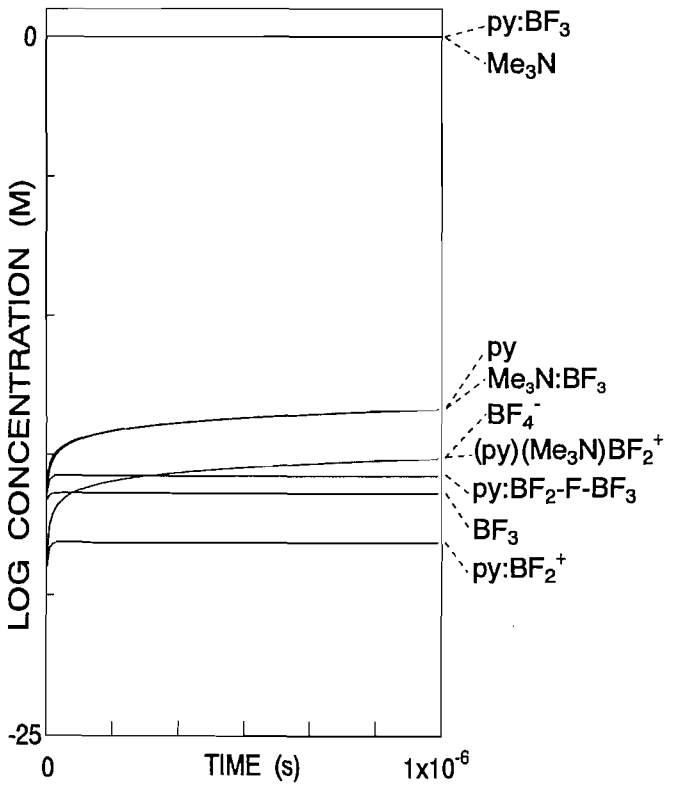

FIG. 6. Calculated log. concentration vs. time curves for the 1:1 reaction of Me_3N with $py:BF_3$. Input rate constants are given in eqs. [15]–[19]. Concentration of $(py)(Me_3N)BF_2^+$ after 1×10^{-6} s is 2.7×10^{-16} M.

strengths in $(Me_3N)_2BF_2^+$, $(Me_3N)(py)BF_2^+$, and $py_2BF_2^+$ are the same as in $Me_3N:BF_3$ and $py:BF_3$.

An abbreviated mechanism for the 1:1 reaction of Me_3N with $py:BF_3$, which includes the essential features of cleavage of B—N and B--F--B bonds, but omits other possible fluorine-bridged intermediates such as $Me_3N:BF_2$--F--BF_3, is shown in eqs. [15]–[19], and the calculated log(conc) vs. time curve is shown in Fig. 6.

$$[15]\quad py:BF_3 \underset{10^9\ M^{-1}\ s^{-1}}{\overset{4.53 \times 10^{-8}\ s^{-1}}{\rightleftharpoons}} py + BF_3$$

$$[16]\quad Me_3N + BF_3 \underset{2.12 \times 10^{-12}\ s^{-1}}{\overset{10^9\ M^{-1}\ s^{-1}}{\rightleftharpoons}} Me_3N:BF_3$$

$$[17]\quad py:BF_3 + BF_3 \underset{2.34 \times 10^{8}\ s^{-1}}{\overset{10^9\ M^{-1}\ s^{-1}}{\rightleftharpoons}} py:BF_2\text{--}F\text{--}BF_3$$

$$[18]\quad py:BF_2\text{--}F\text{--}BF_3 \underset{10^9\ M^{-1}\ s^{-1}}{\overset{4.13 \times 10^{6}\ s^{-1}}{\rightleftharpoons}} py:BF_2^+ + BF_4^-$$

$$[19]\quad py:BF_2^+ + Me_3N \underset{2.12 \times 10^{-12}\ s^{-1}}{\overset{10^9\ M^{-1}\ s^{-1}}{\rightleftharpoons}} (Me_3N)(py)BF_2$$

The reverse reaction of pyridine with $Me_3N:BF_3$ is summarized in eqs. [20]–[24] and the log(conc) vs. time curve is shown in Fig. 7.

$$[20]\quad Me_3N:BF_3 \underset{10^9\ M^{-1}\ s^{-1}}{\overset{2.12 \times 10^{-12}\ s^{-1}}{\rightleftharpoons}} Me_3N + BF_3$$

$$[21]\quad py + BF_3 \underset{4.53 \times 10^{-8}\ s^{-1}}{\overset{10^9\ M^{-1}\ s^{-1}}{\rightleftharpoons}} py:BF_3$$

$$[22]\quad Me_3N:BF_3 + BF_3 \underset{2.34 \times 10^{-8}\ s^{-1}}{\overset{10^9\ M^{-1}\ s^{-1}}{\rightleftharpoons}} Me_3N:BF_2\text{--}F\text{--}BF_3$$

$$[23]\quad Me_3N:BF_2\text{--}F\text{--}BF_3 \underset{10^9\ M^{-1}\ s^{-1}}{\overset{4.13 \times 10^{6}\ s^{-1}}{\rightleftharpoons}} Me_3N:BF_2^+ + BF_4^-$$

$$[24]\quad Me_3N:BF_2^+ + py \underset{4.53 \times 10^{-8}\ s^{-1}}{\overset{10^9\ M^{-1}\ s^{-1}}{\rightleftharpoons}} (Me_3N)(py)BF_2^+$$

Figures 6 and 7 show the concentrations after 1×10^{-6} s. Although equilibrium is far from established, the results do show that the initial concentration of $(py)(Me_3N)BF_2^+$ depends markedly on the order of addition of base, being 2.7×10^{-16} M for addition of Me_3N versus 1.7×10^{-20} M for addition of pyridine, and this increases to 5.6×10^{-14} M and 2.6×10^{-18} M, respectively, after 7.2×10^{-5} s, but longer times were impractical because of the limitation of our kinetic simulation program. An inspection of the rate constants of eqs. [15]–[24] shows clearly that the effect can be attributed mainly to the smaller N—B bond strength of the $py:BF_3$ adduct, which favours dissociation and eventual production of $py:BF_2^+$ and $(Me_3N)(py)BF_2^+$. This dissociation of base:BF_3 to produce free BF_3 is required in eqs. [17] and [22] for the cleavage of boron–fluorine bonds. Another effect may also be important, namely, the relative strength of bridging bonds B--F--B, but the lack of experi-

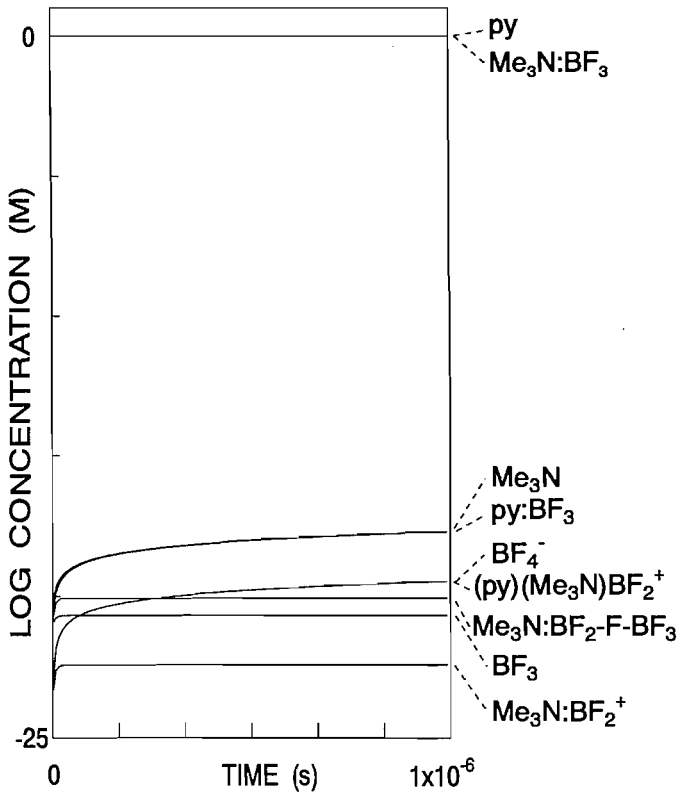

FIG. 7. Calculated log. concentration vs. time curves for the 1:1 reaction of pyridine with $Me_3N:BF_3$. Input rate constants are given in eqs. [20]–[24]. Concentration of $(py)(Me_3N)BF_2^+$ after 1×10^{-6} s is 1.7×10^{-20} M.

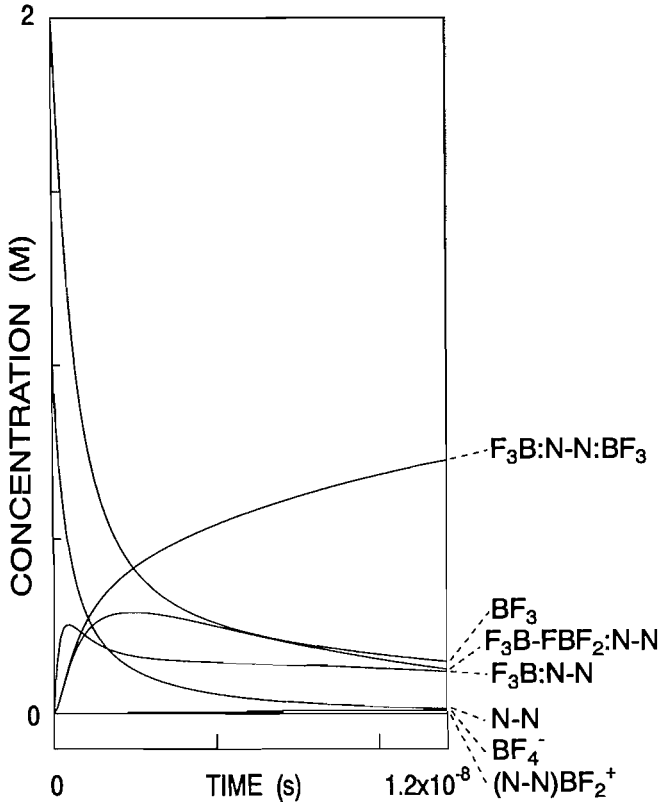

FIG. 8. Calculated concentration vs. time curves for the 2:1 reaction of BF_3 with bidentate ligand, N—N. Input rate constants are given in eqs. [25]–[29]. Concentration of $F_3B:N–N:BF_3$ and $(N–N)BF_2^+$ after 1.2×10^{-8} s is 0.73 M and 0.01 M, respectively.

mental bond strength data prevents a realistic test of this suggestion, although selective cleavage of fluorine-bridging bonds has been described for related systems (1, 2, 20).

$(N–N)BF_2^+$ and n*-center steps*

Entropy effects have been neglected in the analysis of the base–BF_3 systems discussed above, but cyclic *n*-center steps, $+C^{n\text{-center}}$, are strongly favoured by entropy, particularly 3- to 6-center steps where interacting atoms are in close proximity (1), and this introduces the possibility that changes in the ratio of $+C^{n\text{-center}}/+C$ may affect the outcome of a chemical reaction. To estimate a rate constant for ring closure, it may be noted that entropies of gas-phase reactions of BF_3 with acyclic amines are generally negative with $\Delta S = -202 \pm 8$ J mol^{-1} deg^{-1} at 0°C (21). It is also known that formation of a five-membered ring (chelate effect) in a multistep reaction of, say, $Cd^{2+}(aq)$ with ethylenediamine rather than with acyclic $MeNH_2$ leads to enhanced stability because of changes in ΔS from -67.3 to $+14.1$ J mol^{-1} deg^{-1} (22); moreover, the five-membered ring in phosphate esters also accelerates the rate of hydrolysis by factors of 10^6 to 10^8 (23). It is therefore reasonable to assume that ring closure, $+C^{5\text{-center}}$, involves a more positive entropy change than reaction with acyclic bases, +C, and we crudely estimate that entropy changes lead to an increase in the ratio $+C^{5\text{-center}}/+C$ of about 100, thus $k = 10^{11}$ s^{-1} for the ring-closure step of eq. [29].

Pathway P(10,5) and eqs. [25]–[29] may be suggested as a mechanism for reaction of BF_3 with a bidentate ligand N–N, and the question of interest is the relative yield of

$$[25]\quad N–N + BF_3 \underset{8.36 \times 10^{-9}\ s^{-1}}{\overset{10^9\ M^{-1}\ s^{-1}}{\rightleftharpoons}} N–N:BF_3$$

$$[26]\quad F_3B:N–N + BF_3 \underset{8.36 \times 10^{-9}\ s^{-1}}{\overset{10^9\ M^{-1}\ s^{-1}}{\rightleftharpoons}} F_3B:N–N:BF_3$$

$$[27]\quad N–N:BF_3 + BF_3 \underset{2.34 \times 10^{8}\ s^{-1}}{\overset{10^9\ M^{-1}\ s^{-1}}{\rightleftharpoons}} N–N:BF_2\text{--}F\text{--}BF_3$$

$$[28]\quad N–N:BF_2\text{--}F\text{--}BF_3 \underset{10^9\ M^{-1}\ s^{-1}}{\overset{4.16 \times 10^{6}\ s^{-1}}{\rightleftharpoons}} N–N:BF_2^+ + BF_4^-$$

$$[29]\quad N–N:BF_2^+ \underset{8.36 \times 10^{-9}\ s^{-1}}{\overset{10^{11}\ s^{-1}}{\rightleftharpoons}} (N–N)BF_2^+$$

acyclic $F_3B:N–N:BF_3$ versus cyclic $(N–N)BF_2^+$ because the experimental evidence is not clear on this point; some authors have found only acyclic product (12), while others found cyclic cations in high yield (11). If we assume that typical B—N and B--F--B bond strengths of Table 1 apply to this system, with the B—N bond strength equal to that of $Me_3N:BF_3$, then the rate constants of eqs. [25]–[29] can be used to calculate the conc. vs. time curve shown in Fig. 8 for a 2:1 reaction of BF_3 and N–N. The results of Fig. 8 show clearly that $F_3B:N–N:BF_3$ (0.73 M) is favoured over $(N–N)BF_2^+$ (0.01 M) after 1.2×10^{-8} s. These initial concentrations are in agreement with the results of Brown and

Can. J. Chem. Downloaded from www.nrcresearchpress.com by 88.255.202.194 on 09/08/12
For personal use only.

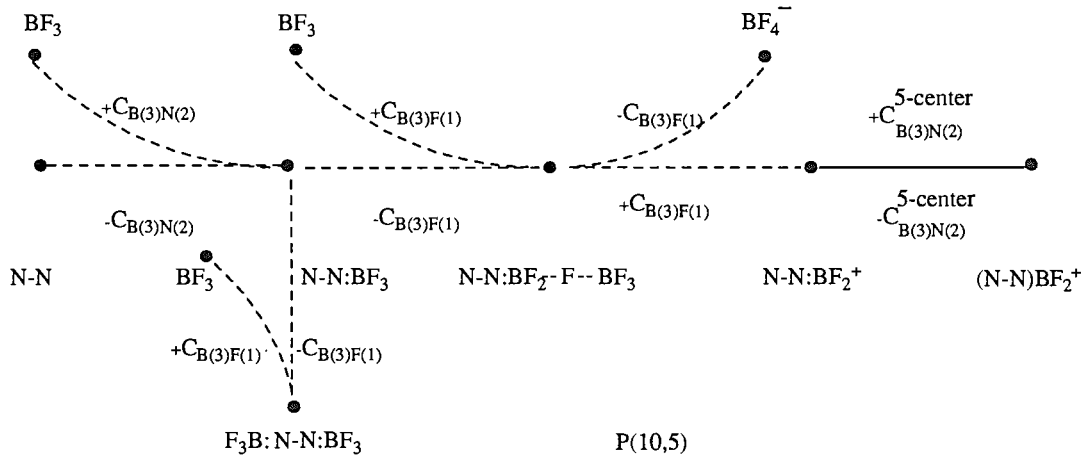

Singaram (12) who found only $F_3B{:}NH_2CH_2CH_2NH_2{:}BF_3$ in their 2:1 reaction of BF_3 with ethylenediamine. An inspection of the rate constants of eq. [26] confirms that $F_3B{:}N{-}N{:}BF_3$ will always be favoured over any competitive reaction with BF_3. Contrary to these calculations, however, are the observations of Wiberg and Buchler (11) who reported high yields (66%) of $(N{-}N)BF_2^+BF_4^-$ in their reaction of BF_3 with the bidentate ligands tetrakis(dimethylamino)ethene and *o*-bis(dimethylamino)benzene. These authors also reported an appreciable amount (13–26%) of $^+HN{-}NH^+2BF_4^-$ among the reaction products, and the latter result leads us to suggest that an additional mechanistic feature may be responsible for the formation of cyclic products, namely, a protected species $F_3B{:}N{-}N{-}H^+$ that prevents the bidentate ligand from further reaction with BF_3, as in eq. [26]; subsequent deprotonation then favours cyclic $(N{-}N)BF_2^+$, as in eq. [29]. The synthesis of a related cyclic cation $(N{-}N)PF_4^+$ is also accompanied by the formation of $N{-}NH^+PF_6^-$, where N–N is bipyridine, 4-fluorobipyridine, and phenanthroline (2), but the simulation of a more complex pathway that includes protonation and deprotonation steps is beyond the capacity of our kinetic program, although analogous systems have been studied by NMR in which protonation–deprotonation is coupled to a rapid 5-center step, e.g., the base–$R_2P(O)OC(CF_3)_2C(CF_3)_2OH$ system (24).

In conclusion, the coordination model of reaction mechanisms has been tested mathematically by comparing calculated with experimental results for the reactions of boron trifluoride with amines and ethers, and the model appears to account in a satisfactory manner for all experimental details, at least in a semi-quantitative manner. This model allows chemical reactions to be analyzed in three stages: firstly, construct a pathway P(*X*,*C*) which specifies the connectivity of all atoms of that pathway; secondly, apply molecular orbital calculations to the postulated intermediates to assist in the task of estimating relative bond strengths and selecting individual steps of multistep pathways; and, thirdly, carry out kinetic simulations of all possible pathways P(*X*,*C*) and obtain the conc. vs. time curves on which further analysis and prediction is based.

Methods

The kinetic simulations were carried out by means of the standard fourth-order Runge–Kutta algorithm (13) here implemented in terms of MathCad software (14). Difficulties associated with the fact that rate constants varied over a wide range, i.e., "stiffness" of the equations, were dealt with by partitioning the time interval into sections and by choosing as large a time interval within each section as was consistent with obtaining an accurate solution. All calculations were carried out on a 386PC using the MathCad 3.1 program, and a typical kinetic simulation of a four-step, nine-species system required 30 min of computational time per time interval.

Ab initio SCF geometries were calculated for $H_3N{:}BF_2{-}F{-}BF_3$ and $py{:}BF_2{-}F{-}BF_3$ using the GAUSSIAN86 program at the 3-21G* level with full optimization, except for pyridine where a fixed geometry was chosen (25).

Acknowledgement

The financial assistance of the Natural Sciences and Engineering Research Council of Canada is gratefully acknowledged. We thank the University of Manitoba for allotment of computer time and Dr. Michael Sowa and Mr. Rudy Sebastian for helpful discussions.

1. A. F. Janzen and M. Jang. Can. J. Chem. **67**, 71 (1989).
2. T. Q. Nguyen, F. Qu, X. Huang, and A. F. Janzen. Can. J. Chem. **70**, 2089 (1992).
3. A. F. Janzen and M. G. Sowa. J. Fluorine Chem. **54**, 179 (1991).
4. M. J. Farquharson and J. S. Hartman. Can. J. Chem. **67**, 1711 (1989).
5. J. S. Hartman and J. M. Miller. Adv. Inorg. Chem. Radiochem. **21**, 147 (1978).
6. (*a*) A. G. Massey. Adv. Inorg. Chem. Radiochem. **10**, 1 (1967); (*b*) Gmelin handbook of inorganic chemistry, boron compounds. 2nd Suppl. Vol. 2. Springer-Verlag, Berlin. 1982. pp. 18–29; Vol. 37. 1976. pp. 114–125; Vol. 46. 1977. pp. 75–170.
7. G. B. Kistiakowsky and R. Williams. J. Chem. Phys. **23**, 334 (1955).
8. A. C. Rutenberg, A. A. Palko, and J. S. Drury. J. Am. Chem. Soc. **85**, 2702 (1963).
9. B. Benton-Jones and J. M. Miller. Inorg. Nucl. Chem. Lett. **8**, 485 (1972).
10. (*a*) J. S. Hartman and G. J. Schrobilgen. Inorg. Chem. **13**, 874 (1974); (*b*) J. S. Hartman and P. Stilbs. J. Chem. Soc. Dalton Trans. 1142 (1980).
11. N. Wiberg and J. W. Buchler. Chem. Ber. **96**, 3000 (1963).
12. H. C. Brown and B. Singaram. Inorg. Chem. **18**, 53 (1979).
13. R. G. Stanton. Numerical methods for science and engineering. Prentice-Hall, Englewood Cliffs, N.J. 1961.
14. MathSoft User's Journal. Vol. 4, No. 2, Spring 1990. p. 4.
15. P. G. Perkins and J. J. Stewart. Inorg. Chim. Acta, **4**, 40 (1970).

Can. J. Chem. Downloaded from www.nrcresearchpress.com by 88.255.202.194 on 09/08/12
For personal use only.

16. D. M. Bishop and K. J. Laidler. J. Chem. Phys. **42**, 1688 (1965).
17. H. C. Brown, P. F. Stehle, and P. A. Tierney. J. Am. Chem. Soc. **79**, 2020 (1957).
18. (*a*) J. S. Hartman and P. Stilbs. J. Chem. Soc. Chem. Commun. 566 (1975); (*b*) S. Brownstein and J. Paasivirta. Can. J. Chem. **43**, 1645 (1965).
19. S. Brownstein, A. M. Eastham, and G. A. Latremouille. J. Phys. Chem. **67**, 1028 (1963).
20. M. Jang and A. F. Janzen. J. Fluorine Chem. **52**, 45 (1991).
21. S. H. Bauer and R. E. McCoy. J. Phys. Chem. **60**, 1529 (1956).
22. F. A. Cotton and G. Wilkinson. Advanced inorganic chemistry. 5th ed. John Wiley & Sons, New York. 1988. p. 46.
23. F. H. Westheimer. Acc. Chem. Res. **1**, 70 (1968).
24. (*a*) D. Schomburg, O. Stelzer, N. Weferling, R. Schmutzler, and W. S. Sheldrick. Chem. Ber. **113**, 1566 (1980); (*b*) A. F. Janzen, A. E. Lemire, R. K. Marat, and A. Queen. Can. J. Chem. **61**, 2264 (1983).
25. M. J. Frisch, J. S. Binkley, H. B. Schlegel, K. Raghavachari, C. F. Melius, R. L. Martin, J. J. P. Stewart, F. W. Bobrowicz, C. M. Rohlfing, L. R. Kahn, D. J. Defrees, R. A. Seeger, R. A. Whiteside, D. J. Fox, E. M. Fleuder, and J. A. Pople. GAUSSIAN86. Carnegie–Mellon Quantum Chemistry Publishing Unit, Pittsburgh, Pa. 1984.
26. S. G. Katalnikov, V. E. Pisarev, and D. I. Frantskevichute. Russ. J. Phys. Chem. **43**, 671 (1969).
27. W. A. G. Graham and F. G. A. Stone. J. Inorg. Nucl. Chem. **3**, 164 (1956).
28. G. C. Pimentel and A. L. McClelland. The hydrogen bond. W. H. Freeman and Company, San Francisco and London. 1960. p. 360.
29. P. A. Kollman and L. C. Allen. J. Am. Chem. Soc. **93**, 4991 (1971).

Can. J. Chem. Downloaded from www.nrcresearchpress.com by 88.255.202.194 on 09/08/12
For personal use only.

Enantioselective synthesis of epoxides via Sharpless epoxidation of alkenylsilanols

T. H. CHAN[1] AND L. M. CHEN
Department of Chemistry, McGill University, Montreal, Que., Canada H3A 2K6

AND

D. WANG[1] AND L. H. LI
Institute of Chemistry, Academia Sinica, Beijing, People's Republic of China

T. H. CHAN, L. M. CHEN, D. WANG, and L. H. LI. Can. J. Chem. **71**, 60 (1993).

Enantioselective synthesis of simple epoxides can be achieved by Sharpless epoxidation of alkenylsilanols followed by protodesilylation of the chiral epoxysilanols. The approach has been applied to the synthesis of frontalin.

T. H. CHAN, L. M. CHEN, D. WANG et L. H. LI. Can. J. Chem. **71**, 60 (1993).

On peut réaliser la synthèse énantiosélective d'époxydes simples en faisant appel à l'époxydation de Sharpless des alcénylsilanols suivie d'une protodésilylation des époxysilanols chiraux. On a appliqué cette approche à la synthèse de la frontaline.

[Traduit par la rédaction]

Can. J. Chem. Downloaded from www.nrcresearchpress.com by 88.255.202.194 on 09/08/12
For personal use only.

Introduction

The Sharpless epoxidation (1) has been hailed as one of the milestones in organic chemistry. The reaction gives chiral epoxides with predictable stereochemistry and high enantiomeric purity. Since its discovery, the reaction has been used in numerous syntheses of natural products (2). The reaction has, however, one serious limitation in that it can only be applied to allylic alcohols. The hydroxy group in the allylic position plays a critical role in assembling the reactants together (3), thus accelerating the reaction as well as conferring high stereoselectivity. For simple alkenes without the pendant hydroxy group, Sharpless epoxidation is not useful. There is no ready method for preparing simple chiral epoxides with high enantioselectivity.[2] In a preliminary report, we outlined an approach to this problem (5).

We previously showed that trimethyl- or triphenyl-silyl epoxides can be protodesilylated in the presence of fluoride ion to give the corresponding epoxides with retention of stereochemistry (6). It seemed to us that alkenylsilanols, which are structurally similar to allylic alcohols, should be amenable to Sharpless epoxidation. The silyl group could then be excised by fluoride ion to give the simple epoxides. The overall transformation (Scheme 1) is then an enantioselective synthesis of simple epoxides. The success of this approach is, however, predicated on the assumption that alkenylsilanols would behave like allylic alcohols in the Sharpless epoxidation reaction, an assumption that remains to be tested.

Results

Preliminary studies

Since silanols are known to dimerize readily to the disiloxanes, we chose β-styryldiphenylsilanol (**1**) as our first example to investigate in the expectation that the more bulky phenyl groups (relative to, e. g., methyl groups) on the silicon may inhibit the dimerization sufficiently to permit the Sharpless epoxidation to take place. Compound **1** was prepared by the reaction of *trans*-β-styryllithium (**2**), generated by metal–halogen exchange of *trans*-β-bromostyrene with *tert*-butyllithium, with diphenyldichlorosilane followed by aqueous hydrolysis. The silanol **1**, obtained in 90% yield, was indeed stable and did not dimerize to disiloxane on flash chromatography. The disiloxane **3** could, however, be obtained from **1** on long standing. Epoxidation of **1** with *m*-chloroperbenzoic acid (MCPBA) gave the corresponding epoxysilanol **4** in 75% yield. Treatment of **4** with tetraethylammonium fluoride hydrate in MeCN gave styrene oxide in excellent yield (Scheme 2).

When **1** was subjected to Sharpless epoxidation conditions [$Ti(O\text{-}i\text{-}Pr)_4$/(+)-diethyl tartrate (DET)/*tert*-butyl hydroperoxide (TBHP)] in CH_2Cl_2 at −40°C, the reaction was very slow. The reaction was faster at −20°C, giving **4** in 70% yield after 48 h. The epoxide **4** was optically active ($[\alpha]_D^{22}$ −4.8 (*c* 0.25, C_6H_6)). The hydroxy group was critical in this reaction as demonstrated by the fact that the disiloxane **3**, though structurally similar to **1**, was not epoxidized under similar conditions even after a prolonged reaction time at a higher temperature. Protodesilylation of **4** by fluoride ion gave (S)-styrene oxide with 7% enantiomeric excess (ee) according to optical rotation as well as ^1H nmr using tris[3-(heptafluoropropylhydroxymethylene)-(+)-camphorato]europium(III), [(+)-Eu(hfc)$_3$]. The use of molecular sieves, as recommended by Sharpless and coworkers (7), improved slightly the rate of epoxidation and increased the ee of the styrene oxide obtained to 20%.

Notwithstanding the rather modest ee obtained in these experiments, the results were considered encouraging. The epoxidation of **1** is likely to have taken place by a mechanism, whatever it may be (8), similar to the allylic alcohol oxidation. This is supported by the fact that the silanol function was necessary for the epoxidation to take place. Furthermore, the absolute configuration of the epoxide **4** was in agreement with the stereochemical model proposed by Katsuki and Sharpless for allylic alcohols (1). We attributed the low stereoselectivity of the reaction to the steric effect of the diphenylsilyl group. While the Sharpless epoxidation has been successful with allylic primary and secondary alcohols, there is little information on the stereoselectivity for allylic tertiary alcohols. We decided to examine the correponding dimethylsilanol **6**.

*Styrene oxide via Sharpless epoxidation of β-styryldimethylsilanol (**6**)*

Compound **6** could not be prepared in good yield by the reaction of β-styryllithium (**2**) with dimethyldichlorosilane

[1]Authors to whom correspondence may be addressed

[2]For asymmetric dihydroxylation and epoxidation of simple alkenes, see ref. 4.

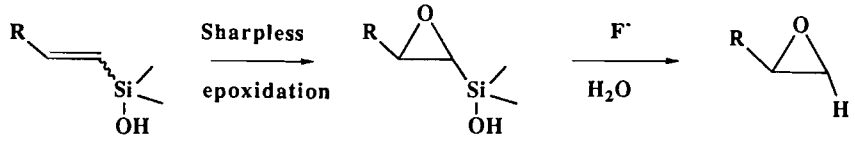

SCHEME 1

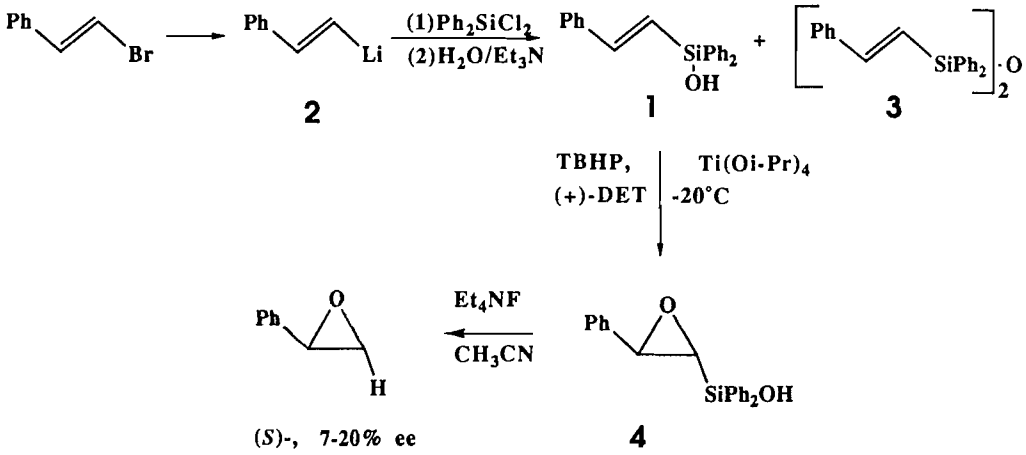

SCHEME 2

or dimethyldiethoxysilane. The difficulty was due to the relative ease of substitution leading to distyryl or disiloxane compounds. Alternative methods of preparing silanols have to be sought. In connection with other research projects in this laboratory, we observed that aminomethylsilyl compounds (9) can be converted to silanols under oxidative conditions (10). Thus, reaction of β-styryllithium with chloromethyldimethylchlorosilane (**7**) gave compound **8** in 82% yield. Heating **8** in pyrrolidine at 80°C for 20 h gave the aminosubstituted silane **9** in 73% yield (Scheme 3). Oxidation of **9** with MCPBA/$CaCO_3$ in CH_2Cl_2 or TBHP/$VO(acac)_2$ in acetone gave a mixture of the silanol **6** and the disiloxane **10** that could be separated by flash chromatography.

Compound **6** can be more conveniently synthesized by an alternative route (Scheme 4). Reaction of β-styryllithium with dimethylchlorosilane (**11**) gave the silane **12** in 92% yield. Oxidation of **12** with silver nitrate/silver oxide in tetrahydrofuran (THF) at room temperature for 9 h gave **6** in good yield (71%). The relative amount of silver nitrate to silver oxide used was critical to the success of the reaction. Too much of either component led to greater amount of the disiloxane **10**, presumably due to the catalytic effect of the acidic or basic nature of the reagents.

Epoxidation of the freshly purified **6** under Sharpless conditions with (+)-DET in CH_2Cl_2 at −20°C for 40 h gave compound **13** in 50% yield. Fluoride ion cleavage of **13** gave (*S*)-styrene oxide (90% yield) with high enantiomeric excess (85–95%, depending on different runs, according to optical rotation and ^1H nmr with (+)-$Eu(hfc)_3$).

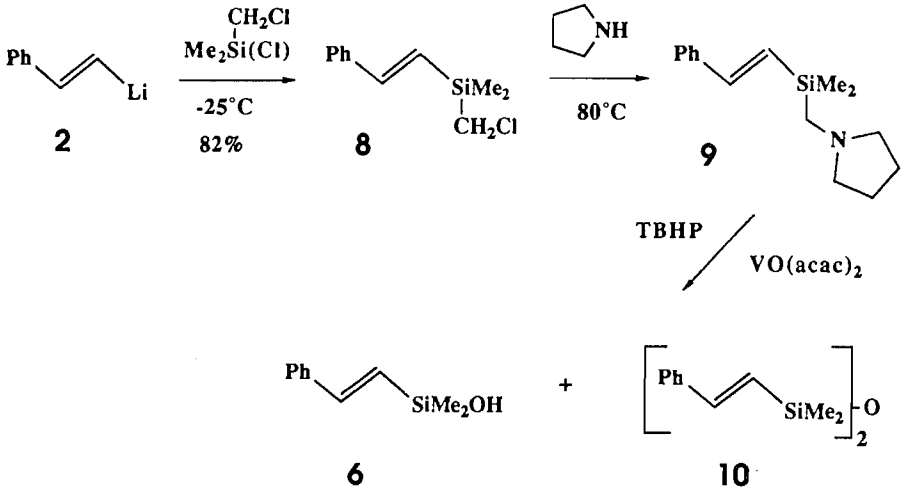

SCHEME 3

Can. J. Chem. Downloaded from www.nrcresearchpress.com by 88.255.202.194 on 09/08/12
For personal use only.

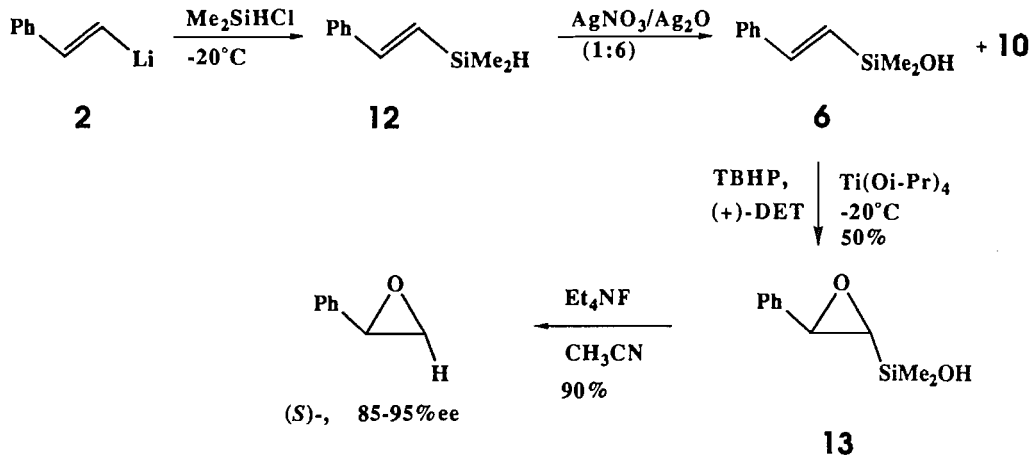

SCHEME 4

1,2-Epoxyheptane (19)

The success in preparing styrene oxide enantioselectively encouraged us to explore the Sharpless epoxidation of other alkenylsilanols. A convenient method of generating the requisite vinylmetallic reagents was by way of hydroalumination of alkynes. Thus, treatment of 1-heptyne with diisobutylaluminium hydride (DIBAL) followed by quenching the mixture with dimethylchlorosilane gave 1-heptenyldimethylsilane (**15**). Oxidation of the silane **15** with $AgNO_3$/Ag_2O gave the silanol **16** in 75% yield (Scheme 5). Epoxidation of **16** with (+)-diisopropyl tartrate (DIPT) and the usual reagents at −20°C gave the epoxysilanol **18**. Compound **18** appeared to be unstable on column chromatography, so the crude product was protodesilylated directly by tetraethylammonium fluoride hydrate in CH_3CN to give (S)-(−)-1,2-epoxyheptane, $[\alpha]_D^{18}$ −18.5 (*c* 0.25, CH_2Cl_2). The ee was determined to be 85% by ^1H nmr using (+)-Eu(hfc)$_3$].

1,2-Epoxy-2-methylundecane (26)

We are interested in extending the generality of this reaction. Compound **26** represents a simple epoxide with two alkyl substituents in one of the epoxide carbon. The precursor silanol **23** was prepared by a general route (Scheme 6) recently developed by us (11). Reaction of (2-methylallyl)-dimethyl-*N*,*N*-diisopropylaminosilane (**20**) with Schlosser's base (*n*-BuLi/*t*-BuOK) (12) generated the carbanion **21**. Quenching the carbanion **21** with *n*-octyl bromide gave a mixture of the γ- and α-alkylation products **22**γ and **22**α in a ratio of 14:1. The crude mixture was hydrolysed and purified at the same time by passing through a column of wet (10% H_2O) alumina to give the silanol **23**. Sharpless epoxidation of **23** using (+)-DET gave the disiloxane **24**, presumably via the silanol **25** first. The crude **24** was treated by fluoride ion to give (S)-(−)-**26**, $[\alpha]_D$ −12.2 (*c* 0.3, EtOH). Its ee was determined to be 90% by ^1H nmr with (+)-Eu(hfc)$_3$.

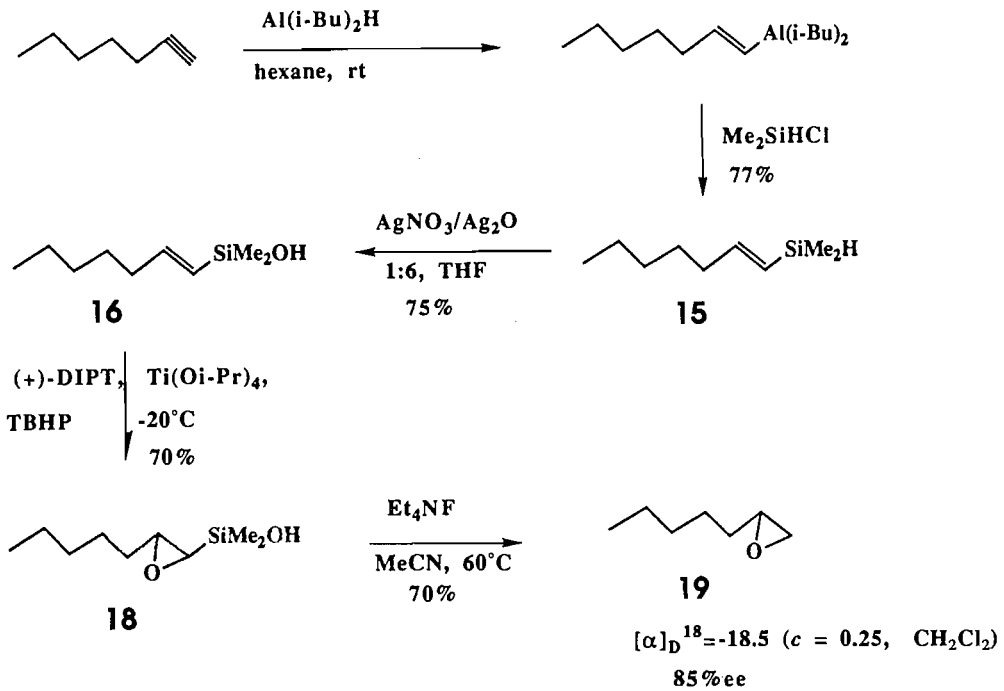

SCHEME 5

Can. J. Chem. Downloaded from www.nrcresearchpress.com by 88.255.202.194 on 09/08/12
For personal use only.

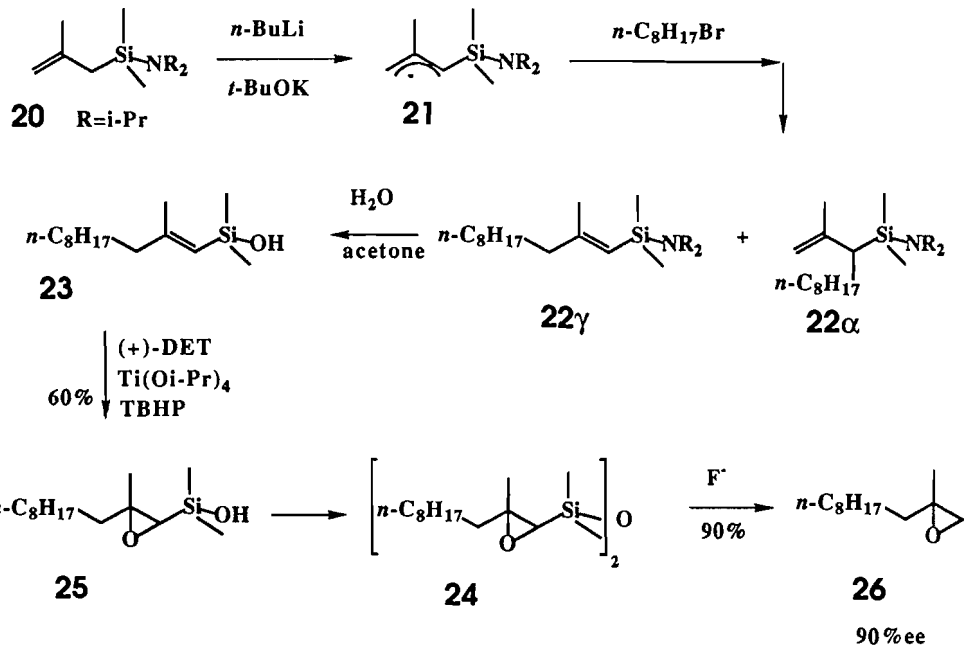

SCHEME 6

Enantioselective synthesis of (S)-(−)-frontalin (33)

We demonstrated the application of the alkenylsilanol methodology by the enantioselective synthesis of (*S*)-(−)-frontalin (**33**), an aggregation pheromone produced by the female southern pine beetle, *Dendroctonus frontalins* (13). Alkylation of the carbanion **21** with the alkyl iodide **27**, followed by mild hydrolysis, gave the silanol **29** (Scheme 7). Epoxidation of **29** under Sharpless conditions using (+)-DET gave the disiloxane **30**, presumably through the dimerization of the silanol **31**. Protodesilylation of **30** under the usual conditions gave the epoxy compound **32**, $[\alpha]_D$ +1.8 (*c* 3, EtOH). The ee of **32** was determined to be 85% using ^{1}H nmr with the Eu chiral shift reagent. Acid-catalysed deketalization of **32** following literature procedure gave (*S*)-(+)-frontalin (**33**) (18).

Discussion

The mechanism of the Sharpless epoxidation is a subject of much discussion (8). An important, and synthetically useful, feature of the asymmetric epoxidation reaction is its ability to accommodate a wide variety of allylic alcohols. The present results suggest that alkenylsilanols can be accommodated in the same manner as allylic alcohols. Presumably, the alkenylsilanol coordinates to the active Ti-tartrate

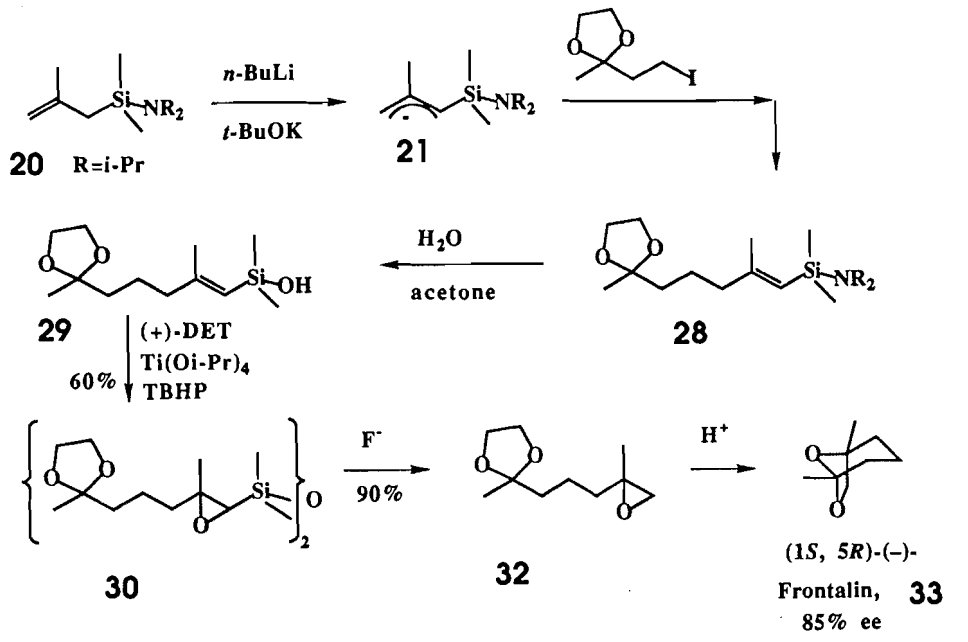

SCHEME 7

Can. J. Chem. Downloaded from www.nrcresearchpress.com by 88.255.202.194 on 09/08/12
For personal use only.

Can. J. Chem. Downloaded from www.nrcresearchpress.com by 88.255.202.194 on 09/08/12
For personal use only.

catalyst together with the alkyl peroxide. It has been argued that the high and consistent enantioselectivity in the epoxidation of allylic alcohols is due to the stereoelectronic orientation required by the olefinic moiety in attacking the coordinated peroxide along the O—O bond axis. Since the atomic radius of silicon is considerably larger than that of carbon, it seems that the stereoelectronic requirement in the epoxidation step may be sufficiently flexible to accommodate the increased bond length of Si—O and Si—C bonds in the alkenylsilanol. This is to be contrasted with the epoxidation of homoallylic alcohols where the enantioselectivity was found to be poor (19). Furthermore, the face selection in the epoxidation of homoallylic alcohol is opposite from that observed for allylic alcohols (19) and alkenylsilanols. This suggests that the facial selection is governed less by the distance between the double bond and the hydroxy group than by the relative angle of the two functionalities.

In any event, the Sharpless epoxidation of alkenylsilanols coupled with fluoride-promoted protodesilylation provides an entry to the enantioselective synthesis of simple epoxides. It remains to be seen whether the silyl moiety in the chiral epoxysilanols can be replaced by electrophiles other than proton. Should that be the case, the synthetic utility would be greatly enhanced.

Experimental[3]

*β-Styryldiphenylsilanol (**1**)*

To a solution of β-bromostyrene (16.0 g, 87.0 mmol) in ether (120 mL), a solution of *tert*-butyllithium (1.7 M in pentane, 60 mL, 92.0 mmol) was added dropwise at −78°C. After stirring for 5 h, diphenyldichlorosilane (21.2 g, 84.0 mmol) was added. The mixture was stirred at room temperature overnight, and then at reflux for 14 h. The resulting suspension was poured into a mixture of triethylamine (1.4 mL), ether (20 mL), and water (40 mL) at 0°C. The mixture was extracted with ether three times and the combined extracts were dried ($MgSO_4$) and concentrated *in vacuo*. The residue was purified by flash chromatography (hexane–$CHCl_3$, 1:3) to give a light yellow oil **1** (27.0 g, 90% yield).Compound **1** had ^{1}H nmr ($CDCl_3$): 2.62 (s, 1H, D_2O exchangeable), 6.72 and 7.20 (AB, 2H, J = 19 Hz), 7.28–7.51 (m, 5H); ms (EI): 302 (31), 224 (74), 199 (46), 180 (100). Exact Mass calcd. for $C_{20}H_{18}OSi$: 302.112; found: 302.117.

*1-(2-Phenyl-1,2-epoxyethyl)diphenylsilanol (**4**)*

A mixture of MCPBA (0.40 g, 2.3 mmol), $NaHCO_3$ (0.80 g), and compound **1** (0.64 g, 2.1 mmol) in CH_2Cl_2 (5 mL) was stirred for 24 h at room temperature. The resulting white solids were removed by filtration and the filtrate was washed with aqueous 5% Na_2SO_3 solution, then aqueous 5% Na_2CO_3 solution, then water, and dried ($MgSO_4$). The solvent was evaporated and the residue was purified by flash chromatography (hexane – ethyl acetate – $CHCl_3$, 8:1:1) to gve a pale yellow oil **4** (0.48 g, 75% yield). Compound **4** had ^{1}H nmr ($CDCl_3$): 1.62 (s, 1H), 2.79 (d, 1H), 2.90 (d, 1H), 7.30–7.8 (m, 5H); ms (CI, NH_3): 336 ($M+NH_4^+$, 17), 319 (MH^+, 48), 318 (M^+, 79), 301.

(S)-Styrene oxide via Sharpless epoxidation of 1

To a mixture of CH_2Cl_2 (30 mL) and 4A molecular sieves (2 g), titanium(IV) isopropoxide (0.50 g, 2.6 mmol) was added followed by a solution of (+)-diethyl L-tartrate (0.50 g, 3.1 mmol) in CH_2Cl_2 (5 mL) at −20°C. The mixture was stirred for 10 min. The silanol **1** (0.77 g, 2.6 mmol) in CH_2Cl_2 (8 mL) and TBHP (3 M in 2,2,4-trimethylpentane, 2.1 mL) were added. The mixture was kept at 0°C and stirred for 24 h. The mixture was filtered to remove the molecular sieves. To the filtrate, an aqueous solution of 10% tartaric acid (8 mL) was added and the mixture was stirred at 0°C for 30 min. The stirring was continued at room temperature until the aqueous layer became clear. The organic phase was then separated, washed with water, and dried ($MgSO_4$). The solvent was removed *in vacuo* and the residue was diluted with ether, followed by addition of 1 N NaOH solution at 0°C. The mixture was stirred for 1 h. The organic phase was separated, washed with brine, dried ($MgSO_4$), and evaporated. The residue was purified by flash chromatography (hexane – ethyl acetate – $CHCl_3$, 6:1:2) to give compound **4** (0.60 g, 71% yield), identical in spectroscopic data with the racemic compound prepared above. A solution of **4** (0.20 g, 0.67 mmol) thus obtained and tetraethylammonium fluoride hydrate (0.16 g, 1.0 mmol) in CH_3CN (8 mL) was stirred for 3 h at room temperature. Water was added and the mixture was extracted with ether. The combined organic phase was dried ($MgSO_4$) and evaporated. The residue was purified by flash chromatography (hexane – ethyl acetate, 100:3) to give (*S*)-styrene oxide (0.07 g, 90% yield) identical in all respects with an authentic sample. It had $[\alpha]_D^{22}$ −8.90° (*c* 0.25, benzene). When the epoxidation was carried out without the 4A molecular sieves, the styrene oxide obtained had $[\alpha]_D^{22}$ −3.70 (*c* 0.25, benzene).

*β-Styryldimethylsilane (**12**)*

To a solution of β-bromostyrene (9.9 g, 50 mmol) in ether (75 mL) was added dropwise a solution of *tert*-butyllithium (1.57 M in pentane, 70 mL) at −20°C. The mixture was stirred for 2 h. Dimethylchlorosilane (5.6 mL) was added slowly at −20°C and the mixture was stirred overnight at room temperature. The mixture was filtered to remove the solids, and water was added to the filtrate. The organic phase was washed with water, dried ($MgSO_4$), and evaporated. The residue was purified by flash chromatography (hexane) to give **12** as a colourless liquid (6.1 g, 92% yield); ^{1}H nmr ($CDCl_3$): 0.22 (d, 6H, J = 3 Hz), 4.20 (m, 1H), 6.45 (A of AB, dd, 1H, J = 19, 3 Hz), 7.01 (B of AB, 1H, J = 19 Hz), 7.28–7.5 (m, 5H); ms (EI): 162 (44), 147 (100). Exact Mass calcd. for $C_{10}H_{14}Si$: 162.087; found: 162.086.

*β-Styryldimethylsilanol (**6**)*

A mixture of 4A molecular sieves (1.0 g), silver nitrate (0.14 g, 0.82 mmol), silver oxide (0.88 g, 3.8 mmol), and **12** (0.60 g, 3.7 mmol) in THF (90 mL) was stirred for 9 h at room temperature. The mixture was filtered through a layer of silica gel and the filtrate evaporated. The residue was purified by flash chromatography (hexane – ethyl acetate, 9:1) to give **6** as a light yellow liquid (0.46 g, 71% yield); ir (film): 3287 cm^{-1}; ^{1}H nmr ($CDCl_3$): 0.30 (s, 6H), 1.66 (s, 1H, D_2O exchangeable), 6.49 and 7.01 (AB, 2H, J = 19 Hz), 7.25–7.35 (m, 5H); ms (EI): 178 (45), 160 (100), 145 (83). Exact Mass calcd. for $C_{10}H_{14}OSi$: 178.081; found: 178.081.

*β-Styrylchloromethyldimethylsilane (**8**)*

To a solution of β-bromostyrene (7.0 mL, 50 mmol) in ether (75 mL) was added dropwise a solution of *tert*-butyllithium in pentane (1.57 M, 70 mL) at −25°C. The mixture was stirred at −25°C for 2 h. Chloromethyldimethylchlorosilane (7.6 g, 50 mmol) was added dropwise to the dark red solution. After the addition was completed, the reaction mixture was allowed to warm to room temperature and stirred overnight. The mixture was filtered and the filtrate was washed with water and dried ($MgSO_4$). Distillation of the solution gave 9.0 g (82% yield) of a colourless liquid **8**, bp 77–80°C/0.08 Torr (1 Torr = 133.3 Pa); ^{1}H nmr ($CDCl_3$): 0.31 (s, 6H), 2.89 (s, 2H), 6.45 and 6.99 (AB, 2H, J = 20 Hz), 7.26–7.52 (m, 5H); ms (EI): 212 (4), 210 (19), 161 (100). Exact Mass calcd. for $C_{11}H_{15}SiCl$: 210.063; found: 210.067.

*β-Styryl-N-pyrrolidinylmethyldimethylsilane (**9**).*

A mixture of **8** (4.9 g, 23 mmol) and pyrrolidine (8 mL) was heated at 80°C in a bomb for 20 h. The reaction mixture was cooled, added to water, and extracted with ether. The ether phase was dried

[3]For experimental details, see refs. 9*a* and 14. The homogeneity of new compounds after flash chromatography was verified by thin-layer chromatography.

Can. J. Chem. Downloaded from www.nrcresearchpress.com by 88.255.202.194 on 09/08/12
For personal use only.

($MgSO_4$) and distilled to give 3.9 g of colourless liquid **9**, bp 96–98°C/0.1 Torr; ^{1}H nmr ($CDCl_3$): 0.24 (s, 6H), 1.76 (m, 4H), 2.16 (s, 2H), 2.49 (m, 4H), 6.51 and 6.94 (AB, 2H, J = 19 Hz), 7.26–7.52 (m, 5H); ms (EI): 245 (11), 230 (3), 145 (14), 84 (100). Exact Mass calcd. for $C_{15}H_{23}NSi$: 245.160; found: 245.162.

*β-Styryldimethylsilanol (**6**) from oxidation of **9***

To a suspension of MCPBA (2.3 g, 13 mmol) and $CaCO_3$ (2.0 g, 20 mmol) in CH_2Cl_2 (40 mL), a solution of **9** (2.7g, 11 mmol) in CH_2Cl_2 (8 mL) was added at −30°C. The reaction mixture was stirred at −30°C and the progress of the reaction was followed by gas chromatography. Upon complete disappearance of the starting material **9**, the mixture was quenched with 5% aqueous Na_2SO_4. The organic phase was washed with water, dried ($MgSO_4$), and evaporated. The residue was purified by flash chromatography (hexane – ethyl acetate, 5:1) to give compound **6** (0.25 g, 13% yield) and the disiloxane **10** (1.4 g, 78% yield). Compound **10** showed no OH absorption in the ir. It had ^{1}H nmr ($CDCl_3$): 0.31 (s, 6H), 6.50 and 7.01 (AB, 2H, J = 19 Hz), 7.28–7.54 (m, 5H); ms (EI): 338 (3), 254 (75), 219 (44), 161 (37), 145 (52), 127 (100). Alternatively, oxidation of **9** could be accomplished by heating **9** (1.9 g, 7.8 mmol), $VO(acac)_2$ (0.03 g), and TBHP (3 M in 2,2,4-trimethylpentane, 6 mL) in acetone (5 mL) at 70°C overnight. Work-up as above gave **6** (0.3 g, 16%) and **10** (0.6 g. 46%).

*1-(2-Phenyl-1,2-epoxyethyl)dimethylsilanol (**13**)*

To a solution of $Ti(O\text{-}i\text{-}Pr)_4$ (0.68 g, 2.4 mmol) in CH_2Cl_2 (20 mL) at −20°C was added a solution of ethyl L-tartrate (0.58 g, 2.9 mmol) in CH_2Cl_2 (10 mL). The mixture was stirred for 10 min. A solution of **6** (0.46 g, 1.8 mmol) in CH_2Cl_2 (10 mL) was added, followed by a solution of TBHP (3 M in 2,2,4-trimethylpentane, 1.6 mL). The mixture was stirred at −20°C for 40 h. To the reaction mixture, saturated Na_2SO_4 solution (5 mL) and ether (150 mL) were added and stirred at room temperature for 4 h. The mixture was filtered through a layer of silica gel (1 cm) and washed thoroughly with ether. To the combined filtrate was added 10% NaOH solution (10 mL) and the mixture was stirred for 15 min at 0°C. The organic phase was washed with brine, dried ($MgSO_4$), and evaporated. The residue was purified by flash chromatography (hexane – ethyl acetate, 8:1) to give the silanol **13** (0.23 g, 50% yield); ir (film): 3390 cm^{-1}; ^{1}H nmr ($CDCl_3$): 0.30 (s, 3H), 0.32 (s, 3H), 1.87 (s, 1H), 2.35 (d, 1H, J =3 Hz), 3.81 (d, 1H, J =3 Hz), 7.25–7.35 (m, 5H); ms (EI): 194 (33), 161 (31), 120 (25), 91 (45), 75 (100). Exact Mass calcd. for $C_{10}H_{14}O_2Si$: 194.076; found: 194.078.

*(S)-(−)-Styrene oxide via **13***

A solution of **13** (0.20 g, 0.67 mmol) and tetraethylammonium fluoride hydrate (0.16 g, 1.0 mmol) in acetonitrile (8 mL) was stirred for 3 h at room temperature. The mixture was partitioned between water and ether. The ether phase was dried ($MgSO_4$) and evaporated. The residue was purified by flash chromatography (hexane–ether, 25:1) to give (*S*)-(−)-styrene oxide (0.11 g, 90% yield), $[\alpha]_D^{18}$ −15.0°C (*c* 0.25, ether).

*1-Heptenyldimethylsilane (**15**)*

To a solution of 1-heptyne (0.9 6g, 10 mmol) in *n*-hexane (4 mL), a solution of DIBAL in toluene (1.5 M, 6.7 mL, 10 mmol) was added dropwise at room temperature over 30 min under an argon atomsphere. The mixture was warmed to 50°C and stirred for 4 h. The mixture was cooled to 0°C and a solution of dimethylchlorosilane (1.1 mL, 10 mmol) in THF (8 mL) was added. The resultant mixture was stirred overnight at room temperature. The mixture was transferred to a solution of 5% sulfuric acid (10 mL) and *n*-hexane (10 mL) cooled with an ice bath. The aqueous phase was washed with ether. The combined organic phase was washed with 10% aqueous sodium bicarbonate solution, dried ($MgSO_4$), and evaporated. The residue was purified by flash chromatography (hexane) to give **15** (1.21 g, 77%) as a colorless liquid; ^{1}H nmr ($CDCl_3$): 0.12 (d, 6H, J = 3 Hz), 0.89 (t, 3H, J = 7 Hz), 1.29 (m, 6H), 4.03 (m, 1H), 5.60 (bd, 1H, J = 19 Hz), 6.17 (dt, 1H, J = 19, 6 Hz); ms(EI): 156 (0.8), 141 (18), 127 (30), 97 (26), 85 (50), 71 (38), 59 (100). Exact Mass calcd. for $C_9H_{20}Si$: 156.133; found: 156.137.

*1-Heptenyldimethylsilanol (**16**)*

A mixture of molecular sieves 4A (1.0 g), silver nitrate (0.10 g, 0.6 mmol), silver oxide (0.60 g, 2.6 mmol), and 1-heptenyldimethylsilane (**15**, 0.40 g, 2.6 mmol) in THF (70 mL) was stirred at 30°C for 9 h. The mixture was filtered through a layer of silica gel. The filtrate was evaporated and the residue was purified by flash chromatography (hexane – ethyl acetate, 9:1) to give **16** as a pale yellow liquid (0.30 g). The disiloxane **17** was also isolated from the column as a pale yellow oil (0.04 g). Compound **16** had ir (film): 3286 cm^{-1}; ^{1}H nmr ($CDCl_3$): 0.98 (s, 6H), 0.88 (t, 3H, J = 7 Hz), 1.29 (m, 6H), 1.54 (s, 1H, D_2O exchangeable), 2.10 (m, 2H), 5.64 (bd, J = 19 Hz, 1H), 6.19 (dt, J = 19, 7 Hz, 1H); ms (EI): 172 (1.0), 157 (100), 101 (28), 97 (21). Exact Mass calcd. for $C_8H_{17}OSi$ $(M-15)^+$: 157.105; found:157.103.

Compound **17**: ir (film), no absorption at 3286 cm^{-1}; ^{1}H nmr ($CDCl_3$): 0.98 (s, 12H), 0.88 (t, 6H, J = 7 Hz), 1.29 (m, 12H), 2.10 (m, 4H), 5.57 (bd, 2H, J = 19 Hz), 6.09 (dt, 2H, J = 19, 7 Hz).

*1-(1,2-Epoxyheptanyl)dimethylsilanol (**18**)*

Diisopropyl L-tartrate (1.1 mL, 5.2 mmol) and 4A molecular sieves (0.5 g) were added sequentially at −20°C to a solution of dichloromethane (8 mL) and titanium isopropoxide (1.3 mL, 4 mmol). The mixture was stirred for 0.5 h. A solution of **16** (0.35 g, 2 mmol) in dichloromethane (4 mL) and a solution of TBHP (3 M, 4 mL) in 2,2,4-trimethylpentane were added sequentially via syringe at −20°C. The mixture was stirred for 44 h at −20°C. A mixture of saturated Na_2SO_4 solution (4 mL) and ether (150 mL) was added and stirred for 4 h. The white solid formed was filtered through a layer of Celite (1 cm) and silica gel (1 cm) and washed thoroughly with ether. To the filtrate was added a solution of 10% sodium hydroxide (15 mL) and the mixture was stirred for 2 h at 0°C. The organic layer was washed with brine and dried over $MgSO_4$. The organic solvent was removed *in vacuo* to give compound **18** (0.30 g, 70%) as a residual oil. Compound **18** appeared to be unstable on column chromatography. The crude product was therefore used directly for the following step without purification. Compound **18** had ir (film): 3390 cm^{-1}; ^{1}H nmr ($CDCl_3$): 0.19 (s, 3H), 0.21 (s, 3H), 0.89 (t, 3H, J = 7 Hz), 1.30 (m, 8H), 1.99 (d, 1H, J = 2 Hz), 2.88 (m, 1H); ms (EI): 188 (1), 158 (25), 131 (55), 116 (49), 75 (100). Exact Mass calcd. for $C_9H_{20}O_2Si$: 188.123; found: 188.123.

*(−)-1,2-Epoxyheptane (**19**)*

A solution of compound **18** (0.10 g, 0.52 mmol) and tetraethylammonium fluoride hydrate (1.2 g, 3.5 mmol) in acetonitrile (2 mL) was stirred at 60°C for 6 h. The mixture was partitioned between water and pentane–ether (20:1) solutions. The organic phase was dried ($MgSO_4$) and the solvent removed by careful distillation. The residue was purified by flash chromatography (pentane–ether, 25:1) to give 1,2-epoxyheptane (0.045 g). It had $[\alpha]_D^{18}$ −18.5 (*c* 0.25, CH_2Cl_2). Its ^{1}H nmr spectrum ($CDCl_3$): 0.89 (t, 3H), 1.30 (m, 4H), 1.49 (m, 2H), 2.45 (dd, 1H, J = 5, 3 Hz), 2.74 (dd, 1H, J = 5, 4 Hz), 2.90 (m 1H) was identical to that of an authentic racemic sample prepared by epoxidation of 1-heptene. The enantiomeric excess (ee) was determined to be 85% by ^{1}H nmr using tris-3-(heptafluoropropylhydroxymethylene)-(−)-camphorato europium(III) as chemical shift reagent (CSR). The proton at 2.74 ppm was split by the chiral CSR (1.5 equiv.) into two peaks and integration of the two peaks in the racemic versus the optically active compounds gave the ee.

*3-(2-Methylpropenyl)-N,N-diisopropylaminodimethylsilane (**20**)*

A solution of freshly prepared 2-methylpropenylmagnesium chloride in THF (1 M, 150 mL) was added to a solution of *N,N*-diisopropylaminodimethylchlorosilane (19.4 g, 0.1 mol) (15) in

Can. J. Chem. Downloaded from www.nrcresearchpress.com by 88.255.202.194 on 09/08/12
For personal use only.

THF (50 mL). The mixture was refluxed overnight. Much of the THF was removed by distillation. The residue was extracted thoroughly with petroleum ether. The combined extracts were distilled under reduced pressure to give 20.1 g (96% yield) of compound **20** as a colourless liquid, bp 118–119°C/45 Torr; ^{1}H nmr (CCl_4): 0.15 (s, 6H), 1.20 (d, 12H, J = 7 Hz), 1.60 (s, 2H), 1.80 (s, 3H), 3.30 (m, 2H), 4.53 (b, 2H); ms (EI): 213 (6), 198 (18), 158 (100). Exact Mass calcd. for $C_{12}H_{27}NSi$: 213.438; found: 213.438.

(E)-1-(2-Methylundec-1-enyl)dimethylsilanol (23)

To a stirred mixture of potassium *tert*-butoxide (2.46 g, 22 mmol) in *n*-hexane (15 mL) at 0°C, was added a solution of *n*-butyllithium in hexane (*c* 1.6 M, 13.6 mL). The mixture was warmed to room temperature and stirred for 30 min. The mixture was then cooled to −78°C. To the cooled mixture was added 10 mL of ether, followed by a solution of **20** (4.26 g, 20 mmol) in ether (10 mL). After addition, the mixture was stirred at room temperature for 4 h. The mixture was again cooled to −-78°C. A solution of octyl bromide (3.86 g, 20 mmol) in ether (10 mL) was added, and the mixture was stirred for 6 h at −78°C and for 12 hr at room temperature. The reaction mixture was quenched with saturated NH_4Cl solution (50 mL). The organic phase was dried ($MgSO_4$), and evaporated to dryness. The crude residue was passed through a column of wet (10% water) alumina, eluting progressively with pet. ether and pet. ether – ether (10:1) to give compound **23** (2.94 g, 61% yield). ^{1}H nmr (CCl_4): 0.16 (s, 6H), 0.9 (t, 3H), 1.3 (m, 14H), 1.83 (s, 3H), 2.10 (t, 2H), 5.10 (s, 1H); ms (EI): 242 (4), 227 (14), 75 (100). Exact Mass calcd. for $C_{14}H_{30}OSi$: 242.207; found: 242.206.

1,1'-Bis[(1S, 2S)-1,2-epoxyundecyl]-1,1,1',1'-tetramethyldisiloxane (24)

To a mixture of 4A molecular sieves (1.0 g), and Ti(O-i-Pr)$_4$ (1.5 g, 5.3 mmol) in CH_2Cl_2 (10 mL) at −20°C was added a solution of diethyl L-tartrate (1.1 g, 5.3 mmol) in CH_2Cl_2 (10 mL). The mixture was stirred for 15 min, and then added to a solution of TBHP in toluene (3.3 M, 4 mL, 13.2 mmol), and stirred for 30 min. A solution of **23** (0.75 g, 3.1 mmol) in CH_2Cl_2 (10 mL) was added and the mixture was stirred for 16 h at −20°C. The mixture was warmed to 0°C. Water (20 mL) was added and stirred for 15 min. A solution of 30% NaOH (6 mL) saturated with NaCl was added and stirred for 1 h. The mixture was warmed to room temperature and partitioned between the aqueous phase and the organic phase. The aqueous phase was extracted three times with CH_2Cl_2 (30 mL). The combined organic phase was dried ($MgSO_4$) and concentrated. The residue was purified by flash chromatography (pet. ether – ether 20:1) to give **24** (0.44 g, 50% yield) as a viscous oil; ^{1}H nmr ($CDCl_3$): 0.20 (s, 12H), 0.85 (t, 6H), 1.24 (m, 32 H), 1.97 (s, 2H); ms (EI): 498 (8), 315 (30), 149 (100).

(S)-1,2-Epoxy-2-methylundecane (26)

A mixture of compound **24** (0.44 g, 0.9 mmol) and tetraethylammonium fluoride hydrate (0.65 g, 2.1 mmol) in acetonitrile (10 mL) was refluxed for 4 h. The mixture was diluted with water (20 mL) and extracted with ether (3 × 15 mL). The combined ether extracts were dried ($MgSO_4$) and evaporated. The residue was purified with flash chromatography (pet. ether – ethyl acetate, 20:1) to give **26** (0.28 g, 91% yield) as a colourless liquid. It had $[\alpha]_D$ −12.2 (*c* 0.3, EtOH); ^{1}H nmr ($CDCl_3$): 0.89 (t, 3H), 1.27 (m, 23H), 2.55 (s, 2H); ms (EI): 184 (5), 169 (37), 85 (6), 70 (100). Exact Mass calcd. for $C_{12}H_{24}O$: 184.183; found: 184.183. Its ee was determined by ^{1}H nmr with (+)-Eu(hfc)$_3$ (1.0 equiv.) to be 90%. In this case, the shift in the 2.55 ppm peak was used.

2-Methyl-(2-iodoethyl)-1,3-dioxolane (27)

The compound was prepared according to literature procedure (16).

(E)-2-Methyl-(6,6-ethylenedioxy-hept-2-enyl)-dimethylsilanol (29).

Compound **29** was prepared according to the same procedure as described for the preparation of **23** using **27** as the alkyl halide. The yield of **29** was 59%. It had ^{1}H nmr (CCl_4): 0.21 (s, 6H), 1.28 (s, 3H), 1.4–1.7 (m, 4H), 1.85 (s, 3H), 2.08 (bt, 2H), 2.23 (s, 1H), 3.85 (m, 4H), 5.15 (s, 1H); ms (EI): 244 (4), 170 (2), 87 (100). Exact Mass calcd. for $C_{12}H_{24}SiO_3$: 244.149; found: 244.148.

(S)-1,2-Epoxy-6,6-ethylenedioxy-2-methylheptane (32)

Compound **29** was epoxidized under Sharpless conditions as described for **24**. Compound **30** was obtained in 63% yield and was subjected to protodesilyation as described above to give **32** in 92% yield. Compound **32** had $[\alpha]_D$ +1.8 (*c* 3, EtOH); ^{1}H nmr (CCl_4): 1.25 (2s, 6H), 1.50 (m, 6H), 2.40 (s, 2H), 3.81 (s, 4H); ms (EI): 171 (M−15, 9), 87 (100). Exact Mass calcd. for $C_9H_{15}O_3$ (M−15): 171.102; found: 171.102. Its ee was determined by ^{1}H nmr with (+)-Eu(hfc)$_3$ (1.5 equiv.) to be 85% by using the shifts of the 2.40 ppm peak.

(S)-(−)-Frontalin (33)

Hydrolysis of **32** (0.20 g) with 2 M H_2SO_4 (2 mL) in THF (4 mL) according to literature (17) procedure gave **33** (0.11 g), identical in spectroscopic data with literature values (18). Alternatively, the hydrolysis could be carried out by mixing **32** (0.20 g) with 2 M H_2SO_4 (0.25 mL), and silica gel (0.5 g) in ether (10 mL) at room temperature and stirring for 4 h. After removal of the solid by filtration, the filtrate was washed with K_2CO_3 solution, dried, and evaporated. The residue was purified by flash chromatography (pet. ether – ether, 20:1) to give **33** (0.14 æ, 91% yield). It had $[\alpha]_D$ −32.6 (*c* 0.15, $CHCl_3$) (lit. (18) $[\alpha]_D$ −50.7 (*c* 1.0, $CHCl_3$). The ee was determined by ^{1}H nmr with (+)-Eu(hfc)$_3$ (2 equiv.) to be 85%. The peak at 3.46 ppm (or 3.92 ppm) was used.

Acknowledgement

We thank the Natural Sciences and Engineering Research Council of Canada (NSERC) and Fonds pour la formation de chercheurs et l'aide à la recherche (FCAR) for financial support of this research. D.W. and L.H.L. thank the National Natural Science Foundation of China for financial support.

1. T. Katsuki and K. B. Sharpless. J. Am. Chem. Soc. **102**, 5974 (1980); K. B. Sharpless. Chem. Tech. 692 (1985).
2. A. Pfenninger. Synthesis, 89 (1986).
3. C. J. Burns, C. A. Martin, and K. B. Sharpless. J. Org. Chem. **54**, 2826 (1989).
4. E. N. Jacobson, I. Marko, W. S. Mungall, G. Schroder, and K. B. Sharpless. J. Am. Chem. Soc. **110**, 1968 (1988); J. S. M. Wai, I.Marko, J. S. Svendsen, M. G. Finn, E. N. Jacobsen, and K. B. Sharpless. J. Am. Chem. Soc. **111**, 1123 (1989); Y. Ogina, H. Chen, E. Manoury, T. Shibata, M. Beller, D. Lubben, and K. B. Sharpless. Tetrahedron Lett. **32**, 5761 (1991); N. H. Lee and E. N. Jacobsen. Tetrahedron Lett. **32**, 6533 (1991); S. L. Colletti and R. Halterman. Tetrahedron Lett. **33**, 1005 (1992); E. N. Jacobsen, W. Zhang, A. R. Muci, J. R. Ecker, and L. Deng. J. Am. Chem. Soc. **113**, 7063 (1991).
5. T. H. Chan, L. M. Chen, and D. Wang. J. Chem. Soc. Chem. Commun. 1280 (1988).
6. T. H. Chan, P. W. K. Lau, and M. P. Li. Tetrahedron Lett. 2667 (1976).
7. Y. Gao, R. M. Hanson, J. M. Klunder, S. Y. Ko, H. Masamune, and K. B. Sharpless. J. Am. Chem. Soc. **109**, 5765 (1987).
8. S. F. Pedersen, J. C. Dewan, R. R. Eckman, and K. B. Sharpless. J. Am. Chem. Soc. **109**, 1279 (1987); K. A. Jorgensen, R. A. Wheeler, and R. Hoffmann. J. Am. Chem.

Soc. **109**, 3240 (1987); E. J. Corey. J. Org. Chem. **55**, 1693 (1990); S. S. Woodard, M. G. Finn, and K. B. Sharpless. J. Am. Chem. Soc. **113**, 106 (1991); M. G. Finn and K. B. Sharpless. J. Am. Chem. Soc. **113**, 113 (1991); B. H. McKee, T. H. Kalanter, and K. B. Sharpless. J. Org. Chem. **56**, 6966 (1991).
9. (*a*) R. F. Horvath and T. H. Chan. J. Org. Chem. **54**, 317 (1989); (*b*) T. H. Chan and D. Wang. Tetrahedron Lett. **30**, 3041 (1989).
10. R. B. Silverman and G. M. Banik. J. Am. Chem. Soc. **109**, 2219 (1987).
11. L. H. Li, D. Wang, and T. H. Chan. Tetrahedron Lett., **32**, 2879 (1991).
12. M. Schlosser, R. Dahan, and S. Cottens. Helv. Chim. Acta, **67**, 284 (1984).
13. C. Meister and H.-D. Scharf. Liebigs Ann. Chem. 913 (1983); A. W. M. Lee. J. Chem. Soc. Chem. Commun. 578 (1984); K. B. Sharpless, C. H. Behrens, T. Katsuki, A. W. M. Lee, V. S. Martin, M. Takatani, S. M. Viti, F. J. Walker, and S. S. Woodard. Pure Appl. Chem. **55**, 589 (1983).
14. T. H. Chan and A. E. Schwerdtfeger. J. Org. Chem. **56**, 3294 (1991).
15. K. Tamao, E. Nakajo, and Y. Ito. Tetrahedron, **44**, 3997 (1988).
16. J. C. Stowell, B. T. King, and J. F. Hauck. J. Org. Chem. **48**, 5381 (1983).
17. N. N. Joshi, V. R. Manadapur, and M. S. Chadha. J. Chem. Soc. Perkin Trans. 1, 2963 (1983).
18. D. R. Hicks and B. Fraser-Reid. J. Chem. Soc. Chem. Commun. 869 (1976); K. Mori. Tetrahedron, **31**, 1381 (1975).
19. B. E. Rossiter and K. B. Sharpless. J. Org. Chem. **49**, 3707 (1984).

Can. J. Chem. Downloaded from www.nrcresearchpress.com by 88.255.202.194 on 09/08/12
For personal use only.

Structural and computational studies of ligands for the glycine binding site on the excitatory amino acid receptor complex: 1. 6,7-Dimethyl and 6,7-dimethoxy 2,3-quinoxalinedione

MACIEJ KUBICKI[1] AND PENELOPE W. CODDING[2]

Departments of Chemistry and of Pharmacology and Therapeutics, University of Calgary, Calgary, Alta., Canada T2N 1N4

Received May 11, 1992

MACIEJ KUBICKI and PENELOPE W. CODDING. Can. J. Chem. **71**, 68 (1993).

The crystal structures of two quinoxalinedione derivatives, 6,7-dimethyl-1,4-dihydro-2,3-quinoxalinedione dihydrate (**1**) and 6,7-dimethoxy-1,4-dihydro-2,3-quinoxalinedione hydrate (**2**), and AM1 molecular orbital computational investigations of electronic properties and hydrogen bond strengths are reported. The space group for **1** is $P\bar{1}$ with a = 7.0109(1) Å, b = 8.5901(3) Å, c = 10.7890(5) Å, α = 112.704(3)°, β = 96.053(3)°, and γ = 107.589(2)°. For **2**, the space group is *Pbca* with a = 12.2769(6) Å, b = 6.9291(3) Å, and c = 25.8644(7) Å. The geometries of these two compounds are similar; small differences are mostly due to the different electronic characters of the substituents and to intermolecular interactions in the crystals. There are two main factors determining the packing schemes of these compounds, π-stacking between neighboring molecules and hydrogen bonds, including bonds with the water molecules of crystallization. The AM1 semi-empirical calculations show differences between net atomic charges and dipole moments. For both structures, calculations confirm the asymmetry of hydrogen bonds that is observed in the crystal structures.

MACIEJ KUBICKI et PENELOPE W. CODDING. Can J. Chem. **71**, 68 (1993).

On a déterminé les structures cristallines de deux dérivés de la quinoxalinedione, le dihydrate de la 6,7-diméthyl-1,4-dihydroquinoxaline-2,3-dione (**1**) et l'hydrate de la 6,7-diméthoxy-1,4-dihydroquinoxaline-2,3-dione (**2**) et on a effectué des calculs moléculaires AM1 de leurs propriétés électroniques et de la force de leurs ponts hydrogènes. Le composé **1** cristallise dans le groupe d'espace $P\bar{1}$, avec a = 7,0109(1), b = 8,5901(3) et c = 10,7890(5) Å, α = 112,704(3)°, β = 96,053(3)° et γ = 107,589(2)° alors que le composé **2** cristallise dans le groupe d'espace *Pbca*, avec a = 12,2769(6), b = 6,929(3) et c = 25,8644(7) Å. Les géométries de ces deux composés sont semblables; les petites différences sont principalement dues aux caractères électroniques différents des substituants et à des interactions intermoléculaires dans les cristaux. Deux facteurs principaux déterminent les schémas d'empilement de ces composés, un empilement π entre des molécules voisines et des liaisons hydrogènes, comprenant des liaisons avec des molécules d'eau de cristallisation. Les calculs semi-empiriques AM1 montrent qu'il existe des différences entres les charges atomiques nettes et les moments dipolaires. Pour les deux structures, les calculs confirment l'asymétrie des liaisons hydrogènes qui est observée dans les structures cristallines.

[Traduit par la rédaction]

Introduction

Excitatory amino acid (EAA) receptors are commonly regarded as the main neutrotransmitter receptors mediating synaptic excitation in the mammalian central nervous system, CNS (1). Because they are involved in many physiological phenomena and their dysfunction leads to neurological disorders, including epilepsy (2) and hypoglycemia (3), their agonists and antagonists are of growing interest as potential therapies for CNS disorders.

The EAA receptors are divided into three subtypes, based on selective agonists for each subtype: *N*-methyl-D-aspartate (NMDA), kainate, and quisqualate (ref. 4, and references therein). A structural analogue of this latter compound, α-amino-3-hydroxy-5-methyl-4-isoxazelopropionic acid (AMPA), was found to be more specific in binding studies, thereby allowing subdivision of the type of quisqualate receptor, Q/AMPA, that is present in mammalian CNS. The number of known NMDA receptor antagonists is extensive (for review, see ref. 5) and it has been shown that glycine is involved in the activation of this receptor and that a strychnine-insensitive glycine binding site is associated with the receptor complex. Quinoxalinedione derivatives were found to be ligands for the glycine site and to be highly potent kainate and AMPA receptor antagonists (6), causing growing interest in this group of compounds. Small structural changes, e.g., changing the position of a nitro group from 6,7-dinitro- to 5,7-dinitro- in the 1,4-dihydro-2,3-quinoxalinediones, can cause large changes in the affinities for the non-NMDA receptors (4). Thus, an extensive study of the structures and intermolecular interactions found in quinoxalinediones was undertaken to account for their activity profiles. Here, we present the results of the X-ray crystallographic studies and semi-empirical molecular orbital calculations on two quinoxalinedione derivatives, 6,7-dimethyl-1,4-dihydro-2,3-quinoxalinedione dihydrate (**1**) and 6,7-dimethoxy-1,4-dihydro-2,3-quinoxalinedione hydrate (**2**), which differ in their ability to inhibit glycine binding.

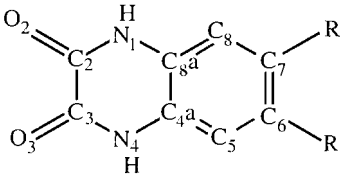

R = Me for **1**, OMe for **2**

Compound **1** has high affinity for the glycine binding site and an IC_{50} value of ca. 7.1 μM while **2** has lower affinity

[1]On leave from Department of Chemistry, Adam Mickiewicz University, 60-780 Poznań, Poland.

[2]Author to whom correspondence may be addressed.

Can. J. Chem. Downloaded from www.nrcresearchpress.com by 88.255.202.194 on 09/08/12
For personal use only.

TABLE 1. Crystal data

Compound	1	2
Formula	$C_{10}H_{10}N_2O_2 \cdot 2H_2O$	$C_{10}H_{10}N_2O_4 \cdot H_2O$
M_r	226.23	240.22
System and space group	Triclinic, $P\bar{1}$	Orthorhombic, *Pbca*
V (Å^3)	552.91(5)	2200.2(1)
Z	2	8
d_x (Mg m^{-3})	1.36	1.45
$\mu(CuK_\alpha)$ (cm^{-1})	8.52	9.62
Crystal dimensions (mm)	0.40 × 0.35 × 0.30	0.45 × 0.35 × 0.20
h,k,l ranges	0,7;−8,8;−11,11	0,15;0,8;0,32
Max sin θ/λ (Å^{-1})	0.63	0.63
No. of unique reflections	2476	2638
No. of observed reflections ($I \geq 2\sigma(I)$)	2097	2018
No. of parameters refined	202	203
Weighting scheme	$w^{-1} = \sigma^2(F) + 0.007F^2$	$w^{-1} = \sigma^2(F)$
Final R	0.043	0.036
Final wR	0.053	0.046
S	1.97	1.87
Maximum shift/error in final cycle	0.001	0.001
Maximum/minimum residual electron density in final ΔF map (e Å^{-3})	0.21/−0.21	0.16/0.16

for the binding site and an IC_{50} value of 113 μM.[3] The focus for this study is the determination of packing modes that may establish the relative importance of different types of potential intermolecular forces: hydrogen bonds, π-stacking, and van der Waals interactions.

Experimental

The samples were provided by ICI Americas Inc., Wilmington, Del. Colorless crystals of both samples were obtained by recrystallization from DMF (**1**) and pyridine (**2**) by a slow evaporation. X-ray intensity data were collected at room temperature on an Enraf–Nonius CAD-4F automated diffractometer with Ni-filtered CuK_α radiation, $\lambda(CuK_\alpha)$ = 1.54178 Å, using an $\omega/2\theta$ scan mode. Accurate unit-cell parameters were obtained by least-squares treatment of the setting angles of 25 reflections (28.68° ≤ θ ≤ 49.35° for **1**, 26.41° ≤ θ ≤ 49.11° for **2**). Three standard reflections, 1,5,−3; 3,4,6; and 3,−1,0 for **1**, and −6,0,0; −5,1,5; and −1,1,1 for **2**, were measured after every 2000 s; they showed no significant changes in their intensities (<1.5% for both compounds) or in their profile shapes. The crystal data not in the abstract are listed in Table 1. Lorentz and polarization corrections were applied.

Both structures were solved by direct methods using SHELXS86 (7). In **1**, the correct solution was obtained in space group $P1$, with two molecules in the asymmetric unit. As they were clearly related by a center of symmetry, the molecular coordinates were then transformed into $P\bar{1}$ and further refinement was performed in this space group. The refinements were done by the full-matrix least-squares method with SHELX-76 (8); in each case, the function $\Sigma w(|F_o| - |F_c|)^2$ was minimized. The non-hydrogen atoms were refined with anisotropic thermal parameters, all hydrogen atoms were found in the subsequent ΔF maps, and both their positional and isotropic thermal parameters were also refined. In each structure, an isotropic extinction correction was made at the final stages of refinement. The empirical extinction parameter x was used to correct F_c according to the formula $F_c' = F_c(1 - xF_c^2/\sin\theta)$; x converged at 5.7(3) × 10^{-7} for **1** and at 4.1(5) × 10^{-7} for **2**. The atomic scattering factors for non-hydrogen atoms were taken from Cromer and Mann (9) and for hydrogen atoms from Stewart *et al.* (10). Other computer programs used were ORTEP (11), PLUTO (12), and CSU88 (13). The final atomic coordinates[4] for both structures are given in Table 2 with the atom labeling as noted on the chemical diagram. The bond distances and angles are listed in Table 3.

Calculation methodology

To obtain further insight into the geometrical differences between those compounds and into the stability of potential intermolecular binding modes, we performed semi-empirical calculations using the AM1 Hamiltonian included in the MOPAC 6.0 program (23, 24). Three calculations were done for each compound; the structures for each calculation were the following: *A*, the isolated molecule; *B*, the quinoxalinedione molecule separated by 6.0 Å from each of four water molecules (which could serve as hydrogen bonding partners); and *C*, the quinoxalinedione molecule hydrogen bonded to each water molecule through a single interaction as shown in Fig. 1*a* for compound **1**. In each calculation, the geometry was optimized; the final hydrogen bonding geometry for *C* is shown in Fig. 1*b* for compound **1**. To evaluate atomic charges, dipole moments, and overlap populations, a stationary point, *ab initio* calculation was done using the GAUSSIAN 90 program (25), the STO-3G basis set, and the optimized AM1 geometry.

Results

In both crystals, hydrogen bonding connects the molecules into three-dimensional structures that have an asymmetrical distribution of bonds around the quinoxalinedione molecules, although each individual quinoxalinedione is

[3]Dr. Linda M. Pullan, ICI Pharmaceuticals, private communication.

[4]Lists of structure factors, anisotropic thermal parameters, torsion angles, bond lengths and angles involving hydrogen atoms, least-squares planes data, and the results of the semi-empirical calculations may be purchased from: The Depository of Unpublished Data, Document Delivery, CISTI, National Research Council Canada, Ottawa, Canada K1A 0S2.

The tables of hydrogen atom fractional coordinates and bond lengths and angles involving hydrogen atoms have also been deposited with the Cambridge Crystallographic Data Centre and can be obtained on request from The Director, Cambridge Crystallographic Data Centre, University Chemical Laboratory, 12 Union Road, Cambridge, CB2 1EZ, U.K.

Can. J. Chem. Downloaded from www.nrcresearchpress.com by 88.255.202.194 on 09/08/12
For personal use only.

Can. J. Chem. Downloaded from www.nrcresearchpress.com by 88.255.202.194 on 09/08/12
For personal use only.

TABLE 2. Non-hydrogen fractional coordinates ($\times 10^4$) and equivalent thermal parameters ($\times 10^4 Å^2$) with their esd's in parentheses

Atom	x/a	y/b	z/c	U_{eq}[a]
Compound **1**				
N1	3637(2)	2839(1)	10077(1)	404(2)
C2	2908(2)	2479(1)	8761(1)	393(2)
O2	3248(1)	3670(1)	8342(1)	516(2)
C3	1645(2)	513(1)	7750(1)	387(2)
O3	961(2)	133(1)	6534(1)	515(2)
N4	1390(2)	−707(1)	8272(1)	393(2)
C4a	2182(2)	−274(1)	9653(1)	367(2)
C5	1881(2)	−1607(2)	10128(1)	440(3)
C6	2672(2)	−1149(2)	11508(1)	464(3)
C61	2296(3)	−2631(2)	11986(2)	641(4)
C7	3783(2)	691(2)	12453(1)	459(3)
C71	4626(3)	1256(3)	13967(2)	640(4)
C8	4094(2)	2005(2)	11966(1)	443(2)
C8a	3311(2)	1528(1)	10579(1)	368(2)
O1w	1198(2)	3312(1)	5748(1)	595(3)
O2w	1025(2)	4355(1)	13508(1)	644(3)
Compound **2**[b]				
N1	3100(1)	3101(2)	22591(4)	318(3)
C2	2278(1)	2657(2)	25816(5)	323(3)
O2	2423(1)	2078(2)	30288(4)	435(3)
C3	1139(1)	2904(2)	23732(5)	331(3)
O3	350(1)	2494(2)	26506(4)	461(3)
N4	1038(1)	3566(2)	18882(4)	332(3)
C4a	2961(1)	3698(2)	17455(5)	293(3)
C5	1744(1)	4445(2)	10436(5)	339(3)
C6	2624(1)	4755(2)	7246(5)	357(3)
O6	2555(1)	5249(2)	2164(4)	478(3)
C61	1499(2)	5266(4)	−113(7)	576(5)
C7	3696(1)	4569(2)	9218(5)	353(3)
O7	4504(1)	4934(2)	5748(4)	494(3)
C71	5596(2)	4712(4)	7513(8)	583(6)
C8	3861(1)	4037(2)	14277(5)	339(3)
C8a	2961(1)	3698(2)	17455(5)	293(3)
O1w	1008(1)	−573(2)	35359(5)	487(3)

[a] U_{eq} is defined as: $U_{eq} = (1/3)\,\Sigma_i\Sigma_j U_{ij} a_i a_j \boldsymbol{a}_i^* \boldsymbol{a}_j^*$.
[b] For **2**, the z coordinates are $\times 10^5$.

TABLE 3. (*a*) Bond lengths (Å) and (*b*) bond angles (deg) with esd's in parentheses

(*a*)

Bond	**1**	**2**
N1—C2	1.336(2)	1.345(2)
N1—C8a	1.399(2)	1.402(2)
C2—O2	1.240(2)	1.237(2)
C2—C3	1.515(1)	1.509(2)
C3—O3	1.224(1)	1.238(2)
C3—N4	1.346(2)	1.341(2)
N4—C4a	1.393(2)	1.399(2)
C4a—C5	1.396(2)	1.394(2)
C4a—C8a	1.386(1)	1.379(2)
C5—C6	1.386(2)	1.376(2)
C6—C61	1.513(3)	
C6—O6		1.361(2)
O6—C61		1.424(2)
C6—C7	1.410(2)	1.417(2)
C7—C71	1.505(2)	
C7—O7		1.362(2)
O7—C71		1.424(2)
C7—C8	1.389(2)	1.374(2)
C8—C8a	1.388(2)	1.397(2)

(*b*)

Bonds	**1**	**2**
C2—N1—C8a	124.5(1)	124.4(1)
N1—C2—O2	123.0(1)	123.1(1)
N1—C2—C3	117.4(1)	116.6(1)
O2—C2—C3	119.6(1)	120.3(1)
C2—C3—O3	119.2(1)	119.5(1)
C2—C3—N4	116.2(1)	117.3(1)
O3—C3—N4	124.6(1)	123.2(1)
C3—N4—C4a	124.6(1)	124.1(1)
N4—C4a—C5	121.8(1)	120.7(1)
N4—C4a—C8a	119.1(1)	118.8(1)
C5—C4a—C8a	119.1(1)	120.5(1)
C4a—C5—C6	121.0(1)	119.5(1)
C5—C6—C61	119.4(1)	
C5—C6—O6		124.8(1)
C5—C6—C7	119.7(1)	119.9(1)
C61—C6—C7	120.9(1)	
O6—C6—C7		115.3(1)
C6—O6—C61		117.2(1)
C6—C7—C71	121.6(1)	
C6—C7—O7		115.0(1)
C6—C7—C8	118.9(1)	120.3(1)
C71—C7—C8	119.6(1)	
O7—C7—C8		124.7(1)
C7—O7—C71		117.1(1)
C7—C8—C8a	120.9(1)	119.2(1)
N1—C8a—C4a	118.2(1)	118.7(1)
N1—C8a—C8	121.3(1)	120.7(1)
C4a—C8a—C8	120.4(1)	120.6(1)

symmetric about a plane perpendicular to the molecular plane. The geometry of these hydrogen bonds is tabulated in Table 4. Thermal-ellipsoid representations of the molecules, together with the hydrogen bonding networks, are presented in Figs. 2 and 3 for **1** and **2**, respectively. In **1**, the molecules are linked to one another directly through a hydrogen bond from N1—H1 to the carbonyl oxygen atom, O2, and indirectly by a hydrogen bonding bridge formed by one of the water molecules of crystallization. This water molecule links the same carbonyl oxygen atom (O2) to the other carbonyl oxygen atom (O3) in a neighboring molecule at $-x$, $-y$, $1-z$. The other amine group (N4—H4) is hydrogen bonded to the other water molecule. The crystallographic center of symmetry generates a cluster of four water molecules, which are interconnected by hydrogen bonds.

In compound **2**, the molecules are again linked directly to one another by a hydrogen bond from an amino group (N1—H1) to a carbonyl oxygen atom and indirectly by a water molecule, providing a hydrogen bonding bridge that is, however, between an amino group and a carbonyl oxygen atom rather than between two carbonyl oxygen atoms as in **1**. The water molecule of crystallization in **2** also bridges one carbonyl oxygen atom to itself to form an infinite chain along the *b* axis.

Overall, in both of these structures the two N—H groups and one of the two carbonyl oxygen atoms are involved in a single hydrogen bond while the other carbonyl oxygen atom is involved in two hydrogen bonds. The singly hydrogen-

Can. J. Chem. Downloaded from www.nrcresearchpress.com by 88.255.202.194 on 09/08/12
For personal use only.

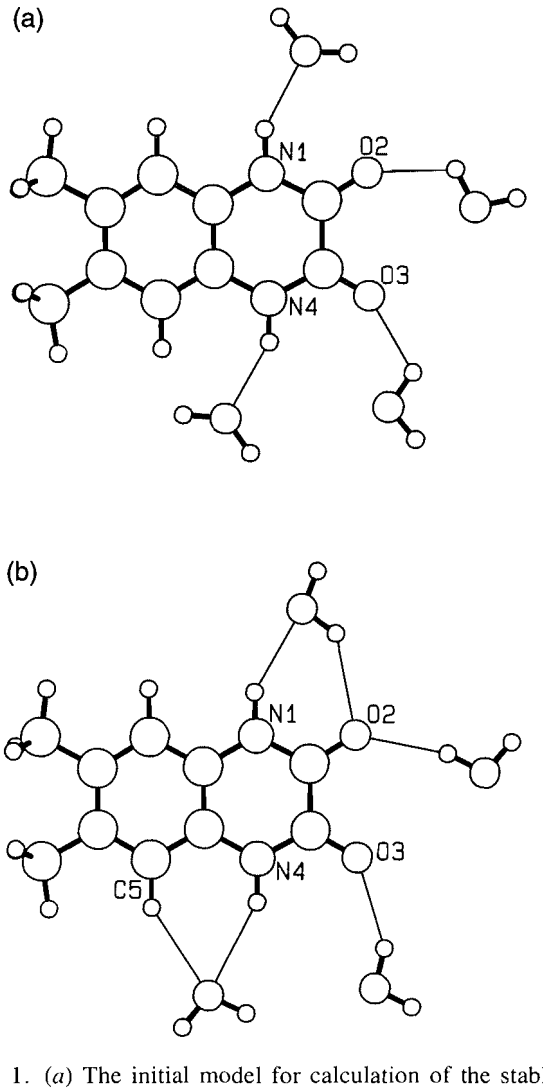

FIG. 1. (*a*) The initial model for calculation of the stable hydrogen bonding pattern for compound **1**, which places one hydrogen bonding partner in contact with each N-H or C=O group in the quinoxalinedione. (*b*) The AM1 optimized hydrogen bonding pattern, which has an unsymmetrical arrangement of hydrogen bonds even though the molecule possesses molecular symmetry.

bonded carbonyl oxygen atom (O3) is also involved in a number of weak, quasi-hydrogen bond interactions, tabulated in Table 4.

The difference in the hydrogen bonding patterns for the two carbonyl oxygen atoms is also reflected in the C=O distances: the greater the involvement in hydrogen bonds, the longer the observed C=O distances. The distance C3—O3 in **1** is 5σ shorter than the other C=O distances. This atom, O3 in **1**, is involved in one hydrogen bond of moderate length (O3···O is 2.828(1) Å). The other singly hydrogen-bonded oxygen atom, O3 in **2**, is involved in a significantly shorter and thus stronger hydrogen bond (O3···H—N4 is 2.805(2) Å). The other two carbonyl oxygen atoms are each involved in two hydrogen bonds.

Another packing interaction important in both structures is π-stacking between neighboring molecules. In **1**, the distances between the plane of the (x,y,z) molecule and the planes of the neighboring molecules $(-x,-y,2-z)$ and $(1-x,-y,2-z)$ are 3.353(2) Å and 3.506(2) Å, respectively. In **2**, the distances between the (x,y,z) molecule and the planes of the neighboring molecules at $(1/2-x,-1/2+y,z)$ and $(1/2-x,1/2+y,z)$ are 3.303(2) Å and 3.330(2) Å, respectively. However, the stacking modes are different in the two structures. In **1**, there is head-to-tail stacking between the molecules connected by the center of symmetry, while in **2** there is head-to-head stacking between the molecules connected by the *b* glide plane, which is stabilized by hydrogen bonds with the water molecule. The molecular packing arrangements for **1** and **2** are presented in Figs. 4 and 5, respectively.

In each compound the quinoxaline is planar, but the deviations from the least-squares plane are greater in **2**. Calculations of the least-squares planes of the constituent rings of the quinoxaline support this difference in planarity; the angle between planes of the 6-carbon atom ring and the 6-membered heterocyclic ring is 1.01(2)° for **1**, and is 2.89(4)° for **2**. The deviations of the carbonyl oxygen atoms, O2 and O3, from the plane of the quinoxaline moiety are also greater for **2**; the values are 0.091(1) Å and 0.104(1) Å for O2 and O3, respectively, while these values are **1** are 0.042(1) Å and −0.010(1) Å. In **2**, the methoxy group at C7 is almost coplanar with the ring system (the dihedral angle C8—C7—O7—C71 is 1.1(2)°); the other methoxy group is slightly tilted out of the plane (the angle C5—C6—O6—C61 is −6.2(2)°) but this tilt still allows significant overlap between the oxygen atom lone pairs and the aromatic system, as shown by the similarity in the C7—O7 and C6—O6 bond distances.

The differences in bond lengths and bond angles between the two structures are mostly due to differences in the substituents. The change of substituents at positions 6 and 7 causes the distances C5—C6 and C7—C8 to differ, between the two structures, by more than $3\sigma_+$ (where σ_+ is defined as $(\sigma_1^2 + \sigma_2^2)^{1/2}$) and the bond angles are different in the substituent region. These differences in bond angles within the carbon rings are similar to those described by Domenicano and Murray-Rust (14) in their studies on the influence of the substituents on the geometry of the benzene ring. These differences include the sharpening of the C5—C6—C7 and C6—C7—C8 angles and widening of the C4a—C5—C6 and C7—C8—C8a angles with the change from a methyl to a methoxy substituent. The greater asymmetry of the exocyclic bond angles around C6 and C7 in **2** is due to the steric effect of the methoxy substituent.

Notable in the geometry of the compounds is the long C2—C3 bond, suggesting significant sigma character to this bond between two sp^2 hybridized atoms. The geometry of the N-C(=O)-C(=O)-N fragment in compounds **1** and **2** is similar to that found for other 1,4-dihydro-2,3-quinoxalinedione derivatives and for the oxamide molecule (18); in these structures the central C—C bond lengths vary from 1.506(6) to 1.522(2) Å, (15–17). However, the longer central C—C bond pattern is not found in quinoxalines lacking the 1,4-dihydro-2,3 dione pattern (19–22). This difference suggests the predominant bonding in this ring is delocalization over the individual amide groups and weak overlap between the groups.

The *ab initio* STO-3G stationary point calculations show that the most significant effect of the change in substituents between **1** and **2** is in the dipole moment, which is 4.431 debye for the methyl compound and 3.315 debye for the methoxy compound. Also, the overlap between C5 and C6

TABLE 4. Hydrogen bond data

D	H	A[a]	D—H (Å)	A...H (Å)	D...A (Å)	D—H...A (deg)
Compound **1**						
N1	H1	O2^{i}	0.97(1)	1.88(1)	2.825(1)	165(2)
N4	H4	O2w^{ii}	0.93(2)	1.88(2)	2.800(1)	170(2)
O1w	H1w1	O3^{iii}	0.85(2)	1.98(2)	2.828(1)	173(3)
O1w	H1w2	O2	0.88(2)	2.02(2)	2.866(2)	162(2)
O2w	H2w1	O1w^{iv}	0.82(3)	2.00(3)	2.828(2)	178(2)
O2w	H2w2	O1w^{v}	0.87(3)	2.10(4)	2.886(2)	149(3)
*O1w[b]	H1w2	O3	0.88(2)	2.55(2)	3.122(2)	124(2)
Compound **2**						
N1	H1	O2^{vi}	0.90(3)	1.94(3)	2.805(2)	160(2)
N4	H4	O1w^{vii}	1.01(3)	1.80(3)	2.805(2)	172(2)
O1w	H1w	O2	0.97(3)	1.97(3)	2.848(2)	150(2)
O1w	H2w	O2^{viii}	1.05(4)	1.80(3)	2.842(2)	170(3)
*C8	H8	O3^{vi}	1.01(2)	2.42(3)	3.189(2)	132(2)
*O1w	H1w	O3	0.97(3)	2.51(3)	3.227(2)	131(2)

[a]Symmetry codes:
[i] $1-x, 1-y, 2-z$ [ii] $-x, -y, 2-z$
[iii] $-x, -y, 1-z$ [iv] $-x, 1-y, 2-z$
[v] $x, y, 1+z$ [vi] $1/2+x, y, 1/2-z$
[vii] $-x, 1/2+y, 1/2-z$ [viii] $1/2-x, -1/2+y, z$
[b]Asterisks denote short contacts, potential weak hydrogen bonds.

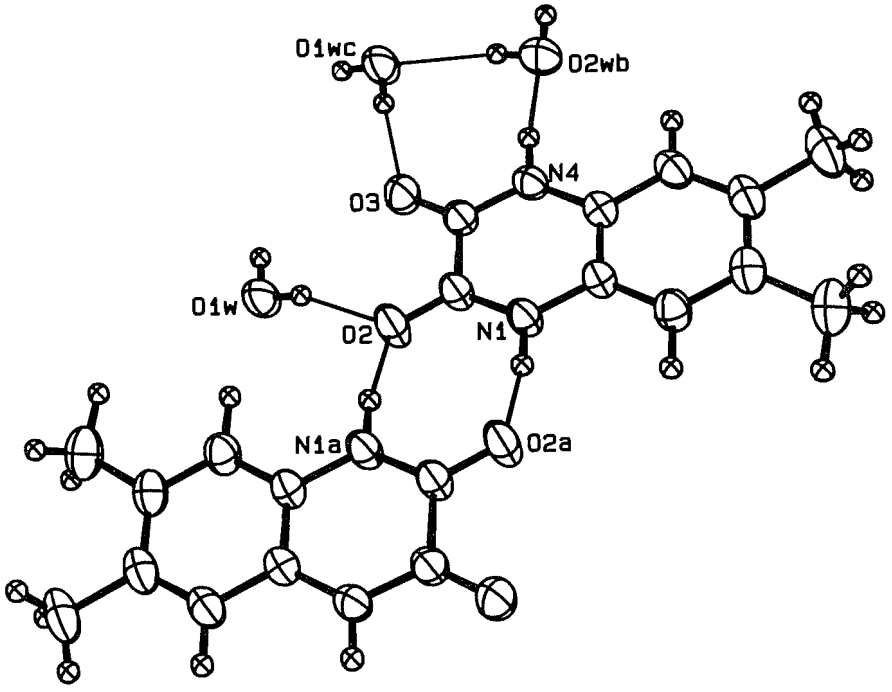

FIG. 2. The hydrogen bonding scheme for **1**. The symmetry codes are (*a*) $-x, -y, 2-z$; (*b*) $x, y, 1+z$; (*c*) $-x, 1-y, 3-z$.

is diminished in the methoxy compound from an overlap population of 0.500 for **1** to 0.475 for **2**.

The optimized AM1 hydrogen-bonded structures reproduce the asymmetrical motif found in the crystal. Differences between the AM1 heats of formation for the nonbonded collection of molecules in *B* and the hydrogen bonding pattern in *C* show that the inactive compound, **2**, forms a slightly more stable hydrogen-bonded network, with a stabilization (difference between structures *B* and *C*) of 14.30 kcal whereas the methyl derivative is stabilized by 13.23 kcal. Although the hydrogen bond energies estimated by AM1 calculations do not compare well with experimental data (26), the relative ordering found for these two very similar systems should be correct.

Mulliken population analysis for the stationary point calculation on *C* (see Fig. 1*b*) shows the induced asymmetry arising from the hydrogen bonding pattern. As shown in Table 5, hydrogen bond formation has the effect of slightly

Can. J. Chem. Downloaded from www.nrcresearchpress.com by 88.255.202.194 on 09/08/12
For personal use only.

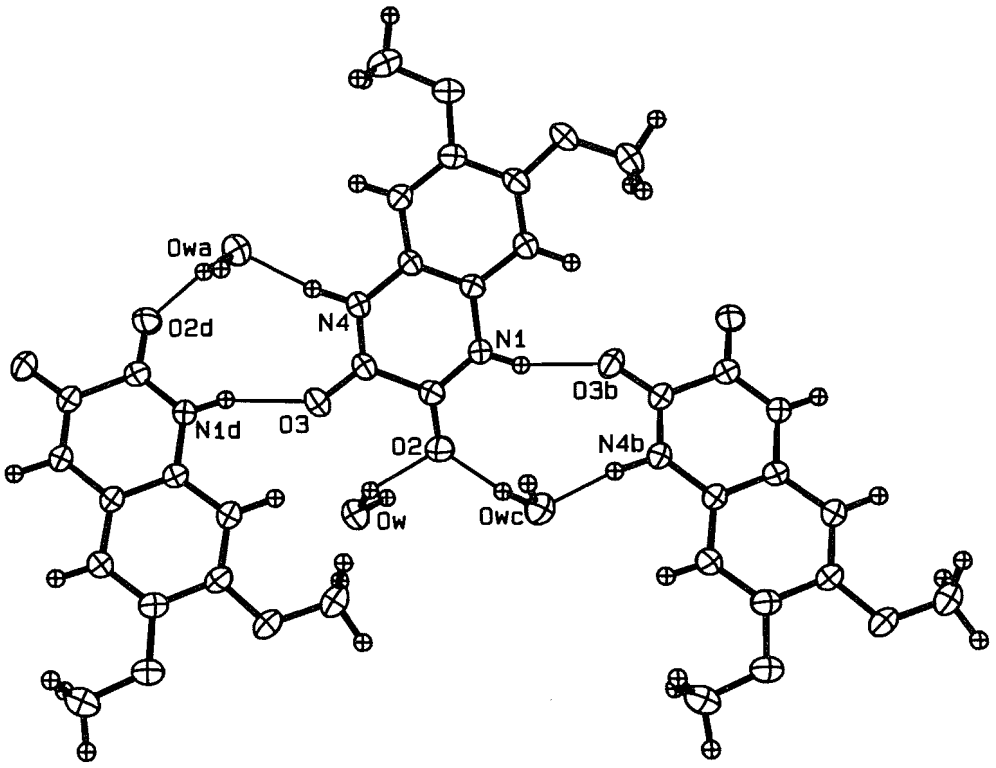

FIG. 3. The hydrogen bonding scheme for **2**. The symmetry codes are (*a*) $-x$, $1/2+y$, $1/2-z$; (*b*) $1/2+x$, y, $1/2-z$; (*c*) $1/2-x$, $1/2+y$, z; (*d*) $-1/2+x$, y, $1/2-z$.

reducing the overlap in the carbonyl bond and the N—H bond and increasing the overlap in the N—C bond of the amide fragment. Thus, the intermolecular interactions favor this resonance form for the amide group:

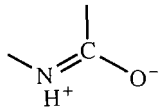

Of the two amides in the heterocyclic ring, the asymmetrical hydrogen bonding pattern induces a greater change in the amide fragment with two hydrogen bonds to the carbonyl oxygen atom. The change in overlap population for this C=O is decreased by three to four times the change in the singly H-bonded carbonyl and the decreases in the N—C and N—H bond overlaps are twice the change for the other amide group. In the hydrogen-bonded structure, in contrast to the isolated molecule, which is symmetrical, the carbonyl oxygen atoms differ in charge by 0.03, with the doubly hydrogen-bonded oxygen atom (O3) more negative.

Discussion

The unsymmetrical distribution of hydrogen bonds found in each crystal, with the carbonyl oxygen atom involded in one hydrogen bond while the other is involved in two hydrogen bonds, was reproduced by the geometric optimization using the AM1 Hamiltonian of the hydrogen-bonded structure in Fig. 1*a* to give the structure in Fig. 1*b*. This pattern appears to be an important interaction motif for these molecules and may model recognition interactions at the EAA receptor. Hydrogen bonding induces asymmetry in the molecule that is evident in the C=O bond lengths and the overlap populations. The two compounds differ slightly in the stabilization gained by the formation of this hydrogen bonding motif; interestingly, the less active compound forms the more stable motif.

The bond distances observed in the crystal structures indicate that the quinoxalinedione comprises two relatively isolated amide groups. This is supported by the Mulliken overlap populations, which show low overlap for the C2—C3 bond (0.353) that is unchanged upon formation of hydrogen bonds so that the amide groups respond separately and differently to the asymmetrical intermolecular environment. The amide involved in two hydrogen bonds to the oxygen atom and one to the N-H group shows the stronger preference for the ionic resonance form.

The geometry and intermolecular interactions found in the two crystal structures and the two sets of calculations are similar and provide little new information regarding the basis for the difference in activity of compounds **1** and **2**. The most important difference between the two compounds is connected to the different substituents on the side of the molecule opposite to the hydrogen bonding region. Structure–activity data (see footnote 3) on this series of compounds indicate that electronegative substituents (in the 5, 6, 7, or 8 positions) — halogen atoms or nitro groups — greatly enhance the activity of the quinoxalinediones; correspondingly, the electron pairs on the ether oxygen of the methoxy groups should cause compound **2** to be more active than the methyl compound. However, the orientation of the methoxy groups, which is somewhat determined by π overlap between the lone pair electrons on the oxygen atom and the aromatic rings, places the bulky methyl groups toward the sides (the 5 and 8 positions) of the quinoxalinedione moiety

Can. J. Chem. Downloaded from www.nrcresearchpress.com by 88.255.202.194 on 09/08/12
For personal use only.

Can. J. Chem. Downloaded from www.nrcresearchpress.com by 88.255.202.194 on 09/08/12
For personal use only.

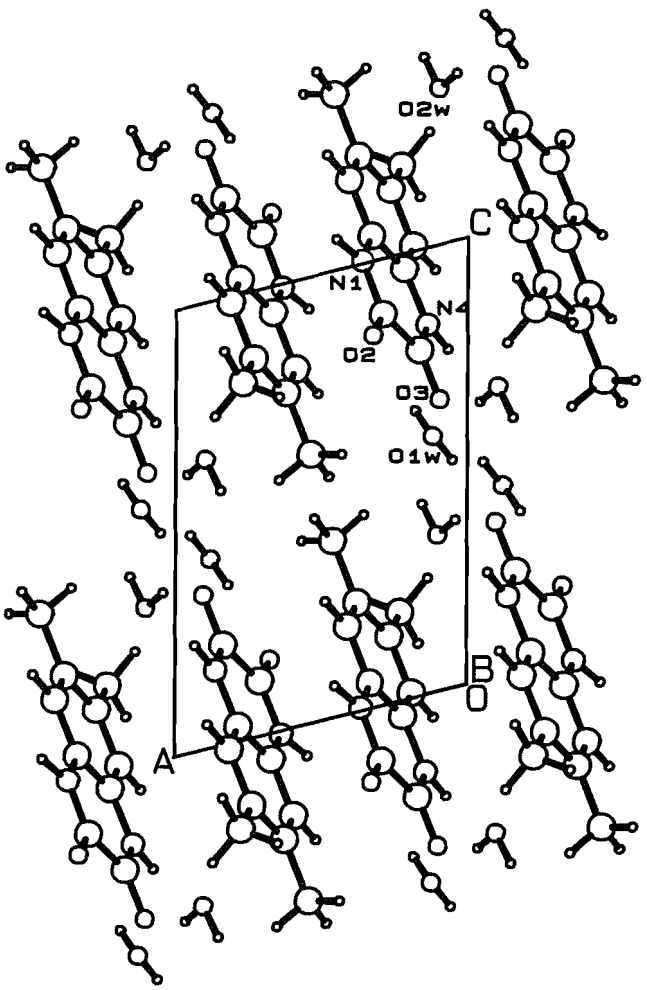

FIG. 4. The molecular packing in the unit cell for **1** as seen along the [010] direction. The molecules stack head-to-tail.

TABLE 5. Overlap populations (GAUSSIAN 90 (ref. 25), see text) condensed to the pairs of atoms

Atom pair		Compound **1**		Compound **2**	
		B	*C*	*B*	*C*
N1	H1	0.358	0.354	0.358	0.355
N1	C2	0.366	0.375	0.366	0.376
N1	C8a	0.373	0.370	0.373	0.371
C2	O2	0.427	0.423	0.427	0.421
C2	C3	0.353	0.353	0.353	0.353
C3	O3	0.427	0.426	0.427	0.425
C3	N4	0.366	0.371	0.366	0.372
N4	H4	0.358	0.356	0.358	0.356
N4	C4a	0.373	0.374	0.373	0.373
C4a	C5	0.503	0.503	0.496	0.495
C4a	C8a	0.491	0.493	0.500	0.500
C5	C6	0.512	0.513	0.511	0.510
C6	C7	0.500	0.499	0.475	0.476
C7	C8	0.512	0.513	0.511	0.511
C8	C8a	0.503	0.501	0.496	0.496
C6	C61	0.388	0.388		
C7	C71	0.388	0.388		
C6	O6			0.291	0.291
C7	O7			0.291	0.291
O6	C61			0.267	0.267
O7	C71			0.267	0.269

(see Fig. 3), possibly obstructing access to the N-H groups or interfering with a recognition point on the binding site. Structure–activity data show that a 5,7-dinitro derivative has the highest activity in this series; thus, the binding site may recognize electronegative groups rather than the methyl portion of the 6,7-dimethoxy substituent in the regions of the 5 and 8 positions.

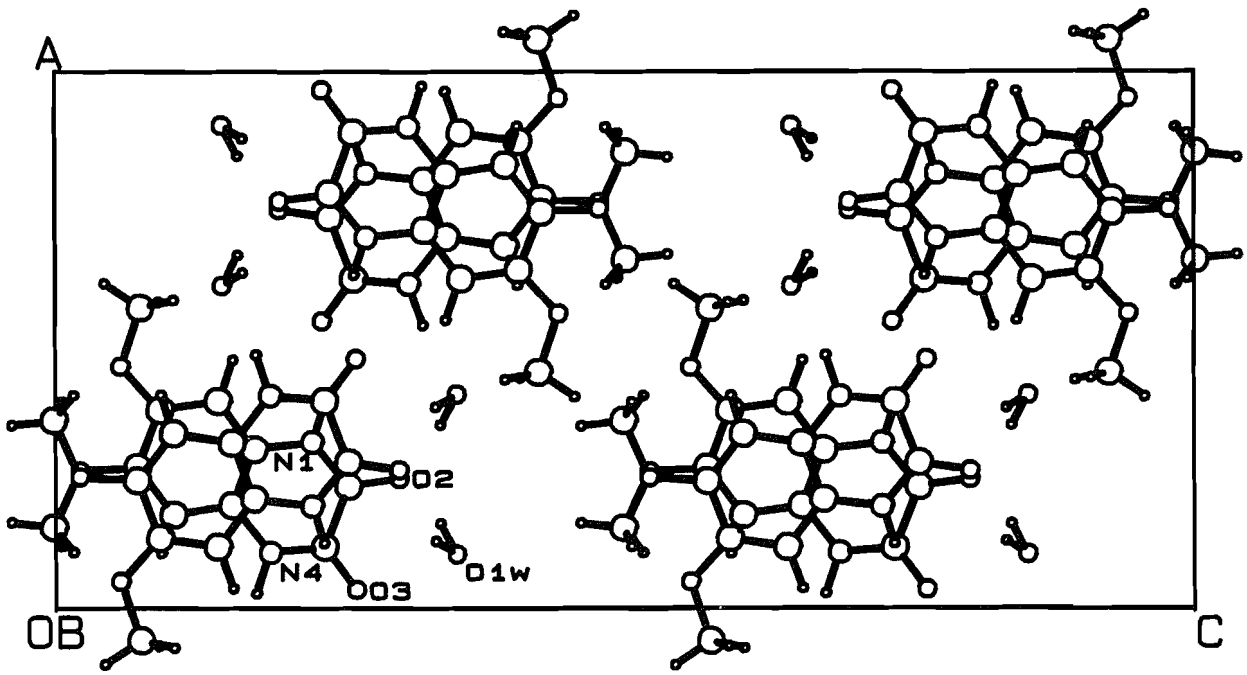

FIG. 5. The molecular packing in the unit cell for **2** as seen along the [010] direction. In contrast to compound **1**, the molecules stack head-to-head.

The charge distributions in the phenyl ring fragments are different in the two compounds; the overall dipole moment is larger by 1 debye for the methyl compound. In the methoxy compound, **2**, the negative charge of the carbonyl oxygen atoms is partially balanced by the charge of the methoxy oxygen and carbon atoms; this could explain the difference in the stacking modes of these compounds as the charge distribution in **2** does not particularly favor head-to-tail stacking.

In conclusion, there are at least two important features present in the crystal structures and the calculated MO structures that provide models for biological recognition. These are the asymmetrical hydrogen bonding pattern displayed by the two amide groups, which could mimic the peptide linkages in glycine and endogenous neurotransmitters, and the distribution of the charge throughout the molecule that determines crystal packing and could determine ligand orientation in the binding site.

Acknowledgments

The authors thank Drs. J. F. Resch and Scott Lehr of ICI Pharmaceuticals for the samples, Mrs. T. Kindopp for the help in crystallization, and the Medical Research Council of Canada (grant to P.W.C.) and ICI Pharmaceutical Group for financial support.

1. J. C. Watkins and R. H. Evans. Annu. Rev. Pharmacol. Toxicol. **21**, 165 (1981).
2. M. J. Croucher, J. F. Collins, and B. S. Meldrum. Science, **216**, 899 (1982).
3. T. Wieloch. Science, **230**, 681 (1985).
4. J. C. Watkins, P. Krogsgaard-Larsen, and T. Honoré. Trends Pharmacol. Sci. **11**, 25 (1989).
5. E. H. F. Wongand and J. A. Kemp. Annu. Rev. Pharmacol. Toxicol. **31**, 401 (1991).
6. T. Honoré, S. N. Davies, J. Drejer, E. J. Fletcher, P. Jacobson, D. Lodge, and F. E. Nielsen. Science, **241**, 701 (1988).
7. G. M. Sheldrick. SHELXS86, program for crystal structure determination. Univ. of Cambridge, Cambridge, England. 1986.
8. G. M. Sheldrick. SHELX-76, program for crystal structure determination. Univ. of Cambridge, Cambridge, England. 1976.
9. D. T. Cromer and J. B. Mann. Acta Crystallogr. Sect. A: Cryst. Phys. Diffr. Theor. Gen. Crystallogr. **A24**, 321 (1968).
10. R. F. Stewart, E. R. Davidson, and W. T. Simpson. J. Chem. Phys. **42**, 3175 (1965).
11. C. K. Johnson. ORTEPII. Report ORNL-5138, Oak Ridge National Laboratory, Oak Ridge, Tenn. 1976.
12. W. D. S. Motherwell and W. Clegg. PLUTO78. Program for drawing molecular and crystal structures. Univ. of Cambridge, Cambridge, England. 1978.
13. I. Vicković. CSU, geometry calculation program for X-ray analysis. Univ. of Zagreb, Zagreb, Yugoslavia. 1988.
14. A. Domenicano and P. Murray-Rust. Tetrahedron Lett. **24**, 2283 (1979).
15. C. Svensson. Acta Chem. Scand. **B30**, 581 (1976).
16. M. J. Grabowski, A. Stepień, M. Cygler, and E. Wajsman. Acta Crystallogr. Sect. B: Struct. Crystallogr. Cryst. Chem. **B33**, 2851 (1977).
17. A. Stępień. Acta Crystallog. Sect. B: Struct. Crystallogr. Cryst. Chem. **B33**, 2854 (1977).
18. E. M. Ayerst and J. R. C. Duke. Acta Crystallogr. **7**, 588 (1954).
19. A. Stępień, M. J. Grabowski, M. Cygler, and E. Wajsman. Acta Crystallogr. Sect. B: Struct. Crystallogr. Cryst. Chem. **B32**, 2048 (1976).
20. G. J. Visser and A. Vos. Acta Crystallogr. Sect. B: Struct. Crystallogr. Cryst. Chem. **B27**, 1793 (1971).
21. A. J. W. A. Vermeulen and C. Huiszoon. Acta Crystallogr. Sect. B: Struct. Crystallogr. Cryst. Chem. **B35**, 3087 (1979).
22. S.-K. Lin and Q.-Z. Cong. J. Mol. Struct. **159**, 279 (1987).
23. J. J. P. Stewart. MOPAC 6.0. Frank J. Seiler Research Laboratory, United States Air Force Academy, Colo. 1990.
24. M. J. S. Dewar, E. G. Zoebisch. E. F. Healy, and J. J. P. Stewart. J. Am. Chem. Soc. **107**, 3902 (1985).
25. M. J. Frisch, M. Head-Gordon, G. W. Trucks, J. B. Foresman, H. B. Schlegel, K. Raghavachari, M. Robb, J. S. Binkley, C. Gonzales, D. J. Defrees, D. J. Fox, R. A. Whiteside, R. Seeger, C. F. Melius, J. Baker, L. R. Kahn, J. J. P. Stewart, S. Topiol, and J. A. Pople. GAUSSIAN 90, Revision I. Gaussian, Inc. Pittsburg, Pa. 1990.
26. G. P. Dado and S. H. Gellman. J. Am. Chem. Soc. **114**, 3138 (1992).

Can. J. Chem. Downloaded from www.nrcresearchpress.com by 88.255.202.194 on 09/08/12
For personal use only.

The synthesis and X-ray structures of the geometric isomers of 1-amino-1,2-cyclopentanedicarboxylic acid

KENNETH CURRY[1] AND HUGH MCLENNAN
Department of Physiology, University of British Columbia, 2146 Health Sciences Mall, Vancouver, B.C., Canada V6T 1Z3

AND

STEVEN J. RETTIG AND JAMES TROTTER
Department of Chemistry, University of British Columbia, 2036 Main Mall, Vancouver, B.C., Canada V6T 1Z1

Received January 21, 1992[2]

KENNETH CURRY, HUGH MCLENNAN, STEVEN J. RETTIG, and JAMES TROTTER. Can. J. Chem. **71**, 76 (1993).

The geometric isomers of 1-amino-1,2-cyclopentanedicarboxylic acid were isolated as the hydrolysis products of 2-cyclopentanecarboxylic acid-5,5′-hydantoin. The hydantoin ester was formed from ethyl -2-oxocyclopentanecarboxylate via a Bucherer–Bergs reaction. Hydrolysis of the hydantoin at elevated temperatures gave a mixture of *trans*- and *cis*-1-amino-1,2-cyclopentanedicarboxylic acids indicating epimerization during hydrolysis. The *trans* product has not been described previously and the *cis* not extensively characterized. X-ray crystallography reveals that both isomers are zwitterionic in the solid state and the *cis* isomer molecules are linked by unusually strong hydrogen bonding. Structures were confirmed by ^{13}C NMR, X-ray crystallography, and elemental analysis. Physical data are also presented.

KENNETH CURRY, HUGH MCLENNAN, STEVEN J. RETTIG et JAMES TROTTER. Can. J. Chem. **71**, 76 (1993).

Les isomères géométriques de l'acide 1-amino-cyclopentane-1,2-dicarboxylique ont été isolés comme produits d'hydrolyse de la 5,5′-hydantoïne de l'acide cyclopentane-2-carboxylique. On a obtenu l'ester hydantoïne par une réaction de Bucherer–Bergs sur le 2-oxocyclopentanecarboxylate d'éthyle. L'hydrolyse de l'hydantoïne à température élevée conduit à un mélange des acides 1-amino-cyclopentane-1,2-dicarboxyliques *trans* et *cis* indiquant qu'une épimérisation se produit au cours de l'hydrolyse. Le produit *trans* n'avait pas été décrit antérieurement alors que le composé *cis* n'avait pas été très bien caractérisé. La cristallographie des rayons X révèle que, dans la phase solide, les deux isomères sont zwitterioniques et que les molécules de l'isomère *cis* sont reliées par des liaisons hydrogènes inhabituellement fortes. On a confirmé les structures par RMN du ^{13}C, par diffraction des rayons X et par analyse élémentaire. On rapporte aussi les données physiques.

[Traduit par la rédaction]

Introduction

Considerable recent interest has been generated in the pharmacology of acidic amino acids related to glutamic and aspartic acids because of the perceived role of these compounds as synaptic transmitters in the mammalian central nervous system. One method of analyzing the receptors that mediate these neuronal events is to produce rigid analogs of glutamic and aspartic acids (1–3). The synthesis of the glutamic acid analogs, *trans*- and *cis*-1-amino-1,3-cyclopentanedicarboxylic acids, has already been described (4) and we report here on the synthesis of the corresponding aspartic acid analogs, *cis*-**4** and *trans*-**5** 1-amino-1,2-cyclopentanedicarboxylic acids (Fig. 1).[3]

Experimental

Melting points were determined on a Fisher–Johns apparatus; UV λ_{max} was determined on an L.K.B. Ultrospec II or a Pye–Unicam SP-8-100 dual beam spectrophotometer.

Ethyl 2-cyclopentanecarboxylate-1-spiro-5-hydantoin, 2

Compound **2** was prepared by a modification of the method of Connors and Ross (5), resulting in two products that were separated by fractional crystallization from chloroform and methanol. After cooling, **2** was isolated as a white solid, 51 g (56%), mp 141°C (lit. (5) mp 145°C), and confirmed by ^{13}C NMR. The second product was determined by ^{13}C NMR to be 2-cyclopentanecarboxylic acid-1-spiro-5-hydantoin **3**. Yield 10.4%. NMR data are presented in Table 1.

2-Cyclopentanecarboxylic acid-1-spiro-5-hydantoin, 3

Hydrolysis of **2** in 4 M hydrochloric acid (HCl) gave 43.5 g of a colorless crystalline material, mp 220°C (lit. (5) mp 225–226°C); UV λ_{max} 307 nm. ^{13}C NMR (Table 1) revealed this to be a single product consistent with the predicted structure of **3**. Anal. calcd. for $C_8H_{10}N_2O_4$: C 48.48, H 5.09, N 14.14; found: C 48.60, H 5.14, N 14.22.

cis- *and* trans-*1-Amino-1,2-cyclopentanedicarboxylic acids, 4 and 5*

Compound **3** (14.0 mmol, 2.8 g) was suspended in 100 mL of 6 M HCl and placed in a pressure reaction vessel. The vessel was sealed and maintained at 155–160°C for 6 h. The vessel was allowed to cool to room temperature and the resulting solution evaporated to dryness *in vacuo* at 60°C to leave a yellow solid. The solid was dissolved in isopropyl alcohol and treated with propylene oxide to remove residual hydrogen chloride. A white solid precipitated on standing and revealed two ninhydrin staining spots running on silica gel 60 TLC and eluting with 90:10 methanol–water, R_f 0.22 (*trans*), 0.48 (*cis*). The two amino acids were separated by fractional crystallization from water and methanol or by column chromatography on silica gel 60 with a gradient of 50:50 to 100:0, methanol–chloroform. In the case of fractional crystallization the first isomer to precipitate was *trans*, mp 220°C, UV λ_{max} 185.4 nm, structure confirmed by ^{13}C NMR and X-ray crystallography (Table 1 and Figs. 2 and 3). The amino acids were prepared for elemental analysis by precipitation from isopropyl alcohol with addition of propylene oxide to solutions of the chloride salts. The powders were then dried *in vacuo* at 70°C for 24 h. Anal. calcd. for $C_7H_{11}NO_4$: C 48.55, H 6.40, N 8.09; found (anhydrous mate-

[1]Author to whom correspondence may be addressed.

[2]Revision received September 10, 1992.

[3]In the *cis* isomer, the C(1)—NH_3^+ and C(2)—CO_2H groups are *cis* (higher priority groups); the carboxyl groups are *trans*. Vice versa for the *trans* isomer.

Can. J. Chem. Downloaded from www.nrcresearchpress.com by 88.255.202.194 on 09/08/12
For personal use only.

TABLE 1. ^{13}C NMR chemical shifts relative to TMS

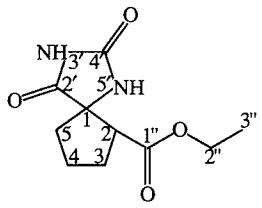

Compound number	Chemical shift (ppm)									
	C1	C2	C3	C4	C5	C2′	C4′	C1″	C2″	C3″
2	70.5	52.3	26.5	22.5	37.3	178.1	180.1	170.6	60.8	13.5
3	72.7	56.1	28.8	23.1	37.3	179.1	191.3	169.3		
4	67.8	53.2	28.6	21.8	36.0	179.8		177.4		
5	68.0	56.2	28.6	22.2	36.2	180.5		179.5		

TABLE 2. Crystallographic data[a]

Compound	*cis*-**4**·H_2O	*trans*-**5**·H_2O
Formula	$C_7H_{11}NO_4 \cdot H_2O$	$C_7H_{11}NO_4 \cdot H_2O$
fw	191.18	191.18
Crystal system	Orthorhombic	Monoclinic
a(Å)	12.366(3)	10.8222(8)
b(Å)	6.516(2)	7.6853(8)
c(Å)	21.005(1)	11.4415(8)
β (deg)	90	109.448(5)
V (Å^3)	1692.5(7)	897.32(13)
Space group	$Pca2_1$	$P2_1/c$
Z	8	4
ρ_c (g/cm^3)	1.50	1.41
F(000)	816	408
μ(Cu-K$_\alpha$) (cm^{-1})	10.53	9.93
Crystal dimensions (mm)	0.08 × 0.25 × 0.30	0.07 × 0.30 × 0.35
Transmission factors	0.88–1.00	0.83–1.00
Scan type	ω–2θ	ω–2θ
Scan range (deg in ω)	1.31 + 0.30 tan θ	1.25 + 0.30 tan θ
Scan speed (deg/min)	32 (up to 8 rescans)	32 (up to 8 rescans)
Data collected	$\pm h$, $+k$, $+l$	$\pm h$, $+k$, $+l$
$2\theta_{max}$ (deg)	155	155
Crystal decay	Negligible	Negligible
Total reflections	3842	1851
Unique reflections	2077	1752
R_{merge}	0.020	0.016
Reflections with $I \geq 3\sigma(I)$	1509	1432
Number of variables	243	155
R	0.040	0.043
R_w	0.052	0.059
S	2.20	2.34
Max. Δ/σ (final cycle)	0.26	0.06
Max. residual density (e/Å^3)	0.16	0.14

[a]Temperature 294 K, Rigaku AFC6S diffractometer, Cu-K$_\alpha$ radiation (λ = 1.54178 Å), graphite monochromator, takeoff angle 6.0°, aperture 6.0 × 6.0 mm at a distance of 285 mm from the crystal, stationary background counts at each end of the scan (scan/background time ratio 2:1, up to 8 recans), $\sigma^2(F^2) = [S^2(C + 4B) + (0.035F^2)^2]/Lp^2$ (S = scan rate, C = scan count, B = normalized background count), function minimized $\Sigma w(|F_o| - |F_c|)^2$ where $w = 4F_c^2/\sigma^2(F_o^2)$, $R = \Sigma||F_o| - |F_c||/\Sigma|F_c|$, $R_w = (\Sigma w(|F_o| - |F_c|)^2/\Sigma w|F_o|^2)^{1/2}$, and $S = [\Sigma w(|F_o| - |F_c|)^2/(m\text{-}n)]^{1/2}$. Values given for R, R_w, and S are based on those reflections with $I \geq 3\sigma(I)$.

Can. J. Chem. Downloaded from www.nrcresearchpress.com by 88.255.202.194 on 09/08/12
For personal use only.

Can. J. Chem. Downloaded from www.nrcresearchpress.com by 88.255.202.194 on 09/08/12
For personal use only.

TABLE 3. Final atomic coordinates (fractional) and equivalent isotropic thermal parameters[a]

Atom	*x*	*y*	*z*	B_{eq}[b]
		cis isomer		
O(1)	0.0022(3)	0.1565(6)	0.3983	4.7
O(2)	−0.0159(2)	0.1453(4)	0.5033(2)	3.3
O(3)	0.2898(3)	0.1543(5)	0.4226(2)	4.3
O(4)	0.3403(2)	0.1117(4)	0.5232(2)	3.0
O(5)	0.2542(3)	0.3311(5)	0.2862(2)	4.7
O(6)	0.2675(2)	0.4537(4)	0.1809(2)	3.3
O(7)	−0.0358(3)	0.3424(5)	0.2649(2)	4.7
O(8)	−0.0866(2)	0.3960(4)	0.1650(2)	3.3
O(9)	0.4736(2)	0.2776(5)	0.3351(2)	3.7
O(10)	−0.2198(2)	0.2237(5)	0.3509(2)	3.7
N(1)	0.1402(3)	0.4617(6)	0.3974(3)	2.4
N(2)	0.1130(3)	0.0325(6)	0.2877(3)	2.6
C(1)	0.1030(2)	0.3946(5)	0.4617(2)	2.0
C(2)	0.1985(3)	0.3415(5)	0.5051(2)	2.0
C(3)	0.2468(3)	0.5511(8)	0.5225(3)	3.1
C(4)	0.1538(4)	0.7056(6)	0.5153(3)	3.1
C(5)	0.0553(3)	0.5807(5)	0.4955(3)	2.6
C(6)	0.0225(3)	0.2163(5)	0.4530(2)	2.3
C(7)	0.2801(3)	0.1924(5)	0.4798(2)	2.3
C(8)	0.1496(2)	0.1023(5)	0.2228(2)	2.1
C(9)	0.0532(3)	0.1601(5)	0.1805(2)	2.1
C(10)	0.0013(3)	−0.0503(8)	0.1645(3)	2.9
C(11)	0.0952(3)	−0.2005(6)	0.1641(3)	3.5
C(12)	0.1954(3)	−0.0814(6)	0.1860(3)	2.8
C(13)	0.2303(3)	0.2794(5)	0.2321(2)	2.4
C(14)	−0.0281(3)	0.3118(5)	0.2075(2)	2.3
		trans isomer		
O(1)	0.0165(1)	0.1141(2)	0.3911(1)	3.9
O(2)	0.2066(1)	0.1562(2)	0.3600(1)	3.9
O(3)	0.1027(1)	0.5130(2)	0.4364(2)	4.7
O(4)	0.3012(1)	0.6122(2)	0.4588(2)	4.8
O(5)	0.1874(2)	0.8112(2)	0.2716(2)	4.9
N	0.0975(1)	0.2205(2)	0.6205(1)	2.6
C(1)	0.2018(1)	0.2018(2)	0.5632(1)	2.3
C(2)	0.2847(2)	0.3686(2)	0.5793(2)	2.7
C(3)	0.4213(2)	0.3077(3)	0.5871(2)	4.0
C(4)[1]	0.4396(4)	0.1527(8)	0.6704(5)	4.9
C(4A)[2]	0.4229(7)	0.1013(11)	0.6078(7)	5.0
C(5)	0.3024(2)	0.0617(3)	0.6308(2)	3.5
C(6)	0.1349(2)	0.1540(2)	0.4261(1)	2.8
C(7)	0.2207(2)	0.5045(2)	0.4839(2)	2.9

[a]Superscripts 1 and 2 refer to site occupancy factors of 0.60 and 0.40, respectively.
[b]$B_{eq} = (8\pi^2/3)\Sigma\Sigma U_{ij} a_i^* a_j^* (\mathbf{a}_i \cdot \mathbf{a}_j)$.

rial): C 48.46, H 6.42, N 8.13. The second was the *cis* isomer, mp 230°C (lit. (5) mp 249°C for NH_4^+ salt), UV λ_{max} 186.8 nm. Found (anhydrous material): C 48.30, H 6.57, N 8.06. Column chromatography gave first **4**, at approximately 70:30, chloroform–methanol, and second, **5**.

*X-ray crystallographic analyses of compounds **4** and **5***

Crystallographic data for *cis*-**4** and *trans*-**5** (both compounds crystallize as monohydrates) are presented in Table 2. Unit-cell parameters were determined by least-squares refinement on diffractometer setting angles for 25 reflections (θ = 42–58° and 28–49° for the *cis* and *trans* isomers, respectively). The data were processed[4] and corrected for Lp and absorption (empirical, azimuthal scans for four reflections).

[4]TEXSAN structure analysis package. Molecular Structure Corp. 1985.

TABLE 4. Bond lengths (Å) and angles (deg)

	cis		
	Molecule A	Molecule B[a]	*trans*
Atoms		Distances	
O(1)—C(6)	1.239(5)	1.220(5)	1.247(2)
O(2)—C(6)	1.248(5)	1.266(5)	1.252(2)
O(3)—C(7)	1.233(5)	1.226(5)	1.212(2)
O(4)—C(7)	1.289(4)	1.273(4)	1.301(2)
N—C(1)	1.492(5)	1.507(6)	1.489(2)
C(1)—C(2)	1.532(4)	1.534(4)	1.540(2)
C(1)—C(5)	1.524(5)	1.533(5)	1.544(2)
C(1)—C(6)	1.540(4)	1.538(4)	1.537(2)
C(2)—C(3)	1.535(5)	1.551(5)	1.525(2)
C(2)—C(7)	1.498(5)	1.520(5)	1.503(3)
C(3)—C(4)	1.536(6)	1.519(6)	1.497(6)
C(3)—C(4A)	—	—	1.603(9)
C(4)—C(5)	1.522(5)	1.533(5)	1.566(5)
C(4A)—C(5)	—	—	1.446(7)
Atoms		Angles	
N—C(1)—C(2)	111.5(3)	111.4(3)	111.3(1)
N—C(1)—C(5)	107.9(3)	109.3(3)	111.0(1)
N—C(1)—C(6)	108.2(3)	107.8(3)	107.7(1)
C(2)—C(1)—C(5)	101.5(3)	100.8(3)	103.6(1)
C(2)—C(1)—C(6)	113.5(3)	113.2(3)	112.3(1)
C(5)—C(1)—C(6)	114.0(3)	114.2(3)	111.0(1)
C(1)—C(2)—C(3)	103.9(3)	103.3(3)	105.5(1)
C(1)—C(2)—C(7)	117.0(3)	117.2(3)	112.5(1)
C(3)—C(2)—C(7)	113.5(3)	112.5(3)	117.3(1)
C(2)—C(3)—C(4)	105.6(3)	104.7(3)	101.6(2)
C(2)—C(3)—C(4A)	—	—	106.0(3)
C(3)—C(4)—C(5)	106.0(3)	106.9(3)	105.0(3)
C(3)—C(4A)—C(5)	—	—	105.6(4)
C(1)—C(5)—C(4)	104.1(3)	104.4(3)	106.1(2)
C(1)—C(5)—C(4A)	—	—	106.9(3)
O(1)—C(6)—O(2)	126.3(3)	126.7(3)	126.0(2)
O(1)—C(6)—C(1)	118.6(3)	118.9(3)	118.1(1)
O(2)—C(6)—C(1)	115.2(3)	114.4(3)	115.9(1)
O(3)—C(6)—O(4)	123.4(3)	125.1(3)	123.3(2)
O(3)—C(6)—C(2)	122.8(3)	121.7(3)	121.7(2)
O(4)—C(6)—C(2)	113.8(3)	113.2(3)	115.0(2)

[a]The atoms O(5–8), N(2), and C(8–14) constituting this molecule correspond, respectively, to atoms O(1–4), N(1), and C(1–7) of molecule A.

Both structures were solved by direct methods. The non-hydrogen atoms of both compounds were refined with anisotropic thermal parameters. For the *cis* isomer the two hydrogen atoms associated with the carboxylic acid moieties (H(7) and H(8)) were refined with isotropic thermal parameters and the remaining hydrogen atoms were fixed in idealized positions (the orientations of the $-NH_3^+$ groups based on observed difference map peaks, O/N/C-H = 0.98 Å, $B_H = 1.2\ B_{bonded\ atom}$). Conformational disorder in the five-membered ring of the *trans* isomer was indicated by anomalous thermal parameters for the atom C(4). A split-atom model for C(4) was refined, the occupancy factors (0.6/0.4) being determined by refinement with fixed isotropic thermal parameters. In the final stages of refinement the occupancy factors were kept fixed and anisotropic thermal parameters were employed for C(4) and C(4A). All ordered hydrogen atoms in the *trans* isomer were refined with isotropic thermal parameters and the disordered hydrogen atom positions were calculated as described above for the *cis* isomer.

The solution of the structure of the *cis* isomer was initiated in the noncentrosymmetric (but racemic) space group $Pca2_1$ on the basis of the *E*-statistics. The two molecules in the asymmetric unit are

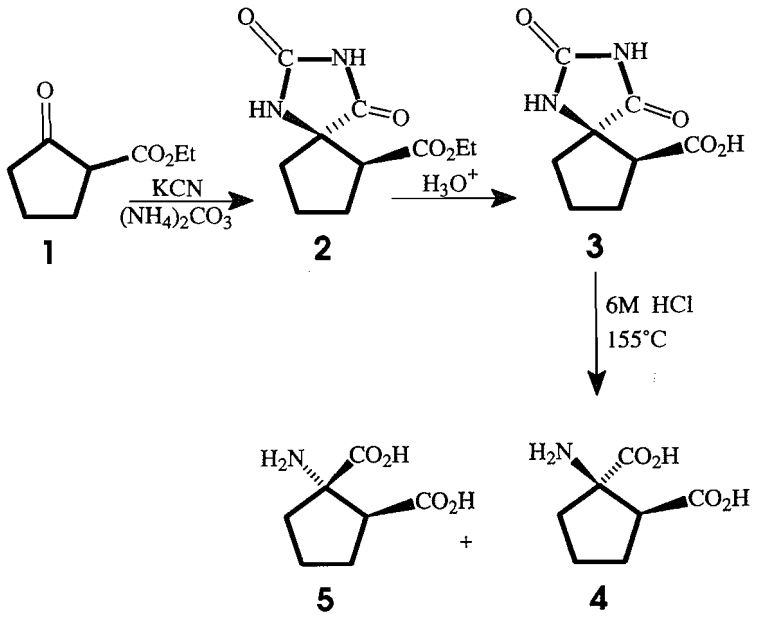

FIG. 1. Schematic for the synthesis of *cis* and *trans*-1-amino-1,2-cyclopentanedicarboxylic acids.

related to one another by a pseudo-inversion centre at approximately (1/8, 1/4, 0.34) (see Table 3). Attempts to refine the structure in the centrosymmetric space group *Pcam* (after appropriate coordinate translations) were unsuccessful. Parallel refinement of the opposite polarity (anomalous dispersion corrections for C, N, O) resulted in marginally higher residuals, the R and R_w ratios being 0.0402/0.0401 = 1.003 and 0.0524/0.0522 = 1.004, respectively. Neutral atom scattering factors for all atoms and anomalous dispersion corrections for the non-hydrogen atoms were taken from the *International tables for X-ray crystallography* (9).

Final atomic coordinates and equivalent isotropic thermal parameters for the non-hydrogen atoms are given in Table 3. Bond lengths and angles, selected torsion angles, and details of the hydrogen bonding are presented in Tables 4–6. Hydrogen coordinates, anisotropic thermal parameters, torsion angles, least-squares planes, intermolecular distances, and structure factors are included as supplementary material.[5]

Results and discussion

Since previous studies had indicated that Bucherer–Bergs hydantoin formation gave one geometric isomer exclusively (5) it was expected that the final product would consist of the *cis* amino acid only. Figure 1 shows the synthetic route and indicates that the most efficient method of hydrolysis with hydrochloric acid leads to epimerization of the final product into *trans* and *cis* amino acids. The *trans* isomer has not been described previously and is of particular interest because the rigidity of the ring and close proximity of the carboxyl groups result in a compound that resembles a folded conformation of glutamic and aspartic acids.

Using a version of the Simplex method (6), the optimum reaction conditions were determined and gave a total yield of approximately 65% for the formation of hydantoin **3** and its ester **2**. The yield of hydantoin was found to be dependent on time, temperature, and concentration of reactants. In particular, the presence of cyanide seemed to suppress the reaction, thus its concentration was kept low by gradual addition over a 24 h period. For unhindered systems, hydantoin formation takes place in 4–6 h; in the present study it was necessary to increase this period to 48 h. As the reaction proceeds, ethyl 2-cyclopentanecarboxylate-1-spiro-5-hydantoin **2** was formed and hydrolyzed *in situ* to give increasing amounts of **3**. The stereospecificity of the Bucherer–Bergs reaction has been discussed in detail with reference to restricted ring systems (7, 8) and, in the present synthesis, conditions are further restrained by the presence of an ester group at C(2) of the cyclic ketone **1**. Alkaline hydrolysis of **3** gave yields that were very low. Refluxing for 48 h in 2 M barium hydroxide gave no product at all while hydrolysis with 2 M sodium hydroxide at 140°C gave only very low yields of the *cis* amino acid (<5%). The best results were obtained with acid hydrolysis using 6 M HCl at 155°C for 6 h. The reaction mixture was found to contain both *cis*-**4** and *trans*-**5** amino acids with a total yield of 46%.

X-ray crystal structure of cis-**4** *and* trans-**5** *1-amino-1,2-cyclopentanedicarboxylic acid monohydrates*

Stereoviews of the asymmetric units (showing atom labeling schemes) of *cis*-**4** and *trans*-**5** (monohydrates) are shown in Fig. 2. The *cis* and *trans* isomers have (1*SR*,2*RS*) and (1*SR*,2*SR*) relative stereochemistries, respectively. Bond lengths and angles in the two isomers (Table 4) are generally as expected. The major structural differences between the two isomers, on the molecular level, can be seen by a comparison of the torsion angles in Table 5. The five-membered rings in both of the crystallographically independent

[5]Supplementary material mentioned in the text may be purchased from the Depository of Unpublished Data, Document Delivery, CISTI, National Research Council Canada, Ottawa, Canada K1A 0R6.

Tables of hydrogen atom coordinates and bond lengths and angles involving hydrogen atoms have also been deposited with the Cambridge Crystallographic Data Centre and can be obtained on request from The Director, Cambridge Crystallographic Data Centre, University Chemistry Laboratory, 12 Union Road, Cambridge CB2 1EZ, U.K.

Can. J. Chem. Downloaded from www.nrcresearchpress.com by 88.255.202.194 on 09/08/12
For personal use only.

Can. J. Chem. Downloaded from www.nrcresearchpress.com by 88.255.202.194 on 09/08/12
For personal use only.

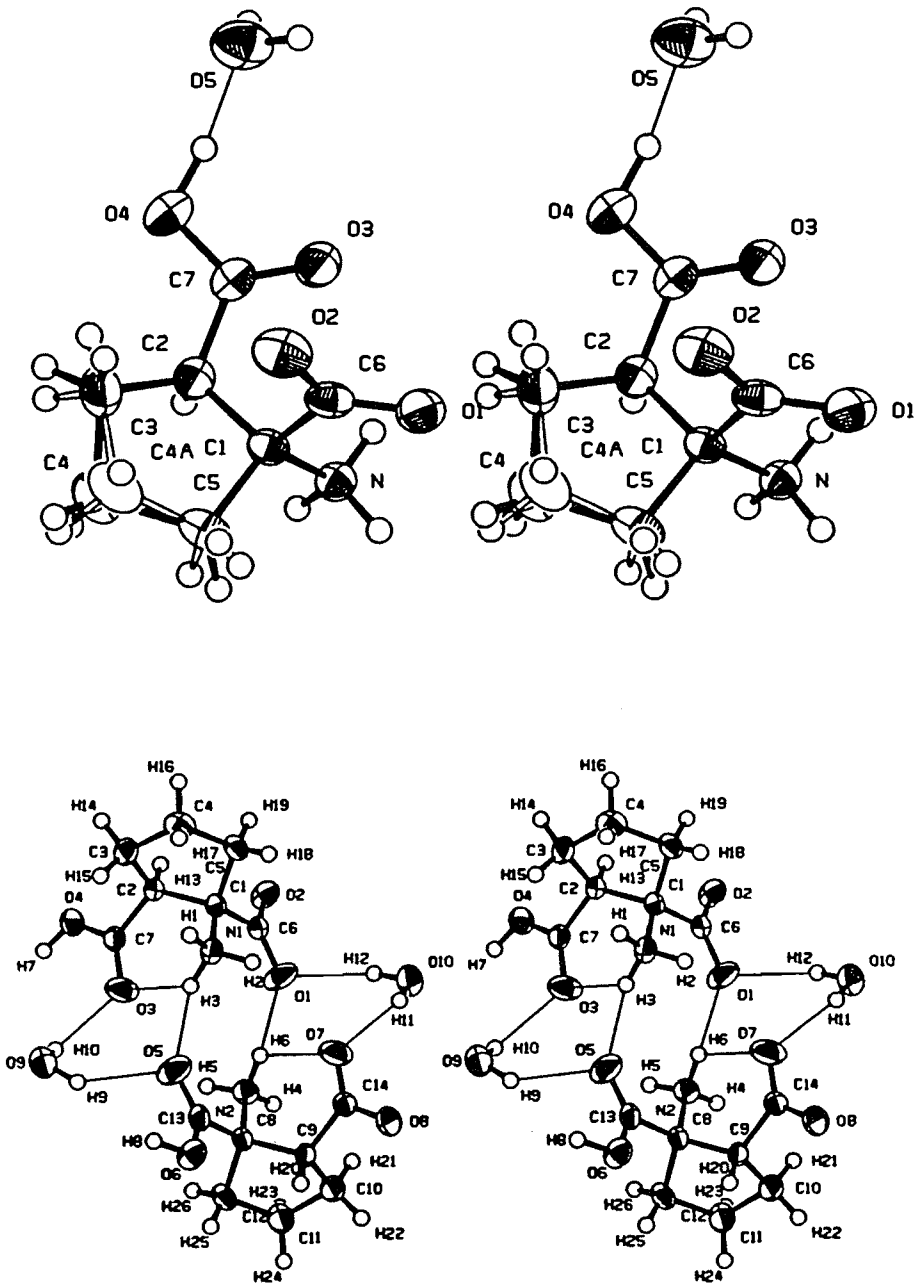

FIG. 2. Stereoviews of *trans*- and *cis*-1-amino-1,2-cyclopentanedicarboxylic acids.

molecules of the *cis* isomer and the minor component of the disordered cyclopentane ring in the *trans* isomer (that containing C(4A)) may be classified as C1-envelopes with varying degrees of irregularity. The conformation of the five-membered ring in the major component of the *trans* isomer is that of a C3-envelope.

Both molecules exist as zwitterions in the solid state. The deprotonated carboxylate group is that bonded to C1 in the *trans* isomer, while for the *cis* isomer the C1-carboxylate group is deprotonated in molecule A (containing N1) and the C1 and C2-carboxylate groups are nearly equivalent and share what is most likely a symmetrically O···H···O hydrogen-bonded proton in molecule B (containing N2) (see below).

Extensive hydrogen bonding dominates the packing arrangements in both crystal structures (see Table 6 and Fig. 3). Both crystal structures contain dimeric units with the individual molecules linked by N—H···O hydrogen bonds about crystallographic (*trans* isomer) or approximate (*cis* isomer) inversion centres. In the *trans* isomer these dimeric units are linked to one another along both the *b* and *c* axes by pairs of N—H···O hydrogen bonds and bridging OH···(H)O—H···O hydrogen-bonded water molecules, forming infinite sheets. In the *trans* isomer the protonated carboxylic acid group is strongly hydrogen-bonded to the water molecule (H···O = 1.57(3), O···O = 2.586(2) Å). The dimeric units in the *cis* isomer are also cross-linked by hydrogen bonds to form infinite sheets parallel to the *ab* plane, but the hydrogen bonding between dimers is different from that

TABLE 5. Torsion angles (deg)[a]

(*a*) Intra-annular

	cis-**4**		*trans*-**5**	
	Mol. A	Mol. B	Major	Minor
C(5)—C(1)—C(2)—C(3)	−41.3(3)	43.9(3)	29.6(2)	29.6(2)
C(1)—C(2)—C(3)—C(4)	24.8(4)	−30.9(4)	−42.9(3)	−13.3(4)
C(2)—C(3)—C(4)—C(5)	1.2(5)	5.6(5)	38.6(4)	−9.1(5)
C(3)—C(4)—C(5)—C(1)	−26.9(4)	21.8(5)	−20.8(4)	28.0(5)
C(4)—C(5)—C(1)—C(2)	41.9(4)	−40.4(4)	−5.5(3)	−36.7(4)

(*b*)

	cis-**4**		
	Mol. A	Mol. B	*trans*-**5**
N(1)—C(1)—C(2)—C(7)	−52.4(4)	52.2(4)	−82.0(2)
N(1)—C(1)—C(2)—C(3)	73.6(4)	−72.0(4)	148.9(1)
N(1)—C(1)—C(2)—H	−173.0	174.0	33.0(1)
C(6)—C(1)—C(2)—C(7)	70.1(4)	−69.5(4)	38.8(2)
C(6)—C(1)—C(2)—C(3)	−163.8(3)	166.3(3)	−90.2(2)
C(6)—C(1)—C(2)—H	−50.0	52.0	154.0(1)
C(5)—C(1)—C(2)—C(7)	−167.1(3)	168.1(3)	158.7(1)
C(5)—C(1)—C(2)—H	72.0	−70.0	−86.0(1)

[a]These angles refer to the 1*S*,2*R* and 1*R*,2*S* isomers, respectively, for the two independent molecules (A and B) of "*cis*-**4**" and to the 1*S*,2*S* isomer for "*trans*-**5**".

TABLE 6. Hydrogen bonding parameters (distance in Å, angles in degrees)

Interaction[a]	N/O—H	O···H	N/O···O	N/O—H···O
		cis Isomer		
N(1)—H(1)···O(10)^{7}	0.98	2.02	2.856(5)	142
N(1)—H(2)···O(9)^{8}	0.98	2.04	2.973(5)	143
N(1)—H(3)···O(3)^{1}	0.98	2.06	2.777(5)	129
N(1)—H(3)···O(5)^{1}	0.98	2.12	2.859(6)	131
N(2)—H(4)···O(9)^{9}	0.98	2.01	2.837(5)	141
N(2)—H(4)···O(10)^{10}	0.98	2.04	2.971(6)	158
N(2)—H(6)···O(1)^{1}	0.98	2.08	2.816(6)	130
N(2)—H(6)···O(7)^{1}	0.98	2.13	2.773(6)	121
O(4)—H(7)···O(2)^{10}	0.98(5)	1.51(5)	2.478(4)	170(5)
O(6)—H(8)···O(8)^{7}	1.08(8)	1.47(8)	2.455(4)	148(7)
O(9)—H(10)···O(5)^{1}	0.98	2.14	2.923(5)	136
O(9)—H(10)···O(3)^{1}	0.98	2.23	3.031(5)	138
O(10)—H(11)···O(7)^{1}	0.98	2.13	3.005(5)	148
O(10)—H(12)···O(1)^{1}	0.98	2.14	2.953(5)	140
O(10)—H(12)···O(3)^{9}	0.98	2.28	2.890(4)	119
		trans Isomer		
O(4)—H(1)···O(5)^{1}	1.04(3)	1.57(3)	2.586(2)	167(3)
N—H(2)···O(1)^{2}	0.98(3)	1.87(3)	2.836(2)	170(2)
N—H(3)···O(2)^{3}	1.04(2)	1.73(2)	2.765(2)	175(2)
N—H(4)···O(3)^{4}	0.96(3)	1.99(3)	2.893(2)	157(2)
O(5)—H(13)···O(1)^{5}	0.86(3)	1.99(4)	2.810(2)	161(3)
O(5)—H(13)···O(2)^{6}	0.90(4)	2.00(4)	2.821(2)	151(3)

[a]Superscripts refer to symmetry operations (1) x, y, z; (2) $-x$, $-y$, 1-z; (3) x, 1/2-y, 1/2+z; (4) $-x$, 1−y, 1-z; (5) $-x$, 1/2+y, 1/2-z; (6) x, 1+y, z; (7) 1/2+x, 1-y, z; (8) x-1/2, 1-y, z; (9) x-1/2, $-y$, z; (10) 1/2+x, $-y$, z.

Can. J. Chem. Downloaded from www.nrcresearchpress.com by 88.255.202.194 on 09/08/12
For personal use only.

Can. J. Chem. Downloaded from www.nrcresearchpress.com by 88.255.202.194 on 09/08/12
For personal use only.

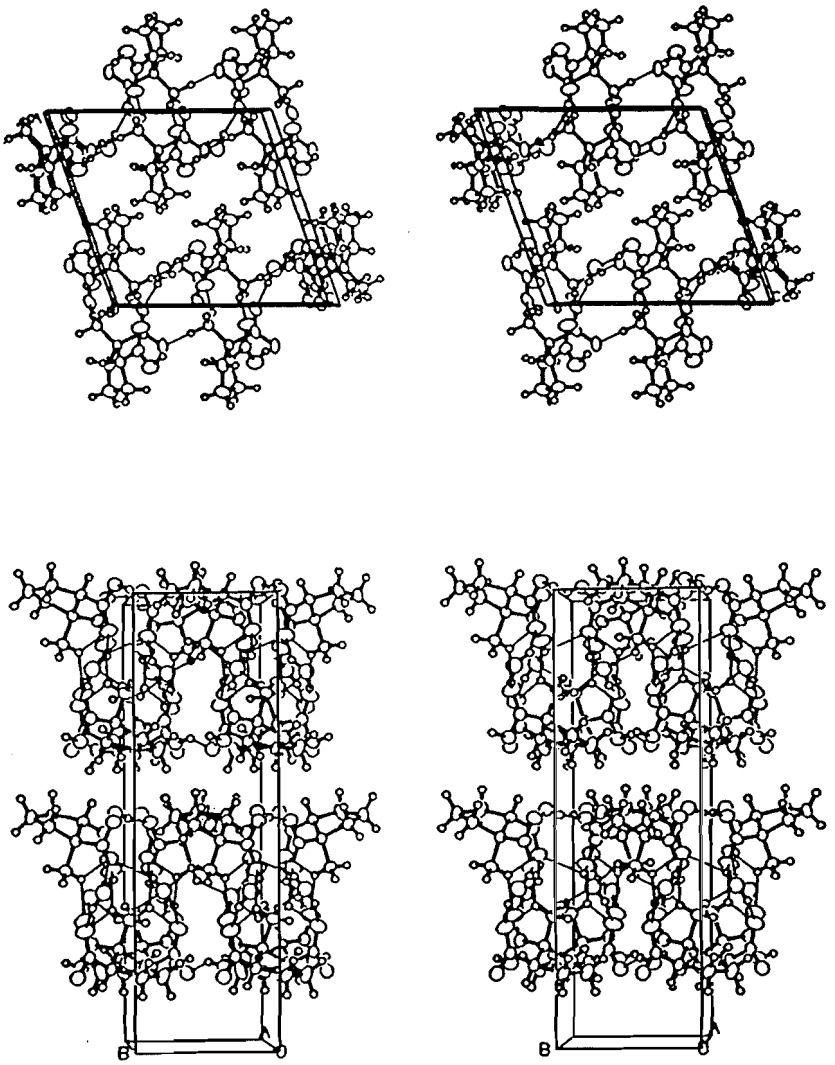

FIG. 3. Packing arrangements for *trans*- and *cis*-1-amino-1,2-cyclopentanedicarboxylic acids.

observed in the structure of the *trans* isomer. Molecules A are linked head-to-tail along *a* by very strong (O···H = 1.51(5), O···O = 2.478(3) Å) hydrogen bonds between protonated and deprotonated carboxylate groups. Molecules B are also linked to one another by the same type of hydrogen bond (O···H = 1.47(8), O···O = 2.455(3) Å), but to dimers translated along the *b* axis with respect to those linked through molecules A. In addition, the dimers in the *cis* isomer are bridged along both *a* and *b* by pairs of bridging $(O\cdots H_2O\cdots HN)_2$ hydrogen-bonded water molecules (O···N = 2.837(5)–2.973(5), O···O = 2.890(4)–3.031(5) Å). The existence of extra bifurcated hydrogen-bonding interactions (1.5 per molecule) in the structure of the *cis* isomer, along with other packing considerations (especially the orientation of the cyclopentane rings with respect to the hydrophobic channels between the hydrogen-bonded layers), is probably responsible for the higher density of the *cis* isomer in the solid state.

As a result of the very strong (O)CO···H···OC(O) hydrogen bonding in the *cis* isomer (see Table 6) the distinction between the COO^- and COOH groups becomes somewhat ambiguous. In molecule A, with the longer O···O distance, the C—O bond lengths (C(7)—O(4) = 1.289(4) and C(6)—O(2) = 1.248(5) Å) and the location of the refined hydrogen atom H(7) (bonded to O(4)) are consistent with protonation of the C(7) carboxylate group. In molecule B, the O···O distance in the strong hydrogen bond is 0.023(5) Å shorter than in molecule A and the two C—O distances involved are not significantly different (C(13)—O(6) = 1.266(5) and C(14)—O(8) = 1.273(4) Å). However, the hydrogen atom H(8) involved in this interaction refined to a position nearer to O(6), the oxygen atom having the shorter C—O bond. In view of the relatively large thermal parameter for H(8) and the near equivalence of the dimensions of the C(13) and C(14) carboxylate moieties, it is likely that the O(6)···H(8)···O(8) interaction is symmetric. The COO^- and COOH functions are clearly distinguished in the *trans* isomer with C—O bond lengths of 1.247(2) and 1.252(2) Å in the former and C—O(H) and C=O distances of 1.301(2) and 1.212(2) Å in the latter.

Acknowledgments

We are indebted to Dr. J. T. Edward for much valuable discussion, to Marrietta Austria for ^{13}C NMR spectra, and

to P. Borda for elemental analysis. This work has been supported by grants to H. McLennan and K. Curry from the Medical Research Council of Canada and by grants to J. Trotter from the Natural Sciences and Engineering Research Council of Canada.

1. K. Curry, D. S. Magnuson, H. McLennan, and M. J. Peet. Neurosci. Lett. **66**, 101 (1986).
2. M. J. Peet, K. Curry, D. S. K. Magnuson, and H. McLennan. Neuroscience, **22**, 563 (1987).
3. K. Curry, D. S. K. Magnuson, H. McLennan, and M. J. Peet. Can. J. Physiol. Pharmacol. **65**, 2196 (1987).
4. K. Curry, M. J. Peet, D. S. K. Magnuson, and H. McLennan. J. Med. Chem. **31**, 864 (1988).
5. T. A. Connors and W. C. J. Ross. J. Chem. Soc. 2119 (1960).
6. F. L. Chubb, J. T. Edward, and S. C. Wong. J. Org. Chem. **45**, 2315 (1980).
7. G. G. Trigo, E. S. Avendano, E. Santos, J. T. Edward, and S. C. Wong. Can. J. Chem. **57**, 1456 (1979).
8. J. T. Edward and C. Jitrangsri. Can. J. Chem. **53**, 3339 (1975).
9. International tables for X-ray crystallography. Vol. IV. Kynoch Press, Birmingham, U.K. (present distributor Kluwer Academic Publishers, Dordrecht, The Netherlands). 1974. pp. 99–102 and 149.

Can. J. Chem. Downloaded from www.nrcresearchpress.com by 88.255.202.194 on 09/08/12
For personal use only.

Cobalt(II) catalyzed oxidation of 2-substituted 1,3-dioxolanes with molecular oxygen[1]

PEI LI AND HOWARD ALPER[2]

Ottawa–Carleton Chemistry Institute, Department of Chemistry, University of Ottawa, Ottawa, Ont., Canada K1N 6N5

PEI LI and HOWARD ALPER. Can. J. Chem. **71**, 84 (1993).

Cobalt(II) chloride catalyzed oxidation of 2-substituted 1,3-dioxolanes in 1,2-dimethoxyethane afforded formate esters and acids in high yields. It was found that the presence of catalytic amounts of $ZnCl_2$ increased the rate of oxidation. A free-radical mechanism is proposed, involving participation of superoxocobalt, and the esterification of the alcohol and acid.

PEI LI et HOWARD ALPER. Can. J. Chem. **71**, 84 (1993).

L'oxydation des 1,3-dioxolanes substitués en position-2, effectuée dans le 1,2-diméthoxyéthane et catalysée par le chlorure de cobalt(II), fournit des esters formiques et des acides avec des rendements élevés. On a trouvé que la présence de quantités catalytiques de $ZnCl_2$ augmente la vitesse d'oxydation. On propose un mécanisme radicalaire impliquant le superoxocobalt et l'estérification de l'alcool et de l'acide.

[Traduit par la rédaction]

Introduction

An impressive part of the chemistry of carbohydrates has dealt with acetals, and especially cyclic acetals. Many studies have focussed on the synthesis of cyclic acetals as temporary protecting groups for aldehydes and ketones. However, during the past few years, the role of acetals has been changing. The cleavage of cyclic acetals to afford synthetically useful derivatives has been investigated in some depth, and some of the routes have already proven to be major tools for structural modifications (1). Therefore, cyclic acetals may now be considered not only as classical protecting groups, but also as reactive functional groups (1, 2).

In 1971, Deslongchamps and Moreau (3) first discovered that ozone reacts readily with acetals to give the corresponding esters in high yield. For example, acetal **1** in dichloromethane or ethyl acetate reacts quantitatively with ozone, in 10 min at −78°C, to give the β-hydroxy ester **2** (eq. [1]).

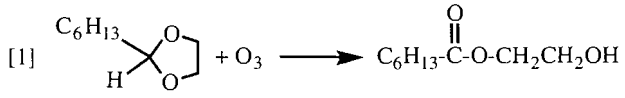

[1] C_6H_{13}-(dioxolane-H)-O + O_3 ⟶ C_6H_{13}-C(=O)-O-CH_2CH_2OH

1 **2** (98%)

The mechanism of the oxidation of acetals by ozone has been extensively studied (4–7), and it has been proposed that ozone inserts into the C—H bond of the acetal to give a hydrotrioxide intermediate, which in turn affords the corresponding hydroxy ester (Scheme 1). More recently, the oxidation of dioxolanes by nitrogen tetroxide (N_2O_4) was reported to give glycol esters in 85–92% yield (8). The reactions are believed to proceed via a free-radical chain mechanism.

There is very little information in the literature about the metal-catalyzed oxidation of acetals. Only one paper by Kuramshin *et al.* (9) reported that homogeneous cobalt catalyzed oxidation of 1,3-dioxacyclanes in the presence of

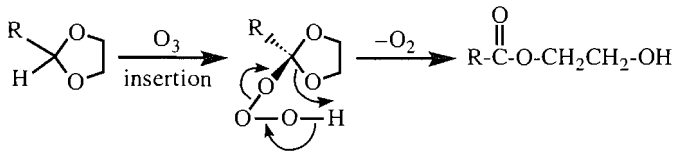

SCHEME 1

acetic acid and chlorobenzene under an oxygen atmosphere resulted in the formation of β-hydroxy esters. Although the oxidation of acetals by ozone or other oxidants has been well established and used in organic syntheses, these methods suffer from one serious drawback, lack of selectivity. For example, if acetal derivatives contain other oxidizable groups, the reactions with ozone usually result in a mixture of products. Furthermore, the noted catalytic oxidation of acetals by cobalt was carried out in an acidic medium. This limits its application to those acetals which are sensitive to the pH of the solution.

The goal of the present research was to develop a catalytic process to selectively oxidize cyclic acetals to the corresponding ester derivatives in a neutral medium under oxygen. The scope and limitation of this new reaction was investigated using a variety of 1,3-dioxolanes.

Results and discussion

Treatment of 1,3-dioxolane with atmospheric oxygen in 1,2-dimethoxyethane (DME) containing a catalytic amount of anhydrous cobalt(II) chloride (substrate:Co^{2+} = 200:1) for 24 h at 60°C gave ethylene glycol monoformate in 61% yield along with 10% ethylene carbonate (eq. [2]).

However, when the oxidation of phenylacetaldehyde ethylene acetal was performed under similar reaction condi-

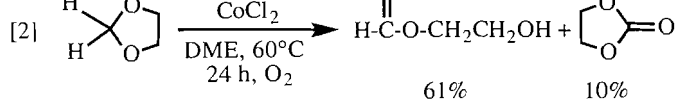

[2] (dioxolane-H)-O $\xrightarrow[\text{DME, 60°C}]{\text{CoCl}_2}$ H-C(=O)-O-CH_2CH_2OH + (dioxolanone)=O

24 h, O_2 61% 10%

tions, but using a 100:1 ratio of substrate:$CoCl_2$, the expected product, ethylene glycol benzoate (**3**), was not the major product. Instead, two new compounds were observed (**4** and **5**).

[1]Dedicated to the memory of Professor Jean-Louis Roustan; an outstanding educator, a sensitive, caring undergraduate-student advisor, and a wonderful colleague.

[2]Author to whom correspondence may be addressed.

Can. J. Chem. Downloaded from www.nrcresearchpress.com by 88.255.202.194 on 09/08/12
For personal use only.

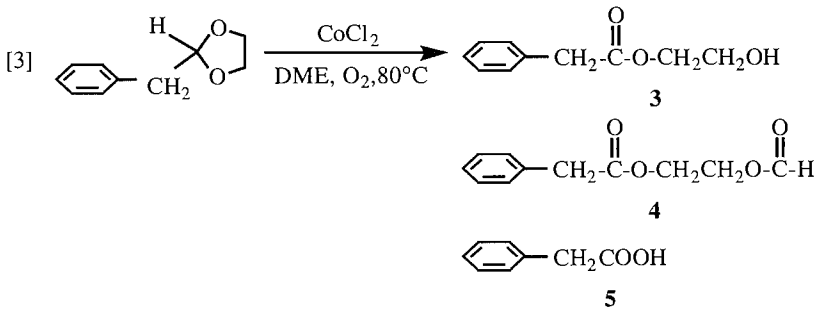

The formation of products **4** and **5** was unexpected, especially **4**, which contains an additional carbon atom. There are two possibilities; either **3** has reacted with solvent (DME) or with itself. As a check, the oxidation of phenylacetaldehyde ethylene acetal was carried out in the presence of 1,4-dioxane instead of DME. It was found that **4** and **5** were still the major products after reaction for 42 h at 85–90°C. This result clearly indicates that the extra carbon of compound **4** was not from DME.

During the reaction, **3** was observed to be the major product formed within 20 h. It slowly disappeared with increasing reaction time and, after 56 h, only **4** and **5** were present. This result indicates that phenylacetaldehyde ethylene acetal can be oxidized to compounds **4** and **5** in a one-step reaction. Such oxidation is very useful because (1) it results in homologation, and (2) two functional groups are introduced simultaneously, one of which is the formate ester. Therefore, research was focussed on determining the optimum reaction conditions to achieve a high yield of **4** and **5**, and the use of such conditions to oxidize a variety of 2-substituted 1,3-dioxolanes to the corresponding formate esters and acids.

Effect of catalyst

A series of metal catalysts were investigated for the oxidation of phenylacetaldehyde ethylene acetal to compounds **4** and **5**. The first group of metal catalysts examined was $FeCl_3$, $CrCl_3$, and $CoCl_2$. It was found that the catalytic effect of these metal complexes increases in the order $FeCl_3 < CrCl_3 < CoCl_2$. In other words, cobalt chloride has reached the highest reactivity towards oxidation. The second group of metal catalysts examined were cobalt complexes containing a variety of ligands including $Co(OAc)_2$, $Co(OCOPh)_2$, $CoCl_2(PPh_3)_2$, $CoBr_2$, $Co(NO_3)_2{\cdot}4H_2O$, and $CoSO_4{\cdot}7H_2O$. Anhydrous $CoCl_2$ was again found to be the most effective catalyst, with $CoSO_4{\cdot}7H_2O$ being inactive. It is noteworthy that $CoBr_2$ results initially at a higher rate than anhydrous $CoCl_2$. For example, after 2 h, reaction in the presence of $CoBr_2$ reached 56% conversion, whereas the use of anhydrous $CoCl_2$ resulted in 45% conversion. However, the catalytic efficiency of $CoBr_2$ as the catalyst apparently decreased after 4 h. As a result, considering the completion of the reaction, $CoCl_2$ is a better catalyst than $CoBr_2$.

Effect of reaction temperature

Increasing the reaction temperature results in a substantial increase in reaction rate (see Table 1). Since the boiling point of DME is 85°C, the oil bath temperature should not exceed 90°C. Otherwise, solvent loss may occur under a flow of oxygen.

TABLE 1. Effect of reaction temperature[a]

T (°C) (oil bath)	Time (h)	Conversion (%)
45–50	28	42
60–65	28	68
85–90	23	100

[a]Reaction conditions: phenylacetaldehyde ethylene acetal (2.5 mmol), anhydrous $CoCl_2$ (0.1 mmol), DME (15 mL).

TABLE 2. Effect of concentration of $CoCl_2$ on the oxidation of phenylacetaldehyde ethylene acetal[a]

Substrate:$CoCl_2$ (mmol)	Time (h)	Conversion (%)	Product ratio[b] (**3**/**4**)
50:1	42	100	1:5
25:1	41	100	1:6
10:1	41	100	1:5.3

[a]Reaction conditions: acetal (5 mmol), DME (15 mL), 85–90°C.
[b]Determined by gas chromatography.

Effect of concentration of anhydrous cobalt chloride

During the oxidation reactions, it was found that the starting material was completely converted after approximately 1 day at 85–90°C. However, the rate of disappearance of glycol ester **3** was quite slow, with 56 h needed to achieve completion of the reaction. Thus it was of interest to determine whether the concentration of $CoCl_2$ influences the rate of disappearance of glycol ester **3**. The results (Table 2) demonstrate that the concentration of cobalt chloride has no significant effect on the rate of further oxidation of glycol ester **3**. Among these experiments, the use of a 25:1 ratio of substrate to $CoCl_2$ seemed to give the best ratio between **3** and **4**.

Effect of additives

Attempts were made to enhance the rate of oxidation of **3** to **4** by the addition of a Lewis acid ($ZnCl_2$), Lewis base (pyridine), or a dehydration agent (4A molecular sieves). The results are presented in Table 3.

It was observed that the addition of a catalytic amount of $ZnCl_2$ dramatically enhanced the rate of oxidation of glycol ester. However, the addition of pyridine and molecular sieves either had no effect or led to negative results. At this point,

Can. J. Chem. Downloaded from www.nrcresearchpress.com by 88.255.202.194 on 09/08/12
For personal use only.

TABLE 3. Effect of additives on further oxidation of the glycol ester **3**[a]

Additives	Substrate:additives	Time (h)	Conversion (%)	Product ratio[b] **3/4**
—	—	41	100	1/16
Pyridine	1:1.2 (mmol)	35	67	1/2
$ZnCl_2$	10/1 (mmol)	28	100	0/1
Molecular sieves	1.6:1 (g)	28	100	1/3.3

[a]Reaction conditions: acetal (5 mmol), $CoCl_2$ (0.2 mmol), DME (15 mL), 85–90°C.
[b]Determined by gas chromatography.

TABLE 4. Oxidation of a variety of 2-substituted 1,3-dioxolanes to their formate esters and acids

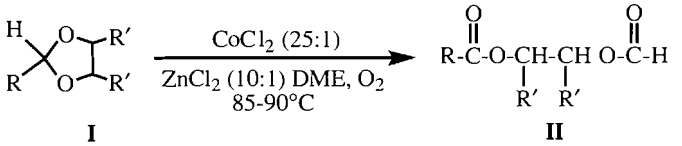

I **II**

+ RCOOH + CO_2

III

Substrates **I**[a] R	R′	T (°C)	Time (h)	Yield (%)[b] **II**	**III**	Other products
C_6H_5	H	85	24	70	85	
$C_6H_5CH_2$	H	90	28	86	91	
n-C_7H_{15}	H	90	30	80	89	
CH_3	H	55	41	79	[c]	
n-C_7H_{15}	CH_3	85	29	38	42	$C_7H_{15}COOCH(CH_3)CH(CH_3)OH$ (34%)
n-C_7H_{15}	*trans*-$COOCH_3$	90	48	No reaction		
trans-C_6H_5CH=CH	H	90	4	—	—	C_6H_5CHO (64%)
			24	—	—	C_6H_5COOH (92%)
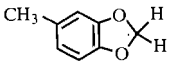		90	48	No reaction		

[a]Ratio of substrate:$CoCl_2$:$ZnCl_2$ was 25:1:2.5.
[b]Isolated yield.
[c]The yield of acetic acid was not determined.

it was necessary to determine whether $CoCl_2$ or $ZnCl_2$ played an essential role in this oxidation. When the oxidation of phenylacetaldehyde ethylene acetal was catalyzed by $ZnCl_2$ (substrate:$ZnCl_2$ = 10:1) in the presence of DME, the rate of oxidation was much slower than that of the reaction catalyzed by $CoCl_2$. Only 21% conversion was obtained after 30 h at 80–90°C. This result indicated that $CoCl_2$ was the key catalyst. The presence of $ZnCl_2$ promoted the rate of further oxidation of the glycol ester.

Results for the conversion of a variety of 2-substituted 1,3-dioxolanes to the corresponding formate esters and acids using a mixed catalyst (substrate:$CoCl_2$:$ZnCl_2$ = 25:1:2.5) system are illustrated in Table 4. Some of the substrates were prepared according to the reaction shown in eq. [4].

The oxidation of 2-phenyl, benzyl, *n*-heptyl, as well as methyl-substituted 1,3-dioxolanes afforded formate esters and acids in high yields. Those 1,3-dioxolanes containing alkyl substituents such as R′ = CH_3 underwent oxidation at a

[4] 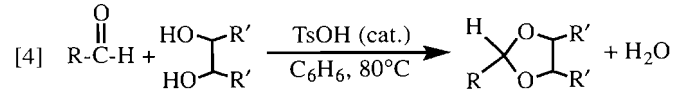

lower rate, and no reaction was observed when electron-withdrawing groups were present. Moreover, when the oxidation of *trans*-cinnamaldehyde ethylene acetal (R = C_6H_5CH=Ch-) was attempted, none of the desired products were observed. Instead, benzoic acid was obtained in 92% yield after 24 h at 90°C. When this reaction was stopped after 4 h, benzaldehyde was produced in 64% yield. Hence, benzoic acid was formed as a result of further oxidation of benzaldehyde. Finally, oxidation of 3,4-(methylenedioxy) toluene did not occur due to the deactivation by the aromatic ring. A possible mechanism for the reaction of 1,3-dioxolanes is outlined in Schemes 2–4. Key to the conversion of the 1,3-dioxolane to the hydroxyester **A** (Scheme 2) is the intermediacy of the 1,3-dioxolanyl radical. The aldehydic

Can. J. Chem. Downloaded from www.nrcresearchpress.com by 88.255.202.194 on 09/08/12
For personal use only.

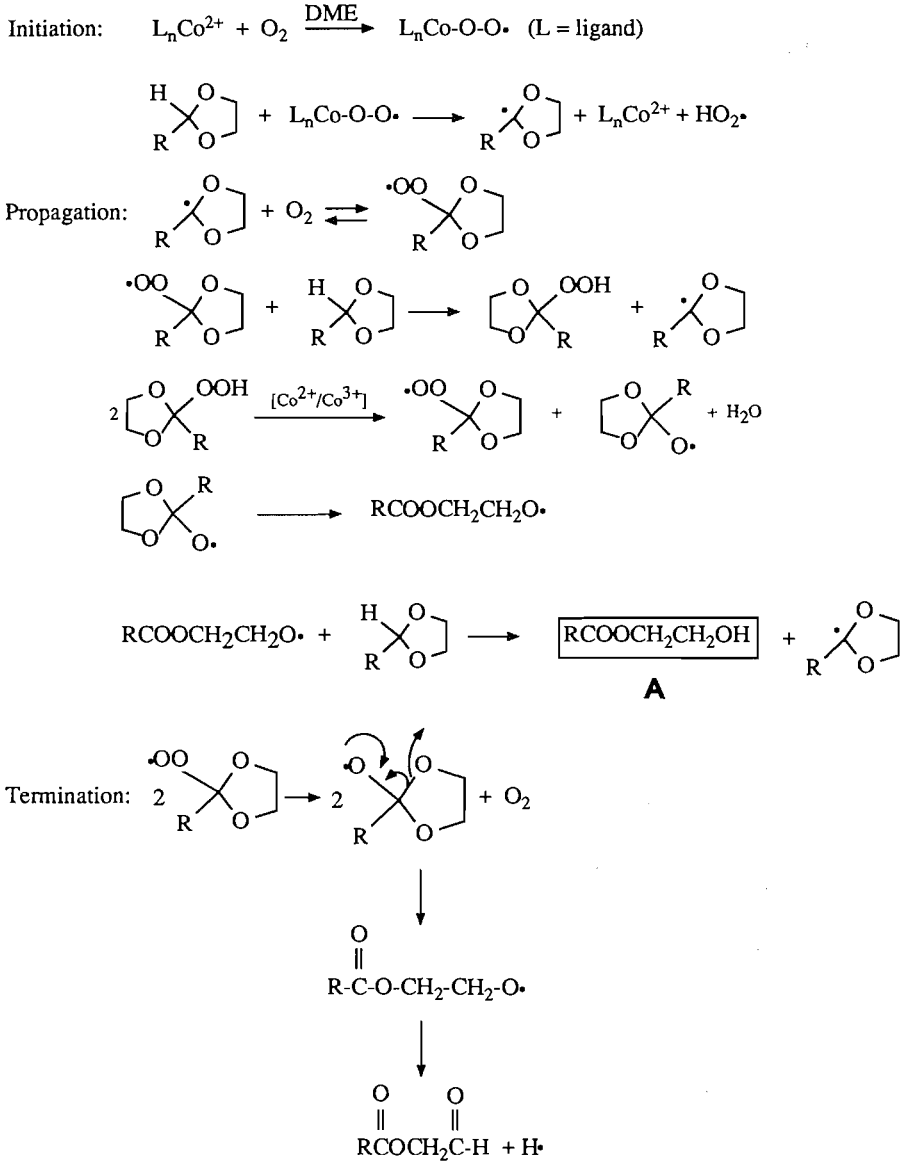

SCHEME 2

ester related to **A**, formed in the termination process, may then be oxidized to **B**. Reaction of the latter with **A** would afford **C** (Scheme 3). Finally the cobalt-induced generation of the radical from **C** followed by fragmentation would form the formate ester and acid (Scheme 4).

A study of the course of these reactions was performed with phenylacetaldehyde ethylene acetal (R = $C_6H_5CH_2$) as substrate. The proposed mechanism receives support from the following evidence:

1. Glycol ester $C_6H_5CH_2COOCH_2CH_2OH$ (**A**, R = Ph-

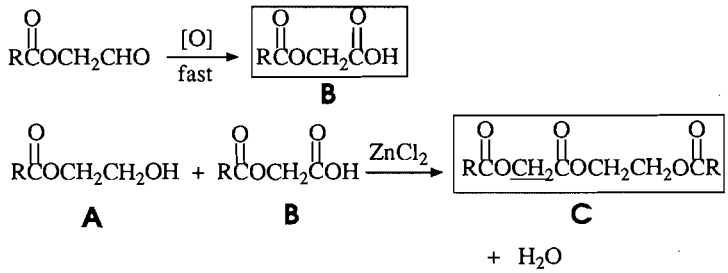

SCHEME 3

Can. J. Chem. Downloaded from www.nrcresearchpress.com by 88.255.202.194 on 09/08/12
For personal use only.

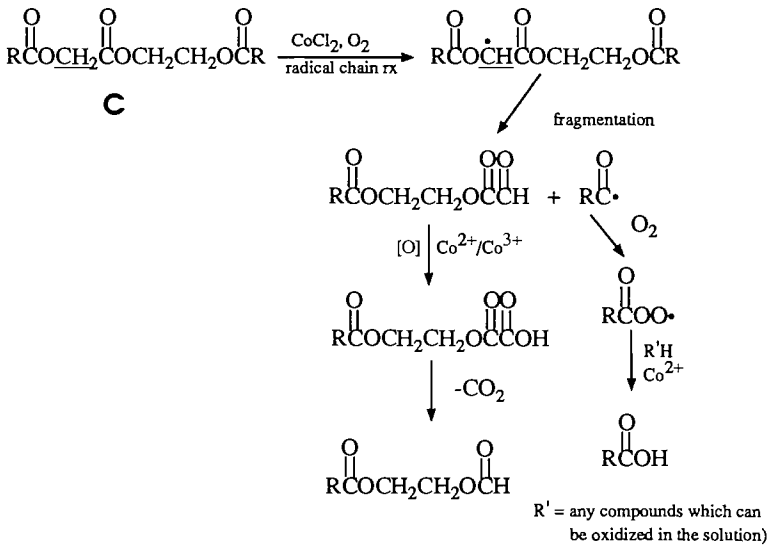

SCHEME 4

CH_2) was isolated as a primary product. When the reaction was carefully followed by GC, it was observed that the peak corresponding to the glycol ester decreased slowly, while those due to the formate ester and acid increased. That is, the glycol ester must be an intermediate and undergo further reaction, affording the formate ester acid.

2. Compound **B** was detected by GC/mass spectrometry: *m/e* 194$[M]^+$; 119$[C_6H_5CH_2CO]^+$; 91$[C_6H_5CH_2]^+$; 59$[CH_2COOH]^+$; 45$[COOH]^+$.

3. Compound **C** was isolated and identified by IR, ^1H NMR, and MS, as well as by elemental analysis. IR($CDCl_3$): $\nu_{C=O}$ 1738, 1730 cm^{-1}; ^1H NMR($CDCl_3$): δ 3.63 (s, 4H, $2C_6H_5\underline{CH_2}$), 4.23 (m, 4H, -$COOCH_2CH_2OCO$-), 4.58 (s, 2H, $PhCH_2\underline{COOCH_2}CO$-), 7.25 (m, 10H, 2Ph). MS: *m/e* 194$[PhCH_2\underline{COO}CH_2COO]^+$, 164$[PhCH_2COOCH_2CH_2]^+$, 118$[C_6H_5CHCO]^+$, 91$[C_6H_5CH_2]^+$.

4. Compounds **B** and **C** disappeared at the end of the reaction.

5. The presence of $ZnCl_2$ greatly enhanced the rate of disappearance of the glycol ester **A**. This result indicated that the glycol ester might react via an esterification process since $SnCl_2$ is known to be an excellent promoter for the esterification step (10).

6. The underlined methylene group in compound **C** could be oxidized by this system. This was tested by the oxidation of a similar type of substrate (ethyl acetoxy acetate). During the oxidation, the decomposition of this compound to smaller molecules was observed with an alcohol intermediate analyzed by GC/MS (*m/e* 89$[CH_3COOCHOH]^+$, 59$[CH_3COO]^+$). The reaction mixture was acidic and CO_2 evolution was determined.

7. Carbon dioxide evolution was determined by bubbling the evolved gases through a solution and a white precipitate of $BaCO_3$ was formed.

In conclusion, 2-substituted 1,3-dioxolanes can be oxidized to the corresponding formate esters and acids in high yields. This process is effectively catalyzed by anhydrous $CoCl_2$ and $ZnCl_2$ (substrate:$COCl_2$:$ZnCl_2$ = 25.1:1:2.5) in the presence of DME, and has the following advantages:

1. Aldehydes can be converted to formate esters and acids via a two-step reaction: (*a*) the preparation of acetal from the aldehyde, and (*b*) the oxidation of the acetal.

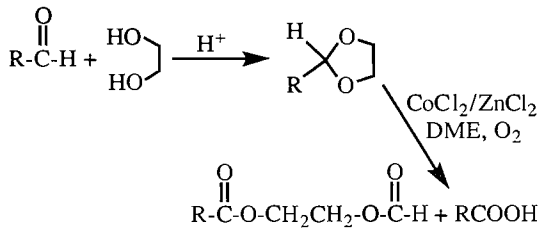

2. The oxidation of acetals is a novel method for preparing synthetically useful products.

Experimental section

Infrared spectra were recorded using a Perkin–Elmer 783 spectrometer. Proton magnetic resonance spectra were obtained with a Varian T60, EM360A, GEMINI 200, or XL300 spectrometer, whereas carbon magnetic resonance spectra were recorded on a Varian XL-300 or GEMINI 200 spectrometer. Mass spectral and gas chromatographic – mass spectrometric determinations were made with a VG-7070E spectrometer and a Varian 3300 chromatograph, fitted with a Megabore DB5 capillary column in tandem with the VG-7070E spectrometer, respectively. Analyses by gas chromatography were carried out with programmable Varian Vista 6000 or 3400 gas chromatographs equipped with flame ionization detectors and a Varian 4270 integrator. Glass columns (3 cm) packed with 3% OV101 or 3% OV-17 on Chromosorb W 80–100 mesh were utilized for gas chromatographic determinations.

The organometallic complexes and most organic chemicals were purchased from Fisher Scientific Company, Alfa Products Company, and Aldrich Chemical Company. They were used as received in almost all cases. Oxygen was obtained from Air Products Company. Solvents employed for extraction were distilled following standard procedures.

General procedure for the oxidation of 2-substituted 1,3-dioxolanes

A mixture of anhydrous $CoCl_2$ (0.027 g, 0.2 mmol) and $ZnCl_2$ (0.068 g, 0.5 mmol) in DME (15 mL) was stirred under oxygen atmosphere at 85–90°C for several minutes. The 2-substituted 1,3-dioxolane (5 mmol) was then added, and stirring was continued until conversion of the substrate was almost complete (GC determina-

Can. J. Chem. Downloaded from www.nrcresearchpress.com by 88.255.202.194 on 09/08/12
For personal use only.

Can. J. Chem. Downloaded from www.nrcresearchpress.com by 88.255.202.194 on 09/08/12
For personal use only.

tion). The following work-up was used in all cases: the reaction mixture was cooled to room temperature, filtered through a small silica column to remove the pink precipitate, and the filtrate was concentrated by rotary evaporation. To the residue was added 20 mL distilled water, and the solution was basified with 5 N NaOH. This solution was then extracted with ether (3 × 20 mL). The organic phase was washed with distilled water (50 mL), and dried ($MgSO_4$). The dried organic phase was concentrated and afforded an oily crude product, which was purified by thin-layer chromatography. The aqueous phase was acidified with dilute hydrochloric acid and extracted with ether (3 × 20 mL). Drying and concentration of this ethereal extract yielded a white solid, which was purified by recrystallization. Pure products were characterized by IR, ^1H and ^{13}C NMR, as well as by mass spectrometry. The results are listed in Table 4.

Several of the products are known materials. Their structures were identified by comparing the spectral data with that for authentic materials. The following data were obtained for the other products.

I, *R* = C_6H_5, *R'* = *H*

*$C_6H_5COOCH_2CH_2OCHO$ (**II**):* IR: $\nu_{C=O}$ 1735, 1720 cm^{-1}, ν_{C-O} 1282, 1170 cm^{-1}; ^1H NMR($CDCl_3$) δ: 3.95 (t, 2H, -CH_2CH_2O-CHO), 4.45 (t, 2H, PhCOOCH_2CH_2-), 7.48 (m, 3H, *meta* and *para* protons), 8.04 (m, 2H, *ortho* protons), 8.10 (s, 1H, -OCHO); MS: *m/e* 194[M]$^+$, 105[C_6H_5CO]$^+$, 77[C_6H_5].

Two other by-products were also isolated. They were identified as follows:

$C_6H_5COOCH_2CH_2OH$ (1% yield): IR($CDCl_3$): ν_{OH} 3440 cm^{-1}, $\nu_{C=O}$ 1720 cm^{-1}, ν_{C-O} 1280, 1122 cm^{-1}; ^1H NMR($CDCl_3$) δ: 2.40 (2, 1H, OH), 3.92 (t, 2H, CH_2OH), 4.43 (t, 2H, $COOCH_2$), 7.43 (m, 2H, *meta* protons), 7.52 (m, 1H, *para* proton), 8.03 (m, 2H, *ortho* protons); ^{13}C NMR($CDCl_3$) δ: 61.19 (-CH_2OH), 66.53 ($COOCH_2$-), 128.43, 129.70, 129.84, 133.22, (aromatic carbons), 167.09 (-COO-); MS *m/e* 148[M − H_2O]$^+$, 105[C_6H_5CO]$^+$, 77[C_6H_5]$^+$.

$C_6H_5COOCH_2CH_2OCH_3$ (1.5% yield): IR($CDCl_3$): $\nu_{C=O}$ 1718 cm^{-1}, ν_{C-O} 1276 cm^{-1}, 1115 cm^{-1}; ^1H NMR($CDCl_3$) δ: 3.42 (s, 3H, OCH_3), 3.71 (t, 2H, CH_2OCH_3), 4.46 (t, 2H, $COOCH_2$), 7.42 (m, 2H, *meta* protons), 7.53 (m, 1H, *para* proton), 8.05 (m, 2H, *ortho* protons); MS *m/e* 105[C_6H_5CO]$^+$, 77(C_6H_5]$^+$.

I, *R* = $C_6H_5CH_2$, *R'* = *H*

*$C_6H_5CH_2COOCH_2CH_2OCHO$(**II** or **4**):* IR(neat): $\nu_{C=O}$ 1730, 1738 cm^{-1}, ν_{C-O} 1255, 1165 cm^{-1}; ^1H NMR($CDCl_3$) δ: 3.64 (s, 2H, $C_6H_5CH_2CO$-), 4.34 (d, 4H, $COOCH_2CH_2O$), 7.29 (m, 5H, Ph), 8.02 (s, 1H, -OCHO); ^{13}C NMR($CDCl_3$) δ: 40.88 ($C_6H_5CH_2$), 61.33, 62.05 ($COOCH_2$, CH_2OCHO), 127.23, 128.63, 129.29, 133.80 (aromatic carbons), 160.67 (OCHO), 171.50 ($C_6H_5CH_2$-COO-); MS: *m/e* 208[M$^+$], 162[M − HCOOH]$^+$, 119[$C_6H_5CH_2$-CO]$^+$, 91[$C_6H_5CH_2$]$^+$.

Glycol ester ($C_6H_5CH_2COOCH_2CH_2OH$): IR($CDCl_3$, **3**): ν_{OH} 3440 cm^{-1}, $\nu_{C=O}$ 1735 cm^{-1}, ν_{C-O} 1161, 1080 cm^{-1}; ^1H NMR($CDCl_3$) δ: 2.48 (s, 1H, OH), 3.65 (s, 2H, $C_6H_5CH_2$-), 3.77 (t, 2H, -CH_2OH), 4.20 (t, 2H, -$COOCH_2$-), 7.28 (m, 5H, C_6H_5). MS: *m/e* 180[M]$^+$, 162[M − H_2O]$^+$, 118[C_6H_5CHCO]$^+$.

I, *R* = n-C_7H_{15}, *R'* = *H*

*$C_7H_{15}COOCH_2CH_2OCHO$ (**II**):* IR(neat): $\nu_{C=O}$ 1735 cm^{-1}, ν_{C-O} 1160 cm^{-1}, 1114 cm^{-1}; ^1H NMR($CDCl_3$) δ: 0.84 (t, 3H, CH_3CH_2-), 1.25 (m, 8H, (-CH_2-)$_4$), 1.58 (m, 2H, -CH_2CH_2COO-), 2.30 (t, 2H, -CH_2CH_2COO-), 4.32 (m, 4H, -$COOCH_2CH_2OCHO$), 8.05(s, 1H, -OCHO); ^{13}C NMR($CDCl_3$) δ: 13.82, 22.36, 24.62, 28.68, 28.83, 31.43, 33.87 (C_7H_{15}), 61.47, 61.53 ($COOCH_2CH_2OCHO$), 160.70 (O-CHO), 173.7 ($C_7H_{15}COO$-); MS: *m/e* 127[$C_7H_{15}CO$]$^+$, 73[CH_2CH_2OCHO]$^+$.

$C_7H_{15}COOH$: IR(neat): ν_{COO-H} 3500–2500 cm^{-1}, $\nu_{C=O}$ 1713 cm^{-1}, ν_{C-O} 1208 cm^{-12}; MS: *m/e* 144[M]$^+$, 60[CH_2=C(OH)$_2$]$^+$.

The intermediate glycol ester ($C_7H_{15}COOCH_2CH_2OH$) was isolated in 3% yield. IR($CDCl_3$): ν_{OH} 3452 cm^{-1}, $\nu_{C=O}$ 1172, 1085 cm^{-1}; ^1H NMR($CDCl_3$) δ: 0.84 (t, 3H, -CH_2CH_3), 1.25 (m, 8H, -(CH$_2$)$_4$-), 1 .58 (m, 2H, -CH_2CH_2COO-), 2.11 (s, 1H, -OH), 2.30 (t, 2H, -CH_2CH_2COO-), 3.76 (t, 2H, $COOCH_2CH_2OH$), 4.16 (t, 2H, -$COOCH_2CH_2OH$); ^{13}C NMR($CDCl_3$) δ: 13.81, 22.36, 24.68, 28.69, 28.86, 31.43, 33.98 (C_7H_{15}), 61.14 (-CH_2OH), 65.77 (-$COOCH_2$), 174.43 (COO); MS: *m/e* 84[CH_2=CH-CH_2CH_2-CH_2CH_3]$^+$.

I, *R* = CH_3, *R'* = *H*

*$CH_3COOCH_2CH_2OCHO$ (**II**):* IR(neat): $\nu_{C=O}$ 1730, 1740 cm^{-1}, ν_{C-O} 1240, 1178 cm^{-1}; ^1H NMR($CDCl_3$) δ: 2.06 (s, 3H, -$COCH_3$), 4.26 (m, 2H, CH_2OCHO), 4.34 (m, 2H, CH_3COOCH_2), 8.02 (s, 1H, OCHO); MS: *m/e* 86[CH_2=CH-O-$COCH_3$]$^+$, 73[$HCOOCH_2CH_2$]$^+$, 43[CH_3CO]$^+$.

I, *R* = n-C_7H_{15}, *R'* = CH_3

*$C_7H_{15}COOCH$—CH—$OCHO$ (**II**):*

IR($CDCl_3$): $\nu_{C=O}$ 1735, 1728 cm^{-1}, ν_{C-O} 1175, 1110 cm^{-1}; ^1H NMR($CDCl_3$) δ: 0.83 (t, 3H, CH_2CH_3), 1.21 (m, 14H, (-CH_2-)$_4$, 2CH_3), 1.58 (m, 2H, -CH_2CH_2COO-), 2.28 (t, 2H, -CH_2CH_2COO-), 5.03 (m, 2H, $CH(CH_3)CH(CH_3)$), 8.05 (s, 1H, OCHO); ^{13}C NMR($CDCl_3$) δ: 13.6, 21.2, 24.9, 28.5, 28.8, 31.5, 34.3 (C_7H_{15}), 15.8 (2CH_3), 70.8, 71.2 [$C_7H_{15}COOCH(CH_3)$ and $CH(CH_3)OCHO$], 160.3 (-OCHO), 172.1 ($C_7H_{15}COOCH(CH_3)$); MS: *m/e* 127[$C_7H_{15}CO$]$^+$.

The β-hydroxy ester [$C_7H_{15}COOCH(CH_3)CH(CH_3)OH$] was also isolated in 34% yield. IR($CDCl_3$): ν_{OH} 3465 cm^{-1}, $\nu_{C=O}$ 1728 cm^{-1}, ν_{C-O} 1170, 1105 cm^{-1}; ^1H NMR($CDCl_3$) δ: 0.83 (t, 3H, -CH_2CH_3), 1.13 (m, 14H, (-CH_2-)$_4$,2-CH_3), 1.56 (m, 2H, $C_5H_{11}CH_2CH_2COO$-), 2.26 (s, 1H, OH), 2.28 (t, 2H, C_6H_{13}-CH_2COO-), 3.69 (m, 1H, -$CH(CH_3)OH$), 4.70 (m, $C_7H_{15}COOCH$-(CH_3)); ^{13}C NMR($CDCl_3$) δ: 13.85, 22.45, 24,95, 28.86, 29.16, 31.46, 334.38 (C_7H_{15}), 16.05, 18.90 (2CH_3), 69.97 ($CH(CH_3)OH$), 75.54 ($C_7H_{15}COOCH(CH_3)$), 173.89 ($C_7H_{15}COO$-); MS *m/e* 127[$C_7H_{15}CO$]+.

1,3-Dioxolane

Ethylene carbonate: IR($CDCl_3$): $\nu_{C=O}$ 1800 cm^{-1}, ν_{C-O} 1280, 1118 cm^{-1}; MS: *m/e* 88[M]$^+$, 43[COOH]$^+$.

Glycol formate ($HCOOCH_2CH_2OH$): IR(neat): ν_{OH} 3400 cm^{-1}, $\nu_{C=O}$ 1720 cm^{-1}, ν_{C-O} 1180, 1078 cm^{-1}; ^1H NMR δ: 3.42 (s, 1H, OH), 3.48 (m, 2H, CH_2OH), 4.33 (m, 2H, $HCOOCH_2$), 8.14 (s, 1H, HCOO); ^{13}C NMR($CDCl_3$) δ: 60.77 (CH_2OH), 65.44 ($HCOOCH_2$), 161.05 (HCOO-); MS(CI): *m/e* 91[M + 1]$^+$.

Acknowledgements

We are grateful to British Petroleum and to the Natural Sciences and Engineering Research Council of Canada for support of this research.

1. J. Gelas. Adv. Carbohydr. Chem. Biochem. **39**, 71 (1981).
2. A. H. Haines. Adv. Carbohydr. Chem. Biochem. **39**, 13 (1981).
3. P. Deslongchanps and C. Moreau. Can. J. Chem. **49**, 2465 (1971).
4. R. J. Taillefer, S. E. Thomas, Y. Nadeau, S. Fliszár, and H. Henry. Can. J. Chem. **58**, 1138 (1980).
5. F. Kovac and B. Plesnicar. J. Chem. Soc. Chem. Commun. 122 (1978).
6. F. Kovac and B. Plesnicar. J. Am. Chem. Soc. **101**, 2677 (1979).
7. E. M. Kuramshin, V. K. Gumerova, L. G. Kulak, S. S. Slotski, and D. L. Rakhmankulov. Zh. Obshch. Khim. **55**, 1611 (1985).
8. E. M. Kuramshin, A. F. Mufteer, S. S. Slotskii, D. L. Rakhmankulov, and Y. M. Paushkin. Dokl. Akad. Nauk SSSR, **293**(1), 120 (1987).
9. E. M. Kuramshin, V. A. Dyachenko, S. S. Zlotskii, and D. L. Rakhmankulov. Oxid. Commun. **4**, 3 (1983).
10. S. Kim, W. J. Lee, and J. I. Lee. Bull. Korean Chem. Soc. **5**, 187 (1984).

The synthesis of esters under microwave irradiation using dry-media conditions

ANDRÉ LOUPY,[1] ALAIN PETIT, MOHAMED RAMDANI, AND CELINE YVANAEFF
Laboratoire des réactions sélectives sur supports, Unité associée 478 du Centre national de la recherche scientifique, Université Paris-Sud, Bâtiment 410, 91405 Orsay CEDEX, France

MUSTAPHA MAJDOUB
Laboratoire de chimie des polymères, Faculté des sciences, 5000 Monastir, Tunisia

AND

BOUCHTA LABIAD AND DIDIER VILLEMIN[1]
Laboratoire de chimie des composés thioorganiques, Institut des sciences de la matière et du rayonnement, Unité associée 480 du Centre national de la recherche scientifique, Université de Caen, 5 Avenue d'Edimbourg, 14032 Caen CEDEX, France

Received January 2, 1992[2]

ANDRÉ LOUPY, ALAIN PETIT, MOHAMED RAMDANI, CELINE YVANAEFF, MUSTAPHA MAJDOUB, BOUCHTA LABIAD, and DIDIER VILLEMIN. Can. J. Chem. **71**, 90 (1993).

Practical and simple techniques are described for using nonmodified domestic microwave ovens as safe and convenient laboratory devices to obtain numerous esters. High pressures are avoided by conducting reactions with reactants impregnated on solid mineral supports in "dry media" or by phase transfer catalysis (PTC) in the absence of organic solvents. Two kinds of microwave effects are involved: (1) displacement of the equilibrium by evaporation of volatile polar molecules (water or alcohols) in esterifications and transesterifications; (2) acceleration of ionic reactions in carboxylate alkylations. As solvents are avoided, there is no need for sealed vessels and water separators.

ANDRÉ LOUPY, ALAIN PETIT, MOHAMED RAMDANI, CELINE YVANAEFF, MUSTAPHA MAJDOUB, BOUCHTA LABIAD et DIDIER VILLEMIN. Can. J. Chem. **71**, 90 (1993).

Nous décrivons ici des techniques simples et pratiques d'utilisation des fours microondes domestiques non modifiés comme procédés sûrs et commodes pour obtenir de nombreux esters. Les hautes pressions sont évitées en effectuant les réactions avec des réactifs imprégnés sur supports minéraux en «milieu sec» ou par catalyse par transfert de phase (CTP) en absence de solvant. Deux types d'effets des microondes sont mis en jeu: (1) déplacement d'équilibre par évaporation de molécules polaires volatiles (eau ou alcools) lors d'estérifications et de transestérifications; (2) accélération des réactions anioniques dans le cas des alkylations de carboxylates. Dans la mesure où les solvants sont évités, il n'est pas nécessaire d'utiliser de la vaisselle scellée et des appareils pour séparer l'eau.

Can. J. Chem. Downloaded from www.nrcresearchpress.com by 88.255.202.194 on 09/08/12
For personal use only.

Esters are among the most important industrial products (1). They are usually synthesized by one of three main methods (2): (*i*) esterification of carboxylic acids, (*ii*) transesterification of methyl or ethyl esters, and (*iii*) alkylation of carboxylate anions. These reactions have been studied widely, but a great need still exists for versatile and simple processes whereby esters may be formed under very mild conditions (3). This is especially so for the two first methods where equilibria are involved.

We have been concerned with microwave activation in "dry media" (4–6) and its application for synthetic and simplificative purposes to the preparation of esters, taking advantage of two possible specific effects: rate enhancements, essentially due to thermal effects (7–9, 39) and displacements of equilibria by removal of volatile polar molecules (water or light alcohols).

Results

Esterification of carboxylic acids

$$RCOOH + R'OH \overset{\text{Acid}}{\rightleftharpoons} RCOOR' + H_2O$$

This type of reaction is generally catalyzed by acids, the equilibrium being shifted to the right by azeotropic removal of water using Dean–Stark apparatus. Acids such as Nafion-H (10, 11), silica–alumina (12), zeolites (13–15), zirconium oxide (16, 17), heteropoly-acids (18), or supported acids on polymers (19) have been used as catalysts.

The influence of microwaves on the rate of esterification in the presence of solvents has been studied (7–9). A large acceleration of the reaction was observed in sealed Teflon vessels due to thermal and pressure effects. However, yields were limited to around 70%. We thought that this limitation with rather heavy alcohols could be removed simply by operating in the absence of any solvent, and consequently by the possibility of evaporation of water due to microwave absorption.

We therefore studied the behaviour of a variety of acids and alcohols, including hindered and long-chain acids with heavy alcohols, which are generally difficult cases. Different acids, including KSF montmorillonite, 13X zeolite (20, 21), and neat *p*-toluenesulfonic acid (PTSA), were tested. In the first case, the effect of isopropenyl acetate as a water scavenger was studied. The results are given in Table 1.

The most favourable reaction conditions involved the use of neat PTSA, which led to good yields under exceptionally mild conditions (3–10 min), in a nonmodified domestic microwave oven. KSF montmorillonite and 13X zeolite were found to be less efficient.

Transesterification of methyl esters

$$RCOOCH_3 + R'OH \overset{\text{Acid or base}}{\rightleftharpoons} RCOOR' + CH_3OH$$

[1]Authors to whom correspondence may be addressed.
[2]Revision received September 1, 1992.

TABLE 1. Esterification under microwave (350 W)

$$RCOOH + R'OH \underset{}{\overset{Acid}{\rightleftharpoons}} RCOOR' + H_2O$$
(4 mM) (4 mM)

R	R′	NMR yield (time, min) KSF[a]	KSF + IA[b]	PTSA[c]	13 X[d]
Ph	nC_8H_{17}	85% (10)	88% (10)	**97%** (3)	54% (10)
	nC_8H_{17}	62% (5)	64% (5)	**82%**[e] (5)	37% (5)
	$nC_{18}H_{37}$	68% (10)	71% (10)	**91%** (10)	41% (10)
$nC_{17}H_{35}$	nC_8H_{17}	65% (5)	67% (5)	**90%** (5)	38% (5)
$nC_{17}H_{35}$	$nC_{18}H_{37}$	71% (10)	74% (10)	**94%** (10)	43% (10)
$nC_{17}H_{35}$		80% (3)	84% (3)	**95%** (3)	52% (3)

[a]Montmorrillonite KSF (4 g).
[b]Montmorrillonite KSF (4 g) and isopropenyl acetate (30 mmol).
[c]Neat *p*-toluenesulfonic acid (2 mM).
[d]Zeolite 13 X (2 g).
[e]PTSA = 0.8 mM, no reaction; PTSA = 4 mM, yield = 45%.

In this case, the reaction can be catalyzed by either acid or base (22). The equilibrium can classically be shifted to the right by azeotropic distillation (23), addition of molecular sieves (24), or by carrying out the reaction under partial vacuum in the absence of organic solvent (25). Under microwave irradiation without solvent, the most volatile component, CH_3OH, could be easily removed by evaporation.

We have studied the acid-catalyzed transesterification of methyl benzoate to octyl benzoate by solid acids, including K10 montmorillonite, Spherosil-S (26), Amberlyst-15 (recommended in this type of reaction) (27, 28), and PTSA, neat or impregnated on alumina or silica gel (29–31) (Table 2).

We also studied base-catalyzed transesterification of methyl to octyl benzoate, testing different bases impregnated on alumina, or in the presence of Aliquat 336 as a phase transfer catalyst (Table 3).

Finally, the most significant results were extrapolated for the most difficult case of methyl mesitoic ester. These results are indicated in Table 4.

From these tables, one can conclude that the best conditions are as follows:

Under acidic catalysis, *neat PTSA* leads to almost quantitative transesterifications, both with benzoic and mesitoic esters; yields obtained from Amberylst-15 (polysulfonic acid ion exchange resin) and Spherosil-S (grafted sulfonic acid on silica) are much lower. PTSA, when impregnated on a solid support, was less efficient and gave a lower yield (Table 2) than did neat PTSA. This fact is significant for silica gel (from 97 to 61%), and dramatic for alumina (<1%) where nonreactive species are generated, and is in disagreement with results of previous studies that claim absorbed PTSA to be an efficient dehydrating agent of alcohols (29–31). In all cases studied, the presence of a support had a negative effect.

Basic catalysis *under solid–liquid phase transfer catalysis (PTC) conditions* is generally more efficient than under conditions using supported bases: K_2CO_3 + Aliquat gives 90% yield, against only 72% for KOH/alumina in the case of methyl benzoate; $KOCH_3$, even in the absence of phase transfer agent, is the most efficient base in promoting mesitoate transesterification.

Carboxylate alkylations

In preliminary work dealing with potassium acetate, we pointed out the possibility of alkylation by microwave irradiation, either in solid–liquid PTC conditions without solvent (32), or by carrying out reactions on solid mineral supports in dry media (5, 33). Extension of this work to the more difficult cases is considered here. Table 5 indicates the results, involving the same esters as above to allow comparison.

It is clear that *PTC conditions are noticeably more efficient than reactions performed on alumina,* as was also apparent in acetate alkylation by classical heating (34). Quantitative yields of esters are always observed using PTC conditions, except in the case of cyclohexylester, where the main pathway is β-elimination.

Discussion

Using microwave irradiation in a domestic oven, in the absence of solvent and under atmospheric pressure, we have demonstrated three efficient and easy-to-perform methods to obtain esters. All of them have operative times of 10 min or less. The synthetic interest is obvious, because it is possible to obtain esters in almost quantitative yields under very mild

Can. J. Chem. Downloaded from www.nrcresearchpress.com by 88.255.202.194 on 09/08/12
For personal use only.

TABLE 2. Acid-catalyzed transesterification under microwave (600 W)

$$\underset{(10\ mM)}{PhCOOCH_3} + \underset{(20\ mM)}{n\ Oct\ OH} \xrightleftharpoons{Acid} PhCOO_nOct + CH_3OH$$

Acid, amount		GC yield (time, min)	Final temperature, °C
Montmorillonite K10	3 g	27% (8)	185
Montmorillonite KSF	3 g	24% (8)	170
Montmorillonite KSF	10 g	14% (8)	200
Spherosil S	0.5 g	3% (3)	148
Spherosil S	3 g	38% (3)	174
Amberlyst 15	0.5 g	18% (4)	170
Amberlyst 15	1.5 g	**61%** (1)	170
Amberlyst 15	3 g	13% (3)	194
PTSA neat	0.5 mM	5% (2)	146
PTSA neat	2 mM	39% (2)	173
PTSA neat	5 mM	**97%** (2)	193
PTSA neat	10 mM	45% (2)	200
PTSA/alumina (1:4)	5 mM	<1% (2–5)	153
PTSA/silicagel 60 (1:4)	5 mM	61% (4)	170

TABLE 3. Base-catalyzed transesterification under microwave (600 W)

$$\underset{(10\ mM)}{PhCOOCH_3} + n\ Oct\ OH \xrightleftharpoons{Base\ (5\ mM)} PhCOO_nOct + CH_3OH$$

Base	Relative amount ester:alcohol	GC yield (time, min)	Final temperature, °C
K_2CO_3/alumina[a]	1:1	30% (5)	167
KOH/alumina[a]	1:1	60% (3)	140
KOH/alumina[a]	1:2	72% (3)	160
KF/alumina[a]	1:1	55% (3)	135
KF/alumina[a]	1:2	**71%** (3)	150
KO*t*Bu/alumina[a]	1:1	49% (5)	165
K_2CO_3 + aliquat 0.5 mM	1:1	54% (3)	180
K_2CO_2 + aliquat 1 mM	1:1	68% (2.5)	181
K_2CO_3 + aliquat 1.5 mM	1:1	70% (2.5)	184
K_2CO_3 + aliquat 1.5 mM	1:2	**90%** (2.5)	186
KOH + aliquat[b]	1:1	40% (3)	180
KF + aliquat[b]	1:1	10% (3)	190
KOtBu + aliquat[b]	1:1	42% (3)	184

[a]Impregnated base on alumina-bases alumina = 1:4 w/w.
[b]Aliquat 336 = 1.5 mM.

conditions with a standard, nonmodified, microwave oven. This is also the case when they are poorly accessible (e.g., double long-chain esters).

Esterification and transesterification

Under microwave irradiation these methods are very efficient; they avoid pervaporation using a water-permeable polyetherimide membrane (35). The effect of microwave irradiation is twofold: (*i*) enhancement of reaction by a thermal effect, and (*ii*) evaporation of water or methanol due to the strong microwave interaction of these materials (cf. final temperatures ≥ 150°C in tables).

Acidic catalysis

Neat PTSA is by far the best agent to promote equilibrium shifting. The maximum yield is obtained when 0.5 mol. equiv. PTSA is used both in esterification and transesterification. Smaller or greater amounts of PTSA lead in both cases to significant reduction in yields.

When impregnated on silica gel, and more so when on alumina, PTSA loses its efficacy. Furthermore, other kinds of supported sulfonic acids, Spherosil-S (grafted on silica) or Amberlyst-15 (exchange resin), also lead to limited yields. The conclusion may be that *when they act as supports the solid acids lose their efficacy*. Certain of them have large specific areas (e.g., K10 = 220–270 m^2/g) or lamellar structures with consequent interfoliar spaces (e.g., montmorillonites). They consequently are able to absorb, either by physisorption or chemisorption, molecules of H_2O or CH_3OH. This absorption can limit evaporation of these molecules. Furthermore, under the microwave effect, the reverse reaction can be promoted.

Another hypothesis is the possibility of ester hydrolysis

Can. J. Chem. Downloaded from www.nrcresearchpress.com by 88.255.202.194 on 09/08/12
For personal use only.

TABLE 4. Transesterification of methyl mesitoic ester under microwave (600 W)

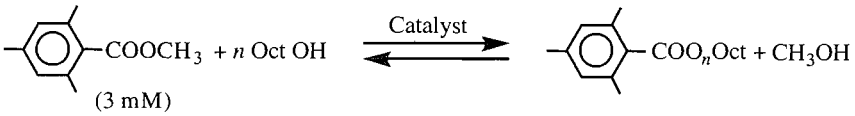

Catalyst	Relative amount ester:alcohol	GC yield (time, min)	Final temperature, °C
KOH + aliquat			
0.5 mM 0.3 mM	1:1	41% (10)	150
1 mM 0.3 mM	1:1	51% (10)	142
1 mM 0.3 mM	1:2	64% (10)	157
KO*t*Bu + aliquat			
1 mM 0.3 mM	1:1	68% (10)	154
$KOCH_3$ + aliquat			
1 mM 0.3 mM	1:1	70% (10)	140
1 mM 0.3 mM	1:2	88% (10)	147
$KOCH_3$			
1 mM	1:1	61% (10)	146
1 mM	1:2	82% (10)	157
1 mM	1:2.5	**89%** (10)	156
Neat PTSA			
1.5 mM	1:1	66% (3)	157
1.5 mM	1:2	88% (10)	177
2 mM	1:1	71% (3)	169
2 mM	1:2	**98%** (10)	186

TABLE 5. Alkylation of carboxylic anions under microwave (600 W)

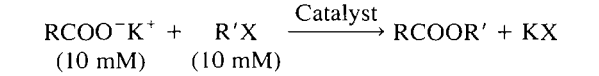

			Aliquat[a]		Alumina[b]	
R	R'	X	Yield (time)	Final temperature, °C	Yield (time, min)	Final temperature, °C
Ph[c]	nC_8H_{17}	Br	**99%** (5 min)[e]	180	47% (12)[e]	175
	nC_8H_{17}	Br	**97%** (30 s)[f]	195	13% (5)[f]	172
	$nC_{18}H_{37}$	Br	**98%** (45 s)[f]	180	10% (5)[f]	165
$nC_{17}H_{35}$	$nC_{18}H_{37}$	Br	**98%** (1 min)[f]	142	20% (5)[f]	160
$nC_{17}H_{35}$	$nC_{18}H_{37}$	Br	**98%** (2 min)[f]	161	11% (5)[f]	145
$nC_{17}H_{35}$		OTs	**40%** (2 min)[d,e]	143	—	—
CH_3	nC_8H_{17}	Br	**98%** (1 min)[e]	187	99% (2)[e]	196

[a]Aliquat 336 = 0.5 mM.
[b]Impregnated salt on alumina. Salt: alumina = 1:4 w/w.
[c]Salt generated *in situ* from RCOOH (10 mM) and K_2CO_3 (10 mM) for R = Ph and KOH (25 mM) for R = mesityl.
[d]Complement is β-elimination.
[e]GC yield.
[f]NMR yield.

Can. J. Chem. Downloaded from www.nrcresearchpress.com by 88.255.202.194 on 09/08/12
For personal use only.

Can. J. Chem. Downloaded from www.nrcresearchpress.com by 88.255.202.194 on 09/08/12
For personal use only.

by intralamellar water molecules present inside montmorillonites (K10 or KSF). To check these possibilities, further work is in progress.

We have to emphasize here the decisive role of microwaves in acidic transesterification, as no reaction can be observed under dynamic or static vacuum in classical conditions (25).

Basic catalysis

The most efficient "dry" systems are those involving PTC conditions rather than supported reagents on mineral supports. This conclusion was drawn for esterifications under traditional heating (34). We verified it here for transesterification with K_2CO_3 either in presence of Aliquat (yield = 88% within 2 h at 55°C) or impregnated on alumina (yield = 50% under the same conditions). One can propose two interpretations for these observations: (*i*) a dilution effect in the support, leading to a loss in reactivity; (*ii*) the PTC system absorbs microwaves more strongly than the alumina. This last assumption is verified in Table 3, as final temperatures due to irradiation are 140–165°C for bases/alumina and 180–190°C for bases + Aliquat.

These results represent a large improvement over experimental conditions that need either partial vacuum (25) or gas–liquid PTC conditions (36), i.e., high temperatures under pressure, to go to completion.

Anionic alkylation

This is the most efficient and simple method where primary alcohols (even very heavy ones) are concerned. Yields are quantitative within 2 min or less of microwave irradiation. The results we obtained represent large improvements when compared to those obtained under traditional heating: for instance, the preparation of octadecyl mesitoate classically needs 8 h at 85°C (37) while comparable yields are obtained in 45 s under microwave irradiation.

Another interesting point is the non-necessity of preforming the anionic species $RCOO^-K^+$ to perform the reaction. One can prepare it *in situ*, as for example in the reaction

$$PhCOOH + K_2CO_3 + n\text{OctBr} \rightarrow PhCOO_n\text{Oct}$$

which gave a 99% yield within 5 min under microwave compared with only 50% after 20 h at 85°C (38). Here, the effect of microwave irradiation is twofold: (*i*) a shifting to the right of the previous acid–base equilibrium by evaporation of H_2O:

$$2\ PhCOOH + K_2CO_3 \rightleftarrows 2\ PhCOO^-K^+ + H_2O + CO_2$$

and (*ii*) an acceleration of benzoate alkylation.

A further advantage lies in the considerable superiority of PTC conditions when compared to supported reactions, except for the alkylation of $CH_3CO_2^-K^+$ where the two methods are equally operative. As before, two assumptions can be made: (*i*) a dilution effect on the support, resulting in reduced reactivity; (*ii*) a diminution in the strength of microwave–material interaction when species are more hindered and heavier (long-chain acids or halides).

Conclusion

We propose here three microwave methods for ester synthesis in dry media. Two of them (esterification and transesterification) need equilibrium shifting of volatile polar molecules (water or methanol), which is here very efficiently and simply conducted *in the absence of solvent and of mineral supports*. Neat *p*-toluenesulfonic acid is used for acid-catalyzed esterification and transesterification, and K_2CO_3 in the presence of a transfer agent (Aliquat 336) is used for base-catalyzed transesterifications. Finally, in the most efficient procedure, alkylations of carboxylic anions are performed quantitatively (≥ 97%) in 1–2 min by simply mixing the potassium salt of the organic acid (possibly generated *in situ*), the alkylating agent (1 mol. equiv.), and a catalytic amount of transfer agent. All three methods are easily used and can be selected, if necessary, according to substituents.

The results described herein, i.e., almost quantitative yields in a few minutes, are characterized by very simple work-up and can be conducted very efficiently at ambient pressure using nonmodified microwave ovens as safe and convenient laboratory devices. These procedures undeniably possess considerable advantages over classical thermal conditions as reaction times are significantly reduced and yields widely enhanced, with apparatus simplified and reduced in cost.

One of the chief limitations of the microwave method is, in general, the difficulty in carrying out reactions safely if larger quantities of products are required. It seems that the dry-media method could achieve this (33, 40). Thus, for reactions on a larger scale (up to 0.5 mol), yields are always excellent (96.5%) for acetate alkylation by *n*-octyl bromide under PTC conditions without solvent; they remain always very acceptable (around 80%) for acid- and base-catalyzed transesterifications and esterifications. Although the reaction rates can be reduced when the reactions are scaled up, large rate enhancements are still observed.

Experimental section

Reaction mixtures (acids or methyl esters + alcohols in presence of catalyst; see below) were introduced in open Erlenmeyer flasks or beakers. They were irradiated (power and reaction times are indicated in the tables) with a Philips Whirlpool 5964 commercial domestic microwave oven operating at 2450 MHz. An approximate temperature measurement was performed by introducing a digital thermometer to the sample at the end of each irradiation. In these temperature evaluations, variations between several readings were less than 5°C. The reaction mixtures were extracted with organic solvent (methanol, diethyl ether or dichloromethane) and filtered. Organic esters were analyzed by gas chromatography and ^1H NMR and comparison made with authentic samples. Yields were evaluated by GC using an internal standard or by NMR. Gas chromatographic analyses were performed on a Carlo Erba Vega 6000 apparatus fitted with a capillary OV1 column (10 or 25 m) under a pressure of 0.4 bar (1 bar = 100 kPa) using helium as carrier gas.

The procedure described below involved from 5 to 20 mmol of standing materials (see tables).

Acid-catalyzed esterifications and transesterifications (Tables 1, 2, and 4)

Reactions with pure PTSA

Carboxylic acid or methyl ester, alcohol, and PTSA were mixed and shaken together in the proportions indicated in the tables and consequently treated as described above.

Reactions on acidic solid supports (montmorillonites, zeolite 13X, Spherosil-S, Amberlyst-15)

Carboxylic acids or methyl esters were impregnated on the support (via solutions in EtOH or CCl_4 in the case of acids and evaporation of solvent under reduced pressure). Alcohols were then added in the amounts indicated in the tables. After mechanical shaking for 1 min, the mixtures were microwaved and treated as previously described.

Impregnated PTSA on alumina or silicagel

PTSA (5 g) was adsorbed on the support (20 g) via a solution in 50 cm^3 EtOH. Solvent was removed by evaporation under reduced pressure. This impregnated PTSA was then used as the acidic solid support as described above.

Base-catalyzed transesterifications (Tables 3 and 4)

Impregnated bases on alumina

The different bases (K_2CO_3, KOH, KF, $KOCH_3$, or KO*t*Bu) were impregnated on basic alumina (alumina 90 type I, 70–230 mesh, Merck) via aqueous or alcoholic solutions (base:alumina = 1:4 w/w) and dried under reduced pressure (1 Torr; 1 Torr = 133.3 Pa) for 2 h at 140°C. Alcohols and esters were then added according to the amounts indicated in the tables. Reactions were carried out as described above.

PTC without solvent

Methyl ester (10 mmol), alcohol (10 or 20 mmol), neat base (5 mmol), and Aliquat 336 (0.5–1.5 mmol) were introduced into a flask and shaken vigorously before irradiation. Treatment remains as previously described..

Carboxylate alkylations (Table 5)

Impregnated salts on alumina

The potassium salts of carboxylic acids were prepared from the acid and a stoichiometric amount of KOH in EtOH and subsequent evaporation of solvent. The salts were impregnated on alumina (1:4 w/w) from ethanolic solutions and dried under reduced pressure (1 Torr). Reactions were then performed by mixing 10 mmol of supported potassium salt and 10 mmol of alkylating agent. After irradiation, treatment and analysis were carried out as described above.

PTC without solvent

The potassium salt (10 mmol), the alkylating agent (10 mmol), and Aliquat 336 (5 mmol) were mixed together and then irradiated. In some cases (cf. Table 5), reactions were performed by generation of the potassium salt *in situ* by reacting the carboxylic acid in the presence of base.

1. J. M. Tedder, A. Nechvatal, and A. H. Jubb. *In* Basic organic chemistry. Part V: Industrial products. Wiley, Chichester. 1975.
2. E. Haslam. Tetrahedron, **36**, 2409 (1980), and references therein.
3. J. M. Khurana, P. B. Sahoo, and G. C. Maikap. Synth. Commun. **20**, 2267 (1990).
4. A. Ben Alloum, B. Labiad, and D. Villemin. J. Chem. Soc. Chem. Commun. 386 (1989).
5. E. Gutierrez, A. Loupy, G. Bram, and E. Ruiz-Hitzky. Tetrahedron Lett. **30**, 945 (1989).
6. (*a*) D. Villemin and B. Labiad. Synth. Commun. **20**, 3207 (1990); **20**, 3213 (1990); (*b*) D. Villemin and A. Ben Alloum. Synth. Commun. **20**, 925 (1990); **20**, 3325 (1990); (*c*) D. Villemin, M. Lalaoui, and A. Ben Alloum. Chem. Ind. 176 (1991).
7. (*a*) R. N. Gedye, F. E. Smith, and K. C. Westaway. Can. J. Chem. **66**, 17 (1988); (*b*) R. N. Gedye, W. Rank, and K. C. Westaway. Can. J. Chem. **69**, 706 (1991).
8. S. D. Pollington, G. Bond, R. B. Moyes, D. A. Whan, J. P. Candlin, and J. R. Jennings. J. Org. Chem. **56**, 1313 (1991).
9. M. S. F. Lie Ken Jie and C. Yan-Kit. Lipids, **23**, 367 (1988).
10. G. A. Olah, T. Keumi, and D. Meidar. Synthesis, 929 (1978).
11. E. A. Olah, P. S. Iyer, and G. K. S. Prakash. Synthesis, 513 (1986).
12. E. Santacesaria, D. Gelosa, P. Danise, and S. Carra. J. Catal. **80**, 427 (1983).
13. E. Santacesaria, S. Carra, and F. Silva. J. Catal. **85**, 519 (1984).
14. Z. T. Chen, J. S. Zhong, Q. F. Li, Y. H. Li, and Z. H. Ou. Sci. China, Ser. B: **32**, 770 (1989).
15. A. Corma, H. Garcia, S. Iborra, and J. Primo. J. Catal. **120**, 78 (1989).
16. M. Hino and K. Arato. Chem. Lett. 1671 (1981).
17. K. Takahashi, M. Shibagaki, and H. Matsushita. Bull. Chem. Soc. Jpn. **62**, 2353 (1989).
18. I. V. Kozhevnikov. Usp. Khim. **56**, 1417 (1987); Russ. Chem. Rev. **56**, 811 (1987), and quoted references.
19. C. Fernandez, J. M. Marinas, and J. V. Sinisterra. Bull. Soc. Chim. Belg. **97**, 17 (1988).
20. W. Hölderich, M. Hesse, and F. Naumann. Angew. Chem. Int. Ed. Engl. **27**, 226 (1988).
21. H. Van Bekkum and H. W. Kouwenhoven. Recl. Trav. Chim. Pays-Bas, **108**, 283 (1989).
22. J. A. Abedi and N. M. Roscher. Synth. Commun. **19**, 1539 (1989).
23. A. Haken. J. Appl. Chem. **13**, 168 (1983).
24. D. P. Roelofsen, J. A. Hagendoorn, and H. Van Bekkum. Chem. Ind. 1622 (1966).
25. J. Barry, G. Bram, and A. Petit. Tetrahedron Lett. **29**, 4567 (1988).
26. B. Mirabel. Actual. Chim. 39 (1980).
27. M. Petrini, R. Ballini, and E. Marcantoni. Synth. Commun. **18**, 847 (1988).
28. R. B. Perni. Synth. Commun. **19**, 2383 (1989).
29. J. W. Apsimon, A. S. Y. Chau, and A. Fruchier. Synth. Commun. **12**, 249 (1982).
30. J. W. Apsimon, A. S. Y. Chau, R. Sampson, H. Tze, and A. Fruchier. Can. J. Chem. **60**, 2002 (1982).
31. F. D'Onofrio and A. Scettri. Synthesis, 1159 (1985).
32. G. Bram, A. Loupy, and M. Majdoub. Synth. Commun. **20**, 125 (1990).
33. G. Bram, A. Loupy, M. Majdoub, E. Gutierrez, and E. Ruiz-Hitzky. Tetrahedron, **46**, 5167 (1990).
34. J. Barry, G. Bram, G. Decodts, A. Loupy, P. Pigeon, and J. Sansoulet. Tetrahedron, **39**, 2673 (1983).
35. H. Kita, S. Sasaki, K. Tanaka, K. I. Okamoto, and M. Yamamoto. Chem. Lett. 2025 (1988).
36. E. Angeletti, P. Tundo, and P. Venturello. J. Org. Chem. **48**, 4106 (1983).
37. A. Loupy, M. Pedoussaut, and J. Sansoulet. J. Org. Chem. **51**, 740 (1986).
38. J. Barry, G. Bram, G. Decodts, A. Loupy, C. Orange, A. Petit, and J. Sansoulet. Synthesis, 40 (1985).
39. A. K. Bose, M. S. Manhas, M. Ghosh, M. Shah, V. S. Raju, S. S. Bari, S. N. Newaz, B. K. Banjk, A. G. Chaudhary, and K. J. Barakat. J. Org. Chem. **56**, 6968 (1991).
40. R. J. Giguere and B. Herberich. Synth. Commun. **21**, 2197 (1991).

Can. J. Chem. Downloaded from www.nrcresearchpress.com by 88.255.202.194 on 09/08/12
For personal use only.

Synthesis, NMR spectroscopy, and crystal structure of [9](*N*6,9)-6-aminopurinophane

ALFREDO CAPRETTA, HOWARD N. HUNTER, CHRISTOPHER S. FRAMPTON,[1] AND RUSSELL A. BELL[2]
Department of Chemistry, McMaster University, Hamilton, Ont., Canada L8S 4M1

Received February 21, 1992[3]

ALFREDO CAPRETTA, HOWARD N. HUNTER, CHRISTOPHER S. FRAMPTON, and RUSSELL A. BELL. Can J. Chem. **71**, 96 (1993).

[9](*N*6,9)-6-Aminopurinophane, **9**, was synthesized by Mitsunobu coupling of 9-azidononanol, **5**, and **6**-chloropurine, **6**. Reduction of the azide allowed for intramolecular nucleophilic displacement of chloride by the resultant amine and cyclization to the cyclophane. Variable temperature proton NMR showed the presence of two conformers below −25°C separated by an activation barrier having a $\Delta G_c^{\neq}$ = 50.2 ± 2.5 kJ mol^{-1}. The conformers arose from partial rotation about the C6—N6 bond, with the *anti* conformation assigned to the major isomer, **9***a*, and the *syn* conformation to the minor, **9***b*. The crystal structure of the [9](*N*6,9)-6-aminopurinophane, $C_{14}H_{21}N_5$, was determined at 173 K. The crystals are monoclinic, of space group $P2_1/n$, with a = 16.941(3) Å, b = 8.512(2) Å, c = 19.300(2) Å, β = 95.90(1)°, V = 2769(1) Å^3, D_c = 1.24 g cm^{-3}, D_m = 1.27 g cm^{-3}, for Z = 8, λ(CuKα) = 1.540598 Å. R_1 = 0.0364, R_2 = 0.0395 for 2846 reflections, ((R_1) = 0.0319, R_2 = 0.0365 for 2556 reflections with $I > 2.5\sigma(I)$). The purine ring shows small but significant distortions from planarity. The N(1)—C(6)—N(6)—C(1′) fragment adopts an *anti* conformation, which is twisted by approximately 35° from the plane of the purine ring, and the exocyclic 6-nitrogen is partially pyramidalized. Such pyramidalization is consistent with the Bader–Wiberg theory of barriers to rotation about bonds.

ALFREDO CAPRETTA, HOWARD N. HUNTER, CHRISTOPHER S. FRAMPTON et RUSSELL A. BELL. Can. J. Chem. **71**, 96 (1993).

On a synthétisé le [9](*N*6,9)-6-aminopurinophane, **9**, par un couplage selon Mitsunobu du 9-azidononanol, **5**, avec la 6-chloropurine, **6**. La réduction de l'azoture permet ensuite un déplacement nucléophile intramoléculaire du chlorure par l'amine qui se forme et conduit à une cyclisation fournissant le cyclophane. La RMN du proton à température variable a mis en évidence, à −25°C, la présence de deux conformères séparés par une barrière d'activation dont le $\Delta G_c^{\neq}$ = 50,2 ± 2,5 kJ mol^{-1}. Les conformères proviennent d'une rotation partielle autour de la liaison C6—N6; on a attribué la conformation *anti* à l'isomère prépondérant, **9***a*, et la conformation *syn* au produit mineur, **9***b*. On a déterminé la structure cristalline du [9](*N*6,9)-6-aminopurinophane, $C_{14}H_{21}N_5$. Les cristaux sont monocliniques, groupe d'espace $P2_1/n$, avec a = 16,941(3), b = 8,512(2) et c = 19,300(2) Å, β = 95,90(1)°, V = 2769(1) Å^3, D_c = 1,24 g cm^{-3}, D_m = 1,27 g cm^{-3}, Z = 8, λ(CuK$_\alpha$) = 1,540598 Å, R_1 = 0,0364 et R_2 = 0,0395 pour 2846 réflexions ((R_1) = 0,0319, R_2 = 0,0365 pour 2556 réflexions avec $I > 2{,}5\sigma(I)$). Le cycle de la purine présente une légère, mais définitive, distorsion par rapport à la planéité. Le fragment N(1)—C(6)—N(6)—C(1′) adopte une conformation *anti* qui dévie par environ 35° par rapport au plan du noyau de purine et l'azote exocyclique en position 6 est partiellement pyramidalysé. Une telle pyramidalisation est en accord avec la théorie de Bader–Wiberg relative aux barrières à la rotation autour des liaisons.
[Traduit par la redaction]

Can. J. Chem. Downloaded from www.nrcresearchpress.com by 88.255.202.194 on 09/08/12
For personal use only.

Introduction

Simple [*n*]-heterocyclophanes have been of continuing interest to oganic chemists because of their structural and spectroscopic properties (1). Emphasis has been placed on the synthesis of cyclophanes with relatively short methylene bridges but, even with the steric and ring strains so introduced, it is remarkable how the chains retain sufficient flexibility to exist in more than one conformation, as, for example, in [8](3,6)-pyridazinophane (2). Our interest has been in utilizing the methylene protons in an [*n*]-cyclophane chain as reporter atoms of the magnetic anisotropy associated with the purine and pyrimidine bases found in ribo- and deoxyribonucleic acids in a manner similar to that employed by Agarwal *et al.* in their study of benzene anisotropy (3). In consequence, the synthetic objectives are molecules that have a methylene chain sufficiently taut to bridge the heteroaromatic ring without introducing severe bending strains into the ring or the chain.

Syntheses of very few [*n*]-cyclophanes of the heteroaromatic purine ring system have been described, although a number of [*m*,*n*]-purinophanes have been prepared (4). Ienaga *et al.* (5) have reported the use of the Dimroth rearrangement to synthesize [*n*](2,6)-6-aminopurinophanes, **1** (*n* = 7,9), and [*n*](2,9)-6-aminopurinophane derivatives, **2**

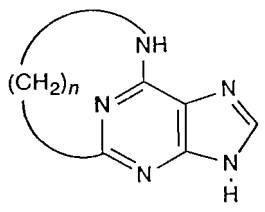

1 *n* = 7, 9, 11

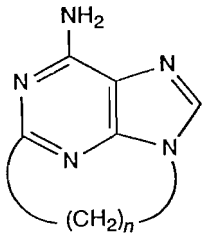

2 *n* = 9, 11

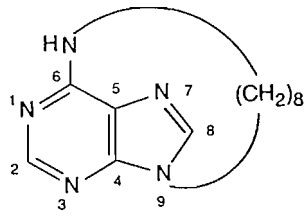

3

[1]Present address: Department of Chemistry, University of Glasgow, Scotland.
[2]Author to whom correspondence may be addressed.
[3]Revision received August 25, 1992.

(n = 9,11). Ienaga and Pfleiderer (6) have recounted the preparation of the corresponding [n](2,*N*6)-adenosine derivatives (n = 7,9,11). A series of heteroatom derivatives, [n](6,9)-6-thiapurinophanes (n = 9,10,11) has been produced by Higuchi *et al.* (7) and an [8](*N*6,9)-6-aminopurinophane, **3**, has been reported by Bell and Hunter (8). Only these latter compounds have their methylene chain constrained to lie directly over the purine ring and, as a consequence, their ^{1}H NMR spectra show a number of highly shielded proton signals.

The crystal structure of [8](*N*6,9)-6-aminopurinophane (9) shows there are appreciable strains present in the molecule, with the N6 and C8′ atoms being moved out of the heteroaromatic plane by 0.314 Å and 0.459 Å, respectively, towards the methylene chain, and the five- and six-membered rings twisted with respect to each other by 5.45°. In view of these distortions we have undertaken the synthesis of [9](*N*6,9)-6-aminopurinophane and report herein its synthesis, NMR spectroscopy, and X-ray crystal structure.

Results and discussion

Synthesis

The strategy for the synthesis of [9](*N*6,9)-6-aminopurinophane, **9**, is outlined in Scheme 1 and, while it follows the methodology developed for the construction of [8](*N*6,9)-6-aminopurinophane (8), a more direct approach has been devised. 1,9-Nonanediol, **4**, and 6-chloropurine, **6**, were the two starting fragments. By use of the elegant procedure of Castro and co-workers (10),[4] 1,9-nonanediol could be routinely converted into 9-azidononanol, **5**, in 85–90% yields. Once reduced, the azido group (effectively a protected amine) provides the nitrogen atom at the 6 position of the cyclophane.

The Mitsunobu reaction (11),[5] which has proved useful in providing good yields of *N*9-alkylated purines, was planned as the procedure for coupling 9-azidononanol to 6-chloropurine. However, the reaction was approached with some caution as one of the reagents, triphenylphosphine, is known to be an efficient reductant of azides (the "other" Staudinger reaction) (12).[6] By carrying out the reaction with prior mixing of the triphenylphosphine, diethylazodicarboxylate (DEAD), and 6-chloropurine, and then addition of 9-azidononanol, a modest yield of 23% of purified 6-chloro-9-(1-azidononyl)purine, **7**, could be obtained. Clearly the lower than normal yield (normal range 65–80%) (11) was a result of unwanted triphenylphosphine reductive processes. No attempt was made to isolate these additional products. Reduction of the azido group to the amine **8** was then readily accomplished with a further 1 mole-equivalent of triphenylphosphine and 1.5 equivalents of water in tetrahydrofuran (THF). Curiously, this reduction proceeded in high yields only if the concentration of **7** was of the order of one molar or greater. The reasons for this behaviour are not entirely clear, but reactions conducted at concentrations of 10–100 mmolar afforded distinctly poorer yields of amine product.

The final, and crucial, cyclization step in the synthesis was an intramolecular nucleophilic aromatic substitution process depicted in the step **8** to **9** in the scheme. While the nonamethylene chain permitted ready access of the amine nitrogen to carbon-6 of the 6-chloropurine, it was anticipated that the reaction rate would be slower than that recorded for the octamethylene chain because of the additional degrees of freedom present with the extra methylene group (13). After refluxing for 48 h in acetonitrile all of the chloro-amine **8** had reacted, as judged by thin-layer chromatography (TLC), but chromatographic purification of the products yielded only 26% of the desired cyclophane. Much of the starting **8** appeared to have degraded, presumably by the presence over the long time period of adventitious water and (or) oxygen.

High-resolution mass spectroscopy (HRMS) together with proton and carbon-13 NMR spectroscopy further confirmed the homogeneity of the [9](*N*6,9)-6-aminopurinophane. Crystallization of a sample of **9** from chloroform–toluene (1:3) yielded large acicular crystals that were found to be suitable for X-ray crystallographic analysis.

NMR spectroscopy

The ^{1}H NMR spectrum of the cyclophane **9** recorded in $CDCl_3$ at 25°C illustrated the pronounced effect the magnetic anisotropy of the purine system had on the bridge protons (see Fig. 1, spectrum (*b*)). With chemical shifts ranging from δ 4.53 to −0.01, many of the nine diastereotopic bridge proton pairs appeared as well-resolved multiplets while others were broadened to various degrees. Such behaviour is characteristic of an exchange process operating in an intermediate rate region and indicated that the methylene chain was undergoing interconversion between two or more conformers. When **9** was heated to 75°C and its spectrum recorded ($CDCl_3$, sealed tube; see Fig. 1, spectrum (*a*)), the majority of the signals became sharp, demonstrating that the fast-exchange limit had been reached. Assignments were made based on 2D-COSY and 2D ^{13}C–^{1}H heteronuclear shift-correlated spectra at the elevated temperature (see Table 1).

The low-temperature ^{1}H NMR spectrum of **9** (CD_2Cl_2:$CFCl_3$ solvent) was especially informative and showed the presence of two "frozen" conformers (see Fig. 1, spectrum (**c**)). At −59.5°C, two species, unequal in population, were clearly evident. Most pronounced were the two sharp singlets between δ 7.7 and 8.4, a set for each conformation, corresponding to H2 and H8 on the purine ring. Signals from the aliphatic chain, at this temperature, ranged from δ 4.84 to −1.30. While the methylene hydrogens of C1′ and C9′ for each conformer were reasonably well resolved, the significant broadening seen in the high-field resonances is likely a result of residual exchange of protons in very different chemical shift environments. The chemical shift dependence of the N6H resonance on temperature was strong, moving from δ ca. 8.0 at −59.9°C to 5.2 at 75°C. Likewise the high-field signal at δ −1.30 moved to ca. δ 0.2 as the temperature was increased.

Assignments for the two conformers observed in the low-temperature spectrum of **9** were made by the analysis of the 2D COSY and the 2D ^{13}C–^{1}H heteronuclear shift-correlated spectra recorded at −59.5°C (see Table 1). Because the two conformers were of unequal population, approximately 75% of the *anti* form **9***a* and 25% of the *syn* form **9***b* as subsequently assigned (see Fig. 2), it was possible to use the 2D ^{13}C–^{1}H experiment to correlate each carbon in the two conformers with its attached geminal pair of diastereotopic hy-

[4]For a review of this reaction, see ref. 10*b*.

[5]For an example of the use of this reaction using 6-chloropurine, see ref. 11*b*.

[6]See ref. 12*b* for a review of this reaction.

Can. J. Chem. Downloaded from www.nrcresearchpress.com by 88.255.202.194 on 09/08/12
For personal use only.

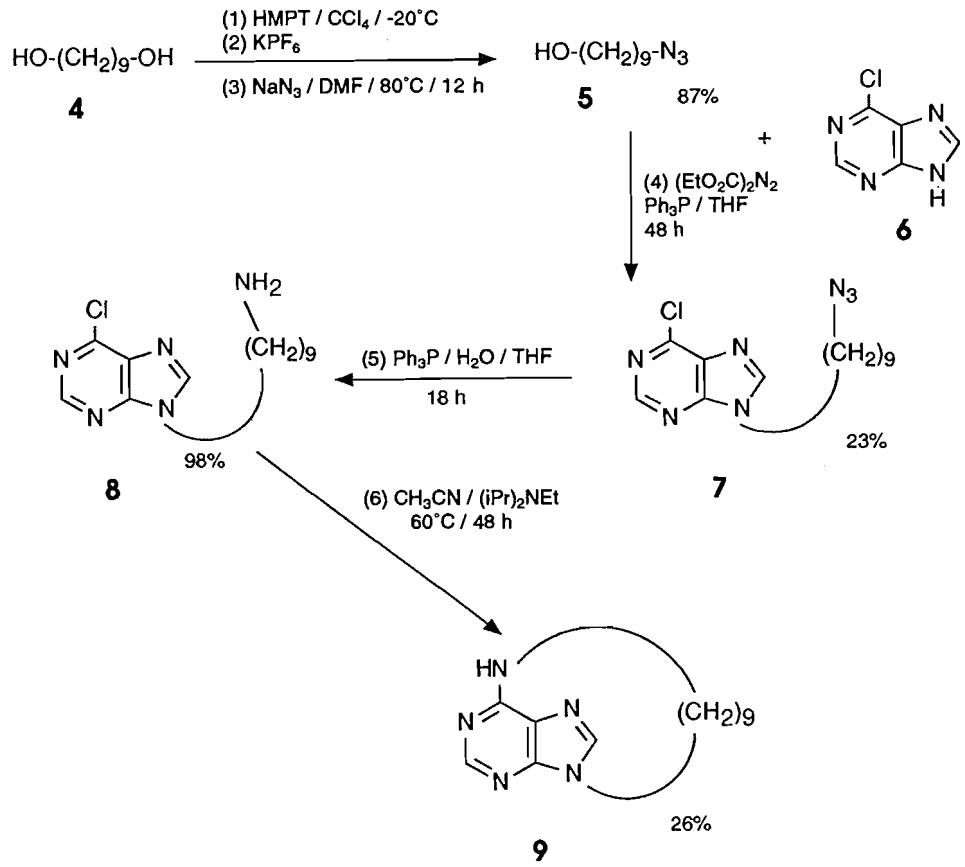

SCHEME 1

drogens; the sole exception was C3′ where the correlation was too weak to be reliably distinguished from noise. The chemical shifts of C1′ and C9′ were defined by comparison with [8](*N*6,9)-6-aminopurinophane, **3**, (C1′ δ 43.03, C8′ δ 45.03), 6-octylaminopurine (C1′ δ 40.72), and 6-chloro-*N*9-octylpurine (N-C1′ δ 44.48) (9), and thence their attached pairs of protons defined. Use was then made of the 2D COSY experiment where each proton could be linked with its neighbours along the chain and allowed each carbon to be assigned. Again the lack of a ^{13}C–^{1}H correlation for C3′ stopped the linking from the C1′ end of the minor conformer but it was possible to proceed uniquely from C9′ to C4′. It should be pointed out that the 2D experiments do not permit the assignment of the *pro-R* and *pro-S* hydrogens in each diastereotopic pair; additional data are required for this, for example the magnitude of the spin–spin coupling constants of a given proton to all of its neighbours and then application of the Karplus equation. Unfortunately, the severe overlaps together with the line broadening of our spectra at −59.5°C did not allow for the derivation of coupling constants of adequate accuracy for unambiguous assignments of *pro-R* and *pro-S* hydrogens. Alternative approaches to this problem are presently being undertaken.

To obtain the activation barrier for interconversion between the two observed conformers, variable temperature NMR experiments were carried out over the range −98.9°C to +30°C. The H2 and H8 protons on the purine ring were the most clearly defined, well-separated, singlets in the spectrum and were used for a line shape analysis (14). A linear chemical shift versus temperature change was noted for both H2 and H8 in proceeding from −98.9°C towards the coalescence temperature of these protons and this change was taken into account in calculating the activation barrier. Coalescence of the signals occurred at −25°C and the Gibbs' energy of activation, $\Delta G_c^{\neq}$, at this temperature was determined to be 50.2 ± 2.5 kJ mol^{-1}. Reitz *et al.* (15) have reported the barrier for rotation about the C6—N6 bond in both 9-benzyl-6-(isopropylamino)purine and 9-benzyl-6-(methylamino)purine to be 54.0 kJ mol^{-1} and the similarity in magnitude to that obtained for **9** strongly suggested that the two observed conformers were the result of partial rotation about the C6—N6 bond where the C1′ carbon may be *anti* (adjacent to N7) or *syn* (adjacent to N1), **9***a* and **9***b* respectively (see Fig. 2). To further confirm this postulate, molecular mechanics calculations (16) were performed on the two proposed conformers and the *anti* conformer was found to be 4–6 kJ mol^{-1} more stable than the *syn* conformer. This relationship was consistent with that observed experimentally if the major conformer was assigned structure **9***a* and the minor conformer structure **9***b*. Final and convincing evidence for these assignments was obtained from the X-ray crystal structure of **9** (see below) where it adopted the lower energy *anti* conformation. Moreover, this structure (see Figs. 3 and 4) and the molecular mechanics model **9***a* were found to be virtually identical, lending strong credence to the conviction that the other observed conformer should be assigned *syn* structure **9***b*.

It is intriguing to note that the previously reported [8]-purinophane, **3**, showed only one conformation to be present in solution (the *anti* form) over a wide temperature range. The addition of one methylene unit has been sufficient to give

Can. J. Chem. Downloaded from www.nrcresearchpress.com by 88.255.202.194 on 09/08/12
For personal use only.

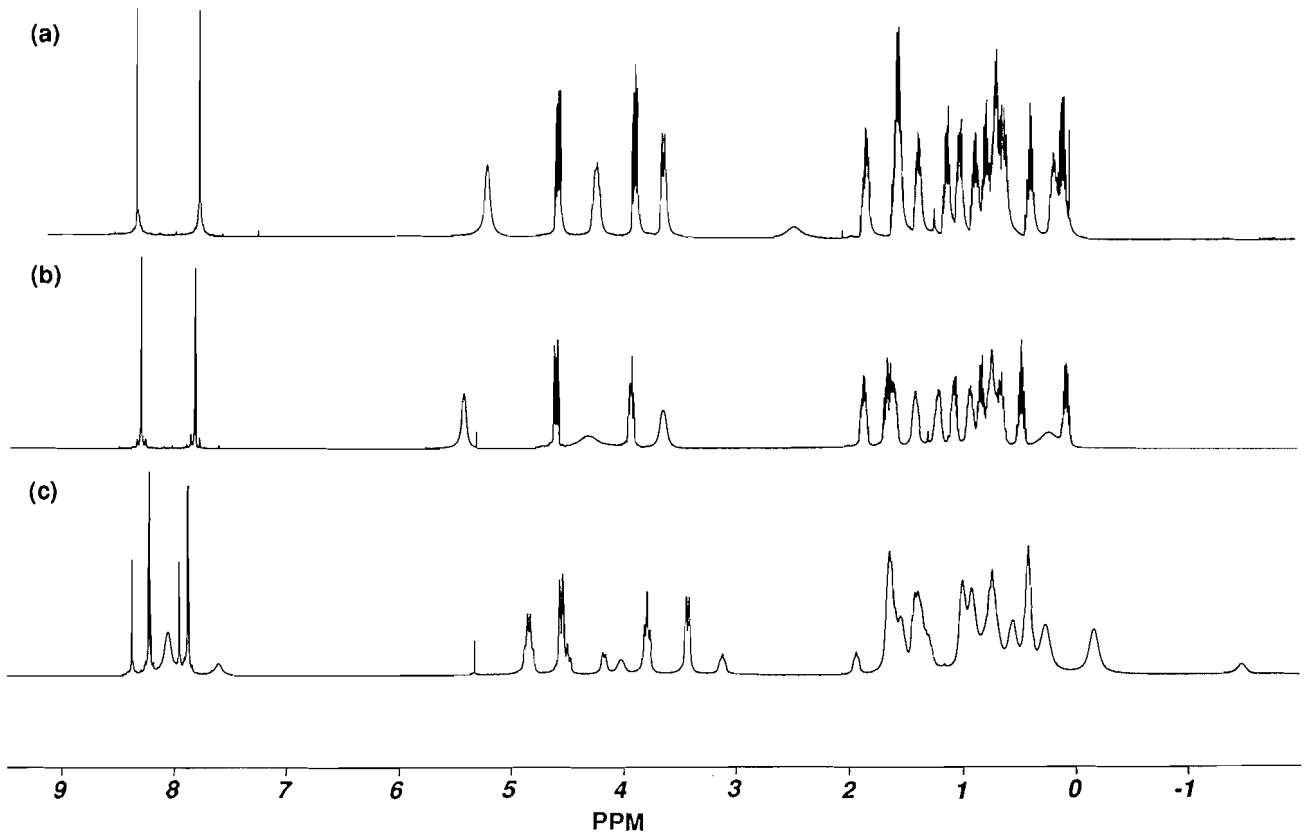

FIG. 1. Proton NMR spectra of [9](*N*6,9)-6-aminopurinophane, **9**, in deuterochloroform at (*a*) 75°C, (*b*) 30°C, and (*c*) −59.9°C.

TABLE 1. Proton and carbon-13 chemical shifts of [9](*N*6,9)-6-aminopurinophane, **9**

	75°C spectrum			−59.5° major, **9***a*			−59.5° minor, **9***b*		
	^{13}C	^{1}H		^{13}C	^{1}H		^{13}C	^{1}H	
C1′	42.87	4.24	3.63	42.04	4.84	3.38	42.60	4.08	3.10
C2′	30.28	1.59	1.38	31.03	1.60	1.43	25.35	1.62	1.03
C3′	24.30	1.02	0.68	24.77	1.00	0.45	21.67	—	—
C4′	26.96	0.72	0.62	25.09	0.45	0.35	27.84	0.93	0.79
C5′	27.35	0.79	0.11	26.50	0.74	−0.09	26.64	0.70	−0.21
C6′	27.74	0.39	0.18	26.91	0.82	0.55	27.84	0.34	−1.30
C7′	24.54	1.14	0.88	22.22	1.32	0.59	25.87	1.20	0.80
C8′	27.90	1.86	1.56	25.52	1.60	1.60	30.49	1.93	1.35
C9′	44.97	4.58	3.88	45.10	4.54	3.79	44.39	4.48	4.15

the aliphatic bridge of the [9]-purinophane enough flexibility to permit rotation about the C6—N6 bond to take place.

Diffraction studies and conformational analysis

The two symmetry-independent molecules of [9](*N*6,9)-6-aminopurinophane (hereafter referred to as molecules A and B),[7] are shown in Figs. 3 and 4 with the atom labelling scheme. Crystal data and other information related to data collection are given in Table 2 while bond lengths and bond angles are shown in Table 3, and dihedral and torsional angles may be found in Table 4. As may be deduced from the latter tables, both molecules A and B are conformationally similar and have essentially the same geometry. It is pertinent to compare the structural results presented in this paper with those obtained (9) for [8](*N*6,9)-6-aminopurinophane, **3**. With the addition of an extra methylene group in the aliphatic chain one would expect the strain energy that was shown to be present in **3** would be slightly less. However, for both molecules A and B there are still a significant number of intramolecular nonbonding contacts less than the accepted van der Waals distances of 3.30 Å, C···C; 3.20–3.25 Å, C···N; 2.90–3.10 Å, C···H; 2.75–3.00 Å, N···H (18). Particularly close approaches by atoms in molecule A are shown by: C(1′)···C(5), 3.02; C(7′)···N(9), 3.00; H(11)···C(6), 2.57; H(72)···C(8), 2.50; H(11)···N(7), 2.38; H(72)···N(9), 2.55 (all in Å); with close approaches between similar atoms in molecule B.

The bond lengths of the adenine moiety are in good agreement with **3** and also agree well with previously pub-

[7]Both the CREDUC and MISSYM outputs from the NRCVAX crystallographic packages (17) failed to detect any additional symmetry.

Can. J. Chem. Downloaded from www.nrcresearchpress.com by 88.255.202.194 on 09/08/12
For personal use only.

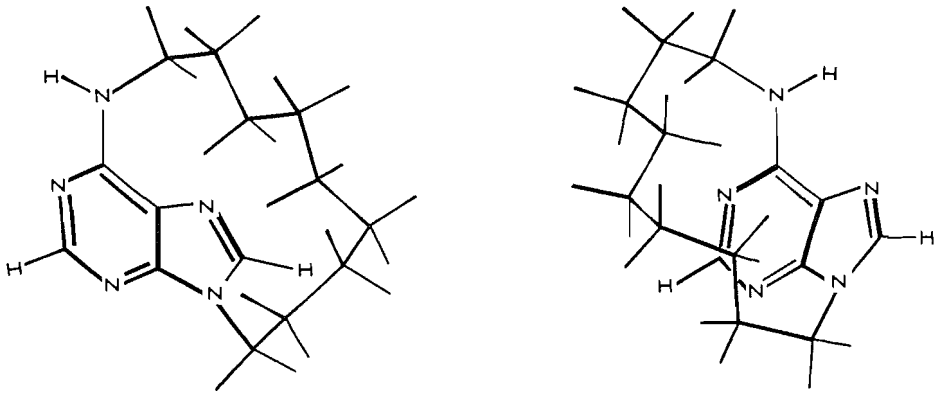

FIG. 2. Molecular mechanics models of *anti*-[9](*N*6,9)-6-aminopurinophane, **9***a*, and *syn*-[9](*N*6,9)-6-aminopurinophane, **9***b*. Bridge methylene protons have been omitted for clarity.

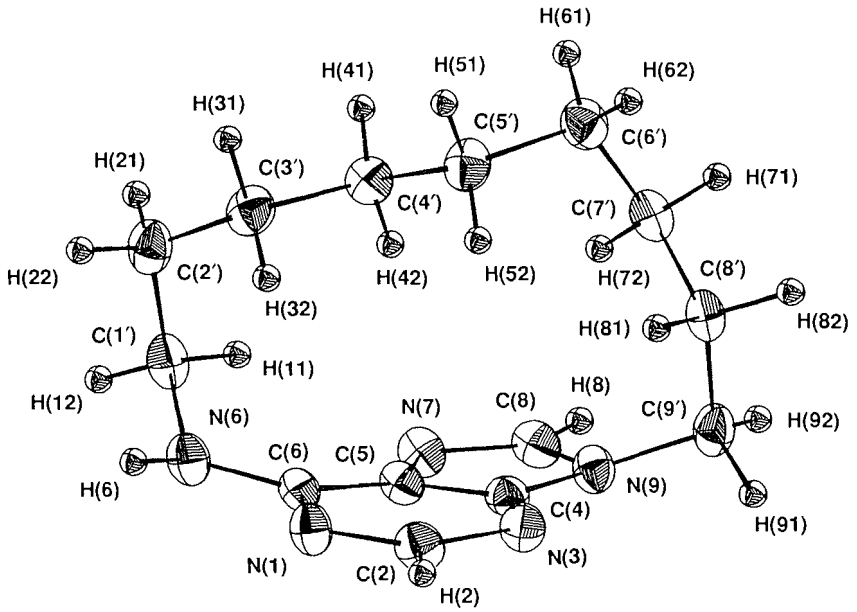

FIG. 3. Molecule A. (*pR*)-[9](*N*6,9)-6-Aminopurinophane showing the complete atom numbering.

lished average values (19) (to within 2.1σ; $\sigma = (\sigma_1^2 + \sigma_2^2)^{1/2}$). Interestingly, the largest deviation found is for C(2)—N(3), 2.1σ (A) and 1.6σ (B), which is consistent with that found for **3**. Similarly, the bond angles are in agreement with previous adenine structures, lying within 2.9σ of the average reported values.

The adenine moiety shows the same pattern of small deviations from planarity as observed in **3**. The dihedral angle between the mean planes through the pyrimidine and imidazole rings is 3.85(6)° (A) and 4.47(6)° (B) (cf. 5.45(9)° for **3**); this reduction in magnitude of the dihedral angle gives the impression that the twisting motion of the adenine group has been somewhat relaxed, leading to a reduction in strain energy in the adenine ring system. In contrast, however, both N(6), N(6B) and C(9′), C(9′B) are displaced out of the plane of the rings to which they are attached (in the direction of the aliphatic chain) to a greater extent than in **3**; (N(6), 0.325(2); N(6B), 0.362(2); C(9′), 0.577(3); C(9′B), 0.624(3); Å). If one examines the N—C—C—C and C—C—C—C torsional angles, deviations from the idealized values of 60, 120, and 180° rarely exceed 10° (average, 9.9° (A) and 11.0° (B)), with the exception, however, of one angle in particular, C(9′)—C(8′)—C(7′)—C(6′), (29.9° (A) and 28.1° (B)). It is at this position that the conformation of the aliphatic chain begins to differ from **3** and is being forced away from the adenine ring system; this, in turn appears to pull C(9′) further out of the mean plane. The N(1)—C(6)—N(6)—C(1′) fragment adopts an *anti* conformation (as does **3**), which is twisted about the N(6)—C(6) bond by approximately 35° from the plane of the purine ring. This twisting motion reduces the overlap of the nitrogen lone pair with the purine π-system. Bond lengths and angles in the aliphatic chain (average values 1.524 Å and 114.9°, respectively, for both A and B) are in very good agreement with average values reported previously (20, 21). A stereoview of the crystal packing is shown in Fig. 5. The view is down *b*. The molecules pack in layers parallel to (−1 0 1). There are no unusual intermolecular contacts and the crystal packing appears to be dominated by van der Waals forces only.

The slightly lower barrier to rotation about C6—N6 in **9**

Can. J. Chem. Downloaded from www.nrcresearchpress.com by 88.255.202.194 on 09/08/12
For personal use only.

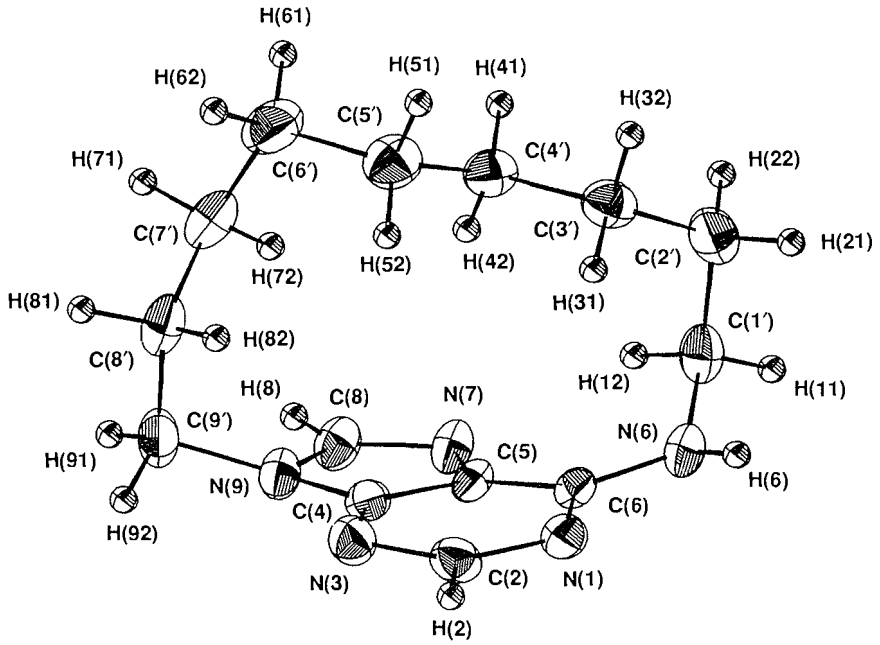

FIG. 4. Molecule B. (*pS*)-[9](*N*6,9)-6-Aminopurinophane showing the complete atom numbering.

TABLE 2. Crystal data for [9](*N*6,9)-6-aminopurinophane

Formula	$C_{14}H_{21}N_5$
Formula weight	259.35
System	Monoclinic
Space group	$P2_1/n$ (No. 14)
a, Å	16.941(3)
b, Å	8.512(2)
c, Å	19.300(2)
β, deg	95.90(1)
V, Å^3	2769(1)
Z	8
D_c, (D_m), g cm^{-3}	1.24, (1.27)
F(000)	1120
μ(Cu K$_\alpha$), cm^{-1}	5.84
Final R_1, R_2[a,c]	0.0364, 0.0395
Weighting scheme	$(\sigma^2F + 0.0005F^2)^{-1}$
Error in observation of unit weight[b]	1.3618
Highest peak, e Å^{-3}; location	0.16; 0.812, 0.538, 0.187
Lowest peak, e Å^{-3}	−0.16

[a] $R_1 = \Sigma||F_o| - |F_c||/\Sigma|F_o|R_2 = [\Sigma\omega(|F_o| - |F_c|)^2/\Sigma\omega F_o^2]^{1/2}$.
[b] $S = [\Sigma\omega(|F_o| - |F_c|)^2/(m\text{-}n)]^{1/2}$; m = number of reflections, n = number of variables.
[c] R_1, R_2 = 0.0319 and 0.0365 for 2556 reflections with $I \geq 2.5\sigma(I)$.

when compared to the noncyclic examples reported by Reitz *et al.* (15) warrants further scrutiny. Inspection of Dreiding models suggested the strain of the cyclophane system should increase the barrier to rotation rather than decrease it. As noted above, however, the H6—N6—C1′ fragment in **9** is twisted about the C6—N6 bond by approximately 35°, whereas in the aliphatic examples studied by Reitz *et al.* (15) the ground state has this fragment essentially planar. Thus, in the [9]-purinophane, the ground state energy of the system has been raised and less energy should be required to achieve rotation about the C6—N6 bond. The magnitude of the decrease is smaller (ca. 4 kJ mol^{-1}) than might be anticipated considering the twist is already 35° and the highest point of the barrier is presumably with a twist of 90°. However, the entire methylene chain must reorganize itself in proceeding from the *anti* to the *syn* conformation and there will be torsional energies associated with this that contribute to the activation barrier and partially offset the increased ground state energy.

The *origin* of the barrier to rotation about the C6—N6 bond of **9** and other *N*6-alkyl substituted purines has been of particular concern to chemists, and the data from the crystallographic structure of **9** offer some insight into this. The barrier is generally considered to arise from destruction of the overlap of the nitrogen atom's lone pair of electrons with the electron-deficient heteroaromatic ring (15, 22). Recently, theoretical studies by Bader *et al.* (23) and Wiberg and Laidig (24) and experimental work by Brown and coworkers (25) on substituted amides suggest that it is the movement apart of the two atoms about which rotation is taking place and the consequent changes in the electron–nucleus attractions and electron–electron repulsions that are the principal contributors to the activation barrier. For a planar amide, rotation about the C—N bond results in lengthening of this bond and pyramidalization of the N atom as the energy maximum is reached. 6-Aminopurines contain an amidine system (N1—C6—N6) and are entirely analogous to an amide. Thus, X-ray crystallographic studies of a number of *N*9-substituted 6-aminopurines show the average length of the C6—N6 bond to be 1.337 Å (26*a*) and show the N and H atoms of the -NH_2 group to be basically coplanar with the heteroaromatic ring, the N atom being only 0.01–0.09 Å out of the C6—H61—H62 plane (26*b–f*). The N6 atom may be regarded as essentially sp^2 hybridized, as its chemical properties testify. Note that a fully pyrimidalized (or sp^3 hybridized) N, as in dimethylamine, places the N atom 0.41 Å out of the basal C—C—H plane. Monosubstitution of N6 with carbon groups causes small changes to this basic geometry (27). The C6—N6—$C_{subst.}$ angle increases slightly to 121–123° while the average C6—N6 bond length becomes 1.341 Å. However, there is no change in the

Can. J. Chem. Downloaded from www.nrcresearchpress.com by 88.255.202.194 on 09/08/12
For personal use only.

TABLE 3. Bond lengths (Å) and bond angles (deg) for [9](*N*6,9)-6-aminopurinophane with estimated standard deviations in parentheses

Molecule A					
N(1)—C(2)	1.338(2)	C(2)—N(3)	1.332(2)	N(3)—C(4)	1.342(2)
C(4)—C(5)	1.392(2)	C(5)—C(6)	1.401(2)	C(6)—N(1)	1.358(2)
C(5)—N(7)	1.392(2)	N(7)—C(8)	1.311(2)	C(8)—N(9)	1.369(2)
N(9)—C(4)	1.372(2)	C(6)—N(6)	1.352(2)	N(6)—C(1′)	1.463(2)
C(1′)—C(2′)	1.515(3)	C(2′)—C(3′)	1.528(3)	C(3′)—C(4′)	1.528(3)
C(4′)—C(5′)	1.522(3)	C(5′)—C(6′)	1.527(3)	C(6′)—C(7′)	1.526(3)
C(7′)—C(8′)	1.523(3)	C(8′)—C(9′)	1.523(3)	C(9′)—N(9)	1.465(2)
C(6)—N(1)—C(2)	118.4(2)	N(1)—C(2)—N(3)	129.2(2)	C(2)—N(3)—C(4)	110.1(1)
N(3)—C(4)—C(5)	127.6(2)	C(4)—C(5)—C(6)	115.8(2)	C(5)—C(5)—N(1)	117.7(2)
N(3)—C(4)—N(9)	126.6(2)	C(5)—C(4)—N(9)	105.8(1)	C(4)—N(9)—C(8)	105.5(1)
N(9)—C(8)—N(7)	114.7(2)	C(8)—N(7)—C(5)	103.2(1)	N(7)—C(5)—C(6)	133.1(2)
N(7)—C(5)—C(4)	110.6(1)	C(5)—C(6)—N(6)	125.3(2)	N(1)—C(6)—N(6)	117.0(2)
C(6)—N(6)—C(1′)	121.8(1)	N(6)—C(1′)—C(2′)	112.3(2)	C(1′)—C(2′)—C(3′)	116.0(2)
C(2′)—C(3′)—C(4′)	116.1(2)	C(3′)—C(4′)—C(5′)	112.5(2)	C(4′)—C(5′)—C(6′)	115.0(2)
C(5′)—C(6′)—C(7′)	115.0(2)	C(6′)—C(7′)—C(8′)	115.5(2)	C(7′)—C(8′)—C(9′)	114.0(2)
C(8′)—C(9′)—N(9)	109.5(1)	C(9′)—N(9)—C(4)	124.3(1)	C(9′)—N(9)—C(8)	125.8(2)
Molecule B					
N(1)—C(2)	1.333(2)	C(2)—N(3)	1.328(2)	N(3)—C(4)	1.343(2)
C(4)—C(5)	1.379(3)	C(5)—C(6)	1.409(2)	C(6)—N(1)	1.355(2)
C(5)—N(7)	1.389(2)	N(7)—C(8)	1.307(3)	C(8)—N(9)	1.366(3)
N(9)—C(4)	1.378(3)	C(6)—N(6)	1.341(2)	N(6)—C(1′)	1.462(2)
C(1′)—C(2′)	1.526(3)	C(2′)—C(3′)	1.518(3)	C(3′)—C(4′)	1.527(3)
C(4′)—C(5′)	1.523(3)	C(5′)—C(6′)	1.519(3)	C(6′)—C(7′)	1.530(3)
C(7′)—C(8′)	1.533(3)	C(8′)—C(9′)	1.516(3)	C(9′)—N(9)	1.464(3)
C(6)—N(1)—C(2)	118.2(2)	N(1)—C(2)—N(3)	129.7(2)	C(2)—N(3)—C(4)	109.8(2)
N(3)—C(4)—C(5)	127.6(2)	C(4)—C(5)—C(6)	116.0(1)	C(5)—C(6)—N(1)	117.3(2)
N(3)—C(4)—N(9)	126.2(2)	C(5)—C(4)—N(9)	106.2(1)	C(4)—N(9)—C(8)	105.1(1)
N(9)—C(8)—N(7)	114.5(2)	C(8)—N(7)—C(5)	103.6(1)	N(7)—C(5)—C(6)	133.4(2)
N(7)—C(5)—C(4)	110.4(1)	C(5)—C(6)—N(6)	125.3(2)	N(1)—C(6)—N(6)	117.4(1)
C(6)—N(6)—C(1′)	122.2(2)	N(6)—C(1′)—C(2′)	112.6(2)	C(1′)—C(2′)—C(3′)	115.2(2)
C(2′)—C(3′)—C(4′)	117.7(2)	C(3′)—C(4′)—C(5′)	112.1(2)	C(4′)—C(5′)—C(6′)	116.2(2)
C(5′)—C(6′)—C(7′)	114.7(2)	C(6′)—C(7′)—C(8′)	114.4(2)	C(7′)—C(8′)—C(9′)	114.3(2)
C(8′)—C(9′)—N(9)	109.8(2)	C(9′)—N(9)—C(4)	124.2(1)	C(9′)—N(9)—C(8)	125.9(2)

slight pyramidalization of the N atom as it ranges from 0.00 Å (27*b*) to 0.05 Å (27*a*) out of the plane defined by C6—H6—$C_{subst.}$. Our purinophane **9** is unique in having a 35° rotational twist enforced upon the C6—N6 bond and, as such, it represents a test of the Bader–Wiberg theory for this class of compounds. From Table 3, the average C6—N6 bond length for molecules A and B of **9** is 1.347 Å, a value at the upper end of the accepted average magnitude for this bond, and scarcely convincing evidence for the theory. However, against this must be set the distinct pyramidalization of N6, which is 0.25 Å out of the C6—H6—C1′ plane in molecule A and 0.22 Å from the corresponding plane in molecule B. That is, N6 is over 50% pyrimidalized, a situation fully consistent with the Bader–Wiberg proposals.

The crystallographic data for [8]-purinophane **3** (9) are also pertinent here because the H6—N6—C1′ fragment of **3** was twisted with respect to the purine ring by 30°. Inspection of the data shows the N6 atom again is pyrimidalized appreciably, being 0.23 Å out of the C6—H6—C1′ plane but, as in the [9]-purinophane, the C6—N6 bond length of 1.349 Å is only marginally longer than the average. Evidently, for this class of compounds rotation about the exocyclic C6—N6 bond is accompanied by strong pyramidalization but the extent of bond lengthening is much less distinctive than is observed for the amide cases (25).

Experimental methods

Melting points were recorded on a Gallenkamp capillary tube melting point apparatus and are uncorrected. Proton magnetic resonance (^{1}H NMR) spectra were recorded on a Varian EM-390, a Bruker AC-200, or a Bruker AM-500 spectrometer with chloroform-*d* as the solvent unless otherwise noted. Unless specified, the usual internal references were tetramethylsilane (TMS) or chloroform. The abbreviations (s) = singlet, (d) = doublet, (t) = triplet, (q) = quartet, (m) = multiplet, and (br) = broad are used in the description of the spin–spin splitting pattern present in the spectra. The natural abundance carbon-13 magnetic resonances (^{13}C NMR) were recorded on an AM-500 (at 125.776 MHz) or AC-200 (at 50.324 MHz) instrument using chloroform-*d* as the solvent and internal reference unless otherwise noted. All ^{13}C spectra were broad band decoupled. Low-resolution mass spectra (MS) and high-resolution mass spectra (HRMS) were obtained on either a VG Micromass 7070F or a VG ZAB-E mass spectrometer with samples being introduced through a direct inlet system. Ions were generated using electron impact (EI) or through chemical ionization (CI) with NH_3 as the reactant gas. Infrared spectra (IR) were recorded on a Perkin–Elmer 283 spectrometer. IR samples were run as neat liquids using NaCl windows. The symbols (s) = strong and (br) = broad were used in the recording of the IR data to indicate the intensity of the recorded bands. Ultraviolet (UV) spectra were recorded on a Perkin–Elmer Lambda 9 UV/VIS/NIR spectrophotometer.

Can. J. Chem. Downloaded from www.nrcresearchpress.com by 88.255.202.194 on 09/08/12
For personal use only.

TABLE 4. Dihedral and torsional angles (deg)

Molecule A			
N(3)—C(4)—C(5)—N(7)	−178.6(2)	C(6)—C(5)—C(4)—N(9)	−171.2(2)
C(5)—C(4)—N(9)—C(9′)	156.7(2)	N(3)—C(4)—N(9)—C(9′)	−22.7(2)
N(7)—C(8)—N(9)—C(9′)	−157.5(2)	C(4)—N(9)—C(9′)—C(8′)	−61.5(2)
C(8)—N(9)—C(9′)—C(8′)	91.9(2)	N(9)—C(9′)—C(8′)—C(7′)	−62.5(2)
C(9′)—C(8′)—C(7′)—C(6′)	150.1(2)	C(8′)—C(7′)—C(6′)—C(5′)	−70.5(2)
C(7′)—C(6′)—C(5′)—C(4′)	−72.3(2)	C(6′)—C(5′)—C(4′)—C(3′)	−174.5(2)
C(5′)—C(4′)—C(3′)—C(2′)	−170.6(2)	C(4′)—C(3′)—C(2′)—C(1′)	66.4(2)
C(3′)—C(2′)—C(1′)—N(6)	56.6(2)	C(2′)—C(1′)—N(6)—C(6)	−89.8(2)
C(1′)—N(6)—C(6)—N(1)	144.5(2)	C(1′)—(N6)—C(6)—C(5)	−35.1(2)
N(6)—C(6)—N(1)—C(2)	−172.1(2)	N(6)—C(6)—C(5)—C(4)	167.7(2)
N(6)—C(6)—C(5)—N(9)	156.5(2)		
Molecule B			
N(3)—C(4)—C(5)—N(7)	176.1(2)	C(6)—C(5)—C(4)—N(9)	172.4(2)
C(5)—C(4)—N(9)—C(9′)	−154.7(2)	N(3)—C(4)—N(9)—C(9′)	26.5(2)
N(7)—C(8)—N(9)—C(9′)	155.4(2)	C(4)—N(9)—C(9′)—C(8′)	61.9(2)
C(8)—N(9)—C(9′)—C(8′)	−90.2(2)	N(9)—C(9′)—C(8′)—C(7′)	63.8(2)
C(9′)—C(8′)—C(7′)—C(6′)	−151.9(2)	C(8′)—C(7′)—C(6′)—C(5′)	72.7(2)
C(7′)—C(6′)—C(5′)—C(4′)	68.9(2)	C(6′)—C(5′)—C(4′)—C(3′)	177.9(2)
C(5′)—C(4′)—C(3′)—C(2′)	171.2(2)	C(4′)—C(3′)—C(2′)—C(1′)	−70.2(2)
C(3′)—C(2′)—C(1′)—N(6)	−56.4(2)	C(2′)—C(1′)—N(6)—C(6)	92.4(2)
C(1′)—N(6)—C(6)—N(1)	−150.8(2)	C(1′)—N(6)—C(6)—C(5)	28.7(2)
N(6)—C(6)—N(1)—C(2)	171.4(2)	N(6)—C(6)—C(5)—C(4)	−166.6(2)
N(6)—C(6)—C(5)—N(9)	−156.7(2)		

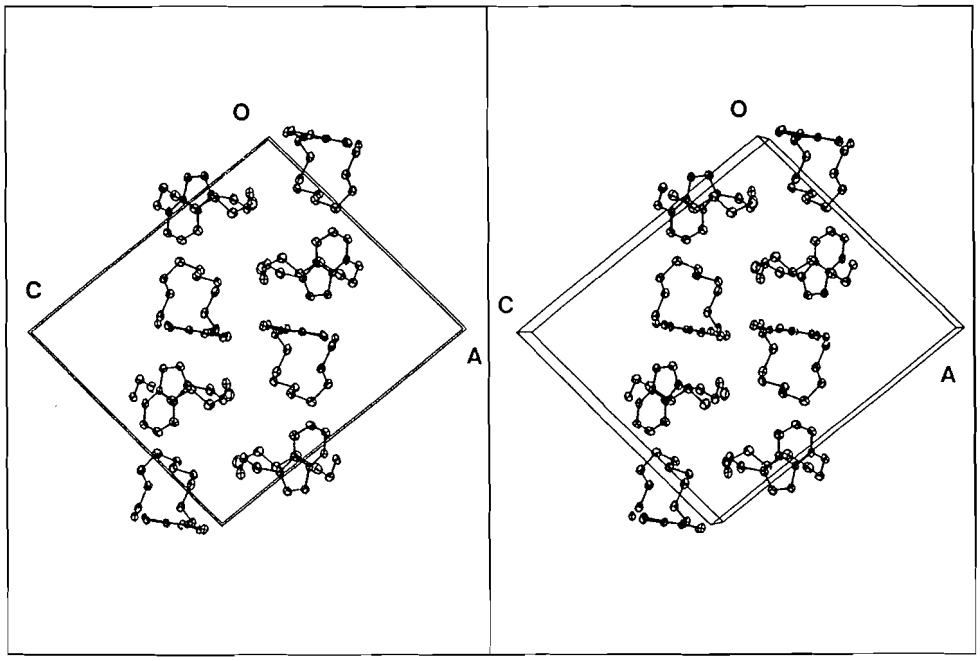

FIG. 5. Stereoview of the crystal packing of [9](*N*6,9)-6-aminopurinophane. The view is down the *b* axis.

Tetrahydrofuran (THF) was dried by refluxing and distilling from sodium and benzophenone under dry nitrogen. THF was collected from the distillation apparatus as required. *N*,*N*-Dimethylformamide (DMF) was refluxed and subsequently distilled from BaO. Acetonitrile was distilled from P_2O_5 followed by distillation from CaH_2, discarding the first 5% and the last 10%. The NMR solvent chloroform-*d* was stored over molecular sieves (4Å) prior to use.

Unless specified, column chromatography was performed by the "flash" method of Still, Kahn, and Mitra (28). The silica gel used for column chromatography (5.0% of 100 mesh up; 47.6% of 100–200 mesh and 47.4% of 200 mesh down) was purchased from Terochem. Silica gel 60 F_{254} (E. Merck Co.) plates of 0.2 mm thickness were used for analytical thin-layer chromatography (TLC). Visualization was achieved using a UV lamp at 254 nm or via treatment of the TLC with either a molybdic acid spray (20 g of molybdic acid and 15 g of ceric sulphate dissolved in 1 L of 10% sulphuric acid) or a ninhydrin spray (0.2% ninhydrin in ethanol) followed by heating.

Synthesis of 9-azidononanol, 5

The procedure followed is similar to that described by Castro (10*b*) or Boigegrain *et al.* (10*a*). 1,9 Nonanediol (2.5 g, 15.6 mmol)

Can. J. Chem. Downloaded from www.nrcresearchpress.com by 88.255.202.194 on 09/08/12
For personal use only.

Can. J. Chem. Downloaded from www.nrcresearchpress.com by 88.255.202.194 on 09/08/12
For personal use only.

TABLE 5. Positional parameters ($\times 10^4$) and U_{eq}(Å^2) ($\times 10^4$) for [9](*N*6,9)-6-aminopurinophane with standard errors in parentheses

Atom	*x*	*y*	*z*	U_{eq}[a]
Molecule A				
N(1)	9737(1)	3284(2)	528(1)	279
C(2)	9664(1)	1740(2)	635(1)	307
N(3)	9125(1)	975(2)	961(1)	285
C(4)	8663(1)	2002(2)	1259(1)	246
C(5)	8702(1)	3634(2)	1244(1)	242
C(6)	9220(1)	4274(2)	799(1)	235
N(7)	8133(1)	4290(2)	1629(1)	287
C(8)	7759(1)	3060(2)	1840(1)	288
N(9)	8045(1)	1645(2)	1639(1)	268
N(6)	9247(1)	5802(2)	611(1)	277
C(1′)	8530(1)	6768(2)	508(1)	293
C(2′)	8145(1)	6708(2)	−236(1)	329
C(3′)	7923(1)	5074(2)	−521(1)	315
C(4′)	7269(1)	4223(2)	−181(1)	302
C(5′)	7179(1)	2516(2)	−410(1)	318
C(6′)	6483(1)	1643(2)	−143(1)	338
C(7′)	6589(1)	1244(2)	632(1)	300
C(8′)	7201(1)	−22(2)	845(1)	289
C(9′)	7603(1)	163(2)	1583(1)	306
Molecule B				
N(1)	5320(1)	6521(2)	−545(1)	301
C(2)	5854(1)	7584(2)	−697(1)	339
N(3)	5948(1)	8277(2)	−1299(1)	343
C(4)	5345(1)	7892(2)	−1775(1)	282
C(5)	4713(1)	6918(2)	−1688(1)	249
C(6)	4757(1)	6075(2)	−1057(1)	262
N(7)	4185(1)	6894(2)	−2289(1)	309
C(8)	4525(1)	7794(2)	−2720(1)	337
N(9)	5230(1)	8430(2)	−2451(1)	307
N(6)	4291(1)	4862(2)	−923(1)	326
C(1′)	3943(1)	3814(2)	−1472(1)	363
C(2′)	4460(1)	2379(2)	−1570(1)	403
C(3′)	5302(1)	2740(2)	−1723(1)	370
C(4′)	5419(1)	3442(3)	−2433(1)	358
C(5′)	6271(1)	3975(3)	−2476(1)	430
C(6′)	6457(1)	4639(3)	−3172(1)	499
C(7′)	6070(1)	6226(3)	−3361(1)	440
C(8′)	6438(1)	7616(2)	−2938(1)	403
C(9′)	5869(1)	8959(2)	−2852(1)	383

[a] $U_{eq} = {}^1/_3(U_{11} + U_{22} + U_{33} + 2\cos\beta U_{13})$.

was dissolved in 15 mL of dry THF under a nitrogen atmosphere and cooled to −20°C. Carbon tetrachloride (6.0 mL, 9.6 g, 62.2 mmol) was added followed by slow dropwise addition of hexamethylphosphorus triamide (HMPT) (3.1 mL, 2.8 g, 17.1 mmol) via a syringe. The reaction mixture was then added to 100 mL of H_2O and washed with 100 mL of diethyl ether. Potassium hexafluorophosphate (5.5 g, 30 mmol) was added to the aqueous solution, which was then extracted with three 100-mL portions of $CHCl_3$. The combined organic extracts were dried over anhydrous Na_2SO_4 and evaporated under reduced pressure. The oily residue was dissolved in 50 mL of DMF and stirred for 12 h in the presence of NaN_3 (5 g, 77 mmol) at 80°C. The solvent was subsequently evaporated under reduced pressure and the residue taken up into 100 mL of H_2O followed by extraction with four 100-mL portions of ether. The ether extracts were dried over Na_2SO_4 and the solvent evaporated under a reduced pressure. The crude product was purified by vacuum distillation. TLC with 5% methanol in $CHCl_3$ using the molybdic acid spray for visualization showed the desired product having an $R_f = 0.54$. The yield was 87% (2.51 g, 13.6 mmol). The compound showed: bp 89°C at 0.01 Torr (1 Torr = 133.3 Pa). IR: 3360 cm^{-1} (br, OH), 2095 cm^{-1} (s, N_3). ^{1}H NMR (200 MHz), δ: 1.22 (m,, 10H, $(CH_2)_5$), 1.49 (m, 4H, CH_2-CH_2-OH and CH_2-CH_2-N_3), 3.16 (t, 2H, J = 6.8 Hz, CH_2-N_3) and 3.51 (t, 2H, J = 6.6 Hz, CH_2-OH). ^{13}C NMR (200 MHz), δ: 25.57 (C3), 26.54 (C5), 28.66 (C6), 28.93 (C7), 29.17 (C4), 29.28 (C8), 32.56 (C2), 51.30 (C9), 62.64 (C1). MS [EI], *m/z* (RI%): 203 $[M + 18]^+$ (17), 186 $[M + 1]^+$ (7), 178 (40), 158 $[M + 1 - N_2]^+$ (65), 70 (60), 56 (40), and 44 (100).

Synthesis of 6-chloro-9-(1-azidononyl)purine, 7

The procedure used was similar to that of Iwakawa *et al.* (11*b*). To a mixture of 6-chloropurine (1.59 g, 10.28 mmol), triphenylphosphine (2.7 g, 10.28 mmol), and diethyl azidocarboxylate (2.20 g, 2 mL, 12.60 mmol) in 40 mL of dry THF was added a solution of 9-azidononanol (2.00 g, 10.80 mmol) in 40 mL of THF. The solution was allowed to stir at room temperature for 48 h, at which time the reaction mixture was concentrated under reduced pressure. The residue was chromatographed on silica gel using 1% methanol in $CHCl_3$, yielding a viscous yellow oil. TLC of the product with 5% methanol in $CHCl_3$ gave an $R_f = 0.52$. The yield was 23% (759 mg, 2.36 mmol). The compound showed: ^{1}H NMR (200 MHz), δ: 1.22 (m, 10H, $(CH_2)_5$), 1.56 (m, 2H, CH_2-CH_2-N_3), 1.92 (m, 2H, CH_2-CH_2-N9), 3.20 (t, 2H, J = 6.5 Hz, CH_2-N_3), 4.27 (t, 2H, J = 7.5 Hz, CH_2-N9), 8.10 (s, 1H, C8H), 8.73 (s, 1H, C2H). ^{13}C NMR (200 MHz), δ: 26.16 (C8′ or C5′), 26.19 (C5′ or C8′), 28.37 (C6′ or C7′), 28.45 (C7′ or C6′), 28.55 (C4′ or C3′), 28.79 (C3′ or C4′), 29.43 (C2′), 44.15 (C9′), 51.00 (C1′), 131.15 (C5), 145.06 (C8), 150.37 (4), 151.39 (C2), 151.52 (C6). HRMS: Exact Mass calcd. for $C_{14}H_{20}N_7Cl$: 321.1468; found: 321.1470. MS [EI], *m/z* (RI%): 321 $[M]^+$ (3), 265 $[M - CH_2N_3]^+$ (41), 209 $[M - (CH_2)_5N_3]^+$ (56), 155 (100).

Synthesis of 6-chloro-9-(1-aminononyl)purine, 8

The procedure used was similar to that of Vaultier *et al.* (12). To 6-chloro-9-(1-azidononyl)purine (500 mg, 1.56 mmol) in 1.6 mL of THF was added triphenylphosphine (410 mg, 1.56 mmol), H_2O (45 μL, 2.34 mmol), and a boiling chip. The evolution of N_2 began immediately. The mixture was left standing at room temperature for 18 h. TLC of the reaction mixture showed the complete disappearance of the azide starting material and the appearance of a ninhydrin positive spot on the baseline. The solution was then concentrated, redissolved in 50 mL of $CHCl_3$, and extracted with three 20-mL portions of 0.01 M HCl. The combined aqueous solutions were adjusted to pH 8 with 1 M NaOH and extracted with three 30-mL portions of $CHCl_3$. These combined organic solutions were dried over anhydrous Na_2SO_4 and evaporated under reduced pressure. The product normally was subjected immediately to cyclization conditions. TLC with 10% methanol in $CHCl_3$ using ninhydrin spray for visualization showed the desired product with an $R_f = 0.05$. The yield of **8** was 98% (451 mg, 1.53 mmol) via NMR. The compound showed: ^{1}H NMR (90 MHz) (hydrochloride salt in D_2O; internal reference: 3-(trimethylsilyl)propionic acid sodium salt), δ: 1.30 (m, 14H, $(CH_2)_7$), 3.00 (t, 2H, CH_2-NH_3^+), 4.38 (t, 2H, CH_2-N9), 7.70 (s, 1H, C2H), and 8.37 (s, 1H, C8H).

Synthesis of [9](N6,9)-6-aminopurinophane, 9

6-Chloro-9-(1-aminononyl)purine (100 mg, 0.338 mmol) was dissolved in 5 mL acetonitrile. Diisopropylethylamine (1 mL, 5.74 mmol) was added and the solution diluted with an additional 45 mL of acetonitrile to give a 6.8 mM solution of **8**. The reaction was left stirring at 60°C for 48 h at which time the solution was evaporated and the resultant residue was chromatographed on silica gel using 5% methanol in $CHCl_3$. Recrystallization from toluene gave analytically pure crystals of the cyclophane. TLC of the product in 10% methanol in $CHCl_3$ gave an $R_f = 0.46$. The yield of **9** was 26% (23 mg, 0.088 mmol). The compound showed: mp 121–123°C. UV: λ_{max} 276.4 (ε = 13 478, methanol). ^{1}H NMR (500 MHz at 75°C; sealed tube with $CDCl_3$), δ: 0.11

Can. J. Chem. Downloaded from www.nrcresearchpress.com by 88.255.202.194 on 09/08/12
For personal use only.

(m, 1H, C5′H), 0.18 (m, 1H, C6′H), 0.39 (m, 1H, C6′H), 0.62 (m, 1H, C4′H), 0.68 (m, 1H, C3′H), 0.72 (m, 1H, C4′H), 0.79 (m, 1H, C5′H), 0.88 (m, 1H, C7′H), 1.02 (m, 1H, C3′H), 1.14 (m, 1H, C7′H), 1.38 (m, 1H, C2′H), 1.56 (m, 1H, C8′H), 1.59 (m, 1H, C2′H), 1.86 (m, 1H, C8′H), 3.64 (m, 1H, C1′H), 3.89 (m, 1H, C9′H), 4.24 (m, 1H, C1′H), 4.58 (m, 1H, C9′H), 5.21 (br, 1H, NH), 7.77 (s, 1H, C2H), and 8.32 (s, 1H, C8H). ^{13}C NMR (500 MHz), δ: 24.30 (C3′), 24.54 (C7′), 26.96 (C4′), 27.35 (5′), 27.74 (C6′), 27.90 (C8′), 30.28 (C2′), 42.89 (C1′), 44.97 (C9′), 121.5 (C5), 142.39 (C8), 152.33 (C2), 158.67 (C6). HRMS: Exact Mass calcd. for $C_{14}H_{21}N_5$: 259.1797; found: 259.1792. MS [CI], *m/z* (RI%): 260 $[M + 1]^+$ (18), 194 (100), and 177 (71).

X-ray crystallography

Crystals of [9](*N*6,9)-6-aminopurinophane were grown from chloroform–toluene (1:3) solution. The density was determined by suspension in an aqueous solution of $ZnCl_2$. Large transparent acicular crystals were examined under a polarizing microscope for homogeneity. A small irregular crystal, 0.10 × 0.20 × 0.40 mm, was cut from a larger crystal and mounted on the tip of a glass fibre with epoxy cement. The crystal was cooled by liquid nitrogen using a device supplied by Molecular Structure Corporation, Texas, and the unit cell parameters were determined at 173 K from a least-squares refinement of the angular positions of 25 reflections with θ in the range $39.7 \leq \theta \leq 40.0°$ recorded on a Rigaku AFC6R diffractometer with use of graphite monochromated CuKα radiation (λ = 1.540 598 Å at 298 K). Intensity data were also recorded on a Rigaku AFC6R diffractometer at 173 K by use of ω–2θ scan for 3232 reflections (*h*,*k*, ± *l*), with $\theta \leq 50.0°$. Three standard reflections were monitored every 150 reflections and showed no sign of instrument instability or crystal decay. Corrections were made for Lorentz-polarization effects but not for absorption. Reflections with $3\sigma_I \geq (I) \geq -3\sigma_I$ were treated by the method of French and Wilson (29). Systematically absent data (264 reflections) were removed and symmetry-equivalent data were averaged to give 2846 independent reflections, $R_{int} = 0.0249$, of which 2556 were within $I \geq 2.5\sigma(I)$. Atomic positional parameters and U_{eq} for non-hydrogen atoms are given in Table 5.[8]

Structure solution

The structure was solved by direct methods based on 494 reflections with $|E| > 1.2$ and 30 sets of starting phases with use of the program SHELXS-86 (30). Full-matrix least-squares refinement of the coordinates of the non-hydrogen atoms followed by a three-dimensional difference electron density synthesis revealed the positional parameters of all the hydrogen atoms. The temperature factors of all of the non-hydrogen atoms were made anisotropic and the hydrogen atoms were assigned a common overall isotropic temperature factor and included in refinement. Further cycles using block-matrix least squares, minimizing $\Sigma\omega(|F_o| - |F_c|)^2$, were terminated when the maximum shift/error reached 0.004. A correction for secondary extinction was made by the method in SHELX-76 (31). Final $R_1 = 0.0364$ and $R_2 = 0.0395$, $S = 1.3618$. Scattering factors were taken from ref. 32. Calculations employed XTAL (33), data reduction and mean planes; SHELX-76 (31), structure refinement; MOLGEOM (34) and CHEM-X (35), molecular geometry; and SNOOPI (36), diagrams running on a VAX 8650 computer.

[8]Tables of anisotropic temperature factors, hydrogen positional parameters, bond lengths and angles involving hydrogen atoms, best planes, and the moduli of F_o and F_c have been deposited. Complete sets of data may be purchased from: The Depository of Unpublished Data, Document Delivery, CISTI, National Research Council Canada, Ottawa, Canada K1A 0S2.

Tables of crystal data, hydrogen positional parameters, and bond lengths and angles involving hydrogen atoms have also been deposited with the Cambridge Crystallographic Data Centre and can be obtained on request from The Director, Cambridge Crystallographic Data Centre, University Chemical Laboratory, 12 Union Road, Cambridge, CB2 1EZ, U.K.

Acknowledgements

The authors acknowledge with thanks the financial support of the Natural Sciences and Engineering Research Council of Canada (NSERC), and the award of an NSERC post-graduate scholarship to A.C.

1. W. W. Paudler and M. D. Bezoari. *In* Cyclophanes. Vol II. *Edited by* P. M. Keehn and S. M. Rosenfeld. Academic Press, New York. 1983. Chap. 6, p. 359.
2. T. Hiyama, S. Hirano, and H. Nozaki. J. Am. Chem. Soc. **96**, 5287 (1974).
3. A. Agarwal, J. A. Barnes, J. L. Fletcher, M. J. McGlinchey, and B. G. Sayer. Can. J. Chem. **55**, 2575 (1977).
4. F. Seyama, K. Akahori, Y. Sakata, S. Misumi, M. Aida, and C. Nagata. J. Am. Chem. Soc. **110**, 2192 (1988), and references therein.
5. K. Ienaga, T. Hasegawa, D. J. Brown, and W. Pfleiderer. J. Chem. Soc. Perkin Trans. 1, 593 (1988).
6. K. Ienaga and W. Pfleiderer. Liebigs Ann. Chem. 1872 (1979).
7. H. Higuchi, M. Mitsuoka, Y. Sakata, and S. Misumi. Tetrahedron Lett. **26**, 3849 (1985).
8. R. A. Bell and H. N. Hunter. Tetrahedron Lett. **28**, 147 (1987).
9. R. A. Bell, R. Faggiani, H. N. Hunter, and C. J. L. Lock. Can. J. Chem. **70**, 186 (1992).
10. (*a*) R. Boigegrain, B. Castro, and C. Selve. Tetrahedron Lett. 2529 (1975); (*b*) B. Castro. Org. React. **29**, Chap. 1 (1983).
11. (*a*) O. Mitsunobu. Synthesis, 1 (1981); (*b*) M. Iwakawa, B. M. Pinto, and W. A. Szarek. Can. J. Chem. **56**, 326 (1978).
12. (*a*) M. Vaultier, N. Knouzi, and R. Carrié. Tetrahedron Lett. **24**, 763 (1983); N. Knouzi, M. Vaultier, and R. Carrié. Bull. Soc. Chim. Fr. 815 (1985); (*b*) Y. G. Gololobov, I. N. Zhmurova, and L. F. Kasukhin. Tetrahedron, **37**, 437 (1981).
13. M. Winnick. Chem. Rev. **81**, 491 (1981).
14. D. A. Kleier and G. Binsch. DNMR3 (1970). Program 165. Quantum Chemistry Program Exchange, Indiana University, Bloomington, Ind.
15. A. B. Reitz, D. W. Graden, A. D. Jordan, Jr., and B. E. Maryanoff. J. Org. Chem. **55**, 5761 (1990).
16. W. C. Still. Macromodel computer program. Version 1.5. Columbia University, New York. 1987.
17. E. J. Gabe, Y. Le Page, J.-P. Charland, F. L. Lee, and P. S. White. NRCVAX. An interactive program system for structure analysis. J. Appl. Crystallogr. **22**, 384 (1989).
18. A. Bondi. J. Phys. Chem. **68**, 441 (1964); N. L. Allinger, J. A. Hirsch, M. A. Miller, I. J. Tyminski, and F. A. VanCatledge. J. Am. Chem. Soc. **90**, 1199 (1968).
19. D. Voet and A. Rich. Prog. Nucleic Acid Res. Mol. Biol. **10**, 183 (1970).
20. F. H. Allen, O. Kennard, D. G. Watson, L. Brammer, G. Orpen, and R. Taylor. J. Chem. Soc. Perkin Trans. 2, S1 (1987).
21. F. J. Zuniga and G. Chapuis. Cryst. Struct. Commun. **10**, 533 (1981).
22. M. Oki. Applications of dynamic NMR spectroscopy to organic chemistry. VCH Publishers Inc., Deerfield, Fla. 1985. Chap. 2.
23. R. F. W. Bader, J. R. Cheeseman, K. E. Laidig, K. B. Wiberg, and C. Breneman. J. Am. Chem. Soc. **112**, 6530 (1990).
24. K. B. Wiberg and K. E. Laidig. J. Am. Chem. Soc. **109**, 5935 (1987).
25. A. J. Bennet, Q.-P. Wang, H. Slebocka-Tilk, V. Somayaji, R. S. Brown, and B. D. Santarsiero. J. Am. Chem. Soc. **112**, 6383 (1990).

26. (*a*) R. Taylor and O. Kennard. J. Mol. Struct. **78**, 1 (1982); (*b*) G. Bunick and D. Voet. Acta Crystallogr. Sect. B: Struct. Crystallogr. Cryst. Chem. **B30**, 1651 (1974); (*c*) T. F. Lai and R. E. Marsh. Acta Crystallogr. Sect. B: Struct. Crystallogr. Cryst. Chem. **B28**, 1982 (1972); (*d*) S. Sprang, D. C. Rohrer, and M. Sundaralingam. Acta Crystallogr. Sect. B: Struct. Crystallogr. Cryst. Chem. **B34**, 2803 (1978); (*e*) T. J. Kistenmacher and M. Rossi. Acta Crystallogr. Sect. B: Struct. Crystallogr. Cryst. Chem. **B33**, 253 (1977); (*f*) W. S. Sheldrick and M. Morr. Acta Crystallogr. Sect. B: Struct. Crystallogr. Cryst. Chem. **B36**, 2328 (1980).
27. (*a*) H. Sternglanz and C. E. Bugg. J. Cryst. Mol. Struct. **8**, 263 (1978); (*b*) U. Thewalt and C. E. Bugg. Acta Crystallogr. Sect. B: Struct. Crystallogr. Cryst. Chem. **B28**, 1767 (1972); (*c*) C. E. Bugg and U. Thewalt. Biochem. Biophys. Res. Commun. **46**, 779 (1972); (*d*) R. K. McMullan and M. Sundaralingam. J. Am. Chem. Soc. **93**, 7050 (1971).
28. W. C. Still, M. Kahn, A. J. Mitra. J. Org. Chem. **43**, 2923 (1978).
29. S. French and K. Wilson. Acta Crystallogr. Sect. A: Cryst. Phys. Diffr. Theor. Gen. Crystallogr. **A34**, 517 (1978).
30. G. M. Sheldrick. SHELXS-86. Program for crystal structure solution. University of Göttingen, Federal Republic of Germany. 1986.
31. G. M. Sheldrick. SHELX-76. Program for crystal structure determination. University of Cambridge, England. 1976.
32. D. T. Cromer and J. B. Mann. Acta Crystallogr. Sect. A: Cryst. Phys. Diffr. Theor. Gen. Crystallogr. **A24**, 321 (1968).
33. J. M. Stewart and S. R. Hall. The XTAL system of crystallographic programs. Tech. Rept. TR-1364. University of Maryland, College Park, Md. 1983.
34. J. Stephens. MOLGEOM adapted from CUDLS. McMaster University, Hamilton, Ont. 1973.
35. K. Davies. CHEM-X. Chemical Design Ltd., Oxford, England. 1986.
36. K. Davies. CHEMGRAF suite: SNOOPI. Chemical Design Ltd., Oxford, England. 1983.

Can. J. Chem. Downloaded from www.nrcresearchpress.com by 88.255.202.194 on 09/08/12
For personal use only.

Reaction de méthanation du gaz de synthèse : Influence de la température de calcination des catalyseurs à base de nickel

M. GHAZI[1] ET J. BARRAULT

Laboratoire de catalyse en chimie organique, Université de Poitiers, Unité de recherche associée 350, Centre national de la recherche scientifique, 40, avenue du Recteur Pineau, 86022 Poitiers CEDEX, France

Reçu le 6 mars 1992

M. GHAZI et J. BARRAULT. Can. J. Chem. **71**, 107 (1993).

En raison de leur activité et sélectivité importantes, les catalyseurs au nickel sont souvent utilisés pour réaliser la réaction de méthanation du gaz de synthèse; cependant le procédé conventionnel basé sur ces solides ne répond plus aux exigences économiques actuelles. Afin d'augmenter leur stabilité, trois catalyseurs à teneur en nickel comparable, ont été étudiés en réaction de méthanation après avoir subi des calcinations à différentes températures. Les résultats obtenus montrent que le solide calciné à haute température (973 K) est le plus prometteur puisqu'il garde une activité appréciable et surtout une stabilité importante même dans des conditions de réactions très sévères (température = 773 K).

M. GHAZI and J. BARRAULT. Can. J. Chem. **71**, 107 (1993).

Due to their important activity and selectivity, nickel catalysts are often used to realize the methanation reaction; however, the usual process based on these catalysts is not fitted for the present economic situation. To raise their stability, three catalysts with similar nickel content but calcinated at different temperatures have been studied for the reaction of methanation. The results obtained show that the catalyst calcinated at the highest temperature (973 K) shows the greatest promise because a great part of its activity and of its stability is preserved even when the reaction conditions are extreme (temperature of 773 K).

[Journal translation]

Can. J. Chem. Downloaded from www.nrcresearchpress.com by 88.255.202.194 on 09/08/12
For personal use only.

Introduction

Les catalyseurs au nickel trouvent des applications industrielles très vastes comme dans l'hydrogénation des composés organiques insaturés, le vaporéformage ou la méthanation du gaz de synthèse. Ils présentent un double intérêt : du point de vue fondamental, le nickel semble mieux se prêter aux études de mécanismes réactionnels, les phases adsorbées sont plus simples à étudier et il y a moins de produits formés. Du point de vue économique, il est possible d'orienter sélectivement la réaction.

Le choix du nickel dans la réaction de méthanation est également justifié par les résultats de Vannice (1) et ceux de notre laboratoire (2, 3) qui montrent que ce métal est l'un des plus actifs après le ruthénium et le fer. Ces derniers ont été écartés, l'un en raison de son prix et l'autre en raison de la facilité de la réaction de dismutation à son contact, réaction qui conduit à un dépôt de carbone et une désactivation plus rapide.

Les catalyseurs au nickel ont cependant une faible résistance aux impuretés contenues dans les charges, en particulier les composés soufrés et azotés. Ces molécules peuvent créer des liaisons de chimisorption suffisamment fortes par l'intermédiaire des doublets libres de l'atome de soufre ou d'azote avec le métal pour avoir un effet toxique très marqué. Généralement, une teneur de 5 ppm en soufre conduit à la désactivation totale du catalyseur.

Le procédé conventionnel de méthanation basé sur l'utilisation de ces catalyseurs ne répond plus aux exigences économiques de la mise en oeuvre de la réaction puisque les catalyseurs au nickel, peu thiorésistants, doivent fonctionner à la température la plus basse possible avec un gaz pur, désulfuré (coûteux) et de composition ajustée. Les progrès dans la réaction de méthanation sur catalyseurs au nickel auront donc deux exigences : (*i*) recherches de catalyseurs stables thermiquement conduisant à une amélioration des rendements énergétiques, et (*ii*) augmentation de la thiorésistance de ces catalyseurs.

Diverses propositions ont été faites dans ce sens pour améliorer la stabilité des catalyseurs au nickel : la modification du nickel par addition de divers promoteurs (3–7); la formation d'alliages entre le nickel et d'autres métaux de type : molybdène, tungstène, iridium (8–11).

Mais c'est la conception du catalyseur et sa préparation qui ont été fondamentalement modifiées à l'exemple des travaux de Kruissink *et al.* (12) ou de Bartholomew *et al.* (13) où les systèmes catalytiques étudiés sont alors des systèmes spinellisés ($NiAl_xO_y$) dont la nature et l'arrangement exact dépendent des processus d'activation.

Dans le but d'améliorer la stabilité thermique des catalyseurs nous avons étudié l'influence de la température de calcination des catalyseurs à teneur en nickel comparable sur leur activité et sélectivité dans la réaction de méthanation du gaz de synthèse.

Partie expérimentale

Appareillage

La réaction d'hydrogénation du monoxyde de carbone est réalisée sous pression ($P < 10$ MPa) à l'aide d'un montage décrit dans des publications antérieures. Les réactifs et produits sont analysés à pression atmosphérique à l'aide d'un chromatographe en phase gazeuse (3, 14).

Préparation des catalyseurs

Une série de catalyseurs au nickel supportés par l'alumine Rhône-Poulenc GFS 400 (extrudés de 1,2 à 2 mm, surface BET = 230 m^2/g) a été étudiée. Ces solides ont été préparés par la technique classique d'imprégnation lente à 353 K de solutions aqueuses du sel correspondant (nitrate de nickel) sur l'alumine. Les poudres obtenues sont ensuite séchées à l'étuve à 393 K puis calcinées sous air à 673 K ou 973 K.

Dans le tableau 1, nous avons résumé les propriétés des catalyseurs étudiés dans la réaction de méthanation du gaz de synthèse. La composition métallique des catalyseurs est donnée en % poids.

Avant la réaction, les catalyseurs sont réduits par l'hydrogène

[1]Auteur à qui adresser toute correspondance.

TABLEAU 1. Les propriétés principales (température de calcination, % de carbone déposé, dispersion, teneur du nickel en % poids . . .) des catalyseurs étudiés

Catalyseurs	Température de prétraitement (K)	Surface BET (m^2/g)	Carbone (%)	Quantité adsorbée H_2 ($\mu mol/g \cdot cat$)	Quantité adsorbée CO ($\mu mol/g \cdot cat$)	Dispersion (CO/Ni)
$Ni(7,9)/Al_2O_3$ GFS 400	393 (séché)	140	2,38	60	140	0,104
$Ni(8,5)/Al_2O_3$ GFS 400	673	140	2,42	50	125	0,086
$Ni(8,6)/Al_2O_3$ GFS 400	973	70	0,56	0	15	0,010

(débit = 10 L/h) à 773 K pendant 10 h après montée linéaire de la température (4°C/min).

Caractérisation des catalyseurs

Les catalyseurs ont été caractérisés par des méthodes simples : l'adsorption de monoxyde de carbone et d'hydrogène et l'analyse des dépôts carbonés par oxydation en température programmée.

Chimisorption du monoxyde de carbone

La technique utilisée est une méthode chromatographique déjà décrite (15) et mise en oeuvre de la façon suivante : un échantillon de catalyseur de masse déterminée est dégazé sous courant d'hélium, puis réduit par l'hydrogène à la température désirée. La réduction est suivie d'un dégazage en présence d'hélium à une température égale à celle de réduction, puis l'échantillon est refroidi à température ambiante. On introduit alors des quantités connues (pulses) de CO ou d'H_2 et on détermine les quantités chimisorbées par le catalyseur à l'aide d'un détecteur à conductivité thermique.

Analyse des dépôts carbonés

La quantité d'espèces carbonées déposées sur le catalyseur au cours de la réaction CO + H_2 est déterminée par oxydation en température programmée. Le gaz carbonique formé est analysé également avec une cellule à conductivité thermique (16).

Conditions de mise en oeuvre de la réaction CO + H_2

La réaction d'hydrogénation du monoxyde de carbone étant fortement exothermique, les grains de catalyseurs sont dilués dans du carbure de silicium (inerte vis-à-vis de la réaction). Les conditions de réaction sont les suivantes : la pression totale = 3 MPa; le rapport molaire H_2/CO = 3; la masse du catalyseur = 5 g; le débit total des réactifs = 30 L/h; la température de réaction est comprise entre 423 K et 773 K de façon à apprécier la stabilité des catalyseurs à haute température.

Resultats et discussion

Influence du prétraitement sur les catalyseurs au nickel

Trois catalyseurs à teneur en nickel comparable et prétraités à différentes températures de calcination (tableau 1) ont été étudiés dans la réaction de méthanation de CO + H_2.

L'évolution de l'activité des catalyseurs au nickel exprimée en taux de transformation global de CO (TTG_{CO} (%)) en fonction du temps de travail (h) est présentée sur la figure 1. Les catalyseurs calcinés à basse température (393 et 673 K) sont actifs initialement mais se désactivent après quelques heures de fonctionnement illustrant ainsi le comportement général des catalyseurs au nickel. Le solide calciné à haute température (973 K) semble au contraire répondre à l'objectif recherché. En effet, jusqu'à une température de réaction de l'ordre de 673 K le catalyseur n'a aucune activité catalytique. Au-delà, l'activité du catalyseur croit rapidement avec la température et le phénomène de vieillissement n'est plus observé et ce, même dans des conditions de réaction très sévères (773 K).

Influence du soufre sur les catalyseurs au nickel

En raison de la désactivation très rapide des catalyseurs au nickel calcinés à basse température au contact du gaz de synthèse, nous n'avons pas pu déterminer sans ambiguïté l'effet du soufre sur l'activité de ces catalyseurs. Il semble toutefois que l'action d'une faible teneur de soufre dans la charge (5 ppm) désactive complètement ces catalyseurs.

Cependant, le comportement du solide calciné à 973 K est très intéressant, puisqu'en plus de sa stabilité à haute température, on constate que sa désactivation en présence de soufre est réversible comme le montre la figure 2. Au cours de cette manipulation, la réaction est d'abord étudiée en l'absence d'H_2S, puis l'impureté soufrée de concentration connue est additionnée aux réactifs (après avoir obtenu une certaine stabilisation de l'activité du catalyseur), enfin l'impureté est supprimée de façon à apprécier la réversibilité de l'empoisonnement. Dans cette première étape nous avons volontairement limité la concentration en H_2S à une valeur inférieure à 50 ppm.

On observe après addition de 10 ou 20 ppm d'H_2S à la charge, une diminution très importante (×6) de l'activité du catalyseur. Lorsqu'on supprime l'H_2S, le catalyseur semble retrouver ses propriétés initiales.

Par rapport au comportement des catalyseurs calcinés à basse température, on met donc en évidence ici deux propriétés particulièrement intéressantes du catalyseur calciné à haute température : (*i*) un effet d'empoisonnement réversible de l'H_2S peu fréquement signalé dans la bibliographie; (*ii*) une stabilité accrue dans des conditions de réactions très sévères (température de réaction = 773 K).

Ces résultats exploratoires de la réaction de méthanation du gaz de synthèse sur un catalyseur conventionnel : nickel/alumine, nous conduisent aux remarques suivantes :

(*a*) Le catalyseur au nickel est actif dans la réaction de méthanation du gaz de synthèse, cependant sa stabilité est très faible. Cette désactivation est souvent attribuée à la formation du carbonyle de nickel $Ni(CO)_4$ (17). Certains auteurs pensent même que l'activité de ces catalyseurs est fonction de la taille des cristallites, à l'exemple de Van Meerten et coll. (18) qui ont montré que la formation (même faible) du carbonyle de nickel durant la réaction accroît la taille des particules entrainant ainsi un changement perpétuel de la surface du nickel.

Une étude très intéressante de Richardson *et al.* (19) sur l'influence de la taille des cristallites montre qu'au cours de la réaction, la distribution des cristallites s'élargit et on voit apparaître différentes tailles de particules variant jusqu'à un facteur 3 en volume. D'après ces mêmes auteurs, lorsque la taille des particules augmente, le degré d'accessibilité des

Can. J. Chem. Downloaded from www.nrcresearchpress.com by 88.255.202.194 on 09/08/12
For personal use only.

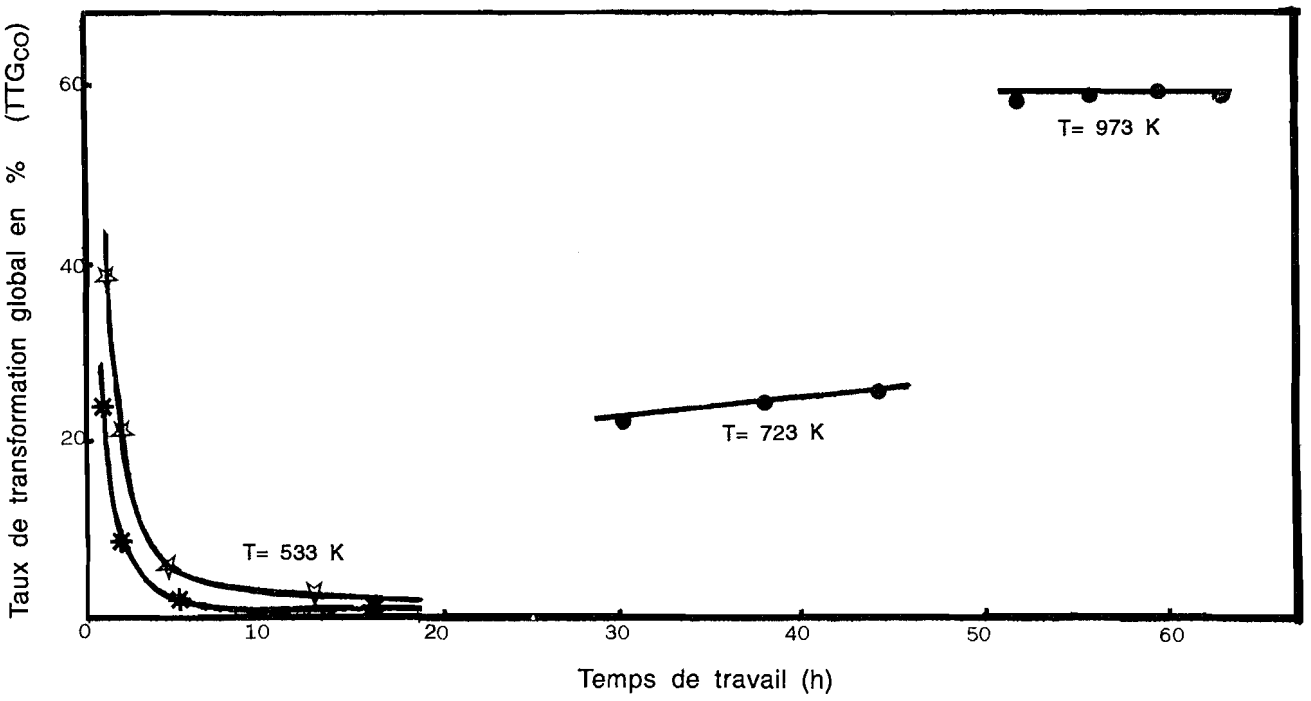

FIG. 1. Evolution de l'activité des catalyseurs au nickel au cours du temps dans la réaction de méthanation de CO + H_2. P = 3 MPa, H_2/CO = 3. Débit total = 30 L/h. (✱) séché à 393 K; (☆) calciné à 673 K; (●) calciné à 973 K.

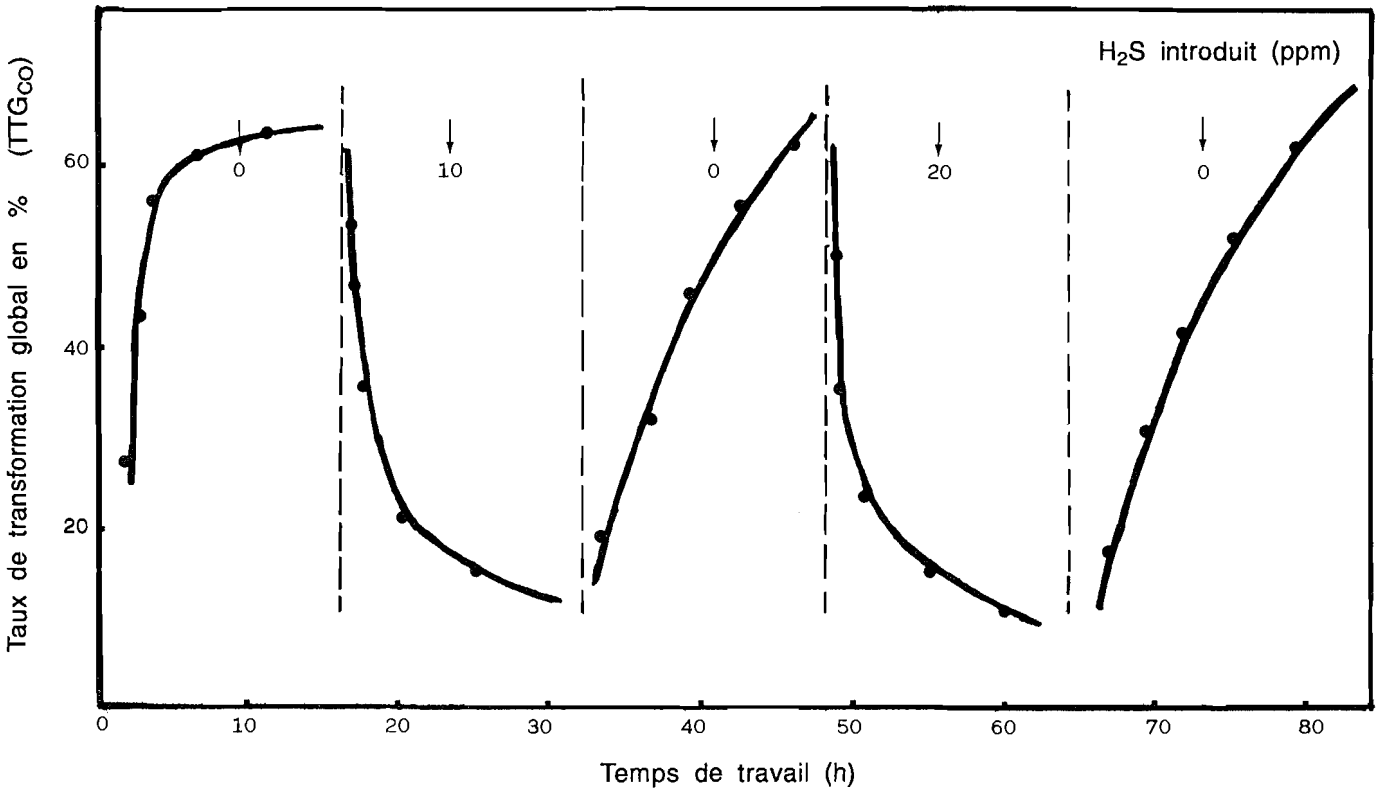

FIG. 2. Influence du soufre sur l'évolution de l'activité du catalyseur Ni(8,6)/Al_2O_3 GFS 400 calciné sous air à 973 K au cours du temps dans la réaction de méthanation de CO + H_2. P = 3 MPa. H_2/CO = 3. Débit total = 30 L/h. Température de réaction = 773 K.

réactifs diminue du même facteur. Les résultats présentés sur la figure 3 semblent aller dans le sens de ces observations. On constate en effet que lorsque la température de calcination passe de 673 à 973 K, la distribution des diamètres moyens des pores s'élargit variant jusqu'à un facteur 2 en volume.

D'autres auteurs (20–23) montrent que sur les catalyseurs au nickel, deux facteurs de désactivation intervien-

Can. J. Chem. Downloaded from www.nrcresearchpress.com by 88.255.202.194 on 09/08/12
For personal use only.

Can. J. Chem. Downloaded from www.nrcresearchpress.com by 88.255.202.194 on 09/08/12
For personal use only.

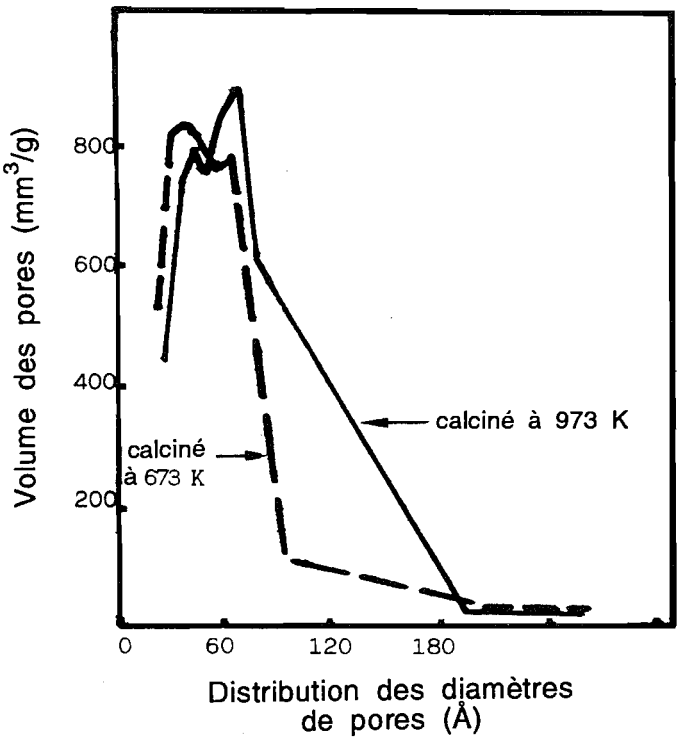

FIG. 3. Influence de la température de prétraitement sur la distribution des diamètres moyens des pores des catalyseurs nickel/alumine.

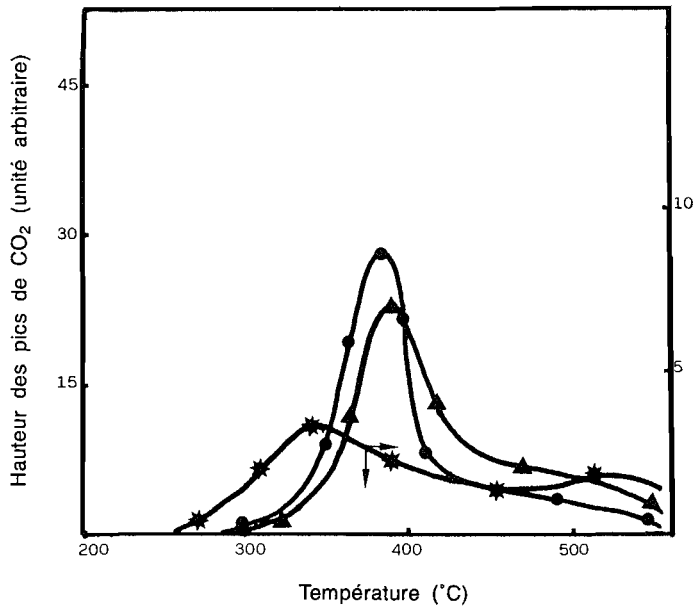

FIG. 4. Comparaison des dépôts carbonés par oxydation en température programmée des catalyseurs nickel/alumine. (●) séché à 393 K; (▲) calciné à 673 K; (✱) calciné à 973 K.

nent simultanément : le frittage de la phase métallique et un dépôt d'espèces carbonées. En fait, le frittage métallique qui explique pour l'essentiel la perte d'activité initiale du catalyseur se stabilise au bout d'un certain temps de réaction et la désactivation ultérieure résulte de l'empoisonnement par le carbone.

L'examen des résultats des analyses de carbone effectuées sur les catalyseurs au nickel présentés dans le tableau 1, montre que la quantité de carbone déposée sur le catalyseur calciné à haute température est diminuée d'un facteur 4. Cette faible valeur est en accord avec l'importante sélectivité en CO_2 observée pour ce catalyseur dans la réaction $CO + H_2$.

D'après les travaux cités précédemment (20, aussi communication orale), la présence du CO_2 dans le mélange réactionnel limite la désactivation en déplaçant l'équilibre de la réaction de dismutation du CO vers la gauche, défavorisant ainsi la formation de carbure ou d'espèces carbonées stables comme le montrent les résultats présentés sur la figure 4. La désactivation des catalyseurs métalliques par le «carbone» est un problème souvent rencontré et de grande importance pour la régénération des catalyseurs. L'analyse globale des dépôts carbonés par oxydation en température programmée (OTP) présentée sur la figure 4 montre que les dépôts carbonés les plus stables se forment au contact des catalyseurs calcinés à basse température (393 et 673 K). Lorsque le solide est calciné à la température de 973 K, on observe une diminution sensible (×4) de la quantité de carbone avec un déplacement du pic principal vers la gauche indiquant une oxydabilité plus facile des espèces carbonées formées. Il est difficile à partir de ces résultats d'établir une relation entre la stabilité des catalyseurs et la teneur ou la nature des dépôts carbonés. Généralement la formation des dépôts carbonés stables correspond à une désactivation plus rapide du catalyseur (24).

(*b*) On note encore une fois, l'extrême sensibilité du nickel à la présence d'impuretés soufrées. Cette propriété est très commentée dans la bibliographie. D'après les travaux de Fitzharris *et al.* (23), il semble que la désactivation rapide d'un catalyseur en présence de soufre est due non pas à un mécanisme «électronique» mais seulement à un blocage «géométrique» des sites actifs du nickel. En effet, ces auteurs en mesurant des énergies d'activation identiques, avec et sans soufre, ont conclu que les atomes de soufre adsorbés paraissent bloquer les sites actifs du nickel à la surface sans affecter les énergies des sites de nickel voisins. Un fait similaire a déjà été observé lors de l'étude de cette réaction sur un nickel déposé sur un film de cuivre (25, 26).

(*c*) Le phénomène évoqué ci-dessus ne semble pas se produire pour le catalyseur au nickel calciné à haute température (973 K), puisque ce dernier est assez actif à haute température et que la désactivation en présence de soufre est réversible. D'après Bartholomew *et al.* (13) ceci pourrait résulter de modifications électroniques ou de la formation de composés mixtes tel un aluminate de nickel ($NiAl_2O_4$) dans lequel les ions Ni^{2+} seraient difficiles à réduire. Le catalyseur résultant serait donc moins sensible aux poisons soufrés et les sites réactionnels ne seraient pas bloqués irréversiblement.

On peut remarquer que les capacités d'adsorption de l'hydrogène et du monoxyde de carbone, présentées dans le tableau 1, sont considérablement diminuées après la calcination à haute température traduisant la formation d'une phase spinelle d'oxydes mixtes de type «aluminate» : $NiAl_xO_y$ signalée précédemment.

Des modifications plus importantes (réduction du support, migration d'espèces partiellement réduites, . . .) pourraient être envisagées puisqu'une différence de comportement importante est mise en évidence par les expériences d'adsorption d'hydrogène et de monoxyde de carbone. Un

tel comportement est à l'origine de la notion de forte intéraction entre métal et support (FIMS) proposé par Tauster *et al.* (27). Il en résulterait la formation de nouveaux centres réactionnels qui favoriseraient l'adsorption dissociative du monoxyde de carbone (28, 29).

Conclusion

La résolution des problèmes de l'activité, la stabilité thermique et la thiorésistance des catalyseurs au nickel reste difficile à réaliser.

Les résultats obtenus montrent cependant que le protocole d'activation à haute température (973 K) où il semble établi que le nickel se trouve impliqué dans une structure spinelle, permet d'obtenir des catalyseurs bien plus stables même à température de réaction élevée ce qui peut présenter un intérêt pour l'objectif recherché dans cette étude et une voie prometteuse qui est en cours d'exploitation.

1. M. A. Vannice. J. Catal. **37**, 447 (1975).
2. P. Villeger. Thèse, Poitiers (1977).
3. M. Ghazi. Thèse, Poitiers (1988).
4. E. B. Maxted. Adv. Catal. **3**, 129 (1951).
5. D. E. Mears et M. Boudart. AIChE J. **12**, 313 (1966).
6. M. Hammer et I. Hakim. Chem. Eng. Technol. **50**, 622 (1978).
7. (*a*) H. Schapper, E. B. M. Doesburg et L. L. Van Reijen. Appl. Catal. **7**, 211 (1983); (*b*) H. Schapper. Thèse, Delft (1984).
8. D. L. Trimm et E. R. Karal. Catal. Proc. Int. Congr. 7th, 1980. p. 517.
9. G. Kadinov, H. Praliaud, M. Primet et G. A. Martin. Appl. Catal. **10**, 63 (1984).
10. R. W. Fowler et C. H. Bartholomew. Ind. Eng. Chem. Prod. Res. Dev. **18**, 339 (1979).
11. P. W. Wentrcek, J. G. McCarty, C. M. Ablow et H. Wise. J. Catal. **61**, 232 (1980).
12. E. C. Kruissink, L. L. Van Reijen et J. R. H. Ross. J. Chem. Soc. Faraday Trans. 1, **77**, 649 (1981).
13. C. H. Bartholomew, C. B. Pannel et R. W. Fowler. J. Catal. **79**, 34 (1983).
14. V. Perrichon, P. Turlier, J. Barrault, C. Forquy et J. C. Menezo. Appl. Catal. **1**, 169 (1981).
15. (*a*) T. R. Hugues, R. J. Houston et R. P. Sieg. Ind. Eng. Chem. Process Des. Dev. **1**, 196 (1962); (*b*) H. L. Gruber. Anal. Chem. **34**, 1828 (1962); (*c*) D. Duprez. J. Chim. Phys. **80**, 487 (1983).
16. G. Corro. Thèse, Poitiers (1983).
17. W. M. Shen, J. A. Dumesic et C. G. Hill. J. Catal. **68**, 152 (1981).
18. J. W. E. Coenen, W. M. T. N. Schats et R. L. C. Van Meerten. Bull. Soc. Chim. Belg. **80**, 435 (1979).
19. (*a*) J. T. Richardson et J. L. Propp. J. Catal. **98**, 457 (1986). (*b*) J. T. Richardson et R. Koveal. J. Catal. **98**, 559 (1986).
20. C. Mirodatos, H. Praliaud et M. Primet. Congrès franco-polonais, Caen, 1985. pp. 99–103.
21. C. Mirotados, G. A. Martin et J. A. Delmon. Catalysis on the energy scene. *Edité par* S. Kaliaguine et Malray. Elsevier, Amsterdam. 1984. p. 505.
22. E. E. Wolf et F. Alfani. Catal. Rev. Sci. Eng. **24**(3), 329 (1983).
23. W. D. Fitzharris, J. R. Katzen et W. H. Manogue. J. Catal. **76**, 369 (1982).
24. C. H. Bartholomew. Catal. Rev. Sci. Eng. **24**, 67 (1982).
25. V. Ponec. Catal. Rev. Sci. Eng. **11**, 41 (1975).
26. V. Ponec et M. Araki. J. Catal. **44**, 439 (1976).
27. S. J. Tauster, S. C. Fung et R. L. Garten. J. Am. Chem. Soc. **100**, 170 (1978).
28. J. S. Rieck et A. T. Bell. J. Catal. **96**, 88 (1985).
29. J. S. Rieck et A. T. Bell. J. Catal. **99**, 278 (1986).

Can. J. Chem. Downloaded from www.nrcresearchpress.com by 88.255.202.194 on 09/08/12
For personal use only.

The structure and vertical excitation energies of the chlorothioformyl radical, ClCS: implications for the photofragmentation of thiophosgene

M. HACHEY AND F. GREIN[1]

Department of Chemistry, University of New Brunswick, Bag Service No. 45222, Fredericton, N.B., Canada E3B 6E2

AND

R. P. STEER

Department of Chemistry, University of Saskatchewan, Saskatoon, Sask., Canada S7N 0W0

Received July 17, 1992

M. HACHEY, F. GREIN, and R. P. STEER. Can. J. Chem. **71**, 112 (1993).

Ab initio CI studies have been performed to determine the geometry of the ground and first electronically excited states of the chlorothioformyl radical, ClCS, and the vertical excitation energies of its ten lowest doublet states and two lowest quartet states. The results are used to construct a more complete energy level correlation diagram for the photofragmentation of Cl_2CS. The lowest excited electronic state of ClCS lies only 0.79 eV (adiabatic) above the ground state. Its discovery indicates that the results of previous photofragmentation experiments may need to be reinterpreted.

M. HACHEY, F. GREIN et R. P. STEER. Can. J. Chem. **71**, 112 (1993).

On a effectué des calculs *ab initio* pour déterminer la géométrie de l'état fondamental et des premiers états électroniquement excités du radical chlorothioformyle, ClCS. On a aussí déterminé les énergies d'excitations verticales des dix états doublets et des deux états quadruplets les plus bas. On a utilisé les résultats pour construire un diagramme de corrélation plus complet des niveaux d'énergie de la photofragmentation du Cl_2CS. L'état électronique excité le plus bas du ClCS ne se trouve qu'à 0,79 eV (adiabatique) au-dessus de l'état fondamental. Cette découverte indique qu'il sera peut-être nécessaire de réinterpréter les résultats antérieurs des expériences de photofragmentation.

[Traduit par la rédaction]

Can. J. Chem. Downloaded from www.nrcresearchpress.com by 88.255.202.194 on 09/08/12
For personal use only.

Introduction

Thiophosgene, Cl_2CS, is one of a small number of interesting tetraatomic molecules known to undergo photodissociation via two parallel channels; a molecular process giving, in this case, Cl_2 + CS ($\tilde{X}^1\Sigma^+$), and a free radical fragmentation yielding Cl + ClCS (1, 2). The free radical process was first described by Okabe (3) who calculated quantum yields of Cl atom production of 0.38, 0.90, and 1.00 in the limit $P = 0$ at λ_{ex} = 435.8, 366.0, and 253.7 nm respectively, on the basis of the yields of HCl obtained from the photolysis of Cl_2CS–heptane mixtures. Okabe also derived a number of thermodynamic quantities relating to the photofragmentation of Cl_2CS, including an estimate of the C—Cl bond dissociation energy in the ground state (D_0^0 = 2.75 ± 0.02 eV; 63.4 ± 0.5 kJ mol^{-1}). This estimate was based on the assumption that the abrupt break-off of $\tilde{A} \rightarrow \tilde{X}$ fluorescence in Cl_2CS (4) observed between λ_{ex} = 455.0 and 447.2 nm is due to predissociation of the $\tilde{A}$ state by an unbound state that yields cold, ground state Cl and ClCS fragments. However, the molecular and free radical dissociation channels in Cl_2CS are almost equi-endothermic (2). Given this, the fact that ϕ_{Cl} is apparently much less than 1 for excitation energies higher than the predissociation limit in the $\tilde{A}$ state, and the knowledge that Okabe would have had great difficulty in detecting a Cl_2 product using his photochemical methods, it appears that there is reason to be cautious in assigning the fluorescence-weakening process in the $\tilde{A}$ state to predissociation through the free radical dissociative channel.

Ondrey and Bersohn (1) investigated the photoframentation of Cl_2CS by exciting at 248 nm in its strong $\tilde{B} \leftarrow \tilde{X}$ absorption system under collision-free conditions in an effusive molecular beam. Free radical dissociation was also found to be the major channel at this wavelength (estimated ϕ = 0.8 ± 0.1), but parallel molecular fragmentation was clearly identified on the basis of the prompt appearance of CS^+ in the time-of-flight ion spectrum. Ondrey and Bersohn interpreted the free radical photofragmentation dynamics by using Okabe's data (3) and assuming that the ClCS fragment was produced in its electronic ground state. They then used a simple impulsive spectator model (5) to predict that about 60% of the available "excess" energy would be released as vibrational excitation of ClCS and about 37% would appear in the translational degrees of freedom of the separating fragments. The latter was, however, only in modest agreement with the experimental result of 29 ± 1%, and led us to question, in particular, the assumption that ClCS was produced in its electronic ground state.

The interpretation of the photofragmentation dynamics of Cl_2CS in its $\tilde{B}$ state is made particularly difficult by the complexity of its $\tilde{B} \leftarrow \tilde{X}$ (uv) spectrum, aspects of which are still not understood (6–8). Although there is agreement that the $^1(\pi,\pi^*)$ excited state of $^1A_1$ symmetry is responsible for the major part of the oscillator strength of the uv absorption, there appear to be several weakly absorbing states at these energies, including one of $n^0\pi^{*2}$ configuration (9, 10). The onset of a $\tilde{B} \rightarrow \tilde{X}$ fluorescence-weakening process (predissociation) is clearly observed at $E_{vib} \sim 1450 \pm 50$ cm^{-1} in the laser-induced fluorescence excitation spectrum of supersonically expanded Cl_2CS, but the nature of the state responsible is essentially unknown.

These features of the spectroscopy and photofragmentation dynamics/energetics of Cl_2CS have led us to reexamine this molecule both theoretically and experimentally. In preparation for further studies of the photofragmentation, we have therefore calculated the structures and electronic ener-

[1]Author to whom correspondence may be addressed.

Can. J. Chem. Downloaded from www.nrcresearchpress.com by 88.255.202.194 on 09/08/12
For personal use only.

gies of the chlorothioformyl radical. Our intent is to determine (*i*) if laser-induced fluorescence spectroscopy might be used as a diagnostic tool for this species, and (*ii*) if the electronically excited states of ClCS need to be considered in interpreting the photofragmentation processes.

Theoretical methods

The geometry of the $\tilde{X}^2A'$ ground state of ClCS, with electron configuration $(1\text{–}15a')^2(1\text{–}4a'')^2 16a'$, was optimized by ROHF, UHF, and UMP2 methods, at various levels of basis sets, using the GAUSSIAN 90 computer programs (11). Later on, a MRD-CI geometry optimization was also performed.

The vertical excitation energies of ClCS were obtained by multireference configuration–interaction calculations, using the MRD-CI programming package of Buenker, Peyerimhoff, and co-workers (12–15). For carbon, the 10*s*6*p* basis set of Huzinaga (16), in the Dunning 5*s*4*p* contraction (17), was augmented by *s* and *p* Rydberg orbitals with α_s = 0.023 and α_p = 0.021, and by a *d*-polarization function with α_d = 0.75 (18). For S and Cl, the (12*s*9*p*/6*s*4*p*) basis sets (19, 20) were augmented by polarization *d*-functions with α = 0.54 for S, and 0.68 for Cl (21). The CI wavefunction was constructed from $\tilde{X}^2A'$ and $1^2A''$ MO's.

Extensive testing showed that $1^2A''$ MO's gave a better description of the ground state and of π^* excited states, due to the occupation of the π^* orbital in $1^2A''$. Only results obtained with $1^2A''$ MO's will be given.

Five roots of both the $^2A'$ and $^2A''$ symmetry species were calculated. Using about 25–50 reference configurations, 5–10 million configurations were generated, of which 22 000–36 000 were selected when using a selection threshold of 10 μh. "Estimated full-CI energies" (a more appropriate term would be quadruples-corrected MRD-CI energies) obtained by the Davidson formula (22) will be given. The molecule is located in the *x*-*y* plane.

Results and discussion

Geometry optimization of ground state $\tilde{X}^2A'$ *and lowest excited state* $1^2A''$

Optimized geometries for the $\tilde{X}^2A'$ state of ClCS, obtained by ROHF, UHF, and UMP2 methods using the 6-31G and 6-31G* basis sets, are given in Table 1. For the latter basis set, UCISD and RCISD results, obtained by Chan and Goddard (23), are also given. It is seen that the 6-31G results differ significantly from the 6-31G* results. With the addition of polarization functions, both R_{CS} and R_{CCl} shorten by 0.04–0.07 Å. Such observations are in line with numerous discussions in the literature on the effect of polarization functions on bond distances (see, for example, refs. 24 and 25). The ClCS bond angle is hardly affected by this change of basis set. Results obtained with 6-31+G* are virtually identical with the 6-31G* results listed in Table 1. There are no experimental geometry parameters for ClCS.

For comparison, the optimized geometry of Cl_2CS, obtained from 6-31G (this work)/6-31G* (ref. 23), is R_{CS} = 1.624/1.591 (1.602) Å, R_{CCl} = 1.781/1.722 (1.728) Å, and α(ClCS) = 124.2/124.0°(124.4), with experimental values (26) in parentheses. Contractions of the CS and CCl bonds similar to those observed for ClCS under the effect of polarization functions are noted.

For ClCS, CISD results using the 6-31G* basis set (from ref. 23, also given in Table 1) lead to R_{CS} = 1.55–1.56 Å, and R_{CCl} = 1.69 Å.

TABLE 1. Optimized geometries for $^2A'$ ground state of ClCS

Method and basis set	R_{CS} (Å)	R_{CCl} (Å)	α(ClCS) (°)
ROHF			
6-31G	1.605	1.754	136.3
6-31G*[a]	1.561	1.685	136.3
UHF			
6-31G	1.658	1.767	133.6
6-316*[a]	1.585	1.691	135.3
UMP2			
6-31G	1.569	1.820	136.9
6-31G*[a]	1.522	1.680	138.0
RCISD			
6-31G*[a]	1.565	1.689	135.8
UCISD			
6-31G*[a]	1.546	1.687	136.9
MRD-CI[b]	1.580	1.688	134.1

[a]Reference 23.
[b]See text for details.

MRD-CI optimizations on the $\tilde{X}^2A'$ state were performed by optimizing the CS and CCl distances and ClCS angle in turn, while keeping the other two parameters fixed at the best previous value. Two full cycles led to R_{CS} = 1.580 Å, R_{CCl} = 1.688 Å, and α(ClCS) = 134.1°. The only significant change relative to the best previous geometry parameters is found for the CS distance, which increases by about 0.02 Å.

MRD-CI geometry optimizations were also performed on the lowest $^2A''$ state of ClCS. CISD/6-31G* optimizations on this state, performed previously by Chan and Goddard (23), gave R_{CS} = 1.553 Å, R_{CCl} = 1.628 Å, and α = 180°. The present MRD-CI optimization resulted in R_{CS} = 1.588 Å, R_{CCl} 1.651 and α = 180°.

According to Walsh's rules (27), the lowest excited state, $1^2A''$, of HCO, HCS, and corresponding halogen compounds is expected to be linear. This is due to the promotion of an electron from n_C, which prefers a bent molecule, to π^*, which is shape-neutral, such that the preference of lower-lying MO's for a linear structure becomes critical. Linearity of the $1^2A''$ state has been confirmed for HCO (28) and HCS (29).

Molecular orbital characteristics

To describe the excited states by their leading configuration, the characteristics of ClCS molecular orbitals will briefly be discussed. Using the valence bond structure Cl—Ċ=S as guideline, one expects a minimal basis set to give one σ(C—Cl) MO, one σ(C—S) and one π(C—S) MO, and the corresponding antibonding orbitals. All σ MO's belong to the *a'*, all π MO's to the *a''* species. The lone pairs on Cl will give two *a'* and one *a''*, whereas the lone pairs on S give two *a'* MO's. The singly occupied orbital is of *a'* type, and is expected to be localized on C. It will be denoted as n_C.

The ordering and principal composition of valence MO's is shown in Table 2. All MO's have some mixing from other AO's not included in this notation.

Can. J. Chem. Downloaded from www.nrcresearchpress.com by 88.255.202.194 on 09/08/12
For personal use only.

TABLE 2. Molecular orbitals of ClCS

MO	Main character
$10a'$	σ(C—Cl)
$11a'$	σ(C—S)
$12a'$	n_{Cl}
$13a'$	n_S
$14a'$	n_{Cl}
$15a'$	n_S
$16a'$	n_C[a]
$17a'$	σ*(C—Cl)
$21a'$	σ*(C—S)[b]
$3a''$	n_{Cl}
$4a''$	π(C—S)
$5a''$	π*(C—S)[c]

[a]Single occupied in ground state.
[b]$18a'$ to $20a'$ are s, p_x, and p_y Rydberg orbitals, respectively.
[c]All higher a'' MO's are of Rydberg type.

TABLE 3. Vertical excitation energies ΔE of ClCS

State	ΔE(eV)	Configuration	
$1^2A'$ $\tilde{X}$	0.00	G.S.[a]	G.S.
$1^2A''$ $\tilde{A}$	1.58[b]	$16a'\rightarrow5a''$	(n_C,π^*)
$2^2A'$ $\tilde{B}$	3.14	$15a'\rightarrow16a'$	(n_S,n_C)
$1^4A''$	3.40	$15a'\rightarrow5a''$	(n_S,π^*)
$1^4A'$	3.55	$4a''\rightarrow5a''$	(π,π^*)
$2^2A''$	3.67	$4a''\rightarrow16a'$	(π,n_C)
$3^2A''$	4.57	$15a'\rightarrow5a''$	(n_S,π^*)
$3^2A'$	4.71	$4a''\rightarrow5a''$	(π,π^*)
$4^2A'$	4.99	$16a'\rightarrow17a'$	$(n_C,\sigma^*(C—Cl))$
$5^2A'$	5.20	$16a'\rightarrow18a'$	(n_C,R_{4s})
$4^2A''$	5.69	$16a'\rightarrow16a''$	(n_C,R_{4p})
$5^2A''$	6.23	$3a''\rightarrow16a'$	(n_{Cl},n_C)

[a]The ground state (G.S.) configuration is $(1\text{–}15a')^2(1\text{–}4a'')^2 16a'$. Excited state configurations are given relative to the G.S.
[b]The calculated adiabatic excitation energy is 0.79 eV. See text for details.

Two Rydberg orbitals appear in the excited state configurations. They are $18a'$, which is R(4s), and $6a''$, which is R(4p_z).

Excitation energies

Vertical excitation energies, calculated at the ground state geometry with R_{CS} = 1.59 Å, R_{CCl} = 1.69 Å, and α(Cl-CS) = 134.1° are given in Table 3. The lowest five $^2A'$ and $^2A''$ states, and the two lowest quartet states $1^4A'$ and $1^4A''$, cover an energy range up to about 6 eV.

Also given are the leading configurations of each state, using the orbital designation of Table 2.

The adiabatic excitation energy, T_e, for the $\tilde{A} \leftarrow \tilde{X}$ transition, is found to be 0.79 eV, which places the lowest electronic transition in the infrared.

For any carbonyl or thiocarbonyl system one expects low-lying excited states of (n,π^*) and (π,π^*) configuration, occurring as singlet and triplet for closed-shell systems, and as doublet and quartet for open-shell systems. For ClCS, these excited states are $3^2A''$ and $1^4A''$, resulting from (n_S,π^*), and $3^2A'$ and $1^4A'$, resulting from (π,π^*). As expected, the quartet states are at lower energy than the corresponding doublet states. All other excited states involve the singly occupied orbital n_C. By removing an electron from n_C, one finds excitations to π^* ($1^2A''$), the lowest excited state, to σ*(C—Cl)($4^2A'$), and to two Rydberg states ($5^2A'$ and $4^2A''$). Furthermore, excitations into n_C occur, originating from n_S ($2^2A'$), π ($2^2A''$), and n_{Cl} ($5^2A''$). Obviously, single excitations out of or into n_C cannot give rise to quartet states, since n_C is either empty or doubly occupied. Therefore, no other quartet states, besides the two calculated ones, are expected at low energies.

Note that excitations into σ*(C—S) occur only at higher energy, since three Rydberg orbitals lie below this orbital ($21a'$).

TABLE 4. Oscillator strengths for transitions from $\tilde{X}^2A'$ state of ClCS, and comparison with literature values for HCO

		ClCS	HCO[a]
$1^2A''$	(n_C,π^*)	0.0003	0.003
$2^2A'$	(n_S,n_C)	0.0183	0.029
$2^2A''$	(π,n_C)	0.0012	0.012
$3^2A''$	(n_S,π^*)	0.0006	0.006
$3^2A'$	(π,π^*)	0.0100	0.041
$4^2A'$	$(n_C,\sigma^*(C—Cl))$	0.0047	
$5^2A'$	(n_C,R_{4s})	0.0362	0.020
$4^2A''$	(n_C,R_{4p})	0.0032	
$5^2A''$	(n_{Cl},n_C)	0.0040	

[a]Reference 30.

Oscillator strengths

Oscillator strengths were calculated (by the dipole length method) for vertical transitions from the ground state to the excited doublet states. They are given in Table 4, and are compared with oscillator strengths calculated for the corresponding transitions in HCO (30).

The transition to (π,π^*) is expected to have the largest f-value, but it is exceeded here by $2^2A' \leftarrow X$ (n_S,n_C) and by one of the Rydberg transitions involving the (n_C,R_{4s}) state. Oscillator strengths for corresponding HCO transitions are always higher.

For H_2CO and H_2CS, the (n,π^*) oscillator strengths are very small, whereas the (π,π^*) oscillator strengths are 0.256 for H_2CO (31) and 0.38 for H_2CS (32). Transitions to Rydberg states have f-values of about 0.04 for s (33) and 0.02–0.04 for p (32).

Discussion

The electronic energies of ClCS (Table 3) now permit us to construct much more complete energy level and photofragmentation correlation diagrams for Cl_2CS. The available data are summarized in Fig. 1, together with correlations for two of the possible photodissociation channels. The electronic energies of Cl_2CS are the electronic origins of the $\tilde{a} \leftarrow \tilde{X}$ (34), $\tilde{A} \leftarrow \tilde{X}$ (35), and $\tilde{B} \leftarrow \tilde{X}$ (6–8) transitions, an estimate of the energy of the origin of the $\tilde{b} \leftarrow \tilde{X}$ transition based upon the electron-impact energy loss spectrum (36), and the origin of a weak transition to a "dark" state near

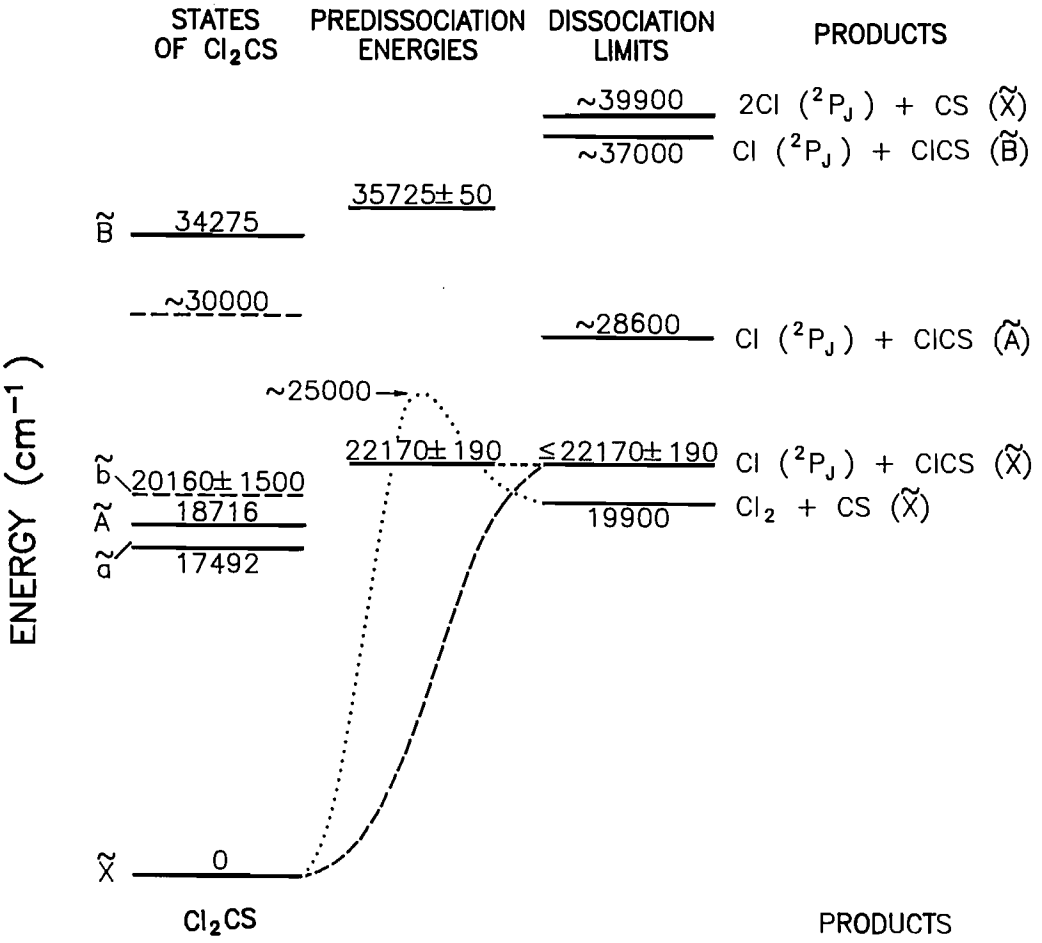

FIG. 1. Energy level and partial state correlation diagram for Cl_2CS and its UV–visible dissociation products. The energies of the electronic states of Cl_2CS are from the origins of the optical absorption spectra. The electronic energy of the $\tilde{b}$ state is estimated from the onset of absorption in the electron energy-loss spectrum (ref. 36). The predissociation energies are from the onsets of fluorescence weakening in the fluorescence excitation spectra. The barrier height on the ground state molecular dissociation path is calculated (ref. 2). The energies of the free radical dissociation products are from the present work. Dissociation limits leading to $Cl_2(^3\Pi)$ have been omitted for clarity.

30 000 cm^{-1} (10). The predissociation energies are those obtained from the onsets of fluorescence-weakening processes in the $\tilde{A}$–$\tilde{X}$ and $\tilde{B}$–$\tilde{X}$ excitation spectra (4, 6).

On the product side, the value of T_e for the adiabatic $\tilde{A}$–$\tilde{X}$ transition in ClCS (0.79 eV, 6400 cm^{-1}) has been used directly. Chan and Goddard's value of 5800 cm^{-1} is slightly lower (23). The lowest possible energy for the $\tilde{B}$ state of ClCS was obtained by optimizing the geometry of the $2^2A'(\tilde{B})$ state using the CIS method and D95 basis set available in the Gaussian 90 package (11). A single-point calculation at this geometry (R_{CS} = 1.976 Å, R_{CCl} = 1.693 Å, α = 139.5°), using MRD-CI, gave an adiabatic transition energy of 1.89 eV (15 200 cm^{-1}) for the $\tilde{B}$ state. The endothermicity of the molecular fragmentation to Cl_2 + CS($\tilde{X}$) is based on good thermodynamic data (2, 3). The energy required for the fragmentation to 2Cl + CS($\tilde{X}$) is obtained by adding to this the ground state dissociation energy of Cl_2 (2.475 eV) (37). Chlorine atoms may be produced in either of two spin-orbit states ($^2P_{3/2}$, $^2P_{1/2}$) separated by 881 cm^{-1} (38). Only the lower of these ($^2P_{3/2}$) is shown in Fig. 1 for clarity. Molecular dissociation channels leading to $Cl_2(^3\Pi)$ have also been omitted.

The $\tilde{X}$ state of Cl_2CS correlates smoothly with the $\tilde{X}$ state of ClCS plus a ground state chlorine atom in the free radical dissociation channels. Ground state Cl + ClCS will also correlate with a repulsive singlet state, which is likely not to be readily observable in the absorption spectrum of the parent molecule (39). Either such a repulsive state or the unbound portion of the ground state surface could be responsible for the observed predissociation of the $\tilde{A}$ state of Cl_2CS some 3400 cm^{-1} above its zero point. Thus, Okabe's suggestion (3) that the fluorescence-weakening process in the $\tilde{A}$ state of Cl_2CS yields ground state Cl and ClCS is probably correct. However, the details of the curve crossing that leads to this fluorescence weakening are unknown. Therefore the predissociation energy in the $\tilde{A}$ state of Cl_2CS only provides an upper limit for the dissociation energy of the ground state, i.e., $D_0 \leq 2.75 \pm 0.02$ eV (22 170 ± 190 cm^{-1}). An *ab initio* calculation places D_0 slightly lower at 2.47 eV (19 940 cm^{-1}) (2). In Fig. 1 the stack of electronic energies of ClCS is placed in relation to the observed electronic energies of Cl_2CS by adding the calculated (or estimated) adiabatic transition energies in ClCS to the upper limit of the ground state Cl-CSCl dissociation energy. If D_0 is actually less than 22 170 cm^{-1}, the whole set of ClCS states should be lowered by the same increment.

The ground state reaction of Cl_2 plus CS to form Cl_2CS is Woodward–Hoffman forbidden. Therefore a barrier exists

Can. J. Chem. Downloaded from www.nrcresearchpress.com by 88.255.202.194 on 09/08/12
For personal use only.

Can. J. Chem. Downloaded from www.nrcresearchpress.com by 88.255.202.194 on 09/08/12
For personal use only.

in the molecular dissociation channel on the ground state surface. H_2CO is similar (40). The height of this barrier for dissociation along a path in which the transition state has C_s symmetry has been calculated by *ab initio* methods (4-31G basis) to be about 25 000 cm^{-1} (2). Although the latter calculation is likely to give only a very crude estimate of the barrier height, the fact that no molecular dissociation products appear on photolysis in the visible (3) suggests that the barrier greatly exceeds the endothermicity of 19 900 cm^{-1}.

Figure 1 reveals that a number of photofragmentation channels are energetically accessible following excitation of Cl_2CS at 248 nm (40 323 cm^{-1}), the wavelength employed by Ondrey and Bersohn (1). Three of these are free radical channels in which the products are Cl atoms plus ClCS in its lowest three electronic states. The Cl + ClCS($2^2A'$) channel is slightly exothermic and would leave only 39 kJ mol^{-1} for the translational, rotational, and vibrational motion of the dissociated fragments. Therefore, this channel can be ruled out on the basis of Ondrey and Bersohn's experiment, where the translational energy alone accounts for 67 kJ mol^{-1}. However, the remaining two free radical channels require careful examination.

For photodissociations involving simple bond scission, the internal energy of the excited molecule minus the bond dissociation energy, D_0, gives E_{avail}, the energy that is available to be partitioned among the translational, rotational, vibrational, and electronic degrees of freedom of the fragments. In Cl_2CS excited at 248 nm, E_{avail} = 233 kJ mol^{-1} if D_0 is taken to be *equal* to 265 kJ mol^{-1} (22 170 cm^{-1}). The average translational energy of ClCS was measured by Ondrey and Bersohn (1) to be 67 kJ mol^{-1}. Thus, if ClCS is produced in its electronic ground state, the fraction of E_{avail} that is partitioned into the translational degrees of freedom of ClCS is f_T = 0.288. On the other hand if ClCS is produced in its $\tilde{A}$ state, 80 kJ mol^{-1} above $\tilde{X}$, then only 154 kJ mol^{-1} is available to be partitioned into the vibrational, rotational, and translational degrees of freedom of the fragments and f_T = 0.438. However, if D_0 is in fact <265 kJ mol^{-1} (as discussed above), then f_T will be <0.438.

We recently calculated the free radical dissociation energy on the ground state surface of Cl_2CS by *ab initio* methods using a 4-31G** basis set and obtained D_0 = 239 kJ mol^{-1} (2). If this value rather than D_0 = 265 kJ mol^{-1} is employed in the calculation of E_{avail}, one obtains f_T = 0.26 if the ClCS radical is assumed to be in its ground state and f_T = 0.37 if ClCS is in its $\tilde{A}$ state. Only f_T = 0.37 is in agreement with the prediction of the impulsive spectator model (1, 5), which gives $(f_T)_{sp}$ = 0.369.

Conclusion

The excellent agreement between $(f_T)_{sp}$ and f_T calculated for D_0 = 239 kJ mol^{-1} and a ClCS ($\tilde{A}$) product may be fortuitous. Nevertheless, the result is sufficiently interesting to encourage us to reinvestigate the photofragmentation dynamics of Cl_2CS experimentally. Although it would be difficult to detect $\tilde{A} \rightarrow \tilde{X}$ emisson from ClCS in the near infrared ($\lambda_{em} \geq 1.49$ μm), laser-induced fluorescence methods might well be used as a diagnostic tool for this species. The strong $\tilde{B}$–$\tilde{X}$ transition in the chlorothioformyl radical, which we predict should be observed in the visible (origin near 575 nm), would appear to be particularly useful in this respect provided the $\tilde{B}$ state is bound.

Acknowledgements

The authors gratefully acknowledge the financial support of the Natural Sciences and Engineering Research Council of Canada. R.P.S. wishes to thank the Center of Excellence for Molecular and Interfacial Dynamics and the Steacie Institute for Molecular Sciences, N.R.C., for support of the photofragmentation experiments, which are now underway. Allocation of computer resources, and first-rate support by the Computing Services Department of UNB, have been instrumental in the pursuit of this work.

1. G. S. Ondrey and R. Bersohn. J. Chem. Phys. **79**, 175 (1983).
2. B. Simard, A. E. Bruno, P. G. Mezey, and R. P. Steer. Chem. Phys. **103**, 75 (1986).
3. H. Okabe. J. Chem. Phys. **66**, 2058 (1977).
4. J. R. McDonald and L. E. Brus. Chem. Phys. Lett. **16**, 587 (1972).
5. A. D. Wilson and R. D. Levine. Mol. Phys. **27**, 1197 (1974).
6. M. Ludwiczak, D. R. Latimer, and R. P. Steer. J. Mol. Spectrosc. **147**, 414 (1991).
7. R. N. Dixon and C. M. Western. J. Mol. Spectrosc. **115**, 74 (1986).
8. R. H. Judge and D. C. Moule. J. Mol. Spectrosc. **80**, 363 (1980).
9. M. Hachey, F. Grein, and R. P. Steer. Chem. Phys. Lett. **183**, 204 (1991).
10. M. Szymanski, A. Maciejewski, and R. P. Steer. Chem. Phys. **165**, 101 (1992).
11. Gaussian 90. M. J. Frisch, M. Head-Gordon, G. W. Trucks, J. B. Foresman, H. B. Schlegel, K. Raghavachari, M. A. Robb, J. S. Binkley, C. Binkley, C. Gonzalez, D. J. Defrees, D. J. Fox, R. A. Whiteside, R. Seeger, C. F. Relins, J. Baker, R. L. Martin, L. R. Kahn, J. J. P. Stewart, S. Topiol, and J. A. Pople. Gaussian, Inc., Pittsburgh, Pa. 1990.
12. R. J. Buenker and S. D. Peyerimhoff. Theor. Chim. Acta, **35**, 33 (1974); **39**, 217 (1975).
13. R. J. Buenker, S. D. Peyerimhoff, and W. Butscher. Mol. Phys. **35**, 771 (1978).
14. R. J. Buenker and R. J. Phillips. J. Mol. Strucut. (Theochem), **123**, 291 (1985).
15. R. J. Buenker. *In* Proc. Workshop Mol. Phys. Quantum Chem. into the 80's. *Edited by* P. B. Burton. In Stud. Phys. Theor. Chem. **21**, 17 (1982).
16. S. Huzinaga. J. Chem. Phys. **42**, 1293 (1965).
17. T. H. Dunning, Jr. J. Chem. Phys. **55**, 716 (1971).
18. T. H. Dunning, Jr. and P. J. Hay. *In* Modern theoretical chemistry. Vol. 3. Methods of electronic structure theory. *Edited by* H. F. Schaefer III. (Plenum Press, New York. 1976).
19. S. Huzinaga. Approximate atomic functions II. Department of Chemistry Report, University of Alberta, Edmonton, Alberta. 1971.
20. A. D. McLean and G. S. Chandler. J. Chem. Phys. **72**, 5639 (1980).
21. B. Roos and P. Siegbahn. Theor. Chim. Acta, **17**, 199 (1970).
22. S. R. Langhoff and E. R. Davidson. Int. J. Quantum Chem. **8**, 61 (1974).
23. W.-T. Chan and J. D. Goddard. Chem. Phys. Lett. **173**, 139 (1990).
24. D. Feller and E. R. Davidson. *In* Reviews in computational chemistry. *Edited by* K. B. Lipkowitz and D. R. Boyd. VCH Publishers, Inc., New York. 1990.
25. W. H. Fink. Int. J. Quantum Chem. **21**, 669 (1987).
26. M. Nakata, T. Fukuyama, and K. Kuchitsa. J. Mol. Struct. **81**, 121 (1982).
27. A. D. Walsh. J. Chem. Soc. 2260 (1953).
28. J. M. Brown and D. A. Ramsay. Can. J. Phys. **53**, 2232 (1975).

29. J. D. Goddard. Chem. Phys. Lett. **102**, 224 (1983); J. Senekowitsh, S. Carter, P. Rosmus, and H. J. Werner. Chem. Phys. **147**, 281 (1990).
30. P. J. Bruna, R. J. Buenker, and S. D. Peyerimhoff. J. Mol. Struct. **32**, 217 (1976).
31. D. J. Clouthier, P. A. Hackett, A. R. Knight, and R. P. Steer. J. Photochem. **17**, 319 (1981), and reference therein.
32. R. H. Judge and G. W. King. Can. J. Phys. **53**, 1927 (1975).
33. J. E. Mental, E. P. Gentien, M. Krauss, and D. Newmann. J. Chem. Phys. **55**, 5471 (1971).
34. D. C. Moule and C. R. Subramaniam. J. Mol. Spectrosc. **48**, 336 (1973).
35. J. C. D. Brand, J. H. Callomon, D. C. Moule, J. Tyrrell, and T. H. Goodwin. Trans. Faraday Soc. **61**, 2365 (1965).
36. W. M. Flicker, O. A. Mosher, and A. Kuppermann. Chem. Phys. Lett. **57**, 183 (1978).
37. G. Herzberg. Spectra of diatomic molecules. 2nd ed. Van Nostrand Reinhold, New York. 1950.
38. C. E. Moore. Natl. Stand. Ref. Data Ser., Natl. Bur. Stand. (U.S.), **35**, 195 (1971).
39. G. Herzberg. Electronic spectra and electronic structures of polyatomic molecules. Van Nostrand Reinhold, New York. 1966. p. 276 ff.
40. M. Dupuis, W. A. Lester, B. H. Lengsfield III, and B. Liu. J. Chem. Phys. **79**, 6167 (1983).

Can. J. Chem. Downloaded from www.nrcresearchpress.com by 88.255.202.194 on 09/08/12
For personal use only.

A model calculation on structures and excitation energies of the hydrated electron

HIROTO TACHIKAWA[1] AND ANDERS LUND
Department of Physics, Linköping University, S-581 83, Linköping, Sweden

AND

MASAAKI OGASAWARA
Hokkaido University of Education, Hakadate 040, Japan

Received May 20, 1992

HIROTO TACHIKAWA, ANDERS LUND, and MASAAKI OGASAWARA. Can. J. Chem. **71**, 118 (1993).

Model calculations were made on the hydrated electron by using the *ab initio* MO method combined with the MR-SD-CI method and the coupled cluster theory. The models used in the calculations were water clusters denoted by $[e^-(H_2O)_n(H_2O)_m]$, where n = 2,3,4, and 6 for the first solvation shell and m = 0–28 for the second and third solvation shells. In these model calculations, the interactions between the excess electron and the water molecules in the first solvation shell are explicitly calculated by *ab initio* MO methods and the water molecules in the second and third solvation shells were represented by the fractional charges obtained at the MP2/D95V** level. The stabilization energies and the solvation radius $r(e^-–O)$, in terms of the distance between the center of the cavity and an oxygen atom of the surrounding water molecules, increased monotonically with the number of water molecules in the first solvation shell. On the other hand, the first excitation energy was not dependent on the number of water molecules in solvation shells, but constant, with the value of ca. 2.0 eV. On the basis of the present calculations, we suggest that (1) the energetic stability of excess electrons depends on both short-range interaction and long-range interaction, (2) the first excitation energy is critically affected by only the short-range interactions, and the excitation is theoretically attributed to the $1s \rightarrow 2p$ transition of the excess electron.

HIROTO TACHIKAWA, ANDERS LUND et MASAAKI OGASAWARA. Can. J. Chem. **71**, 118 (1993).

Des modélisations ont été faites sur l'électron hydraté en utilisant la méthode d'OM *ab initio* en parallèle avec la méthode MR-SD-Cl et la théorie de l'agrégat couplé. Les modèles utilisés dans les calculs sont des agrégats d'eau dénotés $[e^-(H_2O)_n(H_2O)_m]$ où n = 2,3,4 pour la première couche de solvatation et m = 0–28 pour les deuxième et troisième couches. Dans ces calculs, les interactions entre les électrons d'excès et les molécules d'eau dans la première couche de solvatation sont calculées explicitement par des méthodes d'OM *ab initio*; les molécules d'eau dans la deuxième et la troisième couches de solvatation ont été représentées par les charges fractionelles obtenues au niveau MP2/D95V**. Les énergies de stabilisation et le rayon de solvatation $r(e^-–O)$, fonctions de la distance entre le centre de la cavité et un atome d'oxygène des molécules d'eau environnantes, augmentent de façon monotone avec le nombre de molécules dans la première couche de solvatation. D'autre part, la première énergie d'excitation ne s'est pas avérée dépendante du nombre de molécules d'eau dans les couches de solvatation, mais plutôt constante d'une valeur d'environ 2.0 eV. À partir des calculs développés, nous suggérons (1) que la stabilité énergique des électrons d'excès est dépendante des interactions à courte et longue distances et (2) que la première énergie d'excitation n'est affectée que par les interactions à courte portée et que cette excitation est attribuée théoriquement à la transition $1s \rightarrow 2p$ de l'électron d'excès.

Introduction

Significant progress has recently been made in the theoretical treatment of the hydrated electron (1). Information about the solvation structure, electronic properties, and statistical fluctuation of the hydrated electron has been obtained by various kinds of computer experiment. In particular, quantum molecular dynamics (MD) simulation was successful in unraveling the equilibrium and dynamical electronic structure of water cluster anions (1*m*). When the size of cluster $(H_2O)_n$ is small ($8 \leq n \leq 32$), the negative charge is pushed out to the surface of the cluster anion (surface state). The charge is included within the cluster (interior state) when the size is large ($n \leq 32$) (1*e*). Cluster anions with the interior state may be considered models of the hydrated electron. The electron in these clusters is characterized by a localized, roughly spherical, density fluctuation in the ground state, which is very much like a hydrogenic 1*s* state. The average radius for a system comprising 500 water molecules and one electron was found to be 2.05 Å. The existence of three *p*-like states above the ground state was also confirmed. The wave functions corresponding to these states are localized with approximately mutually perpendicular orientation. The most probable energy splitting between the lowest and highest eigenvalue is about 0.8 eV. Above the *p*-like states lies a band of unbound delocalized states of indefinite symmetry.

The present study is aimed at comparing the above picture of the hydyrated electron to that obtained by molecular orbital calculations. The molecular orbital method was first applied to the hydrated electron by Natori and Watanabe (2). Following this pioneering work, *ab initio* MO calculations were made by Newton (3) on the excess electron in a water cluster surrounded by a continuum medium. The results suggested more than four water molecules for capturing an electron effectively. Noell and Morokuma applied their fractional charge MO method to the hydrated systems (4). The system they calculated was composed of an excess electron, the first solvation molecules explicitly considered by molecular orbitals, and surrounding solvent molecules represented by fractional charges. The results favored a six coordination model, rather than a four coordination model, for the first solvation shell around the electron. In 1988, Clark and Illing (5) proposed theoretical models on the basis of *ab initio* HF calculations. They added in their calculations a 31G basis set (hydrogen-atom type) for representing an excess

[1]Author to whom correspondence may be addressed at: Faculty of Engineering, Hokkaido University, Sapporo 060, Japan.

Can. J. Chem. Downloaded from www.nrcresearchpress.com by 88.255.202.194 on 09/08/12
For personal use only.

TABLE 1. Active and frozen orbitals considered in the MR-SD-CI calculations

MO[a]	Group G-I	Group G-II
$n\pi$	2 elec.[b]	2 elec.[b]
$n\sigma$	1 elec.[c]	Frozen

[a]Molecular orbital of coordinating water molecule.
[b]Two-electron excitation is permitted from the Hartree–Fock configuration.
[c]One-electron excitation is permitted from the Hartree–Fock configuration.

electron in the center. The solvation energies calculated for several solvents showed a moderate correlation with the observed maximum wavelength of the absorption spectra.

In the previous study we made *ab initio* calculations on water dimer anions (6); a multi-reference single and double excitation (MR-SD) CI calculation was applied to the excess electron in two water molecules with a surface orbital to represent the surface state *in vacuo*. The results suggested that the first and second electronic excitations were bound–bound and bound–free excitations, respectively (6). In the present study we dealt with models composed of the first solvation shell and surrounding molecules. The calculations were made with special reference to the electronic states in the ground and low-lying excited states. This is the first attempt to study the excited state of hydrated electrons by *ab initio* calculations including electron correlation by the MR-SD-CI and coupled cluster methods. It should be emphasized, however, that this type of calculation has an intrinsic limitation in comparison with the statistical mechanics method. The calculation was made with fixed geometrical nuclear structure of the water structure. Hence, the concept of the first solvation shell and outer solvation shells is only valid in a static condition such as frozen glasses (7).

Method

Models

The solvation shells composed of three layers of water molecules denoted by $[e^-(H_2O)_n(H_2O)_m]$ (n = 2,3,4, and 6, m = 0–28) were considered as model systems for the hydrated electron. Here n is the number of water molecules in the first solvation shell and m is the number in the second and the third solvation shells. The solvent molecules in the first solvation shell denoted by n were explicitly accounted for with molecular orbitals and the geometry of each cluster anion was fully optimized. The second and the third solvation shells composed of m solvent molecules were represented by the fractional charges (q_O = −0.66 and q_H = +0.33 for r(O—H) = 0.962 Å and the H—O—H angle = 104.41°) obtained at the MP2/D95V** level (8). The outer shell molecules were added to the optimized small cluster anions to which each of the molecules is connected by hydrogen bonding (8). We assumed that the hydrogen bonding structure of the water dimer is linear. The distance of the hydrogen bond r(O···HO) and bending angle were 1.867 Å and 21.3°, respectively (6).

MO calculation

In the previous paper, we determined the structure and the electronic states of the water dimer anion by means of *ab initio* Hartree–Fock and MR-SD-CI calculations (6). We applied the same procedure to the present model calculation. Geometry optimizations of equilibrium points were performed by using the energy gradient method based on the Hartree–Fock theory with a 6-31+G basis set (10–12). Energies on the equilibrium points were further refined by Møller–Plesset second-order perturbation theory (13). In the

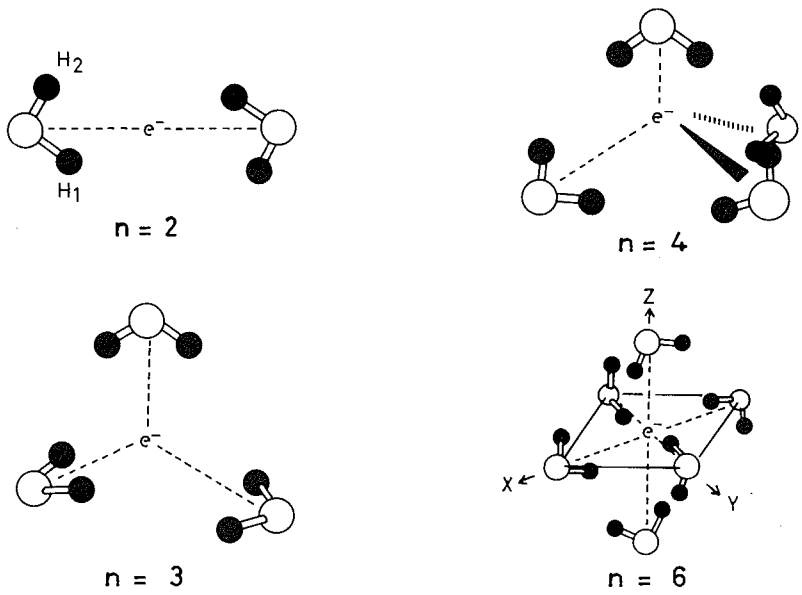

FIG. 1. Model structures for the first coordinating water molecules around the excess electron. The symmetries of the complexes for n = 2, 3, 4, and 6 are assumed to be C_{2h}, C_1, C_s, and C_i, respectively. The hydrogen donated by H_1 is closer to the center of cavity than H_2.

Can. J. Chem. Downloaded from www.nrcresearchpress.com by 88.255.202.194 on 09/08/12
For personal use only.

TABLE 2. Fully optimized parameters calculated at the HF/6-31+G level of $[e^-(H_2O)_n]$ clusters. Bond lengths and angles are in angstrom and in degrees

	n		
	2	3	4
Symmetry	C_{2h}	C_1	C_s
$r(O—e^-)$	2.145	2.564	2.788
$r(O—H_2)^a$	0.953	0.953	0.962
$r(O—H_2)^b$	0.959	0.953	0.953
$\angle H_2—O—e^-$	80.9	55.2	54.4
$\angle H_1—O—H_2$	105.6	108.7	108.5

[a]H_1 is inner hydrogen atom.
[b]H_2 is outer hydrogen atom.

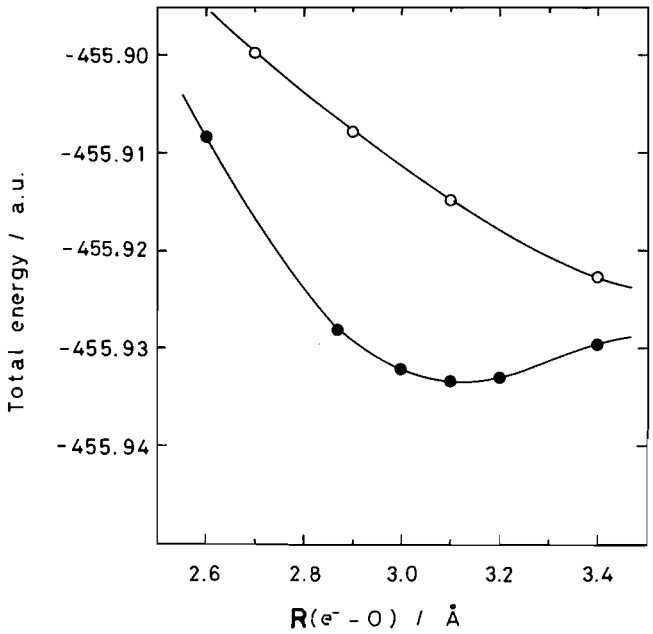

FIG. 2. Potential energy curves for the excess electron system $[e^-(H_2O)_6]$ (—●—) and for the neutral system $[(H_2O)_6]$ (—○—) calculated as a function of $r(e^-–O)$ and the distance between the cavity center and the oxygen atom, respectively. The calculations were performed at the HF/6-31+G level.

calculations of the excitation energies, the coupled cluster method with a 6-31+G basis set and the MR-SD-CI method with Huzinaga's (621/51) basis set were carried out in order to obtain the electron correlations (14–16). We added an *sp*-type diffuse orbital (exponent = 0.0845) to Huzinaga's basis set in this calculation. In the MR-SD-CI calculations, we chose two groups for the active space, as listed in Table 1.

Results and discussion

Structural models

Figure 1 shows the structural models with different coordination numbers (n = 2,3,4, and 6). The structures were fully optimized by means of *ab initio* HF/6-31+G calculations. Table 2 summarizes the corresponding parameters for n = 2, 3, and 4. Three types of geometrical structure, an OH orientation form, a dipole orientation from, and the intermediate form proposed previously by us, were considered as possible orientational forms for the water molecules in the

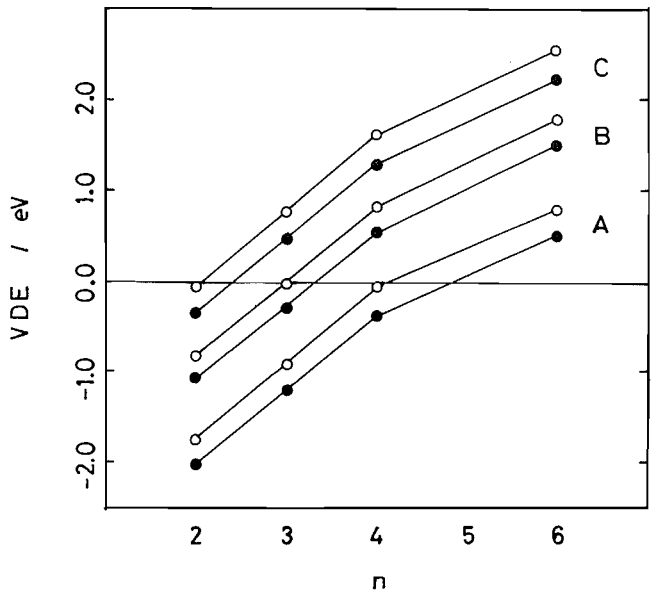

FIG. 3. Vertical detachment energies (VDE's) as a function of the number of coordinating water molecules in the first solvation shell. (*A*) Without the second and third shells. (*B*) Including six water molecules in the second solvation shell. (*C*) Including 28 water molecules in the second and third solvation shells. Open and solid circles denote the HF/6-31+G values and MP2/6-31+G values, respectively.

first solvation shell (6, 7, 17). The dipole orientation form was energetically favored for n = 3 and 4, and the intermediate form was favored for n = 2 within the approximation. The electron–oxygen distance, $r(e^-–O)$, in terms of the distance between the center of the cavity and the nucleus of an oxygen of the first solvation shell molecules, increases monotonically with increasing coordination number n.

For n = 6, we assumed an intermediate form by analogy with the cluster anion with n = 2 and optimized the geometrical structure for $r(e^-–O)$. Figure 2 shows the potential energy curves for the negatively charged system $[e^-(H_2O)_6]$ and the neutral system $[(H_2O)_6]$ calculated as a function of $r(e^-–O)$. The negatively charged system shows a bound state with a potential minimum. To evaluate the vertical electron detachment energy (VDE) of the cluster anion, we calculated the potential energy curve of the neutral system (Fig. 2). In the neutral system, all water molecules are affected by the repulsive interactions due to the hydrogen–hydrogen repulsion force. It means that an excess electron injected into the water cluster composed of six water molecules with the intermediate form plays a role of binding water molecules together. The VDE at the minimum point shows a positive value. The cluster is thus able to capture an electron at the center of the cluster.

Effect of n *and* m *on the VDE*

Figure 3 shows the VDE of the water cluster anions, $[e^-(H_2O)_n(H_2O)_m]$, for m = 0, 6, and 28. The VDE was calculated as a function of the number n of water molecules in the first solvation shell at the HF/6-31+G and MP2/6-31+G levels. The lines *A*, *B*, and *C* correspond to the systems having zero, six, and 28 water molecules in the second and the third solvation shells, respectively. As the differences in

Can. J. Chem. Downloaded from www.nrcresearchpress.com by 88.255.202.194 on 09/08/12
For personal use only.

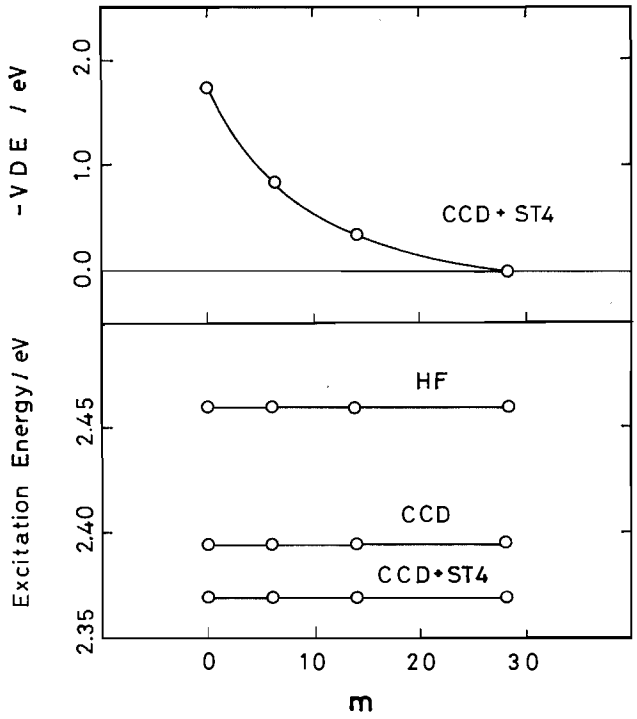

FIG. 4. Excitation energies and the vertical detachment energies (VDE's) of the $[e^-(H_2O)_2(H_2O)_m]$ system calculated as a function of m. The values are obtained by the Hartree–Fock method (HF), Møller–Plesset's perturbation theory (MP2, MP3, and MP4DQ), and the coupled cluster theory (CCD and CCD+ST4) with a 6-31+G basis set.

VDE due to the electron correlation were all found to be 0.28 eV for n = 1–4, the MP2 value for n = 6 was extrapolated from the HF results for the sake of reducing the consumption of CPU time.

Figure 3 shows that the stability of the models depends not only on the number of water molecules in the first solvation shell but on the one in the outer solvation shells as well. It is also suggested that the first solvation shells composed of small numbers of water molecules, two or three molecules for example, may stably trap an excess electron provided that the first solvation shell is surrounded by sufficient numbers of water molecules. However, the stabilization energies for n = 2 and 3 are much smaller than the energy for n = 6. The VDE of the system with the combination of n = 6 and m = 28 is 2.51 eV. This is in good agreement with the calculated value in the framework of the continuum model (3). The model shells composed of the fractional charges of 28 water molecules seem to be energetically equivalent to the continuum model (3). In Kevan's model for trapped electrons, six water molecules surround an excess electron with OH dipole pointing to the cavity center. This model was deduced from the analysis of the two-pulse electron-spin-echo modulation patterns obtained in irradiated 10 M NaOH aqueous glasses at 77 K. The energetics in the present study support Kevan's model, although the molecular dipole properties are slightly merged into the OH form. However, this does not exclude the possibility that the electrons are localized in sites composed of only a few water molecules in frozen matrices; if a potential around the electron is effectively formed, the excess electron could be captured by two or three water molecules, for example, giving rise to the characteristic absorption with its maximum at ca. 700 nm. This possibility is suggested by the result that the electron affinities of the n = 2–3 systems can be positive when sufficient numbers of water molecules exist around the first solvation shell.

According to the results of MD calculations, the first solvation shell of the excess electron in a water cluster is composed of six water molecules with the OH orientation form. It was also suggested that the electron–hydrogen distance $r(e^-–H)$ was 2.05 Å (1m). The distance 2.264 Å (n = 6) obtained in the present study is in reasonable agreement with that value.

Electronic excitation

The excitation energies for the n = 2 systems, $[e^-(H_2O)_2(H_2O)_m]$, were calculated as a function of m. This system was

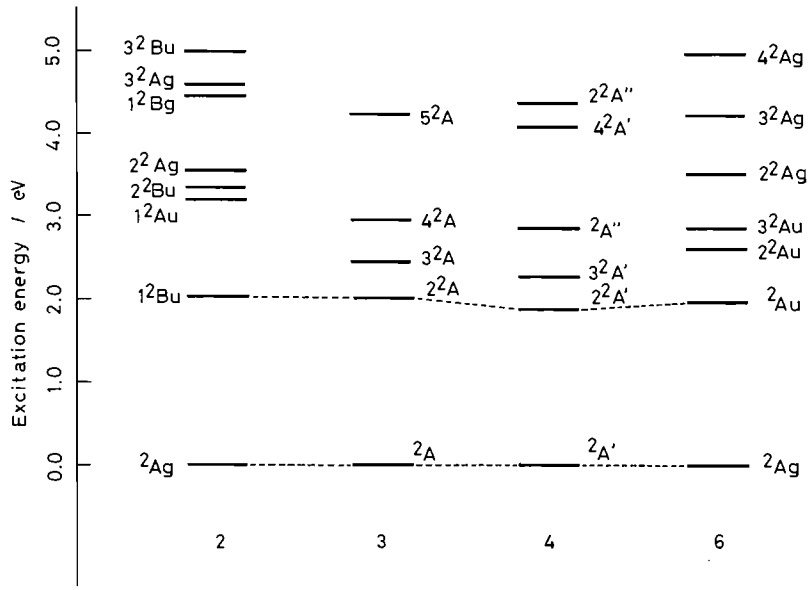

FIG. 5. Low-lying doublet states of the first solvation models $[e^-(H_2O)_n]$ calculated by the MR-SD-CI method.

Can. J. Chem. Downloaded from www.nrcresearchpress.com by 88.255.202.194 on 09/08/12
For personal use only.

TABLE 3. First excitation energies[a] of $[e^-(H_2O)_n]$ clusters calculated by the MR-SD-CI method

n	G-I	G-II
2	2.02	1.97
3	2.02	2.04
4	1.86	1.88
6	1.99	1.98

[a]Values are in eV.

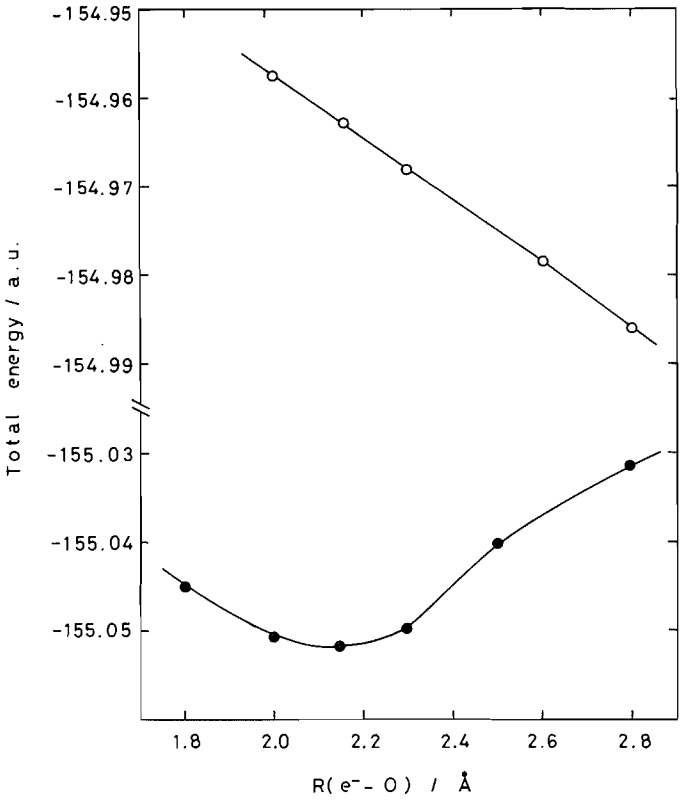

FIG. 6. Potential energy curves of $[e^-(H_2O)_2(H_2O)_{14}]$ at the ground (—●—) and first excited states (—○—) calculated with the coupled cluster theory (CCD/6-31+G) as a function of $r(e^-$–O).

chosen for the sake of simplicity, but the pertinency of the example will be identified in the following paragraph. The results are shown in Fig. 4 together with the VDE's for comparison. The VDE tends to increase with increasing m until it reaches at a constant value at $m = 28$, although the absolute values may not have much sense. In contrast, the excitation energy to the first excited state is constant regardless of the value of m. It is not affected by the number of surrounding solvent molecules in the second and third solvation shells.

Figure 5 shows the energy levels calculated at the MR-SD-CI level of low-lying doublet states for the model systems with $n = 2$, 3, 4, and 6. The first excitation energies calculated with two groups of the active space at the MR-SD-CI level are summarized in Table 3. The results of the MR-SD-CI calculations were not affected by the correction of quadruple electron excitations (MR-SD-CI+Q). The cal-

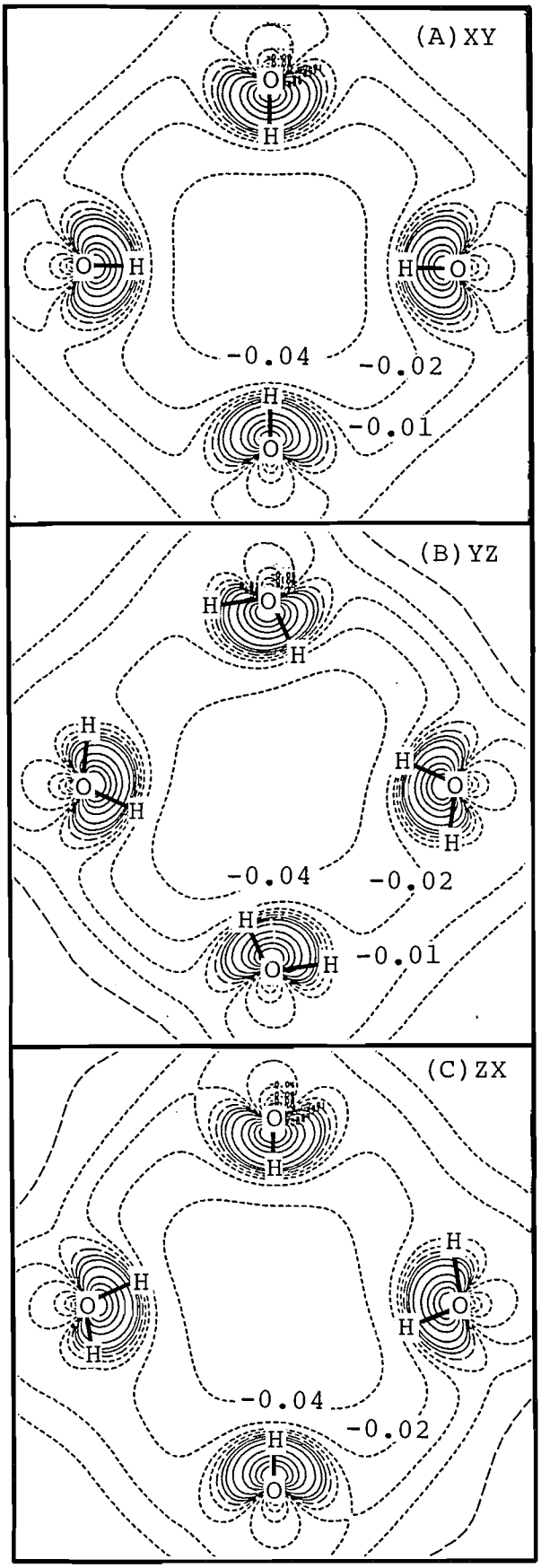

FIG. 7. Contour maps of the spin orbital of the ground state (^2A_g) for the hexacoordination model $[e^-(H_2O)_6]$ calculated by the MR-SD-CI method with Huzinaga's (621/51)+diffuse (sp) basis set.

Can. J. Chem. Downloaded from www.nrcresearchpress.com by 88.255.202.194 on 09/08/12
For personal use only.

Can. J. Chem. Downloaded from www.nrcresearchpress.com by 88.255.202.194 on 09/08/12
For personal use only.

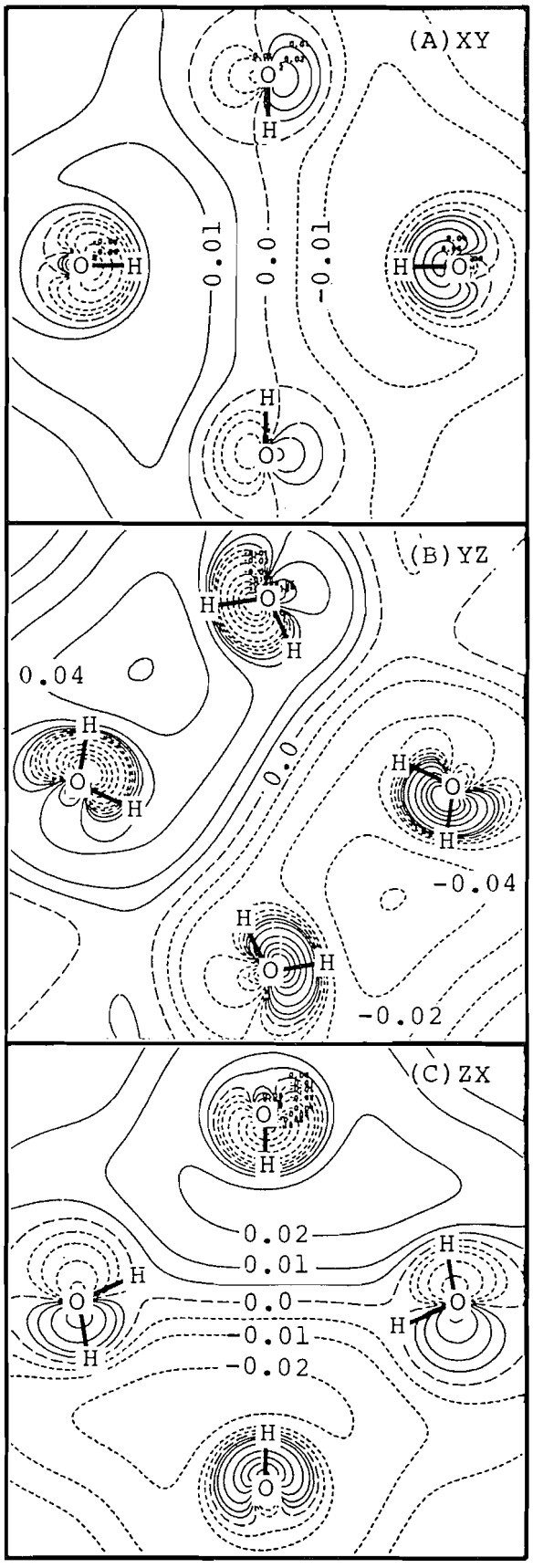

FIG. 8. Contour maps of the singly occupied molecular orbital of the first excited state (^2A_u) for the hexacoordination model [$e^-(H_2O)_6$] calculated by the MR-SD-CI method with Huzinaga's (621/51)+diffuse (*sp*) basis set.

TABLE 4. Spin populations in *s*-type orbitals on hydrogen atoms

Cluster	Atom	*s*-spin population[a]
$[e^-(H_2O)_4(H_2O)_{28}$	H_1	−0.2634
	H_2	−0.2603
$[e^-(H_2O)_6(H_2O)_{28}$	H_1[b]	0.0368[d]
	H_2[c]	−0.0046

[a]The sum of the spin populations on all *s*-type orbitals in the atomic basis.
[b]H_2 is inner hydrogen atom.
[c]H_2 is outer hydrogen atom.
[d]Experimental spin density is 0.004 (ref. 9).

culated values range around 2.0 eV for all the model systems examined.

Figure 6 shows the potential energy curves of $[e^-(H_2O)_2(H_2O)_{14}]$ at the ground and first excited states calculated by the coupled cluster theory (CCD). The potential curve of the ground state has a bound state, but the first excited state is always repulsive. Since the potential curve of the first excited state is substantially steep, the excitation energy is expected to depend sensitively on the geometry of the ground state. In actuality, however, the excitation energies are hardly affected by the number of the coordination water molecules, as shown in Fig. 5.

The effect of the water molecules in the first solvation shell on the excess electron could be regarded as short-range interaction, and that of the molecules in the outer shells as long-range interaction. The present study demonstrated that the solvation energy was, of course, affected by both the short-range interactions and the long-range interactions. On the other hand, the first excitation energy is critically determined only by the short-range interactions.

Contour maps

Figures 7 and 8 show contour maps of the singly occupied molecular orbitals at the ground state (^2A_g) and the first excited state (^2A_u), respectively. The maps were obtained for a hexacoordination form (n = 6) by MR-SD-CI calculations. In the ground state, the orbital occupied by an excess electron is composed of an *s*-like orbital, which is formed by overlapping of the diffuse orbitals of surrounding water molecules. Similar results were obtained previously for methanol cluster anions (18). The excess electron is mainly distributed over the cavity. In the first excited state (^2A_u), however, the corresponding orbital is composed of *p*-like orbitals whose nodal planes go through the cavity center; the orbital spreads over the coordinating water molecules. The first optical excitation is attributed to the transition from 1*s*- to 2*p*-like orbitals of the excess electron. The results are consistent with the picture obtained by MD calculations (1*m*).

Spin population

Table 4 summarizes the spin populations in the *s*-type orbitals of the hydrogen atoms of the model systems. The spin population was obtained from the sum of the spin populations on the *s*-type functions in the atomic basis. The procedure was the same as that employed previously by Clark and Illing (5). In the n = 4 system, the spin populations of all the hydrogen atoms are equal to each other, because the model is a dipole orientation structure with C_s symmetry. The spin populations calculated for the hexacoordination model

($n = 6$) are comparable to the experimental values obtained by Kevan (*7a*, *7b*), but those for the $n = 4$ model (ca. −0.26) are much larger. The sign of the hyperfine constant on the oxygen atoms is positive, in agreement with previous results (3–5). It seems that positive hyperfine coupling constants, which are generally observed in solvated electrons, are caused by the spin polarization mechanism as already pointed out by Clark and Illing (5).

Acknowledgment

The authors thank the National Supercomputer Center at Linkoping University and the Computer Center at the Institute for Molecular Science (IMS) for the use of supercomputers and library programs. One of the authors (H.T.) is indebted to the Japan–Sweden Foundation for a grant for research in Sweden.

1. (*a*) U. Landman, R. N. Bartnett, C. L. Cleveland, D. Scharf, and J. Jortner. J. Phys. Chem. **91**, 4890 (1987); (*b*) R. N. Bartnett, U. Landman, C. L. Cleveland, and J. Jortner. Phys. Rev. Lett. **59**, 811 (1987); (*c*) J. Chem. Phys. **88**, 4421 (1988); (*d*) J. Chem. Phys. **88**, 4429 (1988); (*e*) Chem. Phys. Lett. **145**, 382 (1988); (*f*) R. N. Bartnett, U. Landman, C. L. Cleveland, N. Kestner, and J. Jortner. J. Chem. Phys. **88**, 6670 (1988); (*g*) R. N. Bartnett, U. Landman, and A. Nitzan. J. Chem. Phys. **89**, 2242 (1988); (*h*) J. Schnitker, K. Motakabbir, P. J. Rossky, and R. A. Friesner. Phys. Rev. Lett. **60**, 456 (1988); (*i*) J. Schnitker and P. J. Rossky. J. Chem. Phys. **86**, 3471 (1987); (*j*) A. Wallqvist, D. Thirumalai, and B. J. Berne. J. Chem. Phys. **85**, 1583 (1986); (*k*) W. M. Bartczak, M. Hilczer, and J. Kroh. J. Phys. Chem. **91**, 3834 (1987); (*l*) J. Schnitker, P. J. Rossky, and G. A. Kenny-Wallace. J. Chem. Phys. **85**, 2986 (1986); (*m*) P. J. Rossky and J. Schnitker. J. Phys. Chem. **92**, 4277 (1988).
2. M. Natori and T. Watanabe. J. Phys. Soc. Jpn. **21**, 1573 (1966); M. Natori. J. Phys. Soc. Jpn. **24**, 913 (1968).
3. M. D. Newton. J. Phys. Chem. **79**, 2795 (1975).
4. (*a*) J. O. Noell and K. Morokuma. Chem. Phys. Lett. **36**, 465 (1975); (*b*) J. Phys. Chem. **80**, 2675 (1976); (*c*) J. Phys. Chem. **81**, 2295 (1977).
5. T. Clark and G. Illing. J. Am. Chem. Soc. **109**, 1013 (1987).
6. H. Tachikawa and M. Ogasawara. J. Phys. Chem. **94**, 1746 (1990).
7. (*a*) S. Schlick, P.A. Narayana, and L. Kevan. J. Chem. Phys. **64**, 3153 (1976); (*b*) L. Kevan. J. Phys. Chem. **84**, 1232 (1980); (*c*) P. A. Narayana, M. K. Bowman, L. Kevan, V. F. Yudanov, and Yu.D. Tsvetkov. J. Phys. Chem. **63**, 3365 (1975); (*d*) A. V. Astashkin, S. A. Dikanov, and Yu. D. Tsvetkov. Chem. Phys. Lett. **144**, 258 (1988).
8. H. Tachikawa, S. Lunell, C. Törnkvist, and A. Lund. Int. J. Quant. Chem. **43**, 449 (1992).
9. A. E. Read and T. Clark. Faraday Discuss. Chem. Soc. **85**, 365 (1988).
10. H. F. Schaefer. Applications in electronic structure theory. Vol. 4. *Edited by* H. F. Schaefer. Plenum, New York. 1977. p. 153.
11. M. J. Frish, J. S. Binkley, H. B. Schlegel, K. Raghavachari, C. F. Melius, R. L. Martin, J. J. P. Stewart, F. W. Bobrowicz, C. W. Rohlfing, L. R. Kahn, D. J. DeFrees, R. Seeger, R. A. Whiteside, D. J. Fox, E. M. Fleuder, S. Topiol, and J. A. Pople. *Ab initio* molecular orbital calculation program GAUSSIAN86. Carnegie-Mellon Quantum Chemistry Publishing Unit, Pittsburgh, Pa. 1986.
12. (*a*) J. A. Pople, R. Krishnan, H. B. Schlegel, and J. S. Binkley. Int. J. Quant. Chem. **14**, 545 (1978); (*b*) R. A. Chiles and C. E. Dykstra. Chem. Phys. Lett. **80**, 69 (1981); (c) K. Raghavachari. J. Chem. Phys. **82**, 4607 (1985); (*d*) P. C. Hariharan and J. A. Pople. Theor. Chim. Acta, **28**, 213 (1973).
13. C. Møller and M. S. Plesset. Phys. Rev. **46**, 618 (1934).
14. R. J. Bartlett. J. Phys. Chem. **93**, 1697 (1989). K. Raghavachari. J. Chem. Phys. **82**, 4607 (1985).
15. H. Kashiwagi, T. Takada, E. Miyoshi, S. Obara, and F. Sasaki. RHF calculation program JAMOL4. 1985; A. Murakami, H. Iwaki, H. Terashima, T. Shoda, T. Kawaguchi, and T. Noro. MR-SD-CI calculation program MICA3. 1985.
16. (*a*) S. Huzinaga. Physical science data, Gaussian basis sets. Vol. 16. *Edited by* S. Huzinaga. Elsevier, Amsterdam. 1984; (*b*) H. Tatewaki and S. Huzinaga. J. Comput. Chem. **1**, 205 (1980).
17. S. V. Murphy and D. B. Hibbert. Radiat. Phys. Chem. **28**, 319 (1986).
18. H. Tachikawa, M. Ogasawara, M. Lindgren, and A. Lund. J. Phys. Chem. **92**, 1712 (1988).

Can. J. Chem. Downloaded from www.nrcresearchpress.com by 88.255.202.194 on 09/08/12
For personal use only.

Antibody–oligosaccharide interactions: the synthesis of 2-deoxy-α-L-rhamnose containing oligosaccharide haptens related to *Shigella flexneri* variant Y antigen[1]

H. RIZK HANNA[2] AND DAVID R. BUNDLE[3]

Institute for Biological Sciences, National Research Council of Canada, Ottawa, Ont., Canada K1A 0R6

Received July 6, 1992

H. RIZK HANNA and DAVID R. BUNDLE. Can. J. Chem. **71**, 125 (1993).

A series of di- and trisaccharide glycosides based on the α-L-Rha(1→3)β-D-GlcNAc and α-L-Rha(1→3)α-L-Rha(1→3)β-D-GlcNAc elements have been synthesized to locate the minimal oligosaccharide determinant of the *Shigella flexneri* O-polysaccharide, which is built from a tetrasaccharide repeating unit, [→2) α-L-Rha*p*(1→2)α-L-Rha*p*(1→3)α-L-Rha*p* (1→3)β-D-GlcNAc*p*(1-]$_n$. These compounds also serve to identify the carbohydrate surface of the *Shigella* antigen that interacts with a monoclonal antibody, currently the subject of crystallographic studies. Two strategies utilizing suitably protected glycals **1** and **19** were employed to obtain analogs bearing either terminal or glycosylated 2,6-dideoxy-α-L-*arabino*-hexopyranosyl (2-deoxy-α-L-rhamnopyranosyl) residues. *N*-Iodosuccinimide activation of the glycals in the presence of selectively protected mono- and disaccharide alcohols afforded 2-deoxy-2-iodo-α-L-rhamnopyranosides and these were ultimately reduced during deprotection stages to afford the desired functionality. Di-*O*-acetyl L-rhamnal **1** reacted with monosaccharides **2** and **7**, and with disaccharide **11**, to yield disaccharides **4** and **8**, and trisaccharide **12**, each bearing a terminal 2-deoxy-α-L-rhamnopyranosyl residue. The selectively protected 3-*O*-benzoyl-4-*O*-benzyl-L-rhamnal **19** was synthesized from L-rhamnal and used to prepared trisacceharide **22**, which contained an internal 2-deoxy-2-iodo-α-L-rhamnopyranosyl unit. Removal of protecting groups gave the oligosaccharides **6**, **10**, **14**, and **23**. Oligosaccharides that contained a 2-deoxy-α-L-rhamnopyranosyl residue showed enhanced inhibitory power: in the case of trisaccharide **23** a 1.8 kcal mol^{-1} relative increase in free energy of binding compared to a larger pentasaccharide epitope, α-L-Rha*p*(1→2)α-L-Rha*p*(1→3)α-L-Rha*p*(1→3)β-D-GlcNAc*p*(1→2)α-L-Rha*p*-1→OMe. These data suggest that the rhamnose O-2 hydroxyl of residue **C** points toward and has important interactions with binding site amino acids.

H. RIZK HANNA et DAVID R. BUNDLE. Can. J. Chem. **71**, 125 (1993).

Dans le but déterminer l'oligosaccharide déterminant minimal du O-polysaccharide *Shigella flexneri*, formé à partir du motif de tétrasaccharide [→2) α-L-Rha*p*(1→2)α-L-Rha*p*(1→3)α-L-Rha*p*(1→3)β-D-GlcNAc*p*(1-]$_n$, on a synthétisé une série de glycosides di- et trisaccharides basés sur les éléments α-L-Rha(1→3)β-D-GlcNAc et α-L-Rha(1→3)α-L-Rha(1→3)β-D-GlcNAc. On a utilisé ces composés pour identifier la surface carbohydrate de l'antigène *Shigella* qui interagit avec l'anticorps monoclonal qui fait l'objet d'études cristallographiques. On a utilisé deux stratégies, faisant chacune appel aux glycals **1** et **19** protégés d'une façon appropriés, pour obtenir des analogues des restes 2,6-didésoxy-α-L-*arabino*-hexapyranosyle (2-désoxy-α-L-rhamnopyranosyle) terminal ou glycosé. Une activation des glycals par la *N*-iodosuccinimide en présence d'alcools mono- ou disaccharidiques conduit au 2-désoxy-2-iodo-α-L-rhamnopyranosides qui sont finalement réduits durant les étapes de déprotection pour fournir les fonctionnalités désirées. Le di-*O*-acétyl L-rhamnal **1** réagit avec les monosaccharides **2** et **7** et avec le disaccharide **11** pour conduire aux disaccharides **4** et **8** et au trisaccharide **12** qui portent tous un reste 2-désoxy-α-L-rhamnopyranosyle. On a synthétisé le 3-*O*-benzoyl-4-*O*-benzyl-L-rhamnal sélectivement protégé (**19**) à partir du L-rhamnal et on l'a utilisé pour préparer le trisaccharide **22** qui contient une unité interne de 2-désoxy-2-iodo-α-L-rhamnopyranosyle. L'enlèvement des groupes protecteurs conduit aux oligosaccharides **6**, **10**, **14** et **23** qui contiennent une unité de 2-désoxy-α-L-rhamnopyranosyle et qui présentent une puissance inhibitrice élevée; dans le cas du trisaccharide **23**, on observe une augmentation de 1,8 kcal mol^{-1} de l'énergie libre de liaison par rapport à celle d'un pentasaccharide épitope beaucoup plus important, α-L-Rha*p*(1→2)α-L-Rha*p*(1→3)α-L-Rha*p*(1→3)β-D-GlcNAc*p*(1→2)α-L-Rha*p*-1→OMe. Ces données suggèrent que l'hydroxyle O-2 du rhamnose du reste **C** pointe vers, et interagit d'une façon importante avec, le site de liaison des acides aminés.

[Traduit par la rédaction]

Introduction

Monoclonal antibodies produced in response to immunization of mice with killed cells of *Shigella flexneri* variant Y bacteria exhibit a tendency to bind to structural elements of the cell surface O-antigen that span the junction of biological repeating units (1, 2). The latter structure is a tetrasaccharide, which is polymerized to provide the O-polysaccharide:

[→2)α-L-Rha*p*(1→2)α-L-Rha*p*(1→3)
Units **A** **B**

α-L-Rha*p* (1→3)β-D-GlcNAc*p*(1-]$_n$
C **D**

Mapping of the antibody binding sites that recognize this structure using linear oligosaccharides of different length has identified a residue sequence **BCDA** that frequently appears to be the optimal epitope size for binding (2). A Fab sample from an $IgG_3\kappa$ monoclonal antibody exhibiting these features is now the subject of a high-resolution crystal structure study (3). Characterization of the molecular features of the antigenic determinant that interacts with the antibody surface requires a series of oligosaccharides that have functional group modifications at single sites (4, 5). Chemical synthesis of monodeoxy analogs has been used extensively for this purpose and represents one of the most conservative changes (>CH—OH → >CH_2) that may be used to identify and quantify the incremental contributions of important polar contacts (6).

The disaccharide **CD**, α-L-Rha*p* (1→3) β-D-GlcNAc*p*-1→OMe, was selected as the structural element around which to make functional group replacements, because inhi-

[1]NRCC No. 34293.
[2]NRCC Research Associate 1986–1988.
[3]Author to whom correspondence may be addressed.

Can. J. Chem. Downloaded from www.nrcresearchpress.com by 88.255.202.194 on 09/08/12
For personal use only.

Can. J. Chem. Downloaded from www.nrcresearchpress.com by 88.255.202.194 on 09/08/12
For personal use only.

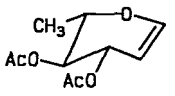

1

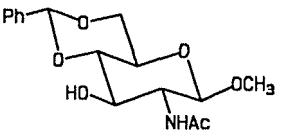

2

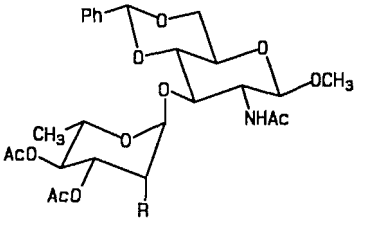

3 R = I
5 R = H

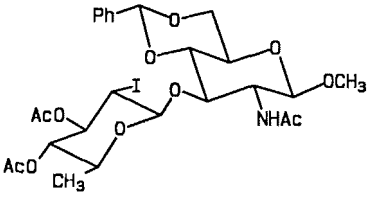

4

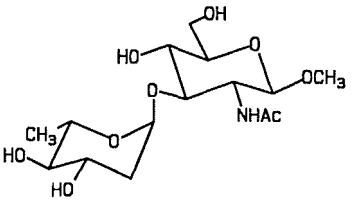

6

bition data with the pentasaccharide **ABCDA** (7), tetrasaccharide **BCDA** (8), and trisaccharides **BCD** (9) and **CDA** suggested that the major contribution to binding occurred in the **BCD** or **CDA** fragments (2). In this study we report the synthesis and relative activities of a series of di- and trisaccharide methyl glycosides centred on this epitope and containing 2-deoxy-α-L-*arabino*-hexopyranosyl residues.

Results and discussion

Di-*O*-acetyl-L-rhamnal **1** was prepared from tri-*O*-acetyl-α-L-rhamnopyranosyl bromide by reaction with magnesium–mercury amalgam (10).[4] Reaction of glycal **1** with the selectively protected monosaccharide alcohol, methyl 2-acetamido-4,6-*O*-benzylidene-2-deoxy-β-D-glucopyranoside **2**, in the presence of *N*-iodosuccinimide (11) provided an epimeric mixture of 1,2-*trans*-2-deoxy-2-iodo glycosides **3** and **4**. Variation of solvent and reaction conditions influenced the yield and ratio of products **3** and **4** (Table 3, experimental section). Extended reaction times in dichloromethane appeared to represent optimal conditions. The major product **3** possessed the α-*manno* configuration judged from ^{1}H and ^{13}C nmr spectral evidence (H-1′ δ 5.26 ppm $^3J_{1,2} < 1$ Hz, $^3J_{2,3} \approx 5$ Hz). A heteronuclear one-bond coupling constant for the anomeric carbon atom of 173 Hz unambiguously established the anomeric configuration of the α-L-rhamnopyranosyl residue (12). Based upon similar considerations (^{1}H nmr $^3J_{1,2}$ 9.0 Hz, $^3J_{2,3}$ 9.2 Hz) the minor product **4** had the β-L-*gluco* configuration. The 2-deoxy-2-iodo-rhamnopyranoside **3** was reduced to the 2-deoxy-*arabino-hexo*-pyranoside **5** in 82% yield following reduction by tributyltin hydride. Alternatively, nickel boride (13) also converted **3** into **5** but in lower yield (68%). Hydrogenation and *trans*-esterification of **5** gave the target disacharide **6**.

In a related series of experiments methyl 3,4-di-*O*-benzyl-α-L-rhamnopyranoside **7** and disaccharide **11** (7) were reacted with di-*O*-acetyl-L-rhamnal **2**. The disaccharide **8** and

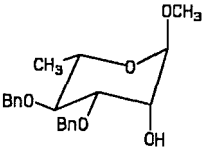

7

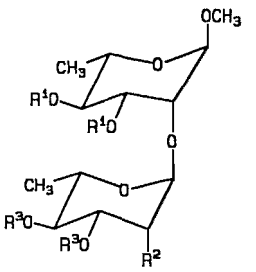

8 R^1 = Bn, R^2 = I, R^3 = Ac
9 R^1 = Bn, R^2 = H, R^3 = Ac
10 R^1 = R^2 = R^3 = H

[4]Application to glycal synthesis is described in ref. 10*b*.

trisaccharide **12** were obtained after chromatography in yields of 56 and 80%. Although use of acetonitrile instead of dichloromethane was not generally advantageous (Table 3), here the reaction time was decreased from 12 days to 30 h and the yield rose to 72%. The corresponding β-L-gluco isomers were not isolated and if present were effectively removed by silica gel chromatography. Compounds **8** and **12** were deprotected by first reducing the 2-iodo moiety to yield compounds **9** and **13**, then the benzyl groups were removed by hydrogenolysis and, finally, acetate esters by transesterification. Trisaccharide **13** was also de-*O*-benzylated by catalytic transfer hydrogenation (14). The purity of the products was indicated by ^{1}H and ^{13}C nmr spectra and the anomeric configuration was unambiguously established by measurement of $^{1}J_{CH}$ values for the anomeric carbon atoms of the deprotected structures **10** and **14**. The native tri-

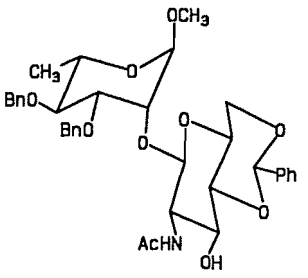

11

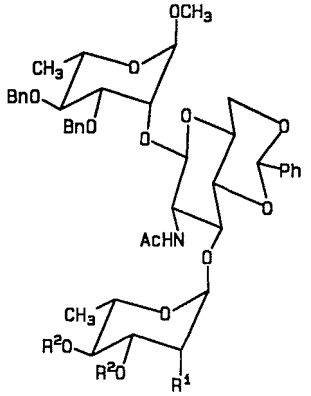

12 R^1 = I, R^2 = Ac
13 R^1 = H, R^2 = Ac

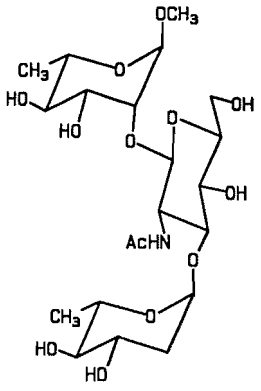

14

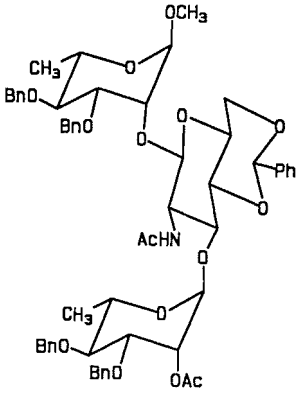

15

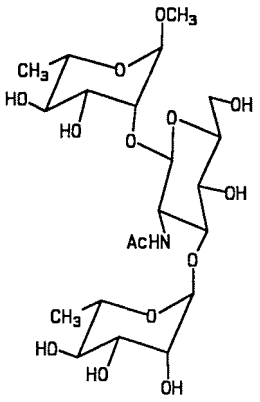

16

saccharide sequence **CDA** was constructed by reaction of disaccharide **11** with 2-*O*-acetyl-3,4-di-*O*-benzyl-α-L-rhamnopyranosyl chloride to give the protected trisaccharide **15** and ultimately trisaccharide **16**.

To introduce an internal 2-deoxy-rhamnose residue, a selectively protected rhamnal derivative was required. L-Rhamnal **17** (15) was selectively benzoylated under controlled conditions to provide 3-*O*-benzoyl-L-rhamnal **18** in 65% yield (16). Benzylation then provided the required intermediate **19**. Methyl 2-acetamido-4,6-*O*-benzylidene-2-deoxy-β-D-glycopyranoside **2** was reacted with the rhamnal **19** for 10 days and, after chromatography, **20** (60%) was obtained as the only disaccharide product. Transesterification afforded the selectively protected disaccharide alcohol **21**, which was glycosylated by tri-*O*-acetyl-α-L-rhamnopyranosyl bromide in the presence of silver triflate promoter.The protected trisaccharide **22** was deblocked in three steps without characterizing the intermediate derivatives. The benzylidene group was removed and the diol was acetylated. Tributyltin hydride reduction gave a 2-deoxy-rhamnose intermediate and transesterification followed by hydrogenolysis then afforded the trisaccharide **23**.

The disaccharides **6** and **10** and the trisaccharides **14**, **16**, and **23** were evaluated as inhibitors for the binding of the *Shigella flexneri* variant Y polysaccharide antigen to monoclonal antibodies, one (GC4) an IgM (17) and the other SYA/J6, an $IgG_3\kappa$. A solid phase assay employing antibody-coated enzyme immunoassay plates and enzyme-labelled polysaccharide antigen was used to obtain association constants for each inhibitor, which permitted the relative inhibitory power to be estimated as well as relative free energies $\Delta(\Delta G)$ for compounds **6**, **10**, **14**, **16**, and **23** (18, 19). In this assay purified antibody is immobilized on the wells of microtiter plates and enzyme- or biotin-labeled an-

Can. J. Chem. Downloaded from www.nrcresearchpress.com by 88.255.202.194 on 09/08/12
For personal use only.

TABLE 1. Direct competitive binding assay (18, 19); inhibition of the binding of enzyme-labelled *O*-polysaccharide to monoclonal antibody SYA/J6 absorbed to EIA plates

Compound	Hapten conc. at 50% inhibition (μmol L^{-1})	Relative potency (%)	$\Delta(\Delta G^0)$ (kcal mol^{-1})
Pentasaccharide **ABCDA**			
αLRha(1→2)αLRha(1→3)αLRha(1→3)βDGlcNAc(1→2)αLRha1→OCH_3	11	100	0
Tetrasaccharide **BCDA**			
αLRha(1→3)αLRha(1→3)βDGlcNAC(1→2)αLRha1→OCH_3	15	73	0.2
Trisaccharides			
CDA			
αLRha(1→3)βDGlcNAc(1→2)αL-Rha1→OCH_3	319	3	2.0
C'DA			
αL2deoxyRha(1→3)βDGlcNAc(1→2)αLRha1→OCH_3	29	38	0.6
BC'D			
αLRha(1→3)αL2deoxyRha(1→3)βDGlcNAc1→OCH_3	0.5	2200	−1.8
Disaccharide			
CD			
αLRha(1→3)βDGlcNAc1→OCH_3	1735	0.006	3.0
C'D			
αL2deoxyRha(1→3)βDGlcNAc1→OCH_3	32	34	0.6

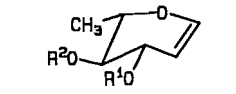

17 $R^1 = R^2 = OH$
18 $R^1 = Bz$, $R^2 = H$
19 $R^1 = Bz$, $R^2 = Bn$

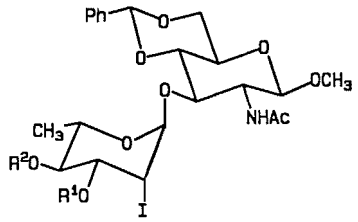

20 $R^1 = Bz$, $R^2 = Bn$
21 $R^1 = H$, $R^2 = Bn$

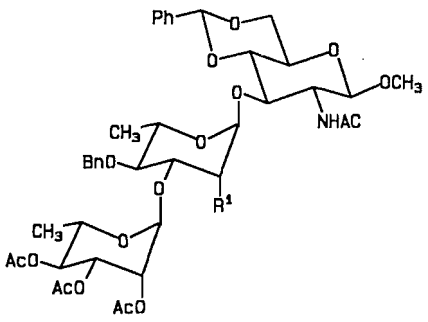

22 $R^1 = I$

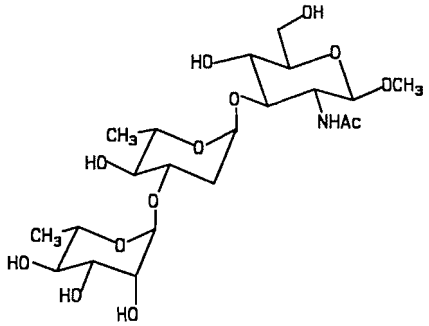

23

tigen is allowed to bind to solid phase antibody in the presence of increasing amounts of inhibitor. Under appropriate conditions it can be shown that the reciprocal antigen concentration at the 50% inhibition point corresponds to the association constant for the antibody–inhibitor pair (18, 19). Even when this does not strictly hold, the relative association constant or binding energy can be related to a reference inhibitor. For the antibody SYA/J6 these data are presented in Table 1 and are related to a native pentasaccharide structure α-L-Rha*p*(1→2)-α-L-Rha*p*(1→3)-β-D-GlcNAc*p*-(1→2)-α-L-Rha*p*-1→OMe, synthesized in other studies (7).

The pentasaccharide **ABCDA'** (7) and tetrasaccharide **BCDA** (8) have comparable activity, suggesting that the

Can. J. Chem. Downloaded from www.nrcresearchpress.com by 88.255.202.194 on 09/08/12
For personal use only.

TABLE 2. Direct competitive binding assay (18, 19); inhibition of the binding of enzyme-labelled *o*-polysaccharide to monoclonal antibody GC-4 absorbed to EIA plates

Compound	Hapten conc. at 50% inhibition (μmol L^{-1})	Relative potency (%)	$\Delta(\Delta G^0)$ (kcal mol^{-1})
Tetrasaccharide **BCDA**			
αLRha(1→3)αLRha(1→3)βDGlNAC(1→2)αLRha1→OCH_3	53	100	0
Trisaccharides			
CDA			
αLRha(1→3)βDGlcNAc(1→2)αL-Rha1→OCH_3	99	53	0.4
BC′D			
αLRha(1→3)αL2deoxyRha(1→3)βDGlcNAc1→OCH_3	20	265	−0.6
Disaccharide			
CD			
αLRha(1→3)βDGlcNAc1→OCH_3	60	88	0.17
C′D			
αL2deoxyRha(1→3)βDGlcNAc1→OCH_3	49	108	−0.1

TABLE 3. Yield of disaccharides in NIS-promoted glycosylations

No.	Solvent	Reaction time	Reaction temperature	Yield of **3** (%)	Yield of side product **4** (%)
1	CH_2Cl_2	7 d	Room temp.	63.00	<4.0
2	CH_2Cl_2	67 h	Reflux	51.00	3.0
3	$CHCl_3$	12 d	Room temp.	42.00	3.0
4	CH_3CN	9 d	Room temp.	62.60	8.4
5	DMF	9 d	Room temp.	11.00	4.0

terminal α-L-Rha residue **A** lies outside the antibody binding site. However, the 1.8 kcal mol^{-1} loss in binding energy when residue **B** is omitted indicates that this residue is a crucial part of the antigenic epitope. Since the tetrasaccharide **ABCD** shows comparable activity to the frame-shifted tetrasaccharide **BCDA′** (data not shown; see ref. 2) the trisaccharide **BCD** is concluded to be the essential recognition element of the bacterial antigen by antibody SYA/J6. Antibody GC-4 (Table 2) shows similar trends although the effective inhibitory power of disaccharide ligands suggests this binding site accommodates a smaller ligand. The relatively weaker activity of trisaccharide **CDA** compared to **BCD** suggests that the **A** residue makes unfavorable contacts with the protein.

The trisaccharides containing a 2-deoxy-rhamnose residue, **C′DA** and **BC′D**, both exhibit enhanced activity with antibodies compared to the corresponding unmodified trisaccharides, a trend that is also seen for the disaccharide analogues. The increased binding strength may be rationalized by assuming that the face of the oligosaccharide that presents the 2-OH group of rhamnose **C** points towards and interacts strongly with protein. Removal of the 2-OH group may then lead to stronger binding by extending nonpolar interactions or by relaxing the requirement of buried OH groups to be paired with an H-bond acceptor (20). The latter interpretation is consistent with more elaborate modelling studies, which are the subject of other publications.

Experimental

General procedures

Solvents were distilled before use and were dried where necessary by literature procedures (21). Reactions performed with dried solvents were conducted under dry nitrogen. Thin-layer chromatography (tlc) was performed on Silica Gel 60 F_{254} (Merck) with detection by uv light and (or) charring with sulphuric acid. Silica Gel 60 (Merck, 70–230 mesh) and redistilled solvents were used for column chromatography. Hexane refers to a mixture of hexanes supplied by Home Oil Company, Wichita, Kansas. Rexyn 101 refers to a strong cation-exchange resin (Fisher Scientific).

Melting points were determined on a Fisher–Johns apparatus and are uncorrected. Optical rotations were measured with a Perkin–Elmer 243 spectropolarimeter.

The ^1H and ^{13}C nmr spectra were recorded with Bruker AM 200 and AM 500 spectrometers. Solutions in organic solvents were referenced to internal tetramethysilane and relative to 1.0% v/v internal acetone (δ_H 2.225 ppm) in D_2O solutions. Internal acetone (δ_C 30.50 ppm) was used as the internal ^{13}C reference for solutions in D_2O. Chemical shifts and coupling constants are first-order values and assignments are based upon homo- and heteronuclear shift correlation spectroscopy.

Enzyme immunoassays were performed according to published procedures (18, 19). *Shigella flexneri* O-polysaccharide was re-

Can. J. Chem. Downloaded from www.nrcresearchpress.com by 88.255.202.194 on 09/08/12
For personal use only.

Can. J. Chem. Downloaded from www.nrcresearchpress.com by 88.255.202.194 on 09/08/12
For personal use only.

ductively aminated and biotinylated (19). Protein A purified antibody was used to coast immunoassay microtiter plates and inhibition assays were conducted as previously described (19).

*1,5-Anhydro-3,4-di-*O*-acetyl-2,6-dideoxy-*L*-*arabino*-hex-1-enitol* ***1***

2,3,4-Tri-*O*-acetyl-α-L-rhamnopyranosyl bromide (102 g, 289 mmol) was dissolved in dry DMF (200 mL distilled over barium oxide). The mixture was cooled with an ice-water bath for 10 min and treated with small portions of magnesium amalgam (200 g) (10). The reaction flask was evacuated for 10 min and the reaction flask closed under vacuum. The ice-water bath was removed after 0.5 h and the reaction mixture stirred vigorously for 2 h. The complete consumption of the starting material, R_F 0.2, to the faster rhamnal derivative, R_F 0.3, was shown by tlc (ethyl acetate: hexanes, 1:3). The reaction mixture was filtered on a bed of Celite and the solvent was removed. The syrupy residue was dissolved in dichloromethane (300 mL) and washed with 0.1 M hydrochloric acid (50 mL), a saturated solution of sodium hydrogen carbonate (100 mL), and water (100 mL). The organic phase was dried over $MgSO_4$, filtered, evaporated, and chromatographed over silica gel, eluting first with hexanes, then ethyl acetate – hexane, 1:7 followed by 1:4. This afforded **1** as a colourless liquid, 48.2 g (78%); $[\alpha]_D$ +64.8 (*c* 1.14, chloroform); (lit. (22) $[\alpha]_D$ 68 ($CHCl_3$)); ^{1}H nmr (200 MHz, $CDCl_3$) δ: 6.4 (dd, 1H, $J_{1,2}$ 6.1 Hz, $J_{1,3}$ 1.4 Hz, H-1), 5.3 (m, 1H, $J_{3,4}$ 6.2 Hz, H-3), 5.00 (dd, 1H, $J_{4,5}$ 8.2 Hz, $J_{3,4}$ 6.2 Hz, H-4), 4.76 (dd, 1H, $J_{2,3}$ 3 Hz, H-2), 4.06 (m, 1H, $J_{4,5}$ 8.2 Hz, H-5), 2.05 (s, 3H, Ac), 2.01 (s, 3H, Ac), 1.28 (d, 3H, $J_{5,6}$ 6.5 Hz, H-6).

*Methyl 2-acetamido-3-*O*-(3′,4′-di-*O*-acetyl-2′-deoxy-2′-iodo-α-*L*-rhamnopyranosyl)-4,6-*O*-benzylidene-2-deoxy-β-*D*-glucopyranoside* ***3*** and *methyl 2-acetamido-3-*O*-(3′,4′-di-*O*-acetyl-2′6′-dideoxy-2′-iodo-β-*L*-glucopyranosyl)-4,6-*O*-benzylidene-2-deoxy-β-*D*-glucopyranoside* ***4***

Methyl 2-acetamido-4,6-*O*-benzylidene-2-deoxy-β-D-glucopyranoside **2** (2.00 g, 6.2 mmol) and 3,4-di-*O*-acetyl-L-rhamnal **1** (2.00 g, 9.3 mmol) were added to a solution of *N*-iodosuccinimide (2.00 g, 9 mmol) in dry dichloromethane (100 mL) in a flask wrapped with aluminum foil. The closed reaction flask was stirred at room temperature for 10 days. The progress of the reaction was monitored by tlc using a solvent mixture of methanol – ethyl acetate – hexanes, 1:10:3. The reaction mixture was then diluted with dichloromethane (100 mL), washed with sodium thiosulfate solution (15%) followed by water, dried, filtered, evaporated, and chromatographed on a silica gel column (ethyl acetate – hexanes, 1:7 followed by 1:1) to give 2.65 g (64.6%) of the 2′-deoxy-2′-iodo-disaccharide **3**: $[\alpha]_D$ −67.6 (*c* 0.88, chloroform); mp 236–239°C (recryst. ethyl acetate); ^{1}H nmr (500 MHz, $CDCl_3$) δ: 7.36 (m, 5H, aromatic), 5.85 (d, 1H, $J_{NH,2}$ 8 Hz, NH), 5.5 (s, 1H, CHPh), 5.26 (bs, 1H, H-1′), 4.96 (q, 1H, $J_{3',4'}$, 9 Hz H-4′), 4.72 (d, 1H, $J_{1,2}$ 8 Hz, H-1), 4.52 (m, 1H, $J_{2',3'}$ 5 Hz, H-2′), 4.51 (q, 1H, $J_{3'4'}$ 9 Hz, H-3′), 4.34 (q, 1H, $J_{6A,6B}$ 10.5 Hz, $J_{5,6}$ 5 Hz, H-6A), 4.25 (t, 1H, H-5), 4.11 (m, 1H, H-5′), 3.75 (t, 1H, H-4), 3.57 (t, 1H, H-3), 3.5 (m, 2H, H-2, H-6B), 2.03 (s, 3H, OAc), 2.01 (s, 3H, OAc), 1.95 (s, 3H, NHAc), 0.7 (d, 3H, $J_{5'6'}$ 6 Hz, H-6′); ^{13}C nmr (500 MHz, $CDCl_3$) δ_C: 101.9 (C-1′, $J_{C,H}$ 173 Hz), 101.8 (CHPh, $J_{C,H}$ 157 Hz), 101.3 (C-1, $J_{C,H}$ 164 Hz), 57.9 (C-2), 57.1 (OMe), 30.1 (C′-2), 23.4 (NHAc), 21.0, 20.7 (2 × OAc), 16.8 (C-6′); the rest of the spectra is in agreement with compound **3**. Anal. calcd. for $C_{26}H_{34}INO_{11}$: C 47.07, H 5.17, I 18.99, N 2.11; found: C 46.86, H 5.21, I 18.88, N 2.02.

A side product was isolated chromatographically from the above reaction as disaccharide **4**: $[\alpha]_D$ −74.95 (*c* 0.86, chloroform); mp 221°C (dec.); ^{1}H nmr (500 MHz, $CDCl_3$) δ: 7.55–7.35 (m, 5H, aromatic), 5.73 (d, 1H, $J_{NH,2}$ 7.4 Hz, NH), 5.58 (s, 1H, CHPh), 5.18 (q, 1H, $J_{2',3'}$ 9.2 Hz, $J_{3',4'}$ 11 Hz, H3′), 5.02 (d, 1H, $J_{1,2}$ 8.4 Hz, H-1), 4.89 (d, 1H, $J_{1',2'}$ 9 Hz, H-1′), 4.67 (t, 1H, Hz, H-4′), 4.51 (t, 1H, H-3), 4.38 (q, 1H, $J_{6A,6B}$ 10.6 Hz, $J_{5,6}$ 5 Hz, H-6A), 3.82–3.76 (m, 2H, H-5, H-2′), 3.73 (t, 1H, H-4), 3.57–3.5 (m, 5H, H-6B, and OMe), 3.18 (m, 1H, H-2), 1.95, 1.99, 2.04 (3s, 9H, 3AcO, 1.195 (d, 3H, $J_{5'6'}$ 6 Hz, H-6′), ^{13}C nmr (200 MHz, $CDCl_3$) δ_C: 101.9 (C-1′), 101.4 (CHPh), 101.2 (C-1), 57.4 (2C, C-2, OMe), 28.2 (C′2), 23.7 (NHAc), 20.6 (2C, 2 × OAc), 17.3 (C-6′). Anal. calcd. for $C_{26}H_{34}INO_{11}$: C 47.07, H 5.17, I 18.99, N 2.11; found: C 46.81, H 5.13, I 18.79, N 1.93.

Table 3 shows the yields of compound **3** and **4** prepared by reaction of **1** with **2** in different solvents.

*Methyl 2-acetamido-3-*O*-(3′,4′-di-*O*-acetyl-2′-deoxy-α-*L*-rhamnopyranosyl)-4,6-*O*-benzylidene-2-deoxy-β-*D*-glycopyranoside* ***5***

A: A mixture of the disaccharide **3** (300 mg, 0.45 mmol), tributyltin hydride (0.2 mL, 0.74 mmol), and benzoyl peroxide (5 mg) in dry toluene (10 mL) was stirred under nitrogen for 45 min at 70°C. The reaction mixture was cooled to room temperature, quenched with methanol (5 mL), evaporated, and chromatographed on a silica gel column (ethyl acetate – hexanes, 1:2 followed by ethyl acetate) to give **5** (200 mg, 82%) as a solid: mp 286–287°C; $[\alpha]_D$ −143.6 (*c* 0.73, chloroform); ^{1}H nmr (200 MHz, $CDCl_3$) δ: 7.37 (m, 5H, aromatic), 6.13 (d, 1H, NH), 5.47 (s, 1H, CHPh), 5.18 (m, 1H, $J_{2'e3}$, 5.7 Hz, $J_{3',2'a}$ 11 Hz, H-3′), 4.95 (bd, 1H, $J_{1',2'a}$ 2.8 Hz, H-1′), 4.7 (d, 1H, $J_{1,2}$ 8.5 Hz, H-1), 4.55 (t, 1H, $J_{3,4}$ 10 Hz, H-4′), 4.27 (m, 2H, H-6 and 5), 4.03 (m, 1H, $J_{4',5'}$ 10 Hz, H5′), 3.74 (t, 1H, H-4), 3.55 (m, 3H, H-3, 2, and 6), 3.45 (s, 3H, OMe), 2.18 (q, 1H, $J_{2'e,3'}$ 5.7 Hz, J_{gem} 11 Hz, H-2′e), 1.94 (bs, 9H, 3Ac), 1.68 (m, 1H, $J_{1,2a}$ 2.8, J_{gem} 11 H, H-2′a), 0.58 (d, 3H, $J_{5'6'}$ 6 Hz, H-6′); ^{13}C nmr (200 MHz, $CDCl_3$) δ_C: 101.7 (CHPh), 101.3 (C-1′), 97.0 (C-1′), 58.0 (C-2), 56.9 (OMe), 35.2 (C-2′), 23.5 (NHAc), 21.0, 20.74 (OAc), 16.7 (C-6′). Anal. calcd. for $C_{26}H_{35}NO_{11}$: C 58.12, H 6.56, N 2.6; found: C 57.88, H 6.43, N 2.51.

B: A solution of nickelous chloride (2 g, 8.4 mmol) in ethanol (15 mL) was treated slowly with sodium borohydride (1 g, 26.4 mmol). Compound **3** (1 g, 1.5 mmol) dissolved in ethanol (35 mL) was added to the black suspension and stirred for 3 h. The mixture was filtered over a bed of Celite and the filtrate was evaporated. The residue was dissolved in dichloromethane (50 mL) and washed with water (20 mL × 2), dried over $MgSO_4$, filtered, and evaporated to give a solid. This solid was recrystallized from hot methanol to give **5** (0.55 g, 68%).

*Methyl 2-acetamido-3-*O*-(2-deoxy-α-*L*-rhamnopyranosyl)-2-deoxy-β-*D*-glucopyranoside* ***6***

A solution of **5** (280 mg, 0.52 mmol) in glacial acetic acid (20 mL) and ethyl acetate (20 mL) was hydrogenated for 4 days at atmospheric pressure over 10% palladium on charcoal. The mixture was filtered and evaporated to dryness. The resultant syrup was taken up in methanol (15 mL) and treated with a catalytic amount of sodium methoxide for 18 h. Sodium ions were removed with Rexyn 101 (H^+) ion-exchange resin. Filtration, evaporation, and chromatographic purification on silica gel with 1:10 (v/v) methanol – ethyl acetate as the eluant gave the disaccharide **6** (104 mg, 55%), recrystallized from methanol – ethyl acetate: mp 273.5°C; $[\alpha]_D$ −97.2 (*c* 0.9, methanol); ^{1}H nmr (500 MHz, D_2O) δ: 5.00 (d, 1H, H-1′), 4.48 (d, 1H, $J_{1,2}$ 10 Hz, H-6), 3.85–3.72 (m, 3H, H-2, 3′, and 6B), 3.56 (m, 1H, H-3), 3.51 (s, 3H, OMe), 3.48 (m, 2H, H-4 and 5), 3.1 (t, 1H, $J_{3',4'}$ 10 Hz, H-4′), 2.04 (s, 3H, Ac), 2.01 (m, 1H, H-2′e), 1.71 (m, 1H, H-2′a), 1.23 (d, 3H, $J_{5',6'}$ 6 Hz, H-6′); ^{13}C nmr (D_2O) δ_C: 102.1 (C-1), 99.5 (C-1′), 82.0 (C-3), 77.3 (C-4′), 76.8 (C-4), 69.4 and 69.3 (C-5′ and C-5), 68.6 (C-3′), 61.6 (C-6), 57.8 (OMe), 56.0 (C-2), 38.2 (C-2′), 22.9 (AcNH), 17.3 (C-6′). Anal. calcd. for $C_{15}H_{27}NO_9$: C 49.30, H 7.45, N 3.83; found: C 49.13, H 7.42, N 3.71.

*Methyl 3,4-di-*O*-benzyl-2-*O*-(3,4-di-*O*-acetyl-2-deoxy-2-iodo-α-*L*-rhamnopyranosyl)-α-*L*-rhamnopyranoside* ***8***

A mixture of methyl 3,4-di-*O*-benzyl-α-L-rhamnopyranosyl **7** (1 g, 2.8 mmol) (23), 3,4-di-*O*-acetyl-L-rhamnal **1** (0.8 g, 3.7 mmol), and *N*-iodosuccinimide (0.8 g, 3.6 mmol) in dry dichloromethane was stirred for 12 days in a flask wrapped with

Can. J. Chem. Downloaded from www.nrcresearchpress.com by 88.255.202.194 on 09/08/12
For personal use only.

aluminum foil. The product, R_f 0.3 (hexane – ethyl acetate), was worked up from the reaction mixture in similar fashion to the previous reaction of compound **3**. The chromatographic purification on silica gel, eluting with hexanes – ethyl acetate 7:1 (v/v), followed by 3:1, gave pure **8** (1.1 g, 56%). Recrystallization from ethyl acetate – hexanes over 48 h at 4°C gave elongated crystals: mp 101–103°C; $[\alpha]_D$ −31.3 (*c* 0.83, chloroform); ^{1}H nmr (200 MHz, $CDCl_3$) δ: 7.3 (m, 10 H, aromatics), 5.32 (s, 1H, H-1′), 5.12 (t, 1H, $J_{3',4'}$ 10 Hz, H-4′), 4.86 (d, 1H, CH_2Ph), 4.75–4.55 (m, 6H, H-1, H-2′, H-3′, and CH_2Ph), 4.06 (m, 1H, H-5′), 3.9 (t, 1H, $J_{2,3}$ 2.5 Hz, H-2), 3.8 (dd, 1H, $J_{3,4}$ 8.8 Hz, H-3), 3.64 (m, 1H, H-5), 3.49 (t, 1H, H-4), 3.3 (s, 3H, OMe), 2.06 (s, 3H, OAc), 2.03 (s, 3H, OAc), 1.2 (d, 3H, $J_{5,6}$ 6 Hz, H-6), 1.18 (d, 3H, $J_{5',6'}$ 6 Hz, H-6′); ^{13}C nmr ($CDCl_3$) δ_C: 102.8 (C-1′), 99.8 (C-1), 54.6 (OMe), 30.5 (C′2), 21.0 (AcO), 20.7 (AcO), 17.9 (C-6), 17.5 (C-6′). Anal. calcd. for $C_{32}H_{39}IO_{10}$: C 53.3, H 5.6, I 18.16; found: C 53.14, H 5.45, I 17.9.

When the above reaction was conducted in acetonitrile instead of dichloromethane, the yield of **8** increased to 72% and the reaction time was reduced to 30 h.

*Methyl 3,4-di-*O*-benzyl-2-*O*-(2-deoxy-3,4-di-*O*-acetyl-α-L-rhamnopyranosyl)-α-L-rhamnopyranoside* ***9***

A mixture of compound **8** (700 mg, 1 mmol), tributyltin hydride (0.4 mL, 1.5 mmol), and benzoyl peroxide (5 mg) in dry toluene (20 mL) was stirred under nitrogen for 1 h at 70°C. The mixture was cooled to room temperature, quenched with methanol (5 mL), and evaporated. The resultant syrup was chromatographed on a silica gel column eluted with ethyl acetate – hexane, 1:10, followed by 1:7, to give 488 mg (85%) of **9**: $[\alpha]_D$ −66.7 (*c* 1.05, chloroform); mp 128–129°C (recryst. methanol); ^{1}H nmr (200 MHz, $CDCl_3$) δ: 7.3 (s, 10 H, aromatics), 5.35 (m, 1H, H-3′), 5.07 (d, 1H, $J_{1',2'a}$ 3.9 Hz, H-1′), 4.9–4.57 (m, 6H, CH_2Ph, H-4′ and H-1), 4.0–3.8 (m, 3H, H-2, H-3, and H-5′), 3.63 (m, 1H, H-5), 3.5 (t, 1H, H-4), 3.3 (s, 3H, OMe), 2.34 (m, 1H, H-2′e), 2.03 (s, 3H, OAc), 2.00 (s, 3H, OAc), 1.7 (m, 1H, H-2′a), 1.32 (d, 3H, $J_{5,6}$ 6 Hz, H-6), 1.15 (d, 3H, $J_{5',6'}$ 6 Hz, H-6′); ^{13}C nmr ($CDCl_3$) δ_C: 100.7 (C-1′), 98.5 (C-1), 54.6 (OMe), 35.3 (C-2′), 21.0 (AcO), 20.6 (AcO), 17.7 (C-6), 17.5 (C-6′). Anal. calcd. for $C_{31}H_{40}O_{10}$: C 65.02, H 7.04; found: C 65.07, H 7.10.

*Methyl 2-*O*-(2-deoxy-α-L-rhamnopyranosyl)-α-L-rhamnopyranoside* ***10***

A mixture of compound **9** (250 mg, 0.437 mmol) in a saturated solution of methanolic ammonia (20 mL) was stirred at room temperature for 18 h. The mixture was evaporated to dryness to give a syrup. A solution of the resultant syrup in ethanol (99%, 15 mL), glacial acetic acid (3 mL), and water (3 drops) was hydrogenated over palladium (on charcoal 10%) catalyst at 70 psi (1 psi = 6.89 kPa) for 5 days. Filtration and evaporation gave a syrup, which was chromatographed on silica gel with 1% methanol in ethyl acetate (v/v) to give **10** as a foam, 108 mg (80%); mp 38–40°C; $[\alpha]_D$ −95.6 (*c* 0.82, methanol); ^{1}H nmr (500 MHz, D_2O) δ: 5.1 (d, 1H, H-1′), 4.73 (s, 1H, H-1), 3.96–3.87 (m, 2H, H-3′ and H-2), 3.77 (m, 2H, H-5′ and H-3), 3.64 (m, 1H, H-5), 3.5 (t, 1H, H-4), 3.4 (s, 3H, OMe), 3.12 (t, 1H, H-4′), 2.33 (m, 1H, H-2′e), 1.7 (m, 1H, H-2′a), 1.32 (d, 3H, H-6), 1.3 (d, 3H, H-6′); ^{13}C nmr (D_2O) δ_C: 100.6 (2C, C-1, C-1′, $^1J_{CH}$ 172 Hz), 78.9 (C-2), 77.4 (C-4′), 73.0 (C-4), 70.9 (C-3), 69.5 (C-5′), 69.3 (C-5), 68.5 (C-3′), 55.7 (OMe), 37.9 (C-2′), 17.5 (C-6), 17.4 (C-6′). Anal. calcd. for $C_{13}H_{24}O_8$: C 50.64, H 7.85; found: C 50.55, H 8.01.

Methyl O*-(3″,4″-di-*O*-acetyl-2″-deoxy-2″-iodo-α-L-rhamnopyranosyl)-(1→3)-*O*-(2′-acetamido-4′,6′-*O*-benzylidene-2′-deoxy-β-D-glucopyranosyl)-(1→2)-3,4-di-*O*-benzyl-α-L-rhamnopyranoside* ***12***

A mixture of the disaccharide **11** (7) (1.00 g, 1.5 mmol), diacetyl rhamnal **1** (0.4 g, 1.87 mmol), and *N*-iodosuccinimide (0.5 g, 2.2 mmol), in a dry solvent mixture of dichloromethane (150 mL) and acetonitrile (50 mL), was stirred in a flask wrapped with aluminum foil for 10 days. The reaction mixture was diluted with dichloromethane (100 mL), washed with a solution of sodium thiosulfate (15%) followed by water, dried over magnesium sulfate, filtered, and evaporated to give a coloured residue. This residue was chromatographed on a silica gel column and eluted with ethyl acetate – hexanes, 1:4 (v/v) followed by 1:2, to collect 1.22 g (80%) of compound **12**: mp 87–89°C; ;$[\alpha]_D$ −38.5 (*c* 0.9, chloroform); ^{1}H nmr (500 MHz, $CDCl_3$) δ: 7.44–7.30 (m, 15H, aromatics), 5.68 (d, 1H, $J_{NH,2}$ 8 Hz, NH), 5.5 (s, 1H, CHPh), 5.02 (s, 1H, H-1″), 4.93 (t, 1H, $J_{3'',4''} + J_{4'',5''}$ = 19 Hz, H-4″), 4.83 (d, 1H, CH_2Ph), 4.74 (d, 1H, CH_2Ph), 4.65 (d, 1H, $J_{1,2} \sim 1$ Hz, H-1), 4.60 (q, 3H, $J_{1',2'}$ 9.5 Hz, H-1′ and CH_2Ph), 4.54 (q, 1H, $J_{2'',3''}$ 4.5 Hz, H-3″), 4.44 (dd, 1H, $J_{1'',2''} < 1$ Hz, H-2″), 4.31 (q, 1H, $J_{6'A\text{-}6'B}$ 11 Hz, $J_{5',6'A}$ 5 Hz, H-6′A), 4.13 (m, 1H, $J_{5'',6''}$ 6 Hz, $J_{4,5''}$ 10 Hz, H-5″), 3.89 (m, 1H, $J_{2,3}$ 3.5 Hz, H-2), 3.87–3.83 (m, 2H, H-2′ and H-3), 3.75 (t, 1H, $J_{6'A,6'B} + J_{5',6'}$ 21 Hz, H-6′B), 3.70–3.61 (m, 2H, H-3′ and H-5), 3.56 (t, 1H, H-4′), 3.38 (m, 1H, H-5′), 3.33 (t, 1H, H-4), 3.3 (s, 3H, OMe), 2.00, 1.93 (2s, 6H, 2 × OAc), 1.69 (s, 3H, NHAc), 1.31 (d, 3H, H-6), 0.76 (d, 3H, H-6″); ^{13}C nmr (200 MHz, $CDCl_3$) δ_C: 103.1 (C-1′), 101.5 (2C, C-1″ and CHPh), 99.7 (C-1), 56.4 (C-2′), 54.3 (OMe), 30.8 (C-2″), 22.6 (NHAc), 20.7, 20.5 (2C, AcO), 17.6, 16.6 (2C, C6 and C6″). When this reaction was conducted in dichloromethane, the yield decreased to 47% and in acetonitrile it similarly decreased to 75%. Anal. calcd. for $C_{46}H_{56}INO_{15}$: C 55.82, H 5.70, N 1.42; found: C 56.06, H 5.76, N 1.77.

Methyl O*-(3″,4″-di-*O*-acetyl-2″-deoxy-α-L-rhamnopyranosyl)-(1→3)-*O*-(2′-acetamido-4′,6′-*O*-benzylidene-2′-deoxy-β-D-glucopyranosyl]-(1→2)-3,4-di-*O*-benzyl-α-L-rhamnopyranoside* ***13***

A mixture of the iodo-trisaccharide **12** (1 g, 1.01 mmol), tributyltin hydride (0.4 mL, 1.52 mmol), and benzoyl peroxide (5 mg) in dry toluene (25 mL) was stirred under nitrogen for 45 min at 70°C. When tlc (ethyl acetate – hexanes, 1.1, (v/v)) of the reaction mixture showed that all the starting material had been consumed, the mixture was cooled to room temperature, quenched with methanol (10 mL), evaporated, and chromatographed on a silica gel column (ethyl acetate – hexanes, 1:5 followed by 1:2) to give 0.84 g (96%) of the trisaccharide **13**: $[\alpha]_D$ −78.8 (*c* 1.03, chloroform); mp 91–93°C; ^{1}H nmr (200 MHz, $CDCl_3$) δ: 2.15 (m, 1H, H-2″e), 1.6 (m, 1H, H-2″a overlapping with NHAc signal); ^{13}C nmr (200 MHz, $CDCl_3$) δ_C: (C-1′), 101.6 (CHPh), 99.9 (C-1), 96.7 (C-1″), 57.1 (C-2′), 54.5 (OMe), 35.2 (C-2″, deoxy), 23.2 (N-Ac), 20.9, 20.7 (2 × Ac), 17.6, 16.8 (C-6 and C-6″). Anal. calcd. for $C_{46}H_{57}NO_{15}$: C 63.44, H 6.74, N 1.64; found: C 63.22, H 6.68, N 1.55.

Methyl O*-2-deoxy-α-L-rhamnopyranosyl-(1→3)-*O*-2-acetamido-2-deoxy-β-D-glucopyranosyl-(1→2)-α-L-rhamnopyranoside* ***14***

A: A solution of the trisaccharide **13** (675 mg, 0.78 mmol) in glacial acetic acid (10 mL) and ethyl acetate (15 mL) was hydrogenolyzed, in the presence of 10% palladium on charcoal, at atmospheric pressure, for 7 days. The mixture was filtered through Celite and the filtrate was evaporated to dryness. The resultant syrup was chromatographed on a silica gel column using 5% methanol in ethyl acetate as eluant. The solid collected (364 mg) was dissolved in saturated methanolic ammonia and let stand overnight at room temperature in a tightly closed flask. The mixture was filtered and evaporated to give 286 mg (72%) of the trisaccharide **14**; $[\alpha]_D$ −59.1 (*c* 0.86, methanol); mp 156–158°C (recryst. ethanol – ethyl acetate); ^{1}H nmr (500 MHz, D_2O) δ: 5.03 (d, 1H, $J_{1'',2''}$ 4 Hz, H-1′), 4.82 (s, 1H, H-1), 4.73 (d, 1H, $J_{1',2'}$ 9 Hz, H-1′), 3.99–3.93 (m, 2H, $J_{4'',5''}$ 10 Hz, $J_{5'',6''}$ 6.5 Hz, H-2 and H-5″), 3.9 (dd, 1H, $J_{6'A,6'B}$ 12.5 Hz, $J_{5'A,6'A}$ 2 Hz, H-6′A), 3.84–3.75 (m, 3H, H-3″, H-2′, and H-3), 3.73 (q, 1H, $J_{6'B,6'A}$ 12.5 Hz, $J_{5',b'B}$ 5.5 Hz, H.-6′B), 3.66–3.57 (m, 2H, H-5 and H-3′), 3.47 (t, 1H, H-4′), 3.43 (m, 1H, H-5′), 3.37 (s, 3H, OMe), 3.3 (t, 1H′, H-4), 3.08 (t, 1H, H-4″), 2.06–2.00 (m, 4H, H-2″e and AcNH), 1.73–1.66

Can. J. Chem. Downloaded from www.nrcresearchpress.com by 88.255.202.194 on 09/08/12
For personal use only.

(m, 1H, H-2″a), 1.26 (d, 3H, $J_{5,6}$ 6.5 Hz, H-6), 1.21 (d, 3H, $J_{5'',6''}$ 6.5 Hz, H-6″); ^{13}C nmr (500 MHz, D_2O) δ_C: 102.6 ($J_{C,H}$ 162.0 Hz, C-1′), 100.4 ($J_{C,H}$ 172.2 Hz, C-1), 99.3 ($J_{C,H}$ 170.0 Hz, C-1″), 81.4 (C-3′), 79.2 (C-2), 77.2 (C-4″), 76.6 (C-5′), 73.0 (C-4), 70.6 (C-3), 69.2 (2C, C-5, C-5″), 69.1 (C-4′), 68.5 (C-3″), 61.4 (C-6′), 56.4 (C-2′), 55.5 (OMe), 38.2 (C-2″), 23.0 (AcNH), 17.4 (C-6), 17.3 (C-6″). Anal. calcd. for $C_{21}H_{37}NO_{13}$: C 49.3, H 7.29, N 2.74; found: C 49.14, H 7.36, N 2.81.

B: The blocked trisaccharide **13** (300 mg, 0.35 mmol) was dissolved in ethanol (99%, 10 mL) and treated with cyclohexene (5 mL) and palladium hydroxide (70 mg) (14). The mixture was refluxed for 60 h, filtered, evaporated, and chromatographed on a silica gel column using 5% methanol in ethyl acetate to give a solid (117 mg). This solid (117 mg) was treated overnight with a saturated methanolic ammonia solution, filtered, and evaporated to give 99 mg (56%) of the deprotected trisaccharide **14**.

Methyl O-*(2″-*O*-acetyl-3″,4″-di-*O*-benzyl-α-L-rhamnopyranosyl)-(1→3)-*O*-(2′-acetamido-4′,6′-O-benzylidene-2′-deoxy-β-D-glucopyranosyl)-(1→2)-3,4-di-*O*-α-L-rhamnopyranoside **15***

A mixture of methyl 2-*O*-(2′-acetamido-4,6-*O*-benzylidene-2′-deoxy - β -D-glucopyranosyl) - 3,4-di- *O*-benzyl-α-L-rhamnopyranoside **11** (0.8 g, 1.23 mmol), 2-*O*-acetyl-3,4-di-*O*-benzyl-α-L-rhamnopyranosyl chloride (1.00 g, 2.47 mmol), 1,1,3,3-tetramethyl urea (0.8 mL, 6.7 mmol), and molecular sieves (4Å, 0.5 g) in anhydrous dichloromethane (45 mL) was stirred under nitrogen and cooled to −30°C. The mixture was then treated, in three portions, with silver trifluoromethane sulphonate (0.52 g, 2.00 mmol) and allowed to warm gradually, overnight, to room temperature. The solid was removed by filtration and the filtrate was washed successively with sodium bicarbonate solution and water. The organic layer was dried ($MgSO_4$), filtered, concentrated, and chromatographed on a silica gel column, using ethyl acetate – hexanes (1:1) as eluant, to give a syrup, 0.95 g (76%), of **15**: $[\alpha]_D$ −18.5 (*c* 1.16, chloroform); ^{1}H nmr (200 MHz, $CDCl_3$) δ: 7.5–7.2 (m, 25H, aromatic), 5.63 (d, 1H, NH), 5.5 (s, 1H), 5.19 (m, 1H), 4.97–4.5 (m, 10H), 4.3 (q, 1H), 4.0–3.3 (m, 16H), 2.1 (s, 3H, OAc), 1.82 (s, 3H, NHAc), 1.35 (d, 3H, H-6), 0.85 (d, 3H, H-6″).

Methyl O-*α-L-rhamnopyranosyl-(1→3)-*O*-2-acetamido-2-deoxy-β-D-glucopyranosyl-(1→2)-α-L-rhamnopyranoside **16***

A solution of the trisaccharide **15** (0.9 g, 0.88 mmol) in 80% aqueous acetic acid (25 mL) was hydrogenolyzed, for 4 days, at 70 psi in the presence of 10% palladium on charcoal. Filtration, repeated co-evaporation with toluene, and chromatographic purification on a silica gel column using ethyl acetate – methanol (7:1) as eluant gave 389 mg of colourless solid. The solid was dissolved in methanol (20 mL) containing a catalytic amount of sodium methoxide and kept at room temperature for 12 h. The sodium ions were removed with Rexyn 101 (H^+) ion-exchange resin. Filtration, followed by evaporation of the solvent, gave 280 mg (60%) of the trisaccharide **16**, $[\alpha]_D$ −57.7 (*c* 0.69, MeOH); mp 160–163°C (recrystallized from MeOH – ethyl acetate); ^{1}H nmr (200 MHz, D_2O) δ: 4.73 (d, 1H, H-1), 4.7 (d, 1H, H-1″), 4.62 (d, 1H, H-1′), 3.9–3.12 (m, 17H), 1.93 (s, 3H, NHAc), 1.13 (d, 3H, H-6), 1.09 (d, 3H, H-6″); ^{13}C nmr (200 MHz, $CDCl_3/CD_3OD$) δ_C: 102.4 (C-1′), 101.3 (C-1″), 99.5 (C-1), 62.6 (C-3′), 79.5 (C-2), 75.7 (C-5′), 72.5 (C-4), 72.0 (C-4″), 70.7 (C-2″), 70.5 (C-3″, C-4′), 68.9 (C-5″), 68.8 (C-3), 67.9 (C-5), 61.1 (C-6′), 55.1 (C-2′), 54.3 (OMe), 22.2 (NHAc), 16.9 (C-6, C-6″). Anal. calcd. for $C_{21}H_{37}NO_{14}$: C 47.81, H 7.01, N 2.66; found: C 47.68, H 6.99, N 2.58.

*1,5-Anhydro-2,6-dideoxy-L-*arabino*-hex-1-enitol **17***

A solution of 3,4-diacetyl-L-rhamnal **1** (20.0 g, 93 mmol) in methanol (50 mL) was treated with a solution of sodium methoxide (2 mL of 0.4 M solution) for 1 h at room temperature, at which point tlc (ethyl acetate – hexanes, 1:1) of the reaction mixture indicated the consumption of all the starting material. Sodium ions were removed with Rexyn 101 (H^+) ion-exchange resin. Filtration, evaporation, and crystallization from ethyl acetate – hexanes gave 10.6 g (87.2%) of L-rhamnal **17**: $[\alpha]_D$ +25.7 (*c* 1.03, chloroform); mp 77–78°C (lit. (15) mp 70–73°C); ^{1}H nmr (200 MHz, $CDCl_3$) δ: 6.26 (dd, 1H, $J_{1,2}$ 5.4 Hz, $J_{1,3}$ 1.4 Hz, H-1), 4.65 (dd, 1H, $J_{2,3}$ 1.4 Hz, H-2), 4.27 (bd, 1H, OH), 4.18 (m, 1H, H-3), 3.9 (bd, 1H, OH), 3.79 (m, 1H, $J_{4,5}$ 10 Hz, $J_{5,6}$ 6 Hz, H-5), 3.35 (m, 1H, $J_{3,4}$ 7.5 Hz, H-4), 1.33 (d, 3H, $J_{5,6}$ 6 Hz, H-6); ^{13}C nmr (200 MHz $CDCl_3$) δ_C: 144.8 (C-1), 102.7 (C-2), 75.2 (C-4), 74.5 (C-5), 70.3 (C-3), 17.2 (C-6). Anal. calcd. for $C_6H_{10}O_3$: C 55.37, H 7.75; found: C 55.28, H 7.68.

*1,5-Anhydro-3-*O*-benzoyl-2,6-dideoxy-L-*arabino*-hex-1-enitol **18***

L-Rhamnal **17** (3.6 g, 27.7 mmol) was dissolved in dry dichloromethane (50 mL) containing anhydrous pyridine. The stirred solution was cooled to −25°C under dry atmosphere and benzoyl chloride (3.55 mL, 30.6 mmol) in dichloromethane solution (20 mL) was added dropwise. The mixture was stirred for 2 h at −20 to −25°C and the reaction was quenched by addition of sodium bicarbonate solution (15 mL). The organic layer was diluted with dichloromethane, then washed successively with sodium bicarbonate solution was water, and dried over magnesium sulfate. Filtration, evaporatiuon of the solvent, and chromatography on a silica gel column using ethyl acetate – hexanes (1:10) as eluant gave 4.2 g (65%) of compound **18**: $[\alpha]_D$ +120.3 (*c* 0.9, chloroform); mp 57–59°C (lit. (16) $[\alpha]_D^{25}$ +120 (*c* 1.0, chloroform); mp 64–65°C); ^{1}H nmr (200 MHz, $CDCl_3$) δ: 8.04 (m, 2H, chloroform), 7.48 (m, 3H, aromatic), 6.46 (dd, 1H, $J_{1,2}$ 6.00 Hz, $J_{1,3}$ 1.5 Hz, H-1), 5.44 (m, 1H, $J_{2,3}$ 2.5 Hz, $J_{3,4}$ 6.3 Hz, H-3), 4.8 (dd, 1H, $J_{2,3}$ 2.5 Hz, H-2), 4.00 (m, 1H, $J_{4,5}$ 9.3 Hz, $J_{5,6}$ 6.3 Hz, H-5), 3.74 (dd, 1H, H-4), 1.43 (d, 3H, H-6); ^{13}C nmr (200 MHz, $CDCl_3$) δ_C: 146.7 (C-1), 133.4, 129.8, 128.4 (aromatic), 98.8 (C-2), 74.8 (C-5), 74.2 (C-3), 72.6 (C-4), 17.1 (C-6).

*1,5-Anhydro-3-*O*-benzoyl-4-*O*-benzyl-2,6-dideoxy-L-*arabino*-hex-1-enitol **19***

A mixture of 3-*O*-benzoyl-L-rhamnal **18** (3.5 g, 14.96 mmol) and benzyl bromide (2.7 mL, 22.7 mmol) in anhydrous DMF (100 mL) was cooled under nitrogen to −40°C and treated at once with sodium hydride (0.44 g, 18.3 mmol). The stirred solution was allowed to warm to −15°C, kept at this temperature for 2 h, and the reaction was quenched with glacial acetic acid (2 mL). The solvents were evaporated to a syrup, which was chromatographed on a silica gel column with ethyl acetate – hexanes (1:10) as eluant. This gave 4.00 g (74%) of pure **19**, $[\alpha]_D$ +182 (*c* 0.96, chloroform); mp 44–45°C; ^{1}H nmr (200 MHz, $CDCl_3$) δ: 8.02 (m, 2H, aromatic), 7.61–7.2 (m, 8H, aromatic), 6.46 (dd, 1H, $J_{1,2}$ 6.2 Hz, $J_{1,3}$ 1.5 Hz, H-1), 5.68 (m, 1H, $J_{3,4}$ 6.0 Hz, H-3), 4.9 (q, $J_{2,3}$ 3.4 Hz, H-2), 4.76 (q, 2H, CH_2Ph), 4.14 (m, 1H, H-5), 3.71 (q, 1H, $J_{4,5}$ 8.2 Hz, H-4), 1.45 (d, 3H, $J_{5,6}$ 6.0 Hz, H-6); ^{13}C nmr (200 MHz, $CDCl_3$ δ_C: 145.95 (C-1), 99.0 (C-2), 78.0 (CH_2Ph), 73.6 (C-5), 73.4 (C-3), 71.1 (C-4), 17.2 (C-6). Anal. calcd. for $C_{20}H_{20}O_4$: C 74.06, H 6.21; found: C 74.03, H 6.28.

*Methyl 2-acetamido-3-*O*-(3′-*O*-benzoyl-4′-*O*-benzyl-2′-deoxy-2′-iodo-α-L-rhamnopyranosyl)-4,6-*O*-benzylidene-2-deoxy-β-D-glucopyranoside **20***

A mixture of compound **2** (1.1 g, 3 mmol), compound **19** (1 g, 3 mmol), and *N*-iodosuccinamide (0.9 g, 4 mmol) in an anhydrous mixture of dichloromethane (50 mL) and acetonitrile (100 mL) was stirred in a stoppered round-bottom flask, wrapped with aluminum foil, for 10 days. The mixture was diluted with dichloromethane (100 mL), washed with sodium thiosulfate solution (15%) followed by water, dried, filtered, evaporated, and chromatographed on a silica gel column (ethyl acetate – hexanes, 1:1) to give 1.43 g (60%) of the 2-deoxy-2-iodo-disaccharide **20**: $[\alpha]_D$ −37.6 (*c* 0.97, chloroform); mp 149–151°C (cryst. methanol); ^{1}H nmr (500 MHz, $CDCl_3$) δ: 8.1–7.08 (m, 15H, aromatic), 6.22 (d, 1H, $J_{NH,H2}$ 8 Hz, NH), 5.53 (s, 1H, CHPh), 5.32 (s, 1H, H-1′), 4.9 (q, 1H, $J_{2',3'}$ 4.2 Hz, $J_{3',4'}$ 8.6 Hz, H-3′), 4.8 (d, 1H,

Can. J. Chem. Downloaded from www.nrcresearchpress.com by 88.255.202.194 on 09/08/12
For personal use only.

$J_{1,2}$ 8 Hz, H-1), 4.71 (dd, 1H, $J_{1',2'}$ 1.4 Hz, H-2'), 4.65 (d, 1H, CH_2Ph), 4.54 (d, 1H, CH_2Ph), 4.33 (m, 2H, H-3, H-6A), 4.21 (m, 1H, $J_{4',5'}$ 9 Hz, $J_{5',6'}$ 6 Hz, H-5'), 3.775 (t, H-4), 3.63–3.46 (m, 7H, H-2, H-5, H-6B, H-4', and OMe), 2.00 (s, 3H, Ac), 0.9 (d, 3H, H-6'); ^{13}C nmr (200 MHz, $CDCl_3$) δ_C: 102.00, 101.7, 101.1 (C-1, C-1', and CHPh), 58.07 (C-2), 57.00 (OMe), 31.64 (C-2'), 23.39 (Ac), 17.35 (C-6'). Anal. calcd. for $C_{36}H_{39}INO_{10}$: C 55.97, H 5.09, I 16.4, N 1.8; found: C 55.78, H 5.21, I 16.38, N 1.73.

Methyl 2-acetamido-3-O-(4'-O-benzyl-2'-deoxy-2'-iodo-α-L-rhamnopyranosyl)-4,6-O-benzylidene-2-deoxy-β-D-glucopyranoside ***21***

The 2-deoxy-2-iodo-disaccharide **20** (3.69 g, 5 mmol) in methanol (150 mL) and dichloromethane (10 mL) was treated with a catalytic amound of sodium methoxide. The reaction mixture was stirred at room temperature for 48 h, when tlc (ethyl acetate – hexanes, 3:1) indicated the consumption of all the starting material. The sodium ions were removed with Rexyn 101 (H^+) ion-exchange resin. Filtration, evaporation, and drying in vacuum over phosphorus pentoxide gave 2.97 g (93%) of **21**, $[\alpha]_D$ −128.7 (*c* 0.99 methanol); mp 198–199°C; ^1H nmr (500 MHz, $CDCl_3$) δ: 7.38–7.2 (m, 10H, aromatic), 6.36 (d, 1H, NH), 5.32 (s, 1H, CHPh), 5.24 (s, 1H, H-1'), 4.74 (d, 1H, H-1), 4.56 (d, 1H, CH_2Ph), 4.5 (d, 1H, CH_2Ph), 4.42 (d, 1H, H-2'), 4.28 (q, 1H, H-3'), 4.04 (m, 2H), 3.74 (m, 2H), 3.52 (m, 2H), 3.36 (s, 3H, OMe), 3.28 (m, 1H), 3.24 (t, 1H), 2.72 (d, OH), 2.08 (s, 3H, Ac), 0.9 (d, 3H, H-6'),; ^{13}C nmr (200 MHz, $CDCl_3/CD_3OD$) δ_C: 102.5, 101.9, 101.5 (C-1, C-1', CHPh), 38.3 (C-2'), 22.4 (AcNH), 17.0 (C-6'). Anal. calcd. for $C_{29}H_{36}INO_9$: C 52.02, H 5.42, N 2.09; found: C 51.90, H 5.56, N 1.98.

Methyl O-(2",3",4"-tri-O-acetyl-α-L-rhamnopyranosyl)-(1→3)-O-(4'-O-benzyl-2'-deoxy-2'-iodo-3'-O-α-L-rhamnopyranosyl)-(1→3)-2-acetamido-4,6-O-benzylidene-2-deoxy-β-D-glucopyranoside ***22***

A mixture of the disaccharide **21** (2.97, 4.44 mmol), 2,3,4-tri-*O*-acetyl-α-L-rhamnopyranosyl bromide (3.2 g, 9.00 mmol), 1,1,3,3-tetramethylura (2.7 mL, 22.6 mmol), and 4Å molecular sieves in anhydrous dichloromethane (200 mL) was stirred under nitrogen and cooled to −60°C. The mixture was then treated, in portions, with silver trifluoromethane sulfonate (2.2 g, 8.6 mmol) and allowed to warm gradually to room temperature. After 24 h the solids were removed by filtration and the filtrate was washed successively with sodium bicarbonate solution and water. The organic layer was dried ($MgSO_4$), filtered, evaporated, and chromatographed on a silica gel columm, using hexanes – ethyl acetate (1:4) as eluant, to give 4.00 g (96%) of **22**: $[\alpha]_D$ −62.2 (*c* 1.00, chloroform); mp 124–126°C; ^1H nmr (500 MHz, $CDCl_3$) δ: 7.46–7.24 (m, 10H, aromatic), 5.92 (d, 1H, $J_{NH,2}$ 8.5 Hz, NH), 5.50 (s, 1H, CHPh), 5.35–5.31 (m, 2H, H-2", H-3"), 5.25 (s, 1H, H-1'), 5.1 (t, 1H, $J_{4",3"} + J_{4",5"}$ = 19.5 Hz, H-4'), 5.01 (d, 1H, $J_{1",2"}$ 1.2 Hz, H-1"), 4.79 (d, 1H, CH_2Ph), 4.53 (d, 1H, CH_2Ph), 4.51 (d, 1H, $J_{1,2}$ 8.5 Hz, H-1), 4.4 (dd, 1H, $J_{1',2'}$ 1.2 Hz, $J_{2',3'}$ 4.0 Hz, H-2'), 4.34 (q, 1H, $J_{5,6A}$ 5.0 Hz, $J_{6A,6B}$ 10.5 Hz, H-6A), 4.2 (m, 1H, H-5"), 4.14–4.01 (m, 3H, H-2, H-5'), 3.75 (m, 1H, H-6B), 3.57–3.46 (m, 2H, H-4, H-5), 3.43–3.35 (m, 5H, H-3', H-4', OMe), 2.08 (s, 6H, 2 × OAc), 2.05 (s, 3H, OAc), 1.98 (s, 3H, NHAc), 1.27 (d, 3H, $J_{5',6'}$ 6.0 Hz, H-6'), 0.86 (d, 3H, $J_{5',6'}$ 6.0 Hz, H-6'); ^{13}C nmr (500 MHz, $CDCl_3$) δ_C: 102.13, 101.68, 101.51, 99.64 (C-1, C-1', C-1", CHPh), 66.16 (C-6), 57.01 (OMe), 56.61 (C-2), 34.75 (C-2'), 23.38 (AcNH), 20.67 (3 AcO), 17.38, 17.14 (C-6', C-6"). Anal. calcd. for $C_{41}H_{52}INO_{16}$: C 52.29, H 5.57, I 13.48, N 1.49; found: C 52.08, H 5.56, I 13.33, N 1.58.

Methyl O-α-L-rhamnopyranosyl-(1→3)-O-2-deoxy-L-rhamnopyranosyl-(1→3)-2-acetamido-2-deoxy-β-D-glucopyranoside ***23***

A solution of the trisaccharide **20** (813 mg, 0.86 mmol) in 80% aqueous acetic acid was heated at 80°C for 1 h. Evaporation of the solvents followed by chromatographic purification on a silica gel column using dichloromethane–methanol (20:1) as eluant gave 420 mg (57%) of a solid. Its ^1H nmr and ^{13}C nmr spectra showed the absence of the benzylidene protecting group.

This trisaccharide (420 mg, 0.492 mmol) was dissolved in pyridine (7 mL) and treated with acetic anhydride (1.00 mL, 10.5 mmol). The mixture was stirred at room temperature (18 h) and the solvents were then evaporated to a colourless syrup. The dried syrup was dissolved in toluene (20 mL) and treated under nitrogen with tributyltin hydride (0.26 mL, 0.97 mmol) and benzoyl peroxide (5 mg). The mixture was heated at 75°C for 2 h and the reaction was quenched with methanol (5 mL). Evaporation of the solvents and chromatographic purification over a silica gel column using dichloromethane–methanol (45:1) as eluant gave 359 mg (90%) of a fully protected 2'-deoxy trisaccharide, identified by its ^1H nmr and ^{13}C nmr spectra.

The trisaccharide (359 mg, 0.44 mmol) in methanol (20 mL) was treated with catalytic amount of sodium methoxide in methanol and stirred at room temperature for 18 h. The mixture was neutralized with Rexyn 101 (H^+) resin and filtered. The filtrate was concentrated to a solid (250 mg), which was dissolved in ethanol (18 mL, 99%) and water (3 mL) and hydrogenated over 10% palladium on carbon at a hydrogen pressure of 70 psi for 5 days. Filtration, evaporation, and chromatographic purification over a silica gel column using ethyl acetate – methanol (10:1) gave 200 mg (88%) of pure **23**: $[\alpha]_D$ −102.1 (*c* 0.76, methanol); mp 277–278°C; ^1H nmr (500 MHz, D_2O) δ: 5.03 (m, 1H, H-1'), 5.00 (s, 1H, H-1"), 4.48 (d, 1H, H-1), 4.04 (m, 1H, H-5'), 4.02 (m, 1H, H-2"), 3.94 (m, 1H, H-6A), 3.87–3.7 (m, 5H, H-2, H-5, H-3', H-3", H-5"), 3.55–3.4 (m, 7H, H-3, H-4, H-6B, H-4", OMe), 3.23 (t, 1H, H-4'), 2.11 (m, 1H, H-2'e), 2.03 (s, 3H, NHAc), 1.85 (m, 1H, H2'a), 1.32 (d, 3H, H-6"), 1.27 (d, 3H, H-6'); ^{13}C nmr (125 MHz, D_2O) δ_C: 102.42 (C-1"), 102.06 (C-1), 99.45 (C-1'), 82.22 (C-4), 77.11 (C-3'), 76.77 (C-4"), 76.13 (C-4'), 72.77 (C-5), 70.95 (C-5'), 70.89 (C-5"), 69.53 (C-3), 69.26 (C-3"), 69.13 (C-2"), 61.55 (C-6), 57.7 (OMe), 55.89 (C-2), 37.38 (C-2'), 22.85 (AcNH), 17.31 (C-6', C-6"). Anal. calcd. for $C_{21}H_{37}NO_{13}$: C 49.31, H 7.29, N 2.74; found: C 49.19, H 7.3, N 2.63.

1. N. I. A. Carlin, D. R. Bundle, and A. A. Lindberg. J. Immunol. **138**, 4419 (1987).
2. D. R. Bundle. Pure Appl. Chem. **61**, 1171 (1989).
3. M. N. Vyas, N. K. Vyas, P. J. Meikle, B. M. Pinto, B. Sinnott, D. R. Bundle, and F. A. Quiocho. J. Biol. Chem. In press.
4. R. U. Lemieux. Chem. Soc. Rev. **18**, 347 (1989).
5. C. P. J. Glaudemans. Chem. Rev. **91**, 25 (1991).
6. I. P. Street, C. R. Armstrong, and S. G. Withers. Biochemistry, **25**, 6021 (1986).
7. B. M. Pinto, D. G. Morrisette, and D. R. Bundle. J. Chem. Soc. Perkin Trans. 1, 9 (1987).
8. H.-P. Wessel and D. R. Bundle. Carbohydr. Res. **124**, 301 (1983).
9. F.-I. Auzanneau and D. R. Bundle. Carbohydr. Res. In press.
10. (*a*) U. Berglund and L. G. Sillen. Acta Chem. Scand. **2**, 116 (1948); (*b*) R. A. Earl. Ph.D. Thesis, University of Alberta, 1970.
11. J. Thiem, H. Karl, and J. Schwenter. Synthesis, 696 (1978).
12. K. Bock and C. Pedersen. J. Chem. Soc. Perkin Trans. 2, 293 (1974).
13. R. B. Boar, D. W. Hawkins, J. F. McGhie, and D. H. R. Barton. J. Chem. Soc. Perkin Trans 1, 654 (1973); J. Thiem and J. Schwentner. Tetrahedron Lett. 459 (1978).
14. V. S. Rao and A. S. Perlin. Can. J. Chem. **61**, 652 (1983).
15. B. Iselin and T. Reichstein. Helv. Chem. Acta, **27**, 1146 (1944).
16. D. Horton, W. Priebe, and O. Varela. Carbohydr. Res. **144**, 317 (1985).

17. N. I. A. Carlin, M. A. J. Gidney, A. A. Lindberg, and D. R. Bundle. J. Immunol. **137**, 2361 (1986).
18. E. Vorberg and D. R. Bundle. J. Immunol. Methods, **132**, 81 (1990).
19. P. J. Meikle, N. M. Young, and D. R. Bundle. J. Immunol. Methods, **132**, 255 (1990).
20. F. A. Quiocho. Pure Appl. Chem. **61**, 1293 (1989).
21. D. D. Perrin, W. L. Armarego, and D. R. Perrin. Purification of laboratory compounds. 2nd ed. Pergamon Press, London. 1980.
22. F. Michael. Berichte, **63B**, 347 (1930).
23. T. Iversen and D. R. Bundle. J. Org. Chem. **46**, 5389 (1981).

Can. J. Chem. Downloaded from www.nrcresearchpress.com by 88.255.202.194 on 09/08/12
For personal use only.

A study of hydrogen abstraction reactions by halogen atoms with HFCO and HClCO: determination of transition state structures, barrier heights, and vibrational frequencies

J. S. FRANCISCO[1] AND N. MINA-CAMILDE
Department of Chemistry, Wayne State University, Detroit, MI 48202, U.S.A.

Received May 11, 1992

J. S. FRANCISCO and N. MINA-CAMILDE. Can. J. Chem. **71**, 135 (1993).

Theoretical barriers and reaction energetics were determined using *ab initio* calculations at the PMP4/6-311++G** level with UMP2/6-311G** optimized geometries for hydrogen abstraction reactions of HFCO and HClCO by fluorine and chlorine atoms. The largest barriers are predicted for fluorine and chlorine atom abstractions of hydrogen from HFCO. Fluorine and chlorine atom abstractions of hydrogen from HClCO are predicted to be barrierless. The predicted barrier for fluorine atom abstraction of hydrogen from HFCO is calculated to be 1.3 kcal mol^{-1} and is in good agreement with the experimental value of 1.8 ± 0.4 kcal mol^{-1}.

J. S. FRANCISCO et N. MINA-CAMILDE. Can. J. Chem. **71**, 135 (1993).

Utilisant des calculs *ab initio* au niveau PMP4/6-311++G** avec des géométries optimisées UMP2/6-311G**, on a déterminé les barrières théoriques et les énergies des réactions d'enlèvement d'hydrogène du HFCO et HClCO par des atomes de fluor et de chlore. Les calculs prédisent que les barrières les plus élevées sont celles de l'enlèvement d'hydrogène du HFCO par les atomes de fluor et de chlore. Les calculs prédisent qu'il n'y a pratiquement pas de barrière à l'enlèvement de l'hydrogène du HClCO par des atomes de fluor et de chlore. On a calculé que la barrière à l'enlèvement de l'hydrogène du HFCO par le fluor est de 1,3 kcal mol^{-1}, ce qui est en bon accord avec la valeur expérimentale de 1,8 ± 0,4 kcal mol^{-1}.

[Traduit par la rédaction]

Introduction

Bimolecular hydrogen exchange reactions of the type

[1] $X + HY \rightarrow HX + Y$

where X and Y are halogen atoms, have been the focus of a number of recent studies. Neumark and co-workers studied several X + HY reactions where X and Y are like and unlike halogen atoms for triatomic systems (1–4). There is also a substantial body of experimental and theoretical work in the literature (5–9) on hydrogen abstraction reactions by halogens from alkanes of the type

[2] $X + RH \rightarrow HX + R$

However, there are few experimental or theoretical investigations of hydrogen abstraction reactions due to halogens from hydrogen carbonyl halides. Such reactions have atmospheric importance since hydrogen carbonyl halides are suggested to be reservoir species resulting from the degradation of alternative halocarbon compounds (10, 11). Consequently, it is of interest to study the reaction of halogen atoms such as F and Cl with HFCO and HClCO. The reaction of Cl atoms with HFCO and HClCO removes active chlorine from ClO_x catalytic cycles that destroy ozone in the stratosphere (12). The reaction of F atoms with HFCO or HClCO also serves to remove F atoms from FO_x catalytic cycles (12). The formation of stable HF and HCl serves as a major sink for halogen atoms such as F and Cl. Unfortunately, few experimental investigations of these reactions have been carried out. Francisco and Zhao (13) made experimental measurements of the reaction rate for the reaction of F + HFCO. Wallington *et al.* (14) measured the first rate coefficient for the reaction of Cl + HFCO. Sanhueza and Heicken (15) measured the room temperature rate for the chlorine atom attack of HClCO. Niki *et al* (16), in a later study, confimed the measurements of Sanhueza and Heicken. To provide insight into the potential energy surfaces that govern the reaction dynamics, we examine the potential energy surface of the X + HYCO system, where X, Y = F, Cl, by means of *ab initio* electronic structure theory. We report the locations of saddle point geometries and vibrational frequencies and the energetics for these reactions.

Computation methodology

All calculations were performed with the GAUSSIAN 88 system of program (17). All equilibrium geometries and transition structures were fully optimized with Schlegel's analytical gradient method (18) of optimization employing unrestricted Hartree–Fock (UHF) and second-order unrestricted Møller–Plesset (UMP2) methods along with 6-31G* and 6-311G** bases (19, 20). Geometries were optimized to better than 0.001 Å for bond distances and 0.1° for bond angles. With a convergence of at least 10^{-9} on the density matrix, the rms force was less than 10^{-4} a.u. for the optimized structures. No symmetry constraints were imposed on the optimization. The fourth-order Møller–Plesset perturbation calculation for single-point energies included single, double, triple, and quadruple excitations (MP4SDTQ) using the frozen core approximation (21). Spin projected energies are denoted by the term PMP4 (22). UMP2/6-311G* calculated values of $\langle s^2 \rangle$ for FCO and ClCO and the hydrogen abstration transition states before spin projection varied from 0.75 to 0.77. Single-point energy calculations of higher order of perturbation and with larger basis set were performed using geometries optimized at the UMP2 level and spin projections were applied to annihilate the highest spin contaminant of the unrestricted wave function. Vibrational frequencies and zero-point energies were obtained at the UHF/6-31G* optimized geometries from analytical second derivatives (23).

[1]Author to whom correspondence may be addressed.

Can. J. Chem. Downloaded from www.nrcresearchpress.com by 88.255.202.194 on 09/08/12
For personal use only.

Can. J. Chem. Downloaded from www.nrcresearchpress.com by 88.255.202.194 on 09/08/12
For personal use only.

TABLE 1. Optimized geometries for reactants and products from the X + HYCO hydrogen abstraction process

Species	Coordinate (Å or deg)	UHF/6-31G*	UMP2/6-31G*	UMP2/6-311G**	Experiment[a]
HF	r(H—F)	0.911	0.934	0.912	0.917
HCl	r(H—Cl)	1.266	1.280	1.274	1.275
FCO	r(C—O)	1.304	1.340	1.329	1.334
	r(C—F)	1.152	1.181	1.170	1.169
	θ(FCO)	128.3	128.1	128.2	127.3
ClCO	r(C—O)	1.840	1.793	1.800	1.75
	r(C—Cl)	1.136	1.175	1.163	1.17
	θ(ClCO)	128.9	128.9	128.8	120
HFCO	r(C—H)	1.081	1.094	1.094	1.100
	r(CF)	1.314	1.352	1.345	1.341
	r(CO)	1.164	1.194	1.183	1.183
	θ(HCO)	126.9	127.6	127.9	129.0
	θ(FCO)	123.0	123.2	123.2	122.7
HClCO	r(C—H)	1.083	1.096	1.096	1.090
	r(C—Cl)	1.756	1.767	1.774	1.765
	r(C—O)	1.165	1.199	1.187	1.182
	θ(HCO)	126.1	126.3	126.7	126.5
	θ(ClCO)	123.2	123.2	123.6	123.1

[a]Sources of experimental geometry: HFCO: ref. 25; HClCO: ref.26; FCO: ref.27; ClCO: ref. 28; all others: ref. 29.

TABLE 2. Optimized transition state geometries for the X + HYCO hydrogen abstraction process

Reaction	Coordinate (Å or degree)	UHF/6-31G*	UMP2/6-31G*	UMP2/6-311G**
F + HFCO → HF + FCO	r(C—O)	1.153	1.185	1.176
	r(C—H)	1.262	1.170	1.153
	r(C—F)	1.296	1.334	1.329
	r(F′—H)	1.163	1.315	1.343
	θ(HCO)	124.3	125.5	126.1
	θ(FCO)	127.4	126.4	126.0
	θ(F′HC)	173.1	162.1	170.9
F + HClCO → HF + ClCO	r(C—O)	1.152	1.186	1.178
	r(C—H)	1.239	1.156	1.142
	r(C—Cl)	1.740	1.751	1.756
	r(F′—H)	1.203	1.373	1.412
	θ(HCO)	123.7	125.1	125.4
	θ(ClCO)	127.3	126.4	125.9
	θ(F′HC)	177.6	171.4	178.1
Cl + HFCO → HCl + FCO	r(C—O)	1.150	1.179	1.170
	r(C—H)	1.405	1.360	1.277
	r(C—F)	1.293	1.325	1.317
	r(Cl′—H)	1.462	1.471	1.523
	θ(HCO)	123.4	124.5	124.4
	θ(FCO)	128.9	129.0	128.4
	θ(Cl′HC)	177.8	174.8	174.3
Cl + HClCO → HCl + ClCO	r(C—O)	1.147	1.179	1.174
	r(C—H)	1.348	1.254	1.189
	r(C—Cl)	1.737	1.737	1.747
	r(Cl′—H)	1.511	1.582	1.686
	θ(HCO)	122.2	123.4	124.5
	θ(ClCO)	128.9	128.7	127.3
	θ(Cl′HC)	177.4	177.8	177.7

TABLE 3. Vibrational frequencies (cm^{-1}) and zero-point energies (kcal mol^{-1}) calculated at the UHF/6-31G* level of theory

Molecules	Vibrational frequencies	Zero-point energy (ZPE)[a]
Reactants and products		
HF	4356	6.2
HCl	3183	4.6
FCO	2140, 1210, 708	5.8
ClCO	2166, 580, 207	4.2
HFCO	3360, 2103, 1539, 1248, 1176, 738	14.5
HClCO	3316, 2043, 1492, 1070, 827, 511	13.2
Transition state structures		
F + HFCO → HF + FCO	2161, 1294, 1206, 967, 774, 430 167, 113, 3562i	10.2
F + HClCO → HF + ClCO	2115, 1231, 926, 864, 542, 391 169, 84, 3594i	9.0
Cl + HFCO → HCl + FCO	2171, 1255, 1096, 977, 761, 313 310, 122, 2250i	10.0
Cl + HClCO → HCl + ClCO	2134, 1183, 997, 808, 522, 298 285, 105, 2325i	9.1

[a]The zero-point energes are unscaled.

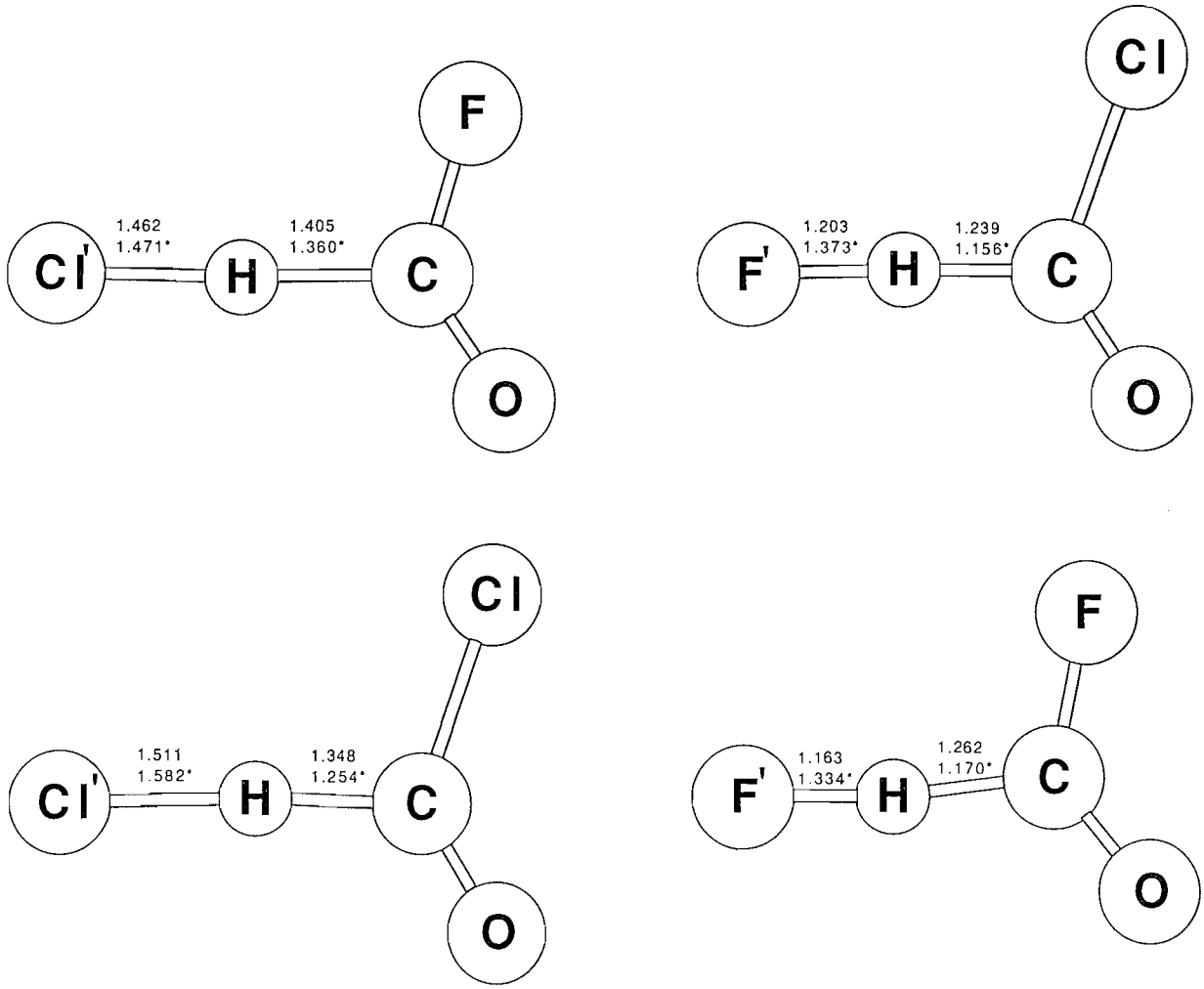

FIG. 1. Transition state structure along with the transition state vector for X + HYCO (where X, Y = F or Cl). Note that UMP2/6-31G* optimized parameters, no asterisk; UMP2/6-311G** optimized parameters, with asterisk; see Table 1 for the complete list of geometrical parameters.

Can. J. Chem. Downloaded from www.nrcresearchpress.com by 88.255.202.194 on 09/08/12
For personal use only.

Can. J. Chem. Downloaded from www.nrcresearchpress.com by 88.255.202.194 on 09/08/12
For personal use only.

TABLE 4. Total energies (hartrees) for optimized species for X + HYCO hydrogen abstraction processes

Species	UHF/6-31G*	UMP2/6-31G*	UMP2/6-311G**	MP4/6-31++G**//MP2/6-31G*	PMP4/6-31++G**//MP2/6-31G*	MP4/6-311++G**//MP2/6-311G**	PMP4/6-311++G**//MP2/6-311G*
Reactants and products							
F	−99.36500	−99.48904	−99.57262	−99.51087	−99.51154	−99.57112	−99.57183
Cl	−459.44796	−459.56206	−459.63376	−459.57162	−459.57209	−459.60377	−459.60455
HF	−100.00291	−100.18416	−100.28608	−100.21477	−100.21477	−100.28621	−100.28621
HCl	−460.05998	−460.20215	−460.29297	−460.22637	−460.22637	−460.26384	−460.26384
FCO	−212.11206	−212.57453	−212.73428	−212.60744	−212.60961	−212.71542	−212.71824
ClCO	−572.16109	−572.59355	−572.74677	−572.62299	−572.62520	−572.70729	−572.71060
HFCO	−212.74784	−213.22926	−213.39753	−213.27249	−213.27249	−213.38119	−213.38119
HClCO	−572.78161	−573.23346	−573.39499	−573.27155	−573.27155	−573.35656	−573.35656
Transition states for hydrogen abstraction							
F + HFCO → HF + FCO	−313.06601	−312.70210	−312.95614	−312.77184	−312.77482	−312.94123	−312.94396
F + HClCO → HF + ClCO	−672.10684	−672.71091	−672.95752	−672.77681	−672.77965	−672.92163	−672.92417
Cl + HFCO → HCl + FCO	−672.14421	−672.76275	−673.01245	−672.81986	−672.82361	−672.96645	−672.96981
Cl + HClCO → HCl + ClCO	−1032.18860	−1032.77878	−1033.01875	−1032.83152	−1032.83466	−1032.95227	−1032.95454

TABLE 5. Literature values for heats of formation for stationary point compounds

Species	$\Delta H^\circ_{f,o}$	Reference
F	18.47 ± 0.07	30
Cl	18.59 ± 0.00	30
HF	−65.1 ± 0.2	30
HCl	−22.02 ± 0.05	30
FCO	−42.9 ± 0.8	31
ClCO	−5.6 ± 0.7	32
HFCO	−93.8 ± 1.5	33
HClCO	−45.5 ± 1.5	33

Results and discussion

Structures and vibrational frequencies

The optimized equilibrium geometries for all reactants, products, and transition structures are listed in Tables 1 and 2.

Calculated structural features for HFCO and HClCO are compared with experimentally derived values. Significant rms (root-mean-square) errors occur at the Hartree–Fock level of theory. The rms error is 0.019 Å for bond lengths and 1.0° for bond angles. Consequently, post Hartree–Fock treatments are necessary for a good description of the bonding of the species involved in the HXCO system. In general, bond lengths and angles are improved with the inclusion of electron correlation, but results of calculations at the UMP2/6-311G** level of theory show the best agreement with the experimental geometries. The rms error calculated at the UMP2/6-311G** level of theory is 0.006 Å for bond lengths and 0.7° for bond angles.

The reaction path for the abstraction of hydrogen involves the approach of the incoming halogen atom along the CH axis of the formyl halide, as shown in Fig. 1. The three atoms involved in the bond-breaking and bond-forming process are not co-linear along the CH axis. An interesting structural feature of these transition states is that the X′HC angle widens as a result of the chlorination of the HXCO for the attack of either fluorine or chlorine atom. For F + HFCO, the FHC angle is 162.1°, while for F + HClCO, the F′HC angle is 171.4°. For the Cl + HFCO and Cl + HClCO systems, the Cl′HC angles are 174.8° and 177.8°, respectively. These results suggest that the attacking halogen experiences the largest interaction with formyl chloride. The difference in the CH bond length in the transition state for the attacking halogen is another interesting structural feature. The CH bond lengths are 1.170 and 1.156 Å for F + HFCO and F + HClCO, respectively, while for Cl + HFCO and Cl + HClCO they are 1.360 and 1.254 Å, respectively. From these results, the transition state for abstraction of hydrogen by fluorine appears to be reactant-like in character since the bond lengths are increased by, at most, only 7%. The transition state for abstraction of hydrogen by chlorine appears to be product-like. The CH bond is elongated by at most 30% of the way from the reactant value. This is in accord with the greater endothermicity of the Cl + HYCO reaction compared with that of the F + HYCO reaction.

The vibrational frequencies for the transition states discussed above, along with those for reactants and products, are collected in Table 3. Vibrational frequencies for all the transition states show one imaginary eigenvalue, which at-

Can. J. Chem. Downloaded from www.nrcresearchpress.com by 88.255.202.194 on 09/08/12
For personal use only.

TABLE 6. Heats of reaction and barrier heights (kcal mol^{-1}) for X

Level of theory	F + HFCO → HF + FCO		F + HClCO → HF + ClCO		Cl + HFCO → HCl + FCO		Cl + HClCO → HCl + ClCO	
	ΔH_f	E_a	ΔH_f	E_a	ΔH_f	E_a	ΔH_f	E_a
UHF/6-31G*	−1.3	29.4	−10.9	25.0	14.9	32.4	5.3	25.7
UMP2/6-31G*	−25.4	10.2	−34.6	7.3	9.2	17.9	−0.1	10.5
UMP2/6-311G**	−31.5	8.8	−40.9	6.3	2.5	11.8	−6.9	6.3
UMP4/6-31++G**//UMP2/6-31G*	−24.4	7.2	−34.7	3.5	6.5	15.2	−3.9	7.3
PMP4/6-31++G**//UMP2/6-31G*	−25.3	5.8	−35.7	2.2	5.4	13.2	−5.0	5.6
UMP4/6-311++G**//UMP2/6-311G**	−30.9	6.9	−41.3	3.8	3.6	11.6	−6.8	5.1
PMP4/6-311++G**//UMP2/6-311G**	−32.3	5.7	−42.9	2.6	2.3	10.0	−8.4	4.1
ΔZPE	−2.5	−4.4	−2.8	−4.2	−4.1	−4.5	−4.4	−4.1
PMP4/6-311++G**//UMP2/6-311G** + ΔZPE	−34.8	1.3	−45.7	−1.5	−1.8	5.5	−12.8	0.0
Experiment	−32.7 ± 1.0	1.8 ± 0.4	−43.7		0.3 ± 1.0		−10.7 ± 1.0	

tests to the fact that the transition structures are first-order saddle points.

Heats of reaction and barrier heights

Reliable heats of formation are available for most of the reactants and products involved in the X + HYCO system. The literature values are given in Table 5. The heats of reaction for pathways calculated with experimental enthalpies are used to assess the reliability of the theoretical calculations. It is interesting to note that to obtain reliable heats of reactions for reactions in the X + HYCO system, electron correlation must be included. This is evidence by the fact that the rms error for the heats of reaction is 27.7 kcal mol^{-1} at the Hartree–Fock level. However, the most significant reduction in rms errors is by the inclusion of higher-order electron correlation at the PMP4SDT level of theory and the use of a large basis set. The use of the 6-311++G** basis set as opposed to the 6-31++G** basis set reduces the heats of reaction by 6.4 kcal mol^{-1} (rms), which suggests that the use of small and medium basis sets in estimation of the energetics has significant basis set superposition errors associated with the results. Nevertheless, compared with experimental results, the rms error in the calculated heats of reaction for all reactions of the H + HYCO system is 2.2 kcal mol^{-1} at the PMP4/6-311++G**//UMP2/6-311G** + ΔZPE level of theory. The average error in calculated heats of reaction for reactions involving fluorine is no different from the errors for reactions involving chlorine. This suggests that the level of theory used is sufficient enough to estimate the energetics for fluorine and chlorine reactions in the H + HYCO system.

There are some interesting trends that emerge from these data. The heats of reaction for the hydrogen abstraction by fluorine atoms are significantly more exothermic than those due to attack by chlorine atoms. It is also noteworthy that the heats of reaction for the hydrogen abstraction processes by either fluorine or chlorine atoms are significantly influenced by chlorination of the HXCO structure. The difference in heats of reaction is ca. 11 kcal mol^{-1}. Nevertheless, on thermodynamical grounds, all the reactions for the X + HYCO system are favored since all are predicted to be exothermic. The kinetics for the X + HYCO system, however, ultimately determine the relative importance and rate ordering of the abstraction process, but this is largely governed by the activation energy. Activation energies for the X + HYCO system are given in Table 6 as determined from the total energies in Table 4.

The only experimental measurement of the activation energy for the X + HYCO system is for the F + HFCO reaction. Francisco and Zhao (13) measured an activation energy of 1.8 ± 0.4 kcal mol^{-1} for this reaction. The calculated activation energy at the PMP4/6-311++G**//UMP2/6-311G** level of theory is 1.3 kcal mol^{-1}. The present result is in better agreement with the experimental measurement than the previous calculation, which ignored the triples contribution to the MP4 energies. In general, Cl atoms are more reactive than OH radicals toward organic compounds. The activation energy (11) for OH + HFCO as calculated at the PMP4/6-311++G**//MP2/6-311G** level of theory is 6.0 kcal mol^{-1}. For chlorine attack of HFCO, the calculated activation energy at the PMP4/6-311++G**//UMP2/6-311G** level is 2.6 kcal mol^{-1}; when zero-point energy corrections are incorporated, the small barrier disappears.

Can. J. Chem. Downloaded from www.nrcresearchpress.com by 88.255.202.194 on 09/08/12
For personal use only.

However, a comparison of the activation energies for the Cl + HFCO and OH + HFCO reactions suggests that chlorine atoms are more reactive than the OH radical because of lower activation energies. An examination of the predicted activation barriers for the F + HClCO and Cl + HClCO reactions shows that they are lower than the corresponding reactions with HFCO. At the UMP2/6-311G** level of theory, the activation energy barrier for F + HClCO is small. The highest level of calculations including spin projection, correlation, and a large basis set. i.e., the PMP4/6-311++G**//UMP2/6-311G** level of the theory, predicts a negligible barrier for the reaction. For the Cl + HClCO reaction, no activation energy barrier is predicted for the abstraction of hydrogen.

Inspection of the activation energies for the X + HYCO system reveals several features: (*i*) the activation energy is largely influenced by the substituent on the HYCO moiety. Fluorination of HYCO increases the activation energy barriers relative to the chlorinated HYCO, regardless of fluorine or chlorine attack of the hydrogen. It can be argued that the increase in the activation barrier for fluorine substitution on HYCO results from a stronger CH bond energy. An examination of the CH bond dissociated energies in HFCO and HClCO, which are 94.4 and 83.8 kcal mol^{-1} at the PMP4/6-311++G**//UMP2/6-311G** level of theory, respectively (24), shows a correlation that does emerge between the activation energies and the CH bond energies. However, a 10.6 kcal mol^{-1} difference in the CH bond dissociation energy between HFCO and HClCO does not reflect a 10 kcal mol^{-1} difference between the activation energies, which suggests that the correspondence between the activation energies and the CH bond dissociation energies is not directly correlated; (*ii*) the activation energy barriers for the attack of fluorine atoms are lower than for the attack of chlorine atoms. Regarding the second feature, this is in accord with the general observation that F atoms are more reactive than Cl atoms toward organic compounds.

Summary

The main conclusions of this work are as follows:

1. Activation energy barriers for chlorine atom abstractions of hydrogen from HFCO are higher than those for the fluorine atom. The present calculation predicts small or no activation energy barriers for the extraction of hydrogen from HClCO by either chlorine or fluorine atoms.

2. Activation energy barriers for fluorine and chlorine atom abstractions of hydrogen from HYCO are influenced by the substituent on HYCO. However, there is no apparent direct or linear correlation between the substituent and the increase in CH bond strength with the activation energy.

1. R. B. Metz, A. Weaver, S. E. Bradforth, T. N. Kitsopoulos, and D. M. Neumark. J. Phys. Chem. **94**, 1377 (1990).
2. A. Weaver, R. B. Metz, S. E. Bradforth, and D. M. Neumark. J. Phys. Chem. **92**, 5558 (1988).
3. S. E. Bradforth, A. Weaver, D. W. Arnold, R. B. Metz, and D. M. Neumark. J. Phys. Chem. **92**, 7205 (1990).
4. I. M. Waller, T. N. Kitsopoulos, and D. M. Neumark. J. Phys. Chem. **94**, 2240 (9190).
5. R. G. Manning, E. R. Grast, E. C. Merrill, N. J. Parks, and J. W. Rout. Int. J. Chem. Kinet. **7**, 39 (1975).
6. D. J. Smith, D. W. Setser, K. C. Kim, and D. J. Bogan. J. Phys. Chem. **81**, 898 (1977).
7. M. A. A. Clyne, D. J. McKenney, and R. F. Walker. Can. J. Chem. **51**, 3596 (1973).
8. G. LeBras, R. Foon, and Combaurien. Chem. Phys. Lett. **73**, 357 (1980).
9. T. N. Truong, D. G. Truhlar, K. K. Baldridge, M. Gordon, and R. Steckler. J. Chem. Phys. **90**, 7137 (1989).
10. World Meteorological Organization Global Ozone Research and Monitoring Project. Report No. 10, Scientific Assessment of Stratospheric Ozone, 1989.
11. T. D. Wallington and O. J. Nielsen. Chem. Phys. Lett. **187**, 33 (1991).
12. F. S. Rowland and M. S. Molina. Res. Geophys. Space Phys. **13**, 1 (1975).
13. J. S. Francisco and Y. Zhao. J. Chem. Phys. **93**, 276 (1990).
14. T. J. Wallington, M. D. Hurley, J. C. Ball, and E. W. Kaiser. Environ. Sci. Technol. In press.
15. E. Sanhucza and J. Heicklen. J. Phys. Chem. **79**, 7 (1975).
16. H. Niki, D. D. Maker, C. M. Savage, and L. P. Breitenbach. Int. J. Chem. Kinet. 12, 915 (1980).
17. GAUSSIAN 88. M. J. Frisch, M. Head-Gordon, H. B. Schlegel, K. Raghavachari, J. S. Binkley, C. Gonzalez, D. J. Defrees, D. J. Fox, R. A. Whiteside, R. Seegar, C. F. Melius, J. Baker, R. Martin, L. R. Kahn, J. J. P. Stewart, E. M. Fluder, S. Topiol, and J. A. Pople. Gaussian, Inc., Pittsburgh, Pa. 1988.
18. H. B. Schlegel. J. Comput. Chem. **3**, 214 (1982).
19. W. J. Hehre, R. Ditchfield, and J. A. Pople. J. Chem. Phys. **56**, 2257 (1972).
20. R. Krishnan, J. S. Binkley, R. Seeger, and J. A. Pople. J. Chem. Phys. **72**, 650 (1980).
21. R. Krishnan and J. A. Pople. Int. J. Quantum Chem. **14**, 91 (1980).
22. H. B. Schlegel. J. Comput. Chem. **84**, 4530 (1986).
23. J. A. Pople, R. Krishnan, H. B. Schlegel, and J. S. Binkley. Int. J. Quantum Chem. Symp. **13**, 225 (1979).
24. J. S. Francisco and Y. Zhao. J. Chem. Phys. **96**, 7593 (1992).
25. O. H. LeBlance, V. W. Laurie, and W. D. Gwinn. J. Chem. Phys. **33**, 598 (1960).
26. R. W. Davis and M. C. Gerry. J. Mol. Spectrosc. **97**, 117 (1983).
27. K. Nagai, C. Yamada, Y. Endo, and E. Hirota. J. Mol. Spectrosc. **90**, 249 (1981).
28. J. M. Brown and D. A. Ramsay. Can. J. Phys. **53**, 2232 (1975).
29. G. Herzberg. Spectra of diatomic molecules. Van Nostrand. New York. 1950.
30. JANAF thermochemical tables. 3rd ed. 1985; M. W. Chase, Jr., C. A. Davies, J. R. Downey, Jr., D. J. Grurip, R. A. McDonald, and A. N. Syverad. J. Phys. Chem. Ref. Data, Suppl. No. 1, Vol. 14. 1985.
31. J. S. Francisco and Y. Zhao. J. Chem. Phys. **93**, 9203 (1990)
32. J. M. Nicovich, K. D. Kreutter, and P. H. Wine. J. Chem. Phys. **92**, 3539 (1990).
33. Y. Zhao and J. S. Francisco. Chem. Phys. Lett. **173**, 551 (1990).

Ab initio SCF and Møller–Plesset studies on hexachlorides of selenium and tellurium and their dianions

MARIUSZ KLOBUKOWSKI

Department of Chemistry, University of Alberta, Edmonton, Alta., Canada T6G 2G2

Received June 24, 1992

MARIUSZ KLOBUKOWSKI. Can. J. Chem. **71**, 141 (1993).

SCF and Møller–Plesset calculations were done for four chalcogen hexahalide systems ($SeCl_6$, $SeCl_6^{2-}$, $TeCl_6$, and $TeCl_6^{2-}$) to study their geometric structures and relative stabilities in their ground electronic states. Flexible all-electron and valence-electron polarized basis sets were used. For some of the basis sets used, the stationary points located on the SCF potential energy surface of the ions in O_h symmetry were found to possess negative eigenvalues of the Hessian matrix; the structural parameters of the corresponding stationary points in C_{3v} symmetry were determined. At the MP2 level, all ions were found to restore the octahedral symmetry.

MARIUSZ KLOBUKOWSKI. Can. J. Chem. **71**, 141 (1993).

Dans le but d'étudier leurs structures géométriques et les stabilités relatives de leurs états électroniques fondamentaux, on a effectué des calculs en champ auto-cohérent et de Møller–Plesset sur quatre hexahalogénures de chalcogène ($SeCl_6$, $SeCl_6^{2-}$, $TeCl_6$ et $TeCl_6^{2-}$). On a utilisé des ensembles de base avec tous les électrons flexibles ou avec les électrons de valence polarisés. Pour certains des ensembles de base utilisés, on a trouvé que les points stationnaires situés sur la surface d'énergie potentielle en champ auto-cohérent des ions de symétrie O_h possèdent des valeurs propres de la matrice de Hessian qui sont négatives; on a déterminé les paramètres structuraux des points stationnaires correspondants de symétrie C_{3v}. Au niveau MP2, on a trouvé que tous les ions retrouvent leur symétrie octaédrique.

[Traduit par la rédaction]

Introduction

The hexachlorotellurate(IV) and hexachloroselenate(IV) ions possess electronic and geometric structure in which the central ion is surrounded by one lone electron pair in addition to the six bonding pairs. According to the valence shell electron pair repulsion theory (VSEPR), such AB_6E systems should possess distorted, non-octahedral geometries in their ground electronic states (1). However, these hexachlorochalcogenate ions were not found to exhibit such structural deviations and appear to exist in regular octahedral geometry (2). Urch (3) attributed this regular geometry to the large size of the ligand compared with the radius of the central ion.

The stereochemically active lone electron pair in the AB_6E systems could lower the O_h symmetry to C_{3v}, C_{2v}, or C_s in its motion from one face of the octahedron to another (4). Of these lower symmetries, the potential minimum is most likely to be of C_{3v} symmetry while the remaining two would correspond to transition states (5). In our previous SCF studies on XeF_6 and isoelectronic systems (6) the stationary points in both C_{3v} and C_{2v} were found. In the concurrent study on the geometry of hexafluorochalcogenate(IV) ions,[1] we found for the TeF_6^{2-} ion that the SCF stationary point of C_{3v} symmetry represents a local minimum, while that of C_{2v} symmetry is a transition state.

In the present work, our previous studies have been extended to explore the possibility of non-octahedral structures in hexachlorochalcogenates. The computational studies involved SCF and Møller–Plesset (restricted to the second-order perturbation expansion, MP2) calculations in the assumed O_h geometry, followed by the evaluation of the Hessian at the stationary points in order to determine whether they are genuine (local) minima on the potential energy surface. In cases when the Hessian was found to possess negative eigenvalues, search for stationary points was done in the symmetry suggested by the symmetry of the harmonic vibrational mode that corresponded to the negative eigenvalue. This procedure was followed both at the SCF and MP2 level. At the MP2 level, instead of the all-electron approach, which proved prohibitively time-consuming, valence-electron calculations were done using effective core potentials; despite earlier warnings (7–9), the nodeless orbitals of the effective core potential method were shown to perform very well in computations of correlation effects (10). In addition to reducing the computation time, the effective core potentials for tellurium, derived from relativistic Hartree–Fock wavefunctions based on the Cowan–Griffin formalism (11), permitted the introduction of some relativistic effects through the use of relativistic effective potentials and corresponding basis sets (12).

All calculations were done on SUN 4/370 and IBM RS/6000 workstations using the GAMESS (13), HONDO 8.1 (14), and Gaussian 90 (15) systems of programs.

Calculations, results, and discussion

Basis sets

For tellurium, in all-electron calculations the largest basis set available in our compilation (16) was used in the double-zeta valence contraction (433321/43321/421), which can be denoted as (6*s*5*p*3*d*); this basis set was identical with the one used in our previous work (6). In the near-Hartree–Fock calculations the well-tempered basis set (23*s*19*p*13*d*) (17) was contracted to (10*s*8*p*3*d*). The valence-electron calculations were done using both the effective-core potentials of Hay and Wadt (18) with the (3*s*3*p*) basis contracted to (21/21) and the compact effective potentials of Stevens *et al.* (19) with (5*s*5*p*) basis contracted to (41/41). All the basis sets for tellurium were augmented with a diffuse *s*-type function whose exponent ($\zeta_s = 0.018$) was optimized in calculations on the ^5S state of $5s^25p^36s^1$ configuration of the atom.

In all-electron calculations, the standard (4333/433/4) basis for selenium (16) was used in contraction (5*s*4*p*2*d*); the primitive well-tempered basis (19*s*14*p*10*d*) was contracted

[1] M. Klobukowski, work in progress.

Can. J. Chem. Downloaded from www.nrcresearchpress.com by 88.255.202.194 on 09/08/12
For personal use only.

Can. J. Chem. Downloaded from www.nrcresearchpress.com by 88.255.202.194 on 09/08/12
For personal use only.

TABLE 1. Equilibrium SCF energies and geometries in O_h symmetry[a]

Method	E_t	r_e	E_t	r_e	ΔE^b
	$SeCl_6$		$SeCl_6^{2-}$		
ECP_1	−96.9934	2.221	−97.1674	2.448	−4.73
CEP_1	−97.0951	2.227	−97.2921	2.442	−5.36
AE-GP_1	−5153.8323	2.227	−5154.0143	2.449	−4.95
AE-WT_1	−5156.8306	2.226	−5157.0094	2.450	−4.86
ECP_2	−97.0045	2.218	−97.1766	2.451	−4.68
CEP_2	−97.1048	2.228	−97.3041	2.445	−5.42
AE-GB_2	−5153.8520	2.226	−5154.0301	2.452	−4.85
AE-WT_2	−5156.8374	2.225	−5157.0127	2.452	−4.77
	$TeCl_6$		$TeCl_6^{2-}$		
ECP_1	−95.9575	2.334	−96.1164	2.586	−4.32
CEP_1	−95.9438	2.355	−96.1271	2.601	−4.99
AE-GB_1	−9363.3117	2.353	−9353.4424	2.616	−3.56
AE-WT_1	−9368.8932	2.346	−9369.0172	2.614	−3.37
ECP_2	−95.9744	2.334	−96.1300	2.587	−4.23
CEP_2	−95.9569	2.353	−96.1392	2.605	−4.96
AE-GB_2	−9363.3386	2.346	−9363.4613	2.616	−3.34

[a]Energies in atomic units, energy differences in eV, bond lengths in angstroms.
[b]$\Delta E = E_t(AB_6^{2-}, O_h) - E_t(AB_6, O_h)$.

TABLE 2. SCF harmonic vibrational frequencies in O_h symmetry[a]

Molecule	Method	Frequencies					
		$\omega_6(t_{2u})$	$\omega_5(t_{2g})$	$\omega_4(t_{1u})$	$\omega_2(e_g)$	$\omega_1(a_{1g})$	$\omega_3(t_{1u})$
$SeCl_6$	ECP_1	163	234	262	327	371	417
	CEP_1	160	230	258	326	365	409
	AE-GB_1	160	229	258	326	368	412
	CEP_2	157	228	254	315	359	392
	AE-GB_2	158	229	255	318	363	397
$TeCl_6$	ECP_1	139	202	216	338	374	401
	CEP_1	133	194	209	333	363	392
	AE-GB_1	133	196	210	339	374	404
	ECP_2	135	199	211	334	373	400
		$\omega_4(t_{1u})$	$\omega_6(t_{2u})$	$\omega_5(t_{2g})$	$\omega_2(e_g)$	$\omega_3(t_{1u})$	$\omega_1(a_{1g})$
$SeCl_6^{2-}$	ECP_1	−27	107	150	236	241	291
	CEP_1	61	108	151	241	247	294
	AE-GB_1	−27	106	149	239	240	291
	CEP_2	60	105	149	239	236	291
	AE-GB_2	−41	105	147	238	231	289
$TeCl_6^{2-}$	ECP_1	39	88	126	225	217	283
	CEP_1	63	86	124	227	223	283
	AE-GB_1	−65	84	120	224	211	280
	ECP_2	26	86	124	225	209	283

[a]All values are in cm^{-1}.

TABLE 3. SCF equilibrium energies and structures of AB_6^{2-} ions in C_{3v} symmetry[a]

System	Method	E_t	$r_e(AB_u)$	$r_e(AB_l)$	$\angle(B_uAB_u)$	$\angle(B_lAB_l)$	ΔE^b
$SeCl_6^{2-}$	ECP_1	−97.1674	2.532	2.374	91.7	89.2	−4.73
	AE-GB_1	−5154.0143	2.534	2.376	91.7	89.2	−4.95
$TeCl_6^{2-}$	AE-GB_1	−9363.4442	2.806	2.465	99.0	87.1	−3.60

[a]Energies in atomic units, energy differences in eV, bond lengths in angstroms, bond angles in degrees.
[b]$\Delta E = E_t(AB_6^{2-}, C_{3v}) - E_t(AB_6, O_h)$.

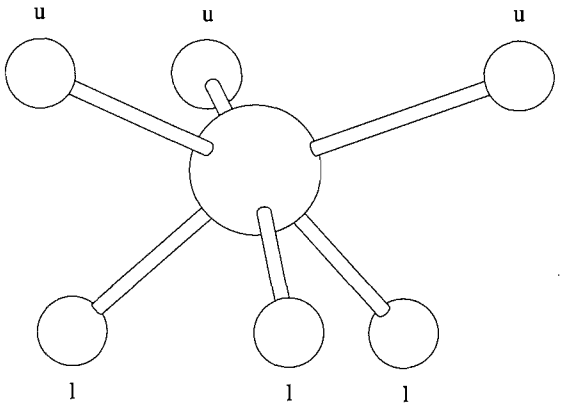

FIG. 1. Geometries of AB_6^{2-} ions in C_{3v} symmetry.

TABLE 4. Equilibrium energies and geometries from MP2 calculations in O_h symmetry[a]

Method	E_t	r_e	E_t	r_e	ΔE[b]
	$SeCl_6$		$SeCl_6^{2-}$		
ECP_1	−97.9781	2.224	−98.1898	2.451	−5.76
CEP_1	−98.0829	2.254	−98.3141	2.445	−6.29
	$TeCl_6$		$TeCl_6^{2-}$		
ECP_1	−96.9041	2.354	−97.0918	2.580	−5.11
CEP_1	−96.8912	2.379	−97.0996	2.596	−5.67
ECP_2	−97.0616	2.358	−97.2646	2.582	−5.47

[a]Energies in atomic units, energy differences in eV, bond lengths in angstroms.
[b]The differences are defined as $\Delta E = E_t(AB_6^{2-},O_h) - E_t(AB_6,O_h)$.

to (9*s*7*p*2*d*). In the valence-electron approach the CEP basis (19) was used, contracted to (41/41). All selenium basis sets were augmented with diffuse *s*- and *p*-type functions (ζ_s = 0.021 and ζ_p = 0.055). The exponent of the *s*-type function was determined by energy minimization of the ^5S state of the $4s^24p^35s^1$ configuration of Se; the exponent of the *p*-type function was obtained from calculations on the ion Se^- in the ^2P state of the configuration $4s^24p^5$.

For chlorine, the all-electron calculations were done using both the more economical (5321/521) basis (16) and the more accurate well-tempered basis (17) in which the (18*s*13*p*) set was contracted to (8*s*6*p*); in the valence-electron calculations, the CEP basis (20) was contracted to (31/31). All chlorine basis sets were augmented with a diffuse *p*-type function with ζ_p = 0.049 (21).

The exponents of both one and two *d*-type polarization functions were taken from our previous work (16).

In the tables of results, the following symbols were used to identify the basis sets: CEP (abbreviated to C in figures) for compact effective potentials both on central atom and on ligands, ECP (E) for effective core potentials on central atom and compact effective potentials on ligands, AE-GB (G) for small, compact all-electron basis sets, and AE-WT (W) for large, well-tempered basis sets. Subscripts (1 or 2) were added to these abbreviations to indicate the number of polarization functions used. For $SeCl_6$ systems, the dimensions of the contracted basis sets with a single polarization function were: 126 (168), 126 (168), 171 (213), and 244 (286) for ECP, CEP, AE-GB, and AE-WT basis sets, respectively (the values in parentheses are dimensions of the basis sets with two polarization functions). For $TeCl_6$, the corresponding contracted basis sets were of dimensions: 123 (165), 123 (165), 178 (220), and 251 (no calculations were done with two polarization functions with the well-tempered basis set; the molecular basis in this case would contain 293 contracted functions).

For the AE-WT basis sets, due to their large size and long expansions of the contracted functions, no analytical gradients could be calculated; these basis sets were used only in single-point calculations in O_h symmetry.

SCF calculations

The energies and bond lengths calculated in the assumed O_h symmetry are shown in Table 1. The bond lengths show satisfactory stability with the change of basis set, especially for the $SeCl_6^q$, q = 0, −2 systems. Slightly stronger variation of bond lengths is seen for the $TeCl_6^{2-}$ ion. The calculated bond lengths are fairly close to the experimental values of 2.411 Å for $SeCl_6^{2-}$ obtained from X-ray studies by Knop *et al.* (22) and 2.54 Å for $TeCl_6^{2-}$, estimated by Gutsev and Boldyrev (23). For the neutral systems, the estimated empirical bond lengths of 2.2 Å for $SeCl_6$ and 2.3 Å for $TeCl_6$ (24) are within 0.5 Å of the present computed values. The structure of the $SeCl_6$ was also studied by Boyd and coworkers (24) who used a STO-3G* basis set and obtained a higher energy of −5101.7898 E_h and a slightly longer bond length of 2.322 Å.

The doubly charged negative ions were found to be more stable than the neutral molecules even at the SCF level, in contrast to the results obtained for hexafluorochalcogenates,[1] where the electron correlation was needed to stabilize anions. There is a significant dependence of the stability on the basis set used. The largest deviation is obtained with the CEP basis set; this effect may be attributed to the presence of more diffuse functions in that basis, which increases the relative stability of the ion. The effect of two polarization functions is very small.

The SCF vibrational frequencies are presented in Table 2: the stationary points for the anions in O_h symmetry are genuine minima except for the ECP and AE-GB basis sets for $SeCl_6^{2-}$ and the AE-GB basis for $TeCl_6^{2-}$.

The stationary points were sought in C_{3v} symmetry; the results are shown in Table 3 and the geometry is defined in Fig. 1. Both the bond lengths and bond angles show smaller deviations from the octahedral values than found previously for hexafluorides.[1] In the previous calculations on the $SeCl_6^{2-}$ ion in C_{3v} symmetry, Boyd (22) obtained the following structural parameters of the stationary point using the STO-3G* basis: $r_e(SeCl_u)$ = 2.488 Å, $r_e(SeCl_l)$ = 2.190 Å, $\angle(Cl_uSeCl_u)$ = 105.5°, and $\angle(Cl_lSeCl_l)$ = 86.2 and the corresponding total energy of −5101.7984 E_h. The differences between these values and the present results are due to the less flexible structure of the STO-3G* basis set.

Møller–Plesset calculations

In the MP2 calculations done in the valence-electron approximation, all valence electrons were correlated using full valence and virtual spaces. The equilibrium total energies and bond lengths obtained in assumed O_h symmetry are collected in Table 4 and shown in Fig. 2. The electron correlation effects increase the bond lengths of the neutral systems,

Can. J. Chem. Downloaded from www.nrcresearchpress.com by 88.255.202.194 on 09/08/12
For personal use only.

Can. J. Chem. Downloaded from www.nrcresearchpress.com by 88.255.202.194 on 09/08/12
For personal use only.

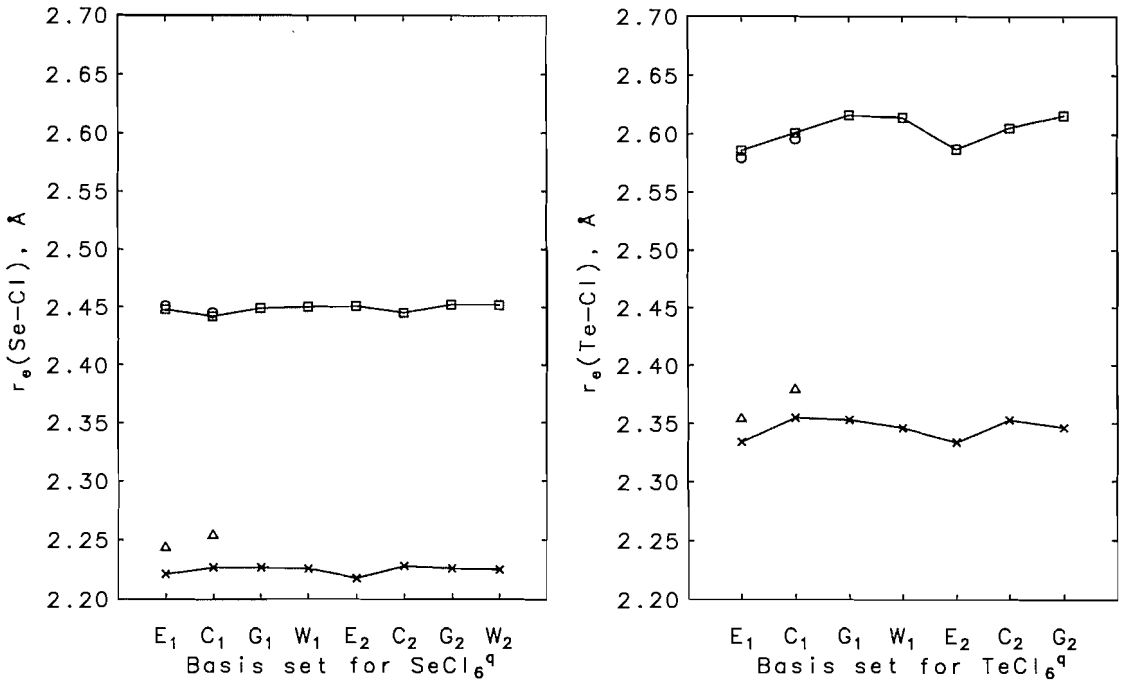

FIG. 2. Equilibrium internuclear distances. ×: SCF ($q = 0$), □: SCF ($q = -2$), △: MP2 ($q = 0$), ○: MP2 ($q = -2$).

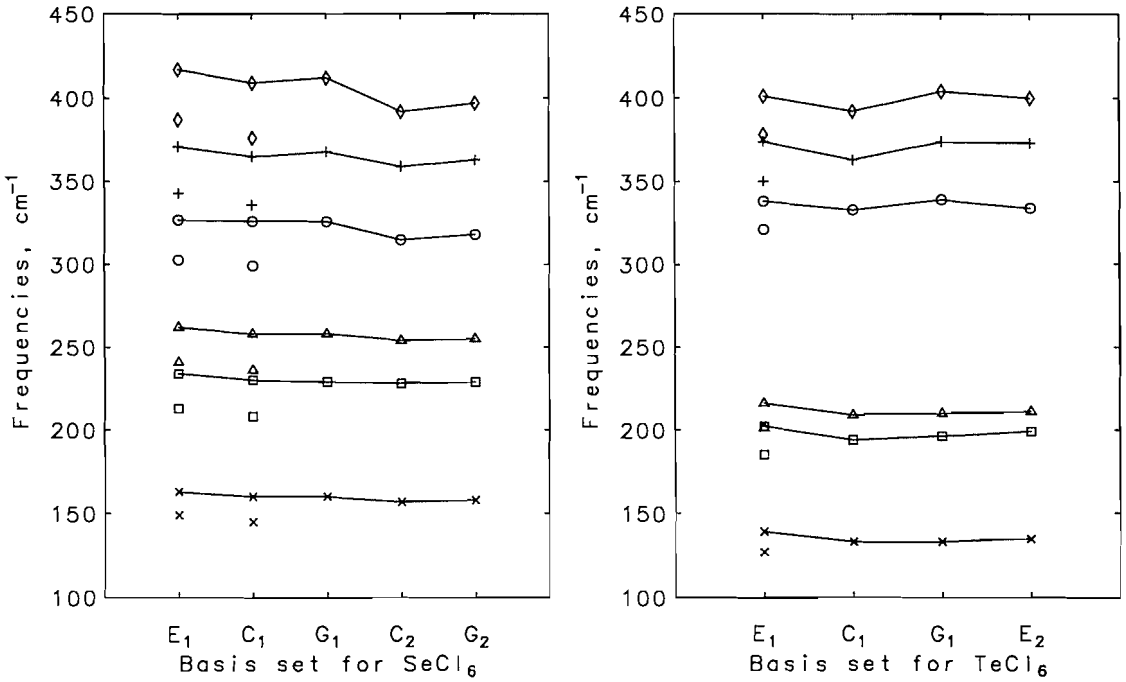

FIG. 3. Calculated harmonic vibrational frequencies of neutral molecules. (The SCF values are joined by straight line segments; MP2 values are shown as isolated points.) ×: $\omega_6(t_{2u})$, □: $\omega_5(t_{2g})$, △: $\omega_4(t_{1u})$, ○: $\omega_2(e_g)$, +: $\omega_1(a_{1g})$, ◇: $\omega_3(t_{1u})$.

leaving them essentially unchanged in the ions. The change is practically independent of the basis set used.

The electron correlation effects increase the stability of the negative ions with respect to the neutral systems by about 1 eV for $SeCl_6^{2-}$ and 0.75 eV for $TeCl_6^{2-}$. The expanded *d*-type polarization set adds about 0.5 eV to the stability of $TeCl_6^{2-}$.

Harmonic vibrational frequencies, calculated in the MP2 approach at the corresponding stationary points using analytical gradients and numerical Hessian, are displayed in Figs. 3 and 4 together with the SCF values and compared in Table 5 with experimental frequencies (25–27). For the neutral systems (Fig. 3), correlation effects reduce the SCF values of the vibrational frequencies by 10–15% and result in an almost uniform shift of the calculated SCF spectrum.

The MP2-induced changes in the SCF vibrational frequencies of the ions are qualitatively different: all vibrations except ω_4 and ω_3, both of t_{1u} symmetry, decrease their

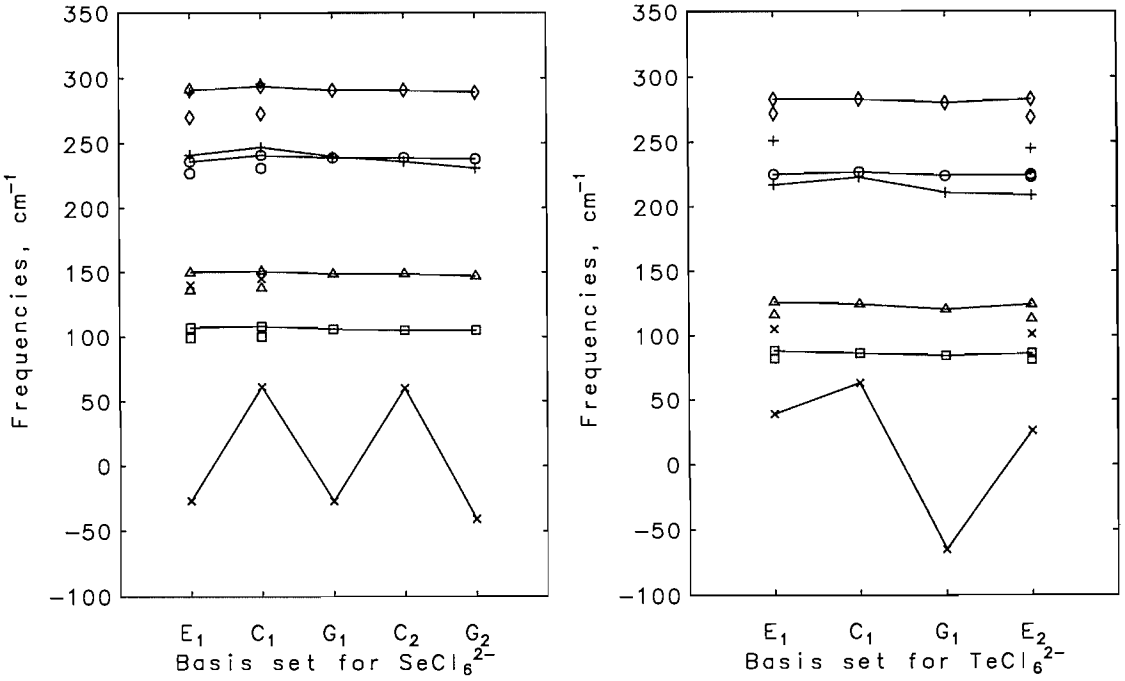

FIG. 4. Calculated harmonic vibrational frequencies of molecular ions. (The SCF values are joined by straight line segments; MP2 values are shown as isolated points.) ×: $\omega_4(t_{1u})$, □: $\omega_6(t_{2u})$, △: $\omega_5(t_{2g})$, ○: $\omega_2(e_g)$, +: $\omega_3(t_{1u})$, ◇: $\omega_1(a_{1g})$.

TABLE 5. MP2 harmonic vibrational frequencies in O_h symmetry[a]

Molecule	Method	Frequencies					
		$\omega_6(t_{2u})$	$\omega_5(t_{2g})$	$\omega_4(t_{1u})$	$\omega_2(e_g)$	$\omega_1(a_{1g})$	$\omega_3(t_{1u})$
$SeCl_6$	ECP_1	149	213	241	303	343	387
	CEP_1	145	208	236	299	336	376
$TeCl_6$	ECP_1	127	185	201	321	350	378
$SeCl_6^{2-}$	ECP_1	99	136	140	227	270	289
	CEP_1	100	138	145	231	273	296
	Expt.	116	165	140–160	255	299	270–280
$TeCl_6^{2-}$	ECP_1	82	116	105	225	272	251
	ECP_2	81	113	101	223	269	245
	Expt.	100	131	120	244	284	235

[a]All values are in cm^{-1}.

frequencies. The electron correlation effects *increase* frequencies of the two t_{1u} modes, with the value of the ω_4 mode increased significantly, reflecting the fact that the stationary points become minima for all basis sets investigated. It is interesting to observe (Fig. 4) that the MP2 values for the various basis sets are very closely spaced even though differences were large at the SCF level. Electron correlation brings about a better agreement with experimental values; however, the ordering of the two highest stretching vibrations differs from that proposed experimentally.

Conclusions

The results of the present calculations indicate that while at the SCF level non-octahedral structures were found for both $SeCl_6^{2-}$ and $TeCl_6^{2-}$ ions, none of these low-symmetry structures survived an improved treatment that included estimating electron correlation effects via the Møller–Plesset method. The non-octahedral geometries found in the SCF calculations are most likely due to instabilities of the Hartree–Fock solutions (28). Thus, on the level of theory used in the present work, hexachloroselenate(IV) and hexachlorotellurate(IV) ions were found to possess the symmetry of a regular octahedron in the ground electronic states. However, to gain any insight into the origin of the non-VSEPR behaviour of the anions, configuration interaction calculations would be required for a definite answer.

The conclusions about the geometry were made on the basis of calculations done in the valence-electron approximation with the outermost *d*-shell electrons treated as a part of the core. However, at least at the SCF level where the all-electron calculations were done, the possible polarization of the *d*-shell does not seem to affect qualitative aspects of this study.

The present work can be improved by: (1) explicitly including *d*-shell electrons in the valence space; (2) adding *f*-type polarization functions; (3) replacing the single-refer-

Can. J. Chem. Downloaded from www.nrcresearchpress.com by 88.255.202.194 on 09/08/12
For personal use only.

ence MP2 scheme by an MC-SCF or MR-CISD approach; (4) preforming fully relativistic calculations instead of using the single-component averaged relativistic effective core potentials for the heavy atoms that were employed in the present work. All of these potential improvements are beyond our present computational possibilities.

Acknowledgments

This work was partly supported by the Natural Sciences and Engineering Research Council of Canada (under Operating Grant No. OGP0046770) and by the Central Research Fund of the University of Alberta (Grant No. 55-48938). Assistance of Drs. Zoila Barandiarán and Luis Seijo and discussions with Professor Sigeru Huzinaga during the pilot calculations are acknowledged with gratitude.

1. R. J. Gillespie and I. Hargittai. The VSEPR model of molecular geometry. Allyn and Bacon, Boston. 1991.
2. B. M. Gimarc, J. F. Liebman, and M. Kohn. J. Am. Chem. Soc. **100**, 2334 (1978).
3. D. S. Urch. J. Chem. Soc. (London), 5775 (1964).
4. L. S. Bartell and R. M. Gavin, Jr. J. Chem. Phys. **48**, 2466 (1968).
5. K. S. Pitzer and L. S. Bernstein. J. Chem. Phys. **63**, 3849 (1975).
6. M. Klobukowski, S. Huzinaga, L. Seijo, and Z. Barandiarán. Theor. Chim. Acta, **71**, 237 (1987).
7. B. Pittel and W. H. E. Schwarz. Chem. Phys. Lett. **46**, 121 (1977).
8. Ch. Teichteil, J. P. Malrieux, and J. C. Barthelat. Mol. Phys. **33**, 181 (1977).
9. E. Miyoshi and Y. Sakai. J. Comput. Chem. **9**, 719 (1988).
10. M. Klobukowski. Theor. Chim. Acta, **83**, 239 (1992).
11. R. D. Cowan and D. C. Griffin. J. Opt. Soc. Am. **66**, 1010 (1976).
12. K. Balasubramanian and K. S. Pitzer. Adv. Chem. Phys. **77**, 287 (1987); M. Krauss and W. J. Stevens. Annu. Rev. Phys. Chem. **35**, 357 (1984).
13. M. W. Schmidt, K. K. Baldridge, J. A. Boatz, J. H. Jensen, S. Koseki, M. S. Gordon, K. A. Nguyen, T. L. Windus, and S. T. Elbert. QCPE Bull. **10**, 52 (1990).
14. M. Dupuis, J. D. Watts, H. O. Villar, and G. J. B. Hurst. QCPE Program No. 544, QCPE Bull. **8**, 79 (1988); M. Dupuis, A. Farazdel, S. P. Karna, and S. A. Maluendes. *In* MOTECC: Modern techniques in computational chemistry. *Edited by* E. Clementi. ESCOM, Leiden. 1990. p. 277.
15. Gaussian 90. M. J. Frisch, M. Head-Gordon, G. W. Trucks, J. B. Foresman, H. B. Schlegel, K. Raghavachari, M. A. Robb, J. S. Binkley, C. Gonzalez, D. J. DeFrees, D. J. Fox, R. A. Whiteside, R. Seeger, C. F. Melius, J. Baker, R. L. Martin, L. R. Kahn, J. J. P. Stewart, S. Topiol, and J. A. Pople. Gaussian, Inc., Pittsburgh, Pa. 1990.
16. J. Andzelm, S. Huzinaga, M. Klobukowski, E. Radzio-Andzelm, Y. Sakai, and H. Tatewaki. Gaussian basis sets for molecular calculations. Elsevier, Amsterdam. 1984.
17. S. Huzinaga and M. Klobukowski. J. Mol. Struct. (Theochem), **167**, 1 (1988).
18. W. R. Wadt and P. J. Hay. J. Chem. Phys. **82**, 284 (1985).
19. W. J. Stevens, M. Krauss, H. Basch, and P. Jasien. Can. J. Chem. **70**, 612 (1992).
20. W. J. Stevens, H. Basch, and M. Krauss. J. Chem. Phys. **81**, 6026 (1984).
21. T. H. Dunning and P. J. Hay. *In* Modern theoretical chemistry. Vol. 3. Methods of electronic structure theory. *Edited by* H. F. Schaefer III. Plenum, New York. 1977.
22. O. Knop, A. Linden, B. R. Vincent, S. C. Choi, T. S. Cameron, and R. J. Boyd. Can. J. Chem. **67**, 1984 (1989).
23. G. L. Gutsev and A. I. Boldyrev. Adv. Chem. Phys. **61**, 169 (1985).
24. G. L. Gutsev and A. P. Klyagina. Chem. Phys. **75**, 243 (1983).
25. T. Barrowcliffe, I. R. Beattie, P. Day, and K. Livingston. J. Chem. Soc. (A), 1810 (1967).
26. R. W. Berg, F. W. Poulsen, and N. J. Bjerrum. J. Chem. Phys. **67**, 1829 (1977).
27. K. Nakamoto. Infrared and Raman spectra of inorganic and coordination compounds. Wiley, New York. 1986.
28. J. Paldus. *In* Self-consistent field: theory and applications. *Edited by* R. Carbó and M. Klobukowski. Elsevier, Amsterdam. 1990. pp. 1–46.

Can. J. Chem. Downloaded from www.nrcresearchpress.com by 88.255.202.194 on 09/08/12
For personal use only.

1992 Merck–Frosst Award Lecture
Orbital symmetry and the photochemistry of cyclobutene[1]

WILLIAM J. LEIGH[2]
Department of Chemistry, McMaster University, Hamilton, Ont., Canada L8S 4M1

Received July 24, 1992

WILLIAM J. LEIGH. Can. J. Chem. **71**, 147 (1993).

Direct photolysis of alkyl-substituted cyclobutene derivatives in solution with monochromatic far-UV light sources results in competing ring opening to the corresponding substituted 1,3-butadiene derivatives and fragmentation to the corresponding alkene and alkyne via formal [2+2] cycloreversion. The excited states leading to the two types of products have been identified. Cycloreversion occurs stereospecifically and arises as a result of excitation of the π,R(3*s*) Rydberg state, which is of comparable energy to the π,π^* state in alkylcyclobutenes. In spite of its stereospecificity, the reaction is nonconcerted; evidence is presented to suggest that it occurs by a mechanism involving [1,2] migration (ring contraction) to yield a cyclopropylcarbene intermediate, which then fragments to yield the alkyne and alkene. The stereochemistry at C3 and C4 in the starting cyclobutene is retained in the alkene produced in the reaction. Ring opening proceeds nonstereoselectively (from the π,π^* singlet state) in well over a dozen systems that have been investigated, and possible mechanisms to account for this are discussed. It is proposed that orbital symmetry plays a role in the reaction, but only in the early stages of ring opening. Bicyclic cyclobutene derivatives in which the cyclobutene double bond is located across the [0] bridge undergo ring opening with a high degree of disrotatory stereoselectivity. Possible reasons for this unusual behavior are discussed in light of recent *ab initio* theoretical results.

WILLIAM J. LEIGH. Can. J. Chem. **71**, 147 (1993).

La photolyse directe de dérivés du cyclobutène substitués par des groupes alkyles, réalisée en solution, à l'aide de sources de lumière UV-lointain monochromatique, conduit à une compétition entre l'ouverture de cycle conduisant aux dérivés buta-1,3-diènes substitués correspondants et une fragmentation conduisant à l'alcène et à l'alcyne correspondants par le biais d'une cycloréversion [2+2] formelle. Les états excités conduisant à ces deux types de produits ont été identifiés. La cycloréversion se produit stéréospécifiquement et elle est le résultat de l'excitation de l'état Rydberg π,R(3*s*) dont l'énergie est comparable à celle de l'état π,π^* des alkylcyclobutènes. Malgré sa stéréospécificité, la réaction n'est pas concertée; on présente des données suggérant qu'elle se produit par un mécanisme impliquant une migration [1,2] (contraction de cycle) qui conduit à un intermédiaire cyclopropène qui se fragmente ensuite pour donner l'alcène et l'alcyne. La stéréochimie en C3 et en C4 du cyclobutène de départ est conservée dans l'alcène qui se forme au cours de la réaction. L'ouverture du cycle se produit d'une façon qui n'est pas stéréospécifique (à partir d'un état singulet π,π^*) dans plus d'une douzaine de systèmes que nous avons examinés; on discute des divers mécanismes possibles pour expliquer les résultats. On propose que la symétrie des orbitales joue un rôle dans la réaction, mais seulement au début de la réaction d'ouverture de cycle. Les cyclobutènes bicycliques dans lesquels la double liaison du cyclobutène se trouve sur le pont [0] subissent la réaction d'ouverture de cycle avec un degré élevé de sélectivité disrotatoire. On discute des raisons possibles de ce comportement inhabituel à la lumière de résultats théoriques *ab initio* récents.

[Traduit par la rédaction]

Can. J. Chem. Downloaded from www.nrcresearchpress.com by 88.255.202.194 on 09/08/12
For personal use only.

Introduction

The thermal and photochemical interconversions of cyclobutene and 1,3-butadiene play a central role in any textbook treatment of orbital symmetry selection rules and pericyclic reactions (1–3). Figure 1 illustrates the classical orbital and state correlation diagrams for the controtatory (C_2 symmetry) and disrotatory (C_s symmetry) interconversion pathways (1). The ground states of cyclobutene and 1,3-butadiene correlate in C_2 symmetry, so that conrotatory interconversion proceeds with no symmetry-imposed barrier. In C_s symmetry, on the other hand, the ground state of the diene correlates with a doubly excited state of cyclobutene (and vice versa); the result is a substantial barrier to ground state disrotatory interconversion owing to orbital symmetry considerations. The barrier results from the avoided crossing of the two surfaces in the intermediate stages of the reaction (see Fig. 1*b*). Since the lowest (π,π^*) excited singlet state of 1,3-butadiene correlates with the π,π^* singlet state of cyclobutene in C_s symmetry, the direct photochemical interconversions are predicted to proceed in disrotatory fashion.

As indicated above, the thermal interconversions are predicted by orbital symmetry to proceed in conrotatory fashion, and there are hundreds of examples in the literature that demonstrate that this is indeed the case (for reviews, see ref. 4). The degree of conrotatory stereospecificity in the thermal interconversions often exceeds 99%. Similarly, there are numerous examples that illustrate the preferred disrotatory stereochemistry of the photochemical ring closure of 1,3-butadiene derivatives to the corresponding cyclobutene (5; also ref. 3*a*, pp. 495–499, and refs. cited). For example, *E*,*E*-2,4-hexadiene (*E*,*E*-**1**) has been reported to yield *cis*-3,4-dimethylcyclobutene (*cis*-**2**) stereospecifically, albeit in low quantum yield owing to competing *cis*,*trans* isomerization, upon direct photolysis in solution (eq. [1]) (5*c*).

Van der Lugt and Oosterhoff proposed that disrotatory ring closure starts in the diene S_1 state, crosses onto the S_2

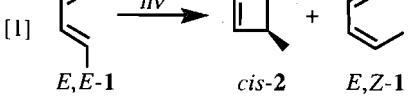

[1]This article is based on the Merck–Frosst Award Lecture delivered by Professor Leigh at the Annual Conference of the Canadian Society for Chemistry, Edmonton, Alberta, June, 1992.

[2]Natural Sciences and Engineering Research Council of Canada University Research Fellow, 1983–1993.

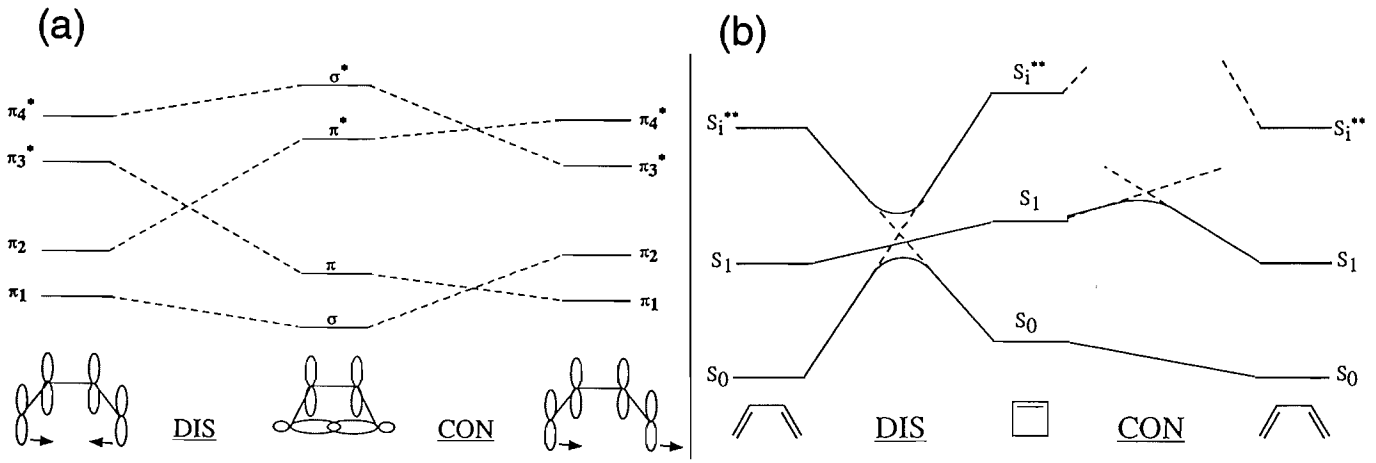

FIG. 1. Orbital (*a*) and state (*b*) correlation diagrams for the con- and disrotatory interconversions of cyclobutene and 1,3-butadiene (1).

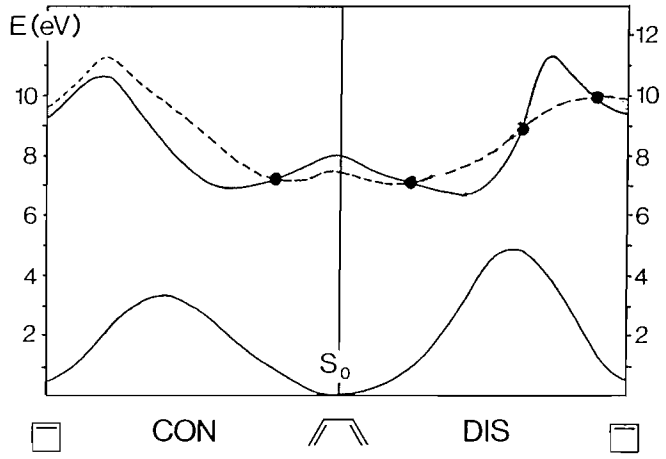

FIG. 2. Calculated (*ab initio*) state correlation diagrams for the con- and disrotatory interconversions of cyclobutene and 1,3-butadiene (9*b*).

potential energy surface and proceeds to a well (the avoided crossing) from which internal conversion to the ground state surface occurs (see Fig. 2) (6). The process cannot occur entirely on the S_1 surface (even though the S_1 state of butadiene correlates directly with the S_1 (π,π^*) state of cyclobutene in C_s symmetry) because the cyclobutene excited singlet state is at least 50 kcal/mol higher in energy than that of the diene (6, 8). The geometry of the reacting molecule at the S_2 energy minimum is similar to that at the transition state for the thermal disrotatory process, so once the excited molecule has entered the ground state surface, it can proceed to cyclobutene or revert to diene. The *ab initio* calculations of Grimbert *et al.* suggested that these general features are common to the ground and excited state energy surfaces for both the conrotatory and disrotatory ring closure reactions (7). However, in the latter case the energy gap between the S_2 and S_0 surfaces is substantially smaller so that the rate of $S_2 \rightarrow S_0$ internal conversion at the avoided crossing is greater for the disrotatory reaction pathway (7). Morihashi *et al.* showed that the probability of the $S_2 \rightarrow S_0$ transition is 10^{12} times greater for the disrotatory pathway than for the conrotatory one (9). The state correlation diagrams for the conrotatory and disrotatory interconversions of cyclobutene and 1,3-butadiene, from the *ab initio* calculations of Morihashi and Kikuchi (9*b*), are summarized in Fig. 2.

Each of the studies described above makes the classical assumption that orbital symmetry is conserved throughout the transformation; i.e., that C_s and C_2 symmetry are maintained in the disrotatory and conrotatory interconversions, respectively. More recent calculations have specified less stringent symmetry requirements for the excited state reaction and explored the possibility that it proceeds asymmetrically. On the basis of semi-empirical (MINDO/3) calculations, Pichko *et al.*, proposed that the photochemical ring closure of 1,3-butadiene occurs by disrotatory closure of the *relaxed* butadiene singlet (10). Thus, following Franck–Condon excitation, butadiene initially relaxes to the allylmethylene biradical geometry, and then undergoes disrotatory terminal-group rotation (over an activation barrier of 8.4 kJ/mol) to reach the geometry at which internal conversion to the ground state surface occurs.

Bernardi and Robb and their co-workers have reported MCSCF *ab initio* calculations (11) that suggest that internal conversion to the ground state surface during ring closure occurs via a conical intersection (12), or a point where ground and excited state surfaces are degenerate. The calculated geometry of the molecule at the conical intersection for ring closure is described as a tetraradicaloid structure in which all π-bonds in the molecule are broken. This more complex mechanism for the reaction will be discussed in more detail later in this account.

Until recently, the *only* example that demonstrates the stereochemistry of photochemical cyclobutene ring opening was that of Saltiel and Ng-Lim, who reported the results of direct photolysis of the tricyclic, isomeric cyclobutene derivatives *cis*- and *trans*-**3** (eqs. [2] and [3]) (13). Diene **4** is the product of (photochemically allowed) disrotatory ring-opening of *cis*-**3**. The apparent failure of *trans*-**3** to yield this product is an indication that ring opening does *not* proceed by the formally forbidden, conrotatory pathway; in this case, the disrotatory pathway is effectively blocked since it must yield the highly strained *cis,trans* isomer of **4**.

The apparent neglect of this prototypical excited state

Can. J. Chem. Downloaded from www.nrcresearchpress.com by 88.255.202.194 on 09/08/12
For personal use only.

pericyclic reaction by photochemists is presumably due to the fact that, in general, phenylated cyclobutenes do not

[2] 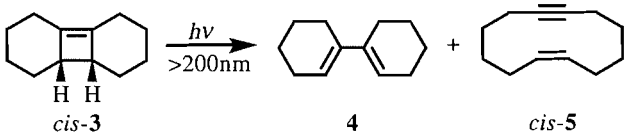

[3] 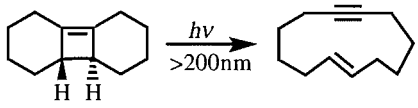

undergo ring opening upon photolysis in solution (14–16).[3] For example, 1,2-diphenylcyclobutene yields only the products of formal [2+2] cycloreversion upon direct photolysis in hydrocarbon solution (14, 16), undergoes solvent addition upon photolysis in methanol solution (15), and fluoresces with high efficiency (16) (see eq. [4]). Evidently,

[4] 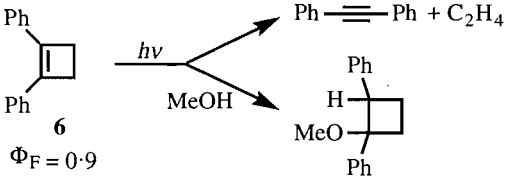

[5] 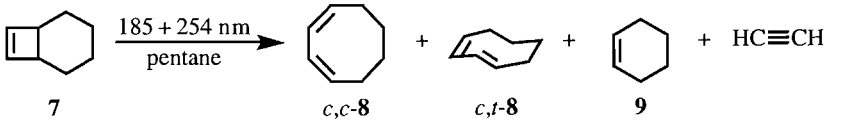

tolysis (185 + 254 nm) of cyclobutene itself in pentane solution results in the formation of 1,3-butadiene, methylenecyclopropane, acetylene, and ethylene in the quantum yields shown in eq. [7] (21).

[6] 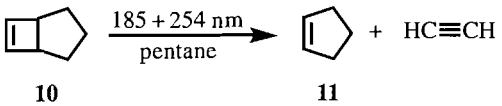

[7] 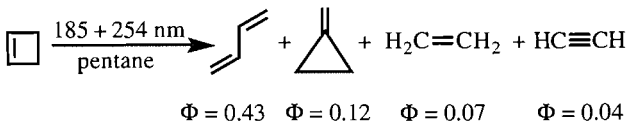

Our interest in this area was initiated by the report of Inoue *et al.* of the photochemistry of **7** and **10**. We originally set about to show simply that photolysis of these molecules with *monochromatic* far-UV radiation, under conditions where the primary diene products *are not* subject to secondary photolysis with the 254 nm component of the low-pressure mercury lamp, would afford results that are both internally consistent and compatible with the earlier report by Saltiel and Ng Lim on the photochemistry of *cis*- and *trans*-**3**. Indeed, photolysis of **10** in pentane with a low-pressure mercury lamp in conjunction with a γ-irradiated LiF crystal filter to remove the 254 nm component of the light source (OD^{185} ~ 0.2; OD^{254} > 5), or with an ArF excimer laser (193 nm), resulted in the formation of 1,3-cycloheptadiene (**12**) and cyclopentene (**11**) in comparable yields (eq. [8]) (22). As expected, the absence of **12** as a product of photolysis of **10** with the unfiltered light source is simply due to its substantial photolability at 254 nm; this diene undergoes photochemical ring closure to yield **10** with a quantum yield of ca. 0.35 (*5d,e*).

[3]Also, W. J. Leigh and A. Postigo, unpublished results.

conjugated cyclobutenes undergo ring opening upon photolysis only if the reaction is accompanied by the relief of ring strain, as for example with the cases of benzocyclobutenes (17) and Dewar aromatics (18). Interestingly, the former have been reported to open nonstereospecifically, while Dewar aromatics yield the corresponding fully aromatic isomer adiabatically from both the singlet and triplet excited states. With unstrained systems, photochemical ring opening evidently occurs only with cyclobutenes bearing nonconjugating substituents, necessitating the use of far-UV photochemical techniques for the study of the reaction.

The photochemistry of alkylcyclobutenes

Inoue *et al.* reported in 1983 that photolysis of bicyclo[4.2.0]oct-7-ene (**7**) in pentane solution with an unfiltered low-pressure mercury lamp (185 + 254 nm) gives rise to *cis,cis*- and *cis,trans*-1,3-cyclooctadiene (**8**), cyclohexene (**9**), and ethylene (eq. [5]) (19). The apparent nonstereospecificity of ring opening was explained by noting that **8** absorbs strongly at 254 nm (the major component of the low-pressure mercury lamp) and undergoes facile *cis,trans* photoisomerization upon photolysis at this wavelength (20). Photolysis of bicyclo[3.2.0]hept-6-ene (**10**) under similar conditions was found to afford only cyclopentene (**11**) and acetylene (eq. [6]) (19). Adam *et al.* later reported that pho-

[8] 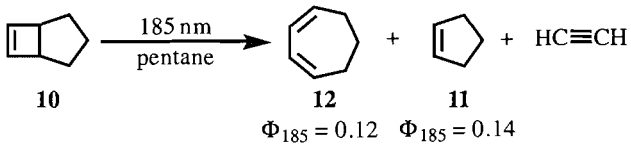

To our considerable surprise, however, photolysis of **7** under similar conditions gave rise to *mixtures* of *cis,cis*- and *cis,trans*-**8**, in addition to cyclohexene (**9**) and small amounts of the methylenecyclopropane derivative **13** (eq. [9]). To demonstrate that the apparent nonstereospecificity of diene formation was not due to secondary photolysis effects, **10** was photolyzed in the presence of small amounts of *c,c*-**8** under the above conditions, and the photolysate was monitored for the formation of the *cis,trans* isomer between 0.3 and 3% conversion. None could be detected within the limits of sensitivity of our analytical method, verifying that secondary diene photolysis does not contribute to the observed product distributions under conditions of monochromatic photolysis to low conversions.

Can. J. Chem. Downloaded from www.nrcresearchpress.com by 88.255.202.194 on 09/08/12
For personal use only.

[9] 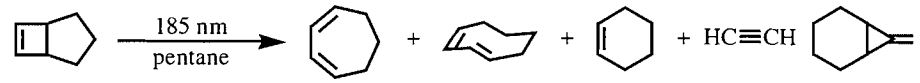

7 *c,c*-**8** *c,t*-**8** **9** **13**

$\Phi_{185} = 0.12$ $\Phi_{185} = 0.04$ $\Phi_{185} = 0.17$ $\Phi_{185} = 0.01$

Even more interesting results were obtained from monochromatic far-UV photolysis of the monocyclic derivatives *cis*- and *trans*-3,4-dimethylcyclobutene (**2**); these afforded mixtures of the three isomeric 2,4-hexadienes weighted in favour of the *formally forbidden* diene isomer(s) in each case (eq. [10]). Similar investigations of the photochemistry of a wide variety of mono-, bi-, and tricyclic alkylcyclobutene derivatives have been reported since our initial study (23–29), and indicate that the nonstereospecificity of the photochemical ring opening reaction is quite general. The results of these studies will be discussed in detail throughout this account.

[10] 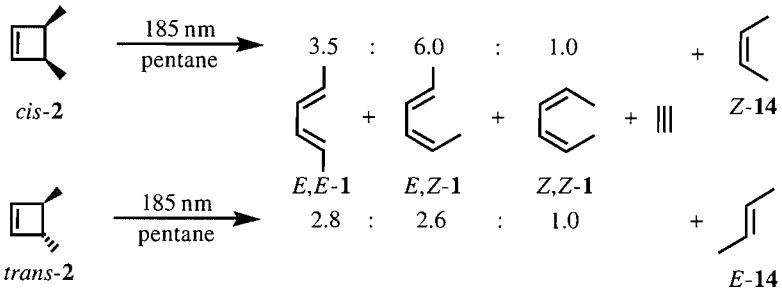

cis-**2** *E,E*-**1** *E,Z*-**1** *Z,Z*-**1** *Z*-**14**

trans-**2** *E*-**14**

Identification of the excited state(s) responsible for ring opening and cycloreversion

It has long been known that population of the triplet state of alkylcyclobutenes through triplet sensitization results in (2+2) dimerization, and does *not* lead to unimolecular isomerization or fragmentation (30; see, however, ref. 18). Thus, it is clear that both ring opening and cycloreversion arise from the excited singlet state manifold. As numerous workers have pointed out (19, 21, 22), there are two excited singlet states of similar energies in simple alkylcyclobutenes, the π,π^* (valence) state and the π,R(3*s*) (Rydberg) state (31). In principle, both could give rise to ring opening and cycloreversion products, though by very different mechanisms.

Since population of the π,R(3*s*) state in simple alkenes involves promotion of a π-electron to a spatially diffuse 3*s* orbital, the classical picture of the electronic structure of this state is that of a semi-ionized species that possesses radical cation character at the C=C bond (32). Since cyclobutene radical cations are known to undergo (thermal) ring opening in the gas phase (33) (the stereochemistry is evidently unknown), it is possible that Rydberg state involvement could account for the nonstereospecificity associated with this aspect of cyclobutene photochemistry, if Rydberg-derived ring opening occurs nonstereospecifically or in conrotatory fashion competitive with π,π^* state-derived disrotatory ring opening. The possibility that the cycloreversion process is derived from Rydberg state excitation is a more concrete one. It is well known that direct photolysis of simple alkenes in solution results in the predominant formation of products derived from carbene intermediates formed via [1,2]-hydrogen or alkyl migrations (32). In simple di-, tri-, and tetrasubstituted alkenes, the π,R(3*s*) state is lower in energy than the π,π^* state in the gas phase as well as in solution (31), and has been conclusively identified as the one responsible for the formation of these types of products (32, 34). With cycloalkenes, ring contraction is often the predominant mode of Rydberg-derived [1,2]-alkyl migration. In the case of cyclobutene, ring contraction would yield cyclopropylcarbene, which is known to fragment to acetylene and ethylene (35). In substituted systems, the alkene that is produced in this process is formed stereospecifically, with the stereochemistry defined by the substitution in the carbene (35). The possible stereospecific formation of *Z*-2-butene from photolysis of *cis*-**2** by this mechanism is illustrated in eq. [11].

[11] 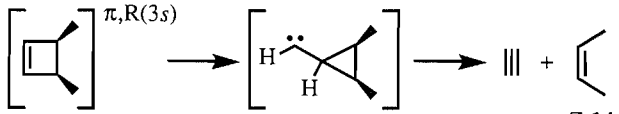

cis-**2** *Z*-**14**

To define the individual contributions of the π,π^* and π,R(3*s*) states to the formation of the various products of cyclobutene photolysis, it is necessary to systematically vary the relative energies of the two states. The obvious ways of doing this involve either preferentially lowering the energy of the π,R(3*s*) state with alkyl substituents at the C=C bond or preferentially lowering the π,π^* state with conjugating substituents at the C=C bond. The first approach was exploited in a study of the photochemistry of the series of monocyclic compounds **2**, **15**, and **16**; unfortunately, there are no regular variations in photoproduct distributions throughout the series that might allow a correlation to be made (27). Since phenylated cyclobutenes do not ring-open upon photolysis, the second approach similarly does not allow identification of the role of the Rydberg state in contributing to the ring opening reaction.

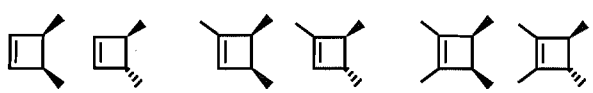

2 **15** **16**

Can. J. Chem. Downloaded from www.nrcresearchpress.com by 88.255.202.194 on 09/08/12
For personal use only.

Can. J. Chem. Downloaded from www.nrcresearchpress.com by 88.255.202.194 on 09/08/12
For personal use only.

The approach we employed for the solution of this problem involved systematically *raising* the energy of the π,R(3*s*) state relative to that of the π,π^* state by trifluoromethyl substitution (28). The strong electron-withdrawing character of this substituent was expected to destabilize the radical-cation-like alkene Rydberg without substantially altering the energy of the π,π^* state (since it is nonconjugative). The gas- and solution-phase UV absorption spectra and π-ionization potentials (measured by photoelectron spectroscopy) of the series of bicyclo[4.2.0]oct-7-ene derivatives **7**, **17**, and **18** verify that trifluoromethyl substitution does indeed have the anticipated effect on the singlet excited state manifold of cyclobutene derivatives, just as it does in simple alkenes such as norbornene (34). Thus, the π,R(3*s*) state is substantially lower in energy than the π,π^* state in **17**, but higher in energy than the π,π^* state in **18** (28).

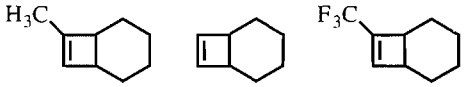

17 **7** **18**

Photolysis of the three compounds in pentane solution with 193 nm light results in competitive ring opening and cycloreversion as shown in eq. [12]. Table 1 lists the quantum yields for formation of dienes and cyclohexene from photolysis of the three compounds, the isomeric diene distributions obtained from each, and the positions of the π,R(3*s*) and π,π^* band maxima from the gas-phase UV-absorption spectra (28).

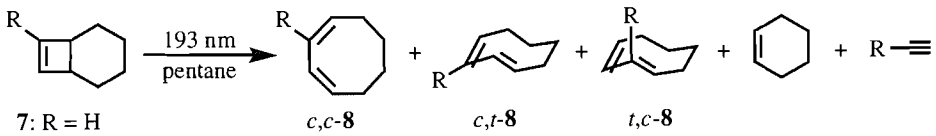

[12] **7**: R = H; **17**: R = CH_3; **18**: R = CF_3 — *c,c*-**8** — *c,t*-**8** (*a*: R = H; *b*: R = CH_3; *c*: R = CF_3) — *t,c*-**8**

TABLE 1. Gas-phase spectroscopic properties and product quantum yields from photolysis (193 nm) of substituted bicyclo[4.2.0]oct-7-enes **7**, **17**, and **18**[a]

	17 (R = CH_3)	**7** (R = H)	**18** (R = CF_3)
π-IP[b]	8.5 ± 0.1	9.0 ± 0.1	9.7 ± 0.2
$E_{\pi,R(3s)}$ (eV)[c]	5.91	6.37	≥6.7
E_{π,π^*}(eV)[c]	6.40	≥6.70	≥6.62
Φ_{dienes}[d]	0.087	0.175	0.292
$\Phi_{cyclohexene}$	0.13	0.14	0.030
c,c/(*c,t* + *t,c*)[e]	1.3	1.3	1.8

[a]Photolysis in deoxygenated pentane solution at 22°C. Relative errors in quantum yields are ca. 5%. Data from ref. 28.
[b]Lowest vertical ionization potential from gas-phase photoelectron spectrum.
[c]Position of absorption band maximum in gas-phase UV absorption spectrum.
[d]Total quantum yield for diene formation.
[e]Ratio of yields of isomeric dienes (error is ca. 10%).

As the data in Table 1 show, the quantum yield for cycloreversion, while substantial in the cases of **7** and **17**, is very small for the trifluoromethyl-substituted compound **18**. This trend indicates that cycloreversion arises nearly exclusively from the Rydberg state. On the other hand, the quantum yields for ring opening *increase* in opposite fashion, indicating that this aspect of cyclobutene photoreactivity is due to π,π^* state excitation. The effect of varying the photolysis wavelength on the observed product distributions from the three compounds is also consistent with these conclusions. Significantly, since ring opening of all three derivatives is nonstereospecific (and yields similar distributions of isomeric dienes), the apparent violation of orbital symmetry selection rules cannot be due to the intervention of more than one singlet excited state.

Scope and mechanism of the cycloreversion reaction

The suggestion that Rydberg-derived cycloreversion proceeds by a mechanism involving initial [1,2]-alkyl migration (ring contraction) to yield a cyclopropylcarbene termediate, which then fragments to yield the corresponding alkyne and alkene (eq. [11]), has been investigated directly (24). Cyclopropylcarbenes are known to undergo *ring contraction* to yield cyclobutenes in addition to fragmenting to an alkene and acetylene. With this in mind, we studied the photochemistry of the isomeric, unsymmetrically substituted cyclobutenes **19** and **20**. The two compounds were found to interconvert in low yield upon photolysis in solution; the most reasonable mechanism for this process is via common cyclopropylcarbene intermediate(s), one of which is shown in eq. [13].

[13]

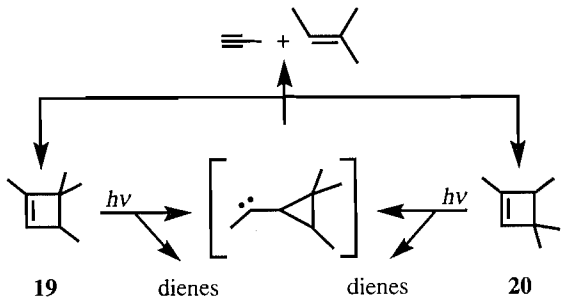

19 dienes dienes **20**

The cycloreversion reaction is suppressed when it must produce a relatively unstable alkene or alkyne product. Thus, photolysis of *cis*- and *trans*-bicyclo[5.2.0]non-8-ene (**21**) yields cycloheptene (**22**) in both cases (eq. [14]), but the quantum yield for formation of this product (185 nm) is ca. five times lower for the *trans* isomer (Φ = 0.26 from *cis*-**21** vs. Φ = 0.05 from *trans*-**21**) (25). The difference is presumably due to the fact that in the latter case, stereospecific "cycloreversion" must produce *trans*-cycloheptene. Even

Can. J. Chem. Downloaded from www.nrcresearchpress.com by 88.255.202.194 on 09/08/12
For personal use only.

[14] 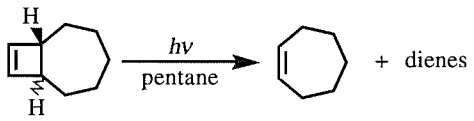

21 22

more remarkably, the fragmentation reaction is completely suppressed in the photolyses of compounds **23**–**25** (30, 29);[4] in these cases, fragmentation would produce highly strained C5–C7 cycloalkynes.

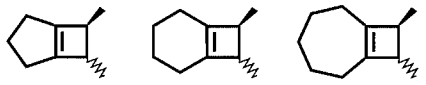

23 24 25

Scope and mechanism of the ring opening reaction

It is clear from the various examples already discussed that, in general, the photochemical ring opening of cyclobutene does not follow orbital symmetry selection rules. Nevertheless, certain observations suggest very strongly that orbital symmetry does (or at least, *can* in certain instances) play a role in the reaction. The most compelling of these is the fact that compounds **23**–**25** consistently open with a high (though not complete) degree of disrotatory stereospecificity (eq. [15]) (ref. 29 and footnote 4). There are a number of structural features present in these compounds that set them apart from the monocyclic and other bicyclic systems that have been studied; the role that these features play in altering the general behavior of cyclobutenes with respect to ring opening will be discussed in more detail later.

[15] 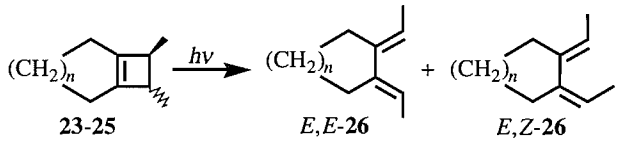

23-25 *E,E*-**26** *E,Z*-**26**

cis: ⟶	72-90%	10-28%
trans: ⟶	10-22%	90-78%

We believe that orbital symmetry *does play a role* in the photochemical ring opening of alkylcyclobutenes, but only in the initial stages of the reaction on the excited state potential energy surface. One piece of supporting evidence for this idea can be obtained from the behavior of *cis*- and *trans*-**3**, whose photochemistry was reinvestigated in light of our results for the numerous other cyclobutenes we have studied (26). It was found that, in fact, both isomers yield ring opening products upon photolysis (214 nm) in solution (eq. [16]). However, *trans*-**3** yields diene with ca. 5 times lower efficiency than does the *cis* isomer. This would be the expected result if disrotatory motions are involved in the initial stages of ring opening; such motions are impeded in *trans*-**3** because the disrotatory pathway leads to the highly strained *cis,trans* isomer of 1,1′-bicyclohexenyl (**4**). Similarly, the permethylated cyclobutene **27** undergoes ring opening with less than half the efficiency of *cis*-**15** (footnote 3); in this case, disrotatory motions are presumably impeded because of the necessity of buttressing two of the methyl groups at C3 and C4 as the rotation occurs.

[4]Also W. J. Leigh, K. Zheng, and A. Postigo, unpublished results.

[16] 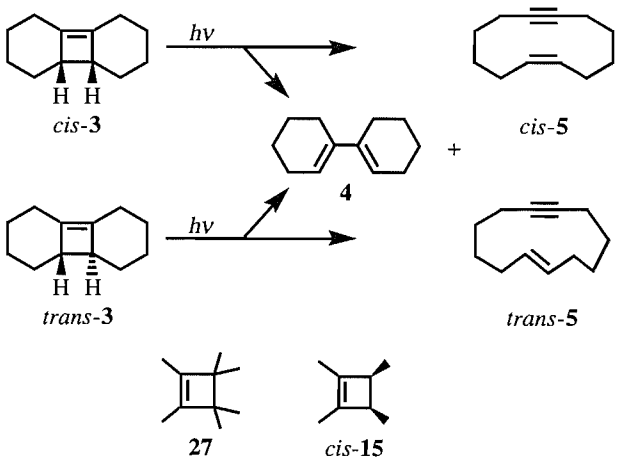

27 *cis*-15

It may also be pertinent to note that the efficiency of photochemical ring opening appears to depend on the bond strength of the C3—C4 bond (25), just as is the case in ground state electrocyclic ring opening reactions (4*d*). This is demonstrated by a comparison of the diene/alkene ratios obtained from photolysis of compounds *cis*-**28** (ca. 1.0) and *cis*-**29** (3.6) (23). Molecular models show that the π-system of the cyclooctenyl C=C bond in *cis*-**29** is almost perfectly coplanar with the fragmenting cyclobutenyl C—C bond. The weakening of the latter in *cis*-**29** compared to the corresponding bond in *cis*-**28** is also manifested in the relative rates of thermal ring opening of the two compounds (23, 36).

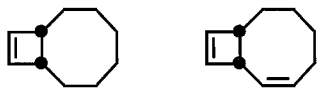

cis-**28** *cis*-**29**

If the above assessment of the initial stages of ring opening is correct, the ultimate loss of stereochemistry must then be due to intervening processes that occur after ring opening is initiated, and which compete with the normal internal conversion processes that are thought to characterize photopericyclic reactions (i.e., internal conversion to the ground state surface at the avoided crossing (6–9)). Several possibilities have been suggested (22, 25): (*i*) internal conversion to upper vibrational levels of ground state cyclobutene, from which conrotatory ring opening occurs; (*ii*) internal conversion to ground state biradical(oid) species; and (*iii*) adiabatic, disrotatory ring opening to yield diene in the first excited singlet state, from which *cis,trans* isomerization ensues. While the first possibility has not yet been investigated experimentally, the results of photolysis of compounds **21** (25) and **29** (23) are consistent with the second, biradical mechanism for ring opening; in both cases, the *cis* and *trans* isomers yield very similar distributions of *cis,cis* and *cis,trans* dienes (eq. [17]), suggesting the involvement of a common set of intermediates, or at least that reaction of the two isomers proceeds through a common point on the excited state surface prior to product formation (25). It is interesting to note that the major diene isomer formed from photolysis of the two isomers of **21** is the less thermodynamically stable *cis,trans* isomer.

The adiabatic ring opening mechanism has been studied in greatest detail, since in this case it is a somewhat more straightforward task to design experiments with which to test

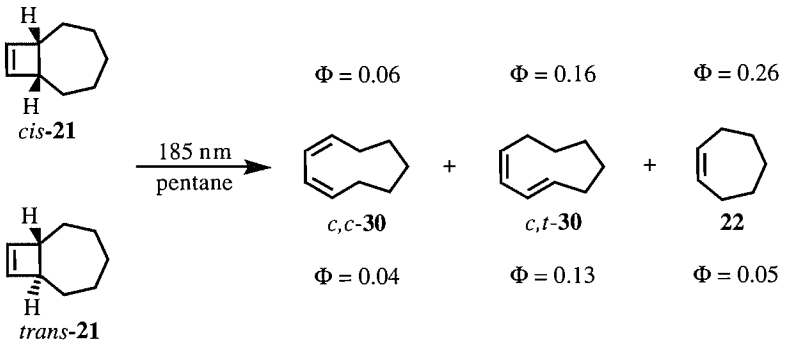

[17]

the mechanism. If ring opening occurs exclusively to yield fully open, excited dienes by the disrotatory pathway, then the observed diene distribution from cyclobutene ring opening would be expected to be dictated by the decay characteristics of the excited dienes, and thus predictable provided that the quantum yields for *cis,trans* isomerization and other photochemical processes of the dienes are known (Scheme 1) (22). While analyses of this type have been carried out for most of the cyclobutene derivatives discussed above, predicted diene distributions very rarely match those actually observed from photolysis of the cyclobutene derivative. In all of these cases, however, the stable ground state conformation of the diene is very different from the planar *s-cis* conformation in which the excited diene would be formed by disrotatory ring opening, so that independent characterization of the excited state behavior of the dienes themselves may not provide a realistic indication of their behaviour when formed by cyclobutene ring opening (22, 25) (the photochemistry of dienes is known to be conformation dependent (37)).

With this in mind, we have studied the photochemistry of the bicyclic cyclobutenes *cis*- and *trans*-**24** (29), whose isomeric dienes are constrained to be *s-cis* (AM1 calculations predict a twist angle of ca. 36° in the parent diene, 1,2-bismethylidenecyclohexane). The work has recently been extended to include the analogous bicyclo[4.2.0]hept-1^5-ene (**23**) and bicyclo[5.2.0]non-1^7-ene (**25**) systems (eq. [15]) (footnote 4). Table 2 lists the observed *EE/EZ* diene ratios from photolysis of these compounds, along with the corresponding ratios calculated from the independently determined quantum yields for *cis,trans* isomerization of the dienes according to the equation given in Scheme 1.

Several interesting trends emerge from these data. First of all, the high degree of disrotatory stereospecificity observed for the ring opening of *cis*- and *trans*-**24** is quite general within this special class of constrained systems. Secondly, these compounds undergo ring opening with considerably higher efficiency than other compounds with dialkyl substitution at the cyclobutene double bond (e.g., **15**). This can be explained conveniently enough by noting that the ancillary ring induces additional strain in the cyclobutenyl ring, as evidenced by the substantially lower activation energies for thermal ring opening of these compounds compared to those of monocyclics (38). Thirdly, the *EE/EZ* diene ratios observed in the photolyses of these compounds are reproduced by the values calculated on the basis of the adiabatic mechanism defined in Scheme 1 in only two cases (*cis*-**23** and *cis*-**24**). We conclude that the adiabatic ring opening pathway cannot account for the nonstereospecificity of the reaction.

Thus, it might be concluded that the general nonstereospecificity of the reaction is due to intervening internal conversion processes that occur before the system reaches the avoided surface crossing for disrotatory ring opening. If this is the case, then the unusually high degree of stereospecificity that is observed for **23–25** might be attributed to structurally induced suppression of these processes. Keeping in mind that the rates of internal conversion processes are affected by rovibrational factors, it is worth noting that the "alkyl substituents" on the C=C bond are more or less locked in **23–25**; furthermore, the isomeric dienes are highly constrained with respect to rotation about the central C—C bond. In principle, either or both of these factors could af-

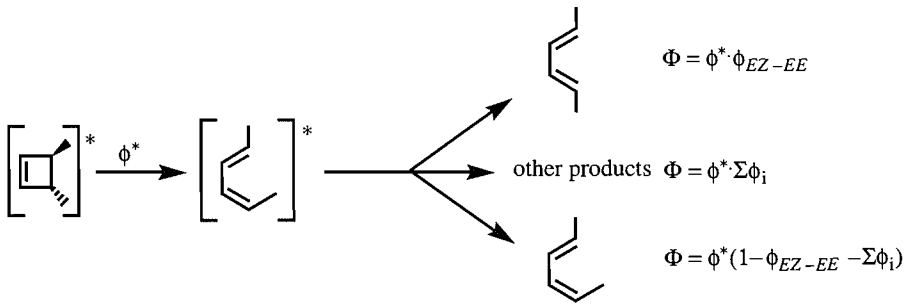

Predicted: $(EE/EZ) = \phi_{EZ-EE}/(1-\phi_{EZ-EE}-\Sigma\phi_i)$

SCHEME 1. The adiabatic mechanism for cyclobutene ring opening.

Can. J. Chem. Downloaded from www.nrcresearchpress.com by 88.255.202.194 on 09/08/12
For personal use only.

TABLE 2. Comparison of observed diene distributions from photolysis (193 nm) of **23–25** with values calculated according to the adiabatic ring opening mechanism[a]

Isomer	Compound	$(EE/EZ)_{obs}$	$(EE/EZ)_{calc}$[b]
cis	**23**	2.5 ± 0.4	2.2 ± 0.4
cis	**24**	3.4 ± 0.6	3.7 ± 0.4
cis	**25**	9.1 ± 1.3	2.9 ± 0.4
trans	**23**	0.11 ± 0.02	0.71 ± 0.09
trans	**24**	0.18 ± 0.03	0.38 ± 0.05
trans	**25**	0.29 ± 0.04	0.19 ± 0.03

[a]Photolysis at 193 nm in pentane solution; 22°C.
[b]Calculated from the quantum yields for photoreaction of the corresponding *E,E*- and *E,Z*-dienes (see eq. [15]), according to the equation in Scheme 1.

fect the rates of internal conversion processes at partially open geometries. Because the rigidity of these compounds varies regularly throughout the series, accompanying variations in the degree of stereospecificity would be expected. However, it is difficult to understand why the variation observed within the series of *cis*-dimethyl compounds (increasing stereospecificity with increasing ancillary ring size) is *opposite* to that observed within the series of *trans*-dimethyl compounds (decreasing stereospecificity with increasing ancillary ring size).

Bernardi and Robb and their co-workers recently reported MCSCF calculations on the photochemical ring opening of 7-methylbicyclo[4.2.0]oct-7-ene (**17**) (39), experimental results for which were discussed earlier. This report follows an earlier study of the photochemical ring closure of 1,3-butadiene, in which was reported the existence of real surface crossings ("conical intersections") between the excited and ground state surfaces for disrotatory conversion of butadiene to cyclobutene (*vide supra*) (11). It was proposed that during the ring closure reaction of 1,3-butadiene, funnelling to the ground state surface occurs at the conical intersection rather than at the avoided surface crossing. The geometry of the reacting species at this stage is one in which all the π-bonds in the molecule are broken, a tetraradicaloid species with the C2—C3 bond twisted by 78°. Excited state ring opening of **17** was proposed to proceed through three such surface crossings; the three conical intersection structures have the common feature of having the (former) cyclobutene double bond twisted by an angle close to 90°. The formation of three isomeric dienes in the reaction is explained as being due to the fact that three different surface crossings exist and, at each one, the reacting species can further relax to give all three of the diene isomers after entering the ground state surface (39).

This theoretical model can adequately explain why ring opening leads to a distribution of isomeric dienes in most of the cyclobutene systems that have been studied experimentally. It might also explain why nearly common distributions of products are formed in systems such as *cis*- and *trans*-**21**, if there is a single conical intersection geometry that is accessible from both isomers of the cyclobutene. Compounds **23–25** are special in that they are prevented from achieving the 80–90° twist angle that characterizes the geometry of the system at the conical intersection. It is possible that in such cases, the system is forced to open largely via the avoided crossing, or perhaps adiabatically, or perhaps via other surface crossings[5] in a pathway that leads predominantly to the disrotatory product(s). It is clear that further study is required in order to develop a complete understanding of the remarkable complexities of this "prototypical" photoelectrocyclic reaction.

Acknowledgments

The work discussed in this account is that of four individuals of whom I am extremely proud: Brad Clark, Nien Nguyen, Zheng Kangcheng, and Al Postigo. I owe an enormous debt to them for their patience and sheer hard work, as I do to my other graduate students who have toiled in our other areas of interest — Brian Fahie, Scott Mitchell, Mark Workentin, Greg Sluggett, Jo-Ann Banisch, and Mike St. Pierre. I am also indebted to the Natural Sciences and Engineering Research Council of Canada for its very generous support of our research through operating and equipment grants, and to the Petroleum Research Fund, which supported some of our work in the cyclobutene area. Finally, I would like to thank the Canadian Society for Chemistry for honouring me with the 1992 Merck–Frosst Centre for Therapeutic Research Lecture Award.

1. R. B. Woodward and R. Hoffman. The conservation of orbital symmetry. Verlag Chemie, Weinheim. 1970.
2. (*a*) F. A. Carey and R. J. Sundberg. Advanced organic chemistry. 2nd ed. Plenum Press, New York. 1984. Part A, Chap. 11; (*b*) T. H. Lowry and K. S. Richardson. Mechanism and theory in organic chemistry. 3rd ed. Harper & Row, New York. 1987. Chap. 11.
3. (*a*) N. J. Turro. Modern molecular photochemistry. 2nd ed. Benjamin-Cummings, New York. 1985. Chap. 7; (*b*) A. Gilbert and J. Baggott. Essentials of molecular photochemistry. CRC Press, Boca Raton, Fla. 1991.
4. (*a*) W. Adam. Chem. Ber. **97**, 1811 (1964); (*b*) R. Criegee, D. Seebach, R. E. Winter, B. Borretzen, and H.-A. Brune. Chem. Ber. **98**, 2339 (1965); (*c*) R. Criegee. Angew. Chem. Int. Ed. Engl. **7**, 559 (1968); (*d*) J. J. Gajewski. Hydrocarbon thermal isomerizations. Academic Press, New York. 1981. pp. 45–58, and references cited therein.
5. (*a*) D. M. Schumate and G. J. Fonken. J. Am. Chem. Soc. **87**, 3996 (1965); **88**, 1073 (1966); (*b*) W. G. Dauben, R. G. Cargill, R. M. Coates, and J. Saltiel. J. Am. Chem. Soc. **88**, 2742 (1966); (*c*) R. Srinivasan. J. Am. Chem. Soc. **90**, 4498 (1968); (*d*) O. L. Chapman, D. J. Pasto, G. W. Borden, and A. A. Griswold. J. Am. Chem. Soc. **84**, 1220 (1962); (*e*) W. G. Dauben and R. L. Cargill. J. Org. Chem. **27**, 1910 (1962).
6. W. Th. A. M. Van der Lugt and L. J. Oosterhoff. J. Am. Chem. Soc. **91**, 6042 (1969).
7. D. Grimbert, G. Segal, and A. Devaquet. J. Am. Chem. Soc. **97**, 6629 (1975).
8. W. G. Dauben. *In* React. Photoexcited Org. Mol. Proc. Conf. Chem. 13th, Brussels, 1965. Wiley–Interscience, New York. 1967. p. 171.
9. (*a*) K. Morihashi, O. Kikuchi, and K. Suzuki. Chem. Phys. Lett. **90**, 346 (1982); (*b*) K. Morihashi and O. Kikuchi. Theor. Chim. Acta, **67**, 293 (1985).
10. V. A. Pichko, B. Ya. Simkin, and V. I. Minkin. J. Mol. Struct. (Theochem), **235**, 107 (1991).
11. F. Bernardi, S. De, M. Olivucci, and M. A. Robb. J. Am. Chem. Soc. **112**, 1737 (1990).
12. (*a*) J. Von Neumann and E. Wigner. Phys. Z. **30**, 467 (1929); (*b*) G. Herzberg and H. C. Longuet-Higgins. Trans. Faraday

[5]M. A. Robb, private communication.

Can. J. Chem. Downloaded from www.nrcresearchpress.com by 88.255.202.194 on 09/08/12
For personal use only.

Soc. **35**, 77 (1963); (*c*) C. A. Mead and D. G. Truhlar. J. Chem. Phys. **70**, 2284 (1979); (*d*) S. P. Keating and C. A. Mead. J. Chem. Phys. **86**, 2152 (1987), and references cited therein.
13. J. Saltiel and L.-S. Ng Lim. J. Am. Chem. Soc. **91**, 5404 (1969).
14. C. D. DeBoer and R. H. Schlessinger. J. Am. Chem. Soc. **90**, 803 (1968).
15. M. Sakuragi and M. Hasegawa. Chem. Lett. 29 (1974).
16. G. Kaupp and M. Stark. Chem. Ber. **111**, 3608 (1978).
17. G. Quinkert, M. Finke, J. Palmowski, and W.-W. Wiersdorff. Mol. Photochem. **1**, 433 (1969).
18. (*a*) N. C. Yang, R. V. Carr, E. Li, J. K. McVey, and S. A. Rice. J. Am. Chem. Soc. **96**, 2297 (1974); (*b*) R. V. Carr, B. Kim, J. K. McVey, N. C. Yang, W. Gerhartz, and J. Michl. Chem. Phys. Lett. **39**, 57 (1976).
19. Y. Inoue, M. Sakae, and T. Hakushi. Chem. Lett. 1495 (1983).
20. W. J. Nebe and G. J. Fonken. J. Am. Chem. Soc. **91**, 1249 (1969).
21. W. Adam, T. Oppenlander, and G. Zang. J. Am. Chem. Soc. **107**, 3921 (1985).
22. K. B. Clark and W. J. Leigh. J. Am. Chem. Soc. **109**, 6086 (1987).
23. W. G. Dauben and J. Haubrich. J. Org. Chem. **53**, 600 (1988).
24. K. B. Clark and W. J. Leigh. Can. J. Chem. **66**, 1571 (1988).
25. W. J. Leigh, K. Zheng, and K. B. Clark. J. Org. Chem. **56**, 1574 (1991).
26. W. J. Leigh and K. Zheng. J. Am. Chem. Soc. **113**, 2163 (1991).
27. W. J. Leigh, K. Zheng, and K. B. Clark. Can. J. Chem. **68**, 1988 (1990).
28. W. J. Leigh, K. Zheng, N. Nguyen, N. H. Werstiuk, and J. Ma. J. Am. Chem. Soc. **113**, 4993 (1991).
29. W. J. Leigh and K. Zheng. J. Am. Chem. Soc. **113**, 4019 (1991); *Errata*: J. Am. Chem. Soc. **114**, 796 (1992).
30. R. Srinivasan. J. Am. Chem. Soc. **84**, 4141 (1962).
31. (*a*) B. B. Loeffler, E. Eberlin, and L. W. Pickett. J. Chem. Phys. **28**, 345 (1958); (*b*) M. B. Robin. Higher excited states of polyatomic molecules. Vol. II. Chap. IV. Academic, New York. 1975.
32. P. J. Kropp. Org. Photochem. **4**, 1 (1979), and references cited therein.
33. (*a*) N. L. Bauld, D. J. Bellville, R. Pabon, R. Chelsky, and G. Green. J. Am. Chem. Soc. **105**, 2378 (1983); (*b*) C. Dass and M. L. Gross. J. Am. Chem. Soc. **109**, 5724 (1987).
34. (*a*) N. Nguyen, K. B. Clark, B. E. Harris, and W. J. Leigh. Can. J. Chem. **68**, 1961 (1990); (*b*) A. T. Wen, A. P. Hitchcock, N. H. Werstiuk, N. Nguyen, and W. J. Leigh. Can. J. Chem. **68**, 1967 (1990).
35. (*a*) M. Jones, Jr. and R. A. Moss. Carbenes. Vol. I. Wiley, New York. 1973, and references cited therein; (*b*) S. S. Olin and R. M. Venable. J. Chem. Soc. Chem. Commun. 104 (1974); 273 (1974); (*c*) R. R. Gallucci and M. Jones, Jr. J. Am. Chem. Soc. **98**, 7704 (1976).
36. (*a*) P. Radlick and W. Fenical. Tetrahedron Lett. 4901 (1967); (*b*) J. J. Bloomfield, S. S. McConaghy, Jr., and A. G. Hartmann. Tetrahedron Lett. 3723 (1969); (*c*) W. G. Dauben and D. M. Michno. J. Am. Chem. Soc. **103**, 2284 (1981).
37. (*a*) J. Saltiel and J. L. Charlton. *In* Rearrangements in ground and excited states. Vol. III. *Edited by* P. de Mayo. Academic, New York. 1980. p. 25, and references cited therein; (*b*) J. Saltiel, J. D'Agostino, E. D. Megarity, L. Metts, K. R. Neuberger, M. Wrighton, and O. U. Zafiriou. Org. Photochem. **3**, 1 (1973); (*c*) L. M. Stephenson and J. I. Brauman. Acc. Chem. Res. **7**, 65 (1974).
38. D. H. Aue and R. N. Reynolds. J. Am. Chem. Soc. **95**, 2027 (1973).
39. F. Bernardi, M. Olivucci, I. N. Ragazos, and M. A. Robb. J. Am. Chem. Soc. **114**, 2752 (1992).

Can. J. Chem. Downloaded from www.nrcresearchpress.com by 88.255.202.194 on 09/08/12
For personal use only.

A new synthesis of castasterone and brassinolide from stigmasterol. A concise and stereoselective elaboration of the side chain from a C-22 aldehyde

THOMAS G. BACK,[1] PETER G. BLAZECKA, AND M. VIJAYA KRISHNA[2]
Department of Chemistry, University of Calgary, Calgary, Alta., Canada, T2N 1N4

Received August 18, 1992

THOMAS G. BACK, PETER G. BLAZECKA, and M. VIJAYA KRISHNA. Can. J. Chem. **71**, 156 (1993).

Brassinolide (**1**) and castasterone (**2**) were prepared from aldehyde **7**, in turn available from stigmasterol (**3**). The addition of (*E*)-1-propenyllithium to **7**, followed by diastereoselective Sharpless epoxidation of allylic alcohol **8** using (L)-(+)-diethyl tartrate, and regioselective epoxide-opening of (*threo*) epoxy alcohol **15** with isopropylmagnesium chloride in the presence of a catalytic amount of cuprous cyanide afforded diol **17**. The epoxidation and cuprate addition steps were investigated in greater detail with the simpler model aldehyde **4**. Hydrolysis of **17** provided **2**, which was converted preferentially into **1** or its regioisomer **22** by Baeyer–Villiger oxidation with trifluoroperoxyacetic acid or peroxyseleninic acids, respectively.

THOMAS G. BACK, PETER G. BLAZECKA et M. VIJAYA KRISHNA. Can. J. Chem. **71**, 156 (1993).

On a préparé le brassinolide (**1**) et la castastérone (**2**) à partir de l'aldéhyde **7** que l'on peut obtenir à partir du stigmastérol (**3**). L'addition du (*E*)-1-propényllithium au composé **7**, suivie par une époxydation diastéréosélective selon Sharpless de l'alcool allylique **8**, utilisant du (L)-(+)-tartrate de diéthyle, et une ouverture régiosélective de l'alcool (*thréo*)-époxydique **15**, à l'aide de chlorure de chlorure d'isopropylmagnésium en présence d'une quantité catalytique de cyanure cuivreux, conduit au diol **17**. Utilisant l'aldéhyde modèle **4**, beaucoup plus simple, on a examiné en détail les étapes d'époxydation et d'addition du cuprate. L'hydrolyse du composé **17** fournit le produit **2** que l'on a transformé d'une façon préférentielle en **1**, ou en son régioisomère **22**, grâce à une oxydation de Baeyer–Villiger avec respectivement de l'acide trifluoroperoxyacétique ou des acides peroxyséléniniques.

[Traduit par la rédaction]

In 1979, Grove, Mandava, and co-workers (1) reported the isolation and structure elucidation of brassinolide (**1**), a novel plant growth-promoter from *Brassica napus* L. pollen. The product was a highly oxygenated steroid with an unprecedented B-ring lactone that displayed activity at concentrations several orders of magnitude lower than those of other plant growth regulators (1–3). In certain plant species, noticeable growth enhancement was observed even at the nanogram level. Field trials in several countries demonstrated substantial improvements in the yields of crops such as wheat, corn, rye, potatoes, and others, when brassinolide or related brassinosteroids were applied, even at low concentrations (3*a*, 3*b*). These compounds also display antiecdysteroid activity in insects (3*c*) and improve the stress resistance of various crops to heat, cold, drought, and salinity (3*d*, 3*e*, 3*f*). The low abundance of brassinolide in natural sources, its potent biological activity, and its intriguing structure have made it and its congeners the targets of several recent syntheses (4). The brassinolide side chain, with its vicinal diol function at C-22 and C-23, and the four contiguous chiral centers at C-20, C-22, C-23, and C-24, presents a special challenge in such endeavours. We now report the preparation of brassinolide (**1**) and its 6-keto analogue, castasterone (**2**), by a simple new approach that elaborates the desired side chain in just three steps from a C-22 aldehyde precursor, which in turn is easily available from inexpensive stigmasterol (**3**).

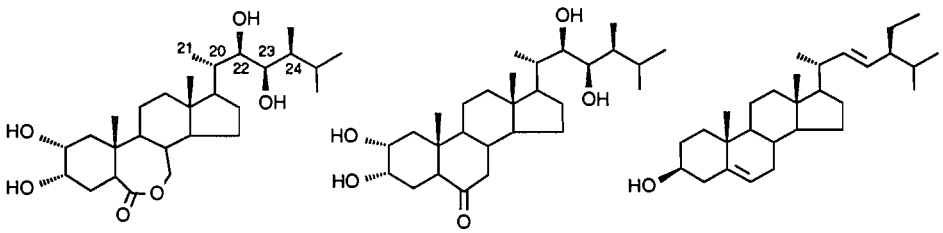

Brassinolide (1) **Castasterone (2)** **Stigmasterol (3)**

Results and discussion

Our general approach to the brassinolide side chain is shown retrosynthetically in Scheme 1. The desired product results from the regio- and stereoselective attack of an isopropyl nucleophile at C-24 of a (*threo*)-23,24-epoxy 22-aldehyde, with inversion of configuration. The key intermediate epoxy alcohol is obtained by the stereoselective epoxidation of the corresponding allylic alcohol, which in turn represents the Cram addition product of a propenyl anion to a C-22 aldehyde.

Both the simple cyclosterol C-22 aldehyde **4** (5) and the more highly elaborated analogue **7** (4*d*, 4*e*) were prepared from stigmasterol (**3**) by literature methods. The former, more readily available aldehyde, was employed as a model sys-

[1]Author to whom correspondence may be addressed.
[2]Present address: Epitope Inc., 8505 SW Creekside Place, Beaverton, OR 97005, U.S.A.

Can. J. Chem. Downloaded from www.nrcresearchpress.com by 88.255.202.194 on 09/08/12
For personal use only.

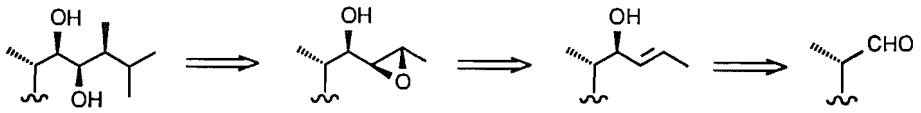

SCHEME 1

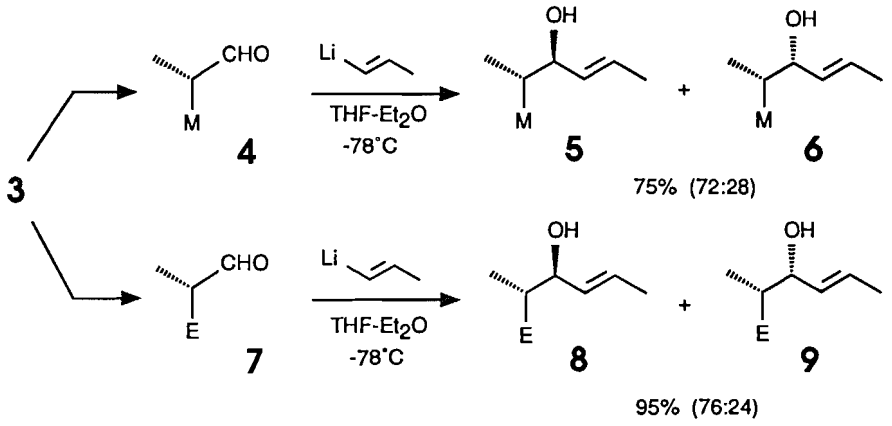

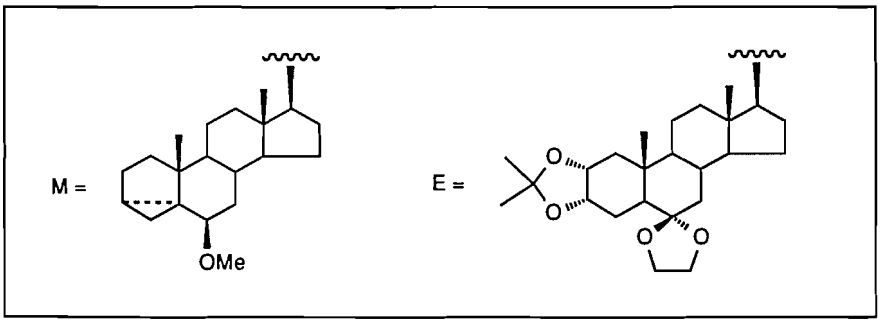

SCHEME 2

tem for the optimization of the three steps in Scheme 1 (see ref. 6 for a preliminary communication), and these were then applied to **7** for the actual preparation of the desired target compounds **1** and **2**. The propenylation of aldehydes **4** and **7** was achieved with (*E*)-1-propenyllithium at −78°C, affording mixtures of the epimeric allylic alcohols **5** and **6**, and **8** and **9**, respectively, as shown in Scheme 2 (M = model steroid nucleus; E = elaborated steroid nucleus). The propenyllithium reagent is easily obtained from (*E*)-1-chloropropene and is known to be configurationally stable (7). As expected, the additions favoured the Cram products **5** and **8** over their anti-Cram isomers **6** and **9** (8).[3] Separation of each epimeric pair was accomplished by routine chromatography. The stereochemical assignments of the known compounds **5** and **6** were previously reported (9), and those of **8** and **9** were made by comparison of their NMR spectra with those of **5** and **6**, and confirmed by the ultimate conversion of **8** into the naturally occurring products **1** and **2**.

The further transformations of allylic alcohol **5** are shown in Scheme 3. Epoxidation of **5** to the corresponding (*threo*) and (*erythro*) epoxy alcohols **10** and **11**, respectively, was investigated under a variety of conditions, summarized in Table 1. *m*-Chloroperbenzoic acid (MCPBA) is an effective epoxidizing agent (10) and, in the case of allylic alcohols, frequently reacts with high stereoselectivity due to complexation of the peracid with the hydroxyl group of the substrate (11). It has been reported that secondary (*E*)-allylic alcohols afford predominantly (*threo*) epoxy alcohols (12), which in the case of **5** would afford the desired diastereomer **10**. Moreover, MCPBA oxidations of the steroidal (*E*)-allylic alcohols **13***a* (4*a*) and **13***b* (4*f*) were reported to afford the corresponding (*threo*) epoxy alcohols **14***a* and **14***b* with excellent diastereoselectivity (eq. [1]). Although the alkene moieties of **13***a,b* are trisubstituted instead of disubstituted as in **5**, in each case the bulkier substituent (i-Pr vs. Me in **13***a,b*; Me vs. H in **5**) is oriented *trans* to C-22. We therefore reasoned that if the side-chain conformations of **13***a,b* and **5** were comparable, then similar stereochemical outcomes might be expected. However, entry 1 in Table 1 reveals that poor stereoselectivity was observed with **5**, unexpectedly favouring the unwanted (*erythro*) isomer **11**. Similarly unsatisfactory results were obtained with *o*-nitrobenzeneperoxyseleninic acid[4] (entry 2), while the urea – hydrogen peroxide complex in the presence of acetic anhy-

[3]For a discussion of and lead references to more recent variations of Cram's rule, see ref. 8*b*. For other methods for controlling the Cram vs. anti-Cram distribution of addition products to steroidal C-22 aldehydes, see ref. 8*c*.

[4]For the use of peroxyseleninic acids in epoxidations, see ref. 13.

Can. J. Chem. Downloaded from www.nrcresearchpress.com by 88.255.202.194 on 09/08/12
For personal use only.

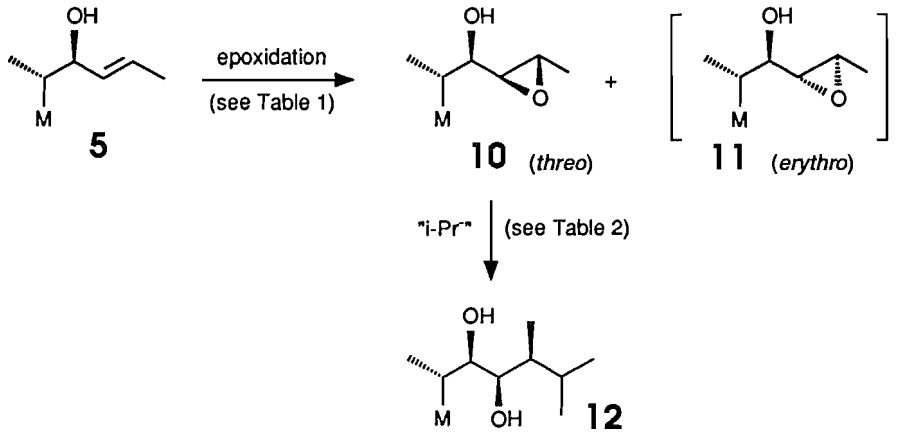

SCHEME 3

TABLE 1. Epoxidation of allylic alcohol **5**

Entry	Oxidant and conditions	Yield[a] (%)	*threo* (**10**):*erythro* (**11**) ratio[b]
1	MCPBA; CH_2Cl_2; 30 min, RT	87	40:60
2	*o*-NO_2PhSeO_2H, H_2O_2, CH_2Cl_2; 48 h, RT	80	31:69
3	Urea–H_2O_2; Ac_2O, $NaHPO_4$, CH_2Cl_2; 100 h, RT	62[c]	57:43
4	*t*-BuOOH; 0.01 equiv. $VO(acac)_2$; toluene; 12 h, RT	90	<5:95
5	*t*-BuOOH; 0.01 equiv. $Mo(CO)_6$; benzene; 4 h, 60°C	—	40:60
6	*t*-BuOOH; 0.1 equiv. $Tl(O\text{-}iPr)_4$; D-DET; mol. sieves, CH_2Cl_2; 6 days, −25°C	96	44:56
7	*t*-BuOOH; 0.1 equiv. $Tl(O\text{-}iPr)_4$; L-DET; mol. sieves, CH_2Cl_2; 6 days, −25°C	95	70:30

[a]Isolated yield unless otherwise indicated.
[b]Ratio determined by NMR integration.
[c]Yield determined by NMR integration.

dride (14) slightly favoured the (*threo*) isomer **10**, but with a lower overall yield (entry 3). Epoxidations of allylic alcohol **5** with *tert*-butyl hydroperoxide in the presence of catalytic amounts of $VO(acac)_2$ or $Mo(CO)_6$ (ref. 15, for a review) were also investigated. The former catalyst is known to produce opposite stereoselectivities to those observed with either the latter catalyst, or with peracids (12). In the present case, the use of $VO(acac)_2$ afforded the (*erythro*) isomer **11** almost exclusively (entry 4), while $Mo(CO)_6$ (entry 5) gave, as expected, similar results to those observed with MCPBA. The tendency of **5** to form substantial or dominant amounts of **11** under all of the conditions in entries 1–5 of Table 1 is possibly due to a preferred side-chain conformation where the face of the C(23)—C(24) π-bond that is required for epoxidation to **10** is directed toward C(16) of the D-ring, resulting in its partial steric protection. The more highly substituted allylic alcohols **13***a* and **13***b* presumably adopt a different side-chain conformation that permits *threo*-selective epoxidation to **14***a* and **14***b*. Further evidence is required, however, for a firm conclusion concerning this point.

[1]

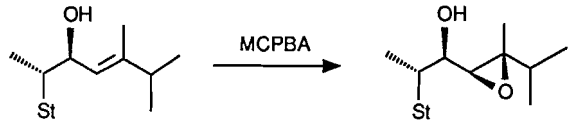

13*a* St= M
13*b* St= E

14*a* St= M (95%)
14*b* St= E (96%)

Finally, we turned our attention to the Sharpless asymmetric epoxidation method (16) employing $Ti(O\text{-}iPr)_4$ in the presence of (D)- or (L)-diethyl tartrate (D-DET or L-DET). While this technique is more commonly employed for the enantioselective epoxidation of prochiral allylic alcohols, we hoped that the tartrate-controlled asymmetric environment of the epoxide-forming transition state could override the propensity of **5** towards diastereoselective formation of the unwanted (*erythro*) isomer **11** with achiral oxidants. Entries 6 and 7 in Table 1 indicate that the use of D-DET affords a similar product distribution to MCPBA, whereas L-DET achieves the desired stereoselectivity favouring the (*threo*)

Can. J. Chem. Downloaded from www.nrcresearchpress.com by 88.255.202.194 on 09/08/12
For personal use only.

TABLE 2. Cuprate additions to (*threo*) epoxy alcohol **10**

Entry	Cuprate	Conditions[a]	Yield (%) of diol **12**[b]
1	iPr_2CuLi	THF; 4 h, 0°C	17[c]
2	$iPr_2Cu(SMe_2)Li$	THF; 4 h, 0°C	15[c]
3	iPrCu(SPh)Li	THF; 18 h, 10°C	15[c]
4	$iPr(2\text{-Th})Cu(CN)Li_2$[d]	THF; 16 h, RT	0
5	$iPr_2Cu(CN)Li_2$	THF; 4 h, 0°C	48[e]
6	$iPr_2Cu(CN)Li_2$	Et_2O; 4 h, 0°C	61[e]
7	i-PrMgCl + CuI (0.1 equiv.)	THF; 6 h, 0°C	38[e]
8	i-PrMgCl + CuI (0.1 equiv.)	Et_2O; 6 h, 0°C	35[e]
9	i-PrMgCl + CuCN (0.1 equiv.)	Et_2O; 6 h, 0°C	76[e]

[a]Reactions were generally commenced at −78°C and then warmed to the indicated temperature.
[b]Mixtures of epoxides **10** and **11** were used; unreacted **11** was recovered. The yield is based on the amount of (*threo*) epoxide **10** present at the start.
[c]Yield determined by NMR integration.
[d]Th = thienyl.
[e]Isolated yield.

isomer **10**. The latter is therefore the method of choice from among those studied.

Ring-opening of epoxides has been reported with both lower order (17) and higher order (18) cuprates, as well as by the Cu(I)-catalyzed reactions of organolithium and Grignard reagents (19). Higher order reagents of general structure $R_2Cu(CN)Li_2$ have been particularly recommended for this type of transformation (20). Previous studies with Me_2CuLi (11*a*, 21) and $Me_2Cu(CN)Li_2$ (22) indicated that 2,3-epoxy alcohols afford principally 1,3-diols instead of their 1,2-diol regioisomers. However, in the present case, we reasoned that the greater steric bulk of the isopropyl group relative to methyl in the cuprate reagent should favour attack at the less hindered epoxide carbon atom (C-24). Thus, preferential vicinal diol formation leading to the required **12** from **10** (Scheme 3) was anticipated. Our results, obtained with various cuprate reagents, are shown in Table 2. We observed that the (*threo*) epoxy alcohol **10** reacted considerably faster than its (*erythro*) isomer **11**, thus obviating the need for the difficult separation of the two diastereomers prior to the reaction of **10** with the cuprate. Instead, the mixture of **10** and **11** was employed directly, thus requiring only the more facile separation of the more polar diol **12** from the unreacted (*erythro*) epoxy alcohol **11**. The yields shown in Table 2 are based on the amount of the (*threo*) isomer present in the starting material. No attempts were made to isolate the corresponding 1,3-diol (i.e., the 22,24-diol using steroid numbering) regioisomer in the examples in Table 2, but there was no evidence to indicate that it was a major product. The reagents in entries 1–3 gave poor yields of **12** because they decomposed faster than they reacted with **10**, resulting in the recovery of both diastereomers **10** and **11**. The more stable 2-thienyl(cyano)-copper lithium (23) reagent in entry 4 failed to react at all. Improved results were obtained with $i\text{-}Pr_2Cu(CN)Li_2$, particularly when using ether as the solvent (entry 6), as recommended by Lipshutz *et al.* (20). Our best results, however, were realized with the CuCN-catalyzed Grignard reaction in entry 9, which cleanly afforded the desired product **12** in high yield. Diol **12** has been prepared by several previous routes (4*a*, 4*m*, 4*s*) and its identical spectral and physical characteristics to those reported in the literature confirm its stereochemistry.

The above protocol was then applied to the more highly elaborated allylic alcohol **8**, as illustrated in Scheme 4. Sharpless epoxidation with L-DET afforded a mixture of (*threo*) and (*erythro*) epoxy alcohols **15** and **16** in the ratio of 63:37, as determined by NMR integration, along with a small amount of recovered starting material. Treatment of the mixture of **15** and **16** with isopropylmagnesium chloride and a catalytic amount of CuCN resulted in the formation of the desired 22,23-diol **17** as the principal product, along with a smaller amount of the regioisomer **18**. The (*erythro*) epoxy alcohol **16** remained virtually unreacted and was recovered intact. Removal of the acetonide and ethylene ketal protecting groups from **17** under standard conditions afforded castasterone (**2**) with properties identical to those reported in the literature (4*c*, 4*f*, 4*k*, 4*q*). The conversion of **2** into brassinolide (**1**) was then completed by the known method of Baeyer–Villiger oxidation of the corresponding tetraacetate **19** with trifluoroperoxyacetic acid to afford predominantly the 7-oxa regioisomer **20**, followed by saponification of the lactone tetraacetate (4*c*). The preferential formation of the desired regioisomer **20** under these conditions is somewhat anomalous, as the migration of the more substituted carbon atom is generally observed in Baeyer–Villiger oxidations. It is interesting to note that, in contrast to the oxidation of **19** with trifluoroperoxyacetic acid, **2** reacted with benzeneperoxyseleninic acid (24) or its *o*-nitro derivative in aqueous THF to produce chiefly the 6-oxa regioisomer **22**, while the tetraacetate **19** failed to react appreciably with either peroxyseleninic acid under similar conditions. Several previous studies (25) of Baeyer–Villiger oxidations of 6-keto steroids have been reported and it was suggested that inductive effects of substituents at C-3, as well as at C-1 and C-2, influence the regiochemistry of these processes (25*a*). Our results indicate that the type of oxidant, as well as the nature of the steroid substituents, plays a key role in determining the regiochemical outcome. Further work is required for a clear understanding of the importance of conformational, steric, and electronic effects, and possibly of complexation between the substituents and the peracid moiety in the Baeyer–Villiger oxidations of 6-keto steroids.

The above approach thus provides a concise, efficient, and stereoselective synthesis of the castasterone and brassinol-

Can. J. Chem. Downloaded from www.nrcresearchpress.com by 88.255.202.194 on 09/08/12
For personal use only.

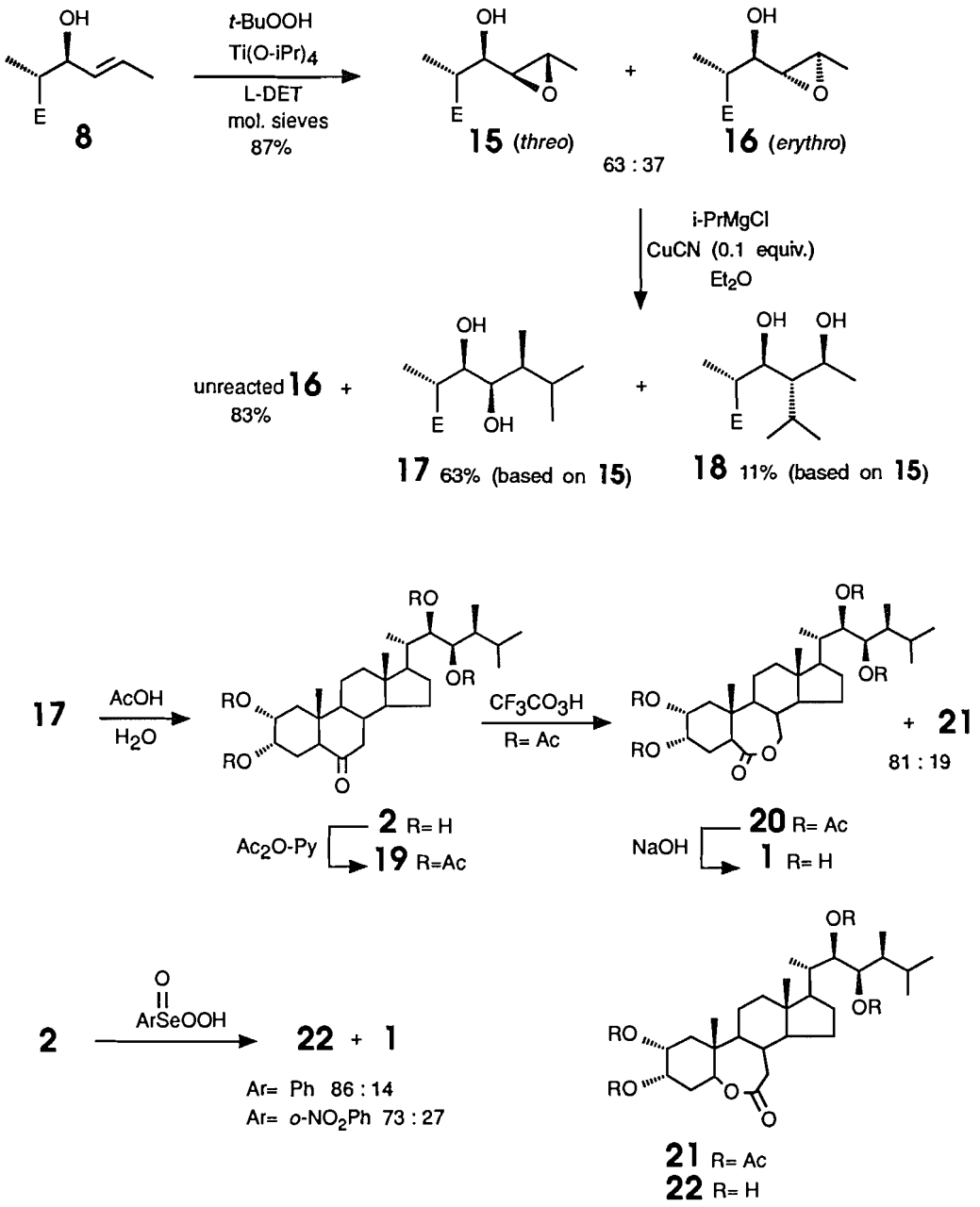

SCHEME 4

ide side chain, affording an overall yield of 22% of castasterone (**2**) from the known aldehyde **7**. Since the procedure employs readily available reagents and the required aldehyde is itself obtained from inexpensive stigmasterol (**3**), this method is one of the most practical routes to brassinosteroids **1** and **2** reported to date.

Experimental section

Melting points were obtained on an A.H. Thomas hot-stage apparatus and are uncorrected. ^1H and ^{13}C NMR spectra were acquired on a Bruker AC-E 200 or AM 400 instrument in deuteriochloroform solvent with either residual chloroform or tetramethylsilane as the internal standard, unless noted otherwise. Analytical TLC was carried out using aluminum sheets coated with 0.2 mm of silica gel and a fluorescent indicator (SG 60 F_{254}, E.M. Merck). Spots were visualized by spraying with a 2% solution of $CeSO_4$ in 12% aqueous H_2SO_4, followed by heating briefly. Flash chromatography was performed on silica gel by the method of Still *et al.* (26).

o-Nitrobenzeneseleninic acid (27), (*E*)-1-propenyllithium (7), and lithium 2-thienyl(cyano)cuprate (2-ThCu(CN)Li) (23) were prepared by literature procedures, and i-$Pr_2Cu(CN)Li_2$ was produced by the same method as employed previously for $Me_2Cu(CN)Li_2$ (20). The other cuprates in entries 1–3 in Table 2 were produced by the addition of i-PrLi (from the reaction of Li powder containing 0.5% Na with i-PrCl in petroleum ether) to CuI, CuBr·SMe_2, or CuSPh, respectively, in THF. Reagents used in the Sharpless asymmetric epoxidations were purified according to published procedures (28). Organolithium compounds were titrated with 2,5-dimethoxybenzyl alcohol (29) or diphenylacetic acid (30) as the indicator prior to use. Ether, THF, and dichloromethane were dried by distillation from CaH_2, $LiAlH_4$, and P_2O_5, respectively. All other reagents were obtained from commercial sources and purified by standard methods as required.

Can. J. Chem. Downloaded from www.nrcresearchpress.com by 88.255.202.194 on 09/08/12
For personal use only.

Can. J. Chem. Downloaded from www.nrcresearchpress.com by 88.255.202.194 on 09/08/12
For personal use only.

*(3β,5α,6β,22S,23E)-6-Methoxy-3,5-cyclo-26,27-dinorcholest-23-en-22-ol (**5**) and its (22R) isomer (**6**)*

A solution of aldehyde **4** (1.943 g, 5.639 mmol) in 12 mL of dry THF was added dropwise over 45 min to a stirred solution of (*E*)-1-propenyllithium (9.93 mL of a 0.71 M solution in ether, 7.1 mmol) at −78°C under argon and stirring was continued for an additional 4 h. The reaction was quenched at this temperature with 20% aqueous NH_4Cl solution and diluted with ether, washed with 5% aqueous $NaHCO_3$, saturated aqueous NaCl, dried ($MgSO_4$), and evaporated under vacuum. The oily residue was flash chromatographed, eluting with 10% ethyl acetate – hexanes, to afford 1.184 g (54%) of the less polar (22*S*) allylic alcohol **5** that crystallized from hexanes, mp 98–100°C (lit. (9) mp 103–104°C); R_f 0.48 (20% EtOAc–hexanes). Further elution afforded 0.464 g (21%) of the more polar (22*R*)-allylic alcohol **6** as a colourless gum; R_f 0.32 (20% EtOAc–hexanes). Both products had spectral properties in accord with those reported in the literature (9).

*(threo)-(3β,5α,6β,22R,23R,24S)-23,24-Epoxy-6-methoxy-3,5-cyclo-26,27-dinorcholestan-22-ol (**10**) and its (erythro) isomer (**11**)*

(+)-L-Diethyl tartrate (L-DET) (107 μL of a 5.00% v/v solution in CH_2Cl_2, 0.0311 mmol) was placed under an Ar atmosphere and cooled to −20°C. The following were then added in the indicated order: powdered 4 Å molecular sieves (14 mg), $Ti(OiPr)_4$ (154 μL of a 5.00% v/v solution in CH_2Cl_2, 0.0259 mmol), and *tert*-butyl hydroperoxide (61 μL of an 8.5 M solution in CH_2Cl_2, 0.52 mmol). The mixture was stirred for 1 h at −20°C, followed by the addition of a solution of the (22*S*)-allylic alcohol **5** (100.2 mg, 0.2592 mmol) in 1 mL of dry CH_2Cl_2. The reaction mixture was allowed to stand at −25°C for 6 days. Four more equivalents of *tert*-butyl hydroperoxide were added at regular intervals over the last 4 days. The reaction was quenched by the addition of 1 mL of 30% aqueous NaOH (saturated with NaCl), diluted with ether, and stirred for 10 min. Magnesium sulfate (1 g) and Celite (0.5 g) were added and the mixture was stirred for another 15 min, followed by filtration through a pad of Celite and removal of the solvent under vacuum. The residue was flash chromatographed, eluting with 30% EtOAc–hexanes, to give 99.4 mg (95%) of a mixture (single spot on TLC, 30% EtOAc–hexanes) of the epoxy alcohols **10** and **11** as a colourless gum with R_f 0.45 (30% EtOAc–hexanes) and a *threo*:*erythro* ratio of 70:30 as determined by NMR integration. The ^1H NMR signals of the (*threo*) isomer **10** in the mixture were assigned on the basis of their literature values (4*m*), while those of the (*erythro*) epoxy alcohol **11** were assigned by comparison of the spectrum of the mixture with that of a pure sample of **11** recovered from the cuprate addition reactions shown in Table 2 (*vide infra*). The *threo*:*erythro* ratio was determined by integration of the signals at δ 3.62 (m, 1 H, H-22) and δ 2.90 (dq, J = 5.2, 2.4 Hz, 1 H, H-24) from **10**, and at δ 3.87 (m, 1 H, H-22) and δ 3.13 (dq, J = 5.3, 2.2 Hz, 1 H, H-24) from **11**.

Other epoxidation methods that were studied for the conversion of **5** into **10** are summarized in Table 1.

*(3β,5α,6β,22R,23R,24S)-6-Methoxy-3,5-cycloergostane-22,23-diol (**12**)*

An ethereal solution of i-PrMgCl (0.54 mL of a 2.0 M solution, 1.1 mmol) was added to a suspension of CuCN (9.7 mg, 0.11 mmol) in 1 mL of ether at −78°C. The turbid grey mixture was stirred for 45 min at this temperature, followed by the addition of a solution of epoxy alcohols **10** and **11** (87.6 mg, 0.218 mmol; *threo*:*erythro* ratio of 52:48). The reaction mixture was stirred for 1 h at −78°C, and then at 0°C for 6 h. The reaction was quenched with 20% aqueous NH_4Cl solution, diluted with ether, the phases were separated, and the aqueous layer was extracted once with ether. The combined ether extracts were washed with 5% aqueous $NaHCO_3$, water, and aqueous NaCl, dried ($MgSO_4$), and evaporated under vacuum. The crude product was flash chromatographed, eluting with 40 → 70% ether–hexanes, to remove unreacted (*erythro*) epoxy alcohol **11** (R_f 0.70, 80% ether–hexanes), followed by 38.5 mg (76% based on the (*threo*) epoxide **10**) of the diol **12** as a colourless gum, recrystallized from chloroform–hexanes to give a white solid with mp 76–79°C (lit (4*a*) mp 70–73°C; lit. (4*s*) mp 84–90°C); R_f 0.50, (80% ether–hexanes); IR (KBr): 3545, 3462, 1246, 1067, 978, 754 cm^{-1}; ^1H and ^{13}C NMR spectra (4*m*), and low-resolution mass spectrum (4*s*) were in close agreement with those reported in the literature. Exact Mass calcd. for $C_{29}H_{50}O_3$: 446.3760; found: 446.3752.

Results with other cuprate reagents that were investigated for the conversion of **10** into **12** are summarized in Table 2.

*(2R,3S,5α,22S,23E)-6,6-Ethylenedioxy-2,3-isopropylidenedioxy-26,27-dinorcholest-23-en-22-ol (**8**) and its (22R) isomer (**9**)*

A solution of the aldehyde **7** (1.057 g, 2.367 mmol) in 15 mL of dry ether was added dropwise over 45 min to a stirred solution of (*E*)-1-propenyllithium (6.45 mL of a 0.55 M solution in ether, 3.6 mmol) at −78°C under argon, and the resulting mixture was stirred at this temperature for an additional 4 h. The reaction was quenched with 20% aqueous NH_4Cl, the phases were separated, and the aqueous layer was extracted once with ether. The combined ether extracts were washed with saturated aqueous $NaHCO_3$ and saturated aqueous NaCl, and dried ($MgSO_4$). Removal of the solvent under vacuum left a white, solid foam that was flash chromatographed, eluting with 5 → 10% acetonitrile–dichloromethane, to afford 78.4 mg (7%) of unreacted **7**, R_f 0.56 (10% acetonitrile–dichloromethane), 256.7 mg (22%) of the less polar (22*R*)-allylic alcohol **9**, R_f 0.39 (10% acetonitrile–dichloromethane), and 839.4 mg (73%) of the more polar (22*S*)-allylic alcohol **8**, R_f 0.31 (10% acetonitrile–dichloromethane).

Compound **8** was a gum with IR (film): 3482, 1669, 1217, 1057, 959, 789, 735 cm^{-1}; ^1H NMR (200 MHz) δ: 5.71–5.44 (complex m, 2 H, H-23 and H-24), 4.24 (m, 1 H), 4.16 (m, 1 H), 4.07 (m, 1 H), 3.91 (m, 3 H), 3.73 (m, 1 H), 1.71 (d, J = 5.1 Hz, 3 H, 25-Me), 1.46 (s, 3 H, acetonide), 1.31 (s, 3 H, acetonide), 0.89 (d, J = 6.0 Hz, 3 H, 21-Me), 0.82 (s, 3 H, 19-Me), 0.67 (s, 3 H, 18-Me); ^{13}C NMR (50.3 MHz) δ: 133.8 (CH), 125.2 (CH), 109.6 (C), 107.5 (C), 74.0 (CH), 72.9 (CH), 72.8 (CH), 65.4 (CH_2), 64.1 (CH_2), 55.7 (CH), 52.9 (CH), 52.4 (CH), 45.4 (CH), 42.6 (CH_2), 42.3 (C), 41.4 (CH), 40.9 (CH_2), 39.5 (CH_2), 37.9 (C), 32.9 (CH), 28.6 (CH_3), 27.6 (CH_2), 26.5 (CH_3), 24.1 (CH_2), 21.9 (CH_2), 20.7 (CH_2), 17.7 (CH_3), 13.3 (CH_3), 11.94 (CH_3), 11.85 (CH_3); mass spectrum, m/z (relative intensity): 488 (M^+, 13), 473 (34), 455 (45), 417 (35), 387 (60), 359 (45), 329 (59), 277 (58), 259 (62), 239 (57), 178 (73), 108 (87), 99 (84), 81 (100). Exact Mass calcd. for $C_{30}H_{48}O_5$: 488.3502; found: 488.3497.

Compound **9** was a gum with IR (film): 3476, 1672, 1217, 1055, 968, 787, 764, 735 cm^{-1}; ^1H NMR (200 MHz) δ: 5.67 (dq, J = 15.3, 6.2 Hz, 1 H, H-24), 5.47 (ddd, J = 15.3, 7.4, 1.2 Hz, 1 H, H-23), 4.25 (m, 1 H), 4.08 (m, 2 H), 3.91 (m, 3 H), 3.74 (m, 1 H), 1.73 (d, J = 6.3 Hz, 3 H, 25-Me), 1.46 (s, 3 H, acetonide), 1.31 (s, 3 H, acetonide), 0.94 (d, J = 6.7 Hz, 3 H, 21-Me), 0.82 (s, 3 H, 19-Me), 0.70 (s, 3 H, 18-Me); ^{13}C NMR (50.3 MHz) δ: 129.6 (CH), 128.3 (CH), 109.6 (C), 107.5 (C), 74.6 (CH), 72.9 (CH), 72.8 (CH), 65.5 (CH_2), 64.2 (CH_2), 55.4 (CH), 53.0 (CH), 52.9 (CH), 45.5 (CH), 42.7 (CH_2 + C), 41.9 (CH), 41.0 (CH_2), 39.5 (CH_2), 38.0 (C), 32.9 (CH), 28.6 (CH_3), 27.5 (CH_2), 26.5 (CH_3), 24.3 (CH_2), 21.9 (CH_2), 20.7 (CH_2), 17.9 (CH_3), 13.3 (CH_3), 12.3 (CH_3), 12.1 (CH_3); mass spectrum, m/z (relative intensity); 488 (M^+, 10), 473 (32), 455 (20), 417 (38), 387 (48), 359 (59), 329 (32), 277 (64), 259 (45), 239 (46), 178 (61), 108 (90), 99 (100), 81 (97). Exact Mass calcd. for $C_{30}H_{48}O_5$: 488.3502; found: 488.3489.

*(threo)-(2R,3S,5α,22R,23R,24S)-6,6-Ethylenedioxy-2,3-isopropylidenedioxy-23,24-epoxy-26,27-dinorcholestan-22-ol (**15**) and its (erythro) isomer (**16**)*

(+)-L-Diethyl tartrate (L-DET) (622 μL of a 5.00% v/v solution in dichloromethane, 0.182 mmol) was added to powdered 4 Å molecular sieves (200 mg) under argon at −20°C, followed by $Ti(O\text{-}iPr)_4$ (901 μL of a 5.00% v/v solution in dichloromethane, 0.151 mmol) and *tert*-butyl hydroperoxide (629 μL of a 4.81 M solution in dichloromethane, 3.03 mmol). The mixture was stirred

Can. J. Chem. Downloaded from www.nrcresearchpress.com by 88.255.202.194 on 09/08/12
For personal use only.

for 1 h at −20°C, after which a solution of the (22*S*)-allylic alcohol **8** (739.3 mg, 1.513 mmol) in 7 mL of dry dichloromethane was added and the reaction mixture was allowed to stand at −25°C for 6 days. An additional 2 equivalents of *tert*-butyl hydroperoxide were added over this period. The reaction was quenched by the addition of 1 mL of water and then stirred for 30 min as the reaction mixture warmed to room temperature. Aqueous NaOH (0.5 mL of a 30% solution) saturated with NaCl was then added and the mixture was stirred vigorously for 1 h. The phases were separated and the aqueous portion extracted twice with dichloromethane. The combined dichloromethane extracts were washed several times with water, once with saturated aqueous NaCl, and dried ($MgSO_4$). Removal of the solvent under vacuum left a white, solid foam, which was flash chromatographed, eluting with 10% acetonitrile–dichloromethane, to afford 30.3 mg (4%) of unreacted allylic alcohol **8**, as evidenced by TLC and ^{1}H NMR spectroscopy, and 663.7 mg (87%) of a mixture of the slightly more polar (*threo*) and less polar (*erythro*) epoxy alcohols **15** (R_f 0.43, 20% acetonitrile–dichloromethane) and **16** (R_f 0.48, 20% acetonitrile–dichloromethane), respectively, with the *threo*:*erythro* ratio of 63:37 as determined by NMR integration. Further chromatography afforded a purer (ca. 90%) sample of the (*threo*) isomer **15**, while a homogeneous sample of (*erythro*)-**16** was recovered from the reaction of the mixture of **15** and **16** with cuprate reagents (*vide infra*).

Compound **15** had ^{1}H NMR (200 MHz) δ: 4.27 (m, 1 H), 4.10 (m, 1 H), 3.92 (m, 3 H), 3.75 (m, 1 H), 3.66 (m, 1 H), 2.93 (dq, J = 5.2, 2.4 Hz, 1 H, H-24), 2.76 (m, 1 H, H-23), 1.48 (s, 3 H, acetonide), 1.33 (s, 3 H, acetonide), 1.33 (d, J = 5.1 Hz, 3 H, 25-Me), 1.02 (d, J = 6.1 Hz, 3 H, 21-Me), 0.84 (s, 3 H, 19-Me), 0.70 (s, 3 H, 18-Me). The *threo*:*erythro* ratio was determined by integration of the signals at δ 2.93 and δ 2.76 from **15**, and at δ 3.15 and δ 2.66 from **16**.

(2R,3S,5α,22R,23R,24S)-6,6-Ethylenedioxy-2,3-isopropylidenedioxyergostane-22,23-diol (17) and (2R,3S,5α,22R,23S,24S)-6,6-ethylenedioxy-2,3-isopropylidenedioxy-23-isopropyl-26,27-dinorcholestane-22,24-diol (18)

Isopropylmagnesium chloride (2.89 mL of a 2.0 M ether solution, 5.8 mmol) was added to a suspension of CuCN (51.7 mg, 0.578 mmol) in 1 mL of ether at −78°C. The mixture was stirred for 1 h at this temperature, followed by the addition of a solution of epoxy alcohols **15** and **16** (583.1 mg, 1.155 mmol; *threo*:*erythro* ratio of 63:37) in 10 mL of ether over 10 min. The reaction mixture was stirred for 2 h at −78°C, and then at 0°C for 3 h. The reaction was quenched with 20% aqueous NH_4Cl solution, the phases separated, and the aqueous layer extracted twice with ether. The combined ether extracts were washed with saturated aqueous $NaHCO_3$, water, and aqueous NaCl, dried ($MgSO_4$), and evaporated under vacuum. The crude product was flash chromatographed, eluting with 30 → 60% ether–hexanes, to afford 64.1 mg (11%) of a compound having ^{1}H and ^{13}C NMR spectra identical to those of the (22*S*)-allylic alcohol **8** (R_f 0.65, 80% ether–hexanes), followed by 179.3 mg (83% recovery) of the pure unreacted (*erythro*) epoxy alcohol **16** (R_f 0.48, 80% ether–hexanes), 44.2 mg (11% based on the (*threo*) epoxide **15**) of the 22,24-diol **18** (R_f 0.37, 80% ether–hexanes), and 252.3 mg (63% based on the (*threo*) epoxide **15**) of the desired 22,23-diol **17** (R_f 0.27, 80% ether–hexanes), identical in all respects to an authentic sample (4*q*).

Compound **16** was a gum with IR (film): 3470, 1217, 1086, 1055, 959, 918, 733 cm^{-1}; ^{1}H NMR (200 MHz) δ: 4.27 (m, 1 H), 4.10 (m, 1 H), 3.92 (m, 4 H), 3.75 (m, 1 H), 3.14 (dq, J = 5.3, 2.3 Hz, 1 H, 24-H), 2.65 (m, 1 H, 23-H), 1.48 (s, 3 H, acetonide), 1.34 (d, J = 5.3 Hz, 3 H, 25-Me), 1.33 (s, 3 H, acetonide), 0.96 (d, J = 6.3 Hz, 3 H, 21-Me), 0.84 (s, 3 H, 19-Me), 0.70 (s, 3 H, 18-Me); ^{13}C NMR (50.3 MHz) δ: 109.6 (C), 107.5 (C), 72.8 (CH), 72.7 (CH), 70.3 (CH), 65.4 (CH_2), 64.1 (CH_2), 61.6 (CH), 55.7 (CH), 52.8 (CH), 52.0 (CH), 51.8 (CH), 45.4 (CH), 42.6 (CH_2), 42.3 (C), 40.9 (CH_2), 39.5 (CH_2), 38.1 (CH), 37.9 (C), 32.9 (CH), 28.6 (CH_3), 27.5 (CH_2), 26.5 (CH_3), 24.0 (CH_2), 21.9 (CH_2), 20.7 (CH_2), 17.0 (CH_3), 13.3 (CH_3), 12.7 (CH_3), 11.8 (CH_3); mass spectrum, m/z (relative intensity); 504 (M^+, 11), 489 (44), 473 (15), 460 (12), 445 (39), 431 (52), 359 (19), 293 (69), 249 (71), 239 (44), 235 (80), 99 (89), 43 (100). Exact Mass calcd. for $C_{30}H_{48}O_6$: 504.3451; found: 504.3440.

Compound **18** was a gum with IR (film): 3461, 1217, 1086, 1055, 756, 735 cm^{-1}; ^{1}H NMR (200 MHz) δ: 4.27 (m, 1 H), 4.10 (m, 1 H), 3.94 (m, 5 H), 3.75 (m, 1 H), 1.48 (s, 3 H, acetonide), 1.33 (s, 3 H, acetonide), 1.27 (d, J = 6.8 Hz, 3 H, 25-Me), 0.95 (d, J = 6.0 Hz, 3 H, 21-Me), 0.90 (d, J = 6.9 Hz, 6 H, isopropyl CH_3 groups), 0.84 (s, 3 H, 19-Me), 0.69 (s, 3 H, 18-H); ^{13}C NMR (50.3 MHz) δ: 109.7 (C), 107.5 (C), 73.4 (CH), 72.9 (CH), 72.8 (CH), 67.4 (CH), 65.5 (CH_2), 64.1 (CH_2), 55.9 (CH), 53.0 (CH), 52.6 (CH), 51.4 (CH), 45.5 (CH), 42.7 (CH_2), 42.4 (C), 41.0 (CH_2), 39.7 (CH_2), 39.2 (CH), 38.0 (C), 33.0 (CH), 28.6 (CH_3), 27.8 (CH), 27.7 (CH_2), 26.5 (CH_3), 25.7 (CH_3), 24.1 (CH_2), 22.0 (CH_2), 20.8 (CH_2), 20.3 (CH_3), 18.1 (CH_3), 13.4 (CH_3), 11.9 (CH_3); mass spectrum, m/z (relative intensity): 548 (M^+, 5), 533 (32), 515 (5.5), 486 (6), 471 (9), 446 (19), 431 (53), 418 (43), 389 (31), 360 (100), 337 (33), 235 (85), 131 (47), 99 (84), 43 (81). Exact Mass calcd. for $C_{33}H_{56}O_6$: 548.4077; found: 548.4101.

Castasterone (2) and brassinolide (1)

The 22,23-diol **17** (201.8 mg, 0.3677 mmol) was hydrolyzed as described previously (4*q*) to afford 150.7 mg (88%) of castasterone (**2**) (R_f 0.43, 10% ethanol–chloroform), mp 248–250°C (from ethyl acetate) (lit. (4*c*) mp 250–252°C; lit (4*q*) mp 248–252°C), identical in all respects to an authentic sample (4*q*).

Acetylation of **2** to the tetraacetate **19** (98%) and oxidation with trifluoroperoxyacetic acid was effected by a literature method (4*d*) to afford an 81% yield of a mixture of 7-oxalactone **20** and 6-oxalactone **21**, obtained in the ratio of 81:19, as determined by NMR integration. Pure **20** was isolated by flash chromatography, eluting with 20 → 30% ethyl acetate – hexanes, and had properties in close agreement with the literature (4*d*). Lactone **21** contained some **20** even after chromatography, but its presence in the mixture was inferred from the ^{1}H NMR signal of its 5α-proton at δ 4.47 (dd, J = 10.9, 5.9 Hz), compared with that of **20** at δ 2.99 (dd, J = 12.3, 4.6 Hz).

Saponification of **20** was achieved with NaOH in methanol water (4*d*), to afford pure brassinolide after flash chromatography and recrystallization from methanol, mp 273–276°C (lit. (1) mp 274–275°C), with spectral properties in accordance with those reported in the literature (1, 4*a*, 4*c*, 4*d*).

Oxidation of castasterone (2) with peroxyseleninic acids

Hydrogen peroxide (37 μL of 30%, 0.36 mmol) was added to a solution of benzeneseleninic acid (4.3 mg, 23 μmol) in 1 mL of THF and 0.5 mL of water at room temperature. A solution of castasterone (**2**) (8.4 mg, 18 μmol) in 2 mL of THF and 0.5 mL of water was then added and the mixture was stirred for 48 h, followed by heating at 75°C for 18 h. An additional 20 equivalents of hydrogen peroxide were added during this time. The reaction mixture was diluted with ether, washed with saturated aqueous $NaHCO_3$, and dried ($MgSO_4$). Removal of the solvent under vacuum gave a residue containing the 7-oxa- and 6-oxalactones **1** and **22** in the ratio of 14:86, as well as some unreacted **2**. The 7-oxa:6-oxa ratio was determined by integration of the ^{1}H NMR signals due to the 5α-protons at δ 3.13 (dd, J = 12.2, 4.5 Hz) from **1**, and at δ 4.61 (dd, J = 11.1, 5.6 Hz) from **22**.

When the above reaction was repeated using *o*-nitrobenzeneseleninic acid in place of benzeneseleninic acid, the ratio of **1**:**22** was 27:73.

Acknowledgement

We thank the Natural Sciences and Engineering Research Council of Canada for financial support.

1. M. D. Grove, G. F. Spencer, W. K. Rohwedder, N. Mandava, J. F. Worley, J. D. Warthen Jr., G. L. Steffens, J. L. Flippen-Anderson, and J. C. Cook, Jr. Nature (London), **281**, 216 (1979).

Can. J. Chem. Downloaded from www.nrcresearchpress.com by 88.255.202.194 on 09/08/12
For personal use only.

2. (*a*) S. C. Chen. Chem. Canada, **35**, 13 (8) (1983); (*b*) H. Singh and T. R. Bhardwaj. Indian J. Chem. Sect. B: **25B**, 989 (1986); (*c*) G. Adam and V. Marquardt. Phytochemistry, **25**, 1787 (1986); (*d*) N. B. Mandava. Annu. Rev. Plant Physiol. Plant Mol. Biol. **39**, 23 (1988); (*e*) V. A. Khripach. Pure Appl. Chem. **62**, 1319 (1990).
3. H. G. Cutler, T. Yokota, and G. Adam (*Editors*). Brassinosteroids: chemistry, bioactivity and applications. American Chemical Society, Washington, D.C. 1991: (*a*) N. Ikekawa and Y. J. Zhao. Chap. 24; (*b*) V. A. Khripach, V. N. Zhabinskii, and R. P. Litvinovskaya. Chap. 5; (*c*) K. Richter and J. Koolman. Chap. 23; (*d*) O. N. Kulaeva, E. A. Burkhanova, A. B. Fedina, V. A. Khokhlova, G. A. Bokebayeva, H. M. Vorbrodt, and G. Adam. Chap. 12; (*e*) G. Schilling, C. Schiller, and S. Otto. Chap. 18; (*f*) R. He, G. Wang, and X. Wang. Chap. 19.
4. (*a*) S. Fung and J. B. Siddall. J. Am. Chem. Soc. **102**, 6580 (1980); (*b*) M. Ishiguro, S. Takatsuto, M. Morisaki, and N. Ikekawa. J. Chem. Soc. Chem. Commun. 962 (1980); (*c*) S. Takatsuto, N. Yazawa, M. Ishiguro, M. Morisaki, and N. Ikekawa. J. Chem. Soc. Perkin Trans. 1, 139 (1984); (*d*) K. Mori, M. Sakakibara, Y. Ichikawa, H. Ueda, K. Okada, T. Umemura, G. Yabuta, S. Kuwahara, M. Kondo, M. Minobe, and A. Sogabe. Tetrahedron, **38**, 2099 (1982); (*e*) M. Sakakibara, K. Okada, Y. Ichikawa, and K. Mori. Heterocycles, **17**, 301 (1982); (*f*) K. Mori, M. Sakakibara, and K. Okada. Tetrahedron, **40**, 1767 (1984); (*g*) M. Sakakibara and K. Mori. Agric. Biol. Chem. **47**, 663 (1983); (*h*) M. J. Thompson, N. B. Mandava, W. J. Meudt, W. R. Lusby, and D. W. Spaulding. Steroids, **38**, 567 (1981); (*i*) J. R. Donaubauer, A. M. Greaves, and T. C. McMorris. J. Org. Chem. **49**, 2833 (1984); (*j*) T. Kametani, T. Katoh, M. Tsubuki, and T. Honda. J. Am. Chem. Soc. **108**, 7055 (1986); (*k*) T. Kametani, T. Katoh, J. Fujio, I. Nogiwa, M. Tsubuki, and T. Honda. J. Org. Chem. **53**, 1982 (1988); (*l*) T. Kametani, M. Kigawa, M. Tsubuki, and T. Honda. J. Chem. Soc. Perkin Trans. 1, 1503 (1988); (*m*) H. Hayami, M. Sato, S. Kanemoto, Y. Morizawa, K. Oshima, and H. Nozaki. J. Am. Chem. Soc. **105**, 4491 (1983); (*n*) V. A. Khripach, V. N. Zhabinskiy, and V. K. Olkhovick. Tetrahedron Lett. **31**, 4937 (1990); (*o*) M. Anastasia, P. Allevi, P. Ciuffreda, A. Fiecchi, and A. Scala. J. Org. Chem. **49**, 4297 (1984); (*p*) M. Anastasia, P. Ciuffreda, and A. Fiecchi. J. Chem. Soc. Perkin Trans. 1, 379 (1983); (*q*) T. G. Back and M. V. Krishna. J. Org. Chem. **56**, 454 (1991); (*r*) T. G. Back, K. Brunner, M. V. Krishna, and E. K. Y. Lai. Can. J. Chem. **67**, 1032 (1989); (*s*) M. Aburatani, T. Takeuchi, and K. Mori. Agric. Biol. Chem. **50**, 3043 (1986); (*t*) Agric. Biol. Chem. **51**, 1909 (1987); (*u*) Z. Wei-Shan, B. Jiang, and X. Pan. J. Chem. Soc. Chem. Commun. 612 (1989); (*v*) S. Zheng-Wu and Z. Wei-Shan. J. Chem. Soc. Perkin Trans. 1, 1765 (1990); (*w*) W.-S. Zhou, B. Jiang, and X. Pan. Tetrahedron, **46**, 3173 (1990); (*x*) W.-S. Zhou, L.-F. Huang, L.-Q. Sun, and X.-F. Pan. Tetrahedron Lett. **32**, 6745 (1991); (*y*) W.-S. Zhou and Z.-W. Shen. J. Chem. Soc. Perkin Trans. 1, 2827 (1991); (*z*) W.-S. Zhou and L.-F. Huang. Tetrahedron, **48**, 1837 (1992); (*aa*) T. Kametani, K. Keino, M. Kigawa, M. Tsubuki, and T. Honda. Tetrahedron Lett. **30**, 3141 (1989); (*ab*) T. Takahashi, A. Ootake, H. Yamada, and J. Tsuji. Tetrahedron Lett. **26**, 69 (1985).
5. (*a*) J. A. Steele and E. Mosettig. J. Org. Chem. **28**, 571 (1963); (*b*) J. J. Pappas, W. P. Keaveney, E. Gancher, and M. Berger. Tetrahedron Lett. 4273 (1966); (*c*) R. F. N. Hutchins, M. J. Thompson, and J. A. Svoboda. Steroids, **15**, 113 (1970); (*d*) W. G. Salmond and M. C. Sobala. Tetrahedron Lett. 1695 (1977).
6. T. G. Back, P. G. Blazecka, and M. V. Krishna. Tetrahedron Lett. **32**, 4817 (1991).
7. (*a*) G. M. Whitesides, C. P. Casey, and J. K. Krieger. J. Am. Chem. Soc. **93**, 1379 (1971); (*b*) G. Linstrumelle, J. K. Krieger, and G. M. Whitesides. Org. Synth. **55**, 103 (1976).
8. (*a*) D. J. Cram and F. A. A. Elhafez. J. Am. Chem. Soc. **74**, 5828 (1952); (*b*) E. P. Lodge and C. H. Heathcock. J. Am. Chem. Soc. **109**, 3353 (1987); (*c*) Y. Yamamoto, H. Abe, S. Nishii, and J. Yamada. J. Chem. Soc. Perkin Trans. 1, 3253 (1991).
9. Y. Hirano and C. Djerassi. J. Org. Chem. **47**, 2420 (1982).
10. N. N. Schwartz and J. H. Blumbergs. J. Org. Chem. **29**, 1976 (1964).
11. (*a*) M. R. Johnson, T. Nakata, and Y. Kishi. Tetrahedron Lett. 4343 (1979); (*b*) M. R. Johnson and Y. Kishi. Tetrahedron Lett. 4347 (1979).
12. (*a*) E. D. Mihelich. Tetrahedron Lett. 4729 (1979); (*b*) B. E. Rossiter, T. R. Verhoeven, and K. B. Sharpless. Tetrahedron Lett. 4733 (1979).
13. (*a*) H. J. Reich, F. Chow, S. L. Peake. Synthesis, 299 (1978); (*b*) P. A. Grieco, Y. Yokoyama, S. Gilman, and M. Nishizawa. J. Org. Chem. **42**, 2034 (1977); (*c*) T. Kametani, H. Nemoto, and K. Fukumoto. Heterocycles, **6**, 1365 (1977); (*d*) T. Hori and K. B. Sharpless. J. Org. Chem. **43**, 1689 (1978).
14. M. S. Cooper, H. Heaney, A. J. Newbold, and W. R. Sanderson. Synlett. 533 (1990).
15. K. B. Sharpless and T. R. Verhoeven. Aldrichimica Acta, **12**, 63 (1979).
16. (*a*) T. Katsuki and K. B. Sharpless. J. Am. Chem. Soc. **102**, 5974 (1980); (*b*) M. G. Finn and K. B. Sharpless. *In* Asymmetric synthesis. Vol. 5. *Edited by* J. D. Morrison. Academic Press, New York. 1985. Chap. 8; (*c*) B. E. Rossiter. *In* Asymmetric synthesis. Vol. 5. *Edited by* J. D. Morrison. Academic Press, New York. 1985. Chap. 7. (*d*) A. Pfenninger. Synthesis, 89 (1986).
17. G. H. Posner. Org. React. **22**, 253 (1975).
18. B. H. Lipshutz, R. S. Wilhelm, and J. A. Kozlowski. Tetrahedron, **40**, 5005 (1984).
19. E. Erdik. Tetrahedron, **40**, 641 (1984).
20. B. H. Lipshutz, R. S. Wilhelm, J. A. Kozlowski, and D. Parker. J. Org. Chem. **49**, 3928 (1984).
21. W. R. Roush, M. A. Adam, and S. M. Peseckis. Tetrahedron Lett. **24**, 1377 (1983).
22. A. B. Smith III, B. A. Salvatore, K. G. Hull, and J. J.-W. Duan. Tetrahedron Lett. **32**, 4859 (1991).
23. B. H. Lipshutz, M. Koerner, and D. A. Parker. Tetrahedron Lett. **28**, 945 (1987).
24. P. A. Grieco, Y. Yokoyama, S. Gilman, and Y. Ohfune. J. Chem. Soc. Chem. Commun. 870 (1977).
25. (*a*) S. Takatsuto and N. Ikekawa. Tetrahedron Lett. **24**, 917 (1983); (*b*) M. S. Ahmad, G. Moinuddin, and I. A. Khan. J. Org. Chem. **43**, 163 (1978); (*c*) R. C. Cookson, R. P. Gandhi, and R. M. Southam. J. Chem. Soc. (C), 2494 (1968).
26. W. C. Still, M. Kahn, and A. Mitra. J. Org. Chem. **43**, 2923 (1978).
27. O. Behaghel and H. Seibert. Chem. Ber. **66B**, 708 (1933).
28. Y. Gao, R. M. Hanson, J. M. Klunder, S. Y. Ko, H. Masamune, and K. B. Sharpless. J. Am. Chem. Soc. **109**, 5765 (1987).
29. M. R. Winkle, J. M. Lansinger, and R. C. Ronald. J. Chem. Soc. Chem. Commun. 87 (1980).
30. W. G. Kofron and L. M. Baclawski. J. Org. Chem. **41**, 1879 (1976).

Synthesis and basicity of 2-*N*-quinolyl- and 2-*N*-isoquinolyl-1,1,3,3-tetramethylguanidines

NASER FOROUGHIFAR[1], KENNETH T. LEFFEK, AND YONG GU LEE[2]
Department of Chemistry, Dalhousie University, Halifax, N. S., Canada B3H 4J3

Received September 18, 1992

NASER FOROUGHIFAR, KENNETH T. LEFFEK, and YONG GU LEE. Can. J. Chem. **71**, 164 (1993).

A series of 2-*N*-quinolyl- and 2-*N*-isoquinolyl-substituted 1,1,3,3-tetramethylguanidines has been synthesized and the pK_a of each has been measured in acetonitrile and water solvents, together with the pK_a of the corresponding aminoquinoline or aminoisoquinoline. The pK_a values in acetonitrile and water fall on the same correlation line as previously determined for 2-*N*-pyridylguanidines and aminopyridines. Replacement substituent constants (σ_a) are reported for several quinolyl and isoquinolyl groups in the two solvents.

NASER FOROUGHIFAR, KENNETH T. LEFFEK et YONG GU LEE. Can. J. Chem. **71**, 164 (1993).

On a synthétisé une série de 1,1,3,3-tétraméthylguanidines substituées par des groupes 2-*N*-quinoléyle et 2-*N*-isoquinoléyle et on a déterminé le pK_a de chacun de ces produits, ainsi que ceux des aminoquinoléines et aminoisoquinoléines correspondantes, dans l'acétonitrile et dans l'eau. Les valeurs des pK_a dans l'acétonitrile et dans l'eau tombent sur la même ligne de corrélation que celle établie antérieurement pour les 2-*N*-pyridylguanidines et pour les aminopyridines. On rapporte les constantes de remplacement des substituants (σ_a) de plusieurs groupes quinoléyles et isoquinoléyles dans les deux solvants.

[Traduit par la rédaction]

Introduction

This work continues the study of the basicity of 2-*N*-substituted 1,1,3,3-tetramethylguanidines (TMG) in water and acetonitrile solvents (1, 2). A series of 2-*N*-quinolyl (**1**) and isoquinolyl (**2**) derivatives have been prepared from the analogous aminoquinoline compounds and their pK_a's determined, together with those of the starting materials. Some quinoline compounds with N-containing basic substituents have been found to be physiologically active as hypertensive agents (3, 4) or antimalarial drugs (5–7), and it is possible that some of the new TMG compounds may show such activity.

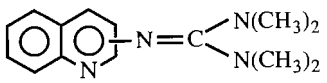

1

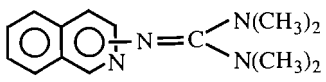

2

The pK_a's of these aminoquinolines and quinolyl TMG's allow a further refinement of the relationship between the basicity in acetonitrile and that in water. They also allow the evaluation of the replacement substituent constants for the quinolyl groups.

Results and discussion

The pK_a values of the conjugate acids of the bases in acetonitrile and water solvents are collated in Table 1. All of the bases are stronger in acetonitrile than in water, as previously observed, reflecting the weaker proton-accepting power of acetonitrile relative to water (2, 10). The solvent effect on the pK_a is consistent with that previously reported (2) and if the 13 compounds in Table 1 are combined with those measured previously, the relationship expressed by eq. [1] is obtained for a total of 51 TMG, pyridine, and quinoline bases, which has the same values for the slope and intercept as previously calculated (2) for 38 of these bases.

$$[1] \quad pK_a^{AN} = (1.11 \pm 0.02)\, pK_a^{W} + 7.0 \pm 0.2$$

This equation, which has a correlation coefficient (c.c.) of 0.986, provides a reliable means of calculating the pK_a of such bases in acetonitrile from that in water with a standard deviation of less than 0.5 pK_a units for a strong base. Within this limit, the pK_a change with solvent for these classes of base is independent of the structure of the base and depends only on the properties of the solvents.

In the series of aminoquinolines, in which the ring nitrogen atom is protonated (11), the strongest base is the 4-amino-2-methylquinoline when the amino group is *para* to the ring N atom, followed by the 1-aminoisoquinoline when the amino group is *ortho* to the ring N atom. These structures allow through-resonance in the protonated molecule between the positively charged ring nitrogen and the amino group, giving these structures an enhanced stability, i.e., increasing the base strength of the amine. Of the remaining structures, only the 5-aminoquinoline allows through-resonance but this compound shows no enhanced basicity over that of the amino group in any other position on the quinoline or isoquinoline ring. A minimum basicity occurs in the 8-aminoquinoline. In contrast to this, in the TMG series in which the 2-*N* atom of the TMG group is protonated, the 2(8′-quinolyl) TMG is the strongest base, indicating the probable involvement of both the TMG N atoms and the ring N atom in the binding of the proton. Protonated TMG bases have the positive charge considerably delocalized over all three N atoms (12) and it is probable that in the protonated 2-(8′-quinolyl) TMG the ring N atom is close enough to the proton that it too is weakly bonded to the proton. The other quinolyl TMG compounds all give approximately the same pK_a. Involvement of the ring N atom and the TMG N atoms in the proton binding may also account for the greater basicity of 2-(1′-isoquinolyl) TMG relative to that of 2-(5′-isoquinolyl) TMG.

Using the Hammett correlations previously determined (2)

[1]Visiting Scientist (1991–1992) from Arak University, Arak, Iran.

[2]Postdoctoral Fellow (1991–1992).

Can. J. Chem. Downloaded from www.nrcresearchpress.com by 88.255.202.194 on 09/08/12
For personal use only.

TABLE 1. pK_a values for derivatives of TMG and quinoline bases in acetonitrile and water solvents

No.	Compound	pK_a^{AN}	pK_a^{W}
1.	3-Aminoquinoline	12.58 ± 0.04	4.86[a]
2.	2-methyl-4-Aminoquinoline	17.98 ± 0.11	9.78 ± 0.15
3.	5-Aminoquinoline	13.04 ± 0.03	5.46[a]
4.	6-Aminoquinoline	13.35 ± 0.14	5.63[a]
5.	8-Aminoquinoline	11.14 ± 0.01	3.99[a]
6.	1-Aminoisoquinoline	15.10 ± 0.06	7.62[a]
7.	5-Aminoisoquinoline	13.21 ± 0.04	5.59[b]
8.	2(3′-Quinolyl) TMG	18.57 ± 0.12	10.32 ± 0.06
9.	2(2′-Methyl-4′-quinolyl) TMG	18.93 ± 0.12	10.45 ± 0.22
10.	2(5′-Quinolyl) TMG	18.69 ± 0.12	10.90 ± 0.04
11.	2(6′-Quinolyl) TMG	18.68 ± 0.15	11.22 ± 0.02
12.	2(8′-Quinolyl) TMG	20.46 ± 0.15	11.74 ± 0.03
13.	2(1′-Isoquinolyl) TMG	—[c]	12.03 ± 0.04
14.	2(5′-Isoquinolyl) TMG	17.68 ± 0.19	10.83 ± 0.07

[a]From ref. 8.
[b]From ref. 9.
[c]Picrate insufficiently soluble in acetonitrile.

TABLE 2. Replacement substituent constants for quinolyl groups in water and acetonitrile solvents

Group	σ_a^{W}	σ_a^{AN}
3-Quinolyl	0.72	0.92
5-Quinolyl	0.37	0.87
6-Quinolyl	0.17	0.87
8-Quinolyl	−0.15	0.10
1-Isoquinolyl	−0.32	—
5-Isoquinolyl	0.41	1.31

for the conjugate acids of 2-*N*-substituted TMG compounds, eqs. [2] (c.c. 0.989) and [3] (c.c. 0.987), a σ_a value may be calculated, i.e., a σ value that the aryl group would show if the group replaces a phenyl group in a molecule (13),

$$[2] \quad pK_a^{AN} = -(2.31 \pm 0.14)\sigma + 20.7 \pm 0.1$$

$$[3] \quad pK_a^{W} = -(1.64 \pm 0.11)\sigma + 11.5 \pm 0.1$$

for each of the aryl groups attached to the TMG. Values of σ_a^{AN} and σ_a^{W} (relative to the phenyl group), calculated from eqs. [2] and [3] respectively, for the quinolyl and isoquinolyl groups are shown in Table 2. A value of $\sigma_a = 0.23$ has been reported (14) for the 6-quinolyl group in water, which is not significantly different from our value of 0.17, given that the standard deviations of the parameters in Table 2 are of the order of ±0.2. In water, the only groups with negative σ_a values (base strengthening) are the 8-quinolyl and 1-isoquinolyl groups where the ring N atom and the TMG N atoms may both be involved with proton binding.

There is a clear solvent effect on σ_a between water and acetonitrile, as is required by eqs. [1], [2], and [3]. Combination of these three equations leads to eq. [4]. Since pK_a^{W} is greater than 10 for all the quinolyl groups in Table 2, σ_a^{AN}

$$[4] \quad \sigma_a^{AN} = \sigma_a^{W} + 0.14\,pK_a^{W} - 1.22$$

should always be greater than σ_a^{W} by more than 0.2 units. Table 2 indicates a solvent effect on σ_a much larger than this but the standard deviation of the σ_a of about ±0.2 precludes a quantitative estimate of the solvent effect. Equation [4] provides a means to smooth the data and yields ($\sigma_a^{AN} - \sigma_a^{W}$) values of 0.2–0.4. The only other example in the literature of a solvent effect on σ_a is for the 2-pyridyl group (15), which showed a change of 0.17 between 56% acetone and 60% DMSO, while the 3-pyridyl and 4-pyridyl groups showed an insignificant change between these solvents.

Experimental

Substituted 2-quinolyl- and 2-isoquinolyl-1,1,3,3-tetramethylguanidines were synthesized using a modification of the procedure of Bredereck, as previously described (16). The aminoquinolines were commercially available (Aldrich) and were dried and purified as necessary.

The picrates of the bases were made by reaction with an equimolar amount of picric acid in 95% ethanol (1, 2), followed by recrystallization from ethanol. The melting points are uncorrected. The ^1H and ^{13}C nmr spectra were run in chloroform-*d* (except where noted) with TMS as the internal standard, using either a Bruker AC 250F or a Nicolet 360 nmr spectrometer, at the Atlantic Resonance Centre, Dalhousie University. The mass spectra were recorded on a modified Du Pont CEC model 21–104 mass spectrometer at 70 eV. The ^{13}C nmr signals are reported in the sequence shown on structures **3** and **4** for the quinoline and isoquinoline compounds, respectively, followed (in one structure) by the ring-substituted methyl group.

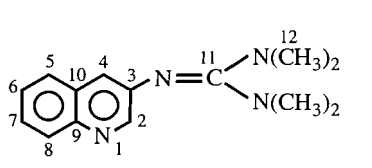

3 **4**

2(3′-Quinolyl)-1,1,3,3-tetramethylguanidine

Yield 65%; mp 43–45°C; ^1H nmr δ: 8.84 (1H, s), 7.99 (1H, d, 8.0 Hz), 7.60 (1H, d, 8.0 Hz), 7.42 (1H, d, 8.0 Hz), 7.39 (1H, d, 8.0 Hz), 7.25 (1H, s), 2.62 (12H, s); ^{13}C nmr δ: 148.4, 145.2, 128.9, 126.1, 125.6, 126.3, 128.6, 149.9, 129.2, 160.8, 39.5; mass spec. (rel. int., %): 242(72), 227(17), 198(100), 183(45), 142(15), 128(22). Picrate: mp 135–136°C; ^1H nmr N^+H δ: 11.32 (1H, bs).

Can. J. Chem. Downloaded from www.nrcresearchpress.com by 88.255.202.194 on 09/08/12
For personal use only.

2(2'-Methyl-4'-quinolyl)-1,1,3,3-tetramethylguanidine

Yield 55%; bp 175–180°C/0.3 Torr (1 Torr = 133.3 Pa); ^{1}H nmr δ: 8.03 (1H, d, 8.0 Hz), 7.9 (1H, d, 8.0 Hz), 7.30 (1H, t, 8.0 Hz) 7.53 (1H, t, 8.0 Hz), 6.28 (1H, s), 2.65 (12H, s), 2.53 (3H, s); ^{13}C nmr δ: 158.7, 127.4, 158.6, 128.5, 128.1, 128.8, 148.7, 156.3, 127.8, 160.8, 39.4, 25.4; mass spec. (rel. int., %): 256(21), 255(100), 212(14), 197(20), 168(28), 142(28). Picrate: mp 163–164°C; ^{1}H nmr N^+H (in pyridine-d_5) δ: 13.46 (1H, bs).

2(5'-Quinolyl)-1,1,3,3-tetramethylguanidine

Yield 55%; mp 175–180°C; ^{1}H nmr δ: 8.82 (1H, dd, 4.0, 1.5 Hz), 8.47 (1H, d, 8.0 Hz), 7.6(1H, d, 8.0 Hz), 7.45 (1H, dd, 8.0, 1.5 Hz), 7.3 (1H, m), 6.61 (1H, d, 8.0 Hz), 2.75 (12H, s); ^{13}C nmr δ: 149.6, 115.2, 132.8, 149.1, 119.1, 120.3, 129.5, 148.8, 123.6, 160.1, 39.3; mass spec. (rel. int., %): 242(100), 198(14), 183(16), 154(22), 128(19). Picrate: mp 171–172°C; ^{1}H nmr N^+H δ: 9.97 (1H, bs).

2-(6'-Quinolyl)-1,1,3,3-tetramethylguanidine

Yield 60%; mp 62–63°C; ^{1}H nmr δ: 8.66 (1H, dd, 4.0, 1.5 Hz), 7.96 (1H, d, 8.0 Hz), 7.94 (1H, d, 8.0 Hz), 7.22 (2H, m), 7.15 (1H, d, 1.5 Hz), 2.66 (12H, s); ^{13}C nmr δ: 146.7, 115.3, 134.4, 120.5, 150.1, 127.1, 129.2, 143.9, 129.9, 160.2, 39.4; mass spec. (rel. int., %): 242(79), 227(19), 198(100), 183(49), 142(18), 128(11). Picrate mp 197–198°C; ^{1}H nmr N^+H δ: 10.70(1H, bs).

2-(8'-Quinolyl)-1,1,3,3-tetramethylguanidine

Yield 53%; bp 170–175°C/0.3 Torr; ^{1}H nmr δ: 8.85 (1H, dd, 4.0, 1.5 Hz), 8.06 (1H, dd, 8.0, 1.5 Hz), 7.29 (1H, t, 8.0 Hz), 7.26 (2H, m), 6.86 (1H, d, 8.0 Hz), 2.72 (12H, s); ^{13}C nmr δ: 147.9, 118.3, 135.3, 126.5, 120.1, 118.1, 149.7, 142.3, 128.8, 160.9, 39.0; mass spec. (rel. int., %): 242(100), 198(89), 154(6), 142(20), 128(16). Picrate mp 153–154°C; ^{1}H nmr N^+H δ: 10.38 (1H, bs).

2-(1'-Isoquinolyl)-1,1,3,3-tetramethylguanidine

Yield 55%; bp 175–180°C/0.3 Torr; ^{1}H nmr δ: 8.34 (1H, d, 3.0 Hz), 8.01 (1H, d, 1.0 Hz), 7.52 (3H, m), 7.00 (1H, d, 1.0 Hz), 2.78 (12H, s); ^{13}C nmr δ: 152.2, 141.7, 117.1, 147.9, 118.8, 119.3, 127.7, 131.3, 129.8, 160.6, 39.6; mass spec. (rel. int., %): 242(79), 227(12), 198(50), 155(29), 143(28), 128(100). Picrate mp 170–172°C; ^{1}H nmr N^+H δ: 9.20 (1H, bs).

2-(5'-Isoquinolyl)-1,1,3,3-tetramethylguanidine

Yield 65%; bp 170–175°C/0.3 Torr; ^{1}H nmr δ: 9.12 (1H, d, 2.5 Hz), 8.40 (1H, d, 2.5 Hz), 7.83 (1H, d, 2.5 Hz), 7.4 (2H, m), 6.79 (1H, t, 2.5 Hz); ^{13}C nmr δ: 152.5, 141.7, 117.1, 147.9, 118.8, 19.3, 127.7, 131.3, 129.8, 160.6, 39.6; mass spec. (rel. int., %): 242(100), 227(20), 198(82), 183(33), 155(31), 142(11). Picrate mp 185–186°C; ^{1}H nmr N^+H δ: 9.90 (1H, bs).

Acetonitrile was purified by the method of O'Donnell *et al.* (17), followed by fractional distillation from P_2O_5 and calcium hydride. Tetraethylammonium perchlorate was recrystallized from benzene and dried in a vacuum oven at 60°C.

The pK_a measurements were carried out as previously described in acetonitrile and water (1, 2).

1. K. T. Leffek, P. Pruszynski, and K. Thanapaalasingham. Can. J. Chem. **67**, 590 (1989).
2. N. Foroughifar, K. T. Leffek, and Y. G. Lee. Can. J. Chem. **70**, 2856 (1992).
3. F. F. Ebetino and G. C. Wright. French Pat. 1 388 756 (1965).
4. A. Winterstein. U.S. Pat. 3 272 806 (1966).
5. A. R. Surrey and H. F. Hammer. J. Am. Chem. Soc. **68**, 113 (1946).
6. E. A. Stock, L. L. Hallock, and A. J. Holland. J. Am. Chem. Soc. **68**, 380 (1946).
7. A. R. Surrey and H. F. Hammer. J. Am. Chem. Soc. **72**, 1814 (1950).
8. A. Albert, R. J. Goldace, and J. N. Phillips. J. Chem. Soc. 2240 (1948).
9. A. Albert. *In* Heterocyclic chemistry. Athlone Press, London. 1968. p. 438.
10. J. F. Coetzee and G. R. Padmanabhan. J. Am. Chem. Soc. **87**, 5005 (1965).
11. D. D. Perrin, B. Dempsey, and E. P. Serjeant. pK_a prediction for organic acids and bases. Chapman and Hall, London. 1981. p. 54.
12. P. Pruszynski, K. T. Leffek, B. Borecka, and T. S. Cameron. Acta Crystallogr. Sect. C: Cryst. Struct. Commun. **C48**, 1638 (1992).
13. O. Exner. Correlation analysis in chemistry. *Edited by* N. B. Chapman and J. Shorter. Plenum Press, New York. 1978. p. 445.
14. H. H. Jaffe and H. L. Jones. Adv. Heterocycl. Chem. **3**, 209 (1964).
15. L. W. Deady and R. A. Shanks. Aust. J. Chem. **25**, 2363 (1972).
16. H. Bredereck and K. Bredereck. Chem. Ber. **94**, 2278 (1961).
17. J. F. O'Donnell, J. T. Ayres, and C. K. Mann. Anal. Chem. **37**, 1161 (1965).

Can. J. Chem. Downloaded from www.nrcresearchpress.com by 88.255.202.194 on 09/08/12
For personal use only.

Influence of the acidity on the kinetics of diphenylamine oxidation by peroxodisulfate anions

M. BALÓN,[1] P. GUARDADO, C. CARMONA, J. HIDALGO, AND M. A. MUÑOZ

Departamento de Química Física, Facultad de Farmacia, Universidad de Sevilla, 41012 Sevilla, Spain

Received June 9, 1992

M. BALÓN, P. GUARDADO, C. CARMONA, J. HIDALGO, and M. A. MUÑOZ. Can. J. Chem. **71**, 167 (1993).

A kinetic study is reported on the oxidation of diphenylamine (DPA) by peroxodisulfate (PDS) anions in H_2SO_4 and buffered acetic acid – acetate 20% v/v methanol–water media. The primary detectable product of the reaction is *N*-phenyl-*p*-benzoquinoneimine (PBQ), which undergoes acid-catalyzed hydrolysis giving different decomposition products. At pH > 4 (acetic acid – acetate buffers) the hydrolytic decomposition is very slow and it does not interfere with PBQ formation, but in H_2SO_4 media of pH < 2.5, PBQ decomposes as it is formed. In these media, the reaction obeys the kinetic rate law:

$$\left[\text{rate} = \frac{a\,[\text{PDS}]\,[\text{DPA}]_T}{1 + b\,[\text{PDS}]}\right]$$

a, the kinetic parameter, being acid dependent. Neither radical promoters (Ag^+) nor radical traps (allyl alcohol) influence the reaction rate. In acetic acid – acetate buffers of pH > 4 the kinetic rate law is simple: first order in each one of the reactants, and acid independent. These results have been interpreted by assuming the formation, in a preequilibrium step, of an *N*-diphenylhydroxylamine-*O*-sulfonate intermediate, which further rearranges to yield PBQ. The rate-determining step of the reaction changes with the protonation state of the intermediate, whose protonation pK_a has been kinetically estimated as 2.4.

M. BALÓN, P. GUARDADO, C. CARMONA, J. HIDALGO et M. A. MUÑOZ. Can. J. Chem. **71**, 167 (1993).

On a réalisé une étude cinétique de l'oxydation de la diphénylamine (DPA) par les anions peroxodisulfate, dans de l'acide sulfurique et dans des solutions tamponnées acide acétique – acétate dans un mélange méthanol–eau à 20% v/v. La *N*-phényl-*p*-benzoquinoneimine (PBQ) est le produit primaire de la réaction qui subit une hydrolyse acidocatalysée conduisant à divers produits de décomposition. À un pH > 4 (tampons acide acétique – acétate), la décomposition par hydrolyse est très lente et elle n'interfère pas avec la formation de la PBQ; toutefois, dans l'acide sulfurique (pH < 2,5), la PBQ se décompose au fur et à mesure de sa formation. Dans ces milieux, la loi de vitesse cinétique de la réaction est:

$$\left[\text{vitesse} = \frac{a\,[\text{PDS}]\,[\text{DPA}]_T}{1 + b\,[\text{PDS}]}\right]$$

dans laquelle *a* est le paramètre cinétique qui dépend de l'acide. Ni les promoteurs de radicaux (Ag^+) ni les pièges à radicaux (alcool allylique) n'influencent la vitesse de réaction. Dans les tampons acide acétique – acétate de pH > 4, la loi de vitesse cinétique est simple; elle est du premier ordre dans chacun des réactifs et elle est indépendante de l'acide. On interprète ces résultats en faisant l'hypothèse qu'il y a formation, dans une étape de prééquilibre, d'un intermédiaire *O*-sulfonate de la *N*-diphénylhydroxylamine qui se transpose par la suite en PBQ. L'étape qui détermine la vitesse de la réaction change avec l'état de protonation de l'intermédiaire dont on a évalué cinétiquement le pK_a de protonation à 2,4.

[Traduit par la rédaction]

Introduction

The oxidation reactions of aromatic amines by peroxodisulfate (PDS) anions have been extensively studied (1). Depending on the experimental conditions and the nature of the amine, the reactions can afford a variety of products derived from competitive mechanisms initially involving PDS attack on the amine nitrogen atom (2). Medium acidity is one of the major factors influencing the partitioning of the products, but its influence on the competitive mechanism is not yet well understood.

In contrast to the extensive literature on these reactions in neutral and basic media, very few reports have appeared on the reactions under acidic conditions. This is because the acidity range accessible for such studies is severely limited by the pK_a's of the amines (typically around 4) (3), since in their protonated forms they do not react with PDS. Diphenylamine (DPA), whose pK_a is 0.78 (3), is therefore of particular value for the study of the influence of the acidity on the kinetics of its reaction with PDS.

The kinetics of the oxidation of DPA by PDS have previously been investigated in aqueous methanol phosphate buffers (4) and in sodium hydroxide – acetonitrile–water media (5). In both solvent systems the reactions were simple, first order in each of the reactants and pH independent, but yielding different reaction products, *ortho*-diphenylamine sulfate and *N*-phenyl-*p*-benzoquinoneimine (PBQ), respectively. In this paper we report a more extensive study of this reaction over a wider acidity range (H_0/pH 0–6).

Experimental

Materials

DPA (>99%) was supplied by Aldrich Quimica and was used as received. Stock solutions of ca. 1×10^{-3} M were prepared in methanol and further diluted in aqueous H_2SO_4 or acetic acid – acetate buffers to obtain final solutions at the desired pH's. Potassium peroxodisulfate and other chemicals were AnalaR grade (Merck) and were used without further purification.

Kinetic measurements

Kinetic measurements were performed spectrophotometrically by monitoring the absorbances of the reaction mixtures with time at the absorption maxima of DPA, 278 nm (sulfuric acid media of

[1]Author to whom correspondence may be addressed.

Can. J. Chem. Downloaded from www.nrcresearchpress.com by 88.255.202.194 on 09/08/12
For personal use only.

TABLE 1. Yield of PBQ for the reaction of PDS, in excess, with DPA

$[DPA]_0 \times 10^4$ (M)	$[PDS]_0 \times 10^3$ (M)	pH	t (°C)	$[PDS]_f^a \times 10^4$ (M)	Yield[b] (%)
1	40	4.57	25	—	47
2	40	4.57	25	—	45
4	30	4.01	25	—	46
4	30	4.57	25	—	46
4	30	5.52	25	—	46
4	50	4.57	25	—	49
4	70	4.57	25	—	49
4	30	4.57	20	—	46
4	30	4.57	30	—	47
4	30	4.57	35	—	48
2	2	4.57	25	2.3	36
4	2	4.57	25	4.8	33
4	1	4.57	25	4.6	35
6	2	4.57	25	7.5	37
8	2	4.57	25	9.8	35

[a]PDS consumed after complete PBQ formation.
[b]Calculated from A_∞ data of several randomly selected kinetic runs followed at the absorption maxima of PBQ at 446 nm (ϵ = 4266 M^{-1} cm^{-1}). Yields are referred to $[DPA]_0$ concentrations.

$H_0 < 2.5$), or at the absorption maxima of the reaction product PBQ, 446 nm (acetic acid – acetate buffers of pH > 4), with a LKB Ultrospec Plus spectrophotometer connected to a Multitech personal computer to control the spectrophotometric system, and the uptake and processing of the data. The temperature control in the cell holder of the spectrophotometer was better than ±0.1°C.

Kinetic runs were carried out under pseudo-first-order conditions in solutions containing PDS in, at least, a tenfold excess. Pseudo-first-order rate constants, k_{obs}, were obtained by a nonlinear least-squares fitting of the absorbance–time data to eq. [1] where A_0, A_∞, and k_{obs} are floating parameters.

$$[1] \quad A_t = A_\infty + (A_0 - A_\infty) \exp(-k_{obs}t)$$

Usually, an excellent agreement between experimental and calculated A_t values was obtained for several half-lives (standard deviation of fitting $< \pm 2.0 \times 10^{-6}$). Rate constants in duplicate runs were reproducible to within better than 8%. In some instances, the reactions exhibited a short induction period. However, when it was eliminated the above treatment was fully satisfactory.

Results

Product analysis

Typical reaction mixtures were monitored by UV–visible spectrophotometry at 25°C in 20% v/v methanol–water media in the H_0/pH region 0–6. At pH > 4 (acetic acid – acetate buffers) the reaction proceeds cleanly with formation of a product absorbing at 446, 285, and 264 nm. In addition, the repetitive spectra exhibit isosbestic points at 300 and 240 nm, indicating that there is no significant buildup of intermediates. This reaction product was isolated as previously described (5) and identified by UV–vis, IR, and ^{13}C NMR spectra as *N*-phenyl-*p*-benzoquinoneimine (PBQ).

PBQ yield was examined as a function of the reactant concentrations, temperature, and pH. As data in Table 1 show, neither the reactant concentrations nor the temperature nor the pH of the reaction media significantly affect the PBQ yield. Conversely, it appears to be markedly dependent on the ratio of the reactant concentrations. Thus, when the DPA:PDS ratio is greater than 10, no PBQ formation could be detected by TLC analysis (Kieselgel 60F Merck plates, 70:30 benzene – petroleum ether). In this case, the reaction follows an entirely different course; *o*- and *p*-diphenylamine sulfate being the reaction products. These typical products of the Boyland–Sims oxidations (16) could not be detected by TLC analysis of reaction mixtures containing PDS in excess over DPA.

Table 1 also presents results on the PDS consumed in the reactions. In these experiments, reaction mixtures containing a moderate excess of PDS over DPA were allowed to go to complete PBQ formation. Different ratios of PDS:DPA were taken and, after the reaction was over, the mixtures were extracted with ether (PBQ slowly reacts with PDS) and the remaining PDS in the aqueous phase was estimated by iodometry. The average number of moles of PDS consumed was 1.2 ± 0.1, based on DPA as the limiting reagent.

Below pH 4, the initial course of the reaction is similar, but PBQ slowly decomposes to a significant extent during the reaction. This reaction is acid catalyzed, so that at pH <2.5 only traces of PBQ could be detected in the spectra of the reaction mixtures. In these media, the spectra of the completed reaction mixtures were comparable with those of PBQ subjected to the same acidic conditions. Furthermore the quantitative transformation of PBQ is demonstrated by the spectra in Fig. 1. In this figure the spectral changes with time for a reaction mixture in H_2SO_4 media are compared with the spectra of a reaction mixture of the same composition at pH = 5 that was further acidified at the end of the reaction until an acid (H_2SO_4) concentration of 0.02 M was reached.

PBQ is known to hydrolyze in acid media (6), the initial products being *p*-benzoquinone and aniline, which can further condense to other polymeric products. This hydrolytic reaction is acid catalyzed with a half-life smaller than 20 s at 25°C in 0.01 M H_2SO_4 20% v/v methanol–water media.

Kinetic studies; rate laws

The kinetics of DPA oxidation by PDS were monitored by UV–visible methods at 25°C in 20% v/v methanol–water media, whose pH's were maintained in the 0–6 H_0/pH region by adding appropriate H_2SO_4 solutions (H_0 ~0–~2.5) or acetic acid – acetate buffer (pH's 4–6) solutions. Throughout these H_0/pH regions the reaction exhibited clean pseudo-first-order kinetics, but in the intermediate pH 2.5–4

Can. J. Chem. Downloaded from www.nrcresearchpress.com by 88.255.202.194 on 09/08/12
For personal use only.

region important deviations from this behaviour were observed due to the interference of PBQ hydrolysis. Attempts to fit the absorbance–time data to a double exponential equation did not give satisfactory results. Therefore, unfortunately, we could not obtain kinetic data in this pH region.

The influence of the acidity on k_{obs} is shown in Fig. 2. In agreement with previous reports (4, 5), we find that above pH 4 the reaction rate is independent of acidity and first order in each of the reagents (Table 2). At 25°C and 20% methanol–water, the overall second-order rate constant has a value of 5.84×10^{-2} M^{-1} s^{-1}, and the activation parameters are $\Delta H^{\neq} = 31 \pm 2$ kJ mol^{-1} and $\Delta S^{\neq} = -181 \pm 6$ J mol^{-1} K^{-1}. Since this reaction was previously investigated by other authors, we have not carried out more extensive studies in this pH region.

The results of the kinetic studies at varying H_2SO_4 and PDS concentrations are collected in Table 3. At fixed $[H_2SO_4]$, k_{obs} increases with [PDS], although plots of k_{obs} vs. [PDS] are curved. Within the range of [PDS], k_{obs} was found to fit the empirical eq. [2].

$$[2] \quad k_{obs} = \frac{a\,[PDS]}{1 + b\,[PDS]}$$

which can be rearranged to give eq. [3].

$$[3] \quad 1/k_{obs} = 1/a\,[PDS] + b/a$$

The linearity of the double reciprocal plots of k_{obs}^{-1} vs. $[PDS]^{-1}$, shown in Fig. 3, confirms the consistency of eq. [2]. The values of the kinetic parameters a and b in eq. [2] collected in Table 4 were obtained from the slopes and intercepts of these plots.

To get a better insight into the reaction mechanism, the effects of Ag^+ ions ($1 \times 10^{-5} - 1 \times 10^{-6}$ M) and allyl alcohol (up to 1% v/v) on the reaction rates were also examined. The former ions are known to be an effective catalyst for radical peroxodisulfate reactions (7, 8), whereas the alcohol is an excellent radical trap (9). Neither of them had a detectable effect on k_{obs} and therefore these results are not reported. This can be taken as evidence for the noninvolvement of radicals in the reaction mechanism. These results, on the other hand, contrast with those reported for the inhibitory effects of allyl alcohol on the reaction rates of this and other related reactions in less acidic media (5, 10). It is also to be noted that the addition of Na_2SO_4 up to 0.1 M did not have an effect on the reaction rates.

Discussion

The results of the product analysis indicate that, under our experimental conditions ([PDS] >> [DPA]), PBQ is the primary detectable reaction product in the oxidation of DPA by PDS. This compound undergoes acid-catalyzed hydrolysis, initially giving *p*-benzoquinone and aniline (6) and further, different, polymeric condensation products. At pH > 4 the hydrolysis of PBQ is very slow and it does not interfere with PBQ formation. However, this hydrolysis is greatly enhanced by acid and at pH < 2.5 PBQ decomposes as it is formed, PBQ formation therefore being the rate-controlling step.

The pH–rate profile of the reaction is complex. As shown in Fig. 2, k_{obs} reaches a maximum value around H_0 1.8, which is flanked by inflection points around H_0 1.3 and pH 2.5, respectively. Before the plateau region at pH > 4 a third inflection point is also expected, but could not be determined due to the previously mentioned kinetic problems. The decrease of k_{obs} at H_0 below the maximum might be clearly imputed to DPA protonation ($pK_a = 0.78$) (3), since the protonated amine is expected to be inert toward oxidation by PDS (2). The further decrease of k_{obs} after the maximum is more difficult to rationalize.

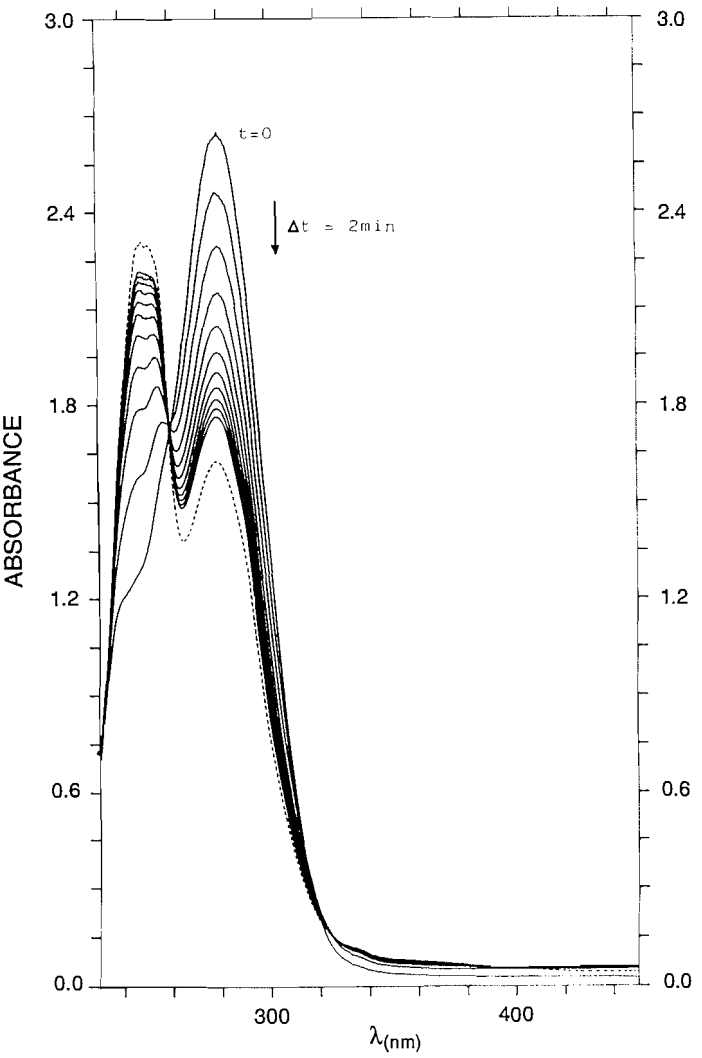

FIG. 1. Spectral changes with time of a reaction mixture ([PDS] = 4×10^{-2} M and [DPA] = 2×10^{-4} M) in 20% v/v methanol–water and 0.02 M H_2SO_4. The dotted line corresponds to the reaction product of a mixture with the same composition, but initially at pH = 5, which at the end of the reaction was acidified until a final H_2SO_4 acid concentration of 0.02 M.

One possible explanation for it might be the PDS protonation ($HS_2O_8^- \rightarrow S_2O_8^{2-} + H^+$), by assuming a greater reactivity for $HS_2O_8^-$ than for $S_2O_8^{2-}$ ions. However, the inflection point in the pH–rate profile at pH ~2.5 is somewhat larger than that expected from the pK_a value of PDS protonation. It has been estimated, although with great uncertainty, to be close to 1 (11). Moreover, PDS protonation equilibria could not explain the further increase of k_{obs} up to the plateau region nor the changeover in the kinetic behaviour of the reaction below pH 2.5 and above pH 4.

Since there are no ionizable functions in the reagents with an expected pK_a value in the vicinity of 3, we then consid-

Can. J. Chem. Downloaded from www.nrcresearchpress.com by 88.255.202.194 on 09/08/12
For personal use only.

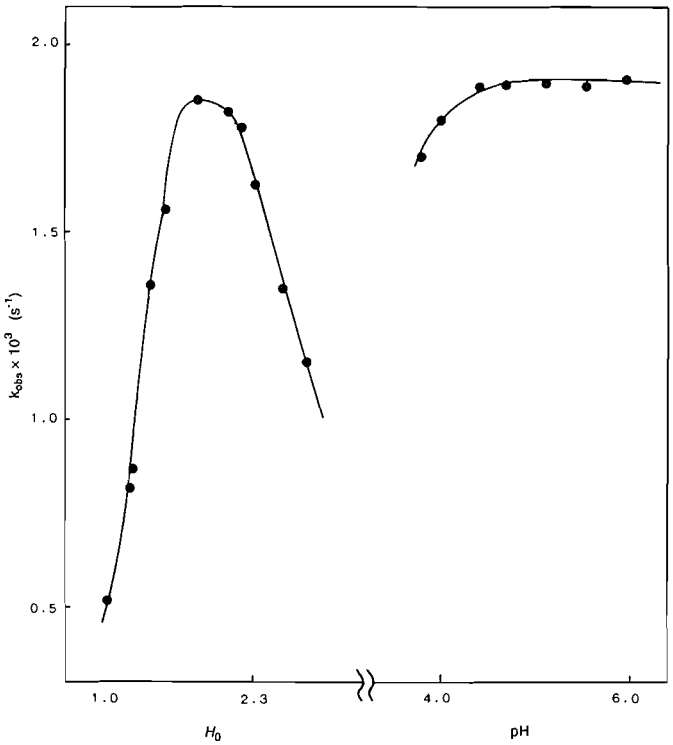

FIG. 2. Rate–pH profile of the DPA–PDS reaction in 20% v/v methanol–water media at 25°C. H_0 values (20% ethanol–water sulfuric acid media) were taken from ref. 3.

TABLE 2. Pseudo-first-order rate constants, k_{obs}, for the DPA–PDS reaction in 20% v/v methanol–water acetic acid – acetate buffers. I = 0.10 M

t (°C)	pH	$10^2 \times$ [PDS] (M)	$10^3 \times k_{obs}$ (s^{-1})
25	4.01	3	1.80
25	4.43	3	1.90
25	4.54	3	1.89
25	4.75	1	0.60
20	4.75	3	1.46
25	4.75	3	1.77
30	4.75	3	2.18
35	4.75	3	2.57
25	4.75	5	2.86
25	4.75	7	4.13
25	5.52	3	1.76

$\Delta H^{\neq}$ = 31 ± 2 kJ mol^{-1}; $\Delta S^{\neq}$ = −181 ± 6 J mol^{-1} K^{-1}.

ered the possible formation of an intermediate having this pK_a value. Thus, the present results of the DPA–PDS reaction can be more easily explained by assuming the formation, in a preequilibrium step, of an intermediate that rearranges to give PBQ. This interpretation also implies, as will be seen below, different rate-controlling steps in the mechanism depending on the protonation state of the intermediate.

The nonlinear form of the rate law [2] obtained in H_2SO_4 media supports the hypothesis of intermediate formation. Furthermore, the existence of an induction period early in the reaction might be taken as evidence that the proposed intermediate is indeed on the reaction coordinate. It can be attributed to the time required for the buildup of the intermediate. In view of the nature of the reagents and

TABLE 3. Pseudo-first-order rate constants, k_{obs}, for the DPA–PDS reaction in 20% v/v methanol–water H_2SO_4 solutions

t (°C)	[H_2SO_4] (M)	$10^2 \times$ [PDS] (M)	$10^3 \times k_{obs}$ (s^{-1})
20	0.0200	7	2.14
		6	1.91
		5	1.62
		4	1.39
		2	0.80
		1	0.42
25		7	2.86
		6	2.56
		5	2.24
		4	1.86
		2	1.05
		1	0.55
30		7	3.61
		6	3.27
		5	2.94
		4	2.51
		2	1.31
		1	0.67
25	0.0100	7	2.80
		6	2.44
		5	2.13
		4	1.80
		3	1.41
		2	0.99
		1	0.54
25	0.0050	7	2.50
		6	2.23
		5	1.96
		4	1.63
		3	1.34
		2	0.97
		1	0.51
25	0.0025	7	2.07
		6	1.83
		5	1.65
		4	1.39
		3	1.13
		2	0.83
		1	0.49
25	0.0010	7	1.67
		6	1.44
		5	1.27
		4	1.16
		3	0.98
		2	0.74
		1	0.46

reaction products, we think that diphenylhydroxylamine-*O*-sulfonate (I) is a reasonable structure for the proposed intermediate. Phenylhydroxylamines, on the one hand, are known to have protonation pK_a's close to that expected for the proposed intermediate (12, 13) and, on the other hand, these compounds experience rearrangement reactions to give aminophenols (Bamberger rearrangement) (12, 14) that are structurally related to PBQ. It must be also noted that similar arylhydroxylamine-*O*-sulfonates were recently proposed

Can. J. Chem. Downloaded from www.nrcresearchpress.com by 88.255.202.194 on 09/08/12
For personal use only.

Can. J. Chem. Downloaded from www.nrcresearchpress.com by 88.255.202.194 on 09/08/12
For personal use only.

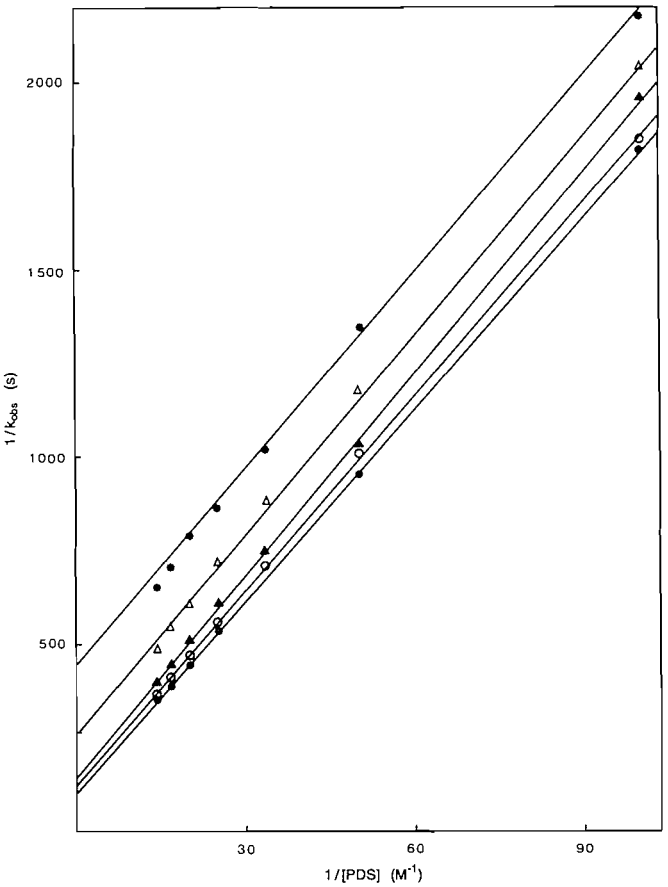

FIG. 3. Plots of k_{obs}^{-1} vs. $[PDS]^{-1}$ for the DPA–PDS reaction in 20% v/v methanol–water media at 25°C. Sulfuric acid concentrations: 2×10^{-2} M (●), 1×10^{-2} M (○), 5×10^{-3} M (▲), 2.5×10^{-3} M (△), and 1×10^{-3} M (*).

as the more probable intermediates in the Boyland–Sims oxidation of aromatic amines by PDS (2, 15).

Scheme 1 outlines a minimal mechanism consistent with the above considerations. Depending on the relative magnitudes of the microscopic constants, this mechanism would give rise to several specific situations, any one of which may occur in the present system.

The rate equation expected from Scheme 1 by assuming the steady-state concentration for the intermediate IH^+ or I is given in eq. [4] where [DPA] is the actual concentration of substrate ($[DPA]_T$ = [DPA] + [I or IH^+]):

$$[4] \quad \text{rate} = \frac{k_1 k_2 [PDS] [DPA]_T}{k_2 + k_{-1} [SO_4^{2-}] + k_1 [PDS]}$$

With [PDS] >> [DPA], the measured first-order rate constant k_{obs} (defined by rate = k_{obs} [DPA]) is given by eq. [5]:

$$[5] \quad k_{obs} = \frac{k_1 k_2 [PDS]}{k_2 + k_{-1} [SO_4^{2-}] + k_1 [PDS]}$$

Equation [5] can be identified with experimental eq. [2] obtained in sulfuric acid media provided that (*i*) $k_{-1} [SO_4^{2-}] << k_2 + k_1 [PDS]$ ($a = k_1^{IH}$ and $b = k_1^{IH}/k_2^{IH}$) or (*ii*) $k_2 << k_{-1} [SO_4^{2-}] + k_1 [PDS]$ ($a = k_2^{IH} K_1^{IH}/[SO_4^{2-}]$ and $b = k_1^{IH}/[SO_4^{2-}]$). Equation [5] predicts a retarding effect of $[SO_4^{2-}]$ ions; therefore, since Na_2SO_4 addition does not affect k_{obs} it may be assumed that situation (*i*) predominates over (*ii*).

TABLE 4. Influence of sulfuric acid concentration and temperature on the kinetic parameters *a* and *b* in eq. [3]

t (°C)	$[H_2SO_4]$ (M)	$10^2 \times a$ (M^{-1} s^{-1})	*b* (M^{-1})
20	0.0200	4.51	7.11
25	0.0200	5.85	6.16
30	0.0200	7.01	4.09
25	0.0100	5.75	7.04
25	0.0050	5.53	8.04
25	0.0025	5.53	14.20
25	0.0010	5.56	22.51

A similar dichotomy of mechanistic possibilities can be envisioned to account for the experimental rate law obtained in media of pH > 4; (*i*) the intermediate, I, is formed in a reversible step but $k_2^I >> k_1^I$, k_1^I being, therefore, the rate-limiting step, and (*ii*) the mechanism operates with $k_{-1}^I [SO_4^{2-}] >> k_2^I$, the rate-controlling constant being $k_2^I k_1^I$. In both cases, the intermediate will be in a steady state and its concentration small relative to the reactants, as it is required by the experimental evidence that the intermediate I does not accumulate. A key observation that can help to decide between the two possibilities is the fact, previously pointed out, that k_{obs} has similar values at high sulfuric acid concentration and in acetic acid – acetate buffers of pH > 4. This fact might be taken as evidence that in both cases the rate-limiting attack is the same; i.e., the PDS attack on DPA, k_1.

Bearing in mind the above assumptions, the kinetic data in Tables 2 and 4 can be analyzed to obtain the microscopic constants in Scheme 1, which are presented in Table 5. A perusal of the data in this table reveals the satisfactory correspondence between k_1^{IH} and k_1^I and among their activation parameters $\Delta H^{\neq}$ and $\Delta S^{\neq}$. The low activation enthalpies and the high negative activation entropies, together with the experimental observations that neither radical promoters nor radical traps have influence on the reaction rates, suggest that the formation of the diphenylhydroxylamine intermediate does not involve a radical mechanism. These results strongly support the formation of the intermediate as a polar mechanism involving nucleophilic displacement of the lone pair of the DPA nitrogen atom on the peroxide group of PDS (16).

On the other hand, the simplest mechanistic interpretation for the rearrangement process, k_2, might be the cleavage of the nitrogen–oxygen bond in the intermediate. However, the experimental evidence supported by the pH–rate curve points clearly to the existence of two separate pathways for each of the conjugate acid–base forms IH^+ and I of the intermediate. The more important difference from a kinetic point of view is that the rearrangement of IH^+ might be slower than that of I and, apparently, acid catalyzed. It means, in other words, that IH^+ is more stable to rearrangement than I. This could be related to the zwitterionic structure of IH^+, which would greatly decrease the leaving tendency of the sulfate group.

The acid dependence of k_2^{IH} resembles the Bamberger rearrangement of phenylhydroxylamines to aminophenols (12, 14) and points to a similar mechanism. This mecha-

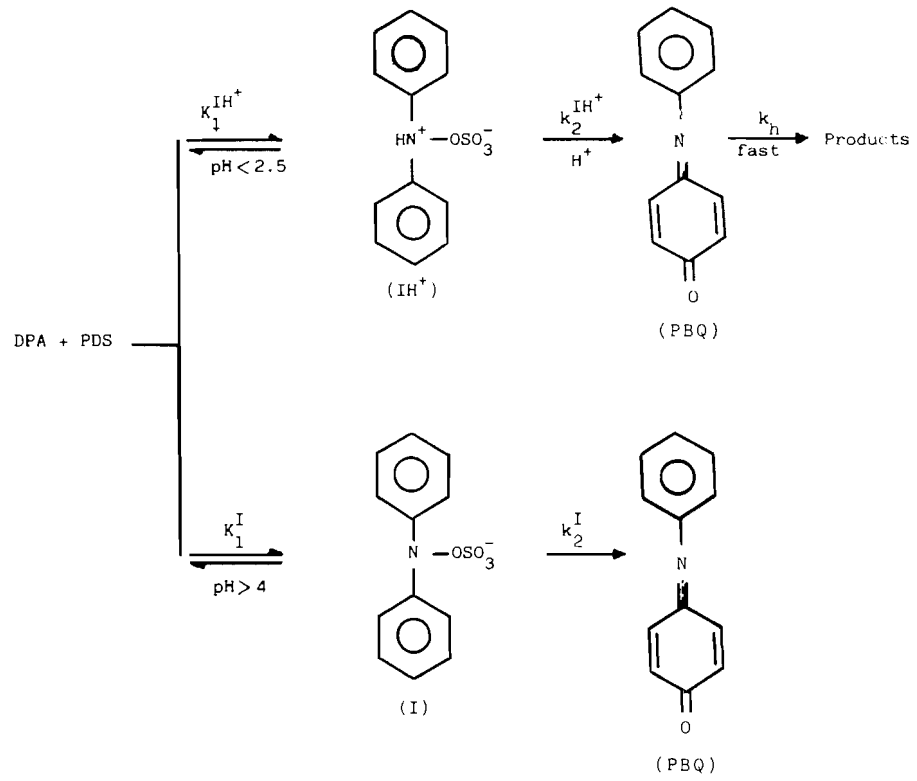

SCHEME 1

TABLE 5. Microscopic constants in Scheme 2 and activation parameters at 25°C

	$10^2 \times k_1$ (M^{-1} s^{-1})	$\Delta H^{\neq}$ (kJ mol^{-1})	$\Delta S^{\neq}$ (J mol^{-1} K^{-1})
I	5.84	31 ± 2	−181 ± 6
IH^+	5.64	35 ± 13	−168 ± 46

	$[H_2SO_4]$				
	0.02 M	0.01 M	0.005 M	0.0025 M	0.001 M
$10^3 \times k_2^{IH^+}$ (s^{-1})	9.5	8.2	6.9	4.4	2.5
	$\Delta H^{\neq}$ = 74 ± 20 kJ mol^{-1}		$\Delta S^{\neq}$ = −45 ± 25 J mol^{-1} K^{-1}		

nism is shown in Scheme 2 and involves the heterolytic cleavage of the N—O bond and the formation of a resonance-stabilized imine ion (14), which reacts with the solvent in fast steps leading to the final product. As in the Bamberger rearrangement, it can be assumed that the reaction proceeds by an S_N1 mechanism and that the active species are not the *N*-protonated ones but the *O*-protonated species (I_OH^+) of the diphenylhydroxylamine sulfate intermediate.

The kinetic rate law previously derived from the Bamberger rearrangement (12, 14) can be adapted to obtain the expression for k_2 in eq. [6]

$$[6] \quad k_2 = \frac{k K_a^N [H^+]}{K_a^O (K_a^N + [H^+])} = \frac{k_N [H^+]}{K_a^N + [H^+]}$$

where $k_N = k K_a^N / K_a^O$, K_a^O and K_a^N being the dissociation constants of the *O*- and *N*-protonated forms of the IH^+ intermediate. As would be expected, the double reciprocal plot of k_2^{-1} vs. $[H^+]^{-1}$ yields a straight line (Fig. 4) from whose slope and intercept the values of 1.1×10^{-2} M^{-1} s^{-1} and 2.4 ± 0.6 can be estimated for k_N and pK_a^N, respectively. These values, as well as the $\Delta H^{\neq}$ value, are of the magnitudes expected for the Bamberger rearrangement (12, 14) of a phenylhydroxylamine derivative. However, the negative activation entropy of −45 ± 25 eu, in the range of the expected value for a bimolecular hydrolysis, is in contrast to the small and usually positive entropies observed for typical unimolecular Bamberger reactions (12). Therefore, although the great uncertainty inherent in the calculation procedure of $\Delta S^{\neq}$ obscures its significance, the possibility of a bimolecular N—O bond cleavage assisted by a water molecule cannot be ruled out.

Because of the lack of kinetic information, the rearrangement mechanism for the unprotonated intermediate I is more difficult to rationalize. However, in spite of the previously assumed differences for the rearrangement reactions of IH^+ and I, their mechanisms are not expected to be very different, since both conjugate species lead to the same rear-

Can. J. Chem. Downloaded from www.nrcresearchpress.com by 88.255.202.194 on 09/08/12
For personal use only.

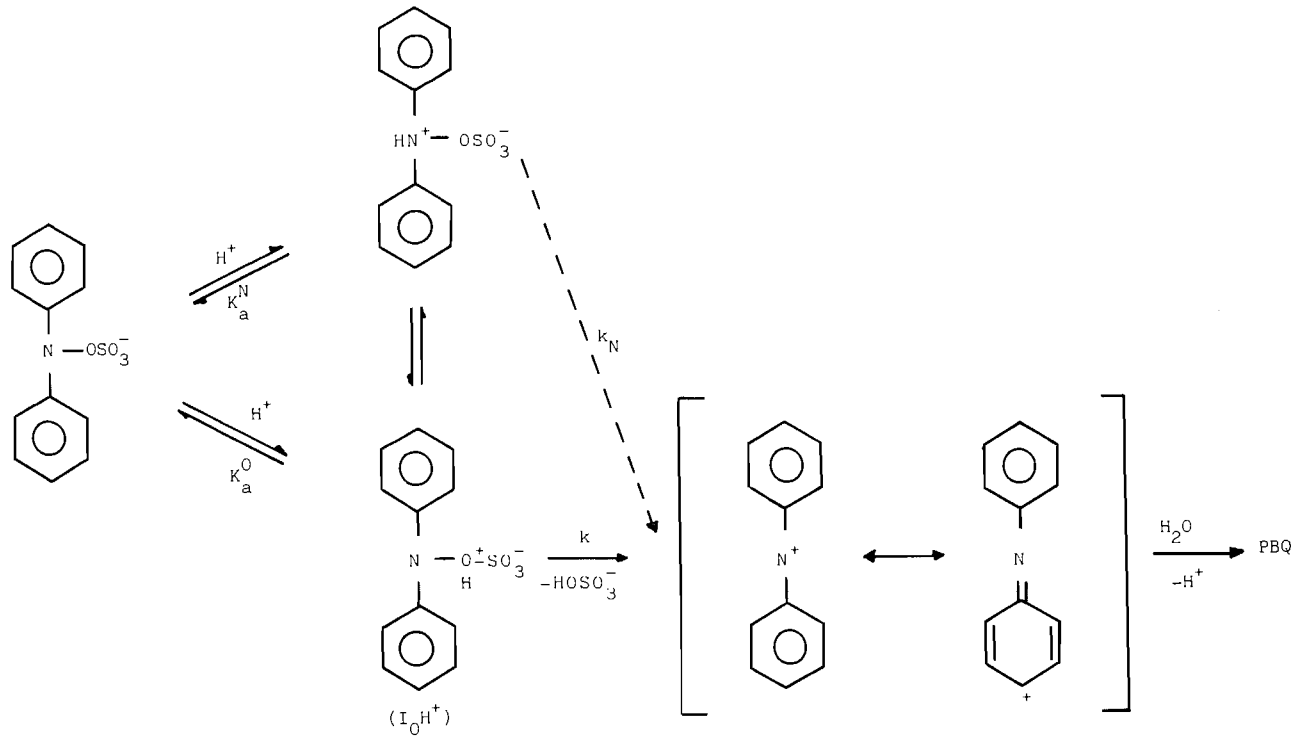

SCHEME 2

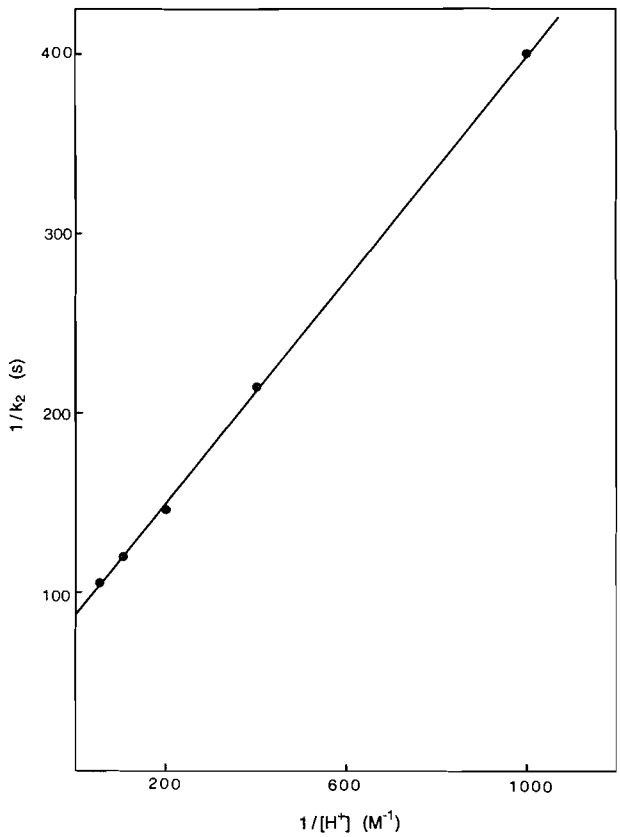

FIG. 4. Plot of k_2^{-1} for the rearrangement of the IH^+ intermediate against $[H^+]^{-1}$ at 25°C.

rangement product. In this sense, the hypothesis that these reaction pathways could be related to the two possible homolytic and heterolytic mechanisms for the N—O cleavage seems to be very attractive. Thus, although for IH^+ the kinetic evidence points to the ionic mechanism depicted in Scheme 2, an alternative radical mechanism for I involving homolytic N—O cleavage is also reasonable. The available trapping data for the reaction in media of pH > 4 could be invoked to support this mechanism. As has been proposed (5, 10), the inhibitory effects of radical traps on the reactions of aromatic amines by PDS involve intermediate radical capture rather than PDS radical reactions. This effect, in turn, may also affect the reaction rates, particularly at high conversion times.

We can now summarize our interpretation of the DPA–PDS reaction mechanism, which has proved to be more puzzling and elusive than we might have conceived at the outset:

1. The reaction of DPA with PDS to give PBQ initially involves the formation of an *N*-diphenylhydroxylamine-*O*-sulfonate intermediate, whose protonation pK_a of 2.4 ± 0.6 has been kinetically estimated. The intermediate further rearranges to give PBQ or, in media of sufficient acidity (pH < 2.5), its hydrolytic decomposition products.

2. The experimental findings strongly suggest that the formation of the proposed intermediate proceeds by a polar mechanism. It involves nucleophilic displacement on the peroxide bond in PDS by the lone electron pair of the DPA nitrogen atom. On the other hand, the intermediate is more stable as a protonated form, IH^+, than as a nonprotonated

Can. J. Chem. Downloaded from www.nrcresearchpress.com by 88.255.202.194 on 09/08/12
For personal use only.

form, I. The zwitterionic structure of IH^+ is apparently responsible for this behaviour.

3. The intermediate rearrangement may be rationalized by a mechanism analogous to that of Bamberger rearrangement of *N*-phenylhydroxylamines to aminophenol, but with separate pathways for each of the acid–base conjugated species IH^+ and I. The latter presumably rearranges via homolytic N—O bond cleavage, the former rearrangement is acid catalyzed and involves an ionic mechanism.

4. The experimental results suggest that, while the rearrangement step may not be rate limiting at pH > 4, it is at least partly limiting at lower pH's. In these more acidic media the intermediate accumulates, being kinetically detectable.

Although we feel that, at present, some aspects of our mechanistic interpretation of the DPA–PDS reaction are rather speculative and therefore should be taken with caution, the interest in the oxidation reactions of aromatic amines by peroxides undoubtedly requires a more extensive experimental effort (including other amines and different peroxides, and medium influence), which will be the subject of future work.

Acknowledgements

We are grateful to the Dirección General de Investigación Cientifica y Técnica (PB89-0643) and the Junta de Andalucia (Research group 3011) for financial support.

1. (*a*) B. Plesnicar. *In* Oxidation in organic chemistry. Part C. *Edited by* W. S. Trahanovsky. Academic Press, London. 1978. Chap. 3; (*b*) E. J. Behrman. *In* Organic reactions. Vol. 35. *Edited by* A. S. Kende. Wiley Interscience, New York. 1988. Chap. 2.
2. E. J. Behrman. J. Org. Chem. **57**, 2266 (1992).
3. D. Dolman and R. Stewart. Can. J. Chem. **45**, 903 (1967).
4. A. Sabesan and N. Venkatasubramanian. Aust. J. Chem. **24**, 1633 (1971).
5. N. Ram and S. Sidhu. Indian J. Chem. **16A**, 195 (1978).
6. W. R. Bansal, S. Puri, and K. S. Sidhu. Bull. Chem. Soc. Jpn. **47**, 2319 (1974).
7. D. A. House. Chem. Rev. **62**, 185 (1962).
8. F. Minisci and A. Citterio. Acc. Chem. Res. **16**, 27 (1983).
9. W. K. Wilmarth and A. Haim. *In* Peroxide reaction mechanisms. *Edited by* J. O. Edwards. Interscience, New York. 1962.
10. R. C. Gupta and S. P. Srivastava. Indian J. Chem. **10**, 706 (1972).
11. E. J. Behrman and J. O. Edwards. Rev. Inorg. Chem. **2**, 179 (1980).
12. T. Sone, Y. Tokuda, T. Sakai, S. Shinkai, and O. Manabe. J. Chem. Soc. Perkin Trans. 2, 298 (1981).
13. T. Sone, K. Hamamoto, Y. Seiji, S. Shinkai, and O. Manabe. J. Chem. Soc. Perkin Trans. 2, 1596 (1981).
14. G. Kohnstan, W. A. Petch, and D. L. Williams. J. Chem. Soc. Perkin Trans. 2, 423 (1984).
15. E. J. Behrman. J. Chem. Soc. Perkin Trans. 1, 305 (1992).
16. E. J. Behrman and J. O. Edwards. Prog. Phys. Org. Chem. **4**, 93 (1967).

Can. J. Chem. Downloaded from www.nrcresearchpress.com by 88.255.202.194 on 09/08/12
For personal use only.

A simple quality test for self-consistent-field atomic orbitals

N. DESMARAIS, G. DANCAUSSE, AND S. FLISZÁR[1]

Département de chimie, Université de Montréal, C.P. 6128, Succ. A, Montréal (Québec), Canada H3C 3J7

Received September 15, 1992

N. DESMARAIS, G. DANCAUSSE, and S. FLISZÁR. Can. J. Chem. **71**, 175 (1993).

A quality test is proposed for SCF atomic orbitals, $\phi_i = \Sigma_k c_{ki}\chi_k^{lm}$, approximated as finite linear combinations of suitable basis functions χ_k^{lm}. The key is in a function, readily derived from the Hartree–Fock equation $\hat{F}\phi_i = \varepsilon_i \phi_i$, which is identically zero for true Hartree–Fock spin orbitals and not so for approximate orbitals. In this way, our test measures how closely approximate orbital descriptions approach the true Hartree–Fock limit and thus provides a quality ordering of orbital bases with respect to one another and with respect to that limit, in a scale uniquely defined by the latter. Moreover, this analysis also holds for atomic subspaces of our choice, e.g., the valence region. Examples are offered for representative collections of Slater- and Gaussian-type orbital expansions.

N. DESMARAIS, G. DANCAUSSE et S. FLISZÁR. Can. J. Chem. **71**, 175 (1993).

On propose un critère pour évaluer la qualité des orbitales atomiques, $\phi_i = \Sigma_k c_{ki}\chi_k^{lm}$, décrites par des combinaisons linéraires finies de fonctions de base χ_k^{lm}. La clé est dans une fonction découlant de l'équation de Hartree–Fock $\hat{F}\phi_i = \varepsilon_i \phi_i$, qui est identiquement nulle pour les vraie orbitales de spin Hartree–Fock, mais non nulle autrement. Ceci permet de mesurer comment la description des orbitales leur permet de se rapprocher de la limite exacte de Hartree–Fock et fournit une appréciation de la qualité des bases dans une échelle définie par cette limite. Cette analyse est également possible pour des sous-espaces atomiques, par exemple la région de valence. Les exemples portent sur une série de fonctions gaussiennes et de Slater.

Can. J. Chem. Downloaded from www.nrcresearchpress.com by 88.255.202.194 on 09/08/12
For personal use only.

1. Introduction

Here we consider analytic Hartree–Fock–Roothaan self-consistent-field (SCF) atomic orbitals

$$[1] \qquad \phi_i = \sum_k c_{ki}\chi_k^{lm}$$

represented as finite linear combinations of appropriately selected basis functions χ_k^{lm}. Of course, to get true Hartree–Fock orbitals, an infinite set of basis functions should be included in eq. [1]. The question is: how closely do finite expansions approach the true Hartree–Fock limit?

This question is usually answered with the help of comparisons between results obtained from selected truncated expansions and results computed from significantly richer expansions, hoping that the latter adequately mirror the Hartree–Fock limit, which calls for a judgement depending also on the property used in this type of comparisons, the total energy, however, offering the primary guideline. Alternatively, fully numerical Hartree–Fock solutions may serve as reference. Either way, some estimate of the exact Hartree–Fock result is required.

The hierarchy of atomic basis sets is nowadays well established, in essence through the vast experience gathered from a wealth of calculations. Here we submit an objective quality test "measuring" how closely atomic SCF wave functions approach the true Hartree–Fock eigenfunctions. This test is self-contained in that it does not require any a priori knowledge of results (e.g., the energy) obtained at (or at least near) the Hartree–Fock limit. Examples are worked out for representative collections of Slater and Gaussian basis functions.

2. Outline of method

Our quality test is rooted in the partitioning of an atom (or ion) into two regions of space: a spherical inner region of radius r_b, centered at the nucleus, and an outer region, extending from r_b to infinity. The Hartree–Fock equation

$$[2] \qquad \hat{F}\phi_i = \varepsilon_i\phi_i$$

is our starting point. Multiplication from the left by ϕ_i^*, integration from r_b to ∞, and summation over all occupied orbitals i leads to

$$[3] \qquad \sum_i \int_{r_b}^{\infty} \nu_i\phi_i^*\hat{F}\phi_i \, d\boldsymbol{r} = \sum_i \int_{r_b}^{\infty} \nu_i\phi_i^*\varepsilon_i\phi_i \, d\boldsymbol{r}$$

where ν_i is the occupation of the normalized orbital with eigenvalue ε_i. No special meaning is attached to any particular radius r_b defining the boundary surface separating the inner and outer regions: r_b can be chosen at will, whether or not this boundary corresponds to a physically meaningful (1) core-valence separation. We shall learn that the validity of eq. [3] depends on whether or not the ϕ_i's are true Hartree–Fock orbitals: approximate solutions, namely those obtained from truncated expansions, eq. [1], do not satisfy eq. [3]. The difference between the left- and right-hand sides of eq. [3] serves as a quality test for these approximations. The better the basis set, the smaller is this difference for any r_b.

Now we transform eq. [3] into something more practical. Let us begin with its right-hand side. The integral

$$[4] \qquad N_i^v = \nu_i \int_{r_b}^{\infty} \phi_i^*\phi_i \, d\boldsymbol{r}$$

represents the number of electrons of orbital i found in the outer region (which we call for simplicity, but admittedly somewhat sketchily, the valence region; hence the superscript v). Equation [3] thus becomes

$$[5] \qquad \sum_i \int_{r_b}^{\infty} \nu_i\phi_i^*\hat{F}\phi_i \, d\boldsymbol{r} = \sum_i N_i^v\varepsilon_i$$

[1]Author to whom correspondence may be addressed.

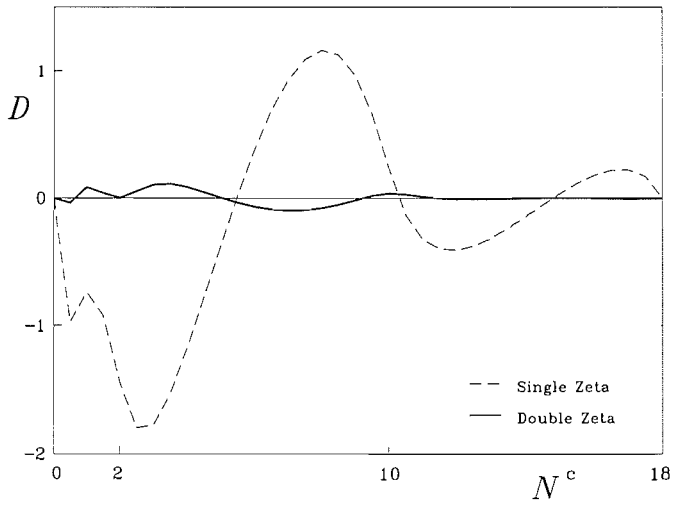

FIG. 1. Argon. Deviations (atomic units) calculated from eq. [12] using the single-ζ and double-ζ Slater bases of Clementi and Roetti (3). The Hartree–Fock limit is represented by the line $D = 0$. $N^c = 0$ and $N^c = 18$ e correspond to $r_b = 0$ and $r_b = \infty$, respectively.

Next, we proceed with the left-hand side of eq. [5]. The evaluation of the monoelectronic integrals occurring in it is straightforward. The nuclear-electronic potential energy of the $\Sigma_i N_i^v$ outer electrons in the field of the nuclear charge Z is

$$[6] \qquad V_{ne}^v = -Z \sum_i \nu_i \int_{r_b}^{\infty} 4\pi r |\phi_i(r)|^2 dr$$

and their kinetic energy is

$$[7] \qquad T^v = \sum_i \nu_i \int_{r_b}^{\infty} \phi_i^* \hat{T} \phi_i d\boldsymbol{r}$$

Now we turn to the bielectronic integrals appearing in the left-hand side of eq. [5]. They require a little attention. Consider the Coulomb operator $\hat{J}_j$ defined by

$$[8] \qquad \hat{J}_j(1)\phi_i(1) = \phi_i(1) \int |\phi_j(2)|^2 \frac{1}{r_{12}} d\tau_2$$

where $d\tau_2 = r_2^2 \sin\theta_2 \, d\theta_2 \, d\varphi_2 \, dr_2$ (with a similar expression for $d\tau_1$). The integral $\int \ldots d\tau_2$ is over all space, but can be separated into two contributions, namely, in short-hand notation,

$$\int_{\tau_2^c} \ldots d\tau_2 + \int_{\tau_2^v} \ldots d\tau_2$$

where the first integral (from 0 to r_b) covers the inner (core) region τ_2^c, whereas the second one (from r_b to ∞) is for the outer (valence) space τ_2^v. Using eq. [8], the integration between r_b and ∞ required by eq. [5] thus gives the following Coulomb repulsion:

$$[9] \qquad \int_{\tau_1^v} \phi_i^*(1)\hat{J}_j(1)\phi_i(1) \, d\tau_1 = \int_{\tau_1^v} \int_{\tau_2^c} \ldots d\tau_2 \, d\tau_1 + \int_{\tau_1^v} \int_{\tau_2^v} \ldots d\tau_2 \, d\tau_1$$

These integrals describe a potential energy of interaction involving the part of electron 1 assigned to the valence space τ^v and a smeared-out electron with density $|\phi_j(2)|^2$. The two terms of the right-hand side of eq. [9] differ from one another because the first integral "sees" only the part of $|\phi_j(2)|^2$ found in the core space τ^c, whereas the second integral concerns only the part of $|\phi_j(2)|^2$ confined within the valence region τ^v.

At last, we can carry out the sum indicated in eq. [5]. This sum also includes a term arising from $\hat{J}_i(2)\phi_j(2)$, whose integral is evaluated as just shown for $\hat{J}_j(1)\phi_i(1)$. As a consequence, the summation over all occupied orbitals counts once again the 1–2 Coulomb interaction confined within the valence space, i.e., the $\int^{\tau_1^v} \int^{\tau_2^v} \ldots d\tau_2 \, d\tau_1$ term already found in eq. [9], and adds the new integral

$$\int_{\tau_1^c} \int_{\tau_2^v} \ldots d\tau_2 \, d\tau_1$$

describing the interaction between the part of electron 2 found in τ^v and the part of electron 1 found in the core region. Briefly, all interactions involving exclusively electron densities assigned to the outer space τ^v are counted twice, whereas the cross interactions between electrons assigned to τ^v and those assigned to τ^c, represented by the appropriate

$$\int_{\tau_1^v} \int_{\tau_2^c} \ldots d\tau_2 \, d\tau_1 + \int_{\tau_1^c} \int_{\tau_2^v} \ldots d\tau_2 \, d\tau_1$$

integrals, are counted only once. The same reasoning applies to the exchange operator

$$\hat{K}_j(1)\phi_i(1) = \phi_j(1) \int \frac{\phi_j^*(2)\phi_i(2)}{r_{12}} d\tau_2$$

and to its integral $\int \ldots d\tau_1$, followed by summation over i. Down the line, taking now all the appropriate Coulomb and exchange integrals into account, it is seen that V_{ee}^{vv} (= electron–electron repulsion involving only the electrons of the outer (valence) region) is counted twice in the left-hand side of eq. [5], whereas V_{ee}^{cv} (= repulsion between the outer (valence) electrons and those of the inner (core) region) is counted only once.

The final result, including now V_{ne}^v and T^v (eqs. [6] and [7], respectively) is thus

$$[10] \qquad \sum_i N_i^v \varepsilon_i = T^v + V_{ne}^v + 2V_{ee}^{vv} + V_{ee}^{cv}$$

The companion formula

$$[11] \qquad \sum_i N_i^c \varepsilon_i = T^c + V_{ne}^c + 2V_{ee}^{cc} + V_{ee}^{cv}$$

where T^c, V_{ne}^c, and V_{ee}^{cc} are the kinetic, the nuclear-electronic, and the interelectronic energies of the $\Sigma_i N_i^c$ core

Can. J. Chem. Downloaded from www.nrcresearchpress.com by 88.255.202.194 on 09/08/12
For personal use only.

Can. J. Chem. Downloaded from www.nrcresearchpress.com by 88.255.202.194 on 09/08/12
For personal use only.

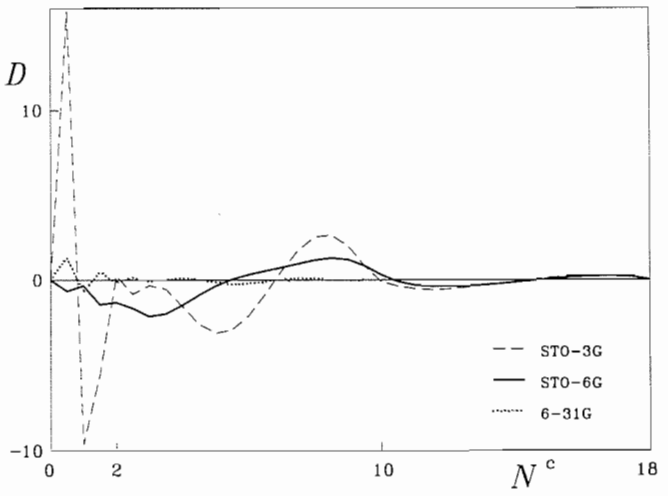

FIG. 2. Argon. Deviations (atomic units) observed for the STO-3G, STO-6G, and 6-31G Gaussian bases of Pople *et al.* (4). The results for STO-4G and STO-5G are intermediate between those shown for the STO-3G and STO-6G bases, namely in the short-range region.

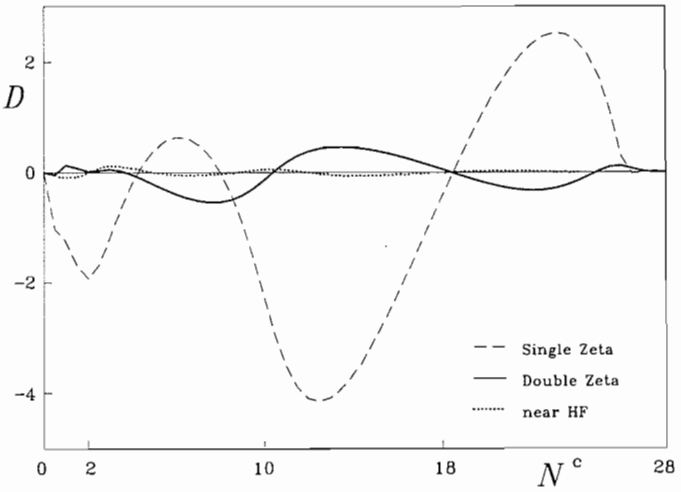

FIG. 3. Nickel. Deviations (atomic units) calculated by means of the Slater bases of ref. 3. The solid line for $D = 0$ represents the Hartree–Fock limit.

electrons, respectively, follows immediately because the individual core and valence terms add up correctly to give the corresponding totals for the entire atom, e.g., $T^{\text{total}} = T^{\text{v}} + T^{\text{c}}$. Remember that all the quantities appearing in eqs. [10] and [11], except ε_i, are functions of r_b, i.e., $N_i^{\text{v}} = N_i^{\text{v}}(r_b)$, $T^{\text{v}} = T^{\text{v}}(r_b)$, etc.

Equation [10] (1) is most convenient for our intended analysis of SCF orbitals, eq. [1]. The first step consists in conventional optimizations of the ϕ_i's (or the selection of the appropriate literature data) and the calculation of the corresponding orbital energies ε_i. The wave functions are used to calculate N_i^{v}, eq. [4], and the sum $\Sigma_i N_i^{\text{v}}\varepsilon_i$ for the r_b of our choice. The V_{ne}^{v} and T^{v} contributions are obtained from eqs. [6] and [7], respectively, and the bielectronic integrals are deduced with the help of the standard expansion of $1/r_{12}$ in terms of spherical harmonics (2) and use of the appropriate limits of integration. The programs were developed both for Slater and Gaussian basis functions.

TABLE 1. Quality indices of single-ζ, double-ζ, and near Hartree–Fock Slater-type atomic orbitals (atomic units)

			Near HF	
Atom	Single-ζ	Double-ζ	CR	Malli
Li	0.061	[a]	0.0006	
Be	0.075	0.008	0.0009	
B	0.084	0.009	0.0010	
C	0.100	0.014	0.0012	
N	0.145	0.019	0.0019	
O	0.257	0.028	0.0034	
F	0.435	0.044	0.0040	
Ne	0.685	0.067	0.0048	
Na	0.728	0.070	0.0019	0.0203
Mg	0.763	0.066	0.0046	0.0041
Al	0.713	0.055	0.0041	0.0051
Si	0.757	0.055	0.0029	0.0082
P	0.773	0.054	0.0042	0.0096
S	0.784	0.055	0.0061	0.0184
Cl	0.793	0.056	0.0130	0.0166
Ar	0.809	0.051	0.0073	0.0549
Ti	0.798	0.063	0.0149	
Cr	0.945	0.139	0.0430	
Fe	1.346	0.178	0.0601	
Ni	2.042	0.284	0.0437	
Zn	3.023	0.425	0.0323	
Ge	3.267	0.421	0.0348	
Se	3.486	0.404	0.0578	
Kr	3.703	0.426	0.0296	

[a] Misprints were detected in the double-ζ basis of Li reported in ref. 3.

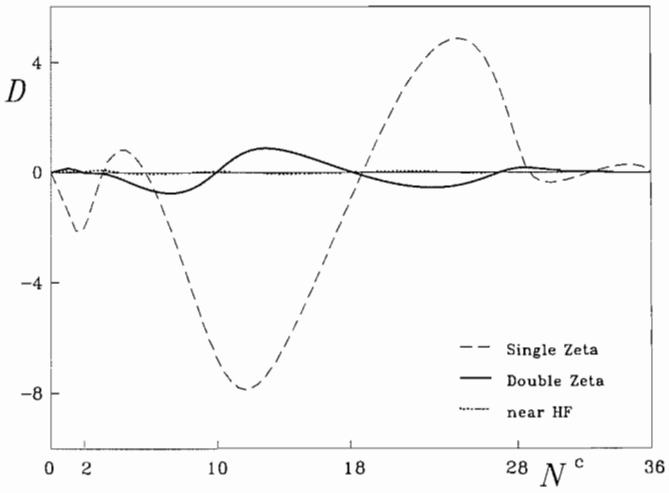

FIG. 4. Krypton. Results (atomic units) obtained with the Slater bases of ref. 3. This example, compared to that given in Fig. 3, illustrates the regularities that are typical for Slater bases.

3. Results

Our results are expressed as the difference, from eq. [10],

$$[12] \quad D = \sum_i N_i^{\text{v}}\varepsilon_i - (T^{\text{v}} + V_{\text{ne}}^{\text{v}} + 2V_{\text{ee}}^{\text{vv}} + V_{\text{ee}}^{\text{cv}})$$

This difference represents what we may call the "noise" of a truncated expansion, with respect to a "base line" that is everywhere identically zero at the true Hartree–Fock limit.

TABLE 2. Quality indices of selected Gaussian-type orbitals, expressed as root-mean-square deviations (atomic units)

Basis	Root-mean-square deviations (au)							
	Be	C	O	Ne	Mg	Si	S	Ar
STO-3G	0.279	0.547	0.889	1.410	1.826	2.348	2.904	3.512
STO-4G	0.187	0.309	0.482	0.902	0.974	1.292	1.486	1.696
STO-5G	0.098	0.139	0.250	0.689	0.705	0.840	0.874	0.898
STO-6G	0.104	0.148	0.254	0.688	0.701	0.832	0.860	0.874
4-31G	0.043	0.212	0.323	0.458				
6-31G	0.025	0.039	0.069	0.137	0.140	0.184	0.216	0.270
6-311G	0.018	0.037	0.056	0.090				
$(10s6p) \rightarrow [5s4p]$	0.012	0.022	0.037	0.057				
$(10s6p)$	0.012	0.023	0.036	0.057				
$(13s8p)^a$	0.0032	0.0056	0.0103	0.017				

[a]Additional results for van Duijneveldt's $(13s8p)$ basis (8) are 0.0038 (B), 0.0082 (N), and 0.0124 a u (F).

TABLE 3. Deviations in the outer atomic regions, assuming a 2e core

Basis[a]	Root-mean-square deviations (au)							
	C	N	O	F	Si	P	S	Ar
STO-3G	0.132	0.142	0.286	0.502	1.019	1.079	1.157	1.336
STO-4G	0.139	0.126	0.267	0.485	0.929	0.945	0.993	1.051
STO-5G	0.132	0.119	0.260	0.476	0.871	0.871	0.898	0.912
STO-6G	0.135	0.117	0.256	0.470	0.850	0.846	0.868	0.868
Single-ζ	0.060	0.129	0.255	0.466	0.776	0.786	0.790	0.801
4-31G	0.033	0.041	0.045	0.058				
6-31G	0.028	0.037	0.056	0.080	0.053	0.064	0.069	0.093
6-311G	0.009	0.013	0.021	0.034				
Double-ζ	0.010	0.018	0.029	0.047	0.057	0.055	0.056	0.050

[a]The Gaussian bases are from ref. 4. The single-ζ and double-ζ Slater bases are from ref. 3.

TABLE 4. Deviations in the valence region of second-row atoms, assuming a 10-electron core

Basis	RMS deviations (atomic units)			
	Si	P	S	Ar
STO-3G	0.309	0.262	0.263	0.320
STO-4G	0.341	0.298	0.291	0.247
STO-5G	0.344	0.302	0.296	0.254
STO-6G	0.339	0.296	0.287	0.241
Single-ζ	0.067	0.090	0.130	0.250
6-31G	0.008	0.008	0.008	0.015
Double-ζ	0.009	0.010	0.009	0.013

This difference is a function of r_b. For each r_b, there is one value of N^c, the number of electrons contained within the sphere of radius r_b. The use of $D = D(N^c)$ allows us to scan the entire atom, thus simplifying the presentation of results by avoiding long tails for large r_b's. At the limits $N^c = 0$ and $N^c = N$ = total number of electrons, it is $D(N^c) = 0$ because $N^c = 0$ corresponds to the entire atom, for which the SCF result is correct, while for $N^c = N$ nothing is left in the "outer" region, meaning that all terms of eq. [10] are naught.

Figures 1 and 2 describe argon and indicate how $D(N^c)$ varies with N^c. The results of Fig. 1 were obtained from the single-ζ and double-ζ Slater bases of Clementi and Roetti (3), those of Fig. 2 from selected popular Gaussian bases developed by Pople and co-workers (4). Figures 3 and 4 display Slater basis results for nickel and krypton, respectively. These examples are typical. The results are self explanatory.

Yet, it seems unpractical to present all our results by means of figures, as was done in the preceding examples. A more compact presentation was selected as follows. The deviations $D(N^c)$ were calculated from eq. [12] at intervals spaced[2] by $\Delta N^c = 0.5$ e, starting from $N^c = 0.5$ up to $N^c = N - 0.5$ e. The final result for each basis set is then conveniently given as the root-mean-square (RMS) of these deviations. While some information is lost in this manner, namely as regards the profile of $D(N_c)$ in the various regions of space, the RMS deviations offer a simple quality index for the bases to which they correspond. The results obtained from Slater orbitals (3, 5) are given in Table 1, for the atoms Li–Kr. Table 2 reports the quality indices calculated for a representative collection of well-known Gaussian-type orbitals (4, 6–8).

4. Discussion and conclusions

The quality indices obtained with the single-ζ, double-ζ, and the near Hartree–Fock Slater-type orbitals of Clementi

[2]The selection of $\Delta N^c = 0.5$ e is arbitrary. It is convenient because it describes the profile of $D(N^c)$ vs. N^c with sufficient accuracy to permit meaningful comparisons. Smaller ΔN^c increments were also considered, with an added computational burden, but tests indicated that the usually minor numerical changes do not affect the overall conclusions reached in this work.

Can. J. Chem. Downloaded from www.nrcresearchpress.com by 88.255.202.194 on 09/08/12
For personal use only.

Can. J. Chem. Downloaded from www.nrcresearchpress.com by 88.255.202.194 on 09/08/12
For personal use only.

and Roetti (3) (Table 1) may serve as a convenient reference.[3] The noise of double-ζ calculations is roughly one tenth that of the single-ζ basis, while in near Hartree–Fock calculations this noise is further reduced by a factor of 10, approximately. Constraints imposed on ζ and the type of expansion to be used for *s*-type orbitals in order to satisfy the cusp condition are included in Malli's bases (5), which is attractive because they give a predominant weight to the description of the charge density at the nucleus. On the whole, these constraints produce a slight deterioration, which, however, seems acceptable.

As regards the familiar Gaussian basis sets of ref. 4 (Table 2), the superiority of the STO-5G and STO-6G sets over STO-3G and STO-4G is seemingly clear-cut. Comparison with Table 1 suggests that the STO-6G basis approaches the quality of a single-ζ Slater basis. The 4-31G basis does not seem to live up to its expectation as a double-ζ basis, which it is by design. We shall return to it a little later. For the first-row atoms, the 6-31G and 6-311G bases, in contrast, tend to approach double-ζ quality. Huzinaga's (10*s*6*p*) basis (6), as well as Dunning's (10*s*6*p*) → [5*s*4*p*] contraction (7), approach this result even better. Interestingly, in contrast with the general trends, with the [5*s*4*p*] basis the noise is systematically somewhat larger, but the energy always slightly better, than what is obtained in Slater double-ζ basis calculations. Finally, van Duijneveldt's (13*s*8*p*) basis (8) leans towards near Hartree–Fock quality.

But this assessment is incomplete. Inspection of Fig. 2 (which is a typical example) shows that the deviations of the STO-3G basis primarily cloud the short-range region. Turning our attention now to the outer atomic regions, beyond a core of 2 electrons, which are of particular interest in molecular problems (bonding, conformational effects, etc.) treated in the LCAO-MO approximation, we ask about the profile of these deviations in the chemically important valence regions. As for the STO-*N*G bases, Table 3 indicates that, for all practical purposes, the quality of the STO-3G and STO-6G expansions is the same, particularly for the first-row elements. It is fair to conclude that, beyond a core of 2 electrons, the profile of STO-*N*G bases is essentially that of single-ζ Slater expansions. It is also clear that in this region the 4-31G and 6-31G bases approach, and that the 6-311G basis surpasses, the quality of double-ζ Slater expansions. Finally, in the valence regions of second-row elements, beyond a core of 10 electrons, all STO-*N*G bases are similar in quality (Table 4), but exhibit a larger noise as the corresponding single-ζ Slater bases. The 6-31G basis, however, comes certainly as close to the true Hartree–Fock result as a double-ζ Slater expansion.

[3]We have examined whether near Hartree–Fock functions given with more significant figures than in ref. 3 would improve on the results of Table 1. This is not the case. We thank Drs. G. Corongiú and E. Clementi for their help in this matter.

All the bases used here as examples are well known, and so are their properties. This has oriented our selection. Therefore, one hardly did expect to learn anything basically new about them. But that was not our intention. The point made here touches the potential of eqs. [3] and [12]: they provide blunt information, unbiased by any a priori knowledge we may have, as to how closely SCF orbital descriptions approach the true Hartree–Fock limit and thus offer a meaningful objective quality ordering of SCF orbital bases with respect to one another and with respect to that limit, in a scale uniquely defined by the latter. In a sense, eq. [12] is but a mechanical device, no replacement for the flair involved in the art of researching good basis functions, yet capable of monitoring and documenting in a simple numerical manner what is otherwise the privilege of intuition supported by vast experience (6, 9). Our approach adds some welcome sharpness from which comparisons between orbital bases should benefit.[4] Extension to molecular LCAO wave functions is in progress.

Acknowledgements

The financial assistance given by le Fonds pour la formation de chercheurs et l'aide à la recherche (FCAR) Québec, and by the Natural Sciences and Engineering Research Council of Canada is gratefully acknowledged.

1. S. Fliszár, N. Desmarais, and G. Dancausse. Can. J. Chem. **70**, 537 (1992).
2. H. Eyring, J. Walter, and G. E. Kimball. Quantum chemistry. Wiley, New York; 1944.
3. E. Clementi and C. Roetti. At. Data, Nucl. Data Tables, **14**, 179 (1974).
4. M. J. Frisch, M. Head-Gordon, G. W. Trucks, J. B. Foresman, H. B. Schlegel, K. Raghavachari, M. Robb, J. S. Binkley, C. Gonzalez, D. J. Defrees, D. J. Fox, R. A. Whiteside, R. Seeger, C. F. Melius, J. Baker, R. L. Martin, L. R. Kahn, J. J. P. Stewart, S. Topil, and J. A. Pople. Gaussian 90, Revision J. Gaussian Inc., Pittsburgh, Pa. 1990.
5. G. Malli. Can. J. Phys. **44**, 3121 (1966); G. Malli and S. Fraga. Can. J. Phys. **44**, 3131 (1966); S. Fraga and G. Malli. Many-electron systems; properties and interactions. W. B. Saunders Co., Philadelphia, London, and Toronto. 1968.
6. S. Huzinaga. J. Chem. Phys. **42**, 1293 (1965).
7. T. H. Dunning, Jr. J. Chem. Phys. **55**, 716 (1971).
8. F. B. van Duijneveldt. Gaussian basis sets for the atoms H–Ne for use in molecular calculations. RJ 945. IBM Research Laboratory, San Jose, Calif. 1971.
9. E. R. Davidson and D. Feller. Chem. Rev. **86**, 681 (1986); R. Ahlrichs and P. R. Taylor. J. Chim. Phys. **78**, 315 (1981); C. Salez and A. Veillard. Theor. Chim. Acta, **11**, 441 (1968); W. J. Hehre, L. Radom, P. V. R. Schleyer, and J. A. Pople. Ab initio molecular orbital theory. John Wiley & Sons, New York. 1986.

[4]The appropriate programs are made available by the authors.

Solid state intermolecular interactions in cyanofunctionalized diselenadiazolyl dimers

WILLIAM M. DAVIS, ROBIN G. HICKS, RICHARD T. OAKLEY,[1] AND BAIYI ZHAO
Guelph–Waterloo Centre for Graduate Work in Chemistry, Department of Chemistry and Biochemistry, University of Guelph, Guelph, Ont., Canada N1G 2W1

AND

NICHOLAS J. TAYLOR
Department of Chemistry, University of Waterloo, Waterloo, Ont., Canada N2L 3G1

Received September 15, 1992

WILLIAM M. DAVIS, ROBIN G. HICKS, RICHARD T. OAKLEY, BAIYI ZHAO, and NICHOLAS J. TAYLOR. Can. J. Chem. **71**, 180 (1993).

The preparation and crystal and molecular structure of the monofunctional 1,2,3,5-diselenadiazolyl radical [RCN_2Se_2] (R = 3,5-dicyanophenyl) are described. Crystals of [$(CN)_2C_6H_3CN_2Se_2$] are triclinic, space group $P\bar{1}$, a = 7.197(2), b = 10.753(3), c = 13.345(5) Å, α = 88.00(3)°, β = 82.05(2)°, γ = 81.00(2)°, MW = 311.1, Z = 4. The structure consists of stacked arrays of radical dimers laced together by networks of short CN---Se contacts, but the steric bulk of the organic ligand leads to a pairwise aggregation of [CN_2Se_2] columns. These structural features are compared with those observed in related dimers, and the results interpreted in the light of extended Hückel band calculations on a series of model structures. The results provide a qualitative correlation between the size and dimensionality of the intermolecular Se---Se network and the degree of crystal orbital dispersion.

WILLIAM M. DAVIS, ROBIN G. HICKS, RICHARD T. OAKLEY, BAIYI ZHAO et NICHOLAS J. TAYLOR. Can. J. Chem. **71**, 180 (1993).

On a préparé le radical monofonctionnel 1,2,3,5-disélénadiazolyle [RCN_2Se_2]$^{\cdot}$ et on a déterminé ses structures cristalline et moléculaire. Les cristaux du [$(CN)_2C_6H_3CN_2Se_2$] sont tricliniques, groupe d'espace $P\bar{1}$, avec a = 7,197(2), b = 10,753(3) et c = 13,345(5) Å, α = 88,00(3)°, β = 82,05(2)° et γ = 81,00(2)°, PM = 311,1 et Z = 4. La structure consiste en des empilements de dimères de radicaux reliés entre eux par des réseaux de contacts CN · · · Se courts; toutefois, le volume stérique des ligands organiques conduit à une agrégation par paire des colonnes de [CN_2Se_2]. On compare ces caractéristiques structurales avec celles observées dans des dimères apparentés et on interprète les résultats en fonction de calculs étendus de la bande de Hückel sur une série de structures modèles. Les résultats fournissent une corrélation qualitative entre la grosseur et la dimension du réseau Se · · · Se intermoléculaire et le degré de dispersion de l'orbitale cristalline.

[Traduit par la rédaction]

Introduction

We recently reported the preparation and structures of the dimers of several 1,2,3,5-diselenadiazolyl radicals, including the 4- and 3-cyanophenyl derivatives **1** and **2** (1). This work resulted from our interest in the design of low-dimensional molecular conductors from neutral radicals (2). In these systems, as elsewhere (3–5), the nitrile moiety serves as a structure-influencing functional group by interacting with the chalcogen atoms of neighbouring radical dimers; the CN---Se contacts so generated link dimers together in ribbon-like (head-to-tail) networks. In the 4-cyanophenyl dimer, adjacent ribbons run in opposite directions, while in the 3-cyanophenyl system the ribbons stack in nearly vertical arrays. All these structures are characterized by extended lateral Se---Se contacts between adjacent ribbons and, where applicable (i.e., **2**), between stacked dimers. The number and magnitude of both vertical and lateral Se---Se interactions have important effects on crystal orbital dispersion (i.e., bandwidth), and hence electronic properties.

To explore further the relationship between crystal structure, bandwidth, and conductivity we have prepared and structurally characterized the 3,5-dicyanophenyl derivative **3**; the structural results from this and previous work are correlated with extended Hückel band structure calculations.

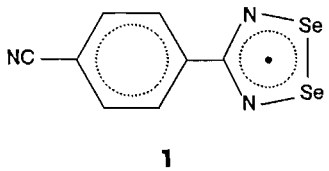

1

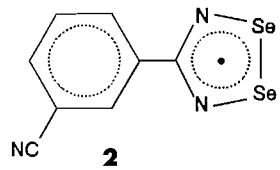

2

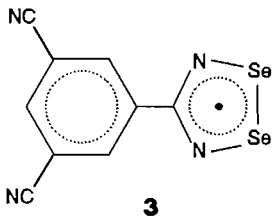

3

Results

Preparation of 3

The precursor to **3**, i.e., the corresponding 1,2,3,5-diselenadiazolium cation, was prepared by the condensation of the *N,N*-bis(trimethylsilyl)-*N'*-lithium salt of 3,5-dicyanobenzamidine with selenium dichloride (eq. [1]). Reduction of the cation with a slight excess of triphenylantimony afforded the crude radical **3**, which was purified by vacuum sublimation at 160°C/10^{-3} Torr (1 Torr = 133.3 Pa) to give dark green crystals.

[1]Author to whom correspondence may be addressed.

Can. J. Chem. Downloaded from www.nrcresearchpress.com by 88.255.202.194 on 09/08/12
For personal use only.

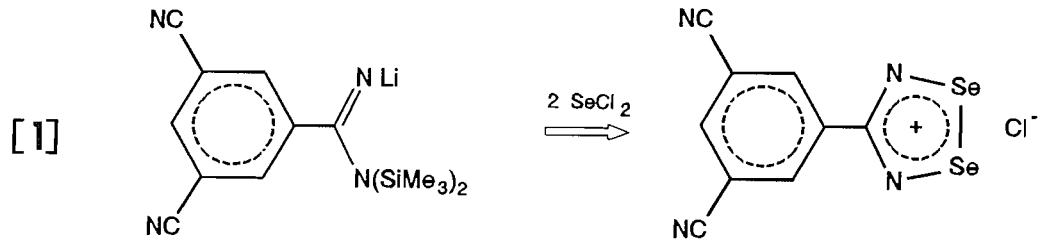

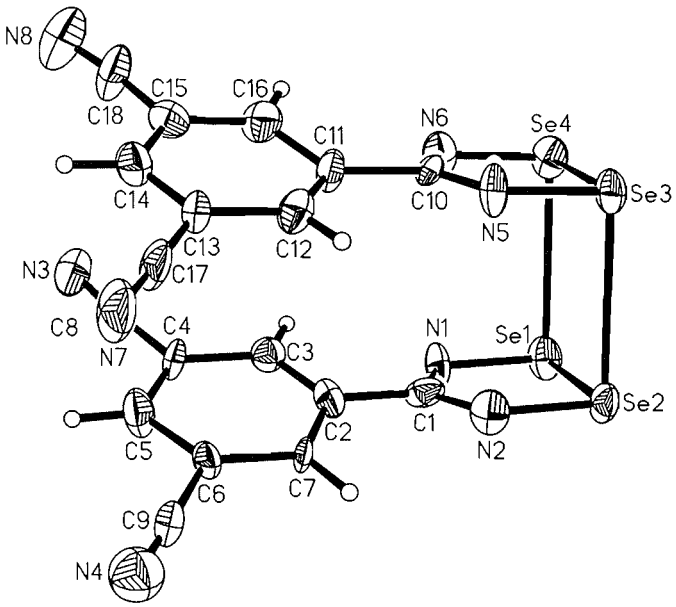

FIG. 1. MOLECULAR PLOT drawing for **3**, showing atom numbering scheme.

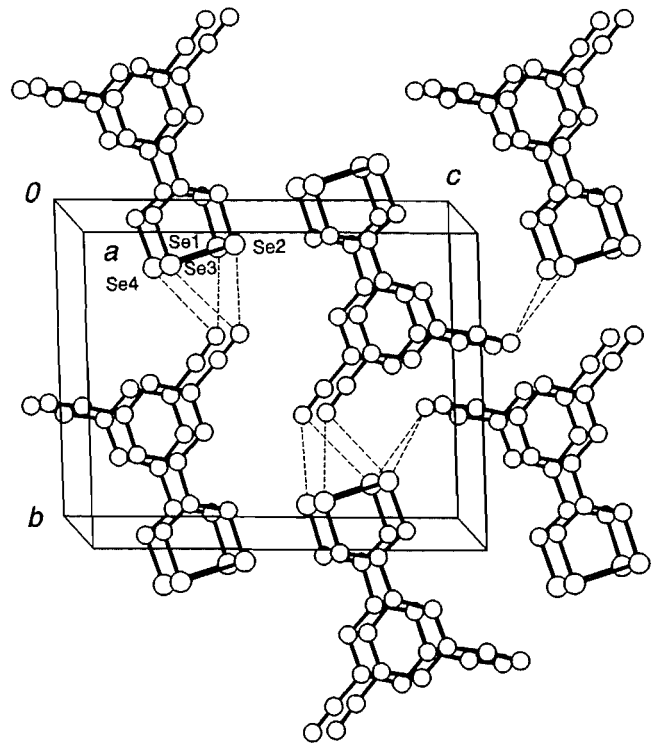

FIG. 2. *yz*-Projection of cell packing in **3**, with Se---NC contacts (dashed lines).

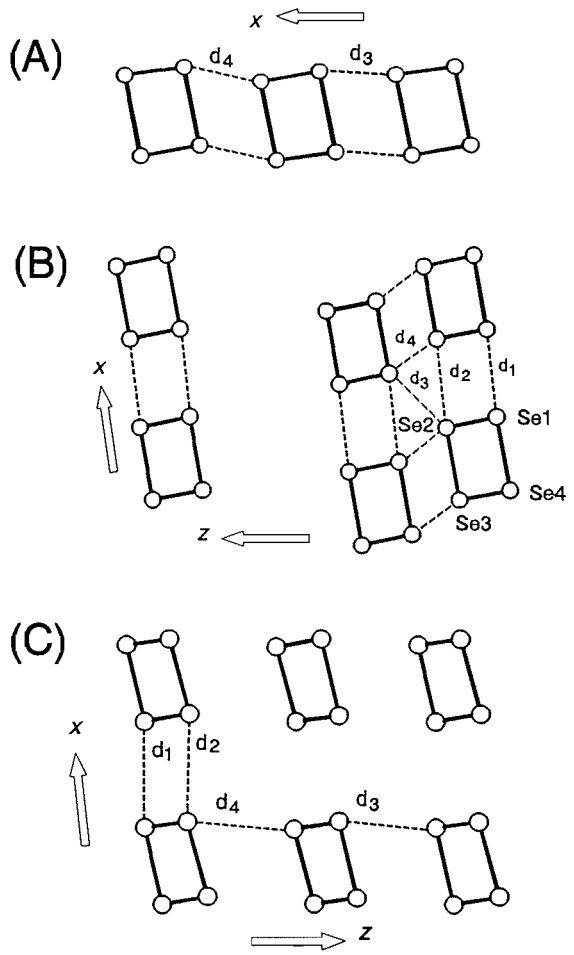

FIG. 3. Stacking of dimer units in **1** (*A*), **3** (*B*), and **2** (*C*), showing lateral and vertical interdimer Se---Se contacts. In **1** there are no vertical contacts, so only one layer is shown.

Crystal structure of **3**

Crystals of **3** belong to the triclinic space group $P\bar{1}$, and consist of radical dimers linked in a cofacial manner through two interannular Se---Se bonds (mean of d_1 and d_2 is 3.239 Å). A drawing of a single dimer unit is shown in Fig. 1. Non-hydrogen coordinates are compiled in Table 1 and internal structural parameters, which are typical for this class of compound, are summarized in Table 2.

The crystal structure of **3** (Fig. 2) consists of rows of radical dimers along *y* linked by CN---Se contacts that are reminiscent of the monocyanophenyl systems. There are also slightly different CN---Se interactions between molecules in adjacent ribbons. The former contacts link a nitrile to two neighbouring selenium atoms within one radical unit (Se1 and Se2 *or* Se3 and Se4), while the latter involve two selenium

Can. J. Chem. Downloaded from www.nrcresearchpress.com by 88.255.202.194 on 09/08/12
For personal use only.

Can. J. Chem. Downloaded from www.nrcresearchpress.com by 88.255.202.194 on 09/08/12
For personal use only.

TABLE 1. Atomic coordinates and equivalent isotropic thermal parameters for **3**; esd's are in parentheses

Atom	x	y	z	U(eq)[a]
Se(1)	0.3995(2)	0.1651(1)	0.2610(1)	36.5(5)
Se(2)	0.3314(2)	0.1064(1)	0.4302(1)	32.5(5)
Se(3)	−0.1178(2)	0.1609(1)	0.4192(1)	30.5(5)
Se(4)	−0.0560(2)	0.2208(1)	0.2502(1)	36.1(5)
N(1)	0.4008(18)	0.0080(11)	0.2206(10)	37(4)
N(2)	0.3312(18)	−0.0526(11)	0.3923(9)	35(4)
N(3)	0.2819(23)	−0.3840(14)	−0.0501(12)	54(6)
N(4)	0.4241(20)	−0.6204(14)	0.4287(11)	51(4)
N(5)	−0.1353(19)	0.0029(10)	0.3840(10)	36(4)
N(6)	−0.0719(20)	0.0671(12)	0.2092(9)	39(5)
N(7)	−0.0669(24)	−0.5628(12)	0.4035(12)	56(6)
N(8)	−0.2377(25)	−0.3225(16)	−0.0575(12)	67(7)
C(1)	0.3684(19)	−0.0759(12)	0.2937(10)	29(5)
C(2)	0.3630(20)	−0.2089(13)	0.2650(11)	33(5)
C(3)	0.3450(19)	−0.2281(13)	0.1647(10)	28(3)
C(4)	0.3408(21)	−0.3541(13)	0.1353(10)	31(5)
C(5)	0.3677(23)	−0.4569(14)	0.2012(11)	40(5)
C(6)	−0.3865(20)	−0.4296(12)	0.3021(12)	31(5)
C(7)	0.3916(17)	−0.3070(11)	0.3326(10)	25(4)
C(8)	0.3060(24)	−0.3760(15)	0.0330(12)	41(6)
C(9)	0.4100(23)	−0.5358(15)	0.3731(12)	39(6)
C(10)	−0.1096(18)	−0.0125(12)	0.2848(11)	28(5)
C(11)	−0.1175(22)	−0.1420(12)	0.2513(11)	31(5)
C(12)	−0.1085(21)	−0.2498(14)	0.3184(11)	34(5)
C(13)	−0.1159(20)	−0.3705(13)	0.2873(11)	32(5)
C(14)	−0.1447(21)	−0.3861(14)	0.1871(12)	38(5)
C(15)	−0.1709(21)	−0.2867(14)	0.1216(11)	35(5)
C(16)	−0.1619(20)	−0.1696(14)	0.1547(12)	37(5)
C(17)	−0.0884(23)	−0.4753(13)	0.3523(12)	37(5)
C(18)	−0.2094(29)	−0.2995(17)	0.0238(14)	55(7)

[a]Equivalent isotropic U defined as one-third of the trace of the orthogonalized U_{ij} tensor.

TABLE 2. Selected intra- and interdimer Se---Se distances (Å)

	Compound		
	1	**2**	**3**
Mean intradimer Se---Se distances[a]			
	3.23(4)	3.27(4)	3.24(4)
Interdimer Se---Se distances[b]			
d_1	—	4.197(5)	4.038(2)
d_2	—	4.105(4)	4.079(2)
d_3	3.890(3)	3.837(3)	3.716(3)
d_4	3.829(3)	3.930(3)	3.846(2)

[a]Numbers in parentheses are ranges.
[b]Numbers in parentheses are esd's.

atoms spanning a dimer (Se1 and Se4). The ribbons stack along x to produce near-vertical arrays of radical dimers. The two interdimer Se---Se contacts within a stack, d_1 (Se1---Se4′) and d_2 (Se2---Se3′) (mean 4.059 Å), are slightly shorter than those found in **2** (mean 4.15 Å). As Fig. 3*B* illustrates, the dimer stacks exist as isolated pairs spanned by the bulky dicyanophenyl ligand. Consequently, Se---Se interactions between stacks are limited to the pairwise contacts d_3 (Se2---Se2′, 3.716 Å) and d_4 (Se2---Se3′, 3.846 Å).

Band structure of 3

The crystal structure of the diselenadiazolyl dimer reported here is, like those of the cyanophenyl derivatives described earlier, strongly influenced by intermolecular CN---Se interactions, which serve to orient dimer units into ribbons or sheets. In the case of the 4-cyanophenyl compound **1**, the antiparallel arrangement of adjacent ribbons affords only lateral Se---Se contacts between dimer units (Fig. 3*A*), while structures **2** and **3** possess stacked assemblies in which dimer units are connected by vertical as well as lateral Se---Se interdimer contacts (Table 2). In the case of **3** these contacts are only pairwise in nature while in **2** they link dimer units into extended networks. Within the context of the design of molecular species that crystallize in a manner which enhances orbital interactions in a multidimensional manner, the series of cyanophenyl structures now in hand provides an opportunity to probe the extent and consequences of intermolecular Se---Se interactions in a systematic manner. To this end we have carried out extended Hückel band structure calculations on a number of model structures related to **1**, **2**, and **3**.

The density of states (DOS) for the structure of **3** is shown in Fig. 4*B*. Also shown are the corresponding DOS diagrams for two model "fragments" related to **3**. The first (Fig. 4*A*) is for a dicyanobenzene structure in which the organic unit is placed in the same positions as are the dicyanophenyl ligands in the unit cell of **3**. The second fragment (Fig.

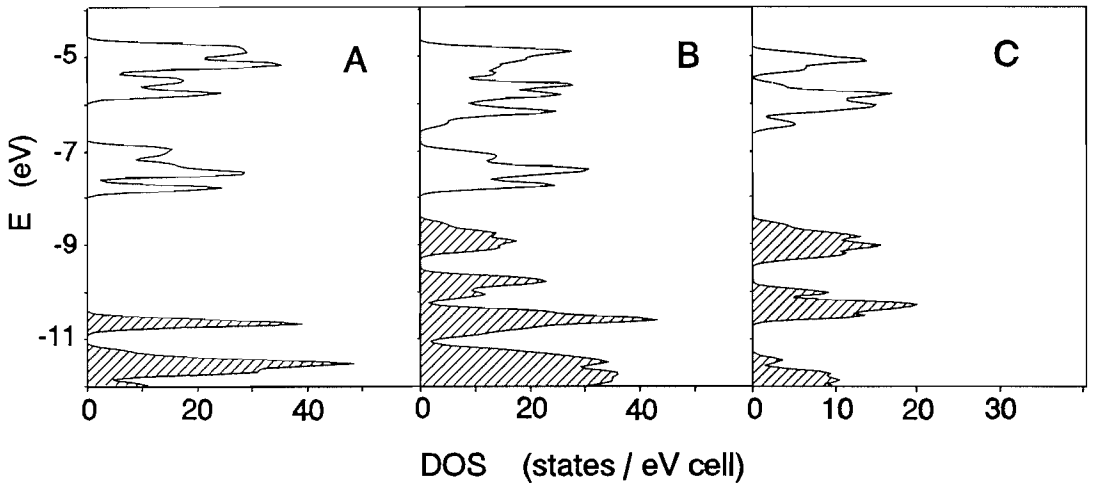

FIG. 4. Density of States (DOS) for (*A*) dicyanobenzene, (*B*) **3**, and (*C*) HCN_2Se_2. The packing pattern is defined by the crystal structure of **3**.

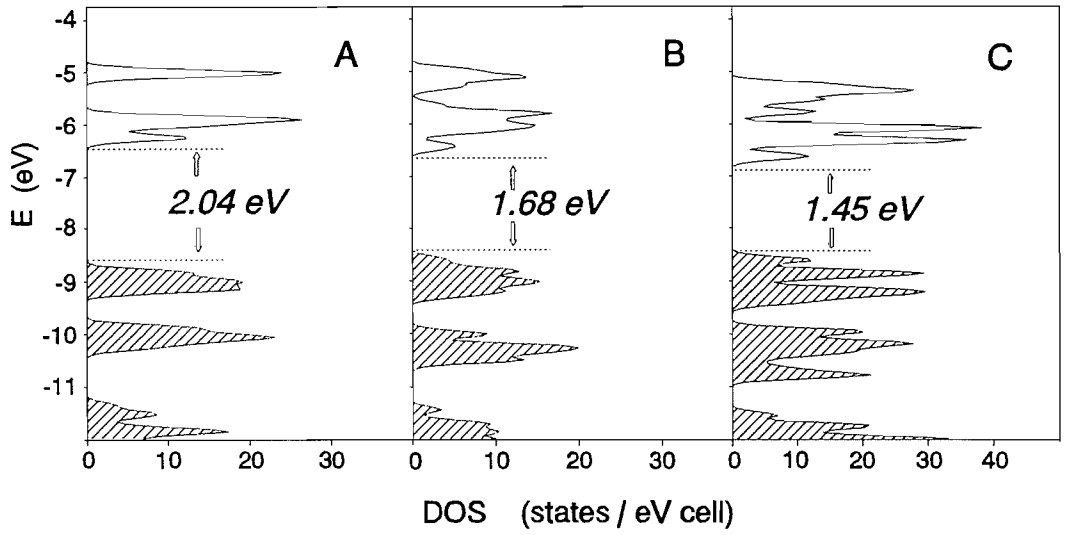

FIG. 5. π-SOMO interactions within and between HCN_2Se_2 radicals, illustrating the development of band-spreading.

4*C*) is HCN_2Se_2, i.e., the basic heterocyclic unit, again located in all the regular positions of the full structure, but with the organic ligand replaced by hydrogen. The combination of the DOS diagrams for the two fragments facilitates a clearer understanding of the origin of the band structure of **3** itself. This approach, i.e., of examining parts of the structure as well as the full structure, is, of course, a routine event in the discussion of molecular electronic structure (6), and was invoked in this case because of the electronic characteristics of the dicyanophenyl group. The low-lying acceptor (vacant) orbitals, which can be loosely described as π^*(CN), generate non-interacting "intruder" states in the full DOS diagram, and can give rise to a false impression of the band gap for the full structure. Correlation of the two fragment DOS diagrams with that of the full structure reveals a relatively clearer picture of the valence and conduction bands associated with the $[HCN_2Se_2]_2$ building blocks. Indeed, insofar as the SOMO orbitals of $[RCN_2Se_2]^{\cdot}$ are nodal at carbon (Fig. 5), it is not surprising that the neither the dispersion nor position of the valence and conduction bands of the model $[HCN_2Se_2]_2$ structure are perturbed by the attachment of the dicyano moiety.

A similar approach, i.e., one using $[HCN_2Se_2]_2$ fragments rather than the full structure, has been applied to analyse the extent of Se---Se interactions in **1** and **2**. The results of these calculations are presented in Fig. 6. Comparison of the dispersion (here approximated by the bandwidth) of the valence and conduction bands from these model systems, and also the valence/conduction band gaps, reveals a satisfying trend that parallels the structural data described above. In **1**, where stacking of dimers is absent, and only lateral interdimer interactions are observed, relatively narrow valence and conduction bands are observed, and the band gap is large. In **3** (Fig. 4*C*), lateral interactions are only pairwise, and band dispersion from such interactions is likely to be small. However, insofar as the structure is stacked, dispersion arising from interactions up and down the stack can be expected to reduce the band gap relative to **1**. For structure **2** extended interactions both within and between columns are observed. Bandwidths accordingly increase, and the va-

Can. J. Chem. Downloaded from www.nrcresearchpress.com by 88.255.202.194 on 09/08/12
For personal use only.

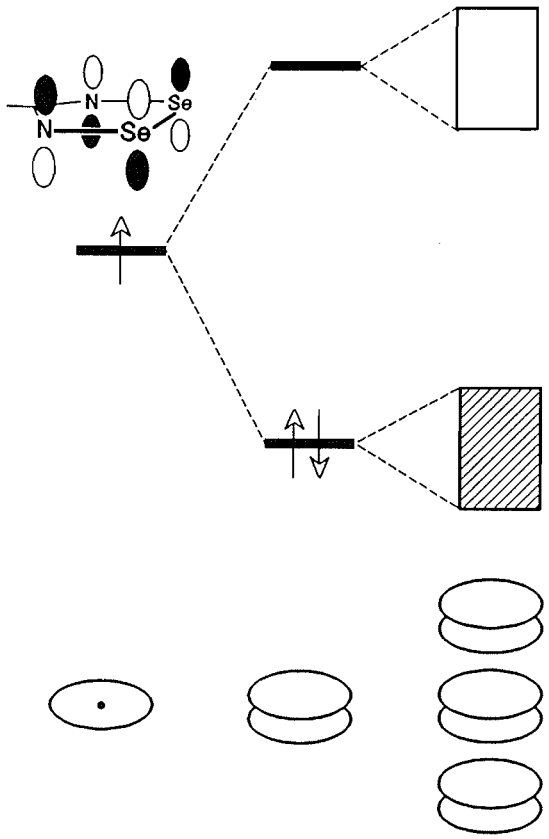

FIG. 6. Density of States (DOS) for HCN_2Se_2 units with packing pattern defined by the crystal structures of **1** (*A*), **3** (*B*), and **2** (*C*).

lence-to-conduction band gap in **2** is less than in either **1** or **3**.

Summary

The three diselenadiazolyl crystal structures under consideration all consist of molecular units, the greater part of which is a cyanoaryl moiety. The heterocyclic radical dimer fragment (i.e., $[\text{-}CN_2Se_2]_2$), which is the "building block" whose solid state properties we wish to probe, constitutes a relatively minor component of the overall molecule. In the polyfunctional diselenadiazolyl radicals we have studied (7–9), the density of the $[\text{-}CN_2Se_2]_2$ blocks within the unit cell is greater, and hence the number and magnitude of the Se---Se contacts is significantly enhanced. As a result of the relatively large size of the organic substituent in the present systems the number and (or) magnitude of significant Se---Se contacts is reduced, and the extent of intermolecular orbital interactions is diminished. Nonetheless the structural differences that are observed along the series **1–3** can be correlated, albeit qualitatively, with band structure calculations on simple model systems related to the three structures.

Insofar as electrical conductivity in these systems can be ascribed to a mechanism involving thermal activation across the valence/conduction band gap, the less extensive solid state networks found in all of **1–3**, and the wider band gaps found for their model counterparts, are all consistent with the poorer conductivity found for these systems compared to the bifunctional compounds previously characterized. Within the group, the relative conductivities appear to be consistent with the trend in the band gaps given above. Both **1** and **3** are insulating, and compound **2** was earlier shown to have a room temperature conductivity near 10^{-9} S cm^{-1}. This value is significantly lower than the conductivities of bifunctional systems.

Experimental

Starting materials and general procedures

1,3,5-Benzenetricarbonyl trichloride, lithium bis(trimethylsilyl)amide, selenium powder, and triphenylantimony were all obtained commercially (Aldrich). 1,3,5-Tricyanobenzene was prepared from the tricarbonyl trichloride according to literature methods (10) and $LiN(SiMe_3)_2$ was converted to its diethyl etherate prior to use. Selenium tetrachloride was prepared by direct oxidation of selenium powder with chlorine (11). Acetonitrile (Fisher HPLC grade) was purified by distillation from P_2O_5, toluene was dried by distillation from sodium, and diethyl ether by distillation from lithium aluminum hydride. All reactions were performed under an atmosphere of nitrogen. Mass spectra (70 eV, EI) were recorded on a Kratos MS890 mass spectrometer. Infrared (CsI optics, Nujol mulls) were obtained on a Nicolet 20SX/C FTIR instrument. Elemental analyses were performed by MHW Laboratories, Phoenix, Arizona.

Preparation of N-*lithio*-N′,N′-*bis(trimethylsilyl)-3,5-dicyanobenzamidine*

This compound was prepared by a modification of the procedure used for tris(trimethylsilyl)amidines (12). A solution of $LiN(SiMe_3)_2 \cdot Et_2O$ (5.60 g, 23.2 mmol) in 50 mL of toluene was added dropwise to a slurry of 1,3,5-tricyanobenzene (3.59 g, 23.4 mmol) in 80 mL of toluene. After stirring for 1 h, the tan-coloured precipitate so produced was filtered, washed with three 20-mL portions of toluene, and pumped to dryness. The *N*-lithiated amidine was obtained in virtually quantitative yield and used in subsequent reactions without further purification.

Preparation of $[3,5\text{-}(CN)_2C_6H_3CN_2Se_2]^{\cdot}$ **3**

Solid *N*-lithio-*N*′,*N*′-bis(trimethylsilyl)-3,5-dicyanobenzamidine (3.21 g, 10.0 mmol) was added to a solution of $SeCl_2$ (generated *in situ* by mixing $SeCl_4$ (2.23 g, 10.0 mmol) and Se powder (0.79 g, 10.0 mmol) in 30 mL of acetonitrile). The mixture was heated to gentle reflux for 1 h, cooled, and filtered to yield crude $[3,5\text{-}(CN)_2C_6H_3CN_2Se_2]^+Cl^-$ as a dark red powder. This solid was slurried in 40 mL of acetonitrile, solid Ph_3Sb (1.80 g, 5.1 mmol) was added, and the mixture was refluxed for 90 min. The resulting dark green solid was filtered, washed with three 10-mL portions of acetonitrile, and dried *in vacuo*. Sublimation of the crude product at 160°C/10^{-3} Torr produced $[3,5\text{-}(CN)_2C_6H_3CN_2Se_2]$ as lustrous metallic green crystals (0.88 g, yield 27%), dec. 280–284°C. IR (2000–200 cm^{-1}): 1465 (vs), 1436 (m), 1377 (s), 1338 (m), 1324 (w), 1214 (m), 1155 (w), 954 (w), 940 (w), 926 (w), 905 (s), 774 (s), 764 (vs), 746 (m), 721 (w), 697 (s), 669 (m), 655 (w), 633 (vs), 616 (w), 545 (s), 471 (w), 390 (s), 291 (s) cm^{-1}. Mass spectrum *m/e*: 327 (M^+, 64%), 174 (Se_2N^+, 100%), 160 (Se_2^+, 30%), 153 ($C_6H_3(CN)_3^+$, 13%), 94 (SeN^+, 11%), 80 (Se^+, 16%). Mass spectral isotope distributions (for selenium) were consistent with the assigned fragments. Anal. calcd. for $C_9H_3N_4Se_2$: C 33.25, H 0.93, N 17.24; found: C 33.27, H 1.08, N 17.13.

X-ray measurements on **3**

X-ray data were collected on a Siemens R3m/V diffractometer at 293 K with monochromated MoK_α (λ = 0.71073 Å) radiation; crystals were mounted on glass fibers with epoxy. The crystals belong to the triclinic space group $P\bar{1}$ and have unit cell parameters a = 7.197(2), b = 10.753(3), c = 13.345(5) Å, α = 88.00(3)°, β = 82.05(2)°, γ = 81.00(2)°, MW = 311.1, Z = 4. Data were collected using a $2\theta/\theta$ method with scan widths from 1.1° below $K_{\alpha 1}$ to 1.1° above $K_{\alpha 2}$. The structure was solved by Patterson and Fourier techniques using Siemens SHELXTL PLUS software and

Can. J. Chem. Downloaded from www.nrcresearchpress.com by 88.255.202.194 on 09/08/12
For personal use only.

refined by full-matrix least squares which minimized $\Sigma(F_o - F_c)^2$. The final R and R_w values of 0.0664 and 0.1071 were based respectively on 2186 observed unique data with $F > 6.0\sigma(F)$. Atoms N2 and C3 were refined isotropically due to data-set limitations.[2]

Extended Hückel band calculations

Extended Hückel calculations were performed with the EHMACC suite of programs, using parameters discussed previously (9). The programs were compiled with the NDP Fortran compiler (version 4.0.2) and implemented under DOS 5.0 on a 486/50 personal computer.

Acknowledgement

Financial support was provided by the Natural Sciences and Engineering Research Council of Canada.

1. A. W. Cordes, R. C. Haddon, R. G. Hicks, R. T. Oakley, and T. T. M. Palstra. Inorg. Chem. **31**, 1802 (1992).
2. (*a*) R. C. Haddon. Nature (London), **256**, 394 (1975); (*b*) Aust. J. Chem. **28**, 2343 (1975); (*c*) A. W. Cordes, R. C. Haddon, and R. T. Oakley. *In* The chemistry of inorganic ring systems. *Edited by* R. Steudel. Elsevier, Amsterdam. 1992. p. 295.
3. (*a*) E. O. Schlemper and D. Britton. Acta Crystallogr. **18**, 419 (1965); (*b*) R. B. Heiart and G. B. Carpenter. Acta Crystallogr. **9**, 889 (1956).
4. T. Suzuki, H. Fujui, Y. Yamashita, C. Kabuto, S. Tanaka, M. Harasawa, T. Mukai, and T. Miyashi. J. Am. Chem. Soc. **118**, 3034 (1992).
5. N. W. Alcock. Adv. Inorg. Radiochem. **15**, 1 (1972).
6. R. Hoffmann. Solids and surfaces, a chemist's view of bonding in extended structures. VCH Publishers, New York. 1988.
7. M. P. Andrews, A. W. Cordes, D. C. Douglass, R. M. Fleming, S. H. Glarum, R. C. Haddon, P. Marsh, R. T. Oakley, T. T. M. Palstra, L. F. Schneemeyer, G. W. Trucks, R. Tycko, J. V. Waszczak, K. M. Young, and N. M. Zimmerman. J. Am. Chem. Soc. **113**, 3559 (1991).
8. A. W. Cordes, R. C. Haddon, R. Hicks. R. T. Oakley, T. T. M. Palstra, L. N. Schneemeyer, J. V. Waszczak, and N. M. Zimmerman. J. Am. Chem. Soc. **114**, 1729 (1992).
9. A. W. Cordes, R. C. Haddon, R. T. Oakley, L. F. Schneemeyer, J. V. Waszczak, K. M. Young, and N. M. Zimmerman. J. Am. Chem. Soc. **113**, 582 (1991).
10. A. S. Bailey, B. R. Henn, and J. M. Langdon. Tetrahedron, **19**, 161 (1963).
11. G. Brauer. Handbook of preparative chemistry. Vol. 1. Academic, New York. 1963. p. 243.
12. R. T. Boeré, R. T. Oakley, and R. W. Reed. J. Organomet. Chem. **331**, 161 (1987).

[2]Tables of crystal data, hydrogen atom parameters, bond lengths and angles, anisotropic thermal parameters, and structure factors for **3** have been deposited as Supplementary Material and may be purchased from: The Depository of Unpublished Data, Document Delivery, CISTI, National Research Council Canada, Ottawa, Canada KIA OS2.

Tables of crystal data, hydrogen atom parameters, and bond lengths and angles have also been deposited with the Cambridge Crystallographic Data Centre and can be obtained from The Director, Cambridge Crystallographic Data Centre, University Chemical Laboratory, 12 Union Road, Cambridge C821 EZ, U.K.

Can. J. Chem. Downloaded from www.nrcresearchpress.com by 88.255.202.194 on 09/08/12
For personal use only.

Nucleic acid related compounds. 77. 2′,3′-Didehydro-2′,3′-dideoxy-2′(and 3′)-methylnucleosides via [3,3]-sigmatropic rearrangements of 2′(and 3′)-methylene-3′(and 2′)-*O*-thiocarbonyl derivatives and radical reduction of a 2′-chloro-3′-methylene analogue[1]

VINCENTE SAMANO AND MORRIS J. ROBINS[2]
Department of Chemistry, Brigham Young University, Provo, UT 84602, U.S.A.

Received August 11, 1992

VINCENTE SAMANO and MORRIS J. ROBINS. Can. J. Chem. **71**, 186 (1993).

Treatment of 5′-*O*-(*tert*-butyldiphenylsilyl)-2′(and 3′)-deoxy-2′(and 3′)-methyleneuridine (and adenosine) derivatives with phenyl chlorothionocarbonate gave the 3′(and 2′)-*O*-phenoxythiocarbonyl intermediates, which underwent spontaneous [3,3]-sigmatropic rearrangement to give the 2′,3′-didehydro-2′,3′-dideoxy-2′(and 3′)-(phenoxycarbonylthio)methyl analogues. These allylic thioesters were subjected to tributylstannane-mediated hydrodesulfurization and deprotection to give 2′,3′-didehydro-2′,3′-dideoxy-2′(and 3′)-methyluridine (and adenosine). Tributylstannane-mediated hydrodehalogenation of a 2′-chloro-2′,3′-dideoxy-3′-methyleneuridine derivative afforded the 2′,3′-didehydro-2′,3′-dideoxy-3′-methyl product of allylic transposition exclusively.

VINCENTE SAMANO et MORRIS J. ROBINS. Can. J. Chem. **71**, 186 (1993).

Le traitement des dérivés 5′-*O*-(*tert*-butyldiphénylsilyl)-2′(et 3′)-désoxy-2′(et 3′)-méthylèneuridine (et adénosine) avec du chlorothionocarbonate de phényle conduit à des intermédiaires 3′(et 2′)-*O*-phénoxythiocarbonyles qui subissent une transposition sigmatropique-[3,3] spontanée fournissant les analogues 2′,3′-didéhydro-2′,3′-didésoxy-2′(et 3′)-(phénoxycarbonylthio)méthyles. On a soumis ces thioesthers allyliques à une hydrodésulfurisation catalysée par le tributylstannane et à une déprotection conduisant à la 2′,3′-didéhydro-2′,3′-didésoxy-2′ (et 3′)-méthyluridine (et adénosine). L'hydrodéshalogénation, catalysée par le tributylstannane, d'un dérive 2′-chloro-2′,3′-didésoxy-3′-méthylèneuridine conduit uniquement au produit 2′,3′-didéhydro-2′,3′-didésoxy-3′-méthyle provenant de la transposition allylique.
[Traduit par la rédaction]

Introduction

A number of 2′,3′-dideoxynucleoside (**A**) and 2′,3′-unsaturated (2′,3′-didehydro) analogue triphosphates cause selective inhibition of the HIV reverse transcriptase in vitro (1). Potent anti-HIV activity has been reported for the 2′,3′-didehydro-2′,3′-dideoxy analogues of cytidine (2) (**B**), thymidine (3, and references therein) (**C**), and carbocyclic

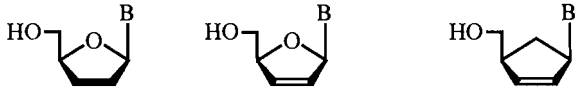

A **B** B = cytosin-1-yl **C** B = thymin-1-yl **D** B = guanin-9-yl

guanosine (4) (**D**). We have reported 2′(and 3′)-deoxy-2′(and 3′)-methylene (**8** and **1**, respectively) pyrimidine (5*a*) and purine (5*b*) nucleosides and their mechanism-based inhibition of ribonucleotide reductase (6) and *S*-adenosyl-L-homocysteine hydrolase (7). We now describe conversions of **1** and **8** into 2′,3′-didehydro-2′,3′-dideoxy-3′(and 2′)-methyl nucleosides (**7** and **14**) via [3,3]-sigmatropic rearrangements of the 2′(and 3′)-*O*-phenoxythiocarbonyl intermediates **3** and **10**, respectively. The endocyclic alkenes **7** and **14** also are produced exclusively by radical dehalogenation of the allylic chloro derivatives **4** and **12**, respectively. During our investigation, Ueda and co-workers (8) reported obtaining the 2′,3′-didehydro-2′,3′-dideoxy-2′(and 3′)-methyl-5-methyluridines via a similar rearrangement of 2′(and 3′)-deoxy-3′(and 2′)-*O*-(imidazol-1-yl)thiocarbonyl-2′(and 3′)-methylene derivatives. Czernecki *et al.* (9) also prepared 2′,3′-didehydro-2′,3′-dideoxy-3′-methyl-5-methyluridine starting from 1,2-*O*-isopropylidene-α-D-xylofuranose via sugar transformations, coupling, and an analogous rearrangement.

Results and discussion

Protection of the 3′-deoxy-3′-methylene nucleosides **1***a* (5*a*) and **1***b* (5*b*) (Scheme 1) with *tert*-butyldiphenylsilyl (TBDPS) chloride/pyridine (10) gave the 5′-*O*-TBDPS derivatives **2***a* (94%) and **2***b* (95%). Treatment of **2**(*a* and *b*) with phenyl chlorothionocarbonate/DMAP/MeCN (11) at ambient temperature resulted in spontaneous conversion into their 2′,3′-didehydro-2′,3′-dideoxy-3′-(phenoxycarbonylthio)methyl analogues **5***a* (80%) and **5***b* (93%). The ^{1}H NMR spectrum of **5***a* (Table 1) had an olefinic proton peak at δ 6.99 for H2′ and an AB system at δ 3.59, 3.89 (J = 15.6 Hz) for the CH_2S group. Similar ^{1}H NMR data were observed for **5***b*. Precedent for the spontaneous [3,3]-sigmatropic rearrangement of the allylic 2′-*O*-phenoxythiocarbonyl intermediates **3***a,b* (observed at lower temperatures by ^{1}H NMR) was noted with allyl *S*-methyl xanthate in 1909 (12), and the mechanism and synthetic applications have been studied (13, and references therein). Tributyltin hydride-mediated hydrodesulfurization (Bu_3SnH/AIBN/toluene/Δ) of **5***a* and **5***b* gave **6***a* (85%) and **6***b* (90%) exclusively, and deprotection with tetrabutylammonium fluoride in tetrahydrofuran (TBAF/THF) and purification gave crystalline 1-(2,3-dideoxy-3-methyl-β-D-*glycero*-pent-2-enofuranosyl)uracil (2′,3′-didehydro-2′,3′-dideoxy-3′-methyluridine) (**7***a*, 60%) and **7***b* (60%), respectively.

Since these exomethylene allylic thioesters, **5**, with an endocyclic double bond gave only the exomethyl endocyclic alkenes, the 2′-chloro-2′-deoxy derivative **4***a* was prepared to evaluate whether initial generation of a radical

[1]For the previous paper in this series see ref. 18.
[2]Author to whom correspondence may be addressed.

Can. J. Chem. Downloaded from www.nrcresearchpress.com by 88.255.202.194 on 09/08/12
For personal use only.

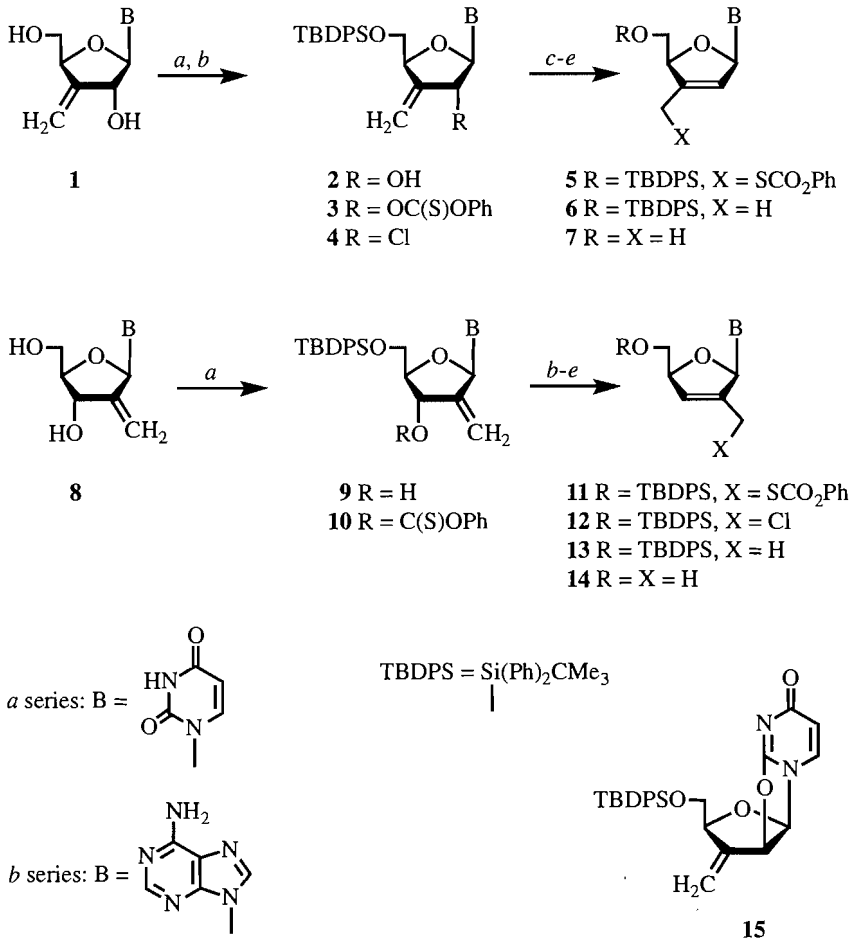

(*a*) TBDPS-Cl/pyridine; (*b*) $SOCl_2$/pyridine; (*c*) PhOC(S)Cl/DMAP; (*d*) Bu_3SnH/AIBN/toluene/100°C; (*e*) Bu_4NF/THF

SCHEME 1

at C2′ would have any effect on product formation. Treatment of **2***a* with thionyl chloride/pyridine/dichloromethane afforded **4***a* (62%) and the cyclonucleoside **15** (14%). O^2,2′-Anhydronucleoside intermediates such as **15** have been identified in various preparations (14) of pyrimidine 2′-deoxy-2′-halonucleosides from 2′-hydroxy precursors. Treatment of **4***a* with Bu_3SnH/AIBN/toluene/Δ gave **6***a* (95%) as the only observed product. Thus, this radical species underwent highly preferential allylic hydrogen transfer at the exocyclic methylene carbon to give the *endo* unsaturated compound, in harmony with the greater thermodynamic stability of 1-methylcyclopentene relative to methylenecyclopentane (15).

The rearrangement/desulfurization/dehalogenation sequence worked equally well with 2′-deoxy-2′-methylene nucleosides. Silylation of **8***a* (5*a*) and **8***b* (5*b*) gave **9***a* (90%) and **9***b* (95%), respectively. Treatment of **9***a* and **9***b* with phenyl chlorothionocarbonate afforded the rearranged products **11***a* (85%) and 9-[5-*O*-(*tert*-butyldiphenylsilyl)-2,3-dideoxy-2-(phenoxycarbonylthio)methyl-β-D-*glycero*-pent-2-enofuranosyl]adenine (**11***b*, 87%). Treatment of **11***a* and **11***b* with Bu_3SnH/AIBN/toluene/Δ gave **13***a* (85%) and **13***b* (84%), which were deprotected to afford **14***a* (95%) and **14***b* (95%), respectively. Compound **14***a* was previously synthesized in low yield from a 2′,3′-didehydro-2′,3′-dideoxy-3′-phenylselenone nucleoside (16).

Treatment of **9***a* with $SOCl_2$/pyridine/CH_2Cl_2 afforded the allylic transposition product **12***a* (89%) in contrast to the results with **2***a* (*vide supra*). Formation of pyrimidine O^2,3′-anhydronucleosides is much less facile than cyclization at the 2′-position (17). Thus, the initially formed 3′-chlorosulfite presumably underwent S_N2' substitution by attack of chloride at the exocyclic 2′-methylene carbon to gave **12***a*. Treatment of **12***a* with Bu_3SnH/AIBN/toluene/Δ again gave the exomethyl endocyclic alkene **13***a* (88%) exclusively.

In summary, we have developed mild conversions of 2′(and 3′)-deoxy-2′(and 3′)-methylenenucleosides into their corresponding 2′,3′-didehydro-2′,3′-dideoxy-2′(and 3′)-methyl analogues via formation of phenyl thionocarbonate esters, spontaneous rearrangement of the latter to allylic thioesters at ambient temperature, and tributylstannane-mediated allylic hydrodesulfurization. We also have demonstrated that the radical-mediated hydrodehalogenations of 5′-*O*-TBDPS-2′-chloromethyl-2′,3′-didehydro-2′,3′-dideoxyuridine and 5′-*O*-TBDPS-2′-chloro-2′,3′-dideoxy-3′-methyleneuridine give the more thermodynamically stable 2′(and 3′)-methyl-2′,3′-didehydro-2′,3′-dideoxyuridine derivatives (exomethyl endocyclic alkenes).

Can. J. Chem. Downloaded from www.nrcresearchpress.com by 88.255.202.194 on 09/08/12
For personal use only.

TABLE 1. ^{1}H NMR spectral data[a]

Compound	H1′[b] (J)	H2′[c] (J)	H3′ ($J_{3'-4'}$)	H4′	H5′[d] ($J_{5'-5''}$)	H5″[d] ($J_{5''-4'}$)	CH_AH_B[e] (J)	CH_AH_B[e] (J)	H5[b](2)[f]	H6[b](8)[f]	NH(NH$_2$)[g]	OH2′[b]/3′[b]/5′[h] ($J_{OH-2'/3'/5'5''}$)	Others
2*a*	5.84 (5.8)	4.64 (1.6)[i,j]		4.76[c]	4.01 (11.4)	3.77 (3.0)	5.17 (2.0)	5.47 (2.2)	5.48 (8.0)	7.76	9.20	3.75[g]	1.01 ($SiCMe_3$) 7.3–7.6 ($SiPh_2$)
2*b*	5.69 (6.4)	5.03 (2.1)[i,j]		4.86[c]	3.88 (11.0)	3.75 (3.5)	5.22 (2.8)	5.48 (2.4)	8.01	8.28	5.75	3.77[g]	0.92 ($SiCMe_3$) 7.2–7.6 ($SiPh_2$)
4*a*	6.14 (6.2)	4.66 (1.8)[j]		4.74[k] (2.2)	4.09 (11.6)	3.81 (2.6)	5.27 (1.8)	5.54 (2.0)	5.39 (8.4)	7.67	8.22		1.04 ($SiCMe_3$) 7.3–7.6 ($SiPh_2$)
5*a*	5.86[g]	6.99		4.87[c]	4.09 (12.0)	3.95 (2.4)	3.59[l] (15.6)	3.89[l]	4.99 (8.2)	7.68	8.40		1.1 ($SiCMe_3$) 7.1–7.6 ($SiPh_2$, OPh)
5*b*	6.06[g]	7.02		4.95[c]	3.91 (11.5)	3.82 (3.5)	3.68[l] (16.0)	3.94[l]	7.94	8.37	5.55		1.01 ($SiCMe_3$) 7.1–7.7 ($SiPh_2$, OPh)
6*a*	5.48[g]	6.92[c] (1.6)		4.63[c]	4.04 (12.0)	3.86 (2.2)			4.90 (8.2)	7.75	8.09		1.1 ($SiCMe_3$) 7.3–7.6 ($SiPh_2$) 1.91[g] (Me3′)
6*b*	5.70[c] (1.5)	6.99 (1.5)		4.74[g]	3.88 (11.6)	3.75 (3.5)			7.99	8.38	5.66		1.06 ($SiCMe_3$) 7.2–7.7 ($SiPh_2$) 1.92[g] (Me3′)
7*a*	5.53[g]	6.71[g]		4.55[g]	3.62[m] (2.7)				5.55 (8.3)	7.86	11.25	4.98 (4.9)	1.81[g] (Me3′)
7*b*	5.75[g]	6.84[g]		4.68[g]	3.62[m]				8.12	8.22	7.25	5.10 (4.8)	1.86[g] (Me3′)
9*a*	6.65[c]		4.83[n] (7.0)	3.78[o]	4.03 (12.0)	3.91 (2.6)	5.42 (1.6)	5.53 (2.0)	5.39 (8.2)	7.50	9.12	2.27 (7.0)	1.05 ($SiCMe_3$) 7.3–7.7 ($SiPh_2$)
9*b*	6.75[k] (1.6)		5.02 (1.5)[i,j]	3.92[c]	3.44[m]		5.39 (1.9)	5.59 (1.6)	7.90	8.34	5.75	3.35[g]	1.05 ($SiCMe_3$) 7.3–7.8 ($SiPh_2$)
11*a*	6.23[g]		7.04[d] (3.4)	4.88[c]	3.99 (12.0)	3.84 (2.8)	3.57[l] (15.4)	3.64[l]	5.20 (8.2)	7.75	9.90		1.09 ($SiCMe_3$) 7.1–7.7 ($SiPh_2$, OPh)
11*b*	6.32[g]		7.02[g]	5.00[g]	3.83[m] (4.5)		3.40[l] (15.5)	3.66[l]	7.99	8.32	6.17		1.05 ($SiCMe_3$) 7.1–7.7 ($SiPh_2$, OPh)
12*a*	6.21[c] (1.4)		7.00[d] (3.6)	4.87[c]	4.10 (12.0)	3.86 (2.8)	4.04[p]		5.20 (8.0)	7.75	8.78		1.03 ($SiCMe_3$) 7.3–7.7 ($SiPh_2$)
13*a*	5.83[k] (1.6)		6.82[g]	4.81[c]	3.93 (11.8)	3.80 (3.0)			5.16 (8.0)	7.60	8.25		1.04 ($SiCMe_3$) 7.3–7.7 ($SiPh_2$) 1.7[g] (Me2′)
13*b*	5.96[k] (1.6)		6.85[g]	4.93[c]	3.77[m] (4.8)				7.85	8.33	5.81		1.05 ($SiCMe_3$) 7.2–7.7 ($SiPh_2$) 1.66[g] (Me2′)
14*a*	6.02[k] (1.6)		6.66[g]	4.73[c]	3.56[m]				5.64 (8.0)	7.75	11.4	4.97 (4.7)	1.60[g] (Me2′)
14*b*	6.05[g]		6.74[g]	4.82[g]	3.57[m,d] (4.5)				8.12	8.21	7.30	5.06 (5.0)	1.60[g] (Me2′)
15	6.17 (2.5)	4.96[g]		4.72[g]	4.29 (12.1)	3.96 (2.5)	5.25[g]	5.54[g]	5.77 (6.9)	8.28			1.05 ($SiCMe_3$) 7.3–7.7 ($SiPh_2$)

[a]Chemical shifts (δ, Me_4Si internal); coupling constants (Hz, in parentheses); solvents: $CDCl_3$ for **2***a*–**6***b* and **9***a*–**13***b*, Me_2SO-d_6 for **7***a*,*b* and **14***a*,*b*.
[b]Doublet (unless noted otherwise).
[c]Multiplet.
[d]Doublet of doublets.
[e]($J_{\text{"apparent"}}$) from incompletely resolved peaks.
[f]Singlet.
[g]Broad singlet.
[h]Triplet (unless noted otherwise).
[i]After D_2O exchange.
[j]Doublet of "apparent" quartets ($J_{\text{"q"}}$).
[k]"Apparent" quartet.
[l]Broad doublet.
[m]H5′,5″ collapsed ($J_{5'-4'}$).
[n]Broad triplet.
[o]Doublet of triplets.
[p]$H_{A,B}$ collapsed.

Can. J. Chem. Downloaded from www.nrcresearchpress.com by 88.255.202.194 on 09/08/12
For personal use only.

TABLE 2. ^{13}C NMR spectral data[a]

Compound	C2	C4	C5	C6	C8	CH_2/CH_3	C1′	C2′	C3′	C4′	C5′
2*a*	152.18	164.27	103.14	140.74		110.64	89.80	77.25	146.04	82.04	66.51
2*b*	153.10	149.50	120.05	156.07	139.17	109.59	91.55	77.50	146.39	83.29	67.01
4*a*	150.68	163.07	103.68	139.72		112.99	89.16	60.63	144.00	81.73	65.99
5*a*	151.19	163.74	102.96	141.30		27.56	88.80	124.73	144.18	87.09	64.02
5*b*	153.87	151.64	120.00	155.90	139.25	27.83	87.66	123.34	144.90	87.37	65.14
6*a*	151.19	163.53	102.67	141.71		13.13	89.09	121.33	144.66	88.94	64.19
6*b*	153.74	150.52	120.00	155.94	139.50	13.04	89.35	120.21	145.20	87.75	65.01
7*a*	151.24	163.70	101.46	141.78		12.28	88.71	120.31	144.49	88.26	60.85
7*b*	152.74	149.31	120.03	156.27	139.00	12.63	89.40	120.26	143.55	87.31	61.62
9*a*	151.38	163.97	103.38	141.23		114.31	85.01	149.05	70.76	84.52	62.81
9*b*	153.77	150.32	120.00	156.00	139.00	114.08	84.85	148.73	71.98	83.33	63.48
11*a*	151.12	163.14	103.47	141.00		26.99	90.00	135.77	132.07	86.81	65.34
11*b*	153.87	150.64	120.25	156.28	139.54	27.07	89.06	134.95	132.05	87.26	66.01
12*a*	151.04	163.17	103.41	141.02		37.34	89.70	136.45	133.18	86.70	65.30
13*a*	151.67	164.02	103.47	140.97		12.05	91.57	135.87	128.34	86.76	65.72
13*b*	153.84	150.79	120.18	156.03	139.44	12.00	90.50	134.99	128.59	87.19	66.48
14*a*	151.37	163.41	102.44	140.94		11.51	90.73	133.94	129.08	86.93	62.66
14*b*	153.04	149.73	119.07	156.43	139.50	11.41	89.97	133.92	128.13	87.53	63.06
15	112.80	167.57	105.72	144.17		114.45	91.93	62.35	142.26	82.19	67.77

[a]δ (Me_4Si internal) in $CDCl_3$ except **7***a,b* and **14***a,b* in Me_2SO-d_6.

Can. J. Chem. Downloaded from www.nrcresearchpress.com by 88.255.202.194 on 09/08/12
For personal use only.

Experimental section

General procedures

Uncorrected melting points were obtained with a capillary melting tube apparatus. Ultraviolet (UV) spectra of MeOH solutions were determined with a Hewlett–Packard 8451A spectrophotometer. ^1H (200 MHz) (Table 1) and ^{13}C (50 MHz) (Table 2) NMR spectra were obtained with a Varian Gemini-200 spectrometer. Low-resolution electron-impact mass spectra (MS) were determined with a Finnigan MAT 8430 spectrometer at 20 eV. Flash evaporations (<35°C bath temperatures) were effected with a rotary evaporator with water aspirator or mechanical oil pump vacuum. Flash chromatography was performed with E. Merck Kieselgel 60, 230–400 mesh. Unless specified otherwise, the solvent for chromatography was hexanes/EtOAc (7:3, v/v). Reagent grade solvents and reagents were distilled prior to use. Pyridine was dried by refluxing with and distillation from CaH_2. MeCN and toluene were distilled from P_4O_{10}. Elemental analyses were determined by M-H-W Laboratories, Phoenix, Ariz.

*1-(5-O-TBDPS-3-deoxy-3-methylene-β-D-*erythro-*pentofuranosyl)uracil* **2**a

Procedure A (10)

TBDPS-Cl (0.40 mL, 0.42 g, 1.56 mmol) was added to a solution of **1***a* (5*a*) (0.25 g, 1.04 mmol) in pyridine (5 mL) and the mixture was stirred at ambient temperature for 18 h. Solvent was evaporated and the residue partitioned between EtOAc (50 mL) and ice-cold 0.01 N HCl/H_2O (30 mL). The aqueous phase was extracted (EtOAc) and the combined organic phase was washed (saturated $NaHCO_3/H_2O$ and brine), dried (Na_2SO_4), and evaporated. The colorless foam (0.55 g) was used without further purification. For characterization, this material was chromatographed (hexane/EtOAc, 1:2) to give **2***a* (0.47 g, 94%) as a colorless solid foam: UV_{max}: 260 nm; MS *m/z*: 420 (10, M − CMe_3 − H), 309 (90, M − CMe_3 − BH), 281 (14, M − CMe_3 − BCHO), 199 (100, Ph_2SiOH).

*9-(5-O-TBDPS-3-deoxy-3-methylene-β-D-*erythro-*pentofuranosyl)adenine* **2**b

Procedure A was applied to **1***b* (5*b*) (0.56 g, 2.13 mmol) to give **2***b* (1.0 g, 95%) as a colorless solid foam: UV_{max}: 260 nm; MS *m/z*: 502 (4, MH^+), 444 (100, M − CMe_3), 309 (18, M − CMe_3 − BH), 199 (75, Ph_2SiOH).

*1-(5-O-TBDPS-2-chloro-2,3-dideoxy-3-methylene-β-D-*erythro-*pentofuranosyl)uracil* **4**a

Procedure B

$SOCl_2$ (37 μL, 60 mg, 0.5 mmol) in CH_2Cl_2 (0.5 mL) was added to **2***a* (50 mg, 0.10 mmol) and pyridine (41 μL, 40 mg, 0.5 mmol) in CH_2Cl_2 (1.5 mL) at 0°C. The mixture was stirred at ambient temperature for 48 h, diluted (CH_2Cl_2, 10 mL), and poured into saturated $NaHCO_3/H_2O$ (5 mL, 0°C). The aqueous phase was extracted (CH_2Cl_2) and the combined organic phase was dried (Na_2SO_4) and evaporated. The residue was chromatographed (hexane/EtOAc, 3:1) to give cyclonucleoside **15** (6.5 mg, 14%) and **4***a* (32 mg, 62%) as a colorless solid foam. **15**: UV_{max}: 306 nm; MS *m/z*: 403 (80, M − CMe_3), 327 (6, M − CMe_3 − Ph), 293 (40, M − CMe_3 − B), 199 (100, Ph_2SiOH). **4***a*: UV_{max}: 259 nm (ε 9000); MS *m/z*: 439 (3, M[^{35}Cl] − CMe_3), 441 (1, M[^{37}Cl] − CMe_3), 403 (40, M − CMe_3 − HCl), 293 (10, M − CMe_3 − Cl − B), 87 (100, M − BCHO − $Ph_2Si(CMe_3)OCH_2$). Anal. calcd. for $C_{26}H_{29}ClN_2O_4Si$: C 62.83, H 5.88, N 5.64; found: C 63.00, H 5.98, N 5.62.

*1-[5-O-TBDPS-2,3-dideoxy-3-(phenoxycarbonylthio)methyl-β-D-*glycero-*pent-2-enofuranosyl]uracil* **5**a

Procedure C (11)

DMAP (0.32 g, 2.7 mmol) was added to a solution of crude **2***a* (0.55 g) in MeCN (25 mL). Phenyl chlorothionocarbonate (0.18 mL, 0.22 g, 1.35 mmol) was added and the mixture was stirred at ambient temperature under N_2 for 18 h. Volatiles were evaporated and the residue was partitioned between EtOAc (50 mL) and brine/H_2O (1:1, 30 mL). The aqueous phase was extracted (EtOAc) and the combined organic phase was washed (saturated $NaHCO_3/H_2O$ and brine), dried (Na_2SO4), and evaporated. Chromatography (hexane/EtOAc, 1:1) gave **5***a* (0.51 g, 80% from **1***a*) as a colorless solid foam: UV_{max}: 260 nm (ε 9700); MS *m/z*: 557 (1, M − CMe_3), 445 (100, M − CMe_3 − BH), 291 (98, M − CMe_3 − BH_2 − PhOCOS). Anal. calcd. for $C_{33}H_{34}N_2O_6SSi$: C 64.47, H 5.57, N 4.56, S 5.22; found: C 64.45, H 5.64, N 4.54, S 5.30.

*9-[5-O-TBDPS-2,3-dideoxy-3-(phenoxycarbonylthio)methyl-β-D-*glycero-*pent-2-enofuranosyl]adenine* **5**b

Procedure C was applied to **2***b* (0.60 g, 1.2 mmol) to give **5***b* (0.70 g, 93%) as slightly colored needles (EtOAc/hexanes): mp 111–112°C; UV_{max}: 260 nm (ε 16 700); MS *m/z*: 580 (10, M −

Can. J. Chem. Downloaded from www.nrcresearchpress.com by 88.255.202.194 on 09/08/12
For personal use only.

CMe_3), 445 (100, M − CMe_3 − BH). Anal. calcd. for $C_{34}H_{35}N_5O_4SSi$: C 64.03, H 5.53, N 10.98; found: C 63.66, H 5.60, N 10.99.

*1-(5-O-TBDPS-2,3-dideoxy-3-methyl-β-D-*glycero*-pent-2-enofuranosyl)uracil* **6**a

Procedure D

AIBN (0.042 g, 0.25 mmol) and Bu_3SnH (0.56 mL, 0.61 g, 2.1 mmol) were added to a solution of **5***a* (0.43 g, 0.70 mmol) in toluene (20 mL). The solution was deoxygenated (N_2) for 20 min and then heated at 100°C under N_2 for 10 h. Volatiles were evaporated and the residue was chromatographed (hexane/EtOAc, gradient 4:1 → 1:1) to give **6***a* (0.27 g, 85%) as a colorless foam: UV_{max}: 260 nm; MS *m/z*: 293 (100, M − CMe_3 − BH), 199 (90, Ph_2SiOH), 187 (60, M − CMe_3 − BCH_2O − Ph). Analogous treatment of **4***a* (17 mg, 0.034 mmol) gave **6***a* (15 mg, 95%) with identical spectral data.

*9-(5-O-TBDPS-2,3-dideoxy-3-methyl-β-D-*glycero*-pent-2-enofuranosyl)adenine* **6**b

Procedure D was applied to **5***b* (0.44 g, 0.69 mmol) to give **6***b* (0.29 g, 90%) as colorless needles (EtOAc/hexane): mp 121–122°C; UV_{max}: 260 nm; MS *m/z*: 428 (95, M − CMe_3), 293 (100, M − CMe_3 − BH), 187 (90, M − CMe_3 − BCH_2O − Ph).

*1-(2,3-Dideoxy-3-methyl-β-D-*glycero*-pent-2-enofuranosyl)uracil (2',3'-didehydro-2',3-dideoxy-3'-methyluridine)* **7**a

Procedure E

Bu_4NF/THF (1 M; 0.54 mL, 0.54 mmol) was added to a solution of **6***a* (0.25 g, 0.54 mmol) in THF (15 mL) at 0°C. After 1 h at 0°C, the solution was evaporated (<25°C) and the residue was chromatographed (Dowex 50 (Na^+) resin/H_2O; elution with H_2O) to give a colorless residue containing uracil (TLC). Chromatography ($CHCl_3$/EtOH, 47:3) and crystallization (acetone/Et_2O) afforded **7***a* (0.072 g, 60%) as a colorless powder: mp 123–124°C; UV_{max}: 260 nm (ε 9600); MS *m/z*: 112 (100, M − BH). Anal. calcd. for $C_{10}H_{12}N_2O_4$: C 53.57, H 5.39, N 12.49; found: C 53.47, H 5.29, N 12.57.

*9-(2,3-Dideoxy-3-methyl-β-D-*glycero*-pent-2-enofuranosyl)-adenine (2',3'-didehydro-2',3'-dideoxy-3'-methyl-adenosine)* **7**b

Procedure E was applied to **6***b* (0.25 g, 0.51 mmol) with evaporation (<25°C) and direct chromatography ($CHCl_3$/EtOH, 93:7) to give **7***b* (0.075 g, 60%) as a colorless solid: mp 110–112°C; UV_{max}: 260 nm (ε 14 000); MS *m/z*: 248 (30, MH^+), 231 (100, MH − OH). Anal. calcd. for $C_{11}H_{13}N_5O_2 \cdot 0.25$ EtOH: C 53.38, H 5.65, N 27.06; found: C 53.35, H 5.36, N 26.82.

*1-(5-O-TBDPS-2-deoxy-2-methylene-β-D-*erythro*-pentofuranosyl)uracil* **9**a

Procedure A was applied to **8***a* (5*a*) (0.70 g, 2.91 mmol) to give **9***a* (1.25 g, 90%) as colorless prisms (EtOAc/hexane): mp 146–147°C; UV_{max}: 260 nm; MS *m/z*: 421 (96, M − CMe_3), 309 (20, M − CMe_3 − BH), 293 (100, M − CMe_3 − B − OH).

*9-(5-O-TBDPS-2-deoxy-2-methylene-β-D-*erythro*-pentofuranosyl)adenine* **9**b

Procedure A was applied to **8***b* (5*b*) (0.37 g, 1.4 mmol) to give **9***b* (0.66 g, 95%) as a colorless solid foam: UV_{max}: 260 nm; MS *m/z*: 444 (100, M − CMe_3), 309 (8, M − CMe_3 − BH).

*1-[5-O-TBDPS-2,3-dideoxy-2-(phenoxycarbonylthio)methyl-β-D-*glycero*-pent-2-enofuranosyl]uracil* **11**a

Procedure C was applied to **9***a* (0.40 g, 0.84 mmol) to give **11***a* (0.43 g, 85%) as a solid foam: UV_{max}: 260 nm (ε 9000); MS *m/z*: 556 (40, M − CMe_3 − H), 445 (100, M − CMe_3 − BH), 351 (30, M − CMe_3 − BH_2 − PhO), 293 (22, M − CMe_3 − B − PhOCOS). Anal. calcd. for $C_{33}H_{34}N_2O_6SSi$: C 64.47, H 5.57, N 4.56, S 5.22; found: C 64.59, H 5.41, N 4.56, S 5.15.

*9-[5-O-TBDPS-2,3-dideoxy-2-(phenoxycarbonylthio)methyl-β-D-*glycero*-pent-2-enofuranosyl]adenine* **11**b

Procedure C was applied to **9***b* (0.40 g, 0.80 mmol) to give **11***b* (0.34 g, 87%) as a colorless solid foam: UV_{max}: 260 nm (ε 18 000); MS *m/z*: 325 (20, M − CMe_3 − B − PhOCO), 293 (22, M − CMe_3 − B − PhOCOS), 199 (100, Ph_2SiOH). Anal. calcd. for $C_{34}H_{35}N_5O_4SSi$: C 64.03, H 5.53, N 10.98; found: C 64.20, H 5.31, N 10.80.

*1-(5-O-TBDPS-2-chloromethyl-2,3-dideoxy-β-D-*glycero*-pent-2-enofuranosyl)uracil* **12**a

Procedure B was applied to **9***a* (50 mg, 0.10 mmol) to give **12***a* (46 mg, 89%) as a colorless solid foam: UV_{max}: 260 nm (ε 9400); MS *m/z*: 403 (12, M − CMe_3 − HCl), 327 (6, M − CMe_3 − BH), 293 (18, M − CMe_3 − BH − Cl), 199 (100, Ph_2SiOH). Anal. calcd. for $C_{26}H_{29}ClN_2O_4Si$: C 62.83, H 5.88, N 5.64; found: C 62.81, H 5.82, N 5.56.

*1-(5-O-TBDPS-2,3-dideoxy-2-methyl-β-D-*glycero*-pent-2-enofuranosyl)uracil* **13**a

Procedure D was applied to **11***a* (0.30 g, 0.48 mmol) to give **13***a* (0.19 g, 85%) as colorless needles (Et_2O/hexane): mp 146–147°C; UV_{max}: 260 nm; MS *m/z*: 405 (5, M − CMe_3), 293 (100, M − CMe_3 − BH), 187 (60, M − CMe_3 − BCH_2O − Ph). Analogous treatment of **12***a* (36 mg, 0.076 mmol) by procedure D gave **13***a* (29 mg, 88%) with identical spectral data.

*9-(5-O-TBDPS-2,3-dideoxy-2-methyl-β-D-*glycero*-pent-2-enofuranosyl)adenine* **13**b

Procedure D was applied to **11***b* (0.35 g, 0.54 mmol) to give **13***b* (0.22 g, 84%) as a colorless solid (EtOAc/hexane): mp 166–167°C; UV_{max}: 260 nm; MS *m/z*: 428 (8, M − CMe_3), 293 (20, M − CMe_3 − BH), 95 (100, M − BH − $Ph_2Si(CMe_3)O$).

*1-(2,3-Dideoxy-2-methyl-β-D-*glycero*-pent-2-enofuranosyl)uracil (2',3'-didehydro-2',3'-dideoxy-2'-methyluridine)* **14**a *(16)*

Procedure E was applied to **13***a* (0.20 g, 0.43 mmol) to afford **14***a* (0.092 g, 95%) as a solid foam: UV_{max}: 259 nm (ε 9200); MS *m/z*: 224 (2, M^+), 193 (30, M − CH_2O), 113 (100, M − B). Anal. calcd. for $C_{10}H_{12}N_2O_4$: C 53.57, H 5.39, N 12.49; found: C 53.73, H 5.49, N 12.29.

*9-(2,3-Dideoxy-2-methyl-β-D-*glycero*-pent-2-enofuranosyl)-adenine (2',3'-didehydro-2',3'-dideoxy-2'-methyl-adenosine)* **14**b

Procedure E was applied to **13***b* (0.185 g, 0.38 mmol) with evaporation (<25°C) followed directly by chromatography ($CHCl_3$/EtOH, 47:3) to give **14***b* (0.085 g, 91%) as a colorless powder: mp 177–178°C; UV_{max}: 259 nm, (ε 14 000); MS *m/z*: 247 (6, M^+), 217 (10, M − CH_2O), 135 (100, BH), 112 (20, M − BH). Anal. calcd. for $C_{11}H_{13}N_5O_2$: C 53.43, H 5.30, N 28.32; found: C 53.27, H 5.47, N 28.10.

Acknowledgments

We thank the American Cancer Society (Grant No. DHP-34) and Brigham Young University Development Funds for generous support and Mrs. Kathryn M. Rollins for assistance with the manuscript.

1. (*a*) H. Mitsuya and S. Broder. Proc. Natl. Acad. Sci. U.S.A. **83**, 1911 (1986); (*b*) E. De Clercq. *In* Antiviral drug development: a multidisciplinary approach. NATO Advanced Study Institutes Series. Vol. A143. *Edited by* E. De Clercq and R. T. Walker. Plenum Press, New York. 1988. pp. 113–118.
2. (*a*) J. Balzarini, R. Pauwels, P. Herdewijn, E. De Clercq, D. A. Cooney, G.-J. Kang, M. Dalal, D. G. Johns, and S. Broder. Biochem. Biophys. Res. Commun. **140**, 735 (1986); (*b*) T.-S. Lin, R. F. Schinazi, M. S. Chen, E. Kinney-Thomas, and W. H. Prusoff. Biochem. Pharmacol. **36**, 311 (1987).
3. C. K. Chu, R. F. Schinazi, M. K. Ahn, G. V. Ullas, and Z. P. Gu. J. Med. Chem. **32**, 612, (1989).

4. R. Vince, M. Hua, J. Brownell, S. Daluge, F. Lee, W. M. Shannon, G. C. Lavelle, J. Qualls, O. S. Weislow, R. Kiser, P. G. Canonico, R. H. Schultz, V. L. Narayanan, J. G. Mayo, R. H. Shoemaker, and M. R. Boyd. Biochem. Biophys. Res. Commun. **156**, 1046 (1988).
5. (*a*) V. Samano and M. J. Robins. Synthesis, 283 (1991); (*b*) J. Org. Chem. **56**, 7108 (1991).
6. C. H. Baker, J. Banzon, J. M. Bollinger, J. Stubbe, V. Samano, M. J. Robins, B. Lippert, E. Jarvi, and R. Resvick. J. Med. Chem. **34**, 1879 (1991).
7. M. J. Robins, V. Samano, W. Zhang, J. Balzarini, E. De Clercq, R. T. Borchardt, Y. Lee, and C.-S. Yuan. J. Med. Chem. **35**, 2283 (1992).
8. (*a*) A. Matsuda, H. Okajima, and T. Ueda. Heterocycles, **29**, 25 (1989); (*b*) A. Matsuda, H. Okajima, A. Masuda, A. Kakefuda, Y. Yoshimura, and T. Ueda. Nucleosides Nucleotides, **11**, 197 (1992).
9. S. Czernecki, A. Ezzitouni, and P. Krausz. Synthesis, 651 (1990).
10. S. Hanessian and P. Lavallee. Can. J. Chem. **53**, 2975 (1975).
11. M. J. Robins, J. S. Wilson, and F. Hansske. J. Am. Chem. Soc. **105**, 4059 (1983).
12. B. Oddo and G. del Rosso. Gazz. Chim. Ital. **39**, 11 (1909); Chem. Abstr. **3**, 1004 (1909).
13. (*a*) D. L. Garmaise, A. Uchiyama, and A. F. McKay. J. Org. Chem. **27**, 4509 (1962); (*b*) F. E. Ziegler and Z. Zheng. Tetrahedron Lett. **48**, 5973 (1987).
14. (*a*) D. M. Brown, D. B. Parihar, and Sir A. Todd. J. Chem. Soc. 4242 (1958); (*b*) J. G. Moffatt. *In* Nucleoside analogues: chemistry, biology, and medical applications. NATO Advanced Study Instiutes Series. Vol. A26. *Edited by* R. T. Walker, E. De Clercq, and F. Eckstein. Plenum Press, New York. 1979. pp. 101–108.
15. K. B. Wiberg, D. J. Wasserman, E. J. Martin, and M. A. Murcko. J. Am. Chem. Soc. **107**, 6019 (1985).
16. J.-C. Wu and J. Chattopadhyaya. Tetrahedron, **46**, 2587 (1990).
17. J. G. Moffatt. *In* Nucleoside analogues: chemistry, biology, and medical applications. NATO Advanced Study Institutes Series. Vol. A26. *Edited by* R. T. Walker, E. De Clercq, and F. Eckstein. Plenum Press, New York. 1979. pp. 122–126.
18. S. F. Wnuk, N. K. Dalley, and M. J. Robins. J. Org. Chem. **58**, 111 (1993).

Can. J. Chem. Downloaded from www.nrcresearchpress.com by 88.255.202.194 on 09/08/12
For personal use only.

Nucleic acid related compounds. 78. Stereocontrolled syntheses of 6′(*E* and *Z*)-halovinyl analogues from uridine-derived vinylsulfones via vinyltin intermediates[1]

STANISLAW F. WNUK AND MORRIS J. ROBINS[2]
Department of Chemistry, Brigham Young University, Provo, UT 84602, U.S.A.

Received August 12, 1992

STANISLAW F. WNUK and MORRIS J. ROBINS. Can. J. Chem. **71**, 192 (1993).

Treatment of the 6′(*E*)-tosylvinyl homonucleoside **1***a* with Bu_3SnH/AIBN/toluene/Δ gave separable mixtures of 6′-vinylstannanes **2***a*(*E*/*Z*) in high yields. Stereospecific halodestannylations with *N*-iodosuccinimide, bromine, and *N*-bromosuccinimide proceeded smoothly to give the 6′(*E* or *Z*)-iodo(and bromo) vinyl compounds with retention of configuration. Chlorine or iodobenzene dichloride effected moderately stereoselective chlorodestannylation. Treatment of **2***a* with NH_4F/MeOH/Δ resulted in carbon–tin bond cleavage to give the free vinyl derivative **4***a*. Aqueous trifluoroacetic acid effected concomitant protiodestannylation and deprotection of **2***a* to give **4***b*. Treatment of **2***a*(*E*) with lead tetraacetate/acetonitrile and deprotection afforded acetylenic derivative **3***b*.

STANISLAW F. WNUK et MORRIS J. ROBINS. Can. J. Chem. **71**, 192 (1993).

Le traitement de l'homonucléoside de 6′(*E*)-tosylvinyle (**1***a*) avec le Bu_3SnH/AIBN/toluène/Δ conduit, avec d'excellents rendements, à des mélanges de 6′-vinylstannanes (**2***a*(*E*/*Z*)) que l'on peut sèparer. Les halodéstannylations stérospécifiques avec de la *N*-iodosuccinimide, du brome ou de la *N*-bromosuccinimide se réalisent facilement et conduisent à des composés 6′(*E* ou *Z*)-iodo(et bromo) vinyliques, avec rétention de configuration. Le chlore ou le dichlorure d'iodobenzène provoquent une chlorodéstannylation modérément stéréosélective. Le traitement du composé **2***a* avec du NH_4F/MeOH/Δ conduit à un clivage de la liaison carbone–étain avec la formation du dérivé vinylique libre **4***a*. L'acide trifluoroacétique aqueux permet d'effectuer la protiodéstannylation concomitante avec la déprotection du composé **2***a* qui fournit le composé **4***b*. Le traitement du composé **2***a*(*E*) avec du tétraacétate de plomb/acétonitrile, suivi d'une déprotection, conduit au dérivé acétylénique **3***b*.

[Traduit par la rédaction]

Introduction

Sulfones (1), vinyl sulfones (2), and vinyltin compounds (3) have recently been incorporated into the sugar moiety of nucleosides and used for a variety of transformations (4–8). Chattopadhyaya and co-workers (4) have prepared 1-(2,3-dideoxy-3-(*p*-toluenesulfonyl)-β-D-*glycero*-pent-2-enofuranosyl)uracil (and adenine) and uracil 2′(and 3′)-phenylselenone analogues and utilized these vinyl sulfones and selenones as Michael acceptors for functionalization of the carbohydrate moiety. Barton *et al.* have developed radical-mediated chemistry at C4′ for the stereocontrolled synthesis of chain-lengthened vinyl sulfones (5*a*) and synthesized sinefungin (5*b*) and its uracil analogue (5*c*).

Oxidation of 2′,3′-*O*-isopropylidene nucleosides and treatment of the resulting 5′-aldehydes with (*p*-toluenesulfonylmethylene)triphenylphosphorane afforded the *E*-vinylsulfone **1***a* (6*a*) and its adenine analogue (6*b*). Michael addition of hydrogen, thiomethanol, and ammonia gave 5′-substituted 5′,6′-dideoxy derivatives, but attempted removal of the tosyl group failed (6*a*) or was difficult (6*b*). Detosylation of the adenine analogue of **1***a* was effected via addition of tributylstannyllithium (6*b*).

Horner–Wittig treatment (7) of 2′-ketonucleosides with diethyl fluoro(phenylsulfonyl)methanephosphonate gave fluorovinyl sulfone diastereomers that were separated and converted into fluorovinylstannanes of retained stereochemistry with tributyltin hydride under free radical conditions. Hydrodestannylation with retention occurred upon protiolysis to give the 2′-deoxy-2′-fluoromethylenecytidines (**A**), which are potent inhibitors (7*b*) of ribonucleoside diphosphate reductase. Sulfonate isosteres of nucleoside monophosphates have been synthesized (8) via Horner–Emmons addition of a sulfonate-stabilized reagent to nucleoside 5′-aldehydes (or carbohydrate 3′-ketones) and incorporated into nonionic dinucleotide analogues.

Other Wittig reactions of nucleoside 5′-aldehydes have provided 6′-substituted hexofuranosyl nucleosides (9, 10), and recently the unsubstituted 5′-deoxy-5′-methyleneadenosine (6*b*) and its neplanocin A analogue (11) were prepared by this route. Hydroboration of a 5′-deoxy-5′-

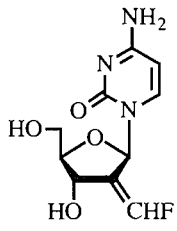

A

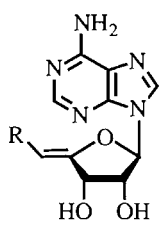

B (R = F or Cl)

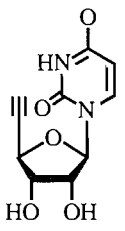

3*b*

methyleneadenosine derivative gave homoadenosine, 9-(5-deoxy-β-D-*ribo*-hexofuranosyl)adenine (12). Treatment of 5′-aldehydes with (dibromomethylene)triphenylphosphorane gave the 5′-(dibromomethylene)-5′-deoxyuridine and thymine analogues. The uracil compound was converted into acetylenic derivative **3***b* (10). The adenine analogue of **3***b* was prepared recently by analogous approaches and found to be a mechanism-based inhibitor of *S*-adenosyl-L-homocysteine hydrolase (13). The 5′(*Z*)-fluoro(and chloro) 4′,5′-unsaturated adenine nucleosides (**B**) also are potent inhibitors of this enzyme (14). Acetylenic and iodomethylene acyclo adenine analogues have been reported recently (15).

We now describe efficient syntheses of uridine-derived 6′(*E* and *Z*)-vinylstannanes **2***a* via radical-mediated detosylation (16) of vinyl sulfone **1***a*. Protiodestannylation gave

[1]For the previous paper in this series see ref. 22.
[2]Author to whom correspondence may be addressed.

Can. J. Chem. Downloaded from www.nrcresearchpress.com by 88.255.202.194 on 09/08/12
For personal use only.

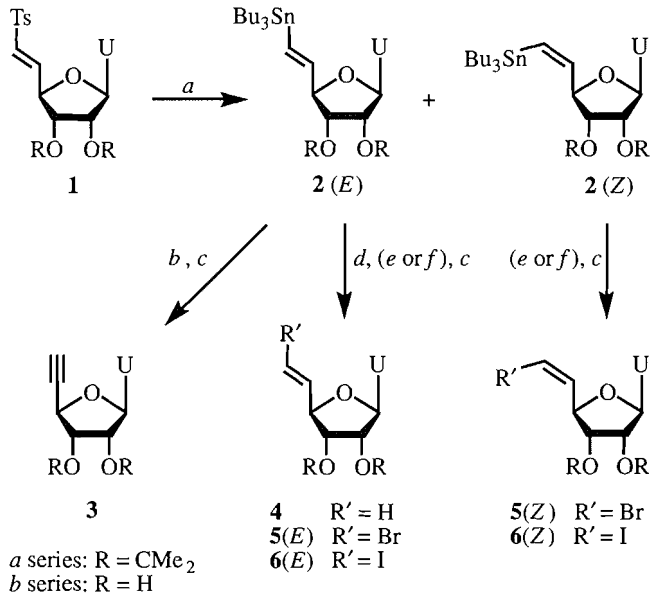

(*a*) Bu_3SnH/AIBN/toluene/Δ; (*b*) $Pb(OAc)_4/CH_3CN$; (*c*) CF_3CO_2H/H_2O; (*d*) NH_4F/MeOH/Δ; (*e*) (Br_2 or NBS/CCl_4/CH_2Cl_2/-40°C; (*f*) (I_2 or NIS)/CCl_4/CH_2Cl_2/-40°C

SCHEME 1

5′-deoxy-5′-methyleneuridine (**4***b*) and oxidative destannylation gave the acetylenic analogue **3***b*. Stereospecific conversion of the **2***a* diastereomers to 6′(*E* and *Z*)-halovinyl derivatives (**5**–**8**) provided convenient access to these 5′-halomethylene analogues, which are difficult to prepare directly.

Results and discussion

The crystalline vinyl sulfone **1***a* was prepared in 85% yield from 2′,3′-*O*-isopropylideneuridine (6*a*). Treatment of **1***a* with Bu_3SnH/AIBN/toluene/Δ gave the 6′-vinylstannanes **2***a* (*E*/*Z*, ~2.8:1; 87%) (Scheme 1). The **2***a*(*E*) ($^3J_{5'-6'}$ = 19.1 Hz) and **2***a*(*Z*) ($^3J_{5'-6'}$ = 12.8 Hz) diastereomers were separated by silica column chromatography. It is noteworthy that no conversion of vinyl sulfone **1***a* to its allylic isomer was observed, since this isomerization had occurred with classical reductive sulfone cleavage methods (6*a*).

Treatment of **2***a* with silica/CH_2Cl_2 (17), CsF/MeOH, or NH_3/MeOH (7*b*) gave the 5′-methylene derivative **4***a* in low yields. However, **4***a* was obtained smoothly (94%) upon treatment of **2***a* with NH_4F/MeOH/Δ, as we recently described for efficient silicon–oxygen bond cleavage (18). Deprotection of **4***a* with aqueous trifluoroacetic acid gave 5′-deoxy-5′-methyleneuridine (**4***b*). Aqueous trifluoroacetic acid effected concomitant protiodestannylation and deprotection of **2***a*(*E*) to give **4***b* (94%). The free 6′-vinylstannane **2***b*(*E*) was obtained (~65%) when unprotected vinyl sulfone **1***b* was treated with Bu_3SnH/AIBN/toluene/*N*,*N*-dimethylacetamide/Δ. Treatment of **2***a*(*E*) with lead tetraacetate (1.25 equiv.) in acetonitrile (19) afforded the acetylenic derivative **3***a* (72%) (plus recovered **2***a*(*E*) (18%)), which was deprotected to give **3***b* (80%).

Bromo(and iodo)destannylation with electrophilic halogen reagents proceeded smoothly to give the 6′-halovinyl derivatives with retention of configuration. Treatment of **2***a*(*E*) with *N*-bromosuccinimide (NBS, 1.02 equiv.) in CCl_4/CH_2Cl_2 (1:1) at −40°C for 10 min gave the 6′(*E*)-bromo derivative **5***a*(*E*). Treatment of **2***a*(*E*) with equimolar bromine also gave **5***a*(*E*) exclusively. Analogous treatment of **2***a*(*Z*) with NBS gave **5***a*(*Z*). The ^{1}H NMR spectra of **5***a*(*E*) and **5***a*(*Z*) had "collapsed" singlet H5′ and H6′ peaks. However, deprotection of **5***a*(*E*) and **5***a*(*Z*) afforded **5***b*(*E*) ($^3J_{6'-5'}$ = 13.5 Hz) and **5***b*(*Z*) ($^3J_{6'-5'}$ = 7.0 Hz), respectively, whose vinyl coupling constants were consistent with the assigned configurations. Analogous treatment of **2***a*(*E*) and **2***a*(*Z*) with *N*-iodosuccinimide (1.03 equiv.) effected iododestannylation to give **6***a*(*E*) and **6***a*(*Z*), which were deprotected to give **6***b*(*E*) (87%) and **6***b*(*Z*) (84%) (two steps), respectively. Stereochemical assignments were in harmony with NMR spectra (Tables 1 and 2).

Treatment of **2***a*(*E*) with *N*-chlorosuccinimide (1–3 equiv.; −40°C–ambient; 15 min – 6 h) in CCl_4/CH_2Cl_2 failed to give the 6′-chloro compounds. Chlorine effected conversions of **2***a*(*E*) to separable mixtures of **7***a*(*E*/*Z*, ~3.2:1; 46%) and the 5,6′-dichloro products **8***a*(*E*/*Z*, ~2.8:1; 33%) (Scheme 2). Similarly, treatment of **2***a*(*Z*) gave **7***a*(*E*/*Z*; ~1:3) plus **8***a*(*E*/*Z*, ~1:3.5) in ~80% combined yields. Lower yields and decreased stereospecificity for chlorodestannylation relative to bromo(and iodo)destannylation reactions have been noted previously (3). Treatment of **2***a*(*E*) and **2***a*(*Z*) with iodobenzene dichloride afforded **7***a*(*E*/*Z*: ~3.3:1 and ~1:3, respectively) in moderate yields without observed formation of the uracil-chlorinated compounds **8**. However, a small quantity of a 6-iodo isomer, **6***b*(*E*), was detected by HPLC (after deprotection) and tentatively identified by ^{1}H NMR comparison. Deprotection, silica column or RP-HPLC separation, and crystallization afforded **7***b*(*E*) and **7***b*(*Z*) (and **8***b*(*E*) and **8***b*(*Z*) when chlorine was used) with NMR data in harmony with the geometric assignments (Tables 1 and 2). ^{13}C NMR peaks for C5′ of the 6′(*E*)-halovinyl derivatives were at lower fields (Δδ 1.81–4.52 ppm) than those of the 6′(*Z*) isomers. Our attempted fluorodestannylation of **2***a*(*E*) with xenon difluoride or *N*-fluoropyridinium triflate (1–2 equiv./CH_2Cl_2/−20°C–ambient/1–6 h) resulted in hydrodestannylation to give the 5′-methylene compound **4***a* in moderate yields. This is consistent with results noted in a very recent report in which the synthesis of vinyl fluorides in low to moderate yields by treatment of vinyl stannanes with xenon difluoride and "silver hexafluorophosphate" was described (20).

In summary, radical-mediated detosylation of the easily accessible 6′(*E*)-vinylsulfone **1***a* with Bu_3SnH/AIBN/toluene/Δ gave separable mixtures of the 6′-vinylstannanes **2***a*(*E*/Z). Stereospecific bromo(and iodo)destannylation proceeded smoothly to give 6′-(bromo or iodo)vinyl derivatives in high yields. Chlorodestannylations proceeded with only moderate stereoselectivity and yields. Attempted fluorodestannylations were not successful. Treatment of the 6′-vinylstannanes with ammonium fluoride in methanol or lead tetraacetate in acetonitrile resulted in carbon–tin bond cleavage to give the unsubstituted-vinyl and acetylenic analogues, respectively.

Experimental section

Uncorrected melting points were determined on a Hoover capillary apparatus. UV spectra of solutions in MeOH were recorded on a Hewlett–Packard 8951A spectrophotometer. ^{1}H (200 MHz) and ^{13}C (50 MHz) NMR spectra were recorded on a Varian

Can. J. Chem. Downloaded from www.nrcresearchpress.com by 88.255.202.194 on 09/08/12
For personal use only.

TABLE 1. ^{1}H NMR spectral data[a,b]

Compound	H1′[c] ($J_{1'-2'}$)	H2′[d] ($J_{2'-3'}$)	H3′[d] ($J_{3'-4'}$)	H4′[d] ($J_{4'-5'}$)	H5′[d] ($J_{5'-6'}$)	H6′[c] ($J_{6'-4'}$)	H5[c] (J_{5-6})	H6[c]	NH[e]	Others[f]
2*a*(*E*)[g]	5.74 (2.1)	4.94 (6.4)	4.72 (4.2)	4.53[h] (6.2)	6.06 (19.1)	6.39[d] (1.1)	5.72[d] (7.9, 2.3[j])	7.28	8.49	0.83–1.55[i] (Bu_3Sn) 1.37, 1.60 (CH_3's)
2*a*(*Z*)[g]	5.63 (2.0)	4.99 (6.5)	4.74 (4.1)	4.33 (8.9)	6.56 (12.8)	6.29	5.72[d] (8.0, 2.4[j])	7.28	8.24	0.84–1.59[i] (Bu_3Sn) 1.38, 1.60 (CH_3's)
2*b*(*E*)	5.74 (4.8)	4.08[h] (5.2)	3.84[h] (4.8)	4.17 (5.5)	6.10 (19.1)	6.26	5.62 (8.1)	7.60	11.40	5.23[c] (5.8,[k] OH3′) 5.46[c] (5.4,[k] OH2′)
3*a*[g]	5.77 (1.3)	5.10 (6.0)	4.94–5.00[i]	4.94–5.00[i]		2.70 (2.1)	5.73 (8.2)	7.55	8.75	1.35, 1.55 (CH_3's)
3*b*	5.83 (5.5)	4.21[h] (4.6)	4.10[h] (3.7)	4.50		3.80 (2.2)	5.76 (8.1)	7.56	11.47	5.63[c] (5.0,[k] OH3′) 5.70[c] (5.5,[k] OH2′)
4*a*[g,l]	5.66 (2.0)	5.02 (6.4)	4.76 (4.3)	4.50–4.56[i] (7.1)	5.99[h] (10.3)	5.27[h] (1.1)	5.74[d] (8.0, 1.9[j])	7.23	8.97	1.35, 1.59 (CH_3's)
4*b*[m]	5.77 (4.8)	4.09[h] (5.2)	3.85[h] (5.3)	4.18–4.24[i] (6.9)	6.03[h] (10.4)	5.23[h] (1.2)	5.67 (8.0)	7.61	11.38	5.29[c] (5.8,[k] OH3′) 5.48[c] (5.5,[k] OH2′)
5*a*(*E*)[g]	5.52 (1.5)	5.10 (6.4)	4.84 (4.4)	4.51 (6.2)	6.40–6.46[i]	6.40–6.46[i]	5.75 (8.0)	7.19	8.76	1.37, 1.6 (CH_3's)
5*a*(*Z*)[g]	5.48 (1.5)	5.16 (6.2)	4.89 (3.3)	5.09 (6.1)	6.35–6.45[i]	6.35–6.45[i]	5.73 (8.0)	7.21	9.01	1.34, 1.58 (CH_3's)
6*a*(*E*)[g]	5.53 (1.5)	5.08 (6.3)	4.83 (4.1)	4.48 (7.4)	6.75 (14.7)	6.54	5.75[d] (8.0, 2.3[j])	7.19	8.52	1.35, 1.58 (CH_3's)
6*a*(*Z*)[g]	5.43[f]	5.09[c] (5.9)	4.79–4.87[i]	4.79–4.87[i] (7.1)	6.43 (7.7)	6.52	5.66 (8.2)	7.15	8.71	1.29, 1.56 (CH_3's)
7*a*(*E*)[g]	5.51 (1.5)	5.09 (6.4)	4.82 (4.2)	4.52 (8.2)	6.14 (13.6)	6.33	5.74[d] (8.1, 2.2[j])	7.19	8.70	1.35, 1.60 (CH_3's)
7*a*(*Z*)[g]	5.50 (1.4)	5.15 (6.3)	4.87 (3.7)	5.17[h] (7.9)	6.03 (7.5)	6.27[d] (1.1)	5.73[d] (7.9, 2.0[j])	7.22	8.48	1.37, 1.58 (CH_3's)
8*a*(*E*)[g]	5.52 (1.2)	5.08 (6.4)	4.82 (4.0)	4.54 (8.1)	6.12 (13.5)	6.35		7.47[f]	9.55	1.33, 1.56 (CH_3's)
8*a*(*Z*)[g,n]	5.53 (1.7)	5.11 (6.5)	4.84 (3.6)	5.17[h] (8.1)	6.00 (7.4)	6.28[d] (1.3)		7.44[f]	9.55	1.31, 1.54 (CH_3's)
5*b*(*E*)	5.74 (4.5)	4.14[h] (5.1)	3.91[h] (5.3)	4.25 (8.1)	6.52 (13.5)	6.74	5.66 (8.1)	7.69	11.40	5.39[c] (5.9,[k] OH3′) 5.52[c] (5.5,[k] OH2′)
5*b*(*Z*)	5.79 (5.5)	4.21[h] (4.2)	3.92[h] (4.0)	4.64 (8.7)	6.55 (7.0)	6.72	5.66 (8.4)	7.70	11.40	5.45[c] (5.1,[k] OH3′) 5.54[c] (5.8,[k] OH2′)
6*b*(*E*)	5.73 (4.5)	4.12[h] (5.2)	3.90[h] (5.3)	4.21 (7.2)	6.82 (14.4)	6.70	5.66 (8.1)	7.67	11.39	5.37[c] (5.1,[k] OH3′) 5.51[c] (5.2,[k] OH2′)
6*b*(*Z*)	5.79 (5.6)	4.20[h] (4.6)	3.93[h] (3.4)	4.45 (7.8)	6.62 (7.9)	6.78	5.66 (8.0)	7.70	11.40	5.44[c] (5.2,[k] OH3′) 5.53[c] (5.3,[k] OH2′)
7*b*(*E*)	5.74 (4.8)	4.14[h] (5.1)	3.89[h] (5.2)	4.28 (8.5)	6.27 (13.2)	6.63	5.66 (8.1)	7.66	11.38	5.38[c] (5.8,[k] OH3′) 5.52[c] (5.3,[k] OH2′)
7*b*(*Z*)	5.78 (5.5)	4.19[h] (5.1)	3.91[h] (4.0)	4.72 (8.6)	6.22 (7.2)	6.56	5.66 (8.0)	7.70	11.41	5.43[c] (5.2,[k] OH3′) 5.52[c] (5.5,[k] OH2′)
8*b*(*E*)	5.73 (5.2)	4.21[h] (5.3)	3.92[h] (4.8)	4.27 (8.6)	6.30 (13.2)	6.62		8.01[f]	11.92	5.37[c] (5.6,[k] OH3′) 5.49[c] (5.3,[k] OH2′)
8*b*(*Z*)	5.77 (5.7)	4.28[h] (5.4)	3.94[h] (3.5)	4.72 (8.7)	6.29 (7.2)	6.57		8.05[f]	11.72	5.43[c] (5.4,[k] OH3′) 5.51[c] (5.6,[k] OH2′)

[a]Chemical shifts (δ, in Me_2SO-d_6 unless otherwise noted) recorded at 200 MHz.
[b]"Apparent" first-order coupling constants (Hz, in parentheses).
[c]Doublet.
[d]Doublet of doublets.
[e]Broad singlet.
[f]Singlet.
[g]In $CDCl_3$.
[h]Doublet of doublets of doublets.
[i]Multiplet.
[j]($^3J_{5\text{-NH}}$).
[k]($^3J_{\text{OH-CH}}$).
[l]δ 5.37 (ddd, $J_{6''-5'}$ = 17.2 Hz (*trans*), $J_{6''-4''}$ = 1.3 Hz, $J_{6''-6'}$ = 1.2 Hz, H6″).
[m]δ 5.34 (ddd, $J_{6''-5''}$ = 17.1 Hz (*trans*), $J_{6''-4''}$ = 1.3 Hz, $J_{6''-6'}$ = 1.3 Hz, H6″).
[n]Signals assigned from a spectrum of the mixture (*E*/*Z* isomers were correlated with integrated intensities.)

Can. J. Chem. Downloaded from www.nrcresearchpress.com by 88.255.202.194 on 09/08/12
For personal use only.

TABLE 2. ^{13}C NMR spectral data[a,b]

Compound	C2	C4	C5	C6	C1′	C2′[c]	C3′[c]	C4′	C5′	C6′
1*b*[d]	150.90	163.42	102.32	142.03[c]	90.32	73.13	72.39	81.08	142.50[c]	132.35
2*a*(*E*)[e]	150.23	163.43	101.94	143.18[c]	91.53	83.99	83.74	89.88	145.66[c]	132.64
2*a*(*Z*)[f]	150.45	163.50	102.10	143.41	92.00[c]	84.39	83.84	90.23[c]	145.63	134.78
2*b*(*E*)[g]	150.81	163.28	102.10	141.24	89.11	73.56	72.77	86.43	146.03	131.32
3*b*	150.82	163.41	102.74	140.60	89.01	73.35	73.21	75.11	81.00	79.36
4*b*	150.83	163.30	102.30	141.26	89.06	73.48	72.82	84.30	136.46	117.84
5*b*(*E*)	150.78	163.42	102.32	141.56	89.28	73.07	72.56	83.29	135.82	110.79
5*b*(*Z*)	150.86	163.52	102.35	141.62	89.02	73.70	72.68	81.45	133.00	112.51
6*b*(*E*)	150.98	163.40	102.38	141.63	89.26	73.01	72.75	83.03[c]	143.48	85.25[c]
6*b*(*Z*)	150.90	163.32	102.34	141.58	88.93[c]	73.68	72.77	85.88[c]	138.96	88.17[c]
7*b*(*E*)	150.77	163.38	102.31	141.52	89.24	73.30	72.62	81.95	131.99	122.34
7*b*(*Z*)	150.86	163.37	102.33	141.61	88.99	73.83	72.60	79.01	130.18	122.25
8*b*(*E*)	150.05	159.20	108.04	138.61	89.53	73.34	72.46	82.41	132.14	122.27
8*b*(*Z*)	150.12	159.16	108.07	138.66	89.26	73.85	72.50	79.43	130.28	122.02

[a]Chemical shifts (δ, in Me_2SO-d_6) recorded at 50 MHz.
[b]Proton-decoupled singlets.
[c]Assignments might be reversed.
[d]Peaks also at δ 21.07 (CH_3), 137.42, 127.67, 130.41, 144.73 (Ar).
[e]Peaks also at δ 9.34, 13.82, 26.84, 28.79 (Bu_3Sn), 25.49, 27.24, 113.61 (CMe_2).
[f]Peaks also at δ 10.44, 13.80, 26.90, 28.79 (Bu_3Sn), 25.51, 27.33, 113.73 (CMe_2).
[g]Peaks also at δ 9.35, 13.82, 26.82, 28.81 (Bu_3Sn).

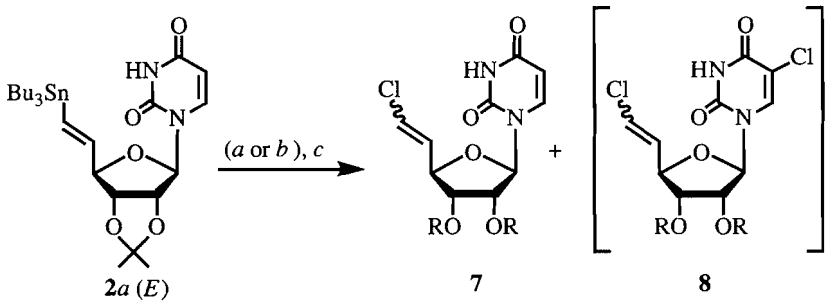

a series: R = CMe_2; *b* series: R = H
(*a*) $Cl_2/CCl_4/CH_2Cl_2$/-50°C; (*b*) $PhICl_2/CCl_4/CH_2Cl_2$/-10°C; (*c*) CF_3CO_2H/H_2O

SCHEME 2

Gemini-200 spectrometer in Me_2SO-d_6 unless otherwise noted. Low-resolution mass spectra (MS) were obtained with a Finnigan MAT 8430 instrument. Elemental analyses were determined by M-H-W Laboratories, Phoenix, Ariz. Reagents and solvents were of reagent quality, and solvents were purified and dried before use. "Diffusion crystallization" was performed with the noted solvent combinations as described (21). Thin-layer chromatography (TLC) was performed on Merck Kieselgel 60 F_{254} sheets with: S_1 (Me_2CO/$CHCl_3$, 1:3), S_2 (EtOAc/hexane, 7:3), or S_3 (MeOH/$CHCl_3$, 1:9) with sample observation under 254 nm light. Column chromatography was performed with Merck Kieselgel 60 (230–400 mesh). Preparative and analytical RP-HPLC were performed with a Spectra Physics SP 8800 ternary pump system and Dynamax C_{18} columns.

*1-[6(*E/Z*)-Tributylstannyl-5,6-dideoxy-2,3*-O-*isopropylidene-β-*D*-*ribo-hex-5-enofuranosyl]uracil* **2**a(E/Z)

A suspension of **1***a* (1.63 g, 3.75 mmol) in toluene (30 mL) was deoxygenated (Ar, 30 min) and Bu_3SnH (4.37 g, 4.02 mL, 15 mmol) was added. Deoxygenation was continued for 15 min and AIBN (66 mg, 0.4 mmol) was added. The solution was refluxed for 4 h (TLC (S_{1-3}) showed less polar products and traces of **1***a*), evaporated, and the residue was column chromatographed. Slow elution (EtOAc/hexane, 3:2 → 4:1) gave **2***a*(*E*) (1.23 g, 58%), **2***a* (*E*/*Z*, ~3:2; 0.19 g, 9%), and **2***a*(*Z*) (0.43 g, 20%). Further elution (EtOAc) gave **1***a* (0.11 g, contaminated with by-products). **2***a*(*E*) (white solid dried at 65°C *in vacuo* for 3 days): mp 82–84°C; UV_{max}: 259 nm (ε 9800), UV_{min}: 233 nm (ε 4200); MS *m*/*z*: 513 (100, M − 57, ^{120}Sn), 511 (74, M − 57, ^{118}Sn), 509 (45, M − 57, ^{116}Sn). **2***a*(*Z*) (viscous oil): MS (CI, CH_4) *m*/*z*: 571 (100, MH^+, ^{120}Sn), 569 (72, MH^+, ^{118}Sn), 567 (43, MH^+, ^{116}Sn).

*1-[6(*E*)-Tributylstannyl-5,6-dideoxy-β-*D*-*ribo-*hex-5-enofuranosyl]uracil* **2**b(E)

A suspension of **1***b* (160 mg, 0.41 mmol) in deoxygenated *N,N*-dimethylacetamide/toluene (1:3, 20 mL), Bu_3SnH (477 mg, 0.44 mL, 1.62 mmol), and AIBN (10 mg, 0.0061 mmol) was refluxed for 6 h. Work-up (as described for **2***a*(*E*/*Z*)) and column chromatography (MeOH/$CHCl_3$, 1:25) gave **2***b*(*E*) (141 mg, ~65%; contaminated with by-products) as a viscous oil: MS (CI, CH_4) *m*/*z*: 531 (31, MH^+, ^{120}Sn), 529 (25, MH^+, ^{118}Sn), 527 (15, MH^+, ^{116}Sn), 473 (100, M − 57, ^{120}Sn), 471 (74, M − 57, ^{118}Sn), 469 (50, M − 57, ^{116}Sn).

1-(6-Deoxy-2,3-O-*isopropylidene-β-*D*-*ribo-hex-5-ynofuranosyl)uracil* **3**a

A solution of **2***a*(*E*) (120 mg, 0.21 mmol) in anhydrous CH_3CN (6 mL) under Ar was treated with $Pb(OAc)_4$ (115 mg, 0.26 mM) and stirred at ~0°C (ice-bath) for 1 h and then an additional 2 h at 0°C–ambient (TLC ($S_{2,3}$) showed more polar **3***a* and **2***a*(*E*)). The

Can. J. Chem. Downloaded from www.nrcresearchpress.com by 88.255.202.194 on 09/08/12
For personal use only.

Can. J. Chem. Downloaded from www.nrcresearchpress.com by 88.255.202.194 on 09/08/12
For personal use only.

mixture was evaporated and the residue was partitioned ($NaHCO_3/H_2O//CHCl_3$). The organic phase was washed ($NaHCO_3/H_2O$ and brine), dried ($MgSO_4$), evaporated, and the residue was column chromatographed (EtOAc) to give **2***a*(*E*) (21 mg, 18%) and **3***a* (42 mg, 72%): MS *m/z*: 263 (24, M − CH_3), 138 (65), 113 (30, BH_2), 80 (100).

*1-(6-Deoxy-β-D-*ribo*-hex-5-ynofuranosyl)uracil* **3**b

A solution of **3***a* (35 mg, 0.12 mmol) in CF_3CO_2H/H_2O (9:1, 5 mL) was stirred at 0°C for 1 h, evaporated, and coevaporated (EtOH). The residue was dissolved (H_2O/MeOH, 4:1; 5 mL), the solution was cooled (ice-bath), and H_2S was gently bubbled through for 30 s. The mixture was filtered through Celite, the filtrate was evaporated, and the residue was column chromatographed (EtOAc → MeOH/EtOAc, 1:9). Diffusion crystallization (EtOH/EtOAc) gave **3***b* (23 mg, 80%): mp 217–218°C (lit. (10) mp 209–211°C); UV_{max}: 261 nm (ε 9600), UV_{min}: 230 nm (ε 2200); MS *m/z*: 238 (M^+, 100).

*1-(5,6-Dideoxy-2,3-*O*-isopropylidene-β-D-*ribo*-hex-5-enofuranosyl)uracil* **4**a

A solution of **2***a* (*E*/*Z*, ~3:2; 0.18 g, 0.32 mmol) and NH_4F (59 mg, 1.6 mmol) in dry MeOH (10 mL) was refluxed for 4 h and evaporated. The white foam was partitioned ($NaHCO_3/H_2O//CHCl_3$) and the organic layer was washed (brine), dried ($MgSO_4$), and evaporated to give **4***a* (97 mg, 108%; contaminated with tin by-products). Column chromatography (EtOAc/hexane, 4:1) gave **4***a* (84 mg, 94%), which failed to crystallize: MS (CI, CH_4) *m/z*: 281 (100, MH^+).

*1-(5,6-Dideoxy-β-D-*ribo*-hex-5-enofuranosyl)uracil (5'-deoxy-5'-methyleneuridine)* **4**b

Method A

A solution of **2***a*(*E*) (91 mg, 0.16 mmol) in CF_3CO_2H/H_2O (9:1, 5 mL) was stirred at ~0°C for 1 h, evaporated, and coevaporated (EtOH). The residue was crystallized (Me_2CO) to give **4***b* (36 mg, 94%): mp 166–167°C; UV_{max}: 261 nm (ε 9800), UV_{min}: 230 nm (ε 2000); MS (CI, CH_4) *m/z*: 241 (18, MH^+), 113 (100, BH_2). Anal. calcd. for $C_{10}H_{12}N_2O_5$ (240.2): C 50.00, H 5.04, N 11.66; found: C 49.90, H 5.18, N 11.66.

Method B

A solution of crude **4***a* (97 mg) in CF_3CO_2H/H_2O (9:1, 5 mL) was stirred at ~0°C for 1 h, evaporated, and coevaporated (EtOH). The residue was chromatographed (Dowex 1 × 2 (OH^-), ~1.0 g of resin; H_2O (~100 mL), MeOH (~100 mL), product eluted with 0.3 M $Et_3NH_2CO_3/H_2O$ (~200 mL)) and the eluate was evaporated followed by additions/evaporations of H_2O (3 × 25 mL) *in vacuo*. The residue was diffusion crystallized (Me_2CO/hexane) to give **4***b* (62 mg, 81% from **2***a*) with identical physical data as in Method A.

*1-[6(*E*)-Bromo-5,6-dideoxy-2,3-*O*-isopropylidene-β-D-*ribo*-hex-5-enofuranosyl]uracil* **5**a(E)

Method A

Bromine (53 mg, 0.33 mmol) in CCl_4 (5 mL) was added dropwise to a stirred solution of **2***a*(*E*) (185 mg, 0.33 mmol) in CH_2Cl_2/CCl_4 (1:1, 15 mL) at ~−50°C. TLC (S_1) indicated that starting material was consumed when the addition of Br_2 was completed. After 5 min the colorless solution was poured into saturated $NaHCO_3/H_2O$ and extracted ($CHCl_3$). The combined organic phase was washed (brine and H_2O), dried ($MgSO_4$), and evaporated to give **5***a*(*E*) (136 mg, 115%; contaminated with tin by-products): mp 149–153°C; MS *m/z*: 360 (20, M^+, ^{81}Br), 358 (21, M^+, ^{79}Br), 112 (100, BH).

Method B

A solution of *N*-bromosuccinimide (37 mg, 0.21 mmol) in CH_2Cl_2/CCl_4 (1:1, 8 mL) was added dropwise to a stirred solution of **2***a*(*E*) (114 mg, 0.2 mmol) in CH_2Cl_2/CCl_4 (1:1, 12 mL) at ~−40°C. After 15 min the mixture was worked up as in Method A and column chromatographed (MeOH/$CHCl_3$, 1:49) to give **5***a*(*E*) (68 mg, 95%).

*1-[6(Z)-Bromo-5,6-dideoxy-2,3-*O*-isopropylidene-β-D-*ribo*-hex-5-enofuranosyl]uracil* **5**a(Z)

Treatment of **2***a*(*Z*) (85 mg, 0.15 mmol) with NBS (28 mg, 0.16 mmol) (as described for **5***a*(*E*), Method B) gave **5***a*(*Z*) (59 mg, 110%; contaminated with tin by-products): mp 167–170°C; MS *m/z*: 360 (34, M^+, ^{81}Br), 358 (35, M^+, ^{79}Br), 112 (100, BH).

*1-[6(*E*)-Bromo-5,6-dideoxy-β-D-*ribo*-hex-5-enofuranosyl]uracil* **5**b(E)

A solution of crude **5***a*(*E*) (136 mg, from Method A) in CF_3CO_2H/H_2O (9:1, 5 mL) was stirred at 0°C for 1 h, evaporated, coevaporated (EtOH), and the residue diffusion crystallized (MeOH/Et_2O) to give **5***b*(*E*) (42 mg). The concentrated mother liquor afforded an additional 41 mg (diffusion crystallization, MeOH/EtOAc//hexane) of **5***b*(*E*) (83 mg, 79% from **2***a*(*E*)) as a white solid: mp 183–184°C; UV_{max}: 261 nm (ε 9200), UV_{min}: 231 nm (ε 1900); MS *m/z*: 320 (8, M^+, ^{81}Br), 318 (8, M^+, ^{79}Br), 190 (52), 188 (53), 162 (54), 160 (52), 141 (90), 113 (100, BH_2). Anal. calcd. for $C_{10}H_{11}BrN_2O_5 \cdot 0.5\ H_2O$ (328.1): C 36.61, H 3.69, N 8.54; found: C 36.85, H 3.80, N 8.34.

*1-[6(Z)-Bromo-5,6-dideoxy-β-D-*ribo*-hex-5-enofuranosyl]uracil* **5**b(Z)

Deprotection of crude **5***a*(*Z*) (59 mg) (as described for **5***b*(*E*)), column chromatography (MeOH/EtOAc; 1:15), and diffusion crystallization (MeOH/EtOAc//hexane) gave **5***b*(*Z*) (39 mg, 81% from **2***a*(*Z*)): mp 194–196°C; UV_{max}: 261 nm (ε 9500), UV_{min}: 231 nm (ε 2000); MS (CI, CH_4) *m/z*: 321 (96, MH^+, ^{81}Br), 319 (100, MH^+, ^{79}Br). Anal. calcd. for $C_{10}H_{11}BrN_2O_5$ (319.1): C 37.64, H 3.47, N 8.78; found: C 37.79, H 3.41, N 8.56.

*1-[5,6-Dideoxy-6(*E*)-iodo-2,3-*O*-isopropylidene-β-D-*ribo*-hex-5-enofuranosyl]uracil* **6**a(E)

A solution of *N*-iodosuccinimide (63 mg, 0.28 mmol) in CH_2Cl_2/CCl_4 (1:1, 10 mL) was added dropwise to a stirred solution of **2***a*(*E*) (142 mg, 0.25 mmol) in CH_2Cl_2/CCl_4 (1:1, 15 mL) at ~−30°C. TLC (S_2) after 25 min indicated complete reaction to give a more polar compound (R_f 0.59; **2***a*(*E*): R_f 0.81). The slightly pink mixture was poured into saturated $NaHCO_3/H_2O$ and extracted ($CHCl_3$). The combined organic phase was washed (very dilute $NaHSO_3/H_2O$ and brine), dried ($MgSO_4$), and evaporated to give **6***a*(*E*) (100 mg, 99%) as a white solid: mp 170–172°C; MS (CI, CH_4) *m/z*: 407 (26, MH^+), 113 (100, BH_2). Treatment of **2***a*(*E*) with I_2 (1.1 equiv.) at ~0°C for 2 h also gave **6***a*(*E*) (85%).

*1-[5,6-Dideoxy-6(Z)-iodo-2,3-*O*-isopropylidene-β-D-*ribo*-hex-5-enofuranosyl]uracil* **6**a(Z)

Treatment of **2***a*(*Z*) (91 mg, 0.16 mmol) with *N*-iodosuccinimide (40 mg, 0.18 mmol) (as described for **6***a*(*E*)) gave **6***a*(*Z*) (63 mg, 97%; TLC (S_2) R_f 0.53, **2***a*(*Z*): R_f 0.75): mp 184–186°C; MS (CI, CH_4) *m/z*: 407 (100, MH^+).

*1-[5,6-Dideoxy-6(*E*)-iodo-β-D-*ribo*-hex-5-enofuranosyl]uracil* **6**b(E)

Deprotection of **6***a*(*E*) (78 mg, 0.19 mmol) (as described for **5***b*(*E*)) gave a colorless solid that was crystallized (MeOH/H_2O, 1:6) to give **6***b*(*E*) (23 mg, 33%) as fine needles. The mother liquor was concentrated and chromatographed ((Dowex 1 × 2 (OH^-) (~2 g of resin); H_2O (100 mL), MeOH (100 mL), product eluted with 0.3 M $Et_3NH_2CO_3/H_2O$ (~300 mL)) and the eluate was evaporated. Additions/evaporations of H_2O (3 × 30 mL) *in vacuo* gave a residue that was crystallized (MeOH/H_2O, 1:12) to give additional **6***b*(*E*) (28 mg; 51 mg, 73%, two crops): mp 202–203°C; UV_{max}: 260 nm (ε 10 500), UV_{min}: 238 (ε 4900); MS (CI, CH_4) *m/z*: 367 (15, MH^+), 239 (32), 113 (100, BH_2). Anal. calcd. for $C_{10}H_{11}IN_2O_5$ (366.1): C 32.81, H 3.03, N 7.65; found: C 33.02, H 3.07, N 7.71.

*1-[5,6-Dideoxy-6(Z)-iodo-β-D-*ribo*-hex-5-enofuranosyl]uracil* **6**b(Z)

Deprotection of **6***a*(*Z*) (61 mg, 0.15 mmol) (as described for **5***b*(*E*)) gave a colorless solid that was column chromatographed

Can. J. Chem. Downloaded from www.nrcresearchpress.com by 88.255.202.194 on 09/08/12
For personal use only.

(MeOH/EtOAc, 1:20) and diffusion crystallized (Me_2CO/hexane) to give **6***b*(*Z*) (39 mg, 71%): mp 203–205°C; UV_{max}: 260 nm (ε 9700), UV_{min}: 237 nm (ε 4400); MS (CI, CH_4) *m/z*: 367 (81, MH^+), 239 (63), 113 (100, BH_2). Anal. calcd. for $C_{10}H_{11}IN_2O_5$ (366.1): C 32.81, H 3.03, N 7.65; found: C 32.79, H 3.09, N 7.71.

1-[6(E/Z)*-Chloro-5,6-dideoxy-2,3*-O-*isopropylidene-β-D*-ribo-*hex-5-enofuranosyl]uracil* **7**a(E/Z) *and 5-chloro-1-[6*(E/Z)*-chloro-5,6-dideoxy-2,3*-O-*isopropylidene-β-D*-ribo-*hex-5-enofuranosyl]uracil* **8**a(E/Z)

Method A

Cl_2 was gently bubbled through a solution of **2***a*(*E*) (285 mg, 0.5 mmol) in CCl_4/CH_2Cl_2 (1:1, 10 mL) at ~−50°C, and stirring was continued at ~−50 to −40°C for 15 min. The solution was washed ($NaHCO_3/H_2O$, dilute $Na_2S_2O_3/H_2O$, and brine), dried ($MgSO_4$), and evaporated. The resulting foam was column chromatographed (EtOAc/hexane, 1:1 → 9:1) to give **8***a*(*E*) (19 mg, 11%; S_2 R_f 0.81), **8***a* (*E/Z*, ~3:2; 38 mg, 22%), **7***a*(*E*) (55 mg, 35%; S_2 R_f 0.48), and **7***a*(*Z*) (17 mg, 11%; S_2 R_f 0.43). **8***a*(*E*): MS (CI, CH_4) *m/z*: 353 (9, MH^+, $^{37}Cl_2$), 351 (50, MH^+, ^{37}Cl, ^{35}Cl), 349 (76, MH^+, $^{35}Cl_2$), 205 (38, M − BH_2, ^{37}Cl), 203 (100, M − BH_2, ^{35}Cl), 149 (18, BH_2, ^{37}Cl), 147 (60, BH_2, ^{35}Cl). **7***a*(*E*): MS *m/z*: 301 (6, M − CH_3, ^{37}Cl), 299 (20, M − CH_3, ^{35}Cl), 144 (100), 138 (62). **7***a*(*Z*): MS (CI, CH_4) *m/z*: 317 (18, MH^+, ^{37}Cl), 315 (53, MH^+, ^{35}Cl), 144 (100), 138 (82).

Product ratios varied in different runs. Treatment of **2***a*(*Z*) under identical conditions gave **7***a*(*E/Z*, ~1:3; 44%) and **8***a*(*E/Z*, ~1:3.5; 36%). Longer reaction times and (or) greater amounts of Cl_2 gave **8***a*(*E/Z*) (~50%).

Method B

$PhICl_2$ (99 mg, 0.36 mM) was added in one portion to a stirred solution of **2***a*(*E*) (171 mg, 0.3 mmol) in CCl_4/CH_2Cl_2 (1:1, 10 mL) at ~−20°C. After 25 min a second portion of $PhICl_2$ (25 mg, 0.09 mM) was added and stirring was continued at ~−20°C for 40 min. Work-up and purification as in Method A gave **7***a*(*E*) (37 mg, 39%) and **7***a*(*Z*) (11 mg, 12%). Analogous treatment of **2***a*(*Z*) with $PhICl_2$ gave **7***a*(*E/Z*, ~1:3: 49%).

1-[6(E)*-Chloro-5,6-dideoxy-β-D*-ribo-*hex-5-enofuranosyl]uracil* **7**b(E)

Deprotection of **7***a*(*E*) (50 mg, 0.16 mmol; from Method A) (as described for **5***b*(*E*)) gave a slightly yellow solid that was column chromatographed (EtOAc/MeOH; 19:1) and diffusion crystallized (MeOH/EtOAc//hexane) to give **7***b*(*E*) (35 mg, 80%): mp 170–172°C (dec.); UV_{max}: 262 nm (ε 10 500), UV_{min}: 229 nm (ε 2000); MS (CI, CH_4) *m/z*: 277 (14, MH^+, ^{37}Cl), 275 (44, MH^+, ^{35}Cl), 113 (100, BH_2). Anal. calcd. for $C_{10}H_{11}ClN_2O_5 \cdot 0.5\ H_2O$ (283.7): C 42.34, H 4.26, N 9.88; found: C 42.66, H 4.55, N 9.49.

Deprotection of **7***a*(*E*) (45 mg, 0.14 mmol; from Method B) (as described for **5***b*(*E*)) and RP-HPLC (preparative column; program: 17% H_2O/CH_3CN for 45 min followed by a gradient of 17–25% for 45 min at 2.7 mL/min) gave **7***b*(*Z*) (2 mg, 5%, R_T = 38 min), **7***b*(*E*) (25 mg, 65%, R_T = 45 min), and **6***b*(*E*) (5 mg, 10%, R_T = 52 min). Compounds **8***b*(*Z*) and **8***b*(*E*) in the same analytical system have R_T = 60 and 67 min, respectively.

1-[6(Z)*-Chloro-5,6-dideoxy-β-D*-ribo-*hex-5-enofuranosyl]uracil* **7**b(Z)

Deprotection of **7***a*(*Z*) (32 mg, 0.1 mmol) (as described for **5***b*(*E*)) gave a slightly yellow solid, which was subjected to RP-HPLC (as described under **7***b*(*E*)) and diffusion crystallized (MeOH/EtOAc//hexane) to give **7***b*(*Z*) (19 mg. 69%): mp 193–194°C; UV_{max}: 261 nm (ε 10 600), UV_{min}: 233 nm (ε 3000); MS *m/z*: 276 (3, M^+, ^{37}Cl), 274 (9, M^+, ^{35}Cl), 113 (100, BH_2). Anal. calcd. for $C_{10}H_{11}ClN_2O_5$ (274.7): C 43.73, H 4.04, N 10.20; found: C 43.85, H 4.15, N 10.12.

5-Chloro-1-[6(E)*-chloro-5,6-dideoxy-β-D*-ribo-*hex-5-enofuranosyl]uracil* **8**b(E)

Deprotection of **8***a*(*E*) (24 mg, 0.07 mmol) (as described for **5***b*(*E*)), column chromatography (EtOAc/MeOH, 19:1), and diffusion crystallization (MeOH/EtOAc//hexane) gave **8***b*(*E*) (15 mg, 70%): mp 198–202°C (dec.); UV_{max}: 275 nm (ε 9800), UV_{min}: 236 nm (ε 1300); MS (CI, CH_4) *m/z*: 313 (0.4, MH^+, $^{37}Cl_2$), 311 (2, MH^+, ^{35}Cl, ^{37}Cl), 309 (3, MH^+, $^{35}Cl_2$), 149 (34, BH_2, ^{37}Cl), 147 (100, BH_2, ^{35}Cl). Anal. calcd. for $C_{10}H_{10}Cl_2N_2O_5$ (309.1): C 38.86, H 3.26, N 9.06; found: C 38.74, H 3.47, N 8.85.

5-Chloro-1-[6(Z)-chloro-5,6-dideoxy-β-D-ribo-*hex-5-enofuranosyl]uracil* **8**b(Z)

Deprotection of **8***a*(*E/Z*, ~1:3.5; 28 mg, 0.08 mmol, from Method A) (as described for **5***b*(*E*)) gave a slightly yellow solid that was purified by RP-HPLC (as described under **7***b*(*E*)) and diffusion crystallized (MeOH/EtOAc//hexane) to give **8***b*(*Z*) (13 mg, 53%; 68% based on **8***a*(*Z*)): mp 148–152°C (dec.); UV_{max}: 274 nm (ε 9600), UV_{min}: 236 nm (ε 1400); MS (CI, CH_4) *m/z*: 313 (1, MH^+, $^{37}Cl_2$), 311 (5, MH^+, $^{35}Cl^{37}Cl$), 309 (8, MH^+, $^{35}Cl_2$), 149 (38, BH_2, ^{37}Cl), 147 (100, BH_2, ^{35}Cl). Anal. calcd. for $C_{10}H_{10}Cl_2N_2O_5$ (309.1): C 38.86, H 3.26, N 9.06; found: C 38.99, H 3.14, N 9.21.

Acknowledgments

We thank the American Cancer Society (Grant No. DHP-34) and Brigham Young University Development Funds for generous support and Mrs. Kathryn M. Rollins for assistance with the manuscript.

1. S. Patai, Z. Rappoport, and C. Stirling (*Editors*). The chemistry of sulphones and sulphoxides. Wiley–Interscience, New York. 1988.
2. N. S. Simpkins. Tetrahedron, **46**, 6951 (1990).
3. M. Pereyre, J.-P. Quintard, and A. Rahm. Tin in organic synthesis. Butterworths, Boston. 1987.
4. (*a*) J.-C. Wu, T. Pathak, W. Tong, J.-M. Vial, G. Remaud, and J. Chattopadhyaya. Tetrahedron, **44**, 6705 (1988); (*b*) J.-C. Wu and J. Chattopadhyaya. Tetrahedron, **45**, 4507 (1989); (*c*) W. Tong, Z. Xi, C. Gioeli, and J. Chattopadhyaya. Tetrahedron, **47**, 3431 (1991).
5. (*a*) D. H. R. Barton, S. D. Géro, B. Quiclet-Sire, and M. Samadi. J. Chem. Soc. Chem. Commun. 1372 (1988); (*b*) J. Chem. Soc. Perkin Trans. 1, 981 (1991); (*c*) D. H. R. Barton, S. D. Géro, F. Lawrence, M. Robert-Gero, B. Quiclet-Sire, and M. Samadi. J. Med. Chem. **35**, 63 (1992).
6. (*a*) S. F. Wnuk, N. K. Dalley, and M. J. Robins. Can. J. Chem. **69**, 2104 (1991); (*b*) S. F. Wnuk and M. J. Robins. Can. J. Chem. **69**, 334 (1991).
7. (*a*) J. R. McCarthy, D. P. Matthews, M. L. Edwards, D. M. Stemerick, and E. T. Jarvi. Tetrahedron Lett. **31**, 5449 (1990); (*b*) J. R. McCarthy, D. P. Matthews, D. M. Stemerick, E. W. Huber, P. Bey, B. J. Lippert, R. D. Snyder, and P. S. Sunkara. J. Am. Chem. Soc. **113**, 7439 (1991).
8. B. Musicki and T. S. Widlanski. Tetrahedron Lett. **32**, 1267 (1991).
9. (*a*) G. H. Jones and J. G. Moffatt. J. Am. Chem. Soc. **90**, 5337 (1968); (*b*) P. Howgate, A. S. Jones, and J. R. Tittensor. Carbohydr. Res. **12**, 403 (1970); (*c*) J. A. Montgomery, A. G. Laseter, and K. Hewson. J. Heterocycl. Chem. **11**, 211 (1974); (*d*) J. M. J. Tronchet and M. J. Valero. Helv. Chim. Acta, **62**, 2788 (1979); (*e*) J.-D. Zhang and L.-H. Zhang. Synthesis, 909 (1990).
10. R. A. Sharma and M. Bobek. J. Org. Chem. **43**, 367 (1978).
11. S. Shuto, T. Obara, M. Toriya, M. Hosoya, R. Snoeck, G. Andrei, J. Balzarini, and E. De Clercq. J. Med. Chem. **35**, 324 (1992).
12. F. Kapper and A. Hampton. *In* Nucleic acid chemistry: improved and new synthetic procedures, methods, and techniques. *Edited by* L. B. Townsend and R. S. Tipson. Wiley, New York. 1991. Part 4, pp. 240–244.
13. (*a*) R. J. Parry, A. Muscate, and L. Askonas. Biochemistry, **30**, 9988 (1991); (*b*) M. L. Edwards, N. J. Prakash, and J. R.

McCarthy. Eur. Pat. Appl. EP. 334,361 (1989); Chem. Abstr. **112**, 99145s (1990).
14. (*a*) J. R. McCarthy, E. T. Jarvi, D. P. Matthews, M. L. Edwards, N. J. Prakash, T. L. Bowlin, S. Mehdi, P. S. Sunkara, and P. Bey. J. Am. Chem. Soc. **111**, 1127 (1989); (*b*) E. T. Jarvi, J. R. McCarthy, S. Mehdi, D. P. Matthews, M. L. Edwards, N. J. Prakash, T. L. Bowlin, P. S. Sunkara, and P. Bey. J. Med. Chem. **34**, 647 (1991); (*c*) M. J. Robins, S. F. Wnuk, K. B. Mullah, N. K. Dalley, R. T. Borchardt, Y. Lee, and C.-S. Yuan. *In* Nucleosides as antitumor and antiviral agents. *Edited by* C. K. Chu and D. C. Baker. Plenum Press, New York. 1993. In press.
15. A. Hasan and P. C. Srivastava. J. Med. Chem. **35**, 1435 (1992).
16. Y. Watanabe, Y. Ueno, T. Araki, T. Endo, and M. Okawara. Tetrahedron Lett. **27**, 215 (1986).
17. G. Stork and R. Mook, Jr. J. Am. Chem. Soc. **109**, 2829 (1987).
18. W. Zhang and M. J. Robins. Tetrahedron Lett. **33**, 1177 (1992).
19. E. J. Corey and R. H. Wollenberg. J. Am. Chem. Soc. **96**, 5581 (1974).
20. M. A. Tius and J. K. Kawakami. Synth. Commun. **22**, 1461 (1992).
21. M. J. Robins, R. Mengel, R. A. Jones, and Y. Fouron. J. Am. Chem. Soc. **98**, 8204 (1976).
22. V. Samano and M. J. Robins. Can. J. Chem. **71**, 186 (1993).

Can. J. Chem. Downloaded from www.nrcresearchpress.com by 88.255.202.194 on 09/08/12
For personal use only.

Studies of the synthesis, structure, and reduction of *trans*-dichloro bis(2,3-dihydro-4- and 7-methylbenzo[*b*]thiophene)palladium(II) complexes

PETER D. CLARK,[1] MARTIN J. KIRK, AND MASSOOD PARVEZ

Department of Chemistry, The University of Calgary, 2500 University Drive N.W., Calgary, Alta., Canada T2N 1N4

Received September 19, 1991[2]

PETER D. CLARK, MARTIN J. KIRK, and MASSOOD PARVEZ. Can. J. Chem. **71**, 199 (1993).

trans-Dichlorobis(2,3-dihydro-4- and -7-methylbenzo[*b*]thiophene)palladium(II), **1***b* and **1***c*, have been prepared by reaction of 2,3-dihydro-4- and -7-methylbenzo[*b*]thiophenes with palladium(II) chloride. Both **1***b* and **1***c* exhibit complex ^1H and ^{13}C NMR spectra as a result of inversion of the sulfur-containing ligands. Their structures were confirmed by single crystal X-ray studies. **1***b* crystallized in the triclinic spacegroup $P\bar{1}$ (a = 7.219(2), b = 8.441(5), c = 8.494(7) Å, α = 61.47(5)°, β = 88.85(4)°, γ = 84.40(3)°, and R = 0.067 for 1372 observed of 1760 unique reflections). **1***c* also crystallized in the triclinic space group $P\bar{1}$ (a = 7.730(3), b = 8.056(3), c = 8.516(4) Å, α = 62.87(3)°, β = 82.31(3)°, γ = 88.82(3)°, and R = 0,040 for 1425 observed of 1825 unique reflections). **1***b* and **1***c* and the complex **1***a* (prepared from 2,3-dihydrobenzo[*b*]thiophene) were unstable in the presence of molecular hydrogen at ambient conditions, liberating the parent dihydrobenzothiophenes and forming elemental palladium. **1***a* was also unstable to the organic hydrogen donor tetrahydronaphthalene, again forming Pd and 2,3-dihydrobenzothiophene. Complexes **1***a–c* were shown to promote the shift of CO/H_2O to hydrogen and CO_2 although most of the hydrogen was consumed by the reduction of Pd(II) to Pd^0.

PETER D. CLARK, MARTIN J. KIRK et MASSOOD PARVEZ. Can. J. Chem. **71**, 199 (1993).

On a préparé les *trans*-dichloro(2,3-dihydro-4- et -7-méthylbenzo[*b*]thiophène)palladium(II), **1***b* et **1***c*, par réaction des 2,3-dihydro-4- et -7-méthylbenzo[*b*]thiophènes avec le chlorure de palladium(II). À cause de l'inversion des ligands contenant du soufre, les produits **1***b* et **1***c* présentent tous les deux des spectres RMN du ^1H et du ^{13}C complexes. On a confirmé les structures par des études de rayons-X sur des cristaux uniques. Le composé **1***b* est triclinique, groupe d'espace $P\bar{1}$, avec a = 7,219(2), b = 8,441(5) et c = 8,494(7) Å, α = 61,47(5)°, β = 88,85(4)° et γ = 84,40(3)° et R = 0.067 pour 1372 des 1760 réflexions uniques. Le composé **1***c* est triclinique, groupe d'espace $P\bar{1}$, avec a = 7,730(3), b = 8,056(3) et c = 8,516(4) Å, α = 62,87(3)°, β = 82,31(3)° et γ = 88,82(3)° et R = 0,040 pour 1425 des 1825 réflexions uniques. Les composés **1***b* et **1***c* ainsi que le complexe **1***a* (préparé à partir du 2,3-dihydrobenzo[*b*]thiophène) sont instables en présence d'hydrogène moléculaire, aux conditions ambiantes; ils libèrent alors les dihydrobenzothiophènes fondamentaux et forment du palladium élémentaire. Le composé **1***a* est aussi instable en présence du donneur d'hydrogène, le tétrahydronaphtalène; il conduit encore à la formation de Pd et du 2,3-dihydrobenzothiophène. On a montré que les complexes **1***a–c* facilitent la transformation de CO/H_2O en CO_2, même si la majorité de l'hydrogène est consommée par la réduction du Pd(II) en Pd^0.

[Traduit par la rédaction]

Introduction

We previously (1) reported the preparation and structural determination of *trans*-dichloro bis(2,3-dihydrobenzo[*b*]thiophene)palladium(II) **1***a*, which was of interest regarding mechanisms for the catalytic hydrodesulfurization of benzo[*b*]thiophene (BT) and the reaction of BT with water at elevated temperatures in the presence of aqueous platinum metal species (2). To unambiguously assign the ^1H NMR spectrum of **1***a*, which is complicated by inversion of the sulfur-containing ligand about the sulfur atom, the 4-methyl derivative **1***b* was prepared and reported (1) but was not characterized fully. In this article, we describe the full NMR and single X-ray characterization of **1***b* and also of the 7-methyl derivative **1***c*.

Since these complexes may model intermediates formed during the catalytic hydrodesulfurization of BT and its methyl-substituted derivatives, we investigated their reactions with molecular hydrogen and with the hydrogen donor tetrahydronaphthalene (THN). Reactions of **1***a–c* with THN are of particular interest since one pathway of desulfurization occurs by interaction of sulfur-containing compounds with organic hydrogen donors that act as vehicles for transfer of gas phase hydrogen (3, 4). In addition, it is shown that complexes **1***a–c* catalyze the shift of CO/H_2O to H_2 and CO_2. This chemistry is relevant to the mechanisms proposed for the desulfurization of BT and related sulfur heterocycles using aqueous platinum metal species (1, 2).

$PdCl_2L_2$

L = 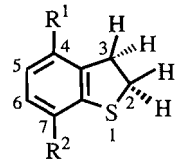

1*a*, R^1, R^2 = H
1*b*, R^1 = CH_3, R^2 = H
1*c*, R^1 = H, R^2 = CH_3

Experimental

Materials

Palladium(II) chloride, organic reagents, and general solvents were purchased from standard chemical suppliers and were used as received. 2,3-Dihydro-4- and -7-methyl-BT have been mentioned (5) as by-products of the Lewis acid catalyzed reactions of BT with aromatics but were not isolated and fully characterized. In this study, these compounds were made by oxidation of 4- and 7-methyl-BTs (prepared by the methods of Elvidge and Foster (6) and Kloetzel *et al.* (7) respectively) to the corresponding sulfones with H_2O_2, reduction of the 2,3-bond of the sulfones with H_2 over Pd on carbon, and removal of the sulfone group with $LiAlH_4$. General procedures for these transformations have been described previously (8). The crude dihydro compounds were purified by

[1]Author to whom correspondence may be addressed.
[2]Revision received May 4, 1992.

Can. J. Chem. Downloaded from www.nrcresearchpress.com by 88.255.202.194 on 09/08/12
For personal use only.

Can. J. Chem. Downloaded from www.nrcresearchpress.com by 88.255.202.194 on 09/08/12
For personal use only.

column chromatography (hexane/silica) and were isolated as oils with the following characteristics.

*2,3-Dihydro-4-methylbenzo[*b*]thiophene*

Isolated as a pale yellow oil in 13% overall yield from 4-methyl-BT; IR (neat), ν(cm^{-1}): 766 (s), 1454 (s), 1578 (s), 2936 (s), and 3057 (m); ^{1}H NMR δ: 2.47 (s, CH_3), 3.38–3.59 (m, CH_2CH_2), 7.06 (dd, H-6), and 7.23–7.27 (m, H-5 and H-7); ^{13}C NMR δ: 141.24, 138.63, and 134.05 (quaternary carbons), 127.33, 125.42, and 119.51 (unsubst. aromatic C), 34.55 and 32.33 (dihydro carbons), and 19.96 (CH_3). Anal. calcd. for $C_9H_{10}S$: C 72.00, H 6.66, S 21.33%; found: C 71.84, H 6.42, S 21.62%.

*2,3-Dihydro-7-methylbenzo[*b*]thiophene*

Isolated as a pale yellow oil in 21% yield from 7-methyl-BT; IR (neat), ν (cm^{-1}): 768 (s), 1059 (s), 1454 (s), 2876 (s), and 3055 (m); ^{1}H NMR δ: 2.60 (s, CH_3), 3.59 (br s, CH_2CH_2), 7.24 – 7.28 (m, H-4, 5, and 6); ^{13}C NMR δ: 141.28, 139.62, and 131.62 (quaternary carbons), 127.79, 124.15, and 121.58 (unsubst. aromatic C), 36.52 and 32.65 (dihydro carbons), and 20.69 (CH_3). Anal. calcd. for $C_9H_{10}S$: C 72.00, H 6.66, S 21.33%; found: C 71.72, H 6.89, 21.01%.

Preparation of palladium complexes **1**b *and* **1**c

Both **1***b* and **1***c* were prepared by adding either 4- or 7-methyl-dihydro-BT (1.5 g, 10 mmol) to a stirred solution of palladium(II) chloride (0.89 g, 5 mmol) in 90% aqueous ethanol (50 mL) at 50°C. After 1 h, the orange solids that had formed were filtered off and were crystallized from ethanol/chloroform.

trans-*Dichloro bis(2,3-dihydro-4-methylbenzo[*b*]thiophene)palladium(II)* **1***b*[3] was isolated as deep orange plates, 41%, mp > 250°C (dec.); IR (KBr), ν (cm^{-1}): 783 (s), 1265 (m), 1419 (m), 1458 (m), and 2362 (m). ^{13}C NMR†, δ:[4] 20.0 (20.39) (CH_3), 34.25 (34.02), 35.51 (35.04) (dihydro carbons), 125.02 (124.13, 124.49), 129.03 (127.97), 130.28 (130.31) (unsubst. aromatic C), 133.31 (132.84), 135.10 (135.19), and 141.59 (141.81) (quaternary C). Anal. calcd. for $C_{18}H_{20}Cl_2PdS_2$: C 45.25, H 4.19, S 13.41%; found: C 44.97, H 3.99, S 13.48%.

trans-*Dichloro bis(2,3-dihydro-7-methylbenzo[*b*]thiophene)palladium(II)* **1***c*[3] was isolated as deep orange plates, 53%, mp > 250°C (dec.); IR (KBr), ν (cm^{-1}): 785 (s), 1261 (m), 1421 (m), 1458 (m), and 2850 (w). ^{13}C NMR† δ: 21.70 (21.49, 21.63) (CH_3), 36.46 (36.16, 36.21), 40.39 (40.56, 41.06) (dihydro carbons), 122.67 (122.58, 122.63), 128.71 (128.23, 128.30), 129.36 (129.42) (unsubst. aromatic C), 132.88 (132.05, 132.18), 137.48 (137.17, 137.54), and 143.73 (143.42, 143.61) (quaternary C). Anal. calcd. for $C_{18}H_{20}Cl_2PdCl_2$: C 45.25, H 4.19, S 13.41%; found: C 45.01, H, 4.06, S, 13.22%.

X-ray structure determinations of **1**b *and* **1**c

Both crystal structures were determined by the same general procedure. Accurate cell dimensions and crystal orientations of suitable crystals placed in Lindemann glass capillaries were determined on an Enraf–Nonius CAD-4 diffractometer by a least-squares refinement of the setting angles of 25 reflections with θ in the range 10–15°. Intensity data were collected by the $\omega/2\theta$ scan method using variable scan speed (1.27–3.30°/min), scan width (1.00 + 0.35 tan θ)°, and monochromatized Mo Kα radiation in the range $2 < \theta < 25°$ with h 0 to 8, k −10 to 10, and l −10 to 10. Three reflections were monitored every two hours of exposure time and showed insignificant variations. The intensities of 1760 (**1***b*) and 1825 (**1***c*) reflections were measured, of which 1372 (**1***b*) and 1425 (**1***c*) had $I > 3\sigma(I)$, where $\sigma^2 I = S + 2B + [0.04(S - B)]^2$, with S = scan count, and B = time averaged background count extended 25% on each side. Data were corrected for Lorentz, polarization, and absorption effects (DIFABS; Walker and Stuart (9)), correction range being 0.676–1.331 for **1***b* and 0.749–1.395 for **1***c*. Crystal data and experimental details are summarized in Table 1.

Both structures were solved by the heavy-atom method. Refinement of the structures used full-matrix least-squares calculations, initially with isotropic, and finally with anisotropic temperature factors for the non-hydrogen atoms. At intermediate stages in the refinements, difference maps revealed all H-atoms which were included in the subsequent cycles at geometrically idealized positions (C—H, 0.95 Å) and at a fixed overall isotropic temperature factor. Refinements converged with $R = 0.067$ and $wR = 0.074$ for **1***b* and $R = 0.040$ and $wR = 0.040$ for **1***c*. In the refinement cycles, weights were derived from the counting statistics. Scattering factors were those of Cromer and Mann (10) and Stewart *et al.* (11) and allowances were made for anomalous dispersions (12). A difference map calculated at the conclusion of the refinement had no chemically significant features. All computer programs used in this study were part of XTAL 2.6 (13) and Figs. 1 and 2 were plotted using ORTEP II (14). Final values of the refined positional parameters, selected bond lengths, and angles are collected in Tables 2, 3, and 4 respectively.

Supplementary tables of hydrogen atom parameters, non-hydrogen thermal parameters, dihedral angles, and observed and calculated structure factors have been deposited with the National Research Council of Canada.[5]

NMR spectra

Variable temperature proton spectra of **1***b* and **1***c* were recorded on a Bruker AM-400 spectrometer in deuterochloroform solution using solvent resonances as internal references. Probe temperatures were determined by reference to methanol and 1,2-dihydroxyethane chemical shift data. Data are summarized in Tables 5 and 6.

Reactions of **1**a–c *with reducing agents*

(a) Hydrogen

All reactions were done at 20°C and at ambient pressure. Hydrogen was admitted to a flask containing a solution of **1***a* or *b* (100 mg) in toluene or dichloromethane (50 mL) that had previously been flushed with nitrogen and evacuated. Hydrogen was taken up rapidly in stirred solutions for experiments conducted in toluene (uptake complete within 15 min) and at a lesser rate (2–16 h) using dichloromethane. No uptake of hydrogen was observed for reactions with **1***c* unless ethanol was used as solvent. In this case reaction was complete after 16 h. Deposition of a palladium mirror on the surfaces of the glassware and disappearance of the characteristic orange coloration of the complex solutions was observed in all experiments. When uptake of hydrogen was complete, the solutions were analyzed for volatile organic products using GC–MS techniques (see ref. 1 for details of this analysis). In each experiment, the corresponding 2,3-dihydro-BT was observed as the only organic product.

(b) THN

A solution of **1***a*, *b*, or *c* (100 mg) in THN was heated under reflux for 16 h. During this time, black particles (later shown to be palladium) deposited from solution. GC–MS analysis of the solution revealed the presence of the 2,3-dihydro-BT compounds originally present in the complexes and traces of naphthalene.

[3]Note: variable temperature NMR data for **1***b* and **1***c* are given in Tables 5 and 6. s, m, and w denote strong, medium and weak absorptions.

[4]†denotes δ ppm from TMS recorded at 293 K; data in parentheses were recorded at 215 K.

[5]Supplementary tables may be purchased from: The Depository of Unpublished Data, Document Delivery, CISTI, National Research Council Canada, Ottawa, Canada K1A 0S2.

Tables of hydrogen atom parameters and dihedral angles have also been deposited with the Cambridge Crystallographic Data Centre and can be obtained on request from The Director, Cambridge Crystallographic Data Centre, University Chemical Laboratory, 12 Union Road, Cambridge, CB2 1EZ, U.K.

Can. J. Chem. Downloaded from www.nrcresearchpress.com by 88.255.202.194 on 09/08/12
For personal use only.

TABLE 1. Summary of crystal data for **1***b* and **1***c*

Parameter	**1***b*	**1***c*
Formula	$C_{18}H_{20}Cl_2PdS_2$	$C_{18}H_{20}Cl_2PdS_2$
Cell dimensions (Å)		
a	7.219(2)	7.730(3)
b	8.441(5)	8.056(3)
c	8.494(7)	8.516(4)
α (deg)	61.47(5)	62.87(3)
β (deg)	88.85(4)	82.31(3)
γ (deg)	84.40(3)	88.82(3)
Cell volume (Å^3)	452.96	467.23
D_c (g cm^{-3})	1.75	1.70
Space group	*P*1	*P*1
λ (Mo Kα) (Å)	0.71069	0.71069
μ (mm^{-1})	1.42	1.37
θ range (deg)	2–25	2–25
ω, scan width (deg)	(1.00 + 0.35 tan θ)	(0.80 + 0.35 tan θ)
Variable scan speed (deg min^{-1})	1.27–3.30	1.25–4.0
Absorption correction:		
minimum	0.067	0.749
maximum	1.331	1.395
Total reflections	1760	1825
Unique data	1588	1641
Data used ($I > 3\ \sigma\ (I)$)	1372	1425
No. of variables	106	106
Data/parameter	12.9	13.4
R, ω*R*	0.067, 0.074	0.040, 0.040
(Δ/σ) max in last cycle	<0.05	0.02
Δ*e* (e Å^{-3}) in final Δ*F* map	0.028	0.94, −0.9

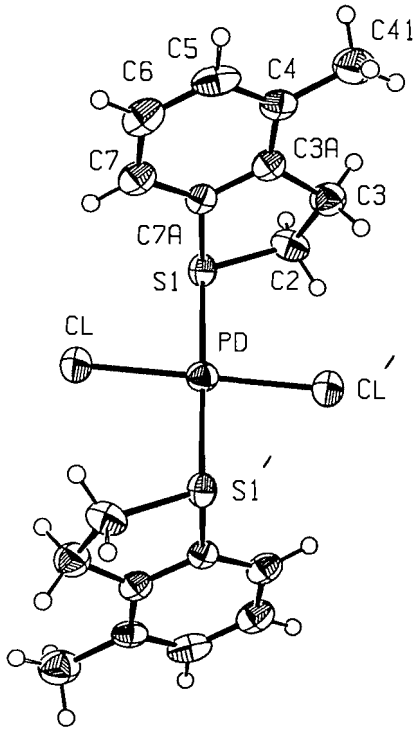

FIG. 1. X-ray structure of **1***b*.

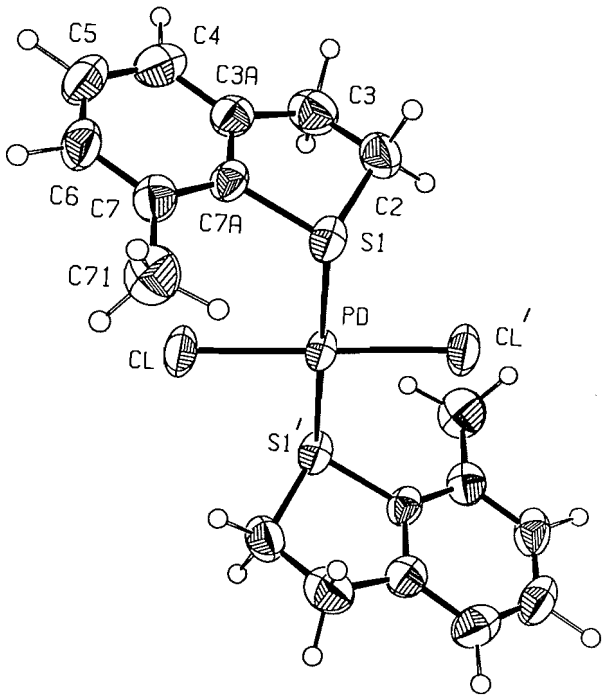

FIG. 2. X-ray structure of **1***c*.

(c) CO/H$_2$O

A solution of **1***a* (220 mg, 0.49 mmol) in 95% ethanol (150 mL) and distilled water (50 mL) was purged with argon to remove dissolved air. A reservoir of 120 mL (5.35 mmol) of CO was connected to the head space over the orange-colored solution and stirring of the solution was commenced. A black precipitate (shown later to be palladium) was formed almost immediately and the orange color faded to give a colorless solution. Analysis of the head space gas showed that CO_2 (0.08 mmol) had been formed (see Discussion for further details) along with traces of hydrogen.

TABLE 2. Positional parameters and U_{eq} for non-hydrogen atoms

Atom	x/a	y/b	z/c	U
		Compound **1***b*		
Pd	0.0000	1.0000	0.0000	0.034(1)
Cl	0.0362(4)	1.1795(4)	0.1316(4)	0.047(3)
S(1)	0.2997(4)	0.8768(3)	0.1130(4)	0.032(3)
C(2)	0.3931(16)	0.7191(15)	0.0368(16)	0.042(7)
C(3)	0.3397(17)	0.5311(15)	0.1637(15)	0.043(7)
C(3A)	0.2935(14)	0.5279(14)	0.3395(15)	0.034(6)
C(4)	0.2723(14)	0.3728(14)	0.5018(15)	0.034(6)
C(41)	0.2993(19)	0.1880(16)	0.5160(18)	0.051(8)
C(5)	0.2228(16)	0.3966(16)	0.6476(15)	0.040(7)
C(6)	0.1891(16)	0.5687(17)	0.6398(16)	0.046(7)
C(7)	0.2119(15)	0.7237(15)	0.4769(16)	0.040(7)
C(7A)	0.2649(13)	0.6963(13)	0.3304(14)	0.029(6)
		Compound **1***c*		
Pd	0.0000	0.0000	0.0000	0.0403(6)
S(1)	0.1335(2)	0.2889(2)	0.7963(2)	0.042(1)
C(1)	0.1528(2)	−0.1636(2)	0.8724(2)	0.057(2)
C(2)	0.2544(9)	0.3621(9)	0.9240(9)	0.057(7)
C(3)	0.4297(9)	0.2761(9)	0.9315(9)	0.058(7)
C(3A)	0.4742(8)	0.2591(8)	0.7632(8)	0.045(6)
C(4)	0.6380(8)	0.2426(9)	0.6821(10)	0.060(7)
C(5)	0.6521(9)	0.2218(9)	0.5279(11)	0.061(7)
C(6)	0.5076(9)	0.2242(9)	0.4514(8)	0.057(7)
C(7)	0.3412(8)	0.2448(8)	0.5228(8)	0.048(6)
C(7A)	0.3308(7)	0.2620(7)	0.6789(8)	0.037(5)
C(71)	0.1823(10)	0.2462(10)	0.4411(9)	0.069(8)

Analysis of the solution using GC–MS indicated that 2,3-dihydro-BT was the only organic product present. Addition of copper(II) chloride (250 mg) to the solution and admission of air to the apparatus caused the black precipitate to redissolve and, after stirring the reaction mixture for 16 h, the orange color of the complex **1***a* was reestablished. Evaporation of the solvents and extraction of the residue with chloroform enabled re-isolation of **1***a*.

Parallel experiments using either **1***b* or **1***c* gave very similar results.

Results and discussion

*Preparation and NMR spectroscopic characterization of 1*b *and 1*c

Both complexes formed readily at 50°C and were isolated as orange-red solids. Analysis of the crude solids by ^{13}C NMR or by reverse phase HPLC showed that only one product had been formed in each experiment. These results follow the general trend (15, 16) that palladium(II) compounds react with thioethers to produce, predominantly, one compound with square planar geometry (X-ray analysis described later confirmed that both **1***b* and **1***c* have a *trans* square planar configuration).

The ^1H NMR spectra of **1***b* (Table 5) and **1***c* (Table 6) taken at ambient temperature displayed very broad signals in all regions of the spectra, most likely because of inversion of the sulfur-containing ligands. Such inversions are commonplace for metal–thioether complexes and have been examined in detail (15–17). As was the case for the unmethylated complex **1***a* (1), the signal for H-4 of **1***b* is well downfield of that of uncomplexed dihydro-BT, most likely because of close contact with the chlorine substituents (see X-ray discussion). At ambient temperature (295 K), the signal due to H-4 consists of two broad lines (*ortho* coupling to H-5, J = 8 Hz), but the expected *meta* coupling was not observed, probably because of the broad nature of the lines. Only at 210 K did the signals for H-4 become sharp but, at this temperature, the signal was much more complex than was expected for an *ortho–meta* coupled aromatic proton, showing eight partly resolved lines consistent with two *ortho–meta* coupled protons. The dihydro protons of **1***b* (at C-2 and C-3) showed the classic coalesence and sharpening behaviour at high and low temperatures, respectively, associated with a dynamic inversion process. Resonances due to the dihydro protons of **1***b* and **1***c* were shifted significantly (both upfield and downfield) in comparison to the signals for the dihydro protons of uncomplexed dihydro-BT ligands (see data in the experimental section and in Tables 5 and 6). X-ray analysis suggests that these shifts may be due to close contact with the chloro ligands. The signals due to the methyl protons of **1***b* and **1***c* were observed as sharp singlets at 315 K and as broader singlets at 295 K that resolved into two singlets of approximately equal intensity at 215 K. This behaviour was completely reversible with no signs of decomposition over the temperature range 215–328 K.

TABLE 3. Interatomic distances (Å) for **1***b* and **1***c*[a]

Compound **1***b*		Compound **1***c*	
Pd—Cl	2.306(4)	Pd—Cl	2.283(2)
Pd—S(1)	2.318(3)	Pd—S(1)	2.330(1)
S(1)—C(7A)	1.78(1)	S(1)—C(2)	1.813(9)
S(1)—C(2)	1.81(2)	S(1)—C(7A)	1.774(6)
C(2)—C(3)	1.52(1)	C(2)—C(3)	1.50(1)
C(3)—C(3A)	1.51(2)	C(3)—C(3A)	1.50(1)
C(3A)—C(7A)	1.38(2)	C(3A)—C(4)	1.39(1)
C(3A)—C(4)	1.39(1)	C(3A)—C(7A)	1.39(1)
C(4)—C(5)	1.38(2)	C(4)—C(5)	1.39(1)
C(4)—C(41)	1.50(2)	C(5)—C(6)	1.36(1)
C(5)—C(6)	1.42(2)	C(6)—C(7)	1.39(1)
C(6)—C(7)	1.40(1)	C(7)—C(7A)	1.39(1)
C(7)—C(7A)	1.41(2)	C(7)—C(71)	1.49(1)

[a]Estimated standard deviations are given in parentheses.

Overall, the spectra described above can be explained by inversion of the sulfur-containing ligands about the sulfur lone pairs. Since the complexes contain two chiral sulfur centers, the complex signals for H-4 and resolution of the methyl signals at 215 K can be ascribed to the presence of diastereomers, which would be observed when inversion at sulfur ceases. Further evidence for the presence of diastereomers at 215 K was given by the observation that many of the signals in a proton-decoupled ^{13}C NMR spectrum of **1***c* taken at 295 K split into two lines when a spectrum was recorded at 215 K. The inequivalence of NMR signals at low temperatures could also be explained on the basis that structurally different isomers arise as a result of hindered rotation around the Pd—S bond. However, inspection of models does not suggest that any particular rotamer should be favored and thus the low-temperature spectra are most probably explained by the presence of diastereomers. The observation of diastereomers as a result of inversion at sulfur bonded to metal species is well documented (18).

Calculation of thermodynamic parameters for inversion using NMR band shape fitting techniques gave values with unacceptable errors. These inaccuracies likely stem from effects of temperature on chemical shift values of the protons of interest.

Can. J. Chem. Downloaded from www.nrcresearchpress.com by 88.255.202.194 on 09/08/12
For personal use only.

TABLE 4. Bond angles for **1***b* and **1***c*

Compound **1***b*		Compound **1***c*	
Cl—Pd—S(1)	95.9(1)	Cl—Pd—S(1)	95.07(7)
C(7A)—S(1)—C(2)	91.4(5)	C(7A)—S(1)—C(2)	91.0(3)
C(7A)—S(1)—Pd	103.7(3)	C(7A)—S(1)—Pd	111.1(2)
C(2)—S(1)—Pd	111.9(4)	C(2)—S(1)—Pd	105.5(2)
C(3)—C(2)—S(1)	109.7(9)	C(3)—C(2)—S(1)	107.2(6)
C(3A)—C(3)—C(2)	106.0(11)	C(3A)—C(3)—C(2)	106.9(6)
C(7A)—C(3A)—C(4)	119.6(12)	C(7A)—C(3A)—C(4)	117.3(7)
C(7A)—C(3A)—C(3)	114.9(9)	C(7A)—C(3A)—C(3)	114.3(6)
C(4)—C(3A)—C(3)	125.4(12)	C(4)—C(3A)—C(3)	128.4(7)
C(5)—C(4)—C(3A)	117.4(12)	C(5)—C(4)—C(3A)	119.9(7)
C(5)—C(4)—C(41)	121.5(9)	C(6)—C(5)—C(4)	120.5(7)
C(3A)—C(4)—C(41)	121.1(13)	C(5)—C(6)—C(7)	122.5(8)
C(4)—C(5)—C(6)	123.7(10)	C(6)—C(7)—C(7A)	115.6(6)
C(7)—C(6)—C(5)	118.6(13)	C(6)—C(7)—C(71)	123.0(7)
C(6)—C(7)—C(7A)	116.8(12)	C(7A)—C(7)—C(71)	121.4(6)
C(3A)—C(7A)—C(7)	123.9(9)	C(7)—C(7A)—C(3A)	124.1(6)
C(3A)—C(7A)—S(1)	113.0(9)	C(7)—C(7A)—S(1)	124.3(5)
C(7)—C(7A)—S(1)	123.2(9)	C(3A)—C(7A)—S(1)	111.6(5)

TABLE 5. ^{1}H NMR data for *trans*-dichloro(2,3-dihydro-4-methylbenzo[*b*]thienyl)palladium (II)[a] (**1***b*)

	Temperature (K)						
Assignment	215	240	270	285	295	300	315
H-7[b]	7.70	7.70					
	7.69	7.69	7.67	7.67	7.66	7.66	7.66
	7.68	7.68	7.66	7.66	7.65	7.65	7.65
	7.67	7.67					
H5-6	7.21–7.25 (m)	7.18–7.22 (m)	7.15–7.18 (m)	7.14–7.18 (m)	7.12–7.18 (m)	7.12–7.17 (m)	7.11–7.17 (m)
H-3[c]	4.02–4.08 (m)	4.05–4.11 (m)	4.08 (brs)	4.09 (brs)	4.00 (brs)	3.9 (vbrs)	3.5 (vbrs)
H-2[c]	3.43–3.56 (m)	3.46–3.53 (m)	3.49 (brs)	3.46 (brs)	3.36 (brs)	3.35 (brs)	3.35 (s)
H-2^{1c}	3.23–3.29 (m)	3.23–3.28 (m)	3.24 (brs)	3.25 (brs)	3.36 (brs)	3.35 (brs)	3.35 (s)
H-3^{1c}	2.96–3.05 (m)	2.97–3.05 (m)	3.00 (brs)	3.00 (brs)	3.05 (brs)	3.2 (vbrs)	3.5 (vbrs)
CH_3[d]	2.34–2.35	2.33–2.34	2.32	2.31	2.31	2.30	2.30

[a]In ppm relative to TMS.
[b]See text for discussion on observation of four lines at low temperature.
[c]Assignments may be reversed.
[d]Two singlets were observed at low temperatures.

X-ray characterization of ***1***b *and* ***1***c

Interatomic distances and bond angles for complexes **1***b* and **1***c* are given in Tables 3 and 4. Each complex has a slightly distorted square planar structure (Cl—Pd—S angles of 95.9(1) and 95.07(7)° for **1***b* and **1***c*, respectively) with the thioether ligands *trans* to each other (Figs. 1 and 2). Pd—S and Pd—Cl bond lengths are very similar to those observed in other Pd–thioether complexes (see ref. 14 for a review of this topic) (Pd—S: 2.318(3) Å for **1***b* and 2.330(1) Å for **1***c*; Pd—Cl: (2.306(4) Å for **1***b* and 2.283(2) Å for **1***b*). Several close contacts exist in each molecule. For **1***b*, through-space distances for Cl—H(21) and Cl—H(71) were 2.747(3) and 3.038(3) Å, respectively. Similar close contacts in solution would explain the downfield shifts observed for these protons in the ^{1}H NMR spectrum. In the 7-methyl complex **1***c*, close contacts were observed for Cl—H(21) (2.840(2) Å) and Cl—H(712) (3.349(2) Å) and again these contacts are useful in rationalizing the proton and carbon chemical shift data.

Reactions of ***1***a–c *with hydrogen and THN*

Since 2,3-dihydro-BT is known to be an intermediate in the catalytic hydrodesulfurization of BT (19–24), it was of interest to determine how the complexes **1***a–c* behaved in the presence of molecular hydrogen or organic donor hydrogen. When a stirred solution of **1***a* in either toluene or dichloromethane was exposed to 1 atmosphere of hydrogen at 20°C (1 atm = 101.3 kPa) there was a rapid uptake of hydrogen and deposition of a palladium mirror on the surface of the apparatus. The reaction was faster in toluene solution but, in either solvent, 2,3-dihydro-BT was the only organic product detected. Similar reactions were noted for the 4- and 7-methyl complexes **1***b* and **1***c* and, in each case, the re-

Can. J. Chem. Downloaded from www.nrcresearchpress.com by 88.255.202.194 on 09/08/12
For personal use only.

TABLE 6. ^{1}H NMR data for *trans*-dichloro(2,3-dihydro-7-methylbenzo[*b*]thienyl)palladium (II)[a] (**1***c*)

	Temperature (K)					
Assignment	215	240	270	290	310	330
H-4[b]	7.08	7.07	7.05			
	7.10	7.08	7.67	7.04	7.03	7.01
	7.12	7.10	7.07	7.06	7.05	7.03
H-6[b]	7.20	7.18				
	7.21	7.19	7.15	7.13	7.11	7.09
	7.22	7.20	7.17	7.15	7.13	7.11
	7.23	7.21				
H-5	7.27	7.26	7.22	7.21	7.19	7.18
	7.30	7.27	7.24	7.23	7.21	7.19
	7.31	7.29	7.26	7.24	7.22	7.21
H-3[b]	3.99–4.04	4.00–4.05	4.02–4.07	4.02–4.07	4.06	4.05
	(dd)	(dd)	(dd)	(dd)	(brs)	(brs)
H-2[b]	3.66–3.72	3.64–3.73	3.65–3.76	3.70	3.69	3.66
	(dd)	(m)	(m)	(brs)	(brs)	(brs)
H-3'[b]	3.36–3.41	3.33–3.40	3.30–3.35	3.28–3.33	3.30	3.30
	(dd)	(dd)	(dd)	(dd)	(brs)	(brs)
H-2'[b]	3.22–3.29	3.20–3.28	3.18–3.26	3.17–3.24	3.21	3.17
	(m)	(m)	(m)	(brs)	(brs)	(brs)
CH_3[c]	2.44	2.44	2.45	2.44	2.45	2.45
	2.41	2.42	2.43			

[a]In ppm relative to TMS.
[b]Assignments for H-6 and H-4 and H-2 and H-3 may be reversed.
[c]Two singlets were observed at low temperatures.

spective 2,3-dihydro compounds were the only organic products. All of the reactions were complete within 30 min with the exception of those with **1***c*, which took several hours to go to completion. No reaction was observed when **1***a–c* were treated with the organic hydrogen donor THN at 20°C. However, when **1***a* was heated with THN at 200°C a palladium mirror was deposited in the apparatus and 2,3-dihydro-BT was formed.

Overall, the major process that occurred when complexes **1***a–c* were exposed to hydrogen was reduction of Pd(II) to Pd^0 and subsequent decomposition of the complexes. Since the thioether sulfur is bonded directly to palladium, it might have been expected that the C—S bonds would have been activated sufficiently to have undergone hydrogenolysis, ultimately producing ethylbenzene as a product. However, careful analysis of the reaction solutions showed that this compound was not formed. This observation may have some implication on the mechanism of catalytic hydrodesulfurization of BT since when Pd catalysts (usually in the form of PdS) are used, it is unlikely that desulfurization of intermediate 2,3-dihydro-BT occurs by coordination to palladium compound sites. Perhaps only in hydrogen atmospheres with high partial pressures of H_2S would complexes of the type **1***a–c* be stable. Note, however, that these statements may not apply when other metal sulfides are used in the catalytic hydrodesulfurization of BT. For example, reduction of MoS_2 by hydrogen is probably a more difficult process than would be the case for PdS. (Note: useful and comparative reduction potentials for metal sulfides absorbed on surfaces are not available but some measure of the stability of PdS and MoS_2 can be ascertained from free energy of formation values (25); ΔG_f^0 PdS = −16 kcal/mol and ΔG_f^0 MoS_2 = −54 kcal/mol). In this case, complexation of 2,3-dihydro-BT with MoS_2-like species may be an important step in the desulfurization of the molecule. A useful review of possible mechanisms for the desulfurization of BT has been given by Gates *et al.* (26).

Reactions of **1***a–c with* CO/H_2O

A variety of metal complexes have been shown to catalyze the water gas shift (WGS) of CO/H_2O to CO_2 and H_2 under very moderate conditions (27–36). A useful collation of recent work is given in ref. 36. However, to our knowledge, complexes incorporating organosulfur ligands have not been used to promote this reaction. The only report concerning the effect of sulfur compounds on the WGS is that of King *et al.* (37), which describes the effect of sodium sulfide on the ability of various metal carbonyls to promote the shift reaction. Consequently, it was of interest to determine if the complexes **1***a–c* catalyzed the WGS. Initial experiments showed that exposure of an aqueous ethanolic solution of any of the complexes **1***a–c* at 20°C resulted in a rapid reaction in which CO_2, H_2, Pd^0, and the free dihydro ligand were produced. No evidence for desulfurization of the ligand was obtained. Very little hydrogen was observed but significant quantities of CO_2 were measured. The percentage of CO_2 in the head space was well above atmospheric levels (up to 1.6%) so there was no doubt that it was produced by chemical reaction. However, much less CO_2 was produced in comparison to the amount of complex used in the experiments (on average, about one fifth the amount). The fact that some H_2 was observed suggests that the shift reaction had occurred but it was observed only in trace quantities. The most likely explanation for the low observed yield of H_2 is that much of it was used to produce the elemental palladium formed in the experiment.

Can. J. Chem. Downloaded from www.nrcresearchpress.com by 88.255.202.194 on 09/08/12
For personal use only.

The overall reactions occurring are thus:

$$PdCl_2L_2 + CO + H_2O \rightarrow Pd(II) + 2Cl^- + H_2 + CO_2 + 2L \quad (\mathbf{1}a\text{–}c)$$

$$Pd(II) + H_2 \rightarrow Pd^0 + 2H^+$$

where L is the dihydro ligand.

Since all of the complexes **1***a*–**1***c* were consumed by exposure to excess CO/H_2O, amounts of CO_2 at least equimolar to the amount of complex originally present should have been produced. The lower than expected amount of CO_2 may be explained by a combination of some CO_2 being dissolved in the aqueous media used and by absorption onto the elemental palladium produced during the experiments (no attempts were made to measure these contributions). The fact that any H_2 was observed suggests that 1 mole of these complexes may have produced more than 1 mole of H_2. However, low yields of H_2 and CO_2 (most likely because of absorption of these gases by the elemental palladium) precludes establishment of precise mechanisms.

By applying the $Cu(II)/O_2$ couple used in the Wacker process (38), it was possible to reform the original complexes. Thus, on addition of $Cu(II)Cl_2$ and admission of air to the apparatus, the deposited palladium was redissolved with formation of the original complex. This confirms that hydrogen produced during the shift of CO was used to reduce palladium rather than desulfurize the ligand. Other metal–thioether complexes in which the metal is less easily reduced might be more useful for the shift of CO. These possibilities are under examination.

Can. J. Chem. Downloaded from www.nrcresearchpress.com by 88.255.202.194 on 09/08/12
For personal use only.

1. P. D. Clark, J. F. Fait, C. G. Jones, and M. J. Kirk. Can. J. Chem. **69**, 590 (1991).
2. P. D. Clark, K. L. Lesage, G. T. Tsang, and J. B. Hyne. Energy Fuels, **2**, 578 (1988).
3. C. J. Collins, V. F. Raaen, B. M. Benjamin, P. H. Maupin, and W. H. Roark. J. Am. Chem. Soc. **101**, 5009 (1979).
4. J. J. de Vlieger, A. P. G. Kieboom, and H. van Bekkum. Fuel, **63**, 334 (1984).
5. P. D. Clark, K. Clarke, D. F. Ewing, R. M. Scrowston, and F. Kerrigan. J. Chem. Res. (S), 307 (1981).
6. J. A. Elvidge and R. G. Foster. J. Chem. Soc. 981 (1964).
7. M. C. Kloetzel, J. E. Little, and D. M. Frisch. J. Org. Chem. **18**, 1511 (1983).
8. F. G. Bordwell and W. H. McKellin. J. Am. Chem. Soc. **73**, 2251 (1951).
9. N. Walker and D. Stuart. Acta. Crystallogr. Sect. A: Found. Crystallogr. **A39**, 158 (1983).
10. D. T. Cromer and J. B. Mann. Acta. Crystallogr. Sect. A: Cryst. Phys. Diffr. Theor. Gen. Crystallogr. **A24**, 321 (1968).
11. R. F. Stewart, E. R. Davidson, and W. T. Simpson. J. Chem. Phys. **42**, 3175 (1965).
12. D. T. Cromer and D. Liberman. J. Chem. Phys. **53**, 1891 (1970).
13. S. R. Hall and J. M. Stewart (*Editors*). XTAL 2.6 User's Manual, Universities of Western Australia and Maryland. 1989.
14. C. K. Johnson. ORTEP II. report ORNL-5138, Oak Ridge National Laboratory, Oak Ridge, Tenn. U.S.A.
15. S. G. Murray and F. R. Hartley. Chem. Rev. **81**, 365 (1981).
16. E. W. Abel, K. G. Orrell, K. B. Qureshi, and V. Sik. Polyhedron, **7**, 1321 (1988); **7**, 1329 (1988).
17. E. W. Abel. Chem. Br. 148 (1990).
18. E. W. Abel, T. P. J. Coston, K. M. Higgins, K. G. Orrell, T. S. Cameron, and V. Sik. J. Chem. Soc. Dalton Trans. 701 (1989).
19. P. Geneste, P. Amblard, M. Bonnet, and P. Graffin. J. Catal. **61**, 115 (1980).
20. R. A. Sanchez-Delgado and E. Gonzalez. Polyhedron, **8**, 1431 (1989).
21. D. Levache, A. Guida, and P. Geneste. Bull. Soc. Chim. Belg. **90**, 1285 (1981).
22. F. P. Daly. J. Catal. **51**, 221 (1978).
23. D. R. Kilanowski, H. Teeuwen, V. H. J. de Beer, B. C. Gates, G. C. A. Schuit, and H. Kwart. J. Catal. **55**, 129 (1978).
24. V. H. J. de Beer, J. G. J. Dahlmans, and J. G. M. Smeets. J. Catal. **42**, 467 (1976).
25. R. C. Weast (*Editor*). Handbook of chemistry and physics. 70th ed. CRC Press, Boca Raton, Fla. 1989–1990. pp. D-75 and D-78.
26. B. C. Gates, J. R. Katzer, and G. C. A. Schuit. *In* Chemistry of catalytic processes. McGraw–Hill Book Company, New York. 1979. Chap. 5.
27. R. M. Laine, R. G. Rinker, and P. C. Ford. J. Am. Chem. Soc. **99**, 252 (1977).
28. C.-H. Cheng, D. E. Hendricksen, and R. Eisenberg. J. Am. Chem. Soc. **99**, 2791 (1977).
29. H. Kang, C. H. Mauldin, T. Cole, W. Slegeir, K. Cann, and R. Pettit. J. Am. Chem. Soc. **99**, 8323 (1977).
30. P. C. Ford, R. G. Rinker, C. Ungermann, R. M. Laine, V. Landis, and S. A. Moya. J. Am. Chem. Soc. **100**, 4595 (1978).
31. R. B. King, C. C. Frazier, R. M. Hanes, and A. D. King. J. Am. Chem. Soc. **100**, 2925 (1978).
32. Y. Yoshida, Y. Ueda, and S. Otsuka. J. Am. Chem. Soc. **100**, 3941 (1978).
33. D. J. Darensburg, B. J. Baldwin, and J. A. Froelich. J. Am. Chem. Soc. **102**, 4688 (1980).
34. A. Spencer. *In* Comprehensive coordination chemistry. Vol. 6. *Edited by* G. Wilkinson. Pergamon, Oxford. 1987. p. 292, and references therein.
35. M. S. Holt, W. C. Wilson, and J. H. Nelson. Chem. Rev. **89**, 11 (1989).
36. M. Kubota. Inorg. Chem. **29**, 574 (1990), and references therein.
37. A. D. King, R. B. King, and D. B. Yang. J. Chem. Soc. Chem. Commun. 529 (1980).
38. P. Wiseman. *In* An introduction to industrial organic chemistry. 2nd ed. Applied Science, London. 1979 p. 116.

Phosphonolipids 4. A phosphonic acid analogue of platelet activating factor[1,2]

YUE-JIN LIU, BURTON E. TROPP, AND ROBERT ENGEL[3]

Department of Chemistry and Biochemistry, Queens College of the City University of New York, Flushing, NY 11367, U.S.A.

Received September 4, 1992

YUE-JIN LIU, BURTON E. TROPP, and ROBERT ENGEL. Can. J. Chem. **71**, 206 (1993).

A phosphonic acid analogue of platelet activating factor (PAF) bearing a backbone that is isosteric with and has stereochemistry corresponding to that of natural PAF has been synthesized. The synthesis uses a route maintaining stereochemical integrity.

YUE-JIN LIU, BURTON E. TROPP et ROBERT ENGEL. Can. J. Chem. **71**, 206 (1993).

On a synthétisé un analogue du facteur activant des plaquettes (FAP) contenant de l'acide phosphonique et comportant un squelette isostère et de la même stéréochimie que le FAP naturel. La synthèse fait appel à une route qui préserve l'intégrité stéréochimique.

[Traduit par la redáction]

Can. J. Chem. Downloaded from www.nrcresearchpress.com by 88.255.202.194 on 09/08/12
For personal use only.

Introduction

Since the discovery (3) of the series of natural ether lipids 1-*O*-alkyl-2-*O*-acetyl-*sn*-glycero-3-phosphorylcholine (**1**), also known by a name describing one of its biological functions, platelet activating factor (PAF), the natural material and structural analogues thereof have been targets of numerous laboratory syntheses (for a review of this area of effort, see ref. 4). These efforts have been stimulated by the particularly intriguing range of biological activities associated with natural PAF (5).

In the continuing efforts of our laboratory toward the preparation and investigation of phosphonic acid analogues of natural phosphate esters, we herein describe the synthesis of a new analogue of **1** which is anticipated to serve as a particularly useful probe of PAF activity. This analogue is one in which are incorporated fundamental structural similarities with **1** while rendering the backbone resistant to hydrolysis at the phosphorus by the incorporation of a carbon–phosphorus bond (6). Specifically, this analogue, illustrated as **2**, bears a backbone that is isosteric with that of **1** and a stereogenic center of the same absolute configuration as found in **1**.

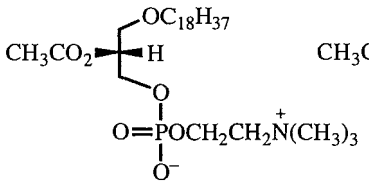

1

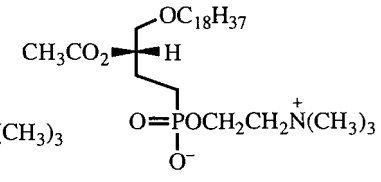

2

Results and discussion

The synthesis of **2** is accomplished starting with (*S*)-malic acid as the source of the stereogenic carbon site. The conversion of (*S*)-malic acid into (*S*)-4-benzyloxy-1,2-butanediol is accomplished in five steps as previously reported (7). Continued conversion of the (*S*)-4-benzyloxy-1,2-butanediol into the target material **2** has been accomplished as illustrated in Scheme 1.

The regiospecificity of the tosylation step, and of the alcohol attack of the epoxide by the alcohol in the presence of boron trifluoride etherate, have been established by prior work of this and other laboratories (2, 8, 9). Once acetylation is accomplished, the remainder of the route involves standard procedures for deprotection of the primary hydroxyl group, conversion to the alkyl chloride, phosphonylation via the Arbuzov reaction, and final functionalization. The selective cleavage of the phosphonate methyl ester groups is accomplished under very mild conditions using bromotrimethylsilane followed by work-up with aqueous tetrahydrofuran (10). Esterification of **10** to generate the target choline derivative **2** was accomplished using a technique previously applied for the preparation of choline derivatives (11).

Experimental

General

All chemicals were of reagent quality and were used without further purification with the following exceptions: chloroform was distilled over phosphorus pentoxide; pyridine was dried over calcium hydride and distilled; dimethylformamide (DMF) and methanol were dried over molecular sieves 4A prior to use. (*S*)-4-Benzyloxy-1,2-butanediol and its precursors were prepared as previously described (7). Thin-layer chromatography (TLC) was performed using Polygram Sil N-HR sheets. Silica gel for flash chromatography was from EM Science (230–300 mesh). Infrared spectra were measured using a Perkin–Elmer 1600 FTIR instrument, and ^{1}H and ^{31}P NMR spectra were measured using an IBM-Bruker WP200SY instrument. Optical rotations were measured using a Jasco DIP-140 digital polarimeter. Elemental analyses were performed by Desert Analytics of Tucson, Arizona, and by Schwarzkopf Microanalytical Laboratories of Woodside, New York.

Preparation of (S)-4-benzyloxy-2-hydroxy-1-tosyloxybutane (3)

In a reaction system under a nitrogen atmosphere the (*S*)-4-benzyloxy-1,2-butanediol (4.20 g, 21.4 mmol) was dissolved in a mixture of chloroform (50 mL) and pyridine (3.6 mL) and the resultant mixture was stirred at 0°C for 5 min. After this time there was added *p*-toluenesulfonyl chloride (4.10 g, 21.4 mmol) in chloroform (5 mL) solution over a period of 2 min. The mixture was stirred at 0°C for 2.5 h, after which time the cooling bath was removed and the mixture was stirred for an additional 2 h at ambient temperature. After this time diethyl ether (200 mL) was added with stirring and the mixture was washed with water (2 × 15 mL). The organic layer was dried over anhydrous calcium chloride, fil-

[1]A preliminary report of this work has been presented, see ref. 1.

[2]Paper 3 in this series is ref. 2.

[3]Author to whom correspondence may be addressed.

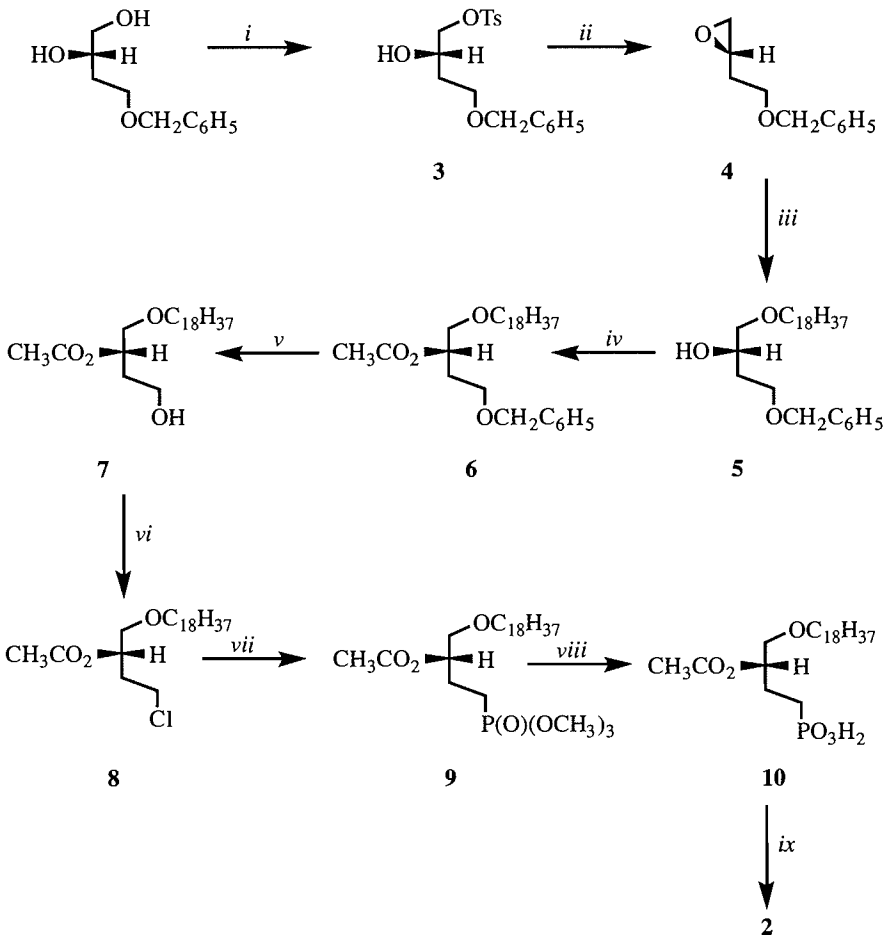

i. TsCl, $CHCl_3$, pyridine, 0°C (~94% yield); *ii*. methanol, anh. K_2CO_3, −10°C (98% yield); *iii*. BF_3 etherate, methylene chloride, 1-octadecanol, 0°C (~95% yield); *iv*. acetic anhydride, methylene chloride, DMAP, 0°C (97% yield); *v*. 95% ethanol, H_2, 5% Pd/C, ambient temp. (97% yield); *vi*. methylene chloride, tetrachloromethane, triphenyl phosphine, ambient temp. (89% yield); *vii*. DMF, trimethyl phosphite, 135°C (59% yield); *viii*. methylene chloride, TMSBr, −10°C; THF/water, ambient temp. (90% yield); *ix*. pyridine, choline tosylate, trichloroacetonitrile, 50°C (39% yield).

SCHEME 1

tered, and the volatile materials were evaporated under reduced pressure to give the desired material (7.00 g, 94%), which exhibited a major spot on TLC (R_f 0.80, hexane ethyl acetate 2:1) with a trace of starting material, and IR and ^{1}H NMR spectra in accord with the proposed structure **3**. Owing to its highly reactive nature, the material was not further purified, but used immediately in the continuing reaction. The IR spectrum (CCl_4) exhibited the following signals (partial) (cm^{-1}): 3500 (broad), 3050–3150, 2900–2990, 1510, 1470, 1400, 1270, 1180, 1100. The ^{1}H NMR spectrum ($CDCl_3$) exhibited the following signals: δ 1.87, multiplet, 2H; δ 2.34, singlet, 3H; δ 2.98, broad singlet, 1H; δ 3.35–3.85, broad multiplet, 4H; δ 4.00, multiplet, 1H; δ 4.51, doublet, 2H, J = 5 Hz; δ 7.25, broad singlet, 5H; δ 7.60, AA'BB', 4H.

Preparation of (S)-4-benzyloxy-1,2-epoxybutane (4)

(*S*)-4-Benzyloxy-2-hydroxy-1-tosyloxybutane (**3**) (3.5 g, 10.0 mmol) was dissolved in dry methanol (30 mL) and cooled to −10°C, and anhydrous potassium carbonate (1.70 g, 12.3 mmol) was added. The reaction mixture was stirred at −10°C for 3 h and allowed to come to room temperature with stirring for an additional 2 h. After this time diethyl ether (50 mL) was added and the resultant precipitate was removed by filtration through a pad of silica gel. The precipitate was washed with diethyl ether (100 mL) and the combined filtrates were evaporated under reduced pressure. The residue was purified by flash chromatography (20 g, 2 cm diameter) eluted using hexane:chloroform mixtures. The fractions exhibiting R_f 0.70 on TLC (hexane:chloroform 2:1) were combined and evaporated under reduced pressure to give the pure desired material (1.65 g, 98.0%), which exhibited IR and ^{1}H NMR spectra in accord with the proposed structure **4**. The IR spectrum (CCl_4) exhibited the following signals (partial) (cm^{-1}): 3010–3050, 2850–2990, 1510, 1480, 1450, 1410, 1350, 1130. The ^{1}H NMR spectrum ($CDCl_3$) exhibited the following signals: δ 1.85, multiplet, 2H; δ 2.51, multiplet, 1H; δ 2.76, multiplet, 1H; δ 3.10, multiplet, 1H; δ 3.62, multiplet, 2H; δ 4.58, singlet, 2H; δ 7.38, broad singlet, 5H. Anal. calcd for $C_{11}H_{14}O_2$: C 74.13%, H 7.92%; found: C 74.49%, H 7.89%. Specific rotation: $[\alpha]_{25}$ = −14.8 (0.08 M, ethanol).

Preparation of (S)-4-benzyloxy-2-hydroxy-1-octadecyloxybutane (5)

In a reaction system under a nitrogen atmosphere a 10% solution of boron trifluoride in methylene chloride (0.5 mL) was added to a mixture of (*S*)-4-benzyloxy-1,2-epoxybutane (**4**) (1.60 g, 9.0 mmol) and 1-octadecanol (2.43 g, 9.0 mmol) in methylene chloride (25 mL) at 0°C. After stirring for 10 min, the reaction mixture was allowed to warm to room temperature and to stir for 24 h. After this time volatile materials were removed under reduced pressure and the residue was purified by flash chromatography (20 g, 2 cm diameter) eluted using hexane:chloroform

Can. J. Chem. Downloaded from www.nrcresearchpress.com by 88.255.202.194 on 09/08/12
For personal use only.

Can. J. Chem. Downloaded from www.nrcresearchpress.com by 88.255.202.194 on 09/08/12
For personal use only.

mixtures. The fractions exhibiting R_f 0.60 (chloroform:hexane 3:1) were combined and evaporated under reduced pressure to give the pure desired material (3.90 g, 97%), which exhibited IR and ^{1}H NMR spectra in accord with the proposed structure **5**. The IR spectrum (CCl_4) exhibited the following signals (partial) (cm^{-1}): 3450 (broad), 3010–3050, 2850–2990, 1480, 1400, 1150. The ^{1}H NMR spectrum ($CDCl_3$) exhibited the following signals: δ 0.91, triplet, 3H, J = 6 Hz; δ 1.12–1.52, broad singlet, 32H; δ 1.80, triplet, J = 6 Hz, 2H; δ 3.25–4.02, broad multiplet, 8H; δ 4.52, singlet, 2H; δ 7.29, singlet 5H. Anal. calcd. for $C_{29}H_{52}O_3$: C 77.62%, H 11.68%; found: C 77.91%, H 11.83%. Specific rotation: $[\alpha]_{25} = -15.7$ (0.022 M, ethanol).

Preparation of (S)-2-acetyloxy-4-benzyloxy-1-octadecyloxybutane (6)

(*S*)-4-Benzyloxy-2-hydroxy-1-octadecyloxybutane (**5**) (3.00 g, 6.68 mmol) was added to a mixture of methylene chloride (15 mL) and acetic anhydride (15 mL). The mixture was stirred at 0°C for 10 min, after which time *p*-(dimethylamino)pyridine (20 mg) was added. The mixture was allowed to warm to room temperature and stirring was continued for 24 h. After this time volatile materials were evaporated under reduced pressure and the liquid residue was purified by flash chromatography (20 g, 2 cm diameter) eluted using hexane: chloroform mixtures. Fractions exhibiting R_f 0.50 (hexane:chloroform 1:1) were combined and evaporated to give the pure desired material (3.20 g, 97%), which exhibited IR and ^{1}H NMR spectra in accord with the proposed structure **6**. The IR spectrum (CCl_4) exhibited the following signals (partial) (cm^{-1}): 3010–3050, 2850–2990, 1740, 1480, 1380, 1290, 1100, 1030. The ^{1}H NMR spectrum ($CDCl_3$) exhibited the following signals: δ 0.90, triplet, 3H, J = 6 Hz; δ 1.15–1.55, broad singlet, 32H; δ 1.82, multiplet, 2H; δ 2.09, singlet, 3H; δ 3.25–3.82, broad multiplet, 7H; δ 4.52, singlet, 2H; δ 7.38, singlet, 5H. Anal. calcd. for $C_{31}H_{54}O_4$: C 75.87%, H 11.09%; found: C 75.61%, H 11.12%. Specific rotation: $[\alpha]_{25} = -14.9$ (0.029 M, ethanol)

Preparation of (S)-3-acetyloxy-1-hydroxy-4-octadecyloxybutane (7)

A mixture of (S)-2-acetyloxy-4-benzyloxy-1-octadecyloxybutane (**6**) (2.02 g, 4.11 mmol) was stirred with 95% ethanol (25 mL) and 5% palladium on charcoal (0.51 g) under a hydrogen atmosphere (1 atm (101.3 kPa)) for 20 h at ambient temperature. After this time the mixture was filtered through a pad of silica gel and the solid was washed with ethanol (75 mL). The combined filtrates were evaporated under reduced pressure and the residue was purified by flash chromatography (20 g, 2 cm diameter) eluted using hexane:ethyl acetate mixtures. The fractions exhibiting R_f 0.72 (hexane:ethyl acetate 3:1) were combined and evaporated under reduced pressure to give the pure desired material (1.60 g, 97%), which exhibited IR and ^{1}H NMR spectra in accord with the proposed structure **7**. The IR spectrum (CCl_4) exhibited the following signals (partial) (cm^{-1}): 3580 (sharp), 3450 (broad), 2850–2990, 1830, 1740, 1480, 1380, 1110. The ^{1}H NMR spectrum ($CDCl_3$) exhibited the following signals: δ 0.89, triplet, 3H, J = 6 Hz; δ 1.28–1.40, broad singlet, 32H: δ 1.71, multiplet, 2H; δ 2.08, singlet, 3H; δ 2.50, broad singlet, 1H; δ 3.30–3.50, broad multiplet, 5H; δ 4.24, multiplet, 2H. Anal. calcd. for $C_{24}H_{48}O_4$: C 71.95%, H 12.08%; found: C 71.63%, H 12.00%. Specific rotation: $[\alpha]_{25} = -9.5$ (0.26 M, ethanol).

Preparation of (S)-3-acetyloxy-1-chloro-4-octadecyloxybutane (8)

To a solution of (*S*)-3-acetyloxy-1-hydroxy-4-octadecyloxybutane (3.90 g, 9.73 mmol) in methylene chloride (5 mL) and tetrachloromethane (3.24 g, 21.1 mmol) was added dropwise a solution of triphenylphosphine (3.57 g, 9.73 mmol) in methylene chloride (6 mL) over a period of 5 h. After completion of the addition, the reaction mixture was stirred at ambient temperature for an additional 2 h, at which time pentane (40 mL) was added, resulting in the formation of a white precipitate. The precipitate was removed by filtration, washed with pentane (50 mL), and the filtrates were combined and volatile materials were evaporated under reduced pressure. The residue was purified by flash chromatography (20 g, 2 cm diameter) eluted using hexane:ethyl acetate mixtures. The fractions exhibiting R_f 0.80 (hexane:ethyl acetate 5:1) were combined and evaporated under reduced pressure to give the pure desired material (3.62 g, 89%), which exhibited IR and ^{1}H NMR spectra in accord with the proposed structure **8**. The IR spectrum (CCl_4) exhibited the following signals (partial) (cm^{-1}): 2850–2990, 1730, 1480, 1360, 1240, 1100, 1040. The ^{1}H NMR spectrum ($CDCl_3$) exhibited the following signals: δ 0.89, triplet, 3H, J = 6 Hz; δ 1.28–1.40, broad singlet, 32H; δ 1.52, multiplet, 2H; δ 2.08, singlet, 3H; δ 3.40–3.60, multiplet, 7H. Anal. calcd. for $C_{24}H_{47}O_3Cl$: C 68.78%, H 11.30%; found: C 68.60%, H 11.20%. Specific rotation: $[\alpha]_{25} = -11.8$ (0.026 M, ethanol).

Preparation of dimethyl (S)-3-acetyloxy-4-octadecyloxybutyl-1-phosphonate (9)

A mixture of (*S*)-3-acetyloxy-1-chloro-4-octadecyloxybutane (**8**) (3.62 g, 8.63 mmol), DMF (10 mL), and trimethyl phosphite (15 g, 120 mmol) was heated at 140°C for 48 h with continual stirring. After that time the volatile materials were evaporated under reduced pressure and the residue was purified by flash chromatography (20 g, 2 cm diameter) eluting with chloroform. In addition to the recovery of unchanged **8** (1.40 g), fractions exhibiting R_f 0.40 (chloroform) were combined and the volatile materials were evaporated to give the pure desired material (2.50 g, 59%), which exhibited IR and ^{1}H NMR spectra in accord with the proposed structure **9**. The IR spectrum (CCl_4) exhibited the following signals (partial) (cm^{-1}): 2850–2990, 1740, 1480, 1230, 1040. The ^{1}H NMR spectrum ($CDCl_3$) exhibited the following signals: δ 0.88, triplet, 3H, J = 6 Hz; δ 1.28–1.40, broad singlet, 32H; δ 1.49–1.65, multiplet, 4H; δ 2.08, singlet, 3H; δ 3.35–3.60, multiplet, 5H; δ 3.80, doublet, 6H, J = 12 Hz. Anal. calcd. for $C_{26}H_{53}O_6P$: C 63.39%, H 10.84%; found: C 63.44%, H 10.84%. Specific rotation: $[\alpha]_{25} = -2.7$ (0.021 M, ethanol).

Preparation of (S)-3-acetyloxy-4-octadecyloxybutyl-1-phosphonic acid (10)

To dimethyl (*S*-3-acetyloxy-4-octadecyloxybutyl-1-phosphonate (**9**) (1.50 g, 3.04 mmol) in methylene chloride (5 mL) solution at −10°C under a nitrogen atmosphere was added bromotrimethylsilane (4.0 g, 26 mmol) and the reaction mixture was stirred for 15 min at −10°C and allowed to come to room temperature for 5 min. After that time the volatile materials were evaporated under reduced pressure, a 9:1 THF:water mixture (15 mL) was added, and the mixture was stirred for 20 min. Again the volatile materials were evaporated under reduced pressure. There was thus isolated the pure material (1.28 g, 90%) of mp 65°C, which exhibited IR and ^{1}H NMR spectra in accord with the proposed structure **10**. The IR spectrum (CCl_4) exhibited the following signals (partial) (cm^{-1}): 3400 (broad), 2850–2990, 1730, 1480, 1380, 1230, 1040 (broad). The ^{1}H NMR spectrum ($CDCl_3$) exhibited the following signals: δ 0.89, triplet, 3H, J = 6 Hz; δ 1.28–140, broad singlet, 32H; δ 1.49–1.65, multiplet, 4H; δ 2.08, singlet, 3H; δ 3.35–3.60, multiplet, 5H; δ 4.74, broad singlet, 2H. Anal. calcd. for $C_{24}H_{49}O_6P$: C 62.04%, H 10.63%; found: C 62.01%, H 10.85%. Specific rotation: $[\alpha]_{25} = -5.0$ (0.011 M, ethanol).

Preparation of (S)-3-acetyloxy-4-octadecyloxybutyl-1-phosphonylcholine (2)

To a solution of (*S*)-3-acetyloxy-4-octadecyloxybutyl-1-phosphonic acid (**10**) (110 mg, 0.237 mmol) in pyridine (5 mL) under a nitrogen atmosphere was added dry choline tosylate (500 mg, 1.82 mmol) and trichloroacetonitrile (1.00 g, 6.92 mmol). The reaction mixture was stirred for 72 h at 50°C, after which time the volatile materials were evaporated under reduced pressure. Acetonitrile (30 mL) was added to the residue and the solid material was isolated by filtration, purified by dissolution in 9:1 THF:water (10 mL), and passed through an ion exchange column (Amberlite MB-3 resin). From the eluent was isolated the pure target material (50.0 mg, 39%), which exhibited IR and ^{1}H and ^{31}P NMR spectra

in accord with the proposed structure **2**. The IR spectrum (CCl_4) exhibited the following signals (partial) (cm^{-1}): 3400 (broad), 2850–2990, 1730, 1480, 1260 (broad), 1080 (broad). The ^1H NMR spectrum ($CDCl_3$) exhibited the following signals: δ 0.88, triplet, 3H, J = 6 Hz; δ 1.18–1.30, broad singlet, 32H; δ 1.36, singlet, 9H; δ 1.49–1.65, multiplet, 4H; δ 2.08, singlet, 3H; δ 3.20–3.65, multiplet, 9H. The ^{31}P NMR spectrum ($CDCl_3$) exhibited a signal at −30 ppm relative to external 85% H_3PO_4. Anal. calcd. for $C_{29}H_{60}NO_6P$: C 63.36%, H 11.00%; found: C 63.71%, H 11.35%. Specific rotation: $[\alpha]_{25}$ = −6.2 (0.01 M, ethanol).

Acknowledgement

This work was supported by grants from the National Institutes of Health (GM 40441) and the PSC-BHE Research Award Program (No. 668261).

1. Y.-j. Liu, B. E. Tropp, and R. Engel, Paper No. 75. Organic Division, 200th National Meeting of the American Chemical Society, Washington, D.C. August 1990.
2. C. Pratt, Y.-j. Liu, T.-y. Chu, K. Melkonian, B. E. Tropp, and R. Engel. Can. J. Chem. **70**, 2135 (1992).
3. (*a*) P. M. Henson. J. Exp. Med. **131**, 287 (1970); (*b*) J. Benveniste, P. M. Henson, and C. G. Cochrane. J. Exp. Med. **136**, 1356 (1972); (*c*) C. A. Demopoulos, R. N. Pinckard, and D. J. Hanahan. J. Biol. Chem. **254**, 9355 (1979); (*d*) D. J. Hanahan, C. A. Demopoulos, J. Liehr, and R. N. Pinckard. J. Biol. Chem. **255**, 5514 (1980); (*e*) J. Polonsky, M. Tence, P. Varenne, B. C. Das, J. Lunel, and J. Benveniste. Proc. Natl. Acad. Sci. U.S.A. **77**, 7019 (1980).
4. L. A. Vargas. *In* Handbook of organophosphorus chemistry. *Edited by* R. Engel. Marcel Dekker, Inc., New York. 1992.
5. (*a*) M. L. Blank, F. Snyder, L. W. Byers, B. Brooks, and E. E. Muirhead. Biochem. Biophys. Res. Commun. **90**, 1194 (1979); (*b*) F. Snyder. Platelet activating factors and related lipid mediators. Plenum Press, New York. 1987; (*c*) M. C. Venuti. Annu. Rep. Med. Chem. **20**, 193 (1985); (*d*) F. Heymans, E. Michel, M.-C. Borrel, B. Wichrowski, J.-J. Godfroid, O. Convert, E. Coeffier, M. Tence, and J. Benveniste. Biochim. Biophys. Acta, **666**, 230 (1981); (*e*) R. L. Wykle, C. H. Miller, J. C. Lewis, J. D. Schmitt, J. A. Smith, J. R. Surles, C. Piantadosi, and J. T. O'Flaherty. Biochem. Biophys. Res. Commun. **100**, 1651 (1981).
6. (*a*) R. Engel. Chem. Rev. **77**, 349 (1977); (*b*) *In* The role of phosphonates in living systems. *Edited by* R. L. Hilderbrand. CRC Press, Inc., Boca Raton, Fla. 1982; (*c*) *In* Handbook of organophosphorus chemistry. *Edited by* R. Engel. Marcel Dekker, Inc., New York. 1992.
7. (*a*) H. Hayashi, K. Nakanishi, C. Brandon, and C. Marmur. J. Am. Chem. Soc. **95**, 8749 (1973); (*b*) K.-C. Tang, B. E. Tropp, and R. Engel. Tetrahedron, **34**, 2873 (1978).
8. S. Ali and R. Bittman. Chem. Phys. Lipids, **50**, 11 (1989).
9. Y.-j. Liu, T.-y. Chu, and R. Engel. Synth. Commun. **22**, 2367 (1992).
10. C. E. McKenna, M. T. Higa, N. H. Cheung, and M.-C. McKenna. Tetrahedron Lett. 155 (1977).
11. (*a*) F. Cramer and G. Weimann. Chem. Ber. **94**, 996 (1961); (*b*) A. F. Rosenthal. J. Lipid Res. **7**, 779 (1966); (*c*) D. Braksmayer, B. E. Tropp, and R. Engel. Chem. Phys. Lipids, **19**, 93 (1977); (*d*) P. W. Schwartz, B. E. Tropp, and R. Engel. Chem. Phys. Lipids, **48**, 1 (1988).

Can. J. Chem. Downloaded from www.nrcresearchpress.com by 88.255.202.194 on 09/08/12
For personal use only.

Reactions of SO_2X mono-substituted arenes with SO_3 in nitromethane: electronic and steric directing effects of the sulfonic acid group and some model substituents[1,2]

HAROLD R. W. ANSINK, ERIK J. DE GRAAF, ERWIN ZELVELDER, AND HANS CERFONTAIN[3]
Laboratory of Organic Chemistry, University of Amsterdam, Nieuwe Achtergracht 129, 1018 WS Amsterdam, The Netherlands

Received June 22, 1992

HAROLD R. W. ANSINK, ERIK J. DE GRAAF, ERWIN ZELVELDER, and HANS CERFONTAIN. Can. J. Chem. **71**, 210 (1993).

The sulfonation of benzene-SO_2X (X = CH_3, OCH_3, OH, and Cl) and of 1- and 2-naphthalene-SO_2X (X = CH_3, OCH_3, and Cl) with sulfur trioxide in nitromethane as solvent has been studied. In the benzene series, substitution only occurs at the 3-position irrespective of X; the reaction rates, which are all within the same order of magnitude, are low. Upon sulfonation of the 1-SO_2X-substituted naphthalenes, the main sulfonation product (58–80%) is the 5-sulfonic acid (5-S); in addition, 6-S and small amounts of 3-S and 7-S are formed. Also, the formation of the intermolecular sulfonic anhydride of 1-(methylsulfonyl)naphthalene-5-S is observed. The 2-SO_2X-substituted naphthalenes all yield the 5-S and 8-S in a ratio of ≅4.9. For both the benzene and naphthalene series, insertion of SO_3 between the SO_2 and X moieties of the chlorosulfonyl and methoxysulfonyl substituents proper takes place. In the benzene series these reactions are fast as compared with the actual ring sulfonation, whereas in the naphthalene series they are, in general, relatively slow. In the naphthalene series the mesomeric directing effect of the SO_2X groups is less important than in the benzene series; the "naphthalene α-effect" also plays an important role.

HAROLD R. W. ANSINK, ERIK J. DE GRAAF, ERWIN ZELVELDER et HANS CERFONTAIN. Can. J. Chem. **71**, 210 (1993).

On a étudié la sulfonation des benzène-SO_2X (X = CH_3, OCH_3, OH et Cl) et des naphtalène-1- et 2-SO_2X (X = CH_3, OCH_3, et Cl) par le trioxyde de soufre dans le nitrométhane. En série benzénique, la substitution ne se produit qu'en position 3, quelle que soit la nature de X; les vitesses de réaction, qui sont toutes du même ordre de grandeur, sont faibles. Lors de la sulfonation des naphtalènes substitués en position par un 1-SO_2X, le principal produit de sulfonation (58–80%) est l'acide 5-sulfonique (5-S); de plus, il se forme du 6-S et de faibles quantités des 3-S et 7-S. De plus, on observe la formation de l'anhydride sulfonique intermoléculaire du 1-(méthylsulfonyl)naphthalène-5-S. Les naphtalènes substitués par un 2-SO_2X conduisent tous aux 5-S et 8-S dans un rapport de ≈4,9. Dans les séries benzénique et naphtalénique, il se produit aussi une insertion du SO_3 entre le SO_2 et le X des substituants chlorosulfonyle et methoxysulfonyle. En série benzénique, ces réactions sont rapides comparées aux réactions de sulfonation du cycle; par contre, en série naphtalénique, elles sont en général relativement plus faibles. En série naphtalénique, l'effet mésomérique directeur des groupes SO_2X est moins important qu'en série benzénique; l'effet-α du naphtalène joue toujours un rôle important.

[Traduit par la rédaction]

Introduction

From studies on the sulfonation of methyl- (1) and methoxy-substituted (2) naphthalenes, it emerged that the electronic directing effect of the activating, "*ortho/para*"-directing CH_3 substituent is large and that this effect is even larger for the OCH_3 substituent. The electronic directing effect of the deactivating "*meta*"-directing sulfonic acid group present in the methyl- and methoxy-substituted naphthalenes is not very apparent; the directing effects of the CH_3 and OCH_3 groups are dominant over that of the sulfonic acid substituent in the further sulfonation of the naphthalenemonosulfonic acid products. In contrast, in the benzene series, the electronic directing effect of a sulfonic acid group appears to be large in most cases (3).[4]

We now report on the SO_3 sulfonation behaviour of a number of SO_2X monosubstituted benzenes and naphthalenes with the objective to monitor, for the two arene systems, the relative importance of the inductive and mesomeric effects on the one hand and the steric effects on the other of the SO_2X substituents, as for the sulfonic acid product mixture composition. Sulfonation of naphthalene-1-sulfonic acid in 98.5% H_2SO_4 occurs at the 5- (58%), 6- (32%), and 7-positions (10%), whereas sulfonation of the 2-isomer occurs at the 4- (4%), 5- (74%), 6- and 7- (4% in total), and 8-positions (18%) (5). The positional reactivity orders for naphthalene-1- and 2-sulfonic acid, predicted on the basis of the electron-withdrawing inductive effect (which will be more pronounced in the ring to which the SO_3H group is attached than in the other), and the mesomeric and steric effect of the sulfonic acid group are $2 < 4 < 3 < 5 \cong 7 < 8 < 6$ and $1 < 3 \cong 4 \cong 6 = 8 < 5 = 7$, respectively (6).

Results and discussion

The sulfonation of benzene-SO_2X (X = CH_3, OCH_3, OH, and Cl) and of 1- and 2-naphthalene-SO_2X (X = CH_3, OCH_3, and Cl) with sulfur trioxide in nitromethane as solvent has been studied, the results of which are compiled in Tables 1 and 2. To obtain more concrete information on the course of the substitution, some of the reactions have been monitored by ^1H NMR using $C^2H_3NO_2$ as solvent.

In the benzene series, substitution very predominantly occurs at the 3-position irrespective of the type of X; the reaction rates, which are all within the same order of magnitude, are low. This implies that all four SO_2X substituents studied (*i*) deactivate the phenyl ring and (*ii*) strongly destabilize the σ-complexes leading to *ortho* and *para* substitution. Furthermore, the chlorosulfonyl and methoxysulfonyl

[1]Aromatic Sulfonation part 117. For part 116, see ref. 2.

[2]For reasons of convenience, all sulfo products have been numbered as the substrates.

[3]Author to whom correspondence may be addressed.

[4]For instance, 3-methylbenzenesulfonic acid, when dissolved in 118.1% sulfuric acid, is sulfonated at the 5-position, i.e., *meta* to the methyl and sulfonic acid groups, for 69.4% (4).

Can. J. Chem. Downloaded from www.nrcresearchpress.com by 88.255.202.194 on 09/08/12
For personal use only.

TABLE 1. Reactions of C_6H_5-SO_2X with sulfur trioxide in nitromethane at ambient temperatures (20–22°C)

Benzene substituent	SO_3 equiv. (± 0.1)	Reaction time (min)	Solvent[a]	Reaction mixture composition (%, ±2)			
				Substrate[b]	C_6H_4-1-SO_2X-3-S[c]	C_6H_5-S	C_6H_4-1,3-S_2
SO_2CH_3	4.0	20	N	≥99	≤1		
		205		96	4		
		1420		82	18		
		4320		70	30		
		13 140		68	32		
	4.0 + 2.0[d]	16 175[e]		67	33		
		20 370[e]		58	42		
SO_2OH	2.0	11 280	N	72	28		
SO_2OCH_3	1.0	1440	W	nd		95	5
	4.0	2880	W	nd		95	5
SO_2Cl	1.0	4560	N	75		25	
	2.0	11 640	W	nd	1	97	2

[a]N and W stand for $C^2H_3NO_2$ and ^2H_2O, respectively.
[b]nd stands for not determined.
[c]S stands for SO_3H when $C^2H_3NO_2$ is the solvent, and for SO_3^- when ^2H_2O is the solvent.
[d]After 16 165 min, 2.0 equiv. of SO_3 were added to the reaction mixture.
[e]The times listed are the total reaction times.

TABLE 2. Reactions of 1- and 2-$C_{10}H_9$-SO_2X with sulfur trioxide in nitromethane at ambient temperatures

Naphthalene substituent	SO_3 equiv. (±0.1)	Reaction time (min)	Solvent[a]	Reaction mixture composition (%, ±2)[b,c]						
				Substrate[d]	3-S	5-S	$(5\text{-}SO_2)_2O$	6-S	7-S	8-S
1-SO_2CH_3	1.0	5	N	63	2	20	7	6	2	
		1128		16	3	65	5	8	3	
		11 446		—	3	84	2	8	3	
		69 000	W[e]		4	83	—	9	4	
	2.0	8	N	—	6	52	27	11	4	
		11 707			6	57	20	11	6	
		69 000	W[e]		6	80	—	11	5	
	4.0	5	N	—	6	43	36	12	3	
		1070			6	50	27	11	6	
		69 000	W[e]		5	78	—	11	6	
1-SO_2Cl[f]	2.0	1380	W	nd	8	58		28	6	
	4.0	16 000	W	nd	6	65		26	3	
	8.0	180	W	nd	5	73		19	3	
1-SO_2OCH_3[g]	1.0	1560	W	nd	6	69		22	3	
	4.0	60	W	nd	11	67		14	8	
	8.0	180	W	nd	10	69		15	5	
2-SO_2CH_3	1.0	5	N	45		46				9
		98		43		47				10
		8781		38		51				11
		68 000	W[e]	nd		81				19
	4.0	8	N	33		56				11
		125		23		64				13
		3135		20		65				15
		13 000	W[e]	nd		80				20
2-SO_2Cl[f]	1.0	60	W	nd		84				16
	2.0	60	W	nd		85				15
	4.0	180	W	nd		83				17
2-SO_2OCH_3[g]	1.0	60	W	nd		81				19
	2.0	1320	W	nd		85				15
	4.0	120	W	nd		83				17

[a]N and W stand for $C^2H_3NO_2$ and ^2H_2O, respectively.
[b]S stands for SO_3H when $C^2H_3NO_2$ is the solvent, and for SO_3^- when ^2H_2O is the solvent.
[c]All compositions are molar!
[d]nd stands for not determined.
[e]Composition obtained after aqueous alkaline work-up of the reaction mixture mentioned above.
[f]In all cases, ≥95% of the SO_2Cl group was converted into a sulfonate group.
[g]In all cases, ≥95% of the SO_2OCH_3 group was converted into a sulfonate group.

Can. J. Chem. Downloaded from www.nrcresearchpress.com by 88.255.202.194 on 09/08/12
For personal use only.

Can. J. Chem. Downloaded from www.nrcresearchpress.com by 88.255.202.194 on 09/08/12
For personal use only.

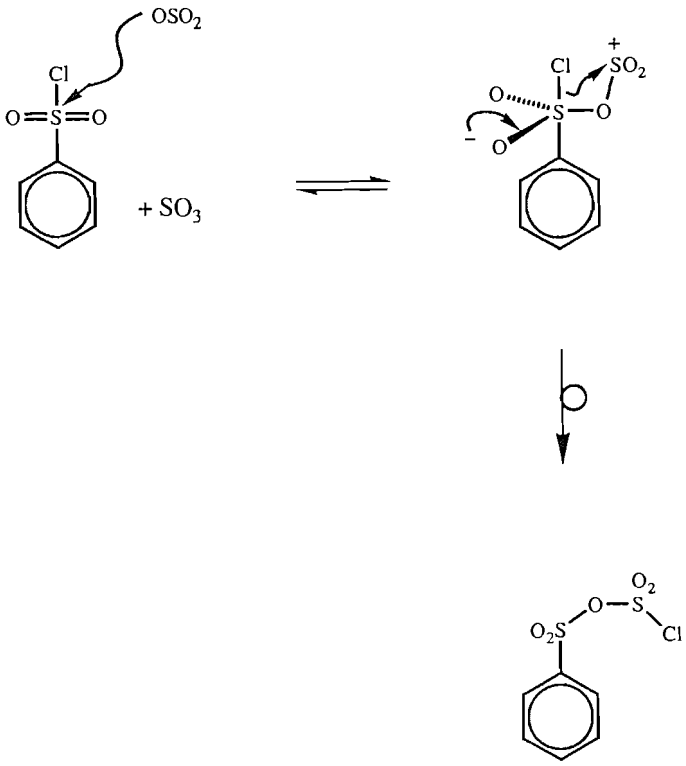

SCHEME 1. Mechanism for the insertion of a SO_3 molecule in between the SO_2 and Cl moieties of (chlorosulfonyl)benzene.

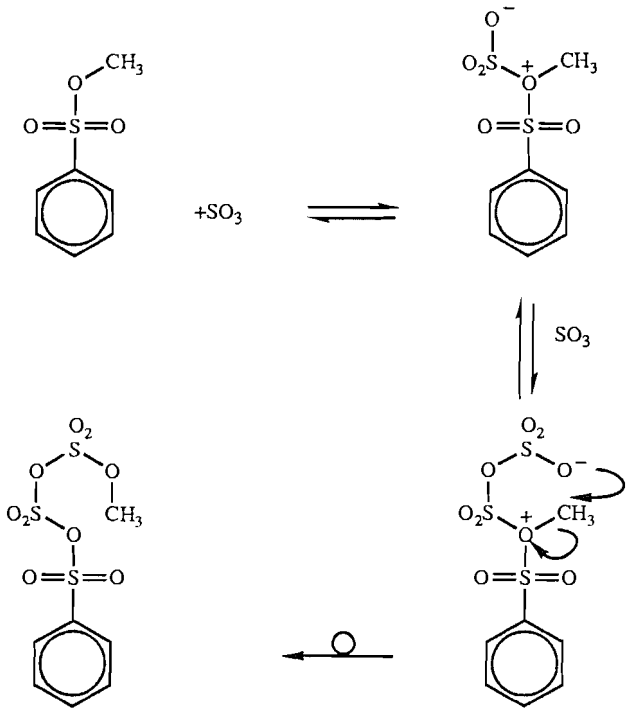

SCHEME 2. Mechanism for the SO_3 insertion in between the SO_2 and OCH_3 moieties of (methoxysulfonyl)benzene.

substituents proper undergo insertion of respectively one and two molecules of SO_3 between the SO_2 and X moieties, reactions that are fast as compared with the actual ring sulfonation. The evidence for these insertions is twofold: first, in the ^1H NMR spectra of the reaction mixtures in fully deuterated nitromethane, signals appear that belong to benzenepyrosulfonic acid rather than to the substrates and, second, after aqueous work-up, potassium benzenesulfonate, containing some dipotassium benzene-1,3-disulfonate, is isolated in all cases. Similar types of SO_3 insertion have been observed for the carbonyl analogues (7, 8) and phenyl methanesulfonates (9). Mechanisms for the insertion of SO_3 between the CO and Cl of the chlorocarbonyl substituent and between the CO and RO of alkoxycarbonyl groups have been proposed (7, 8), with the insertion in the alkoxycarbonyl group being reversible. Mechanisms for the present SO_3 insertions are proposed in Schemes 1[5] and 2[6].

Upon SO_3 sulfonation of the three 1-SO_2X-substituted naphthalenes studied, the 3-, 5-, 6-, and 7-sulfonic acids (3-S, 5-S, 6-S, and 7-S) are formed, of which the 5-S is the major product. A similar product distribution was observed in the sulfuric acid sulfonation of naphthalene-1-S (5). The predominant sulfonation occurs in the ring not containing the (initial) SO_2X substituent. The 5-S is, however, not the main product predicted on the basis of the mesomeric effect of the SO_2X substituents. Apparently, the higher reactivity of the α as compared to the β positions in naphthalenes (the "α-effect") is the dominant factor. Again, sulfodechlorination and sulfodemethylation resulting from SO_3 insertion are the predominant side reactions, although it is not clear at which stage these processes occur. For example, with 1-(methoxysulfonyl)naphthalene, the 5-S derivative was observed in the nitromethane reaction mixture, but only dipotassium naphthalene-1,5-disulfonate is isolated after aqueous alkaline work-up; thus the demethylation had taken place during the alkaline work-up, at least to some extent.

The formation of a substantial amount of the 6-S upon sulfonation of both 1-(methoxysulfonyl)- and 1-(chlorosulfonyl)naphthalene is in contrast to the sulfonation of 1-(methylsulfonyl)naphthalene, for which substrate the amount of 6-S is appreciably smaller. It is thought that the sulfonation σ-complexes for sulfonation at C(3) and C(6) are more stabilized by the chlorosulfonyl and the methoxysulfonyl substituents than by the methylsulfonyl substituent, for the following reason. In the former two σ-complexes, the two carbons adjacent to C(1) are partially positively charged; the electron-rich chlorine atom of the chlorosulfonyl and the methoxy oxygen atom of the methoxysulfonyl substituents are in the vicinity of these two carbons, enabling through-

[5]In the mechanism proposed by Krespan and England (7), the initial step is the electrophilic attack of SO_3 on the carbonyl oxygen; however, we propose that, due to the strong electron-withdrawing power of the chlorine atom, the initial step is *nucleophilic* attack by one of the oxygens of SO_3 on the partially positively charged sulfur atom of the SO_2Cl group, thus avoiding the unlikely four-membered ring intermediate **A** proposed by Krespan and England.

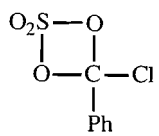

A

[6]A similar mechanism to that in Scheme 2 was proposed for the insertion of SO_3 between the C(sp^2)-bonded oxygen and the sulfur atom of an -OSO_2CH_3 substituent as in 4-(trifluoromethoxy)phenyl methanesulfonate (9*a*) and in dimethyl sulfate (10).

TABLE 3. ^{1}H NMR data of C_6H_5-SO_2X and their reaction products with sulfur trioxide in nitromethane at ambient temperatures

Benzene substituents[a]	Solvent[b]	δ(ppm, ±0.03)[c] 1	2	3	4	5	6
SO_2CH_3	C	3.01	7.90	7.56	7.58		
	N	3.33	8.05	7.76	7.84		
1-SO_2CH_3-3-S	N	3.33	8.55		8.39	8.06	8.39
	W	3.30	8.36		8.18	7.86	8.18
S	N	10.73	8.00	7.64	7.75		
	W		7.83	7.58	7.58		
1,3-S_2	N		8.61		8.44	7.96	8.44
	W		8.20		8.00	7.70	8.00
SO_2OCH_3	N	3.84	7.99	7.73	7.85		
SO_2Cl	N		8.17	7.82	7.96		
1-SO_2Cl-3-S	W		8.48				

[a]S stands for SO_3H when $C^2H_3NO_2$ is the solvent, and for SO_3^- when ^2H_2O is the solvent.
[b]C, N, and W stand for C^2HCl_3, $C^2H_3NO_2$, and ^2H_2O, respectively.
[c]δ relative to virtual internal TMS.

space dipolar stabilization of these σ-complexes (see Fig. 1). As a result, the sulfonation at C(3) and C(6) will be faster than sulfonation at C(5) and C(7) for these two substrates as compared with 1-(methylsulfonyl)naphthalene. In addition, the chloro and methoxy moieties are both electron withdrawing relative to the SO_2 moiety, whereas the methyl group is electron donating. As a result, the sulfonation σ-complexes for sulfonation of 1-(chlorosulfonyl)- and 1-(methoxysulfonyl)naphthalene at the 5- and 7-positions are more destabilized, rendering sulfonation at their 6- and 3-positions relatively more favoured.

The variation in the amounts of 3-, 5-, and especially 6-S formed for X = Cl and OCH_3 upon increasing the relative amount of SO_3 may be explained in terms of the increasing rate of initial complex formation (the first step in Schemes 1 and 2) or SO_3 insertion, thus varying the actual directing effect due to substituent modification. It should, however, be noted that the SO_3-complexed substituents, and the SO_2OSO_2Cl and $SO_2OSO_2OCH_3$ groups resulting from the insertion, will have a similar effect (see Fig. 1) to that originally presented by the SO_2Cl and SO_2OCH_3 groups as they also contain an electron-withdrawing moiety adjacent to the carbon-bonded sulfur atom; thus, the variation will not be very dramatic, as is in fact observed.

Of interest is the conversion of 1-(methylsulfonyl)naphthalene-5-S into its intermolecular anhydride, which is not further sulfonated. Sulfonic anhydride formation is a common secondary reaction in SO_3 sulfonation (11), especially with either substrates of low reactivity, or upon using moderated sulfonating reagents.[7] The ^{1}H NMR absorptions of the aromatic hydrogens are dramatically shifted up-field upon going from the naphthalenesulfonic acid to the corresponding sulfonic anhydride, as is shown in Table 5, as a result of the increase of the electron density due to the proximity of the two naphthalene rings of the sulfonic anhydride.

The formation of a small amount of the 7-S on sulfonation of the 1-SO_2X-naphthalenes with SO_3 is further evidence that the inductive (deactivating) effect is stronger in the ring to which the SO_2X substituent is attached than in the other. The result further compares favourably with the sulfuric acid sulfonation of naphthalene-1-S, which occurs at C(7) for 10% (5).

On sulfonation of the three 2-SO_2X-substituted naphthalenes, the 5-S and 8-S are formed in a ratio of ≅4.9. The 5-S is the product predicted on the basis of the mesomeric and inductive effects of the SO_2X substituents; the formation of ≅17% of the 8-isomer illustrates again the importance of the "α-effect", especially since no β-sulfonation products are observed. Also, the sulfuric acid sulfonation of naphthalene-2-S yields in total only 4% of the 2,6- and 2,7-S_2 (5).

Disulfonation was not observed to occur for any of the substrates, illustrating the large electron-withdrawing effect of both the SO_2X and sulfonic acid substituents. In fact, only when reacting naphthalene with fuming sulfuric acid (containing 105.4% H_2SO_4), naphthalene-1,3,5-, -1,3,6-, and -1,3,7-trisulfonic acid are formed (5).

From the present data it appears that the four SO_2X substituents all behave similarly; the methylsulfonyl substituent seems to be the most suitable model for the sulfonic acid group, as it is stable under both the sulfonation and the aqueous alkaline work-up conditions. The inductive electronic effect diminishes the amount of sulfonation in the ring to which the SO_2X substituent is attached, and the steric effect impedes sulfonation *peri* to an SO_2X group. It appears that the mesomeric directing effect of the SO_2X groups in the naphthalene series is less important than in the benzene series; in addition, the "α-effect" plays an important role.

Experimental

(Chlorosulfonyl)- and (methylsulfonyl)benzene, benzenesulfonic acid, and the (chlorosulfonyl)naphthalenes were obtained commercially and used as such. The methoxysulfonyl derivatives of benzene and naphthalene were synthesized by dissolving the corresponding chlorosulfonyl compounds in methanol. After standing for 8 h, the solvent was removed by vacuum evaporation, the residue dissolved in chloroform, and the resulting solution washed three times with water. After drying over magnesium sulfate and evaporation of the chloroform, the naphthalene products were recrystallized from a 1:1 mixture of diethyl ether and hexane to give 1-(methoxysulfonyl)naphthalene, mp 75°C (lit. (12*a*)

[7]For instance, the sulfonation of 1,7-dimethoxynaphthalene with 4.0 equiv. of SO_3 in $^2H_8$-dioxane yields, as secondary product, the intermolecular anhydride of its 4-S (H.R.W. Ansink, unpublished result).

Can. J. Chem. Downloaded from www.nrcresearchpress.com by 88.255.202.194 on 09/08/12
For personal use only.

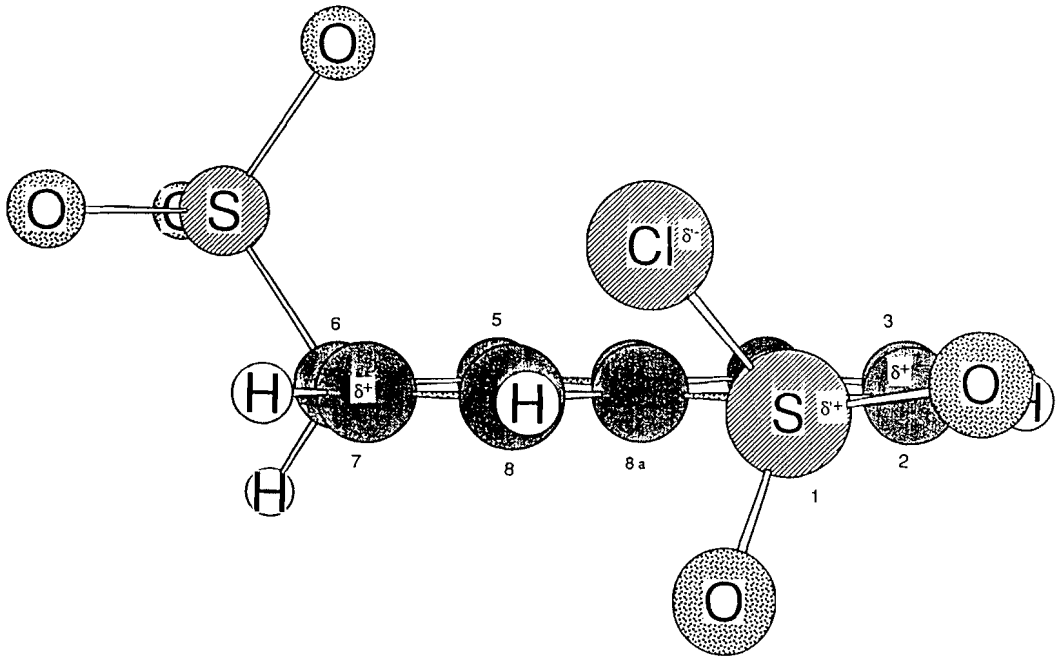

FIG. 1. Through-space stabilization of the partial positive charge at C(2) and C(8a) by the X moieties of the SO_2Cl and SO_2OCH_3 groups, exemplified for the σ-complex structure for sulfonation at C(6) of 1-(chlorosulfonyl)naphthalene as obtained by the Cambridge Scientific Computing "Chem3D plus" calculations. The rotation around the C(1)—S bond is not impeded.

TABLE 4. ^1H NMR data of 1- and 2-$C_{10}H_9$-SO_2X and their reaction products with sulfur trioxide

Naphthalene substituents[a]	Solvent[b]	δ (ppm, ±0.03)[c,d]							
		1	2	3	4	5	6	7	8
1-SO_2CH_3	C	3.23	8.15	7.62	8.35	8.00	7.64	7.74	8.74
	N	3.32	8.31	7.76	8.35	8.16	7.76	7.84	8.76
1-SO_2CH_3-3-S	N		8.66		8.92				
	W		8.50						
1-SO_2CH_3-5-S	W	3.35	8.28	7.78	9.05		8.32	7.82	8.72
	N	3.37	8.52	8.01	9.22		8.52	8.05	9.01
(1-SO_2CH_3-5-SO_2)$_2$O	N	3.35	8.25	7.55	8.87		8.11	7.69	8.55
1-SO_2CH_3-6-S	N					8.76		8.23	8.97
	W					8.47			
1-SO_2CH_3-7-S	N	3.41					8.20		9.42
	W	3.39							9.25
1-SO_2Cl	N		8.42	7.76	8.45	8.17	7.81	7.94	8.78
1-SO_2OCH_3	N	3.80	8.34	7.75	8.36	8.14	7.77	7.86	8.61
1-SO_2OCH_3-5-S	N	3.85	8.01	8.5	9.07[e]		7.97	8.5	8.97[e]
1,3-S_2	W		8.43		8.54				8.67
1,5-S_2	W		8.26	7.77	8.88				
1,6-S_2	W		8.15	7.69	8.22	8.45		8.02	8.76
1,7-S_2	W			7.60		8.07	7.92		9.14
2-SO_2CH_3	C	8.54	3.13	7.91	8.02	7.96	7.69	7.63	7.99
	N	8.58	3.23	7.98	8.19	8.09	7.82	7.76	8.12
2-SO_2CH_3-5-S	N	8.62	3.29	8.15	8.80		8.42	7.81	8.48
	W	8.34	3.30	7.95	8.75		8.03	7.56	8.21
(2-SO_2CH_3-5-SO_2)$_2$O	N		3.32					7.61	
2-SO_2CH_3-8-S	N	9.20	3.31	8.08	8.28	8.31	7.85	8.36	
	W	9.13	3.32	8.04	8.14		7.80		
2-SO_2Cl	N	8.71		8.05	8.22	8.10	7.86	7.80	8.19
2-SO_2OCH_3	N	8.59	3.88	7.92	8.21	8.11	7.83	7.76	8.16

[a]S stands for SO_3H when $C^2H_3NO_2$ is the solvent, and for SO_3^- when ^2H_2O is the solvent.
[b]C, N, and W stand for C^2HCl_3, $C^2H_3NO_2$, and ^2H_2O, respectively.
[c]δ relative to virtual internal TMS.
[d]Due to overlap, not all signals could be assigned.
[e]The assignment may be reversed.

Can. J. Chem. Downloaded from www.nrcresearchpress.com by 88.255.202.194 on 09/08/12
For personal use only.

TABLE 5. Change in the substituent shifts δ on converting the naphthalene-1-sulfonic acid system into its intermolecular sulfonic anhydride[a]

	Δδ (±0.03)							
Solvent[b]	1	2	3	4	5	6	7	8
N	—	−0.41	−0.36	−0.46		−0.27	−0.46	−0.35
D	—	−0.54	−0.34		−0.36		−0.49	−0.37

[a]Calculated from 1-(methylsulfonyl)naphthalene-5-sulfonic acid, 1,7-dimethoxynaphthalene-4-sulfonic acid (taken from ref. 2), 1-mesyloxynaphthalene-4-sulfonic acid (ref. 15), and the corresponding intermolecular sulfonic anhydrides.

[b]N and D stand for $C^2H_3NO_2$ and $^2H_8$-dioxane, respectively.

Can. J. Chem. Downloaded from www.nrcresearchpress.com by 88.255.202.194 on 09/08/12
For personal use only.

mp 75°C) and 2-(methoxysulfonyl)naphthalene, mp 54–55°C (lit. (12*b*) mp 53–54°C). The (methylsulfonyl)naphthalenes were synthesized from the corresponding (chlorosulfonyl)naphthalenes following a described procedure (13). The NMR spectra were recorded using Bruker AC-200 and WM-250 spectrometers. The three-dimensional molecular structures were calculated using the Cambridge Scientific Computing "Chem3D plus" package.

Sulfonation procedures

Method A

A solution of the desired amount of SO_3 in 7.0 mL of nitromethane was added to a homogeneous solution of 1.0 mmol of substrate in 7.0 mL of nitromethane at ambient temperature (≅20°C) in an argon atmosphere. After the appropriate reaction time, 1.0 mL of ^1H_2O was added and the mixture heated to 40°C for 30 min to hydrolyze (most of) the anhydrides. The aqueous layer was isolated and extracted at room temperature three times with 1–2 mL of CH_2Cl_2 to remove any unconverted substrate and remaining nitromethane. The residual CH_2Cl_2 was removed by bubbling N_2 through the aqueous solution for 30 min. The aqueous layer was subsequently neutralized with 10% aqueous potassium hydroxide and the water removed by freeze-drying. Subsequently, an ^1H NMR spectrum of the resulting potassium sulfonate salt mixture dissolved in ^2H_2O was recorded for product assignment and the quantitative analysis.

Method B

A solution of the desired amount of SO_3 in 0.5 mL of $C^2H_3NO_2$ was added to a solution of 0.10 mmol of substrate in 0.5 mL of $C^2H_3NO_2$ at ambient temperature under argon. A sample of the resulting homogeneous reaction mixture was then transferred into an NMR tube and subsequently ^1H NMR and (or) ^{13}C NMR spectra were recorded allowing appropriate time intervals. The reaction mixtures thus obtained were worked up with H_2O and subsequently treated as described in method A.

The structural assignments of the sulfo products of the SO_3 sulfonations were made on the basis of the observed ^1H NMR chemical shifts, absorption area ratios, and coupling constants in combination with the shielding parameters of the SO_3^- and SO_3H substituents. The assignments are compiled in Tables 3 and 4. The compositions of the sulfonation reaction mixtures and the sulfonated product mixtures were determined by multicomponent ^1H NMR analysis on the basis of specific absorptions of the various components (14). The chemical shift changes on converting a 1-naphthalenesulfonic acid group into the corresponding intermolecular anhydride are collected in Table 5.

1. K. Lammertsma and H. Cerfontain. J. Chem. Soc. Perkin Trans. 2, 673 (1979).
2. H. R. W. Ansink, E. J. de Graaf, E. Zelvelder, and H. Cerfontain. Recl. Trav. Chim. Pays-Bas, **111**, 499 (1992).
3. H. Cerfontain. Mechanistic aspects of aromatic sulfonation and desulfonation. Interscience, New York. 1968. pp. 129–130.
4. A. Koeberg-Telder and H. Cerfontain. J. Chem. Soc. Perkin Trans. 2, 633 (1973).
5. P. de Wit and H. Cerfontain. Can. J. Chem. **61**, 1453 (1983).
6. H. Cerfontain. J. Org. Chem. **47**, 4680 (1982).
7. C. G. Krespan and D. C. England. J. Org. Chem. **40**, 2937 (1975).
8. J. Falbe (*Editor*). Surfactants in consumer products. Springer-Verlag, Heidelberg. 1987. pp. 75–77 and references cited therein.
9. H. R. W. Ansink and H. Cerfontain. (*a*) Recl. Trav. Chim. Pays-Bas, **111**, 215 (1992); (*b*) Phosphorus, Sulfur Silicon, **63**, 335 (1991).
10. J. R. v. Wazer, D. Grant, and C. H. Dungan. J. Am. Chem. Soc. **87**, 3333 (1965).
11. A. Koeberg-Telder, C. Ris, and H. Cerfontain. J. Chem. Soc. Perkin Trans. 2, 98 (1974).
12. Elsevier's Encyclopaedia of Organic Chemistry. Ser. III. Vol. 12b. New York. 1950; (*a*) p. 4855; (*b*) p. 4879.
13. L. Field and R. D. Clark. J. Org. Chem. **22**, 1129 (1957).
14. H. Cerfontain, A. Koeberg-Telder, C. Kruk, and C. Ris. Anal. Chem. **46**, 72 (1974).
15. H. R. W. Ansink, E. Zelvelder, and H. Cerfontain. Recl. Trav. Chim. Pays-Bas. In press.

Coincidence electron-scattering experiments: the statistics of coincidence counting

LISA A. GRAHAM, S. J. DESJARDINS, AND A. D. O. BAWAGAN[1]
Ottawa–Carleton Chemistry Institute, Carleton University, Ottawa, Ont., Canada K1S 5B6

Received August 21, 1992

LISA A. GRAHAM, S. J. DESJARDINS, and A. D. O. BAWAGAN. Can. J. Chem. **71**, 216 (1993).

A new coincidence electron-scattering spectrometer for electron momentum spectroscopy (EMS) experiments is described. The new features include the use of a single 360° cylindrical mirror analyzer (CMA) for energy analysis and a coincidence data acquisition system based on a qVt-multichannel analyser and CAMAC electronics. The CMA energy resolution and coincidence time resolution are 0.32 ± 0.03% $\Delta E/E$ fwhm and 3.5 ± 0.5 ns fwhm, respectively. The helium 1*s* orbital binding energy spectrum is obtained at 1000 eV binding energy and 100 eV pass energy, yielding a coincidence binding energy resolution of 1.5 ± 0.2 eV fwhm. The coincidence data analysis procedure that is introduced provides experimental verification of some basic statistics of coincidence counting.

LISA A. GRAHAM, S. J. DESJARDINS et A. D. O. BAWAGAN. Can. J. Chem. **71**, 216 (1993).

On décrit un nouveau spectromètre diffusion des électrons à coïncidence pour des expériences de spectroscopie des moments électroniques. Les nouvelles caractéristiques comprennent l'utilisation d'un analyseur en forme de miroir cylindrique (AMC) de 360° unique pour l'analyse de l'énergie et d'un système à coïncidence d'acquisition de données basé sur un analyseur multicanaux qVt et de l'électronique CAMAC. Les résolutions de l'énergie et du temps de coïncidence par l'AMC sont respectivement de 0,32 ± 0,03% $\Delta E/E$ fwhm et 3,5 ± 0,5 ns fwhm. On a obtenu le spectre d'énergie de liaison de l'orbitale 1*s* de l'hélium à une énergie de liaison de 1000 eV et une énergie de passage de 100 eV qui conduisent à une résolution de la coïncidence de l'énergie de liaison de 1,5 ± 0,2 eV fwhm. La façon d'analyser les données de coïncidence qui est introduite fournit une vérification expérimentale de quelques statistiques fondamentales de la facon de compter les coïncidences.

[Traduit par la rédaction]

Can. J. Chem. Downloaded from www.nrcresearchpress.com by 88.255.202.194 on 09/08/12
For personal use only.

1. Introduction

A coincidence electron-scattering technique called electron momentum spectroscopy (EMS)[2] has emerged as a unique and powerful spectroscopic technique following the pioneering experimental studies of Amaldi *et al.* (1), Camilloni *et al.* (2), and Weigold *et al.* (3) and the insightful theoretical investigations of Neudatchin *et al.* (4) and Glassgold and Ialongo (5). The theoretical framework, originally developed for (p,2p) reactions, was quickly applied to the analysis of (e,2e) experiments. Initial speculations at that time (4–6) indicated the potential of (e,2e) reactions for probing individual orbital electron momentum distributions (MDs) as well as the investigation of correlation effects in atoms, molecules, and thin films. These speculations were soon verified in several experiments around the world (2, 3, 7–9). Since then several reviews have been published and excellent surveys of the literature (10, 11) can be consulted.

The major experimental observables in an EMS experiment are the binding energy spectrum and the experimental momentum profile (XMP). Since EMS is not energy-limited by resonance light sources (e.g., He I limit is 21.2 eV), it is capable of observing spectra over the complete binding energy range including both the outer valence and the inner valence regions. Electron momentum spectroscopy (EMS) and photoelectron spectroscopy (PES) studies in the inner valence region have shown extra structure to what one would expect from the single-particle picture of ionization and these structures are now attributed to correlation states. The understanding of these correlation (many-body) states as well as the accurate prediction of their transition probabilities is fairly recent (12, 13). Nevertheless, the generally semi-quantitative agreement obtained between the experimental binding energy spectra obtained in EMS and the calculated spectrum is quite impressive. It is clear from the studies conducted so far that the breakdown of the single-particle picture of ionization, especially in the inner valence region, is a general phenomenon (13).

Although EMS and PES both give closely related information regarding the correlation state (satellite) intensities, the two techniques are of an entirely different nature because of the different momentum regions sampled by the techniques. In fact, this difference has been the subject of intense investigation and controversy (14).

Electron momentum spectroscopy is one of the experimental techniques capable of probing atomic and molecular momentum distributions. Other techniques include Compton scattering, high-energy electron scattering, and positron annihilation. In EMS the angular correlation spectra obtained for a particular energy-selected state are called experimental momentum profiles (XMPs). The XMP is a well-defined physical observable within the limits defined by the theory of EMS and is proportional to the spherically averaged orbital momentum distribution. Since EMS is orbital selective, it has a *distinct* advantage compared to Compton scattering and high-energy electron scattering, which are experimental techniques that measure a quantity equal to an integral over the total electron momentum distribution.

With the current improvements in momentum resolution, EMS measurements are now providing a sensitive test of the quality of *ab initio* wavefunctions. Collaborative experimental and theoretical studies (15–18) have led to the development of so-called universal wavefunctions in the sense that they are sufficiently accurate to calculate all electronic properties of the molecule with good precision. As opposed to traditional one-electron properties such as the dipole moment, an increasing amount of evidence (15) indicates that XMPs are even more sensitive to the diffuse region of the orbital electron distribution. In addition, the experimental

[1]Author to whom correspondence may be addressed.
[2]Also known as binary (e,2e) spectroscopy.

Can. J. Chem. Downloaded from www.nrcresearchpress.com by 88.255.202.194 on 09/08/12
For personal use only.

investigation of traditional chemical concepts such as inductive effects and hyperconjugation becomes feasible through a comparative study of the outermost valence XMPs of a series of chemically related molecules (19–21).

The present work outlines the construction, calibration, and operation of a new coincidence electron-scattering spectrometer for EMS experiments at Carleton University. The new EMS spectrometer is of a novel design following the early ideas of Cook (22) and Moore *et al.* (8), the ultimate goal being the development of a multichannel EMS spectrometer in the angular plane (ϕ-plane) as opposed to the energy-dispersive plane. Although multichannel EMS spectrometers in the energy-dispersive plane have been utilized extensively in chemical investigations (23), they involve the assembly of several binding energy spectra taken at several azimuthal angles to generate the experimental momentum profiles (XMPs). A multichannel EMS spectrometer in the angular plane will provide the XMPs directly without cumbersome data analysis procedures and is thus of more practical chemical interest. XMPs produced by this type of EMS spectrometer will most likely be less sensitive to instrumental instability because of the shorter data collection times involved.

A further advantage of the present design is the flexibility allowed to perform future (e,3e) triple coincidence experiments, since the larger CMA design would allow the introduction of a third electron energy analyzer (within the inner cylinder) with ease. These (e,3e) experiments are believed (24, 25) to provide a more detailed picture of electron correlations in atoms and molecules.

2. Theoretical background

Electron momentum spectroscopy is based on the (e,2e) reaction,

$$[1] \quad e_0^-(E_0\boldsymbol{p}_0) + M \rightarrow M^+ + e_1^-(E_1\boldsymbol{p}_1) + e_2^-(E_2\boldsymbol{p}_2)$$

where $\boldsymbol{p}_i$, E_i (i = 0, 1, 2) are the momentum and energy of the incoming, scattered, and ejected electrons, respectively. The ion recoil momentum and energy are given by $\boldsymbol{p}_3$ and E_3, respectively. The (e,2e) reaction is also shown in Fig. 1. Early studies (26, 27) have shown that under certain well-defined kinematic conditions the (e,2e) cross section (reaction probability) is largely a measure of the electron momentum distribution of the single-particle orbital from which the electron was ionized or knocked out. It is now established that the necessary conditions are

(*a*) high-impact energy ($E_0 \geq 1000$ eV)
(*b*) symmetric energy sharing ($E_1 = E_2 = E$)
(*c*) large momentum transfer ($|\mathbf{K}| = |\boldsymbol{p}_0 - \boldsymbol{p}_1| \geq 5$ au)
(*d*) non-coplanar ($\theta = 45°$, ϕ = variable)

Under these conditions and within the independent-particle (Hartree–Fock) description of electronic motion, the (e,2e) cross section is given by

$$[2] \quad \sigma_{e,2e} = \text{constant} \cdot (4\pi)^{-1} \int |\psi_j(\mathbf{p})|^2 \, d\hat{p}$$

where $\boldsymbol{p}$ is the momentum of the electron in orbital ψ_j prior to ionization. The momentum distribution is spherically averaged ($d\hat{p}$) to account for the random orientation of the gaseous targets.

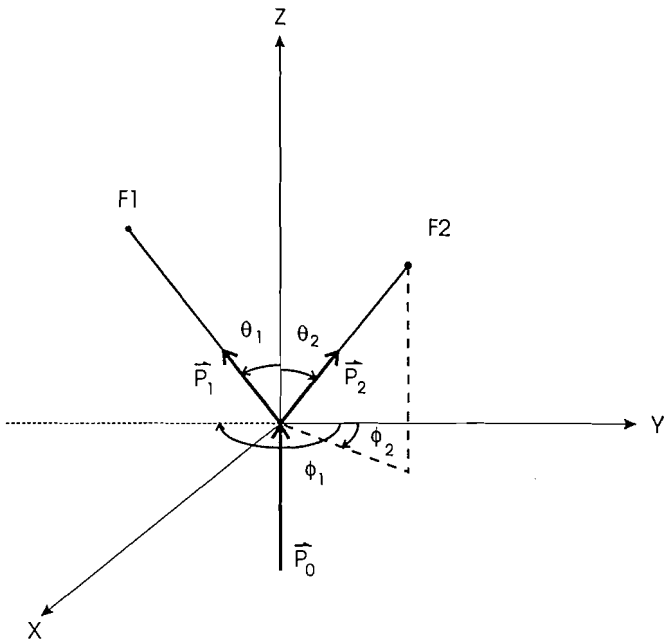

FIG. 1. Vector diagram showing collision geometry for the (e,2e) symmetric non-coplanar scattering kinematics. The experimental parameters are: $\theta_1 = \theta_2 = 45°$, $\phi_1 = 180°$, $\phi_2 = \phi$ = variable.

The expression in eq. [2] follows from energy conservation,

$$[3] \quad E_0 = E_1 + E_2 + E_3 + E_b \sim E_1 + E_2 + E_b$$

and momentum conservation laws,

$$[4] \quad \boldsymbol{p}_0 = \boldsymbol{p}_1 + \boldsymbol{p}_2 + \boldsymbol{p}_3$$

E_3 is the ion recoil energy and is negligible due to the large mass of the ion. E_b is the binding energy (ionization potential) of the orbital electron. The ion recoil momentum, $\boldsymbol{p}_3$ within the conditions (*a*)–(*d*) outlined above is equal in magnitude but opposite in sign to the orbital electron momentum prior to knockout, i.e.,

$$[5] \quad \boldsymbol{p} = -\boldsymbol{p}_3$$

In the symmetric non-coplanar arrangement the magnitude of the orbital electron momentum, $\boldsymbol{p}$, is given by

$$[6] \quad p = p_{\text{nom}} = \{(2p_1 \cos\theta - p_0)^2 + [2p_1 \sin\theta \sin(\phi/2)]^2\}^{1/2}$$

where the scattering angles θ and ϕ are defined in Fig. 1. It should be recognized that eq. [6] is only valid for a *point* source and finite volume effects need to be considered in the assignment of the momentum scale and (or) the incorporation of momentum resolution effects (28–30).

Equation [5] is an approximation that assumes the target to be initially at rest and the ion is a "spectator" in the collision process. The approximations leading to the proportionality relation (eq. [2]) are called the plane wave impulse approximation (PWIA) and the target Hartree–Fock approximation (THFA), both of which were discussed at length in previous publications (26, 27).

Can. J. Chem. Downloaded from www.nrcresearchpress.com by 88.255.202.194 on 09/08/12
For personal use only.

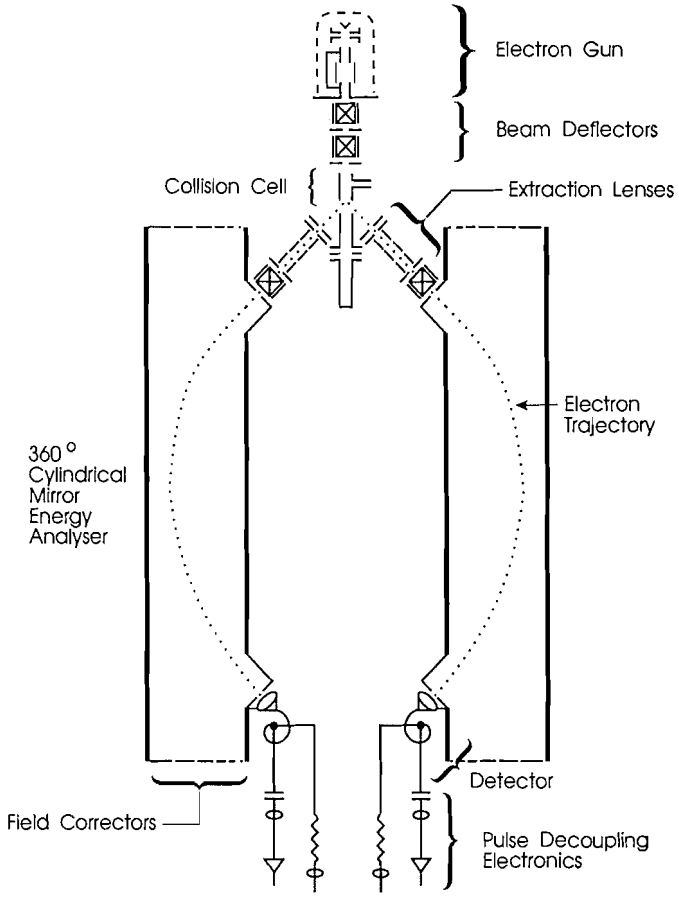

FIG. 2. Illustration of Coincidence Electron Momentum Spectrometer. Note that this illustration is not drawn to scale. Major spectrometer dimensions are indicated in ref. 32.

3. Description of coincidence electron-scattering spectrometer

The coincidence electron-scattering spectrometer for electron momentum spectroscopy (EMS) experiments is shown in Fig. 2. The present EMS spectrometer is of a unique design. It features a *single* 360° cylindrical mirror analyzer (CMA) for the energy analysis of the two outgoing electrons resulting from the (e,2e) reaction (see Fig. 1). A 360° CMA is composed of two concentric cylinders wherein the inner cylinder has entrance and exit slots for the electrons that have to be analysed. Traditionally, most EMS spectrometers have been built with two independent energy analyzers, one for each outgoing electron. In the non-coplanar geometry, one of the energy analyzers is fixed whereas the other is allowed to move (i.e., variable azimuthal angle) to generate the XMP. The present design follows from early ideas (8, 22), where a single energy analyzer is used to select *both* outgoing electrons. With such a design the simultaneous collection of outgoing electrons at several azimuthal angles (ϕ) becomes possible. Thus an experimental momentum profile for an energy-selected molecular orbital can be generated without changing or scanning the azimuthal angles. Clearly, with this kind of design careful calibration studies are necessary to ensure that the collection efficiency across the accessible azimuthal angles is uniform. This requirement places stringent constraints on spectrometer alignment and machining tolerances.

At present, the EMS spectrometer is operated at single-angle mode (i.e., at one fixed azimuthal angle) as a necessary calibration step towards its eventual operation as a multi-angle EMS spectrometer. The spectrometer is described in Sect. 3.1 and preliminary results on the coincidence binding energy spectrum of the He 1*s* orbital are described in Sect. 4.3.

3.1. Physical characteristics of apparatus

Located at the top of the assembly is the electron gun (Cliftronics CE5AH), which uses a thoriated tungsten hairpin filament. The voltage on the filament cathode, which is negative relative to the gas cell (−1000 V), defines the incoming electron impact energy. The filament and its extraction electrodes are housed within a Faraday cage, which is held at large negative potential.

The electron beam passes through a pair of quadrupole beam deflectors for focusing. The electron beam is focused by minimizing the current measured at spray plates 1 and 2 and maximizing the current measured at the Faraday cup. Before reaching the Faraday cup, the electron beam (circular cross section of ~1 mm) passes through a small gas cell where the (e,2e) reaction occurs. The target gas is introduced to the gas cell through a 0.5 mm diameter stainless steel tube. Two sets of three-element cylindrical lenses are used to select those electrons emitted at a 45° polar angle (θ) with respect to the incident beam. These cylindrical lenses are mounted on the legs of a hinge mechanism that rotates about the center axis of the CMA. One leg of the hinge is held stationary while the other hinge can move within a range of azimuthal angles ($-45° \leq \phi \leq +45°$). The angular acceptances of these lenses intersect with the electron beam to define the probed collision volume.

The three-element cylindrical lenses retard and focus the electrons emitted from the collision volume into the CMA for energy analysis. Typically, a 5:1 or 6:1 retarding field is used. In the present application, a 5:1 retarding field is used to retard 500 eV electrons to 100 eV prior to entering the CMA. Thus it is said that the CMA is operating at 100 eV pass energy. Reducing the pass energy to lower values improves the energy resolution up to a point where it is dominated solely by the incoming electron beam energy spread.

The cylindrical mirror analyzer is designed for first-order focusing using the parameters suggested by Risley (31). The base energy resolution R_{base} is given by,

$$[7] \qquad R_{base} = \frac{w_{sz} + w_{ez}}{D}$$

where w_{sz} and w_{ez} are the projections of the source and exit slit widths onto the axis of the analyzer, respectively. D is the linear dispersion of the analyzer. The contributions of angular aberrations to the energy resolution are neglected since these contributions are relatively much smaller in the present application. Using the present experimental parameters,[3] the calculated energy resolution of the present CMA is

$$[8] \qquad R_{base} = \frac{\Delta E_{base}}{E_{pass}} = 0.70\%$$

$$[9] \qquad R_{fwhm} = \frac{\Delta E_{fwhm}}{E_{pass}} = 0.35\%$$

As a result of the high machining tolerances required, both inner and outer cylinders of the CMA are machined from bronze and mounted on high-quality sapphire balls. Concentric rings are placed on the top and bottom ends of the cylinders to correct for fringing field effects. All surfaces traversed by the electron are coated with benzene soot to minimize secondary electron emission. To null the earth's magnetic field, two concentric mu-metal shields (Conetic AA) are placed around the CMA and the electron gun assembly. This reduces the magnetic fields within the CMA to ≤5 mG.

The electrons are detected by identical channel electron multi-

[3]The outer cylinder and inner cylinder radii are 168 and 84 mm, respectively. The entrance and exit aperture diameters are 0.7 and 1.0 mm, respectively. Further details are available in ref. 32.

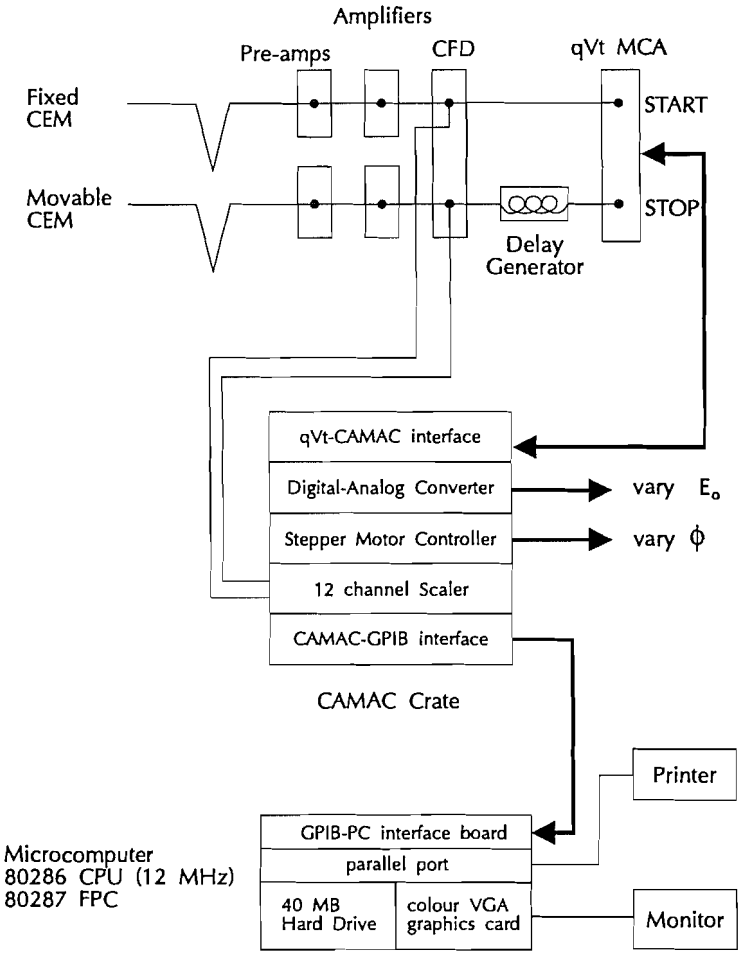

FIG. 3. Schematic diagram of coincidence electronics and computer-controlled data acquisition system.

pliers (Galileo 4318 CEM), which are also located on the same hinge of the corresponding cylindrical lens as shown in Fig. 2. The CEM output pulse is decoupled, amplified, and sent to the coincidence electronics as described in the following section.

The whole coincidence electron-scattering spectrometer is enclosed in a high-vacuum chamber with a base pressure of less than 8×10^{-7} Torr (1 Torr = 133.31 Pa). A baffled oil diffusion pump (Varian VHS 6) with pumping capacity of 2400 L/s is used to maintain this pressure. The diffusion pump is backed by a direct drive roughing pump (Leybold D30A). A second roughing pump is used to evacuate the sample manifold.

3.2. Coincidence timing electronics

Time-correlated pulses are produced by the two electron detectors when the electrons arriving at the detectors arise from the same ionizing event. Electrons that are not from the same ionizing event are also detected, but the time difference between arrival times of these two electrons is randomly distributed. We are interested in distinguishing between the number of true coincidences and the number of random coincidences. The correlated pulses are distinguished by passing one of the CEM pulses through a fixed known time delay and measuring the time delay between the two CEM pulses. Pairs of pulses with a time delay within a certain allowable time spread are considered to be coincident. This time spread is also referred to as the time resolution. Time delays measured outside this range are considered to arise from random events. This classification is accomplished by the coincidence electronics system illustrated in Fig. 3.

The pulses produced by the CEMs are capacitively decoupled and amplified (Ortec 9301, Ortec 474). The amplified pulses are used to trigger the constant fraction discriminators (CFDs, Canberra 2126Q) to produce standard fast timing pulses. These fast timing pulses are then used to trigger the qVt multichannel analyzer (MCA, LeCroy 3001), which measures the time difference between the pulses appearing at its START and STOP inputs. The pulse originating from the fixed detector is used as the START trigger and the pulse originating from the movable detector is passed through a time delay unit (Canberra 2058, τ_d = 32 ns) and used as the STOP trigger. The qVt-MCA is operated in time mode (t) and produces a time spectrum or histogram (counts vs. time difference). At the end of each acquisition time, the time spectrum is transferred from the qVt-MCA to the computer via the qVt-CAMAC interface module (LeCroy 2301).

The time spectrum is a plot of the number of coincidence events occurring with a specific time delay between the two trigger pulses generated by the event, and an example is shown in Fig. 4. The time spectrum can be produced using either the TAC (time to amplitude converter) as used previously (26) or the qVt method (a similar use is outlined in ref. 33) as we have chosen to use. There are advantages and disadvantages as will be explained below. The whole time spectrum is divided into two sections, the coincidence time window and the background time window. The number of true coincidences can therefore be calculated from the number of coincidence counts occurring at both windows and their relative widths.

The ratio of the widths of the coincidence time window to background time window must be known and constant throughout the experiment. In the present qVt method the entire time spectrum is saved at each parameter setting ($E_0 + E_b$ or ϕ), and the data

Can. J. Chem. Downloaded from www.nrcresearchpress.com by 88.255.202.194 on 09/08/12
For personal use only.

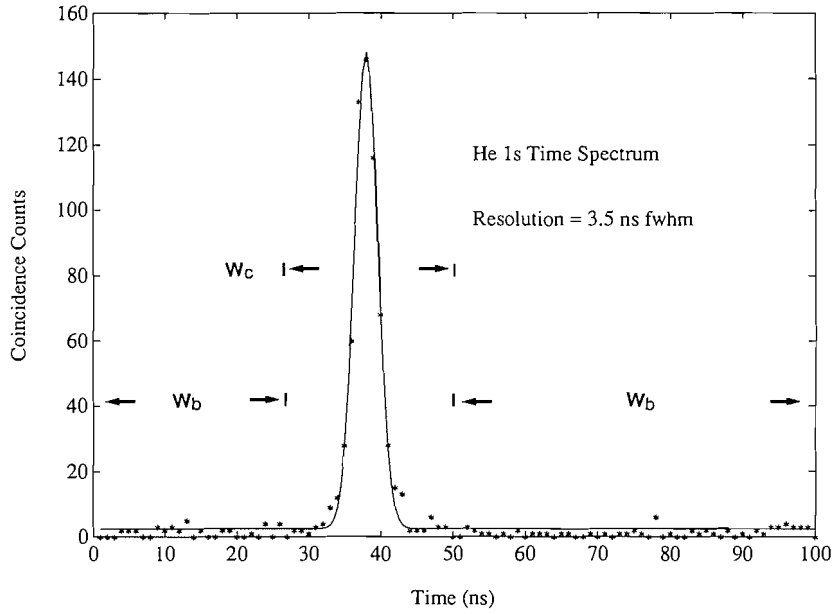

FIG. 4. Typical time delay spectrum observed at $\epsilon \sim \epsilon_b$. The coincidence window and background windows are also indicated. The shift of the peak of the time spectrum from τ_d (32 ns) is due to the inherent time pedestal of the LeCroy qVt. Experimental parameters are: He 1*s* orbital, E_0 = 1000 eV, ϵ = 24.6 eV, E_{pass} = 100 eV.

Can. J. Chem. Downloaded from www.nrcresearchpress.com by 88.255.202.194 on 09/08/12
For personal use only.

analysis is done off-line. The window width ratio is a software parameter that can be chosen to optimize the signal to noise ratio. The window width ratio is therefore known to be constant throughout the data analysis.

In the more popular TAC method, the time difference between the two pulses is converted to a voltage pulse whose amplitude is proportional to the time difference. The TAC output pulse is then connected to two single channel analyzers (SCAs) that count pulses that fall within a specified range of amplitudes. One SCA counts pulses with amplitudes corresponding to the coincidence time window while the second SCA is used to count pulses corresponding to the background time window. The data obtained at each energy parameter are composed of two values, one corresponding to the number of true coincidences plus accidental coincidences and the second value corresponding to the number of random coincidences. The ratio of the coincidence window width and the background window width is determined electronically by the SCAs. Thus in the TAC method this ratio is subject to the temperature and time stability of the electronics (otherwise known as "time walk").

In some cases, elaborate noise veto circuits have to be used with the TAC method to ensure that the pulses being counted arise only from the collision process. If the ambient noise level is high, a significant amount of data collection time is wasted. With the qVt method, the possibility exists for identifying noise interferences that have crept into the data since the full time spectra at different binding energies (or azimuthal angles) are collected. Spurious events occur at specific time delays, often different from τ_d, and can therefore be removed in the data analysis. The recovery of the real coincidence data in the presence of noise interference has recently been demonstrated in our laboratory (32). This is not possible with the TAC method because the counts obtained in the coincidence and background windows are actually *integrated* counts.

3.3 Data acquisition

The binding energy spectrum is a plot of the number of true coincidences versus binding energy ($\varepsilon = E_0 - E_1 - E_2$) with a peak appearing whenever $\varepsilon = E_b$. The impact energy E_0 is scanned using a programmable power supply and a digital to analog converter (Joerger D/A-16). E_1 and E_2 are equivalent and held constant as selected by the CMA.

Rather than using a predetermined, fixed-length, data acquisition time at each energy parameter (or azimuthal angle), the data acquisition time is determined by the sum of the singles count rate of electrons reaching the two detectors. The data acquisition time is determined by counting until a preset number of total singles counts is achieved. Thus the measured true coincidence counts are directly proportional to the EMS triple differential cross section (as defined in eq. [2]) and independent of any fluctuations in incident electron flux and local gas pressure. These fluctuations can be significant especially with the long data collection times (1–4 weeks) characteristic of coincidence-type experiments.

The binding energy spectrum is generated from the time spectra obtained at the different binding energies.[4] First, the coincidence window width (w_c) and background window width (w_b) are assigned. At each binding energy, the total number of counts within the coincidence window (N_c), and the total number of counts in the background window (N_b) are calculated. Within the coincidence window, some of the counts correspond to accidental coincidences (i.e., two electrons from different events arriving at the two detectors at the same time). These counts are subtracted from the total coincidence counts to give the number of true coincidence counts (N_t). The number of true coincidences is therefore given by

$$[10] \quad N_t = N_c - N_b\left(\frac{w_c}{w_b}\right)$$

And the uncertainty of N_t is given by

$$[11] \quad \Delta N_t = (N_c + r^2 N_b)^{1/2}$$

where $r = w_c/w_b$. Statistics can generally be improved by decreasing r and decreasing N_b up to a certain point (33).

A further advantage of having all of the time spectra at different binding energies is that the shape in three dimensions (counts–energy–time) of the coincidence peak may be studied. Any asymmetries in the three-dimensional peak shape would suggest experimental irregularities in timing of the observed coincidences and (or) *new* physical processes in (e,2e) experiments. Verifica-

[4]Likewise, an orbital experimental momentum profile can be generated from the time spectra obtained at different azimuthal angles.

Can. J. Chem. Downloaded from www.nrcresearchpress.com by 88.255.202.194 on 09/08/12
For personal use only.

tion of the randomness of the background at specific binding energies is also possible. Any interferences appearing systematically in the time delay spectra may be dealt with prior to computing the binding energy spectrum.

4. Characterization of EMS spectrometer

4.1. Time resolution

One of the important experimental parameters of an EMS spectrometer is the time resolution. As mentioned in Sect. 3.3, it is necessary to reduce the instrumental time resolution in order to improve the coincidence counting statistics.

The base width of the coincidence peak in the time delay spectrum is generally defined as the time resolution of the system. The analysis of the various contributions to this width as detailed by Volkel and Sandner (33) is used to predict the time resolution of the new EMS spectrometer.

The base width of the coincidence peak is defined as Δt and is the total variation in travel times of both the electrons from collision to detection and any time variations introduced by the signal handling electronics. The width (Δt) is the sum of variations in the total travelling times of both particles.

$$[12] \quad \Delta t = \Delta t_1 + \Delta t_2$$

The contributions to Δt_i ($i = 1, 2$) are as follows:

$$[13] \quad \Delta t_i = \Delta t_{\text{volume}} + \Delta t_{\text{energy}} + \Delta t_{\text{geometric}} + \Delta t_{\text{detector}} + \Delta t_{\text{electronics}}$$

The contribution of Δt_{volume} arises from the time required to travel across the finite collision volume. Assuming a spherical volume, the worst case is that the electron has to traverse the diameter, thus

$$[14] \quad \Delta t_{\text{volume}} = \frac{d}{\sqrt{\frac{2E}{m}}}$$

where d is the diameter of the collision volume (1.0 mm), E is the energy of the electron as it traverses this volume (500 eV), and m is the mass of the electron. Using these values, $\Delta t_{\text{volume}} \approx 80$ ps.

The variation in travelling time due to the finite energy resolution of the energy analyzer is given by

$$[15] \quad \Delta t_{\text{energy}} = \left(\frac{m}{8}\right)^{1/2} \frac{LR}{E^{1/2}}$$

where L is the length of the total flight path from collision point to detector (59.3 cm). The theoretical base resolution of the spectrometer, R, is 0.70% $\Delta E/E$. The energy of the electrons passing through the analyzer, E, is 100 eV. Using these values $\Delta t_{\text{energy}} \approx 150$ ps.

The angular acceptance of the energy analyzer contributes to the time resolution due to the range of allowable launch angles into the energy analyzer. This contribution is given by

$$[16] \quad \Delta t_{\text{geometric}} = \left(\frac{z_0}{\sqrt{\frac{2E}{m}}}\right) \frac{\sin\theta}{\cos^2\theta} \Delta\theta$$

where z_0 is the length of the flight path perpendicular to the electric field in the analyzer (33.6 cm), θ is the polar component of the launch angle (45°), and $\Delta\theta$ is the angular acceptance of the analyzer as defined by the lens apertures (21.74×10^{-3} radians). These values give $\Delta t_{\text{geometric}} \approx$ 720 ps.

The variations in transit time of the charge cloud within the channel electron multiplier are included in $\Delta t_{\text{detector}}$. This transit time variation is on the order of 2 ns (26).

The last contribution is from the time jitter of the electronics and cables used to measure the time difference between the pulses. This was experimentally determined by using a pulse generator and splitting the output to produce two identical pulses. These pulses were connected to the coincidence electronics system instead of the signals from the detectors. The base width of the coincidence peak in the time delay spectrum is a direct measure of $\Delta t_{\text{electronics}}$, which is $\approx$300 ps (35).

Considering the two channels identical, the expected total time resolution of the system is $2\Delta t_1$ or 6.5 ns base width. It is clear from the above estimates that the two largest contributions are from the use of the channel electron multipliers ($\Delta t_{\text{detector}}$) and from the angular acceptance of the energy analyzer ($\Delta t_{\text{geometric}}$). Replacing the CEMs with multichannel plate detectors is expected to reduce $\Delta t_{\text{detector}}$ to 100 ps, giving a predicted lower limit of 2.8 ns (base width).

The experimental time resolution obtained for the present EMS spectrometer is 7 ns base width or 3.5 ns (fwhm) (See Fig. 4). This result is in excellent agreement with the predicted total time resolution ($\Delta t_{\text{base}} = 6.5$ ns).

4.2. CMA energy resolution

Another experimental parameter vital to the performance of an EMS spectrometer is the resolution of its energy analyzer. Energy resolution is defined as the ratio of the energy spread (base width or fwhm) of electrons accepted by the spectrometer to the energy of the electrons as they pass through the spectrometer (see eq. [8]).

Due to the large size of the 360° CMA, possible mechanical misalignments were of main concern. Careful calibration of the CMA deflection voltage and measurement of the energy resolution of the CMA are therefore necessary. The deflection voltage[5] of the CMA determines the electric field between the inner and outer cylinders of the CMA, which determines the energy of the electrons that pass to the detectors. The theoretical deflection voltage V_d required by the CMA for a given pass energy can be calculated from the dimensions of the CMA.

$$[17] \quad V_d = \frac{\ln\left(\frac{b}{a}\right)}{\ln 2.80} E_{\text{pass}}$$

where b is the radius of the outer cylinder, a is the radius of the inner cylinder, and the factor of ln 2.80 is interpolated

[5]Note that in the present design there is only one deflection voltage to focus the two outgoing electrons, in stark contrast to previous EMS designs. A comparison of the experimental and theoretical CMA deflection voltages is therefore a very stringent test of spectrometer alignment.

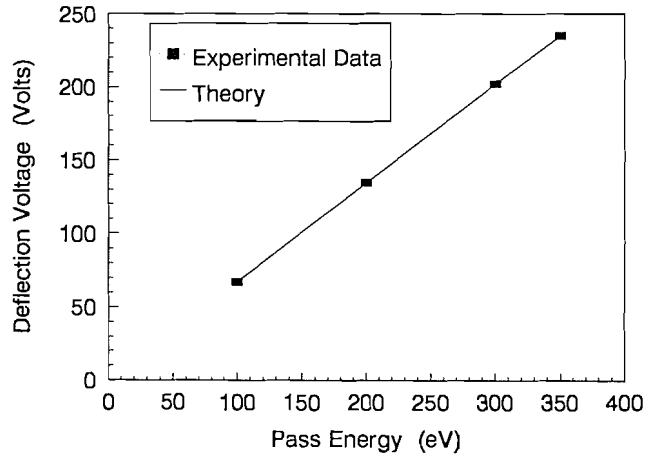

FIG. 5. Calibration of CMA deflection voltage. Scatter of data points for movable and fixed detectors is within the size of the symbols. The solid line is not a fit and indicates the theoretical prediction (eq. [17]).

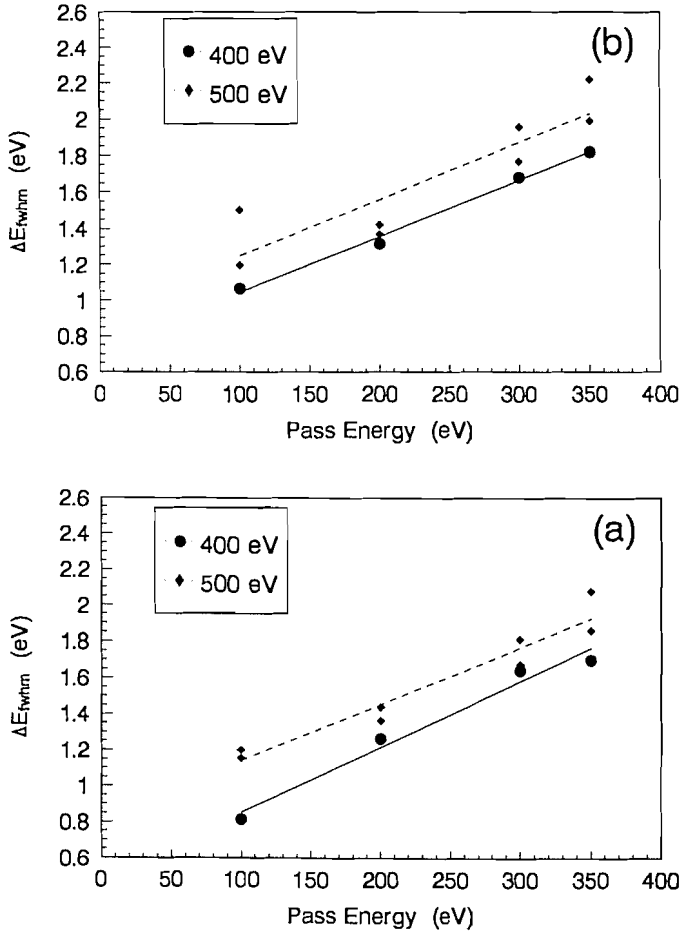

FIG. 6. Determination of experimental energy resolution of CMA. Experimentally measured peak widths obtained from (*a*) movable CEM and (*b*) fixed CEM for the elastic scattering of 400 eV (●) and 500 eV (◆) electrons. The solid and dashed lines are the linear fits to the 400 and 500 eV data, respectively. Note that the relevant curve for the present experiment (E_0 = 1000 eV) is indicated by the 500 eV data (◆).

TABLE 1. Summary of the regression results for determination of the experimental CMA energy resolution

Elastic energy (eV)	Movable R_{fwhm}	Fixed R_{fwhm}	Predicted R_{fwhm}
400	0.00365	0.00310	0.0035
500	0.00314	0.00313	0.0035

from Fig. 4(a) of ref. 31 (with $\theta = 45°$ and $d = 1.0$). The ratio of outer cylinder radius to inner cylinder radius is 2.00.

To calibrate the CMA deflection voltage, elastic scattering experiments at two scattering energies (400 and 500 eV) were done with varying pass energies (100–350 eV) by applying the required retarding voltage to the inner cylinder. The deflection voltage necessary to detect elastically scattered electrons of known kinetic energy (or E_{pass}) was measured. The results of the CMA deflection voltage calibration are shown in Fig. 5. Excellent agreement was obtained between experimental CMA deflection voltages and those predicted by eq. [17]. This result indicates that mechanical misalignments are insignificant.

To experimentally measure the energy resolution of the spectrometer, the full widths at half maximum (ΔE_{fwhm}) of the elastic profiles obtained above were measured for each detector. The energy resolution of the CMA was determined from the slope of a plot of ΔE_{fwhm} versus E_{pass}. These graphs are shown in Fig. 6 for two energies of the elastically scattered electrons (i.e., 400 and 500 eV). The two sets of data points at 500 eV, which represent the actual parameters used in the present experiment, indicate the error limits involved in the measurements of ΔE_{fwhm}. The slope of the regression line obtained from a plot of ΔE_{fwhm} versus E_{pass} is generally associated with the experimental fwhm resolution R_{fwhm} from which the base resolution R_{base} can easily be calculated (31). A summary of the calculated experimental R_{fwhm} for both sections of the CMA and the predicted R_{fwhm} (see Sect. 3.1) are shown in Table 1.

The experimental CMA energy resolution (0.32 ± 0.03% R_{fwhm}) agrees well with the prediction from the design of the CMA (0.35% R_{fwhm}). The results in Table 1 as well as Figs. 5 and 6 clearly indicate that the 360° CMA has been built and assembled to the desired tolerances and is operating at the designed specifications.

4.3. Binding energy spectrum of helium

Coincidence experiments were run at 1000 eV impact energy and $\phi \sim 0°$ using several pass energies from 400 to 100 eV. As expected, energy resolution improved and count rate decreased going from high pass energy to lower pass energies. Figure 7 shows the He 1*s* binding energy spectrum obtained at 100 eV pass energy where the best compromise between energy resolution and coincidence count rate was attained. The background is clearly flat, indicating that the coincidence timing algorithm is functioning as expected. The binding energy peak is Gaussian in shape with a measured coincidence energy resolution of 1.5 ± 0.2 eV fwhm. This resolution is comparable to coincidence energy resolutions obtained in other EMS laboratories (8, 11, 26, 36). Typically, the coincidence energy resolution in an EMS experiment is given (37) by

[18] $$\Delta E_{coinc} = \sqrt{\Delta E^2_{movable} + \Delta E^2_{fixed}}$$

Can. J. Chem. Downloaded from www.nrcresearchpress.com by 88.255.202.194 on 09/08/12
For personal use only.

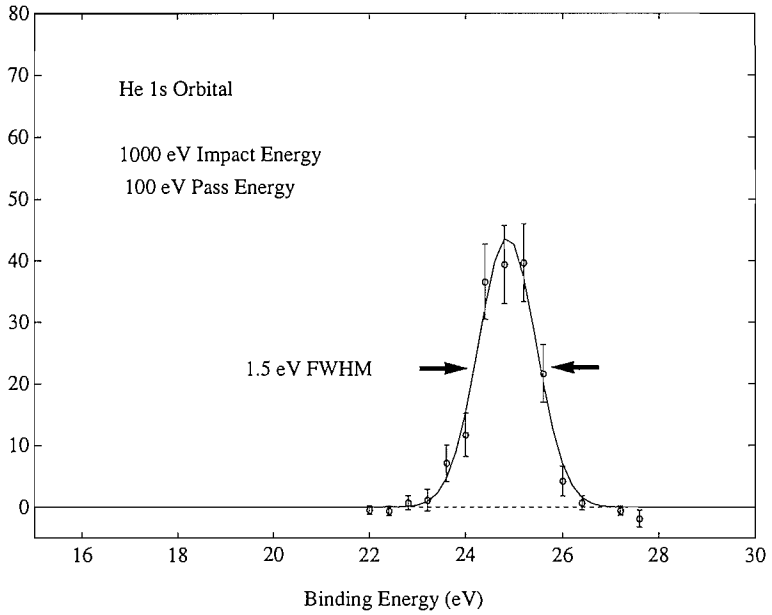

FIG. 7. Binding energy spectrum of helium 1*s* orbital obtained at 1000 eV impact energy, 100 eV pass energy, and $\phi \sim 0°$. Solid line shows Gaussian fit (1.5 ± 0.2 eV fwhm).

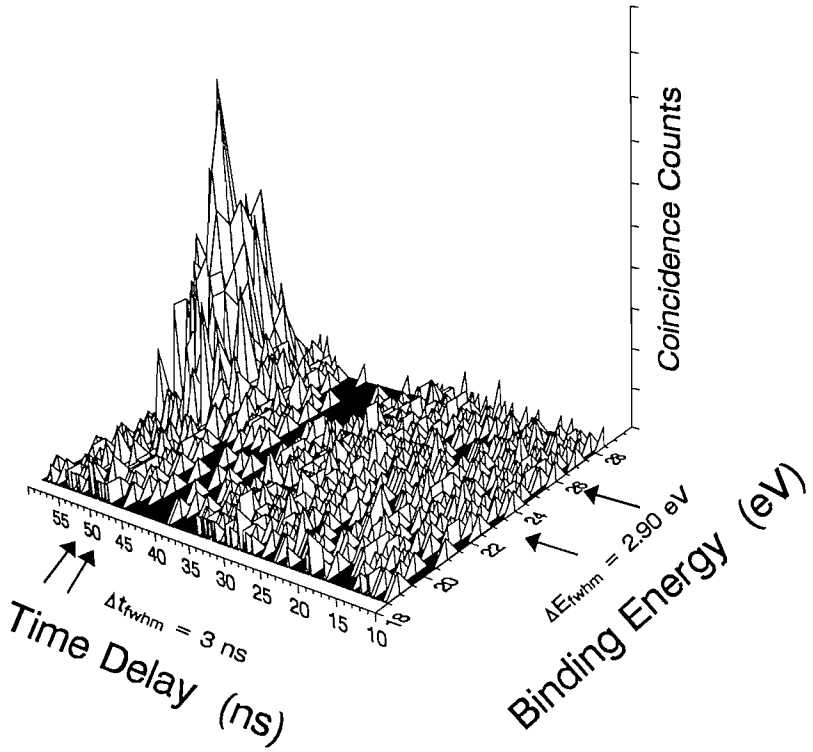

FIG. 8. Three-dimensional surface plot of the He 1*s* (e,2e) binding energy spectrum. Experimental parameters are: E_0 = 1000 eV, E_{pass} = 300 eV, and $\phi \sim 0°$.

where $\Delta E_{movable}$ and ΔE_{fixed} are measured from the elastics experiment described in the previous section.

The measured elastic widths at 100 eV pass energy are 1.0 eV fwhm for both movable and fixed detectors (see Fig. 6), thus the calculated coincidence energy resolution is 1.4 eV fwhm. The measured and calculated coincidence energy resolutions are in reasonable agreement. This suggests that possible misalignments often encountered in 360° cylindrical or spherical analyzers have been dealt with satisfactorily in the present application. This result lends some confidence in future extensions of the coincidence electron-scattering spectrometer to EMS experiments in the multiazimuthal-angle mode.

As discussed earlier, one of the advantages of the present approach to coincidence data collection is the ability to observe the full three-dimensional structure (counts–energy–time) of the coincidence spectra. This is illustrated, for example, in Fig. 8 where the coincidence data were ob-

Can. J. Chem. Downloaded from www.nrcresearchpress.com by 88.255.202.194 on 09/08/12
For personal use only.

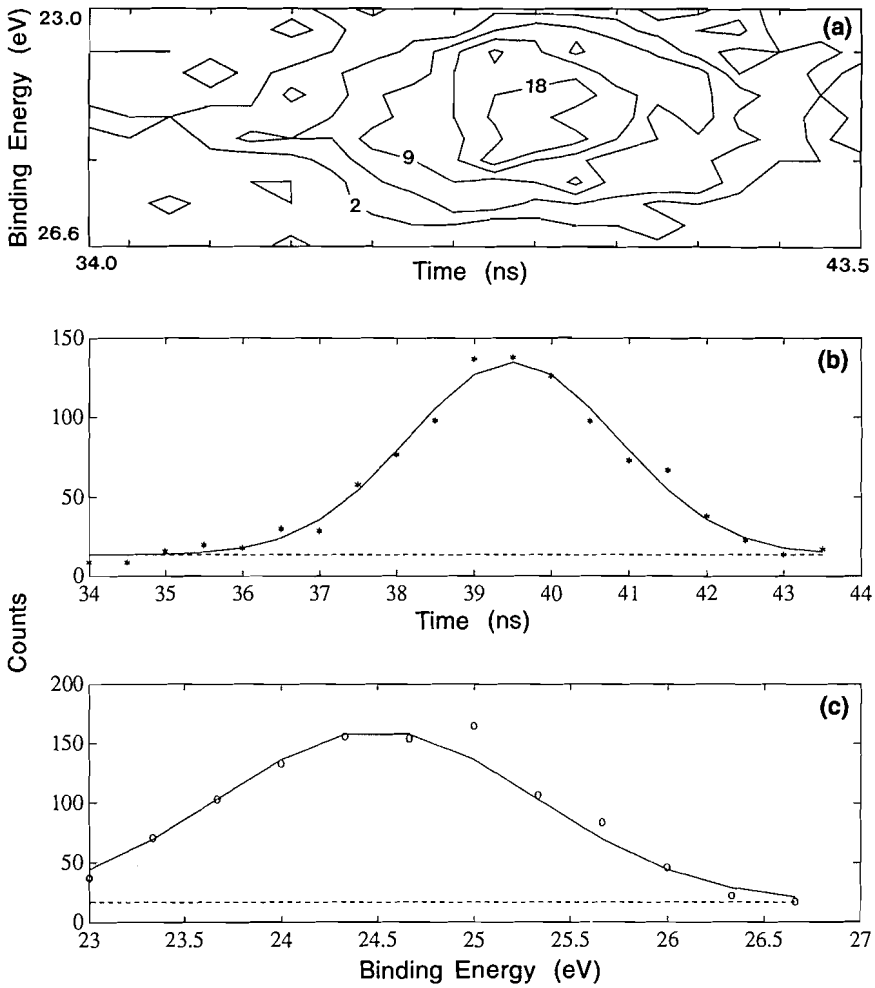

FIG. 9. (*a*) Contour plot of coincidence peak in time delay spectrum of helium 1*s* orbital at E_0 = 1000 eV, E_{pass} = 100 eV, and $\phi \sim 0°$. Contours at 2, 5, 9, 13, and 18 counts. (*b*) Cumulative projection of the coincidence spectrum on the time delay axis. The solid line is a fitted Gaussian curve with 3.5 ns fwhm. (*c*) Cumulative projection of the coincidence spectrum on the binding energy axis. The solid line is a fitted Gaussian curve with 1.9 eV fwhm.

tained at impact energy of 1000 eV + E_b and a pass energy of 300 eV. The high pass energy was necessary to obtain good enough statistics to illustrate the potential of the present approach to a three-dimensional coincidence data analysis. No serious asymmetry is observed in the energy–time plane. The very slight asymmetry at high time delay and the small valley at 40–45 ns are, in fact, artifacts and are not present at lower pass energies (i.e., at 100 eV pass energy, see below).

The distribution of coincidence counts is a function of two variables, namely, the binding energy (E_b) and the time delay (Δt). The most common bivariate distribution (38) is the normal bivariate or normal two-dimensional distribution given by

$$[20]\quad p(E_b, \Delta t) = \frac{1}{2\pi\sigma_{E_b}\sigma_{\Delta t}\sqrt{1-\rho^2}} \exp\left\{-\frac{1}{2(1-\rho^2)}\left[\frac{(E_b-m_{E_b})^2}{\sigma_{E_b}^2} + \frac{(\Delta t-m_{\Delta t})^2}{\sigma_{\Delta t}^2} - \frac{2\rho(E_b-m_{E_b})(\Delta t-m_{\Delta t})}{\sigma_{E_b}\sigma_{\Delta t}}\right]\right\}$$

where m_{E_b}, σ_{E_b}, $m_{\Delta t}$, and $\sigma_{\Delta t}$ are the means and standard deviations of the distributions in E_b and Δt, respectively. ρ is called the "correlation coefficient" for fluctuations in E_b and Δt and is given by

$$[21]\quad \rho = \frac{<(E_b-m_{E_b})(\Delta t-m_{\Delta t})>}{\sigma_{E_b}\sigma_{\Delta t}}$$

ρ measures the degree to which E_b and Δt fluctuate in a mutually dependent manner. If ρ is zero then the normal bivariate distribution (eq. [20]) can be written as a simple product of two one-dimensional normal distributions, i.e., E_b and Δt are statistically independent.

Figure 9*a* shows a contour diagram of the coincidence spectrum as a function of E_b and Δt for the ionization of the helium 1*s* orbital at 1000 eV impact energy and 100 eV pass energy, which are typical EMS operating conditions. The contour diagram (Fig. 9*a*) is clearly Gaussian in shape as can be seen in the cumulative (summed) projections of the

Can. J. Chem. Downloaded from www.nrcresearchpress.com by 88.255.202.194 on 09/08/12
For personal use only.

Can. J. Chem. Downloaded from www.nrcresearchpress.com by 88.255.202.194 on 09/08/12
For personal use only.

coincidence spectrum on both the time delay axis (Fig. 9*b*) and the binding energy axis (Fig. 9*c*).[6] This result verifies a well-known fact that in most physical problems wherein several variables contribute to the experimental observable, the resulting experimental distribution is Gaussian or normal. This result is often attributed to the "central limit theorem". However, a less well-studied aspect of coincidence spectra is the correlation coefficient of the bivariate distribution. As mentioned earlier, most of the previously reported EMS experiments do not save the total coincidence spectra, thus an assessment of the correlation coefficient is not possible in these cases. It is generally assumed, however, that $\rho = 0$ and the bivariate distribution is simply a product of two one-dimensional normal distributions in E_b and Δt. The correlation coefficient for the coincidence spectrum shown in Fig. 9*a* is calculated using eq. [21] and is found to be $\rho = +0.05$ with an estimated uncertainty of ± 0.10. This clearly indicates that E_b and Δt are *statistically independent variables*.

Although it is generally assumed that the coincidence spectrum is a function of statistically independent variables (i.e., the binding energy and the time delay), the present study is the first experimental confirmation of this fact, at least for the helium 1*s* (e,2e) coincidence binding energy spectrum. It is, however, of great interest to verify this statistical independence for a wider range of atomic and molecular systems. Although the present results may appear uninteresting, it is not inconceivable to expect some correlation between binding energy and time delay. One can envision a correlation between binding energy and time delay in cases wherein two or more distinct scattering processes lead to final outgoing electron states similar to the final electron states in the (e,2e) reaction. Since the final state of the ion is never observed in an (e,2e) experiment, there are conceivably many other reaction channels than that illustrated in eq. [1] and assumed in the plane wave impulse approximation (PWIA). Several theoretical and experimental studies (26, 27) indicate that within the present experimental conditions (see Sect. 2), the PWIA is a valid representation of the necessarily complex scattering process. In other words, the PWIA assures us that the coincident electron events detected in an (e,2e) or EMS experiment are *dominated* by single, hard, binary-type collisions and consistent with eq. [1]. The fact that the experimental correlation coefficient (ρ) obtained in the present experiment is effectively *zero* can therefore be viewed as further experimental evidence that the PWIA is a valid framework for the interpretation of EMS experiments.

It is likely that the new coincidence data acquisition methods introduced here may find use in the analysis of other forms of (e,2e) experiments than high-energy, symmetric, non-coplanar kinematics. In addition, the measurement of the correlation coefficient (ρ) in (e,2e) experiments where post-collision interaction effects or resonant channel effects have been observed (39) will be most useful.

5. Acknowledgements

We would like to acknowledge the excellent workmanship and technical help provided by the Science Technology Center (Carleton University). Initial funding for the design and the fabrication of the prototype for this project was generously provided by Carleton University. We would also like to acknowledge the challenging comments of the referees that have contributed to clarifying the main results reported in this paper. This work was funded by the Natural Sciences and Engineering Research Council (NSERC) of Canada.

[6]The slightly large energy resolution compared to Fig. 7 is due to the larger apertures used in this particular experimental run to obtain sufficient statistics.

1. U. Amaldi, Jr., A. Egidi, R. Marconero, and G. Pizella. Rev. Sci. Instrum. **40**, 1001 (1969).
2. R. Camilloni, A. Giardini-Guidoni, R. Tiribelli, and G. Stephani. Phys. Rev. Lett. **29**, 618 (1972).
3. E. Weigold, S. T. Hood, and P. J. O. Teubner. Phys. Rev. Lett. **30**, 475 (1973).
4. V. G. Neudatchin, G. A. Novoskoltseva, and Y. F. Smirnov. Sov. Phys. JETP, **28**, 540 (1969).
5. A. E. Glassgold and G. Ialongo. Phys. Rev. **175**, 151 (1968).
6. V. G. Levin. Phys. Lett. A, **39**, 125 (1972).
7. S. T. Hood, A. Hamnett, and C. E. Brion. Chem. Phys. **39**, 252 (1976).
8. J. H. Moore, M. A. Coplan, T. L. Skillman, Jr., and E. D. Brooks. Rev. Sci. Instrum. **49**, 463 (1978).
9. A. L. Ritter, J. R. Dennison, and R. Jones. Phys. Rev. Lett. **53**, 2054 (1984).
10. K. T. Leung and C. E. Brion. J. Electron. Spectrosc. **35**, 327 (1985).
11. K. T. Leung. *In* Theoretical models of chemical bonding. *Edited by* Z. B. Maksic. Springer, Berlin. 1990.
12. R. L. Martin and D. A. Shirley. J. Chem. Phys. **64**, 3685 (1976).
13. L. S. Cederbaum, W. Domcke, J. Schirmer, and W. von Niessen. Adv. Chem. Phys. **65**, 115 (1986).
14. I. E. McCarthy. J. Electron. Spectrosc. **36**, 37 (1985).
15. A. O. Bawagan, C. E. Brion, E. R. Davidson, and D. Feller. Chem. Phys. **113**, 19 (1987).
16. A. O. Bawagan, R. Muller-Fiedler, C. E. Brion, E. R. Davidson, and C. Boyle. Chem. Phys. **120**, 335 (1988).
17. A. O. Bawagan, C. E. Brion, E. R. Davidson, C. Boyle, and R. Frey. Chem. Phys. **128**, 439 (1988).
18. C. L. French, C. E. Brion, and E. R. Davidson. Chem. Phys. **122**, 247 (1988).
19. A. O. Bawagan and C. E. Brion. Chem. Phys. Lett. **137**, 573 (1987).
20. A. O. Bawagan and C. E. Brion. Chem. Phys. **123**, 51 (1988).
21. S. A. C. Clark, A. O. Bawagan, and C. E. Brion. Chem. Phys. **137**, 407 (1989).
22. J. P. D. Cook. Ph.D. Thesis, University of British Columbia, 1981.
23. J. P. D. Cook, I. E. McCarthy, A. T. Stelbovics, and E. Weigold. J. Phys. B: At Mol. Phys. **17**, 2339 (1984).
24. C. Dupre, A. Lahmann-Benani, and A. Duguet. Meas. Sci. Technol. **2**, 327 (1991).
25. A. Lahmam-Benani. J. Phys. B: At. Mol. Opt. Phys. **24**, 2401 (1991).
26. I. E. McCarthy and E. Weigold. Phys. Rep. C, **27**, 275 (1976).
27. E. Weigold and I. E. McCarthy. Adv. At. Mol. Phys. **14**, 127 (1978).
28. A. O. Bawagan and C. E. Brion. Chem. Phys. **144**, 167 (1990).
29. L. A. Graham and A. D. O. Bawagan. Chem. Phys. Lett. **178**, 441 (1991).
30. P. Duffy, C. E. Brion, M. E. Casida, and D. P. Chong. Chem. Phys. **159**, 347 (1992).

31. J. S. Risley. Rev. Sci. Instrum. **43**, 95 (1972).
32. L. A. Graham. M.Sc. Thesis, Carleton University, 1991.
33. R. Goruganthu, M. Coplan, J. Moore, and J. Tossell. J. Chem. Phys. **89**, 25 (1988).
34. M. Volkel and W. Sandner. J. Phys. E: Sci. Instrum. **16**, 456 (1983).
35. T. S. Kanigan. B.Sc. Thesis, Carleton University, 1990.
36. K. T. Leung and C. E. Brion. Chem. Phys. **82**, 87 (1983).
37. A. Lahmam-Benani, H. F. Wellenstein, A. Duguet, and M. Lecas. Rev. Sci. Instrum. **56**, 43 (1985).
38. B. R. Frieden. Probability, statistical optics and data testing. Springer Verlag, Berlin. 1990. p. 53.
39. L. Avaldi, R. Camilloni, G. C. King, and G. Stefani. Phys. Rev. A, **44**, 4740 (1991).

Can. J. Chem. Downloaded from www.nrcresearchpress.com by 88.255.202.194 on 09/08/12
For personal use only.

The acidity constant of fluorene-9-carboxylic acid in aqueous solution. Determination of the pK_a of a sparingly soluble substance

A. J. KRESGE,[1] I. G. POJARLIEFF,[2] AND E. M. RUBINSTEIN
Department of Chemistry, University of Toronto, Toronto, Ont., Canada M5S 1A1

Received September 3, 1992

A. J. KRESGE, I. G. POJARLIEFF, and E. M. RUBINSTEIN. Can. J. Chem. **71**, 227 (1993).

The acid ionization constant of the carboxylic acid group of fluorene-9-carboxylic acid in aqueous solution at 25°C was determined to be pK_a = 3.61, using a method based upon the increase in solubility of this sparingly soluble substance brought about by its ionization. This corrects an earlier considerably different value of this quantity determined by equating pK_a with the pH measured at half-neutralization. The hazard inherent in the latter method when applied to sparingly soluble substances is discussed.

A. J. KRESGE, I. G. POJARLIEFF et E. M. RUBINSTEIN. Can. J. Chem. **71**, 227 (1993).

Opérant en solution aqueuse, à 25°C, et faisant appel à une méthode basée sur l'augmentation de solubilité de cette substance pratiquement insoluble provoquée par son ionisation, on a déterminé que le pK_a du groupe acide de l'acide fluorène-9-carboxylique est égal à 3,61. Ce résultat corrige une valeur assez différente publiée antérieurement pour cette constante qui avait été déterminée en faisant l'hypothèse que son pK_a est égal au pH mesuré à sa demi-neutralisation. On discute des problèmes potentiels inhérents à cette dernière méthode lorsqu'on l'applique à des produits très peu solubles.

[Traduit par la rédaction]

Can. J. Chem. Downloaded from www.nrcresearchpress.com by 88.255.202.194 on 09/08/12
For personal use only.

In the course of a study of the keto–enol system of fluorene-9-carboxylic acid,[3] we needed to know the pK_a of the carboxylic acid group of this substance in aqueous solution. A value of this quantity has recently been published (1), but it seemed likely that the method used for its determination could have led to significant error. We have therefore carried out a redetermination.

The previous result (1) was based upon a potentiometric titration whose pH value at half-neutralization was taken to be the pK_a. This method assumes that equal amounts of the ionized and unionized forms of the acid exist in solution when half an equivalent of base has been added, but fluorene-9-carboxylic acid is only sparingly soluble in water, and, at the low concentrations that consequently had to be used, significant further ionization of the acid may have taken place; the assumption upon which this method is based may thus have been invalid. We performed our redetermination with a method that is free of this difficulty, and which, in fact, makes use of the sparing solubility of fluorene-9-carboxylic acid (2).

Consider a saturated solution of a sparingly soluble neutral acid, HA, and its anionic conjugate base, A^-. The concentration of HA species in such a solution will be constant, and equal to its solubility S_0, eq. [1], because HA will be in equilibrium with undissolved acid whose activity is constant. The total solubility of the acid, however, will vary with the extent of ionization of the acid because this solubility, S, is equal to the concentration of both HA and A^- species, eq. [2].

$$[1] \quad [HA] = S_0$$

$$[2] \quad [HA] + [A^-] = S$$

The concentration ionization constant of the acid, Q_a, may consequently be expressed in terms of these solubilities and the concentration of hydrogen ions, as in eq. [3], and Q_a may be determined from a knowledge of these solubilities and $[H^+]$.

$$[3] \quad Q_a = [H^+](S - S_0)/S_0$$

We have measured the solubility of fluorene-9-carboxylic acid in a series of aqueous formic acid buffer solutions of known $[H^+]$ and have then determined Q_a by fitting the data to the hyperbolic form of eq. [3] shown as eq. [4].

$$[4] \quad S = S_0 + Q_a S_0/[H^+]$$

Experimental section

Materials

Fluorene-9-carboxylic acid (Aldrich) was recrystallized from ethanol; mp 230–232°C (lit. (3) mp 232°C). All other materials were best available commercial grades and were used as received.

Solubility determinations

Solubilities of fluorene-9-carboxylic acid were determined by measuring its concentration in saturated solutions spectrophotometrically; the absorption maximum at λ = 265 nm, ε = 19 100 M^{-1} cm^{-1}, was used for this purpose. Preliminary experiments showed that considerable oxidation of fluorene-9-carboxylic acid to fluorenone (3) takes place in the times (ca. 1 day) used to ensure equilibration of dissolved with solid acid, and anaerobic conditions were therefore devised. Samples, 10–15 mg, of powdered fluorene-9-carboxylic acid were placed in 25-mL Erlenmeyer flasks, and these were sealed with serum-cap stoppers and purged with argon for 20 min. Formic acid buffer solutions (10 mL), previously purged with argon for 30 min, were then injected into these flasks, and purging was continued for another 20 min. These solutions were allowed to equilibrate in a Precision Dubnoff metabolic shaking incubator equipped with a shallow shaking bath; shaking was first performed at 37°C for 1–2 h and then at 25.0 ± 0.1°C for 24 h. After this period of time, 1.00-mL samples of the equilibrated solutions were withdrawn using pipettes whose tips were wrapped with cotton wool, and these samples were then quenched in 6.00 mL of a mixture consisting of 2 parts methanol and 3 parts 0.1 M aqueous $HClO_4$. The absorbance at λ = 265 nm

[1]Author to whom correspondence may be addressed.

[2]Permanent address: Institute of Organic Chemistry, Bulgarian Academy of Sciences, 1040 Sofia, Bulgaria.

[3]J. Andraos, Y. Chiang, A.J. Kresge, and N.P. Schepp, unpublished work.

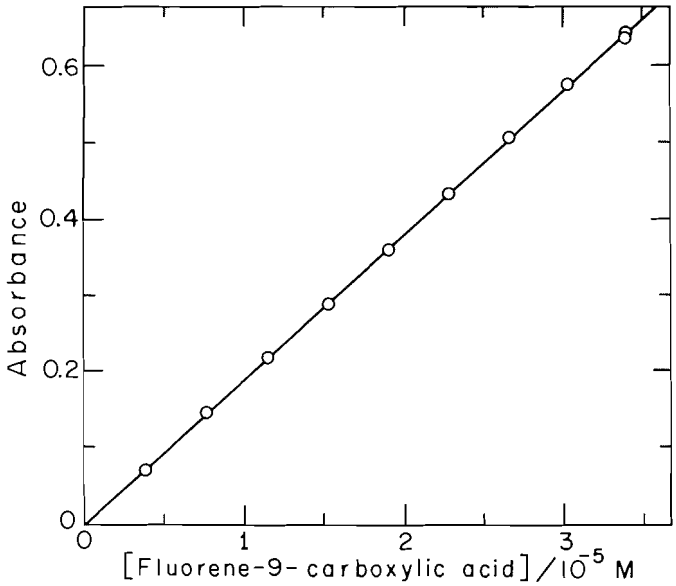

FIG. 1. Beer's Law plot for fluorene-9-carboxylic acid dissolved in the medium used for solubility–absorbance measurements.

TABLE 1. Solubility of fluorene-9-carboxylic acid in aqueous formic acid buffer solutions at 25°C[a]

Buffer ratio[b]	$[H^+]/10^{-4}$ M	$S/10^{-5}$ M
9:1	20.5	7.87
4:1	10.5	8.41
3:1	8.05	9.52
2:1	5.47	10.5
1:1	2.77	14.3
1:2	1.39	23.3
1:3	0.929	30.4
1:4	0.697	40.4
1:5	0.558	48.3

$S/M = (6.33 \pm 0.21) \times 10^{-5} + (2.34 \pm 0.02) \times 10^{-8}/[H^+]$.

[a]Total concentration of buffer = 0.10 M; ionic strength maintained at 0.10 M by adding $NaClO_4$ as required.

[b]Buffer ratio = [acid]: [base].

of these quenched samples was measured with a Cary model 2200 spectrophotometer.

A calibration curve was constructed for the purpose of converting these absorbances into molar concentrations of fluorene-9-carboxylic acid. As Fig. 1 shows, the data obeyed Beer's law accurately: least-squares analysis gave the relationship $A = -(0.85 \pm 2.14) \times 10^{-4} + (1.91 \pm 0.01) \times 10^4 \cdot$ [fluorene-9-carboxylic acid].

Results and discussion

The solubility of fluorene-9-carboxylic acid was measured in nine aqueous formic acid buffer solutions of different buffer ratio and therefore different hydrogen ion concentrations.[4] The data so obtained are summarized in Table 1 and are shown in Fig. 2 plotted according to the relationship of eq. [4]. Nonlinear least-squares fitting of these data to this expression gave $S_0 = (6.33 \pm 0.21) \times 10^{-5}$ M, in good agreement with $S_0 = (6.52 \pm 0.03) \times 10^{-5}$ M measured directly in 0.1 M HCl solution, and $Q_a = (3.70 \pm 0.13) \times 10^{-4}$ M, $pQ_a = 3.43 \pm 0.02$.

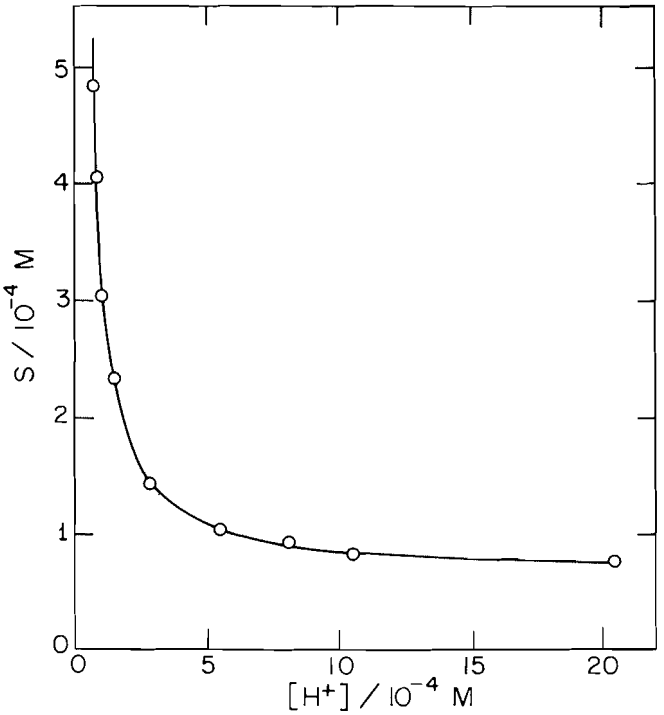

FIG. 2. Solubility of fluorene-9-carboxylic acid in aqueous formic acid buffer solutions plotted according to eq. [4].

This acidity constant is a *concentration quotient*, applicable at the ionic strength of the measurements, μ = 0.10 M. It can be converted into a thermodynamic value, $pK_a = 3.61$, by the use of appropriate activity coefficients (5). This result is considerably less than the value obtained earlier, $pK_a = 4.3$, by equating pK_a with the pH measured at half-neutralization in a potentiometric titration of fluorene-9-carboxylic acid (1).

The difference between this earlier value and the present result can be accounted for in the following way. The previous determination was made by titrating a saturated aqueous solution of fluorene-9-carboxylic acid,[5] (whose stoichiometric concentration of this acid in both forms, HA and A^-, may be estimated as being equal to the saturation solubility of HA (= S_0 as determined in the present work) plus the amount of A^- that would have formed by ionization of HA before the titration had begun. The latter may be calculated as 1.25×10^{-4} M on the basis of the pK_a value (= 3.61) determined here.[6] The total stoichiometric concentration of fluorene-9-carboxylic acid throughout the potentiometric titration was therefore (6.33×10^{-5}) (= S_0) + $(1.25 \times 10^{-4}) = (1.88 \times 10^{-4})$ M. At half-neutralization the stoichiometric concentration of each form, HA and A^-, was half of this, and another calculation using pK_a (= pQ_a) =

[4]Values of $[H^+]$ of these buffers were determined by calculation using the thermodynamic acidity constant of formic acid, $pK_a = 3.75$ (4), and activity coefficients recommended by Bates (5).

[5]E. Krogh, private communication.

[6]This is a good approximation to pQ_a at the very low ionic strength of this solution.

Can. J. Chem. Downloaded from www.nrcresearchpress.com by 88.255.202.194 on 09/08/12
For personal use only.

3.61 gives $[H^+] = 5.8 \times 10^{-5}$ M for this solution. This corresponds to pH = 4.24, which is very close to the half-neutralization pH (= 4.3) taken to be the pK_a of fluorene-9-carboxylic acid in the earlier work (1).

The difficulty with the earlier work may be understood somewhat more clearly by considering the relationship of eq. [5]. Equating pK_a with pH requires the last term of this

$$[5] \quad pK_a = pH + \log ([HA])/[A^-])$$

expression to be zero, or [HA] to be equal to $[A^-]$, but this will be so at half-neutralization only as long as [HA] is sufficiently large to have been able to provide the H^+ represented by pH, which must have come mainly from ionization of HA, without having significantly reduced the value of [HA]. If [HA] is not large enough, it will be reduced when HA ionizes to furnish the necessary H^+; this will bring about a simultaneous increase in $[A^-]$, and, as a result, [HA] will no longer be equal to $[A^-]$ and pK_a will not be correctly represented by pH. This condition was forced upon the earlier determination of the pK_a of fluorene-9-carboxylic acid by the low solubility of this substance: calculations such as those described in the preceding paragraph give $[HA] = 3.95 \times 10^{-5}$ M and $[A^-] = 15.2 \times 10^{-5}$ M at half-neutralization, which makes $\log ([HA])/[A^-]) = -0.63$ and provides a sizeable difference between pK_a and pH.

In the earlier work, the pK_a of fluorene-9-carboxylic acid was also determined in 20% acetonitrile – 80% water, a solvent that allowed a significantly greater substrate concentration to be used than that employed in pure water. The result obtained, $pK_a = 3.9$, supports the presently determined value for pure water, $pK_a = 3.61$, on the basis of the expectation that pK_a's of neutral acids will increase with decreasing polarity of the solvent (6), but it is inconsistent with the earlier result for pure water, $pK_a = 4.3$.

Acknowledgement

We thank Dr. A. T. Baines and Mrs. R. Drangova from the Department of Clinical Biochemistry at the University of Toronto for access to and help in using their Dubnoff shaking incubator, and we are grateful to the Natural Sciences and Engineering Research Council of Canada, the Donors of the Petroleum Research Fund, administered by the American Chemical Society, and the United States National Institutes of Health for financial support of this work.

1. E. Krogh and P. Wan. J. Am. Chem. Soc. **114**, 705 (1992).
2. E. J. King. Acid–base equilibria. Macmillan, New York. 1965. p. 118.
3. W. Wislicenus and A. Ruthing. Ber. **46**, 2770 (1913); A. Jeanes and R. Adams. J. Am. Chem. Soc. **59**, 2609 (1937).
4. H. S. Harned and N. D. Embree. J. Am. Chem. Soc. **56**, 1042 (1934).
5. R. G. Bates. Determination of pH. Theory and practice. Wiley, New York. 1973. p. 49.
6. J. Hine. Structural effects on equilibria in organic chemistry. Wiley, New York. 1975. p. 132; R. Stewart. The proton: applications to organic chemistry. Academic Press, New York. 1985. p. 27.

Can. J. Chem. Downloaded from www.nrcresearchpress.com by 88.255.202.194 on 09/08/12
For personal use only.

Organometallic products from the reaction of the isoelectronic $Mn(CO)_5^-$ and $Cr(CO)_4NO^-$ metallate anions with bis-α-bromocyclopropyl ketone

A. P. MASTERS, M. PARVEZ, T. S. SORENSEN,[1] AND F. SUN

The Department of Chemistry, University of Calgary, Calgary, Alta., Canada T2N 1N4

Received August 27, 1992

A. P. MASTERS, M. PARVEZ, T. S. SORENSEN, and F. SUN. Can. J. Chem. **71**, 230 (1993).

$Mn(CO)_5^-$ and $Cr(CO)_4NO^-$ react with the title ketone to give organometallic products. In the chromium case, a single metallofuran product is produced. In the manganese reaction, one can isolate a series of four complexes, two of which have a structure closely related to the chromium complex. The other two complexes are assigned an acyl manganese structure. The structures of the chromium complex and one of the acyl manganese complexes have been determined by X-ray methods. One finds a distorted octahedral bonding about the metal atom in each case. The chromium complex has bond lengths very similar to those reported for a closely related manganese structure, implying a delocalization of electrons within a metallofuran ring. As expected for this mixed carbonyl nitrosyl complex, the nitrosyl group is positioned *trans* to the oxide bond, representing the weakest and strongest "*trans*-effect" substituents. The acyl manganese structures contain an $Mn(CO)_4$ unit in contrast to the usual $Mn(CO)_5$ acyl complexes, with the $18e^-$ count being provided by an internal chelation with the *n*-electrons of the dicyclopropyl ketone group. The reaction mechanism for the formation of the complexes is postulated to involve initial bromine abstraction (two-electron reduction) by the metallate anion, with the $Cr(CO)_4NO^-$ reaction being much faster compared to $Mn(CO)_5^-$. The resulting organic enolate then "back-reacts" with a carbonyl group of the just-formed metal carbonyl bromide to form a transient anionic Fischer carbene complex. Ultimately this intermediate loses the metal bromide ion with the formation of the neutral complexes.

A. P. MASTERS, M. PARVEZ, T. S. SORENSEN et F. SUN. Can. J. Chem. **71**, 230 (1993).

Le $Mn(CO)_5^-$ et le $Cr(CO)_4NO^-$ réagissent avec la cétone mentionnée dans le titre pour donner des produits organométalliques. Dans le cas du dérivé chromé, il se forme un seul produit organofurane. Dans la réaction du dérivé manganique, on peut isoler une série de quatre complexes dont deux ont des structures très apparentées à celle du complexe du chrome. On a attribué une structure acyle de manganèse aux deux autres complexes. On a déterminé la structure du complexe du chrome et de l'un des complexes du manganèse par des méthodes de rayons X. Dans chaque cas, on observe une liaison octaédrique déformée autour de l'atome métallique. Les longueurs des liaisons dans le complexe du chrome sont très semblables à celles rapportées antérieurement pour une structure manganique très apparentée; ce résultat implique qu'il se produit une délocalisation dans le cycle métallofurane. Comme on pouvait s'y attendre pour un complexe mixte de carbonyle et de nitrosyle, le groupe nitrosyle se trouve en position *trans* par rapport à la liaison oxyde; ces substituants présentent en effet les «effets *trans*» les plus faibles et les plus forts. Par opposition à ce que l'on retrouve généralement avec les complexes acyles de $Mn(CO)_5$, les structures d'acyle manganèse comportent une unité $Mn(CO)_4$ dans laquelle les 18 e^- sont fournis par une chélation interne avec les électrons-*n* du groupe dicyclopropylcétone. On suppose que le mécanisme de la réaction conduisant à la formation des complexes implique un enlèvement initial de brome (réduction à deux électrons) par un anion métallate; cette réaction serait beaucoup plus rapide avec le $Cr(CO)_4NO^-$ qu'avec le $Mn(CO)_5^-$. L'énolate organique qui en résulte «réagit en retour» avec un groupe carbonyle du bromure de carbonyle métallique qui vient de se former et conduit à un complexe carbénique anionique de Fischer transitoire. Pour terminer, cet intermédiaire perd un ion bromure métallique avec la formation de complexes neutres.

[Traduit par la rédaction]

The reaction of selected tri- or tetrasubstituted α,α′-dibromo ketones with transition-metal carbonyl (or carbonyl nitrosyl) anions is a recently discovered low-temperature route to solutions of substituted cyclopropanones[2] (eq. [1]).

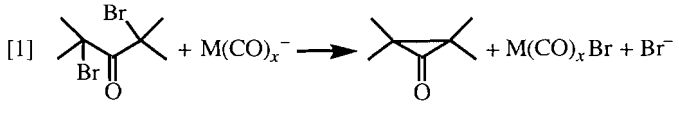

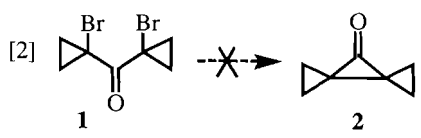

1 2

However, when this reaction was attempted using bis-α-bromocyclopropyl ketone **1**, in the hopes of preparing the unknown bis-spirocyclic cyclopropanone **2** (eq. [2]), unexpected organometallic products were produced instead.

In an attempt to understand why the eq. [2] reaction was being diverted in this case, we isolated and characterized these organometallic products. From these results, one sees that this study has implications as a variant route to Fischer carbene complexes.

Results

The two metallate anions used in this study were the well-known $Mn(CO)_5^-$ (**3**) and a recently described (1) isoelectronic species $Cr(CO)_4NO^-$ (**4**).

Corresponding to the usual cyclopropanone synthetic procedure, the dibromo ketone **1** in methylene chloride solution was added to a solution of **4** PPN^+ (where PPN^+ denotes $(PPh_3)_2N^+$ monocation) in methylene chloride at −78°C. This solution was stirred at −78°C for 4 h and then stored in a freezer for 48 h. Work-up and chromatography gave a 73% crude yield of a single orange crystalline solid that could be recrystallized from *n*-hexane. The mass spectrum indicated a formula $CrC_{11}H_8BrO_6N$, which corresponds to the elements $Cr(CO)_4NO^-$ (**4**) and $C_7H_8OBr_2$ (**1**) with loss of bromide. The infrared spectrum showed strong

[1]Author to whom correspondence may be addressed.

[2]A. P. Masters, T. S. Sorensen, and F. Sun. Manuscript in preparation.

Can. J. Chem. Downloaded from www.nrcresearchpress.com by 88.255.202.194 on 09/08/12
For personal use only.

Can. J. Chem. Downloaded from www.nrcresearchpress.com by 88.255.202.194 on 09/08/12
For personal use only.

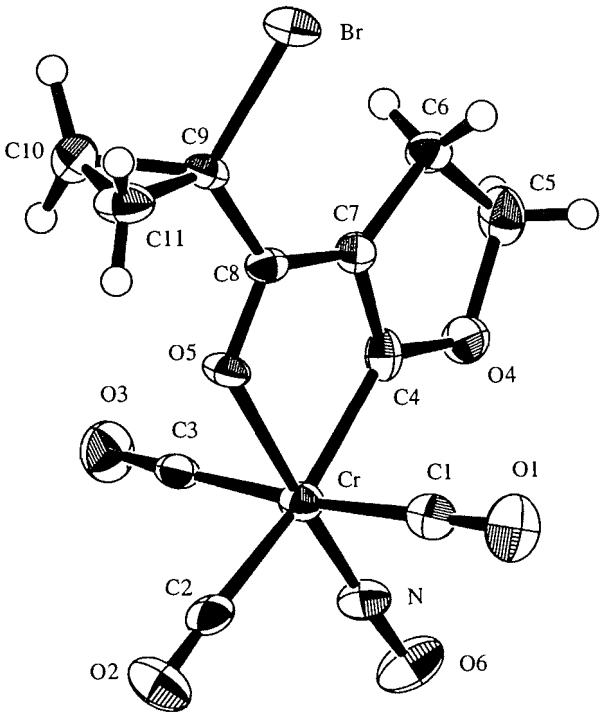

FIG. 1. ORTEP drawing (50% probability level) of the chromium complex **5**.

and characteristic M—C≡O and M—N=O stretching frequencies but there was no sign of organic $\rangle$C=O stretching frequencies, although the M—N=O stretch partially obscures this region. The ^{1}H NMR spectrum showed four peak regions of area 2:2:2:2, indicating symmetry in the molecule. Peak regions centered at 3.03 and 5.02 were mutually coupled triplets, J = 9.0 Hz, characteristic of a partial structure -CH_2-CH_2-O-. The other two peak areas, also mutually coupled, were centered at 1.303 and 1.518, similar to the peaks in the starting ketone **1** and therefore indicative of a $\rangle\!\!<^{Br}$ fragment. In the ^{13}C NMR spectrum, peaks at 20.4 and 29.6 (q) also indicate this latter partial structure. Peaks at 26.5 and 83.2 are in agreement with a -CH_2-CH_2-O fragment. The remaining carbons are all quaternary, located at 128.7, 195.1, 215.1, 217.7, and the unusually low field position of 249.7 ppm. The NMR data clearly suggest that one cyclopropyl ring has opened up, but we were inconclusive about the detailed structure of the complex and therefore a single crystal X-ray analysis was carried out.

The ORTEP structure of the complex **5** is shown in Fig. 1, and bond lengths and angles are given in Tables 1 and 2. Complex **5** is remarkably similar in gross structure to a manganese complex **6** reported by Casey *et al.* (2), obtained by a totally unrelated route.

In structure **5**, atoms Cr—O—C8—C7—C4 form a near planar ring typical of delocalized molecular structures. An average of the resonance hybrid structures **5***a* ↔ **5***b* ↔ **5***c* gives the best representation of the actual bond lengths, as previously reported by Casey *et al.* for **6** (2). Structure **5***a* corresponds to a carbene complex, but it also can be described as a metallofuran. As deduced from the NMR data, the molecule would have a plane of symmetry in solution such that both carbons of the cyclopropane ring are equivalent, as are two of the -C≡O ligands. The nitrosyl ligand is positioned *trans* to the oxide ligand, as expected for the strongest and weakest "*trans*-effect" ligands. The M—C≡O unit *trans* to the carbene carbon is not appreciably different from the other M—C≡O bonds.

The most important structural feature of **5** from a mechanistic viewpoint (see later) is that one original -C≡O ligand on the chromium has been transformed into a carbene center.

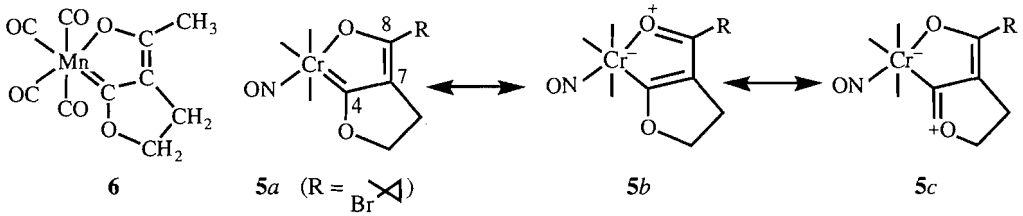

6 **5***a* (R = $\rangle\!\!<_{Br}$) **5***b* **5***c*

The reaction of the dibromo ketone **1** with $Mn(CO)_5^-$ (**3**) was carried out at an initial mixing temperature of −78°C, using a variety of experimental conditions, since this reaction is much more complex than in the chromium anion case. Four organometallic products can be isolated from the reaction, their relative amounts depending on the stoichiometric ratio of the reactants, the counterion of **3**, and the time–temperature cycle used after the initial −78°C addition. These four products will be arbitrarily referred to as **7***a–d*. When a 2:1 molar ratio of **1**:**3** is used, and when the reaction is worked up rapidly after warming the original solution to ca. 0°C, two products, **7***a* and **7***b*, are mainly present. Compound **7***a* is nearly absent when a 1:1 molar stoichiometry is used, and **7***b* is the major product. If the reactions are left at room temperature before work-up, two new products become dominant. Both of these latter compounds are much more mobile on silica gel TLC development than are **7***a* and **7***b*. In most cases, all four complexes are present to some extent in the mixture and the R_F TLC chromatographic order is **7***d* ⩾ **7***c* > **7***a* > **7***b*, using methylene chloride as the developing solvent. Crystalline samples of all four complexes could be obtained using flash chromatography and preparative TLC techniques. Complexes **7***a–d* are relatively air stable. On standing at room temperature for several months, **7***b* was nearly completely transformed into **7***c*. On melting **7***a* (60°C) a small amount of **7***d* was formed and, even on storage in the freezer for prolonged periods, some **7***a* → **7***d* transformation takes place.

From the NMR spectroscopic data, the structures of complexes **7***c* and **7***d* were obviously very similar to each other, and a comparison with the corresponding data for the chromium complex **5** showed that **7***c* and **7***d* were also closely

Can. J. Chem. Downloaded from www.nrcresearchpress.com by 88.255.202.194 on 09/08/12
For personal use only.

TABLE 1. Intramolecular distances[a] for complex **5**

Atom	Atom	Distance	Atom	Atom	Distance
Br	C(9)	1.928(6)	C(5)	C(6)	1.53(1)
Cr	O(5)	2.066(4)	C(5)	H(1)	0.93(6)
Cr	N(1)	1.683(6)	C(5)	H(2)	0.97(6)
Cr	C(1)	1.953(7)	C(6)	C(7)	1.519(9)
Cr	C(2)	1.957(7)	C(6)	H(3)	0.93(6)
Cr	C(3)	1.928(7)	C(6)	H(4)	0.85(6)
Cr	C(4)	2.013(6)	C(7)	C(8)	1.381(8)
O(1)	C(1)	1.129(7)	C(8)	C(9)	1.483(8)
O(2)	C(2)	1.137(7)	C(9)	C(10)	1.509(8)
O(3)	C(3)	1.139(7)	C(9)	C(11)	1.488(9)
O(4)	C(4)	1.334(7)	C(10)	C(11)	1.48(1)
O(4)	C(5)	1.480(9)	C(10)	H(6)	1.05(6)
O(5)	C(8)	1.301(6)	C(10)	H(5)	0.96(5)
O(6)	N(1)	1.189(6)	C(11)	H(7)	0.92(6)
C(4)	C(7)	1.376(8)	C(11)	H(8)	0.83(6)

[a]Distances are in angstroms. Estimated standard deviations in the least significant figure are given in parentheses.

related in structure to this compound. In Table 3, we show the ^{1}H and ^{13}C NMR assignments for **5** and assignments for **7***c* and **7***d* based on the same gross structure. In particular, one notes the characteristic (3) low-field carbene carbon (^{13}C-4) in all three cases, as well as similar δ values for C7 and C8 in each case. The ^{13}C and ^{1}H data for the -O-CH_2-CH_2- region are also very similar among the three structures. Complexes **7***c* and **7***d* differ only in the H vs. Br substitution at C9. This is of course easily seen in the extra ^{1}H peak present in **7***c*. Mass spectral analysis also confirms these structural assignments, showing a molecular ion *m/z* 304 for **7***c* and 382 (^{79}Br) for **7***d*. The infrared spectra in both cases show no typical $\diagdown\!\!\diagup$C=O stretching frequencies, as was also the case for complex **5**.

Complexes **7***c* and **7***d* are thus virtually identical to the complex **6** prepared by Casey *et al.* (2) (methyl substituent at C8 vs. cyclopropyl (**7***c*) and α-bromocyclopropyl (**7***d*). No ^{13}C NMR spectroscopic data were reported for **6** but the ^{1}H values for the C5 and C6 methylene groups of **6** (4.31 and 3.18 ppm) are modestly similar to the ^{1}H data for **7***c* and **7***d*.

Complexes **7***a* and **7***b* also appear to be related to each other. Mass spectral analysis shows that **7***a* has an identical composition to **7***d* (*m/z* 384), while **7***b* is identical to **7***c* (*m/z*) 304). Like **7***c* and **7***d*, **7***a* and **7***b* appear to differ only in the bromine substitution on the α-position of a cyclopropyl group. In contrast to complexes **7***c* and **7***d*, one sees possible $\diagdown\!\!\diagup$C=O stretching frequencies in the infrared spectra of both **7***a* and **7***b*; for example, **7***b* shows absorptions at 1651 and 1584 cm^{-1}, which may indicate the presence of two carbonyl groups. Another major difference between **7***a*, **7***b* and **7***c*, **7***d* is the absence of the -CH_2-CH_2-O- partial structure. In fact, **7***a* and **7***b* appeared from the ^{1}H and ^{13}C NMR data to have two intact, but chemically different, cyclopropyl rings, with each ring having symmetry such that the two carbons in each ring are equivalent. From the spectroscopic data, an acyl manganese structure seemed possible, with the added requirement that the 18e^- count for an $Mn(CO)_4$ acyl structure would require another 2e^- donor, most probably the lone-pair electrons of the ketonic oxygen.

The suppositions were verified by means of a single crystal X-ray structure of **7***b*. The ORTEP structure is shown in Fig. 2 and selected bond lengths and angles are given in Tables 4 and 5. Although the Mn—O—C6—C8—C5 partial structure contains the same bonded atoms in both **7***b* and **7***c*, in **7***b* the C6—O and C5—O bonds have typical carbonyl bond lengths (1.23 and 1.21 Å, respectively). One also sees two intact cyclopropane rings in this structure.

The geometry associated with the spirocyclopropane moiety in **7***b* deserves special mention. One notes that the C8—C7 and C8—C9 bonds are fairly normal (1.53 Å average), whereas the C7—C9 bond is extremely short (1.42 Å). The C6—C8 bond is also very short (1.44 Å). These features are typical of a bisected cyclopropane in which there is extensive delocalization of the electrons from the cyclopropyl ring into the C6=O6 complexed carbonyl group. A comparison with the recent X-ray data of Childs *et al.* (4) reveals that **7***b* has similar bond lengths to those in protonated methyl cyclopropyl ketone. A comparison of bond lengths is provided in Fig. 3, although one should note that structure **7***b* has relatively large bond-length standard deviations. This delocalization has mechanistic implications (see later). Note also that the second cyclopropyl ring shows much more uniform C—C bond lengths (and the cyclopropane ring in **5** even more so).

The assignment of the **7***a* structure as the corresponding α-bromocyclopropyl derivative of **7***b* was made by ^{1}H and ^{13}C NMR spectroscopic comparisons, as shown in Table 6. The correspondence of the ^{1}H NMR data between complexes **7***a* and **7***b* is somewhat divergent. For example, the protons on C7—C9 are deshielded in **7***a* by about 0.4 ppm, compared to **7***b*. However, there is generally good agreement in the ^{13}C shifts; for example, C8 is quite similar, as are the low-field C5 acyl carbons and the C6 ketonic carbons. The infrared spectrum of **7***a* shows a peak at 1657 cm^{-1}, close to the 1651 cm^{-1} peak observed for **7***b*. Both are in a position characteristic of the acyl manganese $\diagdown\!\!\diagup$C=O stretching region. However, **7***a* shows only a very broad peak in the 1566 cm^{-1} region (vs. a sharp peak at 1584 cm^{-1} for **7***b*). There have been several *ortho*-acetylarylmanganese tetracarbonyl X-ray structures reported (5, 6), where the internal ketone coordination provides a 2e^- donation. Structure **7***b* is the first manganese acyl complex to show this feature. The Mn - - - O=C$\diagdown\!\!\diagup$ distance is very similar in all of the reported structures, including **7***b*.

Discussion

Mechanism of formation of the complexes

In both the chromium and manganese complexes, an original metal carbonyl group has been transformed into either an acyl (**7***a*, **7***b*) or an oxycarbene fragment (**5**, **7***c*, **7***d*). In the initial reaction of $Cr(CO)_4NO^-$ or $Mn(CO)_5^-$ with dibromo ketone **1**, there is little doubt that the first reaction is the two-electron reductive cleavage of one of the C—Br bonds, forming the organic enolate and either $Cr(CO)_4NOBr$ or $Mn(CO)_5Br$. For example, in the chromium case, one can entirely quench the organometallic reaction by including trimethylsilyl chloride along with **1** in the original addition of **1** to $Cr(CO)_4NO^-$. A good yield of the silyl enol ether **8**

TABLE 2. Intramolecular bond angles[a] for complex **5**

Atom	Atom	Atom	Angle	Atom	Atom	Atom	Angle
O(5)	Cr	N(1)	174.9(2)	C(4)	C(7)	C(6)	109.9(6)
O(5)	Cr	C(1)	91.4(2)	C(4)	C(7)	C(8)	113.8(6)
O(5)	Cr	C(2)	87.7(2)	C(6)	C(7)	C(8)	136.2(6)
O(5)	Cr	C(3)	85.9(2)	O(5)	C(8)	C(7)	117.5(6)
O(5)	Cr	C(4)	77.0(2)	O(5)	C(8)	C(9)	114.4(5)
N(1)	Cr	C(1)	90.8(3)	C(7)	C(8)	C(9)	128.0(6)
N(1)	Cr	C(2)	96.8(2)	Br	C(9)	C(8)	116.0(4)
N(1)	Cr	C(3)	91.6(3)	Br	C(9)	C(10)	115.8(4)
N(1)	Cr	C(4)	98.6(3)	Br	C(9)	C(11)	115.5(5)
C(1)	Cr	C(2)	90.3(3)	C(8)	C(9)	C(10)	118.6(5)
C(1)	Cr	C(3)	174.7(3)	C(8)	C(9)	C(11)	120.0(5)
C(1)	Cr	C(4)	85.5(2)	C(10)	C(9)	C(11)	59.0(5)
C(2)	Cr	C(3)	94.1(3)	C(9)	C(10)	C(11)	59.8(5)
C(2)	Cr	C(4)	164.0(3)	C(9)	C(11)	C(10)	61.2(5)
C(3)	Cr	C(4)	89.5(2)				
C(4)	O(4)	C(5)	109.2(5)				
Cr	O(5)	C(8)	115.4(4)				
Cr	N(1)	O(6)	176.6(5)				
Cr	C(1)	O(1)	174.0(6)				
Cr	C(2)	O(2)	177.4(6)				
Cr	C(3)	O(3)	176.8(6)				
Cr	C(4)	O(4)	131.1(5)				
Cr	C(4)	C(7)	116.1(5)				
O(4)	C(4)	C(7)	112.7(6)				
O(4)	C(5)	C(6)	106.9(6)				
C(5)	C(6)	C(7)	101.2(6)				

[a]Angles are in degrees. Estimated standard deviations in the least significant figure are given in parentheses.

TABLE 3. ^{1}H and ^{13}C NMR comparisons for complexes **5**, **7***c*, and **7***d*

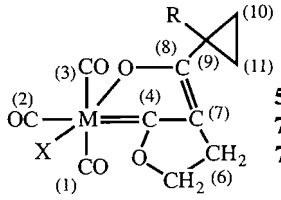

(5)

5 M = Cr, X = NO, R = Br
7*c* M = Mn, X = CO (position 2a), R = H
7*d* M = Mn, X = CO (position 2a), R = Br

	Compound		
^{13}C NMR position	**5** (ppm)	**7***c* (ppm)	**7***d* (ppm)
C1–C3	215.1	209.6	210.9
C2 (and C2a)	217.7	213.1, 218.8	214.5, 219.9
C4	249.7	254.4	267.1
C5	83.2	81.4	84.2
C6	26.5	24.3	28.8
C7	128.7	128.7	131.0
C8	195.1	204.4	199.8
C9	29.4	17.5	31.2
C10–C11	20.4	9.9	22.1
^{1}H NMR position			
H5	5.02(t)[a]	5.01(t)[a]	5.03 (t)[a]
H6	3.03 (t)[a]	2.85 (t)[a]	3.09 (t)[a]
H10–H11	1.52 (m),[b] 1.30 (m)[b]	1.1 (m),[c] 0.9(m)[c]	1.62 (m),[b] 1.33(*m*)[b]
R		1.79 (t,t)[c]	

[a]J = 8.5–9 Hz.
[b]AA′BB′ system.
[c]AA′BB′X system

Can. J. Chem. Downloaded from www.nrcresearchpress.com by 88.255.202.194 on 09/08/12
For personal use only.

Can. J. Chem. Downloaded from www.nrcresearchpress.com by 88.255.202.194 on 09/08/12
For personal use only.

can then be isolated, i.e., this compound is derived from a straightforward reaction between the enolate and the silyl chloride.

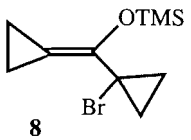

8

In the absence of such enolate traps, the organic enolate must eventually back-react with the metal carbonyl halide, forming an anionic Fischer carbene complex in each case, as shown:

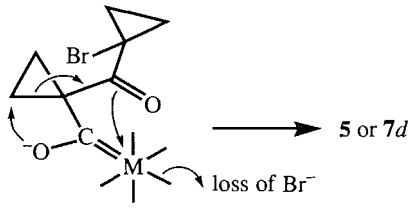

Attack of the nucleophilic oxycarbene on the cyclopropane ring could then lead to complexes **5** or **7***d*, although the details concerning the timing and stereochemistry of the bromide loss are unknown. In the manganese case, a competing reaction of the carbene complex is the simple loss of bromide, forming an acyl complex, i.e., **7***a*.

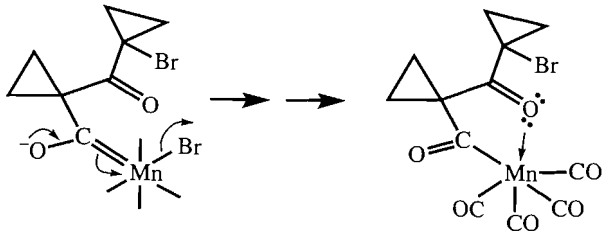

The neutral acyl complexes **7***a* and **7***b* are also thermally rearranged to the complexes **7***d* and **7***c*, respectively, but this process appears to be slower than the rate of formation of **7***c* and **7***d* under the original reaction conditions. This arrangement can be pictured as follows:

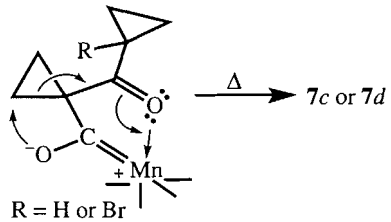

Thus, it appears that the ring-opened products **7***c* and **7***d* may be formed from either the anionic intermediate (in a relatively rapid reaction) or from the neutral complexes **7***a* and **7***b* (in a slow process).

One major difference between $Cr(CO)_4NO^-$ and $Mn(CO)_5^-$ is that the former is considerably more reactive in reduction of the C—Br functionality. One can demonstrate that $Cr(CO)_4NO^-$ reacts slowly with **1** even at −78°C (loss of the deep red color). In contrast, $Mn(CO)_5^-$ almost certainly requires a much higher temperature for the initial reduction to occur. A consequence of this is that the chromium reactions are well separated, i.e., the $Cr(CO)_4NO^-$ is totally consumed in a stoichiometric reaction to form an enolate and $Cr(CO)_4NOBr$ (the latter is only presumed to be formed here, but it is a detectable product of the normal cyclopropanone-forming reaction of eq. [1]). At a much slower rate, the enolate then back-reacts with $Cr(CO)_4NOBr$ to form the complex. The lack of formation of an acyl complex in the chromium case may indicate that the oxycarbene functionality is more nucleophilic than in the manganese case.

For $Mn(CO)_5^-$, it appears that the reduction of the first C—Br bond in **1** is a rate-determining process. After reduction, a faster reaction leads to organometallic complexes, where the remaining bromine in the complex is more reactive than those in **1**. Thus, one gets debrominated complexes **7***b* and **7***c* after work-up (proton source). Also, leaving the reaction at room temperature prior to work-up increases the amount of **7***c* at the expense of **7***b*, an indication that the cyclopropane ring-opening is slowly taking place at this

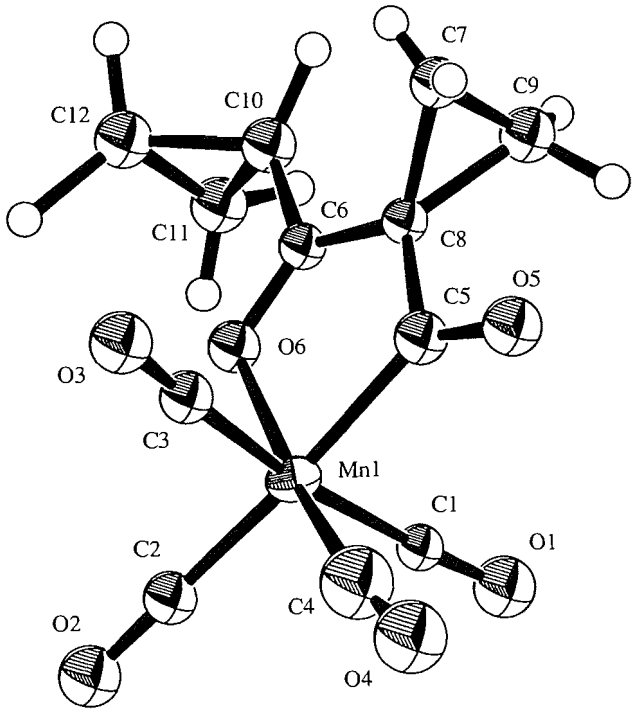

FIG. 2. ORTEP drawing (50% probability level) of the manganese complex **7***b*.

TABLE 4. Intramolecular distances[a] for complex **7***b*

Atom	Atom	Distance	Atom	Atom	Distance
Mn(1)	O(6)	2.066(9)	O(6)	C(6)	1.24(1)
Mn(1)	C(1)	1.85(1)	C(5)	C(8)	1.55(2)
Mn(1)	C(2)	1.79(1)	C(6)	C(8)	1.44(2)
Mn(1)	C(3)	1.84(1)	C(6)	C(10)	1.57(2)
Mn(1)	C(4)	1.79(2)	C(7)	C(8)	1.52(2)
Mn(1)	C(5)	1.97(1)	C(7)	C(9)	1.42(2)
O(1)	C(1)	1.13(1)	C(8)	C(9)	1.54(2)
O(2)	C(2)	1.17(2)	C(10)	C(11)	1.50(2)
O(3)	C(3)	1.16(2)	C(10)	C(12)	1.49(2)
O(4)	C(4)	1.14(2)	C(11)	C(12)	1.47(2)
O(5)	C(5)	1.21(2)			

[a]Distances are in angstroms. Estimated standard deviations in the least significant figure are given in parentheses.

TABLE 5. Intramolecular bond angles[a] for complex **7b**

Atom	Atom	Atom	Angle	Atom	Atom	Atom	Angle
O(6)	Mn(1)	C(1)	89.9(5)	Mn(1)	C(5)	O(5)	135(1)
O(6)	Mn(1)	C(2)	92.2(6)	Mn(1)	C(5)	C(8)	110(1)
O(6)	Mn(1)	C(3)	91.3(5)	O(5)	C(5)	C(8)	115(1)
O(6)	Mn(1)	C(4)	174.8(7)	O(6)	C(6)	C(8)	121(1)
O(6)	Mn(1)	C(5)	82.9(5)	O(6)	C(6)	C(10)	117(1)
C(1)	Mn(1)	C(2)	93.4(6)	C(8)	C(6)	C(10)	121(1)
C(1)	Mn(1)	C(3)	172.1(6)	C(8)	C(7)	C(9)	63(1)
C(1)	Mn(1)	C(4)	89.1(7)	C(5)	C(8)	C(6)	111(1)
C(1)	Mn(1)	C(5)	86.6(5)	C(5)	C(8)	C(7)	117(1)
C(2)	Mn(1)	C(3)	94.3(6)	C(5)	C(8)	C(9)	119(1)
C(2)	Mn(1)	C(4)	93.0(8)	C(6)	C(8)	C(7)	123(1)
C(2)	Mn(1)	C(5)	175.1(7)	C(6)	C(8)	C(9)	121(1)
C(3)	Mn(1)	C(4)	88.9(7)	C(7)	C(8)	C(9)	55.2(9)
C(3)	Mn(1)	C(5)	85.8(6)	C(7)	C(9)	C(8)	61.4(9)
C(4)	Mn(1)	C(5)	91.9(8)	C(6)	C(10)	C(11)	113(1)
Mn(1)	O(6)	C(6)	113.8(9)	C(6)	C(10)	C(12)	116(1)
Mn(1)	C(1)	O(1)	175(1)	C(11)	C(10)	C(12)	59(1)
Mn(1)	C(2)	O(2)	179(1)	C(10)	C(11)	C(12)	60(1)
Mn(1)	C(3)	O(3)	178(1)	C(10)	C(12)	C(11)	61.3(9)
Mn(1)	C(4)	O(4)	171(2)				

[a]Angles are in degrees. Estimated standard deviations in the least significant figure are given in parentheses.

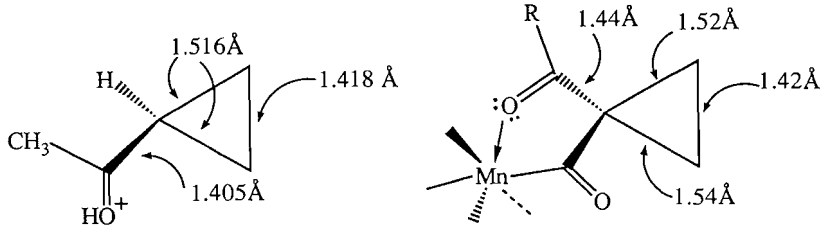

FIG. 3. Comparison of bond lengths for protonated methyl cyclopropyl ketone and complex **7b**.

temperature. Since **7b** and **7c** require two moles of $Mn(CO)_5^-$ in their formation, it is obvious that an initial 1:1 reactant stoichiometry will result in recovered starting dibromo ketone **1**, and this was observed.

One could also explain the formation of acyl products by postulating that $Mn(CO)_5^-$ displaces bromide from **1** in an S_N2 reaction, followed by carbonyl insertion. Although this route is well established with methyl iodide, it is highly unlikely that the tertiary bromines in **1** would undergo such substitution.

Generality of the reactions

The attack of a preformed carbanion on a neutral metal carbonyl is the usual route to transition metal carbenes (7). The unique feature in the present reactions is that one uses the anionic metal complex and an α-bromo carbonyl compound to create the carbanion and a bromo carbonyl metal complex, these then re-reacting by the traditional Fischer route to give an anionic carbene complex intermediate. By having a bromide leaving group on the metal, the reactions leading to the carbene complex are self-quenching after the cyclopropane ring-opening has taken place. Alternatively, if cyclopropane ring-opening does not occur, loss of bromide leads to an acyl complex.

One can note in closing that the failure of eq. [2] in the bis-α-bromocyclopropyl ketone (**1**) case is likely due to the large steric strain involved in forming cyclopropanone **2**, since there is abundant evidence from the structure of the organometallic complexes that the first bromine atom in **1** can be removed without complication.

Experimental

All melting points are uncorrected. NMR spectra were obtained on a Bruker AM-400 (δ values, *J* in Hz). In descriptions of the ^1H NMR spectra, s = singlet, d = doublet, t = triplet, q = quartet, m = multiplet, b = broad. Coupling networks were verified using ^1H COSY 2D spectra and ^{13}C multiplicities were determined from DEPT sequences. Mass spectra were determined with a Kratos MS-80. Infrared spectra were obtained using a Mattson 4030 FT-IR spectrometer. Flash chromatography was performed using silica gel (230–400 mesh) with methylene chloride as the eluting solvent. Thin-layer chromatography (TLC) was performed on precoated silica gel 60 F_{254} plates (Merck 5554) and PTLC was performed on 0.5 mm plates (Merck 5774). Tetrahydrofuran was purified by distillation from sodium benzophenone ketyl. Hexane, pentane, and methylene chloride were dried over 3A molecular sieves. Glassware was oven-dried.

Preparation of complex ***5***

In a small Schlenk tube with a septum and stopcock side-arm, under a nitrogen atmosphere and with magnetic bar stirring, a solution of 0.52 g (0.71 mmol) of $PPN^+Cr(CO)_4NO^-$ (1) in 2 mL methylene chloride was prepared and cooled to −78°C. Dibromo ketone **1** (0.1902 g, 0.710 mmol) in 1 mL of methylene chloride was added dropwise via syringe over 1 min and the mixture stirred for 4 h at −78°C. The reaction mixture was then left at ca. −20°C

Can. J. Chem. Downloaded from www.nrcresearchpress.com by 88.255.202.194 on 09/08/12
For personal use only.

TABLE 6. ^1H and ^{13}C NMR comparisons for complexes *7a* and *7b*

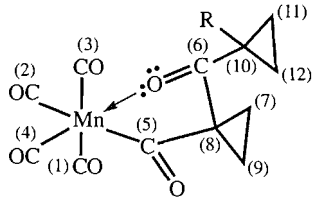

7a R = Br
7b R = H

	Compound	
^{13}C NMR position	*7a* (ppm)	*7b* (ppm)
C1–C3	210.1	210.5
C2	217.9 or 212.4	218.2 or 213.0
C4	212.4 or 217.9	213.0 or 218.2
C5	271.0	274.1
C6	220.2	225.9
C7–C9	25.4	21.8
C8	57.1	55.4
C10	26.7	16.2
C11–C12	21.7	13.8
^1H NMR position		
H7–H9	2.37 (m),[a] 2.07 (m)[a]	1.98 (m),[a] 1.66 (m)[a]
H11–H12	1.70 (m),[a] 1.48 (m)[a]	1.29 (m),[b] 1.15 (m)[b]
R		1.59 (m)[b]

[a]AA'BB' system.
[b]AA'BB'X system.

for 48 h. Pentane (10 mL) was added and the supernatant decanted (orange). The pentane was evaporated, and the residues redissolved in 2 mL pentane and applied to a flash chromatography column (1 × 15 cm, silica gel). Elution with methylene chloride (orange band) gave 0.197 g of crude **5** (73%). Crystallization from *n*-hexane eventually produced needles suitable for X-ray studies, mp 70–72°C. Infrared (CH_2Cl_2): 2092 (m), 2029 (vs), 1707 (vs). The ^1H and ^{13}C NMR spectral data are listed in Table 3. Mass spectrum (^{79}Br) *m/z*: 382 (M^+), 270 (58), 267 (57), 204 (78), 203 (60), 136 (65), 121 (58), 97 (90).

Preparation of complex 7a

Using the same apparatus described above, bis-α-bromocyclopropyl ketone **1** (213 mg, 0.80 mmol) in 1 mL THF was added dropwise to a solution of $Na^+Mn(CO)_5^-$ (prepared from $Mn_2(CO)_{10}$, 80 mg, 0.20 mmol, with 1% Na/Hg amalgam) in 4 mL THF with stirring at −78°C under nitrogen. The reaction mixture was warmed to 10°C during 3 h. Pentane (5 mL) was added and solution decanted from sludge and evaporated. The residue was chromatographed to give 16.4 mg of *7a* (19% yield based on recovered starting material, 151.2 mg), yellow crystals, mp 58–60°C. Infrared (CCl_4): 2091 (w), 2079 (m), 2002 (s), 1985 (s), 1964 (s), 1657 (w). The ^1H and ^{13}C NMR data are listed in Table 6. Mass spectral fragmentation *m/z*: 382 (1), 354 (4), 336 (3), 298 (1), 270 (5), 242 (23), 162 (38), 134 (62), 79 (100). High-resolution mass spectrum calcd. for $C_{12}H_8O_6MnBr$: 381.8889; found: 381.8885.

Preparation of complex 7b

Using the apparatus described above, $PPN^+Mn(CO)_5^-$ (400 mg, 0.54 mmol) in 2 mL methylene chloride was cooled to −78°C. Under a nitrogen atmosphere, dibromo ketone **1** (144 mg, 0.537 mmol) in 1 mL of methylene chloride was added dropwise via syringe. The reaction mixture was slowly warmed to 0°C and then filtered through a short silica gel column (2 g), using methylene chloride washes. After evaporation of the solvent, the residue was applied to a PTLC plate to give 38 mg of *7b* (23%). The yellow solid was recrystallized from hexane to give crystals suitable for X-ray studies, mp 137–139°C. Infrared (KBr plate): 2079 (m), 1977 (s), 1944 (s), 1626 (m), 1574 (m), 1435 (m). The ^1H and ^{13}C NMR data are listed in Table 6. Mass spectral fragmentation *m/z*: 304 (2), 276 (11), 248 (7), 220 (5), 192 (13), 164 (100), 134 (11), 96 (25), and 55 (66). High-resolution mass spectrum calcd. for $C_{12}H_9MnO_6$: 303.9780; found: 303.9790.

Preparation of complex 7c

Using the same apparatus described above, dibromo ketone **1** (170 mg, 0.64 mmol) in 1 mL THF was added to a solution of $PPN^+Mn(CO)_5^-$ (490 mg, 0.67 mmol) in 2 mL THF at −78°C under a nitrogen atmosphere. The reaction mixture was warmed to 20°C during 3 h and stirred for a further 1 h at 20°C. After the same work-up and separation procedure as described for *7b*, 60 mg of *7c* was obtained (31%), yellow crystals, mp 170°C (dec.). Infrared (CCl_4): 2089 (m), 2052 (m), 2000 (s), 1956 (s), 1491 (m). The ^1H and ^{13}C NMR data are listed in Table 3. Mass spectral fragmentation *m/z*: 304 (55), 248 (28), 220 (65), 192 (100), 164 (55), 138 (40), 96 (91), 55 (93). High-resolution mass spectrum calcd. for $C_{12}H_9MnO_6$: 303.9780; found: 303.9783.

Preparation of complex 7d

The reaction was carried out as for *7a*, using a calculated 1:1 stoichiometry of the reactants. The reaction mixture was allowed to warm to 15°C during 2 h, 5 mL of pentane was then added, and the mixture filtered through a short silica gel column (2 g), which was washed with methylene chloride. The solvent was removed and a PTLC separation gave 11.9 mg (8%) of *7d*, together with 8.7 mg of *7c* and 30 mg of *7b*. The compound forms yellow crystals, mp 58–60°C. Infrared (KBr plate): 2090 (m), 1991 (s), 1938 (s), 1462 (m). The ^1H and ^{13}C NMR data are listed in Table 3. Mass spectral fragmentation *m/z*: 382 (13), 354 (2), 328 (6), 300 (31), 272 (76), 230 (46), 190 (47), 136 (59), 97 (60), 55 (100). High-resolution mass spectrum calcd. for $C_{12}H_8O_6MnBr$: 381.8889; found: 381.8885.

Crystal structure determination of 5

Accurate cell dimensions and a crystal orientation matrix were determined on a Rigaku AFC6S diffractometer by a least-squares

Can. J. Chem. Downloaded from www.nrcresearchpress.com by 88.255.202.194 on 09/08/12
For personal use only.

Can. J. Chem. Downloaded from www.nrcresearchpress.com by 88.255.202.194 on 09/08/12
For personal use only.

TABLE 7. Crystal data and experimental details for **5**

A. Crystal data

Empirical formula	$C_{11}H_8O_6BrCrN$
Formula weight	368.08
Crystal color, habit	Yellow, plate
Crystal dimensions	0.090 × 0.260 × 0.400
Crystal system	Monoclinic
No. of reflections used for unit cell determination (2θ range)	25 (20.0–30.0°)
Lattice parameters	a = 13.523(3) Å b = 5.845(2) Å c = 18.488(4) Å β = 110.68(2)°
	V = 1367.2(6) Å^3
Space group	$P2_1/c$ (no. 14)
Z value	4
D_{calc}	1.788 g/cm^3
F_{000}	724.00
μ(MoKα)	37.27 cm^{-1}

B. Intensity measurements

Diffractometer	Rigaku AFC6S
Radiation	MoKα (λ = 0.71069 Å) graphite monochromated
Temperature	−103.0°C
Scan type	ω–2θ
Scan rate	4.0°/min (in ω) (3 rescans)
Scan width	(0.94 + 0.35 tan θ)°
$2\theta_{max}$	50.1°
No. of reflections measured	Total: 3194 Unique: 2678 (R_{int} = 0.045)
Corrections	Lorentz, polarization, absorption (trans. factors: 0.5619–0.9997) Decay (0.77% increase)

C. Structure solution and refinement

Structure solution	Heavy-atom method
Refinement	Full-matrix least squares
Anomalous dispersion	All non-hydrogen atoms
No. of observations ($I > 3.00\ \sigma(I)$)	1537
No. of variables	205
Reflection/parameter ratio	7.50
Residuals: R; Rw	0.036; 0.036
Goodness-of-fit indicator	1.73
Max shift/error in final cycle	0.01
Maximum peak in final diff. map	0.45 e/Å^3
Minimum peak in final diff. map	−0.38 e/Å^3

fit of the setting angles of 25 reflections. Crystal data and experimental details are provided in Table 7. Data were corrected for Lorentz, polarization, and empirical absorption effects (8), transmission factors being in the range 0.5619–0.9997.

The structure was solved by the heavy-atom method. Refinement of the structure was by full-matrix least-squares calculations, initially with isotropic and finally with anisotropic temperature factors for the non-hydrogen atoms. At an intermediate stage in the refinement, a difference map revealed maxima consistent with the positions of hydrogen atoms, which were included in the subsequent cycles of refinement with fixed isotropic temperature factors. Refinement converged with R = 0.036 and Rw = 0.036. In the refinement cycles, weights were derived from the counting statistics. Scattering factors were those of Cromer and Waber (9) and Stewart, Davidson, and Simpson (10) and allowance was made for anomalous dispersion (11). A difference map calculated at the conclusion of the refinement had no chemically significant features. All computer programs used in this study were part of teXsan (12) installed on a Silicon Graphics Personal Iris 4D/35 computer and Fig. 1 was plotted using ORTEP II (13). The positional parameters are given in Table 8.[3]

TABLE 8. Positional parameters and B(eq) for **5**

Atom	x	y	z	B(eq)[a]
Br	0.12203(6)	1.0330(1)	0.28165(4)	2.70(3)
Cr	0.31985(8)	0.7939(2)	0.60148(6)	1.96(4)
O(1)	0.5067(4)	1.0753(8)	0.5911(3)	3.5(2)
O(2)	0.2891(4)	1.1344(8)	0.7199(3)	3.5(2)
O(3)	0.1369(4)	0.4778(9)	0.5968(3)	3.5(2)
O(4)	0.3777(3)	0.4616(8)	0.4948(2)	2.5(2)
O(5)	0.2096(3)	0.9779(7)	0.5146(2)	1.9(2)
O(6)	0.4675(4)	0.4957(8)	0.7104(3)	3.8(2)
N(1)	0.4068(4)	0.6239(10)	0.6671(3)	2.4(2)
C(1)	0.4349(5)	0.9826(11)	0.5938(3)	2.2(3)
C(2)	0.2980(5)	1.0103(12)	0.6752(3)	2.3(3)
C(3)	0.2033(5)	0.6003(12)	0.5991(3)	2.1(3)
C(4)	0.3227(5)	0.6408(11)	0.5047(4)	1.9(3)
C(5)	0.3547(6)	0.4271(13)	0.4111(5)	3.0(3)
C(6)	0.2734(6)	0.6083(12)	0.3686(4)	2.2(3)
C(7)	0.2597(5)	0.7367(11)	0.4359(3)	1.8(3)
C(8)	0.1976(5)	0.9145(11)	0.4445(3)	1.7(3)
C(9)	0.1127(4)	1.0377(11)	0.3833(3)	1.8(2)
C(10)	0.0024(5)	1.0353(15)	0.3858(4)	3.0(3)
C(11)	0.0654(6)	1.2480(14)	0.4028(4)	2.8(3)

[a] $B(\text{eq}) = \frac{8}{3}\pi^2(U_{11}(aa^*)^2 + U_{22}(bb^*)^2 + U_{33}(bb^*)^2 + 2U_{12}aa^*bb^* \cos\gamma + 2U_{13}aa^*cc^* \cos\beta + 2U_{23}bb^*cc^* \cos\alpha)$.

Crystal structure determination of 7b

Accurate cell dimensions and a crystal orientation matrix were determined on a Rigaku AFC6S diffractometer by a least-squares fit of the setting angles of 15 reflections. Crystal data and experimental details are provided in Table 9. Data were corrected for Lorentz, polarization, and empirical absorption effects (8), transmission factors being in the range 0.776–0.997.

The structure was solved by the heavy-atom method. Refinement of the structure was by full-matrix least-squares calculations allowing anisotropic temperature factors for Mn only; carbon and oxygen atoms were allowed isotropic temperature factors. At an intermediate stage in the refinement, a difference map revealed maxima consistent with the positions of hydrogen atoms, which were included in the subsequent cycles at idealized geometries (C—H, 0.95 Å) with fixed isotropic temperature factors. Refinement converged with R = 0.057 and Rw = 0.045. In the refinement cycles, weights were derived from the counting statistics.

[3] A complete set of structure factor listings, anisotropic thermal parameters, torsional angles, and hydrogen atom parameters is available for **5** and **7b** and may be purchased from: The Depository of Unpublished Data, Document Delivery, CISTI, National Research Council Canada, Ottawa, Canada K1A 0S2.

Tables of hydrogen atom parameters have also been deposited with the Cambridge Crystallographic Data Centre and can be obtained on request from The Director, Cambridge Crystallographic Data Centre, University Chemical Laboratory, 12 Union Road, Cambridge, CB2 1EZ, U.K.

TABLE 9. Crystal data and experimental details for **7b**

A. Crystal data	
Empirical formula	$C_{12}H_9O_6Mn$
Formula weight	304.14
Crystal color, habit	Yellow, needle
Crystal dimensions	0.150 × 0.150 × 0.300
Crystal system	Orthorhombic
No. of reflections used for unit cell determination (2θ range)	15 (13.6–22.4°)
Lattice parameters	a = 11.267(6) Å b = 11.784(3) Å c = 9.651(1) Å V = 1281.4(8) Å^3
Space group	$P2_12_12_1$ (no. 19)
Z value	4
D_{calc}	1.576 g/cm^3
F_{000}	616.00
μ(MoKα)	10.06 cm^{-1}
B. Intensity measurements	
Diffractometer	Rigaku AFC6S
Radiation	MoKα (λ = 0.71069 Å) graphite monochromated
Temperature	−123.0°C
Scan type	ω–2θ
Scan rate	4.0°/min (in ω) (3 rescans)
Scan width	(1.78 + 0.35 tan θ)°
$2\theta_{max}$	50.1°
No. of reflections measured	Total: 1742 Unique: 1342 (R_{int} = 0.036)
Corrections	Lorentz, polarization, absorption (trans. factors: 0.7756–0.9965) Decay (0.98% increase) Secondary extinction (coefficient: 2.40e − 07)
C. Structure solution and refinement	
Structure solution	Heavy-atom method
Refinement	Full-matrix least squares
Anomalous dispersion	All non-hydrogen atoms
No. of Observations (I > 3.00σ(I))	667
No. of variables	83
Reflection/parameter ratio	8.0
Residuals: R; Rw	0.057; 0.045
Goodness-of-fit indicator	2.38
Max shift/error in final cycle	0.01
Maximum peak in final diff. map	0.50 e/Å^3
Minimum peak in final diff. map	−0.49 e/Å^3

Other operations were identical to those described for **5**. The positional parameters are given in Table 10.[3]

TABLE 10. Positional parameters and B(eq) for **7b**

Atom	x	y	z	B(eq)[a]
Mn(1)	0.3728(2)	0.1423(2)	0.3881(2)	1.88(9)
O(1)	0.6221(10)	0.2016(8)	0.3164(9)	3.1(2)
O(2)	0.2818(8)	0.1718(8)	0.1028(11)	3.3(2)
O(3)	0.1408(9)	0.0666(8)	0.5090(9)	3.2(2)
O(4)	0.4418(9)	−0.0957(9)	0.3590(12)	4.4(3)
O(5)	0.4778(8)	0.0665(8)	0.6520(9)	2.8(2)
O(6)	0.3364(8)	0.3094(8)	0.4374(9)	2.1(2)
C(1)	0.5256(12)	0.1826(12)	0.3394(13)	1.9(3)
C(2)	0.3173(12)	0.1594(13)	0.2153(15)	2.2(3)
C(3)	0.2298(13)	0.0960(12)	0.4593(15)	2.3(3)
C(4)	0.4111(16)	−0.0036(15)	0.3603(19)	4.7(5)
C(5)	0.4304(11)	0.1372(14)	0.5806(13)	2.2(3)
C(6)	0.3690(13)	0.3370(11)	0.5549(13)	1.9(3)
C(7)	0.3901(13)	0.2571(11)	0.8047(13)	1.9(3)
C(8)	0.4161(11)	0.2550(12)	0.6505(14)	1.9(3)
C(9)	0.5060(15)	0.2900(12)	0.7635(17)	2.7(3)
C(10)	0.3483(12)	0.4640(11)	0.5989(15)	2.5(3)
C(11)	0.3643(15)	0.5465(11)	0.4814(14)	2.7(3)
C(12)	0.2450(15)	0.5216(13)	0.5342(15)	2.8(4)

[a] $B(\text{eq}) = \frac{8}{3}\pi^2(U_{11}(aa^*)^2 + U_{22}(bb^*)^2 + U_{33}(bb^*)^2 + 2U_{12}aa^*bb^* \cos\gamma + 2U_{13}aa^*cc^* \cos\beta + 2U_{23}bb^*cc^* \cos\alpha)$.

Acknowledgement

We thank the Natural Sciences and Engineering Research Council of Canada for generous financial support.

1. D. R. Mantell and W. L. Gladfelter. J. Organomet. Chem. **347**, 333 (1988).
2. C. P. Casey, R. A. Boggs, D. F. Marten, and J. C. Calabrese. J. Chem. Soc. Chem. Commun. 243 (1973).
3. D. K. Thompson, N. Suzuki, L. S. Hegadus, and Y. Satoh. J. Org. Chem. **57**, 1461 (1992).
4. R. F. Childs, M. D. Kostyk, C. J. L. Lock, and M. Mahendran. J. Am. Chem. Soc. **112**, 8912 (1990).
5. (*a*) C. B. Knobler, S. Crawford, and H. D. Kaesz. Inorg. Chem. **14**, 2062 (1975); (*b*) R. J. McKinney, G. Firestein, and H. D. Kaesz. Inorg. Chem. **14**, 2057 (1975).
6. J. M. Cooney, L. H. P. Gommans, L. Main, and B. K. Nicholson. J. Organomet. Chem. **349**, 197 (1988).
7. (*a*) E. O. Fischer and A. Maasböl. Chem. Ber. **100**, 2445 (1967); (*b*) K. H. Dötz and E. O. Fischer. Transition metal carbene complexes. Verlag Chemie, Weinheim, Germany. 1983.
8. A.C.T. North, D. C. Phillips, and F. S. Mathews. Acta Crystallogr. Sect. A: Cryst. Phys. Diffr. Theor. Gen. Crystallogr. **A24**, 351 (1968).
9. D. T. Cromer and J. T. Waber. International tables for X-ray crystallography. Vol. IV. Kynoch Press, Birmingham. 1974. Table 2.2 A, pp. 71–98.
10. R. F. Stewart, E. R. Davidson, and W. T. Simpson. J. Chem. Phys. **42**, 3175 (1965).
11. J. A. Ibers and W. C. Hamilton. Acta Crystallogr. **17**, 781 (1964).
12. teXsan (1992). Single crystal structure analysis software, Version 1.2. Molecular Structure Corporation, The Woodlands, Tex.
13. C. K. Johnson. ORTEP II. Report ORNL-5138, Oak Ridge National Laboratory, Oak Ridge, Tenn. 1976.

Can. J. Chem. Downloaded from www.nrcresearchpress.com by 88.255.202.194 on 09/08/12
For personal use only.

Solid-state chemistry of polycarboxylate crown ether cation complexes: cooperative binding of water and metal ions by flexible chorands

PHILIP J. DUTTON, THOMAS M. FYLES,[1] AND VALIA VEETTIL SURESH
Department of Chemistry, The University of Victoria, Victoria, B.C., Canada V8W 2Y2

AND

FRANK R. FRONCZEK AND RICHARD D. GANDOUR
Department of Chemistry, Louisiana State University, Baton Rouge, LA 70803-1804, U.S.A.

Received August 21, 1991[2]

PHILIP J. DUTTON, THOMAS M. FYLES, VALIA VEETTIL SURESH, FRANK R. FRONCZEK, and RICHARD D. GANDOUR. Can. J. Chem. **71**, 239 (1993).

The solid-state structures of alkali-metal salt complexes of crown ether tetra- and hexa-carboxylic acids (18C6A$_4$ and 18C6A$_6$) have been determined. The sodium salt of 18C6A$_6$ crystallizes as the trihydrate in orthorhombic space group $P2_12_12_1$ (a = 7.6868(12), b = 15.429(3), c = 21.975(2) Å, R = 0.031 for 5192 observed data); the potassium salt of 18C6A$_6$ crystallizes as the the trihydrate in orthorhombic space group $P2_12_12_1$ (a = 7.6711(8), b = 15.709(2), c = 21.966(5) Å, R = 0.035 for 2521 observed data); the thallium(I) salt of 18C6A$_6$ crystallizes as the dihydrate in orthorhombic space group $P2_12_12_1$ (a = 12.0331(10), b = 12.4333(12), c = 17.366(2) Å, R = 0.035 for 4952 observed data); and the cesium salt of 18C6A$_6$ crystallizes as the dihydrate in monoclinic space group $P2_1$ (a = 7.708(3), b = 13.492(2), c = 11.9501(9) Å, β = 94.49(2)°, R = 0.029 for 4480 observed data). The sodium salt of 18C6A$_4$ crystallizes as the dihydrate in monoclinic space group $P2_1$ (a = 11.4368(11), b = 7.7068(11), c = 12.6579(12) Å, β = 98.515(8)°, R = 0.035 for 3000 observed data); the thallium(I) salt of 18C6A$_4$ crystallizes as the dihydrate in monoclinic space group $P2_1$(a = 11.719(2), b = 7.668(2), c = 12.8403(13) Å, β = 99.052(9)°, R = 0.040 for 3981 observed data); and the cesium salt of 18C6A$_4$ crystallizes as the dihydrate in monoclinic space group $P2_1$ (a = 11.787(2), b = 7.637(2), c = 13.001(2) Å, β = 98.705(12)°, R = 0.038 for 3428 observed data). Both chorands exhibit a cooperative relationship of mean cavity radius and guest-ion radius, which closely follows the effective ionic radii of the guests. The hexaacid is a preorganized host for monohydrated cations. It provides a trigonal hydrogen bonding receptor site for the water molecule, and up to nine oxygen donors for cation binding. Guests ranging in size from Na^+ to Cs^+ are accommodated without distortion of the macrocyclic framework. The tetraacid is similarly tolerant of a range of guests, but greater structural reorganization of the ligand is required to optimize contacts with fully dehydrated cations. Skeletal drawings of donor atoms, in conjunction with polar coordinate maps of torsion angles, reveal how the demands of the guest are accommodated by the host.

PHILIP J. DUTTON, THOMAS M. FYLES, VALIA VEETTIL SURESH, FRANK R. FRONCZEK et RICHARD D. GANDOUR. Can. J. Chem. **71**, 239 (1993).

On a déterminé les structures cristallines de complexes de sels de métaux alcalins et d'éthers couronnes tétra- et hexacarboxyliques (18C6A$_4$ et 18C6A$_6$). Le sel de sodium du 18C6A$_6$ cristallise sous la forme d'un trihydrate orthorhombique, groupe d'espace $P2_12_12_1$, avec a = 7,6868(12), b = 15,429(3) et c = 21,975(2) Å et R = 0,031 pour 5192 données observées; le sel de potassium du 18C6A$_6$ cristallise sous la forme d'un trihydrate orthorhombique, groupe d'espace $P2_12_12_1$, avec a = 7,6711(8), b = 15,709(2) et c = 21,966(5) Å et R = 0,035 pour 2521 données observées; le sel de thallium(I) du 18C6A$_6$ cristallise sous la forme d'un dihydrate orthorhombique, groupe d'espace $P2_12_12_1$, avec a = 12,0331(10), b = 12,433(3)(12) et c = 17,366(2) Å et R = 0,035 pour 4952 données observées et le sel de césium du 18C6A$_6$ cristallise sous la forme d'un dihydrate monoclinique, groupe d'espace $P2_1$, avec a = 7,708(3), b = 13,492(2) et c = 11,9501(9) Å, β = 94,49(2)° et R = 0,029 pour 4480 données observées. Le sel de sodium du 18C6A$_4$ cristallise sous la forme d'un dihydrate monoclinique, groupe d'espace $P2_1$, avec a = 11,4368(11), b = 7,7068(11) et c = 12,6579(12) Å, β = 98,515(8)° et R = 0,035 pour 3000 données observées; le sel de thallium(I) du 18C6A$_4$ cristallise sous la forme d'un dihydrate monoclinique, groupe d'espace $P2_1$, avec a = 11,719(2), b = 7,668(2) et c = 12,8403(13) Å, β = 99,052(9)° et R = 0,040 pour 3981 données observées et le sel de césium du 18C6A$_4$ cristallise sous la forme d'un dihydrate monoclinique, groupe d'espace $P2_1$, avec a = 11,787(2), b = 7,637(2) et c = 13,001(2) Å, β = 98,705(12)° et R = 0,038 pour 3428 données observées. Les deux chorands présentent une relation coopérative des rayons moyens de cavité et d'ion invité qui suit de très près celle des rayons ioniques effectifs des invités. L'hexaacide est un hôte préorganisé pour les cations monohydratés. Il fournit aux molécules d'eau un site récepteur pour une liaison hydrogène trigonale et jusqu'à neuf oxygènes donneurs pour des liaisons avec les cations. Les invités dont la taille se situe entre celles du Na^+ et du Cs^+ s'accommodent sans distorsions dans la structure macrocyclique. Le tétraacide tolère aussi une grande variété d'invités; toutefois, une plus grande réorganisation structurale est requise du ligand pour optimiser les contacts avec les cations complètement déshydratés. Des diagrammes du squelette des atomes donneurs utilisés en conjonction avec des cartes en coordonnées polaires des angles de torsion révèlent comment les demandes des invités sont accommodées par l'hôte.

[Traduit par la rédaction]

The search for molecular receptors of the alkali-metal cations has developed from crown ethers via cryptands to spherands (1). Design principles emphasizing ligand cavity size, ligand–cation complementarity, and ligand preorganization have guided syntheses of increasingly complex macrocyclic ligands with highly specific cation binding capabilities (2). Nevertheless, the binding of alkali-metal

[1]Author to whom correspondence may be addressed.
[2]Revision received April 22, 1992.

Can. J. Chem. Downloaded from www.nrcresearchpress.com by 88.255.202.194 on 09/08/12
For personal use only.

cations in aqueous solution remains largely unexplored. Water binds these cations more tightly than simple crown ethers, cryptand binding requires a basic solution to avoid ligand protonation, and the spherands are insoluble in water. In contrast, polycarboxylate crown ethers derived from *R,R*-(+)-tartaric acid (3, 4) bind cations in acidic aqueous solution with stability constants for alkali-metal cations comparable to those for the cryptands.

The structures of polycarboxylate crown ether complexes with alkali-metal cations have been inferred from stability constant data (3, 5, 7) and from UV and ESR spectral changes (8). Analyses of solid-state structures of several derivatives (6, 9–11) have established the main structural features. In particular, the vicinal carboxylates derived from the tartaro units strongly favour an *anti* conformation. All our structural investigations reveal the same.

The purpose of this study is to reveal the structural details of alkali-metal complexation in water by two polycarboxylate crown ethers, an 18-crown-6 tetraacid ($18C6A_4$) (4) and an 18-crown-6 hexaacid ($18C6A_6$) (3).

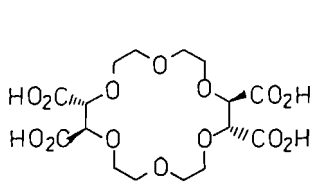

$18C6A_4$

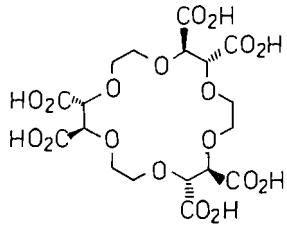

$18C6A_6$

We initially compare the coordination geometries of all the complexes about the cation, especially the relationship of cavity sizes to effective ionic radii of the bound cations. Both ligands are multi-armed lariat ethers, and we follow an earlier analysis of the solid-state structures of neutral lariat ether complexes (12). For each complex, we calculate the mean cavity radius by the procedure of Mathieu *et al.*, which averages the differences between the metal–donor distance and the covalent radius of the donor atom for all donors in the ligand (13). We calculate the guest-ion radius, which includes all donors to the cation, in the same manner as effective ionic radii (14, 15). We then compare both the mean cavity radius and the guest-ion radius with the effective radii of the cations for various coordination numbers. The most striking result is that the $18C6A_6$ complexes contain a water molecule and the guest cation. These hosts complex monohydrated cations rather than dehydrated cations.

We next analyze macrocyclic conformations, a fascination since the earliest reports of macrocycle crystal structures (1, 2). How does macrocyclic conformation influence the complexation of an ion? We describe the detailed reorganizations that the different guest ions provoke in the host and the ways in which those reorganizations may be discerned. We use skeletal drawings, which include only the donor atoms of the ligands (12), to reveal the topographies of the donor atoms about the guest cations. We next present the 18 torsion angles of a macrocycle on a polar-coordinate map (16, 17)[3] to reveal how the host forms the cavity. We have recently used these maps to compare solid-state conformations of many 18-crown-6 metal cation complexes (18). We offer this method as an alternative to the torsion-angle-sequence methods of Stoddart (19) and Dale (20). The polar-coordinate maps permit ready visual comparisons among the maps and reveal how bond rotations may interconvert two conformations. Skeletal drawings and polar-coordinate maps provide complementary perspectives on the cooperative interplay of host and guest.

[3]Also, W. D. Celmer, International Symposium on Medicinal Chemistry, 1986, Berlin; personal communication.

Results

All the salt complexes were formed by simple metathesis reactions of the corresponding metal halide or nitrate and readily crystallized from aqueous solution. Formally, the crystallization generated an equivalent of mineral acid in a strongly acidic solution (3). Large, colourless crystals grew over a period of hours from equimolar mixtures of the ligand ($18C6A_4$ or $18C6A_6$) and cations (Na^+, K^+, Tl^+, Cs^+). The exception was the K^+ complex of $18C6A_4$, which resisted all attempts at crystallization. The corresponding salt complexes of alkaline earth cations failed to crystallize in a form suitable for X-ray analysis; fibrous precipitates immediately formed from mixtures of ligand and salts of the cations (Ca^{2+}, Sr^{2+}, Ba^{2+}). The fibres analyzed as 1:1 complexes.

The structures of seven complexes were determined. For each complex, crystallographic parameters (Tables 1 and 2) and key structural features of the coordination environment of the cation are given (Tables 3 and 4). The structures are illustrated in three ways (Figs. 1–7): a structure with all atoms, a skeletal drawing of all donors to the cation, and a polar-coordinate map of the macrocyclic torsion angles (18). Endocyclic torsion angles are determined with the convention that a positive torsion angle exhibits a clockwise rotation between the front and the rear three atom planes. The macrocycle *bonds* are numbered sequentially: the starting point and direction can be chosen randomly. The torsion angle of each bond is then plotted by bond number on a polar-coordinate system. For 18-crown-6, each bond accounts for 20° (one eighteenth of 360°), and the resultant map is an octadecagon. The torsion angles are plotted from the centre at 0° to the outer edge (360°); negative torsion angles are plotted as 360° plus the negative torsion angles. This plotting convention differs from Ounsworth and Wieler (16), but is useful for crown ethers. It diminishes the small differences about *anti* torsion angles (+175° vs. −175°) and accentuates the equally small differences between *eclipsed* torsion angles (+5° vs. −5°).

Complexes of $18C6A_6^-$

$18C6A_6^- \cdot Na^+$

The Na^+ complex crystallizes from an aqueous 1:1 mixture of the $18C6A_6$ and sodium chloride as the trihydrate (Table 1 and Fig. 1). A water molecule, an oxygen from the carboxylate, and the six macrocyclic oxygens coordinate the Na^+. The macrocyclic oxygens adopt a planar conformation (maximum deviation 0.095(1) Å) with the Na^+ 0.523(1) Å out of this plane, drawn toward the carboxylate. The coordinating water molecule lies above the opposite face of the plane, and hydrogen bonds to three carboxyls of the ligand. The hydrogen bond donor of the ligand utilizes an *anti*

Can. J. Chem. Downloaded from www.nrcresearchpress.com by 88.255.202.194 on 09/08/12
For personal use only.

TABLE 1. Crystal data and data collection parameters for complexes of $18C6A_6$[a]

Parameter	Compound			
	$18C6A_6Na \cdot 3H_2O$	$18C6A_6K \cdot 3H_2O$	$18C6A_6Tl \cdot 2H_2O$	$18C6A_6Cs \cdot 2H_2O$
Formula	$NaC_{18}H_{29}O_{21}$	$KC_{18}H_{29}O_{21}$	$TlC_{18}H_{27}O_{20}$	$CsC_{18}H_{27}O_{20}$
FW	604.4	620.5	767.8	696.3
Crystal system	Orthorhombic	Orthorhombic	Orthorhombic	Monoclinic
Space group	$P2_12_12_1$	$P2_12_12_1$	$P2_12_12_1$	$P2_1$
a, Å	7.6868(12)	7.6711(8)	12.0331(10)	7.708(3)
b, Å	15.429(3)	15.709(2)	12.4333(12)	13.492(2)
c, Å	21.975(2)	21.966(5)	17.366(2)	11.9501(9)
β, deg				94.49(2)
V, Å^3	2606.3(12)	2647.0	2598.1(8)	1240.2(8)
Z	4	4	4	2
d(calc), g cm^{-3}	1.540	1.557	1.963	1.865
T, deg K	295	297	297	297
Abs. coeff., cm^{-1}	13.6	2.9	63.7	15.7
θ lim. for unit cell, deg	25–30	11–13	12–14	10–12
Crystal size, mm	0.38 × 0.48 × 0.58	0.20 × 0.24 × 0.55	0.20 × 0.25 × 0.35	0.12 × 0.15 × 0.28
Radiation	Cu K_α	Mo K_α	Mo K_α	Mo K_α
Min. transmission, %	96.3	91.3	86.4	86.2
Max. transmission, %	100.0	100.0	99.8	99.8
Avg. transmission, %	98.8	96.7	93.3	95.5
Scan rate, deg min^{-1}	1.0–3.3	0.5–4.0	0.5–4.0	0.5–4.0
θ limits, deg.	2–75	1–27.5	1–35	1–30
Min. decay correction			0.9751	1.0000
Max. decay correction			1.000	1.0261
Avg. decay correction			0.9882	1.0124
Unique data	5371	3429	8236	5651
Observed data	5192	2521	4952	4480
Variables	478	402	353	352
F(000), electrons	1264	1296	1504	700
R_{int}	0.009		0.012	0.014
R, obs. data (enantiomer)	0.0307 (0.0312)	0.0352 (0.0353)	0.035 (0.066)	0.029 (0.042)
R, all data	0.038	0.072	0.103	0.060
R_w (enantiomer)	0.0434 (0.0440)	0.0371 (0.0372)	0.035 (0.081)	0.030 (0.048)
GOF (enantiomer)	2.522 (2.561)	1.822 (1.825)	1.675 (3.895)	1.372 (2.168)
Max. residual, e Å^{-3}	0.63	0.32	2.56	0.54
Min. residual, e Å^{-3}	−0.53	−0.26	−2.20	−0.54
Max. shift/σ	0.15	0.17	0.01	0.18
Secondary extinction coeff., g	3.6(1) × 10^{-6}	1.9(4) × 10^{-7}	1.25(5) × 10^{-7}	1.2(3) × 10^{-7}

[a]Definitions are: $R = \Sigma \| |F_o| - |F_c| \| / \Sigma |F_o|$; $R_w = (\Sigma w(|F_o| - |F_c|)^2 / \Sigma w F_o^2)^{1/2}$; GOF = $[\Sigma w(|F_o| - |F_c|)^2 / (N_{obs} - N_{param})]^{1/2}$.

conformation of the carboxylic acid group to form a strong hydrogen bond (2.599(2) Å) with the coordinated water molecule; the other hydrogen bonds to it are longer (2.817(2) and 3.006(2) Å).

$18C6A_6^- \cdot K^+$

The K^+ complex crystallizes from an equimolar mixture of the $18C6A_6$ and potassium chloride in water as the trihydrate (Table 1 and Fig. 2). A water molecule, an oxygen from the carboxylate side arm, an oxygen from a carboxyl side arm, and the six macrocyclic oxygens coordinate the K^+. One of the potential donors, O26, remains uncoordinated to the K^+ at a distance of 3.687(3) Å from the cation. The macrocyclic oxygens adopt a nearly planar conformation (maximum deviation 0.134(2) Å) with the K^+ 0.985(1) Å above this plane on the side of the carboxylate oxygen. On the opposite face, the water molecule is hydrogen bonded to the three carboxyl groups. The hydrogen bond donor of the ligand utilizes an *anti* conformation of the carboxylic acid group to form a strong hydrogen bond (2.592(3) Å) with the coordinated water molecule; the other two hydrogen bonds to it are longer (2.917(4) and 2.994(4) Å).

$18C6A_6^- \cdot Tl^+$

The Tl^+ complex crystallizes from a 1:1 mixture of the $18C6A_6$ and thallium(I) nitrate as the dihydrate (Table 1 and Fig. 3). A water molecule, a carboxylate oxygen, an oxygen from each of two carboxyls, and all six macrocyclic oxygens coordinate the Tl^+. The macrocyclic oxygens adopt a planar conformation (maximum deviation 0.095(5) Å) with the Tl^+ displaced 1.219(1) Å from this plane towards the carboxylate. The water lies below the plane on the opposite face and hydrogen bonds with two carboxyls, O23 (2.667(6) Å) and O35 (2.759(6) Å), and possibly with the third carboxyl O30 (3.096(7) Å). The hydrogen on O23 is in the *anti* conformation.

$18C6A_6^- \cdot Cs^+$

The Cs^+ complex crystallizes from an aqueous solution of the $18C6A_6$ and cesium chloride as the dihydrate (Table 1 and Fig. 4). A water molecule, an oxygen from three intramo-

Can. J. Chem. Downloaded from www.nrcresearchpress.com by 88.255.202.194 on 09/08/12
For personal use only.

Can. J. Chem. Downloaded from www.nrcresearchpress.com by 88.255.202.194 on 09/08/12
For personal use only.

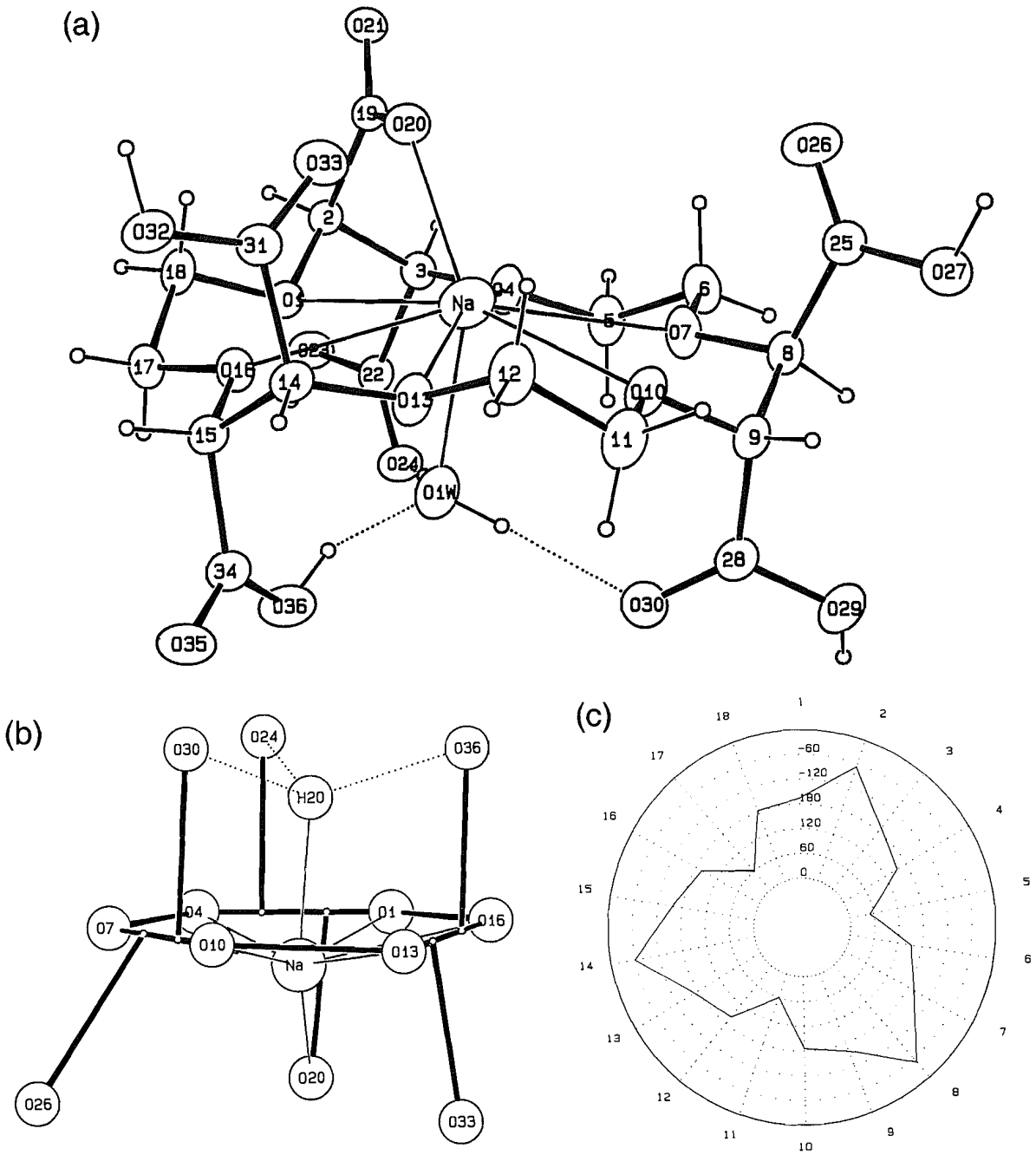

FIG. 1. $18C6A_6^- \cdot Na^+$ complex. (*a*) Structure of the complex showing atom numbering, (*b*) skeletal drawing showing donors to the cation, and (*c*) polar coordinate map of macrocyclic torsion angles.

lecular and two intermolecular carboxyl groups, and the six macrocyclic ether oxygens coordinate the Cs^+. The protonation of the carboxyl groups may be disordered, hence the carboxylate cannot be identified unambiguously. The macrocyclic oxygens adopt a flattened twist-boat conformation with the Cs^+ ion 1.6896(2) Å from their best plane. The Cs^+ and the coordinating water molecule lie on opposite sides of the macrocycle. The water is hydrogen bonded to three carboxyls in a site similar to that in the Na^+, K^+, and Tl^+ complexes. The hydrogen on O23 was not located but is presumed to be in the *anti* conformation as in the other complexes. Like the other complexes, it forms a strong hydrogen bond to the water (2.486(4) Å); the other located hydrogen bonds are longer (2.713(4) and 2.805(4) Å).

Complexes of $18C6A_4^-$

$18C6A_4^+ \cdot Na^+$

The Na^+ complex crystallizes from a mixture of the $18C6A_4$ and 1 equivalent of sodium chloride in water as the dihydrate (Table 2 and Fig. 5). Carbonyl oxygens from two side arms, water, and four ether oxygens ligate the Na^+. The remaining ether oxygens, O4 and O7, reside at 3.074(2) and 3.351(2) Å respectively from the Na^+. The carboxylate group does not participate in the coordination of the cation, but forms two very strong intermolecular hydrogen bonds, 2.490(3) and 2.568(3) Å, with carboxyl groups. The macrocyclic oxygens adopt a flattened twist-boat conformation. The Na^+ lies on one side of the macrocycle, 0.4371(4) Å from the best plane, and the water resides on the opposite side

Can. J. Chem. Downloaded from www.nrcresearchpress.com by 88.255.202.194 on 09/08/12
For personal use only.

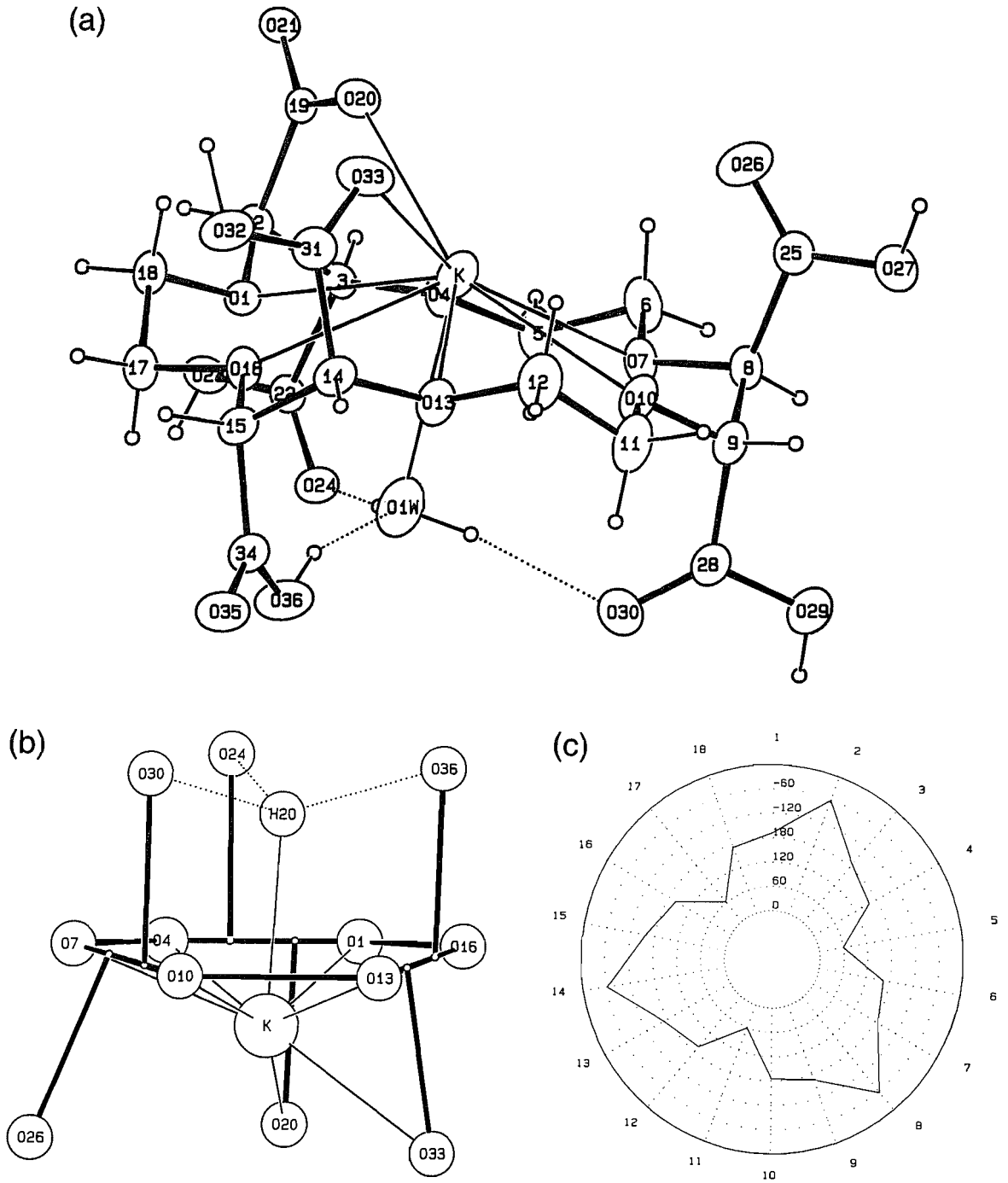

FIG. 2. $18C6A_6^- \cdot K^+$ complex. (*a*) Structure of the complex showing atom numbering, (*b*) skeletal drawing showing donors to the cation, and (*c*) polar coordinate map of macrocyclic torsion angles.

of the macrocycle. The coordinated water molecule has long intramolecular contacts to ether oxygens O7 (2.915(3) Å) and O10 (3.090(3)Å) of the ligand, but forms intermolecular hydrogen bonds to a carboxyl group and to the second water molecule.

$18C6A_4^- \cdot Tl^+$

The Tl^+ complex crystallizes from a mixture of the $18C6A_4$ and thallium nitrate in water, as a hydrate (Table 2 and Fig. 6). The uncertainty in the hydration state results from disorder of the water of crystallization ($x \approx 2$). The Tl^+ is also disordered between two sites with a population ratio of approximately 95:5, separated by 2.36(1) Å. In either site, all six macrocyclic oxygens and an oxygen from each of two side-arm carboxyls coordinate the Tl^+. A coordinated water molecule may lie near the minor Tl′ site. The macrocyclic oxygens adopt a flattened half-chair conformation. The Tl^+ lies 0.9603(1) Å above the best plane of these oxygens.

$18C6A_4^- \cdot Cs^+$

The Cs^+ complex crystallizes from a 1:1 mixture of the $18C6A_4$ and cesium chloride in water as the dihydrate (Table 2 and Fig. 7). All six macrocyclic oxygens, and an oxygen from each of three carboxyls, two intramolecular and one

Can. J. Chem. Downloaded from www.nrcresearchpress.com by 88.255.202.194 on 09/08/12
For personal use only.

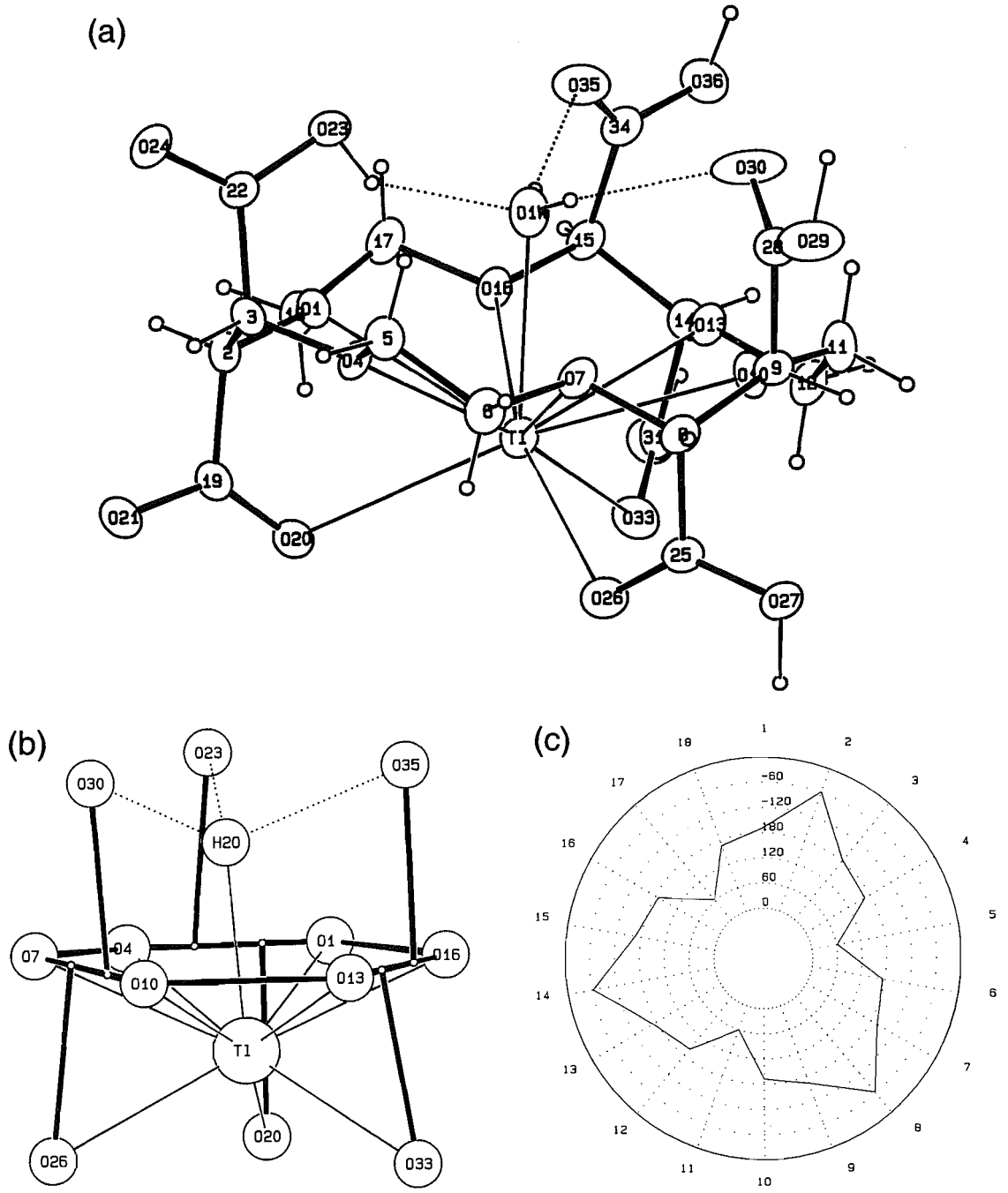

FIG. 3. $18C6A_6^- \cdot Tl^+$ complex. (*a*) Structure of the complex showing atom numbering, (*b*) skeletal drawing showing donors to the cation, and (*c*) polar coordinate map of macrocyclic torsion angles.

intermolecular, coordinate the Cs^+. The carboxylic protons were not located, so the carboxylate is not identified. The macrocyclic oxygens adopt a planar conformation with maximum deviation 0.097(4) Å. The Cs^+ lies 1.4463(1) Å above this plane, and a water molecule lies on the other side. This water molecule does not ligate the cation, but hydrogen bonds to O23 and the other water molecule in the structure.

Discussion

Comparison of 18C6A$_6$ complexes

The threefold symmetry of the arrangement of carboxylic acids, which are attached to the two faces of the macrocycle, is optimal for binding monohydrated cations. All $18C6A_6$ complexes contain a water molecule bound to the metal ion. The water forms three hydrogen bonds to three carboxyl groups on one face of the macrocycle. The water forms two OH...O=C hydrogen bonds, both in the preferred *anti* direction of the carbonyl oxygen (21). The water accepts a hydrogen bond from the third carboxylic acid, which is in the more acidic, but less stable, *anti* conformation about C(O)—OH (22). In the Cs^+ complex, the third carboxyl also donates electron density to a Cs^+ in a neighbouring complex. In addition to the water donor, and the six ether oxygens, the metal ions bind to a carboxylate on the opposite face of the macrocycle. The geometry of the ligand enforces the

Can. J. Chem. Downloaded from www.nrcresearchpress.com by 88.255.202.194 on 09/08/12
For personal use only.

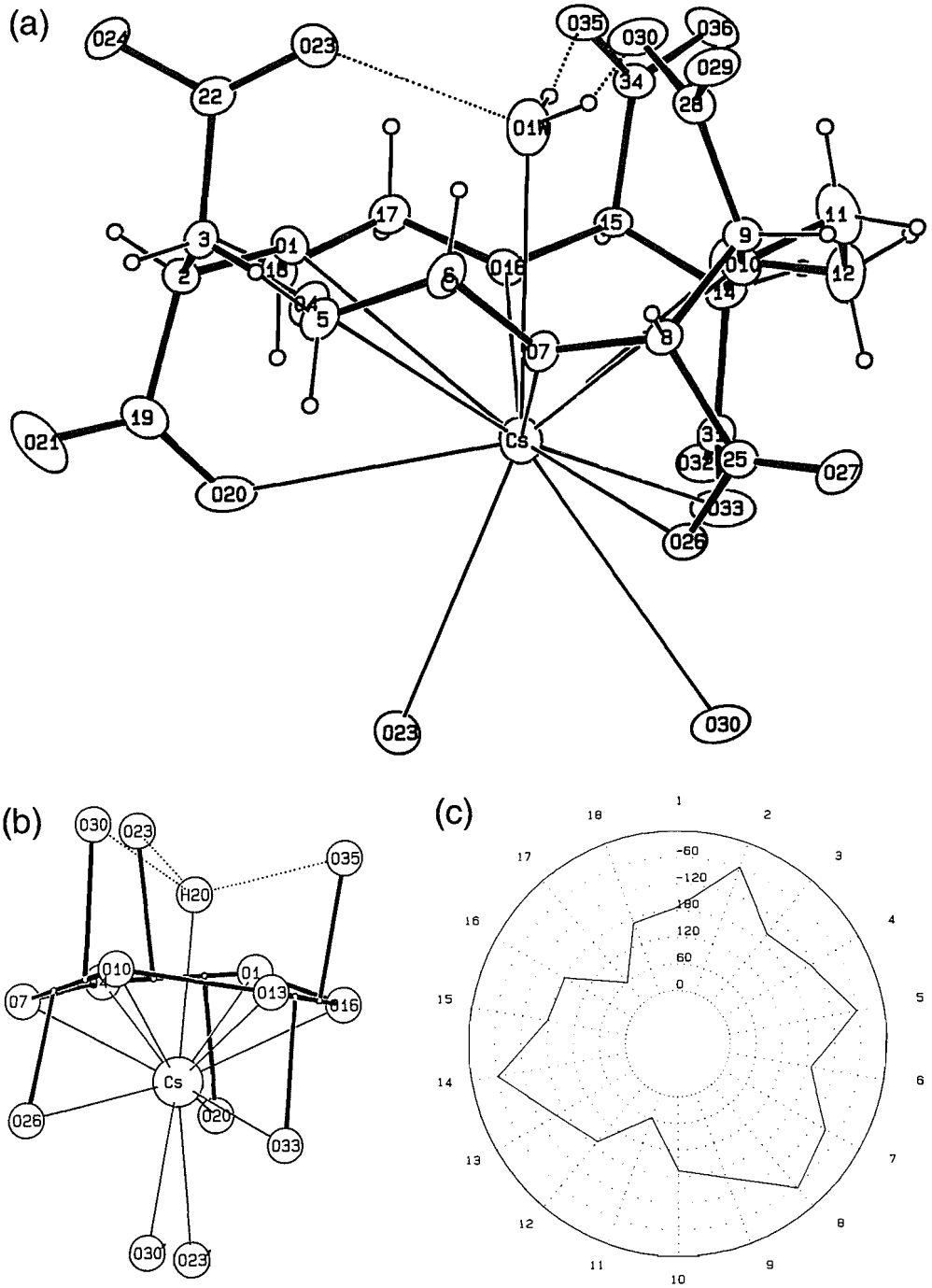

FIG. 4. $18C6A_6^- \cdot Cs^+$ complex. (*a*) Structure of the complex showing atom numbering, (*b*) skeletal drawing showing donors to the cation, and (*c*) polar coordinate map of macrocyclic torsion angles.

less preferred *anti* attachment to the carboxylate for Na^+, K^+, and Tl^+ (23). Cs^+ slightly prefers *direct* and *syn* to *anti* attachment to carboxylate (23). As the size of the cation increases, the remaining two carboxyls donate electron density to the cation. No carboxyls donate to Na^+; one, to K^+; and two, to Tl^+ and Cs^+. Water on one face of the macrocycle and the carboxylate and carboxyls on the other face encapsulate the cations. These complexes resemble bibracchial lariat ether and cryptand complexes (12).

Table 3 summarizes the coordination about each cation. In all cases, the mean cavity radius is the same or slightly larger than the guest ionic radius. This is a minor artifact of calculation because the oxygen radius is a constant (1.4 Å) when calculating the mean cavity radius (13) but increases with increasing coordination number when calculating the guest ionic radius (24). As the ionic size increases, the cation moves away from the mean plane of the macrocyclic oxygens towards the carboxylate. The carboxylate O—M—OH_2 angle also decreases: Na^+(130.0(1)°) > K^+(119.9(1)°) > Tl^+(116.5(1)°) > Cs^+(102.4(1)°). The smaller bite angles involve a nine-atom cycle ($H_2O\cdots$ M$\cdots$O=C-CH-CH-C-O-H$\cdots$), while the larger bite angles involve a 13-atom cycle ($H_2O\cdots M\cdots$O=C-CH-O-CH_2-CH_2-O-CH-C-O-H$\cdots$). In the Na^+ and K^+ complexes, the water

TABLE 2. Crystal data and data collection parameters for complexes of $18C6A_4$[a]

Parameter	Compound		
	$18C6A_4Na \cdot 2H_2O$	$18C6A_4Cs \cdot 2H_2O$	$18C6A_4Tl \cdot 2H_2O$
Formula	$NaC_{16}H_{27}O_{16}$	$CsC_{16}H_{27}O_{16}$	$TlC_{16}H_{27}O_{16}$
FW	498.4	608.3	679.8
Crystal system	Monoclinic	Monoclinic	Monoclinic
Space group	$P2_1$	$P2_1$	$P2_1$
a, Å	11.4368(11)	11.787(2)	11.719(2)
b, Å	7.7068(11)	7.637(2)	7.668(2)
c, Å	12.6579(12)	13.001(2)	12.8403(13)
β, deg.	98.515(8)	98.705(12)	99.052(9)
V, Å^3	1103.4(4)	1156.8(7)	1139.4(6)
Z	2	2	2
d(calc), g cm^{-3}	1.500	1.746	1.981
T, deg K	298	299	298
θ lim. for unit cell, deg	25–30	11–13	12–13
Abs. coeff., cm^{-1}	13.1	16.6	12.3
Crystal size, mm	0.08 × 0.13 × 0.50	0.06 × 0.23 × 0.50	0.23 × 0.25 × 0.30
Radiation	Cu K_α	Mo K_α	Mo K_α
Min. transmission, %	84.0	78.0	69.4
Max. transmission, %	98.9	100.0	99.9
Avg. transmission, %	91.5	92.9	84.2
Scan rate, deg min^{-1}	1.1–3.3	0.5–4.0	0.4–4.0
θ limits, deg	2–75	1–30	1–33
Min. decay correction	0.9642		0.9589
Max. decay correction	1.0728		1.3289
Avg. decay correction	1.0150		1.1226
Unique data	3322	4534	5977
Observed data	3000	3428	3981
Variables	326	297	296
F(000), electrons	524	612	664
R_{int}	0.016	0.020	0.013
R, obs. data (enantiomer)	0.0348 (0.0352)	0.038 (0.039)	0.040 (0.069)
R, all data	0.040	0.066	0.096
R_w (enantiomer)	0.0416 (0.0422)	0.039 (0.041)	0.044 (0.078)
GOF (enantiomer)	1.803 (1.827)	1.748 (1.856)	1.928 (3.419)
Max. residual, e Å^{-3}	0.38	1.68	2.3
Min. residual, e Å^{-3}	−0.30	−0.66	−1.5
Max. shift	0.01	0.06	0.30
Secondary extinction coeff., g	3.2(2) × 10^{-6}		

[a]Definitions are: $R = \Sigma \|\|F_o\| - |F_c\|\|/\Sigma |F_o|$; $R_w = (\Sigma w(|F_o| - |F_c|)^2/\Sigma w F_o^2)^{1/2}$; GOF = $[\Sigma w(|F_o| - |F_c|)^2/(N_{obs} - N_{param})]^{1/2}$.

molecule is held further from the mean plane of the macrocyclic oxygens than in the Cs^+ and Tl^+ complexes. The size of the ion dictates the additional number of intramolecular carboxyl donors: zero (Na^+), one (K^+), or two (Tl^+ and Cs^+). Two intermolecular carboxyls bind to the cation in the Cs^+ complex, which has the only nonplanar skeletal arrangement of macrocyclic oxygens (Fig. 4*b*).

Comparison of 18C6A$_4$ complexes

The $18C6A_4$ complexes show greater structural diversity than the $18C6A_6$ complexes (Table 4). Two oxygens from two carboxyls (or one carboxyl and the carboxylate) attached to the same face of the $18C6A_4$ macrocycle bind to the cation. In the Tl^+ and Cs^+ complexes, the carboxylate is unidentified, but in the Na^+ complex, carboxylate does not contact the cation, but forms two strong intermolecular hydrogen bonds to two carboxyls. Both carboxylic oxygens donate electron density from the *anti* direction. Like other lariat ether complexes, the size of the metal ion affects the skeletal arrangement of the macrocyclic oxygens. The Na^+ complex has a twist-boat arrangement (Fig. 5*b*) that is seen in many Na^+ complexes of 18-crown-6 (18). This arrangement places two macrocyclic oxygens outside bonding distance to the Na^+. The skeletal arrangement of the Tl^+ complex is half chair (Fig. 6*b*), and the Cs^+ complex is planar (Fig. 7*b*).

Comparisons of 18C6A$_6$ and 18C6A$_4$ complexes

The similarity in structure of the $18C6A_6$ complexes contrasts the diversity of the $18C6A_4$ complexes. In both series the *R,R*-tartaro units favour an *anti* conformation for the carboxyls. This conformational bias produces a "stiff" torsion angle in the macrocycle, which resists reorganization to accommodate a guest. The $18C6A_4$ ligand (two tartaro units) is more flexible than $18C6A_6$ (three tartaro units). This flexibility in $18C6A_4$ conforms with the variability of the skeletal arrangements of macrocyclic oxygens in the $18C6A_4$ complexes. The $18C6A_4$ complexes resemble lariat ether complexes, but the $18C6A_6$ complexes resemble cryptates (12). The transannular distances among the macrocyclic oxygens suggest that the $18C6A_4$ macrocycle provides an oval

Can. J. Chem. Downloaded from www.nrcresearchpress.com by 88.255.202.194 on 09/08/12
For personal use only.

Can. J. Chem. Downloaded from www.nrcresearchpress.com by 88.255.202.194 on 09/08/12
For personal use only.

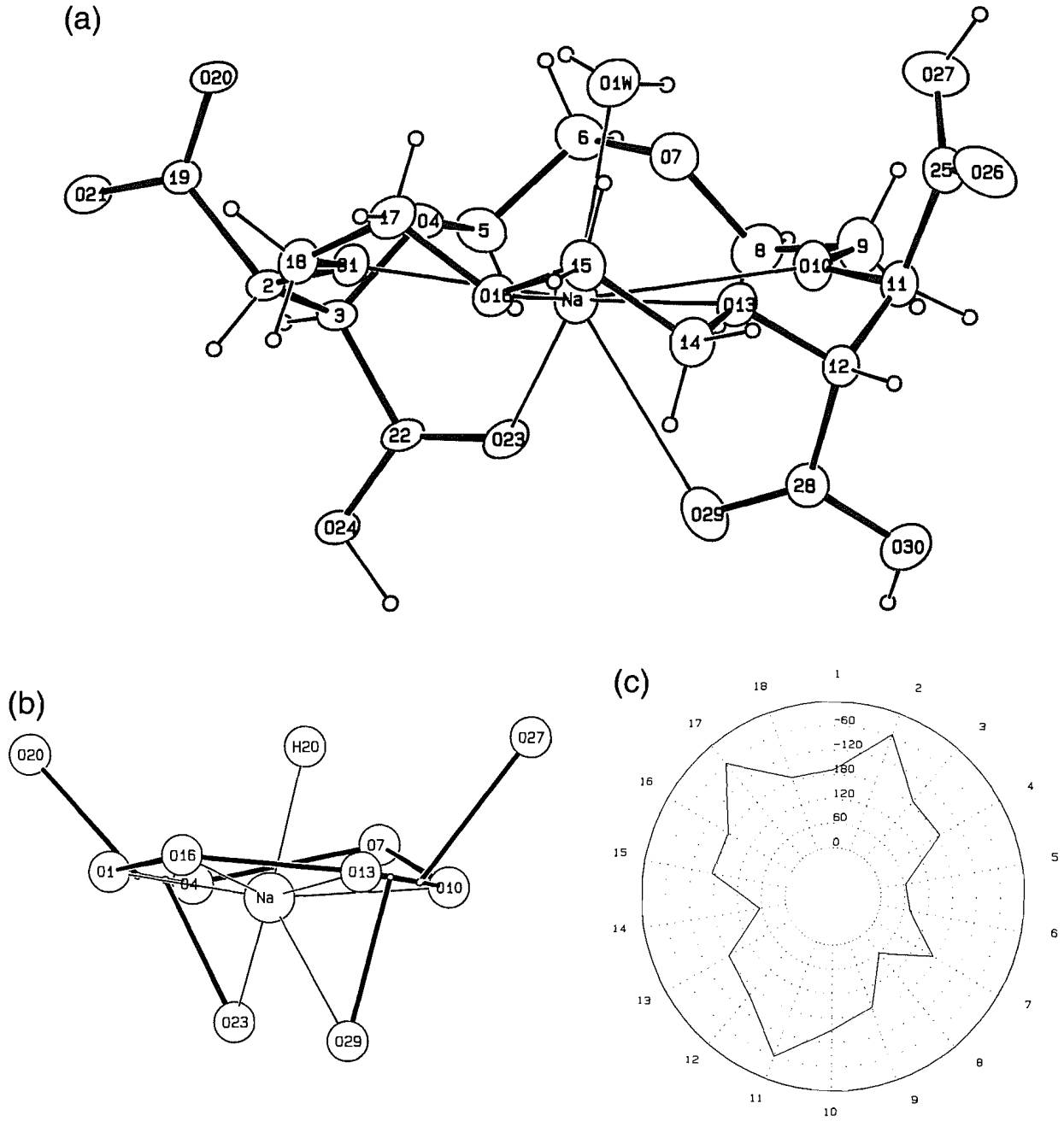

FIG. 5. $18C6A_4^- \cdot Na^+$ complex. (*a*) Structure of the complex showing atom numbering, (*b*) skeletal drawing showing donors to the cation, and (*c*) polar coordinate map of macrocyclic torsion angles.

array of six donor atoms, while the $18C6A_6$ cavity is nearly circular.

Na^+ complexes

A comparison of the Na^+ complexes of $18C6A_4$ and $18C6A_6$ shows that hydrogen bonding to the monohydrating water centres the metal ion in the cavity in the latter. In $18C6A_6$, the M^+—O distances for the macrocyclic oxygens vary only 0.23 Å, but in $18C6A_4$ they vary 0.83 Å. The large spread in the latter results in an ambiguous coordination number of the metal. The carboxylate–metal distance is shorter in $18C6A_4$, but the water–metal distance is shorter in $18C6A_6$. Monohydrated Na^+ is the guest in $18C6A_6$, whereas dehydrated Na^+ is the guest in $18C6A_4$. The guest ionic radius in $18C6A_4$ as either a hepta- or a nona-coordinated complex agrees well with the effective ionic radii. The guest ionic radius in the $18C6A_6$ is larger than the effective ionic radius for octacoordinated Na^+. Mean cavity radii are larger than the guest ionic radii because the solvating water in each complex has a shorter M^+—O distance than all other contacts in the ligand, except for carboxylate.

Tl^+ complexes

A comparison of the Tl^+ complexes shows many similarities in Tl^+—O contacts with the ligand, even though $18C6A_6$ binds a monohydrated Tl^+ and $18C6A_4$ binds only the metal ion (major site; the minor site Tl′ may be hydrated). The mean cavity radii are identical in spite of the additional carboxyl donor in $18C6A_6$. The guest ionic radius of $18C6A_6$ is smaller than that of $18C6A_4$ because the M^+—O distance

Can. J. Chem. Downloaded from www.nrcresearchpress.com by 88.255.202.194 on 09/08/12
For personal use only.

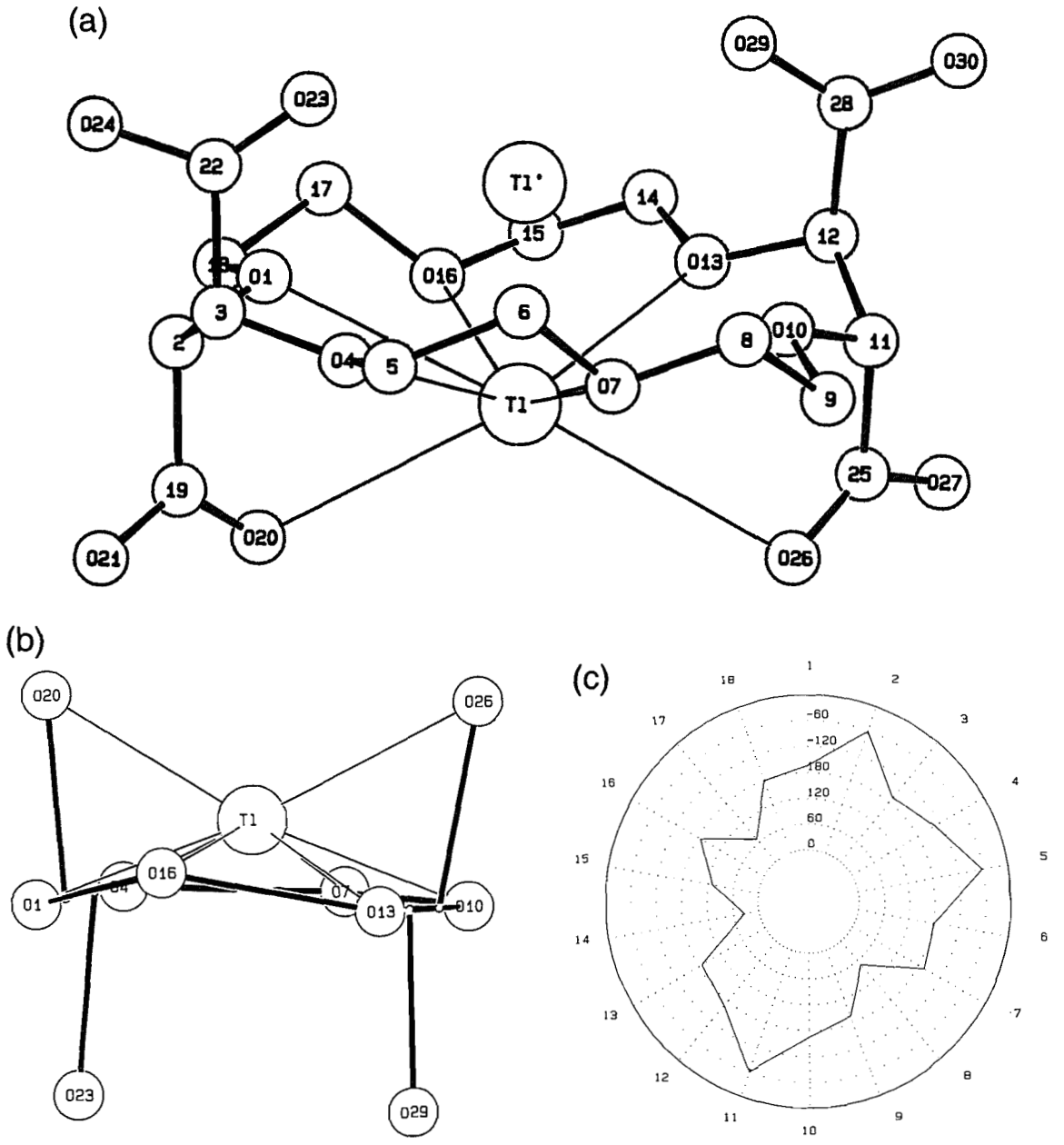

FIG. 6. $18C6A_4^- \cdot Tl^+$ complex. (*a*) Structure of the complex showing atom numbering, (*b*) skeletal drawing showing donors to the cation, and (*c*) polar coordinate map of macrocyclic torsion angles.

for the hydrating water is the shortest contact in the former complex. The close agreement between guest ionic radius in $18C6A_4$ and effective ionic radii for octacoordinated Tl^+ contrasts a similar comparison in $18C6A_6$ with decacoordinated Tl^+.

Cs^+ complexes

The Cs^+ complexes are similar if the two long intercomplex carboxyl contacts in $18C6A_6$ are excluded. Both complexes show close agreement between guest ionic radius and effective ionic radius. The water in the $18C6A_6$ complex has a longer M^+—O distance than any macrocyclic oxygen or intracomplex carboxyl donor. The $18C6A_6$ appears more to act as a host with two loosely coupled guests rather than the tightly coupled guests of the Na^+, K^+, and Tl^+ complexes with this ligand.

Polar maps and skeletal drawings

Clarifying the relationship between macrocyclic conformation and cation binding provides a key to the design of complexing agents with preselected properties. Skeletal drawings focus attention on the topography of the donors of the ligand, revealing the familiar conformations of smaller carbocyclic rings (boat, chair, twist-boat, etc.). The skeletal drawings (Figs. 1*b*–4*b*) reveal a nearly planar array of macrocyclic oxygens in all four $18C6A_6$ complexes. Skeletal drawings of more flexible crown ethers show nonplanar arrangements (12). The conformational restraint of the tartaro units and the three-point binding of the hydrating water partly enforce near planarity of the six macrocyclic oxygens. The rationale for the use of skeletal drawings is that flexible bonds connecting the donors can adjust to give the best arrangement of donors to the cation. If the connecting

Can. J. Chem. Downloaded from www.nrcresearchpress.com by 88.255.202.194 on 09/08/12
For personal use only.

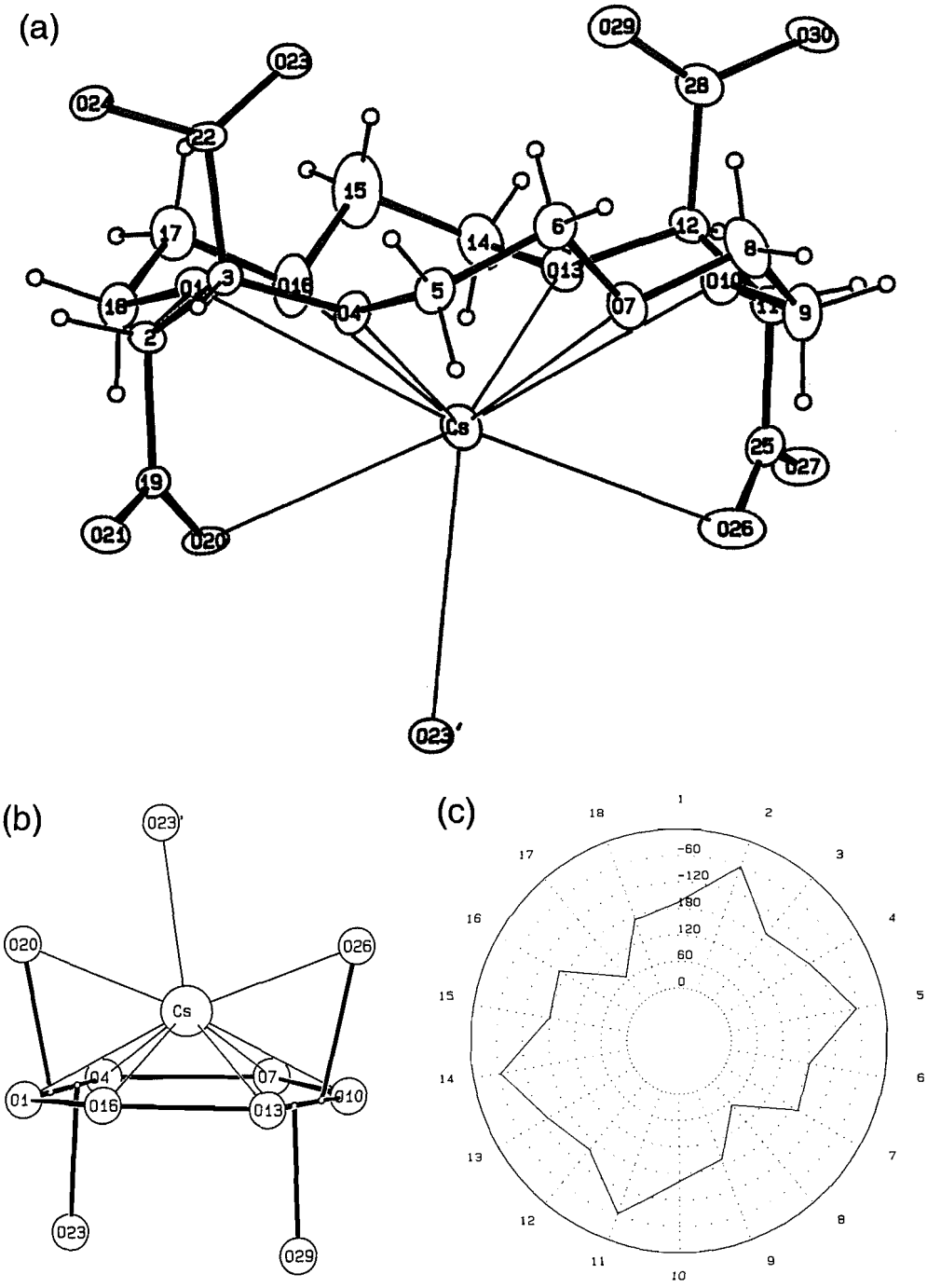

FIG. 7. $18C6A_4^- \cdot Cs^+$ complex. (*a*) Structure of the complex showing atom numbering, (*b*) skeletal drawing showing donors to the cation, and (*c*) polar coordinate map of macrocyclic torsion angles.

bonds are not completely flexible, then there must be a balance between the conformational preference of the host and the optimal donor topography for the guest.

Polar-coordinate maps of macrocyclic torsion angles clearly illustrate the conformations of the macrocycle. For example, compare Figs. 1*c*, 2*c*, and 3*c*. An overlay of the three, Fig. 8, emphasizes the similarity. Now, compare Figs. 1*b*, 2*b*, and 3*b*. All of these skeletal drawings reveal the planar arrangement of the macrocyclic donors. The remaining structure in the series, Fig. 4, has a different skeletal drawing (twist boat) and polar map from the other three $18C6A_6$ complexes. By contrast, the $18C6A_4$ complexes have different polar maps (Figs. 5*c*–7*c*) and skeletal drawings (Figs. 5*b*–7*b*). Polar maps also reflect the difference in symmetry between $18C6A_4$ (twofold) and $18C6A_6$ (threefold) complexes.

Polar-coordinate maps show differences in complexes with similar skeletal drawings. The Na^+ complex of $18C6A_4$ and the Cs^+ complex of $18C6A_6$ have the same skeletal drawing (twist boat). An overlay of the two polar maps, Fig. 9, reveals the similarity. Fifteen of the 18 torsion angles match. One ethylenedioxy unit differs: O4—C5—C6—O7 in $18C6A_4 \cdot Na^+$ and O7—C8—C9—O10 in $18C6A_6 \cdot Cs^+$. In the former, the O—C—C—O torsion angle is *gauche*$^+$

TABLE 3. Coordination environment of the complexes of $18C6A_6^-$

Guest cation	Na^+	K^+	Tl^+	Cs^{+a}	Cs^{+a}
Coordination number	8	9	10	10	12
Ligand donors	7	8	9	9	9
M^+—O distances (Å):					
Carboxylate O	2.367(1)	2.674(2)	2.938(4)	[b]	
H_2O	2.404(1)	2.941(3)	2.794(4)	3.344(3)	
Ether O (short)	2.625(1)	2.761(2)	2.921(4)	3.103(2)	
Ether O (long)	2.854(1)	2.986(2)	3.095(3)	3.363(3)	
Carbonyl O	—	3.085(3)	3.025(5)	3.074(3)	
			3.178(4)	3.239(3)	
				3.266(3)	
					3.469(3)
					3.693(3)
Mean cavity radius (Å)	1.28	1.48	1.61	1.80	1.82
Guest ionic radius (Å)	1.23	1.46	1.55	1.79	1.82
Effective ionic radius (Å)	1.18	1.55	1.81	1.81	1.88
Oxygen skeleton	Planar	Planar	Planar	Twist boat	
Maximum deviation, ether O, from their best plane (Å):	0.095(1)	0.134(2)	0.095(5)	0.331(3)	
Distance to mean plane (Å):					
H_2O	1.847(2)	1.933(3)	1.562(4)	1.643(3)	
Cation	0.523(1)	0.985(1)	1.219(1)	1.6896(2)	
Transannular distances (Å):					
O1—O10	5.381(2)	5.442(3)	5.488(5)	5.350(4)	
O4—O13	5.288(2)	5.429(3)	5.460(5)	5.400(4)	
O7—O16	5.437(2)	5.380(3)	5.448(5)	5.691(4)	
Tartarate torsion angles (°):					
C2—C3	174.8(1)	−176.5(2)	−170.2(4)	−169.6(3)	
C8—C9	−159.3(2)	−166.2(3)	180.0(6)	−167.5(3)	
C14—C15	−175.1(1)	−176.6(3)	179.7(5)	−176.9(3)	

[a]Two coordination spheres considered: deca-coordinate Cs^+ considering only intracomplex donors and dodeca-coordinate Cs^+ include two additional intermolecular donors.
[b]Carboxylate not identified.

(64.3(3)°) while in the latter it is *gauche*$^-$ (−54.0(3)°). The O7—C8—C9—O10 unit in the Cs^+ complex *cannot* be *gauche*$^+$ as this would place the two tartaro carboxyl carbons in a *gauche* conformation. A similar overlay (not shown) exists between the Cs^+ complex of $18C6A_4$ and the Na^+, K^+, and Tl^+ complexes of $18C6A_6$. All four complexes have planar skeletal drawings.

Polar maps also reveal the rotations required to interconvert conformations. For example, an overlay (Fig. 10) of the polar maps of the Tl^+ and Cs^+ complexes of $18C6A_6$ illustrates that the torsion angles about O4—C5—C6—O7 differ in the two complexes. A "crankshaft" rotation, where C3—O4—C5—C6 goes from about 60° to about −60° and C5—C6—O7—C8 goes from about 60° to about 180°, interconverts the two conformations. The end-to-end distance (C3–C8) is the same in the two complexes, but the motion has altered the positions of the carboxyl side arms. The C3—C22 and C9—C28 bonds, which are nearly parallel in the Tl^+ complex, swivel to close the C22 to C28 gap from 6.480(9) to 5.416(6) Å in the Cs^+ complex. The donor at O7 also moves from a position as the longest of the six macrocyclic oxygen–Tl contacts to the shortest of the six macrocyclic oxygen–Cs contacts.

Ligand preorganization

In the absence of metal ions, both ligands crystallize as hydrates (25). The dihydrate of $18C6A_4$ contains water molecules hydrogen bonded to opposite faces of a nearly planar macrocycle, bridging between the carboxylic acid groups. Overlays of the polar-coordinate maps (18) of the $18C6A_4$ hydrate with any of the salt complexes reveal that major conformational changes must occur during complexation. In each case, the formal result is the displacement of the bridging waters and the reorganization of the macrocycle to optimize the coordination environment.

In striking contrast, the tetrahydrate of $18C6A_6$ undergoes minimal net reorganization during the complexation and crystallization processes. The hydrated ligand complexes a water dimer using a six-point hydrogen bond network (25). Three carboxyl donors accept hydrogen bonds in the preferred *anti* direction. The other three host carboxylic acids donate hydrogen bonds in the less preferred, more acidic, *anti* conformation. Substitution of the donor water of the dimer by the cation, accompanied by ionization of one of the carboxylic acids, produces the structure of a salt complex. The hydrogen-bond-accepting water of the dimer coordinates the cation. Consequently, two carboxyls, which hydrogen bond in *anti* conformations to the hydrogen-bond-donating water of the dimer, become carbonyl oxygen donors in the salt complexes and revert to the more stable *syn* conformation. Remarkably, minimal structural reorganization accompanies the formal H_3O^+-by-cation substitution. The polar-coordinate map of the $18C6A_6$–water–dimer complex (18) directly overlaps the polar maps of the Na^+, K^+, and Tl^+ complexes (Fig. 8).

The $18C6A_6$ ligand in water is a rare example of a *chorand* that is preorganized by solvent. Three effects combine

Can. J. Chem. Downloaded from www.nrcresearchpress.com by 88.255.202.194 on 09/08/12
For personal use only.

TABLE 4. Coordination environment of the complexes of $18C6A^{4-}$

Guest cation	Na^{+a}	Na^{+a}	Tl^+	Cs^+
Coordination number	7	9	8	9
Ligand donors	6	8	8	8
M^+—O distances (Å):				
H_2O		2.448(2)	—	—
Ether O (short)		2.456(2)	2.867(6)	3.062(3)
Ether O (long)	2.764(2)	3.351(2)	3.086(6)	3.260(4)
Carbonyl O		2.340(2)	3.059(7)	3.070(4)
		2.804(3)	3.272(9)	3.231(5)
				3.284(4) (intermolecular)
Mean cavity radius (Å)	1.16	1.30	1.61	1.76
Guest ionic radius (Å)	1.13	1.26	1.59	1.74
Effective ionic radius (Å)	1.12	1.24	1.59	1.78
Oxygen skeleton	Twist boat		Half chair	Planar
Maximum deviation, ether O from their best plane (Å):		0.387(2)	0.253(12)	0.097(4)
Distance to mean plane:				
H_2O		1.886(2)	—	3.093(7)
Cation		0.4371(4)	0.9603(1)	1.4463(1)
Transannular distances (Å):				
O1—O10		5.191(2)	5.516(9)	5.577(5)
O4—O13		5.459(3)	5.432(8)	5.438(4)
O7—O16		5.639(3)	5.829(9)	5.816(5)
Tartarate torsion angles (°):				
C2—C3		−170.2(2)	179.9(7)	−173.5(4)
C11—C12		−174.1(2)	−178.4(7)	−179.0(4)

[a]Two coordination spheres considered: hepta-coordinate Na^+ involving only the close interactions illustrated in Fig. 5, and nona-coordinate Na^+ including O4 and O7.

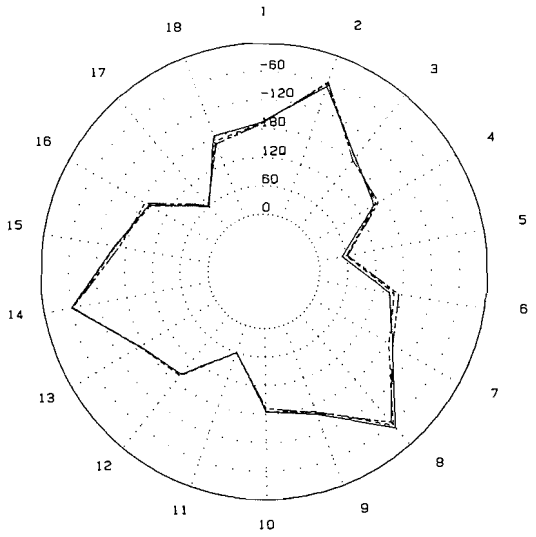

FIG. 8. Overlay of the polar coordinate maps of macrocyclic torsion angles of the Na^+ (solid), K^+ (dashed), and Tl^+ (double dashed) complexes of $18C6A_6$.

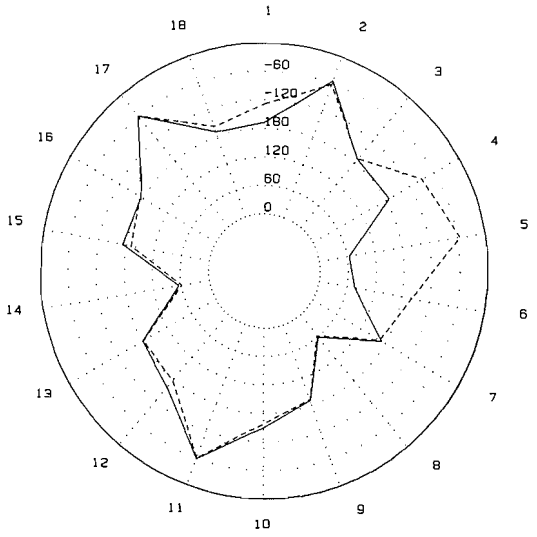

FIG. 9. Overlay of the polar coordinate maps of macrocyclic torsion angles of the Na^+ complex of $18C6A_4$ (solid) and the Cs^+ complex of $18C6A_6$ (dashed). The map of the Cs^+ complex has been rotated by −60° with respect to Fig. 4*c*.

and reinforce one another: (1) the macrocyclic framework adopts the D_{3d} conformation; (2) the tartaro units adopt preferred *anti* conformations; and (3) a bridging water molecule is held by three hydrogen bonds across one face of the molecule. This combination produces a preorganized cavity, which may be occupied either by a second water molecule or a cation.

Relationship of structure to cation binding in solution

Alkali-metal cations in aqueous solutions bind to $18C6A_6$ up to 10^4-fold more strongly than to the parent, 18-crown-6 (3). This structural study implies that $18C6A_6$ could bind monohydrated cations in water. Is there evidence for such a structure in solution? Perhaps there is. Carboxylate electrostatically enhances the stability of a complex (3). In-

Can. J. Chem. Downloaded from www.nrcresearchpress.com by 88.255.202.194 on 09/08/12
For personal use only.

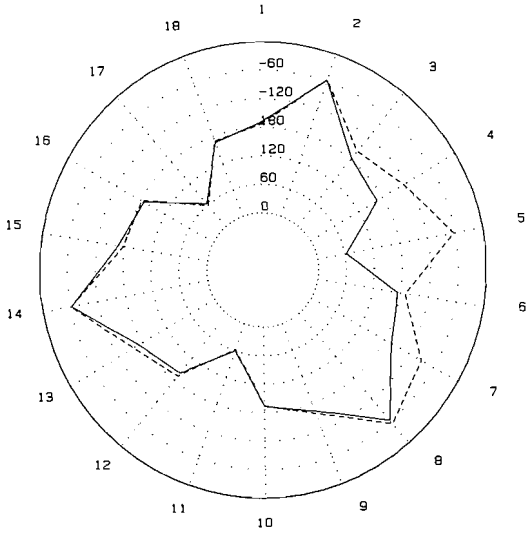

FIG. 10. Overlay of the polar coordinate maps of macrocyclic torsion angles of the Tl^+ (solid) and Cs^+ (dashed) complexes of $18C6A_6$.

creasing the number of carboxylates generally enhances cation binding, but not always. Both the Tl^+ and K^+ complexes of fully deprotonated (6^-) $18C6A_6$ are weaker than the monoprotonated (5^-) forms (3). Such an observation supports the suggestion of monohydrated cations binding to $18C6A_6$ in solution. Optimal binding (three-point attachment) of the water molecule requires at least one carboxyl (protonated carboxylate) to donate a hydrogen bond.

A bound water molecule could enhance complex stability either by preorganizing the ligand, or by altering the energetics of cation desolvation/complex formation. The energy of cation desolvation contributes to the energy of complexation, which can be reduced if a host binds a partly hydrated cation. Dehydration from heptahydrated Na^+ costs 12–16 kJ/mol each for the first five waters[4]. The next water costs 55 kJ/mol and the last 74 kJ/mol. This effect is less with Cs^+ (34 kJ/mol for the last water). Ligand preorganization by bound water or partial cation desolvation have different mechanistic implications, but give the same thermodynamic result. The stability of alkali-metal complexes of $18C6A_6$ results from the host complementing the water–cation guest couple.

Summary

Structural studies of hosts that complex hydrated cations may serve as models of how ions are transported across biological membranes. Carboxylates are frequently located on protein surfaces that contact water. As these studies reveal, a monohydrated sodium or potassium cation could readily move through the 18-crown-6 cavity. Dihydrated cations, if the second water is apical to the first, could conceivably move through as well. Molecular modelling of these complexes may provide further insight into mechanisms of ion transport or confirmation of our speculations about the mechanism of complexation or both.

[4]Experimental data: ref. 26*a*. Computational data: refs. 26 *b–d*.

Experimental

The ligands were prepared and purified as previously described (3, 4). The abbreviations are: $18C6A_6$ = 2*R*,3*R*,8*R*,9*R*,14*R*,15*R*-1,4,7,10,13,16-hexaoxacyclooctadecan-2,3,8,9,14,15-hexacarboxylic acid; $18C6A_4$ = 2*R*,3*R*,11*R*,12*R*-1,4,7,10,13,16-hexaoxacyclooctadecan-2,3,11,12-tetracarboxylic acid. Crystals were grown from aqueous solutions of the ligands (0.5 M) containing an equivalent of the metal halide or nitrate.

Crystal structure determination

Intensity data were collected by ω–2θ scans of variable rate designed to yield measurements of equal relative precision for all significant reflections, using Enraf–Nonius CAD4 diffractometers equipped with Cu Kα (λ = 1.54184 Å) or Mo Kα (λ = 0.71073 Å) radiation and graphite monochromators. Unit-cell dimensions were determined from the setting angles of 25 reflections. A maximum was placed on the scan time spent on any reflection. In several cases more than one unique form of data was collected. Data reduction included correction for absorption by psi scans, background, Lorentz, polarization, and, in several cases, linear intensity decay. Three standard reflections remeasured every 10 000 s monitored the decay. Equivalent data were merged and all reflections having $I > 3\sigma(I)$ were used in the refinements. The structures were solved by heavy atom methods or using coordinates from isomorphous structures. Refinement was carried out by full-matrix least squares minimizing $\Sigma\, w(|F_o|-|F_c|)^2$ with weights $w = \sigma^{-2}(F_o)$, using the Enraf–Nonius SDP programs (27). Scattering factors were those of Cromer and Weber (28), and anomalous coefficients were those of Cromer (29). Except where noted below, non-hydrogen atoms were refined anisotropically, and hydrogen atoms were either located on difference maps and refined isotropically or placed in calculated positions with C—H distance 0.95 Å and $B_{iso} = 1.3B_{eq}$ of the bonded carbon atom. For five of the structures, secondary extinction coefficients, *g*, were refined, where the correction factor $(1 + gI_c)^{-1}$ was applied to F_c. Absolute configuration determinations were attempted, and in all cases, the better refinement agreed with the absolute configuration of the starting materials. Agreement indices for the alternate refinements are given in parentheses in Tables 1 and 2. Crystal and refinement data are given in Table 1 for complexes of $18C6A_6$ and in Table 2 for complexes of $18C6A_4$. Specifics of each refinement are given as follows.[5]

$18C6A_6^- \cdot Na^+$: Two octants of data were collected. All hydrogens were refined.

$18C6A_6^- \cdot K^+$: Isomorphous with the Na^+ complex. Carboxylic acid and water hydrogens refined; all others were fixed.

$18C6A_6^- \cdot Tl^+$: Two octants of data with $\theta < 25°$ were collected. Hydrogen atoms were not refined and those on O2W were not located.

$18C6A_6^- \cdot Cs^+$: One hemisphere of data with $\theta < 25°$ was collected; one quadrant $25° < \theta < 30°$. Carboxylic acid hydrogens and those on uncoordinated water were not located; others were calculated.

$18C6A_4^- \cdot Na^+$: Carboxylic acid and water hydrogens were located and refined; macrocycle hydrogens were fixed. The *B* of one water hydrogen was fixed.

[5]Tables of atomic positional coordinates, hydrogen atom coordinates, anisotropic thermal parameters, bond distances, bond angles, torsion angles, and structure factors have been deposited, and may be purchased from: The Depository of Unpublished Data, Document Delivery, CISTI, National Research Council Canada, Ottawa, Canada K1A 0S2.

Tables of atomic parameters, bond distances, and bond angles have also been deposited with the Cambridge Crystallographic Data Centre and can be obtained on request from The Director, Cambridge Crystallographic Data Centre, University Chemical Laboratory, 12 Union Road, Cambridge, CB2 1EZ, U.K.

Can. J. Chem. Downloaded from www.nrcresearchpress.com by 88.255.202.194 on 09/08/12
For personal use only.

$18C6A_4^- \cdot Cs^+$: The carboxylic acid and water hydrogens were not located; others were calculated and fixed.

$18C6A_4^- \cdot Tl^+$: Isomorphous with the Cs^+ complex. One hemisphere of data with $\theta < 25°$was collected; one quadrant $25° < \theta < 33°$. The Tl^+ is disordered between two sites (95:5). Two water molecules with very high thermal parameters were refined isotropically. These and the high thermal parameters of C15 may be indicative of disorder. Residual peaks around the minor Tl site may indicate partial occupancy by additional water. Values in Table 2 assume the dihydrate. Hydrogen atoms were ignored.

Acknowledgement

T.M.F. gratefully acknowledges the continuing support of the Natural Sciences and Engineering Research Council of Canada.

1. (*a*) C. J. Pedersen. J. Am Chem. Soc. **89**, 7017 (1967); (*b*) J. M. Lehn. Pure Appl. Chem. **50**, 871 (1978); (*c*) D. J. Cram, T. Kaneda, R. C. Helgeson, and G. M. Lein. J. Am. Chem. Soc. **101**, 6752 (1979).
2. (*a*) J. M. Lehn. Struct. Bonding (Berlin), **16**, 1 (1973); (*b*) J. M. Lehn. Science, **227**, 849 (1985); (*c*) D. J. Cram and K. N. Trueblood. Top. Curr. Chem. **98**, 43 (1981); (*d*) D. J. Cram. Angew. Chem. Int. Ed. Engl. **25**, 1039 (1986).
3. P. J. Dutton, T. M. Fyles, and S. J. McDermid. Can. J. Chem. **66**, 1097 (1988).
4. J. P. Behr, J. M. Girodeau, R. C. Hayward, J. M. Lehn, and J. P. Sauvage. Helv. Chim. Acta, **63**, 2096 (1980).
5. (*a*) J. P. Behr, J. M. Lehn, and P. Vierling. Helv. Chim. Acta, **65**, 1853 (1982); (*b*) T. M. Fyles, C. A. McGavin, and D. M. Whitfield. J. Org. Chem. **49**, 753 (1984); (*c*) A. Basak and H. Dugas. Tetrahedron Lett. **27**, 3 (1986); (*d*) J. Desroches, H. Dugas, M. Bouclar, T. M. Fyles, and G. D. Robertson. Can. J. Chem. **65**, 1513 (1987).
6. (*a*) J. P. Behr, C. J. Burrows, R. Heng, and J. M. Lehn. Tetrahedron Lett. **26**, 215 (1985); (*b*) J. P. Behr, J. Bergdoll, B. Chevrier, P. Dumas, J. M. Lehn, and D. Moras. Tetrahedron Lett. **28** 1989 (1987).
7. T. M. Fyles and D. M. Whitfield. Can. J. Chem. **62**, 507 (1984).
8. (*a*) J. D. Behr and J. M. Lehn. Helv. Chim. Acta, **63**, 2112 (1980); (*b*) H. Dugas, P. Keroack, and M. Ptak. Can. J. Chem. **62**, 489 (1984).
9. J. D. Behr, J. M. Lehn, A. C. Dock, and D. Moras. Nature, **295**, 526 (1982); Acta. Crystallogr. Sect. C: Cryst. Struct. Commun. **C39**, 1001 (1983).
10. J. P. Behr, J. M. Lehn, D. Moras, and J. C. Theirry. J. Am. Chem. Soc. **103**, 701 (1981).
11. J. J. Daly, P. Schonholzer, J. P. Behr, and J. M. Lehn. Helv. Chim. Acta, **64**, 1444 (1981).
12. R. D. Gandour, F. R. Fronczek, V. J. Gatto, C. Minganti, R. A. Schultz, B. A. White, K. A. Arnold, D. Mazzocchi, S. R. Miller, and G. W. Gokel. J. Am. Chem. Soc. **108**, 4078 (1986).
13. F. Mathieu, B. Metz, D. Moras, and R. Weiss. J. Am. Chem. Soc. **100**, 4412 (1978).
14. R. D. Shannon. Acta Crystallogr. Sect. A: Cryst. Phys. Diffr. Theor. Gen. Crystallogr. **A32**, 751 (1976).
15. W. H. Baur. Crystallogr. Rev. **1**, 59 (1987).
16. J. P. Ounsworth and L. Weiler. J. Chem. Educ. **64**, 568 (1987).
17. H. Ogura, K. Furuhata, Y. Harada, and Y. Hitaka. J. Am. Chem. Soc. **100**, 6733 (1978).
18. T. M. Fyles and R. D. Gandour. J. Inclusion Phenom. Mol. Recognit. Chem. **12**, 313 (1992).
19. J. F. Stoddart. Chem. Soc. Rev. **8**, 85 (1979).
20. J. Dale. Top. Stereochem. **9**, 199 (1977).
21. E. A. Hillenbrand and S. Scheiner. J. Am. Chem. Soc. **108**, 7178 (1986).
22. M. R. Peterson and I. G. Cszimadia. J. Am. Chem. Soc. **101**, 1076 (1979); K. B. Wiberg and K. W. Laidig. J. Am. Chem. Soc. **109**, 5935 (1987).
23. C. J. Carrell, H. L. Carrell, J. Ehrlebacher, and J. P. Glusker. J. Am. Chem. Soc. **110**, 8651 (1988).
24. F. R. Fronczek and R. D. Gandour. *In* Cation binding by macrocycles: complexation of cationic species by crown ethers. *Edited by* Y. Inoue and G. W. Gokel. Marcel Dekker, New York. 1990. Chap. 7.
25. P. J. Dutton, F. R. Fronczek, T. M. Fyles, and R. D. Gandour. J. Am Chem. Soc. **112**, 8984 (1990).
26. (*a*) I. Dzidic and P. Kebarle. J. Chem. Phys. **74**, 1466 (1970); (*b*) M. M. Probst. Chem. Phys. Lett. **137**, 229 (1987); (*c*) P. Perez, W. K. Lee and E. W. Prohofsky. J. Chem. Phys. **79**, 388 (1983); (*d*) H. Kistenmacher, H. Popkie, and E. Clementi. J. Chem. Phys. **79**, 799 (1974).
27. B. A. Frenz and Y. Okaya. Enraf–Nonius structure determination package. Enraf–Nonius, Delft, The Netherlands. 1980.
28. D. T. Cromer and J. T. Weber. International tables for X-ray crystallography. Vol. IV. Table 2.2B. Kynoch Press, Birmingham. 1974 (present distributor, Kluwer Academic Publishers, Dordrecht).
29. D. T. Cromer. International tables for X-ray crystallography. Vol. IV. Table 2.3.1. Kynoch Press, Birmingham. 1974 (present distributor, Kluwer Academic Publishers, Dordrecht).

Can. J. Chem. Downloaded from www.nrcresearchpress.com by 88.255.202.194 on 09/08/12
For personal use only.

L'azote n'est pas le site basique des amides encombrés

CHRISTIAN LAURENCE ET MARYVONNE HELBERT
Laboratoire de spectrochimie, Université de Nantes, 44072 Nantes CEDEX 03, France

ET

ABDELJALIL LACHKAR
Laboratoire de spectroscopie, Université Cadi Ayyad, BP S15, Marrakech, Maroc

Reçu le 16 octobre 1992

CHRISTIAN LAURENCE, MARYVONNE HELBERT et ABDELJALIL LACHKAR. Can. J. Chem. **71**, 254 (1993).

L'abaissement de la bande carbonyle dans les complexes du diiode avec les amides encombrés i-PrCON(C_6H_{11})$_2$, *t*-BuCON(C_6H_{11})$_2$ ou *t*-BuCON(i-Pr)$_2$ montre que le site de fixation de diiode reste l'atome d'oxygène du carbonyle. Les donneurs de liaison hydrogène *p*-FC_6H_4OH, $CHCl_3$ ou $CHBr_3$ se fixent également sur l'oxygène du carbonyle. Les seules différences entre ces amides encombrés et les amides non encombrés comme $MeCONMe_2$ résident dans des constantes de complexation plus faibles (par exemple 15 L mol^{-1} pour $MeCONMe_2$–I_2, mais 3 L mol^{-1} pour *t*-BuCON(i-Pr)$_2$) et une stoechiométrie inférieure de complexation (par exemple mélanges de complexe 1 : 1 et 1 : 2 pour *t*-BuCON(C_6H_{11})$_2$, alors que $MeCONMe_2$ forme principalement des complexes 1 : 2).

CHRISTIAN LAURENCE, MARYVONNE HELBERT, and ABDELJALIL LACHKAR. Can. J. Chem. **71**, 254 (1993).

The shift of the carbonyl band of the iodine complexes with the hindered amides i-PrCON(C_6H_{11})$_2$, *t*-BuCON(C_6H_{11})$_2$, and *t*-BuCON(i-Pr$_2$) shows that the iodine interacts with the oxygen atom of the carbonyl group. Hydrogen bond donors, such as *p*-FC_6H_4OH, $CHCl_3$, or $CHBr_3$, also interact with the oxygen atom of the carbonyl group. The only differences between these hindered amides and unhindered amides like $MeCONMe_2$ are the lower complexation constants (15 L mol^{-1} for $MeCONMe_2$–I_2 vs. 3 L mol^{-1} for *t*-BuCON(i-Pr$_2$) and a lower stoichiometry of complexation (for example, a mixture of 1:1 and 1:2 complexes is obtained with *t*-BuCON(C_6H_{11})$_2$ while $MeCONMe_2$ forms mainly 1:2 complexes).

[Journal translation]

Introduction

Alors qu'il est généralement admis que la protonation (1), la liaison hydrogène, ou la fixation d'acides de Lewis (2, 3) s'effectuent pour les amides sur l'oxygène du carbonyle, Guihéneuf *et al.* ont récemment émis dans ce journal (4) l'hypothèse que l'azote pourrait devenir le site basique des amides encombrés. Ils ont en effet observé que les constantes de formation des complexes des amides avec l'acide de Lewis I_2 étaient beaucoup plus élevées avec les amides très encombrés comme *t*-BuCON(C_6H_{11})$_2$ qu' avec les amides comme MeCON(Me)$_2$ et qu'elles se rapprochaient de celles des amines correspondantes. Ils ont expliqué ces observations par une déconjugaison stérique des groupes CO et N(C_6H_{11})$_2$ qui réduit la basicité de l'oxygène et augmente celle de l'azote (4).

Dans ce travail nous examinons cette hypothèse séduisante en étudiant par infrarouge la bande carbonyle des amides encombrés et non encombrés en présence de I_2 et également des donneurs de liaison hydrogène comme le *p*-fluorophénol, le chloroforme et le bromoforme.

Partie expérimentale

Produits

Les amides non encombrés, I_2, le *p*-fluorophénol et les solvants sont des produits commerciaux purifiés par les méthodes usuelles (3). Les amides encombrés ont été préparés par action des amines convenables avec les chlorures d'acide correspondants. Leur pureté a été soigneusement vérifiée par spectroscopie IR.

Mesures spectroscopiques

Les spectres infrarouges ont été enregistrés sur un spectromètre à transformée de Fourier Nicolet 510 M avec une résolution de 1 cm^{-1}. Les cellules utilisées sont en CaF_2 et font 0,5 mm d'épaisseur. Les décompositions mathématiques des massifs complexes ont été effectuées avec le logiciel Spectracalc (Galactic).

Constantes d'équilibre

Les constantes de complexation K_c des équilibres dans l'heptane à 25°C :

$$RCONR'_2 + I_2 \leftrightarrows RCONR'_2 \ldots I_2$$

sont déterminées par infrarouge sur la bande carbonyle des amides. Les constantes des équilibres dans CCl_4 à 25°C :

$$RCONR'_2 + p\text{-}FC_6H_4OH \leftrightarrows p\text{-}FC_6H_4OH \ldots RCONR'_2$$

sont déterminées par infrarouge sur la bande ν(OH) du *p*-fluorophénol (6).

Résultats et discussion

Étude de la bande carbonyle des amides encombrés en présence de diiode dans l'heptane

Dans l'heptane les amides tertiaires présentent vers 1650 cm^{-1} une bande fine et très intense. Ainsi le coefficient d'extinction molaire de la bande à 1659 cm^{-1} de MeCON(C_6H_{11})$_2$ vaut 1380 L mol^{-1} cm^{-1}. Cette bande très caractéristique est principalement due à la vibration de valence de la liaison carbonyle.

Drago *et al.* ont montré que la complexation des amides tertiaires avec le diiode ou le phénol s'accompagnait d'un abaissement de plusieurs dizaines de cm^{-1} de la bande carbonyle et que cet abaissement constituait un argument majeur en faveur d'une fixation de ces acides de Lewis sur l'oxygène du carbonyle (2, 3).

Nous avons étudié la bande carbonyle des amides MeCON(C_6H_{11})$_2$, EtCON(C_6H_{11})$_2$, i-PrCON(C_6H_{11})$_2$, *t*-BuCON(C_6H_{11})$_2$ et *t*-BuCON(i-Pr)$_2$ en solution dans l'heptane en ajoutant des quantités croissantes de diiode jusqu'à saturation. Nous observons, comme sur la figure 1 pour

Can. J. Chem. Downloaded from www.nrcresearchpress.com by 88.255.202.194 on 09/08/12
For personal use only.

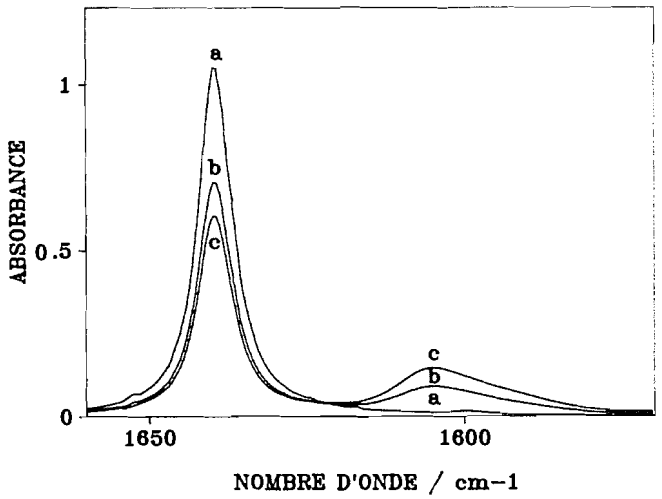

FIG. 1. Spectre IR-TF de *t*-BuCON(C_6H_{11})$_2$ dans l'heptane, seul (*a*) et en équilibre avec son complexe avec le diiode (*b* et *c*); (*a*) *t*-BuCON(C_6H_{11})$_2$ 0,029 M; (*b*) *t*-BuCON(C_6H_{11})$_2$ 0,012 M + I_2 0,027 M; (*c*) *t*-BuCON(C_6H_{11})$_2$ 0,012 M + I_2 à saturation.

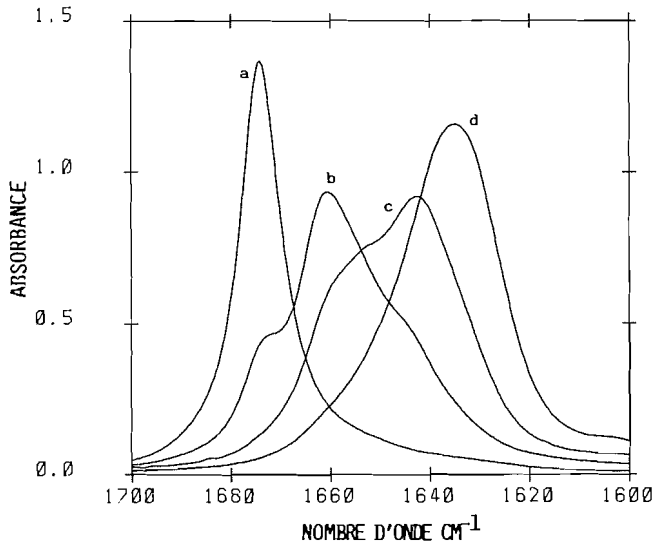

FIG. 2. Spectre IR-TF du *N,N*-diméthylacétamide 0,032 M dans des mélanges chloroforme–hexane; (*a*) fraction molaire *x* de $CHCl_3$ = 0; (*b*) *x* = 0,1; (*c*) *x* = 0,4; (*d*) *x* = 1.

t-BuCON(C_6H_{11})$_2$, que la bande carbonyle de l'amide libre diminue d'intensité et qu'elle est remplacée dans le complexe avec I_2 par une bande plus large aux fréquences plus basses. Ce comportement est caractéristique d'une fixation du diiode sur l'oxygène du carbonyle.

La fixation du diiode sur l'azote de la fonction amide envisagée par Guihéneuf *et al.* devrait s'accompagner de l'apparition d'une bande carbonyle aux fréquences élevées, car alors la participation du doublet de l'azote à la liaison N ... I_2 contrarierait sa conjugaison $n-\pi$ avec le carbonyle. L'examen minutieux, après de nombreuses accumulations spectrales, de solutions heptaniques d'amides saturés en diiode, ne montre aucune nouvelle bande aux fréquences élevées. On peut donc rejeter toute fixation du diiode sur l'azote pour les amides étudiés dans ce travail.

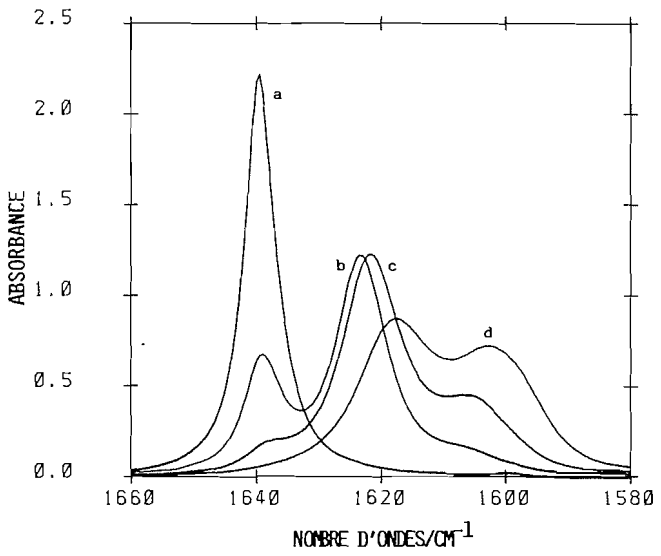

FIG. 3. Spectre IR-TF de *t*-BuCON(C_6H_{11})$_2$ 0,032 M dans des mélanges chloroforme–hexane; (*a*) fraction molaire *x* de $CHCl_3$ = 0; (*b*) *x* = 0,1; (*c*) *x* = 0,4; (*d*) *x* = 1.

Le tableau 1 résume les observations spectrales effectuées dans la région carbonyle, ainsi que la valeur de la constante de complexation K_c. On ne retrouve pas les valeurs très élevées observées par Guihéneuf *et al.* pour i-PrCON(C_6H_{11})$_2$ (1350 L mol^{-1}), *t*-BuCON(C_6H_{11})$_2$ (4300 L mol^{-1}) ou *t*-BuCON(i-Pr)$_2$ (350 L mol^{-1}). Au contraire les constantes K_c diminuent régulièrement dans la série RCON(C_6H_{11})$_2$ de 20 L mol^{-1} pour MeCON(C_6H_{11})$_2$ à 3,5 L mol^{-1} pour *t*-BuCON(C_6H_{11})$_2$ au fur et à mesure que le substituant R sur le carbonyle augmente de volume dans l'ordre Me, Et, i-Pr et *t*-Bu. Ce comportement s'explique bien à partir d'une fixation sur l'oxygène du carbonyle par une augmentation de la tension frontale entre I_2 et le substituant R sur le carbonyle.

Complexes des amides encombrés avec le p*-fluorophénol dans* CCl_4

Le *p*-fluorophénol est un indicateur de référence pour mesurer le pouvoir accepteur de liaison hydrogène des bases (5). Nous avons montré dans un travail précédent (6) que la bande carbonyle des complexes des amides encombrées avec le *p*-fluorophénol est située à une fréquence plus basse ($\Delta\nu$ = 32 cm^{-1} pour *t*-BuCON(C_6H_{11})$_2$) que pour l'amide libre. Ceci caractérise à nouveau une fixation du *p*-fluorophénol sur le groupement carbonyle.

On observe de plus les mêmes effets stériques des substituants alkyles dans les complexes de RCON(C_6H_{11})$_2$ avec le *p*-fluorophénol qu'avec I_2. Les constantes de formation (entre parenthèses en L mol^{-1}) des complexes *p*-fluorophénol–RCON(C_6H_{11})$_2$ diminuent dans l'ordre :

$$\underset{(257)}{\text{MeCON}(C_6H_{11})_2} > \underset{(166)}{\text{EtCON}(C_6H_{11})_2}$$

$$\sim \underset{(174)}{\text{i-PrCON}(C_6H_{11})_2} > \underset{(115)}{t\text{-BuCON}(C_6H_{11})_2}$$

Complexes des amides encombrés avec $CHCl_3$ *et* $CHBr_3$

Le chloroforme est un donneur de liaison hydrogène C—H très utile pour mettre en évidence l'aptitude du groupement

Can. J. Chem. Downloaded from www.nrcresearchpress.com by 88.255.202.194 on 09/08/12
For personal use only.

TABLEAU 1. Fréquences carbonyle (cm^{-1}) des amides libres et complexés par I_2 dans l'heptane et constantes de complexation K_c (L mol^{-1})

Amide	ν(CO)libre	ν(CO)complexe	$\Delta\nu^a$	K_c
$MeCON(C_6H_{11})_2$	1659	1603	56	20
$EtCON(C_6H_{11})_2$	1661[b]	1597[c]	64	10
$i\text{-}PrCON(C_6H_{11})_2$	1654[b]	1608[d]	46	4
$t\text{-}BuCON(C_6H_{11})_2$	1640	1606[d]	34	3,5
$t\text{-}BuCON(i\text{-}Pr)_2$	1641	1606[d]	35	3

[a]$\Delta\nu$ = ν(CO)libre − ν(CO)complexe.
[b]Maximum du doublet causé par l'isomérie de rotation autour des liaisons Et—CO et i-Pr—CO.
[c]Une deuxième bande est observée à 1622 cm^{-1} et est attribuée à une résonance de Fermi avec un harmonique ou une combinaison à 1620 cm^{-1}.
[d]Bande dissymétrique.

TABLEAU 2. Fréquences carbonyle (cm^{-1}) des amides libres et de leurs complexes 1 : 1 et 1 : 2 avec $CHCl_3$ ou $CHBr_3$ dans l'hexane et pourcentage de complexe 1 : 2 dans $CHCl_3$ ou $CHBr_3$ purs

Complexes	ν(CO) libre	ν(CO)[a] 1 : 1	ν(CO)[b] 1 : 2	% de complexe[c] 1 : 2
$MeCONMe_2$–$CHCl_3$	1674	1661	1634	~100
$t\text{-}BuCON(C_6H_{11})_2$–$CHCl_3$	1639	1623	1602	~45
$t\text{-}BuCON(C_6H_{11})_2$–$CHBr_3$	1639	1622	1600	~45

[a]Pour x = 0,1.
[b]Pour x = 1.
[c]En supposant que les coefficients d'extinction molaires des bandes carbonyle des complexes 1 : 1 et 1 : 2 sont voisins.

carbonyle à former des complexes 1 : 2 correspondant à la fixation de deux molécules de $CHCl_3$ sur chacun des doublets libres de l'oxygène du carbonyle (7).

Ainsi pour le *N*,*N*-diméthylacétamide en solution dans des mélanges hexane–$CHCl_3$, l'augmentation progressive de la fraction molaire x de $CHCl_3$ montre la disparition progressive de la bande carbonyle libre (x = 0) à 1674 cm^{-1} au profit d'abord d'un complexe 1 : 1 majoritaire (x = 0,1) à 1661 cm^{-1} puis d'un complexe 1 : 2 majoritaire (x = 0,4) puis unique (x = 1) à 1634 cm^{-1} (figure 2).

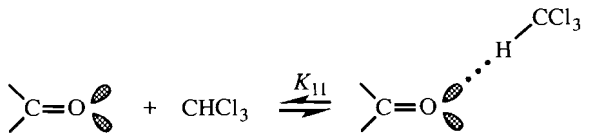

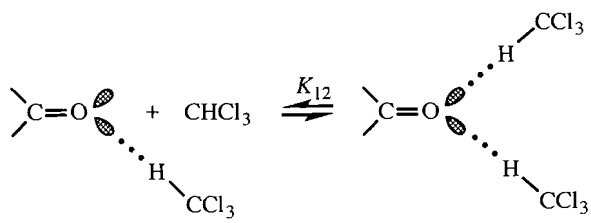

Complexe 1 : 2

Les amides encombrées fixent également le chloroforme sur l'oxygène de carbonyle, puisque l'addition croissante de chloroforme ne fait apparaître de nouvelles bandes de complexes amides–$CHCl_3$ qu'aux basses fréquences (figure 3). Cependant la figure 3 montre que pour une fraction molaire x = 0,4 de chloroforme, le complexe 1 : 2 à 1606 cm^{-1} est devenu minoritaire et que même le chloroforme pur (x = 1) ne réussit pas à complexer totalement $t\text{-}BuCON(C_6H_{11})_2$ avec une stoechiométrie 1 : 2.

Il est clair que la constante de formation K_{12} du complexe 1 : 2 est fortement diminuée par l'effet stérique des substituants sur le carbonyle qui encombrent fortement la paire libre qui leur est proche.

Les mêmes observations ont été effectuées avec le bromoforme. L'ensemble de nos observations spectrales sur la complexation des amides avec $CHCl_3$ et $CHBr_3$ est rassemblé dans le tableau 2.

Conclusion

Les résultats précédents montrent que pour les amides encombrés, comme pour les amides non encombrés, la fixation du diiode et des donneurs de liaison hydrogène s'effectue sur l'oxygène et non pas sur l'azote de la fonction amide. Les resultats de Guihéneuf *et al.* ne peuvent alors s'expliquer que par une pureté insuffisante de certains de leurs produits, des résidus de l'amine servant à leur synthèse pouvant être à l'origine du comportement pseudo-amine des amides encombrés.

1. R. B. Homer et C. D. Johnson. *Dans* The chemistry of amides. J. Zabicky. *Édité par* J. Zabicky. Interscience Publisher, Londres. 1970. Chap. 3.
2. C. D. Schmulbach et R. S. Drago. J. Am. Chem. Soc. **82**, 4484 (1960).

Can. J. Chem. Downloaded from www.nrcresearchpress.com by 88.255.202.194 on 09/08/12
For personal use only.

3. R. S. Drago et D. A. Wenz. J. Am. Chem. Soc. **84**, 526 (1962).
4. G. Guihéneuf, J. L. M. Abboud et A. Lachkar. Can. J. Chem. **66**, 1032 (1988).
5. R. W. Taft, D. Gurka, L. Joris, P. v. R. Schleyer et J. W. Rakshys. J. Am. Chem. Soc. **91**, 4801 (1969).
6. J. Y. Le Questel, C. Laurence, A. Lachkar, M. Helbert et M. Berthelot. J. Chem. Soc. Perkin Trans. 2, 2091 (1992).
7. P. Combelas, C. Garrigou-Lagrangr et J. Lascombe. Ann. Chim. 315 (1970).

Can. J. Chem. Downloaded from www.nrcresearchpress.com by 88.255.202.194 on 09/08/12
For personal use only.

Stereoselective 1,3-debromination reactions

YINGCHUN LIU, TED S. SORENSEN,[1] AND FANG SUN
The Department of Chemistry, University of Calgary, Calgary, Alta., Canada T2N 1N4

Received September 4, 1992

YINGCHUN LIU, TED S. SORENSEN, and FANG SUN. Can. J. Chem. **71**, 258 (1993).

The metallate, $PPN^+Cr(CO)_4NO^-$, was used for the 1,3-debrominative reductive cyclization of the (±) and *meso* isomers of dimethyl 2,4-dibromoglutarate and dimethyl 2,4-dibromo-2,4-dimethylglutarate. In both (±) isomers, the reaction is stereospecific in giving the *trans* cyclopropane product. In the *meso* case, the reaction is unselective in the first case, but distinctly favors the *cis* cyclopropane isomer in the second set of compounds. This (±) and *meso* pair thus represent the first example of near stereospecificity in the debrominations of both 1,3-dibromo diastereomers. Using an enantiomerically enriched dimethyl 2,4-dibromoglutarate, and determining the absolute stereochemistry of the cyclopropane product, it was found that a strict double inversion (⟋⟍) mechanism is involved in the (±) debromination reaction and presumably also in the near-stereospecific *meso* case reported above.

YINGCHUN LIU, TED S. SORENSEN et FANG SUN. Can. J. Chem. **71**, 258 (1993).

On a utilisé le $PPN^+Cr(CO)_4NO^-$ pour provoquer une cyclisation impliquant une débromation réductrice-1,3 des isomères (±) et *méso* des 2,4-dibromoglutarate de diméthyle et 2,4-dibromo-2,4-diméthylglutarate de diméthyle. Avec les deux isomères (±), la réaction est stéréospécifique et elle conduit au cyclopropane *trans*. Avec les isomères *méso*, la réaction n'est pas sélective dans le premier cas, mais elle favorise nettement le cyclopropane *cis* dans le deuxième ensemble de produits. Cette paire d'isomères (±) et *méso* représente donc le premier exemple approchant la stéréospécificité lors de la débromation des deux diastéréoisomères des dérivés 1,3-dibromo. Utilisant un 2,4-dibromoglutarate de diméthyle énantiomériquement enrichi et déterminant la stéréochimie absolue du cyclopropane obtenu, on a trouvé qu'un mécanisme de double inversion stricte (⟋⟍) est impliqué dans la réaction de débromation du produit (±) et que cette conclusion s'applique probablement au cas pratiquement stéréospécifique rapporté plus haut.

[Traduit par la rédaction]

Introduction

1,3-Dehalogenation reactions leading to cyclopropanes have been known for over a century (1). However, compared to their 1,2-dehalogenation counterparts, their stereochemistry and mechanism have received less attention.

Based on several previous studies, it appears that a ⟋⟍-conformation double inversion mechanism (in the Nickon–Werstiuk terminology (2)) is generally involved, although most authors conclude that the reaction is a two-step process, in many cases involving a carbanion intermediate. Previous reagents used for 1,3-debrominations include reducing metals (Zn (3–5), Zn–Cu (6), Mg (6), Na (7), Li/Hg (8)), phosphines (6), $LiAlH_4$ (6), *n*-BuLi (9), iodide ion (6), thiophenoxide ion (6), and electrochemical $2e^-$ reduction (10–12).

Recent work in this laboratory has shown that metallate carbonyl anions are efficient $2e^-$ reductants of C—Br bonds (13–16). Using the PPN^+ ($\phi_3P{=}N^+{=}P\phi_3$) counterion, these metallate salts are soluble in nonpolar organic solvents such as methylene chloride or THF and are often effective at very sub-ambient temperatures, in contrast to most of the reagents listed above. In a preliminary study of 1,2-debromination reactions, we found the stereospecificity of the well-known *anti* elimination product to be comparable to that obtained from the best of the previously described procedures (17). For example, while many reducing reagents give stereospecific *trans*-alkene formation on debromination of *meso*-1,2-dibromides, in the difficult *cis*-alkene cases, such as the formation of *cis*-stilbene from (±)-1,2-dibromo-1,2-diphenylethane, the resulting stereospecificity is often poor or nonexistent (18, 19). However, use of the PPN^+-$Cr(CO)_4NO^-$ metallate (20) at −78°C gave a 19:1 *cis/trans*-stilbene mixture. Furthermore, both *cis* and *trans*-2-butene were taken through the cycle (bromination–debromination)$_2$ with no detectable loss of stereochemistry.

In this paper, we report a study of the stereochemistry associated with the 1,3-debromination of two 2,4-dibromoglutarate ester systems using the metallate anion $Cr(CO)_4NO^-$. These studies were carried out at a temperature of −78°C, or lower (or higher) in a few cases. We previously worked with several other easily obtained metallate anions, e.g., $Mn(CO)_5^-$ and $Fe(CO)_3NO^-$, but the chromium salt is by far the more reactive in these debromination reactions. By using both the (±) and *meso* isomers in the initial reactions, and by using a single enantiomer in a second-stage investigation, the overall reaction is shown to occur with at least a preference for double inversion at both C—Br centers, with the reaction being stereospecific in the (±)-reactant cases.

Results

The 2,4-dibromoglutarate systems **1** and **2** were used in this study.

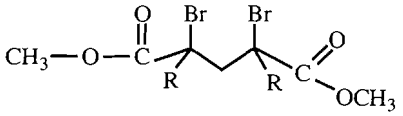

1 R = H **1***a* (±); **1***b meso*
2 R = CH_3 **2***a* (±); **2***b meso*

The acids corresponding to compounds **1***a* and **1***b* were prepared as described by Ingold (21), noting the later revision of the original diastereomer assignments (22). Diastereomeric mixtures of **2***a*–**2***b* were prepared using the method of Chan and Wallace (23). The reaction product consisted of nearly equal amounts of the previously unreported diastereomers. Flash chromatography allowed the isolation of the two nearly pure diastereomers as crystalline

[1]Author to whom correspondence may be addressed.

Can. J. Chem. Downloaded from www.nrcresearchpress.com by 88.255.202.194 on 09/08/12
For personal use only.

TABLE 1. Yields of *cis*- and *trans*-cyclopropanedicarboxylates in the 1,3-debromination reactions

Starting reactant	Temperature (°C)	Solvent	Product(s)	
1*a*	−78	CH_2Cl_2	**3***a*	
1*b*[a]	−78	CH_2Cl_2	**3***a* (46–53%)	**3***b* (43–54%)
1*b*[a]	−78	THF	**3***a* (46–50%)	**3***b* (50–54%)
1*b*[a]	−95	THF	**3***a* (25–40%)	**3***b* (60–75%)
1*b*[a]	−40	CH_3CN	**3***a* (75%)	**3***b* (25%)
2*a*	−78	CH_2Cl_2	**4***a*	
2*b*[a]	−78	CH_2Cl_2	**4***a* (19–25%)	**4***b* (75–81%)
2*b*[a]	−78	THF	**4***a* (10–12%)	**4***b* (88–90%)
2*b*[a]	−95	THF	**4***a* (10–14%)	**4***b* (86–90%)

[a]The data are uncorrected for ca. 2–4% of the (±) isomer as an impurity in the starting material.

compounds. The ^{1}H NMR spectra of **2***a* and **2***b* are distinctive and the assignments unequivocal (an A_2 system for **2***a* and AB for **2***b*, for the H-3 protons).

The reaction of these dibromides with $Cr(CO)_4NO^-$ was carried out on a small scale (0.1–0.4 mmol of dibromide and about a 20% molar excess of the chromium salt). The latter was dissolved in 1 mL of dry methylene chloride under nitrogen, cooled to −78°C or lower, and the dibromide in 1 mL of methylene chloride was added via syringe over about 2 min. All reactions are quite fast and can be monitored visually by noting a marked decrease in the intensity of the deep red color associated with $Cr(CO)_4NO^-$. After work-up (see Experimental), the isolated products were analyzed by ^{1}H NMR spectroscopy and in some cases by GLC. Cyclopropane formation appeared to be the sole reaction product under these experimental conditions. The overall reaction can be written:

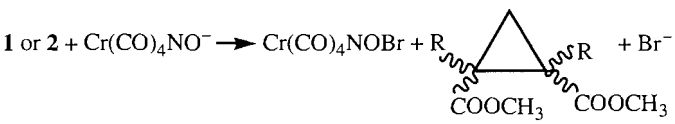

3 R = H (*a*) *trans*; (*b*) *cis*
4 R = CH (*a*) *trans*; (*b*) *cis*

The ^{1}H NMR spectra of all of the possible cyclopropanedicarboxylates have been reported (24, 25), so the ratio of the *cis* and *trans* product isomers was determined by ^{1}H NMR integration, without separation of the *cis* and *trans* diesters in those cases where a mixture was obtained. The experimental results are shown in Table 1.

The results show that the (±) isomers are stereospecifically converted to a *trans*-cyclopropanedicarboxylate. The *meso*-dibromide **2***b* preferentially forms the *cis*-cyclopropanedicarboxylate, while *meso*-dibromide **1***b* forms comparable amounts of both the *cis* and *trans* cyclopropanes.

These results are consistent with a 1,3-debromination mechanism in which both C—Br centers undergo inversion or both involve retention, with the *meso* isomers having some additional mechanistic feature that allows for a further epimerization process.

If one carries out the debromination of either (+)-**1***a* or (−)-**1***a*, then the absolute configuration of the *trans*-cyclopropanedicarboxylate product will differentiate a double inversion (⟋⟍) versus a double retention (∪) mechanism. The optical purity of the product will further offer one a measure of how rigidly the stereochemistry is controlled in the debromination reaction since a *trans* cyclopropane is certainly the thermodynamically stable product (i.e., *trans* > *cis*), but one might conceivably have some loss of optical purity in forming this thermodynamically favourable product.

The preparation of an enantiomer of **1***a* proved somewhat problematic. A literature search revealed that 2,3-dibromosuccinic (26), 2,5-dibromoadipic (27), and 2,6-dibromopimelic acids (27) had long ago been resolved, but 2,4-dibromoglutaric acid was reported (28) to be unstable when the preparation of alkaloidal salts was attempted. We have verified this observation since all attempts to form diastereomeric amine salts produced only the crystalline lactone **5**, even at sub-ambient temperatures (e.g., −78°C), and even under the slightly acidic conditions that prevail when a 1:1 molar ratio of diacid and amine is present. Attempts to effect some kinetic resolution by converting only part of the acid to the lactone using chiral amines was also unsuccessful, as were recrystallizations of the acid from chiral

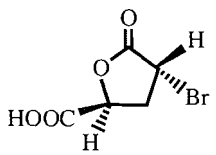

5 (racemic)

solvents. The formation of enantiomeric mono or diesters, followed by resolution, acid hydrolysis, and re-esterification, was considered, but a more practical approach involving the enzymatic hydrolysis of (±) **1***a* was ultimately found, in which the slower hydrolyzing diester enantiomer could be re-isolated and eventually used directly as a reactant.

Initial efforts using pig liver esterase (PLE) gave enantiomeric excesses of a (−)-diester estimated at 6–10% after 40–60% consumption of the racemic diester, assuming an $[\alpha]_D$ value of ca. −76 for the pure enantiomer of **1***a* (estimated from data for the homologous diacids mentioned above). This poor enantiomeric differentiation fits fairly well with that predicted from the Jones active site model (29) for PLE. Candida cylindracea lipase (CCL) proved superior to PLE, giving enantiomeric excesses of the (−)-diester estimated at 20–50% after 40–80% hydrolysis. With this level of enantiomeric excess, it proved possible to further enrich the material, since it was observed that recrystallization of

Can. J. Chem. Downloaded from www.nrcresearchpress.com by 88.255.202.194 on 09/08/12
For personal use only.

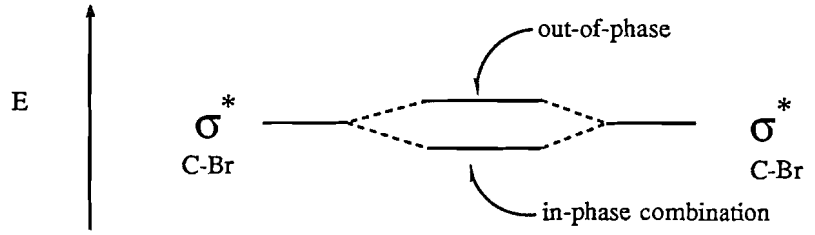

Note: only a W-conformation of the C-Br bond would allow this possible weak back-lobe interaction. For other conformations, the σ* (C-Br) energy level would apply.

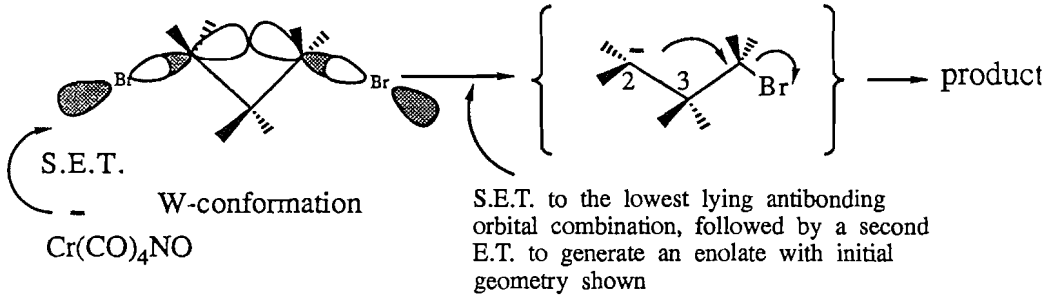

FIG. 1. Proposed mechanistic route for cyclopropane formation.

the diester from hexane preferentially formed crystals of the racemate. After several crystallization crops, a mother liquor diester sample estimated as 85% ee was obtained. Finally, the actual enantiomeric purity was determined by ^{1}H NMR spectroscopy using this diester sample and a chiral shift reagent in deuterocyclohexane solvent, giving a calculated $[\alpha]_D$ of −84, quite close to the estimated value (−76) used in the beginning. The absolute stereochemistry assigned to the laevorotatory diester (2*S*,4*S*) was based on correlations with the known absolute configuration of 2,4-dihydroxyglutaric acid (30) and with the configuration of several mono-α-bromocarboxylic acids or esters.

Reactions of 2*S*,4*S*-**1***a* with $Cr(CO)_4NO^-$, using material that was 78% ee or 34% ee, yielded (+)-dimethyl *trans*-cyclopropanedicarboxylate ((+)-**3***a*) with the same enantiomeric excess, within experimental error, as in the starting material. The $[\alpha]_D$ and absolute configuration of **3***a* are known (31), (+)-**3***a* corresponding to the 1*S*,2*S* configuration. This requires that the 1,3-debromination reaction must have proceeded with strict double inversion.

Discussion

The mechanism by which metallates such as $Cr(CO)_4NO^-$ react with organobromine compounds has not been investigated, although one might anticipate that single electron transfer (S.E.T.) might initially occur, and that this electron transfer would be most facile when the dibromides have already adopted a ⩘ conformation, which allows for back-lobe orbital overlap (an inphase combination of the antibonding C—Br σ*-orbitals that lowers the σ*-orbital energy, see Fig. 1). Independent evidence for a more easily reducible ⩘ conformation of 1,3-dibromides comes from the electrochemical studies of Rifi (10, 32, 33) and the more recent "back-lobe-overlap" concept has been used by a number of authors in discussing dehalogenation reactions. A mechanism for our reactions is pictured in Fig. 1.

We also assume that a second electron transfer occurs before the initially formed radical pair can dissociate. This leads to $Cr(CO)_4NOBr$ and a short-lived enolate intermediate. In the (±) isomers, this enolate has a favorable steric arrangement and *trans*-cyclopropane isomers are generated without any bond-rotation process intervening. In the *meso* isomers, however, an unfavorable geometry can be relieved by a bond rotation (C2—C3 bond), which would necessarily have to be competitive with the actual elimination reaction in order to rationalize our results. The higher specificity observed for **2***b* (vs. **1***b*) is consistent with this picture since there is less driving force for the enolate bond rotation in **2***b* (CH_3 and $COOCH_3$ are somewhat similar in size) and the added methyl group in **2***b* should slightly destabilize the enolate, leading to a more rapid elimination reaction.

In previous work by Fry and Britton (11) on 2,4-dibromopentanes, a ⩘ mechanism has been inferred for the electrochemical reductive cyclization reaction even though the reactions show essentially no stereospecificity (i.e., (±) and *meso* isomers yield nearly the same product mixture). These authors showed, however, that the (+)-dibromide leads to (+)-*trans*-1,2-dimethylcyclopropane (a stereospecific double inversion if one focuses only on this product of the reaction). Schlosser and Fouquet (34) reported similar observations starting with an optically active dibromononane and using lithium amalgam. Bordwell and Jarvis also studied the stereochemistry of the Ramberg–Baeklund reaction (a debromination variant) and provided evidence for a ⩘ double inversion process leading to the episulfone intermediate. Trost *et al.* have shown that (±)- and *meso*-2,4-dibromopentane can be stereoselectively converted to cyclopropanes using *n*-BuLi (*meso* gives mainly *cis*, (±) mainly

Can. J. Chem. Downloaded from www.nrcresearchpress.com by 88.255.202.194 on 09/08/12
For personal use only.

Can. J. Chem. Downloaded from www.nrcresearchpress.com by 88.255.202.194 on 09/08/12
For personal use only.

trans), but covalently bonded lithium intermediates are likely involved.

We believe that the present study is the first one to show that (±)- and *meso*-1,3-dibromo isomers react with at least some stereospecificity *and* that the double inversion mechanism is operative (exclusively with the (±) isomers).

These results for 1,3-debromination can be compared with those for 1,2-debrominations. The latter reactions are usually thought of as strongly concerted (anti-periplanar E2), but clearly the inability to stereospecifically produce *cis*-stilbene from the (±)-dibromide implies some breakdown in this common assumption. It is very likely that 1,3-debrominations are less strongly controlled by stereoelectronic factors, but use of the $Cr(CO)_4NO^-$ salt in this regard may be of advantage since the resulting reactions occur at quite low temperatures and in quite nonpolar solvents where carbanion intermediates are poorly stabilized.

Experimental

Tetrahydrofuran (THF) was purified by distillation from sodium benzophenone ketyl. Hexane, pentane, methylene chloride, and acetonitrile were dried over 3A molecular sieves. ^1H and ^{13}C NMR spectra were obtained on a Bruker ACE 200 (δ values in $CDCl_3$, *J* in Hz). For ^1H NMR, s = singlet, d = doublet, t = triplet, q = quartet. For ^{13}C NMR, q = quaternary; DEPT 90 and 135 experiments were used to determine multiplicities. Mass spectra were determined on a Kratos MS-80, a VG-7070, or an HP 5971A GC–MS system, using a 12.5 m × 0.20 mm (i.d.) DB-1 capillary column. Other GC data were measured on an HP-5890 instrument using 530-μm columns, OV-1. Optical rotations were determined on a Rudolph Autopol III polarimeter, using 5-cm cells. Flash chromatography was performed using silica gel (230–400 mesh). Glassware was oven-dried.

$PPN^+Cr(CO)_4NO^-$

This salt was prepared as described (20) from $Cr(CO)_6$ and $PPN^+NO_2^-$, carrying out all operations under an inert atmosphere.

(±)-2,4-Dibromoglutaric acid and meso*-2,4-dibromoglutaric acid* were prepared as described by Ingold (21). ^1H NMR spectra were in accord with literature values (22). ^{13}C NMR, (±) isomer: 170.0 (C=O), 44.5 (CH), 39.4 (CH_2); *meso* isomer: 169.8 (C—O), 42.9 (CH), 40.3 (CH_2).

Dimethyl (±)- and meso*-2,4-dibromoglutarates (**1**a and **1**b)* were prepared from the acids using diazomethane (ether solvent). These esters have been previously reported (21). During the esterification, and even on storage, a small amount of the *meso* isomer is isomerized to the (±) isomer. For the reaction results shown in Table 1, a *meso* diester of ca. 97% purity was used. These two esters have mutually well-resolved ^1H and ^{13}C NMR spectra.

Dimethyl (±)- and meso*-2,4-dibromo-2,4-dimethylglutarates (**2**a and **2**b)*

To a solution of diisopropylamine (3.54 mL, 0.025 mol) in dry THF (15 mL) was added *n*-butyllithium (10 mL, 0.025 mol) at −30°C under argon. After the reaction mixture was stirred at −30°C for 15 min, a solution of dimethyl 2,4-dimethylglutarate (35) in THF (5 mL) was added dropwise at −78°C. After 15 min, chlorotrimethylsilane (3.24 mL, 0.025 mol) was added and the reaction mixture was slowly warmed to room temperature (2 h). The solvent was removed *in vacuo* and the residue was dissolved with 10 mL of hexane and filtered, using a further 5 mL of hexane wash. The solvent was removed *in vacuo* and *N*-bromosuccinimide (13.5 g, 0.030 mol) in 30 mL of dry CH_2Cl_2 was added. After 12 h, the reaction mixture was poured into a mixture of water and CH_2Cl_2, the organic layer was separated from the aqueous layer, and washed successively with saturated $NaHCO_3$ solution, brine, and water. After drying and evaporation, a residue mixture of the title esters was obtained, 2.1 g (62%). GC–MS showed that the ratio of (±) and *meso* isomers was ca. 1.4:1. The isomers were separated on a silica gel column eluted with hexane – ethyl acetate (50:1 v/v) to give the (±) isomer **2***a* (860 mg, crystallized from hexane), mp 63–64°C, and the *meso* isomer **2***b* (220 mg, crystallized from hexane), mp 53–54°C.

For **2***a*, ^1H NMR: 3.80 (6H, s), 3.43 (2H, s), 1.89 (6H, s). ^{13}C NMR: 171.2 (C=O), 56.6 (q), 53.2 (OCH_3), 52.3 (CH_2); 26.9 (CH_3). MS: 317 (3), 315 (6), 313 (3), 267 (45), 265 (45), 235 (100), 233 (97), 126 (92), 153 (62). Anal. calcd. for $C_9H_{14}Br_2O_4$: C 31.23%, H 4.11%; found: C 31.08%, H 3.95%. For **2***b* (ca. 97% purity), ^1H NMR: 3.82 (6H, s), 3.36, 3.25 (2H, AB system, J = 15.1), 1.96 (6H, s). ^{13}C NMR: 171.3 (C=O), 58.2 (q), 53.5 (OCH_3); 51.6 (CH_2), 28.5 (CH_3). The MS fragmentation pattern is the same as for **2***a*. High-resolution MS, calcd. for $C_9H_{14}{}^{79}Br^{81}BrO_4 - OCH_3$: 314.9055; found: 314.9059.

*Isolation of lactone **5***

Treatment of (±)-2,4-dibromoglutaric acid with one equivalent of (−)-brucine ((−)-cinchonidine or (+)-cinchonine led to similar results) in acetone solution led to a gummy precipitate of brucine · HBr. After decanting/filtering, the acetone solvent was evaporated to give a mixture of solid and oil. This mixture was extracted with hot chloroform, and then some of the chloroform was evaporated to yield, on cooling, crystals of the title lactone, mp 121–123°C, after two recrystallizations from chloroform. ^1H NMR:

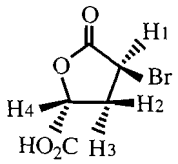

(±) **-5**

H1, 4.86; H2, 2.85; H3, 3.00; H4, 5.20; J_{12} = 5.5; J_{13} = 7.3; J_{23} = 14.4; J_{24} = 7.1; J_{34} = 7.1. ^{13}C NMR: C2, 38.6; C3, 37.4; C4, 75.3; carbonyls, 170.1, 172.6. MS: 208 (0.24), 163 (49), 165 (47), 135 (11), 137 (10), 85 (100), 107 (28), 109 (26). High-resolution MS, calcd. for $C_5H_5O_4{}^{79}Br$: 207.9371; found: 207.9375.

*Enzymatic hydrolysis of **1**a*

Since the PLE hydrolysis yielded inferior results compared to CCL, only the latter reaction is described in detail. To a 1-L round-bottom flask was added a solution of 1.70 g (5.3 mmol) of **1***a* in 200 mL of methanol. This was followed by the addition of 200 mL of tris buffer solution (pH = 8.5, approximately 0.1 M in buffer) and 0.70 g (490 000–1 050 000 units) of Candida cylindracea lipase (CCL) (Sigma Chemical Co.) The resulting mixture was an opaque suspension since the dibromo ester is not water soluble and the enzyme is probably not very soluble in H_2O–CH_3OH. The reaction mixture was stirred (magnetic bar) at room temperature for 26 h. The reaction solution was then acidified by adding concentrated HCl, and extracted with diethyl ether (4 × 100 mL). The extracts were combined, dried over $CaCl_2$, filtered, and the solvent removed on a Rotovap. An ^1H NMR integration of peaks for the unhydrolyzed diester compared to those for lactone **5** and 2,4-dibromoglutaric acid (no mono-ester was observed, presumably because it is more soluble than the diester and more rapidly hydrolyzed) yielded a 45% hydrolysis conversion, but the actual conversion is probably higher since the material balance was less than the theoretical, due likely to the incomplete extraction of the diacid. The residue was subjected to flash chromatographic separation (4:1 v/v hexane–ether) to give 0.37 g (22% recovery) of the diester, $[\alpha]_D^{20}$ −42 (50% ee). Recrystallization of this material from hexane yielded crystals that were mainly the racemic diester. Two more crops of crystals were obtained by concentration of the mother liquors, but the third crop of crystals had an enantiomeric excess similar to that of the filtrate. The final recovered

material was subject to a bulb-to-bulb distillation purification to give an $[\alpha]_D^{20}$ of 65.5. Using this material in cyclohexane-d_{12} with (−)-[Eu(hfc)] (Aldrich Chemical Co.) and integrating the OCH_3 peaks gave a calculated 78% ee determination. Control experiments were performed on (±)-**1***a* and by using (+)-[Eu(hfc)]. The specific rotation, $[\alpha]_D$, of (−)-**1***a* was calculated to be −84°. Control experiments without the enzymes showed no detectable hydrolysis of the diester.

General preparation of the cyclopropanedicarboxylates

Into a small Schlenk tube fitted with a septum and stopcock sidearm, under a nitrogen atmosphere, and with magnetic bar stirring, a solution of 0.10 g (0.14 mmol) of $PPN^+Cr(CO)_4NO^-$ in 1 mL of solvent (see Table 1) was prepared and cooled to the requisite temperature using an external bath. The dibromo ester (0.12 mmol) in 1 mL of solvent was added over a period of ca. 2 min. From the visual color change (considerable loss of intense red color) the reactions appeared to be over almost immediately at −78°C. The reactions were allowed to warm slowly to room temperature and 10 mL of pentane (or hexane) was added. The solutions were recooled to −78°C and stirred for about 40 min. The solution was filtered from the accumulated precipitate (using a $MgSO_4$ column in some instances) while cold, and the solvent was removed on a Rotovap to yield the crude product. Generally, 80–90% crude yield of the cyclopropanedicarboxylates was obtained in the larger scale runs, and the material was further purified by flash chromatography and (or) bulb-to-bulb distillation in some instances. In some cases, total product yields were determined by ^1H NMR integration using a weighed standard. The ratios of the *cis* and *trans* isomers were based on ^1H NMR integrations. In a few cases, GLC peak areas were also determined and these agreed well with the NMR results.

*Conversion of (−)-(2S,4S)-**1**a into (+)-(1S,2S)-**3**a*

A debromination reaction was carried out with 86.0 mg (0.27 mmol) of **1***a* (78% ee) and 400 mg (0.55 mol, a twofold excess) of the $PPN^+Cr(CO)_4NO^-$. After work-up, the crude product was purified by flash chromatography and the residue, after solvent evaporation, was distilled (bulb-to-bulb), yielding the pure diester **3***a*. This sample had $[\alpha]_D^{20}$ +181, which corresponds to 78% ee. Similar results were obtained using (−)-**1***a* of 34% ee.

Acknowledgment

We thank the Natural Sciences and Engineering Research Council of Canada for financial support.

1. A Freund. J. Prakt. Chem. **26**, 367 (1882).
2. A. Nickon and N. H. Werstiuk. J. Am. Chem. Soc. **89**, 3619 (1967).
3. G. J. Östling. J. Chem. Soc. 457 (1912).
4. R. G. Kelso, K. W. Greenlee, J. M. Derfer, and C. E. Boord. J. Am. Chem. Soc. **74**, 287 (1952).
5. R. G. Kelso, K. W. Greenlee, J. M. Derfer, and C. E. Boord. J. Am. Chem. Soc. **77**, 1751 (1955).
6. F. G. Bordwell and B. B. Jarvis. J. Am. Chem. Soc. **95**, 3585 (1973).
7. K. B. Wiberg and G. M. Lampman. Tetrahedron Lett. 2173 (1963).
8. K. Griesbaum and P. E. Butler. Angew. Chem. Int. Ed. Engl. **6**, 444 (1967).
9. B. M. Trost, W. L. Schinski, F. Chen, and I. B. Mantz. J. Am. Chem. Soc. **93**, 676 (1971).
10. M. R. Rifi. J. Am. Chem. Soc. **89**, 4442 (1967).
11. A. J. Fry and W. E. Britton. J. Org. Chem. **38**, 4016 (1973).
12. C. Giomini, A. Inesi, and E. Zeuli. J. Chem. Res. (S), 280 (1983).
13. A. P. Masters, T. S. Sorensen, and T. Ziegler. J. Org. Chem. **51**, 3558 (1986).
14. A. P. Masters, T. S. Sorensen, and P. M. Tran. Can. J. Chem. **65**, 1499 (1987).
15. A. P. Masters and T. S. Sorensen. Can. J. Chem. **68**, 492 (1990).
16. A. P. Masters and T. S. Sorensen. Tetrahedron Lett. **30**, 5869 (1989).
17. I. M. Mathai, K. Schug, and S. I. Miller. J. Org. Chem. **35**, 1733 (1970).
18. W. M. Schubert, B. S. Rabinovitch, N. R. Larson, and V. A. Sims. J. Am. Chem. Soc. **74**, 4590 (1952).
19. W. K. Kwok and S. I. Miller. J. Am. Chem. Soc. **92**, 4599 (1970).
20. D. R. Mantell and W. L. Gladfelter. J. Organomet. Chem. **347**, 333 (1988).
21. C. K. Ingold. J. Chem. Soc. 305 (1921).
22. F. K. Velichko, L. V. Vinogradova, R. A. Amriev, and R. Kh. Freidlina. Dokl. Acad. Nauk SSR, **194**, 1080 (1970).
23. T. H. Chan and I. H. M. Wallace. Tetrahedron Lett. **23**, 799 (1982).
24. D. J. Patel, M. E. Howden, and J. D. Roberts. J. Am. Chem. Soc. **85**, 3218 (1963).
25. A. A. Pavia, J. Wylde, R. Wylde, and E. Arnal. Bull. Soc. Chim. Fr. 2709 (1965).
26. A. McKenzie. J. Chem. Soc. 1196 (1912).
27. L. Schotte. Ark. Kemi, **9**, 407 (1956).
28. L. Schotte. Ark. Kemi, **9**, 423 (1956).
29. E. J. Toone and J. B. Jones. J. Am. Chem. Soc. **112**, 4946 (1990).
30. L. Benoiton, M. Winitz, S. M. Birnbaum, and S. P. Greenstein. J. Am. Chem. Soc. **79**, 6192 (1957).
31. W. van E. Doering and K. Sachdev. J. Am. Chem. Soc. **96**, 1169 (1974).
32. M. R. Rifi. Tetrahedron Lett. 1043 (1969).
33. M. R. Rifi. Collect. Czech. Chem. Commun. **36**, 932 (1971).
34. M. Schlosser and G. Fouquet. Synthesis, 200 (1972).
35. C. R. Noller and C. E. Pannell. J. Am. Chem. Soc. **77**, 1862 (1955).

Can. J. Chem. Downloaded from www.nrcresearchpress.com by 88.255.202.194 on 09/08/12
For personal use only.

Structural studies of organoboron compounds. LVII.[1] Synthesis and structure of bicyclic boron-nitrogen betaines. 1-Methyl-5-(3-nitrophenyl)-4,6,9-trioxa-1-azonia-5-boratabicyclo[3.3.1]nonane and 3,3,4-trimethyl-1-(3-nitrophenyl)-2,6,7-trioxa-3-azonia-1-boratabicyclo[2.2.2]octane

ECKART AHLENSTIEL AND WOLFGANG KLIEGEL
Institut für Pharmazeutische Chemie der Technischen Universität Braunschweig, Beethovenstrasse 55, 3300 Braunschweig, Germany

AND

STEVEN J. RETTIG AND JAMES TROTTER[2]
Department of Chemistry, University of British Columbia, 2036 Main Mall, Vancouver, B.C., Canada V6T 1Z1

Received December 9, 1991[3]

ECKART AHLENSTIEL, WOLFGANG KLIEGEL, STEVEN J. RETTIG, and JAMES TROTTER. Can. J. Chem. **71**, 263 (1993).

The syntheses and structures of the bicyclic boron-nitrogen betaines 1-methyl-5-(3-nitrophenyl)-4,6,9-trioxa-1-azonia-5-boratabicyclo[3.3.1]nonane, **7***a*, and 3,3,4-trimethyl-1-(3-nitrophenyl)-2,6,7-trioxa-3-azonia-1-boratabicyclo[2.2.2]-octane, **14***a*, are reported. Crystals of **7***a* are orthorhombic, $a = 20.256(2)$, $b = 37.652(2)$, $c = 6.642(1)$ Å, $Z = 16$, space group $Fdd2$, and those of **14***a* are orthorhombic, $a = 21.402(2)$, $b = 11.334(3)$, $c = 11.248(2)$ Å, $Z = 8$, space group $Pbca$. The structures were solved by direct methods and were refined by full-matrix least-squares procedures to $R = 0.038$ and 0.045 ($R_w = 0.036$ and 0.053) for 975 and 1646 reflections with $I \geq 3\sigma(F^2)$, respectively. The X-ray analyses establish the bicyclo[3.3.1]nonane and bicyclo[2.2.2]octane "cage" structures for **7***a* and **14***a*, respectively. Bond lengths involving the tetrahedral boron atom are (N)O—B = 1.519(5), (C)O—B = 1.444(6) and 1.443(6), C(aryl)—B = 1.602(5) Å for **7***a*; and (N)O—B = 1.530(3), (C)O—B = 1.446(3) and 1.455(3), C(aryl)—B = 1.608(3) Å for **14***a*. Weak C—H···O interactions are the main feature of the crystal packing arrangements of both compounds.

ECKART AHLENSTIEL, WOLFGANG KLIEGEL, STEVEN J. RETTIG et JAMES TROTTER. Can. J. Chem. **71**, 263 (1993).

On a réalisé la synthèse des bétaïnes bicycliques bore/azote, 1-méthyl-5-(3-nitrophényl)-4,6,9-trioxa-1-azonia-5-boratabicyclo[3.3.1]nonane (**7***a*) et 3,3,4-triméthyl-1-(3-nitrophényl)-2,6,7-trioxa-3-azonia-1-boratabicyclo[2.2.2]-octane (**14***a*) et on en a déterminé les structures. Les cristaux du produit **7***a* sont orthorhombiques, groupe d'espace $Fdd2$, avec $a = 20{,}256(2)$, $b = 37{,}652(2)$ et $c = 6{,}642(1)$ Å et $Z = 16$ alors que ceux du composé **14***a* sont orthorhombiques, groupe d'espace $Pbca$, avec $a = 21{,}402(2)$, $b = 11{,}334(3)$ et $c = 11{,}248(2)$ Å et $Z = 8$. On a résolu les structures par des méthodes directes et on les a affinées par la méthode des moindres carrés (matrice entière) jusqu'à des valeurs de $R = 0{,}038$ et 0,045 ($R_w = 0{,}036$ et 0,053) pour respectivement 975 et 1646 réflexions avec $I \geq 3\sigma(F^2)$. Les déterminations par rayons X ont permis de confirmer les structures en formes de "cage" pour les bicyclo[3.3.1]nonane et bicyclo[2.2.2]octane des composés **7***a* et **14***a* respectivement. Les longueurs des liaisons impliquant un atome de bore tétraédrique sont (N)O—B = 1,519(5), (C)O—B = 1,444(6) et 1,443(6) et C(aryl)—B = 1,602(5) Å pour le composé **7***a* et (N)O—B = 1,530(3), (C)O—B = 1,446(3) et 1,455(3) et C(aryl)—B = 1,608(3) Å pour le composé **14***a*. Pour les deux composés, la caractéristique principale de l'entassement du cristal est un ensemble de faibles interactions C—H···O.

[Traduit par la rédaction]

Introduction

The condensation of bis(2-hydroxyethyl)amines **1** and arylboronic acids leads to 1,3-dioxa-6-aza-2-boracyclooctanes **2** that are known to undergo transannular N → B coordination to form the stable bicyclo[3.3.0]octane ring systems **3**. The structure **3** for these materials has been confirmed by chemical and physical investigations (1), including an X-ray crystallographic analysis of the *N*-unsubstituted derivative **3** (R = H, Ar = C_6H_5) (2). Employing the *N*-oxides **4**, obtained by reaction of **1** with hydrogen peroxide (3, 4), the condensation with an arylboronic acid could result in both the eight-membered cyclic arylboronate **5** and the six-membered chelate **6**.[4] Both products (**5** and **6**) could subsequently cyclize to the bridged-ring compound **7**, the *N*-oxide **5** undergoing an intramolecular O → B coordination and the chelate intermediate **6** by further intramolecular condensation.

The bicyclo[3.3.1]nonane ring system **7** has already been postulated for some phenylboronates of this type (4) but has not been established to date. To achieve this goal, at least for the solid state by single-crystal X-ray analysis, we synthesized several 3-nitrophenylboronates **7** (Ar = 3-$NO_2C_6H_4$). The nitrophenyl substituent was expected primarily to enhance the intramolecular O—B coordination by an inductively increased Lewis acidity (5) of the boronate function, but, as a bonus, produced the derivatives **7***a–c* that formed better crystals than did other analogs. The elemental analyses indicate a complete condensation in each case that is also confirmed by infrared and ^{1}H nmr spectra. The tetracoordination at the boron atom, even in $CDCl_3$ solution, can be deduced (6) from the ^{11}B nmr spectra of **7***a* ($\delta(Et_2OBF_3) = 5.4$ ppm) and **7***b* (5.2 ppm). This evidence strongly supports the intramolecular complex **7** rather than the "open" *N*-oxide **5**, but cannot unambiguously rule out

[1]Previous paper in this series: ref. 26.
[2]Author to whom correspondence may be addressed.
[3]Revision received October 26, 1992.
[4]Type **6** chelates can be isolated under certain conditions (work in progress).

Can. J. Chem. Downloaded from www.nrcresearchpress.com by 88.255.202.194 on 09/08/12
For personal use only.

Can. J. Chem. Downloaded from www.nrcresearchpress.com by 88.255.202.194 on 09/08/12
For personal use only.

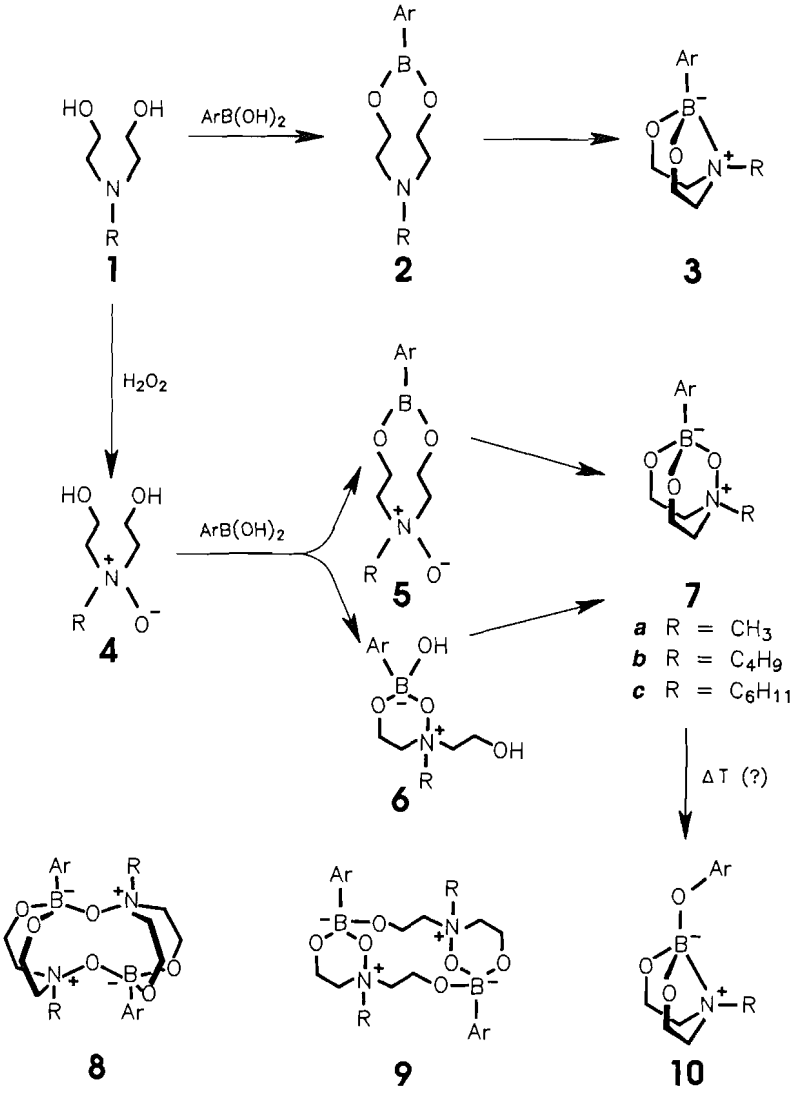

*inter*molecular (polymeric) O—B adducts of **5** or a dimerization product of **5**, like **8**. Similar chemical and spectroscopic features should also be shown by polycondensates of **6** or by the cyclic bis-condensate **9**, which can also be understood as a dimer of **7**. However, the ring sizes of **8** and **9**, and the mass spectral data for **7***a* (EI: 4% M^+; CI: 86% $M^+ + 1$) make these structural alternatives less probable than the monomer **7**. Another isomer of **7** with tetracoordinate boron also had to be considered: the rearrangement product **10** that is conceivable as a result of an intramolecular redox process **7** → **10** causing the oxidation of the boronic acid moiety to a boric acid moiety at the expense of the *N*-oxide function. Comparable findings have been reported for diarylboron chelates of *N*,*N*-dialkyl-*N*-(2-hydroxyalkyl)-amine-*N*-oxides under thermal stress (7, 8). However, a compound of type **10** should be obtainable by condensation of the bis(2-hydroxyethyl)amine **1**, boric acid, and a phenol (Ar-OH). Since we have not yet been able to isolate a crystalline product from this reaction it seemed unlikely that the thermal rearrangement product **10** had been formed. The *N*-methyl derivative **7***a* produced the best crystals for a definitive elucidation of the molecular structure by an X-ray crystallographic analysis.

A problem similar to that detailed above for **7** and its alternatives arises from the condensation of the *N*-oxide **11** with an arylboronic acid. In this case two primary condensates, the six-membered arylboronate **12** and the six-membered chelate **13**, could cyclize to the "cage" compound **14**, either by O → B coordination of the *N*-oxide group to the boronate group in **12**, or by further intramolecular condensation in **13**. In addition to the previously postulated bicyclo[2.2.2]octane ring system **14** (9), possible polyadducts of **12** or the dimer **15**, polycondensates of **13** or the cyclic bis-condensate **16**, and the isomeric rearrangement product **17** had to be considered. The ^{11}B nmr spectra, two of which are reported here,[5] show respective shift values of $\delta(Et_2OBF_3) = 4.0$ and 4.7 ppm for **14***a* (Ar = 3-$NO_2C_6H_4$) and **14***b* (Ar = 4-$CH_3OC_6H_4$). These values are consistent with the presence of a tetracoordinated boron atom (6). Experiments to crystallize a type **17** condensate from the reaction of 2-dimethylamino-2-hydroxymethylpropanol, boric acid, and a phenol have been unsuccessful so far, supporting the

[5] ^{11}B nmr spectra of $CDCl_3$ solutions of **14***a* and **14***b* were determined at 64.21 MHz.

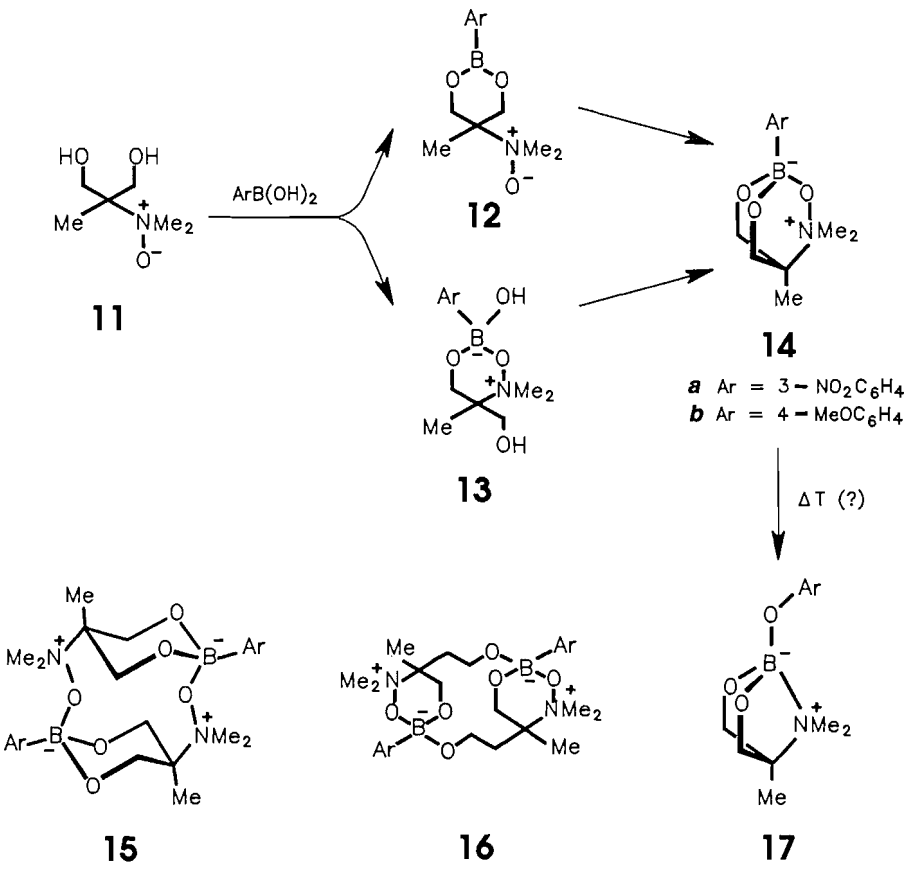

Can. J. Chem. Downloaded from www.nrcresearchpress.com by 88.255.202.194 on 09/08/12
For personal use only.

postulated structure **14**. To establish the structure in the solid state an X-ray crystallographic analysis of **14***a* (Ar = 3-$NO_2C_6H_4$), which forms the best crystals, was undertaken.

Boronate matrices have been shown to be very useful for the separation of various polyfunctional biomolecules, metabolites, and xenobiotics (10–12). Since nitrophenylboronate matrices in particular offer enhanced binding of most molecules having an affinity for such matrices (12), the structural elucidation of the nitrophenylboronate complexes in this work should supply valuable information on the chemical binding and geometry of species resulting from the interaction between polyfunctional ligands and boronic acids. There is also great interest in boronate complexes of polyfunctional compounds with respect to the transfer of reporter reagents into living cells in the area of biomedical research (13) and also in the construction of chiral cavities as specific receptor sites (14), broadening the significance of structural investigations of such boronate complexes.

Experimental

*1-Methyl-5-(3-nitrophenyl)-4,6,9-trioxa-1-azonia-5-boratabicyclo[3.3.1]nonane, 7*a

3-Nitrophenylboronic acid (167 mg, 1 mmol) and 1 mmol of the oily crude *N,N*-bis(2-hydroxyethyl)-*N*-methylamine *N*-oxide **4** (R = CH_3), prepared as described previously for similar *N*-oxides (3, 4, 9), were dissolved in 10 mL of ethanol and heated to the boiling point under reflux for 15 min. The solvent was partially distilled off. Crystallization started spontaneously or upon the addition of diethyl ether. Yield: 165 mg (62%), mp 191–193°C (from ethanol/diethyl ether). Infrared (KBr): 1605 (C=C), 1520 (NO_2, asym), 1350 (NO_2, sym) cm^{-1}; ^1H nmr (90 MHz, $CDCl_3$/TMS), δ (ppm): 3.30 (s, CH_3), 3.65 (t, J = 5 Hz, 2 NCH_2C), 3.9–4.5 (m, 2 OCH_2), 7.40 (t, 5-H of 3-nitrophenyl), 7.80–8.16 (m, 4-H and 6-H of 3-nitrophenyl), 8.40 (d, 2-H of 3-nitrophenyl); ^{11}B nmr (64.2 MHz, $CDCl_3$), δ (Et_2OBF_3): 5.4 ppm ($w_{1/2}$ = 128 Hz). Mass spectrum (EI, 150°C), *m/z*: 266 (4%, M^+), 222 (60%), 144 (100%), 114 (43%); (CI, NH_3, pos., 175°C), *m/z*: 267 (86%, M^+ + 1), 251 (75%), 191 (33%), 118 (100%). Anal. calcd. for $C_{11}H_{15}BN_2O_5$: C 49.66, H 5.68, N 10.53; found: C 49.62, H 5.65, N 10.73.

*1-Butyl-5-(3-nitrophenyl)-4,6,9-trioxa-1-azonia-5-boratabicyclo[3.3.1]nonane, 7*b

3-Nitrophenylboronic acid and *N*-butyl-*N,N*-bis(2-hydroxyethyl)amine *N*-oxide **4** (R = n-C_4H_9) were reacted as described for **7***a*. Yield: 49 mg (16%), mp 128–133°C (from ethanol/diethyl ether). Infrared (KBr): 1605 (C=C), 1520 (NO_2, asym), 1350 (NO_2, sym) cm^{-1}; ^{11}B nmr (64.2 MHz, $CDCl_3$), δ (Et_2OBF_3): 5.2 ppm ($w_{1/2}$ = 170 Hz). Anal. calcd. for $C_{14}H_{21}BN_2O_5$: C 54.57, H 6.87, B 3.51, N 9.09; found: C 54.58, H 7.05, B 3.59, N 9.36.

*1-Cyclohexyl-5-(3-nitrophenyl)-4,6,9-trioxa-1-azonia-5-boratabicyclo[3.3.1]nonane, 7*c

3-Nitrophenylboronic acid and *N*-cyclohexyl-*N,N*-bis(2-hydroxyethyl)amine *N*-oxide **4** (R = C_6H_{11}) were reacted as described for **7***a*. Yield: 200 mg (60%), mp 163–164°C (from ethanol/diethyl ether). Infrared (KBr): 1605 (C=C), 1520 (NO_2, asym), 1350 (NO_2, sym) cm^{-1}. Anal. calcd. for $C_{16}H_{23}BN_2O_5$: C 57.51, H 6.94, B 3.24, N 8.38; found: C 57.08, H 6.92, B 3.18, N 8.29.

3,3,4-Trimethyl-1-(3-nitrophenyl)-2,6,7-trioxa-3-azonia-1-boratabicyclo[2.2.2]octane, ***14***a

This compound was prepared as described previously (9). Additional analytical data: infrared (KBr): 1605 (C=C), 1520 (NO_2, asym), 1350 (NO_2, sym) cm^{-1}; ^1H nmr (90 MHz, DMSO-d_6/

Can. J. Chem. Downloaded from www.nrcresearchpress.com by 88.255.202.194 on 09/08/12
For personal use only.

TABLE 1. Crystallographic data[a]

	7*a*	**14***a*
Formula	$C_{11}H_{15}BN_2O_5$	$C_{12}H_{17}BN_2O_5$
fw	266.06	280.09
Crystal system	Orthorhombic	Orthorhombic
Space group	*Fdd*2	*Pbca*
a, Å	20.256(2)	21.402(2)
b, Å	37.652(2)	11.334(3)
c, Å	6.642(1)	11.248(2)
V, Å^3	5066(2)	2728.5(8)
Z	16	8
ρ_{calc}, g/cm^3	1.395	1.363
F(000)	2240	1184
μ(Cu-K$_\alpha$), cm^{-1}	8.75	8.38
Crystal size, mm	0.10 × 0.20 × 0.25	0.13 × 0.22 × 0.23
Transmission factors (relative)	0.92–1.00	0.73–1.00
Scan type	ω–2θ	ω–2θ
Scan range, deg in ω	1.10 + 0.20 tan θ	1.05 + 0.20 tan θ
Scan speed, deg/min	16	32
Data collected	$+h$, $+k$, $+l$	$+h$, $+k$, $+l$
$2\theta_{max}$, deg	155	155
Crystal decay	7.3%	5.3%
Total unique reflections	1404	2742
Reflections with $I \geq 3\sigma(I)$	975	1646
No. of variables	187	182
R	0.038	0.045
R_w	0.036	0.053
gof	2.62	2.11
Max Δ/σ (final cycle)	0.06	0.02
Residual density e/Å^3	−0.11 to +0.14	−0.19 to +0.21

[a]Temperature 294 K, Rigaku AFC6S diffractometer, Cu-K$_\alpha$ radiation (λ = 1.54178 Å), graphite monochromator, takeoff angle 6.0°, aperture 6.0 × 6.0 mm at a distance of 285 mm from the crystal, stationary background counts at each end of the scan (scan/background time ratio 2:1, up to 8 rescans), $\sigma^2(F^2) = [S^2(C + 4B) + (pF^2)^2]/Lp^2$ (S = scan rate, C = scan count, B = normalized background count, p = 0.00 for 7*a* and 0.02 for **14***a*), function minimized $\Sigma w(|F_o| - |F_c|)^2$ where $w = 4F_o^2/\sigma^2(F_o^2)$, $R = \Sigma||F_o| - |F_c||/\Sigma|F_o|$, $R_w = (\Sigma w(|F_o| - |F_c|)^2/\Sigma w|F_o|^2)^{1/2}$, and gof = $[\Sigma w(|F_o| - |F_c|)^2/(m - n)]^{1/2}$. Values given for R, R_w, and gof are based on those reflections with $I \geq 3\sigma(I)$.

TMS), δ (ppm): 1.14 (s, C-CH_3), 3.36 (s, N(CH_3)$_2$), 4.00 (q, AB, J = 10 Hz, 2 CH_2O), 7.37 (t, 5-H of 3-nitrophenyl), 7.65–8.05 (m, 4-H and 6-H of 3-nitrophenyl), 8.10 (d, 2-H of 3-nitrophenyl); ^{11}B nmr (64.2 MHz, $CDCl_3$), δ (Et_2OBF_3): 4.0 ppm ($w_{1/2}$ = 107 Hz).

Crystals suitable for X-ray analysis were obtained by repeated, very slow, recrystallization from ethanol.

X-ray crystallographic analyses of 7a *and* **14**a

Crystallographic data for 7*a* and **14***a* appear in Table 1. The final unit-cell parameters were obtained by least squares on the setting angles for 25 reflections with 2θ = 40.6–75.9° for 7*a* and 51.9–90.1° for **14***a*. The intensities of three standard reflections, measured every 200 reflections throughout the data collections, showed linear decays of 7.3% for 7*a* and 5.3% for **14***a*. The data were processed,[6] and corrected for Lorentz and polarization effects, decay, and absorption (empirical, based on azimuthal scans for four reflections).

The structures were solved by direct methods, the coordinates of the non-hydrogen atoms being determined from *E*-maps or from subsequent difference Fourier syntheses. The central carbon atoms of the three-atom bridges of the bicyclo[3.3.0]nonane skeleton of 7*a* were refined using a split-atom twofold disordered model. The thermal parameters for the remaining atoms of these two -OCC- moieties and the *N*-methyl carbon atom C(5) suggest minor disordering of these atoms as well. The low number of significant data for this non-centrosymmetric structure and the small separation between components preclude a complete resolution of the disorder. The site occupancy factors for the major component atoms (C(2) and C(4)) were refined, the sums of the occupancies at each site being constrained to equal 1.00. The low-occupancy carbon atom C(2A) in 7*a* was refined isotropically and all other non-hydrogen atoms of both structures were refined with anisotropic thermal parameters. The hydrogen atoms were fixed in idealized positions (C—H = 0.98 Å, B_H = 1.2 $B_{bonded\ atom}$). Corrections for secondary extinction were applied for both structures, the final values of the extinction coefficients being 1.27 × 10^{-6} for 7*a* and 1.11 × 10^{-6} for **14***a*. Neutral atom scattering factors for all atoms and anomalous dispersion corrections for the non-hydrogen atoms were taken from the *International tables for X-ray crystallography* (15). A parallel refinement of the structure of 7*a* having the opposite polarity gave slightly higher residuals, the R and R_w factor ratios being 1.0026 and 1.0028, respectively. Final atomic coordinates and equivalent isotropic thermal parameters, bond lengths, and bond angles appear in Tables 2–4, respectively. Hydrogen atom

[6]TEXSAN/TEXRAY structure analysis package, which includes versions of the following: DIRDIF, direct methods for difference structures, by P. T. Beurskens; ORFLS, full-matrix least squares, and ORFFE, function and errors, by W. R. Busing, K. O. Martin, and H. A. Levy; ORTEP II, illustrations, by C. K. Johnson.

TABLE 2. Final atomic coordinates (fractional) and B_{eq} (Å^2)[a]

Atom	x	y	z	B_{eq}	Occ.
		7*a*			
O(1)	0.63578(10)	0.19026(5)	0.5619	5.0	
O(2)	0.60220(15)	0.14136(8)	0.3500(8)	7.6	
O(3)	0.56439(14)	0.14445(8)	0.6894(8)	7.8	
O(4)	0.3578(2)	0.20898(13)	0.7931(9)	11.5	
O(5)	0.3243(2)	0.24978(14)	0.5868(10)	13.7	
N(1)	0.69290(13)	0.17095(8)	0.6236(8)	5.5	
N(2)	0.3627(2)	0.22578(15)	0.6360(11)	8.6	
C(1)	0.7151(2)	0.14794(11)	0.4521(11)	7.2	
C(2)	0.6620(3)	0.1240(3)	0.3706(12)	7.1	0.85
C(2A)	0.6639(15)	0.1474(11)	0.334(5)	5.0	0.15
C(3)	0.6766(2)	0.15123(13)	0.8140(10)	7.0	
C(4)	0.6115(5)	0.1300(6)	0.816(3)	6.6	0.59
C(4A)	0.6054(8)	0.1512(10)	0.829(3)	6.5	0.41
C(5)	0.7444(2)	0.19783(11)	0.6668(13)	9.0	
C(6)	0.5199(2)	0.18840(8)	0.4377(8)	4.5	
C(7)	0.4675(2)	0.19639(9)	0.5667(8)	5.0	
C(8)	0.4163(2)	0.21771(10)	0.4983(10)	5.5	
C(9)	0.4147(2)	0.23151(10)	0.3078(10)	5.6	
C(10)	0.4657(2)	0.22353(9)	0.1798(9)	5.6	
C(11)	0.5172(2)	0.20240(9)	0.2467(8)	5.1	
B(1)	0.5807(2)	0.16442(10)	0.5108(10)	5.0	
		14*a*			
O(1)	0.24193(7)	0.38083(15)	0.4877(2)	4.8	
O(2)	0.21720(8)	0.5580(2)	0.5953(2)	4.5	
O(3)	0.21281(8)	0.5575(2)	0.3828(2)	4.4	
O(4)	0.01010(11)	0.4314(3)	0.2079(2)	7.1	
O(5)	−0.05112(10)	0.3111(3)	0.2974(2)	8.1	
N(1)	0.30688(9)	0.4083(2)	0.4868(2)	3.4	
N(2)	−0.00474(12)	0.3757(3)	0.2953(3)	5.6	
C(1)	0.31335(11)	0.5448(2)	0.4820(2)	3.4	
C(2)	0.28030(12)	0.5937(2)	0.5923(2)	3.8	
C(3)	0.27643(12)	0.5869(2)	0.3742(2)	3.8	
C(4)	0.38127(12)	0.5822(3)	0.4765(3)	4.6	
C(5)	0.33370(13)	0.3551(2)	0.5961(3)	4.8	
C(6)	0.33380(14)	0.3480(2)	0.3811(3)	5.1	
C(7)	0.13022(11)	0.4405(2)	0.4952(2)	3.3	
C(8)	0.09329(11)	0.4308(2)	0.3940(2)	3.8	
C(9)	0.03388(11)	0.3824(2)	0.4030(3)	4.1	
C(10)	0.00893(12)	0.3438(2)	0.5083(3)	4.5	
C(11)	0.04445(14)	0.3549(2)	0.6088(3)	4.7	
C(12)	0.10394(13)	0.4026(2)	0.6015(3)	4.2	
B(1)	0.20044(12)	0.4908(2)	0.4898(3)	3.2	

[a]$B_{eq} = (8/3)\pi^2\Sigma\Sigma U_{ij}a_i^*a_j^*(\mathbf{a}_i \cdot \mathbf{a}_j)$.

Can. J. Chem. Downloaded from www.nrcresearchpress.com by 88.255.202.194 on 09/08/12
For personal use only.

parameters, anisotropic thermal parameters, torsion angles, intermolecular contacts, and least-squares planes, and measured and calculated structure factor amplitudes for both structures have been supplied as supplementary material.[7]

[7]Supplementary material mentioned in the text may be purchased from: The Depository of Unpublished Data, Document Delivery, CISTI, National Research Council Canada, Ottawa, Canada K1A 0S2.

Tables of hydrogen atom coordinates and bond lengths and angles involving hydrogen atoms have also been deposited with the Cambridge Crystallographic Data Centre and can be obtained on request from The Director, Cambridge Crystallographic Data Centre, University Chemical Laboratory, 12 Union Road, Cambridge CB2 1EZ, U.K.

Results and discussion

The X-ray analyses establish the postulated structures of **7***a* and **14***a* (Fig. 1), both representing examples of bicyclic boron-nitrogen betaines with the anionic borate centre at one of the bridgehead positions and the cationic ammonium nitrogen atoms at the other bridgehead position in **7***a*, and forming part of the bridge itself in **14***a*. Compound **7***a* is a new type of hetero-analog of bicyclo-[3.3.1]nonane (14) containing five hetero atoms in the ring skeleton and bearing substituents at both bridgeheads. As a result of the disordering of the "wing tip" atoms C(2) and C(4) (see experimental section), there are three possible conformations for the bicyclo[3.3.1]nonane skeleton in **7***a*. The most probable conformation (50%, based on the re-

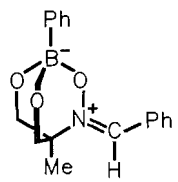

18

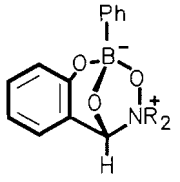

19

(R_2N = piperidino)

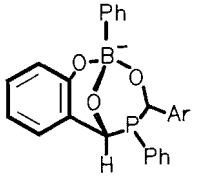

20

(Ar = 2 - HOC_6H_4)

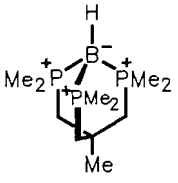

21

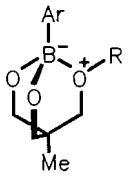

22

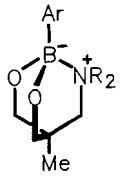

23

TABLE 3. Bond lengths (Å) with estimated standard deviations

Atom	Atom	Distance	Atom	Atom	Distance
			7a		
O(1)	N(1)	1.427(3)	N(2)	C(8)	1.452(6)
O(1)	B(1)	1.519(5)	C(1)	C(2)	1.50(1)
O(2)	C(2)	1.383(6)	C(1)	C(2A)	1.30(3)
O(2)	C(2A)	1.27(3)	C(3)	C(4)	1.54(2)
O(2)	B(1)	1.444(6)	C(3)	C(4A)	1.44(2)
O(3)	C(4)	1.38(1)	C(6)	C(7)	1.396(5)
O(3)	C(4A)	1.27(2)	C(6)	C(11)	1.375(6)
O(3)	B(1)	1.443(6)	C(6)	B(1)	1.602(5)
O(4)	N(2)	1.224(6)	C(7)	C(8)	1.389(5)
O(5)	N(2)	1.236(6)	C(8)	C(9)	1.368(6)
N(1)	C(1)	1.500(6)	C(9)	C(10)	1.370(6)
N(1)	C(3)	1.504(7)	C(10)	C(11)	1.386(5)
N(1)	C(5)	1.481(5)			
			14a		
O(1)	N(1)	1.425(2)	N(2)	C(9)	1.468(4)
O(1)	B(1)	1.530(3)	C(1)	C(2)	1.532(4)
O(2)	C(2)	1.411(3)	C(1)	C(3)	1.524(4)
O(2)	B(1)	1.455(3)	C(1)	C(4)	1.516(3)
O(3)	C(3)	1.405(3)	C(7)	C(8)	1.390(3)
O(3)	B(1)	1.446(3)	C(7)	C(12)	1.389(4)
O(4)	N(2)	1.211(3)	C(7)	B(1)	1.608(3)
O(5)	N(2)	1.234(3)	C(8)	C(9)	1.389(3)
N(1)	C(1)	1.555(3)	C(9)	C(10)	1.371(4)
N(1)	C(5)	1.485(3)	C(10)	C(11)	1.368(4)
N(1)	C(6)	1.488(3)	C(11)	C(12)	1.386(4)

fined site occupancy factors) is the chair–chair arrangement involving the higher-occupancy sites C(2) and C(4). The two possible chair–boat conformations, C(2) and C(4A), C(2A) and C(4), have a combined probability of 44% while the boat–boat form with C(2A) and C(4A) has a 6% probability. For the chair–chair conformation, the O—C—C "wings" appear to be somewhat flattened, probably due to steric repulsions between the *endo* hydrogen atoms at C(2) and C(4). There also appears to be some flattening of the boat components but this may result from errors arising from incomplete modelling of the disorder since the lower-occupancy sites are involved. It is likely that the atoms adjacent to C(2) and C(4) also suffer minor unresolved disorder. In **14***a* the *N*-oxide oxygen–boron coordination (O(1)—B(1)) forces the 1,3-dioxa-2-boracyclohexane ring of the cyclic boronate of type **12** into a somewhat distorted boat conformation.

The tetracoordinated sp^3-boron atoms in both **7***a* and **14***a* show nearly ideal tetrahedral ligand arrangements. Comparable modes of boron coordination have been observed in the intramolecular nitrone adduct **18** (16) and also in a similar cage structure reported for the intramolecular amine *N*-oxide adduct **19** (17). Compound **18** possesses exactly the same heterobicyclo[2.2.2]octane ring system as **14***a*, whereas **19** represents a benzo-fused derivative of an analogous heterobicyclo[3.2.1]octane skeleton. Another related cage structure, containing a tetracoordinated boron atom, has been reported for the bicyclic anion **20** (18).

Within the 1,3-betainic ring segments in **7***a*, **14***a*, **18**, and **19**, the N—O(B) distances in **7***a*, **14***a*, and **19** (17) (1.427(3), 1.425(2), and 1.424(1) Å, respectively) are equal within experimental error and are significantly longer than the N—O bond of 1.352(5) Å in **18** (16), consistent with the retention of some double bond character in the latter case. The (N)O—B bond lengths in **7***a* (1.519(5) Å), **14***a* (1.530(3) Å, and **19** (1.539(2) Å) differ slightly, presumably for steric reasons. The ring system in **7***a* is practically free from angular strain while those in **14***a* and **19** would be expected to have somewhat more strained ring skeletons. The shorter (N)O—B bonds in **7***a* and **14***a* are in accord with the increased Lewis acidity of the boronic acid relative to those in **18** and **19**. The substantially longer (N)O—B bond in **18** (1.601(7) Å) reflects primarily the lower basicity of the azomethine *N*-oxide group compared with that of the amine *N*-oxide group in **14***a*, and perhaps, to a lesser extent, the lower Lewis acidity of the phenylboronic acid relative to that of the 3-nitrophenylboronic acid components of these two compounds.

The B—C(aryl) bond lengths **7***a* (1.602(5) Å) and **14***a* (1.608(3) Å) may be compared with other (sp^3)B—C(aryl) distances that range from 1.581(5) to 1.606(5) Å (19, and references therein). The B—C(aryl) bonds in the present structures are somewhat longer than those in **18**, **19**, and **20** that are all 1.591 (2–8) Å, consistent with stronger binding of the 3-nitrophenylboron moiety to the oxygen atoms of the tridentate ligands. The sums of bond lengths about the boron

Can. J. Chem. Downloaded from www.nrcresearchpress.com by 88.255.202.194 on 09/08/12
For personal use only.

TABLE 4. Bond angles (deg) with estimated standard deviations

Atom	Atom	Atom	Angle	Atom	Atom	Atom	Angle
			7*a*				
N(1)	O(1)	B(1)	109.5(2)	N(1)	C(3)	C(4A)	106(1)
C(2)	O(2)	B(1)	118.4(4)	O(3)	C(4)	C(3)	112(1)
C(2A)	O(2)	B(1)	105(2)	O(3)	C(4A)	C(3)	127(1)
C(4)	O(3)	B(1)	123.3(6)	C(7)	C(6)	C(11)	117.0(3)
C(4A)	O(3)	B(1)	110(1)	C(7)	C(6)	B(1)	121.3(4)
O(1)	N(1)	C(1)	108.6(3)	C(11)	C(6)	B(1)	121.7(4)
O(1)	N(1)	C(3)	108.3(3)	C(6)	C(7)	C(8)	119.4(4)
O(1)	N(1)	C(5)	106.2(3)	N(2)	C(8)	C(7)	118.3(5)
C(1)	N(1)	C(3)	114.8(3)	N(2)	C(8)	C(9)	119.1(4)
C(1)	N(1)	C(5)	109.3(4)	C(7)	C(8)	C(9)	122.6(4)
C(3)	N(1)	C(5)	109.2(5)	C(8)	C(9)	C(10)	118.2(4)
O(4)	N(2)	O(5)	123.5(6)	C(9)	C(10)	C(11)	119.7(4)
O(4)	N(2)	C(8)	119.3(5)	C(6)	C(11)	C(10)	123.0(4)
O(5)	N(2)	C(8)	117.2(6)	O(1)	B(1)	O(2)	109.2(4)
N(1)	C(1)	C(2)	113.9(4)	O(1)	B(1)	O(3)	108.5(4)
N(1)	C(1)	C(2A)	103(2)	O(1)	B(1)	C(6)	105.8(3)
O(2)	C(2)	C(1)	112.2(6)	O(2)	B(1)	O(3)	111.3(3)
O(2)	C(2A)	C(1)	137(3)	O(2)	B(1)	C(6)	110.3(4)
N(1)	C(3)	C(4)	116.9(6)	O(3)	B(1)	C(6)	111.5(4)
			14*a*				
N(1)	O(1)	B(1)	112.9(2)	O(2)	C(2)	C(1)	110.9(2)
C(2)	O(2)	B(1)	111.5(2)	O(3)	C(3)	C(1)	111.9(2)
C(3)	O(3)	B(1)	111.0(2)	C(8)	C(7)	C(12)	116.7(2)
O(1)	N(1)	C(1)	107.7(2)	C(8)	C(7)	B(1)	121.9(2)
O(1)	N(1)	C(5)	106.4(2)	C(12)	C(7)	B(1)	121.4(2)
O(1)	N(1)	C(6)	106.5(2)	C(7)	C(8)	C(9)	119.5(3)
C(1)	N(1)	C(5)	113.5(2)	N(2)	C(9)	C(8)	118.4(3)
C(1)	N(1)	C(6)	113.3(2)	N(2)	C(9)	C(10)	118.5(3)
C(5)	N(1)	C(6)	109.0(2)	C(8)	C(9)	C(10)	123.1(3)
O(4)	N(2)	O(5)	122.4(3)	C(9)	C(10)	C(11)	117.9(2)
O(4)	N(2)	C(9)	119.7(3)	C(10)	C(11)	C(12)	119.9(3)
O(5)	N(2)	C(9)	117.9(3)	C(7)	C(12)	C(11)	122.9(3)
N(1)	C(1)	C(2)	106.9(2)	O(1)	B(1)	O(2)	107.2(2)
N(1)	C(1)	C(3)	107.0(2)	O(1)	B(1)	O(3)	107.9(2)
N(1)	C(1)	C(4)	111.4(2)	O(1)	B(1)	C(7)	104.7(2)
C(2)	C(1)	C(3)	107.0(2)	O(2)	B(1)	O(3)	111.1(2)
C(2)	C(1)	C(4)	112.0(2)	O(2)	B(1)	C(7)	112.6(2)
C(3)	C(1)	C(4)	112.2(2)	O(3)	B(1)	C(7)	112.8(2)

atoms in **7*a*** (6.008 Å)[8] and **14*a*** (6.039 Å) are similar to the values reported for **18** (6.101 Å), **19** (6.099 Å), **20** (6.042 Å), and other compounds having the (aryl)CBO_3 ligand set (19, and references therein) and also that reported for the (alkyl)CBO_3 ligand set of a methylboronate-capped tris(dioximate) complex of Tc(III) (6.093 Å) (20). The bond length sum reflects the overall steric strain at the boron centre.

In addition to the compounds **14*a*** (this work) and **18** (16), which represent the first structurally characterized arylboronates having a bicyclo[2.2.2]octane ring system, one other analogous structure, **21**, derived from a tripodal phosphane, has been reported (21). The larger radius of phosphorus relative to that of oxygen gives rise to a substantial distortion of the bicyclo[2.2.2]octane skeleton, most noticeably affecting the bond angles about the boron atom: the O—B—O angles in **14*a*** range from 107.2(2) to 111.1(2)°, whereas the P—B—P angles in **21** are significantly more acute, ranging from 101.3(5) to 104.6(5)°. Bicyclo[2.2.2]octane skeletons have been postulated for the arylboronates of 2,2-bis(hydroxymethyl)propanal and 2,2-bis(hydroxymethyl)-propanamine derivatives, **22** and **23**, that were believed to be at least partially stabilized by intramolecular coordination. Infrared and nmr (22, 23) as well as FAB mass spectroscopic data (24) indicated a boronate cage structure featuring a tetracoordinated boron atom. The structure of **14*a*** provides additional support for the postulated structures **22** and **23**. The bicyclo[3.3.1]nonane and bicyclo[2.2.2]octane ring skeletons found for the two types of compounds studied here appear to be very stable. Several samples of type **7** and **14** compounds have remained unchanged over a period of 20 years, stored under normal atmospheric conditions in the laboratory.

The most notable features of the crystal packing arrangements of both **7*a*** and **14*a*** are pairs of weak intermolecular C—H···O interactions. In **7*a*** these interactions both involve hydrogen atoms bound to *N*-methylene car-

[8]Due to ligand disordering, the O—B distances in **7*a*** may suffer some degree of foreshortening, resulting in a smaller sum than is actually the case. This sum would nonetheless be expected to be smaller than in the more strained compound **14*a***.

Can. J. Chem. Downloaded from www.nrcresearchpress.com by 88.255.202.194 on 09/08/12
For personal use only.

Can. J. Chem. Downloaded from www.nrcresearchpress.com by 88.255.202.194 on 09/08/12
For personal use only.

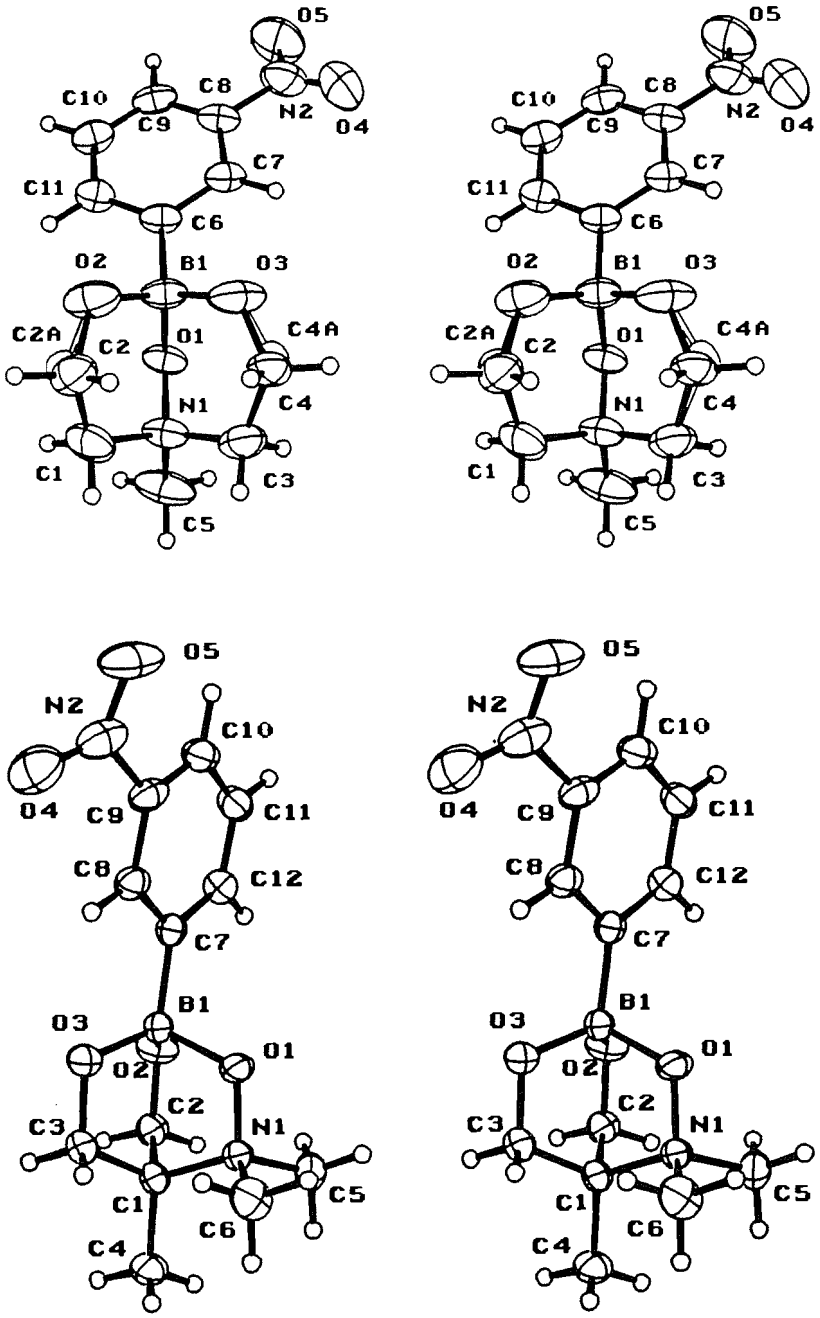

FIG. 1. Stereoviews of **7***a* (top) and **14***a* (bottom); 33% probability thermal ellipsoids are shown for the non-hydrogen atoms.

bon atoms of the chair forms of the 1-aza-2,4-dioxa-3-boracyclohexane rings and (C)O(B) oxygen atoms of the same rings (C(1)—H(1)···O(2)(1/2 + x, 1/4 − y, 1/4 − z) and C(3)—H(6)···O(3)(1/2 + x, 1/4 − y, 1/4 − z), H···O = 2.33 and 2.42 Å, C···O = 3.297(5) and 3.384(5) Å, C—H···O = 168 and 166°, respectively). In **14***a* the C—H···O interactions involve one of the *N*-methyl groups and oxygen atoms of the nitro group and the 1,3-dioxa-2-boracyclohexane ring (C(6)—H(11)···O(3)(1/2 − x, y − 1/2, z) and C(6)—H(13)···O(5)(1/2 + x, y, 1/2 − z), H···O = 2.48 and 2.54 Å, C···O = 3.440(3) and 3.205(4) Å, C—H···O = 166 and 125°, respectively). The C···O distances are less than or near the sum of the van der Waals radii of a methyl group and an oxygen atom (25).

Acknowledgments

We thank the Natural Sciences and Engineering Research Council of Canada and the Fonds der Chemischen Industrie, Frankfurt am Main, for financial support. We are grateful to the Chemische Institute der Technischen Universität Braunschweig for running the ^{11}B nmr and mass spectra.

1. (*a*) H. K. Zimmerman. Adv. Chem. Ser. **42**, 23 (1964); (*b*) I. B. Mazeika, A. G. Gaukhman, I. P. Urtane, G. I. Zelchan, and E. Lukevits. J. Gen. Chem. USSR, **49**, 2233 (1979); (*c*) R. Csuk, N. Müller, and H. Sterk. Z. Naturforsch. **B40**, 987 (1985).
2. S. J. Rettig and J. Trotter. Can. J. Chem. **53**, 1393 (1975).
3. (*a*) M. F. Zienty and H. C. Stalter. U.S. Pat. 3 309 399 (1967);

Chem. Abstr. **67**, 73328 f (1967); (*b*) S. Kida, T. Katayama, and Y. Nishida. Inorg. Chim. Acta, **17**, 55 (1976); (*c*) W. N. Marmer and W. M. Linfield. J. Am. Oil Chem. Soc. **53**, 73 (1976).
4. W. Kliegel. Z. Chem. **10**, 437 (1970).
5. K. Torssell. Prog. Boron Chem. **1**, 369 (1964).
6. H. Nöth and B. Wrackmeyer. Nuclear magnetic resonance spectroscopy of boron compounds. Springer-Verlag, Berlin. 1978.
7. (*a*) W. Kliegel. Liebigs Ann. Chem. **763**, 61 (1972); (*b*) W. Kliegel and E. Ahlenstiel. J. Organomet. Chem. **277**, 173 (1984).
8. E. Ebeling, W. Kliegel, S. J. Rettig, and J. Trotter. Can. J. Chem. **67**, 933 (1989).
9. W. Kliegel and E. Ahlenstiel. Chem. Ber. **110**, 1623 (1977).
10. W. Kliegel. Bor in Biologie, Medizin und Pharmazie. Springer-Verlag, Berlin. 1980.
11. P. G. Dean and F. A. Middle. Affinity chromatography. Marcel Dekker, Basel. 1985.
12. R. P. Singhal, B. Ramamurthy, N. Govindraj, and Y. Sarwar. J. Chromatogr. **543**, 17 (1991).
13. (*a*) P. M. Gallop, M. A. Paz, and E. Henson. Science, **217**, 166 (1982); (*b*) P. M. Gallop, M. A. Paz, E. Henson, and S. A. Latt. BioTechniques, **2**, 32 (1984).
14. N. S. Zefirov and V. A. Palyulin. Top. Stereochem. **20**, 171 (1991).
15. International tables for X-ray crystallography. Vol. IV. Kynoch Press, Birmingham, U.K. (present distributor Kluwer Academic Publishers, Dordrecht, The Netherlands). 1974. pp. 99–102 and 149.
16. W. Kliegel, L. Preu, S. J. Rettig, and J. Trotter. Can. J. Chem. **63**, 509 (1985).
17. W. Kliegel, H.-W. Motzkus, K. Drückler, S. J. Rettig, and J. Trotter. Can. J. Chem. **68**, 64 (1990).
18. I. A. Litvinov. Zh. Strukt. Khim. **31**, No. 2, 194 (1990); J. Struct. Chem. **31**, 359 (1990).
19. W. Kliegel, G. Lubkowitz, S. J. Rettig, and J. Trotter. Can. J. Chem. **70**, 2015 (1992).
20. K. E. Linder, M. F. Malley, J. Z. Gougoutas, S. E. Unger, and A. D. Nunn. Inorg. Chem. **29**, 2428 (1990).
21. H. Schmidbaur, T. Wimmer, G. Reber, and G. Müller. Angew. Chem. **100**, 1135 (1988).
22. J. Bartulin, M. Przybylski, H. Ringsdorf, and H. Ritter. Makromol. Chem. **175**, 1007 (1964).
23. J. Bartulin, M. Zarraga, and H. Zunza. Bol. Soc. Chil. Quim. **27**, 138 (1982); Chem. Abstr. **97**, 92358b (1982).
24. M. E. Rose, C. Longstaff, and P. D. G. Dean. Biomed. Mass Spectrom. **10**, 512 (1983).
25. D. J. Sutor. J. Chem. Soc. 1105 (1963).
26. W. Kliegel, G. Lubkowitz, S. J. Rettig, and J. Trotter. Can. J. Chem. **70**, 2809 (1992).

Can. J. Chem. Downloaded from www.nrcresearchpress.com by 88.255.202.194 on 09/08/12
For personal use only.

Dioxirane formation in ozonolysis of *E*- and *Z*-1,2-dimethoxy-1,2-diphenylethene

KARL R. KOPECKY,[1] YU XIE, AND JOSÉ MOLINA[2]

Department of Chemistry, University of Alberta, Edmonton, Alta., Canada T6G 2G2

Received October 6, 1992

KARL R. KOPECKY, YU XIE, and JOSÉ MOLINA. Can. J. Chem. **71**, 272 (1993).

Addition of ozone to *E*- or *Z*-1,2-dimethoxy-1,2-diphenylethene, *E*- or *Z*-**1**, in inert solvents results in formation of ~1 mole of methyl benzoate, ~0.5 and ~0.1 mole of the corresponding oxiranes **2** and dioxetanes **3**, respectively, and 0.03 mole of 3,6-dimethoxy-3,6-diphenyl-1,2,4,5-tetroxane **4** at −20°C. Product distributions vary with starting material, initial concentration, extent of reaction, and temperature. At −70°C ~0.3 mole of *trans*-**2** and 0.2 mole of *cis*- and *trans*-**4** are formed from *E*-**1**. Addition of *E*- or *Z*-**1** to solutions of excess ozone results in formation of up to 0.7 mole of (methoxy)phenyldioxirane **5**, which is a strong, stereospecific epoxidizing agent.

KARL R. KOPECKY, YU XIE et JOSÉ MOLINA. Can. J. Chem. **71**, 272 (1993).

L'addition d'ozone, à −20°C, aux *E*- et *Z*-1,2-diméthoxy-1,2-diphényléthène, *E*- et *Z*-**1**, dans des solvants inertes, conduit à la formation d'environ 1 mole de benzoate de méthyle, d'environ 0,5 et 0,1 mole respectivement des oxiranes (**2**) et dioxétanes (**3**) correspondants et de 0,03 mole de 3,6-diméthoxy-3,6-diphényl-1,2,4,5-tétroxane (**4**). La distribution des produits varie avec la nature du produit de départ, l'avancement de la réaction et la température. À −70°C, le produit *E*-**1** conduit à la formation d'environ 0,3 mole du produit *trans*-**2** et de 0,2 mole des isomères *cis*- et *trans*-**4**. L'addition des composés *E*- ou *Z*-**1** à des solutions contenant de l'ozone en excès conduit à la formation de jusqu'à 0,7 mole du (méthoxy)phényldioxirane (**5**) qui est un puissant agent d'époxydation stéréospécifique.

[Traduit par la rédaction]

Ozonolysis of tetramethoxyethene results in the formation of mainly tetramethoxy-1,2-dioxetane and methyl trimethoxyacetate with relatively little cleavage product, dimethyl carbonate, eq. [1] (1). This unusual result prompted

[1] $(CH_3O)_2C{=}C(OCH_3)_2 \longrightarrow$ 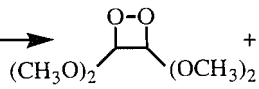 $+ CH_3O_2CC(OCH_3)_3 + (CH_3O)_2CO$

~ 35% ~ 40% ~ 20%

a survey of the ozonolysis of other electron-rich alkenes. Luminescent reaction mixtures, indicative of the presence of 1,2-dioxetanes, were formed from *E*- and *Z*-1,2-dimethoxy-1,2-diphenylethene, *E*- and *Z*-**1**. A detailed study of the ozonolysis of these alkenes showed that large amounts of the noncleavage products, 2,3-dimethoxy-2,3-diphenyloxirane **2** and 3,4-dimethoxy-3,4-diphenyl-1,2-dioxetane **3** were formed in addition to the cleavage products, methyl benzoate and 3,6-dimethoxy-3,6-diphenyl-1,2,4,5-tetroxane **4**. Product distributions vary with starting material, temperature, initial concentration, solvent, and extent of reaction. The dioxetanes and oxiranes are formed stereospecifically. At −20°C, **2, 3**, and methyl benzoate are almost the exclusive products, but at −70°C significant amounts of **4** are also produced, especially from *E*-**1**, Table 1.

Small-scale reactions were carried out by delivering measured amounts of ozone from a gas syringe (1) into CD_2Cl_2 solutions of the alkenes in nmr tubes at −20°C or below. The reaction mixtures were analysed by ^1H nmr spectroscopy at −20°C. The ^1H nmr signals of the OCH_3 groups of the various products are well separated and occur at δ (CD_2Cl_2, −20°C): 3.87, methyl benzoate; 3.24, *trans*-**2**; 3.29, *cis*-**2**; 3.06, *trans*-**3**; 3.36, *cis*-**3**; 3.59, *trans*-**4**; and 3.69, *cis*-**4**. The dioxetanes were identified by comparison of ^1H and ^{13}C signals in the nmr spectra of the reaction mixtures with those of authentic *cis*- and *trans*-**3** prepared by singlet oxygen oxidation of *Z*- and *E*-**1** (2). The oxiranes were identified on the basis of their thermal rearrangement at 20°C to 2,2-dimethoxy-1,2-diphenylethanone **5** (3) and their rapid hydrolysis to benzil. Signals at δ 92.64 and δ 92.74 in the ^{13}C nmr spectra of the reaction mixtures were assigned to *trans*- and *cis*-**2**, respectively. All other ^{13}C nmr signals could be assigned to isolable compounds of known structure. Preparative scale ozonolysis of *E*-**1** resulted in isolable (by thick-layer chromatography on silica gel, 10 developments with 2% ethyl acetate in hexane) amounts of *cis*- and *trans*-**4**. It was necessary first to convert *trans*-**2** to benzil and then treat the resulting mixture briefly with hot methanolic hydroxide ion to convert the benzil to benzilic acid anion. The ^1H nmr signal of the OCH_3 groups of the isomer melting at 145–146°C broadened on cooling and was split into two peaks, δ 3.82 and 3.70 at −65°C. The OCH_3 signal of the isomer melting at 113–114°C remained a sharp singlet down to −65°C. These isomers were thus assigned to be *cis*- and *trans*-**4**, respectively. Both isomers were decomposed to methyl benzoate radical cation and its fragmentation products upon electron impact. However, chemical ionization with

[1]Author to whom correspondence may be addressed.

[2]Recipient of a travel grant from the Consejeria de Education y Ciencias, Junta de Andalucia, 1986.

Can. J. Chem. Downloaded from www.nrcresearchpress.com by 88.255.202.194 on 09/08/12
For personal use only.

TABLE 1. Product distribution from ozonolysis of *E*- and *Z*-**1** in CD_2Cl_2

Alkene	Temperature, °C	Products, moles per mole of **1**				
		$PhCO_2CH_3$	**2**[a]	**3**[a]	**4**[b]	**6**
E-**1**	−20[c]	0.92	0.48	0.01	0.03	0
	−70[c]	1.00	0.28	0.02	0.20	0
	−20[d]	0.86	0.20	0.03	0	0.69
	−70[d]	1.02	0.12	0.02	0.19	0.25
Z-**1**	−20[c]	0.66	0.53	0.12[e]	0.03	0
	−70[c]	0.50	0.47	0.20	0.07	0
	−20[d]	0.50	0.37	0.18	0	0.46
	−70[d]	0.46	0.32	0.23	0.06	0.28

[a]Only *trans* from *E*-**1** and only *cis* from *Z*-**1**.
[b]Equal amounts of *cis* and *trans*.
[c]Normal addition of ozone to ~0.1 M solutions of alkene.
[d]Slow addition of ~0.01 M solutions of alkene to solutions of excess ozone.
[e]None in the presence of 2,5-dimethylfuran.

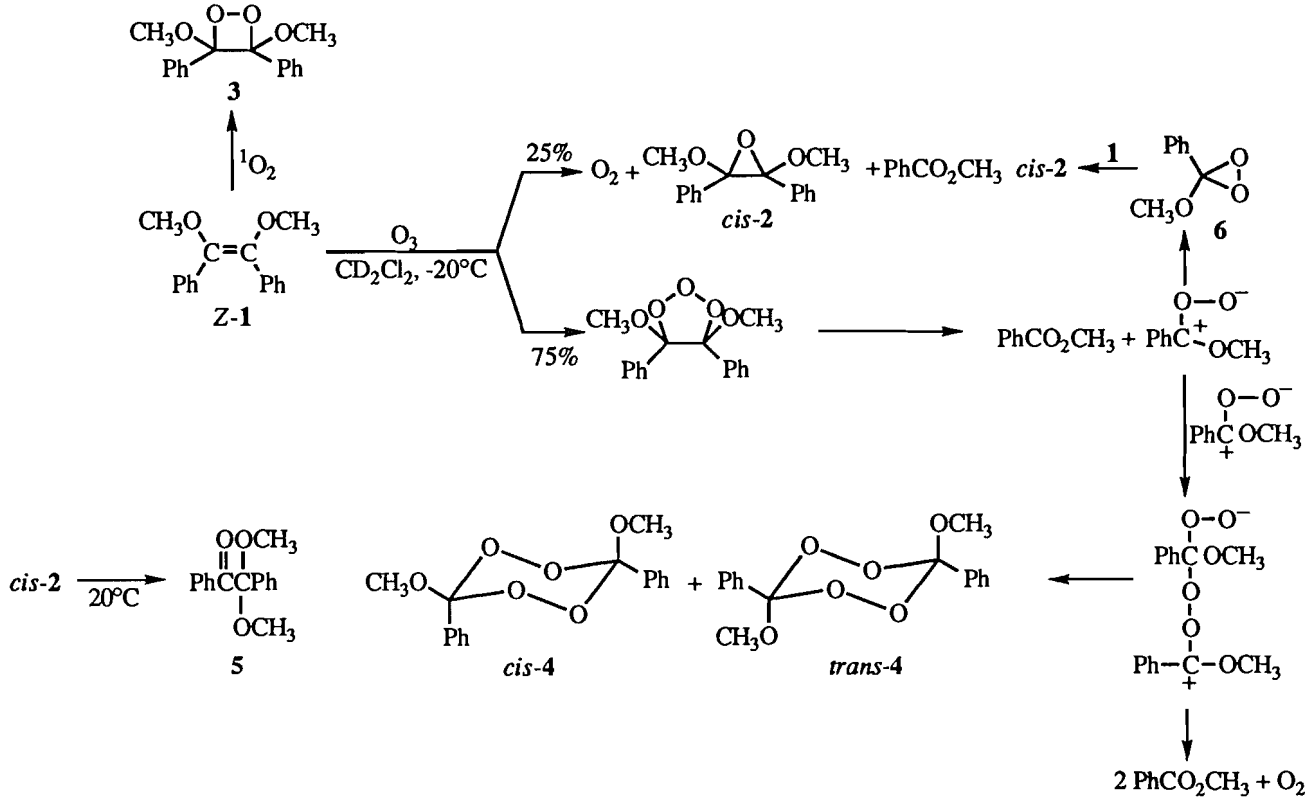

SCHEME 1

$\overset{+}{N}H_4$ afforded the ($M + H^+$) and the $M + \overset{+}{N}H_4$) ions at *m/e* 305 and 322, respectively, from each isomer.

Evidence that the dioxetanes are formed by reaction between singlet oxygen and the alkenes was obtained by carrying out the ozonolysis at −20°C in the presence of some 2,5-dimethylfuran (1). No dioxetane was found although methyl benzoate and oxirane were still formed in similar relative amounts as in the absence of the furan.

At this point it still was not clear how oxirane and singlet oxygen are produced. A possible contribution to oxirane formation from a radical chain oxidation reaction between oxygen and the alkenes (1, 4) could be ruled out. Such a reaction would be unlikely to lead to *cis*-**2** as the only oxirane formed from *Z*-**1**. In fact, when an oxygen-saturated solution of *Z*-**1** containing some di-*tert*-butyl trioxide (5) was allowed to warm slowly from −40° to −20°C a 90:10 mixture of *cis*:*trans*-**2** was formed, along with methyl benzoate, in contrast to the exclusive formation of *cis*-**2** in the ozonolysis reaction.

Attempts to determine whether there is a contribution from a direct reaction between ozone and the alkenes to give oxirane and singlet oxygen (6) resulted in a very enlightening observation. If such a direct reaction occurred, slow addition of alkene to excess ozone should still result in forma-

Can. J. Chem. Downloaded from www.nrcresearchpress.com by 88.255.202.194 on 09/08/12
For personal use only.

tion of large amounts of oxirane. The ^1H nmr spectrum of such a light-yellow ozonolysis reaction mixture from either *E*- or *Z*-**1** at −20°C contained a strong new OCH_3 signal at δ 3.50 (CD_2Cl_2) that decreased slowly in intensity as the signal of the OCH_3 group of methyl benzoate increased in intensity and the yellow color disappeared, when the solution was warmed to 0°C. Relatively much smaller amounts of oxirane and dioxetane were produced than in the normal ozonolyses. Addition at −70°C of *E*- or *Z*-**1** or *E*- or *Z*-2-butene to the reaction mixtures led within a few minutes to the consumption of the new intermediate together with the stereospecific conversion of the alkenes to the corresponding oxiranes. Coincident with the consumption of the intermediate by the alkenes is an equivalent increase in the amount of methyl benzoate and loss of the yellow color. These reactions are strong evidence for the presence of (methoxy)phenyldioxirane **6**. Consistent with this is the presence of a new signal at δ 109.1 in the ^{13}C nmr spectra of reaction mixtures from the inverse ozonolysis of both *E*- and *Z*-**1**. The position of this signal is in the region expected for a carbon atom bound to a phenyl group and three oxygen atoms. The corresponding signal for dimethyldioxirane is at δ 102 (7). Dioxiranes are yellow and are stereospecific epoxidizing agents (7).

The ozonolysis of *E*- and *Z*-**1** thus results in a relatively complex series of reactions, as illustrated in Scheme 1 for *Z*-**1**. There appear to be two initial reactions: one results in formation of oxirane and oxygen, at least some of which must be singlet, the other results in formation of the molozonide. The molozonide fragments in the normal way with formation of methyl benzoate and carbonyl oxide. The latter can either cyclize to dioxirane or dimerize to tetroxane. There must be an energy barrier to cyclization (8), as more tetroxane is formed at −70°C than at −20°C, especially from *E*-**1**. The amount of oxirane formed from the reaction between alkene and dioxirane in the normal ozonolysis reactions is equal to half the moles of methyl benzoate minus the moles of tetroxane. There is always more oxirane than this. The excess must come from the initial reaction between alkene and ozone that also produces oxygen. On this basis the reaction between ozone and *E*-**1** at −20°C results initially in an oxirane:molozonide ratio of about 3:97 and that from *Z*-**1** is about 25:75. Dimerization of the carbonyl oxide to form tetroxane may not be concerted but proceed via a dimeric zwitterion, which could also decompose to form 2 moles of methyl benzoate and oxygen (9). This could be another route to singlet oxygen.

Determination (1) of the stoichiometry of the reaction showed that about 1.4 moles of both *E*- and *Z*-**1** are consumed per mole of ozone at −20°C. This is consistent with the observed product distribution.

This appears to be the first example of dioxirane formation from ozonolysis in solution. Other attempts to find definitive evidence for the presence of dioxiranes from ozonolysis of alkenes or from singlet oxygen oxidation of diazo compounds in solution have been unsuccessful (7, 10).

Acknowledgments

This work was supported by the Natural Sciences and Engineering Research Council of Canada and the University of Alberta.

1. K. R. Kopecky, J. Molina, and R. Rico. Can. J. Chem. **66**, 2234 (1988).
2. G. Rio and J. Berthelot. Bull. Soc. Chim. Fr. 3555 (1971).
3. R. Kuhn and H. Trischmann. Chem. Ber. **94**, 2261 (1961).
4. F. R. Mayo. Acc. Chem. Res. **1**, 193 (1968).
5. P. D. Bartlett and P. Günther. J. Am. Chem. Soc. **88**, 3288 (1966).
6. P. S. Bailey, H. H. Hwang, and C.-Y. Chiang. J. Org. Chem. **50**, 231 (1985).
7. R. W. Murray. Chem. Rev. **89**, 1187 (1989).
8. (*a*) G. Karlstrom and B. O. Roos. Chem. Phys. Lett. **79**, 416 (1981); (*b*) D. Cremer, T. Schmidt, J. Gauss, and T. P. Radhakrishnan. Angew. Chem. Int. Ed. Engl. **27**, 427 (1988); (*c*) M. Rahman, M. L. McKee, P. B. Shevlin, and R. J. Sztyrbicka. J. Am. Chem. Soc. **110**, 4002 (1988).
9. (*a*) S. Fliszar, D. Gravel, and E. Cavalieri. Can. J. Chem. **4**, 1013 (1966); (*b*) S. Fliszar and J. B. Chylinska. Can. J. Chem. **46**, 783 (1968).
10. K. Ishiguro, Y. Hirano, and Y. Sawaki. J. Org. Chem. **43**, 5397 (1988).

Can. J. Chem. Downloaded from www.nrcresearchpress.com by 88.255.202.194 on 09/08/12
For personal use only.

Use of a laboratory robot for repetitive solution NMR sample preparation

MICHAEL A. JEANNOT AND R. STEPHEN REID[1]

Department of Chemistry, University of Saskatchewan, Saskatoon, Sask., Canada S7N 0W0

Received June 29, 1992

MICHAEL A. JEANNOT and R. STEPHEN REID. Can. J. Chem. **71**, 275 (1993).

Observing ligand ^{1}H NMR signals while conditions (e.g., analytical concentrations, pH) are changed in an aqueous metal–proton–ligand system is one of the most potent methods of elucidating the precise details of speciation in such systems. Typically this is performed by changing the conditions in a solution reservoir, while withdrawing a sample for NMR analysis at each stage. However, such sample preparation is tedious and time-consuming. We report here studies, using a Mitsubishi RM-101 laboratory robot, of the feasibility of completely automating such a procedure. A simple acid–base study is used to evaluate performance.

MICHAEL A. JEANNOT et R. STEPHEN REID. Can. J. Chem. **71**, 275 (1993).

L'observation des spectres RMN du ^{1}H des ligands en fonction des conditions (concentrations analytiques, pH, etc.) d'un système aqueux métal–proton–ligand est une des méthodes les plus puissantes pour élucider d'une façon précise les détails de la spéciation dans de tels systèmes. D'une façon typique, on effectue ces études en faisant varier les conditions dans un réservoir de la solution, tout en retirant un échantillon pour analyse RMN à chaque étape. Toutefois, la préparation de ces échantillons est laborieuse et elle demande beaucoup de temps. Dans ce travail, on rapporte des études sur la possibilité d'utiliser un robot de laboratoire Mitsubishi RM-101 pour automatiser complètement une telle procédure. On a utilisé une étude acide–base simple pour évaluer la performance.

[Traduit par la rédaction]

Can. J. Chem. Downloaded from www.nrcresearchpress.com by 88.255.202.194 on 09/08/12
For personal use only.

Introduction

Many methods have been reported in the literature for the determination of metal–ligand speciation data (1, 2). Equilibrium potentiometric studies can yield high-precision complexation constants; however, since potentiometric measurements give no information about the *site* of protonation or deprotonation, a major pitfall is that the data can be fitted to an incorrect model, resulting in statistically valid but chemically meaningless conclusions. By contrast, ^{1}H NMR observation of the ligand in a series of solutions of known proportions of reactants over a range of pH values yields detailed information about the number and type of species present, but gives lower-quality numerical results for the relevant equilibrium constants.

We have found a *combination* of both of these techniques to be a potent method for elucidation of a variety of multi-equilibrium systems (3–7). Details of implementation have been discussed therein; a simple example of the application of NMR studies is given later in this paper (see Performance evaluation).

However, speciation studies of metal–proton–ligand systems using these techniques are hampered by the repetitive, time-consuming nature of the experimental techniques involved in both cases. Development of automated systems, making it possible to collect data without dedicating long hours to manual sample preparation, is therefore a priority. We previously investigated computer-controlled gravimetric titration as a means of automating the potentiometric aspects of the work (8). The possibility of similarly automating the NMR experiments is of obvious interest.

Automatic sample changers for NMR spectrometers, which permit unattended running of multiple samples, have been commercially available for some years; the remaining productivity bottleneck is the preparation of those samples. Here we report preliminary studies of the feasibility of automating the preparation of such samples.

[1]Author to whom correspondence may be addressed.

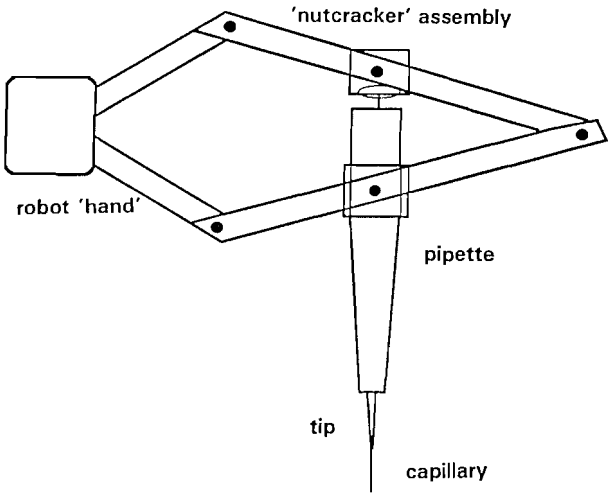

FIG. 1. Robot manipulator for use with automatic pipette.

Experimental

Hardware

A Mitsubishi RM-101 laboratory robot was available for this project. Its basic design is similar to that of a human arm. Control is via six stepping motors: body, shoulder, elbow, wrist (2 motors), and hand. The body motor moves the robot arm around the arc of a circle; full 360-degree coverage is available. The shoulder, elbow, and wrist motors can move the arm up and down over angular ranges roughly similar to a human arm; the wrist can also be used to rotate the hand, again over a 360-degree range. The "hand" has an opposable "finger" and "thumb" and can be opened (about 10 cm maximum separation) and closed.

Delivery of solutions and of samples is accomplished using an automatic plunger-type pipette (Nichiryo, model 5000DG, maximum volume capacity 1 mL). A special adapter for the hand was constructed such that closing the hand motor depresses the plunger of the pipette (see Fig. 1). The mechanism is similar to that of a nutcracker. The pipette is nested near the pivot of the adapter, and the hand squeezes the ends of the "nutcracker." A standard pipette tip was modified to permit entry into a 5 mm o.d. NMR tube

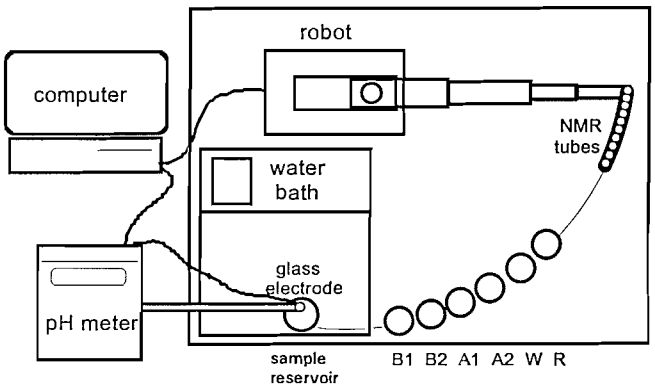

FIG. 2. Layout of apparatus (plan view). Beakers B1, B2, A1, A2, W, and R hold strong base (more and less concentrated), strong acid (more and less concentrated), waste, and rinse water, respectively. See experimental section for further details.

by addition of a glass capillary tube connected with a short length of tubing.

A Fisher Accumet 825 MP pH meter and combination glass electrode were used for pH measurement. The setup was calibrated with standard pH buffers (nominal pH values 4.00 and 7.00), which were periodically standardized against NBS primary standard pH solutions (9). All studies were carried out at 25°C. The temperature was maintained using a water bath equipped with a Haake D1 circulator and a cold-water cooling coil.

The robot, water bath, sample reservoirs, and NMR tubes were secured to a plexiglass sheet (see Fig. 2) The various reservoirs and tubes were placed on the arc of a circle centred on the pivot of the robot body joint. Initially, the joints of the robot arm must be aligned manually to a "home" position (indicated by arrows drawn on the robot body) with the pipette tip 2–5 mm above the centre of the first NMR tube. This is critical for the proper delivery of samples into the tubes; the width of the internal bore of a tube corresponds to only 4–5 steps of the body motor. Initial alignment was performed daily.

Interfacing and software

The robot is interfaced to an AT&T PC6300 8086 microcomputer via a parallel port. Low-level commands are issued by the computer as printer commands; the robot contains a built-in command interpreter. Although the robot is capable of interpreting several different commands, only one of these was used in the control software, the MOVE 1 command. This command simply steps each motor a specified number of steps. (The other commands, such as those to fully open or close the hand, or to adopt a previously defined position, are either not used in this application or, given the "teaching" routine used, offer no advantage over the use of the MOVE 1 command.) The pH meter is interfaced via a serial (RS232C) port; a continuous "print" by the pH meter of the pH reading is polled as required by the controlling software. Control software was written in Turbo Pascal version 5.0. Linear regression and preliminary data analysis were accomplished using QuattroPro on a Dell System 310 80386 microcomputer, and nonlinear least-squares curve fitting using the SigmaPlot scientific graphing software package.

^1H NMR spectroscopic measurements

These were performed on a Bruker AM-300 pulsed Fourier transform NMR spectrometer at an approximate frequency of 300.13 MHz, using a spectral width of 3289 Hz, collecting and transforming 16K points. Sufficient transients were averaged to give a signal-to-noise ratio adequate for precise chemical shift measurement. Typically 16 transients were sufficient. Chemical shifts were measured and are quoted in ppm relative to internal sodium 2,2-dimethyl-2-silapentane-5-sulfonate (DSS), positive shifts to high frequency. A binomial composite ('1331') pulse sequence (10) was used to suppress the intense water resonance.

Chemicals and solutions

All chemicals were of reagent grade and were used as received. Buffers for pH calibration, acetic acid, and sodium chloride were obtained from BDH Inc. (Toronto, Ont.), deuterium oxide (99.9% atom *d*) from the Aldrich Chemical Company Inc. (Milwaukee, Wis.), and DSS from Merck, Sharp and Dohme (Kirkland, Que.). For NMR studies, an aqueous solution of 0.02 M acetic acid containing 10% D_2O to provide a lock signal was used. The solution was also 1 mM in DSS (chemical shift reference) and 0.13 M in NaCl (to adjust the ionic strength); 0.05 M and 0.4 M solutions of sodium hydroxide and of hydrochloric acid were used for pH adjustment. Samples were prepared manually at pH < 2 and pH $>$ 12 to obtain the extreme chemical shift values. Finally, samples were prepared from pH 5.75 to 3.75 in 0.20 pH increments, both manually and using the robot. The allowable discrepancy in pH from the target value was set to ± 0.02 pH units.

Results and discussion

Design considerations

Because both the "independent" (pH) and the dependent (chemical shift) variables are measured, the precision with which solutions can be added does not in fact limit the quality of the experiment. (It is not, for instance, essential that samples be withdrawn at *exactly*, say, 0.5 pH unit intervals, only that they be withdrawn at *approximately* that interval and that the pH in each case be *precisely* known.) For this reason, a simple liquid delivery system based on a single automatic pipette was used, as discussed in the experimental section. By use of water rinsing where appropriate (for instance, when switching from acid delivery to sample collection), the possibility of contamination errors due to the use of a single pipette can be minimized.

Control software

The MOVE 1 commands corresponding to basic motions of the robot, such as moving the pipette tip from one station to another or placing it into an NMR tube, were established using a simple "teaching" routine written in Pascal, as follows. The routine generated a MOVE 1 command from a set of instructions given by the operator, and executed that command. By repeated application of the routine, the operator gradually "taught" the desired motion to the robot; the routine then summed the net change in each stepping motor setting, so that in future MOVE 1 could be executed directly, as a single movement, under computer control. For the relatively simple setup described in this paper, this approach allowed rapid "teaching," and obviated the need for detailed consideration of the position of objects or of a choice of coordinate system to work in. The time-consuming implementation of a kinematic transformation was thus also avoided.

For the hand (pipette), the precise relationship between the number of motor steps the hand opens (from the closed position) and the volume taken up by the pipette had to be determined. This was accomplished by a simple gravimetric calibration. Linear regression was performed to obtain the required relationship (see Fig. 3). The minimum volume that can be added from the linear part of the curve is 0.13 mL; the maximum (determined by the design of the pipette holder) is 0.91 mL.

The robot adjusts the pH of the sample by adding acid or

Can. J. Chem. Downloaded from www.nrcresearchpress.com by 88.255.202.194 on 09/08/12
For personal use only.

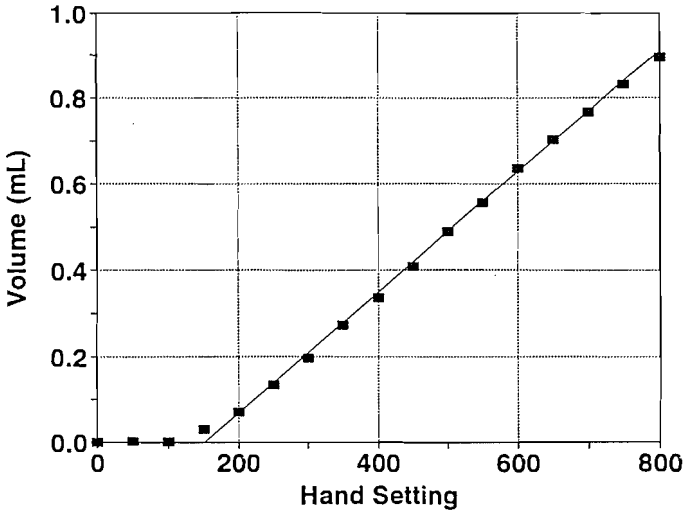

FIG. 3. Pipette calibration (volume delivered as a function of hand stepper motor position). Calibration is linear (correlation coefficient = 0.995) in the range of 0.1–0.9 mL.

base solution using the pipette. Base is used to adjust the pH of the solution upward initially to the highest desired value, acid for the downward adjustment between successive samples, and base also in the case of overshooting the desired pH as adjustment is performed. (Downward pH adjustment is the normal procedure for such studies, since it preserves the ionic strength close to a constant value. For instance, in the sodium acetate – hydrochloric acid titration used in the validation studies, the decline in the moles of acetate ion as the titration proceeds is exactly balanced by the rise in the moles of chloride ion.)

The limited range of volumes of acid the pipette can deliver (0.13–0.91 mL) is a potential problem, since the range of acid volumes necessary in the course of an experiment is likely to be much larger than this. In poorly buffered regions of the titration curve, only very small amounts of acid are required. A single acid solution of sufficiently low concentration to permit 0.13 mL additions near the titration equivalence point would have to be added in unacceptably large volumes in buffered regions of the titration curve. Time-consuming multiple additions would be required and considerable dilution would result. To avoid this problem, two solutions each of acid and base, of differing concentrations, are used. Discussion of the estimation of the optimum concentrations for these solutions lies outside the scope of this paper; typical values are given in the Chemicals section.

Once the pH is within a user-defined tolerance of the nominal target value, the robot withdraws a sample and transfers it to an NMR tube. This process is repeated for the required number of samples. Once a set of operating parameters have been accepted, the system can be left unattended while it prepares the samples.

Control software was written in top-down programming format such that the main loop of the program consists of only a few high-level procedures. Several levels of subroutines are called in turn. A simplified algorithm is as follows:[2]

```
Input parameters (e.g., target pH values)
Read initial pH
Withdraw and deliver first sample
REPEAT:
  Add acid (volume calculation routine)
  REPEAT:
    Read pH meter
    Add acid or base as appropriate (volume
    calculation routine)
  UNTIL pH is within the desired range
  Withdraw and deliver sample
UNTIL pH = lower limit
```

The user has the option of going down by a fixed pH interval between samples, or of entering a list of target pH values. pH data collected during the procedure are stored on disk.

The most difficult part of this procedure is predicting the volume of acid or base solution required to be added in order to change the pH by a given amount. Obviously, this can only be precisely calculated given a detailed knowledge of the equilibria involved — the knowledge the experiment is being performed to elucidate! However, a general prediction method, based on extrapolation of the recent history of the experimental volume added/pH curve, was developed, following the treatment of Smit and Smit (11). It is assumed that small portions of the titration curve may be empirically described by a hyperbolic function defined by the three parameters A, B, and C:

$$[1] \quad \mathrm{pH}(V) = A/(B + V) + C$$

where V is the volume of titrant added. A simple eight-step algorithm can be developed to predict the next volume of acid or base to add in order to reach the next pH value based on the previous three titration points. This algorithm has been incorporated into the control software for the robot.

Performance evaluation

This was accomplished by determination of the pK_a of acetic acid (HA) using both manually and robotically prepared samples. Depending on the pH of the system, varying proportions of HA and the acetate ion A^- will be present at equilibrium. Since the rate of chemical exchange between these two species is rapid on the NMR time scale, the observed methyl proton chemical shift δ_{obs} is the population-weighted average of those of the two species, i.e.,

$$[2] \quad \delta_{obs} = \delta_{HA}\alpha_{HA} + \delta_{A^-}\alpha_{A^-}$$

where δ_i is the chemical shift of a species and α_i its mole fraction. δ_{HA} and δ_{A^-} can be determined at very low and high pH values, respectively. The mole fractions are functions of the hydronium ion concentration[3] and K_a, the acid dissociation constant:

$$[3] \quad \alpha_{HA} = [H_3O^+]/([H_3O^+] + K_a)$$

$$[4] \quad \alpha_{A^-} = K_a/([H_3O^+] + K_a)$$

Samples were prepared over a range of pH values and the resultant chemical shifts measured (see experimental section and Fig. 4 for details). Using the nonlinear least-squares routine Sigmaplot, the value of K_a was refined to obtain the

[2]A copy of the compiled program and a source listing is available from the corresponding author.

[3]Strictly speaking, activity, but we will neglect consideration of activity coefficients here for simplicity, since it is the *comparison* between manually and robotically derived K_a values that is of interest, not the absolute values themselves.

Can. J. Chem. Downloaded from www.nrcresearchpress.com by 88.255.202.194 on 09/08/12
For personal use only.

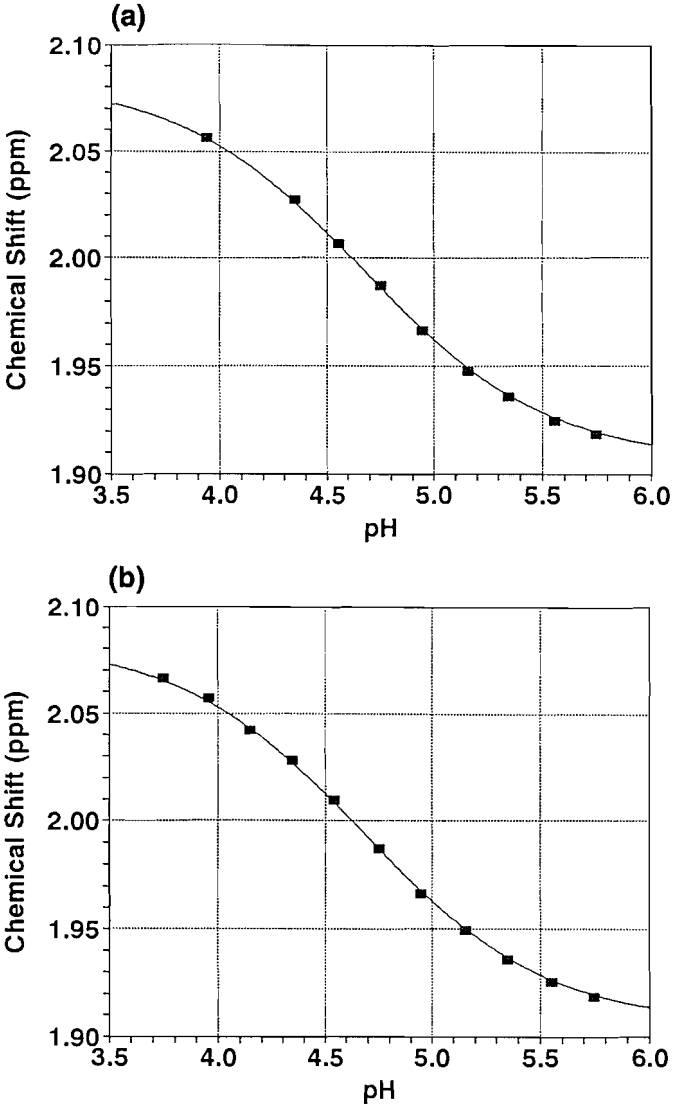

FIG. 4. pH dependence of chemical shift for acetic acid, for (*a*) a set of robotically prepared samples and (*b*) a set of manually prepared samples. The points in each case indicate experimental data and the line the best fit to the model described by eqs. [2], [3], and [4]. See text for further details.

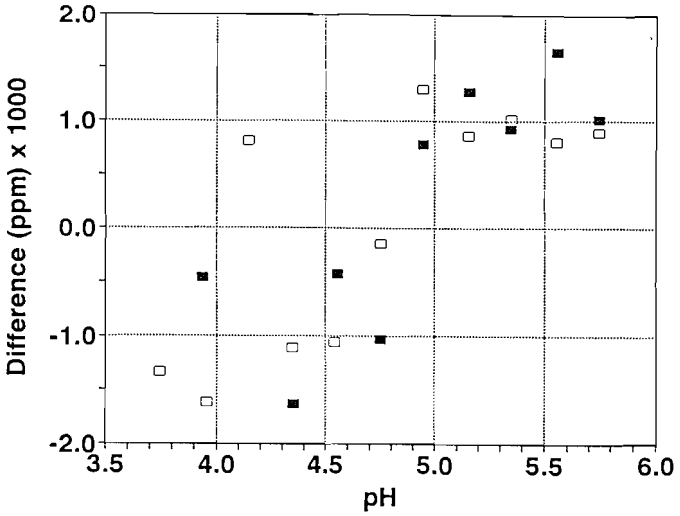

FIG. 5. Differences between experimentally determined chemical shifts and those predicted from the best-fit model for robotically prepared samples (■) and for manually prepared samples (□).

best agreement between experimental and predicted chemical shifts.

Validation results are shown graphically in Fig. 4. The fit, not surprisingly for such a simple equilibrium system, is excellent. A plot of the differences between actual and predicted chemical shifts is given in Fig. 5. A slight systematic trend is apparent. This is probably due to a small error in the pH electrode calibration (slope), to neglect of consideration of activity coefficients, or to an error in one or both of the extreme chemical shift values. Since the frequency difference between points on the digitized NMR spectra is 1.3×10^{-3} ppm, the trend is scarcely significant and further refinement was considered redundant.

A pK_a of 4.669 ± 0.005 (sd) was obtained for the robotically prepared samples, and a pK_a of 4.677 ± 0.005 (sd) was obtained for the manually prepared samples. The standard deviations are based on goodness of fit; allowing for electrode calibration the true standard deviation is approximately 0.02. There is therefore no significant difference between these values.

Overall performance

Typically the setup takes approximately twice as long to prepare a set of samples as an experienced operator would take to perform the job manually; however, the time involved now requires no human intervention, and operator time is freed for other tasks.

The "slack" in the movements of the various joints of the robot does result in some hysteresis effects with respect to volumes of samples delivered to NMR tubes. Although calibration studies (see Fig. 3) indicated that the uncertainty in volume delivered was ±0.01 mL, in practice larger variations in sample volumes were observed. These variations were not normally distributed, and appeared to depend on the recent activities of the arm. In a typical validation run, perhaps two samples were of volume 0.35 mL rather than the expected 0.4 mL. Modern automated NMR spectrometers with computer-controlled shimming facilities can accommodate variations of this magnitude in sample size.

Careful selection of parameters is needed. In particular, the allowable discrepancy between actual and target pH values should not be set too small compared to the pH interval between samples. (This depends upon the titration being performed; typically the discrepancy should be approximately 10% or more of the interval.) If not, although a set of samples will still be prepared, overshooting will occur, resulting in considerable dilution of the reservoir contents during the run. Provided these points are borne in mind, the apparatus performs well.

Acknowledgements

We wish to thank Mr. A. Leyland for assistance in constructing some of the hardware for the system, and Dr. B. Kratochvil for the loan of the robot. Financial support from the Natural Sciences and Engineering Research Council of Canada and the University of Saskatchewan is also gratefully acknowledged.

Can. J. Chem. Downloaded from www.nrcresearchpress.com by 88.255.202.194 on 09/08/12
For personal use only.

1. J. R. Kramer and H. E. Allen. Metal speciation: theory, analysis, and application. Lewis Publishers Inc., Chelsea, Mich. 1988.
2. R. F. Cookson. Chem. Rev. **74**, 5 (1974).
3. A. P. Arnold, A. J. Candy, R. S. Reid, and D. L. Rabenstein. Can. J. Chem. **63**, 2430 (1985).
4. R. S. Reid and B. Podányi. Can. J. Chem. **65**, 1508 (1987).
5. B. Podányi and R. S. Reid. J. Am. Chem. Soc. **110**, 3805 (1988).
6. R. S. Reid and B. Podányi. J. Inorg. Biochem. **32**, 183 (1988).
7. A. Piorko, C. H. Zhang, R. S. Reid, C. C. Lee, and R. G. Sutherland. J. Organomet. Chem. **395**, 293 (1990).
8. R. S. Reid and M. Chen. Can. Res. **21**, 22 (1988).
9. R. G. Bates. Determination of pH, theory and practice. 2nd ed. Wiley, New York. 1973. Chap. 2.
10. P. J. Hore. J. Magn. Reson. **55**, 283 (1983).
11. J. C. Smit and H. C. Smit. Anal. Chim. Acta, **143**, 45 (1982).

Can. J. Chem. Downloaded from www.nrcresearchpress.com by 88.255.202.194 on 09/08/12
For personal use only.

Bifunctional conjunctive reagents: 5-chloro-2-lithio-1-pentene and related substances. A methylenecyclohexane annulation method

EDWARD PIERS,[1] BIK WAH ANISSA YEUNG, AND FRASER F. FLEMING

Department of Chemistry, University of British Columbia, 2036 Main Mall, University Campus, Vancouver, B.C., Canada V6T 1Z1

Received September 28, 1992

EDWARD PIERS, BIK WAH ANISSA YEUNG, and FRASER F. FLEMING. Can. J. Chem. **71**, 280 (1993).

The development of a new, synthetically useful methylenecyclohexane annulation method is described. Transmetallation (MeLi, tetrahydrofuran, −78°C) of 5-chloro-2-trimethylstannyl-1-pentene (**8**) affords the novel bifunctional reagent 5-chloro-2-lithio-1-pentene (**9**), which, at temperatures higher than approximately −50°C, self-destructs to give methylenecyclobutane (**14**). Reagent **9** can be converted into the Grignard reagent **10** and the organocopper(I) species **15**. Conjugate addition of **10** and **15** to a number of cyclic enones (**16–22**), followed by intramolecular alkylation of the resultant adducts (**23–29**), produces the corresponding methylenecyclohexane annulation products (**30–40**).

EDWARD PIERS, BIK WAH ANISSA YEUNG et FRASER F. FLEMING. Can. J. Chem. **71**, 280 (1993).

On décrit le développement d'une nouvelle méthode d'annellation du méthylènecyclohexane qui est utile en synthèse. La transmétallation (MeLi, tétrahydrofurane, −78°C) du 5-chloro-2-triméthylstannylpent-1-ène (**8**) conduit au 5-chloro-2-lithiopent-1-ène (**9**), un nouveau réactif bifonctionnel qui, à des températures plus élevées qu'environ −50°C, s'autodétruit pour donner du méthylènecyclobutane (**14**). On peut transformer le réactif **9** en réactif de Grignard **10** et en l'espèce organocuivrée(I) **15**. L'addition conjuguée des réactifs **10** et **15** à un certain nombre d'énones cycliques (**16–22**), suivie par une alkylation intramoléculaire des adduits qui en résultent (**23–29**), conduit aux produits d'annellation correspondants, soit les méthylènecyclohexanes **30–40**.

[Traduit par la rédaction]

Introduction

A recent paper (1) from this laboratory reported that the novel reagent 4-chloro-2-lithio-1-butene (**2**) can be obtained readily by transmetallation (MeLi, tetrahydrofuran (THF), −78°C) of the vinyl trimethylstannane **1**. Furthermore, it was shown (1) that **2** can be transformed into the lower order heterocuprates **3** and **4** and that the latter substances are effective reagents for the conversion of enones **5** into bicyclic substances of general structure **6**. In these efficient, synthetically useful (1–3) methylenecyclopentane annulation sequences, the conjunctive reagents **3** and **4** serve as synthetic equivalents of the 1-butene d^2,a^4-synthon **7**.

In view of the success derived from the studies summarized above, it was of considerable interest to investigate the transmetallation of 5-chloro-2-trimethylstannyl-1-pentene (**8**), with the aim of determining whether or not the lithio reagent **9**, the corresponding Grignard species **10**, and (or) appropriate copper(I) reagents would serve as stable, viable, bifunctional reagents. We were particularly interested in developing a methylenecyclohexane annulation method shown in general terms by the conversion **5** → **11**. The fact that the methylenecyclohexane moiety is a fairly common structural feature of terpenoid natural products provided additional impetus for developing this new ring-forming method. We report herein the details of this study (4), which showed that **9** and **10**, as well as a related copper(I) reagent, are indeed viable synthetic equivalents of the 1-pentene d^2,a^5-synthon **12**.

Results and discussion

(a) Transmetallation of 5-chloro-2-trimethylstannyl-1-pentene (8). Regarding the stability of 5-chloro-2-lithio-1-pentene (9)

A "large-scale" preparation of the required stannane **8** was achieved, in 68% yield, by reaction of 5-chloro-1-pentyne with $Me_3SnCu \cdot Me_2S$ (**5**) under conditions (THF, −78°C, 6 h) modified from those reported earlier (6). Treatment of **8** with 1.2 equivalents of MeLi in THF at −78°C for 15 min produced a solution of the lithio reagent **9**. Addition of cyclohexanone to this solution, followed by continued stirring for 3 h, appropriate work-up, and product purification, gave the chloro alcohol **13** in 85% yield (Scheme 1, Experiment 1). If the solution of **9** in THF was stirred for an additional 30 min *prior to* addition of cyclohexanone, the yield of **13** was essentially unchanged (84%) (Scheme 1, Experiment 2). Thus, at −78°C in THF, 5-chloro-2-lithio-1-pentene (**9**) is, like its lower homologue **2** (1), a stable reagent.

To obtain additional information regarding the thermal

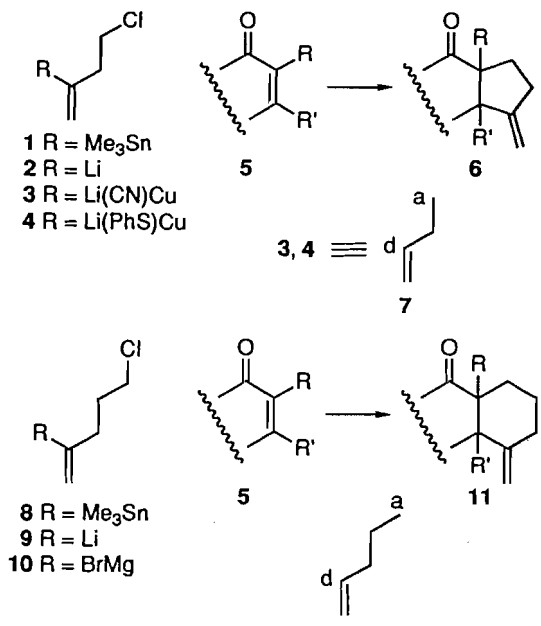

[1]Author to whom correspondence may be addressed.

Can. J. Chem. Downloaded from www.nrcresearchpress.com by 88.255.202.194 on 09/08/12
For personal use only.

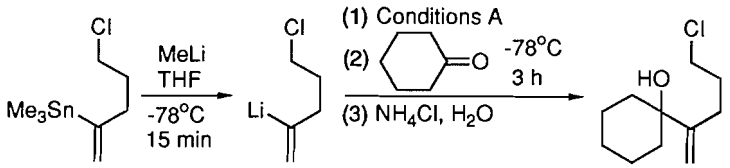

Experiment	Conditions A	Yield of 13(%)
1	--	85
2	-78°C, 30 min	84
3	-63°C, 30 min	76
4	-48°C, 30 min	58
5	-20°C, 30 min	0

SCHEME 1

stability of **9**, Experiments 3–5, Scheme 1, were carried out. The results of these experiments showed that, at −63°C in THF, **9** is still reasonably stable. However, at −48°C, **9** partially decomposes over a period of 30 min and, at −20°C, it completely self-destructs within the same time span. The material isolated from the reaction mixture of Experiment 5, Scheme 1, consisted nearly entirely of one of the starting materials, cyclohexanone.

What is the fate of **9** when a solution of this species is warmed? This question was conveniently answered by means of ^{1}H nmr spectroscopy. A 400 MHz spectrum of an aliquot of a THF solution of **9** that had been warmed to 0°C for 30 min showed, as expected, signals due to Me_4Sn (from transmetallation of **8** with MeLi), Et_2O (from the MeLi solution), and THF. The only other significant signals were obviously due to the presence of methylenecyclobutane (**14**) (7, 8) (eq. [1]). Thus, although the resonance due to the two

[1]

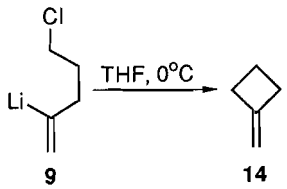

C-3 protons of **14** was hidden under the strong peak for the C-3(C-4) protons of THF, the signals derived from the allylic and olefinic protons of **14** (7, 8) were clearly visible at δ 2.63 (tt, 4H, J = 3, 8 Hz) and 4.61 (quintet, 2H, J = 3 Hz). This experiment was repeated except that, prior to measurement of the ^{1}H nmr spectrum, an internal standard (benzyl benzoate) was added to the reaction mixture. Careful integration of the olefinic protons of **14** and the benzylic protons of benzyl benzoate showed that the conversion of **9** into methylenecyclobutane (**14**) had taken place in essentially quantitative yield. Thus, perhaps not surprisingly, the thermal "decomposition" of 5-chloro-2-lithio-1-pentene (**9**) proceeds via a cyclization process involving elimination of the elements of lithium chloride, accompanied by the formation of the strained carbocycle **14**. It appears that similar cyclizations of analogues of **9** would constitute a useful method for the synthesis of specifically substituted alkylidenecyclobutanes.

(b) Methylenecyclohexane annulations

A number of methods aimed at effecting the conjugate addition of the 2-(5-chloro-1-butenyl) group to cyclic enones were investigated. Eventually, two reasonably effective procedures were found. The first of these (eq. [2], experimental section, general procedure A) involved copper(I)-catalyzed addition of the Grignard reagent **10**, which was readily formed by treatment of a solution of the lithio species **9** with magnesium bromide etherate. The second method (eq. [3], experimental section, general procedure C) was modelled on studies carried out by Noyori and coworkers (9). Addition of a solution of $CuBr \cdot Me_2S$ (1.1 equivalents) and n-Bu_3P (2 equivalents) in Et_2O (−78°C) to a THF solution (−78°C) of the lithio reagent **9** provided a reagent that, for the sake of convenience, may be formulated as shown in **15** (eq. [3]). Reaction of this species with the enone provided the desired conjugate addition product.

[2]

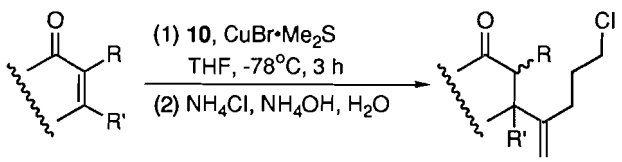

[3]

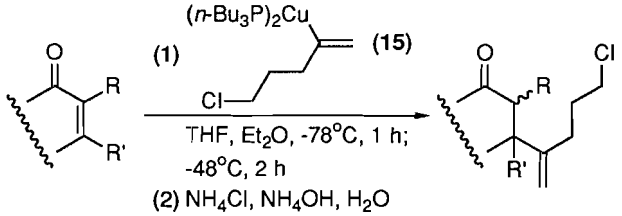

Can. J. Chem. Downloaded from www.nrcresearchpress.com by 88.255.202.194 on 09/08/12
For personal use only.

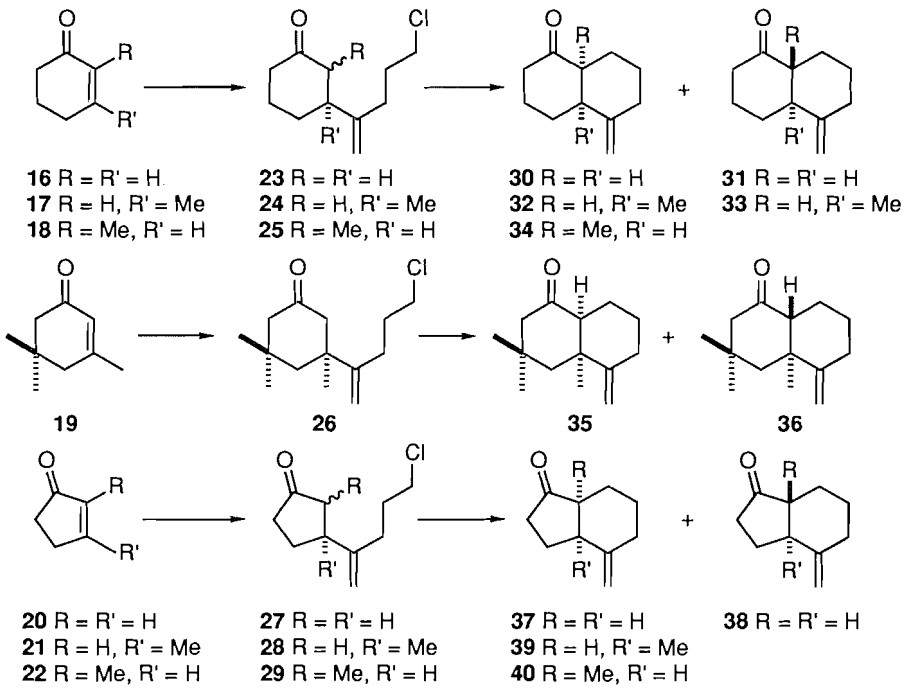

SCHEME 2

TABLE 1. Methylenecyclohexane annulation of cyclic enones

Entry	Enone	Conjugate addition product (procedure,[a] yield (%)[b])	Cyclized product(s)[c] (ratio,[d] yield (%)[b])	Cyclized product(s) (ratio[d] after equilibration[e])
1	**16**	**23** (A, 81; C, 61)	**30**, **31** (1:2, 86)	**30**, **31** (<1:>99)
2	**17**	**24** (B, 37; C, 55)	**32**, **33** (3.5:1, 82)	**32**, **33** (1:2.8)
3	**18**	**25**[f] (B, 56; C, 58)	**34** (—, 78)	
4	**19**	**26** (B, 45; D, 21)	**35**, **36** (8:1, 89)	**35**, **36** (1:2)
5	**20**	**27** (A, 54; C, 65)	**37**, **38** (5:1, 84)	**37**, **38** (5:1)
6	**21**	**28** (B, 54; D, 38)	**39** (—, 83)	(no change)
7	**22**	**29**[f] (B, 33; C, 67)	**40** (—, 90)	

[a]Procedures: A, $CuBr \cdot Me_2S$-catalyzed conjugate addition of the Grignard reagent **10**; B, as procedure A, but in the presence of $BF_3 \cdot Et_2O$; C, conjugate addition of the organocopper(I) reagent **15**; D, as procedure C, but in the presence of $BF_3 \cdot Et_2O$. Details are given in the experimental section of this paper.
[b]Yield of distilled, purified product.
[c]Intramolecular alkylation of the chloro ketones was accomplished with KH in THF.
[d]Ratios were determined by gas–liquid chromatography and (or) by ^1H nmr spectroscopy.
[e]Equilibration was accomplished with NaOMe in refluxing MeOH.
[f]This product consisted of a mixture of epimers.

For enones that are relatively poor substrates for conjugate addition of organocopper(I) reagents, the two procedures (A and C) outlined above were advantageously modified by employing $BF_3 \cdot Et_2O$ (10) to facilitate the process. These methods are designated, respectively, as general procedures B and D (see experimental section).

A number of cyclic enones (**16–22**, see Scheme 2) were subjected to the conjugate addition procedures outlined above and the results are summarized in Table 1. In general, the yields of the addition reactions were satisfactory, but not particularly high. In all cases, the desired chloro ketone could be conveniently purified by a combination of column chromatography on silica gel and distillation. As expected, the products **25** and **29** derived from 2-methyl-2-cyclohexen-1-one (**18**) and the corresponding cyclopentenone **22** (Table 1, entries 3 and 7) consisted of mixtures of epimers. In each case, the ratio of the diastereomeric products varied somewhat from experiment to experiment.

The originally envisaged methylenecyclohexane annulation sequences were completed by carrying out the intramolecular alkylation of each of the chloro ketones **23–29** with excess potassium hydride in dry THF at room temperature. In all cases studied, the yields of the cyclized products were excellent and the desired substances could be obtained in pure form by direct distillation of the crude products.

On the basis of literature reports (11, 12), the *cis*-fused bicyclic ketones would be expected to be the kinetically favored cyclization products. Indeed, in each of the two cases in which subsequent equilibration was not possible (Table 1, entries 3 and 7), a single *cis*-fused annulation product was formed in high yield. The relative configurations of these products (**34**, **40**) were confirmed by ^1H nmr nuclear

Can. J. Chem. Downloaded from www.nrcresearchpress.com by 88.255.202.194 on 09/08/12
For personal use only.

Can. J. Chem. Downloaded from www.nrcresearchpress.com by 88.255.202.194 on 09/08/12
For personal use only.

Overhauser enhancement (nOe) difference experiments. Thus, irradiation at δ 1.10 (three-proton singlet, angular Me signal) in the spectrum of **34** caused enhancement of the resonance (δ 2.25) due to the angular proton. In similar fashion, the resonance (δ 2.49) due to the angular proton in the spectrum of product **40** was enhanced when irradiation was carried out at δ 1.04 (angular Me signal).

During the potassium hydride-induced ring closure of the chloro ketones **23**, **24**, and **26** to produce the corresponding 7-methylenebicyclo[4.4.0]decan-2-ones, the initially formed *cis*-fused products underwent varying degrees of epimerization. Thus, cyclization of **23** produced a mixture in which the *trans*-fused product predominated (Table 1, entry 1), while, in the product mixtures derived from cyclization of substrates **24** and **26**, the *cis*-fused ketones were the major products (Table 1, entries 2 and 4). In each of these cases, the bicyclic products were subjected to equilibration with sodium methoxide in refluxing methanol and the equilibrium ratios were determined (Table 1). Not unexpectedly, the equilibrium between *cis*- (**30**) and *trans*-7-methylenebicyclo[4.4.0]decan-2-one (**31**) favored exclusively the *trans* isomer **31** (Table 1, entry 1). On the other hand, equilbration of the more highly substituted 7-methylenebicyclo[4.4.0]decan-2-ones (**32** ⇌ **33**, **35** ⇌ **36**) gave mixtures in which the *trans* isomers **33** and **36** were only marginally favored (Table 1, entries 2 and 4).

Intramolecular alkylation of the chloro ketone **27** produced a 5:1 mixture of *cis*- (**37**) and *trans*-2-methylenebicyclo[4.3.0]nonan-7-one (**38**). Equilibration (NaOMe, MeOH) of this mixture produced no change, while similar treatment of a pure sample of **37** also furnished a mixture of **37** and **38** in a ratio of 5:1. Thus, the *cis* isomer **37** is somewhat more stable than its *trans* counterpart **38**.

Ring closure of the chloro ketone **28** afforded exclusively *cis*-1-methyl-2-methylenebicyclo[4.3.0]nonan-7-one (**39**). Attempted equilibration of this material produced no detectable amount of the corresponding *trans*-fused isomer.[2]

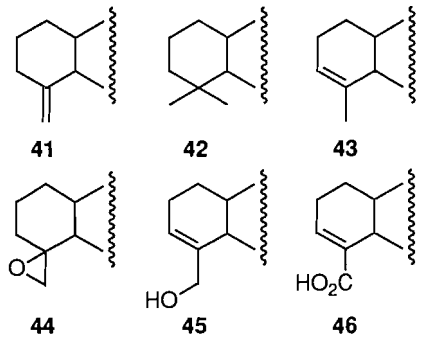

Conclusion

The methylenecyclohexane substructure **41**, as well as, for example, functionalized cyclohexane units represented in general terms by structural formulas **42–46** are quite commonly found in members of the terpenoid family of natural products. It is evident that compounds possessing the part structure **41** should serve as effective synthetic precursors for substances containing the structural features shown in **42–46**. Consequently, the concise methylenecyclohexane annulation method developed in this study should find use in organic synthesis. The details of a number of recent applications will be reported in the near future.[3]

Experimental

General information

Distillation temperatures, which refer to short-path (Kugelrohr) distillations, and melting points are uncorrected. Infrared (ir) spectra were recorded on Perkin–Elmer models 710B or 1710 spectrometers. Proton (^{1}H) and carbon (^{13}C) nuclear magnetic resonance (nmr) spectra were recorded on $CDCl_3$ solutions. Resonance positions are given in parts per million (ppm, δ) relative to the signal for Me_4Si (δ = 0). High-resolution mass spectra were recorded with a Kratos MS-50 mass spectrometer. Gas–liquid chromatography (glc) was performed with gas chromatographs equipped with 12.5 m × 0.21 mm fused silica columns coated with cross-linked OV-210 or SE-54. Analytical thin-layer chromatography was done with commercial aluminum-backed silica gel plates (E. Merck, Type 5554). Column chromatography was carried out with 70–230 mesh silica gel (E. Merck). Reagents and solvents were purified and dried using standard methods.

Aqueous NH_4Cl–NH_4OH (pH 8) was prepared by addition of ~50 mL of aqueous ammonium hydroxide (58%) to 1 L of saturated aqueous ammonium chloride.

Note: Unless otherwise indicated, all reactions were carried out under an atmosphere of dry argon using oven- or flame-dried glassware.

Note: Unless otherwise noted, all substances for which high-resolution mass measurements are given exhibited clean ^{1}H nmr spectra and showed one spot on tlc analysis and essentially one peak on glc analyses.

5-Chloro-2-trimethylstannyl-1-pentene (8)

To a cold (−78°C), stirred solution of $Me_3SnCu \cdot Me_2S$ (5) (38.3 mmol) in dry THF (250 mL) was added 5-chloro-1-pentyne (3.2 mL, 30.2 mmol) and the resultant mixture was stirred at −78°C for 6 h. Acetic acid (3 mL), methanol (3 mL), aqueous NH_4Cl–NH_4OH(pH 8) (200 mL), and diethyl ether (100 mL) were added sequentially. The vigorously stirred mixture was opened to the atmosphere and was allowed to warm to room temperature. The phases were separated and the deep-blue aqueous layer was extracted twice with diethyl ether. The combined organic extracts were washed twice with aqueous NH_4Cl–NH_4OH (pH 8), and then were dried ($MgSO_4$) and concentrated. Column chromatography (450 g silica gel, petroleum ether) of the remaining material, followed by distillation (80–85°C/25 Torr (1 Torr = 133.3 Pa)) of the acquired oil, gave 5.5 g (68%) of the chloro trimethylstannane **8**, a colorless oil that exhibited spectra identical with those recorded previously (6).

Preparation of 5-chloro-2-lithio-1-pentene (9)

To a cold (−78°C), stirred solution of 5-chloro-2-trimethylstannyl-1-pentene (**8**) (1.0 equiv.) in dry THF (~1 mL per 0.1 mmol of **8**) was added a solution of methyllithium (~1.2 equiv.) in diethyl ether. The colorless solution was stirred at −78°C for 15 min before being used.

Experiments to determine the stability of 9. Reactions of 9 with cyclohexanone

Four separate solutions of 5-chloro-2-lithio-1-pentene (**9**) (0.37 mmol) in dry THF (4 mL), each prepared as described above, were stirred at −78, −63, −48, and −20°C for 30 min (experiments A, B, C, and D, respectively). The solutions derived from experiments B–D were recooled to −78°C. Cyclohexanone

[2]Treatment of the **39** with NaOMe–MeOD gave the expected (*cis*-fused) trideuterio ketone. Molecular mechanics calculations (Chem 3D Plus,™ Version 3.0, Cambridge Scientific Computing, Inc., 1991) indicate that **39** is approximately 3 kcal/mol more stable than the corresponding *trans*-fused isomer. We are grateful to Mr. Jacques Roberge for his assistance in performing these calculations.

[3]For preliminary reports, see refs. 13–15.

Can. J. Chem. Downloaded from www.nrcresearchpress.com by 88.255.202.194 on 09/08/12
For personal use only.

(43 μL, 0.41 mmol) was added to each solution and, in each case, the mixture was stirred at −78°C for 3 h. Saturated aqueous NH_4Cl (5 mL) and diethyl ether (10 mL) were added to each reaction mixture, which was then allowed to warm to room temperature. In each case, the phases were separated, the organic solution was washed with saturated aqueous NH_4Cl (2 × 5 mL), and then was dried ($MgSO_4$) and concentrated. Column chromatography (5 g silica gel, 3:2 petroleum ether – diethyl ether) of each of the crude products obtained from experiments A, B, and C, followed by distillation (110–115°C/0.2 Torr) of each of the acquired liquids, provided 64 mg (84%), 57 mg (76%), and 44 mg (58%) of 1-[5-chloro-2-(1-pentenyl)]cyclohexanol (**13**), respectively. The chloro alcohol **13**, a colorless oil, displayed ir (neat): 3431, 3094, 1639, 902 cm^{-1}; ^1H nmr (400 MHz) δ: 1.12–1.30 (m, 2H), 1.50–1.70 (m, 9H), 1.98 (quintet, 2H, J = 7 Hz), 2.24 (t, 2H, J = 7 Hz), 3.36 (t, 2H, J = 7 Hz), 4.82, 5.14 (s, s, 1H each). Exact Mass calcd. for $C_{11}H_{19}{}^{35}ClO$: 202.1124; found: 202.1130.

Analysis (glc, ^1H nmr) of the crude product obtained from experiment D showed that it contained none of the chloro alcohol **13**, but consisted nearly entirely of cyclohexanone.

Cyclization of ***9****. Formation of methylenecyclobutane (****14****)*

A solution of 5-chloro-2-lithio-1-pentene (**9**) (0.43 mmol) in dry THF (4.3 mL) at −78°C, prepared as described above, was allowed to warm to 0°C for 30 min. Benzyl benzoate (80 μL, 0.42 mmol) was added and, after the mixture had been stirred thoroughly, a 50 μL aliquot was removed and dissolved in $CDCl_3$ for ^1H nmr analysis. The ^1H nmr spectrum (400 MHz) showed, in addition to signals due to Me_4Sn, Et_2O (from the MeLi solution used to prepare **9**), and THF, essentially only resonances derived from $PhCO_2CH_2Ph$ and methylenecyclobutane (**14**) (8). The resonance for the C-3 protons of **14** was buried under the signal due to the C-3 + C-4 protons of THF. The four allylic protons of **14** gave rise to a tt (J = 3, 8 Hz) at δ 2.63, while the olefinic protons produced a quintet (J = 3 Hz) at δ 4.61. Careful integration of the signals due to the olefinic protons of **14** and the benzylic protons of benzyl benzoate showed that the conversion of **9** into **14** had taken place quantitatively.

General procedure A. CuBr · Me_2S-catalyzed conjugate addition of the Grignard reagent ***10*** *to enones*

To a cold (−78°C), stirred solution of 5-chloro-2-lithio-1-pentene (**9**) (1.0 equiv.) in dry THF (~1.0 mL per 0.1 mmol of **9**) was added, in one portion, solid magnesium bromide etherate (~1.2 equiv.). The milky solution was stirred at −78°C for 20 min. Solid CuBr · Me_2S complex (~0.25 equiv.) and the enone (1.0 equiv.) were added sequentially and the resultant yellow mixture was stirred at −78°C for 3 h. Aqueous NH_4Cl–NH_4OH (pH 8) (~1.25 mL per 0.1 mmol of enone substrate) and Et_2O (~2.5 mL per 0.1 mmol of enone substrate) were added, the rapidly stirred mixture was opened to the atmosphere, and then was allowed to warm to room temperature. The blue aqueous layer was separated and washed twice with Et_2O. The combined Et_2O solutions were washed twice with aqueous NH_4Cl–NH_4OH (pH 8), dried ($MgSO_4$), and concentrated. The residual material was purified by column chromatography on silica gel (~5 g per 100 mg of crude product, 3:1 petroleum ether – Et_2O) and distillation.

General procedure B. CuBr · Me_2S-catalyzed conjugate addition of the Grignard reagent ***10*** *to enones, in the presence of $BF_3 \cdot Et_2O$*

This procedure was essentially identical with that described above, except that $BF_3 \cdot Et_2O$ (~1.2 equiv.) was added to the reaction mixture immediately after addition of the enone substrate.

General procedure C. Conjugate addition of the organocopper(I) reagent ***15*** *to enones*

Solid CuBr · Me_2S complex (1.1 equiv.) was added to a stirred solution of n-Bu_3P (2.0 equiv.) in dry Et_2O (~1.0 mL per 0.1 mmol of CuBr · Me_2S). After the mixture had been stirred at room temperature for 10 min, all of the solid had dissolved. The solution was cooled to −78°C and then was transferred via cannulation to a cold (−78°C), stirred solution of **9** (1.0 equiv.) in dry THF (~1.0 mL per 0.1 mmol of **9**). The light-yellow solution was stirred at −78°C for 20 min. The enone (1.0 equiv.) was added and the bright-yellow solution was stirred at −78°C for 1 h and at −48°C for 2 h. Work-up as described in general procedure A (*vide supra*) and purification of the crude material by column chromatography on silica gel (~5 g per 100 mg of crude oil, 20:1 to 7:1 petroleum ether – Et_2O) and distillation gave the desired product.

General procedure D. Conjugate addition of the organocopper(I) reagent ***15*** *to enones, in the presence of $BF_3 \cdot Et_2O$*

This procedure was identical with general procedure C, except that $BF_3 \cdot Et_2O$ (1.2 equiv.) was added to the reaction mixture immediately after the enone had been added.

The following compounds were prepared by use of the general procedures described above. The specific procedure employed and the yields obtained are indicated in Table 1.

*3-[2-(5-Chloro-1-pentenyl)]cyclohexanone (****23****)*

Distillation temperature: 82–85°C/0.2 Torr; ir (neat): 3050, 1700, 1630, 900 cm^{-1}; ^1H nmr (400 MHz) δ: 1.52–1.74 (m, 2H), 1.85–2.00 (m, 3H), 2.02–2.14 (m, 1H), 2.15–2.24 (t, 2H, J = 7.0 Hz), 2.24–2.49 (m, 5H), 3.54 (t, 2H, J = 7.0 Hz), 4.85 (br s, 2H). Exact Mass calcd. for $C_{11}H_{17}{}^{35}ClO$: 200.0969; found: 200.0963.

*3-[2-(5-Chloro-1-pentenyl)]-3-methylcyclohexanone (****24****)*

Distillation temperature: 85–90°C/0.2 Torr; ir (neat): 3050, 1700, 1620, 900 cm^{-1}; ^1H nmr (400 MHz) δ: 1.11 (s, 3H), 1.57–1.67 (m, 1H), 1.67–1.80 (m, 1H), 1.80–1.90 (m, 1H), 1.90–2.10 (m, 3H), 2.10–2.36 (m, 5H), 2.60 (br d, 1H, J = 14 Hz), 3.59 (t, 2H, J = 7.0 Hz), 4.87, 4.93 (s, s, 1H each). Exact Mass calcd. for $C_{12}H_{19}{}^{35}ClO$: 214.1126; found: 241.1119.

*3-[2-(5-Chloro-1-pentenyl)]-2-methylcyclohexanone (****25****)*

This material (distillation temperature 93–98°C/0.2 Torr) was shown by gas–liquid chromatographic analysis to consist of a mixture of two diastereomers in a ratio of ~12:1; ir (neat): 3070, 1700, 1635, 900 cm^{-1}; ^1H nmr (400 MHz) δ: 0.95, 1.00 (d, d, 3H total, ratio ~1:12, J = 7.0 Hz in each case), 1.65–1.80 (m, 2H), 1.80–1.97 (m, 3H), 2.21–2.32 (m, 1H), 2.44–2.60 (m, 2H), 2.60–2.70 (m, 1H), 3.55 (t, 2H, J = 7.0 Hz), 4.75, 4.98 (br s, br s, ~0.9 H each), 4.86, 4.89 (br s, br s, ~0.1 H each). In a decoupling experiment, irradiation at δ 1.00 caused the signal at δ 2.60–2.70 to collapse to a d (J = 7.0 Hz). Exact Mass calcd. for $C_{12}H_{19}{}^{35}ClO$: 214.1126; found: 214.1124.

*3-[2-(5-Chloro-1-pentenyl)]-3,5,5-trimethylcyclohexanone (****26****)*

Distillation temperature 82–86°C/0.2 Torr; ir (neat): 3070, 1700, 1630, 900 cm^{-1}; ^1H nmr (400 MHz) δ: 0.97, 1.04, 1.16 (s, s, s, 3H each), 1.58 (d, 1H, J = 14 Hz), 1.90–2.05 (m, 3H), 2.13–2.25 (m, 5H), 2.76 (d, 1H, J = 14 Hz), 3.59 (t, 2H, J = 7.0 Hz). 4.81, 5.04 (br s, br s, 1H each). Exact Mass calcd. for $C_{14}H_{23}{}^{35}ClO$: 242.1437; found: 242.1436.

*3-[2-(5-Chloro-1-pentenyl)]cyclopentanone (****27****)*

Distillation temperature 90–95°C/0.5 Torr; ir (neat): 3050, 1735, 1630, 900 cm^{-1}; ^1H nmr (400 MHz) δ: 1.72–1.86 (m, 1H), 1.93–2.01 (quintet, 2H, J = 7.0 Hz), 2.08–2.32 (m, 5H), 2.34–2.50 (m, 2H), 2.89 (m, 1H), 3.58 (t, 2H, J = 7.0 Hz), 4.86 (br s, 2H). Exact Mass calcd. for $C_{10}H_{15}{}^{35}ClO$: 186.0812; found: 186.0815.

*3-[2-(5-Chloro-1-pentenyl)]-3-methylcyclopentanone (****28****)*

Distillation temperature 76–85°C/0.2 Torr; ir (neat): 3070, 1730, 1630, 900 cm^{-1}; ^1H nmr (400 MHz) δ: 1.20 (s, 3H), 1.85–2.50 (m, 10H), 3.59 (t, 2H, J = 7.0 Hz), 4.82 (br s, 1H), 4.88 (s, 1H). Exact Mass calcd. for $C_{11}H_{17}{}^{35}ClO$: 200.0969; found: 200.0969.

*3-[2-(5-Chloro-1-pentenyl)]-2-methylcyclopentanone (****29****)*

Analysis (glc) showed that this material (distillation temperature 90–95°C/0.2 Torr) consisted of a mixture of two diastereomers in a ratio of ~4:1; ir (neat): 3060, 1730, 1635, 900 cm^{-1}; ^1H nmr (400 MHz) δ: 1.05, 0.88 (d, d, 3H total, ratio ~4:1, J =

Can. J. Chem. Downloaded from www.nrcresearchpress.com by 88.255.202.194 on 09/08/12
For personal use only.

7.0 Hz in each case), 1.60–2.50 (m, ~9.25H), 2.78–2.88 (m, ~0.75H), 3.52–3.63 (m, 2H), 4.78, 4.94 (s, s, ~0.75H each), 4.89–4.92 (m, ~0.5H). Exact Mass calcd. for $C_{11}H_{17}{}^{35}ClO$: 200.0969; found: 200.0975.

General procedure E. Cyclization of chloro ketones

To a stirred solution of KH (~2.5 equiv.) in dry THF (~1 mL per mmol of KH) was added a solution of the chloro ketone (1.0 equiv.) in THF (~1 mL per 0.1 mmol of substrate) and the resultant yellow solution was stirred at room temperature for 2 h. Saturated aqueous NH_4Cl and Et_2O (~2.5 and 5 mL, respectively, per 0.1 mmol of chloro ketone substrate) were added. The aqueous phase was separated and extracted twice with Et_2O. The combined organic extracts were washed with brine, dried ($MgSO_4$), and concentrated. Distillation of the residual oil provided the product(s).

General procedure F. Equilibration of bicyclic ketones

To a stirred solution of NaOMe (4.0 equiv.) in dry MeOH (1.25 mL per mmol of NaOMe) was added a solution of the bicyclic ketone (1.0 equiv.) in dry MeOH (0.5 mL per 0.1 mmol of substrate) and the mixture was refluxed for 18 h. Saturated NH_4Cl and Et_2O (3 and 6 mL, respectively, per 0.1 mmol of substrate) were added. The aqueous layer was separated and extracted twice with Et_2O. The combined organic extracts were washed with brine, dried ($MgSO_4$), and concentrated. The makeup of the crude product was determined by gas–liquid chromatographic analysis or by ^1H nmr spectroscopy. Distillation provided the product(s).

The following compounds were prepared by use of general procedure E. Those substances that contained an angular proton adjacent to the carbonyl group were subjected to equilibration (general procedure F). The results of these experiments are summarized in Table 1.

cis- *and* trans-*7-Methylenebicyclo[4.4.0]decan-2-one (30, 31)*

Cyclization of the chloro ketone **23** (44 mg) provided 31 mg (86%) of a mixture of **30** and **31** (distillation temperature 100–120°C/33 Torr, ratio 1:2, respectively, by ^1H nmr spectroscopy). Column chromatography (10 g silica gel, 12:1 petroleum ether – Et_2O) of this mixture afforded 8 mg of the *cis* isomer **30**, a colorless oil, and 17 mg of the *trans* compound **31**, a white solid.

Compound **30** exhibited ir (neat): 3040, 1700, 1630, 895, cm^{-1}; ^1H nmr (400 MHz) δ: 1.31–1.45 (m, 1H), 1.45–1.64 (m, 2H), 1.64–1.79 (m, 1H), 1.79–1.94 (m, 2H), 2.00–2.19 (m, 3H), 2.19–2.30 (m, 2H), 2.36–2.55 (m, 2H), 2.63–2.72 (m, 1H), 4.66 (t, 1H, J = 1.5 Hz), 4.69 (s, 1H). Exact Mass calcd. for $C_{11}H_{16}O$: 164.1202; found: 164.1205.

The *trans* isomer **31** displayed mp 28–29°C (from petroleum ether); ir ($CHCl_3$): 1700, 1635, 900 cm^{-1}; ^1H nmr (400 MHz) δ: 1.20–1.36 (m, 1H), 1.36–1.52 (m, 1H), 1.60–1.78 (m, 2H), 1.83–2.09 (m, 6H), 2.09–2.21 (m, 1H), 2.23–2.45 (m, 3H), 4.69, 4.75 (s, s, 1H each); ^{13}C nmr (20 MHz) δ: 25.0, 25.3, 26.3, 27.6, 35.8, 41.3, 48.1, 55.5, 75.4, 77.0, 78.6, 105.7, 151.6, 212.5. Exact Mass calcd. for $C_{11}H_{16}O$: 164.1202; found: 164.1202.

Equilibration (general procedure F) of a 1:2 mixture of **30** and **31**, as well as of samples of pure **30** and **31**, gave, in each case, the crystalline *trans*-fused ketone **31** as the only product.

cis- *and* trans-*6-Methyl-7-methylenebicyclo[4.4.0]decan-2-one (32, 33)*

Distillation (100–113°C/33 Torr) of the crude product derived from cyclization of the chloro ketone **24** (22 mg) produced 15 mg (82%) of a mixture of **32** and **33**, in a ratio of 3.5:1, respectively (analysis by glc). Column chromatography of this material on silica gel impregnated with 25% silver nitrate (6 g, 25:1 petroleum ether – Et_2O), followed by distillation of the acquired materials, gave 5 mg of the *cis* isomer **32**, 5 mg of a mixture of **32** and **33**, and 2 mg of the *trans* isomer **33**.

Compound **32** showed ir (neat): 3060, 1700, 1630, 900 cm^{-1}; ^1H nmr (400 MHz) δ: 1.17 (s, 3H), 1.28–1.47 (m, 2H), 1.61–1.70 (m, 1H), 1.75–2.05 (m, 4H), 2.15 (dd, 1H, J = 10, 4 Hz), 2.18–2.40 (m, 4H), 2.43–2.53 (m, 1H), 4.73 (s, 1H), 4.76 (br s, 1H). In a nOe difference experiment, irradiation at δ1.17 caused enhancement of the signals at δ 2.15 (angular proton) and 4.73. Exact Mass calcd. for $C_{12}H_{18}O$: 178.1358; found: 178.1359.

Compound **33** exhibited ir (neat): 3060, 1700, 1630, 895 cm^{-1}; ^1H nmr (400 MHz) δ: 0.95 (s, 3H), 1.20–1.35 (m, 1H), 1.50–1.75 (m, 2H), 1.84–2.40 (m, 10H), 4.70–4.76 (m, 2H). Exact Mass calcd. for $C_{12}H_{18}O$: 178.1358; found: 178.1355.

Equilibration of small samples of each of the pure ketones **32** (11 mg) and **33** (15 mg) gave, in each case, a clean mixture of the two ketones **32** and **33**, in a ratio of 1:2.8 (analysis by glc).

cis-*1-Methyl-7-methylenebicyclo[4.4.0]decan-2-one (34)*

This material (15 mg, colorless oil, distillation temperature 85–92°C/22 Torr) was obtained in 78% yield as the only product from cyclization of the chloro ketone **25** (22 mg). Compound **34** exhibited ir (neat): 3050, 1695, 1635, 895 cm^{-1}; ^1H nmr (400 MHz) δ: 1.10 (s, 3H), 1.19–1.28 (m, 1H), 1.55–1.76 (m, 4H), 1.98–2.37 (m, 7H, including a dd, J = 12, 6 Hz, at 2.25), 2.55–2.67 (m, 1H), 4.69 (t, 1H, J = 1.5 Hz), 4.72 (t, 1H, J = 2 Hz). In a nOe difference experiment, irradiation of δ 1.10 caused enhancement of the resonance at δ 2.25 (angular proton). Exact Mass calcd. for $C_{12}H_{18}O$: 178.1358; found: 178.1357.

cis- *and* trans-*4.4.6-Trimethyl-7-methylenebicyclo[4.4.0]-decan-2-one (35, 36)*

Cyclization of the chloro ketone **26** (77 mg) provided 58 mg (89%) of a mixture of the bicyclic ketones **35** and **36** (distillation temperature 70–86°C/24 Torr, ratio 8:1, respectively, by glc analysis). Column chromatography of this material on silica gel impregnated with 25% silver nitrate (12 g, 25:1 petroleum ether – Et_2O) gave 6 mg of the *cis* isomer **35** (a white solid) and 46 mg of a mixture of **35** and **36**.

Compound **35** displayed mp 56–56.5°C (from petroleum ether); ir ($CHCl_3$): 3070, 1690, 1620, 900 cm^{-1}; ^1H nmr (400 MHz) δ: 1.05, 1.06, 1.26 (s, s, s, 3H each), 1.33 (d, 1H, J = 15 Hz), 1.43 (m, 1H), 1.63–1.76 (m, 2H), 1.92–2.03 (m, 1H), 2.08 (ddd, 1H, J = 14, 1.5, 1.5 Hz), 2.13 (dd, 1H, J = 8, 4.5 Hz), 2.23–2.37 (m, 3H), 2.43 (d, 1H, J = 14 Hz), 4.77 (q, 1H, J = 1.5 Hz), 4.80 (br s, 1H). In a nOe difference experiment, irradiation at δ 1.26 (angular Me group) caused enhancement of the signals at δ 1.06, 2.13 (angular proton), and 4.80. Exact Mass calcd. for $C_{14}H_{22}O$: 206.1672; found: 206.1680.

Equilibration of a sample (54 mg) of an 8:1 mixture of **35** and **36** provided 50 mg (92%) of a mixture of these substances (ratio 1:2, respectively, analysis by glc). Column chromatography of this material on silica gel impregnated with 25% silver nitrate (12 g, 90:1 to 20:1 petroleum ether – Et_2O) gave 11 mg of **35**, 16 mg of a mixture of **35** and **36**, and 17 mg of the *trans*-fused ketone **36** (colorless oil, distillation temperature 72–79°C/24 Torr).

Compound **36** exhibited ir (neat): 3060, 1700, 1623, 900 cm^{-1}; ^1H nmr (400 MHz) δ: 1.04, 1.10, 1.14, (s, s, s, 3H each), 1.19–1.34 (m, 1H), 1.49–1.72 (m, 2H), 1.76–1.91 (m, 2H), 2.01 (d, 1H, J = 13.5 Hz), 2.08–2.20 (m, 2H), 2.20–2.43 (m, 3H), 4.70, 4.73 (br s, br s, 1H each). Exact Mass calcd. for $C_{14}H_{22}O$: 206.1671; found: 206.1675.

cis- *and* trans-*2-Methylenebicyclo[4.3.0]nonan-7-one (37, 38)*

Ring closure of the chloro ketone **27** (37 mg) produced 25 mg (84%) of a colorless oil (distillation temperature 70–85°C/23 Torr) that consisted of a mixture of the bicyclic ketones **37** and **38** in a ratio of ~5:1, respectively (analysis by glc). Column chromatography of this mixture on silica gel impregnated with 25% silver nitrate (6 g, 20:1 petroleum ether – Et_2O) gave 4 mg of the *cis*-fused ketone **37** and 11 mg of a mixture of **37** and **38**.

Compound **37** exhibited ir (neat): 3050, 1730, 1635, 895 cm^{-1}; ^1H nmr (400 MHz) δ: 1.42–1.60 (m, 2H), 1.62–1.80 (m, 2H), 1.85–1.97 (m, 1H), 2.05–2.14 (m, 1H), 2.15–2.37 (m, 3H), 2.37–2.41 (m, 2H), 2.95 (dt, 1H, J = 7.0, 7.0 Hz), 4.79 (s, 1H), 4.80 (br s, 1H). In a nOe difference experiment, irradiation at δ 2.95 (angular allylic proton) caused enhancement of the resonances at

δ 4.79 and 2.37–2.41. Exact Mass calcd. for $C_{10}H_{14}O$: 150.1046; found: 150.1039.

The ^1H nmr spectrum of the mixture of **37** and **38** showed that the alkene protons of the *trans*-fused isomer **38** resonate at δ 4.66 (s) and 4.77 (br s).

Equilibration of a sample (15 mg) of a mixture of **37** and **38** (84.16, respectively), as well as of a sample (15 mg) of pure **37**, produced, in each case, a mixture of **37** and **38** in a ratio of ~5:1, respectively (analyses by glc).

cis-*1-Methyl-2-methylenebicyclo[4.3.0]nonan-7-one (39)*

Cyclization of the chloro ketone **28** (33 mg) gave 22 mg (83%) of a colorless oil (distillation temperature 72–76°C/23 Torr) that, on the basis of analyses by glc and ^1H nmr spectroscopy, consisted of a single compound, the *cis*-fused ketone **39**. This substance displayed ir (neat): 3070, 1735, 1635, 900 cm^{-1}; ^1H nmr (400 MHz) δ: 1.15–1.30 (m, 1H), 1.34 (s, 3H), 1.50–1.61 (m, 3H), 1.97–2.10 (m, 2H), 2.10–2.33 (m, 4H), 2.45 (m, 1H), 4.77, 4.81 (s, s, 1H each). Exact Mass calcd. for $C_{11}H_{16}O$: 164.1202; found: 164.1208.

Attempted equilibration of a sample (11 mg) of **39** gave only the starting material.

cis-*6-Methyl-2-methylenebicyclo[4.3.0]nonan-7-one (40)*

Cyclization of the chloro ketone **29** (37 mg) afforded 27 mg (90%) of the *cis*-fused bicyclic ketone **40**, a colorless oil (distillation temperature 68–73°C/23 Torr) that exhibited ir (neat): 3050, 1730, 1635, 900 cm^{-1}; ^1H nmr (400 MHz) δ: 1.04 (s, 3H), 1.18–1.27 (m, 1H), 1.43–1.56 (m, 2H), 1.60–1.72 (m, 1H), 1.83–1.95 (m, 1H), 1.98–2.12 (m, 1H), 2.12–2.28 (m, 3H), 2.43–2.55 (m, 2H), 4.76–4.83 (m, 2H). In a nOe difference experiment, irradiation at δ 1.04 caused enhancement of the signal at δ 2.49 (dd, J = 12, 8 Hz, angular proton). Exact Mass calcd. for $C_{11}H_{16}O$: 164.1202; found: 164.1205.

Acknowledgements

We gratefully acknowledge financial support from the Natural Sciences and Engineering Research Council of Canada and from Merck Frosst Canada, Inc.

1. E. Piers and V. Karunaratne. Tetrahedron, **45**, 1089 (1989).
2. E. Piers and V. Karunaratne. Can. J. Chem. **67**, 160 (1989).
3. E. Piers and J. Renaud. Synthesis, 74 (1992).
4. E. Piers and B. W. A. Yeung, J. Org. Chem. **49**, 4567 (1984).
5. E. Piers, H. E. Morton, and J. M. Chong. Can. J. Chem. **65**, 78 (1987).
6. E. Piers and J. M. Chong. Can. J. Chem. **66**, 1425 (1988).
7. R. P. Thummel and W. Nutakul. J. Org. Chem. **43**, 3170 (1978).
8. A. I. Dyachenko, E. L. Protasova, A. I. Ioffe, A. Ya. Steinschneider, and O. M. Nefedov. Tetrahedron Lett. 2055 (1979).
9. M. Suzuki, T. Suzuki, T. Kawagishi, and R. Noyori. Tetrahedron Lett. 1247 (1980).
10. A. B. Smith III and P. J. Jerris. J. Org. Chem. **47**, 1845 (1982).
11. J. M. Conia and F. Rouessac. Tetrahedron, **16**, 45 (1961).
12. G. H. Posner, J. J. Sterling, C. E. Whitten, C. M. Lentz, and D. J. Brunelle. J. Am. Chem. Soc. **97**, 107 (1975).
13. E. Piers and J. S. M. Wai. J. Chem. Soc. Chem. Commun. 1342 (1987); 1245 (1988).
14. E. Piers and F. F. Fleming. J. Chem. Soc. Chem. Commun. 1665 (1989).
15. E. Piers and J. Y. Roberge. Tetrahedron Lett. **26**, 5219 (1991).

Can. J. Chem. Downloaded from www.nrcresearchpress.com by 88.255.202.194 on 09/08/12
For personal use only.

On the correlation between electron mobility, free-ion yield, and electron thermalization distance in nonpolar dielectric liquids

JEAN-PAUL JAY-GERIN AND THOMAS GOULET

Groupe du Conseil de recherches médicales du Canada en sciences des radiations et Département de médecine nucléaire et de radiobiologie, Faculté de médecine, Université de Sherbrooke, Sherbrooke (Québec), Canada J1H 5N4

AND

ISABELLE BILLARD

Laboratoire de chimie nucléaire, Centre de recherches nucléaires, B.P. 20, 67037 Strasbourg CEDEX *2, France*

Received September 18, 1992

JEAN-PAUL JAY-GERIN, THOMAS GOULET, and ISABELLE BILLARD. Can. J. Chem. **71**, 287 (1993).

The correlation between the thermal electron mobility, μ_e, the radiation-induced free-ion yield G_{fi} at zero applied electric field, and the most probable thermalization distance b of secondary electrons, is examined for 52 different pure nonpolar dielectric liquids for which data have been reported in the literature. It is shown that, in liquids for which $\mu_e > 10^{-1}$ cm^2 V^{-1} s^{-1}, the variation of G_{fi} with μ_e is well represented by a relation of the type $G_{fi} \propto (\mu_e)^n$, where $n \approx 0.31$. The connection between G_{fi} and μ_e can be described through the product $\varepsilon_s b$, where ε_s is the static dielectric constant of the intervening liquid. In particular, $1/\varepsilon_s b$ is shown to correlate with both μ_e and G_{fi}. Analysis of these correlations allows us to estimate an upper limit of μ_e that can be attained in a room-temperature dielectric liquid, information of utmost importance from the point of view of application to liquid ionization detectors.

JEAN-PAUL JAY-GERIN, THOMAS GOULET et ISABELLE BILLARD. Can. J. Chem. **71**, 287 (1993).

On a évalué la corrélation entre la mobilité des électrons thermiques, μ_e, le rendement G_{fi} en ions libres induit par la radiation à champ électrique appliqué nul et la distance de thermalisation b la plus probable des électrons secondaires de 52 liquides diélectriques non polaires purs différents pour lesquels des données ont été rapportées dans la littérature. On démontre que, dans les liquides pour lesquels $\mu_e > 10^{-1}$ cm^2 V^{-1} s^{-1}, la variation de G_{fi} en fonction de μ_e est bien représentée par une relation du type $G_{fi} \propto (\mu_e)^n$ où $n \approx 0{,}31$. On peut décrire la correspondance entre G_{fi} et μ_e par le produit $\varepsilon_s b$ où ε_s est la constante diélectrique statique du liquide intervenant. En particulier, on a démontré qu'il existe une corrélation entre $1/\varepsilon_s b$ et μ_e ainsi que G_{fi}. Une analyse de ces corrélations nous permet d'évaluer la limite supérieure de μ_e qui peut être atteinte dans un liquide diélectrique à la température ambiante; cette information est d'importance capitale dans l'application aux détecteurs liquides à ionisation.

Can. J. Chem. Downloaded from www.nrcresearchpress.com by 88.255.202.194 on 09/08/12
For personal use only.

The electrical properties of nonpolar dielectric liquids have been actively studied for several decades (for recent reviews, see ref. 1). In particular, electron transport in room-temperature liquids exhibiting high values of the electron mobility has attracted considerable attention in recent years, since these liquids are potential candidates for use in a variety of applications, including liquid ionization detectors (2–5), pulsed-power switches (6), X-ray tomography (7), and high-precision radiotherapy dosimetry (8).

Experimental data on thermal electron mobility μ_e and radiation-induced free-ion yield $G_{fi}(E)$ (measured as a function of applied electric field strength E) are now available in many dielectric liquids (9–14). It is found that μ_e can change by orders of magnitude from one liquid to another, depending strongly on the shape of the constituent molecules. In fact, electron mobilities tend to increase with the degree of sphericity of the molecules (13, 15, 16). Values of μ_e have also been found to correlate with those of G_{fi} at $E = 0$ for liquids of high electron mobilities (5, 17). Despite theoretical efforts (18–20), this correlation remains incompletely understood. Also closely related to the mobility is b, the most probable distance that a secondary electron travels away from its parent ion during its thermalization in the liquid. Values of b are obtained from fitting the field dependence of the experimentally measured yields $G_{fi}(E)$, using various forms of the extended Onsager model (5, 13, 21–25). In fact, there is a correlation between values of b and μ_e in different liquids, the trend being for b to increase with μ_e (13, 26, 27). This correlation is well documented and has been explained on the basis that electrons ejected initially with excess kinetic energy travel the major part of their thermalization distance while having energies of only a few tenths of an electronvolt above thermal (13, 28–31).

In this work, we present a compilation of experimental data available in the literature on the electron mobility, the most probable electron thermalization distance, and the radiolytic zero-field free-ion yield (hereafter simply denoted G_{fi}, for convenience) for a variety of nonpolar liquids, in an attempt to characterize further the interrelationship between these quantities. Values of μ_e, b, and G_{fi} for 52 pure liquids (4, 5, 7, 9, 10, 13, 22, 23, 25–27, 32–57) at room temperature are collected in Table 1, along with the values of the corresponding static dielectric constant ε_s.

In Fig. 1, values of G_{fi} are plotted against log μ_e for all the considered liquids. As we can see, G_{fi} is nearly constant (~0.1 molecule/100 eV) in the range $\mu_e \sim 10^{-2}$–10^{-1} cm^2 V^{-1} s^{-1},[1] whereas it increases with μ_e in higher electron-mobility liquids. Since we are interested by the correlation between G_{fi} and μ_e, we will thus only consider in the following the first 35 liquids of Table 1, for which $\mu_e > 10^{-1}$ cm^2 V^{-1} s^{-1}. A double logarithmic plot of G_{fi} against μ_e is shown in Fig. 2 to examine more quantitatively the re-

[1]Electron mobilities less than 10^{-2} cm^2 V^{-1} s^{-1} are in general observed in polar liquids. The lower mobilities in these liquids are attributed to electron solvation processes; electron migration occurs by an ion-like mechanism rather than by transport through the conduction band (see, for example, refs. 13 and 58.

TABLE 1. Thermal electron mobility (μ_e), most probable electron thermalization distance (b), and free-ion yield (G_{fi}) in various dielectric liquids of static dielectric constant ε_s[a]

Liquid	μ_e ($cm^2\ V^{-1}\ s^{-1}$)	b (Å)	G_{fi}[b] (molecule/100 eV)	ε_s[c]	No.[d]	References
Tetramethylsilane	103	160	0.7	1.92	1	4, 5, 10, 13, 22, 25, 32–35
Tetramethylgermane	102	143	0.66	2.01	2	4, 5, 7, 25, 36, 37
Tetramethylstannane	77.9	115	0.63	2.25	3	4, 5, 13, 22, 25, 36
2,2-Dimethylpropane (neopentane)	69.5	217	1.1	1.78	4	4, 9, 13, 23, 32, 38–41
Ethane	37	222	0.94	1.44	5	42
2,2,4,4-Tetramethylpentane	29	163	0.78	1.98	6	4, 5, 25, 26, 43, 44
Hexamethyldisilane	20	99	0.33	2.16	7	5, 45
2,2-Dimethylbutane (neohexane)	12	120	0.58	1.87	8	13, 43, 46
2,2,5,5-Tetramethylhexane	12	138	0.67	1.97	9	26
2-Methylpropane (isobutane)	7.3	116	0.51	1.74	10	46, 47
2,2,4-Trimethylpentane (isooctane)	6.5	110	0.35	1.94	11	9, 10, 23, 39, 43, 48, 49
2,3-Dimethylbutene-2	6	102	0.44	1.98	12	13, 50
1,4-Cyclohexadiene	6	66	0.23	2.21	13	13, 51
2,2,3,3-Tetramethylpentane	5.2	97	0.42	2.05	14	13, 26
4,4-Dimethyl-*cis*-2-pentene	3.5	79	0.28	2.03	15	13, 46
2-Methyl-2-butene	2.9	72	0.22	1.98	16	13, 46
Propane	2.63	110	0.43	1.65	17	42
cis-Butene-2	2.2	74	0.23	2	18	27, 50
Tetrakis(dimethylamino) ethylene	2.2	62	0.2	2.46	19	52
3,3-Dimethyl-1-butene	1.9	73	0.23	1.98	20	13, 46
4,4-Dimethyl-*trans*-2-pentene	1.8	72	0.21	1.97	21	13, 46
Cyclopentene	1.3	58	0.15	2.08	22	51
Cyclopentane	1.13	75	0.19	1.96	23	9, 13, 36, 51, 53
2,3-Dimethylbutane	1.1	74	0.22	1.89	24	13, 46
Cyclohexene	1.1	62	0.2	2.22	25	13, 27, 51
2-Methylbutane (isopentane)	0.9	78	0.21	1.84	26	9, 13, 40
3,3-Diethylpentane	0.8	73	0.23	2.01	27	13, 46
n-Butane	0.34	73	0.19	1.77	28	42
2-Methylpentane	0.29	71	0.19	1.88	29	13, 46
Cyclohexane	0.28	59	0.15	2.02	30	48, 53, 54
3-Methylpentane	0.2	67	0.18	1.9	31	13, 36, 46
1,3,5-Trimethylbenzene (mesitylene)	0.17	44	0.087	2.27	32	13, 55
n-Pentane	0.154	64	0.15	1.83	33	42
Benzene	0.125	42	0.071	2.28	34	9, 13, 53, 55
cis-Decalin	0.1	50	0.12	2.19	35	53, 54
Methylbenzene (toluene)	0.075	43	0.093	2.38	36	13, 55

Can. J. Chem. Downloaded from www.nrcresearchpress.com by 88.255.202.194 on 09/08/12
For personal use only.

TABLE I (*concluded*)

Liquid	μ_e ($cm^2\ V^{-1}\ s^{-1}$)	b (Å)	G_{fi}[b] (molecule/100 eV)	ε_s[c]	No.[d]	References
n-Hexane	0.074	61	0.14	1.89	37	42
1,4-Dimethylbenzene (*p*-xylene)	0.066	41	0.073	2.26	38	13, 55
1,3-Dimethylbenzene (*m*-xylene)	0.063	41	0.082	2.37	39	13, 55
Methylcyclohexane	0.057	60	0.12	2.02	40	9, 13, 53
n-Heptane	0.051	58	0.13	1.92	41	42
n-Octane	0.038	58	0.13	1.95	42	42
trans-Butene-2	0.029	53	0.08	1.84	43	27, 50
n-Nonane	0.028	56	0.13	1.97	44	42
n-Decane	0.025	57	0.14	1.99	45	42
n-Undecane	0.024	55	0.13	2	46	42
1,2-Dimethylbenzene (*o*-xylene)	0.022	40	0.094	2.56	47	13, 55
1,2,3,4-Tetramethylbenzene	0.02	42	0.11	2.54	48	13, 55
n-Dodecane	0.02	54	0.12	2.01	49	42
n-Tetradecane	0.016	53	0.12	2.04	50	42
trans-Decalin	0.013	50	0.12	2.15	51	53, 54
Hexafluorobenzene	0.011	52	0.08	2.01	52	56, 57
Methane, 122 K	375	510	1	1.65	I	16, 59
Argon, 95 K	447	1630	2.2	1.49	II	60, 61
Xenon, 164 K	1800	1340	4.4	1.93	III	13, 62
Krypton, 129 K	2100	2030	4	1.63	IV	13, 62

[a]Selected values are for room temperature, unless otherwise mentioned. The different liquids are listed in the order of decreasing μ_e.
[b]Values at zero applied electric field strength. Note that G_{fi} is defined as the number of free-ion pairs formed per 100 eV of energy absorbed by the irradiated liquid. Data obtained with low-LET radiations such as γ or X rays, or megavolt electron beams.
[c]Many of the data on ε_s are from ref. 66.
[d]Used in Figs. 1–4.

lationship between those two quantities. A linear correlation is obtained, indicating that the variation of G_{fi} with μ_e can be expressed as

$$[1] \quad G_{fi} = \alpha(\mu_e)^n$$

A least-squares fit of eq. [1] to the log G_{fi} vs. log μ_e data of Fig. 2 (with μ_e in $cm^2\ V^{-1}\ s^{-1}$ and G_{fi} in molecule/100 eV) yields

$$[2] \quad \alpha = 0.21\ (\pm 0.02) \quad \text{and} \quad n = 0.31\ (\pm 0.05)$$

where the values in parentheses indicate the 95% confidence intervals of the estimated parameters calculated using Student's t statistics. The straight line shown in Fig. 2 is calculated from eq. [1] with those parameter values. For the sake of comparison, $G_{fi}(\mu_e)$ data points (13, 16, 59–62) corresponding to low-temperature liquids, namely, liquefied methane and rare gases (see Table 1), are also included in Fig. 2. Rather surprisingly, we note that the fitted line, when extrapolated to higher μ_e and G_{fi} values, also gives a reasonable description of these latter points. This suggests that a general relationship could exist between G_{fi} and μ_e for all dielectric liquids for which $\mu_e > 10^{-1}\ cm^2\ V^{-1}\ s^{-1}$. The physical meaning of the exponent n is not a priori obvious. It is interesting to note, however, that $n \sim 1/3$, which could be indicative that the observed $G_{fi}(\mu_e)$ relationship rests on simple theoretical grounds.

The connection between G_{fi} and μ_e may be seen through the most probable thermalization distance b. This naturally follows from the fact that, on the one hand, liquids with a high μ_e also exhibit a large value of b (13, 26, 27), and that, on the other hand, Onsager's recombination theory (5, 13, 21–25) predicts that high-yield liquids are characterized by high b values. More specifically, the Onsager theory states that in the absence of a collecting electric field, the probability P that an ion pair thermalized at separation r will diffuse apart to become free ions is related to the electron thermalization-distance distribution function $F_b(r)$ by

$$[3] \quad P = \frac{G_{fi}}{G_{tot}} = \int_0^\infty F_b(r) \exp\left[-\frac{e^2}{4\pi\varepsilon_0\varepsilon_s k_B T r}\right] dr$$

where e is the electron charge, ε_0 is the permittivity of vacuum, k_B is Boltzmann's constant, T is the absolute temperature, and G_{tot} is the number of ion pairs initially formed per 100 eV of energy absorbed by the medium.

Can. J. Chem. Downloaded from www.nrcresearchpress.com by 88.255.202.194 on 09/08/12
For personal use only.

Can. J. Chem. Downloaded from www.nrcresearchpress.com by 88.255.202.194 on 09/08/12
For personal use only.

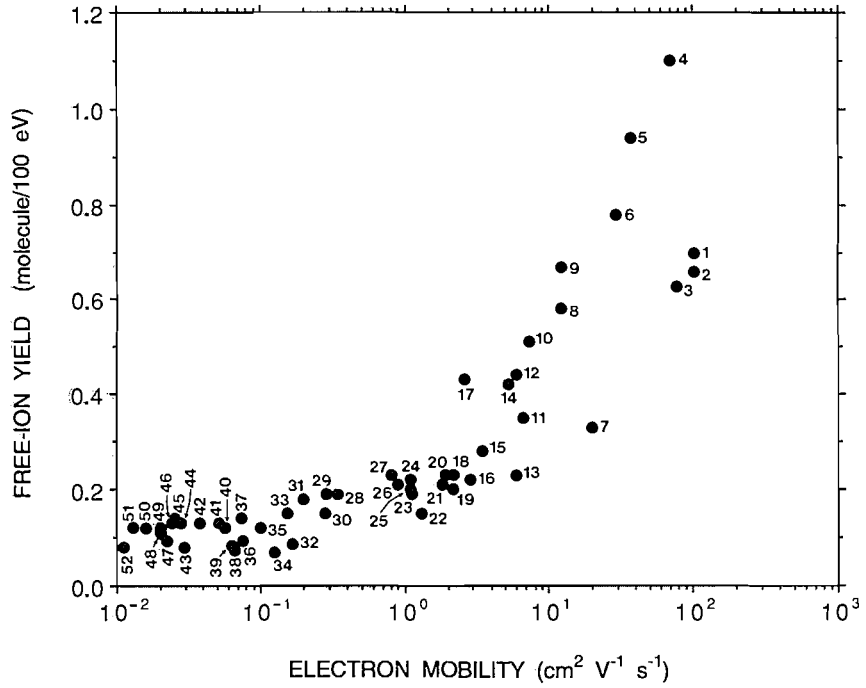

FIG. 1. Free-ion yield G_{fi} as a function of thermal electron mobility μ_e for a variety of pure nonpolar dielectric liquids at room temperature (●). The number for each point refers to the serial number of the liquid in Table 1.

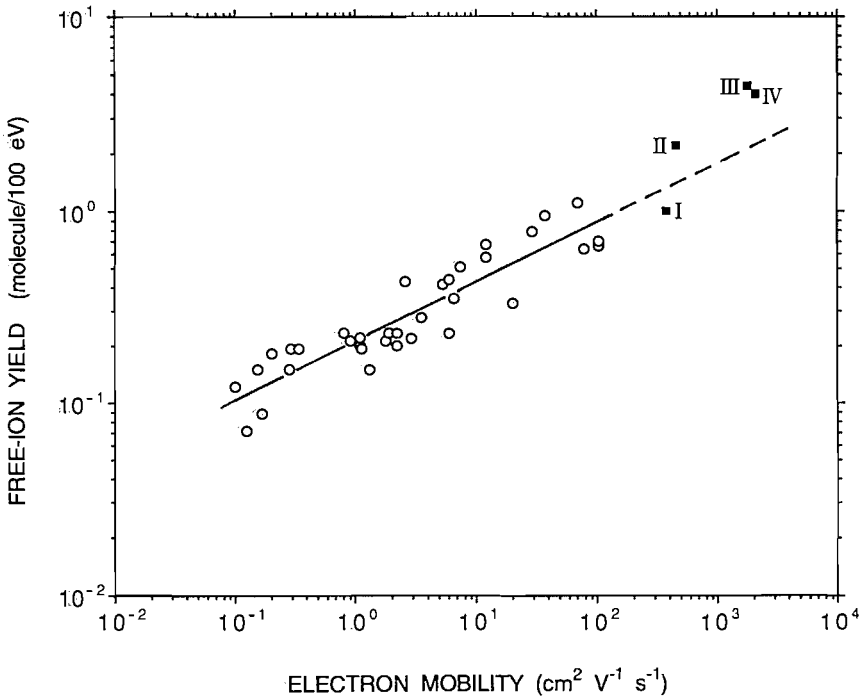

FIG. 2. Double logarithmic plot of free-ion yield against the mobility of thermal electrons for the first 35 liquids listed in Table 1 for which $\mu_e > 10^{-1}$ cm^2 V^{-1} s^{-1} at room temperature (○). The straight line was obtained with eq. [1], using the values of α and n in eq. [2]. The $G_{fi}(\mu_e)$ data points for liquid methane at 122 K, argon at 95 K, xenon at 164 K, and krypton at 129 K (■), included for comparison, are denoted by the numbers I–IV, respectively (see Table 1). The dashed line is an extrapolation of the fitted straight line to higher G_{fi} and μ_e values.

To examine the relationship between G_{fi}, b, and ε_s, a semilog plot of G_{fi} against $1/\varepsilon_s b$ is shown in Fig. 3. A good linear correlation is obtained, indicating that the variation of G_{fi} can be described by a simple equation of the form

$$[4] \quad G_{fi} = G_\infty \exp(-B/\varepsilon_s b)$$

which includes the essential elements of eq. [3]. A least-squares fit of eq. [4] to the log G_{fi} vs. $1/\varepsilon_s b$ data yields

$$[5] \quad G_\infty = 2.1\ (\pm 0.3)\ \text{molecule/100 eV}$$

and $B = 324\ (\pm 22)$ Å

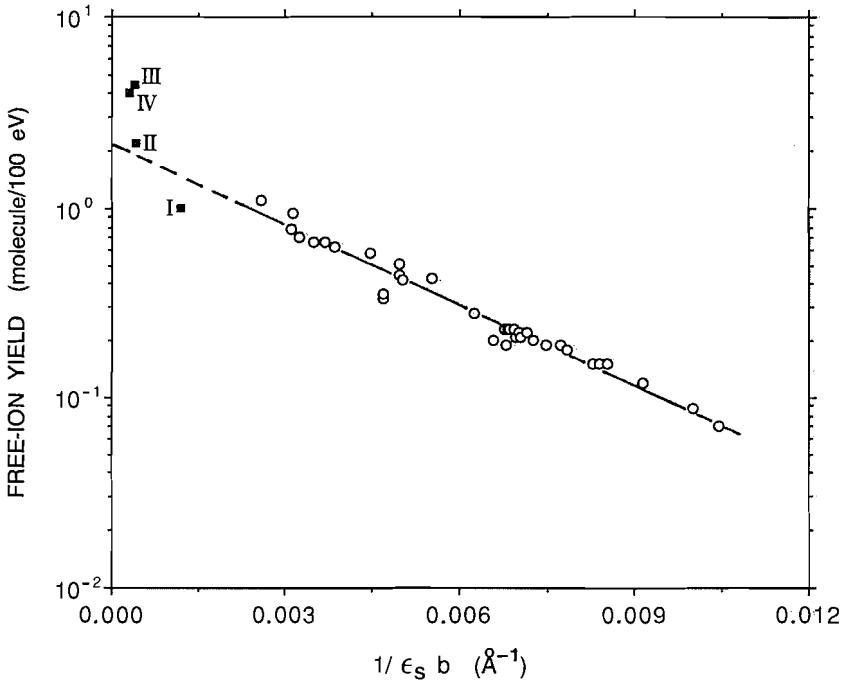

FIG. 3. Plot of the free-ion yield G_{fi} as a function of $1/\varepsilon_s b$ for the same liquids as those in Fig. 2 (○). The straight line was obtained with eq. [4], using the values of G_∞ and B in eq. [5]. The dashed line is an extrapolation of the fitted straight line to $1/\varepsilon_s b \rightarrow 0$. The corresponding data points for liquid methane at 122 K, argon at 95 K, xenon at 164 K, and krypton at 129 K (■), denoted by the numbers I–IV, respectively (see Table 1), are included for comparison.

for the parameters and their 95% confidence intervals (values in parentheses). The solid line shown in Fig. 3 is calculated from eq. [4] with these parameter values. The low-temperature $G_{fi}(1/\varepsilon_s b)$ data points corresponding to liquefied methane and rare gases (see Table 1) are also included in Fig. 3 for comparison. Extrapolation of the fitted line to $1/\varepsilon_s b \rightarrow 0$ passes again through these latter points, but the dispersion is rather large. No indication can be seen here of the existence of anomalous behavior in the variation of G_{fi} with $1/\varepsilon_s b$ in going from the region of electron mobilities considered in this study to higher μ_e values. This does not preclude, however, the breakdown of the Onsager theory that has been predicted for high-electron-mobility liquids (63) since all the b values reported here were obtained with the explicit assumption that this theory remains applicable.

One should note that G_∞, the limiting value of G_{fi} as $1/\varepsilon_s b \rightarrow 0$, cannot be interpreted as the average value of G_{tot} for the various liquids considered. Similarly, B does not represent the term $e^2/4\pi\varepsilon_0 k_B T$ (equal to 560.7 Å at T = 298 K) that appears in the Onsager recombination model (see eq. [3]) (5, 13, 21–25). In fact, eq. [4] is purely empirical and does not attempt to account for the actual electron thermalization-distance distribution function $F_b(r)$ (which peaks at $r = b$) for each liquid. In that sense, the quality of the fit obtained is somewhat surprising, but makes this simple empirical relation quite useful.

If we use eq. [3] with the well-known distribution function YGP (consisting of a three-dimensional Gaussian function extended to larger r values by the addition of a power function tail (13, 50)) in a nonlinear least-squares fit to the $G_{fi}(1/\varepsilon_s b)$ data of Table 1, we find an average total ionization yield $\bar{G}_{tot}$ = 3.7 (±0.5). This value is significantly lower than the commonly accepted gas-phase G_{tot} value of 4.3 molecule/100 eV (64), which has been used in the literature for a variety of hydrocarbon liquids (13, 65). Interestingly, a "universal" value of G_{tot} of 4.3 has also been questioned recently by Holroyd *et al.* (5). In fact, these authors concluded from their analyses of free-ion yields in several room-temperature tetraalkyl liquids containing silicon, germanium, or tin atoms, that G_{tot} values close to 3 ion pairs per 100 eV deposited seemed more appropriate than values near 4 (5).

Combining eqs. [1] and [4] readily yields

$$[6] \quad 1/\varepsilon_s b = C - D \ln \mu_e$$

in agreement with the linear correlation that one can see in the plot of $1/\varepsilon_s b$ against log μ_e of Fig. 4. The best fit to the data (with b in Å and μ_e in $cm^2\ V^{-1}\ s^{-1}$) is obtained with $C = (7.2 \pm 0.3) \times 10^{-3}\ Å^{-1}$ and $D = (9.6 \pm 1.2) \times 10^{-4}\ Å^{-1}$. The extrapolation of the fitted straight line to $1/\varepsilon_s b \rightarrow 0$ again provides a reasonable description (within the statistical uncertainties) of the corresponding $1/\varepsilon_s b(\mu_e)$ data points for liquefied methane and rare gases.

A few words should finally be said about the physical significance of $(\mu_e)_\infty = \exp(C/D) = 1800\ (\pm 1580)\ cm^2\ V^{-1}\ s^{-1}$, the extrapolated value of the fitted straight line in Fig. 4 to $1/\varepsilon_s b \rightarrow 0$. $(\mu_e)_\infty$ appears as an upper limiting value of the mobility of an excess electron in an "ideal" room-temperature liquid in which the most probable thermalization distance would be infinity. A knowledge of $(\mu_e)_\infty$ is therefore of utmost importance from the point of view of application to liquid ionization detectors since it gives us an estimate of the upper limit of μ_e that it is possible to attain in a dielectric liquid at room temperature.

In conclusion, we have presented as complete a compilation as possible of literature values of thermal electron mobilities, radiolytic free-ion yields, and thermalization distances of secondary electrons in a variety of pure non-

Can. J. Chem. Downloaded from www.nrcresearchpress.com by 88.255.202.194 on 09/08/12
For personal use only.

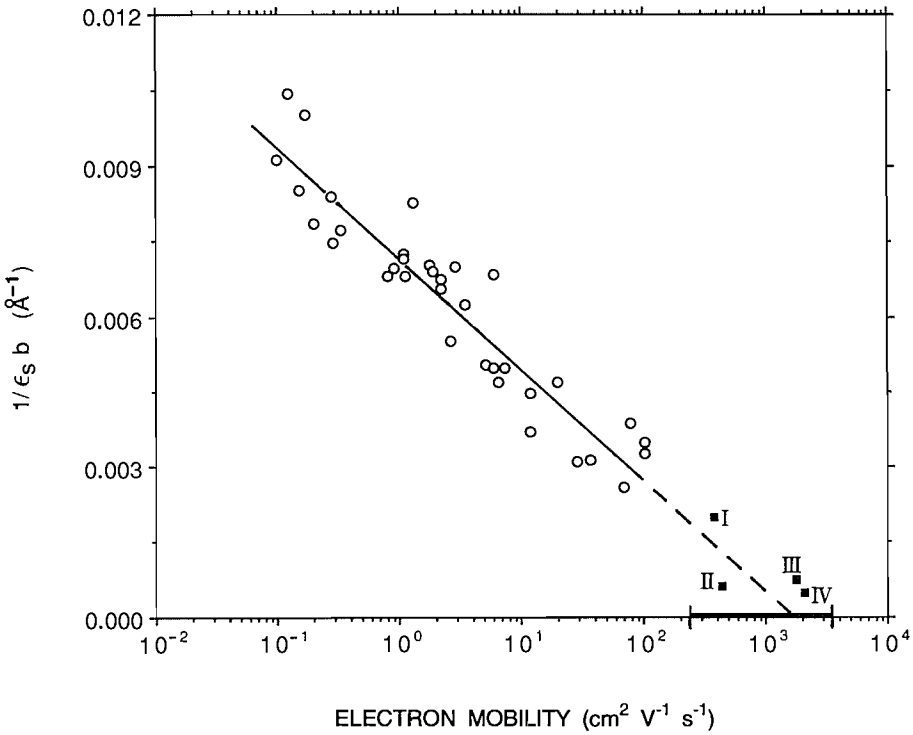

FIG. 4. Plot of $1/\varepsilon_s b$ as a function of the thermal electron mobility μ_e for the same liquids as those in Fig. 2 (○). The straight line was obtained with eq. [6], using the values $C = 7.2 \times 10^{-3}$ Å^{-1} and $D = 9.6 \times 10^{-4}$ Å^{-1}. The dashed line is an extrapolation of the fitted straight line to $1/\varepsilon_s b \rightarrow 0$. The error bar on $(\mu_e)_\infty$ at $1/\varepsilon_s b = 0$ indicates the 95% confidence interval on this parameter. The data points for liquid methane at 122 K, argon at 95 K, xenon at 164 K, and krypton at 129 K (■), denoted by the numbers I–IV, respectively (see Table 1), are included for comparison.

polar liquids at room temperature. On this basis, we have quantitatively described certain correlations that exist between these values. We hope that the present results will contribute to favor further developments of a coherent theory of electron transport and geminate ion–electron recombination in dielectric liquids.

Acknowledgments

We wish to thank Professor C. Ferradini and Dr. J.-Ch. Abbé for a critical reading of the manuscript and for valuable discussions. Financial support from the Medical Research Council of Canada and the Natural Sciences and Engineering Research Council of Canada is gratefully acknowledged.

1. R. C. Muñoz. *In* Excess electrons in dielectric media. *Edited by* C. Ferradini and J.-P. Jay-Gerin. CRC Press, Boca Raton, Fla. 1991. p. 161; R. A. Holroyd and W.F. Schmidt. Annu. Rev. Phys. Chem. **40**, 439 (1989); L. Nyikos and R.Schiller. *In* The chemical physics of solvation. Part C. *Edited by* R. R. Dogonadze, E. Kálmán, A. A. Kornyshev, and J. Ulstrup. Elsevier, Amsterdam. 1988. p. 329.
2. W. F. Schmidt. IEEE Trans. Electr. Insul. **26**, 560 (1991).
3. M. Krammer (For the UA1 Collaboration). Nucl. Instrum. Methods Phys. Res. Sect. A: **A283**, 630 (1989); A. Gonidec. *In* Conference record of the 10th international conference on conduction and breakdown in dielectric liquids, Grenoble, France, 10–14 September 1990. *Edited by* P. Atten and R. Tobazeon. IVR, Grenoble. 1990. p. 120.
4. H. Faidas, L. G. Christophorou, and D. L. McCorkle. IEEE Trans. Electr. Insul. **26**, 568 (1991); H. Faidas, L. G. Christophorou, D. L. McCorkle, and J. G. Carter. Nucl. Instrum. Methods Phys. Res. Sect. A: **A294**, 575 (1990); H. Faidas and L. G. Christophorou. Nucl. Instrum. Methods Phys. Res. Sect. A: **A320**. 608 (1992).
5. R. A. Holroyd, S. Geer, and F. Ptohos. Phys. Rev. B, **43**, 9003 (1991); S. Geer, R. A. Holroyd, and F. Ptohos. Nucl. Instrum. Methods Phys. Res. Sect. A: **A287**, 447 (1990).
6. L. G. Christophorou and H. Faidas. Appl. Phys. Lett. **55**, 948 (1989).
7. F. Mathy, S. Lepert, and G. Thomas. IEEE Trans. Electr. Insul. **26**, 631 (1991); S. Lepert. Rev. Sci. Instrum. **61**, 3456 (1990).
8. G. Wickman and H. Nyström. Phys. Med. Biol. **37**, 1789 (1992).
9. A. O. Allen. Yields of free ions formed in liquids by radiation. Natl. Stand. Ref. Data Ser. Natl. Bur. Stand. (U.S.). Report No. 57. U.S. Government Printing Office, Washington, D.C. 1976.
10. A. O. Allen. Drift mobilities and conduction band energies of excess electrons in dielectric liquids. Natl. Stand. Ref. Data Ser. Natl. Bur. Stand. (U.S.). Report No. 58. U.S. Government Printing Office, Washington, D.C. 1976.
11. W. F. Schmidt. IEEE Trans. Electr. Insul. **EI-19**, 389 (1984).
12. L. G. Christophorou and K. Siomos. *In* Electron–molecule interactions and their applications. Vol. 2. *Edited by* L. G. Christophorou. Academic, Orlando. 1984. p. 221.
13. G. R. Freeman. *In* Kinetics of nonhomogeneous processes. *Edited by* G.R. Freeman. Wiley, New York. 1987. p. 19.
14. Y. Tabata, Y. Ito, and S. Tagawa (*Editors*). Handbook of radiation chemistry. CRC Press, Boca Raton. Fla. 1991. pp. 293 and 395.
15. I. György and G. R. Freeman. J. Chem. Phys. **70**, 4769 (1979).
16. M. A. Floriano and G.R. Freeman. J. Chem. Phys. **85**, 1603 (1986).

Can. J. Chem. Downloaded from www.nrcresearchpress.com by 88.255.202.194 on 09/08/12
For personal use only.

17. A. Mozumder. IEEE Trans. Nucl. Sci. **NS-26**, 129 (1979).
18. R. Schiller and S. Vass. Int. J. Radiat. Phys. Chem. **7**, 193 (1975), and references cited therein; R. Schiller. *In* Proceedings of the fifth international congress of radiation research, Seattle, Wash., U.S.A., 14–20 July 1974. *Edited by* O. F. Nygaard, H. I. Adler, and W. K. Sinclair. Academic, New York. 1975. p. 388.
19. H. Sano and A. Mozumder. J. Chem. Phys. **66**, 689 (1977).
20. K. Funabashi and T. Kajiwara. J. Phys. Chem. **76**, 2726 (1972).
21. L. Onsager. Phys. Rev. **54**, 554 (1938).
22. W. F. Schmidt and A. O. Allen. J. Chem. Phys. **52**, 2345 (1970).
23. J. Casanovas, R. Grob, J. Ortet, and A. Shamsaldin. J. Chim. Phys. **80**, 325 (1983).
24. G. Ramanan, N. Gee, and G. R. Freeman. Can. J. Phys. **68**, 925 (1990).
25. R. C. Muñoz, A. Ferrando, D. Drijard, and E. Torrente-Luján. *In* Conference record of the 10th international conference on conduction and breakdown in dielectric liquids, Grenoble, France, 10–14 September 1990. *Edited by* P. Atten and R. Tobazeon. IVR, Grenoble. 1990. p. 110.
26. J.-P. Dodelet and G. R. Freeman. Can. J. Chem. **50**, 2667 (1972).
27. J.-P. Dodelet, K. Shinsaka, and G. R. Freeman. J. Chem. Phys. **59**, 1293 (1973).
28. A. Hummel, A. O. Allen, and F. H. Watson, Jr. J. Chem. Phys. **44**, 3431 (1966).
29. A. Mozumder and J. L. Magee. J. Chem. Phys. **47**, 939 (1967).
30. J.-P. Dodelet. Can. J. Chem. **55**, 2050 (1977), and references cited therein.
31. G. R. Freeman. *In* Proceedings of the workshop on the interface between radiation chemistry and radiation physics, Argonne, Ill., U.S.A., 9–10 September 1982. Report ANL-82-88. *Edited by* M. A. Dillon, R. J. Hanrahan, R. Holroyd, Y.-K. Kim, M. C. Sauer, Jr., and L. H. Toburen. Argonne National Laboratory, Argonne. 1983. p. 9.
32. G. Bakale and W. F. Schmidt. Chem. Phys. Lett. **175**, 319 (1990).
33. R. C. Muñoz and G. Ascarelli. Chem. Phys. Lett. **94**, 235 (1983).
34. R. C. Muñoz and R. A. Holroyd. Chem. Phys. Lett. **137**, 250 (1987).
35. R. A. Holroyd and W. F. Schmidt. Nucl. Instrum. Methods Phys. Res. Sect. A: **A311**, 631 (1992).
36. W. F. Schmidt. Can. J. Chem. **55**, 2197 (1977).
37. I. Lopes and W. F. Schmidt. Z. Naturforsch. A: Phys. Sci. **45**, 832 (1990).
38. K. Shinsaka and G. R. Freeman. Can. J. Chem. **52**, 3556 (1974).
39. J. Casanovas, J. P. Guelfucci, and M. Terrissol. Radiat. Phys. Chem. **32**, 361 (1988).
40. I. György and G. R. Freeman. J. Chem. Phys. **86**, 681 (1987).
41. R. M. Minday, L. D. Schmidt, and H. T. Davis. J. Phys. Chem. **76**, 442 (1972).
42. N. Gee, P. C. Senanayake, and G. R. Freeman. J. Chem. Phys. **89**, 3710 (1988).
43. K. Itoh, R. C. Muñoz, and R. A. Holroyd. J. Chem. Phys. **90**, 1128 (1989).
44. T. G. Ryan and G. R. Freeman. J. Chem. Phys. **68**, 5144 (1978).
45. S. S. Takeda, N. E. Houser, and R. C. Jarnagin. J. Chem. Phys. **54**, 3195 (1971).
46. J.-P. Dodelet, K. Shinsaka, and G. R. Freeman. Can. J. Chem. **54**, 744 (1976).
47. N. Gee and G. R. Freeman. Phys. Rev. A, **32**, 525 (1985).
48. T. Tezuka, H. Namba, Y. Nakamura, M. Chiba, K. Shinsaka, and Y. Hatano. Radiat. Phys. Chem. **21**, 197 (1983).
49. C. A. M. van den Ende, J. M. Warman, and A. Hummel. Radiat. Phys. Chem. **23**, 55 (1984).
50. J.-P. Dodelet, K. Shinsaka, U. Kortsch, and G. R. Freeman. J. Chem. Phys. **59**, 2376 (1973).
51. K. Shinsaka, J.-P. Dodelet, and G. R. Freeman. Can. J. Chem. **53**, 2714 (1975).
52. R. A. Holroyd, S. Ehrenson, and J. M. Preses. J. Phys. Chem. **89**, 4244 (1985).
53. J. M. Warman. *In* The study of fast processes and transient species by electron pulse radiolysis. *Edited by* J. H. Baxendale and F. Busi. D. Reidel, Dordrecht. 1982. p. 433; M. P. de Haas. *In* Book of abstracts of the international workshop on liquid state electronics, Berlin, Germany, 7–10 November 1988. *Edited by* W. F. Schmidt. Hahn-Meitner-Institut, Berlin. 1988. p. 73.
54. N. Gee and G. R. Freeman. J. Chem. Phys. **96**, 586 (1992).
55. K. Shinsaka and G. R. Freeman. Can. J. Chem. **52**, 3495 (1974).
56. N. Gee and G. R. Freeman. Can. J. Phys. **68**, 930 (1990).
57. C. A. M. van den Ende, L. Nyikos, J. M. Warman, and A. Hummel. Radiat. Phys. Chem. **19**, 297 (1982).
58. J.-P. Jay-Gerin and C. Ferradini. *In* Excess electrons in dielectric media. *Edited by* C. Ferradini and J.-P. Jay-Gerin. CRC Press, Boca Raton, Fla. 1991. p. 259.
59. I. György and G. R. Freeman. J. Appl. Phys. **60**, 3188 (1986).
60. S. S.-S. Huang, N. Gee, and G. R. Freeman. Radiat. Phys. Chem. **37**, 417 (1991).
61. S. S.-S. Huang and G. R. Freeman. Phys. Rev. A, **24**, 714 (1981).
62. S. S.-S. Huang and G. R. Freeman. Can. J. Chem. **55**, 1838 (1977).
63. M. Tachiya. Radiat. Phys. Chem. **32**, 37 (1988); J. Chem. Phys. **89**, 6929 (1988); M. Tachiya and W. F. Schmidt. J. Chem. Phys. **90**, 2471 (1989).
64. Average energy required to produce an ion pair. ICRU Report No. 31. International Commission on Radiation Units and Measurements, Washington, D.C. 1979.
65. W. F. Schmidt and A. O. Allen. J. Phys. Chem. **72**, 3730 (1968).
66. J. A. Riddick, W. B. Bunger, and T. K. Sakano. Organic solvents. 4th ed. Wiley, New York. 1986; J. A. Dean. Handbook of organic chemistry. McGraw–Hill, New York. 1987. pp. 4–45; Handbook of chemistry and physics. 1st student edition. CRC Press, Boca Raton, Fla. 1988. p. E-43.

Can. J. Chem. Downloaded from www.nrcresearchpress.com by 88.255.202.194 on 09/08/12
For personal use only.

Processus élémentaires en solution : Apports et limites de la théorie du complexe activé dans le cas d'un prééquilibre rapide d'échange protonique entre réactifs

B. SOLASTIOUK, A. MERLIN ET X. DEGLISE[1]

Université de Nancy I, Laboratoire de photochimie appliquée (Unité associée au Centre nationale de la recherche scientifique n° 328), Boîte Postale n° 239, 54506 Vandoeuvre les Nancy CEDEX, France

Reçu le 15 juillet 1992

B. SOLASTIOUK, A. MERLIN et X. DEGLISE. Can. J. Chem. **71**, 294 (1993).

L'étude cinétique des réactions de N-chloration en milieu aqueux de différentes molécules azotées (amines secondaires, imides, acide cyanurique . . .) nous a montré que le comportement acido-basique faible en solution aqueuse des réactifs implique, du fait d'un échange rapide de proton, une indétermination sur le mécanisme exact de chloration. Nous avons généralisé ce résultat à des réactifs de charge quelconque susceptibles d'échanger rapidement un proton. Cette généralisation nous a montré que ce sont les hypothèses de la théorie de l'état de transition qui imposent cette indétermination.

B. SOLASTIOUK, A. MERLIN, and X. DEGLISE. Can. J. Chem. **71**, 294 (1993).

The kinetic study of N-chlorination reactions in the aqueous phase of different nitrogenized molecules (secondary amines, imides, cyanuric acid, etc . . .) shows that the correct chlorination mechanism has not yet been determined because fast proton exchange causes weak acido-basic behaviour of the reagents in aqueous solution. We extended this result to reagents of any charge capable of fast proton exchange. This generalization demonstrates that the indeterminate nature of the mechanism is imposed by the hypotheses of transition state theory.

Can. J. Chem. Downloaded from www.nrcresearchpress.com by 88.255.202.194 on 09/08/12
For personal use only.

Introduction

Nous intéressant à l'étude cinétique des réactions de N-chloration en milieu aqueux de différentes fonctions azotées (amines secondaires, succinimide et triazine trione) et des réactions d'hydrolyse des dérivés N-chlorés correspondants, il nous est apparu que le comportement acido-basique faible du chlore et de molécules azotées en solution aqueuse implique, du fait d'un échange rapide de proton,

$$HOCl \leftrightarrows ClO^- + H^+ \text{ pour le chlore}$$

et

$$R_3NH^+ \leftrightarrows R_3N + H^+ \text{ pour les molécules azotées}$$

une indétermination sur le mécanisme exact de la réaction de chloration (1–3).

Dans le cas où la réaction peut concerner les formes acides et basiques de façon croisée, par exemple pour une amine secondaire :

$$R_2NH + ClOH \rightarrow \text{produits}$$

ou

$$R_2NH^+ + ClO^- \rightarrow \text{produits}$$

ces deux mécanismes (pourtant ionique pour l'un ou moléculaire pour l'autre) rendent compte du point de vue théorique de tout résultat expérimental qu'il s'agisse des influences du pH ou de la force ionique sur ces coefficients d'activité qui sont des effets classiquement utilisés en cinétique homogène en solution.

Ce phénomène a déjà été noté par Morris et Weil (4) à propos également de la cinétique de réactions de N-chloration et analysé par Pearson pour la réaction de conversion de cyanate d'ammonium en urée (5–7) où, de façon analogue, les deux mécanismes :

$$NH_3 + CNOH \rightarrow CO(NH_2)_2$$

ou

$$NH_4^+ + CNO^- \rightarrow CO(NH_2)_2$$

sont cinétiquement indiscernables.

Notre objectif est de généraliser ce résultat, a priori surprenant, à des réactifs de charge quelconque susceptibles d'échanger rapidement un proton et de montrer que les hypothèses de l'état de transition imposent cette indétermination.

Constantes de vitesse expérimentales

Hypothèses et expressions générales

Considérons une réaction en solution aqueuse du type :

$$AX + B \underset{V_b}{\overset{V_f}{\rightleftharpoons}} \text{produits}$$

où X représente un atome ou un groupe d'atomes. Les produits peuvent être du type A + XB (substitution, cas de la N-chloration) ou du type A × B (addition, cas de la conversion cyanate d'ammonium-urée), la nature de ces produits n'ayant pas d'influence sur le raisonnement qui suit.

Nous supposons d'une part que la réaction est étudiée suffisamment loin de son état d'équilibre pour que la vitesse de retour V_b soit négligeable devant celle du sens direct V_f et d'autre part qu'il a été observé un ordre 1 par rapport à chacun des réactifs AX et B. Le processus limitant du mécanisme est soit bimoléculaire soit monomoléculaire avec un intermédiaire (C) en équilibre rapide avec AX et B :

$$AX + B \leftrightarrows C^{\neq} \rightarrow \text{produits}$$

$$AX + B \leftrightarrows C \leftrightarrows C^{\neq} \rightarrow \text{produits}$$

Le fait de considérer le cas d'une processus élémentaire limitant bimoléculaire ne nuit en rien à la généralisation des résultats; en effet, supposer un intermédiaire réactionnel en équilibre rapide avec les réactifs d'une part et le composé activé d'autre part n'influe pas sur le raisonnement que nous allons développer.

[1]Auteur à qui adresser toute correspondance.

Can. J. Chem. Downloaded from www.nrcresearchpress.com by 88.255.202.194 on 09/08/12
For personal use only.

AX et B possèdent de plus propriétés acido-basiques et se répartissent selon le pH en espèces protonées ou non selon les équilibres suivants :

$$HAX^{(Z_{AX})} \leftrightarrows AX^{(Z_{AX}-1)} + H^+ \qquad (K_a^{AX})$$

$$HB^{(Z_B+1)} \leftrightarrows B^{(Z_B)} + H^+ \qquad (K_a^{B})$$

Les charges Z_i des espèces correspondantes sont quelconques, positives, négatives ou nulles.

Nous admettrons que ces équilibres sont rapides devant la cinétique de la réaction étudiée.

Dans ces conditions sont conservés, quelque soit l'avancement de la réaction, les lois d'action de masse et les bilans suivants :

[1] $$C_{AX} = [HAX] + [AX]$$

avec C_{AX} : concentration totale de AX.

[2] $$C_B = [BH] + [B]$$

avec C_B : concentration totale de B.

[3] $$K_a^{AX} = \frac{(AX)(H^+)}{(HAX)} = \frac{[AX](H^+)}{[HAX]} \frac{f_{(AX)}}{f_{(HAX)}}$$

[4] $$K_a^{B} = \frac{(B)(H^+)}{(BH)} = \frac{[B](H^+)}{[BH]} \frac{f_{(B)}}{f_{(BH)}}$$

Les concentrations molaires courantes de chaque espèce s'écrivent donc à tout instant de la réaction :

[5] $$[HAX] = \frac{(H^+) f_{(AX)}}{(H^+) f_{(AX)} + K_a^{AX} f_{(HAX)}} C_{AX}$$

[6] $$[AX] = \frac{K_a^{AX} f_{(HAX)}}{(H^+) f_{(AX)} + K_a^{AX} f_{(HAX)}} C_{AX}$$

[7] $$[BH] = \frac{(H^+) f_{(B)}}{(H^+) f_{(B)} + K_a^{B} f_{(BH)}} C_B$$

[8] $$[B] = \frac{K_a^{B} f_{(BH)}}{(H^+) f_{(B)} + K_a^{B} f_{(BH)}} C_B$$

L'expérimentation en cinétique doit, à partir de la mesure d'une vitesse globale $V_{(observée)}$, conduire, par une méthode quelconque, à la détermination d'une constante de vitesse expérimentale $k^{(exp)}$ à partir de la relation :

[9] $$V_{(observée)} = k^{(exp)} C_{AX} C_B = -\frac{d C_{AX}}{dt} = -\frac{d C_B}{dt}$$

Cette relation s'applique à une expérience menée dans un réacteur fermé, isotherme, isochore et parfaitement agité.

La constante de vitesse ainsi déterminée dépend de tous les paramètres expérimentaux (pH, température, force ionique . . .) auxquels la réaction est sensible.

Pour remonter au mécanisme de la réaction et à une constante de vitesse qui ne dépende que de la température, il faut, à partir de l'inventaire de tous les mécanismes possibles, comparer les variations de la constante de vitesse expérimentale $k^{(exp)}$ aux variations attendues dans l'hypothèse de l'un ou l'autre des mécanismes.

Dans notre cas, compte tenu de la bimolécularité de la réaction et sans tenter de décrire les états de solvatation des réactifs, quatre mécanismes différents sont envisageables :

$$\mathcal{P}_1 : HAX^{(Z_{AX})} + B^{(Z_B)} \xrightarrow{k_1} \text{produits}$$

$$\mathcal{P}_2 : AX^{(Z_{AX}-1)} + HB^{(Z_B+1)} \xrightarrow{k_2} \text{produits}$$

$$\mathcal{P}_3 : HAX^{(Z_{AX})} + HB^{(Z_B+1)} \xrightarrow{k_3} \text{produits}$$

$$\mathcal{P}_4 : AX^{(Z_{AX}-1)} + B^{(Z_B)} \xrightarrow{k_4} \text{produits}$$

En faisant l'hypothèse de la participation exclusive d'un seul de ces mécanismes, l'expression de la vitesse devient pour chacune des hypothèses :

[10] $$\mathcal{P}_1 : V_{(observée)} = k^{(exp)} C_{AX} C_B = k_1[HAX^{(Z_{AX})}] [B^{(Z_B)}]$$

[11] $$\mathcal{P}_2 : V_{(observée)} = k^{(exp)} C_{AX} C_B = k_2[AX^{(Z_{AX}-1)}] [HB^{(Z_B+1)}]$$

[12] $$\mathcal{P}_3 : V_{(observée)} = k^{(exp)} C_{AX} C_B = k_3[HAX^{(Z_{AX})}] [HB^{(Z_B+1)}]$$

[13] $$\mathcal{P}_4 : V_{(observée)} = k^{(exp)} C_{AX} C_B = k_4[AX^{(Z_{AX}-1)}] [B^{(Z_B)}]$$

avec pour une solution réelle :

[14] $$k_i = k_i^0 \frac{f_{(AX)} f_{(B)}}{f_i^{\neq}}$$

k_i^0 est la constante de vitesse dans des conditions où les coefficients d'activité (f_i) sont égaux à 1. $f_i^{\neq}$ exprime le coefficient d'activité du complexe activé du processus $\mathcal{P}_i$.

À partir des relations [5]–[14], nous obtenons quatre expressions théoriques de la constante de vitesse expérimentale :

[15] $$\mathcal{P}_1 : k^{(exp)} = k_1^0 \frac{K_a^{B}}{f_1^{\neq}} \left[\frac{(H^+) f_{(AX)} f_{(HAX)} f_{(B)} f_{(BH)}}{\mathcal{A}}\right]$$

[16] $$\mathcal{P}_2 : k^{(exp)} = k_2^0 \frac{K_a^{AX}}{f_2^{\neq}} \left[\frac{(H^+) f_{(AX)} f_{(HAX)} f_{(B)} f_{(BH)}}{\mathcal{A}}\right]$$

[17] $$\mathcal{P}_3 : k^{(exp)} = k_3^0 \frac{1}{f_3^{\neq}} \left[\frac{(H^+)^2 f_{(AX)} f_{(HAX)} f_{(B)} f_{(BH)}}{\mathcal{A}}\right]$$

[18] $$\mathcal{P}_4 : k^{(exp)} = k_4^0 \frac{K_a^{AX} K_a^{B}}{f_4^{\neq}} \left[\frac{f_{(AX)} f_{(HAX)} f_{(B)} f_{(BH)}}{\mathcal{A}}\right]$$

avec

$$\mathcal{A} = [(H^+) f_{(AX)} + K_a^{AX} f_{(HAX)}] [(H^+) f_{(B)} + K_a^{B} f_{(BH)}]$$

La figure 1 représente ces fonctions sur le domaine de pH des solutions aqueuses avec des paramètres arbitraires.

Il apparaît clairement que si les processus $\mathcal{P}_3$ et $\mathcal{P}_4$ sont facilement discernables par une simple étude de l'influence du pH sur la constante de vitesse expérimentale, il n'en est pas de même pour les processus $\mathcal{P}_1$ et $\mathcal{P}_2$ dont les variations théoriques de la constante de vitesse en fonction du pH sont strictement identiques à coefficients d'activité constants. Ce second cas est observé par les réactions de N-chloration d'amines (2) ou d'isomérisation du cyanate d'alkylammonium en phase aqueuse (5).

En milieu neutre et basique, les variations de la constante de vitesse expérimentale de chloration de la diéthylamine

Can. J. Chem. Downloaded from www.nrcresearchpress.com by 88.255.202.194 on 09/08/12
For personal use only.

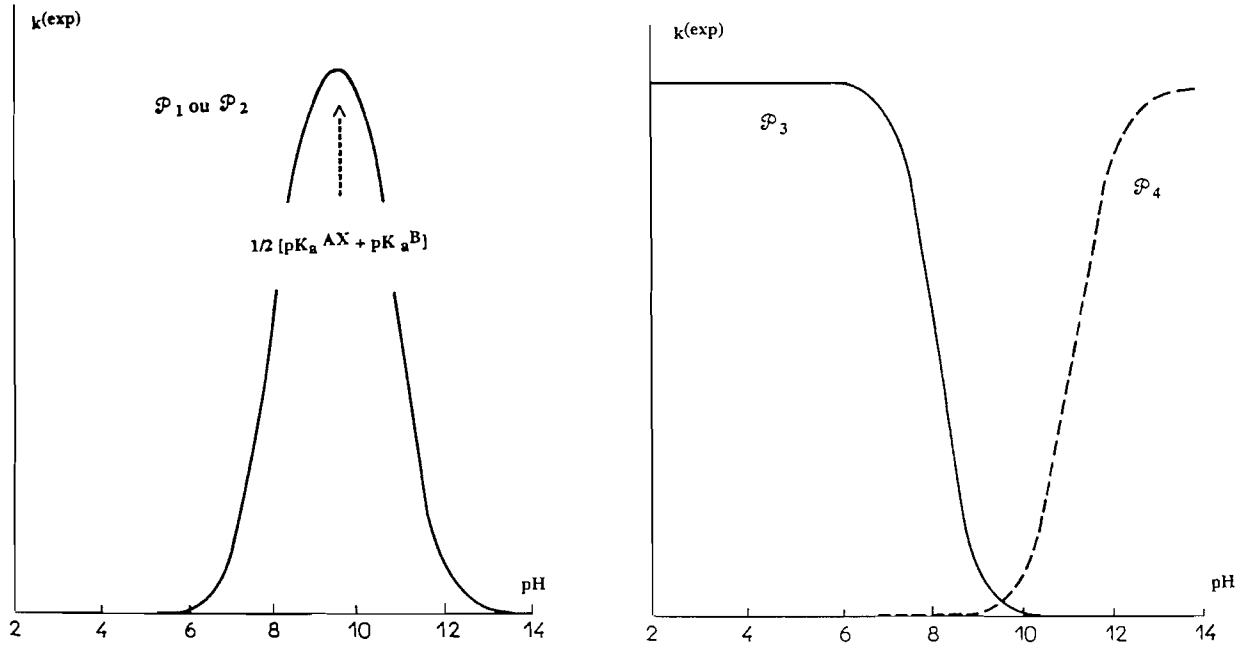

FIG. 1. Variations théoriques de la constante de vitesse expérimentale pour chaque processus en fonction du pH.

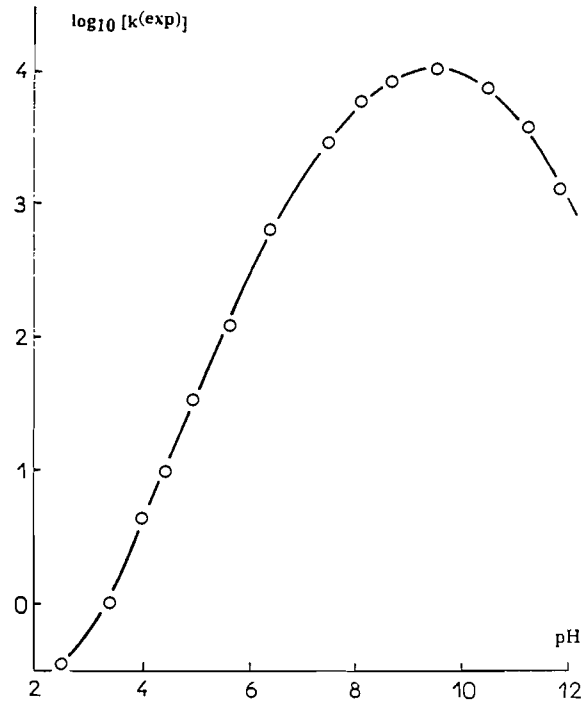

FIG. 2. Variation de la constante de vitesse expérimentale de la *N*-chloration de la diéthylamine.

(figure 2) montrent que ces cinétiques correspondent au cas $\mathcal{P}_1$ et $\mathcal{P}_2$ avec les deux processus équivalents :

$$R_2NH + ClOH \xrightarrow{k_1} \text{produits}$$

$$R_2NH_2^+ + ClO^- \xrightarrow{k_2} \text{produits}$$

En milieu acide, nous observons une chloration par le chlore moléculaire. Une étude spécifique de cette réaction a montré que cette cinétique est limitée par la diffusion des réactifs et se fait sur l'amine non protonée (2) :

$$R_2NH + Cl_2 \xrightarrow{k_{Cl_2}} R_2NCl + H^+ + Cl^-$$

Formes limites et effets de la force ionique

Dans la mesure où l'effet de pH ne permet pas de différencier les processus $\mathcal{P}_1$ et $\mathcal{P}_2$, il semble logique, dans ce but, d'étudier l'effet de la force ionique du milieu sur la vitesse de réaction.

Pour ces processus, en posant :

$$[19] \quad W = \frac{(H^+) f_{(AX)} f_{(HAX)} f_{(B)} f_{(BH)}}{\mathcal{A}}$$

nous obtenons pour $\mathcal{P}_1$:

$$[20] \quad k^{(exp)} = k_1^0 \frac{K_a^B}{f_1^{\neq}} W$$

pour $\mathcal{P}_2$:

$$[21] \quad k^{(exp)} = k_2^0 \frac{K_a^{AX}}{f_2^{\neq}} W$$

Les constantes de vitesse k_i^0 et d'équilibre K_a ne dépendent que de la température. Ainsi, une différence observable sur les constantes de vitesse expérimentale $k^{(exp)}$ à température constante obtenue pour une variation des paramètres ne peut provenir que d'un comportement différent de la valeur du coefficient d'activité du complexe activé de chacun des processus.

En fait, ceux-ci sont constitués du même nombre d'atomes et portent la même charge :

$$\mathcal{P}_1 : HAX^{(Z_{AX})} + B^{(Z_B)} \leftrightarrows (HAX...B)^{(Z_1^{\neq})} \rightarrow \text{produits}$$

$$\mathcal{P}_2 : AX^{(Z_{AX}-1)} + HB^{(Z_B+1)} \leftrightarrows (AX...BH)^{(Z_2^{\neq})} \rightarrow \text{produits}$$

$$Z_2^{\neq} = (Z_{AX} - 1) + (Z_B + 1) = Z_{AX} + Z_B = Z_1^{\neq}$$

Can. J. Chem. Downloaded from www.nrcresearchpress.com by 88.255.202.194 on 09/08/12
For personal use only.

Dans ces conditions, il est difficile d'attendre une influence différente du milieu sur la valeur du coefficient d'activité de l'un ou l'autre de ces complexes activés.

Même s'il ne permet pas de différencier ces deux processus, l'effet de la force ionique sur les constantes de vitesse expérimentales est intéressant à analyser, en particulier en milieu fortement acide ou basique où les expressions de ces constantes prennent des formes simplifiées (tableau 1).

Ces formes limites sont représentées par des droites de pente +1 en milieu acide et −1 en milieu basique en portant $\log_{10}(k^{(exp)})$ en fonction du pH (figure 3).

Dans les domaines de concentration et de force ionique où la loi de Debye–Hückel peut être appliquée, les coefficients d'activité se déduisent de la relation $\log_{10}(f) = -\alpha Z^2\sqrt{I}$ avec I la force ionique du milieu et $\alpha \approx 0{,}5$ pour l'eau à 298 K. Nous avons alors pour toutes les espèces en présence :

$$\log_{10}[f_{(HAX)}] = -\alpha(Z_{AX})^2\sqrt{I}$$

$$\log_{10}[f_{(AX)}] = -\alpha(Z_{AX} - 1)^2\sqrt{I}$$

$$\log_{10}[f_{(B)}] = -\alpha(Z_B)^2\sqrt{I}$$

$$\log_{10}[f_{(BH)}] = -\alpha(Z_B + 1)^2\sqrt{I}$$

et pour les complexes activés :

$$\log_{10}(f_1^{\neq}) = \log_{10}(f_2^{\neq}) = -\alpha(Z_{AX} + Z_B)^2\sqrt{I}$$

On en déduit les expressions suivantes de la constante de vitesse, en milieu acide :

$$\log_{10}(k^{(exp)}) = C^{te} - \alpha[1 + 2Z_B - 2Z_{AX}Z_B]\sqrt{I}$$

en milieu basique :

$$\log_{10}(k^{(exp)}) = C^{te} - \alpha[1 - 2Z_{AX} - 2Z_{AX}Z_B]\sqrt{I}$$

qui sont valables pour les deux processus $\mathcal{P}_1$ et $\mathcal{P}_2$.

Pour $Z_{AX} = Z_B = 0$ (par exemple $\mathcal{P}_1$: ClOH + R_2 NH et $\mathcal{P}_2$: ClO^- + $R_2NH_2^+$), la pente attendue de la droite représentant la variation de $\log_{10}(k^{(exp)})$ en fonction de $\sqrt{I}$ est de $-\alpha$ pour $\mathcal{P}_1$ et $\mathcal{P}_2$ alors que, si l'on ne tient compte que de l'effet de sel primaire, elle devrait être de $2\alpha Z_{AX}Z_B$ donc nulle pour $\mathcal{P}_1$ et de -2α pour $\mathcal{P}_2$. En effet, dans ce dernier cas, on ne prend plus en compte les propriétés acido-basiques des espèces AX et B. D'après les relations [10], [11] et [14], on aura, pour $\mathcal{P}_1$:

$$k^{(exp)} = k_1^0 \frac{f_{(HAX)}f_{(B)}}{f_1^{\neq}}$$

soit

$$\log_{10}(k^{(exp)} = C^{te} + 2\alpha Z_{AX}Z_B\sqrt{I}$$

pour $\mathcal{P}_2$:

$$k^{(exp)} = k_2^0 \frac{f_{(AX)}f_{(BH)}}{f_2^{\neq}}$$

soit

$$\log_{10}(k^{(exp)}) = C^{te} + 2\alpha(Z_{AX} - 1)\,(ZB + 1)\sqrt{I}$$

Le raisonnement précédent montre que l'analyse des variations des constantes expérimentales en fonction des paramètres du milieu ne permet pas de différencier les processus du type $\mathcal{P}_1$ et $\mathcal{P}_2$.

Pour poursuivre plus loin une tentative de différenciation de ces processus, il nous faut exprimer les constantes de vitesse absolues (k_i^0) dans les hypothèses de la théorie du complexe activé.

Utilisation de la théorie du complexe active

Pour qu'une réaction qui n'est pas limitée par la diffusion ait lieu de part et d'autre d'un processus élémentaire, on doit supposer qu'il existe une configuration correspondant au point d'énergie maximum entre l'état de réactif et l'état de produit.

La théorie du complexe activé prête à cet état transitoire les propriétés thermodynamiques d'une molécule normale. Sa concentration, par exemple, peut être calculée par la thermodynamique statistique. On suppose de plus que la vitesse de réaction est égale au produit de cette concentration $C^{\neq}$ par sa fréquence de dissociation $\nu^{\neq}$ (8).

Formellement, ces hypothèses ne s'appliquent qu'à l'équilibre entre réactifs et produits mais son extension à des systèmes hors équilibre n'est généralement pas remise en cause.

À l'équilibre entre réactifs et produits, la concentration en complexe activé est constante.

Dans ces conditions, en reprenant le formalisme utilisé par Hall (9) et en notant $C_f^{\neq}$ la concentration en complexe provenant des réactifs et p_f la probabilité qu'ont ceux-ci de reformer les réactifs, une fraction $\frac{1}{1 + p_f}$ donne les produits alors qu'une fraction $\frac{p_f}{1 + p_f}$ reforme les réactifs. Alors la vitesse dans le sens direct s'écrit :

$$[22] \quad V_f = \nu^{\neq}\left(\frac{1 - p_f}{1 + p_f}\right) C_f^{\neq}$$

De la même façon, en indiçant par b les valeurs symétriques concernant le sens direct de la réaction :

$$[23] \quad V_b = \nu^{\neq}\left(\frac{1 - p_b}{1 + p_b}\right) C^{\neq}$$

À l'équilibre, $V_f = V_b$ et comme $C^{\neq} = C_f^{\neq} = C_b^{\neq}$, on en déduit l'équation de la vitesse :

$$[24] \quad V_f = \kappa\,\nu^{\neq}\frac{C^{\neq}}{2}$$

où

$$\kappa = \frac{(1 - p_f)\,(1 - p_b)}{1 - p_f p_b}$$

est le coefficient de transmission du processus.

On admet en solution réelle que la concentration en complexe activé dépend d'une constante d'équilibre soit, pour une réaction bimoléculaire du type qui nous intéresse (8, 9) :

$$[25] \quad K^{\neq} = \frac{a^{\neq}}{(AX)\,(B)} = \frac{C^{\neq}}{[AX]\,[B]}\frac{f^{\neq}}{f_{(AX)}f_{(B)}}$$

Can. J. Chem. Downloaded from www.nrcresearchpress.com by 88.255.202.194 on 09/08/12
For personal use only.

TABLEAU 1. Formes limites des constantes de vitesse expérimentales en milieu fortement acide ou basique

	Milieu acide	Milieu basique
$\mathcal{P}_1$	$k^{(exp)} = k_1^0 \frac{K_a^B}{(H^+)} \frac{f_{(HAX)} f_{(BH)}}{f_1^{\neq}}$	$k^{(exp)} = k_1^0 \frac{(H^+)}{K_a^{AX}} \frac{f_{(AX)} f_{(B)}}{f_1^{\neq}}$
$\mathcal{P}_2$	$k^{(exp)} = k_2^0 \frac{K_a^{AX}}{(H^+)} \frac{f_{(HAX)} f_{(BH)}}{f_2^{\neq}}$	$k^{(exp)} = k_2^0 \frac{(H^+)}{K_a^B} \frac{f_{(AX)} f_{(B)}}{f_2^{\neq}}$

où $a^{\neq}$ est l'activité du complexe activé. L'utilisation d'une telle constante d'équilibre sous-entend que le complexe activé est normalement solvaté donc que la réorganisation du solvant autour du complexe en collision est rapide par rapport à la durée du processus.

À partir de l'expression de $C^{\neq}$ déduite de la relation [25], la vitesse de réaction devient :

$$[26] \quad V_f = \kappa \frac{\nu^{\neq}}{2} K^{\neq} \frac{f_{(AX)} f_{(B)}}{f^{\neq}} [AX] [B]$$

Par identification à la relation [14], k^0 prend la forme :

$$[27] \quad k^0 = \kappa \frac{\nu^{\neq}}{2} K^{\neq}$$

Dans le cas AX + B, il est habituel de considérer la fréquence de dissociation du complexe activé comme le rapport d'une vitesse moyenne (v) de déplacement de X sur une coordonnée privilégiée de l'espace des configurations dite coordonnée de réaction et d'une longueur δ définissant le complexe activé sur cette coordonnée. Par définition du complexe activé, sur cette longueur δ, X n'est soumis à aucun grandient de potentiel et ne possède qu'une énergie de translation. Dans cette situation, on assimile X à une molécule de gaz parfait et on peut donc lui attribuer une vitesse moyenne calculée par la théorie cinétique :

$$v = \sqrt{\frac{2k_B T}{\pi m}} \qquad (k_B \text{ constante de Boltzmann})$$

ainsi qu'une fonction de partition de translation :

$$Q^x_{trans} = \frac{\delta}{h} \sqrt{2 \pi m k_B T}$$

Il en découle l'expression habituelle de k^0 :

$$k^0 = \kappa \frac{k_B T}{h} K^* \text{ avec } K^* = \frac{K^{\neq}}{Q^x_{trans}}$$

K^* ne représente pas, au contraire de $K^{\neq}$, une valeur thermodynamique «normale».

À partir des relations [15], [16] et [27], nous obtenons les expressions des constantes de vitesse expérimentales pour les processus $\mathcal{P}_1$ et $\mathcal{P}_2$:

$$\mathcal{P}_1 : \quad k^{(exp)} = \frac{k_1}{2} \frac{\nu_1^{\neq}}{f_1^{\neq}} K_1^{\neq} K_a^B W$$

$$\mathcal{P}_2 : \quad k^{(exp)} = \frac{k_2}{2} \frac{\nu_2^{\neq}}{f_2^{\neq}} K_2^{\neq} K_a^{AX} W$$

En exprimant les constantes d'équilibre en fonction des activités des espèces, le rapport des produits $K_1^{\neq} K_a^B$ et $K_2^{\neq} K_a^{AX}$ apparaît comme égal au rapport des activités des complexes activés donc à une constante d'équilibre $K_{12}^{\neq}$:

$$[28] \quad \frac{K_1^{\neq} K_a^B}{K_2^{\neq} K_a^{AX}} = \frac{a_1^{\neq}}{a_2^{\neq}} = K_{12}^{\neq}$$

Ceci découle de nos hypothèses car, si l'on veut comparer les vitesses dues respectivement à $\mathcal{P}_1$ et $\mathcal{P}_2$, il faut admettre un triple équilibre :

$$(B...HAX)^{\neq} \leftrightarrows B + HAX \leftrightarrows BH + AX \leftrightarrows (BH...AX)^{\neq}$$

et donc indirectement un équilibre entre les deux complexes activés.

On aura donc égalité de leurs potentiels chimiques :

$$\mu_1^{\neq} = \mu_2^{\neq}$$

soit :

$$\mu_1^{0\neq} + RT \ln(a_1^{\neq}) = \mu_2^{0\neq} + RT \ln(a_2^{\neq})$$

La relation [28] devient alors :

$$K_{12}^{\neq} = \frac{K_1^{\neq} K_a^B}{K_2^{\neq} K_a^{AX}} = \exp\left(\frac{\mu_2^{0\neq} - \mu_1^{0\neq}}{RT}\right)$$

En admettant $\nu_1^{\neq} = \nu_2^{\neq}$ et $\kappa_1 = \kappa_2$ ou que ces valeurs sont proportionnelles d'un facteur β qui ne dépend pas du milieu $\kappa_2 \nu_2^{\neq} = \beta \kappa_1 \nu_1^{\neq}$, nous avons (avec $\beta = 1$) :

$$\mathcal{P}_1 : \quad k^{(exp)} = k_1^0 \frac{K_a^B}{f_1^{\neq}} W$$

$$\mathcal{P}_2 : \quad k^{(exp)} = k_1^0 \frac{K_a^B}{f_2^{\neq}} W \exp\left(\frac{\mu_2^{0\neq} - \mu_1^{0\neq}}{RT}\right)$$

soit :

$$[29] \quad k_{(\mathcal{P}_1)}(exp) = k_{(\mathcal{P}_2)}(exp) K_{12}^{\neq}$$

Il existe donc un facteur de proportionnalité entre les deux constantes de vitesse qui ne dépend que des énergies standards des complexes activés. Dans ces conditions, seul un effet comme celui du solvant qui pourrait avoir une influence différente sur ces niveaux selon le processus et la nature du complexe activé correspondant peut être envisagé pour différencier $\mathcal{P}_1$ de $\mathcal{P}_2$.

La relation [29] montre que toute différence d'effet attendue dans l'une ou l'autre de ces hypothèses ne peut se mesurer que par les potentiels standards des complexes activés. Pour dire si la réaction se fait par l'un ou l'autre des processus, il faut que ces potentiels soient nettement différents (un seul des processus participe à la réaction). Pour le prouver, il faut trouver un paramètre qui agisse théoriquement différemment sur les énergies libres standards de ces états. Ceci implique de faire d'abord une hypothèse sur la structure des complexes activés ce qui peut être délicat en solution.

Effet de solvant

L'effet de solvant sur les vitesses de réaction (12) est décrit à partir de l'expression de la variation d'énergie libre pour amener une sphère de rayon r contenant des charges à répartition non uniforme (possédant un moment dipolaire ρ)

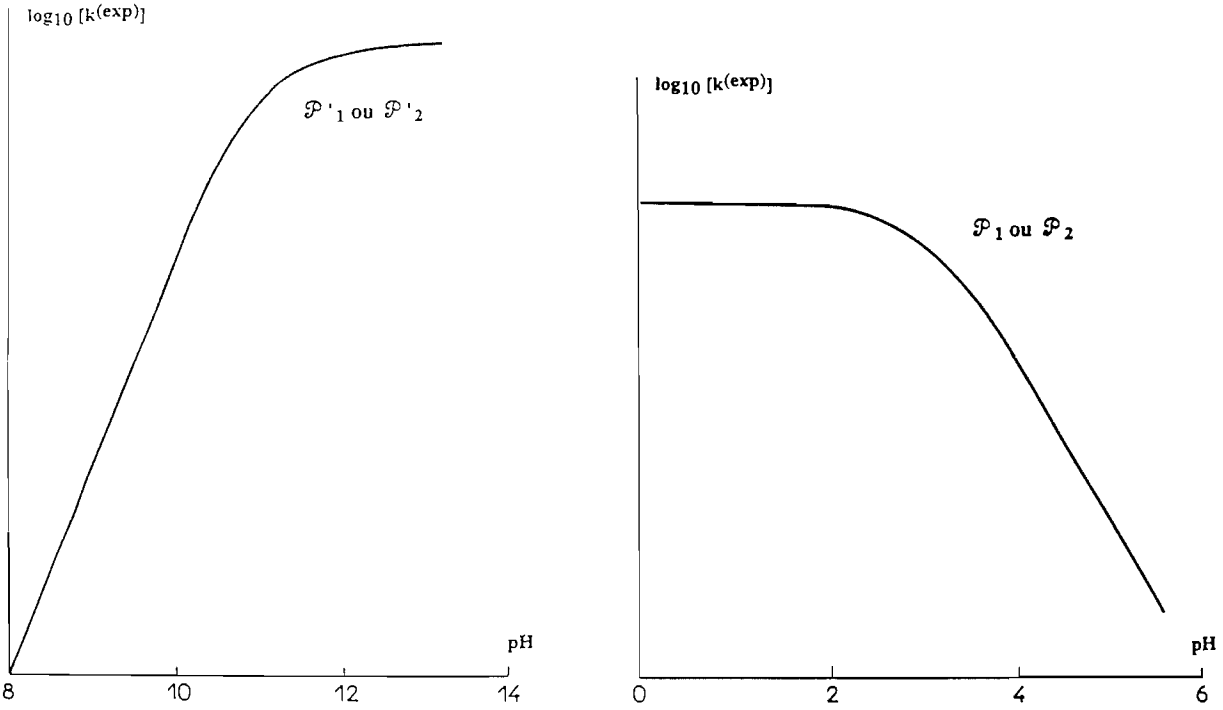

FIG. 3. Variations théoriques du logarithme décimal de la constante de vitesse expérimentale pour chaque processus en fonction du pH.

d'un milieu de constante diélectrique égal à 1 dans un milieu de constante diélectrique ε.

$$\Delta G = \frac{z^2 e^2}{2r}\left(\frac{1}{\varepsilon} - 1\right) + \frac{3\rho^3}{8r^3}\left(\frac{1-\varepsilon}{1+\varepsilon}\right)$$

Pour les deux complexes activés $z^{\neq} = z_{AX} + z_B$, leurs rayons sont du même ordre de grandeur ($r_1^{\neq} = r_2^{\neq}$). Quant à leurs moments dipolaires, si l'on prend comme exemple la N-chloration de l'ammoniac NH_3 :

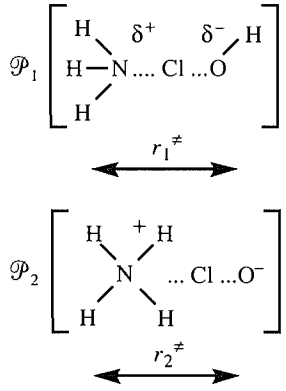

du fait de la structure proche des complexes activés, ceux-ci sont nécessairement de même grandeur ($\rho_1^{\neq} \approx \rho_2^{\neq}$). On peut donc admettre que la variation d'energie libre due au passage d'un solvant (S) à un solvant (S') est quasiment égale pour les deux complexes activés :

$$\Delta G_1^{\neq 0}(S \rightarrow S') = \Delta G_2^{\neq 0}(S \rightarrow S')$$

et donc :

[30] $$K_{12(S)}^{\neq} = K_{12(S')}^{\neq}$$

Cet exemple montre qu'il est extrêmement peu probable de trouver un cas où l'effet de solvant puisse jouer de façon suffisamment différente et mesurable sur deux complexes activés dont la nature ne diffère que de la position d'un proton. Néanmoins, un tel cas ne peut être généralisé et cet effet ne peut être analysé qu'au cas par cas. Dans des situations favorables, il permet en théorie de tirer des conclusions mais cela ne peut être que dans les hypothèses décrites précédemment. Une analyse partielle peut conduire à des déductions erronées comme l'a montré Pearson et Frost (5) à propos d'études sur la réaction de conversion du cyanate d'ammonium en urée.

Les relations [29] et [30] indiquent que ces constantes de vitesse expérimentales pour l'un ou l'autre des processus sont proportionnelles d'un terme ne dépendant pas des conditions expérimentales. Dans les hypothèses de la théorie du complexe activé, ces deux processus nous apparaissent comme indiscernables par l'analyse formelle des effets du milieu sur la cinétique de réaction.

Approche du mécanisme par corrélation entre reactions similaires

Il est possible par comparaison de deux séries de réactions voisines, dont l'une ne présente pas d'ambiguïté de mécanisme, d'obtenir des indications sur la nature des mécanismes dans l'autre série. Jensen (6), par exemple, a pu corréler de façon évidente les constantes de vitesse de réactions d'amines avec l'acide cyanique et celles des mêmes amines avec le dioxyde de carbone pour former des carbamates (réaction qui ne présente pas d'ambiguïté de mécanisme; l'hydratation de CO_2 étant lente par rapport à celle-ci).

$$R\,NH_2 + CO_2 \xrightarrow{k_{CO_2}} R\,NH\,CO_2H$$

$$R\,NH_2 + CNOH \xrightarrow{k_{CNOH}} R\,NH\,CO\,NH_2$$

Can. J. Chem. Downloaded from www.nrcresearchpress.com by 88.255.202.194 on 09/08/12
For personal use only.

avec

$$\log_{10}(k_{CNOH}/1\ M^{-1}\ s^{-1}) = \log_{10}(k_{CO_2}/1\ M^{-1}\ s^{-1}) - 1{,}08$$

alors qu'il n'existe pas de corrélation pour les valeurs de constantes de vitesse calculées dans l'hypothèse du processus :

$$R\,NH_2^+ + CNO^- \xrightarrow{k_{CNO^-}} R\,NH\,CO\,NH_2$$

Pour les N-chlorations, le fait qu'en présence de dichlore (Cl_2), nous ayons (2) :

$$R_2NH + Cl_2 \xrightarrow{k_{Cl_2}} R_2N\,Cl + H^+ + Cl^-$$

permet de penser que le mécanisme le plus probable pour la chloration par l'acide hypochloreux est

$$R_2NH + Cl\,OH \xrightarrow{k_{ClOH}} R_2N\,Cl + H_2O$$

Il n'est malheureusement pas possible de corréler les valeurs de k_{Cl_2} et de k_{ClOH}, la chloration des amines par Cl_2 en milieu aqueux présentant une cinétique limitée par la diffusion (2, 13).

De plus, contrairement au cas des réactions des amines avec CNOH, les constantes de vitesse de N-chloration sont directement liées au pK_a de l'amine. La relation liant k_{ClOH} à k_{ClO^-} étant

$$k_{ClOH} = \frac{K_2}{K_a} k_{ClO^-}$$

toute corrélation concernant l'une des constantes de vitesse sera aussi valable pour l'autre.

Ces comparaisons, ou des hypothèses sur la structure la plus probable d'un complexe activé, ne donnent que des indications et ne constituent pas des preuves irréfutables sur la nature du processus élémentaire limitant.

Cas particulier de l'hydrolyse

Les réactions d'hydrolyse de composés acides ou bases faibles représentent un cas particulier du type de réaction présenté précédemment. Deux cas sont possibles :
Hydrolyse «acide» :

$$SH + H_2O \leftrightarrows S^- + H_3O^+$$

$\mathcal{P}_1$: $S^- + H_3O^+ \rightarrow$ produits

$\mathcal{P}_2$: $SH + H_2O \rightarrow$ produits

Hydrolyse «basique» :

$$S^- + H_2O \leftrightarrows SH + OH^-$$

$\mathcal{P}'_1$: $S^- + H_2O \rightarrow$ produits

$\mathcal{P}'_2$: $SH + OH^- \rightarrow$ produits

Dans le premier cas, les vitesses s'expriment selon le processus envisagé :

$$[31] \quad v = k_1^0 \frac{f_{(H)} f_{(S^-)}}{f_1^0} [S^-]\,[H_3O^+]$$

$$[32] \quad v = k_2^0 \frac{f_{(H_2O)} f_{(HS)}}{f_2^{\neq}} [SH]\,[H_2O]$$

En appliquant les principes définis précédemment, nous obtenons les constantes de vitesse expérimentales :

$$[33] \quad \mathcal{P}_1 : \quad k^{(exp)} = k_1^0 \frac{k_a^S}{f_1^{\neq}} \left(\frac{(H^+) f_{(S^-)} f_{(SH)}}{[(H^+) f_{(S^-)} + K_a^S f_{(SH)}]} \right)$$

$$[34] \quad \mathcal{P}_2 : \quad k^{(exp)} = k_2^0 \frac{(H_2O)}{f_2^{\neq}} \left(\frac{(H^+) f_{(S^-)} f_{(SH)}}{[(H^+) f_{(S^-)} + K_a^S f_{(SH)}]} \right)$$

Pour le milieu basique :

$$[35] \quad v = k_1'^0 \frac{f_{(H_2O)} f_{(S^-)}}{f_1^{\neq}} [S^-]\,[H_2O]$$

$$[36] \quad v = k_2'^0 \frac{f_{(OH^-)} f_{(SH)}}{f_2^{\neq}} [SH]\,[OH^-]$$

Soit, en posant $K_W = (H_3O^+)\,(OH^-)$:

$$[37] \quad \mathcal{P}'_1 : \quad k^{(exp)} = k_1'^0 \frac{(H_2O) K_a^S}{f_1'^{\neq}} \left(\frac{f_{(S^-)} f_{(SH)}}{[(H^+) f_{(S^-)} + K_a^S f_{(SH)}]} \right)$$

$$[38] \quad \mathcal{P}'_2 : \quad k^{(exp)} = k_2'^0 \frac{K_W}{f_2'^{\neq}} \left(\frac{f_{(S^-)} f_{(SH)}}{[(H^+) f_{(S^-)} + K_a^S f_{(SH)}]} \right)$$

L'activité de l'eau est équivalente à la constante d'acidité du proton solvaté :

$$H_2O + H_3O^+ \leftrightarrows H_3O^+ + H_2O$$

soit avec les conventions habituelles :

$$H_3O^+ \leftrightarrows H_2O + H^+$$

et

$$K_a^{H_2O} = \frac{(H^+)\,(H_2O)}{(H_3O^+)} = (H_2O)$$

Cette valeur est généralement sous-entendue sous celle de k^0 (en milieu tamponné, ces cinétiques sont du pseudo-premier ordre par rapport à S).

La figure 4 montre les variations de ces constantes de vitesse en fonction du pH.

Contrairement aux cas précédents, ces courbes ne présentent pas de maximum mais là aussi, il persiste une indétermination du mécanisme réel. Ces exemples de réaction de ce type sont nombreux. Ainsi, au cas acide, correspondent les hydrolyses des amides (de pK_a suffisamment élevé) avec, comme prééquilibre :

$$R\,CO\,NH_3^+ + H_2O \leftrightarrows R\,CO\,NH_2 + H_3O^+$$

En milieu basique, nous avons rencontré cette situation (10) à propos de l'hydrolyse du dérivé monochloré de l'acide cyanurique (H_3Cy) avec l'équilibre d'échange protonique. Deux processus sont possibles :

Can. J. Chem. Downloaded from www.nrcresearchpress.com by 88.255.202.194 on 09/08/12
For personal use only.

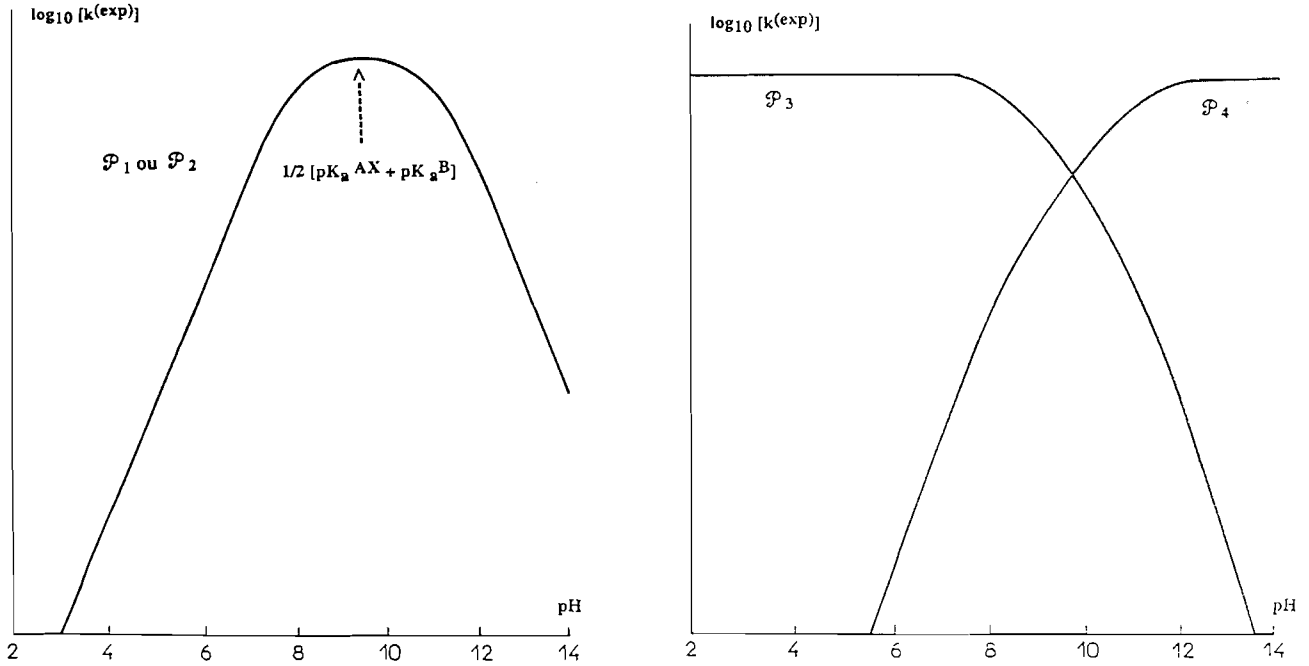

FIG. 4. Variations du logarithme de la constante de vitesse expérimentale de l'hydrolyse de bases ou d'acides faibles en fonction du pH.

$$\mathcal{P}_1 : \quad Cy\,Cl\,H^- + OH^- \rightarrow Cy\,H_2^- + ClO^-$$

$$\mathcal{P}_2 : \quad Cy\,Cl^{2-} + H_2O \rightarrow Cy\,H_2^- + ClO^-$$

avec ici une totale ambiguïté puisque les deux processus sont imaginables du point de vue de la structure du complexe activé.

Indétermination ou équivalence?

Les raisonnements précédents reposent sur l'hypothèse que les processus $\mathcal{P}_1$ et $\mathcal{P}_2$ sont élémentaires. En fait, en solution, la notion de processus élémentaire est moins facilement définie qu'en phase gazeuse. L'effet cage par exemple impose un état physique supplémentaire des réactifs. Pour une réaction limitée cinétiquement par cette barrière, l'étape de diffusion et de formation des paires solvatées n'est pas limitante et n'a pas d'influence sur la cinétique de réaction.

L'existence d'une paire solvatée a une influence si l'on admet le modèle proposé par Bell (11) pour le mécanisme d'échange de proton pour un équilibre acido-basique :

$$HAX + B \underset{k_{ba}}{\overset{k_{ab}}{\rightleftarrows}} HAX\,B \underset{k_{cb}}{\overset{k_{bc}}{\rightleftarrows}} AX\,BH \underset{k_{dc}}{\overset{k_{cd}}{\rightleftarrows}} AX + BH$$

où le signe barre symbolise les espèces réunies dans une même cage de solvant. On admet que $k_{ba} < k_{bc}$ et $k_{cd} < k_{cb}$ ce qui signifie que le proton s'échange de nombreuses fois entre les deux espèces avant que le phénomène de difffusion n'intervienne. Si la fréquence de cet échange est élevée par rapport à la vitesse de diffusion des réactifs, c'est que la quasi-totalité des collisions dans la cage de solvant le provoque, alors que le processus d'échange de X est moins fréquent (cinétique limitée par la barrière).

Ainsi, à l'échelle de temps du processus étudié, la position du proton sur AX ou sur B dans la paire solvatée serait indépendante de l'origine de celle-ci (AXH + B ou AX + BH).

Dans une telle optique, si l'on prend comme exemple la N-chloration des amines, en admettant, comme c'est probable, que l'étape limitante de la cinétique est l'attaque nucléophile de l'amine non protonée sur ClOH, nous avons le schéma réactionnel suivant :

$$ClOH + R_2NH \leftrightarrows \overline{ClOH\,R_2NH} \leftrightarrows [H\,R_2N \ldots Cl - OH]^{\neq} \xrightarrow[V_f]{}$$

$$\Updownarrow$$

$$ClO^- + R_2NH_2^+ \leftrightarrows \overline{ClO^-\,R_2NH_2^+}$$

Il apparaît équivalent d'écrire la vitesse en fonction des concentrations de ClO^- et $R_2NH_2^+$ ou ClOH et R_2NH, expressions globales qui cachent la nature de l'acte élémentaire limitant.

Conclusions

Les succès de la théorie du complexe activé en solution sont liés aux hypothèses thermodynamiques qu'elle implique. Le principe de l'état final et initial permet d'écrire toute cinétique comme pour les réactions en phase gazeuse :

$$A + B \leftrightarrows AB^{\neq} \rightarrow \text{produits}$$

En général cette simplification est utile et permet une analyse simple des réactions en solution mais elle cache la réalité physique de la suite de processus qui peuvent intervenir en solution.

Une analyse plus fine des réactions en solution pose un certain nombre de problèmes (14) que l'on peut difficilement résoudre. Néanmoins, la théorie du complexe activé reste, pour l'expérimentateur, un outil puissant pour l'ana-

Can. J. Chem. Downloaded from www.nrcresearchpress.com by 88.255.202.194 on 09/08/12
For personal use only.

lyse et la prévision des cinétiques en phase liquide. Il apparaît cependant nécessaire d'en connaître les limites en particulier pour interpréter les phénomènes expérimentaux.

1. B. Solastiouk et X. Deglise. Can. J. Chem. **66**, 2188 (1988).
2. D. Matte, B. Solastiouk, A. Merlin et X. Deglise. Can. J. Chem. **67**, 786 (1989).
3. D. Matte, B. Solastiouk, A. Merlin et X. Deglise. Can. J. Chem. **68**, 307 (1990).
4. J. C. Morris et I. Weil. J. Am. Chem. Soc. **71**, 1664 (1949).
5. R. H. Pearson et W. Frost. Kinetics and mechanism. John Wiley and Sons Inc., New York. 1962. Chap. 12, Part B.
6. M. B. Jensen. Acta Chem. Scand. **2**, 13 (1959).
7. P. Johncolk, G. Kohnstam et D. J. Speight. J. Chem. Soc. 2544 (1958).
8. H. Eyring et D. W. Urry. J. Chem. Phys. **67**, 731 (1963).
9. D. G. Hall. J. Chem. Soc. Faraday Trans. 2, **82**, 1297 (1986).
10. B. Solastiouk. Thèse de Doctorat de l'Université de Nancy I. 1989.
11. R. P. Bell. The proton in chemistry. Chapman and Hall, London. 1973.
12. K. J. Laidler. Chemical kinetics. Tata McGraw–Hill Publishing Company Ltd., New Delhi. 1973.
13. M. S. Chao. J. Electrochem. Soc. **115**, 1172 (1968).
14. D. G. Truhlar, W. L. James et J. T. Hynes. J. Am. Chem. Soc. **87**, 2664 (1983).

Can. J. Chem. Downloaded from www.nrcresearchpress.com by 88.255.202.194 on 09/08/12
For personal use only.

Ab initio study of the structure of the hydrogen maleate anion

MIGUEL A. RÍOS AND JESÚS RODRÍGUEZ[1]

Departamento de Química Física, Facultade de Química, Universidade de Santiago, 15706 Santiago de Compostela, Galicia, Spain

Received September 28, 1992

MIGUEL A. RÍOS and JESÚS RODRÍGUEZ. Can. J. Chem. **71**, 303 (1993).

The hydrogen maleate ion was studied by *ab initio* methods with complete optimization at the 3-21G, 6-31G, 6-31G**, and 6-31+G(2*d*,1*p*) levels. To study the influence of electron correlation, MP2 calculations have been done for the 6-31G** geometry. All calculations at the HF level predicted an asymmetric hydrogen bond with a double minimum potential governing transfer between the two equivalent structures. Moreover, both asymmetry and proton transfer barrier increase systematically with the power of the basis set used, with calculated barrier heights of 0.12 (3-21G), 1.59 (6-31G), 1.64 (6-31G**), and 2.00 kcal/mol (6-31+G). Only the introduction of the electron correlation at the MP2 level seems to predict a single minimum potential.

MIGUEL A. RÍOS et JESÚS RODRÍGUEZ. Can. J. Chem. **71**, 303 (1993).

On a étudié l'ion maléate d'hydrogène par des méthodes *ab initio* des optimisations complètes, aux niveaux 3-21G, 6-31G, 6-31G** et 6-31+G(2*d*,1*p*). Afin d'étudier l'influence de la corrélation électronique, on a effectué des calculs MP2 sur la géométrie 6-31G**. Tous les calculs au niveau HF prédisent une liaison hydrogène asymètrique pour laquelle le transfert entre les deux structures équivalentes implique un double minimum de potentiel. De plus, l'asymétrie et la barrière au transfert de proton augmentent tous les deux systématiquement avec la puissance de l'ensemble de base utilisé; les hauteurs calculées de la barrière sont 0,12 (3-21G), 1,59 (6-31G), 1,64 (6-31G**) et 2,00 kcal/mol (6-31+G). Seule l'introduction d'une corrélation électronique au niveau MP2 semble prédire un seul minimum du potentiel.

[Traduit par la rédaction]

Introduction

One of the fundamental issues when studying intramolecular hydrogen bonds is to determine whether the potential energy surface governing the motion of the hydrogen atom has just a single minimum (*a*) or two distinct minima (*b*):

X--H--X X-H---X ⇌ X---H-X

(*a*) (*b*)

Assuming that the two electronegative atoms are identical (which implies that the molecular fragments linked by the hydrogen bond are identical), then in the former case the two X—H distances will be equal.

In the double-minimum case there will generally be two distinct asymmetric structures that, depending on the characteristics of the potential surface, may or may not be interconverted by intramolecular proton transfer. When the double-minimum surface is completely symmetric, proton transfer does take place (in fact tunnelling through the potential barrier is observed (see, for example, refs. 1 and 2)) but even a small energy difference between the two tautomers can hinder or totally prevent proton transfer, leading to one tautomer predominating over the other (3).

The hydrogen bond is asymmetric in most of the compounds showing this kind of interaction. However, the hydrogen maleate and hydrogen phthalate anions (Fig. 1) have usually been considered as paradigms of symmetric hydrogen bonding (for review, see ref. 4), and for the former this notion has been supported experimentally by X-ray (5) and neutron diffraction (6) studies (which, while not locating the position of the hydrogen atom, have shown that the heavy atom skeleton is symmetric, implying that the hydrogen bond also should be symmetric) and by nmr experiments (7, 8). Even for the asymmetric chloro hydrogen maleate, practically equal OH distances (1.206 and 1.199 Å) have been found (9). Recently, there have been reports that the position of the hydrogen atom in hydrogen maleate is in fact not totally symmetric (10–14), the reported asymmetry, however, being slight: Table 1 lists the hydrogen bond geometries determined by X-ray and neutron diffraction studies using the potassium (5, 6, 9), sodium (10), calcium (11), zinc (12), lithium (12), and magnesium (13) salts of hydrogen maleate. The greatest asymmetry in the hydrogen bond (Δ_{OH} = 0.288 Å, the difference between the two OH distances) is found in the sodium salt. The differences among the studies must evidently depend on the different cations present, and in some cases on the presence of water molecules in the crystal lattice. In all cases the crystal environment affects the position of the hydrogen atom more than it does the heavy skeleton, which is never very asymmetric: even in the salt with greatest Δ_{OH}, "equivalent" bond lengths differ by less than 0.03 Å and "equivalent" angles by much less than 1°. The reported O---O distances are all very similar, ranging between 2.403 and 2.445 Å. Although these data are for crystals rather than the free anion, they suggest that any asymmetry in the hydrogen bond of the latter cannot be very pronounced. Theoretical 4-21G level calculations with complete geometry optimization (13) do not

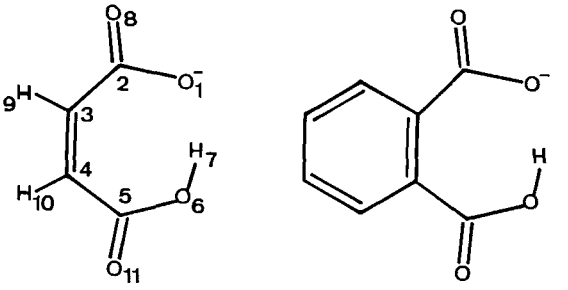

FIG. 1. Hydrogen maleate and hydrogen phthalate anions.

[1]Author to whom correspondence may be addressed.

Can. J. Chem. Downloaded from www.nrcresearchpress.com by 88.255.202.194 on 09/08/12
For personal use only.

TABLE 1. Experimental hydrogen bond geometries (distances in Å, angle in degrees) of hydrogen maleate anion

	O—H	O---H	Δ_{OH}	O---O	OHO
Potassium salt, ref. 5	[a]	[a]	—	2.437	[a]
Potassium salt, ref. 6	[a]	[a]	—	2.44	[a]
Potassium salt, ref. 9	1.199	1.206	0.007	2.403	175.4
Sodium salt, ref. 10	1.079	1.367	0.288	2.445	176.1
Calcium salt, ref. 11	1.121	1.305	0.184	2.424	175.9
Zinc salt, ref. 12	1.097	1.317	0.220	2.410	174.7
Lithium salt, ref. 12	1.074	1.360	0.286	2.432	175.9
Magnesium salt, ref. 13	1.186	1.228	0.042	2.414	176.0

[a]Position of the hydrogen atom was not reported in this study.

TABLE 2. Optimized geometries of the hydrogen maleate anion obtained with the various basis sets (distances in Å, angles in degrees)

Atoms	3-21G	4-31G[a]	6-31G	6-31G**	6-31+G	Expt.[b]
C(2)—O(1)	1.280	1.272	1.276	1.251	1.245	1.26–1.29
C(3)–C(2)	1.525	1.515	1.516	1.531	1.530	1.49–1.51
C(4)—C(3)	1.321	1.326	1.332	1.328	1.328	1.33–1.35
C(5)—C(4)	1.506	1.490	1.492	1.502	1.501	1.49–1.51
O(6)–C(5)	1.305	1.314	1.319	1.297	1.293	1.28–1.30
H(7)—O(6)	1.089	1.017	1.012	1.004	0.999	1.07–1.20
O(8)–C(2)	1.230	1.237	1.243	1.218	1.217	1.23–1.25
H(9)–C(3)	1.073	1.073	1.074	1.078	1.077	0.95–1.10
H(10)—C(4)	1.073	1.073	1.074	1.077	1.076	0.97–1.10
O(11)—C(5)	1.221	1.221	1.225	1.202	1.198	1.22–1.24
O(1)—H(7)	1.323	1.464	1.479	1.475	1.494	1.21–1.37
O(1)—O(6)	2.403	2.464	2.473	2.475	2.489	2.40–2.44
C(3)—C(2)—O(1)	117.9	117.9	118.0	117.6	117.8	118.0–120.3
C(4)—C(3)—C(2)	131.0	131.5	131.4	131.6	131.7	129.5–130.7
C(5)—C(4)—C(3)	131.1	131.8	131.9	131.6	131.6	129.5–130.6
O(6)—C(5)—C(4)	118.8	119.9	120.1	119.4	119.6	120.0–121.0
H(7)—O(6)—C(5)	115.3	115.8	115.7	112.3	111.9	110.4–111.8
O(8)—C(2)—C(3)	115.3	114.8	114.7	114.2	114.2	116.0–118.8
H(9)—C(3)—C(2)	110.6	111.3	111.5	111.8	111.8	111.0–113.8
H(10)—C(4)—C(3)	118.9	118.2	118.0	118.1	118.0	115.8–117.7
O(11)—C(5)—C(4)	117.3	118.2	118.2	118.2	118.2	117.0–118.6
O(1)—H(7)—O(6)	169.7	166.1	165.7	173.2	173.2	174.7–176.1
C(2)—O(1)—H(7)	116.1	117.0	117.2	114.4	114.0	112.0–114.0

[a]Reference 16.
[b]References 5, 6, 9, 10–13.

contradict the above conclusion, the predicted OH distances (1.080 and 1.365 Å) yielding a value of Δ_{OH} of 0.285 Å, which is within the experimental range. Also *ab initio* vibrational analysis (15) suggested a low barrier height for the proton potential. However, 4-31G level calculations (16) indicate that both the heavy skeleton and the hydrogen bond of the free anion are clearly asymmetric, with OH distances of 1.017 and 1.464 Å (Δ_{OH} = 0.447 Å).

To obtain a clearer picture of the situation, we have now used a number of basis sets of differing complexity for *ab initio* geometrical optimizations of the hydrogen maleate anion and investigation of the potential curve governing proton transfer and the transition state.

Computation

All calculations were performed at the HF level, with complete geometry optimizations. The basis sets 3-21G (17), 6-31G (18), 6-31G** (19), and 6-31+G(2*d*,1*p*) (20) were used; the last includes the next diffuse functions: 2*d* functions on heavy atoms (scaled up and down by a factor of 2 from the standard single-*d* value), *p*-functions on hydrogen, and a set of diffuse *sp* functions on heavy atoms. Moreover, single-point MP2 calculations were carried out for the HF/6-31G** optimized geometries. Computations were performed with the GAUSSIAN 88 program (21).

Results and discussion

Table 2 shows the optimized geometric parameters of the anion as calculated using the basis sets mentioned above. All the optimized structures are planar, showing C_S symmetry. Data of this table show that a slight asymmetry in the molecular skeleton gives rise to a clear asymmetry in the O--H--O fragment.

The salient feature of Table 2 is the systematic increase in the asymmetry of the hydrogen bond with the complexity of the basis set used: Δ_{OH} is given as 0.234 Å by 3-21G,

Can. J. Chem. Downloaded from www.nrcresearchpress.com by 88.255.202.194 on 09/08/12
For personal use only.

TABLE 3. Optimized geometries of the C_{2v} structures of the hydrogen maleate anion obtained with the various basis sets (distances in Å, angles in degrees)

Atoms	3-21G	4-31G[a]	6-31G	6-31G**	6-31+G
C(2)—O(1)	1.292	1.292	1.296	1.272	1.268
C(3)—C(2)	1.515	1.502	1.504	1.515	1.514
C(4)—C(3)	1.320	1.325	1.331	1.327	1.327
H(7)—O(6)	1.192	1.187	1.186	1.178	1.179
O(8)—C(2)	1.225	1.229	1.233	1.210	1.207
H(9)—C(3)	1.073	1.073	1.074	1.077	1.076
O(1)—O(6)	2.376	2.363	2.361	2.355	2.358
C(3)—C(2)—O(1)	118.2	118.3	118.4	118.0	118.1
C(4)—C(3)—C(2)	130.8	130.7	130.6	130.4	130.3
H(7)—O(6)—C(5)	115.8	116.3	116.4	113.6	113.3
O(8)—C(2)—C(3)	116.3	116.7	116.6	116.4	116.4
H(9)—C(3)—C(2)	110.4	111.1	111.3	111.6	111.7
O(1)—H(7)—O(6)	170.3	169.3	169.2	176.0	176.4

[a]Reference 16.

Can. J. Chem. Downloaded from www.nrcresearchpress.com by 88.255.202.194 on 09/08/12
For personal use only.

0.447 Å by 4-31G (ref. 15), 0.467 Å by 6-31G, 0.417 Å by 6-31G**, and 0.495 Å by 6-31+G(2*d*,1*p*). Only 3-21G calculations predict a slightly asymmetric hydrogen bond, the larger asymmetry corresponding to the calculations including diffuse functions (which in principle should give accurate results for anions). Although to make an accurate comparison it would be necessary to dispose of experimental data in the gaseous phase, according to the crystallographic data reviewed above the hydrogen bond seems to be symmetric or nearly symmetric. Only the value of Δ_{OH} predicted using 3-21G is within the experimental range; all the others are considerable greater.

The O---O distance also increases systematically with the size and complexity of the basis, and it is again 3-21G that gives the only value in the experimental range, 2.40–2.44 Å (7–13).

The hydrogen maleate anion is not the only species for which the above trend has been observed. Similar results have been reported for malonaldehyde (22–24) and for salicylaldehyde and its derivatives (25, 26), for which the best Hartree–Fock predictions of the characteristics of the hydrogen bond are likewise provided by 3-21G, and for which increasing the power of the basis set again systematically increases the O---O distance, causing it and the rest the hydrogen bond geometry to deviate from the experimental value.

The angle OHO formed by the hydrogen bond is almost linear according to the experimental data, with values in the neighbourhood of 175°. This feature is adequately predicted by all the theoretical calculations, although the predicted angles are slightly narrower.

It is not only regarding the hydrogen bond that the 3-21G optimized geometry is more symmetric than the others; the experimental finding that the rest of the anion is very close to exact symmetry is likewise best predicted by 3-21G. The greatest discrepancy between the 3-21G and experimental geometries concerns the angles C3—C2—O1 and C4—C5—O6, for which the 3-21G values are rather smaller; the O---O distance is, however, not affected because the narrowing of angles C3—C2—O1 and C4—C5—O6 is compensated by a slight widening of the C2—C3—C4 and C5—C4—C3 angles. Similarly, the above-mentioned narrowing of the OHO angle is compensated by the widening of the two COH angles.

In malonaldehyde (24), salicylaldehyde (25, 26), and tropolone (27), intramolecular hydrogen bonding favours the existence of a "pseudoaromatic" ring in which the difference in length between the single and double bonds is considerably less than usual. For the hydrogen maleate anion, this phenomenon is supported by neither the experimental nor the theoretical data: two of the C—C bonds have lengths of around 1.5 Å, i.e., in the normal range for a single bond, while C3—C4 is clearly a typical double bond. π-Delocalization is thus practically limited to the O—C—O regions.

All the basis sets used lead to the prediction of an asymmetric structure, so that there are two C_S related tautomers that in principle are interconvertible by intramolecular proton transfer. Assuming C_{2v} symmetry, we optimized the corresponding transition state using each of the basis sets, obtaining barrier heights of 0.12 (3-21G), 1.37 (4-31G, ref. 15), 1.59 (6-31G), 1.64 (6-31G**), and 2.00 (6-31+G(2*d*,1*p*)) kcal/mol. Improving the basis set thus raises the potential barrier, which is in keeping with the increased asymmetry of the more stable structure.

To illustrate the effect of electron correlation, MP2 calculations were performed. The MP2/6-31G**//HF/6-31G** energies of the C_S and C_{2v} geometries were −453.51352 and −453.51459 au respectively. The C_{2v} geometry is thus 0.7 kcal/mol more stable than the C_S geometry, supporting the hypothesis of a single minimum potential energy curve, contrary to the findings from HF calculations.

Table 3 shows the geometries of the calculated transition states. Contrary to the trend exhibited by the C_S tautomer, the O---O distance decreases as the basis set improves. The difference between the O---O distances of the C_S (minimum) and C_{2v} (transition state) structures, $\Delta(O---O)_{C_S\text{-}C_{2v}}$, is, however, found to increase as the basis set improves. This can be related to the increase in the asymmetry of the C_S form, and results in an increase in the separation between the minimum and the transition state, i.e., an increase in the breadth of the potential barrier. Improving the basis set therefore tends to establish a potential with two minima that are increasingly deep and increasingly farther apart. The potential calculated using 3-21G has practically a single minimum, the

height of the barrier being only 0.12 kcal/mol (much less than the thermal energy) and the C_S and C_{2V} structures being very close.

Conclusions

Our results show that for hydrogen maleate anion, calculations at the HF level predict an asymmetric structure for the hydrogen bond. Moreover, the improvement of the basis set systematically increases the asymmetry and the height barrier for the motion of the hydrogen atom between the two oxygen atoms. However, MP2 single-point calculations seem to predict a single minimum potential. This trend has been already reported for other compounds, therefore it could be generalizable to compounds with similar kinds of intramolecular hydrogen bond. As a result of this trend, the acceptable behaviour of the 3-21G calculations (which give a very slight asymmetry and a potential curve virtually with a single minimum) seems to be due to mutual cancellation of errors.

1. (*a*) Rossetti, R. C. Haddon, and L. E. Brus. J. Am. Chem. Soc. **102**, 6913 (1980); (*b*) R. Rossetti, R. Rayford, R. C. Haddon, and L. E. Brus. J. Am. Chem. Soc. **103**, 4303 (1981).
2. (*a*) E. M. Fluder and J. R. De la Vega. J. Am. Chem. Soc. **100**, 373 (1978); (*b*) T. Carrington, Jr. and W. H. Miller. J. Chem. Phys. **84**, 4364 (1986).
3. J. Emsley. Struct. Bonding (Berlin), **57**, 147 (1984).
4. (*a*) F. Hibbert. Adv. Phys. Org. Chem. **22**, 113 (1986); (*b*) J. Emsley. Chem. Soc. Rev. **9**, 91 (1980). (*c*) P. Shuster, G. Zundel, and C. Sandorfy. *In* The hydrogen bond: recent developments in theory and experiments. North Holland, Amsterdam. 1976.
5. S. F. Darlow and W. Cochram. Acta Crystallogr. **14**, 1250 (1961).
6. S. W. Peterson and H. A. Levy. J. Chem. Phys. **29**, 948 (1958).
7. G. Gunnarson, H. Wennerstrom, W. Egan, and S. Forsen. Chem. Phys. Lett. **38**, 96 (1976).
8. L. J. Altman, D. Laungani, G. Gunnarson, H. Wennerstrom, and S. Forsen. J. Am. Chem. Soc. **100**, 8264 (1978).
9. R. D. Ellison and H. A. Levy. Acta Crystallogr. **19**, 260 (1965).
10. G. Olovsson, I. Olovsson, and M. S. Lehmann. Acta Crystallogr. Sect. C: Cryst. Struct. Commun. **C40**, 1521 (1984).
11. B. Hsu and E. O. Schlemper. Acta Crystallogr. Sect. B: Struct. Crystallogr. Cryst. Chem. **B36**, 3017 (1980).
12. P. Popelier, A. T. H. Lenstra, and H. J. Geise. Acta Crystallogr. Sect. C: Cryst. Struct. Commun. **C45**, 1024 (1989).
13. F. Vanhouteghem, A. T. H. Lenstra, and P. Schweiss. Acta Crystallogr. Sect. B: Struct. Sci. **B43**, 523 (1987).
14. C. L. Perrin and J. D. Thoburn. J. Am. Chem. Soc. **111**, 8010 (1989).
15. F. Avbelj, M. Hodoscek, and D. Hadzi. Spectrochim. Acta, **41A**, 89 (1985).
16. P. George, C. W. Bock, and M. Tratchtman. J. Chem. Phys. **87**, 1839 (1983).
17 J. S. Binkley, J. A. Pople, and W. J. Hehre. J. Am. Chem. Soc. **102**, 939 (1980).
18. W. J. Hehre, R. Ditchfield, and J. A. Pople. J. Chem. Phys. **56**, 2257 (1972).
19. P. C. Hariharan and J. A. Pople. Chem. Phys. Lett. **66**, 217 (1972).
20. (*a*) T. Clark, J. Chandrasekar, G. W. Spitznagel, and P. v. R. Schleyer. J. Comput. Chem. **4**, 294 (1983); (*b*) M. J. Frisch, J. A. Pople, and J. S. Binkley. J. Chem. Phys. **80**, 3265 (1984); (*c*) Z. Latjka and S. Schneiner. Chem. Phys. Lett. **105**, 435 (1984).
21. M. J. Frisch, M. Head-Gordon, H. B. Schlegel, K. Raghavachari, J. S. Binkley, C. González, D. J. Defrees, D. J. Fox, R. A. Whiteside, R. Seeger, C. F. Melius, J. Baker, R. L. Martin, L. R. Kahn, J. J. P. Stewart, E. M. Fluder, S. Topiol, and J. A. Pople. Gaussian, Inc., Pittsburgh, Pa. 1988.
22. J. Bicerano, H. F Schaefer III, and W. H. Miller. J. Am. Chem. Soc. **105**, 2250 (1983).
23. M. J. Frisch, A. C. Scheiner, H. F. Schaefer III, and J. S. Binkley. J. Chem. Phys. **82**, 4194 (1985).
24. M. A. Ríos and J. Rodríguez. J. Mol. Struct. (Theochem), **228**, 149 (1991).
25. A. M. Graña, M. A. Ríos, and J. Rodríguez. Struct. Chem. **2**, 575 (1991).
26. C. M. Estévez, M. A. Ríos, and J. Rodríguez. Struct. Chem. **3**, 381 (1992).
27. M. A. Ríos and J. Rodríguez. Can. J. Chem. **69**, 201 (1991).

Can. J. Chem. Downloaded from www.nrcresearchpress.com by 88.255.202.194 on 09/08/12
For personal use only.

Reactions of Ni(II) and its complexes with free radicals derived from thymine

S. CHAKRABARTI, P. C. MANDAL, AND S. N. BHATTACHARYYA[1]

Nuclear Chemistry Division, Saha Institute of Nuclear Physics, 1/AF, Bidhannagar, Calcutta-700064, India

Received February 20, 1992[2]

S. CHAKRABARTI, P. C. MANDAL, and S. N. BHATTACHARYYA. Can. J. Chem. **71**, 307 (1993).

The effects of nickel(II) ions and its complexes on the products arising from the γ-radiolysis of thymine were studied. The decomposition of the pyrimidine base and formation of different radiolytic products indicate that nickel(II) ions or its complexes have little effect on the radiosensitivity of thymine. The transient hydroxyl adduct of thymine reacts with Ni(II) with the formation of a complex having a nickel–carbon bond. The rate constants for the reactions are of the order of 10^6 dm^3 mol^{-1} s^{-1}. Possible mechanisms for the formation of different products in the radiolysis of thymine in the presence of nickel(II) compounds are discussed.

S. CHAKRABARTI, P. C. MANDAL et S. N. BHATTACHARYYA. Can. J. Chem. **71**, 307 (1993).

On a étudié l'influence des ions du nickel(II) et de ses complexes sur les produits provenant de la radiolyse γ de la thymine. La décomposition de la pyrimidine et la formation de divers produits radiolytiques indiquent que les ions nickel(II) ou ses complexes n'ont que peu d'effet sur la radiosensibilité de la thymine. L'adduit hydroxylé transitoire de la thymine réagit avec le Ni(II) avec formation d'un complexe comportant une liaison nickel–carbone. Les constantes de vitesse pour les réactions sont de l'ordre de 10^6 dm^3 mol^{-1} s^{-1}. On discute des mécanismes possibles pour la formation des divers produits de radiolyse de la thymine en présence de composés du nickel(II).

[Traduit par la rédaction]

Introduction

In connection with studies on the effects of transition metal ions on the radiosensitivity of nucleic acid components, the effects of Cu(II) and Fe(III) ions on the radiation-induced degradation of thymine were investigated earlier in dilute aqueous solutions (1–3). It was observed that both Cu(II) and Fe(III), whether present as simple salts or as complexed ions, could enhance the radiation-induced degradation of the nucleic acid base. The increased radiosensitivity of thymine depends on the reactivity of transient adducts of thymine, e.g., TOH$^\cdot$, TH$^\cdot$, T$^-$, and UCH$_2^\cdot$ (where both T and UCH$_3$ represent thymine), with the metal ions. This reactivity was earlier reported to be dependent on the one-electron reduction potential of the metal ion couple ($M^{n+}/M^{(n-1)+}$) and on the redox properties of the transient radicals of thymine. The one-electron reduction potential of Ni^{2+}/Ni^{1+} ($E_0 = -2.7$ V) (4) is much lower than that of Cu^{2+}/Cu^{1+} ($E_0 = 0.16$ V) (5) or Fe^{3+}/Fe^{2+} ($E_0 = 0.77$ V) (5). Hence it is very difficult to reduce Ni^{2+}. It is also very difficult to oxidize Ni^{2+} in its complex with EDTA (E_0(Ni(III)EDTA/Ni(II)EDTA) = 1.9 V) (6). Although the redox properties of the reducing or oxidizing thymine adducts are too weak to cause reductive or oxidative interaction with Ni^{2+} or its complexes, some of the nickel(II) complexes have been found to be radiosensitizing (7). Hence a detailed study of the effects of Ni(II) ions/complexes on the radiosensitivity of molecules like thymine may shed light on the reactivity of the thymine transients with the Ni^{2+} ions. The present investigation describes the results of studies on the reaction of Ni(II) ions and their complexes with transient thyminyl radicals. The rate constants for the reactions were studied using flash photolysis whereas the stable products arising from the degradation of thymine were ascertained in steady-state radiolysis experiments.

Experimental

Materials

Thymine (Koch Light) was recrystallized three times from triply distilled water. 2-^{14}C-thymine was procured from BARC, Bombay. The nickel(II) complexes of EDTA, NTA, and IDA were prepared by the usual methods as described earlier (8–10). EDTA, NTA, and IDA represent ethylenediamine tetraacetic acid, nitrilotriacetic acid, and iminodiacetic acid, respectively. All other chemicals and reagents were of analytical reagent grade. Nitrous oxide and argon gas were of extra pure grade.

γ-Irradiation

γ-Irradiation was carried out with ^{60}Co γ-rays. The dose rate (10.4 Gy/min) was measured by Fricke dosimeter taking $G(Fe^{3+})$ = 15.5. (1 G unit = 1.036×10^{-7} mol J^{-1}.)

Analysis

The products of radiolysis arising from the degradation of thymine were measured after separation by bidimensional thin-layer chromatography using the solvent systems chloroform:methanol:water (4:2:1) and ethyl acetate:isopropanol:water (75:16:9) as described earlier (3). Since the Ni(II) complexes and most of the products of radiolysis (except 5-hydroxymethyluracil, which, however, is only present in insignificant amounts) do not absorb at the wavelengths where thymine absorbs, they can also be measured using spectrophotometry. Formaldehyde was measured by the chromotropic acid method (11) and glyoxalic acid by its reaction with 2,4-dinitrophenylhydrazine (12).

Flash photolysis

Kinetics for the decay of the transient thyminyl radicals (TH$^\cdot$ and TOH$^\cdot$) in the presence of various nickel(II) compounds were studied by flash photolysis. The flash photolysis apparatus (model KN-020) was supplied by Applied Photophysics Ltd. The path length of the photolysis cell is 10 cm. Two flash lamps (LR 16) connected in series were operated at 15 kV, which gives a light flash of 10 μs duration (FWHM). The digitized transient signal from the oscilloscope (Iwatsu TS-8123) was fed into a PC through a GPIB interface and the absorption vs. time data were analysed for first-order and second-order fits by least-squares methods.

Results and discussion

Reaction between TOH$^\cdot$ and Ni(II) compounds

Flash photolytic study

TOH$^\cdot$ was generated by the flash photolysis of an aqueous deaerated solution of 2×10^{-3} mol dm^{-3} thymine (T) in the

[1]Author to whom correspondence may be addressed.

[2]Revision received November 13, 1992.

Can. J. Chem. Downloaded from www.nrcresearchpress.com by 88.255.202.194 on 09/08/12
For personal use only.

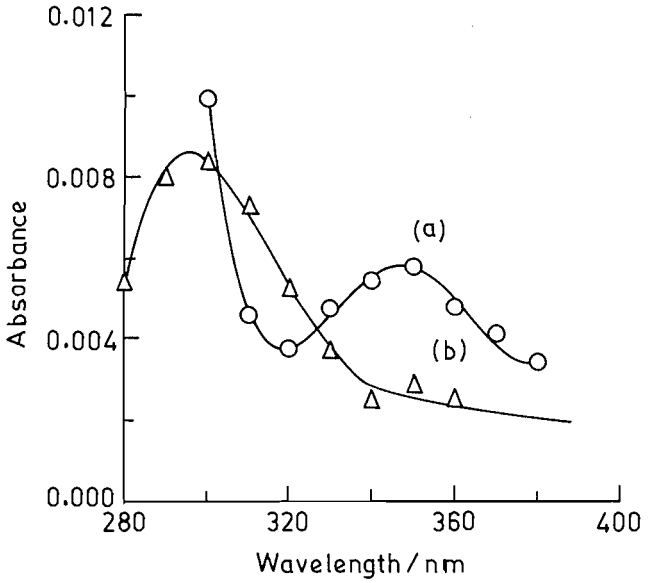

FIG. 1. (*a*) Transient spectrum of TOH$^{\bullet}$ obtained 200 μs after the flash in the flash photolysis of 2×10^{-3} mol dm^{-3} thymine and 10^{-2} mol dm^{-3} H_2O_2 in the presence of 10^{-5} mol dm^{-3} Ni(II)EDTA under deaerated conditions at neutral pH. (*b*) The absorption spectrum of the products formed after the reaction of TOH$^{\bullet}$ with Ni(II)EDTA. The spectrum was taken 5 ms after the flash.

presence of 10^{-2} mol dm^{-3} H_2O_2. When light is absorbed by H_2O_2, the OH$^{\bullet}$ radical is produced.

$$[1] \quad H_2O_2 \xrightarrow{h\nu} 2OH^{\bullet}$$

This OH radical then undergoes reactions [2] and (predominantly) [3] ($k_2 = 2 \times 10^7$ dm^3 mol^{-1} s^{-1} and $k_3 = 6.4 \times 10^9$ dm^3 mol^{-1} s^{-1}) (13).

$$[2] \quad OH^{\bullet} + H_2O_2 \xrightarrow{k_2} H_2O + HO_2^{\bullet}$$

$$[3] \quad T + OH^{\bullet} \xrightarrow{k_3} TOH^{\bullet}$$

Figure 1*a* shows that the spectrum of transients formed 200 μs after the flash is very similar to that of TOH$^{\bullet}$ reported earlier (14). OH$^{\bullet}$ adds to thymine, producing C_5-OH and C_6-OH adducts, which have similar absorption spectra but different absorption maxima (15). Contrary to the uracil system where the C_5-UOH adduct (82%) predominates over the C_6-UOH adduct (18%) (15), in the case of thymine the C_6-TOH adduct is formed in 30% yield and C_5-TOH adduct in 60% yield. The observed spectrum was found to be similar to the composite spectrum of both OH adducts of 1,3-dimethylthymine reported earlier by Deeble and von Sonntag (16).

The absorption spectrum of the product formed after the reaction of TOH$^{\bullet}$ with Ni(II)EDTA is shown in Fig. 1*b*. The uv part of the spectrum is very similar to that of Ni(III)EDTA formed by oxidation of the Ni(II)EDTA complex to the Ni(III) state (17). It can be surmised that TOH$^{\bullet}$ radicals formed in reaction [3] are reacting with Ni(II)EDTA, forming Ni(III)EDTA or a species having similar absorption. Note that the C_5-OH adduct of thymine is known to be reducing while the C_6-OH adduct is oxidizing (18). However, consideration of the redox potentials of Ni(II)/Ni(I) (4) and Ni(III)/Ni(II) (6) indicates that oxidation of C_5-TOH$^{\bullet}$ (19) and reduction of C_6-TOH$^{\bullet}$ (20) by Ni(II) compounds is unlikely.

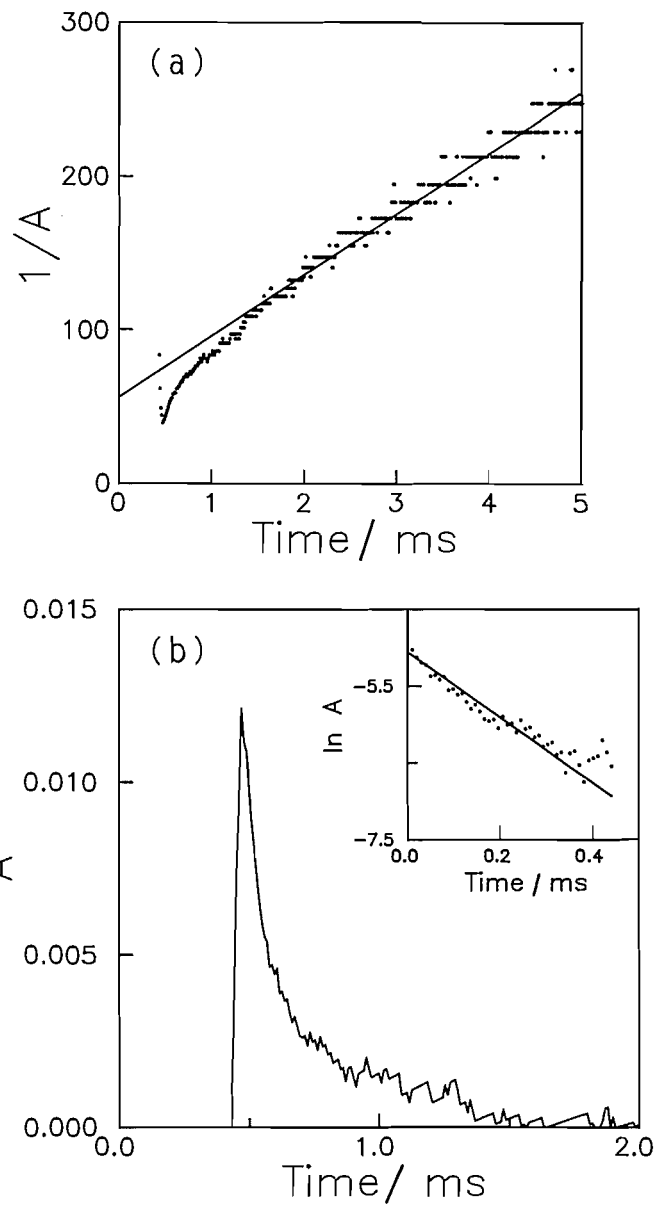

FIG. 2. (*a*) Second-order kinetic fitting of the absorbance (*A*) vs. time data for the decay of TOH$^{\bullet}$ formed by the photolysis of deaerated solutions of 2×10^{-3} mol dm^{-3} thymine and 10^{-2} mol dm^{-3} H_2O_2 in the presence of 4×10^{-4} mol dm^{-3} $NiSO_4$. (*b*) *A* vs. time curve for the decay of TOH$^{\bullet}$ at 360 nm after subtracting the contribution for the second-order component from the absorbance–time data. Inset: fitting of the data by an integrated equation based on first-order kinetics.

When the decay of TOH at 360 nm was followed in the presence of Ni(II)EDTA or other Ni(II) complexes, the absorbance did not show first-order or second-order decay but was best described as due to concurrent pseudo-first-order and second-order processes (Fig. 2). An apparent second-order rate constant was determined by plotting $1/A$ vs. time. Its value ($\sim 10^9$ dm^3 mol^{-1} s^{-1}) was found to be that observed for bimolecular TOH$^{\bullet}$ decay in the absence of metal

Can. J. Chem. Downloaded from www.nrcresearchpress.com by 88.255.202.194 on 09/08/12
For personal use only.

Can. J. Chem. Downloaded from www.nrcresearchpress.com by 88.255.202.194 on 09/08/12
For personal use only.

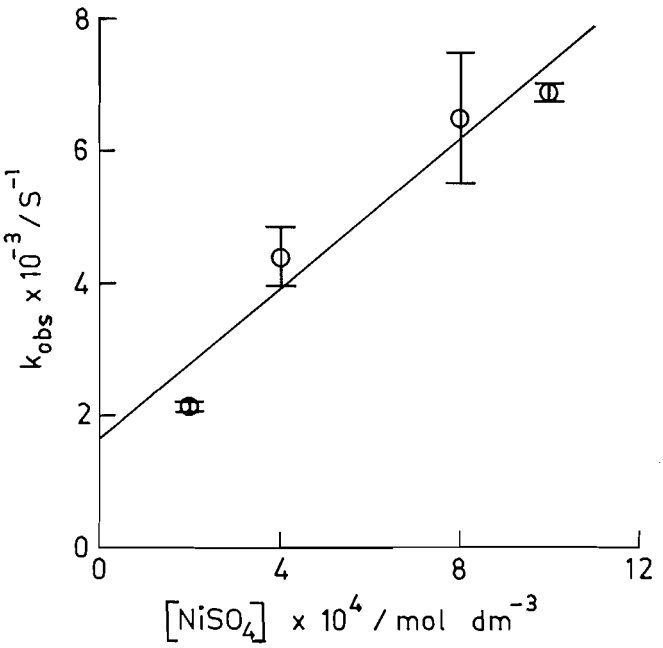

FIG. 3. Observed pseudo-first-order rate constants (k_{obs}) for the decay of TOH radical vs. [$NiSO_4$].

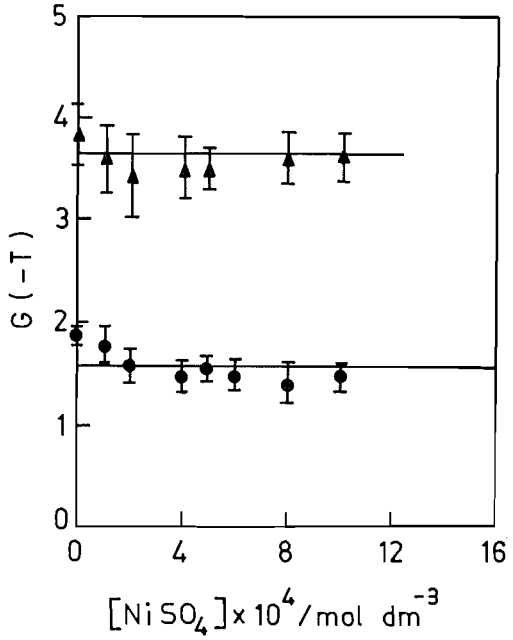

FIG. 4. Effect of [$NiSO_4$] on G(-T): (●), argon saturation, and (▲), N_2O-saturated condition. [T] = 2×10^{-3} mol dm^{-3}.

TABLE 1. Rate constants[a] for the reactions of $TOH^{\bullet}$ and $TH^{\bullet}$ with Ni(II) compounds. [Thymine] = 2×10^{-3} mol dm^{-3}; [dihydrothymine] = 10^{-3} mol dm^{-3}; [H_2O_2] = 10^{-2} mol dm^{-3}

Ni(II) compound	$k_{TOH+Ni(II)}$ ($dm^3\ mol^{-1}\ s^{-1}$)	$k_{TH+Ni(II)}$ ($dm^3\ mol^{-1}\ s^{-1}$)
$NiSO_4$	5.6×10^6	7.8×10^5
Ni(II)EDTA	2.8×10^6	1.0×10^6
Ni(II)NTA	5.5×10^6	8.1×10^5
$Ni(II)(IDA)_2$	2.8×10^6	8.8×10^5

[a]Estimated error is within ±15%.

ions (21). Subtraction of this slow second-order component yielded a fast exponential decay of TOH in the presence of Ni(II) compounds. The corresponding second-order rate constants, k, were determined from the observed dependence of the pseudo-first-order rate constants on the concentrations of Ni(II) compounds. A typical plot is shown in Fig. 3 and the relevant rate constants are listed in Table 1. This plot shows a large intercept, a behaviour typical for an equilibrium where the slope represents the rate constant for the forward reaction. These data can thus be interpreted as due to complex formation between $TOH^{\bullet}$ and Ni(II) compounds.

[4] $TOH^{\bullet} + Ni(II)EDTA \rightleftarrows TOH\text{--}NiEDTA$

Such a complex might contain a nickel–carbon bond. Formation of a metal–carbon bond has been reported in the reactions of some alcohol radicals with metal ions (22–24). The complexes containing a Ni—C bond are rather long lived (25) and the absorption spectrum observed 5 ms after the flash (spectrum (*b*) in Fig. 1) is probably due to such a species.

γ-Radiolytic study

In γ-irradiated dilute aqueous solutions, the OH radical formed in the radiolysis of water reacts with thymine, forming TOH radicals (reaction [3]) (15). However, when Ni(II) ions are present they compete with thymine for primary radicals, depending upon the respective concentrations and rate constants (13).

The absence of a dependence of the decomposition of thymine, G(-T), on the concentration of $NiSO_4$ in the γ-radiolysis of 2×10^{-3} mol dm^{-3} thymine in N_2O-saturated solution is shown in Fig. 4. The base decomposition yields, G(-T), determined under different conditions are tabulated in Table 2. From Table 2 and Fig. 4, it is evident that the Ni(II) ions have no influence on the radiosensitivity of thymine. The study was extended to various Ni(II) complexes of aminopolycarboxylic acids, the resulting G(-T) values also being shown in Table 2. It follows that the G(-T) values observed with Ni(II) complexes are comparable to those obtained with $NiSO_4$. Analysis of the products arising from the degradation of thymine in the presence of Ni(II) ions and their complexes showed that they are similar to those obtained without Ni(II) compounds (Table 3).

The observed G(-T) values in N_2O-saturated solution were nearly double those observed under argon-saturated conditions (Table 2). In N_2O-saturated solution e_{aq}^- formed in the radiolytic system is converted to an equivalent amount of OH radical.

[5] $e_{aq}^- + N_2O \rightarrow OH^{\bullet} + OH^- + N_2$

Hence it can be argued that the base degradation is primarily due to the reaction of TOH radicals. This was verified by carrying out the radiolysis in the presence of 0.4 mol dm^{-3} *tert*-butyl alcohol under N_2O-saturated conditions where G(-T) values were negligibly small.

From these observations one can conclude that the degradation of thymine is due to OH radicals only. It must be pointed out that the electron adduct of thymine, T^-, must be present in appreciable amount under argon-saturated conditions. Why the disappearance of T^- does not lead to degradation of thymine is not immediately clear.

TABLE 2. Yields in the radiolysis of thymine[a] in the presence of different Ni(II) compounds[b] at neutral pH

Ni(II) compound	Condition	G(-T)	G(HCHO)	G(OHC.COOH)	G(>C=O)[c]
None	Argon satd.	1.9	0.0	0.0	0.0
None	N_2O satd.[d]	3.9	0.0	0.0	0.0
None	Aerated[e]	2.7	0.0	0.0	0.0
$NiSO_4$	Argon satd.	1.6	0.0	0.0	0.0
$NiSO_4$	N_2O satd.[d]	3.5	0.0	0.0	0.0
$NiSO_4$	Aerated[e]	2.6	0.0	0.0	0.0
Ni(II)EDTA	Argon satd.	1.6	0.5	0.2	0.7
Ni(II)EDTA	N_2O satd.[d]	2.7	0.6	0.5	1.1
Ni(II)EDTA	Aerated[e]	2.7	0.0	0.0	0.0
Ni(II)NTA	Argon satd.	1.6	0.0	0.4	0.4
Ni(II)NTA	N_2O satd.[d]	3.3	0.1	0.6	0.7
Ni(II)NTA	Aerated[e]	2.8	0.0	0.0	0.0
Ni(II)IDA	Argon satd.	1.5	0.1	0.0	0.1
Ni(II)IDA	N_2O satd.[d]	3.2	0.2	0.2	0.4
Ni(II)IDA	Aerated[e]	2.8	0.0	0.0	0.0
$Ni(II)(IDA)_2$	Argon satd.	1.5	0.1	0.2	0.3
$Ni(II)(IDA)_2$	N_2O satd.[d]	3.2	0.0	1.2	1.2
$Ni(II)(IDA)_2$	Aerated[e]	2.6	0.0	0.0	0.0

[a][Thymine] = 2×10^{-3} mol dm^{-3}.
[b][Ni] = 5×10^{-4} mol dm^{-3}.
[c]Total carbonyl yield.
[d][N_2O] = 2.5×10^{-2} mol dm^{-3}.
[e][O_2] = 2.7×10^{-4} mol dm^{-3}.

TABLE 3. Radiolytic yields[a] of different products in the radiolysis of thymine in the presence and in the absence of Ni(II) compounds at neutral pH. [T] = 2×10^{-3} mol dm^{-3}; [Ni(II) compounds] = 5×10^{-4} mol dm^{-3}

	Condition[b]							
G(products)	A	B	C	D	E	F	G	H
G(dimer)	0.3	0.7	0.4	0.6	0.3	0.6	0.3	0.6
G(*cis*-thymine glycol)	0.3	0.7	0.3	0.5	0.1	0.3	0.2	0.3
G(*trans*-thymine glycol)	0.1	0.2	0.1	0.1	0.1	0.1	0.1	0.1
G(5,6-dihydrothymine)	0.3	0.1	0.1	0.0	0.4	0.2	0.3	0.2
G(6-hydroxydihydrothymine)	0.1	0.2	0.2	0.4	0.1	0.2	0.2	0.2
G(5-hydroxydihydrothymine)	0.0	0.1	0.1	0.4	0.1	0.2	0.2	0.2
G(5-hydroxymethyluracil)	0.2	0.6	0.1	0.5	0.1	0.4	0.1	0.3
G(5-methylbarbituric acid)	0.2	0.3	0.2	0.4	0.2	0.2	0.2	0.3
G(unidentified products)	0.2	0.3	0.2	0.0	0.1	0.1	0.2	0.2
G(-thymine)[c]	1.8	3.8	1.7 (1.6)	3.3 (3.5)	1.6 (1.6)	2.7 (2.7)	1.5 (1.5)	3.1 (3.2)

[a]Yields were determined spectrophotometrically. Error in the estimation of yields of various products is ±10%.
[b]A: in the absence, and C, E, and G: in the presence of $NiSO_4$, Ni(II)EDTA, and Ni(II)IDA, respectively, under argon-saturated conditions. B: in the absence, and D, F, and H: in the presence of $NiSO_4$, Ni(II)EDTA, and Ni(II)IDA, respectively, under N_2O-saturated conditions.
[c]Values in parentheses are those obtained spectrophotometrically.

When thymine is irradiated in N_2O-saturated solutions in the presence of Ni(II) aminopolycarboxylates, formation of carbonyl compounds, such as formaldehyde and glyoxalic acid, was observed; the yields are shown in Table 2. In argon-saturated solutions these yields are much lower. No carbonyl products were observed when the radiolysis was carried out in the presence of $NiSO_4$ or in the absence of any metal ion, or in aerated solutions. Thus it appears that the carbonyl products arise from degradation of the aminopolycarboxylate ligand in the complex. In this context a possible contribution of C_5-TOH$^\bullet$ to the formation of carbonyl compounds by abstracting hydrogen from the nickel complexes was checked, since the reducing C_5-OH adduct of uracil or thymine has been reported (26, 27) to abstract hydrogen from polyuridylic or polythymidylic acid. However, the absence of carbonyl compounds during radiolysis of dihydrothymine (where mainly reducing radical C_5-TH is formed) in the presence of Ni(II)EDTA in N_2O-saturated solution indicates that in our system no such abstraction of hydrogen from the ligands of nickel complexes takes place. The degradation of the ligand therefore may be thought of as arising from the interaction between C_6-TOH$^\bullet$ and Ni(II) complexes.

Can. J. Chem. Downloaded from www.nrcresearchpress.com by 88.255.202.194 on 09/08/12
For personal use only.

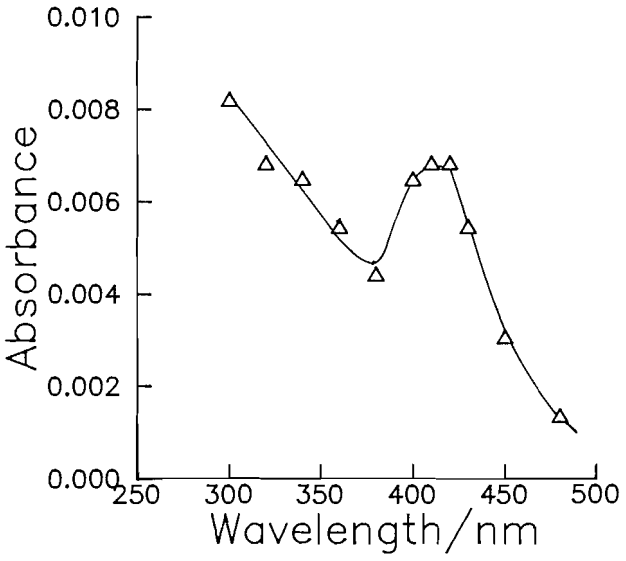

FIG. 5. Absorption spectrum of TH radical formed after flash photolysis of an aqueous solution containing 10^{-3} mol dm^{-3} dihydrothymine and 10^{-2} mol dm^{-3} hydrogen peroxide under argon saturated conditions.

It was reported earlier (28) that the C_6-OH adduct of uracil oxidizes the Ni(II) aminopolycarboxylates to Ni(III) species, which then give rise to carbonyl products arising from the degradation of ligands by Ni(III) in the complexes. But as discussed earlier, the C_6-OH adduct of thymine does not oxidize Ni(II) to Ni(III); rather, it seems to form a complex having a Ni—C bond that exists in equilibrium with the reactants.

Thus from the flash photolytic as well as γ-radiolysis experiments of thymine in the presence of Ni(II) it is quite clear that the electron transfer reaction, which leads to the enhanced oxidation of the C_5-TOH radical with previously studied metal ions such as Cu(II) (1, 2) or Fe(III) (3), does not occur in the nickel system.

Reactions of TH$^{\bullet}$ and Ni(II) compounds

Flash photolytic study

TH radicals were generated through reactions of 10^{-3} mol dm^{-3} dihydrothymine (TH_2) with OH$^{\bullet}$ radicals produced by flash photolysis of 10^{-2} mol dm^{-3} H_2O_2 under deaerated conditions. The rate constant (29) for the reaction of OH$^{\bullet}$ with TH_2 is $\sim 1 \times 10^9$ dm^3 mol^{-1} s^{-1}. Hence under these conditions all the OH radicals would react with TH_2 to give TH$^{\bullet}$.

[6] $TH_2 + OH^{\bullet} \rightarrow TH^{\bullet} + H_2O$

Figure 5 shows that the spectrum of the transient obtained during flash photolysis under argon-saturated conditions is similar to the spectrum of the TH$^{\bullet}$ radical produced by pulse radiolysis (30). Ni(II) compounds increase the decay rate of the absorption peak at 420 nm. The absorption data were fitted in a similar way as those in Fig. 2. From the variation of the pseudo-first-order rate constants with the concentration of the Ni(II), the second-order rate constants for the reactions of TH$^{\bullet}$ with Ni(II) compounds shown in Table 1 were determined.

The plot of the variation of the Ni(II) concentration with k_{obs} shows an intercept (plot not shown), indicating that the TH radical forms a complex with the Ni(II) ions. The TH radical formed by OH attack on dihydrothymine is a reducing species (31–33), but its redox potential is not high enough to reduce Ni(II) to Ni(I) (19). Hence it can be assumed that the intermediate Ni(II)–TH complex does not undergo electron transfer but stabilizes through some bimolecular process (30).

γ-Radiolytic study

H and e_{aq}^- formed in the γ-irradiated deaerated dilute aqueous solution react with thymine, forming TH and T^- radicals (15, 34).

[7] $T + H \rightarrow TH^{\bullet}$

$k_7 = 5.7 \times 10^8$ dm^3 mol^{-1} s^{-1} (13)

The addition of hydrogen atom occurs mainly (60%) at the C(6) position of the thymine ring (15, 35).

[8] $T + e_{aq}^- \rightarrow T^-$

$k_8 = 1.8 \times 10^{10}$ dm^3 mol^{-1} s^{-1} (13)

T^- cannot reduce Ni(II) to Ni(I), since the redox potential of T^- is only in the order of −1.0 V (36) while that of the Ni(II)/Ni(I) equals −2.7 V. The electron adduct of thymine, T^-, protonates at oxygen to form mainly the reducing C_4-TOH radical (37). The protonation in neutral solution is relatively slow ($k < 2 \times 10^{-4}$ s^{-1}) (15) but the protonation by H^+ is quite fast ($k = 2.6 \times 10^{10}$ dm^3 mol^{-1} s^{-1}) (38). A slower protonation at the C_6 position occurs in the presence of phosphate buffer, producing oxidizing C_6-TH$^{\bullet}$ ($k = 3.7 \times 10^6$ dm^3 mol^{-1} s^{-1}) (38). The protonated form of the electron adduct of thymine, T^-, is, however, ultimately converted to the oxidizing C_6-TH radical (36). H and e_{aq}^- adducts of thymine therefore lead to C_5 and C_6-TH adducts. The former is reducing but its redox potential is not sufficiently high to reduce Ni(II) to Ni(I) (19). Thus when dihydrothymine is radiolysed in the presence and in the absence of various Ni(II) compounds under N_2O-saturated conditions, the amount of thymine generated ($G(T) \simeq 1.35 \pm 0.15$) from TH was found to be identical under all conditions. The C_6-TH radical is oxidizing (18), but the C_6-TH adduct has a much lower oxidative power (39) than the corresponding C_6-TOH radical. Hence it can be presumed that the C_6-TH radical does not oxidize Ni(II) to Ni(III) species and probably disappears through bimolecular decay ($2k_{TH+TH} = 10^9$ dm^3 mol^{-1} s^{-1}) (30).

Radiolysis of thymine in the presence of Ni(II) in an aerated medium

In an aerated medium the decomposition of thymine takes place only due to OH radicals, because hydrated electrons and H atoms are converted to unreactive O_2^- and HO_2, respectively.

[9] $e_{aq}^- + O_2 \rightarrow O_2^-$

$k_9 = 1.9 \times 10^{10}$ dm^3 mol^{-1} s^{-1} (13)

[10] $H + O_2 \rightarrow HO_2$

$k_{10} = 2.1 \times 10^{10}$ dm^3 mol^{-1} s^{-1} (13)

In fact, the observed yield of thymine decomposition in the presence of Ni(II) compounds closely resembles $G_{OH} \sim 2.7$ (Table 2). Since no carbonyl compounds are formed during the radiolysis of thymine in presence of nickel(II) complexes in aerated medium, the TOH radicals do not

Can. J. Chem. Downloaded from www.nrcresearchpress.com by 88.255.202.194 on 09/08/12
For personal use only.

undergo reaction with Ni(II) ions, but react with molecular oxygen to give peroxy radicals that ultimately give rise to thymine degradation products.

It can therefore be concluded that, unlike the case of Cu(II) and Fe(III), no electron transfer from the hydroxyl radical adduct of thymine to Ni(II) occurs, in conformity with the redox potentials of the metal ions.

Acknowledgement

The authors are grateful to the referees for their valuable suggestions in revising the manuscript.

1. S. N. Bhattacharyya, P. C. Mandal, and S. Chakrabarti. Anticancer Res. **9**, 1181 (1989).
2. S. N. Bhattacharyya, P. C. Mandal, and S. Chakrabarti. Radiat. Phys. Chem. **37**, 347 (1991).
3. S. N. Bhattacharyya, P. C. Mandal, and S. Chakrabarti. Bull. Chem. Soc. Jpn. **63**, 3001 (1990).
4. J. H. Baxendale and R. S. Dixon. Z. Phys. Chem. **43**, 161 (1964).
5. N. A. Lange. Handbook of chemistry. McGraw-Hill, New York. 1961. p. 1212.
6. P. C. Mandal, D. K. Bardhan, S. Sarkar, and S. N. Bhattacharyya. J. Chem. Soc. Dalton Trans. 1457 (1991).
7. K. A. Skov. Radiat. Res. **112**, 217 (1987).
8. S. N. Bhattacharyya and K. P. Kundu. Radiat. Res. **51**, 45 (1972).
9. N. C. Saha. Ph.D. Thesis, University of Calcutta, 1978.
10. E. V. Srisankar and S. N. Bhattacharyya. J. Chem. Soc. Dalton Trans. 675 (1980).
11. C. E. Bricker and H. R. Johnson. Ind. Eng. Chem. Anal. Ed. **17**, 400 (1945).
12. T. E. Friedmann and G. E. Haugen. J. Biol. Chem. **147**, 415 (1943).
13. G. V. Buxton, C. L. Greenstock, W. P. Hellman, and A. B. Ross. J. Phys. Chem. Ref. Data, **17**, 513 (1988).
14. J. Planinic and Lj. Planinic. Radiochem. Radioanal. Lett. **46**, 13 (1981).
15. C. von Sonntag and H. P. Schuchmann. Int. J. Radiat. Biol. **49**, 1 (1986).
16. D. J. Deeble and C. von. Sonntag. Z. Naturforsch. **40C**, 925 (1985).
17. J. Lati and D. Meyerstein. Int. J. Radiat. Phys. Chem. **7**, 611 (1975).
18. S. Fujita and S. Steenken. J. Am. Chem. Soc. **104**, 2540 (1981).
19. F. Busi, V. Concialini, O. Tubertini, and M. D.'Angelantonio. Radiat. Phys. Chem. **34**, 857 (1989).
20. S. Nishimoto, H. Ide, K. Nakamichi, N. Otsuki, and T. Kagiya. Chem. Lett. 1441 (1983).
21. R. V. Bensasson, E. J. Land, and T. G. Truscott. Flash photolysis and pulse radiolysis. Pergamon Press, New York. 1983. p. 131.
22. H. Cohen and D. Meyerstein. J. Chem. Soc. Faraday Trans. 1, **84**, 4157 (1988).
23. M. Kelm, J. Lilie, A. Henglein, and E. Janata. J. Phys. Chem. 78, 882 (1974).
24. M. Freiburg and D. Meyerstein. J. Chem. Soc. Faraday Trans. 1, **76**, 1825 (1980).
25. S. N. Bhattacharyya and P. C. Mandal. J. Chem. Soc. Faraday Trans. 1, **79**, 2613 (1983).
26. D. G. E. Lemaire, E. Bothe, and D. Schulte-Frohlinde. Int. J. Radiat. Biol. **45**, 351 (1984).
27. L. R. Karam, M. Dizdaroglu, and M. G. Simic. Radiat. Res. **116**, 210 (1988).
28. S. N. Bhattacharyya and P. C. Mandal. J. Chem Soc. Faraday Trans. 1, **80**, 1205 (1984).
29. H. R. Haysom, J. M. Philips, J. Richards, G. Scholes, and R. L. Wilson. *In* Fast processes in radiation chemistry and biology. *Edited by* G. E. Adams, E. M. Fielden, and B. D. Michael. The Institute of Physics and John Wiley and Sons, London. 1975. p. 241.
30. Jr. L. S. Myers and M. L. Theard. J. Am. Chem. Soc. **92**, 2868 (1970).
31. M. N. Schuchmann, M. Al-Sheikhly, C. von Sonntag, A. Garner, and G. Scholes. J. Chem. Soc. Perkin Trans. 2, 1777 (1984).
32. M. I. Al-sheikhly, A. Hissung, H. P. Schuchmann, M. N. Schuchmann, C. Von Sonntag, A. Garner, and G. Scholes. J. Chem. Soc. Perkin Trans. 2, 601 (1984).
33. M. N. Schuchmann, S. Steenken, J. Wroblewski, and C. von Sonntag. Int. J. Radiat. Biol. **46**, 225 (1984).
34. S. Nishimoto, H. Ide, T. Wada, and T. Kagiya. Int. J. Radiat. Biol. **44**, 585 (1983).
35. S. Das, D. J. Deeble, and C. von Sonntag. Z. Naturforsch. **40C**, 292 (1985).
36. S. Steenken, J. P. Telo, H. M. Novais, and L. P. Candeias. J. Am. Chem. Soc. **114**, 4701 (1992).
37. S. Das, D. J. Deeble, M. N. Schuchmann, and C. von Sonntag. Int. J. Radiat. Biol. **46**, 7 (1984).
38. D. J. Deeble, S. Das, and C. von Sonntag. J. Phys. Chem. **89**, 5784 (1985).
39. V. Jagannadham and S. Steenken. J. Phys. Chem. **92**, 111 (1988).

Can. J. Chem. Downloaded from www.nrcresearchpress.com by 88.255.202.194 on 09/08/12
For personal use only.

Diatomic centrifugal distortion constants for large orders at any level: application to the $XO_g^+-I_2$ state

MAHMOUD KOREK[1]

Department of Physics, Concordia University, 1455 de Maisonneuve Blvd W., Montreal, Qué., Canada H3G 1M8

AND

HAFEZ KOBEISSI

Faculty of Science, Lebanese University, and the Group of Molecular and Atomic Physics at the National Research Council, Beirut, Lebanon

Received May 15, 1992

MAHMOUD KOREK and HAFEZ KOBEISSI. Can. J. Chem. **71**, 313 (1993).

The determination of the centrifugal distortion constants (CDC) of a diatomic molecule is sought for high orders. When the vibrational energy $e_0 = E_v$ is known for a vibrational level v, the use of Rayleigh–Schrödinger perturbation theory gives the rotational constant $e_1 = B_v = \langle\Phi_0 R\Phi_0\rangle$ (with $R = 1/r^2$), and the CDC $e_2 = -D_v = \langle\Phi_0 R\Phi_1\rangle$, $e_3 = H_v = \langle\Phi_0 R\Phi_2\rangle$, ..., $e_n = \langle\Phi_0 R\Phi_{n-1}\rangle$, ... where $\Phi_n(r)$ is the solution of the nth rotational Schrödinger equation. The problem of the determination of a function Φ_n is solved by deriving exact analytical expressions for the initial values $\Phi_n(r_0)$ and $\Phi_n'(r_0)$ at an arbitrary "origin" r_0, the determination of any $\Phi_n(r)$ becoming as easy as that of $\Phi_0(r)$ when e_0 is known; that of e_n becomes as easy as that of $e_1 = B_v = \langle\Phi_0 R\Phi_0\rangle$. The application of the present formulation to the model Lennard–Jones potential function allows the numerical computation of D_v, H_v, L_v, M_v, N_v, O_v, P_v, Q_v for low and high v; the CDC beyond M_v are given for the first time; higher order CDC may be reached. The results for the four lowest order constants are in good agreement with those from previously confirmed methods. Appropriate tests for all orders show that the present method provides an elegant and competitive solution to the diatomic CDC problem even for large orders and high levels (near dissociation). Similar good results are obtained for an RKR potential of the $XO_g^+-I_2$ state bounded by 109 levels.

MAHMOUD KOREK et HAFEZ KOBEISSI. Can. J. Chem. **71**, 313 (1993).

On a cherché à déterminer les constantes de distorsion de centrifugation (CDC) d'une molécule diatomique, aux ordres élevés. Lorsqu'on connait l'énergie de vibration $e_0 = E_v$ d'un niveau de vibration v, l'utilisation de la théorie des perturbations de Rayleigh–Schrödinger fournit la constante rotationnelle $e_1 = B_v = \langle\Phi_0 R\Phi_0\rangle$ (avec $R = 1/r^2$) et les CDC $e_2 = -D_v = \langle\Phi_0 R\Phi_1\rangle$, $e_3 = H_v = \langle\Phi_0 R\Phi_2\rangle$, ..., $e_n = \langle\Phi_0 R\Phi_{n-1}\rangle$, dans lesquelles $\Phi_n(r)$ est la solution de la $n^{\text{ième}}$ équation rotationnelle de Schrödinger. On a résolu le problème de la détermination d'une fonction Φ_n en dérivant les expressions analytiques exactes pour les valeurs initiales $\Phi_n(r_0)$ et $\Phi_n'(r_0)$ à une «origine» arbitraire, r_0: la détermination de chacune des $\Phi_n(r)$ devient aussi facile que celle de $\Phi_0(r)$ lorsqu'on connait e_0 et celle de e_n devient aussi facile que celle de $e_1 = B_v = \langle\Phi_0 R\Phi_0\rangle$. L'application de cette formulation à la fonction de potentiel modèle de Lennard–Jones permet de faire des calculs numériques de D_v, H_v, L_v, M_v, N_v, O_v, P_v et Q_v pour des valeurs tant élevées que basses de v. On rapporte pour la première fois des valeurs des CDC au-delà de M_v; on pourrait atteindre des ordres plus élevés. Les résultats obtenus pour les quatre constantes les plus basses sont en bon accord avec celles obtenues antérieurement avec des méthodes confirmées. Des essais appropriés effectués pour tous les ordres démontrent que la méthode rapportée ici présente une solution élégante et compétitive pour la solution du problème des CDC de molécules diatomiques, même pour des ordres et des niveaux élevés (près de la dissociation). On a aussi obtenu de bons résultats pour un potentiel RKR d'un état $XO_g^+-I_2$ délimité par 109 niveaux.

[Traduit par la rédaction]

1. Introduction

The centrifugal distortion constants (CDC) D_v, H_v, L_v, . . ., (1) are usually needed, together with the vibrational energy E_v and the rotational constant B_v, to describe the state of a diatomic molecule characterized by the vibrational quantum number v.

By using a perturbation approach, Hutson (2) elaborated an algorithm to compute the constants $e_1 = B_v$, $e_2 = -D_v$, $e_3 = H_v$, $e_4 = L_v$, $e_5 = M_v$, when v and $e_0 = E_v$ are given. These are given by the expressions:

$$[1.1] \quad e_1 = B_v = \langle\Phi_0 R\Phi_0\rangle$$

$$[1.2] \quad e_2 = -D_v = \langle\Phi_0 R\Phi_1\rangle$$

$$[1.3] \quad e_3 = H_v = \langle\Phi_1|R - e_1|\Phi_1\rangle$$

$$[1.4] \quad e_4 = L_v = \langle\Phi_1|R - e_1|\Phi_2\rangle - e_2\langle\Phi_1\Phi_1\rangle$$

$$[1.5] \quad e_5 = M_v = \langle\Phi_2|R - e_1|\Phi_2\rangle - 2e_2\langle\Phi_1\Phi_2\rangle - e_3\langle\Phi_1\Phi_1\rangle$$

where Φ_0, Φ_1, Φ_2 are the successive solutions of the equations

$$\Phi_0'' + (e_0 - U)\Phi_0 = 0$$

$$\Phi_1'' + (e_0 - U)\Phi_1 = -(e_1 - R)\Phi_0$$

$$\Phi_2'' + (e_0 - U)\Phi_2 = -(e_1 - R)\Phi_1 - e_2\Phi_0$$

with $R = 1/r^2$, r the internuclear variable, and $U(r)$ the potential characterizing the molecule in a given electronic state.

Other recent works presented improvements (3, 4), or alternatives (5, 6), over Hutson's method.

In all these works, the computed CDC were limited to $e_5 = M_v$, i.e., to "low-order" distortion constants. The main reason for this limitation is the common belief that "there is little need for the higher order CDC" (3). A second reason

[1]Author to whom correspondence may be addressed. Permanent address: Department of Physics, American University of Beirut, 850 Third Avenue, 18th Floor, New York, NY10022, U.S.A.

Can. J. Chem. Downloaded from www.nrcresearchpress.com by 88.255.202.194 on 09/08/12
For personal use only.

Can. J. Chem. Downloaded from www.nrcresearchpress.com by 88.255.202.194 on 09/08/12
For personal use only.

is that the algorithm presented by Hutson was not extended to higher orders ($e_6 = N_v$, $e_7 = O_v$, ...).

However, in a recent publication (4), Coxon noticed for some diatomic hydrides that when the dissociation limit is approached by increasing v, constants beyond $e_5 = M_v$ appear to be needed, and that "the perturbation in the wavefunction needs to be calculated to approximately fourth order to provide agreement within the experimental uncertainties" (4). In a more recent work (7), Coxon asserts: "Additional constants beyond M_v are required to describe the high rotational levels of high v. A computational algorithm for this purpose has not yet been developed".

The aim of the present work is to make use of the compact form $e_n = \langle \Phi_0 R \Phi_{n-1} \rangle$ of a CDC of any order n (Sect. 2), where Φ_n is the solution of the differential equation $\Phi_n'' + f(r)\Phi_n = s(r)$, $f(r)$ and $s(r)$ are given, as well as the initial values $\Phi_n(r_0)$ and $\Phi_n'(r_0)$ at an arbitrary origin r_0 (Sect. 3). In Sect. 4 we show that one simple routine is sufficient to compute $e_1 = B_v$, up to $e_6 = N_v$, $e_7 = O_v$, etc. Thus higher order CDC are computed as easily as their low-order counterparts.

2. Theory

Within the framework of the vibrating rotator model, the vibrational–rotational motion of the diatomic molecule is governed by the radial Schrödinger equation

$$[2] \qquad \psi_{v\lambda}'' + (E_{v\lambda} - U - \lambda R)\psi_{v\lambda} = 0$$

where $\lambda = J(J+1)$, J is the rotational quantum number, and $\lambda R(r) = \lambda / r^2$ is the rotational contribution to the potential $U(r)$ (1).

According to the Rayleigh–Schrödinger perturbation theory (8), $\lambda R(r)$ may be considered as a perturbation; $E_{v\lambda}$ and $\psi_{v\lambda}(r)$ are expanded in powers of λ,

$$[3] \qquad E_{v\lambda} = \sum_{n=0}^{\infty} e_n \lambda^n$$

$$[4] \qquad \psi_{v\lambda} = \sum_{n=0}^{\infty} \Phi_n(r) \lambda^n$$

where $\Phi_0(r)$ is the solution of the "vibrational" Schrödinger equation

$$[5] \qquad \Phi_0'' + (e_0 - U)\Phi_0 = 0$$

and $\Phi_n(r)$ are the solutions of the "rotational Schrödinger equations" (2–9):

$$[6.1] \qquad \Phi_1'' + (e_0 - U)\Phi_1 = -(e_1 - R)\Phi_0$$

$$[6.2] \qquad \Phi_2'' + (e_0 - U)\Phi_2 = -(e_1 - R)\Phi_1 - e_2\Phi_0$$

$$[6.n] \qquad \Phi_n'' + (e_0 - U)\Phi_n = -(e_1 - R)\Phi_{n-1} - \sum_{m=2}^{n} e_m \Phi_{n-m}$$

By making use of the well-known properties of $\Phi_n(r)$ (continuity at any r, boundary conditions similar to those of the vibrational wavefunction $\psi_v = \Phi_0$ (2–9)), one can derive the expressions [1] found by Hutson (2), or the expressions

$$[7.1] \qquad e_1 = \langle \Phi_0 R \Phi_0 \rangle$$

$$[7.2] \qquad e_2 = \langle \Phi_0 R \bar{\Phi}_1 \rangle - e_1 \langle \Phi_0 \bar{\Phi}_1 \rangle$$

$$[7.3] \qquad e_3 = \langle \Phi_0 R \bar{\Phi}_2 \rangle - e_1 \langle \Phi_0 \bar{\Phi}_2 \rangle - e_2 \langle \Phi_0 \bar{\Phi}_1 \rangle$$

$$[7.n] \qquad e_n = \langle \Phi_0 R \bar{\Phi}_{n-1} \rangle - \sum_{m=1}^{n-1} e_m \langle \Phi_0 \bar{\Phi}_{n-m} \rangle$$

---

as presented in a recent work (6). Φ_n and $\bar{\Phi}_n$ are both solutions of eq. [6.n], but Φ_n is, as taken by Hutson (2), orthogonal to Φ_0, while $\bar{\Phi}_n$ is free from this constraint (6).

In theory, expressions [7] differ from expressions [1] only in minor details: (*i*) eqs. [7] have a more compact form; (*ii*) up to e_5, eqs. [1] and eqs. [7] are "identical"; (*iii*) eqs. [1] give e_5 in terms of Φ_0, Φ_1, Φ_2 only, while eqs. [7] give e_5 in terms of Φ_0, $\bar{\Phi}_1$ up to $\bar{\Phi}_4$; (*iv*) eqs. [7] provide an extension to any order n (>5).

In practice, the computation of e_1–e_5 is quite different by using eqs. [7] or eqs. [1]. Details of the two algorithms are already known (2, 6), and we note here only that Hutson (2) used a matrix method to integrate eqs. [5], [6.1], and [6.2] all together, while Kobeissi *et al.* (6) repeated the same routine for eqs. [5], [6.1], [6.2], [6.3], . . . successively, till the required order.

Another approach giving more compact (and more elegant) expressions is one that requires $\bar{\Phi}_n$ orthogonal to Φ_0 ($n > 0$) in eqs. [7]; one then obtains

$$[8.1] \qquad e_1 = \langle \Phi_0 R \Phi_0 \rangle$$

$$[8.2] \qquad e_2 = \langle \Phi_0 R \bar{\Phi}_1 \rangle$$

$$[8.3] \qquad e_3 = \langle \Phi_0 R \bar{\Phi}_2 \rangle$$

$$[8.n] \qquad e_n = \langle \Phi_0 R \bar{\Phi}_{n-1} \rangle$$

The computation of e_n is here too reduced to that of $\Phi_n(r)$, i.e., to that of the numerical integration of the "rotational Schrödinger equations" [6]. These equations, as well as eq. [5], are all of the form

$$[9] \qquad y'' + f(r)y = s(r)$$

where only $s(r)$ changes from one equation to another. For given $f(r)$ ($f(r) = e_0 - U(r)$) and $s(r)$, the solution $y(r)$ is easily obtained by standard techniques, provided the initial values $y(r_0)$ and $y'(r_0)$ (at a given point r_0) are known. This "initial value" problem is treated in the next section.

3. The Φ_n initial values

We write eq. [6.n] in the form

$$[10] \qquad \Phi_n'' + f\Phi_n = s_n$$

where $f = e_0 - U$ and

$$[11] \qquad s_n = R\Phi_{n-1} - \sum_{m=1}^{n} e_m \Phi_{n-m}$$

The coefficient $f(r)$ is given, while $s_n(r)$ is deduced from the successive integration of eq. [10] with increasing values of n.

Can. J. Chem. Downloaded from www.nrcresearchpress.com by 88.255.202.194 on 09/08/12
For personal use only.

For the numerical integration of eq. [10] one may use the boundary conditions for $\Phi_n(r)$ (and for $\Phi_n'(r)$)

[12] $\Phi_n(0) = 0$

[12′] $\Phi_n(r) \to 0 \quad \text{as} \quad r \to \infty$

and proceed as follows.

We begin the integration at a starting point $r_s \sim 0$, where we take $\Phi_n(r_s) = 0$ and $\Phi'(r_s) = c$ (a small arbitrary constant). As is usual in such problems, eq. [10] is replaced by a convenient difference equation (that of Numerov (10), for example); we step on towards infinity and stop at a (final) point $r_f \sim \infty$ according to a convenient numerical criterion to detect the numerical convergence of $\Phi_n(r)$ at infinity (11).

An alternative to this simple method is one inspired by the Cooley algorithm (12) used for the vibrational eigenvalue problem. It is sufficient to start at "convenient" r_s and r_f, and to integrate simultaneously in opposite directions, till an arbitrary point r_0 ($r_s < r_0 < r_f$), where the solution $\Phi_n(r)$ is reached.

These two procedures are simple, yet they suffer from a well-known weakness (2, 3, 6, 11) described by Tellinghuisen (3) as "nuisance instabilities in the non-classical regions". These instabilities appear mainly for high v.

We already showed (6) that these instabilities are removed by using exact initial values of Φ_n at an arbitrary "origin" r_0 located in the classical region. In this previous work $\Phi_n(r_0)$ and $\Phi_n'(r_0)$ were derived for the solution $\bar{\Phi}_n(r)$ appearing in eqs. [7]. We extend this work to the present case, i.e., to the function $\Phi_n(r)$ (orthogonal to $\Phi_0(r)$) appearing in eqs. [8] adopted here for the expressions of e_n.

We multiply eq. [10] by Φ_0 and integrate between r_0 and ∞; we obtain, by making use of eq. [5],

$$\int_{r_0}^{\infty} (\Phi_n'' \Phi_0 - \Phi_n \Phi_0'') \, dr = \int_{r_0}^{\infty} s_n(r)\Phi_0(r) \, dr$$

We then make use of the boundary conditions for Φ_0 and Φ_n at $r \sim \infty$, and find

[13] $$\Phi_n'(r_0)\Phi_0(r_0) - \Phi_n(r_0)\Phi_0'(r_0) = -\int_{r_0}^{\infty} s_n(r)\,\Phi_0(r)dr$$

When $e_0 = E_v$ is given, $\Phi_0(r_0)$ and $\Phi_0'(r_0)$ are well determined by the canonical functions methods (13). Equation [13] gives the exact value of $\Phi_n'(r_0)$ for an arbitrary given value of $\Phi_n(r_0)$. Note that this expression for $\Phi_n'(r_0)$ implies the Φ_n boundary condition at infinity, and that a similar one,

[13′] $$\Phi_n'(r_0)\Phi_0(r_0) - \Phi_n(r_0)\Phi_0'(r_0) = \int_0^{r_0} s_n(r)\Phi_0(r)dr$$

implies the Φ_n boundary condition at $r = 0$. Note also that one may take $r_0 = \infty$ in eq. [13′], or $r_0 = 0$ in eq. [13], and get

[14] $$\int_0^{\infty} s_n(r)\Phi_0(r) \, dr = 0$$

Substituting for s_n from eq. [11], and taking account of the orthogonality of the functions Φ_n ($n > 0$) with Φ_0, one can verify that eq. [14] leads to eq. [8.n].

The last point in this treatment is to specify $\Phi_0(r_0)$ for the "orthogonal" $\Phi_n(r)$ (verifying the condition $\langle\Phi_0\Phi_n\rangle = 0$). This can be done by considering again a function $\bar{\Phi}_n(r)$, with an arbitrary $\bar{\Phi}_n(r_0)$, and by noticing that the "orthogonal" Φ_n is related to $\bar{\Phi}_n$ by the relation (2)

[15] $$\Phi_n(r) = \bar{\Phi}_n(r) + c_n\Phi_0(r)$$

where the condition $\langle\Phi_0\Phi_n\rangle = 0$ gives for c_n

[16] $$c_n = -\langle\Phi_0\bar{\Phi}_n\rangle$$

Thus the initial values at r_0 of the "orthogonal" Φ_n are

[17] $$\Phi_n(r_0) = \bar{\Phi}_n(r_0) - \langle\Phi_0\bar{\Phi}_n\rangle\Phi_0(r_0)$$

[18] $$\Phi_n'(r_0)\Phi_0(r_0) = \Phi_n(r_0)\Phi_0'(r_0) + \int_0^{r_0} s_n(r)\Phi_0(r) \, dr$$

Since $\bar{\Phi}_n(r_0)$ is taken arbitrarily, we may take

[19] $$\bar{\Phi}_n(r_0) = 0, \; \bar{\Phi}_n'(r_0)\Phi_0(r_0) = \int_0^{r_0} s_n(r)\Phi_0(r) \, dr$$

[19′] $$\Phi_n(r_0) = -\langle\Phi_0\bar{\Phi}_n\rangle\Phi_0(r_0)$$
$$\Phi_n'(r_0) = \bar{\Phi}_n'(r_0) - \langle\Phi_0\bar{\Phi}_n\rangle\Phi_0'(r_0)$$

4. The numerical treatment

In the previous section we adopted for the CDC e_{n+1}, the expression $e_{n+1} = \langle\Phi_0 R\Phi_n\rangle$, and showed that Φ_n is the solution of the equation $\Phi_n'' + f\Phi_n = s_n$ (f and s_n are known), orthogonal to Φ_0, and having the initial values given by eqs. [19] and [19′].

Apparently, one faces an "initial value problem" for the computation of Φ_n: it is first necessary to compute $\bar{\Phi}_n(r)$ (with $\bar{\Phi}_n(r_0) = 0$ and $\Phi_0'(r_0) = \int_0^{r_0} s_n\Phi_0 \, dr/\Phi_0(r_0)$) and then to deduce the Φ_n initial values (eq. [19′]), implying the computation of the integral $\langle\Phi_0\bar{\Phi}_n\rangle$. In fact, this preliminary work may be avoided by proceeding as follows:

The equation $\Phi_n'' + f\Phi_n = s_n$ is integrated for the "arbitrary solution" $\bar{\Phi}_n$, the integral $\langle\Phi_0\bar{\Phi}_n\rangle$ being obtained in the same run, as well as the Φ_n initial values ($\Phi_n(r_0) = -\langle\Phi_0\bar{\Phi}_n\rangle\Phi_0(r_0)$ and $\Phi_n'(r_0) = \bar{\Phi}_n'(r_0) - \langle\Phi_0\bar{\Phi}_n\rangle\Phi_0'(r_0)$).

By making use of the relation $\Phi_n = \bar{\Phi}_n - \langle\Phi_0\bar{\Phi}_n\rangle\Phi_0$, e_{n+1} becomes

[20] $$e_{n+1} = \langle\Phi_0 R\Phi_n\rangle = \langle\Phi_0 R\bar{\Phi}_n\rangle - \langle\Phi_0\bar{\Phi}_n\rangle\langle\Phi_0 R\Phi_0\rangle$$

Thus the integration of the equation $\Phi_n'' + f\Phi_n = s_n$ for the "arbitrary solution" $\bar{\Phi}_n$ allows one to find e_{n+1} along with the Φ_n initial values, these being necessary to compute s_{n+1} appearing in the next equation $\Phi_{n+1}'' + f\Phi_{n+1} = s_{n+1}$, which is used to compute e_{n+2}.

Thus the CDC e_{n+1} is given by eq. [20], in which $\bar{\Phi}_n$ is an "arbitrary" solution" of the corresponding rotational Schrödinger equation (i.e., arbitrary initial value $\bar{\Phi}_n(r_0)$). In this computation of $\bar{\Phi}_n$, the functions Φ_i ($1 \leqq i \leqq n-1$) appearing in s_n are taken orthogonal to Φ_0, i.e., the appropriate $\Phi_i(r_0)$ and $\Phi_i'(r_0)$ are used.

According to this outline, and once $e_0 = E_v$ is given, the description of the computation of e_1, e_2, . . . may be presented as follows:

(*i*) The initial values $\Phi_0(r_0)$ and $\Phi_0'(r_0)$ (then $\Phi_0(r)$) can be obtained by using the "canonical functions" method as out-

TABLE 1. Centrifugal distortion constants of the first four orders for several vibrational levels of the model Lennard–Jones potential (all values in units of the well depth)

v	$-D_v \times 10^9$	$-H_v \times 10^{14}$	$-L_v \times 10^{19}$	$-M_v \times 10^{28}$
0	0.293 427 036 531	0.350 081 726 148	0.768 573 442 866	0.218 222 652 746
4	0.461 820 586 952	0.937 419 238 719	3.439 462 930 74	1.611 203 623 60
8	0.758 781 432 793	2.631 149 075 07	1.611 893 748 92 × 10	1.253 417 382 49 × 10
12	1.332 167 809 01	8.535 332 031 30	9.711 506 965 04 × 10	1.419 072 325 10 × 10^2
16	2.639 382 159 57	3.873 947 520 89 × 10	1.063 247 668 23 × 10^3	3.837 893 425 16 × 10^3
20	7.253 570 427 91	4.822 355 269 33 × 10^2	6.693 290 386 49 × 10^4	1.253 738 312 03 × 10^5

TABLE 2. Centrifugal distortion constants of higher orders for several vibrational levels of the model Lennard–Jones potential (all values in units of the well depth)

v	$-N_v \times 10^{28}$	$-O_v \times 10^{32}$	$-P_v \times 10^{37}$	$-Q_v \times 10^{41}$
0	0.716 515 556 158	0.258 514 024 713	0.996 757 231 458	0.403 829 915 430
4	8.644 767 929 83	5.058 989 808 61	3.147 734 643 35 × 10	2.048 801 324 80 × 10
8	1.116 007 632 17 × 10^2	1.085 638 731 63 × 10^2	1.124 616 304 69 × 10^3	1.221 261 410 67 × 10^3
12	2.395 046 716 83 × 10^3	4.441 850 054 08 × 10^4	8.806 477 480 96 × 10^4	1.835 170 045 79 × 10^5
16	1.616 730 613 45 × 10^5	7.524 620 646 92 × 10^5	3.757 236 100 64 × 10^7	1.977 686 157 36 × 10^8
20	2.775 814 771 71 × 10^8	6.857 389 476 02 × 10^9	1.832 554 539 57 × 10^{12}	5.198 203 544 83 × 10^{13}

TABLE 3. Centrifugal distortion constants of the first four orders for several vibrational levels of the RKR potential of the state XO_g^+–I_2 (all values in units of the well depth)

v	D_v	H_v	L_v	M_v
20	5.262 614 210 03 (−9)	−1.232 656 298 95 (−15)	−1.001 915 610 26 (−21)	−1.092 301 921 93 (−27)
40	6.988 956 048 61 (−9)	−3.840 311 112 04 (−15)	−5.348 249 498 18 (−21)	−9.201 400 705 70 (−27)
60	1.225 901 378 84 (−8)	−1.708 776 106 39 (−14)	−4.551 606 019 76 (−20)	−1.531 671 836 15 (−25)
80	3.178 259 108 37 (−8)	−2.445 063 620 10 (−13)	−4.386 243 931 30 (−19)	3.292 383 896 65 (−22)
100	1.233 522 760 80 (−7)	−3.957 501 848 15 (−12)	2.586 418 372 00 (−16)	3.102 547 370 16 (−20)

Can. J. Chem. Downloaded from www.nrcresearchpress.com by 88.255.202.194 on 09/08/12
For personal use only.

lined in the appendix of ref. 6. The rotational constant $e_1 = \langle\Phi_0 R\Phi_0\rangle$ is deduced, as well as the $\bar{\Phi}_1(r)$ initial values, i.e., $\Phi_1(r_0) = 0$, $\bar{\Phi}_1'(r_0) = \int_0^{r_0} s_1(r)\Phi_0(r)\,dr/\Phi_0(r_0)$ (eq. [19]) with $s_1(r) = (R - e_1)\Phi_0$.

(*ii*) The initial values $\bar{\Phi}_1(r_0)$ and $\bar{\Phi}_1'(r_0)$ being in hand, $\bar{\Phi}_1(r)$ is deduced from eq. [6.1], as well as $c_1 = -\langle\Phi_0\bar{\Phi}_1\rangle$, $e_2 = \langle\Phi_0 R\Phi_1\rangle + c_1 e_1$, $\Phi_1(r) = c_1\Phi_0(r_0)$, $\Phi_0'(r_0) = \bar{\Phi}_1'(r_0) + c_1\Phi_1'(r_0)$ (eq. [19′]), $\Phi_2'(r_0) = \int_0^{r_0} s_2(r)\Phi_0(r)\,dr/\Phi_0(r_0)$, and $\Phi_2(r_0) = 0$ with $s_2(r) = (R - e_1)\Phi_1 - e_2\Phi_0$. Note that, in s_2, Φ_1 is the "orthogonal function".

(*iii*) As in (*ii*), the initial values $\bar{\Phi}_2(r_0)$ and $\bar{\Phi}_2'(r)$ allow the computation of $\Phi_2(r)$ (eq. [6.2]), $c_2 = -\langle\Phi_0\bar{\Phi}_2\rangle$ and $e_3 = \langle\Phi_0 R\bar{\Phi}_2\rangle + c_2 e_2$, $\Phi_2(r_0) = c_2\Phi_0(r_0)$, $\Phi_2'(r_0) = \bar{\Phi}_2'(r) + c_2\Phi_0'(r_0)$, $\bar{\Phi}_3(r_0) = 0$, $\Phi_3'(r_0)\int_0^{r_0} s_3(r)\Phi_0(r)\,dr/\Phi_0(r_0)$.

(*iv*) . . . and so on . . .

According to this procedure the computation of one CDC requires: (*i*) the integration of one linear second-order differential equation (with given coefficients and given initial values); (*ii*) the computation of simple integrals of the types $\int_0^{r_0}\Phi_n\Phi_0\,dr$, $\int_0^{r_0}\Phi_n R\Phi_0\,dr$ (used for the $\bar{\Phi}_{n+1}$ initial values).

We deduce that one simple routine is needed: the numerical integration of the equation $y'' + fy = s$, and the numerical computation of simple integrals of the form $I = \int_0^a y(r)g(r)\,dr$ ($a = r_0$, or ∞, $g(r)$ stands for Φ_0 or $R\Phi_0$). This routine is repeated when the order n of e_n increases, and is exactly the same for low or for higher orders.

The method was tested for the commonly used Lennard–Jones model potential and for the Rydberg–Klein–Rees (RKR) potential of the XO state of I_2. In Table 1 we give the low order CDC ($e_2 = -D_v$, $e_3 = H_v$, $e_4 = L_v$, $e_5 = M_v$) for the Lennard–Jones potential; these values have been computed previously (2, 3, 5, 6). In Table 2 we give the higher order CDC ($e_6 = N_v$, $e_7 = O_v$, $e_8 = P_v$, $e_9 = Q_v$), which are reported here for the first time. Similarly Tables 3 and 4 are presented for the XO–I_2 potential constructed by Martin *et al.* (15). The results of Table 3 may be compared to other previous results (14, 15), whereas those in Table 4 are new.

5. Discussion

By comparing the results of Table 1 with those of our previous work (6), we find an agreement to seven significant figures or better; the same result holds in the comparison of the results of Table 3 with those of ref. 14. The previous results were critically tested and showed high accuracy (6, 14). We consider this agreement as a confirmation of the validity of the results of Tables 1 and 3.

Since the results in Tables 2 and 4 are published here for the first time, no comparison with other results is available. However, we may assume that the higher order CDC of Tables 2 and 4 are as accurate as the low-order CDC of Tables 1 and 3, since they are obtained by using the same routine and the same highly accurate numerical techniques (the details may be found in ref. 6).

Moreover we applied the "continuity test" to all the CDC computed here (for the Lennard–Jones potential). This is, for e_1, for example,

TABLE 4. Centrifugal distortion constants of higher orders for several vibrational levels of the RKR potential of the state XO_g^+–I_2 (all values in units of the well depth)

v	N_v	O_v	P_v	Q_v
20	−5.104 619 726 62 (−33)	3.104 062 819 07 (−38)	4.723 897 554 11 (−43)	−3.585 650 211 75 (−48)
40	−5.722 594 992 64 (−32)	3.554 567 287 71 (−38)	1.139 000 860 12 (−41)	−2.062 543 842 27 (−47)
60	−4.377 499 600 90 (−31)	−3.632 249 814 09 (−35)	3.378 373 565 07 (−38)	−2.865 586 898 48 (−41)
80	1.237 781 528 38 (−26)	−7.698 483 261 27 (−32)	2.083 773 893 68 (−35)	−6.930 778 711 89 (−40)
100	−1.606 589 564 09 (−23)	−1.171 978 621 06 (−27)	3.309 698 188 99 (−31)	1.385 915 544 00 (−35)

TABLE 5. Variation of the "continuity index" $\Delta_n = f(e_n)$ when the parameter e_n takes the values $e_n = e_n^* + kh_n$, where e_n^* is the computed CDC given in Tables 1 and 2; $k = 0, \pm1, \pm2$; h_n is an arbitrary step-size. The values are given for $v = 12$. All values are dimensionless.

n	$e_n^* - 2h_n$	$e_n^* - h_n$	e_n^*	$e_n^* + h_n$	$e_n^* + 2h_n$	h_n
2	−5.21(−12)[a]	−2.60(−12)	−1.15(−15)	2.60(−12)	5.21(−12)	10^{20}
3	−5.65(−13)	−2.82(−13)	6.96(−16)	2.83(−13)	5.66(−13)	10^{23}
4	6.22(−14)	3.13(−14)	3.72(−16)	−3.05(−14)	−6.14(−14)	10^{27}
5	−6.77(−13)	−3.39(−13)	−7.85(−16)	3.37(−13)	6.74(−13)	10^{30}
6	7.27(−14)	3.61(−14)	−8.45(−16)	−3.80(−14)	−7.50(−14)	10^{34}
7	−8.02(−14)	−3.98(−14)	3.38(−16)	4.07(−14)	8.09(−14)	10^{36}
8	8.83(−14)	4.44(−14)	−7.21(−16)	−4.33(−14)	−8.72(−14)	10^{40}
9	−9.61(−14)	−4.82(−14)	−2.55(−16)	4.76(−14)	9.55(−14)	10^{43}

[a]Number between parentheses stands for a multiplicative power of 10.

$$\Delta_1(e_1) = (l_1^+ - l_1^-)/(l_1^+ + l_1^-)$$

where, according to eqs. [13] and [13′]

$$l_1^+ = \left[\Phi_1(r_0) - \int_{r_0}^{\infty} s_1(r)\Phi_0(r)\,dr\right] \Big/ \Phi_0(r_0) = \Phi_1'(r_0)|_{r>r_0}$$

$$l_1^- = \left[\Phi_1(r_0) + \int_{0}^{r_0} s_1(r)\Phi_0(r)\,dr\right] \Big/ \Phi_0(r_0) = \Phi_1'(r_0)|_{r<r_0}$$

with $s_1(r) = (R - e_1)\Phi_0(r)$. We know that $l_1^+ = l_1^-$ only when e_1 is the "exact" constant, say e_1^*, otherwise $l_1^+ \neq l_1^-$ and $\Delta_1(e_1) \neq 0$. Thus the quantity $\Delta_1(e_1)$ is an index measuring the "numerical" continuity (or discontinuity) of the function $\Phi_1(r)$ at r_0.

In Table 5 we give the results of the "continuity test" (for $v = 12$, for example) for all the CDC given in Table 1 (low order) and in Table 2 (high order). The index $\Delta_n(e_n)$ is computed for several values of e_n given by: $e_n = e_n^* + kh_n$, where e_n^* is the computed CDC (Tables 1 or 2), k is an integer (positive or negative), h_n is a convenient step.

The results of Table 5 show that for all values of n, the computed CDC, e_n^*, gives the "best" continuity index Δ_n, i.e., that closest to zero. This provides strong evidence for our assumption that the higher-order CDC are as accurate as the low-order values.

6. Conclusion

The problem of the determination of the diatomic centrifugal distortion constants for large orders was considered.

By using a non-conventional version of perturbation theory, we see that the CDC given by the expression $e_n = \langle\Phi_0 R \Phi_{n-1}\rangle$ is easily computed, for any order n, by using a simple method for the computation of the functions Φ_n, as successive solutions of the "rotational Schrödinger equations". This is done by taking Φ_n orthogonal to Φ_0 (the vibrational wavefunction), and by deriving exact values of $\Phi_n(r_0)$ and $\Phi_n'(r_0)$, the initial values of Φ_n at an arbitrary point r_0.

The numerical application of the present method to the model Lennard–Jones potential allowed us to obtain the same CDC for low orders (D_v, H_v, L_v, M_v) as already calculated by other methods, as well as for large orders (N_v, O_v, P_v, Q_v) given here for the first time. We believe that larger order CDC may be obtained, if needed, in the same manner. A similar application to the RKR potential of the XO_g^+ state of I_2 is presented for several vibrational levels up to dissociation.

1. G. Herzberg. Spectra of diatomic molecules. Van Nostrand, Toronto. 1950.
2. J. Hutson. J. Phys. B: At. Mol. Phys. **14**, 851 (1981).
3. J. Tellinghuisen. J. Mol. Spectrosc. **122**, 455 (1987).
4. J. A. Coxon and P. G. Hajigeorgiou. J. Mol. Spectrosc. **139**, 84 (1990).
5. P. Pajunen. J. Mol. Spectrosc. **124**, 185 (1987).
6. H. Kobeissi, M. Korek, and M. Dagher. J. Mol. Spectrosc. **138**, 1 (1989).
7. J. A. Coxon and P. G. Hajigeorgiou. J. Mol. Spectrosc. **142**, 254 (1990).
8. A. Messiah. Mécanique Quantique. Vol. II. Dunod, Paris. 1972.
9. H. Kobeissi. J. Phys. Lett. **42**, L215 (1981).
10. B. Numerov. Publ. Obs. Cent. Astrophys. Russ. **2**, 188 (1933).
11. H. Kobeissi, A. El-Hajj, and M. Kobrosi. J. Comput. Phys. **96**, 470 (1991).
12. J. W. Cooley. Math. Comput. **15**, 363 (1961).
13. H. Kobeissi. J. Phys. B: At. Mol. Phys. **15**, 693 (1982).
14. M. Korek and H. Kobeissi. J. Mol. Spectrosc. **145**, 448 (1991).
15. F. Martin, R. Bacis, S. Churassy, and J. Vergès. J. Mol. Spectrosc. **116**, 71 (1986).

Can. J. Chem. Downloaded from www.nrcresearchpress.com by 88.255.202.194 on 09/08/12
For personal use only.

Charge transfer complexes of Schiff bases derived from 2-aminobenzothiazole with some acidic and nonacidic acceptors

AMANY M. A. IBRAHIM
Department of Chemistry, Faculty of Science, University of Ain Shams, Cairo, Egypt

Received September 18, 1992

AMANY M. A. IBRAHIM. Can. J. Chem. **71**, 318 (1993).

When Schiff bases derived from 2-aminobenzothiazole were reacted with di- and trinitrobenzene derivatives as acidic and nonacidic acceptors in the ratio of 1:1, stable coloured charge transfer complexes (CTC's) were obtained. The structure and stoichiometry of the CTC's were studied by elemental analysis as well as by electronic absorption and infrared and nuclear magnetic resonance spectra. The CTC's derived from nonacidic acceptors were stabilized via intermolecular $\pi-\pi^*$ and $n-\pi^*$ transitions while those derived from acidic acceptors were formed by intermolecular $\pi-\pi^*$ transitions and a proton transfer stabilized by resonance. The ionization potentials of the Schiff bases and the electron affinities of the nitrobenzene derivatives were calculated.

AMANY M. A. IBRAHIM. Can. J. Chem. **71**, 318 (1993).

Lorsqu'on fait réagir des bases de Schiff du 2-aminobenzothiazole avec une mole de dérivés du di- et du trinitrobenzène agissant comme accepteurs acides et non acides, on obtient des CTC's colorés stables. On a étudié la structure et la stoechiométrie des CTC's par le biais d'analyses élémentaires ainsi que par leurs spectres infrarouge, résonance magnétique nucléaire et d'absorption électronique. Les CTC's dérivés d'accepteurs non acides sont stabilisés par des transitions intermoléculaires $\pi-\pi^*$ et $n-\pi^*$ alors que ceux dérivés des accepteurs acides se forment par des transitions intermoléculaires $\pi-\pi^*$ et un transfert de proton stabilisé par résonance. On a calculé les potentiels d'ionisation des bases de Schiff et les affinités électroniques des dérivés du nitrobenzène.

[Traduit par la rédaction]

Introduction

A lot of interest in molecular charge transfer complexes (CTC's) has stemmed from their technological potential. The most important applications of charge transfer complexes are the adsorption of electron acceptors on metal oxides to characterize the electron donor properties of these metal oxides (1–3), their use in current-controlled electrically switched memory (4, 5), the determination of critical micelle concentrations (6), their use as conducting single crystals in the microcircuitry of electronic devices (7, 8), as components of solar cells (9) and in the printing industry (10), and in applications making use of their high electrical conductivity (11, 12).

The present work is devoted to the study of CTC's of Schiff bases derived from 2-aminobenzothiazole with some di- and trinitrobenzene derivatives. The choice of Schiff bases as donors was mainly because they contain the azomethine group, the same group that occurs in rhodopsin, the visual pigment extracted from rod cells (13), while pyridoxal forms Schiff bases with various amino compounds found in the cell, including natural substrates of many B_6 enzymes (14). The CTC's of aromatic nitro compounds have been studied with various aromatic donor compounds (15–18), while few studies have been concerned with CTC's of benzylidene derivatives (19, 20). On the other hand, the behaviour of Schiff bases as donors towards acceptors other than the aromatic nitro compounds was the subject of several investigations (21–23). This study was also extended to investigate the stoichiometry and the structure of the molecular complexes and to identify the types of bonding contributing to their formation.

Experimental

Reagents and preparation of Schiff bases

The Schiff bases (**I–IX**) having the general structure:

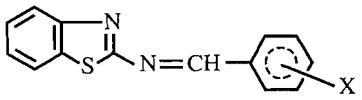

where X = H (**I**), *p*-$N(CH_3)_2$ (**II**), *p*-OCH_3 (**III**), *p*-OH (**IV**), *o*-OH (**V**), *p*-Cl (**VI**), *m*-Cl (**VII**), *p*-Br (**VIII**), and *p*-NO_2 (**IX**), were prepared using the method described by Vogel (24). The products were recrystallized several times from ethanol and dried under vacuum. Their purity was checked by thin-layer chromatography, elemental analysis, ir spectra, and melting points, Table 1.

The acceptors used in the present investigation are 1,3-dinitrobenzene (**1**), 3,4-dinitrotoluene (**2**), 2,4-dinitrophenol (**3**), 3,4-dinitrobenzoic acid (**4**), 3,5-dinitrobenzoic acid (**5**), 3,5-dinitrosalicylic acid (**6**), picric acid (**7**), and trinitrobenzene (**8**). Unless otherwise stated, all the chemicals and solvents used in this investigation were of the purest grade and purchased from either BDH (England) or Aldrich Chemical Company, Inc. (U.S.A.).

Preparation of the CTC's

The CTC's were prepared by mixing a saturated solution of Schiff base (0.01 mol dm^{-3} in ethanol) with a similar solution of the acceptor at 40°C. The solid CTC's were separated at once or after cooling and then filtered off and recrystallized from ethanol. Insoluble CTC's were purified by heating them with ethanol several times to remove any contaminants. The complexes were filtered off, dried in vacuum, and preserved in closed tubes over $CaCl_2$. The purity and stoichiometry of the CTC's were checked by thin-layer chromatography, mp (95–205°C), colour (yellow, greenish yellow, orange, brown, or reddish brown), elemental analysis (C,H,N, and S content), and ir and nmr spectra. The data revealed that the Schiff bases (**I–IX**) give mainly 1:1 CTC's with di- and trinitrobenzene derivatives (**1–8**), Table 2.

Instruments

The working procedure and instruments used for electronic absorption, and for the ir and ^1H nmr spectra were as described previously (15). The electronic absorption and ir spectra were measured in Nujol mulls and as KBr discs, respectively. The ^1H nmr spectra were obtained using DMSO-d_6 as solvent and TMS as internal standard.

Can. J. Chem. Downloaded from www.nrcresearchpress.com by 88.255.202.194 on 09/08/12
For personal use only.

TABLE 1. Colour, melting point, elemental analysis, and some of the ir bands of Schiff bases (**I–IX**)

Schiff base no.	Colour	Melting point (°C)	Elemental analysis calcd./found (%)				Infrared bands (cm^{-1})	
			C	H	N	S	$\nu_{C=N}$	$\gamma_{CH=N}$
I	Buff	122	70.38 70.10	4.22 4.34	11.75 11.82	13.87 13.50	1643	1005
II	Orange	162	68.15 67.90	5.36 5.20	14.90 14.30	11.58 11.50	1650	1010
III	Pale yellow	200	66.99 66.78	4.49 4.42	10.42 10.38	12.14 12.00	1646	1010
IV	Yellow	215	65.96 65.40	3.95 4.10	10.98 10.80	12.81 12.90	1648	1008
V	Orange	145	65.96 66.70	3.95 4.00	10.98 10.90	12.81 12.30	1645	995
VI	Buff	132	61.51 61.50	3.32 3.80	10.25 10.30	11.95 12.10	1628	1000
VII	Orange	110	61.51 60.90	3.32 3.50	10.25 10.38	11.95 12.00	1640	1005
VIII	Orange	190	52.91 52.60	2.85 2.80	8.81 8.60	10.27 10.35	1640	996
IX	Yellow	219	59.23 59.00	3.19 3.30	14.80 14.50	11.50 11.50	1638	992

Can. J. Chem. Downloaded from www.nrcresearchpress.com by 88.255.202.194 on 09/08/12
For personal use only.

Results and discussion

Electronic absorption spectra

The electronic absorption spectra of the CTC's include, in addition to the absorption bands of the Schiff bases and nitrobenzene derivatives, one more band in the case of CTC's derived from acidic acceptors (**3–7**) and two more bands for CTC's derived from nonacidic acceptors (**1**, **2**, and **8**), Fig. 1 and Tables 3 and 4. The first band displays relatively high absorbance and appears as a broad shoulder at 340–460 nm, interacting with the long wavelength band of the Schiff base, which suffers a blue shift on complex formation. The second band observed in the spectra of CTC's derived from nonacidic acceptors appears as a very shallow broad absorption at 420–470 nm and disappears on adding few drops of HCl, Fig. 1. The two bands belong to intermolecular CT of the $\pi-\pi^*$ and $n-\pi^*$ type transitions, respectively.

The spectra reveal a blue shift for the long wavelength band of the Schiff bases at 340–415 nm due to $\pi-\pi^*$ intramolecular CT within the benzylidine moiety (25) and a red shift for the ^1L_a and ^1L_b bands of the nitrobenzene derivatives (26). Thus, the nonacidic acceptors interact with Schiff bases **I–IX** through $\pi-\pi^*$ transitions from the HOMO of the benzal ring to the LUMO of the nitrobenzene molecule, in addition to $n-\pi^*$ transitions from the nitrogen atom of the azomethine group or of the $-N(CH_3)_2$ group in the case of Schiff base **II**. Donation from the benzal ring rather than the benzothiazole moiety is supported by the linear free energy relationship (LFER) between λ_{CT} ($\pi-\pi^*$) and Hammett σ-constants, Fig. 2. The magnitude of the shift to longer wavelength is larger in the case of electron-donating substituents than in the case of electron-acceptor substituents, while with λ_{CT} ($n-\pi^*$) a straight line is observed.

π-Donation from the benzal ring is further supported by calculating the ionization potential of the HOMO of the Schiff bases using the equation given by Briegleb (27):

$$[1] \quad I_p = 5.11 + 0.701\, h\nu_D$$

where $h\nu_D$ is the energy of the band at 340–415 nm of the Schiff bases. This band suffers a red shift on increasing the electron-donating or -accepting character of the substituent, Fig. 2. The ionization potential values of Schiff bases, Table 3, are lower than those of benzothiazole (8.58 eV), 2-aminobenzothiazole (8.64 eV) (15), or thiazole and 2-aminothiazole (9.50 and 8.45 eV, respectively) (28). Also, for one and the same donor, the variation of λ_{CT} ($\pi-\pi^*$) with the electron affinity values of di- and trinitrobenzene derivatives, Table 4, is given by broken or straight lines with positive slopes, Fig. 3. These electron affinity values were calculated using eq. [2]:

$$[2] \quad h\nu_1 - h\nu_2 = E_{A_2} - E_{A_1}$$

where $h\nu_1$ and $h\nu_2$ are the energies of the two acceptors **1** and **2** having electron affinities E_{A_1} and E_{A_2}, respectively (27), and using the reported available E_A values of acceptors **1**, **2**, and **8** (27, 29). The broken lines indicate that there are other factors, in addition to the conventional factors, affecting the stability of the CTC's. In this case, they are mainly proton transfer from the acidic acceptors to the basic center of the Schiff bases and the symmetry properties that affect the molecular orientations of the acceptor and the donor to form segregated or mixed stakes (30).

The calculated values of the energy of the CT band, using the relation given by Briegleb *et al.* (31),

$$[3] \quad E_{CT} = I_p - E_A + C_1 + \frac{C_2}{I_p - E_A + C_1}$$

TABLE 2. Colour, melting point, and elemental analysis of some CTC

CTC	Colour	Melting point (°C)	Elemental analysis calcd./found (%) C	H	N	S	CTC	Colour	Melting point (°C)	Elemental analysis calcd./found (%) C	H	N	S
$\mathbf{I}_1$	Orange	108	59.84 59.40	3.51 3.38	13.95 14.50	7.98 8.40	V_2	Yellow	130	58.46 59.00	3.73 4.00	12.98 12.50	7.43 8.60
$\mathbf{I}_3$	Yellow	155	57.55 56.90	3.80 3.16	13.42 13.90	7.68 8.00	V_4	Canary Yellow	171	54.66 54.90	3.05 3.60	12.14 11.80	6.94 7.40
$\mathbf{I}_5$	Pale yellow	132	56.63 57.10	3.60 4.11	12.58 12.90	7.19 7.30	V_6	Greenish yellow	118	52.83 52.20	2.95 3.40	11.73 11.80	6.71 6.80
$\mathbf{II}_3$	Yellow	109	56.76 56.50	4.2 3.88	15.04 14.90	6.88 7.10	VI_1	Orange	166	55.12 55.20	3.00 3.10	12.85 13.00	7.35 7.80
$\mathbf{II}_5$	Buff	184	55.97 55.90	3.88 3.80	14.19 14.40	6.49 7.20	VI_8	Reddish brown	101	49.96 50.80	2.93 3.50	14.56 14.20	6.66 6.30
$\mathbf{II}_6$	Reddish brown	205	54.22 54.80	3.75 3.90	13.74 13.20	6.29 6.40	VII_6	Reddish brown	128	50.87 50.10	3.04 4.00	11.29 12.20	6.46 6.80
$\mathbf{II}_7$	Yellow	106	51.76 51.50	3.55 3.80	16.46 16.30	6.28 6.60	VII_7	Yellow	98	48.35 49.80	2.84 3.20	14.09 14.60	6.45 6.70
$\mathbf{III}_2$	Greenish yellow	121	59.32 58.20	4.07 4.90	12.57 13.10	7.19 7.90	$VIII_1$	Red	156	50.01 50.40	2.73 3.10	11.66 11.30	6.67 6.60
$\mathbf{III}_4$	Yellow	106	55.58 56.10	3.39 3.70	11.78 11.90	6.74 6.80	$VIII_3$	Yellow	134	48.40 48.50	2.64 2.90	11.28 11.40	6.45 6.90
$\mathbf{III}_8$	Brown	95	52.94 53.00	3.17 3.90	14.70 14.50	6.72 6.80	$VIII_5$	Buff	123	48.10 47.90	2.49 2.70	10.68 10.50	6.11 6.00
$\mathbf{IV}_1$	Orange	160	57.55 57.70	3.39 3.70	13.42 13.20	7.68 7.80	IX_1	Golden yellow	137	53.81 52.50	3.38 3.80	15.68 16.20	7.18 7.70
$\mathbf{IV}_3$	Golden yellow	148	58.20 58.00	3.25 4.00	12.92 12.70	7.39 7.70	IX_3	Orange	111	51.95 51.80	2.83 3.80	15.14 15.10	6.93 6.20
$\mathbf{IV}_7$	Canary yellow	122	50.21 50.70	2.73 3.80	14.64 14.30	6.70 7.10	IX_5	Yellow	141	51.43 50.90	2.67 3.20	14.28 14.00	6.53 6.80
$\mathbf{V}_1$	Yellow	128	57.55 58.10	3.38 3.90	13.42 13.40	7.68 7.70	IX_7	Greenish yellow	103	47.34 47.40	2.38 3.00	16.56 16.50	6.31 6.50

where C_1 and C_2 are constants for a given acceptor (27, 31), are equal to (2.70–3.85 eV) and in good agreement with the experimental values (2.69–3.65 eV), thus supporting the intermolecular CT nature of the first band.

On the other hand, the acidic acceptors interact with Schiff bases through π–π^* transitions, as indicated by the presence of the intermolecular CT band. The absence of the band due to n–π^* transitions reveals that the n–π^* interaction is absent due to blocking of the lone pair of electrons on the nitrogen atom by the proton transferred from the hydroxy or the carboxy group to the basic centre of the Schiff base.

The structure of the CTC's, the infrared and nuclear magnetic resonance spectra

The characteristic ir bands of Schiff bases due to $\nu_{C=N}$ at 1650–1638 cm^{-1}, $\nu_{CH=N}$ and $\gamma_{CH=N}$ at 3030 and 1010 cm^{-1}, respectively, and ν_{C-N} at 1250 cm^{-1} exhibit shifts to lower frequencies on CTC formation. Also, the ν_{asym} of the NO_2 group of acceptors appearing as a group of bands at 1550, 1540, and 1530 cm^{-1} and the ν_{sym} NO_2 band at 1340–1350 cm^{-1} are shifted to lower frequencies due to the increased polarization of the nitro group. On the other hand, the ν_{CH} and γ_{CH} of the acceptors are shifted to higher frequencies, supporting the intermolecular π–π^* interaction between the Schiff bases as donors and the nitrobenzene derivatives as acceptors. This is further supported by the ^1H nmr spectra of the CTC's, Table 5, which show that the resonances due to the Schiff base moieties are shifted downfield, whereas the resonances due to the acceptors are moved to a higher field. The indication from the electronic spectra that the π-donation comes from the benzal ring rather than the benzothiazole moiety is also confirmed by the large magnitude of the shift of the ν_{CH} and γ_{CH} ir bands, as well as the nmr signals around 7.30 ppm of the benzal ring of the CTC's relative to those of the Schiff bases, compared to those of the benzothiazole moiety.

In the case of nonacidic acceptors, the n–π^* transitions play an important role, in addition to the intermolecular π–π^* transitions, for stabilizing the CTC's. A large shift to lower frequencies was observed for the $\nu_{CH=N}$ and $\nu_{C=N}$ ir bands of CTC's (from 3030 to 3010 cm^{-1} and from 1650–1638 to 1640–1625 cm^{-1}, respectively) relative to those of the Schiff bases. Also, the proton chemical shifts of the azomethine group at 9.65–10.45 ppm, which vary linearly with the Hammett σ-constants, Fig. 2, suffer a downfield shift in the nmr spectra of the CTC's, Table 5. This indicates the participation of the lone pair of electrons of the azomethine group

Can. J. Chem. Downloaded from www.nrcresearchpress.com by 88.255.202.194 on 09/08/12
For personal use only.

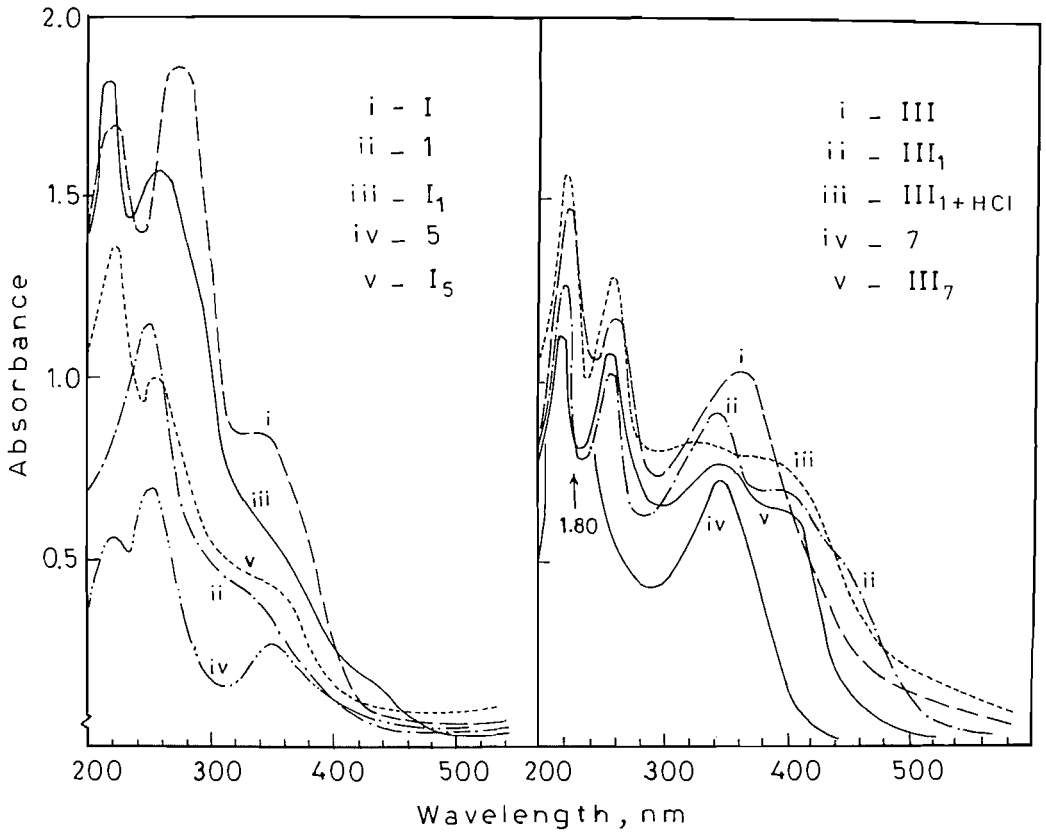

FIG. 1. The electronic absorption spectra of Schiff bases **I** and **III**, acceptors **1**, **5**, and **7**, and their CTC's $\mathbf{I_1}$, $\mathbf{I_5}$, $\mathbf{III_1}$, and $\mathbf{III_7}$, in Nujol mull.

TABLE 3. The ionization potential values of Schiff bases (SB) and the CT bands of some CTC's

SB no.	π–π^* Transition of SB			λ_{max}(nm) of CTC derived from acceptors **1**		**3**	**7**
	λ_{max}(nm)	E (eV)	I_p (eV)	π–π^*	n–π^*	π–π^*	π–π^*
I	340	3.65	7.66	360	440	365	380
II	415	2.99	7.21	420	470	425	430
III	365	3.40	7.49	400	455	385	395
IV	360	3.44	7.52	360	450	370	385
V	380	3.26	7.39	390	448	373	390
VI	350	3.54	7.59	360	435	360	372
VII	355	3.49	7.55	365	438	363	380
VIII	348	3.56	7.61	355	440	365	376
IX	370	3.35	7.45	360	410	360	368

TABLE 4. The electron affinity values of the di- and trinitrobenzene derivatives (**1**–**8**) and CTC bands of some CTC's

Acceptor no.	λ_{max}(nm) of acceptors $^1L_b \leftarrow {}^1A$	E_A (eV)	λ_{max}(nm) of CTC's derived from SB's **I**	**II**	**V**	**VIII**
1	344	1.30 ± 0.06	360,440	420,470	390,448	355,440
2	340	1.09 ± 0.05	350,430	430,440	375,420	360,445
3	350	1.15 ± 0.05	365	425	370	365
4	300	1.00 ± 0.06	340	450	360	383
5	350	0.81 ± 0.07	360	460	350	375
6	320	1.23 ± 0.06	365	418	380	350
7	350	1.50 ± 0.06	380	430	390	376
8	340	1.77 ± 0.06	395,440	450,470	405,435	400,450

Can. J. Chem. Downloaded from www.nrcresearchpress.com by 88.255.202.194 on 09/08/12
For personal use only.

Can. J. Chem. Downloaded from www.nrcresearchpress.com by 88.255.202.194 on 09/08/12
For personal use only.

TABLE 5. The ^{1}H nmr data (δ, ppm) of the Schiff bases, di- and trinitrobenzene derivatives (**1–8**),[a] and some CTC's

CTC	SB moiety	Acceptor moiety
SBI	10.10(s),8.05(m),7.25(m)	
I_2	10.23(s),8.10(m),7.35(m)	7.90(m),2.50(s)
I_6	10.30(s),8.15(m),7.38(m),5.70(bs)	9.40(s),8.65(d)
SB_{II}	9.70(s),7.85(m),6.90(m),3.00(s)	
II_1	9.80(s),7.90(m),7.15(m),3.25(s)	8.65(m),7.85(dd)
II_3	9.75(s),7.90(m),7.20(m),6.00(bs),3.15(s)	10.45(s),8.70(d),8.35(dd),7.35(dd)
II_7	9.80(s),7.95(m),7.35(m),5.50(b),3.20(s)	8.60(s)
SB III	9.95(s),7.90(m),7.10(m)	
III_2	10.05(s),8.15(m),7.30(m)	7.95(m),2.45(s)
III_6	10.10(s),8.10(m),7.30(m),6.00(bs)	9.45(s),8.73(d)
SB IV	10.00(s),8.9(bs),8.10(m),7.20(m)	
IV_1	10.20(s),10.10(s),8.10(m),7.4(m)	8.70(m),7.90(dd)
IV_3	10.20(s),8.00(m),7.35(m),6.5(bs)	8.70(d),8.30(dd),7.30(dd)
IV_5	10.20(s),8.50(bs),8.15(m),7.30(m)	9.90(b),9.10(d),9.00(d)
IV_7	10.40(s),8.20(m),7.50(m),6.00(bs)	8.65(s)
SB V	10.65(s),9.65(s),7.90(m),7.15(m)	
V_1	10.60(s),9.75(s),8.00(m),7.40(m)	8.70(m),7.90(dd)
V_3	9.70(s),7.95(m),7.85(bs),7.35(m)	10.40(s),8.72(d),8.35(dd)
V_7	9.80(s),9.60(bs),7.90(m),7.50(m)	8.65(s)
SB VI	10.25(s),7.80(m),7.20(m)	
VI_1	10.30(s),8.0(m),7.60(m)	8.68(m),7.85(dd)
SB VII	10.30(s),7.90(m),7.30(m)	
VII_5	10.45(s),9.40(bs),7.92(m),7.5(m)	11.25(s),9.00(dd),8.80(dd)
SB VIII	10.17(s),7.85(m),7.25(m)	
$VIII_1$	10.20(s),8.00(m),7.55(m)	8.65(m),7.90(dd)
$VIII_3$	10.25(s),7.95(m),7.45(m),5.60(bs)	10.65(s),8.75(m),8.40(dd)
$VIII_5$	10.35(s),8.10(bs),7.90(m),7.40(m)	10.81(bs),9.05(dd),8.83(dd)
SB IX	10.45(s),8.40(m),7.40(m)	
IX_2	10.50(s),8.40(m),7.55(m)	7.85(m),2.50(s)
IX_4	10.60(s),8.45(m),7.90(bs),7.60(m)	13.60(bs),8.50(d),8.35(d)
IX_5	10.60(s),8.45(m),8.10(bs),7.65(m)	9.00(dd),8.90(dd)
IX_7	10.55(s),9.70(bs),8.50(m),7.60(m)	8.60(s),6.10(bs)

[a]The ^{1}H nmr data for the di- and trinitrobenzenes: (**1**) 8.85(m),8.0(dd); (**2**) 8.10(m),2.55(s); (**3**) 10.68(bs),8.78(d),8.43(dd),7.40(d); (**4**) 13.40(bs),8.62(s),8.45(d),8.37(d); (**5**) 9.14(d),9.05(d); (**6**) 9.62(s),8.80(d),8.92(d); (**7**) 13.90(s)8.72(s); (**8**) 9.28(s). s, singlet; bs, broad singlet; d, doublet; dd, doublet of doublet; m, multiplet.

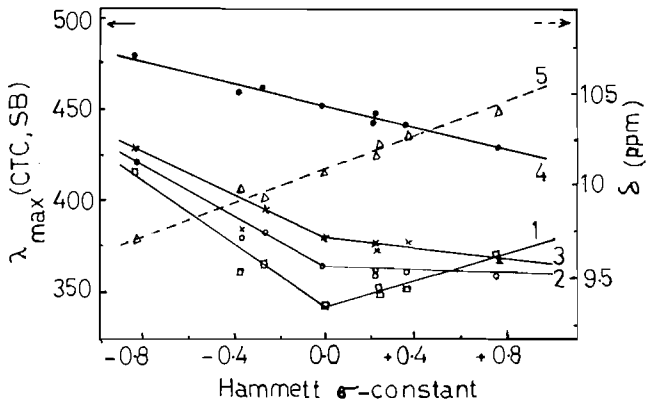

FIG. 2. The variation of λ_{CT} ($\pi-\pi^*$ transitions) of (1) SB; (2) CTC's (**I–IX**)$_3$; (3) CTC's (**I–IX**)$_7$; (4) CT ($n-\pi^*$ transitions) of CTC's (**I–IX**)$_1$; (5) with the proton chemical shifts of the azomethine group of SB, with the Hammett σ-constant.

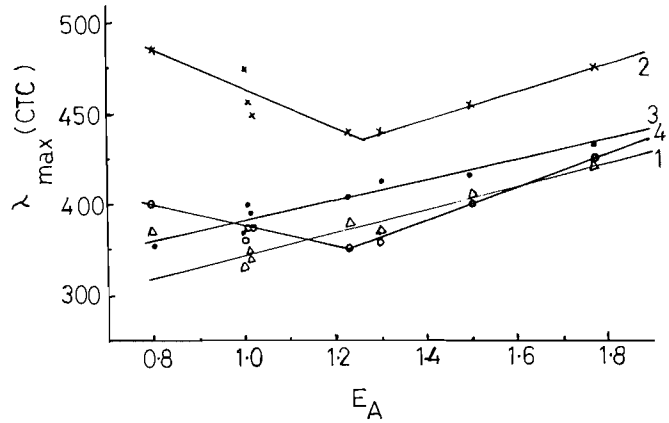

FIG. 3. The variation of λ_{CT} ($\pi-\pi^*$ transitions) of CTC's (1) $\mathbf{I}_{1-8}$; (2) $\mathbf{II}_{1-8}$; (3) $\mathbf{V}_{1-8}$; (4) $\mathbf{VII}_{1-8}$ with the electron affinity values of di- and trinitrobenzene derivatives.

in complex formation. On the other hand, the *n*-donation in CTC's derived from Schiff base **II** comes from the -N(CH$_3$)$_2$ group, as implied by the shifts of the ir bands due to ν_{CH_3} from 2960 to 2945 cm^{-1} and δ_{CH_3} from 1460 to 1450 cm^{-1}, as well as the downfield shift of the strong singlet of the methyl protons from 3.0 to 3.25 ppm on CTC formation, Scheme 1. The interaction between the acidic acceptors (**3–7**) and Schiff bases is achieved by intermolecular $\pi-\pi^*$ transitions

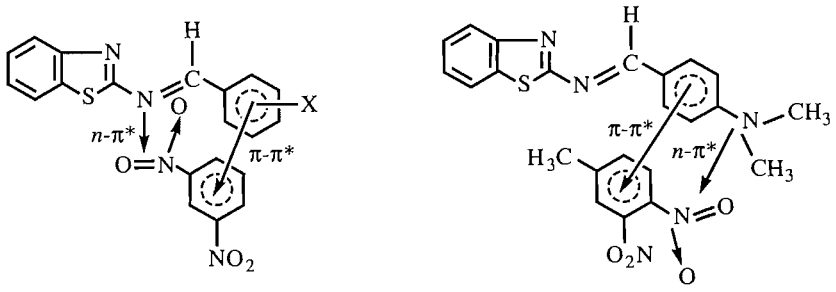

SCHEME 1

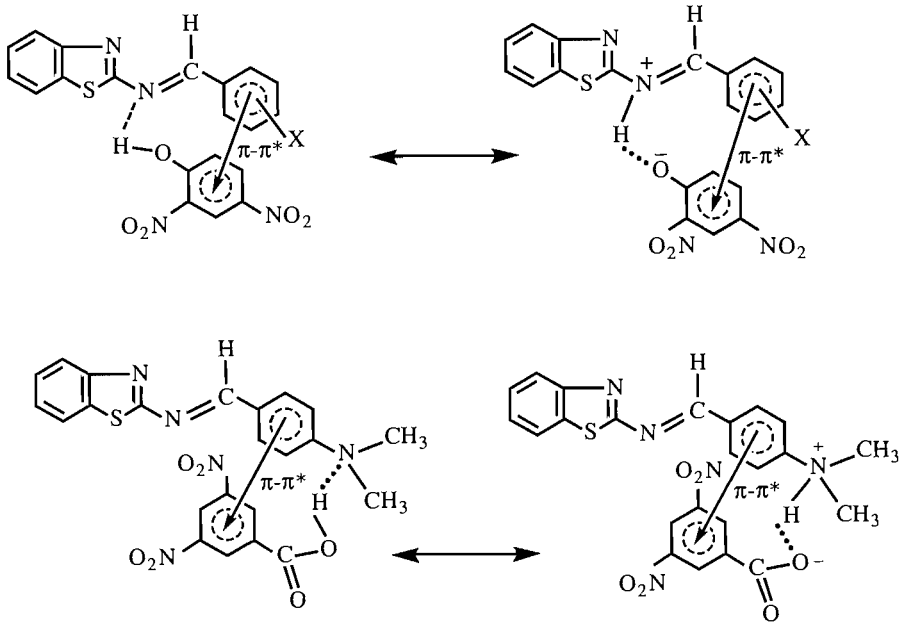

SCHEME 2

and proton transfer, Scheme 2. Proton transfer from the hydroxy or carboxy group to the basic centre of the Schiff base can be concluded by the presence of the ν^{+}_{NH} and δ^{+}_{NH} bands at 3220 and 1640 cm^{-1}, respectively, and the ν_{COO^-} band at 1610 cm^{-1} in addition to the bands due to ν_{OH} and $\nu_{C=O}$ at 2560 and 1700 cm^{-1}, respectively, with a relatively weak intensity and a shift to lower frequencies. The ^1H nmr spectra of the CTC's show that the signal due to the hydroxy and carboxy groups disappears, or in some cases appears as a weak broad signal at variable positions, Table 5. The spectra reveal a new broad signal, in the 5.50–9.60 ppm region, which disappears on deuteration. This new signal could be due to the protonation of the basic center of the Schiff base. In these CTC's the n–π^* transitions seem to be ruled out and complete permanent proton transfer is not believed to occur; rather, partial protonation stabilized by resonance seems to be the convenient route to complex formation, Scheme 2.

1. K. Esumi and K. Meguro. Shikizai Kyokaishi, **48**, 535 (1975); **48**, 544 (1975).
2. H. Hosaka, T. Fujiwara, and K. Meguro. Bull. Chem. Soc. Jpn. **44**, 2616 (1971).
3. B. D. Flockhart, I. R. Leith, and R. C. Pine. Trans. Faraday Soc. **65**, 542 (1969); **66**, 469 (1970).
4. R. S. Potember and T. O. Poehler. Synth. Met. **4**, 371 (1982).
5. F. Gutmann, A. M. Hermann, and A. Rembaum. J. Electrochem. Soc. **114**, 323 (1967).
6. O. A. Elseoud, M. J. DA Silva, and M. I. Elseoud. J. Colloid Interface Sci. **62**, 119 (1977).
7. L. J. Pace, J. Martinson, A. Ulman, B. M. Hoffman, and J. A. Ibers. J. Am. Chem. Soc. **105**, 2612 (1983), and references therein.
8. C. J. Schramm, R. P. Scaringe, D. R. Stojakovic, B. M. Hoffman, J. A. Ibers, and T. J. Marks. J. Am. Chem. Soc. **102**, 6702 (1980).
9. G. A. Chamberlain. Sol. Cells, **8**, 47 (1983).
10. E. M. Engler, F. B. Kaufman, and B. A. Scott. Ger. Patent. 2 627 828 (1977); Chem. Abstr. **86**, 180, 744C (1977).
11. T. B. Torrance, J. E. Vazquez, J. T. Mayerle, and V. Y. Lee. Phys. Rev. Lett. **46**, 253 (1981), and references therein.
12. D. Jérome, A. Mazond, M. Rimbault, and K. Bech-gaard. J. Phys. Lett. **41**, L.95 (1980).
13. G. Massig, M. Stockburger, W. Gärtner, D. Oesterhelt, and P. Towner. J. Raman Spectrosc. **12**, 287 (1982).
14. R. Raunio, T. Korpela, and E. Näsi. Finn. Chem. Lett. 23 (1975).
15. R. M. Ramadan, A. M. El Atrash, and A. M. A. Ibrahim. Spectrochim. Acta, **46A**, 1305 (1990).
16. M. R. Bryce, A. S. Secco, J. Trotter, and L. Weiler. Can. J. Chem. **60**, 2057 (1982).
17. G. Briegleb and H. Delle. Ber. Bunsen-Ges. Phys. Chem. **64**, 347 (1960).

Can. J. Chem. Downloaded from www.nrcresearchpress.com by 88.255.202.194 on 09/08/12
For personal use only.

18. R. M. Issa and M. M. El-Essawey. Z. Phys. Chem. (Leipzig), **253**, 96 (1973).
19. A. M. Hindawey, Y. M. Issa, R. M. Issa, and H. F. Rizk. Acta Chim. Hung. **112**, 415 (1983).
20. R. M. Issa, M. Gaber, A. L. El-Ansary, and H. F. Rizk. Bull. Soc. Chim. Fr. 2, 173 (1985), and references therein.
21. Y. M. Issa, A. E. El-Kholy, and A. L. El-Ansary. Acta Chim. Hung. **118**, 43 (1985).
22. A. F. E. Mourad and A. M. Nour ElDin. Spectrochim. Acta, **39A**, 533 (1983).
23. Y. M. Issa. Spectrochim. Acta, **40A**, 137 (1984).
24. A. I. Vogel. A textbook of practical organic chemistry — including qualitative organic analysis. 3rd ed. Longman, London. 1975.
25. M. Belletéte and G. Durocher. Can. J. Spectrosc. **24**, 87 (1979), and references therein.
26. S. H. Etaiw, R. Farag, A. M. El-Atrash, and A. M. A. Ibrahim. Spectrochim. Acta, **48A**, 1503 (1992).
27. G. Briegleb. Angew. Chem. Int. Ed. Engl. **76**, 326 (1964).
28. T. V. Mutzger. Comprehensive heterocyclic chemistry. Vol. 6. Part 4B. *Edited by* A. R. Katritzky, C. W. Rees, and K. T. Potts. Pergamon Press, Oxford. 1984.
29. M. Batley and L. E. Lyons. Nature, **196**, 573 (1962).
30. M. Meneghetti, R. Bozio, C. Bellitto, and C. Pecile. J. Chem. Phys. **89**, 2704 (1988).
31. G. Briegleb. J. Czekalla, and A. Hauser. Z. Phys. Chem. **21**, 99 (1959).

Can. J. Chem. Downloaded from www.nrcresearchpress.com by 88.255.202.194 on 09/08/12
For personal use only.

Reduction mechanism of 4-nitrobenzophenone in tetrahydrofuran. Influence of added proton donors

J. C. GARD AND Y. MUGNIER[1]

Laboratoire de synthèse et d'électrosynthèse organométalliques associé au Centre national de la recherche scientifique (Unité de recherche associée n° 33), Faculté des Sciences, 6, Boulevard Gabriel, 21000 Dijon, France

AND

Y. HUANG AND J. LESSARD[1]

Laboratoire d'électrochimie, Département de chimie, Université de Sherbrooke, Sherbrooke (Québec), Canada J1K 2R1

Received July 1, 1992

J. C. GARD, Y. MUGNIER, Y. HUANG, and J. LESSARD. Can. J. Chem. **71**, 325 (1993).

In tetrahydrofuran, with tetrabutylammonium hexafluorophosphate as supporting electrolyte, 4-nitrobenzophenone is reduced to the radical anion and, at a more negative potential, to the dianion. These two species are stable even on the time scale of electrolysis. In the presence of proton donors of increasing strength, the dianion is protonated to $ArNO_2H^-$ but the radical anion is protonated to $ArNO_2H^{\cdot}$ only with the strongest acids. These species react further and the different mechanisms are discussed.

J. C. GARD, Y. MUGNIER, Y. HUANG et J. LESSARD. Can. J. Chem. **71**, 325 (1993).

Dans du tétrahydrofurane contenant de l'hexafluorophosphate de tétrabutylammonium comme électrolyte-support, la 4-nitrobenzophénone est d'abord réduite en son radical anion et, à un potentiel plus négatif, au dianion. Ces deux espèces sont stables à l'échelle de temps d'une électrolyse. En présence de donneurs de protons d'acidités différentes, le dianion est toujours protoné pour donner $ArNO_2H^-$ tandis que le radical anion n'est protoné que par les acides les plus forts pour donner $ArNO_2H^{\cdot}$. Les mécanismes des réactions subséquentes de ces deux intermédiaires sont discutés.

Can. J. Chem. Downloaded from www.nrcresearchpress.com by 88.255.202.194 on 09/08/12
For personal use only.

Introduction

The electrochemical behavior of aromatic nitro compounds and more particularly of nitrobenzene has been extensively studied in aqueous or in aprotic medium (see refs. 1–10 for reviews). In aprotic solvents such as DMF (11) and in liquid ammonia (12), nitrobenzene is reduced reversibly to the anion radical and, at a more negative potential, to the dianion. In liquid ammonia, on the coulometric time scale, the dianion reacts slowly with the solvent; in the presence of isopropyl alcohol, the dianion of nitrobenzene is protonated and then rapidly eliminates a hydroxyl ion to give nitrosobenzene.

In this paper, we report the results of an investigation of the electrochemical behavior of 4-nitrobenzophenone (**1**) in tetrahydrofuran (THF). Due to the presence of two electron-withdrawing groups, the anionic species generated should be less basic than in the case of nitrobenzene, and we have examined the reactivity of these anionic species towards proton donors of increasing strength.

Experimental

Tetrahydrofuran was purified by distillation from sodium benzophenone ketyl under argon. The supporting electrolyte was tetrabutylammonium hexafluorophosphate (0.2 M) in all cases; the salt (Fluka) was recrystallized twice from ethanol, then dried and deoxygenated before use. 4-Nitrobenzophenone, fluorene, diethyl malonate, phenol, and benzoic acid were all commercial products.

Apparatus and general procedures

All the experiments were carried out under an atmosphere of argon using Schlenck techniques. In voltammetry, the working electrode was a platinum disc (diameter: 1.2 mm) and for the controlled potential electrolyses, a platinum grid. In each case the reference electrode was a saturated calomel electrode (sce) separated from the solution by a sintered glass disc. The auxiliary electrode was a platinum wire. For thin-layer cyclic voltammetry (tlcv), the platinum disc electrode was lowered until it came into contact with the flat floor of the electrolytic cell so that only a thin layer of solution existed between them. The reagents (4-nitrobenzophenone and proton donors) in THF solution were added with a syringe previously purged with argon. For the rotating disc experiments, a three-electrode Tacussel Tipol polarograph was used. The cyclic voltammetry experiments were conducted with a Tacussel UAP4 unit connected to a Tektronix 5115 oscilloscope or a Sefram TGM 164 X-Y recorder. The macroelectrolyses were carried out with an Amel 552 potentiostat equipped with a Tacussel IG5 integrator.

[1]Authors to whom correspondence may be addressed.

Results and discussion

In THF with Bu_4NPF_6 as supporting electrolyte, the voltammogram of **1** ($ArNO_2$) on a Pt rotating disc electrode (rde) shows two reduction waves A and B (Fig. 1*a*); the second wave is smaller than the first because the diffusing species is $ArNO_2^{\cdot-}$, which has a smaller diffusion coefficient than $ArNO_2$. The half-wave potentials are respectively −1.0 and −1.6 V vs. sce. The cyclic voltammogram (Fig. 2) shows the two corresponding reversible systems of peaks, A/A′ and B/B′, which correspond to the redox reactions [1] and [2] respectively. No modification of the cyclic voltammogram was observed within the temperature range −30°C to 25°C.

$$[1] \quad ArNO_2 \overset{+e^-}{\rightleftharpoons} ArNO_2^{\cdot-} \qquad A/A'$$

$$[2] \quad ArNO_2^{\cdot-} \overset{+e^-}{\rightleftharpoons} ArNO_2^{2-} \qquad B/B'$$

The electrolysis of **1** at −1.2 V (plateau of wave A) and at 0°C consumed one equivalent of electrons. The rde voltammogram of the green electrolysis solution (Fig. 1*b*) exhibited the oxidation wave A′ and a reduction wave at a lower cathodic potential than the initial wave B; these two waves have nearly the same height but are smaller than the

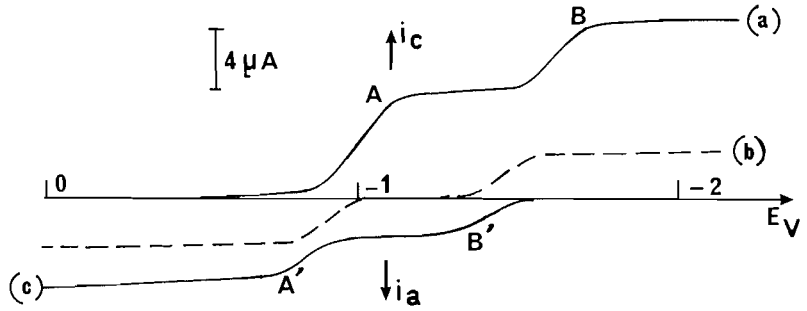

FIG. 1. Rotating disk electrode voltammograms of **1** in THF (*a*) before electrolysis; (*b*) after one-electron reduction at −1.2 V; (*c*) after two-electron reduction at −1.7 V.

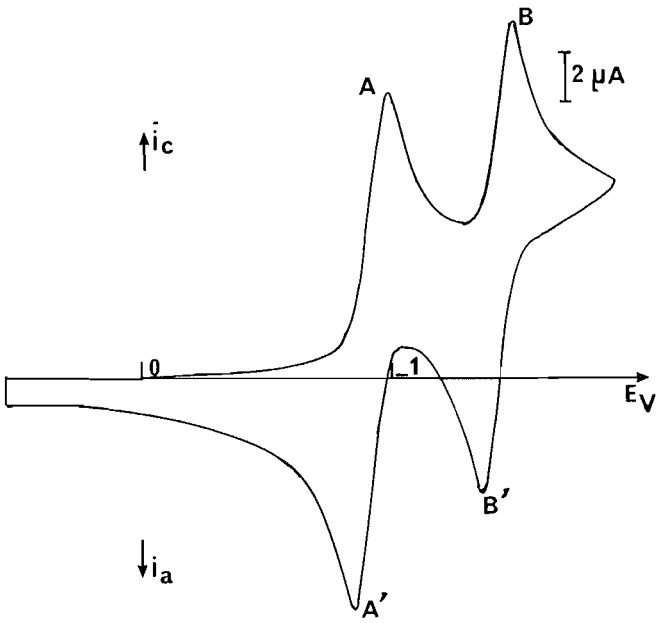

FIG. 2. Cyclic voltammogram of **1**; starting potential +0.6 V; sweep rate 0.05 V s^{-1}.

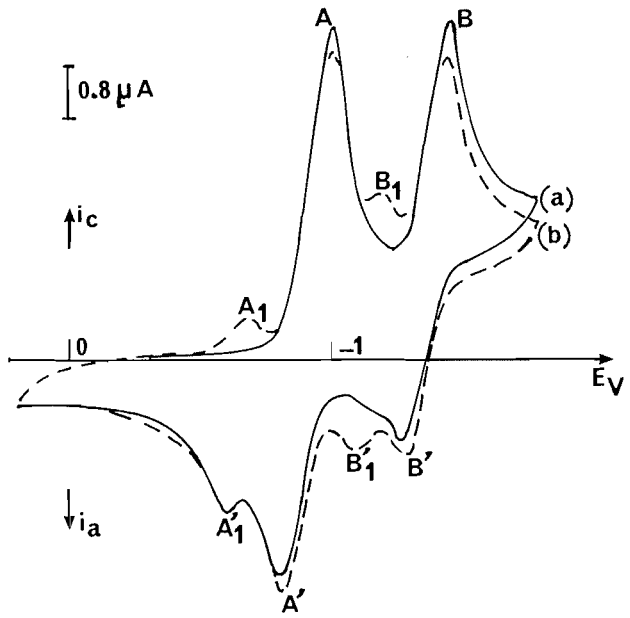

FIG. 3. Thin-layer voltammograms of **1** in THF in the presence of excess of water. Starting potential +0.2 V; sweep rate 0.02 V s^{-1}. (*a*) First scan; (*b*) second scan.

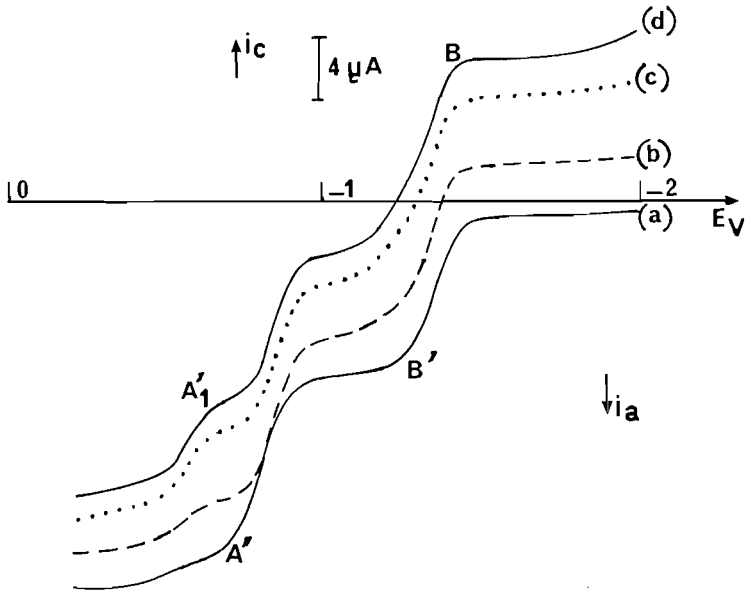

FIG. 4. (*a*) Rotating disk electrode voltammograms of the dianion $ArNO_2^{2-}$; (*b*) after addition of seven equivalents of water; (*c*) after addition of 12 equivalents of water; (*d*) after 30 min.

Can. J. Chem. Downloaded from www.nrcresearchpress.com by 88.255.202.194 on 09/08/12
For personal use only.

TABLE 1. pK_a values of added proton donors

	pK_a	Solvent	Reference
Water	31.4	Me_2SO	14
Fluorene	22.6	Me_2SO	15
Phenol	18	Me_2SO	16
Diethyl malonate	16.4	Me_2SO	17
Benzoic acid	11	Me_2SO	15

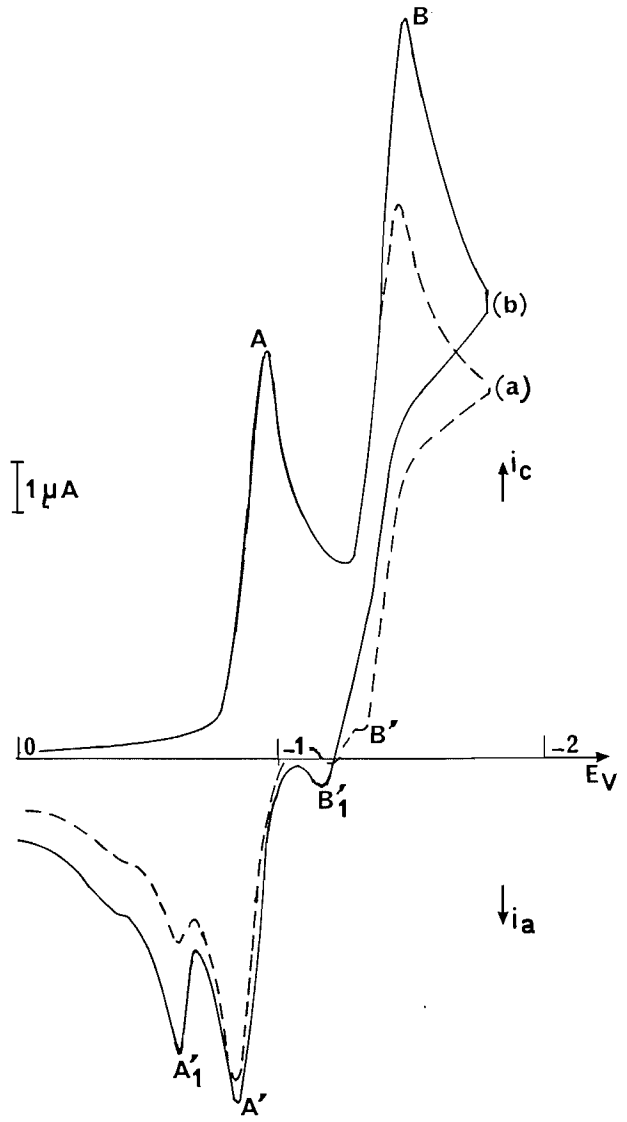

FIG. 5. Cyclic voltammograms of **1** in THF (*a*) in the presence of two equivalents of FlH_2; (*b*) after addition of 10 equivalents of FlH_2. Starting potential 0 V. Sweep rate 0.05 V s^{-1}.

initial waves A and B. The electron spin resonance (esr) spectrum of the electrolysis solution showed the signals characteristic of the anion radical $ArNO_2^{\cdot-}$ (13). There was no starting product left: absence of the $\nu_{(C=O)}$ band at 1670 cm^{-1}. The anion radical was stable in the electrolysis medium since no modification of the rde voltammogram occurred when the temperature was increased from 0 to 30°C. The one-electron oxidation at −0.8 V (plateau of wave A′) gave back the initial voltammogram. Further reduction of the

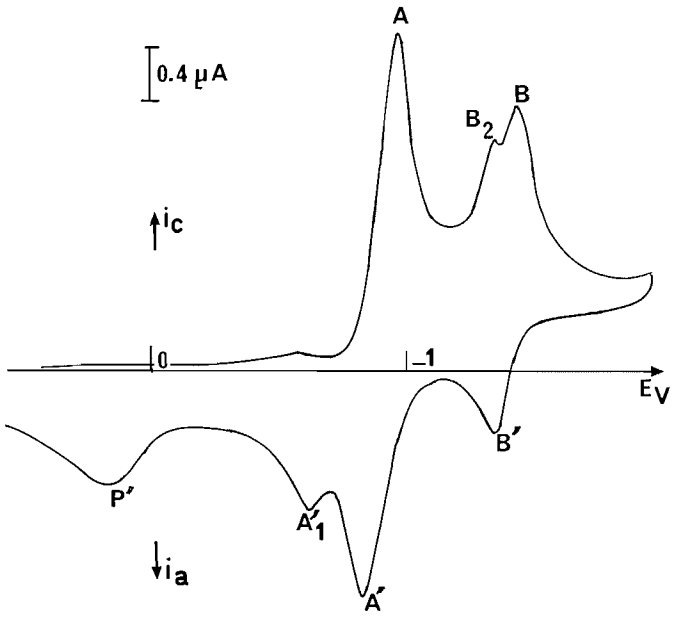

FIG. 6. Thin-layer voltammogram of **1** in THF in the presence of one equivalent of PhOH. Starting potential +0.6 V. Sweep rate 0.02 V s^{-1}.

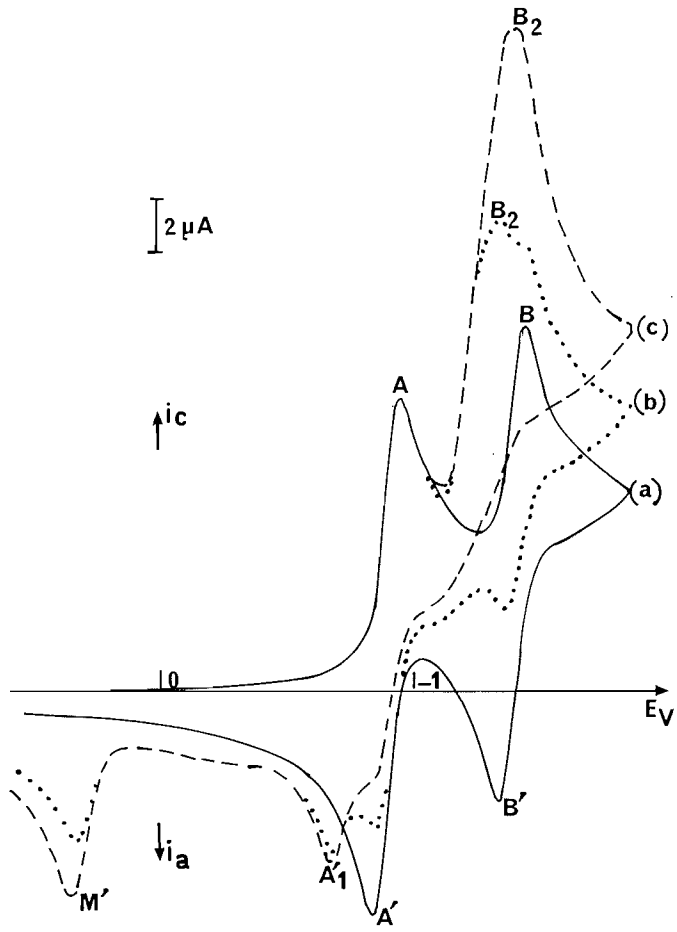

FIG. 7. Cyclic voltammograms of **1** in THF: (*a*) **1** alone; (*b*) **1** in the presence of one equivalent of diethyl malonate; (*c*) in the presence of two equivalents of diethyl malonate. Starting potential +0.6 V. Sweep rate: 0.05 V s^{-1}.

Can. J. Chem. Downloaded from www.nrcresearchpress.com by 88.255.202.194 on 09/08/12
For personal use only.

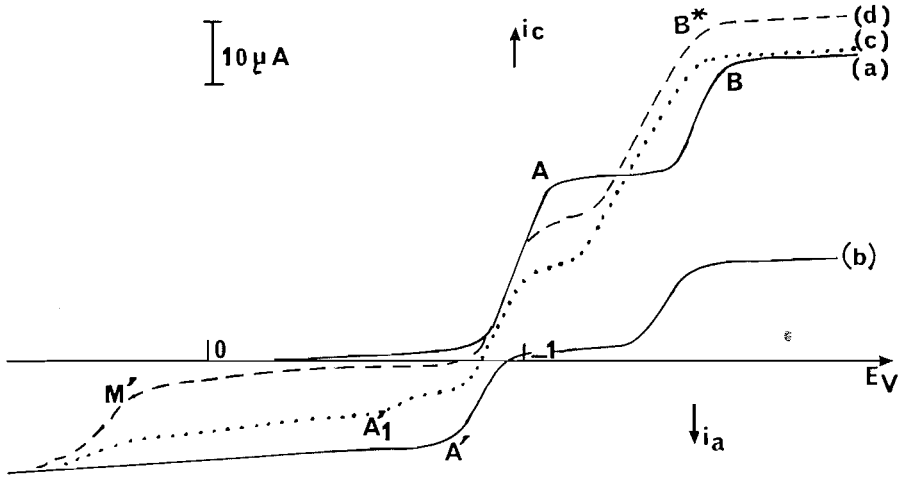

FIG. 8. Rotating disk electrode voltammograms of **1** in THF on platinum electrode (*a*) before electrolysis; (*b*) after one-electron reduction at −1.2 V; (*c*) immediately after addition of one equivalent of diethyl malonate; (*d*) after heating at 50°C.

radical anion at −1.7 V (plateau of the second wave B) and at 0°C consumed one equivalent of electrons. The rde voltammogram of the resulting green solution showed two oxidation waves B′ and A′ of equal height (Fig. 1*c*) corresponding to the oxidation of the dianion to $ArNO_2^{\cdot-}$ and of $ArNO_2^{\cdot-}$ to $ArNO_2$ respectively. The same voltammogram was obtained when a two-electron reduction of **1** was performed directly at −1.7 V. No signal was detected by esr spectroscopy and the band at 1670 cm^{-1} was absent in the ir spectrum. The dianion was stable at 0°C in the electrolysis medium since no modification of the rde voltammogram occurred after several hours. A two-electron oxidation at +0.75 V (plateau of wave A′) gave back the initial voltammogram.

Behavior with added proton donors

The various proton donors studied and their pK_a values in DMSO are shown in Table 1.

Water

No modification in the cyclic voltammogram of **1** occurs when one equivalent of water is added. In the presence of an excess of water, system A/A′ is not modified when the scan is reversed after peak A. In thin-layer voltammetry, two new oxidation peaks B'_1 and A'_1 appear when the potential scan is reversed after peak B (Fig. 3); in the second scan, two other reduction peaks A_1 and B_1 are obtained. This shows that $ArNO_2^{\cdot-}$ does not react with water on the time scale of cyclic voltammetry whereas $ArNO_2^{2-}$ reacts slowly. So we have examined the reactivity of the electrogenerated dianion towards water. Figure 4 shows the rde voltammogram of the dianion $ArNO_2^{2-}$ at room temperature (two oxidation waves B′ and A′). When water (7 equiv.) is added to the solution, reduction wave B appears immediately (Fig. 4*b*). The height of wave B increases and the oxidation wave A'_1 becomes well defined when the proportion of water increases (Fig. 4*c*) or when the solution is stored under argon. This suggests that wave A'_1 corresponds to the oxidation of $ArNO_2^{\cdot-}$ and wave B to the reduction of $ArNO_2^{\cdot-}$. The formation of $ArNO^{\cdot-}$ can be accounted for by reactions [3] (AH = H_2O) – [5]. The systems A_1/A'_1 and B_1/B'_1 of Fig. 3 correspond to the redox reactions [6] and [7].

$$[3]\quad ArNO_2^{2-} + AH \xrightarrow[\text{slow}]{} ArN(O)OH^-$$

$$[4]\quad ArN(O)OH^- \xrightarrow[\text{fast}]{} ArNO + OH^-$$

$$[5]\quad ArNO + ArNO_2^{2-} \rightarrow ArNO^{\cdot-} + ArNO_2^{\cdot-}$$

$$[6]\quad ArNO \overset{e^-}{\rightleftharpoons} ArNO^{\cdot-} \qquad A_1/A'_1$$

$$[7]\quad ArNO^{\cdot-} \overset{e^-}{\rightleftharpoons} ArNO^{2-} \qquad B_1/B'_1$$

Fluorene

Figure 5 shows the cyclic voltammogram of **1** in the presence of two and 10 equivalents of fluorene (FlH_2). The dianion $ArNO_2^{2-}$ reacts more rapidly with fluorene than with water to give ArNO (reactions [3] (AH = FlH_2) and [4]). By adding an excess of FlH_2 to the electrogenerated radical anion $ArNO_2^{\cdot-}$, no modification of the rde voltammogram was observed even at 50°C thus showing that $ArNO_2^{\cdot-}$ is not basic enough to react with FlH_2.

Phenol and diethyl malonate

The thin-layer voltammogram of **1** in the presence of one equivalent of phenol (Fig. 6) exhibits the reduction peaks A and B, a new reduction peak B_2, and the four oxidation peaks B′, A′, A'_1, and P′. We have verified that peak P′ corresponds to the oxidation of PhO^- (in THF, PhONa is oxidized at the potential of peak P′). When increasing the concentration of PhOH, the height of peaks A and B_2 increases and peak B_2 is shifted towards a less negative potential. Peak B_2 corresponds to the reduction of $ArNO_2^{\cdot-}$ followed by the fast protonation of the electrogenerated dianion (EC process) yielding ArNO, which is immediately reduced first to $ArNO^{\cdot-}$ (oxidation peak A'_1), then to $ArNO^{2-}$. The fact that peak B'_1 due to the oxidation of the dianion $ArNO^{2-}$ is absent suggests that its protonation by phenol must be very fast;[2] $ArNO^{2-}$ should be a stronger base than $ArNO_2^{2-}$, the oxidation peak of which, peak B′, is present.

The influence of added diethyl malonate on the electro-

[2]Alternatively, according to a referee's suggestion, the absence of peak B'_1, although peak A'_1 due to the oxidation of $ArNO_2^{\cdot-}$ is present, could be explained by the relative rates of formation of ArNO and the comproportionation reaction $ArNO^{2-} + ArNO \rightarrow 2ArNO^{\cdot-}$.

Can. J. Chem. Downloaded from www.nrcresearchpress.com by 88.255.202.194 on 09/08/12
For personal use only.

Can. J. Chem. Downloaded from www.nrcresearchpress.com by 88.255.202.194 on 09/08/12
For personal use only.

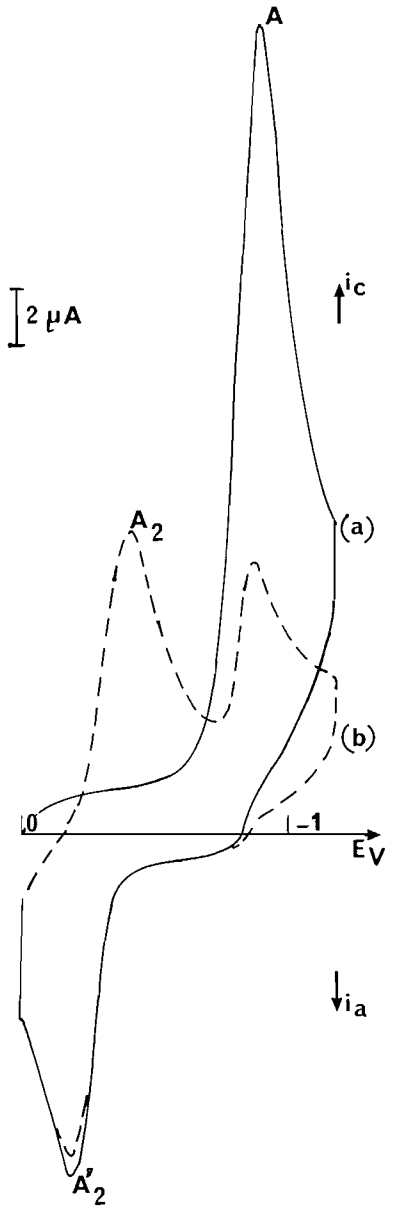

FIG. 9. Thin-layer voltammograms of **1** in THF in the presence of one equivalent of benzoic acid. Starting potential 0 V; sweep rate 0.02 V s^{-1}. (*a*) First scan; (*b*) second scan.

chemical behavior of **1** is shown in Fig. 7. Upon the addition of one equivalent of diethyl malonate, the height of peak B increases, the reduction peak B_2 appears, the oxidation peak B'_1 is absent as in the presence of phenol, and four oxidation peaks B′, A′, A'_1, and M′ are observed (Fig. 7*b*). Peak M′ corresponds to the oxidation of the malonate anion. With two equivalents of diethyl malonate, peaks B and B′ disappear, the height of peak B_2 increases, and that of peak A′ decreases (Fig. 7*c*). The radical anion $ArNO_2^{\cdot-}$ is relatively stable and the dianion $ArNO_2^{2-}$ reacts rapidly with diethyl malonate on the time scale of cyclic voltammetry. However, when adding one equivalent of diethyl malonate to the electrogenerated green solution of the anion radical $ArNO_2^{\cdot-}$, the oxidation waves A'_1 and M′ appear and **1** is regenerated as shown by waves A and B* (ill-defined wave). When this solution is heated at 50°C, the oxidation wave A'_1 disappears. The above results can be explained by reactions [8]–[11]. First, the radical anion is protonated (eq. [8]). Then the protonated anion radical leads to the starting material and the dihydroxylamine derivative $ArNO_2H_2$ by disproportionation (reaction [9]). The loss of water (eq. [10]) or hydroxide ion (eq. [4]) gives ArNO, which is then reduced by $ArNO_2^{\cdot-}$ to $ArNO^{\cdot-}$ (eq. [11]). Peak A'_1 corresponds to the oxidation of $ArNO^{\cdot-}$. Upon heating, $ArNO^{\cdot-}$ probably gives the azoxy derivative according to a process (eq. [12]) similar to the formation of azoxybenzene from the nitrosobenzene radical anion (18); ArN(O)NAr is probably reduced at the potential of wave B* (see Fig. 8).

[8] $ArNO_2^{\cdot-} + AH \rightarrow ArNO_2H^{\cdot} + A^-$

[9] $2ARNO_2H^{\cdot} \rightarrow ArNO_2 + ArNO_2H_2$

[10] $ArNO_2H_2 \rightarrow ArNO + H_2O$

[11] $ArNO + ArNO_2^{\cdot-} \rightarrow ArNO^{\cdot-} + ArNO_2$

[12] $2ArNO^{\cdot-} + 2AH \rightarrow ArN(O)NAr + 2A^- + H_2O$

The decrease in height of wave A is in keeping with the mechanism proposed, to which corresponds the global reaction [13] that shows that two thirds of the initial $ArNO_2$ is regenerated.

[13] $6ArNO_2 + 6AH + 6e^- \rightarrow 4ArNO_2 + ArN(O)NAr + 6A^- + 3H_2O$

Benzoic acid

Upon the addition of one equivalent of benzoic acid, in thin-layer voltammetry, the reduction peak A becomes higher, an oxidation peak A'_2 appears, and, during the second scan, reduction peak A_2 is observed (Fig. 9). ArNHOH is obtained from a four-electron reduction of $ArNO_2$, leading to anionic species ($ArNO_2^{\cdot-}$, $ArNHO_2^-$, $ArNO^{\cdot-}$, $ArNHO^-$) that are quickly protonated in the presence of benzoic acid. Peak A'_2 corresponds to the oxidation of the hydroxylamine derivative in the presence of electrogenerated $PhCO_2^-$ according to the global reaction [14]. Peak A_2 corresponds to the reduction of the nitroso derivative under the influence of benzoic acid (eq. [15]).

[14] $ArNHOH - 2e^- + 2PhCO_2^- \rightarrow ArNO + 2PhCO_2H$

[15] $ArNO + 2e^- + 2PhCO_2H \rightarrow ArNHOH + 2PhCO_2^-$

After a four-electron reduction of **1** at −1.1 V in the presence of six equivalents of $PhCO_2H$, the hydroxylamine ArNHOH was obtained in a nearly quantitative yield as determined by polarography (the height of wave A'_2 being twice as small as the initial reduction wave).

Conclusion

We have shown that, on the time scale of voltammetry, the radical anion $ArNO^{\cdot-}$ is stable in the presence of water or fluorene, but is slowly protonated by phenol or diethyl malonate. In the presence of benzoic acid, $ArNO_2^{\cdot-}$ is rapidly protonated and further reductions and protonations give the hydroxylamine. The anion radical of the nitroso derivative was formed by adding water to the electrogenerated dianion $ArNO_2^{2-}$ (eqs. [3]–[5]). A disproportionation reaction of $ArNO_2H^{\cdot}$ (eq. [9]) was observed when diethyl malonate was added to the electrogenerated anion radical $ArNO_2^{\cdot-}$.

Acknowledgements

We are grateful to M. T. Compain for her technical assistance and we acknowledge financial support from the Ministère des Affaires Étrangères de France, the Ministère des Relations Internationales du Québec (coopération franco-québécoise), the Fonds FCAR du Québec, and the Natural Sciences and Engineering Research Council of Canada.

1. R. C. Snowdon. J. Phys. Chem. **15**, 797 (1991).
2. C. J. Brockman. Electroorganic chemistry. Wiley Interscience, New York. 1928. pp. 185–259.
3. F. Fichter. Organische Electrochemie. Theodor Steinkopff Verlag, Leipzig. 1942. Chap. 10.
4. B. Kastening. *In* Progress in polarography. Vol. 3. *Edited by* P. Zuman and L. Meites. Wiley Interscience, New York. 1972. pp. 259–267.
5. W. Kemula and T. M. Krygowski. *In* Encyclopedia of electrochemistry of the elements. Vol. 13. *Edited by* A. J. Bard and H. Lund. Marcel Dekker, New York. 1979. Chap. 2.
6. A. J. Fry. *In* The chemistry of amino, nitroso and nitro compounds and their derivatives. *Edited by* S. Patai. John Wiley, New York. 1982. p. 319.
7. H. Lund. *In* Organic electrochemistry. *Edited by* M. M. Baizer and H. Lund. Marcel Dekker, New York. 1983. pp. 295–306.
8. A. P. Tomilov, S. G. Mairanovskii, M. Y. Fioschin, and V. A. Smirnov. Elektrokhimiya Organicheskikh Soedinienii. Izdat. Khimiya, Leningrad. 1968. Chap. 5; Electrochemistry of organic compounds. Halsted Press, New York. 1972. Chap. 5.
9. F. D. Popp and H. P. Schultz. Chem. Rev. **19**, 62 (1962).
10. A. Cyr, P. Huot, J. F. Marcoux, G. Belot, E. Laviron, and J. Lessard. Electrochim. Acta, **34**, 439 (1989).
11. B. S. Jensen and V. D. Parker. J. Chem. Soc. Chem. Commun. 367 (1974).
12. W. H. Smith and A. J. Bard. J. Am. Chem. Soc. **97**, 5203 (1975).
13. S. Miertus and O. Kysec. Collect. Czech. Chem. Commun. **45**, 369 (1980).
14. W. N. Olmstead, Z. Margolin, and F. G. Bordwell. J. Org. Chem. **45**, 3295 (1980).
15. W. S. Matthews, J. E. Bares, J. E. Bartmess, J. E. Bordwell, F. G. Bordwell, F. J. Cornforth, G. E. Drucker, Z. Margolin, R. J. McCallum, G. J. McCallum, and N. R. Vanier. J. Am. Chem. Soc. **97**, 7006 (1975).
16. F. G. Bordwell, J. C. Bianca, D. L. Hughes, and W. N. Olmstead. J. Org. Chem. **45**, 3305 (1980).
17. W. N. Olmstead and F. G. Bordwell. J. Org. Chem. **45**, 3299 (1980).
18. G. A. Russell and E. J. Geels. J. Am. Chem. Soc. **87**, 122 (1965); G. A. Russell, E. J. Geels, F. J. Smentowski, K. Y. Chang, J. Reynolds, and G. Kaupp. J. Am. Chem. Soc. **89**, 3821 (1967).

Can. J. Chem. Downloaded from www.nrcresearchpress.com by 88.255.202.194 on 09/08/12
For personal use only.

Low-temperature X-ray diffraction studies on $[Cu(4\text{-}Xpz)_2]_x$ linear chain polymers (where X = Cl, Br, CH_3, H; pz = pyrazolate)

MARTIN K. EHLERT, ALAN STORR,[1] AND ROBERT C. THOMPSON[1]
Department of Chemistry, University of British Columbia, Vancouver, B.C., Canada V6T 1Z1

AND

FREDERICK W. B. EINSTEIN AND RAYMOND J. BATCHELOR
Department of Chemistry/Biochemistry, Simon Fraser University, Burnaby, B.C., Canada V5A 1S6

Received July 10, 1992

MARTIN K. EHLERT, ALAN STORR, ROBERT C. THOMPSON, FREDERICK W. B. EINSTEIN, and RAYMOND J. BATCHELOR. Can. J. Chem. **71**, 331 (1993).

Room temperature and low-temperature (110–140 K) powder diffractograms have been obtained for the polymeric compounds $[Cu(4\text{-}Xpz)_2]_x$ (where X = H, CH_3, Cl, and Br), and values of the unit cell parameters (orthorhombic, space group *Ibam*) *a*, *b*, and *c* have been obtained at both high and low temperatures. A single crystal X-ray diffraction study of the X = H compound at 116 K was completed and the results compared with a published study done at room temperature. The structures of these complexes involve extended chains of pyrazolate-bridged copper ions extending along the *c* crystallographic axis. The X-ray studies indicate little change in the *c* parameter with decreasing temperature and small but significant changes in the *a* or *b* parameters reflecting changes in interchain packing. This study permits some evaluation of how structural parameters are affected by these variations in interchain packing and how these variations may be affecting the magnitude of magnetic exchange in the compounds.

MARTIN K. EHLERT, ALAN STORR, ROBERT C. THOMPSON, FREDERICK W. B. EINSTEIN et RAYMOND J. BATCHELOR. Can. J. Chem. **71**, 331 (1993).

On a déterminé les spectres de diffraction, à la température ambiante et à basse température (110–140 K), de poudres polymériques des composés $[Cu(4\text{-}Xpz)_2]_x$ (dans lesquels X = H, CH_3, Cl et Br) et on a déterminé les paramètres *a*, *b* et *c* de la maille (orthorhombique, groupe d'espace *Ibam*) aux températures tant élevée que basses. On a réalisé une analyse complète de la diffraction des rayons X, à 116 K, par un cristal unique du composé où X = H et on a comparé les résultats obtenus avec ceux rapportés dans la littérature pour une étude faite à la température ambiante. Les structures de ces complexes impliquent de longues chaînes d'ions cuivres reliés par des ponts pyrazolates et s'étendant le long de l'axe cristallographique *c*. Les études de rayons X indiquent qu'un abaissement de la température ne provoque que peu de changements dans le paramétre *c*; on observe toutefois de faibles changements significatifs dans les paramètres de *a* ou de *b* qui sont le reflet de changements dans l'empilement interchaîne. Cette étude permet d'évaluer la façon dont les paramètres structuraux sont affectés par ces variations dans l'empilement interchaîne et comment ces variations peuvent affecter l'amplitude de l'échange magnétique de ces composés.

[Traduit par la rédaction]

Introduction

Binary copper(II) pyrazolates and substituted pyrazolates adopt structures in which copper ions are doubly bridged by pyrazolate ligands to form extended linear chain polymers (1–3). The compounds show relatively strong antiferromagnetic coupling with values of *J*, the exchange coupling constant, in the range -58 to -105 cm^{-1} (3). The shortest intrachain copper–copper separations in these compounds are of the order of 3.9 Å, too large for direct metal–metal interactions and requiring therefore a ligand-mediated mechanism for exchange (4). A comparison of magnetic and structural parameters between these compounds has revealed that relatively small differences in structural parameters involving the bridging ligands lead to small but significant differences in the magnitude of the exchange (2). The magnetic characterization of these complexes involves the measurement of magnetic susceptibilities over a wide temperature range (2–300 K) and the possibility that minor structural changes with temperature could be occurring in these systems with consequent effects on their magnetic properties prompted the current investigation.

Some evidence for structural change in pyrazolates of copper(II), on cooling, is already available. Several of these polymers exhibit thermochromism and two compounds, $[Cu(4\text{-}Clpz)_2]_x$ (green form) and $[Cu(4\text{-}Brpz)_2]_x$ (where pz = pyrazolate), show discontinuities in their magnetic susceptibility versus temperature plots (2). Accordingly, we have recorded the X-ray powder diffraction patterns of the compounds $[Cu(4\text{-}Xpz)_2]_x$, where X = H, CH_3, Cl, and Br, at room temperature and at low temperature (~110–140 K). We have also completed a single crystal X-ray diffraction study of $[Cu(4\text{-}Hpz)_2]_x$ at 116 K for comparison with the published study (1) done at room temperature.

Experimental

Descriptions of the preparations of the compounds were given previously (2, 3). The powder diffractograms were recorded using a Rigaku Rotaflex rotating anode X-ray diffractometer (graphite monochromator, CuK_α radiation). Low-temperature measurements on this instrument were achieved by equipping the diffractometer with a custom-designed copper cold stage cooled with liquid nitrogen. The samples were deposited as an octane slurry on a glass slide that was mounted on the cold stage. Temperatures were measured using a copper–constantan thermocouple and a Fluke 8120A digital voltmeter. The thermocouple was imbedded in the copper cold stage immediately behind the sample slide.

Unit cell parameters for these compounds derived from powder diffractograms were obtained by least-squares refinement of diffraction peaks to which Miller indices could be unambiguously assigned. For the $[Cu(4\text{-}Xpz)_2]_x$ compounds, the temperature, the

[1]Authors to whom correspondence may be addressed.

Can. J. Chem. Downloaded from www.nrcresearchpress.com by 88.255.202.194 on 09/08/12
For personal use only.

TABLE 1. Fractional atomic coordinates and isotropic temperature factors (Å^2) for $[Cu(4\text{-}Hpz)_2]_x$ at 116 K

Atom	x	y	z	B_{eq}[a]
Cu	1/2	0	1/4	0.854
N	0.32992(14)	0.05847(9)	0.08735(15)	0.98
C(1)	0.19767(17)	0.12540(12)	0.13994(20)	1.21
C(2)	0.1108 (3)	0.17064(17)	0	1.31
H(1)	0.165 (3)	0.1404 (25)	0.262 (3)	1.34
H(2)	0.024 (4)	0.232 (3)	0	1.50

[a]B_{eq} is the mean of the principal axes of the thermal ellipsoid (in the case of the H atoms B_{eq} is the assigned B_{iso}).

number of powder diffraction data observed, and the number of data used in least-squares refinement (in parentheses) are as follows: X = H: 298 K, 22(18); 110 K, 20(13); X = CH_3: 298 K, 26(21); 109 K, 25(18); X = Cl: 298 K, 36(18); 110 K, 30(25); X = Br: 298 K, 23(15); 140 K 38(20).

The low-temperature single crystal X-ray diffraction study of $[Cu(4\text{-}Hpz)_2]_x$ was done using an Enraf–Nonius CAD-4F diffractometer (graphite monochromatized MoK_α radiation) equipped with an in-house modified low-temperature attachment. A crystal, mounted on a Pyrex filament with epoxy resin as adhesive, was cooled to 116 K. The unit cell was determined from 25 well-centred reflections in the range $38° \leq 2\theta \leq 50°$. Two intensity standards were measured hourly and showed no systematic variations in intensity throughout data acquisition ($2\theta_{max} = 70°$). The data were corrected empirically for the effects of absorption (5). Data reduction included corrections for Lorentz and polarization effects.

The room temperature and this low-temperature study lead to isostructural models (1). Parameters included in the final refinement were coordinates for all atoms and anisotropic thermal parameters for the non-hydrogen atoms. The hydrogen atoms were assigned isotropic temperature factors dependent on the thermal parameters of the carbon atoms to which they were bonded. A weighting scheme, based on counting statistics, was applied such that $\langle w(|F_o| - |F_c|)^2 \rangle$ was approximately constant as a function of either $|F_o|$ or $(\sin\theta)/\lambda$. Final full-matrix least-squares refinement of 33 parameters from 643 observations ($I_o \geq 2.5\sigma(I_o)$) converged at $R_F = 0.027$.

The NRCVAX (6) system of crystallographic programs was used for data reduction and structure refinement. Complex scattering factors for neutral atoms (7) were used in the calculations. All computations were performed with a MicroVax-II computer.

The final atomic coordinates are listed in Table 1, and the unit cell parameters (116 K) are included in Table 2. Supplementary material is available, including experimental details, anisotropic thermal parameters, and observed and calculated structure factors.[2]

Results and discussion

The $[Cu(4\text{-}Xpz)_2]_x$ compounds[3] are orthorhombic, space group *Ibam*; values of the cell parameters are given in Table 2. Comparisons between cell parameters determined by the single crystal and powder methods at equivalent temperatures reveal that most agree to within 3σ, with the largest deviation 6σ. The crystal structures reveal chains of pyrazolate-bridged copper ions extending along the *c* axis (1, 2). Changing the temperature would be expected to have the largest effect on the interchain interactions and hence more effect on the *a* and *b* lattice constants than on *c*. Consistent with this, the cell parameter *c* shows the smallest change on cooling in all four compounds (Table 2), ranging from no change in the X = CH_3 compound to a change of 10σ in the X = H derivative. On the basis of the change in the other two cell parameters the four compounds fall into two groups. The X = H and CH_3 compounds exhibit significant decreases in the *b* parameter on cooling, 77σ and 26σ, respectively. These compounds also show smaller changes in *a* on cooling. For X = H, *a* decreases by 24σ while for X = CH_3 it increases by 3σ. For the other derivatives it is the *a* parameter that is most affected by changing the temperature. For X = Cl and Br the *a* parameter decreases by 49σ and 38σ, respectively, on cooling. On lowering the temperature the *b* parameter shows small increases of 7σ and 6σ, respectively, for X = Cl and Br.

A comparison of the low-temperature single crystal X-ray diffraction study of $[Cu(4\text{-}Hpz)_2]_x$ done here with the previous room temperature study (1) shows how bonding parameters in this compound are affected by changing the temperature. The study also provides some insight into how temperature-induced changes in bond angles and lengths are related to changes in lattice constants in these compounds. Values of selected bond distances and angles are given in Tables 3 and 4. Bond distances are virtually unaffected by the temperature change; the largest change involves the C(1)—C(2) distance, which increases by 0.015 Å or ~4σ on cooling. (These could of course be partially accounted for by thermal motion.) All other changes are smaller and no particular significance can be attached to changes in these bond distances. Bond angles involving only the pyrazolate ligand atoms are also not affected significantly by the temperature change. Some angles involving copper show small, barely significant, changes, notably the N—Cu—N^d angle, which decreases by 0.50° (4.5σ), and the C(1)—N—Cu angle, which also decreases by 0.50° (3.5σ). These changes in angles are necessarily tied to more significant changes in pyrazolate ring dihedral angles (*vide infra*). The most significant changes are seen in the dihedral angle between fused $Cu(N—N)_2Cu$ and N_2C_3 rings and the dihedral angle between consecutive $Cu(N—N)_2Cu$ planes. These are the angles labelled α and β, respectively, in Fig. 5 of ref. 2. The angle α increases from 9.10(3)° to 9.87(5)° (13σ) on cooling while β increases from 126.10(3)° to 127.62(3)° (38σ) on cooling.

Changes in the α and β dihedral angles would be expected to affect the dimensions of the polymer perpendicular to the chain direction and therefore the interchain packing and the *a* and *b* cell parameters. The net effect of the increase of 0.77° in α and 1.5° in β on the dimensions of the polymer chain perpendicular to the chain axis can be seen by examining the changes in the *x* and *y* atomic coordinates of C(1) and C(2) on cooling. These represent an increase of the *x* component of Cu.....C by 0.008 and 0.018 Å, respectively, and a decrease of the *y* component by 0.015 and 0.009 Å, respectively. In effect, on cooling, the polymer chains become slightly compressed along *y* and elongated

[2]A complete set of data may be purchased from: The Depository of Unpublished Data, Document Delivery, CISTI, National Research Council Canada, Ottawa, Canada K1A 0S2.

A table of crystallographic data has also been deposited with the Cambridge Crystallographic Data Centre and can be obtained on request from the Director, Cambridge Crystallographic Data Centre, University Chemical Laboratory, 12 Union Road, Cambridge, CB2 1EZ, U.K.

[3]Distinct green and brown forms of the X = Cl compound have been identified (2). The work described in this paper is on the green form.

Can. J. Chem. Downloaded from www.nrcresearchpress.com by 88.255.202.194 on 09/08/12
For personal use only.

TABLE 2. Unit cell parameters[a] for $[Cu(4\text{-}Xpz)_2]_x$ compounds

X	Temperature (K)	*a*	*b*	*c*
H	294[b]	7.917(1)	11.491(2)	7.778(1)
	298[c]	7.944(9)	11.530(10)	7.798(8)
	116[b]	7.870(2)	11.259(2)	7.807(3)
	110[c]	7.910(10)	11.320(10)	7.800(10)
	Δ[d]	−0.047(2)	−0.232(3)	0.029(3)
CH_3	294[b]	9.7436(6)	12.6106(8)	7.7482(6)
	298[c]	9.777(8)	12.630(8)	7.748(7)
	109[c]	9.765(7)	12.458(6)	7.743(6)
	Δ[d]	0.021(7)	−0.153(6)	−0.005(6)
Cl	294[b]	9.155(4)	12.968(6)	7.715(5)
	298[c]	9.152(6)	13.021(7)	7.734(8)
	110[c]	8.813(6)	13.036(8)	7.780(10)
	Δ[d]	−0.342(7)	0.068(10)	0.065(10)
Br	298[c]	9.44(1)	13.32(2)	7.70(1)
	140[c]	9.06(1)	13.49(2)	7.77(1)
	Δ[d]	−0.38(1)	0.17(3)	0.07(1)

[a]Estimated standard deviations in last figure are given in parentheses.
[b]Single crystal data: for X = H, room temperature data from ref. 1, low temperature data, this work; for X = CH_3 and Cl, data from ref. 2.
[c]Powder diffraction data: for X = Br, room temperature data from ref. 2; all other data, this work.
[d]Δ = difference in cell parameters (low temperature data − room temperature data): X = H using single crystal data; X = CH_3, Cl using single crystal data for room temperature; all other data from powders.

TABLE 3. Bond lengths (Å), with estimated standard deviations in parentheses, for $[Cu(4\text{-}Hpz)_2]_x$ at 294 and 116 K

		Distance				Distance	
Atom	Atom	294 K	116 K	Atom	Atom	294 K	116 K
Cu	N	1.957(2)	1.959(2)	C(1)	H(1)	1.02(3)	1.00(2)
N	C(1)	1.345(3)	1.349(2)	C(1)	C(2)	1.371(3)	1.386(2)
N	N[a]	1.359(3)	1.364(2)	C(2)	H(2)	0.80(6)	0.97(4)

[a]$x, y, -z$.

along *x*. As might be anticipated, these changes in the dimensions of the chains perpendicular to the chain axis coincide with changes in chain packing as evidenced by changes in the *a* and *b* unit cell parameters. Specifically, in this case, chain packing becomes more efficient with a decrease in *b* by 0.232(3) Å and a much smaller decrease in *a* by 0.047(2) Å. This latter decrease could arise solely because of decreased thermal motion. It should be noted that there appears to be no simple correlation between the nature of the chain distortion and the effect on individual cell parameters. Hence, while the compression in *y* coincides with a decrease in *b*, the elongation in *x* also coincides with a decrease, albeit very small, in the relevant cell parameter *a*.

Although low-temperature single crystal X-ray diffraction studies are not available for the other three compounds studied here, the changes in their unit cell parameters on cooling, as measured by the powder method, are considered here in relation to possible change in the α and β dihedral angles. The *a* and *b* parameters of the X = CH_3 compound change on cooling in a manner similar to that observed for the X = H compound, although the changes are smaller. In this case the change in *a* is not significant. Such changes would be consistent with small α and β dihedral angle changes like those observed for X = H. The changes in the cell parameters for the X = Cl and Br compounds are very different from those observed for the other two compounds. For these halogen derivatives it is the *a* parameter that decreases significantly on cooling while the *b* parameter shows a small but significant increase (rather than the expected decrease due to thermal effects). The analysis of the X = H compound showed that it is not possible to predict the nature of the distortion perpendicular to the chain axis solely on the basis of the changes in *a* and *b*. Nevertheless the clear difference in the changes in the cell parameters for the two groups of compounds strongly suggests, although it certainly does not prove, that the distortions taking place are fundamentally different. It is possible that in the case of the halogen derivatives the chains are compressed along *x* and elongated along *y*, opposite to the distortion seen in the X = H compound. This form of distortion for the halogen complexes could arise from a decrease in the β dihedral angle and (or) an increase in α.

We turn now to a discussion of how these structural changes might be expected to affect the magnetic properties of these compounds. It was argued previously (2) that the strength of magnetic coupling might be expected to in-

Can. J. Chem. Downloaded from www.nrcresearchpress.com by 88.255.202.194 on 09/08/12
For personal use only.

TABLE 4. Bond angles (deg) with estimated standard deviations in parentheses, for $[Cu(4\text{-}Hpz)_2]_x$ at 294 and 116 K

Atom	Atom	Arom	Angle 294 K	Angle 116 K	Atom	Atom	Atom	Angle 294 K	Angle 116 K
N	Cu	N[b]	99.4(1)	99.19(5)	H(1)	C(1)	N	128(2)	125(2)
N	Cu	N[c]	139.5(1)	140.72(5)	H(1)	C(1)	C(2)	122(2)	124(2)
N	Cu	N[d]	94.3(1)	93.80(5)	N	C(1)	C(2)	110.4(2)	110.3(2)
C(1)	N	N[a]	107.4(1)	107.7(1)	H(2)	C(2)	C(1)	127.4(5)	127.4(3)
C(1)	N	Cu	121.7(1)	121.2(1)	C(1)	C(2)	C(1)[a]	104.3(3)	104.1(2)
N[a]	N	Cu	130.28(5)	130.41(8)					

[a] $x, y, -z$.
[b] $1 - x, -y, z$.
[c] $1 - x, y, 0.5 - z$.
[d] $x, -y, 0.5 - z$.

crease with increasing β and decreasing α. For the X = H compound α and β both increase on cooling. The counter-complimentary effect of these changes probably results in no significant change in the strength of the magnetic coupling on cooling and probably accounts for the fact that the magnetic data for this compound were reasonably well fitted to a model for exchange employing a single J value for the whole temperature region studied (2–300 K). For the X = CH_3 compound similar, probably smaller, changes are suggested in the α and β angles and, consistent with this, the magnetic data for this compound were also reasonably well fitted to a single J model (2). If our conclusion is correct, i.e., that the change on cooling in the a and b cell parameters of the X = Cl and Br compounds is a consequence of a decrease in β and (or) an increase in α, then the magnetic anomalies observed in these systems are readily understood. As discussed previously (2), such changes in the dihedral angles should result in a decrease in the magnitude of exchange coupling. This could account for the poor fit of the 2–300 K magnetic data for these compounds and, more importantly, would explain the discontinuity in the χ_M vs. T plots (2).

In summary, these studies have shown that in copper(II) pyrazolate extended-chain polymers interchain distances may be affected by changes in temperature. This appears to have little effect on intrachain bond lengths and angles but may significantly alter the dihedral angle between fused $Cu(N—N)_2Cu$ and N_2C_3 rings and the dihedral angle between consecutive $Cu(N—N)_2Cu$ planes. Previous studies indicated that changes in these dihedral angles may measurably alter the magnitude of the exchange coupling. Hence the assumption of a single exchange coupling constant value, J, valid over a wide range of temperatures, in the magnetic modelling of these systems may not be totally correct. Such structural effects may contribute to the variation in the quality of fit between experiment and theory for different compounds (2, 3). They also provide an explanation for features such as the discontinuities observed in the χ_M vs. T plots for $[Cu(4\text{-}Clpz)_2]_x$ and $[Cu(4\text{-}Brpz)_2]_x$ (2). Finally, the difficulty in fitting the low-temperature magnetic data for some compounds, which has been ascribed to inadequacies in modelling paramagnetic impurity in the sample (2, 3), may be due at least in part to these structural effects.

Acknowledgements

This research is supported, in part, by grants from the Natural Sciences and Engineering Research Council of Canada.

1. M. K. Ehlert, S. J. Rettig, A. Storr, R. C. Thompson, and J. Trotter. Can. J. Chem. **67**, 1970 (1989).
2. M. K. Ehlert, S. J. Rettig, A. Storr, R. C. Thompson, and J. Trotter. Can. J. Chem. **69**, 432 (1991).
3. M. K. Ehlert, A. Storr, and R. C. Thompson. Can. J. Chem. **70**, 1121 (1992).
4. C. J. O'Connor. *In* Progress in inorganic chemistry. Vol. 29. *Edited by* S. J. Lippard. John Wiley and Sons, New York. 1982. p. 203.
5. A. C. T. North, D. C. Phillips, and F. S. Mathews. Acta. Crystallogr. Sect. A: Cryst. Phys. Diffr., Theor. Gen. Crystallogr. **A24**, 351 (1968).
6. E. J. Gabe, Y. Lepage, J-P Charland, F. J. Lee, and P. S. White. NRCVAX—An interactive program system for structure analysis. J. Appl. Crystallogr. **22**, 384 (1989).
7. International tables for X-ray crystallography. Vol. IV. Kynoch Press, Birmingham. 1975. p. 99.

Can. J. Chem. Downloaded from www.nrcresearchpress.com by 88.255.202.194 on 09/08/12
For personal use only.

Ab initio studies on the reaction $SN^+ + SNS^+ \rightarrow S_3N_2^{2+}$

F. GREIN

Department of Chemistry, University of New Brunswick, Fredericton, N.B., Canada E3B 6E2

Received October 22, 1992

F. GREIN. Can. J. Chem. **71**, 335 (1993).

The reaction $SN^+ + SNS^+ \rightarrow S_3N_2^{2+}$ has been studied by *ab initio* SCF methods. Geometry optimizations with the 3-21G(*) basis set were followed by 6-31G* single-point calculations. The barrier of $S_3N_2^{2+}$ to dissociation is 10.9 kcal/mol with 3-21G(*), and 19.7 kcal/mol with the (single-point) 6-31G* basis set. The transition structure is cyclic (C_s), and is similar to the optimized C_{2v} structure of $S_3N_2^{2+}$. The relative orientation of the two approaching cations is governed by electrostatic forces rather than electronic (frontier orbital) effects. The product lies 99.3 (3-21G(*)) and 95.2 (6-31G*) kcal/mol higher than the reactants.

F. GREIN. Can. J. Chem. **71**, 335 (1993).

Faisant appel à des méthodes *ab initio* en champ auto-cohérent, on a étudié la réaction $SN^+ + SNS^+ \rightarrow S_3N_2^{2+}$. Après avoir effectué des optimisations de la géométrie à l'aide de l'ensemble 3-21G(*), on a effectué des calculs 6-31G* en point unique. La barrière à la dissociation de l'ion $S_3N_2^{2+}$ est égale à 10,9 kcal/mol lorsqu'on utilise l'ensemble 3-21G(*) alors qu'elle est égale à 19,7 kcal/mol avec l'ensemble 6-31G* (point unique). La structure de transition est cyclique (C_s) et elle est semblable à la structure C_{2v} optimisée de l'ion $S_3N_2^{2+}$. L'orientation relative des deux cations qui s'approchent est plutôt déterminée par des forces électrostatiques que des effects électroniques (orbitales frontières). Suivant les ensembles utilisés, l'énergie du produit est 99,3 (3-21G(*)) et 95,2 (6-31G*) plus élevée que celle des réactifs.

[Traduit par la rédaction]

Introduction

$S_3N_2^{2+}$, in the form of the heterocycle $\overline{SNSNS}^{2+}$, structure **1**, has recently been characterized by Passmore and coworkers (1). Crystalline material of $S_3N_2^{2+}(AsF_6^-)_2$ is formed by the symmetry-allowed cycloaddition reaction

[1] $SNS^+ + SN^+ \rightarrow \overline{SNSNS}^{2+}$

Although in the gas phase $S_3N_2^{2+}$ is about 100 kcal/mol less stable than the reactants $SNS^+ + SN^+$, in the solid state it is stabilized by the large difference in crystal lattice energy between $S_3N_2(AsF_6)_2$ (355.5 kcal/mol) and $SNAsF_6 + SNSAsF_6$ (253.6 kcal/mol), as estimated in ref. 1. In solution, **1** decomposes back to $SNS^+ + SN^+$.

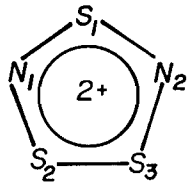

1

C_{2v} *min.*

Geometry optimizations at the 6-31G* level on **1**, as well as on SNS^+ and SN^+, have previously been reported by us (1) and by Gimarc and Warren (2). The results are summarized in Table 1. The optimized geometry of **1**, shown in Fig. 1*a*, is remarkably close to the structure found by X-ray crystallography (1), also given in Table 1.

The detailed mechanism of reaction [1], which is highly endothermic in the gas phase but exothermic in the solid state, is of interest. For this reason, the path of reaction [1] (obviously restricted to the gas phase) has been followed by *ab initio* studies.

SNS^+ is a three-atom, four-electron π system, and is similar to 1,3-dipoles (3). Both the π_g-HOMO and the π_u-LUMO of SNS^+ have suitable symmetry to interact with the π^*-LUMO and the π-HOMO of SN^+, respectively. Since HOMO(SNS^+) and LUMO(SN^+) lie closer in energy than the opposite pair of frontier orbitals, the cycloaddition reaction [1] can be seen as proceeding from the HOMO of SNS^+ to the LUMO of SN^+. It therefore resembles "type I" cycloadditions as classified by Sustmann (in ref. 3). Mulliken charges, to be given later, will confirm this predicted charge transfer from SNS^+ to SN^+.

Since the LUMO of SN^+ has a larger orbital coefficient on S than on N, an initial approach of SNS^+ to SN^+ via the terminal sulfur atoms, $S^{(+)}NS^{(+)}\cdots S^+N$, is expected if the approach is orbital controlled. However, the positive charge of each reactant is mainly located on the sulfur atoms, causing strong electrostatic repulsion of the sulfurs. Based on electrostatic arguments one therefore predicts as initial approach $S^{(+)}NS^{(+)}\cdots NS^+$ or a T-shaped version with the two nitrogens being closest.

In performing the reaction path calculations, both approaches, the orbital-controlled and the electrostatic repulsion-controlled one, have been considered. The cycloaddition reaction prefers the latter approach, as will be shown.

A well-studied example in the literature of a dictation reaction is the dissociation

$$CH_4^{2+} \rightarrow CH_3^+ + H^+$$

which is calculated to be exothermic by about 100 kcal/mol, and has a barrier to dissociation of about 17 kcal/mol (4, 5).

Methods

Geometry optimizations on the supermolecule $SNS^+ \cdot SN^+$ were performed with the GAUSSIAN 86 program (6) using the 3-21G(*) basis set. Here, polarization functions are added to the S, but not to the N atoms. The geometries of $S_3N_2^{2+}$, SNS^+, and SN^+ were reoptimized using this smaller basis set, and the results, also given in Table 1 and Fig. 1*b*, show that the optimized geometry parameters, as well as energy differences, are close to the 6-31G* results. The S—N distances differ by less than 0.01 Å, while the S—S distance differs by about 0.06 Å.

Due to the large number of geometries that had to be studied (see

Can. J. Chem. Downloaded from www.nrcresearchpress.com by 88.255.202.194 on 09/08/12
For personal use only.

Can. J. Chem. Downloaded from www.nrcresearchpress.com by 88.255.202.194 on 09/08/12
For personal use only.

TABLE 1. Optimized geometries (distances in Å, angles in degree), energies E (in hartree), and energy differences ΔE (in kcal/mol), of $S_3N_2^{2+}(C_{2v})$, $SNS^+(D_{\infty h})$, and SN^+. For numbering of atoms see structure **1**

	3-21G(*)	6-31G*	Expt.[a]
$S_3N_2^{2+}$			
R(S2—S3)	2.152	2.092	2.093
R(S1—N1)	1.601	1.596	1.591
R(N1—S2)	1.529	1.535	1.532
α(S1—N2—S3)	127.84	124.34	122.6
β(S2—S3—N2)	94.24	96.24	96.8
γ(N1—S1—N2)	95.85	98.84	101.5
E	−1294.371078	−1300.504033	
SNS^+			
R(S—N)	1.478	1.474	1.501[b](1.480)[c]
E	−845.110452	−849.090238	
SN^+			
R(S—N)	1.401	1.397	1.42[b](1.361)[c]
E	−449.418766	−451.565526	
ΔE[d]	99.3	95.2	

[a]Reference 1.
[b]Corrected for thermal effects.
[c]Uncorrected value.
[d]$S_3N_2^{2+}$ less stable than $SNS^+ + SN^+$ by this amount.

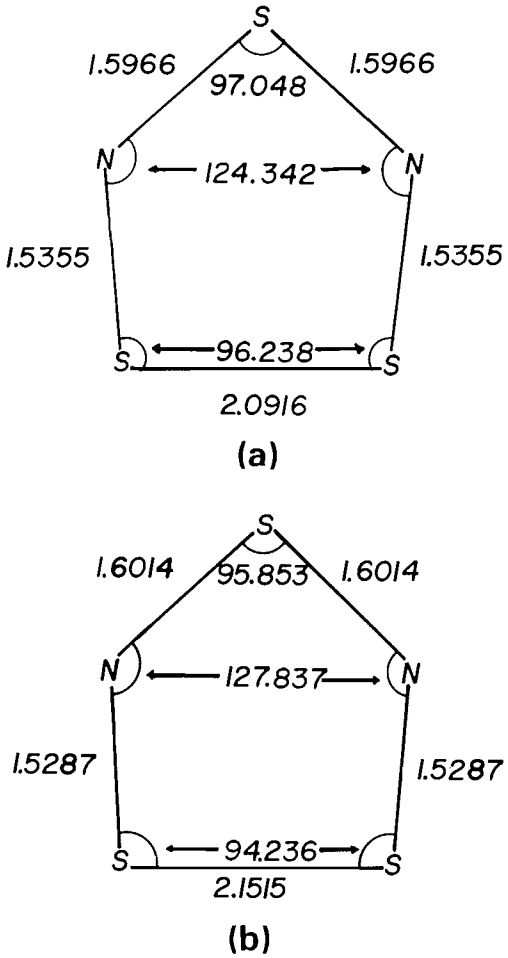

FIG. 1. Optimized geometry of $S_3N_2^{2+}$. (*a*) 6-31G* basis set; (*b*) 3-21G(*) basis set.

below), use of a basis set larger than 3-21G(*) for the bulk of the calculations would have made the computations prohibitively expensive.

The procedure for obtaining the transition structure (TS) was complicated because no single internal coordinate could serve as reaction coordinate, in the sense that varying such a coordinate from large to small values would bring the system smoothly from the separated reactants over the transition structure to the product. The procedure used will be outlined in the next section. Planar symmetry (C_s) was maintained throughout the reaction path.

Procedure and results

Midpoint approach

The distance between the midpoints of SNS^+ and SN^+, called R_{MM}, was taken as the initial reaction coordinate (see structure **2**). The potential curve with respect to R_{MM} is shown

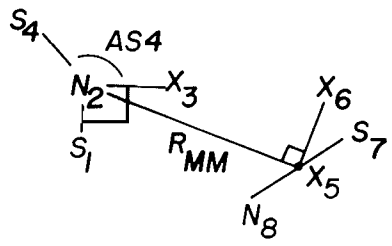

2

in Fig. 2. According to the classification presented in the Introduction, this choice of reaction path allows the molecule to orient itself under the influence of electrostatic forces (as well as frontier orbital interactions). It is more flexible than the S—S approach to be discussed in the next section.

For R_{MM} values above 3 Å, the supermolecule forms a C_{2v} structure, **3** (Scheme 1), with the two nitrogens facing each other. This can be ascribed to minimization of the electro-

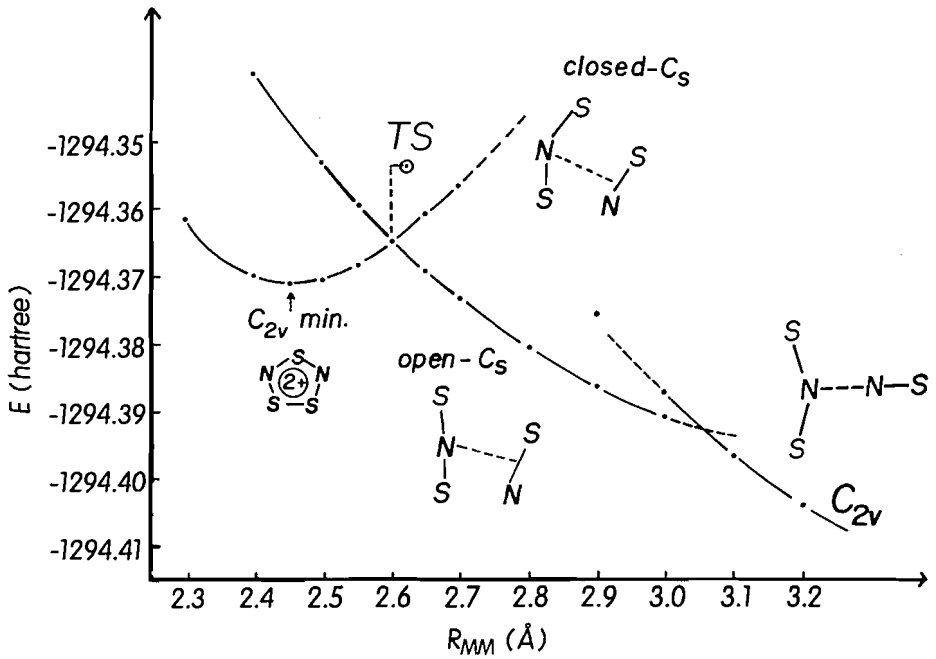

FIG. 2. Minimum energy path for reaction $SNS^+ + SN^+ \rightarrow S_3N_2^{2+}$, using R_{MM} (as defined in structure **2**) as reaction coordinate.

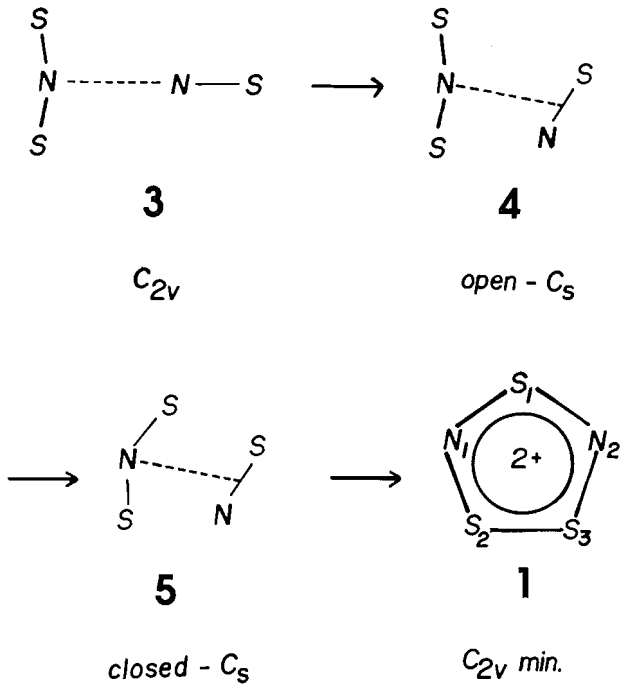

SCHEME 1

static repulsion between SNS^+ and SN^+ since the two nitrogens carry the least positive charge. At R_{MM} = 3 Å it is possible to optimize both a C_{2v} and a C_s structure. The latter, shown in **4** for about 3 Å, has slightly lower energy. It will be designated as the "open-C_s" structure, as contrasted to the "closed-C_s" structure **5** to become important at smaller values of R_{MM}. Figure 2 shows that the C_{2v} and open-C_s curves cross around 3.05 Å.

As R_{MM} decreases, the open-C_s energy increases, until the open-C_s curve crosses the closed-C_s curve around 2.6 Å. In the vicinity of 2.6 Å, both an open-C_s and a closed-C_s structure can be optimized. For example, at 2.55 Å the two structures differ in energy by 5.57 kcal/mol, with the closed-C_s being more stable. With further lowering of R_{MM}, the closed-C_s energy decreases, until it reaches a minimum of C_{2v} symmetry, corresponding to the most stable structure of $S_3N_2^{2+}$, as found earlier. Open and closed C_s energies for selected values of R_{MM} around 2.6 Å are given in Table 2. There is no change of electronic configuration when going from the open-C_s to the closed-C_s structure.

TABLE 2. Relative energies ΔE (in kcal/mol) for the reaction $SNS^+ + SN^+ \rightarrow S_3N_2^{2+}$. See structure **2** for definition of R_{MM}

R_{MM} (Å)	ΔE closed-C_s	ΔE open-C_s
2.152[a]	0	—
2.5	0.40	11.0
2.55	1.71	7.28
2.6	3.73	3.98
2.7	8.70	−1.54
2.8	—	−5.97

[a] C_{2v} symmetry.

At, or close to, 2.6 Å the lowest-energy structure changes abruptly (when seen as function of R_{MM}) from open to closed-C_s. It is obvious that in a smooth structural change, e.g., by varying the angle AS4 in **2** from the open to the closed value, the energy has to go over a barrier. With this in mind, AS4 was chosen as the second reaction coordinate. Keeping R_{MM} at a fixed value, e.g., 2.6 Å, and varying AS4, all other geometry parameters were optimized. As shown in Fig. 3, for R_{MM} at 2.6 Å a maximum is obtained for AS4 = 60°, 7.2 kcal/mol above the closed-C_s energy at 2.6 Å. The potential curves for closing the molecule at 2.5 and 2.7 Å are also shown in Fig. 3. The maximum shifts to 70° and 50°, respectively, and is higher in energy than for R_{MM} = 2.6 Å.

Can. J. Chem. Downloaded from www.nrcresearchpress.com by 88.255.202.194 on 09/08/12
For personal use only.

Can. J. Chem. Downloaded from www.nrcresearchpress.com by 88.255.202.194 on 09/08/12
For personal use only.

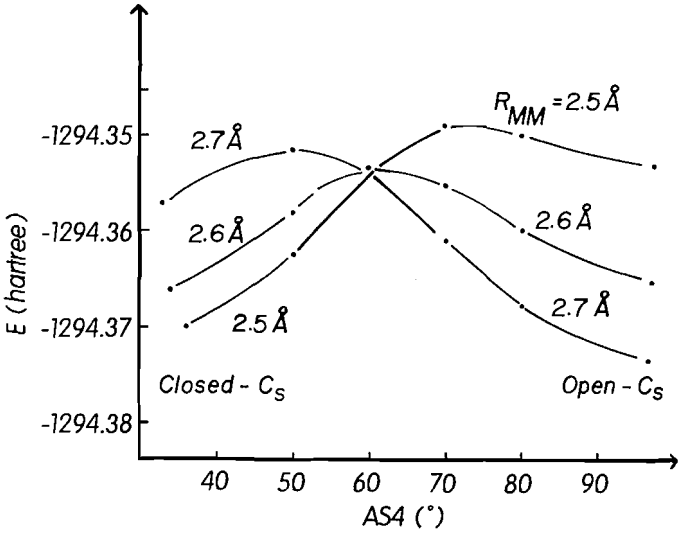

FIG. 3. Potential energies of $S_3N_2^{2+}$, for transition from open to closed C_s structure, as function of angle AS4 (as defined in structure **2**). The distances labeling each curve are the R_{MM} parameters.

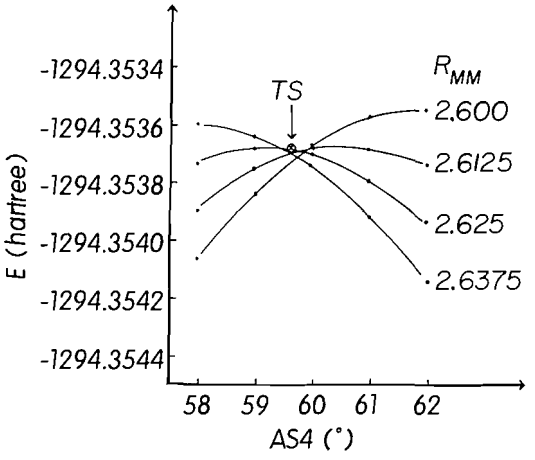

FIG. 4. Refined potential energies as function of angle AS4.

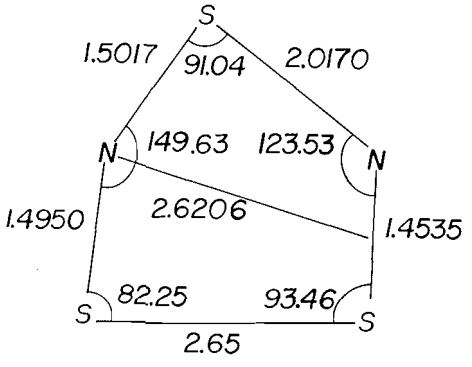

FIG. 5. Optimized geometry of transition structure of $S_3N_2^{2+}$.

A series of calculations for a grid of R_{MM}/AS4 values, with R_{MM} close to 2.6 Å and AS4 close to 60°, was performed in order to refine the potential curves for ring closure and to locate the transition structure. In Fig. 4, potential curves are shown for R_{MM} between 2.6 and 2.6375 Å, and AS4 angles

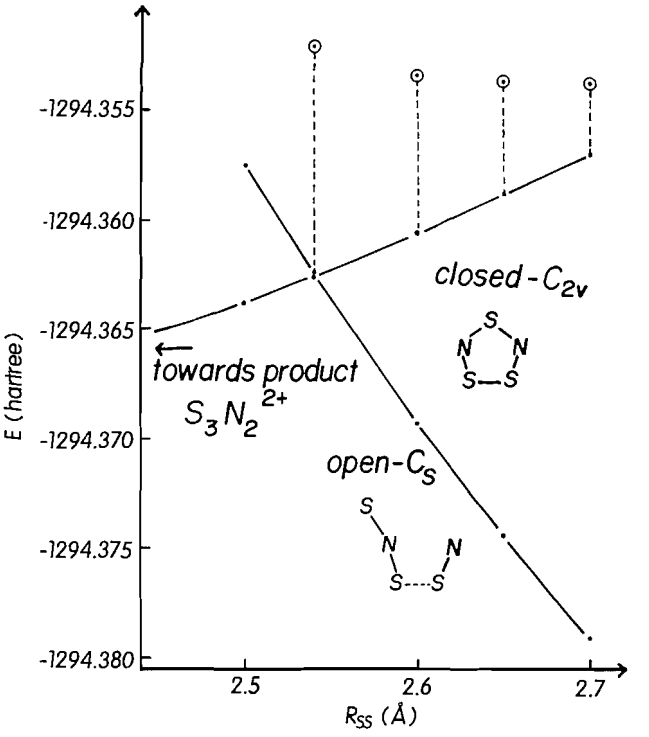

FIG. 6. Minimum energy path for reaction $SNS^+ + SN^+ \rightarrow S_3N_2^{2+}$, using R_{SS} (structure **6**) as reaction coordinate.

from 58° to 62°. The lowest barrier now occurs between 2.6125 Å (~60.5°) and 2.625 Å (~59°). Further refinement leads to a TS with R_{MM} = 2.620625 Å and AS4 = 59.625°, having an energy 7.19 kcal/mol above the closed-C_s energy at 2.6 Å, and 10.92 kcal/mol above the C_{2v} minimum product structure. The geometry of this transition structure is shown in Fig. 5.

S—S approach

Both HOMO of SNS^+ and LUMO of SN^+ are π^*-type orbitals. The HOMO of SNS^+ has, for symmetry reasons, no atomic orbital on N. The LUMO of SN^+ is more pronounced on S than N. Using frontier orbital arguments only, one would expect that the two cations approach each other via the terminal sulfur atoms. Accordingly, another series of

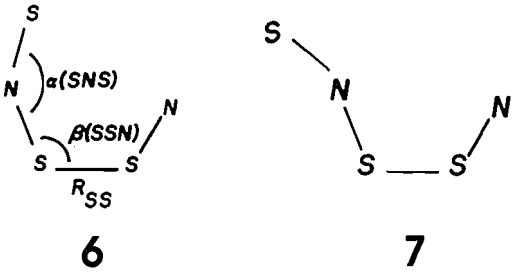

calculations was performed to find the reaction pathway and transition state of reaction [1]. Now the initial reaction coordinate was chosen to be R_{SS}, the distance between the terminal S atoms of SNS^+ and SN^+ (structure **6**).

At large R_{SS} values, a T-shaped C_{2v} structure, as discussed above, has (for a given R_{SS}) a higher energy than the open-C_s structure **7**. As shown in Fig. 6, the open-C_s energy increases as R_{SS} decreases, and a crossing occurs around 2.54 Å with a closed-C_{2v} structure (and probably also a closed-C_s structure). The closed-C_s curve reaches a mini-

TABLE 3. Mulliken charges for atoms of $SNS^+ + SN^+$. For numbering of atoms see structure **2**

R_{MM} (Å)	S1	N2	S4	SNS^+	S7	N8	SN^+
3.5, $-C_{2v}$	0.657	−0.313	0.657	1.001	0.997	0.001	0.998
3.0, $-C_{2v}$	0.670	−0.307	0.670	1.033	1.002	−0.034	0.968
3.0, $-C_s$	0.774	−0.354	0.613	1.033	0.940	0.027	0.967
2.8, $-C_s$	0.818	−0.368	0.634	1.084	0.909	0.007	0.916
2.6206, −TS	1.067	−0.415	0.772	1.424	0.857	−0.281	0.576
2.152, $-C_{2v}$	1.223	−0.467	0.856	1.612	0.856	−0.467	0.389

mum at R_{SS} = 2.152 Å for the product $S_3N_2^{2+}$. At the crossing point an abrupt change from open-C_s to cyclic C_{2v} occurs, and a second reaction coordinate had to be chosen. For a selected value of R_{SS}, the angle α(SNS) (**6**) was varied from the open-C_s to the closed-C_{2v} value. The energy maximum for a given R_{SS} is indicated in Fig. 6 by a vertical bar. It is seen that the transition structure lies between R_{SS} = 2.65 and 2.70 Å. A third reaction coordinate was needed for which the angle β(SSN) (**6**) was chosen. Finally, the TS was located at R_{SS} = 2.65 Å, α = 149.73°, and β = 82.25°, 10.92 kcal/mol above the C_{2v} minimum. The transition structures obtained by the two methods are (fortunately) identical.

The last-described procedure, which starts with R_{SS} instead of R_{MM} as the initial reaction coordinate, suffers from the same problem as the first method, namely, that there is no suitable single reaction coordinate. It is actually more complicated, since energies over a three-dimensional rather than a two-dimensional grid of geometry parameters had to be evaluated. The choice of R_{SS} led to a nonsymmetrical separation of the product into reactants, whereas the midpoint-to-midpoint approach shows $S_3N_2^{2+}$ to separate into $SNS^+ + SN^+$ having T-shaped C_{2v} symmetry.

Discussion

The transition structure of eq. [1] was found by calculating the energies in a two-dimensional (or three-dimensional) grid. A transition state optimization was not possible since the minimum energy path cannot be described as a function of any one internal coordinate as defined here, but goes diagonally through a grid involving distances and angles. For the same reason, frequency calculations at the TS could not be performed. Due to the low level of basis set used in the optimizations, zero point energy corrections were not found to be helpful. It is intended to carry out 6-31G* geometry optimization if and when better computing resources become available.

All optimizations were performed on planar $S_3N_2^{2+}$. A nonplanar TS cannot be ruled out. It could further lower the energy barrier. Exploratory calculations on nonplanar structures close to the TS were performed. While by no means conclusive, they showed in each case a preference (lower energy) for the planar structure.

The energy of the TS lies 10.9 kcal/mol above the optimized $S_3N_2^{2+}$ structure, and 110.2 kcal/mol above the energy of the reactants $SNS^+ + SN^+$. Single point 6-31G* calculations at the optimized 3-21G(*) geometries of the product and the TS led to an energy difference of 19.7 kcal/mol. However, due to the lack of 6-31G* geometry optimization of the TS, the above number is not considered to be as trustworthy as the 3-21G(*) value.

The transition structure, Fig. 5, is basically cyclic. The SNS^+ and SN^+ units are clearly discernible. Within the SNS^+ unit the bond distances are slightly longer than in free SNS^+ (by about 0.02 Å), whereas the bond angle has changed from 180° to 149.7°. For SN^+ the bond distance is about 0.05 Å larger than in free SN^+. The distances separating SNS^+ and SN^+ are large, 2.65 Å for S—S and 2.02 Å for N—S. The major structural change seen in the TS relative to the reactants is the bending of SNS^+.

At large distances, SNS^+, essentially linear, stands at right angles to SN^+, with the nitrogens, the least positive elements, facing each other. The reasons for this geometry are purely electrostatic. As the distance between the two units decreases, the T-shaped C_{2v} configuration cannot be maintained, and the open-C_s structure, with the two terminal S atoms pointing away from each other, results. Around R_{MM} = 2.6206 Å, the value for the TS (R_{TS}), the open-C_s structure has to become cyclic, which is accomplished by bending SNS^+ towards SN^+. At R_{MM} values below R_{TS}, the supermolecule moves towards the product $S_3N_2^{2+}$, having C_{2v} symmetry.

Using frontier orbital arguments, and neglecting electrostatic repulsions, an initial approach of one of the terminal S atoms of SNS^+ to the S atom of SN^+ would have been predicted. The calculated energies and geometries show that electrostatic repulsions play a more important role than electronic efforts at least in the initial approach of two cations.

In Table 3, the Mulliken charges are given for some typical values of R_{MM}, starting with the C_{2v} structure at 3.5 Å, going to the C_{2v} and open-C_s structures at 3 Å, the open-C_s structure at 2.8 Å, the transition structure, and finally the C_{2v} product. Consistent with frontier orbital arguments, the positive charge on SNS^+ (HOMO) increases, whereas it decreases on SN^+ (LUMO) as one moves from the reactants towards the product. An astonishing amount of charge (0.6 units in the Mulliken picture) is transferred from SNS^+ to SN^+.

Looking at the internal charge distribution, at large separation SN^+ has all positive charge located on S, whereas SNS^+ has N negative (−0.313), and each S therefore positive by more than 0.5 charge units. At the minimum of $S_3N_2^{2+}$, the N's are even more negative. Starting again from the reactants, N2 and N8 (**2**) become more negative, the charge on N2 going from −0.313 to −0.467, and on N8 from 0 to −0.467. Therefore, the S atoms together have to become more positive. S1 and S4, originally associated with SNS^+, go from 0.657 to 1.223 for S1, and from 0.657 to 0.856 for S4. On the other hand, S7 (of SN^+) started out with a charge of 1, and goes to 0.856, becoming thereby less positive.

Can. J. Chem. Downloaded from www.nrcresearchpress.com by 88.255.202.194 on 09/08/12
For personal use only.

Considering that the geometrical structures change several times when going from reactants to product (C_{2v} reactants, open-C_s, closed-C_s, C_{2v} product), the charges vary smoothly over the reaction path. The dominant feature of reaction [1], as far as charges are concerned, is the gradual accumulation of negative charge on the nitrogens, and the associated depletion of electrons from the sulfurs. The pattern of sulfur charges is consistent with the S...F cation–anion contacts in the crystal, as reported by Passmore and co-workers (7). S1 has the strongest contact (0.62 valence units, calculated charge of 1.223) while the base sulfur atoms have contacts of 0.5 valence units (charge of 0.856).

In an experimental study on cycloadditions of SNS^+ to alkynes, nitriles, and thiazyl halides, Parsons *et al.* (8) state that, at least for the nitrile cycloadditions, steric factors are found to be unimportant, implying "a highly asynchronous, early transition state." The gas-phase reaction $SNS^+ + SN^+$ is also asynchronous, but has a late transition state in agreement with Hammond's postulate, since the reactants are at much lower energy than the product. The TS itself looks like a slightly distorted blown-up version of the product. Due to the large electrostatic repulsion between the two fragments, a late transition state is expected for the gas phase reaction.

Summary and conclusion

Due to the strong Coulomb repulsions, the formation of the dictation $S_3N_2^{2+}$ from two cations SN^+ and SNS^+ is expected and found to be highly endothermic with an energy of 95–99 kcal/mol, depending on basis set. The barrier to dissociation of $S_3N_2^{2+}$ is calculated to be 10.9 kcal/mol.

$S_3N_2^{2+}$ is known in crystal form as $S_3N_2(AsF_6)_2$ but dissociates in solution, and does not exist in the gas phase.

The transition structure looks similar to the $S_3N_2^{2+}$ product, as expected from Hammond's postulate. The dissociation of $S_3N_2^{2+}$ occurs via distortion from the C_{2v} minimum to a closed-C_s structure, further by ring-opening to an open-C_s structure, and finally at large distances to a symmetric C_{2v} structure, with a T-shaped $SNS^+...NS^+$ having the two nitrogen atoms face each other. The electrostatic interaction between the two cations, rather than frontier orbital considerations, dominate the reaction path.

The cation SNS^+ has been found to undergo many novel chemical reactions, and further theoretical work on reactions of SNS^+ with other systems is of interest.

Acknowledgements

The author is much indebted to Jack Passmore for suggesting this project and for his continuous support and interest in this work. Special thanks go to Simon Parsons for carefully reading the manuscript and for making valuable suggestions towards its improvement. Robert Mawhinney is thanked for drawing several of the structures.

Financial support by the Natural Sciences and Engineering Research Council of Canada (NSERC) and allocation of computing resources by the University of New Brunswick are gratefully acknowledged.

1. W. V. F. Brooks, T. S. Cameron, F. Grein, S. Parsons, J. Passmore, and M. J. Schriver. J. Chem. Soc. Chem. Commun. **16**, 1079 (1991).
2. B. M. Gimarc and D. S. Warren. Inorg. Chem. **30**, 3276 (1991).
3. R. Huisgen. *In* 1,3-dipolar cycloaddition chemistry. *Edited by* A. Padwa. John Wiley, New York. 1984.
4. J. A. Pople, B. Tidor, and P. v. R. Schleyer. Chem. Phys. Lett. **88**, 533 (1982).
5. P. E. M. Siegbahn. Chem. Phys. **66**, 443 (1982).
6. M. J. Frisch, J. S. Binkley, H. B. Schlegel, K. Raghavachari, C. F. Melius, R. L. Martin, J. J. P. Stewart, F. W. Bobrowicz, C. M. Rohlfing, L. R. Kahn, D. J. Defrees, R. Seeger, R. A. Whiteside, D. J. Fox, E. M. Fleuder, and J. A. Pople. Gaussian 86. Carnegie Mellon Quantum Chemistry Publishing Unit, Pittsburgh, Pa. 1984.
7. W. V. F. Brooks, T. S. Cameron, S. Parsons, J. Passmore, and M. J. Schriver. Inorg. Chem. Submitted.
8. S. Parsons, J. Passmore, M. J. Schriver, and X. Sun. Inorg. Chem. **30**, 3342 (1991).

Can. J. Chem. Downloaded from www.nrcresearchpress.com by 88.255.202.194 on 09/08/12
For personal use only.

The dipole oscillator strength distribution and predicted dipole properties for ammonia

GORDON R. BURTON, WING FAT CHAN, GLYN COOPER, AND C. E. BRION[1]
Department of Chemistry, The University of British Columbia, Vancouver, B.C., Canada V6T 1Z1

AND

ASHOK KUMAR[2,3] AND WILLIAM J. MEATH[3]
Department of Chemistry, The University of Western Ontario, London, Ont., Canada N6A 5B7

Received October 14, 1992

GORDON R. BURTON, WING FAT CHAN, GLYN COOPER, C. E. BRION, ASHOK KUMAR, and WILLIAM J. MEATH. Can. J. Chem. **71**, 341 (1993).

Newly available and highly accurate oscillator strength data, extending over the continuous energy range from the first excitation threshold to 200 eV, are used together with mixture rule estimates and other photoabsorption data to construct a refined dipole oscillator strength distribution to infinite photon energy using Thomas–Reiche–Kuhn sum rule and molar refractivity constraints. This constrained dipole oscillator strength distribution has been used to calculate a wide range of related dipole properties (S_k, k = 2, 1, 0, −1/2, −1, −3/2, −2, −5/2, −3, −4, −5, −6, −8, −10, −12; L_k and I_k, k = 2, 1, 0, −1, −2). The theoretical analysis and associated consistency checks support the high accuracy of the newly available absolute oscillator strengths for the photoabsorption of NH_3.

GORDON R. BURTON, WING FAT CHAN, GLYN COOPER, C. E. BRION, ASHOK KUMAR et WILLIAM J. MEATH. Can. J. Chem. **71**, 341 (1993).

Faisant appel à la règle des sommes de Thomas–Reiche–Kuhn et à des contraintes de réfractivité molaire, et utilisant une combinaison de nouvelles données très précises relatives à la force d'oscillateur dipolaire couvrant l'ensemble continue des énergies allant du seuil de la première excitation jusqu'à 200 eV avec des évaluations de la règle de mélange et d'autres données de photoabsorption, on a construit une distribution raffinée de la force d'oscillateur dipolaire jusqu'à une énergie photonique infinie. On a utilisé cette distribution de la force d'oscillateur dipolaire pour calculer un grand ensemble de propriétés dipolaires apparentées (S_k, k = 2, 1, 0, −1/2, −1, −3/2, −2, −5/2, −3, −4, −5, −6, −8, −10 et −12; L_k et k = 2, 1, 0, −1 et −2). L'analyse théorique et des vérifications de la cohérence associée supportent la grande exactitude des nouvelles forces absolues d'oscillateurs dipolaires pour la photoabsorption du NH_3.
[Traduit par la rédaction]

1. Introduction and background

Ammonia has been observed in the interstellar medium, molecular clouds (1, 2), and in the atmospheres of Saturn and Jupiter (3) and is of importance in photochemistry, being a low-energy source of NH_2 and NH radicals (4). Therefore the absolute photoabsorption oscillator strengths (cross sections) for NH_3 over the entire electromagnetic spectrum, and the related dipole properties, are of interest to astrophysicists and others wishing to model the interaction of energetic radiation and particles with this molecule. There is also considerable interest in the possibility of using additivity concepts and mixture rules to estimate the quantitative aspects of the interaction of energetic electromagnetic radiation with large and complex molecules and to evaluate the properties of these molecules from those of smaller, related species (5–9). Therefore the present analysis for NH_3 will be used to provide a foundation that will be extended in subsequent work[4] to include the absolute photoabsorption oscillator strength distributions and dipole properties for monomethylamine (methanamine), dimethylamine (*N*-methylmethanamine), trimethylamine (*N*,*N*-dimethylmethanamine), and also the higher *n*-alkylamines. By comparing the oscillator strength distributions and dipole properties of ammonia and the methylamines an indication of the effect on the oscillator strength distribution, and the dipole properties, of adding methyl or amino groups to larger molecules can be assessed.

The discrete region of the valence-shell photoabsorption spectrum of ammonia has been the subject of numerous experimental studies, presumably owing to the wealth of spectral features below the first ionization threshold. The earliest experiments used photographic techniques and were performed primarily to determine the energy positions of the various observed electronic, vibrational, and rotational transitions rather than transition probabilities. A variety of experiments using conventional light sources or synchrotron radiation have been aimed at also obtaining absolute photoabsorption cross-section data for the valence shell of ammonia (11–28). Electron-impact based techniques have also proved useful in determining the optical oscillator strengths for the photoabsorption of the lowest energy transition in NH_3, by the tedious method of extrapolation of a series of generalized oscillator strength measurements for each transition to zero momentum transfer (29). Absolute total photoabsorption and also partial photoionization oscillator strengths (cross sections) for molecular and dissociative photoionization of NH_3, as well as for the production of electronic states of ions, have been obtained directly over wide energy ranges in the VUV and soft X-ray region at low

[1]Author to whom correspondence may be addressed.
[2]Permanent address: Department of Physics, Meerut University, Meerut 250004, India.
[3]Associated with the Centre for Interdisciplinary Studies in Chemical Physics, University of Western Ontario, London. Ont., Canada N6A 5B7.
[4]A. Kumar, W. J. Meath, G. R. Burton, G. Cooper, W. F. Chan, and C. E. Brion. Manuscript in preparation.

Can. J. Chem. Downloaded from www.nrcresearchpress.com by 88.255.202.194 on 09/08/12
For personal use only.

Can. J. Chem. Downloaded from www.nrcresearchpress.com by 88.255.202.194 on 09/08/12
For personal use only.

resolution by the techniques of dipole (e,e), (e,e+ion), and (e,2e) spectroscopy, respectively (30–32). These dipole techniques, using the broad spectral range and constant flux of the virtual photon field created by a fast inelastically scattered electron, at negligible momentum transfer, provide a direct route to obtaining reliable absolute optical oscillator strengths for photoabsorption and photoionization processes over wide energy ranges up to several hundreds of electron volts (27, 33, 34). In these dipole experiments (27, 33) the absolute photoabsorption oscillator strength scale has usually been established using a valence-shell adapted Thomas–Reiche–Kuhn (TRK) sum rule with allowance for the Pauli-excluded transitions from inner shells to the already occupied valence orbitals. This method of establishing the absolute scale avoids difficulties such as determinations of absolute target density and photon flux that are required in traditional optical methods for absolute cross-section scale determinations. These fast electron impact techniques have proven to be an extremely viable and completely independent alternative to direct optical methods for the measurement of photoabsorption oscillator strengths in the VUV and soft X-ray regions (27). In particular, the problems of contributions from higher-order electromagnetic radiation, which can occur with monochromated synchrotron radiation, are avoided and measurements can be obtained at a constant energy resolution over a wide spectral range. Furthermore, since the electron impact process is non-resonant, and because no logarithmic transform is involved, the high-resolution optical oscillator strength spectrum determined with dipole (e,e) spectroscopy in the region of discrete excitation will be free of the "line-saturation" (i.e., bandwidth) effects that can often seriously perturb intensities obtained in discrete photoabsorption spectra using Beer–Lambert Law techniques (35, 36).

The reliable direct experimental determination or *ab initio* calculation of most of the dipole properties for molecules the size of NH_3 is not at present feasible. However, these properties can be evaluated if globally reliable molecular dipole oscillator strength distributions (DOSDs) are available for all values of the excitation energy from the electronic photoabsorption threshold to very high energy. Such DOSDs can be constructed, by using quantum mechanical constraint techniques (37–42), if sufficient photoabsorption oscillator strength (cross section) and accurate molar refractivity data are available for the molecules of interest. Using this approach a constrained DOSD can be constructed and used to reliably compute a wide variety of dipole properties (43, 44) including the mean excitation energies, and other dipole properties associated with the Lamb shift, and with the straggling, stopping, and total inelastic scattering of fast charged particles in matter (7, 8, 44). Nitrogen-containing organic compounds are of importance in the latter context because of their occurrence in molecules of biological and radiological interest. The presently determined DOSD and dipole properties of ammonia, and the subsequent studies of the methylamines,[4] will provide a fundamental foundation for the investigation of the interaction of larger nitrogen-containing molecules with energetic electromagnetic radiation at UV and X-ray energies.

The constrained least-squares method used here to construct the DOSD, and to evaluate the dipole properties, for ammonia was previously used with considerable success for a variety of molecules (37, 38, 45–51). The previous DOSD studies of NH_3 (37) were, of course, based on the then available absolute photoabsorption oscillator strength data. While they were reasonably successful, the results were limited by inconsistencies between, and the limited energy ranges of, the various available oscillator strength data sets; for details see ref. 37. Recent DOSD analyses,[5] which served as a preliminary basis for the study reported here, have confirmed the inconsistencies and limitations of the currently available absolute photoabsorption oscillator strength data for ammonia and indicated the need for new comprehensive measurements over as wide an energy range as possible. New measurements should also include the valence-shell discrete excitation spectrum at high resolution since no reliable continuous absolute data set is available throughout this low-energy region.

In this paper we make a constrained DOSD analysis of new high- and low-resolution measurements of the absolute oscillator strengths for NH_3 over the entire energy range from the first excitation threshold to 200 eV. A detailed account of the experimental data, including extensive tabular data, together with a spectral analysis of these comprehensive measurements, is to be published elsewhere.[6] The low- and high-resolution oscillator strength data measurements are presented in Fig. 1 and, as integrals over suitable energy blocks, in Table 1. They are used together with molar refractivity data (54–56) to obtain constrained DOSDs, which in turn are used to calculate results of improved reliability for a wide variety of the dipole properties of NH_3. The relatively recent oscillator strength data of Samson *et al.* (26), for 11.07–150 eV, are also included explicitly in the DOSD analysis for NH_3. However, it should be noted that the latter data (26) do not include the discrete excitation region below the first ionization potential. The results obtained in the present work provide updated values of the dipole properties of ammonia, relative to those reported earlier by Zeiss *et al.* (37), and provide the most reliable values yet available for many of the dipole properties of NH_3.

2. Experimental details and results

The dipole (e,e) spectrometers and procedures used to determine the absolute photoabsorption oscillator strengths (cross sections) at both low resolution (~1 eV fwhm) and at high resolution (0.048 eV) have been described previously (36, 57–63, and footnote 6), so only a brief description of the methods will be given. The low resolution (LR) measurements of ammonia were made using an unmonochromated, high incident energy (8000 eV), electron beam in an electron energy-loss spectrometer. The absolute photoabsorption oscillator strengths were obtained by Bethe–Born conversion and valence-shell TRK sum-rule normalization of the background-subtracted electron energy-loss spectrum obtained at a mean scattering angle of zero degrees (acceptance angle of 1.4×10^{-4} sr) (57). The data were obtained from the electronic excitation threshold at 5.5–200 eV. The relative valence-shell optical oscillator strength spectrum was

[5]A. Kumar, W. J. Meath, G. R. Burton, G. Cooper, W. F. Chan, and C. E. Brion. Unpublished work.

[6]G. R. Burton, W. F. Chan, G. Cooper, and C. E. Brion. To be published.

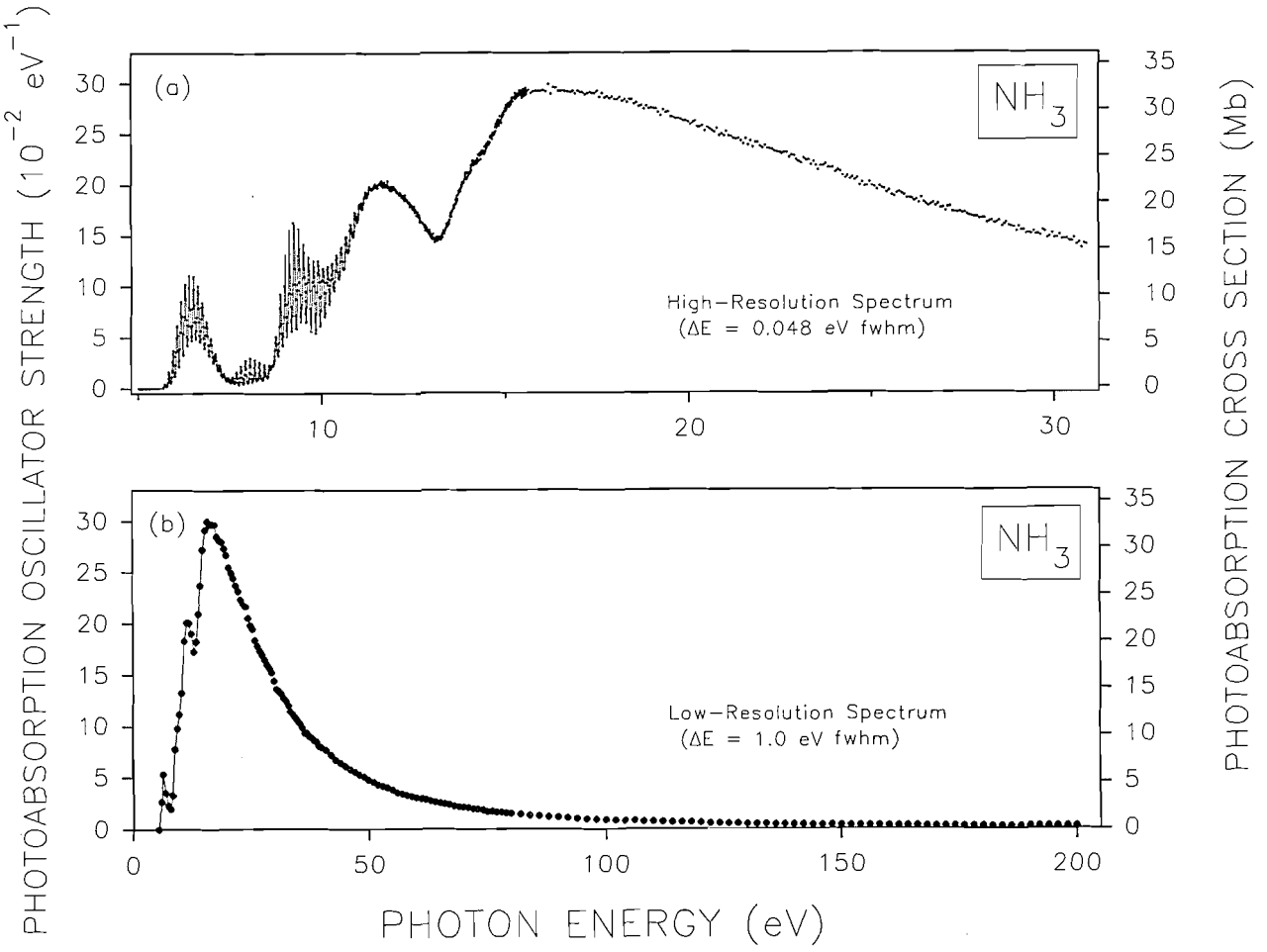

FIG. 1. Absolute photoabsorption oscillator strengths for ammonia: (*a*) the valence-shell region from 5 to 31 eV measured at high resolution (0.048 eV fwhm); (*b*) the valence-shell region from 5.5 to 200 eV measured at low resolution (~1 eV fwhm). These data were determined using dipole (e,e) spectroscopy (see footnote 6 for details).

placed on an absolute scale by first fitting a curve to the high-energy tail from 90 to 200 eV. Using this curve there is estimated to be 4.5% of the total valence-shell oscillator strength above 200 eV. The fitted curve was then extrapolated to infinity and the total area under the whole spectrum was normalized to 8.13. The same value was used to normalize the previously reported low-resolution dipole (e,e) data of Wight *et al.* (31). The value 8.13 corresponds to the eight valence-shell electrons in NH_3 plus a small estimated contribution of 0.13 to account for Pauli-excluded transitions from the nitrogen 1*s* shell to the already occupied valence orbitals (64).[7]

The high-resolution (HR) measurements for ammonia were obtained using a high-resolution electron energy-loss spectrometer, with an incident electron energy of 3000 eV (61). This instrument was recently calibrated to obtain the appropriate Bethe–Born conversion factor so as to be able to produce relative optical oscillator strength distributions from the background-subtracted, zero degree electron energy-loss spectrum (36, 63). The relative oscillator strength spectrum was put on an absolute scale by single point normalization to the presently reported low-resolution photoabsorption oscillator strength spectrum (see above) in the smooth continuum region. The reliability of the presently used dipole (e,e) techniques has been confirmed by the excellent agreement between the previously measured oscillator strengths and high-level *ab initio* calculations for He (36) and H_2 (62).

The sample of ammonia used in this work was obtained from a Matheson lecture bottle and was of a minimum stated purity of 99.99%. The gas sample was used without further purification and no impurity peaks could be detected in the high-resolution electron energy-loss spectrum.

The newly measured absolute differential photoabsorption oscillator strength data for NH_3, obtained as described above, are presented in Fig. 1. Figure 1*a* shows the high-resolution spectrum from 5 to 31 eV at a resolution of 0.048 eV fwhm. The figure gives a detailed and accurate view of the highly structured portion of the differential oscillator strength spectrum in the vibrationally resolved pre-edge region of discrete excitation. The low-resolution spectrum in Fig. 1*b* provides a global view of the absolute photoabsorption oscillator strength distribution from 5 to 200 eV at a resolution of 1 eV fwhm. At this modest resolution the pre-edge excitation region is only partially re-

[7]M. Inokuti. Private communication.

Can. J. Chem. Downloaded from www.nrcresearchpress.com by 88.255.202.194 on 09/08/12
For personal use only.

TABLE 1. Integrated dipole oscillator strengths in selected photon energy ranges for NH_3. This table contains the constrained integrated oscillator strengths and also the integrated oscillator strengths obtained from unmodified experimental or mixture rule data. The integrated DOSs obtained from the recommended DOSD of Zeiss *et al.* (37) are shown for comparison

Energy region (eV)	Integrated oscillator strength[a] Constrained values DOSDA[b]	Constrained values DOSDB[b,c]	Constrained values DOSDC[b]	High-resolution data[d]	Low-resolution data[c,d]	Samson *et al.* (26) PhAbs.	Mixture rule	Zeiss *et al.* (37) DOSD
5.685–7.563	8.278(−2)	7.349(−2)[e]	8.197(−2)	7.384(−2)	7.122(−2)[e]			8.023(−2)
7.563–8.590	1.334(−2)	2.622(−2)[e]	1.333(−2)	1.324(−2)	2.613(−2)[e]			1.141(−2)
8.590–10.19	1.418(−1)	1.445(−1)[e]	1.408(−1)	1.359(−1)	1.429(−1)[e]			1.460(−1)
10.19–11.07	1.231(−1)	1.322(−1)[e]	1.225(−1)	1.201(−1)	1.314(−1)[e]			1.267(−1)
11.07–12.40	2.677(−1)	2.645(−1)	2.936(−1)	2.574(−1)	2.618(−1)	2.873(−1)		2.769(−1)
12.40–13.08	1.136(−1)	1.251(−1)	1.152(−1)	1.121(−1)	1.246(−1)	1.145(−1)		1.161(−1)
13.08–14.06	1.736(−1)	1.855(−1)	1.709(−1)	1.707(−1)	1.845(−1)	1.695(−1)		1.765(−1)
14.06–18.05	1.187(0)	1.146(0)	1.166(0)	1.105(0)	1.119(0)	1.124(0)		1.170(0)
18.05–22.03	1.084(0)	1.069(0)	1.063(0)	1.040(0)	1.050(0)	1.040(0)		1.077(0)
22.03–25.09	6.657(−1)	6.729(−1)	6.663(−1)	6.532(−1)	6.657(−1)	6.592(−1)		6.731(−1)
25.09–28.02	5.371(−1)	5.275(−1)	5.235(−1)	5.304(−1)	5.232(−1)	5.197(−1)		5.353(−1)
28.02–30.88	4.403(−1)	4.311(−1)	4.347(−1)	4.365(−1)	4.283(−1)	4.323(−1)		4.167(−1)
30.88–40.0	9.647(−1)	9.639(−1)	9.644(−1)		9.504(−1)	9.541(−1)	8.820(−1)	9.096(−1)
40.0–50.0	6.245(−1)	6.255(−1)	6.236(−1)		6.199(−1)	6.198(−1)	5.967(−1)	6.011(−1)
50.0–60.0	3.835(−1)	3.841(−1)	3.912(−1)		3.820(−1)	3.898(−1)	4.414(−1)	4.339(−1)
60.0–80.0	4.363(−1)	4.373(−1)	4.474(−1)		4.346(−1)	4.457(−1)	5.554(−1)	5.414(−1)
80.0–100.0	2.328(−1)	2.332(−1)	2.417(−1)		2.324(−1)	2.412(−1)	2.991(−1)	2.955(−1)
100.0–124.4	1.691(−1)	1.693(−1)	1.738(−1)		1.689(−1)	1.735(−1)	1.913(−1)	1.907(−1)
124.4–150.0	1.152(−1)	1.153(−1)	9.772(−2)		1.515(−1)	9.764(−2)	1.199(−1)	1.196(−1)
150.0–200.0	1.421(−1)	1.423(−1)	1.422(−1)		1.420(−1)		1.341(−1)	1.335(−1)
200.0–400.0	1.672(−1)	1.679(−1)	1.678(−1)				1.667(−1)	1.663(−1)
400.0–425.0	2.623(−1)	2.639(−1)	2.637(−1)			2.610(−1)[f]	1.543(−1)	1.543(−1)
425–1000.0	1.289(0)	1.314(0)	1.311(0)				1.268(0)	1.268(0)
1000.0–10^4	3.802(−1)	3.814(−1)	3.812(−1)				3.793(−1)	3.795(−1)
10^4–10^6	3.301(−3)	3.301(−3)	3.301(−3)				3.301(−3)	3.300(−3)
10^6–∞	5.832(−8)	5.832(−8)	5.832(−8)				5.832(−8)	5.830(−8)

[a]Power of ten is in parentheses, e.g., 8.278(−2) = 8.278 × 10^{-2}.
[b]Present work.
[c]Involves low-resolution data. As discussed in the text, the integrated oscillator strengths in the discrete excitation region (below 11.07 eV) may not be reliable due to resolution effects, whereas the *total* integrated oscillator strength from 5.685 to 11.07 eV is reliable.
[d]Experiment, present work, see also footnote 6 for further details.
[e]Akimov *et al.* (68) nitrogen K-shell photoabsorption data.

Can. J. Chem. Downloaded from www.nrcresearchpress.com by 88.255.202.194 on 09/08/12
For personal use only.

solved and thus cannot provide accurate *differential* oscillator strength information. However, the integrated oscillator strength over the entire discrete excitation region is consistent with the high-resolution data. In the smooth continuum region the high- and low-resolution differential oscillator strength distributions exhibit the same shape and can thus be compared directly. The overall consistency of the newly reported high- and low-resolution valence-shell oscillator strength measurements can be seen from Fig. 2 where the complete data sets are conveniently displayed in a single diagram on a wavelength scale (Å).

3. Constrained dipole oscillator strength distributions and related properties

3.1. Computational methods

The dipole oscillator strength distribution (DOSD) for a molecule is given by the molecular differential dipole oscillator strength, (df/dE), as a function of photon energy E, from the photoabsorption threshold, E_0, to very high energy. Many important molecular dipole properties (37, 43, 44) can be evaluated if the DOSD for the given molecule is available. Those of particular interest for this paper include the dipole oscillator strength sums S_k, the analogous logarithmic dipole sums L_k, and the related mean excitation energies I_k, defined by

$$[1] \quad S_k = \int_{E_0}^{\infty} \left(\frac{E}{E_H}\right)^k \left(\frac{df}{dE}\right) dE$$

$$[2] \quad L_k = \int_{E_0}^{\infty} \left(\frac{E}{E_H}\right)^k \left(\frac{df}{dE}\right) \ln(E) dE$$

$$[3] \quad I_k = E_H \exp\left[L_k/S_k\right]$$

where E_0 is the electronic absorption threshold for the molecule, and E_H is 27.212 eV (the Hartree unit of energy). The index k can take many different values (e.g., k = 5/2, 2, 1, 0, −1/2, −1, −3/2, −2, −3, −4, ...) and each choice corresponds to a different molecular property with respect to eqs. [1]–[3]. For example, $\alpha_d = a_0^3 S_{-2}$ is the static dipole polarizability of the molecule, where a_0 is the Bohr radius. A further example is the Thomas–Reiche–Kuhn (TRK) sum rule, $S_0 = N$, where N is the total number of electrons in the atom or molecule being studied. Furthermore, the mean excitation energies I_k, for k = 1, 0, and −1, are the average

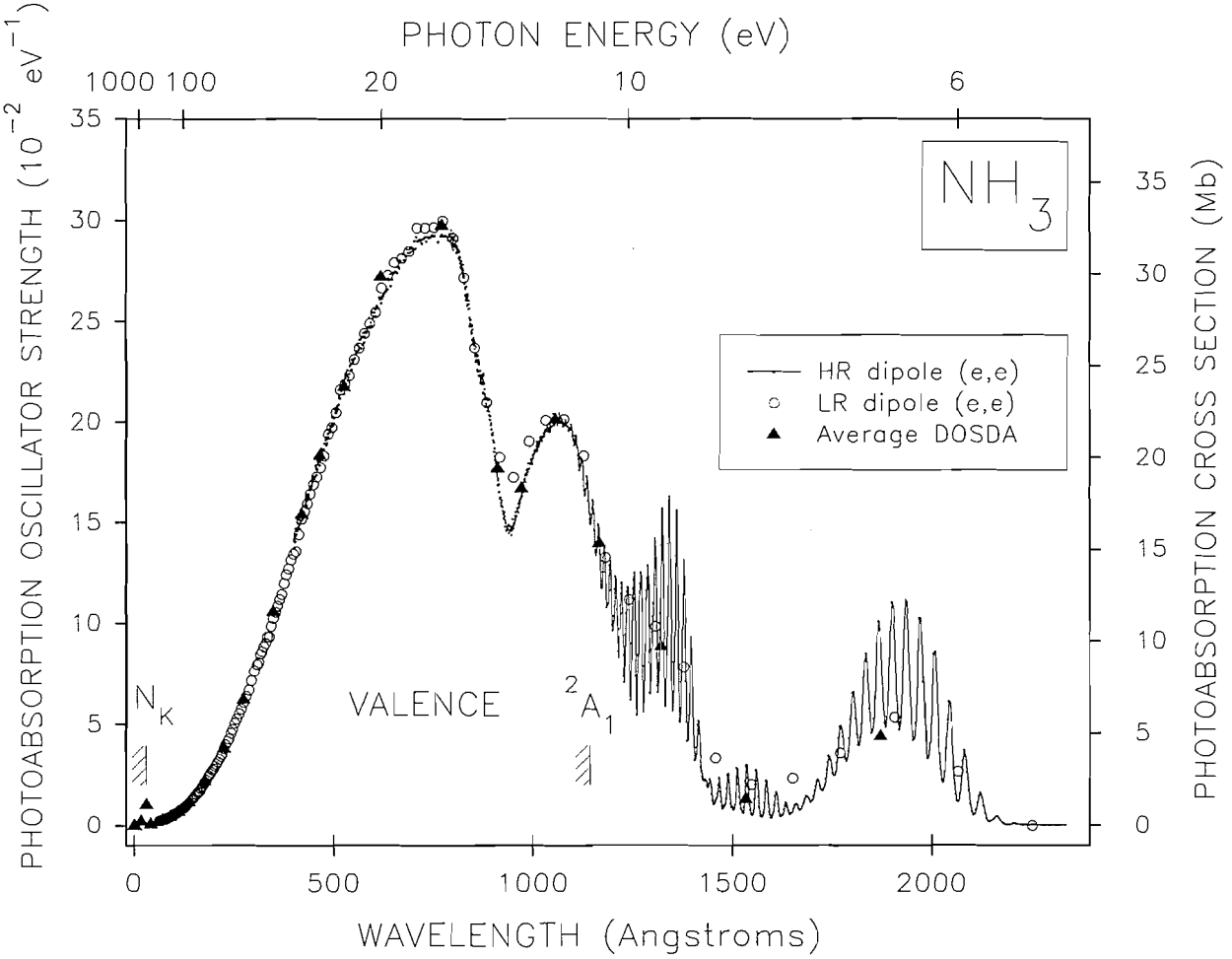

FIG. 2. Absolute experimental low-resolution (~1 eV fwhm) and high-resolution (0.048 eV fwhm) photoabsorption data for NH_3 as a function of wavelength. The hatched lines indicate the positions of the lowest energy valence-shell vertical ionization potential (VIP) and the nitrogen K-shell VIP. The average constrained DOSD data points, calculated for each energy block in the valence- and nitrogen K-shell regions, are taken from DOSD A (Table 1). The energy position of each of these data points is the midpoint of the energy region over which the particular integrated oscillatory strength value was determined and the associated differential oscillator strength value for these data points is the integrated oscillator strength value divided by the width of the energy region.

energies associated with straggling, stopping, and total inelastic cross sections for fast charged particles in matter, respectively. Another important property related to molecular DOSDs is the molar refractivity, R_λ, of a dilute molecular gas. R_λ is related to the refractive index, $n(\lambda)$, and the dynamic dipole polarizability, $\alpha(\lambda)$, of the gas at wavelength λ by

$$[4]\quad R_\lambda = \frac{1}{\rho}\left[\frac{n^2(\lambda)-1}{n^2(\lambda)+2}\right] = \frac{4\pi}{3}\mathcal{N}(E_H)^2 a_0^3 \int_{E_0}^{\infty} \frac{(df/dE)}{E^2-(hc/\lambda)^2}\,dE = \frac{4\pi}{3}\mathcal{N}\,\alpha(\lambda)$$

where ρ is the molar density of the gas, h is Planck's constant, $\mathcal{N}$ is Avogadro's number, and c is the speed of light (42, 43, 66).

The constrained least-squares methods used to construct the DOSD for a given molecule, from an initial data base of (df/dE) versus E values, have been discussed and applied in the literature previously (37, 38). In summary, the excitation energies for the molecule are divided into N_0 energy regions from threshold to very large values of E. The initial differential dipole oscillator strength data for the ith spectral region are modified according to

$$[5]\quad (df/dE)^i_{mod} = (1+a_i)(df/dE)^i_{initial}, \qquad i = 1, 2, \ldots, N_0$$

such that the total modified DOSD satisfies constraints through the choice of the $\{a_i\}$. The constraints used in the present work are the molar refractivity, R_λ, for two well-spaced (47, 49) λ values, and the TRK sum rule, S_0.

A DOSD can be constructed for each initial data base for a given molecule. The amount of modification of the initial (df/dE) versus E data that is required to satisfy the constraints can be represented by the standard deviation (STD) defined by

$$[6]\quad (\mathrm{STD}) = \left[\sum_{i=1}^{N_0}(a_i-\bar{a})^2/N_0\right]^{1/2}$$

where $\bar{a}$ is the mean of the a_i values.

Can. J. Chem. Downloaded from www.nrcresearchpress.com by 88.255.202.194 on 09/08/12
For personal use only.

Can. J. Chem. Downloaded from www.nrcresearchpress.com by 88.255.202.194 on 09/08/12
For personal use only.

Each adopted DOSD is represented by a set of data points, E_l and $(df/dE)_l$, for $l = 1, 2, \ldots, N_p >> N_0$, and a set of interpolating functions to connect the points; $N_p = 2538$ for ammonia. For very high photon energies, i.e., $E \geq 10^9$ eV, the (df/dE) are represented by the Born dipole formula (67), $AE^{-3.5}$. The dipole properties represented in eqs. [1]–[4] are readily evaluated using this representation of the DOSDs.

3.2. Dipole oscillator strength distribution of ammonia

A DOSD for NH_3 was constructed some time ago (1977) by Zeiss *et al.* (37) who employed methods that are the precursor to those used in this paper. Such photoabsorption, or equivalent data, as were available at the time were considered. However, because of substantial disagreements amongst the available experimental data sets, and due to the lack of NH_3 data for higher photon energies, the DOSD was based on the (H_2, N_2) mixture rule above 33 eV. It was noted (37) that the dipole oscillator strength (DOS) data (4–100 eV) of Van der Wiel and Brion (30) generally agreed with the mixture rule values to within 10%. In this section we construct new DOSDs for NH_3 based on new NH_3 oscillator strength data (see refs. 26 and 68 and the present new experimental work) that has become available since the original DOSD work on ammonia (37) was carried out. We then compare the dipole properties obtained from the resulting constrained DOSDs with those (37) evaluated from the DOSD of Zeiss *et al.* (37). The sources of DOS data discussed and analyzed in ref. 37 are not considered explicitly in the construction of the DOSD for NH_3 reported below. The data subsequently reported by Wight *et al.* (31) over the range 10–60 eV are also not considered explicitly in what follows since it is now apparent that adequate background subtraction procedures were not employed. This was confirmed by preliminary work (see footnote 5), which indicated that the data of Wight *et al.* (31) are too high relative to the new (background-subtracted) measurements reported in Sect. 2.

The following experimental dipole oscillator strength data are considered for the construction of the DOSDs for NH_3: 5.685–30.88 eV (high-resolution data of Sect. 2); 5.685–200 eV (low-resolution data of Sect. 2); 11.07–150.0 eV (Samson *et al.* (26)); 400–425 eV (Akimov *et al.* (68)). This experimental molecular NH_3 data is augmented by employing the following mixture rule, particularly for photon energies $E \geq 150$ eV,

$$[7] \quad (df/dE)(NH_3) = \frac{1}{2}(df/dE)(N_2) + \frac{3}{2}(df/dE)(H_2)$$

The input for this mixture rule uses the recommended N_2 and H_2 DOSDs of Zeiss *et al.* (37).

To construct the DOSD, the photoabsorption spectrum is divided into 26 energy intervals as suggested by the structure of the spectrum and by the photon energy regions corresponding to the various sources of DOS input data. The integrated DOSs for each individual source, and for each relevant energy interval, are given in Table 1, which also contains the analogous results calculated from the adopted DOSD of Zeiss *et al.* (37). The constraints used for constructing the DOSDs for NH_3 from the initial DOS input data are provided by $S_0 = 10$ and by the experimental molar refractivity data of Frivold *et al.* (54) and Friberg (55) at $\lambda = 2753$ Å and $\lambda = 5462$ Å, respectively. These are the same constraints as employed by Zeiss *et al.* (37).

We have constructed three new DOSDs by taking the following combinations of the initial dipole oscillator strength data:

DOSDA : 5.685–30.88 eV (present high-resolution data); 30.88–200 eV (present low-resolution data); 400–425 eV (Akimov *et al.* (68)); all other energy regions (mixture rule).

DOSDB : 5.685–200 eV (present low-resolution data); then as in DOSDA.

DOSDC : 11.07–150 eV (Samson *et al.* (26)); then as in DOSDA.

Each of these initial DOSDs was modified, through requiring the constraints to be satisfied, by using the constrained least-squares procedure discussed earlier. The values of the standard deviation (STD), see eq. [6], for the resulting distributions are 2.68, 0.90, and 2.19, respectively. The STDs for all three DOSDs compare favorably with those for many other DOSDs constructed using the methods employed here.

The constraints used to construct the DOSDs involve integrals over the DOSDs, weighted by simple functions of E, and therefore are effective in a "global" sense over a range of photon energies (46). The constraints used are sensitive to different ranges of photon energies (7, 47, 49). For example, the energy region 5.685–50.0 eV yields ~98% of the molar refractivity constraints while ~100% of S_0 is due to the energy region 5.685–10^4 eV with ~92% arising from the 11.07–10^3 eV region. Therefore the constrained DOSDs are generally reliable in the sense of yielding accurate results for various related dipole properties, but not in the sense of providing accurate DOS values at specific local energies or over narrow energy regions (46). In the present context, while the smaller values of STD imply that less modification of the initial DOS data is required to satisfy the constraints, this cannot be used to discriminate between the input data since the STDs are all small. The difference between the STDs for DOSDA and DOSDB is essentially due to the energy region 5.685–7.563 eV, which contributes only ~1% of S_0 and ~10% of the molar refractivity constraints. The integrated oscillator strengths corresponding to all the input data, and to the constrained DOSDs A, B, and C, are compared in Table 1, which also contains the corresponding previously unpublished results obtained from the recommended DOSD (STD = 2.64) of Zeiss *et al.* (37).

For common energy regions above 11.07 eV, the integrated DOSs obtained directly from the presently reported high- and low-resolution data (estimated error ±5%) agree with each other, and are in essential agreement with those obtained from the data of Samson *et al.* (26) (estimated error ±3%), to within their combined experimental errors. Exceptions are the results obtained from the data of Samson *et al.* (26) for 11.07–12.40 eV and 124.4–150 eV, which are ~12% and ~15% higher and lower, respectively, than the present experimental work over the same energy ranges. For photon energies below 11.07 eV our high- and low-resolution integrated oscillator strengths also agree well with each other except apparently in the 7.563–8.590 eV region where the low-resolution data are larger by a factor of two. Of course in this narrow energy range the low-resolution data are not realistic, since the fine structure (Fig. 1*a*) in the discrete excitation region cannot be resolved. Thus local oscillator strength values in the discrete region of the low-resolution spectrum where sharp structures exist are likely to be severely modified by the "filling in of valleys" and

Can. J. Chem. Downloaded from www.nrcresearchpress.com by 88.255.202.194 on 09/08/12
For personal use only.

"clipping of peaks" that occurs at low resolution. However, the *integrated* oscillator strengths over the entire discrete region, obtained from the two sets of measurements at high and low resolution, may be compared with each other. For example, over the energy range 5.685–13.08 eV the high- and low-resolution integrated oscillator strengths are 0.7125 and 0.7580, respectively; the corresponding results from 5.685–30.88 eV are 4.649 and 4.728.

The integrated oscillator strengths obtained from the constrained DOSDs generally agree to within the estimated experimental error with the corresponding integrated DOSs obtained from the experimental NH_3 data. The largest difference (~11%) occurs in the 5.685–7.563 eV region for DOSDs A and C. Also the raw mixture data, used to construct the constrained DOSDs for most energies greater than 200 eV, are only modified by a few percent by the constraint procedures. Furthermore, the raw mixture data predict results for the integrated oscillator strengths between 150 and 200 eV that differ by only ~6% from the values obtained from the constrained DOSDs. The integrated oscillator strengths for the constrained DOSDs A, B, and C agree very well over the whole energy domain with the largest disagreements being ~12% between DOSDs A and C and DOSDB for 5.685–7.563 eV and ~11% and 15% between DOSDs A and B and DOSDC for 11.07–12.40 eV and 124.4–150 eV, respectively. The oscillator strength input used to construct the adopted DOSD of Zeiss *et al.* (37) differs significantly from that used to obtain the constrained DOSDs A, B, and C for the energy regions 5.685–150 eV and 400–425 eV and this results in the differences that occur between the relevant integrated oscillator strengths in Table 1.

The photoabsorption cross sections reported by Akimov *et al.* (68) in the K-edge region exhibit a structure with four peaks occurring at photon energies of 400.9, 402.4, 403.6, and 404.5 eV and the cross sections at these energies are 1.398, 4.025, 1.525, and 1.751 Mb (10^{-18} cm^2), respectively. The use of the mixture rule, which was based on atomic nitrogen data at high energies, in this energy region yields a single absorption edge at E = 401.5 eV (i.e., the K-edge of N) with a cross section of 0.7670 Mb; the K-edge of N is very close to the average (401.6 eV) of the energies associated with the two most significant absorption peaks in the molecular K-edge measurements. The mixture rule absorption maximum is about five times smaller than the highest molecular K-edge maximum (68). For the energy region 400–425 eV, around the K-edge, the integrated DOSs for the mixture rule data and the data reported by Akimov *et al.* (68) are 1.543(−1) and 2.610(−1), respectively. However, at 400 eV, and for $E \geq 420$ eV, the mixture rule and molecular DOSs agree to within 10 and 20% respectively; the estimated experimental error in the molecular cross section of Akimov *et al.* (68) is about 15%.

The disagreement between the mixture rule and the ammonia experimental data at, and close to, the K-edge reflects the very different photoabsorption effects occurring in atomic nitrogen and NH_3 at these photon energies. An analogous effect has also been discussed by Kumar and Meath (49) for the L_1 absorption of HCl (see also Eberhardt *et al.* (69) and Yates *et al.* (9)). In general, mixture rules, which are based on additivity principles (5–8), work reasonably well for photon energies greater than about 60 eV and become more reliable for high photon energies, except near photoabsorption edges where significant deviations from additivity can occur due to specific molecular effects; examples can be taken from Table 1 and refs. 38 and 45–50.

The averaged oscillator strength results obtained from constrained DOSDA, calculated for each energy block in Table 1, are compared with the initial high- and low-resolution valence-shell oscillator strengths in a global perspective over the entire spectral range in Fig. 2. Figure 3 provides an alternative representation of the integrated DOSDA (Table 1) on a linear scale in the region below 200 eV. These figures show that the *averaged* constrained DOSD data provide an effective representation of the experimental data from 5.685 to 200 eV.

3.3. *Dipole properties for ammonia*

The results for the S_k, $-12 \leq k \leq 2$, and the L_k and I_k, for $-2 \leq k \leq 2$, evaluated by using the constrained DOSDs A and B, and the initial DOSDA, are compared with the results of Zeiss *et al.* (37) in Table 2. The results for the constrained DOSDC are not included in the table since they differ insignificantly from those of constrained DOSDA and DOSDB. The dipole properties obtained from the constrained DOSDs agree very well with each other and certainly to well within the estimated errors in the present results for the dipole properties (these are discussed later in this section). Nominally we choose the results for the dipole properties obtained from constrained DOSDA as recommended values since they are derived using spectroscopically more reliable oscillator strength input data, especially in the low-photon-energy region of the NH_3 photoabsorption spectrum. The results for the molar refractivity of NH_3 evaluated using constrained DOSDA are compared with experiment (54–56) in Table 3 as a function of wavelength; analogous results were not obtained in ref. 37. It is clear that the calculated results for R_λ are in excellent agreement with experiment with the maximum discrepancy being only ~0.07%. The dipole property S_{-2} is related to the static dipole polarizability, which in turn is proportional to R_∞. Our recommended result of S_{-2} = 14.56 can be compared with values obtained from refractivity measurements (70), 14.57, and from dielectric constant measurements (71, 72), 14.71 and 14.2.

The results for the dipole properties (Table 2) evaluated using the initial (unmodified) DOSDA, leading to our constrained DOSDA for NH_3, agree reasonably well with the recommended properties, which indicates the high quality of the input DOSs. The effect of applying the constraint procedure is only 0.3% for S_2, ~1% for S_1, ~2% for S_0, and increases as k decreases, to ~3.5% for S_{-1}, ~4.5% for S_{-2}, and ~9.5% for S_{-12}. For the L_k the differences are ≤1% for $k \geq 0$ and ~7% for $k = -1$ and -2. Berkowitz (73) analyzed the absolute photoabsorption data available before 1979 for NH_3 and used atomic additivity (Henke *et al.* (74)) to extend the molecular data for $E \geq 62$ eV. The dipole sums so obtained are S_0 = 9.38, S_{-1} = 8.70, and S_{-2} = 14.04, which are ~6.2, 6.6, and 3.6% lower than our recommended values. Samson *et al.* (26) obtained S_0 = 9.78 by combining their DOS data from 11 to 150 eV with that used by Berkowitz below 11 eV and above 150 eV.

Our recommended results for the dipole properties of NH_3 (Table 2) generally agree with the results of Zeiss *et al.* (37) to within their estimated errors; this is partly due to the use of the same constraints in the construction of the corre-

Can. J. Chem. Downloaded from www.nrcresearchpress.com by 88.255.202.194 on 09/08/12
For personal use only.

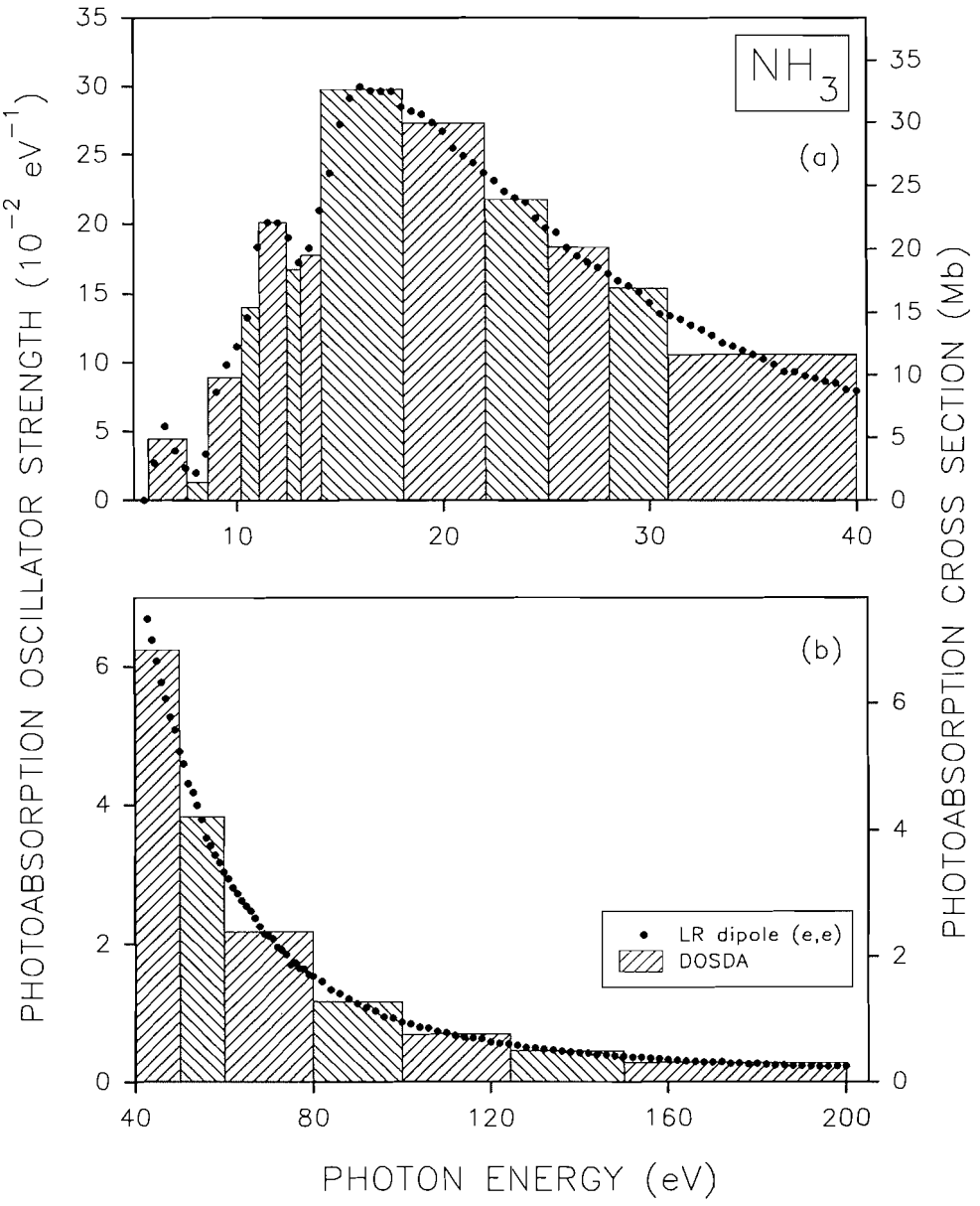

FIG. 3. Absolute experimental low-resolution (~1 eV fwhm) oscillator strengths (filled circles) and constrained DOSD A results (hatched blocks): (*a*) 5.5–40 eV; (*b*) 40–200 eV. Each integrated oscillator strength value (Table 1) is represented by a hatched block with a base that spans the energy range over which the value was determined and with an area equal to the integrated oscillator strength value.

sponding DOSDs. For the S_k the discrepancies are ~2.3% for $k = 1$, ≤0.5% for $k = 2$ and $-12 \leq k \leq 0$; for I_k they are ≤2% for all k. Error estimates were not given for the L_k in ref. 37; the differences in the two sets of values are ≤1% for $k = 2$, -1, -2, and ~2.5% for $k = 1$ and 0, respectively.

There are a number of *ab initio* calculations available for the electronic static dipole polarizability, $\alpha(\lambda = \infty) = a_0^3 S_{-2}$, of NH_3. A coupled Hartree–Fock calculation (75), using an extended complete neglect of differential overlap (CNDO) basis set, yielded $S_{-2} = 15.39$ while a value of $S_{-2} = 13.43$ was obtained (76) using an CNDO/2-FPP (finite perturbation plus polarization) approach. There are also *ab initio* calculations at the SCF level and these correspond to Hartree–Fock, $S_{-2} = 12.71$ (77), coupled Hartree–Fock, $S_{-2} = 12.90$ (78) and 12.80 (79), time-dependent coupled Hartree–Fock, $S_{-2} = 12.95$ (80) and derivative Hartree–Fock, $S_{-2} = 12.83$ (81), treatments. These results do not include the small vibrational averaging effect and are much smaller than the present recommended result of $S_{-2} = 14.56$. Only the calculations of Werner and Meyer (82) include vibrational averaging effects. Their pseudo natural orbital configuration interaction and coupled electron pair approximation results are $S_{-2} = 14.55$ and 14.96, respectively; the former is in excellent agreement with the present recommended result, the latter is ~2.5% higher. Diercksen and Sadlej (10) have used fourth-order many-body perturbation theory to compute S_{-2} and their result, including the vibrational averaging correction (0.26) evaluated by Werner and Meyer (82), is 14.63. Correlation contributions to S_{-2} have also been considered by Maroulis (52) and by Wormer and Hettema (53) using many-body perturbation theory meth-

TABLE 2. The dipole sums S_k, logarithmic dipole sums L_k, and mean excitation energies I_k for NH_3 calculated from various DOSDs. The previously reported results of Zeiss *et al.* (37) are shown for comparison. The values obtained from the constrained DOSDA are recommended.

Property	Initial DOSDA[a]	Constrained DOSDA	Constrained DOSDB	Zeiss *et al.* DOSDA (37)	Property	Initial DOSDA	Constrained DOSDA	Constrained DOSDB	Zeiss *et al.* DOSD (37)
S_2	6.175(3)	6.193(3)	6.214(3)	6.156(3)	S_{-12}	2.457(6)	2.746(6)	2.898(6)	2.758(6)
S_1	7.257(1)	7.329(1)	7.393(1)	7.162(1)					
S_0	9.772(0)	1.000(1)	1.000(1)	1.000(1)					
$S_{-1/2}$	8.341(0)	8.602(0)	8.581(0)	8.625(0)	L_2	3.846(4)	3.853(4)	3.861(4)	3.842(4)
S_{-1}	8.975(0)	9.310(0)	9.290(0)	9.319(0)	L_1	2.377(2)	2.395(2)	2.417(2)	2.340(2)
$S_{-3/2}$	1.077(1)	1.123(1)	1.122(1)	1.123(1)	L_0	6.970(0)	6.962(0)	7.049(0)	6.796(0)
S_{-2}	1.391(1)	1.456(1)	1.456(1)	1.456(1)	L_{-1}	−2.480(0)	−2.671(0)	−2.681(0)	−2.641(0)
$S_{-5/2}$	1.906(1)	2.004(1)	2.006(1)	2.005(1)	L_{-2}	−7.962(0)	−8.466(0)	−8.496(0)	−8.479(0)
S_{-3}	2.757(1)	2.913(1)	2.915(1)	2.916(1)					
S_{-4}	6.687(1)	7.140(1)	7.120(1)	7.144(1)	I_2(eV)	1.380(4)	1.370(4)	1.359(4)	1.397(4)
S_{-5}	1.921(2)	2.073(2)	2.056(2)	2.071(2)	I_1(eV)	7.195(2)	7.143(2)	7.151(2)	7.134(2)
S_{-6}	6.287(2)	6.855(2)	6.768(2)	6.840(2)	I_0(eV)	5.553(1)	5.459(1)	5.507(1)	5.369(1)
S_{-8}	8.633(3)	9.547(3)	9.468(3)	9.527(3)	I_{-1}(eV)	2.064(1)	2.043(1)	2.039(1)	2.050(1)
S_{-10}	1.404(5)	1.564(5)	1.588(5)	1.565(5)	I_{-2}(eV)	1.535(1)	1.521(1)	1.518(1)	1.520(1)

[a]Power of ten in parentheses e.g. 6.175(3) = 6.175×10^3.

TABLE 3. Values of the molar refractivity of NH_3 (ideal gas at STP, 0°C and 1 atm) evaluated using the constrained DOSD A, and a comparison with previously reported experimental data (54–56)

	Molar refractivity			Molar refractivity	
λ (Å)	Constrained DOSD A	Experiment	λ (Å)	Constrained DOSD A	Experiment
6709.0	5.571	5.570[a]	3861.0	5.876	5.878[b]
6564.0	5.577	5.581[c]	3544.0	5.976	5.978[b]
6440.0	5.583	5.582[a]	3342.0	6.060	6.062[b]
5895.0	5.612	5.615[c]	2968.0	6.292	6.290[b]
5792.0	5.618	5.618[a]	2926.0	6.327	6.326[b]
5771.0	5.620	5.619[a]	2894.0	6.356	6.356[b]
5462.0	5.642[d]	5.642[a,b,c]	2857.0	6.391	6.391[b]
5210.0	5.663	5.663[a]	2760.0	6.496	6.495[b]
5087.0	5.675	5.675[a]	2753.0	6.504[d]	6.504[b]
4917.0	5.693	5.697[c], 5.694[b]	2675.0	6.607	6.606[b]
4801.0	5.707	5.708[a]	2577.0	6.765	6.766[b]
4359.0	5.770	5.773[c]	2464.0	7.010	7.006[b]
4109.0	5.818	5.820[b]	2447.0	7.055	7.052[b]
3985.0	5.845	5.848[b]	2346.0	7.393	7.392[b]

[a]Cuthbertson and Cuthbertson (56), normalized to Frivold *et al.* (54) at λ = 5462.0 Å.
[b]Friberg (55), normalized to Frivold *et al.* (54) at λ = 5462.0 Å.
[c]Frivold *et al.* (54).
[d]Used as constraints in constructing the DOSD.

ods and these calculations yield values of 14.01 and 14.136, respectively.

Reinsch (65) has computed the dynamic polarizability $\alpha(\lambda)$, see eq. [4], of NH_3 for $\lambda = \infty$ and $2278.2 \leq \lambda \leq 9112.7$ Å, using a time-dependent Hartree–Fock approach and the basis set B of Warner and Meyer (82). The values obtained by Reinsch (65) for $\lambda = \infty$ and $\lambda = 9112.7$ Å are ~5% lower than the present results obtained using constrained DOSDA and the discrepancy increases to ~20% at $\lambda = 2278.2$ Å.

3.4. *The reliability of calculated dipole properties*

The uncertainties in our recommended values of the dipole properties of ammonia can be estimated by employing procedures discussed previously (37, 38, 49). The approach is to compare the adopted results with those derived from alternative DOSDs satisfying the same constraints. The uncertainty estimates thus obtained are less reliable for those properties that do not depend significantly on the spectral regions that dominate the constraints, namely, the properties corresponding to $k = 2$, and to a lesser extent $k = 1$ and $k < -4$. A detailed discussion of the photon energy dependence of the dipole properties can be found in refs. 7, 47, and 49. For $k \geq 1$, the uncertainties in the dipole properties are influenced by the uncertainties in the very high energy DOS data used in constructing the DOSD, which are generally a few percent.

Using the results for various alternate DOSDs constructed for NH_3 (this work, ref. 37, and footnote 5) we es-

Can. J. Chem. Downloaded from www.nrcresearchpress.com by 88.255.202.194 on 09/08/12
For personal use only.

timate the uncertainties in the recommended results for the dipole properties to be ≤3% for S_2, S_1, L_2, L_1, and I_2, ≤1% for S_k, $0 \leq k \leq -5$, and for L_2, I_{-1}, and I_{-2}, ≤1–2% for S_k, $-6 \leq k \leq -10$, L_{-1} and I_1, and ~3–4% for S_{-12}. The uncertainty of ~3% in L_0, and hence in I_0, is relatively high because of a partial cancellation (49) between the positive and negative parts of L_0; for NH_3, L_0 ($E \leq E_H$) ~ −1.9 while $L_0(E \geq E_H) \sim 8.4$. The uncertainties in the recommended results for the dipole properties of NH_3 are also based on the assumption that the molar refractivities, used as constraints in the construction of the DOSDs, have experimental errors associated with accurate measurements, namely, a few tenths of a percent.

The application of the constrained DOSD method to NH_3 results in relatively little modification of the high- and low-resolution oscillator strength data of this work, or of the data of Samson *et al.* (26). These three measurements are in close agreement over most of their common energy regions. The high quality of the experimental DOSD data used to construct the ammonia DOSDs is further exemplified by the comparison, made earlier, of the dipole properties obtained from the initial DOSDA with those from the constrained DOSDA. Relative to many other applications of the constrained DOSD method, very little modification of the initial data is required to satisfy the constraints, and the differences between the two sets of dipole properties, see Table 2, are relatively small. The recommended dipole properties of this paper, as obtained from constrained DOSDA, show only small differences from the results of the original calculations of Zeiss *et al.* (37). However, the values obtained here are to be (nominally) preferred since they are based on newer, more reliable DOS input data, which span a much wider energy range than the data available to Zeiss *et al.* (37). On the other hand, the integrated oscillator strengths for DOSDA and constrained DOSDA are clearly preferred relative to those obtained from the recommended DOSD of ref. 37. The excellent agreement between our recommended dipole properties and those of ref. 37 is a good example of the usefulness of the constrained DOSD approach for evaluating molecular *properties*. Very similar properties are obtained from different sets of DOS input data provided that they are in agreement by ~10–20%. For example, the recommended DOSD of Zeiss *et al.* (37) was based on the mixture rule DOS data for photon energies above 33 eV, which are significantly different from the other input DOS data considered here for 30.88–100 eV.

4. Acknowledgements

This collaborative research project received financial support from the Canadian National Networks of Centres of Excellence (Centres of Excellence in Molecular and Interfacial Dynamics) and from the Natural Sciences and Engineering Research Council (NSERC) of Canada. A Graduate Fellowship from the University of British Columbia (W.F.C.) and an NSERC Postgraduate Scholarship (G.R.B.) are gratefully acknowledged.

1. T. W. Harquist (*Editor*). Molecular astrophysics—a volume honouring Alexander Dalgarno. Cambridge Press, Cambridge. 1990.
2. T. Watanabe, I. Shimamura, M. Shimizu, and Y. Itikawa (*Editors*). Molecular processes in space. Plenum Press, New York. 1990.
3. E. I. Minor. Phys. Today, **43**, 40 (1990).
4. M.-J. Hubin-Franskin, J. Delwiche, F. Tollet, M. Furlan, and J. E. Collin. J. Phys. B: At. Mol. Opt. Phys. **21**, 189 (1988).
5. G. D. Zeiss, W. J. Meath, J. C. F. MacDonald, and D. J. Dawson. Mol. Phys. **39**, 1055 (1980).
6. W. J. Meath, D. J. Margoliash, B. L. Jhanwar, A. Koide, and G. D. Zeiss. *In* Intermolecular forces. *Edited by* B. Pullman. Reidel, Dordrecht. 1981. p. 101.
7. G. D. Zeiss, W. J. Meath, J. C. F. MacDonald, and D. J. Dawson. Radiat. Res. **70**, 284 (1977).
8. B. L. Jhanwar, W. J. Meath, and J. C. F. MacDonald. Radiat. Res. **96**, 20 (1983); **106**, 288 (1986).
9. B. W. Yates, D. M. Shinozaki, A. Kumar, and W. J. Meath. J. Polym. Sci. Part B: Polym. Phys. **30**, 185 (1992).
10. G. H. F. Diercksen and A. J. Sadlej. Mol. Phys. **57**, 509 (1986).
11. R. J. Thompson and A. B. F. Duncan. J. Chem. Phys. **14**, 573 (1946).
12. E. Tannenbaum, E. M. Coffin, and A. J. Harrison, J. Chem. Phys. **21**, 311 (1953).
13. K. Watanabe. J. Chem. Phys. **22**, 1564 (1954).
14. H. Sun and G. L. Weissler. J. Chem. Phys. **23**, 1160 (1955).
15. W. C. Walker and G. L. Weissler. J. Chem. Phys. **23**, 1540 (1955).
16. A. D. Walsh and P. A. Warsop. Trans. Faraday Soc. **57**, 345 (1961).
17. B. A. Thompson, P. Harteck, and R. R. Reeves, Jr. J. Geophys. Res. **68**, 6431 (1963).
18. P. H. Metzger and G. R. Cook. J. Chem. Phys. **41**, 642 (1964).
19. K. Watanabe and S. P. Sood. Sci. Light (Tokyo), **14**, 36 (1965).
20. R. G. Schmitt and R. K. Brehm. Appl. Opt. **5**, 1111 (1966).
21. L. de Reilhac and N. Damany. Spectrochim. Acta, **26A**, 801 (1970).
22. S. Durmaz, J. N. Murrell, J. M. Taylor, and R. Suffolk. Mol. Phys. **19**, 533 (1970).
23. K. A. Dick and A. O. Ziko. Astrophys. J. **182**, 609 (1973).
24. C. Bertrand, G. Collin, and H. Gagnon. J. Chim. Phys. Phys.-Chim. Biol. **72**, 719 (1975).
25. M. Suto and L. C. Lee. J. Chem. Phys. **78**, 4515 (1983).
26. J. A. R. Samson, G. N. Haddad, and L. D. Kilcoyne. J. Chem. Phys. **87**, 6416 (1987).
27. J. W. Gallagher, C. E. Brion, J. A. R. Samson, and P. W. Langhoff. J. Phys. Chem. Ref. Data, **17**, 9 (1988).
28. T. J. Xia, T. S. Chien, C. Y. R. Wu, and D. L. Judge. J. Quant. Spectrosc. Radiat. Transfer, **45**, 77 (1991).
29. W. R. Harshbarger, A. Skeberle, and E. N. Lassettre. J. Chem. Phys. **54**, 3784 (1971).
30. M. J. Van der Wiel and C. E. Brion. J. Electron Spectrosc. Relat. Phenom. **1**, 443 (1972/73).
31. G. R. Wight, M. J. Van der Wiel, and C. E. Brion. J. Phys. B: At. Mol. Phys. **10**, 1863 (1977).
32. C. E. Brion, A. Hamnett, G. R. Wight, and M. J. Van der Wiel. J. Electron Spectrosc. Relat. Phenom. **12**, 323 (1977).
33. C. E. Brion. Comments At. Mol. Phys. **16**, 249 (1985).
34. M. Inokuti. Rev. Mod. Phys. **43**, 297 (1971).
35. R. D. Hudson. Rev. Geophys. Space Phys. **9**, 305 (1971).
36. W. F. Chan, G. Cooper, and C. E. Brion. Phys. Rev. A, **44**, 186 (1991).
37. G. D. Zeiss, W. J. Meath, J. C. F. MacDonald, and D. J. Dawson. Can. J. Phys. **55**, 2080 (1977).
38. A. Kumar, G. R. G. Fairley, and W. J. Meath. J. Chem. Phys. **83**, 70 (1985), and some of the references therein.
39. H. Margerau. Phys. Rev. **37**, 1425 (1931); **56**, 1000 (1939).
40. A. Dalgarno and N. Lynn. Proc. Phys. Soc. **70**, 802 (1957).
41. A. Dalgarno and A. E. Kingston. Proc. Phys. Soc. **72**, 1053 (1958); **73**, 455 (1959); **78**, 607 (1961).

Can. J. Chem. Downloaded from www.nrcresearchpress.com by 88.255.202.194 on 09/08/12
For personal use only.

42. P. J. Leonard and J. A. Barker. Theor. Chem. (NY), **1**, 117 (1975).
43. J. O. Hirschfelder, W. Byers Brown, and S. T. Epstein. Adv. Quantum Chem. **1**, 255 (1964).
44. U. Fano and J. W. Cooper. Rev. Mod. Phys. **40**, 441 (1968); **41**, 724 (1969).
45. G. F. Thomas and W. J. Meath. Mol. Phys. **34**, 113 (1977).
46. B. L. Jhanwar and W. J. Meath. Chem. Phys. **67**, 185 (1982).
47. B. L. Jhanwar, W. J. Meath, and J. C. F. MacDonald. Can. J. Phys. **59**, 185 (1981); **61**, 1027 (1983).
48. B. L. Jhanwar and W. J. Meath. Can. J. Chem. **62**, 373 (1984).
49. A. Kumar and W. J. Meath. Can. J. Phys. **63**, 417 (1985); Can. J. Chem. **63**, 1616 (1985).
50. R. J. Pazur, A. Kumar, R. A. Thuraisingham, and W. J. Meath. Can. J. Chem. **66**, 615 (1988).
51. A Kumar and W. J. Meath. Mol. Phys. **75**, 311 (1992).
52. G. Maroulis. Chem. Phys. Lett. **195**, 85 (1992).
53. P. E. S. Wormer and H. Hettema. J. Chem. Phys. **97**, 5592 (1992).
54. O. E. Frivold, O. Hassel, and S. Rustad. Phys. Z. **38**, 191 (1937).
55. S. Friberg. Z. Phys. **41**, 378 (1927).
56. C. Cuthbertson and M. Cuthbertson. Philos. Trans. R. Soc. London, A: **213**, 1 (1913).
57. C. Backx, R. R. Tol, G. R. Wight, and M. J. Van der Wiel. J. Phys. B: At. Mol. Phys. **8**, 2050 (1975).
58. C. Backx and M. J. Van der Wiel. J. Phys. B: At. Mol. Phys. **8**, 3020 (1975).
59. F. Carnovale and C. E. Brion. Chem. Phys. **74**, 253 (1983).
60. Y. Iida, F. Carnovale, S. Daviel, and C. E. Brion. Chem. Phys. **105**, 211 (1986), and references therein.
61. S. Daviel, C. E. Brion, and A. P. Hitchcock. Rev. Sci. Instrum. **55**, 182 (1984).
62. W. F. Chan, G. Cooper, and C. E. Brion. Chem. Phys. **168**, 375 (1992).
63. W. F. Chan, G. Cooper, X. Guo, and C. E. Brion. Phys. Rev. A, **45**, 1420 (1992).
64. J. A. Wheeler and J. A. Bearden. Phys. Rev. **46**, 755 (1934).
65. E.-A. Reinsch. J. Chem. Phys. **83**, 5784 (1985).
66. H. A. Kramers and W. Heisenberg. Z. Phys. **31**, 681 (1925).
67. H. A. Bethe and E. E. Salpeter. Quantum mechanics of one- and two-electron atoms. Springer-Verlag, Berlin. 1957.
68. V. N. Akimov, A. S. Vinogradov, and A. V. Zhadenov. Opt. Spektrosk. **65**, 349 (1988).
69. W. Eberhardt, T. K. Sham, R. Carr, S. Krummancher, M. Strogin, S. L. Weng, and D. Wesner. Phys. Rev. Lett. **50**, 1038 (1983).
70. E. A. Moelwyn-Hughes. Physical chemistry. 2nd ed. Pergamon Press, New York. 1964.
71. F. U. Wolf. Hand- und Jahrbuch der Chemischen Physik, Band 6, Abschn. I. Leipzig, Germany. 1935. p. 262.
72. J. M. A. De Bruyne and C. P. Smyth. J. Am. Chem. Soc. **57**, 1203 (1935).
73. J. Berkowitz. Photoabsorption, photoionization and photoelectron spectroscopy. Academic Press, New York. 1979.
74. B. L. Henke, R. L. Elgin, R. E. Lent, and R. B. Ledingham. Norelco Rep. **14**, 112 (1967).
75. M. Grupta and S. Bhattacharyya. J. Chem. Soc. Faraday Trans. 2, **80**, 1405 (1984).
76. R. M. Metzger and C. H. Rhee. Mol. Cryst. Liq. Cryst. **85**, 81 (1982).
77. R. D. Amos, N. C. Handy, P. J. Knowles, J. E. Rice, and A. J. Stone. J. Phys. Chem. **89**, 2186 (1985).
78. P. Lazzeretti and R. Zanasi. J. Chem. Phys. **74**, 5216 (1981).
79. J. G. C. M. Van Duijneveldt-Van De Rijdt and F. B. Van Duijneveldt. J. Mol. Struct. **89**, 185 (1982).
80. M. Bulski, P. E. S. Wormer, and A. Vander Avoid. J. Chem. Phys. **94**, 491 (1991).
81. S. Y. Liu, C. E. Dykstra, K. Kolenbrander, and J. M. Lisy. J. Chem. Phys. **85**, 2077 (1986).
82. H.-J. Werner and W. Meyer. Mol. Phys. **31**, 855 (1976).

Can. J. Chem. Downloaded from www.nrcresearchpress.com by 88.255.202.194 on 09/08/12
For personal use only.

High-pressure Raman studies of triquinacene and dodecahedrane

S. H. BERTZ,[1] G. A. KOUROUKLIS,[2] AND A. JAYARAMAN[3]
AT&T Bell Laboratories, Murray Hill, NJ 07974, U.S.A.

AND

G. LANNOYE AND J. M. COOK
Department of Chemistry, University of Wisconsin–Milwaukee, Milwaukee, WI 53201, U.S.A.

Received August 20, 1992

S. H. BERTZ, G. A. KOUROUKLIS, A. JAYARAMAN, G. LANNOYE, and J. M. COOK. Can. J. Chem. **71**, 352 (1993).

The dimerization of triquinacene ($C_{10}H_{10}$) to dodecahedrane ($C_{20}H_{20}$) has been a goal of organic chemists for more than three decades. An attempted synthesis of dodecahedrane from triquinacene using high pressure and near-UV radiation was not successful, but both hydrocarbons survived the 15 GPa treatment. There is no evidence for a pressure-induced transition in either of the materials. The results of high-pressure Raman spectroscopic investigations to 20 GPa on triquinacene and dodecahedrane are reported. Liquid triquinacene crystallizes near 0.2 GPa at 295 K and the Raman peaks associated with the molecular modes sharpen strikingly. In the crystal the external mode peaks exhibit a large pressure dependence, as expected, but the surprising fact is that the C—H stretching modes behave likewise. In dodecahedrane a similar effect is observed for the C—H stretching modes, but no external mode peaks are observed. The Raman data on dodecahedrane are compared with earlier results and calculations, which support the I_h symmetry for the molecule and an fcc lattice for the crystal.

S. H. BERTZ, G. A. KOUROUKLIS, A. JAYARAMAN, G. LANNOYE et J. M. COOK. Can. J. Chem. **71**, 352 (1993).

La dimérisation du triquinacène ($C_{10}H_{10}$) en dodécaédrane ($C_{20}H_{20}$) a été un des objectifs des chimistes organiciens depuis plus de trois décennies. Un essai de synthèse du dodécaédrane à partir du triquinacène en faisant appel à une radiation du proche UV, à haute pression, n'a pas été couronné de succès; toutefois, les deux hydrocarbures ont survécu au traitement à 20 GPa. On n'a pas de données suggérant une transition induite par la pression de ces composés. On rapporte les résultats d'études par spectroscopie Raman à haute pression, allant jusqu'à 15 GPa, du triquinacène et du dodécaédrane. Le triquinacène liquide cristallise à 295 K, à 0,2 GPa, et les bandes Raman associées avec les modes moléculaires sont fortement affinées. Dans le cristal, comme on pouvait s'y attendre, les bandes du mode externe varient beaucoup en fonction de la pression; toutefois, il est surprenant de réaliser que les modes d'élongation C—H se comportent de la même manière. Dans le dodécaédrane, on observe un effet similaire pour les modes de vibration C—H; toutefois, on n'observe aucune bande du mode externe. On compare les données Raman relatives au dodécaédrane avec les résultats obtenus antérieurement ainsi qu'avec des calculs qui supportent la symétrie I_h pour la molécule et un réseau fcc pour le cristal.

[Traduit par la rédaction]

Can. J. Chem. Downloaded from www.nrcresearchpress.com by 88.255.202.194 on 09/08/12
For personal use only.

Introduction

Triquinacene is a $C_{10}H_{10}$ hydrocarbon with C_{3v} symmetry, consisting of three multiply fused cyclopentene rings in a unique cup-shaped geometry (1). It is a liquid at room temperature but freezes to a clear crystalline solid at about 18°C. The crystal structure of triquinacene has been determined (2) to be in space group $R\bar{3}$ with six molecules per hexagonal unit cell (a = 7.272(5) Å and c = 23.557(13) Å). The molecules in the crystal are arranged in layers perpendicular to the c-axis, and contacts between molecules are top-to-top (convex faces) and bottom-to-bottom (concave faces) in alternate layers. The molecules are not juxtaposed; they are shifted in the plane perpendicular to the c-axis.

Our interest in triquinacene was stimulated by the expectation that application of high pressure on a triquinacene crystal might lead to a direct synthesis of dodecahedrane by the dimerization of bottom-to-bottom pairs of molecules. For this reaction to take place the two molecules have to move a small amount for proper overlap, and the six double bonds have to open and fuse into six new single bonds (Scheme 1). In fact, attempts to synthesize dodecahedrane by application of 5 GPa (1 GPa = 10 kbar) pressure on a *para*-triquinacenophane by Roberts, Srivastava, and le Noble (3) were unsuccessful. However, we thought we could use much higher pressures with the diamond cell and also use photochemistry, since the concerted 12-electron π-bond rearrangement of two triquinacenes to dodecahedrane is photochemically allowed by the Woodward–Hoffmann rules (4).

Pressurization of triquinacene to nearly 20 GPa in a diamond cell and exposure to 248 and 308 nm ultraviolet radiation at 5 GPa failed to produce any detectable dodecahedrane. In the process we studied the effect of pressure on the Raman modes of both triquinacene and dodecahedrane in order to characterize these two unique molecules. We believe that our high-pressure Raman results are of interest to those in the areas of high-pressure Raman scattering and high-pressure organic chemistry.

Experimental procedures

High pressure was generated in a gasketed diamond anvil cell (5) and triquinacene liquid was introduced directly via syringe into the gasket hole, which also contained a ruby chip for pressure calibration (6). Dodecahedrane is a solid at room temperature and argon was employed as the pressure medium for high-pressure Raman

[1]Author to whom correspondence may be addressed. Current address: Molecular Complexity Study Center, 80 E. Main St., Mendham, NJ 07945, U.S.A.

[2]Permanent address: Physics Division, School of Technology, Aristotle University of Thessaloniki, Thessaloniki 54006, Greece.

[3]Current address: Hawaii Institute of Geophysics, University of Hawaii at Manoa, Honolulu, HA 96822, U.S.A.

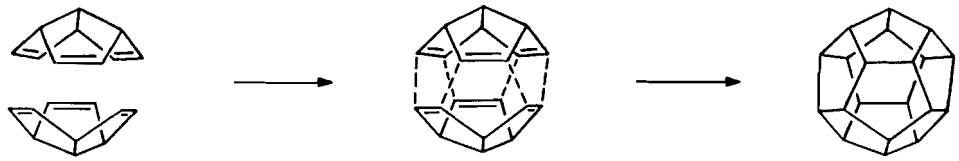

SCHEME 1

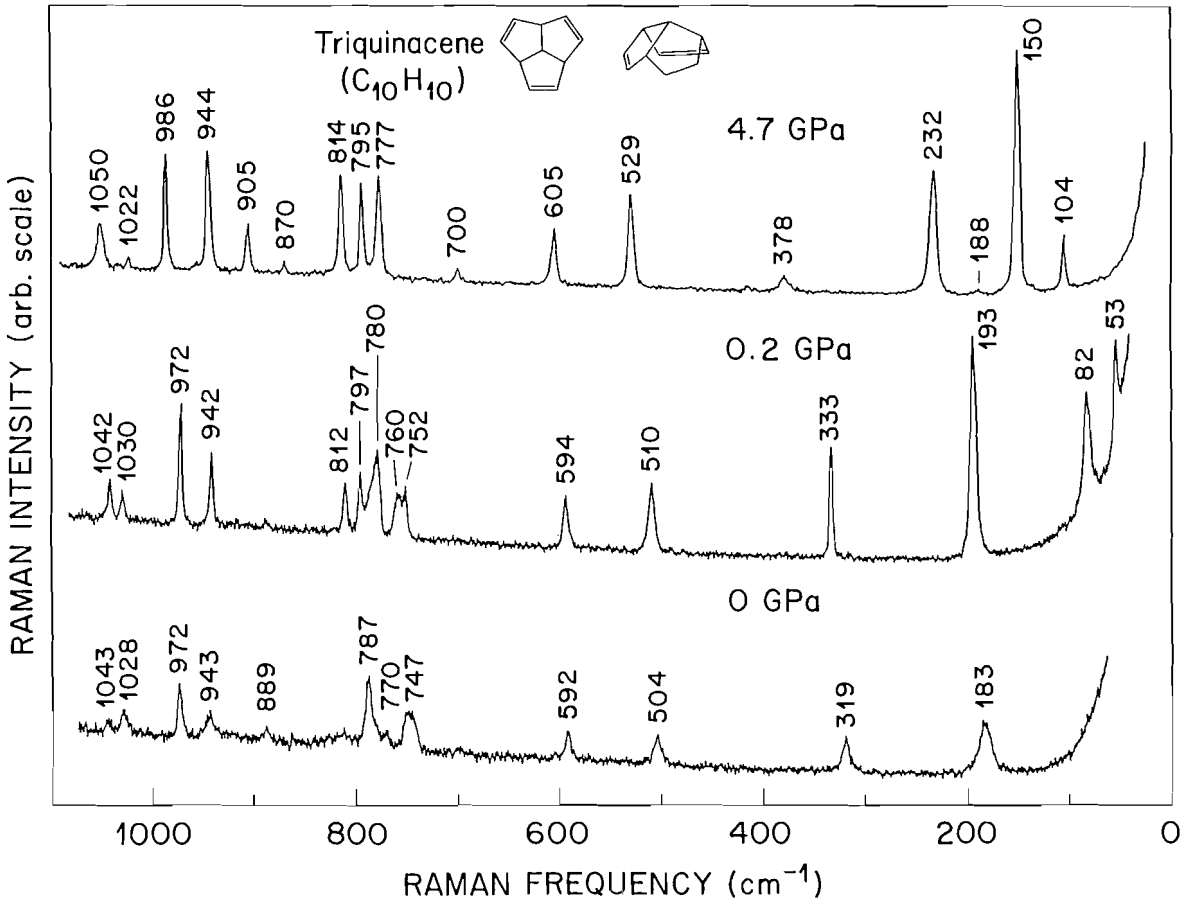

FIG. 1. Raman spectra of liquid (0 GPa) and solid triquinacene at 0.2 and 4.7 GPa in the 0–1100 cm^{-1} region. Raman peaks narrow and become intense in passing from the liquid to the crystalline state.

studies of this material. Raman spectra of samples in the diamond cell were recorded in the back-scattering geometry using a Spex double monochromator equipped with a conventional photon-counting system. For excitation the 488- or the 514.5-nm laser lines from an argon-ion laser were used at a power level of 40–60 mW. All the spectra were recorded at room temperature (~25°C). After each high-pressure experiment, the material in the cell was removed via syringe with ~2–4 μL of benzene and analyzed by GC–MS on a Finnigan 8230 high-resolution mass spectrometer interfaced with a Varian 3400 capillary GC, using on-column injection of the entire sample. A J&W Scientific DB-1 GC column (15 m, 0.32 mm i.d., 0.25 μm film) was used with the following temperature program: 50°C/3 min followed by a 30°C/min ramp to 320°C. Photolyses were carried out at 248 and 308 nm with KrF (Lumonics Hyperex 460) and XeCl (Lambda Physik EMG 201 MSC) lasers, respectively.

Results

Figures 1 and 2 show the Raman spectra of both liquid (0 GPa) and crystalline (0.2 and 4.7 GPa) triquinacene. The liquid sample crystallizes between 0.1 and 0.2 GPa pressure. By slow application of pressure the crystal growth can be controlled and watched through a microscope, and crystals with well-formed facets can be grown. It was also found that the hole in the gasket can be filled with a single crystal by manipulating the pressure on the sample while crystallization is in progress.

All the Raman peaks become much narrower for the triquinacene crystal and, further, two external modes of the molecule appear in the low-frequency end of the spectrum at 53 and 82 cm^{-1}. The observed Raman peaks and their intensities are presented in Table 1 for both the liquid and crystalline triquinacene (near 0.2 GPa). In general, the frequencies of the Raman peaks increase upon crystallization, with two exceptions: 1121 → 1113 cm^{-1} and 1280 → 1270 cm^{-1}. The highest frequency Raman peak of the liquid at 3054 cm^{-1} is quite broad, but in the crystal it becomes a sharp double peak with frequencies of 3063 and 3050 cm^{-1}. These peaks are assigned to vinylic and aliphatic C—H stretching, respectively.

Can. J. Chem. Downloaded from www.nrcresearchpress.com by 88.255.202.194 on 09/08/12
For personal use only.

Can. J. Chem. Downloaded from www.nrcresearchpress.com by 88.255.202.194 on 09/08/12
For personal use only.

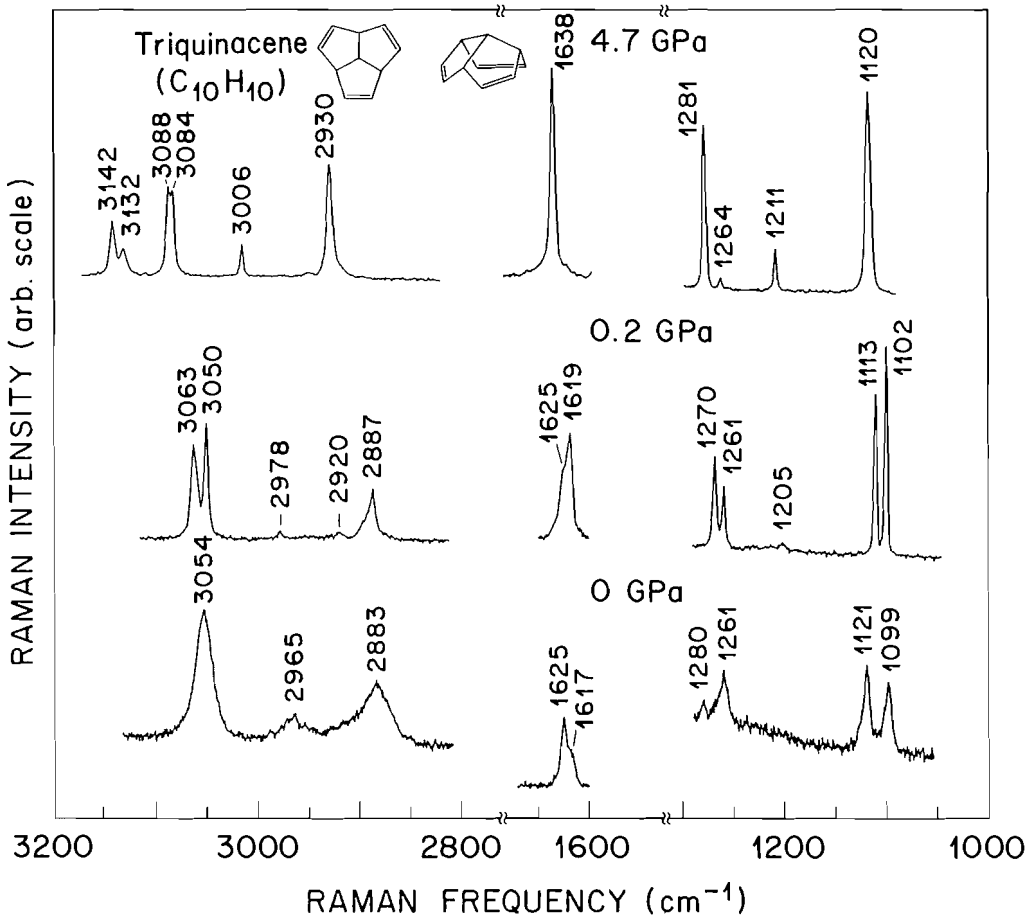

FIG. 2. Raman spectra of liquid (0 GPa) and solid triquinacene at 0.2 and 4.7 GPa in the 1000–3200 cm^{-1} region. Note the narrowing of the Raman peaks and the intensity changes upon crystallization. Some peaks show splittings.

The pressure dependence of the Raman modes is presented in Figs. 3 and 4. With increasing pressure the frequencies of almost all the Raman peaks of the crystal increase. The peak at 3063 cm^{-1} (see Fig. 2, 0.2 GPa spectrum) shifts anomalously and splits (compare the 0.2 and 4.7 GPa spectra in Fig. 2). The 3050 cm^{-1} peak also splits. At pressures higher than 6 GPa the Raman peaks are broadened, presumably due to nonhydrostatic pressure distribution.

The crystalline sample of dodecahedrane was strongly luminescent; however, we were able to record several Raman peaks over the luminescence background with the 514.5-nm laser line excitation. The observed peaks are listed in Table 2 along with the previously reported Raman lines (7). The pressure dependence of the modes is shown in Fig. 5. The strongest and sharpest peak in the Raman spectrum of dodecahedrane is at 679 cm^{-1} at ambient pressure. We assign this peak to a "breathing" mode of the molecule.

Discussion

The synthesis of dodecahedrane is a classic problem in organic chemistry. The successful synthesis (8*a*) in 23 steps by Paquette *et al.* in 1982 has been acclaimed as a great achievement.[4] Our expectation that pressure (up to 17 GPa) with or without photochemistry (248 and 308 nm, 5 GPa) could lead to a direct synthesis of dodecahedrane from triquinacene (1*a*, 1*b*, 9) was not realized.[5] Triquinacene has a negligible extinction coefficient beyond 230 nm (1*a*); nevertheless, we felt photolysis with the high photon flux of eximer lasers might result in a measurable amount of product. The diamonds we used did not transmit light at 222 nm (KrCl laser).

Our high-pressure Raman data on both triquinacene and dodecahedrane reveal some interesting features. We have not been able to find any published account of the Raman spectrum of triquinacene; consequently, this study appears to be the first. We will not present a detailed analysis of the spectra from the point of view of symmetry and the possible vibrational modes of the molecule, as this would be a complicated task. Rather, we identify the group frequencies and comment upon their behavior.

Firstly, the Raman peaks in the liquid spectra of triquinacene are broad, and all of them become strikingly narrower upon crystallization. In the liquid the molecules can have subtle conformational differences. Such a state can give rise to chemical environments that differ from one molecule to another, resulting in a spread of force constants and a corresponding spread in the frequencies of the stretching and

[4]For another successful route see ref. 8*b*.

[5]Small amounts of several triquinacene dimers were observed by GC–MS at retention times less than that of authentic dodecahedrane on a boiling point column.

TABLE 1. Triquinacene Raman frequencies

Liquid[a]	Solid[b]		dω/dP(cm^{-1}/GPa)
	53 s	Lattice	11.3
	82 s	modes	16.2
183 m	193 vs	Breathing	8.6
319 w	333 s		9.9
504 w	510 m		4.3
592 w	594 m		2.4
747 w	752 m	Skeletal	5.8
	760 m	deformation	7.0
770 vw	780 m	and bending	3.2
787 m	797 m	modes	3.8
	812 w		0.6
889 vw	890 vw		3.5
943 w	942 m		0.4
972 w	972 s		3.0
1028 w	1030 w	Bending	4.4
1043 vw	1042 w	modes	1.9
1099 m	1102 s	C—C	3.9
1121 m	1113 s	stretching	1.3
	1205 vw		1.8
1261 w	1261 m	Bending	1.0
1280 vw	1270 m	modes	2.5
1617 m	1619 m	C=C	3.5
1625 m	1625 m	stretching	
2883 m	2887 w	Bending	9.6
	2920 vw	modes	7.0
2965 w	2978 vw		8.4
3054 s	3050 s	—C—H	7.9
	3063 m	=C—H stretching	16.3

[a]Abbreviations: vs = very strong, s = strong, m = medium, w = weak, vw = very weak.
[b]Solid spectrum at 0.2 GPa.

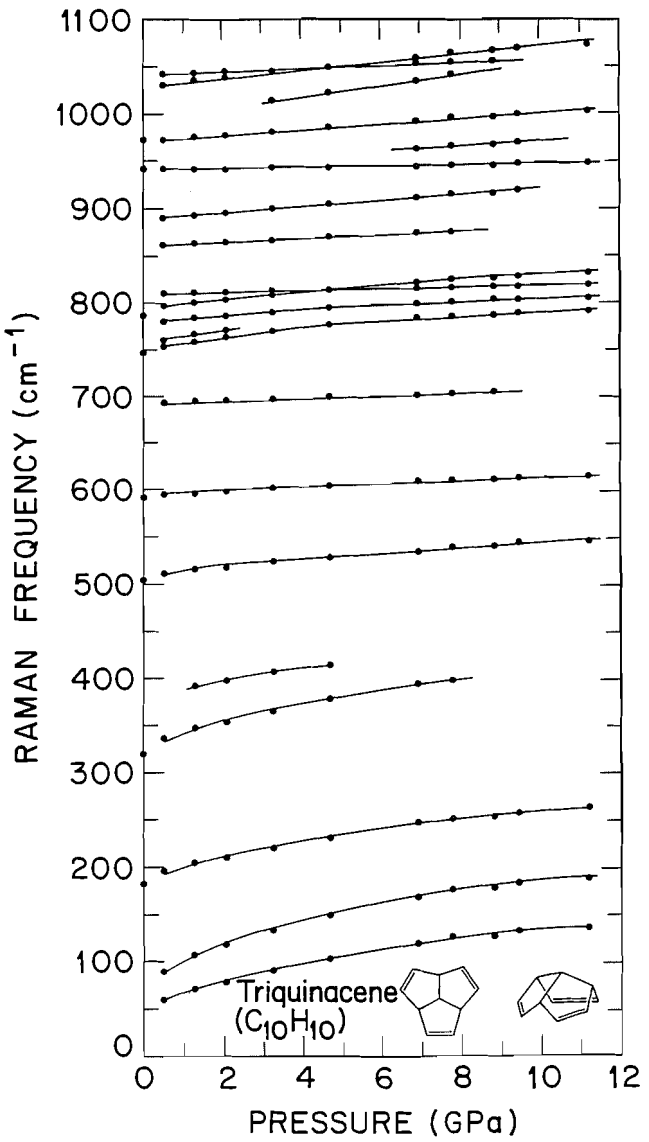

FIG. 3. Pressure dependence of the Raman peaks of triquinacene (see also Fig. 4).

bending modes of the molecule. In the crystal, only a small number of conformations — sometimes just one — are possible, leading to narrower Raman frequencies.

We have indicated in Table 1 the types of stretching modes that can be expected for triquinacene, and many bending modes are evidently possible. The two strong low-frequency peaks at 53 and 82 cm^{-1} are the lattice modes and, as expected of an organic system, they show a strong pressure dependence. There are two mode crossing situations involving the 797 and 812 cm^{-1} modes and the 1030 and 1042 cm^{-1} modes. No phase transition is indicated in our studies up to 11 GPa. A surprising result is that the two high-frequency C—H stretching modes at 3050 and 3063 cm^{-1} exhibit a large pressure dependence. Usually these are relatively insensitive to pressure in an organic crystal.

Dodecahedrane has been described as a beautiful molecule with I_h symmetry (10). It is a highly stable hydrocarbon (8). In Table 2 we have compared our Raman data with Raman peaks reported in an earlier study (8*a*) as well as with the theoretically calculated frequencies (10). In our studies up to 10 GPa there is no evidence for any phase transition and, surprisingly, the high-frequency vibrations (2988 and 2962 cm^{-1}) show a large increase in frequency with pressure. These are assigned to the C—H stretching and bending modes, respectively. There were doubts whether dodecahedrane would form a crystalline lattice; however, a recent X-ray diffraction study has shown that it does crystallize and that the unit cell is face-centered cubic (*FM* 3) (11). For an fcc lattice no Raman-active lattice mode is expected.

Summary and conclusions

We were not successful in synthesizing dodecahedrane from triquinacene by application of pressures up to 17 GPa. Also, exposure to near-UV radiation while the sample was under pressure was ineffective. We find a remarkable narrowing of all the Raman peaks of triquinacene in going from the liquid to the crystalline state. The large changes in the C—H frequencies with pressure in both triquinacene and dodecahedrane is a surprising result. The dodecahedrane molecule is believed to possess I_h symmetry and the crystal the fcc arrangement. The Raman peaks are consistent with these features.

Can. J. Chem. Downloaded from www.nrcresearchpress.com by 88.255.202.194 on 09/08/12
For personal use only.

TABLE 2. Observed Raman peaks of dodecahedrane and calculated frequencies

ω_R(obsd.)[a]		ω_R[b]	ω_R(calcd.)[c]	$d\omega/dP$(cm^{-1}/GPa)[a]
479	Skeletal	480		2.6
679	deformation	672	732 A_g	6.6
	modes			
843		840	846 H_g	3.1
1094	C—C	1092	1101 H_g	6.4
1168	stretching	1164	1166 H_g	16.4
2906	C—H		2899 A_g	3.3
2930	bending			6.0
	modes	2938		
2947				11.7
		2954		
2962	C—H			24.4
2988	stretching			24.0

[a]From the present study.
[b]Reference 8*a*.
[c]Reference 10.

Can. J. Chem. Downloaded from www.nrcresearchpress.com by 88.255.202.194 on 09/08/12
For personal use only.

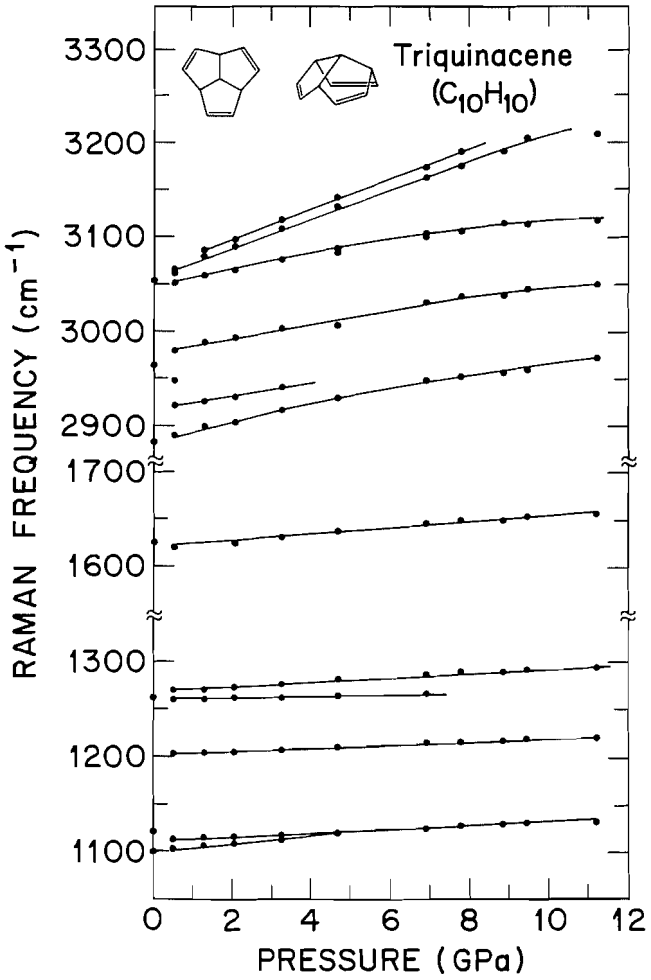

FIG. 4. Pressure dependence of the Raman peaks of triquinacene, high-frequency modes. The pressure dependencies of the two C—H stretching modes, near the top, are unusually large.

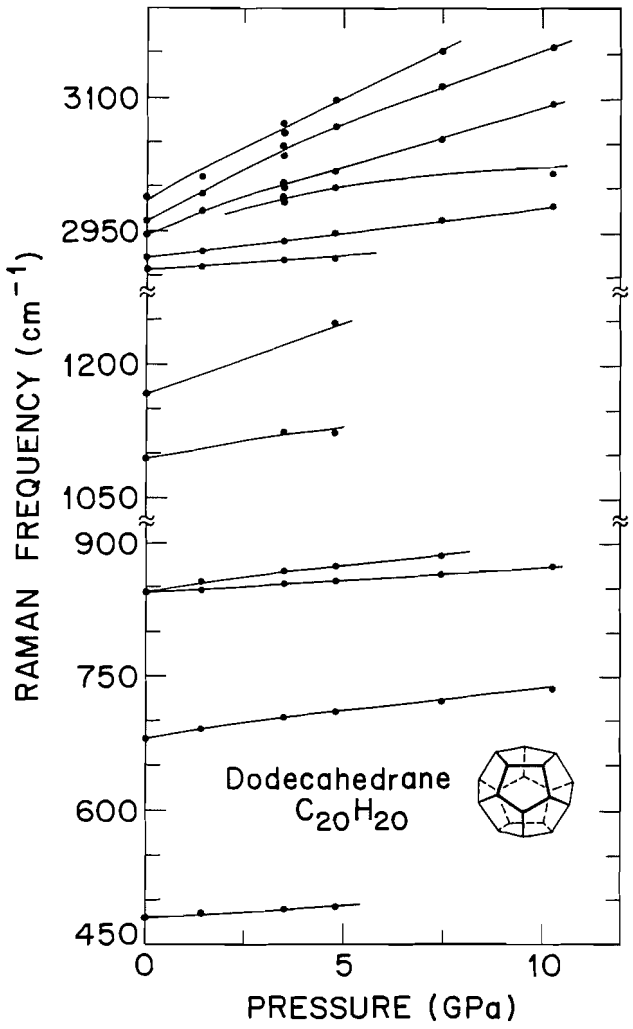

FIG. 5. Pressure dependence of the Raman peaks in dodecahedrane. The C—H stretching mode shows a large pressure dependence.

Acknowledgment

We thank Professor L. A. Paquette for the authentic sample of dodecahedrane he generously provided. We appreciate the assistance of V. Donnelly and T. Nakano with the laser photochemistry experiments. The GC—MS analysis of the diamond cell contents would not have been possible without the expert assistance of Dr. Thomas Hartman of Rutgers University – Centre for Advanced Food Technology.

1. (*a*) R. B. Woodward, T. Fukunaga, and R. C. Kelly. J. Am. Chem. Soc. **86**, 3162 (1964); (*b*) T. Jacobson. Acta Chem. Scand. **21**, 2235 (1967); (*c*) A. de Meijere, D. Kaufmann, and O. Schallner. Angew. Chem. Int. Ed. Engl. **10**, 417 (1971); (*d*) C. Mercier, P. Soucy, W. Rosen, and P. Deslongchamps. Synth. Commun. **3**, 161 (1973); (*e*) M. J. Wyvratt and L. A. Paquette. Tetrahedron Lett. 2433 (1974); (*f*) S. H. Bertz, G. Lannoye, and J. M. Cook. Tetrahedron Lett. **26**, 4695 (1985).
2. E. D. Stevens, J. D. Kramer, and L. A. Paquette. J. Org. Chem. **41**, 2266 (1976).
3. W. P. Roberts, S. Srivastava, and W. J. LeNoble. Ind. Chem. News, August, 24 (1984).
4. R. B. Woodward and R. Hoffmann. The conservation of orbital symmetry. Verlag Chemie, Weinheim. 1971.
5. G. J. Piermarini and S. Block. Rev. Sci. Instrum. **46**, 973 (1975).
6. J. D. Barnett, S. Block, and G. J. Piermarini. Rev. Sci. Instrum. **44**, 1 (1973).
7. S. C. Stinson. Science, August 16, 25 (1982).
8. (*a*) L. A. Paquette, R. J. Ternansky, W. Balogh, and G. Kentgen. J. Am. Chem. Soc. **105**, 5446 (1983); (*b*) W. D. Fessner, B. A. R. C. Murty, J. Wörth, D. Hunkler, H. Fritz, H. Prinzbach, W. D. Roth, P. von R. Schleyer, A. B. McEwen, and W. F. Maier. Angew. Chem. Int. Ed. Engl. **26**, 452 (1987); J.-P. Melder, R. Pinkos, H. Fritz, J. Worth, and H. Prinzbach. J. Am. Chem. Soc. **114**, 10213 (1992).
9. D. M. Muller. Chem. Weekbl. **59**, 334 (1963).
10. O. Ermer. Angew. Chem. Int. Ed. Engl. **16**, 411 (1977).
11. J. C. Gallucci, C. W. Doecke, and L. A. Paquette. J. Am. Chem. Soc. **108**, 1343 (1986).

Can. J. Chem. Downloaded from www.nrcresearchpress.com by 88.255.202.194 on 09/08/12
For personal use only.

The crystal and molecular structures of *N*,*N*′-di(2-acetylcyclohexenyl)ethylenediamine and its copper(II) complex

JUAN N. FERNÁNDEZ-G.,[1] RAÚL G. ENRÍQUEZ, AMALIA TOBÓN-CERVANTES, MARGARITA I. BERNAL-URUCHURTU, AND RENÉ VILLENA-I.

Instituto de Química, Universidad Nacional Autónoma de México, Circuito Exterior, Ciudad Universitaria, Coyoacán 04510, México, D.F. México

AND

WILLIAM F. REYNOLDS AND JI-PING YANG

Department of Chemistry, University of Toronto, 80 St. George Street, Toronto, Ont., Canada M5S 1A1

Received June 10, 1992

JUAN M. FERNÁNDEZ-G., RAÚL G. ENRÍQUEZ, AMALIA TOBÓN-CERVANTES, MARGARITA I. BERNAL-URUCHURTU, RENÉ VILLENA-I., WILLIAM F. REYNOLDS, and JI-PING YANG. **71**, 358 (1993).

The crystal structures of *N*,*N*′-di(2-acetylcyclohexenyl)ethylenediamine (L_1) and its copper(II) complex, which crystallizes with one solvent molecule of chloroform ($Cu(L_1\text{-}2H) \cdot CHCl_3$), were determined. Crystallographic details are as follows: L_1 is monoclinic, space group $P2_1/c$, with a = 8.280(2), b = 11.692(2), and c = 9.355(2) Å, β = 114.10(2)°, V = 826.7(3) Å^3, Z = 2; ρ_c = 1.22 g cm^{-3}, μ(Cu Kα) = 5.93 cm^{-1}, with the final residual indices of R = 0.046 and R_w = 0.070 for 991 unique reflections. $Cu(L_1\text{-}2H) \cdot CHCl_3$ is triclinic, space group $P\bar{1}$, with a = 11.121(3), b = 11.713(3), and c = 8.974(2) Å, α = 99.35(2)°, β = 110.83(2)°, γ = 82.33(2)°, V = 1074(1) Å^3, Z = 2; ρ_c = 1.50 g cm^{-3}, μ(Cu Kα) = 50.74 cm^{-1}, with the final residual indices of R = 0.048 and R_w = 0.077 for 2369 unique reflections. The X-ray diffraction study shows that in the crystal state the ligand L_1 is in the methylketone–cyclohexanonenamine isomeric form. For the copper complex $Cu(L_1\text{-}2H) \cdot CHCl_3$, the geometry around the metal atom is distorted square planar, and the angle between the chelate ring planes in the complex is 15.1°. An NMR study shows that L_1 in solution has the same structure as that observed in the solid state by X-ray diffraction.

JUAN M. FERNÁNDEZ-G., RAÚL G. ENRÍQUEZ, AMALIA TOBÓN-CERVANTES, MARGARITA I. BERNAL-URUCHURTU, RENÉ VILLENA-I., WILLIAM F. REYNOLDS et JI-PING YANG. **71**, 358 (1993).

On a déterminé les structures cristallines de la *N*,*N*-di(2-acétylcyclohexényl)éthylènediamine (L_1) et de son complexe avec le cuivre(II) qui cristallisent avec une molécule de solvant (chloroforme) ($Cu(L_1\text{-}2H) \cdot CHCl_3$). Les détails cristallographiques sont les suivants : L_1 est monoclinique, groupe d'espace $P2_1/c$, avec a = 8,280(2), b = 11,692(2) et c = 9,355(2) Å, β = 114,10(2)°, V = 826,7(3) Å^3, Z = 2; ρ_c = 1.22 g cm^{-3}, μ(Cu K$_\alpha$) = 5,93 cm^{-1}, R = 0,046 et R_w = 0,070 pour 991 réflexions uniques alors que $Cu(L_1\text{-}2H) \cdot CHCl_3$ est triclinique, groupe d'espace $P\bar{1}$, avec a = 11,121(3), b = 11,713(3) et c = 8,974(2) Å, α = 99,35(2)°, β = 110,83(2)°, γ = 82,33(2)°, V = 1074(1) Å^3, Z = 2; ρ_c = 1,50 g cm^{-3}, μ(Cu K$_\alpha$) = 50,74 cm^{-1}, R = 0,048 et R_w = 0,077 pour 2369 réflexions uniques. L'étude de diffraction des rayons-X montre que, à l'état cristallin, le ligand L_1 est dans la forme isomère méthylcétone–cyclohexanoneamine. Pour le complexe cuivrique $Cu(L_1\text{-}2H) \cdot CHCl_3$, la géométrie autour de l'atome métallique est plan carré déformé et l'angle entre les plans des cycles du chélate est égal à 15,1°. Une étude par RMN montre que, en solution, le ligand L_1 possède la même structure que celle observée à l'état solide par diffraction des rayons X.

[Traduit par la rédaction]

Introduction

With the aim of obtaining a tricyclic compound derived from "cyclam" (1,4,8,11-tetrazaacyclotetradecane), in which the 6–7 and 12–13 positions are shared with cyclohexane rings and having a methyl radical on the 5,14 positions, we prepared the Schiff base *N*,*N*′-di(2-acetylcyclohexenyl)-ethylenediamine (L_1) and its corresponding copper(II) complex ($Cu(L_1\text{-}2H)$), as possible intermediates for that macrocycle. Both the ligand and its copper complex were already reported by Moss and Robinson in 1973 (1). They proposed that the condensation site between ethylenediamine and the β-diketone occurred at the side-chain carbonyl group of the cyclohexane ring (Fig. 1). In agreement with this consideration, it has been accepted that polyamines condense very readily at the carbonyl carbon of an acetyl group whether it be a diketone or a triketone (2). However, a careful inspection of the mass spectrum of L_1 suggested to us that its structure might be wrongly assigned because of the presence of a fragment ion of m/e 43 with relative intensity of 42%, indicating that a methyl ketone group might be present in the ligand. This observation prompted us to establish unambiguously the structure of L_1 by an X-ray diffraction single crystal determination.

In this paper, we describe the crystal and molecular structures of the Schiff base ligand L_1 and its corresponding copper(II) complex $Cu(L_1\text{-}2H) \cdot CHCl_3$, in order to elucidate the conformation and structure of this ligand and to examine the conformational differences between it and its copper complex. Finally, ^{1}H and ^{13}C nmr analyses were also carried out to make an unambiguous assignment of signals and to confirm that the solution and crystal structures of the ligand were identical.

Experimental

Melting points were determined on a Fisher–Johns apparatus and are uncorrected; 2-acetylcyclohexanone, ethylenediamine, and copper acetate dihydrate were from Aldrich. The ir spectra were recorded on a Perkin–Elmer model 203-B spectrometer. The ^{1}H and ^{13}C nmr spectra and COSY, APT, HETCOR, FLOCK spectra were obtained on a Varian XL-400 spectrometer using $CDCl_3$ or a 1:1 mixture of $CDCl_3$ and C_6D_6, and TMS as internal standard. Mass

[1]Author to whom correspondence may be addressed.

Can. J. Chem. Downloaded from www.nrcresearchpress.com by 88.255.202.194 on 09/08/12
For personal use only.

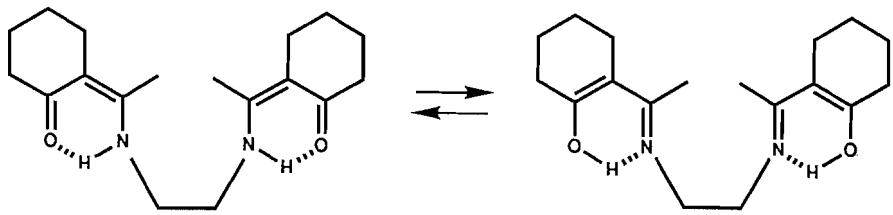

FIG. 1. Proposed tautomeric structures for L_1 in solution.

TABLE 1. Summary of crystal and intensity collection data for L_1 and $Cu(L_1\text{-}2H) \cdot CHCl_3$

Parameter	Compound	
	L_1	$Cu(L_1\text{-}2H) \cdot CHCl_3$
Molecular formula	$C_{18}H_{28}N_2O_2$	$C_{19}H_{27}N_2O_2Cl_3Cu$
M_R	304.21	485.34
Crystal system	Monoclinic	Triclinic
Space group	$P2_1/c$	$P\bar{1}$
Cell dimensions		
a (Å)	8.280(2)	11.121(3)
b (Å)	11.692(2)	11.713(3)
c (Å)	9.355(2)	8.974(2)
α (°)	90	99.35(2)
β (°)	114.10(2)	110.83(2)
γ (°)	90	82.33(2)
Cell volume (Å^3)	826.7(3)	1074(1)
Z	2	2
d_{calc} (g cm^{-3})	1.22	1.50
$F(000)$	332	502
μ CuKα (cm^{-1})	5.93	50.74
Crystal dimensions (mm)	0.34 × 0.38 × 0.4	0.28 × 0.54 × 0.56
T (K)	296	296
$2\theta_{min}$,°	3	3
$2\theta_{max}$,°	110.0	110.1
No. reflections measd.	1037	2927
No. unique reflections ($I > 3\sigma(I)$)	991	2369
σ limit ($F > n\sigma(F)$, n	3	3

spectra were obtained on a Hewlett–Packard instrument model 5985, operating at an ionizing potential of 70 eV.

The ligand was prepared as previously described (1) as very pale yellow crystals from hexane–dichloromethane, mp 139–141°C (lit. (1) mp 142–142.5°C).

The complex was obtained as follows: to a stirred solution of 0.304 g (1 mmol) of the Schiff base in dry methanol (100 mL) was added a solution of 2.5 g (30.48 mmol) of sodium acetate in water (25 mL) followed by 0.200 g (1 mmol) of copper(II) acetate monohydrate in water (25 mL). The resulting solution was stirred for 15 min after which time deep red–purple crystals formed, mp 197–199°C (lit. (1) mp 202–204°C).

The ir spectra were in agreement with those reported by Moss and Robinson; the mass spectrum of L_1 showed the following fragments: m/e (relative intensity) 304(13) M^+, 165(17), 152(100), 138(24), 110(10), 69 (5), 43(42). The mass spectrum of $Cu(L_1\text{-}2H)$ showed the molecular ion with the characteristic isotopic contribution of the copper atom: 367(25.6) [M^+ + 2], 365(56) M^+, 216(38.5), 214(100), 150(72), 138(10), 136 (5), 43(37).

Single crystals of L_1 were grown by slow evaporation of an ethyl acetate – hexane mixture while those of $Cu(L_1\text{-}2H)$ were grown by diffusion of ethyl acetate into a chloroform solution. However, the shining dark-red crystals of the complex decompose in the solid state to an opaque solid over the course of 3 h after removal from solution, probably due to loss of the crystallization solvent. Consequently, to avoid decomposition, all the faces of freshly cropped suitable crystals were covered with epoxy resin.

The data for the two compounds were collected on a Nicolet R3m four-circle diffractometer with graphite monochromated CuKα radiation (λ = 1.54178 Å) using an ω-scan mode with variable scan rate from 4 to 30 deg/min and a scan width of 1.0°. Crystal data and additional data collection parameters are given in Table 1. Cell dimensions for L_1 and $Cu(L_1\text{-}2H) \cdot CHCl_3$ were determined by least squares from 25 reflections (11.7° < 2θ < 29.58° and 7.7° < 2θ < 26.55°, respectively). Corrections were applied for Lorentz and polarization effects. Data for $Cu(L_1\text{-}2H) \cdot CHCl_3$ were corrected for absorption using the Ψ scan method.

The structures were solved by direct methods and subsequent use of Fourier difference maps. They were refined by the full-matrix least-squares method using anisotropic thermal parameters for all non-hydrogen atoms. The H atoms of the CH_2 and CH_3 groups were allowed to ride on bonded C atoms with a fixed isotropic temperature factor, U = 0.06 Å^2. The H atoms bonded to N atoms were found from a difference Fourier map at an advanced stage of anisotropic refinement and their coordinates refined. For L_1, the function minimized was $\Sigma w|\Delta F|^2$ with a weighting scheme $w = [\sigma^2(F_o) + G(F_o)^2]^{-1}$, where σ is the esd, based on counting statistics, and G an adjustable variable, final G = 0.00633. The final R and R_w were 0.046 and 0.070 (where $R_w = \Sigma w^{1/2}||F_o| - |F_c||/\Sigma w^{1/2}(|F_o|)]$. For $Cu(L_1\text{-}2H) \cdot CHCl_3$, the function minimized was $\Sigma w(|F_o| - |F_c|)^2$ with a weighting scheme $w = 1/\sigma^2(F)$ based on counting statistics, including a factor (p = 0.09) to downweight the intense reflexions. The final R and R_w were 0.048 and 0.077.

Can. J. Chem. Downloaded from www.nrcresearchpress.com by 88.255.202.194 on 09/08/12
For personal use only.

Can. J. Chem. Downloaded from www.nrcresearchpress.com by 88.255.202.194 on 09/08/12
For personal use only.

The largest peaks in the final difference map for L_1 and $Cu(L_1\text{-}2H) \cdot CHCl_3$ were 0.75 and 0.17 e/Å^3, respectively.

The atomic scattering factors were taken from International Tables for X-ray Crystallography (3). Solution and refinement of L_1 were carried out using SHELTXL (4) on a Nova 4S computer while $Cu(L_1\text{-}2H) \cdot CHCl_3$ was solved and refined on a Vax station ILI using the TEXSAN–TEXRAY structure analysis package (5).

Results and discussion

Final positional parameters for compounds L_1 and $Cu(L_1\text{-}2H) \cdot CHCl_3$ are given in Table 2, while Table 3 contains selected bond lengths and bond angles.[2] The molecular structures of the compounds, including atom-numbering schemes, are illustrated in Figs. 2 and 3, respectively.

The X-ray structure determination of L_1 (Fig. 2) shows unequivocally that the structure is the result of a nucleophilic attack on the carbonyl of the cyclohexanone ring, which eliminates the structure shown in Fig. 1. In the crystalline state, L_1 is composed of two $C_9H_{14}NO$ halves, which are related to each other by a crystallographic center of inversion as shown in Fig. 2. The ligand is found in the tautomeric enamine–ketone form with an N—H distance of 0.84(2) Å, which is similar to the values observed for other N—H bonds in related compounds (6, 7). The corresponding O · · · · H distance is 1.91(2) Å and the O · · · · H—N angle is 138.8°. Bond lengths in the molecule suggest an electronic delocalization in the N(1)—C(1)—C(2)—C(7)—O(1) bonds. The C(1)—N(1) distance (1.346(3) Å) is slightly longer but in the same range as the C—N distance observed in *N,N'*-ethylenebis(acetylacetoneimine) [en(acacH)$_2$] (7) (mean, 1.331(3) Å), the C(7)—O(1) bond length (1.258(3) Å) is similar to the value observed for the corresponding C=O bond (mean, 1.243(4) Å) in the same compound, and the C(1)—C(2) and C(2)—C(7) bonds have similar lengths (1.394(3) and 1.427(2) Å) to the corresponding C—C bonds in en(acacH)$_2$ (1.393(5) and 1.440(6) Å). In L_1 the torsion angles around the C(1)—N(1)—C(9)—C(9a), C(9)—C(9a), and C(9)—C(9a)—N(1a)—C(1a) bonds are −92.3, 180, and 92.3°, respectively.

The X-ray diffraction analysis of $Cu(L_1\text{-}2H) \cdot CHCl_3$ shows the copper to be four-coordinate and to be involved in a slightly distorted square planar structure. As expected, the ligand undergoes changes upon coordination similar to those found in similar complexes (7–10) and follows the same trend as that observed in the latter complexes, i.e., shortening of the C(1)—N(1) and C(2)—C(7) bonds and a lengthening of the C(7)—O(1) and C(1)—C(2) bonds (see Table 3), which is the result of a greater conjugation in the chelate rings of the metal complex. The chloroform molecules are not interacting directly with the metal atom, but the hydrogen atom of the chloroform does make a close approach, 2.380 and 2.477 Å, to the O(1a) and O(1b) atoms while the carbon atom of chloroform is, respectively, 3.235(6) and 3.294(5) Å from the same oxygen atoms. The angle between the two coordination chelate planes defined by O(1b)—Cu—N(1b) and O(1a)—Cu—N(1a) is 15.1°.

The solution structure of the ligand, L_1, and the ^1H and ^{13}C nmr spectral assignments were confirmed by a series of one-dimensional (^1H, ^{13}C, APT) and two-dimensional (HETCOR, FLOCK, and COSY) nmr experiments. The experiments were carried out in both $CDCl_3$ and a 1:1 mixture of $CDCl_3$ and C_6D_6. The latter solution was required because the two sets of allylic methylene proton signals overlapped in $CDCl_3$,

TABLE 2. Positional parameters and equivalent isotropic thermal parameters (Å^2 × 10^3) for (*a*) L_1 and (*b*) $Cu(L_1\text{-}2H) \cdot CHCl_3$ (esd's in parentheses refer to the least significant digit printed)

(*a*) L_1

Atom	*x*	*y*	*z*	U_{eq}[a]
C(1)	0.7789(2)	−0.0213(1)	0.1679(2)	38(1)
C(2)	0.7505(2)	0.0084(2)	0.3000(2)	38(1)
C(3)	0.6421(3)	−0.0689(2)	0.3580(2)	50(1)
C(4)	0.5395(2)	−0.1603(2)	0.2419(2)	54(1)
C(5)	0.6588(3)	−0.2182(2)	0.1785(2)	55(1)
C(6)	0.7145(3)	−0.1326(2)	0.0839(2)	49(1)
C(7)	0.8316(2)	0.1074(2)	0.3899(2)	42(1)
C(8)	0.8130(3)	0.1291(2)	0.5421(2)	55(1)
O(1)	0.9209(2)	0.1785(1)	0.3515(2)	57(1)
N(1)	0.8683(2)	0.0482(1)	0.1111(2)	45(1)
C(9)	0.9098(2)	0.0284(2)	−0.0232(2)	47(1)

(*b*) $Cu(L_1\text{-}2H) \cdot CHCl_3$

Atom	*x*	*y*	*z*	U_{eq}[a]
Cu	0.95273(4)	0.21020(4)	0.90959(5)	42.1(4)
Cl(1)	0.5382(1)	0.1158(1)	0.8932(3)	105(2)
Cl(2)	0.6314(2)	0.2914(2)	1.1590(2)	118.5(2)
Cl(3)	0.4774(2)	0.3553(2)	0.8506(2)	115.0(1)
O(1a)	0.7889(3)	0.1945(2)	0.7499(3)	56.4(2)
O(1b)	0.8800(2)	0.3417(2)	1.0107(3)	51.7(2)
N(1b)	1.1238(3)	0.2383(3)	1.0480(4)	47.1(2)
N(1a)	1.0221(3)	0.0637(3)	0.8292(4)	50.6(2)
C	0.5949(4)	0.2559(5)	0.9532(7)	74.6(3)
C(1b)	1.1614(4)	0.3324(4)	1.1515(4)	48.1(2)
C(1a)	0.9603(4)	−0.0128(3)	0.7106(5)	53.7(2)
C(2a)	0.8308(4)	0.0101(4)	0.6101(5)	54.3(2)
C(2b)	1.0742(4)	0.4173(3)	1.1970(4)	47.7(2)
C(3a)	0.7677(6)	−0.0815(5)	0.4705(6)	78.3(3)
C(3b)	1.1239(5)	0.5171(4)	1.3305(6)	66.8(3)
C(4a)	0.833(1)	−0.2025(6)	0.4907(9)	114.0(5)
C(4b)	1.2657(7)	0.5055(6)	1.4191(8)	102.8(5)
C(5a)	0.9678(8)	−0.2057(5)	0.5278(8)	92.9(4)
C(5b)	1.3368(6)	0.4681(7)	1.3124(7)	105.6(5)
C(6a)	1.0344(5)	−0.1278(4)	0.6821(5)	69.6(3)
C(6b)	1.3051(4)	0.3468(5)	1.2241(6)	69.3(3)
C(7a)	0.7576(4)	0.1099(4)	0.6331(5)	58.0(2)
C(7b)	0.9419(4)	0.4168(3)	1.1249(4)	48.4(2)
C(8a)	0.6209(5)	0.1347(5)	0.5148(7)	77.7(3)
C(8b)	0.8527(5)	0.5123(4)	1.1751(6)	68.3(3)
C(9b)	1.2165(4)	0.1521(4)	1.0038(5)	58.8(2)
C(9a)	1.1538(4)	0.0392(4)	0.9335(5)	60.0(3)

[a]The equivalent isotropic *U* defined as one third of the trace of the orthogonalized U_{ij} tensor.

[2]Supplementary material for the ligand L_1 and $Cu(L_1\text{-}2H) \cdot CHCl_3$ (packing arrangement; atom coordinates; complete bond lengths and angles; anisotropic temperature factors, and hydrogen coordinates; observed and calculated structures factors) may be purchased from: The Depository of Unpublished Data, Document Delivery, CISTI, National Research Council of Canada, Ottawa, Canada K1A 0S2.

Tables of bond lengths and angles and atomic coordinates, and diagrams of the packing arrangement have also been deposited with the Cambridge Crystallographic Data Centre and can be obtained on request from The Director, Cambridge Crystallographic Data Centre, University Chemical Laboratory, 12 Union Road, Cambridge, CB2 1EZ, U.K.

TABLE 3. Selected bond lengths (Å) and angles (°) for (*a*) L_1 and (*b*) $Cu(L_1\text{-}2H)\cdot CHCl_3$ with esd's in the least significant figure given in parentheses

(*a*) L_1

C(1)—C(2)	1.394(3)	C(1)—C(6)	1.500(2)
C(1)—N(1)	1.346(3)	C(7)—O(1)	1.258(3)
C(2)—C(7)	1.427(2)	C(7)—C(8)	1.515(3)
N(1)—C(9)	1.450(3)	C(9)—C(9a)	1.526(4)
C(2)—C(1)—C(6)	121.8(2)	C(2)—C(1)—N(1)	121.2(2)
C(6)—C(1)—N(1)	116.9(2)	C(1)—C(2)—C(3)	120.4(2)
C(1)—C(2)—C(7)	121.0(2)	C(2)—C(3)—C(4)	113.8(2)
C(1)—C(6)—C(5)	113.1(2)	C(2)—C(7)—C(8)	119.0(2)
C(2)—C(7)—O(1)	123.9(2)	C(8)—C(7)—O(1)	117.1(2)
C(1)—N(1)—C(9)	127.5(2)	N(1)—C(9)—C(9a)	112.0(2)

(*b*) $Cu(L_1\text{-}2H)\cdot CHCl_3$

Cu—O(1a)	1.885(3)	C(1a)—C(2a)	1.418(6)
Cu—O(1b)	1.894(3)	C(1a)—C(6a)	1.517(6)
Cu—N(1b)	1.904(3)	C(2a)—C(7a)	1.364(6)
Cu—N(1a)	1.924(3)	C(2a)—C(3a)	1.534(6)
O(1b)—C(7b)	1.290(5)	C(2b)—C(7b)	1.381(6)
O(1a)—C(7a)	1.302(5)	C(1b)—C(6b)	1.517(6)
N(1b)—C(9b)	1.458(5)	C(1b)—C(2b)	1.411(6)
N(1b)—C(1b)	1.329(5)	C(7b)—C(8b)	1.515(6)
N(1a)—C(1a)	1.320(5)	C(7a)—C(8a)	1.535(7)
N(1a)—C(9a)	1.450(6)	C(9b)—C(9a)	1.516(7)
O(1a)—Cu—O(1b)	88.5(1)	C(7a)—C(2a)—C(1a)	123.0(4)
O(1a)—Cu—N(1b)	171.1(1)	C(7b)—C(2b)—C(1b)	122.9(4)
O(1a)—Cu—N(1a)	92.4(1)	C(2a)—C(7a)—C(8a)	121.2(4)
O(1b)—Cu—N(1b)	92.6(1)	C(2b)—C(7b)—C(8b)	120.6(4)
O(1b)—Cu—N(1a)	171.3(1)	C(7a)—O(1a)—Cu	126.2(3)
N(1b)—Cu—N(1a)	87.9(1)	C(7b)—O(1b)—Cu	126.7(2)
C(1b)—N(1b)—Cu	127.1(3)	C(1b)—N(1b)—C(9b)	121.5(3)
C(1b)—N(1a)—Cu	127.7(3)	C(1a)—N(1a)—C(9a)	122.4(4)
N(1b)—C(1b)—C(2b)	122.9(3)	C(9b)—N(1b)Cu	110.3(2)
N(1b)—C(1b)—C(6b)	117.7(4)	C(9a)—N(1a)—Cu	109.4(3)
N(1a)—C(1a)—C(2a)	122.6(4)	C(2b)—C(1b)—C(6b)	119.4(4)
N(1a)—C(1a)—C(6a)	117.3(4)	C(2a)—C(1a)—C(6a)	120.2(4)
C(2a)—C(7a)—C(8a)	121.2(2)	O(1a)—C(7a)—C(2a)	127.6(4)
C(2b)—C(7b)—C(8b)	120.6(4)	O(1a)—C(7a)—C(8a)	121.2(4)
O(1b)—C(7b)—C(2b)	126.8(3)	N(1b)—C(9b)—C(9a)	109.1(3)
O(1b)—C(7b)—C(8b)	112.6(4)	N(1a)—C(9a)—C(9b)	109.4(3)

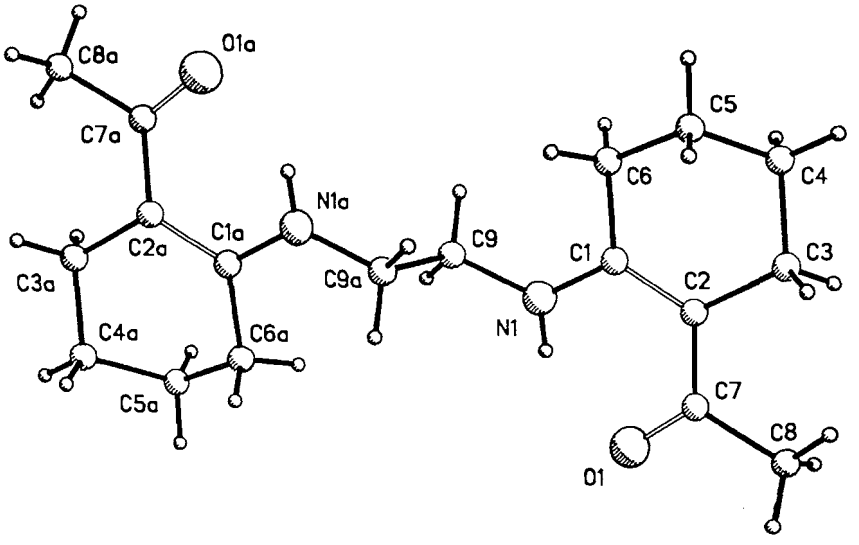

FIG. 2. A view of a single molecule of L_1 showing the atom labelling.

Can. J. Chem. Downloaded from www.nrcresearchpress.com by 88.255.202.194 on 09/08/12
For personal use only.

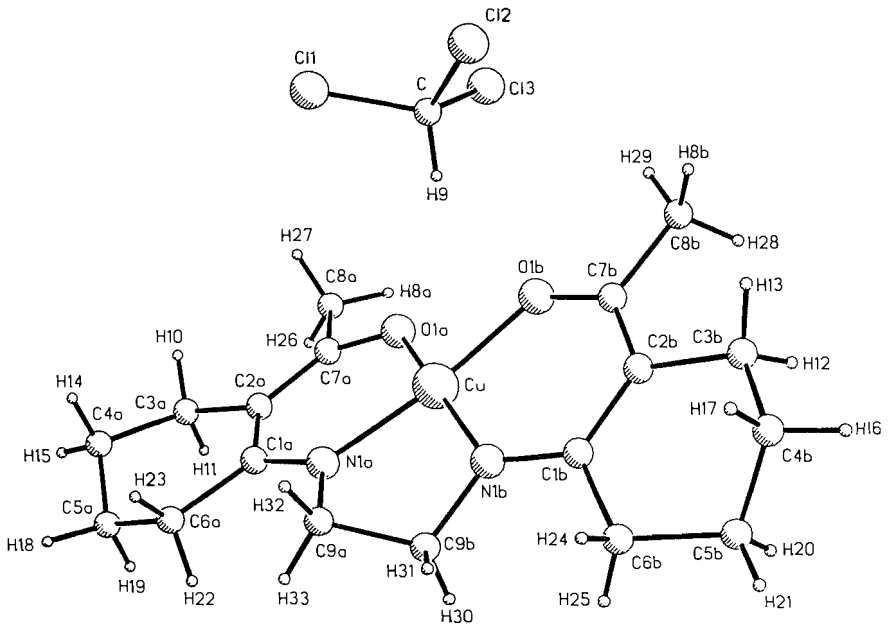

FIG. 3. A view of a molecule of $Cu(L_1\text{-}2H) \cdot CHCl_3$ showing the atom labelling.

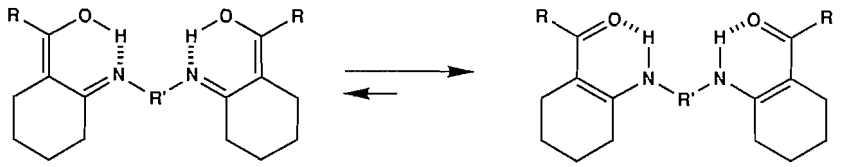

FIG. 4. Structure **1** shows the NH tautomer of L_1 that is the major form in solution.

TABLE 4. The nmr data of L_1 in $CDCl_3$ and a 1:1 mixture of $CDCl_3$–C_6D_6.

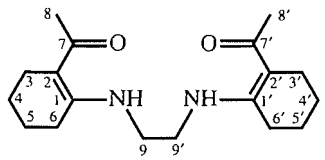

Carbon	δ_C[a] (ppm)		δ_H[a] (ppm)	
1,1′	161.26	(160.97)	—	—
2,2′	100.86	(100.92)	—	—
3,3′	26.01	(26.12)	2.32	(1.94)
4,4′	21.71	(22.12)	1.60	(1.36)
5,5′	22.84	(23.27)	1.60	(1.38)
6,6′	26.06	(26.42)	2.32	(2.12)
7,7′	196.43	(196.25)	—	—
8,8′	27.48	(27.74)	2.08	(2.00)
9,9′	42.52	(42.67)	3.35	(2.86)
N—H	—	—	11.55	(10.75)

[a]Values in parentheses are for a 1:1 mixture of $CDCl_3$ and C_6D_6.

as did the other two ring-proton methylene signals (H:3 and H:4). Spectral assignments are summarized in Table 4. The key observation was provided by a FLOCK experiment that determines *n*-bond $^{13}C—^1H$ (n = 2 or 3) (11). In this experiment the methyl ^1H singlet (H-8) showed cross peaks with a carbonyl ^{13}C signal at δ 196 ppm and an olefinic carbon at δ 101 ppm. This confirms the proposed structure with the acetyl group unreacted. With the alternative structure reported by Moss and Robinson, one would expect methyl ^1H cross peaks to the two olefinic carbons but none to the carbonyl carbon.

As previously reported (1), the CH_2–CH_2 bridge appeared as a distorted triplet with approximately 2:1:2 peak intensities. This collapsed to a singlet when the broad peak at δ 11.55 ppm was irradiated. The presence of coupling to the N-H proton confirms that L_1 exists in solution as the N-H (enamine) tautomer rather than the alternative O-H (imine) tautomer (see Fig. 4). This was also observed in the solid state.

The unusual appearance of the methylene envelope can be attributed to virtual coupling. The HN—CH_2—CH_2—NH unit forms an AA′A″A‴XX′ spin system. Since the four methylene protons are strongly coupled, they appear to be coupled almost equally to both NH protons, even though the four-bond coupling is actually near zero.

Based on the X-ray diffraction data and the nmr data, there can be no doubt that L_1 has the structure **1** shown in Fig. 4. Because of the limited data reported in the earlier publication of Moss and Robinson (1), it is impossible to determine whether, as they claimed, they actually synthesized and isolated the isomer corresponding to the reaction of diami-

Can. J. Chem. Downloaded from www.nrcresearchpress.com by 88.255.202.194 on 09/08/12
For personal use only.

noethane with the acetyl group of 2-acetylcyclohexanone or whether they isolated L_1 but misassigned its structure. Their assignment was entirely based on mass spectral fragmentation patterns that, with the exception of the peak at m/e 43, corresponded closely to those we observed for L_1. We previously demonstrated that use of mass spectral fragmentation patterns can lead to errors in structural assignments (12). To better understand the reactivity of 2-ketocycloalkanones with diaminoalkanes, we are undertaking a more systematic investigation of this reaction.

Acknowledgments

The authors thank Quim. R. A. Toscano and Mr. Abelardo Cuellar for technical assistance.

1. K. C. Moss and F. P. Robinson. Can. J. Chem. **51**, 505 (1973).
2. P. Zanello, S. Tamburini, P. A. Vigato, and G. A. Mazzochin. Coord. Chem. Rev. **77**, 165 (1987).
3. International tables for X-ray crystallography. Vol. IV. Kynoch Press, Birmingham. 1974.
4. G. M. Sheldrick. SHELXTL Version 3. An integrated system for solving, refining and displaying crystal structures from diffraction data. Univ. of Göttingen, Germany. 1981.
5. TEXSAN–TEXRAY. Structure Analysis Package. Molecular Structure Corporation, Tex. 1985.
6. E. Acevedo-Arauz, J. M. Fernández-G, M. J. Rosales-Hoz, and R. A. Toscano. Acta Crystallogr. Sect. C: Cryst. Struct. Commun. **C48**, 115 (1992)
7. N. Bresciani-Pahor, M. Calligaris, G. Nardin, L. Randaccio, and D. Viterbo. Acta Crystallogr. Sect. B: Struct. Crystallogr. Cryst. Chem. **B35**, 2776(1979).
8. D. Hall, A. D. Rae, and T. N. Waters. J. Chem. Soc. 5897 (1963).
9. R. Cea-Olivares, I. Rodríguez, M. J. Rosales, and A. Toscano. Aust. J. Chem. **37**, 879 (1984).
10. H. C. Allen, G. I. Hillhouse, and D. J. Hodgson. Inorg. Chim. Acta, **37**, 37 (1979).
11. W. F. Reynolds, S. McLean, M. Perpick-Dumont, and R. G. Enríquez. Magn. Reson. Chem. **27**, 162(1989).
12. S. McLean, M. Perpick-Dumont, W. F. Reynolds, H. Jacobs, and S. S. Lachmansing. Can. J. Chem. **65**, 2519 (1987).

Can. J. Chem. Downloaded from www.nrcresearchpress.com by 88.255.202.194 on 09/08/12
For personal use only.

The chemistry of 5β,6β-epoxy-4,4-dimethylcholest-1-en-3-one. Approaches to the synthesis of 1α,5α-cyclosteroids. Part II[1]

PARIS E. GEORGHIOU[2] AND YI REN
Department of Chemistry, Memorial University of Newfoundland, St. John's, Nfld., Canada, A1B 3X7

Received September 24, 1992

PARIS E. GEORGHIOU and YI REN. Can. J. Chem. **71**, 364 (1993).

Epoxidation of 4,4-dimethylcholesta-1,5-dien-3-one (**9**) with MCPBA gives a mixture of the corresponding epimeric 5α,6α and 5β,6β epoxides. The major product is the 5β,6β epimer **6**, in contradiction to what has been reported by others. The unambiguous assignment of the structures of these epoxides is based upon NMR NOED experiments. The chemistry of the 5β,6β epoxide is described in the context of unsuccessful attempts at synthesizing the corresponding 1α,5α cyclosteroids. Reductive methods using lithium – liquid ammonia, lithium–ethylamine, or tri-*n*-butyl- or triphenyltin–AIBN gave products in which the α,β-unsaturated carbonyl system and the epoxide were reduced. When **6** was treated with BF_3·etherate a *B*-nor derivative **27** was formed, presumably via a pinacol-type rearrangement.

PARIS E. GEORGHIOU et YI REN. Can. J. Chem. **71**, 364 (1993).

L'époxydation de la 4,4-diméthylcholesta-1,5-dièn-3-one (**9**) par l'AMCPB conduit à un mélange des époxydes épimères correspondants 5α,6α et 5β,6β. Contrairement à ce qui a été rapporté par d'autres, le produit majeur est l'épimère 5β,6β (**6**). L'attribution non-ambiguë des structures de ces époxydes est basée sur des expériences de RMN «NOED». On décrit la chimie de l'époxyde 5β,6β dans le contexte d'essais infructueux de synthèse des 1α,5α cyclostéroïdes correspondants. Les réductions à l'aide de lithium – ammoniac liquide, de lithium–èthylamine ou des tri-*n*-butyl- ou triphényl-étain–AIBN conduisent à des produits dans lesquels le système carbonyle α,β-insaturé et l'èpoxyde sont réduits. Le traitement du produit **6** par du BF_3·ether conduit à la formaton du dérivé *B*-nor **27**, probablement par un réarrangement de type pinacolique.

[Traduit par la rédaction]

Introduction

The 1α,5α cyclocholesterols are relatively rare. Laing and Sykes (1, 2) reported the synthesis of 1α,5α-cyclocholest-2-ene (**1**), and 3β-acetoxy-1α,5α-cyclocholestan-6-one (**2**) (3). The synthesis of **2** could not, however, be duplicated (4). Christensen and Reusch (5) synthesized 1-hydroxy-1α,5α-cyclocholestan-7-one (**3**) via lithium – liquid ammonia reduction of cholest-5-ene-1,7-dione. More recently we succeeded in synthesizing 4,4-dimethyl-1α,5α-cyclocholestane-3,7-dione (**4**) via an intramolecular reductive coupling of the *bis*-α,β-unsaturated diketone **5** (6).

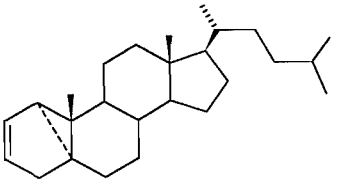

1

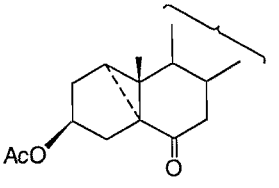

2

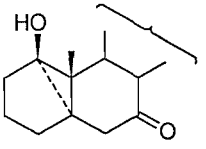

3

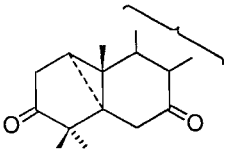

4

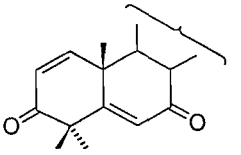

5

5β,6β-Epoxy-4,4-dimethylcholest-1-en-3-one (**6**) can be envisioned as a potential precursor for the synthesis of the cyclosteroid **7**. As depicted in Scheme 1, **7** could in principle be formed via an intramolecular ring opening of the epoxy group by the intermediate dianion **8** generated by metal – liquid ammonia reduction (7). We were unable to synthesize **7** but the results of our experiments on the chemistry of **6** form the subject of this paper.

Results and discussion

4,4-Dimethylcholesta-1,5-dien-3-one (8) (**9**) was prepared by benzeneselenenic anhydride (8) oxidation of 4,4-dimethylcholest-5-en-3-one (**10**). Reaction of **9** with

[1]Part I, see ref. 22.
[2]Author to whom correspondence may be addressed.

Can. J. Chem. Downloaded from www.nrcresearchpress.com by 88.255.202.194 on 09/08/12
For personal use only.

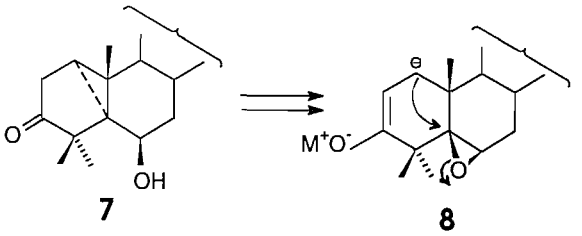

7 8

SCHEME 1

m-chloroperoxybenzoic acid (MCPBA) in refluxing dichloromethane solution for 4 h gave a mixture of the 5β,6β and 5α,6α epoxides, **6** and **11**, respectively, and a small amount (12%) of the epoxy-lactone **12**. The mixture comprised the major product **6** (71%) and the 5α,6α epoxide **11** (only 9%). The assignment of structures to the epimeric epoxides was initially based on the observations of Cross (9) and Halsall *et al.* (10) of the C-6 proton chemical shift values of other 5β,6β and 5α,6α epoxides. The major product had the lower field chemical shift value for the C-6 proton and was assigned structure **6**. Nuclear Overhauser effect difference (NOED) experiments on both epoxides were in agreement with this assignment. Separate, selective irradiation of both the α and β C-4 methyl groups of the 5α,6α epoxide at δ 0.93 and 1.36, respectively, each enhanced the C-6 proton signal at δ 3.10 (16% and 3%, respectively). By contrast, only when the α C-4 methyl group of the 5β,6β epoxide at δ 0.94 was irradiated was there any enhancement of the C-6 proton signal at δ 3.32 (20%). No corresponding enhancement was observed when the β C-4 methyl group at δ 1.33 on **6** was irradiated.

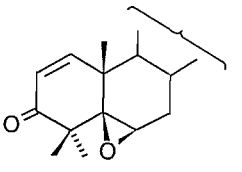

6

Brynjolffssen *et al.* (11) reported obtaining a 60% yield of **11** when they treated **9** with MCPBA in refluxing dichloromethane. The melting point and NMR data of what they presumed to be the 5α,6α epoxide were identical with our data for **6**. In addition to our NOE data, direct proof by X-ray crystallographic analysis was obtained. Although both **6** and **11** were crystalline, only crystals of **11** were suitable for X-ray crystallography. The structure obtained[3] confirmed our original assignment that **11** was indeed that 5α,6α epoxide and that the assignment of Brynjolffssen *et al.* was incorrect. Using their conditions **11** was obtained only as a minor product. The major product was different from the expected 5β,6β epoxide **6**. Spectral and mass data of this compound were consistent with it being the epoxy-lactone **12**. Compound **12** is most likely formed by a Baeyer–Villager oxidation of **6** since the MCPBA used is in excess.

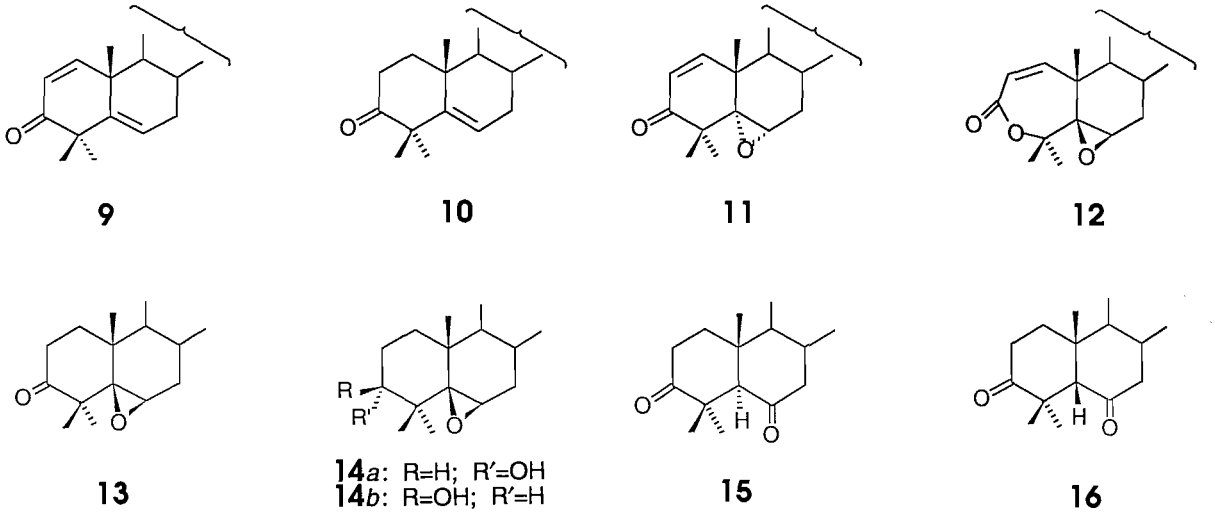

9 **10** **11** **12**

13 **14***a*: R=H; R'=OH **14***b*: R=OH; R'=H **15** **16**

Epoxide **6** was reacted with lithium in liquid ammonia under several different conditions, each giving the same results. These were mixtures that could be separated by flash chromatography to afford 5β,β-epoxy-4,4-dimethylcholestan-3-one (**13**), and a mixture of the corresponding epimeric 3α and 3β alcohols **14***a* and **14***b*. Reaction of **6** with ytterbium in liquid ammonia (12) gave the same results as were found with lithium in liquid ammonia. Thus, although the α,β-unsaturated carbonyl system could be reduced, presumably via the dicarbanion **8**, cyclization to **7** via transannular opening of the epoxide did not occur.

The desired intramolecular cyclization can be envisioned as an example of a favoured 3-*exo-tet* or 5-*exo-tet* ring closure (13). It is possible, however, that cyclization did not occur because pyramidalization of the carbanion at C-1 was preferentially formed on the β-face as a result of interactions (14) with the σ-framework.

Reductions employing sodium or lithium in ethylamine can yield different results than when they are employed in liquid ammonia (15, 16). Hallsworth and Henbest (16) found that the course of reductive ring opening of 5β,6β-epoxycholestane could be altered when ethylamine was used with

[3]X-ray crystallographic analysis on **11** confirmed the assigned structure (P. E. Georghiou, Y. Ren, and J. N. Bridson, unpublished data).

Can. J. Chem. Downloaded from www.nrcresearchpress.com by 88.255.202.194 on 09/08/12
For personal use only.

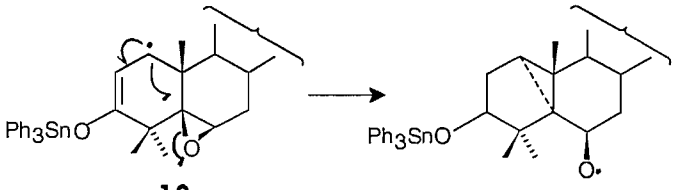

18

SCHEME 2

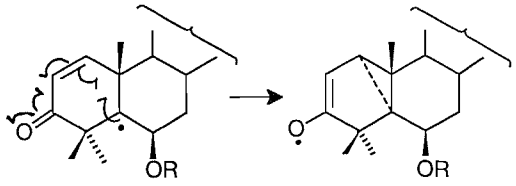

SCHEME 3

lithium. They proposed that the C-5 carbanion was formed directly by the reductive ring opening of the epoxide under these conditions.

Epoxide **6** was therefore treated with lithium in ethylamine at 0°C. A more complex mixture was obtained than those from the corresponding lithium – liquid ammonia reductions. The mixture could be simplified considerably by oxidation with pyridinium chlorochromate (PCC) to afford only three compounds, none, however, being the desired cyclosteroid. The compounds identified were the C-5 epimeric 4,4-dimethylcholestane-3,6-diones (**15**, **16**) and 4,4-dimethylcholest-5-en-3-one (**10**). The 5α dione **15** was the major product (50%). The 5β dione **16** was obtained in 32% yield. Thus, both the α,β-unsaturated carbonyl system and the epoxide were reduced under these conditions.

The complex mixture that was initially formed resulted from the fact that a new stereogenic centre at C-3 is produced and two of the existing ones at C-5 and C-6 are modified during the reduction. PCC oxidation removed the two stereogenic centres at C-3 and C-6 by converting the epimeric alcohols into the corresponding ketones. That **10** was obtained indicated that an elimination of the epoxy oxygen had also occurred during this reaction. Hallsworth and Henbest (17) reported an analogous finding with 5β,6β-epoxycholesterol under similar conditions. In our case, reduction of the epoxide ring was observed but it is likely that the α,β-unsaturated ketone was reduced more rapidly, thereby precluding the intramolecular Michael addition of a C-5 carbanion. Carbanion formation at C-5 would not be inhibited as was presumed to have been the case with 5β,6β-epoxycholesterol (17) because the enolate oxyanion at C-3 of the intermediate **17** is sufficiently distant from C-5. However, it is recognized that the desired cyclization in this case would have required a type of ring closure that can be viewed as being both a disfavoured 5-*endo-trig* and a favoured 3-*exo-trig* type.

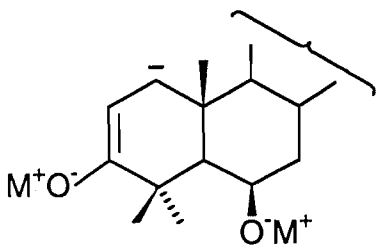

17

Triphenyltin hydride (TPTH) and tri-*n*-butyltin hydride (TBTH) reduce α,β-unsaturated ketones via a radical mechanism (18, 19). It was therefore of interest to determine whether a radical-induced intramolecular cyclization (20) could be effected with our system via a tin enolate radical **18** (see Scheme 2). When a dilute solution of **6** was treated with TPTH and azobisisobutyronitrile (AIBN), a mixture of four compounds was obtained. The major product surprisingly was the epoxide **19** (76%), followed by the keto-epoxide **13** (14%) and small amounts (3 and 4%, respectively) of the corresponding epoxide ring-opened products, the dihydroxy **20** and the hydroxy-ketone **21**. The fact that **20** and **21** were obtained, albeit in small amounts, indicated that the epoxide ring could be opened by TPTH/AIBN.

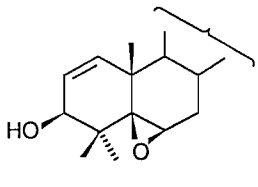

19

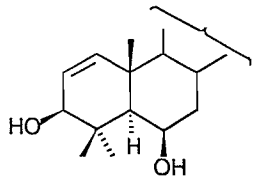

20

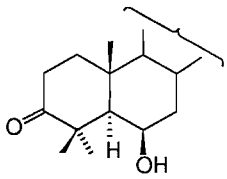

21

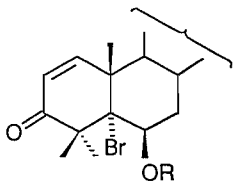

22 R = H
23 R = Ac

Since we were unable to effect transannular cyclization using reductive methods on the α,β-unsaturated ketone-epoxide **6**, we explored the potential for a more typical radical cyclization–coupling (21) route as depicted in Scheme 3. Reaction of **6** with HBr in acetic acid gave the bromohydrin **22**, its corresponding acetate **23**, and the 6α-bromo-5β-hydroxy bromohydrin **24**. Since the bromohydrins were unstable the crude bromohydrin mixture was isolated and, without purification, was treated with TBTH/AIBN in dilute refluxing benzene. The resulting product mixture consisted of three compounds whose spectral properties are consistent with the structures **21**, **25**, and **26**, and an unstable fourth compound that could not be characterized. The major product (48%) was identical with **21**, indicating that the bromine atom of the bromohydrin could indeed be removed by TPTH to afford a radical at C-5 but that it did not add internally to the α,β-unsaturated ketone at C-1—C-3. It is possible that the α,β-unsaturated ketone was reduced first. However, as **25** and **26** were also isolated, this could imply that radical formation occurred at C-5 from bromohydrin **21** and at C-6 from bromohydrin **24**, respectively, whilst the α,β-unsaturated ketone was still present. Cycli-

Can. J. Chem. Downloaded from www.nrcresearchpress.com by 88.255.202.194 on 09/08/12
For personal use only.

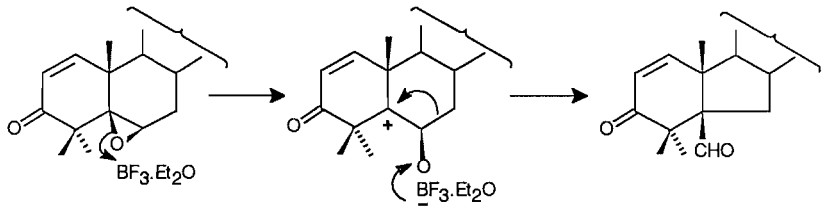

SCHEME 4

zation could apparently not be effected under these conditions either, for similar reasons to those proposed above for **17**. Compound **26** was presumably formed from **24**, which would have been formed as the minor product of the HBr-induced ring opening of **6**. Compound **26** was found to be inert to PCC oxidation, confirming the presence of a tertiary hydroxy group. It is interesting that when the 5β,6β epoxide group was present as in **6**, the major product of TPTH reduction was that in which the C-3 carbonyl group was reduced. Without the epoxide group present, however, normal reduction of the carbon–carbon double bond was preferred.

The reaction of **6** with BF_3·etherate was also examined during the course of our investigations. A mixture of several compounds was obtained, the major one (77%) being the *B*-nor-enone-5β aldehyde **27** presumably formed via a pinacol-type rearrangement. A similar *B*-nor keto-aldehyde was obtained by Halsall *et al.* (10) and Blunt *et al.* (23) with

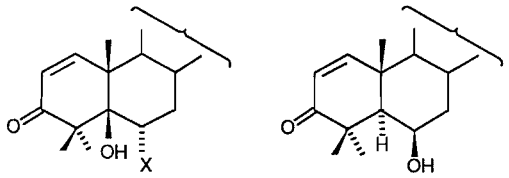

24 X=Br
26 X=H

25

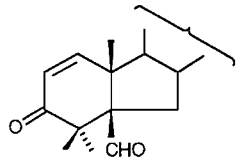

27

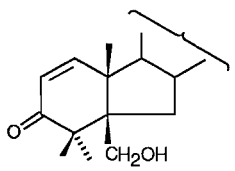

28

5β,6β-epoxy-4,4-dimethylcholestan-3-one **13**. These authors, however, did not unambiguously assign the stereochemistry to the aldehyde at C-5.

Since the crystals of **27** that were obtained were not suitable for X-ray crystallography, NOED experiments on **27** were undertaken. Irradiation of the signal due to the aldehyde proton at δ 9.57 enhanced the signals due to both the C-19 methyl and the β C-4 methyl groups by 1%. This evidence ruled out the possibility of an α configuration for the aldehyde group since in this case only the 4α-methyl could be expected to be positively enhanced. However, since the C-19 and β C-4 methyl signals overlap and only a small NOED was observed, the aldehyde **27** was selectively reduced with $NaBH_4$ to the corresponding carbinol **28**. NOED experiments on **28** confirmed the structure assigned. Irradiation of the signal due to the methylene protons of the carbinol group at δ 3.71 enhanced the signals due to the C-19 methyl group at δ 1.21 and the β C-4 methyl group at δ 1.09 by 1.7 and 2.3%, respectively. A likely mechanism for the formation of **27** can be envisioned in Scheme 4, and is in agreement with the mechanism proposed by Blunt *et al.* (23).

In summary, we have shown that epoxidation of 4,4-dimethylcholesta-1,5-dien-3-one with MCPBA leads to the formation of 5β,6β epoxide **6** as the major product. This is in contrast to what was previously reported by others. We were unable to transform this epoxide into the corresponding 1α,5α cyclosteroid **7** using several alternative reductive methods. It is likely that the α,β-unsaturated carbonyl system undergoes reduction more rapidly than intramolecular cyclization occurs, or that the cyclization is reversible, favouring the uncyclized carbanion **8**, or radical **18**.

Experimental

Melting points (mp) were determined on a Fisher–Johns apparatus and are uncorrected. Infrared (IR) spectra were recorded on a Mattson Polaris FT instrument. Mass spectral (MS) data were from a V.G. Micromass 7070HS instrument. ^{1}H NMR spectra were recorded with a GE GN-300NB spectrometer at 300 MHz. ^{13}C NMR spectra were recorded with the same instrument at 75.47 MHz. The solvents used are noted in the experimental details. Proton nuclear Overhauser effect difference (NOED) spectra were obtained from zero-filled 32K data tables to which a 1–2 Hz exponential line-broadening function had been applied. A set of four "dummy" scans was employed to equilibrate the spins prior to data acquisition. No relaxation delay was applied between successive scans of a given frequency. Ultraviolet (UV) spectra were determined on a Unicam SP.800 ultraviolet spectrophotometer. Microanalyses were performed by the Canadian Microanalytical Service Ltd., Delta, B.C.

5β,6β-Epoxy-4,4-dimethylcholest-1-en-3-one (6) and 5α,6α-epoxy-4,4-dimethylcholest-1-en-3-one (11)

A solution of dienone **9** (8) (1.05 g, 2.55 mmol) in 20 mL CH_2Cl_2 was refluxed under argon. *m*-Chloroperoxybenzoic acid, 50–60% (865 mg, 2.76 mmol), in 20 mL CH_2Cl_2 was added dropwise over 0.5 h. The mixture was stirred at reflux for 4 h. The solution was extracted with ether (×4) and the combined organic layers were washed with 10% $NaHCO_3$ (×3) and saturated NaCl (×4), dried ($MgSO_4$), and concentrated. Chromatography (10% benzene in hexane over aluminium oxide, Grade III) yielded the lactone **12** (142 mg, 12%), 5β,6β epoxide **6** (776 mg, 71%), and 5α,6α epoxide **11** (99 mg, 9%). For **6**, mp 101–102°C; $\nu_{max}(CCl_4)/cm^{-1}$: 1687 (α,β-unsaturated ketone); δ_H (300 MHz; $CDCl_3$): 0.67(3H, s, 18-Me), 0.86(3H, d, J = 6.6 Hz, 26-Me), 0.86(3H, d, J = 6.6 Hz, 27-Me), 0.90(3H, d, J = 6.5 Hz, 21-Me), 1.77–1.90(1H, m), 0.94(3H, s, 4α-Me), 1.27(3H, s, 19-Me), 1.33(3H, s, 4β-Me), 2.01(1H, dt, J = 3.4, 12.7 Hz), 2.14(1H, ddd, J = 2.2, 4.3, 14.9 Hz, 7-H), 3.32(1H, s, 6-H), 5.93(1H, d, J = 10.5 Hz, 2-H), 6.90(1H, d, J = 10.5 Hz, 1-H); *m/z*(%): 426(65, M^+), 398(25), 383(15), 356(10), 339(4), 295(5), 247(17), 161(19), 136(82), 107(58), 81(61), 43(100). Anal. calcd. for $C_{29}H_{46}O_2$: C 81.63; H, 10.87%; found C 81.79 H 10.44%. For α-epoxide **11**, mp 132.0–

Can. J. Chem. Downloaded from www.nrcresearchpress.com by 88.255.202.194 on 09/08/12
For personal use only.

Can. J. Chem. Downloaded from www.nrcresearchpress.com by 88.255.202.194 on 09/08/12
For personal use only.

135.0°C; $\nu_{max}(CCl_4)/cm^{-1}$: 1681(α,β-unsaturated ketone); δ_H(300 MHz; $CDCl_3$): 0.65(3H, s, 18-Me), 0.86(3H, d, J = 6.6 Hz, 26-Me), 0.86(3H, d, J = 6.6 Hz, 27-Me), 0.90(3H, d, J = 6.6 Hz, 21-Me), 0.93(3H, s, 4α-Me), 1.31(3H, s, 19-Me), 1.36(3H, s, 4β-Me), 3.10(1H, d, J = 3.6 Hz, 6-H), 6.00(1H, d, J = 10.3 Hz, 2-H), 7.11(1H, d, J = 10.3 Hz, 1-H); m/z(%): 426(21, M^+), 411(9), 383(13), 365(4), 343(3), 300(3), 275(10), 247(15), 43(100). Anal. calcd. for $C_{29}H_{46}O_2$: C 81.63; H, 10.87%; found C 81.69 H 10.79%.

*5β,6β-Epoxy-4,4-dimethyl-4-oxa-*A*-homocholest-1-en-3-one lactone (**12**)*

A solution of dienone **9** (51 mg, 0.12 mmol) in 10 mL CH_2Cl_2 was refluxed under argon. *m*-Chloroperoxybenzoic acid, 50–60% (300 mg, ca. 0.96 mmol), in 10 mL CH_2Cl_2 was added dropwise over 0.5 h. The mixture was stirred at reflux for 12 h. The solution was extracted with ether (×4) and the combined organic layers were washed with 10% $NaHCO_3$ (×3) and saturated NaCl (×4), dried ($MgSO_4$), and concentrated. Chromatography (10% benzene in hexane over aluminium oxide) yielded the lactone **12** (27 mg, 48%), and a mixture containing 5α,6α epoxide **11** (6 mg, 12%). For lactone **12**, mp 177.5–178.5°C; $\nu_{max}(CCl_4)/cm^{-1}$: 1754 (ε-lactone); δ_H(300 MHz; $CDCl_3$): 0.64(3H, s, 18-Me), 0.86(3H, d, J = 6.6 Hz, 26-Me), 0.86(3H, d, J = 6.6 Hz, 27-Me), 0.89(3H, d, J = 6.6 Hz, 21-Me), 1.19(3H, s, Me), 1.31(3H, s, Me), 1.40(3H, s, Me), 1.77–1.90(1H, m), 1.98(1H, dt, J = 3.4, 12.6 Hz), 2.13(1H, dt, J = 3.2, 14.0 Hz, 7-H), 3.20(1H, br d, J = 1.9 Hz, 6-H), 5.19(1H, d, J = 7.3 Hz, 2-H), 6.26(1H, d, J = 7.3 Hz, 1-H); m/z(%): 442(1, M^+), 427(3), 399(13), 371(10), 353(2), 329(3), 287(3), 262(7), 175(6), 153(25), 123(40), 43(100). Anal. calcd. for $C_{29}H_{46}O_3$: C 78.68; H, 10.47%; found C 78.24 H 10.09%.

*5β,6β-Epoxy-4,4-dimethylcholestan-3-one (**13**)*

Freshly condensed ammonia (30 mL, dried over sodium at −78°C) was allowed to distill into a stirring suspension of lithium (20 mg, 2.9 mmol) in anhydrous THF (5 mL) at −78°C and the stirring continued until the metal had dissolved. A solution of 5β,6β epoxide (**6**) (190 mg, 0.45 mmol) in anhydrous THF (5 mL) was added dropwise over 1 h and the solution stirred at −78°C for another 1 h. Sufficient NH_4Cl was added to discharge the blue colour and the ammonia was allowed to evaporate. Upon the addition of 30 mL of ether and 20 mL of water the aqueous layer was extracted with ether. The combined ether solutions were washed, dried, and evaporated as usual. Chromatography of the residue and gradient elution with hexane – ethyl acetate yielded 5β,6β-epoxy-4,4-dimethylcholestan-3-one (**13**) (124 mg, 65%) and a mixture of the corresponding epimeric 3α and 3β alcohols **14*a***, **14*b*** (48 mg, 25%). For compound **13**, mp 197.0–198.0°C (needles from hexane–methanol (lit. (10) mp 197–200°C); $\nu_{max}(CCl_4)/cm^{-1}$: 1716 (saturated ketone); δ_H(300 MHz; $CDCl_3$): 0.64(3H, s, 18-Me), 0.86(3H, d, J = 6.6 Hz, 26-Me), 0.87(3H, d, J = 6.6 Hz, 27-Me), 0.87(3H, s, Me), 0.89(3H, s, Me), 0.90(3H, d, J = 6.4 Hz, 21-Me), 1.21(3H, s, Me), 1.78–1.90(1H, m), 1.98(1H, dt, J = 3.4, 12.5 Hz), 2.01–2.06(2H, m), 2.15(1H, dt, J = 3.2, 14.2 Hz, 7-H), 2.40–2.58(2H, m), 3.07(1H, s, 6-H); m/z(%): 428(32, M^+), 400(15), 385(10), 343(14), 330(9), 301(2), 273(4), 247(9), 137(100), 107(47), 81(50), 55(94).

*PCC oxidation of **14**a and **14**b*

The mixture of the epimeric 3α and 3β alcohols **14*a*** and **14*b*** (40 mg, 0.09 mmol) was suspended in anhydrous CH_2Cl_2 (10 mL) and pyridinium chlorochromate (41 mg, 0.19 mmol) was added in one portion to the stirred solution. After 2 h the reaction solution was put on the top of a short silica gel column and was washed by a sufficient amount of ether. Evaporation of the ether yielded 5β,6β-epoxy-4,4-dimethylcholestan-3-one (**13**) (34 mg, 84%).

*Hydrogenation of 5β,6β epoxide **6***

To a solution of 5β,6β epoxide **6** (51 mg, 0.12 mmol) in ethyl acetate (100 mL) was added Pd–C (5%, 15 mg) and the mixture stirred under a H_2 atmosphere (1 atm; (= 101.3 kPa)) for 2 h. The reaction solution was applied onto a silica gel column and eluted with sufficient ether. Evaporation of the ether gave 5β,6β-epoxy-4,4-dimethylcholestan-3-one (**13**) in quantitative yield.

*Reaction of **6** with lithium–ethylamine*

Lithium (108 mg, 15.5 mmol) was added to a solution of 5β,6β epoxide **6** (200 mg, 0.47 mmol) in ethylamine (anhydrous, 99%, 15 mL) with stirring at 0°C. The mixture was stirred at 0°C for 1.5 h and then moist ether was added to discharge the blue colour. After the addition of 30 mL of ether and 20 mL of water the aqueous layer was extracted with ether. The combined ether solutions were washed, dried, and evaporated as usual. Thin-layer chromatography (TLC) showed the residue to be a complex mixture that was difficult to separate. The crude residue was suspended in CH_2Cl_2 (10 mL) and PCC (700 mg, 3.25 mmol) and CH_3COONa (200 mg, 2.44 mmol) were added together in one portion to the stirred solution. After 2 h the reaction mixture was placed directly onto a short silica gel column and was eluted with ether. Evaporation of the ether yielded a mixture of three major products. Silica gel chromatography using a gradient solvent system of hexane – ethyl acetate gave 4,4-dimethylcholest-5-en-3-one (**10**) (21 mg, 11%), 4,4-dimethyl-5α-cholestane-3,6-dione (**15**) (100 mg, 50%), and 4,4-dimethyl-5β-cholestane-3,6-dione (**16**) (65 mg, 32%). For **15**, mp 139.5–140.5°C (plates from acetone–methanol) (lit. (10) mp 141–142°C); $\nu_{max}(CCl_4)/cm^{-1}$: 1714 (saturated ketones); δ_H(300 MHz; $CDCl_3$): 0.68(3H, s, 18-Me), 0.86(3H, d, J = 6.6 Hz, 26-Me), 0.87(3H, d, J = 6.6 Hz, 27-Me), 0.91(3H, d, J = 6.5 Hz, 21-Me), 1.12(3H, s, Me), 1.13(3H, s, Me), 1.50(3H, s, Me), 1.95(1H, t, J = 12.5 Hz, 7α-H), 2.22(1H, ddd, J = 2.8, 4.2, 14.4 Hz, 2α-H), 2.31(1H, dd, J = 4.2, 12.5 Hz, 7β-H), 2.40(1H, s, 5-H), 2.81(1H, dt, J = 5.9, 14.6 Hz, 2β-H); m/z(%): 428 (37, M^+), 413(9), 400(3), 371(35), 315(9), 273(11), 262(4), 231(9), 165(40), 137(67), 43(100). For **16**, mp 118–119°C (lit. (10) mp 112–114°C); $\nu_{max}(CCl_4)/cm^{-1}$: 1707 (saturated ketones); δ_H(300 MHz; $CDCl_3$): 0.67(3H, s, 18-Me), 0.86(3H, d, J = 6.6 Hz, 26-Me), 0.87(3H, d, J = 6.6 Hz, 27-Me), 0.91(3H, d, J = 6.5 Hz, 21-Me), 0.96(3H, s, Me), 1.15(3H, s, Me), 1.17(3H, s, Me), 1.93–2.09(3H, mm), 2.38(1H, d, J = 1.5 Hz, 5-H), 2.44(1H, t, J = 4.2 Hz), 2.50(1H, dd, J = 1.7, 4.2 Hz). m/z(%): 428(17, M^+), 400(5), 373(2), 331(100), 302(3), 273(10), 247(8), 191(15), 83(62), 43(74).

*Epimerization of **16** to **15***

To a solution of **16** (20 mg) in dry methanol (50 mL) was added sodium and and the mixture was stirred at room temperature for 3 h. Water (10 mL) was added in to quench the reaction. The solution was extracted with ether and the combined ether layers were washed, dried, and evaporated to gave the 5α epimer **15** in quantitative yield.

*Reaction of 5β,6β epoxide **6** with triphenyltin hydride*

A solution of 5β,6β epoxide **6** (113 mg, 0.265 mmol) in dry benzene (50 mL) was refluxed under argon while triphenyltin hydride (TPTH) (435 mg, 1.24 mmol) and a trace amount of AIBN (7 mg, 0.04 mmol) in dry benzene (30 mL) was added dropwise over 20 h. The mixture was stirred at reflux for 50 h. A small amount of water was then added to quench the reaction. The residue obtained after evaporating the solvent was placed directly onto a silica gel column. Elution, first with pure benzene, removed the TPTH derivatives completely. Subsequent elution using a hexane – ethyl acetate gradient solvent system gave, in the following order: 5β,6β-epoxy-4,4-dimethylcholestan-3-one (**13**) (15 mg, 14%); 6β-hydroxy-4,4-dimethylcholestan-3-one (**21**) (5 mg, 4%); 3β-hydroxy-5β,6β-epoxy-4,4-dimethylcholest-1-ene (**19**) (87 mg, 76%); and 3β,6β-dihydroxy-4,4-dimethylcholest-1-ene (**20**) (3 mg, 3%). For **19**, mp 158.0–159.0°C; $\nu_{max}(CCl_4)/cm^{-1}$: 3632, 3611 (O-H); δ_H(300 MHz; $CDCl_3$): 0.63(3H, s, 18-Me), 0.86(3H, d, J = 6.6 Hz, 26-Me), 0.86(3H, d, J = 6.8 Hz, 27-Me), 0.88(3H, s, Me), 1.02(3H, s, Me), 1.08(3H, s, Me), 1.76–1.88(1H, m), 1.96(1H, dt, J = 3.4, 12.6 Hz), 2.14(1H, ddd, J = 2.1, 4.4,

Can. J. Chem. Downloaded from www.nrcresearchpress.com by 88.255.202.194 on 09/08/12
For personal use only.

14.8 Hz, 7-H), 3.28(1H, s, 6-H), 4.08(1H, s, 3-H), 5.50(1H, dd, J = 1.4, 10.4 Hz, 2-H), 5.87(1H, dd, J = 2.5, 10.4 Hz); m/z(%): 428(9, M^+), 410(8), 395(4), 360(7), 331(3), 273(2), 227(3), 175(7), 121(43), 95(52), 43(100). Anal. calcd. for $C_{29}H_{48}O_2$: C 81.25, H 11.29%; found: C 81.37, H 11.18%. For **20**, $\nu_{max}(CCl_4)/cm^{-1}$: 3624 (two free O-H); δ_H(300 MHz; $CDCl_3$): 0.70(3H, s, 18-Me), 0.86(3H, d, J = 6.6Hz, 26-Me), 0.86(3H, d, J = 6.6 Hz, 27-Me), 0.91(3H, d, J = 6.5 Hz, 21-Me), 1.09(3H, s, Me), 1.14(3H, s, Me), 1.28(3H, s, Me), 1.76(1H, s, 5α-H), 1.78–1.83(2H, m), 2.01(1H, dt, J = 3.4, 12.6 Hz), 3.81(1H, d, J = 8.2 Hz, 3-H), 4.41(1H, s, 6-H), 5.36(1H, dd, J = 1.6, 10.4 Hz, 1-H), 5.74(1H, dd, J = 2.3, 10.4 Hz, 2-H). For **21**, mp 152.5–153.5°C; $\nu_{max}(CCl_4)/cm^{-1}$: 3621(free O-H), 1707(saturated ketone); δ_H(300 MHz, $CDCl_3$): 0.71(3H, s, 18-Me), 0.86(3H, d, J = 6.6 Hz, 26-Me), 0.87(3H, d, J = 6.6 Hz, 27-Me), 0.91(3H, d, J = 6.5 Hz, 21-Me), 1.15(3H, s, Me), 1.38(3H, s, Me), 1.43(3H, s, Me), 1.68(1H, s), 1.75–1.86(3H, mm), 1.95(1H, ddd, J = 3.0, 6.0, 13.1 Hz), 2.01(1H, dt, J = 3.3, 12.8 Hz), 2.26(1H, ddd, J = 3.0, 4.6, 14.9 Hz, 2-H), 2.76(1H, dt, J = 6.0, 14.6, 14.6 Hz, 2-H), 4.34(1H, s, 6-H); m/z(%): 430(4, M^+), 412(18), 397(4), 357(4), 327(3), 257(12), 187(17), 145(15), 107(27), 81(36), 43(100). Anal. calcd. for $C_{29}H_{50}O_2$: C 80.87, H 11.70%; found: C 81.00, H 11.54%.

Sodium borohydride reduction of 5β,6β epoxide ***6***

To a solution of **6** (100 mg, 0.24 mmol) in methanol (30 mL) was added $NaBH_4$ (53 mg, 1.4 mmol) and $CeCl_3 \cdot 7H_2O$ (100 mg, 0.27 mmol). The mixture was stirred at room temperature for 45 min before a small amount of water was added to quench the reaction. The mixture was extracted with ether and the combined ether layers were washed, dried, and evaporated as usual. Silica gel chromatography of the residue and elution with a hexane – ethyl acetate gradient solvent system yielded 3β-hydroxy-5β,6β-epoxy-4,4-dimethylcholest-1-ene (**19**) (89 mg, 87%).

PCC oxidation of hydroxy-ketone ***21***

To a solution of 6β-hydroxy-4,4-dimethylcholestan-3-one (**21**) (10 mg, 0.024 mmol) in anhydrous CH_2Cl_2 (10 mL) was added PCC (10 mg, 0.049 mmol) in one portion and the mixture was stirred at room temperature for 2 h. The reaction solution was placed onto a silica gel column and was eluted with ether. Evaporation of the ether yielded 4,4-dimethyl-5α-cholestane-3,6-dione (**15**) (9 mg, 92%).

Preparation of bromohydrin acetate ***23***

To a solution of **6** (100 mg, 0.24 mmol) in dry glacial acetic acid (10 mL) with stirring at 10°C was added a solution of hydrogen bromide (3.7%) in acetic acid (9 mL, 0.41 mmol) by syringe over 30 min. After stirring at 10°C for 8 h, the reaction mixture was poured onto ice-water and extracted with ether. The combined ether layers were washed, dried, and evaporated as usual. Silica gel chromatography of the residue and elution with a hexane – ethyl acetate gradient solvent system afforded **6** (89 mg, 85%), bromohydrin acetate **23** (13 mg, 10%), and a compound (5 mg) whose structure was not determined. For **23**, mp 180–182°C (needles from acetone–water); $\nu_{max}(CCl_4)/cm^{-1}$: 1747(ester carbonyl), 1692(α,β-unsaturated ketone); δ_H(300 MHz, $CDCl_3$): 0.73(3H, s, 18-Me), 0.86(3H, d, J = 6.6 Hz, 26-Me), 0.87(3H, d, J = 6.6 Hz, 27-Me), 0.92(3H, d, J = 6.5 Hz, 21-Me), 1.45(3H, s, Me), 1.52(3H, s, Me), 1.69(3H, s, Me), 2.09(1H, dt, J = 3.3, 12.8 Hz), 2.14(3H, s, acetate methyl), 2.20–2.34(2H, m), 5.59(1H, br s, 6-H), 5.94(1H, d, J = 10.3 Hz, 2-H), 6.83(1H, d, J = 10.5 Hz, 1-H); m/z(%): 426(2, M^+-Br,CH_3CO), 410(7), 408(8), 395(3), 393 (6), 367(3), 365(5), 339(5), 337(2), 149(11), 147(8), 81(38), 79(24), 43(100).

In-situ *reaction of* ***21*** *with triphenyltin hydride*

To a solution of **6** (100 mg, 0.24 mmol) in dry glacial acetic acid (10 mL) with stirring at 10°C was added a solution of hydrogen bromide (3.7%) in glacial acetic acid (0.8 mL, 0.37 mmol) by syringe over 30 min. After stirring at 10°C for 90 min, the reaction mixture was poured onto ice-water. The precipitate was filtered and washed with ice-water to remove all traces of acetic acid. The colourless residue was vacuum-dried and then was dissolved in dry benzene (50 mL) and refluxed. Tri-*n*-butyltin hydride (TBTH) (97%, 0.06 mLl, 0.22 mmol) in dry benzene (10 mL), and a catalytic amount of AIBN were then added dropwise over 1 h. The mixture was stirred at reflux for 2 h. A small amount of water was added to the reaction solution to quench the reaction. The residue after evaporation of the solvent was placed directly onto a silica gel column. Elution, first with pure benzene removed the TBTH derivatives. Subsequent elution with the hexane – ethyl acetate gradient solvent system gave 6β-hydroxy-4,4-dimethylcholestan-3-one (**21**) (49 mg, 48%), 6β-hydroxy-4,4-dimethyl-5α-cholest-1-en-3-one (**25**) (3 mg, 3%), 5β-hydroxy-4,4-dimethylcholest-1-en-3-one (**26**) (18 mg, 18%), and an unstable compound (17 mg, 17%). For **25**, $\nu_{max}(CCl_4)/cm^{-1}$: 3622 (free O-H), 1676 (α,β-unsaturated ketone); δ_H(300 MHz, $CDCl_3$): 0.74(3H, s, 18-Me), 0.86(3H, d, J = 6.6 Hz, 26-Me), 0.87(3H, d, J = 6.6 Hz, 27-Me), 0.92(3H, d, J = 6.5 Hz, 21-Me), 1.22(3H, s, Me), 1.39(3H, s, Me), 1.41(3H, s, Me), 1.64(1H, d, J = 1.4 Hz, 5-H), 1.77–1.90(2H, m), 2.07(1H, dt, J = 3.3, 3.3, 12.9 Hz, 8-H), 4.40(1H, s, 6-H), 5.82(1H, d, J = 10.3 Hz, 2-H), 6.97(1H, d, J = 10.3 Hz, 1-H). For **26**, $\nu_{max}(CCl_4)/cm^{-1}$: 3626(free O-H), 1686(α,β-unsaturated ketone); δ_H(300 MHz, $CDCl_3$): 0.70(3H, s, 18-Me), 0.86(3H, d, J = 6.6 Hz, 26-Me), 0.86(3H, d, J = 6.6 Hz, 27-Me), 0.91(3H, d, J = 6.5 Hz, 21-Me), 1.22(3H, s, Me), 1.30(3H, s, Me), 1.37(3H, s, Me), 2.03(1H, dt, J = 3.3, 12.9 Hz), 2.14(1H, ddd, J = 2.1, 4.5, 14.1 Hz), 5.88(1H, d, J = 10.5 Hz, 2-H), 6.56(1H, d, J = 10.4 Hz, 1-H).

*4,4-Dimethyl-3-oxo-*B*-norcholest-1-ene-5-carboxaldehyde (27)*

To a solution of **6** (110 mg, 0.26 mmol) in dry benzene (5 mL) with stirring at room temperature was added boron trifluoride etherate (0.1 mL, 0.8 mmol) by syringe. After stirring at room temperature for 30 min, the reaction mixture was quenched by pouring into $NaHCO_3$ solution (3%) and extracted with ether. The combined ether extracts were washed, dried, and evaporated as usual. Silica gel chromatography using the hexane – ethyl acetate gradient solvent system yielded the *B*-nor aldehyde **27** (86 mg, 77%), and two other products that could not be characterized due to their instability. For **27**, mp 103.5–104.5°C (plates from ethanol–water); $\nu_{max}(CCl_4)/cm^{-1}$: 1729 (aldehyde), 1688 (α,β-unsaturated ketone); δ_H(300 MHz, $CDCl_3$): 0.64(3H, s, 18-Me), 0.86(3H, d, J = 6.6 Hz, 26-Me), 0.86(3H, d, J = 6.6 Hz, 27-Me), 0.91(3H, d, J = 6.5 Hz, 21-Me), 1.04(3H, s, 4β-Me), 1.04(3H, s, 19-Me), 1.11(1H, dd, J = 11.2, 13.0 Hz, 7-H), 1.17(3H, s, 4α-Me), 1.83–1.90(1H, m), 2.04(1H, dt, J = 2.8, 12.9 Hz), 2.41(1H, dd, J = 7.0, 13.0 Hz, 7-H), 5.94(1H, d, J = 10.2 Hz, 2-H), 6.63(1H, d, J = 10.2 Hz, 1-H), 9.57(1H, s, 6-H); HRMS for $C_{29}H_{46}O_2$, calcd.: 426.3495; found: 426.3495; m/z(%): 426(7, M+), 397(7), 356(5), 313(3), 261(9), 243(3), 149(35), 43(100). Anal. calcd. for $C_{29}H_{46}O_2$: C 81.63, H 10.87%; found: C 81.51, H 10.78%.

Sodium borohydride reduction of 27

To a solution of the *B*-nor aldehyde **27** (51 mg, 0.12 mmol) and $CeCl_3 \cdot 7H_2O$ (56 mg, 0.15 mmol) was added $NaBH_4$ in small portions over 4 h until the starting material almost disappeared according to TLC. The reaction mixture was stirred at room temperature for an additional hour before a small amount of water was added to quench the reaction. The reaction mixture was extracted with ether and the combined ether layers were washed, dried, and evaporated as usual. Chromatography of the residue and elution with the hexane – ethyl acetate gradient solvent system gave 5β-hydroxymethyl-4,4-dimethyl-*B*-norcholest-1-en-3-one (**28**) (45 mg, 88%). For **28**, mp 150–151°C; $\nu_{max}(CCl_4)/cm^{-1}$: 3630 (free O-H), 3493 (intermolecular and weakly bonded O-H), 1685

(α,β-unsaturated ketone); δ_H(300 MHz, $CDCl_3$): 0.66(3H, s, 18-Me), 0.86(3H, d, J = 6.6 Hz, 26-Me), 0.87(3H, d, J = 6.6 Hz, 27-Me), 0.92(3H, d, J = 6.5 Hz, 21-Me), 1.09(3H, s, 4β-Me), 1.12–1.16(1H, m, 7α-H), 1.21(3H, s, 19-Me), 1.22(3H, s, 4α-Me), 1.35(1H, br s, 7β-H), 1.65–1.75(1H, m), 1.81–1.93(1H, m), 2.04(1H, dt, J = 3.2, 12.8 Hz, 12β-H), 3.71(2H, br s, 6-methylene), 5.82(1H, d, J = 10.2 Hz, 2-H), 6.54(1H, d, J = 10.2 Hz, 1-H); m/z(%): 428(23.6, M^+), 413(8), 410(7), 398(14), 397(34), 385(7), 358(22), 261(12), 166(14), 149(43), 121(66), 43(100). Anal. calcd. for $C_{29}H_{48}O_2$: C 81.25, H 11.29%; found: C 81.05; H 11.17%.

Acknowledgements

The authors wish to express their sincerest appreciation to Dr. C. R. Jablonski and Ms. N. Brunet for their generous contributions in the form of numerous high-quality high-resolution nmr spectra. We thank Dr. D. J. Burnell for many suggestions and for his ongoing encouragement, Dr. B. Gregory and Ms. M. Baggs for their mass spectral contributions, and Dr. J. N. Bridson for X-ray crystallographic analyses. The Department of Chemistry and Memorial University are thanked for their financial assistance in the form of graduate student support to one of us (Y.R.).

1. S. B. Laing and P. J. Sykes. J. Chem. Soc.(C), 421 (1968).
2. S. B. Laing and P. J. Sykes. J. Chem. Soc.(C), 653 (1968).
3. S. B. Laing and P. J. Sykes. J. Chem. Soc.(C), 937 (1968).
4. P. E. Georghiou and G. Just. J. Chem. Soc. Perkin Trans. 1, 70 (1973).
5. J. R. Christensen and W. E. Reusch. J. Org. Chem. **48**, 3741 (1983).
6. P. E. Georghiou, Y. Ren, and J. N. Bridson. J. Org. Chem. **58**, 827 (1993).
7. D. Caine. Org. React. **23**, 1 (1976).
8. D. H. Barton, D. J. Lester, and S. V. Ley. J. Chem. Soc. Perkin Trans. 1, 2209 (1980).
9. A. D. Cross. J. Am. Chem. Soc. **84**, 3206 (1962).
10. T. G. Halsall, E. R. H. Jones, E. L. Tan, and G. R. Chaudhry. J. Chem. Soc.(C), 1374 (1966).
11. J. Brynjolffssen, J. Midgley, and W. B. Whalley. J. Chem. Soc. Perkin Trans. 1, 812 (1977).
12. J. D. White and G. L. Larson. J. Org. Chem. **43**, 4555 (1978).
13. J. E. Baldwin. J. Chem. Soc. Chem. Commun. 738 (1976).
14. S. K. Pradhan. Tetrahedron, **42**, 6351 (1986).
15. R. A. Benkeser, R. E. Robinson, D. M. Sauve, and O. H. Thomas. J. Am. Chem. Soc. **77**, 3230 (1975).
16. A. S. Hallsworth and H. B. Henbest. J. Chem. Soc. 4604 (1957).
17. A. S. Hallsworth and H. B. Henbest. J. Chem. Soc. 3571 (1960)
18. M. Pereyre, J.-P. Quintard, and A. Rahm. Tin in organic synthesis, Butterworths, Kent. 1987, and references therein.
19. H. Laurent, P. Esperling, and G. Baude. Liebigs Ann. Chem. 1996 (1983).
20. V. H. Rawal, R. C. Newton, and V. Krishnamurthy. J. Org. Chem. **55**, 5181 (1990).
21. V. M. A. Chambers, W. R. Jackson, and G. W. Young. J. Chem. Soc.(C), 2075 (1971).
22. P. E. Georghiou and M. A. MacDiarmid. Can. J. Chem. **58**, 1759 (1980).
23. J. W. Blunt, M. P. Hartshorn, and D. N. Dirk. J. Chem. Soc. (C), 635 (1968).

Can. J. Chem. Downloaded from www.nrcresearchpress.com by 88.255.202.194 on 09/08/12
For personal use only.

Électrodes à membrane indicatrices de surfactifs cationiques. Variation des propriétés électriques de la membrane en fonction de sa composition

M. P. GLOTON, M. TURMINE, A. MAYAFFRE ET P. LETELLIER[1]

Laboratoire d'energétique et réactivité aux interfaces, Université Pierre et Marie Curie, boîte 39, 4 place Jussieu, 75252 Paris, France

Reçu le 23 mars 1992[2]

M. P. GLOTON, M. TURMINE, A. MAYAFFRE et P. LETELLIER. Can. J. Chem. **71**, 371 (1993).

Les électrodes membranaires indicatrices d'ions amphiphiles cationiques utilisent le plus souvent comme capteur de potentiel une membrane spécifique constituée d'un mélange de polymère tel que le PVC, d'un plastifiant et d'un transporteur de l'ion amphiphile. Pour un polymère donné, il existe un grand nombre de plastifiants pouvant convenir à la préparation de membranes spécifiques. Nous avons exploré ce domaine, en préparant différentes membranes à partir de deux polymères (PVC : haut et bas poids moléculaire), de quatre plastifiants utilisés en diverses proportions, et d'un transporteur de l'ion dodécyltriméthylammonium. Ces membranes ont été montées sur des corps d'électrode et utilisées comme électrode spécifique. Nous montrons que tous les mélanges entre ces constituants ne permettent pas la réalisation d'électrodes spécifiques. Peu, en fait, permettent d'obtenir une réponse «nernstienne». Ainsi, les mélanges les plus riches en polymère sont hétérogènes; les réponses de l'électrode ne sont pas reproductibles d'un échantillon à l'autre d'un même mélange. L'introduction d'un modèle de transport des ions à travers la membrane qui suppose une diffusion par transporteur pour l'ion amphiphile et une diffusion non spécifique du sel par les défauts créés par l'hétérogénéité du support permet de rendre compte, de manière qualitative, de la variation de la pente de réponse de l'électrode avec la composition de la membrane.

M. P. GLOTON, M. TURMINE, A. MAYAFFRE, and P. LETELLIER. Can. J. Chem. **71**, 371 (1993).

Amphiphilic-cation-specific electrodes most often use, as captor of potential, a specific membrane composed of a mixture of a polymer such as PVC, a plasticizer, and a carrier of the amphiphilic ion. For a given polymer, various plasticizers can be used to make "plastisols" that can be suitable for the preparation of specific membranes. We prepared different membranes using two polymers (PVC: high and low molecular weight), four plasticizers in various proportions, and a carrier of the dodecyltrimethylammonium ion. These membranes were mounted on an electrode support and used as ion-selective electrodes. We show that none of these component mixtures can allow the design of specific electrodes. Only a few of them give a "Nernstian" response. Thus, the mixtures rich in polymer lead to heterogeneous plastisols; the electrode responses cannot be reproduced with different samples of the same mixture. We use a model of ion transport through the membrane that assumes a diffusion by carrier for the amphiphilic ion and nonspecific diffusion of the salt through the flaws created by the heterogeneity of the plastisols. The introduction of this model allows us to explain qualitatively the variation of the slope of the electrode response with the membrane composition.

Can. J. Chem. Downloaded from www.nrcresearchpress.com by 88.255.202.194 on 09/08/12
For personal use only.

Introduction

La mise en oeuvre des électrodes membranaires indicatrices d'agents tensio-actifs cationiques, anioniques et neutres a fait l'objet depuis quelques années de nombreuses études et il est décrit, dans la littérature, différentes manières de réaliser des membranes spécifiques aux amphiphiles (1–6). Le plus souvent, ces membranes sont réalisées à partir d'un mélange de polymère et de plastifiant que l'on convient de nommer «plastisol» (7–17). La présence d'un transporteur de l'ion à doser confère à la membrane sa sélectivité.

On peut constater en consultant la littérature sur ce sujet, qu'en général, la nature des constituants de la membrane et les compositions proposées par les différents auteurs sont relativement proches les unes des autres, sans doute parce que de tels systèmes fournissent des réponses de potentiel tout à fait convenables pour la majorité des applications envisagées. Il nous a cependant semblé intéressant d'examiner les réponses électriques de membranes contenant d'autres mélanges de plasifiant et de polymère et en diverses proportions. Il existe en effet, pour un polymère donné, comme le chlorure de polyvinyl, PVC, un grand nombre de plastifiants qui conduisent à des supports «solides» sur une gamme très étendue de composition, le plus souvent entre 0 et 90% en masse de plastifiant.

L'étude suivante concerne donc les mélanges entre deux polymères, les PVC haut et bas poids moléculaire, et quatre plastifiants différents pour diverses compositions. Nous exposerons tout d'abord les techniques opératoires mises en oeuvre.

I. Techniques expérimentales

I-1. Les solvants

L'eau est de qualité ultrapure. Le méthanol de même que le tétrahydrofuranne utilisé comme solvant du PVC sont des produits Merck.

I-2. Les gels de polymère

Le polymère

Nous avons utilisé deux types de polymères présentant des propriétés chimiques proches : (*i*) le PVC haut poids moléculaire (PVC-hpm) de masse molaire supérieure à 1 500 000 g mol^{-1} et (*ii*) le PVC bas poids moléculaire (PVC-bpm) dont la masse molaire est de 48 000 g mol^{-1}.

Le plastifiant

C'est un solvant organique qui confère au polymère sa malléabilité. Quatre plastifiants (Fluka) ont été utilisés pour la fabrication des supports : le dinonylphtalate (DNP) de formule $C_{26}H_{42}O_4$; le nitrophényloctyléther (NPOE) de formule $C_{24}H_{21}O_3N$; le dioctyladipate (DOA) de formule $C_{22}H_{42}O_4$; le dioctylsébacate (DOS) de formule $C_{26}H_{50}O_4$.

Préparation de la membrane

La membrane sélective. Elle est constituée d'un mélange entre un polymère et un plastifiant (plastisol). L'ajout d'un transporteur

[1]Auteur à qui adresser toute correspondance.

[2]Révision reçue le 18 décembre 1992.

Can. J. Chem. Downloaded from www.nrcresearchpress.com by 88.255.202.194 on 09/08/12
For personal use only.

du cation amphiphile à basse concentration lui donne ses propriétés de sélectivité :

Nous avons utilisé comme cation amphiphile le dodécyltriméthylammonium que nous conviendrons de noter DTA^+. La valeur de la concentration micellaire critique de cet agent tensio-actif dans l'eau est égale à $1{,}6 \times 10^{-2}$ mol L^{-1} à 298 K. Le tétraphénylborure de DTA^+ (ϕ_4B^-,DTA^+) insoluble dans l'eau est, en revanche, soluble dans les solvants organiques. Ce sel est introduit à la même concentration dans toutes les membranes préparées. Il est plus ou moins dissocié dans la matrice selon la nature du plastifiant. L'ion ϕ_4B^- assure le transport de DTA^+ dans la membrane.

Préparation des membranes. (*a*) On mélange en proportions variables du PVC et du plastifiant (masse totale environ 2 g) dans 10 mL de tétrahydrofuranne, THF. À 3 mL de cette solution, on ajoute 0,2 mL d'une solution du transporteur ($DTAB\phi_4$) dans le THF à une concentration de 10^{-2} mol L^{-1}. On dépose ce mélange dans un cristallisoir à fond plat de 25 cm^2 de surface et on laisse évaporer le solvant pendant 12 h à la température ambiante. Avant évaporation du THF, la concentration de transporteur dans la membrane est égale à $6{,}25 \times 10^{-4}$ mol L^{-1}.

(*b*) On prépare le sel du transporteur de la manière suivante : on mélange 5×10^{-3} mol de chacun des deux sels (DTABr et $NaB\phi_4$) dans 50 mL de dichlorométhane. Après 3–4 h d'agitation, ce mélange est filtré sur papier et on obtient un filtrat limpide dont le solvant est évaporé sous hotte. Les cristaux résultants sont lavés à l'eau puis recristallisés deux fois dans un mélange d'éther et de quelques gouttes de méthanol. Cette membrane, d'une épaisseur moyenne de 0,2 mm, constitue le capteur de potentiel de l'électrode (18).

I-3. Le montage électrochimique

L'électrode de mesure

La membrane est découpée à l'emporte-pièce et collée à l'extrémité d'un tube de verre qui constitue le corps de l'électrode. Une électrode à calomel protégée par un pont agar-agar de la diffusion de l'agent tensio-actif constitue la référence interne de l'électrode. Le liquide de remplissage est une solution aqueuse de DTABr à une concentration inférieure à la concentration micellaire critique (cmc).

L'électrode de référence

Les électrodes de référence sont des électrodes à calomel saturées en KCl, protégées de la diffusion des cations amphiphiles par une solution de KCl de concentration égale à 2 mol L^{-1} gélifiée par de l'agar-agar, contenue dans un capillaire de Téflon. Il est très important pour obtenir des mesures reproductibles de renouveler souvent la jonction au cours des manipulations, la diffusion des cations amphiphiles étant très rapide.

La chaîne électrochimique

Toutes les mesures sont effectuées en utilisant la même chaîne électrochimique schématisée ci-dessous :

référence : calomel | solution interne | membrane | solution de mesure | référence : calomel

Étalonnage des électrodes

Les variations de concentration de DTA^+ dans la solution de mesure sont obtenues par une méthode d'ajouts. Chaque étalonnage est effectué sur plusieurs échantillons d'une même préparation de membrane.

II. Étude électrochimique

II-1. Comportement électrochimique des plastisols

Le fonctionnement des électrodes spécifiques membranaires repose sur la mesure d'un potentiel intermembranaire que s'établit de part et d'autre d'une interface séparant deux phases contenant des électrolytes de concentrations et parfois de nature différentes. Lorsque par exemple cette interface sépare deux solutions, 1 et 2, d'un même sel M^+X^- aux concentrations respectives C_1 et C_2, dans deux solvants identiques, il s'établit une différence de potentiel entre les deux compartiments égale à $\Delta\phi$ tel que :

$$[1] \qquad \Delta\phi = (1 - 2t^+)\frac{RT}{F}\ln\frac{C_2}{C_1}$$

où t^+ est le nombre de transport du cation.

Si l'on interpose entre les deux solutions une membrane sélective au cation M^+ ($t^+ = 1$), la différence de potentiel prend la forme :

$$[2] \qquad \Delta\phi = \frac{RT}{F}\ln\frac{C_2}{C_1}$$

La différence de potentiel aux bornes de la pile suivante,

Reference calomel, KCl sat.	solution interne $M^+ : C_1$ constante	Membrane	solution de mesure $M^+ : C_2$ variable	Reference calomel, KCl sat.
$\phi 1$	ϕ sol. 1	ϕ m	ϕ sol. 2	$\phi 2$

s'écrit :

$$\Delta E = \phi 1 - \phi 2 = \phi 1 - \phi \text{ sol. } 1 + \phi \text{ sol. } 1 - \phi \text{ m} + \phi \text{ m} - \phi \text{ sol. } 2 + \phi \text{ sol. } 2 - \phi 2$$

On peut supposer que les deux différences de potentiel ϕ 1 $-$ ϕ sol. 1 et ϕ 2 $-$ ϕ sol. 2 correspondantes aux électrodes à calomel sont constantes. L'expression de la f.e.m. de la pile se résume alors en :

$$[3] \qquad \Delta E = \text{constante} + \phi \text{ sol. } 1 - \phi \text{ sol. } 2 = \text{constante} - \Delta\phi = \text{constante}' + \frac{RT}{F}\ln C_2$$

ΔE varie linéairement avec $\ln C_2$ avec, à 25°C, une pente de 59 mV/dec (pente dite nernstienne).

II-2. Résultats expérimentaux

Avant de présenter l'ensemble des résultats obtenus avec les deux polymères et les quatre plastifiants pour différentes compositions de plastisols, nous avons décrit ci-dessous le comportement d'une électrode réputée pour bien fonctionner, afin de disposer d'un élément de comparaison permettant de juger du comportement des autres électrodes.

Comportement de comparaison : la membrane PVC-hpm 20% | DNP 80%

Un grand nombre d'électrodes indicatrices de surfactifs cationiques proposées dans la littérature utilisent une mem-

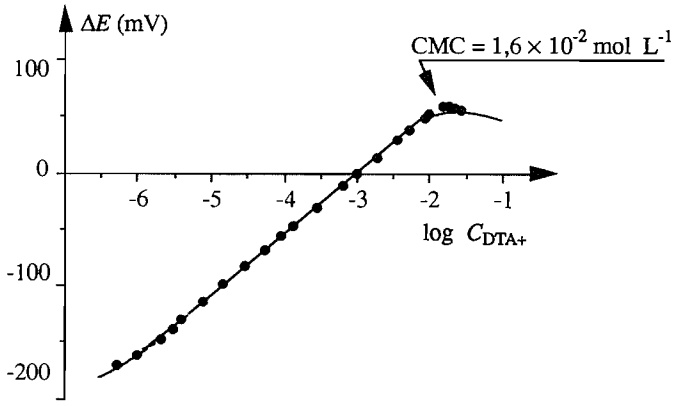

FIG. 1. Comportement de l'électrode de comparaison indicatrice de DTA^+ utilisant une membrane d'un plastisol contenant du DNP 80% – PVC-hpm 20%.

TABLEAU 1. Caractéristiques électrochimiques des électrodes à membranes réalisées avec le mélange PVC-hpm–plastifiant. Les membranes hétérogènes sont signalées par la lettre H

Pourcentage en plastifiant	Pente ±1 (mV/dec)			
	NPOE	DOS	DOA	DNP
80	59	59	60	59
60	58	55	54	52
50	57	49	47	45
45	—	H	H	31
40	55	H	H	H
30	56	H	H	H
25	32	H	H	H

TABLEAU 2. Caractéristiques électrochimiques des électrodes à membranes réalisées avec le mélange PVC-bpm–plastifiant. Les membranes hétérogènes sont signalées par la lettre H

Pourcentage en plastifiant	Pente ±1 (mV/dec)			
	NPOE	DOS	DOA	DNP
80	60	58	59	60
60	57	56	57	60
50	54	54	54	57
40	50	51	44	34
30	49	H	H	H
20	44	H	H	H

brane de PVC-hpm contenant 80% en masse de DNP comme capteur de potentiel (4, 5, 9, 19–23). L'excellente réponse aux agents tensio-actifs cationiques des électrodes sélectives réalisées à partir de cette membrane a pu être vérifiée au laboratoire (18). Une courbe d'étalonnage obtenue avec le DTA^+ est représentée sur la figure 1.

Les électrodes fabriquées à l'aide de cette membrane présentent une cassure très nette au niveau de la cmc. La réponse de l'électrode est linéaire entre la cmc et une concentration en surfactif de l'ordre de 10^{-6} mol L^{-1}. La valeur de la pente de la droite, déterminée par une régression linéaire à partir d'une cinquantaine de points, est égale à la valeur théorique de 59 ± 1 mV/dec. La stabilité des mesures est de ±0,5 mV.

Nous avons caractérisé les autres membranes par les valeurs des pentes des parties linéaires relatives aux concentrations inférieures à la cmc. Ces valeurs sont également déterminées au moyen d'une régression linéaire portant sur une cinquantaine de points.

II-2-1. Plastisols à base de PVC haut poids moléculaire
Mélanges PVC-hpm–plastifiant

Nous avons regroupé dans le tableau 1, les valeurs des pentes des droites caractéristiques des différentes membranes.

Plastifiant : NPOE. On constate qu'entre 80 et 50% en masse de NPOE, la réponse de l'électrode est pratiquement nernstienne. Lorsque la teneur en plastifiant devient inférieure à 30%, on observe une brusque diminution de la valeur de la pente.

Pour des pourcentages encore inférieurs (10 et 20% en NPOE), les mesures deviennent très instables et les valeurs des pentes des parties linéaires diffèrent selon l'échantillon de membrane prélevé. Il apparaît à l'évidence qu'en dessous de 30% les *plastisols sont hétérogènes.*

Plastifiants : DOS, DOA, DNP. Contrairement au cas des mélanges avec le NPOE, on constate que la valeur de la pente de l'électrode diminue dès que le pourcentage en plastifiant devient inférieur à 80%. Seul ce dernier pourcentage pour les trois plastifiants conduit à une pente nersnstienne de l'électrode.

Pour des membranes contenant moins de 40% de ces plastifiants la valeur de la pente dépend de l'échantillon de membrane prélevé. Ces membranes sont hétérogènes.

II-2-2. Plastisols à base de PVC bas poids moléculaire

Nous avons regroupé dans le tableau 2, les valeurs des pentes des droites caractéristiques des différentes membranes.

Mélanges PVC-bpm–plastifiant

Plastifiant : NPOE, DOS, DOA. En ce qui concerne le NPOE, contrairement aux plastisols de ce même plastifiant préparés avec du PVC haut poids moléculaire, on constate que la pente de l'électrode diminue dès que la composition en plastifiant devient inférieure à 80%.

La membrane contenant 10% en NPOE donne des réponses électrochimiques différentes selon l'échantillon utilisé. Ces compositions conduisent à des plastisols hétérogènes. On retrouve un comportement identique pour les deux autres plastifiants.

Plastifiant : DNP. On retrouve, avec ce plastisol, un comportement proche de celui que nous avons observé pour le PVC-hpm et le NPOE, mais sur un domaine de composition plus étroit. Entre 80 et 50% la pente de l'électrode est pratiquement nernstienne.

En revanche pour des compositions inférieures à 30%, les valeurs de pente diffèrent selon l'échantillon utilisé. Ces membranes sont hétérogènes.

Discussion

Les mesures précédentes[3] montrent que l'on dispose en fait d'un nombre restreint de plastisols permettant de fabriquer des électrodes sélectives aux agents tensio-actifs cationiques dont les valeurs des pentes sont égales à 59 mV/dec.

[3]Série complète de données peut être acheté de : Dépôt des données non publiées, Service de fourniture de documents, ICIST, Conseil national de recherches Canada, Ottawa, Canada K1A 0S2.

Can. J. Chem. Downloaded from www.nrcresearchpress.com by 88.255.202.194 on 09/08/12
For personal use only.

Can. J. Chem. Downloaded from www.nrcresearchpress.com by 88.255.202.194 on 09/08/12
For personal use only.

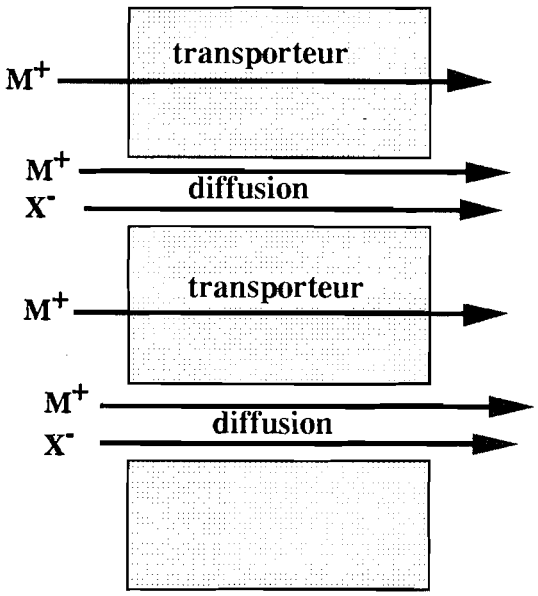

FIG. 2. Modèle de membrane «mosaïque» pour rendre compte du comportement des membranes de plastisol dans le domaine hétérogène.

Ce sont tous des mélanges relativement riches en plastifiant.

En fait, le choix d'un plastisol particulier pour fabriquer une électrode dépend essentiellement de l'utilisation que l'on projette d'en faire, des milieux d'études et des propriétés mécaniques recherchées pour le plastisol. Ainsi, les mélanges PVC-hpm–NPOE constituent un excellent choix pour la réalisation de membranes si l'on ne considère que le large domaine de composition conduisant à des pentes nernstiennes. Ils possèdent, en revanche, l'inconvénient de conduire à des électrodes dont la réponse électrique est fortement influencée par le pH de la solution, ce qui n'est pas le cas des autres plastisols (18); les membranes au NPOE sont donc essentiellement utilisables pour des études à acidité contrôlée de la solution.

Il apparaît ainsi que l'importance du domaine de composition conduisant à une réponse nernstienne n'est pas le seul critère de choix.

Les résultats précédents sont également intéressants sur un tout autre plan. Le fait que, pour certains domaines de composition, la valeur de la pente de l'électrode devient inférieure à la valeur théorique signifie que le nombre de transport des anions dans les plastisols cesse d'être nul (cf. sect. II-1). Ce comportement implique un mode de transport différent de l'amphiphile dans la membrane. Cette conclusion peut être étayée par la constatation que les plastisols de faible teneur en plastifiant sont hétérogènes, ce qui suppose au sein de la structure membranaire la présence de défauts. Cette propriété a déjà été évoquée dans la littérature (24), où l'existence d'agrégats de PVC dans certains plastisols a été montrée.

La création de défauts au sein du support conduit inévitablement à un régime de diffusion hétérogène. Sous l'effet de son gradient de potentiel électrochimique, le transfert de l'ion M^+ peut se réaliser par l'intermédiaire du transporteur, l'ion tétraphénylborure (transport sélectif), mais aussi par diffusion, associé à X^- (transport non-sélectif), en empruntant les chemins ménagés par les défauts du support.

On peut rendre compte de ce comportement en modélisant la membrane de plastisol sous la forme d'une membrane «mosaïque» résultant de la juxtaposition de domaines possédant des propriétés différentes de transfert. On considèrera ainsi, que la membrane est constituée de deux domaines interpénétrés :

(*i*) parfaitement sélectif à l'ion M^+. On conviendra d'appeler θ le rapport de l'aire de ce domaine sur l'aire totale. Le transfert du cation se réalise par l'intermédiaire du transporteur. On conviendra de noter la mobilité de M^+, ω_{mt}. Le flux de cation est alors J_{mt}.

(*ii*) parfaitement non sélectif. M^+ et X^- diffusent dans les chemins ménagés au sein du support par les défauts ou les «volumes libres». Le rapport de l'aire de ce domaine sur l'aire totale est $1 - \theta$. On conviendra de noter les mobilités de M^+ et de X^-, respectivement ω_{md} et ω_{xd}. Les flux respectifs sont J_{md} et J_{xd}.

Le modèle est schématisé sur la figure 2.

On peut alors écrire les flux des deux ions à travers la membrane en tenant compte des deux modes de transfert :
Pour M^+ :

$$[4] \quad Jm = \theta J_{mt} + (1 - \theta) J_{md}$$

Pour X^- :

$$[4'] \quad Jx = (1 - \theta) J_{xd}$$

Chaque flux répond à l'équation suivante :

$$[5] \quad J_{mt} = -\frac{1}{T} \omega_{mt} \text{ grad } \tilde{\mu}_M$$

$$[5'] \quad J_{md} = -\frac{1}{T} \omega_{md} \text{ grad } \tilde{\mu}_M$$

$$[5''] \quad J_{xd} = -\frac{1}{T} \omega_{xd} \text{ grad } \tilde{\mu}_X$$

où $\tilde{\mu}_M$ et $\tilde{\mu}_X$ sont les potentiels électrochimiques de M^+ et de X^-. Le respect de l'électroneutralité lors du transfert permet d'écrire :

$$[6] \quad [\theta \omega_{mt} + (1 - \theta) \omega_{md}] \text{ grad } \tilde{\mu}_M = (1 - \theta) \omega_{xd} \text{ grad } \tilde{\mu}_X$$

À partir de l'expression du potentiel électrochimique des espèces,

$$\tilde{\mu}_i = \mu i + zi F \phi$$

où ϕ est le potentiel de la phase qui contient i, zi la valence algébrique de i, et F le faraday, on établit la relation :

$$[7] \quad F \, d\phi \, [\theta\omega_{mt} + (1 - \theta) (\omega_{md} + \omega_{xd})] = (1 - \theta) \omega_{xd} d\mu_X - [\theta\omega_{mt} + (1 - \theta)\omega_{md}] \, d\mu_M$$

Pour les solutions diluées, on peut indentifier les nombres qui mesurent les concentrations et les activités. Les concentrations en M^+ et X^- sont égales à C, la concentration de MX.

En développant les expressions des potentiels chimiques, on obtient la relation différentielle :

$$[8] \quad d\phi = \frac{RT}{F} \frac{(1 - \theta) (\omega_{xd} - \omega_{md}) - \theta\omega_{mt}}{(1 - \theta) (\omega_{md} + \omega_{xd}) + \theta\omega_{mt}} d \ln C$$

Une fois intégrée entre les compartiments 1 et 2, dans lesquelles les concentrations de MX sont respectivement C_1 et C_2, on établit que la différence de potentiel transmembranaire s'écrit sous la forme :

$$[9] \quad \Delta\phi = \phi 2 - \phi 1 = \frac{RT}{F} \frac{(1-\theta)(\omega_{xd} - \omega_{md}) - \theta\omega_{mt}}{(1-\theta)(\omega_{md} + \omega_{xd}) + \theta\omega_{mt}} \ln \frac{C_2}{C_1}$$

Si l'on introduit le nombre de transport de M^+ dans la phase membranaire, tel que

$$t_m = \frac{\omega_{md}}{\omega_{md} + \omega_{xd}}$$

on peut alors écrite la relation précédente sous la forme :

$$[10] \quad \Delta\phi = \phi 2 - \phi 1 = \frac{RT}{F} \left[\frac{2}{\frac{1}{1-t_m} + \left(\frac{\theta}{1-\theta}\right)\frac{\omega_{mt}}{\omega_{xd}}} - 1 \right] \ln \frac{C_2}{C_1}$$

La différence de potentiel aux bornes de la pile est alors de la forme :

$$[11] \quad \Delta E = \text{constante} + \frac{RT}{F} \left[1 - \frac{2}{\frac{1}{1-t_m} + \left(\frac{\theta}{1-\theta}\right)\frac{\omega_{mt}}{\omega_{xd}}} \right] \ln C_2$$

On conviendra d'appeler $\frac{RT}{F}\alpha$ le terme prélogarithmique

$$\Delta E = \text{constante} + \frac{RT}{F}\alpha \ln C_2$$

On constate ainsi que la pente de la droite de réponse de l'électrode est liée aux valeurs de trois paramètres :

(*i*) le nombre de transport de l'anion caractéristique du phénomène de diffusion passive à travers les défauts du support;

(*ii*) le rapport $r = \omega_{mt}/\omega_{xd}$ entre la mobilité du cation lorsqu'il est associé au transporteur et la mobilité de l'anion pour la partie diffusive du transport;

(*iii*) le rapport des aires associées aux deux phénomènes de transport.

Les deux premiers paramètres sont caractéristiques de la nature de la membrane et des propriétés du transporteur vis-à-vis de l'amphiphile. Le troisième est directement lié à la composition du support. On peut en effet supposer en considérant les résultats expérimentaux que la quantité de défauts de la membrane s'accroît lorsque la concentration en plastifiant diminue. Ceci implique que θ et la proportion de plastifiant sont deux paramètres qui varient dans le même sens.

Nous avons reporté sur la figure 3, à titre d'illustration, les variations de α en fonction de θ pour différentes valeurs de r. Nous avons retenu pour t_m la valeur de 0,3 qui caractérise le transport de l'ion amphiphile dans l'eau en présence de l'anion bromure (18). Ce choix est purement formel et n'a

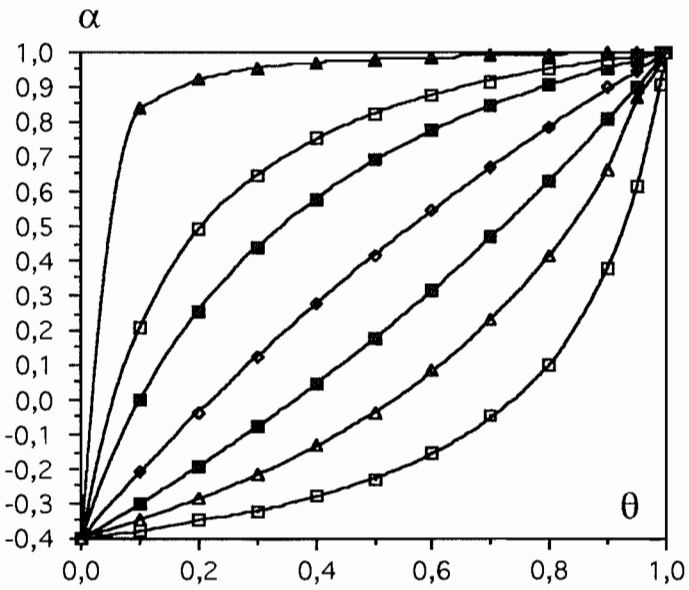

FIG. 3. Variation du paramètre α en fonction de la contribution θ (transfert par transporteur) au transport de M^+ à travers la membrane. De bas en haut : ⊡ $r = 0{,}2$; △ $r = 0{,}5$; ■ $r = 1$; ◇ $r = 2$; ■ $r = 5$; □ $r = 10$; ▲ $r = 100$.

que peu d'importance dans l'analyse suivante qui reste essentiellement qualitative.

Lorsque le rapport r est très grand, c'est-à-dire lorsque la mobilité de l'anion est faible (cf $r = 100$), l'électrode possède une réponse nernstienne sur un très large domaine de composition. Ce comportement correspond tout à fait au cas des plastisols PVC-hpm–NPOE et PVC-bpm–DNP dont on peut donc supposer, soit qu'ils possèdent peu de défauts (θ petit), soit que la mobilité de X^- (ω_{xd}) y est faible.

Pour des valeurs de r plus petites, de l'ordre de 5 à 10, qui supposent qu'une partie non négligeable du transport de M^+ s'effectue par diffusion libre, on retrouve le comportement observé pour l'ensemble des autres plastisols, c'est-à-dire une diminution de la valeur de la pente de l'électrode dès que le milieu s'appauvrit en plastifiant.

Nous avons également reporté sur la figure 3 les comportements limites correspondant au cas où le transfert de M^+ s'effectue essentiellement par diffusion libre $r = 0$; on retrouve bien entendu le cas de la jonction libre.

Bien qu'interprété de manière essentiellement qualitative, ce modèle rend bien compte de la diminution de la pente de l'électrode en supposant l'existence de micro-hétérogénéités permettant une diffusion des sels à travers la membrane.

Conclusion

L'étude présentée avait pour objectif d'explorer les propriétés de différents plastisols en vue de leur utilisation comme capteurs de potentiel. Les résultats obtenus montrent, qu'en fait, peu de plastisols, préparés à température ambiante, conduisent à des milieux homogènes permettant la réalisation d'électrodes sélectives aux surfactifs cationiques possédant une pente nernstienne. Les meilleurs résultants sont toujours obtenus avec les gels les plus riches en plastifiant (60–80%), dans des zones de composition où le support présente des propriétés proches de celles des membranes liquides. Dès que l'on enrichit le milieu en po-

Can. J. Chem. Downloaded from www.nrcresearchpress.com by 88.255.202.194 on 09/08/12
For personal use only.

lymère, on crée des défauts dans la membrane par lesquels vont pouvoir diffuser les ions. La membrane perd alors sa sélectivité assurée par le transporteur.

Les caractéristiques des électrodes obtenues avec les différents plastisols montrent que l'emploi du PVC-bpm est intéressant. Ce polymère permet de réaliser des membranes homogènes possédant d'excellentes réponses sélectives aux ions amphiphiles, dans des domaines de composition en plastifiant beaucoup plus larges que ceux permis par le PVC-hpm. En particulier, les mélanges PVC-bpm–DNP constituent un bon choix.

Cette étude élargit ainsi grandement les possibilités d'utilisation des plastisols pour la réalisation d'électrodes membranaires sélectives.

1. G. H. Fricke. Anal. Chem. **52**, 259R (1980).
2. M. A. Arnold et R. L. Solsky. Anal. Chem. **58**, 85R (1986).
3. J. Koryta. Ion-selective electrodes. Cambridge Physical Chemistry Monographs. W. Clowes & Sons Ltd., Cambridge University Press. 1975.
4. R. D. Armstrong et G. Horvai. Electrochim. Acta, **35**, 1 (1990).
5. C. Gavach et P. Seta. Anal. Chim. Acta, **50**, 407 (1970).
6. M. Muratsugu, N. Kamo, K. Kurihara et Y. Kobatake. Biochim. Biophys. Acta, **464**, 613 (1977).
7. G. Geminet. Ann. Biol. **15**, 449 (1976).
8. S. Cutler, P. Meares et D. G. Hall. J. Electroanal. Chem. **85**, 145 (1977).
9. A. G. Fogg, A. S. Pathan et D. Thorburn Burns. Anal. Chim. Acta, **69**, 238 (1974).
10. T. Shinbo, N. Kamo, K. Kurihara et Y. Kobatake. Arch. Biochem. Biophys. **187**, 414 (1978).
11. C. R. Martin et H. Freiser. Anal. Chem. **52**, 562 (1980).
12. L. Cunningham et H. Freiser. Anal. Chim. Acta, **132**, 43 (1981).
13. S. S. Davis et O. Olejnik. Anal. Chim. Acta, **132**, 51 (1981).
14. L. Cunningham et H. Freiser. Anal. Chim. Acta, **180**, 271 (1986).
15. C. Davidson, P. Meares et D. G. Hall. J. Membr. Sci. **36**, 511 (1988).
16. I. Kasahara, M. Kanai, M. Taniguchi, A. Kakeka, N. Hata, S. Taguchi et K. Goto. Anal. Chim. Acta, **219**, 239 (1989).
17. W. C. Campbell et C. J. Dowie. Brit. Patent 2 207 250 A (1989).
18. D. Jezequel. Thèse de Doctorat de l'Université Pierre et Marie Curie, Paris. 1991.
19. D. Jezequel, A. Mayaffre et P. Letellier. J. Chim. Phys. **88**, 391 (1991).
20. D. Jezequel, A. Mayaffre et P. Letellier. Can. J. Chem. **69**, 1865 (1991).
21. G. J. Moody, R. B. Oke et J. D. R. Thomas. Analyst, **95**, 910 (1970).
22. K. Vytras, M. Remes et H. Kubesova-Svoboda. Anal. Chim. Acta, **124**, 91 (1981).
23. G. H. Zhang, T. Imato, Y. Asano, T. Sonoda, H. Kobayashi et N. Ishibashi. Anal. Chem. **62**, 1644 (1990).
24. P. L. Soni, P. H. Geil et E. A. Collins. J. Macromol. Sci. Phys. **B20**, 479 (1981).

Can. J. Chem. Downloaded from www.nrcresearchpress.com by 88.255.202.194 on 09/08/12
For personal use only.

Characterization of the 2,2′-bipyridine chelates of lanthanum(III) in acetonitrile. A ^{1}H, ^{13}C, ^{17}O, and ^{139}La NMR study

MONIQUE FRÉCHETTE

Ottawa–Carleton Chemistry Institute, University of Ottawa Campus, Ottawa, Ont., Canada K1N 6N5

Received July 7, 1992

MONIQUE FRÉCHETTE. Can. J. Chem. **71**, 377 (1993).

We have investigated the reaction between $La(NO_3)_3 \cdot 6H_2O$ and 2,2′-bipyridine (bipy) in acetonitrile by means of ^{139}La, ^{17}O, ^{13}C, and ^{1}H NMR spectroscopy. The ^{139}La spectra show up to three different sites with variable intensities attributed to solvated La(III) ions and to two complex species with one or two bipy moieties in the La(III) coordination sphere. ^{17}O NMR indicates that during the complexation reaction, the coordinated water is totally displaced from the coordination sphere whereas the nitrate groups remain coordinated. Proton NMR data confirm the water expulsion. In addition, the proton chemical shifts of bipy, in comparison with the ^{13}C NMR data, clearly show an anisotropic shielding when two bipy are coordinated to La(III). Therefore, the two bipy molecules are in close proximity in the coordination sphere. From the NMR results it has been shown that, during the complexation process, five different La(III) species are formed: $[La(NO_3)_3(CH_3CN)_4]$, $[La(NO_3)_3(CH_3CN)_3(H_2O)]$, $[La(NO_3)_3(bipy)(CH_3CN)_2]$, $[La(NO_3)_3(bipy)(CH_3CN)(H_2O)]$, and $[La(NO_3)_3(bipy)_2]$. Each La(III) complex has a coordination member of 10, with NO_3^- and bipy acting as chelating ligands. Furthermore, the structure of the $La(NO_3)_3(bipy)_2$ complex in solution shows similarities with the solid state compound. Finally, comparisons are made with the La(III) complexes previously obtained with 1,10-phenanthroline.

MONIQUE FRÉCHETTE. Can. J. Chem. **71**, 377 (1993).

On a étudié par RMN du ^{139}La, ^{17}O, ^{13}C et ^{1}H la réaction entre $La(NO_3)_3 \cdot 6H_2O$ et la bipyridine-2,2′ (bipy) en milieu acétonitrile. Les spectres de ^{139}La indiquent la présence de trois sites différents dont les intensités varient avec des quantités croissantes de bipy. Ces sites correspondent aux ions solvatés La(III) ainsi qu'à deux espèces complexes avec une et deux molécules de bipy appartenant à la sphère de coordination du La(III). La RMN de ^{17}O montre que l'eau initialement coordinée aux ions La(III) est complètement expulsée lors de la complexation alors que les nitrates restent coordinés. La RMN du proton confirme l'expulsion de l'eau et indique la présence d'une contribution anisotropique lorsque deux bipy sont coordinées; les deux molécules de bipy sont donc à proximité dans la sphère de coordination. En combinant l'ensemble des résultats de RMN, on a pu démontrer que cinq espèces différentes de La(III) sont formées : $[La(NO_3)_3(CH_3CN)_4]$, $[La(NO_3)_3(CH_3CN)_3(H_2O)]$, $[La(NO_3)_3(bipy)(CH_3CN)_2]$, $[La(NO_3)_3(bipy)(CH_3CN)(H_2O)]$ et $[La(NO_3)_3(bipy)_2]$. Chaque ion La(III) a une coordination de 10 avec NO_3^- et bipy agissant comme ligands chélatants. De plus, la structure du complexe $La(NO_3)_3(bipy)_2$ en solution montre des similarités avec le complexe isolé à l'état solide. Enfin, des comparaisons sont faites avec les complexes des ions La(III) précédemment obtenus avec la phénanthroline-1,10.

Can. J. Chem. Downloaded from www.nrcresearchpress.com by 88.255.202.194 on 09/08/12
For personal use only.

Introduction

The existence of stable lanthanide(III) complexes, having only nitrogens as coordinating centers, was proved previously (1–3). Such complexes were observed with macrocyclic N-donor ligands (3, 4) and aliphatic amines (5–8), as well as with aromatic and heterocyclic amines (9–11) in organic solvents of low donicity number. In these media, the competing strength of the solvent molecules for the coordination sites on the Ln(III) ions is significantly decreased in comparison with water or other highly basic solvents, improving the chances for the formation of the corresponding amino complexes.

Although the choice of the solvent plays a crucial role in the amino complex stabilization, the type of anion associated with the Ln(III) ions also has a decisive effect on the stability and stoichiometric composition of the resulting amino complexes. Anions can form, to varying degrees, inner sphere complexes with the Ln(III) ions and then act as additional competitors (2, 6, 12, 13).

In a stepwise attempt to characterize and understand the amino Ln(III) complexes in solution, we recently reported a multi-NMR analysis that successfully gave structural and thermodynamic information about the mono- and bis-phen complexes obtained from the reaction of $La(NO_3)_3 \cdot 6H_2O$ and 1,10-phenanthroline (phen) in CH_3CN (14). In the present paper, 2,2′-bipyridine (bipy) is used instead of phen in the complexation reaction. Bipy has a more flexible structure than phen with the possibility that the two pyridyl rings rotate along the C(2)—C(2′) bond. Therefore, interesting differences in the complex stability and in the stoichiometric composition of the species present in solution can be observed.

Until now, nothing has been reported about the bipy complexes of La(III) in solution and only a little is known about the bipy complexes of some other rare earths in water and methanol (15, 16). The solid bipy complexes have been investigated a little more fully. The mixed $La(NO_3)_3(bipy)_2$ crystal was fully studied by Al-Karaghouli and Wood (17), and Sinha characterized some bipy complexes of rare earths from their infrared, fluorescence, and reflection spectra (18, 19).

In the course of this investigation, the ^{139}La, ^{17}O, ^{13}C, and ^{1}H NMR properties of CH_3CN solutions containing bipy and $La(NO_3)_3 \cdot 6H_2O$ are reported and analyzed. The nature of the interactions between the La(III) ions and the various potentially coordinating compounds in solution are discussed and compared with those recently obtained for the phen complexes of La(III) in the same medium (14).

Experimental section

Materials and samples

$La(NO_3)_3 \cdot 6H_2O$ (Aldrich, 99.99%) was kept in a desiccator over Drierite and used as received. 2,2′-Bipyridine (Aldrich, 99+%) was recrystallized in hexane, vaccum dried (44°C) over P_2O_5 for at least

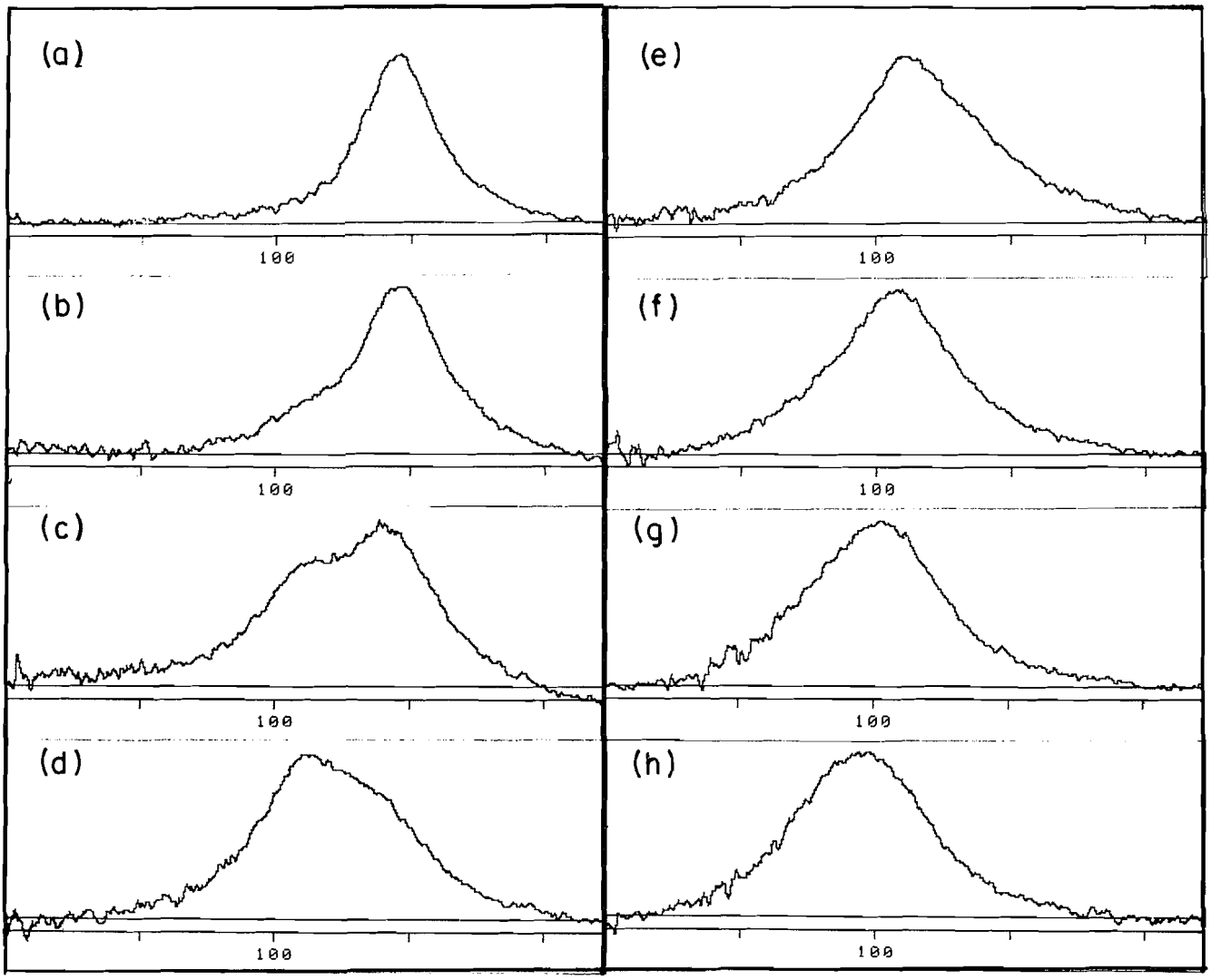

FIG. 1. ^{139}La NMR spectra, at 42.37 MHz, of $La(NO_3)_3 \cdot 6H_2O$ in CH_3CN in the presence of increasing concentration of bipy; $\rho = [bipy]_0/[La(III)]_0$ with $[La(III)]_0 = 5.14 \times 10^{-3}$ M. (*a*) $\rho = 0$, (*b*) $\rho = 0.25$, (*c*) $\rho = 0.50$, (*d*) $\rho = 0.75$, (*e*) $\rho = 1.01$, (*f*) $\rho = 1.26$, (*g*) $\rho = 1.51$, (*h*) $\rho = 1.76$.

20 h, and kept in a desiccator over Drierite. Acetonitrile (CH_3CN) (BDH) was dried as previously described (14). Acetonitrile-d_3 (Aldrich, 99% D) was used as received.

The NMR samples were prepared as previously reported (14). Most of the spectra recorded were of freshly prepared samples because precipitation occurred on standing, especially if $\rho = [bipy]_0/[La(III)]_0 > 1.0$.

NMR measurements

^{139}La, ^{17}O, ^{13}C, and ^1H NMR spectra were recorded at 25.0 ± 0.5°C on a Varian XL-300 spectrometer using resonance frequencies of 42.37, 40.66, 75.43, and 299.94 MHz, respectively. No lock was used (except for proton NMR), the field drift being negligible. The experimental conditions and references used were fully described in a previous paper (14).

The ^{139}La spectral lineshapes, showing the superposition of two or three Lorentzian signals, were decomposed by using a curve-fitting program. From 22 different NMR samples, 35 La NMR spectra were recorded and 62 decompositions were performed. Intensities (I), linewidths ($\upsilon_{1/2}$), and chemical shifts (δ) characterizing the decomposed Lorentzian lines were also derived from that analysis. Because of residual baseline distortions and large linewidth values, non-negligible errors are associated with the I, $\upsilon_{1/2}$, and δ values. Indeed, it was observed that small variations in the phase parameters LP and RP led in some cases to dramatic changes in I, $\upsilon_{1/2}$, and δ even if very good curve fittings were obtained.

The ^{17}O NMR nitrate signal of the $La(NO_3)_3 \cdot 6H_2O$ solutions was only visible at higher concentrations after overnight accumulations. The nitrate resonance of the CH_3CN solutions saturated with KNO_3 and NH_4NO_3 needed at least 36 h to be observable.

Results

^{139}La NMR data

The ^{139}La NMR spectra of $La(NO_3)_3 \cdot 6H_2O$ in CH_3CN were recorded in the presence of increasing amounts of bipy so that $0 < \rho = [bipy]_0/[La(III)]_0 < 1.8$ with $[La(III)]_0 = 5.14 \times 10^{-3}$ M (see Fig. 1). In the presence of bipy, the ^{139}La NMR spectra of the solutions show a single Lorentzian line characterized by a chemical shift (δ) of 9 ± 2 ppm and a linewidth value ($\upsilon_{1/2}$) of 2.75 ± 0.10 kHz, in excellent agreement with the values previously reported (14).

In adding bipy to the La(III) solutions, the ^{139}La spectral lineshapes first show an additional site appearing downfield (82 ± 6 ppm) and associated with the 1:1 complex formation, $La(bipy)^{3+}$ (s) ($\rho < 0.75$). Then for larger bipy concentrations ($\rho > 0.88$), the ^{139}La spectra clearly indicate

Can. J. Chem. Downloaded from www.nrcresearchpress.com by 88.255.202.194 on 09/08/12
For personal use only.

TABLE 1. Chemical shift, δ, and linewidth, $\upsilon_{1/2}$, of the ^{139}La NMR resonances in CH_3CN

Species	δ (ppm)	$\upsilon_{1/2}$ (kHz)
La^{3+} (s)[a]	10 ± 4	2.9 ± 0.2
$La(phen)^{3+}$ (s)[a]	80 ± 4	2.35 ± 0.15
$La(phen)_2^{3+}$ (s)[a]	150 ± 6	2.06 ± 0.09
La^{3+} (s)	10 ± 5	2.9 ± 0.3
$La(bipy)^{3+}$ (s)[b]	82 ± 6	>3.0
$La(bipy)_2^{3+}$ (s)[b]	150	—

[a]From ref. 14.
[b]$La(bipy)^{3+}$ (s) and $La(bipy)_2^{3+}$ (s) resonances collapse in a single Lorentzian line when ρ = 1.76 when δ = 110 ppm and $\upsilon_{1/2}$ = 5.17 kHz.

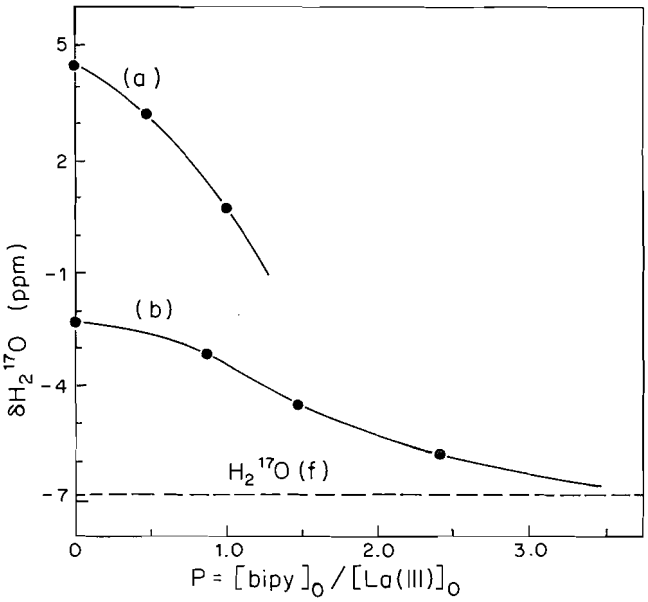

FIG. 2. ^{17}O NMR chemical shift of H_2O in CH_3CN as a function of ρ and for different $La(NO_3)_3 \cdot 6H_2O$ concentrations. (*a*) $[La(III)]_0 = 2.67 \times 10^{-2}$ M, (b) $[La(III)]_0 = 5.24 \times 10^{-3}$ M.

TABLE 2. Chemical shift, δ, and linewidth, $\upsilon_{1/2}$, of the ^{17}O NMR resonances of H_2O and NO_3^- in CH_3CN

Compound	δH_2O[a] (ppm)	δNO_3^-[b] (ppm)	$\upsilon_{1/2}(NO_3^-)$ (kHz)
KNO_3 (satd.)	−6.16	427	0.15
NH_4NO_3 (satd.)	−6.01	423	0.15
H_2O (f) (0.05 M)	−6.88	—	—
$La(NO_3)_3 \cdot 6H_2O$ (2.62×10^{-2} M) + bipy[c]			
0	4.53	425 ± 1	1.3 ± 0.2
0.43	3.24	427	wide
0.99	0.70	426	wide
$La(NO_3)_3 \cdot 6H_2O$ (5.24×10^{-3} M) + bipy			
0	−2.26	—	—
0.72	−3.18	—	—
1.45	−4.52	—	—
2.41	−5.90	—	—

[a]Deviation better than ±0.10 ppm.
[b]Averaged value: 425 ± 3 ppm.
[c]$\rho = [bipy]_0/[La(III)]_0$.

steadily faster exchange conditions and the presence of a third ^{139}La site, again more downfield (150 ppm). The result is increasingly broad and deshielded non-Lorentzian spectral lines. Finally for ρ = 1.76, the ^{139}La resonances merge in a Lorentzian signal whose corresponding chemical shift is 110 ppm. This signal appears at a weight-averaged position between the δ values characterizing $La(bipy)^{3+}$ (s) and $La(bipy)^{3+}$ (s).

The ^{139}La NMR lineshapes resulting from the overlap of two or three Lorentzian signals were decomposed by using a curve-fitting program in order to find out the respective spectral contributions and characteristics of each species. Although large errors are possible, particularly regarding the intensities (*I*) and linewidths ($\upsilon_{1/2}$) (see experimental part), fair chemical shift values (δ) were obtained. Data are summarized in Table 1.

^{17}O NMR data

The ^{17}O NMR spectra of 5.24×10^{-3} M and 2.62×10^{-2} M $La(NO_3)_3 \cdot 6H_2O$ in CH_3CN were recorded with increasing concentrations of bipy. As $[bipy]_0$ increases, the water peak appears as a well-resolved triplet (20) steadily resonating at lower frequencies and gradually drawing nearer to the chemical shift of free water in CH_3CN (Fig. 2). This behaviour clearly indicates the presence of free and coordinated water in solution under fast exchange conditions according to the ^{17}O NMR time scale. Data also show that coordinated water is expelled from the coordination sphere of La(III) during the complexation.

The ^{17}O NMR spectra of 2.62×10^{-2} M $La(NO_3)_3 \cdot 6H_2O$ solutions in CH_3CN also show a broad signal associated with the NO_3^- resonance. Its chemical shift and linewidth of 426 ± 2 ppm and 1.3 ± 0.2 kHz, respectively, remain unchanged with the addition of bipy, indicating no change in the nature of the interactions of the NO_3^- species in the medium. Comparison with the ^{17}O NMR properties of free NO_3^- obtained from saturated solutions of KNO_3 and NH_4NO_3 in CH_3CN (see Table 2) reveals identical chemical shift values (426 ± 3 ppm) for both the coordinated and free NO_3^- species. However, a much narrower linewidth value (0.15 kHz instead of 1.3 kHz) is associated with free NO_3^- (Table 2). This linewidth difference does indicate that the three nitrate groups are initially coordinated to La(III) and are not displaced during the complexation with bipy.

No nitrate NMR signal was observable with the 5.24×10^{-3} M $La(NO_3)_3 \cdot 6H_2O$ solutions after an overnight accumulation due to the low natural abundance of ^{17}O and the large NO_3^- linewidth.

^{13}C NMR data

The ^{13}C NMR spectra of 1.26×10^{-2} M bipy solutions were recorded with increasing concentrations of $La(NO_3)_3 \cdot 6H_2O$ in CH_3CN so that $R = [La(III)]_0/[bipy]_0 < 3.7$. All ^{13}C NMR spectra consist, as expected, of five resonance lines whose observed chemical shift (δ) results from fast exchange conditions on the ^{13}C NMR time scale. The carbon assignment is in agreement with the study of Marker *et al.* (21).

The variation of the ^{13}C chemical shifts as a function of *R* (Fig. 3) indicates the formation of $La(bipy)_2^{3+}$ (s) because of plateaus when $R = 0.5$. For $R > 0.5$, no additional ^{13}C NMR shifts were observed, indicating the absence of additional bipy sites. However, the ^{139}La NMR data clearly show the formation of $La(bipy)^{3+}$ (s). Consequently, we do con-

Can. J. Chem. Downloaded from www.nrcresearchpress.com by 88.255.202.194 on 09/08/12
For personal use only.

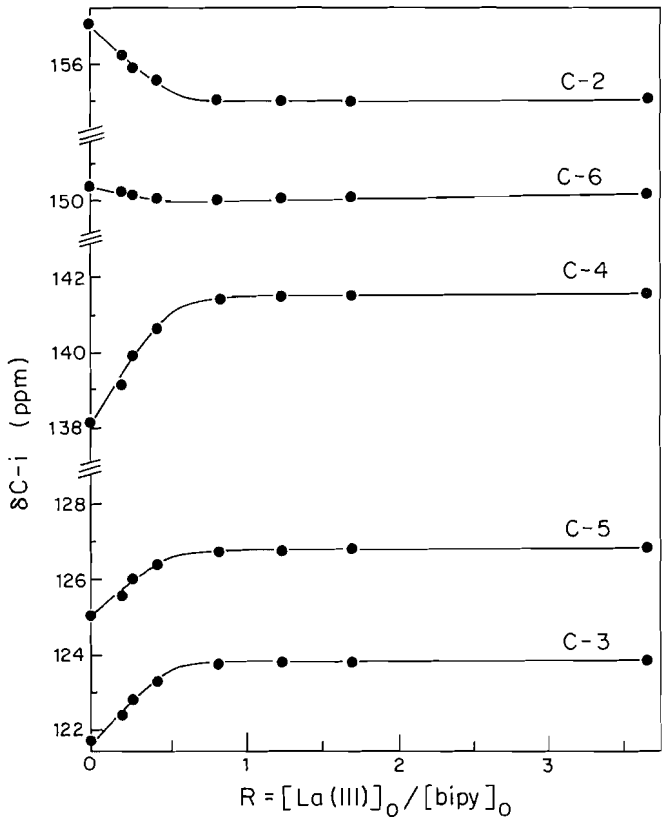

FIG. 3. ^{13}C NMR chemical shifts of bipy in CH_3CN in the presence of increasing concentration of $La(NO_3)_3 \cdot 6H_2O$. $R = [La(III)]_0/[bipy]_0$ with $[bipy]_0 = 1.27 \times 10^{-2}$ M.

clude that the chemical shifts of the coordinated bipy in both $La(bipy)^{3+}$ (s) and $La(bipy)_2^{3+}$ (s) are identical. Similar behaviour was previously observed for the complexation of La(III) with phen under identical experimental conditions (14). The ^{13}C NMR spectral data of free and coordinated bipy are summarized in Table 3.

^1H NMR data

Figure 4 shows the ^1H NMR chemical shifts of bipy (2.63×10^{-3} M) (δH_i) and H_2O) (δH_2O) in CD_3CN in the presence of increasing amounts of $La(NO_3)_3 \cdot 6H_2O$ so that $R < 4.0$. Our proton assignment for the uncomplexed bipy agrees with literature data (22). Both bipy and H_2O are in fast exchange on the ^1H NMR time scale so that their observed δ values appear at weight-averaged positions between those characterizing the free and coordinated ligands.

For $0 < R < 0.4$, the $La(bipy)_2^{3+}$ (s) complex is exclusively present and water-free. Indeed, δH_2O is constant at 2.22 ± 0.01 ppm and very close to the value obtained for the residual H_2O ($H_2O(f)$) in the bipy solution for which $R = 0$ and $\delta H_2O(f) = 2.21$ ppm. For $R > 0.4$, δH_2O appears increasingly downfield, in agreement with the formation of $La(bipy)^{3+}$ (s) and La^{3+} (s), which both have coordinated H_2O.

The ^1H NMR titration curves of bipy with increasing La(III) concentrations differ greatly from the corresponding ^{13}C NMR curves. The ^1H NMR curves, especially those of H-3, H-4, and H-5, reach a plateau around $R = 1.0$ rather than for $R = 0.5$ as observed by ^{13}C NMR, suggesting that only the $La(bipy)^{3+}$ (s) species is formed. For H-6, the sigmoid titration curve can only be explained by the successive formation of $La(bipy)_2^{3+}$ (s) and $La(bipy)^{3+}$ (s) if different δH_i values characterized the coordinated bipy in each complex.

TABLE 3. ^{13}C and ^1H NMR spectral data[a] for the complexation of La(III) with La(III) 2,2′-bipyridine in CH_3CN

Position	2,2′	3,3′	4,4′	5,5′	6,6′
^{13}C NMR data					
bipy (s)					
^1J (Hz)	—	165	163	164	175
δ (ppm)	157.00	121.72	138.15	125.06	150.32
bipy (c)[b]					
^1J (Hz)	—	158	167	160	185
δ (ppm)	155.00	123.85	141.54	126.86	150.13
^1H NMR data					
bipy (s)					
δ (ppm)	—	8.47	7.95	7.44	8.72
bipy (1:1)					
δ (ppm)	—	8.38	8.20	7.70	8.87
bipy (1:2)					
δ (ppm)	—	8.41	8.08	7.56	8.74
σ_i(ani)	—	0	−0.12	−0.14	−0.13

[a]Chemical shifts: deviation better than ±0.03 ppm.
[b]The chemical shifts of complexed bipy in the 1:1 and 1:2 complexes are undistinguishable.

The differences between the ^{13}C and ^1H titration curves are attributed to an anisotropic contribution that is only experimentally observable by using ^1H NMR. Indeed, as previously reported for the complexation of La(III) with phen (14), Ru(II) with polypyridines (23), and Ln(III) with alkyl-substituted bipyridines (24), the protons of bipy in the 1:2 complex can interact with the aromatic system of the other coordinated bipy. These interactions are a source of high-field shift and when present, as suspected here in $La(bipy)_2^{3+}$ (s), lead to lower δH_i values. Consequently, the ^1H NMR titration curves show various patterns that depend on the magnitude of these anisotropic contributions as well as on the magnitude of the coordination shifts.

The δH_i values for free bipy and coordinated bipy in $La(bipy)^{3+}$ (s), $\delta H_i(f)$ and $\delta H_i(1:1)$, respectively, were determined from the titration curves for $R = 0$ and for $R > 2.0$. δH_i of bipy in $La(bipy)_2^{3+}$ (s), $\delta H_i(1:2)$, were calculated from eq. [1] for $R = 0.156$ and 0.312 because, according to the δH_2O values, only the uncomplexed bipy and the $La(bipy)_2^{3+}$ (s) species are present in solution.

$$[1] \quad \delta H_i = X(1:2)\delta H_i(1:2) + X(f)\delta H_i(f)$$

$X(1:2)$ and $X(f)$ are, respectively, the populations of the coordinated and free bipy. Then, the anisotropic contributions, σ(ani), were estimated from eq. [2].

$$[2] \quad \sigma_i(ani) = \delta H_i(1:2) - \delta H_i(1:1)$$

These ^1H NMR data are given in Table 3.

Discussion

The ^{139}La NMR data (Table 1) indicate a constant downfield shift of 70 ppm for each bipy molecule added in the coordination sphere of La(III). As suggested in previous work (14, 25, 26), such steady chemical shift variations are observed when the same molecules are expelled from the co-

Can. J. Chem. Downloaded from www.nrcresearchpress.com by 88.255.202.194 on 09/08/12
For personal use only.

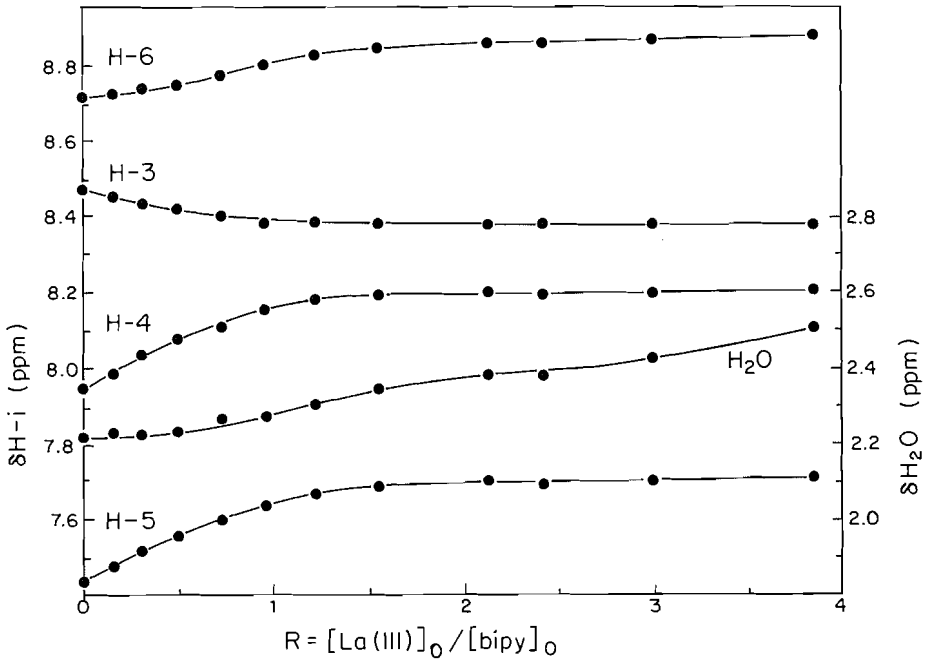

FIG. 4. ^{1}H NMR chemical shifts of bipy and H_2O in CH_3CN in the presence of increasing concentration of $La(NO_3)_3 \cdot 6H_2O$. R = $[La(III)]_0/[bipy]_0$ with $[bipy]_0 = 2.63 \times 10^{-3}$ M.

ordination sphere of La(III) with successive additions of the new ligand. In the present case, CH_3CN and H_2O are the species simultaneously expelled from the coordination sphere of La(III) as a result of the addition of bipy.

The constant downfield shift variation suggests that the coordination number of the La(III) species remains unchanged during the course of the complexation. This is hypothesized according to a study of Evans and Missen (26) that reported a dramatic break in the direction of the ^{139}La chemical shift variation when increasing amounts NO_3^- were added to $La(ClO_4)_3$ in CH_3CN. The break, which occurred with the addition of 4 to 5 NO_3^- molecules, was attributed to a change in the coordination number (C.N.) of La(III), the small size of NO_3^- favouring a higher C.N. value. No such variations are usually observed when C.N. is supposedly unchanged, as clearly indicated by the stepwise addition of H_2O, ethylenediamine, and diethylenetriamine to $La(ClO_4)_3$ solutions in CH_3CN (26).

The results reported in Table 1 also show a marked similarity between the ^{139}La chemical shifts of the bipy complexes of La(III) with those obtained with phen under the same experimental conditions. This similarity strongly suggests that the nature of the interactions between La(III) and the ligand as well as the stoichiometry of the La(III) species are identical with both bipy and phen.

The $\upsilon_{1/2}$ values reported for the bipy complexes of La(III) are quite large in comparison to the corresponding values reported for the phen chelates. Indeed, the similarity of the phen and bipy complexes in solution and in the solid state (14, 17) suggests that the $\upsilon_{1/2}$ values should decrease with the successive complexation of La(III) with bipy, resulting in greater electronic symmetries at the ^{139}La nuclei (14). Considering the present results, the anticipated decrease in the $\upsilon_{1/2}$ values may be obscured by the line broadening contribution, which is a result of the moderate exchange rate of the bipy moieties between the different ^{139}La sites.

The ^{17}O chemical shifts of the free and coordinated NO_3^- are very similar (426 ± 2 ppm). However, their respective $\upsilon_{1/2}$ values are adequate indicators of the behaviour of the NO_3^- counterions during the complexation process. The linewidth values of NO_3^- remain constant at 1.3 ± 0.2 kHz, but are much broader than the corresponding $\upsilon_{1/2}$ value characterizing the free NO_3^- (0.15 ± 0.01 kHz). Therefore we must conclude that the three nitrate groups remain coordinated to La(III) all along the complexation. The presence of the three NO_3^- groups in the La(III) coordination sphere is in agreement with the ^{139}La NMR study of Evans and Missen (26) and the calorimetric works of Forsberg and co-workers using more basic N-donor chelating ligands (6–8).

In comparison to NO_3^-, the H_2O initially coordinated to La(III) is expelled with the addition of bipy. The amount of coordinated water should be very low because in quintupling $[La(III)]_0$ (see Table 2), the ^{17}O chemical shift of water is dramatically changed. According to the thermodynamics of equilibrium, this important variation of the water chemical shifts can only occur if less than one molecule of water is coordinated. This low content in coordinated H_2O has been mathematically proved and will be reported in another paper[1] (the populations of La(III) ions having coordinated water are 24 ± 6% and 60 ± 13% if $[La(III)]_0$ are 5.24×10^{-3} M and 2.62×10^{-3} M, respectively).

When bipy is added to the La(III) solution, the water expulsion causes decreases in the H_2O resonating frequency. For ρ values higher than 1.3, data indicate that some water is still coordinated (see Fig. 2). Therefore the inner coordination sphere of $La(bipy)^{3+}$ (s) must contain coordinated water as well because no more uncomplexed La(III) ions are present in these solutions according to the ^{139}La NMR data. Finally, the $La(bipy)_2^{3+}$ (s) species should be water-free be-

[1]M. Fréchette. Results to be published.

Can. J. Chem. Downloaded from www.nrcresearchpress.com by 88.255.202.194 on 09/08/12
For personal use only.

Can. J. Chem. Downloaded from www.nrcresearchpress.com by 88.255.202.194 on 09/08/12
For personal use only.

cause, in the presence of large quantities of bipy ($\rho = 2.4$), the ^{17}O chemical shift of free water in CH_3CN has almost been reached. Proton NMR data also confirm the water expulsion because for R values lower than 0.4 the ^1H NMR water shift is identical to the chemical shift of residual water in the bipy solution. The complete expulsion of water from the coordination sphere of the La(III) ions when the $La(bipy)_2^{3+}$ (s) species is exclusively present in solution is in agreement with previous results obtained with phen (14) and with the X-ray crystallographic analysis of $La(bipy)_2(NO_3)_3$ (17). Therefore, according to the ^{17}O and ^1H water chemical shifts, the $La(bipy)_2^{3+}$ (s) is anhydrous whereas H_2O is present in both La^{3+} (s) and $La(bipy)^{3+}$ (s).

Results in Table 2 also show discrepancies of 0.87 and 0.72 ppm between the chemical shift of water dissolved in acetonitrile and the values obtained from the saturated solutions of NH_4NO_3 and KNO_3, respectively. These discrepancies are a likely result of specific interactions between H_2O and NO_3^-, K^+, or NH_4^+.

A description of the La(III) species present in solution during the complexation process is possible by using a combination of the ^{139}La and ^{17}O NMR data.

We confirm the existence of the water-free bis(bipy)La(III) species as $[La(NO_3)_3(bipy)_2]$. The coordination number is 10 with two chelating bipy and three bidentate NO_3^-, just as found for the crystalline complex (17). The main evidence for a C.N. of 10 is (1) the high similarity between the bis(bipy) complex in solution and in the solid state, and (2) the constant downfield shift variation of the ^{139}La NMR signals, with the addition of each bipy then suggesting no variation of the C.N. value. Although the expulsion of H_2O has been proved by ^{17}O and ^1H NMR data, no direct information was obtained for the expulsion of CH_3CN. However, because H_2O is a very good competitor with respect to CH_3CN (despite the huge difference in their concentrations) and because the bis(bipy)La(III) complex is water-free, the CH_3CN molecules should also be absent from the La(III) coordination sphere.

The two other species, La^{3+} (s) and $La(bipy)^{3+}$ (s), are better described by an equilibrium between an aquo and a water-free species because of the low degree of participation of water in the inner sphere of La(III). For each species, the coordination number should be 10 because no change in the C.N. value is expected according to the ^{139}La NMR results. Therefore, because the three NO_3^- are also coordinated, the resulting molecular formulae are $[La(NO_3)_3(CH_3CN)_4]$ in equilibrium with $[La(NO_3)_3(CH_3CN)_3(H_2O)]$ for La^{3+} (s), and $[La(NO_3)_3(bipy)(CH_3CN)_2]$ in equilibrium with $[La(NO_3)_3(bipy)(CH_3CN)(H_2O)]$ for $La(bipy)^{3+}$ (s).

The ^{13}C NMR data do not allow the differentiation of bipy in the 1:1 and 1:2 complexes and only show two different bipy sites associated with the free and coordinated bipy. In comparison, ^1H NMR data are more sensitive to the molecular structures of the La(III) species, and bipy in the 1:1 and 1:2 complexes can be differentiated. Bipy in the 1:1 complex is not subject to special perturbing influences other than the deshielding (shielding for H-3) expected from the electron-withdrawing inductive effect of coordination. However, protons of bipy in the 1:2 complex are subject to an additional high-field shift caused by interaction of its protons with the aromatic system of the other coordinated bipy. Consequently, information about the three-dimensional structure of the chelates can be obtained from ^1H NMR data.

If it is assumed that a similar structure is adopted by $[La(NO_3)_3(bipy)]_2$ in solution and in the solid state (17), the two halves of the bipy ligand are not magnetically equivalent. One pyridine ring is influenced by the adjacent bipy moieties due to the partial superposition of two bipy while the other pyridine only behaves as in $La(bipy)^{3+}$ (s). According to our ^1H NMR data in solution, we do have an anisotropic contribution but no inequivalence of the proton resonance is observed. This suggests an intramolecular configurational equilibrium between a species, analogous to that depicted for $[La(NO_3)_3(bipy)_2]$ in the solid state (17) and its mirror image. The inequivalence should be associated with a rapid exchange of configuration as previously reported for the alkyl-substituted bipyridine complexes of lanthanides (24). According to these facts, we believe that the three-dimensional structures of the 1:2 complex in solution and in the solid state are very close, in agreement with the results previously reported for $[La(NO_3)_3(phen)_2]$ (14).

Because of large errors in the determination of the populations of the La(III) species from the ^{139}La NMR spectra, the apparent constants of stability of the $La(bipy)^{3+}$ (s) and $La(bipy)_2^{3+}$ (s) complexes were not calculated. However, the general trend of the results indicates that these complex species are slightly less stable than the corresponding La–phen complexes (14). Furthermore, results clearly indicate that the bipy moieties are exchanged more rapidly than are the phen from one ^{139}La site to another.

In conclusion, the present results demonstrate the efficiency with which a multi-NMR analysis can establish the behaviour of chelates towards La(III) ions in solution. This multi-NMR study not only indicated the presence of interactions between La(III) and bipy but also provided the number and type of coordinates as well as the possible molecular geometry. Obviously, many more different La(III) species were identified in solution than those isolated in the solid state. Further work is presently in progress in the hope of collecting data with different nitrogen donor ligands that are potentially able to displace the nitrate groups from the coordination sphere and to change the coordination number.

Acknowledgements

Operating grants from le Conseil de l'Éducation Franco-Ontarienne (CEFO) and the Development Fund of the Faculty of Science of the University of Ottawa are gratefully acknowledged. I also thank Prof. C. Detellier for sharing his laboratory space with me.

1. J. H. Forsberg. Coord. Chem. Rev. **10**, 195 (1973).
2. S. P. Sinha. *In* Complexes of the rare earths. Pergamon Press Ltd., Toronto. 1966. pp. 24–35.
3. L. M. Vallarino. *In* Handbook on the physics and chemistry of rare earths. Vol. 15. *Edited by* K. A. Gschneidner, Jr. and L. Eyring. Elsevier Science Publishers, Amsterdam. 1991. pp. 443–512.
4. F. Benetollo, G. Bombieri, K. K. Fonda, A. Polo, J. R. Quagliano, and L. M. Vallarino. Inorg. Chem. **30**, 1345 (1991).
5. E. R. Birbaum and S. Stratton. Inorg. Chem. **12**, 379 (1973).
6. J. H. Forsberg and C. A. Wathen. Inorg. Chem. **10**, 1379 (1971).
7. J. H. Forsberg and T. Moeller. Inorg. Chem. **8**, 883 (1969).
8. J. H. Forsberg and T. Moeller. Inorg. Chem. **8**, 889 (1969).
9. J. Selbin, N. Ahmad, and N. Bhacca. Inorg. Chem. **10**, 1383 (1971).

10. Q. Jaradat and T. Akasheh. Polyhedron, **6**, 175 (1987).
11. S. Gurriere, S. Musumeci, E. Rizzarelli, and A. Seminara. J. Inorg. Nucl. Chem. **38**, 259 (1976).
12. P. L. Rinaldi, S. A. Khan, G. R. Choppin, and G. C. Levy. J. Am. Chem. Soc. **101**, 1350 (1979).
13. J. C. G. Bunzli, A. E. Merbach, and R. M. Nielson. Inorg. Chim. Acta, **139**, 151 (1987).
14. M. Fréchette, I. R. Butler, R. Hynes, and C. Detellier. Inorg. Chem. **31**, 1650 (1992).
15. K. Bukietynska and P. N. Thuy. Inorg. Chim. Acta, **132**, 21 (1987).
16. V. L. Ermolaev and V. P. Gruzdev. Inorg. Chim. Acta, **95**, 179 (1984).
17. A. R. Al-Karaghouli and J. S. Wood. Inorg. Chem. **11**, 2293 (1972).
18. S. P. Sinha. J. Inorg. Nucl. Chem. **27**, 115 (1965).
19. S. P. Sinha. Spectrochim. Acta, **20**, 879 (1964).
20. J. P. Kintzinger. *In* NMR. Basic principles and progress. Oxygen-17 and silicon-29. *Edited by* P. Diehl, E. Fluck, and R. Kosfeld. Springer, New York. 1981. pp. 4, 37.
21. A. Marker, A. J. Canty, and R. T. C. Brownbi. Aust. J. Chem. **31**, 1255 (1978).
22. S. Castellano, H. Gunther, and S. Ebersole. J. Phys. Chem. **31**, 4166 (1965).
23. F. E. Lytle, L. M. Petrosky, and L. R. Carlson. Anal. Chim. Acta, **57**, 239 (1971).
24. F. A. Hart, J. E. Newberry, and D. Shaw. J. Inorg. Nucl. Chem. **32**, 3585 (1970).
25. Y. Ducommun, L. Holm, G. Laurenczy, and A. E. Merbach. Magn. Reson. Chem. **26**, 1023 (1988).
26. D. E. Evans and P. H. Missen. J. Chem. Soc. Dalton Trans. 1929 (1982).

Can. J. Chem. Downloaded from www.nrcresearchpress.com by 88.255.202.194 on 09/08/12
For personal use only.

Activity coefficients of $NaNO_3$ in (Mg, Ca, Sr, and Ba)$(NO_3)_2$ + H_2O systems at 298 K by EMF methods

STEPHEN N. SMITH, S. SARADA,[2] AND RAMAMURTHY PALEPU[1]

Department of Chemistry, University College of Cape Breton, Sydney, N.S., Canada B1P 6L2

Received September 3, 1992

STEPHEN N. SMITH, S. SARADA, and RAMAMURTHY PALEPU. Can. J. Chem. **71**, 384 (1993).

The activity coefficients of $NaNO_3$ in $Mg(NO_3)_2$, $Ca(NO_3)_2$, $Sr(NO_3)_2$, and Ba $(NO_3)_2$ were determined at constant total ionic strength of 0.1, 0.5, 0.75, 1.0, 1.5, and 2.0 mol kg^{-1} at 298 K using EMF methods. The experimental activity coefficients were analyzed using four different formalisms, namely, Reilly–Wood–Robinson, Scatchard, Pitzer, and Harned equations, and the interaction parameters were evaluated. Excess Gibbs free energy of mixing and trace activity coefficients were calculated and the results are discussed.

STEPHEN N. SMITH, S. SARADA et RAMAMURTHY PALEPU. Can. J. Chem. **71**, 384 (1993).

Opérant à 298 K, et faisant appel à des méthodes de FÉM, on a déterminé les coefficients d'activité du $NaNO_3$ dans les sels suivants : $Mg(NO_3)_2$, $Ca(NO_3)_2$, $Sr(NO_3)_2$ et $Ba(NO_3)_2$ à des forces ioniques totales constantes de 0,1, 0,5, 0,75,1,0, 1,5 et 2,0 mol kg^{-1}. On a analysé les coefficients d'activité expérimentaux à l'aide de quatre formalismes, soit les équations de Reilly–Wood–Robinson, Scatchard, Pitzer et Harned et on a évalué les paramètres d'interaction. On a calculé l'énergie libre de mélange de Gibbs en excès et les coefficients d'activité de trace et on discute des résultats.

[Traduit par la rédaction]

Can. J. Chem. Downloaded from www.nrcresearchpress.com by 88.255.202.194 on 09/08/12
For personal use only.

Thermodynamic properties of multicomponent electrolyte mixtures in water have received considerable attention in the literature (1–5). Such solutions are found to be important in various geological, biological, and industrial processes. Knowledge of the value of the activity coefficient of each component in the mixture is essential. Ion selective electrodes (ISE) have been used extensively in the determination of activity coefficients of multicomponent electrolyte systems (6). However, very few studies have been made using the ion-exchange base nitrate ISE in the determination of activity coefficients (7). In the present study, the activity coefficients of $NaNO_3$ in ternary mixtures of $NaNO_3$ + $M(NO_3)_2$ + H_2O where M = Mg, Ca, Sr, and Ba were determined at 298 K and total ionic strengths of 0.1, 0.5, 1.0, 1.5, and 2.0 molal.

Experimental

Analytical grades of sodium, calcium, magnesium, strontium, and barium nitrates (either Baker Analyzed or B.D.H.) were used without further purification. All solutions were prepared by using distilled water that was passed through a NANO pure (Barnstead) ion-exchange apparatus.

The cell used consisted of a Ross sodium glass ISE (model 84-11) and an Orion nitrate ion-exchange ISE (model 93-07) immersed in a mixture of $NaNO_3$ and $M(NO_3)_2$ solution in a double-walled cell. The solutions were stirred at a constant rate with an air-driven magnetic stirrer and the temperature was maintained at 25.0 ± 0.1°C. The cell arrangement is as follows:

Na ion selective electrode	$NaNO_3$ (m_A) + $M(NO_3)_2$ (m_B)	NO_3 ion selective electrode

where m_A and m_B are the molalities of $NaNO_3$ and $M(NO_3)_2$ solutions, respectively. The emf values were recorded using an Accumet 925 pH meter (Fisher) after adding aliquots of m_B to m_A or vice versa at regular intervals. The accuracy of the emf measurements was ±0.1 mV. The potential of the cell was observed to be stable to within ±0.5 mV for periods of time from 0.5 to 1 h. A titration procedure was used to alter the composition of the mixture, so that the cell was undisturbed during the experimentation. Two sets of potential measurements were made at each ionic strength to test the reproducibility and accuracy of the measurements. In the first set, the potentials were measured by taking a $NaNO_3$ solution and using a $M(NO_3)_2$ solution as titrant, and in the second set the order was reversed. In the central region of composition the two runs overlap and this is used as a test for the reproducibility of the data.

Results and discussion

The potentials of the cell in the $NaNO_3$ + $M(NO_3)_2$ mixtures are described by the equation:

$$[1] \quad E_{cell} = E^0 + K \log [a_{Na} a_{NO_3} + K' a_M^{1/2} a_{NO_3}]$$

where K' is the selectivity coefficient of the Na ISE for M^{2+} ions and K is the Nernstian slope.

At each ionic strength, the emf values of the cell were first measured with pure $NaNO_3$ solution in order to calibrate the electrodes. The values of E^0 and K were determined by plotting the cell emf values against log a_{NaNO_3}. The values of the activity coefficients of $NaNO_3$ were taken from N.B.S. data (8). The emf of pure $M(NO_3)_2$ solutions were then measured to evaluate the selective coefficient (K') values. The values of K' were found to be in the range of 10^{-5}–10^{-4} at all the ionic strengths studied. The term $K'(\sqrt{a_M})a_{NO_3}$ in eq. [1] can be neglected and the equation is modified as follows:

$$[2] \quad E_{cell} = E^0 + K \log [a_{Na} a_{NO_3}]$$

By substituting $m_+\gamma_+$ for a_{Na} and $m_-\gamma_-$ for a_{NO_3}, eq. [2] can be rearranged as follows:

$$[3] \quad \gamma_\pm^2 = \frac{1}{m_{Na} m_{NO_3}} [10^{(E_{cell} - E^0)/K}]$$

The mean activity coefficient values[3] of $NaNO_3$ in the mix-

[1]Author to whom correspondence may be addressed.

[2]Postdoctoral Fellow, Department of Chemistry, University of Delaware, Delaware, U.S.A.

[3]Four pages of experimental data of log $\gamma_\pm$ as a function of y_B at different ionic strengths have been deposited as supplementary material and may be purchased from: The Depository of Unpublished Data, Document Delivery, CISTI, National Research Council Canada, Ottawa, Canada K1A 0S2.

Can. J. Chem. Downloaded from www.nrcresearchpress.com by 88.255.202.194 on 09/08/12
For personal use only.

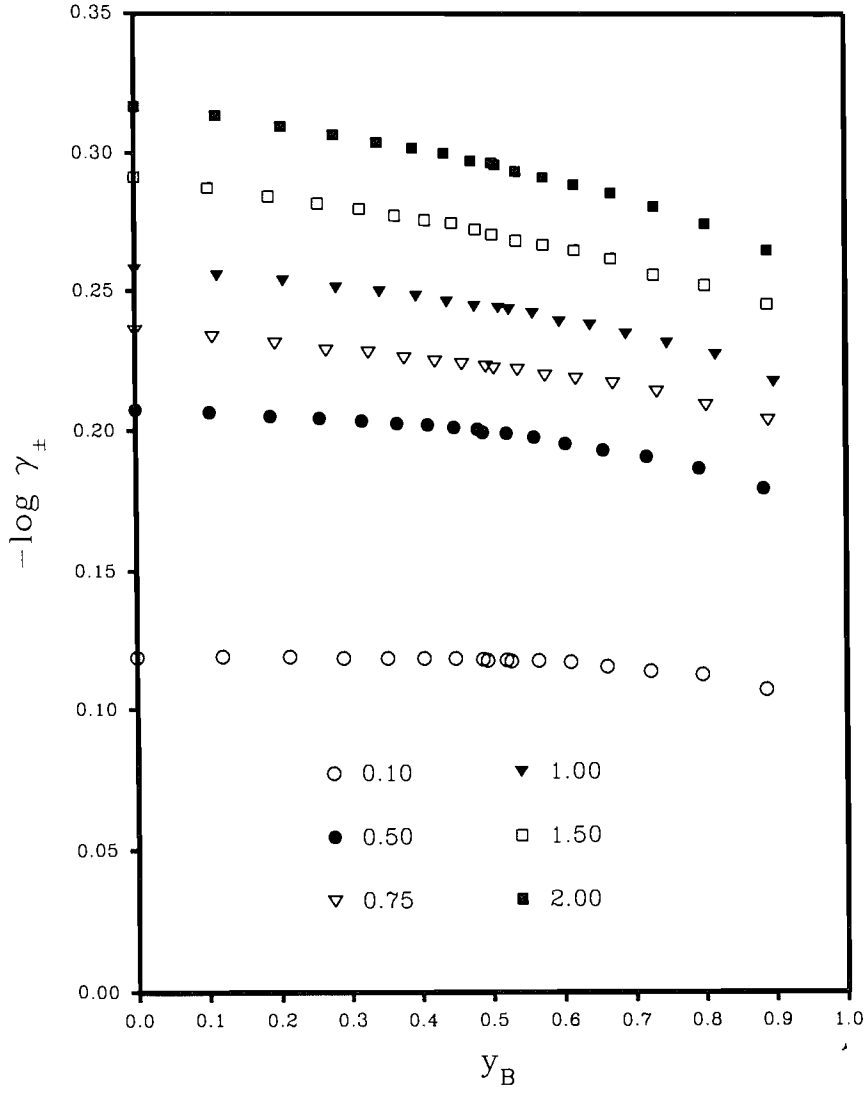

FIG. 1. Plot of log $\gamma_{\pm}$ ($NaNO_3$) vs. y_B at various ionic strengths for the $NaNO_3$ + $Ca(NO_3)_2$ + H_2O system.

TABLE 1. Harned coefficients for the system $NaNO_3$ + $M(NO_3)_2$ + H_2O at 25°C

Ionic strength	Mg			Ca		
	α_{AB}	β_{AB}	RMSD	α_{AB}	β_{AB}	RMSD
0.10	2.632×10^{-3}	-1.841×10^{-2}	6.4×10^{-4}	8.824×10^{-3}	-2.23×10^{-2}	7.7×10^{-4}
0.50	-1.383×10^{-2}	-2.089×10^{-2}	6.9×10^{-4}	5.833×10^{-4}	-3.42×10^{-2}	6.6×10^{-4}
0.75	-3.550×10^{-2}	-9.901×10^{-3}	9.3×10^{-4}	-1.731×10^{-2}	-1.92×10^{-2}	7.0×10^{-4}
1.00	-3.850×10^{-2}	-2.212×10^{-2}	1.4×10^{-3}	-1.001×10^{-2}	-3.56×10^{-2}	9.0×10^{-4}
1.50	-5.312×10^{-2}	-3.127×10^{-2}	5.4×10^{-4}	-2.908×10^{-2}	-2.51×10^{-2}	6.3×10^{-4}
2.00	-5.536×10^{-2}	-5.852×10^{-2}	4.2×10^{-4}	-2.386×10^{-2}	-3.75×10^{-2}	6.3×10^{-4}
	Sr			Ba		
	α_{AB}	β_{AB}	RMSD	α_{AB}	β_{AB}	RMSD
0.10	1.804×10^{-2}	-3.015×10^{-2}	8.8×10^{-4}	1.393×10^{-2}	-2.803×10^{-2}	5.6×10^{-4}
0.50	4.535×10^{-3}	-3.671×10^{-2}	8.6×10^{-4}	2.986×10^{-3}	4.326×10^{-3}	3.9×10^{-4}
0.75	1.057×10^{-2}	-2.732×10^{-2}	6.2×10^{-4}	8.049×10^{-3}	-3.895×10^{-3}	9.1×10^{-4}
1.00	-1.038×10^{-2}	-1.499×10^{-2}	7.3×10^{-4}	7.194×10^{-3}	-4.759×10^{-3}	8.1×10^{-4}
1.50	-1.235×10^{-2}	-2.141×10^{-2}	5.8×10^{-4}			
2.00	-1.312×10^{-2}	-4.530×10^{-2}	9.2×10^{-4}			

TABLE 2. Scatchard, RWR, Pitzer, and modified Harned parameters for the system $NaNO_3 + M(NO_3)_2 + H_2O$ at 25°C

M	Scatchard	RWR	Pitzer	Modified Harned
Mg	$b^{0,1} = -8.018 \times 10^{-2}$ $b^{0,2} = 4.861 \times 10^{-2}$ $b^{0,3} = 7.234 \times 10^{-3}$ RMSD = 4.920×10^{-3}	$g_0 = -5.588 \times 10^{-2}$ $g_1 = -6.755 \times 10^{-2}$ $g_0' = 1.343 \times 10^{-1}$ RMSD = 1.831×10^{-3}	$S_\theta = -2.411 \times 10^{-1}$ $\psi = 7.985 \times 10^{-2}$ RMSD = 4.515×10^{-3}	$\alpha' = -3.212 \times 10^{-2}$ $\beta' = -2.614 \times 10^{-2}$ RMSD = 2.388×10^{-3}
Ca	$b^{0,1} = 3.828 \times 10^{-2}$ $b^{0,2} = 5.973 \times 10^{-3}$ $b^{0,3} = -1.371 \times 10^{-2}$ RMSD = 2.754×10^{-3}	$g_0 = 3.394 \times 10^{-2}$ $g_1 = -1.246 \times 10^{-2}$ $g_0' = -1.660 \times 10^{-2}$ RMSD = 2.148×10^{-3}	$S_\theta = 3.220 \times 10^{-2}$ $\psi = -3.691 \times 10^{-2}$ RMSD = 2.671×10^{-3}	$\alpha' = -1.384 \times 10^{-2}$ $\beta' = -2.283 \times 10^{-2}$ RMSD = 3.645×10^{-3}
Sr	$b^{0,1} = -7.527 \times 10^{-2}$ $b^{0,2} = 4.861 \times 10^{-2}$ $b^{0,3} = 7.234 \times 10^{-3}$ RMSD = 4.920×10^{-3}	$g_0 = -1.213 \times 10^{-1}$ $g_1 = -8.935 \times 10^{-2}$ $g_0' = 2.123 \times 10^{-1}$ RMSD = 3.216×10^{-3}	$S_\theta = -1.657 \times 10^{-1}$ $\psi = 1.170 \times 10^{-1}$ RMSD = 5.478×10^{-3}	$\alpha' = -5.189 \times 10^{-3}$ $\beta' = -2.252 \times 10^{-2}$ RMSD = 3.284×10^{-3}
BA	$b^{0,1} = 8.237 \times 10^{-2}$ $b^{0,2} = -5.028 \times 10^{-1}$ $b^{0,3} = 4.437 \times 10^{-1}$ RMSD = 1.904×10^{-3}	$g_0 = -8.135 \times 10^{-2}$ $g_1 = -7.427 \times 10^{-2}$ $g_0' = 2.309 \times 10^{-1}$ RMSD = 5.656×10^{-4}	$S_\theta = 6.272 \times 10^{-2}$ $\psi = 3.645 \times 10^{-2}$ RMSD = 8.513×10^{-4}	$\alpha' = 4.853 \times 10^{-3}$ $\beta' = 3.221 \times 10^{-3}$ RMSD = 1.142×10^{-3}

tures at various ionic strengths were obtained by substituting the values of E_{cell}, E^0, and K into eq. [3]. A typical plot of $\gamma_\pm$ for $NaNO_3$ in $NaNO_3 + Ca(NO_3)_2$ as a function of the ionic strength fraction y_B where

$$[4] \quad y_B = \frac{3m_B}{m_A + 3m_B}$$

is presented in Fig. 1. The activity coefficient data were fitted to the Harned equation (9) in the following form:

$$[5] \quad \log \gamma_A = \log \gamma_A^0 - \alpha_{AB} y_B - \beta_{AB} y_B^2$$

where γ_A^0 is the activity coefficient of pure A at the same ionic strength and α_{AB} and β_{AB} are the Harned coefficients, calculated using regression methods. The values of α_{AB} and β_{AB}, along with the root-mean-square deviations, are listed in Table 1. The fact that quadratic terms are needed to fit the experimental data indicates the importance of cation–cation and ternary interactions.

The activity coefficient data were analyzed further using the following three equations available in the literature: (1) The Reilly, Wood, and Robinson (R.W.R.) treatment (10, 11), which expresses the activity coefficient of $NaNO_3$ in ternary mixtures as

$$[6] \quad \log \gamma_A = \log \gamma_A^0 - \frac{1}{2 \ln 10}[(2\phi_A^0 - \phi_B^0 - 1)y_B - (g_0 I + 2g_1 I^2 + g_0' I^2)y_B + (3g_1 + g_0')I^2 y_B^2]$$

where g_0 is identified with binary interaction parameters and g_0' represents the change in the value of g_0 with ionic strength. (2) The Scatchard equation (12, 13) for the activity coefficients of $NaNO_3$ in $M(NO_3)_2$ solutions can be written as

$$[7] \quad \log \gamma_A = \log \gamma_A^0 + \frac{1}{2 \ln 10}\left[(\phi_B^0 - 2\phi_A^0 + 1)y_B + (b^{0,1} I + b^{0,2} I^2 + b^{0,3} I^3)y_B + (b^{1,2} I^2 + b^{1,3} I^3)y_B - \left(0.5 b^{0,2} I^2 + \left(\frac{2}{3}\right) b^{0,3} I^3\right) y_B^2\right]$$

where $b^{0,1}$ can be identified with interactions between ions of the same charge, and $b^{0,2}$ with the ternary interactions. In the present study the higher order parameters $b^{1,2}$ and $b^{1,3}$ were set equal to zero. The Scatchard equation uses different coefficients of $\sqrt{I}$ to account for the different distances of closest approach for the solute components. (3) The Pitzer treatment (14–16), which contains fewer adjustable parameters even after the inclusion of the higher order interaction terms of E_θ and E_θ'. The relevant Pitzer equation for $\gamma_\pm$ of $NaNO_3$ is given by:

$$[8] \quad \ln \gamma_A = \ln \gamma_A^0 - \frac{4}{3} I y_B B_{NaNO_3} + \frac{I y_B}{3} B_{M(NO_3)_2} + \frac{I^2}{18}(7y_B^2 - 30y_B) C^\phi_{NaNO_3} + \frac{I^2 y_B}{3\sqrt{2}} \frac{(1 - y_B)}{3} C^\phi_{M(NO_3)_2} + \frac{I y_B}{3} \theta_{Na-M} + \frac{I^2 y_B}{3} \frac{(1 - 2y_B)}{3} \Psi_{Na-M-NO_3} + \frac{I^2 y_B}{3}(y_B - 4) B'_{NaNO_3} + \frac{I^2 y_B}{3} \frac{(1 - y_B)}{3} B'_{M(NO_3)_2} + \frac{I^2 y_B}{3}(1 - y_B) \theta'_{Na-M}$$

where $\theta_{NaM} = S_{\theta_{NaM}} + E_\theta$ and $\theta'_{NaM} = E'_{\theta_{NaM}}$. The value of S_θ represents the binary interaction between ions of the same charge,

Can. J. Chem. Downloaded from www.nrcresearchpress.com by 88.255.202.194 on 09/08/12
For personal use only.

TABLE 3. Friedman parameters for the system $NaNO_3$ + $M(NO_3)_2$ + H_2O at 25°C

Ionic strength	g_0				g_1			
	Mg	Ca	Sr	Ba	Mg	Ca	Sr	Ba
0.10	−0.6781	−1.227	−0.2651	0.7541	−0.1218	0.4185	−0.06078	0.1234
0.50	−0.7008	−0.4383	−0.3592	0.2346	−0.1338	0.02356	−0.08322	0.03339
0.75	−0.6181	−0.3430	−0.2866	0.2041	−0.1162	0.001284	−0.06727	0.03065
1.00	−0.5590	−0.2890	−0.2312	0.1917	−0.1020	−0.008687	−0.05251	0.03153
1.50	−0.4805	−0.2276	−0.1498		−0.0792	−0.01601	−0.02910	
2.00	−0.4321	−0.1971	−0.09255		−0.06087	−0.02258	−0.009105	

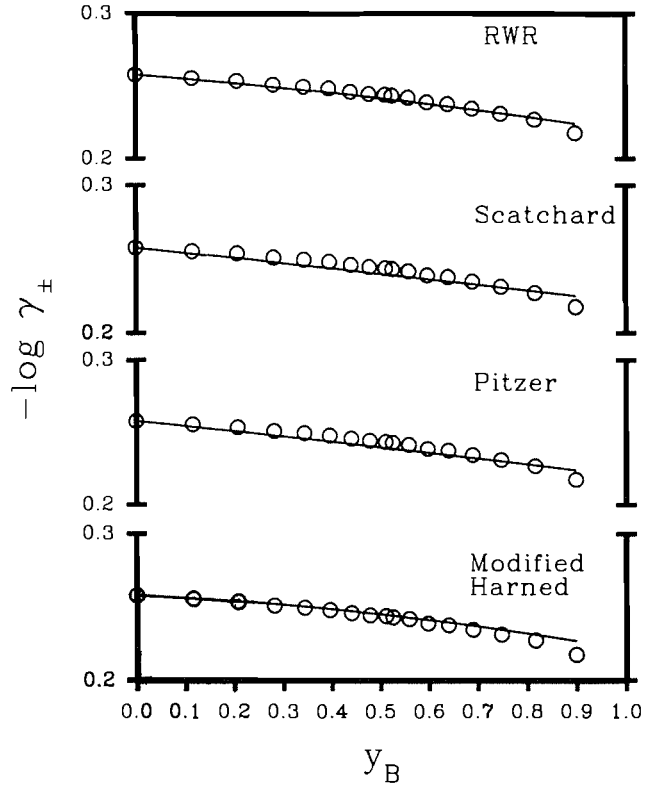

FIG. 2. Plot of log $\gamma_{\pm}$ ($NaNO_3$) vs. y_B at I = 1.0 for ternary mixtures of $NaNO_3$ + $Ca(NO_3)_2$ + H_2O using eqs. [6]–[9].

Ψ represents the ternary interactions, and all other terms have their usual significance. All the data required for the analysis using the Pitzer equation were taken from the work of Kim and Frederick (17).

The experimental activity coefficient data were fitted with a single nonlinear least-squares program and solved for values of the interaction parameters. The interaction parameters along with the RMSD are presented in Table 2. The experimental data were also analyzed using a modified Harned equation of the form (18)

$$[9] \quad \log \gamma_A = \log \gamma_A^0 - \alpha'_{AB} I y_B - \beta'_{AB} I y_B^2$$

The values of α'_{AB} and β'_{AB} are also included in Table 2. The binary interaction parameters $b^{0,1}$, g_0, S_0, and α'_{AB} obtained by solving these equations are of the same sign in all cases except for g_0 in the $NaNO_3$ + $Ba(NO_3)_2$ + H_2O system. In Fig. 2, the experimental activity coefficients of $NaNO_3$ in the mixture $NaNO_3$ + $Ca(NO_3)_2$ + H_2O at I = 1.0 are plotted against y_B and the continuous curves were generated with the

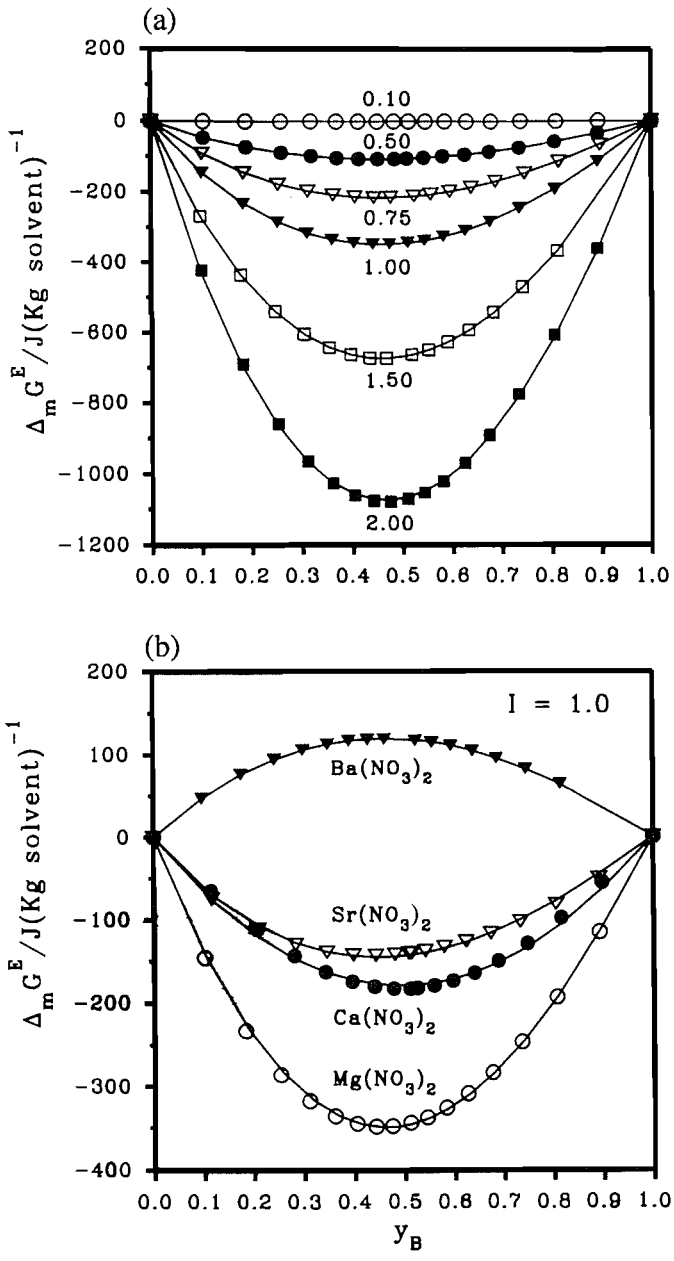

FIG. 3. (*a*) Plot of $\Delta_m G^E$ vs. y_B for the $NaNO_3$ + $Mg(NO_3)_2$ + H_2O system at 298 K at various ionic strengths. (*b*) Plot of $\Delta_m G^E$ vs. y_B at I = 1.0 for the system $NaNO_3$ + $M(NO_3)_2$ + H_2O.

Can. J. Chem. Downloaded from www.nrcresearchpress.com by 88.255.202.194 on 09/08/12
For personal use only.

Can. J. Chem. Downloaded from www.nrcresearchpress.com by 88.255.202.194 on 09/08/12
For personal use only.

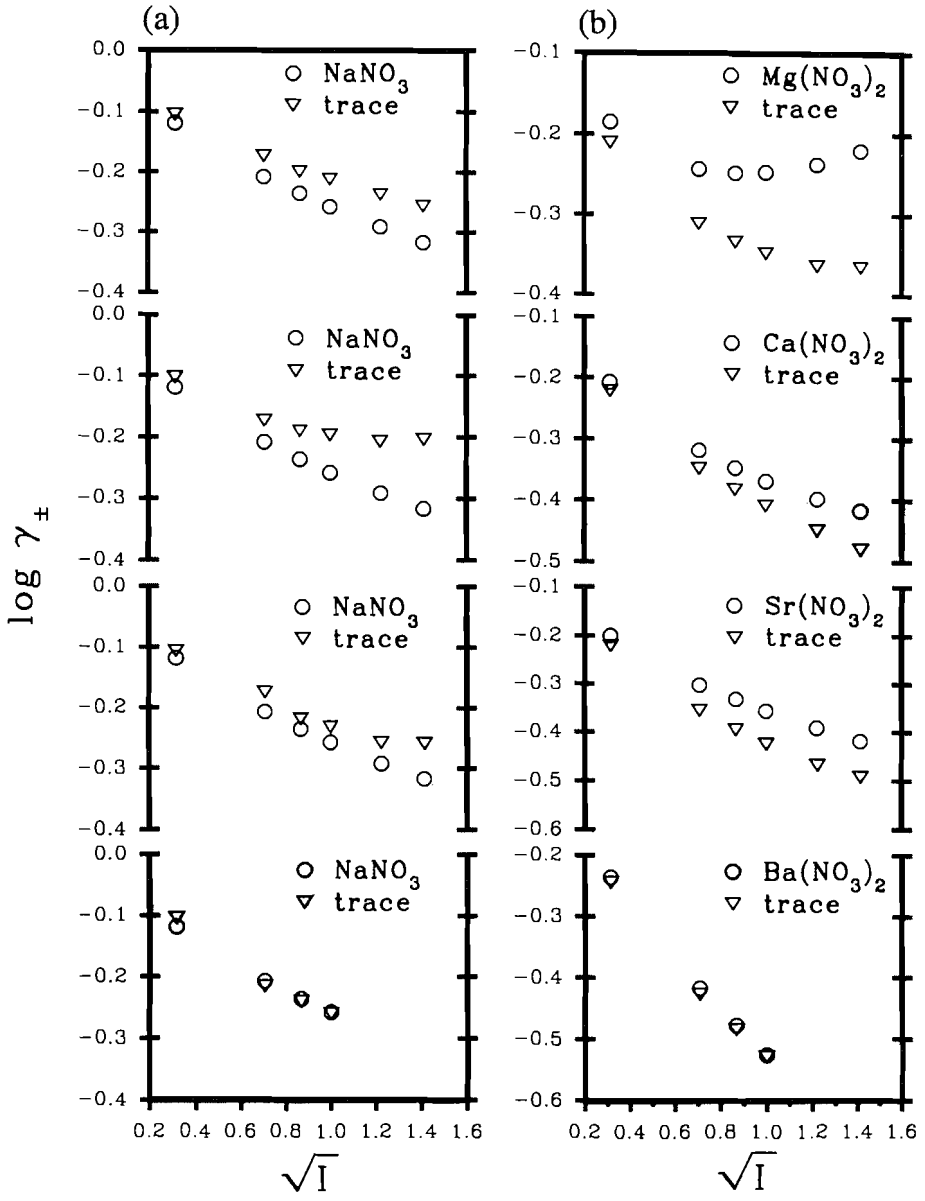

FIG. 4. Plots of log γ^{trace} vs. $\sqrt{I}$. (*a*) $NaNO_3$. (*b*) $M(NO_3)_2$.

aid of the values of the binary coefficients in Table 2. It is apparent that the figure shows good agreement between the R.W.R., Scatchard, Pitzer, and modified Harned treatments and the experimental data. By comparing the coefficients of y_B in the equations of Pitzer, Scatchard, and R.W.R. with the Harned equation, one can calculate α_{AB} and β_{AB} from the values of the interaction parameters in Table 2. The calculated values agree well with the values in Table 1 only at $I \geq 1.5$. At lower ionic strengths the agreement is poor and improves when interaction parameters are obtained by solving these equations individually at each ionic strength.

Values of the Gibbs energy of mixing ($\Delta_m G^E$) were calculated from the experimentally determined activity coefficients and the calculated osmotic coefficients from the Pitzer parameters, using the following equation:

$$[10] \quad \Delta_m G^E = Y_A[\ln(\gamma_A/\gamma_A^0) + (\phi_A - \phi_m)] + Y_B[\ln(\gamma_B/\gamma_B^0) + (\phi_B - \phi_m)]$$

$$[11] \quad Y_A = \nu_A y_A m_A RT \quad \text{and} \quad Y_B = \nu_B y_B m_B RT$$

where ϕ_A and ϕ_B are the osmotic coefficients of the pure components at the same ionic strength as the mixture. The values of ϕ_m and γ_B at various ionic strengths were calculated according to Pitzer equation (14–16). The values of $\Delta_m G^E$ were found to be negative for all the systems except $Ba(NO_3)_2$. Also the values of $\Delta_m G^E$ decrease with increasing ionic strength (Fig. 3*a*) and at a given ionic strength the $\Delta_m G^E$ values varies in the order $Ba(NO_3)_2 > Sr(NO_3)_2 > Ca(NO_3)_2 > Mg(NO_3)_2$ (Fig. 3*b*). The positive $\Delta_m G^E$ on mixing AX and BX_2 solutions implies that replacing A–A and B–B interactions produces an increase in the free energy of the system. This suggests that such replacements will take place less frequently than expected on a purely random basis (19). A negative $\Delta_m G^E$ would require that formation of A–B pairs be more favoured than would be expected from statistical encounters (19). Our results indicate that formation of A–B pairs is definitely favoured at higher ionic

strengths in all the mixtures except for the $Ba(NO_3)_2$ system.

These excess Gibbs energies were fitted to the Friedman (20) equation, which is applicable to a mixture of two electrolytes with a common ion.

$$[12] \quad \Delta_m G^E = I^2 RT y_B (1 - y_B)[g_0 + (1 - 2y_B)g_1]$$

The Friedman coefficients were obtained by solving eq. [12] and the parameters are listed in Table 3. The continuous curves in Figs. 3*a* and *b* were generated with the aid of these parameters. These g_0 and g_1 coefficients represent the changes in the configuration and environments of ion pairs and ion triplets in the solution and are therefore sensitive to both the total salt concentration and composition. As indicated in Fig. 3*a*, $\Delta_m G^E$ changes markedly with ionic strength and this is reflected in the g_0 parameters. All the curves were fairly symmetrical and this is reflected in the g_1 parameter.

The trace activity coefficients of $NaNO_3$ and $M(NO_3)_2$ in the mixtures were calculated using eqs. [13] and [14];

$$[13] \quad \log \gamma^{trace}_{NaNO_3} = \log \gamma^{0}_{NaNO_3} - \alpha_{AB} - \beta_{AB}$$

$$[14] \quad \log \gamma^{trace}_{M(NO_3)_2} = \log \gamma^{0}_{M(NO_3)_2} - \alpha_{BA} - \beta_{BA}$$

and presented in Figs. 4*a* and *b*. Trace activity coefficient values facilitate a more detailed comparison of the effect of one electrolyte on the other in the mixture (21, 22). In ternary mixtures of the $NaNO_3 + M(NO_3)_2 + H_2O$ systems the relative values of log γ^{trace} to the log γ values of the pure salt depend upon two major factors: (1) ion–ion interactions and (2) ion–solvent interactions. An increase in ion–ion interaction causes a fall in log γ whereas an increase in ion–solvent interaction results in a rise in log γ. Examination of Figs. 4*a* and *b* indicates that ion–solvent interactions play a major role in the case of $NaNO_3$ in the presence of $M(NO_3)_2$ (Fig. 4*a*), resulting in an increase in log γ^{trace} above the values for the pure $NaNO_3$. In the case of activity coefficients of $M(NO_3)_2$ in the presence of $NaNO_3$, ion–ion interactions dominate over the ion–solvent interactions, resulting in a decrease in log γ^{trace} below the curves for the pure $M(NO_3)_2$ (Fig. 4*b*). These effects are more pronounced in the mixtures of Mg and Ca nitrates with $NaNO_3$ and minimal in the barium nitrate with $NaNO_3$ mixtures.

Can. J. Chem. Downloaded from www.nrcresearchpress.com by 88.255.202.194 on 09/08/12
For personal use only.

Acknowledgements

We are grateful to the Natural Sciences and Engineering Research Council of Canada and the University College of Cape Breton for financial support of this work. We would also like to acknowledge the partial funding, in the form of a salary supplement for Mr. S. Smith, from the Department of Economic Development of the Nova Scotia Provincial Government.

1. M. Whitefield. Geochem. Cosmochem. Acta, **39**, 1545 (1975).
2. J. Ananthaswamy and G. Atkinson. J. Solution Chem. **11**, 509 (1982).
3. T. M. Hanna and G. Atkinson. J. Phys. Chem. **89**, 4884 (1985).
4. R. N. Roy, J. J. Gibbons, J. K. Trower, and G. A. Lee. J. Solution Chem. **9**, 535 (1980).
5. D. R. White, R. A. Robinson, and R. G. Bates. J. Solution Chem. **9**, 457 (1980).
6. S. Sarada. Ph.D. dissertation, Osmania University, Hyderabad, India. 1990.
7. R. G. Bates, A. Dickson, M. Gratzi, A. Hrabeczy-Pall, E. Linder, and E. Pungor. Anal. Chem. **55**, 1275 (1983).
8. W. J. Hamer and Y-C Wu. J. Phys. Chem. Ref. Data, **1**, 1047 (1974).
9. H. S. Harned and B. B. Owen. The physical chemistry of electrolyte solutions. 3rd ed. Reinhold, New York. 1958.
10. P. J. Reilly, R. H. Wood, and R. A. Robinson. J. Phys. Chem. **75**, 1305 (1971).
11. T. K. Lim, C. Y. Chan, and K. H. Khoo. J. Solution Chem. **9**, 507 (1980).
12. G. Scatchard. J. Am. Chem. Soc. **83**, 2636 (1961).
13. R. M. Rush and J. S. Johnson. J. Phys. Chem. **72**, 767 (1961).
14. K. S. Pitzer and J. J. Kim. J. Am. Chem. Soc. **96**, 5701 (1974).
15. K. S. Pitzer. J. Phys. Chem. **77**, 268 (1973).
16. K. S. Pitzer. J. Solution Chem. **4**, 249 (1975).
17. H. T. Kim and W. J. Frederick, Jr. J. Chem. Eng. Data, **33**, 177 (1988).
18. H. S. Harned and R. A. Robinson. Multicomponent electrolyte solutions. Pergamon, Oxford. 1968 p. 60.
19. G. E. Boyd. J. Solution Chem. **6**, 135 (1977).
20. H. L. Friedman. Ionic solution theory. Interscience Publishers, New York. 1962.
21. R. A. Robinson and H. S. Harned. Chem. Rev. **28**, 419 (1941).
22. F. Frank and D. J. G. Ives. Q. Rev. Chem. Soc. **66**, 1 (1966).

Molecular modelling of photoactive pigments in the solid state: Investigations of polymorphism

ANDREW J. MCKERROW AND ERWIN BUNCEL[1]
Department of Chemistry, Queen's University, Kingston, Ont., Canada K7L 3N6

AND

PETER M. KAZMAIER[1]
Xerox Research Centre of Canada, Mississauga, Ont., Canada L5K 2L1

Received July 17, 1992

ANDREW J. MCKERROW, ERWIN BUNCEL, and PETER M. KAZMAIER. Can. J. Chem. **71**, 390 (1993).

The application of molecular mechanics calculations to the study of solid state organic photoconductors has been investigated. Using X-ray crystallographic information for a series of four *N,N'*-dialkylperylene pigments, **1**–**4**, lattices of these molecules were modelled using the Dreiding force field. Comparison of the resulting lattices with the experimental data demonstrated that both molecular and physical features of the perylenes could be accurately reproduced in these calculations. When systematic deviations in molecular geometry occurred, these errors could be attributed to the generic nature of the force field. We have extended the computational studies to the problem of polymorphism since this is known to have a profound effect on photoconduction. To model enthalpic polymorphs of *N,N'*-dimethylperylene, **1**, the symmetry relationships and atomic coordinates from the crystal structure of *N,N'*-di-*n*-pentylperylene, **4**, were utilized. By truncating the pentyl substituents to methyl groups and applying external stresses to the resulting lattice during minimization it was possible to identify two likely polymorphs of **1**. The inclusion of Gasteiger's partial equalization of orbital electronegativity (PEOE) charges on the perylenes was not found to be beneficial in locating suitable polymorphs. These computational methods have been successful in modelling perylene pigments in the solid state and have been shown to be useful in investigating polymorphism.

ANDREW J. MCKERROW, ERWIN BUNCEL et PETER M. KAZMAIER. Can J. Chem. **71**, 390 (1993).

On a évalué la possibilité d'utiliser des calculs de mécanique moléculaire pour l'étude de photoconducteurs organiques à l'état solide. Utilisant des informations cristallographiques obtenues par diffraction des rayons X pour une série de quatre pigments *N,N'*-dialkylpérylène, **1**–**4**, et faisant appel au champ de force de Dreiding, on a développé un modèle de ces molécules. Une comparaison des réseaux qui en résultent avec les données expérimentales démontre que ces calculs permettent de reproduire fidèlement les caractéristiques tant moléculaires que physiques des pérylènes. Lorsque des déviations systématiques dans la géométrie moléculaire se produisent, on peut attribuer ces erreurs à la nature générique du champ de force. Sachant que le polymorphisme affecte profondément la photoconduction, on a examiné le polymorphisme du pérylène par des méthodes de calcul. Comme modèle du polymorphisme enthalpique du *N,N'*-diméthylpérylène, **1**, on a utilisé les relations de symétrie et les coordonnées atomiques de la structure cristalline du *N,N'*-di-*n*-pentylpérylène, **4**. En tronquant les substituants pentyles en méthyles et en appliquant des stress externes au réseau qui en résulte durant la minimisation, il a été possible d'identifier deux polymorphes possibles du composé **1**. On n'a pas trouvé que l'inclusion de charges PEOE de Gasteiger sur les pérylènes avait des effets bénéfiques pour détecter des polymorphes appropriés. On a utilisé ces méthodes de calcul avec succès dans le modelage de pigments du pérylène à l'état solide et on a montré qu'elles sont utiles dans l'étude du polymorphisme.

[Traduit par la rédaction]

Introduction

The study of organic molecules in the solid state has traditionally utilized X-ray crystallography as a means to obtained detailed information concerning molecular structure, i.e., bond lengths, angles, and conformations. Increasingly, the study of organic solids has been directed wards understanding the factors controlling the packing of molecules in the crystalline state. The nature of this packing is of interest as an example of a highly specific recognition phenomenon, as well as in situations in which the chemical and physical properties of the organic compounds are affected by the nature of the solid state packing. Examples of the former are found in investigations of the intermolecular interactions that occur in the crystalline state as these studies can yield insights into the nature of similar interactions in biological systems (1). Effects due to solid state packing are significant in the design of organic molecules with nonlinear optical properties (2), therapeutic drugs (3), and organic photoconductors.

Our interest in the organic solid state results from studies of organic photoconductors. Previous investigations have demonstrated that photoconduction in organic materials is dependent on molecular properties such as fluorescence quantum yield (4). Further studies from our laboratories have shown that photosensitivity is also strongly dependent on interactions that occur in the solid state (5). This is clearly illustrated in the study by Weigl *et al.* in which different photosensitivities were associated with the α, β, and *x* polymorphs of metal-free phthalocyanine (6).

From these examples it is clear that efforts directed towards the development of organic compounds for applications such as photoconduction must not only be concerned with the molecular characteristics of these materials, but also with their solid state properties.

Molecular modelling of photoreceptor pigments presents problems endemic to the pigment area as a whole. Photogenerator pigments by design are very insoluble so it is very difficult, if not impossible, to obtain single crystal X-ray diffraction information on most systems. Furthermore, the chemist designing new pigment structures would like to

[1]Authors to whom correspondence may be addressed.

Can. J. Chem. Downloaded from www.nrcresearchpress.com by 88.255.202.194 on 09/08/12
For personal use only.

Can. J. Chem. Downloaded from www.nrcresearchpress.com by 88.255.202.194 on 09/08/12
For personal use only.

predict the effect of molecular changes on the packing of the pigment in the solid state; thus the force field and software program must perform equally effectively at the molecular level as well as on the aggregate or crystal lattice level of calculation. Finally, the coupling of the calculation to readily available information such as X-ray powder diffraction must eventually be achieved.

Our strategy is to start with a generic force field capable of predicting the molecular structure and demonstrate that it can be used to reproduce the lattice and crystal parameters on a known series of photogenerator pigments where single crystal X-ray data are available. Having demonstrated the efficacy of the force field, one could then calculate a series of polymorphs for a particular compound and use this structural information to calculate a series of X-ray powder diffraction spectra. Once these are in hand, the experimental exploration of the relationship between the barriers to polymorphic interconversion and the energy window of polymorph stability could be explored. Our focus in this paper will be on the first two of these objectives, that is to say, the qualification of the force field and the calculation of polymorph energies and geometries.

Of the computational methods which we examined for modelling organic molecules in the solid state, calculations based on the atom–atom potential method (7) were one possibility. These empirical intermolecular force fields are used to calculate crystal packing energies and have been used to predict crystal structures for low-polarity organic compounds (8). This method, however, was shown to be unsuccessful in modelling crystals featuring heteroatoms (9). As organic photoconductors generally incorporate heteroatoms in the molecular framework, an alternative modelling technique was necessary.

Molecular mechanics force fields are routinely used in the study of organic molecules, yet their application to crystalline photoconductors has in the past been limited. With traditional force fields the treatment of molecules with unusual functionality has required considerable effort in order to parametrize the force field to model this functionality. Application of a suitable force field to the study of crystalline systems has been further hindered by difficulties in efficiently calculating the large number of nonbonded interactions occurring in such systems. The recent development of the Dreiding force field has provided possible solutions to these limitations.

The Dreiding force field models molecular structures using parameters that are based on hybridization considerations (10). Although this is not anticipated to be as accurate as customized force fields, the Dreiding method is ideal for studying molecules with non-routine functionality, as compound-specific parametrization is not necessary. The application of this force field to modelling crystalline systems has been rendered computationally feasible through the development of an accuracy-controlled accelerated convergence method for aiding in the calculation of nonbonded interactions (11).

As the Dreiding force field was not previously used to study crystalline organic photoconductors, our initial studies focused on determining if both molecular and physical features of a series of four *N,N'*-dialkylperylene-3,4:9,10-bis(dicarboximide) pigments, **1–4**, could be accurately modelled with this method. This computational approach was subsequently used, in conjunction with crystallographic data, in the search for likely enthalpic polymorphs of *N,N'*-dimethylperylene, **1** (12).[2]

TABLE 1. Crystallographic data for the *N,N'*-dialkylperylenes

Substituent	Unit cell	*Z*	Space group
Methyl	Monoclinic	2	$P2_1/c$
n-Propyl	Triclinic	2	$P\bar{1}$
n-Butyl	Monoclinic	2	$P2_1/c$
n-Pentyl	Triclinic	1	$P\bar{1}$

Force field validation — calculations

Hädicke and Graser carried out an X-ray structural analysis of a series of photoconductive *N,N'*-dialkyl perylene-3,4:9,10-bis(dicarboximide) pigments (13). Their data for the perylenes **1–4** was hence chosen in this work as a starting point for investigating the ability of the Dreiding force field to model crystalline systems.

For each of the perylenes **1–4**, Hädicke and Graser's coordinates of the atoms in the asymmetric unit were used to construct an unit cell according to the symmetry operations dictated by the experimentally determined space group. As the hydrogen atom positions were not available from Hädicke and Graser's study, these atoms were explicitly added to the pigment molecules using default carbon–hydrogen bond lengths and angles from the Dreiding force field. Periodic boundary conditions were imposed on all faces of the unit cell in order to model an infinite crystalline environment.

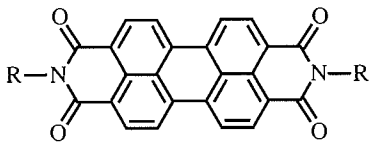

R Substituents
1 Methyl
2 *n*-Propyl
3 *n*-Butyl
4 *n*-Pentyl

As with other molecular mechanics force fields, the Dreiding method calculates potential energy on the basis of molecular geometry and this energy comprises contributions from bonded and nonbonded interactions. In our studies it was anticipated that evaluation of the electrostatic contribution to the nonbonded interactions could cause problems due to difficulties in accurately determining atomic charges on large molecular systems. To gauge the impact of these interactions on our investigations, parallel studies were carried out in which electrostatic terms were either evaluated based on atomic charges derived from the partial equalization of orbital electronegativity (PEOE) charging scheme of Gasteiger and Marsili (14), or these interactions were omitted.

In minimizing the energy of the lattices generated for perylenes **1–4**, all atoms in the lattice were free to adjust and a cutoff function was used in calculating the nonbonded intereactions so as to exclude interactions between atoms separated by more than 9.25 Å. Studies were carried out in which the unit cell parameters were either allowed to optimize or they were fixed at the experimental values. In both cases, the conjugate gradient method was used to minimize the total energy until the RMS force per degree of freedom

[2]Portions of this work were communicated in a preliminary form at the 10th International Conference on the Chemistry of the Organic Solid State, July 7–12, 1991, Vancouver, British Columbia.

TABLE 2. RMS errors in molecular geometry from perylene modelling studies

Substituent	Charges	Bond length (angstroms)	Angles (degrees)	Torsion angles (degrees)
Methyl	None	0.038	2.421	2.013
n-Propyl	None	0.039	2.116	1.507
n-Butyl	None	0.036	2.093	1.627
n-Pentyl	None	0.039	2.058	1.108
Avg. error	None	0.038	2.172	1.564
Methyl	PEOE	0.040	2.474	1.814
n-Propyl	PEOE	0.039	2.185	1.352
n-Butyl	PEOE	0.037	2.131	1.679
n-Pentyl	PEOE	0.038	2.111	1.076
Avg. error	PEOE	0.039	2.225	1.480
Mayo *et al.*[a]		0.035	3.224	8.948

[a]Errors in molecular geometry based on a study of 76 organic compounds by Mayo *et al.* (10).

was less than 0.16 kcal mol^{-1}. All calculations were carried out on a Silicon Graphics 4D25 workstation using version 2.10 of the Polygraf Polymer Simulation Program.[3]

Force field validation — discussion

A summary of Hädicke and Graser's crystallographic data for compounds **1–4** is given in Table 1. Changes in the perylene alkyl substituents that are minor on a molecular basis lead to major changes in the nature of the crystal packing. The dimethyl, di-*n*-butyl, and di-*n*-pentylperpylenes crystallized with one half of a molecule in the asymmetric unit, while the di-*n*-propylperylene crystallized with two half molecules in the asymmetric unit that differ from each other in conformation. These differences in crystal packing reinforce the notion that it can be misleading to predict solid state packings based on similarities in molecular structure.

A comparison between the minimized lattices and Hädicke and Graser's experimental lattices was carried out in order to evaluate the accuracy of the Dreiding force field in modelling molecular structure. For perylenes **1–4**, molecules were extracted from both the minimized and experimental lattices so that bond lengths, angles, and torsion angles could be compared. The RMS errors in these molecular structural parameters were found to be small in studies including and excluding electrostatic interactions, Table 2. The magnitude of the errors in Table 2 was similar to that reported in Dreiding modelling studies of a series of 76 organic compounds (10).

Further examination of these deviations revealed that the force field could accurately reproduce the perylene carbon skeleton, with the exception of bonds between carbon and nitrogen. The carbon–nitrogen bonds were consistently 5–6% shorter than the literature values and this systematic error was attributed to the generic nature of the Dreiding parameters. As previously mentioned, with the Dreiding method geometric parameters and force constants are selected solely on the basis of the hybridization state of atoms. Using this generic approach it is possible to study molecules, such as perylene dicarboximides, that contain non-routine functionality without having to initially parametrize the force field for such functionality. It is hence inferred that the errors in carbon–nitrogen bond lengths were a direct manifestation of employing such a generic approach, as the default resonant nitrogen parameters used in the perylene studies imparted too much double bond character to all imide nitrogen–carbon bonds.

Optimization of the unit cell parameters in these modelling calculations led to only small deviations from the experimental unit cell parameters, Table 3. The minimized unit cells of the *N,N'*-dialkylperylenes **1–4** are shown in Figs. 1–4. Comparison of the optimized lattices with perylenes minimized in fixed unit cells showed that the former were more stable by 1.88–6.58 kcal mol^{-1}. This energy decrease appeared to be the result of compensatory motion in the lattice as in each case the increase in stability was accompanied by a slight increase in unit cell volume, 1.3–3.8%. The inclusion of electrostatic interactions led to a similar conclusion but the degree of stabilization in the optimized lattices decreased slightly, 1.41–6.29 kcal mol^{-1}.

Based on these results it was concluded that the Dreiding force field could accurately model both molecular and crystalline features of perylenes **1–4**.

Studies of polymorphism — calculations

A central difficulty in the development of novel organic photoconductors is the occurrence of polymorphism in the solid state. Variations in intermolecular interactions that occur in polymorphic forms of these materials are observed to affect their photoconductive properties. As experimental studies of polymorphism with most photoconductive dyes and pigments are difficult, we sought to study this phenomenon using our computational methods.

Polymorphism in organic solids can be the result of entropic and (or) enthalpic factors (ref. 9, pp. 285–299). Variations in crystal packing that result from disorder, i.e., entropic polymorphism, cannot easily be investigated with the computational methods used in this study due to the symmetry constraints that are imposed when generating the unit cell. Crystalline forms of compounds that are characterized by different periodic packings and stabilities are known as enthalpic polymorphs. If crystallographic information was available concerning enthalpic polymorphs of perylenes, the Dreiding modelling techniques could be used to study them and characterize their relative stabilities. As

[3]The Polygraf Polymer Simulation Program is available from Molecular Simulations Inc., 16 New England Executive Park, Burlington, MA 01803-5297, U.S.A.

Can. J. Chem. Downloaded from www.nrcresearchpress.com by 88.255.202.194 on 09/08/12
For personal use only.

Can. J. Chem. Downloaded from www.nrcresearchpress.com by 88.255.202.194 on 09/08/12
For personal use only.

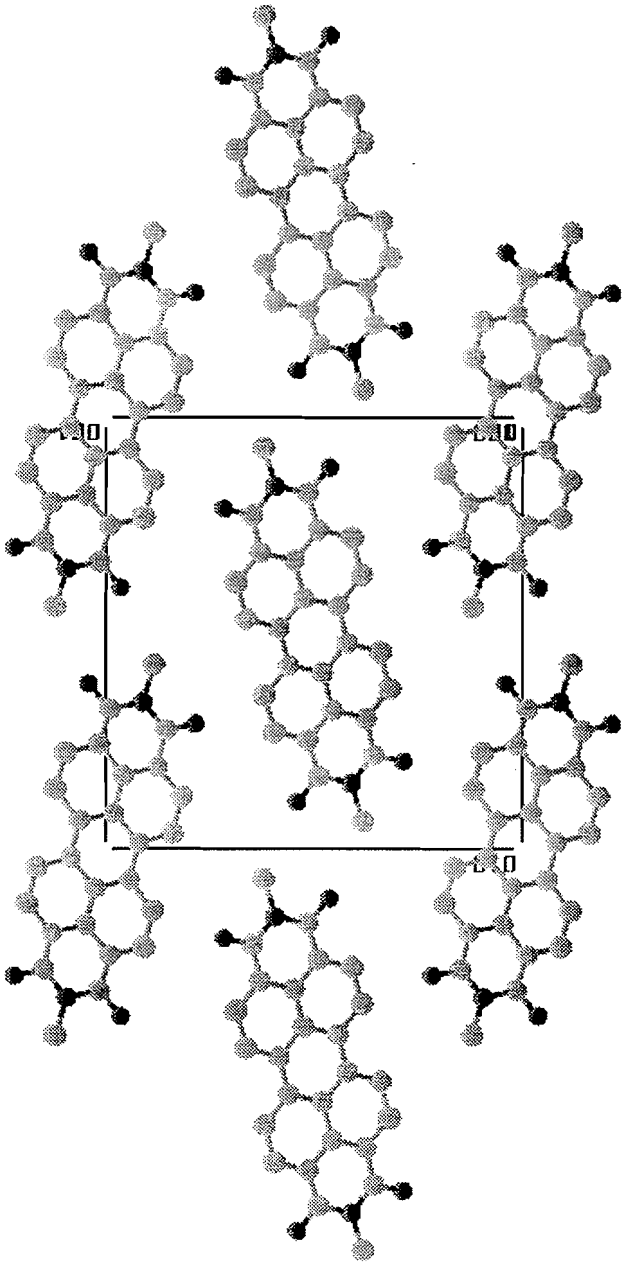

FIG. 1. Minimized unit cell of *N,N'*-dimethylperylene, **1**, (projection along the *a* axis).

TABLE 3. RMS errors in unit cell parameters from perylene modelling studies

Substituent	Charges	RMS error in cell lengths (Å)	RMS error in cell angles (degrees)
Methyl	None	0.267	0.663
n-Propyl	None	0.197	1.195
n-Butyl	None	0.362	1.236
n-Pentyl	None	0.324	1.257
Methyl	PEOE	0.088	0.691
n-Propyl	PEOE	0.218	0.825
n-Butyl	PEOE	0.338	1.197
n-Pentyl	PEOE	0.268	0.913

TABLE 4. Stress-annealed triclinic polymorphs of *N,N'*-dimethylperylene calculated using PEOE charges

Direction of stress	Stress (GPa)	Energy (kcal mol^{-1})	Optimized density
XX[a]	1	83.29	0.737[b]
YY	1	73.51	1.115
ZZ	1	74.03	1.095
YZ	1	72.78	1.212
XZ	1	70.79	1.327
XY	1	78.49	0.962
XX	−1	71.07	1.348
YY	−1	74.03	1.151
ZZ	−1	72.52	1.244
YZ	−1	73.63	1.141
XZ	−1	74.30	1.124
XY	−1	79.63	1.045

[a]The *XX* designation refers to the application of a direct stress to a surface perpendicular to the *X* axis in the *X* direction. Shear stresses are simulated when the direction in which force is applied differs from the site of application, i.e., *XY*.

[b]The minimized monoclinic $P2_1/c$ unit cell had an energy of 63.00 kcal mol^{-1} and a density of 1.54 g cm^{-3} when PEOE charges were included.

TABLE 5. Stress-annealed triclinic polymorphs of *N,N'*-dimethylperylene calculated without PEOE charges

Direction of stress	Stress (GPa)	Energy (kcal mol^{-1})	Optimized density
XX	1	91.99	0.769
YY	1	82.84	1.093
ZZ	1	83.25	1.076
YZ	1	78.68	1.330
XZ	1	79.68	1.404
XY	1	85.91	1.117
XX	−1	74.52	1.476[a]
YY	−1	84.26	1.170
ZZ	−1	76.14	1.474[a]
YZ	−1	76.68	1.386
XZ	−1	79.45	1.404
XY	−1	82.44	1.299

[a]These polymorphs can be compared with the minimized monoclinic $P2_1/c$ polymorph, which had an energy of 72.84 kcal mol^{-1} and a density of 1.533 g cm^{-3}.

such information has apparently not been reported, we sought to locate enthalpic polymorphs of perylenes computationally for comparison with the experimentally observed crystal forms.

Our strategy for studying polymorphism in perylenes is based on the following suppositions. Perylenes have very high lattice energy dictated primarily by the interaction of the aromatic rings in the solid state. In one well-studied system, several polymorphs were identified by X-ray powder diffraction but the structure could not be assigned because X-ray powder diffraction alone provides insufficient information to completely determine the structure (5).

In the work of Graser and Hädicke many perylenes are reported that differ only in the substituent on the side chain. It is not clear if the single crystals that were isolated are the thermodynamically favoured polymorphs or if they are produced by kinetic control. Nevertheless it seems to be a rea-

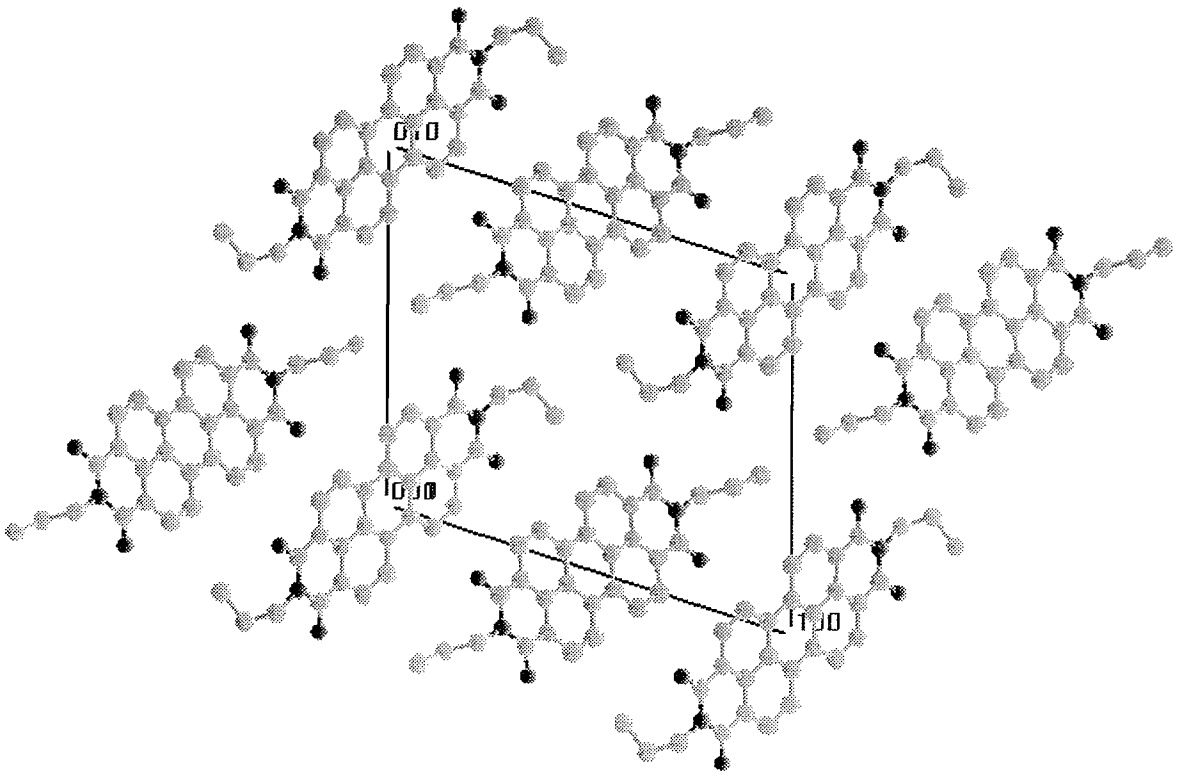

FIG. 2. Minimized unit cell of *N,N'*-di-*n*-propylperylene, **2**, (projection along the *c* axis).

sonable assumption that, for a single compound, all these crystal packings represent a polymorphic packing arrangement for that compound and the side chains act to modify the relative thermodynamic stability of the polymorph. If this assumption is correct, then one could use this experimental series of crystal packings to act as a template for the optimization of the pigment system to a new polymorphic arrangement without having to grapple with the enormous number of degrees of freedom and the many local minima inherent in an optimization without any symmetry constraints.

N,N'-Dimethylperylene, **1**, was chosen as a model compound for these studies as its *N*-alkyl substituents lack the conformational freedom of pigments **2**–**4** that can lead to entropic polymorphism. Furthermore, we have endeavoured to identify polymorphs of *N,N'*-dimethylperylene that occur in triclinic $P\bar{1}$ lattices, as these represent one of the simplest packing motifs for molecular crystals, with only one perylene molecule per unit cell. To simplify this modelling process we used crystallographic data from one of the perylenes that had been found to crystallize in a $P\bar{1}$ lattice. Specifically, the atomic coordinates and symmetry relationships of *N,N'*-di-*n*-pentylperylene, **4**, were used to model theoretical $P\bar{1}$ polymorphs of *N,N'*-dimethylperylene.

The coordinates for the atoms in the asymmetric unit of *N,N'*-di-*n*-pentylperylene, **4**, were edited so as to truncate the alkyl chains to methyl groups. A unit cell was constructed based on the original unit cell parameters with an inversion centre characteristic of the $P\bar{1}$ space group. Periodic boundary conditions were imposed to simulate a crystalline environment. Energy minimizations of this lattice, either with or without electrostatic interactions, yielded high-energy polymorphs with unrealistic densities. For these calculations to be successful it would have been necessary for molecules in the lattice to be drawn together to remove the considerable void volume in the unit cell. This process would presumably have resulted from attractive interactions modelled by the nonbonded component of the Dreiding force field. At the large interatomic separations found in the truncated lattice these interactions were not found to vary markedly on optimization of the atomic positions. This observation supports the supposition that the packing energy is to a large extent governed by the packing of the aromatic nucleus and that the complexity of the aromatic system leads to multiple local minima. The lack of a driving force that would lead to crystal annealing resulted in the system minimizing into unacceptable local minima.

An attractive concept for overcoming this multiple minima problem takes advantage of the shape of the van der Waals potential. Lattices that contain a large void volume are in a regime where the forces that would reduce the void volume are weak while the barriers to reorganization are relatively high because of the strong interaction of the planar pi (π) moieties. On the other hand, if the system could be over-compressed onto the steep portion of the van der Waals repulsion curve, this high potential energy would be sufficient to drive the packing to a minimum that has little if any void volume left. To state it another way, all of the high-energy local minima occur on the low-density side of the minimized structure because the van der Waals attractions at these distances are weak enough to allow these false minima to exist.

Thus, application of external stresses to the initial triclinic *N,N'*-dimethylperylene unit cell during the energy minimizations was an approach that was investigated as a means of annealing the lattice. Direct and shear stresses were

Can. J. Chem. Downloaded from www.nrcresearchpress.com by 88.255.202.194 on 09/08/12
For personal use only.

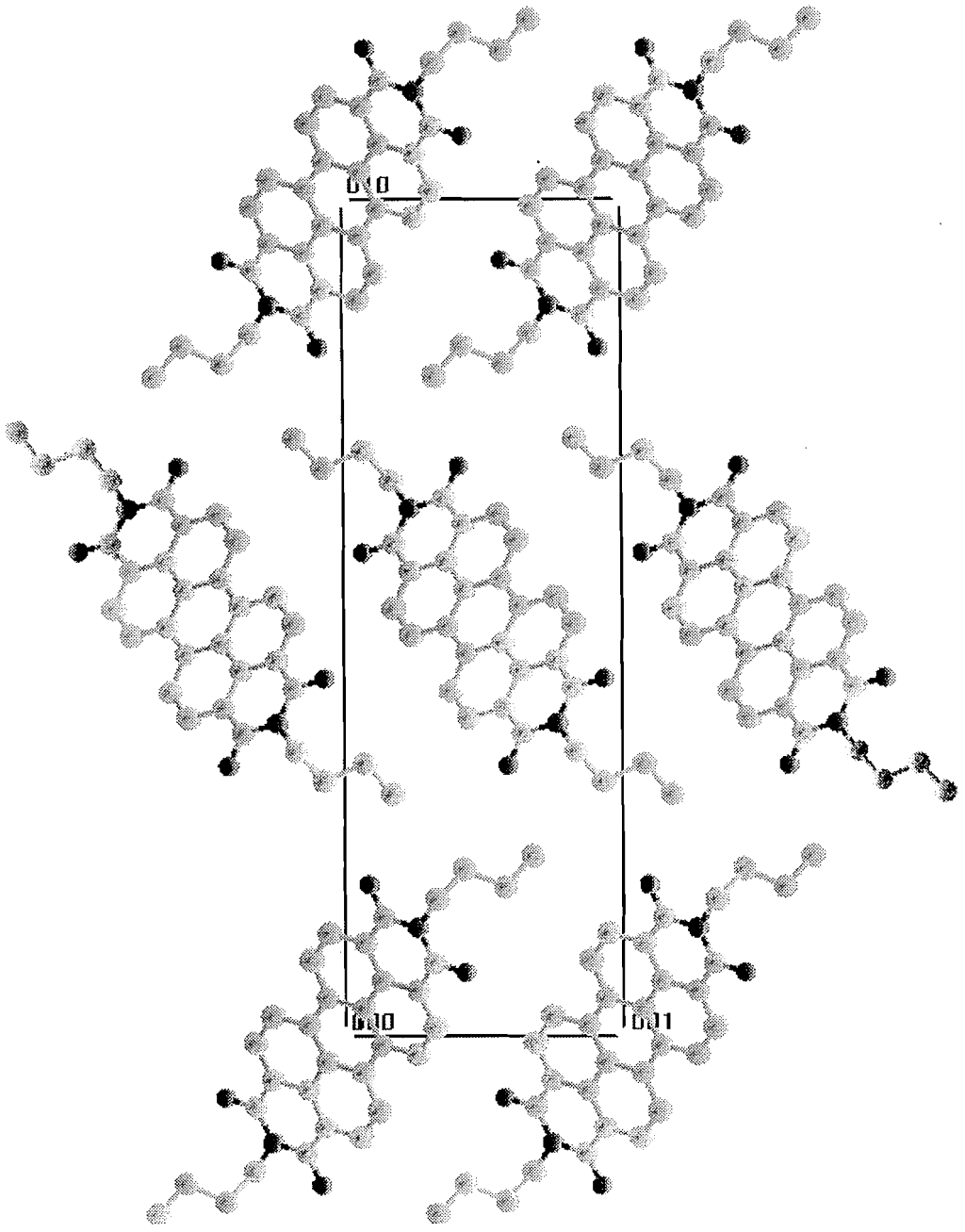

FIG. 3. Minimized unit cell of *N,N'*-di-*n*-butylperylene, **3**, (projection along the *a* axis).

applied to the three faces of the unit cell using either compressive or expansive stresses of 1 GPa during the energy minimizations. These calculations were interrupted after 1000 cycles and the resulting lattices minimized *without any external stresses being applied*. Once again, two sets of calculations were carried out in which electrostatic interactions were either included based on PEOE charge estimates, or these interactions were omitted.

The densities and energies of the lattices generated in these stressed-minimization studies are presented in Table 4 for calculations carried out with PEOE charges. The corresponding information for studies without charges is presented in Table 5. Based on a comparison of these data with the properties of the monoclinic *N,N'*-dimethylperylene, two likely theoretical triclinic polymorphs of this compound have been identified.

Studies of polymorphism — discussion

In the studies incorporating charges, the stressed-minimization procedure did not locate theoretical triclinic polymorphs of *N,N'*-dimethylperylene with densities and energies that compared favourably with the experimentally observed monoclinic polymorph (Table 4). Continued minimization of the stressed lattices beyond 1000 cycles did not significantly increase the density of the polymorphs.

The failure to locate a reasonable triclinic polymorph of *N,N'*-dimethylperylene may be due to limitations in facets of our computational method. Gasteiger's PEOE charging scheme is solely dependent on topology and, as a result, the static atomic charges are not affected by the immediate chemical environment. In crystalline systems it is anticipated that a dynamic charging scheme that was influenced

Can. J. Chem. Downloaded from www.nrcresearchpress.com by 88.255.202.194 on 09/08/12
For personal use only.

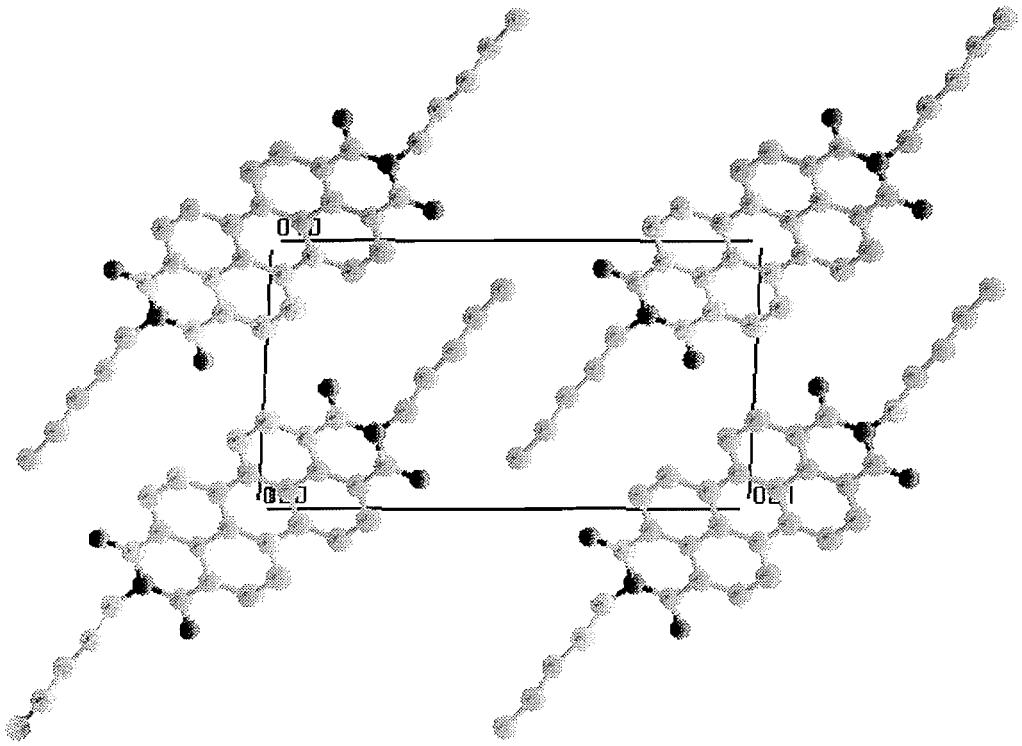

FIG. 4. Minimized unit cell of *N,N'*-di-*n*-pentylperylene, **4**, (projection along the *a* axis).

TABLE 6. Packing characteristics of minimized *N,N'*-dimethylperylene

Polymorph	Monoclinic	Triclinic *X*	Triclinic *Z*
Surface area (Å^2)	493.3	334.0	317.6
Molecular volume (Å^3)	595.5	319.1	317.9
Unit cell volume (Å^3)	906.4	470.6	471.3
Packing coefficient (C_K)	0.657	0.678	0.674

by neighbouring molecules would be better for modelling the annealing process examined in the polymorphism studies. Such a charging scheme has in fact been developed (15) and would be useful to apply in future studies.

Analysis of the lattices generated without PEOE charges revealed situations in which the coupling of energy minimization with the application of external stresses yielded reasonable triclinic *P*1 polymorphs of *N,N'*-dimethylperylene (Table 5). The application of direct compressive stresses to either the X or Z faces of the unit cell yielded polymorphs, hereafter referred to as the Triclinic **X** and Triclinic **Z** polymorphs, respectively, with calculated densities of 1.476 and 1.474 g cm^{-3}, respectively. These values compare favourably with the experimentally observed density of 1.533 g cm^{-3} for the monoclinic polymorph and are well within the range of densities observed for perylenes in general (1.33–1.62 g cm^{-3}). The minimized energies of these theoretical triclinic polymorphs also compare favourably with the energy of the minimized monoclinic polymorph *N,N'*-dimethylperylene. On visual examination the Triclinic **X** and Triclinic **Z** polymorphs appear to be almost identical (Fig. 5). The observation that none of the local minima generated in Table 5 simultaneously combines energies that are too high and densities that are too high validates the supposition that the local minima lie on the *low density side* of the energy hyperspace.

Using a uniform finite element analysis (16) it was possible to calculate the molecular volumes and surface areas of the contents in the minimized monoclinic unit cell and the two hypothetical triclinic *N,N'*-dimethylperylene unit cells (Table 6). The ratio of the molecular volume to the unit cell volume per molecule is known as the Kitaigorodskii packing coefficient, C_K, and for most close-packed organic compounds it is found to be in the range 0.65–0.75 (17). The Kitaigorodsky packing coefficients for the Triclinic **X** and Triclinic **Z** polymorphs lie within this range and compare favourably with the experimental monoclinic polymorph, indicating that all three are close-packed systems.

Conclusions

The study of organic molecules in the solid state is useful in situations in which intermolecular interactions are likely to have an impact on the physical and chemical properties of the compound. As a class, photoconductors are known to be highly dependent on such interactions and therefore our modelling studies have focused on the solid state.

It has been found in this work that the Dreiding force field, as incorporated in Polygraf, can successfully perform molecular mechanics calculations on crystalline solids. Our studies using the solved crystal structures of a series of four *N,N'*-dialkylperylenes, **1**–**4**, verified that this method could

Can. J. Chem. Downloaded from www.nrcresearchpress.com by 88.255.202.194 on 09/08/12
For personal use only.

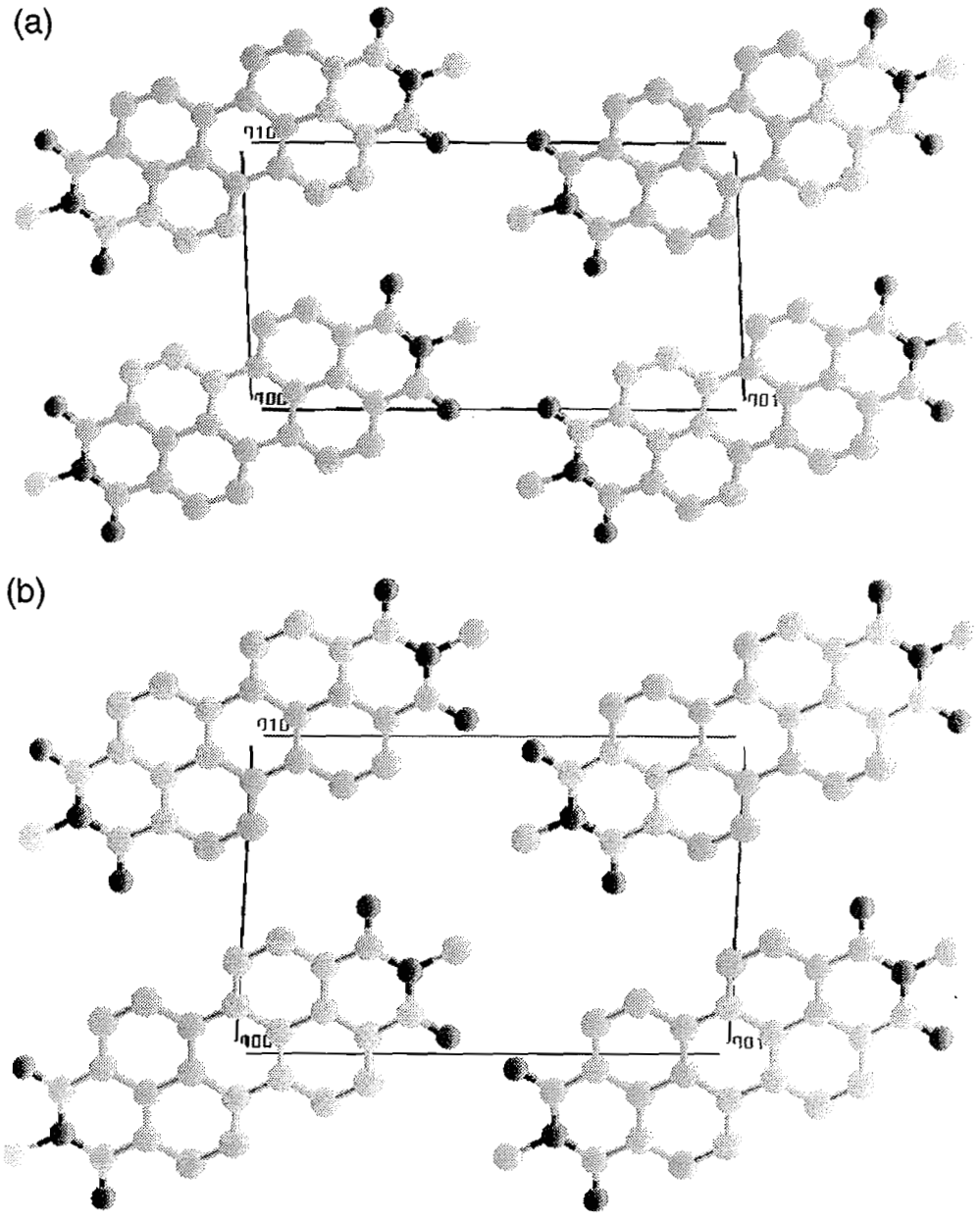

FIG. 5. (*a*) Minimized unit cell for the Triclinic **X** polymorph and (*b*) minimized unit cell for the Triclinic **Z** polymorph (both projections along the *a* axis).

reproduce accurately most molecular features of the perylenes and their unit cell parameters. Where this method was found to deviate from molecular geometries, the discrepancies were attributed to the generic nature of the force field.

Polymorphism is of importance in the study of materials where solid state packing is likely to affect properties such as photosensitivity. As part of our efforts to gain insights into this phenomenon, we have examined polymorphism in perylenes with the Dreiding force field. Using existing crystallographic information we carried out energy minimizations on lattices that were subjected to external stresses. Studies in which atomic charges were included did not yield chemically reasonable perylene polymorphs and this failure is believed to be related to limitations in the charging scheme. In studies in which these charges were omitted it was possible to generate two theoretical enthalpic polymorphs of *N*,*N*′-dimethylperylene, **1**, with reasonable chemical properties and packing parameters.

Acknowledgments

Financial support for this research was provided by the Natural Sciences and Engineering Research Council of Canada, through a University–Industry Cooperative Research Development Grant, and by the Xerox Research Centre of Canada. The award to A.J.M. of a Graduate Award by Queen's University is gratefully acknowledged.

1. T. Sakaki, M. Inoue, S. Senda, and K. Tomita. Biochem. Biophys. Res. Commun. **83**, 21 (1978).
2. P. N. Prasad and D. J. Williams. Introduction to nonlinear optical effects in molecules and polymers. John Wiley and Sons, New York. 1991. pp. 59–82.

Can. J. Chem. Downloaded from www.nrcresearchpress.com by 88.255.202.194 on 09/08/12
For personal use only.

3. S. R. Byrn. Solid-state chemistry of drugs. Academic Press, New York. 1982. pp. 79–146.
4. R. O. Loutfy and J. H. Sharpe. J. Phys. Chem. **83**, 1208 (1979).
5. R. O. Loutfy, A. M. Hor, and P. M. Kazmaier. Front. Macromol. Sci. Proc. IUPAC Int. Symp. Macromol. 32nd, 1988, Kyoto. Blackwell, Boston. 1989. p. 437; R. O. Loutfy, A. M. Hor, P. Kazmaier, and M. Tam. J. Imaging Sci. **33**, 151 (1989).
6. J. W. Weigl, J. Mammino, G. L. Whittaker, R. W. Radler, and J. F. Byrne. *In* Current problems in electrophotography. *Edited by* W. F. Berg and K. Hauffe. Walter de Gruyter, New York. 1972. pp. 285–300.
7. A. J. Pertsin and A. I. Kitaigorodskii. The atom–atom potential method. Springer, Berlin. 1987.
8. A. Gavezzotti. J. Am. Chem. Soc. **113**, 4622 (1991).
9. G. R. Desiraju. Crystal Engineering. The design of organic solids. Elsevier, Amsterdam. 1989. pp. 27–56.
10. S. L. Mayo, B. D. Olafson, and W. A. Goddard III. J. Phys. Chem. **94**, 8897 (1990).
11. N. Karasawa and W. A. Goddard III. J. Phys. Chem. **93**, 7320 (1989).
12. E. Buncel, A. J. McKerrow, and P. M. Kazmaier. Mol. Cryst. Liquid Cryst. **211**, 415 (1992).
13. E. Hädicke and F. Graser. Acta Crystallogr. Sect. C: Cryst. Struct. Commun. **C42**, 189 (1986); **C42**, 195 (1986); G. Klebe, F. Graser, E. Hädicke, and J. Berndt. Acta Crystallogr. Sect. B: Struct. Sci. **B45**, 69 (1989).
14. J. Gasteiger and M. Marsili. Tetrahedron. **36**, 3219 (1980).
15. A. K. Rappé and W. A. Goddard III. J. Phys. Chem. **95**, 3358 (1991).
16. T. R. Stouch and P. C. Jurs. J. Chem. Inf. Comput. Sci. **26**, 4 (1986).
17 A. I. Kitaigorodskii. Molecular crystals and molecules. Academic Press, New York. 1973.

Can. J. Chem. Downloaded from www.nrcresearchpress.com by 88.255.202.194 on 09/08/12
For personal use only.

Preparation and characterization of the osmium cluster complexes $H_2Os_3(CO)_8L(EtFcPCMe)$ (L = CO or PEt_2Fc) and $H_2Os_3(CO)_8[(\eta\text{-}C_5H_3PEt_2)Fe(\eta\text{-}C_5H_4)]$

WILLIAM R. CULLEN,[1] STEVEN J. RETTIG, AND TU CAI ZHENG

Department of Chemistry, University of British Columbia, 2036 Main Mall, Vancouver, B.C., Canada V6T 1Z1

Received July 7, 1992

WILLIAM R. CULLEN, STEVEN J. RETTIG, and TU CAI ZHENG. Can. J. Chem. **71**, 399 (1993).

Thermolysis of $Os_3(CO)_{11}(PEt_2Fc)$ (Fc = $(\eta\text{-}C_5H_4)Fe(\eta\text{-}C_5H_5)$) in octane for 8 h affords $H_2Os_3(CO)_9(EtFcPCMe)$, **10**, and $H_2Os_3(CO)_8[(\eta\text{-}C_5H_3PEt_2)Fe(\eta\text{-}C_5H_4)]$, **9***e*, in 15 and 65% yield, respectively. Heating $Os_3(CO)_{12}$ and PEt_2Fc in 1:2 molar ratio in xylene for 10 h gives two isomers of $H_2Os_3(CO)_8(PEt_2Fc)(EtFcPCMe)$, **11**, in about 40% yield. Two crystalline modifications of the complex **9***e* have been obtained from the same solvent: **9***e*A, triclinic, a = 15.653(1), b = 15.799(1), c = 11.257(1) Å, α = 90.388(7)°, β = 109.740(6)°, γ = 82.445(6)°, Z = 4 (two molecules per asymmetric unit), space group $P\bar{1}$; and **9***e*B, monoclinic, a = 9.889(2), b = 13.632(3), c = 18.927(4) Å, β = 97.36(2)°, Z = 4, space group $P2_1/n$. The structures were solved by heavy atom methods and were refined by full-matrix least-squares procedures to R = 0.033 and 0.037 for 8131 and 5145 reflections with $I \geq 3\sigma(I)$, respectively.

WILLIAM R. CULLEN, STEVEN J. RETTIG et TU CAI ZHENG. Can. J. Chem. **71**, 399 (1993).

La thermolyse du $Os_3(CO)_{11}(PEt_2Fc)$(Fc = $(\eta\text{-}C_5H_4)Fe(\eta\text{-}C_5H_5)$) dans de l'octane pendant 8 h conduit au $H_2Os_3(CO)_9(EtFcPCMe)$ (**10**) et au $H_2Os_3(CO)_8[(\eta\text{-}C_5H_3PEt_2)Fe(\eta\text{-}C_5H_4)]$ (**9***e*) avec des rendements respectifs de 15 et 65%. Le chauffage du $Os_3(CO)_{12}$ avec du PEt_2Fc, dans un rapport molaire de 1 : 2, dans du xylène pendant 10 h conduit à deux isomères du $H_2Os_3(CO)_8(PEt_2Fc)(EtFcPCMe)$ (**11**) avec un rendement d'environ 40%. On a obtenu les deux formes cristallines du complexe **9***e* à partir du même solvant : **9***e*A est triclinique avec a = 15,653(1), b = 15,799(1) et c = 11,257(1) Å, α = 90,388(7)°, β = 109,740(6)° et γ = 82,445(6)°, Z = 4 (deux molécules par unité asymétrique) et groupe d'espace $P\bar{1}$ alors que **9***e*B est monoclinique avec a = 9,889(2), b = 13,642(3) et c = 18,927(4) Å, β = 97,36(2)°, Z = 4 et groupe d'espace $P2_1/n$. On a résolu les structures par les méthodes des atomes lourds et on les a affinées par les méthodes des moindres carrés jusqu'à des valeurs de R de 0,033 et 0,037 pour respectivement 8131 et 5145 réflexions avec $I \geq 3\sigma(I)$.

[Traduit par la rédaction]

Introduction

Thermolysis of the triruthenium and triosmium cluster complexes $M_3(CO)_{12-n}L_n$ (M = Ru or Os, L = monodentate tertiary phosphine or arsine, n = 1, 2, 3, L = bidentate di(tertiary phosphine), n = 2, 4) generally leads to oxidative cleavages of C—H and (or) C—P(As) bonds (1–23). The ease of both these reactions generally follows the order $sp > sp^2 > sp^3$ for hybridization at carbon atoms (1–3). Thus thermolysis of $Os_3(CO)_{11}(PMePh_2)$ results in aryl C—H and C—P cleavage to give $HOs_3(CO)_9(PMePhC_6H_4)$, **1**, $Os_3(CO)_{10}(PMeC_6H_4)$, **2**, and $Os_3(CO)_9(PMe)(C_6H_4)$, **3** (17, 18, 23). Similarly $Os_3(CO)_{11}(PMe_2Ph)$ affords $HOs_3(CO)_9(PMe_2)(C_6H_4)$, **4**, as a result of one aryl C—H and one aryl C—P bond cleavage (12). Thermolysis of $Os_3(CO)_{11}(PMe_3)$ results in double alkyl C—H oxidative addition from one methyl group to form $H_2Os_3(CO)_9(Me_2PCH)$, **5***a* (15). Complexes of ethylphosphines PEt_xPh_{3-x} (x = 1–3) generally behave similarly, but the pyrolysis of $Os_3(CO)_{11}(PEt_2Ph)$ afforded a complex **6** resulting from two alkyl C—H bond cleavages and one aryl C—P cleavage (Scheme 1) (16). The

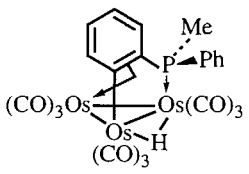

1

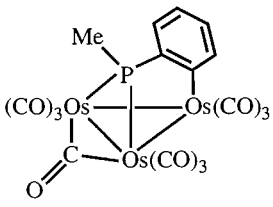

2

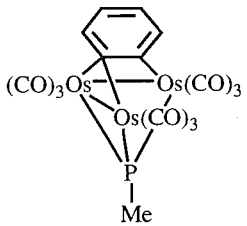

3

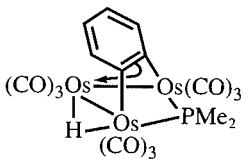

4

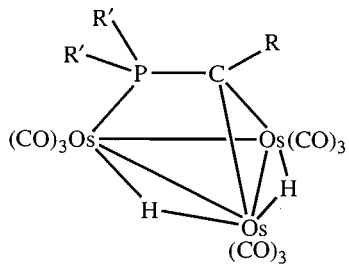

5*a* R = H, R′ = Me
5*b* R = Me, R′ = Et

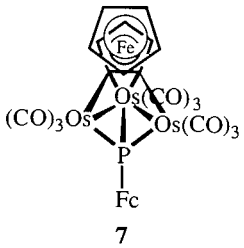

7

[1]Author to whom correspondence may be addressed.

Can. J. Chem. Downloaded from www.nrcresearchpress.com by 88.255.202.194 on 09/08/12
For personal use only.

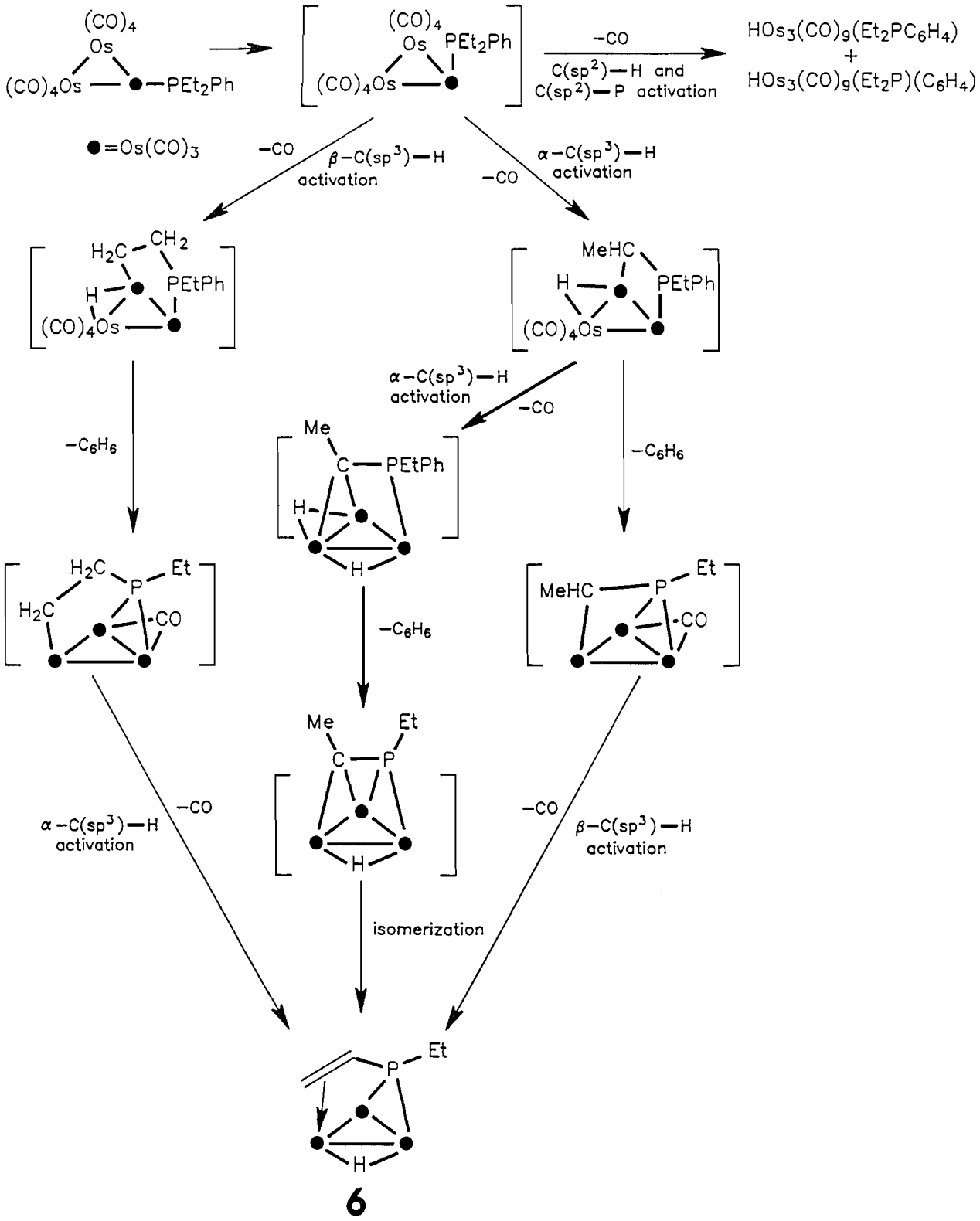

SCHEME 1. Plausible reaction pathways leading to complex **6**.

formation of **6** possibly involves one alkyl α-C—H cleavage to yield $HOs_3(CO)_{10}(EtPPhCHCH_3)$ as the first step. However, instead of undergoing a further alkyl α-C—H cleavage to yield a complex $H_2Os_3(CO)_9(EtPPhCCH_3)$, analogous to **5**, a reductive elimination of benzene occurs to give $Os_3(CO)_{10}(EtPCHCH_3)$, enabling a second alkyl C—H bond cleavage to take place at the β carbon to give the isolated product **6**. This reaction sequence is summarized in Scheme 1. Two plausible alternative sequences, one involving double α-C—H activation and the other β-C—H activation of an ethyl group are also presented in the scheme.

In our recent investigations of the thermolytic reactions of

Can. J. Chem. Downloaded from www.nrcresearchpress.com by 88.255.202.194 on 09/08/12
For personal use only.

Can. J. Chem. Downloaded from www.nrcresearchpress.com by 88.255.202.194 on 09/08/12
For personal use only.

TABLE 1. Crystallographic data[a]

Compound	**9***e*A	**9***e*B
Formula	$C_{22}H_{19}FeO_8Os_3P$	$C_{22}H_{19}FeO_8Os_3P$
fw	1068.81	1068.81
Color, habit	Red-orange, prism	Red-orange, prism
Crystal size, mm	0.08 × 0.20 × 0.30	0.40 × 0.40 × 0.45
Crystal system	Triclinic	Monoclinic
Space group	$P\bar{1}$	$P2_1/n$
a, Å	15.653 (1)	9.889 (2)
b, Å	15.799 (1)	13.642 (3)
c, Å	11.257 (1)	18.927 (4)
α, °	90.388 (7)	90
β, °	109.740 (6)	97.36 (2)
γ, °	82.445 (6)	90
V, Å^3	2595.4 (4)	2532.3 (9)
Z	4	4
ρ_{calc}, g cm^{-3}	2.735	2.803
F(000)	1936	1936
μ(Mo-K_α), cm^{-1}	153.08	156.89
Relative transmission factors	0.22–1.00	0.65–1.00
Scan type	ω–2θ	ω–2θ
Scan range, deg in ω	1.05 + 0.35 tan θ	1.15 + 0.35 tan θ
Scan rate, deg min^{-1}	32	16
Data collected	$+h, \pm k, \pm l$	$+h, +k, \pm l$
$2\theta_{max}$, deg	60	60
Crystal decay	Negligible	Negligible
Total no. of reflections	15630	9879
No. of unique reflections	15109	9419
R_{merge}	0.046	0.064
Reflections with $I \geq 3\sigma(I)$	8131	5145
No. of variables	632	317
R	0.033	0.037
R_w	0.031	0.036
gof	1.53	1.86
Max Δ/σ (final cycle)	0.03	0.07
Residual density e Å^{-3}	−1.18 to +1.10	−1.49 to +1.59 (near Os)

[a]Temperature 294 K, Rigaku AFC6S diffractometer, Mo-K_α radiation (λ = 0.71069 Å), graphite monochromator, takeoff angle 6.0°, aperture 6.0 × 6.0 mm at a distance of 285 mm from the crystal, stationary background counts at each end of the scan (scan/background time ratio 2:1, up to 8 rescans), $\sigma^2(F^2) = [S^2(C + 4B) + (0.01F^2)^2]/Lp^2$ (S = scan rate, C = scan count, B = normalized background count), function minimized $\Sigma w(|F_o| - |F_c|)^2$ where $w = 4F_o^2/\sigma^2(F_o^2)$, $R = \Sigma \||F_o| - |F_c|\|/\Sigma |F_o|$, $R_w = (\Sigma w(|F_o| - |F_c|)^2/\Sigma w|F_o|^2)^{1/2}$, and gof = $[\Sigma w(|F_o| - |F_c|)^2/(m - n)]^{1/2}$. Values given for R, R_w, and gof are based on those reflections with $I \geq 3\sigma(I)$.

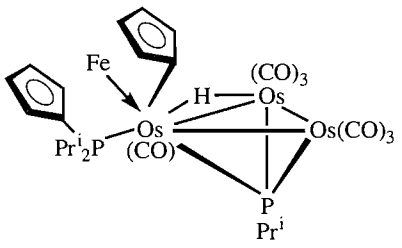

8

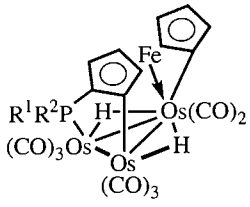

9*a* $R^1 = R^2 = Ph$ *c* $R^1 = Fc, R^2 = Et$
b $R^1 = Fc, R^2 = Ph$ *d* $R^1 = R^2 = Pr^i$
e $R^1 = R^2 = Et$

ferrocenylphosphine-substituted Ru_3 and Os_3 carbonyl-cluster complexes, we characterized a number of novel complexes such as the ferrocyne derivative **7** in addition to an extensive range of compounds such as **8** and **9***a–d* that contain strong Fe→Os interactions (8–10, 20, 21, 24–26). Previously known compounds that show Fe→M bonding of this type were confined to M = group 10 or 11 metals (27–30). We expect to discover an interesting chemistry of these cluster compounds once high-yield routes are available for their preparation, and the work presented in the present paper is directed towards this objective.

The pyrolysis of $Os_3(CO)_{11}(PFcPr^i_2)$ affords at least five products including **9***d* as a result of extensive C—H and C—P cleavages (ref. 25 and footnote 2). The pyrolysis of alkyl-bis(ferrocenyl)phosphine complexes such as $Os_3(CO)_{11}$-$(PEtFc_2)$ affords even more complicated mixtures.[2] On this basis we expected that the pyrolysis of $Os_3(CO)_{11}(PEt_2Fc)$ should afford **9***e* in high yield because complications resulting from the presence of a second Fc group are avoided and

[2]W. R. Cullen and T. C. Zheng, unpublished results.

TABLE 2. Final atomic coordinates (fractional) and B_{eq} (Å^2) for **9e**

Atom	x	y	z	B_{eq}[a]
		Triclinic form		
Os(1)	0.72276(2)	0.26953(2)	0.40194(4)	2.91(2)
Os(2)	0.66854(2)	0.42586(2)	0.21598(3)	2.52(2)
Os(3)	0.85337(2)	0.34092(2)	0.32371(3)	2.57(2)
Fe(1)	0.75361(9)	0.37360(9)	0.6156(1)	2.97(6)
P(1)	0.7143(1)	0.5220(1)	0.3833(2)	2.6(1)
O(1)	0.8461(6)	0.1156(5)	0.5519(9)	6.6(5)
O(2)	0.5952(6)	0.1572(5)	0.2363(8)	6.9(5)
O(3)	0.7332(6)	0.5321(5)	0.0469(8)	5.7(4)
O(4)	0.4668(5)	0.4992(6)	0.1320(7)	6.5(5)
O(5)	0.6372(5)	0.2867(5)	0.0208(7)	5.5(4)
O(6)	0.9680(5)	0.4863(5)	0.3459(8)	5.3(4)
O(7)	1.0215(5)	0.2107(5)	0.4504(8)	5.8(4)
O(8)	0.8597(5)	0.3084(5)	0.0591(7)	5.7(5)
C(1)	0.8374(5)	0.3758(5)	0.5028(8)	2.4(4)
C(2)	0.7926(5)	0.4601(5)	0.5201(8)	2.6(4)
C(3)	0.8209(6)	0.4781(6)	0.6500(8)	2.9(4)
C(4)	0.8806(6)	0.4059(6)	0.7165(8)	3.4(4)
C(5)	0.8891(6)	0.3443(6)	0.6328(9)	3.4(4)
C(6)	0.6648(7)	0.2955(6)	0.538(1)	3.6(5)
C(7)	0.6143(6)	0.3771(6)	0.543(1)	3.5(5)
C(8)	0.6401(7)	0.4044(7)	0.669(1)	4.5(6)
C(9)	0.7020(8)	0.3366(8)	0.749(1)	5.1(6)
C(10)	0.7135(7)	0.2696(7)	0.670(1)	4.6(6)
C(11)	0.7740(6)	0.6071(6)	0.353(1)	3.7(5)
C(12)	0.8129(8)	0.6621(7)	0.466(1)	5.8(6)
C(13)	0.6253(6)	0.5834(6)	0.434(1)	3.3(4)
C(14)	0.5705(7)	0.6583(6)	0.341(1)	4.4(5)
C(15)	0.7982(7)	0.1743(7)	0.496(1)	4.4(6)
C(16)	0.6464(7)	0.2000(7)	0.300(1)	4.7(5)
C(17)	0.7093(7)	0.4930(7)	0.112(1)	3.9(5)
C(18)	0.5417(6)	0.4735(7)	0.1661(9)	3.8(5)
C(19)	0.6490(7)	0.3376(7)	0.095(1)	3.7(5)
C(20)	0.9234(6)	0.4331(7)	0.336(1)	3.8(5)
C(21)	0.9586(7)	0.2613(6)	0.406(1)	3.6(5)
C(22)	0.8558(6)	0.3199(7)	0.157(1)	3.6(5)
Os(4)	0.32185(3)	0.09560(2)	0.25994(4)	3.10(2)
Os(5)	0.26497(2)	0.22076(2)	0.02755(4)	2.64(2)
Os(6)	0.13495(3)	0.15972(3)	0.12437(4)	3.30(2)
Fe(2)	0.31450(8)	−0.05002(8)	0.1114(1)	2.79(6)
P(2)	0.2329(1)	0.1071(1)	−0.1167(2)	2.6(1)
O(9)	0.3029(7)	0.0023(6)	0.4792(8)	7.7(6)
O(10)	0.4462(6)	0.2048(6)	0.4352(8)	7.6(5)
O(11)	0.1050(5)	0.3385(5)	−0.1557(8)	6.0(4)
O(12)	0.4209(5)	0.2776(5)	−0.0439(8)	5.6(4)
O(13)	0.2968(6)	0.3527(5)	0.2338(8)	6.3(5)
O(14)	−0.0322(5)	0.1782(6)	−0.1171(9)	6.9(5)
O(15)	0.0370(7)	0.0692(7)	0.268(1)	9.0(7)
O(16)	0.0740(6)	0.3425(6)	0.188(1)	7.4(5)
C(23)	0.1917(6)	0.0352(6)	0.081(1)	3.5(5)
C(24)	0.2155(6)	0.0198(5)	−0.0320(8)	2.7(4)
C(25)	0.2187(6)	−0.0683(6)	−0.0577(8)	3.0(4)
C(26)	0.2002(6)	−0.1098(6)	0.042(1)	3.8(5)
C(27)	0.1847(6)	−0.0480(6)	0.1253(9)	3.2(4)
C(28)	0.4156(6)	−0.0041(6)	0.243(1)	3.6(4)
C(29)	0.4377(6)	−0.0116(6)	0.126(1)	3.5(4)
C(30)	0.4388(6)	−0.0987(6)	0.093(1)	3.6(5)
C(31)	0.4234(6)	−0.1456(6)	0.188(1)	3.8(4)
C(32)	0.4123(7)	−0.0889(7)	0.2803(9)	4.1(5)
C(33)	0.1289(6)	0.1270(7)	−0.259(1)	4.0(5)
C(34)	0.1081(7)	0.0498(7)	−0.343(1)	4.8(5)
C(35)	0.3192(6)	0.0670(6)	−0.1883(9)	3.3(4)
C(36)	0.3268(7)	0.1290(7)	−0.286(1)	4.4(5)
C(37)	0.3113(8)	0.0382(8)	0.395(1)	5.0(6)

Can. J. Chem. Downloaded from www.nrcresearchpress.com by 88.255.202.194 on 09/08/12
For personal use only.

TABLE 2 (*concluded*)

Atom	*x*	*y*	*z*	B_{eq}[a]
C(38)	0.3948(8)	0.1657(7)	0.371(1)	4.6(5)
C(39)	0.1651(7)	0.2945(6)	−0.088(1)	3.8(5)
C(40)	0.3635(6)	0.2530(6)	−0.0202(9)	3.2(4)
C(41)	0.2862(7)	0.3014(7)	0.158(1)	4.1(5)
C(42)	0.0320(7)	0.1681(6)	−0.029(1)	4.2(5)
C(43)	0.0742(8)	0.1038(7)	0.217(1)	5.4(6)
C(44)	0.0980(7)	0.2736(8)	0.166(1)	5.1(6)
		Monoclinic form		
Os(1)	0.55397(3)	0.11602(3)	0.25031(2)	2.00(1)
Os(2)	0.40894(3)	0.17386(3)	0.10263(2)	1.81(1)
Os(3)	0.69324(3)	0.21031(3)	0.14787(2)	1.90(1)
Fe(1)	0.4895(1)	0.2957(1)	0.31230(7)	2.42(5)
P(1)	0.3784(2)	0.3393(2)	0.1385(1)	1.78(9)
O(1)	0.7900(8)	0.0731(8)	0.3625(5)	7.0(5)
O(2)	0.5017(8)	−0.0990(5)	0.2327(5)	4.6(4)
O(3)	0.439(1)	0.2471(7)	−0.0458(4)	5.7(5)
O(4)	0.1070(8)	0.1197(8)	0.0780(5)	6.5(5)
O(5)	0.4974(9)	−0.0351(5)	0.0743(4)	4.5(4)
O(6)	0.7524(7)	0.3893(6)	0.0612(5)	5.2(4)
O(7)	0.9790(7)	0.1928(6)	0.2271(5)	4.8(4)
O(8)	0.7668(8)	0.0796(6)	0.0272(4)	4.3(4)
C(1)	0.6156(8)	0.2970(6)	0.2298(4)	1.6(3)
C(2)	0.4967(8)	0.3599(6)	0.2168(4)	1.9(3)
C(3)	0.499(1)	0.4323(7)	0.2709(6)	2.9(4)
C(4)	0.616(1)	0.4161(9)	0.3203(6)	3.8(5)
C(5)	0.686(1)	0.3330(8)	0.2970(5)	3.1(4)
C(6)	0.4349(9)	0.1605(8)	0.3272(5)	2.8(4)
C(7)	0.314(1)	0.2150(8)	0.3098(5)	3.1(4)
C(8)	0.308(1)	0.290(1)	0.3599(6)	4.1(5)
C(9)	0.428(1)	0.282(1)	0.4114(6)	4.3(6)
C(10)	0.501(1)	0.198(1)	0.3944(6)	4.1(5)
C(11)	0.2116(9)	0.3741(7)	0.1613(5)	2.8(4)
C(12)	0.102(1)	0.386(1)	0.0951(6)	4.2(5)
C(13)	0.409(1)	0.4369(7)	0.0752(5)	2.7(4)
C(14)	0.390(1)	0.5406(7)	0.1000(6)	3.5(5)
C(15)	0.698(1)	0.0883(8)	0.3208(6)	3.5(5)
C(16)	0.525(1)	−0.0168(8)	0.2380(6)	3.4(5)
C(17)	0.426(1)	0.2188(7)	0.0105(6)	3.1(4)
C(18)	0.219(1)	0.1415(9)	0.0876(6)	3.8(5)
C(19)	0.462(1)	0.0416(7)	0.0835(5)	2.5(4)
C(20)	0.725(1)	0.3212(8)	0.0941(6)	3.6(5)
C(21)	0.8730(8)	0.2031(7)	0.1976(6)	3.4(4)
C(22)	0.739(1)	0.1287(8)	0.0713(6)	3.0(4)

[a] $B_{eq} = (8/3)\ \pi^2 \Sigma \Sigma\ U_{ij} a_i^* a_j^* (a_i \cdot a_j)$.

alkyl β-C—H and P—C cleavage are minimized. We have realized this expectation with the isolation of $H_2Os_3(CO)_8[(\eta\text{-}C_5H_3PEt_2)Fe(\eta\text{-}C_5H_4)]$, ***9e***, in 65% yield. Two other complexes are also described.

Experimental

All reactions were carried out under an argon atmosphere. Solvents were distilled prior to use. Thermolysis reaction was carried out in a flask fitted with a bubbler. ^{31}P and ^1H NMR chemical shifts are given in ppm from 85% H_3PO_4 and TMS, respectively, and NMR spectra were recorded in $CDCl_3$ by using Bruker AC-200 or Varian XL-300 spectrometers. Mass spectra were obtained on a Kratos MS-50 (EI) or an AEI MS-9 (FAB) spectrometer. Elemental analysis were performed by Mr. Peter Borda of this department. Diethylchlorophosphine was purchased from Strem Chemicals Inc. and *n*-butyllithium (1.6 M, hexanes) was obtained from Aldrich Chemical Co.

Preparation of diethylferrocenylphosphine, PEt_2Fc

Ferrocene (5.2 g, 0.028 mol) in diethyl ether (20 mL) was placed in a Schlenk tube equipped with a magnetic stirrer. To the stirred suspension was added *n*-butyllithium (12.8 mL, 0.02 mol) and the solution was left stirring for 60 h. After cooling the reaction mixture in a Dry Ice – acetone bath, diethylchlorophosphine (2.0 g, 0.016 mol) was added dropwise. The reaction mixture was allowed to warm slowly to room temperature and was left stirring for a further 2 h. Water (20 mL) was added to the solution; the oganic layer was separated, reduced in volume by using a rotary evaporator, and pumped to dryness. The residue was chromatographed on silica gel (20:1 petroleum ether:diethyl ether as eluent) and the pure product eluted in the second band. It was obtained in 30% yield (1.3 g) as a reddish yellow oil. $^{31}P\{^1H\}$ NMR δ: 26.1. ^1H NMR δ: 4.28 (m, 2H), 4.20 (m, 2H), 4.10 (s, 5H), 1.58 (m, 4H), 1.04 (td, 6H, J_{P-H} = 20.0 Hz). Mass spectrum (EI), *m/e* (relative intensity): 274(P^+, 40.6), 245(23.9), 218(13.6), 217(100.0), 186(19.8),

Can. J. Chem. Downloaded from www.nrcresearchpress.com by 88.255.202.194 on 09/08/12
For personal use only.

Can. J. Chem. Downloaded from www.nrcresearchpress.com by 88.255.202.194 on 09/08/12
For personal use only.

TABLE 3. Selected bond lengths (Å) with standard deviations for **9*e***

Atom	Atom	Triclinic		Monoclinic
		Molecule 1	Molecule 2	
Os(1)	Os(2)	3.0857(6)	3.0951(6)	3.0765(9)
Os(1)	Os(3)	2.8397(5)	2.8531(6)	2.8274(7)
Os(1)	Fe(1)	2.844(1)	2.826(1)	2.826(2)
Os(1)	C(6)	2.04(1)	2.06(1)	2.08(1)
Os(1)	C(15)	1.87(1)	1.84(1)	1.86(1)
Os(1)	C(16)	1.83(1)	1.85(1)	1.84(1)
Os(2)	Os(3)	2.8763(5)	2.8789(6)	2.8754(8)
Os(2)	P(1)	2.389(2)	2.400(2)	2.387(2)
Os(2)	C(17)	1.90(1)	1.91(1)	1.88(1)
Os(2)	C(18)	1.92(1)	1.92(1)	1.91(1)
Os(2)	C(19)	1.92(1)	1.91(1)	1.93(1)
Os(3)	C(1)	2.172(9)	2.17(1)	2.168(8)
Os(3)	C(20)	1.91(1)	1.91(1)	1.87(1)
Os(3)	C(21)	1.89(1)	1.92(1)	1.904(9)
Os(3)	C(22)	1.92(1)	1.92(1)	1.93(1)
Fe(1)	C(1)	2.114(9)	2.12(1)	2.120(8)
Fe(1)	C(2)	2.019(9)	2.028(8)	2.019(9)
Fe(1)	C(3)	2.039(9)	2.033(8)	2.03(1)
Fe(1)	C(4)	2.059(8)	2.048(9)	2.06(1)
Fe(1)	C(5)	2.05(1)	2.09(1)	2.065(9)
Fe(1)	C(6)	1.958(9)	1.982(8)	1.95(1)
Fe(1)	C(7)	2.048(9)	2.052(9)	2.05(1)
Fe(1)	C(8)	2.06(1)	2.07(1)	2.11(1)
Fe(1)	C(9)	2.05(1)	2.069(9)	2.05(1)
Fe(1)	C(10)	2.00(1)	2.033(9)	2.04(1)
Fe(1)	Cp(1)[a]	1.661(4)	1.668(5)	1.659(5)
Fe(1)	Cp(2)[a]	1.619(5)	1.643(5)	1.644(5)
C(1)	C(2)	1.47(1)	1.45(1)	1.45(1)
C(1)	C(5)	1.47(1)	1.44(1)	1.45(1)
C(2)	C(3)	1.42(1)	1.42(1)	1.42(1)
C(3)	C(4)	1.41(1)	1.43(1)	1.41(1)
C(4)	C(5)	1.37(1)	1.41(1)	1.43(1)

[a]Here and elsewhere, Cp(1) and Cp(2) refer to the unweighted centroids of the C(1–5) and C(6–10) cyclopentadienyl rings (or their equivalents for molecule 2, triclinic form).

151(11.2), 121(90.0), 56(18.9). Anal. calcd. for $C_4H_{19}FeP$: C 61.20, H 6.86; found: C 61.34, H 6.99.

Preparation of $Os_3(CO)_{11}(PEt_2Fc)$

The preparation is based on a literature method (31) but does not involve the isolation of $Os_3(CO)_{11}(MeCN)$. To triosmium dodecacarbonyl (454 mg, 0.5 mol) in dichloromethane (40 mL) in a two-necked flask was added acetonitrile (2 mL, excess) and trimethylamine oxide (38 mg, 0.5 mmol). After stirring the mixture for 2 h, the phosphine PEt_2Fc (137 mg, 0.50 mmol) dissolved in a small amount of dichloromethane was added. After a further 2 h at 20°C, the solvent was removed *in vacuo* and the residue was applied to a column for chromatographic separation (SiO_2, 3:1 petroleum ether:CH_2Cl_2 as eluent). Pure product eluted in the second band; the first contained unreacted $Os_3(CO)_{12}$. Solvent removal afforded orange crystalline $Os_3(CO)_{11}(PEt_2Fc)$ in 80% yield (460 mg). $P\{^1H\}$ NMR δ: −17.0. ^1H NMR δ: 4.50 (m, 2H), 4.30 (m, 7H), 2.24 (m, 4H), 1.10 (td, 6H, J_{P-H} = 24.1 Hz). Mass spectrum (FAB), *m/e*: 1154 (P^+, base peak), 1126, 1098, 1070, 1042, 1014, 984, 955, 928. Anal. calcd. for $C_{25}H_{19}FeO_{11}Os_3P$: C 26.36, H 1,80; found: C 26.05, H 1.66.

*Thermolysis of $Os_3(CO)_{11}(PEt_2Fc)$ and preparation of **9**e and **10***

$Os_3(CO)_{11}(PEt_2Fc)$ (100 mg, 0.086 mmol) in octane (30 mL) was refluxed for 8 h. TLC monitoring of the reaction mixture in association with $^{31}P\{^1H\}$ NMR studies revealed one major product, one in medium quantity, and three in trace quantities. Some starting material was also present. The residue was chromatographed on a silica gel column with 3:1 petroleum ether:CH_2Cl_2 as eluent. The first minor band contained $Os_3(CO)_{12}$, the second contained complex **10** (15 mg, 15%), the third band was $Os_3(CO)_{11}(PEt_2Fc)$, and the fourth orange band proved to be complex **9*e*** (64 mg, 65%). **10**, $^{31}P\{^1H\}$ NMR δ: −50.9. ^1H NMR δ: 4.50 (m, 1H), 4.38 (m, 2H), 4.20 (m, 1H), 4.16 (s, 5H), 2.88 (m, 1H), 2.52 (m, 1H), 2.24 (d, 3H, J_{P-H} = 24.2 Hz), 1.50 (td, 3H, J_{P-H} = 24.0 Hz), −15.1 (d, 1H, J_{P-H} = 11.1 Hz), −19.6 (d, 1H, J_{P-H} = 12.4 Hz). Mass spectrum (FAB), *m/e*: 1096 (P^+, base peak), 1068, 1040, 1012, 983, 955, 927, 913, 899, 883, 876, 854, 841, 827, 813. Anal. calcd. for $C_{23}H_{19}FeO_9Os_3P$: C 25.19, H 1.75; found: C 25.40, H 1.72. **9*e***, $^{31}P\{^1H\}$ NMR δ: −22.7. ^1H NMR δ: 5.16 (m, 1H), 5.02 (m, 1H), 4.70 (m, 1H), 4.18 (m, 2H), 4.06 (m, 1H), 3.06 (m, 1H), 2.16 (m, 1H), 1.86 (m, 2H), 1.28 (m, 1H), 0.90–1.04 (bm, 6H), −12.2 (d, 1H, J_{P-H} = 4.5 Hz), −17.4 (d, 1H, J_{P-H} = 11.0 Hz). Mass spectrum (FAB), *m/e*: 1068 (P^+), 1040, 1012 (base peak), 984, 956, 928, 900, 870, 840, 812. Anal. calcd. for $C_{22}H_{19}FeO_8Os_3P$: C 24.72, H 1.79; found: C 24.99, H 1.92.

*Thermolysis of $Os_3(CO)_{12}$ with PEt_2Fc and preparation of **11***

Triosmium dodecacarbonyl (272 mg, 0.30 mmol) and diethylferrocenylphosphine (160 mg, 0.60 mmol) in *p*-xylene (40 mL) were refluxed for 10 h. The solvent was removed *in vacuo* and the residue chromatographed on a silica column by using 3:1 petroleum ether:CH_2Cl_2 as eluent. The first fraction contained unreacted $Os_3(CO)_{12}$, the second one contained mainly **11*a*** together with some **11*b*** (**11*a***:**11*b*** > 20:1), and the third one contained almost equal amounts of **11*a*** and **11*b***. The two isomers were separated by careful repeated chromatography. **11*a***, $^{31}P\{^1H\}$ NMR δ: −24.6, −62.7. ^1H NMR δ: 4.49 (m, 3H), 4.34 (m, 1H), 4.28 (m, 4H), 4.23 (s, 5H), 4.17 (s, 5H), 2.97 (m, 1H), 2.72 (m, 1H), 2.42 (dd, 3H, J_1 = 18 Hz, J_2 = 5 Hz), 2.20 (bm, 4H), 1.57 (m, 3H), 1.25 (bm, 6H), −14.82 (pt, 1H, $J_1 = J_2$ = 9.9 Hz), −20.42 (pt, 1H, $J_1 = J_2$ = 11.0 Hz). Mass spectrum (FAB), *m/e*: 1342 (P^+), 1314, 1286 (base peak), 1258, 1230, 1200, 1172, 1142. Anal. calcd. for $C_{36}H_{38}Fe_2O_8Os_3P_2$: C 32.20, H 2.85; found: C 31.85, H 2.70. **11*b***, $^{31}P\{^1H\}$ NMR δ: −25.8, −62.1. ^1H NMR δ: 4.5–4.3 (m, 8H), 4.28 (s, 5H), 4.22 (s, 5H), 2.83 (m, 1H), 2.72 (m, 1H), 2.55 (dd, 3H, J_1 = 18 Hz, J_2 = 5 Hz), 2.20 (bm, 4H), 1.57 (m, 3H), 1.25 (bm, 6H), −15.13 (pt, 1H, $J_1 = J_2$ = 10.0 Hz), −20.60 (dd, 1H, J_1 = 11.0 Hz, J_2 = 8.8 Hz). Anal. calcd. for $C_{36}H_{38}Fe_2O_8Os_3P_2$: C 32.30, H 2.85; found: C 32.02, H. 2.74.

*Crystal structure determination of **9**e*

Suitable crystals for X-ray diffraction studies were obtained by evaporation of the solvent from the appropriate chromatographic fraction. Two different forms of crystals were found and both were subjected to crystallographic analyses.

Crystallographic data for the two crystal forms of $\{\mu_3:\eta^4\text{-}[(\eta^5\text{-}C_5H_4)Fe(\eta^5\text{-}C_5H_3)]P(C_2H_5)_2\text{-}Fe,P,C,C,\}(\mu\text{-}H)_2Os_3(CO)_8$, **9*e***, appear in Table 1. The final unit-cell parameters were obtained by least squares on the setting angles for 25 reflections with 2θ = 37.2–44.1° for **9*e***A and 35.0–44.6° for **9*e***B. The intensities of three standard relections, measured every 200 reflections throughout the data collections, remained constant for both data sets. The data were processed (32) and corrected for Lorentz and polarization effects, and for absorption (empirical, based on azimuthal scans for four reflections).

Both structures were solved by heavy atom methods, the coordinates of the Os and Fe atoms being determined from the Patterson functions and those of the remaining non-hydrogen atoms from subsequent difference Fourier syntheses. The structure analysis of **9*e***A was initiated in the centrosymmetric space group $P\bar{1}$, this choice being confirmed by the subsequent successful solution and refinement of the structure. All non-hydrogen atoms of both com-

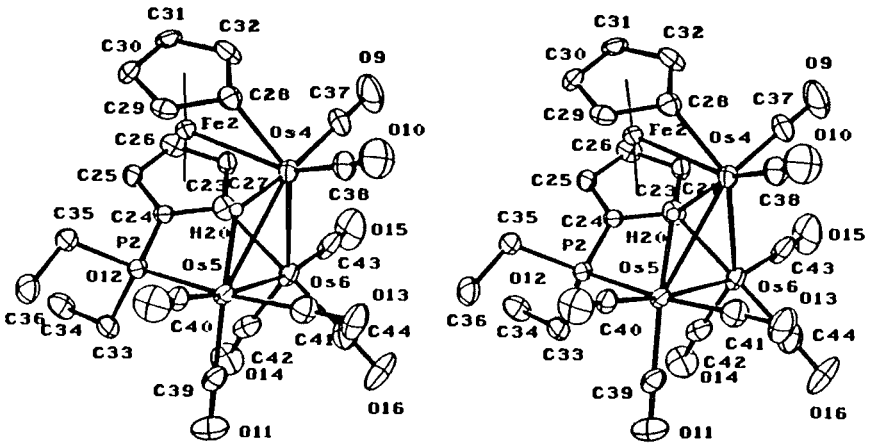

FIG. 1. Stereo ORTEP diagram of 9*e*A.

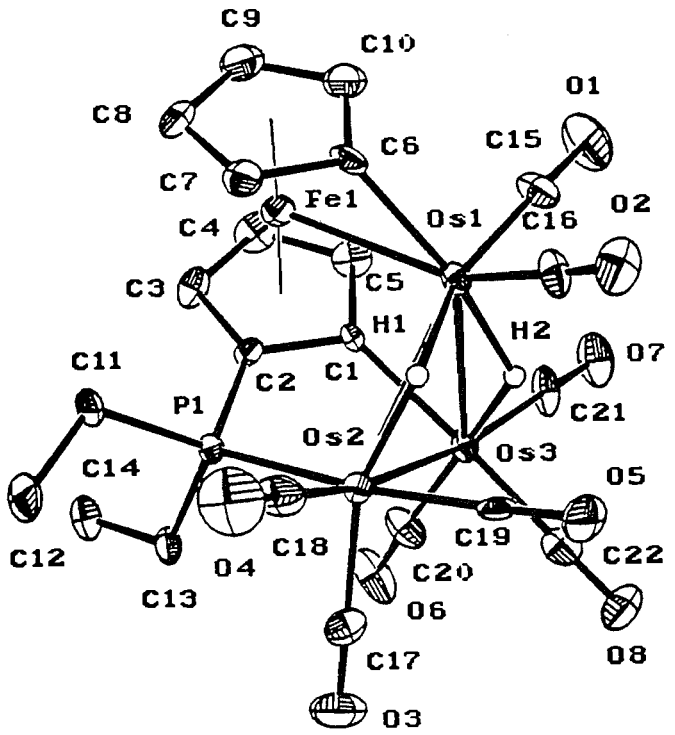

FIG. 2. ORTEP diagram of 9*e*B.

plexes were refined with anisotropic thermal parameters. The metal hydride atoms in both crystal forms, except for one of those associated with the Os(4) molecule in 9*e*A, were included in difference map positions but were not refined. All other hydrogen atoms were fixed in idealized positions (methyl groups staggered, C—H = 0.98 Å, $B_H = 1.2\ B_{\text{bonded atom}}$). Corrections for secondary extinction were applied, the final values of the extinction coefficient being 1.68×10^{-7} for 9*e*A and 2.17×10^{-7} for 9*e*B. Neutral atom scattering factors for all atoms and anomalous dispersion corrections for the non-hydrogen atoms were taken from the *International tables for X-ray crystallography* (33). Final atomic coordinates and equivalent isotropic thermal parameters, selected bond lengths, and selected bond angles appear in Tables 2–4, respectively. Hydrogen atom parameters, anisotropic thermal parameters, complete tables of bond lengths and bond angles, torsion angles, intermolecular contacts, least-squares planes, and measured and calculated structure factor amplitudes are included as supplementary material.[3]

Results and discussion

The complex $Os_3(CO)_{11}(PEt_2Fc)$ is readily prepared via the reaction of $Os_3(CO)_{11}(MeCN)$ with the phosphine PEt_2Fc. The analytical and spectroscopic results support the formulation of this new ligand and its complex.

When $Os_3(CO)_{11}(PEt_2Fc)$ is heated in refluxing octane for 8 h, two main products **9***e* and **10** can be isolated in 65 and 15% yields, respectively. The molecular formula $H_2Os_3(CO)_8[(C_5H_3PEt_2)Fe(C_5H_4)]$ is established for **9***e* on the basis of the spectroscopic and analytical data and by comparing these with those of **9***a–d*. The $^{31}P\{^1H\}$ NMR resonance of **9***e* at −22.7 ppm is only 5.7 ppm shifted from that of the parent complex $Os_3(CO)_{11}(PEt_2Fc)$, while two hydrides are clearly derived from the ferrocenyl moiety. The structure of **9***e* is confirmed by an X-ray diffraction study. Interestingly, two different forms of crystals of **9***e* were found and they were obtained from the same solvent. A stereoview of 9*e*A from the triclinic system and an ORTEP diagram of 9*e*B from the monoclinic system are shown in Figs. 1 and 2, respectively. Since the structure and bonding parameters of the two molecules are very close, metrical remarks will be confined to the structure 9*e*B from the monoclinic system.

The structure of **9***e* is very similar to those of **9***a–d* previously described (20, 25). It consists of a triangular array of three osmium atoms with one face capped by an axial phosphine and a doubly metalated ferrocenyl moiety. Both

[3]Hydrogen atom parameters, anisotropic thermal parameters, complete tables of bond lengths and bond angles, torsion angles, intermolecular contacts, least-squares planes, and measured and calculated structure factor structure amplitudes for 9*e*A and 9*e*B are available as supplementary material and may be purchased from: The Depository of Unpublished Data, Document Delivery, CISTI, National Research Council Canada, Ottawa, Canada K1A 0S2.

Hydrogen atom parameters and complete tables of bond lengths and angles have also been deposited with the Cambridge Crystallographic Data Centre and can be obtained on request from The Director, Cambridge Crystallographic Data Centre, University Chemical Laboratory, 12 Union Road, Cambridge, CB2 1EZ, U.K.

Can. J. Chem. Downloaded from www.nrcresearchpress.com by 88.255.202.194 on 09/08/12
For personal use only.

TABLE 4. Selected bond angles (deg) with standard deviations for **9*e***

Atom	Atom	Atom	Triclinic		Monoclinic
			Molecule 1	Molecule 2	
Os(2)	Os(1)	Os(3)	57.90(1)	57.72(1)	58.11(2)
Os(2)	Os(1)	Fe(1)	92.58(3)	93.00(3)	92.92(3)
Os(2)	Os(1)	C(6)	108.4(3)	109.6(3)	108.8(2)
Os(2)	Os(1)	C(15)	156.5(3)	158.1(4)	158.2(3)
Os(2)	Os(1)	C(16)	97.4(3)	95.4(3)	95.2(3)
Os(3)	Os(1)	Fe(1)	92.04(3)	92.11(3)	92.62(3)
Os(3)	Os(1)	C(6)	135.0(2)	136.2(2)	135.8(3)
Os(3)	Os(1)	C(15)	99.1(3)	101.3(4)	100.9(3)
Os(3)	Os(1)	C(16)	121.2(4)	119.1(3)	116.3(3)
Fe(1)	Os(1)	C(6)	43.5(2)	44.5(2)	43.7(3)
Fe(1)	Os(1)	C(15)	93.4(3)	94.3(4)	94.1(4)
Fe(1)	Os(1)	C(16)	145.4(4)	147.1(4)	149.8(3)
C(6)	Os(1)	C(15)	91.5(4)	89.9(5)	90.4(4)
C(6)	Os(1)	C(16)	102.1(4)	103.0(4)	106.3(4)
C(15)	Os(1)	C(16)	90.5(4)	89.6(5)	89.1(5)
Os(1)	Os(2)	Os(3)	56.76(1)	56.92(1)	56.60(2)
Os(1)	Os(2)	P(1)	92.34(6)	92.18(6)	92.60(5)
Os(1)	Os(2)	C(17)	144.5(3)	144.4(3)	147.1(3)
Os(1)	Os(2)	C(18)	114.4(3)	115.9(3)	114.2(3)
Os(1)	Os(2)	C(19)	81.5(3)	80.9(3)	79.9(3)
Os(3)	Os(2)	P(1)	84.65(6)	85.04(6)	84.61(5)
Os(3)	Os(2)	C(17)	88.3(3)	87.9(3)	91.0(3)
Os(3)	Os(2)	C(18)	170.7(3)	172.8(3)	170.8(3)
Os(3)	Os(2)	C(19)	86.8(3)	88.0(3)	86.5(3)
P(1)	Os(2)	C(17)	90.4(3)	89.9(3)	89.2(3)
P(1)	Os(2)	C(18)	93.3(3)	95.7(3)	95.9(4)
P(1)	Os(2)	C(19)	171.2(3)	172.1(3)	170.6(3)
C(17)	Os(2)	C(18)	100.8(4)	99.2(4)	98.2(4)
C(17)	Os(2)	C(19)	91.1(4)	93.6(4)	94.1(4)
C(18)	Os(2)	C(19)	94.9(4)	90.7(4)	92.4(5)
Os(1)	Os(3)	Os(2)	65.34(1)	65.36(1)	65.29(2)
Os(1)	Os(3)	C(1)	60.5(2)	60.9(2)	60.6(2)
Os(1)	Os(3)	C(20)	147.1(3)	149.3(3)	150.7(4)
Os(1)	Os(3)	C(21)	99.4(3)	100.9(4)	98.2(3)
Os(1)	Os(3)	C(22)	118.5(3)	113.8(3)	115.7(3)
Os(2)	Os(3)	C(1)	84.3(2)	83.7(2)	83.4(2)
Os(2)	Os(3)	C(20)	102.1(3)	98.7(3)	101.9(3)
Os(2)	Os(3)	C(21)	164.2(3)	166.3(4)	162.4(3)
Os(2)	Os(3)	C(22)	89.5(3)	90.6(3)	89.4(3)
C(1)	Os(3)	C(20)	88.9(4)	92.6(4)	92.8(4)
C(1)	Os(3)	C(21)	91.6(4)	89.1(4)	93.9(4)
C(1)	Os(3)	C(22)	173.5(4)	173.5(4)	172.8(3)
C(20)	Os(3)	C(21)	93.0(4)	93.2(5)	95.6(4)
C(20)	Os(3)	C(22)	90.4(4)	91.3(5)	89.2(5)
C(21)	Os(3)	C(22)	94.9(4)	95.8(5)	92.8(4)
Os(1)	Fe(1)	Cp(1)	97.4(1)	97.6(2)	97.4(2)
Os(1)	Fe(1)	Cp(2)	85.3(2)	85.3(2)	85.6(2)
Cp(1)	Fe(1)	Cp(2)	177.1(2)	177.2(2)	176.8(3)
Os(3)	C(1)	C(2)	121.9(6)	123.4(7)	123.7(6)
Os(3)	C(1)	C(5)	131.8(6)	128.6(7)	129.5(6)
C(2)	C(1)	C(5)	102.8(8)	104.9(8)	103.7(7)

Os(2) and Os(3) are bound to three terminal carbonyls and Os(1) to two. The Os—Os bonds show large variations with Os(1)—Os(2) at 3.0765(9) Å being the longest and Os(1)—Os(3) at 2.8274(7) Å the shortest; the remaining Os(2)—Os(3) bond is of intermediate length, 2.8754(8) Å. The longest and shortest Os—Os bonds are each bridged by a hydride, which was located but not refined. One ortho- and one heteroannular C—H bond of the ferocenyl group is cleaved and one Fe→Os bond is established in forming **9*e***. The Fe→Os bond length, 2.826(2) Å, is similar to that found for the other compounds **9** (20, 25).

The C(1)—Os(3) and C(6)—Os(1) distances at 2.168(8) and 2.08(1) Å, respectively, are typical of carbon–osmium σ-bonds, but there is probably also some interaction between C(1) and Os(1) since this distance of 2.584(9) Å is not extreme. The C(1)—C(5) plane, Cp(1), makes an angle of 78.62° with the Os_3 plane. The two Cp rings have a very small ring tilt angle of 1.44° despite the C—Os and Fe→Os

Can. J. Chem. Downloaded from www.nrcresearchpress.com by 88.255.202.194 on 09/08/12
For personal use only.

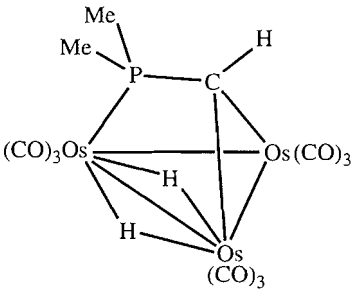

(A)

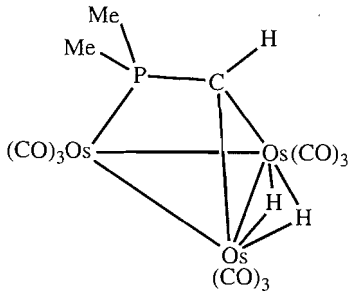

(B)

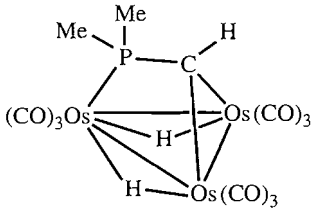

(C)

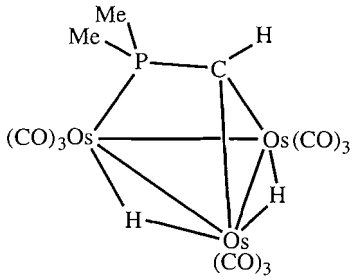

(D)

bonding interactions, and the rings are slightly staggered with the torsion angle C(1)Os(3)Os(1)C(6) being 12.1(4)°. P(1) is almost coplanar with Cp(1) (0.0118 Å away) and, as for the other structures **9** (20, 25), the Fe(1)—C(1) bond at 2.120(8) Å is slightly longer than the other four (avg. 2.044 Å) in Cp(1), while the Fe(1)—C(6) bond at 1.95(1) Å is slightly shorter than the other four (avg. 2.063 Å) in Cp(2). Carbonyl C—Os and C—O bond distances are not unusual and all Os—C—O vectors are close to linear.

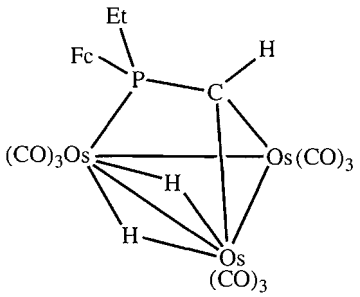

10*a*

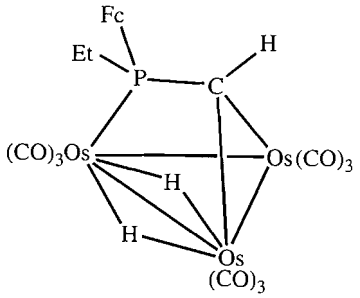

10*b*

The mass spectrum of **10** suggests the loss of two carbonyls from the parent complex and the analytical data are consistent with this formulation. The $^{31}P\{^1H\}$ NMR resonance at −50.9 ppm indicates that the C—P bonds remain intact. The ^1H NMR spectrum clearly establishes that the two hydrides are derived from the α position of one ethyl group. Generally the spectrum of **10** is very similar to that of $H_2Os_3(CO)_9(Et_2PCMe)$, **5*b*** (15). However, the two hydride signals in **10** are sharp and well separated at room temperature, indicating that the hydride exchange found in **5*b*** is largely suppressed in **10**. The resonances of the two α-hydrogen atoms of the PEt group of **10** are non-equivalent since the P atom is chiral and they are shifted downfield from those in $Os_3(CO)_{11}(PEt_2Fc)$. The methyl attached to the methylene carbon has a chemical shift of 2.24 ppm, a downfield shift of 1.14 ppm from that in the parent complex.

The structure of **10** is not obvious. Table 5 lists the chemical shifts and coupling constants of the hydride resonances for complexes **5**, **10**, **11**, **12**, **13**, and also **9*e***. It seems reasonable to assume that all these complexes, except **9*e***, have a similar hydride arrangement.

For complex **5*a*** four types of hydride arrangements may be considered. Type (C) is symmetrical for **5*a*** and is not consistent with the inequivalency of the two hydrides. Type (D) is not consistent with the almost equal J_{P-H} couplings since one hydride is three bonds and the other two bonds away from the P atom. Support for this statement is provided by complex **9*e*** for which hydrides were located in the crystal structure. This complex shows a coupling of ca. 4 Hz for the hydride that is three bonds away from the P atom and a coupling of ca. 12 Hz for the one that is two bonds away. Type (B) is inconsistent with the fact that the two methyl groups in **5*a*** are found to be inequivalent; two methyl resonances are seen in the ^1H NMR spectrum (15). Moreover the hydride–phosphorus couplings observed for **5*a***, Table 5, are much larger than the ca. 4 Hz expected for a three-bond coupling. Therefore, although Deeming and Underhill (15) favour a type (D) structure for **5**, we prefer a type (A) hydride arrangement as this structure seems to be more consistent with the NMR data. Such a double hydride bridge is

Can. J. Chem. Downloaded from www.nrcresearchpress.com by 88.255.202.194 on 09/08/12
For personal use only.

TABLE 5. Hydride NMR resonances for complexes **5**, **10**, **11**, **12**, **13**, and **9*e***

Compound	Hydride chemical shifts and coupling constants	
$H_2Os_3(CO)_9(PMe_2CH)$ **5*a***	−15.75, J = 10.8	−20.08, J = 6.2
$H_2Os_3(CO)_9(PEt_2CMe)$ **5*b***	−15.19, J = 9.4	−20.05, J = 8.0
$H_2Os_3(CO)_8(PMe_3)$ (PMe_2CH) **12*a***	−15.68, J = 11.2, 11.2	−20.44, J = 12.0, 8.0
$H_2Os_3(CO)_8(PMe_3)$ (PMe_2CH) **12*b***	−16.06, J = 11.2, 11.2	−19.25, J = 24.7, 8.9
$H_2Os_3(CO)_8(PEt_3)$ (PEt_2CMe) **13**	−15.30, J = 10.0, 10.0	−20.75, J = 11.0, 9.0
10	−15.13, J = 9.6	−19.72, J = 10.0
11*a*	−14.82, J = 9.9, 9.9	−20.42, J = 11.0, 11.0
11*b*	−15.13, J = 10.0, 10.0	−20.60, J = 11.0, 8.8
9*e*	−12.22, J = 4.4	−17.39, J = 11.4

known and the magnitude of the difference of hydride chemical shifts is not unreasonable (35).

If complex **10** has the same hydride arrangement as **5**, two isomers are possible depending on whether the hydrides are *syn* to the Fc group or to the Et group. It is possible that **10** is a mixture of these rapidly interconverting isomers, but we prefer to believe that it has a structure with two hydrides *syn* either to the Fc or to the Et group, with the latter being more likely since the hydride chemical shifts and couplings are close to those of **5*b***. However, there is no rational explanation to account for the absence of the other isomer.

The relative yields of **9*e*** and **10** suggest that C—H activation of the ferrocenyl moiety is easier than that of the ethyl, and that ferrocenyl and ethyl C—P cleavages are not as facile as phenyl C—P cleavage, as we surmised earlier (20). The good yield of **9*e*** obtained from $Os_3(CO)_{11}(PEt_2Fc)$ will allow its chemistry to be explored in future work. However, because of the ready formation of the complexes **9**, as yet unknown, but plausible, ferrocyne complexes such as $HOs_3(CO)_9(\mu\text{-}PR_2)[\mu_3\text{-}(C_5H_3)Fe(C_5H_5)]$ (R = alkyl, cf. **4** (12, 16, 34)) might have to be prepared by routes other than the pyrolysis of $Os_3(CO)_{11}(PFcR_2)$.

When $Os_3(CO)_{12}$ is refluxed in *p*-xylene with PEt_2Fc in 1:2 molar ratio, only one major product, **11**, is formed. This can be isolated as two isomeric forms **11*a*** and **11*b***. The spectroscopic and analytical data for **11** establish the formulation as $H_2Os_3(CO)_8(PEt_2Fc)(PEtFcCMe)$. These data are similar to those reported for $H_2Os_3(CO)_8(PMe_3)(PMe_2CH)$ **12** and $H_2Os_3(CO)_8(PEt_3)(PEt_2CMe)$ **13**.

From Table 5 it is clear that both complexes **11*a*** and **11*b***, which contain two phosphine moieties, are very similar to **12*a*** and **13**, but not to **12*b***. Complexes **12*a*** and **12*b*** interconvert in solution. Deeming and Underhill (15) considered three possible coordination sites for the PMe_3 ligand as shown, and suggested that the two isomers differ in the sites occupied by the phosphine PMe_3, a–c.

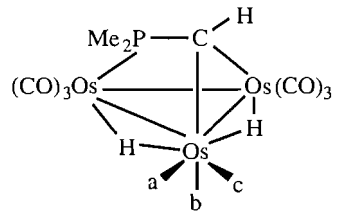

12

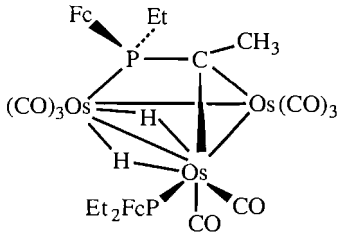

11*a*

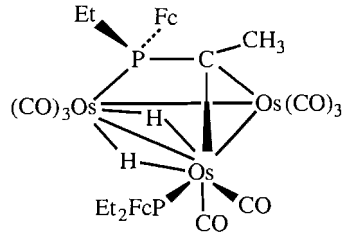

11*b*

In solution, **11*a*** and **11*b*** do not equilibrate over several weeks at room temperature, indicating that they do not differ in the site of PEt_2Fc substitution. Since the hydrides

Can. J. Chem. Downloaded from www.nrcresearchpress.com by 88.255.202.194 on 09/08/12
For personal use only.

couple to two phosphorus atoms approximately equally, the PEt_2Fc ligand must be bonded to the osmium atom that is bridged by the two hydrides. One of the possible structures is shown in **11**. It should be noted that both the P and the C atoms in **11** are chiral, thus two diastereomers result, and these account nicely for the two isomers obtained.

Acknowledgement

The authors gratefully acknowledge the financial support of the Natural Sciences and Engineering Research Council of Canada (W.R.C) and the award of a Graduate Fellowship (T.C.Z) by the University of British Columbia.

1. A. J. Deeming. Adv. Organomet. Chem. **26**, 1 (1986), and references therein.
2. P. E. Garrou. Chem. Rev. **85**, 171 (1985), and references therein.
3. A. J. Carty. Pure Appl. Chem. **54**, 113 (1982), and references therein.
4. M. I. Bruce, G. Shaw, and F. G. A. Stone. J. Chem. Soc. Dalton Trans. 2094 (1972).
5. N. Lugan, G. Lavigne, and J.-J. Bonnet. Inorg. Chem. **25**, 7 (1986).
6. S. A. R. Knox, B. R. Lloyd, A. G. Orpen, J. M. Vinâs, and M. Weber. J. Chem. Soc. Chem. Commun. 1498 (1987).
7. W. R. Cullen, S. J. Rettig, and H. Zhang. Organometallics, **10**, 2965 (1991).
8. W. R. Cullen, S. T. Chacon, M. I. Bruce, F. W. B. Einstein, and R. H. Jones. Organometallics, **7**, 2273 (1988).
9. M. I. Bruce, W. R. Cullen, P. A. Humphrey, O. B. Shawkataly, M. R. Snow, and E. R. T. Tiekink. Organometallics, **9**, 2910 (1990).
10. W. R. Cullen, S. J. Rettig, and T. C. Zheng. Organometallics, **11**, 853 (1992).
11. C. W. Bradford and R. S. Nyholm. J. Chem. Soc. Dalton Trans. 529 (1973).
12. A. J. Deeming, R. E. Kimber, and M. Underhill. J. Chem. Soc. Dalton Trans. 2589 (1973).
13. J. A. Clucas, D. F. Foster, M. M. Harding, and A. K. Smith. J. Chem. Soc. Chem. Commun. 949 (1984).
14. P. A. Jackson, B. F. G. Johnson, J. Lewis, A. D. Massey, D. Braga, C. Gradella, and F. Grepioni. J. Organomet. Chem. **391**, 225 (1990).
15. A. J. Deeming and M. Underhill. J. Chem. Soc. Dalton Trans. 2727 (1973).
16. A. J. Deeming, J. Organomet. Chem. **128**, 63 (1977).
17. A. J. Deeming, S. E. Kabir, N. I. Powell, P. A. Bates, and M. B. Hursthouse. J. Chem. Soc. Dalton Trans. 1529 (1987).
18. S. C. Brown, J. Evans, and L. E. Smart. J. Chem. Soc. Chem. Commun. 1021 (1980).
19. A. J. Deeming, N. I. Powell, A. J. Arce, Y. De Sanctis, and J. Manzur. J. Chem. Soc. Dalton Trans. 3381 (1991).
20. W. R. Cullen, S. J. Rettig, and T. C. Zheng. Organometallics, **11**, 277 (1992).
21. W. R. Cullen, S. J. Rettig, and T. C. Zheng. Organometallics, **11**, 928 (1992).
22. S. R. Hodge, B. F. G. Johnson, J. Lewis, and P. R. Raithby. J. Chem. Soc. Dalton Trans. 931 (1987).
23. A. J. Deeming, J. E. Marshall, D. Nuel, G. O'Brien, and N. I. Powell. J. Organomet. Chem. **384**, 347 (1990).
24. W. R. Cullen, S. J. Rettig, and T. C. Zheng. Can. J. Chem. **70**, 2215 (1992).
25. W. R. Cullen, S. J. Rettig, and T. C. Zheng. Organometallics. **11**, 3434 (1992).
26. W. R. Cullen, S. J. Rettig, and T. C. Zheng. Organometallics. In press.
27. D. Seyferth, B. W. Hames, T. G. Rucker, M. Cowie, and R. S. Dickson. Organometallics, **2**, 472 (1983).
28. S. Akabori, T. Kumagai, T. Shirahige, S. Sato, K. Kowazoe, S. Tamura, and M. Sato. Organometallics, **6**, 2105 (1987).
29. A. N. Nesmeyanov, E. G. Perevalova, K. I. Grandberg, D. A. Lemenovskii, T. V. Baukova, and O. B. Afanasova. J. Organomet. Chem. **65**, 131 (1974).
30. A. N. Nesmeyanov, Y. T. Struchkov, N. N. Sedova, V. G. Andrianov, Y. V. Volgin, and V. A. Suzonova. J. Organomet. Chem. **137**, 217 (1977).
31. B. F. G. Johnson, J. Lewis, and D. A. Pippard. J. Chem. Soc. Dalton Trans. 407 (1981).
32. TEXSAN/TEXRAY structure analysis package. Molecular Structure Corporation (1985).
33. International tables for X-ray crystallography. Vol. IV. Kynoch Press, Birmingham, U.K. (present distributor: Kluwer Academic Publishers, Dordrecht, The Netherlands). 1974. pp. 99–102 and 149.
34. A. J. Arce, and A. J. Deeming. J. Chem. Soc. Dalton Trans. 1155 (1982).
35. A. C. Willis, F. W. B. Einstein, R. M. Ramadan, and R. K. Pomeroy. Organometallics, **2**, 935 (1983).

Can. J. Chem. Downloaded from www.nrcresearchpress.com by 88.255.202.194 on 09/08/12
For personal use only.

SO_2 extrusion in 1,2,6-thiadiazine 1,1-dioxides: a novel synthesis of pyrazoles

JEAN F. KLEIN, JEAN CLAUDE POMMELET, AND JOSSELIN CHUCHE[1]

Laboratoire de chimie organique, Unité associée du Centre national de la recherche scientifique, n° 459, Université de Reims, 51062 Reims CEDEX, France

AND

JOSÉ ELGUERO, PILAR GOYA, AND ANA MARTINEZ[1]

Instituto de Quimica Médica (CSIC), Juan de la Cierva 3, 28006 Madrid, Spain

Received October 2, 1992

JEAN F. KLEIN, JEAN CLAUDE POMMELET, JOSSELIN CHUCHE, JOSÉ ELGUERO, PILAR GOYA, and ANA MARTINEZ. Can. J. Chem. **71**, 410 (1993).

A novel synthesis of the pyrazole ring involving SO_2 extrusion by flow vacuum pyrolysis in the 1,2,6-thiadiazine 1,1-dioxide system is described. The reaction has potential industrial significance for routes to pyrazoles or functionalized pyrazoles that do not involve hydrazines.

JEAN F. KLEIN, JEAN CLAUDE POMMELET, JOSSELIN CHUCHE, JOSÉ ELGUERO, PILAR GOYA et ANA MARTINEZ. Can. J. Chem. **71**, 410 (1993).

On décrit une nouvelle synthèse du noyau de pyrazole faisant appel à l'extrusion de SO_2 au moyen de la pyrolyse éclair à partir de 1,1-dioxydes de 1,2,6-thiadiazines. Cette méthode a un possible intérêt industriel pour la préparation de pyrazoles ou des pyrazoles fonctionalisés en évitant l'usage d'hydrazines.

Can. J. Chem. Downloaded from www.nrcresearchpress.com by 88.255.202.194 on 09/08/12
For personal use only.

Introduction

Heterocyclic compounds containing the N-SO_2-N moiety, such as 1,2,6-thiadiazine 1,1-dioxides and fused systems, have been the subject of different studies concerning their biological and physico-chemical aspects (1). We now wish to report their use for the synthesis of pyrazoles through a novel thermal extrusion of the SO_2 group. The N—N bond formation by extrusion of small stable fragments such as sulphur or sulphur monoxide from this heterocycle has already been described, but all attempts to eliminate the SO_2 moiety adjacent to two nitrogen atoms have up to now failed (2) (for a recent review on extrusion of SO_2 from heterocyclic compounds see ref. 3).

In the present case a flow vacuum pyrolysis technique (4) was applied successfully to the synthesis of pyrazoles from 1,2,6-thiadiazine 1,1-dioxides. The starting thiadiazine 1,1-dioxides are readily available by reactions involving condensation of sulfamides with suitable three-carbon fragments (1). On the other hand, the corresponding N-S-N and N-SO-N bridged derivatives are much more difficult to prepare.

Results and discussion

Flow vacuum pyrolysis (5) of *N*-alkyl derivatives **1***a* and **1***b* carried out in C_6D_6 afforded pyrazoles **2***a* and **2***b* as a result of the extrusion of an SO_2 molecule, in yields that increased with temperature (Scheme 1, Table 1). Thermolysis of **1***a* (700°C) and **1***b* (650°C) began at a temperature of 550–600°C and was complete by 650–700°C. A preparative thermolysis carried out in benzene solutions of **1***a* and **1***b* allowed the isolation of **2***a* and **2***b* in 66 and 47% yield, respectively.

Thiadiazine **1***c* showed a completely different thermal behaviour. Thermolysis began at a lower temperature and, at 500°C, 45% of the starting material had already disappeared. This reaction was more complicated and in the crude reaction product, besides unchanged thiadiazine **1***c*, three new products could be identified by NMR: pyrazole **2***c*, thiadiazine **1***d*, and cyclohexene. By 600°C, all the starting material had completely disappeared. A preparative thermolysis of **1***c*, carried out at this temperature, afforded compounds **2***c* and **1***d* (which were separated by silica gel chromatography) in 50 and 35% yield, respectively.

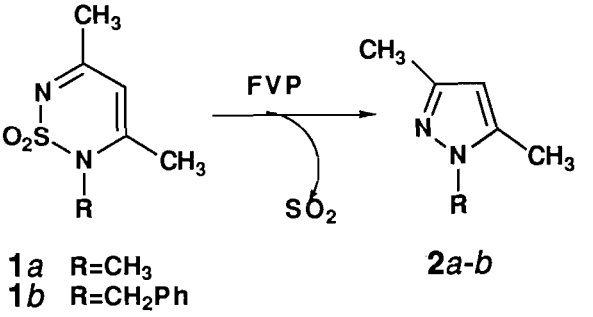

SCHEME 1

TABLE 1. Thermolysis of **1***a* and **1***b*

T (°C)	**1***a* (%)	**2***a* (%)	**1***b* (%)	**2***b* (%)
550	—	—	100	0
600	80	20	55	45
650	92	8	0	100
700	0	100	—	—

Two competitive reactions occur in the thermolysis of **1***c*: (*i*) an SO_2 elimination similar to that of **1***a* and **1***b*; (*ii*) an elimination of cyclohexene from **1***c*. At this point, it should be mentioned that cyclohexene could also result from the pyrolysis of **2***c*, since it has been shown (6) that *N*-alkyl pyrazoles bearing at least two carbon atoms on the alkyl chain afford alkenes by thermolysis.

To verify this hypothesis, thermolysis of **2***c* was carried out at 600°C under the same conditions. Since at this temperature only traces of cyclohexene and pyrazole **2***d* were

[1]Authors to whom correspondence may be addressed.

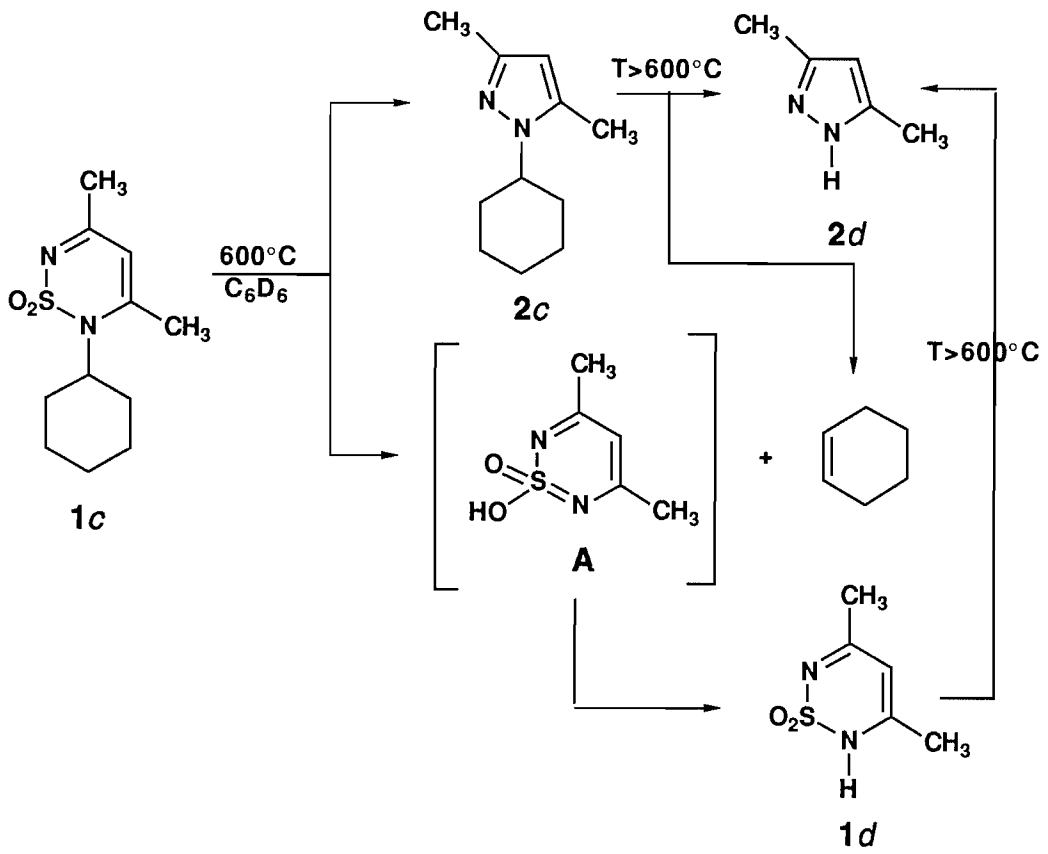

SCHEME 2

observed, it can be concluded that cyclohexene is formed essentially from **1***c*. However, at higher temperatures, there is a considerable increase of pyrolysis products (cyclohexene, **2***d*, and **2***c* in a 2:2:1 ratio at 700°C).

To complete this study, the thermal behaviour of **1***d*, which is also capable of losing an SO_2 molecule to afford pyrazole **2***d*, has been investigated. At 600°C, compound **1***d* remained practically unchanged and only traces of pyrazole **2***d* could be detected. At higher temperatures, the reaction became more complicated; at 630°C a considerable increase of **2***d* was observed, together with the appearance of several unidentified products. At 700°C, thiadiazine **1***d* had completely disappeared.

All the experimental results observed in the thermolysis of **1***c* are gathered in Scheme 2. It should be mentioned that the formation of **1***d* is likely to occur through a retroene type reaction (4) with the participation of the S=O double bond to give cyclohexene and the precursor **A** shown in Scheme 2.

The structures of all the products were established by comparison of the NMR data (^1H and ^{13}C) with authentic samples of the corresponding pyrazoles prepared by standard procedures (7).

Conclusions

This unambiguous synthesis of pyrazoles by SO_2 extrusion from 1,2,6-thiadiazine 1,1-dioxides could be very useful to introduce substituents in the five-membered aromatic ring, considering the different reactivity of the two heterocycles, and especially that referring to the 4-position (1).

Experimental

^1H and ^{13}C NMR spectra were recorded on a Bruker AC 250F spectrometer operating at 250 and 60 MHz, respectively, with TMS as internal standard.

Synthesis and characterization of thiadiazines and pyrazoles

Most compounds described in this work were already known (8): **1***a*, **1***b*, **1***d*, **2***a*, **2***b*, and **2***d*.

1-Cyclohexyl-3,5-dimethyl-1,2,6-thiadiazine 1,1-dioxide **1***c*

A solution of cyclohexylsulfamide (1.1 g, 0.011 mol) in ethanol (50 mL) was saturated with hydrogen chloride and then acetylacetone was added. The reaction mixture was refluxed for 4 h, the solvent evaporated *in vacuo*, and the residue recrystallized from water to give 1.8 g (67%) of **1***c*; mp 106–108°C; ^1H NMR ($CDCl_3$) δ: 5.65 (s, 1H, CH-4), 4.01 (m, 1H, -CH-N), 2.27 (s, 3H, CH_3-3), 2.1 (s, 3H, CH_3-5), 1.96–1.21 (m, 10H, CH_2); ^{13}C NMR ($CDCl_3$) δ: 172.74 (C-5), 157.81 (C-3), 103.91 (C-4), 61.62 (CH), 31.88 (CH_2), 26.96 (CH_2), 25.43 (CH_3-5), 25.27 (CH_2) 22.32 (CH_3-3). Anal. calcd. for $C_{11}H_{18}N_2O_2S$: C 54.54, H 7.43, N 11.57, S 13.22; found: C 54.61, H 7.79, N 11.32, S 13.17.

Flow pyrolysis of thiadiazines **1***a–c. General procedure*

Thermolyses were performed in the gas phase by passing the product through a 750 × 18 mm vertical quartz column heated by an electric Hermann–Moritz oven. The column was filled with small quartz cylinders (5 × 0.2 mm) and was connected to the pumping system ($p = 10^{-2}$ Torr; 1 Torr = 133.3 Pa).

In preparative thermolyses, the derivatives **1***a–c* (500 mg) were dissolved in benzene (25 mL) and introduced into the column dropwise. The emergent vapors were collected in a receiver cooled with liquid nitrogen. The solvent was evaporated under reduced pressure and the residue was chromatographed on a silica gel column using chloroform as eluent.

In analytical runs, thermolyses of **1***a–d* and **2***c* (50 mg) at var-

Can. J. Chem. Downloaded from www.nrcresearchpress.com by 88.255.202.194 on 09/08/12
For personal use only.

ious temperatures were carried out in benzene-d_6 solutions (2 mL). Crude products of reaction were directly characterized by ^{1}H NMR spectroscopy and the relative percentage established by integration of the well-separated singlets of pyrazoles and thiadiazine 1,1-dioxides.

1-Cyclohexyl-3,5-dimethylpyrazole **2**c*:* liquid (this compound is mentioned in an article about thin-layer chromatography of pyrazoles (9)); ^{1}H NMR (C_6D_6) δ: 5.75 (s, 1H, CH-4), 3.65 (m, 1H, CH), 2.32 (s, 3H, CH_3-5), 1.91 (s, 3H, CH_3-3), 1.4–2.2 (m, 10H, CH_2); ^{13}C NMR (C_6D_6) δ: 146.48 (C-5), 136.82 (C-3), 104.58 (C-4), 57.10 (CH), 33.32 (CH_2), 25.98 (CH_2), 25.68 (CH_2), 14.02 (CH_3-5), 10.60 (CH_3-3). Anal. calcd. for $C_{11}H_{18}N_2$: C 74.15, H 10.11, N 15.73; found: C 73.92, H 10.21, N 15.54.

Acknowledgements

The financial support of the project by grant no. FAR 90-0761 (Spain) is gratefully acknowledged. J.F.K. thanks the Region Champagne-Ardenne for a doctoral fellowship.

1. V. Aran, P. Goya, and C. Ochoa. Adv. Heterocycl. Chem. **44**, 81 (1988).
2. J. Barluenga, J. F. Lopez-Ortiz, M. Tomas, and V. Gotor. J. Chem. Soc. Perkin Trans. 1, 1891 (1981).
3. A. Aitken. Prog. Heterocycl. Chem. **4**, 1 (1992).
4. F. C. Brown. Pyrolytic methods in organic chemistry. Academic Press, New York. 1980. pp. 23 and 238.
5. C. Pale-Grosdemange and J. Chuche. Tetrahedron, **45**, 3397 (1989).
6. J. D. Perez, G. I. Yranzo, and L. M. Phagouape. Bull. Soc. Chim. Fr. 129 (1986).
7. J. Elguero. *In* Comprehensive heterocyclic chemistry. Vol. 5. *Edited by* A. R. Katritzky and C. W. Rees. Pergamon Press, Oxford. 1984. pp. 167–303.
8. J. Elguero, C. Ochoa, M. Stud, C. Esteban-Calderon, M. Martinez-Ripoll, J. P. Fayet, and M. C. Vertut. J. Org. Chem. **47**, 536 (1982).
9. A. N. Kost, G. K. Faizova, and I. I. Grandberg. Zh. Obshch. Khim. **33**, 533 (1963).

Can. J. Chem. Downloaded from www.nrcresearchpress.com by 88.255.202.194 on 09/08/12
For personal use only.

Synthesis of 2′-deoxy-2′-spirocyclopropyl cytidine as potential inhibitor of ribonucleotide diphosphate reductase

STANISLAS CZERNECKI,[1] LAURENCE MULARD, AND JEAN-MARC VALÉRY
Laboratoire de chimie des glucides, Université Pierre et Marie Curie, T74, 4, Place Jussieu, F-75005 Paris, France

AND

ALAIN COMMERÇON
Rhône-Poulenc Rorer, Centre de recherches de Vitry-Alforville, 13, Quai Jules Guesde, B.P. 14, F-94403 Vitry-sur-Seine CEDEX, France

Received October 1, 1992

STANISLAS CZERNECKI, LAURENCE MULARD, JEAN-MARC VALÉRY, and ALAIN COMMERÇON. Can. J. Chem. **71**, 413 (1993).

Based on the mechanism of action of ribonucleoside diphosphate reductase (RDPR), a new class of nucleosides that may act as inhibitors of this enzyme was designed. Starting from uridine, a 2′-deoxy-2′-spirocyclopropyl derivative of cytosine was prepared. The key step of the synthesis is the condensation of diazomethane with a suitably protected 2′-methylene nucleoside. Light-induced nitrogen extrusion affords the cyclopropane ring.

STANISLAS CZERNECKI, LAURENCE MULARD, JEAN-MARC VALÉRY et ALAIN COMMERÇON. Can. J. Chem. **71**, 413 (1993).

En se basant sur le mécanisme d'action de la réductase du diphosphate de ribonucléoside (RDPR), on a mis au point une nouvelle classe de nucléosides qui peuvent agir comme inhibiteurs de cet enzyme. Utilisant l'uridine comme produit de départ, on a préparé un dérivé 2′-désoxy-2′-spirocyclopropylé de la cytosine. L'étape clé de la synthèse est la condensation du diazométhane avec un 2′-méthylène nucléoside protégé d'une façon appropriée. Sous l'influence de la lumière, il y a extrusion d'azote et formation du noyau cyclopropane.

[Traduit par la rédaction]

Can. J. Chem. Downloaded from www.nrcresearchpress.com by 88.255.202.194 on 09/08/12
For personal use only.

Ribonucleoside diphosphate reductase (RDPR) is a key enzyme in the *de novo* production of deoxynucleoside precursors for DNA synthesis and is tightly linked to neoplastic transformation and progression (1). Accordingly, RDPR appears as a very attractive target for new anticancer agents and much research has been aimed at better understanding its mechanism of action (2) and at devising selective inhibitors (3). Among them, 2′-deoxy-2′-halogenated cytidine derivatives such as 2′-deoxy-2′,2′-difluorocytidine (4) and 2′-deoxy-2′-methylidenecytidine (5) are the more promising.

Since the extensive study of the molecular mechanism of this enzyme by Stubbe *et al.* (2*a*), a tyrosinyl radical is suspected to be the initiator of the enzymatic reaction by abstraction of H-3′. The resulting radical then undergoes a series of transformations to afford the 2′-deoxynucleotide with concomitant regeneration of the tyrosinyl radical.

We thought that it could be possible to design inhibitors utilizing this radical processing.[2] Since radical rearrangements involving β-scission of a cyclopropylmethyl moiety are known to be extremely rapid, they were used as mechanistic probes in reaction pathways implicating radical intermediates (7). Consequently, we decided to prepare a nucleoside derivative bearing a cyclopropyl ring at C-2′ that may act as an in vivo irreversible inhibitor of RDPR. Since the more active inhibitors are found in the cytidine series, 2′-deoxy-2′-spirocyclopropyl cytidine was chosen as target molecule.

The 3′,5′-*O*-protected derivative **1** (8) was smoothly oxidized by the pyridinium dichromate (PDC) – acetic acid reagent (9). This system, which requires only 1.5 molar equivalent of chromium species, was found to be superior to other reagents widely used for the oxidation of nucleosides (10). Further Wittig reaction on the 2′-keto nucleoside **2** was conducted with triphenylmethylene phosphorane generated from methyltriphenyl phosphonium iodide and *sec*-butyllithium in THF at −78°C to −30°C. This technique avoids the use of DMSO as in the procedure of Sano *et al.* (11) and compares favorably with the "salt-free" conditions successfully employed by Samano and Robins (10). Thus we were able to obtain the 2′-deoxy-2′-methylene uridine derivative **3***a* in 70% yield from uridine.

Despite numerous attempts, the samarium-promoted cyclopropanation reaction failed both on the free and on the protected methylene nucleoside although this method had been claimed to work well on various allylic alcohols (12). Deoxyspirocyclopropyl pentoses have previously been prepared by cycloaddition of diazomethane followed by photoinduced nitrogen extrusion from the resulting isomeric spiropyrazolines (13).

Treatment of compound **3***a* by diazomethane in ether at ambient temperature resulted only in the formation of uracil-methylated nucleosides **4** and **5**, together with a very small amount of presumed spiropyrazolines, and this whatever the excess of diazomethane was. Cyclopropanation of allyloxy- and allylamino derivatives was recently carried out with diazomethane in the presence of bisbenzonitrile dichloropalladium (14). Treatment of **3***a* under these conditions afforded **4** and **5** (90:10) together with unreacted starting material.

Nevertheless, we decided to carry out this experiment on the uracil-protected methylene nucleoside **6***b*. The 4-*O*-ethyl protection was chosen because this group could be further replaced by 4-amino, thus leading to cytosine-1-yl derivatives (15). Insufficient stability of the TPDS group during the nucleophilic displacement of the unstable 4-*O*-tosyl derivative (16) required the use of another protective group before activation and transformation at the 4-position of the uracil

[1]Author to whom correspondence may be addressed.

[2]While this paper was in preparation, a similar approach involving 2′-deoxy-2′-spirocyclopropyl derivatives of uridine and adenosine was reported: see ref. 6.

Can. J. Chem. Downloaded from www.nrcresearchpress.com by 88.255.202.194 on 09/08/12
For personal use only.

residue (See Scheme 1). Diacetylated 2′-deoxy-2′-methylene derivative **3***b* was efficiently prepared from **3***a* (92%), and transformed into **6***a* (72% yield), which was further acetylated in nearly quantitative yield to get the soluble derivative **6***b*.

Treatment of **6***b* with excess diazomethane in ether for 16 h at ambient temperature gave a separable mixture of isomeric 2′-deoxy-2′-spiropyrazoline derivatives **7** (59%) and **8** (15%). The stereochemistry of the major compound **7** (2′*R*) was deduced from variable temperature ^{1}H NMR experiments, which demonstrated restricted rotation of the uracil residue around the glycosidic bond at ambient temperature due to the steric hindrance of the methylene groups of the pyrazoline ring, resulting in low resolution of the signals. At 50°C, a well-resolved spectrum was obtained, indicating the restoration of free rotation of the base. Such a phenomenon was not observed for the minor isomer **8**. Moreover, diazomethane approach from the less-hindered α side of **6***b* seems to be favored, as was previously noticed for the dihydroxylation of the double bond (11).

Exposure of neat **7** and **8** (or their mixture) to daylight during ca. 1 week resulted in the formation of **9***a* by extrusion of nitrogen. The structure of **9***a* was confirmed by mass spectroscopy and the appearance of signals of the cyclopropyl ring between 0.5 and 1 ppm in the ^{1}H NMR spectrum.

Treatment of **9***a* by a methanolic solution of ammonia at room temperature afforded the deacetylated 2′-spirocyclopropyl-2′-deoxyuridine derivative **9***b*. The target molecule **9***c* was obtained by treatment of **9***a* with the same solution at 100°C.

The biological evaluation of this compound is in progress (Dr. F. Lavelle, Rhône-Poulenc Rorer).

Experimental

Microanalyses were performed at the Service de Microanalyse de l'Université Pierre et Marie Curie. Melting points were determined with a Thomas–Hoover apparatus and are uncorrected. Optical rotations were measured with a Perkin–Elmer model 141 polarimeter. The ^{1}H NMR spectra were recorded on a Bruker AM-250 spectrometer with TMS as internal standard. Reactions were monitored by analytical TLC using 2×5 cm precoated aluminum plates and silica gel 60 F_{254} (Merck), and detection by UV light and charring with H_2SO_4. For column chromatography, Merck silica gel 60 (230–400 mesh) and anhydrous solvents were used. Solvents and reagents were purified and dried by standard procedures.

*2′-Keto-3′,5′-*O*-(1,1,3,3-tetraisopropyldisiloxane-1,3-diyl)-β-*D*-uridine (2)*

To a stirred mixture of **1** (8) (4.86 g, 10 mmol), pyridinium dichromate (5.65 g, 15 mmol), and 4 Å molecular sieves (8 g) in CH_2Cl_2 (50 mL), acetic acid (1 mL, 1.75 mmol) is added. Stirring in continued at room temperature for 18 h. Celite (5 g) is added and the mixture is filtered and the solvent evaporated under reduced pressure. To the residue is added a large volume of Et_2O (100 mL) to precipitate most of the chromium salts. The ether solution is dried and slowly filtered through a column containing silica gel and Florisil (1:1). After evaporation pure **2** is obtained (4.11 g, 85%); mp 78–80°C; $[\alpha]_D^{20}$ −25.2 (*c* = 1, $CHCl_3$). Anal. calcd. for $C_{21}H_{36}N_2O_7Si_2$ (484,68): C 52.07, H 7.44, N 5.78; found: C 52.45 H 7.60 N 5.43. The ^{1}H NMR data of **2** are identical with the reported values (17).

*2′-Deoxy-2′-methylene-3′,5′-di-*O*-(1,1,3,3-tetraisopropyldisiloxane-1,3-diyl)-β-*D*-uridine (3a)*

Under a pressure of argon, *sec*-butyllithium in hexane (1.4 N, 6.45 mL, 9 mmol) is added to a suspension of triphenylmethyl phosphonium iodide (4.54 g, 11.2 mmol) in THF (20 mL) cooled at −78°C. The homogeneous orange solution is allowed to warm to −30°C and a solution of **2** (2.17 g, 4.5 mmol) in THF (7 mL) is transferred to this mixture under a pressure of argon. After warming to room temperature, stirring is continued for 24 h. THF is evaporated and replaced by CH_2Cl_2 (250 mL), water is added (20 mL), and the solution is neutralized with a cooled solution of 2% HCl. The organic layer is washed with H_2O (20 mL), 5% aqueous $NaHCO_3$ (20 mL), H_2O to neutrality, and brine (10 mL). After drying (Na_2SO_4), the solvent is evaporated *in vacuo* to give **3***a* (2.0 g), which is chromatographed on a silica gel column. Elution with light petroleum ether – ethyl acetate (7:3) affords pure **3***a* (1.78 g, 82%); mp 174–176°C (lit. (11) mp 130–133°C); $[\alpha]_D^{20}$ +26 (*c* = 1, $CHCl_3$).

*3′,5′-Di-*O*-acetyl-2′-deoxy-2′-methylene-β-*D*-uridine (3b)*

A 1 M solution of Bu_4N^+, F^- in THF (11.12 mL, 11.12 mmol) containing **3***a* (2.68 g, 5.56 mmol) is stirred at room temperature for 15 min. THF is evaporated *in vacuo* and acetonitrile (5 mL), Et_3N (7.7 mL, 56 mmol), and, after cooling at 0°C, acetic anhydride (2.62 mL, 55.6 mmol) are added to the reaction mixture. After evaporation to dryness, the residue is partitioned between AcOEt (50 mL) and aqueous $NaHCO_3$ (10 mL), water, and brine (10 mL). After drying (Na_2SO_4), the solvent is evaporated and the crude product is chromatographed. Elution with AcOEt – pet. ether (4:6) affords pure **3***b* (1.68 g, 92%); $[\alpha]_D^{20}$ −32.6 (*c* = 0.65, MeOH). ^{1}H NMR ($CDCl_3$) δ: 9.48 (br s, 1H, H-3), 7.24 (d, 1H, $J_{5,6}$ = 8.6 Hz, H-6), 6.73 (br s, 1H, H-1′), 5.78 (d, 1H, H-5), 5.64 (br s, 2H, methylene), 5.36 (br s, 1H, H-3′), 4.33 (m, 1H, $J_{5',5''}$ = 12.2 Hz, H-5′,H-5″), 4.2 (m, 1H, $J_{4',5'}$ = 4.2 Hz, $J_{4',5'}$ = 3.9 Hz, H-4′), 2.14 (s, 3H, CH_3CO), 2.03 (s, 3H, CH_3CO). Anal. calcd. for $C_{14}H_{16}N_2O_7$ (324.28): C 51.85, H 4.94, N 8.64; found: C 51.77, H 5.01, N 8.53.

*1-(2-Deoxy-2-methylene-*erythro*-β-*D*-pentofuranosyl)-4-*O*-ethyluracil (6a)*

A suspension of K_2CO_3 (590 mg, 5.9 mmol) in a solution of **3***b* (1.29 g, 3.93 mmol) and *p*-toluenesulfonyl chloride (900 mg, 4.72 mmol) in CH_3CN (15 mL) is heated at 85°C for 2 h. After cooling, the solvent is evaporated *in vacuo* and the residue is treated with NaOEt (1.5 M, 26 mL, 40 mmol) in EtOH (20 mL). The solid is filtered off and washed with EtOH. The ethanolic solution is neutralized with Amberlite IRN-77 (H^+ form). After filtration and evaporation of the solvent, the solid obtained is chromatographed. Elution with $CHCl_3$–methanol (9:1) affords pure **6***a*; yield: 640 mg (60%); mp 115–116°C; $[\alpha]_D^{20}$ +24.7 (*c* = 0.7, CH_3OH). ^{1}H NMR (DMSO-*d*6) δ: 7.9 (d, 1H, $J_{5,6}$ = 7.6 Hz, H-6), 651 (s, 1H, H-1′), 6.02 (d, 1H, H-5), 5.68 (d, 1H, $J_{3',OH}$ = 6.4 Hz, 3′-OH), 5.35 (s, 1H, H-2′), 5.24 (s, 1H, H-2″), 5.06 (t, 1H, $J_{6',OH}$ = $J_{6'',OH}$ = 5.1 Hz, 5′-OH), 4.52 (dd, 1H, $J_{3',4'}$ = 6.8 Hz, H-3′), 4.27 (9, 2H, *J* = 7 Hz, O-CH_2), 3.67 (m, 1H, H-4′), 3.71 (d, 1H, $J_{5',5''}$ = 12.4 Hz, H-5′), 3.57 (d, 1H, H-5″), 1.25 (t, 3H, CH_3).

*1-(3′,5′-Di-*O*-acetyl-2′-deoxy-2′-methylene-*erythro*-β-*D*-pentofuranosyl)-4-*O*-ethyl-uracil (6b)*

A solution of **6***a* (269 mg, 1 mmol) and acetic anhydride (570 mL, 6 mmol) in anhydrous pyridine (5 mL) is stirred at room temperature for 16 h. Solvent is evaporated and the residue is partitioned between $CHCl_3$ (50 mL) and water (10 mL). The organic layer is washed successively with 5% HCl (5 mL) and water, dried (Na_2SO_4), filtered, and evaporated. Compound **6***b* (360 mg, 100%) is homogeneous in TLC (R_f 0.62, $CHCl_3$–MeOH, 95:5; R_f 0.51, AcOEt – pet. ether, 7:3) and is characterized as follows. ^{1}H NMR (400 MHz, $CDCl_3$) δ: 7.5 (d, 1H, $J_{5,6}$ = 8 Hz, H-6), 6.9 (br s, 1H, H-1′), 5.92 (d, 1H, $J_{5,6}$ = 8 Hz, H-5), 5.68 (m, 1H, $J_{3',4'}$ = 5 Hz, H-3′), 5.6 (br s, 1H, H-2″a), 5.38 (br s, 1H, H-2″b), 4.48 (q, 2H, CH_2O ethyl), 4.38 (d, 2H, H-5′, H-5″), 4.24 (dd, 1H, $J_{4',5'}$ = 5 Hz, H-4′), 2.18 (s, 3H, CH_3CO-), 2.10 (s, 3H, CH_3CO-), 1.38 (t, 3H, CH_3 ethyl). MS (EI) *m/z*: 352 ($M^{+\cdot}$), 293 ($M^{+\cdot}$ −OAc), 227. ($M^{+\cdot}$ −BH^+). Anal. calcd. for $C_{16}H_{20}N_2O_7$ (352.34): C 54.54, H 5.72, N 7.94; found: C 54.71, H 5.65, N 7.80.

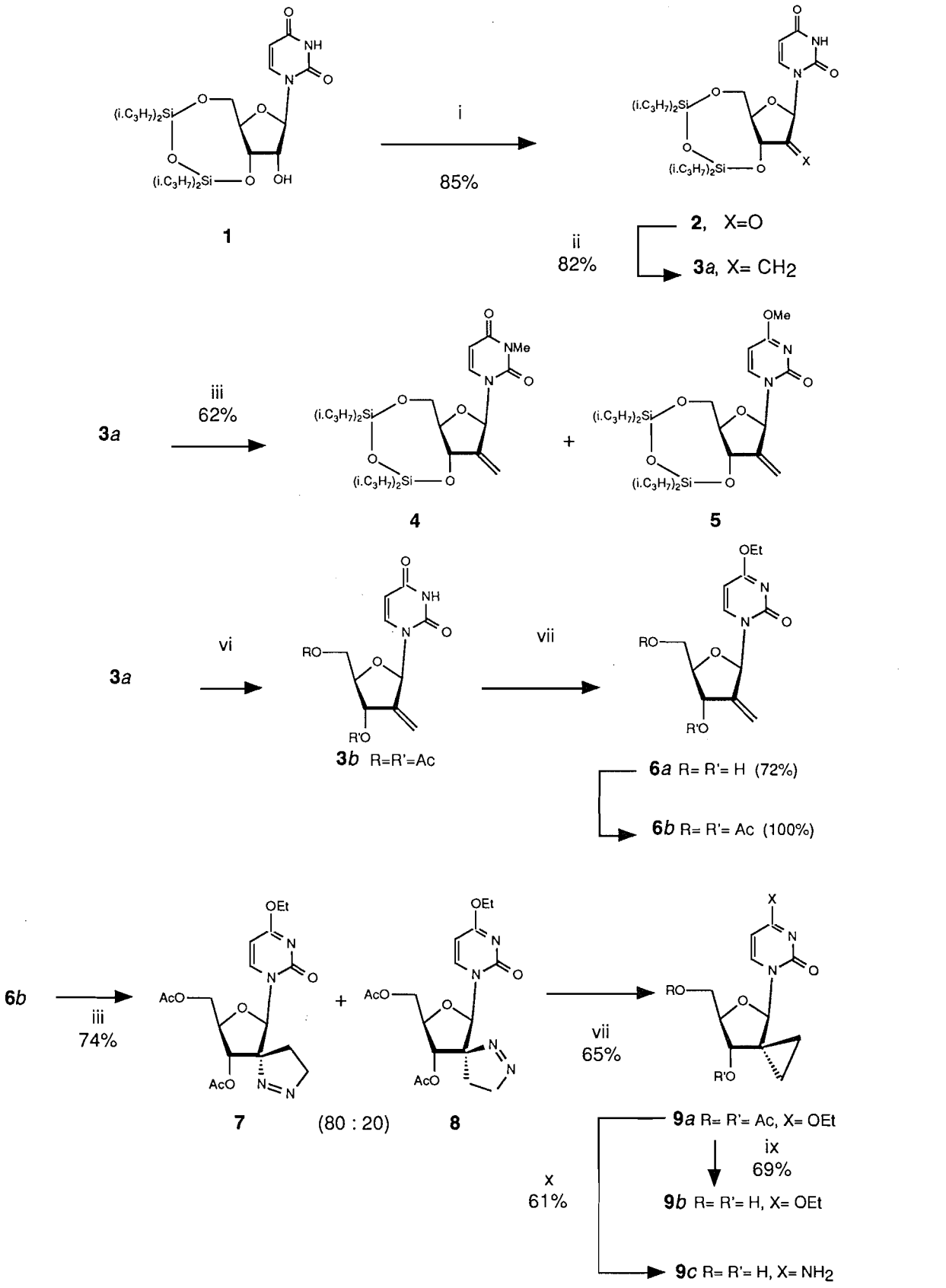

(i) PDC/AcOH/3 Å mol. sieves/CH_2Cl_2; (ii) Ph_3P^+, I^-/*s*BuLi 2.3 equiv./THF/ −30°C, then room temp.; (iii) CH_2N_2/Et_2O/room temp.; (vi) (1): Bu_4NF/THF; (2): $Ac_2O/Et_3N/CH_3CN$; (vii) (1): $TsCl/K_2CO_3/CH_3CN$; (2): 1 M NaOEt/EtOH; (viii) *hν*, neat, room temp.; (ix) NH_3/MeOH/room temp.; (x) NH_3/MeOH/100°C

SCHEME 1

Can. J. Chem. Downloaded from www.nrcresearchpress.com by 88.255.202.194 on 09/08/12
For personal use only.

Can. J. Chem. Downloaded from www.nrcresearchpress.com by 88.255.202.194 on 09/08/12
For personal use only.

*1-[3',5'-Di-*O*-acetyl-2'-deoxy-2'-(*S*)-spiro-4"-(1"-pyrazoline)-*erythro-*β-*D*-pentofuranosyl]-4-*O*-ethyl-uracil (**7**) and its 2'-(*R*) epimer (**8**)*

Compound **6** (100 mg, 0.28 mmol) is reacted with an excess of a solution of diazomethane in diethyl ether (4 equiv., 5 mL). Completion of the reaction is indicated by TLC ($CHCl_3$–MeOH, 98:2) and the mixture is chromatographed after evaporation *in vacuo*. Elution with $CHCl_3$–MeOH (98:2) affords **7** and **8**; yield: 82 mg (74%). The two epimers can be separated with AcOEt – pet. ether (120:130) as eluent and are characterized as follows:

Compound **7**, 2'-(*S*): ^{1}H NMR (400 MHz, $CDCl_3$, 50°C) δ: 7.9 (d, 1H, $J_{5,6}$ = 8 Hz, H-6), 6.04 (br s, 1H, H-1'), 5.96 (d, 1H, H-5), 5.52 (d, 1H, $J_{3',4'}$ = 9 Hz, H-3'), 5.0 (dd, 1H, $J_{4',5'}$ = $J_{4',5'}$ = 3 Hz, H-4'), 4.45–4.7 (m, 6H, CH_2-O, CH_2-N, H-5', H-5"), 2.20 (s, 3H, CH_3CO-), 2.05 (CH_3CO-), 1.62 and 1.42 (m, 2H, CH_2 pyrazoline), 1.39 (t, 3H, J = 7 Hz, CH_2- ethyl).

Compound **8**, 2'-(*R*): ^{1}H NMR (400 MHz, $CDCl_3$) δ: 7.88 (d, 1H, $J_{5,6}$ = 8 Hz, H-6), 6.6 (s, 1H, H-1'), 5.9 (d, 1H, H-5), 5.08 (d, 1H, $J_{3',4'}$ = 4 Hz, H-3'), 4.72 (dd, 1H, $J_{5',5''}$ = 12 Hz, $J_{5',4'}$ = 8 Hz, H-5'), 4.64 (dd, 1H, $J_{4'5''}$ = 4 Hz, H-5"), 4.4–4.52 (m, 5H, CH_2-O ethyl, CH_2-N, H-4'), 2.22 (m, 1H, H-4"a pyrazoline), 2.20 (s, 3H, CH_3CO-), 2.19 (s, 3H, CH_3CO-), 1.78 (m, 1H, H-4" pyrazoline). MS (Cl, NH_3) *m/z*: 395 (M+1).

*1-(3',5'-Di-*O*-acetyl-2'-deoxy-2',2'-spirocyclopropyl-*erythro-β-*D*-pentofuranosyl)-4-*O*-ethyl-uracul (**9**a)*

Compounds **7** and **8** (82 mg, 0.21 mmol) are exposed to sunlight in a round-bottom flask for several days (ca. 1 week). The transformation works better without any solvent, but is also effected in chloroform solution and exposure to a tungsten-filament lamp. Completion of nitrogen extrusion is indicated by TLC ($CHCl_3$–MeOH, 95:5); the resulting product is chromatographed on a silica gel column. Elution with AcOEt – pet. ether (1:1) affords pure **9***a*; yield: 43 mg (65%). ^{1}H NMR (400 MHz) $CDCl_3$) δ: 7.76 (d, 1H, $J_{5,6}$ = 8 Hz, H-6), 6.60 (s, 1H, H-1'), 5.95 (d, 1H, H-5), 4.92 (d, 1H, $J_{3',4'}$ = 3 Hz, H-3'), 4.32–4.50 (m, 1H, CH_2O, H-4', H-5', and H-5"), 2.17 (s, 3H, CH_3CO-), 2.16 (s, 3H, CH_3CO-), 1.38 (t, 3H, CH_3-CH_2), 1.06, 0.78, and 0.56 (3m, 2H, 1H, and 1H, cyclopropane). MS(EI) *m/z*: 366 (M^+), 307 ($M^{+\bullet}$ – OAc), 227 ($M^{+\bullet}$ – BH^+). Anal. calcd. for $C_{17}H_{20}N_2O_7$ (364.32): C 56.04, H 5.53, N 7.68; found: C 56.12, H 5.50, N 7.59.

*1-(2'-Deoxy-2'-spirocyclopropyl-*erythro-β-*D*-pentofuranosyl)-4-*O*-ethyl-uracil (**9**b)*

Compound **9***a* (50 mg, 0.13 mmol) is dissolved in methanol presaturated with ammonia (5 mL). After 24 h at room temperature, the solvent is evaporated and the residue purified by flash chromatography using chloroform–methanol (19:1) as eluent. Yield: 36 mg (69%) as a colorless syrup. ^{1}H NMR (DMSO-d_6) δ: 8.24 (d, 1H, $J_{5,6}$ = 7.39 Hz, H-6), 6.04 (d, 1H, H-5), 6.00 (s, 1H, H-1'), 5.19 (d, 1H, $J_{H,OH}$ = 5.84 Hz, 3'-OH), 5.10 (t, 1H, $J_{H,OH}$ = 5.34 Hz, 5'-OH), 4.27 (q, 2H, J = 7.05 Hz, -OCH_2), 4.05 ("t", 1H, $J_{3',4'}$ = 6.05 Hz, H-3'), 3.58–3.83 (m, 3H, H-4', H-5', H-5"), 1.27 (t, 3H, CH_3), 1.03, 0.58, and 0.47 (3m, 1H, 1H, and 2H, cyclopropane). MS (CI/NH_3) *m/z*: 300 (M+18), 283 (M+1).

*2'-Deoxy-2'-spirocyclopropyl cytidine (**9**c)*

Compound **9***a* (180 mg, 0.49 mmol) is dissolved in methanol presaturated with ammonia (40 mL). The mixture is heated in a stainless steel bomb at 100°C for 6 h. The solvent is evaporated and the residue purified as above with chloroform–methanol (2.6:1) as eluent. Yield: 76 mg (61%) as an amorphous solid. ^{1}H NMR (DMSO-d_6) δ: 7.77 (d, 1H, $J_{5,6}$ = 7.37 Hz, H-6), 6.00 (s, 1H, H-1'), 5.72 (d, 1H, H-5), 5.13 (d, 1H, $J_{H,OH}$ = 5.83 Hz, 3'-OH), 4.99 (t, 1H, $J_{H,OH}$ = 5.24 Hz, 5'-OH), 3.97 ("t", 1H, $J_{3',4'}$ = 5.84 Hz, H-3'), 3.72–3.56 (m, 3H, H-4', H-5', H-5"), 0.98 and 0.46 (2m, 1H and 3H, cyclopropane). MS (CI/NH_3) *m/z*: 271 (M+18), 254 (M+1).

Acknowledgements

We are grateful to the Rhône-Poulenc Company for financial support and a grant to one of us (L.M.). We acknowledge the assistance of Dr. M. Vuilhorgne (Rhône-Poulenc Rorer) for recording the 400 MHz ^{1}H NMR spectra.

1. (*a*) H. L. Elford, M. Freese, E. Passamani, and H. P. Morris. J. Biol. Chem. **245**, 5228 (1970); (*b*) E. Takeda and G. Weber. Life Sci. **28**, 1007 (1981); (*c*) G. Weber. Cancer Res. **43**, 3466 (1983).
2. (*a*) J. Stubbe, M. Ator, and T. Krenitsky. J. Biol. Chem. **258**, 1625 (1983); (*b*) J. Stubbe. J. Adv. Enzymol. **63**, 349 (1990).
3. C. H. Baker, J. Banzon, J. M. Bollinger, J. Stubbe, V. Samano, M. J. Robins, B. Lippert, E. Jarvi, and R. Resvich. J. Med. Chem. **34**, 1879 (1991).
4. L. Thelander, A. Graslund, and M. Thelander. Biophys. Res. Commun. **110**, 859 (1986).
5. (*a*) K. Takenuki, A. Matsuda, T. Ueda, T. Sasaki, and A. Fuji. J. Med. Chem. **31**, 1063 (1988); (*b*) T. Ueda, A. Matsuda, Y. Yoshimura, and K. Takenuki. Nucleosides Nucleotides, **8**, 743 (1989).
6. V. Samano and M. J. Robins. J. Am. Chem. Soc. **114**, 4007 (1992).
7. C. J. Suckling. Angew. Chem. Int. Ed. Engl. **27**, 537 (1988).
8. W. T. Markiewicz. J. Chem. Res. (S) 24 (1979).
9. S. Czernecki, C. Georgoulis, C. L. Stevens, and K. Vijayakumaran. Tetrahedron Lett. **26**, 1699 (1985).
10. V. Samano and M. J. Robins. Synthesis, 283 (1991).
11. T. Sano, S. Shuto, H. Inoue, and T. Ueda. Chem. Pharm. Bull. **33**, 3617 (1985).
12. G. A. Molander and J. B. Etter. J. Org. Chem. **52**, 3942 (1987).
13. J. M. J. Tronchet, B. Gentile, and J. Tronchet. Helvetica Chim. Acta, **58**, 1817 (1975).
14. Y. V. Tomilov, A. B. Kostitsyn, E. V. Shulishov, and O. M. Nefedov. Synthesis, 246 (1990).
15. A. Matsuda, H. Itoh, T. Takenuki, T. Sasaki, and T. Ueda. Chem. Pharm. Bull. **36**, 945 (1988).
16. M. Kawada, K. Matsumoto, and M. Tsurushima. Eur. Patent App. 204,264, (10 Dec. 1986), Jpn. App. 85/121, 786 (4 Jun 1985); Chem. Abstr. **106**, 214307m (1987).
17. F. Hansske, D. Madej, and M. J. Robins. Tetrahedron, **40**, 125 (1984).

A deuterium NMR study of molecular dynamics and geometry in two classes of onium salts: $(CH_3)_3E^+X^-$ and $C_6H_5M(CH_3)_3{}^+I^-$

GLENN H. PENNER,[1] JAMES M. POLSON,[2] STEPHEN I. DALEMAN,[3] AND KARA REID[3]

Guelph–Waterloo Centre for Graduate Work in Chemistry, Department of Chemistry and Biochemistry, University of Guelph, Guelph, Ont., Canada N1G 2W1

Received August 6, 1992

GLENN H. PENNER, JAMES M. POLSON, STEPHEN I. DALEMAN, and KARA REID. Can. J. Chem. **71**, 417 (1993).

Deuterium NMR measurements are reported for two types of onium salts: $(CH_3)_3E^+I^-$, where E = O (counterion is BF_4^-), S, Se, or Te, and $C_6H_5M(CH_3)_3{}^+I^-$, where M = N, P, or As. Within each class of compounds the activation energy for rotation of the trimethyl groups about the C_3' axis increases with increasing size of the central atom. In the first class of compounds the C—E—C bond angle decreases with the size of the atom E. In addition the magnitude of the quadrupolar coupling constant, χ, varies with E, ranging from 160 kHz for E = O to 190 kHz for E = Te. This is in qualitative agreement with molecular orbital calculations of the electric field gradients. At low temperatures the ^2H NMR spectrum of $C_6H_5N(CH_3)_3{}^+I^-$ can only be rationalized with a model in which trimethyl rotation is faster than methyl rotation. The ^2H NMR of ring (predominantly *ortho* and *para*)-deuterated $C_6H_5N(CH_3)_3{}^+I^-$ is consistent with rapid n-site ($n \geq 3$) rotation of the phenyl ring above 390 K. Below 390 K spectra characteristic of two-site, 180°, flips of the phenyl ring are observed. Below 280 K the motion of the phenyl ring is in the rigid lattice limit.

GLENN H. PENNER, JAMES M. POLSON, STEPHEN I. DALEMAN et KARA REID. Can. J. Chem. **71**, 417 (1993).

On a effectué des mesures de RMN du deutérium pour deux types de sels onium : $(CH_3)_3E^+I^-$ dans lesquels E = O (le contre-ion est le BF_4^-), S, Se ou Te, et $C_6H_5M(CH_3)_3$ dans lesquels M = N, P ou As. Dans chacune de ces classes de composés, l'énergie d'activation de la rotation des groupes méthyles autour de l'axe C_3' augmente avec une augmentation de la taille de l'atome central. Dans la première classe de composés, l'angle de la liaison C—E—C augmente avec une augmentation de la taille de l'atome E. De plus, l'amplitude de la constante de couplage quadripolaire, χ, varie avec E; elle varie de 160 kHz pour E = O à 190 kHz pour E = Te. Ce résultat est en accord qualitatif avec les calculs d'orbitales moléculaires des gradients des champs électriques. À basses températures, on ne peut rationaliser les spectres RMN du ^2H du $C_6H_5N(CH_3)_3{}^+I^-$ qu'à l'aide d'un modèle dans lequel la rotation de triméthyle est plus rapide que celle du méthyle. Le spectre RMN du ^2H du cycle $C_6H_5N(CH_3)_3{}^+I^-$ deutéré (principalement en *ortho* et *para*) est en accord avec la rotation rapide de n-sites ($n \geq 3$) du cycle phényle à des températures supérieures à 390 K. À des températures inférieures à 390 K, on observe des spectres caractéristiques de rotations rapides des noyaux phényles sur deux sites, 180°. En-dessous de 280 K, les déplacements du noyau phényle se font dans les limites d'un réseau rigide.

[Traduit par la rédaction]

Introduction

An important application of solid state NMR spectroscopy is in the study of molecular dynamics. A detailed analysis of NMR spectral lineshapes at different temperatures can provide information on the type of motion and on the energetics of that motion. For powdered samples the change in lineshape is most sensitive to the exchange rate of the dynamic process when this rate is comparable to the inhomogeneous linewidth.

Deuterium (^2H) NMR spectroscopy has developed rapidly as a tool for examining dynamic processes in solids (1–3). It is often relatively easy to introduce ^2H into a variety of molecular systems (4), and ^2H NMR techniques can be used to study molecular dynamics with exchange rates, k, ranging from 10^{-2} to 10^9 s^{-1} (1). The molecular motions of numerous solid trimethyl systems of the type $(CH_3)_3M$, where M is CSH (5), CBr (6), CCl, Cl, CCHO (7), NH^+, $NCH_3{}^+$ (8, 9), $S{=}O^+$ (10), N (11), and CC_6H_5 (12), have been studied by deuterium NMR spectroscopy.

Solid state deuterium NMR spectral lineshapes are dominated by the quadrupolar interaction. The quadrupolar interaction is due to the coupling between the deuterium quadrupole moment, eQ, and the electric field gradient, eq_{zz}, at the deuteron. Two measurable parameters are obtained from the deuterium NMR lineshape: the deuterium quadrupole coupling, $\chi = e^2q_{zz}Q/h$, and the asymmetry parameter, η. The asymmetry parameter is defined as the difference between the other two principle components (eq_{xx}, eq_{yy}) of the electric field gradient tensor, V, (eq. [1] in the principal axis system of the tensor) and has absolute values between 0 and 1.

$$[1] \quad V = \begin{bmatrix} eq_{xx} & 0 & 0 \\ 0 & eq_{yy} & 0 \\ 0 & 0 & eq_{zz} \end{bmatrix}$$

The ^2H NMR spectra of a powder sample containing static C—D bonds is characterized by three separations, $\Delta\nu_{11}$, $\Delta\nu_{22}$, and $\Delta\nu_{33}$, as shown in Figs. 1*a* and 1*b*. These are related to χ and η according to eqs. [2] and [3].

$$[2a] \quad \Delta\nu_{11} = \frac{3}{4}\chi(1 - \eta)$$

$$[2b] \quad \Delta\nu_{22} = \frac{3}{4}\chi(1 + \eta)$$

$$[2c] \quad \Delta\nu_{33} = \frac{3}{2}\chi$$

$$[3] \quad \eta = \frac{\Delta\nu_{22} - \Delta\nu_{11}}{\Delta\nu_{33}}$$

[1]Author to whom correspondence may be addressed.

[2]Present address: Department of Physics, University of British Columbia, Vancouver, B.C., Canada.

[3]Undergraduate Research Participant.

Can. J. Chem. Downloaded from www.nrcresearchpress.com by 88.255.202.194 on 09/08/12
For personal use only.

Can. J. Chem. Downloaded from www.nrcresearchpress.com by 88.255.202.194 on 09/08/12
For personal use only.

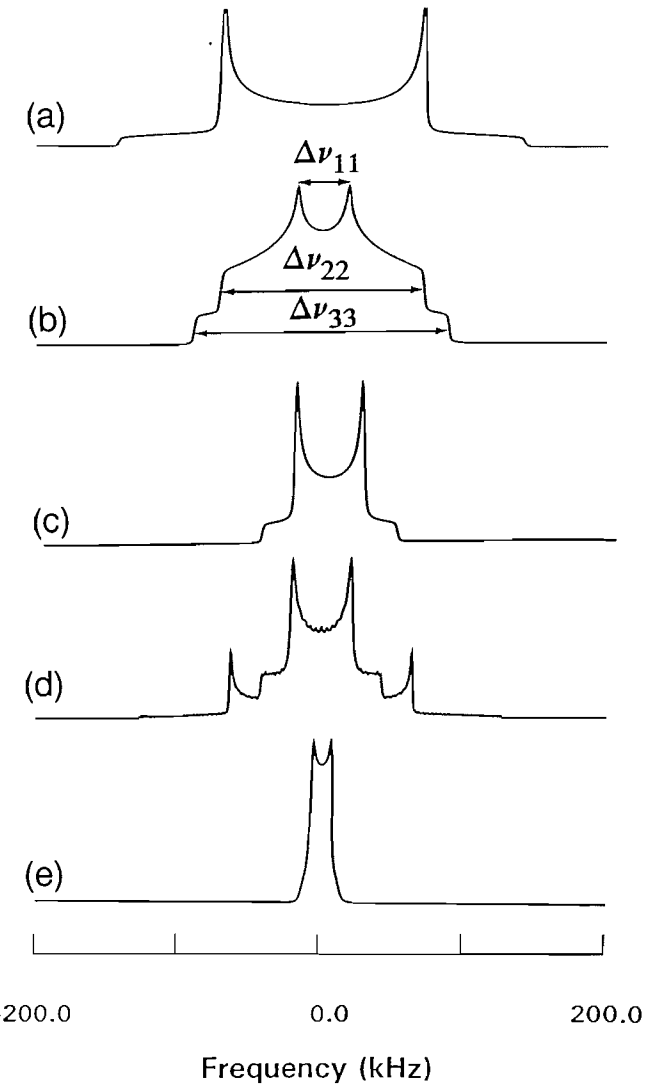

FIG. 1. Calculated deuterium NMR spectra. (*a*) χ = 190 kHz and η = 0.05; typical for a static phenyl ring deuteron. (*b*) χ = 190 kHz and η = 0.05 with rapid 180° flips of the phenyl ring yielding χ_{eff} = 114 kHz and η_{eff} = 0.6 for *ortho* and *meta* deuterons. (*c*) χ = 175 kHz and η = 0 with rapid 3-fold exchange of the methyl deuterons yielding χ_{eff} = 58 kHz and η_{eff} = 0.0. Tetrahedral geometry is assumed for the methyl carbon. (*d*) Same parameters as (*c*) with additional exchange between the three methyl groups of a trimethyl group; tetrahedral methyl and trimethyl geometries are assumed. (*e*) Same parameters as (*c*) but with slow methyl rotation and rapid trimethyl rotation.

Typically η = 0 for methyl deuterons and the spectrum is characterized by a quadrupolar splitting $\Delta\nu$ of $3\chi/4$ and an outer separation of $3\chi/2$. The value of χ normally lies between 160 and 180 kHz, for methyl deuterons (13).

Molecular reorientation in systems of the type $(CH_3)_3M$ usually consists of three-site exchange between the C—D bonds of the methyl groups, often referred to as C_3 rotation, and three-site exchange between the methyl groups, referred to as C_3' rotation.

Rapid ($k > 10^7$ s^{-1}) methyl rotation reduces $\Delta\nu$ by a factor of $\frac{1}{2}(3\cos^2\theta_{CD} - 1)$, where θ_{CD} is the angle between the C—D bonds and the rotational axis, and additional rapid trimethyl rotation ($k' > 10^7$ s^{-1}) further reduces $\Delta\nu$ by a factor of $\frac{1}{2}(3\cos^2\theta_{MC} - 1)$ where θ_{MC} is the angle between the M—C bonds and the C_3' rotational axis. Therefore rapid methyl and trimethyl rotation reduces $\Delta\nu$ according to eq. [4].

$$[4] \qquad \Delta\nu = \frac{3}{16}\chi\,(3\cos^2\theta_{CD} - 1)(3\cos^2\theta_{MC} - 1)$$

Typical spectra for methyl deuterons undergoing rapid C_3 and for trimethyl deuterons undergoing rapid C_3 plus C_3' rotation are shown in Figs. 1*c* and 1*d*, respectively. If C_3' rotation is fast while C_3 rotation is slow ($k < 10^3$ s^{-1}) the orientation of one C—D bond in each methyl group will not change with respect to the C_3 axis while the other two experience a three-site exchange. The resulting spectrum is simulated in Fig. 1*e*. Spectra for intermediate exchange rates (10^3–10^6 s^{-1}) are more complex in appearance but the lineshapes can be simulated if the correct geometry (θ_{CD} and θ_{MC}) and exchange rates (k and k') are provided (14, 15).

We have undertaken a deuterium NMR study of the methyl and trimethyl rotational dynamics in two classes of solid onium salts:

1. The series of cations $(CH_3)_3E^+$ where E is Te, Se, S, or O (compounds **1**, **2**, **3**, and **4**); and where the counterion is I^-; except for **4** where Y^- is BF_4^-.

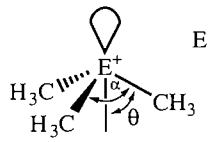

2. The series of cations $C_6H_5M(CH_3)_3{}^+I^-$, where M = N, P, or As (compounds **5**, **6**, and **7**).

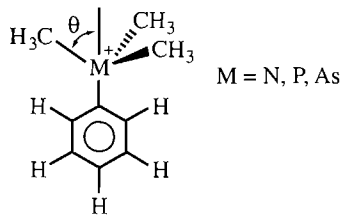

In addition, since **7** was easily deuterated in the phenyl ring positions, the dynamics of the phenyl ring were also studied by ^{2}H NMR. It is worth noting at this point that whereas the geometry about M in **5**, **6**, and **7** is expected to be tetrahedral or nearly tetrahedral, the structure of the $(CH_3)_3E^+$ cation changes significantly with E (16–19).

Experimental

Deuterated samples of trimethyltelluronium-d_3 iodide, trimethylselenonium-d_3 iodide, and trimethylsulfonium-d_9 iodide were synthesized according to eq. [5] by direct addition of iodomethane-d_3 to dimethyltelluride, dimethylselenide, and dimethylsulfide-d_6, respectively (19).

$$[5] \qquad (CH_3)_2\,E + CH_3\,I \rightarrow (CH_3)_3E^+I^-$$

Trimethyloxonium-d_3 tetrafluoroborate was prepared by condensation of excess dimethyl ether into a suspension of silver tetrafluoroborate in an iodomethane-d_3/dichloromethane solution at −78°C (20). The reaction mixture was allowed to warm to room temperature, under an inert nitrogen atmosphere, and any remaining iodomethane, dimethyl ether, or solvent was removed under vacuum.

$$[6] \qquad (CH_3)_2O + CH_3\,I \xrightarrow{AgBF_4} (CH_3)_3O^+\,BF_4^- + AgI$$

Can. J. Chem. Downloaded from www.nrcresearchpress.com by 88.255.202.194 on 09/08/12
For personal use only.

No attempt was made to separate the oxonium salt from the silver iodide. Methyl-deuterated samples of phenyltrimethylammonium-d_3 iodide, phenyltrimethylphosphonium-d_3 iodide, and phenyltrimethylarsonium-d_3 iodide were prepared by addition of iodomethane-d_3 to dimethylaniline, dimethylphenylphosphine, and dimethylphenylarsine, respectively.

[7] $C_6H_5M(CH_3)_2 + CH_3I \rightarrow C_6H_5M(CH_3)_3{}^+I^-$

Phenyl-ring-deuterated **7** was prepared by refluxing dimethylaniline in a 35% DCl/D_2O solution overnight. The product was neutralized with $NaOD/D_2O$ solution and extracted with ether. This was methylated by the above-mentioned procedure. The product is deuterated predominantly in the *ortho* and *para* positions. The samples were ground and sealed in 7 mm (300 mg) or 8 mm (500 mg) o.d. tubes. The oxonium sample was ground and sealed in a dry box under an argon atmosphere. Sample purity was checked by high-resolution solution (solvent: D_2O) ^1H (**1**, **2**, **5**–**7**) and ^{13}C (**3**, **4**) NMR spectroscopy.

Deuterium NMR spectra were obtained at 30.7 MHz on a Bruker CXP-200 or at 41.3 MHz on a home-built spectrometer. Spectra at liquid nitrogen temperature (77 K) were obtained on a Bruker CXP-200 using a home-built probe. The small size of the liquid nitrogen reservoir and potential for damage to the magnet severely limited the total collection time for each spectrum. Spectra were obtained by using the quadrupolar echo (21) pulse sequence: $(\pi/2)_x$–τ_Q–$(\pi/2)_y$–τ_Q-acquire, followed by Fourier transformation. Typically the length of the $\pi/2$ pulse was 3.5–4.0 μs and a τ_Q value of 40 μs was used.

Lineshape simulations of the spectra, partially narrowed by molecular motion, were simulated by standard methods using the program MXQET (15). These computations employed an IBM 3081-K mainframe. Simulated spectra were visually matched to experimental lineshapes. Molecular orbital calculations employed the Gaussian 90 program (22) on a Silicon Graphics Power Series 8 computer.

Results and discussion

Trimethyltelluronium iodide-d_3 ***(1)***

At temperatures between 77 and 423 K the ^2H spectrum of **1** is consistent with that expected for C_3 rotation of the methyl groups. There is no evidence for C_3' rotation in this temperature range. The observed quadrupolar splitting in this temperature range is 47.5 ± 0.5 kHz and, if the methyl groups are assumed to have a tetrahedral geometry, this corresponds to a χ value of 190 ± 2 kHz.

An X-ray diffraction study of **1** indicates that the iodide anions are situated in such a way that secondary bonding may occur between tellurium and the iodine (19). Tellurium ··· iodine secondary bonding has also been reported for β-dimethyltellurium di-iodide, $[Me_3Te]^+$ $[MeTeI_4]^-$ (23). The secondary Te ··· I contacts are approximately *trans* to the Te—C bonds. The existence of these secondary bonds would significantly hinder any C_3' rotation of the cation. Secondary Te ··· X bonds in $Me_3TeCl{\cdot}H_2O$, Me_3TeCl, Me_3TeBr, and Me_3TeI are responsible for scalar ^{125}Te—X *J*-coupling (X = ^{35}Cl, $^{79/81}Br$, ^{127}I) in the ^{125}Te CP/MAS spectra (19), although the internuclear distances are large enough that no dipolar coupling is observed in the static ^{125}Te powder spectra.

Trimethylselenonium iodide-d_3 ***(2)***

Deuterium NMR spectra were obtained for **2** in the temperature range 292–378 K. At the lowest temperature the cation is experiencing only C_3 rotation. Assuming a tetrahedral geometry for each methyl group, the quadrupolar splitting of 45.0 kHz corresponds to a χ value of 180.0 kHz. At temperatures above 378 K the cation is undergoing fast C_3 and C_3' rotation. The reduction in $\Delta\nu$ due to C_3' rotation corresponds to a θ_{SeC} angle of 62.0 ± 0.5°. The polar angle, θ_{EC}, between the E—C bonds and the C_3' rotational axis is related to the C—E—C bond angle, α, by eq. [8],

[8] $\cos(\alpha) = \cos^2(\theta) + \sin^2(\theta)\cos(\phi)$

where φ is the projection angle of the C—E—C bonds onto a plane perpendicular to the C_3' rotational axis.

For all the onium cations considered here, φ = 120°. Then

[9] $\alpha = \cos^{-1}[\cos^2(\theta_{EC}) - 0.5\sin^2(\theta_{EC})]$

The bond angle α is calculated to be 99.8 ± 0.5°, which is in good agreement with the X-ray diffraction crystal structure value of 98.5 ± 1° (18).

Now that the quadrupolar coupling constant, χ, and the polar angle, θ_{SeC}, have been determined from the lowest and highest temperature spectra, respectively, the only parameter that must be varied in order to match simulated and experimental spectra in the intermediate temperature region is the rate constant, k'. The best-fit simulations of spectra for the intermediate C_3' exchanges rates, together with the observed spectra, are shown in Fig. 2. The resulting eight $\ln k'$ versus $1/T$ points were fit to a straight line. The activation energy for C_3' exchange between methyl groups is 78 ± 3 kJ/mol.

The ability of the $(CH_3)_3Se^+$ cation to undergo C_3' rotation at lower temperatures than the $(CH_3)_3Te^+$ ion is a result of the weaker Se···I interaction in $(CH_3)_3SeI$ compared to three relatively strong Te···I interactions in $(CH_3)_3TeI$. The reported linebroadening in the ^{77}Se CP/MAS spectra of $(CH_3)_3SeI$ due to ^{77}Se-^{127}I *J*-coupling is much less severe than that due to ^{125}Te-^{127}I *J*-coupling in $(CH_3)_3TeI$ (19); this implies a weaker Se···I interaction in $(CH_3)_3SeI$.

Trimethylsulfonium iodide-d_9 ***(3)***

Deuterium NMR spectra of solid **3** were obtained at temperatures between 247 and 323 K. At 247 K and below, only methyl rotation is narrowing the lineshape and the measured $\Delta\nu$ value is 43.3 kHz. This yields a quadrupolar coupling constant, χ, of 173 kHz. The spectra at 323 K and above display fast C_3 and C_3' rotation. Assuming a tetrahedral geometry for the methyl groups, the best simulation of the spectrum at 323 K gives a polar angle, θ_{SC}, of 65.0 ± 0.5. The corresponding C—S—C bond angle is 103.4 ± 0.5°. This is in excellent agreement with the crystal structure value of 103 ± 1° (16). Simulations of the spectra in the intermediate exchange regime are shown, together with the experimental spectra, in Fig. 3. An Arrhenius plot of $\ln k'$ versus $1/T$ yields an activation energy of 65 ± 3 kJ/mol for C_3' cation rotation.

Trimethyloxonium-d_3 *tetrafluoroborate* ***(4)***

At temperatures above 240 K the ^2H spectrum of solid **4** is a smooth Lorentzian-like peak of half-maximum width 50 Hz. At lower temperatures a broad component appears. The lineshape of this broad component is consistent with the spectrum expected for fast C_3 and C_3' rotation. The quadrupolar splitting is 15 kHz. The lineshape of the broad component begins to change at 186 K and continues to change as the temperature is lowered. The narrow component begins to broaden at 157 K and by 138 K appears to contribute very little to the overall spectral intensity. The broad component of the ^2H spectrum could be successfully simu-

Can. J. Chem. Downloaded from www.nrcresearchpress.com by 88.255.202.194 on 09/08/12
For personal use only.

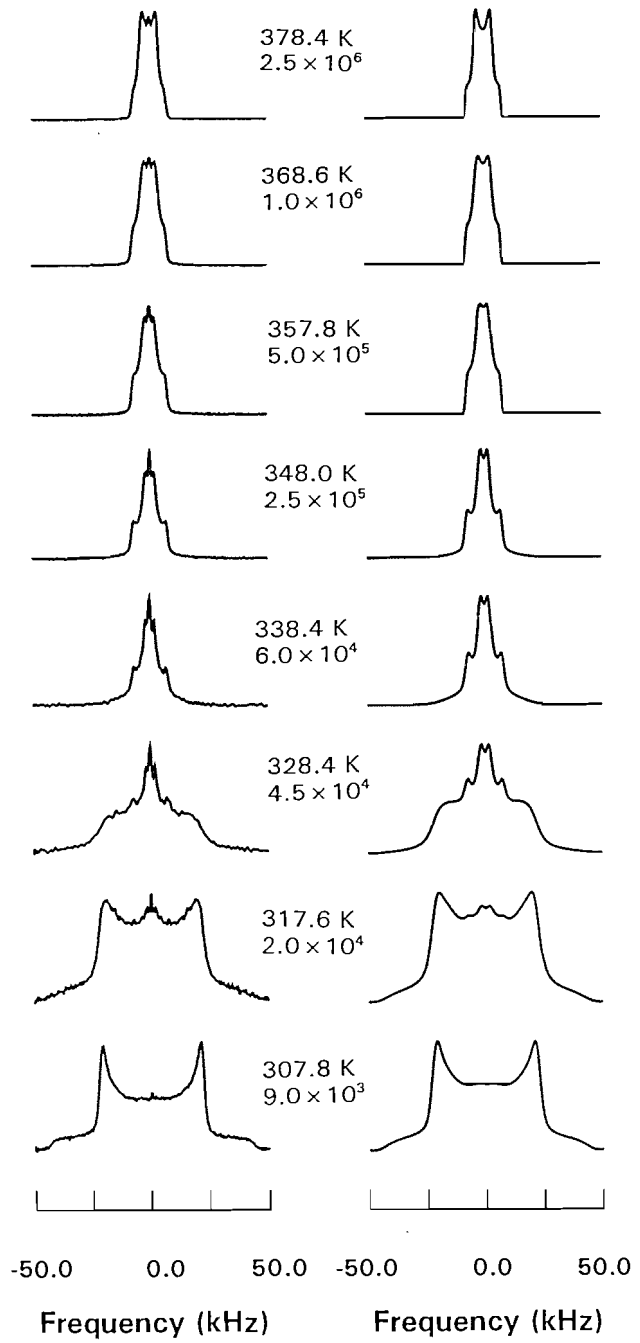

FIG. 2. Deuterium NMR spectra for trimethylselenium-d_3 iodide at various temperatures together with the best-fit simulated spectra.

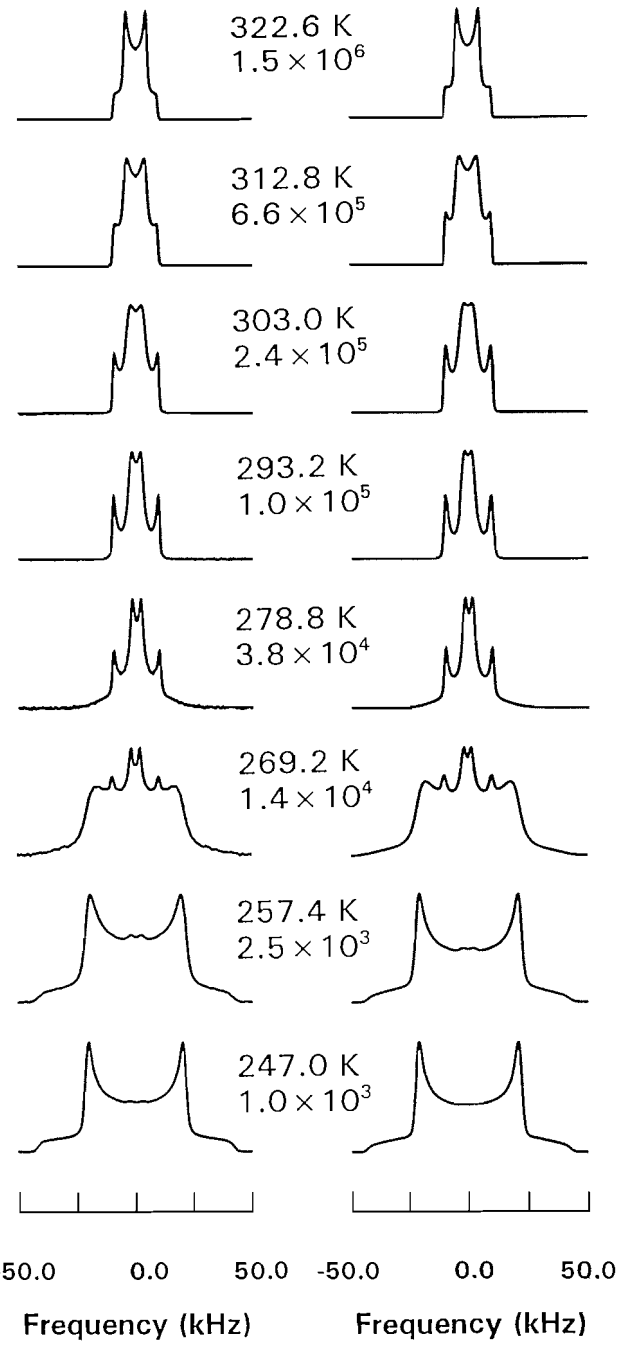

FIG. 3. Deuterium NMR spectra for trimethylsulfonium-d_9 iodide at various temperatures together with the best-fit simulated spectra.

lated using trimethyl rotational rates ranging from 1×10^3 s^{-1} at 119 K to 1.5×10^6 s^{-1} at 186 K. Simulated and experimental spectra are shown in Fig. 4. To satisfactorily simulate the spectrum at 119 K a methyl rotational rate of 4×10^6 s^{-1} was employed. At temperatures above 119 K the methyl C_3 rotation is in the fast exchange limit and the spectral lineshape is independent of the methyl exchange rate. The spectra were simulated with a χ value of 160 kHz and an angle, θ_{OC}, of 73.5°; the methyl groups were assumed to be tetrahedral ($\theta_{CD} = 70.5°$). An X-ray crystal structure is not available for **4** although a C—O—C bond angle of 112.7 ± 2.5° has been found for $(CH_3CH_2)_3O^+PF_6^-$ (16). This is in close agreement with our value of 112.2 ± 1.0°. An Arrhenius plot of the C_3' rotational rates of the oxonium cation versus inverse temperature gave an activation energy of 31 ± 2 kJ/mol.

It is evident that the sample of **4** consists of two components. We have identified one component as due to the oxonium cation undergoing varying rates of methyl rotation and trimethyl rotation below 240 K. The component that remains narrow over a larger temperature range is either a coexisting phase of **4** or an impurity. The ^{13}C spectrum of the solid showed only one resonance of peak width 800 Hz (8 ppm). Two possible impurities, due to the hydrolysis of

Can. J. Chem. Downloaded from www.nrcresearchpress.com by 88.255.202.194 on 09/08/12
For personal use only.

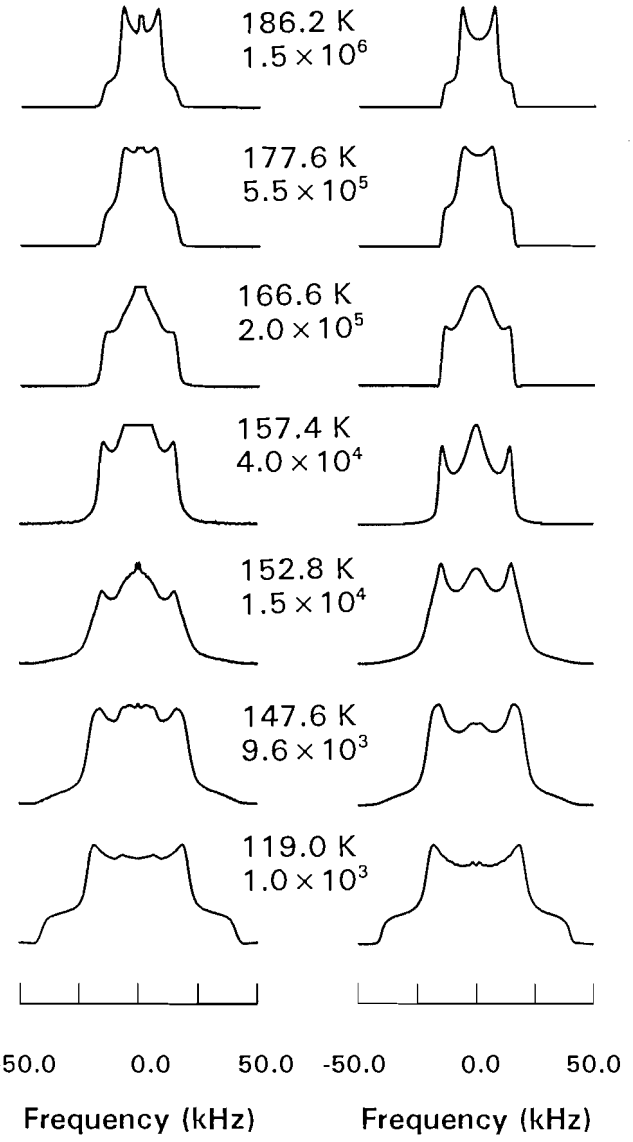

FIG. 4. Deuterium NMR spectra for trimethyloxonium-d_3 tetrafluoroborate at various temperatures. Simulations of the broad component are shown on the right-hand side.

4, are dimethyl ether and methanol. These impurities have ^{13}C chemical shifts that are easily resolved from that for **4**: ($\delta((CH_3)_3O^+)$ = 79 ppm, $\delta((CH_3)_2O)$ = 60 ppm, and $\delta(CH_3OH)$ = 49 ppm. We therefore suggest that some of the trimethyloxonium cations in solid $(CH_3)_3O^+BF_4^-$ can exist in a motionally different regime. Figure 5 shows a spectrum of **4** at 77 K. The spectrum consists of a component with a quadrupolar splitting of 40.5 ± 2 kHz and a component with a splitting of 124 ± 6 kHz, suggesting that at 77 K one component is in the rigid lattice limit and the other is undergoing C_3 rotation.

Oxonium cations may also undergo inversion about the oxygen atom. Rapid inversion would introduce a non-zero asymmetry ($\eta > 0$) and reduce the effective quadrupolar coupling constant. These effects are not observed in the broad component of the deuterium NMR spectrum of **4**. The high-temperature narrow component is likely due to isotropic random reorientation of the trimethyloxonium cation; additional inversion will not change the spectral lineshape. Molecular orbital calculations at the MP2/6-31G** level yield an inversion barrier of 20.9 kJ/mol. The only reported inversion barrier for an oxonium salt in solution is that for **8**. A proton dynamic NMR study of **8** yields an inversion barrier of 42 ± 8 kJ/mol (24). These values suggest that for the broad component the inversion barrier in the solid is higher than those for the gas or solution phases.

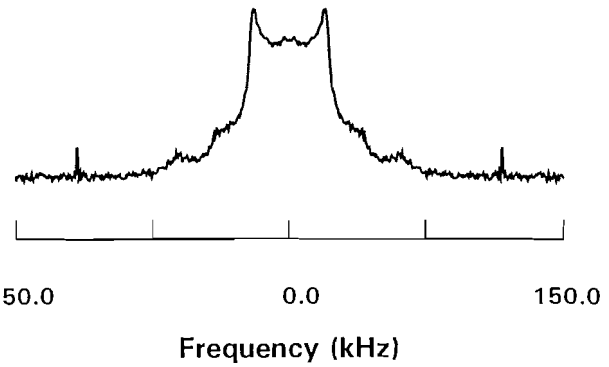

FIG. 5. The deuterium NMR spectrum of trimethyloxonium-d_3 tetrafluoroborate at 77 K.

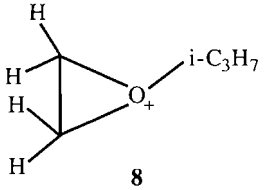

8

Variation of χ in the series $(CH_3)E^+$

The deuterium quadrupolar coupling constant, χ, in the series $(CH_3)_3E^+$ shows a rather significant change with atom E. The value increases steadily from 160 kHz for E = O to 190 kHz for E = Te. Molecular orbital calculations of the electric field gradient, q_{zz}, at the deuterium sites can provide theoretical χ values if the nuclear quadrupolar moment, Q, is known. Equation [10] relates the three quantities,

$$[10] \quad \chi = 235Q\,q_{zz}$$

where q_{zz} is in atomic units, Q has units of 10^{-28} m^2, and χ has units of MHz. Molecular orbital calculations of χ using the STO-3G* basis set are given in Table 1. Although the χ values are not quantitatively reproduced, the trend of decreasing χ with decreasing size of the E-atom is apparant. It has been shown that χ values calculated with large basis sets (e.g., 6-31G*) and at levels where second-order correlation effects are taken into account (e.g., MP2 or CI) are in good aggreement with those obtained from gas phase experiments (e.g., microwave spectroscopy) (25–27). The large size of the Se and Te atoms has restricted our calculations to the STO-3G* basis; therefore electron correlation effects are not taken into account. Also, our experiments were carried out in the solid state. Nevertheless, a qualitative comparison between experiment and theoretical calculation can be made. There are two factors that can affect χ in molecules of the type $(CH_3)_3E^+$: the size of the central atom and the molecular geometry about the central atom. To test the first effect, q_{zz} was calculated for oxygen and sulfur central atoms with the angle θ_{EC} held at 65°. The value of χ increased from 196.7 kHz (E = O) to 199.3 kHz (E = S).

TABLE 1. Activation energies for C_3' motion, bond angles, and deuterium quadrupolar coupling constants for various $(CH_3)_3E^+$ salts

Variable	$(CH_3)_3TeI$	$(CH_3)_3SeI$	$(CH_3)_3SI$	$(CH_3)_3OBF_4$
E_a (kJ/mol)	—	78 ± 3	65 ± 3	31 ± 2
θ_{EC} (deg)	—	62.0 ± 0.5	65.0 ± 0.5	73.5 ± 1.0
α_{EC} (deg)	—	99.8 ± 0.5	103.4 ± 0.5	112.2 ± 1.0
$\alpha_{X\text{-}ray}$	94.2 ± 0.1	98.5 ± 1	103 ± 1	112.7 ± 2.5[a]
χ_{obs} (kHz)	190 ± 2	180 ± 2	173 ± 2	160 ± 2
χ_{MO} (kHz)	203.5	201.8	200.8	196.7

[a]For triethyloxonium hexafluorophosphate (16).

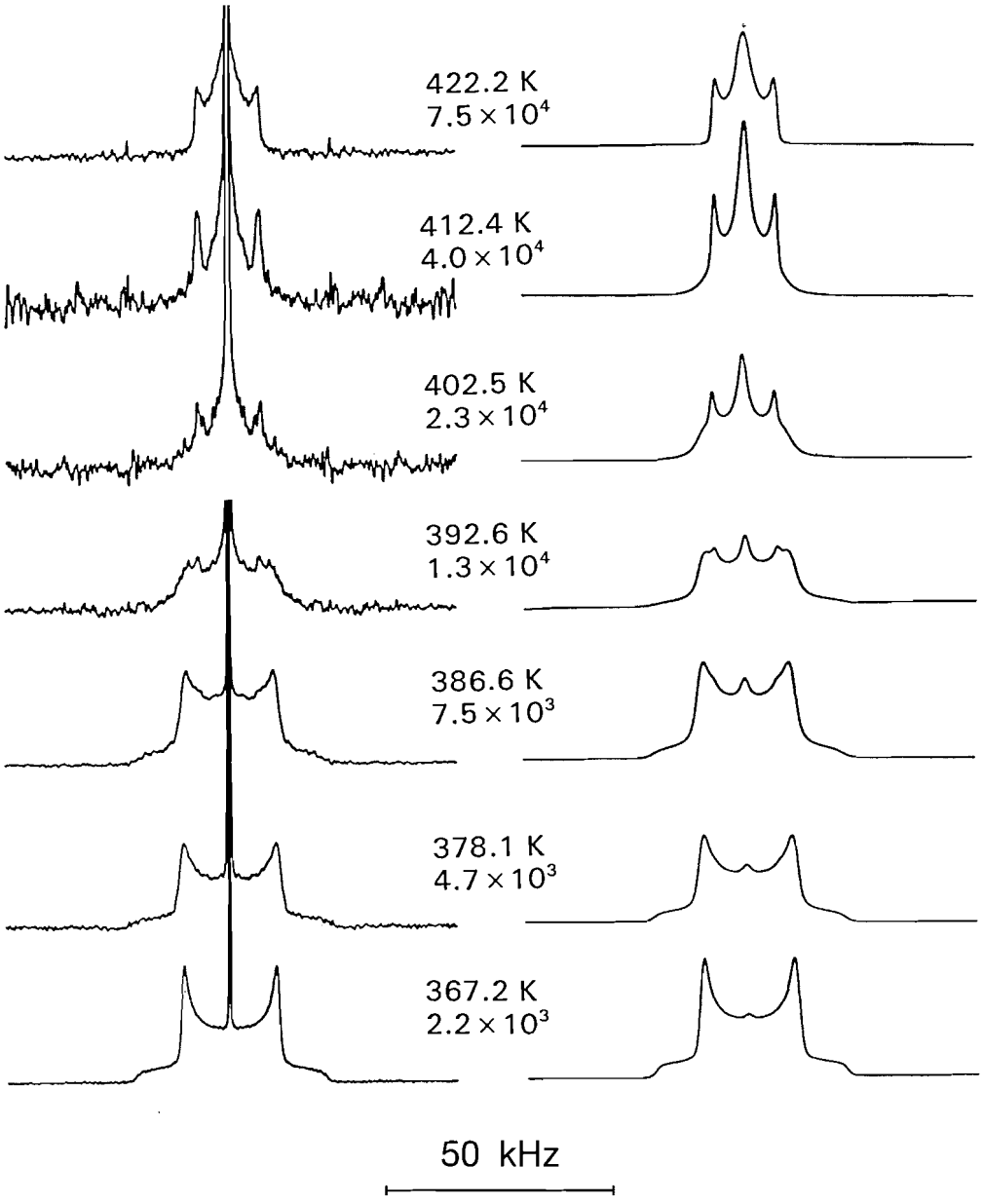

FIG. 6. Deuterium NMR spectra for phenyltrimethylarsoniun-d_3 iodide at various temperatures together with simulated spectra.

Calculations of χ for both the oxygen and sulfur compounds were performed while varying θ_{EC} from 90° to 45°. For both molecules the magnitude of q_{zz} and hence χ increased. These calculations suggest that as one descends group VIB the increasing size of the E-atom and the decreasing angle θ_{EC} each yield an increase in the quadrupolar coupling constant for the methyl deuterons. One factor that cannot be assessed by standard molecular orbital calculations is the intermolecular

Can. J. Chem. Downloaded from www.nrcresearchpress.com by 88.255.202.194 on 09/08/12
For personal use only.

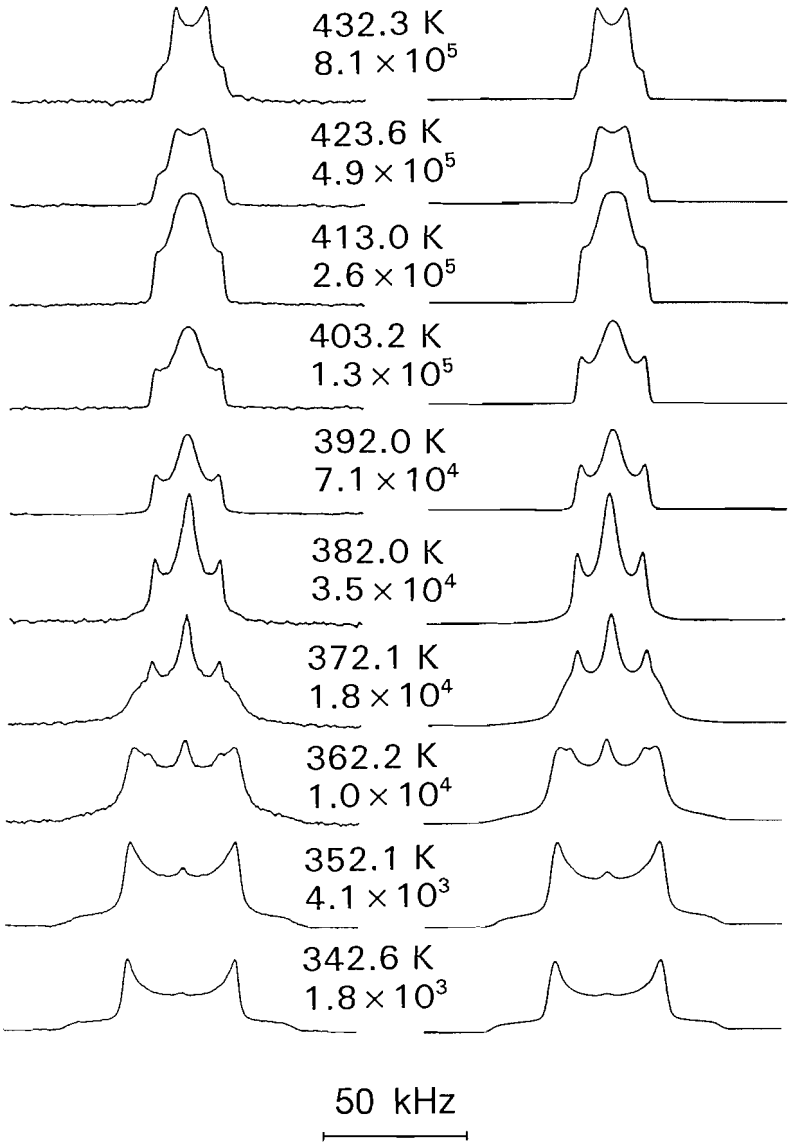

FIG. 7. Deuterium NMR spectra for phenyltrimethylphosphonium-d_3 iodide at various temperatures together with simulated spectra.

Can. J. Chem. Downloaded from www.nrcresearchpress.com by 88.255.202.194 on 09/08/12
For personal use only.

contribution to χ due to the neighboring atoms in the crystalline material. To our knowledge the χ value of 190 kHz for **1** is the largest reported for a methyl deuteron.

Phenyltrimethylarsonium-d_3 *iodide (**5**)*

The ^{2}H NMR lineshapes for **5** are shown in Fig. 6. At temperatures below 367 K there is only evidence of methyl rotation. At higher temperatures the lineshape changes in a way characteristic of that expected for intermediate C_3' rotational rates. It is evident that even at the highest attainable temperature (422 K) the trimethyl rotation is not in the fast exchange limit. The central component, which increases in intensity with increasing temperature, is due to decomposition products. Despite relatively poor signal to noise, the lineshape could be simulated with χ = 59 kHz, θ_{As-C} = 70.5, and trimethyl exchange rates between 2.2 kHz (367 K) and 75 kHz (422 K). Simulations are also shown in Fig. 6. The Arrhenius activation energy for reorientation of the $(CH_3)_3As$ group is 96.6 ± 4.6 kJ/mol.

Phenyltrimethylphosphonium-d_3 *iodide (**6**)*

The ^{2}H NMR spectra of **6** are displayed in Fig. 7. The appearance of the spectra below 345 K is consistent with rapid rotation of the methyl groups. Attempts were made to simulate the higher temperature, intermediate C_3' exchange, spectra by varying only k'. Although the general lineshapes could be simulated, the experimental linewidth became progressively narrower with increasing temperature. The reduction of linewidth with increasing temperature is due to a third reorientational motion of the methyl deuterons. This motion is likely a wobbling of the phenyltrimethylphosphonium cation, with the amplitude of the motion increasing with temperature. At the highest attainable temperature (432 K) the trimethyl rotation is not yet in the fast exchange regime. The wobbling motion is taken into account in the simulations by simply reducing the effective quadrupolar coupling constant as the temperature increases. A precessional wobble has been used to explain the decrease in χ_{eff} with increasing temperature for deuterated CH_3NH_3 cations

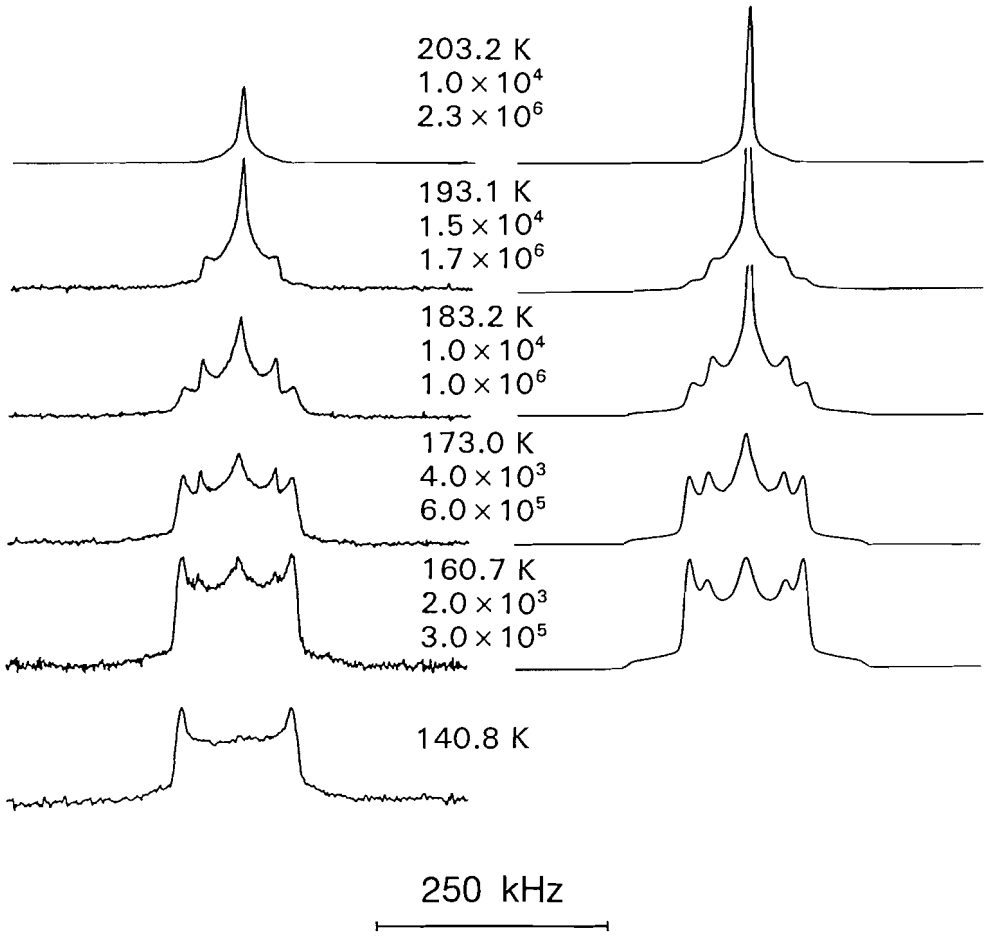

FIG. 8. Deuterium NMR spectra for phenyltrimethyl ammonium-d_3 iodide at various temperatures together with simulated spectra.

in methylammonium salts (28, 29). At temperatures between 343 and 432 K effective χ values ranging from 159 to 146 kHz were employed. The activation energy for trimethyl rotation in **6** is 84.3 ± 0.6 kJ/mol.

Phenyltrimethylammonium-d_3 *iodide (7)*

At temperatures above 300 K the ^{2}H NMR series of **7** indicate that the trimethylammonium group is undergoing both fast methyl and trimethyl rotation. The quadrupolar splitting is about 11 kHz. At temperatures below 150 K both methyl and trimethyl rotation are in the rigid lattice limit. The quadrupolar splitting is 128 ± 5 kHz, yielding a χ value of 171 ± 7 kHz. Therefore, if the geometries about the methyl carbons and ammonium nitrogen are tetrahedral, fast C_3 and C_3' rotation should yield quadrupolar splitting of 14 kHz. This is larger than the observed value of 11 kHz. The observed splitting does not decrease with an increase with temperature; therefore a temperature-dependent wobbling motion similar to that proposed for the phosphonium cation is unlikely. The alternative explanation is a distortion of either the methyl groups or the trimethylammonium group from tetrahedral geometries. A crystal structure is available for phenyltrimethylammonium chloride; the average C(1)—N—CH_3 bond angle, θ_{NC}, is 110.8° (30). If tetrahedral methyl groups are assumed, then eq. [4] yields a reduction of about 1 kHz in $\Delta\nu$. The deviation may be larger for **7**, the iodide salt. An average bond angle, θ_{NC}, of 113.5° is required to give a splitting of 11 kHz. The N—C—H bond angles of the methyl groups, θ_{CD}, may also be greater than 109.5°, yielding a decrease in $\Delta\nu$. The crystal structure of the chloride salt does not provide accurate positions for the methyl hydrogens.

As the temperature of the sample is lowered, the sharp peaks (which define the quadrupolar splitting) become less well defined and, by 233 K, have vanished completely leaving only a smooth Lorentzian-like curve with a width at half maximum of ≈8 kHz. A broad component of low intensity appears at 203 K. As the temperature is further lowered the intensity of the broad component increases at the expense of that of the narrow peak and, by 140 K, the spectrum indicates that the rigid lattice limit has been reached. The spectra for temperatures between 140 and 203 K are shown in Fig. 8. The spectra shown in Fig. 8 are typical of those expected when C_3 and C_3' rotation are of comparable rate (11). Previous work by Ripmeester and Ratcliffe (8, 9) demonstrated that, in trimethyl and tetramethylammonium salts, both C_3' and C_3 rotation may be in the intermediate exchange region at low temperatures. It was also shown that in some $(CH_3)_3CX$ systems C_3' rotation is rapid at low temperatures, whereas C_3 rotation is slow (7, 12). In principle it should be possible to reproduce the spectra shown in Fig. 7, given the correct geometry for the trimethylammonium group (θ_{MC} and θ_{CD}) and the correct combination of k and k'. Any simulations that resembled the observed spectra required that k' be larger than k. Unfortunately these simulations yield a central peak that is too intense. Adjusting the angle θ_{NC}, such that the 11 kHz splitting is reproduced at

Can. J. Chem. Downloaded from www.nrcresearchpress.com by 88.255.202.194 on 09/08/12
For personal use only.

Can. J. Chem. Downloaded from www.nrcresearchpress.com by 88.255.202.194 on 09/08/12
For personal use only.

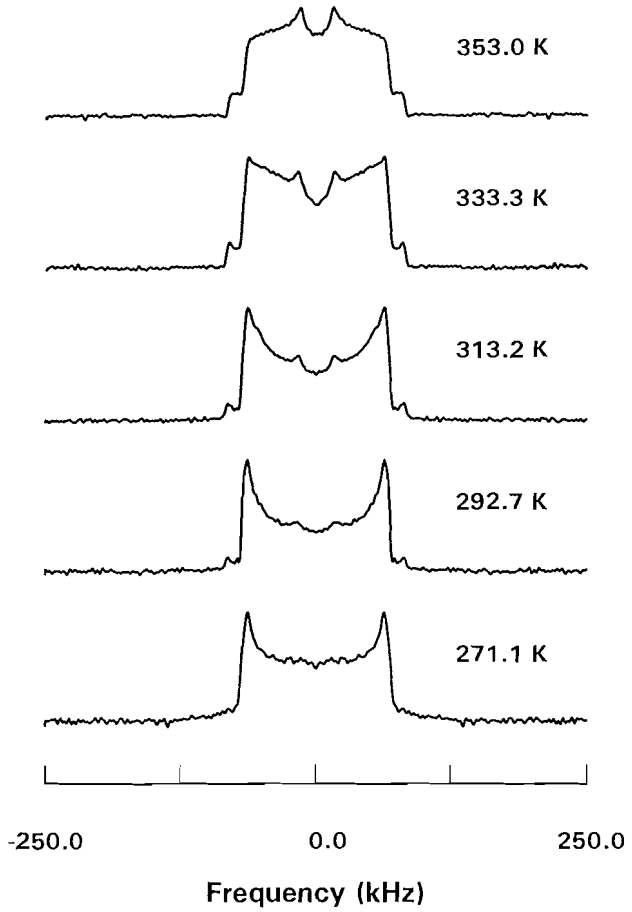

FIG. 9. Low-temperature deuterium NMR spectra for ring-deuterated phenyl-d_3-trimethyl ammonium iodide.

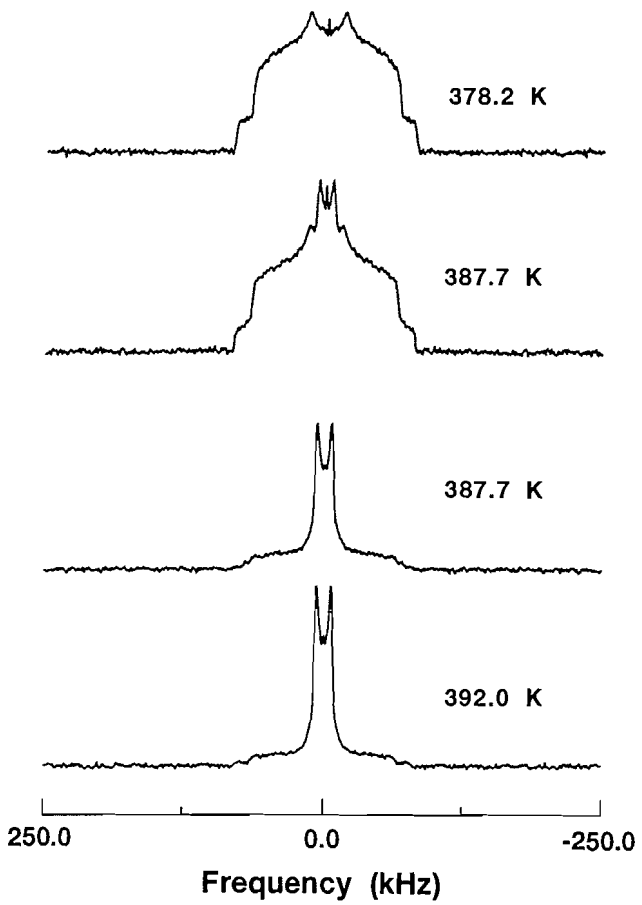

FIG. 10. Deuterium NMR spectra for ring-deuterated phenyl-d_3-trimethyl ammonium iodide near the transition temperature.

higher temperatures, yields some improvement in the fit of the broad component, although the narrow resonance is still too intense. The best-fit simulations are also displayed in Fig. 8. A less significant improvement in the simulations is obtained if one of the methyl groups is allowed to be rotationally inequivalent. With both models k' was required to be about two orders of magnitude greater than k. The former model gave activation energies for methyl and trimethyl rotation of 18.8 ± 1.5 and 13.3 ± 0.4 kJ/mol, respectively. The error quoted is simply the standard deviation obtained from a least-squares fit to the equation $\ln k = E_a/RT + \ln k_0$ and does not reflect the uncertainty associated with the flexibility in the combinations of k and k' that gave reasonable simulated spectra. A satisfactory analysis of the ^2H spectra of methyl-deuterated **7** may well require that the angle θ_{CD} as well as the rotational rates differ for each of the three methyl groups. Analysis of such a nine-site dynamic system (7 variables, with χ and methyl geometry fixed) would be too time consuming and has not been undertaken.

Phenyl-d_3 *trimethylammonium iodide (7)*

The ^2H spectra for **7** deuterated in the *ortho* and *para* positions are shown in Figs. 9 and 10. The lowest temperature spectrum (271 K) is consistent with a rigid phenyl ring. As the temperature is increased the lineshape changes and takes on the appearance of that expected for a superposition of the spectrum for the *para* deuteron, which is not reorienting, and the spectrum for the *ortho* deuterons, which are undergoing two-site exchange. The spectral lineshape changes as the rate of ring reorientation increases with increasing temperature. By about 378 K the rate of ring flipping is in the fast exchange limit. At higher temperature (388 K) a doublet with a splitting of 16 kHz begins to appear. After an additional 15 min at 388 K the broad signal is nearly gone and the intensity of the doublet has increased. After heating the sample to 392 K (the upper temperature limit for our spectrometer) the relative intensity of the narrow doublet has further increased. The appearance of a narrow doublet with a quadrupolar splitting of 16 kHz suggests that the sample goes through a transition to a phase in which the phenyl ring is jumping between n ($n \geq 3$) equivalent sites. Molecular

TABLE 2. Activation energies for C_3' rotation for some trimethyl-M groups

M	E_a (kJ/mol)	Reference
O^+	31 ± 2	This work
S^+	65 ± 3	This work
Se^+	78 ± 3	This work
Te^+	>100	This work
$S{=}O^+$	46 ± 4	10
P=S	41 ± 4	42
N	33 ± 7	11
$N\text{-}C_6H_5^+$	13.3 ± 0.4	This work
$P\text{-}C_6H_5^+$	84.3 ± 0.6	This work
$As\text{-}C_6H_5^+$	96.6 ± 4.6	This work

reorientation has been studied in a large number of solid ammonium salts (8, 9, 28, 29, 31–39). Ratcliffe and Dunell have used proton spin-lattice relaxation times to investigate the reorientation motion of the $-NH_3^+$ and phenyl moieties in solid anilinium chloride, bromide, iodide, and sulphate salts (40). In an ^{123}I NQR study of $C_6H_6NH_3^+I^-$ Fecher and Weiss suggest the possibility of phenyl ring motion (41).

Although there have been numerous investigations of trimethyl rotation by ^1H and ^2H NMR spectroscopy, very few activation energies are reported. There are a number of reasons for this, the most serious being the difficulty in separating contributions to T_1, second moment, or lineshape due to methyl and trimethyl rotation when the two motions have similar activation energies. In some cases additional motions (5–7, 8, 9) make the analysis difficult. A number of investigations were reported before computer lineshape simulation programs capable of reproducing intermediate exchange rate spectra were commonly available. Activation energies for C_3' rotation in several trimethyl compounds are given in Table 2.

Rotation of trimethyl groups can be influenced by a number of intermolecular interactions such as secondary bonding, hydrogen bonding, and the relative proximity and orientation of adjacent molecules (crystal packing). It is extremely difficult to predict the influence of each of these factors without good crystal structures. For example, the extent of secondary bonding influences the trimethyl rotation in $(CH_3)_3E^+$ cations, whereas it is unclear what factors contribute to the hindered rotation for $(CH_3)_3MC_6H_5^+$ cations.

In this study, deuterium NMR spectral lineshape techniques were employed to determine the dynamics of trimethyl groups in $(CH_3)_3E^+$ and $(CH_3)_3MC_6H_5^+$ cations. It is shown that for the former the C—E—C bond angle decreases and the magnitude of the quadrupolar coupling constant increases. For both series of compounds the lineshape analyses show that the trimethyl rotational barrier increases with size of the central atom, E or M. Trimethyl rotation is slower and has a higher activation energy than methyl rotation for all compounds except $(CH_3)_3NC_6H_5^+$.

Acknowledgements

We thank the National Sciences and Engineering Research Council of Canada (NSERC) for financial support. We are very grateful to Dr. J. K. Jeffrey for access to the home-built spectrometer. We also thank the University of Guelph for allocations of computer time.

1. H. W. Spiess. Adv. Polym. Sci. **60**, 23 (1985).
2. R. G. Griffin. Methods Enzymol. **72**, 108 (1981).
3. J. H. Davis. *In* Isotopes in the physical and biomedical science. Vol. 3. *Edited by* E. Buncel and J. R. Jones. Elsevier, Amsterdam. 1991.
4. A. F. Thomas. Deuterium labelling in organic chemistry. Meredith Corp., New York. 1971.
5. S. Mooibroek and R. E. Wasylishen. Can. J. Chem. **63**, 2926 (1989).
6. B. A. Pettitt, J. S. Lewis, R. E. Wasylishen, W. Danchura, and E. Tomchuck. J. Magn. Reson. **44**, 508 (1981).
7. S. Mooibroek, R. E. Wasyishen, J. B. MacDonald, C. I. Ratcliffe, and J. A. Ripmeester. Can. J. Chem. **66**, 734 (1988).
8. C. I. Ratcliffe and J. A. Ripmeester. Can. J. Chem. **64**, 1348 (1986).
9. J. A. Ripmeester and C. I. Ratcliffe. *In* Dynamics of molecular crystals. *Edited by* J. Lascombe. Elsevier Science Publishers, Amsterdam. 1987.
10. L. J. Schwartz, E. Meirovitch, J. A. Ripmeester, and J. H. Freed. J. Phys. Chem. **87**, 4457 (1983).
11. A. J. Vega and Z. Luz. J. Chem. Phys. **86**, 1803 (1987).
12. G. H. Penner, J. M. Polson, C. Stuart, G. Ferguson, and B. Kaitner. J. Chem. Phys. **96**, 5121 (1992).
13. H. H. Mantsch, H. Saito, and I. C. P. Smith. Prog. NMR Spectrosc. **11**, 211 (1977).
14. R. J. Wittebort, E. T. Olejniczac, and R. G. Griffin. J. Chem. Phys. **86**, 5411 (1987).
15. M. S. Greenfield, A. D. Ronemus, R. L. Vold, R. R. Vold, P. D. Ellis, and T. R. Raidy. J. Magn. Reson. **72**, 89 (1987).
16. M. I. Watkins, W. M. Ip, G. A. Olah, and R. Bau. J. Am. Chem. Soc. **104**, 2365 (1982).
17. D. E. Zuccaro and J. D. McCullough. Z. Kristallogr. **112**, 26 (1959).
18. H. Hope. Acta. Crystallogr. **20**, 610 (1966).
19. M. J. Collins, J. A. Ripmeester, and J. F. Sawyer. J. Am. Chem. Soc. **110**, 8583 (1988).
20. G. A. Olah, H. Doggweiler, and J. D. Felberg. J. Org. Chem. **49**, 2112 (1984).
21. J. H. Davis, K. R. Jeffrey, M. Bloom, M. I. Valic, and T. P. Higgs. Chem. Phys. Lett. **42**, 390 (1976).
22. M. J. Fisch, M. Head-Gordon, G. W. Trucks, J. B. Foresman, H. B. Schlegal, K. Raghavachari, M. Robb, J. S. Binkley, C. Gonzales, D. J. DeFrees, D. J. Fox, R. A. Whiteside, R. Seeger, C. F. Melius, J. Baker, R. L. Martin, L. R. Kahn, J. J. D. Stewart, S. Topiol, and J. A. Pople. Gaussian 90, Revision F. Gaussian Inc., Pittsburg, Pa. 1990.
23. F. Einstein, J. Trotter, and C. Williston. J. Chem. Soc. A, 2018 (1967).
24. J. B. Lambert and D. H. Johnson. J. Am. Chem. Soc. **90**, 1349 (1968).
25. M. H. Palmer. Z. Naturforsch. **45A**, 357 (1990).
26. M. H. Palmer. Z. Naturforsch. **41A**, 1471 (1986).
27. G. H. Penner, S. I. Daleman, and A. R. Custodio. Can. J. Chem. **70**, 2420 (1992).
28. M. Körfer, R. Kind, and H. Fuess. Z. Naturforsch. **44A**, 1177 (1989).
29. M. L. H. Gruwel and R. E. Wasylishen. Z. Naturforsch. **45A**, 55 (1990).
30. V. V. Krug and U. Mueller. Acta. Crystallogr. **C45**, 2022 (1989).
31. J. Tsau and D. F. R. Gilson. Can. J. Chem. **48**, 717 (1970).
32. H. Ishida, T. Iwachido, N. Hayama, R. Ikeda, M. Terashima, and D. Nakamura. Z. Naturforsch. **44A**, 741 (1989).
33. K. Hirokawa and Y. Furukawa. Z. Naturforsch. **43A**, 187 (1988).
34. A. Kobayashi, Y. Yoshioka, N. Nakamura, and H. Chihara. Z. Naturforsch. **43A**, 233 (1988).
35. Y. Furukawa and D. Nakammura. Z. Naturforsch. **44A**, 112 (1989).
36. Q. Xu, T. Eguchi, H. Nakayama, N. Nakamura, and M. Kishita. Z. Naturforsch. **46A**, 240 (1991).
37. H. Ishida, S. Inada, N. Hayama, D. Nakamura, and R. Ikeda. Z. Naturforsch. **46A**, 265 (1991).
38. C. I. Ratcliffe. J. Phys. Chem. **94**, 152 (1990).
39. R. Ikeda, A. Kubo, and C. A. McDowell. J. Phys. Chem. **93**, 7315 (1989)
40. C. I. Ratcliffe and B. A. Dunell. Faraday Disc. Chem. Soc. Faraday Symp. **13**, 142 (1979).
41. G. Fecher and A. Weiss. Ber. Bunsenges. Phys. Chem. **90**, 10 (1986).
42. G. R. Hays, Ph.D. Thesis, University of East Anglia, 1978.

Can. J. Chem. Downloaded from www.nrcresearchpress.com by 88.255.202.194 on 09/08/12
For personal use only.

Preparation and reactions of bromo-2-nitro- and bromo-2-aminoimidazoles

SALIM F. FARAH AND ROBERT A. MCCLELLAND[1]
Department of Chemistry, University of Toronto, Toronto, Ont., Canada M5S 1A1

Received October 23, 1992

SALIM F. FARAH and ROBERT A. MCCLELLAND. Can. J. Chem. **71**, 427 (1993).

Treatment of 1-methyl-2-nitroimidazole with bromine in water resulted in rapid dibromination to give 4,5-dibromo-1-methyl-2-nitroimidazole. In dioxane, the bromination was slower, and could be controlled to give 4-bromo-1-methyl-2-nitroimidazole **5** and 5-bromo-1-methyl-2-nitroimidazole **6** in a 4:1 ratio. In an attempt to displace the bromine, the monobromo compounds were treated with cysteamine hydrochloride. In each case the nitro group was displaced instead, the 4-bromo **5** resulting in 2-[(2-aminoethyl)thio]-4-bromo-1-methylimidazole **9** as sole product, and the 5-bromo **6** giving two products identified as the monosubstituted 2-[(2-aminoethyl)thio]-5-bromo-1-methylimidazole **13** and the disubstituted 2,5-bis[2-(aminoethyl)thio]-1-methylimidazole **12**. The latter product forms by further reaction of the former and was the sole material observed at long reaction times. A fraction of **12** may also originate from an initial displacement of bromine giving 5-[(2-aminoethyl)thio]-1-methyl-2-nitroimidazole **14**, although this cannot be observed due to a rapid further displacement of its nitro group. The bromonitroimidazoles **5** and **6** were reduced to 4-bromo-2-amino-1-methylimidazole **25** and 5-bromo-2-amino-1-methylimidazole **26** with Zn/HCl. On reflux in water, in the presence or absence of cysteamine hydrochloride, these undergo a protodebromination resulting in the same product, 2-amino-1-methylimidazole **17**. In D_2O the 4-bromo isomer was demonstrated to react specifically to give 2-amino-4-deuterio-1-methylimidazole **27**. Attempted preparation of the bromoaminoimidazoles **25** and **26** by bromination of 2-amino-1-methylimidazole in water resulted in the clean formation of *cis* and *trans* 2-amino-4,5-dihydro-4,5-dihydroxyimidazolium ions **18**.

SALIM F. FARAH et ROBERT A. MCCLELLAND. Can. J. Chem. **71**, 427 (1993).

Le traitement du 1-méthyl-2-nitroimidazole avec du brome dans l'eau conduit à une dibromation rapide, avec formation du 4,5-dibromo-1-méthyl-2-nitroimidazole. Dans le dioxane, la bromation est plus lente et elle peut être contrôlée pour conduire à la formation des 4-bromo- (**5**) et 5-bromo- (**6**) 1-méthyl-2-nitroimidazoles, dans un rapport de 4 : 1. Dans un effort pour déplacer le brome, on a traité les composés monobromés avec de chlorhydrate de la cystéinamine. Dans chaque cas, c'est plutôt le groupe nitro qui a été déplacé; le dérivé 4-bromé (**5**) conduit uniquement au 2-[(2-aminoéthyl)thio]-4-bromo-1-méthylimidazole (**9**) alors que le composé 5-bromé (**6**) fournit deux produits identifiés comme le 2-[(2-aminoéthyl)thio]-5-bromo-1-méthylimidazole (**13**) monosubstitué et le 2,5-bis-[2-(aminoéthyl)thio]-1-méthylimidazole (**12**) disubstitué. Ce dernier composé se forme par réaction ultérieure du premier; il est le seul produit à se former après des temps de réactions prolongés. Une partie du composé **12** peut aussi provenir d'un déplacement initial du brome conduisant au 5-[(2-aminoéthyl)thio]-1-méthyl-2-imidazole (**14**); toutefois, on ne peut pas observer sa formation à cause de la substitution rapide du groupe nitro. On a réduit les bromonitroimidazoles **5** et **6** avec du Zn/HCl et on a obtenu les 4-bromo- (**25**) et 5-bromo- (**26**) 2-amino-1-méthylimidazoles. Par reflux dans de l'eau, en présence ou en l'absence du chlorhydrate de cystéinamine, ces composés subissent tous les deux une protodébromation conduisant au même composé, le 2-amino-1-méthylimidazole (**17**). Dans le D_2O, il a été démontré que l'isomère 4-bromé réagit spécifiquement pour donner le 2-amino-4-deutéro-1-méthylimidzole (**27**). Des essais de préparation des bromoaminoimidazoles **25** et **26** par bromation du 2-amino-1-méthylimidazole dans l'eau à conduit à la formation propre des ions 2-amino-4,5-dihydro-4,5-dihydroxyimidazolium *cis* et *trans* (**18**).

[Traduit par la rédaction]

As part of a program of study of the reduction products of 2-nitroimidazoles (1), we desired independent routes to imidazole derivatives of the structure **3** and **4**.

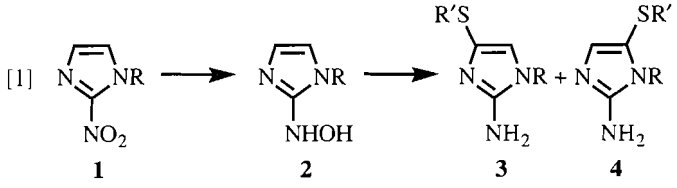

Such compounds have been characterized in mixtures after the reduction of the 2-nitroimidazole misonidazole (**1**, R = $CH_2CHOHCH_2OCH_3$) following treatment with the thiol glutathione (γ-glutamylcysteinylglycine) (2, 3). They are also observed by reacting an isolated sample of the product of four-electron reduction, the 2-hydroxylaminoimidazole **2**, with thiols such as cysteamine and glutathione (4–6). Misonidazole depletes intracellular glutathione selectively under hypoxic conditions (7), and this chemistry provides a model for the effect. Indeed, the formation of the adducts **3** and **4** has been implicated in biological systems (8–10). There are, however, uncertainties that would be answered through the availability of pure authentic material, particularly with respect to the exact structures of these adducts (11), and to the structures of the metabolites that are being observed in cells.

As an initial approach to these compounds we envisaged the reaction of bromo-2-nitroimidazoles with an appropriate thiol, to be followed by reduction of the nitro group to the amine.

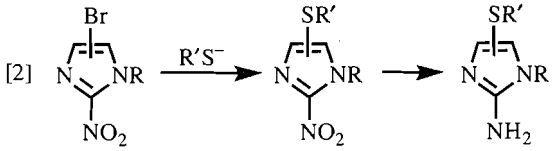

Nitro groups situated at positions 4 and 5 of an imidazole are known to activate adjacent halogens to nucleophilic

[1]Author to whom correspondence may be addressed.

Can. J. Chem. Downloaded from www.nrcresearchpress.com by 88.255.202.194 on 09/08/12
For personal use only.

substitution (12–15), and there is a recent example, the conversion of 4,5-dibromo-1-methyl-2-nitroimidazole to 4-bromo-5-morphilino-1-methyl-2-nitroimidazole (16), that offers precedent in the case of a 2-nitro compound. This plan obviously required a convenient route to the bromonitroimidazoles. An examination of the literature revealed a 4-bromo derivative of misonidazole (**4**, R = CH_2CHOH-CH_2OCH_3), prepared by bromination of the parent nitro compound with Br_2 in dioxane (17), and, more recently, 4-bromo-1-methyl-2-nitroimidazole, prepared by treatment of the nitro compound with *N*-bromosuccinimide (NBS) in dioxane (16). Neither of these studies mentioned the presence of the 5-bromo isomer, although the latter did prepare 4,5-dibromo-1-methyl-2-nitroimidazole. This was achieved by methylation of the N1-unsubstituted compound, as obtained by NBS treatment of azomycin (**1**, R = H), a reaction that could not be stopped at the monobromo stage.

In this paper we report conditions where both 4-bromo and 5-bromo isomers of 1-methyl-2-nitroimidazole are obtained from the bromination of the nitro compound. We further describe the outcome of the treatment of these compounds with the thiol cysteamine. This reaction disappointingly proceeds with displacement of the nitro group rather than the halogen. We also report further novel results encountered in our examination of these systems: a protodebromination of 4-bromo- and 5-bromo-2-aminoimidazoles that offers a convenient route to specifically deuterated 2-aminoimidazoles, and an attempted bromination of a 2-aminoimidazole that leads to 4,5-dihydro-4,5-dihydroxyimidazolium ions.

Results and discussion

4-Bromo- and 5-bromo-1-methyl-2-nitroimidazoles

Our route to these compounds involved the reaction of molecular bromine with 1-methyl-2-nitroimidazole. In water the reaction was very fast, and although the monobromo derivatives are presumably intermediate, the reaction could not be stopped at this stage, the product even with stoichiometric amounts of bromine being the dibromo compound plus unreacted starting material. Use of excess bromine did, however, provide the 4,5-dibromo derivative in good yield in a single reaction step.

Reaction in 1,4-dioxane was slower, and by monitoring the products by ^1H NMR, the monobromo species could be observed to form as intermediates, followed by their subsequent conversion to the dibromide that had been previously characterized from the aqueous reaction. Moreover, it was clear from the NMR spectra taken at intermediate stages that two monosubstituted products were forming, in that two singlets could be observed in the aromatic region. Separate methyl signals corresponding to these isomers could also be observed, along with the methyl signal of the dibromide. Optimal conditions for the preparation of the monobromides were found to be 6 days at room temperature, at which time the product mixture corresponded to that given below, with 5% unreacted starting material also present. At this point the products could be separated to obtain pure samples of the two monobromo compounds.

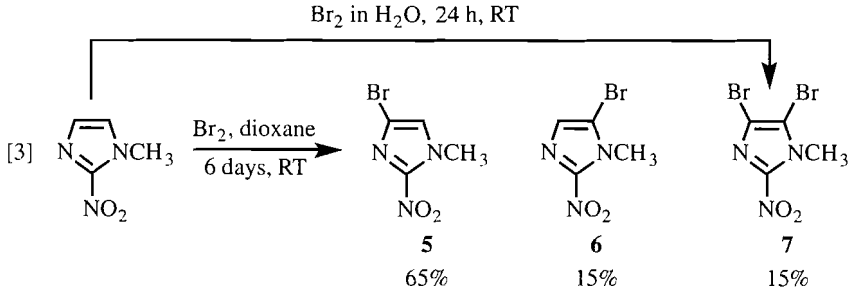

The isomers were distinguished by the patterns of C4 and C5 in their ^1H-coupled ^{13}C NMR spectra. With the major product, the signals for these two carbons were at 114.2 and 128.4 ppm (in acetone-d_6), with the former splitting into a doublet with J = 9 Hz in the ^1H-coupled spectrum, and the latter a doublet of quartets with J = 200 and 5 Hz. The former signal can be assigned to the carbon bearing the bromine, with the small splitting arising from coupling with the proton on the adjacent carbon. The large splitting for the signal at 128.3 ppm indicates that this is the carbon bearing the remaining hydrogen. The further smaller splitting into the quartet represents long-range coupling with the N-methyl protons, indicating that this carbon is C5. Thus, this compound must be the 4-bromo isomer. The minor product had signals at 129.4 and 112.3 ppm, the former splitting into a clean doublet with J = 193 Hz, the latter, a doublet of quartets with J = 14 and 4 Hz. Thus, the carbon bearing the hydrogen is again at lower field as in the major isomer, but now there is no long-range coupling to the methyl protons. Such coupling is exhibited by the carbon bearing the bromine. In consequence, this isomer can be assigned the 5-bromo structure.

Reaction of bromo-1-methyl-2-nitroimidazoles with cysteamine

The bromonitroimidazoles were treated with cysteamine, employing a weakly acidic aqueous solution (pH 5.5) to minimize the direct hydrolysis that occurs in more basic solution (18–22). With 4-bromo-1-methyl-2-nitroimidazole the reaction produced a single new compound, whose ^1H NMR spectrum showed a singlet in the aromatic region corresponding to the ring hydrogen, the N-CH_3 singlet, plus a pair of triplets near 3 ppm associated with a cysteamine substituent. Integration of these peaks indicated that this was a product of monosubstitution. The mass spectrum, however, showed the characteristic doubling of peaks associated with the presence of a bromine atom, with molecular ions at m/e 235/237 indicating that it is the nitro group that has been displaced. The UV spectrum offered further corroboration of this assignment. 2-Nitroimidazoles such as the starting

Can. J. Chem. Downloaded from www.nrcresearchpress.com by 88.255.202.194 on 09/08/12
For personal use only.

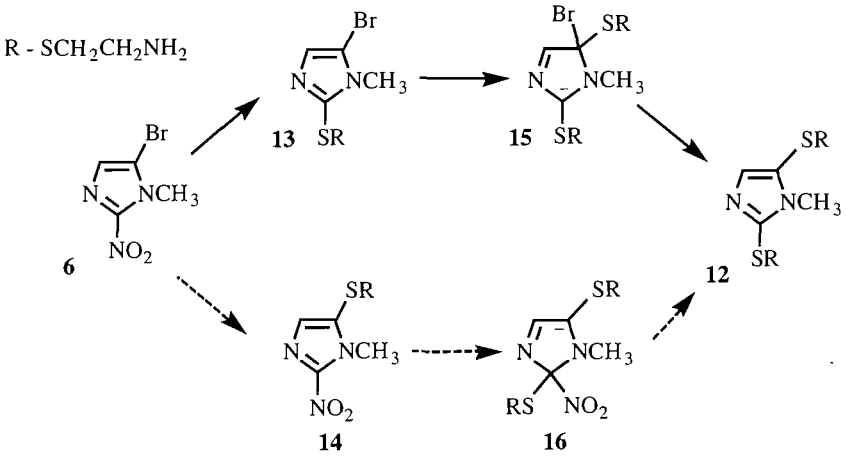

SCHEME 1

[4] 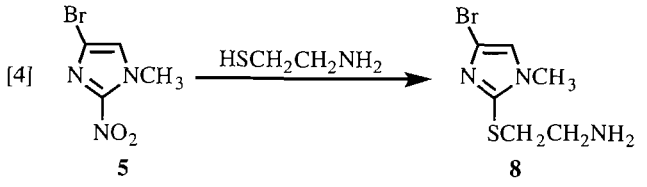

material (λ_{max} = 340 nm) typically absorb above 300 nm. With the product the λ_{max} had been reduced to 240 nm.

Treatment of misonidazole with cysteamine, under conditions similar to those of the present study, was previously found to lead to nucleophilic substitution of the 2-nitro group (22).[2]

[5] 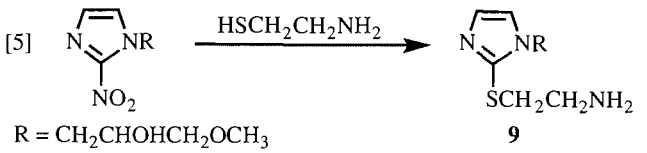

With the 4-bromo-2-nitro compound, the reaction obviously followed the same course. Although there is an additional leaving group, reaction still occurs at the 2-position. This is perhaps not surprising, since the intermediate **10** formed by addition of a nucleophile at the 4-position does not have the negative charge directly conjugated with the nitro group.

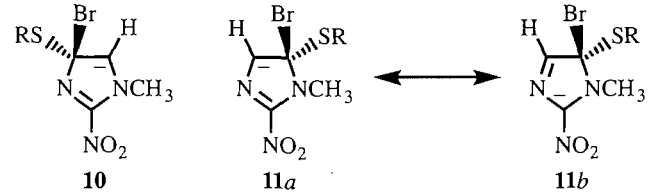

With the 5-bromo isomer, such conjugation does exist (see **11***b*), leading to the anticipation of bromine displacement. The reaction proved to be more complex than in the case of 4-bromo, in that two new products appeared on treatment with cysteamine. These products were characterized by two new singlets at δ 7.88 and 7.59, downfield from the aromatic peak for the starting material at 7.37 ppm. Corresponding peaks for the N-CH_3 group could also be observed, at 4.12 ppm for the starting material, and 3.98 and 3.92 ppm for the products with aromatic signals at 7.88 and 7.59 ppm, respectively. With time, it became apparent that the product with the signals at lower field was unstable, being converted into the product with the higher field signals such that at long reaction times the latter became the only species present. A sample was isolated and the NMR and mass spectra indicated a disubstituted compound **12** with both nitro and bromo groups displaced by cysteamine. The other product, which must then be monosubstituted, could not be isolated in pure form. A mass spectrum recorded on a mixture indicated that it still retained its bromine, with peaks at *m/e* 235/237 consistent with a product **13** (Scheme 1) where the nitro group had been displaced.

Thus, both 4-bromo- and 5-bromo-2-nitroimidazoles undergo nucleophilic displacement of the nitro group at the C2 position rather than at C4 or C5. This can be explained by a greater electrophilicity at C2, due to the presence of the powerful electron-withdrawing nitro group coupled with the two electronegative nitrogens of the imidazole ring. The further reaction of the monosubstituted adduct **13** with the 5-bromo substituent can be rationalized in terms of the sulfur located at C2 stabilizing the anionic intermediate, as in **15**. As noted above, such a resonance contributor cannot be written for the 4-bromo analog.

Interestingly, the disubstituted **12** formed in significant amounts (25–30% of total **12** + **13**) even at short reaction times, that is, under conditions where there would be little formation of this product from the monosubstituted **13**. Thus, it appears that some of the disubstituted **12** is an immediate product of the reaction of cysteamine with the bromonitroimidazole **6**. This can arise if a portion of the initial substitution actually occurs through displacement of the bromo group giving the desired product **14**, followed by the rapid reaction of this with a second equivalent of cysteamine. The conversion of **14** to **12** couples the electrophilicity of C2 in a 2-nitroimidazole with sulfur stabilization of the anionic intermediate (as in **16**). This process, therefore, is expected to be fast relative to the other displacements that occur in this system.

Bromination of 2-amino-1-methylimidazole

Having observed a displacement of a 5-bromo substituent in the conversion of **13** to **12**, we turned to the possibility

[2]This study also established that, under some conditions, the substitution can also occur via an electron transfer pathway.

Can. J. Chem. Downloaded from www.nrcresearchpress.com by 88.255.202.194 on 09/08/12
For personal use only.

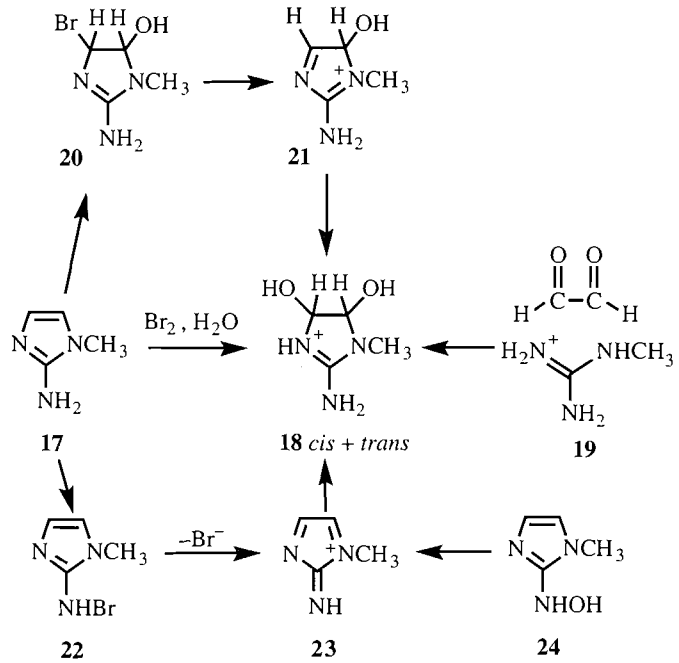

SCHEME 2

of directly reacting a bromo-2-aminoimidazole with a thiol. Our initial approach to the required starting material involved the bromination of the readily available 2-amino-1-methylimidazole **17**. To our surprise this reaction in water proceeded cleanly to give products that we had previously characterized following the reaction of glyoxal and the methylguanidinium ion **19** (4, 23, 24), a *cis*:*trans* mixture of the 2-amino-4,5-dihydro-4,5-dihydroxy-1-methylimidazolium ion **18**.

This unusual reaction can be explained (Scheme 2) by the formal addition of BrOH across C4,C5 to produce **20** (or its isomer with the bromine at C5), whose bromine would be labile to water displacement because of the presence of the ring nitrogens (see **21**). Imidazoles lacking a 2-NH_2 group, however, give substitution products upon bromination (see above and refs. 16, 25, 26), suggesting that the external amino substituent in **17** may play a direct role. *N*-Bromination, for example, results in an *N*-bromoimidazole **22**, where loss of bromide would lead to the cation **23** and hence to **18**. The cation **23** has previously been implicated as an intermediate in the aqueous decomposition of the imidazole-2-hydroxylamine **24**, a reaction where **18** is also the product (4, 6, 23).

Preparation and reaction of bromo-2-aminoimidazoles

With the failure to obtain samples by direct bromination, we turned to reduction of the previously prepared **5** and **6**. Flockhart *et al.* have reported the catalytic six-electron hydrogenation of misonidazole over Adam's catalyst (27). Similar reactions with **5** and **6** failed, as indicated by no uptake of hydrogen and unchanged NMR spectra. Misonidazole was verified to be reduced to the corresponding amine under the same conditions. Hydrogenation of **5** and **6** using Pd/charcoal in methanol also failed. Finally, we turned to reduction with Zn/HCl and this was successful.

Attempted displacement of the bromine in the reduction products **25** and **26** with cysteamine hydrochloride, however, did not work. Refluxing in water did result in loss of

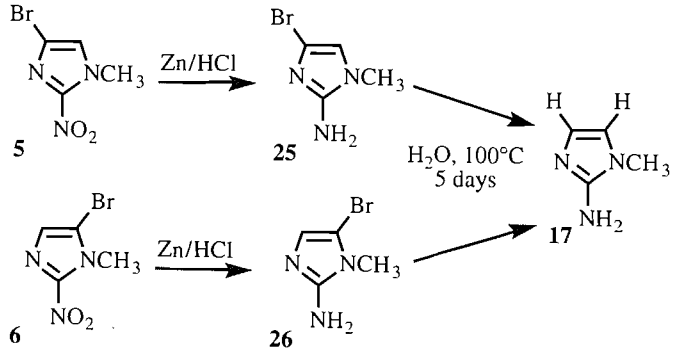

SCHEME 3

bromine, but to our surprise the two bromoaminoimidazoles gave the same product, with an NMR spectrum identical to that of 2-amino-1-methylimidazole **17** (Scheme 3). The same reaction product was obtained under identical conditions even in the absence of thiol.

The implication of these experiments is that bromine exchanges with the protons from the solvent, presumably by electrophilic substitution into the electron-rich imidazole.

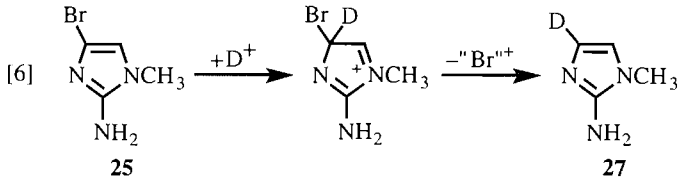

This reaction results in release of an electrophilic bromine. In the case of the reaction with the thiols present this would be taken up by oxidizing these species to disulfides, as is observed. The fate of the bromine in the reaction without the thiol was not determined.

To verify the location of the incoming hydrogen, the displacement with the 4-bromo derivative **25** was carried out in refluxing D_2O. This resulted in a product with deuterium at a single ring position, as evident from the appearance of one singlet at 6.77 ppm in the ^1H NMR spectrum in water. The ^1H-decoupled ^{13}C NMR spectrum showed signals at 149.1, 120.3, 114.9 (and 34.7 ppm for CH_3), with the signal at 114.9 ppm appearing as a weak triplet and representing the carbon bearing the deuterium. In the ^1H-coupled spectrum the signal at 120.3 for the carbon bearing the hydrogen appeared as a doublet. This showed further small splitting into quartets due to long-range coupling with the N-methyl, demonstrating that this carbon was C5 and that the product therefore was the 4-deuterio derivative **27**.

Experimental section

4,5-Dibromo-1-methyl-2-nitroimidazole (7)

1-Methyl-2-nitroimidazole (18, 19) (0.5 g) was dissolved in 150 mL of water and 3 mL of bromine was added with vigorous stirring. The resulting solution was left standing in the dark overnight, at which time the unreacted bromine was driven out of the solution by bubbling with air. Water was removed, and the resulting yellow solid was chromatographed on silica gel (200 mesh) using a mixture of 1:2 ethyl acetate: *n*-hexane. The solvents were evaporated to yield 0.57 g (70%) of product as yellow needles, mp 144–145°C (lit. (5) mp 143–145°C); ^1H NMR (DMSO-d_6) δ: 4.15 (s).

Can. J. Chem. Downloaded from www.nrcresearchpress.com by 88.255.202.194 on 09/08/12
For personal use only.

Can. J. Chem. Downloaded from www.nrcresearchpress.com by 88.255.202.194 on 09/08/12
For personal use only.

*4-Bromo-1-methyl-2-nitroimidazole (**5**) and 5-bromo-1-methylimidazole (**6**)*

1-Methyl-2-nitroimidazole (0.5 g) was dissolved in 70 mL of 1,4-dioxane and 1 mL of bromine was added with vigorous stirring. The mixture was left standing at room temperature, with the progress being monitored by withdrawing small aliquots, evaporating the solvent, and recording a ^{1}H NMR spectrum in DMSO-d_6. The mixture was characterized by doublets at 7.12 and 7.62 ppm due to starting material, singlets at 7.83 and 7.40 ppm due to the monobromo products, and a cluster of four singlets near 4 ppm due to the methyl groups of these three species, plus the dibromo isomer. After 6 days, 95% of starting material was consumed with minimal formation of dibromide, and the reaction was stopped by evaporating the excess bromine and solvent. To ensure removal of all the Br_2, the resulting oil was twice dissolved in 100 mL of fresh 1,4-dioxane, followed by evaporation. The material so obtained was chromatographed on silica gel (200 mesh) using 2:3 (v:v) ethyl acetate:hexane as eluant. An initial fraction containing the dibromide was discarded. The two monobromo compounds, which were not separated on this column, were collected together as a second fraction. After solvent removal, these were separated on preparative thin-layer chromatography plates (alumina GF, 2 mm thickness) eluted with 1:1 ethyl acetate:hexane. The solids obtained after evaporation of the solvent were recrystallized from water to yield pale yellow needles of the products.

4-Bromo-1-methyl-2-nitroimidazole (0.43 g, 65%): mp 139–141°C (lit. (5) mp 142–144°C); R_f in 1:1 ethyl acetate:hexane, 0.47. ^{1}H NMR (DMSO-d_6) δ: 7.83 (s, 1 H), 3.94 (s, 3 H). MS (EI, methanol): 206/204 (100), 176/174 (79), 160/158 (19), 137/135 (36), 119/117 (20), 80 (60). Anal. calcd. for $C_4H_4N_3O_2Br$: C 23.32, H 1.96, N 20.40, Br 38.79; found: C 23.26, H 2.03, N 20.07, Br 39.03.

5-Bromo-1-methyl-2-nitroimidazole (0.12 g, 15%): mp 117–119°C; R_f in 1:1 ethyl acetate:hexane, 0.31. ^{1}H NMR (DMSO-d_6) δ: 7.40 (s, 1 H), 4.22 (s, 3 H). MS (EI, methanol): 206/204 (56), 176/174 (38), 160/158 (9), 135/133 (76), 121/119 (26), 80 (100). Anal. calcd. for $C_4H_4N_3O_2Br$: C 23.32, H 1.96, N 20.40, Br 38.79; found: C 23.51, H 2.13, N 20.27, Br 38.93.

*Reaction of 4-bromo-1-methyl-2-nitroimidazole (**5**) with cysteamine 2-[(2-Aminoethyl)thio]-4-bromo-1-methylimidazole (**8**)*

To a suspension of 0.1 g of 4-bromo-1-methyl-2-nitroimidazole in 100 mL of oxygen-free water at pH 5.5 was added 1.1 g of cysteamine hydrochloride. The mixture was refluxed for 2 days, at which time the solution was cooled and water removed by lyophilization. The resulting oil was taken up in 100 mL of 3 M NaOH, followed by extraction with 2 × 100 mL of chloroform. The combined chloroform layers were exhaustively washed with 7 × 200 mL of 0.5 M NaOH to effect the complete removal of cysteamine, followed by 3 × 150 mL of distilled water. After drying ($MgSO_4$) and filtration, the solvent was evacuated to give a yellow liquid: ^{1}H NMR ($CDCl_3$) δ: 7.62 (s, 1H), 3.93 (s, 3H), 3.28 (t, 2H, J = 9 Hz), 3.12 (t, 2H, J = 9 Hz). MS (EI, neat): 235/237 (12), 105/207 (76), 175/177 (55), 134/136 (100), 80 (66). HRMS m/e: 235.1430 ($C_6H_{10}{}^{79}BrNS_3$ requires 235.1438).

*Reaction of 5-bromo-1-methyl-2-nitroimidazole (**6**) with cysteamine*

5-Bromo-1-methyl-2-nitroimidazole (0.1 g) was treated with varying amounts of cysteamine hydrochloride as described above. The course of the reaction was monitored by periodically withdrawing a small sample, removing water by lyophilization, dissolving in D_2O, and recording 200 MHz ^{1}H NMR spectra. In an experiment with a 10-fold excess of cysteamine, reaction had gone to completion after refluxing for 10 days, producing a single species that was isolated as described in the previous paragraph. This product had spectra consistent with 2,5-bis[2-(aminoethyl)thio]-1-methylimidazole **12**: ^{1}H NMR (D_2O) δ: 7.58 (s, 1H), 3.92 (s, 3H), 3.40 (two overlapping t's, 6H), 3.09 (t, 6H, J = 9 Hz). HRMS m/e: 212.1577 ($C_8H_{16}N_4S_2$ requires 212.1565). The initial product could not be isolated in pure form. After 6 days of refluxing with a sevenfold excess of cysteamine, a time sufficient for complete disappearance of the NMR signals of the starting material, a 1:3 mixture of monosubstituted:disubstituted compounds was obtained. A mass spectrum of this mixture showed peaks at m/e 235/237 consistent with 2-[(2-aminoethyl)thio]-5-bromo-1-methylimidazole **13** as the structure of the monosubstituted product.

Reaction of 2-amino-1-methylimidazolium chloride with bromine in water

Bromine was slowly added to a solution of 2-amino-1-methylimidazolium chloride (28) (1 g) in 200 mL of water. The bromine color was immediately discharged during this addition, which was continued until a faint orange color persisted. The solvent and excess bromine were removed by evaporation under reduced pressure and lyophilization, the resulting solid was taken up in 35 mL methanol, and then precipitated by addition of 350 mL of ice-cold diethyl ether. After filtration, the ^{1}H NMR spectrum was recorded in D_2O. The only signals observed corresponded to those of a 1:5 *cis*:*trans* ratio of **18**: *cis* **18**, δ 5.37 (d, 1H, J = 5.8 Hz), 5.23 (d, 1H, J = 5.8 Hz), 2.99 (s, 3H) and *trans* **18**, δ 5.18 (d, 1H, J = 0.8 Hz), 5.04 (d, 1H, J = 0.8 Hz), 3.03 (s, 3H). A sample of **18** prepared by the reaction of glyoxal and methylguanidinium chloride (23) was added to the NMR tube to establish the exact correspondence of the signals from the two preparations.

Preparation and reactions of bromoaminoimidazoles

4-Bromo-1-methyl-2-nitroimidazole **5** (0.2 g) and 5-bromo-1-methyl-2-nitroimidazole **6** (50 mg) were dissolved in 100 mL of 0.1 M HCl and zinc dust (1 g) added. The suspension was stirred for 1 h, solids separated by filtration, and the water removed by lyophilization. NMR spectra recorded in D_2O showed the presence of two singlets in a 1:3 ratio in each case, 2-amino-4-bromo-1-methylimidazole hydrochloride at δ 6.79 (1H), 3.51 (3H); 2-amino-5-bromo-1-methylimidazole hydrochloride at δ 6.81 (1H), 3.49 (3H).

These two products were refluxed in water, with and without cysteamine hydrochloride, for 2–5 days. The solvent was removed by lyophilization and NMR spectra recorded in D_2O. Both isomers produced the same product, showing a 2H doublet of doublets with δ 6.83 and δ 6.77, and a 3H singlet at δ 3.53. The identity of the two products was further indicated by the absence of any change in the ^{1}H NMR spectra when the two were mixed together. Addition of authentic 2-amino-1-methylimidazolium chloride also resulted in superimposable peaks.

Acknowledgements

Support for this research from the National Cancer Institute of Canada and the Natural Sciences and Engineering Research Council of Canada is gratefully acknowledged.

1. R. A. McClelland. *In* Selective activation of drugs by redox processes. *Edited by* G. Adams, A. Breccia, E. M. Fielden, and P. Wardman. Plenum Press, New York. 1990. pp. 125–136.
2. A. J. Varghese. Biochem. Biophys. Res. Commun. **112**, 1013 (1983).
3. E. Chacun, C. J. Morrow, A. A. Leon, J. L. Born, and B. R. Smith. Biochem. Pharmacol. **37**, 361 (1988).
4. R. A. McClelland, R. Panicucci, and A. M. Rauth. J. Am. Chem. Soc. **107**, 1762 (1985).
5. R. Panicucci. Ph.D. Thesis, University of Toronto, 1988.
6. J. L. Bolton and R. A. McClelland. J. Am. Chem. Soc. **111**, 8172 (1989).
7. E. A. Bump, Y. C. Taylor, and J. M. Brown. Cancer Res. **44**, 997 (1983).
8. A. J. Varghese. Int. J. Radiat. Oncol. Biol. Phys. **10**, 1341 (1984).

9. B. R. Smith and J. L. Born. Int. J. Radiat. Oncol. Biol. Phys. **10**, 1365 (1984).
10. A. J. Varghese and G. F. Whitmore. Int. J. Radiat. Oncol. Biol. Phys. **12**, 1223 (1986).
11. S. F. Farah. Ph.D. Thesis, University of Toronto, 1990.
12. I. J. Stratford, S. Hoe, G. E. Adams, and C. Williamson. Int. J. Radiat. Biol. **43**, 31 (1983).
13. B. Iddon, N. Khan, and B. L. Lim. J. Chem. Soc. Perkin Trans. 1, 1437 (1987).
14. S. Kulkarni, M. R. Grinett, L. R. Hanton, and J. Simpson. Aust. J. Chem. **40**, 1399 (1987).
15. S. Kulkarni and M. R. Grinett. Aust. J . Chem. **40**, 1415 (1987).
16. B. D. Palmer and W. A. Denny. J. Chem. Soc. Perkin Trans. 1, 95 (1989).
17. J. S. Rasey, K. A. Krohn, and S. Freauff. Radiat. Res. **91**, 1015 (1982).
18. A. G. Beaman, W. Tautz, T. Gabriel, O. Keller, V. Toome, and R. Duschinsky. Antimicrob. Agents Chemother. 469 (1965).
19. A. G. Beaman, W. Tautz, and R. Duschinsky. Antimicrob. Agents Chemother. 520 (1967).
20. Y. Takeuchi, H. J. C. Yeh, K. L. Kirk, and L. A. Cohen. J. Org. Chem. **43**, 3565 (1978).
21. Y. Takeuchi, K. L. Kirk, and L. A. Cohen. J. Org. Chem. **43**, 3570 (1978).
22. P. Goldman and J. D. Wuest. J. Am. Chem. Soc. **103**, 6224 (1981).
23. R. A. McClelland, R. Panicucci, and A. M. Rauth. J. Am. Chem. Soc. **109**, 4308 (1987).
24. R. Panicucci and R. A. McClelland. Can. J. Chem. **67**, 2128 (1989).
25. I. E. Balaban and F. L. Pyman. J. Chem. Soc. 947 (1922); 1564 (1924).
26. I. E. Balaban. J. Chem. Soc. 2423 (1932).
27. I. R. Flockhart, P. Large, S. L. Malcolm, T. R. Marten, and D. Troup. Xenobiotica, **8**, 97 (1978).
28. B. T. Storey, W. W. Sullivan, and C. L. Moyer. J. Org. Chem. **29**, 3118 (1964).

Can. J. Chem. Downloaded from www.nrcresearchpress.com by 88.255.202.194 on 09/08/12
For personal use only.

Manifestations of noncovalent interactions in the solid state. 3.[1] X-ray crystal structures of $[H_4(cyclam)][FeCl_5(OH_2)](Cl)_2$ and $[H_4(cyclam)][CF_3COO]_4$, two network hydrogen bonded solids

S. SUBRAMANIAN AND MICHAEL J. ZAWOROTKO[2]

Department of Chemistry, Saint Mary's University, Halifax, N. S., Canada B3H 3C3

Received October 21, 1992

S. SUBRAMANIAN and MICHAEL J. ZAWOROTKO. Can. J. Chem. **71**, 433 (1993).

$FeCl_2$ or $FeCl_3$ react with cyclam (cyclam = 1,4,8,11-tetraazacyclotetradecane) in an acidic medium (4 M HCl) to afford dark orange-red plates of $[H_4(cyclam)][FeCl_5(OH_2)](Cl)_2$ (**1**). **1** crystallizes in a polar space group (orthorhombic, $Pc2_1b$) with a = 10.7730(6), b = 13.3418(10), c = 14.4564(10) Å, V = 2077.84(24) Å^3, and D_{calc} = 1.68 g cm^{-3} for Z = 4. Final values of R = 0.031 and Rw = 0.034 were obtained for 1950 independent observed ($I > 3\sigma(I)$) reflections. Cyclam reacts with neat trifluoroacetic acid to afford a colourless salt, $[H_4(cyclam)][CF_3COO]_4$ (**2**). **2** crystallizes in a centric space group (monoclinic, $P2_1/c$), with a = 8.7442(11), b = 10.5121(11), c = 15.2469(20) Å, β = 102.526(15)°, V = 1368.1(3) Å^3, and D_{calc} = 1.593 g cm^{-3} for Z = 2. Final values of R = 0.059 and Rw = 0.067 were obtained for 1336 independent observed ($I > 3\sigma(I)$) reflections. Extensive interionic hydrogen bonding between the cyclam cations, which adopt exodentate conformations, and anions results in network polymeric hydrogen bonding (1-D for **1**, 2-D for **2**). The networking in **1** is intrinsically polar because one chloride anion and the $[FeCl_5(OH_2)]^{2-}$ complex anion are involved in networking between the $H_4(cyclam)^{4+}$ cations. The implications of the crystal structures are discussed from the perspective of rational design of polar solids.

S. SUBRAMANIAN et MICHAEL J. ZAWOROTKO. Can. J. Chem. **71**, 433 (1993).

En milieu acide (4 M HCl), le $FeCl_2$ ou le $FeCl_3$ réagissent avec le cyclame (cyclame = 1,4,8,11-tétraazacyclotétradécane) pour conduire à des plaques rouge-orange foncé de $[H_4(cyclame)][FeCl_6(OH_2)](Cl)_2$ (**1**). Le composé **1** cristallise dans un groupe d'espace polaire (orthorhombique, $Pc2_1b$) avec a = 10,7730(6), b = 13,3418(10) et c = 14,4564(10) Å, V = 2077,84(24) Å^3 et D_{calc} = 1,68 g cm^{-3} pour Z = 4. On a obtenu les valeurs finales de R = 0,031 et R_w = 0,034 pour 1950 réflexions indépendantes observées avec $I = \geq 3\sigma(I)$. Le cyclame réagit aussi avec l'acide trifluoroacétique pur pour conduire à un sel incolore de $[H_4(cyclame)][CF_3COO]_4$ (**2**). Le sel **2** cristallise dans un groupe d'espace centré (monoclinique, $P2_1/c$) avec a = 8,7442(11), b = 10.5121(11) et c = 15,2469(20) Å, β = 102,526(15)°, V = 1368,1(3) Å^3 et D_{calc} = 1,593 g cm^{-3} pour Z = 2. On a obtenu les valeurs finales de R = 0,059 et R_w = 0,067 pour 1336 réflexions indépendantes observées avec $I \geq 3\sigma(I)$. Des liaisons hydrogènes interioniques importantes entre les anions et les cations du cyclame, qui adoptent des conformations exocoordinés, conduisent à l'existence de réseaux de liaisons hydrogènes polymériques (1-D pour **1** et 2-D pour **2**). Le réseau que l'on peut observer dans **1** est intrinsèquement polaire parce qu'un anion chlorure et l'anion complexe $[FeCl_5(OH_2)]^{2-}$ sont impliqués dans le réseau entre les cations $H_4(cyclame)^{4+}$. On discute des implications des structures cristallines dans la perspective de la création rationnelle de solides polaries.

[Traduit par la rédaction]

Introduction

Rational design of solids, crystal engineering, is an aspect of chemistry that is of growing interest to synthetic and materials chemists (2). A particularly topical application of crystal engineering concerns design and preparation of solids that exhibit second-order nonlinear optical properties such as second harmonic generation, SHG (2–5). An important criterion for construction of such materials is that they crystallize in a noncentrosymmetric or polar space group (2–6). In this context, the importance of intermolecular network hydrogen bonding cannot be overemphasized. The prototypal inorganic SHG-active solid, KH_2PO_4, is a three-dimensional diamondoid solid that becomes SHG active when the hydrogen bonds align at low temperatures (7). Organic cation $H_2PO_4^-$ analogues are also SHG active (8). Furthermore, analysis of crystallographic databases has recently revealed that there is strong correlation between whether or not a solid is a polymeric network and space group centrosymmetry (6). Therefore, although it is now realized that SHG activity is possible in as wide an array of materials as KH_2PO_4, organics (e.g., polarizable donor–acceptor compounds such as *p*-nitroaniline), and organometallics (e.g., ferrocene derivatives, acetylides), the necessity for crystallizing in a polar space group remains. Moieties that are capable of engaging in network hydrogen bonding are therefore of more than passing interest since they are likely to be predisposed towards polar space groups.

Polyazamacrocyclic molecules have been primarily a subject of interest for their coordination properties (9). In a macrocyclic ligand such as cyclam (1,4,8,11-tetraazacyclotetradecane) the nitrogen atoms typically adopt an endodentate conformation and are therefore oriented for complexation of metal ions within the macrocyclic cavity. Thus, the chemistry of cyclam itself is rather dominated by cation complexation and formation of discrete molecules and ions (10–12). Nevertheless, polyazamacrocyclic ligands and their complexes are capable of forming ordered solids, but not as a direct result of the ligand engaging in intermolecular interactions (13–16). The protonated polyammonium derivatives of cyclam are known but have received much less attention, although complexation of anions by polyammonium and macrocyclic cations has been of interest from structural (17–20), photochemical (21), and analytical (22) perspectives. In this contribution we present the first crystal structures of compounds containing the fully protonated form of cyclam, $[H_4(cyclam)]^{4+}$, a moiety that we expect to be

[1]For parts 1 and 2, see refs. 1*a* and 1*b*, respectively.

[2]Author to whom correspondence may be addressed.

Can. J. Chem. Downloaded from www.nrcresearchpress.com by 88.255.202.194 on 09/08/12
For personal use only.

Can. J. Chem. Downloaded from www.nrcresearchpress.com by 88.255.202.194 on 09/08/12
For personal use only.

TABLE 1. Crystal data and summary of intensity data collection and structure refinement for compounds **1** and **2**

Parameter	Compound	
	$FeCl_7ON_4C_{10}H_{30}$, **1**	$F_{12}O_8N_4C_{18}H_{28}$, **2**
Color	Orange red	Colorless
Formula wt.	526.4	656.4
Crystal system	Orthorhombic	Monoclinic
Space group	$Pc2_1b$	$P2_1/c$
Temp. °C	17	17
Cell constants[a]		
a, Å	10.7730(06)	8.7442(11)
b, Å	13.3418(10)	10.5121(11)
c, Å	14.4564(10)	15.2469(20)
β, °		102.526(15)
Cell volume, Å^3	2077.84(24)	1368.1(3)
F(000)	1088	672
Z	4	2
D_{calc}, g cm^{-3}	1.68	1.59
μ_{calc}, cm^{-1}	16.4	1.9
Scan type	ω/2θ	ω/2θ
Radiation	Graphite Monochromated MoK_α (λ = 0.70930Å)	
Max. crystal dimensions, mm	0.15 × 0.85 × 0.85	0.20 × 0.50 × 0.50
Scan width	0.80 + 0.35 tan θ	0.80 + 0.35 tan θ
Transmission range	0.697, 0.999	0.775, 1.000
Decay of standards	±2%	±2%
Reflections measured	3195	1860
2θ range, °	2–50	2–45
Unique reflections	2253	1787
Reflections observed[b]	1950	1336
Computer programs[c]	NRCVAX (ref. 23)	NRCVAX (ref. 23)
Structure solution	Direct	Direct
Number parameters	208	244
Weight modifier, k	0.00001	0.00005
G.O.F.	3.26	4.65
R_f	0.031	0.059
R_w	0.034	0.067
Final diff. map(max) (e/Å^3)	0.41	0.26

[a]Least-squares refinement of $((\sin\theta)/\lambda)^2$ for 24 reflections $\theta > 16°$.
[b]$I > 3.0\sigma(I)$. Corrections: Lorentz-polarization and absorption (empirical psi scan).
[c]All the non-hydrogen atoms were refined anisotropically. For **1** all the methylene hydrogens were fixed in calculated positions with idealized angles (d_{C-H} = 1.08 Å) and hydrogen atoms on the hetero atoms were located from the difference map and fixed. For **2** all hydrogen atom positions were calculated (d_{C-H} = 1.08 Å).

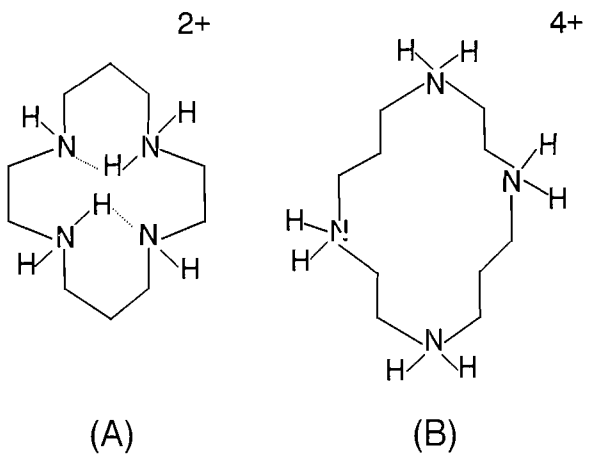

FIG. 1. Conformation of di (A) and tetra (B) cations of cyclam and intramolecular hydrogen bonding in the dication.

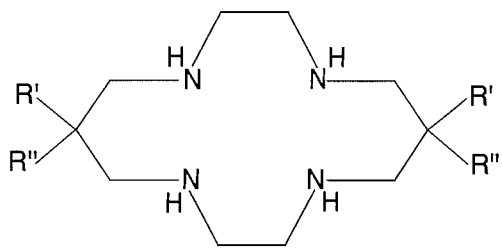

capable of promoting network hydrogen bonding and therefore of potential relevance in crystal engineering.

Experimental

$FeCl_3 \cdot 6H_2O$, $FeCl_2 \cdot 4H_2O$, and concentrated HCl were purchased from Fisher Scientific Co., cyclam was purchased from

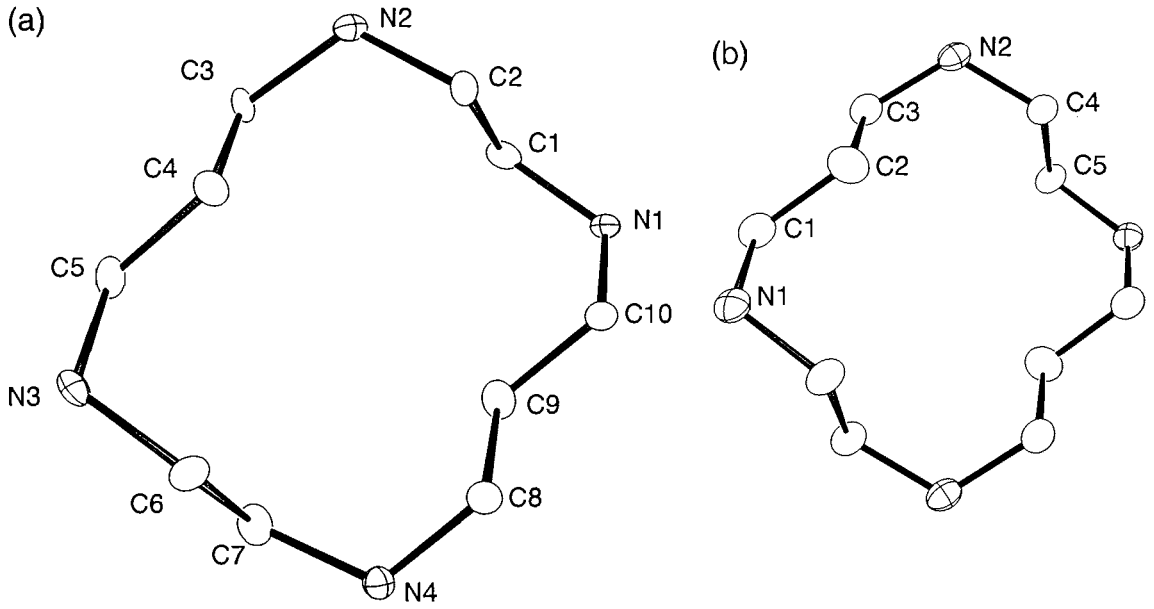

FIG. 2. ORTEP perspective views of the $[H_4(cyclam)]^{4+}$ cations in (*a*) **1** and (*b*) **2**.

Strem Chemicals, Inc., and trifluoroacetic acid was purchased from Aldrich Chemical Co. All reagents were used as received. Microanalysis was performed by Canadian Microanalytical Services Ltd., B.C. IR spectra were recorded on a Perkin–Elmer 1600 Series FTIR using the solid reflectance technique (KBr crystals). Melting points were recorded on a Fisher–John apparatus and were not corrected.

*Preparation of [H_4(cyclam)][$FeCl_5(OH_2)$][$Cl)_2$ (**1**)*

To a solution of 0.20 g (1.0 mmol) of $FeCl_2 \cdot 4H_2O$ in 20 mL of water, 0.20 g (1.0 mmol) of cyclam in 20 mL of aqueous ethanol (1:1) was added. Initially, a dark green precipitate was formed. However, within minutes it turned brown in the presence of air. Concentrated HCl was added dropwise under stirring to dissolve this precipitate and the resulting bright yellow solution, approximately 4 M in HCl, was allowed to evaporate and afforded large orange-red crystals (0.42 g, 0.80 mmol, 80%) of **1**. Melting point: slowly darkens above 195°C and decomposes at 250°C. IR, cm^{-1}: 3125 (O-H, broad), 3024 (C-H, broad), 2674 (-NH_2-$^+$ cation), sharp peaks at 1634 (N-H), 1570, 1469, 1373, 1298, 1199, 1155, 1128, 1078, 1030, 1007, 952, 910, 850, 816, and 742. Anal. calcd. for $FeCl_7ON_4C_{10}H_{30}$: C 22.81, H 5.70, N 10.64; found: C 22.95, H 5.59, N 10.61.

1 can also be obtained following an identical procedure except that $FeCl_2 \cdot 4H_2O$ is replaced with $FeCl_3 \cdot 6H_2O$.

*Preparation of [H_4(cyclam)][$CF_3COO]_4$ (**2**)*

Cyclam (0.100 g, 0.499 mmol) was dissolved in 15 mL of trifluoroacetic acid. The resulting solution was allowed to slowly evaporate at room temperature and afforded large colourless crystals of **2**. Yield: 0.310 g (0.472 mmol, 94.6%). **2** melts sharply at 147°C into a clear liquid with decomposition. IR, cm^{-1}: 3307, 3146 (N-H, sharp), 2936 (C-H), 2534 (NH_2^+ cation), 1795, 1734 (C=O), 1654 (N-H), 1580, 1453, 1355, 1307, 1258, 1202, 1147, 1052, 940, 851, 750.

X-ray structure determinations

Single crystals suitable for X-ray crystallography were obtained directly from the reaction mixtures. Suitable crystals were mounted and sealed in thin-walled glass capillaries and diffraction data were collected on an Enraf–Nonius CAD4 diffractometer. The experimental parameters used for the data collection and structure refinement are presented in Table 1. The function $R = \Sigma(F_o - F_c)/(F_o)$, was minimized and values of $Rw = [(\Sigma w(F_o - F_c)^2/\Sigma wF_o^2]^{1/2}$ and GOF = $[\Sigma w(F_o - F_c)^2/$(no. of reflns. − no. of parameters)$]^{1/2}$ are also presented. Weights based on counting statistics were used, the weight modifier, k, being determined experimentally via statistical analysis of the variation in intensity of the standard reflections. Final fractional coordinates and selected interatomic distances and angles are presented in Tables 2–5.[3] The only unusual aspects of structure refinement concern **2**. The CF_3 groups were found to be disordered. It was possible to refine two independent CF_3 moieties for each anion (sets A and B, each with site occupancy factors of 0.5 and identified as such in Table 4). The fluorine atoms exhibited high thermal motion, presumably accounting for the relatively high R values obtained, although thermal motion was observed to be low elsewhere, particularly within the cation. The $[H_4(cyclam)]^{4+}$ in **2** was found to lie around a crystallographic inversion center (1, 1/2, 0) whereas the CF_3COO^- anions were located in general positions. All crystallographic calculations were effected using the PC version of the NRCVAX suite of programs (23). Neutral atom scattering factors and corrections for anomalous dispersion were taken from ref. 24. To determine the enantiomorph for **1**, data were collected from −12, to 12 in h, −2 to 15 in k, and −17 to 17 in l, the merging R value of equivalent intensities being 0.014. The enantiomorph was determined using the Rogers method (25).

Results and discussion

Cyclam forms stable complexes with both the common and the uncommon oxidation states of 3*d*, 4*d*, and 5*d* transition metal ions (9–12, 26) and Fe(II) and Fe(III) complexes of cyclam are known (27, 28). However, solvent and acid concentration of the reaction media play very important roles and, under the conditions we employed, formation

[3]Listings of complete atom positional parameters and anisotropic thermal parameters for **1** and **2** (4 pages) and observed and calculated structure factors for **1** and **2** (19 pages) may be purchased from: The Depository of Unpublished Data, Document Delivery, CISTI, National Research Council Canada, Ottawa, Canada K1A 0S2.

Tables of atom positional parameters have also been deposited with the Cambridge Crystallographic Data Centre and can be obtained on request from The Director, Cambridge Crystallographic Data Centre, University Chemical Laboratory, 12 Union Road, Cambridge, CB2 1EZ, U.K.

Can. J. Chem. Downloaded from www.nrcresearchpress.com by 88.255.202.194 on 09/08/12
For personal use only.

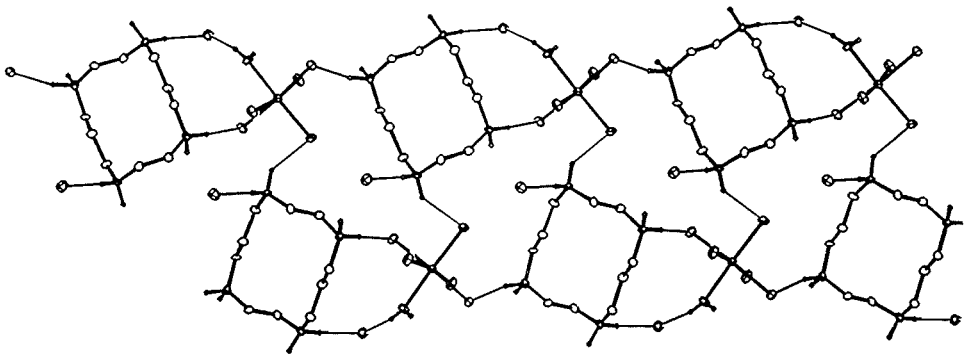

FIG. 3. ORTEP diagram showing a portion of the polymeric chain in **1**.

TABLE 2. Atomic parameters x,y,z and B_{iso} for $[H_4(cyclam)][FeCl_5(OH_2)](Cl)_2$

Atom	x	y	z	B_{iso}[a]
Fe	0.24590(10)	0.25816	0.01478(6)	1.73(4)
Cl1	0.15166(16)	0.12594(19)	−0.07482(12)	2.33(8)
Cl2	0.44247(17)	0.19001(20)	−0.02362(14)	2.66(8)
Cl3	0.34138(15)	0.38139(19)	0.11277(12)	2.07(7)
Cl4	0.05242(16)	0.31522(20)	0.07078(13)	2.86(9)
Cl5	0.24415(23)	0.36697(20)	−0.10868(13)	4.26(11)
Cl6	0.06036(16)	0.01151(20)	0.21646(12)	2.58(8)
Cl7	0.51458(15)	−0.43506(21)	−0.23303(13)	2.74(8)
OW	0.2510 (4)	0.1620 (4)	0.1338 (3)	2.31(21)
N1	0.1990 (5)	−0.1871 (5)	0.1982 (4)	1.82(24)
N2	0.1594 (5)	0.5642 (5)	0.0700 (4)	1.74(24)
N3	0.3057 (5)	−0.2815 (4)	−0.2281 (4)	1.67(23)
N4	0.3621 (5)	−0.0379 (5)	−0.0937 (4)	1.90(25)
C1	0.1336 (6)	0.7282 (5)	0.1508 (5)	1.9 (3)
C2	0.2218 (6)	0.6416 (6)	0.1281 (5)	1.9 (3)
C3	0.1292 (6)	0.5927 (6)	−0.0290 (4)	1.7 (3)
C4	0.2421 (6)	0.6286 (6)	−0.0809 (5)	2.0 (3)
C5	0.2005 (6)	0.6696 (6)	−0.1753 (5)	2.0 (3)
C6	0.3761 (6)	−0.1979 (6)	−0.1809 (5)	2.0 (3)
C7	0.2938 (6)	−0.1086 (6)	−0.1573 (5)	2.2 (3)
C8	0.3899 (7)	−0.0730 (5)	0.0026 (5)	2.0 (3)
C9	0.2742 (6)	−0.1061 (6)	0.0528 (5)	2.2 (3)
C10	0.3088 (6)	−0.1451 (6)	0.1494 (5)	2.1 (3)

[a] B_{iso} is the mean of the principal axes of the thermal ellipsoid.

of $[H_4(cyclam)]^{4+}$ and $[FeCl_5(OH_2)]^{2-}$ is favoured over Fe(cyclam) moieties. Indeed, **1** is not the only product that can be recrystallized from the crude reaction mixture.[4] Under other reaction conditions oxidative dehydrogenation of the ligand can occur and both monomeric and dimeric Fe(II) complexes containing unsaturated ligands have been isolated (29, 30). A reasonable mechanism under the conditions we employed is that cyclam, being a strong base (31), converts hydrolyzed $FeCl_2$ to ferrous hydroxide, which in turn undergoes aerial oxidation to form ferric hydroxide. Subsequent addition to acid results in the formation of the tetracation, $[H_4(cyclam)]^{4+}$, and the complex dianion, aquapentachloroferrate(III), $[FeCl_5(OH_2)]^{2-}$. Salts of both the di- and tetracations of cyclam and its derivatives have been reported (20, 31, 32); However, only the perchlorate salt of the dication, $[H_2(cyclam)]^{+2}$, has been characterized by X-ray crystallography (31). Another relevant macrocyclic cation that has been characterized by X-ray crystallography is the hexacyanoferrate(III) salt of the tetracation $[H_4(\mathbf{3})]^{+4}$ (**3** = 6,13-dimethyl-1,4,8,11-tetraazacyclotetradecane-6,13-diamine) (20). In both $[H_2(cyclam)]^{2+}$ and $[H_4(\mathbf{3})]^{4+}$ only two of the four nitrogen atoms of the macrocyclic rings (*trans* to each other) are protonated, with the two primary amino groups being protonated in the latter. The ethylene bridges adopt a *gauche* and the propylene bridges adopt a *syn* conformation. Hence, the 14-membered macrocyclic rings in both these cations adopt a conformation in which the nitrogen atoms are endodentate. Such a conformation is also enhanced by strong intramolecular hydrogen bonding (Fig. 1).

An ORTEP (33) diagram of $[H_4(cyclam)]^{4+}$ is presented in Fig. 2*a* and a portion of the polymeric chain in Fig. 3. The atomic coordinates and important lengths and angles are

[4] If the ratio of water and ethanol used for recrystallization is different, a hydrate of **1**, $[H_4(cyclam)][FeCl_5(OH_2)]Cl_2 \cdot H_2O$, is obtained. The structure of this compound has also been solved: space group triclinic, $P\bar{1}$, a = 7.8092(11), b = 10.1643(18), c = 15.001(4) Å, α = 102.30(3)°, β = 94.21(4)°, γ = 106.08(2)°, V = 1106.7(4) Å^3, Z = 2, R = 0.033, Rw = 0.040 for 2505 independent observed reflections. Full details will be published elsewhere.

Can. J. Chem. Downloaded from www.nrcresearchpress.com by 88.255.202.194 on 09/08/12
For personal use only.

TABLE 3. Interatomic distances (Å) and angles (°) for $[H_4(cyclam)][FeCl_5(OH_2)](Cl)_2$

Distances			
Fe—Cl1	2.4126(23)	N3—C6	1.512(9)
Fe—Cl2	2.3706(22)	N4—C7	1.509(9)
Fe—Cl3	2.4016(22)	N4—C8	1.500(9)
Fe—Cl4	2.3621(21)	C1—N1	1.499(9)
Fe—Cl5	2.3008(22)	C1—C2	1.531(10)
Fe—OW	2.147(5)	C3—C4	1.506(10)
N1—C1	1.499(9)	C4—C5	1.537(10)
N1—C10	1.487(9)	C5—N3	1.516(9)
N2—C2	1.491(9)	C6—C7	1.523(10)
N2—C3	1.515(8)	C8—C9	1.508(10)
N3—C5	1.516(9)	C9—C10	1.536(10)
Cl1....N4	3.160(6)	Cl6....N1	3.053(6)
Cl3....N2	3.190(6)	Cl7....N3	3.044(6)
Cl6....OW	3.111(5)	Cl5....N3a	3.151(6)
Angles			
Cl1—Fe—Cl2	88.27(7)	C1—N1—C10	116.1(5)
Cl1—Fe—Cl3	175.94(8)	C2—N2—C3	117.1(5)
Cl1—Fe—Cl4	92.77(8)	C5—N3—C6	117.7(5)
Cl1—Fe—Cl5	92.37(9)	C7—N4—C8	117.8(6)
Cl1—Fe—OW	90.25(15)	N1—C1—C2	112.1(5)
Cl2—Fe—Cl3	91.04(8)	N2—C2—C1	111.3(5)
Cl2—Fe—Cl4	172.83(9)	N2—C3—C4	112.1(5)
Cl2—Fe—Cl5	93.88(9)	C3—C4—C5	108.6(5)
Cl2—Fe—OW	86.32(14)	N3—C5—C4	112.5(5)
Cl3—Fe—Cl4	87.43(7)	N3—C6—C7	112.7(5)
Cl3—Fe—Cl5	91.67(8)	N4—C7—C6	110.0(5)
Cl3—Fe—OW	85.71(15)	N4—C8—C9	111.9(6)
Cl4—Fe—Cl5	93.17(9)	C8—C9—C10	109.7(6)
Cl4—Fe—OW	86.58(14)	N1—C10—C9	111.5(5)
Cl5—Fe—OW	177.37(16)		

a: x, $0.5 + y$, $-0.5 + z$

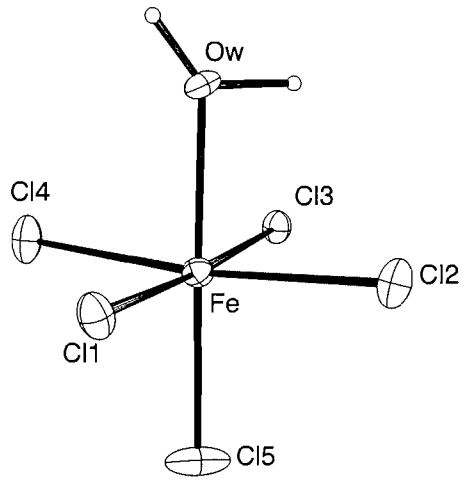

FIG. 4. ORTEP perspective view of the $[FeCl_5(OH_2)]^{2-}$ in **1**.

presented in Tables 2 and 3, respectively. The salient feature of the structure concerns the conformation adopted by $[H_4(cyclam)]^{4+}$, which is dramatically different from that adopted by cyclam and $[H_2(cyclam)]^{2+}$. $[H_4(cyclam)]^{+4}$ adapts a conformation such that the ammonium centers are positioned as far away as possible from each other (presumably to minimize electrostatic repulsions). As a result, the ethylene bridges adopt a *transoid* conformation and the propylene bridges, adapt a "W" ($^{N}\backslash_{C}/^{C}\backslash_{C}/^{N}$) conformation. Thus, the endodentate orientation (31) of the nitrogens observed in the dication, $[H_2(cyclam)]^{+2}$, is lost in the tetracation, $[H_4(cyclam)]^{+4}$. The consequence of this geometry is that the nitrogen hydrogen atoms are now predisposed towards network interionic hydrogen bonding. In the case of **1** this facilitates the formation of a one-dimensional polymer with the counterions, two chlorides and an aquapentachloro-ferrate(III).

The network hydrogen bonding is illustrated in Fig. 3. This view was generated by assuming that significant hydrogen bonding occurs when Cl....X (X = O,N) distances are <3.2 Å when corresponding Cl....H distances are <2.3 Å. There are numerous weak interionic interactions that were considered to be insignificant in the context of determining the nature of the networking. Figure 3 illustrates how the $[FeCl_5(OH_2)]^{2-}$ anion and one chloride anion are involved in hydrogen bonding such that they bridge adjacent cations. The remaining chloride ion, Cl7, is terminally hydrogen bonded to the cation through H31. The closest interionic contacts (Cl....O and Cl....N) vary in the range 3.044(6)–3.190(6) Å and are at the short end of the range found in other amine hydrochloride salts (34–36). Hydrogen bonds between $[FeCl_5(OH_2)]^{2-}$ ions, with an average O....Cl distance of 3.20(4) Å, were observed in the crystal structures of $M_2[FeCl_5(OH_2)]$ (M = Cs^+, NH_4^+, and OH_3^+) (37–39);

Can. J. Chem. Downloaded from www.nrcresearchpress.com by 88.255.202.194 on 09/08/12
For personal use only.

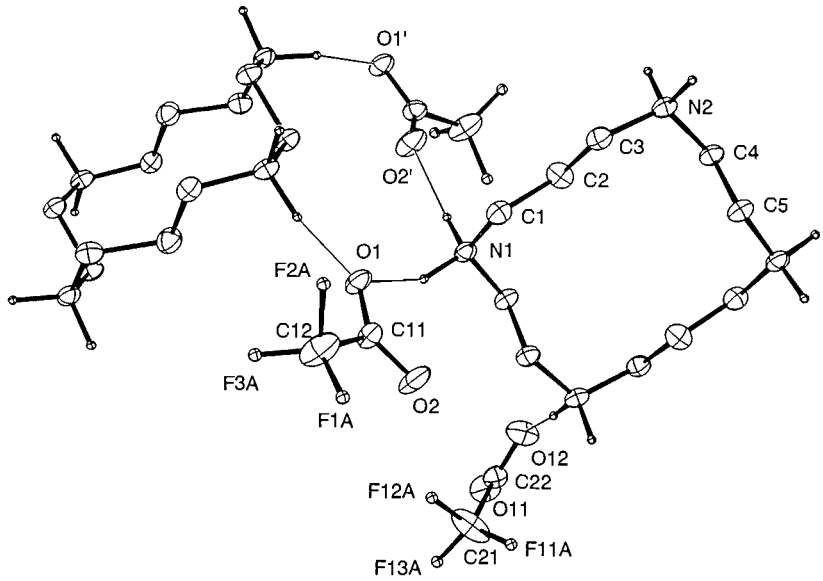

FIG. 5. ORTEP diagram showing a portion of the polymeric chain in **2**. For the sake of clarity, only one set of fluorine atoms is illustrated.

TABLE 4. Atomic parameters x,y,z and B_{iso} for $[H_4(cyclam)][CF_3COO]_4$

Atom	x	y	z	B_{iso}[a]
N1	0.9403(4)	0.6452(3)	0.16935(21)	2.64(16)
N2	0.7530(4)	0.3337(3)	0.07163(22)	2.60(16)
C1	1.0980(5)	0.6410(4)	0.1462 (3)	2.99(20)
C2	1.0913(5)	0.6703(4)	0.0476 (3)	3.46(20)
C3	1.2522(5)	0.6531(4)	0.0268 (3)	2.88(18)
C4	0.8596(5)	0.4214(4)	0.1343 (3)	2.67(18)
C5	0.8146(4)	0.5610(4)	0.1148 (3)	2.70(19)
C11	0.1210(5)	0.4978(4)	0.3713 (3)	3.06(19)
C12	0.2393(6)	0.4707(5)	0.4582 (4)	5.5 (3)
F1A	0.2880(9)	0.3597(5)	0.4658 (5)	8.5 (4)
F1B	0.3184(8)	0.3644(7)	0.4534 (6)	10.4 (4)
F2A	0.3703(12)	0.5374(13)	0.4485 (13)	24.8 (13)
F2B	0.3399(6)	0.5574(4)	0.4845 (4)	5.1 (3)
F3A	0.2140(14)	0.5135(11)	0.5263 (6)	17.7 (8)
F3B	0.1561(8)	0.4529(9)	0.5236 (4)	8.6 (5)
O1	0.0970(3)	0.6131(3)	0.35089(19)	3.46(14)
O2	0.0564(4)	0.4060(3)	0.32962(21)	4.74(16)
C21	0.4358(7)	0.2469(7)	0.2083 (4)	6.9 (3)
C22	0.3669(5)	0.3366(4)	0.1311 (3)	3.28(20)
F11A	0.5246(14)	0.1617(9)	0.1878 (9)	16.3 (8)
F11B	0.5713(8)	0.2081(11)	0.2057 (6)	15.0 (7)
F12A	0.5489(12)	0.3072(13)	0.2656 (6)	15.8 (7)
F12B	0.4280(12)	0.2975(13)	0.2867 (5)	14.6 (8)
F13A	0.3609(12)	0.2212(13)	0.2576 (7)	16.6 (8)
F13B	0.3380(9)	0.1384(6)	0.2045 (5)	8.3 (4)
O11	0.2257(3)	0.3544(3)	0.11887(24)	4.95(18)
O12	0.4595(3)	0.3806(3)	0.08876(23)	4.79(17)

[a] B_{iso} is the mean of the principal axes of the thermal ellipsoid.

however, these hydrogen bonds are interanionic. The N-H...Cl and O-H...Cl distances in $(NH_4)_2[FeCl_5(OH_2)]$ and $(OH_3)_2[FeCl_5(OH_2)]$ are 3.53(4) and 3.306(8) Å, respectively. The nature of the network hydrogen bonding, which is a direct consequence of the ability of $H_4(cyclam)^{4+}$ to hydrogen bond, makes the two directional senses of the polymeric network geometrically and physically different. This direction of the crystal is therefore polar and hence **1** crystallizes in a polar space group.

The aquapentachloroferrate(III) anion is well known (40). This study agrees well with the earlier X-ray crystallographic reports (36–39). The Fe atom exists in a distorted octahedral environment (Fig. 4). The distortion presumably results from repulsive interactions between the chlorines, which would be expected to be greater than those between the chlorine atoms and water. This is reflected in the Cl—Fe—Cl and O—Fe—Cl angles (see Table 3). The Fe—Cl distances are not equivalent. Specifically, the Fe—Cl

Can. J. Chem. Downloaded from www.nrcresearchpress.com by 88.255.202.194 on 09/08/12
For personal use only.

TABLE 5. Interatomic distances (Å) and angles (°) for $[H_4(cyclam)][CF_3COO]_4$

Distances			
N1—C1	1.497(5)	C12—F2A	1.378(17)
N1—C5	1.512(5)	C12—F2B	1.269(7)
N2—C3a	1.498(5)	C12—F3A	1.195(14)
N2—C4	1.498(5)	C12—F3B	1.368(9)
C1—C2	1.523(6)	C21—C22	1.527(7)
C2—C3	1.518(6)	C21—F11A	1.268(11)
C3—N2a	1.498(5)	C21—F11B	1.262(8)
C4—C5	1.531(6)	C21—F12A	1.330(12)
C11—C12	1.520(7)	C21—F12B	1.323(11)
C11—O1	1.258(5)	C21—F13A	1.132(9)
C11—O2	1.224(5)	C21—F13B	1.419(9)
C12—F1A	1.239(8)	C22—O11	1.223(5)
C12—F1B	1.324(10)	C22—O12	1.230(5)
N1..O1b	2.830(4)	N2..O1d	2.797(4)
N1..O2c	2.742(4)	N2..O12	2.681(4)
Angles			
C1—N1—C5	116.7(3)	F1B—C12—F3B	107.0(6)
C3a—N2—C4	117.5(3)	F2A—C12—F3A	102.5(9)
N1—C1—C2	112.7(3)	F2B—C12—F3B	108.1(6)
C1—C2—C3	110.0(3)	C22—C21—F11A	113.9(7)
N2a—C3—C2	111.7(3)	C22—C21—F11B	113.0(5)
N2—C4—C5	111.6(3)	C22—C21—F12A	109.0(7)
N1—C5—C4	109.2(3)	C22—C21—F12B	111.1(7)
C12—C11—O1	116.2(4)	C22—C21—F13A	118.1(6)
C12—C11—O2	117.1(4)	C22—C21—F13B	109.3(5)
O1—C11—O2	126.6(4)	F11A—C21—F12A	95.2(9)
C11—C12—F1A	114.4(5)	F11A—C21—F13A	118.0(9)
C11—C12—F1B	112.0(5)	F11B—C21—F12B	113.0(8)
C11—C12—F2A	103.6(8)	F11B—C21—F13B	107.5(8)
C11—C12—F2B	115.7(5)	F12A—C21—F13A	97.6(10)
C11—C12—F3A	117.8(7)	F12B—C21—F13B	102.2(7)
C11—C12—F3B	106.9(5)	C21—C22—O11	115.4(4)
F1A—C12—F2A	102.3(7)	C21—C22—O12	116.2(4)
F1A—C12—F3A	113.4(8)	O11—C22—O12	128.4(4)
F1B—C12—F2B	106.8(5)		

a: $2 - x$, $1 - y$, $-z$
b: $1 + x$, y, z
c: $1 - x$, $0.5 + y$, $0.5 - z$
d: $1 - x$, $-0.5 + y$, $0.5 - z$

bond that is *trans* to the water molecule is consistently shorter than the other four Fe—Cl distances, presumably a manifestation of *trans* influence.

Compound **2** was crystallized directly from a solution of cyclam in trifluoroacetic acid. An ORTEP (33) diagram of the $[H_4(cyclam)]^{4+}$ cation is presented in Fig. 2*b* and a portion of the polymeric chain in Fig. 5. The atomic coordinates and important bond lengths and angles are presented in Tables 4 and 5, respectively. The geometry of the cation is almost identical to that of the cation in **1** and network hydrogen bonding is once again observed. As was observed in **1**, not all of the anions are involved in the network but the networking is less complex. There are two pairs of crystallographically equivalent anions. One pair of CF_3COO^- anions forms terminal hydrogen bonds through one oxygen atom to the cation (O12....N2, 2.681(4) Å). The other pair of CF_3COO^- moieties bridges three separate cations through both oxygen atoms (O1....N2, 2.797(4) Å; O1....N1 of a second cation, 2.830(4) Å; and O2....N1 of a third cation, 2.742(4) Å). The net result is a two-dimensional network that contains inversion centers. **2** therefore crystallizes in a centrosymmetric space group.

To conclude, under the highly acidic conditions employed in this study, formation of $[H_4(cyclam)]^{4+}$ is facilitated. $[H_4(cyclam)]^{4+}$ adopts an exodentate conformation that favours network hydrogen bonding and, in the case of **1**, a polar one-dimensional network of hydrogen bonds. Materials that are polar in their crystalline state have been shown to possess a number of useful and interesting physical properties, particularly as SHG-active materials. $[H_4(cyclam)]^{4+}$ therefore has potential relevance as a bridging group in crystal engineering of SHG-active materials.

Acknowledgement

We thank the Natural Sciences and Engineering Research Council of Canada (NSERC) (operating grant to M.J.Z.) and Saint Mary's University for purchasing the X-ray diffractometer.

Can. J. Chem. Downloaded from www.nrcresearchpress.com by 88.255.202.194 on 09/08/12
For personal use only.

1. (*a*) S. Copp, S. Subramanian, and M. J. Zaworotko. J. Am. Chem. Soc. **114**, 8719 (1992); (*b*) J. S. Wilkes and M. J. Zaworotko. Supramol. Chem. In press.
2. G. R. Desiraju. *In* Crystal engineering; the design of organic solids. Elsevier Science Publishing Company, Inc., New York. 1989.
3. S. R. Marder, J. E. Sohn, and G. D. Stucky (*Editors*). Materials for nonlinear optics; chemical perspectives. ACS Symp. Ser. American Chemical Society, Washington, D.C. 1991.
4. R. A. Hann and D. Bloor (*Editors*). Organic materials for nonlinear optics. Royal Society of Chemistry, London. 1989.
5. (*a*) S. R. Marder, J. W. Perry, B. G. Tiemann, R. E. Marsh, and W. P. Schaefer. Chem Mater. **2**, 685 (1990); (*b*) L-T. Cheng, W. Tam, S. H. Stevenson, G. R. Meredith, G. Rikken, and S. R. Marder. J. Phys. Chem. **95**, 10631 (1991); (*c*) L-T. Cheng, W. Tam, S. R. Marder, A. E. Stiegman, G. Rikken, and C. W. Spangler. J. Phys. Chem. **95**, 10643 (1991).
6. (*a*) G. M. Frankenbach and M. C. Etter. Chem. Mater. **4**, 272 (1992); (*b*) M. C. Etter and K-S. Huang. Chem. Mater. **4**, 824 (1992).
7. S. Endo, T. Chino, S. Tsuboi, and K. Koto. Nature, **340**, 452 (1989), and references therein.
8. C. B. Aakeroy, P. B. Hitchcock, B. D. Moyle, and K. R. Seddon. J. Chem. Soc. Chem. Commun. 1856 (1989).
9. L. F. Lindoy. *In* The chemistry of macrocyclic ligand complexes. Cambridge University Press, Cambridge. 1989.
10. B. Bosnich, C. K. Poon, and M. L. Tobe. Inorg. Chem. **4**, 1102 (1965).
11. B. Bosnich, M. L. Tobe, and G. A. Webb. Inorg. Chem. **4**, 1109 (1965).
12. E. J. Bounsall and S. R. Koprich. Can. J. Chem. **48**, 1481 (1970).
13. K. Toriumi, M. Yamashita, H. Ito, and T. Ito. Acta. Crystallogr. Sect. C: Cryst. Struct. Commun. **C42**, 963 (1986).
14. F. Brisse, M. G. Simard, H. Dugas, and A. Basak. Acta. Crystallogr. Sect. C: Cryst. Struct. Commun. **C47**, 1683 (1991).
15. A. McAuley, S. Subramanian, and M. J. Zaworotko. J. Chem. Soc. Chem. Commun. 1321 (1992).
16. D. K. Towle, S. K. Hoffmann, W. E. Hatfield, P. Singh, and P. Chaudhury, Inorg. Chem. **27**, 394 (1988).
17. J. Cullinane, R. I. Gelb, T. N. Margulis, and L. J. Zompa. J. Am. Chem. Soc. **104**, 3048 (1982).
18. A. Bianchi, E. Garbia-Espana, M. Micheloni, and P. Paoletti. Inorg. Chim. Acta, **L9**, 102 (1985).
19. F. Peter, M. Gross, M. W. Hosseini, J-M. Lehn, and R. B. Sessions. J. Chem. Soc. Chem. Commun. 1067, (1981).
20. P. V. Bernhardt, G. A. Lawrance, B. W. Skelton, and A. H. White. Aust. J. Chem. **42**, 1035 (1989).
21. M. F. Manfrin, L. Setti, and L. Moggi. Inorg. Chem. **31**, 2768 (1992), and references therein.
22. S. A. Van Arman and A. W. Czarnik. J. Am. Chem. Soc. **112**, 5376 (1990).
23. E. J. Gabe, Y. Le Page, J-P. Charland, F. L. Lee, and P. S. White. J. Appl. Crystallogr. **22**, 384 (1989).
24. International tables for X-ray crystallography. Kynoch Press, Birmingham, England, 1974. Distributor: D. Reidel, Dordrecht, The Netherlands.
25. D. Rogers. Acta Crystallogr. Sect. A: Cryst. Phys. Diffr. Theor. Gen. Crystallogr. **A37**, 734 (1981).
26. (*a*) L. Fabbrizzi. Comments Inorg. Chem. **4**, 33 (1985); (*b*) M. O. Kostner and A. L. Allred. J. Am. Chem. Soc. **94**, 7189 (1972); (*c*) C-M. Che and C-K. Poon. Pure Appl. Chem. **60**, 1201 (1988).
27. D. D. Watkins, Jr., D. P. Riley, J. A. Stone, and D. H. Busch. Inorg. Chem. **15**, 387 (1976).
28. P-K. Chan and C-K. Poon. J. Chem. Soc. Dalton Trans. 858 (1976).
29. (*a*) J. C. Dabrowiak, P. H. Merrel, and D. H. Busch. Inorg. Chem. **11**, 1979 (1972); (*b*) C. J. Hipp, L. F. Lindoy, and D. H. Busch. Inorg. Chem. **11**, 1988 (1972); (*c*) J. C. Dabrowiak, F. V. Lovecchio, V. L. Geodken, and D. H. Busch. J. Am. Chem. Soc. **94**, 5502 (1972).
30. H. S. Mountford, L. O. Spreer, J. W. Otvos, M. Calvin, K. J. Brewer, M. Ritcher, and B. Scott. Inorg. Chem. **31**, 718 (1992).
31. C. Nave and M. R. Truter. J. Chem. Soc. Dalton Trans. 2351 (1974).
32. N. F. Curtis. J. Chem. Soc. 2644 (1964).
33. C. K. Johnson. ORTEP, a Fortran thermal ellipsoid plot program. Technical Report ORNL-5138, Oak Ridge, Tenn. 1976.
34. M. D. Joesten and L. J. Schadd. Hydrogen bonding. Marcel Dekker, Inc. New York. 1974.
35. (*a*) M. V. Gaudet, M. J. Zaworotko, and P. S. White. Inorg. Chem. **28**, 1191 (1989); (*b*) R. H. Dubois, M. J. Zaworotko, and P. S. White. Inorg. Chem. **28**, 2019 (1989); (*c*) J. M. Martell and M. J. Zaworotko. J. Chem. Soc. Dalton Trans. 1495 (1991).
36. A. McAuley, K. Beveridge, S. Subramanian, and T. W. Whitcombe. Can. J. Chem. **67**, 1657 (1989).
37. J. E. Greedan, D. C. Hewitt, R. Faggiani, and I. D. Brown. Acta Crystallogr. Sect. B: Struct. Crystallogr. Cryst. Chem. **B36**, 1927 (1980).
38. C. J. O'Connor, B. S. Deaver, and E. Sinn. J. Chem. Phys. **70**, 5161 (1979).
39. B. N. Figgis, C. L. Raston, R. P. Sharma, and A. H. White. Aust. J. Chem. **31**, 2717 (1978).
40. I. Lindqvist. Ark. Kemi Mineral. Geol. **24**, 1 (1947).

Can. J. Chem. Downloaded from www.nrcresearchpress.com by 88.255.202.194 on 09/08/12
For personal use only.

Stereoisomerism of oxotrichlorobis(triphenylphosphine)rhenium(V), $ReOCl_3(PPh_3)_2$: a reinvestigation

ANNE-MARIE LEBUIS AND ANDRÉ L. BEAUCHAMP[1]

Département de chimie, Université de Montréal, C.P. 6128, Succ. A, Montréal (Québec), Canada H3C 3J7

Received August 26, 1992

ANNE-MARIE LEBUIS and ANDRÉ L. BEAUCHAMP. Can. J. Chem. **71**, 441 (1993).

The various preparative procedures described in the literature for $ReOCl_3(PPh_3)_2$ were repeated. The standard methods were found to yield a yellow triclinic material ($P\bar{1}$, a = 11.793, b = 14.300, c = 16.422 Å, α = 64.04°, β = 84.31°, γ = 87.32°, R = 0.064). The unit cell contains three discrete monomeric molecules with the *trans*-bis(phosphine) configuration, one of which has its Cl-Re=O unit disordered over two opposite directions. Recrystallization in CH_2Cl_2 yielded crystals of the bright green monoclinic polymorph ($C2/c$, a = 24.347, b = 9.604, c = 15.666 Å, β = 116.77°, R = 0.025) containing the same monomeric molecule, but with a different conformation of the PPh_3 ligands and a different packing pattern. These two polymorphs actually correspond to "isomers" 1 and 2 described by Johnson, Lock, and Wilkinson in 1964. Attempts to prepare their third "isomer" yielded powders containing $ReOCl_3(PPh_3)_2$ (green polymorph) and $ReNCl_2(PPh_3)_2$. The IR and ^{31}P NMR spectra of these samples are discussed.

ANNE-MARIE LEBUIS et ANDRÉ L. BEAUCHAMP. Can. J. Chem. **71**, 441 (1993).

Les différentes méthodes de préparation décrites dans la litterature pour $ReOCl_3(PPh_3)_2$ ont été répétées. Les méthodes courantes conduisent à un produit triclinique jaune ($P\bar{1}$, a = 11,793, b = 14,300, c = 16,422 Å, α = 64,04°, β = 84,31°, γ = 87,32°, R = 0,064). La maille élémentaire renferme trois molécules individuelles ayant une configuration *trans*-bis(phosphine), dont l'une possède un motif Cl-Re=O désordonné selon deux directions opposées. La recristallisation dans CH_2Cl_2 donne des cristaux du polymorphe monoclinique vert brillant ($C2/c$, a = 24,347, b = 9,604, c = 15,666 Å, β = 116,77°, R = 0,025) renfermant la même molécule monomère, mais la conformation des ligands PPh_3 et l'empilement cristallin sont différents. Ces deux polymorphes correspondent aux «isomères» 1 et 2 décrits par Johnson, Lock et Wilkinson en 1964. Des tentatives pour préparer leur troisième «isomère» ont conduit à des poudres contenant $ReOCl_3(PPh_3)_2$ (polymorphe vert) et $ReNCl_2(PPh_3)_2$. Les spectres IR et RMN ^{31}P de ces échantillons sont discutés.

Introduction

$ReOCl_3(PPh_3)_2$ is extensively used as a starting compound in the coordination chemistry of rhenium (1). It was first identified as a yellow material in a short paper by Lock and Wilkinson in 1962 (2). Shortly after, Chatt and Rowe (3, 4) proposed the *mer-trans* structure **A** for this compound on the basis of the dipole moment. In a more detailed report, Johnson, Lock, and Wilkinson (5) described three varieties of $ReOCl_3(PPh_3)_2$, which they labelled "isomers" 1, 2, and 3.[2] They could be differentiated by their color and Re=O stretching band in infrared, but no structure was assigned to any of these materials. More recently, tested procedures were proposed to prepare the yellow complex (6, 7). The products obtained by these methods correspond to the compound studied by Chatt and Rowe (4) and to "isomer" 1 of Johnson *et al.* (5), but its stereochemistry is not explicitly identified. Hence, although the existence of stereoisomers for $ReOCl_3(PPh_3)_2$ has been mentioned (5, 6, 8), this question has apparently not yet received a satisfactory answer.

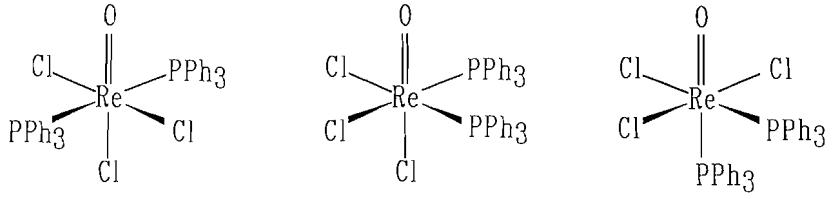

The present paper reports X-ray diffraction and ^{31}P NMR results showing that two distinct varieties of $ReOCl_3(PPh_3)_2$ indeed exist in the solid state, but that they are polymorphs of the same compound with configuration **A**. No evidence could be found for configurations **B** and **C**.

Experimental section

Reactants and methods

$KReO_4$ and PPh_3 were used as received from Aldrich. Samples of $ReOCl_3(PPh_3)_2$ were prepared by the various methods available in the literature (4–7). $ReNCl_2(PPh_3)_2$ and $ReOCl_3(PPh_3)(OPPh_3)$ were synthesized by published methods (9, 10) and checked by IR and ^1H and ^{31}P NMR spectroscopies.

IR spectra (4000–250 cm^{-1}) were recorded as CsI pellets on a Perkin–Elmer 783 spectrophotometer. UV–visible spectra (220–750 nm) were obtained on a Varian Instruments DMS 100S spec-

[1]Author to whom correspondence may be addressed.

[2]Throughout this paper, the term "isomer" will be used strictly to refer to these three materials described by Wilkinson and coworkers.

Can. J. Chem. Downloaded from www.nrcresearchpress.com by 88.255.202.194 on 09/08/12
For personal use only.

Can. J. Chem. Downloaded from www.nrcresearchpress.com by 88.255.202.194 on 09/08/12
For personal use only.

TABLE 1. Crystallographic data for the two polymorphs of $ReOCl_3(PPh_3)_2$

Parameter	Polymorph	
	Monoclinic	Triclinic
Formula	$C_{36}H_{30}OP_2Cl_3Re$	$C_{36}H_{30}OP_2Cl_3Re$
Formula weight	833.15	833.15
Space group	$C2/c$	$P\bar{1}$
a, Å	24.347(9)	11.793(5)
b, Å	9.604(5)	14.300(8)
c, Å	15.666(6)	16.422(9)
α, deg	90.0	64.04(4)
β, deg	116.77(3)	84.31(4)
γ, deg	90.0	87.32(4)
V, Å^3	3270(2)	2477(2)
D_{calc}	1.692	1.675
Z	4	3
λ, Å	0.71069	0.71069
μ, cm^{-1}	41.09	40.96
Crystal size, mm (faces)	0.18 ($101/\bar{1}0\bar{1}$)	0.028 ($111/\bar{1}\bar{1}\bar{1}$)
	0.17 ($11\bar{1}/\bar{1}11$)	0.122 ($1\bar{1}0/\bar{1}10$)
	0.16 ($\bar{1}11/1\bar{1}\bar{1}$)	0.114 ($\bar{1}01/10\bar{1}$)
	0.06 ($100/\bar{1}00$)	
Transmission range	0.54–0.78	0.65–0.89
$2\theta_{max}$, deg	50	45
No. unique reflections	2881	6498
No. observed reflections (n)	2109	2021
Rejection criterion, $I/\sigma(I) <$	3.0	3.0
R^a	0.025	0.064
$R_w{}^a$	0.026	0.058
Goodness-of-fit, S^a	0.74	1.27
No. parameters refined (v)	197	306
Residual on final ΔF map, e/Å^3		
Maximum	0.26 (near Re and P)	1.24 (near Re(2))
General background	±0.20	±1.1

$^aR = \Sigma| |F_o| - |F_c| |/\Sigma|F_o|$; $R_w = [\Sigma w(|F_o| - |F_c|)^2/\Sigma w|F_o|^2]^{1/2}$; $S = [\Sigma w(|F_o| - |F_c|)^2/(n - v)]^{1/2}$.

trophotometer. ^{1}H NMR spectra (in CD_2Cl_2) were recorded at 300 MHz on a Varian VXR-300 spectrometer. The residual solvent signal (δ 5.320 ppm) served as internal standard. The ^{31}P solution and solid-state spectra were recorded at 121.42 MHz with the same instrument. For the solids, the relaxation delays and spin rates were respectively 10 s and 2.5 kHz for $ReNCl_2(PPh_3)_2$, 4s and 4 kHz for the other samples. The spectra were referenced to external D_3PO_4 85% in D_2O (δ 0 ppm). X-ray powder patterns were taken with a Debye–Scherrer camera (radius 57.3 mm) using Ni-filtered CuKα̃ radiation (1.54178 Å).

X-ray work — monoclinic polymorph

Bright green, roughly hexagonal, platelets were obtained by recrystallization of the yellow powder in CH_2Cl_2. The crystallographic work was done at room temperature on an Enraf–Nonius CAD-4 diffractometer using graphite monochromatized MoKα̃ radiation. The reduced cell (a_r = 9.63, b_r = 13.10, c_r = 15.71 Å, α_r = 63.44°, β_r = 71.95°, γ_r = 68.48°) was determined from 15 centered reflections located from a preliminary polaroid photograph and checked with long-exposure axial photographs about the three axes. A Laue mirror plane perpendicular to the a_r axis and the Niggli parameters suggested a non-primitive monoclinic lattice. The reduced cell was first transformed to an I-monoclinic cell with matrix 27 (11), and then the usual transformation to a conventional C-centered cell ($\boldsymbol{a}_C = \boldsymbol{a}_I + \boldsymbol{c}_I$, $\boldsymbol{b}_C = \boldsymbol{b}_I$, $\boldsymbol{c}_C = -\boldsymbol{a}_I$) was applied. As expected, the a_r axis, for which a Laue mirror had been observed, has now become the unique b axis of the monoclinic cell. The accurate cell parameters given in Table 1 were obtained by refinement on a new set of 25 centered high-angle reflections ($20° < 2\theta < 22°$).

Intensity data ($2\theta \leq 50°$) were collected by the ω scan technique over a range $\Delta\omega = (1.00 + 0.35 \tan\theta)°$. Option FLAT was used to adjust the ψ angle so that absorption is minimized for the plate-shaped crystal. Orientation was monitored every 200 measurements and intensity was checked every hour with seven standard reflections. Intensity fluctuations remained within ±1.2%. A total of 5704 reflections with $h + k = 2n$ were measured in octants hkl, $h\bar{k}l$, $hk\bar{l}$, and $h\bar{k}\bar{l}$. The data were corrected for absorption (Gaussian integration, 10 × 10 × 10 grid). Averaging of the equivalent $+k/-k$ pairs (R_{av} = 0.037) yielded a set of 2881 unique reflections, of which 2109 with $I \geq 3.0\ \sigma(I)$ were retained for structure determination and refinement. The usual corrections for the effects of Lorentz and polarization were finally applied.

Monoclinic Laue symmetry and systematic absences (hkl, $h + k \neq 2n$; $h0l$, $l \neq 2n$) were consistent with space groups Cc and $C2/c$. The structure was solved in the centric $C2/c$ space group by the heavy-atom method. The Re atom was located from a Patterson map and all other non-hydrogen atoms were found from successive difference Fourier (ΔF) maps. Refinement was done by full-matrix least-squares procedures. The function minimized was $\Sigma w(|F_o| - |F_c|)^2$, with weights w based on counting statistics ($w = 1/\sigma^2(F) + 0.001\ F^2$). The non-hydrogen atoms were refined anisotropically. Hydrogens were fixed at idealized positions (C—H = 0.95 Å, U = 0.065 Å^2). Their parameters were not refined, but the coordinates were recalculated after each cycle. There

Can. J. Chem. Downloaded from www.nrcresearchpress.com by 88.255.202.194 on 09/08/12
For personal use only.

were no indications, such as high thermal motion or large residuals in the final ΔF map, to suggest that the space group could be *Cc* instead of $C2/c$.

X-ray work — triclinic polymorph

Suitable crystals of this yellow polymorph were not readily obtained. Conversion of the raw material to the monoclinic polymorph occurred in polar solvents (acetone, CH_2Cl_2, THF). Benzene reproducibly yielded the yellow polymorph, but the crystals obtained were very small and often twinned. Slow vapour diffusion of light petroleum ether into a saturated benzene solution gave the best results. The specimen used for X-ray work was the largest available that was not twinned. A set of precession and cone-axis photographs indicated a triclinic unit cell and provided starting cell parameters. The rest of the X-ray work was carried out on a Syntex $P\bar{1}$ diffractometer using graphite monochromatized MoK$\bar{\alpha}$ radiation. The reduced cell obtained as above from 15 reflections was identical to the one deduced from precession work. Lattices of symmetry higher than triclinic were ruled out by the Niggli parameters. The final cell parameters given in Table 1 were obtained by refinement on a new set of 15 centered reflections in the range $18° < 2\theta < 24°$.

Intensity data ($2\theta \leq 45°$) were collected at room temperature by the $\omega/2\theta$ scan technique over a range $\Delta\omega = (0.90 + 0.35 \tan\theta)°$. Three standard reflections checked every 75 measurements showed fluctuations within ±3.0% during data collection. A total of 6498 *hkl*, $h\bar{k}l$, $hk\bar{l}$, and $h\bar{k}\bar{l}$ reflections was measured, of which 2021 with $I \geq 3.0\,\sigma(I)$ were retained for structure determination and refinement. The data were corrected as above for the effects of absorption, Lorentz, and polarization.

The structure was solved in the centric space group $P\bar{1}$ by the heavy-atom method. Structure resolution was not straightforward, since the Re positions introduced pseudosymmetry that could be removed only at a late stage in the refinement. Since the unit cell contained three formula units, at least two independent types of Re atoms had to be present. The Patterson map readily revealed the positions of a Re(1) atom in special position (0, 0, 0) and a pair of Re(2) atoms in general positions near (1/3, 1/3, 1/3) and 2/3, 2/3, 2/3). The Cl and P atoms could be located from a ΔF map, but they did not remove pseudosymmetry. The nine independent phenyl rings were laboriously extracted from the overlapping images in a series of ΔF maps. It is only after this model was isotropically refined that Re could be refined anisotropically and clear features emerged for the oxygens.

Re(1) being situated on an inversion center, the necessarily noncentric $ReOCl_3(PPh_3)_2$ molecule had to be disordered. However, no evidence of disorder was found in the phosphine and the Cl(12) atom *cis* to oxygen. When full occupancy was assumed for the *trans* Cl(11) position extracted from the ΔF map, an abnormally high temperature factor was obtained and a new peak, closer to Re(1), appeared in the map. Thus, this region (and its centrosymmetry-related counterpart) had to be statistically occupied by oxygen and chlorine atoms, leading to two opposite orientations of the Cl(11)-Re(1)=O(1) bonds. However, there were no indications of disorder at Re(1) itself, which was kept at the origin. Since coalescence occurred when the O(1) and Cl(11) half-atoms were simultaneously refined, O(1) was fixed on the Re(1)-Cl(11) line at 1.66 Å from Re (the distance found in the monoclinic polymorph), and only Cl(11) was refined. In the other molecule, geometric constraints were not applied. The structure was refined by least-squares procedures as above: Re, Cl, and P anisotropically, remaining non-hydrogen atoms isotropically, hydrogens fixed. Although disorder was not detected for the molecule sitting in general position, the presence of a small amount of disorder in the $ReOCl_3$ plane cannot be totally ruled out, considering the limitations imposed by poor crystal quality.

The scattering factors used were those of Cromer and Liberman (12), except for hydrogen (13). Anomalous dispersion was included in structure factor calculations for Re, Cl, and P (14). The computer programs used are listed elsewhere (15). The refined coordinates for the non-hydrogen atoms are listed in Tables 2 and 3.[3]

TABLE 2. Final coordinates ($\times 10^4$, Re, Cl and P $\times 10^5$) and equivalent isotropic temperature factors ($Å^2 \times 10^3$) for the monoclinic polymorph

	x	*y*	*z*	U_{eq}
Re(1)	0	16320(3)	25000	25
Cl(1)	5462(6)	17198(16)	42104(8)	40
Cl(2)	0	41138(10)	25000	36
P(1)	9715(5)	17091(15)	23053(8)	26
O(1)	0	−100(5)	2500	36
C(1A)	1220(2)	−103(5)	2414(3)	28
C(2A)	819(2)	−1072(5)	1763(4)	37
C(3A)	969(3)	−2476(6)	1870(4)	47
C(4A)	1511(3)	−2910(6)	2628(5)	54
C(5A)	1901(3)	−1983(6)	3261(4)	56
C(6A)	1758(3)	−570(6)	3159(4)	41
C(1B)	897(2)	2334(5)	1159(3)	28
C(2B)	768(3)	3727(5)	941(4)	48
C(3B)	733(3)	4265(6)	100(5)	59
C(4B)	811(3)	3415(7)	−541(4)	49
C(5B)	929(3)	2044(6)	−336(4)	48
C(6B)	976(2)	1488(6)	506(3)	39
C(1C)	1627(2)	2719(5)	3139(3)	31
C(2C)	1598(2)	3529(6)	3848(3)	35
C(3C)	2107(3)	4321(6)	4447(4)	42
C(4C)	2634(3)	4286(6)	4354(4)	48
C(5C)	2669(3)	3495(7)	3653(4)	56
C(6C)	2176(3)	2711(7)	3046(4)	50

Results and discussion

Wilkinson's "isomers" 1 and 2

Samples of $ReOCl_3(PPh_3)_2$ were prepared following the two tested methods described in Inorganic Synthesis (6, 7). The earlier procedures reported by Johnson *et al.* (5) and by Chatt and Rowe (4) were also repeated. These various runs allowed us to isolate in pure form a yellow triclinic and a bright green monoclinic material.

The product obtained by the standard methods consists of a yellow powder or microcrystalline solid. The approach used by Parshall *et al.* (7), which was adapted from Chatt and Rowe (4), consists of reacting Re_2O_7 or $KReO_4$ with excess PPh_3 in a HCl–ethanol mixture. Although some KCl is present if $KReO_4$ is used, it can be removed by washing with small amounts of water. In the method proposed by Johnson *et al.* (6), which corresponds to one of the approaches they

[3]The supplementary material includes a view of the unit cell of $ReNCl_2(PPh_3)_2$, *d*-spacings from powder patterns of $ReNCl_2(PPh_3)_2$, $ReOCl_3(PPh_3)_2$, and "isomer" 3, crystallographic results (lists of observed and calculated structure factor amplitudes, anisotropic thermal parameters, hydrogen coordinates, torsion angles, distances and angles in phosphine, and atom-to-plane distances for both structures) (59 pages). Complete set of data may be purchased from: The Depository of Unpublished Data, Document Delivery, CISTI, National Research Council Canada, Ottawa, Canada K1A 0S2.

Calculated powder patterns, stereoview of the unit cell, and tables of hydrogen atom coordinates and distances and angles in PPh_3 ligands have also been deposited with the Cambridge Crystallographic Data Centre and can be obtained on request from The Director, Cambridge Crystallographic Data Centre, University Chemical Laboratory, 12 Union Road, Cambridge, CB2 1EZ, U.K.

Can. J. Chem. Downloaded from www.nrcresearchpress.com by 88.255.202.194 on 09/08/12
For personal use only.

TABLE 3. Final coordinates ($\times 10^3$, Re, Cl and P $\times 10^4$) and equivalent isotropic temperature factors (Å^2 $\times 10^3$) for the triclinic polymorph

	x	y	z	U_{eq}
Re(1)	0	0	0	40
Re(2)	3470(2)	3437(2)	3320(2)	34
Cl(11)	−152(16)	1268(14)	489(13)	62
Cl(12)	188(8)	1288(8)	−1514(6)	62
Cl(21)	2994(8)	4608(8)	3933(7)	67
Cl(22)	3424(8)	2184(8)	4865(7)	67
Cl(23)	3869(8)	2034(8)	2929(7)	64
P(1)	2134(8)	41(7)	−126(6)	41
P(2)	5638(7)	3482(7)	3327(7)	45
P(3)	1314(7)	3215(8)	3360(6)	42
O(1)[a]	11	−92	−36	39
O(2)	349(1)	437(2)	220(1)	40
C(11A)	273(3)	96(3)	22(2)	59
C(12A)	237(3)	203(3)	−31(2)	40
C(13A)	273(3)	284(3)	−12(2)	58
C(14A)	348(2)	256(2)	57(2)	39
C(15A)	380(3)	156(3)	104(2)	51
C(16A)	349(3)	77(3)	84(2)	54
C(11B)	289(2)	34(2)	−126(2)	29
C(12B)	386(3)	90(3)	−151(3)	64
C(13B)	447(3)	102(3)	−233(3)	70
C(14B)	404(3)	64(3)	−286(2)	55
C(15B)	317(3)	7(3)	−260(3)	72
C(16B)	251(3)	−6(3)	−173(2)	61
C(11C)	276(2)	−115(2)	65(2)	30
C(12C)	350(3)	−175(3)	36(2)	48
C(13C)	400(3)	−271(3)	97(3)	80
C(14C)	378(3)	−302(3)	187(3)	65
C(15C)	310(3)	−255(3)	222(3)	79
C(16C)	252(3)	−156(3)	161(2)	47
C(21A)	634(2)	341(2)	231(2)	27
C(22A)	607(4)	413(3)	145(3)	87
C(23A)	650(3)	423(3)	62(2)	45
C(24A)	739(4)	351(4)	66(3)	103
C(25A)	764(3)	285(3)	139(2)	58
C(26A)	727(3)	270(3)	237(2)	61
C(21B)	628(3)	240(3)	428(2)	62
C(22B)	600(3)	146(3)	438(3)	64
C(23B)	646(3)	58(3)	509(3)	62
C(24B)	711(3)	78(3)	566(3)	80
C(25B)	724(3)	176(3)	552(3)	65
C(26B)	684(3)	258(3)	483(3)	69
C(21C)	613(2)	473(2)	333(2)	38
C(22C)	570(3)	523(3)	379(2)	62
C(23C)	617(3)	606(3)	380(2)	49
C(24C)	712(3)	641(3)	325(2)	56
C(25C)	764(3)	601(3)	280(3)	66
C(26C)	717(3)	517(3)	272(3)	65
C(31A)	79(2)	433(2)	239(2)	36
C(32A)	2(3)	415(3)	183(2)	49
C(33A)	−33(3)	508(3)	105(3)	83
C(34A)	3(3)	599(3)	92(2)	57
C(35A)	75(3)	619(3)	139(2)	59
C(36A)	110(3)	535(3)	216(2)	60
C(31B)	82(2)	214(2)	333(2)	33
C(32B)	123(2)	192(2)	261(2)	38
C(33B)	84(3)	105(3)	246(2)	54
C(34B)	0(3)	35(3)	312(2)	60
C(35B)	−46(3)	60(3)	384(3)	73
C(36B)	−5(3)	152(3)	386(2)	51
C(31C)	54(3)	325(3)	437(3)	64
C(32C)	−30(3)	394(3)	433(2)	53
C(33C)	−97(3)	416(3)	493(3)	65
C(34C)	−63(3)	346(3)	581(2)	56
C(35C)	18(4)	276(4)	603(3)	94
C(36C)	85(3)	249(3)	526(3)	76

[a]Fixed (see experimental section).

used to obtain their "isomer" 1 (5), $HReO_4$ is the source of rhenium and the reaction is carried out in acetic acid. The same product is also obtained by these authors by reacting $ReO(OEt)Cl_2(PPh_3)_2$ with HCl. All these methods were found to give good yields of the same yellow powder, identified by the strong Re=O stretching band at 969 cm^{-1} in infrared.

Yellow triclinic crystals were obtained when this material was recrystallized from benzene – petroleum ether. The X-ray work described hereafter shows that it contains monomeric molecules with the *mer-trans* configuration **A**. The yellow crystals and the powder have superimposable infrared spectra. As a further check that they are the same phase, the idealized X-ray powder pattern was calculated (16) from the refined coordinates of Table 3. The *d*-spacings (Table S-11, supplementary material) were found to be in excellent agreement with those observed in the Debye–Scherrer pattern recorded with the powder.

In the papers describing the tested preparation methods, the authors do not mention which stereoisomer is obtained, but they apparently take for granted that the yellow material corresponds to configuration **A**. This is the stereochemistry preferred by Chatt and Rowe (4), who based their conclusion on preliminary single-crystal X-ray film work and a dipole moment. It should be noted, however, that the X-ray results are found here *not* to correspond to the yellow material (see below). Therefore, the only evidence for structure **A** was the comparison of the dipole moment with those of stereoisomers **A** and **B** of $ReOCl_3(PPhEt_2)_2$ (4), whose structures are known from X-ray diffraction studies (17, 18). The dipole moment of 2.5 D for the PPh_3 complex was regarded as more consistent with the *mer-trans* molecule **A** (1.7 D) than with the *cis* species **B** (10.8 D). This interpretation is now found to be correct from the complete single-crystal X-ray diffraction work described hereafter.

Upon refluxing the yellow material in acetone or CH_2Cl_2, Johnson *et al.* (5) obtained a green crystalline solid (their "isomer" 2), whose Re=O band is shifted to 981 cm^{-1} (our value 978 cm^{-1}). The X-ray diffraction work below shows that it contains the same stereoisomer **A** as the yellow form, but with a different arrangement of phenyl rings in the phosphine and a completely different packing. The X-ray powder pattern (Table S-11) calculated from the data of Table 2 differs markedly from that of the yellow material, and corresponds with the Debye–Scherrer diagram obtained on the green material. Thus, the green monoclinic phase ("isomer" 2 of Johnson *et al.*) (5) and the yellow triclinic phase ("isomer" 1) are polymorphs of the same compound of structure **A**.

The X-ray diffraction results briefly mentioned by Chatt and Rowe (4) as evidence for the presence of structure **A** call for some comments. These authors obtained a set of X-ray Weissenberg films indicating a *C*-monoclinic cell with the following parameters: a = 24.55(5), b = 9.56(2), c =

Can. J. Chem. Downloaded from www.nrcresearchpress.com by 88.255.202.194 on 09/08/12
For personal use only.

TABLE 4. ^{31}P NMR Data[a]

	δ (ppm)
$ReOCl_3(PPh_3)_2$	−15.8
$ReNCl_2(PPh_3)_2$	26.7
$ReOCl_3(OPPh_3)(PPh_3)$	52.5[b]
	−30.8
$ReOCl_3(OPPh_3)_2$	60.4
	49.3
$OPPh_3$	30.5
PPh_3	−2.3

[a]In CD_2Cl_2, vs. external 85% D_3PO_4.
[b]$^3J(^{31}P–^{31}P)$ = 4.7 Hz.

15.80(4) Å, β = 117.2(1)°. Even though the crystals used are claimed to be those of the yellow phase, they actually correspond to the bright green polymorph, as can be seen from the crystal data in Table 1. In addition, as pointed out by Lock and Turner (19), the proposed interpretion was not completely rigorous. The systematic absences revealed by the films were considered to identify space group *C*2/*c*, but it was not mentioned that space group *Cc* was equally possible. With the density indicating the presence of four molecules per unit cell, no useful conclusions concerning stereochemistry could be drawn for space group *Cc*, since the molecule would sit in general position. It is only if the space group is *C*2/*c* that a special position on a crystallographic twofold axis is available to accommodate a molecule with the *trans*-phosphine structure **A**. Fortunately, the *C*2/*c* space group retained by the authors is now found to be correct and the molecule in the *green* polymorph does lie on a crystallographic twofold axis.

The IR spectra of both $ReOCl_3(PPh_3)_2$ polymorphs show the series of bands expected for triphenylphosphine (20). Besides the ν(Re=O) vibration discussed earlier, the spectra include bands at 310 (broad) and 265 cm^{-1}. On the basis of assignments proposed by Fergusson and Heveldt (21) for analogous compounds with other phosphines, the former band is believed to include the two stretching modes for the Re—Cl bonds *cis* to Re=O, whereas the low-frequency band should correspond to Re—P stretching. The Re—Cl_{trans} band is expected to show below 250 cm^{-1}.

The yellow and the green polymorphs, when dissolved in CH_2Cl_2, give identical UV–visible spectra, consisting of bands at 420 nm (ε = 7.5 × 10^2), 319 nm (ε = 3.2 × 10^3), and 271 nm (ε = 2.2 × 10^4). Similarly, the ^{31}P NMR spectra in CD_2Cl_2 both show a single resonance at −15.8 ppm (Table 4), shifted upfield from free PPh_3 (−2.3 ppm). This is consistent with structure **A**, although structure **B** is not ruled out, since it also contains two equivalent phosphines. However, structure **C** is excluded, since inequivalent phosphines should yield distinct signals (unless a fast exchange process takes place). The solids are indefinitely stable and CD_2Cl_2 solutions in closed NMR tubes show no appreciable decomposition after 24 h, even when they had not been degassed. When air is freely admitted in the tube, a pair of doublets at 52.5 and −30.8 ppm, with 4.7 Hz coupling, is visible after 60 h: these signals correspond with those of an authentic sample of $ReOCl_3(PPh_3)(OPPh_3)$. Under similar conditions, a solution of this new species also decomposes slowly to yield two signals of the same intensity at 60.4 and 49.3 ppm, which are most probably due to $ReOCl_3(OPPh_3)_2$. The structures of these two molecules are not known but, in the related complex $ReOCl_3(PPhEt_2)(OPPhEt_2)$, the OPR_3 ligand is *trans* to the Re=O bond (18). As to the $ReOCl_3(OPPh_3)_2$ species, it must adopt the *mer-cis* structure of type **C**, since the two other structures would give a single ^{31}P signal.

Crystal structures

ORTEP drawings of the $ReOCl_3(PPh_3)_2$ molecules in the two polymorphs are given in Fig. 1. In both cases, the *trans*-bis(phosphine) stereoisomer **A** is present. Structure refinement for the bright green monoclinic crystals grown from CH_2Cl_2 raised no particular problems. On the other hand, the crystals of the yellow phase were small and of poor quality, so that relatively few observed reflections were accessible. Structure resolution was further complicated by disorder and pseudo-symmetry problems. Although the overall structure can be regarded as well established despite these problems, distances and angles are much less reliable. Only the values derived from the monoclinic structure will be discussed.

The principal distances and angles are given in Table 5. In the monoclinic compound, the perfectly linear Cl(2)-Re=O(1) unit lies on a crystallographic twofold axis. Angular deformation about the metal is small: the *cis* angles deviate from 90° by <3.4°, the *cis* Cl and P atoms being displaced away from O(1), but less than in $ReO(OEt)Cl_2(PPh_3)_2$ (22).

The Re—P distance of 2.519(1) Å is on the short side of the range (2.519–2.553 Å) found for the three ethoxo-halogen derivatives $ReO(OEt)X_2(PPh_3)_2$ (22–24). In the nitride $ReNCl_2(PPh_3)_2$ (25), the shorter distance (2.448(2) Å) can be ascribed to the coordination number being reduced from six to five. The much shorter distances (2.444–2.478 Å) observed for a series of related compounds with the less bulky $PPhEt_2$ ligand (17, 18) point to the primary role of steric effect.

The Re—Cl distances lie in the range (2.37–2.44 Å) found for a series of $ReOCl_3(PR_3)_2$ compounds (17). The presence of chlorine, instead of an ethoxo group, *trans* to Re=O renders the *cis* Re—Cl bonds (2.397(1) Å) somewhat shorter than in $ReO(OEt)Cl_2(PPh_3)_2$ (2.422 Å) (22). The Re—Cl bond *trans* to the oxo group (2.383(2) Å) is identical with the one recently found for the mixed-halide compound *trans*-*trans*-$ReOClI_2(PPh_3)_2$ (26). It is roughly equal to or slightly shorter than Re—Cl_{cis},[4] even though the oxo group has been reported to lengthen the opposite Re—Cl bond in related compounds. For instance, in *trans*-$ReOCl_3(PPhEt_2)_2$ (17), the Re—Cl_{trans} distance (2.445(3) Å) is greater than the *cis* distances (2.380(3), 2.420(4) Å). Phosphine displacement from the axial directions toward the Cl_{trans} side (P—Re—P = 161°) perhaps contributes to increasing the Re—Cl_{trans} bond length. For $ReOCl_3$(diphos) (18), the extent of distortion cannot be evaluated, since the structure is reported very briefly without crystallographic coordinates. On the other hand, the possibility has to be considered that the Re—Cl_{trans} distance observed here is artificially short because of a replacement of some of the Re—Cl by Re=O bonds in the crystal. A

[4]X-ray data were collected altogether on three specimens, for which refinement converged to *R* = 0.025 (reported here), 0.031, and 0.051, respectively. The individual and mean Re—Cl distances found are: Re—Cl_{trans}: 2.383(2), 2.394(3), 2.387(4), mean 2.388 Å; Re—Cl_{cis}: 2.397(1), 2.395(4), 2.390(3), mean 2.394 Å. Hence, Re—Cl_{trans} is not longer than Re—Cl_{cis}.

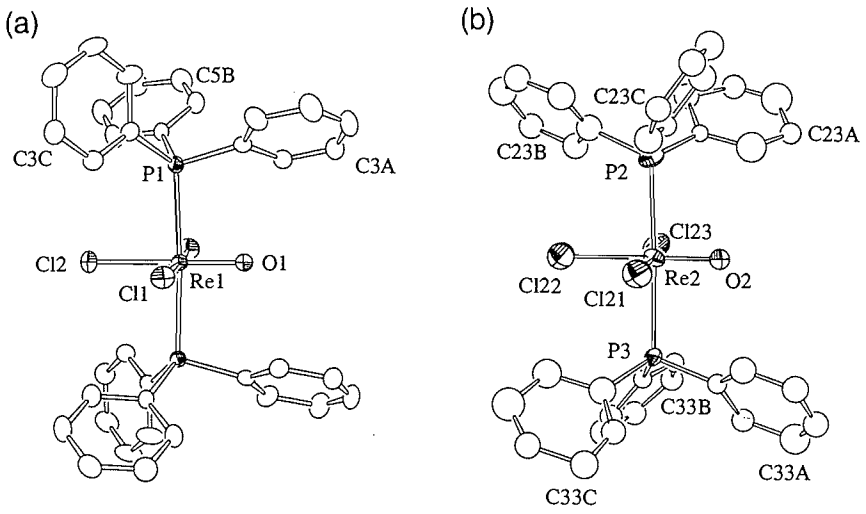

FIG. 1. ORTEP drawings of the $ReOCl_3(PPh_3)_2$ molecules found in the two polymorphs: (*a*) monoclinic form, crystallographic twofold axis along O(1)=Re-Cl(2); (*b*) triclinic form, molecule 2 in general position. Conformation is similar for the disordered molecule 1 in the triclinic polymorph. Hydrogens are omitted for simplicity. Ellipsoids correspond to 50% probability. In the symbols used for the carbon atoms, the letter identifies the ring, the first digit identifies the ligand, and the second digit corresponds to the position around the ring starting with 1 for the P-bonded atom. For the monoclinic compound containing only one type of ligand, the first digit is omitted.

TABLE 5. Selected bond lengths (Å) and angles (deg) in the $ReOCl_3(PPh_3)_2$ compounds

		Triclinic	
	Monoclinic	Molecule 1	Molecule 2
Re—O	1.663(5)	1.66[a]	1.73(2)
Re—Cl_{trans}	2.383(2)	2.28(2)	2.378(10)
Re—Cl_{cis}	2.397(1)	2.354(9)	2.326(12)
			2.375(12)
Re—P	2.519(1)	2.506(9)	2.562(9)
O—Re—Cl_{trans}	180.0	180.0	178.8(7)
P—Re—P	176.63(4)	180.0	174.9(3)
Cl_{cis}—Re—Cl_{cis}	175.97(5)	180.0	170.9(4)
O—Re—P	91.68(10)	87.6(2)	90.1(7)
		92.4(2)	92.9(7)
Cl_{trans}—Re—P	88.32(4)	92.4(5)	87.5(3)
		87.6(5)	89.6(3)
O—Re—Cl_{cis}	92.02(10)	90.3[a]	94.5(7)
		89.7[a]	94.2(7)
Cl_{trans}—Re—Cl_{cis}	87.98(4)	89.5(6)	86.9(4)
		90.5(6)	84.3(4)
P—Re—Cl_{cis}	93.21(5)	95.3(3)	98.0(4)
	86.68(5)	84.7(3)	86.0(3)
			84.0(3)
			91.6(3)

[a]Oxygen position fixed, see text.

related case of Mo complexes forming solid solutions has been discussed recently (27): when part of the *fac*-$MoCl_3(PR_3)_3$ molecules are replaced by isostructural Mo-$OCl_2(PR_3)_3$ molecules, resolved positions are not detected for the two types of atoms in the electron density map, but the apparent Mo—(Cl/O) distance based on the refined Cl/O position significantly decreases. One way to make our Re—Cl_{trans} bond artificially short would be a small amount of orientation disorder interchanging the direction of the Cl(2)-Re=O(1) unit. However, the Re=O(1) bond would then be simultaneously stretched, which is not the case: our Re=O(1) distance of 1.663(5) Å, comparable with those of the related Re-oxo compounds mentioned earlier, lies just below the range reported by Mayer (28) for a series of mono-oxo compounds of Re(V). The normal Re=O(1) and the short Re—Cl_{trans} distances could be explained by a substitution disorder involving a species like *trans-trans*-Re-$O_2Cl_2(PPh_3)_2$. However, judging from the "distance vs. composition" curve reported for the Mo systems (27), ~40% substitution by Re=O would be required to decrease the

Can. J. Chem. Downloaded from www.nrcresearchpress.com by 88.255.202.194 on 09/08/12
For personal use only.

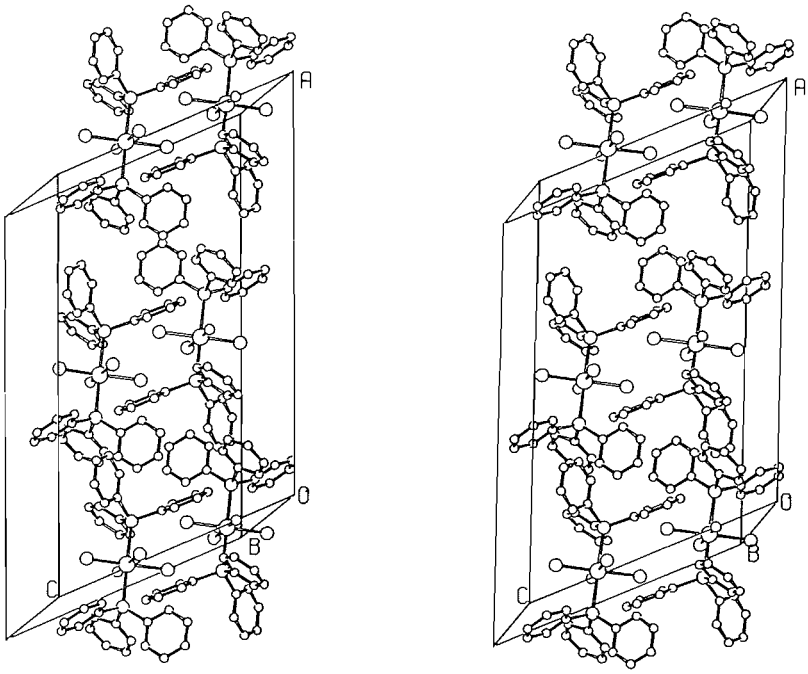

FIG. 2. Stereoview of the unit cell of the monoclinic polymorph. Atoms are represented by spheres of arbitrary size: Re > Cl ~ P > O ~ C. Hydrogens are omitted.

Re—Cl_{trans} distance by ~0.05 Å. There are no warnings to this end from either the X-ray or the spectroscopic results. Nevertheless, in such systems, where the metal can access oxidation states one unit greater or lower and the shape of the molecule is controlled by bulky phosphines, substitution disorder of the type observed with the Mo compounds remains a definite possibility. Studies underway on $ReOCl_3(PR_3)_2$ compounds with related phosphines should cast more light on this problem.

Details on the geometry of the coordinated phosphine are provided in the supplementary material. The P—C distances are normal (mean 1.823(5) Å). As usual, coordination increases the C—P—C angles (mean 105.1°) above the value found in uncoordinated phosphine (mean 102.6°) (29).

Each PPh_3 ligand introduces four conformational degrees of freedom in the complex, that is, three rotations about P—C bonds and one about the Re—P bond. The corresponding torsion angles are listed in the supplementary material. As can be seen from Fig. 1*a*, phenyl ring C is almost coplanar with the Re—P(1) bond (Re—P(1)—C(1C)—C(2C) = −4.3(5)°) and an *ortho* hydrogen is near the $ReOCl_3$ plane. Its projection in the plane is roughly the bisector of Cl(1)—Re—Cl(2), to minimize steric hindrance, but short intramolecular contacts remain between H(2C) and Cl(1) (2.60 Å) and Cl(2) (2.87 Å). An extra intermolecular contact of 2.94 Å is found between Cl(2) and H(4B). Steric effect is also revealed by the pattern of Re—P—C angles: the Re—P(1)—C(1B) (116.5(2)°) and Re—P(1)—C(1C) angles (119.8(2)°), on the side of these interactions, are greater than Re—P(1)—C(1A) (104.5(2)°). Ring A is above O(1), making the Re=O(1) and P(1)—C(1A) bonds nearly eclipsed. The crystallographic twofold axis repeats the same pattern on the other side of the plane, so that O(1) is nearly coplanar with two Re—P(1)—C(1A) units in a *cisoid* arrangement.

The distances and angles in the triclinic polymorph (Table 5) are much less accurate, but consistent with those of the above green material. The two independent $ReOCl_3(PPh_3)_2$ molecules have similar, although not superimposable, conformations, which differ strikingly from that observed in the monoclinic compound. The coordinated phosphine adopts a more classic 60°/60°/40° pattern of Re—P—C_P—C_{ortho} torsion angles (30) (see supplementary material), in contrast with the previous case, where one of these angles was near 0°. There are no short contacts of *ortho* hydrogens with the $ReOCl_3$ plane. In molecule 2, the conformation is such that the P(2)—C(21B) and P(2)—C(21C) bonds are nearly eclipsed with the Re—Cl(22) and Re—Cl(21) bonds, respectively, whereas similar orientations are found, on the other side of the $ReOCl_3$ plane, for the P(3)—C(31A) and P(3)—C(31B) bonds with respect to Re—O(2) and Re—Cl(23), respectively. In this case, the arrangement is close to being centrosymmetric, but this is not imposed by crystallographic symmetry. For molecule 1, disordered on the origin, the P(1)—C(11A) bond of one ligand is eclipsed with the Re=O(1) bond, whereas the same bond in the other phosphine is eclipsed with the Re—Cl(11) bond: the disorder results from atoms O(1) and Cl(11) exchanging their role and leading to statistical distribution over two centrosymmetry-related orientations of the O(1)=Re(1)—C(11) unit.

Views of the unit cells are given in Figs. 2 and 3. In both cases, all molecules have their P—Re—P bonds oriented along the same direction, roughly parallel to the *a* axis. However, the different van der Waals envelopes resulting from phosphine conformation generate distinct packing patterns. In the monoclinic polymorph, the *trans* Cl—Re=O bonds all lie on the crystallographic twofold axes along *b* but, for any molecule, the nearest neighbours have their Cl—Re=O direction inverted. In the triclinic polymorph, for the two molecules in general position inside the unit cell, the Cl—Re=O directions are parallel (along the bisector of *c* and −*b*) and opposite. As to the molecule sitting on the

Can. J. Chem. Downloaded from www.nrcresearchpress.com by 88.255.202.194 on 09/08/12
For personal use only.

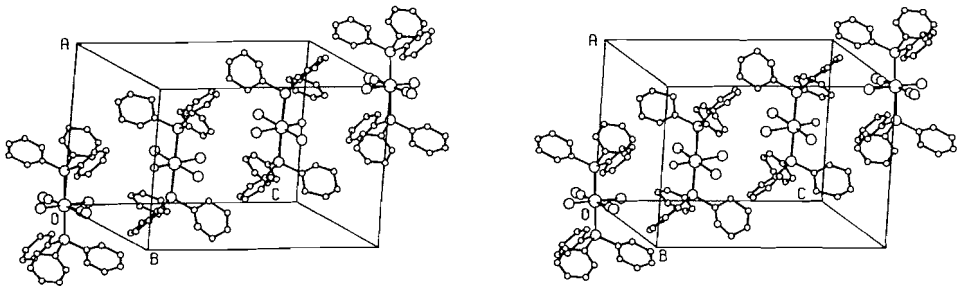

FIG. 3. Stereoview of the unit cell of the triclinic polymorph. Atoms are represented by spheres as in Fig. 2. Molecules of type 2, inside the unit cell, are not disordered. In molecules of type 1, sitting on the origin, both disordered sets of positions for O(1) and Cl(11) are shown.

Can. J. Chem. Downloaded from www.nrcresearchpress.com by 88.255.202.194 on 09/08/12
For personal use only.

inversion center at the origin, the Cl—Re=O bonds are aligned differently, roughly parallel to the *b* axis, and they are statistically disordered over the two opposite orientations.

Judging from the relatively large size of the phosphine and overall shape of the molecule, it can be anticipated that phosphine conformation should have considerable influence on packing. In this respect, it is interesting to note that our monoclinic polymorph and the nitride complex $ReNCl_2(PPh_3)_2$ have very similar structures, even though they are chemically different. The crystallographic work on the nitride complex was done by Doedens and Ibers (25), who solved the structure in space group $I2/a$, an alternative definition of $C2/c$. When this cell is redefined in a C-centered monoclinic lattice, its dimensions (a = 24.01, b = 9.53, c = 15.71 Å, β = 116.1°) are almost equal to those of $ReOCl_3(PPh_3)_2$ (Table 1). Furthermore, the van der Waals envelopes of the molecules are very similar and the P—Re—P directions are also oriented along the *a* axis (stereoview and torsion angles in supplementary material). Therefore, because of their small volume, the $ReNCl_2$ or $ReOCl_3$ planes seem to have relatively little effect on packing, which is largely guided by nonbonded interactions of the bulky phenyl rings. This point will be further discussed below in connection with "isomer" 3.

Wilkinson's "isomer" 3

The third "isomer" of $ReOCl_3(PPh_3)_2$ described by Johnson *et al.* (5) is puzzling. It was obtained when hydrazinium dihydrochloride was reacted with $HReO_4$ in dry ethanol – HCl, thorough drying being achieved by distilling out H_2O via the benzene–ethanol–water azeotrope. This same material was later obtained when Chatt *et al.* (8) reacted yellow $ReOCl_3(PPh_3)_2$ or $ReO(OEt)Cl_2(PPh_3)_2$ with hydrazinium hydrochloride in dry ethanol or THF. Exclusion of moisture in the ethanol solution was identified as a necessary condition to isolate a $ReOCl_3(PPh_3)_2$ complex, since the nitride $ReNCl_2(PPh_3)_2$ was obtained when the ethanol was wet. In fact, these methods are very similar to those leading to the nitride (8, 9).

We were unable to obtain the yellow plates described by Johnson *et al.* (5). In all cases, the material was an orange-brown powder. The ^{31}P NMR spectrum in CD_2Cl_2 showed only two roughly equal singlets, whose chemical shifts were identical with those of authentic samples of $ReNCl_2(PPh_3)_2$ and $ReOCl_3(PPh_3)_2$, respectively (Table 4). The IR spectrum was also a superposition of the spectra of both compounds, with the Re=O band at 978 cm^{-1} identical in shape and position with that of our monoclinic form. It should be pointed out that in contrast with most other $ReNCl_2(PR_3)_2$ complexes, the PPh_3 compound does not exhibit a strong characteristic Re≡N stretching vibration near 1050 cm^{-1} (8). This may explain that the nitride went unnoticed as a component of "isomer" 3. In the low-frequency region, Chatt *et al.* (8) reported bands at 343 (s), 322 (m), and 308 (m) for $ReNCl_2(PPh_3)_2$. In our spectrum, only two bands were observed in the 250–400 cm^{-1} region, at 332 (s) and 311 cm^{-1} (w), respectively. For our samples of "isomer" 3, the low-frequency region is a superposition of those we observed for $ReNCl_2(PPh_3)_2$ and $ReOCl_3(PPh_3)_2$. The ^{31}P CP/MAS NMR spectra were also recorded for $ReNCl_2(PPh_3)_2$, our green polymorph of $ReOCl_3(PPh_3)_2$, and "isomer 3". Although the signals were broad, the spectrum of "isomer" 3 does correspond to a simple summation of those of both pure compounds. Finally, the powder pattern observed for "isomer" 3 was compared with those of pure $ReNCl_2(PPh_3)_2$ and both polymorphs $ReOCl_3(PPh_3)_2$ (supplementary material, Table S-11): it was found to be similar to those calculated for the nitride and the monoclinic polymorph.

Although $ReNCl_2(PPh_3)_2$ and $ReOCl_3(PPh_3)_2$ are identified as the two components of the bulk sample, the above methods cannot distinguish between simple mixtures and solid solutions of the type reported for the $MoOCl_2(PMe_2Ph)_3$–$MoCl_3(PMe_2Ph)_3$ pair (27). A related example of solid solution in Re chemistry is the deep violet material originally formulated as $Re(OH)Cl_3(PPhEt_2)_2$ and subsequently shown to contain *mer-trans*-$ReOCl_3(PPhEt_2)_2$ and *trans*-$ReCl_4(PPhEt_2)_2$ (31). In the present case, with such similar molecular geometries and packing patterns, it is conceivable that co-crystallization of $ReNCl_2(PPh_3)_2$ and $ReOCl_3(PPh_3)_2$ under suitable conditions could lead to a mixed phase. However, from the results available, no definitive conclusion can be drawn as to the intimate structure of our orange-brown material.

Conclusion

Of the three "isomers" of $ReOCl_3(PPh_3)_2$ described in the literature, the present work shows that two are actually polymorphs of the *mer*-trichloro-*trans*-bis(phosphine) molecule **A**. The two phases differ mainly by molecular packing, which is largely controlled by nonbonded interactions of phenyl rings. As to "isomer" 3, our results are consistent with the presence of the monoclinic polymorph of $ReOCl_3(PPh_3)_2$ and of $ReNCl_2(PPh_3)_2$ in the sample. Therefore, there is no evidence whatsoever for the presence of structures **B** and **C** in this case, even though one of the *cis* isomers has been shown to exist for $ReOCl_3(PPhEt_2)_2$. The

greater cone angle (32) of PPh_3 probably makes either *cis* molecule more difficult to isolate because of steric hindrance.

Acknowledgments

We wish to thank M. Simard for assistance in collecting data for the green polymorph, and F. D. Rochon who kindly collected the data for the yellow polymorph. We would also like to thank S. Boisvenue, C. Roux, and C. Pearson for preparing some of the samples.

1. K. A. Conner and R. A. Walton. Comprehensive coordination chemistry. *Edited by* G. Wilkinson, R. D. Gillard and J. A. McCleverty. Pergamon, Oxford. 1987. Chap. 43.
2. C. J. L. Lock and G. Wilkinson. Chem. Ind. 40 (1962).
3. J. Chatt and G. A. Rowe. Chem. Ind. 92 (1962).
4. J. Chatt and G. A. Rowe. J. Chem. Soc. 4019 (1962).
5. N. P. Johnson, C. J. L. Lock, and G. Wilkinson. J. Chem. Soc. 1054 (1964).
6. N. P. Johnson, C. J. L. Lock, G. Wilkinson, J. L. Booker, and R. J. Thompson. Inorg. Synth. **9**, 145 (1967).
7. G. W. Parshall, L. W. Shive, and F. A. Cotton. Inorg. Synth. **17**, 110 (1977).
8. J. Chatt, C. D. Falk, G. J. Leigh, and R. J. Paske. J. Chem. Soc. A, 2288 (1969).
9. J. Chatt, J. D. Garforth, N. P. Johnson, and G. A. Rowe. J. Chem. Soc. 1012 (1964).
10. G. Rouschias and G. Wilkinson. J. Chem. Soc. A, 993 (1967).
11. International tables for X-ray crystallography. Vol. 1. Kynoch Press, Birmingham. 1969.
12. D. T. Cromer and D. Liberman. J. Chem. Phys. **53**, 1891 (1970).
13. R. F. Stewart, E. R. Davidson, and W. T. Simpson. J. Chem. Phys. **42**, 3175 (1965).
14. D. T. Cromer. Acta Crystallogr. **18**, 17 (1965).
15. M. Authier-Martin and A. L. Beauchamp. Can. J. Chem. **55**, 1213 (1977).
16. E. J. Gabe, F. L. Lee, and Y. Le Page. The NRCVAX crystal structure system. *In* Crystallographic computing 3: data collection, structure determination, proteins, and databases. *Edited by* G. M. Sheldrick, C. Kruger, and R. Goddard. Clarendon Press, Oxford. 1985. p. 167.
17. V. S. Sergienko and M. A. Porai-Koshits. Koord. Khim. **8**, 251 (1982) (Engl. Trans. 130); H. W. W. Ehrlich and P. G. Owston. J. Chem. Soc. 4368 (1963).
18. V. S. Sergienko, M. A. Porai-Koshits, V. E. Mistryukov, and K. V. Kotegov. Koord. Khim. **8**, 230 (1982) (Engl. Transl. 119).
19. C. J. L. Lock and G. Turner. Can. J. Chem. **55**, 333 (1977).
20. G. B. Deacon and J. H. S. Green. Spectrochim. Acta, **24A**, 845 (1967).
21. J. E. Fergusson and P. F. Heveldt. J. Inorg. Nucl. Chem. **38**, 2231 (1976).
22. R. Graziani, U. Caselatto, R. Rossi, and A. Marchi. J. Crystallogr. Spectrosc. Res. **15**, 573 (1985).
23. A. M. Lebuis, C. Roux, and A. L. Beauchamp. Acta Crystallogr. Sect. C: Cryst. Struct. Commun. **C49**, 33 (1993).
24. G. F. Ciani, G. D'Alfonso, P. F. Romiti, A. Sironi, and M. Freni. Inorg. Chim. Acta, **72**, 29 (1983).
25. R. J. Doedens and J. A. Ibers. Inorg. Chem. **6**, 204 (1967).
26. S. Rossi, S. Bélanger, A. M. Lebuis, and A. L. Beauchamp. Acta Crystallogr. In press.
27. K. Yoon, G. Parkin, and A. L. Rheingold. J. Am. Chem. Soc. **114**, 2210 (1992).
28. J. M. Mayer. Inorg. Chem. **27**, 3899 (1988).
29. J. J. Daly. J. Chem. Soc. 3799 (1964); P. G. Jones. J. Chem. Soc. Chem. Commun. 1031 (1980); D. Fenske, R. Basoglu, J. Hachgenei, and F. Rogel. Angew. Chem. Int. Ed. Engl. **23**, 160 (1984); A. Albinati, C. G. Anklin, F. Ganazzoli, H. Ruegg, and P. S. Pregosin. Inorg. Chem. **26**, 503 (1987).
30. W. DeW. Horrocks, Jr. and E. S. Greenberg. Inorg. Chem. **10**, 2190 (1971).
31. J. Chatt, J. D. Garforth, N. P. Johnson, and G. A. Rowe. J. Chem. Soc. 601 (1964).
32. C. A. Tolman. Chem. Rev. **77**, 313 (1977).

Can. J. Chem. Downloaded from www.nrcresearchpress.com by 88.255.202.194 on 09/08/12
For personal use only.

The photochemical nucleophile–olefin combination, aromatic substitution (photo-NOCAS) reaction (Part 4): methanol–olefins, methyl 4-cyanobenzoate[1]

KEVIN MCMAHON AND DONALD R. ARNOLD[2]
Department of Chemistry, Dalhousie University, Halifax, N.S., Canada B3H 4J3

Received August 13, 1992

KEVIN MCMAHON and DONALD R. ARNOLD. Can. J. Chem. **71**, 450 (1993).

Dicyanobenzene-1,4 (**1**) and -1,2 are known to undergo substitution upon irradiation, in the presence of an olefin, in acetonitrile–methanol (3:1) solution. The products are 1:1:1 (methanol:olefin:aromatic) adducts, substituted on the aromatic ring with loss of a cyano group. This reaction, referred to as the photo-NOCAS (nucleophile–olefin combination, aromatic substitution) reaction, has been shown to be fairly general with regard to the olefin and the nucleophile that can be incorporated. Less is known about the scope of the reaction incorporating other electron-withdrawing substituted aromatic molecules. The purpose of this study was to determine if methyl 4-cyanobenzoate (**10**) would also take part in this reaction, to form 4-substituted aromatic esters. Irradiation of acetonitrile–methanol solutions of **10** and olefins 2,3-dimethyl-2-butene (**2**) and 1-methylcyclohexene (**5**) gave cyclic imine esters, **11** and **13**, respectively, instead of photo-NOCAS products. The photo-NOCAS products were obtained when the codonor biphenyl (**4**) was added to the irradiation mixture. Formation of the cyclic imine ester is attributed to excitation of the charge-transfer complex formed between **10** and the olefin. The addition of biphenyl (**4**) serves to generate the contact radical ion pair (CRIP) upon irradiation of the charge-transfer complex between **10** and **4**. This CRIP can dissociate to the solvent-separated radical ions, the radical cation of **4** can accept an electron from the olefin, and the olefin radical cation can go on to give the photo-NOCAS products. Irradiation of a solution of **10** and **2** in nonpolar solvent (benzene) gave the oxetane, believed to arise from the exciplex. In addition to photo-NOCAS products from **10**, 4-cyanophenylketones **17** and **23** are also formed by attack of the β-alkoxyalkyl radical at the carboxyl carbonyl. The differences in behaviour between 1,4-dicyanobenzene (**1**) and methyl 4-cyanobenzoate (**10**) under these reaction conditions are described and explained.

KEVIN MCMAHON et DONALD R. ARNOLD. Can. J. Chem. **71**, 450 (1993).

Il est connu que les 1,4-(**1**)- et 1,2-dicyanobenzènes subissent une réaction de substitution lors de leur irradiation, en solution dans un mélange 3 : 1 d'acétonitrile–méthanol, en présence d'une oléfine. Les produits sont des adduits 1 : 1 : 1 (méthanol : oléfine : produit aromatique) dans lesquels le noyau aromatique a subit une substitution avec perte du groupe cyano. Cette réaction, connue comme une photo-SACON (substitution aromatique avec combinaison d'une oléfine et d'un nucléophile) est reconnue comme une réaction assez générale par rapport aux oléfines et aux nucléophiles potentiels. On connaît moins de choses concernant l'étendue de la réaction avec d'autres molécules aromatiques portant des groupes électroaffinitaires. Le but du présent travail était de déterminer si le 4-cyanobenzoate de méthyle (**10**) donnerait cette réaction pour former des esters aromatiques substitués en position 4. Irradiation du produit **10**, en solution dans un mélange d'acétonitrile–méthanol avec des oléfines 2,3-diméthylbut-2-ène (**2**) ou 1-méthylcyclohexène (**5**), conduit, suivant le cas, aux esters imines cycliques **11** ou **13**, plutôt qu'aux produits de photo-SACON. On n'a obtenu les produits de photo-SACON que lorsqu'on a ajouté du biphényle (**4**) comme codonneur au mélange réactionnel. On attribue la formation des esters imines cycliques à l'excitation du complexe de transfert de charge que se forme entre le produit **10** et l'oléfine. L'addition du biphényle (**4**) sert à générer la paire ion-radical de contact (PIRC) lors de l'irradiation du complexe de charge des composés **10** et **4**. Cette PIRC peut se dissocier en ions radicaux séparés par le solvant, le cation radical de **4** peut accepter un électron de l'oléfine et le cation radical de l'oléfine peut alors donner les produits de photo-SACON. L'irradiation d'une solution des produits **2** et **10** dans un solvant non polaire (benzène) a donné l'oxétanne qui doit être formé à partir de l'exciplex. En plus des produits de photo-SACON du produit **10**, il y a aussi formation des 4-cyanophénylcétones **17** et **23** par attaque du radical β-alkoxyalkyle sur le carbonyle du carboxyle. On décrit les différences de comportement entre le 1,4-dicyanobenzène (**1**) et le 4-cyanobenzoate de méthyle (**10**) dans ces conditions réactionnelles et on les explique.

[Traduit par la rédaction]

Introduction

The photochemical nucleophile–olefin combination, aromatic substitution (photo-NOCAS) reaction is a potentially useful synthetic procedure. Readily available starting materials (a nucleophile, an olefin, and an aromatic molecule) are combined to make a more complex bifunctional product in one simple step; two new bonds are made during the process. The utility of this procedure for the synthesis of *para*-cyanophenyl β-alkyl ethers has been amply demonstrated (e.g., reactions [1] and [2]) and a mechanism has been proposed that is consistent with all of the observations (Scheme 1) (2). Reaction occurs when an acetonitrile–methanol solution of 1,4-dicyanobenzene (**1**) and the olefin is irradiated through Pyrex; the efficiency and yield of photo-NOCAS product may be significantly increased when a codonor, e.g., biphenyl (**4**), is added to the reaction mixture.[3]

Nucleophiles that have been incorporated include methanol, water, and cyanide ion. The reaction has been shown to be fairly general with respect to the olefin; both acyclic

[1]This is also Part 29 of the series Radical Ions in Photochemistry. Previous publications in these series are refs. 1*a*,*b*.

[2]Author to whom correspondence may be addressed.

[3]Yields are based upon the aromatic molecule; the olefin is generally present in excess. Side products include the following: 1:1 (olefin:aromatic) adducts formally resulting from substitution by the allylic radical, formed upon deprotonation of the olefin radical cation, on the aromatic ring; dimers of the olefin resulting from coupling of the allylic radicals; and ethers resulting from the addition of methanol to the olefin radical cation.

Can. J. Chem. Downloaded from www.nrcresearchpress.com by 88.255.202.194 on 09/08/12
For personal use only.

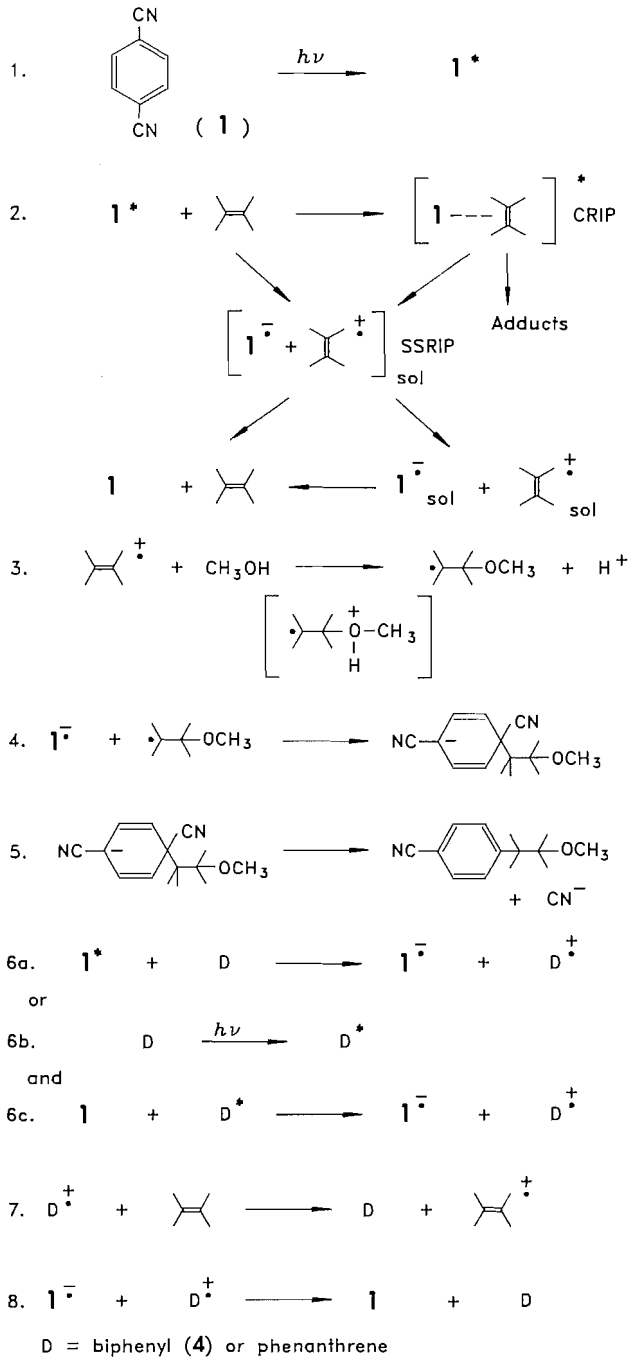

SCHEME 1

and cyclic olefins react regio- and stereoselectively to give predominately *anti*-Markovnikov products.[4] Previous work has emphasized 1,4- and 1,2-dicyanobenzene as the electron-accepting aromatic reactant (1*a*, 2). While the *para*- or *ortho*-cyano group incorporated in the product is useful functionality for further synthetic modification, for many applications it will be desirable to have some other functional group. Consideration of the mechanism leads to the

[4]The designation of regiochemistry as *anti*-Markovnikov is in keeping with the original definition. The methanol (anion) is attached at the less-substituted ethenoid carbon atom. The designation *cis* or *trans* refers to the relative orientation of the aryl and methoxyl groups.

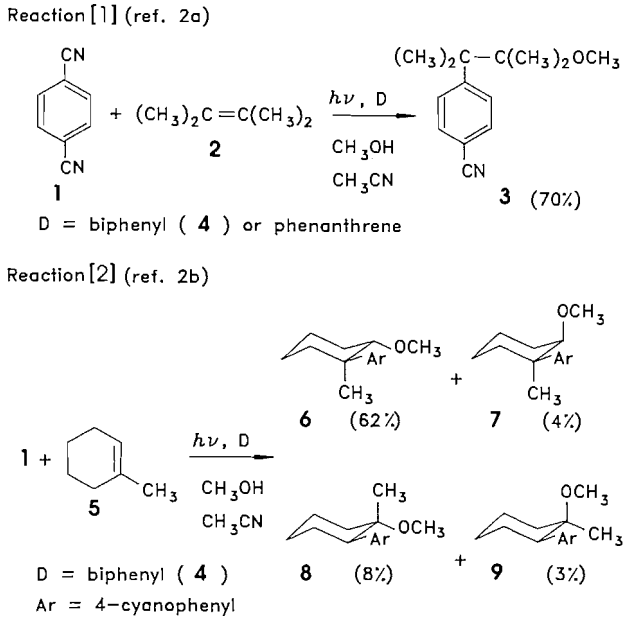

suggestion that the reaction may incorporate other electron-withdrawing substituted aromatic molecules. The main objective of this study was to determine the reactivity of such an alternative, methyl 4-cyanobenzoate (**10**), under these conditions. While there are some obvious similarities between 1,4-dicyanobenzene (**1**) and methyl 4-cyanobenzoate (**10**), there are also important differences (Table 1) (3). Comparison of the behaviour of the two (**1** and **10**) under these reaction conditions has led to a more complete understanding of the mechanism.

Results

Irradiation of an acetonitrile–methanol (3:1) solution of methyl 4-cyanobenzoate (**10**) and 2,3-dimethyl-2-butene (**2**)

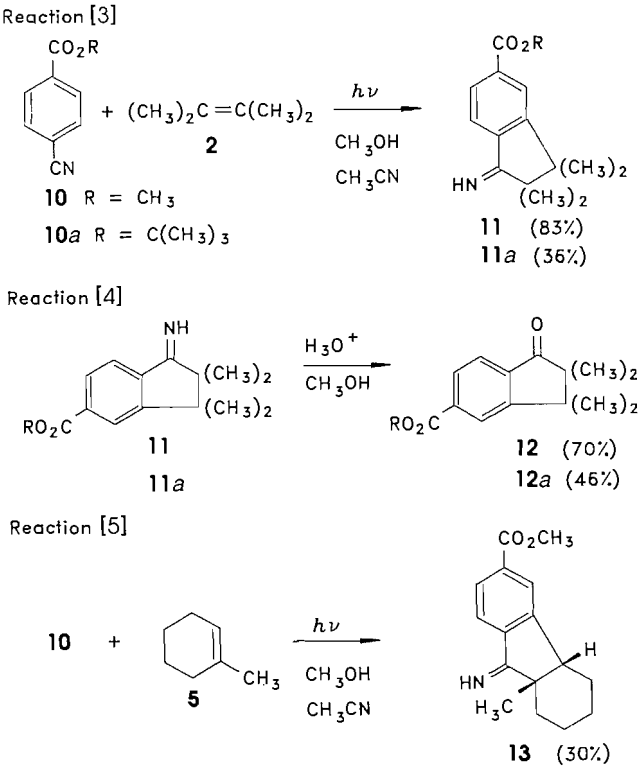

Can. J. Chem. Downloaded from www.nrcresearchpress.com by 88.255.202.194 on 09/08/12
For personal use only.

TABLE 1. Comparison of some photophysical properties of 1,4-dicyanobenzene (**1**) and methyl 4-cyanobenzoate (**10**)

	λ_{max} [a]	$E^{S}_{,0-0}$ [b]	τ_s [c]	$E^{red}_{1/2}$ [d]	$E^{T}_{,0-0}$ [e]
1,4-Dicyanobenzene (**1**)	286 (3.15)	408.4[f]	9.73[f]	−1.66[i]	296.6[j]
Methyl 4-cyanobenzoate (**10**)	285 (3.13)	395.6[f]	<1.0[h]	−1.76[f]	301.2[g]

[a]Long wavelength (^1L_b) absorption maximum, nm (log ε), in acetonitrile–methanol (3:1).
[b]Excited singlet state energy (kJ mol^{-1}).
[c]Singlet excited state lifetime (ns).
[d]Reduction potential (V, vs. sce) in acetonitrile (0.1 TEAP).
[e]Triplet energy (kJ mol^{-1}) taken from the 0–0 band of the phosphorescence emission spectrum (EtOH:MeOH, 4:1, at 77 K).
[f]Reference 3*a*.
[g]Reference 3*b*.
[h]Too short to measure by single photon counting (see also ref. 3*d*).
[i]Reference 2*a*.
[j]Reference 3*c*.

gave the cyclic imine (**11**) as the only significant volatile product (83% yield based upon **10**, reaction [3]). There was no evidence (capillary column gas chromatography with mass selective detection, gc/ms) for formation of the photo-NOCAS product. Imine **11** was readily hydrolysed to ketone **12**, under mild conditions, by treatment with aqueous acidic methanol (reaction [4]). Reactions [3] and [4] were repeated using *tert*-butyl 4-cyanobenzoate (**10***a*) instead of the methyl ester. The resulting *tert*-butyl ester imine (**11***a*) and *tert*-butyl ester ketone (**12***a*) were fully characterized; **12***a* was converted to **12** upon transesterification.

When an acetonitrile–methanol solution of methyl 4-cyanobenzoate (**10**) and 1-methylcyclohexene (5) was irradiated, the analogous imine (**13**) was obtained (30%, reaction [5]). Analysis (gc/ms) of the crude photolysate indicates that **13** was the only isomer formed in appreciable amounts; less than 1% of any regio- or stereoisomer was detected, and there were no photo-NOCAS products. Imine **13** gave ketone **14** under mild hydrolysis conditions (reaction [6]). More rigorous hydrolysis of ketone **14** gave the keto acid, isolated as a crystalline ammonium salt **15** (reaction [7]).

Reaction [6]

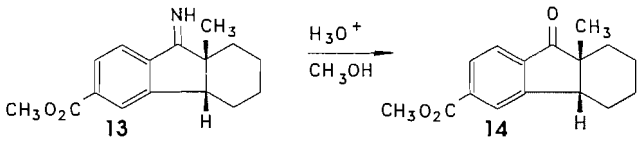

Reaction [7]

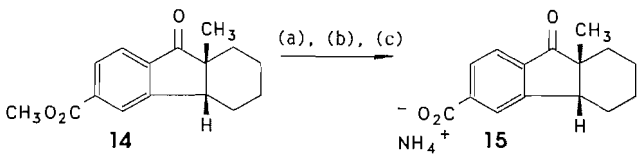

(a) NaOH, H_2O
(b) H_3O^+
(c) NH_3, ether

The addition of biphenyl (4) to these reaction mixtures has a profound effect. Irradiation of an acetonitrile–methanol solution of methyl 4-cyanobenzoate (**10**), 2,3-dimethyl-2-butene (**2**), and biphenyl (**4**) gave photo-NOCAS

Reaction [8]

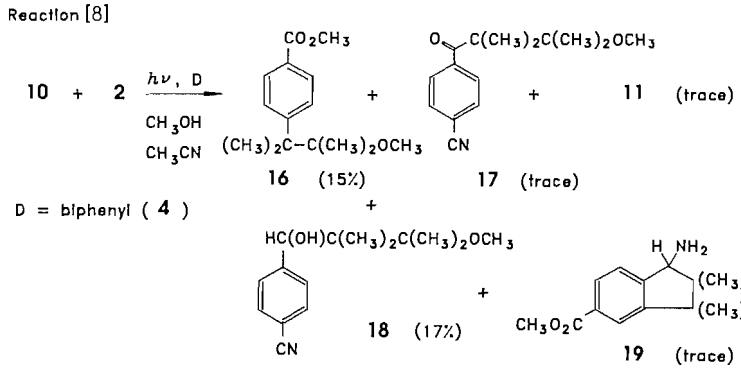

Reaction [9]

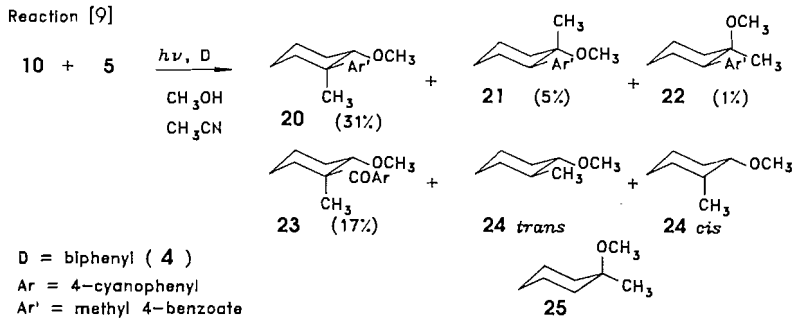

Can. J. Chem. Downloaded from www.nrcresearchpress.com by 88.255.202.194 on 09/08/12
For personal use only.

TABLE 2. Mass spectral data for the ethers *cis*- and *trans*-**24** and **25** formed during the photo-NOCAS reaction of methyl 4-cyanobenzoate (**10**) with 1-methylcyclohexene (**5**) in acetonitrile–methanol-*O*-*d* (reaction [9])

	Ions m/z[a]								
	trans-**24**			*cis*-**24**			**25**		
	128	129	130	128	129	130	128	129	130
Theoretical[b]	100	8.8	0.6	100	8.8	0.6	100	8.8	0.6
Authentic sample	100	8.2	0.5	100	7.8	0.7	100	8.5	—
In $CH_3CN:CH_3OH$	100	10	1	100	8	0.6	100	10	—
In $CH_3CN:CH_3OD$	100	31	3	100	43	4	100	17	2
d-Incorporation (%)		18			25			7	

[a]Analysis of the molecular ions using the selective ion monitoring programme (gc/ms).
[b]Relative intensity calculated on the basis of natural abundance of ^{13}C and ^{2}H.

Can. J. Chem. Downloaded from www.nrcresearchpress.com by 88.255.202.194 on 09/08/12
For personal use only.

product **16** (15%) along with alcohol **18** (17%, reaction [8]). When this irradiation was carried out to low conversion, ketone **17** was also obtained in low yield. This ketone was not detected in the photolysate when the irradiation was carried out to high conversion. Only trace amounts of imine **11** and amine **19** were formed under these conditions.

Photo-NOCAS products were also obtained upon irradiation of acetonitrile–methanol solutions of methyl 4-cyanobenzoate (**10**) and 1-methylcyclohexene (**5**) when biphenyl (**4**) was added to the reaction mixture (reaction [9]). Three isomeric esters (**20–22**) (combined yield, 37%) were isolated and characterized. The major product (**20**) has the *trans* configuration of the *anti*-Markovnikov regiochemistry. Also isolated from the reaction mixture was the 4-cyanophenyl ketone (**23**) with the *trans anti*-Markovnikov structure. Substantial amounts of ethers: 2-methoxy-1-methylcyclohexane (**24** *cis* and *trans*) and 1-methoxy-1-methylcyclohexane (**25**), were formed. This reaction was repeated using acetonitrile–methanol-*O*-*d* as solvent. Ethers *cis*- and *trans*-**24** and **25** were analyzed (gc/ms) for deuterium incorporation. These results are summarized in Table 2.

Cyclohexene (**26**) was incorporated into a photo-NOCAS product; irradiation of an acetonitrile–methanol solution of **10**, **4**, and **26** gave the *trans* 1:1:1 adduct **27** (8%, reaction [10]). The major product was the 1:1 (olefin:aromatic) adduct, 3-(methyl 4-benzoate)cyclohexene (**28**, 12%).

Reaction [10]

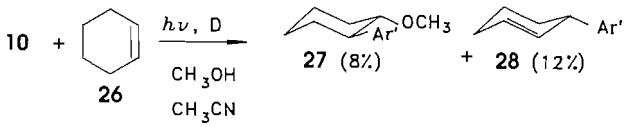

D = biphenyl (**4**)
Ar' = methyl 4–benzoate

All of the photochemical reactions described so far were carried out using acetonitrile–methanol (3:1) as solvent; irradiations were also performed in benzene solution in order to assess the importance of solvent polarity. Irradiation of a benzene solution of methyl 4-cyanobenzoate (**10**) and 2,3-dimethyl-2-butene (**2**) gave oxetane **29** (12%) along with a trace of imine **11** (reaction [11]). Similar irradiation of the *tert*-butyl ester (**10***a*) gave only the imine (**11***a*); there was no evidence for formation of an oxetane in this case. Acid-catalyzed cleavage of oxetane **29** gave ketones **30** and **31** (reaction [12]).

When a benzene solution of **10** and 2-methylpropene (**32**) was irradiated, the expected oxetane analogous to **29** was not detected. The only volatile product was oxetane **33**, isolated in low yield (reaction [13]).

Reaction [11]

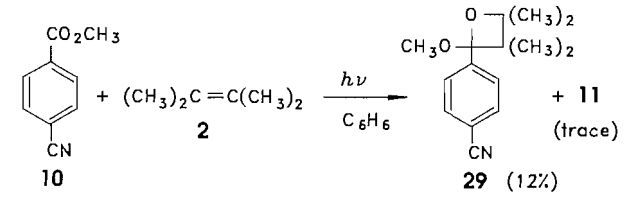

Reaction [12]

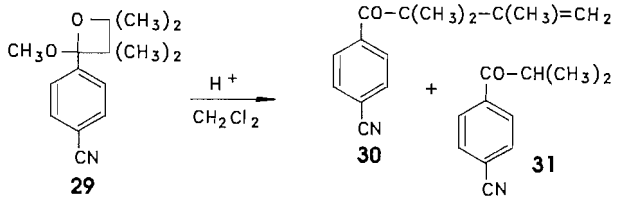

Reaction [13]

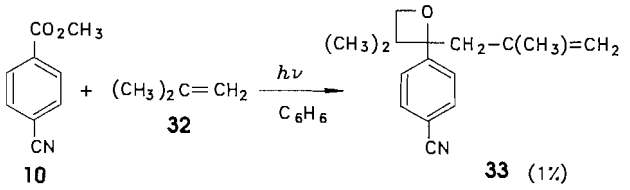

Reactions of methyl 4-cyanobenzoate (**10**) and 1,4-dicyanobenzene (**1**) with methyl and *tert*-butyl Grignard and lithium reagents were studied in order to gain a better understanding of the addition step (Scheme 1, step 4) in the proposed mechanism. That is, should this step be viewed as an alkyl radical adding to an aromatic radical anion, or as an alkyl anion adding to the neutral aromatic? Products obtained with the Grignard reagent are shown in reactions [14]–[17]. Imines **39** and **41** obtained in reactions [16] and [17] were hydrolysed to ketones, **35** and 4-cyanoacetophenone (**42**), respectively, during work-up. These results are summarized in Table 3.

Ultraviolet absorption spectra of 1,4-dicyanobenzene (**1**), methyl 4-cyanobenzoate (**10**), and biphenyl (**4**) are shown in Fig. 1. The long-wavelength ultraviolet absorption of

TABLE 3. Reactions of 1,4-dicyanobenzene (**1**) and methyl 4-cyanobenzoate (**10**) with *tert*-butyl and methyl Grignard and lithium reagents

Reagents	Product yield (%)[a]						
	34	35	36	37	38	40	42
10 + *tert*-BuMgCl (reaction [14])	23	5	13	—	—	—	—
10 + *tert*-BuLi	13	20	12	—	—	—	—
10 + *tert*-BuLi[b]	100	—	—	—	—	—	—
10 + CH_3MgBr (reaction [15])	—	—	—	97	—	—	—
10 + CH_3Li	—	—	—	25	—	—	44
1 + *tert*-BuMgCl (reaction [16])	—	23[c]	—	—	42	25	—
1 + *tert*-BuLi	—	—	—	—	77	23	—
1 + CH_3MgBr (reaction [17])	—	—	—	—	—	—	87[c]
1 + CH_3Li	—	—	—	—	—	—	58[c]

[a]Yields (gc/fid) based on consumed **1** and **10**; conversion >50%. Details of reaction conditions are given in the experimental section.
[b]Reaction stopped after 1% conversion of **10**.
[c]Initially formed imine hydrolysed to the ketone upon work-up.

solutions of **1** and **10**, and varying concentrations of 2,3-dimethyl-2-butene (**2**) and 1-methylcyclohexene (**5**), are indicative of ground state charge-transfer complex formation. Spectra for **10** are shown in Fig. 2. Bensei–Hildebrand plots of $[A]_0/A$ against $1/[D]_0$ for a series of acetonitrile–methanol (3:1) solutions of **10** with varying concentrations of **2** and **5** are shown in Fig. 3 (4). Association constants (K_x^{AD}) for the charge-transfer complex involving **10** are 0.36 ± 0.02 with **2**, and 0.4 ± 0.2 with **5**. Similar results were observed for **1**; for the charge-transfer complex between **1** and **2**, $K_x^{AD} = 0.15 \pm 0.01$. Details are given in the experimental section.

Reaction [14]

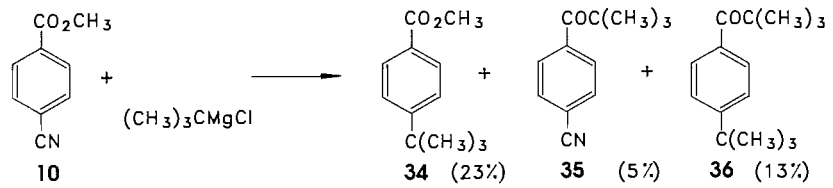

10 **34** (23%) **35** (5%) **36** (13%)

Reaction [15]

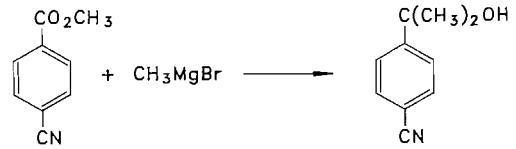

10 **37** (97%)

Reaction [16]

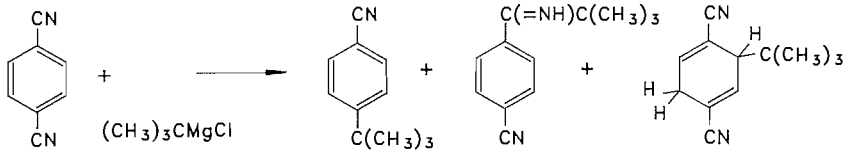

1 **38** (42%) **39** (23%) **40** (25%)

Reaction [17]

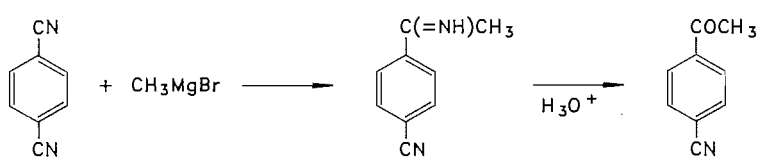

1 **41** (87%) **42**

Can. J. Chem. Downloaded from www.nrcresearchpress.com by 88.255.202.194 on 09/08/12
For personal use only.

Can. J. Chem. Downloaded from www.nrcresearchpress.com by 88.255.202.194 on 09/08/12
For personal use only.

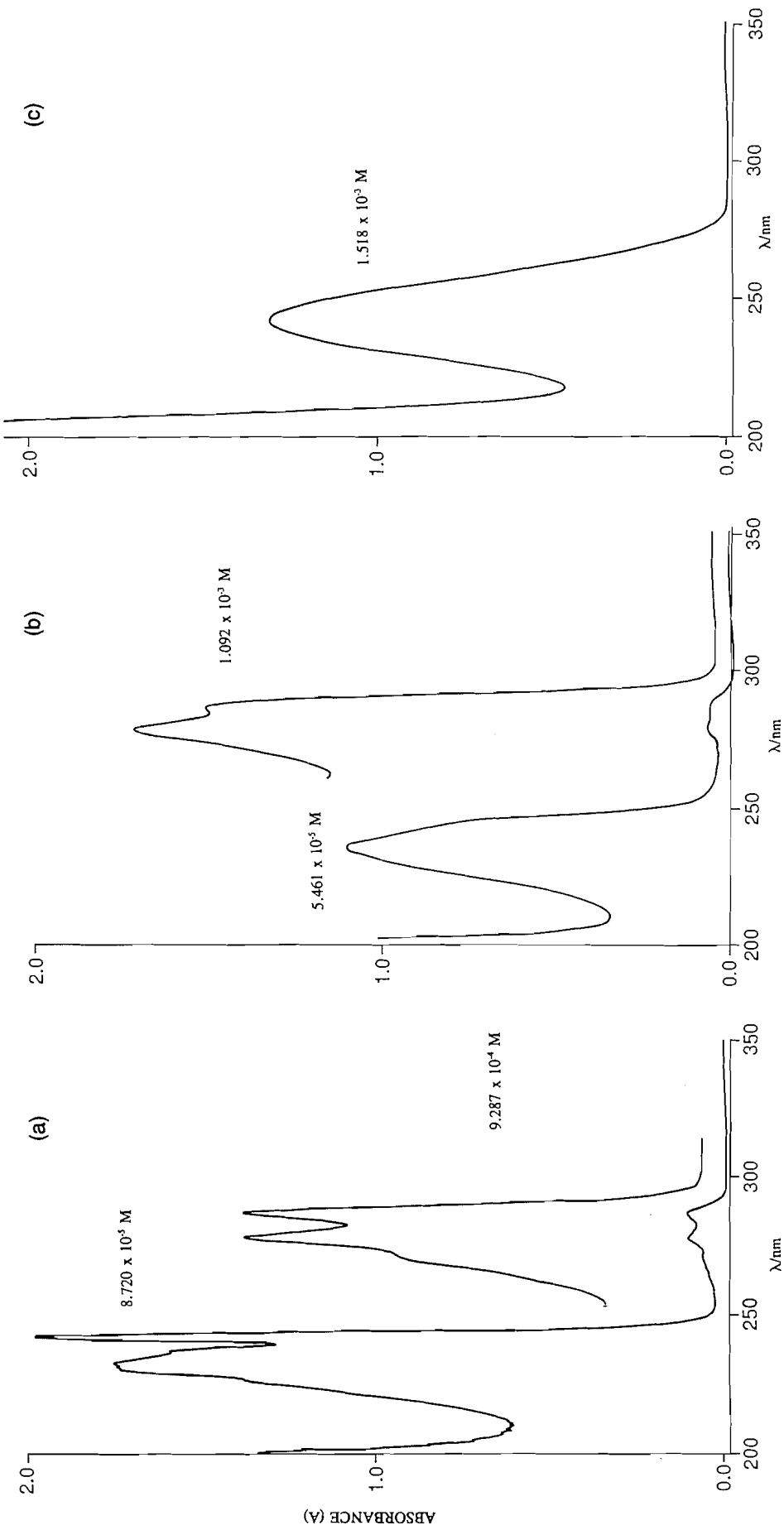

FIG. 1. The ultraviolet absorption spectra of (*a*) 1,4-dicyanobenzene (**1**); (*b*) methyl 4-cyanobenzoate (**10**); and (*c*) biphenyl (**4**) in acetonitrile–methanol.

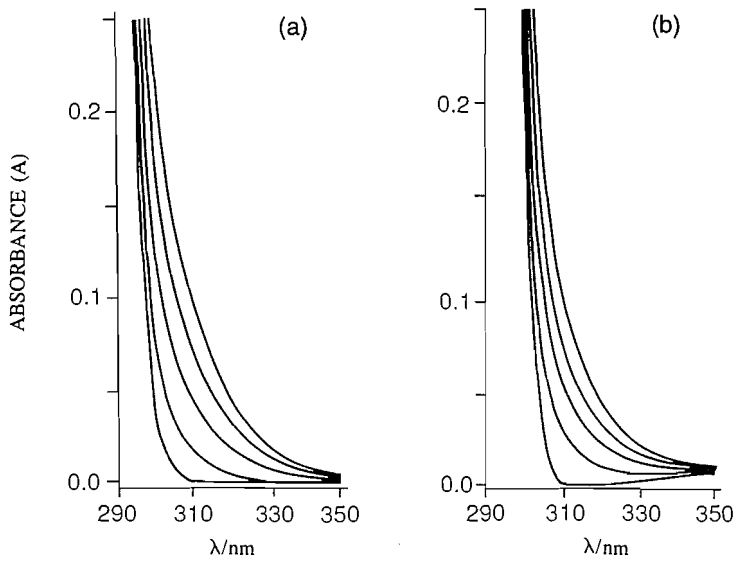

FIG. 2. The long-wavelength ultraviolet absorption spectra of solutions (acetonitrile–methanol) of (*a*) 1,4-dicyanobenzene (1); (*b*) methyl 4-cyanobenzoate (**10**) and varying concentrations of 2,3-dimethyl-2-butene (**2**).

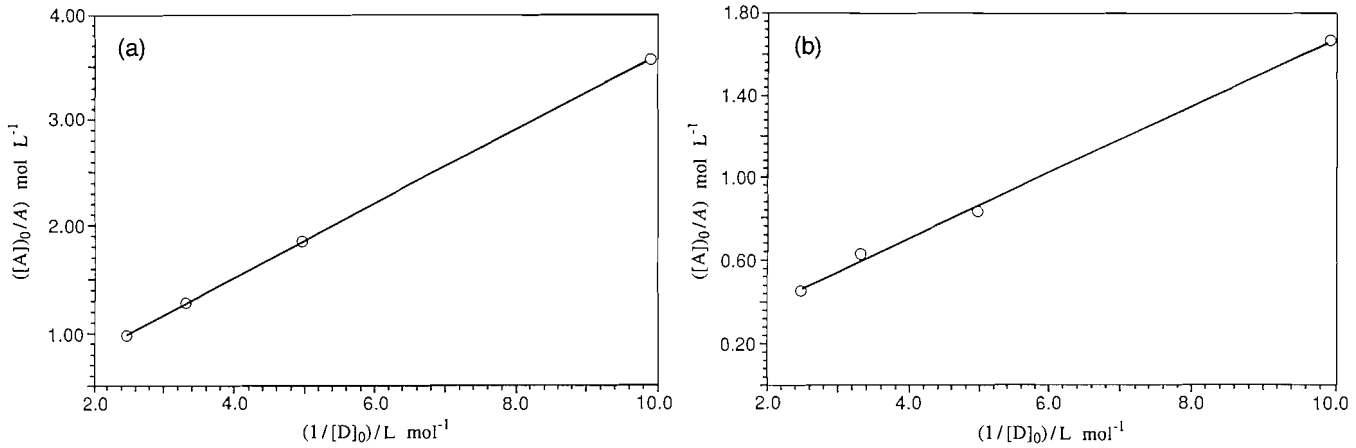

FIG. 3. Benesi–Hildebrand plots of $[A]_0/A$ against $1/[D]_0$ for a series of acetonitrile–methanol (3:1) solutions of methyl 4-cyanobenzoate (**10**) with varying concentrations of (*a*) 2,3-dimethyl-2-butene (**2**); (*b*) 1-methylcyclohexene (**5**).

Spin and charge distributions on the radical anions of 1,4-dicyanobenzene (**1**) and methyl 4-cyanobenzoate (**10**) were calculated. *Ab initio* molecular orbital calculations were carried out with the Gaussian 90 series of programmes (5). Carbon atoms of the aromatic ring and the atoms directly attached were constrained to a plane, and the methyl group of the ester was not allowed to rotate; the remaining structural features were fully optimized at the UHF/STO-3G level. Spin density were taken as the square of the coefficient at the atomic p_z-orbital in the singly occupied molecular orbital (SOMO) and the charge distribution was calculated by Mulliken population analysis (6). The limitations of this method have been discussed (7). These data are summarized in Figs. 4 and 5.

Structural determination

Imine **11** (reaction [3]) was labile towards hydrolysis, but could be isolated and characterized. A broad band was observed in the infrared spectrum at 3400 cm^{-1} attributed to the N–H stretching frequency. There was a strong absorption band at 1645 cm^{-1} due to carboxyl carbonyl, but no absorption in the region of the nitrile stretching frequency. An exchangeable (D_2O) proton was observed at 8.6 ppm in the ^1H nmr spectrum. Signals due to three hydrogens were clearly resolved in the aromatic region of the ^1H nmr spectrum, with three corresponding doublets in the aromatic region of the coupled ^{13}C nmr spectrum. The two pairs of equivalent methyl groups were evident in the ^1H nmr spectrum as sharp singlets at 1.19 and 1.10 ppm.

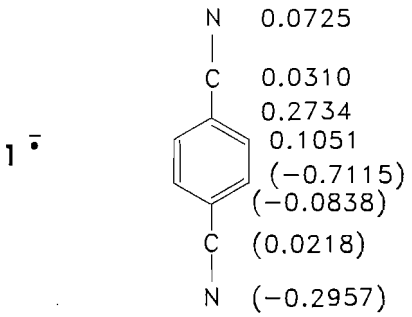

FIG. 4. Calculated (STO-3G) (spin) and charge densities on the radical anion of 1,4-dicyanobenzene (**1**).

Can. J. Chem. Downloaded from www.nrcresearchpress.com by 88.255.202.194 on 09/08/12
For personal use only.

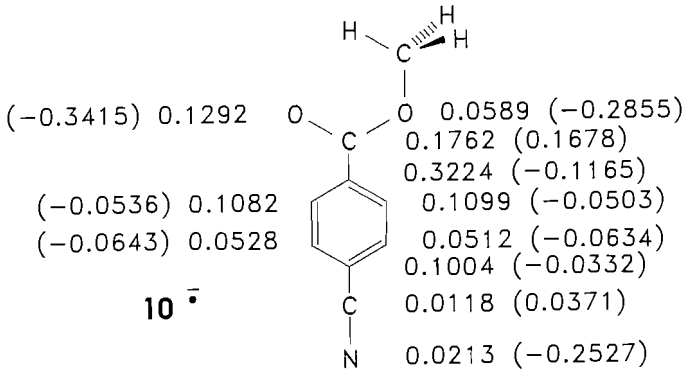

FIG. 5. Calculated (STO-3G) (spin) and charge densities on the radical anion of methyl 4-cyanobenzoate (**10**).

After hydrolysis (reaction [4]), the spectra of ketone **12** were similar to those of imine **11**, with some important differences. The band due to the N–H stretching frequency, observed in the infrared, and the signal attributed to the exchangeable proton in the ^{1}H nmr spectra of the imine were no longer present. Two sharp singlets at 1.26 ppm and 1.10 ppm were attributed to the two pairs of equivalent methyl groups. The singlet resonance observed at 188.23 ppm in the ^{13}C nmr spectrum of **11**, attributed to the carbon of the imine group, was shifted to 210.59 ppm, indicative of a ketone carbonyl carbon. The mass spectrum of **12** also showed the expected increase by one mass unit in the molecular ion and in the base peak (loss of CH_3.).

Structures assigned to the *tert*-butyl ester imine **11***a* and ketone **12***a*, similar to those of the analogous methyl ester, were consistent with the observed spectra.

The assignment of the regio- and stereochemistry of structures **13** and **14** (reaction [5] and [6]), from the ^{1}H and ^{13}C nmr spectra, was not as straightforward and was ultimately achieved by X-ray analysis of a single crystal of the ammonium salt of the carboxylic acid derivative **15**. Trisubstitution of the aromatic ring in **14** was apparent from the three distinct signals due to aromatic hydrogens (8.13, 8.04, and 7.80 ppm) in the ^{1}H nmr spectrum, and three doublets in the aromatic region of the ^{13}C nmr spectrum (128.60, 124.25, and 125.59 ppm). An apparent triplet (J = 5.24 Hz) due to a single hydrogen was observed at low field (3.08 ppm). Acid- and base-catalyzed deuterium exchange experiments were carried out to determine if this hydrogen was exchangeable and therefore adjacent to the carbonyl at the junction between the 5- and 6-membered rings. An attempt was also made to alkylate the enolate anion. These reactions were carried out using conditions found to be effective for the exchange and alkylation at the carbon α to the carbonyl of 1-indanone. However, there was no evidence (^{1}H nmr and gc/ms, with single ion monitoring) for deuterium exchange or alkylation of **14**. These results provided the first indication that the low-field signal (3.08 ppm) was due to a benzylic hydrogen (not a hydrogen α to a carbonyl group) and thus established the regiochemistry of the cycloaddition.

The ^{1}H nmr spectrum of ester **14** was recorded in benzene-d_6 and in chloroform-*d*; the variation in chemical shift for the signals due to the methyl and the benzylic hydrogens was compared. Benzene is known to interact with electron-deficient sites on the solute molecule (8). Orientation of the solute–solvent complex is governed by local dipolar interactions and the benzene will be remote from the negative end of the solute molecule. This distortion causes a change in the total screening constant (σ), which has a contribution from the solute–solvent interaction. The "carbonyl plane rule" has been proposed as a method for assigning the position of a hydrogen (or a group of hydrogens) relative to a plane drawn through the carbonyl carbon perpendicular to the C—O bond (9). Hydrogens that lie on the oxygen side of this plane will have a negative difference in chemical shift ($\Delta = \delta_{CDCl_3} - \delta_{C_6D_6}$), while those on the other side of the plane will be shifted positively. Hydrogens in the reference plane will be relatively unaffected. In the case of **14** a much larger difference in chemical shifts was observed for the single hydrogen (+0.55 ppm) than for the methyl group (+0.19 ppm). This suggests that the methyl group is nearer the reference plane, and therefore α to the carbonyl group. Again, this is indicative of the regiochemistry of the ring juncture; however, the stereochemistry of the ring juncture was still uncertain. Therefore, **14** (an oil) was converted into a crystalline derivative for X-ray analysis.

Ester **14** was hydrolysed to the acid under basic conditions. The acid was readily converted to the crystalline ammonium salt (**15**) (reaction [7]), which was used for X-ray analysis. The results clearly show that the methyl group is α to the carbonyl group, and the 5- and 6-membered rings are fused in a *cis* juncture (Fig. 6). Interatomic distances, bond angles, and torsional angles are listed in the appendix (Depository of Unpublished Data).[5]

Identification of the products from reaction [8]: the peak characteristic of the nitrile stretching frequency was not observed in the infrared spectrum of photo-NOCAS product **16**. The ^{1}H nmr spectrum of **16** is indicative of a symmetric structure: an A_2X_2 pattern in the aromatic region confirms the 1,4 ring substitution. Two low-field peaks assigned to the methyl groups on oxygen, as well as two peaks due to six equivalent hydrogens of the two pairs of methyl groups, are observed.

Ketone **17** was easily identified. The ^{1}H nmr spectrum showed the methyl groups as two singlets indicative of the symmetric structure. The carbonyl group was detected in the infrared spectrum (the carbonyl stretching frequency at 1680 cm^{-1}) and in the ^{13}C nmr spectrum (a singlet due to the carbonyl carbon at 210.65 ppm). The nitrile stretching frequency (2240 cm^{-1}) in the infrared spectrum and the symmetric pattern in the aromatic region of the ^{1}H nmr spectrum confirm the 4-cyano substitution on the aromatic ring.

For compound **18**, the presence of the hydroxyl group was indicated by a broad, exchangeable (D_2O), low-field (5.72 ppm), absorption due to the hydroxyl proton in the ^{1}H nmr spectrum, and a peak due to the O–H stretching frequency observed at 3450 cm^{-1} in the infrared spectrum. The presence of a chiral centre renders the geminal methyl groups

[5]These data may be purchased from: The Depository of Unpublished Data, Document Delivery, CISTI, National Research Council Canada, Ottawa, Canada K1A 0S2.

Details of data collection, structural analysis and refinement, and tables of interatomic distances and bond angles have also been deposited with the Cambridge Crystallographic Data Centre and can be obtained on request from the Director, Cambridge Crystallographic Data Centre, University Chemical Laboratory, 12 Union Road, Cambridge, CB2 1EZ, U.K.

Can. J. Chem. Downloaded from www.nrcresearchpress.com by 88.255.202.194 on 09/08/12
For personal use only.

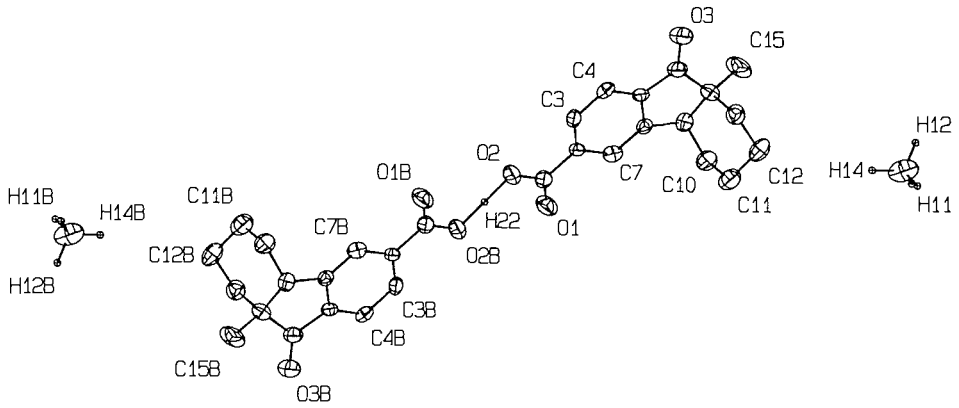

FIG. 6. X-ray crystal structure (Chemgraf) of ammonium salt **15**.

heterotopic; four distinct singlets are observed in the ^{1}H nmr spectrum. The signal due to the benzylic hydrogen geminal to a hydroxyl group occurs as a singlet at 4.98 ppm (compare with the signal due to the benzylic hydrogen of benzyl alcohol, which occurs at 4.58 ppm). The nitrile stretching frequency (2260 cm^{-1}) is observed in the infrared spectrum and an AA′XX′ pattern in the aromatic region of the ^{1}H nmr spectrum confirms the 1,4 disubstitution.

The four methyl groups in the spectrum of the product assigned to amine **19** appear as distinct singlets in the ^{1}H nmr spectrum, indicative of a chiral molecule. The benzylic hydrogen shows up as a singlet at low field (4.10 ppm). The primary amine function is indicated by a broad exchangeable (D_2O) singlet equivalent to two hydrogens at 1.46 ppm in the ^{1}H nmr spectrum, attributed to the protons on nitrogen, and by a broad band centred at 3400 cm^{-1} in the infrared spectrum due to the N–H stretching frequency. The mass spectrum gives a molecular ion with an odd mass (m/z = 247) and a major fragment (72%) resulting from loss of one mass unit, indicative of a molecular ion of an amine that loses the α-hydrogen (C*H*-NH_2) to give the nitrogen-stabilized cation. The aromatic region of the ^{1}H nmr spectrum is consistent with a trisubstituted aromatic ring — three distinct resonances with the expected couplings.

Structure proof of the photo-NOCAS products from methyl 4-cyanobenzoate (**10**) and 1-methylcyclohexene (**5**) (reaction [9]) was aided by comparison of spectra with those from the analogous cyano compounds **6**–**9** reported earlier (2*b*). The distinction between Markovnikov and *anti*-Markovnikov adducts was made on the basis of the chemical shift due to the single proton multiplet at low field, geminal to either the phenyl ring or the methoxy group. On this basis, adduct **20** (low-field dd at 3.48 ppm, hydrogen α to oxygen) and ketone **23** (dd at 3.58 ppm) were assigned the *anti*-Markovnikov structure, while **21** (higher field dd at 2.86 ppm, therefore a benzylic hydrogen) and **22** (dd at 2.47 ppm) are Markovnikov adducts. Additional evidence for these assignments comes from the ^{13}C nmr spectrum where signals due to carbon adjacent to the ether oxygen also appear at lower field than benzylic carbons. Low-field doublets at 84.12 (J = 139.3 Hz) and 81.92 (J = 143.1 Hz) ppm are consistent with the assigned structures, **20** and **23**, respectively. The signal due to the carbon of the methoxy group in these spectra is observed as a quartet of doublets, showing long-range coupling (J^3_{C-H} = 4.3 Hz for **20** and 4.2 Hz for **23**) to the hydrogen geminal to the methoxy group. Signals due to the carbon of the methoxy group in **21** and **22** were simply quartets; there was no evidence of long-range coupling.

Having established the regiochemistry of these products (**20**–**23**), the stereochemistry was determined on the basis of vicinal proton–proton and proton–carbon coupling; axial–axial coupling is relatively large (10). The ^{1}H nmr spectrum of isomer **20** shows a large vicinal coupling in the signal due to the proton geminal to the methoxy group (J^3_{H-H} = 9.6 and 3.6 Hz) indicative of axial–axial and axial–equatorial coupling. The methoxy group is therefore in the equatorial position. A similar coupling is observed in the signal due to the proton geminal to the methoxy group in the spectrum of ketone **23** (J^3_{H-H} = 10.1 and 3.9 Hz); in this case also, the methoxy group is assigned to the equatorial position. For isomer **20** and ketone **23**, the relative position of the methyl and aryl groups was determined by examining the long-range coupling between the methyl carbon and the vicinal hydrogens in the coupled ^{13}C nmr spectra. One of the central lines of the quartet due to the carbon of the methyl group was expanded, and a measure of the width at half-height gave an indication of the magnitude of the coupling. This long-range hydrogen–carbon coupling generally can be related to the vicinal proton–proton coupling by the empirical relationship shown in eq. [18].

$$[18] \quad \text{(ref. 11)} \qquad J^3_{C-H} = 1.2 \times J^3_{H-H} - 3.5 \text{ Hz}$$

Central lines of the quartet due to the methyl group in the ^{13}C nmr spectrum of isomer **20** are broad (13.5 Hz). Similar broad lines (14.4 Hz) are observed in the spectrum of ketone **23**. The methyl groups in **30** and **23** are therefore in the axial position. Signals in the ^{1}H nmr spectrum due to the benzylic hydrogens of isomers **21** and **22** are broad; large coupling constants (**21**, 11.7 and 4.0 Hz; **22**, 12.8 and 3.3 Hz) indicate that these protons are in the axial position. The coupled ^{13}C nmr spectrum of isomer **21** also showed a large J^3_{C-H} coupling (12.9 Hz) indicative of an axial methyl group. The structure of isomer **22**, with an axial benzylic hydrogen, was therefore assigned with an equatorial methyl group and an axial methoxy group.

The ethers **24** *cis* and *trans*, and **25** are known compounds, positively identified by direct comparison (gc/ms, retention times, and mass spectra) with authentic samples.

The structure of the photo-NOCAS product (**27**), formed in reaction [10], was determined in much the same manner as that for **20**. In the ^{1}H nmr spectrum of **27**, the signal for the hydrogen adjacent to the methoxy group appears at low

Can. J. Chem. Downloaded from www.nrcresearchpress.com by 88.255.202.194 on 09/08/12
For personal use only.

field (3.27 ppm) as an apparent triplet of doublets (J = 10.2 and 4.2 Hz). This corresponds to two coincidentally equivalent large axial–axial and one smaller axial–equatorial couplings. The methoxy group is therefore in the equatorial position, adjacent to the equatorial aryl group. Substitution product **28** is clearly a 1:1 (olefin:aromatic) adduct. Only one signal (3.90 ppm) for a methoxy group was observed in the ^{1}H nmr spectrum, and this is associated with the carbonyl group; hence, there was no incorporation of methanol. Two olefinic hydrogens were evident from signals in the vinyl region (5.69 and 5.92 ppm). The high-field signal is clearly coupled to two other hydrogens with one large geminal coupling (9.9 Hz) to the other vinyl hydrogen and one smaller coupling (2.0 Hz) to the benzylic proton. Hence, the aryl group is attached at the allylic position of the olefin.

Strong absorption in the infrared spectra, at 1020 cm^{-1} for **29** and 955 cm^{-1} for **33**, is characteristic of the C–O stretching frequency of the oxetanes formed in reactions [11]

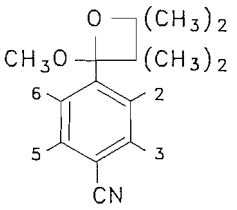

29

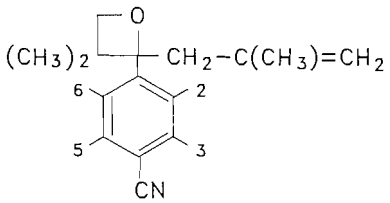

33

and [13] (12). The ^{1}H nmr spectra of these oxetanes are particularly interesting (Figs. 7 and 8). There is clear evidence, from the multiplicity of peaks in the aromatic region, that there is a significant barrier to rotation of the 4-cyanophenyl group. In the spectrum of **29**, at −70°C, the signals assigned to H5 and H6 are coincidentally equivalent (7.79 ppm) while H2 and H3 appear as an AB quartet (7.34 ppm, J = 8.2 Hz, and 7.73 ppm, J = 8.1 Hz). As the temperature is increased, H3 and H5 coalesce at −20°C and H2 and H6 coalesce at +10°C. Analysis of this data indicates that the barrier to rotation of the 4-cyanophenyl group is 54.4 ± 0.9 kJ mol^{-1} (13.0 ± 0.2 kcal mol^{-1}) (13). Results for **33** are similar: at −70°C, the signals due to H5 and H6 overlap at 7.71 ppm and H2 and H3 appear as an AB quartet (6.97 ppm, J = 8.3 Hz, and 7.60 ppm, J = 8.3 Hz). Signals due to H3 and H5 coalesce at −20°C while the signals due to H2 and H6 coalesce at +10°C. The barrier to rotation of the 4-cyanophenyl group in **33** is 53.18 ± 0.97 kJ mol^{-1} (12.7 ± 0:2 kcal mol^{-1}).

Structures for the products from reactions [14]–[17] were established by analysis of ^{1}H and ^{13}C nmr spectra. Imines **39** and **41** were hydrolysed to ketones, *tert*-butyl (4-cyanophenyl) ketone (**35**) and 4-cyanoacetophenone (**42**), which were fully characterized. The structure of the product that results from addition of the *tert*-butyl Grignard reagent to the ring of **1** (**40**, reaction [16]) was evident from the ^{1}H nmr spectrum; signals due to the vinyl hydrogens on C2 and C5 (3.03 and 2.95 ppm) are not coupled to each other.

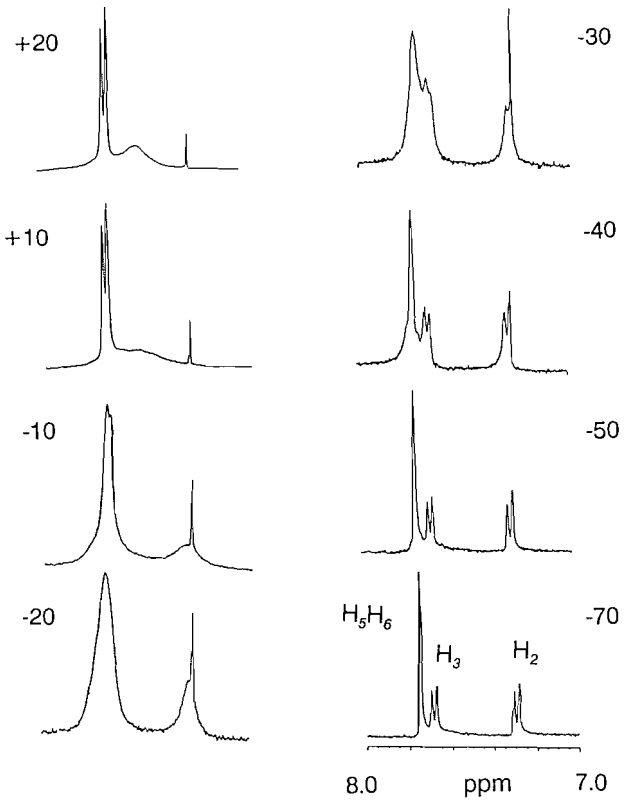

FIG. 7. Variable temperature ^{1}H NMR (360 MHz) study of oxetane **29**.

Discussion

Like 1,4-dicyanobenzoate (**1**), methyl 4-cyanobenzoate (**10**) can be an effective electron-accepting aromatic component in the photo-NOCAS reaction, **but only when the irradiation is carried out in the presence of a codonor, e.g., biphenyl (4)**. This reaction can be used for the synthesis of 4-substituted benzoate esters (reactions [8]–[10]). However, there are major differences in the behaviour of 1,4-dicyanobenzene (**1**) and methyl 4-cyanobenzoate (**10**):

(*i*) While irradiation of acetonitrile–methanol solutions of **1** and an olefin leads to formation of photo-NOCAS products, cyclic imines are obtained from **10** under these conditions. Addition of biphenyl (**4**) to the irradiation mixture of **1** and an olefin increases the efficiency of the formation of photo-NOCAS products; in marked contrast, no photo-NOCAS products are formed upon irradiation of acetonitrile–methanol solutions of **10** and an olefin unless **4** has been added to the solution.

(*ii*) In these reactions involving 1,4-dicyanobenzene (**1**), attack of the intermediate β-alkoxyalkyl radical occurs exclusively at the *ipso* position of **1**$^{\cdot-}$; there is no evidence for attack directly on the cyano group. With methyl 4-cyanobenzoate (**10**) the photo-NOCAS products, which result from attack of the β-alkoxyalkyl radical on the position *ipso* to the cyano group, are accompanied by products resulting from attack directly on the carboxyl carbonyl.

The mechanism (Scheme 1), which is consistent with all of the results for 1,4-dicyanobenzene (**1**), obviously is in-

Can. J. Chem. Downloaded from www.nrcresearchpress.com by 88.255.202.194 on 09/08/12
For personal use only.

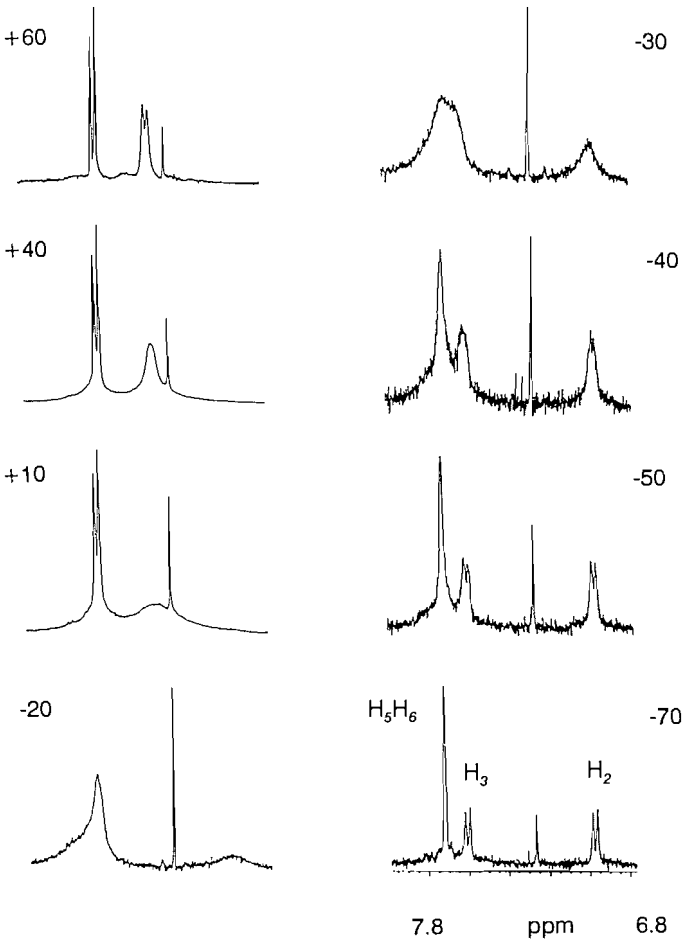

FIG. 8. Variable temperature ^{1}H NMR (360 MHz) study of oxetane **33**.

adequate for reactions of methyl 4-cyanobenzoate (**10**); deficiencies arise within the first two steps.

Step 1: Excitation of 1,4-dicyanobenzene (**1**), in the long-wavelength ultraviolet region (>280 nm), leads to the lowest excited singlet state (^1L_b) (14). In this excited state **1** is a powerful oxidant; based upon the Weller equation (eq. [19] (ref. 15)), this state will accept an electron at the rate of formation of the collision encounter complex (ca. 1.7×10^{10} M^{-1} s^{-1} in acetonitrile (2*a*)) from any prospective donor having an oxidation potential less than ca. 2.4 V (vs. sce) when $\Delta G_{et} = -20$ kJ mol^{-1} (2*a*).

[19] (ref. 15) $\Delta G_{et} = F[E^{ox}_{1/2}(D) - E^{red}_{1/2}(A) - e/\epsilon\alpha] - E_{0,0}(A)$

Step 2: The measured lifetime of the ^1L_b state of **1** is 9.7 ns (Table 1). Stern–Volmer studies show that fluorescence from **1** is indeed quenched by olefin **2** ($E^{ox}_{1/2}$ = 1.62 V, vs. sce) at the diffusion-controlled rate ($k_q = 1.5 \times 10^{10}$ M^{-1} s^{-1} (2*a*)). Therefore, under the usual conditions for the photo-NOCAS reaction, i.e., 0.1 M concentration of olefin, electron transfer leading directly to formation of the solvent-separated radical ion pair (SSRIP) is competitive with unimolecular deactivation (intersystem crossing and internal conversion) of the singlet excited state of **1**. Formation of the solvent-separated radical ion pair is necessary for reaction; the SSRIP may proceed subsequently to the individually solvated radical ions, and the mechanism continues.

The long-wavelength absorption band of methyl 4-cyanobenzoate (**10**) also involves excitation of the ^1L_b transition. The first contrast in the behaviour of **1** and **10** lies in the singlet excited state lifetime. Attempts to measure the singlet lifetime of **10** have so far failed. We, and others (3*d*), have been unable to detect fluorescence emission from **10**. The singlet excited state lifetime of **10** must be significantly less than 1 ns, the limit of our detection system. Even though the singlet of **10** should undergo electron transfer at the diffusion-controlled rate with olefins **2** and **5**, ΔG_{et} = −78.0 kJ mol^{-1} for **2** and −48.1 kJ mol^{-1} for **5**, this bimolecular reaction cannot compete with unimolecular deactivation. Involvement of a triplet state also seems unlikely. The triplet of **10** (301.2 kJ mol^{-1}) will be quenched (energy transfer) by olefins. Deactivation of the olefin π,π^* triplet is rapid (the "free-rotor") effect).

We propose that formation of the cyclic imines, **11** and **13** in reactions [3] and [5], can be accounted for by excitation of the ground state charge-transfer complex formed between **10** and olefins **2** and **5**.[6] The increased absorption on the long-wavelength tail of the ^1L_b band of **10**, as a function of olefin concentration (Fig. 2), is indicative of ground state charge-transfer complex formation. Excitation of this charge-transfer complex in polar solvent leads directly to the excited state of the charge-transfer complex which can accurately be described as a contact radical ion pair (CRIP); electron transfer is exergonic. In terms of the Mulliken description of the excited charge-transfer complex, the contribution of the "no bond" wavefunction involving locally excited states is small relative to that of the "dative bond" wavefunction (4*d*). Reaction of the contact radical ion pair leads to cyclic imine formation. The sequence of bond-forming events leading to the imine is not known; however, the regiochemistry of **13** (reaction [5]) is indicative of initial bonding between the carbon *ortho* to the cyano group and the olefin.

When the irradiation of **10** and **2** is carried out in non-polar solvent (benzene), the dative bond wavefunction contributes less to the nature of the excited state of the charge-transfer complex and the oxetane **29** is formed instead (reaction [11]).

There is a veritable plethora of reactions that are known to occur upon irradiation of cyanoaromatics in the presence of an olefin (17–27).[7] In addition to the photo-NOCAS reaction (1*a*, 2, 17), other reactions that may occur include (*a*) formation of 1:1:1 (nucleophile:olefin:aromatic) adducts without loss of cyanide ion (18); (*b*) formation of 1:1 (olefin:aromatic) adducts by addition of the allylic radical to the ring (19); (*c*) cycloaddition of the olefin to the cyanoaromatic, across the nitrile bond (20) or (*d*) across the ring (either *ortho* or *meta*) (21). Furthermore, the cyanoaromatic may act as a photosensitizer leading to (*a*) *anti*-Markovnikov addition of nucleophilic solvent to the olefin (22); (*b*) cyclic dimers, [2e + 1e] and [4e + 1e], of the olefin (23); (*c*) *cis–trans* isomerization of the olefin (24); (*d*) rearrangement of the olefin (25); or (*e*) tautomerization of the olefin (26).

[6]There are several reports of bimolecular reactions of similar benzoate esters attributed to the singlet excited state (16). This interpretation seems improbable in view of the short singlet excited state lifetime of these compounds. Excitation of ground state charge-transfer complexes may be involved in these cases as well.

[7]Many of these references (17–27) discuss more than one type of reaction.

Can. J. Chem. Downloaded from www.nrcresearchpress.com by 88.255.202.194 on 09/08/12
For personal use only.

Can. J. Chem. Downloaded from www.nrcresearchpress.com by 88.255.202.194 on 09/08/12
For personal use only.

Despite this considerable effort to define the reactivity of cyanoaromatics irradiated in the presence of olefins, there are few reported examples of cyclic imine formation analogous to that observed here (reactions [3] and [5]). This type of product has not been observed previously with either **1** or with **10**. Irradiation of acetonitrile solutions of 1,3,5-tricyanobenzene and 2,3-dimethyl-2-butene (**2**), and of 2-cyanopyridine and 2-methyl-2-butene, leads to cyclic imine formation (27). Electron transfer, from the olefin to the singlet excited state of these cyanoaromatics, is exergonic in both these cases. Ground state charge-transfer complex formation is also likely; the mechanism for imine formation has not been defined in either case.

1,4-Dicyanobenzene (**1**) also forms a ground state charge-transfer complex with olefins; for example, with **2**, $K_x^{AD} = 0.15 \pm 0.01$. Nevertheless, cyclic imines have never been detected (gc/ms) following irradiation of acetonitrile–methanol solutions of **1** and olefins; with **2**, only photo-NOCAS products are formed (reaction [1]). The implication is that following formation of the CRIP obtained upon irradiation of the ground state charge-transfer complex between **1** and **2** (and other olefins), the rate of reaction leading to cyclic imine is slow relative to solvent separation of the radical ions. Irradiation of the charge-transfer complex between **10** and **2** leads to a CRIP which reacts to give the cyclic imine more rapidly than solvent separation.

Photo-NOCAS products are observed from methyl 4-cyanobenzoate (**10**) when biphenyl (**4**) has been added to the reaction mixture (reactions [8]–[10]). Photo-NOCAS adduct **16** is a major product, formed upon irradiation of an acetonitrile–methanol solution of methyl 4-cyanobenzoate (**10**), 2,3-dimethyl-2-butene (**2**), and biphenyl (**4**); imine **11** and amine **19** are minor products under these conditions (reaction [8]). Ketone **17** and alcohol **18** are also major products. Products **18** and **19** may result from secondary photolysis, reduction of the primary products **17** and **11**. We believe this reduction involves electron transfer from the initially formed radical anion $\mathbf{10}^{-\cdot}$ to the ketone **17** and imine **11**, followed by protonation of the radical anion and disproportionation. The reduction potential of ketone **17** will be significantly less negative than that of **10** (compare, for example, 4-cyanoacetophenone, $E_{1/2}^{red} = -0.65$ V (28)). Direct photochemical reduction of ketone **17** involving intermolecular hydrogen abstraction by the carbonyl n,π^* triplet state seems unlikely; intramolecular hydrogen abstraction should be more favourable. Alternatively, the imine may be reduced by chemical sensitization, i.e., hydrogen atom transfer (29).

Reaction involving the unsymmetric olefin 1-methylcyclohexene (**5**) provides more insight into the mechanism; the regio- and stereochemistry are diagnostic. The three isomeric photo-NOCAS products **20**, **21**, and **22**, formed from methanol, 1-methylcyclohexene (**5**), and methyl 4-cyanobenzoate (**10**), when biphenyl (**4**) is present (reaction [9]), are produced in the expected ratio; the *trans-anti*-Markovnikov adduct **20** is the major product. In this case also, the 4-cyanophenyl ketone (**23**) is a major product.

The photo-NOCAS adduct **27** is also formed upon irradiation of an acetonitrile–methanol solution of **10**, **4**, and cyclohexene (**26**) (reaction [10]). Only the *trans* isomer was isolated. The major product from this reaction is the 1:1 (olefin:aromatic) adduct 3-(methyl 4-benzoate)cyclohexene (**28**). This product results from attack of the 3-cyclohexenyl radical, which is formed upon deprotonation of the radical cation of cyclohexene, at the *ipso* position of the methyl 4-cyanobenzoate radical anion. Similar results were observed from 1,4-dicyanobenzene (**1**) and cyclohexene (**26**) upon irradiation under these conditions (2*b*). The radical cation of cyclohexene is particularly prone to deprotonation.

The role of biphenyl (4)

The singlet energy of biphenyl (**4**) ($E_{0,0}$ = 399.6 kJ mol^{-1} (30)) is higher than that of methyl 4-cyanobenzoate (**10**). The long-wavelength absorption tail of this transition does not extend much beyond 280 nm; therefore, most of the initial excitation must involve either methyl 4-cyanobenzoate (**10**) or the methyl 4-cyanobenzoate (**10**) – biphenyl (**4**) charge-transfer complex. Excitation of the charge-transfer complex of **10** and **4** will generate the CRIP, which can subsequently separate. The oxidation potential of biphenyl (**4**) ($E_{1/2}^{ox}$ = 1.9 V (31)) is similar to that of the olefins, and the effectiveness of the biphenyl radical cation ($\mathbf{4}^{+\cdot}$), serving as a codonor for reactions of olefins (Scheme 1, step 7), is well documented (2, 32). The olefin radical cation generated in this way is then free to react with nucleophile (methanol) (Scheme 1, step 3) and the mechanism continues. The fact that photo-NOCAS products are produced under these conditions is additional evidence that irradiation in the absence of added biphenyl (**4**) does not generate the solvated olefin radical cation.

Step 4 in the proposed mechanism (Scheme 1) is depicted as an attack of an alkyl radical at the *ipso* position, bearing the cyano group, of the radical anion. This process is related to the mechanism involving attack of a carbanion on the neutral molecule by single electron transfer (SET). A related duality of mechanism has received considerable attention in connection with reactions of Grignard and alkyl lithium reagents (33). The observation of ketonic products in reactions [8] and [9] now takes on additional significance. Should attack of the β-alkoxyalkyl moiety on the aromatic be considered as a radical attack on the radical anion or as an attack of a carbanion on the neutral molecule? Reactions of **1** and **10** with Grignard and alkyl lithium reagents are shown in reactions [14]–[17] and the results are summarized in Table 3. Differences observed can be correlated with the oxidation potentials of the Grignard and alkyl lithium reagents and the reduction potentials of **1** and **10** (33*d*).

Consider first the reactions of 1,4-dicyanobenzene (**1**). Reaction of **1** with the methyl Grignard (reaction [17]) or methyllithium reagents gives imine **41**, the product expected from nucleophilic attack of the methyl carbanion directly on the nitrile. No *ipso* attack, substitution of methyl for cyano on the aromatic ring, was observed. A major product from the analogous *tert*-butyl reagents, on the other hand, results from attack at the *ipso* position and displacement of cyanide ion, to give 4-*tert*-butylbenzonitrile (**38**). The product resulting from attack at the *ortho* position (**40**), was also formed in significant amounts. Attack of the *tert*-butyl reagent directly on the nitrile is a relatively minor pathway.

This difference in reactivity can be explained in terms of the relative oxidation potentials of the methyl and *tert*-butyl reagents. The oxidation potentials of Grignard and alkyl lithium reagents have been measured (34). There are complications involved in making and interpreting these measurements in terms of the redox couple $R^-/R^\cdot$: structures of

Can. J. Chem. Downloaded from www.nrcresearchpress.com by 88.255.202.194 on 09/08/12
For personal use only.

these reagents are complex, they are known aggregates, involvement of the counter cation is difficult to assess, values are usually reported in ethereal solution and these reagents form complexes with this solvent, and the electrochemical process is not reversible. Nevertheless, the results do provide a reasonably good relative scale of potentials even though the absolute values have no thermodynamic significance and they should only be used in a qualitative sense.

Oxidation potentials for the methyl reagents (CH_3MgBr, $E^{ox}_{1/2} = -0.25$ V; CH_3Li, $E^{ox}_{1/2} = -0.5$ V) are relatively low. The significantly more negative reduction potential of 1,4-dicyanobenzene (**1**) ($E^{red}_{1/2} = -1.66$ V ensures that the methyl reagents exhibit anionic reactivity. Carbanion nucleophilic attack occurs directly on the nitrile group forming the imine (**41**). The oxidation potentials of the *tert*-butyl analogues are much more negative (*tert*-BuMgBr, $E^{ox}_{1/2} = -1.07$ V; *tert*-BuLi, $E^{ox}_{1/2} = -2.30$ V); SET from the alkyl reagent to **1** is now possible, and reaction involving alkyl radical attack on the radical anion ($\mathbf{1}^{-\bullet}$) can now compete with carbanion attack directly on the nitrile.

Ab initio calculations on $\mathbf{1}^{-\bullet}$, at the STO-3G level (Fig. 4), show that spin density is highest at the *ipso* positions, with significant spin also at the *ortho* positions, and very little spin density on the carbons of the nitriles. Coupling of the *tert*-butyl radical at positions of high spin density can account for formation of the major products (**38** and **40**). The minor product, imine **39**, may result from competitive attack of the *tert*-butyl anionic reagent on the nitrile.

The 1,4-diene (**40**) resembles products normally obtained upon Birch reduction of the aromatic (35). Addition of *tert*-butyl radical to the *ortho* position of $\mathbf{1}^{-\bullet}$ gives the carbanion intermediate, which may be stabilized by interaction with the metal counterion. Protonation during work-up gives **40**.

Reactions of methyl 4-cyanobenzoate (**10**) with the Grignard and alkyl lithium reagents are somewhat more complex. The methyl reagents again show exclusive nucleophilic attack at the carboxyl carbonyl expected of anionic species.[8] The methyl Grignard reagent gives a good yield of alcohol **37**, formed by further reaction of the initial product, 4-cyanoacetophenone (**42**). Methyllithium gives a mixture of **37** and ketone **42**. The reduction potential of **10** ($E^{red}_{1/2} = -1.76$ V) is even more negative than that of **1**; the methyl reagents react as anions. Nucleophilic attack occurs exclusively at the carboxyl carbonyl.

The *tert*-butyl reagents attack at both the carbonyl group and at the *ipso* position. The disubstituted product **36** is formed as a secondary product from **34**. Reactions of the *tert*-butyl reagents are again dominated by single electron transfer, followed by *tert*-butyl radical attack at the *ipso* position of the radical anion $\mathbf{10}^{-\bullet}$.

Ab initio calculations on $\mathbf{10}^{-\bullet}$ (Fig. 5) show that spin density is high at the *ipso* positions. Single electron transfer from the *tert*-butyl reagents to **10**, followed by attack of the *tert*-butyl radical at the *ipso* position bearing the cyano group of $\mathbf{10}^{-\bullet}$ can account for the formation of the major products **34** and **36**. The spin density is also high on the carboxyl carbonyl carbon; therefore formation of ketone **42** may involve either (or both) radical–radical anion coupling or anionic attack at the carboxyl carbonyl. Complexation by the metal ion at the carbonyl oxygen may further increase spin density at the carbonyl carbon.

Step 3 (Scheme 1) yields the β-alkoxyalkyl radical; step 4 begins with the radical attacking the radical anion. Electrochemical measurements of the reduction potential of alkyl radicals have been reported (37). Standard potentials of the $R^{\bullet}/R^{-}$ couple are bracketed by (V vs sce, DMF): *tert*-butyl, −1.48, −1.60; *sec*-butyl, −1.38, −1.50; *n*-butyl, < −1.30, −1.42. These values are (perhaps surprisingly) not very different from the values determined for the oxidation of the Grignard and alkyl lithium reagents. Clearly, equilibrium SET involving the β-alkoxy *sec*- or *tert*-alkyl radicals and the radical anions $\mathbf{1}^{-\bullet}$ and $\mathbf{10}^{-\bullet}$ is thermochemically feasible; step 4 can be viewed as a radical attack on the radical anion. Spin density is high (0.27) on the *ipso* positions of the 1,4-dicyanobenzene radical anion ($\mathbf{1}^{-\bullet}$) and there is very little spin density on the cyano group (Fig. 4). In marked contrast, the spin density on the carbon *ipso* to the cyano group in the radical anion of methyl 4-cyanobenzoate ($\mathbf{10}^{-\bullet}$) is relatively small (0.10) and a larger fraction of the spin density is associated with the carbonyl group (Fig. 5). It is reasonable to suggest that coupling of the β-alkoxylalkyl radical and $\mathbf{10}^{-\bullet}$ will occur at both the *ipso* position and at the carbonyl carbon. While the results can be explained in terms of a reaction of the equilibrium concentration of β-alkoxyalkyl radical and carbanion, it is also possible that SET from the anion radical to the radical may, in fact, be slow relative to attack of the radical on the radical anion. Solvent reorganization and configurational change, associated with conversion from a planar alkyl radical to a tetrahedral carbocation, contribute to an intrinsic barrier for SET as high as 0.58 eV (37, 38). Therefore, product mixtures may be controlled either by kinetics or by the equilibrium of SET.

Deuterium incorporation in the ethers *cis*- and *trans*-**24** and **25**, isolated from reaction [9] when the irradiation is carried out in acetonitrile–methanol-*O*-*d* (Table 2), provides good evidence that SET does occur. Photosensitized (electron transfer) *anti*-Markovnikov addition of alcohols to alkenes is a well-known reaction (22). Two mechanisms have been recognized. After the alkene radical cation reacts with alcohol: the resulting β-alkoxyalkyl radical may be reduced by SET, followed by protonation of the carbanion, or the radical may abstract a hydrogen atom, either by disproportionation or from the allylic position of the starting alkene. Deuterium incorporated in the product ether when the irradiation is carried out in methanol-*O*-*d* is evidence for the SET, protonation (deuteration) of the β-alkoxy carbanion. The fact that deuterium is incorporated in *cis*- and *trans*-**24** and **25** provides strong support for the SET, deuteration sequence. The fact that the percentage of deuterium incorporation is not high indicates that the radical mechanism is also occurring. An alternative mechanism for formation of **25**, addition of methanol to *trans*-1-methylcyclohexene, may contribute. But this mechanism also requires deuterium incorporation and it is, therefore, not a major process.

Conclusions

1. In contrast with 1,4-dicyanobenzene, the singlet excited state (^1L_b) of methyl 4-cyanobenzoate is too short-lived for diffusion-controlled bimolecular reactions.

2. Irradiation of the ground state charge-transfer complex between methyl 4-cyanobenzoate and olefins, in polar solvent, leads to cyclic imine formation. The intermediate

[8]The carboxyl carbonyl is more susceptible to nucleophilic attack than is the nitrile (36).

Can. J. Chem. Downloaded from www.nrcresearchpress.com by 88.255.202.194 on 09/08/12
For personal use only.

excited state of the charge-transfer complex can be described as a contact radical ion pair (CRIP).

3. Irradiation of methyl 4-cyanobenzene and an olefin in nonpolar solvent (e.g., benzene) leads to oxetane formation. In nonpolar solvent the excited state of the charge-transfer complex is dominated by the "no-bond" wavefunction involving locally excited states.

4. When irradiation of methyl 4-cyanobenzoate and an olefin is carried out in acetonitrile–methanol and in the presence of a codonor (e.g., biphenyl) the solvent-separated methyl 4-cyanobenzoate radical anion and olefin radical cation can be obtained and photo-NOCAS products result. This reaction is a useful synthetic procedure for the synthesis of benzoate esters.[9]

5. Attack of an alkyl radical on a radical anion and the attack of a carbanion on a neutral molecule are complimentary/competitive processes, related by single electron transfer (SET). A key step in the photo-NOCAS reaction of methyl 4-cyanobenzoate is depicted as a β-alkoxyalkyl radical attack on the radical anion. Attack may occur at both the *ipso* position, bearing the cyano group, and at the carboxyl carbonyl; both are positions of high spin density.

6. Attack of a carbanion (e.g., the methyl Grignard or methyllithium reagent) on methyl 4-cyanobenzoate occurs exclusively at the carboxyl carbonyl. The *tert*-butyl carbanion (e.g., *tert*-BuMgBr and *tert*-BuLi) is relatively easy to oxidize, SET gives the *tert*-butyl radical and methyl 4-cyanobenzoate radical anion, and alkyl radical attack on the radical anion occurs at the *ipso* position.

Experimental

General information

^{1}H and ^{13}C nmr spectra were recorded on a Nicolet 360 NB, a Varian EM-360L, or a Bruker 300 MSL spectrometer. Chemical shifts are reported in parts per million (ppm) downfield relative to tetramethylsilane. Infrared spectra (ir) were recorded on an air-purged Perkin–Elmer 180 grating spectrometer and are reported in wavenumbers (cm^{-1}). The spectra were calibrated against the 1601.4 cm^{-1} absorption band of polystyrene film. Mass spectra were recorded on a Hewlett–Packard 5970 series mass selective detector and are reported as m/z with the relative intensities in parentheses. Exact mass determinations were carried out using a ZAB-E spectrometer. Elemental analyses were carried out by Canadian Microanalytical Service Ltd., B.C. Melting points were determined using a Cybron Corporation Thermolyne apparatus linked to a digital thermocouple, and are corrected. Ultraviolet absorption spectra were recorded on a Cary Varian 219 spectrometer and are reported in nm. Product analyses were determined by gas chromatography (gc) using either a Hewlett–Packard 5890 gc, fitted with a 5% phenyl methyl silicone fused silica WCOT column (25 m × 0.20 mm, 0.33 μm film thickness), coupled to a H–P mass selective detector (gc/ms), or a H–P 5890 gc, fitted with a DB 1701 fused silica WCOT column (30 m × 0.25 mm, 0.25 μm film thickness), with a flame ionization detector (gc/fid). Preparative gc was carried out using Varian Aerograph models A-700 and 920, fitted with either a 10% FFAP SW 60/80 or 10% QF-1 Chromasorb P 60/80 column. Preparative medium-pressure liquid chromatography (mplc) was carried out using a 2.5 cm × 1 m column packed with tlc grade silica gel (without binder) (Merck, Kieselgel 60 PF_{254}) at 15 psi helium (1 psi = 6.9 kPa). The chromatograms were generally developed with a hexanes–dichloromethane linear solvent gradient and the eluent was monitored and collected by a uv spectrometer – fraction collector. Dry column flash (dcfc) and flash chromatography (fc) were performed using tlc grade silica gel (Merck) and silica gel (Aldrich, 230–400 mesh 60A) respectively (39).

Irradiations were carried out at 10°C using either a CGE 1-kW or an Hanovia 450-W medium-pressure mercury vapour lamp contained in a quartz immersion well. Solutions were degassed by nitrogen ebullition prior to irradiation.

Materials

Solvents were fractionally distilled immediately before use. Acetonitrile was purified by the reported method (40). Anhydrous diethyl ether (Mallinckrodt) was used without further purification. Tetrahydrofuran (Anachemia, ACS grade) was refluxed for 24 h over lithium aluminum hydride, then fractionally distilled directly into reaction vessels under nitrogen. Thiophene-free benzene was distilled from sodium/benzophenone under nitrogen. Hexane used for uv studies was stirred with sulphuric acid (conc.) to remove alkenes, washed with water, dried over magnesium sulphate, and fractionally distilled from sodium hydride. The olefins 2,3-dimethyl-2-butene (**2**), 1-methylcyclohexene (**5**), and cyclohexene (**26**) were obtained from Aldrich and were fractionally distilled from calcium hydride prior to use. Methyl 4-cyanobenzoate (**10**) (Aldrich) was sublimed and recrystallized twice from methanol. 1,4-Dicyanobenzene (**1**) (Aldrich) was purified by the previously reported method (40). Biphenyl (**4**), 1-methylcyclohexanol, 2-methylcyclohexanol (*cis* and *trans*), and the Grignard and lithium reagents were obtained from Aldrich, and were used as received. 2-Methylpropene was obtained from Matheson.

*Irradiation of methyl 4-cyanobenzoate (**10**) and 2,3-dimethyl-2-butene (**2**) in acetonitrile–methanol (reaction [3])*

A solution of methyl 4-cyanobenzoate (**10**) (0.65 g, 4 × 10^{-3} mol) and 2,3-dimethyl-2-butene (**2**) (1 mL, 8.4 × 10^{-3} mol) in acetonitrile–methanol (3:1, 40 mL) was terminated through quartz using the 450-W lamp. The irradiation was irradiated after 70 h (35.6% conversion, based on unrecovered **10**). Volatile components were removed from the photolysate by distillation at reduced pressure, leaving a yellow oil, which was separated (fc, silica gel, dichloromethane – ethyl acetate). Imine **11** (0.20 g, 83%) was characterized immediately; ir (liq. film) ν: 3400(m, broad), 3240(m), 2960(s), 2870(m), 1720(s), 1645(s), 1590(m), 1380(s); ^{1}H nmr (60 MHz, $CDCl_3$) δ: 8.6(b, 1H, exch.), 8.2–7.7(m, 3H), 3.9(s, 3H), 1.2(s, 6H), 1.1(s, 6H); ^{1}H nmr (361.027 MHz, $CDCl_3$) δ: 8.03(s, 1H), 8.01(m, 1H), 7.78(m, 1H), 3.94(s, 3H), 1.19(s, 6H), 1.10(s, 6H); ^{13}C nmr (90.79 MHz, $CDCl_3$) δ: 188.23(s), 166.75(s), 156.84(s), 139.12(s), 133.34(d, J = 5.0 Hz), 128.62(d, J = 163.3 Hz), 124.29(d, J = 167.2 Hz), 122.42(d, J = 165.9 Hz), 52.28(q, J = 147.1 Hz), 52.01(s), 46.35(s), 25.68(q, J = 127.4 Hz), 25.40(q, J = 126.6 Hz); m/z: 246(3), 245($M^{+\cdot}$, 18), 244(3), 231(39), 230(100), 215(24), 171(23), 128(10), 115(10), 77(5).

*Hydrolysis of imine **11** to ketone **12** (reaction [4])*

Hydrolysis of **11** (0.29 g) was carried out in aqueous methanol (50 mL) and HCl (1 mL, 6 M). The solvent was removed by distillation at reduced pressure, and the residue was diluted with water (50 mL) and extracted with dichloromethane (3 × 25 mL). The combined organic layers were washed with aqueous sodium bicarbonate and water, dried over magnesium sulphate, and evaporated to give a yellow oil. Ketone **12** was isolated (fc, silica gel, dichloromethane) as a colourless solid (0.20 g, 69%). Recrystallization of **12** from 95% ethanol afforded fine needles; mp 69.4–70.4°C; ir (KBr) ν: 2980(m), 2940(m), 2880(w), 1730(vs), 1625(w), 1595(w), 1450(m), 1340(m), 1290(s), 1250(s), 1200(s), 985(s), 760(s); ^{1}H nmr (361.03 MHz, $CDCl_3$) δ: 8.15(s, 1H), 8.03(d, 1H, J = 8.1 Hz), 7.76(d, 1H, J = 8.1 Hz), 3.97(s, 3H), 1.26(s, 6H),

[9]Our study of the scope of the photo-NOCAS reaction has been extended to include 4-(methylsulphonyl)benzonitrile, 4-(trifluoromethyl)benzonitrile, 4-fluorobenzonitrile, (4-cyanophenyl)trimethylammonium iodide, 4-cyanobenzaldehyde, and 4-cyanobenzophenone. Only with 1,4-dicyanobenzene and methyl 4-cyanobenzoate were photo-NOCAS products formed (D. R. Arnold and K. McMahon, unpublished results).

Can. J. Chem. Downloaded from www.nrcresearchpress.com by 88.255.202.194 on 09/08/12
For personal use only.

1.10(s, 6H); ^{13}C nmr (90.79 MHz, $CDCl_3$) δ: 210.59(s), 166.47(s), 161.45(s), 136.73(s), 135.47(s), 128.69(d, J = 164.0 Hz), 124.68(d, J = 163.5 Hz), 123.88(d, J 164.1 Hz), 54.15(s), 52.49(q, J = 147.4 Hz), 44.95(s), 26.22(q, J = 127.0 Hz), 21.57(q, J = 127.5 Hz); ms m/z: 247(5), 246($M^{+\cdot}$, 25), 232(19), 231(100), 215(5), 172(6), 128(11), 155(11), 91(5). Anal. calcd. for $C_{15}H_{18}O_3$: C 73.15, H 7.35; found: C 73.14, H 7.37.

Irradiation of tert*-butyl 4-cyanobenzoate (**10**a) and 2,3-dimethyl-2-butene (**2**) in acetonitrile–methanol*

A solution of **10***a* (1.8 g, 8×10^{-3} mol) and **2** (2.14 mL, 1.8×10^{-2} mol) in acetonitrile–methanol (3:1, 90 mL) was irradiated through Pyrex (450 W) for 120 h. The photolysate was concentrated at reduced pressure to give a residual red solid mixture that was separated using dcfc. Elution using 20% ethyl acetate – dichloromethane solvent gave the starting ester (1.7 g, 7.7% conversion) and the cyclic imine **11***a* (0.07 g, 2.4×10^{-4} mol, 36%). **11***a*: ir (liq. film, NaCl) ν: 3240(w, broad), 2980(m), 2980(m), 1720(vs), 1700(m), 1370(m), 1300(s), 1250(s), 1165(vs), 1115(m), 835(w); ^{1}H nmr (361.01 MHz, $CDCl_3$) δ: 7.98(m, 2H, Ar-H and N-H), 7.84(d, 1H, J = 7.80 Hz), 7.77–7.76(m, 1H), 1.63(s, 9h), 1.20(s, 6H), 1.13(s, 6H); ^{13}C nmr (75.47 MHz, DEPT, $CDCl_3$) δ: 188.96(s), 165.39(s), 157.19(s), 138.11(s), 135.70(s), 128.52(d), 124.06(d), 122.70(d), 81.49(s), 52.15(s), 46.49(s), 28.15(s), 28.15(q, *t*-Bu), 25.42(q), 22.58(q); ms m/z: 288(4), 287($M^{+\cdot}$, 18), 272(28), 231(10), 217(39), 216(100), 214(24), 171(20), 57(24).

Imine **11***a* (0.03 g, 1.08×10^{-4} mol) was stirred at room temperature in acetone (5 mL) with a trace of hydrochloric acid (1 M) for 15 m. The sample was evaporated at reduced pressure, dissolved in dichloromethane (2 mL), and passed down a short silica column (Sep-pak). Further elution with dichloromethane (5 mL) gave ketone **12***a* (0.015 g, 5.20×10^{-5} mol, 50%).

12*a*, colourless oil: ir (liq. film, NaCl) ν: 2980(m), 2940(w), 1720(vs), 1370(m), 1310(m), 1285(m), 1255(m), 1165(s), 960(w); ^{1}H nmr (361.01 MHz, $CDCl_3$) δ: 8.09(s, br, 1H), 7.97(dd, 1H, J = 8.00 Hz, J = 1.04 Hz), 7.73(d, 1H, J = 8.00 Hz), 1.62(s, 9H), 1.25(s, 6H), 1.09(s, 6H); ^{13}C nmr (90.78 MHz, $CDCl_3$) δ: 210.82(s), 165.18(s), 161.39(s), 137.42(s), 136.32(s), 128.53(d, J = 165.30 Hz), 124.42(d, J = 161.43 Hz), 123.70(d, J = 165.30 Hz), 81.87(s), 54.16(s), 44.93(s), 28.15(q, J = 127.31 Hz), 26.22(q, J = 129.15 Hz), 21.61(q, J = 128.06 Hz); ms m/z: 289(5), 288($M^{+\cdot}$, 24), 232(36), 218(24), 217(100), 215(24), 172(16), 129(18), 128(24), 115(21), 57(40).

The *tert*-butyl ester (**12***a*) was converted to the methyl ester (**12**) by heating in methanolic hydrochloric acid (1 M) at 70°C for 24 h. The product was identical (gc/ms, retention time, and mass spectrum) with an authentic sample of **12**.

*Irradiation of methyl 4-cyanobenzoate (**10**) and 1-methylcyclohexene (**5**) in acetonitrile–methanol (reaction [5])*

An acetonitrile–methanol (3:1, 250 mL) solution of **10** (3.2 g, 0.02 mol) and **5** (4.7 mL, 0.04 mol) was degassed and irradiated through quartz at 10°C using the 450-W lamp for 17 h. Dilute aqueous HCl (10 mL) was added and the solution was stirred at room temperature for 7 h until the imine (**13**) hydrolysed (gc/ms). The solution was then concentrated under reduced pressure and the residual oil was chromatographed (mplc, silica gel, 90% hexanes – ethyl acetate eluent). Ketone **14** was isolated as a colourless oil (0.45 g, 17.5%, at 50% conversion of the ester **10**).

14: ir (liq. film) ν: 2955(s), 2800(m), 1735(vs), 1630(w), 1600(w), 1500(s), 1455(s), 1210(s), 1100(m), 980(w), 765(m); ^{1}H nmr (361.01 MHz, $CDCl_3$) δ: 8.13(s, 1H), 8.04(d, 1H, J = 7.94 Hz), 7.80(d, 1H, J = 7.79 Hz), 3.97(s, 3H), 3.08(t, 1H, J = 5.24 Hz), 2.03–1.94(m, 2H), 1.58–1.20(m, 6H), 1.28(s, 3H); ^{13}C nmr (90.78 MHz, $CDCl_3$) δ: 209.93(s), 166.43(s), 155.36(s), 138.62(s), 135.09(s), 128.60(d, J = 167.04 Hz), 124.25(d, J = 165.91 Hz), 125.59(d, J = 163.43 Hz), 52.43(q, J = 147.34 Hz), 50.22(s), 45.60(d, J = 132.10), 31.52(t, J = 127.40 Hz), 26.14(t, J = 127.31 Hz), 21.14(tm), 21.01(tm), 21.66(q, J = 127.34 Hz); ms m/z: 260(2), 259(13), 258($M^{+\cdot}$, 84), 244(17), 243(100), 240(21), 229(41), 227(19), 225(13), 217(41), 216(21), 203(21), 181(50), 171(16), 143(15), 142(12), 141(21), 129(25), 128(43), 127(19), 115(48), 77(19), 75(12), 59(24). Exact Mass calcd. for $C_{16}H_{18}O_3$: 258.1256; found: 258.1256.

*Preparation of ammonium salt **15** from keto ester **14** (reaction [7])*

An aqueous sodium hydroxide solution (0.5 mL, 6.2 M) of the keto ester **14** (0.10 g, 3.9×10^{-4} mol) was heated under reflux for 20 min, after which time the ester had dissolved. The solution was cooled in an ice-bath, and water (0.5 mL) was added. This solution was then acidified using hydrochloric acid (conc.). A pale yellow solid was collected by filtration and washed with water. This solid was dissolved in dichloromethane and dried over magnesium sulphate. Evaporation of the solvent gave the acid, 0.08 g (88%), as a colourless solid. The ^{1}H nmr spectrum showed the presence of an exchangeable hydrogen and the absence of the ester methoxy group; ^{1}H nmr (361.01 MHz, $CDCl_3$) δ: 8.214(s, 1H), 8.136(d, 1H, J = 7.95 Hz), 7.856(d, 1H, J = 7.95 Hz), 3.115(t, 1H, J = 5.32 Hz), 2.060–1.930(m, 2H), 1.298(s, 3H), 1.628–1.204(m, 6H). An exchangeable proton was detected (EM-360L) at 8.6 ppm (this peak was not evident in the high-field spectrum (Nicolet)); ^{13}C nmr (90.784 MHz, acetone-d_6) δ: 170.42, 155.47, 139.40, 134.09, 129.28, 126.25, 124.49, 50.38, 45.65, 31.56, 26.24, 21.72, 21.21.

Ammonium salt **15** was formed by bubbling ammonia through a diethyl solution of the acid at room temperature. The salt immediately precipitated from solution. The mixture was filtered; the solid was washed with diethyl ether to remove traces of unreacted acid, and dried under vacuum. The resulting colourless solid was then recrystallized from methanol, to give a sample (mp 183.4–184.8°C) from which a crystal was chosen for X-ray analysis.

*The photo-NOCAS reaction: methanol, 2,3-dimethyl-2-butene (**2**), methyl 4-cyanobenzoate (**10**), and biphenyl (**4**) (reaction [8])*

An acetonitrile–methanol (3:1, 20 mL) solution of ester **10** (0.32 g, 2.0×10^{-3} mol), biphenyl (**4**) (0.31 g, 2.0×10^{-3} mol), and olefin **2** (0.5 mL, 4.2×10^{-3} mol) was degassed and irradiated through quartz using the 450-W lamp. The reaction was stopped after 35 h, at 91.5% conversion of the ester. After the volatile components of the reaction mixture were removed under vacuum, the crude yellow oil was chromatographed using dcfc. Biphenyl (**4**) was recovered (84%) using hexane as the eluent. The photo-NOCAS product (**16**) eluted with 5% diethyl ether – hexane as a colourless solid, 0.068 g (15%). Alcohol **18** was also isolated as a solid, 0.077 g (17%), using 10% acetone–dichloromethane eluent.

16: recrystallized from methanol to give fine needles, mp 66.8–67.4°C; ir (KBr) ν: 3000(m), 2970(w), 1720(s), 1600(w), 1445(m), 1280(s), 1200(m), 1120(m), 1105(s), 1060(m), 1015(m), 770(m), 705(m); ^{1}H nmr (361.11 MHz, $CDCl_3$) δ: 7.92(d, 2H, J = 8.49 Hz), 7.52(d, 2H, J = 8.51 Hz), 3.89(s, 3H), 3.10(s, 3H), 1.39(s, 6H), 1.00(s, 6H); ^{13}C nmr (90.78 MHz, $CDCl_3$) δ: 167.28(s), 153.06(s), 128.62(d, J = 159.46 Hz), 128.10(d, J = 128.12 Hz), 127.20(s), 78.82(s), 51.90(q, J = 146.56 Hz), 49.46(q, J = 140.40 Hz), 45.79(s), 24.35(q, J = 126.65 Hz), 19.88(q, J = 125.31 Hz); ms m/z: no mol, ion, 235(1.5), 219(0.7), 178(2.1), 163(3.2), 118(2.5), 117(2.5), 115(2.7), 103(1.5), 102(1.6), 91(2.5), 74(5.0), 73(100), 51(1.4). Anal. calcd. for $C_{15}H_{22}O_3$: C 71.97, H 8.86, O 19.17; found: C 71.71, H 8.87.

18: recrystallized from methanol, mp 132.7–133.4°C; ir (KBr) ν: 3450(b), 3055(m), 2970(m), 2260(s), 1625(m), 1490(m), 1415(m), 1390(w), 1340(w), 1220(m), 1075(s), 1020(m), 875(s), 860(s), 790(s), 640(s); ^{1}H nmr (361.01 MHz, $CDCl_3$) δ: 7.60–7.58(d, 2H, J = 8.45 Hz), 7.49–7.47(d, 2H, J = 8.14 Hz), 5.72(s, 1H, exch.), 4.98(s, 1H), 3.31(s, 3H), 1.42(s, 3H), 1.20(s, 3H), 0.90(s, 3H), 0.63(s, 3H); ^{13}C nmr (90.78 MHz, $CDCl_3$) δ: 147.64(s), 131.01(d, J = 165.17 Hz), 129.44(d, J = 162.93 Hz), 119.08(s), 110.67(s), 83.24(s), 78.46(d, J = 143.97 Hz), 40.03(q,

Can. J. Chem. Downloaded from www.nrcresearchpress.com by 88.255.202.194 on 09/08/12
For personal use only.

J = 142.02 Hz), 44.02(s), 22.95(q, J = 125.18 Hz), 19.70(q, J = 125.60 Hz), 19.40(q, J = 125.59 Hz), 14.74(q, J = 126.35 Hz); ms m/z: no mol. ion, 130(12), 115(22.4), 104(8.5), 102(8.6), 85(12.5), 84(100), 83(28), 77(9.8), 73(89.7), 69(58.2). Anal. calcd. for $C_{15}H_{21}NO_2$: C 72.84, H 8.56, N 5.66; found: C 72.65, H 8.57, N 5.59.

When the irradiation described above was carried out to lower conversion (43% of the ester (**10**) consumed after 3.5 h), along with **16** and **18**, two additional products, **17** and **19**, were detected.

Amine **19** was isolated as a colourless oil (13.4% yield) (dcfc, ethyl acetate eluent); ir (liq. film, NaCl) ν: 3900(w, broad), 2960(s), 1720(s), 1615(w), 1585(w), 1435(m), 1290(s), 1240(m), 750(m); ^{1}H nmr (361.01 MHz, $CDCl_3$) δ: 7.92(dd, 1H, J = 7.78, 1.55 Hz), 7.79(d, 1H, J = 13.6 Hz), 7.35(d, 1H, J = 7.86 Hz), 4.10(s, 1H), 3.90(s, 3H), 1.46(br s, 2H, exch. D_2O), 1.24(s, 3H), 1.078(s, 3H), 1.06(s, 3H), 0.64(s, 3H); ^{13}C nmr (90.78 MHz, $CDCl_3$) δ: 167.40(s), 151.14(s), 149.83(s), 129.38(s), 128.38(d, J = 164.07 Hz), 123.24(d, J = 159.93 Hz), 122.82(d, J = 159.67 Hz), 63.26(d, J = 135.58 Hz), 51.98(q, J = 146.96 Hz), 50.34(s), 46.27(s), 25.90(q, J = 125.67 Hz), 22.062(q, J = 125.06 Hz), 19.95(q, J = 125.16 Hz), 17.74(q, J = 125.97 Hz); ms m/z: 248(10), 247($M^{+\cdot}$, 68), 246(72), 232(62), 216(39), 215(100), 190(52), 188(38), 183(36), 171(25), 156(73), 155(29), 143(26), 141(29), 131(29), 130(38), 129(35), 128(38), 115(38), 70(31), 59(31), 58(29). Exact Mass calcd. for $C_{15}H_{21}NO_2$: 247.1572; found: 247.1572.

Ketone **17** (4% yield) was isolated from the reaction mixture (dcfc, 30% diethyl ether – hexane). Recrystallization from methanol (3×) gave **17** as fine needles, mp 64.5–65.5°C; ir (liq. film, NaCl) ν: 2980(s), 2960(m), 2240(s), 1725(m), 1680(s), 1475(m), 1395(m), 1370(m), 1260(s), 1145(s), 1070(s), 975(m), 970(m), 855(m), 740(m); ^{1}H nmr (361.01 MHz, $CDCl_3$) δ: 7.77(d, 2H, J = 8.59 Hz), 7.64(d, 2H, J = 8.46 Hz), 3.22(s, 3H), 1.25(s, 6H), 1.21(s, 6H); ^{13}C nmr (90.78 MHz, $CDCl_3$) δ: 210.65(s), 145.66(s), 131.40(d, J = 167.45 Hz)), 128.48(d, J = 166.64 Hz), 118.48(s), 113.16(s), 80.30(s), 54.75(s), 48.91(q, J = 141.24 Hz), 23.56(q, J = 126.95 Hz), 19.56(q, J = 125.28 Hz); ms m/z: no mol. ion, 230(1), 214(0.1), 131(8), 130(86), 115(9), 102(37), 84(48), 83(24), 75(10), 74(8), 73(100), 69(28), 55(25). Anal. calcd. for $C_{15}H_{19}NO_2$: C 73.44, H 7.81, N 5.71, O 13.04; found: C 73.22, H 7.58, N 5.68.

*The photo-NOCAS reaction: methanol, 1-methylcyclohexene (**5**), methyl 4-cyanobenzoate (**10**), and biphenyl (**4**) (reaction [9])*

A solution of **10** (0.65 g, 4.03 × 10^{-3} mol), **4** (0.62 g, 4.02 × 10^{-3} mol), and **5** (1 mL, 8.45 × 10^{-3} mol) in acetonitrile–methanol (3:1, 40 mL) was degassed and irradiated through quartz (1 kW). Progress of the reaction was followed by gc/fid and when conversion of the ester was essentially complete (12 h) the reaction was stopped. Removal of the volatile components of the mixture by distillation under reduced pressure gave a yellow oil (2.10 g). This mixture was separated using mplc. When necessary, combined fractions were further purified using dcfc. The isomeric photo-NOCAS products **20**–**22** and the ketone **23** were obtained.

Isomer **20**, 31%: ir (liq. film, NaCl) ν: 2970(m), 2930(s), 2860(m), 2810(w), 1725(vs), 1610(s), 1440(s), 1280(vs), 1190(s), 1105(vs), 760(s), 700(s); ^{1}H nmr (300.13 MHz, $CDCl_3$) δ: 7.99(d, 2H, J = 8.5 H z), 7.49(d, 2H, J = 8.5 Hz), 3.88(s, 3H), 3.48(dd, 1H, J = 9.6 Hz, 3.6 Hz), 3.14(s, 3H), 1.88–1.46(m, 8H), 1.31(s, 3H); ^{13}C (75.47 MHz, $CDCl_3$) δ: 167.12(s). 154.89(s), 129.37 (dd, J = 161.8 Hz, J = 6.0 Hz), 127.49(s), 126.22(dd, J = 157.2 Hz, J = 6.8 Hz), 84.12(d, J = 139.3 Hz), 57.02 (qd, J = 140.6 Hz, J = 4.3 Hz), 51.88(q, J = 147.0 Hz), 43.37(s), 37.88(t, J = 126.8 Hz), 25.90(t, J = 127.4 Hz), 23.73(t, J = 125.4 Hz), 21.78(t, J = 125.4 Hz), 19.54(qm, J = 127.1 Hz); ms m/z: 263(11), 262($M^{+\cdot}$, 71), 231(36), 230(100), 176(43), 145(42), 143(87), 115(33), 91(22), 71(76), 59(22). Anal. calcd. for $C_{16}H_{22}O_3$: C 73.25, H 8.45; found: C 72.99, H 8.51.

Isomer **21**, 5%: ir (liq. film, NaCl) ν: 2950(s), 2880(m), 2840(w), 1740(vs), 1620(m), 1450(m), 1290(vs), 1200(m), 1130(s), 1080(m), 780(m), 720(m); ^{1}H nmr (300.13 MHz, $CDCl_3$) δ: 7.93(d, 2H, J = 8.4 Hz), 7.29(d, 2H, J = 8.4 Hz), 3.89(s, 3H), 3.13(s, 3H), 2.86(dd, 1H, J = 11.7 Hz, 4.0 Hz), 1.98–1.26(m, 8H), 1.02(s, 3H); ^{13}C nmr (75.47 MHz, $CDCl_3$) δ: 167.34(s), 148.51(s), 129.55(d, J = 159.6 Hz), 128.69(d, J = 161.9 Hz), 127.94(s), 76.84(s), 51.89(q, J = 146.8 Hz), 51.80(d, J = 133.0 Hz), 48.52(q, J = 140.3 Hz), 37.01(t, J = 127.8 Hz), 29.53(t, J = 127.1 Hz), 26.28(t, J = 127.1 Hz), 23.81(t, J = 127.3 Hz), 16.94(qm, J = 124.9 Hz); ms m/z: 262($M^{+\cdot}$, 21) 231(18), 230(63), 188(25), 171(22), 131(19), 129(48), 128(19), 115(14), 85(100), 72(37), 59(14), 55(24). Exact Mass calcd. for $C_{16}H_{22}O_3$: 262.1569; found: 262.1567.

Isomer **22**, 1%: ir (liq. film, NaCl) ν: 2950(s), 2880(m), 2845(w), 1735(vs), 1625(m), 1450(m), 1290(s), 1120(m), 1090(m), 780(m); ^{1}H nmr (300.13 MHz, $CDCl_3$) δ: 7.91(d, 2H, J = 8.3 Hz), 7.38(d, 2H, J = 8.3 Hz), 3.89(s, 3H), 3.11(s, 3H), 2.47(dd, 1H, ^3J = 12.8 Hz, 3.3 Hz), 2.18–2.04(m, 2H), 1.83–1.13(m, 6H), 0.88(s, 3H); ^{13}C nmr (75.47 MHz, $CDCl_3$) δ: 167.25, 149.59, 129.74, 128.83, 127.75, 74.26, 55.25, 51.87, 48.28, 34.01, 28.99, 26.52, 23.42, 21.57; ms m/z: 263(7), 262(42), 247(2), 231(24), 230(74), 219(11), 188(37), 187(10), 171(18), 131(12), 129(48), 128(12), 115(12), 103(8), 91(10), 85(100), 77(10), 72(39), 55(21). Exact Mass calcd. for $C_{16}H_{22}O_3$: 262.1569; found: 262.1569.

Ketone **23**, 17%: ir (liq. film, NaCl) ν: 3000(m), 2960(vs), 2890(s), 2840(w), 2260(s), 1700(vs), 1110(vs), 1475(m), 1280(m), 1260(m), 960(s), 850(s); ^{1}H nmr (300.13 MHz, $CDCl_3$) δ: 7.70(d, 2H, J = 8.3 Hz), 7.58(d, 2H, J = 8.2 Hz), 3.58(dd, 1H, J = 10.1 Hz, 3.9 Hz), 3.26(s, 3H), 1.97–1.62(m, 4H), 1.54–1.28(m, 4H), 1.24(s, 3H); ^{13}C nmr (75.47 MHz, $CDCl_3$) δ: 210.86(s), 144.84(s), 131.81(d, J = 167.8 Hz), 127.23(d, J = 172.2 Hz), 118.21(s), 113.46(s), 81.92(d, J = 143.1 Hz), 56.31(qd, J = 141.1 Hz, J = 4.2 Hz), 53.42(s), 34.70(t, J = 128.4 Hz), 24.85(t, J = 125.9 Hz), 23.44(t, J = 127.4 Hz), 20.91(t, J = 127 87 Hz), 16.01(qm, J = 127.7 Hz); ms m/z: 257($M^{+\cdot}$, 6), 225(67), 196(34), 127(25), 130(56), 95(100), 102(54), 71(54), 67(29), 59(50), 55(29). Anal. calcd. for $C_{16}H_{19}NO_2$: C 74.94, H 7.49, N 5.43; found: C 74.68, H 7.44, N 5.44.

Ethers *cis*- and *trans*-**24** and **25** were isolated from the volatile components of the photolysate and were identified by direct comparison (ir, gc/ms) with authentic samples.

Reaction [9] was repeated using acetonitrile–methanol-*O*-*d* (3:1) as solvent. The ethers (*cis*- and *trans*-**24**, and **25**) were analyzed by gc/ms, using selective ion monitoring, to determine the percent of deuterium incorporation. The results are shown in Table 2.

Preparation of ethers: cis- *and* trans-*1-methoxy-2-methylcyclohexane (**24**) and 1-methoxy-1-methylcyclohexane (**25**)*

Ethers *cis*- and *trans*-**24** and **25** were made from commercially available alcohols using published procedures (41). The alcohol was treated with sodium hydride in tetrahydrofuran, and then with an excess of methyl iodide. After work-up, the ethers were purified using prep-gc (QF1 column).

1-Methoxy-1-methylcyclohexane (**25**); ^{1}H nmr (361.01 MHz, $CDCl_3$) δ: 3.18(s, 3H, OCH_3), 1.69–1.21(m, 10H), 1.11(s, 3H, CH_3).

cis-1-Methoxy-2-methylcyclohexane (*cis*-**24**); ^{1}H nmr (361.01 MHz, $CDCl_3$) δ: 3.31(s, 3H, OCH_3), 3.21(m, 1H), 1.79–1.25(m, 9H), 0.92(d, 1H, J = 7.19 Hz).

trans-1-Methoxy-2-methylcyclohexane (*trans*-**24**); ^{1}H nmr (361.01 MHz, $CDCl_3$) δ: 3.35(s, 3H, OCH_3), 2.65(td, 1H, J_{aa} = 9.75, 9.75 Hz, J_{ae}= 4.02 Hz), 2.11–2.06(m, 1H), 1.78–1.03(m, 8H), 0.98(d, 3H, CH_3, J = 6.48 Hz).

*The photo-NOCAS reaction: methanol, cyclohexene (**26**), methyl-4-cyanobenzoate (**10**), and biphenyl (**4**) (reaction [10])*

A solution of **10** (1.61 g, 1.0 × 10^{-2} mol), **4** (1.55 g, 1.0 × 10^{-2} mol), and **26** (2.1 mL, 1.8 × 10^{-3} mol) in acetonitrile–

Can. J. Chem. Downloaded from www.nrcresearchpress.com by 88.255.202.194 on 09/08/12
For personal use only.

methanol (3:1, 110 mL) was degassed and irradiated (1 kW) through Pyrex. After 206 h the reaction was stopped (38.6% conversion of **10**). Separation (mplc) of the photolysate gave photo-NOCAS product **27**, 0.08 g (8% yield), and the 1:1 adduct **28**, 0.10 g (12%), both as colourless oils.

27: ir (liq. film, NaCl) ν: 2940(s), 2880(m), 2840(w), 1735(vs), 1620(m), 1030(w), 775(m), 710(m); ^{1}H nmr (361.03 MHz, $CDCl_3$) δ: 7.97(d, 2H, J = 8.32 Hz), 7.29(d, 2H, J = 8.30 Hz), 3.89(s, 3H), 3.27(td, 1H, J = 10.19, 10.18, 4.17 Hz), 3.09(s, 3H), 2.62–2.54(m, 1H), 2.29–2.24(m, 1H), 1.90–1.72(m, 3H), 1.53–1.20(m, 4H); ^{13}C nmr (90.79 MHz, $CDCl_3$) δ: 167.18, 150.47, 129.60(d, J = 162.7 Hz), 128.02, 127.58(d, J = 158.4 Hz), 82.97(d, J = 141.41), 56.65(q, J = 140.9 Hz), 51.92(q, J = 146.5 Hz), 51.24(d, J = 128.5 Hz), 34.10(t, J = 131.7 Hz), 31.30(t, J = 126.7 Hz), 25.98(t, J = 126.7 Hz), 24.90(t, J = 128.8 Hz); ms m/z: 249(7), 248($M^{+\cdot}$, 39), 217(15), 216(39), 157(24), 131(22), 129(48), 115(15), 103(13), 77(14), 71(100), 58(14). Exact Mass calcd. for $C_{15}H_{20}O_3$: 248.1412; found: 248.1415.

28: ir (liq. film, NaCl) ν: 3030(w), 2940(s), 2870(m), 1730(m), 1620(m), 1410(m), 1285(s), 1110(m), 1025(w), 845(w), 765(m); ^{1}H nmr (361.01 MHz, $CDCl_3$) δ: 7.96(d, 2H, J = 8.24 Hz), 7.28(d, 2H, J = 8.22 Hz), 5.92(m, 1H, J = 9.93, 2.50 Hz), 5.69(dd, 1H, J = 9.93, J = 2.02 Hz), 3.90(s, 3H), 3.46(m, 1H), 2.10–1.49(m, 6H); ^{13}C nmr (90.78 MHz, $CDCl_3$) δ: 167.11(s), 152.08(s), 129.60(d, J = 165.86 Hz), 129.15(d, J = 153.54 Hz), 128.96(d, J = 162.88 Hz), 127.77(s), 127.71(d, J = 166.27 Hz), 51.96(q, J = 146.90 Hz), 41.85(d, J = 125.78 Hz), 32.36(t, J = 128.94 Hz), 24.92(t, J = 125.78 Hz), 21.04(t, J = 128.39 Hz); ms m/z: 218(1), 217(12), 216($M^{+\cdot}$, 66), 201(17), 185(17), 158(12), 157(88), 142(14), 131(16), 130(13), 129(100), 128(44), 115(32), 91(33), 79(13), 77(22), 59(14). Exact Mass calcd. for $C_{14}H_{16}O_2$: 216.1150; found: 216.1151.

*Irradiation of methyl 4-cyanobenzoate (**10**) and 2,3-dimethyl-2-butene (**2**) in benzene (reaction [11])*

A solution of **10** (2.40 g, 0.015 mol) and **2** (3.5 mL, 0.029 mol) in benzene (150 mL) was irradiated through Pyrex for 186 h. Separation of the resulting mixture by mplc (20% diethyl ether – hexanes gave oxetane **29** as a colourless oil (0.20 g, 8.3×10^{-4} mol, 12% at 45% conversion of the ester). The oxetane was quantitatively converted into ketones **30** and **31** (**30**:**31**, 1:1.3), which were fully characterized.

29: ir (liq. film, NaCl) ν: 3020(m), 2980(s), 2950(m), 2255(s, sharp), 1485(w), 1410(m), 1395(m), 1285(s), 1180(m), 1115(vs), 1040(m), 1020(s), 1005(s), 970(s), 945(m), 845(vs); ^{1}H nmr (361.01 MHz, $CDCl_3$) δ: 7.67(d, 2H, J = 8.22 Hz), 7.55(br, 2H), 3.00(s, 3H, OCH_3), 1.53(s, 3H), 1.29(s, 3H), 1.21(s, 3H), 0.67(s, 3H); ^{13}C nmr (75.47 MHz, $CDCl_3$, DEPT) δ: 144.95(s), 131.85(d), 127.62(d), 118.77(s), 111.80(s), 108.32(s), 85.07(s), 49.25(q), 46.58(s), 26.31(q), 24.55(q), 22.46(q), 17.79(q); ms m/z: 230($M^{+\cdot}$, 0.1), 214(2), 187(48), 186(37), 172(24), 156(9), 130(74), 116(23), 102(72), 84(100), 83(21), 75(20), 69(98), 55(32), 51(18).

30: ir (liq. film, NaCl) ν: 2990(m), 2940(w), 2235(s), 1685(vs), 1640(m), 1380(m), 1245(s), 960(m), 880(m), 835(m); ^{1}H nmr (361.01 MHz, $CDCl_3$) δ: 8.33(d, 2H, J = 8.3 Hz), 7.67(d, 2H, J = 8.3 Hz), 5.11(s, 1H), 5.07(s, 1H), 1.75(s, 3H), 1.39(s, 6H); ^{13}C nmr ($CDCl_3$, 75.47 MHz) δ: 202.86(s), 148.69(s), 140.23(s), 131.97(d), 129.30(d), 118.04(s), 115.36(s), 111.75(t), 53.06(s), 25.54(q), 20.37(q); ms m/z: 214(3), 213($M^{+\cdot}$, 15), 198(27), 170(7), 130(66), 102(43), 83(100), 75(14), 55(88). Exact Mass calcd. for $C_{14}H_{15}NO$: 213.1154; found: 213.1150.

31: mp 46.9–48.3°C (lit. (42) mp 45–47°C); ^{1}H nmr ($CDCl_3$, 361.006 MHz) δ: 8.04(d, 2H, J = 8.1 Hz), 7.78(d, 2H, J = 8.1 Hz), 3.53(septet, 1H, J = 6.8 Hz), 1.23(d, 6H, J = 6.8 Hz); ^{13}C nmr ($CDCl_3$, 90.784 MHz) δ: 202.90(s), 139.46(s), 132.51(d), 128.71(d), 117.89(s), 116.21(s), 35.91(d), 18.83(q); ms m/z: 173(12), 131(16), 130(100), 103(22), 102(57), 76(16), 75(21), 51(18).

The irradiation of tert*-butyl 4-cyanobenzoate (**10**a) and 2,3-dimethyl-2-butene (**2**) in benzene*

A solution of **10***a* (1.6 g, 0.008 mol) and **2** (0.016 mol) in dry benzene (80 mL) was irradiated (1-kW lamp) through Pyrex for 105 h (9.6% conversion of the ester). Analysis (gc/ms) of the reaction mixture showed only the presence of cyclic imine **11***a* and ketone **12***a*.

*Irradiation of methyl-4-cyanobenzoate (**10**) and 2-methylpropene (**32**) in benzene (reaction [13])*

A solution of **10** (1.45 g, 9.02×10^{-3} mol) and **32** (2.0×10^{-2} mol) in benzene (90 mL) was irradiated through Pyrex. Analysis of the photolysate indicated that an inefficient reaction had occurred. The product, isolated in low yield (1%) as a colourless oil by dcfc, has been assigned structure **33**; ir (liq. film, NaCl) ν: 2980(s), 28880(m), 2240(s, sharp), 1605(m), 955(s), 820(m); ^{1}H nmr (361.01 MHz, $CDCl_3$) δ: 7.64(d, 2H, J = 7.76 Hz) (variable temperature studies are described in the results section), 7.35(broad signal, 2H), 4.56(s, 1H), 4.42(s, 1H), 4.46(d, 1H, J = 5.51 Hz), 4.12(d, 1H, J = 5.51 Hz), 3.16(d, 1H, J = 13.95 Hz), 2.56(d, 1H, J = 14.01 Hz), 1.45(s, 3H), 1.34(s, 3H), 0.78(s, 3H); ^{13}C nmr (75.47 MHz, DEPT, $CDCl_3$) δ: 148.74(s), 141.21(s), 131.55(d), 126.00(d), 119.07(s), 114.95(t), 110.25(s), 92.94(t), 44.44(t), 42.88(s), 25.94(q), 23.75(q), 21.85(q); ms m/z: 241($M^{+\cdot}$, 0.1), 211(5), 196(22), 186(86), 168(20), 131(19), 130(100), 116(24), 102(83), 75(16), 56(49), 55(20), 51(19).

Alkyl Grignard and lithium study

Typical reaction

The electron acceptor (1,4-dicyanobenzene (**1**) or methyl 4-cyanobenzoate (**10**)) was dissolved in freshly distilled tetrahydrofuran and cooled to −84°C (ETOAc – liquid nitrogen slush bath). The Grignard or alkyl lithium reagent was added dropwise under a nitrogen atmosphere. The resulting solution was stirred at low temperature for 1 h and then at room temperature for 1 h. The reaction was quenched by the addition of saturated aqueous ammonium chloride solution. The mixture was stirred for 15 min and extracted with CH_2Cl_2. The combined extracts were washed with H_2O and dried over $MgSO_4$. The solution was filtered and concentrated by rotary evaporation, and the crude mixture was made up to 250 mL with CH_2Cl_2. A 25-mL aliquot, with a known amount of cyclododecane (ca. 0.013 g), was made up to 50 mL with CH_2Cl_2. This solution was then analyzed (gc/fid).

The following samples, isolated from the reaction mixtures, were prepared for calibration of the gc/fid. 1-(4-Cyanophenyl)-2,2-dimethyl-1-propanone (**35**): ir (liq. film, NaCl) ν: 2980(m), 2245(m), 1685(s), 1480(m), 1280(m), 1195(m), 1175(w), 950(m), 840(m); ^{1}H nmr ($CDCl_3$, 361.03 MHz) δ: 7.72(s, 4H), 1.34(s, 9H); ms m/z: 187($M^{+\cdot}$, 5), 131(19), 130(28), 103(22), 130(28), 103(22), 102(24), 75(12), 57(100).

40: recrystallization from methanol affords needles, mp 86.6–87.3°C; ir (KBr) ν: 2940(m), 2840(m), 2200(s), 1605(s), 1460(s), 1405(m), 1355(m), 1275(m), 1200(s), 1015(m), 995(m), 950(s), 900(s), 815(s); ^{1}H nmr ($CDCl_3$, 300.13 MHz) δ: 6.83(m, 1H), 6.75–6.74(m, 1H, J = 4.7 Hz), 3.05–3.00(m, 2H), 2.97–2.92(m, 1H), 1.06(s, 9H); ^{13}C nmr ($CDCl_3$, 90.785 MHz) δ: 143.94(d, J = 165.1 Hz), 142.38(d, J = 166.4 Hz), 119.16(s), 117.73(s), 113.13(s), 110.20(s), 48.61(d, J = 129.2 Hz), 39.20(s), 29.12(t, J = 132.6 Hz), 27.50(q, J = 125.2 Hz); ms m/z: no $M^{+\cdot}$, 184(0.2, loss of H_2), 169(1.5), 130(5), 129(16), 128(10), 102(11), 76(5), 75(6), 57(100), 51(8). The multiplets due to olefinic hydrogens collapse to two singlets upon irradiation of the alkyl hydrogens. This observation, along with the uv spectrum, which showed no long-wavelength absorption, is indicative of a 1,4-diene. Anal. calcd. for $C_{12}H_{14}N_2$: C 77.38, H 7.58, N 15.04; found: C 76.98, H 7.48, N 14.87.

Methyl 4-*tert*-butylbenzoate (**34**): ^{1}H nmr ($CDCl_3$, 361.03 MHz) δ: 7.97(d, 2H, J = 8.7 Hz), 7.43(d, 2H, J = 8.7 Hz), 3.88(s, 3H), 1.32(s, 9H); ms m/z: 193($M^{+\cdot}$, 4), 192(32), 178(24), 177(100),

161(21), 149(44), 145(10), 118(12), 117(16), 115(18), 105(24), 93(12), 91(25), 77(13), 59(21), 51(10).

*Preparation of 1-[4-(1,1-dimethylethyl)phenyl]-2,2-dimethyl-1-propanone (**36**)*

The procedure followed was that used by Pearson (43). Dry magnesium (2.43 g, 0.1 mol) and 1-bromo-4-*tert*-butylbenzene (21.7 g, 0.1 mol) in diethyl ether (75 mL) were placed in an ultrasonic bath for 1 h until all the metal had dissolved. Trimethylacetonitrile (8.3 g, 0.1 mol) in diethyl ether (10 mL) was added dropwise to the solution. The mixture was refluxed for 2 h; an off-white precipitate formed. The mixture was poured onto ice/HCl (6 M, 200 mL) and allowed to stand overnight. The organic layer was separated and the aqueous layer was extracted with ether (3 × 100 mL). The combined organic layers were washed with dilute HCl (2 × 100 mL), saturated sodium bicarbonate (2 × 100 mL), and H_2O (2 × 100 mL). The solution was dried and concentrated at reduced pressure to give a yellow liquid. Fractional distillation at reduced pressure gave the desired ketone in 34% yield; bp 90–95°C, 0.1 Torr (1 Torr = 133.3 Pa) (lit. (43) mp 103–106°C, 1 Torr) ir (liq. film, NaCl) ν: 2980(m), 2880(m), 1660(s), 1600(m), 1460(s), 1390(m), 1355(s), 1270(s), 1200(m), 1170(s), 1100(m), 945(s), 830(s); ^{1}H nmr ($CDCl_3$, 361.027 MHz) δ: 7.40(d, 2H, J = 8.5 Hz), 7.73(d, 2H, J = 8.5 Hz), 1.36(s, 9H), 1.31(s, 9H), ms m/z: 218($M^{+\cdot}$, 3), 162(48), 161(100), 146(25), 118(24), 117(12), 115(12), 105(11), 91(24), 77(12), 57(21).

2-(4-Cyanophenyl)-2-propanol (**37**): ir (liq. film) ν: 3450(s, broad), 2990(m), 2250(s), 1600(m), 1170(m), 1090(m), 945(m), 823(s); ^{1}H nmr ($CDCl_3$, 60 MHz) δ: 7.6(s, 4H), 2.9(s, 1H, exch.), 1.6(s, 6H); ms m/z: 161($M^{+\cdot}$, 2), 147(11), 146(100), 102(11), 75(11), 59(14), 51(11).

Ultraviolet absorption studies

Ultraviolet absorption spectra were recorded in acetonitrile–methanol (3:1) solution, the solvent system used in the photo-NOCAS reaction, to determine if there were charge-transfer (CT) complexes present under the irradiation conditions. A stock solution of acceptor (0.1 M) was used for this study. The absorptions were studied at 310 nm, where **1**, **10**, and **10*a*** show no absorbance at this concentration. The absorbance was studied as a function of increasing olefin concentration (0.0 M–2.0 M).

To carry out the determination of the association constant, the concentration of the acceptor was made 0.010 M while the concentration of the olefin was varied over the range 0.101–0.404 M in keeping with the assumption used in the derivation of the Benesi–Hildebrand equation (4). To maintain constant solvent characteristics, the total number of moles added to the stock solutions was kept constant by the coaddition of *n*-hexane. The total concentration of added alkene and hexane was 0.404 M.

Acknowledgements

This work was supported by a grant from the Natural Sciences and Engineering Research Council of Canada. We thank Dr. D. L. Hooper at the Atlantic Regional Magnetic Resonance Centre at Dalhousie University for the high-field NMR spectra and for help in the preparation of the manuscript. Exact mass measurements were carried out by Mr. D. Embree at the Institute for Marine Biosciences, Halifax. We also thank Dr. T. S. Cameron at Dalhousie for the X-ray analysis of **15**.

1. (*a*) D. R. Arnold and X. Du. J. Am. Chem. Soc. **111**, 7666 (1990); (*b*) A. L. Perrott and D. R. Arnold. Can. J. Chem. **70**, 272 (1992).
2. (*a*) R. M. Borg, D. R. Arnold, and T. S. Cameron. Can. J. Chem. **62**, 1785 (1984); (*b*) D. R. Arnold and M. S. Snow. Can. J. Chem. **66**, 3012 (1988).
3. (*a*) D. R. Arnold and A. J. Moroulis. J. Am. Chem. Soc. **98**, 5931 (1976); (*b*) D. R. Arnold, J. R. Bolton, and J. A. Pederson. J. Am. Chem. Soc. **94**, 2872 (1972); (*c*) P. J. Wagner and E. J. Siebert. J. Am. Chem. Soc. **103**, 7329 (1981); (*d*) N. Yamasaki, Y. Inoue, T. Yokoyama, A. Ishida, and S. Takamuku. J. Am. Chem. Soc. **113**, 1933 (1991).
4. (*a*) R. Foster. Organic charge-transfer complexes. Academic Press, New York. 1969; (*b*) R. Foster. *In* Molecular complexes. Vol. 2. Edited by R. Foster. Elek Science, London. 1974. p. 107. (*c*) R. Foster and C. A. Fyfe. Trans. Faraday Soc. **61**, 1626 (1965); (*d*) R. S. Mulliken. J. Am. Chem. Soc. **72**, 610 (1950).
5. M. J. Frisch, M. Head-Gordon, G. W. Trucks, J. B. Foresman, H. B. Schlegel, K. Raghavachari, M. A. Robb, J. S. Binkley, C. Gonzalez, D. J. DeFrees, D. J. Fox, R. A. Whiteside, R. Seeger, C. F. Melius, J. Baker, R. L. Martin, L. R. Kahn, J. J. P. Stewart, S. Topiol, and J. A. Pople. Gaussian 90, Gaussian, Inc. Pittsburgh, Pa. 1990.
6. R. S. Mulliken. J. Chem. Phys. **23**, 1833 (1955); **23**, 1841 (1955); **23**, 2338 (1955); **23**, 2343 (1955).
7. (*a*) W. J. Hehre, L. Radom, P.v.R. Schleyer, and J. A. Pople. Ab initio molecular orbital theory. Wiley, New York. 1986; (*b*) J. B. Collins and A. Streitwieser. J. Comput. Chem. **1**, 81 (1980); (*c*) H. P. Luthi, J. H. Ammeter, J. Almlof, and K. Faegri. J. Chem. Phys. **77**, 2002 (1982).
8. (*a*) R. A. Y. Jones. Annu. Rev. NMR Spectrosc. **2** (1969); (*b*) J. Ronayne and D. H. Williams. Annu. Rev. NMR Spectrosc. **2** (1969).
9. D. H. Williams and N. S. Bacca. Tetrahedron, **21**, 2021 (1965).
10. (*a*) L. M. Jackman and S. Sternhell. Applications of nuclear magnetic resonance spectroscopy in organic chemistry. 2nd ed. Pergamon Press, New York. 1969; (*b*) J. B. Stothers. Carbon-13 NMR spectroscopy. Academic Press, New York. 1972; (*c*) J. L. Marshall. Carbon–carbon and carbon–proton NMR coupling: application to organic stereochemistry and conformational analysis. Verlag Chemie International, Deerfield Beach, Fla. 1983.
11. T. P. Forrest and S. Sukumar. Can. J. Chem. **55**, 3686 (1977).
12. D. R. Arnold, R. L. Hinman, and A. H. Glick. Tetrahedron Lett. 1425 (1964).
13. J. Sandstrom. Dynamic NMR spectroscopy. Academic Press, London. 1982.
14. H. H. Jaffe and M. Orchin. Theory and applications of ultraviolet spectroscopy. John Wiley and Sons, New York. 1962. Chap. 12.
15. (*a*) D. Rehm and A. Weller. Isr. J. Chem. **8**, 259 (1970); (*b*) H. Leonhardt and A. Weller. Ber. Bunsen-Ges. Phys. Chem. **63**, 791 (1963).
16. (*a*) Y. Inoue, S. Takamuku, Y. Kunitomi, and H. Sakurai. J. Chem. Soc. Perkin Trans. 2, 1672 (1980); (*b*) Y. Inoue, T. Yokoyama, Y. Yamasaki, and A. Tai. J. Am. Chem. Soc. **111**, 6480 (1989); (*c*) S. Goto, S. Takamuku, H. Sakurai, Y. Inoue, and T. Hakushi. J. Chem. Soc. Perkin Trans. 2, 1678 (1980); (*d*) Y. Shigemitsu, H. Nakai, and Y. Odaira. Tetrahedron, **25**, 3039 (1969); (*e*) Y. Katsuhara, Y. Shigemitsu, and Y. Odaira. Bull. Chem. Soc. Jpn. **44**, 1169 (1971); (*f*) T. S. Cantrell and A. C. Allen. J. Org. Chem. **54**, 135 (1989); (*g*) T. S. Cantrell, A. C. Allen, and H. Ziffer. J. Org. Chem. **54**, 140 (1989).
17. (*a*) S. L. Mattes and S. Farid. J. Am. Chem. Soc. **108**, 7356 (1986); (*b*) T. Majima, C. Pac, A. Nakasone, and H. Sakurai. J. Am. Chem. Soc. **103**, 4499 (1981); (*c*) C. Pac, A. Nakasone, and H. Sakurai. J. Am. Chem. Soc. **99**, 5806 (1977).
18. (*a*) J. J. McCullough, R. C. Miller, and W.-S. Wu. Can. J. Chem. **55**, 2909 (1977); (*b*) K. Mizuno, C. Pac, and H. Sakurai. J. Am. Chem. Soc. **96**, 2993 (1974); (*c*) C. Pac and

Can. J. Chem. Downloaded from www.nrcresearchpress.com by 88.255.202.194 on 09/08/12
For personal use only.

H. Sakurai. Chem. Lett. 1067 (1976); (*d*) F. D. Lewis and R. J. DeVoe. Tetrahedron, **38**, 1069 (1982); (*e*) M. Melia, E. Fasani, and A. Albini. J. Photochem. Photobiol. A: **59**, 297 (1991).
19. (*a*) D. R. Arnold, P. C. Wong, A. J. Maroulis, and T. S. Cameron. Pure Appl. Chem. **52**, 2609 (1980); (*b*) D. Bryce-Smith, B. Foulger, J. Forrester, A. Gilbert, B. H. Orger, and H. M. Tyrrell. J. Chem. Soc. Perkin Trans. 1, 55 (1980).
20. (*a*) T. S. Cantrell. J. Am. Chem. Soc. **94**, 5929 (1972); (*b*) J. Org. Chem. **42**, 4238 (1977); (*c*) N. C. Yang, B. Kim, W. Chiang, and T. Hamada. J. Chem. Soc. Chem. Commun. 729 (1976).
21. (*a*) G. Buchi, J. G. Atkinson, D. E. Ayer, and E. W. Robb. J. Am. Chem. Soc. **85**, 2257 (1963); (*b*) J. J. McCullough, R. C. Miller, D. Fung, and W. S. Wu. J. Am. Chem. Soc. **97**, 5942 (1975); (*c*) R. A. Caldwell and L. Smith. J. Am. Chem. Soc. **96**, 2994 (1974).
22. (*a*) R. A. Neunteufel and D. R. Arnold. J. Am. Chem. Soc. **95**, 4080 (1973); (*b*) Y. Shigemitsu and D. R. Arnold. J. Chem. Soc. Chem. Commun. 407 (1975); (*c*) A. J. Maroulis, Y. Shigemitsu, and D. R. Arnold. J. Am. Chem. Soc. **100**, 6383 (1979); (*d*) D. R. Arnold, X. Du, and K. M. Henseleit. Can. J. Chem. **69**, 839 (1991); (*e*) P. G. Gassman and K. J. Bottorff. Tetrahedron Lett. **28**, 5449 (1987); (*f*) J. Am. Chem. Soc. **109**, 7547 (1987); (*g*) P. G. Gassman and S. A. De Silva. J. Am. Chem. Soc. **113**, 9870 (1991).
23. (*a*) D. R. Arnold, R. M. Borg, and A. Albini. J. Chem. Soc. Chem. Commun. 138 (1981); (*b*) H. D. Roth and M. L. M. Schilling. J. Am. Chem. Soc. **102**, 4303 (1980); (*c*) M. Mella, E. Fasani, and A. Albini. Tetrahedron, **47**, 3137 (1991).
24. (*a*) F. D. Lewis, J. R. Petisce, J. D. Oxman, and M. J. Nepras. J. Am. Chem. Soc. **107**, 203 (1985); (*b*) F. D. Lewis, A. M. Bedell, R. E. Dykstra, J. E. Elbert, I. R. Gould, and S. Farid. J. Am. Chem. Soc. **112**, 8055 (1990).
25. (*a*) P. G. Gassman and K. D. Olson. Tetrahedron Lett. **24**, 19 (1983).
26. (*a*) D. R. Arnold and S. A. Mines. Can. J. Chem. **65**, 2312 (1987); (*b*) Can. J. Chem. **67**, 689 (1989).
27. (*a*) N. Ohashi, N. Aoyagi, T. Miyama, S. Kyushin, and S. Yamada. J. Chem. Soc. Perkin Trans. 1, 189 (1990); (*b*) I. Saito, K. Shimozono, and T. Matsuura. J. Org. Chem. **47**, 4356 (1982).
28. A. J. Bard and H. Lund (*Editors*). Encyclopedia of electrochemistry of the elements. Vol. 12. Marcel Dekker, New York. 1978. p. 58.
29. (*a*) A. Padwa, W. Bergmark, and D. Pashayan. J. Org. Chem. **40**, 1896 (1975); (*b*) J. Am. Chem. Soc. **91**, 2653 (1969).
30. R. O. Loutfy and R. O. Loutfy. Can. J. Chem. **54**, 1454 (1976).
31. L. Eberson and K. Nyberg. J. Am. Chem. Soc. **88**, 1686 (1966).
32. (*a*) A. P. Schaap, L. Lopez, and S. D. Gahnon. J. Am. Chem. Soc. **105**, 663 (1983); (*b*) T. Majima, C. Pac, A. Nakasone, and H. Sakurai. J. Am. Chem. Soc. **103**, 4499 (1981); (*c*) S. Mattes and S. Farid. Org. Photochem. **6**, 233 (1983).
33. (*a*) C. Walling. J. Am. Chem. Soc. **110**, 6846 (1988); (*b*) E. C. Ashby, J. Laemmle, and H. M. Newmann. Acc. Chem. Res. **7**, 272 (1974); (*c*) E. C. Ashby. Pure Appl. Chem. **52**, 545 (1980); (*d*) T. Holm. Acta Chem. Scand. Ser. B: **B37**, 567 (1983); (*e*) L. H. Kristensen and H. Lund. Acta Chem. Scand. Ser. B: **B33**, 735 (1979).
34. L. Eberson. Electron transfer reactions in organic chemistry. Springer-Verlag, New York. 1987.
35. (*a*) A. J. Birch and G. Subba Rao. Adv. Org. Chem. **8**, 1 (1972); (*b*) A. J. Birch and D. Nasipuri. Tetrahedron, **6**, 148 (1972).
36. H. O. House. Modern synthetic reactions. 2nd ed. W. A. Benjamin Inc., Menlo Park, Calif. 1972. p. 72.
37. C. P. Andrieux. D. Gallardo, and J.-M. Saveant. J. Am. Chem. Soc. **111**, 1620 (1989).
38. (*a*) R. Fuhlendorff, D. Occhialini, S. U. Pedersen, and H. Lund. Acta Chem. Scand. **43**, 803 (1989); (*b*) G. D. Sargent and G. A. Lux. J. Am. Chem. Soc. **90**, 7162 (1968).
39. (*a*) L. M. Harwood. Aldrichimica Acta, **18**, 25 (1985); (*b*) W. C. Still, M. Kahn, and A. Mitra. J. Org. Chem. **43**, 2923 (1978); (*c*) J. T. Sharp, I. Gosney, and A. G. Rowley. Practical organic chemistry. Chapman and Hall, New York. 1989.
40. A. Okamoto, M. S. Snow, and D. R. Arnold. Tetrahedron, **42**, 6175 (1986).
41. A. H. Haines and M. S. Shandiz. J. Chem. Soc. Perkin Trans. 1, 1671 (1981).
42. G. A. Russell and F. Ros. J. Am. Chem. Soc. **107**, 2506 (1985).
43. D. E. Pearson. J. Am. Chem. Soc. **72**, 4169 (1950).

Can. J. Chem. Downloaded from www.nrcresearchpress.com by 88.255.202.194 on 09/08/12
For personal use only.

Solvation and metal ion effects on structure and reactivity of phosphoryl compounds. Part 2.[1] Alkali metal ion catalysis in the demethylation of methyl di(3-nitrophenyl)phosphinate by iodide ion

AGNES M. MODRO AND TOMASZ A. MODRO[2]

Centre for Heteroatom Chemistry, Department of Chemistry, University of Pretoria, Pretoria 0002, South Africa

Received September 18, 1992

AGNES M. MODRO and TOMASZ A. MODRO. Can. J. Chem. **71**, 469 (1993).

Second-order rate constants for the demethylation of methyl di(3-nitrophenyl)phosphinate by iodide in acetone-d_6 at 25°C have been measured. For a series of iodide salts the rate increased in the order: $NBu_4I < KI \leq NaI < LiI$. The addition of crown ethers or D_2O has a retarding effect on the reaction rate. The results are discussed in terms of the increase of the nucleofugality of the phosphinate group via the complexation of metal ions with the phosphoryl function.

AGNES M. MODRO et TOMASZ A. MODRO. Can. J. Chem. **71**, 469 (1993).

On a mesuré les constantes de vitesse du deuxième ordre de la réaction de déméthylation du di(3-nitrophényl)-phosphinate de méthyle par l'iodure dans l'acétone-d_6, à 25°C. Pour une série d'iodures, la vitesse augmente dans l'ordre $NBu_4I < KI \leq NaI < LiI$. L'addition d'éthers couronnes ou de D_2O diminue la vitesse de la réaction. On discute des résultats en fonction de l'augmentation du caractère nucléofuge du groupe phosphinate via une complexation des ions métalliques par la fonction phosphoryle.

[Traduit par la rédaction]

Can. J. Chem. Downloaded from www.nrcresearchpress.com by 88.255.202.194 on 09/08/12
For personal use only.

Methyl phosphotriester analogues of polynucleotides attract increasing attention (2), while nucleophilic removal of the methyl group from the POMe function (see, for example, ref. 3) represents the final step in the "phosphotriester" method of oligonucleotide synthesis. Various nucleophiles can be employed in the dealkylation, and the utility of halide ions as reagents for selective removal of alkyl groups in phosphate esters was recognised 40 years ago by Zervas and Dilaris (4), as well as by Todd in his classic studies on phosphorylation (5). Although the effect of the counterion of the halide salt on the reaction rate was never the subject of an investigation, it was reported in one of Todd's papers (6) that the yield of debenzylation of benzyl diphenylphosphate by M^+I^- increases in the order: $M^+ = C_6H_{11}NH_3^+ < Na^+ < Li^+$. The participation of the Li^+ ion in the demethylation of phosphoric esters was postulated by van Lier and co-workers (7), followed by their nmr spectroscopic study of the interactions between Li^+ and phosphoryl substrates (8). On the other hand, Winstein (9) and others (10) demonstrated that the rate of dealkylation of alkyl arenesulfonates by halide ions in acetone or HMPTA is independent of the cation used.

In a recent series of papers on the nucleophilic displacement at phosphorus and sulfur centers, Buncel and co-workers demonstrated for the first time, and quantitatively assessed, alkali metal ion catalysis in the displacement at the phosphoryl centre by oxygen nucleophiles (11). The catalysis, increasing in the order: $K^+ < Na^+ < Li^+$, was interpreted in terms of the association of the metal ion and the transition state. Our own studies on the effect of metal ions (K^+, Na^+, Li^+, Mg^{2+}) on nmr spectroscopic parameters and the conformational preferences of phosphonic esters (1) gave evidence for strong interactions between the metal ion and the PO_3R_2 group. In this work we report our results on the O-demethylation of methyl di(3-nitrophenyl)phosphinate **1** by iodide salts in acetone (Scheme 1), which show, to our knowledge for the first time, metal ion catalysis in an S_N2 process with the phosphate-derived ion, $X_2PO_2^-$, as a leaving group.

Results and discussion

Methyl di(3-nitrophenyl)phosphinate (**1**) was prepared by nitration of methyl diphenylphosphinate and the pure bis-*meta* isomer was isolated by column chromatography. The rate of reaction of **1** with iodide salts in acetone-d_6 at 25°C was studied by ^{31}P nmr spectroscopy, following the disappearance of the signal due to the substrate (δ_P 28.8) and the appearance of the signal due to the di(3-nitrophenyl)phosphinate ion (δ_P 7–14). The observed second-order rate constants (k_{obs}) were calculated in the usual way from the conversion values and the initial concentrations of **1** and the (total) iodide salt. The values obtained for the alkali metal (K^+, Na^+, Li^+) and the ammonium (NH_4^+, NBu_4^+) iodides are listed in Table 1. For the kinetic runs with [**1**]/[MI] = 1, some curvature of the second-order rate plots was obtained due to the change in concentration of the free ions with the degree of conversion. The k_{obs} values determined for low conversions (given in parentheses in the fourth column of Table 1) were not, however, significantly different from the average values obtained from the whole runs. As in all cases involving ion-pairing nucleophiles in S_N2 reactions (12), the observed rate constants decrease with increase in salt concentration due to the supression of the dissociation of the ion pairs into free ions. Using the available (13) dissociation constants for the iodides studied, the specific second-order rate constants for the free iodide ion, k_{I^-}, were calculated and are given in the last column of Table 1. It is clear that the rate of the demethylation depends on the counterion introduced with the nucleophile, the reactivity of the salts increasing in the order: $NBu_4I \approx NH_4I < KI \leq NaI < LiI$. Taking for each cation the average value of k_{I^-}, the catalytic effect of the alkali metal ions relative to the rate obtained with NBu_4^+ as a counterion (no catalysis, $k_{rel} = 1.0$) is approximately $k_{rel} = 3.9$, 4.5, and 30.7, for K^+, Na^+, and Li^+, respectively. The order and the magnitude of the rate acceleration obtained for these three

[1]For previous papers of this series see ref. 1.

[2]Author to whom correspondence may be addressed.

SCHEME 1

TABLE 1. Kinetic data on the reaction of **1** with iodide salts, MI, in acetone-d_6 at 25°C; [**1**] = 0.0497 M

M^+	$[MI]_o$ (M)	K_d[a] 10^3(M)	k_{obs}[b] 10^4(M^{-1} s^{-1})	k_{I^-}[c] 10^4(M^{-1} s^{-1})
NBu_4^+	0.0497	6.5	0.70 (0.74; 8%)	2.32
	0.248		0.47	3.15
NH_4^+	0.0497	7.9[d]	0.71 (0.61; 15%)	2.18
K^+	0.0497	9.1	3.00 (2.28; 10%)	8.67
	0.248		1.85	10.9
	0.497		1.62	12.8
Na^+	0.0497	13.0	4.80 (4.12; 19%)	12.1
	0.248		2.46	12.0
	0.497		1.83	12.3
Li^+	0.0497	6.9	27.0 (31.7; 28%)	87.2
	0.248		12.1	78.8

[a]Taken from ref. 13.
[b]For [**1**]/[MI] = 1, the values obtained for low conversions, together with the conversions, are given in parentheses.
[c]$k_{I^-} = k_{obs}/a$, where a is a fraction of free I^- ion in solution.
[d]Since no K_d value for NH_4I in acetone was available, the value reported for NEt_4I was taken for comparison.

TABLE 2. Kinetic data on the effect of adding crown ethers to the reaction of **1** with MI in acetone-d_6 at 25°C; [**1**] = [MI] = 0.0497 M

M^+	Crown ether	[CE]/[MI]	k_{obs} 10^4(M^{-1} s^{-1})
K^+	DCH18C6	5	2.24
		7.5	2.44
	18C6	7.5	2.79
Na^+	DCH18C6	5	1.86
		7.5	1.70
	15C5	5	1.06
		7.5	1.00
Li^+	12C4	5	1.90
		7.5	1.17

TABLE 3. Effect of D_2O on the rate of demethylation of **1** by MI in acetone-d_6 at 25°C; [**1**] = [MI] = 0.0497 M

M^+	10^4 k_{obs} (M^{-1} s^{-1}) in acetone-d_6/D_2O (%D_2O, v/v)				Decelerating factor[a]
	(0.0)	(5.0)	(10.0)	(17.0)	
NBu_4^+	0.70	0.41	0.20	0.062	3.5
K^+	3.00	1.30	0.22		13.6
Na^+	4.80	0.74	0.16		30.0
Li^+	27.0	0.54	0.23		117.4

[a]k_{obs}(acetone)/k_{obs}(acetone/D_2O, 9:1, v/v).

alkali metal ions parallel the results reported by Buncel and co-workers (11) for nucleophilic displacement at the phosphinyl centre by ethoxide salts.

Catalysis by the alkali metal ions in the nucleophilic displacement of the phosphinate ester was confirmed by the effect of complexing agents on the reaction rate (Table 2). When the reaction was carried out in the presence of 5–7.5 mol-equivalent of crown ethers, a decrease in the rate was observed; again, the effect increased in the order: $K^+ < Na^+ < Li^+$. Under those conditions the rate constants reached approximately the same value for all three metal ions (10^4 $k_2 = 1.80 \pm 0.63$), and are in reasonable agreement with the value of k_{I^-} obtained for the ammonium salts (Table 1, 10^4 $k_{I^-} = 2.55 \pm 0.52$), for which no cation catalysis should be expected.

The addition of protic solvents often has a decelerating effect in S_N2 reactions (14); for example, exchange of the halide ions between benzyl iodide and NaI in acetone is decelerated by the addition of water, by a factor of ca. 0.4 at a [water]/[acetone] ratio of 0.1 (15). The retarding effect is attributed to the hydrogen bonding of the halide ion, decreasing the latter's nucleophilic activity. We have measured the effect of water (D_2O) on the demethylation of **1** and the results are given in Table 3. As expected, the addition of D_2O decreased the rate of the reaction, with the retarding effect increasing in the order: $NBu_4^+ < K^+ < Na^+ < Li^+$. In the medium containing 10% (v/v) of D_2O all salts react with approximately the same rate (10^4 $k_{obs} = 0.20 \pm 0.03$). This result is consistent with an assumption that under those conditions (molar ratio D_2O/MI $\approx 10^2$) the ions of the iodide salts are fully hydrated, and any catalytic effects of the metal ions are therefore absent. The observed rate constant is ca. 10 times smaller than k_{I^-} obtained for ammonium iodides in acetone (Table 1), reflecting the decelerating effect of the hydrogen bonding of the iodide ion to the molecules of water.

In their interpretation of catalysis in the nucleophilic displacement at phosphorus, Buncel and co-workers (11) proposed a model according to which ". . . bond formation between the alkoxide oxygen and the phosphorus atom . . . occurs concomitantly with association of the phosphinyl oxygen with M^+ . . ." We would like to extend this model to the nucleophilic displacement at the α-carbon atom of a phosphinyl center by introducing the mechanism (Fig. 1) in which the departure of the leaving group is enhanced by coordination of the metal ion to the phosphinyl oxygen atoms that develop negative charge in the transition state. The metal-ion-assisted pathway can involve free ions (Fig. 1*a*), as well as the ion pair (Fig. 1*b*); in the latter case the delivery of the iodide ion to the methyl carbon should be facilitated by coordination to the phosphoryl oxygen.

In acetone solution the reaction product, diarylphosphinate ion, interacts strongly with the counterion and probably exists as a tight ion pair. ^{31}P nmr chemical shift of the phosphinate salt varied significantly with the counterion, and

Can. J. Chem. Downloaded from www.nrcresearchpress.com by 88.255.202.194 on 09/08/12
For personal use only.

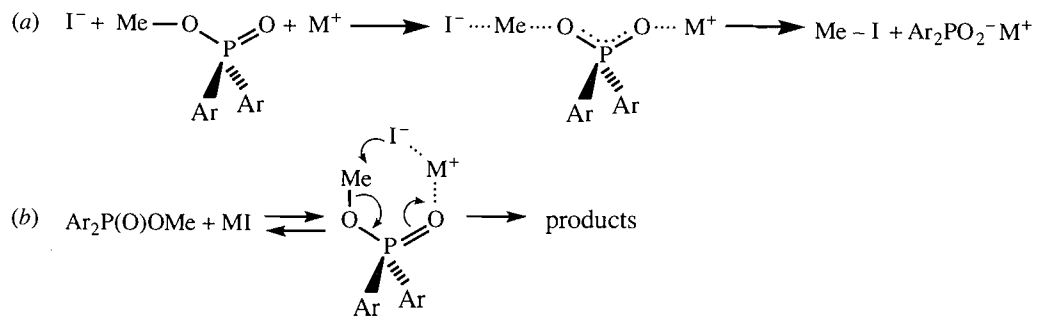

FIG. 1. Proposed models for the metal-ion catalysis in the nucleophilic displacement of phosphinate ester.

Can. J. Chem. Downloaded from www.nrcresearchpress.com by 88.255.202.194 on 09/08/12
For personal use only.

decreased in the order: δ_P = 13.7, 11.5, 11.4, 10.7, and 7.1, for Li^+, Na^+, K^+, NH_4^+, and NBu_4^+, respectively. In the case of the Li^+ salt, the ^{31}P nmr signal was very broad, indicating strong association that eventually led to the precipitation of lithium phosphinate from the acetone solution. In the medium consisting of 90% of acetone-d_6 and 10% of D_2O (v/v), on the other hand, all phosphinate salts gave rise to the ^{31}P nmr signal at the same field (δ_P 12.3 ± 0.7) irrespective of the nature of the cation.

We believe that we have demonstrated that alkali metal ions can play a role in the nucleophilic displacement at carbon of a phosphoric ester via the complexation of the phosphoryl group in a similar way to their effects on the phosphorylation (11), or on the conformational equilibria (1). Our further investigations are aimed at the evaluation of such catalytic effects in systems containing a larger number of oxygen atoms at the phosphoryl center, i.e., the phosphonic and the, biologically more related, phosphoric esters.

Experimental section

Solvents and commercially available reagents were purified by standard methods immediately before use. Acetone-d_6 (Aldrich, 99.5 at.% D) was dried over molecular sieves. The salts were dried in an oven at 120°C and stored in a desiccator over P_4O_{10}. The nmr spectra were recorded on a Bruker AC 300 MHz spectrometer at a probe temperature of 30°C. Chemical shifts are given relative to $SiMe_4$ (^1H) or 85% H_3PO_4 (^{31}P). Coupling constants are given in Hz. The mass spectrum was recorded on a Varian MAT-212 double-focusing direct-inlet spectrometer at an ionization potential of 70 eV. Only the molecular ion data are included.

Methyl diphenylphosphinate was prepared from diphenylphosphinic chloride and methanol in the presence of triethylamine (16) and purified by bulb-to-bulb distillation (oven temp. 250°C/0.2 Torr; 1 Torr = 133.3 Pa). δ_H ($CDCl_3$): 3.77 (3 H, d, J_{HP} 11.1, OMe), 7.42–7.52 (6 H, m, *meta* and *para* H's of Ph), 7.78–7.82 (4 H, m, *ortho* H's of Ph). δ_P: 33.7.

Methyl di(3-nitrophenyl)phosphinate **1** was prepared by nitration of methyl diphenylphosphinate according to the following procedure, reported (17) for a similar synthesis.

To a solution of the substrate (2.50 g, 10.77 mmol) in glacial acetic acid (15 mL) a solution of nitric acid (100%, freshly distilled from conc. H_2SO_4, 30 mL) in glacial acetic acid (7.5 mL) was added dropwise with stirring and cooling in an ice bath. The solution was left at room temperature for 70 h and poured on ice (750 g). The first fraction of a crude product (1.54 g, 44.5%) was collected by filtration and dissolved in chloroform. The aqueous filtrate was extracted with chloroform (3 × 30 mL), the combined chloroform solutions were dried ($MgSO_4$), and the solvent was removed under reduced pressure. Crude **1** was obtained as a pale yellow solid, 3.46 g (98%), and was purified by column chromatography (silica gel, $CHCl_3$), followed by crystallization from benzene – ethyl acetate – acetone. Colorless crystals, mp 127–128°C; δ_H ($CDCl_3$): 3.87 (3 H, d, J_{HP} 11.3, OMe), 7.71 (1 H, dt, J_{ortho} 9.0, J_{HP} 5.0, H-5), 8.16 (1 H, dddd, J_{HP} 11.7, J_{ortho} 7.6, J_{meta} 1.8, 1.1, H-6), 8.41 (1 H, ddd, J_{ortho} 9.1, J_{meta} 2.0, 1.8, H-4), 8.64 (1 H, ddd, J_{HP} 12.9, J_{meta} 1.8, 0.5, H-2); δ_P: 27.3; ms, m/z: 332 (M^+, 2%).

Sodium di(3-nitrophenyl)phosphinate

A sample of **1** was incubated at room temperature in aqueous methanolic solution containing 1 mol-equivalent of NaOH, and the progress of the hydrolysis was followed by TLC. After all **1** was consumed, the solution was evaporated to dryness under reduced pressure, the residue was washed several times with ether, and dried. Yield: quantitative; white powder, δ_P (D_2O) 18.7.

Kinetic measurements

Solutions of substrates in acetone-d_6 (or in acetone-d_6/D_2O) were transferred to an nmr tube and incubated in a thermostatted water bath at 25 ± 0.2°C. Tubes were withdrawn at selected time intervals and the ^{31}P nmr spectra of the reaction mixtures were recorded immediately. The concentration changes of the reaction product, measured from the integrated peak areas of **1** and of the reaction product, followed second-order kinetics. In cases when the ^{31}P nmr signal of the product was broad (lithium salts), the internal standard (benzyltriphenylphosphonium tetrafluoroborate, δ_P = 25.0) was used. The runs were carried out to at least 80% conversion. Good second-order linear plots were obtained, with values of r^2 = 0.9945–0.9999.

Acknowledgment

Financial support from the University of Pretoria and the Foundation for Research Development is gratefully acknowledged.

1. (*a*) A. M. Modro, P. L. Wessels, and T. A. Modro. J. Chem. Res. (S), 224 (1991); (*b*) M. P. Belciug, A. M. Modro, T. A. Modro, and P. L. Wessels. J. Phys. Org. Chem. **5**, 787 (1992).
2. L. H. Coole, H. M. Moody, N. L. H. L. Broeders, P. J. L. M. Quaedflieg, W. H. A. Kuijpers, M. H. P. van Genderen, A. J. J. M. Coenen, S. van der Wal, and H. M. Buck. J. Org. Chem. **54**, 1657 (1989).
3. D. J. H. Smith, K. K. Ogilvie, and M. F. Gillen. Tetrahedron Lett. **21**, 861 (1980).
4. L. Zervas and I. Dilaris. J. Am. Chem. Soc. **77**, 5354 (1955).
5. V. M. Clark and A. Todd. J. Chem. Soc. 2030 (1950), and the following papers of this series.
6. R. J. W. Cremlyn, G. W. Kenner, J. Mather, and A. Todd. J. Chem. Soc. 528 (1958).
7. M. M. C. F. Castelijns, D. van Aken, P. Schipper, J. J. C. van Lier, and H. M. Buck. Recl. Trav. Chim. Pays-Bas, **99**, 380 (1980).

8. J. J. C. van Lier, L. J. M. van de Ven, J. W. de Haan, and H. M. Buck. J. Phys. Chem. **87**, 3501 (1983).
9. S. Winstein, L. G. Savedoff, S. Smith, I. D. R. Stevens, and J. S. Gall. Tetrahedron Lett. 24 (1960).
10. P. Muller and B. Siegfried. Helv. Chim. Acta, **55**, 2965 (1972).
11. (*a*) E. J. Dunn and E. Buncel. Can. J. Chem. **67**, 1440 (1989); (*b*) E. J. Dunn, R. Y. Moir, E. Buncel, J. G. Purdon, and R. A. B. Bannard. Can. J. Chem. **68**, 1837 (1990).
12. I. P. Beletskaya. Russ. Chem. Rev. **44**, 1067 (1975).
13. G. J. Janz and R. P. T. Tomkins. Nonaqueous electrolytes handbook. Vol. I. Academic Press, New York. 1972.
14. C. Reichardt. Solvent effects in organic chemistry. Verlag Chemie, Weinheim. 1979. Chap. 5.
15. J. A. Leary and M. Kahn. J. Am. Chem. Soc. **81**, 4173 (1959).
16. K. D. Berlin, T. H. Austing, and M. Nagabhushanam. J. Org. Chem. **30**, 1267 (1965).
17. O. G. Piskunova, A. I. Bokanov, and B. I. Stepanov. J. Gen. Chem. USSR, Engl. Transl. **48**, 1201 (1978).

Can. J. Chem. Downloaded from www.nrcresearchpress.com by 88.255.202.194 on 09/08/12
For personal use only.

Aryl 1,5-dithia-2,4,6,8-tetrazocines. A synthetic, electrochemical, and structural investigation

RENÉ T. BOERÉ,[1] KLAUS H. MOOCK,[2] SEAN DERRICK, WILLIAM HOOGERDIJK, KATHRYN PREUSS, AND JUDY YIP

Department of Chemistry, University of Lethbridge, Lethbridge, Alta., Canada T1K 3M4

AND

MASOOD PARVEZ

Department of Chemistry, University of Calgary, Calgary, Alta., Canada T2N 1N4

Received November 9, 1992

Can. J. Chem. Downloaded from www.nrcresearchpress.com by 88.255.202.194 on 09/08/12
For personal use only.

RENÉ T. BOERÉ, KLAUS H. MOOCK, SEAN DERRICK, WILLIAM HOOGERDIJK, KATHRYN PREUSS, JUDY YIP, and MASOOD PARVEZ. Can. J. Chem. **71**, 473 (1993).

New preparative routes to the title compounds are reported in which the yields are substantially improved over previous methods. In one method, reaction of O_2 with a mixture of $XC_6H_4CN_2S_2^+Cl^-$ and Ph_3Sb leads to the products in 40–60% yield. In another, the reaction of the same salts with silylated amidines $XC_6H_4C\{NSiMe_3\}N(SiMe_3)_2$ in a 1:1 mol ratio leads to the same compounds in 18–65% yield. The syntheses of 3,7-$(XC_6H_4)_2\{CN_2S_2N_2C\}$, X = H, 4-$CH_3$, 4-$CH_3O$, 4-Cl, 4-$CF_3$, and 3-$CF_3$, are reported. Mixed derivatives were also prepared, but not isolated as pure compounds. The crystal structure of the 4-CF_3 compound has been determined by X-ray diffraction; triclinic, $P\bar{1}$ with Z = 1; cell dimensions: a = 6.835(2), b = 9.936(3), c = 6.320(2) Å, α = 96.44(3)°, β = 102.88(3)°, γ = 88.42(3)°. R = 3.4%, R_w = 3.5% for 1100 data. The eight-membered ring is flat with equivalent bond lengths between any two types of atoms, indicative of a delocalized electron distribution. The 10π central aromatic rings have been oxidized and reduced in CH_2Cl_2 using voltammetric methods. The reversible one-electron reduction step gives stable 11π species. The resistance to oxidation of the title compounds is contrasted to the ease of oxidizing 3,7-$[(CH_3)_2N]_2\{CN_2S_2N_2C\}$, in accordance with earlier chemical studies.

RENÉ T. BOERÉ, KLAUS H. MOOCK, SEAN DERRICK, WILLIAM HOOGERDIJK, KATHRYN PREUSS, JUDY YIP et MASOOD PARVEZ. Can. J. Chem. **71**, 473 (1993).

On a développé de nouvelles voies de synthèse des composés mentionnés dans le titre qui donnent des rendements de beaucoup supérieurs à ceux rapportés antérieurement. Dans une méthode, la réaction du O_2 avec un mélange de $HC_6H_4CN_2S_2^+Cl^-$ et de Ph_3Sb conduit aux produits avec des rendements allant de 40 à 60%. Dans une autre méthode, la réaction des mêmes sels avec les amidines silylées $XC_6H_4C\{NSiMe_3\}N(SiMe_3)_2$, dans un rapport molaire de 1 : 1, conduit aux mêmes produits avec des rendements allant de 18 à 65%. Donc on rapporte la synthèse des 3,7-$(XC_6H_4)_2\{CN_2S_2N_2C\}$, X = H, 4-$CH_3$, 4-$CH_3O$, 4-Cl, 4-$CF_3$ et 3-CF_3. On a aussi préparé des dérivés mixtes; toutefois, il n'a pas été possible de les isoler à l'état pur. On a déterminé la structure cristalline du composé 4-CF_3 par diffraction des rayons X; triclinique, $P\bar{1}$, avec a = 8,835(2), b = 9,936(3) et c = 6,320(2) Å, α = 96,44(3)°, β = 102,88(3)° et γ = 88,42(3)°, Z = 1. R = 3,4% et R_w = 3.5% pour 1100 données. Le cycle à huit chaînons est plat alors que les longueurs des liaisons sont équivalentes entre tous les atomes pris deux à deux; ce résultat indique que la distribution électronique est délocalisée. Utilisant des méthodes voltampérométriques et opérant dans le CH_2Cl_2, on a oxydé et réduit les cycles aromatiques à 10 électrons π. La réduction réversible par un électron conduit à des espèces stables à 11 électrons π. En accord avec les études chimiques antérieures, les composés mentionnés dans le titre sont beaucoup plus difficiles à oxyger que le 3,7-$[(CH_3)_2N]_2\{CN_2S_2N_2C\}$.

[Traduit par la rédaction]

Introduction

1,5-Dithia-2,4,6,8-tetrazocine heterocycles **4** are structurally and theoretically interesting molecules that may exist either in the planar, 10π aromatic structure I or in the folded structure II, in which the two halves are planar. Since their discovery in 1981 (1), there have been numerous studies on the synthesis (2–4), UV photoelectron spectra (5, 6), magnetic circular dichroism (7), and MO electronic structure of these compounds (6, 8, 9). This class of compound has been placed in context in a recent comprehensive review (10).

The type II compounds have interesting chemical reactivity in oxidation reactions, and as ligands to low-valent metal complexes (11–13). However, the chemistry of the type I compounds is less developed. We have reported the complete resistance of these compounds towards both polar and radical oxidants (12), while Amin and Rees were able to degrade the eight-membered ring by reaction with ozone (3). A major limitation towards further chemical studies has been the lack of a synthetic method for the preparation of reasonable quantities of the type I compounds. Amin and Rees investigated more than 10 methods and variations for the preparation of **4***a* (see Scheme 1), without managing to increase the yield above 10%.

Recently we discovered a higher yield route to type I derivatives through the reaction of 4-aryl-1,2,3,5-dithiadiazolyl dimers **3** with dioxygen (14). This is a novel and unexpected reaction, and in this paper we provide the full details of this investigation. Starting from here we have developed a much higher yield synthetic method with a simple work-up for the preparation of **4***a–f*. Both existing and new compounds have been prepared by this route, and the products have been fully characterized. The ^1H and ^{13}C NMR spectra have been recorded and shown to be quite diagnostic. The single-crystal X-ray structure of **4***e* is also reported.

[1]Author to whom correspondence may be addressed.

[2]Feodor-Lynen Fellow of the Alexander von Humboldt Foundation, Bonn, Germany.

Structures I

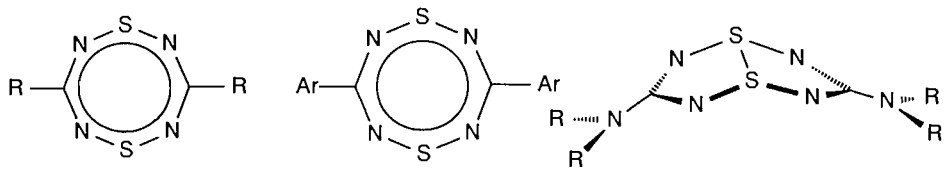

4 TYPE I TYPE II

Can. J. Chem. Downloaded from www.nrcresearchpress.com by 88.255.202.194 on 09/08/12
For personal use only.

There is a claim in the literature that **4***a,b,e,g* can be prepared in high yield by the reaction of **1***a,b,e,g* with 1.5 equivalents of SCl_2 in toluene (4). However, the physical properties of the products reported do not agree with those we have determined, and we believe that the yields in this report are in error.[3] Amin and Rees demonstrated that both benzamidine and its persilylated analogue *N,N,N'*-tris(trimethylsilyl)benzamidine react with sulfur dichloride or sulfur monochloride in CH_2Cl_2 to give a large amount of **2***a* and simultaneously a small amount of **4***a* (less than 10%) (2, 3). We were intrigued by these conflicting reports and speculated about the origin of two products from such a simple condensation reaction. In this paper we also demonstrate a second viable synthetic route to aryl dithiatetrazocines by the reaction of purified salt **2** with another equivalent of amidine **1**.

We have probed the previously noted difference in the reactivity of the type I and II compounds through a detailed electrochemical study. Cyclic voltammetry and phase-sensitive alternating-current voltammetry measurements of **4***a–f* are reported and discussed in the light of molecular orbital calculations. Our results improve the understanding of the electronic structure of these interesting compounds. These results are contrasted to the voltammetric behaviour of the type II compound with R = Me, i.e., $Me_2N\text{-}CN_2S_2N_2C\text{-}NMe_2$, **9**.

Experimental section

Starting materials and general procedures

Silylated amidines **1***a–g* were prepared by the literature methods (15), as were the known dithiatetrazocines $^tBu\text{-}CN_2S_2N_2C\text{-}^tBu$, **5**, and **9** (1, 6). **5** was purified by sublimation at 10^{-2} Torr (1 Torr = 133.3 Pa) at ambient temperature (7). Chlorine (Matheson), triphenylantimony, *p*-nitrobenzonitrile, and magnesium (Aldrich) were obtained commercially and used as received. NBu_4PF_6 (Aldrich) was vacuum dried before use and handled in a glove box. Sulfur dichloride (Aldrich) was distilled from PCl_3 immediately before use. Solvents were Fisher reagent grade, or better, and were distilled from P_2O_5 (CCl_4, $CHCl_3$, CH_3Cl_2) and Na wire (diethyl ether). CH_3CN was double-distilled from P_2O_5 and CaH_2. O_2 gas was passed through a 30-cm Drierite column before use. Unless otherwise indicated, all procedures were performed under an atmosphere of purified N_2 using a dry-box, Schlenk-ware, and vacuum-line techniques. Infrared spectra were recorded on a Bomem MB102 Fourier transform spectrometer as Nujol mulls between CsI plates and are reported in the 1700–200 cm^{-1} region only, unless otherwise indicated. NMR spectra were recorded on a Bruker AC-F 250 MHz FT spectrometer. NMR data are collected in Table 1. Electronic absorption spectra were obtained in 1.00-cm quartz cuvettes on a Varian DMS 100S spectrophotometer. Data are collected in Table 2. Mass spectra were recorded by the Mass Spectrometry Centre, University of Alberta. Elemental analyses were performed by MHW Laboratories, Phoenix Ariz.

Preparation of **2**a–g

2*a* was prepared by the published procedure (16, 17). The IR spectrum agreed with that reported previously (18).

2*b*: From 2.1 g (6.1 mmol) of **1***b* and 2.5 mL SCl_2 (excess) in 100 mL CH_3CN; yield 0.93 g, 64% as deep orange needles. An analytical sample was obtained by recrystallizing from acetonitrile, mp 160°C. IR: 1604(m), 1413(w), 1296(w), 1259(w), 1211(w), 1198(w), 1155(w), 1041(w), 1026(w), 924(m), 901(m), 847(m), 825(w), 725(m), 686(w), 547(w), 493(w), 289(w). Mass spectrum (EI, 70 eV), high resolution: 195.0052 (calcd.: 195.0051); *m/z*: 195 ($RCN_2S_2^+$, R = $CH_3C_6H_4$, 98%), 149 ($RCNS^+$, 38%), 117 (RCN^+, 30%), 116 (RCN − H^+, 38%), 78 (S_2N^+, 100%). Anal. calcd. for $C_8H_7ClN_2S_2$: C 41.64, H 3.06%, N 12.14%; found: C 41.79, H 3.20, N 12.28%.

2*c*: From 3.5 g of (9.5 mmol) of **1***c* and 1.5 mL SCl_2 (excess) in 20 mL CH_3CN; yield 1.8 g, 76% as a dark solid. An analytical sample was obtained by recrystallizing from acetonitrile, mp 218°C. IR: 1674(s), 1601(s), 1574(m), 1520(w), 1427(m), 1393(vs), 1323(m), 1306(w), 1269(s), 1198(w), 1173(vs), 1121(w), 1015(s), 919(m), 891(s), 859(s), 848(m), 820(m), 793(w), 743(m), 723(w), 691(m), 631(w), 600(m), 550(m), 532(w), 484(w), 407(w), 286(w), 228(w). Mass spectrum (EI, 70 eV) *m/z*: 211 ($RCN_2S_2^+$, R = $CH_3OC_6H_4$, 100%), 165 ($RCNS^+$, 48%), 133 (RCN^+, 71%), 78 (S_2N^+, 100%). Anal. calcd. for $C_8H_7ClN_2OS_2$: C 38.94, H 2.90, N 11.53%; found: C 39.15, H 2.90, N 11.53%.

2*d*: From 5.0 g of (13.5 mmol) of **1***d* and 2.0 mL SCl_2 (excess) in 50 mL CH_3CN; yield 2.7 g, 80% as orange needles. The infrared spectrum matched that reported in the literature (18).

2*e*: From 5.0 g (12.4 mmol) of **1***e* and 2.0 mL SCl_2 (excess) in 40 mL CH_3CN; yield 2.84 g, 81% as orange plates. An analytical sample was obtained by recrystallizing from acetonitrile, mp 208–210°C. IR: 1680(w), 1518(w), 1414(vs), 1404(s), 1329(vs), 1321(s), 1260(m), 1221(m), 1171(vs), 1155(s), 1124(vs), 1067(vs), 1015(m), 927(w), 891(m), 858(s), 845(s), 801(w), 752(w), 698(m), 691(m), 596(w), 547(m), 384(w), 278(w), 224(m). Mass spectrum (EI, 70 eV) *m/z*: 249 ($RCN_2S_2^+$, R = $CF_3C_6H_4$, 100%), 230 (*M* − F^+, 6%), 203 ($RCNS^+$, 30%), 171 (RCN^+, 33%), 152 (RCN − F^+, 25%), 121 ($FC_6H_4CN^+$, 24%), 78 (S_2N^+, 98%). Anal. calcd. for $C_8H_4ClF_3N_2S_2$: C 33.75, H 1.42, N 9.84%; found: C 29.07, H 1.59, N 8.36%.

2*f*: From 5.0 g (12.4 mmol) of **1***f* and 2.0 mL SCl_2 (excess) in 40 mL CH_3CN; yield 3.0 g, 85% as yellow crystals. An analytical sample was obtained by recrystallizing from acetonitrile, mp 195–197°C. IR: 1613(w), 1391(vs), 1292(s), 1217(w), 1157(m), 1123(s), 1092(m), 1074(m), 949(m), 918(w), 891(w), 851(w), 826(w), 725(m), 696(m), 552(w), 385(w), 265(w). Mass spectrum (EI, 70 eV) *m/z*: 249 ($RCN_2S_2^+$, R = $CF_3C_6H_4$, 64%), 230 (*M* − F^+, 7%), 203 ($RCNS^+$, 40%), 171 (RCN^+, 23%), 152

[3]We find that the IR spectrum and the mp point of **4***b*, as well as the mp and NMR data of **4***e* reported in ref. 4 differ greatly from our own results (see Experimental and Table 1). Although we have not found a reliable method for the preparation of **4***g*, the samples we obtained with a mass spectrum fitting **4***g* had quite different NMR parameters from those reported in ref. 4.

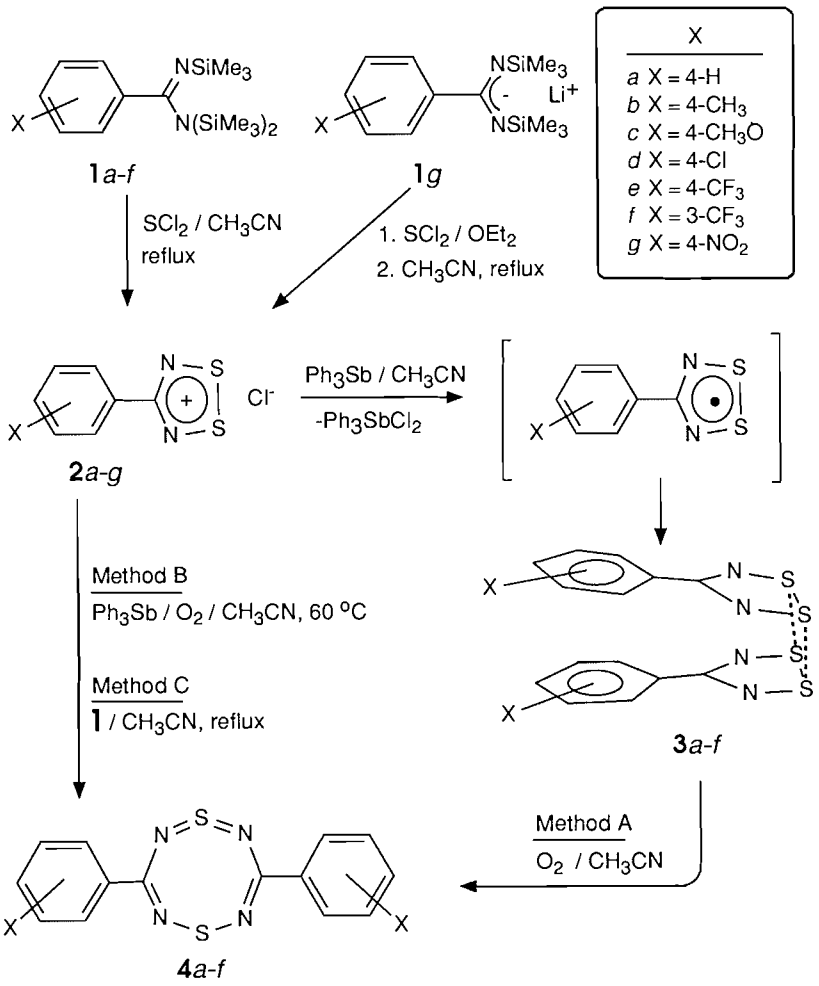

SCHEME 1

(RCN − F$^+$, 24%), 121 ($FC_6H_4CN^+$, 21%), 78 (S_2N^+, 100%). Anal. calcd. for $C_8H_4ClF_3N_2OS_2$: C 38.94, H 2.90, N 11.53%; found: C 42.12, H 1.65, N 12.01%.

2*g*: To a solution prepared by stirring *p*-$NO_2C_6H_4CN$ (10.0 g, 67.5 mmol) and $LiN(SiMe_3)_2 \cdot Et_2O$ (16.30 g, 67.5 mmol) in 250 mL diethyl ether for 12 h was added dropwise 15.4 mL of SCl_2 in 20 mL ether while cooling the solution with an ice bath. After a further 30 min, 100 mL of CH_3CN was added, the ether was distilled off, and the resulting solution refluxed for 30 min, cooled, and filtered. Yield 16.1 g of impure **2***g* (containing LiCl). An analytical sample was obtained by dissolving a small sample in hot PhCN, filtering off the LiCl, and cooling. The resulting crystalline solid lost crystallinity on vacuum drying. It was therefore rinsed exhaustively with CH_3CN, and vacuum dried to a yellow powder, mp 213–217°C. IR: 1603(w), 1521(s), 1514(s), 1489(w), 1348(vs), 1330(vs), 1259(w), 1138(w), 1117(s), 1107(s), 1010(s), 926(w), 898(w), 866(m), 851(m), 785(s), 727(s), 714(vs), 698(m), 664(m), 565(m), 534(m), 507(m), 496(w), 453(w), 438(m). Mass spectrum (EI, 70 eV) *m/z*: 249 ($RCN_2S_2^+$, R = $NO_2C_6H_4$, 100%), 180 ($RCNS^+$, 36%), 148 (RCN^+, 11%), 134 (RC^+, 15%), 102 ($C_6H_4CN^+$, 30%), 78 (S_2N^+, 72%). Anal. calcd. for $C_7H_4ClN_2O_2S_2$: C 32.13, H 1.5, N 16.06%; found; C 32.23, H 1.72, N 16.02%.

Preparation of **3**a–g

3*a* was prepared as described in the literature (16, 17). Its physical and spectroscopic properties agreed with those reported previously (18). A similar approach was used to prepare the rest.

3*b*: From 0.58 g of **2***b* (2.5 mmol) and 1.16 g Ph_3Sb (2.5 mmol) in 25 mL of CH_3CN. The solution had to be filtered hot to remove a yellow precipitate, then cooled to room temperature. Dark crystals were collected. These were sublimed for 48 h at 80°C under high vacuum. Yield 0.12 g of **3***b* (0.61 mmol *as the monomer*, 24%), mp 140°C. IR: 1608(w), 1456(s), 1416(w), 1314(w), 1260(m), 1238(w), 1182(w), 1173(w), 1132(m), 1109(m), 1022(m), 822(s), 806(s), 775(s), 729(w), 674(w), 652(m), 509(m), 482(w). Mass spectrum (EI, 70 eV), high resolution: 195.0050 (calcd.: 195.0051); *m/z*: 195 ($RCN_2S_2^+$, R = $CH_3C_6H_4$, 100%), 149 ($RCNS^+$, 20%), 117 (RCN^+, 15%), 116 (RCN − H^+, 13%), 78 (S_2N^+, 90%). Anal. calcd. for $C_8H_7N_2S_2$: C 49.20, H 3.61, N 14.34, S 32.84%; found: C 49.46, H 3.65, N 14.23, S 32.89%.

3*c*: From 3.38 g of **2***c* (13.7 mmol) and 2.55 g Ph_3Sb (7.20 mmol) in 50 mL of CH_3CN. A copious, fibrous crystalline product formed in the hot solvent, was cooled at room temperature, and filtered. Yield 2.44 g of **3***c* (11.6 mmol *as the monomer*, 84%), mp 131°C. IR: 1602(w), 1514(w), 1508(w), 1302(w), 1256(s), 1192(w), 1185(w), 1171(m), 1128(w), 1105(w), 1020(w), 833(w), 802(w), 791(w), 775(w), 727(w), 654(w), 596(w), 519(w), 280(w). Mass spectrum (EI, 70 eV) *m/z*: 211 ($RCN_2S_2^+$, R = $CH_3OC_6H_4$, 100%), 165 ($RCNS^+$, 38%), 133 (RCN^+, 85%), 90 (CNS_2^+, 41%), 78 (S_2N^+, 87%), 64 (S_2^+, 47%). Anal. calcd. for $C_8H_7N_2OS_2$: C 45.48, H 3.34, N 13.26, S 30.35%; found: C 44.05, H 4.60, N 12.62, S 17.85%.

3*d*: From 2.97 g **2***d* (11.2 mmol) in 80 mL and 3.95 g Ph_3Sb (11.2 mmol) in 20 mL. Hot filtered to remove yellow precipi-

Can. J. Chem. Downloaded from www.nrcresearchpress.com by 88.255.202.194 on 09/08/12
For personal use only.

TABLE 1. ^{1}H,[a,c] ^{13}C,[b,c] and ^{19}F NMR data for **4**

Compound	H_2	H_3	X (H_4)	C_1'	C_1	C_2	C_3	C_4	X
4*a*	8.55 dd (8.5,1.2)	7.545–7.60 m	7.46–7.51 m	138.0	137.9	128.8*	128.0*	—	—
4*b*	8.41 d (8.3)	7.34 d (8.3)	2.44 s	138.6	139.9†	129.5*	127.9*	135.3†	21.3
4*c*	8.45 d (9.0)	7.05 d (9.0)	3.90 s	140.7	130.4	129.7	114.1	161.1	55.5
4*d*	8.48 d (8.6)	7.52 d (8.6)	—	137.1	136.3†	129.3*	129.0*	136.1†	—
4*e*[d]	8.67 d (8.2)	7.81 d (8.2)	−63.29[e]	136.7	140.9	128.3	125.9 q (3.8)	131.7 q (32.9)	124.1 q (273)
4*f*[d,f]	8.81 s	$H_{4,5}$: 7.64–7.75 m H_6: 8.73 d (7.4)	−63.20[e]	136.7	138.5	124.9* q (3.9)	131.4 q (32.5)	126.4* q (3.6)	124.1 q (272)
4*g*	8.42 d (8.8)	8.07 d (8.8)							

[a]In $CDCl_3$, except **4***g* in DMSO-d_6; format: δ (ppm), multiplicty, *J* (Hz).
[b]Numbering scheme:

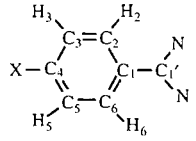

Assignments marked *,†,‡ are interchangeable.
[c]Saturated soln. in $CDCl_3$; 6000–20 000 scans required for acceptable S/N.
[d]^{13}C spectrum obtained with 6 s delay.
[e]δ(^{19}F), relative to external CF_3COOH at −77.00 ppm.
[f]δ(^{13}C): C_5 129.4‡; C_6 131.2‡ ppm.

TABLE 2. Electronic absorption spectra of **4**[a]

Compound	λ_1 ϵ_1	λ_2 ϵ_2	λ_3 ϵ_3	λ_4 ϵ_4	λ_5 ϵ_5	λ_6 (nm) ϵ_6
4*a*	412 4 400	322(sh) 16 500	311 22 100	299 19 200	282(sh) 18 400	276 18 700
4*b*	422 7 300	327(sh) 34 900	316 46 300	304(sh) 39 300	291(sh) 31 800	282(sh) 29 900
4*c*[b]	439 4 000	335(sh) 31 900	323 40 700	312(sh) 35 400	291(sh) 32 100	282(sh) 32 900
4*d*	414 9 400	330 44 000	317 62 000	306(sh) 47 000	—	275 34 500
4*e*	400 10 400	325 37 000	313 46 700	303(sh) 43 900	—	274 31 500
4*f*	402 11 900	322 42 800	310 53 700	300(sh) 39 100	—	273 39 200

[a]All spectra were recorded using 1-cm quartz cuvettes in dry $CHCl_3$. Literature values for **4***a,c* are available for 95% EtOH and dioxane solutions, respectively (1).
[b]An additional peak appears for this compound at 367 nm (7100), which was not reported in dioxane solution (1).

tate, cooled to room temperature and 1.02 g of purple needles (5.19 mmol *as the monomer*, 46%) filtered off, mp 123–124°C. IR: 1591(w), 1576(w), 1549(w), 1487(m), 1400(m), 1269(s), 1225(s), 1173(w), 1134(m), 1089(s), 1014(s), 962(w), 905(w), 837(s), 808(s), 777(s), 740(w), 718(m), 669(w), 648(m), 629(w), 509(m), 484(m).[4] Mass spectrum (EI, 70 eV) *m/z* (mass calculated on ^{35}Cl): 215 ($RCN_2S_2^+$, R = ClC_6H_4, 97%), 169 ($RCNS^+$, 46%), 137 (RCN^+, 47%), 78 (S_2N^+, 100%). Anal. calcd. for $C_7H_4ClN_2S_2$: C 38.98, H 1.87, S 29.73%; found: C 39.14, H 1.74, S 29.47%.

[4]**3***d* is a known, but insufficiently characterized, compound. Our infrared spectroscopic data are qualitatively similar to the published spectrum (19).

3*e*: From 2.0 g **2***e* (7.0 mmol) in 30 mL CH_3CN and 2.5 g Ph_3Sb (7.0 mmol) in 20 mL CH_3CN. Cooled to −30°C, and collected crude product. Sublimed at 60°C under high vacuum. Yield 0.60 g of a deep purple solid (2.41 mmol, 34%), mp 110–115°C. IR: 1689(w), 1615(m), 1549(w), 1412(w), 1323(w), 1260(w), 1238(w), 1171(s), 1134(s), 1067(m), 1017(m), 851(m), 804(w), 779(w), 735(w), 685(w), 656(w), 592(w), 529(w), 509(w), 451(w). Mass spectrum (EI, 70 eV) *m/z*: 249 ($RCN_2S_2^+$, R = $CF_3C_6H_4$, 100%), 230 (*M* − F^+, 12%), 203 ($RCNS^+$, 41%A), 171 (RCN^+, 15%), 152 (RCN − F^+, 25%), 121 ($FC_6H_4CN^+$, 25%), 78 (S_2N^+, 98%). Anal. calcd. for $C_8H_4F_3N_2S_2$: C 38.55, H 162, N 11.24, S 25.73%; found: C 38.73, H 1.76, N 11.12, S 25.63%.

3*f*: From 2.0 g **2***f* (7.0 mmol) in 30 mL CH_3CN and 2.5 g Ph_3Sb

Can. J. Chem. Downloaded from www.nrcresearchpress.com by 88.255.202.194 on 09/08/12
For personal use only.

TABLE 3. Experimental details

A. Crystal data	
Empirical formula	$C_{16}H_8F_6N_4S_2$
Formula weight	434.38
Crystal color, habit	Yellow, plate
Crystal dimensions	0.230 × 0.360 × 0.070
Crystal system	Triclinic
No. of reflections used for unit cell determination (2θ range)	14 (20.1–33.4°)
Omega scan peak width at half-height	0.36°
Lattice parameters	a = 6.835(2) Å b = 9.936(3) Å c = 6.320(2) Å α = 96.44(3)° β = 102.88(3)° γ = 88.42(3)° V = 415.8(2) Å^3
Space group	$P\bar{1}$ (No. 2)
Z value	1
D_{calc}	1.735 g/cm^3
F_{000}	218.00
$\mu_{(MoK\alpha)}$	3.79 cm^{-1}
B. Intensity measurements	
Diffractometer	Rigaku AFC6S
Radiation	MoKα (λ = 0.71069 Å) graphite monochromated
Take-off angle	6.0°
Detector aperture	6.0 mm horizontal 6.0 mm vertical
Crystal to detector distance	40 mm
Temperature	−103.0°C
Scan type	ω–2θ
Scan rate	2.0°/min (in omega) (3 rescans)
Scan width	(1.52 + 0.35 tan θ)°
$2\theta_{max}$	50.2°
No. of reflections measured	Total: 1616 Unique: 1481 (R_{int} = 4.54)
Corrections	Lorentz–polarization Absorption (trans. factors: 0.8978–1.0000) Decay (−4.36% decline)
C. Structure solution and refinement	
Structure solution	Direct methods (SAPI91)
Refinement	Full-matrix least-squares
Least-squares weights	$1/\sigma^2F + 0.000134F^2$)
Anomalous dispersion	All non-hydrogen atoms
No. observations ($I > 3.00\sigma(I)$)	1100
No. variables	173
Reflection/parameter ratio	6.4
Residuals: R; Rw	0.034; 0.035
Max shift/effor in final cycle	0.13
Maximum peak in final diff. map	0.22 e/Å^3
Minimum peak in final diff. map	−0.20 e/Å^3

(7.0 mmol) in 10 mL CH_3CN. Cooled to −30°C, and filtered crude product. Sublimed at 60–70°C onto a water-cooled finger. Yield 0.90 g of purple solid (3.6 mmol, 51%), mp 142–145°C. IR: 1559(w), 1335(m), 1260(s), 1231(w), 1171(m), 1134(s), 1072(m), 932(w), 910(w), 835(w), 804(m), 787(w), 772(w), 733(w), 691(m), 648(w), 600(w), 509(w), 383(w), 204(s). Mass spectrum (EI, 70 eV) m/z: 249 ($RCN_2S_2^+$, R = $CF_3C_6H_4$, 82%), 230 ($M - F^+$, 10%), 203 ($RCNS^+$, 34%), 171 (RCN^+, 13%), 152 ($RCN - F^+$, 20%), 121 ($FC_6H_4CN^+$, 17%), 78 (S_2N^+, 100%).

Preparation of **4**a–f

Three routes, A, B, and C, to these compounds have been developed, as outlined below for **4***a*. Purity was established in all cases

Can. J. Chem. Downloaded from www.nrcresearchpress.com by 88.255.202.194 on 09/08/12
For personal use only.

Can. J. Chem. Downloaded from www.nrcresearchpress.com by 88.255.202.194 on 09/08/12
For personal use only.

by ^{1}H NMR (Table 1). The other compounds were prepared in an analogous manner.

Method A: Dry O_2 was bubbled through a suspension of 0.12 g (0.66 mmol) of **3***a* in 25 mL of dry CH_3CN warmed to 60°C for 3 h. The initially black solution slowly turned dark brown, then orange and dark yellow. The solvent was removed (Rotovap), and the residue extracted with hot toluene to give a bright yellow solution. After removal of the solvent, the residue was shown by ^{1}H NMR to be a mixture containing some **4***a*. The residue was purified by column chromatography (20 × 2 cm dimensions, 200–400 mesh, Terrochem). A bright yellow band was elluted with 1:1 toluene:ethyl acetate. After removal of solvent, the bright yellow solid was shown by ^{1}H NMR to be pure **4***a*. Yield 9%. The identity of **4***a* was confirmed by comparing the IR spectrum (KBr disk) of a pure sample with that reported in the literature (1), and by comparing the ^{1}H NMR parameters with those reported in the literature (3).

Method B: To a suspension of 0.50 g **2***a* (3.4 mmol) in 15 mL of CH_3CN saturated with O_2 was added dropwise 1.20 g (3.4 mmol) of Ph_3Sb in 5 mL CH_3CN. The solution was then heated in an O_2 atmosphere to 60°C for 1.5 h, cooled to room temperature, and the precipitate that formed was filtered off and shown by ^{1}H NMR to be pure **4***a*. Yield 0.22 g of yellow powder (0.74 mmol, 43%).

Method C: To a suspension of 0.090 g of **2***a* in 10 mL of CH_3CN was added 0.139 g of **1***a*. The orange suspension was heated to reflux for 3 h, then cooled to room temperature. The resulting yellow crystals were filtered, and the filtrate reduced to dryness. Analysis by ^{1}H NMR showed the precipitate to be pure **4***a*, while the residue was a mixture of several components.

4*b*: Method A: 20% yield after chromatography on silica gel. Method B: From 0.50 g of **2***b* in 15 mL CH_3CN and 0.77 g Ph_3Sb in 5 mL CH_3CN. The precipitate was pure **4***b*, 0.16 g (0.48 mmol, 45% yield). Method C: From 0.25 g **2***b* and 0.38 g **1***b* in 15 mL CH_3CN. The precipitate was pure **4***b*, 0.80 g, 23% yield. An analytical sample was prepared by recrystallizing from hot CH_3CN, mp 267°C. IR (KBr disk): 1369(s), 1340(w), 1319(w), 1261(w), 1229(w), 1173(m), 1128(w), 1111(w), 1067(w), 1018(w), 943(w), 826(m), 720(w), 650(s), 617(w), 592(w), 526(w), 488(w), 369(s), 319(w). Mass spectrum (EI, 70eV) *m/z*: 326 ($RCN_2S_2N_2CR^+$, R = $CH_3C_6H_4$, 36%), 281 (RCN_2SNCRH^+, 7%), 163 (RCN_2S^+, 12%), 149 ($RCNS^+$, 100%), 117 (RCN^+, 39%), 46 (SN^+, 32%), 28 (N_2, 89%). Anal. calcd: for $C_{16}H_{14}N_4S_2$: C 58.87, H 4.32, N 17.16, S 19.64%; found: C 58.51, H 4.76, N 17.07, S 19.39%.

4*c*: Method A: 10% yield after chromatography on silica gel. Method B: From 0.50 g of **2***c* in 15 mL CH_3CN and 0.72 g Ph_3Sb in 5 mL CH_3CN. The precipitate was almost pure **4***c*, 0.14 g (0.40 mmol, 39% yield). A pure sample, as judged by ^{1}H NMR, was prepared by recrystallizing from hot CH_3CN. The IR spectrum (KBr disk) of the recrystallized material matched that reported in the literature (1).

4*d*: Method A: 7% yield after chromatography on silica gel. Method B: From 0.50 g of **2***d* in 15 mL CH_3CN and 0.67 g Ph_3Sb in 5 mL CH_3CN. The precipitate was pure **4***d*, 0.19 g (0.52 mmol, 55% yield). Method C: From 0.25 g **2***d* and 0.37 g **1***d* in 30 mL CH_3CN. The precipitate was pure **4***d*, 0.10 g, 40% yield. An analytical sample was prepared by recrystallizing from hot CH_3CN, mp 238–239°C. IR (KBr disk): 1593(m), 1487(m), 1404(w), 1373(s), 1281(w), 1225(w), 1173(w), 1105(w), 1098(s), 1013(m), 941(w), 833(s), 826(m), 729(w), 719(m), 650(s), 637(m), 525(w), 501(w), 482(w). Mass spectrum (EI, 16eV) *m/z* (reported on ^{35}Cl): 366 ($RCN_2S_2N_2CR^+$, R = ClC_6H_4, 49%), 169 ($RCNS^+$, 82%), 92 ($S_2N_2^+$, 100%). Anal. calcd. for $C_{14}H_8Cl_2N_4S_2$: C 45.78, H 2.20, N 15.25, S 17.46%; found: C 45.52, H 2.73, N 14.90, S 17.21%.

4*e*: Method A: product hydrolyzed under chromatographic workup. Method B: From 0.50 g of **2***e* in 15 mL CH_3CN and 0.62 g Ph_3Sb in 5 mL CH_3CN. The precipitate was pure **4***e*, 0.12 g (0.28 mmol, 32% yield). Method C: From 0.25 g **2***e* and 0.36 g **1***e* in 30 mL CH_3CN. The precipitate was pure **4***e*, 0.069 g, 18% yield. An analytical sample was prepared by recrystallizing from hot CH_3CN, mp 226–228°C. IR (KBr disk): 1412(w), 1369(m), 1315(vs), 1262(w), 1240(w), 1181(m), 1171(m), 1135(m), 1109(m), 1065(s), 1015(m), 942(w), 851(m), 685(w), 655(m), 644(m), 590(W), 528(w), 448(w). Mass spectrum (EI, 70 eV) *m/z*: 434 ($RCN_2S_2N_2CR^+$, R = $CF_3C_6H_4$, 17%), 415 ($RCN_2S_2N_2CR - F^+$, 7%), 263 ($RCN_3S_2^+$, 4%), 249 ($RCN_2S_2^+$, 1%), 203 ($RCNS^+$, 100%), 46 (SN^+, 31%), 28 (N_2, 77%). Anal. calcd. for $C_{16}H_8F_6N_4S_2$: C 44.24, H 1.86, N 12.90, S 14.76%; found: C 44.40, H 1.69, N 13.05, S 14.58%.

4*f*: Method B: From 0.50 g of **2***f* in 15 mL CH_3CN and 0.62 g Ph_3Sb in 5 mL CH_3CN. The precipitate was pure **4***f*, 0.23 g (0.53 mmol, 60% yield). Method C: From 0.25 g **2***f* and 0.36 g **1***f* in 30 mL CH_3CN. The precipitate was pure **4***f*, 0.25 g, 66% yield. An analytical sample was prepared by recrystallizing from hot CH_3CN, mp 201–203°C. IR (KBr disk): 1638(m), 1616(m), 1489(m), 1445(m), 1371(s), 1325(vs), 1290(s), 1240(m), 1206(s), 1173(s), 1128(vs), 1094(m), 1072(s), 972(m), 930(w), 910(m), 808(s), 787(w), 696(s), 689(s), 640(s), 598(m), 530(m), 364(w). Mass spectrum (EI, 70 eV) *m/z*: 434 ($RCN_2S_2N_2CR^+$, R = $CF_3C_6H_4$, 9%), 415 ($RCN_2S_2N_2CR - F^+$, 4%), 263 ($RCN_3S_2^+$, 3%), 249 ($RCN_2S_2^+$, 1%), 203 $RCNS^+$, 100%), 171 (RCN^+, 15%), 152 ($RCN - F^+$, 19%), 46 (SN^+, 56%), 28 (N_2, 13%). Anal. calcd. for $C_{16}H_8F_6N_4S_2$: C 44.24, H 1.86, N 12.90, S 14.76%; found: C 44.38, H 1.79, N 13.07, S 14.61%.

Crystal structure determination

Accurate cell dimensions and a crystal orientation matrix were determined on a Rigaku AFC6S diffractometer by a least-squares fit of the setting angles of 14 reflections. Experimental details are provided in Table 3. Data were corrected for Lorentz, polarization, and empirical absorption effects (20), transmission factors being in the range 0.8978–1.0000.

The structure was solved by direct methods using SAPI91 (21). Refinement of the structure was by full-matrix least-squares calculations, initially with isotropic and finally with anisotropic temperature factors for the non-hydrogen atoms using SHELX-76 (22). Fluorine atoms of the CF_3 group were found to be disordered; F-atoms were allowed to refine with anisotropic temperature factors along with their site occupancy factors. At an intermediate stage in the refinement, a difference map revealed maxima consistent with the positions of the hydrogen atoms, which were included in the subsequent cycles of refinement with fixed isotropic temperature factors. Refinement converged at $R = 0.034$ and $Rw = 0.035$. In the refinement cycles, weights were derived from the counting statistics. Scattering factors were those of Cromer and Mann (23) and Stewart, Davidson, and Simpson (24), and allowance was made for anomalous dispersion (25). A difference map calculated at the conclusion of the refinement had no chemically significant features. The computer programs used for data reduction were part of TEXSAN (26) installed on a Silicon Graphics Personal Iris 4D/35 computer, and Fig. 1 was plotted using ORTEP II (27). Experimental details are summarized in Table 3, fractional coordinates and U_{eq} in Table 4, and important interatomic distances in Table 5.[5]

Electrochemistry

Cyclic voltammetric studies (scan rates ν = 20–1000 mV s^{-1}) and phase-sensitive alternating current (a.c.) measurements (ω = 615 Hz, ν = 10 mV s^{-1}) were made with a PAR 173 potentiostat

[5]Tables of bond lengths and angles (S1), anisotropic thermal parameters (S2), and observed and calculated structure factors (S3) for the crystal structure may be purchased from: The Depository of Unpublished Data, Document Delivery, CISTI, National Research Council Canada, Ottawa, Canada, K1A 0S2.

Tables of bond lengths and angles have also been deposited with the Cambridge Crystallographic Data Centre and can be obtained on request from The Director, Cambridge Crystallographic Data Centre. University Chemical Laboratory, 12 Union Road, Cambridge, CB2 1EZ, U.K.

TABLE 4. Final fractional coordinates (S, N, C × 10^4; F and H × 10^3) and U_{eq} (Å^2 × 10^3) with esd's in parentheses

Atom	x	y	z	s.o.f.	U_{eq}[a]
S(1)	7580(1)	11007(1)	−275(1)		38(1)
F(1)	630(3)	474(1)	741(2)	0.56(4)	90(7)
F(2)	521(3)	641(1)	906(3)	0.68(3)	154(12)
F(3)	818(1)	569(2)	1005(2)	0.55(3)	89(7)
F(4)	460(2)	578(3)	763(3)	0.33(2)	84(10)
F(5)	715(7)	624(3)	1025(2)	0.47(4)	148(18)
F(6)	697(5)	464(1)	785(6)	0.43(4)	148(15)
N(1)	7956(3)	9952(2)	1432(4)		34(1)
N(2)	8991(3)	11318(2)	−1789(4)		33(1)
C(1)	9272(4)	9048(3)	2275(4)		28(2)
C(2)	8684(4)	8301(3)	3973(4)		29(2)
C(3)	6861(4)	8588(3)	4567(5)		35(2)
C(4)	6237(5)	7832(3)	6009(5)		38(2)
C(5)	7420(4)	6806(3)	6875(4)		35(2)
C(6)	9276(5)	6547(3)	6378(5)		40(2)
C(7)	9895(5)	7294(3)	4914(5)		37(2)
C(8)	6689(5)	5913(3)	8309(5)		46(2)
H(31)	614(4)	923(3)	401(5)		43(4)
H(41)	494(4)	804(3)	631(5)		43(4)
H(61)	1008(4)	591(3)	698(5)		43(4)
H(71)	109(4)	710(3)	450(5)		43(4)

[a] $U_{eq} = (U11 + U22 + U33)/3$.

Can. J. Chem. Downloaded from www.nrcresearchpress.com by 88.255.202.194 on 09/08/12
For personal use only.

in combination with a PAR 175 programmer and EGG 9209 lock-in amplifier and recorded on a Houston Graphics 2000 XY plotter. Electrochemical experiments were performed on a platinum three-electrode system with the platinum working electrode either a Pt wire or a 0.5 mm diameter Pt micro-tip. The vacuum-tight all-glass cell has an integrated cooling finger for studies at low temperatures. The cell was charged with electrolyte (0.4 M NBu_4PF_6), and the solvent, dry degassed CH_2Cl_2, transferred on a vacuum line. Samples and ferrocene as an internal reference were added to the cell using break-seal techniques. The ferricenium/ferrocene couple appeared in this system at 0.48 V vs. SCE at 25°C in CH_2Cl_2.

Results and discussion

Synthetic method

The preparation of salts **2** and radicals **3** follows a well-established route (16, 17). We found that the best solvent for the preparation of the rather insoluble chloride salts **2** is indeed acetonitrile. Amin and Rees used methylene chloride, and reported a 60% yield of **2***a* from the reaction of **1***a* and SCl_2 in this solvent (3). They also obtained about 6% of **4***a* in this reaction. To see if the switch to the even less polar solvent toluene might change these relative yields dramatically, we repeated the reaction of **1***a* with freshly distilled SCl_2 according to the exact stoichiometry reported in ref. 4. A copious yellow precipitate is indeed obtained, but ^{1}H NMR analysis failed to detect any appreciable amount of **4***a*, and the IR spectrum of the bulk material matched that of **2***a*. Since **2** are readily hydrolysed (for example, this occurs by preparing an NMR sample with $CDCl_3$ from a freshly opened bottle), it is not surprising that these workers detected **4** by mass spectroscopy, or that, by extensive washing, materials with approximately the correct chemical analysis were obtained. Based on our experience and the results of ref. 3, it seems clear that the reaction of SCl_2 with silylated amidines in low-polarity solvents consistently leads to **2** as the major product and **4** as the minor product (reaction [1]). We recommended the use of hot acetonitrile and excess SCl_2 for the preparation of **2**.

TABLE 5. Important interatomic distances (Å) and angles (deg) for **4***a*,*c*,*e*[a]

	Compound		
	4*e*	**4***a*[b]	**4***c*[b]
Space Group	$P\bar{1}$	$P2_1/c$	*Pbca*
Site symmetry	C_i	C_i	C_i
N_1—S_1	1.563(2)	1.559[c]	1.559(2)
N_2—S_1	1.561(2)	1.569[c]	1.564(2)
C_1—N_1	1.322(3)	1.319[c]	1.330(3)
C_1—N_2'	1.323(3)	1.327[c]	1.328(3)
C_1—C_2	1.501(3)	1.495[c]	1.497(3)
N_1—S_1—N_2	126.8(1)	127.0(2)	127.2(1)
C_1—N_1—S_1	142.4(2)	140.9(2)	142.2(2)
C_1—N_2'—S_1'	141.6(2)	142.9(2)	142.2(2)
N_1—C_1—N_2'	129.2(2)	129.2(3)	128.5(2)
C_2—C_1—N_1	115.5(2)	115.1(3)	115.9(2)
C_2—C_1—N_2'	115.4(2)	115.7(3)	115.7(2)

[a] Atomic numbering scheme is that of **4***e* as defined in Fig. 1.
[b] Reference 1.
[c] Uncertainty in distance of 0.004–0.006 Å.

*Reaction of **3** with dioxygen*

Method A

Our entry into this chemistry was the serendipitous discovery that **4***b* was formed as a by-product in the synthesis of **3***b* from **2***b* by reduction with Ph_3Sb (14). The hypersensitivity of **3***b* towards O_2 may well be caused by its much greater solubility compared to that of **3***a*. We had to go to quite extraordinary lengths in degassing our solvent to suppress this side reaction. After realizing what was occurring, we deliberately exposed solutions of **3** to dry O_2 in warm acetonitrile. We observed in all cases the slow disappear-

ance of the dark black or purple colour of solutions of **3** and the corresponding monomers over the space of 1–3 h. The final solutions were usually pale orange. After removal of the solvent, ^{1}H NMR analysis showed that the residues in all cases were complex mixtures, with as few as four and as many as eight or 10 different constituents containing the aromatic ring from **3**. Nonetheless, column chromatography using a 1:1 toluene:ethyl acetate eluant produced samples of pure **4** in yields at least as good as the best previously reported (9% for **4***a*), and in some cases substantially higher (e.g., **4***b*, 20%).

A similar reaction occurs for **3***a,e* in the melt. A small quantity of pure **3** (consisting of black or purple flakes) was placed in a porcelain boat (1 × 10 cm) inside a Pyrex tube, and heated either with a hot-air blower or with a tube furnace. Dry O_2 was passed through the tube for 2–3 h. Upon cooling, the melt solidified to a yellow solid, which had a honeycomb appearance under the microscope, with bright yellow regions interspersed with other, lighter coloured regions. Chromatographic work-up and NMR analysis showed that yields of **4***a,e* similar to those from the solution-phase reactions with O_2 were obtained.

[1] 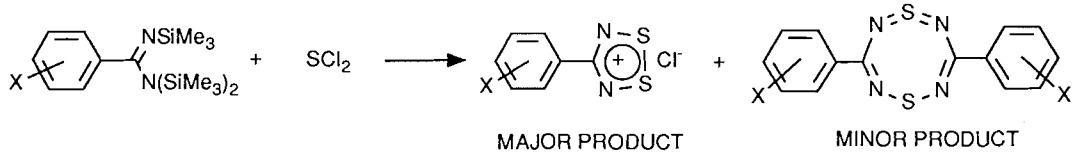

Method B

Since many of the by-products were colourless, somewhat water-soluble, solids, we reasoned that they represented over-oxidation at sulfur, and speculated that if the reaction could be slowed down, higher yields of **4** might be obtained. We thus developed Method B (see experimental), in which we added the reducing agent Ph_3Sb dropwise to a solution of salts **2** in warm CH_3CN that had been saturated in O_2. This method indeed led to substantially higher yields of **4**, and of course avoided the difficult preparation of pure samples of the dimers **3**. Moreover, the work-up is greatly simplified, and the yields reported in the Experimental section (40–60%) refer to the amount of pure **4** that precipitated from CH_3CN on cooling to room temperature. In several instances there was ^{1}H NMR evidence for more product in the filtrate, but we judged the recovery of this contaminated product to be more effort than it was worth.

Amidine coupling reactions

Method C

We were intrigued by the fact that both **2** and **4** seemed to be formed in the reaction of **1** with SCl_2 in less polar solvents, as discussed above. We reasoned that this could simply be a kinetically controlled phenomenon: the reaction of SCl_2 with **1** could be much faster than the further reaction of already formed **2** with **1**. We therefore attempted the reaction of purified **2** (i.e., filtered and rinsed with fresh CH_3CN) with a further equivalent of **1** (Method C, Scheme 1). Indeed we discovered that this is also a viable route to **4**. Yields of precipitated **4** range from 18 to 66%, and have not been optimized. We believe that this methodology could be developed into large-scale, "one-pot" syntheses, by which crude **2**, made from **1**, is filtered, rinsed back into the same flask, and converted to **4**.

Characterization of dithiatetrazocine ring compounds

The new compounds **4***b,d–f* have been fully characterized by elemental analysis and all have consistent mass spectra. **4***a,c* are well-characterized known compounds (1). However, apart from the ^{1}H NMR spectrum of **4***a* (2), little is known about their NMR spectra. Since we found that NMR was an essential tool in monitoring the progress of the reactions and the purity of the products from the various preparative routes, we present the full ^{1}H, ^{13}C, and, where relevant, ^{19}F NMR parameters for **4** in Table 1. The compounds were insufficiently soluble, in any solvent tried, to enable measurement of the ^{14}N spectra. In a few specific cases, an almost complete assignment of the ^{13}C resonances was possible (e.g., for **4***a,e,f*). In our opinion the endocyclic ^{13}C resonance should be assigned to the signals found in the range 136–141 ppm. While complete certainty is not possible, we note that in ^{t}BuCN$_2$S$_2$N$_2$C^{t}Bu, **5**, the endocyclic resonance can be indisputably assigned as 144.8 ppm (6). This resonance is also the least intense, either due to a long relaxation time or to line broadening from the adjacent nitrogen atoms.

We note that the ^{1}H resonances of $H_{2,6}$ (see Table 1) are found in the range 8.4–8.8 ppm, i.e., very far downfield. For comparison, the *ortho* protons in biphenyl occur at 7.4 ppm. Only in the bay region of polyaromatics such as phenanthrene are such shifts surpassed, e.g., 8.93 ppm (28). In the related heterocycle **6**, the *ortho* protons are at 7.966 ppm, while in **7** they are found at 8.08 and 8.61 ppm. Presumably there are two contributors to this deshielding: inductive or through-space effects from the neighbouring N—C—N functional group, and the ring current of the dithiatetrazocine ring. An excellent probe for these effects is found in the NMR spectrum of a mixed substituent 3-dimethylamino-7-phenyl-1,5-dithia-2,4,6,8-tetrazocine, **8**, which has a type II structure according to its electronic absorption spectrum (3). The $H_{2,6}$ resonance in this compound is found at 8.17 ppm (dd, J = 1.5 and 8.5 Hz), i.e., 0.38 ppm further upfield than in **4***a*. While these protons in **8** should experience a very similar inductive influence from the N—C—N group to that in **4***a*, they will not be subject to a ring current, since the aromaticity of the type II structures has been quenched (10). Thus the downfield shift of about 1.4 ppm from the position in benzene of the *ortho* protons in **4***a* caused by the dithiatetrazocine "substituent" is about two thirds due to inductive effects, and one third due to ring current.

The $H_{3,4,5}$ chemical shifts are found in the correct relative positions expected for being *ortho* to the X substituent in XC_6H_4- (28). However, all the resonances are shifted 0.3–0.4 ppm downfield. We attribute this shift to the dithiatetrazocine ring. By comparing the shifts in **4***a* with that in **8** (m, 7.35–7.5 ppm), we see that the downfield shift effect on these protons by the 10π ring current is only about one

Can. J. Chem. Downloaded from www.nrcresearchpress.com by 88.255.202.194 on 09/08/12
For personal use only.

Structures II

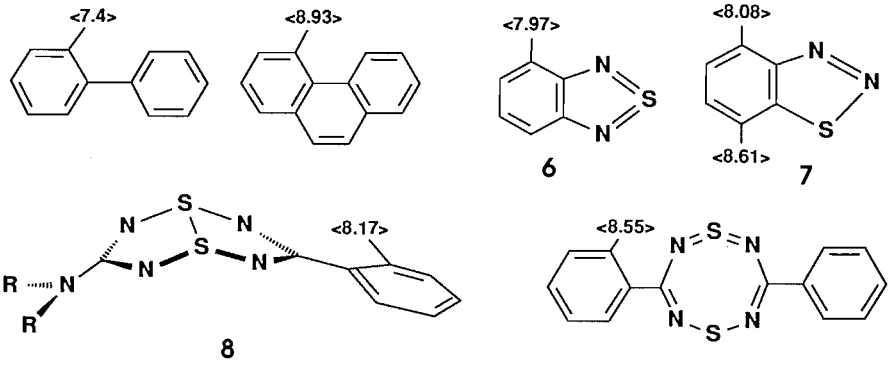

quarter of the total. In conclusion, we suggest that the chemical shift of protons on aryl rings *ortho* to a planar dithiatetrazocine ring will characteristically be found in the range 8.4–8.8 ppm, and that such shifts are diagnostic of the type I structure.

Structure

The electronic absorption spectra of **4***a* and the type II dithiatetrazocine **9** are quite distinct and, as has already been mentioned, this fact can be used with confidence to assign structure (1, 3, 10). The spectral data are summarized in Table 2, and it is clear that **4***a–f* have very similar spectra, and can thus be assigned a common type I structure.

Since there is some dispute about the spectral and physical properties of **4***e* (4), we have also determined its structure by X-ray crystallography. An ORTEP illustration of the structure is given in Fig. 1, and the crystallographic parameters are found in Tables 3–5. **4***e* does indeed have the planar structure first noted for **4***a,c*. The appearance of disorder in the CF_3 atom positions is not unexpected for such a rod-like molecule, whose twofold symmetry axis is at odds with the threefold axis in the CF_3 group. A simple disorder model accounts for this quite effectively, although the C—F bond distances are somewhat unrealistic as a result. In Table 5, the metric parameters relevant to the eight-membered ring are collected for the three crystallographically characterized compounds of this type. **4***e,a,c* represent aryl dithiatetrazocines with electron-withdrawing, neutral, and electron-donating substituents, respectively. The influence of these remote substituents is not apparent in the structural parameters. A statistical treatment of the three structures shows that while the bonds should not be averaged, they are not definitely different either. In general there is as much variation in similar bond lengths within any of these structures as there is between them (29).

The rod-like molecules of **4***e* stack side-by-side and end-to-end in long ribbons, approximately along the (111) plane of the crystal, as shown in Fig. 2. Since there is only one molecule per unit cell, this stacking is completely ordered. It is interesting to note that although the crystals of **4***a,c,e* each belong to a different space group, the molecules are all located at sites with inversion symmetry.

In conclusion, the similarity in the electronic spectra of **4***a–f*, the consistent crystal structures of **4***a,c,e*, as well as the similarity in mass-spectral fragments suggest that all these aryl-1,5,3,4,6,8-dithiatetrazocines have a similar geometry

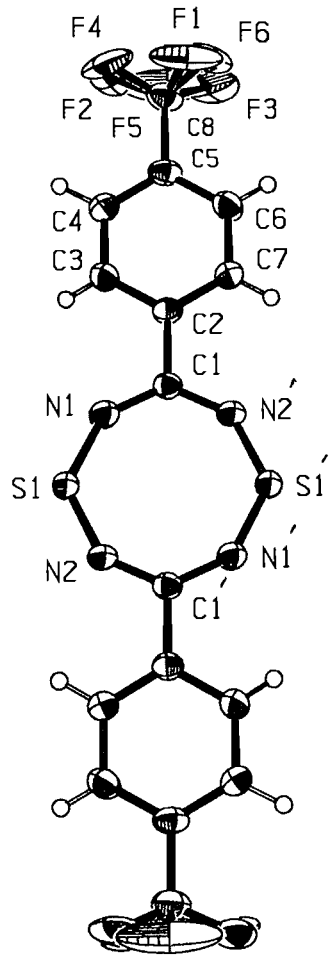

FIG. 1. ORTEP illustration of **4***e*, showing the atom numbering scheme. The hydrogen atoms are shown with artificially small temperature factors for clarity.

and are type I structures. We have not characterized any material corresponding to the 1,3,2,4,6,8 isomer (30).

Electrochemistry and electronic structure

4 are sufficiently soluble in the noncoordinating solvent CH_2Cl_2 to be studied by d.c. and a.c. voltammetric methods. Figure 3 contrasts the cyclic voltammetry of the 10π aromatic type I heterocycle **4***a* with the folded, nonaromatic

Can. J. Chem. Downloaded from www.nrcresearchpress.com by 88.255.202.194 on 09/08/12
For personal use only.

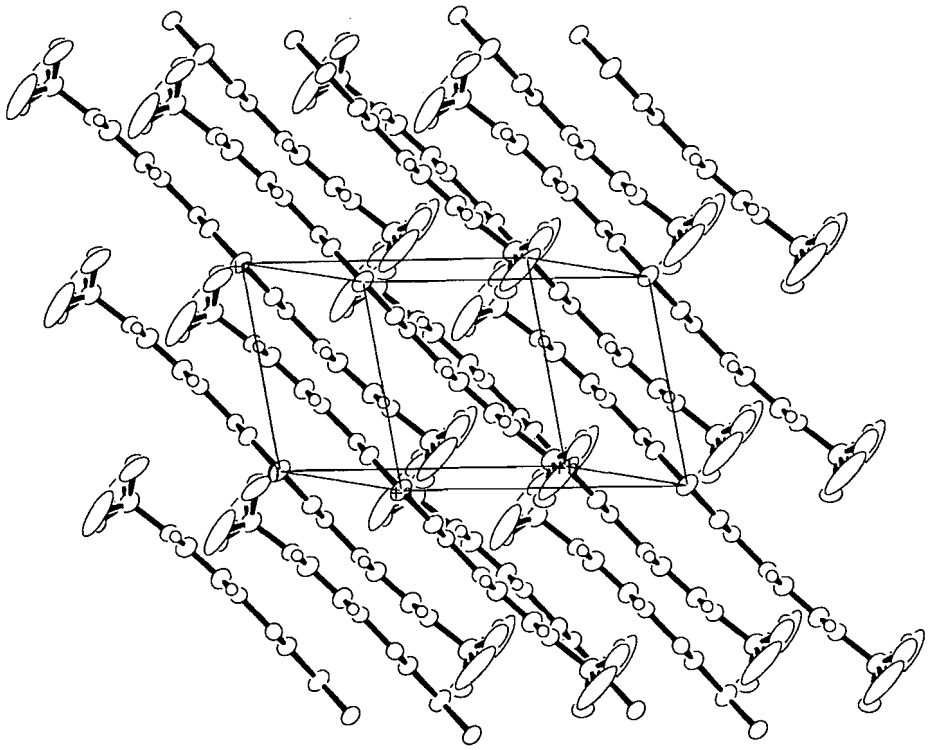

FIG. 2. Packing diagram for **4***e* in the crystal. Ribbons of end-to-end dithiatetrazocine molecules are packed side-by-side in sheets along the (111) plane.

type II compound **9** at room temperature. All the type I and type II compounds that we have studied were found to undergo a fully reversible one-electron reduction, except for **5** where quasi-reversible conditions were observed. The type I aryl-substituted systems **4***a–f* are reduced over the narrow potential range of −0.90 to −1.02 V vs. SCE, while the 'Bu derivative **5** at $\mathscr{E}_{1/2} = -1.14$ V has the lowest reduction potential of the type I compounds, distinct from the aryl compounds. The type II compound **9** has a much lower reduction potential than the others (−1.36 V).

None of the oxidation processes studied is reversible at ambient temperature and slower scan rates. The anodic peak potentials of type I structures **4***a–f* and **5** are strongly substituent dependent, varying from +1.54 for **4***c* to + 2.05 for **4***e*. Irreversible oxidation of **9** occurs at $\mathscr{E}_a = +1.28$ V, making it far easier to oxidize than the type I compounds. A quasi-reversible response of the oxidation step of **4***a,b,c,e* could be obtained using fast-scan techniques and by working at lower temperatures. Scheme 2 illustrates the principle electrode processes of the 10π ring system. All electrode potentials measured in this study, together with the conditions chosen to achieve Nernstian behaviour, are listed in Table 6.

The electrochemical results for **4** are in agreement with simple MO arguments. The HOMO (b_{1u}) and LUMO (b_{2g}) of the model compound $HCN_2S_2N_2CH$ are both π orbitals. (Fig. 4). The LUMO, to which electrons are added in the reduction of **4**, posseses a node at the C atoms, so that the effect of substituents on the energy of this orbital is negligible. This result is unchanged for the diaryl-substituted ring (8). Consistently, the reduction potentials for all these compounds are highly similar, and even that of **5**, in which the aryl group is completely replaced by *tert*-butyl, is only slightly more negative. The HOMO has a large coefficient at the C atoms, and should be much more greatly influenced by substituents bearing p–π orbitals. Thus the lower oxidation potential of **4***a* versus **5** can be explained by extension of conjugation in the former.

A more dramatic effect on the oxidation $\mathscr{E}_a$ occurs upon substitution of the aryl ring. This shows that π-donating substituents, in particular, have a large influence on the oxidation step, leading to lowering of the redox potential, while inductively withdrawing substituents have a smaller effect in raising the potential. A very similar trend is observed in the position of λ_1 in the electronic absorption spectrum (Table 2). This transition has been identified as the HOMO–LUMO transition by magnetic circular dichroism (7). The latter study also concluded that "the extension of conjugation due to the presence of the two phenyl rings (in **4***a*) can hardly be viewed as a minor perturbation." Our voltammetric study strongly substantiates this comment.

The remarkably large thermodynamic stability "window" within which the type I compounds resist oxidation or reduction is fully consistent with their description as aromatic species. The width of this window ranges from 2.49 to 2.96 V, depending on substituents. Although the folded compound **9** has a similar window width (2.63 V), the whole is shifted towards negative potentials. Thus it is by far the most easily oxidized of the series, and the most difficult to reduce. These results are fully consistent with our previous chemical studies, in which we observed **4***a* to be completely resistant to chemical oxidation by chlorine, SO_2Cl_2, and the powerful radical oxidant $(CF_3)_2NO$. On the other hand, **9** reacted readily with these reagents (11, 12).

Can. J. Chem. Downloaded from www.nrcresearchpress.com by 88.255.202.194 on 09/08/12
For personal use only.

Can. J. Chem. Downloaded from www.nrcresearchpress.com by 88.255.202.194 on 09/08/12
For personal use only.

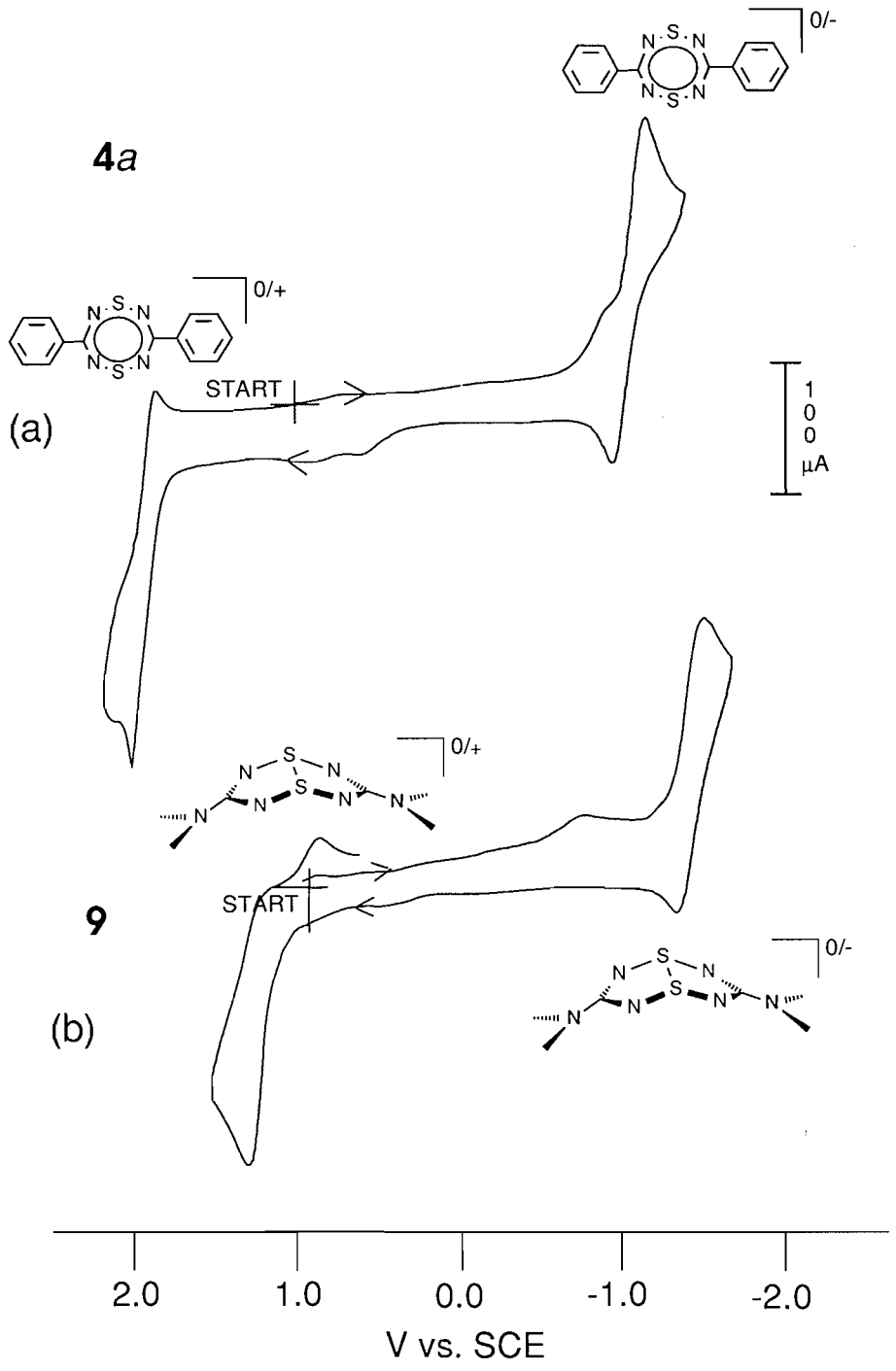

FIG. 3. Cyclic voltammograms for **4***a* and **9** in CH_2Cl_2 containing 0.4 M NBu_4PF_6, run at 50 mV s^{-1} at 25°C. (*a*) $\mathscr{E}_{1/2}$ (10π–11π) = −1.02 V, $\mathscr{E}_{1/2}$ (10π–9π) = +1.86 V; (*b*) $\mathscr{E}_{1/2}$ = −1.36 V, anodic peak at +1.28 V.

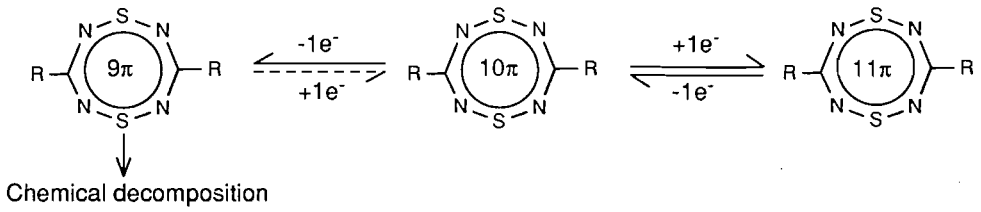

SCHEME 2

TABLE 6. Voltammetric data for some type I and type II dithiatetrazocines

Compound	Reduction $\mathscr{E}_{1/2}$/V[a]	Oxidation $\mathscr{E}_a$/V[c]	Oxidation $\mathscr{E}_{1/2}$/V
4*c*	−0.95	+1.54	+1.50[d]
4*d*	−0.98	+1.69	Irreversible
4b	−0.90	+1.74	+1.70[e]
4*a*	−1.02	+1.91	+1.86[f]
4*f*	−0.91[b]	+1.98	+1.93[g]
4*e*	−0.91	+2.05	Irreversible
5	−1.14[h]	+1.74	Irreversible
9	−1.36[b]	+1.28	Irreversible

[a]At a Pt electrode in CH_2Cl_2/0.4 M NBu_4PF_6 solutions under reversible conditions, referenced to SCE such that $\mathscr{E}_{1/2}$ = +0.48 V for $[Fe(C_5H_5)_2]^{+/0}$ at a scan rate ν = 50 mV s^{-1}.

[b]Reversible conditions confirmed by a.c. voltammetry at ν = 10 mV s^{-1}.

[c]Anodic peak potentials.

[d]Separation of anodic ($\mathscr{E}_a$) and cathodic ($\mathscr{E}_c$) peak = 80 mV at ν = 200 mV s^{-1} and −20°C.

[e]$\mathscr{E}_a - \mathscr{E}_c$ = 120 mV at ν = 500 mV s^{-1} and −10°C.

[f]$\mathscr{E}_a - \mathscr{E}_c$ = 100 mV at ν = 200 mV s^{-1} and 0°C.

[g]$\mathscr{E}_a - \mathscr{E}_c$ = 100 mV at ν = 200 mV s^{-1} and −10°C.

[h]Quasi-reversible conditions, $\mathscr{E}_a - \mathscr{E}_c$ = 120 mV, also confirmed by a.c. voltammetry.

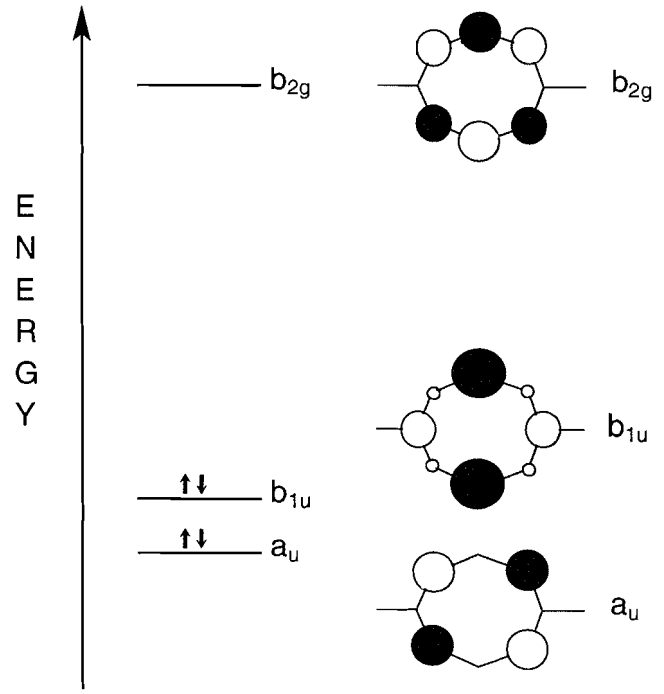

FIG. 4. Frontier orbitals of the model compound 1,5,2,4,6,8-dithiatetrazocine, $HCN_2S_2N_2CH$, from an MNDO calculation. Orbital topologies of the π-orbitals are shown.

Attempts to prepare other compounds

We have attempted to extend methods B and C to the preparation of some non-aryl dithiatetrazocines. For many of these, silylated amidines analogous to **1** are not available. This restricts us to method B. We have accordingly reacted X-$CN_2S_2^+Cl^-$ **10** (**10***a* X = CH_3 (18), **10***b* ^{t}Bu (31), **10***c* Cl (32), and **10***d* Me_2N (33)) with Ph_3Sb/O_2 in warm acetonitrile. However, no precipitates formed in these reactions, as might be expected for the much greater solubility anticipated for the corresponding dithiatetrazocines. In fact it proved impossible to separate the product(s) of these reactions from Ph_3SbCl_2. The latter compound was impossible to separate by column chromatography, being found in *every* fraction collected. We were able to prepare the type II dithiatetrazocine **9** in an atmosphere of O_2 from **10***d* using fine Mg powder as the reducing agent. However, the yield was only 5%. Our attempts to prepare **5** by this route from **10***b* also failed, only S_8 being isolated.

We also applied method C in an attempt to prepare mixed aryl-substituted derivatives of **4**. For example, the chloride salt **2***d* was refluxed in a minimum volume of CH_3CN with one equivalent of **1***e*. We were quite surprised to see clear evidence in the NMR spectra for the appearance of all three products resulting from a scrambling process, i.e., **4***d*, **4***e*, as well as {4-$CF_3C_6H_4$}$CN_2S_2N_2C${4-C_6H_4Cl}. Allowing for differences in solubility both in the reaction solvent and in the NMR solvent, we judge these products to be formed in about equal quantity, and the overall yield is at least 50%. We also investigated the residues that did not precipitate on cooling the reaction mixture. ^{1}H NMR analysis after removal of the solvent indicated the presence of many different compounds, including the three products identified in the precipitate.

Since the mixed product **8** had been prepared by others, albeit in very low yield (3), we reacted **1***a* with **10***b*. Again, the three possible products were formed, as judged by the known NMR parameters of these compounds. These reactions do not fall within the scope of this paper as simple preparative routes, and we have not attempted the separation of these mixtures. However, we consider these results to be mechanistically significant.

Mechanistic considerations

The mechanism for the reactions of methods A and B are not clear. Since radicals are involved, NMR monitoring of the reaction is not feasible. And since the reaction mixture is saturated with dioxygen, following the course of the reaction by ESR is also not feasible. The rate and product distribution for method A does not seem to be greatly affected by concentration; e.g., much the same yields and times are found for the melt reactions as for reactions in acetonitrile or toluene. Presumably this means that the presence of dimers **3** is not a requirement for this reaction. One conceivable reaction of O_2 with a radical momomer is the formation of SO_2, leaving a four-membered ring radical $RCN_2S^{\cdot}$. Dimerization of this latter species would lead directly to **4**. Such four-membered ring species have been implicated in solution in equilibrium with the type II heterocycles $R_2PN_2Se_2N_2PR_2$ (34).

Method C starts with sulfur in the +II oxidation state. As Amin and Rees have already noted, this reaction requires a change in oxidation state to S(III) (i.e., the average oxidation state of the two sulfur atoms in one canonical structure of **4**).

It is possible to imagine a simple condensation reaction of **11** with **2**, leading to chain intermediate **12** (Scheme 3). Ring closure leads to the reduced ring **13**, which can undergo elimination of disilane to produce **4**. A precedent is again known in selenium chemistry where, even in the absence of aromatization of the eight-membered ring, elimination of alkyl groups from $Ph_2PN_2(SeR)_2N_2PPh_2$ (R = Me, Et) occurs to give the type II compound $Ph_2PN_2Se_2N_2PPh_2$ (35).

Can. J. Chem. Downloaded from www.nrcresearchpress.com by 88.255.202.194 on 09/08/12
For personal use only.

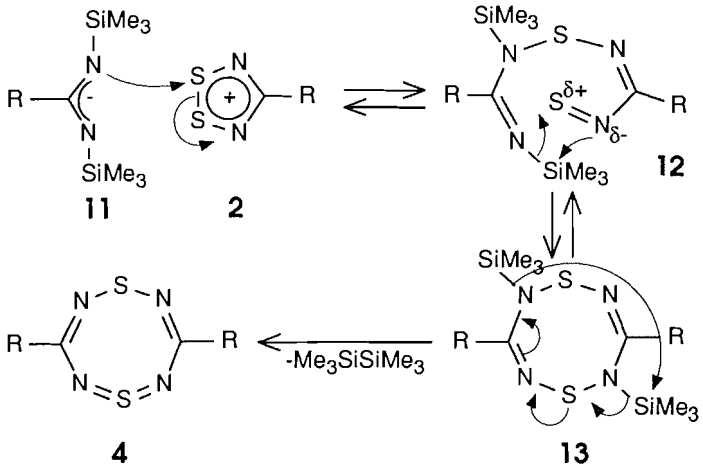

SCHEME 3

This elimination could be preceded by a variety of possible silyl-migration steps. The result of using mixed substituents in this reaction gives credence to such a migration process. Indeed, if the initial condensation reaction leading to **12** as well as the formation of **13** is reversible, then the observed scrambling reaction is certainly feasible. According to this model, the silane elimination must be a slow step. Once elimination occurs, the process is no longer reversible. To test this we heated **4***d* and **4***e* together under reflux in acetonitrile as well as in the presence of 10 equivalents of $ClSiMe_3$. There was no evidence of the mixed-substituent species being formed. In an attempt to see if the elimination step could be enhanced by external conditions, we performed the mixed-substituent reactions in an atmosphere of both O_2 and Cl_2, but found no enhancement or retardation of the process.

Conclusions

We have developed two higher yield synthetic routes to 1,5-dithiatetrazocines with greatly simplified work-up. These methods further illustrate the utility of silylated amidines as an entry into sulfur nitrogen heterocyles. We have properly characterized **4***b,e*, for which the previously reported physical and spectroscopic properties are partly in error. We have prepared and characterized three previously unknown dithiatetrazocines. However, for reasons that remain unclear, but may be related to solubility, the method appears to work only for aryl derivatives. Thus the route described in the literature for *tert*-butyl remains the only viable way to prepare this ring. Finally, for the bent type II rings, the method originally reported is far superior to those reported here.

Our voltammetric studies have confirmed the stability of the aromatic 10π electronic structure of **4**. The width of the redox stability window is directly comparable to the wavelength of the lowest energy (HOMO–LUMO) transition in the electronic spectrum. Thus we have confirmed electrochemically the extension of conjugation in aryl-1,5-dithiatetrazocines first noted in electronic and magnetic circular dichroism spectroscopic studies (7).

We are currently investigating the feasibility of preparing novel mixed-substituent dithiatetrazocines by the reactions described here. It seems likely that such species will be more reactive than the symmetrical compounds. The preparation of benzene rings disubstituted with dithiatetrazocines is also being investigated.

Acknowledgements

We thank the Natural Sciences and Engineering Research Council of Canada (NSERC) for support in the form of an operating grant (R.T.B.) and an equipment grant for the infrared spectrometer, as well as the University of Lethbridge for the purchase of the NMR spectrometer. K.H.M. acknowledges the award of a Feodor-Lynen Fellowship by the A. v. Humboldt Foundation, Bonn, Germany. W.H. was the recipient of an NSERC summer research scholarship, and K.P. was supported through the University of Lethbridge Research Fund.

1. I. Ernst, W. Holick, G. Rihs, D. Schomburg, G. Shoham, D. Wenkert, and R. B. Woodward. J. Am. Chem. Soc. **103**, 1540 (1981).
2. M. Amin and C. W. Rees. J. Chem. Soc. Chem. Commun. 1137 (1989).
3. M. Amin and C. W. Rees. J. Chem. Soc. Perkin Trans. 1, 2495 (1989).
4. U. Scholz, H. W. Roesky, J. Schimkowiak, and M. Noltemeyer. Chem. Ber. **122**, 1067 (1989).
5. J. P. Boutique, R. Lazzaroni, J. Riga, J. J. Verbist, G. Pfister-Guillouzo, J. Delhalle, J. G. Fripiat, R. C. Haddon, and M. D. Kaplan. J. Chem. Soc. Perkin Trans. 2, 259 (1987).
6. R. Gleiter, R. Bartetzko, and D. Cremer. J. Am. Chem. Soc. **106**, 3437 (1984).
7. H. P. Klein, R. T., Oakley, and J. Michl. Inorg. Chem. **25**, 3194 (1986).
8. J. P. Boutique, J. Riga, J. J. Verbist, J. Delhalle, J. G. Fripiat, R. C. Haddon, and M. D. Kaplan. J. Am. Chem. Soc. **106**, 312 (1984).
9. S. Millefiori, A. Millefiori, and G. Granozzi. Inorg. Chim. Acta, **90**, L55 (1984).
10. R. T. Oakley. Prog. Inorg. Chem. **36**, 299 (1988).
11. R. T. Boeré, A. W. Cordes, R. T. Oakley, and R. W. Reed. J. Chem. Soc. Chem. Commun. 655 (1985).
12. R. T. Boeré, A. W. Cordes, S. L. Craig, R. T. Oakley, and R. W. Reed. J. Am. Chem. Soc. **109**, 868 (1987).
13. T. Chivers, K. S. Dhathathreyan, and T. Ziegler. J. Chem. Soc. Chem. Commun. 86 (1989).
14. R. T. Boeré, K. Larsen, J. Fait, J. Yip, and K. H. Moock. Phosphorus Sulfur Silicon Relat. Elem. **65**, 143 (1992).

Can. J. Chem. Downloaded from www.nrcresearchpress.com by 88.255.202.194 on 09/08/12
For personal use only.

15. R. T. Boeré, R. T. Oakley, and R. W. Reed. J. Organomet. Chem. **331**, 161 (1987).
16. P. D. Bel Belluz, A. W. Cordes, E. M. Kristof, P. V. Kristof, S. W. Liblong, and R. T. Oakley. J. Am. Chem. Soc. **111**, 9276 (1989).
17. A. W. Cordes, R. C. Haddon, R. T. Oakley, L. F. Schneemeyer, J. V. Waszczak, K. M. Young, and N. M. Zimmerman. J. Am. Chem. Soc. **113**, 582 (1991).
18. A. J. Banister, N. R. M. Smith, and R. G. Hey. J. Chem. Soc. Perkin Trans. 1, 1181 (1983).
19. A. J. Banister, M. I. Hansford, Z. V. Hauptman, S. T. Wait, and W. Clegg. J. Chem. Soc. Dalton Trans. 1705 (1989).
20. A. C. T. North, D. C. Phillips, and F. S. Mathews. Acta Crystallogr. Sect. A: Cryst. Phys. Diffr. Theor. Gen. Crystallogr. **A24**, 351 (1968).
21. H.-F. Fan. SAPI91: Structure Analysis Programs with Intelligent Controls. Rigaku Corporation, Tokyo. 1991.
22. G. M. Sheldrick. SHELX-76. A program for crystal structure determination. University of Cambridge, Cambridge, U.K. 1976.
23. D. T. Cromer and J. B. Mann. Acta Crystallogr. Sect. A: Cryst. Phys. Diffr. Theor. Gen. Crystallogr. **A24**, 321 (1968).
24. R. F. Stewart, E. R. Davidson, and W. T. Simpson. J. Chem. Phys. **42**, 3175 (1965).
25. D. T. Cromer and D. Liberman. J. Chem. Phys. **53**, 1891 (1970).
26. TEXSAN. Single crystal structure analysis software, Version 1.2. Molecular Structure Corporation, The Woodlands, Tex. 1992.
27. C. K. Johnson. ORTEP II. Report ORNL-5138. Oak Ridge National Laboratory, Tenn. 1976.
28. R. M. Silverstein, G. C. Bassler, and T. C. Morrill. Spectrometric identification of organic compounds. 5th ed. Wiley, New York. 1991.
29. G. H. Stout and L. H. Jensen. X-ray structure determination; a practical guide. 2nd ed. Wiley, New York 1989.
30. T. Chivers, J. F. Richardson, and N. R. M. Smith. Inorg. Chem. **25**, 47 (1986).
31. G. C. Alange, A. A. Banister, B. Bell, and P. W. Millen. Inorg. Nucl. Chem. Lett. **13**, 143–144 (1977).
32. H.-U. Höfs, R. Mews, W. Clegg, M. Noltemeyer, M. Schmidt, and G. M. Sheldrick. Chem. Ber. **116**, 416 (1983).
33. A. W. Cordes, J. D. Goddard, R. T. Oakley, and N. P. C. Westwood. J. Am. Chem. Soc. **111**, 6147 (1989).
34. T. Chivers and D. D. Doxsee. Phosphorus Sulfur Silicon Relat. Elem. **64–65**, 317 (1992).
35. T. Chivers, D. D. Doxsee, and J. F. Fait. J. Chem. Soc. Chem. Commun. 1703 (1989).

Can. J. Chem. Downloaded from www.nrcresearchpress.com by 88.255.202.194 on 09/08/12
For personal use only.

Secondary metabolites of the aspen fungus *Stachybotrys cylindrospora*

WILLIAM A. AYER[1] AND SHICHANG MIAO
Department of Chemistry, University of Alberta, Edmonton, Alta., Canada T6G 2G2

Received November 24, 1992

WILLIAM A. AYER and SHICHANG MIAO. Can. J. Chem. **71**, 487 (1993).

The secondary metabolites produced by the fungus *Stachybotrys cylindrospora*, which is known to be strongly antagonistic to the blue-stain fungus *Ceratocystiopsis crassivaginata*, have been examined. The compounds responsible for the antifungal activity are trichodermin (**5**) and trichodermol (**6**), two previously known mycotoxins belonging to the trichothecene family. The other metabolites, stachybotrydial (**1**), stachybotramide (**8**), and 6,8-dihydroxy-3,5,7-trimethylisochroman (**7**), although not active against *C. crassivaginata*, are new natural products. The structures of the new compounds were established by spectroscopic techniques.

WILLIAM A. AYER et SHICHANG MIAO. Can. J. Chem. **71**, 487 (1993).

On a étudié les métabolites secondaires produits par le champignon *Stachybotrys cylindrospora* qui est connu pour être un antagoniste puissant du champignon à teinte bleue *Ceratocystiopsis crassivaginata*. Les composés responsables de l'activité antifongique sont la trichodermine (**5**) et le trichodermol (**6**), deux mycotoxines isolées antérieurement appartenant à la famille du trichothécène. Les autres métabolites, les stachybotrydial (**1**), stachybotramide (**8**) et 6,8-dihydroxy-3,5,7-triméthylisochromane (**7**) qui ne sont pas actifs contre le *C. crassivaginata* sont de nouveaux produits naturels. On a déterminé les structures des nouveaux composés à l'aide de techniques spectroscopiques.

[Traduit par la rédaction]

Introduction

The decay and staining of aspen (*Populus tremuloides* Michaux) caused by fungi is a serious problem associated with aspen utilization in Canada (1, 2). For aspen lumber and wood products such as chipboard and chopsticks, even small amounts of rot or stain can drastically reduce product quality and make it unmarketable (1). Two of the most important staining fungi are the so-called blue-stain fungi *Ceratocystiopsis crassivaginata* (H. D. Griffin) Upadhyay (NOF1509)[2] and *Ophiostoma piliferum* (Fr.: Fr.) Syd. and Syd. (1). Another fungal pathogen of aspen, *Stachybotrys cylindrospora* C. N. Jensen (NOF1828) (3), isolated from aspen has been found to be strongly antagonistic to the blue-stain fungus *C. crassivaginata* when grown on malt extract agar plates.[3] In this paper, we report several secondary metabolites produced when *S. cylindrospora* is grown in malt extract liquid culture. Two of these compounds, trichodermin (**5**) and trichodermol (**6**), which have been previously reported as mycotoxins, are responsible for the above-mentioned antagonistic activity. The other compounds, stachybotrydial (**1**), stachybotramide (**8**), and 6,8-dihydroxy-3,5,7-trimethylisochroman (**7**), albeit not active against *C. crassivaginata*, are new natural products.

Results and discussion

Stachybotrys cylindrospora was grown in malt extract/yeast extract liquid culture. The culture broth of the first and fourth fermentations was extracted with ethyl acetate to provide a large quantity of metabolites that did not exhibit antagonistic activity against *C. crassivaginata*. The major compound present is a new natural product (**1**), which we have named stachybotrydial. A portion of the crude extract was acetylated to produce the corresponding diacetate (**2**) of **1**. The remaining portion of the extract decomposed to produce an artifact (**3**) that was inseparable from the original compound (**1**). Since the original compound was an aldehyde, it could be reduced by sodium borohydride to the corresponding alcohol (**4**), which could then be separated from the artifact (**3**). All other fermentations have produced metabolites that show antifungal activity against *C. crassivaginata*. It was found that still cultures produce more of the bioactive metabolites than do shake cultures. The active extract was fractionated on Sephadex LH20. The bioactivity was located in the early fraction, which after repeated chromatography on silica gel yielded two pure compounds, **5** and **6**. The remaining fractions were subjected to repeated silica gel chromatography to give pure compounds: compound **7** from the second fraction, compound **3** from the third fraction, orsellinic acid from the fourth fraction, compound **8** (as its acetylated derivative **9**) from the fifth fraction.

Stachybotrydial diacetate (2)

Compound **2** was obtained as a pale yellow solid. The molecular formula $C_{27}H_{34}O_7$ was determined by HREIMS and indicates 11 unsaturations. A literature search based on the spectroscopic data of compound **2** revealed that its unacetylated parent compound, **1**, for which we propose the name stachybotrydial, is the 2-deoxy analog of a previously reported fungal metabolite, K-76 (**10**) (4, 5). The IR spectrum of compound **2** displays a strong band at 1690 cm^{-1} corresponding to the phthalaldehyde functionality as well as two bands at 1773 and 1728 cm^{-1} corresponding to the two acetoxy groups. The aldehyde absorption is similar to that reported for K-76 (4). The ^1H NMR spectrum (Table 1) of compound **2** displays very characteristic signals at 10.55 (s) and 10.61 (s) ppm for the phthalaldehyde moiety. The ^{13}C NMR chemical shifts for compound **2** (Table 3) are very similar to those reported for K-76 (5*b*) except for C2 (22.15 ppm) and for the carbons of the two acetoxy groups (3-OAc: 21.10. 170.45; 2′-OAc: 20.76, 167.25 ppm). A COSY experiment, assisted by a HETCOR experiment, clearly identified the two spin systems in ring A and ring B of the

[1]Author to whom correspondence may be addressed.

[2]Cultures are deposited in the fungal culture collection at the Northern Forestry Center (NOF 1824), Forestry Canada, Edmonton, and the University of Alberta Microfungus Herbarium (UAMH 7122), Edmonton.

[3]L. J. Hutchison and Y. Hiratsuka, Northern Forestry Center, Edmonton, Canada, personal communication.

Can. J. Chem. Downloaded from www.nrcresearchpress.com by 88.255.202.194 on 09/08/12
For personal use only.

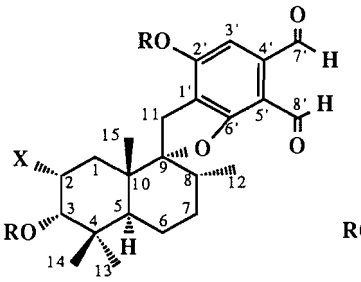

1 R=X=H
2 R=Ac X=H
10 R=H X=OH

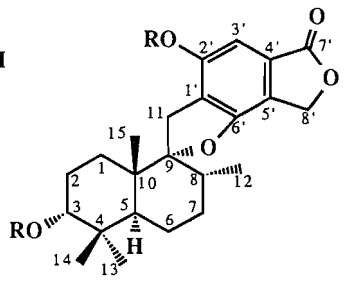

3 R=H
11 R=Ac

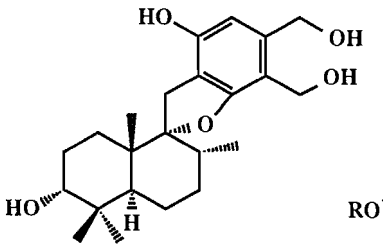

4

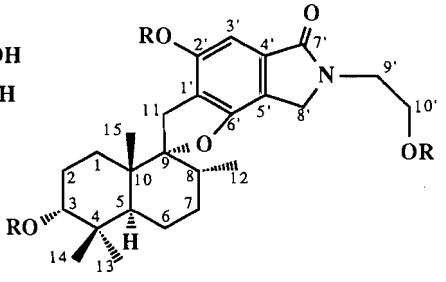

8 R=H
9 R=Ac

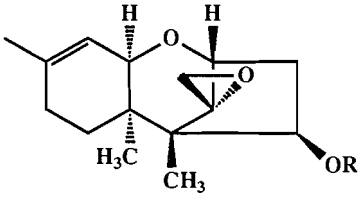

5 R=Ac
6 R=H

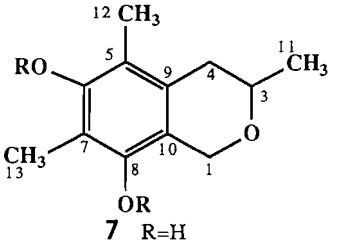

7 R=H
12 R=Ac

drimane moiety. For example, in ring A, the signal for H3β (4.62, br s) is coupled to a methylene pair at 1.82 and 1.62 ppm, and these in turn are coupled to another methylene pair at 1.12 and 1.65 ppm. In a long-range COSY experiment, H3′ (7.14 ppm) was found to couple with one (10.55 ppm) of the aldehyde protons. This long-range benzylic coupling accounts for the fact that the aldehyde peak at 10.55 ppm is broader than the aldehyde proton at 10.61 ppm. All of the observed nuclear Overhauser enhancements (Fig. 1) are consistent with the proposed structure for compound **1**. The HREIMS fragmentation pattern (Fig. 2) is also in good agreement with the proposed structure. For example, the base peak at 190.1716 is attributed to the drimane fragment arising from cleavage a. Another cleavage, a′, produces the phthalaldehyde fragment that accounts for the peak at 220.0371. The strong peaks at 272.0681 ($C_{15}H_{12}O_5$) and 230.0579 ($C_{13}H_{10}O_4$) are attributed to cleavage b across ring B.

Compound 3

Compound **3**, believed to be an artifact formed from stachybotrydial (**1**), was separated from **1** as a white crystalline solid after **1** was reduced to the corresponding diol (**4**). Examination of its NMR data suggested that its structure is **3**; the dialdehyde moiety in stachybotrydial (**1**) is transformed into a lactone. The spectroscopic evidence supporting this proposal is as follows. The HREIMS revealed that the molecular formula is $C_{23}H_{30}O_5$, identical with that of the dialdehyde, **1**. In the IR spectrum, the aromatic aldehyde absorption is replaced by a band at 1742 cm^{-1}, appropriate for an α,β-unsaturated γ-lactone. The ^1H (Table 1) and ^{13}C NMR (Table 3) signals corresponding to the dialdehyde functionality are replaced by methylene signals at 5.23 and 5.17 ppm (J = 14.7) in the ^1H NMR and at δ 67.84 (t) and 171.29 in the ^{13}C NMR. A COSY experiment (Table 1) together with an HMQC (6) experiment identified the two spin systems in the drimane nucleus. An HMBC experiment (Table 1) was employed to establish the regiochemistry of the lactone system. Thus a three-bond correlation from H3′ (6.76 ppm) to the carbonyl at 171.29 ppm unambiguously indicates that the lactone carbonyl is located at C7′ rather than C8′. The correlations from the lactone methylene protons (5.23 and 5.17 ppm) to C5′ (128.07 ppm), C4′ (119.22 ppm), and C6′ (155.47 ppm) indicate that the methylene is located at C8′, while the correlation from the same methylene protons to the lactone carbonyl confirmed the presence of a γ-lactone. All of the observed HMBC correlations are consistent with structure **3** for this compound.

The spontaneous transformation of stachybotrydial (**1**) in

Can. J. Chem. Downloaded from www.nrcresearchpress.com by 88.255.202.194 on 09/08/12
For personal use only.

TABLE 1. NMR data for compounds **2** and **3**

Position	Compound **2**	Compound **3**		
	^{1}H (400 MHz, $CDCl_3$)	^{1}H (400 MHz, acetone-d_6)	COSY	Selected HMBC[b] (for J = 7 Hz)
1	α: 1.65 β: 1.12	α: 1.90 β: 1.06	H1β, H2α,β H1α,H2α,β	
2	α: 1.82 β: 1.62	α: 1.60 β: 1.44	H1α,β,H3,H2β H1α,β,H3,H2α	
3	β: 4.62, br s	β: 3.32, br s	H2α, β	C1, C5
5	α: 2.11,dd,12.3,2.5	2.17,dd,11.6,2.7	H6α,β	C6,C10
6	α: 1.45 β: 1.60	α: 1.46 β: 1.55	H5,H6β.H7α,β H5,H6α,H7α,β	
7	α: 1.67 β: 1.52	α: 1.60 β: 1.45	H6α,β,H7β,H8 H6α,β,H7a,H8	
8	β: 1.85	β: 1.86	H12, H7α,β	
11	a:[a] 3.13, d, 17.6 b:[a] 2.82, d, 17.6	a:[a] 3.26, d, 17.3 b:[a] 2.90, d, 17.3	H11b H11a	C8,C9,C10,C1′,C2′,C6′ C8,C9,C10,C1′,C2′,C6′
12	α: 0.79, d, 6.5; 3H	α: 0.72, d, 6.5	H8	C7, C8, C9
13	α: 0.91; 3H	α: 0.97, s		C3,C4,C5,C14
14	β: 0.92; 3H	β: 0.86, s		C3,C4,C5,C13
15	β: 1.01; 3H	β: 1.06, s		C1, C5, C9, C10
3′	7.14, s	6.76, s		C1′, C5′, C7′
7′	10.55, s			
8′	10.61, s	a: 5.23, d, 14.7 b: 5.17, d, 14.7	H8b H8a	C4′, C5′, C6′, C7′ C4′, C5′, C6′, C7′
3-OAc	1.94, s; 3H			
2′-OAc	2.32, S; 3H			

[a]H11a is defined as the proton on the side of C10, while H11b is on the side of C8 (Fig. 1).
[b]Heteronuclear Multiple Bond Connectivity.

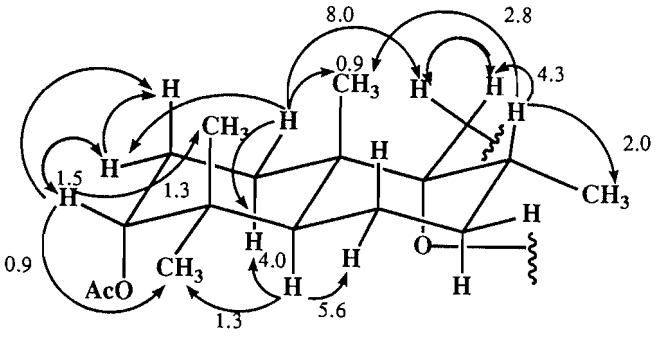

FIG. 1. Selected nOes for stachybotrydial diacetate (**2**).

organic solvents into the corresponding lactone (**3**) results from an intramolecular Cannizzaro reaction, which normally requires alkaline conditions. However, no alkali was used during the isolation. Stachybotrydial diacetate (**2**) underwent the same transformation in $CDCl_3$ when kept in the fridge for several weeks. This transformation has not been reported for K-76 (**10**) (4, 5*a*, 5*b*).

Stachybotramide (8)

Another new compound, **8**, for which we propose the name stachybotramide, was isolated in its acetylated form (**9**) as a white amorphous solid. Stachybotramide triacetate (**9**) has the molecular formula $C_{31}H_{41}NO_8$ according to HREIMS. The similarity between the NMR data of stachybotramide triacetate (**9**) and those of the lactone diacetate (**11**) (Table 2) suggests that **9** possesses the same phenylspirodrimane skeleton. The COSY and TOCSY (7) spectra of compound **9** clearly identified the three spin systems in the drimane moiety, i.e., C1-C2-C3 in ring A, C5-C6-C7-C8-C12 in ring B, and the C11 methylene. Long-range H/C correlations provided by an HMBC experiment are fully consistent with the proposed structure (see Table 2). A proton spin system that is not present in **11**, $>NCH_2CH_2O$- (^{1}H δ: 3.85, 4.32 ppm; ^{13}C δ: 41.86, 62.25 ppm), was also identified by COSY and TOCSY. Both the proton and carbon signals of the C8′ methylene were shifted significantly upfield to 4.46 and 4.34 ppm and 48.18 ppm, respectively. This is accounted for by the replacement of the oxygen atom on C8′ of **11** by the nitrogen in **9**. Both the IR absorption at 1696 cm^{-1} and ^{13}C NMR signal at δ 167.99 ppm are consistent with the presence of a γ-lactam. An HMBC experiment (Table 2) optimized for J = 4 Hz provided unambiguous evidence for the attachment of the $>NCH_2CH_2O$- fragment to C7′ and C8′. For example, the C9′ methylene protons (3.85 ppm) showed long-range correlations to both C7′ and C8′ as well as to C10′ (62.25 ppm); the C10′ methylene

Can. J. Chem. Downloaded from www.nrcresearchpress.com by 88.255.202.194 on 09/08/12
For personal use only.

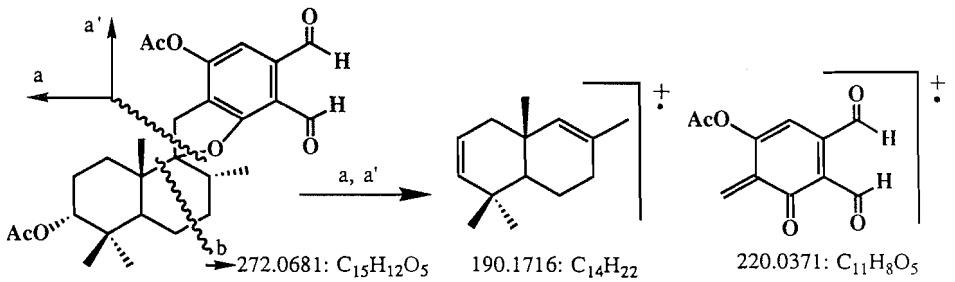

FIG. 2. HREIMS fragmentation pattern for stachybotrydial diacetate (**2**).

TABLE 2. NMR data for compounds **11** and **9** (both in $CDCl_3$)

Position	Compound **11**	Stachybotramide triacetate (**9**)			
	^{1}H (500 MHz)	^{1}H (400 MHz)	COSY	Selected HMBC (for J = 7 Hz)	Selected HMBC (for j = 4 Hz)
1	α: 1.65 β: 1.11	α: 1.66 β: 1.12	H1β, H2α,β H1α, H2α,β	C3, C5, C15	C15
2	α: 1.84 β: 1.62	α: 1.86 β: 1.63	H1α,β, H3, H2β H1α,β, H3, H2α	C3, C4, C10	C10
3	β: 4.63, t, 3.0	β: 4.64, br s	H2α,β	C2, C5, 3-OAc	
5	α: 2.05	α: 2.05	H6α,β	C4,C10,C14,C15	
6	α: 1.58 β: 1.43	α: 1.62 β: 1.47	H5, H6β, H7a,b H5, H6α, H7a,b		
7	a: 1.60 b: 1.50	a: 1.60 b: 1.50	H6α,β, H7b, H8 H6α,β, H7a, H8		
8	β: 1.80	β: 1.82	H12, H7a,b		
11	a:[a] 3.18, d, 17.3	a:[a] 3.16, d, 17.0	H11b	C8, C9, C10 C1′, C2′, C6′	C8, C9, C10 C1′, C2′, C6′
	b:[a] 2.82, d, 17.3	b:[a] 2.78, d, 17.0	H11a	C8, C9, C10 C1′, C2′, C6′	C8, C9, C10 C1′, C2′, C6′
12	α: 0.76,d,6.5	α: 0.75,d,6.5	H8	C7, C8, C9	C7, C8, C9
13	α: 0.91, s	α: 0.92, s		C3,C4,C5,C14	C3,C4,C5,C14
14	β: 0.92, s	β: 0.93, s		C3,C4,C5,C13	C3,C4,C5,C13
15	β: 1.00, s	β: 1.00, s		C1, C9, C10	C1, C9, C10
3′	7.11, s	7.05, s		C1′,C2′,C4′,C7′	C1′,C2′,C4′
8′	a: 5.32,d,15.0 b: 5.16,d,15.0	a: 4.46,d,16.6 b: 4.34,d,16.6	H8′b H8′a	C4′, C5′, C7′ C4′, C5′, C7′	C4′, C5′, C7′ C4′, C5′, C7′
9′		3.85, m; 2H	H10′		C7′,C8′,C10′
10′		4.32, m; 2H	H9′		C9′,10′-OAc
3-OAc	2.03, s; 3H	2.03, s; 3H		3-OAc (C=O)	3-OAc (C=O)
2′-OAc	2.32, s; 3H	2.31, s; 3H		2′-OAc (C=O)	2′-OAc (C=O)
10′-OAc		2.06, s; 3H		10′-OAc (C=O)	10′-OAc (C=O)

[a]H11a is defined as the proton on the side of C10, while H11b is on the side of C8.

protons showed long-range correlations to C9′ (41.86 ppm) and an acetoxy carbonyl carbon (170.69 ppm), indicating that the oxygen in the $>NCH_2CH_2O$- fragment is acetylated. Thus stachybotramide possesses structure **8**.

Trichothecenes (5, 6)

Compound **5** was obtained as a colorless oil, $[\alpha]_D$ −9.3, IR ν_{max}: 1735, 1374, 1244, 1081 cm^{-1}. The molecular formula $C_{17}H_{24}O_4$ was determined by HREIMS. Extensive NMR studies including ^{1}H, ^{13}C, COSY, HMQC, and HMBC revealed that compound **5** is identical with trichodermin, a known mycotoxin belonging to the trichothecene family.[4] The spectroscopic data are consistent with those reported for trichodermin (8). Compound **6**, slightly more polar than com-

[4]For reviews on the chemistry and biological activities of trichothecenes, see ref. 8.

Can. J. Chem. Downloaded from www.nrcresearchpress.com by 88.255.202.194 on 09/08/12
For personal use only.

TABLE 3. ^{13}C NMR data for compounds **2**, **3**, **9** (100 MHz)

Position	Compound **2** ($CDCl_3$)	Compound **3** (acetone-d_6)	Compound **9** ($CDCl_3$)
1	24.92, t	24.91, t	24.84, t
2	22.15, t	21.60, t	22.32, t
3	77.42, d	75.21, d	77.76, d
4	36.71, s	38.29, s	36.79, s
5	41.10, d	40.65, d	41.02, d
6	20.57, t	25.91, t	20.69, t
7	30.94, t	31.81, t	30.85, t
8	36.84, d	37.78, d	37.06, d
9	101.08, s	100.00, s	99.16, s
10	42.26, s	43.09, s	42.11, s
11	31.63, t	32.53, t	32.44, t
12	15.46, q	15.86, q	15.51, q
13	27.83, q	28.94, q	27.80, q
14	21.71, q	22.80, q	21.89, q
15	15.98, q	16.36, q	16.05, q
1′	115.28, s	120.72, s	123.65, s
2′	150.59, s	156.65, s	147.09, s
3′	114.57, d	103.00, d	108.53, d
4′	137.91, s	119.22, s	118.23, s
5′	127.57, s	128.07, s	134.55, s
6′	166.39, s	155.47, s	156.01, s
7′	188.43, d	171.29, s	167.99, s
8′	191.21, d	67.84, t	48.18, t
9′			41.86, t
10′			62.25, t
3-OAc	21.10, q; 170. 45, s		20.90*, q; 170.26, s
2′-OAc	20.76, q; 167.25, s		21.24*, q; 168.32, s
10′-OAc			20.83*, q; 170.69, s

*These assignments may be interchanged.

pound **5**, was obtained as an amorphous white solid, $[\alpha]_D$ −22, IR ν_{max}: 3458, 1625, 1070 cm^{-1}. The molecular formula is $C_{15}H_{22}O_3$ according to HREIMS, C_2H_2O less than that of compound **5**. NMR studies established that compound **6** is the desacetyl form of compound **5**, known as trichodermol, a well-known mycotoxin in the trichothecene family (8).

Bioassays against the blue-stain fungus *C. crassivaginata* indicate that trichodermin (**5**) and trichodermol (**6**) are responsible for the antifungal activity.[5] Trichothecenes have been isolated from various species of *Fusarium, Myrothecium, Trichothecium, Cephalosporium, Verticimonosporium, Stachybotrys, Trichoderma*, and *Cylindrocarpon*. Many trichothecenes possess a variety of significant biological activities such as toxicity, antifungal activity, enzyme inhibition, and immunosuppresion (8). This is the first report of the isolation of trichothecenes from *S. cylindrospora*.

6,8-Dihydroxy-3,5,7-trimethylisochroman (7)

Compound **7** was isolated as an amorphous yellow solid. HREIMS revealed the molecular formula $C_{12}H_{16}O_3$. The IR spectrum displayed a broad band at 3412 cm^{-1}, suggesting the presence of hydroxy groups. The ^1H NMR spectrum of compound **7** (Table 4) displays singlets at 7.00 and 6.94 ppm, a methylene AB system at 4.83 and 4.52 ppm (J = 14.7), methyl singlets at 2.13 and 2.06 ppm, and a $(Ar)CH_2CH(O)CH_3$ fragment. The proton signals at 7.00 and 6.94 ppm are replaced by aromatic acetyl methyl signals (2.34, 2.30 ppm) upon acetylation (compound **12**), indicating the presence of two phenolic hydroxyls in **7**. The carbon spectrum (Table 4) of compound **7** contains six aromatic singlets between 152.44 and 109.63 ppm, indicating that four of the five unsaturations of the molecule may be accounted for by a fully substituted benzene ring. The substituents are two hydroxyls, two methyls, one methylene, and the $CH_2CH(O)CH_3$ fragment. The latter two fragments must be *ortho* related and connected through the oxygen atom to create a ring which accounts for the fifth unsaturation. The substitution pattern of the methyls and hydroxyls on the benzene ring was determined by a series of nOe irradiations (Fig. 3). Thus the structure of compound **7** is established as 6,8-dihydroxy-3,5,7-trimethylisochroman. Long-range H/C correlations (Table 4) provided by an HMBC experiment are fully consistent with the proposed structure **7**. For example, the correlations from both the C1 methylene and the C4 methylene protons to C9 (131.08 ppm) and C10 (115.25 ppm) established the *ortho* relationship between these two groups. The correlation between the C1 methylene protons and C3 (71.23 ppm) confirmed the ether linkage between C1 and C3.

In conclusion, the investigation of the metabolites of the aspen fungus *Stachybotrys cylindrospora* has led to the isolation and identification of three types of compounds, namely, the phenylspirodrimanes (stachybotrydial (**1**) and stachybotramide (**8**)), the trichothecenes (trichodermin (**5**) and trichodermol (**6**)), and 6,8-dihydroxy-3,5,7-trimethylisochroman (**7**). Trichodermin (**5**) and trichodermol (**6**) are responsible for the antifungal activity of *S. cylindrospora*

[5]P. Chakravarty and Y. Hiratsuka, Northern Forestry Center, Edmonton, Canada, personal communication.

Can. J. Chem. Downloaded from www.nrcresearchpress.com by 88.255.202.194 on 09/08/12
For personal use only.

TABLE 4. NMR data for compound **7** (acetone-d_6)

Position	^{1}H (400 MHz)	^{13}C (100 MHz)	HMBC
1	a: 4.52, d, 14.7	65.57, t	C3, C8, C9, C10
	b: 4.83, d, 14.7		C8, C9, C10
3	3.64, m	71.23, d	
4	a: 2.58, dd, 16.4, 2.5	34.65, t	C9, C10
	b: 2.29, dd, 16.4, 10.8		C3, C9, C10, C11
5		114.21, s	
6		152.44, s	
7		109.63, s	
8		149.55, s	
9		131.08, s	
10		115.25, s	
11	1.28, d, 6.2; 3H	22.14, q	C3, C4
12	2.06, s; 3H	10.92, q	C5, C6, C9
13	2.13, s; 3H	9.06, q	C6, C7, C8
6-OH	6.94, br s		
8-OH	7.00, br s		

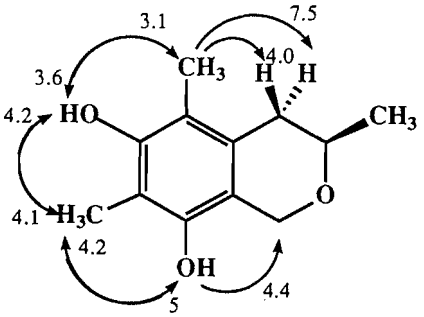

FIG. 3. Selected nOes for compound **7**.

against the blue-stain fungus *Ceratocystiopsis crassivaginata*. Compounds **1**, **7**, and **8** are new natural products.

Experimental

General

All solvents used were distilled prior to use. ^{1}H NMR spectra were recorded on either a Bruker AM400 or Varian Unity-500 spectrometer. All ^{13}C NMR spectra were recorded on a Bruker AM400 spectrometer. All COSY and LR-COSY experiments were performed by using standard Bruker or Varian Unity programs. All HMQC and HMBC experiments were performed on a Varian Unity-500 spectrometer, with 2K data points in the F2 domain and 256 increments, and optimized for $^1J_{H/C}$ = 140 Hz and $^{2-3}J_{H/C}$ = 7 Hz unless otherwise stated in the text.

Culture conditions for S. Cylindrospora

Stachybotrys cylindrospora was cultured in 5 or 10 L malt extract/yeast extract liquid medium (20 g malt extract/1 g yeast extract in 1 L double-distilled water) for 3 weeks. The early batches were shake cultures (100 rpm) while the later batches were still cultures, which were found to produce larger amounts of the active compounds (**5** and **6**). Details of culturing techniques have been described previously (9).

Work-up and isolation procedures

1. Procedures for batches 1 and 4. The mycelium was removed by filtration through cheese cloth to give 5 L yellow broth, which was then concentrated to 1/10 volume under reduced pressure. The concentrate was extracted with ethyl acetate three times. The organic extract was dried over sodium sulfate and concentrated under reduced pressure to yield an orange solid (1.2 g), which contained mainly one compound, **1**. A portion (120 mg) of the extract was acetylated with Ac_2O/pyridine to yield 30 mg of compound **2** as a white amorphous solid after purification on a silica gel column (solvent: 10–20% acetone/hexanes). The remaining portion of the extract partially decomposed to give compound **3**, which was inseparable from compound **1**; 119 mg of this mixture was treated with 250 mg $NaBH_4$ (in 20 mL CH_3CH/H_2O, 30 min at 0°C, 3 h at room temperature). The reaction mixture was acidified with AcOH, diluted with water, and extracted with EtOAc. The organic extract was chromatographed on silica gel (25–50% acetone/hexanes) to yield 16 mg compound **3** and 40 mg compound **4**.

2. Procedures for the other culture batches. The broth (10 L) was separated from the mycelium by filtration through cheese cloth and either extracted with EtOAc or passed through an XAD-16 column, which was then eluted with acetone. The crude extract was partitioned over Sephadex LH20 (acetone) to give five fractions. Fraction 1 was biologically active and repeatedly chromatographed on silica gel (step 1: preparative TLC: 1:1 acetone/hexanes; step 2: 3% acetone/CH_2Cl_2 for the first active TLC fraction and 5% MeOH/CH_2Cl_2 for the second active TLC fraction) to yield two pure compounds, **5** (6.5 mg) and **6** (2.1 mg). Fraction 2 was purified by silica gel chromatography (15–100% acetone/hexanes) to yield 25 mg compound **7**. Fraction 3 was chromatographed on silica gel (preparative TLC: 1:1 acetone/hexanes) to give 2.0 mg compound **3** and a small amount of compound **7**. Fraction 4 was fractionated on a silica gel column (0.5% AcOH–5% MeOH/CH_2Cl_2) to yield 25 mg orsellinic acid. Fraction 5 was acetylated with Ac_2O/pyridine to give 4 mg stachybotramide triacetate (**9**) after chromatography over silica gel (15–40% acetone/hexanes).

Stachybotrydial diacetate (2): obtained as a white amorphous solid; $[\alpha]_D$ −69 (*c* 0.063, $CHCl_3$); IR ($CHCl_3$) ν_{max}: 2930, 1773, 1728, 1690, 1595, 1403, 1257, 1247, 1190, 1093 cm^{-1}; UV (MeOH) λ_{max}: 230 (14 000), 252 (sh, 9400), 282 (4300), 357 (4300) nm; HREIMS *m/z*: 470.2306 ($C_{27}H_{34}O_7$, Δmmu = 0.2, 2%), 410.2117 ($C_{25}H_{30}O_5$, 40%), 368.1976 ($C_{23}H_{28}O_4$, 10%), 272.0681 ($C_{15}H_{12}O_5$, 10%), 230.0579 ($C_{13}H_{10}O_4$, 56%), 190.1716 ($C_{14}H_{22}$, 100%), 178.0263 ($C_9H_6O_4$, 29%); ^{1}H NMR (400 MHz, $CDCl_3$), see Table 1; ^{13}C NMR (100 MHz, $CDCl_3$), see Table 3.

Compound 3: obtained as a white or pale yellow crystalline solid; mp 280°C (dec.); $[\alpha]_D$ −6.4 (*c* 0.09, acetone); IR ($CHCl_3$) ν_{max}: 3600–3100, 2939, 1742, 1623, 1469, 1389, 1356, 1332, 1079, 954, 943, 772, 737 cm^{-1}; UV (MeOH) λ_{max}: 218 (28 000), 268 (5300), 309 (2600) nm; HREIMS *m/z*: 386.2095 ($C_{23}H_{30}O_5$, Δmmu = 0.1, 53%), 368.1977 ($C_{23}H_{28}O_4$, 11%), 353.1753 ($C_{22}H_{25}O_4$, 9%), 244.0730 ($C_{14}H_{12}O_4$, 9%), 230.0579 ($C_{13}H_{10}O_4$, 100%), 217.0499 ($C_{12}H_9O_4$, 18%), 207.1747 ($C_{14}H_{23}O$, 38%),

Can. J. Chem. Downloaded from www.nrcresearchpress.com by 88.255.202.194 on 09/08/12
For personal use only.

189.1642 ($C_{14}H_{21}$, 35%); ^{1}H NMR (400 MHz), see Table 1; ^{13}C NMR (100 MHz), see Table 3.

Compound 4: obtained as a pale yellow solid; IR (MeOH) ν_{max}: 3500–3200, 2939, 1623, 1451, 1385, 1361, 1116, 990 cm^{-1}; ^{1}H NMR (400 MHz, DMSO-d_6) δ: 9.23 (br s), 6.30 (s), 4.95 (t, 5.4), 4.42 (m, 4H), 4.31 (t, 5.0), 4.09 (br s), 4.00 (d, 3.5), 3.02 (d, 16.2), 2.66 (d, 16.2), 2.05 (br d, 11.0), 1.82–1.68 (m, 3H), 1.50–1.35 (m, 5H), 0.97 (s, 3H), 0.92 (s, 3H), 0.88 (m), 0.79 (s, 3H), 0.65 (d, 6.4, 3H) ppm; ^{13}C NMR (100 MHz, DMSO-d_6) δ: 160.64 (s), 152.17 (s), 141.80 (s), 110.56 (s), 110.37 (s), 106.37 (d), 95.41 (s), 73.50 (d), 60.95 (t), 54.39 (t), 41.77 (s), 39.43 (d), 37.22 (s), 36.44 (d), 31.63 (t), 30.93 (t), 28.64 (q), 24.90 (t), 23.91 (q), 20.55 (t), 15.73 (q), 15.60 (q) ppm; HREIMS *m/z*: 390.2402 ($C_{23}H_{34}O_5$, Δmmu = −0.4, 7%), 372.2283 ($C_{23}H_{32}O_4$, 16%), 218.0939 ($_{13}H_{14}O_3$, 26%), 207.1748 ($C_{14}H_{23}O$, 36%), 189.1641 ($C_{14}H_{21}$, 7%).

Stachybotramide triacetate (9): obtained as a white amorphous solid; $[\alpha]_D$ −36 (*c* 0.048, $CHCl_3$); IR ($CHCl_3$) ν_{max}: 2960, 2937, 2876, 1767, 1742, 1696, 1613, 1461, 1371, 1321, 1248, 1201, 1075, 1066, 893 cm^{-1}; UV (MeOH) λ_{max}: 219 (25 000), 256 (5200), 290 (2500), 300 (2700) nm; HREIMS *m/z*: 555.2831 ($C_{31}H_{41}NO_8$, Δmmu = 0.0, 19%), 495.2622 ($C_{29}H_{37}NO_6$, 100%), 480.2382 ($C_{28}H_{34}NO_6$, 11%), 453.2505 ($C_{27}H_{35}NO_5$, 26%), 305.0899 ($C_{15}H_{15}NO_6$, 20%), 263.0795 ($C_{13}H_{13}NO_5$, 9%); ^{1}H NMR (400 MHz, $CDCl_3$), see Table 2; ^{13}C NMR (100 MHz, $CDCl_3$) see Table 3.

Trichodermin (5): obtained as a colorless oil; $[\alpha]_D$ −9.3 (*c* 0.10, $CHCl_3$) (lit. (8*c*) $[\alpha]_D$ −10.2 (*c* 1.0, $CHCl_3$); IR ($CHCl_3$) ν_{max}: 2970, 1735, 1374, 1244, 1220, 1081, 1031, 996, 970 cm^{-1}; ^{1}H NMR (400 MHz, $CDCl_3$) δ: 5.56 (dd, 7.8, 3.6), 5.40 (br d, 4.2), 3.82 (d, 5.3), 3.60 (br d, 5.5), 3.12 (d, 4.0), 2.82 (d, 4.0), 2.53 (dd, 15.4, 7.8), 2.08 (s, 3H), 2.02–1.95 (m, 3H), 1.91 (dd, 11.5, 6.0), 1.71 (br s, 3H), 1.41 (br d, 10.0), 0.93 (s, 3H), 0.71 (s, 3H) ppm; HREIMS *m/z*: 292.1676 ($C_{17}H_{24}O_4$, Δmmu = 0.2, 100%), 277.1441 ($C_{16}H_{21}O_4$, 78%), 217.1230 ($C_{14}H_{17}O_2$, 10%).

Trichodermol (6): obtained as a white amorphous solid, $[\alpha]_D$ −22 (*c* 0.015, $CHCl_3$) (lit. (8*c*) $[\alpha]_D$ −33 (*c* 1.1, $CHCl_3$)); IR ($CHCl_3$) ν_{max}: 3458, 2970, 2885, 1625, 1441, 1384, 1279, 1070, 965, 955, 752, 644, cm^{-1}; ^{1}H NMR (400 MHz, $CDCl_3$) δ: 5.39 (br d, 5.6), 4.33 (td, 8.6, 2.9), 3.82 (d, 5.4), 3.51 (br d, 5.2), 3.10 (d, 3.9) 2.81 (d, 4.0), 2.60 (dd, 15.6, 7.4), 2.00–1.90 (m, 4H), 1.71 (br s, 3H), 1.55 (d, 10), 1.44 (m), 0.85 (s, 3H), 0.80 (s, 3H) ppm; HREIMS *m/z*: 250.1569 ($C_{15}H_{22}O_3$; Δmmu = 0.0, 16%), 235.1335 ($C_{14}H_{19}O_3$, 27%), 207.1384 ($C_{13}H_{19}O_2$, 50%), 188.1200 ($C_{13}H_{16}O$, 50%).

6,8-Dihydroxy-3,5,7-trimethylisochroman (7): obtained as a yellow amorphous solid; mp 183–186°C; $[\alpha]_D$ +103 (*c* 0.36, CH_3CN); UV (CH_3CN) λ_{max}: 202 (38 000), 225 (sh, 8000), 275 (1100), 281 (1400) nm; IR ($CHCl_3$) ν_{max}: 3600–3100, 1595, 1465, 1450 cm^{-1}; HREIMS *m/z*: 208.1091 ($C_{12}H_{16}O_3$, Δmmu = 0.2, 79%), 193.0861 ($C_{11}H_{13}O_3$, 25%), 164.0836 ($C_{10}H_{12}O_2$, 79%); ^{1}H NMR (400 MHz), see Table 4; ^{13}C NMR (100 MHz), see Table 4.

Compound 12: obtained as a white amorphous solid; $[\alpha]_D$ +85 (*c* 0.075, $CHCl_3$); UV (MeOH) λ_{max}: 220 (11 000), 264 (1000) nm; IR ($CHCl_3$) ν_{max}: 2972, 2933, 1763, 1461, 1368, 1202, 1130, 1081, 756 cm^{-1}; ^{1}H NMR (400 MHz, $CDCl_3$) δ: 4.71 (br d, 15.0), 4.54 (br d, 15.0), 3.75 (m), 2.62 (dd, 16.5, 3.0), 2.44 (dd, 16.5, 10.7), 2.34 (s, 3H), 2.30 (s, 3H), 2.00 (s, 3H), 1.91 (s, 3H), 1.36 (d, 6.2; 3H) ppm; ^{13}C NMR (100 MHz, $CDCl_3$) δ: 168.72 (s), 168.46 (s), 146.69 (s), 143.39 (s), 131.74 (s), 126.14 (s), 124.87 (s), 120.59 (s). 70.42 (d), 64.26 (t), 33.53 (t), 21.60 (q), 20.37 (q), 20.23 (q), 11.72 (q), 9.90 (q) ppm; HREIMS *m/z*: 292.1308 ($C_{16}H_{20}O_5$, Δmmu = −0.3, 5%), 250.1202, ($C_{14}H_{18}O_4$, 13%), 233.1171 ($C_{14}H_{17}O_3$, 28%), 232.1100 $C_{14}H_{16}O_3$, 21%), 208.1094 ($C_{12}H_{16}O_3$, 80%), 191.1067 ($C_{12}H_{15}O_2$, 50%), 164.0837 ($C_{10}H_{12}O_2$, 100%).

Acknowledgements

The financial support from the Natural Sciences and Engineering Research Council of Canada through strategic and operating grants is gratefully acknowledged. We thank Drs. Y. Hiratsuka, L. J. Hutchison, and P. Chakravarty of the Northern Forestry Center, Edmonton, and L. Sigler of University of Alberta Microfungus Collection and Herbarium for fungal cultures, bioassays, and valuable discussion. We also thank Dr. T. T. Nakashima and his staff of the High Resolution NMR Laboratory for technical assistance.

1. Y. Hiratsuka, D. A. Gibbard, O. Bakowsky, and G. B. Maier. Classification and measurement of the aspen decay and stain in Alberta. Forestry Canada, Information Report NOR-X-314. 1990.
2. E. B. Peterson and N. M. Peterson. Ecology, management, and use of aspen and balsam poplar in the Prairie Provinces, Canada. Forestry Canada. 1992.
3. S. C. Jong and E. E. Davis. Mycotaxon, **3**, 409 (1976).
4. H. Kaise, M. Shinohara, W. Miyazaki, T. Izawa, Y. Nakano, M. Sugawara, K. Sugiura, and K. Sasaki. J. Chem. Soc. Chem. Commun. 726 (1979).
5. (*a*) E. J. Corey and J. Das. J. Am. Chem. Soc. **104**, 5551 (1982); (*b*) J. E. McMurry and M. D. Erion. J. Am. Chem. Soc. **107**, 2712 (1985).
6. A. Bax and M. F. Summers. J. Am. Chem. Soc. **108**, 2093 (1986).
7. A. Bax and D. Davis. J. Magn. Reson. **65**, 355 (1985).
8. (*a*) Y. Ueno (*Editor*). Trichothecenes: chemical, biological and toxicological aspects. Kodansha Ltd., Japan. 1983; (*b*) S. P. Swanson, C. Helaszek, and H. D. Rood. *In* Microbial toxins in foods and feeds. *Edited by* A. E. Pohland, V. R. Dowell, Jr., and J. L. Richard. Plenum Press, New York. 1990. pp. 467–481; (*c*) Ch. Tamm and M. Tori. *In* Mycotoxins: production, isolation, separation and purification. *Edited by* V. Betina. Elsevier Science Publishers, New York. 1984. pp. 131–182.
9. W. A. Ayer, P. A. Craw, and J. Neary. Can. J. Chem. **70**, 1338 (1992).

Can. J. Chem. Downloaded from www.nrcresearchpress.com by 88.255.202.194 on 09/08/12
For personal use only.

Squaraine chemistry. A new approach to symmetrical and unsymmetrical photoconductive squaraines. Characterization and solid state properties of these materials

KOCK-YEE LAW[1] AND F. COURT BAILEY

Xerox Webster Research Center, 800 Phillips Road, 0114-39D, Webster, NY 14580, U.S.A.

Received September 15, 1992

KOCK-YEE LAW and F. COURT BAILEY. Can. J. Chem. **71**, 494 (1993).

A new approach to 1-(*p*-dimethylaminophenyl)-2-hydroxycyclobutene-3,4-dione (**4**), a precursor for the synthesis of symmetrical and unsymmetrical photoconductive squaraines, is described. *In situ* generation of *p*-nitrophenyl ketene, by the reaction of *p*-nitrophenylacetyl chloride and triethylamine in the presence of tetraethoxyethylene in anhydrous ether, results in a (2+2) cycloaddition between the ketene and the electron-rich olefin. The cycloadduct generated, **6**, was hydrolyzed to give 1-(*p*-nitrophenyl)-2-hydroxycyclobutene-3,4-dione (**5**) in 51% yield. Reductive alkylation of **5** by hydrogen in the presence of formaldehyde in DMF at 50–60°C affords **4** in 81% yield. The overall yield of **4** is 41% from tetraethoxyethylene and is significantly better than other preparative procedures of **4** based on a partial Friedel–Crafts reaction or an arylation reaction of a squaric acid derivative with an aniline, where yields ranging from 8.5% to 24% were reported. Condensations of **4** with 2 equivalents of *N*,*N*-dimethylaniline and its derivatives in refluxing 2-propanol in the presence of 6 equivalents of tributyl orthoformate yield symmetrical squaraine **1***a* and unsymmetrical squaraines **1***b*–**1***e*. The synthesis is accomplished by a (2+2) cycloaddition – reductive alkylation – condensation reaction sequence and represents a new, cost-effective synthesis for photoconductive squaraines where the expensive squaric acid reactant is bypassed. The spectroscopic and the solid state properties of **1***a*–**1***e* have been studied. Results show that the properties exhibited by **1***a*–**1***e* are essentially identical to those exhibited by other photoconductive, symmetrical squaraines that are synthesized by other known processes. From the resemblance in solid state properties, **1***a*–**1***e* are expected to be photoconductive. This has indeed been observed in preliminary experiments.

KOCK-YEE LAW et F. COURT BAILEY. Can. J. Chem. **71**, 494 (1993).

On décrit une nouvelle approche pour la préparation de la 1-(*p*-diméthylaminophényl)-2-hydroxycyclobutène-3,4-dione (**4**), un précurseur dans la synthèse de squaraïnes photoconductrices symétriques et non-symétriques. La génération *in situ* du *p*-nitrophényl cétène, par la réaction du chlorure de *p*-nitrophénylacétyle avec la triéthylamine en présence de tétraéthoxyéthylène dans l'éther anhydre, conduit à une cycloaddition (2+2) du cétène et de l'oléfine riche en électrons. L'hydrolyse du cycloadduit, **6**, ainsi généré conduit à la 1-(*p*-nitrophényl)-2-hydroxycyclobutène-3,4-dione (**5**) avec un rendement de 51%. L'alkylation réductrice de **5** par de l'hydrogène en présence de formaldéhyde dans de DMF, à 50–60°C, fournit le composé **4** avec un rendement de 81%. Le rendement global de **4** est de 41% à partir du tétraéthoxyéthylène et ce rendement est supérieur à ceux obtenus lors de préparations impliquant une réaction de Friedel–Crafts partielle ou une réaction d'arylation d'un dérivé de l'acide squarique avec de l'aniline alors que les rendements rapportés sont de l'ordre de 8,5 à 24%. Les condensations de **4** avec deux équivalents de *N*,*N*-diméthylaniline et de ses dérivés, dans du propan-2-ol, en présence de 6 équivalents d'orthoformate de tributyle conduisent à la squaraïne symétrique **1***a* et aux squaraïnes non-symétriques **1***b*–**1***e*. La synthèse est réalisée par une séquence de réactions de cycloaddition (2+2) – alkylation réductrice – condensation et elle représente une nouvelle synthèse efficace du point de vue du prix de squaraïnes photoconductrices dans laquelle l'acide squarique qui est très chère n'est pas impliquée. On a étudié les propriétés spectroscopiques et les propriétés à l'état solide des composés **1***a*–**1***e*. Les résultats montrent que les propriétés de ces composés sont essentiellement identiques à celles d'autres squaraïnes symétriques photoconductrices qui ont été synthétisées par d'autres procédés connus. En se basant sur la ressemblance des propriétés à l'état solide des produits **1***a*–**1***e*, on peut s'attendre à ce qu'ils soient photoconducteurs. C'est ce qui a été observé dans des expériences préliminaires.

[Traduit par la rédaction]

Introduction

Bis(4-dimethylaminophenyl)squaraine (**1***a*) and many of its derivatives are photoconductive pigments known to be useful for xerographic diode laser printers (1). The traditional synthesis, which involves the condensation of one equivalent of squaric acid, and two equivalents of an *N*,*N*-dimethylaniline derivative in an azeotropic solvent, is very straightforward and versatile (2); a large number of squaraine derivatives have been synthesized by this procedure (2–8).

Squaraines synthesized by this procedure are, however, often found to exhibit low charge-accepting properties and high dark-conductivity in bilayer xerographic devices (1). Because of their low solubility in organic solvents, a conventional purification procedure to improve their xerographic properties has yet to be developed. Two modified procedures, using the mono- and the dialkyl esters of squaric acid as precursors for the squaraine synthesis, have been

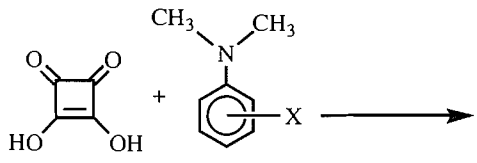

squaric acid

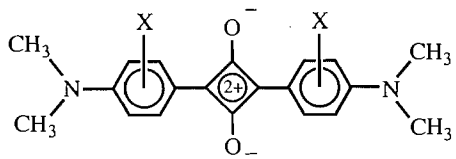

1*a*, X = H

[1]Author to whom correspondence may be addressed.

Can. J. Chem. Downloaded from www.nrcresearchpress.com by 88.255.202.194 on 09/08/12
For personal use only.

developed to circumvent the performance problem (9, 10). The common starting material for these procedures is squaric acid, a relatively expensive chemical. It is thus advantageous from the viewpoint of cost reduction to develop new procedures for squaraines, so that low-cost starting materials can be used.

With this research direction in mind, a new approach to photoconductive unsymmetrical squaraines, based on a (2+2) cycloaddition – condensation reaction sequence, has been developed (11, 12). The essence of this approach involves the preparation of intermediate **2** by a (2+2) cycloaddition reaction between *p*-methoxyphenyl ketene and tetraethoxyethylene, followed by an acid hydrolysis reaction, and the condensation of **2** and an *N*,*N*-dimethylaniline derivative to form unsymmetrical squaraine **3** or its derivatives.

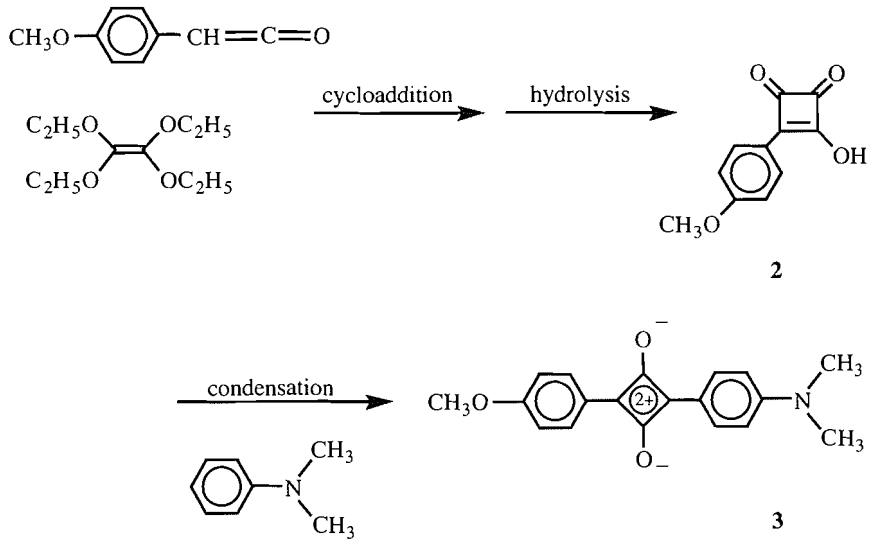

Since no squaric acid is used and since both cycloaddition and condensation reactions appear to be efficient, the goals of developing a new procedure for squaraines with cost reduction and synthetic simplification are accomplished.

The aim of this report is to describe our investigation of the extension of the above concept to synthesize squaraines, such as **1***a* and its derivatives, that are known to be photoconductive in device applications.[2] Here, the synthesis of **1***a* and its unsymmetrical analogs **1***b*–**1***e* by a (2+2) cycloaddition – reductive alkylation – condensation reaction sequence is reported. The merit and the limitations of the synthesis will be discussed. The spectroscopic and the solid state properties of **1***a*–**1***e* are presented and are found to be similar to those exhibited by squaraines that are photoconductive.

Experimental

Materials

p-Nitrophenylacetic acid (97%), phosphorus pentachloride, triethylamine (99+%), palladium (10%) on activated carbon, formaldehyde (37% solution in water), and *N*,*N*-dimethylaniline were purchased from Aldrich. Tributyl orthoformate was bought from Pfaltz & Bauer. Acetone, ether (anhydrous), toluene, methanol, *N*,*N*-dimethylformamide, tetrahydrofuran, 2-propanol, and *n*-heptane were certified grade from Fisher; concentrated hydrochloric acid was reagent grade, also from Fisher. All these materials were used as received. Substituted *N*,*N*-dimethylanilines were synthesized by methylating the corresponding aniline with trimethyl phosphate (14).

General techniques

Melting points were taken on a capillary melting point apparatus (Thomas Hoover) and were uncorrected. Infrared spectra were determined on a Perkin–Elmer model 1750 FTIR. Proton NMR spectra were recorded either on a Bruker WP-80 spectrometer or a Bruker AM360 spectrometer. Absorption spectra were taken on a Cary 17 spectrophotometer or on a Hewlett Packard 8451 diode array spectrophotometer. Mass spectra were recorded on a Varian VG 7035 mass spectrometer at the University of Rochester. Elemental analyses were performed by Galbraith Laboratories. X-ray powder diffraction patterns were performed in-house on a Scintag PAD V X-ray diffractometer.

Synthesis of p*-nitrophenylacetyl chloride*

p-Nitrophenylacetic acid (60.6 g) and phosphorus pentachloride (74.4 g) were placed in a 1-necked 1-L flask. The two solid compounds were mixed gently with a glass rod and an exothermic reaction was observed, which was accompanied by the formation of phosphorus oxychloride. As soon as the exotherm subsided, the mixture was brought to reflux at an oil-bath temperature of ~120°C for ~2 h. The mixture was cooled to ~60°C and phosphorus oxychloride was removed under reduced pressure. The crude product was then recrystallized from *n*-heptane (~1.5 L), yield pure *p*-nitrophenylacetyl chloride (white solid), 53.6 g (83%); mp 47.5–49°C (lit. (15) mp 46–47°C). IR (KBr): ~1800 cm^{-1} (C=O).

*Synthesis of 1-(*p*-nitrophenyl)-2-hydroxycyclobutene-3,4-dione*

Tetraethoxyethylene (51.3 g), which was freshly prepared according to procedures described by Bellus *et al.* (16), triethylamine (54.8 g), and diethyl ether (1.6 L) were placed in a 3-necked 3-L flask, which was equipped with a nitrogen inlet and a mechanical stirrer. An ethereal solution containing 105.2 g of *p*-nitrophenylacetyl chloride in 800 mL of ether was slowly added to the tetraethoxyethylene solution at room temperature over a 2-h period. A light brown precipitate was formed during the addition. The product mixture was then kept at 25–30°C by a warm water

[2]A preliminary account of this work has appeared in ref. 13.

Can. J. Chem. Downloaded from www.nrcresearchpress.com by 88.255.202.194 on 09/08/12
For personal use only.

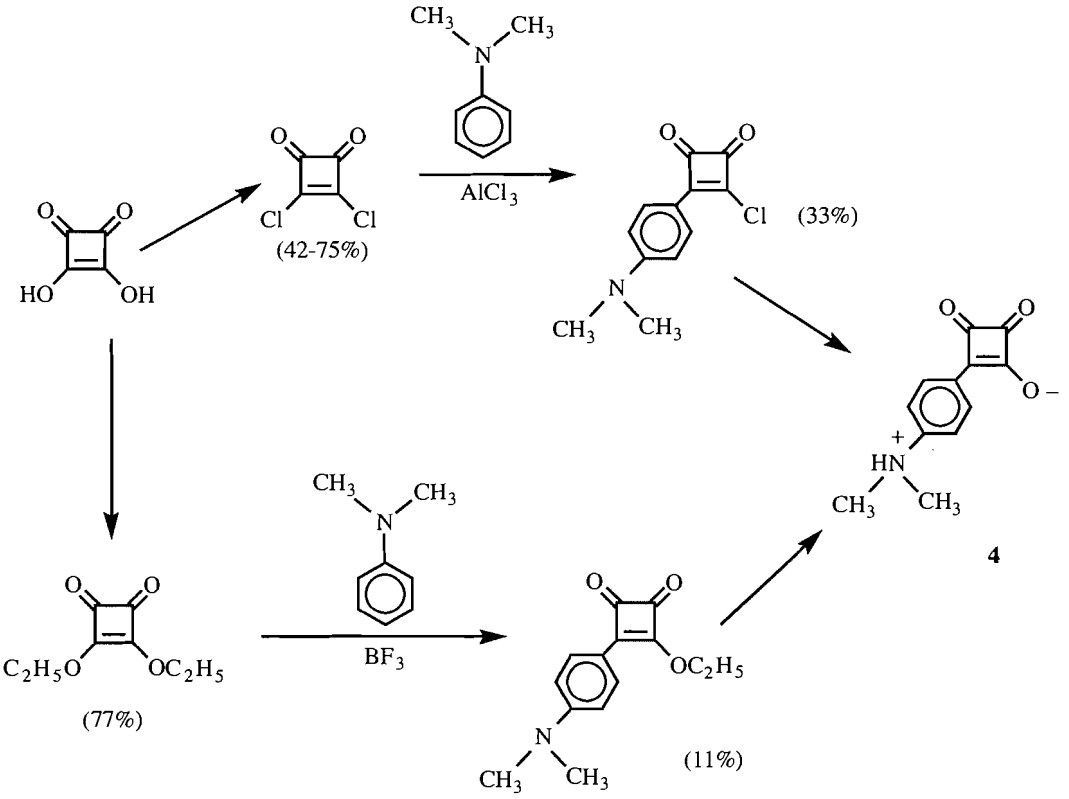

SCHEME 1

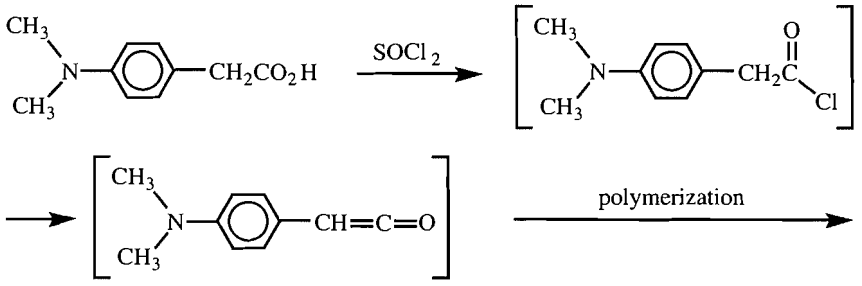

SCHEME 2

bath for a further 4 h. The product, which was soluble in diethyl ether, was isolated by filtration. The insoluble precipitate was washed with another litre of ether. The filtrate was combined. After solvent evaporation, 83.2 g of yellow residue was obtained. The yellow residue was then hydrolyzed by 150 mL of 18% hydrochloric acid at reflux for 4.5 h. Hydrochloric acid was evaporated under reduced pressure, yield 46.5 g crude product (a tan-colored gum). The crude product was then digested with boiling *n*-hexane and was recrystallized from a mixture of acetone and toluene. A light yellow solid, 1-(*p*-nitrophenyl)-2-hydroxycyclobutene-3,4-dione (**5**) was obtained, yield 28.2 g (51%); mp 162–163°C (dec.) (lit. (17) mp 187°C, (18) mp 160°C (dec.), (19) mp 188°C). IR (KBr): 1822, 1790, and 1724 cm^{-1}. ^1H NMR (DMSO-d_6) δ: 8.05–8.40 (AB quartet). MS (*m/z*): 219 (M^+). Anal. calcd. for $C_{10}H_5NO_5$: C 54.81, H 2.30, N 6.39; found: C 54.91, H 2.86, N 6.57.

*Synthesis of 1-*p*-dimethylaminophenyl-2-hydroxycyclobutene-3,4-dione*

A solution containing 8.77 g of 1-(*p*-nitrophenyl)-2-hydroxycyclobutene-3,4-dione in 160 mL of DMF was placed in a 500-mL Parr bottle. Formaldehyde (8.8 mL, 37% in water) and 2.4 g catalyst (10% palladium on carbon) were added. The bottle was then placed on a Parr apparatus and the mixture was hydrogenated at a pressure of ~60 psi (1 psi = 6.89 kPa) at ~50°C for ~1.5 h. The catalyst was removed by filtration and the solvent was evaporated under reduced pressure. The resulting orange-brown residue was then digested with acetone. After vacuum drying, 7.02 g (80.8%) of orange solid, 1-(*p*-dimethylaminophenyl)-2-hydroxycyclobutene-3,4-dione (**4**), was obtained; mp >300°C. IR (KBr): 1766, 1756, and 1707 cm^{-1}. ^1H NMR (DMSO-d_6) δ: 3.04 (s, 6H, NCH_3), 6.86 (d, J = 9.6 Hz, 2H), and 7.87 (d, J = 9.6 Hz, 2H). MS (*m/z*): 217 (M^+). Anal. calcd. for $C_{12}H_{11}NO_3$: C 66.35, H 5.10, N 6.45; found: C 64.61, H 5.17, N 6.95.

Synthesis of symmetrical and unsymmetrical squaraines

N,N-Dimethylaniline (0.35 mL, 2.76 mmol), 2-propanol (25 mL), and tributyl orthoformate (2 mL) were placed in a 3-necked 100-mL flask, which was equipped with a magnetic stirbar and a nitrogen inlet. The mixture was stirred and was brought to reflux. A solution containing 1-(*p*-dimethylaminophenyl)-2-hydroxycyclobutene-3,4-dione (0.3 g, 1.38 mmol) in ~4 mL of DMF was added slowly through a pressure-equalizing funnel over a 3-h period. After the addition was completed, the product mixture was

Can. J. Chem. Downloaded from www.nrcresearchpress.com by 88.255.202.194 on 09/08/12
For personal use only.

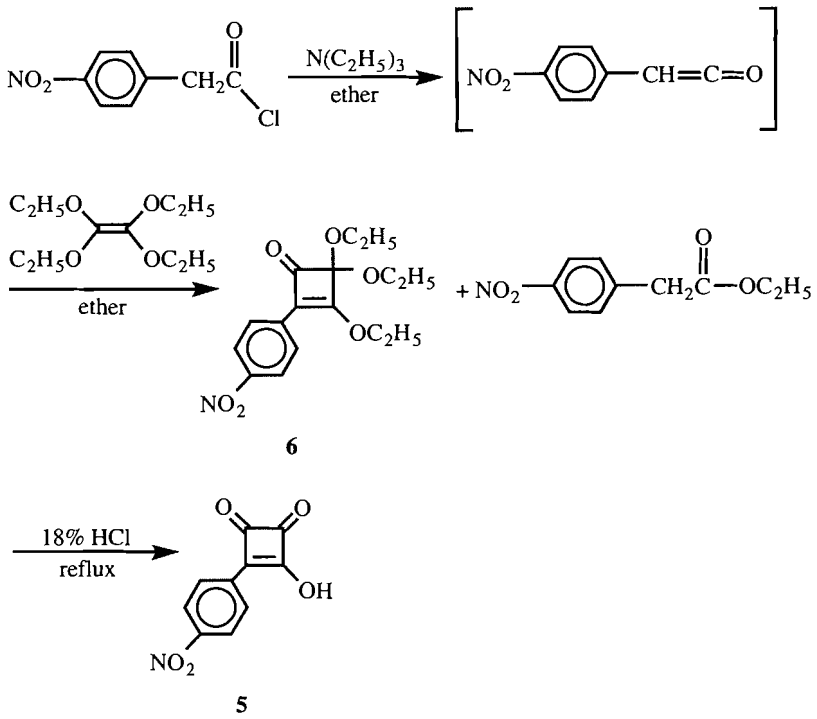

SCHEME 3

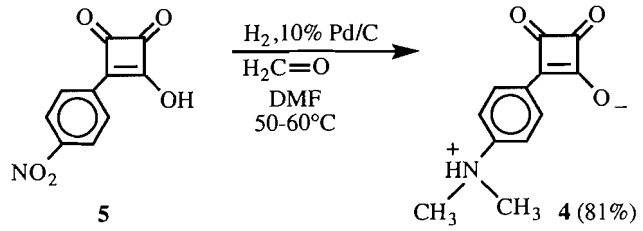

SCHEME 4

kept at reflux for a further 3 h. A blue precipitate was formed and was isolated by filtration. After washing with methanol and ether and vacuum drying, 0.20 g of a blue solid, which was subsequently identified as bis(4-dimethylaminophenyl)squaraine (**1***a*), was obtained (46%).

Unsymmetrical squaraines were analogously synthesized by condensing 1-(*p*-dimethylaminophenyl)-2-hydroxycyclobutene-3,4-dione and an appropriate aniline. The yields, the physical properties, and the spectral data of these materials are summarized in Tables 1–3.

Results and discussion

*Precursor, 1-(*p*-dimethylaminophenyl)-2-hydroxycyclobutene-3,4-dione (**4**)*

Strategy and synthesis

As noted earlier, squaraines can be synthesized from squaric acid, and the mono- as well as the dialkyl ester of squaric acid. Regardless of the precursors in these syntheses, the final squaraine formation step involves the condensation of **4** and an *N*,*N*-dialkylaniline (9). It becomes obvious that if one can develop an independent synthesis of **4**, one would not only be able to optimize the reaction condition for the squaraine formation step, but also have access to unsymmetrical squaraines when an appropriate aniline reactant is chosen. Kazmaier *et al.* (20) proposed that **4** could either be synthesized by a partial Friedel–Crafts reaction between the acid dichloride of squaric acid and *N*,*N*-dimethylaniline, followed by hydrolysis of the resulting mono-acid chloride to **4**, or by mono-arylation of the diethyl ester of squaric acid with *N*,*N*-dimethylanine, followed by hydrolysis of the subsequent monoethyl ester to **4**. These reaction schemes are summarized in Scheme 1.

The synthetic yields for the acid dichloride and the diethyl ester were reported to be 42–75% (21, 22) and 77% (23), respectively, from squaric acid. Assuming that both hydrolysis reactions in Scheme 1 are quantitative, the overall yield of **4** (from squaric acid) would be in the range of 8.5–24%, due to the low yields obtained in the Friedel–Crafts reaction (33%) and the arylation reaction (11%). The low synthetic yield of **4** and the need of using squaric acid as a precursor are major obstacles to the further development of the synthetic concepts in Scheme 1.

We recently reported the synthesis of **2**, an analog of **4**, using a (2+2) cycloaddition reaction (11, 12). The intention here is to extend the cycloaddition approach to synthesize **4**. Initial attempts to synthesize *p*-dimethylaminophenylacetyl chloride, a precursor for the (2+2) cycloaddition to synthesize **4**, consistently produced a brown polymeric material. Since *p*-dimethylaminophenylacetyl chloride consists of an acid chloride group and a dimethylamino group, the formation of a polymeric product is then attributable to the polymerization reaction of *p*-dimethylaminophenyl ketene, which is generated as soon as the acid chloride is formed owing to its self-reaction (Scheme 2).

The strategy in this work is to use a nitro group as a masking group and then regenerate the dimethylamino group by a reductive-alkylation process. The acid chloride for the (2+2) cycloaddition process is *p*-nitrophenylacetyl chloride, which can be synthesized by a direct reaction between *p*-nitrophenylacetic acid and phosphorus pentachloride.

Can. J. Chem. Downloaded from www.nrcresearchpress.com by 88.255.202.194 on 09/08/12
For personal use only.

Can. J. Chem. Downloaded from www.nrcresearchpress.com by 88.255.202.194 on 09/08/12
For personal use only.

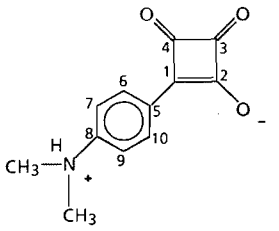

carbon	δ (ppm)	
	in DMSO - d_6	solid
1	173.8	172.2
2	194.8	195.8
3		210.8
4	194.9	200.3
5		133.2
6	127.5	129.0*
7,9	112.3	~122.9
8	151.3	144.4
10	127.5	~122.9*

(*may be interchanged)

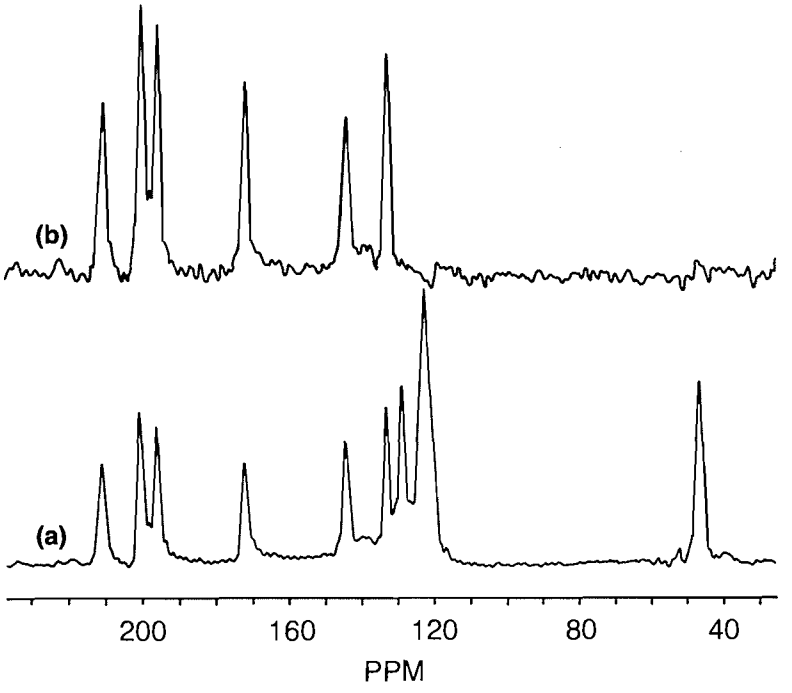

FIG. 1. Solid state ^{13}C NMR spectra of **4**; (*a*) full ^{13}C spectrum; (*b*) nonprotiated ^{13}C spectrum; inset: chemical shift data of **4**.

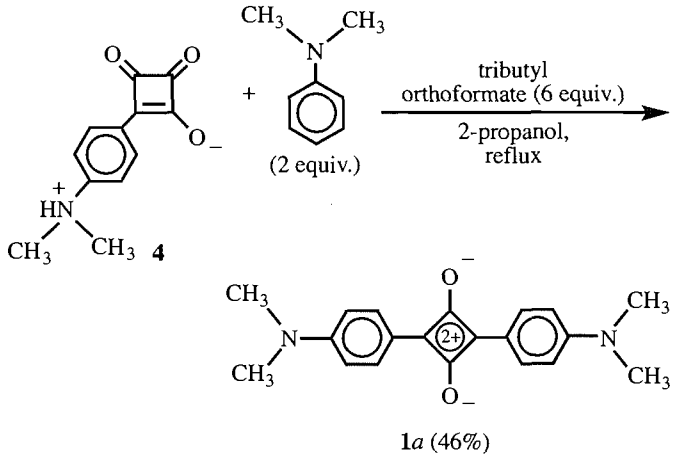

SCHEME 5

Addition of an ethereal suspension of *p*-nitrophenylacetyl chloride to an ethereal solution of tetraethoxyethylene in the presence of triethylamine leads to a (2+2) cycloaddition reaction between *p*-nitrophenyl ketene and the electron-rich olefin. The product mixture exhibits strong vibrational bands at 1735, 1748, and 1764 cm^{-1} in the IR spectrum. By comparing with the frequency of the C=O stretch of ethyl *p*-nitrophenylacetate, which is at 1735 cm^{-1}, and the C=O stretches of products of similar cycloaddition reactions (12), the bands at 1748 and 1764 cm^{-1} can be assigned to cycloadduct **6**. This assignment is confirmed by proton NMR spectral data of the product mixture. For instance, after subtracting proton signals corresponding to ethyl *p*-nitrophenylacetate, proton signals at δ 1.27 (t, J = 8.7 Hz), 1.55 (t, J = 8.7 Hz), 3.5–4.1 (two overlapped quartets), 7.93 (d, J = 11.2 Hz), and 8.25 (d, J = 11.2 Hz) of approximate ratio of 6:3:6:2:2 are observed. Since proton signals of **6** dom-

TABLE 1. Synthesis and physical properties of squaraines

	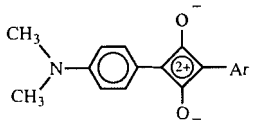	Isolated yield (%)	Melting point (°C)	Elemental analysis			
					C	H	N
1*a*	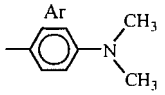	46	275–276 (lit. (7) 276)	Calcd.	74.98	6.29	8.74
				Found	74.47	6.38	8.27
1*b*	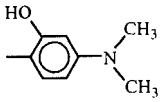	52	286–287	Calcd.	71.41	5.99	8.33
				Found	71.05	5.90	8.44
1*c*	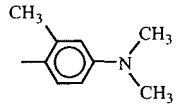	22	244–245	Calcd.	75.43	6.63	8.38
				Found	74.93	6.77	7.93
1*d*	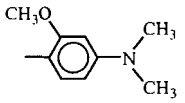	33	229(dec.)	Calcd.[a]	71.98	6.33	7.99
				Found	70.88	6.50	7.86
1*e*	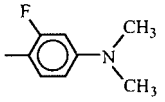	3.8	270(dec.)	Calcd.	70.99	5.66	8.28
				Found	70.36	5.73	7.85

[a]Assuming that **1***d* is hydrated with half a water molecule, the calculated values would be C 70.22, H 6.45, N 7.80.

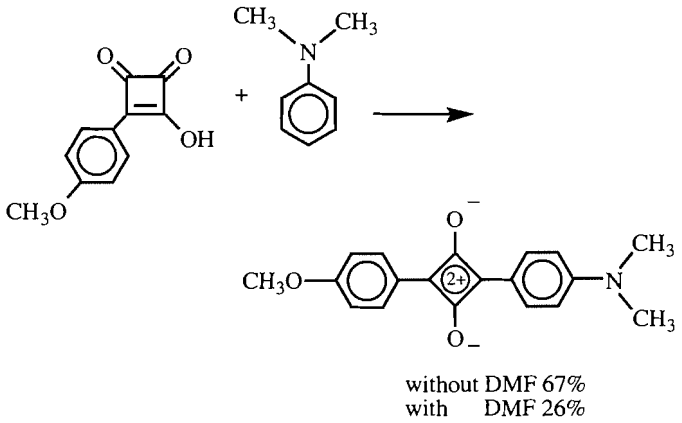

SCHEME 6

inate the NMR spectrum, our data indicate that **6** is the major cycloadduct for the cycloaddition reaction. The side product is ethyl *p*-nitrophenylacetate. Hydrolysis of the crude cycloaddition mixture in refluxing 18% HCl results in the formation of 1-*p*-nitrophenyl-2-hydroxycyclobutene-3,4-dione (**5**), which is isolated and purified in 51% yield after recrystallization from a mixture of acetone and toluene. The reaction sequence is summarized in Scheme 3.

The use of the cycloaddition between *p*-nitrophenyl ketene and tetraethoxyethylene for **5** was advanced by Bellus (18). The reported yield was 25%. The yield improvement obtained in this work is attributable to the use of ether rather than hexane as a reaction solvent for the cycloaddition. Compound **5** was also reported to be synthesized in an overall yield of 44% by a (2+2) cycloaddition reaction between *p*-nitrophenylacetylene and trifluorochloroethylene, followed by acid hydrolysis with sulfuric acid and an oxidation reaction (17). More recently, **5** was reported to be synthesized in 58% yield by reacting semisquaric acid with 4-nitrobenzene-1-diazonium chloride (19). The procedure reported here appears to be more attractive for practical use, because of the simplicity of the synthesis and the use of low-cost starting materials.

The dimethylamino group in **4** is regenerated by reductive alkylation of **5** under an atmospheric pressure of hydrogen in the presence of >2 equivalents of formaldehyde and a catalyst (10% Pd on charcoal). Initial attempts were carried out using the reductive-alkylation condition of *p*-nitrophenylacetic acid, where ethanol was used as the reaction solvent (24). By comparing the hydrogen consumption of the model reaction, only 10% of the expected hydrogen was consumed in the reductive-alkylation reaction of **5**. It is worth pointing out that the hydrogen uptake was stopped after the initial small exotherm. TLC analysis of the reaction mixture (after removing the catalysts) revealed that the major component is **5**. A minute amount of insoluble brown solid was isolated by concentrating the product solution. This brown solid was identified as **7** by mass spectrometry, where an intense peak at *m/z* 189 attributed to the molecular ion of **7** was observed.

The fact that there was no further uptake of hydrogen after the initial reaction and that most of **5** could be recovered from the reaction mixture suggests that the catalyst used in the hydrogenation process was poisoned as soon as the reduction occurred. Since it is known from the literature that hydroxy groups of squaric acid derivatives are highly acidic (pK_a ranges from +0.2 to −1.1) (18), the reduced product **7** and the reductive-alkylation product **4** are therefore expected to

Can. J. Chem. Downloaded from www.nrcresearchpress.com by 88.255.202.194 on 09/08/12
For personal use only.

TABLE 2. IR, VIS-absorption, and ^{1}H NMR spectral data of **1***a*–**1***e*

Squaraine	IR[a]	λ_{max}[b] (log ε_{max})[c]	^{1}H NMR (ppm from TMS)[d]
1*a*	1590 1620	623.9 (5.43) lit. (32) 624 (5.48)	3.20 (s, 12H, NCH_3), 6.77 (d, J = 9.2 Hz, 4H), and 8.41 (d, J = 9.2 Hz, 4H).
1*b*	1595 1625	626.1 (5.08)	[e]
1*c*	1590	632.5 (5.30)	2.93 (s, 3H, CH_3), 3.19 (s, 12H, NCH_3), 6.55 (d, J = 2.7 Hz, 1H), 6.60 (ABq, J_A = 9.0 Hz, J_B = 2.7 Hz, 1H), 6.76 (d, J = 9.3 Hz, 2H), 8.45 (d, J = 9.3 Hz, 2H), and 8.95 (d, J = 9.0 Hz, 1H)
1*d*	1592 1620	627.3 (5.07)	3.17 (s, 6H, NCH_3), 3.21 (s, 6H, NCH_3), 4.02 (s, 3H, OCH_3), 6.02 (d, J = 2.1 Hz, 1H), 6.42 (ABq, J_A = 9.2 Hz, J_B = 2.1 Hz, 1H), 6.75 (d, J = 9.0 Hz, 2H), 8.43 (d, J = 9.0 Hz, 2H), and 8.76 (d, J = 9.2 Hz, 1H)
1*e*	1592 1620	6.25 (5.03)	3.06 (s, 6H, NCH_3), 3.16 (s, 6H, NCH_3), 6.36 (d, J = 13.4 Hz, 1H), 6.48 (ABq, J_A = 9.1 Hz, J_B = 2.5 Hz, 1H), 6.71 (d, J = 9.2 Hz, 2H), 8.40 (d, J = 9.2 Hz, 2H), and 8.53 (m, 1H)

[a]In KBr, frequency expressed in cm^{-1}.
[b]In $CHCl_3$, wavelength expressed in nm.
[c]In cm^{-1} M^{-1}.
[d]In $CDCl_3$;
[e]The solubility of compound **1***b* in $CDCl_3$ is too low for solution spectrum.

TABLE 3. Mass spectral data of squaraines

			m/z (relative intensity)					
Squaraine	M^+	M + $CH_2^{\cdot+}$	a		b	M + $H_2^{\cdot+}$	c	Base peak
1*a*	320 (22)	334 (33)	148 (11)		161 (23)	322 (57)	134 (100)	**c**
Lit. (3)	320 (13)	334 (95)	148 (13)		161 (37)	322 (48)	134 (100)	**c**
1*b*	336 (61)	—	X = H	148 (27)	161 (20)	—	134 (100)	**c**
			X = OH	—	—		—	
1*c*	334 (69)	348 (46)	X = H	148 (67)	—	336 (90)	134 (100)	**c**
			X = CH_3	—	—		148 (67)	
1*d*	350 (27)	364 (60)	X = H	148 (21)	—	352 (60)	134 (100)	**c**
			X = OCH_3	178 (18)	—		164 (55)	
1*e*	—	352 (100)	X = H	—	161 (71)	—	134 (62)	M + $CH_2^{\cdot+}$
			X = F	—	—		152 (48)	

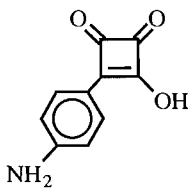

7

exist as zwitterions due to the protonation of the -NH_2 and -$N(CH_3)_2$ groups. We believe that the catalyst poisoning is the result of the precipitation of **7** and **4** onto the surface of the catalyst, because of their low solubility in ethanol. To circumvent the solubility problems and to minimize the effect of catalyst poisoning, we modify the reductive-alkylation condition in this work by using (*a*) DMF as the reaction solvent, (*b*) a large excess of catalyst (×6 of the model reaction), and (*c*) an elevated reaction temperature (50–60°C). This modification has resulted in a tremendous improvement in the reductive alkylation of **5**, and an isolated yield of 81% has been obtained for **4**. The overall yield of **4** is 41% from tetraethoxyethylene and is significantly higher than the processes shown in Scheme 1. More importantly, **4** is synthesized without using squaric acid, indicating a definite cost saving and a probable synthetic simplification for the squaraine synthesis developed in this work.

Structural characterization

Compound **4** is a high-melting orange solid. Unlike its methoxy analogs, which are soluble in slightly polar (acetone, THF) and polar (DMF, DMSO) solvents, **4** is only slightly soluble in DMSO and DMF. Since the hydroxy groups in squaric acid derivatives are known to be highly acidic (18), **4** should exist as a zwitterion; its insolubility in THF and acetone is therefore reasonable. This structural assignment is further supported by the IR spectrum of **4**. For instance, **4** exhibits broad C=O bands consisting of a doublet at 1756 and 1766 cm^{-1} and a band at 1707 cm^{-1}. The fre-

Can. J. Chem. Downloaded from www.nrcresearchpress.com by 88.255.202.194 on 09/08/12
For personal use only.

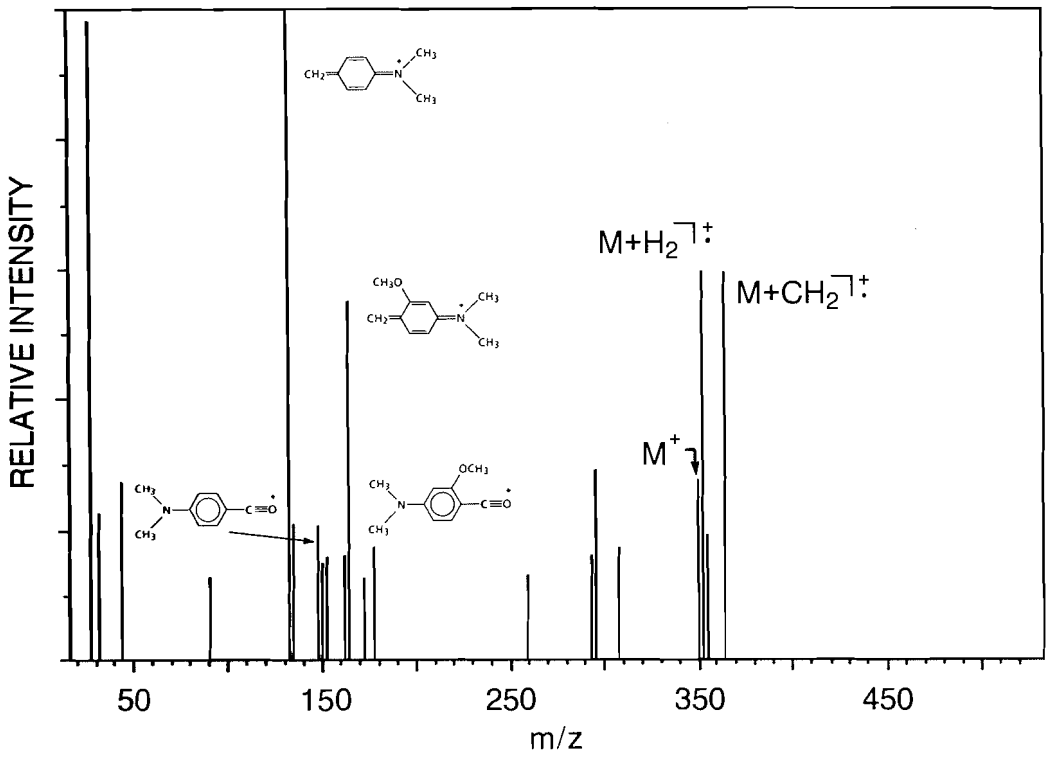

FIG. 2. Electron impact mass spectrum of **1***d*.

quency and the pattern are very similar to the deprotonated form of **2** (12).

In DMSO solution, **4** exhibits a singlet at 3.04 ppm for the six *N*-methyl protons and two doublets at 6.86 and 7.87 ppm for the four aromatic protons in the proton NMR spectrum. Due to the low solubility, acquisition of a good solution ^{13}C NMR spectrum for **4** requires at least an overnight scan, even on a Bruker AM360 instrument. The long scan time improves the signal-to-noise ratio of the spectrum, but **4** was found to decompose slowly during the overnight scan. The appearance of peaks from the decomposition product makes detailed chemical shift assignment of the solution ^{13}C NMR spectrum of **4** not probable. However, in a short (20 min) scan, ^{13}C signals at 44.3, 45.0, 112.3, 127.5, 151.3, 173.8, 194.8, and 194.9 ppm are clearly observable. From the ^{13}C NMR spectral data of **2**[3] and of *N*,*N*-dimethylaniline,[4] these signals can be assigned to *N*-methyl, *N*-methyl, C7 and C9, C6 and C10, C8, C1, and C2 and C4 of **4**, respectively (see inset of Fig. 1 for labelling). The observation of two peaks for the two *N*-methyl groups and two peaks for C2 and C4 suggests that the C—N bond in **4** is not freely rotated in DMSO solution. However, ^{13}C signals for C3 and C5 are within the noise level and could not be positively identified.

In this work, we further characterize **4** by solid state CP MAS ^{13}C NMR spectroscopy.[5] Figure 1*a* shows the full ^{13}C NMR spectrum of **4** and Fig. 1*b* shows the ^{13}C spectrum of the nonprotiated carbons of **4**. Six nonprotiated carbons are observed. The spectral result is consistent with the structure of **4** and also indicates that C2 and C4 are also not equivalent in the solid. The three downfield ketonic protons at 210.8, 200.3, and 195.8 ppm are assigned to C3, C4, and C2, respectively, based on their ketonic character in the resonance structure (27). It is worth pointing out that while the chemical shift difference between C2 and C4 is only 0.1 ppm in DMSO, the difference becomes 4.5 ppm in the solid state. The increase in nonequivalency between C2 and C4 is presumably due to rigidity of the entire carbon skeleton of **4** in the solid state. The nonprotiated carbons at 172.2, 144.4, and 133.2 ppm are assigned to C1, C8, and C5, respectively, based on the solution ^{13}C data of **2**, **4**, and *N*,*N*-dimethylaniline.

Two protiated carbon peaks at 129.0 and ~122.9 ppm with a ratio of ~1:3 are observed by subtracting Fig. 1*b* from Fig. 1*a*. From the solution data, C7 and C9 would be at ~122.9 ppm. C6 and C10 become magnetically nonequivalent in the solid state. We tentatively assign C10 at ~122.9 ppm because of its proximity to the negative charge. The chemical shift data are summarized in the inset of Fig. 1.

Squaraine synthesis

Squaraines can be synthesized by directly condensing **4** with an *N*,*N*-dimethylaniline derivative. The condition for the condensation reaction is investigated using **4** and *N*,*N*-dimethylaniline as reactants. The squaraine product is **1***a*; the quality of the product obtained can be compared with other **1***a* samples (9). Results showed that, when **4** and *N*,*N*-dimethylaniline were condensed in refluxing 1-butanol (2), 1-heptanol (under reduced pressure) (4), or 2-propanol (in the presence of tributyl orthoformate) (11, 12), a greenish-blue

[3]Using the labelling system of **4** (Fig. 1), the ^{13}C chemical-shift assignments of **2** are (in ppm, in DMSO-d_6) 55.4 (OCH_3), 114.7 (C7 and C9), 122.2 (C5), 127.9 (C6 and C10), 161.4 (C8), 172.6 (C1), 195.3 (C2 and C4), and 199.5 (C3).

[4]The chemical shifts of the carbons in *N*,*N*-dimethylaniline are 150 (C1), 113 (C2 and C6), 128.9 (C3 and C5), and 117 (C4); data taken from ref. 25.

[5]For details of the procedure for acquiring the CP MAS ^{13}C spectrum, see ref. 26.

Can. J. Chem. Downloaded from www.nrcresearchpress.com by 88.255.202.194 on 09/08/12
For personal use only.

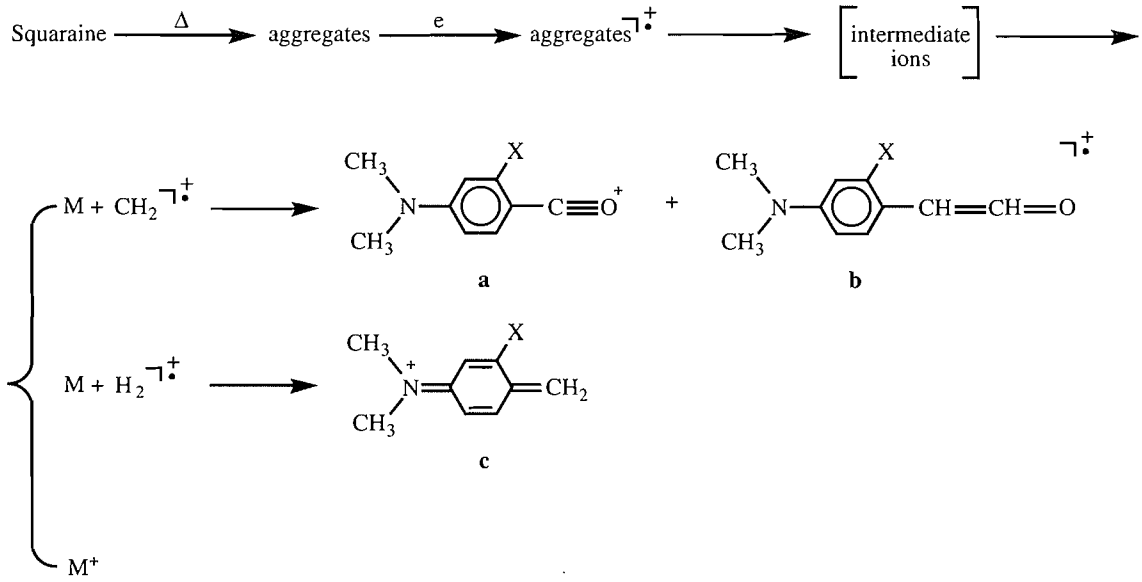

SCHEME 7

solid was obtained. VIS-absorption, TLC, and IR analysis indicated that the greenish-blue solid is a mixture of **1***a* and **4**. The incomplete consumption of **4** is somewhat surprising because the major side reaction in these condensation media is the esterification reaction of **4** to form an alkyl ester (4, 9, 12). We attribute the incomplete reaction to the low solubility of **4** in alcoholic solvents.

To circumvent the low solubility, we introduce **4** into the condensation media as a saturated DMF solution. According to the mechanism of the squaraine synthesis, **4** is the key reaction intermediate and is usually present at a very low concentration (9). In this work, we attempt to stimulate this condition by adding the DMF solution of **4** very slowly (over a period of 3 h) into the condensing medium. Our data show that the optimal condition for the synthesis of **1***a* is to add a saturated DMF solution of **4** into a refluxing 2-propanol solution containing 6 equivalents of tributyl orthoformate. The isolated yield of pure **1***a* was ~46% and is comparable to the yields obtained from other processes (9) (Scheme 5). The significance here is that, since **4** is synthesized by a cycloaddition – reductive alkylation process, the squaraine synthesis described thus represents a new and general approach to squaraine in which the use of squaric acid as a precursor is bypassed.

Using the above optimal conditions, several unsymmetrical squaraines (**1***b*–**1***e*) were synthesized. The yields and the physical properties of these materials are summarized in Table 1. The isolated yields of **1***b*–**1***e* are in the range of 3.8–52%, depending on the reactivity of the aniline reactant. In comparison with the yields of similar reactions (9), the yields reported in Table 1 appear to be relatively low. Thus, even though novel unsymmetrical squaraines have been synthesized by the present process, work is still needed to improve the efficiency of the condensation reactions.

The major difference between the condensation of **4** and *N*,*N*-dimethylaniline and that reported earlier between **2** and *N*,*N*-dimethylaniline is the use, in this work, of DMF in introducing **4**. Thus we also examined the effect of DMF on the condensation of **2** and *N*,*N*-dimethylaniline. The results are given in Scheme 6. Our results confirm that DMF exhibits a strong, adverse effect on the condensation reaction. The relatively low yields of **1***a*–**1***e* in Table 1 are attributable to the adverse effect exhibited by DMF in the condensation reaction. Future direction for yield improvement should thus be focussed on identifying a solvent for **4** that would at least be neutral to the condensation reaction.

Finally, condensations of 1-aryl-2-hydroxycyclobutene-3,4-diones with primary and secondary amines are known to form the corresponding 1,3-disubstituted unsymmetrical squaraine products (28–30). A similar reaction has also been reported for a pyrrole derivative (31). However, none of these squaraines is known to possess useful photoconductivity. The present study, as well as our previous work (11, 12), represents an extension of these condensation reactions to teritary aromatic amines. The resulting compounds are intensely absorbing in the visible region and are found to be photoconductive in xerographic devices.

Spectroscopic properties

IR spectra

Results in Table 2 show that all squaraines synthesized exhibit intense bands at ~1600 cm^{-1}. The absence of any C=O stretchings at ~1700 cm^{-1} is very characteristic for squaraine (3, 4, 12). The spectral results here suggest that, even though there is asymmetrical charge distribution in the two phenyl rings as revealed by proton NMR spectroscopy, the electrons in the central C_4O_2 unit are fully delocalized.

VIS spectra

The visible absorption spectrum of **1***a* synthesized in this work was found to be identical to the **1***a* sample that was synthesized by other processes (32). In the case of unsymmetrical squaraines **1***b*–**1***e*, all exhibit intense and sharp absorption bands in dilute chloroform solutions with λ_{max} ranging from 625 to 633 nm. Their molar extinction coefficients are typical of squaraines, in the order of 10^5 cm^{-1} M^{-1} (32, 33). Substituents are known to have an effect on the λ_{max}. In the case of **1***b*–**1***e*, it is interesting to point out that the substituent effect on their λ_{max} is smaller than on the λ_{max} of their symmetrical, disubstituted analogs (33). For instance, when the squaraine is substituted with two hydroxy groups

Can. J. Chem. Downloaded from www.nrcresearchpress.com by 88.255.202.194 on 09/08/12
For personal use only.

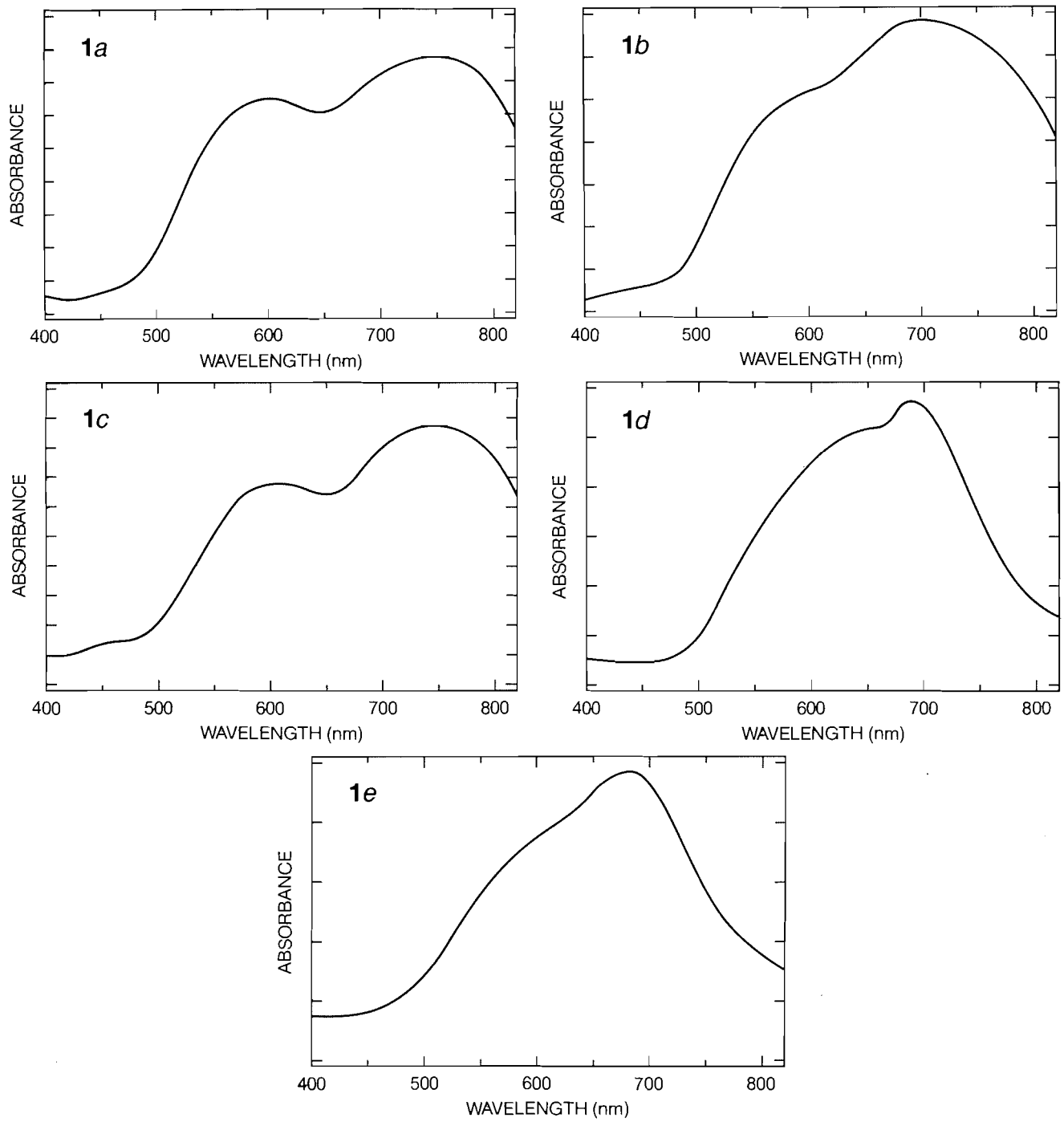

FIG. 3. Solid state (in KBr) absorption spectra of squaraines **1***a*–**1***e*.

Can. J. Chem. Downloaded from www.nrcresearchpress.com by 88.255.202.194 on 09/08/12
For personal use only.

in the positions adjacent to the central C_4O_2 unit, the λ_{max} is at 635.9 nm (33). The λ_{max} of **1***b* is at 626.1 nm and is midway between those of **1***a* and the dihydroxy compound.

^1H NMR spectra

Despite the low solubility, most of the squaraines synthesized in this work (except **1***b*) can be examined in $CDCl_3$ on a 360 MHz spectrometer. The results in Table 2 show that **1***a* exhibits a singlet at δ 3.20 and two doublets at δ 6.77 and 8.41 in a ratio of 3:1:1. They can be assigned to the *N*-methyl protons, the aromatic protons adjacent to the *N*,*N*-dimethylamino group, and the aromatic proton adjacent to the C_4O_2 unit, respectively (4, 34).

In the cases of unsymmetrical squaraines **1***c*–**1***e*, there are five magnetically nonequivalent aromatic protons. All five of them are identifiable by their chemical shifts, their coupling pattern, and their relative intensity.

Electron-impact mass spectra

Squaraines have been reported to exhibit anomalous electron-impact mass spectrometric behavior (3). For instance, owing to strong intermolecular donor–acceptor charge-transfer interactions in the solid state, squaraines vaporize thermally as molecular aggregates in the mass spectrometer. Ionization of these aggregates by electron impact results predominantly in intermediate fragment ions of formula

Can. J. Chem. Downloaded from www.nrcresearchpress.com by 88.255.202.194 on 09/08/12
For personal use only.

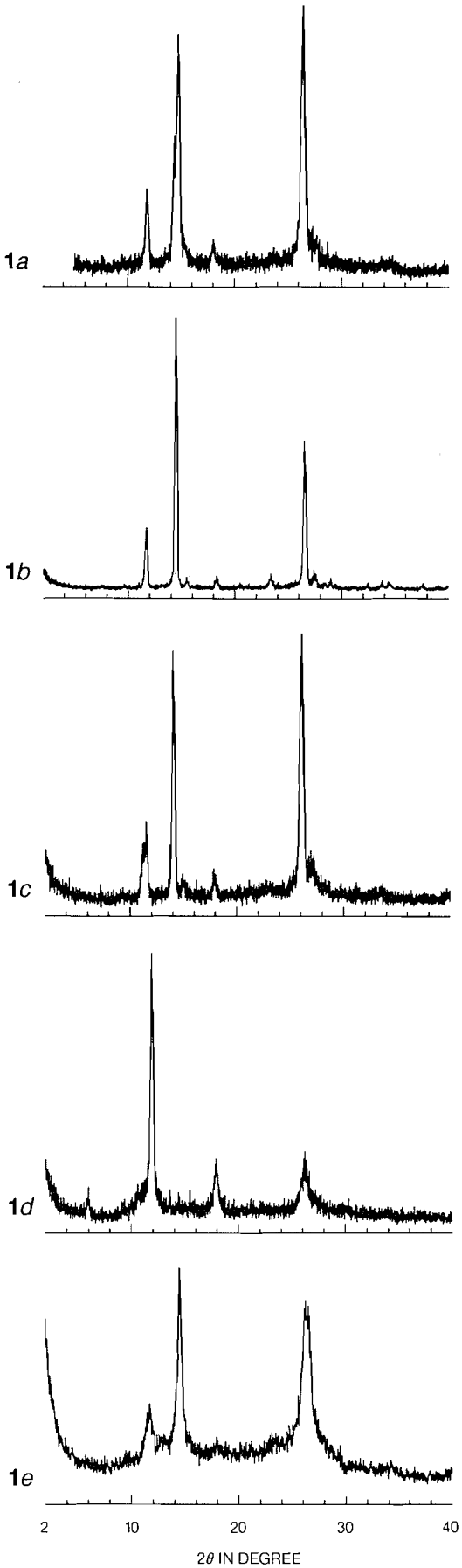

FIG. 4. X-ray powder diffraction patterns of squaraines **1***a*–**1***e*.

weight higher than the molecular weight of squaraine. In the case of **1***a*, fragmentation of the intermediate fragment ion leads to an alkylated ion M + $CH_2^{\square+}$, a dihydrogenated ion M + $H_2^{\square+}$, and the molecular ion M^+. Further fragmentation of these ions in the mass spectrometer results in the formation of characteristic rearranged ions, types **a**, **b**, and **c** (Scheme 7). Mechanistic details of their formation have been described previously (3). The mass spectral data of **1***a* are tabulated in Table 3 and are found to be identical to previous spectral data of **1***a* (3), for which a different synthetic route was used.

In the cases of **1***b*–**1***e*, more fragment ions are anticipated due to the unsymmetrical structure. The mass spectral data are listed in Table 3. A typical mass spectrum of an unsymmetrical squaraine (**1***d*) is depicted in Fig. 2. Comparing the spectral data of **1***b*–**1***e* with those of **1***a* indicates that all unsymmetrical squaraines have a similar set of mass spectral reactions (Scheme 7).

Solid state properties

The photoconductivity and the spectral response of squaraines are shown to be governed by the state of aggregation of squaraine molecules in their microcrystalline state (35). The photoactive aggregates are characterized by the broad and panchromatic solid state absorption, which typically consists of two bands, one in the visible (500–650 nm) and the other in the near IR (~700 nm) (36), and by the characteristic powder pattern with diffraction lines at 2θ 11.5°, 14.5°, and 26° (1). The solid state absorption spectra and X-ray powder diffraction patterns of **1***a*–**1***e* are given in Figs. 3 and 4, respectively. The solid state absorption spectrum and the X-ray powder pattern of **1***a* are found to be identical to those of the **1***a* samples synthesized by other processes (1, 36), suggesting that the **1***a* synthesized in this work exhibits solid state properties identical to previous **1***a* samples. Thus, the **1***a* sample prepared here should be photoconductive in xerographic photoreceptor devices and this has indeed been verified experimentally (37).

The data in Figs. 3 and 4 also suggest that the solid state properties of **1***b*–**1***e* are similar to those of **1***a*, despite their unsymmetrical structures. These results are not unexpected in view of similar results obtained from other symmetrical and unsymmetrical squaraines and in view of the small substituent effect on the solid state properties (1, 12, 38). Studies of the photoconductivities of these compounds are underway.

Concluding remarks

This work reports a new, general approach to the synthesis of squaraines based on a (2+2) cycloaddition – reductive alkylation – condensation reaction sequence. The goal of synthesizing squaraines at a lower cost, e.g., without using squaric acid, was accomplished. Due to the low solubility of the precursor compound (**4**) in alcoholic solvents, DMF, which was shown to have a detrimental effect on the yield of the condensation reaction, had to be used. Future investigation to improve the efficiency of the condensation reaction, such as identifying a substitute for DMF, is needed to enhance the practical value of the new synthetic approach described here.

One symmetrical and four unsymmetrical squaraines were synthesized. These compounds are shown to exhibit spectroscopic and solid state properties very similar to those of

their symmetrical analogs. Their solid state properties indicate that these squaraines should be photoconductive in xerographic devices. Very encouraging results have been obtained.

Acknowledgements

The authors thank Mr. R. Crandall for recording the CP MAS ^{13}C NMR spectrum of **4**, and Drs. P. M. Kazmaier and A. Paine for helpful discussion.

1. K. Y. Law and F. C. Bailey. J. Imaging Sci. **31**, 172 (1987), and references therein.
2. H. E. Sprenger and W. Ziegenbein. Angew. Chem. Int. Ed. Engl. **6**, 553 (1967).
3. K. Y. Law, F. C. Bailey, and L. J. Bluett. Can. J. Chem. **64**, 1607 (1986).
4. K. Y. Law and F. C. Bailey. Dyes Pigm. **9**, 85 (1988).
5. A. Treibs and K. Jacob. Liebigs Ann. Chem. **712**, 123 (1968); **699**, 153 (1966).
6. W. Ziegenbein and H. E. Sprenger. Angew. Chem. Int. Ed. Engl. **5**, 893 (1966).
7. H. Sprenger and W. Ziegenbein. Angew. Chem. Int. Ed. Engl. **5**, 894 (1966).
8. A. Treibs and K. Jacob. Angew. Chem. Int. Ed. Engl. **4**, 694 (1965).
9. K. Y. Law and F. C. Bailey. Can. J. Chem. **64**, 2269 (1986).
10. K. Y. Law. U. S. Patent 4,524,219 (1985).
11. K. Y. Law and F. C. Bailey. J. Chem. Soc. Chem. Commun. 863 (1990).
12. K. Y. Law and F. C. Bailey. J. Org. Chem. **57**, 3278 (1992).
13. K. Y. Law and F. C. Bailey. J. Chem. Soc. Chem. Commun. 1156 (1991).
14. A. I. Vogel. Textbook of practical organic chemistry. 4th ed. *Revised by* B. S. Furniss, A. J. Hannaford, V. Roger, P. W. G. Smith, and A. R. Tatchell. Longman, London and New York. 1978. Chap. IV.
15. J. Buckingham and S. M. Donaghy. Dictionary of organic compounds. 5th ed. Chapman and Hall, New York. 1982. p. 4270.
16. D. Bellus, P. Martin, H. Sauter, and T. Winkler. Helv. Chim. Acta, **63**, 1130 (1980).
17. W. Ried, A. H. Schmidt, and W. Kuhn. Chem. Ber. **104**, 2622 (1971).
18. D. Bellus. *In* Oxocarbons. *Edited by* R. West. Academic Press, New York. 1980. p. 178.
19. A. H. Schmidt, G. Schmidt, and H. Diedrich. Synthesis, 579 (1990).
20. P. M. Kazimaier, R. A. Burt, and G. Baranyi. U. S. Patent 4,624,904 (1986).
21. A. H. Schmidt. Synthesis, 961 (1980).
22. R. C. De Selms, C. J. Fox, and R. C. Riordan. Tetrahedron Lett. 781 (1970).
23. S. Cohen and S. G. Cohen. J. Am. Chem. Soc. **88**, 1533 (1966).
24. H. Baumgarten (*Editor in chief*). Org. Synth. Collect. Vol. **5**, 555 (1973).
25. E. Breitmaier, G. Haas, and W. Voelter. Atlas of ^{13}C NMR data. Heyden & Son Ltd., London. 1979.
26. K. Y. Law, I. W. Tarnawskyj, and S. Kaplan. Dyes Pigm. **17**, 41 (1991).
27. E. Breitmaier and W. Voelter. Carbon-13 NMR spectroscopy. VCH, New York. 1987.
28. W. Ried, W. Kunkeland, and G. Isenbruck. Chem. Ber. **102**, 2688 (1969).
29. W. Ried, A. H. Schmidt, G. Isenbruck, and F. Batz. Chem. Ber. **105**, 325 (1972).
30. W. Ried and G. Isenbruck. Chem. Ber. **105**, 337 (1972).
31. A. Treib and K. Jacob. Liebigs Ann. Chem. **712**, 123 (1968).
32. K. Y. Law. Chem. Phys. Lett. **150**, 357 (1988).
33. K. Y. Law. J. Phys. Chem. **91**, 5184 (1987).
34. K. Y. Law. J. Phys. Chem. **93**, 5925 (1989).
35. K. Y. Law. J. Phys. Chem. **92**, 4226 (1988).
36. K. Y. Law, J. S. Facci, J. F. Yanus, and F. C. Bailey. J. Imaging Sci. **34**, 31 (1990).
37. K. Y. Law and F. C. Bailey. U. S. Patent 5,004,661 (1991).
38. K. Y. Law. J. Imaging Sci. Technol. **36**, 567 (1992).

Can. J. Chem. Downloaded from www.nrcresearchpress.com by 88.255.202.194 on 09/08/12
For personal use only.

Dynamic behaviour of oxidized glutathione in solution investigated by nuclear magnetic resonance

CLAUDIO ROSSI,[1] ALESSANDRO DONATI, SERGIO ULGIATI, AND MARIA ROSARIA SANSONI
Department of Chemistry, University of Siena, Pian dei Mantellini, 44-53100 Siena, Italy

Received March 17, 1992[2]

CLAUDIO ROSSI, ALESSANDRO DONATI, SERGIO ULGIATI, and MARIA ROSARIA SANSONI. Can. J. Chem. **71**, 506 (1993).

In view of the important biological functions of oxidized glutathione (GSSG), we investigated the correlation between dynamic and conformational properties and biological activity. Anisotropic molecular motion characterizes different GSSG molecular districts. This information, obtained by NMR carbon relaxation investigations, suggests that the peptide does not independently assume any stable structure in solution. Analysis of the effects of the addition of a stable spin label to the solution confirmed the absence of conformation of GSSG in D_2O. Moreover, the paramagnetic effects observed on proton and carbon nuclei of oxidized glutathione suggest that the dipolar term is the main source of paramagnetic relaxation.

CLAUDIO ROSSI, ALESSANDRO DONATI SERGIO, ULGIATI et MARIA ROSARIA SANSONI. Can. J. Chem. **71**, 506 (1993).

Considérant les fonctions biologiques importantes du glutathion oxydé (GSSG), on a examiné la corrélation entre les propriétés dynamiques et conformationnelles et l'activité biologique. Un mouvement moléculaire anisotropique caractérise les différentes portions moléculaires du GSSG. Cette information, obtenue par des études de relaxation en RMN du carbone, suggère que, d'une façon indépendante, le peptide n'assume aucune structure stable en solution. L'analyse des effets de l'addition d'un marqueur de spin à la solution a confirmé l'absence de conformation dans le GSSG dans le D_2O. De plus, les effets paramagnétiques observés sur le proton et les noyaux de carbone du glutathion oxydé suggèrent que le terme dipolaire est la principale source de relaxation paramagnétique.

[Traduit par la redaction]

Can. J. Chem. Downloaded from www.nrcresearchpress.com by 88.255.202.194 on 09/08/12
For personal use only.

Introduction

Glutathione (GSH), *N*(*N*-γ-L-glutamyl-L-cysteinyl-glycine), is the most abundant intracellular non-protein thiol. Under normal circumstances its oxidized form (GSSG) accounts for 1% of GSH concentrations. It is mainly formed in cells as a consequence of the protective activity of GSH against hydroperoxides (1). Oxidized glutathione is not solely the result of the reductive activity of GSH; in fact several metal ion – GSSG complexes seem to be involved in biological reactions. The copper and zinc complexes of GSSG in particular are believed to play an important role in promoting GSSG reduction (2) and the Cu(II)–GSSG complex acts as an inhibitor of the opiate receptor site (3). GSH and GSSG peptides are important in the vital functions of cells and biological fluids (4), and several papers have been published on their conformations (5, 6) and those of their metal complexes (7–13). Cyclic peptides frequently assume a definite conformation in solution (14–19). This does not occur in linear peptides since the intramolecular non-covalent interactions necessary for stabilizing any conformation are less probable. In oxidized glutathione, a disulphide bridge between the cisteine residues could promote specific structure in solution. This makes oxidized glutathione an interesting semilinear peptide molecule for evaluating the conformational effects induced by structural constraints.

In this paper proton and carbon NMR spin-lattice relaxation rate measurements were used to study the dynamic motion conditions of the peptide. The soluble spin label, TEMPOL, was used for further inspection of conformational properties. Soluble spin labels have been used (20–24) to investigate the solvent-exposed vs. solvent-shielded protons of biopolymers. Here we report: (*a*) the effects of the addition of a spin label on the proton spin-lattice relaxation rates of the peptides; (*b*) the extension of these measurements to carbon nuclei for a more accurate description of the interaction between spin label and oxidized glutathione; (*c*) the use of nitroxide-enhanced spin-lattice relaxation rates as quantitative criteria of the exposure of the peptide backbone and side-chain hydrogens and carbons.

Experimental

Oxidized glutathione, GSSG (Fig. 1), *N*,*N*′-[dithiobis[1-[(carboxymethyl) carbamoyl]ethylene]]diglutamine, and TEMPOL (ethyl-4-hydroxy-piperidin-1-oxyl) were purchased from Sigma Chemical Co. and used without any further purification. $Mg(ClO_4)_2 \cdot 6H_2O$ was obtained from Aldrich.

The measurements performed on the GSSG diamagnetic system were obtained using a 0.15 mol dm^{-3} D_2O (99.9%) solution at pH 5.5. The final TEMPOL concentration was in the range $5 \times 10^{-3} - 4 \times 10^{-2}$ mol dm^{-3}. All the experiments, when not otherwise indicated, were run at 25°C.

NMR spectra were recorded on a Varian XL-200 spectrometer with an "ADVANCE" computer system, operating at 200.058 and 50.03 MHz for ^1H and ^{13}C respectively. Proton and carbon spin-lattice relaxation rates were obtained using the $(180°–\tau–90°–t)_n$ pulse sequence and subsequent three-parameters exponential regression analysis of the longitudinal magnetization recovery curves. In general, the recovery of proton longitudinal magnetization after a 180° pulse is not a single exponential, due to the sum of different relaxation terms. To account for this, proton spin-lattice relaxations were calculated using the initial slope approximation, considering only the first part of the recovery curves (25, 26). A maximum experimental error of ±6% was calculated for the relaxation measurements. The paramagnetic contributions R_{1p} were obtained from the expression:

$$R_{1p} = R_{1\,\mathrm{exp}} - R_{1\,\mathrm{blank}}$$

where $R_{1\,\mathrm{blank}}$ is the relaxation rate measured in the absence, and $R_{1\,\mathrm{exp}}$ that measured in the presence of nitroxide.

The EPR spectra were recorded with a Bruker ER 200-tt spectrometer operating in the X-band (ω_0 = 9.78 GHz).

[1]Author to whom correspondence may be addressed.
[2]Revision received January 21, 1992.

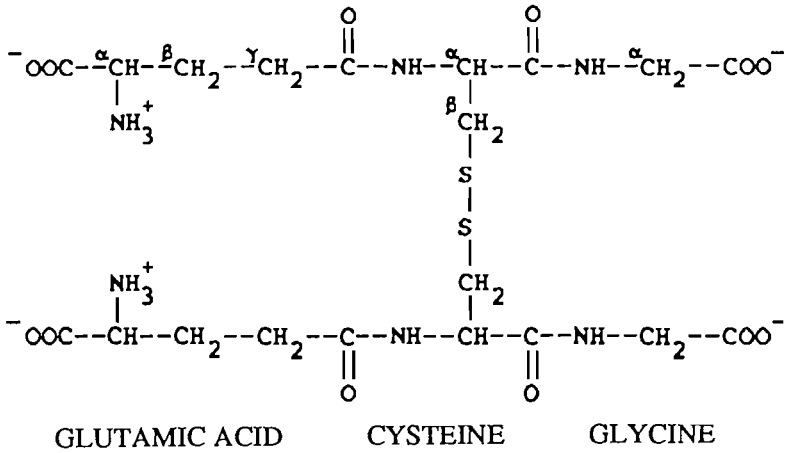

FIG. 1. Structure of oxidized glutathione.

TABLE 1. Proton and carbon spin-lattice relaxation rates and effective correlation times of 0.15 mol dm^{-3} of oxidized glutathione in D_2O at 25°C and pH 5.5

Carbon	δ/ppm	R_1 (s^{-1})	$\tau_{C_{eff}\times 10^{10}}$ s	Proton	δ/ppm	R_1 (s^{-1})
Gly-COOH	175.174	0.09	—	Cys-Hα	4.41	1.00
Glu-CO	173.885	0.30	—	Gly-Hα	3.45	2.00
Glu-COOH	173.253	0.19	—	Glu-Hα	3.40	1.25
Cys-CO	170.702	0.26	—	Cys-$H\beta_1$	2.99	5.26
Glu-Cα	52.971	2.10	1.00	Cys-$H\beta_2$	2.64	5.00
Cys-Cα	51.418	4.40	2.22	Glu-Hγ	2.20	3.23
Gly-Cα	42.330	3.10	0.73	Glu-Hβ	1.82	3.00
Cys-Cβ	37.546	8.60	2.15			
Glu-Cγ	30.254	3.60	0.85			
Glu-Cβ	25.255	3.90	0.92			

TABLE 2. Paramagnetic effects observed on proton spin-lattice relaxation rates, R_1, of oxidized glutathione 0.15 mol dm^{-3} in D_2O at 25°C

		Relaxation rates $R_1(s^{-1})$ at different TEMPOL concentrations (mol dm^{-3})				
Proton	δ/ppm	0	5×10^{-3}	10^{-2}	2×10^{-2}	4×10^{-2}
Cys Hα	4.41	1.00	2.5	3.85	6.70	13.10
Gly Hα	3.45	2.00	2.90	3.80	5.60	9.20
Glu Hα	3.40	1.25	2.22	3.20	5.35	9.05
Cys $H\beta_1$	2.99	5.26	7.20	9.25	12.95	20.10
Cys $H\beta_2$	2.64	5.00	6.84	8.86	12.79	20.39
Glu Hγ	2.20	3.23	4.95	6.65	10.00	16.60
Glu Hβ	1.82	3.30	4.50	5.95	8.50	13.80

Results and discussion

The conformational and dynamic properties of oxidized glutathione were analyzed by proton and carbon NMR relaxation studies, as well the effects induced on proton and carbon R_1, by the addition of water-soluble spin label TEMPOL to the GSSG solution.

Dynamic analysis

The dynamic properties of oxidized glutathione were investigated by analyzing the proton and carbon spin-lattice relaxation rates of GSSG. It is well known that the relaxation rates of carbon nuclei are dominated by the proton–carbon dipolar interactions. For protonated carbons the short proton–carbon internuclear distance makes this process extremely efficient. Since the C*i*—H*i* distance is constant, the correlation time modulating the dipolar interaction can be determined from the equation (27):

$$[1]\quad R_1^{DD} = \frac{1}{10}\frac{N\gamma_H^2\gamma_C^2\hbar^2}{r_{Ci-Hi}^6}\left[\frac{3\tau_c}{1+\omega_C^2\tau_c^2} + \frac{6\tau_c}{1+(\omega_H+\omega_C)^2\tau_c^2} + \frac{\tau_c}{1+(\omega_H-\omega_C)^2\tau_c^2}\right]$$

Can. J. Chem. Downloaded from www.nrcresearchpress.com by 88.255.202.194 on 09/08/12
For personal use only.

TABLE 3. Paramagnetic effects observed on carbon spin-lattice relaxation rates, R_1, of 0.15 mol dm^{-3} of oxidized glutathione in D_2O

Carbon	δ/ppm	Relaxation rates $R_1(s^{-1})$ at different TEMPOL concentrations (mol dm^{-3})				
		0	5×10^{-3}	10^{-2}	2×10^{-2}	4×10^{-2}
Gly COOH	175.174	0.09	0.17	0.25	0.41	0.70
Glu CO	173.885	0.30	0.41	0.51	0.70	1.08
Glu COOH	173.253	0.19	0.27	0.33	0.50	0.77
Cys CO	170.702	0.26	0.36	0.45	0.63	0.98
Glu Cα	52.971	2.10	2.22	2.32	2.55	2.92
Cys Cα	51.418	4.40	4.58	4.77	5.16	5.93
Gly Cα	42.330	3.10	3.23	3.36	3.58	4.05
Cys Cβ	37.546	8.60	8.80	9.01	9.36	10.20
Glu Cγ	30.254	3.90	4.07	4.26	4.59	5.32
Glu Cβ	25.255	3.60	3.74	3.86	4.15	4.65

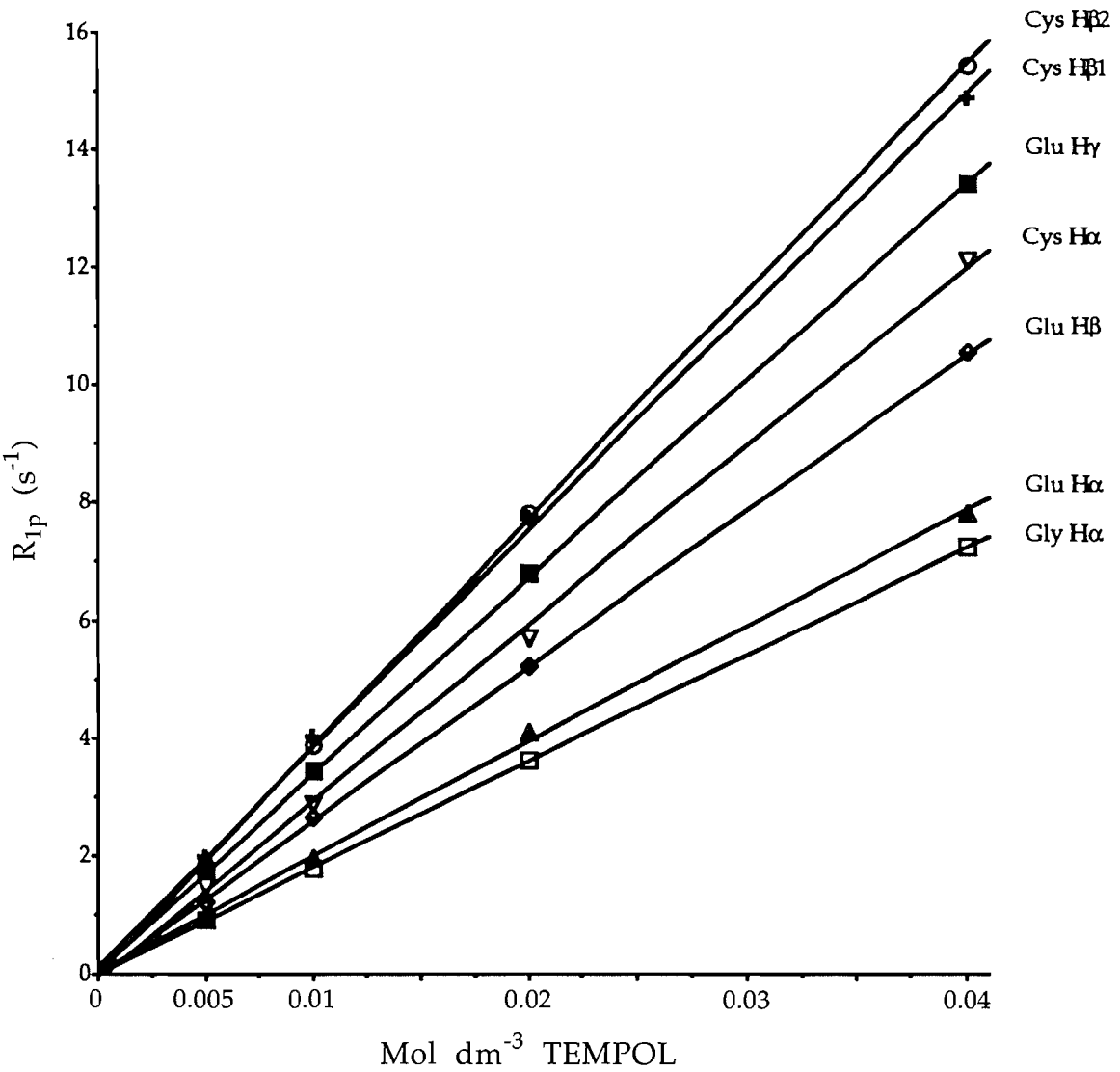

FIG. 2. Dependence of proton R_{1p} on TEMPOL concentration for 0.15 mol dm^{-3} oxidized glutathione in D_2O at 25°C.

where N is the number of proton nuclei directly bonded to the carbon nucleus, γ_H and γ_C and ω_H and ω_C are the proton and carbon magnetogyric ratios and Larmor frequencies, respectively, τ_c the rotational correlation time, and r_{ij} the proton–carbon distance. Table 1 gives the carbon spin-lattice relaxation rates and the effective correlation time $\tau_{c_{eff}}$, calculated assuming a carbon and covalent bonded proton distance of 1.09 Å. The results reported in Table 1 show that

Can. J. Chem. Downloaded from www.nrcresearchpress.com by 88.255.202.194 on 09/08/12
For personal use only.

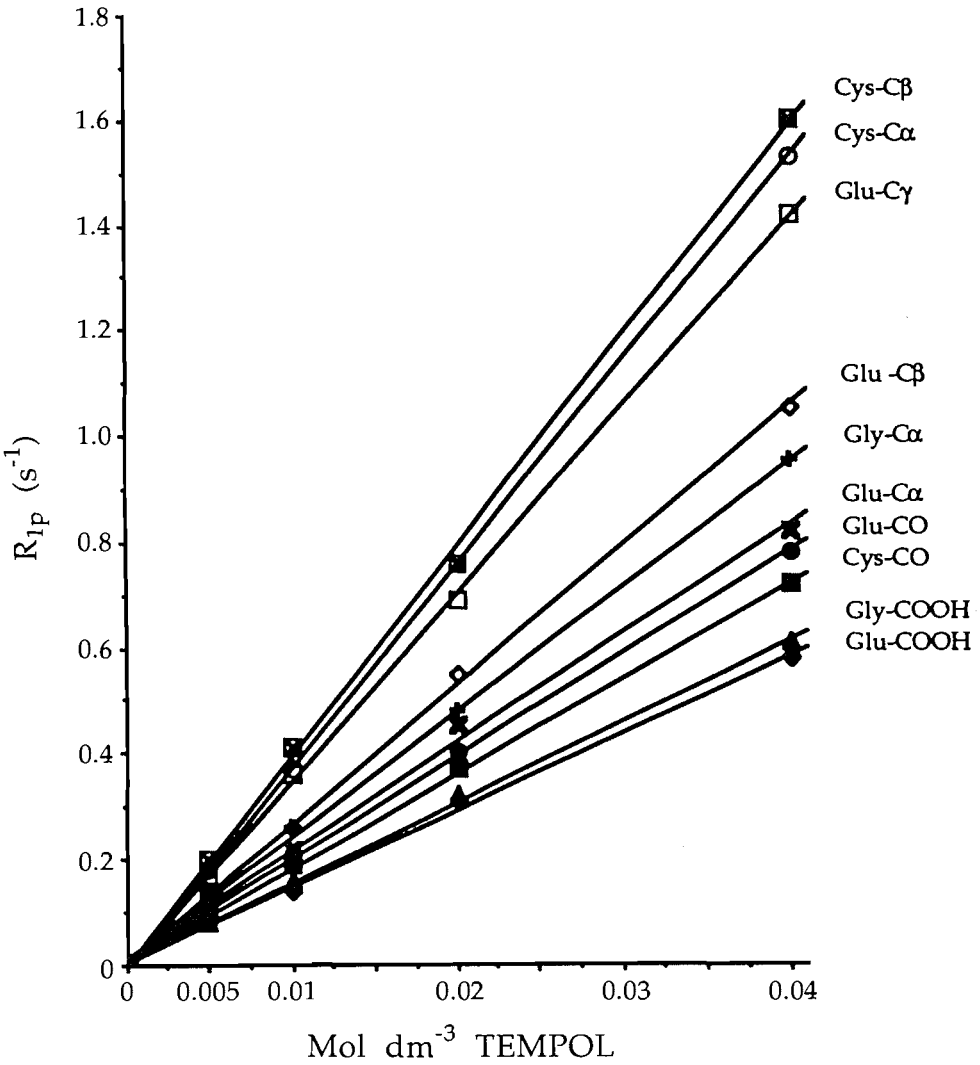

FIG. 3. Dependence of carbon R_{1p} on TEMPOL concentration for 0.15 mol dm^{-3} oxidized glutathione in D_2O at 25°C.

the region subject to the most restricted molecular motion in GSSG is the cysteine moiety, whereas the glycine region is characterized by faster motion. In the glutamic side chain, Glu Cγ is subject to faster motion than Glu Cα, but to slower motion than Glu C_β. The presence of a correlation time distribution along the molecule also suggests that GSSG does not assume any specific stable conformation in solution but rather that the amino acid side chains are subject to random motion around specific allowed spatial positions. For structured peptides, a more uniform correlation time is expected due to constraints determined by non-covalent interaction between amino acid moieties.

In contrast, whenever a molecule consists of unstructured rigid and mobile moieties, the degree of the segmental motion is greatest at the end of the side chains, decreasing steadily towards the centre, as previously shown in phospholipids (28).

The correlation time values calculated by carbon relaxation analysis can be confirmed by the proton relaxation data reported in Table 1. In particular, confirmation of the effective correlation time $\tau_{c_{eff}}$ calculated from carbon relaxation can be obtained from the analysis of proton relaxation rates of Gly Hα, Cys $H\beta_{1,2}$, Glu Hγ, and Glu H_β methylene groups. The calculated values were 7.4×10^{-11}, 2.42×10^{-10}, 2.30×10^{-10}, 1.26×10^{-10}, and 1.29×10^{-10}, respectively. These values, calculated taking into account the dominant geminal methylene H—H interaction, confirm the presence in the molecule of regions with different dynamic properties. Nevertheless the values obtained from proton spin-lattice relaxation rates appear to be overestimated. This is presumably due to contributions (which were not considered) of vicinal protons to the proton R_1 of the methylene groups.

GSSG – spin label interaction

The analysis of the correlation time values obtained from carbon, R_1, suggests that oxidized glutathione does not assume specific structure in solution.

To have more information on the dynamic and structural properties of oxidized glutathione in solution and on the interaction process between GSSG and nitroxide free radicals, the relaxation effect of TEMPOL on GSSG was analyzed. As previously shown, nitroxides may be used to induce paramagnetic perturbation on R_1 and R_2 relaxation rates of peptide protons in solution (20–22). These results were used to delineate the inner and outer protons, i.e., those exposed to, and shielded from, the solvent.

Oxidized glutathione is an interesting molecule for studying the induction of proton and carbon relaxation enhance-

Can. J. Chem. Downloaded from www.nrcresearchpress.com by 88.255.202.194 on 09/08/12
For personal use only.

Can. J. Chem. Downloaded from www.nrcresearchpress.com by 88.255.202.194 on 09/08/12
For personal use only.

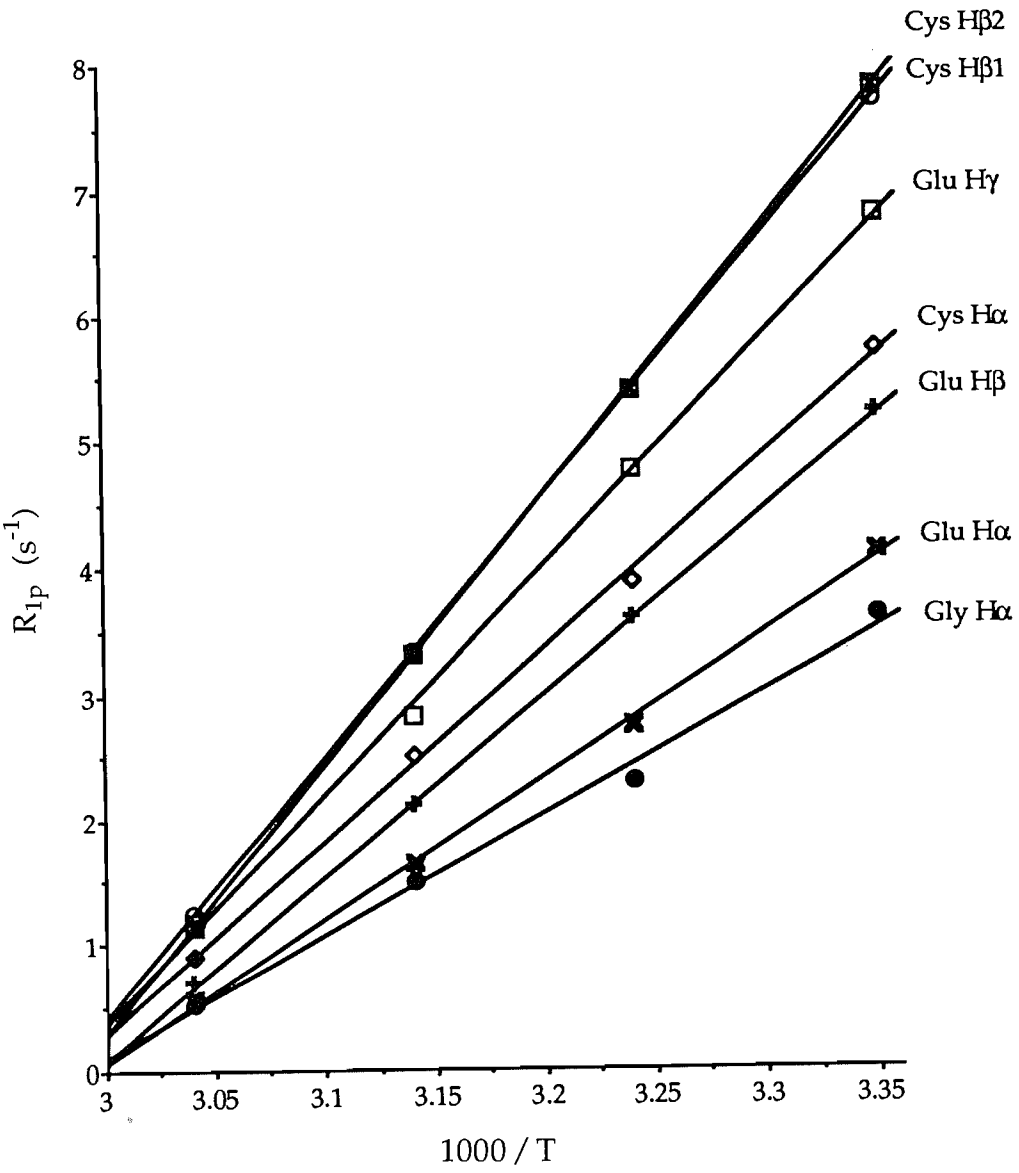

FIG. 4. Dependence of proton $R_{1\rho}$ on $1000/T$(K) for 0.15 mol dm^{-3} oxidized glutathione in D_2O. The temperature was varied from 25°C to 55°C. The concentration of TEMPOL was 2×10^{-2} mol dm^{-3}.

TABLE 4. Paramagnetic effects observed on carbon spin-lattice relaxation rates, R_1, in the Mg(II)-GSSG system at pH = 5.5. [Mg(II)] = [GSSG] = 0.15 mol dm^{-3}. Temperature = 25°C

		Relaxation rates $R_1(s^{-1})$ at different TEMPOL concentrations (mol dm^{-3})				
Carbon	δ/ppm	0	5×10^{-3}	10^{-2}	2×10^{-2}	4×10^{-2}
Gly COOH	175.174	0.15	0.23	0.30	0.43	0.97
Glu CO	173.885	0.37	0.47	0.55	0.75	1.31
Glu COOH	173.253	0.36	0.41	0.44	0.55	0.84
Cys CO	170.702	0.32	0.41	0.46	0.59	1.03
Glu Cα	52.971	2.30	2.41	2.50	2.68	3.22
Cys Cα	51.418	4.80	4.99	5.17	5.58	6.70
Gly Cα	42.330	3.70	3.72	3.88	4.10	4.65
Cys Cβ	37.546	9.20	9.52	9.87	10.61	12.62
Glu Cγ	30.254	4.00	4.25	4.49	5.02	6.40
Glu Cβ	25.255	4.30	4.42	4.55	4.77	5.54

ments by the addition of soluble spin-label reagents. In fact, using this peptide it is possible to compare the paramagnetic effects on the proton and carbon nuclei, to investigate the paramagnetic relaxation mechanisms, and to derive conformational information. Tables 2 and 3 show the proton and carbon spin-lattice relaxation rates of GSSG in D_2O at different TEMPOL concentrations. The dependence of R_{1p} on TEMPOL concentration for GSSG protons and carbons is shown in Figs. 2 and 3, respectively. The temperature dependence of proton R_{1p} was also investigated. Figure 4 shows the plot of proton R_{1p} vs. $1000/T(K)$. The positive slope shown for all the GSSG protons indicates a condition of fast chemical exchange between the peptide and the spin label. Moreover, the linearity of these plots shows that nuclear relaxation is mainly a diffusion-limited process, proportional to the mean diffusion coefficient of the radical and the peptide and consistent with Hubbard's "outer sphere" mechanism (29, 30). Besides the collisional mechanism, other contributions, such as the one arising from peptide–nitroxide transient complexes, could be of some importance in determining the relaxation of proton and carbon peptide nuclei (31).

To have more evidence of the nature of the GSSG–nitroxide interaction, the EPR spectra of the nitroxide and GSSG–nitroxide systems were recorded. The typical three-line EPR spectrum of TEMPOL in D_2O was indistinguishable from that of the GSSG–TEMPOL system, indicating a nitroxide isotropic rotational correlation time of $\tau_c < 1 \times 10^{-11}$ s (30, 32). The absence of linewidth broadening and a small reduction in the intensity of the EPR spectrum suggested that the presence of the peptide did not significantly affect the solution behaviour of the nitroxide molecules.

A different experiment was then performed. The paramagnetic contribution to carbon spin-lattice relaxation induced by TEMPOL on the Mg(II)–GSSG system was analyzed. As shown in Table 4, the presence of the Mg(II) ion did not significantly change the experimental R_{1p} values. Nevertheless, an increase in R_{1p} values with respect to solutions without Mg(II) ions was observed for all proton and carbon nuclei of oxidized glutathion. This could be the result of two effects: (*i*) the change in the diffusion coefficient of GSSG on complexation and (*ii*) the neutralization of the carboxylic negative charge by the magnesium ion, facilitating the approach of the nitroxide to the peptide molecule. Our results suggest that: (*i*) in both GSSG – nitroxide and GSSG – Mg(II) nitroxide systems, the main source of paramagnetic relaxation is related to the formation of collisional complexes ("outer-sphere"); and (*ii*) the spread of R_{1p} among proton and carbon nuclei of GSSG excludes the presence of completely shielded nuclei. However, the presence of different paramagnetic terms suggests some specificity in GSSG–nitroxide interaction.

Can. J. Chem. Downloaded from www.nrcresearchpress.com by 88.255.202.194 on 09/08/12
For personal use only.

1. L. Flohé, W. A. Gunzler, and R. Ladenstein. *In* Glutathione: metabolism and function. *Edited by* I. M. Arias and W. B. Jakoby. Raven Press, New York. 1976.
2. M. Fareggi and J. G. Leopold. Radiat. Res. **65**, 238 (1976).
3. G. Marzullo and A. J. Friedhoff. Life Sci. **21**, 1559 (1977).
4. M. Jouini, G. Lapluye, J. Haret, R. J. Ferradini, and C. Ferradini. J. Inorg. Biochem. **26**, 269 (1986).
5. S. Fujiwara, G. F. Kozlowska, and H. Kozlowski. Bull. Chem. Soc. Jpn. **50**, 3131 (1977).
6. M. J. York, G. R. Beilharz, and P. W. Kuchel. Int. J. Peptide Protein Res. **29**, 638 (1987).
7. B. J. Fuhr and D. L. Rabenstein. J. Am. Chem. Soc. **95**, 6944, (1973).
8. H. J. Wigand, H. Ottenwälder, and H. M. Bolt. Arch. Toxicol. Suppl. **8**, 319 (1985).
9. K. Várnagy, I. Sovago, and H. Kozlowski. Inorg. Chim. Acta, **151**, 171 (1988).
10. B. Birgersson, R. E. Carter, and T. Drakenberg. J. Magn. Reson. **28**, 299 (1977).
11. B. Podányi and R. S. Reid. J. Am. Chem. Soc. **110**, 3805 (1988).
12. M. J. Blais and G. Berthan. J. Chem. Soc. Dalton Trans. 1803 (1982).
13. W. S. Postal, E. J. Vogel, C. M. Young, and F. T. Greenway. J. Inorg. Biochem. **25**, 25 (1985).
14. C. Ramakrishnan and K. P. Sarathy. Biochim. Biophys. Acta, **168**, 402 (1968).
15. Y. A. Ovchinnikov and V. T. Ivanov. Tetrahedron, **31**, 2177 (1975).
16. C. M. Deber, V. Madison, and E. R. Blout. Acc. Chem. Res. **9**, 106 (1976).
17. K. D. Kopple and A. Go. J. Am. Chem. Soc. **99**, 7698 (1977).
18. D. H. Rich and R. D. Jasensky. J. Am. Chem. Soc. **102**, 1112 (1980).
19. H. R. Loosli, H. Kessler, H. Oschkinat, H. P. Weber, T. J. Petcher, and A. Widmer. Helv. Chim. Acta, **68**, 682 (1985).
20. N. Niccolai, G. Valensin, C. Rossi, and W. A. Gibbons. J. Am. Chem. Soc. **104**, 1534 (1982).
21. N. Niccolai, C. Rossi, G. Valensin, P. Mascagni, and W. A. Gibbons. J. Phys. Chem. **88**, 5689 (1984).
22. N. Zhou, P. Mascagni, W. A. Gibbons, N. Niccolai, C. Rossi, and H. Wyssbrod. J. Chem. Soc. Perkin Trans. 2, 581 (1985).
23. K. D. Koppler and T. J. Schamper. J. Am. Chem. Soc. **99**, 7698 (1977).
24. Z. W. Qiu, D. M. Grant, and R. J. Pugmire. J. Am. Chem. Soc. **104**, 2747 (1982).
25. I. D. Campbell and R. Freeman. J. Magn. Reson. **11**, 143 (1973).
26. R. Freeman, D. W. Hill, B. Tomlison, and L. D. Hall. J. Chem. Phys. **61**, 4466 (1974).
27. A. Allerhand and R. A. Komoroski. J. Am. Chem. Soc. **95**, 8288 (1973).
28. R. J. Abraham and P. Loftus. *In* Proton and carbon-13 NMR spectroscopy. Heyden, London. 1978. pp. 136–138.
29. P. S. Hubbard. Proc. R. Soc. London, **291**, 537 (1966).
30. R. A. Dwek. *In* NMR in biochemistry. Clarendon Press, Oxford. 1979. pp. 285–327.
31. I. Solomon and N. Bloembergen. J. Chem. Phys. **25**, 261 (1956).
32. G. I. Likhtenshtein. *In* Spin labeling methods in molecular biology. J. Wiley, New York. 1976. pp. 1–21.

An *ab initio* study on the reaction of $CH(X^2\pi)$ with CH_4

ZHONGHUA YU, CONGXIANG CHEN, AND MINGBAO HUANG[1]

Department of Modern Chemistry, University of Science and Technology of China, Hefei, Anhui 230026, China

Received October 5, 1992

ZHONGHUA YU, CONGXIANG CHEN, and MINGBAO HUANG. Can. J. Chem. **71**, 512 (1993).

The mechanism of the reaction $CH(X^2\pi) + CH_4$ has been investigated by *ab initio* molecular orbital calculations. Addition, insertion, and abstraction–addition reaction paths have been examined by, in total, five methods of approach. The addition reaction path has a rather high energy barrier. Our calculations have implied that the assumed insertion reaction path does not seem to exist for the reaction $CH + CH_4$, and a two-step mechanism (abstraction–addition reaction path) was then proposed. For the abstraction–addition reaction, the reactants, transition state, intermediates, and products were optimized at the HF/3-21G and HF/6-31G* levels, and vibrational frequencies were calculated at the HF/3-21G level. Electronic correlation energy was estimated by means of the Møller–Plesset perturbation theory and configuration interaction method. The excited-state abstraction reaction was also studied in some detail.

ZHONGHUA YU, CONGXIANG CHEN et MINGBAO HUANG. Can. J. Chem. **71**, 512 (1993).

Faisant appel à des calculs d'orbitales moléculaires *ab initio*, on a étudié le mécanisme de la réaction $CH(X^2\pi) + CH_4$. On a examiné cinq voies réactionnelles différentes, dont l'addition, l'insertion et l'arrachement–addition. La réaction d'addition implique une énergie relativement élevée. Nos calculs impliquent que la réaction d'insertion ne semble pas exister pour la réaction $CH + CH_4$; on propose donc un mécanisme en deux étapes (voie d'arrachement–addition). Pour cette voie d'arrachement–addition, on a optimisé les réactifs, l'état de transition, les intermédiaires et les produits aux niveaux HF/3-21G et HF/6-31G* et on a calculé les fréquences vibrationnelles au niveau HF/3-21G. On a évalué l'énergie de corrélation électronique à l'aide de la théorie perturbationelle de Møller–Plesset et par la méthode des interactions de configuration. On a aussi étudié la voie d'arrachement du état excité en détail.

[Traduit par la rédaction]

Introduction

Carbynes are presently attracting the attention of experimentalists and theoreticians, and methylidine (CH), the simplest member of this family of monovalent carbon radicals, is known to be one of the most reactive of all free radicals (1). For the CH radical, many reactions with such small molecules as H_2, O_2, N_2, H_2O, NH_3, CH_2O, oxides of carbon and nitrogen, and a number of saturated and unsaturated hydrocarbons, have been studied in kinetic experiments (1). However, very few theoretical studies of CH reactions have been reported. In 1977, Brooks and Schaefer (2) carried out CI calculations for the simple $CH + H_2$ reaction. For the insertion reaction with the $CH_3(^2A_2)$ radical as the product, the least-motion path, where the CH radical is perpendicular to the H_2 molecule, was found to have an energy barrier of about 75 kcal/mol. However, for the "non-least-motion" path, where the CH radical is parallel to the H—H bond, there was little or no energy barrier.

In 1986, Dunning *et al.* (3) presented a comprehensive theoretical description of the $CH + H_2$ reaction based on their GVB and CI calculations and pointed out a new reaction pathway. Strausz and co-workers (4) carried out *ab initio* calculations for the $CH(X^2\pi) + C_2H_4(X^1A_g)$ addition and insertion reactions using the ROHF SCF method with configuration interaction, and their results indicated that, in agreement with experiment, the energy barrier for the addition reaction was zero if an asymmetric non-least-motion path was followed. On the other hand, their computed barrier for the insertion reaction path was very high (15 kcal/mol). These important studies somehow imply that in theoretical studies for the CH reactions unexpected situations and complexities may occur. In 1990, Vegiri and Farantos (5) calculated potential energy surfaces for the reaction $CH(A^2\Delta) + H_2$ using the MRDCI method.

[1]Author to whom correspondence may be addressed.

Because of their importance in combustion and planetary atmospheric chemistry, the reactions of CH with a number of saturated and unsaturated hydrocarbons have been studied experimentally (1). For the reaction of $CH(X^2\pi)$ with CH_4, detailed kinetic experiments have been performed (6–9). Using the laser-photolysis/LIF technique, Berman and Lin (9) found that, in the temperature range 167–652 K and at a fixed total pressure of 100 Torr (1 Torr = 133.3 Pa), the measured activation energy was −0.4 kcal/mol, and that at 297 K the measured rate constants were independent of the total pressure. On the basis of the above facts and thermochemistry data, they proposed the following reaction mechanism (1, 9):

$$[1]\quad CH(X^2\pi) + CH_4 \xrightarrow{(a)} C_2H_5 \xrightarrow{(b)} C_2H_4 + H$$

(0.0 kcal/mol) (−94.5 kcal/mol) (−59.0 kcal/mol)

$$[2]\quad CH(X^2\pi) + CH_4 \rightarrow CH_2 + CH_3$$

(0.0 kcal/mol) (2.6 kcal/mol)

According to their proposed mechanism, in the first reaction a vibrationally hot ethyl radical is the product of the insertion of the CH radical into a methane C—H bond and is a long-lived intermediate complex. Reaction [1] was considered (1) as the dominant channel since it is strongly exothermic. On the other hand, reaction [2] is slightly endothermic and therefore could not compete with the first reaction because of its weak endothermicity (1).

We have noticed that no theoretical studies for the CH reaction with CH_4 have been reported. We believe that a detailed theoretical study of this reaction may be of very fundamental significance for CH reactions with organic molecules (at least, with paraffinic molecules). We therefore directed our attention to the first reaction (a) above and performed *ab initio* calculations. In this paper we report our theoretical results and draw some conclusions about the

Can. J. Chem. Downloaded from www.nrcresearchpress.com by 88.255.202.194 on 09/08/12
For personal use only.

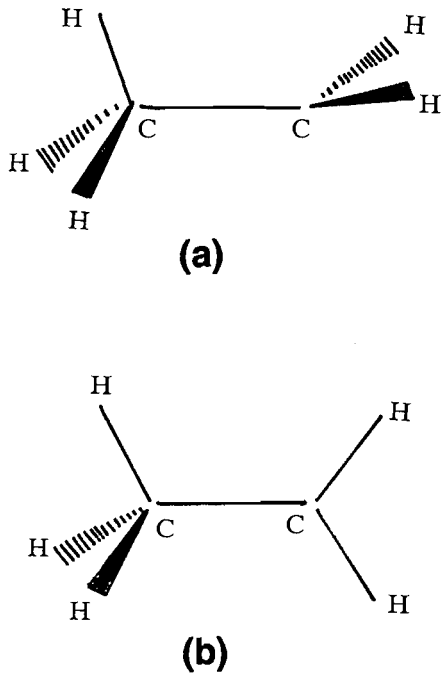

FIG. 1. The two conformations of the ethyl radical: (*a*) staggered; (*b*) eclipsed.

mechanism of the CH + CH_4 reaction. Step (b) of reaction [1] has already been studied by Schlegel (10).

Calculation methods and details

We performed *ab initio* calculations[2] with the GAUSSIAN82 program (12), using extended 3-21G and polarized 6-31G* basis sets. All equilibrium geometries and transition-state structures were fully optimized with the analytical gradient method at the Hartree–Fock level and, in some cases, at the MP2 level. Electronic correlation energy was estimated by using Møller–Plesset perturbation theory up to fourth order (MP4SDTQ, full) and using configuration interaction theory (CISD, full). Vibrational frequencies were obtained from analytical second derivatives calculated at the HF/3-21G level.

For the reaction CH + CH_4, we examined addition, insertion, and abstraction–addition reaction paths in turn. The 3-21G basis was employed in the overall scans of the reaction paths, and the total energies as functions of the reaction coordinates were calculated by optimizing all the rest of the geometric parameters of the reaction system. The polarized 6-31G* basis was also used in calculations for the critical points of the reaction paths. For the ethyl radical C_2H_5, previous experimental and theoretical studies (13) indicated that the potential energy curve for internal rotation about the C—C bond is very flat and the staggered conformer (see Fig. 1(*a*)) corresponds to the energy minimum. The eclipsed conformer (see Fig. 1(*b*)) is only 0.14 kcal/mol (MP2/6-31G*//HF/6-31G*) less stable than the staggered one. In the three reaction paths we examined, the reaction system was assumed to have a symmetry plane. Thus, the expected product C_2H_5 would be in the eclipsed conformation ($^2A''$) in the addition and insertion paths, while it would be in the staggered conformation ($^2A'$) in the abstraction–addition path, as will be described clearly below.

[2]A general description of the calculation methods and basis sets is given in ref. 11.

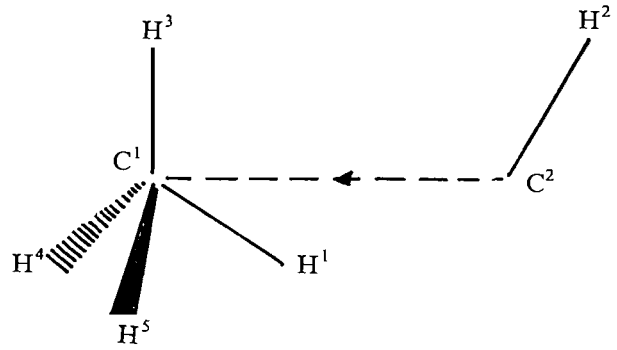

FIG. 2. Addition reaction path.

Results

To study the mechanism of the reaction CH + CH_4, we considered three reaction paths by, in total, five methods of approach.

1. Addition reaction path

For the addition reaction path (see Fig. 2), we assumed that methylidyne, with its carbon atom C^2, attacks methane directly at the carbon C^1, and the C^1—C^2 distance was taken as the reaction coordinate *Z*. We further assumed that the CH radical approached between the C^1H^1 and C^1H^3 bonds of methane and within the plane $H^1C^1H^3$, so the system had only C_s symmetry. Such a reaction path was proposed in imitation of the route considered for insertion of the CH radical into C_2H_4, adopted by Strausz and co-workers (4), and of the C atom reaction with CH_4, adopted by Lebrilla and Maier (14). We hoped that, as the *Z*-value decreased, the changes in geometric parameters would show migration of one methane hydrogen (H^1 or H^3) to the methylidyne carbon C^2, finally leading to the eclipsed conformation ($^2A''$) of the C_2H_5 radical. The HF/3-21G potential energy curve for the addition path was calculated starting at $Z = 4.0$ Å, but we stopped the calculations at $Z = 1.80$ Å. At $Z = 1.80$ Å, the values of the C^2H^1, C^2H^3, C^1H^1, and C^1H^3 distances were 2.04, 1.38, 1.07, and 1.15 Å, respectively, indicating that significant hydrogen migration in that geometry had not yet taken place. However, the energy value was already 46 kcal/mol higher than the sum of the HF/3-21G energies of the reactants, which implies that the addition reaction path is not energetically favourable.

2. Insertion reaction paths

For the insertion reaction, we considered two paths (a) and (b), which are shown in Fig. 3(*a*) and (*b*), respectively. In both cases, the CH radical was assumed to approach within the $H^1C^1H^3$ plane (an assumed symmetry plane of the system) at the center, denoted as X, of the C^1H^1 bond of methane, and the C^2X distance (*Z*) was taken as the reaction coordinate. In path (a), the $H^2C^2XH^1$ part was in a *trans* form. Such an insertion reaction path was proposed in imitation of the method adopted by Gordon and Gano (15) in their *ab initio* study of the insertion of singlet methylene into the C—H bond of methane, and we hoped that, as the *Z*-value decreased, the H^1 atom would migrate to C^2 and the optimized C^1–C^2 distance would become shorter, finally lead-

Can. J. Chem. Downloaded from www.nrcresearchpress.com by 88.255.202.194 on 09/08/12
For personal use only.

Can. J. Chem. Downloaded from www.nrcresearchpress.com by 88.255.202.194 on 09/08/12
For personal use only.

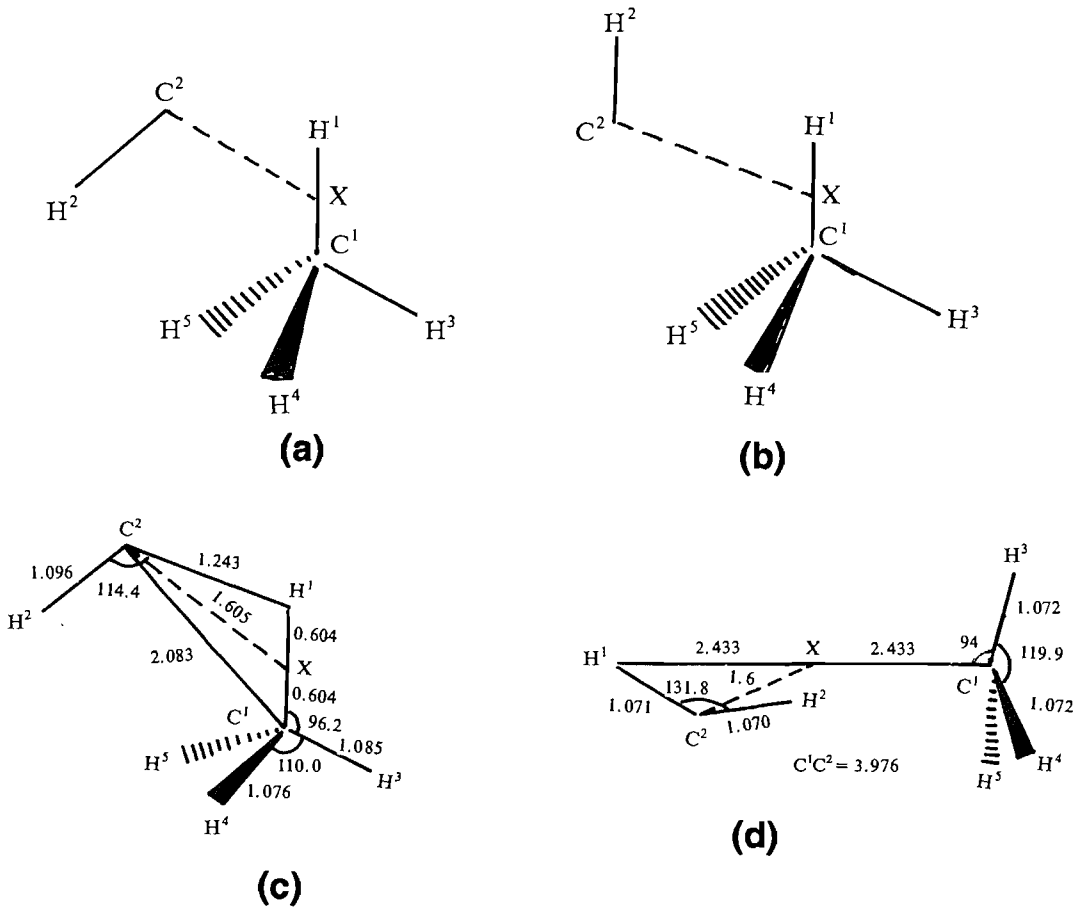

FIG. 3. (*a*) Insertion reaction path with the $H^2C^2XH^1$ part in a *trans* form. X denotes the midpoint of the C^1H^1 distance. (*b*) Insertion reaction path with the $H^2C^2XH^1$ part in a *cis* form. (*c*) The geometry corresponding to the point B in Fig. 4. (*d*) The geometry corresponding to the point C in Fig. 4.

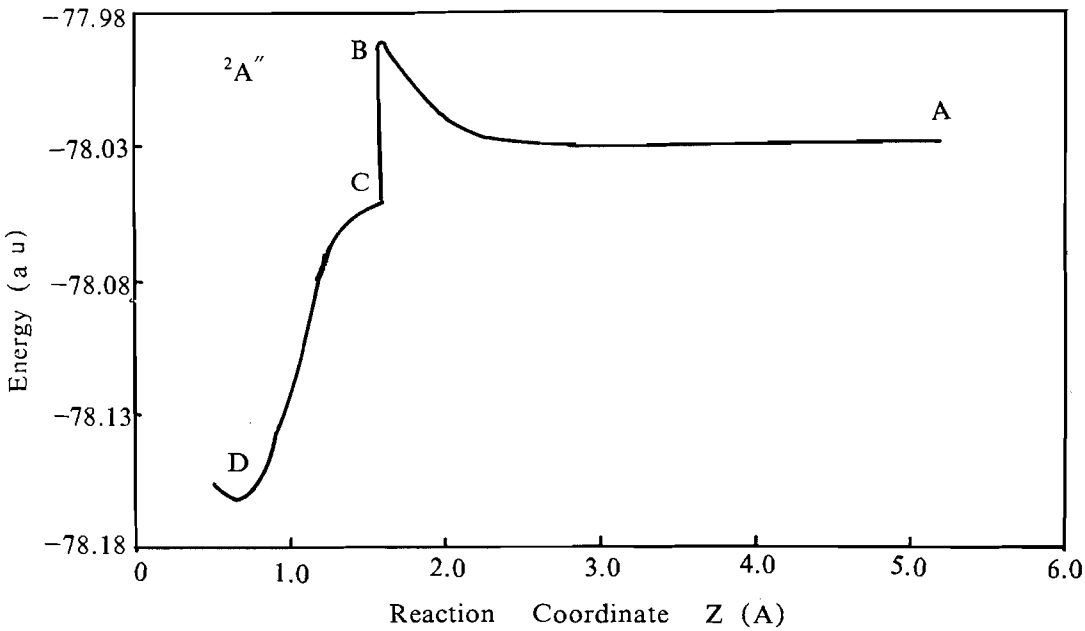

FIG. 4. Potential energy curve for the insertion reaction path (*a*) at the HF/3-21G level.

Can. J. Chem. Downloaded from www.nrcresearchpress.com by 88.255.202.194 on 09/08/12
For personal use only.

ing to the eclipsed conformation ($^2A''$) of C_2H_5. The HF/3-21G energy curve $E(Z)$ for the insertion reaction path (a) is shown in Fig. 4. This curve appears discontinuous and seems to consist of three sections: A ($Z = \infty$, the reactants) – B (Z = 1.605 Å), B–C (Z = 1.600 Å), and C–D (Z = 0.66 Å, the product). However, it should be emphasized that the electronic state ($^2A''$) and electronic configuration (α,β-electron occupation numbers in the MOs of A' and A'' symmetries) were kept unchanged throughout the curve from A to D.

The geometry evolution along the AB part of the curve seemed quite optimistic, H^1 migrating and the C–C distance being shortened. In the geometry corresponding to point B, shown in Fig. 3(*c*), the decreased C–C distance has a value of 2.083 Å and both the C^1H^1 and C^2H^1 distances are longer than 1.2 Å, which indicates that at Z = 1.605 Å the C^1H^1 bond has broken and the C^2H^1 bond has not yet formed. This geometry should be close to the transition-state geometry, which was not located exactly. The HF/3-21G energy at point B is 23.3 kcal/mol higher than the energy sum of the reactants (point A).

It was unexpected that the C–C distance would be much elongated as the system went along the curve from B to C in Fig. 4. The geometry corresponding to point C (shown in Fig. 3(*d*)) indicates that, at Z = 1.600 Å, H^1 has completed its migration and the system can be viewed as two separate fragments, $H^1C^2H^2$ and $C^1H^3H^4H^5$, due to the long C–C distance of 3.976 Å. The bent geometry of the $H^1C^2H^2$ fragment is very close to the HF/3-21G geometry of the triplet ground state ($^3B_1$) of CH_2 (d_{C-H} = 1 .071 Å and ∠HCH = 131.3°), while the flat geometry of the $C^1H^3H^4H^5$ fragment is close to the HF/3-21G geometry of CH_3 ($^2A_2$) (d_{C-H} = 1.072 Å and ∠HCH = 120.0°). The sums of the calculated atomic spin densities on the atoms of the $H^1C^2H^2$ and $C^1H^3H^4H^5$ fragments are 2.16 and −1.12, respectively. The energy of the system at the point C, −78.0524 au, is approximately equal to the sum of the HF/3-21G energies of CH_2 ($^3B_1$) and CH_3 ($^2A_2$), −78.0518 au. The above analyses of the geometries, atomic spin densities, and energies suggest that the ABC part of the energy curve for the insertion reaction path (a) represents the following reaction step,

$$CH(X^2\pi) + CH_4 \rightarrow CH_2(^3B_1) + CH_3(^2A_2)$$

From C to D along the curve in Fig. 4, the energy decreases monotonically and without any energy barrier. Point D represents the product C_2H_5 in its eclipsed conformation ($^2A''$). At the HF/3-21G level, the energy difference between the eclipsed and staggered conformations of C_2H_5 is only 2.1 kcal/mol, which is almost negligible compared with the energy difference of about 70 kcal/mol between E(C) and E(D). Actually the CD part of the energy curve for the insertion reaction path (a) represents the following reaction step.

$$CH_2(^3B_1) + CH_3(^2A_2) \rightarrow C_2H_5(^2A'')$$

We also performed HF/6-31G* calculations around the critical points A, B (Z = 1.605 Å), C (Z = 1.600 Å), and D, and the skeleton of the HF/6-31G* potential energy curve is similar to the HF/3-21G curve shown in Fig. 4. The HF/6-31G* energy difference between E(B) and E(A) is 21.4 kcal/mol, which is slightly smaller than the HF/3-21G difference (23.3 kcal/mol).

In the insertion reaction path (b), shown in Fig. 3(*b*), the $H^2C^2XH^1$ part was in a *cis* form, which was proposed in imitation of the non-least-motion paths of the insertion reaction $CH(X^2\pi) + H_2 \rightarrow CH_3$, adopted by Brooks and Schaefer (2), and of the reaction $CH_2(^1A_1) + H_2 \rightarrow CH_4$, adopted by Sosa and Schlegel (16). Our calculated HF/3-21G energies at Z = 2.40 Å and 2.00 Å were both about 3 kcal/mol higher than the corresponding energies in path (a), which implies that path (b) is less favourable than path (a). We then stopped the calculations for path (b).

3. Abstraction–addition reaction path

Based on analyses of the results described above, we propose an abstraction–addition reaction path, explicitly considering a two-step mechanism as implied by the curve in Fig. 4. The first step is an abstraction reaction $CH + CH_4 \rightarrow CH_2(^3B_1) + CH_3$ (see Fig. 5(*a*)), and the second step is an addition reaction $CH_2(^3B_1) + CH_3(^2A_2'') \rightarrow C_2H_5$ (staggered) (see Fig. 1(*a*)).

In the study of the first step of the abstraction–addition reaction path, we first optimized the geometry of the transition state (identified by performing frequency analysis calculations), then we calculated the potential energy curve ABC. This is shown in Fig. 6, the points A, B, and C representing the reactants, transition state, and products of this step, respectively. We took the distance C^2H^1 as the reaction coordinate Z in the B–A part of the curve, and the distance C^1H^1 as Z in the B–C part. The system along the curve A–B–C is in the $^2A''$ electronic state and we denote the transition state as $^2A''$TS. The optimized geometry of $^2A''$TS is shown in Fig. 5(*c*), the unique imaginary frequency being 2507i cm^{-1}. At the HF/3-21G level, the predicted energy barrier (E(B)–E(A)) is 15.5 kcal/mol, which is the lowest of all the paths we considered. Our energetic results therefore imply that the abstraction reaction path is the most favourable, which is unexpected.

The second step of the abstraction–addition reaction path is an addition reaction to form the final product C_2H_5 in its staggered conformation ($^2A'$). The reaction system was assumed to have a staggered geometry (see Fig. 1(*a*)) and the C–C distance was taken as the reaction coordinate Z. The HF/3-21G potential energy curve (D–F) is shown in Fig. 6, the electronic state being $^2A'$. Both points D and C in Fig. 6 denote $CH_2(^3B_1) + CH_3$ ($Z = \infty$), and the point F the final product. No energy barrier was found along the curve D–F, and this step was predicted to be strongly exothermic.

For the critical points along the abstraction–addition path, we also carried out higher level calculations rather than the HF/3-21G level. The HF/6-31G* transition-state optimization calculations predicted an $^2A''$TS geometry, which is similar to the HF/3-21G geometry, both sets of the optimized geometric parameters being given in Fig. 5(*c*). Table 1 gives total energies for the critical points along the abstraction–addition reaction path. Relative energies are collected in Table 2. At the HF/3-21G and HF/6-31G* levels, the first reaction step was predicted to be exothermic by 14.4 and 12.8 kcal/mol (E(C)–E(A)), respectively, while, based on thermochemistry data, it should be weakly endothermic. As shown in Table 2, inclusion of correlation energies is important for narrowing the energy gap between A and C. At the MP4SDTQ/6-31G*//HF/6-31G* level, the first reaction step was predicted to be endothermic by 2.8 kcal/mol, which is in agreement with experiment (1). At this level, the

Can. J. Chem. Downloaded from www.nrcresearchpress.com by 88.255.202.194 on 09/08/12
For personal use only.

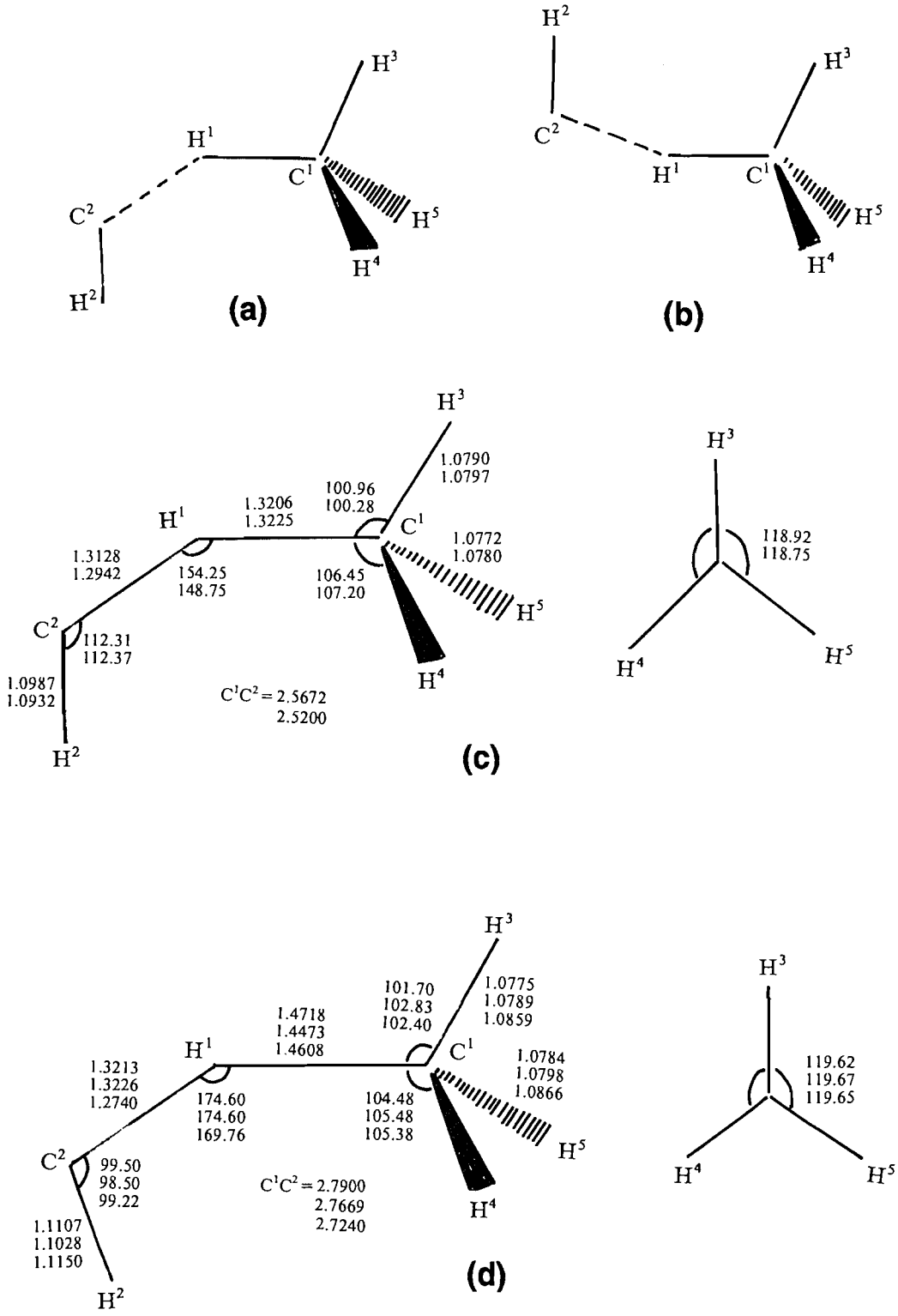

FIG. 5. (*a*) The first step of abstraction–addition reaction path. (*b*) Another method of approaching the first step of the abstraction–addition reaction path (it was tested and is less favourable than the method given in Fig. 5(*a*)). (*c*) The optimized $^2A''$TS geometries for the first step of the abstraction–addition reaction path. The upper values are the HF/3-21G results, and the lower values the HF/6-31G* results. Bond distances in Å and angles in degree. (*d*) The optimized $^2A'$TS geometries for the excited-state abstraction reaction. The upper, mid, and lower values are the HF/3-21G, HF/6-31G*, and MP2/6-31G* results, respectively.

energy barrier (E(B)–E(A)) for the first step was predicted to be 13.7 kcal/mol. The experimental value for the heat of the (whole) reaction is −94.5 kcal/mol, and our calculations at all the levels gave large values (−84.6 and −103.6 kcal/mol) for the energy difference (E(F) − E(A)) (see Table 2).

For the first step, we also tested another pathway, shown in Fig. 5(*b*). However, the calculated energies (HF/3-21G)

Can. J. Chem. Downloaded from www.nrcresearchpress.com by 88.255.202.194 on 09/08/12
For personal use only.

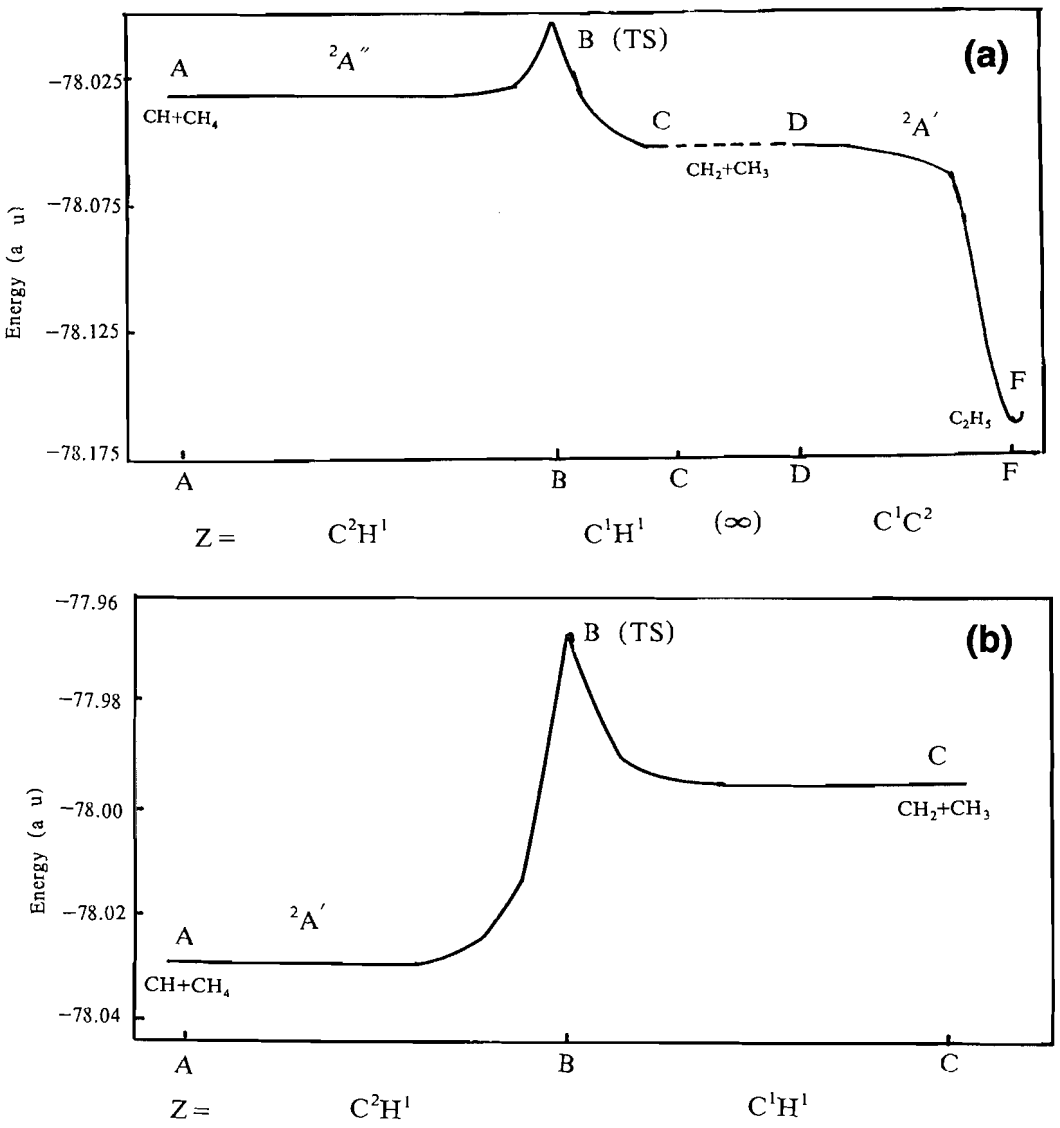

FIG. 6. (*a*) A schematic diagram of the HF/3-21G potential energy curves for the abstraction–addition reaction path. (*b*) A schematic diagram of the HF/3-21G potential energy curve for the excited-state abstraction reaction.

TABLE 1. Energetics (total energy) of the abstraction–addition reaction path CH + CH_4 → $CH_2(^3B_1)$ + CH_3 → C_2H_5 (staggered)

Level	Total energy (au)[a]			
	CH + CH_4	$^2A''$TS	CH_2 + CH_3	C_2H_5
HF/3-21G	−78.02879	−78.00412	−78.05168	−78.16365
MP2/3-21G//HF/3-21G	−78.17510	−78.15580	−78.18280	−78.33097
MP3/3-21G//HF/3-21G	−78.19987	−78.17818	−78.20518	−78.35184
MP4SDQ/3-21G//HF/3-21G	−78.20755	−78.18606	−78.21095	−78.35763
MP4SDTQ/3-21G//HF/3-21G	−78.20943	−78.18896	−78.21222	−78.36068
CISD/3-21G//HF/3-21G	−78.20635	−78.17887	−78.21057	−78.34798
HF/6-31G*	−78.46011	−78.43174	−78.48049	−78.59715
MP2/6-31G*//HF/6-31G*	−78.67927	−78.65890	−78.68032	−78.84443
MP3/6-31G*//HF/6-31G*	−78.71164	−78.68821	−78.71008	—
MP4SDQ/6-31G*//HF/6-31G*	−78.71949	−78.69590	−78.71578	—
MP4SDTQ/6-31G*//HF/6-31G*	−78.72290	−78.70105	−78.71841	—
CISD/6-31G*//HF/6-31G*	−78.71438	−78.67933	−78.71188	—

[a]1 au = 627.5 kcal/mol.

TABLE 2. Energetics (relative energy, in kcal/mol) of the abstraction–addition reaction path

Level	CH + CH_4	$^2A''$TS	CH_2 + CH_3	C_2H_5
HF/3-21G	0.0	15.5	−14.4	−84.6
MP2/3-21G//HF/3-21G	0.0	12.1	−4.8	−97.8
MP3/3-21G//HF/3-21G	0.0	13.6	−3.3	−95.4
MP4SDQ/3-21G//HF/3-21G	0.0	13.5	−2.1	−94.2
MP4SDTQ/3-21G//HF/3-21G	0.0	12.8	−1.8	−94.9
CISD/3-21G//HF/3-21G	0.0	17.3	−2.7	−89.0
HF/6-31G*	0.0	17.8	−12.8	−86.0
MP2/6-31G*//HF/6-31G*	0.0	12.8	−0.7	−103.6
MP3/6-31G*//HF/6-31G*	0.0	14.7	1.0	—
MP4SDQ/6-31G*//HF/6-31G*	0.0	14.8	2.3	—
MP4SDTQ/6-31G*//HF/6-31G*	0.0	13.7	2.8	—
CISD/6-31G*//HF/6-31G*	0.0	22.0	1.6	—
Experimental			2.6[a]	−94.5[a]

[a]Reference 1.

TABLE 3. Energetics of the excited-state abstraction reaction CH + $CH_4 \rightarrow CH_2(^1A_1)$ + CH_3 (R.E. = relative energy, in kcal/mol)

	CH + CH_4		$^2A'$TS		$CH_2(^1A_1)$ + CH_3	
Level	*E*(au)	R.E.	E(au)	R.E.	E(au)	R.E.
HF/3-21G	−78.02879	0.0	−77.96587	39.5	−77.99446	21.5
MP2/3-21G//HF/3-21G	−78.17510	0.0	−78.11953	34.9	−78.13793	23.3
MP3/3-21G//HF/3-21G	−78.19987	0.0	−78.14491	34.5	−78.16371	22.7
MP4SDQ/3-21G//HF/3-21G	−78.20755	0.0	−78.15353	33.9	−78.17092	23.0
MP4SDTQ/3-21G//HF/3-21G	−78.20943	0.0	−78.15618	33.4	−78.17253	23.2
CISD/3-21G//HF/3-21G	−78.20635	0.0	−78.14464	38.7	−78.17085	22.3
HF/6-31G*	−78.46011	0.0	−78.39564	40.5	−78.43136	18.0
MP2/6-31G	−78.67944	0.0	−78.62474	34.3	−78.64704	20.3
Experimental						22.1[a]

[a]The sum of the $^3B_1$–$^1A_1$ energy separation of CH_2, 19.5 kcal/mol (16), and the heat of the ground-state abstraction reaction, 2.6 kcal/mol (1).

at several large *Z* values were higher than those for the approach shown in Fig. 5(*a*); we then stopped the calculations.

4. The excited-state abstraction reaction

We also studied the excited-state abstraction reaction $CH(X^2\pi)$ + $CH_4 \rightarrow CH_2(^1A_1)$ + $CH_3(^2A_2)$ in the $^2A'$ electronic state, and the corresponding HF/3-21G potential energy curve A–B′–C′ is shown in Fig. 6(*b*). The optimized geometry of the transition state (B), denoted as $^2A'$TS, is shown in Fig. 5(*d*). This transition state was characterized by an imaginary frequency of 2535i cm^{-1} at the HF/3-21G level. In Fig. 5(*d*), it is seen that calculations of the three different levels predicted very similar geometries for $^2A'$TS. The geometries of $^2A''$TS and $^2A'$TS are quite different. The $\angle H^1C^2H^2$ angle in the $^2A''$TS geometry is about 12° larger than that in the $^2A'$TS geometry, which is consistent with the fact that the ground-state abstraction reaction ($^2A''$) leads to the triplet $CH_2(^3B_1)$ ($\angle HCH$ = 131.2°) while the excited-state reaction leads to the singlet $CH_2(^1A_1)$ ($\angle HCH$ = 102.4°) product. The $\angle C^2H^1C^1$ angle in the $^2A'$TS geometry is about 20° larger than that in the $^2A''$TS geometry.

At the HF/3-21G level, this excited-state reaction was predicted to be endothermic by 21.5 kcal/mol, and all the energetic results for this reaction are given in Table 3. The effect of inclusion of *d*-functions on carbon atoms is very small. Correlation energy corrections with Møller–Plesset perturbation theory decrease the energy barrier by 5–6 kcal/mol. At the MP2/6-31G* level, the energy barrier for this reaction was predicted to be 34.3 kcal/ mol. At this level, the reaction was predicted to be endothermic by 20.3 kcal/mol, which is in agreement with the experimental value, 22.1 kcal/mol. The latter value is the sum of the $^3B_1$–$^1A_1$ energy separation of CH_2, 19.5 kcal/mol (17), and the heat of the ground-state abstraction reaction, 2.6 kcal/mol (1).

Discussion

Because the assumed insertion reaction CH + $CH_4 \rightarrow C_2H_5$ is strongly exothermic and the measured activation energy for the reaction CH + CH_4 is negative, −0.4 kcal/mol, Berman and Lin (9) suggested that the insertion reaction path was the dominant channel for the reaction $CH(X^2\pi)$ + CH_4. We examined addition, insertion, and abstraction–addition reaction paths using, in total, five methods of approach. Our calculations indicated that the addition path has a very high energy barrier. Our calculation results for the assumed insertion path implied just a two-step mechanism — the abstraction–addition reaction path, for which we performed detailed calculations. Based on our calculations, we would conclude that the abstraction–addition reaction path is the most favourable channel for the reaction CH + CH_4, which is not in line with Lin's proposal. How to rationalize the

Can. J. Chem. Downloaded from www.nrcresearchpress.com by 88.255.202.194 on 09/08/12
For personal use only.

discrepancy between theoretical indications and experimental results seems to be a difficult problem.

Our predicted energy barrier for the first step, 13.7 kcal/mol, is relatively high compared with the experimental activation energy of −0.4 kcal/mol. We expect that inclusion of *p*-functions on the hydrogen atoms and geometry optimizations at the MP levels will considerably lower the calculated energy barrier, but the calculated energy barrier will not disappear due to the weak endothermicity of the abstraction reaction step.

Our study indicates that the reaction $CH(X^2\pi) + CH_4$ cannot be a synchronous or concerted reaction. This is also supported by Dewar's opinion (18) that multibond reaction cannot normally be synchronous.

Summary

Our detailed theoretical studies for the reaction $CH(X^2\pi) + CH_4$ indicate that the insertion reaction path does not seem to be feasible, and we have proposed a two-step mechanism (abstraction–addition path) for this reaction. However, our predicted energy barrier for the first step is relatively high compared with the experimental value. More sophisticated experimental *and* theoretical studies are both required.

Acknowledgement

We appreciate the financial support for this work that was provided by the National Natural Science Foundation Committee of China.

1. W. A. Sanders and M. C. Lin. *In* Chemical kinetics of small organic radicals. Vol. III (Reactions of special radicals). *Edited by* Z. Alfassi. CRC Press, Boca Raton, Fla. 1988. Chap. 14.
2. B. R. Brooks and H. F. Schaefer. J. Chem. Phys. **67**, 5146 (1977).
3. T. H. Dunning, L. B. Harding, R. A. Bair, R. A. Eades, and R. L. Shepard, J. Phys. Chem. **90**, 344 (1986).
4. R. K. Gosavi, I. Safarik, and O. P. Strausz. Can. J. Chem. **63**, 1689 (1985).
5. A. Vegiri and S. C. Farantos. Chem. Phys. Lett. **167**, 278 (1990).
6. J. E. Butler, J. W. Fleming, L. P. Goss, and M. C. Lin. Chem. Phys. **56**, 355 (1981).
7. M. W. Bosnali and D. Perner. Z. Naturforsch. A: Phys., Phys. Chem. Kosmophys. **26A**, 1768 (1971).
8. W. Braun, J. R. McNesby, and A. M. Bass. J. Chem. Phys. **46**, 2071 (1967).
9. M. R. Berman and M. C. Lin. Chem. Phys. **82**, 435 (1983).
10. H. B. Schlegel. J. Phys. Chem. **86**, 4878 (1982).
11. W. Hehre, L. Radom, P. V. R. Schleyer and J. A. Pople. Ab initio molecular orbital theory. Wiley, New York. 1986.
12. J. S. Binkley, M. J. Frisch, D. J. DeFrees, K. Raghavachari, R. A. White, H. B. Schlegel, E. M. Fluder, and J. A. Pople. GAUSSIAN82, Department of Chemistry, Carnegie-Mellon University, Pittsburgh, Pa.
13. J. Pacansky and M. Dupuis. J. Am. Chem. Soc. **104**, 415 (1982).
14. C. B. Lebrilla and W. F. Maier. Chem. Phys. Lett. **105**, 183 (1984).
15. M. S. Gordon and D. R. Gano. J. Am. Chem. Soc. **106**, 5421 (1984).
16. C. Sosa and H. B. Schlegel. J. Am. Chem. Soc. **106**, 5847 (1984).
17. P. F. Zittel, G. B. Ellison, S. V. O'Neil, E. Herbst, W. C. Lineberger, and W. P. Reinhardt. J. Am. Chem. Soc. **98**, 3731 (1976).
18. M. J. S. Dewar. J. Am. Chem. Soc. **106**, 209 (1984).

Can. J. Chem. Downloaded from www.nrcresearchpress.com by 88.255.202.194 on 09/08/12
For personal use only.

An ^{1}H NMR conformational analysis of 3-phenylpentane in solution

TED SCHAEFER[1] AND LINA B.-L. LEE
Department of Chemistry, University of Manitoba, Winnipeg, Man., Canada R3T 2N2

Received October 20, 1992

TED SCHAEFER and LINA B.-L. LEE. Can. J. Chem. **71**, 520 (1993).

Some 30 proton chemical shifts and proton–proton coupling constants are reported for a 4.7 mol% solution of 3-phenylpentane in a CS_2/C_6D_{12}/TMS solvent mixture at 300 K. The long-range coupling constant over six formal bonds between the methine and *para* protons is used to deduce an apparent twofold barrier of 15.0 ± 0.3 kJ/mol to rotation about the Csp^2—Csp^3 bond, at least twice as large as that for isopropylbenzene in solution. AM1 computations agree with experiment in finding the conformation of lowest energy as that in which the methine C—H bond is situated in the phenyl plane, but predict a barrier height of only 13.9 kJ/mol. The vicinal coupling constants are consistent with a fractional population, 0.38(2), of the TT conformer, that in which all the carbon atoms of the alkyl chain lie in a plane. A doubly degenerate conformer, $TG^+(G^-T)$, in which one methyl group is twisted away from the phenyl substituent, then has a fractional population of 0.62(2). The assumption that only these three conformers are present is tested with the signs and magnitudes of the four different coupling constants over four bonds. These coupling constants are consistent with the absence of significant proportions of the other six all-staggered conformers. These six are characterized by a close approach of the methyl groups (1,5 interactions) or by proximity of the methyl and phenyl moieties.

TED SCHAEFER et LINA B.-L. LEE. Can. J. Chem. **71**, 520 (1993).

Opérant à 300 K, on a déterminé quelques 30 déplacements chimiques et constantes de couplage proton–proton du 3-phénylpentane en solution à 4,7 mol% dans un mélange des solvants CS_2/C_6H_{12}/TMS. On utilise la constante de couplage à longue distance à travers six liaisons entre les protons méthine et *para* pour déduire une barrière binaire apparente de 15,0 ± 0,3 kJ/mol pour la rotation autour de la liaison Csp^2—Csp^3; cette valeur est deux fois plus grande que celle observée pour l'isopropylbenzène en solution. Des calculs AM1 sont en accord avec le fait que la conformation de plus basse énergie est celle dans laquelle la liaison C—H du méthine se trouve dans le plan du phényle; toutefois, ces calculs prédisent une barrière de seulement 13,9 kJ/mol. Les constantes de couplage vicinales sont en accord avec une population fractionnaire de 0,38(2) pour le conformère TT, celui dans lequel tous les atomes de carbone de la chaîne alkyle sont dans un plan. Un conformère doublement dégénéré, $TG^+(G^-T)$, dans lequel un méthyle est éloigné du substituant phényle, possède donc une population fractionnaire de 0,62(2). On a évalué l'hypothèse selon laquelle ces trois conformères sont présents en faisant appel aux signes et aux amplitudes des quatre constantes de couplage différentes à travers quatre liaisons. Ces constantes de couplage sont en accord avec l'absence des six autres conformères complètement décalés. Ces six conformères sont caractérisés par un rapprochement des groupes méthyles (interactions 1,5) ou par une proximité des portions méthyle et phényle.

[Traduit par la rédaction]

Can. J. Chem. Downloaded from www.nrcresearchpress.com by 88.255.202.194 on 09/08/12
For personal use only.

Introduction

Of the nine all-staggered conformers of 3-phenylpentane shown in Scheme 1, only the TT and the $TG^+(G^-T)$ are thought to exist in the liquid or in solution. Two bands in the infrared spectrum of the liquid are assigned to these conformers (1). The temperature dependence of the intensities of these bands indicates an enthalpy difference of 1.7 kJ/mol between these conformers. In the solid form, one of the bands is absent. The remaining band is assigned to the less stable $TG^+(G^-T)$ conformers. An early ^{1}H nmr investigation (1) employs an approximate analysis of the spectrum of the methylene protons at two temperatures of liquid 3-phenylpentane to deduce an enthalpy of 1.5 kJ/mol favoring the TT form over the $TG^+(G^-T)$ forms. The assumption underlying this deduction, that only these three conformers are present, is supported by some molecular mechanics calculations reported in that investigation (1). Presumably the other conformers are energetically unfavorable because of close approaches of phenyl and methyl groups (G^+T), of the two methyl groups (G^-G^+), or because of the presence of both of these repulsive interactions (G^+G^-).

With modern nmr instrumentation, higher dispersion and resolution are possible. A proper analysis of a current ^{1}H nmr spectrum will yield additional spectral parameters helpful in the conformational characterization of this molecule. Thus, the long-range coupling constants between the methine and ring protons can provide an estimate of the barrier to rotation about the Csp^2—Csp^3 bond as well as the preferred conformation of the phenyl group relative to the alkyl backbone. Again, the coupling constants over four bonds, three of them between the protons in the two methylene groups, and one between the methine and methyl protons, are very likely sensitive in sign and magnitude to the presence of the various conformers.

Accordingly, the precise analysis of the ^{1}H nmr spectrum of 3-phenylpentane is reported here. The ensuing spectral parameters allow the indicated, more detailed, characterization of the conformational behaviour of 3-phenylpentane.

Experimental

A 4.7 mol% solution of 3-phenylpentane (K & K Laboratories) in a CS_2/C_6D_{12}/TMS solvent mixture (see Table 1 for details) was filtered through cotton wool into a 5 mm o.d. nmr sample tube. The tube was degassed by five cycles of the freeze–pump–thaw procedure and was then flame-sealed under vacuum to produce a reasonably symmetric top.

The ^{1}H nmr spectra were acquired in the way described before (2). A typical acquisition time for a free induction decay was 41 s, of which as many as 64 were accumulated on a Bruker AM300 spectrometer. A digital resolution of not less than about 0.025 Hz/point was used and the induction decays were zero-filled twice or four times before Fourier transformation. Moderate amounts of resolution enhancement were also applied.

[1]Author to whom correspondence may be addressed.

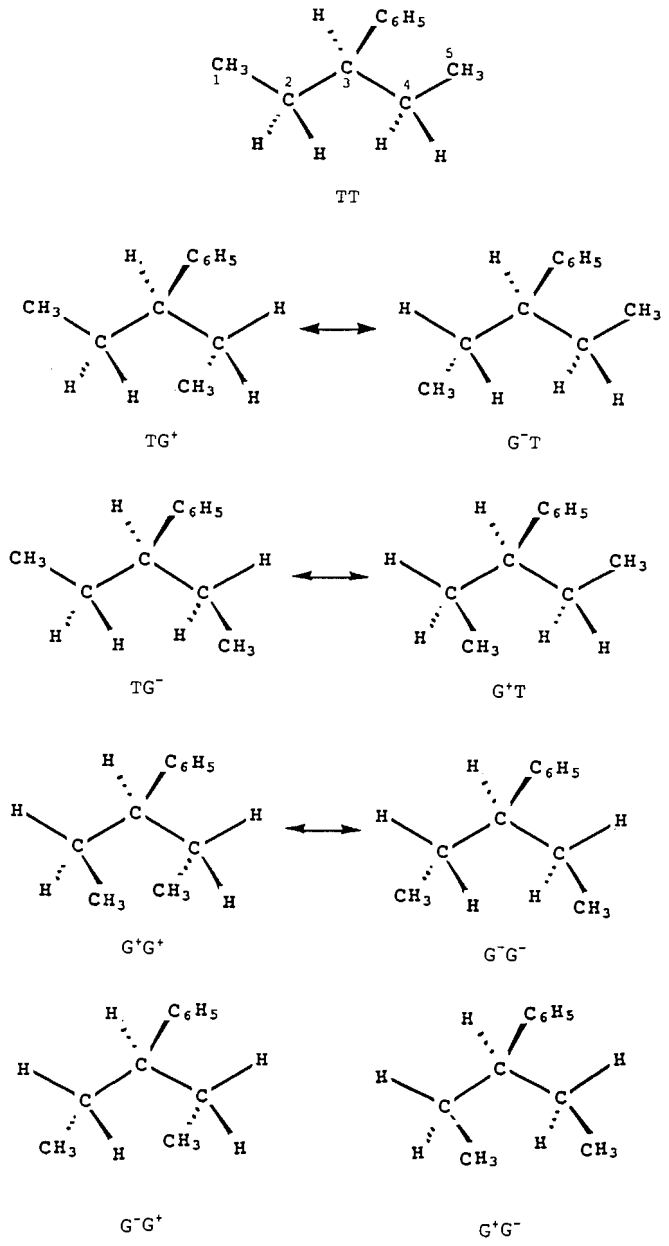

SCHEME 1

AM1 computations (3) used the algorithms in GAUSSIAN 86 (4). During rotation about the Csp^2—Csp^3 bond at fixed intervals of the torsion angle, all bond angles and lengths were allowed to relax, with the constraint, however, that the atoms of the phenyl group remain in a plane.

Results and discussion

Spectral analyses

The complete ^1H nmr spectrum of 3-phenylpentane corresponds to a 16-spin system. The program NUMARIT (5), as extensively modified by R. Sebastian in this laboratory, accommodates 12 spins only. Accordingly, the spectrum of the alkyl protons was analyzed as an $A_3A'_3BB'CC'D$ system, the methylene protons being magnetically nonequivalent. The spectrum of the aromatic protons, which couple to the methine and methyl protons, yielded to an analysis based on the spin system $A_6BCC'DD'E$. The peaks in the methine proton region of the spectrum were not assigned; the methine proton couples significantly to 15 protons. Table 1 presents the spectral parameters obtained from the composite analyses. As a simple example of how the complexity of the total spectrum yielded the signs of coupling constants, Fig.

TABLE 1. The ^1H nmr spectral parameters for a 4.7 mol% solution of 3-phenylpentane in CS_2/C_6D_{12}/TMS[a] at 300 K

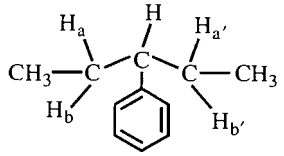

Parameter	Value
$\nu(CH_3)$	224.319(1)[b,c]
$\nu(H_a = H'_a)$	454.936(1)
$\nu(H_b = H'_b)$	494.989(1)
$\nu(CH)$	673.600[d]
$\nu(H2 = H6)$	2107.425(1)
$\nu(H3 = H5)$	2149.092(0)
$\nu(H4)$	2117.605(1)
$^3J(CH_3, H_a = H_b)$	7.356(2)
$^3J(CH_3, H_b = H'_b)$	7.387(2)
$^4J(CH_3, CH)$	−0.273(2)
$^5J(CH_3, H_a = H'_a)$	−0.001(0)
$^5J(CH_3, H_b = H'_b)$	−0.001(0)
$^6J(CH_3, H2 = H6)$	0.054(0)
$^7J(CH_3, H3 = H5)$	−0.001(0)
$^4J(H_a, H'_a)$	−0.233(3)
$^2J(H_a, H_b) = {}^2J(H'_a, H'_b)$	−13.476(3)
$^4J(H_a, H'_b) = {}^4J(H'_a, H_b)$	−0.231(0)
$^4J(H_b, H'_b)$	−0.228(2)
$^3J(H_a = H'_a, CH)$	9.207(3)
$^3J(H_b = H'_b, CH)$	5.250(2)
$^4J(CH, H2 = H6)$	−0.454(1)
$^5J(CH, H3 = H5)$	0.279(1)
$^6J(CH, H4)$	−0.107(1)
$^3J(H2, H3)$	7.710(1)
$^4J(H2, H4)$	1.269(1)
$^4J(H2, H6)$	1.925(1)
$^3J(H3, H4)$	7.395(1)
$^4J(H3, H5)$	1.461(1)
$^5J(H3, H6)$	0.576(0)

Transitions calculated	2596[e]	1689[f]
Transitions assigned	740	1200
Peaks observed	170[g]	
Largest absolute difference	0.031	0.026
RMS deviation	0.016	0.010

[a]Containing 10.0 mol% of C_6D_{12} and 0.5 mol% of tetramethylsilane.

[b]In Hz at 300.135$_2$ MHz to high frequency of internal TMS.

[c]Numbers in parentheses are standard deviations in the last significant digit.

[d]Not optimized in the analysis.

[e]Number of transitions calculated for the side-chain region, there being many degenerate transitions.

[f]Number of transitions calculated for the ring proton region, there being many degenerate transitions.

[g]Total number of peaks observed for the complete spectrum.

Can. J. Chem. Downloaded from www.nrcresearchpress.com by 88.255.202.194 on 09/08/12
For personal use only.

Can. J. Chem. Downloaded from www.nrcresearchpress.com by 88.255.202.194 on 09/08/12
For personal use only.

1 displays the sensitivity of the relatively simple methyl proton region to the sign of $^4J(H,CH_3)$.

The motion about the Csp^2—Csp^3 *bond*

^6J(H-4, C-H) = ^6J in toluene derivatives is given by $^6J = {}^6J_{90} \sin^2\theta$, in which θ is the angle by which the α C—H bond twists out of the plane of the phenyl group (6). In toluene, $^6J_{90}$ is −1.204(4) Hz, that is, when the C—H bond lies in a plane perpendicular to the phenyl plane (2). An electronegative substituent on the side chain polarizes the α C—H bond and thereby decreases the hyperconjugative overlap between the C—H and π orbitals. It has been shown, for example, that $^6J_{90}$ is −0.95 Hz in benzyl fluoride (7). From previous work on the ethyl and isopropyl derivatives of benzene (8, 9) it follows that $-1.12 \geq J_{90} \geq -1.16$ Hz holds for 3-phenylpentane, where ^6J is −0.107(1) Hz (Table 1). Therefore the expectation value of $\sin^2\theta$ obeys $0.094(1) \leq \langle\sin^2\theta\rangle \leq 0.096(1)$ at 300 K. A hindered rotor model or a classical average then yields an apparent twofold barrier of $15.0_5(2_5)$ kJ/mol for rotation about the sp^2—sp^3 bond. The conformation of lowest energy is characterized by θ = 0, as previously assumed (1).

The barrier magnitude is more than twice as large as that in isopropylbenzene, 6.6(7) kJ/mol (9). The relatively large magnitude in 3-phenylpentane very likely arises from the close approach of the methyl groups to the *ortho* C—H bonds as rotation occurs in the TT and $TG^+(G^-T)$ conformers. In the all-staggered arrangements the hydrogen atoms of the alkyl and aromatic C—H bonds would move to within about 0.8 Å of each other for a θ of 90°, whereas in isopropylbenzene this distance would be about 2 Å.

The proximity of the hydrogen atoms of the *ortho* and methyl C—H bonds during some part of the torsional motions is also consistent with the relatively large through-space coupling between their protons, formally over six bonds, its magnitude being 0.054 Hz (Table 1). This coupling magnitude is an average over the potential surface for two *ortho* protons and six methyl protons. The coupling constant is large when the hydrogen atoms come within the sums of their van der Waals radii.

Of course, the severe repulsive interactions will be relieved somewhat by compensatory twisting about the Csp^3—Csp^3 bonds in the side chain, which, however, is also hindered because, for example, the internal barrier in ethane is 12.1 kJ/mol. It appears that a compromise is reached in which the torsion about the Csp^2—Csp^3 bond is considerably more hindered than in isopropylbenzene. The measured ^6J represents an average over all occupied conformers in Scheme 1 and hence cannot yield a barrier for the individual conformers.

The geometry-optimized AM1 computations give a barrier height of 13.9 kJ/mol for rotation about the Csp^2—Csp^3 bond in 3-phenylpentane and 6.6 kJ/mol for isopropylbenzene. The relatively good agreement with the apparent twofold barriers in solution may be accidental because the AM1 value for the internal barrier in ethane, 5.2 kJ/mol, is much too low, so that the twist energy about the C—C bonds in the side chain of 3-phenylpentane, necessary to relieve steric strain, is presumably underestimated.

It may be noted that an analysis of Raman line-shapes for *meso* 2,4-diphenylpentane in chloroform solution indicates the sp^2—sp^3 barrier as 13.8 ± 1.3 kJ/mol in magnitude (10). A precise analysis of the ^{1}H nmr spectrum of this compound would be of interest; it would also be difficult.

The populations of the TT and $TG^+(G^-T)$ *conformers*

If only the cited conformers are present then (see **1** and **2**) the following analysis is possible. Because of symmetry,

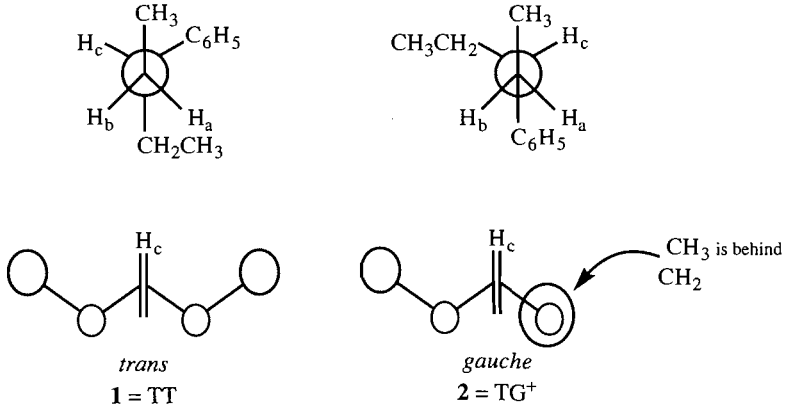

one need discuss the protons in only one methylene group.

$$[^3J_{ac} = P(TT)J_t + P(TG^+)J_g + P(G^-T)J_t]$$

$$[^3J_{bc} = P(TT)J_g + P(TG^+)J_t + P(G^-T)J_g]$$

These equations assume that J_t and J_g do not vary between conformers. Because $P(TG^+) = P(G^-T)$, $P(TT) + 2P(TG^+) = 1$. It follows that $^3J_{ac} + {}^3J_{bc} = J_t + J_g = 14.457(5)$ Hz and that $^3J_{ac} - {}^3J_{bc} = [1-2P(TG^+)](J_t - J_g) = 3.957(5)$ Hz. The fractional populations depend on $J_t - J_g$. A recent discussion of ^3J in ethane-like fragments shows the unlikelihood that J_g is larger than 2 Hz (11). If J_g is taken as 2.0 Hz, then $2P(TG^+)$ is 0.62. Hence the free energy difference is 1.22 kJ/mol at 300 K, favoring the *gauche* conformers.

The double degeneracy of the *gauche* conformer implies an enthalpy difference of 0.5 kJ/mol between the conformers, the TT conformer having the greater stability. The error in ΔH^0, in this treatment, depends on the error in J_g, which, if it amounts to 10%, implies that ΔH^0 is 0.5(1) kJ/mol. This value is 1 kJ/mol less than that obtained from the differences between J_{ac} and J_{bc} at 293 and 453 K for the liquid (1). The disagreement can be traced to 3.2 Hz (error not stated) given for $J_{ac} - J_{bc}$ at 293 K (1). Judging by the difference of more than 0.3 Hz between the ^2J(H,H) values in the two

TABLE 2. Computed ^4J(H, H) for the conformers of 2-phenylpentane[a]

Conformer	^4J(aa')[b]	^4J(bb')[b]	^4J(ab)	^4J(H, CH_3)
TT	−0.49	−0.49	−0.16	−0.22
TG^+, G^-T	−0.16	−0.02	−0.26	−0.22
TG^-, G^+T	−0.02	−0.16	−0.26	−0.13
G^+G^+, G^-G^-	−0.02	−0.02	−0.68	−0.13
G^-G^+	−0.49	1.52	−0.02	−0.22
G^+G^-	1.52	−0.49	−0.02	0.49
Experimental	−0.233(3)	−0.228(2)	−0.23(0)	−0.273(2)
Predicted[c]	−0.28	−0.20	−0.22	−0.22

[a]Using columns D in Tables 2 and 3 of ref. 16.

[b]^4J(aa') and ^4J(bb') are interchangeable. Attempts at identification of a and b protons on the basis of shifts induced by the diamagnetic anisotropy of the phenyl group proved unsuccessful.

[c]P(TT) = 0.38, $P(TG^+) = P(G^-T) = 0.31$.

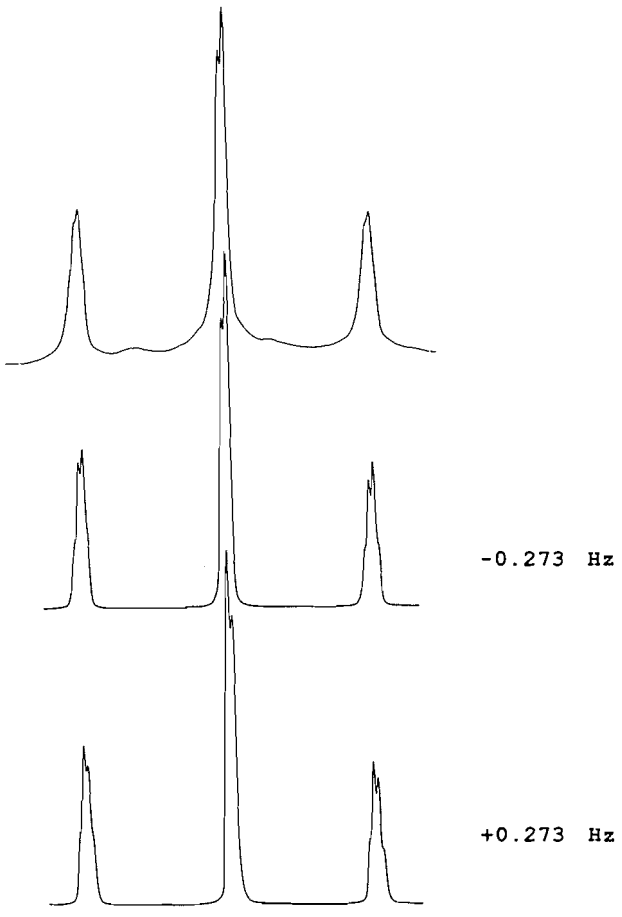

FIG. 1. The ^{1}H nmr spectrum of the methyl protons is displayed for a 4.7 mol% solution of 3-phenylpentane in CS_2/C_6D_{12} at 300 K and 300 MHz. The calculated spectra take $^4J(H,CH_3)$ as −0.273 and +0.273 Hz. There occur many transitions within the components of the "triplet" because the vicinal coupling constants to the neighbouring methylene protons are not identical and also because (Table 1) there occurs additional coupling to the *ortho* protons of the phenyl group. In consequence, the width of the components is substantial. The computed spectra are given somewhat narrow peaks to emphasize the asymmetry introduced by $^4J(H,CH_3)$.

analyses, the uncertainty in $J_{ac} - J_{bc}$ in the previous analysis might be as large as 0.6 Hz. It is unlikely (8, 9, 12, 13) that the conformational equilibrium is markedly solvent dependent.

The *gauche* form of the parent, pentane, is 3.5 kJ/mol less stable than the *trans* conformer (14). Comparison with present results for 3-phenylpentane suggests that, in the TT conformer, there occurs a repulsive interaction between the methyl and phenyl groups; one C—H bond of the methyl group approaches the ipso carbon atom to within 2 Å. The large barrier to rotation about the Csp^2—Csp^3 bond, relative to that in isopropylbenzene, must surely arise, in part at least, from methyl–phenyl repulsions. At least for 3-phenylpentane there appears to be no evidence for so-called attractive CH/π forces (15).

Conformational information from ^{4}J(H,H)

In the propanic fragment, ^4J(H,H) depends on two dihedral angles, φ and φ', indicated in **3** (16).

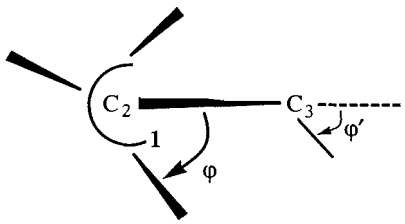

3

The reasonably successful theory (16) of ^4J(H,H), particularly of $^4J(H,CH_3)$, is here used to calculate the four ^4J(H,H) values for the alkyl chain in 3-phenylpentane. Table 2 presents the theoretical numbers for the various conformers, appropriate averages of ^4J(H,H) for the various dihedral angles being employed. These angles were taken as ideal or regular angles for the staggered conformations in Scheme 1, that is, values such as 60°, 120°, and 180°.

Comparison between the calculated ^4J(H,H) and the experimental values, also given in Table 2, suggests that the assumption of a predominance of the TT and TG^+,G^-T conformers at 300 K is essentially correct. For example, the absence of G^-G^+ is indicated by the three ^4J(H,H) values for the methylene protons, whereas that of G^+G^- is consistent

Can. J. Chem. Downloaded from www.nrcresearchpress.com by 88.255.202.194 on 09/08/12
For personal use only.

with $^4J(H,CH_3)$. Furthermore, the theoretical value of $^4J(H,CH_3)$ for the predominant TT and TG^+,G^-T forms becomes fully consistent with experiment when it is noted (Fig. 4 of ref. 16) that the theoretical values of $^4J(H,CH_3)$ for the appropriate dihedral angles are about 0.05 Hz too small in magnitude compared to the available experimental data. Again, significant amounts of G^+G^-,G^-G^+ can be excluded on the basis of all four coupling constants, while three of the coupling constants strongly suggest that TT is not the most populated conformer in the sense that the sum of the fractional populations of the isoenergetic TG^+ and G^-T conformers is 0.62.

Exact agreement between predicted and measured coupling constants is not to be expected, of course, for a number of reasons. Among them are the likely deviations from pure all-staggered bond arrangements and the neglect of intermediate rotational states of the methyl group. Nevertheless, the present results illustrate that precise analyses of good spectra can be important in conformational analysis.

Acknowledgments

We thank the Natural Sciences and Engineering Research Council of Canada for a grant-in-aid of research. A referee is thanked for his comments, which led to a clearer manuscript.

1. J. Stokr, H. Pivcova, B. Schneider, and S. Dirlikov. J. Mol. Struct. **12**, 45 (1972).
2. T. Schaefer, R. Sebastian, and G. H. Penner. Can. J. Chem. **63**, 2597 (1985).
3. M. J. S. Dewar, E. J. Zoebisch, E. F. Healy, and J. J. P. Stewart. J. Am. Chem. Soc. **107**, 3902 (1985).
4. M. J. Frisch, J. S. Binkley, H. B. Schlegel, K. Raghavachari, C. F. Melius, R. L. Martin, J. J. P. Steward, F. W. Bobrowicz, C. F. Rohlfing, L. R. Kahn, D. J. Defrees, R. Seeger, R. A. Whiteside, D. J. Fox, E. M. Fluder, and J. A. Pople. Carnegie-Mellon Quantum Publishing Unit, Pittsburgh, Pa. 1984.
5. J. S. Martin, A. R. Quirt, and K. F. Worvill. The NMR program library, Daresbury Laboratory, Daresbury, U.K.
6. W. J. E. Parr and T. Schaefer. Acc. Chem. Res. **13**, 400 (1980).
7. T. Schaefer, C. Beaulieu, R. Sebastian, and G. H. Penner. Can. J. Chem. **68**, 581 (1990).
8. T. Schaefer, G. H. Penner, and R. Sebastian. Can. J. Chem. **65**, 873 (1987).
9. T. Schaefer, R. Sebastian, and G. H. Penner. Can. J. Chem. **66**, 1495 (1988).
10. S. Koda, H. Nomura, and Y. Miyahara. Bull. Chem. Soc. Jpn. **52**, 1828 (1979).
11. M. Barfield and W. B. Smith. J. Am. Chem. Soc. **114**, 1574 (1992).
12. W. L. Jorgensen, J. D. Madura, and C. J. Swenson. J. Am. Chem. Soc. **106**, 6638 (1984).
13. F. A. Bovey, F. P. Hood III, E. W. Anderson, and L. C. Snyder. J. Chem. Phys. **42**, 3900 (1965).
14. K. B. Wiberg and M. A. Murcko. J. Am. Chem. Soc. **110**, 8029 (1988).
15. M. Nishio and M. Hirota. Tetrahedron, **45**, 7201 (1989).
16. M. Barfield, A. M. Dean, C. J. Fallick, R. J. Spear, S. Sternhell, and P. W. Westerman. J. Am. Chem. Soc. **97**, 1482 (1975).

Can. J. Chem. Downloaded from www.nrcresearchpress.com by 88.255.202.194 on 09/08/12
For personal use only.

Carbon-13 nuclear magnetic resonance study of phenyl derivatives of B, Si, Sn, P, and Te fluorides

CHENGRUI WANG AND YUXIANG MO
Department of Chemistry, Wuhan University, Wuhan, China 430072

AND

MEEHAE JANG AND ALEXANDER F. JANZEN[1]
Department of Chemistry, University of Manitoba, Winnipeg, Man., Canada R3T 2N2

Received June 15, 1992[2]

CHENGRUI WANG, YUXIANG MO, MEEHAE JANG, and ALEXANDER F. JANZEN. Can. J. Chem. **71**, 525 (1993).

^{13}C nuclear magnetic resonance data for a variety of phenyl derivatives of boron, silicon, tin, phosphorus, and tellurium fluorides are presented. Neutral, anionic, and cationic complexes are included and the coordination number of the central element varies from 3 to 6. Empirical equations of the ^{13}C chemical shifts of the benzene ring have been deduced by taking into consideration the charge density, dipole moment, and binding energy, and the ^{13}C chemical shifts calculated from these equations deviate from the experimental values by up to 1.4 ppm, but mostly less than 0.7 ppm.

CHENGRUI WANG, YUXIANG MO, MEEHAE JANG et ALEXANDER F. JANZEN. Can. J. Chem. **71**, 525 (1993).

On présente de données de résonance magnétique nucléaire du ^{13}C pour une variété de dérivés phénylés de fluorures de bore, de silicium, d'étain, de phosphore et de tellure comprenant des complexes neutres, anioniques et cationiques pour lesquels le nombre de coordination de l'élément central varie de 3 à 6. On a déduit les équations empiriques des déplacements chimiques du ^{13}C du benzène en prenant en considération la densité de charge, le moment dipolaire et l'énergie de liaison, et les déplacements chimiques du ^{13}C calculés diffèrent des valeurs expérimentales par des valeurs allant jusqu'à 1,4 ppm; toutefois, ces différences sont généralement inférieures à 0,7 ppm.

[Traduit par la rédaction]

Can. J. Chem. Downloaded from www.nrcresearchpress.com by 88.255.202.194 on 09/08/12
For personal use only.

Halogen exchange occurs rapidly in systems such as $PhPF_4$–$PhPF_5^-$ (*1*, *2*)

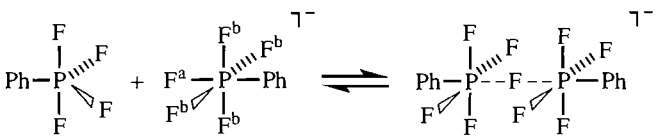

9 **10**

or $PhPCl_4$–$PhPCl_5^-$ (3), and related systems (4), and this intermolecular exchange, sometimes initiated by common impurities, as well as axial–equatorial ligand exchange in trigonal bipyramidal molecules, may complicate spectral identification if ^{19}F nmr is used to monitor fluorine site exchange. It was therefore decided to record the ^{13}C nmr spectra of the non-labile phenyl substituent of a variety of B, Si, Sn, P, and Te fluorides in which the coordination number of the central element varies from 3 to 6 in neutral, anionic, or cationic complexes.

The ^{13}C nmr data for phenyl-element fluorides **1**–**15** are given in Table 1. All the compounds contain the structural unit

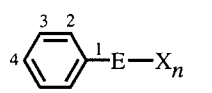

E = B, C, Si, Sn, P, Te
X = F, Cl
n = 2-5

However, *mer*-Ph_3TeF_3 **12** has nonequivalent phenyl rings, as expected for the *mer* structure, which has been established by X-ray crystallography (5), and the carbons C1′–C4′ are assigned to the phenyl ring *trans* to F^a.

The ^{13}C nmr spectra of $Ph_3TeF_2^+$ **11**, Ph_3TeFCl^+ **13**, and $Ph_3SnF_2^-$ **15** show equivalent phenyl groups, as expected for

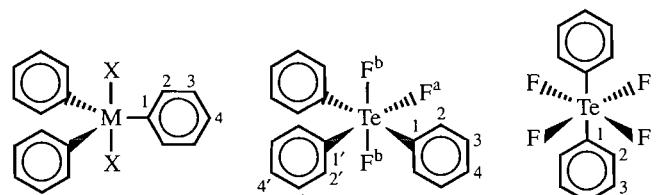

11 $Ph_3TeF_2^+$
13 Ph_3TeFCl^+
15 $Ph_3SnF_2^-$

12 *mer*-Ph_3TeF_3

14 *trans*-Ph_2TeF_4

a trigonal bipyramidal geometry with three phenyls in the equatorial plane, and the two phenyl substituents in *trans*-Ph_2TeF_4 **14** are also equivalent. For $PhSiF_4^-$ **8** and $PhPF_4$ **9**, which undergo rapid axial–equatorial exchange, carbons are coupled equally to four fluorines, but different couplings from carbon to nonequivalent fluorines F^a and F^b can be observed in "rigid" $PhPF_5^-$ **10** and *mer*-Ph_3TeF_3 **12**. The assignments of C1–C4 peaks in the ^{13}C spectra of phenyl-element fluorides are based on relative intensities, carbon–fluorine couplings, and related nmr spectra reported in the literature (6).

We have included for comparison purposes the published data for $PhCF_2^+$ **5** (7) and $PhCF_3$ **6** (8); the other ^{13}C nmr spectra were recorded for this study although the spectra of $PhBF_2$ and $PhBF_3^-$ have been reported previously (9).

The distribution of the chemical shifts of compounds **1**–**12** is shown in Fig. 1 and it can be seen that the chemical shift of C1 moves consistently downfield by 15.6 to 25.7 ppm as F^- is added to various phenyl-element fluorides. There is an opposite effect on carbons C2–C4, which move upfield as F^- is added, with the exception of C2 of $PhSiF_3$ **7**. In the case of $Ph_3TeF_2^+$ **11**, the addition of F^- produces a larger shift in phenyl carbons C1–C4, which are *cis* to F^a, than on carbons C1′–C4′, which are *trans* to F^a.

Figure 1 shows that chloride ion has an effect similar to

[1]Author to whom correspondence may be addressed.
[2]Revision received January 22, 1993.

TABLE 1. ^{13}C nuclear magnetic resonance data for some phenyl derivatives of B, C, Si, Sn, P, and Te fluorides[a]

Compound	δC1	δC2	δC3	δC4	^2J(C1,F)[b]	^3J(C2,F)	^4J(C3,F)	^5J(C4,F)
1 $PhBF_2$	124.8	136.9	129.1	134.8	36.3	4.8	0	1.2
2 $PhBF_3^-$	150.1	131.8	126.8	125.6	49.2	1.8	0	0.7
3 $PhBCl_2$	128.5	137.0	128.3	135.2				
4 $PhBCl_3^-$	148[c]	131.7	126.9	126.3				
5 $PhCF_2^+$[d]	111.2	145.5	134.1	159.5	8.2	10.7	1	5.7
6 $PhCF_3$[e]	131.0	125.2	128.8	131.8	32.2	3.9	—	1.4
7 $PhSiF_3$	120.8	134.8	128.9	133.6	25.6	1.3	0.8	0.4
8 $PhSiF_4^-$	141.8	137.7	127.2	128.8	34.9	3.2	0	0
9 $PhPF_4$	125.9	137.4	129.8	136.2	20.0	4.8	$\omega_{1/2}$ 3.2	0
10 $PhPF_5^-$	151.6	131.1	126.8	126.6	46.2(F^b)	4.0(F^b)	$\omega_{1/2}$ 2.2(F^b)	0(F^b)
					0(F^a)	0(F^a)	0(F^a)	0(F^a)
11 $Ph_3TeF_2^+$	129.6	133.3	133.2	137.6	3.1	5.6	1.5	1.0
12 Ph_3TeF_3	151.2	129.7	130.8	129.9	49.1(F^a)	2.7(F^a)	2.5(F^a)	0.9(F^a)
					16.5(F^b)	1.2(F^b)	2.5(F^b)	0(F^b)
C1′–C4′	145.2	131.6	131.9	132.2	23.7(F^a)	0.4(F^a)	0(F^a)	0(F^a)
					1.7(F^b)	2.5(F^b)	0(F^b)	0.7(F^b)
13 Ph_3TeFCl^+	132.2	132.5	133.1	136.8	4.9	5.0	1.3	1.1
14 Ph_2TeF_4	148.8	130.6	130.6	133.9	16.0	2.7	1.5	0.5
15 $Ph_3SnF_2^-$	146.9	136.1	125.6	126.1	24.9	3.0	2.0	0

Chemical shifts in ppm and coupling constants in Hz.
[b]See diagrams in text for labelling of fluorine and carbon atoms.
[c]Broad peak.
[d]Reference 7.
[e]Reference 8.

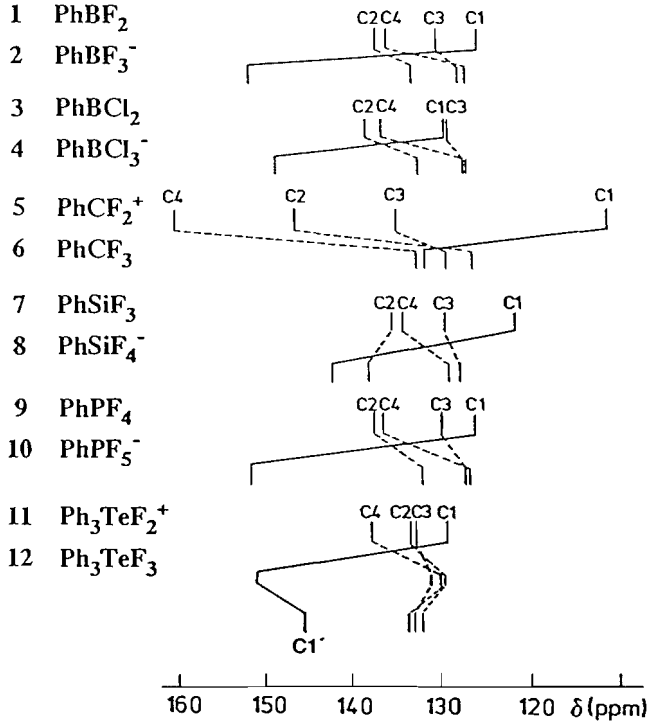

FIG. 1. Distribution of ^{13}C chemical shifts of compounds **1**–**12**. Data are taken from Table 1.

that of fluoride, and addition of Cl^- to $PhBCl_2$ results in a downfield shift of C1 of 19.5 ppm as $PhBCl_3^-$ is formed. Similar changes have been observed on addition of Cl^- to triphenyltin chloride (10), i.e., Ph_3SnCl (δC1 137.1 ppm) versus $Ph_3SnCl_2^-$ (δC1 147.5 ppm), or on addition of $C_6H_5^-$ to triphenylboron (11), i.e., Ph_3B (δC1 144.9 ppm) versus Ph_4B^- (δC1 164.8 ppm).

TABLE 2. $\Delta\delta^{13}C$ of some phenyl-element fluorides (ppm)[a]

Compound	C1	C2	C3	C4
1 $PhBF_2$	+0.6	+0.7	0	+0.1
2 $PhBF_3^-$	−1.4	−0.3	+0.3	+0.4
3 $PhBCl_2$	−0.6	−0.5	+0.7	0
6 $PhCF_3$[b]	+1.1	+0.1	−0.5	−0.3
9 $PhPF_4$	+0.1	−0.2	−0.4	0
10 $PhPF_5^-$	+1.0	+0.2	+0.2	−0.3

[a]$\Delta\delta^{13}C = \delta^{13}C(\text{calcd.}) - \delta^{13}C(\text{expt.})$
[b]Experimental value from ref. 8.

A similar result might be expected with donor solvents, although a dynamic equilibrium may give only a weighted average value for δC1, and this effect has been observed by other workers (12) who found a downfield shift in δC1 of only 3.7 ppm as acetonitrile was added to $PhSnCl_3$. Any competition between donor solvents and halide ions could mask differences between δC1 of various species in solution, as illustrated by the very similar chemical shifts in p-$PhC_6H_4TeCl_3$ (δC1 145.5 ppm) and p-$PhOC_6H_4TeCl_4^-$ (δC1 146.7 ppm) if both are dissolved in DMSO solution (13).

These changes in δC1 are thus a useful indicator of changes in coordination number and electron count of the central element E as ligands such as F^-, Cl^-, or $C_6H_5^-$ are added, and the ^{13}C nmr of the non-labile phenyl substituent may complement nmr studies of systems undergoing rapid ligand exchange.

Can. J. Chem. Downloaded from www.nrcresearchpress.com by 88.255.202.194 on 09/08/12
For personal use only.

TABLE 3. CNDO/2 calculated valence charge density, VCD, binding energy, BE (au), and dipole moments, DM (debye) of some phenyl-element fluorides

Compound	VCD					BE	DM
	C1	C2	C3	C4	E		
1	4.1300	3.9253	4.0189	3.9500	2.5173	−7.2831	3.27534
2	4.0893	3.9819	4.0146	4.0181	2.5465	−7.5322	7.06203
3	4.0560	3.9347	4.0169	3.9505	2.7959	−7.2901	3.00721
6	4.0436	3.9716	3.9959	3.9974	3.4145	−7.7812	2.69120
9	4.0352	3.9503	3.9934	3.9976	4.1689	−6.9349	3.52916
10	4.0782	3.9682	4.0148	4.0039	4.1688	−7.1408	8.76378

The coupling constants J(C,F) are given in Table 1 and in each case there is an increase in ^2J(C1,F) of 9.9 to 46.1 Hz as F^- is added; furthermore, J(C,F) depends significantly on stereochemical changes in these "rigid" complexes, but rapid intermolecular fluorine exchange would result in loss of coupling between carbon and fluorine.

Calculated chemical shifts

The phenyl-element fluorides discussed above show significant differences in their structure, coordination number, and electron count and these differences will influence the chemical environment of the central atom, which in turn will affect the carbon atoms of the benzene ring.

The relationship between the ^{13}C chemical shifts of the benzene ring and the characteristics of the substituted group has been studied for a long time, but often the chemical shift of the *para* carbon (δC4) is related to a single parameter such as total charge density, Hammett σ constant, or dual substituent parameter, and the empirical equations for the chemical shifts of the *ortho* (δC2) and *meta* (δC3) carbons often do not show a good correlation (6). We therefore derived empirical equations of chemical shifts and compared the calculated and measured ^{13}C chemical shifts.

The chemical shift of a nucleus is determined by its chemical environment and the atom in a molecule can be distinguished from the same atom in the free state by the partial shift of its valence electrons, which means the change of the valence charge density. Hence the valence charge density will definitely be one of the major factors affecting the chemical shift. Moreover, since the applied magnetic field in nmr affects all the atoms of the molecule, the chemical shift should be related to the charge distribution of the whole molecule, and the dipole moment of the molecule, $\boldsymbol{\mu} = e \int\psi^*\gamma\psi \, d\tau$, where ψ is the wave function of the system, the physical property that describes the charge distribution of the whole molecule. Thus, there should be a dipole moment term in the empirical equation of chemical shifts. Since the nucleus will be shielded not only by its own electrons but also by the other electrons in the molecular system, then, considered from the view of energy, it may be stated that chemical shifts will also be related to the binding energy.

For these reasons we used the three parameters of valence charge density (ρ) (where ρ_E = ρ of atom E in the molecule), dipole moments (μ), and binding energy (BE), and carried out a multivariable, step-by-step regression analysis to get the empirical equations [1]–[4] for the ^{13}C chemical shifts of the monosubstituted benzene ring.

$$[1]\quad \delta C1 = -4.871866 * \rho^2 + 4.912487 * \mu - 12.43392 * BE + 101.8069$$

$$[2]\quad \delta C2 = -3.98671 * \rho_E - 0.4117336 * \mu + 18.01284 * BE + 280.1893$$

$$[3]\quad \delta C3 = 1.522819 * BE - 0.03860589 * \mu^2 + 140.476$$

$$[4]\quad \delta C4 = 7.141028 * BE - 15.3116\rho - 1.599473 * \mu + 252.6104$$

The correlation coefficients of the regression equations [1]–[4] are 0.9955, 0.9956, 0.961, and 0.9993, respectively. We used these four equations to calculate the ^{13}C chemical shifts for the molecules and anions **1**–**3**, **6**, **9**, **10**, and the differences between calculated and experimental values of ^{13}C chemical shifts are listed in Table 2.

As seen in Table 2, the maximum absolute deviation is 1.4 ppm, but the relative deviation is 1% and the data in most cases deviate by less than 0.7 ppm or 0.5%. We have used eqs. [1]–[4] to calculate the ^{13}C chemical shifts for the molecule $PhCF_3$ **6**, and compared the results with experimental results from the literature (8); as seen in Table 2, the deviations for $PhCF_3$ **6** are also within the range established for the other compounds.

A CNDO/2 program was used to calculate the charge density, dipole moments, and binding energy, and these data (Table 3) were used for the calculation of ^{13}C chemical shifts. Molecular configurations were obtained from standard sources (14).

Experimental

$PhBCl_2$ **3** (Alfa) and *n*-Bu_4NF in THF (Aldrich) were obtained commercially. A solution of *n*-Pr_4NF in acetonitrile was made by diluting *n*-Pr_4NOH (30 mL of 10% aq. sol.) to 3% and neutralizing the solution to pH 7 with dilute hydrofluoric acid; the resulting solution was reduced to a thick oil on a rotary evaporator and 80 mL of CH_3CN was added.

$PhBF_2$ **1** (15), $PhSiF_3$ **7** (16), *n*-$Pr_4N^+PhSiF_4^-$ **8** (17), $PhPF_4$ (18), *n*-$Pr_4N^+PhPF_5^-$ **10** (1), $Ph_3TeF_2^+PF_6^-$ **11** (5), *mer*-Ph_3TeF_3 **12** (5), $Ph_3TeFCl^+PF_6^-$ **13** (4), *trans*-Ph_2TeF_4 **14** (19), and *n*-$Bu_4N^+Ph_3SnF_2^-$ **15** (20) were prepared according to literature methods.

n-$Bu_4N^+PhBF_3^-$ **2** was prepared by slowly adding $PhBF_2$ (1.33 g, 10.6 mmol) to a solution of *n*-Bu_4NF (2.16 g of 1 M THF solution) with stirring, followed by removal of solvent with rotary evaporator and filtration under vacuum to give white crystals identified as *n*-$Bu_4N^+PhBF_3^-$ (3.4 g, 83% yield, mp 193–195°C) by ^{19}F, ^{11}B, and ^{13}C nmr. $Et_4N^+PhBCl_3^-$ **4** (21) was prepared by slowly adding $PhBCl_2$ (5 g, 31 mmol), with stirring, to a cooled (−78°C) solution of Et_4NCl (5 g, 30 mmol) in CH_2ClCH_2Cl (150 mL); removal of solvent by rotary evaporator and filtration gave white crystals, which were dried under vacuum and identified as $Et_4N^+PhBCl_3^-$ **4** (1.27 g, 13%) by ^{11}B and ^{13}C nmr.

Can. J. Chem. Downloaded from www.nrcresearchpress.com by 88.255.202.194 on 09/08/12
For personal use only.

All ^{13}C (proton-decoupled) nmr spectra were recorded at ambient temperature on a Bruker WH90 spectrometer at 22.63 MHz, except for tellurium and tin compounds **11**–**15**, which were recorded on a Bruker AM300 spectrometer at 75.4 MHz. The samples were dissolved in $CDCl_3$ or CD_2Cl_2 (30%, w/w) in 10-mm tubes (internal reference: $CDCl_3$ δC 79.73 ppm, CD_2Cl_2 δC 53.90 ppm) and degassed and sealed.

Acknowledgement

The financial assistance of the Natural Sciences and Engineering Research Council of Canada, and the National Natural Science Foundation of China, is gratefully acknowledged.

1. C. Wang and A. F. Janzen. Can. J. Chem. **62**, 1563 (1984).
2. R. Appel, I. Ruppert, and F. Knoll. Chem. Ber. **105**, 2492 (1972).
3. K. B. Dillon, R. N. Reeve, and T. C. Waddington. J. Chem. Soc. Dalton Trans. 1318 (1978).
4. (*a*) A. F. Janzen and M. Jang. Can. J. Chem. **67**, 71 (1989); (*b*) T. Q. Nguyen, F. Qu, X. Huang, and A. F. Janzen. Can. J. Chem. **70**, 2089 (1992); (*c*) A. F. Janzen. Coord. Chem. Rev. In press.
5. A. S. Secco, K. Alam, B. J. Blackburn, and A. F. Janzen. Inorg. Chem. **25**, 2125 (1986).
6. (*a*) G. C. Levy, R. L. Lichter, and G. L. Nelson. Carbon-13 nuclear magnetic resonance spectroscopy. 2nd ed. John Wiley & Sons, New York. 1980; (*b*) D. G. Farnum. Adv. Phys. Org. Chem. **11**, 123 (1975); (*c*) H. Sterk and W. Fabian. Org. Magn. Reson. **7**, 274 (1975).
7. R. J. Spear, D. A. Forsyth, and G. A. Olah. J. Am. Chem. Soc. **98**, 2493 (1976).
8. (*a*) R. A. Newmark and J. R. Hill. Org. Magn. Reson. **9**, 589 (1977); (*b*) C. W. Fong. Aust. J. Chem. **33**, 1291 (1980).
9. J. D. Odom, T. F. Moore, R. Goetze, H. Nöth, and B. Wrackmeyer. J. Organomet. Chem. **173**, 15 (1979).
10. J. Holecek, M. Nadvornik, K. Handlir, and A. Lycka. J. Organomet. Chem. **241**, 177 (1983).
11. B. R. Gragg, W. J. Layton, and K. Niedenzu. J. Organomet. Chem. **132**, 29 (1977).
12. G. Matsubayashi and T. Tanaka. Spectrochem. Acta, **30A**, 869 (1974).
13. R. K. Chadha and J. M. Miller. Can. J. Chem. **60**, 596 (1982).
14. J. A. Pople and D. L. Beveridge. Approximate molecular orbital theory. McGraw–Hill, New York. 1970.
15. P. A. McCusker and H. S. Makowski. J. Am. Chem. Soc. **79**, 5185 (1957).
16. W. J. E. Parr, T. Schaefer, and K. Marat. Can. J. Chem. **55**, 3243 (1977).
17. R. K. Marat and A. F. Janzen. Can. J. Chem. **55**, 3845 (1977).
18. (*a*) R. Schmutzler. Inorg. Chem. **3**, 410 (1964); (*b*) C. Wang, E. Bock, J. Peeling, and A. F. Janzen. Phosphorus, Sulfur Silicon, **57**, 123 (1991).
19. M. Jang and A. F. Janzen. J. Fluorine Chem. **52**, 45 (1991).
20. A. C. Sau, L. A. Carpino, and R. R. Holmes. J. Organomet. Chem. **197**, 181 (1980).
21. I. Y. Ahmed and C. D. Schmulbach. Inorg. Chem. **8**, 1411 (1969).

Can. J. Chem. Downloaded from www.nrcresearchpress.com by 88.255.202.194 on 09/08/12
For personal use only.

Reactions of 5-cyano-1,4-diphenylpyridazino[4,5-*a*]indolizines with dimethyl acetylenedicarboxylate: regioselective formation of 1:2 Michael type adducts

KIYOSHI MATSUMOTO[1] AND YUKIO IKEMI
Graduate School of Human and Environmental Studies, Kyoto University, 606-01 Japan

MOTOO SHIRO
Research Department, Rigaku Corporation, Akishima, Tokyo 196, Japan

TAKANE UCHIDA
Faculty of Education, Fukui University, Fuki 910, Japan

AND

JAMES WILLIAM LOWN[1]
Department of Chemistry, University of Alberta, Edmonton, Alta., Canada T6G 2G2

Received December 7, 1992

KIYOSHI MATSUMOTO, YUKIO IKEMI, MOTOO SHIRO, TAKANE UCHIDA, and JAMES WILLIAM LOWN. Can. J. Chem. **71**, 529 (1993).

Reactions of 5-cyano-1,4-diphenylpyridazino[4,5-*a*]indolizines with dimethyl acetylenedicarboxylate afforded the 1:2 adducts regioselectively and, unexpectedly, in a Michael fashion rather than in a 1,3-dipolar manner. The structure of the products was established by X-ray crystallography. Regiospecific formation of the observed product **3** can be explained by the higher nucleophilicity of the nitrogen at the 2 position than at the 3 position of the 5-cyano-1,4-diphenylpyridazino[4,5-*a*]indolizine **1** owing to the contribution of a resonance structure **5** to the hybrid. This favors two successive Michael additions to two equivalents of dimethyl acetylenedicarboxylate affording the observed 1:2 adducts **3**.

KIYOSHI MATSUMOTO, YUKIO IKEMI, MOTOO SHIRO, TAKANE UCHIDA et JAMES WILLIAM LOWN. Can. J. Chem. **71**, 529 (1993).

Les réactions des 5-cyano-1,4-diphénylpyridazino[4,5-*a*]indolizines avec l'acétylènedicarboxylate de diméthyle fournit d'une façon inattendue et régiosélective les adduits 1 : 2 d'une réaction de Michael plutôt ceux d'une réaction 1,3-dipolaire. On a déterminé la structure de produits par diffraction des rayons X. On peut expliquer la formation régiospécifique observée des produits **3** en faisant appel au caractère nucléophile plus grand de l'azote en position 2 (par rapport à celui en position 3) du 5-cyano-1,4-diphénylpyridazino[4,5-*a*]indolizine **1** qui est dû à la contribution d'une structure de résonance de **5** à l'hybride. Cette orientation favorise deux additions successives de Michael à deux équivalents de l'acétylènedicarboxylate de diméthyle conduisant aux adduits-1,2 observés, **3**.

[Traduit par la rédaction]

Introduction

Bicyclic bridgehead nitrogen-containing heterocycles such as indolizines (1) and azapentalenes (2), the resonance hybrids of which involve an ylide structure, could serve as a bicycloimmonium or masked azomethine ylide (Scheme 1). Indeed, several indolizines (3–5) undergo [8+2]π cycloaddition with electron-deficient alkynes to afford the cycl[2.2.3]azines (6). Furthermore, investigations of addition reactions of acetylenic esters to nitrogen-containing heterocycles have been stimulated because of the problems involved in unraveling the novel types of reactions and structures sometimes observed (7, 8). Annulation of the benzene ring at the 1,2 position proved to activate 3-cyanoindolizines as 1,3-dipolar species, probably because of aromatic stabilization in favor of the azomethine ylide structure (Scheme 1). Thus, 6-cyanobenz[*a*]indolizines undergo 1,3-dipolar cycloaddition smoothly with activated alkynes such as dibenzoylacetylene (4) and dialkyl acetylenedicarboxylate (9). Therefore, we expected that annulation of a heteroaromatic ring at the 1,2 position of 3-cyanoindolizine would also favor the azomethine ylide structure by means of aromatic stabilization. Since 1,2-pyridazine-fused 3-cyanoindolizines are readily available by 1,3-dipolar cycloaddition reactions of dicyanomethylides with dibenzoylacetylene, followed by treatment with hydrazine (Scheme 2) (4), we have examined the reactions of 1,4-diphenylpyridazino[4,5-*a*]indolizines with dimethyl acetylenedicarboxylate (DMAD).

Results and discussion

Reaction of 5-cyano-1,4-diphenylpyridazino[4,5-*a*]indolizine (**1***a*) with four equimolar amounts of DMAD in refluxing toluene for 14 h gave yellow crystals, mp 282–283°C. The mass spectral and microanalytical analysis established that the compound had a 1:2 adduct structure. Similarly, the corresponding 1:2 adducts were obtained in low to moderate yields from **1***b*–**1***f* with excess DMAD. The results are presented in Table 1. Initially, we expected that the compounds would have the structure **2**, and could be formed by successive Michael-type additions and subsequent cyclization (Scheme 3). There are precedents for this type of 1:2 structure being formed from nitrogen heterocycles such as azapentalenes (10) and azaazulenes (11).

However, the ^{13}C value (6) of δ 116 does not appear to be at high enough field for an sp^3 secondary carbon. Furthermore, all attempts to convert the compounds to the corresponding [2.2.4]cyclazines failed. Fortunately, the 1:2 adduct obtained from the 1,4,8-triphenylpyridazino[4,5-*a*]indolizine (**1***d*) formed crystals suitable for an X-ray

[1]Authors to whom correspondence may be addressed.

Can. J. Chem. Downloaded from www.nrcresearchpress.com by 88.255.202.194 on 09/08/12
For personal use only.

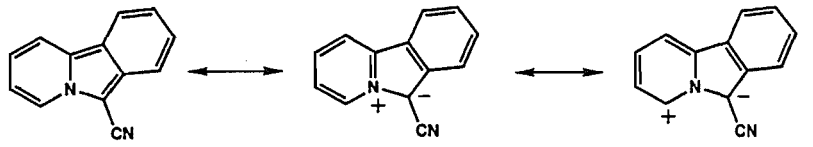

SCHEME 1

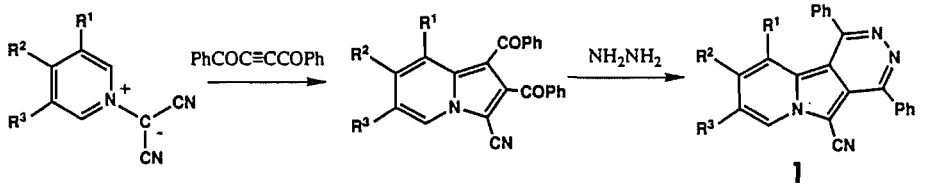

SCHEME 2

TABLE 1. 1:2 Adducts from 5-cyano-1,4-diphenylpyridazino[4,5-*a*]indolizines (**1**) and DMAD

1	R^1	R^2	R^3	Time (h)	Yield (%)	Melting point (°C)
a	H	H	H	14	43	282–283
b	H	Me	H	14	47	253–254
c	Me	H	Me	14	25	243–244
d	H	Ph	H	41	40	284–285
e	H	COPh	H	37	25	260–261
f	CH_2=CH—CH=CH_2		H	21	15	303–304

analysis. An analysis of this adduct established that the compound had structure **3***d* as shown in Fig. 1 (7). No regioisomers of type **4** could be isolated in our hands.

Regiospecific formation of **3** could be explained by the higher nucleophilicity of the nitrogen at the 2 position than at the 3 position owing to the contribution of resonance hybrid **5**, since the adducts probably arise from successive Michael additions as shown in Scheme 4. In agreement with this interpretation, neither 3-chloro-6-phenylpyridazine nor 3-chloro-6-methoxypyridazine reacted with DMAD under comparable conditions. Neither were Diels–Alder adducts across the pyridazine ring observed. This latter observation is in agreement with the previous result that the reaction of the dihydropyridazine **6** with DMAD showed no tendency to add in a Diels–Alder fashion to give **7** but instead added the ester in a Michael manner, affording **8** (Scheme 5) (12).

Finally, reaction of 7-azaindolizine **9** with DMAD took place in a similar fashion to give the 1:2 adduct **10** (Scheme 6). This type of structure is well documented in the reactions of pyridines with DMAD (7). Thus, **9** behaved as a nucleophile rather than as a 1,3-dipole. In contrast, 2-phenyl-1-azaindolizine (13) and 7-methyl-2-phenyl-6-azaindolizine (14) with DMAD were reported to give the corresponding azacycl[2.2.3]azines.

Experimental

General

Melting points were taken on a Yanagimoto micro melting point apparatus and are uncorrected. The ^{1}H NMR spectra were measured on one of the following: a Hitachi R40 (90 MHz), a Jeol JNM FX90Q (90 MHz), a Varian VX200 (200 MHz), or a Jeol JNE-EX270 (270 MHz) instrument. ^{13}C NMR spectra were recorded either on a Jeol JNJ-FX90Q or a JNM-EX270 pulsed Fourier transform spectrometer operating at 22.49 MHz and 67.80 Hz, respectively. Chemical shifts are expressed in parts per million downfield from internal tetramethylsilane. Partial proton decoupling was used to distinguish between individual carbon atoms. Preparative medium-pressure liquid chromatography was carried out using a column (25 × 310 mm) prepacked with silica gel (Lobar, LiChroprep Si60, Merck).

Reaction of 5-cyano-1,4-diphenylpyridazino[4,5-a]indolizine (1) with DMAD: general procedure

A solution of **1** (9) (0.85 mmol) and DMAD (3.39 mmol) in toluene (30 mL) was heated under reflux for 40 h. After evaporation of the solvent, the residue was chromatographed on silica (Wako Gel C-200) using benzene – ethyl acetate as eluent (from 39:1 to 17:3 in a gradient fashion) giving the 1:2 adducts **3**. The analytical samples were obtained by recrystallization from ethanol–dichloromethane.

*8-Cyano-7,13c-diphenyl-1,2,3,4-tetramethoxycarbonyl-13c*H*-pyrido[1′,2′:2,3]pyridazino[4,5-a]indolizine (3a; R^1 = R^2 = R^3 = H)*

^{1}H NMR (90 MHz) δ: 3.45, 3.65, 3.86, 3.88 (s each, 3H each), 6.80–6.96 (m, 2H), 7.15–7.35 (m, 5H), 7.50–7.65 (m, 4H), 7.66–7.77 (m, 2H), 8.19–8.24 (m, 1H). ^{13}C NMR (22.49 MHz) δ: 54.2, 53.3, 54.1, 54.2 (q each), 65.3, 91.6, 103.5, 109.5, 115.8, 118.1, 128.5, 133.0, 134.4, 141.8, 141.8, 144.5, 145.7 (s each), 116.1, 119.9, 126.0, 126.5, 128.7, 128.8, 129.5, 131.2, 132.6 (d each), 165.0, 165.1, 166.2, 168.5 (s each). Anal. calcd. for $C_{35}H_{26}N_4O_8$: C 66.66, H 4.16, N 8.89; found: C 66.60, H 4.16, N 8.50.

*8-Cyano-7,13c-diphenyl-12-methyl-1,2,3,4-tetramethoxycarbonyl-13c*H*-pyrido[1′,2′:2,3]pyridolizine (3b; R^1 = R^3 = H, R^2 = Me)*

^{1}H NMR (90 MHz) δ: 2.17, 3.40, 3.57, 3.81, 3.83 (s each, 3H each), 6.59 (dd, *J* = 2, 7 Hz, 1H), 6.85 (bs, 1H), 7.10–7.31 (m, 4H), 7.37–7.895 (m, 6H), 8.01 (bd, *J* = 7 Hz, 1H). ^{13}C NMR

Can. J. Chem. Downloaded from www.nrcresearchpress.com by 88.255.202.194 on 09/08/12
For personal use only.

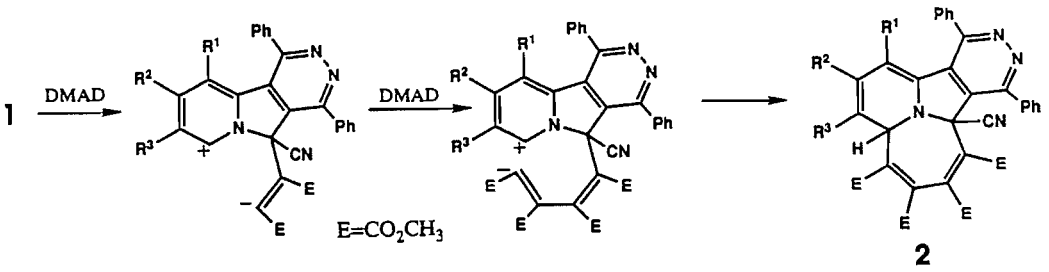

SCHEME 3

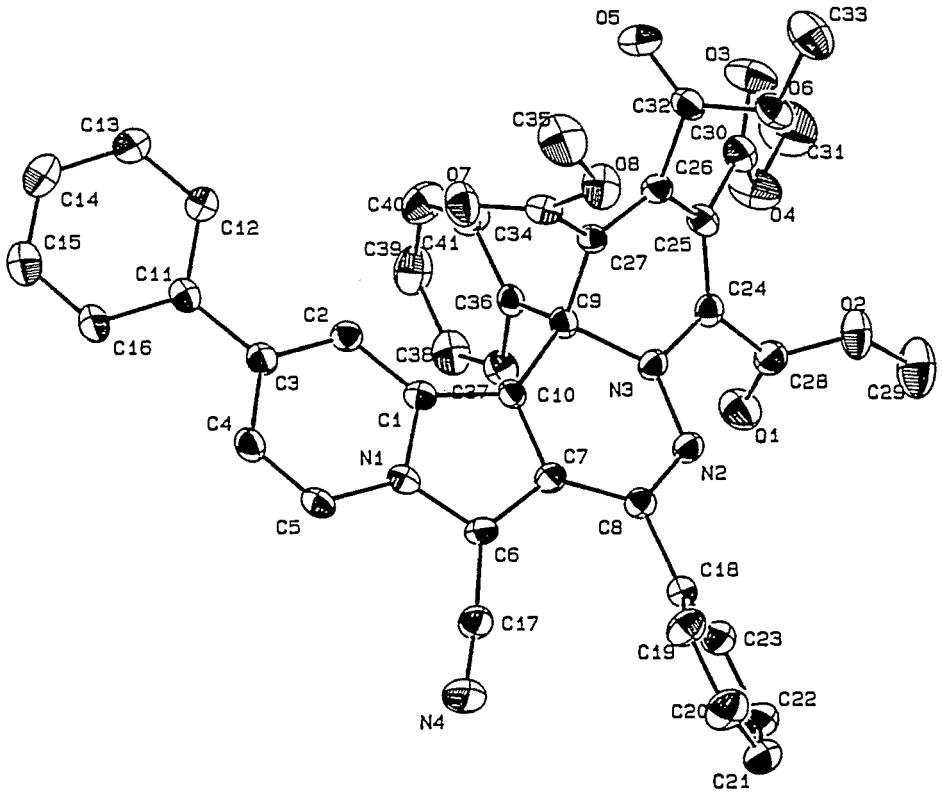

FIG. 1. ORTEP drawing of compound **3*d***.

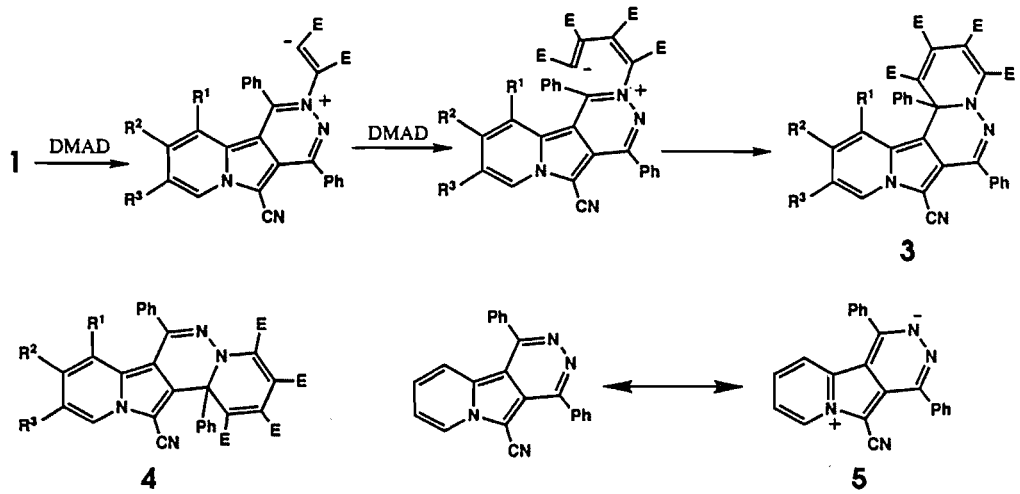

SCHEME 4

Can. J. Chem. Downloaded from www.nrcresearchpress.com by 88.255.202.194 on 09/08/12
For personal use only.

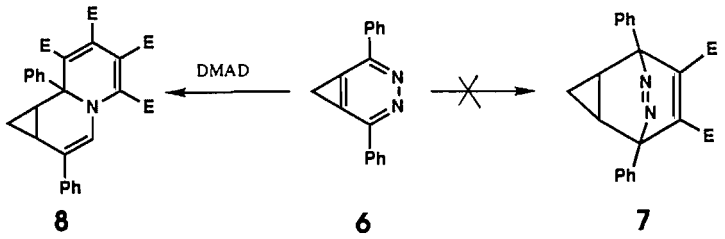

SCHEME 5

TABLE 2. Crystal data for *3d*

Formula	$C_{42}H_{32}N_4O_8Cl_2$
Crystal dimensions (mm)	0.5 × 0.10 × 0.10
M (amu)	791.64
Monoclinic space group	$P2_1/c$ (no. 14)
a (Å)	15.005(2)
b (Å)	8.9852(9)
c (Å)	29.129(1)
β	100.92(1)
U (Å^3)	3856.2(9)
Z	4
D_0 (g cm^{-3})	1.363
μ (cm^{-1})	20.14
F (000)	1640
Radiation Cu-Kα, graphite monochromatized	λ = 1.54178 Å
Diffractometer	Rigaku AFC5R
Orienting reflections, range	25.8, 37.57° < 2θ < 41.96°
T (K)	296
Scan method	ω–2θ
Data collection range	3.0° < 2θ < 110.1°
No. unique reflections	5243
No. of observed reflections with $I > 3\sigma(I)$	3001
No. of parameters	506
R^a	5.3%
$R_w{}^b$	7.1%
Largest shift/esd, final cycle	0.42
Largest positive peak (e Å^{-3})	0.43
Largest negative peak (e Å^{-3})	−0.52

$^aR = [\Sigma|F_0| - |F_c|/\Sigma|F_0|$.
$^bR_w = \{[\Sigma w(|F_0| - |F_c|)^2]/\Sigma w(|F_0|)^2]\}^{1/2}$. Weighting scheme: $w = 1.000/]\sigma^2F + 0.0036F]$.

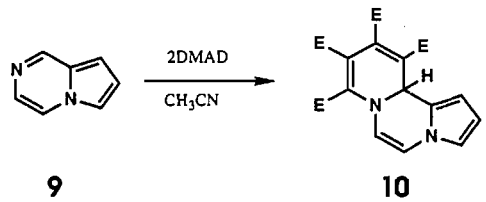

SCHEME 6

(22.49 MHz) δ: 21.3, 52.0, 52.2, 52.7, 52.9 (q each), 65.6, 91.5, 104.4, 108.0, 112.4, 116.2, 117.2, 130.4, 132.6, 133.9, 134.4, 142.6, 143.6, 143.7 (s each), 117.8, 118.2, 124.8, 126.5, 128.0, 128.3, 128.7 (d each), 163.2, 163.5, 165.2, 166.8 (s, each). Anal. calcd. for $C_{36}H_{28}N_4O_8$: C 67.07, H 4.37, N 8.69; found: C 66.7, H 4.16, N 8.50.

*8-Cyano-11,13-dimethyl-7,13c-diphenyl-1,2,3,4-tetramethoxycarbonyl-13c*H*-pyrido[1′,2′:2,3]pyridazino[4,5-a]indolizine c (3c; $R^1 = R^3 = Me$, $R^2 = H$)*

^{1}H NMR (90 MHz) δ: 1.76, 2.17, 3.33, 3.59, 3.68, 3.89 (s each, 3H each), 7.11–7.63 (m, 10H), 7.90 (bs, 1H). ^{13}C NMR (67.80 MHz) δ: 18.6, 21.5, 53.8, 54.0, 54.2, 54.5 (q each), 55.1, 84.6, 108.5, 108.7, 112.7, 116.9, 128.6, 131.7, 133.0, 134.8, 136.2, 137.6, 145.7, 152.7, 155.0 (s each), 125.5, 126.5, 129.4, 129.6, 130.2, 130.9, 131.0, 134.0 (d each), 160.4, 161.9, 165.2, 165.9 (d each). MS (*m/z*) calcd. for $C_{37}H_{30}N_4O_8$: 658.2064; found: 658.2035.

*8-Cyano-7,13c-diphenyl-12-phenyl-1,2,3,4-tetramethoxycarbonyl-13c*H*-pyrido[1′2′:2,3]pyridazino[4,5-a]indolizine (3d; $R^1 = R^3 = H$, $R^2 = Ph$)*

^{1}H NMR (90 MHz) δ: 3.33, 3.56 (s each, 3H each), 3.82 (s, 6H), 7.03 (dd, J = 2, 7 Hz, 1H), 7.12–7.67 (m, 16H), 8.14 (bd, J = 7 Hz, 1H). ^{13}C NMR (22.49 MHz) δ: 51.9, 52.3, 52.7, 52.9 (q each), 64.5, 91.8, 105.2, 109.7, 112.2, 117.1, 117.6, 132.3, 133.2, 133.9, 135.9, 142.3, 142.7, 143.0, 143.5 (s each), 116.6, 126.4, 126.6, 128.1, 128.4, 128.7, 128.8, 129.2, 130.4 (s each), 163.2, 163.4, 165.4, 166.6 (s each). Anal. calcd. for $C_{41}H_{30}N_4O_8$: C 69.67, H 4.27, N 7.92; found: C 69.51, H 4.17, N 7.91.

*8-Cyano-7,13c-diphenyl-12-benzoyl-1,2,3,4-tetramethoxycarbonyl-13c*H*-pyrido[1′,2′:2,3]pyridazino[4,5-a]indolizine (3e; $R^1 = R^3 = H$, $R^2 = COPh$)*

^{1}H NMR (90 MHz) δ: 3.37, 3.56, 3.78, 3.81 (s each, 3H each), 7.07–7.17 (m, 3H), 7.28–7.66 (m, 14H), 8.19 (d, J = 7 Hz, 1H). ^{13}C NMR (22.49 MHz) δ: 52.1, 52.4, 52.7, 53.0 (q each), 64.74,

Can. J. Chem. Downloaded from www.nrcresearchpress.com by 88.255.202.194 on 09/08/12
For personal use only.

94.13, 106.1, 111.4, 113.2, 117.0, 118.2, 132.2, 132.8, 136.2, 142.3, 142.3, 142.5, 143.5 (s each), 114.5, 124.6, 125.4, 126.6, 128.4, 128.5, 129.6, 130.6, 131.1, 132.7, 133.0 (d each), 163.1, 163.3, 164.6, 166.4, 192.8 (s each). Anal. calcd. for $C_{42}H_{30}N_4O_9$: C 68.65, H 4.11, N 7.62; found: C 68.49, H 4.13, N 7.43.

*8-Cyano-7,13c-diphenyl-12,13-benzo-1,2,3,4-tetramethoxycarbonyl-13c*H*-pyrido[1′,2′:2,3]pyridazino[4,5-a]indolizine (**3f**; R^1 = -CH = CH-CH = CH- = R^2, R^3 = H)*

^{1}H NMR (90 MHz) δ: 3.60, 3.66, 3.87, 3.92 (s each, 3H each), 6.80–7.60 (m, 15H), 7.98 (d, J = 7 Hz, 1H). ^{13}C NMR (67.80 MHz) δ: 52.2, 52.4, 52.7, 3.2 (q each), 66.5, 97.9, 106.5, 111.8, 115.1, 116.2, 123.0, 126.5, 129.0, 130.2, 133.7, 135.5, 137.9, 142.7, 147.4 (s each), 122.1, 127.1, 128.0, 128.7, 129.3, 130.6 (d each), 162.8, 163.5, 164.3, 167.3 (s each). Anal. calcd. for $C_{39}H_{28}N_4O_8$: C 68.81, H 4.14, N 8.23; found: C 68.55, H 3.95, N 7.97.

*Reaction of 7-azaindolizine **9** with DMAD*

To a solution of 7-azaindolizine **9** (14) (1 g, 8.5 mmol) in acetonitrile (30 cm^3) was added dropwise DMAD (3 g, 21 cm^3) at room temperature. After 15 min, **9** was no longer detected by TLC. The solvent and excess of DMAD were removed *in vacuo* and the residue was chromatographed on silica (benzene – ethyl acetate) and further purified by recrystallization from ethanol to give 8,9,10,11-tetramethoxycarbonyl-11a*H*-pyrazino[1,2-*a*]pyrro[2,1-*c*]pyrazine **10** (440 mg, 13%) as orange crystals, mp 171–175°C. IR: 1720, 1697 and 1612 (C=O) cm^{-1}; ^{1}H NMR (90 MHz) δ: 3.66, 3.71 (3H × 2, each s, OCH_3), 3.88 (s, 6H, OCH_3), 5.77–5.87 (m, 1H, H-1), 5.95–6.07 (m, 1H, H-2), 6.18 (br t, 1H, J = 4 Hz, H-3), 6.64–6.80 (m, 2H, 5, H-11a), 7.31 (d, 1H, J = 9 Hz, H-6). ^{13}C NMR (22.49 Hz; $CDCl_3$) δ: 52.1, 52.2, 52.5, 53.3 (q each, OCH_3), 5.49 (d, C-11a), 96.3 (s, C-9), 110.9 (s, C-10), 125.6 (s, C-11), 138.6 (s, C-8), 148.0 (s, C-121b), 107.2 (d, C-1), 109.7 (d, C-2), 112.3 (d, C-6), 117.1 (d, C-5), 119.8 (d, C-3), 162.7, 163.5, 164.3, 167.2 (s each, C=O). Anal. calcd. for $C_{19}H_{18}N_2O_8$: C 56.71, H 4.51, N 6.96; found: C 56.96, H 4.59, N 6.72.

Crystal structure determination

The 1:2 adduct **3*d*** was recrystallized from hexane–dichloromethane giving yellow, prismatic crystals that proved to be crystalline complexes with dichloromethane. A summary of the crystal data and structure refinement details are given in Table 2.[2] The structure was solved by a direct method (15), and refined by full-matrix least squares. The atoms other than hydrogen were refined anisotropically. The atomic scattering factors for all atoms and the anomalous dispersion correction factors for atoms other than hydrogen were taken from the literature (16–18). All calculations were performed using the TEXSAN (19) crystallographic software package of the Molecular Structure Corporation.

Acknowledgments

This work was supported in part by a Grant-in-Aid (to K. M.) for Scientific Research from the Ministry of Education, Science, and Culture, Japan (No. 04453023) and a grant (to J. W. L.) from the Natural Sciences and Engineering Research Council of Canada (No. A-2305). We thank Dr. M. Toda (Kyoto University) and Professor A. Kakehi (Shinshu University) for helpful assistance in the preliminary stage of this work.

[2]Tables of atomic coordinates, fractional atomic coordinates, bond lengths, bond angles, and thermal parameters have been deposited. Complete sets of data may be purchased from: The Depository of Unpublished Data, Document Delivery, CISTI, National Research Council Canada, Ottawa, Canada, K1A 0S2.

Tables of atomic coordinates and of bond lengths and angles have also been deposited with the Cambridge Crystallographic Data Centre and can be obtained on request from The Director, Cambridge Crystallographic Data Centre, University Chemical Laboratory, 12 Union Road, Cambridge, CB2 1EZ, U.K.

1. D. Leaver. *In* Rodd's chemistry of carbon compounds. Suppl. 2nd ed. Vol IVH. Elsevier, Amsterdam. 1987. p. 33; W. Flitsch. *In* Comprehensive heterocyclic chemistry. Vol. 4. *Edited by* A. R. Katritzky and C. W. Rees. Pergamon, Oxford. 1984. p. 443: F. J. Swinbourne, J. H. Hunt, and G. Klinkert. Adv. Heterocycl. Chem. **23**, 103 (1978); T. Uchida and K. Matsumoto. Synthesis, 209 (1976).
2. C. A. Ramsden. Tetrahedron, **33**, 3202 (1977); W. D. Ollis, S. P. Stanforth, and C. A. Ramsden. Tetrahedron, **41**, 2239 (1985).
3. A. Galbraith, T. Small, R. A. Barnes, and V. Boekelheide. J. Am. Chem. Soc. **83**, 453 (1961).
4. K. Matsumoto, T. Uchida, K. Aoyama, M. Nishikawa T. Kuroda, and T. Okamoto. J. Heterocycl. Chem. **25**, 1793 (1988).
5. W. Flitsch and J. Heinrich. Tetrahedron Lett. **21**, 3673 (1980).
6. D. Leaver. *In* Rodd's chemistry of carbon compounds. Suppl. 2nd ed. Vol IVH. Elsevier, Amsterdam. 1987. p. 45; W. Flitsch. *In* Comprehensive heterocyclic chemistry. Vol. 4. *Edited by* A. R. Katritzky and C. W. Rees. Pergamon, Oxford. 1984. p. 478; W. Flitsch and U. Kramer. Adv. Heterocycl. Chem. **22**, 322 (1978); K. Matsumoto, T. Uchida, and J. Yamauchi. Yuki Gosei Kagaku Kyokai Shi, **35**, 739 (1977).
7. R. M. Acheson. Adv. Heterocycl. Chem. **1**, 125 (19965); R. M. Acheson and N. F. Elmore. Adv. Heterocycl. Chem. **23**, 263 (1978).
8. D. E. Pereira and N. J. Leonard. Tetrahedron Lett. **27**, 4129 (1986); P. J. Dunn and C. W. Rees. J. Chem. Soc. Perkin Trans. 1, 1579 (1987); H. Marley, K. J. MacCullough, P. N. Preston, and S. H. B. Wright. J. Chem. Soc. Chem. Commun. 112 (1987); R. N. Butler, D. Cunningham, E. G. Marren, and P. McArdle. J. Chem. Soc. Chem. Commun. 706 (1987); T. Yamasaki, E. Kawaminami, T. Yamada, T. Okawara, and M. Furukawa. J. Chem. Soc. Perkin Trans. 1, 991 (1991); K. Matsumoto, T. Uchida, H. Yoshida, M. Toda, and A. Kakehi. J. Chem. Soc. Perkin Trans. 1, 2437 (1992).
9. K. Matsumoto, T. Uchida, T. Kato, M. Toda, K. Aoyama, and H. Konishi. Heterocycles, **31**, 593 (1980).
10. O. Tsuge and H. Samura. Tetrahedron Lett. 597 (1973); K. T. Potts and J. L. Marshall. J. Org. Chem. **41**, 129 (1976).
11. N. Abe, Y. Tanaka, and T. Nishiwaki. J. Chem. Soc. Perkin Trans. 1, 1924 (1977).
12. G. Maier and U. Heep. Chem. Ber. **101**, 1371 (1968).
13. V. Boekelheide and A. Miller. J. Org. Chem. **26**, 431 (1961).
14. V. Boekelheide and S. Kerteli. J. Org. Chem. **28**, 3212 (1963).
15. MITHRIL: C. J. Gilmore. J. Appl. Crystallogr. **17**, 42 (1984); DIFDIR: P. T. Beurkens. Technical Report 1984/1, Crystallography Laboratory, Toernooiveld, 6525 Ed Nijmegen, Netherlands.
16. D. T. Cromer and J. T. Weber. International tables for X-ray crystallography. Vol. IV. The Kynoch Press, Birmingham. 1974. Table 2.2A.
17. J. A. Ibers and W. C. Hamilton. Acta Crystallogr. **17**, 781 (1964).
18. D. T. Cromer. International tables for X-ray crystallography. Vol. IV. The Kynoch Press, Birmingham. 1974. Table 2.3.1.
19. TEXRAY structure analysis package, Molecular Structure Corporation. 1985.

Can. J. Chem. Downloaded from www.nrcresearchpress.com by 88.255.202.194 on 09/08/12
For personal use only.

Application of thioglycoside chemistry to the synthesis of trisaccharides and deoxy-trisaccharides related to the *Shigella flexneri* Y polysaccharide[1]

FRANCE-ISABELLE AUZANNEAU AND DAVID R. BUNDLE[2]
Institute for Biological Sciences, National Research Council of Canada, Ottawa, Ont., Canada K1A OR6

Received November 30, 1992

FRANCE-ISABELLE AUZANNEAU and DAVID R. BUNDLE. Can. J. Chem. **71**, 534 (1993).

The *Shigella flexneri* lipopolysaccharide has a biological repeating unit, →2)α-L-Rha*p*(1→2)α-L-Rha*p*(1→3)α-L-Rha*p*(1→3)β-D-GlcNAc*p*(1→ ABCD, but the residue segment BCD suffices to fill the binding site of an O-antigen specific monoclonal antibody, SYA/J6. Synthetic modifications to this trisaccharide have been designed to investigate the involvement in binding of the acetamido moiety, the 4- and 6-OH groups of the GlcNAc residue D, the 4′-OH group of the Rha residue C, and the 3″- and 4″-OH groups of the Rha residue B. Sequential chain extension provided the protected trisaccharides **18**, **24**, **26**, **28**, **30**, **32**, and **35** using thioglycoside glycosyl donors activated by iodonium ions generated *in situ* from *N*-iodosuccinimide and triflic acid. Trisaccharides each monodeoxygenated in either ring B **25** and **27** or ring C **29** were accessed by the use of 3,6-dideoxy or 4,6-dideoxy glycosyl donors **14** and **17** and when these were used in sequential steps trisaccharides **31** and **33**, each deoxygenated at double sites in adjacent residues, were obtained. Selective protection of the glucosamine residue as its *N*-benzyloxycarbonyl derivative provided a facile route to the trisaccharide amino compound **20**, from which *N*-acetyl **21**, *N*-propionyl **22**, and *N*-trifluoroacetyl **23** derivatives were directly prepared. Orthoester intermediates were detected in several glycosylation reactions and culminated in an orthoacetate **34** as a major product rather than the target trisaccharide **35**. When triflic acid concentration was increased these products were avoided but acid-catalyzed migration of a 2-*O*-acetyl group led to both 1→2 and 1→3 linked trisaccharides **35** and **37**. To avoid similar undesirable 1,2-linked products, a block synthetic strategy using the 2-*O*-benzoylated disaccharide glycosyl donor **40** was chosen so that the propensity for orthoester formation was minimized in reactions leading to the trisaccharide analogue deoxygenated at C-6 of the glucosamine unit D.

FRANCE ISABELLE AUZANNEAU et DAVID R. BUNDLE. Can. J. Chem. **71**, 534 (1993).

Le tétrasaccharide →2)-α-L-Rha*p*(1→2) α-L-Rha*p*(1→3) α-L-Rha*p*(1→3)β-D-GlcNAc*p*, ABCD constitue l'unité biologique répétitrice du lipopolysaccharide de *Shigella flexneri*, mais le segment BCD suffit à remplir le site de reconnaissance de l'anticorps monoclonal SYA/J6 spécifique de cet antigène-O. La préparation de trisaccharides modifiés a été effectuée afin d'évaluer l'importance pour la reconnaissance des groupes acétamido, 4- et 6-OH du résidu GlcNAc ainsi que des groupes 4′-, 3″- et 4″-OH des résidus rhamnosyles C et B. Les trisaccharides protégés **18**, **24**, **26**, **28**, **30**, **32** et **35** ont été obtenus en suivant une stratégie d'élongation de chaîne séquentielle utilisant comme donneurs de glycosyles des thioglycosides activés par des ions iodonium générés *in situ* depuis la *N*-iodosuccinimide et l'acide triflique. Les trisaccharides monodésoxygénés sur les résidus B **25**, **27** ou C **29** furent obtenus en utilisant les thioglycosides 3,6- ou 4,6-didésoxy **14** et **17**, dont l'emploi séquentiel combiné permit également l'accès aux trisaccharides **31** et **33** chacun didésoxygénés sur les résidus adjacents B et C. La protection sélective de la glucosamine par un groupe *N*-benzyloxycarbonyle permit d'obtenir facilement le trisaccharide amino **20**, précurseur des composés *N*-acétyl **21**, *N*-propionyl **22** et *N*-trifluoroacétyl **23**. La formation intermédiaire d'orthoesters, détectée au cours de plusieurs glycosylations, fut culminante durant la synthèse du trisaccharide **35** à l'issue de laquelle l'orthoacétate **34** fut isolé majoritairement. Sa formation fut évitée en augmentant la concentration d'acide triflique, mais la migration acido-catalysée du groupe 2-*O*-acétyl conduisit, dans ces conditions, à la formation des trisaccharides **37** et **35** respectivement 1→2 et 1→3 liés. Pour éviter la formation indésirable de composés similaires 1,2 liés, l'analogue **46**, désoxygéné en C-6 de l'unité de glucosamine D, fut préparé en suivant une stratégie de synthèse par bloc, utilisant un disaccharide 2-*O*-benzoylé comme donneur de glycosyle afin de minimiser sa tendance à former un orthoester.

Introduction

In our studies of the antibody combining sites that are generated by immunization of mice with killed vaccines of variant Y *Shigella flexneri*, we have concentrated on two antibodies that are typical of the majority that bind to the Y polysaccharide antigen, an IgM GC-4 and an IgG SYA/J6 (1–3). In their binding patterns with native antigen and glycoconjugates both exhibit a specificity that is directed toward an epitope occurring at the junction of the biological repeating unit (1). Preliminary investigations were based on enzyme immunoassay (EIA) screening with synthetic ligands coupled to BSA and a limited set of modified oligosaccharides (1). These results identified the probable extent of the oligosaccharide–protein contacts and, of the four residues that make up the biological repeating unit of the bacterial *O*-antigen:

[→2)-α-L-Rha*p*(1→2)-α-L-Rha*p*(1→3)-α-L-Rha*p*(1→3)-β-D-GlcNAc*p*(1−]
A B C D

it seemed most probable that the residue sequence BCDA represented the extent of the oligosaccharide epitope. Although the contribution to the binding by the A residue was estimated to be very small (1), we did not properly consider the possibility that the trisaccharide BCD rather than the tetrasaccharide BCDA filled the binding site. Conclusions that the acetamido group of residue D was exposed to

[1]Issued as NRCC No. 34287.
[2]Author to whom correspondence may be addressed.

Can. J. Chem. Downloaded from www.nrcresearchpress.com by 88.255.202.194 on 09/08/12
For personal use only.

Can. J. Chem. Downloaded from www.nrcresearchpress.com by 88.255.202.194 on 09/08/12
For personal use only.

solvent were based on the use as inhibitor of partially *N*-deacetylated trisaccharide BCD. The residual activity of the trisaccharide α-L-Rha*p*(1→3)-α-L-Rha*p*(1→3)-β-D-GlcNAc*p*-1→*O*Me, which was a 40% contaminant of the intended α-L-Rha*p*(1→3)-α-L-Rha*p*(1→3)-β-D-GlcNH$_2$*p*-1→*O*Me inhibitor, led to an erroneous conclusion that the acetamido group was not a contact residue in the site. To complete the mapping of the SYA/J6 binding site a reliable synthesis of these two trisaccharides as well as various *N*-acylated derivatives was required, together with a complete investigation via monodeoxy derivatives of the hydroxyl groups that form hydrogen bonds to the antibody. The results of this study will provide an important comparison with the detailed oligosaccharide–antibody interactions that should be available now that the crystal structures have been solved for antibody SYA/J6 Fab cocrystallized with penta- and trisaccharide ligands (4).

In this report, we describe the use of the *N*-benzyloxycarbonyl protecting group to provide the amino congener of the naturally occurring trisaccharide Rha→Rha→GlcNAc, as well as other acylamido analogues. Early work (1) had suggested that the B residue contributed some 1.5–2.0 kcal/mol of binding energy but its attribution to hydrogen bonding involving the 3- or 4-hydroxyl groups was not investigated. It was also suggested that a hydrogen bond involving the 4-hydroxyl group of the glucosamine unit was crucial to the binding of the antigen to SYA/J6 but that neither the 6-OH group of unit D, or the 4-OH group of residue C were involved in important polar contacts ($\Delta(\Delta G) < 0.5$ kcal/mol). However, the latter results were measured using monodeoxydisaccharide analogues (1) of CD and therefore had to be confirmed using analogues of the trisaccharide BCD that represents the smallest antigen epitope that could fill the SYA/J6 IgG binding site.

To identify the trisaccharide hydroxyl groups that form the most important polar contacts with the protein, five monodeoxy analogues involving various positions within units B, C, or D were synthesized. Two dideoxygenated trisaccharides were also prepared to evaluate the additivity effects to binding energy when changes were made in both the units B and C.

The 11 trisaccharide target compounds were synthesized from thioglycosides. These are flexible and stable intermediates that are well suited for oligosaccharide chemistry since the thioalkyl group can be easily converted to glycosyl halide under mild conditions or activated, *in situ*, by thiophilic reagents (5). Sequential chain extension strategies involving activation of thioglycosides with iodonium ions generated, *in situ*, from *N*-iodosuccinimide and triflic acid (6, 7) were employed for most of these oligosaccharide syntheses.

Results

The known (8) disaccharides **1**, **4**, **7**, and **9** were employed as precursors of the glycosyl acceptors needed to prepare the protected trisaccharides **18**, **24**, **26**, **28**, **30**, **32**, and **35**. The triacetates **1** and **4** were transesterified to the triol derivatives **2** and **5**. Regioselective acetylations of **2**, **4**, and **9** to give respectively the acceptors **3**, **6**, and **10** were then accomplished in three steps. Reaction of the triols with trimethylorthoacetate gave 2′,3′-orthoesters that were acetylated at OH-4 prior to acid-catalyzed regioselective opening

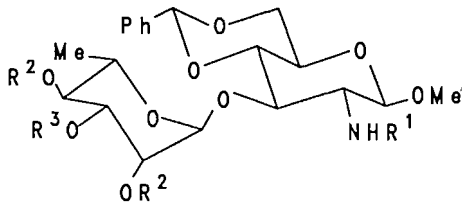

1 $R^1 = CO_2CH_2Ph$, $R^2 = R^3 = Ac$
2 $R^1 = CO_2CH_2Ph$, $R^2 = R^3 = H$
3 $R^1 = CO_2CH_2Ph$, $R^2 = Ac$, $R^3 = H$
4 $R^1 = R^2 = R^3 = Ac$
5 $R^1 = Ac$, $R^2 = R^3 = H$
6 $R^1 = R^2 = Ac$, $R^3 = H$

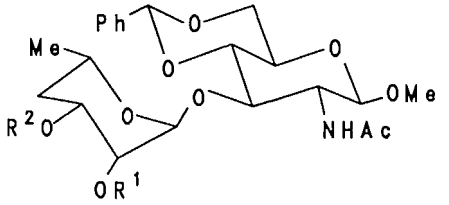

7 $R^1 = R^2 = H$
8 $R^1 = Ac$, $R^2 = H$

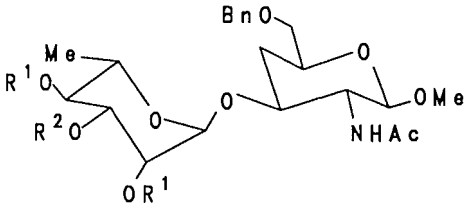

9 $R^1 = R^2 = H$
10 $R^1 = OAc$, $R^2 = H$

to O-2 by treatment in aqueous acetic acid. The diol **7** was converted into the acceptor **8** analogously by formation of a 2′,3′-orthoacetate and regioselective opening to the axial position with mild acidic treatment.

The thioethylrhamnopyranoside **11**, and the thioethyldideoxyhexopyranosides **14** and **17** were used as glycosyl donors. Preparation of a rhamnosyl donor deoxygenated at C-3 was accomplished from methyl 2-*O*-benzoyl-3,6-dideoxy-α-L-*arabino*-hexopyranoside (9) **12**. The glycoside was converted by acetolysis to a mixture of anomeric acetates **13** (α) and **15** (β) from which the α anomer crystallized from hexanes. Reaction of **13** with ethanethiol in the presence of BF_3–etherate gave the α-L and β-L thioglycosides **14** (75%) and **16** (11%), which were separated by chromatography.

Ethyl tri-*O*-acetyl-1-thio-α-L-rhamnopyranoside (10–12) **11** activated by iodonium ions (6) generated *in situ* from *N*-iodosuccinimide and triflic acid (0.13 equivalent) reacted

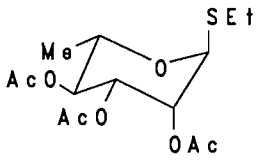

11

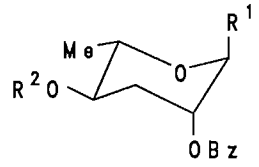

12 $R^1 = OMe$, $R^2 = H$
13 $R^1 = OAc$, $R^2 = Ac$
14 $R^1 = SEt$, $R^2 = Ac$

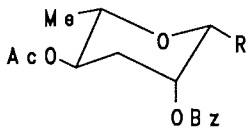

15 R = OAc
16 R = SEt

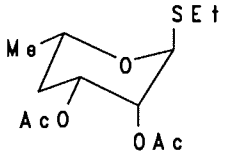

17

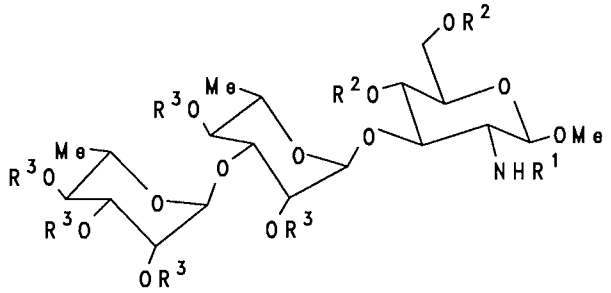

18 $R^1 = CO_2CH_2Ph$, $R^2 = >CHPh$, $R^3 = Ac$
19 $R^1 = CO_2CH_2Ph$, $R^2 = R^3 = H$
20 $R^1 = R^2 = R^3 = H$
21 $R^1 = COCH_3$, $R^2 = R^3 = H$
22 $R^1 = COCH_2CH_3$, $R^2 = R^3 = H$
23 $R^1 = COCF_3$, $R^2 = R^3 = H$

with the disaccharide acceptor **3** to give the protected trisaccharide **18** (84%). Using identical reaction conditions glycosylation of the *N*-acetylated disaccharide **6** with the 3,6-dideoxythiohexoside **14** required further addition of both glycosyl donor and triflic acid to afford the trisaccharide **24** in only 57% yield. Consequently, glycosylation of disaccharide **6** with the thioglycoside **17** was started using more triflic acid (0.26 equivalent) than for the preparation of **18** and gave trisaccharide **26** (86%) without further addition of acid. In view of this result, the same glycosylation conditions were employed to condense the acceptor deoxydisaccharide **8** with the thioglycosides **11**, **14**, and **17**. When **14** and **17** were reacted with **8**, trisaccharides **30** and **32** were isolated in good yields (respectively 82% and 89%). Surprisingly, glycosylation of **8** with the triacetate **11** gave the trisaccharide **28** in only 55% yield. In this case TLC monitoring of the reaction showed complete disappearance of the glycosyl acceptor with simultaneous consumption of the

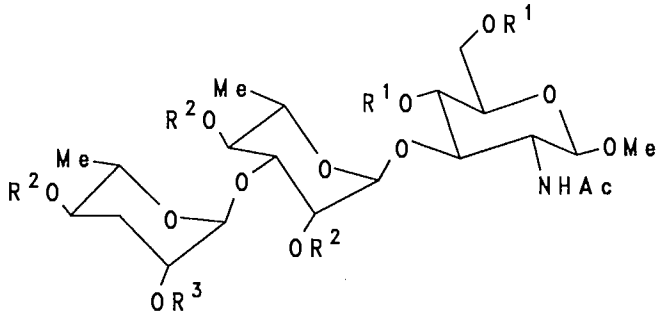

24 $R^1 = >CHPh$, $R^2 = Ac$, $R^3 = Bz$
25 $R^1 = R^2 = R^3 = H$

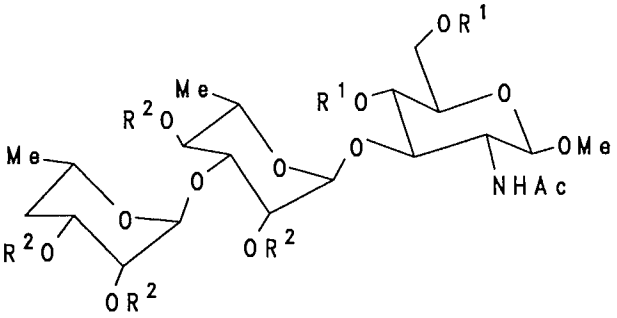

26 $R^1 = >CHPh$, $R^2 = Ac$
27 $R^1 = R^2 = H$

rhamnosyl donor but formation of two UV-absorbent compounds. Upon further addition of triflic acid the less polar product was converted into the more polar compound, which was isolated and identified as the desired trisaccharide **28**. These observations suggested the formation of an orthoester intermediate that rearranged to give **28**. Similarly, when disaccharide **10** was glycosylated with the triacetate **11**, the formation of two products was observed. Work-up and chromatography of the reaction mixture afforded the orthoester **34** (54%) and the target trisaccharide **35** (11%). Their structures were assigned on the basis of ^1H and ^{13}C NMR spectra (Tables 6 and 7). The orthoester **34** showed signals at 26.4 ppm (^{13}C) and 1.63 ppm (^1H) characteristic of an orthoacetate C-CH_3 group (13). As well, the typical signal of a quaternary carbon at 124.7 ppm was evident, while only five signals corresponding to quaternary carbons of carbonyl groups were observed. Since only one stereoisomer was observed, and as the nucleophilic attack of an alcohol on an intermediate 1,2-cyclic acyloxonium ion is sterically favored from the side *trans* (*exo*) to the pyranose ring (14), it is most likely that compound **34** has the *exo* configuration. As expected, the formation of this orthoester could be avoided by adding twice as much triflic acid (0.56 equivalent) when starting the glycosylation. Under these conditions a TLC homogenous mixture (75:25) of the isomeric trisaccharides **35** (53%) and **37** (18%) was obtained. The formation of trisaccharide **37** can be explained by the acid-catalyzed (2′→3′) migration of the 2′-*O*-acetyl group in disaccharide **10** leading to a glycosyl acceptor with a 2-hydroxy group on the rhamnose unit, which can be easily glycosylated by the

Can. J. Chem. Downloaded from www.nrcresearchpress.com by 88.255.202.194 on 09/08/12
For personal use only.

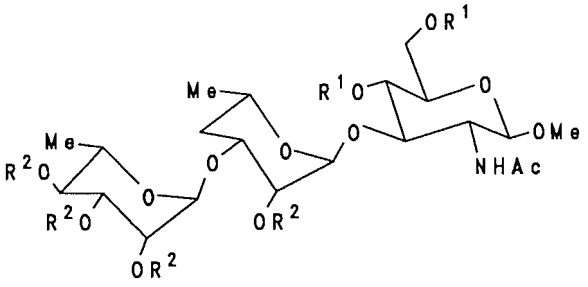

28 $R^1 = >CHPh$, $R^2 = Ac$
29 $R^1 = R^2 = H$

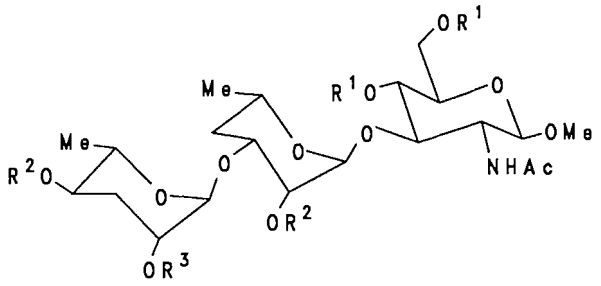

30 $R^1 = >CHPh$, $R^2 = Ac$, $R^3 = Bz$
31 $R^1 = R^2 = R^3 = H$

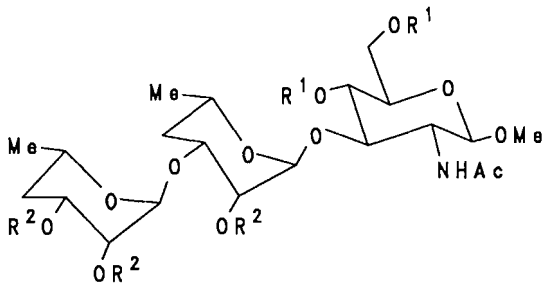

32 $R^1 = >CHPh$, $R^2 = Ac$
33 $R^1 = R^2 = H$

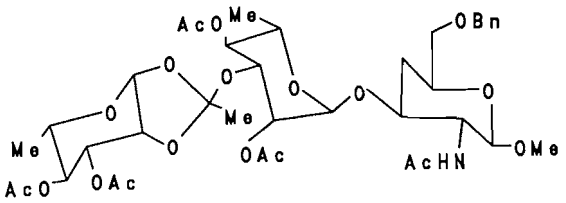

34

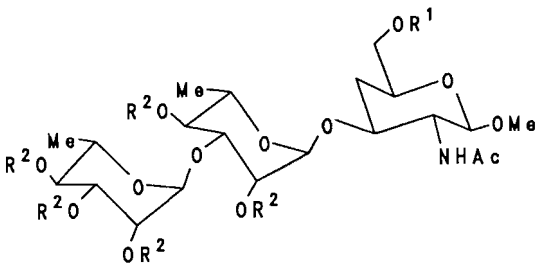

35 $R^1 = Bn$, $R^2 = Ac$
36 $R^1 = R^2 = H$

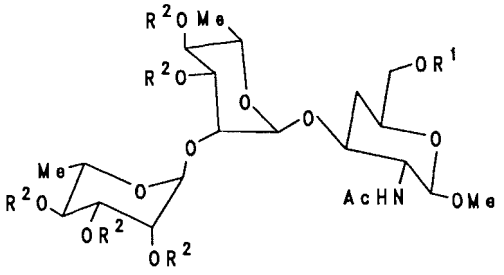

37 $R^1 = Bn$, $R^2 = Ac$
38 $R^1 = R^2 = H$

activated donor **11**. The results described above showed that the success of the iodonium-catalyzed glycosylation of analogous disaccharides such as **3**, **6**, **8**, or **10** was dependent on the structure of both acceptors and donors. Ethyl thiorhamnopyranosides with a 2-*O*-acetyl group react with the acceptor alcohols to form the glycosidic linkage via an orthoacetate, which may be stable in the weakly acidic reaction medium. This observation led us to investigate a block synthetic strategy to prepare trisaccharide **42**, the precursor of the 6-deoxy trisaccharide **46**. The alcohol **39** (12) was glycosylated with acetobromorhamnose (15) (AgOTf) to give disaccharide **40**, which was condensed with monosaccharide **41** (16) under iodonium ion catalysis. As no acetyl group migration was likely to occur when using **41** as glycosyl acceptor, the glycosylation was performed with 0.5 equivalent of triflic acid to avoid orthoester formation and trisaccharide **42** was isolated in 71% yield. The disaccharide donor **40** avoids troublesome orthoester products (17) and thus provides a more convenient route to trisaccharides that are modified in the Glc*N*Ac residue D.

The *N*-benzyloxycarbonyl derivative **19** was obtained as an analytically pure white powder after acetal hydrolysis and transesterification of the protected trisaccharide **18**. Removal of the benzyloxycarbonyl group was accomplished by hydrogenolysis of a methanolic solution of **19** and the amine **20** was precipitated as its hydrochloride salt. Each of the trisaccharides **21**–**23** was prepared from **19** by hydrogenolysis of the *N*-protecting group and *N*-acylation of the crude amine **20**. A methanolic solution of **20** was treated with acetic or propionic anhydride to give **21** (85%) and **22** (73%). The acetylation proceeded much faster than the propionylation, which required the addition of triethylamine to reach completion. Trifluoroacetylation was achieved by treating a solution of **20** in anhydrous pyridine with an excess of trifluoroacetic anhydride, followed by the *in situ* hydrolysis of the *O*-trifluoroacetyl groups, by adding water to the crude reaction mixture. The *N*-trifluoroacetate **23** (50%) was pu-

Can. J. Chem. Downloaded from www.nrcresearchpress.com by 88.255.202.194 on 09/08/12
For personal use only.

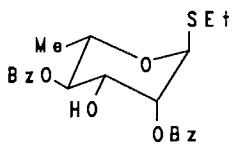

39

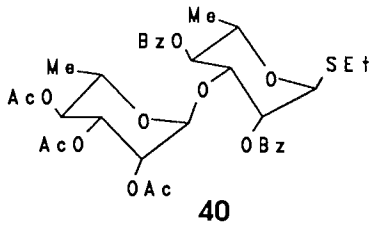

40

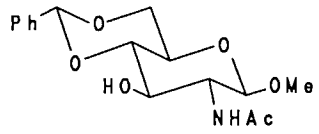

41

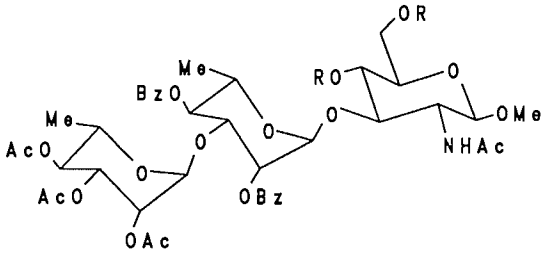

42 R = > CHPh
43 R = H

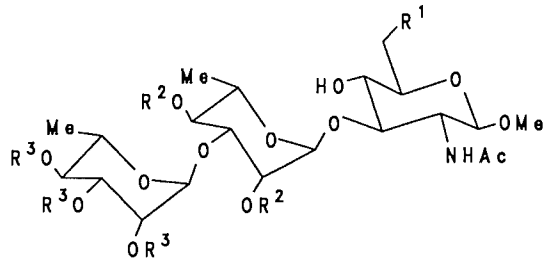

44 R^1 = Br, R^2 = Bz, R^3 = Ac
45 R^1 = H, R^2 = Bz, R^3 = Ac
46 $R^1 = R^2 = R^3 = H$

rified by chromatography and obtained free of salt by gel permeation chromatography on a Biogel P2 column eluted with water.

The 3″-, 4″-, and 4′-monodeoxygenated trisaccharides **25**, **27**, and **29** as well as the dideoxy analogues **31** and **33** were obtained by a two-step procedure from the protected trisaccharides **24**, **26**, **28**, **30**, and **32**. The transesterification of the *O*-acyl groups in methanol was followed by the hydrogenolysis of the benzylidene acetal. The latter reaction was preferred to an acid hydrolysis in order to preserve the acid-labile dideoxyhexopyranoside linkages. An analogous sequence of reactions was applied to the mixture of **35** and **37** to obtain the deprotected trisaccharides **36** and **38** that were separated by reversed-phase HPLC.

Deoxygenation at C-6 of the glucosamine unit was achieved in four steps from the protected trisaccharide **42**. Hydrolysis of the benzylidene acetal gave the diol **43**, which was selectively brominated at C-6 using conditions analogous to those described by Garegg *et al.* for the selective chlorination of sugar (18). The brominated trisaccharide **44** (55%) was then reduced to give the 6-deoxy derivative **45**, which, upon transesterification of the acyl groups, led to the deprotected analogue **46** (84%, from **44**).

New compounds and intermediates were fully characterized by ^{1}H NMR spectroscopy (Tables 1 and 3–6). Glycosylation and bromination products as well as final compounds were also characterized by ^{13}C NMR spectroscopy (Tables 2 and 7) and the configurations of the anomeric linkages were assigned according to the heteronuclear coupling constants measured between anomeric carbons and protons (19). The spectroscopic data were in full accord with the proposed structures.

Discussion

The synthesis of 11 trisaccharides reported here underscores the convenience and efficacy of thioglycosides in both block and sequential oligosaccharide synthesis, especially when the glycosyl donors are activated by *N*-iodosuccimide/triflic acid (6). The acidic conditions of activation are sufficiently mild that intermediate orthoesters are observed under typical glycosylation conditions, e.g., synthesis of **34** from reaction of the donor **11** with the acceptor disaccharide **10**. In several reactions TLC monitoring suggested the formation of intermediate orthoesters that rearranged during the normal reaction period, 4–7 h. The formation of orthoester was minimized by increasing the acidity of the reaction mixture; however, in general this is potentially hazardous because of the likelihood of acyl group migration, especially when acetate esters are employed for selective protection. The simplest explanation for the formation of both the 1,2- and 1,3-linked trisaccharide products **35** and **37** was the acid-catalyzed migration of an acetate from *O*-2 to *O*-3 of the terminal rhamnose residue of disaccharide **10**.

Orthoester formation in the *manno* series is well documented (13) and it could be anticipated that the formation of acetoxonium ions following activation of the acylated thioglycoside would lead to orthoester formation under appropriate circumstances of donor and acceptor reactivity (17, 20).

Can. J. Chem. Downloaded from www.nrcresearchpress.com by 88.255.202.194 on 09/08/12
For personal use only.

Can. J. Chem. Downloaded from www.nrcresearchpress.com by 88.255.202.194 on 09/08/12
For personal use only.

The use of functional group replacement, particularly monodeoxy analogues to map protein binding sites and to draw conclusions about three-dimensional features of the carbohydrate–protein binding sites (21), assumes that only minor perturbations of the conformational equilibria about glycosidic linkages result from these synthetic changes. An initial indication of the validity of this assumption may be drawn from an examination of the ^{1}H NMR and ^{13}C NMR chemical shift changes that accompany the modifications. Carbon-13 chemical shifts of anomeric and aglyconic carbon atoms have been shown to be sensitive to torsional and valence angle changes (22–24). Proton NMR shifts are also diagnostic of predominant conformations (24, 25).

Examination of the ^{1}H NMR chemical shifts for D_2O solutions of the modified and deprotected trisaccharides relative to the native trisaccharide **21** shows a consistent pattern of chemical shifts. Both α-L-rhamnopyranose residues B and C adopt the typical $^1C_4$(L) chair conformation as judged by the ^3J values, and in similar fashion the β-D-GlcNAc residue D has ^1J coupling constants consistent with the $^4C_1$(D) chair conformation (Table 1). The ^{13}C NMR chemical shifts also show closely related values and a consistent pattern for the native trisaccharide and its cogeners. Together, the chemical shift similarities suggest that the conformational equilibria of each trisaccharide are closely related. This is in agreement with calculations that predict closely related potential energy surfaces for each glycosidic linkage of the series of monodeoxy derivatives and, furthermore, shows no indication of substantially shifted conformational equilibria. This conclusion then provides a sound basis for direct comparison of the inhibitory power of each structure and its correlation with a three-dimensional model for the epitope bound to its antibody.

Experimental

General methods

The methods employed were described in an earlier publication (8). NMR data are presented in tables, ^{1}H NMR in Tables 1 and 3–6, ^{13}C NMR in Tables 2 and 7.

*Methyl 2-amino-4,6-*O*-benzylidene-2-*N*-benzyloxycarbonyl-2-deoxy-3-*O*-(α-L-rhamnopyranosyl)-β-D-glucopyranoside (2)*

A solution of the protected disaccharide **1** (8) (2.02 g, 2.94 mmol) in methanolic NaOMe (0.1 M, 200 mL) was stirred for 1 h at room temperature and deionized with Amberlite IR-120 (H^+) resin. The solution was filtered and concentrated to give the triol **2** (1.61 g, 98%) as a white powder that was isolated by filtration from Et_2O: mp 222–224°C (dec.); $[\alpha]_D^{25}$ −99.2 (*c* 0.6, MeOH). Anal. calcd. for $C_{28}H_{35}NO_{11}$: C 59.9, H 6.3, N 2.5; found: C 59.6, H 6.3, N 2.3.

*Methyl 2-amino-3-*O*-(2′,4′-di-*O*-acetyl-α-L-rhamnopyranosyl)-4,6-*O*-benzylidene-2-*N*-benzyloxycarbonyl-2-deoxy-β-D-glucopyranoside (3)*

Trimethylorthoacetate (520 μL, 1.5 mol-equiv.) was added to a suspension of the triol **2** (1.53 g, 2.72 mmol) in anhydrous CH_3CN (60 mL) containing *p*-toluenesulfonic acid (87 mg), and the mixture was stirred for 1 h under N_2 at room temperature. NEt_3 (5 mL) was added, the solution was concentrated to dryness, and residual traces of MeOH were coevaporated with a mixture of anhydrous pyridine–NEt_3 (4:1, 25 mL). *N*,*N*-Dimethylaminopyridine (40 mg) and acetic anhydride (520 μL, 2 mol-equiv.) were then added to a stirred solution of the residue in anhydrous pyridine (60 mL). After 1 h at room temperature more anhydride (100 μL) was added and stirring was continued for another hour. MeOH (200 μL) was added to destroy excess reagent, solvents were evaporated, and the residue, dissolved in EtOAc (200 mL), was washed successively with 1 M HCl (50 mL), saturated aqueous $NaHCO_3$ (50 mL), saturated aqueous NaCl (50 mL), and dried. The solid obtained after concentration was dissolved in aqueous 80% acetic acid (100 mL), stirred 30 min at room temperature, and solvents were evaporated at 25°C under high vacuum. Residual traces of acid were coevaporated with toluene (3 × 20 mL), and flash chromatography ($CHCl_3$–acetone, 10:1.5) of the residue gave the alcohol **3** (1.3 g, 73%), which crystallized on standing: mp 221.6°C; $[\alpha]_D^{25}$ −45.3 (*c* 0.7, $CHCl_3$). Anal. calcd. for $C_{32}H_{39}NO_{13}$: C 59.5, H 6.1, N 2.2; found: C 59.1, H 6.2, N 2.2.

*Methyl 2-acetamido-4,6-*O*-benzylidene-2-deoxy-3-*O*-(α-L-rhamnopyranosyl)-β-D-glucopyranoside (5)*

Deacetylation of disaccharide **4** (8) (1.25 g, 2.1 mmol), as well as work-up of the reaction, was performed in the same manner as the preparation of disaccharide **2**. Triol **5** was obtained as a pure white powder (951 mg, 96%) by crystallization from Et_2O: mp 232.5–234.2°C; $[\alpha]_D^{25}$ −112.5 (*c* 1.0, MeOH). Anal. calcd. for $C_{22}H_{31}NO_{10}$: C 56.3, H 6.7, N 3.0; found: C 55.8, H 6.7, N 3.3.

*Methyl 2-acetamido-3-*O*-(2′,4′-di-*O*-acetyl-α-L-rhamnopyranosyl)-4,6-*O*-benzylidene-2-deoxy-β-D-glucopyranoside (6)*

Selective acetylation of triol **5** (860 mg, 1.83 mmol) was performed in three steps, using conditions similar to those used to prepare the alcohol **3**. The alcohol **6** was crystallized from MeOH–Et_2O and obtained as a white powder (904 mg, 89%): mp 255–257°C (dec.); $[\alpha]_D^{25}$ −46.2 (*c* 0.55, $CHCl_3$). Anal. calcd. for $C_{26}H_{35}NO_{12}$: C 56.4; H 6.4, N 2.5; found: C 56.2, H 6.4, N 2.3.

*Methyl 2-acetamido-3-*O*-(2′-*O*-acetyl-4′-deoxy-α-L-*lyxo*-hexopyranosyl)-4,6-*O*-benzylidene-2-deoxy-β-D-glucopyranoside (8)*

Treatment of the diol **7** (8) (763 mg, 1.68 mmol) with trimethylorthoacetate and acid opening of the intermediate 2′,3′-orthoacetate using identical conditions to those used to prepare the alcohol **3** gave the alcohol **8** as an amorphous white solid isolated by filtration from EtOAc (687 mg, 82%); $[\alpha]_D^{25}$ −76.0 (*c* 0.7, DMSO). Anal. calcd. for $C_{24}H_{33}NO_{10}$: C 58.2, H 6.7, N 2.8; found: C 58.3, H 6.7, N 2.8.

*Methyl 2-acetamido-3-*O*-(2′,4′-di-*O*-acetyl-α-L-rhamnopyranosyl)-6-*O*-benzyl-2,4-dideoxy-β-D-*xylo*-hexopyranoside (10)*

Triol **9** (8) (444 mg, 0.97 mmol) was selectively acetylated in the conditions used to prepare alcohol **3**. The alcohol **10** was isolated as a white solid (290 mg, 55%) from MeOH–Et_2O. Chromatography of the mother liquors ($CHCl_3$–MeOH; 40:1, 150 mL; 30:1, 90 mL; 20:1, 80 mL) gave more alcohol (101 mg, 19%), which was also filtered off in MeOH–Et_2O: mp 212.3–212.9°C (dec.); $[\alpha]_D^{25}$ −23.2 (*c* 0.6, $CHCl_3$). Anal. calcd. for $C_{26}H_{37}NO_{11}$: C 57.9, H 6.9, N 2.6; found: C 57.5, H 6.8, N 2.6.

*1,4-Di-*O*-acetyl-2-*O*-benzoyl-3-deoxy-α-L-*arabino*-hexopyranoside (13) and 1,4-di-*O*-acetyl-2-*O*-benzoyl-3-deoxy-β-L-*arabino*-hexopyranoside (15)*

A solution of sulfuric acid in glacial acetic acid (0.47 M, 5 mL) was added dropwise to a stirred solution of the glycoside **12** (9) (2.21 g, 8.7 mmol) in a mixture of glacial acetic acid and acetic anhydride (2:5, 185 mL). After 1 h at 20°C (water bath) NaOAc (5 g) was added and the reaction mixture was poured slowly into an ice-cold saturated solution of $NaHCO_3$ (250 mL). The product was extracted in EtOAc (2 × 250 mL), washed with saturated aqueous NaCl (200 mL), dried, and concentrated. Chromatography (hexanes–EtOAc, 7:3) of the oily residue gave a mixture (2.5 g) of the α-(**13**) and β-(**15**) anomers (94:6). Monosaccharide **13** crystallized from hexanes (2.0 g, 71%): mp 90.2–90.8°C; $[\alpha]_D^{25}$ −31.7 (*c* 0.95, $CHCl_3$). Anal. calcd. for $C_{17}H_{20}O_7$: C 60.7, H 6.0; found: C 60.7, H 6.0.

*Ethyl 4-*O*-acetyl-2-*O*-benzoyl-3-deoxy-1-thio-α-L-*arabino*-hexopyranoside (14) and ethyl 4-*O*-acetyl-2-*O*-benzoyl-3-deoxy-1-thio-β-L-*arabino*-hexopyranoside (16)*

The di-*O*-acetate **13** (1.80 g, 5.35 mmol) dissolved in dry CH_2Cl_2 (100 mL) was reacted for 30 min at room temperature with EtSH

TABLE 1. ^{1}H NMR chemical shifts for D_2O solutions of the trisaccharides

Protons (J, Hz)	**21**	**20**	**22**	**23**	**25**	**27**	**29**	**31**	**33**	**36**	**46**	**38**
α-L-Rha unit B												
H-1	5.01	5.06	5.02	5.01	4.85	5.05	4.94	4.78	4.99	4.99	5.01	4.87
($J_{1,2}$)	(1.5)		(1.5)	(1.5)						(1.5)	(1.0)	(1.0)
H-2	4.05	4.08	4.05	4.05	4.05	3.89	3.93	3.93	3.76	4.05	4.05	4.05
($J_{2,3}$)	(3.5)		(3.5)	(3.0)	(3.0)	(~3.5)	(3.0)		(3.5)	(3.0)	(3.5)	(3.0)
H-3	3.82	3.85	3.82	3.81	1.87	4.08	3.79	1.84	4.05	3.82	3.82	3.77
($J_{3,4}$)	(9.0)	(10.0)	(10.0)	(9.5)	(~11.5)	(12.0)	(9.5)		(12.0)	(9.5)	(9.5)	(9.5)
($J_{3,3'}$)					(~12.0)			(13.5)				
H-3′					2.04			2.03				
($J_{2,3'}$)								(~3.5)				
($J_{3',4}$)					(4.5)			(~3.5)				
H-4	3.45	3.47	3.47	3.45	3.61	1.60	3.44	3.61	1.59	3.45	3.46	3.45
($J_{4,5}$)	(10.0)	(10.0)	(10.0)	(9.5)	(~11.5)	(12.0)	(9.5)		(12.0)	(9.5)	(9.5)	(9.5)
H-4′						1.76			1.75			
($J_{3,4'}$)						(~3.5)			(4.5)			
($J_{4,4'}$)						(12.0)			(12.0)			
H-5	3.78	3.85	3.77	3.73	3.76	4.04	3.74	3.73	3.99	3.77	3.78	3.72
($J_{5,6}$)	(6.5)	(6.5)	(6.5)	(6.0)	(6.0)	(6.5)	(6.0)	(6.0)	(6.5)	(6.5)	(6.0)	(6.0)
H-6	1.30	1.30	1.31	1.29	1.27	1.24	1.30	1.27	1.23	1.29	1.30	1.28
α-L-Rha unit C												
H-1	4.81	4.99	4.82	4.78	4.82	4.82	4.87	4.88	4.87	4.83	4.80	4.99
($J_{1,2}$)	(~1.5)	(~1.0)	(~1.5)						(1.0)	(~1.5)		
H-2	3.86	4.20	3.86	3.82	3.89	3.85	3.71	3.74	3.70	3.86	3.85	3.72
($J_{2,3}$)	(~2.5)		(~2.0)	(3.5)	(3.0)		(~4.0)	(~4.0)		(~2.5)	(3.0)	(3.5)
H-3	3.78	3.84	3.78	3.76	3.80	3.76	4.01	4.04	4.00	3.76	3.77	3.82
($J_{3,4}$)		(10.0)	(10.0)	(9.5)	(9.5)	(~9.0)	(12.0)	(12.0)		(9.5)	(10.0)	(10.0)
H-4	3.52	3.58	3.52	3.53	3.52	3.49	1.57	1.58	1.56	3.50	3.51	3.45
($J_{4,5}$)		(10.0)	(10.0)				(12.0)	(12.0)	(12.0)	(9.5)	(10.0)	(9.5)
H-4′							1.85	1.85	1.85			
($J_{3,4'}$)							(~4.0)	(~3.5)				
($J_{4,4'}$)							(12.0)	(12.0)	(12.0)			
H-5	4.03	3.99	4.04	4.02	4.04	4.03	4.23	4.24	4.23	3.80	4.05	3.72
($J_{5,6}$)	(6.0)	(6.0)	(6.5)	(6.5)	(6.5)	(6.5)	(6.0)	(6.5)	(6.0)	(6.5)	(6.0)	(6.0)
H-6	1.24	1.29	1.23	1.24	1.24	1.24	1.18	1.18	1.18	1.27	1.23	1.27
β-D-GlcNAc unit D												
H-1	4.47	4.68	4.48	4.58	4.47	4.47	4.47	4.48	4.47	4.41	4.45	4.45
($J_{1,2}$)	(8.5)	(8.5)	(8.5)	(8.5)	(8.5)	(8.5)	(8.5)	(8.5)	(8.5)	(8.5)	(8.5)	(8.5)
H-2	3.82	3.20	3.83	3.92	3.82	3.82	3.80	3.81	3.81	3.65	3.81	3.62
($J_{2,3}$)	(9.5)	(9.0)	(10.0)	(~9.0)	(~9.5)	(9.0)	(10.0)	(10.0)	(10.0)		(9.5)	(9.5)
H-3	3.58	3.86	3.60	3.69	3.59	3.58	3.57	3.58	3.58	3.77	3.52	3.74
($J_{3,4}$)	(9.0)	(~9.5)	(10.0)	(10.0)	(9.5)	(9.0)				(11.5)	(9.5)	(10.5)
($J_{3,4'}$)												(4.0)
H-4	3.52	3.66	3.52	3.58	3.52	3.52	3.50	3.50	3.49	1.59	3.28	1.58
($J_{4,5}$)		(~9.5)	(10.0)	(10.0)						(11.5)	(9.5)	(12.5)
H-4′										2.07		2.04
($J_{4,4'}$)										(11.5)		(12.5)
H-5	3.47	3.54	3.48	3.50	3.47	3.46	3.47	3.48	3.48	3.71	3.49	3.71
H-6	3.76	3.78	3.76	3.77	3.76	3.75	3.75	3.75	3.74	3.64	1.33	3.64
($J_{6,5}$)	(6.0)	(5.5)	(6.0)	(6.0)		(~6.0)					(6.0)	
H-6′	3.94	3.95	3.95	3.96	3.94	3.94	3.94	3.94	3.94	3.71		3.71
($J_{6',5}$)	(2.0)	(2.0)	(1.5)	(1.5)	(~1.0)	(~2.0)						
($J_{6,6'}$)	(12.5)	(12.0)	(12.0)	(12.5)	(12.0)	(11.5)			(13.0)			
OCH_3	3.51	3.60	3.51	3.53	3.52	3.51	3.51	3.52	3.51	3.51	3.49	3.52
NCOC*H*R	2.03		2.30		2.05	2.04	2.05	2.06	2.05	2.04	2.05	2.06
NCOCCH_3			1.13									

(700 μL, 1.8 mol-equiv.) and BF_3–etherate (800 μL, 1.2 mol-equiv.). NEt_3 (1.1 mL) was added slowly and the solution was concentrated to dryness. The residue dissolved in EtOAc (200 mL) was washed successively with saturated aqueous $NaHCO_3$ (2 × 100 mL), saturated aqueous NaCl (100 mL), and dried. Concentration and flash chromatography (hexanes–EtOAc; 9:1, 400 mL; 8:2, 400 mL) gave the α-L-thioglycoside **14** (1.36 g, 75%), which crystallized on standing: mp 84.3–84.8°C; $[\alpha]_D^{25}$ −103.9 (*c* 0.9, $CHCl_3$). Anal. calcd. for $C_{17}H_{22}O_5S$: C 60.3, H 6.6; found: C 60.1, H 6.7.

Can. J. Chem. Downloaded from www.nrcresearchpress.com by 88.255.202.194 on 09/08/12
For personal use only.

TABLE 2. ^{13}C NMR chemical shifts for D_2O solutions of the trisaccharides[a]

Carbon	21	20	22	23	25	27	29	31	33	36	46	38
α-L-Rha unit B												
C-1	103.2	103.5	103.1	103.1	102.0	103.9	99.2	98.0	99.8	103.2	103.2	103.5
($J_{C,H}$)	(172)	(172)	(172)	(172)	(171)	(171)	(171)	(169)	(170)	(172)	(172)	(168)
C-2	71.0	71.0	70.9	70.8	68.2	68.6	71.3	68.5	68.9	71.0	71.0	70.9
C-3	71.0	70.8	70.9	70.8	34.2	65.9	71.0	34.2	65.9	71.0	71.0	70.9
C-4	72.8	72.8	72.7	72.8	67.8	35.4	72.9	67.8	35.3	72.8	72.8	72.9
C-5	69.9	70.0	69.8	69.8	70.9	66.4	69.8	70.9	66.5	69.8	69.9	70.0
C-6	17.5	17.5	17.5	17.1	17.6	20.9	17.5	17.6	20.9	17.5	17.5	17.4
α-L-Rha unit C												
C-1	102.2	102.0	102.1	102.3	102.2	102.2	103.0	103.0	103.0	102.6	102.2	101.2
($J_{C,H}$)	(170)	(171)	(170)	(170)	(170)	(171)	(170)	(170)	(170)	(170)	(170)	(171)
C-2	71.3	70.9	71.2	71.2	71.4	71.4	68.9	68.9	68.9	71.1	71.3	80.5
C-3	79.0	79.4	78.9	78.7	78.8	78.8	72.0	71.9	71.8	78.8	79.1	70.5
C-4	72.1	71.9	72.1	72.0	72.1	72.0	32.4	32.6	32.5	72.2	72.1	72.9
C-5	69.9	70.6	69.8	69.8	69.8	69.8	66.5	66.5	66.4	69.9	69.8	69.8
C-6	17.3	17.5	17.1	17.1	17.3	17.3	20.7	20.7	20.7	17.4	17.2	17.7
β-D-GlcNAc unit D												
C-1	102.2	100.6	102.2	101.4	102.2	102.1	102.2	102.2	102.2	102.7	102.2	102.4
($J_{C,H}$)	(162)	(161)	(162)	(163)	(162)	(162)	(163)	(162)	(162)	(162)	(162)	(162)
C-2	55.9	55.8	55.8	56.4	55.9	55.9	55.9	55.9	55.9	56.4	56.1	56.6
C-3	82.6	82.2	82.4	82.5	82.5	82.5	82.6	82.6	82.5	78.6	82.4	78.7
C-4	69.3	69.5	69.3	69.2	69.3	69.3	69.4	69.4	69.4	34.6	74.5	34.6
C-5	76.9	76.9	76.8	76.9	76.8	76.8	76.8	76.8	76.8	73.3	72.9	73.3
C-6	61.6	61.3	61.6	61.4	61.6	61.6	61.6	61.6	61.6	64.4	17.5	64.4

[a]The numbers in parentheses denote the one-bond $^{13}C-^{1}H$ coupling constants for the anomeric carbon atoms (Hz).

Can. J. Chem. Downloaded from www.nrcresearchpress.com by 88.255.202.194 on 09/08/12
For personal use only.

Further elution of the column gave the β-anomer **16** (200 mg, 11%) as a colourless oil: $[\alpha]_D^{25}$ +36.6 (*c* 1.0, $CHCl_3$). Anal. found: C 60.1, H 6.6.

Methyl 2-amino-3-O-[2',4'-di-O-acetyl-3'-O-(2",3",4"-tri O-acetyl-α-L-rhamnopyranosyl)-α-L-rhamnopyranosyl]-4,6-O-benzylidene-2-N-benzyloxycarbonyl-2-deoxy-β-D-glucopyranoside (18)

A mixture of the alcohol **3** (585 mg, 0.91 mmol) and the glycosyl donor **11** (350 mg, 1.2 mol-equiv.) in anhydrous CH_2Cl_2 (30 mL) containing powdered activated molecular sieves 4Å (2 g) was stirred under N_2 for 18 h at room temperature. *N*-Iodosuccinimide (262 mg, 1.3 mol-equiv.) and a saturated solution of triflic acid in CH_2Cl_2 (0.15 M, 785 μL, 0.13 mol-equiv.) were added to the mixture, which was protected from light, and stirred 30 min at room temperature. NEt_3 (800 μL) was added to the reaction mixture, and solids were removed by filtration and rinsed with EtOAc (75 mL). The combined organic solutions were washed successively with a 5% solution of sodium thiosulfate in aqueous 0.5 M NaOH (3 × 50 mL), 1 M HCl (50 mL), saturated aqueous $NaHCO_3$ (50 mL), saturated aqueous NaCl (50 mL), and then dried. Concentration and flash chromatography (toluene–EtOAc, 7:3) gave the trisaccharide **18** (697 mg, 84%) as a white powder: mp 119–123°C (dec.); $[\alpha]_D^{25}$ −40.6 (*c* 0.9, $CHCl_3$). Anal. calcd. for $C_{44}H_{55}NO_{20}$: C 57.6, H 6.0, N 1.5; found: C 57.4, H 6.1, N 1.8.

Methyl 2-amino-2-N-benzyloxycarbonyl-2-deoxy-3-O-[3'-O-(α-L-rhamnopyranosyl)-α-L-rhamnopyranosyl]-β-D-glucopyranoside (19)

A solution of the trisaccharide **18** (647 mg, 0.7 mmol) in 60% acetic acid (35 mL) was stirred for 45 min at 100°C and concentrated to a syrup. Residual acid was removed by evaporating a mixture of toluene–MeOH (1:1, 2 × 20 mL). The dry residue was dissolved in a 0.06 M methanolic solution of NaOMe (30 mL) and was stirred for 18 h at room temperature. The reaction mixture was deionized with Amberlite IR-120 (H^+) resin, filtered, and the filtrate was concentrated. The deprotected trisaccharide **18** was obtained as a white powder from EtOH–acetone (397 mg; 91%); mp 210–213°C (dec.); $[\alpha]_D^{25}$ −55.1 (*c* 0.5, H_2O). Anal. calcd. for $C_{27}H_{41}NO_{15}$: C 52.3, H 6.7, N 2.3; found: C 51.9, H 6.5, N 2.2.

Methyl 2-amino-2-deoxy-3-O-[3'-O-(α-L-rhamnopyranosyl)-α-L-rhamnopyranosyl]-β-D-glucopyranoside (20)

A solution of the trisaccharide **19** (56 mg, 0.09 mmol) in MeOH (5.5 mL) containing Pd–C catalyst (10%, 19 mg) was stirred for 2 h at room temperature under a hydrogen atmosphere. The catalyst was removed by filtration, rinsed with MeOH (10 mL), and the combined filtrates were concentrated to dryness. The residue was dissolved in H_2O (2 mL), the pH lowered to 4 by addition of 0.1 M HCl, and the solution was concentrated. The pure trisaccharide **20** was then precipitated (EtOH–acetone) as the hydrochloride salt, centrifuged, washed (acetone 2 × 1 mL), and dried (38 mg, 82%); $[\alpha]_D^{25}$ −56.4 (*c* 0.4 MeOH). Anal. calcd. for $C_{19}H_{36}ClNO_{13}$: C 43.7, H 6.9, N 2.7; found: C 43.6, H 6.8, N 2.5.

Methyl 2-acetamido-2-deoxy-3-O-[3'-O-(α-L-rhamnopyranosyl)-α-L-rhamnopyranosyl]-β-D-glucopyranoside (21)

Hydrogenolysis of the trisaccharide **19** (34 mg, 0.05 mmol) was performed as described for the preparation of **20**. Acetic anhydride (200 μL) was added to the crude reaction mixture, which was stirred for 1 h at room temperature, then filtered and concentrated. The trisaccharide **21** was purified by elution from a Biogel P-2 column (H_2O) and it was obtained as a white powder by freeze-drying (24.6 mg, 85%); $[\alpha]_D^{25}$ −74.9 (*c* 0.4, MeOH). Anal. calcd. for $C_{21}H_{37}NO_{14}$: C 47.8, H 7.1, N 2.6; found: C 47.6, H 7.0, N 2.8.

Methyl 2-deoxy-2-methylacetamido-3-O-[3'-O-(α-L-rhamnopyranosyl)-α-L-rhamnopyranosyl]-β-D-glucopyranoside (22)

The amine obtained from **19** (53.9 mg, 0.09 mmol) by hydrogenolysis was dissolved in MeOH (4 mL) and treated with propionic anhydride (200 μL). After 1 h at room temperature, more

TABLE 3. ^{1}H NMR data for compounds **2**, **3**, **5**, **6**, **8**, and **10**

Protons (J, Hz)	**2**[a]	**3**[a]	**5**[b]	**6**[c]	**8**[a]	**10**[d]
α-L-Rha unit C						
H-1	4.76	4.82	4.77	4.75	4.76	4.87
($J_{1,2}$)						(~1.0)
H-2	3.59	4.97	3.73	4.78	4.67	4.92
($J_{2,3}$)		(~3.0)	(~2.5)	(3.0)		(3.5)
H-3	3.40	3.79	3.64	3.90	3.78	3.96
($J_{3,4}$)	(9.0)	(10.0)	(10.0)	(10.0)	(9.0)	(9.5)
H-4	3.10	4.59	3.26	4.68	1.32	4.81
($J_{4,5}$)	(~9.5)	(10.0)	(10.0)	(10.0)	(12.0)	(10.0)
H-4′					1.41	
($J_{4',4}$)					(12.0)	
H-5	3.66	3.92	3.74	4.86	3.95	3.84
($J_{5,6}$)	(6.0)	(6.0)	(6.0)	(6.0)	(6.0)	(6.5)
H-6	0.70	0.49	0.64	0.52	0.56	1.15
β-D-GlcNAc unit D						
H-1	4.37	4.35	4.58	4.55	4.38	4.70
($J_{1,2}$)	(8.5)	(8.5)	(8.5)	(8.5)	(8.0)	(8.5)
H-2	3.44	3.52	3.90	3.62	3.74	3.12
($J_{2,3}$)	(9.5)	(10.0)	(9.5)	(9.0)		(11.0)
H-3	3.74	3.74	3.81	3.93	3.72	4.20
($J_{3,4}$;$J_{3,4'}$)	(9.0)	(10.0)	(9.5)	(~9.0)	(9.0)	(11.0, 5.2)
H-4	3.57	3.65	3.72	3.50	3.56	1.52
($J_{4,5}$)	(9.0)	(9.5)	(9.0)	(9.5)	(9.0)	(11.5)
H-4′						2.04
($J_{4,4'}$;$J_{4',5}$)						(11.5; 5.0)
H-5	3.37	3.39	3.60	3.44	3.42	3.69
H-6	3.76	3.77	3.86	3.71	3.75	3.50
($J_{5,6}$)	(~10.0)	(10.5)	(9.0)	(10.0)	(10.0)	(5.0)
H-6	4.22	4.25	4.36	4.28	4.23	3.59
($J_{5,6'}$;$J_{6,6'}$)	(5.0, 10.0)	(5.0, 10.1)	(5.0, 10.5)	(5.0, 10.5)	(5.0, 10.5)	(5.5. 10.0)
OCH_3	3.36	3.36	3.50	3.42	3.33	3.47
N*H*R	7.5					5.58
C*H*Ph	5.62	5.67	5.67	5.44	5.63	
CH_2Ph	5.01, 5.07	4.84, 5.06				4.56
OAc		1.96, 2.00		1.98, 1.99	1.83	2.11, 2.12
NAc			2.05	2.04	2.01	2.02

[a]In $(CD_3)_2SO$.
[b]In 1:1 CD_3OD–D_2O at 310 K.
[c]In 9:1 $CDCl_3$–CD_3OD.
[d]In $CDCl_3$.

anhydride (100 μL) was added and the reaction mixture was stirred for an additional hour. As a TLC (EtOAC–MeOH–H_2O, 6:3:1, R_f (product) 0.6) showed that the reaction was not proceeding further, NEt_3 (600 μL) and propionic anhydride (200 μL) were added to the solution stirred at 18°C (water bath). The acylation was completed within 1 h. Solvents were evaporated and the residual NEt_3 was coevaporated with MeOH (2 × 2 mL). The residue dissolved in MeOH (1 mL) was deionized on a mixed bed column (20 × 1.5) (top half Rexyn 201 (OH^-) and bottom half Amberlite IR-120 (H^+)). Elution with MeOH and concentration of the effluent gave the trisaccharide **22** as a white powder (35 mg, 73%) that was centrifuged from an acetone suspension (2 mL) and dried; $[\alpha]_D^{25}$ −76.9 (*c* 0.4, MeOH). Anal. calcd. for $C_{22}H_{39}NO_{14}$: C 48.8, H 7.3, N 2.6; found: C 48.6, H 7.3, N 2.4.

*Methyl 2-deoxy-3-*O*-[3′-*O*-(α-L-rhamnopyranosyl)-α-L-rhamnopyranosyl]-2-trifluoroacetamido-β-D-glucopyranoside (**23**)*

The amine obtained by hydrogenolysis of the trisaccharide **19** (21 mg, 0.03 mmol) was filtered, concentrated, evaporated with anhydrous pyridine (2 × 2 mL), and a solution of the dry residue in anhydrous pyridine (1.5 mL) containing trifluoroacetic anhydride (60 μL) was stirred 48 h at 40°C. Water (100 μL) was added to the reaction mixture, which was concentrated, and residual pyridine was coevaporated with H_2O (2 × 1 mL). Flash chromatography (EtOAc–MeOH–H_2O, 8:1.2:1) of the oily residue gave the trisaccharide **23**, subsequently obtained free of salts by chromatography on a Biogel P2 column (H_2O). Freeze-drying of the appropriate fractions gave **23** as an amorphous white powder (9.6 mg, 50%); $[\alpha]_D^{25}$ −79.2 (*c* 0.4, MeOH). Anal. calcd. for $C_{21}H_{34}F_3NO_{14}$: C 43.4, H 5.9, N 2.4; found: C 43.3, H 5.8, N 2.3.

*Methyl 2-acetamido-4,6-*O*-benzylidene-2-deoxy-3-*O*-[2′,4′-di-*O*-acetyl-3′-*O*-(4″-*O*-acetyl-2″-*O*-benzoyl-3″-deoxy-α-L-arabino-hexopyranosyl)-α-L-rhamnopyranosyl]-β-D-glucopyranoside (**24**)*

A mixture of the alcohol **6** (216 mg, 0.4 mmol), the thioglycoside **14** (153 mg, 1.3 mol-equiv.), and activated powdered molecular sieves 4Å (1.1 g) in anhydrous CH_2Cl_2 (15 mL) was stirred for 2 h under N_2 at room temperature. *N*-Iodosuccinimide (120 mg,

Can. J. Chem. Downloaded from www.nrcresearchpress.com by 88.255.202.194 on 09/08/12
For personal use only.

TABLE 4. ^{1}H and ^{13}C NMR data[a] for compounds **13**, **14**, and **16**

Proton (J Hz)	^{1}H NMR			^{13}C NMR[b]			
	13	**14**	**16**	Carbon	**13**	**14**	**16**
L-Rhamnopyranose derivatives							
H-1	6.06	5.29	4.77	C-1	89.8	82.1	84.0
($J_{1,2}$)				($J_{C,H}$)	(176)	(166)	(152)
H-2	5.15	5.28	5.38	C-2	68.9	72.1	71.4
($J_{2,3}$;$J_{2,3'}$)	(−, ~3.5)	(~3.0, −)	(~3.0, ~4.0)				
H-3	2.05	2.02	1.81	C-3	29.5	30.5	34.6
($J_{3,3'}$;$J_{3,4}$)	(13.5, 10.5)	(14.0, 11.5)	(14.0, 11.0)				
H-3′	2.36	2.31	2.50				
($J_{3',4}$)	(4.5)	(~4.5)	(4.5)				
H-4	4.92	4.96	4.83	C-4	69.5	70.2	69.5
($J_{4,5}$)	(10.5)	(~11.0)	(11.0)				
H-5	3.92	4.22	3.56	C-5	68.9	67.0	76.7
($J_{5,6}$)	(6.0)	(6.0)	(6.0)				
H-6	1.23	1.23	1.29	C-6	17.7	17.6	18.1
OAc	2.07, 2.14	2.06	2.0	OAc	20.7, 21.2	21.1	20.9
SCH_2CH_3		2.67	2.71	SCH_2CH_3		25.3	25.5
SCH_2CH_3		1.31	1.25	SCH_2CH_3		15.1	14.8

[a]In $CDCl_3$.
[b]The numbers in parentheses denote the one-bond ^{13}C–^{1}H coupling constants for the anomerics (Hz).

Can. J. Chem. Downloaded from www.nrcresearchpress.com by 88.255.202.194 on 09/08/12
For personal use only.

1.3 mol-equiv.) and a saturated solution of triflic acid in CH_2Cl_2 (0.15 M, 400 μL, 0.15 mol-equiv.) were added to the reaction mixture, which was stirred for 30 min in the dark at room temperature. More glycosyl donor (10.8 mg, 0.2 mol-equiv.) in CH_2Cl_2 (120 μL), and more acid (3 × 200 μL) were added during the following 2 h. NEt_3 (900 μL) was then added to the reaction mixture and work-up was carried out as described for the preparation of **18**. Flash chromatography ($CHCl_3$–MeOH, 30:1) gave the pure trisaccharide **24** (148 mg, 46%) as a colourless glass. Preparative TLC (Silica Gel 60 F254, Merck, 2-mm plate, $CHCl_3$–MeOH, 20:1) of impure fractions gave another 37 mg (11%) of pure **24**; $[\alpha]_D^{25}$ −40.7 (*c* 0.7, $CHCl_3$). Anal. calcd. for $C_{41}H_{51}NO_{17}$: C 59.3, H 6.2, N 1.7; found: C 59.1, H 6.4, N 1.9.

*Methyl 2-acetamido-2-deoxy-3-*O*-[3′-*O*-(3″-deoxy-α-*L*-*arabino*-hexopyranosyl)-α-*L*-rhamnopyranosyl]-β-*D*-glucopyranoside (25)*

A solution of the protected trisaccharide **24** (46 mg, 0.055 mmol) in methanolic NaOMe (3.2 mL, 0.07 M) was stirred 18 h at room temperature, deionized with Amberlite IR-120 (H^+) resin, and filtered. The resin was rinsed with MeOH (5 mL) and the combined filtrates were concentrated to dryness. A solution of the residue in aqueous acetic acid (90%, 3 mL) was hydrogenated 18 h at 60 psi (1 psi = 6.89 kPa) in the presence of 10% Pd–C catalyst (54 mg). The reaction mixture was filtered, the catalyst rinsed with MeOH, and the combined filtrates concentrated. Chromatography (EtOAc–MeOH–H_2O, 7:2:1) of the residue gave the trisaccharide **25**, finally purified on a Biogel P2 column (H_2O) and obtained as a white amorphous powder by freeze-drying (19 mg, 68%); $[\alpha]_D^{25}$ −92.8 (*c* 0.4, H_2O). Anal. calcd. for $C_{21}H_{37}NO_{13}$: C 49.3, H 7.3, N 2.7; found: C 49.1, H 7.4, N 2.8.

*Methyl 2-acetamido-3-*O*-[2′,4′-di-*O*-acetyl-3′-*O*-(2″,3″-di-*O*-acetyl-4″-deoxy-α-*L*-*lyxo*-hexopyranosyl)-α-*L*-rhamnopyranosyl]-4,6-*O*-benzylidene-2-deoxy-β-*D*-glucopyranoside (26)*

A mixture of the alcohol **6** (100.4 mg, 0.18 mmol), the thioglycoside **17** (8) (62.5 mg, 1.3 mol-equiv.), and activated powdered molecular sieve 4Å (550 mg) in anhydrous CH_2Cl_2 (7 mL) was stirred 18 h under N_2 at room temperature. *N*-Iodosuccinimide (56 mg, 1.4 mol-equiv.) and a saturated solution of triflic acid in CH_2Cl_2 (320 μL, 0.26 mol-equiv.) were added to the reaction mixture, which was protected from light and stirred 3.5 h at room temperature. NEt_3 was added and work-up was carried out as described for the preparation of **18**. The trisaccharide **26** was purified by flash chromatography ($CHCl_3$–MeOH, 30:1) and obtained as a colourless glass (119 mg, 86%); $[\alpha]_D^{25}$ −49.5 (*c* 0.8, $CHCl_3$). Anal. calcd. for $C_{36}H_{49}NO_{17}$: C 56.3, H 6.4, N 1.8; found: C 56.1, H 6.4, N 1.5.

*Methyl 2-acetamido-2-deoxy-3-*O*-[3′-*O*-(4″-deoxy-α-*L*-*lyxo*-hexopyranosyl)-α-*L*-rhamnopyranosyl]-β-*D*-glucopyranoside (27)*

The trisaccharide **26** (96 mg, 0.125 mmol) was deprotected using the conditions employed to prepare trisaccharide **25**. Flash chromatography (EtOAc–MeOH–H_2O; 7:1.5:1, 150 mL; 7:2:1, 50 mL) gave trisaccharide **26**, finally purified on a Biogel P2 column (H_2O) and obtained as a white amorphous powder by freeze-drying (47 mg, 73%); $[\alpha]_D^{25}$ −86.4 (*c* 0.8, H_2O). Anal. calcd. for $C_{21}H_{37}NO_{13}$: C 49.3, H 7.3, N 2.7; found: C 49.0, H 7.3, N 2.6.

*Methyl 2-acetamido-3-*O*-[2′-*O*-acetyl-4′-deoxy-3′-*O*-(2″,3″,4″-tri-*O*-acetyl-α-*L*-rhamnopyranosyl)-α-*L*-*lyxo*-hexopyranosyl]-4,6-*O*-benzylidene-2-deoxy-β-*D*-glycopyranoside (28)*

Glycosylation of the disaccharide **8** (102 mg, 0.2 mmol) with the glycosyl donor **11** (85 mg, 1.22 mol-equiv.) was started in the same conditions as those used to prepare the trisaccharide **26**. After 4 h at room temperature more acid (150 μL, 0.11 mol-equiv.) was added, and the reaction was allowed to proceed during an additional 3 h at room temperature and quenched by addition of NEt_3 (50 μL). Work-up was carried out as described for the preparation of **18** and the trisaccharide **28** was purified by flash chromatography ($CHCl_3$–MeOH, 50:1) to yield a colourless glass (87 mg, 55%); $[\alpha]_D^{25}$ −62.6 (*c* 0.5, $CHCl_3$). Anal. calcd. for $C_{36}H_{49}NO_{17}$: C 56.3, H 6.4, N 1.8; found: C 56.5, H 6.5, N 2.0.

*Methyl 2-acetamido-2-deoxy-3-*O*-[4′-deoxy-3′-*O*-(α-*L*-rhamnopyranosyl)-α-*L*-*lyxo*-hexopyranosyl]-β-*D*-glucopyranoside (29)*

The trisaccharide **28** (70 mg, 0.1 mmol) was deprotected as described for **25**. Flash chromatography (EtOAc–MeOH–H_2O, 7:1.5:1) gave trisaccharide **29**, finally purified on a Biogel P2 column (H_2O) and isolated as a white powder by freeze-drying (34 mg, 72%); $[\alpha]_D^{25}$ −92.9 (*c* 0.4, H_2O). Anal. calcd. for $C_{21}H_{37}NO_{13}$: C 49.3, H 7.3, N 2.7; found: C 49.2, H 7.4, N 2.7.

TABLE 5. ^{1}H NMR data for compounds **18**, **19**, **24**, **26**, **28**, **30**, and **32**

Protons (J, Hz)	**18**[a]	**19**[b]	**24**[c]	**26**[c]	**28**[c]	**30**[c]	**32**[c]
α-L-Rha unit B							
H-1	~4.89	5.01	4.89	4.90	4.84	4.91	4.88
H-2	~4.94	4.05	4.96	4.84	5.10	5.04	4.93
($J_{2,3}$)		(3.5)			(3.5)	(3.0)	(3.0)
H-3	~4.94	3.83	1.96	5.06	5.19	1.98	5.13
($J_{3,4}$)		(10.5)			(10.0)		(11.5)
($J_{3,3'}$)						(13.5)	
H-3′			2.20			2.21	
($J_{2,3'}$)						(~3.5)	
($J_{3',4}$)						(~3.5)	
H-4′	~4.90	3.45	4.88	1.66	5.01	4.87	1.68
($J_{3,5}$)	(10.0)	(10.0)		(12.0)	(10.0)		
H-4				1.73			1.69
($J_{3,4'}$)							
($J_{4,4'}$)				(12.0)			
H-5	3.87	3.73	3.79	3.91	3.83	3.84	3.93
($J_{5,6}$)	(6.0)	(6.0)	(6.0)	(6.0)	(6.0)	(6.0)	(6.0)
H-6	1.13	1.26	1.15	1.17	1.15	1.17	1.18
α-L-Rha unit C							
H-1	~4.90	4.87	4.81	4.77	4.86	4.87	4.83
H-2	5.10	3.87	5.07	5.04	4.89	4.94	4.90
($J_{2,3}$)	(3.0)	(3.0)	(3.5)	(3.5)		(~4.0)	
H-3	4.01	3.78	4.06	3.99	4.03	4.10	4.01
($J_{3,4}$)	(10.0)	(10.0)	(10.0)	(10.0)			
H-4	4.76	3.52	4.84	4.90	~1.55	~1.57	~1.52
($J_{4,5}$)	(10.0)	(11.0)	(10.0)	(8.5)			
H-4′					~1.55	~1.58	~1.52
H-5	3.98	4.04	3.94	3.93	3.96	3.99	3.97
($J_{5,6}$)	(6.0)	(6.0)	(6.0)	(6.0)	(6.0)	(6.0)	(6.0)
H-6	0.49	1.24	0.58	0.57	0.65	0.65	0.64
β-D-GlcNAc unit D							
H-1	4.36	4.45	4.95	4.92	4.83	4.85	4.83
($J_{1,2}$)	(8.5)	(8.0)	(8.5)	(8.0)	(9.0)	(~8.5)	(7.5)
H-2	3.54	~3.50	3.14	3.19	3.30	3.27	3.28
($J_{2,3}$)	(10.0)	(9.0)	(~9.0)	(9.5)	(9.5)	(9.5)	(9.5)
H-3	3.76	3.59	4.46	4.42	4.29	4.32	4.28
($J_{3,4}$)	(9.0)	(9.0)	(~9.0)	(9.5)	(9.5)	(9.5)	(9.5)
H-4	3.68	~3.50	3.47	3.48	3.46	3.46	3.45
($J_{4,5}$)	(9.0)		(~10.0)	(9.5)	(9.0)	(9.5)	(9.0)
H-5	3.41	3.45	3.54	3.54	3.53	3.53	3.53
H-6	3.74	3.74	3.73	3.74	3.73	3.73	3.73
($J_{6,5}$)	(9.5)	(6.5)	(10.5)	(10.0)	(10.0)	(10.0)	(10.0)
H-6′	4.24	3.94	4.34	4.34	4.33	4.33	4.33
($J_{5,6'}$)	(5.0)		(5.0)	(5.0)	(5.0)	(4.5)	(4.5)
($J_{6,6'}$)	(10.0)	(12.0)	(10.5)	(10.5)	(10.5)	(10.0)	(10.0)
OCH_3	3.36	3.49	3.47	3.48	3.44	3.43	3.43
N*H*R			5.71	5.70	5.81	5.89	5.88
C*H*Ph	5.67		5.49	5.49	5.46	5.46	5.46
CH_2Ph	4.96, 5.09	5.13, 5.19					
NAc			2.00	1.98	2.08	1.99	1.98
OAc	1.94–2.08		2.04–2.13	1.96–2.09	1.95–2.10	2.04, 2.08	1.95–2.10

[a]In $(CD_3)_2SO$.
[b]Solution: ~2.5 mg in 0.5 mL D_2O.
[c]In $CDCl_3$.

Methyl 2-acetamido-3-O-[2′-O-acetyl-4′-deoxy-3′-O-(4″-O-acetyl-2″-O-benzoyl-3″-deoxy-α-L-arabino-hexopyranosyl)-α-L-lyxo-hexopyranosyl]-4,6-O-benzylidene-2-deoxy-β-D-glucopyranoside (30)

Glycosylation of the alcohol **8** (101 mg, 0.2 mmol) by the glycosyl donor **14** (85 mg, 1.25 mol-equiv.), as well as work-up of the reaction, were performed according to the conditions used to prepare trisaccharide **26**. The trisaccharide **30** was purified by flash chromatography ($CHCl_3$–MeOH, 50:1) and isolated as a colourless glass (127 mg, 82%); $[\alpha]_D^{25}$ −46.9 (*c* 0.7, $CHCl_3$). Anal. calcd. for $C_{39}H_{49}NO_{15}$: C 60.7, H 6.4, N 1.8; found: C 60.2, H 6.4, N 1.9.

Can. J. Chem. Downloaded from www.nrcresearchpress.com by 88.255.202.194 on 09/08/12
For personal use only.

TABLE 6. ^{1}H NMR data for $CDCl_3$ solutions of compounds **34**, **35**, **37**, **40**, and **42–45**

Protons (J, Hz)	**34**	**35**	**37**	**40**	**42**	**43**	**44**	**45**
α-L-Rha unit B								
H-1	5.47	4.84	4.74	4.86	4.91	4.92	4.93	4.91
($J_{1,2}$)	(1.0)				(1.5)	(2.0)		
H-2	4.70	5.03	5.24	4.86	4.83	4.89	4.88	4.87
($J_{2,3}$)		(3.0)	(3.5)	(3.0)	(3.5)	(3.0)	(3.5)	(3.5)
H-3	4.72	5.12	5.32	5.03	5.07	5.04	5.04	5.03
($J_{3,4}$)	(9.5)	(10.0)	(10.0)	(10.0)	(10.0)	(10.0)	(10.0)	(9.5)
H-4	5.00	5.00	5.02	4.84	4.84	4.84	4.84	4.83
($J_{4,5}$)	(9.5)	(10.5)	(10.0)	(10.0)	(10.0)	(10.0)	(10.0)	(10.0)
H-5	3.45	3.80	3.92	3.81	3.76	3.73	3.73	3.72
H-6	1.21	1.13	1.19	1.01	0.91	0.94	0.94	0.93
($J_{5,6}$)	(6.0)	(~6.0)	(6.5)	(6.0)	(6.0)	(6.0)	(6.5)	(6.0)
α-L-Rha unit C								
H-1	4.67	4.80	4.86	5.40	5.06	5.04	5.03	5.03
($J_{1,2}$)				(1.0)	(1.5)	(~2.0)		
H-2	4.92	5.03	3.91	5.48	5.31	5.35	5.35	5.34
($J_{2,3}$)	(3.0)	(3.5)	(~3.0)	(3.0)	(3.0)	(3.5)	(3.0)	(3.0)
H-3	4.07	4.00	5.11	4.29	4.31	4.34	4.33	4.34
($J_{3,4}$)	(10.0)	(10.0)	(~10.0)	(9.5)	(10.0)	(9.5)	(9.5)	(9.5)
H-4	4.90	5.03	5.01	5.48	5.34	5.48	5.48	5.48
($J_{4,5}$)	(10.0)		(~10.0)	(9.5)	(10.0)	(9.5)	(9.5)	(9.5)
H-5	3.81	3.80	3.85	4.33	4.21	4.24	4.23	4.25
H-6	1.13	1.13	1.18	1.28	0.68	1.30	1.30	1.30
($J_{5,6}$)	(6.5)	(~6.0)	(6.5)	(6.0)	(6.0)	(6.0)	(6.0)	(6.0)
β-D-GlcNAc unit D								
H-1	5.15	4.66	4.76		4.96	4.73	4.74	4.61
($J_{1,2}$)	(8.5)	(8.5)	(8.5)		(8.5)	(8.5)	(8.5)	(8.5)
H-2	2.73	3.12	2.90		3.31	3.46	3.45	3.49
($J_{2,3}$)	(10.5)	(10.0)	(~10.0)		(~8.0)	(8.5)	(8.0)	(8.5)
H-3	4.48	4.18	4.44		4.49	4.01	4.05	3.90
($J_{3,4}$)	(10.5)	(10.5)	(~10.5)			(10.0)		(10.0)
($J_{3,4'}$)	(5.5)	(5.0)	(5.0)					
H-4	1.53	1.50	1.50		3.59	3.56	3.47	3.20
($J_{4,5}$)	(~12.5)	(12.0)	(~12.0)			(10.0)		(9.0)
H-4′	1.97	2.02	2.07					
($J_{4,4'}$)	(~12.5)	(12.0)	(~12.0)					
H-5	3.74	3.67	3.70		3.59	3.40	3.47	3.34
H-6	3.53	3.48	3.48		3.79	3.83	3.56	1.33
($J_{6,5}$)	(4.5)	(5.5)	(5.5)			(4.5)		(6.0)
H-6′	3.58	3.57	3.57		4.38	3.93	3.77	
($J_{6',5}$)	(5.5)	(5.5)	(~5.5)			(3.5)		
($J_{6,6'}$)	(11.0)	(10.0)	(~10.0)		(10.5)	(12.0)	(11.0)	
OCH_3	3.49	3.45	3.45		3.51	3.50	3.50	3.47
N*H*Ac	7.26	5.60	5.64		5.82	5.69	5.85	5.86
C*H*Ph					5.58			
CH_2Ph	4.58	4.54	4.54					
SCH_2CH_3				2.68				
SCH_2CH_3				1.30				
NAc	1.99	1.98	1.97		2.07	2.07	2.07	2.07
OAc	2.03–2.18	1.94–2.14	1.94–2.10	1.80–1.86	1.81–1.90	1.82–1.92	1.81–1.91	1.80–1.90
CCH_3	1.63							

*Methyl 2-acetamido-2-deoxy-3-*O*-[4′-deoxy-3′-*O*-(3″-deoxy-α-L-*arabino*-hexopyranosyl)-α-L-*lyxo*-hexopyranosyl]-β-D-glucopyranoside (**31**)*

The trisaccharide **30** (106 mg, 0.14 mmol) was deprotected using the conditions described for trisaccharide **25**. Flash chromatography (EtOAc–MeOH–H_2O, 7:1.5:1) and gel permeation chromatography (Biogel P2, H_2O) gave pure trisaccharide **31** (56 mg, 82%) isolated as a lyophilized white powder: $[\alpha]_D^{25}$ −110.7 (*c* 0.6, H_2O). Anal. calcd. for $C_{21}H_{37}NO_{12}$: C 50.9, H 7.5, N 2.8; found: C 50.9, H 7.6, N 2.8.

*Methyl 2-acetamido-3-*O*-[2′-*O*-acetyl-4′-deoxy-3′-*O*-(2″,3″-di-*O*-acetyl-4″-deoxy-α-L-*lyxo*-hexopyranosyl)-α-L-*lyxo*-hexopyranosyl]-4,6-*O*-benzylidene-2-deoxy-β-D-glucopyranoside (**32**)*

Glycosylation of the alcohol **8** (101 mg, 0.2 mmol) by the glycosyl donor **17** (71 mg, 1.3 mol-equiv.), as well as work-up of the

Can. J. Chem. Downloaded from www.nrcresearchpress.com by 88.255.202.194 on 09/08/12
For personal use only.

TABLE 7. ^{13}C NMR data[a] for $CDCl_3$ solutions of compounds **18**, **19**, **24**, **26**, **28**, **30**, **32**, **34**, **35**, **37**, **40**, **42**, **44**

Carbon	18	19	24	26	28	30	32	34	35	37	40	42	44
α-L-Rha unit B													
C-1	97.7	103.3	98.2	99.8	96.4	95.2	97.2	97.4	98.8	99.3	99.2	98.9	99.1
($J_{C,H}$)	(175)	(172)	(171)	(171)	(170)	(169)	(170)	(176)	(171)	(171)	(168)	(172)	(172)
C-2	69.3	71.0	70.4	68.1	70.3	70.8	68.2	75.1	70.0	70.0	69.7	69.9	69.5
C-3	68.2	71.0	29.3	66.5	68.8	29.3	66.6	72.7	68.6	68.6	68.4	68.4	68.4
C-4	69.9	72.9	69.6	33.2	70.9	69.8	33.3	69.8	70.8	71.2	70.9	70.9	70.9
C-5	66.8	70.0	67.4	65.1	67.0	67.3	64.9	68.5	—[b]	66.8	67.2	67.2	67.2
C-6	17.0	17.5	17.5	20.9	17.3	17.7	20.9	17.2	17.3	17.4	17.2	17.1	17.1
α-L-Rha unit C													
C-1	98.2	102.2	97.4	97.5	98.5	98.5	98.6	98.5	98.8	99.9	82.1	97.3	99.6
($J_{C,H}$)	(175)	(171)	(173)	(174)	(172)	(172)	(172)	(174)	(171)	(171)	(169)	(175)	(172)
C-2	70.8	71.5	72.1	71.9	69.6	70.0	69.7	71.4	71.4	77.2	74.0	72.4	72.1
C-3	73.9	79.1	75.5	75.3	71.4	70.9	70.9	67.7	75.7	70.4	76.0	76.3	75.7
C-4	72.1	72.2	72.1	72.1	33.3	33.4	33.2	71.4	71.9	71.4	73.5	72.7	72.2
C-5	65.8	70.0	66.4	66.6	64.5	64.6	64.5	66.7	—[b]	67.1	67.5	66.6	68.3
C-6	16.5	17.3	16.4	16.5	20.3	20.3	20.3	17.4	17.3	17.2	17.6	16.7	17.7
β-D-GlcNAc unit D													
C-1	102.3	102.7	100.8	100.9	101.1	101.0	101.1	100.0	100.7	100.4		101.0	100.4
($J_{C,H}$)	(164)	(163)	(165)	(165)	(164)	(164)	(164)	(164)	(162)	(164)		(163)	(163)
C-2	57.3	58.1	58.8	59.0	58.5	58.6	58.5	60.5	58.6	59.5		59.0	56.4
C-3	77.6	82.6	75.1	75.1	75.5	75.3	75.5	74.0	76.1	75.1		74.8	85.0
C-4	79.0	69.5	80.3	80.3	80.3	80.4	80.3	36.0	35.8	35.9		80.3	72.2
C-5	66.0	76.9	66.1	66.1	66.1	66.1	66.1	70.5	70.9	70.9		66.1	74.5
C-6	67.9	61.7	68.8	68.8	68.8	68.8	68.8	72.2	72.2	72.2		68.9	32.5

[a]The numbers in parentheses denote the one-bond ^{13}C–^{1}H coupling constants for the anomerics (Hz).
[b]Unresolved 67.2 or 66.9.

Can. J. Chem. Downloaded from www.nrcresearchpress.com by 88.255.202.194 on 09/08/12
For personal use only.

reaction, followed the procedure described for the synthesis of trisaccharide **26**. The trisaccharide **32** was purified by flash chromatography ($CHCl_3$–MeOH, 50:1) and isolated as a colourless glass (129 mg, 89%); $[\alpha]_D^{25}$ −65.2 (*c* 0.65, $CHCl_3$). Anal. calcd. for $C_{34}H_{47}NO_{15}$: C 57.5, H 6.7, N 2.0; found: C 57.2, H 6.5, N 1.8.

*Methyl 2-acetamido-2-deoxy-3-*O*-[4'-deoxy-3'-*O*-(4"-deoxy-α-L-*lyxo*-hexopyranosyl)-α-L-*lyxo*-hexopyranosyl)-β-D-glucopyranoside (**33**)*

The trisaccharide **32** (107 mg, 0.15 mmol) was deprotected in similar fashion to trisaccharide **24**. Flash chromatography (EtOAc–MeOH–H_2O, 7:1.5:1) and gel permeation chromatography (Biogel P2, H_2O) gave pure trisaccharide **33** (58 mg, 77%) isolated as a white lyophilized powder; $[\alpha]_D^{25}$ −99.8 (*c* 0.5, H_2O). Anal. calcd. for $C_{21}H_{37}NO_{12}$: C 50.9, H 7.5, N 2.8; found: C 51.0, H 7.5, N 2.7.

*3,4-Di-*O*-acetyl-1,2-*O*-[2',4'-di-*O*-acetyl-1'-*O*-(2"-acetamido-6"-*O*-benzyl-2",4"-dideoxy-1"-*O*-methyl-β-D-*xylo*-hexopyranos-3"-yl)-α-L-rhamnopyranos-3'-yl orthoacetyl)-α-L-rhamnopyranose (**34**), methyl 2-acetamido-3-*O*-[2',4'-di-*O*-acetyl-3'-*O*-(2",3",4"-tri-*O*-acetyl-α-L-rhamnopyranosyl)-α-L-rhamnopyranosyl]-6-*O*-benzyl-2,4-dideoxy-β-D-*xylo*-hexopyranoside (**35**), and methyl 2-acetamido-3-*O*-[3',4'-di-*O*-acetyl-2'-*O*-(2",3",4"-tri-*O*-acetyl-α-L-rhamnopyranosyl)-α-L-rhamnopyranosyl]-6-*O*-benzyl-2,4-dideoxy-β-D-*xylo*-hexopyranoside (**37**)*

Method A

Glycosylation of the disaccharide **9** (109 mg, 0.2 mmol) by the glycosyl donor **11** (82 mg, 1.2 mol-equiv.) initially used conditions similar to the synthesis of trisaccharide **26**. After 1.5 h at room temperature more acid (175 μL, 0.13 mol-equiv.) was added and the reaction proceeded for 2 h at room temperature, after which it was quenched by addition of NEt_3 (100 μL). Work-up followed the procedure described for **18**. Flash chromatography (EtOAc–hexanes; 7:3, 100 mL; 8:2, 100 mL) gave the orthoester **34** (87 mg, 54%). Further elution of the column gave the trisaccharide **35** as a colourless glass (18 mg, 11%). Both compounds were characterized by NMR spectroscopy (Tables 6 and 7).

Method B

A mixture of the disaccharide **10** (103 mg, 0.3 mmol), the donor **11** (71 mg, 1.12 mol-equiv.), and activated powdered 4Å molecular sieves (400 mg) in anhydrous CH_2Cl_2 (7 mL) was stirred 18 h under N_2 at room temperature. *N*-Iodosuccinimide (59 mg, 1.4 mol equiv.) and a saturated solution of triflic acid (0.15 M, 740 μL, 0.56 mol-equiv.) were added to the mixture, which was protected from light, and stirred 6 h at room temperature. NEt_3 (100 μL) was added to the mixture and work-up was carried out as described for the preparation of **18**. Flash chromatography ($CHCl_3$–MeOH, 50:1) gave a mixture (75:25, 110 mg, 71%) of trisaccharides **35** and **37** that could not be separated. They were characterized by NMR spectroscopy (Tables 6 and 7).

*Methyl 2-acetamido-2,4-dideoxy-3-*O*-[3'-*O*-(α-L-rhamnopyranosyl)-α-L-rhamnopyranosyl]-β-D-*xylo*-hexopyranoside (**36**) and methyl 2-acetamido-2,4-dideoxy-3-*O*-[2'-*O*-(α-L-rhamnopyranosyl)-α-L-rhamnopyranosyl]-β-D-*xylo*-hexopyranoside (**38**)*

The mixture of trisaccharides **35** and **37** (75:25, 110 mg) was dissolved in anhydrous MeOH (9 mL) and a solution of NaOMe (1 M, 200 μL) in MeOH was added. The mixture was stirred 18 h at room temperature, deionized with amberlite IR-120 (H+) resin, and filtered. The resin was rinsed with MeOH (3 mL) and the combined filtrates were concentrated. Pd–C catalyst (10%, 50 mg) was added to a solution of the residue in MeOH (9 mL) and the mixture was hydrogenated for 18 h at 60 psi. The catalyst was fil-

Can. J. Chem. Downloaded from www.nrcresearchpress.com by 88.255.202.194 on 09/08/12
For personal use only.

tered off, rinsed with MeOH (3 mL), and the combined filtrates were concentrated. Reversed-phase HPLC (C-18 column, H_2O) gave the pure trisaccharide **36** (43 mg, 84%), isolated as a white powder upon freeze-drying; $[\alpha]_D^{25}$ −73.1 (*c* 0.45, MeOH). Anal. calcd. for $C_{21}H_{37}NO_{13}$: C 49.3, H 7.3, N 2.7; found: C 49.0, H 7.3, N 2.8.

Further elution of the column gave the pure trisaccharide **38** (13 mg, 75%) isolated as a white powder upon freeze-drying; $[\alpha]_D^{25}$ −71.6 (*c* 0.5, MeOH). Anal. found: C 49.0, H 7.4, N 2.9.

*Ethyl 3-O-(2',3',4'-tri-O-acetyl-α-L-rhamnopyranosyl)-2,4-di-O-benzoyl-1-thio-α-L-rhamnopyranoside (**40**)*

A solution of the alcohol **39** (12) (522 mg, 1.25 mmol) in anhydrous CH_2Cl_2 (50 mL) containing powdered activated molecular sieve 4Å (2 g) and silver trifluoromethanesulfonate (651 mg, 2 mol-equiv.) was stirred 2 h in the dark under N_2 and cooled to −75°C. A solution of tri-*O*-acetyl-α-L-rhamnopyranosyl bromide (15) (598 mg, 1.35 mol-equiv.) in anhydrous CH_2Cl_2 (5 mL) was added dropwise and the mixture was allowed to reach −50°C over 2 h, at which temperature it was left for an additional 0.5 h. NEt_3 (270 μL) was added to the reaction mixture and solids were filtered off on Celite. The solids were rinsed with CH_2Cl_2 (150 mL), and the combined filtrates washed with saturated aqueous $NaHCO_3$ (50 mL), H_2O (50 mL), and dried. Concentration and chromatography (hexanes–EtOAc; 6:2, 200 mL; 6:3, 400 mL) gave the disaccharide **40** (620 mg, 72%) as a colourless glass; $[\alpha]_D^{25}$ −1.09 (*c* 1.1, $CHCl_3$). Anal. calcd. for $C_{34}H_{40}O_{13}S$: C 59.3, H 5.8; found: C 59.4, H 6.0.

*Methyl 2-acetamido-3-O-[2',4'-di-O-benzoyl-3'-O-(2",3",4"-tri-O-acetyl-α-L-rhamnopyranosyl)-α-L-rhamnopyranosyl]-4,6-O-benzylidene-2-deoxy-β-D-glucopyranoside (**42**)*

A mixture of the acceptor **41** (274 mg, 0.85 mmol) (16), the disaccharide thioglycoside **40** (698 mg, 1.2 mol-equiv.), and powdered activated molecular sieves 4Å (1.6 g) in anhydrous CH_2Cl_2 (40 mL) was stirred 18 h under N_2 at room temperature. *N*-Iodosuccinimide (259 mg, 1.35 mol-equiv.) and a saturated solution of triflic acid (0.15 M, 2.6 mL, 0.5 mol-equiv.) in CH_2Cl_2 were added to the mixture, which was protected from light and stirred 2 h under N_2 at room temperature. NEt_3 (200 μL) was then added and work-up was carried out as described for the preparation of **18**. Flash chromatography (EtOAc–hexanes, 65:35) gave the pure trisaccharide **42** (544 mg, 67%) as a colourless glass. Combined impure fractions containing mostly **42** were subjected to reversed-phase HPLC (C-18 column, CH_3CN–H_2O 6:4) and gave additional pure trisaccharide **42** (31 mg, 4%); $[\alpha]_D^{25}$ −6.1 (*c* 0.8, $CHCl_3$). Anal. calcd. for $C_{48}H_{55}NO_{19}$: C 60.7, H 5.8, N 1.5; found: C 60.6, H 5.7, N 1.42.

*Methyl 2-acetamido-3-O-[2',4'-di-O-benzoyl-3'-O-(2",3",4"-tri-O-acetyl-α-L-rhamnopyranosyl)-α-L-rhamnopyranosyl]-2-deoxy-β-D-glucopyranoside (**43**)*

A solution of the acetal **42** (895 mg, 0.94 mmol) in 60% acetic acid (30 mL) was stirred 1 h at 100°C, cooled to room temperature, and concentrated. Residual acid was coevaporated with a mixture of toluene–MeOH (10:1, 3 × 10 mL) and flash chromatography ($CHCl_3$–MeOH, 30:1) of the dry residue gave the pure diol **43** (637 mg, 78%) as a white powder; $[\alpha]_D^{25}$ +31.0 (*c* 0.3, $CHCl_3$). Anal. calcd. for $C_{41}H_{51}NO_{19}$: C 57.1, H 6.0, N 1.6; found: C 57.3, H 6.0, N 1.8.

*Methyl 2-acetamido-6-bromo-3-O-[2',4'-di-O-benzoyl-3'-O-(2",3",4"-tri-O-acetyl-α-L-rhamnopyranosyl)-α-L-rhamnopyranosyl]-2,6-dideoxy-β-D-glucopyranoside (**44**)*

Imidazole (125 mg, 8 mol-equiv.), triphenylphosphine (238 mg, 4 mol-equiv.), and carbon tetrabromide (757 mg, 10 mol-equiv.) were added to a stirred solution of the diol **43** (196 mg, 0.22 mmol) in a mixture of anhydrous CH_3CN and anhydrous pyridine (1:1, 6 mL). After 22 h at room temperature MeOH (400 μL) was added, solvents were evaporated, and the residue dissolved in EtOAc (100 mL) was washed successively with 1 M aqueous HCl (2 × 50 mL), saturated aqueous $NaHCO_3$ (50 mL), and H_2O (50 mL). The washings were reextracted with EtOAc (2 × 50 mL) and the combined organic phases were dried and concentrated. Chromatography ($CHCl_3$–MeOH, 60:1) of the residue gave the trisaccharide **44** contaminated with triphenylphosphine oxide (124 mg) and the pure trisaccharide **44** (58 mg, 27%). Rechromatography (solvent as above) of the impure trisaccharide again yielded a contaminated fraction (80 mg) and the pure trisaccharide **44** (36 mg, 17%). The remaining contaminated trisaccharide was finally isolated pure (21 mg, 11%) by preparative TLC (solvent as above). The trisaccharide **44** was isolated as a colourless glass, $[\alpha]_D^{25}$ +35.0 (*c* 0.83, $CHCl_3$). Anal. calcd. for $C_{41}H_{50}BrNO_{18}$: C 53.2, H 5.4, N 1.5; found: C 53.1, H 5.6, N 1.3.

*Methyl 2-acetamido-2,6-dideoxy-3-O-[3'-O-(α-L-rhamnopyranosyl)-α-L-rhamnopyranosyl]-β-D-glucopyranoside (**46**)*

A solution of the brominated trisaccharide **44** (115 mg, 0.14 mmol) in EtOH (9 mL) containing NEt_3 (50 μL, 2.6 mol-equiv.) was hydrogenated 18 h at 60 psi in the presence of Pd–C catalyst (10%, 100 mg). More catalyst (20 mg) was added and hydrogenolysis was continued during another 8 h at 60 psi. The catalyst was filtered off, rinsed with dichloromethane (20 mL), and the combined filtrates were concentrated. A solution of the residue in CH_2Cl_2 (30 mL) was washed successively with 1 M HCl (25 mL), saturated aqueous $NaHCO_3$ (20 mL), and H_2O (20 mL). The washings were reextracted with CH_2Cl_2 (2 × 20 mL) and the combined organic phases were dried and concentrated to give the pure trisaccharide **45**, characterized by ^1H NMR spectroscopy (Table 6). Compound **45** was used directly in the next step. It was concentrated from anhydrous MeOH (2 × 3 mL), dissolved in anhydrous MeOH (6 mL), and a solution of NaOMe, 1 M in MeOH (600 μL), was added. The mixture was stirred 18 h at room temperature, more NaOMe was added portionwise over 3 h (2 × 200 μL), and stirring was continued during 2 h. The solution was deionized with Amberlite IR-120 (H^+) resin, diluted with MeOH (8 mL), filtered and the resin was washed with MeOH (10 mL). The combined filtrates were concentrated to dryness and chromatography (EtOAc–MeOH–H_2O, 7.5:1.5:1) gave **46**, which was finally purified on a Biogel P-2 column (H_2O). The trisaccharide **46** was obtained pure (53 mg, 84%) as a white solid by evaporation from MeOH; $[\alpha]_D^{25}$ −74.9 (*c* 0.6, MeOH). Anal. calcd. for $C_{21}H_{37}NO_{13}$: C 49.3, H 7.3, N, 2.7; found: C 48.9, H 7.5, N 2.8.

1. D. Bundle. Pure Appl. Chem. **61**, 1171 (1989).
2. N. I. A. Carlin, M. A. J. Gidney, A. A. Lindberg, and D. R. Bundle. J. Immunol. **137**, 2361 (1986).
3. N. I. A. Carlin, D. R. Bundle, and A. A. Lindberg. J. Immunol. **138**, 4419 (1987).
4. M. N. Vyas, N. K. Vyas, P. J. Meikle, B. M. Pinto, D. R. Bundle, and F. A. Quiocho. J. Mol. Biol. In press.
5. P. Fügedi, P. J. Garegg, H. Lönn, and T. Norberg. Glycoconj. J. **4**, 97 (1987).
6. G. H. Veeneman, S. H. Van Leewen, H. Zuurmond, and J. H. Van Boom. J. Carbohydr. Chem. **9**, 783 (1990).
7. P. Konradsson, D. R. Motoo, R. E. McDevitt, and B. Fraser-Reid. J. Chem. Soc. Chem. Commun. 270 (1990).
8. F.-I. Auzanneau, H. R. Hanna, and D. R. Bundle. Carbohydr. Res. **240**, 161 (1993).
9. D. R. Bundle and S. Josephson. Can. J. Chem. **56**, 2686 (1978).
10. J. Kihlberg, D. Leigh, and D. R. Bundle. J. Org. Chem. **55**, 2860 (1990).
11. A. K. Ray, U. B. Maddali, A. Roy, and N. Roy. Carbohydr. Res. **197**, 93 (1990).
12. F.-I. Auzanneau and D. R. Bundle. Carbohydr. Res. **212**, 13 (1991).
13. A. S. Perlin. Can. J. Chem. **41**, 399 (1963).
14. R. U. Lemieux and J. D. T. Cipera. Can. J. Chem. **34**, 906 (1956).

15. E. Fisher, M. Bergmann, and A. Rabe. Ber. Dtsch. Chem. Ges. **53**, 2362 (1920).
16. W. Roth and W. Pigman. J. Am. Chem. Soc. **92**, 4608 (1960).
17. P. J. Garegg and T. Norberg. Acta Chem. Scand. **B33**, 116 (1979).
18. P. J. Garegg, R. Johansson, and B. Samuelson. Synthesis, 168 (1984).
19. K. Bock and C. Pedersen. J. Chem. Soc. Perkin Trans. 2, 293 (1974).
20. J. Banoub and D. R. Bundle. Can. J. Chem. **57**, 2091 (1979).
21. R. U. Lemieux. Chem. Soc. Rev. **18**, 347 (1989).
22. R. U. Lemieux and S. Koto. Tetrahedron, **30**, 1933 (1974).
23. K. Bock, A. Brignole, and B. W. Sigurskjold. J. Chem. Soc. Perkin Trans. 2, 1711 (1986).
24. K. Bock, J. F.-B. Bolanos, and R. Norrestam. Carbohydr. Res. **179**, 97 (1989).
25. R. U. Lemieux and K. Bock. Arch. Biochem. Biophys. **221**, 125 (1983).

Can. J. Chem. Downloaded from www.nrcresearchpress.com by 88.255.202.194 on 09/08/12
For personal use only.

Preparation and structure of 7-azaindolium salts containing unusual chloro-copper(II) anionic units

JACQUES POITRAS, MARTIN LEDUC, AND ANDRÉ L. BEAUCHAMP[1]

Département de chimie, Université de Montréal, C.P. 6128, Succ. A, Montréal (Québec), Canada H3C 3J7

Received June 23, 1992[2]

JACQUES POITRAS, MARTIN LEDUC, and ANDRÉ L. BEAUCHAMP. Can. J. Chem. **71**, 549 (1993).

Dark-red crystals of $(H_2aza)_5[Cu_5Cl_{14}(H_2O)_4]Cl$ were obtained by addition of HCl to equimolar amounts of 7-azaindole (Haza) and $CuCl_2 \cdot 2H_2O$ in methanol. They were shown by X-ray diffraction (triclinic, $P\bar{1}$, a = 9.396(1), b = 9.894(1), c = 15.958(1), Å, α = 106.10(1)°, β = 98.25(1)°, γ = 105.56(1)°, Z = 1, R = 0.031) to contain infinite chains in which the basic $[Cu_5Cl_{14}(H_2O)_4]^{4-}$ pattern is built up from *trans*-$CuCl_2(H_2O)_2$, $[CuCl_3(H_2O)]^-$, and dichloro-bridged $[Cu_2Cl_6]^{2-}$ species. In the idealized chain, these units occur in the 1:2:1 ratio, but disorder is present and some of the $CuCl_2(H_2O)_2$ units are randomly replaced by $[CuCl_3(H_2O)]^-$. The Cu atoms have a roughly square-planar primary coordination, and connection along the chain is achieved by weaker apical Cu–Cl bridging interactions. All azaindole molecules are present as uncoordinated N7-protonated monocations. A related $(H_2aza)_3[Cu_3Cl_8(H_2O)_3]Cl$ salt was obtained as a side-product of the reaction of 7-azaindole with excess $CuCl_2 \cdot 2H_2O$ in methanol without acid. In these brown crystals (triclinic, $P\bar{1}$, a = 9.308(1), b = 9.964(1), c = 19.212(4) Å, α = 76.67(1)°, β = 79.35(1)°, γ = 75.27(1)°, Z = 2, R = 0.046), the $[Cu_6Cl_{16}(H_2O)_6]^{4-}$ pattern of the chain contains the same three building units as above, but in the 2:2:1 ratio. In both salts, the polymeric chloro-copper chains are parallel and separated by azaindolium cations stacked along the same direction. The structures are stabilized by networks of hydrogen bonds involving the azaindolium cations, the chlorine atoms, and water molecules in the chloro-copper chain, and a noncoordinated Cl^- ion. Most of the azaindolium cations are disordered. The influence of N7-protonation on the infrared spectrum of azaindole is discussed.

JACQUES POITRAS, MARTIN LEDUC et ANDRÉ L. BEAUCHAMP. Can. J. Chem. **71**, 549 (1993).

Les cristaux rouge sombre de $(H_2aza)_5[Cu_5Cl_{14}(H_2O)_4]Cl$ ont été obtenus par addition de HCl à des quantités équimolaires de 7-azaindole (Haza) et de $CuCl_2 \cdot 2H_2O$ dans le méthanol. La diffraction des rayons X (triclinique, $P\bar{1}$, a = 9.396(1), b = 9.894(1), c = 15.958(1) Å, α = 106.10(1)°, β = 98.25(1)°, γ = 105.56(1)°, Z = 1, R = 0.031) démontre la présence de chaînes infinies dans lesquelles le motif de base $[Cu_5Cl_{14}(H_2O)_4]^{4-}$ est constitué d'espèces *trans*-$CuCl_2(H_2O)_2$, $[CuCl_3(H_2O)]^-$ et $[Cu_2Cl_6]^{2-}$ à double pont chlore. La chaîne idéalisée renferme ces motifs selon un rapport 1 : 2 : 1, mais la présence de désordre entraîne le remplacement aléatoire de quelques segments $CuCl_2(H_2O)_2$ par $[CuCl_3(H_2O)]^-$. Les atomes de Cu possèdent une coordination primaire à peu près plan carré et la connexion le long de la chaîne est assurée par des interactions axiales Cu–Cl pontantes. Toutes les molécules d'azaindole sont sous forme de monocations protonés en N7 et non coordonnés. Un sel analogue $(H_2aza)_3[Cu_3Cl_8(H_2O)_3]Cl$ a été obtenu comme produit secondaire de la réaction du 7-azaindole avec un excès de $CuCl_2 \cdot 2H_2O$ dans le méthanol sans acide. Ces cristaux bruns (triclinique, $P\bar{1}$, a = 9.308(1), b = 9.964(1), c = 19.212(4) Å, α = 76.67(1)°, β = 79.35(1)°, γ = 75.27(1)°, Z = 2, R = 0.046) contiennent des chaînes dont le motif $[Cu_6Cl_{16}(H_2O)_6]^{4-}$ renferme les trois mêmes espèces que ci-haut, mais selon un rapport 2 : 2 : 1. Dans les deux sels, les chaînes polymères chloro-cuivriques sont parallèles et séparées par des cations azaindolium empilés selon la même direction. Les structures sont stabilisées par un réseau de liaisons hydrogène impliquant les cations azaindolium, les chlores et l'eau de la chaîne chloro-cuivrique, et un anion Cl^- non coordonné. La plupart des cations azaindolium sont désordonnés. L'influence de la protonation en N7 sur le spectre infrarouge de l'azaindole est discutée.

Introduction

In many of the complexes of 7-azaindole (Haza, Scheme 1) reported so far, the ligand monoanion plays a bridging role similar to that of carboxylates in stabilizing dinuclear units. For instance, copper(II) azaindolate has been found to contain discrete $Cu_2(aza)_4$ dimeric units with the "windmill" tetra(azaindolate)dimetal structure of copper(II) acetate (1). A similar bridging role has been observed in compounds with several other metals (2–4). As yet, unidentate binding of the anionic form has been observed only in the $[CH_3Hg(aza)]$ molecule, which was recently shown to exist as an N1-bonded monomer (4–6). Because azaindole is a much weaker acid, adduct formation with the neutral molecule is anticipated to occur more commonly than with carboxylic acids. Nevertheless, when this work was undertaken, only a few simple adducts had been structurally characterized, e.g., those with CH_3Hg^+ (4, 6), $ZnCl_2$ (7), and $Rh_2(carboxylate)_4$ (8, 9). In a previous paper (10), we reported on the reactions of

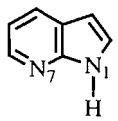

SCHEME 1

azaindole with copper(II) chloride in methanol, under conditions that favored ligand binding in the neutral form. To complete our survey of the $CuCl_2$–azaindole system, some experiments were run in slightly acidic solution, conditions that were known to lead to N7-protonated azaindolium salts with $ZnCl_2$ (7). This was intended to yield salts of simple chloro-copper anions that would provide routine infrared diagnostics to distinguish between coordinated and protonated azaindole. However, the composition of the material obtained did not correspond to any known type of halo-copper(II) anions (11). We also isolated another salt of unusual composition as a by-product of reactions in neutral solution. The crystallographic work below provides the first examples of chlorine-bridged chains built from *three* types of chloro-copper(II) units with different compositions.

[1]Author to whom correspondence may be addressed.

[2]Revision received January 25, 1993.

Can. J. Chem. Downloaded from www.nrcresearchpress.com by 88.255.202.194 on 09/08/12
For personal use only.

Can. J. Chem. Downloaded from www.nrcresearchpress.com by 88.255.202.194 on 09/08/12
For personal use only.

TABLE 1. Crystal data and conditions for data collection

	$(H_2aza)_5[Cu_5Cl_{14}(H_2O)_4]Cl$	$(H_2aza)_3[Cu_3Cl_8(H_2O)_3]Cl$
Formula	$C_{35}H_{43}Cu_5Cl_{15}N_{10}O_4$	$C_{21}H_{27}Cu_3Cl_9N_6O_3$
Formula weight	1517.3	921.2
Crystal system	Triclinic	Triclinic
Space group	$P\bar{1}$	$P\bar{1}$
a, Å	9.396(1)	9.308(1)
b, Å	9.894(1)	9.964(1)
c, Å	15.958(1)	19.212(4)
α, deg	106.10(1)	76.67(1)
β, deg	98.25(1)	79.35(1)
γ, deg	105.56(1)	75.27(1)
V, Å^3	1334.5	1661.7
D_{calc}, g cm^{-3}	1.888	1.841
Z	1	2
Radiation, λ (Å)	MoKα, 0.71069	CuKα, 1.54178
$F(000)$	755	918
μ, cm^{-1}	27.8	93.7
Crystal size, mm (faces)	0.12 (010–0$\bar{1}$0)	0.15 (1$\bar{1}$0–$\bar{1}$10)
	0.08 (100–$\bar{1}$00)	0.07 (010–0$\bar{1}$0)
	0.20 (001–00$\bar{1}$)	0.19 (001–00$\bar{1}$)
Scan type	ω/2θ	ω/2θ
Scan range Δω, deg	1.00 + 0.35 tan θ	0.80 + 0.14 tan θ
Scan speed, deg(ω) min^{-1}	3.3	3.3
2θ max, deg	50.0	140.0
No. unique reflections measured	4684	6300
No. observed reflections	3317	5168
Rejection criterion, $I/\sigma(I)$ <	3.00	3.00
T, K	293	293
No. parameters refined	363	491
R^a	0.031	0.046
$R_w{}^a$	0.036	0.061
Goodness-of-fit ratio, S	1.71	2.14

$^aR = \Sigma||F_o| - |F_c||/\Sigma|F_o|$; $R_w = [\Sigma w(|F_o| - |F_c|)^2/\Sigma w|F_o|^2]^{1/2}$.

Experimental section

$CuCl_2 \cdot 2H_2O$ (BDH) and 7-azaindole (Aldrich) were used as received. The methanol used was of reagent grade. Infrared spectra (4000–250 cm^{-1}) were recorded as KBr pellets with a Perkin–Elmer 783 spectrophotometer.

Reactions

$(H_2aza)_5[Cu_5Cl_{14}(H_2O)_4]Cl$

To a solution of 1.16 g (10 mmol) of 7-azaindole in 30 mL of methanol was added a solution of 1.71 g (10 mmol) of $CuCl_2 \cdot 2H_2O$ in 30 mL of methanol. A light brown mixture of $CuCl_2(Haza)_2$ and $Cu_4OCl_6(Haza)_4$ precipitated immediately, and redissolved instantly on addition of concentrated HCl (1 mL) to give a lime-green solution. Dark-red prismatic crystals appeared over 2 days, as the solvent slowly evaporated. Yield: 2.06 g (69%).

$(H_2aza)_3[Cu_3Cl_8(H_2O)_3]Cl$

To 3.41 g (20 mmol) of $CuCl_2 \cdot 2H_2O$ in 30 mL of methanol was added 0.59 g (5 mmol) of 7-azaindole in 20 mL of the same solvent. The mixture was stirred for several minutes and filtered to remove 0.58 g of the light-green precipitate of $CuCl_2(Haza)_2$. The filtrate was left at room temperature for slow evaporation, and after 10 days a small amount of dark-brown crystals of $(H_2aza)_3[Cu_3Cl_8(H_2O)_3]Cl$ mixed with a brown powder of $Cu_4OCl_6(Haza)_4$ was obtained.

Crystallographic measurements and structure determination

The crystallographic work was carried out with an Enraf–Nonius CAD-4 diffractometer following similar methods for both compounds. The reduced triclinic cell was determined from a set of 25 randomly distributed reflections, generated by the automatic search routine of the CAD-4 software and centred in the counter aperture. The Niggli coefficients unambiguously ruled out all lattices of symmetry higher than triclinic, leaving $P\bar{1}$ and $P1$ as possible space groups.

The crystal data are collected in Table 1. The intensities were measured as described earlier (12). Six standard reflections were monitored for crystal decay every hour and for misorientation every 200 reflections. In the case of $(H_2aza)_3[Cu_3Cl_8(H_2O)_3]Cl$, a half-sphere of data (hkl, $h\bar{k}l$, $\bar{h}kl$, $\bar{h}\bar{k}\bar{l}$) was collected (6300 reflections). The data were corrected for absorption (Gaussian integration, transmission range = 0.26–0.54). For $(H_2aza)_5[Cu_5Cl_{14}(H_2O)_4]Cl$, the whole sphere was measured (9368 reflections) and averaging (R_{av} = 0.016) yielded a set of 4684 independent hkl, $\bar{h}kl$, $h\bar{k}l$, and $hk\bar{l}$ data. An absorption correction was not deemed necessary, considering the low absorption coefficient and small size of the crystal. The intensities were corrected for the effects of Lorentz and polarization.

Similar strategies were applied to refine both structures. The centric $P\bar{1}$ space group was clearly favored in both cases by the slightly hypercentric distribution of the normalized structure factors. Full-matrix least squares were used to refine all non-hydrogen atoms isotropically. The function minimized was $\Sigma w(|F_o| - |F_c|)^2$, with individual weights w based on counting statistics. The Cl and Cu atoms were then allowed to refine anisotropically, while the remaining non-hydrogen atoms were kept isotropic. At this stage, occupancy factors were determined for the disordered azaindole rings. Hydrogens were introduced at idealized positions (C(N)—H = 0.95 Å, U_{iso} = 0.05 Å^2). Their parameters were not refined, but their coordinates were recalculated after each least-squares cycle. Anisotropic temperature factors were finally refined for the non-hydrogen atoms. The scattering curves were taken

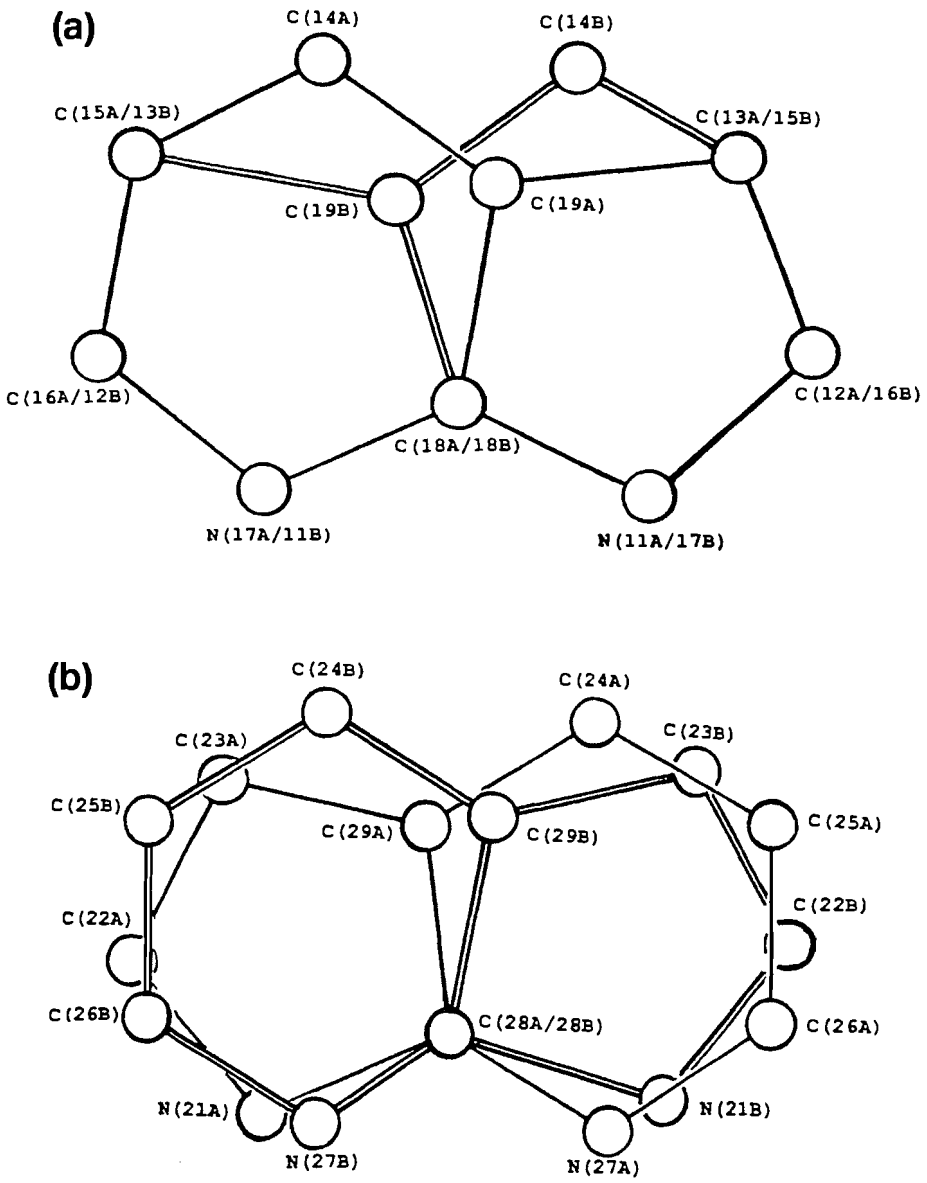

FIG. 1. Disorder of the azaindolium cations in $(H_2aza)_3[Cu_3Cl_8(H_2O)_3]Cl$. (*a*) Cation 1 (occupancies = 0.80(A)/0.20(B)). (*b*) Cations 2 (0.50/0.50) and 3 (0.70(A)/0.30(B)). Pattern *a* (0.80(A)/0.20(B)) is also found for cation 1 in $(H_2aza)_5[Cu_5Cl_{14}(H_2O)_4]Cl$.

from standard sources (13). The contributions of Cu and Cl to anomalous dispersion were those of Cromer (14).

Structure resolution of $(H_2aza)_3[Cu_3Cl_8(H_2O)_3]Cl$

The three independent Cu atoms were located by the direct methods of SHELX-86 (15). Interpretation was continued with the SHELX-76 package (16). From a difference Fourier (ΔF) map, the atoms attached to Cu, an uncoordinated Cl^- ion, and non-hydrogen atoms for three independent azaindolium cations could be identified. They were all refined by full-matrix least-squares procedures. When convergence was reached with this model (R = 0.166), abnormally high thermal parameters indicated that the azaindolium ions were all disordered. Inspection of the ΔF map revealed that most of the strongest residual peaks were partners of azaindolium atoms already located. For ion 1 (Fig. 1*a*), the five-membered ring of one individual was roughly superimposed with the six-membered ring of the other, and vice versa. This pattern was encountered with free azaindole (4) and $Mo_2(acetate)_2(azaindolate)_2 \cdot 2DMF$ (2). The nitrogen atoms were identified from the positions and distances to hydrogen-bond acceptors. The unresolved atoms were assigned full occupancies, whereas the resolved C(14A), C(14B), C(19A), and C(19B) positions were temporarily assigned half-occupancies. The coordinates and isotropic temperature factors were refined. The temperature factors of the resolved components were then fixed at 0.07 Å^2 (~mean of unresolved atoms). The occupancy factors were refined, but those of fractional atoms belonging to the same disordered individual were constrained to be equal. The refined occupancies of 1.25 for C(14A) and C(19A) and 0.29 for C(14B) and C(19B) were scaled down to 0.80 and 0.20, respectively, and fixed for the rest of the refinement. The coordinates and temperature factors of these fractional atoms were finally refined individually, together with those of the remaining non-hydrogen atoms. Disorder for azaindolium 2 followed a different pattern (Fig. 1*b*). All atoms were disordered over two resolved sites, except C(28A/28B), which was assigned full occupancy. By applying constraints as above, the normalized occupancies were found to be 0.50/0.50. The same pattern was observed for cation 3 with occupancy factors of 0.70/0.30.

For the final least-squares cycles, hydrogen atoms with appropriate occupancies were fixed at idealized positions, which were recalculated after each cycle. The water hydrogens were not located. The final residuals were R = 0.046 and R_w = 0.061. The

Can. J. Chem. Downloaded from www.nrcresearchpress.com by 88.255.202.194 on 09/08/12
For personal use only.

Can. J. Chem. Downloaded from www.nrcresearchpress.com by 88.255.202.194 on 09/08/12
For personal use only.

background in the final ΔF map was within ±0.6 e Å^{-3}. The refined coordinates are listed in Table 2.[3]

Attempts were made to refine the structure in the non-centric group, but the regions disordered in $P\bar{1}$ remained disordered in $P1$, and refinement was extremely unstable and erratic because of very high correlations. The $P\bar{1}$ model was retained.

Structure resolution of $(H_2aza)_5[Cu_5Cl_{14}(H_2O)_4]Cl$

The SHELX-86 package (15) revealed the presence of three independent Cu atoms, one of which occupied the inversion centre at the cell origin. A ΔF map (16) provided positions for all chlorine and oxygen atoms. Three independent azaindolium cations could also be recognized in the map, two of them showing extensive peak doubling due to disorder. One set of peaks defining a reasonable geometry was first introduced with full occupancy. Isotropic refinement by full-matrix least squares converged to R = 0.067. Strong residual peaks were found in the ΔF map near azaindolium cations. Disorder for ion 1 followed the pattern encountered for ion 1 in the previous compound (Fig. 1*a*). Cation 2 was not disordered, but ion 3 showed a new type of disorder with all atomic positions resolved (Fig. 2). No site could be assigned to nitrogen exclusively, since the N(37/C34)–N(31/C33) and the C(34/N37)–C(33/N31) pairs could participate equally well in hydrogen bonding and no indications were provided by ΔF peaks or temperature factors. Thus, the cation had to be statistically distributed over two orientations with the N1–N7 and C3–C4 sides interchanged by 180° rotation about an axis through C(32/C32) and the inversion center. Average "half-C half-N" scattering curves were used for mixed positions. This cation was further disordered by the crystallographic inversion centre over two equally populated orientations, in which the six- and the five-membered rings were interchanged. Thus, any cation can adopt altogether four possible arrangements. The refined coordinates likely represent averages of unresolved, but not exactly coincident, atomic positions. For any given cation, the N1-H group is probably slightly closer to its hydrogen-bond acceptor, thereby lengthening the intermolecular contacts involving C3-H.

All non-hydrogen atoms were refined anisotropically. Hydrogens were introduced at idealized positions with appropriate occupancy factors. The coordinates were recalculated after each least-squares cycle. Water hydrogens were not located. The final residuals were R = 0.031 and R_w = 0.036. The final ΔF map had a background below ±0.4 e Å^{-3}. The refined coordinates are listed in Table 3. As above, attempts to refine a non-centric $P1$ model failed.

Although agreement with the X-ray data is excellent, the distance obtained for Cu(1)—O(11) is unusually long (2.19 Å): the apparent "stretch" corresponds to ~70% of the difference between the normal Cu—OH_2 and Cu—Cl bond lengths (~1.99 and ~2.27 Å, respectively). This large distance and the O(11) thermal ellipsoid elongated along the Cu—O bond suggest that the O(11) site is partly occupied by chlorine, so that some of the $CuCl_2(H_2O)_2$ units around Cu(1) would actually be $[CuCl_3(H_2O)]^-$ (disordered over two orientations across the inversion centre). However, any chlorine transferred near Cu(1) has to be removed from somewhere else in the structure to keep the charge balanced. Since the Cu—Cl bonds are all normal, the source of chlorine is probably the free anion site Cl(0), where the Cl^- ion is presumably replaced by water. Thus, the overall effect is a balanced transfer of water and chlorine to the Cl(0) and O(11) sites, respectively.

Various attempts were made to estimate the extent of exchange. First, the final cycles of refinement were rerun assuming full transfer (that is, Cl(0) occupied by oxygen, O(11) by chlorine). The rest of the structure remained essentially unchanged, but the temperature factor became negative for Cl(0) and extremely large for the O(11) site. Therefore, the description with these sites as initially populated was close to reality. Similarly, assuming no exchange and keeping U_{iso} of O(11) and Cl(0) fixed at 0.07 Å^2, refinement of occupancies yielded values close to unity for these atoms, again indicating that the extent of exchange was relatively small. At first glance, a small amount of substitution seems to be inconsistent with the large Cu—(O/Cl) distance observed, but the results reported recently for a related substitution disorder in $MoCl_3(PR_3)_3$/$MoOCl_2(PR_3)_3$ solid solutions (17) indicate that there is no contradiction. As for the present structure, resolved peaks did not appear in the Fourier map for the two types of atoms. The "apparent" Mo—(O/Cl) distance was found to increase, as expected, when the Mo=O bond of $MoOCl_2(PR_3)_3$ was replaced by the Mo—Cl bond of the isostructural $MoCl_3(PR_3)_3$ molecule. Because of the higher atomic number of chlorine, the Mo—(O/Cl) distance increased rapidly as a function of substitution at low substitution levels. The "distance vs. composition" curve (Fig. 10 of ref. 17) reveals that ~25% substitution of O by Cl is enough to "stretch" the Mo=O bond by 70% of the difference between the Mo=O and Mo—Cl bond lengths. Since extensive disorder in other parts of the present Cu structure precludes any reliable evaluation of the extent of exchange from X-ray data alone, it will be assumed that the observed 70% "stretch" of our Cu—O(11) distance is also produced by ~25% substitutions of Cu—OH_2 by Cu—Cl bonds. A final check was done by refining the structure with occupancies adjusted to fit the average number of electrons (1.14 for O(11), 0.87 for Cl(0)). Refinement converged to the same R and R_w factors, the rest of the structure remained unaffected, and the coordinates of O(11) and Cl(0) did not shift significantly. The changes were picked up by the temperature factors: U_{eq} = 0.088 Å^2 for O(11) and 0.047 Å^2 for Cl(0). Thermal motion for O(11) is slightly high, but not unreasonable considering that O(11) spans two unresolved positions ~0.28 Å apart.

Results and discussion

In a previous paper (10), we reported on the green *trans*-$CuCl_2(Haza)_2$ and $[CuCl_2(Haza)_2][Cu(Haza)_4]Cl_2$ compounds obtained from methanol solutions containing $CuCl_2 \cdot 2H_2O$ and excess azaindole. Under appropriate conditions, equimolar mixtures led to the tetranuclear μ_4-oxide cluster $Cu_4OCl_6(Haza)_4$ in pure form. When no special precautions were taken, some $CuCl_2(Haza)_2$ precipitated first and was difficult to remove from the brown compound.

This part of our study on $CuCl_2 \cdot 2H_2O$ reactions with azaindole was intended to provide azaindolium salts from which infrared features characteristic of this cation could be identified. A 1:1 methanol solution was prepared and concentrated HCl was added. The light-brown mixture of $CuCl_2(Haza)_2$ and $Cu_4OCl_6(Haza)_4$ redissolved instantly and a lime-green solution resulted. By evaporation, dark-red prismatic crystals of $(H_2aza)_5[Cu_5Cl_{14}(H_2O)_4]Cl$ were isolated in good yield.

A small amount of crystals, first believed to be of the same material, was obtained from a reaction with excess $CuCl_2 \cdot 2H_2O$ without added acid. After the initially formed

[3]The supplementary material includes a table of infrared frequencies for azaindolium salts and crystallographic results (refined temperature factors, hydrogen coordinates, distances and angles in the azaindole rings, distances and angles for hydrogen bonds, least-squares plane calculations and structure factor amplitudes) for both structures (68 pages). Complete set of data may be purchased from: The Depository of Unpublished Data, Document Delivery, CISTI, National Research Council Canada, Ottawa, Canada K1A 0S2.

Tables of hydrogen coordinates, distances and angles in the azaindole rings, and distances and angles for hydrogen bonds have also been deposited with the Cambridge Crystallographic Data Centre and can be obtained on request from the Director, Cambridge Crystallographic Data Centre, University Chemical Laboratory, 12 Union Road, Cambridge, CB2 1EZ, U.K.

TABLE 2. Refined Coordinates ($\times 10^4$, Cu, Cl $\times 10^5$) and equivalent isotropic temperature factors ($Å^2 \times 10^3$) for $(H_2aza)_3[Cu_3Cl_8(H_2O)_3]Cl$

Atom	x	y	z	U_{eq}
Cu(1)	11373(6)	6456(6)	40753(3)	38
Cu(2)	30006(6)	19494(6)	22813(3)	38
Cu(3)	53829(6)	34758(6)	6423(3)	35
Cl(0)	37380(11)	−5296(11)	60243(6)	44
Cl(11)	18854(12)	27158(11)	36636(6)	45
Cl(12)	3729(12)	−13997(11)	45564(6)	47
Cl(21)	34117(11)	41611(11)	17670(6)	46
Cl(22)	27112(12)	−2738(10)	28238(6)	45
Cl(23)	6855(11)	25191(11)	19208(7)	45
Cl(31)	39710(12)	43570(11)	−2959(6)	46
Cl(32)	48656(12)	13232(11)	8070(7)	49
Cl(33)	73890(10)	26168(11)	12831(6)	42
O(11)	3087(3)	−211(3)	4485(2)	38
O(12)	−650(3)	1457(3)	3555(2)	45
O(21)	5107(3)	1337(4)	2495(2)	51
N(11A/17B)	10333(4)	12(4)	1068(2)	47
N(17A/11B)	8252(4)	−628(4)	732(2)	52
C(12A/16B)	11815(5)	−572(5)	1118(3)	53
C(13A/15B)	12266(5)	−1873(5)	933(3)	57
C(14A)[a]	10418(8)	−3092(7)	510(4)	64
C(15A/13B)	8998(6)	−2820(6)	409(3)	69
C(16A/12B)	7912(5)	−1680(6)	501(3)	56
C(18A/18B)	9681(5)	−837(4)	850(2)	41
C(19A)[a]	10836(6)	−2104(5)	742(3)	43
C(14B)[b]	11756(18)	−2663(18)	748(9)	24[f]
C(19B)[b]	10205(18)	−2140(19)	669(10)	27[f]
N(21A)[c]	6047(8)	3230(8)	5930(5)	49
N(27A)[c]	3770(8)	2780(8)	5716(5)	50
C(22A)[c]	6384(12)	4430(12)	6044(6)	62
C(23A)[c]	5204(10)	5503(9)	6026(6)	49
C(24A)[c]	2542(10)	5603(9)	5818(5)	49
C(25A)[c]	1716(10)	4719(11)	5666(6)	56
C(26A)[c]	2272(10)	3338(11)	5632(5)	52
C(28A/28B)	4402(6)	3536(5)	5829(3)	61
C(29A)[c]	4023(9)	4986(7)	5901(4)	35
N(21B)[c]	3197(9)	2850(7)	5673(4)	52
N(27B)[c]	5618(9)	3005(8)	5908(5)	53
C(22B)[c]	1816(12)	3789(12)	5619(7)	67
C(23B)[c]	1836(12)	5047(11)	5766(6)	65
C(24B)[c]	4155(12)	5723(11)	6017(7)	65
C(25B)[c]	5651(10)	5206(11)	6122(6)	60
C(26B)[c]	6387(11)	3878(13)	6054(6)	66
C(29B)[c]	3354(10)	4907(9)	5869(5)	48
N(31A)[d]	−2302(6)	5209(5)	2094(3)	51
N(37A)[d]	−62(6)	5600(5)	2363(3)	51
C(32A)[d]	−3761(8)	6016(10)	2065(4)	66
C(33A)[d]	−3873(7)	7269(8)	2271(4)	59
C(34A)[d]	−1770(8)	8176(7)	2616(4)	57
C(35A)[d]	−239(8)	7783(8)	2705(4)	56
C(36A)[d]	557(7)	6504(8)	2574(4)	52
C(38A/38B)	−1426(5)	5981(5)	2302(2)	46
C(39A)[d]	−2425(7)	7278(6)	2408(4)	46
N(31B)[e]	155(12)	5852(12)	2417(7)	42[f]
N(37B)[e]	−2002(14)	5236(14)	2138(7)	50[f]
C(32B)[e]	367(19)	7092(19)	2577(10)	59[f]
C(33B)[e]	−941(16)	8019(16)	2647(8)	46[f]
C(34B)[e]	−3504(16)	7838(16)	2402(9)	45[f]
C(35B)[e]	−4258(17)	6941(17)	2223(9)	50[f]
C(36B)[e]	−3444(16)	5678(16)	2124(9)	48[f]
C(39B)[e]	−2059(13)	7383(13)	2483(7)	32[f]

Occupancy factors: [a]0.80, [b]0.20, [c]0.50, [d]0.70, [e]0.30.
[f]Isotropic temperature factor.

Can. J. Chem. Downloaded from www.nrcresearchpress.com by 88.255.202.194 on 09/08/12
For personal use only.

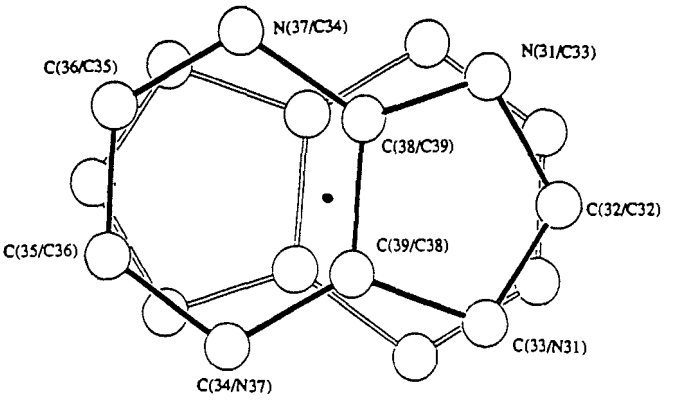

FIG. 2. Disorder of azaindolium cation 3 in $(H_2aza)_5[Cu_5Cl_{14}(H_2O)_4]Cl$ (occupancies = 0.50/0.50). The crystallographic inversion centre is indicated by a black dot.

$CuCl_2(Haza)_2$ complex was filtered, the green solution was allowed to evaporate in open air, whereupon a brown powder shown to be $Cu_4OCl_6(Haza)_4$ appeared, mixed with brown crystals. The latter crystals were expected to contain the azaindolium cation, since two H^+ ions were liberated for each $Cu_4OCl_6(Haza)_4$ molecule formed. Preliminary X-ray work showed cell parameters different from those of the above dark-red compound. The composition of this material was shown by X-ray diffraction to be $(H_2aza)_3[Cu_3Cl_8(H_2O)_3]Cl$.

Crystal structures of $(H_2aza)_3[Cu_3Cl_8(H_2O)_3]Cl$ and $(H_2aza)_5[Cu_5Cl_{14}(H_2O)_4]Cl$

Although the formulas look very different, these compounds are actually closely related. In both cases, azaindole is present only as the uncoordinated N7-protonated cation and the unit cell includes free Cl^- anions. Infinite chains of chlorine-bridged copper atoms are generated from *three* kinds of square-planar units, namely *trans*-$CuCl_2(H_2O)_2$ about Cu(1), $[CuCl_3(H_2O)]^-$ about Cu(2), and chlorine-bridged $[Cu_2Cl_6]^{2-}$ dimers containing Cu(3). The preference of copper(II) for square-planar primary coordination is well established, as well as its ability to form one or two weaker bridging axial bonds with halogens of adjacent units, resulting in square-pyramidal [4+1] or elongated octahedral [4+2] overall coordinations (11). In the case of $(H_2aza)_3[Cu_3Cl_8(H_2O)_3]Cl$, the tris-copper asymmetric unit is repeated by crystallographic inversion centres at both the Cu(1) and the Cu(3) ends, generating the infinite chain of Fig. 3, in which the basic repetition pattern (within braces) is ···Cu(3)-{Cu(3)-Cu(2)-Cu(1)-Cu(1)-Cu(2)-Cu(3)}Cu(3)···. In the case of $(H_2aza)_5[Cu_5Cl_{14}(H_2O)_4]Cl$ (Fig. 4), the basic pattern is ···Cu(3){Cu(3)-Cu(2)-Cu(1)-Cu(2)-Cu(3)}Cu(3)···, with only one Cu(1) centre instead of two. This compound shows evidence for a small amount of disorder about Cu(1), on which we will comment below. The present discussion deals with the pattern of Fig. 4 representing the major part of the structure.

Polymeric arrangements are often observed for chloro-Cu(II) species in the solid state. For instance, chain or layer structures are found for salts of the $[CuCl_4]^{2-}$ ion (18, 19). Various salts of composition A^ICuCl_3 consist of $[CuCl_3]^-$ units or chlorine-bridged $[Cu_2Cl_6]^{2-}$ dimers connected into a linear chain (20–24). Salts of $[CuCl_3(H_2O)]^-$ are also known (25). A number of infinite one-dimensional structures resulting from stacking of higher chloro-Cu(II) oligomers have also been described (20, 26, 27). Chains are known for $CuCl_2L_2$ compounds with ligands L such as imidazoles (28) and pyridines (29). In most of these materials, the chains are constructed from a single square-planar Cu(II) monomer. Only a few examples of arrangements created from two copper units alternating along the chain are known (30–32). To our knowledge, periodic chains of the types observed here, based on *three* different ligand compositions, are unprecedented. The distances and angles around copper for the two structures are listed in Table 4.

(a) Cu(1): trans-*$CuCl_2(H_2O)_2$*

The Cu—OH_2 (mean 2.006 Å) and the short Cu—Cl bonds (2.267(1)Å) in $(H_2aza)_3[Cu_3Cl_8(H_2O)_3]Cl$ are similar to those found for the same unit in other compounds (18, 31, 33). In $(H_2aza)_5[Cu_5Cl_{14}(H_2O)_4]Cl$, the same distance is obtained for the short Cu—Cl bonds, but the observed Cu—OH_2 distance is ~0.18 Å longer. This value is artificially high because some $CuCl_2(H_2O)_2$ units are statistically replaced by $[CuCl_3(H_2O)]^-$ along the chain (see experimental part and (*f*) below). Cu(1) occupies an inversion centre, so that all *trans* angles are exactly 180° and the square plane is rigorously planar, whereas departure from 90° in the *cis* angles is small (< 2.2°). In $(H_2aza)_3[Cu_3Cl_8(H_2O)_3]Cl$, Cu(1) has no local symmetry. The *cis* angles between the four strong bonds (89.2°–92.3°) are close to 90°. The atom-to-plane distances (Table S-5, supplementary material) indicate a small, but significant, tetrahedral distortion, which is also reflected by the *trans* angles being appreciably different from 180°.

(b) Cu(2): $[CuCl_3(H_2O)]^-$

The structures observed for this ion in the two compounds are very similar, although distortion is a little greater in $(H_2aza)_5[Cu_5Cl_{14}(H_2O)_4]Cl$. The Cu—Cl bonds in the square plane (mean 2.284 Å) are comparable to those found earlier (25), as are the Cu—OH_2 bonds (mean 1.992 Å). The *cis* angles range from 87.1° to 92.2°. The water molecule is displaced from the $CuCl_3$ plane by 0.2–0.3 Å on the Cl(32) side (supplementary material), distorting the Cl(23)—Cu(2)—O(21) angle to 173.1(1)° in $(H_2aza)_3[Cu_3Cl_8(H_2O)_3]Cl$ and to 169.8(1)° in $(H_2aza)_5[Cu_5Cl_{14}(H_2O)_4]Cl$. A normal bridging bond of ~2.8 Å is formed with Cl(11), but the sixth neighbour Cl(32), completing the elongated octahedron, is much more distant (~3.2 Å). Weaker interaction in the latter case is also reflected by the greater departure from 90° or 180° for the bonds involving this atom. It is not clear whether the Cu(2)–Cl(32) interaction should be described as a weak bond to a [4+2]-coordinated metal or an extra intermolecular contact with a [4+1] square-pyramidal entity. In any event, Cl(32) efficiently blocks the region of the sixth apex of a distorted octahedron around Cu(2).

(c) Cu(3): $[Cu_2Cl_6]^{2-}$

Two centrosymmetry related Cu(3) atoms define a dichloro-bridged dimer of the type found in various A^ICuCl_3 salts (20–23). The four short Cu—Cl bonds around Cu(3) (2.249(1)–2.309(1) Å) are comparable with those found in related salts (21, 22, 24). Within the bridge, the angles at Cu(3) and Cl(31) (mean values 82.8° and 97.2°, respectively) are typical of this type of bridging. A [4+1] square-pyramidal overall coordination around each Cu(3) centre is completed by an axial Cu(3)—Cl(21) bond of ~2.66 Å. Cu(3) is displaced by ~0.12 Å from the plane of the four strongly bonded Cl atoms, toward the apical Cl(21) atom, which is a common feature in square pyramids. This results

Can. J. Chem. Downloaded from www.nrcresearchpress.com by 88.255.202.194 on 09/08/12
For personal use only.

TABLE 3. Refined coordinates ($\times 10^4$, Cu, Cl $\times 10^5$) and equivalent isotropic temperature factors (Å^2 $\times$ 10^3) for $(H_2aza)_5[Cu_5Cl_{14}(H_2O)_4]Cl$

Atom	x	y	z	U_{eq}
Cu(1)	0	0	0	29
Cu(2)	23075(6)	5354(6)	21691(4)	26
Cu(3)	51910(6)	8384(6)	41833(4)	22
Cl(0)	50000	0	0	61
Cl(11)	8216(14)	−16411(13)	5156(8)	47
Cl(21)	29312(13)	−10996(13)	28101(8)	45
Cl(22)	17843(16)	21212(16)	14525(10)	61
Cl(23)	2238(13)	4169(13)	27426(8)	46
Cl(31)	40321(13)	9297(13)	53690(8)	44
Cl(32)	46530(14)	28342(13)	39982(8)	48
Cl(33)	69510(12)	10022(13)	33243(8)	43
O(11)	−1772(5)	−273(4)	749(3)	76
O(21)	4318(3)	972(4)	1850(2)	52
N(11A/17B)	10038(5)	3834(4)	3675(3)	45
C(12A/16B)	11523(6)	4409(6)	3630(3)	50
C(13A/15B)	11997(6)	5929(6)	3882(3)	53
C(14A)[a]	10316(7)	7605(7)	4431(4)	50
C(14B)[b]	11569(32)	6872(29)	4130(17)	37[d]
C(15A/13B)	8913(7)	7440(7)	4548(4)	64
C(16A/12B)	7808(6)	6159(7)	4405(3)	55
N(17A/11B)	8101(5)	4869(4)	4107(3)	46
C(18A/18B)	9483(5)	4956(5)	3961(3)	39
C(19A)[a]	10664(9)	6323(8)	4112(5)	37
C(19B)[b]	10140(32)	6483(39)	4200(21)	29[d]
N(21)	7170(6)	7481(5)	2473(3)	63
C(22)	5694(8)	6698(10)	2476(4)	80
C(23)	5467(7)	5135(9)	2208(4)	93
C(24)	7559(9)	3940(7)	1768(4)	82
C(25)	8947(10)	4284(9)	1693(4)	78
C(26)	9807(7)	5645(9)	1868(4)	70
N(27)	9331(5)	6770(5)	2128(3)	61
C(28)	7920(6)	6509(6)	2222(3)	46
C(29)	6964(7)	5014(6)	2038(3)	57
N(31/C33)[c]	5705(16)	3321(17)	9658(10)	77
C(32/C32)[c]	7061(16)	4353(19)	9695(10)	65
C(33/N31)[c]	7137(17)	5761(17)	9941(11)	61
C(34/N37)[c]	5019(16)	6802(16)	10331(10)	64
C(35/C36)[c]	3491(14)	6300(14)	10351(10)	73
C(36/C35)[c]	2675(16)	4831(17)	10221(9)	54
N(37/C34)[c]	3299(15)	3711(12)	9976(9)	61
C(38/C39)[c]	4861(15)	4151(17)	9891(12)	50
C(39/C38)[c]	5668(15)	5711(16)	10059(9)	42

Occupancy factors: [a]0.80, [b]0.20, [c]0.50.
[d]Isotropic temperature factor.

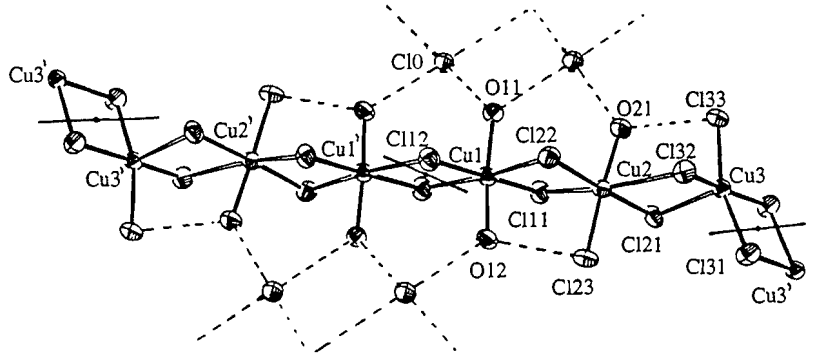

FIG. 3. ORTEP drawing of the $[Cu_3Cl_8(H_2O)_3]^{2-}$ unit. The asymmetric tris-copper segment limited by the thin lines is repeated by crystallographic inversion centres at both ends, generating the six-copper basic pattern of the infinite chain. Cl(0) is the uncoordinated Cl^- ion. Thermal ellipsoids correspond to 50% probability. Dashed lines represent hydrogen bonds.

Can. J. Chem. Downloaded from www.nrcresearchpress.com by 88.255.202.194 on 09/08/12
For personal use only.

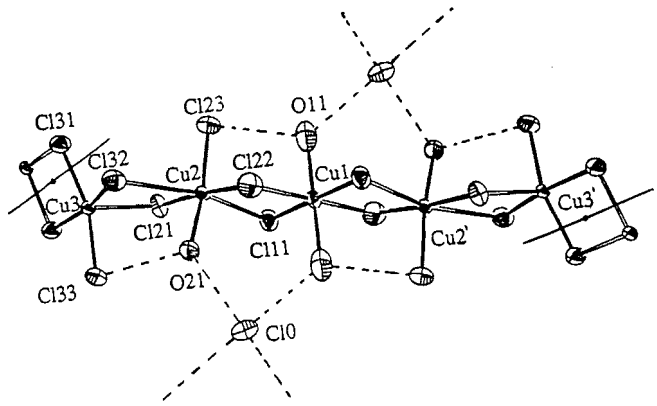

FIG. 4. ORTEP drawing of the $[Cu_5Cl_{14}(H_2O)_4]^{4-}$ unit. The asymmetric tris-copper segment is repeated by crystallographic inversion centres on Cu(1) and near Cu(3), generating the five-copper basic pattern of the infinite chain. Cl(0) is the uncoordinated Cl^- ion. Thermal ellipsoids correspond to 50% probability. Dashed lines represent hydrogen bonds.

in the angles between *trans* ligands being decreased to 163° and 170°.

(d) Azaindolium cations

The unit cell of $(H_2aza)_3[Cu_3Cl_8(H_2O)_3]Cl$ includes three symmetry-independent azaindolium cations, all disordered over two orientations. This flat molecule is prone to disorder, because its van der Waals envelope does not change drastically if the five- and six-membered rings are interchanged by a 180° rotation about C8—C9. In both orientations, N1 and N7 remain properly oriented toward their hydrogen-bond acceptors. The kind of disorder found for cations of type 1 (Fig. 1*a*) has been observed in other structures where the N1–N7 side is firmly anchored to metal atoms (1, 2) or to hydrogen-bond acceptors (4). For cations of types 2 and 3 (Fig. 1*b*), the relative orientation of the two individuals is less constrained and only the C8 atoms remain unresolved. In $(H_2aza)_5[Cu_5Cl_{14}(H_2O)_4]Cl$, one of the three independent cations (type 2) shows no evidence of disorder. Ion 1 shows the disorder pattern of Fig. 1*a*. Ion 3 is involved in a new, more complex, type of disorder (Fig. 2), in which four equally probable atomic distributions are obtained by interchanging the five- and six-membered rings, and the N1–N7 and C3–C4 sides.

The distances and angles in the azaindolium ions are listed in the supplementary material. Considering that apparent distortion results from the refined unresolved positions describing not exactly coincident atoms, the geometry is in reasonable agreement with those observed for free azaindole (4) or the azaindolium ion (7). The cations are planar within experimental error.

(e) Packing

A stereoview of the unit cell of $(H_2aza)_3[Cu_3Cl_8(H_2O)_3]Cl$ is shown in Fig. 5. It includes the six-copper basic pattern of Fig. 3 for two adjacent chains. These parallel chains, translated along the *a* axis, define infinite layers, which also contain the uncoordinated Cl^- ions, near the $CuCl_2(H_2O)_2$ units. Between the layers, oriented in the same direction as the chloro-copper chains and just above the region occupied by the Cl^- ions, are found slanted stacks of azaindolium cations, separated by ~3.45 Å.

Cohesion between these components is provided to a large extent by hydrogen bonding. Within the chains (Fig. 3), both hydrogens of each water molecule form O—H···Cl bonds of 3.05–3.20 Å (normal range: 2.86–3.21 Å) (34) with favourably oriented Cl^- ions or coordinated chlorines (Table 5). Two adjacent chains provide each of the two nearby Cl^- ions in the middle of the cell with four roughly coplanar and orthogonal hydrogen bonds. Above this plane, a type 2 azaindolium cation forms an extra N—H···Cl bond of 3.20 Å (normal range: 2.91–3.52 Å) (34). A number of other hydrogen bonds are formed by other azaindolium ions with coordinated chlorines (Table S-4, supplementary material).

In the case of $(H_2aza)_5[Cu_5Cl_{14}(H_2O)_4]Cl$ (Fig. 6), the infinite chloro-copper chains, represented by the five-copper pattern of Fig. 4, similarly form infinite layers with Cl^- ions inserted between $CuCl_2(H_2O)_2$ units of adjacent chains. The slanted stacks of azaindolium cations are also positioned between the layers, above the region of the Cl^- ions.

This structure can be regarded as derived from $(H_2aza)_3[Cu_3Cl_8(H_2O)_3]Cl$ by removing one of the central $CuCl_2(H_2O)_2$ units, a Cl^- anion, and an imidazolium cation. This can be done without loss of the local stabilizing interactions along the chains. For instance, inside the chain, all water molecules form the same number of O—H···Cl bonds, the two symmetry-equivalent O—H···Cl(23) bonds being provided now by the same, instead of two distinct, $CuCl_2(H_2O)_2$ units (Fig. 4 and Table 6). Cutting one $CuCl_2(H_2O)_2$ unit removes two water molecules making hydrogen bonds with the Cl^- ions in the previous compound, but these are no longer needed, since a Cl^- ion has also been removed. The five-copper chain is ~3.45 Å shorter than the six-copper one, but since the imidazolium rings are roughly 3.45 Å thick, removing one cation shortens the stack by the same amount. Hence, each remaining azaindolium ion is facing the same pattern of hydrogen-bond acceptors as before and maintains similar interactions with the chain, without sacrificing inter-ring stacking stabilization.

(f) Substitution disorder in $(H_2aza)_5[Cu_5Cl_{14}(H_2O)_4]Cl$

In this compound, some of the central $CuCl_2(H_2O)_2$ units (Fig. 4) are replaced by $[CuCl_3(H_2O)]^-$ groups, as a result of a partial interchange of Cl^- ions and water molecules between the O(11) and Cl(0) sites. Substitution does not appreciably affect the geometry about Cu(1), except for the "apparent" Cu—O(11) distance of 2.187(4) Å (Table 4), which is greater than for a normal Cu—OH_2 bond (~1.99 Å), although less than that of a Cu—Cl bond (~2.27 Å). By comparing with a related case of substitution disorder (17), the extent of interchange was estimated to be ~25% (see experimental section). As revealed by careful inspection of molecular packing (Fig. 6), mutual O(11)/Cl(0) substitution can take place without greatly affecting the overall structure, because water and chloride ions can play the same roles as ligands to Cu(1) and hydrogen-bond acceptors, whereas the O—H···Cl(0) bonds they form to one another are always retained. It is not clear, however, why no such substitution disorder is detected in $(H_2aza)_3[Cu_3Cl_8(H_2O)_3]Cl$.

Infrared spectra of the azaindolium salts

A list of frequencies and tentative assignments for 7-azaindole and its protonated Cl^-, ClO_4^-, and $[Cu_5Cl_{14}(H_2O)_4]^{4-}$ salts are provided in the supplementary material. The infrared spectrum of azaindole has been discussed elsewhere (2, 6, 10). Protonation can be detected from new bands and significant shifts in the spectra. The N–H vibrations in

Can. J. Chem. Downloaded from www.nrcresearchpress.com by 88.255.202.194 on 09/08/12
For personal use only.

TABLE 4. Interatomic distances (Å) and bond angles (deg) in the $[Cu_3Cl_8(H_2O)_3]^{2-}$ and $[Cu_5Cl_{14}(H_2O)_4]^{4-}$ units

Atoms	$[Cu_3Cl_8(H_2O)_3]^{2-}$	$[Cu_5Cl_{14}(H_2O)_4]^{4-}$
	Distances	
Cu(1)—Cl(11)	2.267(1)	2.267(1)
Cu(1)—Cl(12)	2.267(1)	—
Cu(1)—O(11)	2.018(3)	2.187(4)
Cu(1)—O(12)	1.995(3)	—
Cu(1)—Cl(22)	2.792(1)	2.624(2)
Cu(1)—Cl(12)[a]	2.908(1)	—
Cu(2)—Cl(21)	2.294(1)	2.294(1)
Cu(2)—Cl(22)	2.281(1)	2.293(2)
Cu(2)—Cl(23)	2.279(1)	2.266(1)
Cu(2)—O(21)	1.990(3)	1.994(4)
Cu(2)—Cl(11)	2.868(1)	2.780(1)
Cu(2)—Cl(32)	3.142(1)	3.214(1)
Cu(3)—Cl(31)	2.303(1)	2.307(1)
Cu(3)—Cl(32)	2.256(1)	2.249(1)
Cu(3)—Cl(33)	2.299(1)	2.296(1)
Cu(3)—Cl(31)[b]	2.306(1)	—
Cu(3)—Cl(31)[c]	—	2.309(1)
Cu(3)—Cl(21)	2.661(1)	2.671(1)
Cu(1)—Cu(1)[a]	3.906(1)	—
Cu(1)—Cu(2)	3.667(1)	3.630(1)
Cu(2)—Cu(3)	3.751(1)	3.780(1)
Cu(3)—Cu(3)[b]	3.452(1)	—
Cu(3)—Cu(3)[c]	—	3.467(1)
Cu(1)—Cl(0)	4.598(1)	4.698
Cu(1)—Cl(0)[a]	4.609(1)	—
Cu(1)—Cl(0)[b]	—	4.698
Cu(2)—Cl(0)[b]	4.600(1)	—
Cu(2)—Cl(0)[c]	—	4.569(1)
	Angles	
Cl(11)—Cu(1)—Cl(12)	176.50(5)	—
Cl(11)—Cu(1)—Cl(11)[d]	—	180.00
Cl(11)—Cu(1)—O(11)	89.41(9)	88.48(11)
Cl(11)—Cu(1)—O(11)[d]	—	91.52(11)
Cl(11)—Cu(1)—O(12)	89.21(9)	—
Cl(11)—Cu(1)—Cl(12)[a]	93.96(4)	—
Cl(11)—Cu(1)—Cl(22)	88.75(4)	88.08(5)
Cl(11)—Cu(1)—Cl(22)[d]	—	91.92(5)
Cl(12)—Cu(1)—O(11)	89.44(9)	—
Cl(12)—Cu(1)—O(12)	92.32(10)	—
Cl(12)—Cu(1)—Cl(22)	94.44(4)	—
Cl(12)—Cu(1)—Cl(12)[a]	82.77(4)	—
O(11)—Cu(1)—O(12)	173.08(13)	—
O(11)—Cu(1)—Cl(22)	84.69(9)	87.85(11)
O(11)—Cu(1)—Cl(12)[a]	91.72(9)	—
O(12)—Cu(1)—Cl(12)[a]	95.14(9)	—
Cl(11)—Cu(2)—Cl(32)	167.09(4)	167.55(4)
Cl(21)—Cu(2)—Cl(22)	176.74(5)	175.79(6)
Cl(21)—Cu(2)—Cl(23)	91.95(4)	92.18(5)
Cl(21)—Cu(2)—O(21)	89.28(10)	89.33(11)
Cl(21)—Cu(2)—Cl(32)	80.53(4)	79.91(4)
Cl(21)—Cu(2)—Cl(11)	92.56(4)	94.02(5)
Cl(22)—Cu(2)—Cl(23)	91.26(4)	91.68(5)
Cl(22)—Cu(2)—O(21)	87.60(10)	87.16(11)
Cl(22)—Cu(2)—Cl(11)	86.65(4)	83.89(5)
Cl(22)—Cu(2)—Cl(32)	99.64(4)	101.44(5)
Cl(23)—Cu(2)—O(21)	173.12(10)	169.79(11)
Cl(23)—Cu(2)—Cl(32)	97.26(4)	94.71(4)
Cl(23)—Cu(2)—Cl(11)	93.83(4)	96.39(5)
O(21)—Cu(2)—Cl(11)	92.89(10)	93.58(10)
O(21)—Cu(2)—Cl(32)	76.25(10)	75.61(10)
Cl(21)—Cu(3)—Cl(31)[b]	94.98(4)	—

Can. J. Chem. Downloaded from www.nrcresearchpress.com by 88.255.202.194 on 09/08/12
For personal use only.

TABLE 4 (*concluded*)

Atoms	$[Cu_3Cl_8(H_2O)_3]^{2-}$	$[Cu_5Cl_{14}(H_2O)_4]^{4-}$
Cl(21)—Cu(3)—Cl(31)[c]	—	95.75(5)
Cl(31)—Cu(3)—Cl(32)	91.90(5)	91.98(5)
Cl(31)—Cu(3)—Cl(33)	162.04(5)	163.81(5)
Cl(31)—Cu(3)—Cl(31)[b]	83.00(4)	—
Cl(31)—Cu(3)—Cl(31)[c]	—	82.62(5)
Cl(31)—Cu(3)—Cl(21)	102.07(4)	101.42(5)
Cl(32)—Cu(3)—Cl(33)	92.86(5)	92.55(5)
Cl(32)—Cu(3)—Cl(31)[b]	171.40(5)	—
Cl(32)—Cu(3)—Cl(31)[c]	—	169.72(5)
Cl(32)—Cu(3)—Cl(21)	92.85(4)	93.88(5)
Cl(33)—Cu(3)—Cl(31)[b]	89.99(4)	—
Cl(33)—Cu(3)—Cl(31)[c]	—	90.38(5)
Cl(33)—Cu(3)—Cl(21)	94.99(4)	93.77(5)
Cu(1)—Cl(11)—Cu(2)	90.35(4)	91.40(4)
Cu(1)—Cl(12)—Cu(1)[a]	97.23(4)	—
Cu(2)—Cl(21)—Cu(3)	98.14(4)	98.89(5)
Cu(1)—Cl(22)—Cu(2)	92.01(4)	94.91(6)
Cu(3)—Cl(31)—Cu(3)[b]	97.00(5)	—
Cu(3)—Cl(31)—Cu(3)[c]	—	97.38(5)
Cu(2)—Cl(32)—Cu(3)	86.40(4)	85.64(4)

[a] $-x, -y, 1 - z$.
[b] $1 - x, 1 - y, -z$.
[c] $1 - x, -y, 1 - z$.
[d] $-x, -y, -z$.

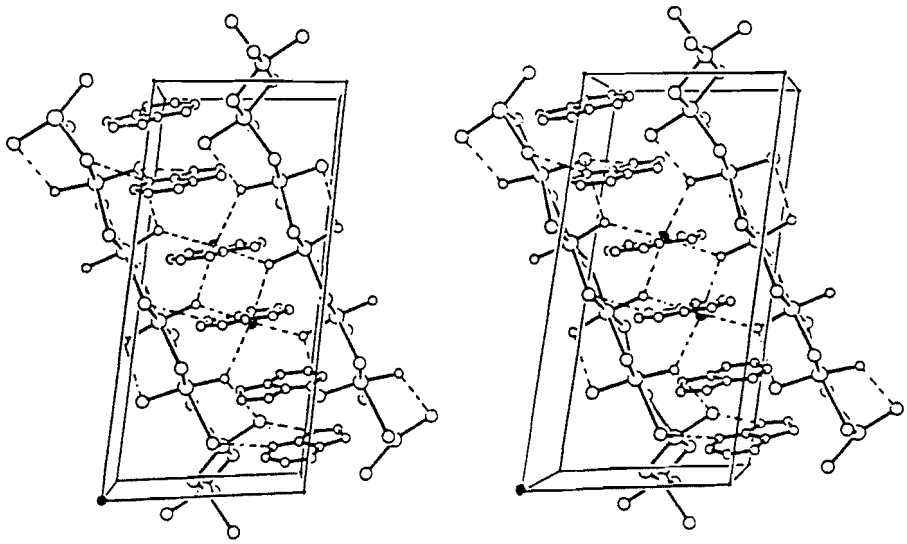

FIG. 5. Stereoview of the unit cell of $(H_2aza)_3[Cu_3Cl_8(H_2O)_3]Cl$. Axes *a* (horizontal, right) and *c* (vertical, up) are in the plane of the figure, whereas *b* points away from the reader. Atoms are represented by spheres of arbitrary size: C ~ N ~ O < Cl < Cu. The uncoordinated Cl^- ion is shown as a black sphere and hydrogen bonds as dashed lines. The atoms in the chain can be identified from Fig. 3. Only the most abundant orientations of the disordered azaindolium cations are shown.

the salts introduce a broad feature at 3300–3600 cm^{-1}, whereas the maximum of the azaindole massif at 2900 cm^{-1} is displaced to 3100 cm^{-1} in the Cl^- and ClO_4^- salts, and to 3280 cm^{-1} in $(H_2aza)_5[Cu_5Cl_{14}(H_2O)_4]Cl$. A general shift to higher frequency is also noted in the 1650–1470 cm^{-1} range containing ring stretching modes. The ligand bands at 1600, 1583, and 1498/1480 cm^{-1} are displaced to 1634, 1613, and 1505/1492 cm^{-1}, respectively, in the salts, whereas a new weak band appears at 1524 cm^{-1}. Bands at 878 and 762 cm^{-1} lose intensity and shift to 884 and 749 cm^{-1}, respectively, in the salts. In the low-frequency region, the ligand out-of-plane ring mode at 559 cm^{-1} is displaced to 546 cm^{-1}, whereas the doublet at 428/419 cm^{-1} moves to 410/400 cm^{-1}. These spectral changes are different from those found for complexes containing N7-coordinated neutral (6, 10) or N1–N7-bridged anionic azaindole (2). Hence, they provide good diagnostics to identify the N7-protonated cation.

The ligand shows no vibrations in the 250–400 cm^{-1} range. This spectral region for $(H_2aza)_2[Cu_5Cl_{14}(H_2O)_4]Cl$ exhibits bands at 280, 250, and 235 cm^{-1}, which are probably due to Cu–Cl stretching modes (35).

Can. J. Chem. Downloaded from www.nrcresearchpress.com by 88.255.202.194 on 09/08/12
For personal use only.

TABLE 5. Distances (Å) and angles (deg) for the hydrogen bonds in the $[Cu_3Cl_8(H_2O)_3]^{2-}$ unit

Atoms		Atoms	
O(11)—H···Cl(0)	3.057(3)	O(12)—H···Cl(0)^b	3.149(3)
O(11)—H···Cl(0)^a	3.153(3)	O(21)—H···Cl(33)	3.121(3)
O(12)—H···Cl(23)	3.196(3)	O(21)—H···Cl(0)^a	3.087(3)
Cl(0)—O(11)—Cl(0)^a	86.32(8)	Cu(1)—O(12)—Cl(23)	104.91(12)
Cl(23)—O(12)—Cl(0)^b	122.68(10)	Cu(1)—O(12)—Cl(0)^b	125.78(13)
Cl(33)—O(21)—Cl(0)^a	111.49(10)	Cu(2)—O(21)—Cl(33)	113.77(13)
Cu(1)—O(11)—Cl(0)	128.75(13)	Cu(2)—O(21)—Cl(0)^a	128.63(14)
Cu(1)—O(11)—Cl(0)^a	130.01(13)		

$^a 1 - x, y, 1 - z.$
$^b -x, -y, 1 - z.$

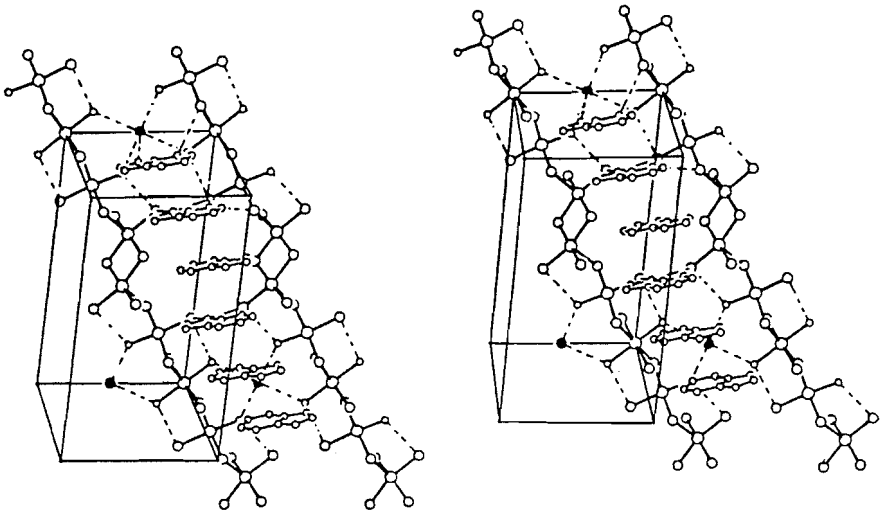

FIG. 6. Stereoview of the unit cell of $(H_2aza)_5[Cu_5Cl_{14}(H_2O)_4]Cl$. Axes *a* (horizontal, left) and *c* (vertical, up) are in the plane of the figure, whereas *b* points toward the reader. The atoms, represented by spheres as in Fig. 5, can be identified from Fig. 4. Hydrogen bonds are shown as dashed lines.

TABLE 6. Distances (Å) and angles (deg) for the hydrogen bonds in the $[Cu_5Cl_{14}(H_2O)_4]^{4-}$ unit

Atoms		Atoms	
O(11)—H···Cl(0)^a	3.206(4)	O(21)—H···Cl(33)	3.148(4)
O(11)—H···Cl(23)	3.240(4)	O(21)—H···Cl(0)	3.058(3)
Cl(23)—O(11)—Cl(0)^a	133.81(14)	Cl(0)—O(21)—Cl(33)	109.87(11)
Cu(1)—O(11)—Cl(23)	101.29(14)	Cu(2)—O(21)—Cl(0)	128.28(15)
Cu(1)—O(11)—Cl(0)^a	119.99(16)	Cu(2)—O(21)—Cl(33)	113.00(14)

$^a -1 + x, y, z.$

Concluding remarks

In the two structures described here, 7-azaindole cannot act as a ligand, since both of its nitrogen donors are protonated. However, as the counter-cation, it plays a determining role in stabilizing an unusual type of chloro-copper(II) chains based on a square-planar building block of three different compositions. Two varieties of periodic chains, respectively based on five- and six-copper patterns, have been found. Both contain the -Cu(2)-Cu(3)-Cu(3)-C(2)- sequence, that is, a dichloro-bridged $[Cu_2Cl_6]^{2-}$ dimer in the middle and $[CuCl_3(H_2O)]^-$ units at each end. Such segments are connected by a single *trans*-$CuCl_2(H_2O)_2$ unit in $(H_2aza)_2[Cu_5Cl_{14}(H_2O)_4]Cl$, but by two such units in $(H_2aza)_3[Cu_3Cl_8(H_2O)_3]Cl$. The extra $CuCl_2(H_2O)_2$ unit in the latter case extends the chain by ~3.45 Å, but this does not lead to disruption of the structure. An extra Cl^- ion is simultaneously added, filling the space in the layer between the new $CuCl_2(H_2O)_2$ in adjacent chains and acting as hydrogen-bonding acceptor for the coordinated water molecules. Also, introducing an extra azaindolium ion extends the cationic stack by the same amount, while providing contributions to stabilization via extra hydrogen bonding and inter-

Can. J. Chem. Downloaded from www.nrcresearchpress.com by 88.255.202.194 on 09/08/12
For personal use only.

ring stacking interactions. Features that likely contribute to the azaindolium ion playing this specific role are the relatively large aromatic system that favours stacking and the orientation of N—H bonds on the same side of the molecule. Judging from the structures observed here, it can be anticipated that increased water content at crystallization time could lead to chains based on a longer basic pattern, in which more than two consecutive $CuCl_2(H_2O)_2$ units could be inserted between the -Cu(2)-Cu(3)-Cu(3)-C(2)- sequences. However, a $CuCl_2(H_2O)_2$–$CuCl_3(H_2O)$ substitution disorder of the type representing ~25% of the structure of the $[Cu_5Cl_{14}(H_2O)_4]^{4-}$ chain is a definite possibility in such systems, because of the similar roles of water and Cl^- as ligands to Cu(II) and hydrogen-bond acceptors.

Acknowledgments

We wish to thank M. Simard and F. Bélanger-Gariépy for their assistance in solving the X-ray structures, and one of the reviewers for helpful suggestions concerning disorder in the $[Cu_5Cl_{14}(H_2O)_4]^{4-}$ chain. The support of the Natural Sciences and Engineering Research Council of Canada is gratefully acknowledged.

1. S. M. Peng and Y. N. Lin. Acta Crystallogr. Sect C: Cryst. Struct. Commun. **C42**, 1725 (1986); S. M. Peng and C. H. Lai. J. Chin. Chem. Soc. (Taipei), **35**, 325 (1988).
2. F. Allaire and A. L. Beauchamp. Inorg. Chim. Acta, **156**, 241 (1989).
3. J. J. H. Edema, S. Gambarotta, A. Meetsma, F. Van Bolhuis, A. L. Spek, and W. J. J. Smeets. Inorg. Chem. **29**, 2147 (1990); L. A. Oro, M. A. Ciriano, B. E. Villaroya, A. Tiripicchio, and F. J. Lahoz. J. Chem. Soc. Dalton Trans. 1891 (1985); F. A. Cotton, D. G. Lay, and M. Millar. Inorg. Chem. **17**, 186 (1978).
4. P. Dufour, Y. Dartiguenave, M. Dartiguenave, N. Dufour, A. M. Lebuis, F. Bélanger-Gariépy, and A. L. Beauchamp. Can. J. Chem. **68**, 193 (1990).
5. R. J. Kline, L. F. Sytsma, and D. R. Shackle. Inorg. Nucl. Chem. Lett. **7**, 311 (1971).
6. N. Dufour, A.-M. Lebuis, M.-C. Corbeil, A. L. Beauchamp, P. Dufour, Y. Dartiguenave, and M. Dartiguenave. Can. J. Chem. **70**, 2914 (1992).
7. W. S. Sheldrick. Z. Naturforsch. B: Anorg. Chem. Org. Chem. **37B**, 653 (1982).
8. F. A. Cotton and T. R. Felthouse. Inorg. Chem. **20**, 600 (1981).
9. F. Allaire and A. L. Beauchamp. Manuscript in preparation.
10. J. Poitras and A. L. Beauchamp. Can. J. Chem. **70**, 2846 (1992).
11. B. J. Hathaway. Comprehensive coordination chemistry. *Edited by* G. Wilkinson, R. D. Gillard, and J. A. McCleverty. Pergamon Press, New York. 1987. Chap. 53.
12. F. Bélanger-Gariépy and A. L. Beauchamp. J. Am. Chem. Soc. **102**, 3461 (1980).
13. International tables for X-ray crystallography. Vol. 3. Kynoch Press, Birmingham. 1968; D. T. Cromer and J. T. Waber. Acta Crystallogr. **18**, 104 (1965); R. F. Stewart, E. R. Davidson, and W. T. Simpson. J. Chem. Phys. **42**, 3175 (1965).
14. D. T. Cromer. Acta Crystallogr. **18**, 17 (1965).
15. G. Sheldrick. SHELX-86. Crystallographic program system. Institute für Anorganische Chemie der Universität Gottingen, Germany. 1986.
16. G. Sheldrick. SHELX-76. Crystallographic program system. Cambridge University, U.K. 1976.
17. K. Yoon, G. Parkin, and A. L. Rheingold. J. Am. Chem. Soc. **114**, 2210 (1992).
18. M. Bukowska-Strzyzewska and J. Skoweranda. Acta Crystallogr. Sect. C: Cryst. Struct. Commun. **C43**, 2290 (1987).
19. J. P. Steadman and R. D. Willett. Inorg. Chim. Acta, **4**, 367 (1970); D. N. Anderson and R. D. Willett. Inorg. Chim. Acta, **8**, 167 (1974).
20. U. Geiser, R. D. Willett, M. Lindbeck, and K. Emerson. J. Am. Chem. Soc. **108**, 1173 (1986).
21. S. A. Roberts, D. R. Bloomquist, R. D. Willett, and H. W. Dodgen. J. Am. Chem. Soc. **103**, 2603 (1981).
22. U. Geiser, R. M. Gaura, R. D. Willett, and D. X. West. Inorg. Chem. **25**, 4203 (1986).
23. B. Scott and R. Willett. Inorg. Chim. Acta, **141**, 193 (1988).
24. M. Bukowska-Strzyzewska, A. Tosik, T. Glowiak, and J. Wnek. Acta Crystallogr. Sect. C: Cryst. Struct. Commun. **C41**, 1184 (1985).
25. G. Valle and R. Ettorre. Acta Crystallogr. Sect. C: Cryst. Struct. Commun. **C48**, 919 (1992); L. K. Thompson, T. C. Woon, D. B. Murphy, E. J. Gabe, F. L. Lee, and Y. Le Page. Inorg. Chem. **24**, 4719 (1985); T. Manfredini, G. C. Pellacani, A. Bonamartini-Corradi, L. P. Battaglia, G. T. Guardini, J. G. Giusti, G. Pon, R. D. Willett, and D. X. West. Inorg. Chem. **29**, 2221 (1990).
26. L. Antolini, G. Marcotrigiano, L. Menabue, and G. C. Pellacani. J. Am. Chem. Soc. **102**, 5506 (1980).
27. T. E. Grigereit, B. L. Ramakrishna, H. Place, R. D. Willett, G. C. Pellacani, T. Manfredini, L. Menabue, A. Bonamartini-Corradi, and L. P. Battaglia. Inorg. Chem. **26**, 2235 (1987).
28. B. K. S. Lundberg. Acta Chem. Scand. **26**, 3977 (1972).
29. B. Morosin. Acta Crystallogr. Sect. B: Struct. Crystallogr. Cryst. Chem. **B31**, 632 (1975); V. H. Crawford and W. E. Hatfield. Inorg. Chem. **16**, 1336 (1977).
30. M. R. Bond, R. D. Willett, and G. V. Rubenacker. Inorg. Chem. **29**, 2713 (1990).
31. R. S. Sager and W. H. Watson. Inorg. Chem. **7**, 2035 (1968).
32. C. P. Landee, A. Djili, D. G. Mudgett, M. Newhall, H. Place, B. Scott, and R. D. Willett. Inorg. Chem. **27**, 620 (1988); M. Studer, A. Reisen, and T. A. Kaden. Helv. Chim. Acta, **72**, 1253 (1989); I. Vasilevesky, N. R. Rose, R. Stenkamp, and R. D. Willett. Inorg. Chem. **30**, 4082 (1991).
33. S. W. Peterson and H. A. Levy. J. Chem. Phys. **26**, 220 (1957).
34. G. H. Stout and L. H. Jensen. X-ray structure determination, a practical guide. Macmillan, London. 1968. p. 303.
35. B. De Castro, C. Freire, D. Domingues, and J. Gomes. Polyhedron, **10**, 2541 (1991); J. A. C. Van Ooijen and J. Reedijk. Inorg. Chim Acta, **25**, 131 (1977); J. E. Ruede and D. A. Thornton. J. Mol. Struct. **34**, 75 (1976); P. T. T. Wong and D. G. Brewer. Can. J. Chem. **46**, 139 (1968); R. J. H. Clark and C. S. Williams. Inorg. Chem. **4**, 350 (1965).

Can. J. Chem. Downloaded from www.nrcresearchpress.com by 88.255.202.194 on 09/08/12
For personal use only.

2-Acylidene-3,5-diaryl-2,3-dihydro-1,3,4-thiadiazoles and related compounds: a question of hypervalent S...O interactions

NARESH PANDYA, ANTHONY J. BASILE, AJAY K. GUPTA, PATRICK HAND, CINDY L. MACLAURIN, TAJ MOHAMMAD, ELAREF S. RATEMI, MARTIN S. GIBSON,[1] AND MARY FRANCES RICHARDSON[1]

Department of Chemistry, Brock University, St. Catharines, Ont., Canada L2S 3A1

Received July 28, 1992

NARESH PANDYA, ANTHONY J. BASILE, AJAY K. GUPTA, PATRICK HAND, CINDY L. MACLAURIN, TAJ MOHAMMAD, ELAREF S. RATEMI, MARTIN S. GIBSON, and MARY FRANCES RICHARDSON. Can J. Chem. **71**, 561 (1993).

A new synthesis of **1** by selective deacetylation of **2** is reported. The acylation step implied in earlier syntheses of **1** and related compounds is exemplified by direct acylations of **3** to give **4***a* and **4***b*. Several new 2-acylidene-3-(2,4-dibromophenyl)-5-phenyl-2,3-dihydro-1,3,4-thiadiazoles (**11**) and thioacylidene analogues (**12**) are described. The crystal structures of **11***a*, **11***b*, **11***c*, and **11***d* reveal a hypervalent interaction, ca. 2.45–2.7 Å long, between the sulfur and carbonyl oxygen atoms. The dibromophenyl ring is nearly perpendicular to the thiadiazole ring plane in the crystal structures, and NMR data suggest that this conformation is maintained in solution. Molecular mechanics calculations show that the S...O interaction need only be a few kilocalories in order to stabilize the observed acylidene side chain configuration over other possible isomers. Crystals of **11***a* are triclinic, $P\bar{1}$, with cell dimensions a = 12.937(2), b = 13.429(2), c = 13.489(2) Å, α = 60.14(1)°, β = 74.59(1)°, γ = 58.70(1)°, Z = 4, and R = 0.044 for 3287 observed reflections. Crystals of **11***b* are monoclinic, $P2_1/c$, with cell dimensions a = 10.512(1), b = 12.084(2), c = 16.268(4) Å, β = 96.91(1)°, Z = 4, R = 0.050 for 1938 observed reflections. Crystals of **11***c* are monoclinic, $P2_1/c$, with cell dimensions a = 17.492(4), b = 16.979(1), c = 14.962(1) Å, β = 106.46(1)°, Z = 8, R = 0.057 for 3112 observed reflections. Crystals of **11***d* are monoclinic, $P2_1/c$, with cell dimensions a = 11.749(1), b = 8.533(1), c = 22.670(4) Å, β = 100.17(1)°, Z = 4, and R = 0.059 for 2265 observed reflections.

NARESH PANDYA, ANTHONY J. BASILE, AJAY K. GUPTA, PATRICK HAND, CINDY L. MACLAURIN, TAJ MOHAMMAD, ELAREF S. RATEMI, MARTIN S. GIBSON et MARY FRANCES RICHARDSON. Can. J. Chem. **71**, 561 (1993).

On décrit une nouvelle synthèse du composé **1** réalisée par une désacétylation sélective du composé **2**. L'étape d'acylation impliquée dans les synthèses antérieures du composé **1** et de ses composés apparentés est démontrée par des acylations directes de **3** qui donnent **4***a* et **4***b*. On décrit plusieurs nouveaux 2-acylidène-3-(2,4-dibromophényl)-5-phényl-2,3-dihydro-1,3,4-thiadiazoles (**11**) et leurs analogues thioacylidènes (**12**). Les structures cristallines des composés **11***a*, **11***b*, **11***c* et **11***d* révèlent l'existence d'une interaction hypervalente, d'une longueur d'environ 2,45–2,7 Å, entre le soufre et l'oxygène du carbonyle. Dans les structures cristallines, le noyau dibromophényle est pratiquement perpendiculaire au plan du noyau thiadiazole et les données de la RMN suggèrent que cette conformation est maintenue en solution. Des calculs de mécanique moléculaire montrent qu'il suffit d'une interaction S···O de quelques kilocalories pour stabiliser la configuration observée pour la chaîne latérale par rapport aux autres isomères possibles. Les cristaux du produit **11***a* sont tricliniques, groupe d'espace $P\bar{1}$, avec a = 12,937(2), b = 13,429(2) et c = 13,489(2) Å, α = 60,14(1)°, β = 74,59(1)° et γ = 58,70(1)°, Z = 4 et R = 0,044 pour 3287 réflexions observées. Les cristaux du produit **11***b* sont monocliniques, groupe d'espace $P1_1/c$, avec a = 10,512(1), b = 12,084(2) et c = 16,268(4) Å, β = 96,91(1)°, Z = 4 et R = 0,050 pour 1938 réflexions observées. Les cristaux du produit **11***c* sont monocliniques, groupe d'espace $P1_1/c$, avec a = 17,492(4), b = 16,979(1) et c = 14,962(1) Å, β = 106,46(1)°, Z = 8 et R = 0,057 pour 3112 réflexions observées. Les cristaux du produit **11***d* sont monocliniques, groupe d'espace $P1_2/c$, avec a = 11,749(1), b = 8,533(1) et c = 22,670(4) Å, β = 100,17(1)°, Z = 4 et R = 0,059 pour 2265 réflexions observées.

[Traduit par la rédaction]

Introduction

We previously described syntheses of a number of 2-acylidene-3,5-diaryl-2,3-dihydro-1,3,4-thiadiazoles such as **1** from a variety of substituted thiohydrazides (1) and 1,3,4-thiadiazolium salts (2). We now report a further synthesis of **1** by acidic hydrolysis of the acetylacetonylidene derivative **2**.

Compounds such as **1** can be regarded as acyl derivatives of methine bases, and, in our view, a reactive methine base is generated *in situ* in the earlier syntheses (1, 2) and then intercepted by the acylating agent present. We have now demonstrated the acylation step for a representative methine base **3** by reaction with two aroyl chlorides to give **4***a* and **4***b*. The enaminic character of **3** is further indicated by its reaction with iodomethane and with trichloroacetic acid to give **5** and **6**, respectively, so providing a parallel with the benzothiazole series (3). We noted, however, that attempted acetylation of **7** gave dimer **8** although the parent thiadiazolium salt reacted normally to give **9**. This behavior recalls that of methine bases in the 1,3,4-oxadiazole series, which form rearranged dimers on attempted acetylation (4). We tried to trap one such methine base, generated *in situ*, but obtained the rearranged dimer **10** (4).

2-Acylidene-3,5-diaryl-2,3-dihydro-1,3,4-thiadiazoles (**11**) and the thioacylidene analogs (**12**) (5) are of interest from a number of points of view. Formally, geometrical isomerism is possible, yet in all syntheses to date only one isomer has

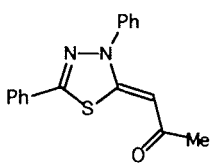

1

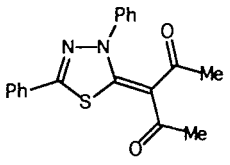

2

[1]Authors to whom correspondence may be addressed.

Can. J. Chem. Downloaded from www.nrcresearchpress.com by 88.255.202.194 on 09/08/12
For personal use only.

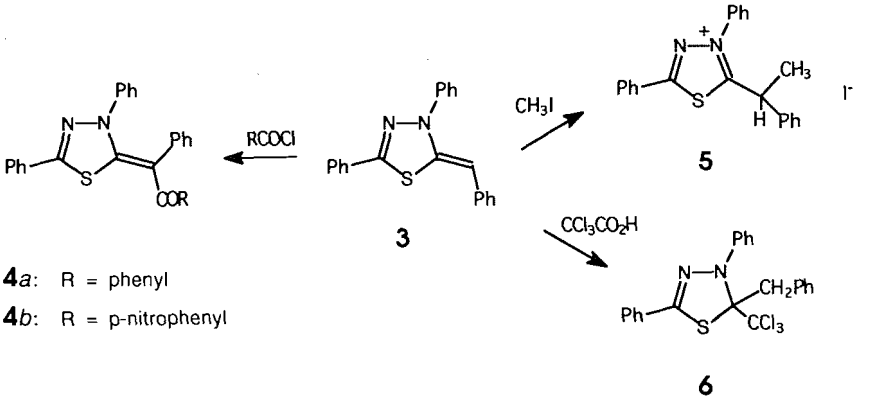

4*a*: R = phenyl
4*b*: R = p-nitrophenyl

3

5

6

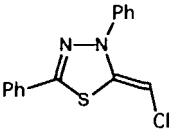

7

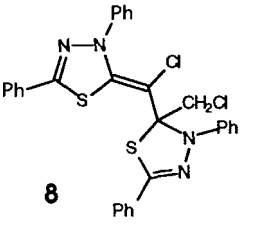

8

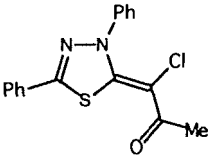

9

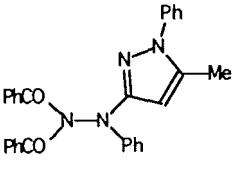

10

been isolated (6). We early suspected that these compounds possessed (*Z*) geometry and might be bicyclic as in **13** (5). We have since prepared a number of acyl compounds **11** (and thioacyl analogues **12**) in which the methine proton is replaced by alkyl in order to determine the overall geometry and the effect of alkyl size on the interatomic S—X (X = O,S) distance and hence the extent of S...X interaction. This paper reports the crystal structures of four acyl compounds **11***a*–**11***d* and interprets the short S...O distance as a hypervalent interaction that stabilizes the (*Z*) configuration.

Experimental section

Instrumentation

The following instruments were used: Analect FX-6220 FT IR spectrophotometer for IR spectra; Bruker WP-60 FT and WP-80 CW spectrometers for ^{1}H NMR spectra (tetramethylsilane was used as an internal standard); DMS 100 UV–visible spectrophotometer for UV spectra (log ε values given in parentheses); AEI MS30 double-beam instrument for mass spectra. Melting points are uncorrected.

Hydrolysis of **2** *(7)*

Compound **2** (1) (50 mg, 0.15 mmol) was refluxed in concentrated HCl (5 mL) for 50 min. When cool, the mixture was neutralized with 1 M NaOH solution, and the solid was collected. Crystallization from absolute EtOH gave **1** (20 mg, 45%), mp 147–149°C, identified by mp and spectral correlation with a reference sample (1).

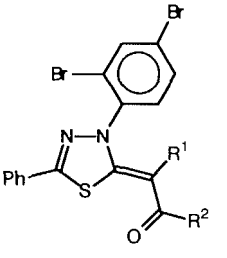

11*a*: R^1 = H, R^2 = Me
11*b*: R^1 = H, R^2 = Ph
11*c*: R^1 = Me, R^2 = Ph
11*d*: R^1 = Et, R^2 = Ph

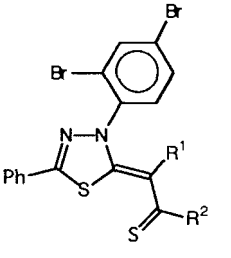

12*a*: R^1 = H, R^2 = Ph
12*b*: R^1 = Me, R^2 = Ph
12*c*: R^1 = Et, R^2 = Ph

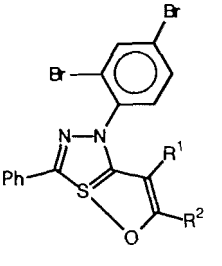

13

Can. J. Chem. Downloaded from www.nrcresearchpress.com by 88.255.202.194 on 09/08/12
For personal use only.

Can. J. Chem. Downloaded from www.nrcresearchpress.com by 88.255.202.194 on 09/08/12
For personal use only.

Reactions of 2-benzylidene-2,3-dihydro-3,5-diphenyl-1,3,4-thiadiazole (3) (8)

(a) Acylation

A solution of the methine base **3** (0.33 g, 1 mmol) in dry benzene (10 mL) containing triethylamine (0.1 g, 1 mmol) and freshly distilled benzoyl chloride (0.14 g, 1 mmol) was refluxed under nitrogen for 2.5 h. The triethylamine hydrochloride was filtered off and the filtrate was evaporated to give a brown solid (0.42 g). Purified by chromatography on silica, the benzoyl derivative **4***a* crystallized from 95% ethanol as yellow prisms (0.39 g, 90%), mp 171–173 °C; UV (MeCN): 242 (4.28) and 387 (4.26) nm; IR (KBr): 1585 (C=O) cm^{-1}; mass spectrum *m/z*: 432 (M^+, base peak). Anal. calcd. for $C_{28}H_{20}N_2OS$: C 77.77, H 4.62, N 6.48; found: C 77.54, H 4.51, N 6.33.

Similarly prepared (2 mmol scale), the *p*-nitrobenzoyl derivative **4***b* crystallized from chloroform–methanol as deep orange needles (0.74 g, 77%), mp 237–240°C; UV (MeCN): 248 (4.31) and 398 (4.16) nm; IR (KBr): 1595 (C=O) cm^{-1}; mass spectrum *m/z*: 477 (M^+, base peak). Anal. calcd. for $C_{28}H_{19}N_3O_3S$: C 70.44, H 3.98, N 8.81; found: C 70.28, H 4.07, N 9.01.

(b) Methylation

A solution of **3** (0.5 g, 1.5 mmol) in MeI (8 mL) was refluxed for 72 h, and excess MeI was then evaporated *in vacuo*. Crystallization from MeCN gave 2-(1-phenethyl)-3,5-diphenyl-1,3,4-thiadiazolium iodide (**5**) as a yellow crystalline solid (0.4 g, 56%), mp 233–235°C; UV (MeCN): 247 (4.32) and 285 (4.00) nm; ^1H NMR (CD_3CN) δ: 1.98 (d, *J* 7 Hz, 3H, CH_3), 4.80 (q, *J* 7 Hz, 1H, CH), and 7.26–8.06 (m, 15H, arom H); mass spectrum *m/z*: 342 (M^+ − HI). Anal. calcd. for $C_{22}H_{19}IN_2S$: C 56.17, H 4.04, I 27.02, N 5.96; found: C 55.99, H 4.11, I 27.31, N 6.02.

(c) Reaction with trichloroacetic acid

A solution of **3** (0.5 g, 1.5 mmol) in dry benzene (10 mL) containing freshly distilled trichloroacetic acid (0.25 g, 1.5 mmol) was refluxed under nitrogen for 1.5 h. The solvent was evaporated *in vacuo* and the residual gum was crystallized from 95% EtOH to give 2-benzyl-2,3-dihydro-3,5-diphenyl-2-trichloromethyl-1,3,4-thiadiazole (**6**) as a yellow crystalline solid (0.55 g, 81%), mp 45–50°C; UV (MeCH): 232 (4.22) and 342 (3.92) nm; ^1H NMR ($CDCl_3$) δ: 3.70 (d, *J* 16 Hz, 1H), 4.10 (d, *J* 16 Hz, 1H), and 7.10–7.75 (m, 15H, arom H); mass spectrum *m/z*: 328 (M^+ − $CHCl_3$). Anal. calcd. for $C_{22}H_{17}Cl_3N_2S$: C 58.86, H 3.79, N 6.24; found: C 59.15, H 3.88, N 6.26.

Attempted acetylation of 7

Compound **7** (8) (0.2 g, 0.7 mmol) was added in portions to a stirred mixture of acetyl chloride (0.1 mL, ca. 1.4 mmol) and dry pyridine (3 mL) at 0°C. The solution was stirred at 0°C for 1 h, and then at room temperature for 4 h. The reaction mixture was poured into water and was extracted with chloroform. The combined organic extracts were washed with water and dried (Na_2SO_4). Evaporation *in vacuo* gave a red solid (0.18 g), which was identified as **8** (8) by comparison with an authentic specimen (mp and mixture mp; ^1H NMR spectrum).

2-(1-Chloroacetonylidene)-2,3-dihydro-3,5-diphenyl-1,3,4-thiadiazole (9)

2-Chloromethyl-3,5-diphenyl-1,3,4-thiadiazolium perchlorate (8) (0.5 g, 1.3 mmol) was added in portions to a stirred mixture of acetyl chloride (0.15 mL, ca. 2.1 mmol) and dry pyridine (5 mL) at 0°C. The resulting dark red mixture was stirred at 0°C for 1 h, and then at room temperature for 30 min. The reaction mixture was poured into water (50 mL) and left overnight. The separated solid was filtered off, washed with water, and dried. Two crystallizations from absolute EtOH gave **9** as a pale yellow crystalline solid (0.20 g, 47%), mp 142–146°C; UV (MeCN): 237 (4.31) and 369 (4.25) nm; IR (KBr): 1600 (C=O) cm^{-1}; ^1H NMR ($CDCl_3$) δ: 2.43 (s, 3H, CH_3) and 7.38–8.13 (m, 10H, arom H); mass spectrum (rel. int.) *m/z*: 328 (M^+, 14%), and 103 (base peak). Anal. calcd. for $C_{17}H_{13}ClN_2OS$: C 62.19, H 3.96, N 8.53; found: C 62.34, H 4.09, N 8.50.

3,5-Diphenyl-2-methyl-1,3,4-oxadiazolium perchlorate and 10

A mixture of *N*-phenylbenzohydrazide (1.0 g, 44 mmol) and acetonitrile (0.3 mL, ca. 53 mmol) in acetic acid (2 mL) and 70% perchloric acid (1 mL) was refluxed for 5 min. When cool, water (20 mL) was added with stirring; the suspension cleared, and the oxadiazolium salt slowly separated as a white crystalline solid (1.5 g, 99%), mp 188–190°C (lit. (4) mp 191–192.5°C).

Treatment of this salt in acetonitrile with triethylamine, alone or in conjunction with acetic or benzoic anhydride, gave 3-(*N'*,*N'*-dibenzoyl-*N*-phenylhydrazino)-5-methyl-1-phenylpyrazole (**10**), identified by correlation of mp and spectral data with published values (4).

2-Acylidene-3,5-diaryl-2,3-dihydro-1,3,4-thiadiazoles (11)

*(a) 11*c

A stirred mixture of *N'*-(2,4-dibromophenyl)-*N'*-propionylbenzothiohydrazide (1) (2.20 g, 5.0 mmol) and benzoic anhydride (6.0 g, 26.5 mmol) in MeCN (15 mL) was refluxed for 3 h. After cooling, 10% aqueous NaOH (75 mL) was added, and the mixture was stirred for 2 h. The separated solid was filtered off, washed with water, and dried. Crystallization from chloroform – light petroleum gave **11**c as a light brown crystalline solid (2.0 g, 76%), mp 199–201°C; UV (MeCN): 237 and 380 nm; IR (KBr): 1595 (C=O) cm^{-1}; ^1H NMR ($CDCl_3$) δ: 1.60 (s, 3H, CH_3) and 7.30–8.00 (m, 13H, arom H); mass spectrum (rel. int.) *m/z*: 526 (M^+, 4%) and 105 (base peak). Anal. calcd. for $C_{23}H_{16}Br_2N_2OS$: C 52.27, H 3.03, N 5.30; found: C 51.96, H 3.04, N 5.05. Crystals were grown from ethyl acetate.

*(b) 11*d

Similarly prepared (1.1 mmol scale), **11***d* crystallized from MeCN as light brown prisms (0.425 g, 72%), mp 153–155°C; UV (MeCN): 238 (4.34) and 375 (4.21) nm; IR (KBr): 1595 (C=O) cm^{-1}; ^1H NMR ($CDCl_3$) δ: 0.57 (t, *J* 7 Hz, 3H, CH_3), 1.94–2.33 (m, 2H, CH_2), and 7.39–7.92 (m, 13H, arom H); mass spectrum (rel. int.) *m/z*: 540 (M^+, 9%) and 105 (base peak). Anal. calcd. for $C_{24}H_{18}Br_2N_2OS$: C 53.14, H 3.32, N 5.17; found: C 53.09, H 3.32, N 4.99. Crystals were grown from acetonitrile.

3,5-Diaryl-2,3-dihydro-2-thioacylidene-1,3,4-thiadiazoles (12)

*(a) 12*b

To a stirred solution of 3-(2,4-dibromophenyl)-2-ethyl-5-phenyl-1,3,4-thiadiazolium perchlorate (2) (0.5 g, 1.5 mmol) and thiobenzoylthioglycollic acid (1.0 g, 4.7 mmol) in absolute EtOH (15 mL) was added triethylamine (0.3 mL). The resulting mixture was refluxed for 20 h. The solvent was evaporated *in vacuo* and the residue was dissolved in chloroform (75mL). The chloroform solution was washed with 5% aqueous NaOH (2 × 25 mL) and water (2 × 25 mL), then dried over Na_2SO_4. Evaporation of chloroform and chromatography on silica gave **12***b*, which crystallized from chloroform–hexane as a brick-red crystalline solid (0.25 g, 48%), mp 303–304°C (dec. after changing colour to yellow-green at 185°C); UV (MeCN): 235 (4.40) and 447 (4.16) nm; ^1H NMR ($CDCl_3$) δ: 1.70 (s, 3H, CH_3) and 7.28–7.91 (m, 13H, arom H); mass spectrum (rel. int.) *m/z*: 542 (M^+, 2%) and 103 (base peak). Anal. calcd. for $C_{23}H_{16}Br_2N_2S_2$: C 50.73, H 2.94, N 5.14; found: C 50.44, H 3.27, N 4.93. Crystals were grown from chloroform.

*(b) 12*c

A stirred suspension of **11***d* (0.75 g, 1.4 mmol) and phosphorus pentasulfide (0.8 g, 3.6 mmol) in dry benzene (25 mL) was refluxed for 30 min. The product was isolated as described for **12***b*.

TABLE 1. Crystal data

	11*a*	**11***b*	**11***c*	**11***d*
Formula	$C_{17}H_{12}Br_2N_2OS$	$C_{22}H_{14}Br_2N_2OS$	$C_{23}H_{16}Br_2N_2OS$	$C_{24}H_{18}Br_2N_2OS$
Formula weight	452.16	514.23	528.26	542.29
Crystal size, mm	—[a]	—[a]	0.34 × 0.15 × 0.11	—[a]
Crystal system	Triclinic	Monoclinic	Monoclinic	Monoclinic
Space group	$P\bar{1}$	$P2_1/c$	$P2_1/c$	$P2_1/c$
Cell dimensions determined from 25 reflections with:	$9° < \theta < 19°$	$10° < \theta < 18°$	$8° < \theta < 16°$	$8° < \theta < 20°$
a, Å	12.937(2)	10.512(1)	17.492(4)	11.749(1)
b, Å	13.429(2)	12.084(2)	16.979(1)	8.533(1)
c, Å	13.489(2)	16.268(4)	14.962(1)	22.670(4)
α, °	60.14(1)	90	90	90
β, °	74.59(1)	96.91(1)	106.46(1)	100.17(1)
γ, °	58.70(1)	90	90	90
V, Å^3	1736.5	2054.5	4261.5	2236.9
Z	4	4	8	4
ρ_{calc}, ρ_{obs} (g cm^{-3})	1.73, —	1.66, —	1.65, 1.62	1.61, —
μ, cm^{-1}	50.6	42.9	41.4	39.5
Reflections collected, max 2θ	$h,\pm k,\pm l$, 50°	$\pm h,k,l$, 40°	$h,k,\pm l$, 50°	$h,\pm k,\pm l$, 50°
Standard reflection, deviation	−1,2,0; ±1.1% −3, 0, 5; ±2.1%	0,3,1; ±0.9%	1,0,6; ±1.6%	2,3,0; −4%
No. of reflections collected	6576	3965	8178	8324
No. of unique reflections	6101	3075	7498	3939
No. of observed reflections	3287 ($I > 2\ \sigma(I)$)	1938 ($I > 3\ \sigma(I)$)	3112 ($I > 3\ \sigma(I)$)	2265 ($I > 3\ \sigma(I)$)
No. of parameters refined	420	254	343	273
Final R, R_w	0.044, 0.046	0.050, 0.053	0.057, 0.059	0.059, 0.065
Final shift/error, max	0.02	0.08	0.06	0.03
Final difference map, max, min (e Å^{-3})	0.74, −0.73	0.87, −0.89	1.16, −1.15	0.91, −0.69
p in weighting scheme, $[\sigma^2(F) + pF^2]^{-1}$	0.0010	0.0010	0.0005	0.0007

[a]Irregular; maximum dimension 0.3 mm.

Crystallization from absolute EtOH gave **12***c* as an orange-red crystalline solid (0.45 g, 58%), mp 265–268°C (dec. after darkening at 150°C); UV (MeCN): 232 (4.45) and 444 (4.09) nm; ^{1}H NMR ($CDCl_3$) δ: 0.63 (t, J 7 Hz, 3H, CH_3), 1.99–2.40 (m, 2H, CH_2), and 7.30–7.94 (m, 13H, arom H); mass spectrum (rel. int.) m/z: 556 (M^+, 6%) and 103 (base peak). Anal. calcd. for $C_{24}H_{18}Br_2N_2S_2$: C 51.61, H 3.22, N 5.01; found; C 50.83, H 3.21, N 4.76. Crystals were grown from acetonitrile.

Crystal structure determinations

Crystals of **11***c* and **11***d* were obtained as described above; **11***a* and **11***b* were prepared in previous work (1). Unit cell dimensions were determined from the angular setting of 25 reflections measured with graphite-monochromatized MoKα radiation (λ = 0.71069 Å). Intensities were measured by the ω–2θ technique at room temperature (293–298 K) with an Enraf–Nonius CAD4 single-crystal diffractometer and corrected for Lorentz and polarization effects but not for absorption. The structures were solved by Patterson methods and refined by full-matrix least-squares techniques (**11***b* and **11***d*) or by block-diagonal least squares (**11***a* and **11***c*) with each block containing all of the atoms in one independent molecule plus the sulfur and bromine atoms in the second. Hydrogen atom positions were calculated. Anisotropic displacement parameters were assigned to all atoms except hydrogen in **11***a*, **11***b*, and **11***d*. The phenyl carbons and the hydrogens in **11***c* were refined with isotropic displacement parameters; the remaining atoms were refined with anisotropic displacement parameters. Scattering factors, including the real and imaginary parts of the anomalous scattering, were taken from the *International tables for X-ray crystallography* (9). The weighting scheme was $w = [\sigma^2(F) + p\,F^2]^{-1}$ with a value of p assigned to minimize the variance as a function of reflection intensity. Programs used included SHELX-76 (10) and ORTEP (11). The largest peaks and holes on the final difference maps (ca. ±1 e Å^{-3}) were located near the bromines, and are due to the lack of an absorption correction. The crystal data and experimental details are listed in Table 1. The final parameters are given in Tables 2–5.[2]

Molecular mechanics

Molecular mechanics calculations were carried out with Chem3D Plus (Cambridge Scientific Computing, Cambridge, Mass.), which implements Allinger's MM2 force field (12) with automatic π-calculation. A few new parameters were introduced and standard parameters were modified slightly to reproduce the structure of **11***a*; the full parameter set is given in the Supplementary Material.

Results and discussion

Syntheses and characterization

Syntheses of **11***a* and **11***b* were described previously (1); compounds **11***c* and **11***d* were prepared from the corresponding *N'*-acyl-*N'*-(2,4-dibromophenyl)benzothiohydra-

[2]Packing diagrams, anisotropic displacement parameters, hydrogen atom positions, short contact distances, bond distances and angles in the phenyl rings and side chains, least-squares planes, and structure factor tables for **11***a*–**11***d*, as well as molecular mechanics parameters and the results of the Cambridge Crystallographic Database Search, may be purchased from: The Depository of Unpublished Data, CISTI, National Research Council Canada, Ottawa, Canada K1A 0S2.

Packing diagrams and tables of hydrogen atom positions, short contact distances, and bond distances and angles have also been deposited with the Cambridge Crystallographic Data Centre and can be obtained on request from The Director, Cambridge Crystallographic Data Centre, University Chemical Laboratory, 12 Union Road, Cambridge, CB2 1EZ, U.K.

Can. J. Chem. Downloaded from www.nrcresearchpress.com by 88.255.202.194 on 09/08/12
For personal use only.

Can. J. Chem. Downloaded from www.nrcresearchpress.com by 88.255.202.194 on 09/08/12
For personal use only.

TABLE 2. Fractional coordinates and displacement parameters for **11***a*

Atom	*x*	*y*	*z*	U_{eq}[a]
Br(1A)	0.10616(7)	0.07036(7)	0.43421(7)	0.071
Br(2A)	0.49743(8)	−0.22301(7)	0.73461(7)	0.080
S(A)	−0.0484(1)	0.5090(1)	0.3037(1)	0.048
O(A)	−0.2023(4)	0.5443(4)	0.4759(4)	0.063
N(1A)	0.1690(4)	0.3349(4)	0.2895(4)	0.046
N(2A)	0.1352(4)	0.2973(4)	0.4044(4)	0.046
C(1A)	0.0946(5)	0.5086(5)	0.1022(5)	0.044
C(2A)	−0.0017(6)	0.6194(6)	0.0348(6)	0.055
C(3A)	0.0116(7)	0.6757(7)	−0.0803(7)	0.069
C(4A)	0.1220(8)	0.6190(7)	−0.1329(6)	0.071
C(5A)	0.2160(7)	0.5103(7)	−0.0679(6)	0.068
C(6A)	0.2046(6)	0.4549(6)	0.0506(6)	0.056
C(7A)	0.0817(5)	0.4440(5)	0.2265(5)	0.042
C(8A)	0.2187(5)	0.1760(5)	0.4830(5)	0.046
C(9A)	0.2200(6)	0.0619(6)	0.5039(5)	0.048
C(10A)	0.3042(6)	−0.0566(6)	0.5782(5)	0.054
C(11A)	0.3836(5)	−0.0607(6)	0.6323(5)	0.053
C(12A)	0.3812(6)	0.0523(7)	0.6130(6)	0.062
C(13A)	0.2987(6)	0.1697(6)	0.5383(6)	0.059
C(14A)	0.0244(5)	0.3744(5)	0.4320(5)	0.046
C(15A)	−0.0250(5)	0.3554(6)	0.5381(5)	0.049
C(16A)	−0.1380(6)	0.4438(6)	0.5569(6)	0.052
C(17A)	−0.1859(6)	0.4168(7)	0.6774(6)	0.067
Br(1B)	0.39394(7)	0.61055(7)	0.06589(7)	0.072
Br(2B)	0.00260(8)	1.00916(8)	−0.23459(7)	0.080
S(B)	0.5488(1)	0.7643(2)	0.1959(1)	0.048
O(B)	0.7039(4)	0.8168(4)	0.0259(4)	0.062
N(1B)	0.3317(4)	0.7929(5)	0.2114(4)	0.047
N(2B)	0.3645(4)	0.8365(5)	0.0970(4)	0.049
C(1B)	0.4063(5)	0.7056(5)	0.3967(5)	0.045
C(2B)	0.5013(6)	0.6532(6)	0.4644(6)	0.056
C(3B)	0.4868(8)	0.6072(7)	0.5811(7)	0.070
C(4B)	0.3799(8)	0.6080(7)	0.6324(6)	0.072
C(5B)	0.2846(7)	0.6611(7)	0.5651(6)	0.069
C(6B)	0.2934(6)	0.7119(6)	0.4484(6)	0.057
C(7B)	0.4180(5)	0.7534(5)	0.2727(5)	0.042
C(8B)	0.2821(5)	0.8779(6)	0.0156(5)	0.048
C(9B)	0.2790(6)	0.7878(6)	−0.0049(5)	0.050
C(10B)	0.1971(6)	−0.8265(6)	0.0813(5)	0.055
C(11B)	0.1171(6)	0.9544(6)	−0.1314(5)	0.053
C(12B)	0.1192(6)	1.0450(6)	−0.1139(6)	0.060
C(13B)	0.2004(6)	1.0070(6)	−0.0408(6)	0.063
C(14B)	0.4769(5)	0.8303(6)	0.0690(6)	0.047
C(15B)	0.5254(6)	0.8685(6)	−0.0381(6)	0.050
C(16B)	0.6387(6)	0.8624(6)	−0.0561(6)	0.051
C(17B)	0.6848(6)	0.9093(7)	−0.1785(6)	0.066

[a]$U_{eq} = 1/3\ \Sigma\Sigma U_{ij} a_i^* a_j^* \mathbf{a}_i \cdot \mathbf{a}_j$.

TABLE 3. Fractional coordinates and displacement parameters for **11***b*

Atom	*x*	*y*	*z*	U_{eq}[a]
Br(1)	0.47093(9)	0.29353(7)	−0.00406(7)	0.086
Br(2)	0.16454(7)	0.64116(6)	0.08684(7)	0.087
S	0.2522(2)	−0.0544(1)	0.0165(1)	0.044
O	0.0794(5)	−0.0855(4)	−0.1123(3)	0.057
N(1)	0.3458(5)	0.1121(4)	0.1036(4)	0.043
N(2)	0.2492(5)	0.1503(4)	0.0445(3)	0.042
C(1)	0.4577(7)	−0.0558(5)	0.1477(4)	0.042
C(2)	0.4318(8)	−0.1608(6)	0.1754(5)	0.054
C(3)	0.5285(10)	−0.2183(7)	0.2241(5)	0.071
C(4)	0.6452(9)	−0.1717(8)	0.2451(5)	0.072
C(5)	0.6694(7)	−0.0650(8)	0.2187(5)	0.066
C(6)	0.5755(7)	−0.0075(6)	0.1690(4)	0.051
C(7)	0.3582(6)	0.0065(5)	0.0947(4)	0.039
C(8)	0.2232(6)	0.2668(5)	0.0473(4)	0.039
C(9)	0.3168(6)	0.3424(5)	0.0330(4)	0.043
C(10)	0.3009(7)	0.4533(5)	0.0433(4)	0.047
C(11)	0.1864(7)	0.4882(5)	0.0682(4)	0.048
C(12)	0.0889(6)	0.4147(5)	0.0819(4)	0.045
C(13)	0.1101(7)	0.3029(5)	0.0718(4)	0.043
C(14)	0.1905(6)	0.0760(5)	−0.0088(4)	0.036
C(15)	0.0964(6)	0.0994(5)	−0.0725(4)	0.044
C(16)	0.0460(6)	0.0118(5)	−0.1260(4)	0.043
C(17)	−0.0500(6)	0.0391(6)	−0.1990(4)	0.046
C(18)	−0.1201(8)	−0.0471(7)	−0.2375(5)	0.065
C(19)	−0.2138(9)	−0.0234(8)	−0.3055(6)	0.074
C(20)	−0.2313(8)	0.0793(9)	−0.3340(6)	0.077
C(21)	−0.1623(8)	0.1668(8)	−0.2972(5)	0.070
C(22)	−0.0694(7)	0.1464(6)	−0.2300(5)	0.051

[a]$U_{eq} = 1/3\ \Sigma\Sigma U_{ij} a_i^* a_j^* \mathbf{a}_i \cdot \mathbf{a}_j$.

zide and benzoic anhydride. Of the corresponding thioacyl derivatives, **12***a* was prepared from thiobenzoylthioglycollic acid and the required thiadiazolium salt by the literature method (2). This method was successfully extended to the preparation of **12***b*, although a small amount of PhCSOEt was also apparently formed. However, PhCSOEt emerged as the main product (IR, NMR, and mass spectral identification) recovered from the complex mixture obtained when a similar synthesis of **12***c* was attempted. This compound was therefore prepared, though not in analytically pure condition, from **11***d* and phosphorus pentasulfide (5); Lawesson's reagent (13), as an alternative reagent to phosphorus pentasulfide, proved unsuitable for this purpose. We did not obtain crystals suitable for X-ray structure determinations for any of the thioacyl compounds.

As noted, we early suspected that compounds such as **1** and their thioacyl analogues possessed (*Z*) geometry and might even be bicyclic structures such as **13** (5). For compounds like **1**, our suspicions were aroused by the somewhat low frequency (ca. 1600 cm^{-1}) observed for carbonyl absorption in the IR spectra (for similar quinoline derivatives **14** with R = Me or Et, the carbonyl absorption band is at 1635 cm^{-1} (14)). For the thioacyl compounds, our suspicions were based on mass spectra; for example, **11***b* shows *m/z* 105 (PhCO) as base peak, whereas **12***a* shows *m/z* 103 (PhCN) as base peak, with a peak at *m/z* 425 (12%) (M − PhCN) that suggests S–S interaction. Similar features are exhibited by compounds **11***c* and **11***d*, and by **12***b* and **12***c*, though the last does not show a detectable (M − PhCN) fragment.

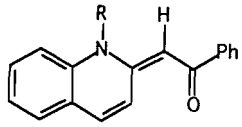

14

Molecular structures

The structures of **11***a*–**11**d are shown in Figs. 1–4, and important distances and angles are listed in Table 6. Bond distances lie within the range of values established for similar structural fragments (15). The six independent mole-

Can. J. Chem. Downloaded from www.nrcresearchpress.com by 88.255.202.194 on 09/08/12
For personal use only.

TABLE 4. Fractional coordinates and displacement parameters for **11***c*

Atom	*x*	*y*	*z*	*U* or U_{eq}[a]
Br(1A)	0.19227(7)	0.48704(7)	0.37576(10)	0.064
Br(2A)	0.19769(8)	0.16801(7)	0.27568(9)	0.070
S(A)	0.4161(1)	0.5841(1)	0.5586(2)	0.032
O(A)	0.4439(3)	0.6619(3)	0.4308(3)	0.041
N(1A)	0.3662(4)	0.4508(3)	0.4955(4)	0.031
N(2A)	0.3647(4)	0.4462(4)	0.5882(4)	0.035
C(1A)	0.3971(4)	0.5275(4)	0.7269(5)	0.029(2)
C(2A)	0.4149(5)	0.6018(6)	0.7633(8)	0.055(3)
C(3A)	0.4217(6)	0.6166(6)	0.8579(8)	0.062(3)
C(4A)	0.4146(6)	0.5573(6)	0.9146(9)	0.070(4)
C(5A)	0.3941(8)	0.4821(8)	0.8770(10)	0.083(4)
C(6A)	0.3885(6)	0.4668(6)	0.7848(8)	0.064(3)
C(7A)	0.3903(4)	0.5132(5)	0.6272(5)	0.033
C(8A)	0.3261(4)	0.3858(4)	0.4395(5)	0.030(2)
C(9A)	0.2481(5)	0.3913(4)	0.3842(5)	0.036(2)
C(10A)	0.2104(5)	0.3266(5)	0.3335(6)	0.044(3)
C(11A)	0.2500(5)	0.2572(5)	0.3395(5)	0.036(2)
C(12A)	0.3285(5)	0.2496(5)	0.3948(5)	0.035(2)
C(13A)	0.3658(5)	0.3152(4)	0.4446(5)	0.036(3)
C(14A)	0.3910(4)	0.5189(4)	0.4635(6)	0.031
C(15A)	0.3981(5)	0.5364(5)	0.3773(5)	0.033
C(16A)	0.4232(4)	0.6149(5)	0.3640(5)	0.030
C(17A)	0.4252(4)	0.6437(4)	0.2710(5)	0.027(2)
C(18A)	0.4894(5)	0.6880(4)	0.2662(6)	0.036(3)
C(19A)	0.4923(5)	0.7203(5)	0.1816(6)	0.050(3)
C(20A)	0.4311(5)	0.7068(5)	0.1023(6)	0.048(3)
C(21A)	0.3670(5)	0.6639(5)	0.1057(6)	0.046(3)
C(22A)	0.3636(5)	0.6300(5)	0.1892(6)	0.042(3)
C(23A)	0.3851(5)	0.4750(5)	0.3014(6)	0.038(3)
Br(1B)	0.08038(9)	0.33024(7)	0.48870(11)	0.079
Br(2B)	0.36453(7)	0.15489(9)	0.61649(10)	0.084
S(B)	−0.1416(2)	0.1348(2)	0.3945(2)	0.047
O(B)	−0.1824(3)	0.0902(3)	0.5319(4)	0.054
N(1B)	0.0052(4)	0.1648(4)	0.4468(5)	0.047
N(2B)	−0.0150(4)	0.1811(4)	0.3529(5)	0.053
C(1B)	−0.1301(5)	0.1792(5)	0.2169(6)	0.042(3)
C(2B)	−0.2108(5)	0.1950(5)	0.1867(6)	0.046(3)
C(3B)	−0.2471(6)	0.2048(5)	0.0910(6)	0.048(3)
C(4B)	−0.2037(6)	0.1993(5)	0.0307(8)	0.055(3)
C(5B)	−0.1240(6)	0.1832(5)	0.0579(8)	0.059(3)
C(6B)	−0.0862(6)	0.1728(5)	0.1535(6)	0.049(3)
C(7B)	−0.0894(5)	0.1681(5)	0.3177(6)	0.045
C(8B)	0.0899(5)	0.1633(5)	0.4912(6)	0.046(3)
C(9B)	0.1331(5)	0.2325(5)	0.5123(6)	0.043(3)
C(10B)	0.2153(5)	0.2306(5)	0.5518(6)	0.050(3)
C(11B)	0.2520(5)	0.1588(5)	0.5674(6)	0.050(3)
C(12B)	0.2113(6)	0.0893(6)	0.5463(6)	0.057(3)
C(13B)	0.1286(5)	0.0919(6)	0.5088(6)	0.053(3)
C(14B)	−0.0523(5)	0.1410(5)	0.4862(6)	0.040
C(15B)	−0.0477(5)	0.1240(5)	0.5762(6)	0.046
C(16B)	−0.1178(6)	0.0959(5)	0.5968(8)	0.048
C(17B)	−0.1182(5)	0.0720(5)	0.6902(6)	0.048(3)
C(18B)	−0.1820(6)	0.0922(6)	0.7235(8)	0.062(3)
C(19B)	−0.1855(8)	0.0699(8)	0.8112(9)	0.083(4)
C(20B)	−0.1270(8)	0.0248(6)	0.8666(9)	0.076(4)
C(21B)	−0.0630(6)	0.0013(6)	0.8364(8)	0.068(4)
C(22B)	−0.0593(6)	0.0244(6)	0.7482(8)	0.064(3)
C(23B)	0.0252(6)	0.1471(6)	0.6559(8)	0.057(3)

[a] $U_{eq} = 1/3\ \Sigma\Sigma U_{ij} a_i^* a_j^* \mathbf{a}_i \cdot \mathbf{a}_j$.

TABLE 5. Positional parameters and equivalent isotropic displacement parameters for **11***d*

Atom	*x*	*y*	*z*	U_{eq}[a]
Br(1)	0.37918(9)	0.28258(10)	0.44335(5)	0.070
Br(2)	0.46580(11)	0.90190(12)	0.38269(6)	0.103
S	0.0274(2)	0.0940(2)	0.3304(1)	0.046
O	0.0769(5)	−0.0271(7)	0.2396(2)	0.064
N(1)	0.0843(6)	0.3280(9)	0.4008(3)	0.060
N(2)	0.1492(6)	0.3367(8)	0.3557(3)	0.059
C(1)	−0.0592(6)	0.1692(9)	0.4359(3)	0.046
C(2)	−0.1360(7)	0.0470(10)	0.4247(4)	0.065
C(3)	−0.2070(8)	0.0048(11)	0.4649(4)	0.075
C(4)	−0.2011(9)	0.0881(12)	0.5164(4)	0.074
C(5)	−0.1254(8)	0.2123(12)	0.5293(4)	0.075
C(6)	−0.0541(8)	0.2513(10)	0.4886(4)	0.062
C(7)	0.0186(6)	0.2105(10)	0.3939(3)	0.047
C(8)	0.2257(7)	0.4665(10)	0.3603(3)	0.048
C(9)	0.3284(7)	0.4647(8)	0.3978(3)	0.044
C(10)	0.4006(7)	0.5925(9)	0.4049(3)	0.051
C(11)	0.3653(8)	0.7249(9)	0.3724(4)	0.058
C(12)	0.2609(8)	0.7317(10)	0.3368(4)	0.063
C(13)	0.1887(8)	0.6045(12)	0.3301(3)	0.064
C(14)	0.1338(6)	0.2212(9)	0.3132(3)	0.050
C(15)	0.1880(7)	0.1999(10)	0.2641(3)	0.056
C(16)	0.1522(6)	0.0636(9)	0.2280(3)	0.045
C(17)	0.2090(6)	0.0245(9)	0.1753(3)	0.049
C(18)	0.2885(8)	−0.0959(13)	0.1789(4)	0.080
C(19)	0.3365(8)	−0.1394(14)	0.1283(5)	0.084
C(20)	0.3072(8)	−0.0609(12)	0.0766(4)	0.069
C(21)	0.2274(9)	0.0545(12)	0.0716(4)	0.078
C(22)	0.1774(8)	0.0992(11)	0.1200(4)	0.063
C(23)	0.2780(12)	0.3271(18)	0.2395(6)	0.129
C(24)	0.3847(18)	0.2785(20)	0.2651(6)	0.164

[a] $U_{eq} = 1/3\ \Sigma\Sigma U_{ij} a_i^* a_j^* \mathbf{a}_i \cdot \mathbf{a}_j$.

cules exhibit several common features: a short S...O contact (2.463–2.691 Å), essentially planar thiadiazole rings with the C(15)—C(16)—O side chain deviating only slightly from the plane of the thiadiazole ring, and the dibromophenyl ring nearly perpendicular to the thiadiazole ring (N(1)—N(2)—C(8)—C(9) torsion angles of 63.1–97.0°). The C(14)—C(15) and C(15)—C(16) distances, intermediate between single and double bond lengths, show that there is delocalization in the C(14)—C(15)—C(16)—O moiety. However, the C(16)—O distances are not significantly longer than the expected distance for a C=O bond (15).

The S...O contacts in all six independent molecules in **11***a*–**11***d* adhere closely to the geometry observed by Rosenfield, Parthasarathy, and Dunitz (16) for the approach of nucleophiles to divalent sulfur: the C(7)—S...O and S...O—C(16) angles of ≈165° and 100°, respectively, are consistent with a hypervalent interaction in which a pair of electrons from the carbonyl donates to a C—S σ* orbital (16), or with σ-bond coupling between a filled oxygen *p*-orbital with an empty sulfur $d_{x^2-y^2}$ orbital (17). Both bonding models explain the shift of the carbonyl stretching frequency to ≈1600 cm^{-1}, and both are consistent with a structure lying along the reaction coordinate that connects the monocyclic **11** and the bicyclic **13** (18). The S...O distance varies with the substituents, and is longest when R^1 = H (**11***a*, **11***b*). Replacement of the methine proton by methyl (**11***c*) or ethyl (**11***d*) shortens the S...O distance by ca. 0.20 Å. The shortening can be interpreted in terms of steric crowding, as the N(2)—C(14)—C(15) and C(15)—C(16)—C(17) angles increase to accommodate the bulkier alkyl groups.

There are also trends in the C(15)—C(16) distance and C(14)—C(15)—C(16) angle with substituent: when R^2 =

Can. J. Chem. Downloaded from www.nrcresearchpress.com by 88.255.202.194 on 09/08/12
For personal use only.

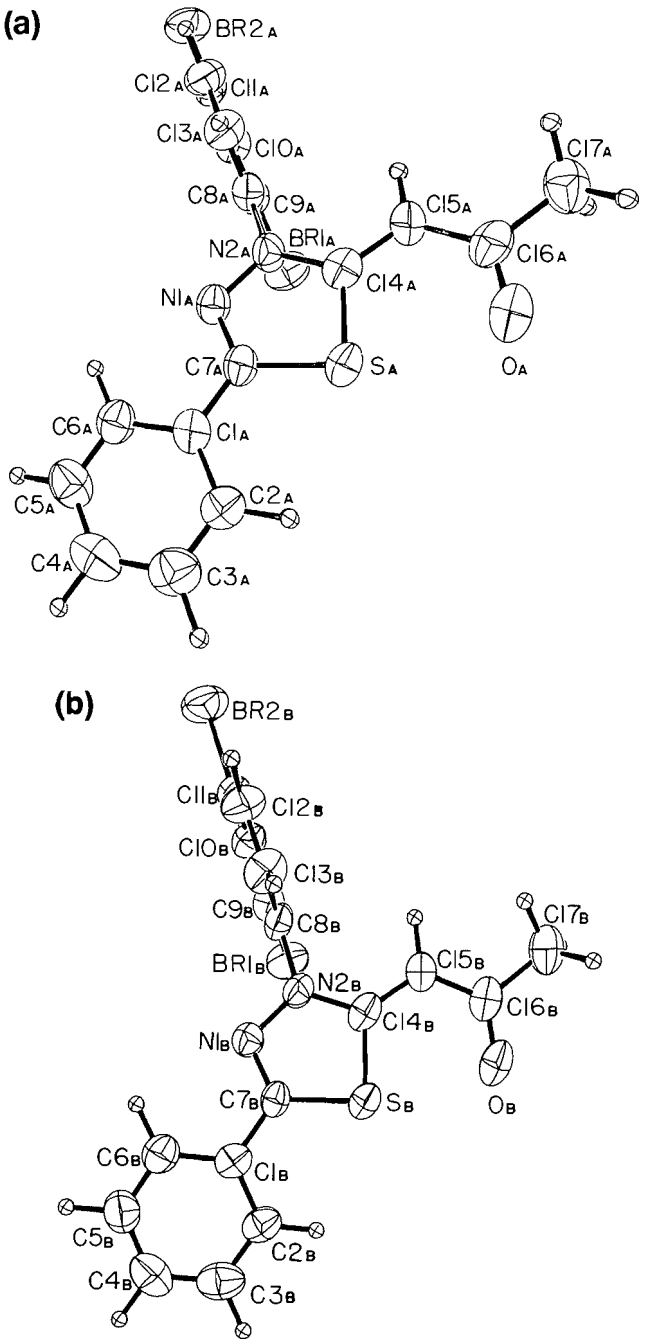

FIG. 1. Independent molecules (*a*) A and (*b*) B in the structure of **11***a*.

methyl (**11**a), C(15)—C(16) is ca. 0.05 Å shorter and C(14)—C(15)—C(16) is ca. 3° larger than when R^2 = phenyl (**11***b*, **11***c*, **11***d*). These changes, which are due to electronic effects, also affect the S...O distance so that it is nearly the same in **11***a* and **11***b*.

The orientation of the dibromophenyl ring nearly perpendicular to the thiadiazole plane was unexpected since phenyl rings do not normally twist greatly out of the plane of another delocalized ring system (e.g., note the N(1)—C(7)—C(1)—C(2) torsion angles in the present structures; Table 6). A search of the Cambridge Crystallographic Database (ref. 19; see supplementary information) yielded eight structures having 2-bromophenyl rings attached to planar atoms in 5- or 6-membered rings. Of the eight, only one had a dihedral angle less than 50°. That such a large dihedral angle is maintained across a spectrum of different compounds is an indication that it reflects the most favorable conformation of a 2-bromophenyl ring. This is an important point since below we shall interpret NMR spectra in terms of the differing phenyl and dibromophenyl ring conformations in **7**, **11**, and **12** and their corresponding nonbrominated analogues.

Two of the structures (**11***a* and **11***c*) have two independent molecules in the asymmetric unit. This phenomenon occurs with reasonable frequency in lower-symmetry space groups (20), and sometimes the independent molecules have essentially identical conformations (21). The conformations of molecules A and B in **11***c* are quite different (note the N(1)—N(2)—C(8)—C(9), N(1)—C(7)—C(1)—C(2), and C(15)—C(16)—C(17)—C(18) torsion angles in Table 6), whereas molecules A and B in **11***a* are essentially identical. We checked carefully for higher symmetry in **11***a*, especially since there is a pseudo-monoclinic C-centred cell that can be derived from the triclinic cell. However, nominally equivalent reflections in the monoclinic cell did not have the same intensity, and the final structure showed that molecules A and B are not related by a monoclinic symmetry element.

In every structure, the C(12)—H and (or) C(13)—H groups in the dibromophenyl ring make short contacts with carbonyl oxygens in adjacent molecules. Some of these contacts are short enough to be regarded as C—H...O hydrogen bonds (22).

Molecular mechanics, isomerism, and conformations

Molecular mechanics allows a semiquantitative estimate of the relative energies of isomers and conformers of a given molecule. The accuracy of the calculated structure and the steric energy depend on the quality of the parameters, which are less well established for molecules such as **11***a*–**11***d* than for simpler compounds. For example, the MM2 minimization of **11***a* gave structures with the dibromophenyl ring included at an angle of ≈32° with respect to the thiadiazole plane, and a corresponding energy of 1–5 kcal less than the observed conformation with the dibromophenyl ring perpendicular to the plane. The final torsion angle of the dibromophenyl ring depended on the parameters associated with the lone pair on N(1). The S...O and other distances varied with the orientation of the dibromophenyl ring and, in order to produce consistent results, minimizations were carried out with the N(1)—N(2)—C(8)—C(9) torsion angles fixed at the values observed in the crystal structures.

Scheme 1 shows the possible isomers/conformers of **11**, designated as if there were no delocalization in the side chain. In **11***a* (R^1 = H, R^2 = CH_3), the two (*Z*) conformers in Scheme 1 both have lower steric energies (21.7 and 21.8 kcal) than the two (*E*) conformers (23.7 and 27.2 kcal). The steric energies of (*Z*) conformers 1 and 2 remain similar as R^2 is changed to phenyl, but the steric energy of (*E*) conformer 2 increases sharply unless the R^2CO group is rotated out of the thiadiazole plane. The similar steric energies of both of the (*Z*) conformers is an additional argument for a hypervalent S...O interaction, whose energy need be no more than a few kilocalories to account for the overwhelming predominance of conformer 1. These results are consistent with quantum chemical calculations that show the

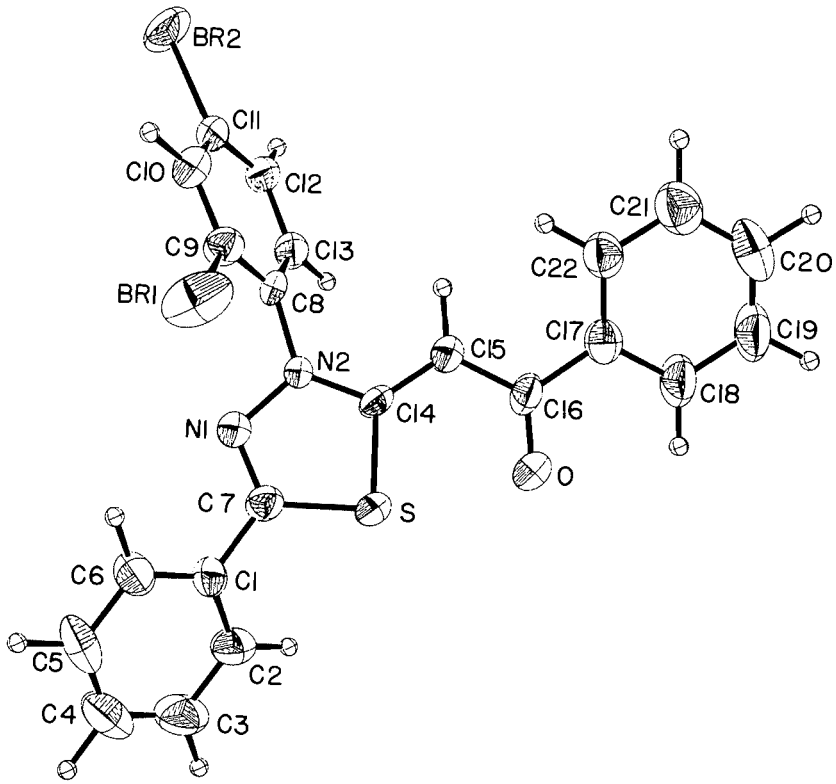

FIG. 2. The structure of **11***b*.

S...O interaction in $CH_3SCH{=}CHCHO$ to be equivalent to about 10% of a usual single bond (23).

The minimized "single-ring" structures shown as (*Z*) conformer 1 in Scheme 1 had S...O distances ≈0.2 Å longer than observed in the crystal structures. Decreasing the S—O distance (by changing the angles at C(14), C(15), and C(16)) resulted in increased van der Waals repulsions of several kilocalories. When the MM2 parameter set was changed to allow for an additional bond between S and O, the minimized structures more closely resembled the observed structures. The MM2 calculations reproduced the bond angle changes in bond angles and S...O distances that occurred as R^1 and R^2 were varied, thus substantiating the proposal that substituent effects in the series **11***a*–**11***d* are steric rather than electronic in nature.

Calculations for **11***d* show that the ethyl group is tightly sandwiched between the phenyl and dibromophenyl rings. Rotation of the ethyl group results in severe high-energy strain in the rest of the molecule. Hindered rotation is thus very likely the cause of the complex ^{1}H NMR spectrum for the CH_2 group in **11***d* and **12***c*, as well as for the apparent disorder of the ethyl group in the crystal structure of **11***d*. (The large displacement parameters and the uncertainty in the positions suggest disorder; unfortunately the difference map did not clearly reveal a second position for the methyl carbon C(24).)

NMR spectra and conformations in solution

It is interesting to recall that the ^{1}H NMR spectra of compounds such as **11***a* and **11***b*, which contain an *ortho* substituent in the N-aryl group, display the methine proton signal ca. 0.6 ppm upfield from that for analogous compounds containing no such *ortho* substituent (8). This is compatible with (*Z*) geometry and a conformation in solution in which the N-aryl group is twisted out of the plane of the thiadiazole ring. This implies that the conformation in solution is similar to the structure in the crystal, and that it is not simply a crystal packing effect that holds the dibromophenyl rings nearly perpendicular to the thiadiazole ring plane. Similar shifts have been noted for thioacyl derivatives **12**, from which (*Z*) geometry and a perpendicular dibromophenyl ring may also be inferred, as well as for chloromethylene derivatives like **7**. Indeed the close similarity in ^{1}H NMR spectra of **11***b*–*d* and **12***a*–*c*, respectively, implies similar conformations and thus a significant hypervalent S...S interaction in the thioacylidene series of compounds **12**. A hypervalent S...Cl interaction may additionally stabilize compounds such as **7**.

The ^{1}H NMR spectrum of **2**, run at ambient temperature, is also of interest in that the methyl protons appear as a singlet (1). This suggests appreciable single bond character for the carbon–carbon "double bond", analogous to the C(14)—C(15) bonds in **11***a*–**11***d*, with a low barrier to rotation. This is borne out by a low-temperature study. The ^{1}H NMR spectrum of **2** (in CD_2Cl_2) at 183 K shows two distinct singlets at δ 1.85 and 2.23 for the protons of the two methyl groups. As the temperature is raised, the intensities of these two signals decrease and the signals broaden. By 213 K, the two signals have collapsed to a broad hump that continues to sharpen, and by 303 K only one sharp signal is observed for the two methyl groups, at δ 2.04. Lowering of this rotational barrier is thus associated with (electrophilic) acetylation of **1** to give 2 (1). This is relevant to electrophilic substitution in the 1,6,6a-trithiapentalene series where ring opening – rotation – alternative ring closure reactions have been observed during nitrosation (24) and treatment with aryl diazonium ions (25); 1-oxa-6,6a-dithiapentalenes behave similarly in the latter reaction (25).

Can. J. Chem. Downloaded from www.nrcresearchpress.com by 88.255.202.194 on 09/08/12
For personal use only.

Can. J. Chem. Downloaded from www.nrcresearchpress.com by 88.255.202.194 on 09/08/12
For personal use only.

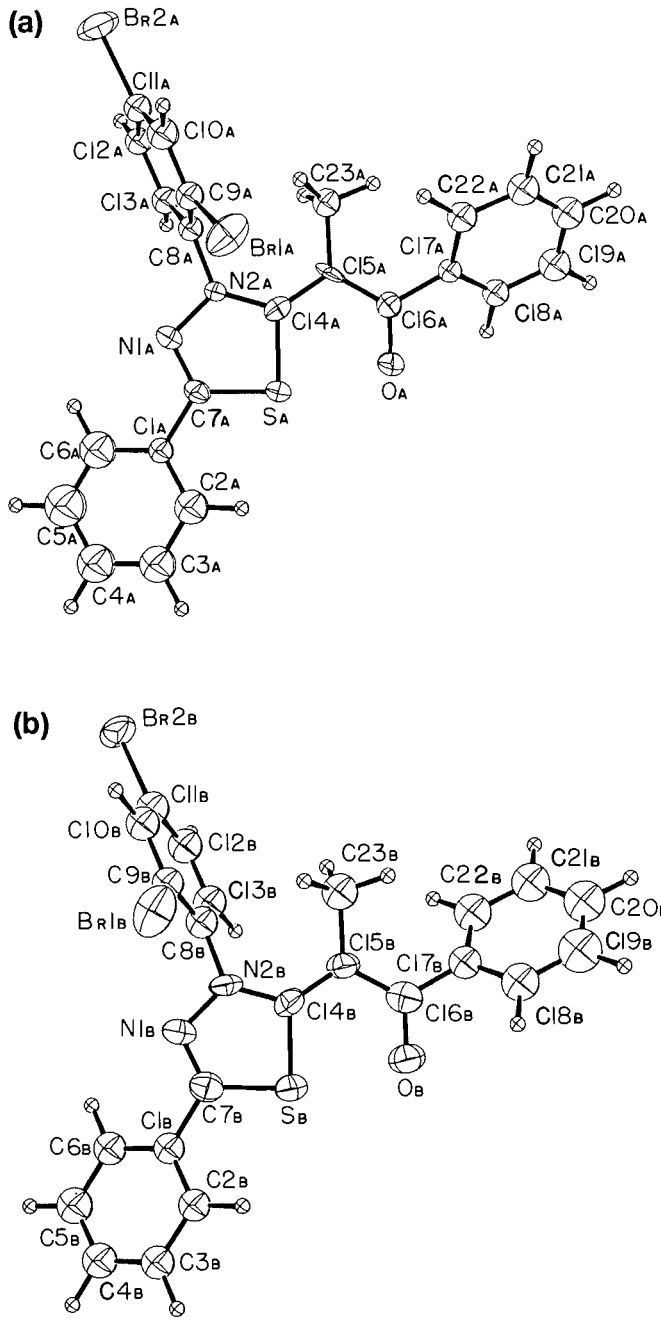

FIG. 3. Independent molecules (*a*) A and (*b*) B in the structure of **11***c*.

aryl diazonium ions (25); 1-oxa-6,6a-dithiapentalenes behave similarly in the latter reaction (25).

The ^{1}H NMR spectrum of **11***d* is interesting in that the signal due to the CH_2 protons appeared as a multiplet rather than a quartet, suggesting that these protons might be diastereotopic with respect to the dibromophenyl ring because of restricted rotation. No simplification was observed when the spectrum was run at 56.5°C, nor was there clear evidence of simplification when the CH_3 triplet was irradiated at ambient temperature. Similar data were obtained from the spectrum run in pyridine-d_5, even at temperatures of 57, 69, and 82°C.

Finally we wish to comment further on the ^{1}H NMR spectra of **15***a* and **15***b*. The spectrum of **15***a*, originally

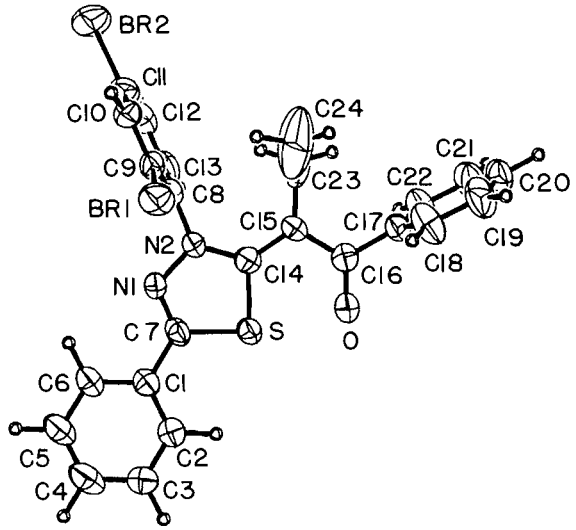

FIG. 4. The structure of **11***d*.

measured at 60 MHz, was reported to exhibit the CH_2 proton signal as a multiplet, suggestive of restricted rotation

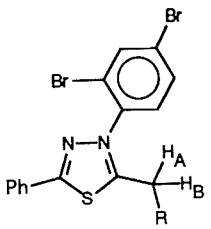

15*a*: R = Me
15*b*: R = Ph

about the N-aryl bond (2). We have rerun this spectrum several times (at 80 and 200 MHz in CD_3CN, CD_3COCD_3, and in $(CD_3)_2SO$) on more modern instruments and can confirm that this signal appears at ambient temperatures as a quartet; typically, the compound shows δ (CD_3CN): 1.38 (t, *J* 7 Hz, 3H, CH_3) and 3.25 (q, *J* 7 Hz, 2H, CH_2), and saturation of the CH_3 protons causes the quartet to collapse to a singlet. To determine whether N-aryl rotation might become restricted at lower temperatures, we scanned the ^{1}H NMR spectrum (200 MHz) of **15***a* in CD_3COCD_3 over the temperature range 303–213 K. At 253 K, the CH_2 quartet shows signs of splitting as a result of differentiation of A and B protons as an AB system. This becomes clearer as the temperature is lowered, and from the spectrum at 233 K we calculate J_{AB} 7.3 Hz. By 213 K the methylene proton signal is a multiplet (ABX_3 system). By this temperature, interconversion of enantiomeric conformers through N-aryl rotation has become very slow.

We have also noted that the CH_2 signal in the ^{1}H NMR spectrum (80 MHz) of **15***b* in CD_3CN at ambient temperatures is a slightly broadened singlet (8). However, the spectrum at 200 MHz of this salt in $(CD_3)_2SO$ (with perchloric acid added to suppress dissociation to the methine base) shows the methylene protons clearly discriminated as an AB system with signals at δ: 4.13 (d, *J* 18 Hz, 1H) and 4.76 (d, *J* 18 Hz, 1H). Evidently there is restricted N-aryl rotation in **15***b* under these conditions.

TABLE 6. Selected bond distances (Å), bond angles (°), and torsion angles (°)

	11*a* mol. A	**11***a* mol. B	**11***b*	**11***c* mol. A	**11***c* mol. B	**11***d*
S...O	2.691(5)	2.683(5)	2.648(5)	2.483(6)	2.478(7)	2.463(5)
S—C(7)	1.768(6)	1.770(6)	1.760(7)	1.723(10)	1.752(12)	1.768(7)
S—C(14)	1.769(5)	1.749(8)	1.737(6)	1.758(9)	1.766(9)	1.751(8)
C(7)—N(1)	1.302(6)	1.283(10)	1.293(8)	1.299(12)	1.277(13)	1.259(10)
N(1)—N(2)	1.392(7)	1.384(7)	1.400(7)	1.396(11)	1.376(12)	1.380(8)
N(2)—C(14)	1.351(7)	1.371(9)	1.350(8)	1.369(12)	1.363(15)	1.370(9)
C(14)—C(15)	1.356(9)	1.363(9)	1.383(9)	1.363(14)	1.356(16)	1.387(10)
C(15)—C(16)	1.382(8)	1.385(11)	1.435(9)	1.434(14)	1.430(17)	1.442(10)
C(16)—O	1.247(7)	1.263(10)	1.240(8)	1.250(11)	1.267(12)	1.238(9)
C(7)—S...O	162.2(2)	162.7(3)	163.4(2)	166.5(6)	165.7(6)	166.7(3)
C(14)—S...O	73.2(2)	73.8(3)	74.6(2)	76.8(3)	76.9(3)	77.9(3)
C(16)—O...S	98.1(4)	97.4(4)	99.5(4)	101.5(5)	101.9(4)	101.5(5)
C(7)—S—C(14)	89.1(3)	88.9(3)	89.0(3)	89.7(5)	88.8(5)	88.9(4)
S—C(7)—N(1)	114.6(4)	115.3(5)	115.5(5)	117.3(7)	116.4(8)	115.2(6)
C(7)—N(1)—N(2)	110.1(4)	110.1(5)	108.9(5)	107.2(8)	108.9(9)	111.0(6)
N(1)—N(2)—C(14)	118.4(4)	117.9(6)	118.0(5)	119.4(7)	119.5(7)	117.5(6)
N(2)—C(14)—S	107.9(4)	107.8(4)	108.6(5)	106.3(7)	106.3(7)	107.4(5)
N(2)—C(14)—C(15)	127.4(5)	126.8(7)	125.9(6)	129.7(9)	130.4(9)	129.6(7)
S—C(14)—C(15)	124.8(4)	125.4(6)	125.5(5)	124.0(7)	123.3(8)	123.0(6)
C(14)—C(15)—C(16)	122.5(5)	121.5(7)	119.5(6)	118.1(9)	118.1(9)	115.6(7)
C(15)—C(16)—O	121.3(6)	121.8(6)	120.7(6)	120.9(9)	119.5(1.0)	122.0(7)
C(15)—C(16)—C(17)	119.4(5)	118.0(7)	119.3(6)	121.7(8)	122.5(9)	120.3(7)
N(1)—N(2)—C(8)—C(9)	−83.8	−82.1	63.1	97.0	76.6	80.2
N(1)—C(7)—C(1)—C(2)	175.0	174.6	141.9	−172.0	−154.6	175.0
C(15)—C(16)—C(17)—C(18)	N/A	N/A	−164.5	−138.0	139.2	104.2

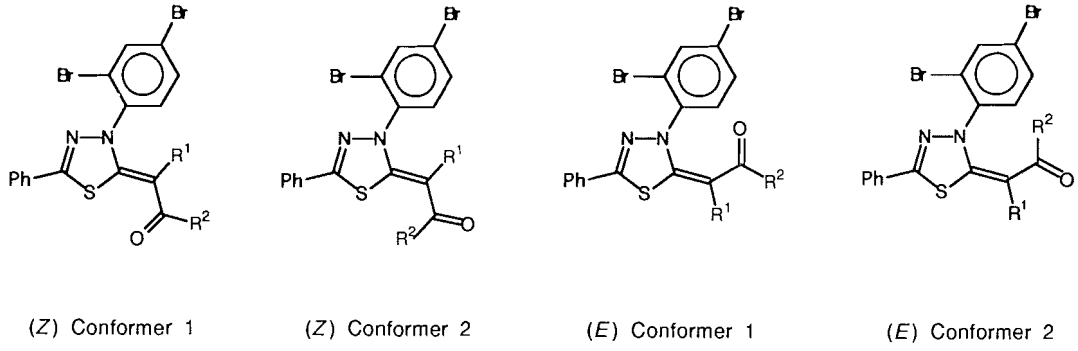

SCHEME 1

Acknowledgements

We are grateful to the Natural Sciences and Engineering Research Council of Canada for financial support of this work.

1. P. D. Callaghan, A. J. Elliott, S. S. Gandhi, M. S. Gibson, H. Mastalerz, and D. J. Vukov. J. Chem. Soc. Perkin Trans. 1, 2948 (1981).
2. H. Mastalerz and M. S. Gibson. J. Chem. Soc. Perkin Trans. 1, 245 (1983).
3. G. H. Alt. J. Org. Chem. **33**, 2858 (1968).
4. G. V. Boyd and S. R. Dando. J. Chem. Soc. C, 2314 (1971); 1397 (1970).
5. H. Mastalerz and M. S. Gibson. J. Chem. Soc. Perkin Trans. 1, 2952 (1981).
6. H. Mastalerz, T. Mohammad, and M. S. Gibson. Can. J. Chem. **65**, 2713 (1987).
7. L. G. S. Brooker, G. H. Keyes, H. H. Sprague, R. H. van Dyke, E. van Lare, G. van Zandt, and F. L. White. J. Am. Chem. Soc. **73**, 5326 (1951).
8. T. Mohammad and M. S. Gibson. Phosphorus, Sulfur, Silicon, **70**, 243 (1992).
9. International tables for X-ray crystallography. Vol. IV. Kynoch Press, Birmingham. 1968.
10. G. Sheldrick. SHELX76 program for crystal structure determination. University of Cambridge. 1976.
11. ORTEP II. Report ORNL-5138. Oak Ridge National Laboratory, Tenn. 1976.
12. U. Burkert and N. L. Allinger. Molecular mechanics. ACS Monograph 177, American Chemical Society, Washington, D. C. 1982.
13. A. Z. Khan and J. Sandström. J. Chem. Soc. Perkin Trans. 1, 2085 (1988).
14. (*a*) G. Fukata, C. O'Brien, and R. A. M. O'Ferrall. J. Chem. Soc. Perkin Trans. 2, 792 (1979); (*b*) N. Lozac'h. Adv. Heterocycl. Chem. **13**, 161 (1971); A. Kucsman and I. Kapovits. Studies in organic chemistry. Vol. 19. Organic sulfur

Can. J. Chem. Downloaded from www.nrcresearchpress.com by 88.255.202.194 on 09/08/12
For personal use only.

chemistry. *Edited by* F. Bernardi, I. G. Csizmadia, and A. Mangini. Elsevier, Amsterdam. 1985. Chap. 4.
15. F. H. Allen, O. Kennard, D. G. Watson, L. Brammer, A. G. Orpen, and R. Taylor. J. Chem. Soc. Perkin Trans. 2, S1 (1987).
16. R. E. Rosenfield, R. Parthasarathy, and J. D. Dunitz. J. Am. Chem. Soc. **99**, 4860 (1977).
17. C. Cohenaddad, M. S. Lehmann, P. Becker, L. Parkanyi, and A. Kalman. J. Chem. Soc. Perkin Trans. 2, 191 (1984).
18. H. B. Burgi and J. D. Dunitz. Acc. Chem. Res. **16**, 153 (1983).
19. F. H. Allen, O. Kennard, and R. Taylor. Acc. Chem. Res. **16**, 146 (1983).
20. N. Padmaja, S. Ramakumar, and M. A. Viswamitra. Acta Crystallogr. Sect. A: Found. Crystallogr. **A46**, 725 (1990).
21. V. Sona and N. Gautham. Acta Crystallogr. Sect. B: Struct. Sci. **B48**, 111 (1992).
22. J. A. R. P. Sarma and G. Desiraju. Acc. Chem. Res. **19**, 222 (1986).
23. J. G. Angyan, R. A. Poirier, A. Kucsman, and I. G. Csizmadia. J. Am. Chem. Soc. **109**, 2237 (1987).
24. R. M. Christie, A. S. Ingram, D. H. Reid, and R. G. Webster. J. Chem. Soc. Perkin Trans. 1, 722 (1974), and references cited therein.
25. R. M. Christie and D. H. Reid. J. Chem. Soc. Perkin Trans. 1, 880 (1976).

Can. J. Chem. Downloaded from www.nrcresearchpress.com by 88.255.202.194 on 09/08/12
For personal use only.

Generalization of an empirical model for bond dissociation energies

YU-RAN LUO AND PHILIP D. PACEY[1]
Department of Chemistry, Dalhousie University, Halifax, N.S., Canada B3H 4J3

Received July 16, 1991[2]

YU-RAN LUO and PHILIP D. PACEY. Can. J. Chem. **71**, 572 (1993).

A relationship between homolytic bond dissociation energies (BDEs) of C—X bonds and the electronegativity of X and the degree of methyl substitution of C has been extended. The range of leaving groups, X, now includes SiH_3, GeH_3, and PH_2 and a variety of C-, N-, and O-centred radicals. Alkyl groups with ethyl and propyl chains attached to the radical centre have been incorporated. Steric effects, including those in bulky silanes, have been treated. The method is believed to be generally applicable where resonance and ring strain are not significant. BDEs for 73 bonds have been calculated; in the 42 cases where experimental data are available, the average deviation is 0.7 kcal/mol.

YU-RAN LUO et PHILIP D. PACEY. Can. J. Chem. **71**, 572 (1993).

On a étendu une relation entre les énergies de dissociation homolytique des liaisons (EDL) C—X, l'électronégativité de X et le degré de substitution méthyle du C. Les groupes qui partent comprennent maintenant le SiH_3, le GeH_3 et le PH_2 ainsi qu'une variété de radicaux centrés sur les atomes de C, N et O. On a incorporé des groupes alkyles dans lesquels des chaînes éthyles et propyles sont attachées au centre radicalaire. On a traité des effets stériques, y compris ceux des silanes volumineux. On croit que la méthode est générale et applicable dans tous les cas où la résonance et les tensions de cycle ne sont pas importantes. On a calculé les EDL de 73 liaisons; dans les 42 cas où des données expérimentales sont disponibles, la déviation moyenne est de 0,7 kcal/mol.

[Traduit par la rédaction]

1. Introduction

Knowledge of bond dissociation energies (BDEs) is fundamental to our understanding of chemical reactions. Most available BDEs have been obtained from gas kinetic measurements, which are restricted to volatile compounds. There is a need to develop dependable methods for estimating BDEs for larger molecules.

Recently Luo and Benson (1) were able to correlate BDEs of simple alkyl substituents, RX, with the degree of methyl substitution, m, of the radical, R, and the electronegativity, V_X, of the substituent, X. In this article we shall attempt to generalize these findings to a wider range of fragments, R and X. In the next section we will establish a hierarchy of interactions. In Sect. 3, the range of substituents, X, will be extended to include C_2H_5, CN, CH_3CO, ONO, i-C_3H_7O, ON, O_2N, SiH_3, GeH_3, and PH_2. In Sects. 4 and 5 the range of radicals R will be extended to include longer linear and branched alkyl radicals, respectively.

Most heats of formation of organic molecules used in this work have been taken from ref. 2. The heats of formation of methyl, ethyl, isopropyl, and *tert*-butyl radicals are the same as those used in ref. 1. Heats of formation of *n*-propyl and *sec*-butyl radicals have been taken from ref. 3, but have been adjusted upward by 0.6 kcal/mol to conform to the revised (1) heat of formation of methyl, which was used as a standard in ref. 3. The BDEs of CH_3—SiH_3, CH_3—GeH_3, and CH_3—PH_2 are from refs. 4, 5, and 6. Heats of formation of leaving groups X are from refs. 7–9.

2. Hierarchy of forces

The strong correlation between BDEs of R—X bonds and electronegativity was demonstrated in ref. 1. This suggests the presence of electrostatic forces that are propagated either though bonds by the inductive effect or through space as the field effect. We consider each of these effects separately elsewhere (10, 11). For now we will merely note that electrical effects decline with increasing distance, as illustrated in Fig. 1.

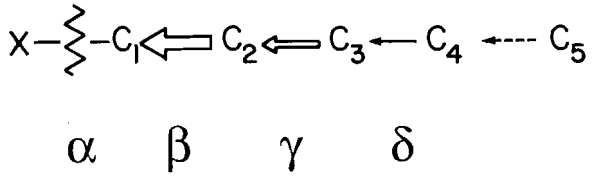

FIG. 1. Hierarchy of interactions. Replacement of H by CH_3 at position C_2 gives rise to the β effect, and a similar replacement at position C_3 to the γ effect.

Among the hierarchy of forces in the figure, the strongest interaction is the direct bond between X and atom C_1 (10, 11). The non-bonding interaction between the next-nearest neighbours X and C_2 is still strong (1–5 kcal/mol). This interaction, which will be called the β-effect, was the subject of ref. 1. The next-next-nearest neighbouring interaction between C_3 and X is predicted to be weaker, and will be called the γ-effect. Longer range electrical forces would be weaker still.

Some molecules involve other types of forces, such as resonance and steric effects. We have limited the effect of resonance in this article by considering only singly bonded alkyl groups, R. Steric effects will be considered in Sect. 5.

3. The effect of methyl substitution at the β position

Recently, Luo and Benson (1) described the methyl substituent effect on bond dissociation energies, DH.

$$[1]\quad DH^0(X—C(CH_3)H_{3-m}) = DH^0(X—CH_3) - m\frac{6.33 + 0.36\,m - V_x}{0.67 + 0.21\,m}$$

Here $C(CH_3)_mH_{3-m}$ is an ethyl, isopropyl, or *tert*-butyl group when m = 1, 2, or 3, respectively. In eq. [1], V_X is the co-

[1]Author to whom correspondence may be addressed.
[2]Revision received November 18, 1992.

Can. J. Chem. Downloaded from www.nrcresearchpress.com by 88.255.202.194 on 09/08/12
For personal use only.

TABLE 1. Estimated BDEs of Si—C, Ge—C, and P—C bonds, in kcal/mol

X	V_X	CH_3	C_2H_5	i-C_3H_7	t-C_4H_9
SiH_3	3.41	88.5 ± 1.5[a]	84.8	81.8	79.1
GeH_3	3.27	82.6[b]	78.7	75.7	73.1
PH_2	4.55	73.0 ± 2.5[b]	70.6	68.4	66.4

[a]Observed value from refs. 4 and 5.
[b]Observed values based on ref. 6.

valent potential, a new scale of electronegativity. The covalent potential is defined as

[2] $V_X = n_X/r_X$

Here n_X is the number of valence electrons in the bonding atom in X and r_X is its covalent radius. Equation [1] provides a convenient manner of estimating the homolytic BDEs of X—R bonds.

Luo and Benson did not estimate BDEs for cases in which X is SiH_3, GeH_3, or PH_2, because data for heats of formation of these compounds were not available. Nevertheless, eq. [1] should be valid for these cases. Therefore, we may estimate the BDEs for these bonds from those for X—CH_3, as shown in Table 1. Values of V_X were reported in ref. 5.

In the particular case that X is CH_3, eq. [1] reduces to a simple form:

[3] $DH^0(CH_3—C(CH_3)_mH_{3-m}) = DH^0(CH_3—CH_3) - 1.7\,m$

Each extra methyl group attached to one end of a C—C bond weakens the bond by 1.7 kcal/mol. Since both ends of the C—C bond in ethane are identical, the same reduction must apply, irrespective of which end of the molecule has the methyl group added. Thus the C—C bonds in propane have an experimental BDE of 88.5 kcal/mol, 1.7 kcal/mol less than that in ethane, as listed in Table 2. Furthermore, the central C—C bond in butane, with an experimental BDE of 86.8 kcal/mol, is observed to be 1.7 kcal/mol weaker than the C—C bonds in propane. In the case of butane the substituent X is the same as the radical R.

Estimation of the effect of substitution at the β position in the substituent X is not possible using eq. [1] when X is not an alkyl group. Table 2 lists BDEs for several other substituents for which the central atom is C, O, or N. Replacement of three β hydrogen atoms in CH_3 by an N atom in CN gives a much stronger bond to another CH_3. In all the other cases, replacement of β hydrogen atoms by other elements leads to much weaker bonds. In several of these cases the radical formed would be stabilized by resonance, a phenomenon not explicitly considered in the present approach. We will leave the effect of β substitution in X, except for alkyl groups, to future work.

We note that the present approach uses experimental values of the BDEs in CH_3X as reference values, eliminating any need to estimate them.

The effect of substitution of a hydrogen atom by a methyl group at the β position in R is shown in the third full column (headed C_2H_5) in Table 2. The numbers in the first row for each X are experimental. The numbers in parentheses below these were calculated using eq. [1], taking V_x as the electronegativity of the central atom in group X in each case. There is good agreement between experiment and eq. [1]. The average absolute error in this column is 0.2 kcal/mol, with a maximum error of 0.9 kcal/mol for aminoethane. Replacement of CH_3 by C_2H_5 weakens C—C bonds by 1.7 kcal/mol, strengthens C—O bonds by 1.6 kcal/mol, and makes no difference to C—N bonds.

The last two columns in this table will be discussed in Sect. 5.

4. The effect of methyl substitution at the γ position and beyond in derivatives of normal alkanes

The effect of a methyl group at the β position on the BDE lies between −4.5 kcal/mol for C—H bonds and +1.6 kcal/mol for C—O bonds. According to the hierarchy in Sect. 2, we expect that methyl groups farther from the breaking bond would have lesser effects.

The experimental thermochemistry has been established for very few radicals with a methyl group at the γ position. In Table 3 we can see a comparison between experimental BDEs for C_2H_5—X and n-C_3H_7—X. The extra γ-methyl group leaves BDEs unchanged within a standard deviation of ±0.2 kcal/mol, a negligible amount compared to the average experimental uncertainty of 1.3 kcal/mol. For s-C_4H_9—X compared to i-C_3H_7—X, the extra methyl group weakens the C—X bonds by an average of 0.8 ± 0.7 kcal/mol.

We conclude that there is insufficient experimental evidence to support assignment of a γ-effect at present and we will assume that electrostatic effects at the γ position and beyond are negligible.

5. Steric effects

The hierarchy in Fig. 1 assumes that interactions become weaker as one proceeds farther along a chain of carbon atoms. This is probably valid for normal alkanes and their derivatives. However, for ring compounds or highly branched alkanes, atoms farther along the chain may be forced to a position a short distance from atoms on the other side of the breaking bond. In this case, one would expect van der Waals forces between the nearby atoms.

van der Waals forces exist even between next-nearest neighbouring atoms and in molecules like CH_3X. Such forces are automatically subtracted out in $DH^0(CH_3X)$ or incorporated into the β-effect in eq. [1]. We seek an expression for the van der Waals interaction between groups separated by three or more bonds. This could correspond to an interaction between two β-methyl groups in X and R or interactions between groups separated further still. The same problem arose when the group additivity scheme was being established (12). Next-nearest neighbouring interactions were automatically incorporated in the group parameters, but less direct interactions were counted separately as steric effects. The magnitudes of these interactions were determined empirically by comparing the heats of formation of molecules with and without groups in close proximity, but separated by three or more bonds. The approach was not extended to radicals or bond dissociation energies. In the present article we have adopted the steric terms for molecules from the group additivity scheme and have extended the approach to radicals.

For noncyclic saturated hydrocarbons, the group additivity method identified two types of steric repulsive interactions: the 1,4-*gauche* interaction and the 1,5-H repulsion (12).

Can. J. Chem. Downloaded from www.nrcresearchpress.com by 88.255.202.194 on 09/08/12
For personal use only.

TABLE 2. BDEs of R—C, R—N and R—O bonds, kcal/mol[a]

Group centre	X	CH_3	C_2H_5	i-C_3H_7	t-C_4H_9
C	CH_3 (35.1 ± 0.1)	90.2 ± 0.2	88.5 ± 0.5 (88.5)	87.2 ± 0.6 (86.8)	85.2 ± 0.7 (85.1)
	C_2H_5 (28.4 ± 0.4)	88.5 ± 0.5 (88.5)	86.8 ± 0.5 (86.8)	85.1 ± 0.8 (84.3)	82.8 ± 1.0 (81.8)
	CN (104 ± 2)	121.5 ± 2.1	120.1 ± 0.7 (119.8)	118.4 ± 0.7 (118.1)	114.5 ± 0.8 (116.4)
	CH_3CO (−5.8 ± 0.4)	81.2 ± 0.5	79.7 ± 0.6 (79.5)	76.9 ± 0.7 (77.3)	73.6 ± 0.8 (75.1)
O	OH (9.4)	92.7 ± 0.2	94.0 ± 0.5 (94.3)	94.5 ± 0.6 (94.6)	94.0 ± 0.6 (94.3)
	ONO (7.9 ± 0.2)	59.1	60.5 (60.7)	59.8 (61.0)	58.8 (60.7)
	i-C_3H_7O (−12.4 ± 0.5)	82.9 ± 0.6	(84.5)	83.9 ± 0.8 (84.3)	83.0 ± 1.6 (82.0)
N	H_2N (45.9 ± 0.2)	86.5 ± 0.3	85.6 ± 0.5 (86.5)	85.9 ± 0.6 (85.9)	84.7 ± 0.7 (84.8)
	ON (21.6)	40.0 ± 0.9	(40.0)	38.9 ± 3.1 (39.3)	35.5–41.0 (38.3)
	O_2N (7.9 ± 0.2)	60.8 ± 0.4	60.8 ± 0.6 (60.8)	61.2 ± 0.8 (60.2)	60.1 ± 0.8 (59.1)

[a]$\Delta_f H^0$ of free radicals, listed under X, are from refs. 7–9. Values without parentheses are experimental, values in parentheses are estimated using eqs. [1] or [5].

TABLE 3. The effect of next-next-nearest neighbors on observed BDEs, in kcal/mol

X	$DH^0(C_2H_5—X)$	$DH^0(n\text{-}C_3H_7—X)$	Δ^a	DH^0(i-C_3H_7—X)	$DH^0(s\text{-}C_4H_9—X)$	Δ^a
OH	94.0 ± 0.5	93.9 ± 1.0	−0.1	94.5 ± 0.6	94.0 ± 1.1	−0.5
Cl	84.2 ± 0.5	84.0 ± 1.0	−0.2	83.6 ± 0.6	82.1 ± 2.3	−1.5
NH_2	85.6 ± 0.5	86.2 ± 1.0	+0.6	85.9 ± 0.6	84.0 ± 1.5	−1.9
Br	69.9 ± 0.6	71.0 ± 1.0	+0.1	70.5 ± 0.8	70.1 ± 1.2	−0.4
SH	73.5 ± 0.7	73.7 ± 1.0	+0.2	72.2 ± 0.7	71.8 ± 1.1	−0.4
CH_3	88.5 ± 0.5	88.6 ± 1.1	+0.1	87.2 ± 0.6		
C_2H_5	86.8 ± 0.7	87.0 ± 1.2	+0.2			
n-C_3H_7	87.0 ± 1.2	86.9 ± 1.5	−0.1			
H	100.5 ± 0.5	100.6 ± 1.0	+0.1	97.1 ± 0.5	96.9 ± 1.1	−0.2

[a]Difference between numbers in previous two columns, the γ effect. Heats of formation of n-C_3H_7 and s-C_4H_9 are from ref. 3, adjusted as described in Sect. 1.

The 1,4-*gauche* interaction occurs when there are two methyl groups at positions 1 and 4, separated by three C—C bonds, oriented in the *gauche* conformation about the bond joining C_2 to C_3. This conformation forces two H atoms (at positions 0 and 5) very close. Benson (12) found such an interaction raised the heats of formation of hydrocarbons by 0.8 kcal/mol on average. Since the effect is repulsive, such conformations are avoided by internal rotation, if possible. The number of unavoidable 1,4-*gauche* interactions about bond C_2—C_3 is

$$[4] \quad g_{2,3} = (n_2 - 1)(n_3 - 2)$$

where n_2 is the number (1–4) of alkyl groups attached to the less substituted carbon and n_3 is the number attached to the more substituted carbon. Note that $n = 2$ for a secondary carbon, 3 for tertiary, and 4 for quaternary and is equal to m (from eq. [1]) plus one.

In ethers, where either atom 2 or 3 is oxygen, we follow Benson (12) in assigning 0.5 kcal/mol for each *gauche* interaction between methyl groups.

In radicals and ketones, the bond angles about one carbon atom increase to 120°, allowing the repelling hydrogen atoms to separate and reducing any interaction. Accordingly we have taken 1,4-methyl interactions involving sp^2 centres as 0.5 kcal/mol, as Benson did for alkene centres (12).

Where there are five carbon atoms in a chain and both atoms 2 and 4 are quaternary, two pairs of hydrogen atoms on carbons 1 and 5 are forced to a short internuclear separation. This results in two 1,5-H repulsions, estimated (12) at 1.5 kcal/mol each. We have adopted the same value here.

Can. J. Chem. Downloaded from www.nrcresearchpress.com by 88.255.202.194 on 09/08/12
For personal use only.

TABLE 4. The BDEs of typical C—C bonds in kcal/mol

R_1	R_2	ΔV_s	$DH^0(R_1—R_2)$ Estd.[a]	Obsd.[b]	Δ[c]
i-C_3H_7	i-C_3H_7	−1.6	81.8	82.6 ± 0.9	0.8
i-C_3H_7	t-C_4H_9	−3.2	78.5	78.8 ± 1.0	0.3
t-C_4H_9	t-C_4H_9	−4.8	75.2	73.7 ± 1.0	−1.5
i-C_3H_7	n-C_3H_7	−0.8	84.3	85.3 ± 1.2	1.0
s-C_4H_9	n-C_3H_7	−1.6	83.5	83.8 ± 1.5	0.3
t-C_4H_9	n-C_3H_7	−1.6	81.8	82.6 ± 1.3	0.8
CH_3	s-C_4H_9	−0.8	86.0	86.4 ± 1.2	0.4
C_2H_5	s-C_4H_9	−1.6	83.5	84.1 ± 1.2	0.6
i-C_3H_7	s-C_4H_9	−2.4	81.0	82.1 ± 1.2	1.1
s-C_4H_9	s-C_4H_9	−3.2	80.2	80.1 ± 1.5	−0.1
t-C_4H_9	s-C_4H_9	−4.0	77.7	77.1 ± 1.3	−0.6
CH_3	i-C_4H_9	−0.8	87.7		
C_2H_5	i-C_4H_9	−0.8	86.0		
n-C_3H_7	i-C_4H_9	−0.8	86.0		
i-C_3H_7	i-C_4H_9	−1.6	83.5		
i-C_4H_9	i-C_4H_9	−1.6	85.2		
s-C_4H_9	i-C_4H_9	−2.4	82.7		
t-C_4H_9	i-C_4H_9	−3.9	79.5		
CH_3	n-C_4H_9		88.5		
C_2H_5	n-C_4H_9		86.8		
n-C_3H_7	n-C_4H_9		86.8		
i-C_3H_7	n-C_4H_9	−0.8	84.3		
n-C_4H_9	n-C_4H_9		86.8		
i-C_4H_9	n-C_4H_9	−0.8	86.8		
s-C_4H_9	n-C_4H_9	−1.6	83.5		
t-C_4H_9	n-C_4H_9	−1.6	81.8		

[a]Based on eq. [5].
[b]The observed values are based on experimental heats of formation of free alkyls and hydrocarbons. The data on free radicals are from refs. 1 and 3; those on hydrocarbons are from ref. 2.
[c]These are the differences between the observed and estimated BDEs.

We can now obtain a more general expression for the BDE of an X—R bond

$$[5]\quad DH^0(X—R) = DH^0(X—CH_3) - m\frac{6.33 + 0.36\,m - V_x}{0.67 + 0.21\,m} + \Delta V_s$$

Here ΔV_s is the change in the steric interaction. Where this includes only 1,4-*gauche* interactions in alkanes,

$$[6]\quad \Delta V_s = (0.8\,\Delta g)\ \text{kcal/mol}$$

Here Δg is the change in the total number of *gauche* interactions from R—X to R and X. This includes the sum of *gauche* interactions across all bonds, not just the dissociating bond. Where other types of steric interactions are involved, ΔV_s is the sum of the steric interactions in R and X minus the sum of the steric interactions in RX. It is generally negative.

We will first apply this principle to C—C bonds in alkanes. With no 1,5-H repulsions, eq. [5] can be simplified as follows:

$$[7]\quad DH^0(R_1—R_2) = (90.2 - 1.7\beta + 0.8\,\Delta g)\ \text{kcal/mol}$$

Here 90.2 is the BDE of the C—C bond in ethane and β is the total number of alkyl groups attached to the two ends of the breaking bond.

Three examples of estimations of the BDEs of C—C bonds are given below:

1. DH^0 (C(C)(C)—C(C)(C)—C)$_{est}$ = 90.2 − (1.7 × 5) − (0.8 × 4)
= 78.5 kcal/mol

The experimental value is 78.8 ± 1.0 kcal/mol, as in Table 4.

2. An example, in which 1,5-H repulsion energy is significant, is the BDE of a C_2—C_3 bond in 2,2,4,4-tetramethyl pentane. There are four carbon atoms at the β positions in the radicals, and four *gauche* conformations and two 1,5-H repulsions in the parent molecule. The BDE of the C—C bond is predicted to be

DH^0 (C(C)(C)—C(C)(C)—C)$_{est}$
= 90.2 − (1.7 × 4) − (0.8 × 4) − (1.5 × 2)
= 77.2 kcal/mol

This bond strength has not been determined experimentally.

3. The estimated BDEs of four C—C bonds in 2,2,4-trimethyl pentane are as follows:

C_1----C_2(C)----C_3----C_4----C_5

$DH^0(C_1—C_2)_{est}$ = 90.2 − (1.7 × 3) − (0.8 × 2) − 1.5 + 0.5 = 82.5 kcal/mol

$DH^0(C_2 - C_3)_{est}$ = 90.2 − (1.7 × 4) − (0.8 × 3) − 1.5 = 79.5 kcal/mol

$DH^0(C_3 - C_4)_{est}$ = 90.2 − (1.7 × 3) − (0.8 × 3) − 1.5 = 81.2 kcal/mol

$DH^0(C_4—C_5)_{est}$ = 90.2 − (1.7 × 2) − 0.8 − 1.5 = 84.5 kcal/mol

There are no observed values available for comparison.

The predictions of eq. [5] are compared with experimental results in Table 4. For 11 cases where a comparison is possible, the difference between prediction and experiment, listed in the last column, has an average value of ±0.7 kcal/mol, with a maximum value of −1.5 kcal/mol for tetramethylbutane, which is the only case where the difference exceeds the experimental uncertainty.

Positive deviations occur in Table 4 for small values of Δg; the three negative values occur in cases where Δg is −4 to −6. Where there are few *gauche* interactions, the bond angles can adjust to weaken the van der Waals repulsion. Where there are many interactions, as in tetramethylbutane, the *gauche* repulsions are difficult to escape.

The table continues with predictions of BDEs for bonds involving the i-C_4H_9 and n-C_4H_9 radicals, for which accurate experimental heats of formation are not available.

Equation [5] has been applied to C-, O-, and N-centred leaving groups, X, bonded to isopropyl and *tert*-butyl groups

Can. J. Chem. Downloaded from www.nrcresearchpress.com by 88.255.202.194 on 09/08/12
For personal use only.

Can. J. Chem. Downloaded from www.nrcresearchpress.com by 88.255.202.194 on 09/08/12
For personal use only.

in the last two columns in Table 2. The average absolute deviation between experimental values and the predictions of eq. [5] is 0.5 kcal/mol. The greatest deviation is 1.9 kcal/mol for *tert*-butyl cyanide.

The steric correction can be extended to H—Si bonds. Griller and co-workers (13, 14) found anomalously low values for highly substituted silanes. In two molecules, $HSiEt_3$ and $HSi(Me)_2Si(Me)_3$, the distances between the hydrogen atoms involved in either 1,4-*gauche* or 1,5-H interactions are larger than 2.6 Å. That means there is no steric repulsion of these types in these two molecules. But in the staggered structure of $HSi(SiMe_3)_3$, the distance between hydrogen atoms involved in the 1,5-H interaction is about 1.8 Å. This is about equal to the distances between hydrogens involved in the 1,4-*gauche* interactions in tetramethylbutane. Therefore we suggest that the contribution to steric repulsion from each 1,5-H pair in $HSi(SiMe_3)_3$ is about 0.8 kcal/mol. The total steric compression release due to cleaving of the H—Si bond is about 4.8 kcal/mol for six pairs of 1,5-H repulsions. Combining this with the results of our previous work (15), we obtain

$$DH^0(H—SiEt_3)_{est} \approx DH^0(H—SiH_3) = 90.3 \pm 1.2 \text{ kcal/mol}$$

$$DH^0(H—Si(Me)_2SiMe_3)_{est} \approx DH^0(H—Si_2H_5) = 86.3 \pm 2 \text{ kcal/mol}$$

$$DH^0(H—Si(SiMe_3)_3)_{est} \approx DH^0(H—Si_2H_5) - 4.8 = 81.5 \pm 2 \text{ kcal/mol}$$

The values of the BDEs of H—Si bonds in SiH_4 and Si_2H_6 were taken from refs. 4 and 16. The observed values (13, 14) were 90.1 ± 2.0, 85.3 ± 2.0, and 79.0 ± 2.0 kcal/mol, respectively. This explains the fact that BDEs of H—Si bonds are not sensitive to alkyl substitution, unlike H—C bonds in hydrocarbons, but that H—Si bonds are sensitive to substitution by $SiMe_3$ groups.

6. Discussion

Equation [5], the central result in this work, is empirically based but has considerable predictive power. It contains four numerical constants, which were found in the earlier work (1) by examining data on eight leaving groups, X, and four alkyl groups, methyl, ethyl, isopropyl, and *tert*-butyl. Five parameters are contained in the steric term, ΔV_s, for five different types of steric interaction. The steric parameters, except those for radicals, ketones, and silanes, are taken from the work of Benson (12). To calculate the BDEs given in this paper, 12 values of $DH^0(X—CH_3)$ and six values of the covalent potential, V_X, are also needed. Since V_X is calculated from covalent bond lengths, not BDEs, it is really a semi-empirical, as opposed to empirical, parameter. In total, 21 empirical parameters and six semi-empirical parameters were used to estimate 73 BDEs in the tables in this article. For comparison, in the group additivity method (12), it would be necessary to supply 54 parameters to calculate these BDEs.

The key to this approach is the covalent potential, V_X. Of all available electronegativity scales, V_X gives the best correlation for the effect of methyl substitution on heats of formation and BDEs of organic molecules (17). It has also been shown to correlate well with group parameters (18), atomic ionization potentials (19), Lewis acid strengths (20), divalent state stabilization energies (21), heterolytic bond dissociation energies (22), and heats of formation of organic cations (23). It is also linearly related to theoretical electronegativity scales, such as the Mulliken electronegativity of the valence state, the electronic chemical potential, and the central electrostatic potential (24).

The method is based on the BDEs of methyl derivatives, for which most values have been determined with high precision. In this way, calculation of the direct interaction in C—X bonds has been avoided, and we have been able to focus on the weaker interactions in Fig. 1.

The numerical constants appearing in eq. [5] are derived from the heats of formation of the prototypical alkyl radicals. There has, recently, been some controversy (25–30) surrounding these values. The basic features of eq. [5] and the main conclusions of this work would be valid even if these input parameters were adjusted. If we had taken the values from Gutman's (27), Tsang's (29), or Griller's (30) groups, the estimated γ-effect and higher order interactions would still be small quantities, less than the current experimental uncertainty. If Gutman's (27) negative activation energies and the resulting thermochemistry had been accepted, eq. [5] would have changed a little:

$$[8] \quad DH^0(X—R) = DH^0(X—CH_3) - (3.8 + 3.9\,m) + \frac{mV_X}{0.67 + 0.21\,m} + \Delta V_s$$

This equation would behave very much like eq. [5].

Equation [1] was originally developed to correlate the BDEs of 24 bonds involving eight substituents, X, and three alkyl groups, R. The present work has extended the applicability of this equation in several ways. The range of substituents, X, has been enlarged to include SiH_3, GeH_3, and PH_2 in Table 1, seven new C-, O-, and N-centred groups in Table 2, and four new alkyl groups with methyl groups at the γ or δ positions relative to the radical centre in Tables 3 and 4. Section 5 also discusses three cases where R contains silicon atoms. Equation [5] and Table 4 incorporate steric effects. For the 42 cases where a comparison is possible between predicted and observed BDEs, the average absolute error is 0.7 kcal/mol, less than the average uncertainty of 1.1 kcal/mol in the experimental values. Of these 42 cases, 33 are discussed for the first time. Equation [5] may be used to predict other organic BDEs where resonance effects and ring strain are not important. It may also provide a step toward a better theoretical understanding of bond strengths.

Acknowledgements

The authors wish to thank the Natural Sciences and Engineering Research Council of Canada for financial support. Y. R. Luo thanks the Dorothy Killam Trust for the award of an Izaak Walton Killam Memorial Scholarship.

1. Y. R. Luo and S. W. Benson. J. Phys. Chem. **93**, 3304 (1989).
2. J. B. Pedley, R. D. Naylar, and S. P. Kirby. Thermochemical data of organic compounds. 2nd ed. Chapman and Hall, London. 1986.
3. A. L. Castelhano and D. Griller. J. Am. Chem. Soc. **104**, 3655 (1982).
4. R. Walsh. *In* The chemistry of organic silicon compounds. Part 1. *Edited by* S. Patai and Z. Rappoport. Wiley, Chichester. 1989. p. 371.

5. Y. R. Luo and S. W. Benson. J. Phys. Chem. **93**, 3791 (1989).
6. Y. R. Luo and S. W. Benson. J. Am. Chem. Soc. **111**, 2486 (1989).
7. L. Batt. Int. Rev. Phys. Chem. **6**, 53 (1987).
8. J. A. Kerr. *In* Handbook of chemistry and physics. 71st ed. CRC Press, Boca Raton, Fla. 1990–1991.
9. W. R. Anderson. J. Phys. Chem. **93**, 530 (1989).
10. Y. R. Luo. Ph.D thesis, Dalhousie University, 1991.
11. N. Laurencelle and P. D. Pacey. J. Am. Chem. Soc. **115**, 625 (1993).
12. S. W. Benson. Thermochemical kinetics. 2nd ed. John Wiley, New York. 1976.
13. J. M. Kanabus-Kaminska, J. A. Hawari, D. Griller, and C. Chatgilialoglu. J. Am. Chem. Soc. **109**, 5267 (1987).
14. D. Griller and D. D. M. Wayner. Pure Appl. Chem. **61**, 717 (1989).
15. Y. R. Luo and P. D. Pacey. J. Phys. Org. Chem. **4**, 562 (1991).
16. R. Walsh. Acc. Chem. Res. **14**, 246 (1981).
17. Y. R. Luo and S. W. Benson. J. Phys. Chem. **94**, 914 (1990).
18. Y. R. Luo and S. W. Benson. J. Phys. Chem. **93**, 3306 (1989).
19. Y. R. Luo and S. W. Benson. J. Phys. Chem. **93**, 7355 (1989).
20. Y. R. Luo and S. W. Benson. Inorg. Chem. **30**, 1670 (1991).
21. R. Walsh. Organometallics, **8**, 1973 (1989).
22. Y. R. Luo and P. D. Pacey. J. Phys. Chem. **95**, 9470 (1991).
23. Y. R. Luo and P. D. Pacey. Int. J. Mass Spectrom. Ion Processes, **112**, 63 (1992).
24. Y. R. Luo and P. D. Pacey. J. Am. Chem. Soc. **113**, 1465 (1991).
25. Y. Chen, A. Rauk, and E. Tschuikow-Roux. J. Phys. Chem. **94**, 6250 (1990).
26. O. Dobis and S. W. Benson. J. Am. Chem. Soc. **113**, 6377 (1991).
27. D. Gutman. Acc. Chem. Res. **23**, 375 (1990).
28. A. B. McEwen and D. M. Golden. J. Mol. Struct. **224**, 357 (1990).
29. W. Tsang. J. Am. Chem. Soc. **107**, 2872 (1985).
30. D. D. M. Wayner and D. Griller. Adv. Free Radical Chem. (Greenwich, Conn.), **1**, 159 (1990).

Can. J. Chem. Downloaded from www.nrcresearchpress.com by 88.255.202.194 on 09/08/12
For personal use only.

The vibrational spectra (100–1500 cm^{-1}) of a series of bicyclo[3.2.1]octanes assigned by means of scaled 3-21G *ab initio* harmonic force fields[1]

THOMAS EGGIMANN, NAN IBRAHIM, R. ANTHONY SHAW, AND HAL WIESER[2]
Department of Chemistry, University of Calgary, Calgary, Alta., Canada T2N 1N4

Received July 31, 1992

THOMAS EGGIMANN, NAN IBRAHIM, R. ANTHONY SHAW, and HAL WIESER. Can. J. Chem. **71**, 578 (1993).

The infrared absorption (vapor phase and solution) and Raman (liquid phase) spectra of bicyclo[3.2.1]octane, 8-oxabicyclo[3.2.1]octane, 6-oxabicyclo[3.2.1]octane, 6,8-dioxabicyclo[3.2.1]octane, and the 7,7-dideutero-substituted derivatives of the last two compounds are reported in the region 100–1500 cm^{-1} for the first time. The vibrational spectra are assigned almost completely with the guidance of *ab initio* 3-21G geometries and scaled force fields. A total of 14 force-field scale facors are transferred from smaller molecules, predicting the frequencies with an average error of 7.6 cm^{-1} (1.2%) for 196 assigned transitions. After optimizing the factors in an overlay refinement involving all six molecules, the frequencies are within 5.7 cm^{-1} (0.75%) of experiment. The *ab initio* absorption and Raman intensities are calculated with the 3-21G basis set and are demonstrated to be of such accuracy as to be useful for the spectral assignments. These intensities are calculated with uniformly and nonuniformly scaled force fields and compared to the experimental spectra. The intensities derived from the latter force fields are superior, meaning that nonuniform scaling is preferable at this level of theory for both vibrational frequencies and normal mode descriptions.

THOMAS EGGIMANN, NAN IBRAHIM, R. ANTHONY SHAW et HAL WIESER. Can. J. Chem. **71**, 578 (1993).

On a déterminé pour la première fois les spectres d'absorption (100–1500 cm^{-1}) infrarouge (phase vapeur et solution) et Raman (phase liquide) des bicyclo[3.2.1]octane, 8-oxabicyclo[3.2.1]octane, 6-oxabicyclo[3.2.1]octane, 6,8-dioxabicyclo[3.2.1]octane et des dérivés 7,7-dideutérés des deux derniers composés. On a attribué les bandes des spectres de vibration en faisant appel presqu'uniquement aux géométries *ab initio* 3-21G et aux champs de force. Utilisant des molécules plus petites, on a transféré un total de 14 facteurs d'échelle de champs de force et on a ainsi pu prédire les fréquences avec une erreur moyenne de 7,6 cm^{-1} (1,2%) pour les 196 transitions attribuées. Après avoir optimisé les facteurs à l'aide d'un affinement impliquant les six molécules, les fréquences calculées sont à 5,7 cm^{-1} (0,75%) des valeurs expérimentales. On a calculé l'absorption et les intensités Raman *ab initio* à l'aide de l'ensemble 3-21G et on a démontré que les valeurs calculées sont d'une telle exactitude qu'elles peuvent être utiles pour attribuer des spectres. On a calculé ces intensités à l'aide de champs de force à échelles uniformes et non uniformes et on les a comparées à celles des spectres expérimentaux. Les intensités obtenues à l'aide des derniers champs de force sont supérieurs, c'est-à-dire que, pour les fréquences vibrationnelles ainsi que pour les descriptions des modes normaux, les échelles non uniformes sont préférables à ce niveau de la théorie.

[Traduit par la rédaction]

Introduction

In recent years the assignment of the vibrational spectra of small molecules by means of *ab initio* calculated geometries and harmonic force fields has become almost a routine procedure. The *ab initio* calculations can be performed at various levels of theory with a choice of many different basis sets. The accuracy of the results is largely limited by the size of the molecule and the available computing power. In attempting to reproduce experimental frequencies as accurately as possible, more or less severe corrections are applied to the *ab initio* geometries and force fields, depending on the level of approximation.

We are interested in the vibrational dynamics of monocyclic and bicyclic molecules with low symmetry and seek conceptually simple ways to interpret the experimental infrared absorption, Raman, and vibrational circular dichroism (VCD) spectra (1–6). Our approach is to calculate harmonic *ab initio* force fields (3-21G, or higher if possible) from the uncorrected geometries optimized with the same basis set. The force constants are transformed to appropriate local symmetry coordinates, then scaled with a small set of factors for particular types of modes. These procedures are basically equivalent to the standard scaled quantum mechanical (SQM) force field, originally developed and recommended by Pulay *et al.* (7), with the difference that we prefer not to correct the *ab initio* geometries. Such scale factors, in our experience, when judiciously selected and transferred from similar moieties, lead to frequency predictions with errors well below 2% on average. Even quite complex spectra can then be assigned with high confidence. Simultaneously, the scale factors can be refined in a least-squares fit of the frequencies in overlay refinements involving series of molecules. Finely tuned factors are thus obtained that are again suitable for transfer to the corresponding local symmetry modes of other classes of molecules with similar structural elements. Such refinements of scale factors are significant, as a dependence on the chemical or structural environment has been noted for the factors of certain modes. For the C—O stretching mode, for example, values of 0.903 (dimethyl ether) (1), 0.851 (2-methyloxetane) (2*a*), and 0.845 (7-oxanorbornane) (5) were found, indicating unequal overestimations of the *ab initio* C—O stretching force constants for different molecules, possibly depending on the C—O—C bond angle. It is essential therefore to explore scale factors for local symmetry modes in a variety of different environments, thereby rendering them more suitable for a transfer to new structures.

A good fit of the frequencies by nonuniform scaling and refining does not guarantee that the normal mode descriptions are correctly calculated. Moreover, the solutions of the refinements need not be unique. It is therefore even more

[1]Based in part on the Ph.D. thesis of T. Eggimann, The University of Calgary, 1991.

[2]Author to whom correspondence may be addressed.

Can. J. Chem. Downloaded from www.nrcresearchpress.com by 88.255.202.194 on 09/08/12
For personal use only.

Can. J. Chem. Downloaded from www.nrcresearchpress.com by 88.255.202.194 on 09/08/12
For personal use only.

important to start out with a set of scale factors that are already close to the optimized values and to perform the refining procedure very carefully. To judge the quality of scaling it is essential to investigate both the frequencies and the normal mode descriptions of the vibrations. The latter cannot be observed directly, but their accuracy appears with great sensitivity in the calculated intensities of the absorption, Raman, and even more in the VCD spectra. We demonstrate in this work that nonuniform scaling of force fields does not deteriorate the *ab initio* eigenvectors if enough care is taken in the process of transferring and refining the factors. It is also shown that in spite of using the primitive 3-21G basis set, the *ab initio* absorption and Raman intensities reflect the experimental spectra sufficiently accurately that, at the very least, the intensities can assist in the assignments. This aspect is of particular importance for this series of molecules, two of which have C_s symmetry and the remaining four are asymmetric, as the most useful and unambiguous experimental data, namely vapor phase band shapes and Raman polarization ratios, are helpful only for very few bands. The properties that are available to guide the spectral assignments other than the frequencies are then the calculated absorption and Raman intensities. In addition, the method of scaling and simultaneously optimizing several force fields with the same set of factors is indispensable for this series of sufficiently similar molecules, since the wealth of combined experimental data that can be fitted with just a few parameters helps to resolve a number of ambiguities that otherwise would be intractable.

We report below the vibrational spectra from 100 to 1500 cm^{-1} and corresponding assignments based on *ab initio* 3-21G harmonic force fields for bicyclo[3.2.1]octane (BCO), and the 8-oxa (8OXA), 6-oxa (6OXA), 7,7-d_2-6-oxa (6OXA-d_2), 6,8-dioxa (DIOXA), and 7,7-d_2-6,8-dioxa (DIOXA-d_2) analogues (Figs. 1, 2). The investigation of the VCD spectrum of DIOXA described earlier (6) was based on these assignments. Of interest for further VCD studies are the vibrational spectra and assignments of several mono- and dimethyl substituted analogues of DIOXA, to be reported in a subsequent publication.

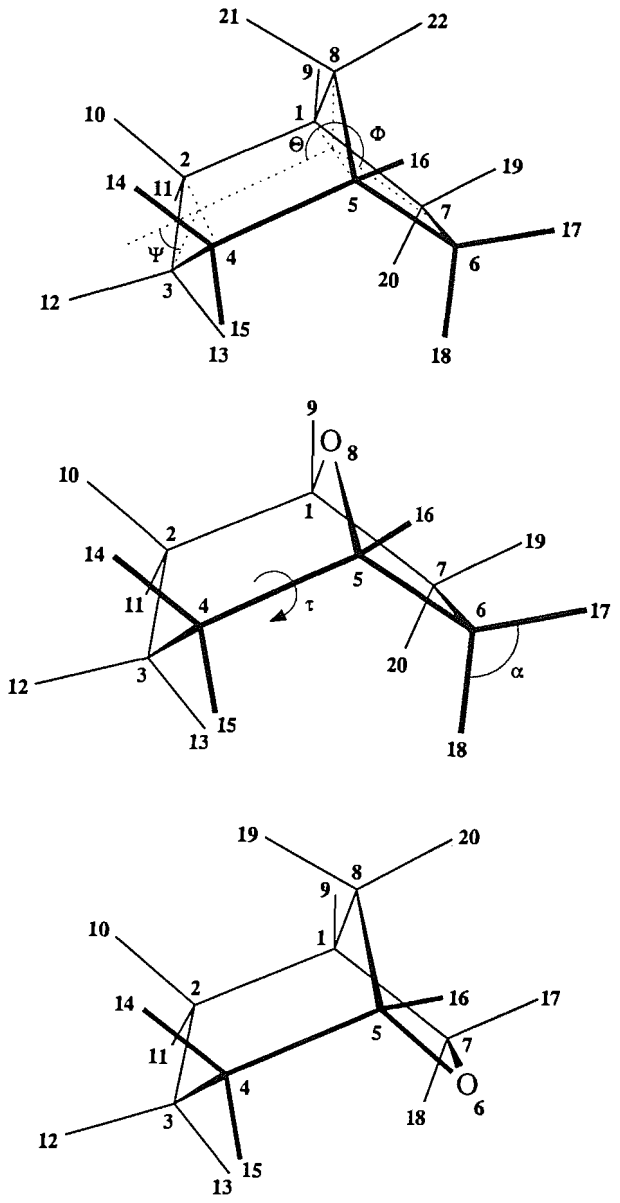

FIG. 1. Structures of bicyclo[3.2.1]octane (BCO), (top); 8-oxabicyclo[3.2.1]octane (8OXA), (middle); and 6-oxabicyclo-[3.2.1]octane (6OXA), (bottom). Numbers correspond to atom numbering used in Tables 7 and 8–10.

Syntheses

The synthesis of DIOXA has been described elsewhere (8). All the compounds were further purified to >98% by vacuum sublimation before recording their spectra. The purities were confirmed by gas chromatography.

Bicyclo[3.2.1]octane (BCO)

Following a known procedure (9), dichlorocarbene was added to norbornene to form *exo*-3,3-dichlorotricyclo[3.2.1.$0^{2,4}$]octane, which upon heating rearranged to *exo*-3,4-dichlorobicyclo[3.2.1]-oct-2-ene with an overall yield of 19%. This dichloride was dechlorinated using a method recommended for a similar compound (10). A mixture of dry THF (400 mL), sodium metal (1.6 mol, cut into small pieces), and *tert*-butanol (0.57 mol) was stirred vigorously and heated under a nitrogen atmosphere. When reflux of the solvent started, 3,4-dichlorobicyclo[3.2.1]oct-2-ene (0.17 mol) was added dropwise. After stirring and refluxing for 40 h, the product was separated and purified as recommended (10). Bicyclo-[3.2.1]oct-2-ene was obtained in 44% yield.

In a hydrogenation flask were placed bicyclo[3.2.1]oct-2-ene (37 mmol), absolute ethanol (30 mL), and 5% Pd/C (100 mg). The addition was carried out in a Parr hydrogenator applying an initial pressure of 70 psi (1 psi = 6.9 kPa) of hydrogen. The pressure dropped quickly and the reaction was stopped after 4 h. The mixture was filtered through Celite and the BCO precipitated by adding a large volume of water. The yield of crude product after filtration was 2.4 g (59%). The structures of the products in every step were confirmed by ^1H nmr.

8-Oxabicyclo[3.2.1]octane (8OXA)

This synthesis has been reported by other workers and is therefore given in short form only. From cyclopentanone and pyrrolidine the enamine (1-(*N*-pyrrolidinyl)cyclopentene was prepared, which was reacted with acrolein to form 2-(*N*-pyrrolidinyl)-bicyclo[3.2.1]octan-8-one (11, 12). The methyl iodide of this amine was converted to 4-cycloheptenecarboxylic acid by base-induced ring opening (11–13). Lead tetraacetate decarboxylation of the acid, followed by the reduction of the acetate with $LiAlH_4$, gave 4-cycloheptenol (14). Ring closure to 8-oxabicyclo[3.2.1]octane-2-mercurial iodide was achieved by treatment with mercury acetate (15). Treatment with iodine gave 2-iodo-8-oxabicyclo[3.2.1]octane, which, upon reduction with $LiAlH_4$, afforded the desired

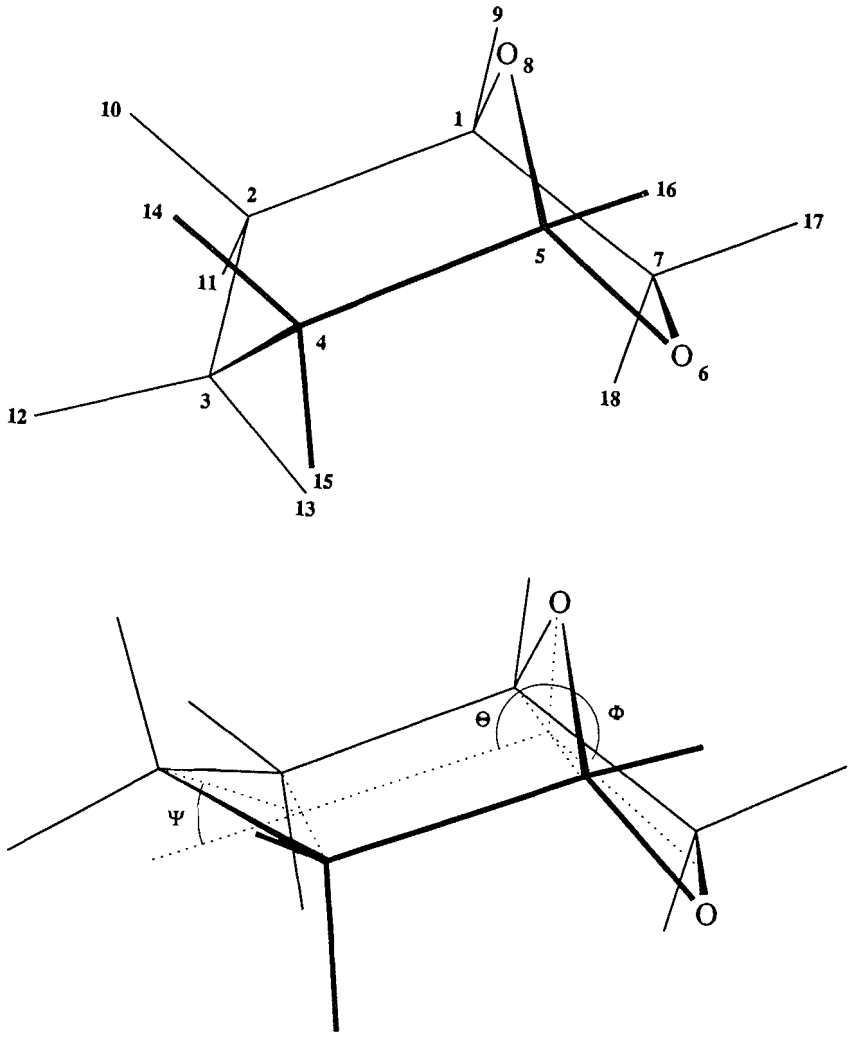

FIG. 2. Structures of the chair (upper) and boat (lower) conformers of 6,8-dioxabicyclo[3.2.1]octane (DIOXA). Numbers correspond to atom numbering used in Tables 7 and 11.

8OXA (15). In all steps the yields were comparable to values reported in the stated references. The products were always checked by their ^{1}H nmr spectra.

6-Oxabicyclo[3.2.1]octane (6OXA)

The precursor, 4-hydroxymethylcyclohexene, was obtained from cyclohexene-4-carboxaldehyde (Aldrich) by reduction with sodium borohydride in methanol, following a published procedure for a similar compound (16). The yield after work-up was 84%.

Ring closure of the alcohol to the bicyclic structure was achieved analogously to 8OXA (15). A solution of mercury acetate (40 mmol) and sodium acetate (40 mmol) in 50 mL of water was stirred. The alcohol (40 mmol) was added within 5 min and stirring was maintained at ambient temperature for 15 min. A solution of potassium iodide (52 mmol) and sodium hydroxide (40 mmol) in 50 mL water was added dropwise, causing the product to precipitate. After stirring for another 15 min, the supernatant liquid was decanted and the solid 6-oxabicyclo[3.2.1]octane-2-mercurial iodide was dried under vacuum at room temperature and used as such for the following step.

The mercury was eliminated by stirring the mercurial iodide (40 mmol) with an equimolar amount of iodine in 250 mL of carbon tetrachloride for 28 h. The work-up was carried out as described (15), yielding 6.8 g of crude iodide (71% relative to 4-hydroxymethylcyclohexene).

The iodide was reduced with $LiAlH_4$ in ether (15). After the usual work-up, 6OXA was distilled at aspirator vacuum and obtained with 50% yield. Its ^{1}H nmr spectrum was identical to the reported spectrum (17).

7,7-d_2-6-Oxabicyclo[3.2.1]octane (6OXA-d_2)

Following a published procedure (18), *m*-hydroxybenzoic acid was hydrogenated with sodium in boiling absolute ethanol. When all the sodium had reacted, water was added and the mixture was neutralized with hydrochloric acid. The alcohol was evaporated and after adding an excess of hydrochloric acid the solution was extracted continuously with ether for 8 h. The extract was dried with $MgSO_4$ and the ether was evaporated to give a residue containing *cis*- and *trans*-3-hydroxycyclohexanecarboxylic acid. The mixture was heated at 170°C for 40 min to convert the *cis* isomer to 6-oxabicyclo[3.2.1]octan-7-one (25% yield after distillation).

6OXA-d_2 was prepared by a modification of a published procedure (17). A solution of the lactone (24 mmol) in ether (50 mL) was added dropwise to a stirred slurry of $LiAlD_4$ (38 mmol) in ether (90 mL). The mixture was refluxed for 2.5 h. After work-up an oil was recovered containing the *cis*-3-hydroxycyclohexyl-1,1-dideuteromethanol, which was used without further purification. The crude diol and *p*-toluenesulfonic acid were mixed and heated to 150°C (oil bath temperature) in a distillation apparatus at aspirator vacuum. The fraction boiling at 50–80°C was collected and redistilled. The 6OXA-d_2 was obtained in 20% overall yield; ^{1}H nmr

Can. J. Chem. Downloaded from www.nrcresearchpress.com by 88.255.202.194 on 09/08/12
For personal use only.

Can. J. Chem. Downloaded from www.nrcresearchpress.com by 88.255.202.194 on 09/08/12
For personal use only.

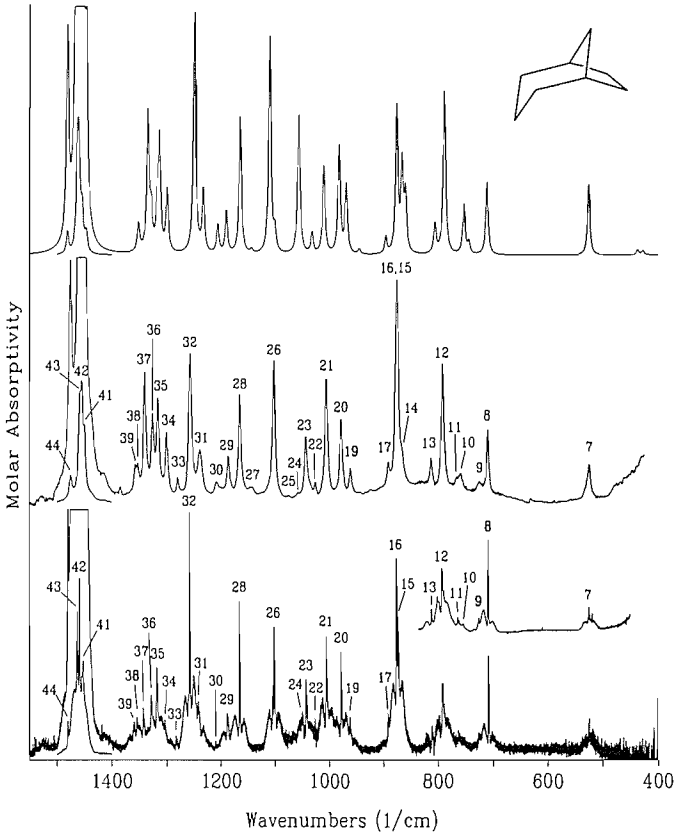

FIG. 3. Calculated (top) and observed solution (middle) and vapor phase (bottom) absorption spectra of bicyclo[3.2.1]octane (BCO). The solution and theoretical spectra are on the same scale. For experimental conditions see text. The insert vapor phase spectrum (450–830 cm^{-1}) was recorded with 0.5 cm^{-1} resolution (500 scans). Numbers correspond to "Band nos." in Tables 1 and 13.

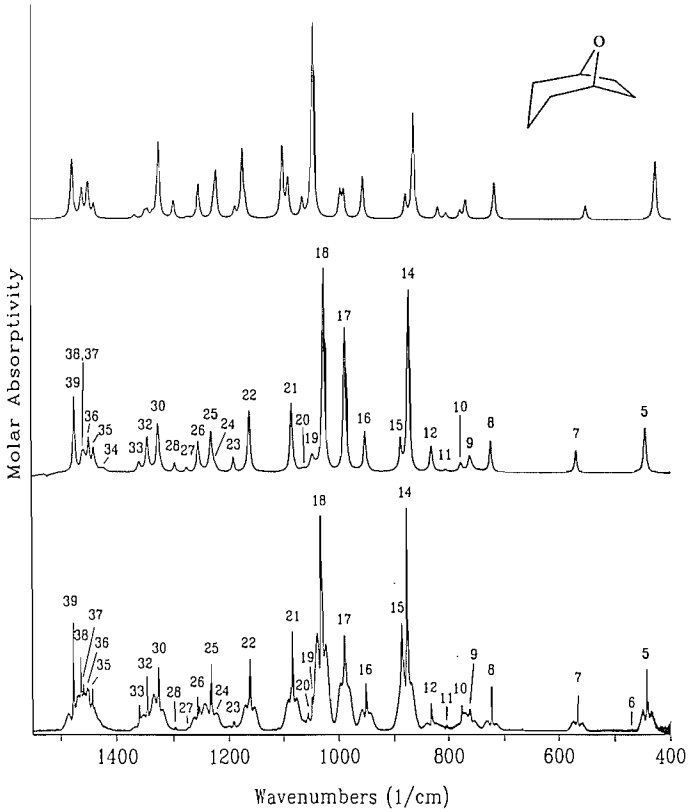

FIG. 4. Calculated (top) and observed solution (middle) and vapor phase (bottom) absorption spectra of 8-oxabicyclo[3.2.1]-octane (8OXA). The solution and theoretical spectra are on the same scale. For experimental conditions see text. Numbers correspond to "Band nos." in Tables 2 and 14.

(Bruker AC 200, 200 MHz, $CDCl_3$) δ: 1.5–1.9 (m, 8H), 2.36 (s, br, 1H, C1-H), 4.31 (t, 1H, C5-H).

7,7-d_2-6,8-Dioxabicyclo[3.2.1]octane (DIOXA-d_2)

3,4-Dihydro-2*H*-pyran-2-carboxylate ethyl ester (8) was reduced with an equimolar amount of $LiAlD_4$ by stirring for 2 h to yield 3,4-dihydro-2*H*-pyran-2-(1,1-dideutero)-methanol after decomposition (88% after distillation, F = 85–87°C, asp. vacuum). For cyclization, the alcohol (26 mmol) was refluxed for 1 h in *p*-toluenesulfonic acid (30 mg) and benzene (30 mL). The mixture was neutralized with sodium methanolate, filtered, and distilled. DIOXA-d_2 was collected at 68–74°C (asp. vacuum) in 79% yield; ^1H nmr (Bruker AC 200, 200 MHz, $CDCl_3$) δ: 1.5–2.0 (m, 6H), 4.49 (s, 1H, C1-H), 5.51 (s, 1H, C5-H).

Experimental

The absorption spectra were measured with a Nicolet 8000 FT-IR interferometer using a MCT detector with a cutoff at 400 cm^{-1}. The condensed phase spectra (400–1500 cm^{-1}) were recorded from solutions in CS_2 (700–840 cm^{-1}) and CCl_4 (remaining parts of the spectra) with typical concentrations of 0.5 mol/L (0.8 mol/L for BCO) and with 0.1 mm path length. To obtain adequate signal-to-noise for Fourier self-deconvolution, 2000 scans were coadded at 1 cm^{-1} resolution. For the mid-infrared vapor phase spectra (400–1500 cm^{-1}), the compounds were evaporated into a Wilks variable-path gas cell adjusted to approximately 5 m path length using pressures of typically 1.4 Torr (1 Torr = 133.2 Pa), except for BCO for which 12 Torr were required. In all cases 500 scans were collected with 0.12 cm^{-1} resolution (unapodized). The water lines in the spectrum of BCO were diminished by subtracting a spectrum of water recorded with identical instrumental settings. The spectra are displayed in Figs. 3–8.

The far-infrared vapor phase spectra (80–400 cm^{-1}) were recorded for BCO, 8OXA, 6OXA, 6OXA-d_2, and DIOXA with 0.12 cm^{-1} resolution. The spectra exhibit well-resolved sequences of *Q*-branches for many fundamentals resulting from skeletal anharmonicities. While the details are published elsewhere (19), peak positions of the fundamentals are included here for the sake of completeness. For BCO, the absence of significant transition dipole moments results in very weak absorptions, obscured in addition by water lines. Nonetheless, two bands located at 262.5 and 358.1 cm^{-1} could be identified and assigned to A' fundamentals.

The Raman spectra of the neat melted compounds (Figs. 9–14) were measured between 100 cm^{-1} and 1500 cm^{-1} with a Jarrell–Ash model 25-100 double grating monochromator, utilizing for excitation the 514.5-nm line of an argon ion laser (Coherent Radiation) with 300 mW power at the sample. The photomultiplier detector was interfaced to a microcomputer, which allowed coaddition of 8 scans for each spectrum with a scanning step size of 2 cm^{-1} and a time constant of 1 s. The slits were adjusted to an effective spectral width of 5 cm^{-1} at 1000 cm^{-1}. Since the samples have relatively high vapor pressures, they were sealed into capillary tubes and melted with a stream of hot air (50–150°C) in a specially designed apparatus. The laser beam was focused into the samples from the bottom of the capillary tubes. The frequencies were calibrated against the CCl_4 peaks. The measured intensities were not corrected for the frequency-dependent response of the photomultiplier tube. The resulting errors are estimated to be within 15% maximally over the whole reported spectral region, and

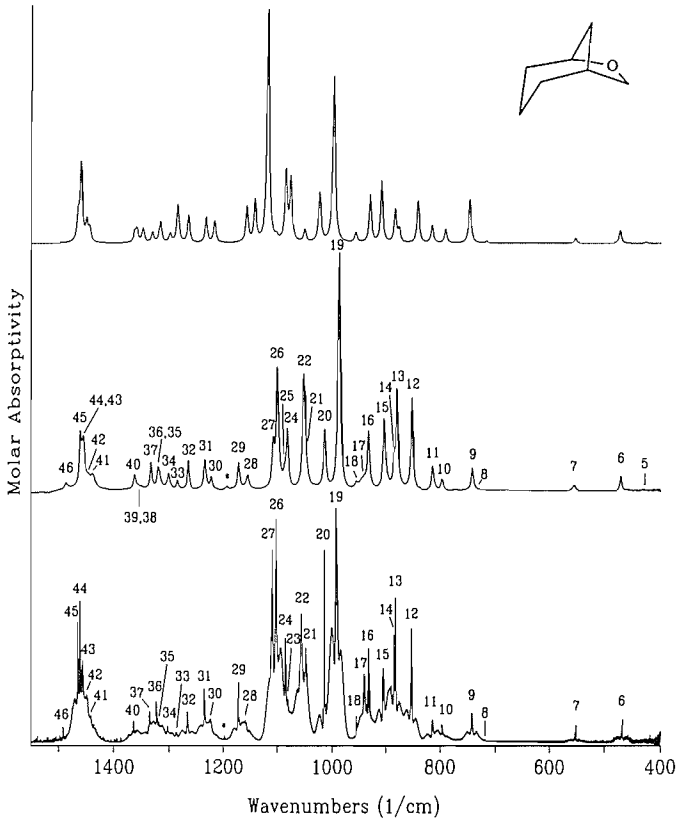

FIG. 5. Calculated (top) and observed solution (middle) and vapor phase (bottom) absorption spectra of 6-oxabicyclo[3.2.1]-octane (6OXA). The solution and theoretical spectra are on the same scale. For experimental conditions see text. Numbers correspond to "Band nos." in Tables 3 and 15. Asterisks indicate bands that are believed to arise from impurities.

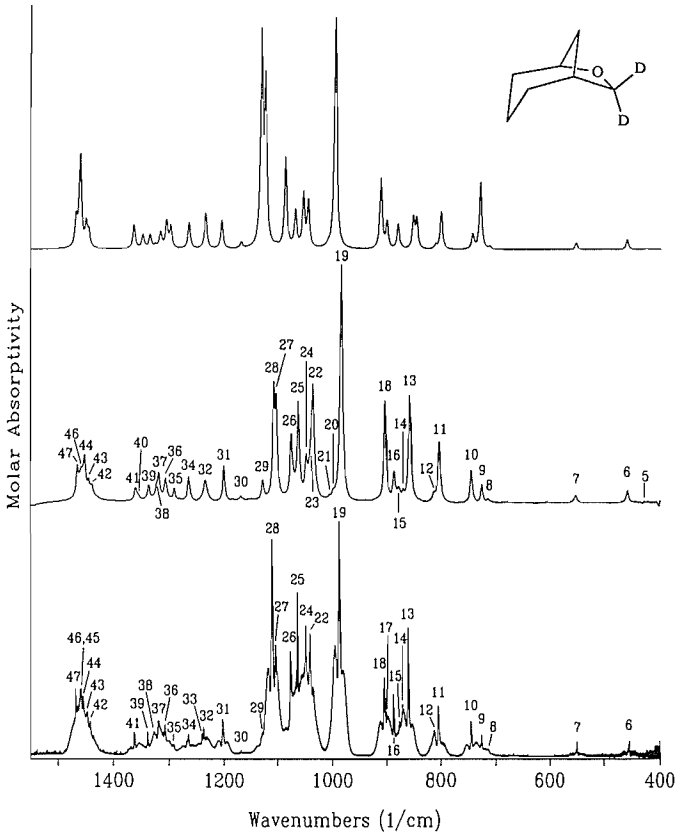

FIG. 6. Calculated (top) and observed solution (middle) and vapor phase (bottom) absorption spectra of 7,7-d_2-6-oxabicyclo[3.2.1]octane (6OXA-d_2). The solution and theoretical spectra are on the same scale. For experimental conditions see text. Numbers correspond to "Band nos." in Tables 4 and 16.

appreciably less in narrower regions of specific group frequencies within which intensity comparisons are invariably made in the following text for the purpose of assisting with assignments.

Observed vibrational frequencies and absorption intensities (expressed as dipole strengths) are listed in Tables 1–6. Selected portions of the condensed phase absorption spectra were subjected to Fourier self-deconvolution (20) in order to resolve partially overlapped bands and to check for transitions that might be completely hidden by other bands. Accurate frequencies were thus measured for a number of bands that otherwise would have been uncertain or left unnoticed. Such bands are marked with the label "dcn" in Tables 1–6. Absorption intensities were determined from the solution spectra by fitting Lorentzian band-shape functions and measuring band heights and widths at half height. The results obtained by visual and least-squares methods and for different solutions usually varied between 2 and 10%. The errors in the experimental intensities are thus estimated to lie in this range for most bands, while for a few of the very weak and overlapped lines the errors may be above 20%.

Calculations

Ab initio *calculations*

The geometries of BCO, 8OXA, 6OXA, and DIOXA were fully optimized and their harmonic force fields calculated by analytical second differentiation of the energies at the equilibrium geometries. The computations were carried out at the SCF-RHF level of theory using the programs GAUSSIAN 82 implemented on a CDC Cyber 205 (STO-3G basis set), and GAUSSIAN 86 (21) running on a Convex C120 (3-21G basis set). The atomic polar tensors and the polarizability derivatives were computed using the 3-21G basis set. BCO and 8OXA were restricted C_S symmetry. The existence of a true minimum in the potential hypersurface at the stationary point was ensured in every instance by confirming that all diagonal force constants were positive. Proof of good convergence was supplied by the fact that the lowest vibrational frequencies, which would be most affected by insufficient convergence of the energy, are calculated with an average error of 10.8 cm^{-1} (5.7%), which is within the expected error for the unscaled force fields. Contrary to Pulay's advocated standard procedure (7, 22), according to which corrected geometries afford more accurate force fields, we prefer to obtain the force fields at the uncorrected *ab initio* geometries. The practice of calculating Cartesian force fields at distorted theoretical geometries would require nonlinear transformations to other coordinate systems in order to account for the non-vanishing forces. For the bicyclic structures investigated, any correctional variations of the bond lengths and angles would unavoidably lead to distortions in the ring segments, and these distortions would be dependent on the choice of the valence coordinates in which the corrections are carried out.

The calculations utilizing STO-3G force fields are not presented here since they are clearly inferior to the 3-21G results. Information, however, can be obtained from the authors. Selected structural parameters and the RHF energies of all four parent molecules are given in Table 7 for the two

Can. J. Chem. Downloaded from www.nrcresearchpress.com by 88.255.202.194 on 09/08/12
For personal use only.

Can. J. Chem. Downloaded from www.nrcresearchpress.com by 88.255.202.194 on 09/08/12
For personal use only.

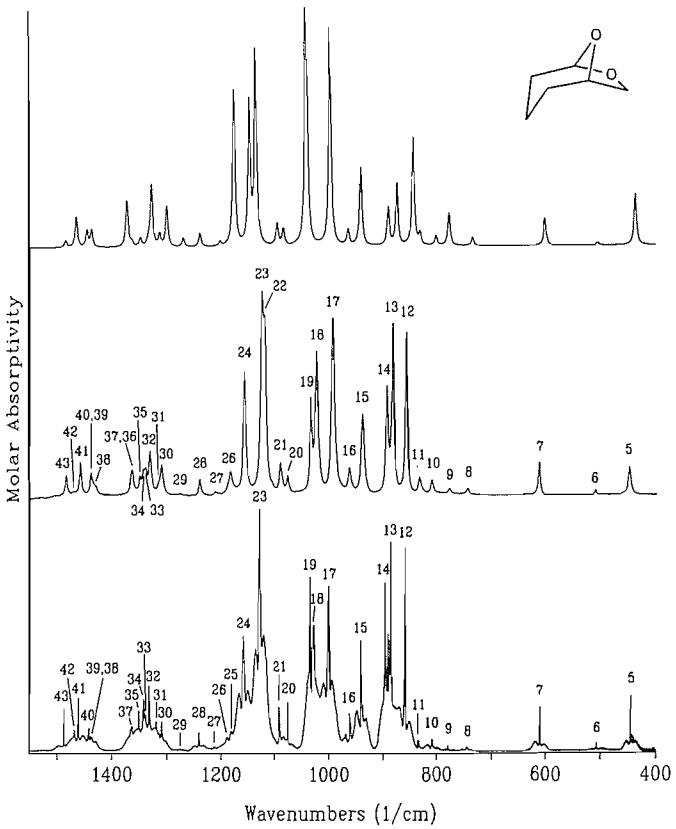

FIG. 7. Calculated (top) and observed solution (middle) and vapor phase (bottom) absorption spectra of 6,8-dioxabicyclo-[3.2.1]octane (DIOXA). The solution and theoretical spectra are on the same scale. For experimental conditions see text. Numbers correspond to "Band nos." in Tables 5 and 17.

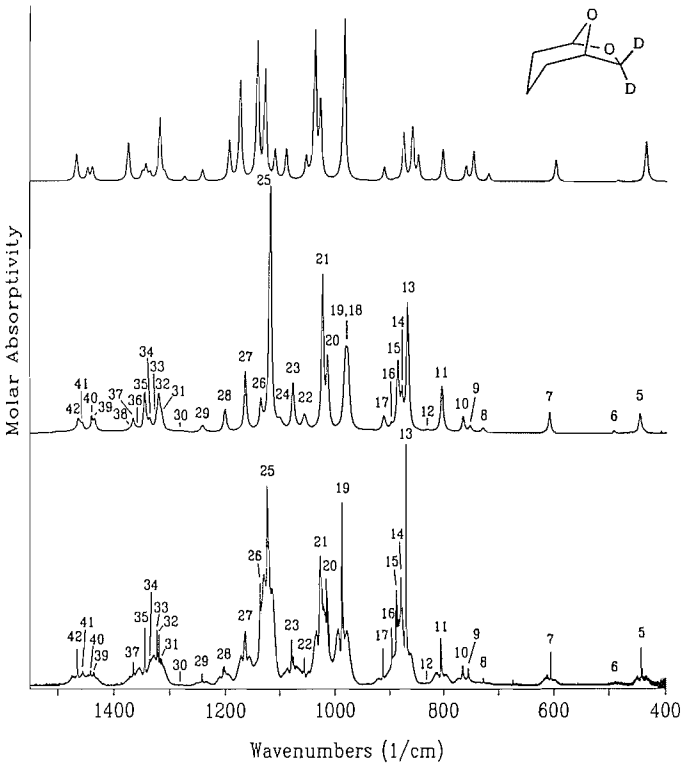

FIG. 8. Calculated (top) and observed solution (middle) and vapor phase (bottom) absorption spectra of 7,7-d_2-6,8-dioxabicyclo[3.2.1]octane (DIOXA-d_2). The solution and theoretical spectra are on the same scale. For experimental conditions see text. Numbers correspond to "Band nos." in Tables 6 and 18.

basis sets. For each of these bicyclics, two stable conformers may be expected to exist, which may be described by the chair and boat forms of the six-membered ring segment. All four structures converged to the chair conformation (Figs. 1, 2) in the geometry optimizations. To better characterize the potential surface of the ring inversion, the boat conformer of DIOXA was relaxed, converging at the 3-21G level in a local minimum higher in energy by 1577 cm^{-1} (18.9 kJ/mol) compared to the chair (Fig. 2). The chair to boat inversion is accompanied by other changes, involving considerable lengthening of the bonds C1—C2 and C4—C5, as well as an increase of the twist in the seven-membered ring segment, as expressed by the dihedral angle δ(1-7-6-5) in Table 7. The STO-3G calculation in addition proposes a remarkable expansion of the O6—C7 bond. Although no similar calculations for the other compounds were carried out, we suspect that they all possess similar highly asymmetric double minimum potentials for the inversion of the six-membered ring. The vibrational analysis of the boat conformers of the two DIOXA isotopomers revealed a number of transitions that should be observable distinctively among those of the chairs, but none were detected in the experimental spectra. This is in accord with the calculated population (0.04%, neglecting the zero-point vibrational energy) of the boat at the experimental conditions. Experimental structures have been published for 8OXA from a microwave study (23) and for BCO from electron diffraction (24). In both cases the agreement with the calculated geometries is reasonably good. These experimental studies confirm for both molecules the strong preponderance of the chair form at ambient temperatures.

Scaling and refining of ab initio *force fields*

These procedures, which were also described in previous publications (1, 2*a*, 4, 5), were carried out with a program developed by Shaw (25). The harmonic *ab initio* Cartesian force constants were transformed to a nonredundant set of local symmetry coordinates (LSCs), defined as linear combinations of internal coordinates following Pulay *et al.* (22) and listed in Tables 8–11 for the four parent molecules. The transformed force constants K_{ij} were then scaled with factors c_i and c_j associated with the local symmetry modes i and j, respectively, according to $F_{ij} = (c_i c_j)^{1/2} K_{ij}$, where the F_{ij} are the scaled force constants (26). The scale factors for the individual LSCs were transferred from similar molecules (see Table 12) and subsequently optimized stepwise in overlay refinements including all six compounds by least-squares fitting of the calculated frequency parameters, $\lambda_k = (2\pi c\bar{\nu}_k)^2$, to the observed values after weighting by $(1/\lambda_k^{obs})^2$.

Three vibrational calculations are presented here which differ in the way the *ab initio* force fields were scaled. The three scaling techniques were analyzed for the resulting accuracy in reproducing the experimental spectra in an attempt to find the most favorable force-field correction method. The simplest scheme, namely uniform scaling, consists of multiplying all diagonal and off-diagonal force constants by the same factor, which is subsequently refined. These results are found in column 1 under "Calculated wavenumbers" in Tables 13–18. The other two

Can. J. Chem. Downloaded from www.nrcresearchpress.com by 88.255.202.194 on 09/08/12
For personal use only.

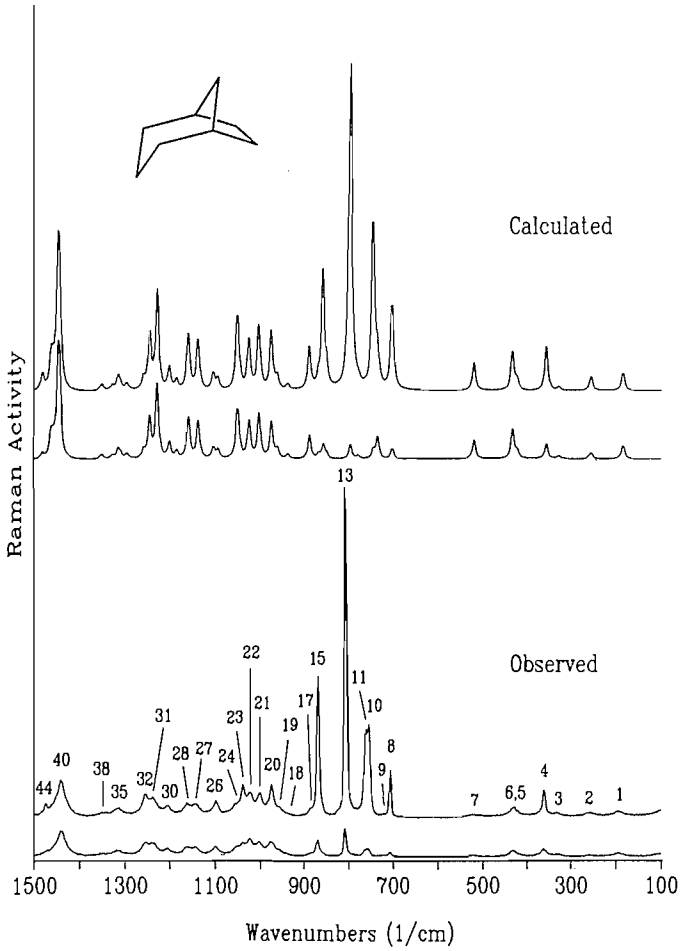

FIG. 9. Observed and calculated Raman spectra of liquid bicyclo[3.2.1]octane (BCO). The two traces correspond to the parallel ($I^{\parallel}$, upper) and perpendicular ($I^{\perp}$, lower) polarization measurements. For experimental conditions see text. Numbers correspond to "Band nos." in Tables 1 and 13.

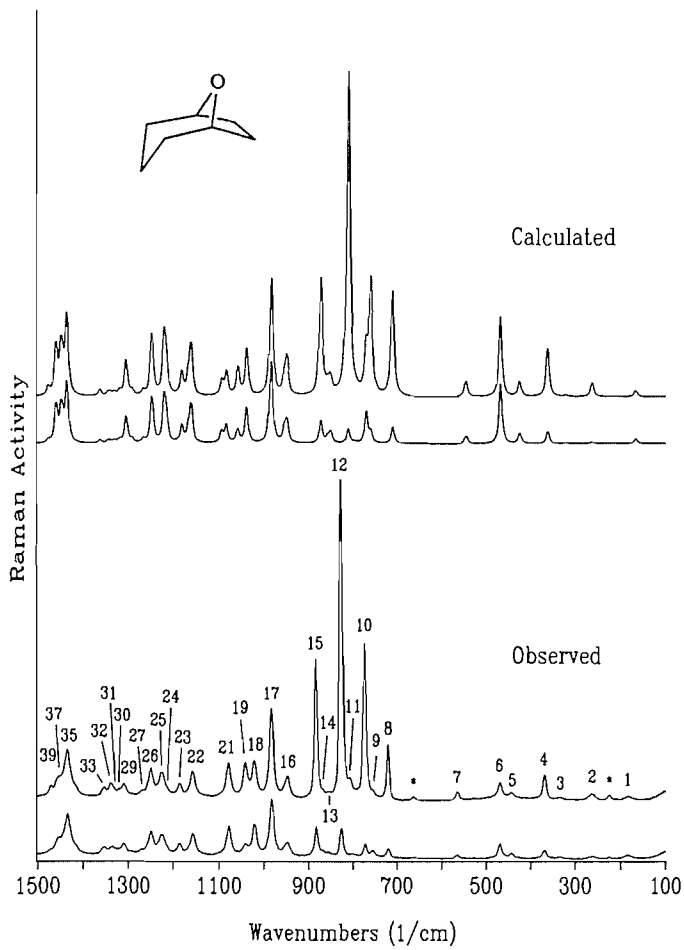

FIG. 10. Observed and calculated Raman spectra of liquid 8-oxabicyclo[3.2.1]octane (8OXA). The two traces correspond to the parallel ($I^{\parallel}$, upper) and perpendicular ($I^{\perp}$, lower) polarization measurements. For experimental conditions see text. Numbers correspond to "Band nos." in Tables 2 and 14. Asterisks indicate bands that are believed to arise from impurities.

calculations adopt the method of nonuniform scaling, applying and adjusting several factors, separately scaling the force constants for different types of LSCs as outlined above. Tables 13–18 contain the resulting wavenumbers using 14 factors directly transferred from other molecules (column 2, see discussion below), and fully refined (column 3). The factors applied to the three scaling schemes are listed in Table 12.

Intensity calculations

The absorption and Raman intensities listed in Tables 13–18 were derived from the refined nonuniformly scaled force fields. The dependence of the intensities on the scaling method is analysed below in the Discussion. The theoretical absorption intensities were computed by the standard expression for the dipole strength D_i (in units of esu^2 cm^2) of the ith fundamental (27, 28):

$$[1]\quad D_i = \frac{h}{8\pi^2\nu_i}\left|\sum_a \left(\frac{\partial \underline{\mu}}{\partial \underline{x}_a}\right)_0 \left(\frac{\partial \underline{x}_a}{\partial q_i}\right)\right|^2 = \frac{3(2303)hc}{8\pi^3 N_0}\int_{\text{band}} \frac{\epsilon(\nu)\,d\nu}{\nu}$$

where the symbols, h, c, N_0, and ν_i refer, respectively, to Planck's constant, the speed of light, Avogadro's number, and the vibrational frequency of normal mode i, in cgs units. The atomic polar tensor $(\partial \underline{\mu}/\partial \underline{x}_a)_0$ is the *ab initio* molecular dipole moment derivative with respect to the Cartesian position vector $\underline{x}_a$ of atom a, evaluated at the equilibrium geometry, and $(\partial \underline{x}_a/\partial q_i)$ is the Cartesian eigenvector for atom a in normal coordinate q_i as obtained from the Wilson GF formalism (29). The right-hand side of the equation defines the connection to the experimentally available molar absorptivity $\epsilon(\nu)$ if used in units of M^{-1} cm^{-1}.

The Raman scattering activities may be obtained to a good approximation from the derivatives of the molecular polarizability with respect to the normal coordinates $\partial \underline{\underline{\alpha}}/\partial q_i)$ if the electronic ground state is nondegenerate, and if the Raman frequency shifts ν_i are small compared to the frequency ν_0 of the incident light and compared to $\nu_E - \nu_0$, where ν_E is the lowest electronic absorption frequency (28*a*, 29). All these conditions are satisfied for the title compounds. The desired quantities can be calculated using:

$$[2]\quad \left(\frac{\partial \underline{\underline{\alpha}}}{\partial q_i}\right) = \sum_a \left(\frac{\partial \underline{\underline{\alpha}}}{\partial \underline{x}_a}\right)_0 \left(\frac{\partial \underline{x}_a}{\partial q_i}\right)$$

Can. J. Chem. Downloaded from www.nrcresearchpress.com by 88.255.202.194 on 09/08/12
For personal use only.

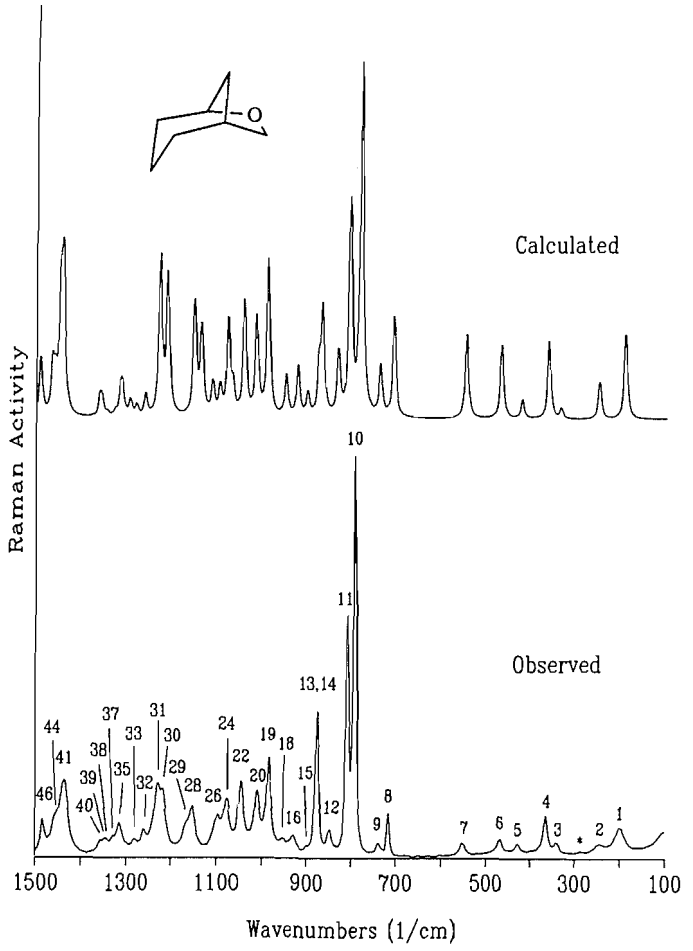

FIG. 11. Observed and calculated total Raman intensities (I^T) of liquid 6-oxabicyclo[3.2.1]octane (6OXA). For experimental conditions see text. Numbers correspond to "Band nos." in Tables 3 and 15. Asterisks indicate bands that are believed to arise from impurities.

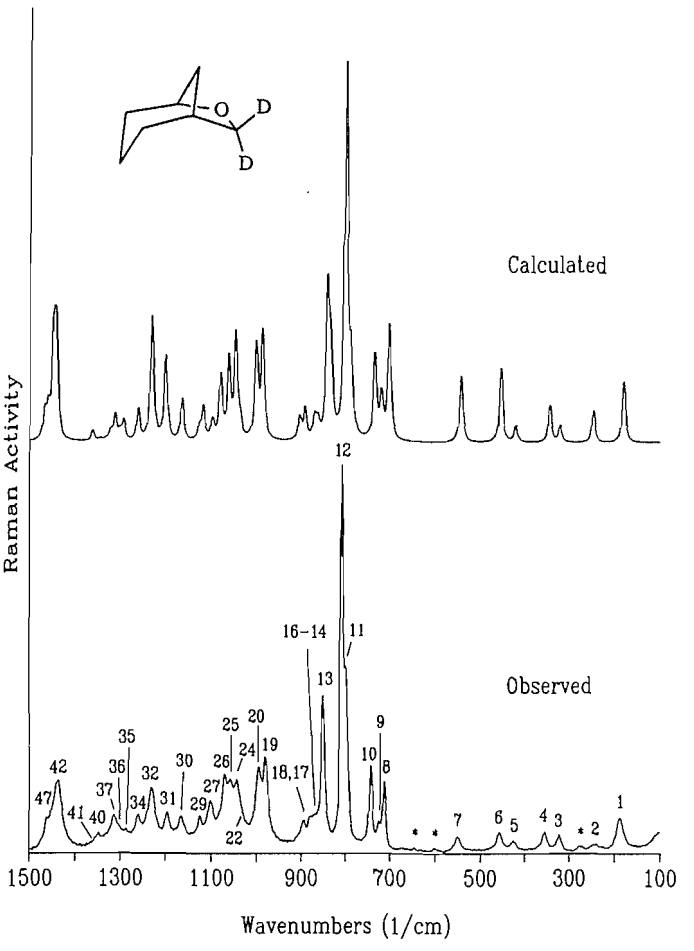

FIG. 12. Observed and calculated total Raman intensities (I^T) of liquid 7,7-d_2-6-oxabicyclo[3.2.1]octane (6OXA-d_2). For experimental conditions see text. Numbers correspond to "Band nos." in Tables 4 and 16. Asterisks indicate bands that are believed to arise from impurities.

where the polarizability derivatives with respect to Cartesian atomic coordinates $(\partial\underline{\alpha}/\partial x_a)_0$ are generated *ab initio* in the GAUSSIAN86 program. The mean value $\bar{\alpha}_i$ and the anisotropy γ_i^2 of the polarizability derivative tensors are then substituted into the standard classical equations for the Raman intensity of fundamentals (28*a*, 29, 30). For our experimental setup, which is collecting the scattered light at 90° from the progagation direction and perpendicularly to the electric field vector of the incident plane-polarized laser beam, these expressions are

$$[3] \quad S^T_i = 45\bar{\alpha}_i^2 + 7\,\gamma_i^2$$

$$[4] \quad S^{\parallel}_i = 45\bar{\alpha}_i^2 + 4\,\gamma_i^2$$

$$[5] \quad S^{\perp}_i = 3\,\gamma_i^2$$

$$[6] \quad \rho_i = 3\,\gamma_i^2/(45\bar{\alpha}_i^2 + 4\,\gamma_i^2)$$

where S^T_i designates the total intensity of the scattered light in the stated direction, $S^{\parallel}_i$ and $S^{\perp}_i$ are the parallel and perpendicular polarized components, respectively, and ρ_i is the depolarization ratio of normal mode *i*. The Raman data listed in Tables 13–18 were calculated using eqs. [3] and [6]. These quantities, although commonly reported, are not proportional to the experimental Raman activities. To allow direct comparison to observed intensities, the pertinent theoretical equations [3]–[5] must be multiplied with the factor $(\nu_0 - \nu_i)^4/\nu_i$ and another term correcting for the relative populations of the vibrational levels as derived from the Boltzmann distribution law (30, 31):

$$[7] \quad I_i = C\,\frac{(\nu_0 - \nu_i)^4}{\nu_i}\,[1 - \exp(-h\nu_i/kT)]^{-1}\,S_i$$

Here, C is a constant, k is Boltzmann's constant, and T is the absolute temperature. The expression in square brackets implicitly includes a summation over the population-weighted fundamental and hot band transitions, which is significant for the lowest vibrations. Equation [7] was utilized for the theoretical Raman spectra plotted in Figs. 9–14. The constant C is irrelevant here because the Raman spectra were not measured on an absolute scale, and only the relative Raman band strengths could be compared.

Basis set tests

After the assignments and force field refinements described below had been completed, the *ab initio* geometries, force fields, and intensity parameters were also

Can. J. Chem. Downloaded from www.nrcresearchpress.com by 88.255.202.194 on 09/08/12
For personal use only.

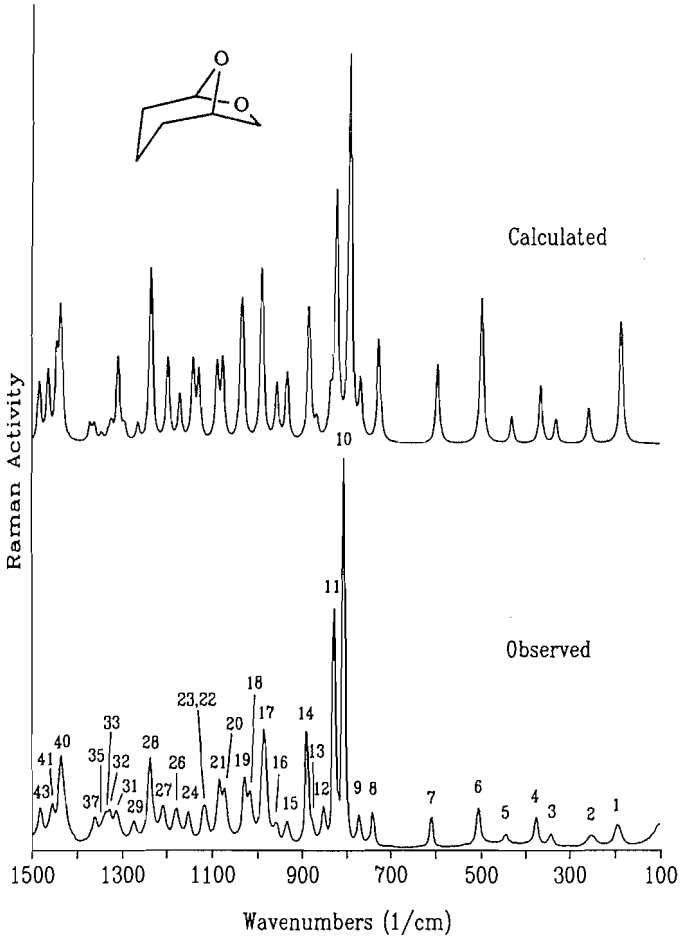

FIG. 13. Observed and calculated total Raman intensities (I^T) of liquid 6,8-dioxabicyclo[3.2.1]octane (DIOXA). For experimental conditions see text. Numbers correspond to "Band nos." in Tables 5 and 17.

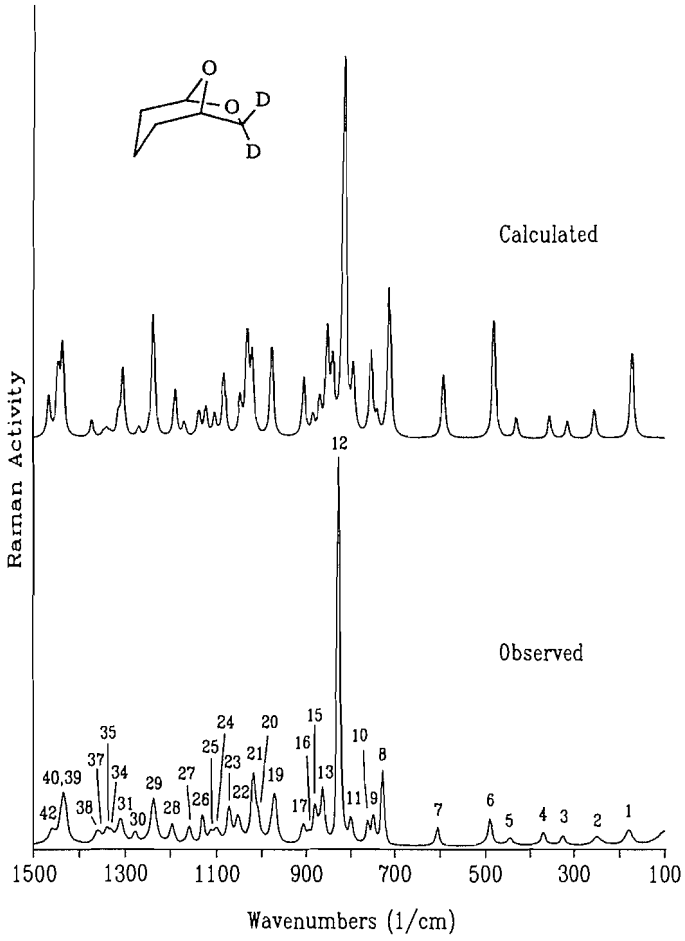

FIG. 14. Observed and calculated total Raman intensities (I^T) of liquid 7,7-d_2-6,8-dioxabicyclo[3.2.1]octane (DIOXA-d_2). For experimental conditions see text. Numbers correspond to "Band nos." in Tables 6 and 18.

computed for DIOXA with the basis sets 6-31G, 6-31G*, 6-31*$^{(0.3)}$, and 6-31G**. The 6-31G*$^{(0.3)}$ basis set (32) derives from the standard 6-31G* by reducing the exponents for the *d* functions from 0.8 to 0.3, thus rendering the polarization functions considerably more diffuse. This or very similar modifications have been recommended by several authors for calculating dipole moments and polarizabilities and their derivatives (7*a*, 32, 33). These force fields were scaled with the refined 3-21G factors (Table 12), which were then optimized again for each force field, based on the 72 assigned band positions of DIOXA and DIOXA-d_2. The band assignments for the two molecules suggested by the 3-21G results (Tables 17, 18) were confirmed by the higher level calculations. To allow proper comparison, the 3-21G scale factors were also refined once more using the data of the two DIOXA isotopomers only, changing the factors by small amounts. The average error in the frequency predictions reduced to 0.52% with the 6-31G calculation as compared to 0.70% for 3-21G. The improvement of the eigenvectors was also reflected in the better agreement of the absorption and Raman intensities. However, addition of polarization functions with the 6-31G* and 6-31G** basis sets did not give rise to any further improvements in the frequencies or intensities. In fact, the last two basis sets yielded virtually identical results after the scale factor refinements (wavenumbers agreed within 0.025%, absorption intensities within 6%, and Raman within 5%). Even the 6-31G*$^{(0.3)}$ basis set, although designed for absorption and Raman intensities, did not provide significantly improved results.

It was found that, when employing the same eigenvectors in combination with the APTs and polarizability derivatives from the various basis sets, the theoretical absorption and Raman intensities were the same throughout. That is, the *ab initio* calculated intensity parameters were insensitive to the basis set applied, except for small changes in the absolute intensities (6-31G* intensities were largest). The distribution of the relative intensities among the vibrational modes was completely governed by the eigenvectors. The basis set dependence of the eigenvector was further traced back to the force fields. While there was also a small dependence on the geometry, the accuracy of the vibrational intensities attainable by the split-valence and the polarized basis sets was thus primarily determined by the quality of the force field. The tests also suggest that the quality of the scaled 3-21G force field closely approaches the scaled 6-31G force field, which is as accurate as the scaled 6-31G* and 6-31** force fields. Among the basis sets tested, the 6-31G calculation appeared to have the best performance-to-cost ratio. Compar-

TABLE 1. Observed band positions (cm^{-1}) and dipole strengths for bicyclo[3.2.1]octane

Band nos.[a]	Infrared absorption		Raman[d]	Symmetry	Dipole strengths[e]
	Vapor[b]	Solution[c]			
1			195 w		
2	262.5[f]		261 w, pol	A′	
3			332 w		
4	358.1[f]		361 w, pol	A′	
5			421 w, sh		
6			430 w		
7	525.0	523.7 w	523 w		5.49
8	709.4	709.3 w (CS_2)	707 m, pol	A′	4.25
9	726.3	724.7 w (CS_2)	718 w		1.18
10	755.0	758.5 w (CS_2)	757 m, pol	A′	1.39
11	764.7	765.8 w, sh (CS_2)	763 m, pol	A′	0.99
12	795.0 (B)	790.5 m (CS_2)		A″	9.25
13	812.4	811.3 w (CS_2)	809 s, pol	A′	1.75
14		863.8 w, sh, dcn			3.25
15	872.9	872.5 m, sh, dcn	869 s, pol	A′	8.03
16	876.3	874.8 m, dcn			8.53
17	892.3	890.1 w	887 w, sh		1.45
18			938 w, sh		
19	963.4	960.9 w	959 w, sh		1.15
20	979.6	977.7 w	975 m, pol	A′	4.19
21	1006.5	1004.6 m	1001 m, pol	A′	6.75
22	1026.9	1025.0 w	1022 m		0.32
23	1044.1	1042.2 w	1039 m, pol	A′	3.89
24	1050.4	1056.1 w, sh	1052 w		0.18
25		1074.0 w			0.06
26	1102.5	1101.2 m	1098 w, pol	A′	7.22
27		1143.9 w	1142 w		0.82
28	1167.0	1164.6 m	1161 w		4.39
29	1188.7 (B)	1185.5 w		A″	1.72
30	1211.3	1207.7 w	1204 w		0.55
31	1243.9	1238.4 w	1237 m		2.92
32	1259.9	1256.7 m	1253 m, pol	A′	6.76
33	1284.4	1279.7 w			0.26
34	1305.2	1299.8 m			2.56
35	1319.6	1315.7 m	1315 w		4.01
36	1329.7	1325.3 m			3.04
37	1344.3	1339.5 m			4.78
38	1355.5	1352.4 w	1349 w		0.87
39	1360.6	1356.7 w			0.92
40			1441 m		
41	1453.8	1449.0 s, sh, dcn			11.1
42	1460.2	1453.7 s, dcn			30.3
43	1464.2	1458.4 s, sh, dcn			26.7
44	1481.2	1474.8 s	1473 w, pol	A′	8.85

[a]Numbers correspond to labels in observed spectra (Figs. 3, 9).
[b]Observed band contours are in parentheses if discernible.
[c]Measured in CCl_4 unless labelled (CS_2). Abbreviations: s = strong, m = medium, w = weak, sh = shoulder, dcn = band position measured after Fourier self-deconvolution.
[d]Measured from neat liquid phase. Abbreviations: s = strong, m = medium, w = weak, sh = shoulder, pol = clearly polarized band ($\rho < 0.75$).
[e]Units of 10^{-40} esu^2 cm^2.
[f]From ref. 19.

Can. J. Chem. Downloaded from www.nrcresearchpress.com by 88.255.202.194 on 09/08/12
For personal use only.

ing these results to similar studies on smaller molecules (*7a*, *7b*, 34), it appears that the basis set dependencies of the vibrational intensities encountered here are less severe, particularly for the polarized basis sets. The conclusions derived from these tests apply strictly only to the DIOXA isotopomers. Similar results may be found for other large molecules with related structures.

Assignments and scaling of force fields

General procedure

In general, the complexity of the spectra prevented straightforward assignments based only on observed features. The majority of the bands had to be assigned on the basis of the theoretical frequencies. In the cases where such assignments were ambiguous, the calculated absorption in-

TABLE 2. Observed band positions (cm^{-1}) and dipole strengths for 8-oxabicyclo[3.2.1]octane

Band nos.[a]	Infrared absorption		Raman[d]	Symmetry	Dipole strengths[e]
	Vapor[b]	Solution[c]			
1			184 w		
2	263.9[f,g]		263 w, pol	A′	
3	332.2[g] (B)		337 w	A″	
4	368.3[g]		371 m, pol	A′	
5	443.5	445.6 m	446 w		93.6
6	470.8		471 w		
7	566.0	567.7 w	567 w, pol	A′	30.8
8	724.0	723.6 m (CS_2)	722 m, pol	A′	30.3
9	763.2 (B)	760.3 w (CS_2)	758 w, sh	A″	24.2
10	777.5	776.6 w (CS_2)	775 s, pol	A′	10.3
11	803.7	803.2 w (CS_2)	809 w		1.93
12	832.7	829.3 m (CS_2)	828 s, pol	A′	27.6
13			856 w		
14	877.2	871.8 s	870 w		175
15	886.9	886.1 m	885 s, pol	A′	27.8
16	951.5	950.7 m	949 w		37.7
17	990.5	987.1 s	984 m, pol	A′	124
18	1032.6	1025.1 s	1023 m		170
19	1049.8	1045.7 w	1043 m, pol	A′	25.0
20	1056.8	1060.2 w			2.72
21	1084.6	1083.1 m	1081 m		54.3
22	1162.4	1160.2 m	1159 m		44.7
23	1192.6 (B)	1189.4 w	1186 w	A″	7.60
24	1223.7 (B)	1222.7 w, sh, dcn	1220 w, sh	A″	5.41
25	1231.9	1229.3 m	1226 m		29.4
26	1257.2	1252.3 m	1250 m		20.8
27	1275.2 (B)	1273.4 w	1268 w, sh	A″	3.08
28	1297.6 (B)	1295.1 w		A″	4.62
29			1312 w		
30	1327.3	1324.3 m	1323 w, sh		32.2
31			1333 w, sh		
32	1347.1	1343.0 m	1341 w, pol	A′	22.0
33	1361.0	1357.6 w	1355 w		6.67
34		1421.5 w	1416 w, sh		4.94
35	1444.5	1439.2 w	1436 m		15.0
36	1453.7	1447.8 m			15.4
37	1460.6	1456.3 w, dcn	1456 w, sh		16.4
38	1465.0	1459.9 w, sh, dcn			3.86
39	1478.6	1473.4 m	1472 w, pol	A′	29.8

[a]Numbers correspond to labels in observed spectra (Figs. 4, 10).
[b]Observed band contours are in parentheses if discernible.
[c]Measured in CCl_4 unless labelled (CS_2). Abbreviations: s = strong, m = medium, w = weak, sh = shoulder, dcn = band position measured after Fourier self-deconvolution.
[d]Measured from neat liquid phase. Abbreviations: s = strong, m = medium, w = weak, sh = shoulder, pol = clearly polarized band ($\rho < 0.75$).
[e]Units of 10^{-40} esu^2 cm^2.
[f]From ref. 23.
[g]From ref. 19.

tensities, and Raman activities and polarization ratios turned out to be very helpful guides, assuming that at least the order of magnitude of the calculated intensities was correct. The validity of this assumption will be demonstrated in the Discussion. In general, therefore, band assignments were initially based on the mode symmetries as deduced from Raman polarization ratios and gas phase absorption band shapes where applicable, and on the frequencies, which are the most reliable theoretical predictions with the 3-21G basis set. The intensities usually were consulted only for transitions that were observed or calculated less than 10 cm^{-1} apart (which is in the same range as the uncertainly in the predicted band positions) and only on a semi-quantitative basis, that is, if the absorption or Raman intensities of the involved bands were sufficiently different, to provide a safe criterion to differentiate between them. A few bands were assigned despite remaining uncertainties, if the predicted frequencies were in good agreement with the frequencies of observed bands that appeared to correspond to the normal modes in question. This was done to ensure that there were sufficient data to guarantee stability in the refinement of the force field. Even if a few of these assignments were incorrect, the ef-

Can. J. Chem. Downloaded from www.nrcresearchpress.com by 88.255.202.194 on 09/08/12
For personal use only.

TABLE 3. Observed band positions (cm^{-1}) and dipole strengths for 6-oxabicyclo[3.2.1]octane

Band nos.[a]	Infrared absorption		Raman[c]	Dipole strengths[d]
	Vapor	Solution[b]		
1	198.8[e]		200 w	
2	249.5[e]		242 w	
3	338.3[e]		340 w	
4	363.6[e]		364 m	
5		429.8 w	426 w	1.9
6	467.7	470.3 w	466 w	17.8
7	551.3	554.1 w	552 w	9.54
8	719.7	718.5 w (CS_2)	714 m	0.49
9	743.2	741.6 m (CS_2)	738 w	21.6
10	796.7	796.0 w (CS_2)	792 s	10.4
11	814.1	813.0 m (CS_2)	808 s	22.2
12	852.5	850.8 s	846 w	71.2
13	882.8	878.9 s	876 s	72.2
14	885.8	884.4 m, sh, dcn		17.2
15	905.5	903.0 m	898 w	61.0
16	933.8	932.8 m	928 w	45.0
17	942.6	942.9 w, sh, dcn (broad)		23.0
18	956.3	955.1 w	954 w	4.14
19	993.5	987.3 s	984 m	180
20	1015.2	1013.0 m	1010 m	40.6
21	1048.6	1047.7 m, sh, dcn		27.7
22	1056.5	1051.4 s, dcn	1046 m	66.9
23	1081.0			
24	1085.8	1080.6 m, dcn	1076 m	34.9
25		1085.5 m, sh, dcn		11.8
26	1102.5	1099.7 s	1096 m	86.7
27	1109.9	1106.8 m		24.5
28	1160.1	1154.8 w	1152 m	10.7
29	1172.6	1171.4 m	1166 w, sh	15.9
30	1224.0	1222.0 w	1220 m	7.16
31	1236.0	1233.9 m	1230 m	19.3
32	1267.6	1265.0 m	1260 w	13.8
33	1288.5	1285.1 w	1280 w	4.26
34	1303.9	1301.1 w		9.85
35	1319.8	1317.2 w, sh	1314 w	8.08
36	1323.7	1320.0 m		6.92
37	1336.1	1332.5 m	1328 w, sh	11.6
38		1348.0 w	1342 w	0.75
39		1355.7 w, sh, dcn	1348 w	2.80
40	1364.6	1361.7 w	1356 w	6.73
41	1442.8	1437.6 w, dcn	1436 m	14.8
42	1450.0	1445.8 w, sh, dcn		4.83
43	1456.8	1454.7 m, dcn		28.1
44	1462.0	1458.1 m, sh, dcn	1456 m, sh	6.04
45	1466.0	1460.9 m, dcn		17.1
46	1492.9	1486.4 w	1482 m	3.75

[a]Numbers correspond to labels in observed spectra (Figs. 5, 11).
[b]Measured in CCl_4 unless labelled (CS_2). Abbreviations: s = strong, m = medium, w = weak, sh = shoulder, dcn = band position measured after Fourier self-deconvolution.
[c]Measured from neat liquid phase. Abbreviations: s = strong, m = medium, w = weak, sh = shoulder.
[d]Units of 10^{-40} esu^2 cm^2.
[e]From ref. 19.

fect on the optimized scale factors was negligible because the frequency errors were always small.

Initially, the force fields were scaled with 11 factors, 10 of which (factors 1, 2, and 4–11 in Table 12) were transferred from the norbornane series (4) (from refinement "A" in that reference, where the ring out-of-plane deformation factor of norbornane was used) and applied to the corresponding local symmetry modes of the bicyclo[3.2.1]-octanes. The C—O stretching factor (3 in Table 12) was taken from 7-oxanorbornane (5). Previous experience from the assignment of the vibrational spectrum of 2-methyloxetane (2*a*) suggests that different scale factors may be required for certain methylene deformation modes if the CH_2 group is located next to an oxygen atom, and for methyne

Can. J. Chem. Downloaded from www.nrcresearchpress.com by 88.255.202.194 on 09/08/12
For personal use only.

TABLE 4. Observed band positions (cm^{-1}) and dipole strengths for 7,7-d_2-6-oxabicyclo[3.2.1]octane

Band nos.[a]	Infrared absorption		Raman[c]	Dipole strengths[d]
	Vapor	Solution[b]		
1	184.5[e]		187 w	
2	245.5[e]		240 w	
3	320.1[e]		322 w	
4	353.6[e]		355 w	
5		~427 w	423 w	
6	455.6	458.5 w	456 w	15.6
7	549.7	550.7 w	549 w	9.78
8	715.3	714.6 w (CS_2)	712 m	3.56
9	726.8	726.0 w (CS_2)	723 w	14.6
10	746.3	745.3 m (CS_2)	742 m	27.4
11	804.7	802.2 m (CS_2)	800 m, sh	46.9
12	811.7	811.7 w, sh (CS_2)	808 s	5.40
13	860.0	855.7 s	851 m	79.7
14	869.9	867.9 w, sh		3.21
15	876.1	876.7 w, sh	870 w, sh (broad)	9.19
16	887.1	885.7 m		19.0
17	900.8		895 w	
18	904.9	903.0 s		67.1
19	988.3	983.5 s	980 m	157
20		997.6 w, sh	994 m	2.40
21		1004.7 w		0.34
22	1041.5	1035.0 s	1030 w, sh	78.7
23		1040.0 m, sh, dcn		14.5
24	1049.1	1047.3 m	1043 m	18.8
25	1064.7	1061.9 s	1058 m	53.6
26	1077.5	1075.0 m	1070 m	37.9
27	1104.7	1102.2 s	1101 w	44.8
28	1110.7	1106.4 s		45.9
29	1129.3	1127.3 w	1124 w	8.80
30	1168.8	1167.7 w	1164 w	2.33
31	1202.9	1199.5 m	1194 w	16.0
32	1238.5	1234.0 w (broad)	1230 m	18.2
33	1241.5			
34	1266.2	1264.3 w	1259 w	11.4
35	1293.4	1289.7 w	1286 w	3.84
36	1308.2	1305.4 w	1304 w, sh	10.0
37	1319.7	1317.4 m	1313 w	10.8
38	1327.3	1321.6 w, sh, dcn		4.28
39	1338.4	1335.3 w		6.25
40		1354.6 w, sh, dcn	1348 w	3.15
41	1362.7	1359.1 w, dcn	1356 w, sh	4.39
42	1442.7	1438.1 w, sh, dcn	1436 m	6.38
43	1448.7	1444.5 w, sh, dcn		5.52
44	1455.7	1451.7 m, dcn		13.9
45	1459.4			
46	1461.3	1457.9 m, sh, dcn		22.5
47	1469.5	1465.2 m, dcn	1460 w, sh	9.38

[a]Numbers correspond to labels in observed spectra (Figs. 6, 12).
[b]Measured in CCl_4 unless labelled (CS_2). Abbreviations: s = strong, m = medium, w = weak, sh = shoulder, dcn = band position measured after Fourier self-deconvolution.
[c]Measured from neat liquid phase. Abbreviations: s = strong, m = medium, w = weak, sh = shoulder.
[d]Units of 10^{-40} esu^2 cm^2.
[e]From ref. 19.

deformations if an adjacent C—O bond is located approximately in the plane of the CH bend. Two special factors for the CH_2 wag and twist (12 and 13 in Table 12) were therefore transferred from 2-methyloxetane (2*a*) and used for the corresponding modes on C7 of 6OXA, DIOXA, and their isotopomers. Factor 14 was taken from the same source and used for all "in-plane" (i/p) and "out-of-plane" (o/p) methyne CH bends for which an adjacent oxygen atom lies approximately in the plane of the motion of the hydrogen atom (C1 and C5 o/p in 8OXA, C5 i/p in 6OXA and

Can. J. Chem. Downloaded from www.nrcresearchpress.com by 88.255.202.194 on 09/08/12
For personal use only.

TABLE 5. Observed band positions (cm^{-1}) and dipole strengths for 6,8-dioxabicyclo[3.2.1]octane

Band nos.[a]	Infrared absorption		Raman[c]	Dipole strengths[d]
	Vapor	Solution[b]		
1	188.2[e]		196 w	
2	252.3[e]		251 w	
3	338.6[e]		342 w	
4	372.8[e]		376 w	
5	445.2	447.7 m	446 w	79.1
6	506.4	508.3 w	506 m	8.14
7	610.0	611.4 m	609 w	49.9
8	746.5	743.9 w (CS_2)	741 w	8.51
9	779.8	776.8 w (CS_2)	773 w	6.14
10	808.8	808.8 w (CS_2)	807 s	21.2
11	833.5	832.2 w	828 s	26.1
12	858.9	856.7 s	853 m	175
13	886.4	882.1 s	885 w, sh	216
14	896.8	893.1 m	890 m	120
15	942.0	938.5 m	935 w	120
16	962.5	962.1 m	960 w	32.6
17	1000.4	992.6 s	987 m	249
18	1030.3	1022.4 s	1019 m	191
19	1035.0	1032.8 m	1031 m	77.4
20	1076.7	1075.6 w	1073 m	17.0
21	1092.5	1088.7 m	1085 m	33.4
22		1118.6 s, sh, dcn	1119 m	206
23	1129.1	1123.9 s, dcn		172
24	1158.9	1156.5 s	1153 w	126
25	1181.3			
26	1190.1	1182.2 w	1179 w	34.4
27	1213.1	1210.7 w	1208 m	
28	1242.7	1240.0 w	1237 m	11.5
29	1276.6	1275.7 w	1274 w	0.78
30	1310.5	1309.5 m		28.1
31	1320.7	1314.8 w, sh, dcn	1313 w	5.84
32	1333.5	1330.6 m, dcn	1328 w	37.6
33	1340.4	1338.2 m, dcn	1335 w, sh	11.4
34	1343.7	1342.6 m, dcn		21.8
35	1352.3	1349.1 w, dcn	1350 w, sh	8.33
36		1362.2 w, dcn	1361 w	14.9
37	1364.7	1364.9 w, dcn		11.1
38	1437.3	1429.6 w, sh, dcn		6.72
39	1439.3	1434.6 w, sh, dcn	1435 m	5.81
40	1442.7	1438.3 w, dcn		11.9
41	1462.7	1457.6 m	1455 m	20.7
42	1469.5	1469.1 w		3.92
43	1488.5	1483.5 w	1482 w	13.1

[a]Numbers correspond to labels in observed spectra (Figs. 7, 13).
[b]Measured in CCl_4 unless labelled (CS_2). Abbreviations: s = strong, m = medium, w = weak, sh = shoulder, dcn = band position measured after Fourier self-deconvolution.
[c]Measured from neat liquid phase. Abbreviations: s = strong, m = medium, w = weak, sh = shoulder.
[d]Units of 10^{-40} esu^2 cm^2.
[e]From ref. 19.

6OXA-d_2, C1 o/p, C5 i/p and o/p in DIOXA and DIOXA-d_2).

The frequency predictions that resulted from this first correction of the force field with the 14 factors led to the unambiguous assignment of 55 bands for the six molecules in the methylene scissoring (1400–1500 cm^{-1}) and the low frequency (100–600 cm^{-1}) regions. The assignments in the latter were straightforward. Except for BCO, the seven lowest modes for each molecule were identified in either or both the absorption and Raman spectra simply by consulting the frequencies. Additional confirmation was obtained for BCO and 8OXA from the Raman polarization ratios, clearly establishing A′ symmetry for a number of vibrations. The factors for the dominant local symmetry modes (factors 4, 10, and 11) were then refined. Next, bands from 600 to about 1050 cm^{-1} were included and the factors 1, 3, and 5 were floated together with 4, 10, and 11, fitting a total of 123 frequencies. The assignment of the rest of the spectra turned

Can. J. Chem. Downloaded from www.nrcresearchpress.com by 88.255.202.194 on 09/08/12
For personal use only.

TABLE 6. Observed band positions (cm^{-1}) and dipole strengths for 7,7-d_2-6,8-dioxabicyclo[3.2.1]octane

Band nos.[a]	Infrared absorption		Raman[c]	Dipole strengths[d]
	Vapor	Solution[b]		
1			180 w	
2			246 w	
3			325 w	
4			369 w	
5	443.6	445.7 m	443 w	72.0
6	489.4	491.4 w	491 w	7.01
7	605.8	607.2 m	604 w	45.3
8	729.1	728.9 w (CS_2)	726 m	9.42
9	755.9	752.2 w (CS_2)	748 m	11.0
10	764.4	764.6 w (CS_2)	762 w	25.5
11	805.0	802.3 m (CS_2)	800 w	77.2
12	830.1	829.3 w (CS_2)	826 s	1.35
13	870.1	866.4 s	862 m	201
14	879.8	877.1 m		51.3
15	888.6	884.4 m	880 m	98.0
16	897.3	896.5 w sh	892 w	5.81
17	913.6	910.1 w	906 w	26.7
18		975.5 m, sh, dcn		102
19	987.1	979.9 m dcn	971 m	128
20	1016.1	1012.8 m	1015 m, sh	89.8
21	1026.8	1021.9 s	1018 m	192
22	1056.4	1054.8 w	1052 m	33.5
23	1079.4	1075.1 m	1070 m	66.3
24		1098.1 w, sh, dcn	1100 w	20.1
25	1122.8	1116.5 s	1111 w	315
26	1137.2	1133.6 m	1130 m	36.7
27	1163.5	1162.1 m	1158 w	68.5
28	1202.0	1198.8 m	1196 w	31.8
29	1242.7	1239.7 w	1236 m	10.6
30	1280.5	1280.6 w	1278 w	2.11
31	1315.5	1312.8 w, sh, dcn	1310 w	18.6
32	1319.4	1318.0 m, dcn		37.8
33	1323.2	1322.0 w, sh, dcn		7.42
34	1336.5	1333.8 w	1330 w	11.5
35	1345.6	1342.9 m	1340 w	39.2
36		1357.2 w, sh, dcn		2.38
37	1365.9	1363.5 w, dcn	1359 w	12.7
38		1369.6 w, sh, dcn		1.88
39	1436.8	1432.8 w	1434 m	11.0
40	1441.9	1438.0 w		10.6
41	1456.9	1456.0 w, sh, dcn		9.03
42	1466.4	1462.4 w, dcn	1458 w	13.5

[a]Numbers correspond to labels in observed spectra (Figs. 8, 14).
[b]Measured in CCl_4 unless labelled (CS_2). Abbreviations: s = strong, m = medium, w = weak, sh = shoulder, dcn = band position measured after Fourier self-deconvolution.
[c]Measured from neat liquid phase. Abbreviations: s = strong, m = medium, w = weak, sh = shoulder.
[d]Units of 10^{-40} esu^2 cm^2.

out to be more difficult because of congested bands. However, it was possible to assign with relatively high confidence a number of bands in the remaining parts of the spectra, followed by the third refinement cycle including the factors 6–9 and 12–14. With a total of 196 assigned transitions, all the factors except the one for the C—H stretch were finally optimized simultaneously, converging to the set listed in Table 12 as "Refined factors" with an average error of 5.7 cm^{-1} (0.75%).

Tables 13–18 list in bold lettering the assignments included in the refinements, and the frequencies calculated with the three scaling methods. Also listed are dipole strengths, Raman intensities and depolarization ratios, and the strongest contributors to the potential energy distribution (PED) of the normal modes, all of which have been calculated with the fully refined, nonuniformly scaled force fields. The following paragraphs contain an outline of the rationales used for the most problematic band assignments, as well as discussions about spectral details that are interesting for other reasons. In some instances, plausible assignments are suggested for bands that were not included in the refinement cycles; they are listed in Tables 13–18 in italic lettering.

Can. J. Chem. Downloaded from www.nrcresearchpress.com by 88.255.202.194 on 09/08/12
For personal use only.

Can. J. Chem. Downloaded from www.nrcresearchpress.com by 88.255.202.194 on 09/08/12
For personal use only.

TABLE 7. Selected *ab initio* 3-21G and STO-3G structural parameters and energies of BCO, 8OXA, 6OXA, and DIOXA[a]

Structure parameters[b]	BCO		8OXA[c]		6OXA		DIOXA (chair)		DIOXA (boat)	
	3-21G	STO-3G	3-21G	STO-3G	3-21G	STO-3G	3-21G	STO-3G	3-21G	STO-3G
1–2	1.542	1.549	1.531	1.554	1.544	1.549	1.530	1.553	1.552	1.561
2–3	1.544	1.548	1.545	1.547	1.548	1.549	1.547	1.549	1.542	1.549
3–4					1.543	1.549	1.546	1.547	1.544	1.546
4–5					1.532	1.555	1.519	1.559	1.532	1.570
5–6	1.554	1.554	1.548	1.557	1.459	1.448	1.446	1.446	1.449	1.444
6–7	1.568	1.558	1.561	1.552	1.458	1.449	1.456	1.420	1.453	1.444
1–7					1.540	1.552	1.537	1.556	1.531	1.561
1–8	1.542	1.544	1.452	1.443	1.541	1.542	1.458	1.443	1.460	1.444
5–8					1.535	1.543	1.432	1.435	1.436	1.435
1–9	1.083	1.089	1.078	1.094	1.082	1.088	1.077	1.093	1.076	1.092
2–10	1.086	1.088	1.084	1.088	1.086	1.088	1.084	1.088	1.083	1.087
2–11	1.086	1.088	1.085	1.088	1.086	1.088	1.085	1.088	1.083	1.087
3–12	1.085	1.088	1.084	1.088	1.084	1.088	1.083	1.088	1.081	1.087
3–13	1.084	1.087	1.084	1.087	1.082	1.087	1.082	1.087	1.083	1.088
4–14					1.085	1.088	1.083	1.088	1.083	1.086
4–15					1.084	1.088	1.082	1.087	1.081	1.088
5–16					1.079	1.094	1.074	1.099	1.074	1.098
6(7)–17	1.083	1.087	1.081	1.086	1.082	1.095	1.079	1.095	1.080	1.094
6(7)–18	1.083	1.087	1.081	1.086	1.080	1.094	1.078	1.093	1.077	1.094
8–21(19)	1.084	1.086			1.081	1.086				
8–22(20)	1.086	1.087			1.084	1.086				
∠1–2–3	111.3	111.7	110.5	110.6	111.5	111.3	110.8	110.4	109.4	109.6
∠2–3–4	111.9	112.7	110.7	111.1	112.2	112.9	111.1	111.3	111.0	111.6
∠3–4–5					109.2	110.9	108.6	110.1	108.8	109.9
∠4–5–6	111.3	111.9	112.4	112.6	108.7	110.5	109.1	111.4	109.0	111.0
∠5–6–7	105.2	105.3	103.6	103.0	109.3	107.0	108.0	104.9	108.0	104.6
∠6–7–1					104.9	107.3	103.0	105.8	101.8	104.9
∠7–1–2					111.1	111.9	112.6	112.6	111.8	113.1
∠1–8–5	101.1	100.8	104.1	102.5	99.47	98.48	103.2	100.8	102.5	100.6
∠2–1–8	108.7	108.7	107.7	109.0	108.7	109.0	107.6	109.1	109.1	109.4
∠7–1–8	102.4	102.5	103.7	104.6	100.4	99.93	100.8	100.8	99.51	101.8
∠4–5–8					109.8	109.0	108.4	109.4	109.0	110.2
∠6–5–8					103.7	105.2	105.1	106.8	104.9	106.3
Ψ	42.74		42.47		43.02		42.58		−44.05	
Θ	115.9		113.0		115.3		112.4		114.3	
Φ	132.9		135.1		135.0		137.2		135.7	
δ(1–7–6–5)	0.000	0.000	0.000	0.000	8.222	2.948	10.11	1.636	17.73	4.865
-*E*(RHF)[d]	309.393236	307.485504	345.010370	342.749721	345.009257	342.744242	380.629852	378.013607	380.622665	378.008601

[a]Structures are displayed in Figs. 1,2.
[b]Bond lengths (Å), angles, and dihedral angle δ (deg). For definitions of atom numberings and angles Ψ, Θ, and Φ, see Figs. 1, 2.
[c]See also ref. 23.
[d]Hartree–Fock SCF energies in units of hartrees.

TABLE 8. Definitions of local symmetry coordinates for bicyclo[3.2.1]octane[a]

1	C—C stretch		C(1)—(C(2)
2			C(2)—C(3)
3			C(3)—C(4)
4			C(4)—C(5)
5			C(5)—C(6)
6			C(6)—C(7)
7			C(7)—C(1)
8			C(1)—C(8)
9			C(5)—C(8)
24	CH_2 scissor		C(2) 5α(10-2-11) + α(1-2-3)
25			C(3) 5α(12-3-13) + α(2-3-4)
26			C(4) 5α(14-4-15) + α(3-4-5)
27			C(6) 5α(17-6-18) + α(5-6-7)
28			C(7) 5α(19-7-20) + α(1-7-6)
29			C(8) 5α(21-8-22) + α(1-8-5)
30	CH_2 rock		C(2) α(10-2-1) + α(10-2-3) − α(11-2-1) − α(11-2-3)
31			C(3) α(12-3-2) + α(12-3-4) − α(13-3-2) − α(13-3-4)
32			C(4) α(14-4-5) + α(14-4-3) − α(15-4-5) − α(15-4-3)
33			C(6) α(17-6-5) + α(17-6-7) − α(18-6-5) − α(18-6-7)
34			C(7) α(19-7-1) + α(19-7-6) − α(20-7-1) − α(20-7-6)
35			C(8) α(21-8-1) + α(21-8-5) − α(22-8-1) − α(22-8-5)
36	CH_2 twist		C(2) α(10-2-1) − α(10-2-3) − α(11-2-1) + α(11-2-3)
37			C(3) α(12-3-2) − α(12-3-4) − α(13-3-2) + α(13-3-4)
38			C(4) α(14-4-5) − α(14-4-3) − α(15-4-5) + α(15-4-3)
39			C(6) α(17-6-5) − α(17-6-7) − α(18-6-5) + α(18-6-7)
40			C(7) α(19-7-1) − α(19-7-6) − α(20-7-1) + α(20-7-6)
41			C(8) α(21-8-1) − α(21-8-5) − α(22-8-1) + α(22-8-5)
42	CH_2 wag		C(2) α(10-2-1) − α(10-2-3) + α(11-2-1) − α(11-2-3)
43			C(3) α(12-3-2) − α(12-3-4) + α(13-3-2) − α(13-3-4)
44			C(4) α(14-4-5) − α(14-4-3) + α(15-4-5) − α(15-4-3)
45			C(6) α(17-6-5) − α(17-6-7) + α(18-6-5) − α(18-6-7)
46			C(7) α(19-7-1) − α(19-7-6) + α(20-7-1) − α(20-7-6)
47			C(8) α(21-8-1) − α(21-8-5) + α(22-8-1) − α(22-8-5)
48	C—H def. (i/p)		C(1) α(9-1-2) − α(9-1-7)
49			C(5) α(16-5-4) − α(16-5-6)
50	C—H def. (o/p)		C(1) 2α(9-1-8) − α(9-1-2) − α(9-1-7)
51			C(5) 2α(16-5-8) − α(16-5-4) − α(16-5-6)
52	Ring def. (i/p)	A′	α(1-8-5) − α(8-5-4) + α(5-4-3) − α(4-3-2) + α(3-2-1) − α(2-1-8)
53		A′	2α(1-8-5) − α(8-5-4) − α(5-4-3) + 2α(4-3-2) − α(3-2-1) − α(2-1-8)
54		A″	α(8-5-4) − α(5-4-3) + α(3-2-1) − α(2-1-8)
55	Ring def. (o/p)	A′	τ(3-2-1-8) − τ(2-1-8-5) + τ(1-8-5-4) − τ(8-5-4-3) + τ(5-4-3-2) − τ(4-3-2-1)
56		A′	τ(2-1-8-5) − τ(1-8-5-4) + τ(5-4-3-2) − τ(4-3-2-1)
57		A″	2τ(3-2-1-8) − τ(2-1-8-5) − τ(1-8-5-4) + 2τ(8-5-4-3) − τ(5-4-3-2) − τ(4-3-2-1)
58	Bridge wag	A′	α(7-1-8) + α(6-5-8) − α(7-1-2) − α(6-5-4)
59	Bridge twist	A″	α(7-1-8) − α(6-5-8) − α(7-1-2) + α(6-5-4)
60	Bridge rock	A″	α(1-7-6) − α(5-6-7)

[a]For atom numbering see Fig. 1. C—H stretching coordinates nos. 10–23 are omitted. Labels i/p and o/p refer to deformations in-plane and out-of-plane with respect to the six-membered ring segment.

Can. J. Chem. Downloaded from www.nrcresearchpress.com by 88.255.202.194 on 09/08/12
For personal use only.

Bicyclo[3.2.1]octane (BCO)

There are only four CH_2 scissoring modes apparent in the spectrum of BCO. Band 44 is separated from the rest and exhibits strong polarization in the Raman spectrum (Figs. 3 and 9). It clearly corresponds to ν_{10} (Table 13). The remaining three observed bands (41–43) can be assigned to ν_{39}, ν_{12}, and ν_{11} by noting that the last two scissoring modes, ν_{13} and ν_{40}, are predicted with much smaller absorption intensities by comparison. The latter two transitions, not included in the refinement, are predicted to give rise to the strongest Raman lines of all scissoring modes, and are therefore likely to be the principal if not the only significant contributors to band 40 in Fig. 9.

The region between 1050 and 1400 cm^{-1} is quite congested. The modes ν_{46} and ν_{50} cannot be found in the spectrum. They are both predicted with very low infrared intensities near prominent fundamentals (32 and 26, respectively) and are therefore likely to be completely hidden. There is one unassigned band (25 in Fig. 3) that could be identified with ν_{50}, but the large discrepancy in frequency makes this assignment problematic. Some of the bands in the wagging region (1280–1350 cm^{-1}) were assigned, although not with absolute confidence. Band 34 with the lowest frequency and band 37 with the highest intensity were ascribed to ν_{44} and ν_{42}, respectively. For the three fundamentals predicted between these two, namely ν_{15}, ν_{16}, and ν_{43}, there are only two observed absorptions (bands 35 and 36). One plausible assignment is suggested in Table 13. The remaining two bands at the highest frequencies in this region (38 and 39) were included in the refinement by virtue of their

TABLE 9. Definitions of local symmetry coordinates for 8-oxabicyclo[3.2.1]octane[a]

1	C—C stretch		C(1)—(C(2)
2			C(2)—C(3)
3			C(3)—C(4)
4			C(4)—C(5)
5			C(5)—C(6)
6			C(6)—C(7)
7			C(7)—C(1)
8	C—O stretch		C(1)—O(8)
9			C(5)—O(8)
22	CH_2 scissor		C(2) 5α(10-2-11) + α(1-2-3)
23			C(3) 5α(12-3-13) + α(2-3-4)
24			C(4) 5α(14-4-15) + α(3-4-5)
25			C(6) 5α(17-6-18) + α(5-6-7)
26			C(7) 5α(19-7-20) + α(1-7-6)
27	CH_2 rock		C(2) α(10-2-1) + α(10-2-3) − α(11-2-1) − α(11-2-3)
28			C(3) α(12-3-2) + α(12-3-4) − α(13-3-2) − α(13-3-4)
29			C(4) α(14-4-5) + α(14-4-3) − α(15-4-5) − α(15-4-3)
30			C(6) α(17-6-5) + α(17-6-7) − α(18-6-5) − α(18-6-7)
31			C(7) α(19-7-1) + α(19-7-6) − α(20-7-1) − α(20-7-6)
32	CH_2 twist		C(2) α(10-2-1) − α(10-2-3) − α(11-2-1) + α(11-2-3)
33			C(3) α(12-3-2) − α(12-3-4) − α(13-3-2) + α(13-3-4)
34			C(4) α(14-4-5) − α(14-4-3) − α(15-4-5) + α(15-4-3)
35			C(6) α(17-6-5) − α(17-6-7) − α(18-6-5) + α(18-6-7)
36			C(7) α(19-7-1) − α(19-7-6) − α(20-7-1) + α(20-7-6)
37	CH_2 wag		C(2) α(10-2-1) − α(10-2-3) + α(11-2-1) − α(11-2-3)
38			C(3) α(12-3-2) − α(12-3-4) + α(13-3-2) − α(13-3-4)
39			C(4) α(14-4-5) − α(14-4-3) + α(15-4-5) − α(15-4-3)
40			C(6) α(17-6-5) − α(17-6-7) + α(18-6-5) − α(18-6-7)
41			C(7) α(19-7-1) − α(19-7-6) + α(20-7-1) − α(20-7-6)
42	C—H def. (i/p)		C(1) α(9-1-2) − α(9-1-7)
43			C(5) α(16-5-4) − α(16-5-6)
44	C—H def. (o/p)		C(1) 2α(9-1-8) − α(9-1-2) − α(9-1-7)
45			C(5) 2α(16-5-8) − α(16-5-4) − α(16-5-6)
46	Ring def. (i/p)	A′	α(1-8-5) − α(8-5-4) + α(5-4-3) − α(4-3-2) + α(3-2-1) − α(2-1-8)
47		A′	2α(1-8-5) − α(8-5-4) − α(5-4-3) + 2α(4-3-2) − α(3-2-1) − α(2-1-8)
48		A″	α(8-5-4) − α(5-4-3) + α(3-2-1) − α(2-1-8)
49	Ring def. (o/p)	A′	τ(3-2-1-8) − τ(2-1-8-5) + τ(1-8-5-4) − τ(8-5-4-3) + τ(5-4-3-2) − τ(4-3-2-1)
50		A′	τ(2-1-8-5) − τ(1-8-5-4) + τ(5-4-3-2) − τ(4-3-2-1)
51		A″	2τ(3-2-1-8) − τ(2-1-8-5) − τ(1-8-5-4) + 2τ(8-5-4-3) − τ(5-4-3-2) − τ(4-3-2-1)
52	Bridge wag	A′	α(7-1-8) + α(6-5-8) − α(7-1-2) − α(6-5-4)
53	Bridge twist	A″	α(7-1-8) − α(6-5-8) − α(7-1-2) + α(6-5-4)
54	Bridge rock	A″	α(1-7-6) − α(5-6-7)

[a]For atom numbering see Fig. 1. C—H stretching coordinates nos. 10–21 are omitted. Labels i/p and o/p refer to deformations in-plane and out-of-plane with respect to the six-membered ring segment.

predicted positions and infrared intensities as corresponding to ν_{41} and ν_{14}, respectively, although their ordering may be reversed.

Many assignments in the 600–1050 cm^{-1} region were guided by the Raman spectrum, which exhibits intense, strongly polarized lines. The two fundamentals ν_{28} (A′) and ν_{57} (A″) were not assigned as there are three observed bands (9–11) in the vicinity. The predicted frequencies would suggest bands 10 and 11 as the fundamentals. This is contradicted by the Raman spectrum, which shows both as strongly polarized. Accordingly, band 9 should be assigned to the A″ fundamental ν_{57}, while the bands 10 and 11 may possibly result from Fermi resonance involving ν_{28} (A′). Although the three bands near 870 cm^{-1} (14–16) were not included in the refinement, a plausible assignment may be suggested. Of the three fundamentals ν_{25}, ν_{26}, and ν_{55}, the second is predicted to give rise to a polarized Raman line with much greater intensity than the other two, while the first should have the highest infrared intensity. Accordingly, ν_{26} most likely corresponds to band 15, and bands 16 and 14 to ν_{25} and ν_{55}, respectively.

8-Oxabicyclo[3.2.1]octane (8OXA)

The highest and the lowest frequency CH_2 scissoring bands 39 and 35 (Figs. 4, 10) are assigned to ν_8 (A′) and ν_{36} (A″), respectively (Table 14). Besides the clear separation from others, band 39 is readily distinguished by the relatively high infrared intensity, and the low Raman depolarization ratio, as predicted for ν_8. The assignment of band 35 is supported mainly by the pronounced observed and calculated Raman intensities. The remaining three scissoring modes cannot be clearly assigned, but must correspond to bands 36–38. They have therefore not been included in the refinements.

Also left unassigned was ν_{17}, as it may correspond either to band 20, in which case the calculated frequency and intensity would be completely wrong, or it may coincide with ν_{45} (band 21). The second alternative is consistent with the

Can. J. Chem. Downloaded from www.nrcresearchpress.com by 88.255.202.194 on 09/08/12
For personal use only.

TABLE 10. Definitions of local symmetry coordinates for 6-oxabicyclo[3.2.1]octane[a]

1	C—C stretch	C(1)—(C(2)
2		C(2)—C(3)
3		C(3)—C(4)
4		C(4)—C(5)
5	C—O stretch	C(5)—O(6)
6		O(6)—C(7)
7	C—C stretch	C(7)—C(1)
8		C(1)—C(8)
9		C(5)—C(8)
22	CH_2 scissor	C(2) 5α(10-2-11) + α(1-2-3)
23		C(3) 5α(12-3-13) + α(2-3-4)
24		C(4) 5α(14-4-15) + α(3-4-5)
25		C(7) 5α(17-7-18) + α(1-7-6)
26		C(8) 5α(19-8-20) + α(1-8-5)
27	CH_2 rock	C(2) α(10-2-1) + α(10-2-3) − α(11-2-1) − α(11-2-3)
28		C(3) α(12-3-2) + α(12-3-4) − α(13-3-2) − α(13-3-4)
29		C(4) α(14-4-5) + α(14-4-3) − α(15-4-5) − α(15-4-3)
30		C(7) α(17-7-1) + α(17-7-6) − α(18-7-1) − α(18-7-6)
31		C(8) α(19-8-1) + α(19-8-5) − α(20-8-1) − α(20-8-5)
32	CH_2 twist	C(2) α(10-2-1) − α(10-2-3) − α(11-2-1) + α(11-2-3)
33		C(3) α(12-3-2) − α(12-3-4) − α(13-3-2) + α(13-3-4)
34		C(4) α(14-4-5) − α(14-4-3) − α(15-4-5) + α(15-4-3)
35		C(7) α(17-7-1) − α(17-7-6) − α(18-7-1) + α(18-7-6)
36		C(8) α(19-8-1) − α(19-8-5) − α(20-8-1) + α(20-8-5)
37	CH_2 wag	C(2) α(10-2-1) − α(10-2-3) + α(11-2-1) − α(11-2-3)
38		C(3) α(12-3-2) − α(12-3-4) + α(13-3-2) − α(13-3-4)
39		C(4) α(14-4-5) − α(14-4-3) + α(15-4-5) − α(15-4-3)
40		C(7) α(17-7-1) − α(17-7-6) + α(18-7-1) − α(18-7-6)
41		C(8) α(19-8-1) − α(19-8-5) + α(20-8-1) − α(20-8-5)
42	C—H def. (i/p)	C(1) α(9-1-2) − α(9-1-7)
43		C(5) α(16-5-4) − α(16-5-6)
44	C—H def. (o/p)	C(1) 2α(9-1-8) − α(9-1-2) − α(9-1-7)
45		C(5) 2α(16-5-8) − α(16-5-4) − α(16-5-6)
46	Ring def. (i/p)	α(1-8-5) − α(8-5-4) + α(5-4-3) − α(4-3-2) + α(3-2-1) − α(2-1-8)
47		2α(1-8-5) − α(8-5-4) − α(5-4-3) + 2α(4-3-2) − α(3-2-1) − α(2-1-8)
48		α(8-5-4) − α(5-4-3) + α(3-2-1) − α(2-1-8)
49	Ring def. (o/p)	τ(3-2-1-8) − τ(2-1-8-5) + τ(1-8-5-4) − τ(8-5-4-3) + τ(5-4-3-2) − τ(4-3-2-1)
50		τ(2-1-8-5) − τ(1-8-5-4) + τ(5-4-3-2) − τ(4-3-2-1)
51		2τ(3-2-1-8) − τ(2-1-8-5) − τ(1-8-5-4) + 2τ(8-5-4-3) − τ(5-4-3-2) − τ(4-3-2-1)
52	Bridge wag	α(7-1-8) + α(6-5-8) − α(7-1-2) − α(6-5-4)
53	Bridge twist	α(7-1-8) − α(6-5-8) − α(7-1-2) + α(6-5-4)
54	Bridge rock	α(1-7-6) − α(5-6-7)

[a]For atom numbering see Fig. 1. C—H stretching coordinates nos. 10–21 are omitted. Labels i/p and o/p refer to deformations in-plane and out-of-plane with respect to the six-membered ring segment.

Can. J. Chem. Downloaded from www.nrcresearchpress.com by 88.255.202.194 on 09/08/12
For personal use only.

Raman spectrum where band 20 has no analog. A similar situation holds for ν_{16} (left unassigned) and ν_{44}, both of which likely contribute to band 22 in the infrared and Raman spectra. The ordering of ν_{15} and ν_{42} (bands 25 and 24, respectively) was reversed based on the absorption intensities and the apparent B-type contour of band 24 (not visible in Fig. 4). In the wagging region, band 30 can be assigned confidently to ν_{13} based on the observed and calculated infrared intensities, while band 33 must correspond to ν_{11} by virtue of the observed and calculated positions. Mode ν_{39} is absent in the absorption spectra, but is observed in the Raman (band 29). The last remaining A′ wagging mode, ν_{12}, must correspond to the partially polarized Raman line 32, while the remaining two A″ frundamentals, ν_{38} and ν_{37}, cannot be assigned unambiguously. The former may give rise to band 31 (in the Raman only), while the latter may be hidden under band 32.

Although ν_{24} and ν_{51} are predicted in the wrong order, their assignment is unambiguous based on the apparent B-type contour of the latter (band 9 in gas phase infrared) and the clearly polarized Raman line 10 corresponding to the former. The location of ν_{48} remains uncertain as evidently it is too weak to be observed in the absorption spectra. The slight asymmetry of Raman band 16 may indicate the presence of ν_{48} there. Band 17 probably contains ν_{19} (A′) and ν_{47} (A″), both of which are calculated with equally strong absorption intensities. Moreover, ν_{19} is predicted to give rise to a dominant polarized Raman line, which is consistent with the observed spectrum, justifying inclusion of ν_{19} in the refinement, while ν_{47} was not added to the certain assignments.

6-Oxabicyclo[3.2.1]octane (6OXA) and 7,7-d_2-6-oxabicyclo[3.2.1]octane (6OXA-d_2)

The spectra of these two isotopically related molecules are similar in several respects and are therefore discussed

TABLE 11. Definitions of local symmetry coordinates for 6,8-dioxabicyclo[3.2.1]octane[a]

1	C—C stretch	C(1)—(C(2)
2		C(2)—C(3)
3		C(3)—C(4)
4		C(4)—C(5)
5	C—O stretch	C(5)—O(6)
6		O(6)—C(7)
7	C—C stretch	C(7)—C(1)
8	C—O stretch	C(1)—O(8)
9		C(5)—O(8)
20	CH_2 scissor	C(2) 5α(10-2-11) + α(1-2-3)
21		C(3) 5α(12-3-13) + α(2-3-4)
22		C(4) 5α(14-4-15) + α(3-4-5)
23		C(7) 5α(17-7-18) + α(1-7-6)
24	CH_2 rock	C(2) α(10-2-1) + α(10-2-3) − α(11-2-1) − α(11-2-3)
25		C(3) α(12-3-2) + α(12-3-4) − α(13-3-2) − α(13-3-4)
26		C(4) α(14-4-5) + α(14-4-3) − α(15-4-5) − α(15-4-3)
27		C(7) α(17-7-1) + α(17-7-6) − α(18-7-1) − α(18-7-6)
28	CH_2 twist	C(2) α(10-2-1) − α(10-2-3) − α(11-2-1) + α(11-2-3)
29		C(3) α(12-3-2) − α(12-3-4) − α(13-3-2) + α(13-3-4)
30		C(4) α(14-4-5) − α(14-4-3) − α(15-4-5) + α(15-4-3)
31		C(7) α(17-7-1) − α(17-7-6) − α(18-7-1) + α(18-7-6)
32	CH_2 wag	C(2) α(10-2-1) − α(10-2-3) + α(11-2-1) − α(11-2-3)
33		C(3) α(12-3-2) − α(12-3-4) + α(13-3-2) − α(13-3-4)
34		C(4) α(14-4-5) − α(14-4-3) + α(15-4-5) − α(15-4-3)
35		C(7) α(17-7-1) − α(17-7-6) + α(18-7-1) − α(18-7-6)
36	C—H def. (i/p)	C(1) α(9-1-2) − α(9-1-7)
37		C(5) α(16-5-4) − α(16-5-6)
38	C—H def. (o/p)	C(1) 2α(9-1-8) − α(9-1-2) − α(9-1-7)
39		C(5) 2α(16-5-8) − α(16-5-4) − α(16-5-6)
40	Ring def. (i/p)	α(1-8-5) − α(8-5-4) + α(5-4-3) − α(4-3-2) + α(3-2-1) − α(2-1-8)
41		2α(1-8-5) − α(8-5-4) − α(5-4-3) + 2α(4-3-2) − α(3-2-1) − α(2-1-8)
42		α(8-5-4) − α(5-4-3) + α(3-2-1) − α(2-1-8)
43	Ring def. (o/p)	τ(3-2-1-8) − τ(2-1-8-5) + τ(1-8-5-4) − τ(8-5-4-3) + τ(5-4-3-2) − τ(4-3-2-1)
44		τ(2-1-8-5) − τ(1-8-5-4) + τ(5-4-3-2) − τ(4-3-2-1)
45		2τ(3-2-1-8) − τ(2-1-8-5) − τ(1-8-5-4) + 2τ(8-5-4-3) − τ(5-4-3-2) − τ(4-3-2-1)
46	Bridge wag	α(7-1-8) + α(6-5-8) − α(7-1-2) − α(6-5-4)
47	Bridge twist	α(7-1-8) − α(6-5-8) − α(7-1-2) + α(6-5-4)
48	Bridge rock	α(1-7-6) − α(5-6-7)

[a]For atom numbering see Fig. 2. C—H stretching coordinates nos. 10–19 are omitted. Labels i/p and o/p refer to deformations in-plane and out-of-plane with respect to the six-membered ring segment.

Can. J. Chem. Downloaded from www.nrcresearchpress.com by 88.255.202.194 on 09/08/12
For personal use only.

together. Of the methylene scissoring modes of 6OXA, ν_{13} is separated from the rest and must correspond to band 46 (Figs. 5, 11, Table 15). It clearly disappears on deuteration (Figs. 6, 12, Table 16), confirming the assignment to C7 scissoring. Another prominent feature in the congested region is the strong Raman line labelled as 41 and 42 for the two compounds, respectively (Figs. 11 and 12). For 6OXA a connection between this band and ν_{17} is readily made with confidence. For the isotopomer, the infrared band is not as neatly separated and therefore was not included in the refinement, although the assignment to ν_{16} is nonetheless reasonable by comparison. Since ν_{16} and ν_{15} in the two compounds, respectively, also are predicted to exhibit relatively strong Raman lines, they probably contribute significantly to lines 41 and 42, respectively, while being clearly resolved in the absorption spectra and labelled as band 42 in Fig. 5 and band 43 in Fig. 6. The last relatively certain assignment in this region is band 47 in the infrared spectrum of 6OXA-d_2 (Fig. 6) that we believe must correspond to ν_{13} in this compound. By comparison, the same mode in 6OXA, ν_{14}, can probably be associated with band 45 in Fig. 5. For the last scissoring mode in both compounds, several choices of observed bands are possible and the fundamental cannot be located unambiguously.

The abundance of bands with undistinguished intensities in the region of 1280–1380 cm^{-1} seemingly confuses their assignment. The region contains the CH_2 wagging and CH bending modes variously coupled. Their predicted intensities are not expected to be very reliable, since small differences in force constants may subtly alter the eigenvectors. Nonetheless, a one-to-one correspondence between predicted and observed band positions exists for both derivatives. The assignment, therefore, of ν_{18}–ν_{25} to bands 40–33, respectively, in 6OXA, and ν_{17}–ν_{23} to bands 41–35 in 6OXA-d_2, can be made with little hesitation, although for the sake of refining the scale factors only ν_{18}, ν_{24}, and ν_{25} in 6OXA, and ν_{17} and ν_{21}–ν_{23} in 6OXA-d_2, were included as firm.

For ν_{35} of 6OXA, the predicted position and intensities provided reasonable grounds for association with band 22. The predicted intensities for ν_{31}–ν_{34} appeared unreasonably different from those of bands 24–27 to which presumably these modes should correspond. They were therefore not

TABLE 12. Sets of force field scale factors

Nos.[a]	Local symmetry coordinate[b]	Transferred factors[c]	Refined factors[d]	(uncertainties)
1	C—C stretch	0.907	0.925	(07)
2	C—H stretch	0.82	[0.82]	(not refined)
3	C—O stretch	0.845	0.838	(13)
4	CH_2 scissor	0.78	0.771	(05)
5	CH_2 rock	0.81	0.802	(10)
6	CH_2 wag	0.776	0.763	(09)
7	CH_2 twist	0.768	0.765	(08)
8	C—H bend i/p	0.78	0.784	(25)
9	C—H bend o/p	0.773	0.799	(30)
10	Ring bend	0.812	0.886	(06)
11	Ring torsion	0.989	0.853	(06)
12	CH_2 wag (C7)[e]	0.802	0.802	(26)
13	CH_2 twist (C7)[e]	0.797	0.768	(25)
14	C—H bend[f]	0.822	0.814	(11)
	All coordinates (uniform scaling)		*0.827*	*(03)*

[a]Numbers as used in text.
[b]Definitions of coordinates are found in Tables 8–11.
[c]As described in text.
[d]Following the procedure explained in text.
[e]When adjacent to oxygen.
[f]If oxygen atom is in plane of bend.

TABLE 13. Assignments and calculated vibrational wavenumbers (cm^{-1}) and intensities for bicyclo[3.2.1]octane

	Observed		Calculated (3-21G)						
			Wavenumbers[c]				Raman		
ν	Band position[a]	Band nos.[b]	(1)	(2)	(3)	Dipole strengths[d]	Intensities[e]	ρ[f]	Approximate PEDs[g]
A′									
1			2979.1	2966.2	2966.2	81.95	89.6	0.72	
2			2961.3	2948.5	2948.6	119.27	50.8	0.46	
3			2958.3	2945.8	2945.9	29.94	268.8	0.03	
4			2953.9	2941.2	2941.2	7.12	97.1	0.34	
5			2934.7	2922.2	2922.2	61.35	54.4	0.58	
6			2930.2	2917.7	2917.6	97.85	74.6	0.28	
7			2920.5	2907.7	2907.9	26.40	134.8	0.32	
8			2912.6	2900.0	2900.1	33.38	53.9	0.40	
9			2900.0	2887.5	2887.5	18.95	72.2	0.26	
10	**1481.2**	**44**	1531.8	1487.6	1479.4	7.40	4.6	0.32	0.5 C6/C7 sci + 0.3 C3 sci
11	**1464.2**	**43**	1512.8	1469.5	1461.5	30.01	5.4	0.71	0.5 C3 sci + 0.3 C8 sci
12	**1460.2**	**42**	1510.8	1467.2	1459.2	27.04	6.9	0.73	0.5 C6/C7 sci + 0.4 C2/C4 sci
13	*1441.0 (R)*	*40*	1497.2	1454.2	1446.5	5.31	27.6	0.75	0.6 C8 sci + 0.3 C2/C4 sci
14	**1360.6**	**39**	1387.9	1352.0	1351.4	1.13	1.8	0.69	0.3 C2/C4 wag + 0.3 CH bend o/p
15	*1329.7*	*36*	1356.8	1325.8	1328.8	1.43	1.2	0.70	0.2 CH bend o/p + 0.2 CH bend i/p
16	*1319.6*	*35*	1336.6	1310.6	1314.3	4.53	1.3	0.68	0.4 C2/C4 wag + 0.3 C—C str. (1+4)
17	**1259.9**	**32**	1286.7	1254.0	1250.4	10.52	14.0	0.73	0.6 C2/C4 twist + 0.2 C6/C7 wag
18	**1211.3**	**30**	1233.3	1218.8	1207.0	1.29	5.2	0.73	0.5 C6/C7 wag + 0.2 C—C str. (5+7)
19	**1167.0**	**28**	1197.6	1161.9	1165.5	6.44	12.3	0.75	0.5 C6/C7 twist + 0.1 CH bend o/p
20	**1102.5**	**26**	1117.7	1113.3	1110.8	10.70	3.0	0.67	0.2 C2/C4 rock + 0.2 CH bend i/p
21	**1044.1**	**23**	1032.6	1045.6	1057.4	7.10	6.8	0.61	0.3 ring def. i/p (52) + 0.1 C—C str. (1+4)
22	**1006.5**	**21**	1014.7	1003.3	1011.8	4.73	10.0	0.70	0.2 C6/C7 twist + 0.1 C8 rock
23	**979.6**	**20**	958.9	981.2	983.9	5.94	8.4	0.63	0.2 C—C str. (6) + 0.2 C3 rock
24	**892.3**	**17**	880.9	897.1	898.0	1.03	4.7	0.56	0.3 C8 rock + 0.2 C—C str. (5+7)
25	*876.3*	*16*	842.6	869.4	877.5	9.04	0.7	0.72	0.5 C—C str. (8+9) + 0.2 C—C str. (6)
26	*872.9*	*15*	833.0	861.5	868.0	5.37	8.8	0.11	0.4 C—C str. (6) + 0.2 C—C str. (5+7)
27	**812.4**	**13**	790.3	803.8	808.4	1.97	19.6	0.04	0.4 C—C str. (2+3) + 0.2 C6/C7 rock
28	*755.0*	*10*	741.0	755.4	757.0	3.58	8.5	0.05	0.6 C6/C7 rock + 0.1 C—C str. (1+4)
29	**709.4**	**8**	702.2	713.1	715.0	5.58	4.1	0.12	0.3 C3 rock + 0.2 C2/C4 rock
30	**525.0**	**7**	517.0	517.7	527.7	7.38	1.1	0.69	0.5 ring def. i/p (53) + 0.3 ring def. i/p (52)

Can. J. Chem. Downloaded from www.nrcresearchpress.com by 88.255.202.194 on 09/08/12
For personal use only.

TABLE 13 (*concluded*)

	Observed		Calculated (3-21G) Wavenumbers[c]				Raman		
ν	Band position[a]	Band nos.[b]	(1)	(2)	(3)	Dipole strengths[d]	Intensities[e]	ρ[f]	Approximate PEDs[g]
31			422.9	441.6	429.9	0.55	0.2	0.70	0.7 ring def. o/p (55) + 0.3 ring def. i/p (53)
32	**358.1**	**4**	350.9	348.0	362.0	1.15	0.6	0.34	0.7 bridge wag (58) + 0.2 ring def. i/p (53)
33	**262.5**	**2**	255.4	277.4	259.4	0.60	0.1	0.43	2.0 ring def. o/p (56) + 0.8 ring def. o/p (55)
A″									
34			2956.5	2943.7	2943.7	5.34	77.9	0.75	
35			2947.2	2934.5	2934.4	152.60	14.1	0.75	
36			2932.1	2919.3	2919.4	12.36	63.1	0.75	
37			2923.4	2910.7	2910.8	8.99	31.1	0.75	
38			2901.3	2888.8	2888.8	50.70	37.5	0.75	
39	**1453.8**	**41**	1504.8	1461.6	1453.7	13.68	2.4	0.75	0.6 C6/C7 sci + 0.4 C2/C4 sci
40	*1441.0 (R)*	*40*	1498.6	1455.2	1447.6	1.09	31.6	0.75	0.6 C2/C4 sci + 0.4 C6/C7 sci
41	**1355.5**	**38**	1385.8	1348.4	1347.3	0.03	0.0	0.75	0.3 C3 wag + 0.3 CH bend i/p
42	**1344.3**	**37**	1379.8	1342.8	1334.6	5.61	0.3	0.75	0.5 C2/C4 wag + 0.1 C3 wag
43			1358.8	1318.9	1318.0	1.36	3.8	0.75	0.3 C3 wag + 0.1 CH bend o/p
44	**1305.2**	**34**	1340.6	1306.8	1300.4	2.59	1.7	0.75	0.3 C6/C7 wag + 0.2 C8 wag
45	**1284.4**	**33**	1330.7	1293.4	1291.7	0.02	0.2	0.75	0.5 C6/C7 wag + 0.2 CH bend o/p
46			1283.6	1258.6	1263.3	0.001	2.8	0.75	0.3 C—C str. (8-9) + 0.2 C2/C4 twist
47	**1243.9**	**31**	1272.2	1233.6	1234.2	2.73	25.2	0.75	0.5 C6/C7 twist + 0.2 C3 twist
48	**1188.7**	**29**	1211.4	1188.4	1191.3	1.92	2.2	0.75	0.2 C6/C7 twist + 0.2 C6/C7 rock
49	**1143.9 (sol)**	**27**	1175.8	1141.7	1144.6	0.19	10.7	0.75	0.3 CH bend i/p + 0.2 C8 twist
50			1136.6	1100.5	1101.3	1.02	2.1	0.75	0.3 CH bend o/p + 0.2 C2/C4 wag
51	**1050.4**	**24**	1056.2	1054.5	1058.6	0.11	6.4	0.75	0.4 C—C str. (2-3) + 0.3 C8 twist
52	**1026.9**	**22**	1015.6	1028.5	1033.3	1.07	8.4	0.75	0.2 C2/C4 twist + 0.2 C6/C7 rock
53	**963.4**	**19**	956.9	967.1	971.2	3.83	1.8	0.75	0.4 C6/C7 rock + 0.3 C—C str. (8-9)
54	**938.0 (R)**	**18**	913.3	940.3	947.6	0.29	0.7	0.75	0.5 C—C str. (5-7) + 0.2 C—C str. (1-4)
55	*863.8 (sol)*	*14*	871.2	863.6	862.0	3.55	0.5	0.75	0.7 C2/C4 rock + 0.1 bridge rock (60)
56	**795.0**	**12**	755.5	785.9	791.7	11.29	0.4	0.75	0.4 C—C str. (1-4) + 0.2 C—C str. (5-7)
57	*726.3*	*9*	722.8	727.0	748.3	0.84	2.4	0.75	0.5 bridge rock (60) + 0.2 C—C str. (8-9)
58			425.6	422.8	439.3	0.64	1.1	0.75	0.7 ring def. i/p (54) + 0.4 bridge twist (59)
59	**332.0**	**3**	325.1	332.1	333.3	0.06	0.1	0.75	0.7 bridge twist (59) + 0.4 ring def. o/p (57)
60	**195.0**	**1**	183.9	194.1	188.0	0.02	0.1	0.75	0.6 ring def. o/p (57) + 0.1 bridge twist (59)
Average error of calculations			*23.8 (2.3%)*	*5.4 (0.72%)*	*5.4 (0.65%)*				

[a]Measured from vapour phase absorption unless designated sol (absorption of solution) or R (Raman).
[b]As listed in Table 1 and Figs. 3 and 9.
[c]Calculated with uniformly scaled force field (1), transferred scale factors (2), and fully refined scale factors (3); see text.
[d]In units of 10^{-40} esu^2 cm^2, from fully refined force field.
[e]S^T_i (eq. [3] in text) in units of Å^4 amu^{-1}, from fully refined force field.
[f]Depolarization ratios ρ_i (eq. [6] in text), from fully refined force field.
[g]Most important contributors to potential energy distribution (PED) of the normal modes. Numbers in parentheses refer to coordinate definitions in Table 8.

TABLE 14. Assignments and calculated vibrational wavenumbers (cm^{-1}) and intensities for oxabicyclo[3.2.1]octane

	Observed		Calculated (3-21G) Wavenumbers[c]				Raman		
ν	Band position[a]	Peak nos.[b]	(1)	(2)	(3)	Dipole strengths[d]	Intensities[e]	ρ[f]	Approximate PEDs[g]
A′									
1			3002.4	2989.5	2989.5	79.95	109.6	0.20	
2			2993.5	2980.7	2980.8	0.22	178.8	0.19	
3			2970.1	2957.3	2957.3	103.52	40.1	0.73	
4			2955.5	2943.0	2943.1	28.27	118.6	0.15	
5			2946.8	2934.0	2934.1	40.66	91.7	0.50	
6			2929.3	2916.6	2916.7	29.58	150.6	0.11	

Can. J. Chem. Downloaded from www.nrcresearchpress.com by 88.255.202.194 on 09/08/12
For personal use only.

TABLE 14 (*concluded*)

	Observed		Calculated (3-21G)						
			Wavenumbers[c]			Raman			
ν	Band position[a]	Peak nos.[b]	(1)	(2)	(3)	Dipole strengths[d]	Intensities[e]	ρ[f]	Approximate PEDs[g]
7			2917.3	2904.7	2904.8	7.93	59.7	0.51	
8	**1478.6**	**39**	1527.6	1483.4	1475.2	33.50	2.2	0.34	0.5 C6/C7 sci + 0.5 C3 sci
9			1509.7	1466.4	1458.4	16.16	17.0	0.75	0.5 C6/C7 sci + 0.5 C3 sci
10			1498.2	1455.1	1447.5	10.92	10.8	0.70	1.0 C2/C4 sci + 0.1 C3 sci
11	**1361.0**	**33**	1395.5	1367.8	1363.6	2.23	1.6	0.50	0.5 CH bend o/p + 0.2 C2/C4 wag
12	**1347.1**	**32**	1371.6	1350.6	1341.8	4.59	0.7	0.48	0.3 CH bend i/p + 0.3 C2/C4 wag
13	**1327.3**	**30**	1345.2	1320.2	1322.8	48.81	1.2	0.63	0.4 C2/C4 wag + 0.3 C—C str. (1+4)
14	**1257.2**	**26**	1287.2	1254.9	1252.0	22.96	16.0	0.74	0.6 C2/C4 twist + 0.2 C6/C7 wag
15	**1231.9**	**25**	1248.0	1233.2	1220.9	30.72	5.5	0.74	0.6 C6/C7 wag + 0.1 C—C str. (5+7)
16			1199.0	1169.4	1168.0	9.64	10.8	0.75	0.5 C6/C7 twist + 0.1 CH bend o/p
17			1092.3	1097.8	1090.8	28.24	4.4	0.74	0.2 C2/C4 rock + 0.2 ring def. o/p (49)
18	**1049.8**	**19**	1052.9	1055.0	1065.7	14.23	4.2	0.46	0.3 ring def. i/p (46) + 0.2 C2/C4 rock
19	**990.5**	**17**	963.7	981.7	991.1	21.98	17.5	0.69	0.3 C—C str. (1+4) + 0.2 C—C str. (6)
20	**951.5**	**16**	936.2	948.4	957.3	36.73	4.6	0.59	0.3 C—C str. (6) + 0.2 C3 rock
21	**886.9**	**15**	857.7	873.8	879.5	21.56	9.6	0.19	0.3 C—C str. (6) + 0.3 C—C str. (5+7)
22	**877.2**	**14**	846.9	865.1	865.1	101.97	0.8	0.75	0.6 C—O str. + 0.2 C—C str. (2+3)
23	**832.7**	**12**	804.5	816.9	819.9	12.07	20.0	0.04	0.4 C—C str. (2+3) + 0.2 C6/C7 rock
24	**777.5**	**10**	752.9	770.7	770.9	20.19	6.3	0.08	0.5 C6/C7 rock + 0.1 C—C str. (1+4)
25	**724.0**	**8**	703.0	723.0	720.3	42.36	5.4	0.15	0.2 C3 rock + 0.2 C—C str. (5+7)
26	**566.0**	**7**	545.2	550.2	553.6	20.18	0.6	0.50	0.4 ring def. i/p (46) + 0.2 bridge wag
27	**443.5**	**5**	420.9	434.3	430.6	115.17	0.4	0.68	0.7 Ring def. i/p (47) + 0.6 ring def. o/p (49)
28	**368.3**	**4**	356.5	355.1	367.6	24.65	0.7	0.24	0.7 bridge wag + 0.2 ring def. o/p (50)
29	**263.9**	**2**	261.5	282.9	265.7	14.45	0.1	0.11	1.8 ring def. o/p (50) + 0.8 ring def. o/p (49)
A″									
30			2990.8	2977.9	2978.0	75.58	108.9	0.75	
31			2976.9	2964.1	2964.0	17.99	16.2	0.75	
32			2958.3	2945.4	2945.5	12.93	44.2	0.75	
33			2943.9	2931.2	2931.4	21.37	24.8	0.75	
34			2920.7	2908.1	2908.1	58.05	37.5	0.75	
35			1499.2	1456.1	1448.3	9.71	5.7	0.75	0.9 C6/C7 sci + 0.1 C2/C4 sci
36	**1444.5**	**35**	1488.0	1445.0	1437.4	7.74	27.7	0.75	0.9 C2/C4 sci + 0.1 C6/C7 sci
37			1382.5	1347.8	1346.0	3.92	0.9	0.75	0.4 CH bend i/p + 0.3 C3 wag
38			1381.3	1342.0	1333.3	2.55	0.9	0.75	0.6 C2/C4 wag + 0.2 C3 wag
39	**1312.0 (R)**	**29**	1348.8	1311.4	1309.1	0.52	10.1	0.75	0.2 C3 wag + 0.2 CH bend i/p
40	**1297.6**	**28**	1338.1	1305.3	1296.2	11.23	1.4	0.75	0.9 C6/C7 wag + 0.1 C—C str. (5-7)
41	**1275.2**	**27**	1285.7	1274.7	1271.0	1.23	1.2	0.75	0.6 CH bend o/p + 0.1 C—C str. (5-7)
42	**1223.7**	**24**	1264.0	1226.3	1224.8	9.57	14.0	0.75	0.7 C6/C7 twist + 0.1 C3 twist
43	**1192.6**	**23**	1205.8	1183.3	1186.8	7.14	5.1	0.75	0.2 C3 twist + 0.2 C—C str. (2-3)
44	**1162.4**	**22**	1201.2	1174.5	1173.4	48.31	2.9	0.75	0.4 C2/C4 twist + 0.1 C—O str.
45	**1084.6**	**21**	1088.9	1096.8	1100.3	53.39	2.8	0.75	0.2 C—C str. (1-4) + 0.2 C—O str.
46	**1032.6**	**18**	1043.0	1044.8	1046.5	157.65	8.2	0.75	0.4 C—O str. + 0.2 C2/C4 twist
47	*990.5*	*17*	994.9	997.1	996.9	22.11	0.6	0.75	0.4 C6/C7 rock + 0.1 C—C str. (2-3)
48			928.2	956.8	962.3	0.18	2.2	0.75	0.5 C—C str. (5-7) + 0.2 C—C str. (2-3)
49	**856.0 (R)**	**13**	864.8	859.3	859.3	2.49	1.6	0.75	0.7 C2/C4 rock + 0.2 bridge rock
50	**803.7**	**11**	775.7	798.1	805.0	5.99	0.1	0.75	0.4 C—C str. (1-4) + 0.2 C—C str. (5-7)
51	**763.2**	**9**	754.7	760.4	780.4	8.62	3.8	0.75	0.4 bridge rock + 0.1 C—O str.
52	**470.8**	**6**	459.3	456.6	473.9	0.60	2.6	0.75	0.7 ring def. i/p (48) + 0.3 bridge twist
53	**332.2**	**3**	319.4	326.1	326.8	4.14	0.0	0.75	0.7 bridge twist + 0.4 ring def. o/p (51)
54	**184.0 (R)**	**1**	166.5	175.3	170.2	2.03	0.0	0.75	0.6 ring def. o/p (51) + 0.2 bridge twist
Average error of calculations			*22.2 (2.6%)*	*7.5 (1.3%)*	*7.0 (1.0%)*				

[a]Measured from vapour phase absorption unless designated R (Raman).
[b]As listed in Table 2 and Figs. 4 and 10.
[c]Calculated with uniformly scaled force field (1), transferred scale factors (2), and fully refined scale factors (3); see text.
[d]In units of 10^{-40} esu^2 cm^2, from fully refined force field.
[e]S^T_i (eq. [3] in text) in units of Å^4 amu^{-1}, from fully refined force field.
[f]Depolarization ratios ρ_i (eq. [6] in text), from fully refined force field.
[g]Most important contributors to potential energy distribution (PED) of the normal modes. Numbers in parentheses refer to coordinate definitions in Table 9.

Can. J. Chem. Downloaded from www.nrcresearchpress.com by 88.255.202.194 on 09/08/12
For personal use only.

TABLE 15. Assignments and calculated vibrational wavenumbers (cm^{-1}) and intensities for 6-oxabicyclo[3.2.1]octane

	Observed		Calculated (3-21G)						
			Wavenumbers[c]			Raman			
ν	Band position[a]	Peak nos.[b]	(1)	(2)	(3)	Dipole strengths[d]	Intensities[e]	ρ[f]	Approximate PEDs[g]
1			2990.0	2977.2	2977.2	41.44	60.9	0.49	
2			2988.6	2975.9	2976.0	64.31	173.6	0.16	
3			2983.4	2970.4	2970.5	61.01	92.4	0.68	
4			2977.4	2964.5	2964.6	24.58	28.6	0.70	
5			2969.6	2956.9	2956.8	75.01	108.2	0.17	
6			2953.6	2940.8	2940.9	29.81	75.1	0.66	
7			2937.4	2924.8	2924.8	65.09	64.8	0.36	
8			2935.9	2923.2	2923.3	4.32	196.1	0.23	
9			2932.6	2919.9	2920.1	115.73	18.3	0.65	
10			2932.2	2919.6	2919.7	20.99	77.1	0.34	
11			2917.6	2905.0	2905.1	29.03	50.9	0.51	
12			2906.1	2893.6	2893.6	37.87	63.3	0.31	
13	**1492.9**	**46**	1542.7	1498.4	1490.8	0.17	10.7	0.58	C7 sci
14	*1466.0*	*45*	1516.6	1473.0	1464.8	11.53	8.0	0.67	0.6 C3 sci + 0.2 C4 sci
15			1510.7	1467.3	1459.4	37.68	4.5	0.73	0.4 C3 sci + 0.3 C8 sci
16	*1450.0*	*42*	1500.1	1456.9	1449.1	9.52	17.7	0.75	0.6 C2 sci + 0.2 C4 sci
17	**1442.8**	**41**	1494.1	1451.4	1443.8	6.22	24.0	0.75	0.5 C4 sci + 0.4 C8 sci
18	**1364.6**	**40**	1389.1	1367.9	1361.8	5.06	2.7	0.66	0.5 C5 CH bend i/p + 0.2 C7 wag
19	*1355.7 (sol)*	*39*	1387.9	1354.9	1358.1	6.38	2.0	0.74	0.4 C7 wag + 0.2 C5 CH bend o/p
20	*1348.0 (sol)*	*38*	1383.2	1351.2	1347.3	7.39	0.5	0.74	0.3 C1 CH bend i/p + 0.3 C3 wag
21	*1336.1*	*37*	1371.6	1336.9	1330.7	5.49	0.7	0.75	0.4 C2 wag + 0.2 C4 wag
22	*1323.7*	*36*	1355.2	1320.5	1319.3	1.76	2.9	0.73	0.2 C1 CH bend o/p + 0.2 C3 wag
23	*1319.8*	*35*	1336.2	1311.6	1316.5	10.71	3.3	0.70	0.3 C4 wag + 0.2 C—C str. (4)
24	**1303.9**	**34**	1330.7	1301.6	1299.5	4.70	2.1	0.74	0.3 C8 wag + 0.1 C2 wag
25	**1288.5**	**33**	1306.7	1288.1	1286.0	21.19	1.4	0.75	0.3 C7 wag + 0.2 C5 CH bend i/p
26	**1267.6**	**32**	1283.6	1258.2	1266.3	15.54	2.6	0.73	0.2 C—C str. (8) + 0.1 C—C str. (9)
27	**1236.0**	**31**	1262.7	1234.6	1233.4	14.75	19.0	0.71	0.3 C4 twist + 0.2 C2 twist
28	**1224.0**	**30**	1238.6	1216.5	1217.5	12.57	16.2	0.75	0.3 C3 twist + 0.2 C7 twist
29	**1172.6**	**29**	1184.9	1164.2	1157.8	21.89	11.8	0.75	0.2 C8 twist + 0.1 C5 CH bend i/p
30	**1160.1**	**28**	1175.8	1153.6	1143.1	25.92	8.7	0.75	0.5 C7 twist + 0.1 C7 rock
31	*1102.5*	*26*	1138.8	1130.1	1119.4	149.71	3.0	0.60	0.2 ring def. o/p (49) + 0.1 C—O str. (5)
32	*1109.9*	*27*	1125.0	1102.3	1103.5	2.43	2.4	0.74	0.2 C1 CH bend o/p + 0.2 C3 wag
33	*1085.8*	*24*	1086.4	1082.0	1086.0	45.69	8.4	0.73	0.2 C7 rock + 0.1 bridge wag
34			1062.1	1059.6	1077.2	41.35	2.2	0.42	0.4 ring def. i/p (46) + 0.1 C8 rock
35	**1056.5**	**22**	1026.5	1045.6	1051.8	8.25	9.7	0.75	0.2 C—C str. (2) + 0.2 C—C str. (3)
36	**1015.2**	**20**	1013.0	1019.7	1025.1	34.56	7.8	0.70	0.2 C—C str. (9) + 0.1 C2 twist
37	**993.5**	**19**	988.4	996.8	1000.0	119.96	11.9	0.63	0.3 C—O str. (6) + 0.2 C—C str. (8)
38	*942.6*	*17*	948.0	957.8	959.8	7.31	2.8	0.60	0.2 C7 rock + 0.2 C—C str. (7)
39	**933.8**	**16**	910.7	929.3	933.3	36.59	3.2	0.74	0.2 C—C str. (7) + 0.2 C7 rock
40	**905.5**	**15**	902.2	914.9	911.6	48.38	1.4	0.75	0.3 C8 rock + 0.2 C—O str. (6)
41	*882.8*	*13*	883.6	884.2	886.3	26.07	2.5	0.57	0.2 C—O str. (5) + 0.1 C2 rock
42	*885.8*	*14*	849.1	873.4	879.0	10.66	5.9	0.13	0.2 C—C str. (8) + 0.1 C3 rock
43	**852.5**	**12**	838.4	845.0	843.8	36.07	3.2	0.49	0.2 C—O str. (6) + 0.2 C4 rock
44	**814.1**	**11**	782.3	812.9	817.9	15.32	10.4	0.09	0.3 C—C str. (4) + 0.3 C—C str. (3)
45	**796.7**	**10**	756.2	786.4	793.7	12.39	16.2	0.05	0.3 C—C str. (1) + 0.3 C—C str. (2)
46	**743.2**	**9**	728.5	733.0	750.3	41.68	2.0	0.69	0.5 bridge rock + 0.1 C—C str. (9)
47	**719.7**	**8**	707.6	715.1	719.6	1.78	3.7	0.08	0.3 C3 rock + 0.1 C2 rock
48	**551.3**	**7**	543.2	541.6	555.3	6.17	1.8	0.67	0.5 ring def. i/p (47) + 0.3 bridge wag
49	**467.7**	**6**	461.0	460.9	474.9	19.15	1.1	0.74	0.5 ring def. i/p (48) + 0.4 bridge twist
50	**426.0 (R)**	**5**	421.6	438.2	428.6	1.90	0.2	0.35	0.7 ring def. o/p (49) + 0.3 ring def. i/p (47)
51	**363.6**	**4**	356.8	353.9	367.8	8.88	0.7	0.50	0.6 bridge wag + 0.2 ring def. i/p (47)
52	**338.3**	**3**	331.0	336.2	340.2	61.33	0.1	0.70	0.5 bridge twist + 0.3 ring def. o/p (51)
53	**249.5**	**2**	248.9	270.2	252.7	3.59	0.2	0.43	2.2 ring def. o/p (50) + 1.0 ring def. o/p (49)
54	**198.8**	**1**	191.8	203.5	195.9	156.43	0.2	0.71	0.7 ring def. o/p (51) + 0.1 bridge twist
Average error of calculations			*17.6 (1.9%)*	*6.9 (1.2%)*	*4.9 (0.65%)*				

[a]Measured from vapour phase absorption unless designated R (Raman).
[b]As listed in Table 3 and Figs. 5 and 11.
[c]Calculated with uniformly scaled force field (1), transferred scale factors (2), and fully refined scale factors (3); see text.
[d]In units of 10^{-40} esu^2 cm^2, from fully refined force field.
[e]S^T_i (eq. [3] in text) in units of Å^4 amu^{-1}, from fully refined force field.
[f]Depolarization ratios ρ_i (eq. [6] in text), from fully refined force field.
[g]Most important contributors to potential energy distribution (PED) of the normal modes. Numbers in parentheses refer to coordinate definitions in Table 10.

Can. J. Chem. Downloaded from www.nrcresearchpress.com by 88.255.202.194 on 09/08/12
For personal use only.

TABLE 16. Assignments and calculated vibrational wavenumbers (cm^{-1}) and intensities for 7,7-d_2-6-oxabicyclo[3.2.1]octane

	Observed		Calculated (3-21G)						
			Wavenumbers[c]				Raman		
ν	Band position[a]	Peak nos.[b]	(1)	(2)	(3)	Dipole strengths[d]	Intensities[e]	ρ[f]	Approximate PEDs[g]
1			2989.9	2977.0	2977.1	46.95	53.8	0.55	
2			2988.3	2975.6	2975.6	62.12	162.6	0.19	
3			2980.4	2967.5	2967.5	31.57	49.4	0.67	
4			2968.2	2955.5	2955.4	58.98	99.5	0.25	
5			2953.6	2940.8	2940.9	28.83	75.3	0.66	
6			2937.5	2924.9	2924.9	70.62	59.3	0.40	
7			2935.6	2922.9	2923.0	10.50	155.6	0.22	
8			2932.3	2919.6	2919.7	45.74	64.6	0.37	
9			2917.6	2905.1	2905.1	30.35	50.6	0.52	
10			2906.1	2893.6	2893.6	38.09	64.5	0.31	
11			2215.6	2205.8	2206.1	44.89	34.7	0.75	
12			2134.6	2125.7	2126.5	82.10	50.2	0.15	
13	**1469.5**	**47**	1518.6	1475.0	1466.7	11.03	5.6	0.53	0.5 C3 sci + 0.2 C2 sci
14			1510.9	1467.5	1459.6	37.56	5.4	0.73	0.5 C3 sci + 0.3 C8 sci
15	*1448.7*	*43*	1500.0	1456.8	1449.0	9.31	17.6	0.75	0.6 C2 sci + 0.2 C4 sci
16	*1442.7*	*42*	1494.4	1451.7	1444.1	6.22	22.3	0.75	0.6 C4 sci + 0.4 C8 sci
17	**1362.7**	**41**	1388.9	1365.4	1361.2	10.44	1.9	0.67	0.4 C5 CH bend i/p + 0.2 C5 CH bend o/p
18	*1354.6 (sol)*	*40*	1387.4	1349.9	1345.3	5.85	0.4	0.74	0.3 C3 wag + 0.2 C1 CH bend i/p
19	*1338.4*	*39*	1377.7	1341.1	1332.8	5.98	0.3	0.75	0.3 C2 wag + 0.3 C4 wag
20	*1327.3*	*38*	1355.6	1319.1	1323.7	1.43	1.4	0.74	0.3 C5 CH bend o/p + 0.1 C4 twist
21	**1319.7**	**37**	1340.6	1313.7	1314.9	7.02	4.4	0.75	0.2 C1 CH bend o/p + 0.2 C3 wag
22	**1308.2**	**36**	1330.6	1303.0	1304.3	12.00	1.3	0.62	0.2 C4 wag + 0.2 C1 CH bend i/p
23	**1293.4**	**35**	1318.6	1299.3	1297.1	9.68	3.2	0.73	0.4 C8 wag + 0.2 C3 twist
24	**1266.2**	**34**	1283.0	1256.2	1264.3	12.20	4.9	0.73	0.2 C—C str. (8) + 0.1 C2 twist
25	**1238.5**	**32**	1266.3	1235.0	1234.4	17.14	18.9	0.71	0.3 C4 twist + 0.2 C2 twist
26	**1202.9**	**31**	1216.6	1198.5	1204.4	14.06	12.1	0.75	0.2 C8 twist + 0.2 C3 twist
27	**1168.8**	**30**	1195.1	1169.2	1168.0	3.07	5.5	0.75	0.2 C3 twist + 0.2 C1 CH bend i/p
28	**1129.3**	**29**	1147.4	1144.4	1130.6	109.22	1.2	0.71	0.3 C—C str. (7) + 0.2 C7 wag
29	**1110.7**	**28**	1138.9	1124.3	1123.3	83.77	4.0	0.51	0.5 C7 sci + 0.1 ring def. o/p (49)
30	**1104.7**	**27**	1129.7	1102.3	1103.6	0.79	2.1	0.75	0.2 C1 CH bend o/p + 0.2 C3 wag
31	**1077.5**	**26**	1080.8	1076.6	1086.3	49.76	7.2	0.65	0.2 ring def. i/p (46) + 0.1 C2 rock
32	**1064.7**	**25**	1065.6	1058.8	1068.4	20.32	8.6	0.75	0.2 ring def. i/p (46) + 0.1 C8 rock
33	**1049.1**	**24**	1046.5	1049.2	1053.6	30.26	11.0	0.75	0.3 C8 twist + 0.2 C—C str. (3)
34	**1041.5**	**22**	1023.9	1038.5	1044.8	26.08	1.3	0.73	0.2 C7 wag + 0.2 C—O str. (5)
35	**997.6 (sol)**	**20**	996.6	1003.7	1008.9	1.35	9.0	0.75	0.2 C—C str. (9) + 0.1 C8 wag
36	**988.3**	**19**	984.9	993.0	995.6	140.03	10.0	0.65	0.2 C—O str. (6) + 0.2 C3 rock
37	*900.8*	*17*	904.4	916.1	912.0	46.14	1.7	0.74	0.3 C8 rock + 0.2 C—O str. (6)
38	*904.9*	*18*	888.8	896.2	901.0	17.10	2.3	0.67	0.1 C7 wag + 0.1 C—C str. (1)
39	**887.1**	**16**	875.0	878.2	880.0	16.63	1.4	0.42	0.2 C—C str. (8) + 0.1 C—C str. (2)
40	**876.1**	**15**	860.9	870.8	873.4	0.71	1.1	0.73	0.2 C4 rock + 0.1 C—C str. (9)
41	*860.0*	*13*	844.8	853.1	851.5	21.33	9.4	0.34	0.2 C7 rock + 0.2 C—O str. (6)
42	*860.0*	*13*	839.1	849.1	845.5	20.27	5.1	0.40	0.4 C7 twist + 0.3 C7 rock
43	**811.7**	**12**	801.8	804.7	811.1	3.01	22.5	0.06	0.3 C—C str. (3) + 0.2 C—C str. (4)
44	**804.7**	**11**	773.9	802.4	801.1	28.02	3.5	0.66	0.2 C7 twist + 0.2 C2 rock
45	**746.3**	**10**	730.8	743.6	745.3	11.60	4.2	0.26	0.2 C—C str. (1) + 0.1 C7 rock
46	**726.8**	**9**	709.6	716.1	731.2	55.31	2.0	0.61	0.5 bridge rock + 0.1 C—C str. (8)
47	**715.3**	**8**	701.6	709.2	714.4	1.88	5.3	0.07	0.3 C3 rock + 0.1 C—C str. (1)
48	**549.7**	**7**	540.5	539.0	552.6	7.12	1.8	0.68	0.4 ring def. i/p (47) + 0.2 bridge wag
49	**455.6**	**6**	448.5	451.6	461.1	12.81	1.4	0.71	0.5 ring def. i/p (48) + 0.3 bridge twist
50	**423.0 (R)**	**5**	419.8	433.4	427.2	1.53	0.2	0.34	0.7 ring def. o/p (49) + 0.3 ring def. i/p (47)
51	**353.6**	**4**	339.7	338.1	349.9	46.10	0.4	0.56	0.6 bridge wag + 0.1 ring def. i/p (47)
52	**320.1**	**3**	319.4	326.4	327.1	20.83	0.1	0.53	0.5 bridge twist + 0.4 ring def. o/p (51)
53	**245.5**	**2**	245.8	265.9	249.6	8.14	0.2	0.42	2.1 ring def. o/p (50) + 1.0 ring def. o/p (49)
54	**184.5**	**1**	179.1	188.9	183.1	146.13	0.2	0.69	0.6 ring def. o/p (51) + 0.1 bridge twist
Average error of calculations			*15.1 (1.6%)*	*6.6 (1.1%)*	*4.0 (0.56%)*				

[a]Measured from vapour phase absorption unless designated sol (absorption of solution) or R (Raman).
[b]As listed in Table 4 and Figs. 6 and 12.
[c]Calculated with uniformly scaled force field (1), transferred scale factors (2), and fully refined scale factors (3); see text.
[d]In units of 10^{-40} esu^2 cm^2, from fully refined force field.
[e]S^T_i (eq. [3] in text) in units of Å^4 amu^{-1}, from fully refined force field.
[f]Depolarization ratios ρ_i (eq. [6] in text), from fully refined force field.
[g]Most important contributors to potential energy distribution (PED) of the normal modes. Numbers in parentheses refer to coordinate definitions in Table 10.

Can. J. Chem. Downloaded from www.nrcresearchpress.com by 88.255.202.194 on 09/08/12
For personal use only.

TABLE 17. Assignments and calculated vibrational wavenumbers (cm^{-1}) and intensities for 6,8-dioxabicyclo[3.2.1]octane

	Observed		Calculated (3-21G)						
			Wavenumbers[c]				Raman		
ν	Band position[a]	Peak nos.[b]	(1)	(2)	(3)	Dipole strengths[d]	Intensities[e]	ρ[f]	Approximate PEDs[g]
1			3032.3	3019.4	3019.6	60.10	156.7	0.17	
2			3014.3	3001.4	3001.4	52.04	109.1	0.45	
3			3008.0	2995.1	2995.1	33.51	66.5	0.48	
4			2989.1	2976.1	2976.1	53.13	38.3	0.75	
5			2973.9	2960.8	2961.0	16.81	57.2	0.71	
6			2959.5	2946.7	2946.8	40.50	109.3	0.37	
7			2957.7	2944.9	2945.1	30.87	72.7	0.37	
8			2945.3	2932.7	2932.8	41.75	158.2	0.07	
9			2936.5	2923.9	2923.9	32.66	43.7	0.75	
10			2923.2	2910.6	2910.7	28.40	65.7	0.36	
11	**1488.5**	**43**	1535.1	1491.1	1483.5	5.01	9.6	0.64	C7 sci
12	**1462.7**	**41**	1516.1	1472.5	1464.4	22.16	10.8	0.74	C3 sci
13	**1442.7**	**40**	1495.7	1452.7	1445.1	12.02	11.7	0.72	0.6 C2 sci + 0.3 C4 sci
14			1487.3	1444.5	1436.8	12.38	19.0	0.75	0.6 C4 sci + 0.4 C2 sci
15	**1364.7**	**37**	1397.3	1378.9	1372.1	35.70	2.4	0.66	0.3 C5 CH bend i/p + 0.3 C5 CH bend o/p
16	**1352.3**	**35**	1386.3	1368.6	1363.5	3.31	2.2	0.74	0.4 C7 wag + 0.2 C5 CH bend i/p
17	**1343.7**	**34**	1385.1	1352.5	1348.3	6.51	0.9	0.73	0.3 C1 CH bend i/p + 0.3 C3 wag
18	**1340.4**	**33**	1378.5	1343.2	1334.2	4.70	0.8	0.74	0.4 C2 + wag 0.2 C4 wag
19	**1333.5**	**32**	1348.3	1328.5	1328.2	49.51	2.1	0.52	0.3 C4 wag + 0.1 C2 wag
20	**1320.7**	**31**	1345.3	1317.8	1313.4	9.78	10.5	0.75	0.3 C3 wag + 0.2 C3 twist
21	**1310.5**	**30**	1314.4	1303.1	1300.5	33.34	1.7	0.64	0.4 C7 wag + 0.2 C—C str. (7)
22	**1276.6**	**29**	1284.8	1275.0	1270.5	7.60	2.0	0.66	0.3 C5 CH bend o/p + 0.3 C1 CH bend o/p
23	**1242.7**	**28**	1269.9	1244.2	1240.1	11.67	19.1	0.74	0.3 C4 twist + 0.2 C2 twist
24	**1190.1**	**26**	1224.9	1203.0	1202.3	4.03	8.4	0.75	0.3 C3 twist + 0.2 C7 twist
25	**1158.9**	**24**	1202.3	1180.7	1176.4	143.05	4.4	0.75	0.2 C2 twist + 0.2 C4 twist
26	**1129.1**	**23**	1179.1	1156.6	1147.8	132.26	7.1	0.72	0.3 C7 twist + 0.1 C1 CH bend i/p
27	**1118.6 (sol)**	**22**	1129.2	1143.5	1135.8	182.33	5.9	0.69	0.2 C—O str. (5) + 0.1 C4 twist
28	**1092.5**	**21**	1098.1	1098.9	1095.6	21.19	6.1	0.66	0.2 C4 rock + 0.2 ring def. o/p (43)
29	**1076.7**	**20**	1067.1	1082.5	1084.4	15.71	6.3	0.75	0.2 C—C str. (1) + 0.1 C—C str. (2)
30	**1030.3**	**18**	1034.9	1038.9	1043.4	137.53	3.5	0.56	0.3 ring def. i/p (40) + 0.1 C7 rock
31	**1035.0**	**19**	1026.7	1026.4	1041.8	134.28	7.7	0.72	0.2 C—O str. (8) + 0.2 C—O str. (9)
32	**1000.4**	**17**	988.8	997.9	998.6	234.82	11.7	0.60	0.5 C—O str. (6) + 0.1 C—O str. (5)
33	**962.5**	**16**	951.5	964.1	965.6	17.25	3.5	0.72	0.3 C—C str. (7) + 0.2 C7 rock
34	**942.0**	**15**	922.8	938.5	942.8	88.47	4.1	0.75	0.2 C—C str. (2) + 0.1 C—O str. (5)
35	**896.8**	**14**	885.2	891.5	892.2	45.57	7.0	0.31	0.2 C—C str. (5) + 0.2 C3 rock
36	**886.4**	**13**	869.4	876.2	876.1	75.09	0.9	0.39	0.3 C—O str. (8) + 0.2 C—O str. (9)
37	**858.9**	**12**	844.6	847.4	845.2	136.88	1.7	0.72	0.3 C—O str. (9) + 0.2 C4 rock
38	**833.5**	**11**	801.6	828.6	832.5	14.58	11.1	0.14	0.3 C—C str. (3) + 0.2 C—C str. (4)
39	**808.8**	**10**	766.2	796.1	802.9	12.84	16.1	0.05	0.3 C—C str. (2) + 0.3 C—C str. (1)
40	**779.8**	**9**	761.6	762.1	779.7	44.82	2.1	0.73	0.5 bridge rock + 0.1 C—O str. (8)
41	**746.5**	**8**	723.5	741.5	737.2	12.22	3.6	0.19	0.2 C3 rock + 0.1 C—O str. (5)
42	**610.0**	**7**	590.7	593.1	602.9	49.06	1.8	0.52	0.2 bridge wag + 0.2 ring def. i/p (40)
43	**506.4**	**6**	491.4	490.4	505.3	6.21	2.3	0.75	0.4 ring def. i/p (42) + 0.3 bridge twist
44	**445.2**	**5**	427.4	440.0	437.7	126.50	0.3	0.75	0.8 ring def. i/p (41) + 0.5 ring def. o/p (43)
45	**372.8**	**4**	360.1	359.1	370.8	65.52	0.5	0.40	0.6 bridge wag + 0.2 ring def. o/p (44)
46	**338.6**	**3**	328.1	332.2	336.5	47.34	0.2	0.40	0.7 bridge twist + 0.3 ring def. o/p (45)
47	**252.3**	**2**	257.2	278.5	261.2	2.14	0.1	0.20	2.0 ring def. o/p (44) + 0.9 ring def. o/p (43)
48	**188.2**	**1**	185.6	197.2	189.5	155.73	0.3	0.60	0.7 ring def. o/p (45) + 0.1 bridge twist
Average error of calculations			*22.4 (2.3%)*	*9.9 (1.4%)*	*6.7 (0.76%)*				

[a]Measured from vapour phase absorption unless designated sol (absorption of solution).
[b]As listed in Table 5 and Figs. 7 and 13.
[c]Calculated with uniformly scaled force field (1), transferred scale factors (2), and fully refined scale factors (3); see text.
[d]In units of 10^{-40} esu^2 cm^2, from fully refined force field.
[e]S^T_i (eq. [3] in text) in units of Å^4 amu^{-1}, from fully refined force field.
[f]Depolarization ratios ρ_i (eq. [6] in text), from fully refined force field.
[g]Most important contributors to potential energy distribution (PED) of the normal modes. Numbers in parentheses refer to coordinate definitions in Table 11.

Can. J. Chem. Downloaded from www.nrcresearchpress.com by 88.255.202.194 on 09/08/12
For personal use only.

TABLE 18. Assignments and calculated vibrational wavenumbers (cm^{-1}) and intensities for 7,7-d_2-6,8-dioxabicyclo[3.2.1]octane

	Observed		Calculated (3-21G)						
			Wavenumbers[c]				Raman		
ν	Band position[a]	Peak nos.[b]	(1)	(2)	(3)	Dipole strengths[d]	Intensities[e]	ρ[f]	Approximate PEDs[g]
1			3023.3	3019.2	3019.4	59.58	150.1	0.20	
2			3012.3	2999.4	2999.5	41.58	97.6	0.37	
3			2989.2	2976.3	2976.3	53.44	43.4	0.75	
4			2973.9	2960.9	2961.0	14.43	60.9	0.70	
5			2958.8	2946.0	2946.1	17.72	77.8	0.71	
6			2945.3	2932.7	2932.8	39.47	166.5	0.07	
7			2936.5	2923.9	2923.9	33.62	44.8	0.74	
8			2923.3	2910.7	2910.7	28.93	67.9	0.35	
9			2238.6	2228.8	2229.1	34.96	32.6	0.74	
10			2151.5	2142.7	2143.4	54.09	49.1	0.15	
11	**1466.4**	**42**	1516.9	1473.2	1465.0	24.91	8.4	0.71	C3 sci
12	**1441.9**	**40**	1495.9	1452.9	1445.2	11.42	12.4	0.72	0.6 C2 sci + 0.3 C4 sci
13	**1436.8**	**39**	1487.3	1444.6	1436.8	12.42	17.9	0.75	0.7 C4 sci + 0.4 C2 sci
14	**1365.9**	**37**	1397.5	1379.3	1372.2	37.72	3.2	0.67	0.4 C5 CH bend i/p + 0.3 C5 CH bend o/p
15	**1345.6**	**35**	1386.1	1352.0	1347.5	8.12	0.7	0.74	0.3 C3 wag + 0.2 C1 CH bend i/p
16	**1336.5**	**34**	1380.8	1349.9	1341.5	15.34	1.3	0.57	0.2 C5 CH bend o/p + 0.2 C4 wag
17	**1323.2**	**33**	1362.7	1342.9	1334.1	7.28	0.7	0.75	0.3 C2 wag + 0.3 C4 wag
18	**1319.4**	**32**	1341.9	1319.6	1316.9	65.27	3.0	0.72	0.2 C4 wag + 0.2 C2 wag
19	**1315.5**	**31**	1328.0	1308.0	1307.9	6.29	11.3	0.75	0.3 C1 CH bend i/p + 0.3 C3 twist
20	**1280.5**	**30**	1286.4	1276.6	1272.3	4.99	1.4	0.51	0.4 C1 CH bend o/p + 0.3 C5 CH bend o/p
21	**1242.7**	**29**	1271.0	1244.3	1240.3	12.60	18.3	0.74	0.4 C4 twist + 0.2 C2 twist
22	**1202.0**	**28**	1210.3	1189.1	1191.8	45.28	6.4	0.75	0.2 C3 twist + 0.1 C—C str. (2)
23	**1163.5**	**27**	1197.6	1174.1	1172.4	117.04	1.8	0.73	0.2 C3 twist + 0.1 C4 twist
24	**1137.2**	**26**	1148.7	1145.2	1141.0	164.27	3.0	0.45	0.1 C—O str. (5) + 0.1 C2 twist
25	**1122.8**	**25**	1124.1	1125.0	1126.8	130.96	3.3	0.69	0.2 C7 wag + 0.2 C—C str. (7)
26	**1098.1 (sol)**	**24**	1102.2	1111.2	1108.3	36.20	2.4	0.72	0.6 C7 sci + 0.1 C—O str. (6)
27	**1079.4**	**23**	1091.4	1089.3	1088.0	39.14	6.9	0.65	0.2 C4 rock + 0.2 C2 rock
28	**1056.4**	**22**	1045.4	1051.4	1052.6	27.73	3.7	0.74	0.2 C7 wag + 0.1 C—C str. (2)
29	**1026.8**	**21**	1032.8	1036.6	1037.5	193.28	9.6	0.75	0.3 C—O str. (8) + 0.2 C—O str. (9)
30	**1016.1**	**20**	1001.0	1007.8	1027.7	98.59	7.3	0.70	0.3 ring def. i/p (40) + 0.1 C—C str. (4)
31	**987.1**	**19**	979.1	983.5	984.2	226.65	7.9	0.64	0.5 C—O str. (6) + 0.2 C—O str. (5)
32	**913.6**	**17**	899.7	907.4	910.9	20.63	4.4	0.75	0.2 C7 wag + 0.2 C—C str. (4)
33	**897.3**	**16**	887.2	891.8	890.8	1.89	1.3	0.72	0.2 C4 rock + 0.1 C2 rock
34	*888.6*	*15*	871.8	876.7	875.6	74.86	2.2	0.26	0.2 C—O str. (8) + 0.1 C—O str. (9)
35	*879.8*	*14*	859.7	860.0	859.4	84.03	6.6	0.50	0.2 C—O str. (9) + 0.2 C—C str. (7)
36	*870.1*	*13*	851.7	854.6	848.3	38.12	4.1	0.61	0.4 C7 twist + 0.3 C7 rock
37	**830.1**	**12**	803.6	818.6	823.5	1.83	22.8	0.06	0.3 C—C str. (3) + 0.2 C—C str. (2)
38	**805.0**	**11**	789.7	803.0	803.4	54.47	3.4	0.75	0.2 C2 rock + 0.1 C—O str. (9)
39	**764.4**	**10**	748.1	762.8	762.8	25.26	4.3	0.49	0.2 C7 twist + 0.1 C—C str. (1)
40	**755.9**	**9**	737.1	736.2	749.6	53.92	0.9	0.48	0.5 bridge rock + 0.1 C—O str. (5)
41	**729.1**	**8**	705.3	723.7	722.2	14.46	6.8	0.17	0.2 C3 rock + 0.2 C—C str. (7)
42	**605.8**	**7**	587.7	589.9	599.7	48.31	2.0	0.55	0.2 bridge wag + 0.2 ring def. i/p (40)
43	**489.4**	**6**	474.6	474.6	486.7	3.44	2.3	0.72	0.4 ring def. i/p (42) + 0.2 bridge twist
44	**443.6**	**5**	426.6	438.6	437.0	126.33	0.3	0.75	0.8 ring def. i/p (41) + 0.5 ring def. o/p (43)
45	**369.0 (R)**	**4**	350.4	349.8	360.6	105.16	0.2	0.43	0.5 bridge wag + 0.2 ring def. o/p (44)
46	**325.0 (R)**	**3**	313.1	320.6	320.1	8.80	0.1	0.37	0.6 bridge twist + 0.4 ring def. o/p (45)
47	**246.0 (R)**	**2**	253.6	273.2	257.7	0.79	0.2	0.20	1.8 ring def. o/p (44) + 0.8 ring def. o/p (43)
48	**180.0 (R)**	**1**	171.9	181.2	175.6	142.39	0.2	0.54	0.6 ring def. o/p (45) + 0.1 bridge twist
Average error of calculations			*20.4 (2.3%)*	*9.0 (1.3%)*	*5.8 (0.82%)*				

[a]Measured from vapour phase absorption unless designated sol (absorption of solution) or R (Raman).
[b]As listed in Table 6 and Figs. 8 and 14.
[c]Calculated with uniformly scaled force field (1), transferred scale factors (2), and fully refined scale factors (3); see text.
[d]In units of 10^{-40} esu^2 cm^2, from fully refined force field.
[e]S^T_i (eq. [3] in text) in units of $Å^4$ amu^{-1}, from fully refined force field.
[f]Depolarization ratios ρ_i (eq. [6] in text), from fully refined force field.
[g]Most important contributors to potential energy distribution (PED) of the normal modes. Numbers in parentheses refer to coordinate definitions in Table 11.

Can. J. Chem. Downloaded from www.nrcresearchpress.com by 88.255.202.194 on 09/08/12
For personal use only.

Can. J. Chem. Downloaded from www.nrcresearchpress.com by 88.255.202.194 on 09/08/12
For personal use only.

included in the refinement. Bands 24, 27, and 26 may be ascribed to ν_{33}, ν_{32}, and ν_{31}, respectively, based on approximately matching intensities. The location of ν_{34} is left uncertain unless it gives rise to band 22, in which case ν_{35} could be reassigned to band 21; however, the calculated frequency of ν_{34} appears unreasonably high. Evidently, band 23 and possibly band 25 are not fundamental transitions. The corresponding normal modes ν_{29}–ν_{34} in 6OXA-d_2 are readily assignable to bands 28–22, respectively, from the point of view of the frequencies, but appreciable differences in the absorption intensities emerge. A similar competition between position and intensity is found also for ν_{28} in the same compound (band 29 in Fig. 6). From the point of view of the former, the assignment given in Table 16 seems the most reasonable and was adopted as firm only in the very last refinement cycle on that basis. The scale factors as a result changed very little. From the point of view of the intensities, however, it would seem better if ν_{28}, ν_{29}, and ν_{30} were assigned to bands 28, 27, and 30, respectively, thereby clearly introducing major discrepancies in the frequencies. This dilemma remains unresolved.

Bands 13 and 14 in 6OXA, which must correspond to one or the other of ν_{41} and ν_{42}, were originally not assigned and hence not included in the refinement. In retrospect, ν_{41} is predicted to be the stronger of the two in absorption, while ν_{42} should be stronger in the Raman (Figs. 5 and 11). The assignment suggested in Table 15 is based on the relative intensities in the infrared spectra. The corresponding fundamentals in 6OXA-d_2 are thought to be nearly coincident, together giving rise to band 13 (Fig. 6). The last remaining ambiguity concerns bands 17 and 18 for both compounds. Only one normal mode (ν_{38}) is at disposal for assigning the two bands for 6OXA. While band 17 appears prevalent in the infrared, the Raman experiment suggests band 18 as the fundamental. Bands 17 and 18 in the isotopomer may be ascribed to ν_{37} and ν_{38} as a nearly coincident pair.

6,8-Dioxabicyclo[3.2.1]octane (DIOXA) and 7,7-d_2*-6,8-dioxabicyclo[3.2.1]octane (DIOXA-*d_2*)*

The methylene scissoring bands 43, 41, and 40 of DIOXA (Figs. 7, 13) were readily assigned to ν_{11}, ν_{12}, and ν_{13}, respectively (Table 17). Near the predicted position of ν_{14}, the two bands 38 and 39 are observed with about equal intensities, preventing firm identification of the fundamental. One of the bands 38 or 39 and also 42, therefore, are likely to arise from higher order transitions. The normal mode descriptions for the three methylene scissors ν_{11}–ν_{13} of DIOXA-d_2 (Table 18) are essentially the same as for the corresponding modes (ν_{12}–ν_{14}) in DIOXA. The vibrations are identified for DIOXA-d_2 as bands 39, 40, and 42 (Figs. 8, 14) by comparison with the spectrum of DIOXA, and confirmed by the predictions of the frequencies and intensities.

The methylene wagging and methyne bending regions for both molecules were completely assigned on the basis of the good agreement of predicted frequencies and intensities with the observed absorption spectra, although some ambiguities remain. The band ordering may be wrong for the modes ν_{20} and ν_{21} and for ν_{17} and ν_{18} for DIOXA, and for ν_{15} and ν_{16} for the isotopomer. The C5 C—H bending vibration of DIOXA (ν_{15}) is observed to be split into the two bands 36 and 37, while the corresponding mode of DIOXA-d_2 (ν_{14}) has shoulders on either side (bands 36, 38) that are not fundamentals. The Raman spectra confirm the assignments to a satisfactory degree.

Presuming that bands 22 and 23 are both fundamental transitions, the calculations suggest bands 22–24 of DIOXA to correspond to ν_{27}–ν_{25} despite large errors in the frequencies, but leave uncertain the correct ordering of ν_{27} and ν_{26}. Bands 25 and 27 cannot be fundamentals. Bands 25 and 26 of DIOXA-d_2 must be attributed to ν_{25} and ν_{24} even though their calculated intensities are in error in absorption and Raman scattering. Similar discrepancies were encountered in the same region for DIOXA (bands 23 and 22, Fig. 7), 6OXA-d_2 (bands 28 and 29, Fig. 6), and 6OXA (bands 26 and 27, Fig. 5). None of these bands was assigned firmly.

The region 600–1050 cm^{-1} is reproduced unambiguously by the theory for both molecules except for a few congested lines. For DIOXA, the pair of bands 18 and 19 (ν_{30}, ν_{31}), which are calculated only 1.6 cm^{-1} apart, are tentatively assigned in the reverse order using the Raman intensities as a criterion. The correct ordering of ν_{36}, ν_{35}, and ν_{34} for the deuterated isotopomer cannot be resolved due to the differences between experiment and the predictions of frequencies and intensities in both the absorption and Raman spectra, preventing any firm interpretation of bands 13–15. The transition ν_{31} of DIOXA-d_2 involving C—O stretching is split into a doublet (bands 18 and 19) with about equal inensities in the solution absorption spectrum, while the splitting is not evident in the gas phase and Raman.

Discussion

The detailed analysis of the absorption spectra described above revealed the presence of a number of transitions that cannot be fundamentals, many of them with considerable intensities, likely due to mixing with fundamentals by Fermi resonance. Such bands have repeatedly confused definitive identifications of fundamentals in this study. Recurring examples are the lines in the CH_2 scissoring region at approximately 1440 and 1465 cm^{-1} and a mode around 1080 cm^{-1}. While an investigation of the origin of these transitions would be of great interest, such endeavor is beyond the scope of this work as it would require anharmonic force fields. Some vapor phase bands exhibit series of Q-branches that probably arise from coupling to excited vibrational states of low energy vibrations of anharmonic skeletal deformations. This observation and the occurrence of Fermi resonances are evidence for high anharmonicity in the potentials of certain vibrations, in particular the ones involving skeletal deformations.

Force-field scaling and refining

The average errors of the frequency predictions for all six bicyclo[3.2.1]octanes after uniform scaling is 20.4 cm^{-1} (2.2%), which is lowered to 7.6 cm^{-1} (1.2%) and 5.7 cm^{-1} (0.75%), respectively, upon nonuniform scaling with the transferred and refined sets of factors (see Table 12). Tables 13–18 contain the corresponding errors for the six individual molecules, among which 8OXA has the largest deviation in the frequency predictions after refinement (1.0%), and also has the worst fit after uniform scaling (2.6%). The excellent fit of the frequencies in general and the qualitative agreement of the intensities strongly support the assignments listed in Tables 13–18 in bold letters as firm, except for a small number of bands that are discussed in the previous section. Difficulties were encountered especially for clusters of closely spaced bands with similar intensities. In some cases, such modes were tentatively assigned to cal-

culated transitions despite uncertainties and may therefore be incorrect. Nevertheless, the success of the spectral assignments is also reflected in the refined scale parameters, which deviate only slightly from the transferred values, demonstrating as well the validity of transferring the parameters. The comparatively large changes for the ring bend (+9.1%) and ring torsion (−13.8%) factors may be rationalized by the smaller ring strain of the bicyclo[3.2.1]octane system compared to the bicyclo[2.2.1]octane (norbornane) system from which these parameters were taken, and also by the presence of one or two oxygen atoms in the rings, since the C—O—C and the C—C—C bending force constants were not scaled differently. Vibrational anharmonicities may also account in part for the differences as they influence the magnitudes of the scale factors.

The necessity of special scale factors for deformations of methylene groups adjacent to oxygen atoms is confirmed for the wagging mode, but not for the twisting mode. The "normal" CH_2 wagging and twisting factors converge to similar values as observed previously for norbornane (2*a*). The "special" factor for wagging does not change upon refinement and is found still considerably higher than the normal value. However, the "special" twist factor converges back to its original value. Whether this trend is real or not is not clear at this stage as the uncertainty of the refined value is relatively large. The most ambiguous scale factors in this work are the ones used for the methyne deformations. The problem apparently lies in their strong dependence on neighboring substituents and bonding, necessitating three separate factors that are then supported only by a relatively small number of experimental data. This naturally leads to large uncertainties in the refinement process. Removal of any one of the CH bending factors leads to appreciably worse frequency fits.

Intensities

In general, the calculated absorption intensities and, perhaps even more surprisingly, the Raman activities and depolarization ratios of the title compounds are predicted very satisfactorily using the 3-21G basis set. All intensity data are certainly accurate enough to be useful in a qualitative manner for spectral interpretations. Other workers have reported before that simple split-valence basis sets afford absorption intensities that are correct in the order of magnitude (7*b*, 22, 26, 35). The calculated absorption intensities in this study appear to surpass this order of magnitude accuracy as will be demonstrated below with a statistical analysis of the data. Raman activities have been reported to be even more susceptible to basis set truncation (7*b*, 22, 36). Large *ab initio* basis sets extended by polarization functions were deemed necessary for reasonable predictions (37). In this study, the relative intensities agree in the order of magnitude or better (Figs. 9–14). The calculated relative Raman intensities and depolarization ratios appear to be about as accurate as the absorption intensities. With theoretical predictions of such quality at hand, it would be worthwhile now for the purpose of spectral assignments to measure Raman depolarization ratios even for asymmetric molecules, as these properties can be calculated with reasonable accuracy. Furthermore, our results for DIOXA and DIOXA-d_2 from various *ab initio* calculations indicate that the APTs and polarizability derivatives are only slightly basis-set dependent in the domain of the split-valence and the 6-31G*, 6-31G*$^{(0.3)}$, and 6-31G** basis sets. The relative absorption and Raman intensities were found to be governed only by the accuracy of the normal mode descriptions.

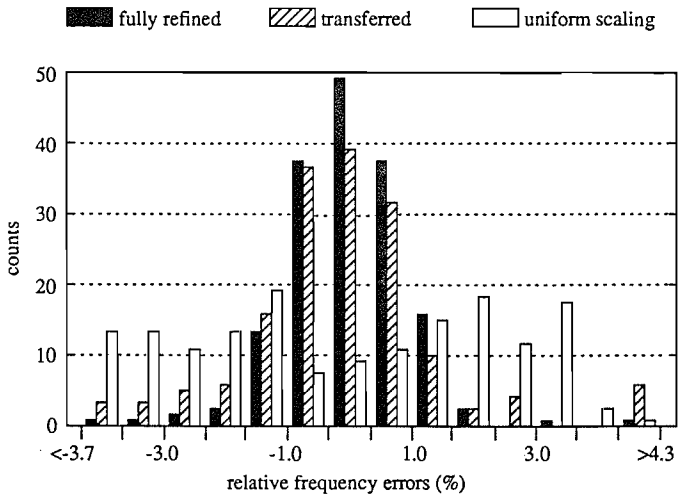

FIG. 15. Error distributions of the calculated frequencies for all six molecules using the three different force fields (fully refined nonuniform, transferred nonuniform, and uniform scaling).

Accuracy of eigenvectors

Some recently reported analyses of vibrational spectra have adopted uniform scaling methods, multiplying the entire force field by only one parameter. In the same studies, the nonuniform correction procedures used for SQM force fields were found to deteriorate the *ab initio* vibrational eigenvectors (38). Uniform scaling was preferred by these authors because it does not change the composition of the *ab initio* normal modes. These observations conflict with the findings by other workers that different local symmetry coordinates need different scale factors to obtain good frequency fits, which originally led to the idea of nonuniform scaling (39). The abundance of data for the series of molecules in this work permits a statistical analysis of the errors in the calculated intensities which rely partly on the underlying eigenvectors. This should allow some conclusions to be drawn about the preferable approach to scale force fields. To reexamine the validity of our approach and to gauge the accuracy of the scaled force fields, tests were carried out based on the assignments of the bicyclo[3.2.1]octanes as outlined above, probing the quality of our scaling method against uniform scaling. Figure 15 displays histograms that compare the distributions of the relative errors in the calculated frequencies for the force fields obtained by scaling with the fully refined and transferred multiple set of factors, and with the uniform parameter, respectively. The standard deviations of the errors of the 196 firmly assigned transitions are found at 1.1%, 2.0%, and 2.6%, respectively, assuming Gaussian distributions. The apparent superiority of the nonuniformly scaled force field in predicting the vibrational frequencies does not guarantee that the eigenvectors also are calculated more accurately. To judge the effect of nonuniform vs. uniform scaling on the normal mode compositions, the accuracy of the calculated absorption intensities was also investigated. Due to the large error margins on the intensities, distributions using relative errors for the abscissa of the histograms are not symmetric. The error in absorption intensity for every assigned transition is therefore mea-

Can. J. Chem. Downloaded from www.nrcresearchpress.com by 88.255.202.194 on 09/08/12
For personal use only.

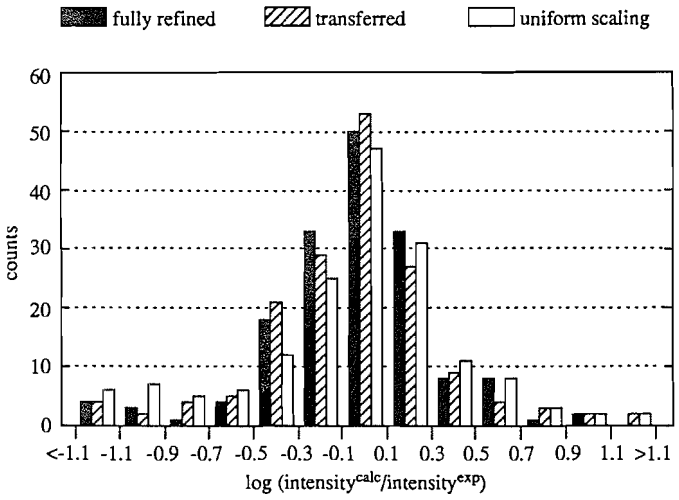

FIG. 16. Error distributions of the calculated absorption intensities for all six molecules using the three different force fields (fully refined nonuniform, transferred nonuniform, and uniform scaling).

sured here by the ratio of the calculated and the experimental intensity of the band ($f_k = I_k^{calc}/I_k^{exp}$). A histogram using $\log(f_k)$ for the abscissa is approximately symmetric and does reflect a Gaussian distribution (Fig. 16). The standard deviations calculated in this fashion are then found at $f_k = 2.5$, 2.7, and 3.2, respectively, for refined nonuniform, transferred nonuniform, and uniform scaling. The error distributions demonstrate clearly that nonuniform scaling certainly does not deteriorate but rather slightly improves the intensities. The Raman spectra did not allow a similar test as the experimental absolute intensities were not measured. However, a qualitative comparison of the relative calculated Raman intensities with the spectra leads to the same conclusion.

Conclusions

It appears that for these compounds and probably also for a large set of other moieties the *ab initio* eigenvectors are generally not deteriorated by nonuniform scaling if the factors are transferred from appropriate molecules and then carefully refined. This statement holds for the 3-21G basis set that was utilized here and can probably be extended to all split-valence basis sets. Even the intensities predicted by the transferred, unrefined set of scale parameters are notably superior to the calculations based on the uniformly scaled force field. It is known that similar calculations closer to the Hartree–Fock limit utilizing large basis sets require fewer scale factors. Consequently, if more sophisticated basis sets are used, uniform scaling will give more favorable results compared to this study, or may even be superior to nonuniform scaling (40). Some very recent theoretical work suggests that the Hartree–Fock-limit force field for a given molecule can be corrected with one factor only (41). However, due to basis set truncation, calculations at the 3-21G level are significantly less accurate and require nonuniform scaling as demonstrated theoretically (41) and confirmed here.

In principle, the errors in the intensities originate from two possible sources, firstly from deficiencies in the eigenvectors and secondly from inaccurate atomic polar tensors and polarizability derivatives. If a principal part of these intensity deviations originates from poor eigenvectors, some degree of correlation between the frequency errors and the intensity errors would be expected. However, linear regression of the errors from the above analysis shows no correlation at all, meaning that the intensity errors encountered here are basically independent of the remaining inaccuracies of the force field. When properly scaled force fields are utilized, the deviations from the observed values of the intensities must therefore originate from deficiencies in the APTs and polarizability derivatives, and cannot be substantially improved with more accurate force fields. Deficiencies in the force fields would obviously become more evident if the APTs and polarizability derivatives were obtained with sophisticated basis sets. However, the scaled force fields developed here are probably almost as accurate as any other harmonic *ab initio* force field, except if very large basis sets or electron correlation methods were used, which in any case are not yet feasible or are very expensive for molecules of this size. The basis set tests carried out with the DIOXA isotopomers not only demonstrate that the intensity parameters remain largely unchanged up to the 6-31G** basis set, but also that, after scaling, the 3-21G force field is only slightly inferior to the force fields from the considerably larger basis sets. This study fully justifies using the 3-21G basis set for the vibrational calculations for the title compounds. Application of the 6-31G basis set may be recommended, which appears to produce improved force constants without much increase of computational costs.

In connection with reports that favor uniformly scaled harmonic *ab initio* force fields, the following comments seem appropriate. It is crucial to realize that the fine tuning of several scale factors is important for large molecules with low symmetry, as even very small frequency shifts of normal modes will cause considerable remixing among modes of similar energies and hence subtle redistributions of intensities, more so than for small and highly symmetric molecules where the modes perturb each other to a lesser degree. For the latter, scaling with a very small set of independent factors may be preferable for the sake of simplicity or because of lack of sufficient experimental data, but the eigenvectors will almost certainly be less accurate than they could be using a full set of scale factors. Such inaccuracies in the predicted normal modes, if present for large molecules, will likely prevent or confuse numerous band assignments in the congested regions of the spectra. A judicious nonuniform scaling with a full set of factors, as demonstrated above, will yield more reliable predictions, allowing for firmer band assignments.

Finally, according to the standard deviation of the intensity errors, 95.5% of the calculated absorption intensities lie within a factor of 5 of the measured values. This validates the approach to utilize theoretical intensities from 3-21G *ab initio* calculations as an aid for spectral assignments, especially if only orders of magnitude are required. The theoretical relative Raman intensities are judged qualitatively to be comparably accurate. The 3-21G intensities are particularly gratifying when compared to the calculations carried out with the polarized and diffuse basis sets, all of which are only marginally more accurate. The successful performance of the 3-21G basis set for the absorption and Raman intensities may be connected to the large size of these molecules. Despite the small number of basis functions per atom, the overall sum of the functions applied in these molecules is considerable

Can. J. Chem. Downloaded from www.nrcresearchpress.com by 88.255.202.194 on 09/08/12
For personal use only.

and may permit a sufficiently detailed description of the electron densities and the connected properties. In terms of the accuracy of the theoretical predictions, applying a simple split-valence basis set to large molecules may therefore be equivalent to utilizing more sophisticated basis sets for small molecules.

Summary

We have assigned 196 observed bands as fundamental transitions in the vibrational spectra (100–1500 cm^{-1}) of six bicyclo[3.2.1]octane analogs. More assignments are suggested that could not be unambiguously confirmed by the available data. All assignments were based on the theoretical *ab initio* RHF geometries, harmonic force fields, and absorption and Raman intensities calculated with the 3-21G basis set. To correct for the deficiencies in the predicted frequencies, three methods for scaling force constants were tested, namely, multiplication by a uniform optimized factor, scaling with a set of parameters originally transferred from other molecules, and, finally, optimization by least-squares fitting of the frequency parameters. The three procedures produced frequency predictions with average errors of 2.2%, 1.2%, and 0.75%, respectively. To assess the accuracy of the vibrational eigenvectors resulting from the differently scaled force fields, the errors in the theoretical absorption intensities were analyzed in detail. The error distributions demonstrate that the absorption intensities are reproduced most accurately with nonuniformly corrected force fields and after refining the scale factors. A qualitative inspection of the theoretical Raman spectra indicates a similar trend. We conclude that for the most accurate predictions of frequencies and normal mode descriptions, scaling with multiple factors followed by refinement is preferable provided that the scale parameters are judiciously selected and transferred from other molecules and then refined with great care. We believe that this applies to all *ab initio* RHF force fields derived from split-valence basis sets. Accurate predictions of vibrational frequencies and intensities are crucial, particularly for large molecules, since the spectra become considerably more congested, which aggravates the problem of identifying the vibrations. In addition, the mixing of the modes is more pronounced such that even small deviations of the frequencies may result in erroneous normal mode descriptions and intensities.

The 3-21G calculated absorption intensities and the Raman data agree very satisfactorily with the experiments. The observed intensities are reproduced by the theory considerably better than just in order of magnitude. The intensity predictions are therefore extremely valuable in guiding the spectral assignments. The theoretical Raman depolarization ratios are particularly useful for this purpose since they can be applied to molecules with no symmetry. While a better force field for DIOXA was obtained by applying the 6-31G basis set, the intensity parameters remained essentially unchanged. Calculations using the 6-31G* and 6-31G** basis sets did not further improve the 6-31G frequencies and intensities.

Acknowledgements

This work was supported by an Operating Grant from the Natural Sciences and Engineering Research Council of Canada. We gratefully acknowledge the generous support from the Academic Computing Services and Supercomputer Committee of the University of Calgary to access the Honeywell Multics, the Convex C120, and the Cyber 205 supercomputer. We are further indebted to Drs. A. Rauk and R. Dutler for their assistance with the mainframe computers and the associated programs.

1. R. A. Shaw, C. Ursenbach, A. Rauk, and H. Wieser. Can. J. Chem. **66**, 1318 (1988).
2. (*a*) R. A. Shaw, N. Ibrahim, and H. Wieser. J. Phys. Chem. **93**, 3920 (1989); (*b*) J. Phys. Chem. **94**, 125 (1990).
3. (*a*) R. A. Shaw, C. Castro, N. Ibrahim, and H. Wieser. J. Phys. Chem. **92**, 6528 (1988); (*b*) R. A. Shaw, N. Ibrahim, and H. Wieser. Can. J. Chem. **68**, 90 (1990); (*c*) Can. J. Chem. **69**, 345 (1991).
4. R. A. Shaw, C. Castro, R. Dutler, A. Rauk, and H. Wieser. J. Chem. Phys. **89**, 716 (1988).
5. R. A. Shaw, N. Ibrahim, and H. Wieser. Can. J. Chem. **67**, 535 (1989).
6. T. Eggimann, R. A. Shaw, and H. Wieser. J. Phys. Chem. **95**, 591 (1991).
7. (*a*) P. Pulay, G. Fogarasi, X. Zhou, and P. W. Taylor. Vib. Spectrosc. **1**, 159 (1990); (*b*) G. Fogarasi and P. Pulay. *In* Vibrational spectra and structure. Vol. 14. *Edited by* J. R. Durig. Elsevier, Amsterdam. 1985. pp. 125–219; (*c*) Annu. Rev. Phys. Chem. **35**, 191 (1984).
8. N. Ibrahim, T. Eggimann, E. A. Dixon, and H. Wieser. Tetrahedron, **46**, 1503 (1990).
9. W. R. Moore, W. R. Moser, and J. E. Laprade. J. Org. Chem. **28**, 2200 (1963).
10. P. G. Gassman and J. L. Marshall. Org. Synth. (Collect. Vol.) **V**, 424 (1973).
11. G. Stork and H. K. Landesman. J. Am. Chem. Soc. **78**, 5129 (1956).
12. R. A. Appleton, K. H. Baggaley, C. Egan, J. M. Davies, S. H. Graham, and D. O. Lewis. J. Chem. Soc. (C), 2032 (1968).
13. A. C. Cope and G. L. Woo. J. Am. Chem. Soc. **85**, 3601 (1963).
14. A. C. Cope, C. H. Park, and P. Scheiner. J. Am. Chem. Soc. **84**, 4862 (1962).
15. L. A. Paquette, I. R. Dunkin, J. P. Freeman, and P. C. Storm. J. Am. Chem. Soc. **94**, 8124 (1972).
16. F. Sweet and R. K. Brown. Can. J. Chem. **46**, 2289 (1968).
17. S. W. Baldwin, R. J. Doll, and S. A. Haut. J. Org. Chem. **39**, 2470 (1974).
18. E. J. Boorman and R. P. Linstead. J. Chem. Soc. 258 (1935).
19. (*a*) T. L. Smithson. Ph.D. Thesis, The University of Calgary. 1982; (*b*) T. L. Smithson and H. Wieser. Unpublished results.
20. J. K. Kauppinen, D. J. Moffatt, H. H. Mantsch, and D. G. Cameron. Appl. Spectrosc. **35**, 271 (1981).
21. M. J. Frisch, J. S. Binkley, H. B. Schlegel, K. Raghavachari, C. F. Melius, L. R. Martin, J. J. P. Stewart, F. W. Bobrowicz, C. M. Rohlfing, L. R. Kahn, D. J. Defrees, R. Seeger, R. A. Whiteside, D. J. Fox, E. M. Fluder, and J. A. Pople. Carnegie–Mellon Publishing Unit, Pittsburgh, Pa. 1984.
22. P. Pulay, G. Fogarasi, F. Pang, and J. E. Boggs. J. Am. Chem. Soc. **101**, 2550 (1979).
23. T. Eggimann, T. L. Smithson, H. Wieser, P. Lorenčak, P. Bergquist, H. Badawi, S. P. Sibley, and R. L. Kuczkowski. Can. J. Chem. **68**, 267 (1990).
24. V. S. Mastryukov, E. L. Osina, L. V. Vilkov, and R. L. Hilderbrandt. J. Struct. Chem. **22**, 190 (1981).
25. R. A. Shaw. Ph.D. Thesis, The University of Calgary. 1986.
26. P. Pulay, G. Fogarasi, G. Pongor, J. E. Boggs, and A. Vargha. J. Am. Chem. Soc. **105**, 7037 (1983).
27. W. B. Person and J. H. Newton. J. Chem. Phys. **61**, 1040 (1974).
28. (*a*) G. Zerbi. *In* Vibrational intensites in infrared and Raman

Can. J. Chem. Downloaded from www.nrcresearchpress.com by 88.255.202.194 on 09/08/12
For personal use only.

spectroscopy. *Edited by* W. B. Person and G. Zerbi. Elsevier, Amsterdam. 1982. pp. 23–64; (*b*) W. B. Person. *In* Vibrational intensites in infrared and Raman spectroscopy. *Edited by* W. B. Person and G. Zerbi. Elsevier, Amsterdam. 1982. pp. 67–95.
29. E. B. Wilson, Jr., J. C. Decius, and P. C. Cross. Molecular vibrations. McGraw–Hill, New York. 1955.
30. R. E. Hester. *In* Molecular spectroscopy. Vol. 2. The Chemical Society, London. 1974. pp. 439–465.
31. J. A. Koningstein. Introduction to the theory of the Raman effect. Reidel, Dordrecht (Holland). 1972.
32. A. Rauk and D. Yang. J. Phys. Chem. **96**, 437 (1992).
33. J. G. C. M. Van Duijneveldt and F. B. Van Duijneveldt. J. Mol. Struct. **89**, 185 (1982).
34. A. Rauk, T. Eggimann, H. Wieser, and D. Yang. Can. J. Chem. **70**, 464 (1992).
35. C. Pouchan, A. Dargelos, and M. Chaillet. J. Chim. Phys. Phys.-Chim. Biol. **75**, 595 (1978).
36. B. A. Hess, L. J. Schaad, P. Čársky, and R. Zahradník. Chem. Rev. **86**, 709 (1986).
37. P. L. Polavarapu. J. Phys. Chem. **94**, 8106 (1990).
38. (*a*) P. K. Bose and P. L. Polavarapu. Chem. Phys. Lett. **152**, 39 (1988); (*b*) P. L. Polavarapu. Chem. Phys. Lett. **163**, 576 (1989).
39. (*a*) C. E. Blom, P. J. Slingerland, and C. Altona. Mol. Phys. **31**, 1359 (1976); (*b*) C. E. Blom and C. Altona. Mol. Phys. **31**, 1377 (1976).
40. R. Dutler and A. Rauk. J. Am. Chem. Soc. **111**, 6957 (1989).
41. V. I. Pupyshev, Y. N. Panchenko, C. W. Bock, and G. Pongor. J. Chem. Phys. **94**, 1247 (1991).

Can. J. Chem. Downloaded from www.nrcresearchpress.com by 88.255.202.194 on 09/08/12
For personal use only.

Diastereoselective intramolecular Diels–Alder reactions of the furan diene: the synthesis of (±)-1,4-epoxycadinane

CHRISTINE ROGERS AND BRIAN A. KEAY[1]

Department of Chemistry, University of Calgary, Calgary, Alta., Canada T2N 1N4

Received October 9, 1992

CHRISTINE ROGERS and BRIAN A. KEAY. Can. J. Chem. **71**, 611 (1993).

The diastereoselective intramolecular Diels–Alder reactions of the furan diene (IMDAF), in which the side arm comprises four carbon atoms and is substituted by a methyl group adjacent to, or one carbon removed from, the furan ring, are described. Adducts are formed in moderate to excellent yields when treated with either Florisil in methylene chloride at room temperature or methylaluminum dichloride in methylene chloride at −78°C. Florisil is most effective for substrates containing unsubstituted dienophiles. An equimolar quantity (1.1 equivalents) of methylaluminum dichloride is most effective for precursors having methacrolein-type dienophiles, while a catalytic quantity (0.1 equivalent) is effective for crotonaldehyde-type dienophiles. Only the adducts with the side arm orientated *syn* with respect to the oxygen bridge are detected and isolated. The major diastereomer is the one in which the methyl group (initially on the side arm) is situated equatorially on the newly formed six-membered ring. An application of the diastereoselective IMDAF reaction to the synthesis of (±)-1,4-epoxycadinane is described, beginning with 2-methylfuran.

CHRISTINE ROGERS et BRIAN A. KEAY. Can. J. Chem. **71**, 611 (1993).

On décrit les réactions diastéréosélectives de Diels–Alder intramoléculaires du furane (DAIMF) agissant comme diène et dans lequel la chaîne latérale comporte quatre atomes de carbone et est substituée par un groupe méthyle sur le carbone en α ou en β par rapport au noyau furanique. Les adduits se forment avec des rendements allant de moyens à excellents lorsqu'on les traite soit avec du Florisil dans le chlorure de méthylène à la température ambiante soit avec du dichlorure de méthylaluminium dans le chlorure de méthylène à −78°C. Le Florisil est le plus efficace pour les substrats contenant des diénophiles qui ne sont pas substitués. Une quantité équimolaire (1,1 équivalents) de dichlorure de méthylaluminium est le plus efficace pour des diénophiles précurseurs du type méthacroléine alors qu'une quantité catalytique (0,1 équivalent) est efficace pour les diénophiles du type crotonaldéhyde. On n'a détecté et isolé que les adduits dont la chaîne latérale est orientée en *syn* par rapport au pont oxygéné. Le diastéréoisomère principal est celui dans lequel le groupe méthyle (initialement dans la chaîne latérale) est en position équatoriale dans le cycle à six chaînons nouvellement formé. On décrit une application de la réaction diastéréosélective Diels–Alder intramoléculaire du furane pour la synthèse du (±)-1,4-époxycadinane à partir du 2-méthylfurane.

[Traduit par la rédaction]

The intramolecular Diels–Alder reaction of the furan diene (IMDAF) has been studied by many groups since it was first reported in 1978 (1). These investigations have attempted to define the scope and limitations of the IMDAF reaction with respect to (*i*) the effect of varying the length of the tether linking the diene and dienophile,[2,3] (*ii*) the effect of substituting heteroatoms for carbon on the tether,[2,3] (*iii*) the effect of varying the type and placement of substituents on both the furan ring and dienophile,[2,3] (*iv*) the development of methods to overcome the unfavourable equilibrium towards product,[2,3] and, lastly, (*v*) utilization of the adducts in the synthesis of natural products (7).

Our efforts have concentrated on defining the scope and limitations of the IMDAF reaction of systems containing a four-carbon-atom side arm (8–10). Precursors containing substituted dienophiles have an equilibrium favouring starting material, and therefore we examined methods to shift the equilibrium toward adduct formation. We recently showed (9) that the IMDAF reaction of precursors having a four-carbon-atom side arm was accelerated by methylaluminum dichloride in methylene chloride at −78°C (Scheme 1). The oxatricyclo adducts were obtained in good to excellent yield after only 2–8 h. In addition, the reaction was shown to be 100% stereoselective; only the adducts in which the side arm was orientated *syn* with respect to the oxygen bridge were isolated. Thus, adducts were prepared containing up to four asymmetric centres of known stereochemistry depending on the substituent pattern of the dienophile (i.e., Scheme 1: R^1 = Me, R^2 = H, R^3 = H or Me).

Placement of a single substituent on the side arm of the IMDAF precursor could lead to two diastereomers. The major isomer was expected to be that with the substituent in the equatorial position of the newly formed six-membered ring (Scheme 1: R^1 = H, R^2 = R^3 = Me), since the above IMDAF reactions were shown to be under thermodynamic control. This modification would result in adducts having up to five asymmetric centres of known relative stereochemistry (i.e., Scheme 1: R^1 = R^2 = R^3 = Me), which would be useful as intermediates for the synthesis of natural products, such as 1,4-epoxycadinane **1**.

We recently reported (11) that stirring various IMDAF precursors possessing a methyl-substituted four-carbon-atom tether with Florisil in methylene chloride for 0.5–19 days provided oxatricyclo adducts in which the major diastereomer had the methyl group situated in the equatorial position on the newly formed six-membered ring.[4] The adducts with the side arm *syn* to the oxygen bridge were the only isomers detected (by ^{1}H NMR) and isolated (i.e., Scheme 1: R^1 = H, R^2 = R^3 = Me). Since methylaluminum dichloride is an effective Lewis acid for accelerating the IMDAF reaction, we studied the effect of methylaluminum dichloride on the diastereomeric ratios of a number of IMDAF precursors having monosubstituted tethers. We herein provide (*i*) a full

[1]Author to whom correspondence may be addressed.

[2]For reviews, see ref. 2.

[3]For work reported on IMDAF reactions containing side arms with (*a*) heteroatoms, (*b*) three carbon atoms, (*c*) four carbon atoms, and (*d*) five carbon atoms, see refs. 3, 4, 5, and 6, respectively.

[4]Related diastereoselective IMDAF reactions have since been reported, see refs. 4*a*, 7*g*, and 12.

Can. J. Chem. Downloaded from www.nrcresearchpress.com by 213.200.69.106 on 09/08/12
For personal use only.

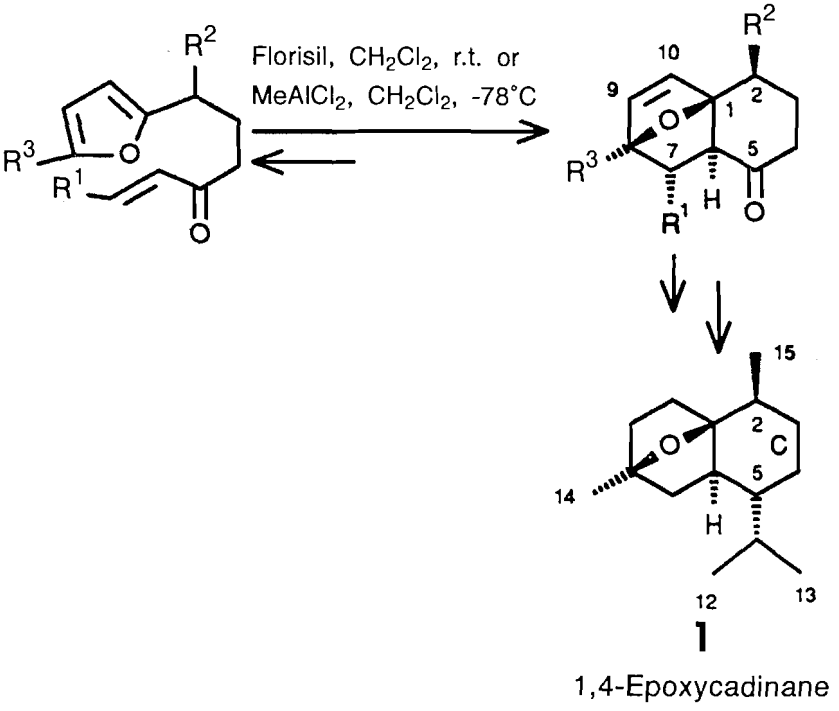

SCHEME 1

account of both the effect of Florisil and methylaluminum dichloride on the IMDAF reaction of precursors containing a single substituent on the tether, and (*ii*) the application of this methodology to the synthesis of (±)-1,4-epoxycadinane **1** (Scheme 1).[5]

Preparation of monosubstituted IMDAF precursors

The synthesis of the precursors with monosubstituted tethers was accomplished as outlined in Scheme 2. Friedel–Crafts alkylation (13) of 2-methylfuran **2** with either methacrolein or crotonaldehyde, in the presence of a trace of concentrated sulfuric acid, provided aldehydes **3** (53%) and **4** (36%), respectively. Although the yields were low, the starting materials are inexpensive, the reactions could be run on large scale, and the products were easily purified by distillation. The aldehydes **3** and **4** were converted into their respective iodides **5** and **6** by (*i*) reduction of the aldehydes with sodium borohydride in ethanol to the corresponding alcohols, (*ii*) conversion of the alcohols into tosylates, and (*iii*) displacement of the tosylate moiety by iodide in refluxing acetone. Treatment of iodides **5** and **6** with 2.2 equivalents of *tert*-butyllithium at −78°C (14), followed by trapping of the resulting carbanion with either acrolein, methacrolein, or crotonaldehyde, provided the allylic alcohols **7**–**12** in good yield. Alcohols **7**, **8**, **10**, and **11** were isolated as mixtures of diastereomers that were not separated, but were oxidized under Swern conditions (15) to provide enones **13**, **14**, **16**, and **17**, respectively. Alcohols **9** and **12** were oxidized to enones **15** and **18**, respectively, with Fétizon's reagent (16), since the Swern conditions provided low yields of the desired enones and a mixture of unidentified by-products.

IMDAF reactions with Florisil in methylene chloride

A study was performed to determine the optimum quantity of Florisil necessary for accelerating the IMDAF reaction. Compound **13** was studied as a model since previous work had shown (8, 9*c*) that the IMDAF reaction of precursors with unsubstituted dienophiles and side chains was accelerated by Florisil. Thus, furan **13** (100 mg) was treated with various quantities of Florisil (100–200 mesh) at room temperature, and aliquots were removed at various intervals to determine the ratio of starting material to adduct (SM : A) by integration of the ^1H NMR spectrum of the mixture. Gas chromatography was not used since some of the adducts cyclo-reversed on the column. The results of this study are summarized in Table 1 and several points are noteworthy. First, the presence of Florisil was required for the IMDAF reaction to occur. Secondly, two isomeric products **19**e and **19**a were formed, with the proportion of **19**e increasing over time. Both isomers had the side chain orientated *syn* with respect to the oxygen bridge (at C-6)[6] due to an *exo* mode of attack; however, the methyl group at C-2 was positioned equatorially (*syn* to the oxygen bridge) in the major isomer (**19**e) and axially (*anti* to the oxygen bridge) in the minor isomer (**19**a) (*vide infra*). Thirdly, equilibrium was attained more rapidly as the quantity of Florisil was increased; however, the use of greater than 10 weight equivalents led to low recoveries. Finally, the equilibrium was shifted completely toward adduct formation when 10 weight equivalents of Florisil were employed, and the reaction was stirred for 19 days.

Precursors **14**–**18** were therefore treated under the optimized conditions in methylene chloride at room temperature. The results are summarized in Table 2. The IMDAF

[5]The numbering of all oxatricyclo adducts in this paper will follow the IUPAC nomenclature rules. The natural product 1,4-epoxycadinane was originally numbered as a decahydronaphthalene system and thus the "1,4" numbering in the name does not follow the IUPAC numbering.

[6]See ref. 9*c* for details regarding the assignment of the stereochemistry of the side arm relative to the oxygen bridge in oxatricyclo adducts.

Can. J. Chem. Downloaded from www.nrcresearchpress.com by 213.200.69.106 on 09/08/12
For personal use only.

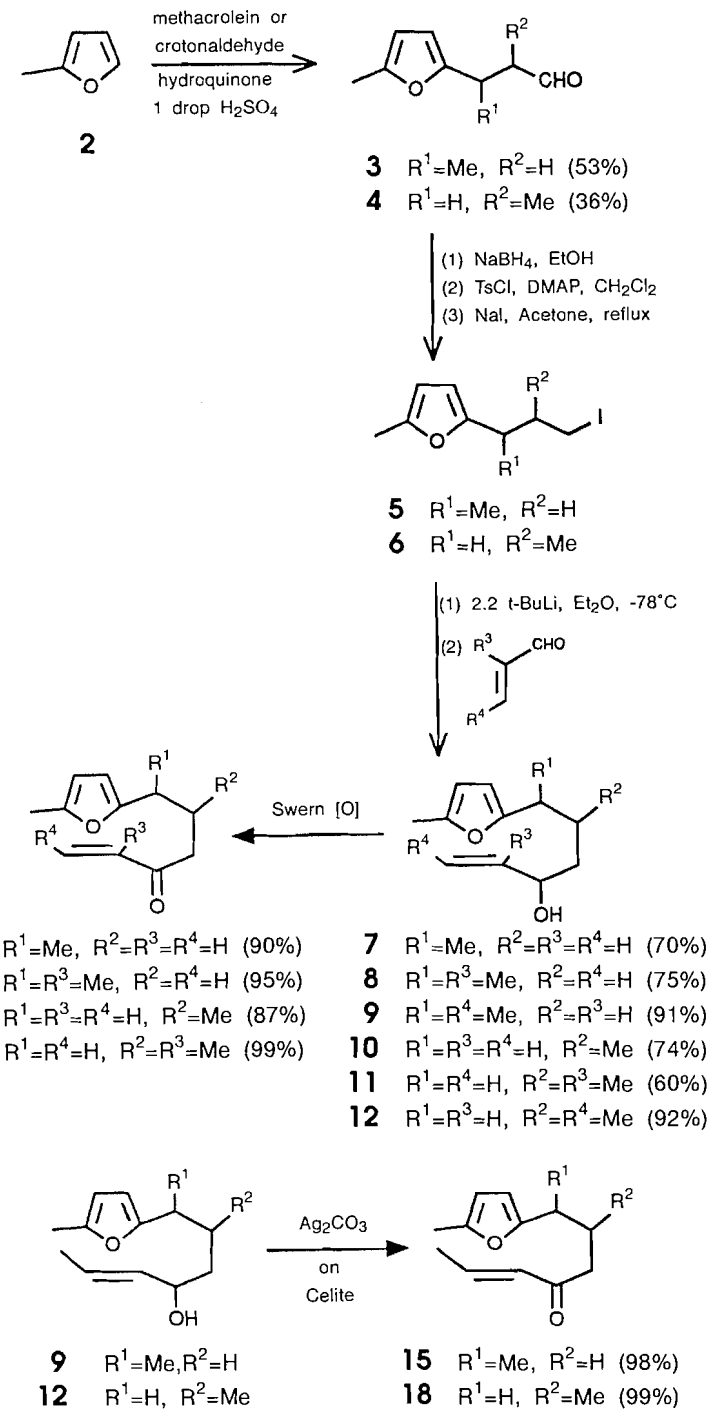

SCHEME 2

reactions of precursors **13–15** were less diastereoselective than those of the corresponding precursors **16–18** (diastereoselectivity will refer to the stereocenter on the side chain (i.e., C-2 or C-3)). Only the adducts in which the side chain was orientated *syn* to the oxygen bridge (at C-6) were detected (by ^{1}H NMR) and isolated.

Precursors **13–15** always provided a mixture of two diastereomers with the major isomer having the side-chain methyl equatorially positioned (*syn* to the oxygen bridge). The stereochemistry of the C-2 methyl group was determined as follows, using adducts **19**e and **19**a as representative examples. Irradiation of the C-2 methyl doublet resulted in the collapse of the C-2 hydrogen signal to a doublet of doublets and a triplet for compounds **19**e and **19**a, respectively. The measured coupling constants of 4.5 Hz (axial–equatorial) and 13.0 Hz (axial–axial) for the C-2 proton in compound **19**e indicated that it was axial. The coupling constant of 4.6 Hz (equatorial–equatorial and equatorial–axial) for the triplet indicated that the C-2 hydrogen was equatorial in compound **19**a.

Compounds **16–18** yielded only one isomer in which the methyl on the side chain was equatorially positioned (*anti* to the oxygen bridge). The stereochemistry of the C-3 methyl group was determined as follows using adduct **22**e as an ex-

Can. J. Chem. Downloaded from www.nrcresearchpress.com by 213.200.69.106 on 09/08/12
For personal use only.

TABLE 1. Optimization of quantity of Florisil

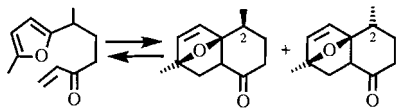

13 19e 19a

Quantity of Florisil (g)	Time (h)	Ratio **13**:**19e**:**19a**
0.0	2	100:0:0
	4	100:0:0
	9	100:0:0
	24	100:0:0
0.1	2	100:0:0
	4	78:12:10
	9	82:9:9
	24	64:20:16
0.5	2	71:12:17
	4	68:17:15
	9	44:27:29
	24	36:29:35
	48	22:41:37
	72	25:43:32
	480	18:66:16
1.0	24	30:37:33
	48	25:46:29
	456	0:87:13

ample. Since the C-3 hydrogen was "buried" in the 300 MHz ^{1}H NMR spectrum, the stereochemistry of the C-3 hydrogen atom was assigned by measuring the vicinal coupling constants of the adjacent C-2 and C-4 protons. For example, the doublet of doublets (12.0 Hz to H-3 and 14.5 Hz (germinal)) at δ 1.92 was assigned to H-2α by a combination of one- and two-dimensional NMR techniques. The large vicinal coupling constant of 12.0 Hz indicated that the C-3 hydrogen was axial, thus placing the methyl group equatorial.

A possible reason for the increased diastereoselectivity observed with compounds **16**–**18** may be due to an unfavourable 1,3-diaxial interaction, which would exist between the C-3 side-chain methyl group and the oxygen atom of the ether bridge if the methyl group were axial in adducts **22**–**24** (Fig. 1); this 1,3-diaxial interaction is absent in adducts **19**–**21**. This unfavourable interaction may promote the retro-Diels–Alder reaction, and thus equilibration occurs to provide the thermodynamically more stable equatorially substituted adduct.

The IMDAF reactions of precursors **14** and **17** also resulted in the formation of the desired adducts, although the SM:A ratios were in favour of starting material. The lower SM:A ratios relative to those of **13** and **16** may be a result of either unfavourable steric interactions in the transition state due to substitution of the dienophile, or decreased reactivity of the dienophile, which would be more electron rich than the unsubstituted dienophile due to the electron-donating methyl group (17). Substitution of the tether with a single methyl group accelerated the IMDAF reaction relative to that of the corresponding unsubstituted precursors, which showed no reaction in the presence of Florisil (8, 9*c*). Again, the IMDAF reaction of precursor **17** was more diastereoselective than that of compound **14** (*vide supra*). A higher proportion of equatorial to axial isomers was obtained for product **20** relative to adduct **19** (12:1 for compound **20** versus 7:1 for compound **19**). A very strong 1,3-diaxial interaction exists in adduct **20**a between the C-2 and C-6 methyl groups (Fig. 1), which could promote the retro-Diels–Alder reaction and thus favour equilibration to the equatorial isomer **20**e.

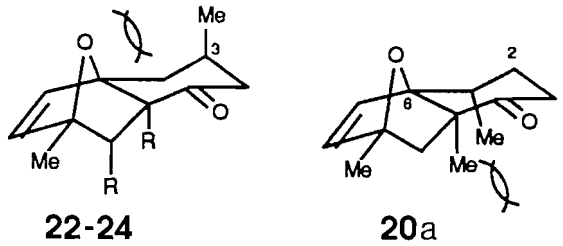

22-24 20a

FIG. 1. 1,3-Diaxial interaction in compounds **22**–**24** and **20**a.

Compounds **15** and **18** showed even less propensity to undergo the IMDAF reaction than the methacrolein precursors **14** and **17**. The reduced reactivity is likely due to steric interaction between the methyl groups on the terminus of the dienophile and on the 5-position of the furan ring in the transition state. Again, the major adducts produced (**21**e and **24**e, respectively) had the methyl group oriented equatorially on the newly formed six-membered ring.

It is interesting to note that heating precursors **13**, **17**, and **18** to 40°C resulted in acceleration of the rate at which the IMDAF equilibrium was attained. This result is in contrast to the behaviour of the adducts derived from precursors with unsubstituted side arms, which revert to starting material upon heating (8, 9*c*). This method provided equilibrium ratios within 1 day similar to those obtained at room temperature after 19 days and is therefore more synthetically useful.

IMDAF reactions with methylaluminum dichloride in methylene chloride

We have reported that methylaluminum dichloride accelerates the IMDAF reaction of precursors having unsubstituted side chains (9). Both 1.1 and 0.1 equivalents of methylaluminum dichloride were shown to be effective; precursors with a substituted dienophile provided a higher ratio of adduct when the catalytic quantity of methylaluminum dichloride was employed. Precursors **13**–**15**, **17**, and **18** were therefore treated with methylaluminum dichloride, and the results are summarized in Table 2. The use of 1.1 equivalents of methylaluminum dichloride was found to be very effective for accelerating the IMDAF reaction of compounds **13**, **14**, and **17**. The products were formed stereoselectively in favour of the adduct with the methyl group situated equatorially on the newly formed cyclohexanone ring. In all cases the side chain was orientated *syn* with respect to the oxygen bridge due to an *exo* mode of attack. The reaction was complete within 15 min at −78°C compared to the 4–14 days required for equilibrium to be achieved with Florisil (Table 2), and provided the adducts in excellent yields (81–88%). Thus methylaluminum dichloride is much superior to Florisil in accelerating the IMDAF reaction.

Precursors **15** and **18**, having a terminally substituted dienophile, provided SM:A ratios of 79:21 and 42:58, respectively, with 1.1 equivalents of methylaluminum dichloride. The ratios were improved to 17:79 and 11:89 by treating precursors **15** and **18** with 0.1 equivalent of

Can. J. Chem. Downloaded from www.nrcresearchpress.com by 213.200.69.106 on 09/08/12
For personal use only.

TABLE 2. IMDAF reaction of monosubstituted precursors with Florisil and $MeAlCl_2$ (MAC)

Starting material	Lewis Acid	Time	Temperatures	SM: Adduct ratio (SM:Eq.:Ax.)	Yield[a] (%)	Adduct
13	Florisil	13 d	rt	0:87:13	70	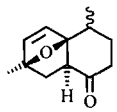
	Florisil	24 h	40°C	<1:84:16	67	
	Florisil	48 h	40°C	7:75:18	60	
	MAC					
	1.1 equiv.	15 min	−78°C	0:90:10	88	**19**e and **19**a
14	Florisil	24 h	rt	73:27:<1	22	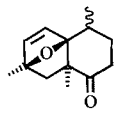
	Florisil	4 d	rt	65:35:<1	28	
	Florisil	13 d	rt	48:47:4	38	
	MAC					
	1.1 equiv.	5 min	−78°C	9:88:3	81	**20**e and **20**a
15	Florisil	24 h	rt	93:6:0	—	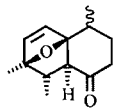
	Florisil	4 d	rt	89:11:<1	9	
	Florisil	13 d	rt	73:19:8	15	
	MAC					
	1.1 equiv.	5 min	−78°C	79:16:5	15	
	0.1 equiv.	2 h	−65°C	17:75:4	74	**21**e and **21**a
16	Florisil	6 d	rt	0:100:0	85	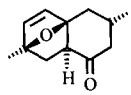 **22**e
17	Florisil	5 d	rt	62:38:0	—	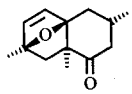
	Florisil	9 d	rt	52:48:0	—	
	Florisil	19 d	rt	50:50:0	40	
	Florisil	24 h	40°C	62:38:0	—	
	Florisil	48 h	40°C	56:44:0	37	
	MAC					
	1.1 equiv.	5 min	−78°C	11:89:0	88	**23**e
18	Florisil	5 d	rt	85:15:0	—	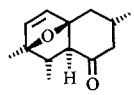
	Florisil	8 d	rt	80:20:0	16	
	Florisil	24 h	40°C	85:15:0	13	
	MAC					
	1.1 equiv.	5 min	−65°C	61:31:8	30	
	0.1 equiv.	2 h	−65°C	11:87:2	83	**24**e

[a]Isolated yield of the major adduct.

methylaluminum dichloride at −65°C for 2 h.[7,8] The major adducts (**21**e and **24**e) were those with the methyl group on the side arm in the equatorial position on the newly formed six-membered ring. The major adducts were formed in excellent yield (73% and 85%, respectively) and were easily separated from the minor adduct and starting material by flash chromatography.

Conclusions

The Florisil-mediated diastereoselective IMDAF reaction was optimized with 10 weight equivalents of Florisil in methylene chloride. Optimized results with methylaluminum dichloride were obtained at −78°C when 1.1 equivalents were employed with either unsubstituted or α-substituted dienophiles; β-substituted dienophiles gave the best results with 0.1 equivalent of methylaluminum dichloride. The IMDAF reactions with Florisil and methylaluminum dichloride were highly diastereoselective. Only the adducts with the side arm orientated *syn* with respect to the oxygen bridge were detected and isolated. In addition, the major adduct had the methyl substituent in the equatorial position of the newly formed six-membered ring, and reactions that resulted in the substituent in the C-3 position were more diastereoselective than those with the substituent in the C-2 position. Finally, the use of methylaluminum dichloride was superior to that of Florisil since the reaction time was reduced from up to 19 days with Florisil to a couple of hours with methylaluminum dichloride. In addition, higher yields of the adducts were obtained and lower temperatures were required when methylaluminum dichloride was employed. The reaction time with

[7]Catalytic quantities of $MeAlCl_2$ were not used on compounds **14** and **17** since the results with 1.1 equivalents provided the adducts in excellent yield.

[8]A paper describing competitive complexation NMR studies with $MeAlCl_2$ has recently been submitted, which provides evidence to support our hypothesis (ref. 9) on why catalytic quantities of $MeAlCl_2$ provide higher ratios of adduct to starting material than when 1.1 equivalents of $MeAlCl_2$ are used.

Can. J. Chem. Downloaded from www.nrcresearchpress.com by 213.200.69.106 on 09/08/12
For personal use only.

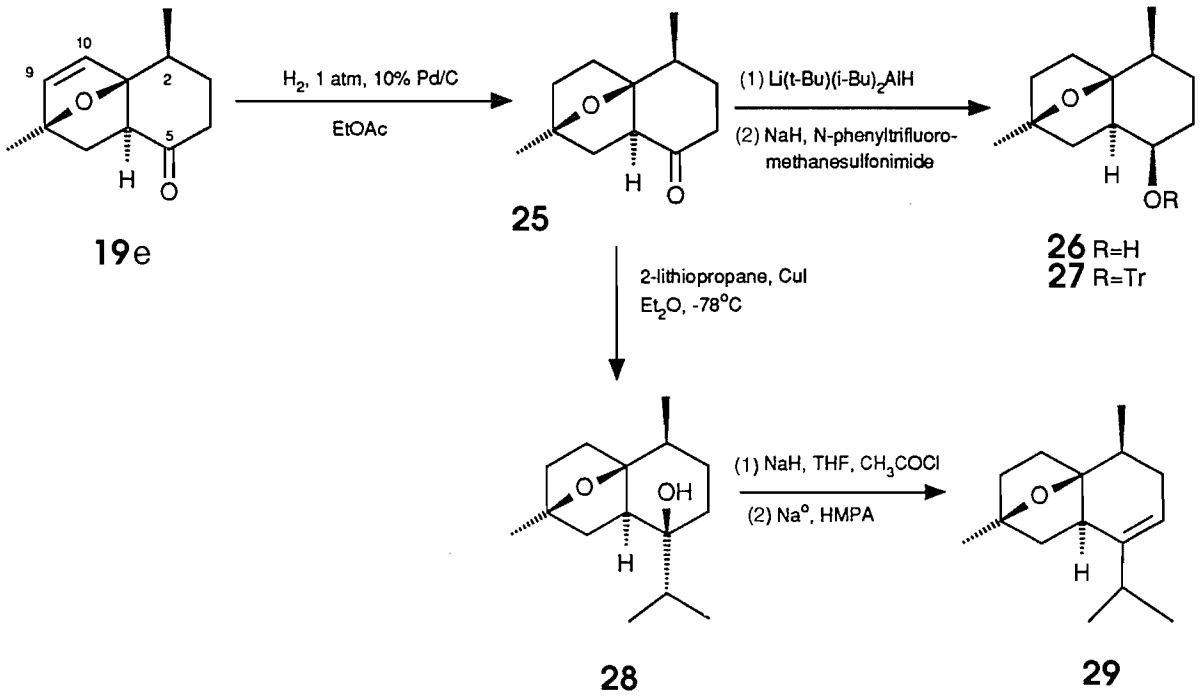

SCHEME 3

Florisil, however, could be reduced from 19 days to 1 day by refluxing the mixture at 40°C in methylene chloride.

Thus, these reactions constitute the first examples of diastereoselective IMDAF reactions with the diene and dienophile connected by a four-carbon-atom tether. In addition, adducts containing up to five asymmetric centers, all of known relative stereochemistry, were formed in one step from an acyclic precursor. The accompanying synthesis of 1,4-epoxycadinane illustrates the synthetic usefulness of the above IMDAF reactions.

The synthesis of (±)-1,4-epoxycadinane

The natural product 1,4-epoxycadinane **1** (Scheme 1) was isolated as a crystalline, optically active, solid from the brown alga *Dilophus fasciola* in 1979 (18*a*). 1,4-Epoxycadinane **1** is a sesquiterpene containing the cadinane ring (18*b*, 18*c*) system with five asymmetric centres and an oxygen ether linkage between carbons 1 and 8 (IUPAC numbering). While there have been many reported syntheses of natural products containing the cadinane ring system, 1,4-epoxycadinane has not been synthesized (19).

The methyl group at C-2 and the isopropyl group at C-5 are both equatorially positioned on ring C of 1,4-epoxycadinane. In addition, the C-2 methyl group and C-6 hydrogen are *syn* and *anti*, respectively, to the oxygen bridge. Since the IMDAF reaction of precursor **13** provided adduct **19**e, which contains four of the five asymmetric centres present in 1,4-epoxycadinane, as the major product (Table 2), we investigated the conversion of adduct **19**e into 1,4-epoxycadinane. The synthesis of 1,4-epoxycadinane would therefore entail (1) reduction of the C9—C10 double bond and (2) stereoselective conversion of the C-5 ketone into the equatorially positioned isopropyl group.

The first step in the synthesis of 1,4-epoxycadinane was routine. Compound **19**e was hydrogenated using 10% palladium on carbon in ethyl acetate to provide compound **25** in 95% yield (Scheme 3) (20). The absence of the vinyl protons at δ 6.08 and 6.18 in the ^{1}H NMR spectrum indicated the carbon–carbon double bond had been reduced, while the presence of the absorption at 1713 cm^{-1} in the IR spectrum confirmed that the ketone had not been reduced to the alcohol.

The conversion of the carbonyl moiety into the equatorially positioned isopropyl group proved to be more troublesome than initially expected. Our first approach involved (1) a stereoselective reduction of the ketone to an axial alcohol, (2) conversion of the alcohol into a good leaving group, and (3) an S_N2 displacement of the leaving group with an isopropyl moiety. Reduction of ketone **25** with lithium *tert*-butyldiisobutylaluminum hydride in THF at −78°C provided a single compound **26** in which the alcohol group was axial (Scheme 3). The attempted conversion of alcohol **26** into the triflate **27**, employing a variety of conditions (21), provided only starting material upon work-up, although TLC indicated that the alcohol had reacted. Since it was possible that the triflate was being hydrolyzed during work-up, the above reaction was repeated and the mixture added directly to an ethereal solution of isopropylmagnesium chloride in the presence of copper(I) iodide to attempt an *in situ* displacement of the triflate. Again, only starting material was recovered. Attempts to prepare the tosylate of alcohol **26** were equally unsuccessful under a variety of conditions (22). An alternative approach was therefore required.

Since the bulky reducing agent lithium *tert*-butyldiisobutylaluminum hydride reduced the ketone in compound **25** exclusively from the α face, attack by isopropyl nucleophile should provide alcohol **28** having the isopropyl group in the equatorial position (Scheme 3). Removal of the tertiary hydroxyl group with retention of stereochemistry would then complete the synthesis. Although compound **25** did not react with isopropylmagnesium chloride (quantitative recovery of starting material) it did react smoothly with the less basic, higher order, cuprate (23) of 2-lithiopropane (24)

Can. J. Chem. Downloaded from www.nrcresearchpress.com by 213.200.69.106 on 09/08/12
For personal use only.

Can. J. Chem. Downloaded from www.nrcresearchpress.com by 213.200.69.106 on 09/08/12
For personal use only.

(prepared by adding 2-lithiopropane (8 equivalents) to copper(I) iodide (3 equivalents)) in ether at 0°C to provide a single alcohol **28**. Treatment of compound **28** under a variety of conditions reported for the deoxygenation of tertiary alcohols (25) did not provide 1,4-epoxycadinane. Either starting material **28** was recovered or eliminated product **29** was isolated and was inert to catalytic hydrogenation (H_2, PtO_2, or 10% Pd/C) (Scheme 3).

Since the shorter synthetic routes for the conversion of the ketone carbonyl into an isopropyl group failed, a longer sequence was utilized (Scheme 4). This synthetic strategy takes advantage of the fact that the presence of the oxygen bridge in compound **25** does not allow the adjacent cyclohexanone ring to undergo chair interconversions. Thus, elaboration of the ketone in compound **25** to an aldehyde group via Wittig chemistry should provide an equatorially disposed aldehyde under thermodynamic conditions (see compound **31**, Scheme 4). The aldehyde (at C-5) would therefore be *trans* to the methyl group at C-2, thus providing the correct relative stereochemistry at C-5.

Wittig reaction of ketone **25** with the ylid of (methoxymethyl)triphenylphosphonium chloride provided compound **30** (82%) as a 2:3 mixture of double bond isomers. No attempt was made to separate these isomers. The mixture was treated immediately with dilute HCl in THF to provide aldehyde **31** (63%) as a single isomer (26). The stereochemistry of the aldehyde was determined by decoupling experiments. Irradiation of the aldehyde signal resulted in a collapse of the signal centered at δ 2.18 to a doublet (3.3 Hz) of triplets (10.9 Hz). These coupling constants are indicative of a vicinal axial–equatorial and two axial–axial couplings, respectively. Therefore the C-5 hydrogen was axial, establishing the aldehyde in the desired equatorial position.

The aldehyde **31** was converted into the methyl ketone **33** in two steps. Treatment of **31** with excess methyllithium at −78°C for 1.5 h provided compound **32** (97%) as a 7:3 mixture of diastereomers. The mixture was smoothly oxidized to the methyl ketone **33** (90%) under Swern conditions (15). The stereochemistry at C-5 was again confirmed by measuring the coupling constants of the C-5 hydrogen (δ 2.3, doublet of triplets). The single coupling constant of 3.1 Hz (doublet, axial–equatorial) and two 10.4 Hz couplings (triplet, axial–axial) established that the C-5 hydrogen in compound **33** was axial.

Wittig reaction of ketone **33** with a 20-fold excess of the ylid of methylenetriphenylphosphorane (27) provided compound **34** (74%) and some unreacted starting material (20%). The mixture was easily separated and the unreacted starting material was recycled. Finally, vinyl compound **34** was hydrogenated (H_2, PtO_2, 1 atm (1 atm = 101.3 kPa)) to provide 1,4-epoxycadinane in 93% yield. Although the ^{13}C and ^1H NMR spectra of synthetic 1,4-epoxycadinane agreed very well with the data reported for the authentic sample (Table 3), irradiation of the proton at δ 1.81 did not result in a collapse of the methyl doublets at δ 0.73 and δ 0.89 as reported by Fattorusso *et al.* (i.e., the isopropyl methine hydrogen) (18*a*). Through 2D-NMR techniques the isopropyl methine hydrogen was assigned to the signal at δ 1.58. Fattorusso informed us that the reported irradiation of the peak at δ 1.81 was a typographical error and should have been δ 1.58.

Thus, (±)-1,4-epoxycadinane was synthesized in 14 steps from 2-methylfuran in 9% overall yield. The relative stereochemistry of four of the five stereocentres was controlled by the IMDAF reaction, while the rigidity of the oxatricyclo adduct was used effectively to control the stereochemistry of the fifth stereocentre. This synthesis clearly illustrates the synthetic usefulness of the IMDAF reaction for the preparation and control of remote stereocentres.

Experimental

General methods

Melting points were determined using an Electrothermal melting point apparatus and are uncorrected. Boiling points refer to the air-bath temperature using Kugelrohr distillation apparatus, and are also uncorrected. Infrared spectra were obtained as thin films (oils) on either NaCl or KBr plates or as KBr pellets (solids). The infrared spectra were recorded on either a Nicolet 5-DX FT-IR spectrophotometer or a Mattson model 4030 FT-IR.

Nuclear magnetic resonance spectra were obtained on one of three instruments: Bruker AC-300 (^1H 300 MHz, ^{13}C 75 MHz), Bruker ACE-200 (^1H 200 MHz, ^{13}C 50 MHz), or a Bruker AM-400 spectrometer (^1H 400 MHz). Deuterochloroform was used both as the solvent, and as the internal standard (^1H, δ 7.27, ^{13}C, δ 77.0), unless otherwise stated. All ^1H NMR spectra listed will have the following format: chemical shift (in ppm), (multiplicity, number of protons, coupling constants (Hz), assignment). The abbreviations used to describe the multiplicities are as follows: br = broadened, s = singlet, d = doublet, t = triplet, q = quartet, and ABq refers to a quartet due to an AB spin system. The ^{13}C NMR spectra listed will have the following format: chemical shift (in ppm), (number of attached protons as determined by DEPT experiments).

Low-resolution mass spectra were recorded using either a Varian CH5 spectrometer or a VG 7070 instrument. The data are listed as mass (*m/e*), (relative intensity, assignment). The spectra were obtained either by the electron-impact (EI) method or field ionization (FI), and the method will only be listed if FI was used. High-resolution mass spectra were recorded on a Kratos MS80. Microanalyses were performed either by Guelph Chemical Laboratories Limited, Guelph, Ontario, or by Mrs. D. Fox, Department of Chemistry, University of Calgary.

Solvents were either dried by standard methods (28), then distilled prior to use, or were purchased as anhydrous solvents in Sure-Seal® bottles from the Aldrich Chemical Company. THF was dried over sodium and benzophenone, as was diethyl ether. Methylene chloride, diisopropyl amine, and triethylamine were dried over CaH_2. Methanol was refluxed with Mg^0 metal for 12 h, then distilled. DMSO was dried over NaOH. Acetonitrile, DMF, and diethyl ether were purchased as anhydrous solvents, and HPLC-grade acetone was used.

All glassware and syringes were dried in a 120°C oven for at least 4 h, then cooled under a stream of argon, or in a desiccator containing Drierite. Reactions that were sensitive to moisture or atmospheric conditions were performed under an argon atmosphere. Compounds were purified by flash chromatography using various ratios of petroleum ether and ethyl acetate.

The experimental procedures for the preparation of compounds **3–17** have been deposited as Supplementary Material.[9]

General procedure 1: IMDAF reactions in Florisil

The freshly distilled enone (1 mmol) was dissolved in dry CH_2Cl_2 (15 mL) and placed in an argon-purged round-bottom flask. To this was added Florisil (100–200 mesh, 10 weight equivalents to the enone). The reaction was wrapped in foil and stirred at the appropriate temperature for the required length of time. The reaction was then filtered, the Florisil washed well with EtOAc (20 mL), and the

[9]Supplementary material mentioned in the text may be purchased from: The Depository of Unpublished Data, Document Delivery, CISTI, National Research Council Canada, Ottawa, Canada K1A 0S2.

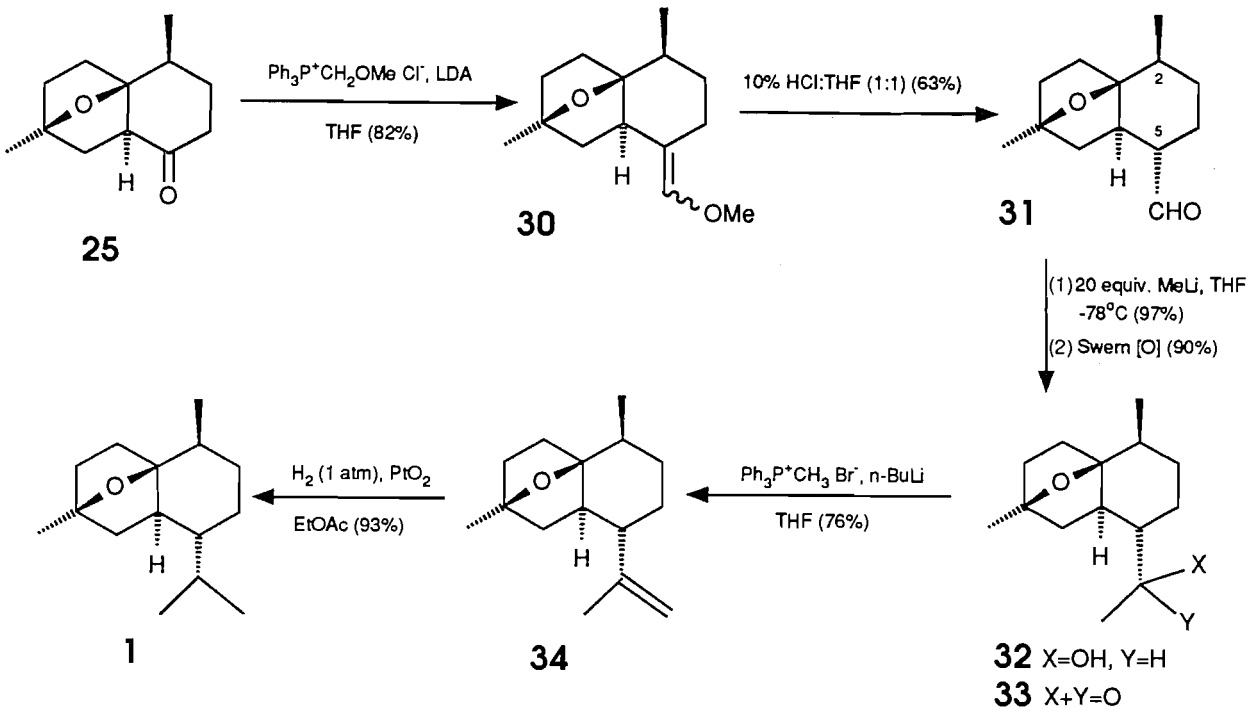

SCHEME 4

TABLE 3. A comparison of the ^{13}C and ^{1}H NMR spectra of natural and synthetic 1,4-epoxycadinane **1**

Multiplicity	Natural product	Synthetic product
	^{13}C NMR data	
Quartet	15.96	15.99
Quartet	16.22	16.22
Quartet	21.61	21.61
Quartet	21.79	21.83
Triplet	24.46	24.37
Triplet	31.84	31.81
Triplet	34.69	34.64
Triplet	37.54	37.50
Triplet	44.76	44.68
Doublet	27.47	27.38
Doublet	34.82	34.78
Doublet	48.15	48.08
Doublet	48.66	48.60
Singlet	83.32	83.27
Singlet	88.02	86.97
	Selected ^{1}H NMR data	
Me-12	0.73	0.74
Me-13	0.89	0.89
Me-15	1.05	1.06
Me-14	1.44	1.45

solvent removed *in vacuo* without external heating to provide the crude product, which could be purified by flash chromatography (pet. ether: EtOAc).

General procedure 2: IMDAF reactions using Lewis acid

The freshly distilled enone (0.2 mmol) was dissolved in dry CH_2Cl_2 (10 mL), placed in an argon-purged 3-necked flask, and cooled to the appropriate temperature. Methylaluminum dichloride (1.0 M in hexane) was added to the cooled enone solution, and the reaction was stirred for the appropriate length of time. The reaction was quenched with 10% $NaHCO_3$ (10 mL), and warmed until no frozen material remained. The aqueous layer was extracted with CH_2Cl_2 (4 × 10 mL), then the organic layer was washed with H_2O (15 mL), dried over Na_2SO_4, filtered, and the solvent removed *in vacuo* without external heating to provide the crude product, which was purified by flash chromatography (pet. ether: EtOAc).

*(6αH)-2β,8β-Dimethyl-11-oxatricyclo[6.2.1.0^{1,6}]undec-9-en-5-one (**19e**) and (6αH)-2α,8β-dimethyl-11-oxatricyclo[6.2.1.0^{1,6}]undec-9-en-5-one (**19a**)*

Enone **13** (380.1 mg) was stirred with Florisil (4.0 g) according to general procedure 1 for 13 days at room temperature under argon to provide a mixture of **13**:**19e**:**19a** in a ratio of 0:87:13. The isolated yields were **19e**: 70% (239 mg) and **19a**: 71% (29 mg).

Enone **13** (48.8 mg, 0.254 mmol) was treated with excess $MeAlCl_2$ (280 μL, 0.280 mmol) according to general procedure 2 at −78°C for 15 min to provide a mixture of **13**:**19e**:**19a** in a ratio of 0:90:10 with quantitative recovery (**19e**: 88% (40 mg); **19a**: 90% (4.2 mg)). The above mixtures were separated using flash chromatography (9:1, pet. ether: EtOAc).

*Compound **19e** (colourless oil)*: IR (neat): 1709, 1108 cm^{-1}; ^{1}H NMR (300 MHz) δ: 1.06(d, 3H, J = 7.0 Hz, C-2-CH_3), 1.52(s, 3H, C-8-CH_3), 1.55(dd, 1H, $J_{7\alpha,6\alpha}$ = 8.3 Hz, J_{gem} = 11.8 Hz, H-7α), 1.73(dq, 1H, $J_{3\beta,4\beta}$ = 5.6 Hz, $J_{3\beta,2\alpha}$ = 13.0 Hz, $J_{3\beta,4\beta}$ = 13.0 Hz, J_{gem} = 13.0 Hz, H-3β), 1.88(ddd, 1H, $J_{3\alpha,2\alpha}$ = 4.5 Hz, J_{gem} = 13.0 Hz, H-3α), 2.10(dd, 1H, $J_{7\beta,6\alpha}$ = 3.4 Hz, J_{gem} = 11.8 Hz, H-7β), 2.28(dd, 1H, $J_{6\alpha,7\beta}$ = 3.4 Hz, $J_{6\alpha,7\alpha}$ = 8.3 Hz, H-6α), 2.35(ddq, 1H, $J_{2\alpha,3\alpha}$ = 4.5 Hz, $J_{2\alpha,12}$ = 7.0 Hz, $J_{2\alpha,3\beta}$ = 13.0 Hz, H-2α), 2.28–2.45(overlapping m, 2H, H-4α and H-4β), 6.07 and 6.17(ABq, 2H, J = 5.5 Hz, H-9 and H-10); ^{13}C NMR (75 MHz) δ: 16.32(q), 18.68(q), 29.68(t), 33.58(d), 35.65(t), 41.61(t), 53.46(d), 85.61(s), 93.62(s), 137.17(d), 140.89(d), 209.70(s); mass spectrum, *m/e*: 192(4, M^+), 122(100, $M-C_4H_6O$, retro IMDAF–McLafferty rearrangement); HRMS (EI) calcd. for $C_{12}H_{16}O_2$: 192.1151; found: 192.1154.

*Compound **19a** (colourless oil)*: IR (neat): 1710 cm^{-1}; ^{1}H NMR (300 MHz) δ: 1.30(d, 3H, $J_{12,2\beta}$ = 7.2 Hz, C-2-CH_3), 1.52(s, 3H, C-8-CH_3), 1.58(dd, 1H, $J_{7\alpha,6\alpha}$ = 8.4 Hz, J_{gem} = 11.8 Hz, H-7α), 1.69(m, 1H, $J_{3\alpha,2\beta}$ = 4.4 Hz, $J_{3\alpha,4\beta}$ = 4.4 Hz, $J_{3\alpha,4\alpha}$ = 5.6 Hz,

Can. J. Chem. Downloaded from www.nrcresearchpress.com by 213.200.69.106 on 09/08/12
For personal use only.

Can. J. Chem. Downloaded from www.nrcresearchpress.com by 213.200.69.106 on 09/08/12
For personal use only.

J_{gem} = 13.6 Hz, H-3α), 2.10(dd, 1H, $J_{7\beta,6\alpha}$ = 3.4 Hz, J_{gem} = 11.7 Hz, H-7β), 2.10(overlapping ddt, 1H, H-3β), 2.32(dt, 1H, $J_{4\beta,3\alpha}$ = 4.6 Hz, $J_{4\beta,3\beta}$ = 4.6 Hz, J_{gem} = 15.3 Hz, H-4β), 2.34(m, 1H, H-2β), 2.37(dd, 1H, $J_{6\alpha,7\beta}$ = 3.4 Hz, $J_{6\alpha,7\alpha}$ = 8.4 Hz, H-6α), 2.51(ddd, 1H, $J_{4\alpha,3\alpha}$ = 5.5 Hz, $J_{4\alpha,3\beta}$ = 11.8 Hz, J_{gem} = 15.5 Hz, H-4α), 6.22 and 6.29(ABq, 2H, J = 5.7 Hz, H-9 and H-10); ^{13}C NMR (75 MHz) δ: 16.18(q), 18.64(q), 27.85(t), 30.35(d), 35.79(t), 36.63(t), 51.32(d), 85.61(s), 93.71(s), 135.04(d), 141.44(d), 210.41(s); mass spectrum, *m/e*: 192(10, $M^{+\cdot}$), 122(100, M−C_4H_6O. retro IMDAF–McLafferty rearrangement); HRMS (EI) calcd. for $C_{12}H_{16}O_2$: 192.1151; found: 192.1147.

*2β,6α,8β-Trimethyl-11-oxatricyclo[6.2.1.0^{1,6}]undec-9-en-5-one (**20e**)*

Enone **14** (108.0 mg) was stirred with Florisil (1.1 g) according to general procedure 1 for 13 days at room temperature under argon to provide a mixture of **14**:**20**e:**20**a in a ratio of 48:47:4 in quantitative yield. The starting material **14** could be separated from the adducts by flash chromatography (9:1); however, the minor isomer **20**a could not be completely separated from the major isomer **20**e. Only the major isomer could therefore be characterized.

Enone **14** (79.5 mg, 0.385 mmol) was treated with excess $MeAlCl_2$ (424 μL, 0.424 mmol) according to general procedure 2 at −78°C for 5 min to provide a mixture of **14**:**20**e:**20**a in a ratio of 9:88:3 with quantitative recovery. IR (KBr): 1707 cm^{-1}; ^{1}H NMR (400 MHz) δ: 1.07(s, 3H, C-6-CH_3), 1.07(d, 3H, J = 6.8 Hz, C-2-CH_3), 1.12(d, 1H, J_{gem} = 11.7 Hz, H-7α), 1.52(s, 3H, C-8-CH_3), 1.76(m, 1H, $J_{3\beta,4\beta}$ = 3.0 Hz, $J_{3\beta,2\alpha}$ = 11.7 Hz, $J_{3\beta,4\alpha}$ = 13.1 Hz, J_{gem} = 13.1 Hz, H-3β), 1.82–1.89(m, 1H, H-3α), 2.38(ddq, 1H, $J_{2\alpha,3\alpha}$ = 4.2 Hz, J = 6.8 Hz, $J_{2\alpha,3\beta}$ = 11.7 Hz, H-2α), 2.40(dt, 1H, $J_{4\beta,3\alpha}$ = 4.1 Hz, $J_{4\beta,3\beta}$ = 4.1 Hz, J_{gem} = 14.6 Hz, H-4β), 2.54(d, 1H, J_{gem} = 11.7 Hz, H-7β), 2.65(dt, 1H, $J_{4\alpha,3\alpha}$ = 6.0 Hz, $J_{4\alpha,3\beta}$ = 14.3 Hz, J_{gem} = 14.3 Hz, H-4α), 6.13 and 6.26(ABq, 2H, J = 5.6 Hz, H-9 and H-10); ^{13}C NMR (50 MHz) δ: 16.59(q), 18.95(q), 22.40(q), 29.19(t), 38.31(t), 30.39(d), 44.03(t), 57.17(s), 85.55(s), 95.29(s), 135.37(d), 141.30(d), 213.72(s); mass spectrum, *m/e*: 206(5, $M^{+\cdot}$), 122(100, M−C_5H_8O, retro IMDAF–McLafferty rearrangement); HRMS (EI) calcd. for $C_{13}H_{18}O_2$: 206.1307; found: 206.1306.

*(6αH)-2β,7α,8α-Trimethyl-11-oxatricyclo[6.2.1.0^{1,6}]undec-9-en-5-one (**21e**) and (6αH)-2α,7α,8α-trimethyl-11-oxatricyclo[6.2.1.0^{1,6}]undec-9-en-5-one (**21a**)*

Enone **15** (95.4 mg) was stirred with Florisil® (0.95 g) according to general procedure 1 for 13 days at room temperature under argon to provide a mixture of **15**:**21**e:**21**a in a ratio of 73:19:8 in quantitative yield.

Enone **15** (145.2 mg, 0.704 mmol) was treated with excess $MeAlCl_2$ (774 μL, 0.774 mmol) according to general procedure 2 at −78°C for 5 min to provide a mixture of **15**:**21**e:**21**a in a ratio of 79:16:5 with quantitative recovery.

Enone **15** (350.1 mg, 1.70 mmol) was treated with catalytic $MeAlCl_2$ (170 μL, 0.17 mmol) at −65°C for 2 h to provide a mixture of **15**:**21**e:**21**a in a ratio of 17:75:4 with 98% recovery. Flash chromatography (9:1) provided the compounds **15** (4.0 mg), and **21**e (250 mg) and **21**a (2.0 mg).

*Major isomer **21e**:* mp 55–56°C; IR (neat): 1709 cm^{-1}; ^{1}H NMR (400 MHz) δ: 0.94(d, 3H, J = 7.0 Hz, C-7-CH_3), 1.10(d, 3H, J = 6.9 Hz, C-2-CH_3), 1.52(s, 3H, C-8-CH_3), 1.73(dq, 1H, $J_{3\beta,4\beta}$ = 3.9 Hz, $J_{3\beta,2\alpha}$ = 13.6 Hz, $J_{3\beta,4\alpha}$ = 13.6 Hz, J_{gem} = 13.6 Hz, H-3β), 1.83(d, 1H, $J_{6\alpha,7\beta}$ = 4.2 Hz, H-6α), 1.89(m, 1H, $J_{3\alpha,4\beta}$ = 3.3 Hz, $J_{3\alpha,2\alpha}$ = 5.0 Hz, $J_{3\alpha,4\alpha}$ = 5.0 Hz, J_{gem} = 13.6 Hz, H-3α), 2.33(m, 1H, $J_{2\alpha,3\alpha}$ = 4.2 Hz, J = 6.9 Hz, $J_{2\alpha,3\beta}$ = 13.6 Hz, H-2α), 2.41(dq, 1H, $J_{7\beta,6\alpha}$ = 4.2 Hz, J = 7.0 Hz, H-7β), 2.30–2.42(m, 1H, H-4α), 2.49(dt, 1H, $J_{4\beta,3\alpha}$ = 3.6 Hz, $J_{4\beta,3\beta}$ = 3.6 Hz, J_{gem} = 14.4 Hz, H-4β), 6.17 and 6.23 (ABq, 2H, J = 5.6 Hz, H-9 and H-10); ^{13}C NMR(50 MHz) δ: 16.21(q), 17.07(q), 17.15(q), 29.42(t), 33.66(d), 41.60(t), 43.47(d), 61.36(d), 88.41(s), 93.07(s), 138.38(d), 138.66(d), 210.28(s); mass spectrum, *m/e*: 206(14, $M^{+\cdot}$), 122(100, M−C_5H_7O, retro IMDAF–McLafferty rearrangement); HRMS (EI) calcd. for $C_{13}H_{18}O_2$: 206.1307; found: 206.1315.

*Minor isomer **21a**:* IR (neat): 1708 cm^{-1}; ^{1}H NMR (400 MHz) δ: 0.96(d, 3H, J = 7.0 Hz, C-7-CH_3), 1.31(d, 3H, J = 7.3 Hz, C-2-CH_3), 1.52(s, 3H, C-8-CH_3), 1.70–1.80(m, 1H), 1.92(d, 1H, $J_{6\alpha,7\beta}$ = 4.2 Hz, H-6α), 2.00–2.20(overlapping m, 2H), 2.30(m, 1H, $J_{2\alpha,3\alpha}$ = 4.8 Hz, $J_{2\alpha,3\beta}$ = 4.8 Hz, J = 7.3 Hz, H-2β), 2.30–2.44(overlapping m, 2H), 2.40(dq, 1H, $J_{7\beta,6\alpha}$ = 4.2 Hz, J = 7.2 Hz, H-7β), 2.45–2.56(m, 1H), 6.22(d, 1H, $J_{10,9}$ = 5.7 Hz, H-10), 6.45(d, 1H, $J_{9,10}$ = 5.7 Hz, H-9); ^{13}C NMR(50 MHz) δ: 16.26(q), 17.08(q), 17.16(q), 29.70(t), 36.62(t), 30.67(d), 43.69(d), 65.82(d), 88.22(s), 93.19(s), 136.24(d), 139.09(d), 210.85(s); mass spectrum, *m/e*: 206 (23, $M^{+\cdot}$); HRMS (EI) calcd. for $C_{13}H_{18}O_2$: 206.1307; found: 206.1301.

*(6αH)-3α,8α-Dimethyl-11-oxatricyclo[6.2.1.0^{1,6}]undec-9-en-5-one (**22e**)*

Enone **16** (372.8 mg) was stirred with Florisil (3.79 g) according to general procedure 1 for 6 days at room temperature under argon to provide a mixture of **16**:**22**e in a ratio of 0:100 in 75% yield after purification by flash chromatography (3:1). The product was obtained as a white crystalline solid (280.0 mg), mp 62–64.5°C; IR (KBr): 1700 cm^{-1}; ^{1}H NMR (300 MHz) δ: 1.05(d, 3H, J = 6.1 Hz, C-3-CH_3), 1.56(s, 3H, C-8-CH_3), 1.59(dd, 1H, $J_{7\alpha,6\alpha}$ = 8.2 Hz, J_{gem} = 11.8 Hz, H-7α), 1.92(dd, 1H, $J_{2\alpha,3\beta}$ = 12.0 Hz, J_{gem} = 14.5 Hz, H-2α), 2.12–2.20(m, 2H, H-3β and H-4α), 2.18(dd, 1H, $J_{7\beta,6\alpha}$ = 3.4 Hz, J_{gem} = 11.8 Hz, H-7β), 2.30(dd, 1H, $J_{6\alpha,7\beta}$ = 3.4 Hz, $J_{6\alpha,7\alpha}$ = 8.2 Hz, H-6α) 2.38(dt, 1H, $J_{2\beta,3\beta}$ = 3.2 Hz, $J_{2\beta,4\beta}$ = 3.2 Hz, J_{gem} = 14.5 Hz, H-2β), 2.45(ddd, 1H, $J_{4\beta,2\beta}$ = 2.2 Hz, $J_{4\beta,3\beta}$ = 3.2 Hz, J_{gem} = 10.2 Hz, H-4β), 6.15 and 6.21(ABq, 2H, J = 7.9 Hz, H-9 and H-10); ^{13}C NMR (75 MHz) δ: 18.67(q), 21.94(q), 29.08(d), 35.42(t), 37.15(t), 50.02(t), 52.87(d), 85.99(s), 90.36(s), 137.61(d), 141.15(d), 209.19(s); mass spectrum, *m/e*: 192(4, $M^{+\cdot}$), 122(100 M−C_4H_6O, retro IMDAF–McLafferty rearrangement); HRMS (EI) calcd. for $C_{12}H_{16}O_2$: 192.1151; found: 192.1148.

*3α,6α,8α-Trimethyl-11-oxatricyclo[6.2.1.0^{1,6}]undec-9-en-5-one (**23e**)*

Enone **17** (75.7 mg) was stirred with Florisil (760 mg) according to general procedure 1 for 19 days at room temperature under argon to provide a mixture of **17**:**23**e in a ratio of 50:50 in quantitative recovery.

Enone **17** (79.5 mg, 0.385 mmol) was treated with excess $MeAlCl_2$ (424 μL, 0.424 mmol) according to general procedure 2 at −78°C for 5 min to provide a mixture of **17**:**23**e in a ratio of 11:89 with quantitative recovery. Flash chromatography (9:1) provided the compounds **17** (4.5 mg), and **23**e (84.7 mg) as a white crystalline solid, mp 45–49°C; IR (KBr): 1705 cm^{-1}; ^{1}H NMR (400 MHz) δ: 1.04(d, 3H, J = 6.2 Hz, C-3-CH_3), 1.08(s, 3H, C-6-CH_3), 1.14(d, 1H, J_{gem} = 11.8 Hz, H-7α), 1.51(s, 3H, C-8-CH_3), 1.89(dd, 1H, $J_{2\alpha,3\beta}$ = 12.0 Hz, J_{gem} = 14.1 Hz, H-2α), 2.18(m, 1H, $J_{3\beta,2\beta}$ = 4.2 Hz, $J_{3\beta,4\beta}$ = 4.2 Hz, J = 6.2 Hz, $J_{3\beta,2\alpha}$ = 12.0 Hz, $J_{3\beta,4\alpha}$ = 12.0 Hz, H-3β), 2.23(dt, 1H, $J_{2\beta,4\beta}$ = 2.1 Hz, $J_{2\beta,3\beta}$ = 4.2 Hz, J_{gem} = 14.1 Hz, H-2β), 2.32(t, 1H, $J_{4\alpha,3\beta}$ = 12.3 Hz, J_{gem} = 12.3 Hz, H-4α), 2.38(ddd, 1H, $J_{4\beta,2\beta}$ = 2.1 Hz, $J_{4\beta,3\beta}$ = 4.2 Hz, J_{gem} = 13.6 Hz, H-4β), 2.57(d, 1H, J_{gem} = 11.7 Hz, H-7β), 6.14 and 6.29(ABq, 2H, J = 5.6 Hz, H-9 and H-10); ^{13}C NMR (50 MHz) δ: 18.78(q), 21.87(q), 22.12(q), 28.02(d), 34.43(t), 43.40(t), 46.52(t), 85.68(s), 91.79(s), 135.74(d), 141.53(d), 212.89(s); mass spectrum, *m/e*: 206(3, $M^{+\cdot}$), 122(100, M−C_5H_8O, retro IMDAF–McLafferty rearrangement); HRMS (EI) calcd. for $C_{13}H_{18}O_2$: 206.1307; found: 206.1316.

*(6αH)-3α,7α,8α-Trimethyl-11-oxatricyclo[6.2.1.0^{1,6}]undec-9-en-5-one (**24e**)*

Enone **18** (233.8 mg) was stirred with Florisil (2.4 g) according to general procedure 1 for 8 days at room temperature under argon to provide a mixture of **18**:**24**e in a ratio of 80:20 in 68% yield.

Enone **18** (103.6 mg, 0.500 mmol) was treated with excess $MeAlCl_2$ (552 μL, 0.552 mmol) according to general procedure 2

Can. J. Chem. Downloaded from www.nrcresearchpress.com by 213.200.69.106 on 09/08/12
For personal use only.

at −65°C for 5 min to provide a **18**:**24**e ratio of 42:58 with 96% recovery. Flash chromatography (9:1) provided the compounds **18** (32.8 mg), and **24**e (37.8 mg) as oils.

Enone **17** (60.5 mg, 0.293 mmol) was treated with catalytic $MeAlCl_2$ (30 μL, 0.03 mmol) at −65°C for 9 min to provide, after flash chromatography (9:1), **17** (41.6 mg), **24**e (12.5 mg), and **24**a (2.5 mg) with 93% recovery. Compound **24**a was always contaminated with compound **24**e and therefore could not be characterized. Compound **24**e: IR (neat): 1710 cm^{-1}; ^1H NMR (400 MHz) δ: 0.94(d, 3H, J = 7.1 Hz, C-7-CH_3), 1.05(d, 3H, J = 6.2 Hz, C-3-CH_3), 1.50(s, 3H, C-8-CH_3), 1.82(d, 1H, $J_{6\alpha,7\beta}$ = 4.1 Hz, H-6α), 1.85(dd, 1H, $J_{2\alpha,3\beta}$ = 11.9 Hz, J_{gem} = 14.6 Hz, H-2α), 2.07(dd, 1H,$J_{4\alpha,3\beta}$ = 13.0 Hz, J_{gem} = 13.0 Hz, H-4α), 1.90–2.16(m, 1H, H-3β), 2.33(dt, 1H, $J_{2\beta,3\beta}$ = 3.1 Hz, $J_{2\beta,4\beta}$ = 3.1 Hz, J_{gem} = 14.6 Hz, H-2β), 2.45(dt, 1H, $J_{4\beta,2\beta}$ = 3.1 Hz, $J_{4\beta,3\beta}$ = 3.1 Hz, J_{gem} = 13.0 Hz, H-4β), 2.46(dq, 1H, $J_{7\beta,6\alpha}$ = 4.1 Hz, J = 7.1 Hz, H-7β), 6.20 and 6.23(ABq, 2H, J = 5.6 Hz, H-9 and H-10); ^{13}C NMR (50 MHz) δ: 16.96(q), 17.02(q), 21.91(q), 28.77(d), 37.30(t), 43.17(d), 49.94(t), 60.65(d), 88.69(s), 89.87(s), 138.72(d), 138.84(d), 209.48(s); mass spectrum, *m/e*: 206(2, $M^{\cdot+}$), 122(100, $M-C_5H_8O$, retro IMDAF–McLafferty rearrangement); HRMS (EI) calcd. for $C_{13}H_{18}O_2$: 206.1307; found: 206.1307.

(6αH)-2β,8α-Dimethyl-11-oxatricyclo[6.2.1.0^{1,6}]undecan-5-one (25)

Ketone **19**e (0.13 g, 0.65 mmol) was dissolved in EtOAc (10 mL) and a small spatula tip of 10% palladium on carbon was added. The flask was evacuated, then filled with hydrogen gas three times via a hydrogen-filled balloon attached to a three-way stopcock. The reaction was stirred at room temperature for 1 h, filtered through Celite®, and the solvent removed *in vacuo* to produce the hydrogenated ketone **25** (0.12 g, 0.62 mmol) as a colourless oil in 95% yield, bp 58–62°C/0.025 Torr (1 Torr = 133.3 Pa), IR (neat): 1713, 1088 cm^{-1}; ^1H NMR (300 MHz) δ: 1.10(d, 3H, J = 6.9 Hz, C-2-CH_3), 1.42(s, 3H, C-8-CH_3), 1.45–2.00(overlapping m, 7H), 2.11(ddq, 1H, $J_{2\alpha,3\alpha}$ = 4.4 Hz, J = 6.9 Hz, $J_{2\alpha,3\beta}$ = 12.4 Hz, H-2α irradiation of methyl doublet at δ 1.10 resulted in collapse of signal to dd), 2.00–2.20(m, 1H), 2.30–2.50(overlapping m, 3H); ^{13}C NMR (75 MHz) δ: 15.21(q), 20.94(q), 30.93(t), 33.94(t), 37.24(t), 37.62(t), 41.42(t), 33.94(d), 57.04(d), 83.26(s) 89.87(s), 210.61(s); mass spectrum, *m/e*: 194(73, $M^{\cdot+}$); Anal. calcd. for $C_{12}H_{18}O_2$: C 74.19, H 9.34; found: C 74.29, H 9.51.

(E)- and (Z)-(6αH)-2β,8α-Dimethyl-5-(methoxymethylene)-11-oxatricyclo[6.2.1.0^{1,6}]undecane (30)

(Methoxymethyl)triphenylphosphonium chloride (0.82 g, 2.38 mmol) was suspended in dry THF (30 mL) and cooled to −78°C. To this was added LDA (1.59 mL, 2.38 mmol), and the reaction was stirred for 10 min at −78°C, then warmed to 0°C for 30 min and subsequently to room temperature for 30 min before being cooled to 0°C once more. Ketone **25** (0.11 g, 0.54 mmol) was dissolved in THF (6 mL), added dropwise to the anion, and stirred overnight. The reaction was quenched with wet Et_2O (10 mL), and the solvent was removed *in vacuo* to yield a crude brown oil. The product was purified by a filter column (5:1), then flash chromatography (9:1), then distillation to yield compound **30** as a clear, colourless oil (98.4 mg, 0.44 mmol) in 82% yield as a mixture of isomers, bp 56–60°C/0.06 Torr; IR (neat): 1676, 1102 cm^{-1}; ^1H NMR (300 MHz) δ: 1.02 and 1.03(d, 3H each, J = 6.9 Hz, C-2-CH_3), 1.41 and 1.44(s, 3H each, C-8-CH_3), 1.20–2.80(overlapping multiplets, 24H), 3.47 and 3.51(s, 3H each, vinyl methoxy CH_3), 5.65 and 5.58(m, 1H each, vinyl-H); ^{13}C NMR (75 MHz) δ: 16.06(q), 16.22(q), 21.35(q), 21.46(q), 24.20(t), 25.85(t), 30.21(t), 30.29(t), 30.87(t), 32.12(t), 36.21(t), 37.01(t), 42.06(t), 43.81(t), 34.23(d), 34.40(d), 46.08(d), 46.33(d), 59.28(q), 59.40(q), 82.56(s), 82.89(s), 88.00(s), 88.20(s), 125.49(s), 119.57(s), 140.37(d), 141.37(d); mass spectrum, *m/e*: 222(1, $M^{\cdot+}$); HRMS calcd. for $C_{14}H_{22}O_2$: 222.1621; found: 222.1624.

(6αH)-2β,8α-Dimethyl-11-oxatricyclo[6.2.1.0^{1,6}]undecane-5-carboxaldehyde (31)

The mixture of methyl enol ethers **30** (98.4 mg, 0.44 mmol) was dissolved in THF (4 mL) and 10% HCl (3 mL) and stirred at room temperature for 1 h. The solution was neutralized to pH 7 (monitored with universal pH paper) with saturated Na_2CO_3, then the aqueous layer was extracted with Et_2O (3 × 10 mL). The organic layer was dried (over Na_2SO_4), filtered, and the solvent was removed *in vacuo* to yield a crude yellow oil. Distillation yielded compound **31** (57.8 mg, 0.28 mmol) as a clear, colourless oil (62%), bp 60°C/0.03 Torr; IR (neat): 2706, 1722, 1094 cm^{-1}; ^1H NMR (300 MHz) δ: 1.05(d, 3H, J = 6.6 Hz, C-2-CH_3), 1.17(dt, 1H, J = 3.0 Hz, J = 3.0 Hz, J = 12.4 Hz), 1.30–1.50(overlapping m, 4H), 1.43(s, 3H, C-8-CH_3), 1.52–1.78(overlapping m, 3H), 1.80–2.05(overlapping m, 3H), 2.18(dddd, 1H, $J_{5\beta,11}$ = 1.6 Hz, $J_{5\beta,4\beta}$ = 3.4 Hz, $J_{5\beta,6\alpha}$ = 10.5 Hz, $J_{5\beta,4\alpha}$ = 12.4 Hz, H-5β, assignment confirmed since irradiation of H-11 at δ 9.57 caused collapse to ddd with 1.6 Hz coupling removed), 9.57(d, 1H, J = 1.6 Hz, H-11); ^{13}C NMR (75 MHz) δ: 15.76(q), 21.32(q), 25.26(t), 30.58(t), 33.91(t), 37.67(t), 44.19(t), 34.06(d), 44.07(d), 56.62(d), 83.93(s), 85.90(s), 204.31(d); mass spectrum, *m/e*: 208(9, $M^{\cdot+}$), 179(100, M−CHO); Anal. calcd. for $C_{13}H_{20}O_2$: C 74.96, H 9.68; found: C 74.81, H 9.73.

(6αH)-5α-(1-Hydroxyethyl)-2β,8α-dimethyl-11-oxatricyclo[6.2.1.0^{1,6}]undecane (32)

Freshly distilled aldehyde **31** (49.2 mg, 0.24 mmol) was dissolved in THF (5 mL) and the solution was cooled to −78°C. Methyllithium (1.00 mL, 1.40 mmol) was added; the reaction was stirred for 1.5 h at −78°C, then was allowed to warm to room temperature and was quenched with saturated NH_4Cl (5 mL). The aqueous layer was extracted with EtOAc (3 × 10 mL), the organic layer was dried over Na_2SO_4, filtered, and the solvent was removed *in vacuo*. The resulting crude oil was purified by flash chromatography (5:1) to produce compound **32** (51.6 mg, 0.23 mmol) as a mixture of two isomers in 97% yield, bp 80°C/0.024 Torr (data listed for 1 isomer only); IR (neat): 3422, 1092 cm^{-1}; ^1H NMR (300 MHz) δ: 1.02(d, 3H, J = 6.6 Hz, C-2-CH_3), 1.15(d, 3H, J = 6.5 Hz), 1.41(s, 3H, C-8-CH_3), 3.68(dq, 1H, J = 1.2 Hz, J = 6.5 Hz), 1.10–1.40(overlapping m, 6H), 1.41–1.75(overlapping m, 6H), 1.80–1.92(overlapping m, 2H); ^{13}C NMR (75 MHz) δ: 16.03(q), 21.69(q), 21.88(q), 23.31(t), 31.32(t), 34.50(t), 37.64(t), 44.66(t), 34.61(d), 46.71(d), 49.42(d), 67.66(d), 83.55(s), 87.05(s); mass spectrum, *m/e*: 224 ($M^{\cdot+}$); HRMS (EI) calcd. for $C_{14}H_{24}O_2$: 224.1777; found: 224.1780.

(6αH)-2β,8α-Dimethyl-5α-(1-oxoethyl)-11-oxatricyclo[6.2.1.0^{1,6}]undecane (33)

Oxalyl chloride (11 mmol) was dissolved in dry CH_2Cl_2 (25 mL) and cooled to −60°C (Dry Ice/chloroform) in an argon-purged 3-neck round-bottom flask equipped with a dropping funnel. Freshly distilled alcohol **32** (21.6 mg, 10 mmol) was dissolved in dry CH_2Cl_2 (10 mL) and placed in the dropping funnel. DMSO (22 mmol) was added neat (by syringe) to the oxalyl chloride solution, the reaction was stirred for 2 min, and then the alcohol solution was added within 5 min. The mixture was stirred an additional 15 min; then Et_3N (50 mmol) was added and stirring was continued for another 5 min before warming the reaction to room temperature. Water (50 mL) was added, and the aqueous layer was extracted with CH_2Cl_2 (5 × 25 mL). The combined organic layers were washed with 5% HCl (15 mL), 5% Na_2CO_3 (15 mL), and water (15 mL), dried over Na_2SO_4, filtered, and the solvent removed *in vacuo* to provide the crude product. This was purified by flash chromatography, then distilled to provide compound **33** (19.2 mg, 0.086 mmol) as a clear, colourless oil in 90% yield after purification by flash chromatography (5:1), bp 58–60°C/0.03 Torr; mp 63.5–64.5°C; IR (neat): 1702, 1087 cm^{-1}; ^1H NMR (300 MHz) δ: 0.97(dt, 1H, $J_{7\beta,6\alpha}$ = 2.9 Hz, $J_{7\beta,9\beta}$ = 2.9 Hz, J_{gem} = 11.8 Hz, H-7β), 1.04(d, 3H, J = 6.6 Hz, C-2-CH_3), 1.21(dq, 3H, J = 2.6 Hz, J = 12.8 Hz, J = 12.8 Hz), 1.30–

Can. J. Chem. Downloaded from www.nrcresearchpress.com by 213.200.69.106 on 09/08/12
For personal use only.

1.49(overlapping m, 3H), 1.41(s, 3H, C-8-CH_3), 1.50–1.72(overlapping m, 3H), 1.80–1.95(overlapping m, 3H), 2.00(ddd, 1H, $J_{6\alpha,7\beta}$ = 2.9 Hz, $J_{6\alpha,7\alpha}$ = 8.1 Hz, $J_{6\alpha,5\beta}$ = 10.6 Hz, H-6α), 2.10(s, 3H, $COCH_3$), 2.31(ddd, 1H, $J_{5\beta,4\beta}$ = 3.1 Hz, $J_{5\beta,6\alpha}$ = 10.2 Hz, $J_{5\beta,4\alpha}$ = 13.1 Hz, H-5β); ^{13}C NMR (75 MHz) δ: 15.76(q), 21.42(q), 29.31(q), 28.61(t), 31.39(t), 34.00(t), 37.70(t), 44.74(t), 34.00(d), 45.57(d), 57.75(d), 83.73(s), 86.09(s), 211.83(s); mass spectrum, *m/e*: 222(28, $M^{\cdot+}$), 179(38, M−MeCO); HRMS (EI) calcd. for $C_{14}H_{22}O_2$: 222.1621; found: 222.1625.

(6αH)-2β,8α-Dimethyl-5α-(1-methylethenyl)-11-oxatricyclo[6.2.1.0^{1,6}]undecane (34)

Methyltriphenylphosphonium bromide (Aldrich Chemical Co.) was purified by washing with hot toluene, then dried under high vacuum for 8 h. The purified phosphonium salt (0.88 g, 2.45 mmol) was suspended in dry THF (10 mL), and cooled to 0°C. Butyllithium (0.98 mL, 2.48 mmol) was added dropwise by syringe, and the reaction was warmed to room temperature and stirred for 20 min. A solution of ketone **33** (27.6 mg, 0.124 mmol) in THF (3 mL) was added to the orange anion solution, and the reaction was refluxed overnight. The reaction was cooled, quenched with wet Et_2O (10 mL), and the solvent was removed *in vacuo*. The crude compound was purified by flash chromatography (5:1) to yield starting material (9.0 mg) and product **34** (30.9 mg) as a mixture with an aromatic-containing impurity. The mixture was further purified by flash chromatography (20:1) to yield compound **34** (20.8 mg, 71%), bp 50–60°C/0.04 Torr; IR (KBr): 1088 cm^{-1}; ^{1}H NMR (300 MHz) δ: 0.90–1.4(overlapping m, 6H), 1.04(d, 3H, J = 6.6 Hz, C-2-CH_3), 1.42(s, 3H, C-8-CH_3), 1.48–1.82 (overlapping m, 5H), 1.85–1.96(m, 1H), 1.62(m, 3H, J = 1.0 Hz, vinyl-CH_3), 4.63 and 4.67(m, 2H, J_{gem} = 1.4 Hz, J = 2.5 Hz); mass spectrum, *m/e*: 220(15, $M^{\cdot+}$); HRMS (EI) calcd. for $C_{15}H_{24}O$: 220.1828; found: 220.1827.

(6αH)-2β,8α-Dimethyl-5α-(1-methylethyl)-11-oxatricyclo[6.2.1.0^{1,6}]undecane (epoxycadinane) (1)

Compound **34** (8.8 mg, 0.04 mmol) was dissolved in absolute ethanol (5 mL). Platinum(IV) oxide (28.5 mg, 0.126 mmol) was added, then the flask was evacuated and filled with hydrogen gas three times by way of a hydrogen-filled balloon attached to a three-way stopcock. The reaction was stirred at room temperature for 1 h; then the catalyst was removed by filtration and the solvent was removed *in vacuo* to yield compound **1** (6.0 mg, 0.027 mmol) as a colourless oil in 93% yield, bp 42–50°C/0.06 Torr; IR (neat): 2964–2869, 1376, 1367, 1094 cm^{-1}; ^{1}H NMR (300 MHz), see Table 4; ^{13}C NMR (75 MHz), see Table 4; mass spectrum, *m/e*: 222(3, $M^{\cdot+}$), 179(100, M−$CHMe_2$); HRMS (EI) calcd. for $C_{15}H_{26}O$: 222.1984; found: 222.1986.

Acknowledgments

We thank the Natural Sciences and Engineering Research Council of Canada (NSERC) and the University of Calgary Research Board for financial support. In addition we thank NSERC for a postgraduate scholarship (to C.R.).

1. K. A. Parker and M. R. Adamchuk. Tetrahedron Lett. **19**, 1689 (1978).
2. D. Craig. Chem. Soc. Rev. **16**, 187 (1987); K. Hayakawa and K. Kanematsu. J. Synth. Org. Chem. Jpn. **44**, 109 (1986); D. F. Taber. Intramolecular Diels–Alder reactions and Alder ene reactions. Springer-Verlag, New York. 1984; E. Ciganek. Org. React. **32**, 1 (1984); A. G. Fallis. Can. J. Chem. **62**, 183 (1984); R. Sustman and J. Sauer. Angew. Chem. Int. Ed. Engl. **19**, 779 (1980); G. Brieger and J. N. Bennett. Chem. Rev. **80**, 63 (1980).
3. (*a*) W. Blokzul, M. R. Blandamer, and J. B. F. N. Engberts. J. Am. Chem. Soc. **113**, 4241 (1991); (*b*) M. E. Jung and J. Gervay. J. Am. Chem. Soc. **113**, 224 (1991); (*c*) M. E. Jung. Synlett, 186 (1990); (*d*) K. H. Dotz, R. Noack, K. Harms, and G. Muller. Tetrahedron, **46**, 1235 (1990); (*e*) H. Finch, L. M. Harwood, G. M. Robertson, and R. C. Sewell. Tetrahedron Lett. **30**, 2585 (1989); (*f*) Y. Yamaguchi, H. Yamada, K. Hayakawa, and K. Kanematsu. J. Org. Chem. **52**, 2040 (1987); (*g*) W. M. Best and D. Wege. Aust. J. Chem. **39**, 635 (1986); **39**, 647 (1986); (*h*) J. Moursounidis and D. Wege. Tetrahedron Lett. **27**, 3045 (1986).
4. (*a*) B. L. Feringa, O. J. Gelling, and L. Meesters. Tetrahedron Lett. **31**, 7201 (1990); (*b*) K. Fischer and S. Hunig. J. Org. Chem. **52**, 564 (1987); (*c*) A. P. Kozikowski and W. Tuckmantel. J. Org. Chem. **56**, 2826 (1991); (*d*) A. Padwa, Y. S. Kulkarni, and L. W. Terry. J. Org. Chem. **55**, 2478 (1990); (*e*) T. Ghosh and H. Hart. J. Org. Chem. **54**, 5073 (1989); (*f*) S. Cauwberghs, P. J. De Clercq, B. Tinant, and J. P. Declercq. Tetrahedron Lett. **29**, 2493 (1988); (*g*) D. D. Sternbach, D. M. Rossana, and K. D. Onan. Tetrahedron Lett. **26**, 591 (1985); (*h*) B. M. Trost, M. Lautens, M.-H. Hung, and C. S. Carmichael. J. Am. Chem. Soc. **106**, 7641 (1984); (*i*) D. D. Sternbach, D. M. Rossana, and K. D. Onan. J. Org. Chem. **49**, 3427 (1984).
5. (*a*) L. M. Harwood, S. A. Leeming, N. S. Isaacs, G. Jones, J. Pickard, R. M. Thomas, and D. A. Watkin. Tetrahedron Lett. **29**, 5017 (1988); (*b*) L. M. Harwood, G. Jones, J. Pickard, R. M. Thomas, and D. Watkin. Tetrahedron Lett. **29**, 5825 (1988); (*c*) P. Missiaen and P. J. De Clercq. Bull. Soc. Chem. Belg. **96**, 105 (1987); (*d*) L. A. Van Royen, R. Mijngheer, and P. J. De Clercq. Tetrahedron, **41**, 4667 (1985); (*e*) L. A. Van Royen, R. Mijngheer, and P. J. De Clercq. Bull. Soc. Chem. Belg. **93**, 1019 (1984).
6. S. J. Burrell, A. E. Derome, M. S. Edenborough, L. M. Harwood, S. A. Leeming, and N. S. Isaacs. Tetrahedron Lett. **26**, 2229 (1985), and refs. 4*a*, 4*b*, and 3*a* above.
7. (*a*) F. Nuyttens, G. Appendino, and P. J. De Clercq, Synlett, 526 (1991); (*b*) L. M. Harwood, T. Ishikawa, H. Phillips, and D. Watkin. J. Chem. Soc. Chem. Commun. 527 (1991); (*c*) P. Missiaen and P. J. De Clercq. Bull. Soc. Chem. Belg. **99**, 271 (1990); (*d*) L. M. Harwood, B. Jackson, G. Jones, K. Prout, R. M. Thomas, and F. J. Witt. J. Chem. Soc. Chem. Commun. 608 (1990); (*e*) L. M. Harwood, G. Jones, J. Pickard, R. M. Thomas, and D. Watkin. J. Chem. Soc. Chem. Commun. 605 (1990); (*f*) G. Appendino, J. Hoflack, P. J. De Clercq. G. Chiari, and M. Calleri. Tetrahedron, **44**, 4605 (1988); (*g*) S. G. Cawberghs and P. J. De Clercq. Tetrahedron Lett. **29**, 6501 (1988); (*h*) W. M. Grootaert and P. J. De Clercq. Tetrahedron Lett. **27**, 1731 (1986); (*i*) W. M. Grootaert and De Clercq. Tetrahedron Lett. **23**, 3291 (1982).
8. B. A. Keay. J. Chem. Soc. Chem. Commun. 419 (1987).
9. (*a*) C. Rogers and B. A. Keay. Synlett, 353 (1991); (*b*) Tetrahedron Lett. **32**, 6477 (1991); (*c*) Can. J. Chem. **70**, 2929 (1992).
10. P. W. Dibble and B. A. Keay. Tetrahedron Lett. **30**, 1045 (1989).
11. C. Rogers and B. A. Keay. Tetrahedron Lett. **30**, 1349 (1989).
12. E. Bovenschulte, P. Metz, and G. Henkel. Angew. Chem. Int. Ed. Engl. **28**, 202 (1989).
13. Y. K. Yur'ev, N. S. Zefirov, and A. A. Shteinman. Chem. Abstr. **59**, 11395d (1963).
14. W. F. Bailey, T. T. Nurmi, J. J. Patricia, and W. Wang. J. Am. Chem. Soc. **109**, 2442 (1987).
15. A. J. Mancuso and D. Swern. Synthesis, 165 (1981).
16. A. McKillop and D. W. Young. Synthesis, 401 (1979).
17. W. G. Dauben and H. O. Krabbendroft. J. Am. Chem. Soc. **98**, 1992 (1976).
18. (*a*) E. Fattorusso, S. Magno, and L. Mayol. Gazz. Chim. Ital. **109**, 589 (1979); (*b*) M. Bordoloi, V. S. Shukla, S. C. Nath, and R. P. Sharma. Phytochemistry, **28**, 2007 (1989); (*c*) B. M. Fraga. Nat. Prod. Rep. **9**, 217 (1992).
19. T.-L. Ho. Enantioselective synthesis. Wiley Interscience, New York. 1992. pg. 226; H. Irie, R. Matsumoto, M. Nishimura, and Y. Zhang. Chem. Pharm. Bull. **38**, 1852 (1990); B. S.

Davidson, K. A. Plavcan, and J. Meinwald. J. Org. Chem. **55**, 3912 (1990); J. ApSimon. Total Synth. Nat. Prod. **5**, 157 (1983); B. M. Fraga. Nat. Prod. Rep. **9**, 557 (1992).
20. R. A. Augustine. Catalytic hydrogenation. M. Dekker, New York. 1965.
21. J. A. Hendrickson and R. Bergeron. Tetrahedron Lett. **46**, 4607 (1973).
22. E.-I. Negishi, L. D. Boardman, H. Sawada, V. Bagheri, A. T. Stoll, J. M. Tour, and C. L. Rand. J. Am. Chem. Soc. **110**, 5383 (1988).
23. B. H. Lipshutz, R. S. Wilhelm, and J. A. Kozlowski. Tetrahedron, **40**, 5005 (1984).
24. H. Gilman, W. Langham, and F. W. Moore. J. Am. Chem. Soc. **62**, 2327 (1940).
25. R. E. Ireland, D. C. Muchmore, and U. Hengartner. J. Am. Chem. Soc. **94**, 5098 (1972); S. C. Dolan and J. MacMillan. J. Chem. Soc. Chem. Commun. 1588 (1985); A. G. M. Barrett, C. R. A. Godfrey, D. M. Hollinshead, P. A. Prokopiou, D. H. R. Barton, R. B. Boar, L. Joukhadar, J. F. McGhie, and S. C. Misra. J. Chem. Soc. Perkin Trans. 1, 1501 (1981); A. G. M. Barrett, P. A. Prokopiou, D. H. R. Barton, R. B. Boar, and J. F. McGhie. J. Chem. Soc. Chem. Commun. 1173 (1979); W. Hartwig. Tetrahedron, **39**, 2609 (1983); G. Hofle, W. Steglich, and H. Vorbruggen. Angew. Chem. Int. Ed. Engl. **17**, 5691 (1978); H. Deshayes, J.-P. Pete, C. Portella, and D. Scholler. J. Chem. Soc. Chem. Commun. 439 (1975); H. Deshayes and J.-P Pete. J. Chem. Soc. Chem. Commun. 567 (1978).
26. L. A. Paquette, P. C. Bulman-Page, P. D. Pansegrau, and P. E. Wiedeman. J. Org. Chem. **53**, 1450 (1988).
27. E. Piers and G. L. Jung. Can. J. Chem. **63**, 996 (1985).
28. D. D. Perrin and W. L. F. Armarego. Purification of laboratory chemicals. 3rd ed. Pergamon Press, Toronto. 1988.

Can. J. Chem. Downloaded from www.nrcresearchpress.com by 213.200.69.106 on 09/08/12
For personal use only.

Étude de la conformation de dérivés pyrroliques

BOUALEM OUSSAID, CATHY HUBERT, LEILA MOEINI ET BERNARD GARRIGUES[1]

Unité de recherche associée au Centre national de la recherche scientifique, n° 454, Université Paul Sabatier, Laboratoire de synthèse, structure et réactivité de molécules phosphorées, 118 Route de Narbonne, 31062 Toulouse CEDEX, France

ET

JEAN-PIERRE FAYET

Unité de recherche associée 1311, Université Paul Sabatier, Laboratoire de chimie des matériaux inorganiques, 118 Route de Narbonne, 31062 Toulouse CEDEX, France

Reçu le 6 août 1992

BOUALEM OUSSAID, CATHY HUBERT, LEILA MOEINI, BERNARD GARRIGUES et JEAN-PIERRE FAYET. Can. J. Chem. **71**, 623 (1993).

La conformation de dérivés pyrroliques (**1**, **2**, **3***a*,*b*, **4***a*,*b*, **5**, **6** et **7**) a été étudiée à partir de calculs théoriques de mesures de moments dipolaires, de l'utilisation du couplage stéréospécifique à travers cinq liaisons et des expériences d'effets Overhauser (**6**).

BOUALEM OUSSAID, CATHY HUBERT, LEILA MOEINI, BERNARD GARRIGUES, and JEAN-PIERRE FAYET. Can. J. Chem. **71**, 623 (1993).

The conformations of pyrrole derivatives (**1**, **2**, **3***a*,*b*, **4***a*,*b*, **5**, **6**, and **7**) have been elucidated from theoretical investigations, dipole moment measurements, use of stereospecific coupling through five bonds, as well as Overhauser experiments (**6**).

Can. J. Chem. Downloaded from www.nrcresearchpress.com by 213.200.69.106 on 09/08/12
For personal use only.

Introduction

De nombreux travaux ont été effectués afin de déterminer en solution la conformation des dérivés pyrroliques. Ces études (1) ont été menées à partir de mesures de moments dipolaires, par infrarouge, micro-ondes, par calculs théoriques et surtout par RMN ^{1}H, grâce à la stéréospécificité (2) d'un couplage entre cinq liaisons qui impose une disposition en zigzag et la planéité de la molécule.

Le 2-formyl pyrrole a été particulièrement étudié par différentes techniques. Les premiers travaux remontent à 1954 (3) où une étude par mesure de moment dipolaire conclut à la stabilisation du conformère 2*c* (NH, O *cis*), stabilisé par liaison hydrogène. Ce résultat a éte confirmé par infrarouge (4, 5) et par des études de RMN ^{1}H : à partir des constantes de couplages, il a été établi qu'il y avait 95% de la forme 2*c* (6). À −70°C, ces mêmes auteurs ont pu mettre en évidence la présence des deux conformères (6). De nombreux calculs théoriques ont confirmé la prépondérance de la forme (2*c*) chelatée (7, 8), avec une barrière à la rotation de 39,2 kJ mol^{-1} (9). Pour une série de *N*-alkyl 2-formyl pyrroles (alkyl : méthyle, éthyle, isopropyle, tertiobutyle), la valeur de la constante de couplage $^5J_{CHO-H(5)}$ de l'ordre de 1,2 Hz permet de conclure à la prépondérance de la forme 2*c* (NR, O *cis*) (10).

L'étude de la conformation du 3-formylpyrrole fait apparaître une absence de convergence. Les travaux effectués à partir de la RMN (6, 11) et des mesures de moments dipolaires (7, 12) sont en bon accord : la forme 3*t* (NH, O *trans*) est prépondérante 95–100%. À partir de calculs théoriques, certains auteurs ont montré que la structure 3*c* (NH, O *cis*) était favorisée (8, 9).

Il n'existe qu'une seule étude concernant les imines pyrroliques (13). L'étude des quatre imines : la 2-méthyliminométhyl pyrrole (R = H, R′ = CH_3), la 2-*n*-butyliminométhyl pyrrole (R = H, R′ = *n*-C_4H_9), la 2-méthyliminométhyl *N*-méthyl pyrrole (R = CH_3, R′ = CH_3) et la 2-*n*-butyliminométhyl *N*-méthyl pyrrole (R = CH_3, R′ = *n*-C_4H_9) a été effectuée par RMN à température variable. Ces études excluent la présence d'une isomérie rotationnelle. Les valeurs des couplages stéréospécifiques à travers cinq liaisons prouvent que la conformation *s-trans* est la seule qui existe.

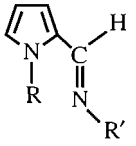

Des études théoriques de la conformation de 2-vinyl pyrroles ont abouti à des conclusions divergentes (8, 14). Enfin, le 2-pyrrole carboxylate de méthyle existe de façon préférentielle, en solution, majoritairement sous la conformation plane 2*c* (NH, O *cis*) (12).

La conformation de *N*-alkyl 2 ou 3 carboxylate ou des 2,4 ou 2,5 *N*-alkyl dicarboxylate a été étudiée par infrarouge (15); par exemple : les *N*-alkyl 2-carboxylate existent majoritairement sous un seul rotamère probablement *syn–s-trans* (15).

Nous nous proposons dans ce travail d'étudier à partir de calculs théoriques MNDO (16), de mesures de moments dipolaires et par RMN la conformation d'aldéhydes, d'imines, d'éthyléniques et d'esters pyrroliques non encore abordée dans la littérature.

Partie expérimentale

Généralités

Points de fusion, non corrigés, en capillaires (appareil Tottoli, Büchi). Spectres IR : entre lames CaF_2, enregistrés sur un spectromètre Perkin–Elmer 257. Spectres de RMN ^{1}H : déplacements chimiques en ppm par rapport au TMS; constantes de couplage en Hz : appareil Bruker AC 250.

Les spectres ^{1}H ont été enregistrés avec une résolution digitale de 0,15 Hz/point. Celle des spectres ^{13}C est de 0,46 Hz/point.

[1]Auteur à qui adresser toute correspondance.

Can. J. Chem. Downloaded from www.nrcresearchpress.com by 213.200.69.106 on 09/08/12
For personal use only.

TABLEAU 1. Grandeurs intermédiaires pour la détermination des moments dipolaires expérimentaux

	α	β	R_{MD}	$P_{2\infty}$	μ_D
1	17,53	~0	31,89	448,05	4,51
2	9,39	−0,20	42,46	350,56	3,95
3*a*	1,46	−0,10	42,67	73,83	1,23
3*b*	6,40	−0,22	48,39	234,33	3,01
4*a*	11,90	−0,30	28,73	233,18	3,16
4*b*	2,50	~0	37,58	110,48	1,88
5	4,31	~0	39,58	147,81	2,55
6	4,13	−0,50	52,71	178,30	2,48
7	11,39	~0	49,39	524,55	4,82

Les expériences 2D-NOESY ont été réalisées dans des conditions tout à fait classiques, avec un temps de mélange $t_m \sim T_1$. D'autre part, pour permettre une relaxation optimum, nous avons choisi dans tous les cas un délai entre deux accumulations légèrement supérieur à $5\times T_1$.

Les analyses élémentaires ont été effectuées par le service de microanalyse de l'École nationale supérieure de chimie de Toulouse.

Synthèse des dérivés

Les composés **1**, **2**, **3***a*, **6** et **7** ont été préparés, respectivement, à partir des références 17, 18, 19, 20 et 21.

Synthèse des dérivés **3**b, **4**a,b *et* **5**

On mélange à température ambiante soit 0,01 mol de 2-formyl *N*-phényl pyrrole (**3***b*) préparé d'après la référence 18, soit 0,01 mol de 3-formyl pyrrole (**4***a*,*b*), soit 0,01 mol de 2,5-diformyl pyrrole préparé d'après la référence 20 avec 0,05 mol d'amine, en solution dans 30 mL d'acétonitrile anhydre, sous argon. L'évolution de la réaction est suivie par RMN ^{1}H. Lorsque la réaction est terminée, le mélange réactionnel est évaporé à sec. On obtient un produit analytiquement pur sour forme d'huile pour **3***b* et **5**, solide pour **4***a* (F = 158°C), **4***b* (F = 90°C). Ces imines, peu stables, se décomposent par purification sur colonne de silice.

2-Méthyliminométhyl N*-phényl pyrrole :* **3**b. Rdt = 89%. IR (entre lames) : 1638 (C=N) cm^{-1}. RMN ^{1}H ($CDCl_3$) 7,98 (m, 1H, HC=N); 7,50–7,30 (m, 5H, arom.); 6,95 (dd, 1H, $^3J_{34}$ = 3,8, $^4J_{35}$ = 1,7, H3); 6,91 (dd, 1H, $^4J_{35}$ = 1,7, $^3J_{45}$ = 2,6, H5); 6,33 (ddd, 1H, $^3J_{34}$ = 3,8, $^3J_{45}$ = 2,6, $^5J_{H(4)-HCN}$ = 0,6, H4); 3,36 (d, 3H, ^4J = 1,5, CH_3). RMN ^{13}C {^{1}H} ($CDCl_3$) : 152,8 (s, C=N); 139,1 (s, arom.); 130,8 (s, C2 pyr.); 129,2 (s, arom.); 128.2 (s, arom.); 127,7 (s, arom.); 125,5 (s, C5 pyr.); 111,5 (s, pyr.); 110,1 (s, pyr.); 48,5 (s, CH_3). Anal. calc. pour $C_{12}H_{12}N_2$ (MM = 184,2) : C 78,22; H 6,57; N 15,27; tr. : C 77,86; H 6,48; N 15,46.

3-Méthyliminométhyl pyrrole : **4**a. Rdt = 95%. IR (entre lames) : 3119 (NH); 1641 (C=N) cm^{-1}. RMN ^{1}H ($CDCl_3$) : 8,16 (m, 1H, CH=N); 7,06 (dd, 1H, $^4J_{25}$ = 1,7, $^4J_{24}$ = 1,5, H2); 6,74 (ddd, 1H, $^5J_{H(5)-CHN}$ = 0,6, $^3J_{45}$ = 2,7, $^4J_{25}$ = 1,7, H5); 6,43 (dd, 1H, $^3J_{45}$ = 2,7, $^4J_{24}$ = 1,5, H4); 3,30 (d, 3H, ^4J = 0,7, CH_3). RMN ^{13}C {^{1}H} (DMSO) : 156,64 (s, C=N); 122,6 (s, C3 pyr.); 121,3 (s, pyr.); 119,2 (s, pyr.); 105,6 (s, pyr.); 47,3 (s, CH_3). Anal. calc. pour $C_6H_8N_2$ (MM = 108,1) : C 66,45; H 7,44; N 25,84; tr. : C 65,75; H 7,24; N 25,41.

3-Isopropyliminométhyl pyrrole : **4**b. Rdt = 91%. IR (entre lames) : 3126 (NH); 1639 (C=N) cm^{-1}. RMN ^{1}H (C_6D_6) : 9,75 (s, 1H, NH); 8,25 (s, 1H, CH=N); 7,26 (dd, 1H, $^4J_{24}$ = 1,5, $^4J_{25}$ = 2,0, H2); 6,76 (dd, 1H, $^4J_{25}$ = 2,0, $^3J_{45}$ = 2,8, H5); 6,56 (dd, 1H, $^3J_{45}$ = 2,8 $^4J_{24}$ = 1,5, H4); 3,44 (hept, 1H, ^3J = 6,3, CH); 1,24 (d, 6H, ^3J = 6,3, CH_3). RMN ^{13}C {^{1}H} (C_6D_6) : 153,9 (s, C=N); 122,9 (s, C3 pyr.); 121,2 (s, pyr.); 119.5 (s, pyr.); 107,2 (s, pyr.); 81,6 (s, CH-C); 24,4 (s, CH_3). Anal. calc. pour $C_8H_{12}N_2$ (MM = 136,2) : C 70,54; H 8,89; N 20,57; tr. : C 70,24; H 8,75; N 20,27.

2,5-Bis[(méthylimino)methyl]pyrrole : **5**. Rdt = 88%. IR (entre lames) : 1642 (C=N) cm^{-1}. RMN ^{1}H ($CDCl_3$) : 8,02 (q, 2H, ^4J = 1,5, HC=N); 6,42 (s, 2H, HC=C); 3,40 (d, 6H, ^4J = 1,5, CH_3). RMN ^{13}C {^{1}H} ($CDCl_3$) 152,5 (s, C=N); 132,7 (s, C-NH); 113,7 (s, C=C); 47,7 (s, CH_3). Anal. calc. pour $C_8H_{11}N_3$ (MM = 149,19) : C 64,40; H 7,43; N 28,16; tr. : C 63,95; H 7,66; N 28,40.

Les moments dipolaires des composés étudiés sont mesurés dans le dioxanne à 25°C (tableau 1). La formule de Debye est utilisée ainsi que la méthode d'extrapolation d'Halverstadt et Kumler (22) pour calculer la polarisation totale avec $\alpha = (d\varepsilon/d\omega_2)\omega_2 \rightarrow 0$, $\beta = (dv/d\omega_2)\omega_2 \rightarrow 0$ et $0{,}001 < \omega_2 < 0{,}05$. ε est la constante diélectrique, ω_2 la fraction massique de l'échantillon et v le volume massique. Les polarisations électroniques sont assimilées aux refractions moléculaires R_{MD}.

Les calculs théoriques ont été effectués pour l'ensemble des conformations des 11 dérivés pyrroliques. Les approximations de base dans la méthode MNDO inclue un modèle semi-empirique pour les intégrales à deux centres (16).

Pour juger de la fiabilité de cette méthode on peut comparer les valeurs calculées en MNDO aux valeurs expérimentales (23) pour les chaleurs de formation, les géométries moléculaires, les potentiels d'ionisation et les moments dipolaires; on constate le bon accord ce qui justifie l'utilisation de la méthode.

Résultats et discussion

Nous nous sommes tout d'abord intéressés à l'étude conformationnelle en solution des aldéhydes **1** et **2**.

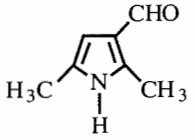

1

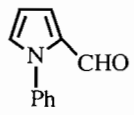

2

Le 2,5-diméthyl 3-formyl pyrrole **1** peut exister en solution soit sous la conformation 3*c* (NH, O *cis*) soit sous la conformation 3*t* (NH, O, *trans*).

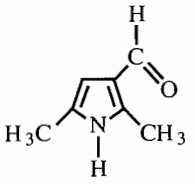

3*c*

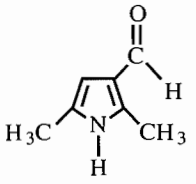

3*t*

Les calculs MNDO montrent que les énergies des formes 3*c* (−1551, 40 eV) et 3*t* (−1551, 46 eV) sont très proches.

La valeur expérimentale du moment dipolaire mesuré dans le benzène à 25°C (μ_{ex} = 4,51 D) indique la prépondérance de la forme 3*c* qui a un moment théorique de 4,65 D alors que la forme 3*t* a un moment de 3,49 D. Ceci peut s'expliquer par la formation d'une liaison hydrogène possible entre un hydrogène du groupe méthyle et l'oxygène du carbonyle. Cette structure est analogue à celle obtenue pour la forme céto-énolique, majoritaire des β dicétones.

Nous avons étudié la conformation du 2-formyl *N*-phenyl pyrrole **2**, qui peut exister soit sous la conformation 2*c* (N, O *cis*) soit 2*t* (N, O *trans*).

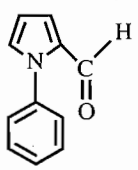

2*c*

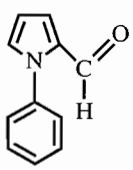

2*t*

Can. J. Chem. Downloaded from www.nrcresearchpress.com by 213.200.69.106 on 09/08/12
For personal use only.

Nous avons par calcul optimisé la position du phényle en le faisant tourner autour de la liaison phényle–azote. Dans le cas où la molécule serait plane, nous avons obtenu pour une valeur de $\phi = 0°$ (ϕ = angle entre le plan du phényle et du pyrrole) des valeurs de l'énergie pour 2*c* (−2051,03 eV) et pour 2*t* (−2056,06 eV). L'énergie a été optimisée à $\phi = 90°$ avec des valeurs très proches respectivement de −2058,02 eV pour 2*c* et −2058,08 eV pour 2*t*. Les mesures de moments dipolaires nous ont permis de préciser le pourcentage respectif de chacun des conformères. La valeur théorique, avec le phényle perpendiculaire au plan du pyrrole, des conformations 2*c* (1,26 D) et 2*t* (4,55 D), comparée à la valeur expérimentale mesurée dans le benzène à 20°C (μ = 3,95 D) permet de préciser qu'il existe un équilibre conformationnel entre ces deux structures déplacé vers la forme 2*t* (73%). La structure 2*t* est favorisée, car dans la zone des électrons π du noyau benzénique il est préférable d'avoir un hydrogène positivé que l'oxygène du carbonyle chargé négativement.

Nous avons étudié par calcul, mesure de moments dipolaires et RMN les imines pyrroliques **3***a*,*b*, **4***a*,*b* et **5**.

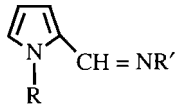

3*a* R = H, R′ = *t*Bu
3*b* R = C_6H_5, R′ = CH_3

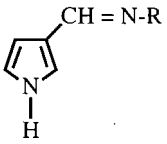

4*a* R = CH_3
4*b* R = iPr

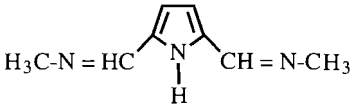

5

Les composés **3***a*,*b* peuvent se présenter sous l'une des quatre conformations possibles : 2*c trans*, 2*c cis*, 2*t trans* et 2*t cis*.

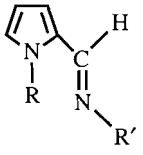

2*c trans*

2*c cis*

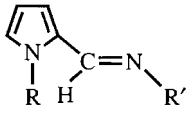

2*t trans*

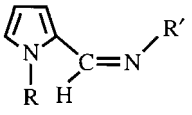

2*t cis*

L'examen des énergies dans le cas de **3***a* montre que les conformations 2*c trans* (−1756,64 eV) et 2*t trans* (−1756,58 eV) sont les plus basses en énergie (tableau 2). Pour la conformation 2*c cis*, l'encombrement stérique ne permet pas de calculer l'énergie et la valeur théorique du moment dipolaire. La valeur expérimentale du moment dipolaire (μ = 1,23 D), mesurée à 25°C dans le dioxanne, permet de préciser l'existence d'un équilibre entre ces deux conformations 2*c trans* et 2*t trans* dans un rapport 80 : 20 (tableau 2).

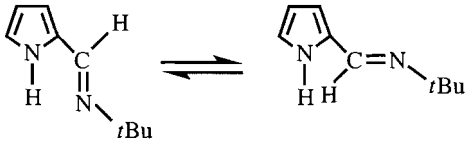

80% 20%

La molécule étant plane, il doit exister un couplage stéréospécifique entre protons séparés par cinq liaisons, dans une disposition zigzag (proton de la fonction imine et H5). Dans le spectre de RMN ^{1}H, il existe un tel couplage $^5J_{HCN-H(5)}$ = 0,75 Hz ce qui confirme bien la prépondérance de la conformation 2*c trans*, stabilisée par une liaison hydrogène intramoléculaire, comme cela avait déjà été montré pour des molécules appartenant à cette famille (14).

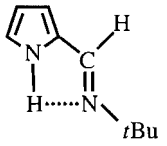

Nous avons étudié la conformation du 2-méthyliminométhyl *N*-phényl pyrrole **3***b*. Les différentes conformations ont été calculées dans le cas où la molécule est coplanaire ($\phi = 0°$) et optimisées en faisant tourner le plan du phényl. Nous avons obtenu une énergie minimale à $\phi = 90°$ correspondant aux formes 2*c trans* (−2113,22 eV) et 2*t trans* (−2113,25 eV) très proches en énergie (tableau 2).

La valeur expérimentale du moment dipolaire mesurée dans le dioxanne (3,01 D) permet de conclure à l'existence en solution d'un équilibre entre les deux conformations 2*c trans* et 2*t trans* (le phényle étant perpendiculaire au pyrrole) avec un pourcentage respectif de 39% et 61% (tableau 2).

Nous nous sommes intéressés à la conformation du 3-méthyliminométhyl pyrrole **4***a* (R=CH_3) et du 3-isopropyliminométhyl pyrrole **4***b* (R=iPr). Ces molécules peuvent exister sous l'une des quatre conformations 3*c trans*, 3*c cis*, 3*t trans* et 3*t cis*.

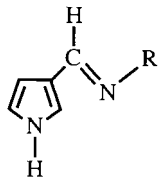

3*c trans*

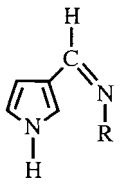

3*c cis*

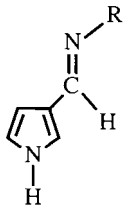

3*t trans*

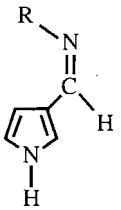

3*t cis*

Les quatre conformations ont été calculées. Comme on peut le voir dans le tableau 3, il existe pour ces deux dé-

TABLEAU 2. Valeur des énergies (eV) et des moments dipolaires (D) des conformations **3***a* et **3***b*

	R	R′	N°	2*c trans*	2*t trans*	2*t cis*	2*c cis*
E	H	*t*Bu	**3***a*	−1756,64	−1756,58	−1748,12	[a]
μ_{th}	H	*t*Bu	**3***a*	1,12	1,61	2,33	[a]
E (θ = 0)	C_6H_5	CH_3	**3***b*	−2105,34	−2111,22	−2108,22	[a]
E (θ = 90)	C_6H_5	CH_3	**3***b*	−2113,22	−2113,25	−2110,22	−2093,83
μ_{th} (θ = 90)	C_6H_5	CH_3	**3***b*	0,90	3,79	3,38	2,17

[a]Incompatibilité stérique.

TABLEAU 3. Valeur des énergies (eV) et des moments dipolaires (D) pour les quatre conformations des composés **4***a* et *b*

	R	N°	3c *trans*	3c *cis*	3t *trans*	3t *cis*	μ_{exp}
E	Me	**4***a*	−1293,42	−1289,67	−1293,37	−1289,66	
μ_{th}	Me	**4***a*	1,79	4,07	3,16	4,38	3,16
E	iPr	**4***b*	−1606,06	−1602,27	−1606,01	−1602,27	
μ_{th}	iPr	**4***b*	1,84	3,92	3,11	4,54	1,88

rivés deux conformations qui sont les plus basses en énergie et très proches : respectivement les conformations 3*c trans* (−1293,42 eV pour **4***a* et −1606,06 eV pour **4***b*) et 3*t trans* (−1293,37 eV pour **4***a* et −1606,01 eV pour **4***b*). La valeur expérimentale du moment dipolaire, mesurée dans le dioxanne à 25°C pour **4***a* (μ = 3,16 D) et dans le benzène à 25°C pour **4***b* (μ = 1,88 D) a permis de préciser que dans le cas de **4***a* la conformation 3*t trans* est prépondérante (μ_{th} = 3,16) et que dans le cas de **4***b* c'est au contraire la conformation 3*c trans* qui est majoritaire (μ_{th} 1,84) (tableau 3).

Ces conclusions ont pu être confirmées par le spectre de RMN ^{1}H. Dans le case de **4***a*, la conformation majoritaire étant 3*t trans*, on doit observer dans le spectre un couplage stéréospécifique, à cause de la disposition zigzag, entre les protons de la fonction imine et le proton H5. En effet, un tel couplage $^5J_{HCN-H(5)}$ = 0,6 Hz est observé. Dans le cas de **4***b*, la conformation priviligiée étant 3*c trans*, l'absence d'un tel couplage confirme les conclusions précédentes. Il est à noter que l'on n'observe pas de modifications des spectres de RMN lorsqu'on refroidit à −60°C.

Nous avons étudié la conformation du 2,5-bis(méthyliminométhyl) pyrrole **5**. La simplicité du spectre de RMN ^{1}H de ce composé, dans un domaine de température de −60°C à +60°C ne peut s'expliquer que par la présence d'un plan de symétrie passant par l'atome d'azote. Cela entraîne qu'il n'existe que quatre conformations planes possibles 2*c* 5*c trans*, 2*t* 5*t trans*, 2*t* 5*t cis* et 2*c* 5*c cis*; cette dernière pour des raisons d'encombrement stérique n'a pas pu être calculée.

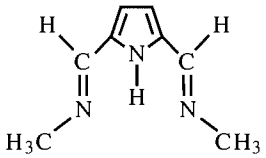

2*c* 5*c trans*

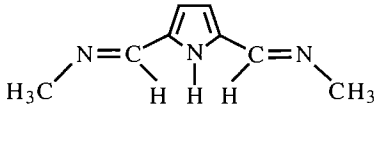

2*t* 5*t trans*

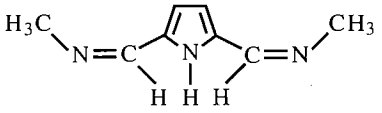

2*t* 5*t cis*

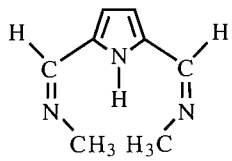

2*c* 5*c cis*

TABLEAU 4. Valeurs des énergies (eV) et du moment dipolaire (D) pour les trois conformations de **5**

	2*c* 5*c trans*	2*t* 5*t trans*	2*t* 5*t cis*
E	−1793,44	−1791,66	−1789,96
μ_{th}	2,58	2,52	0.02

Un calcul théorique MNDO, effectué pour les trois conformations, montre (tableau 4), que la conformation 2*c* 5*c trans* est la plus basse en énergie (−1793,44 eV). La mesure du moment dipolaire expérimental, effectuée dans le dioxanne à 25°C (2,55 D) est compatible avec la valeur théorique de la conformation 2*c* 5*c trans* (2,58 D).

Le spectre de RMN ^{1}H, confirme que le 2,5-bis(méthyliminométhyl) pyrrole **5** existe de façon prépondérante sous la conformation 2*c* 5*c trans*. En effet, dans cette conformation, on n'a pas de disposition zigzag entre le proton de la fonction imine et le proton du cycle pyrrolique, donc pas de couplage ^5J stéréospécifique entre protons séparés par cinq liaisons. Ceci exclut donc les conformations 2*t* 5*t trans* et 2*t* 5*t cis*.

La conformation privilégiée 2*c* 5*c trans* peut s'expliquer facilement si l'on admet une stabilisation par liaison hydrogène intramoléculaire.

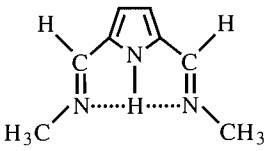

Nous avons étudié la conformation du composé **6**

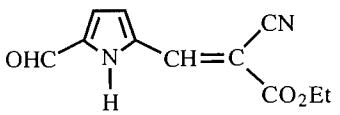

6

Dans le spectre de RMN ^{1}H on n'observe pas de couplage stéréospécifique ^5J entre le proton aldéhydique et le proton H3 du cycle ce qui est en faveur d'une conforma-

Can. J. Chem. Downloaded from www.nrcresearchpress.com by 213.200.69.106 on 09/08/12
For personal use only.

TABLEAU 5. Valeur des énergies (eV) et du moment dipolaire (D) des conformations de **6** et **7**

	N°	*a*	*b*	*c*	*d*	*e*
E	**6**	−2913,17	−2904,90	−2920,85	−2920,80	
μ_{th}	**6**	2,76	4,18	0.53	3,71	
E	**7**	−2955,52	−2935,07	−2940,10	−2893,84	−2942,39
μ_{th}	**7**	4,92	10,88	1,72	9,58	8,03

tion (O, NH, *cis*). Il existe un couplage stéréospécifique $^5J_{HC=C-H(4)}$ = 0,7 Hz compatible avec une conformation dans laquelle la fonction éthylénique est en *trans* par rapport au NH.

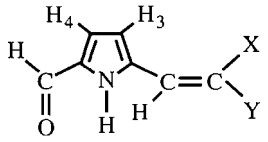

Cette géométrie a été confirmée dans le spectre de RMN ^{2}D NOESY par une très forte tache de correlation entre les protons H4 et aldéhydique et une absence de tache de correlation entre H3 et le proton éthylénique.

Nous avons effectué des calculs théoriques MNDO pour les quatre conformations ci-dessous **6***a*, **6***b*, **6***c*, **6***d* en choisissant une conformation *s-trans* pour la fonction ester comme cela a été clairement établi dans la littérature (16).

L'examen des énergies (tableau 5) montre que les conformations **6***c* et **6***d* sont les plus basses en énergies et ont

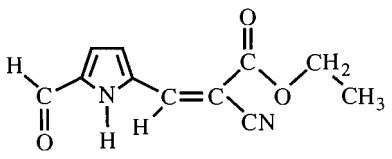

6*a*

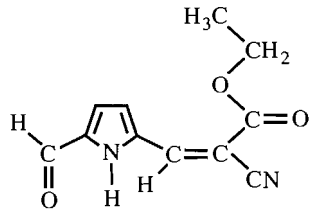

6*b*

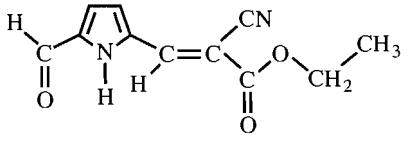

6*c*

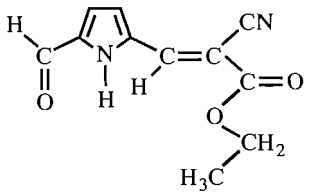

6*d*

des valeurs très proches, respectivement −2920,85 eV et −2920,80 eV. Les formes **6***a* (−2913,17 eV) et **6***b* (−2904,90 eV) peuvent être éliminées. La valeur expérimentale du moment dipolaire, mesurée dans le dioxanne à 25°C (2,48 D), est en faveur de la prépondérance de la conformation **6***d*. Cette structure est favorisée, car elle permet de former deux liaisons hydrogènes : l'une entre le NH et le carbonyle aldéhydique, l'autre entre le proton éthylénique et l'oxygène de l'éthoxy du groupe ester.

Enfin, nous avons étudié la conformation du 3,4-carbethoxy pyrrole **7**. La simplicité du spectre de RMN ^{1}H ne s'explique que par l'existence d'un plan de symétrie passant par l'atome d'azote. Nous n'avons pas observé de modification du spectre lorsque la solution est refroidie à −60°C. Si l'on compare la valeur des énergies du tableau 5, il est clair que l'énergie la plus basse correspond à la conformation **7***a* (−2955,52 eV) dans laquelle les deux carboxyles sont en *trans* de l'azote, les deux fonctions esters sont *s-trans*. En faisant tourner le CH_3 autour de la liaison O—C, l'énergie minimale correspond à une disposition *s-trans*. Le moment dipolaire expérimental mesuré dans le benzène à 25°C (4,82 D) est en parfait accord avec la valeur théorique calculée pour **7***a* (4,92 D) (tableau 5). Dans ce dernier cas il n'y a pas de liaison hydrogène possible ni d'encombrement stérique. Il est alors normal que les deux doubles liaisons conjugées soient *s-trans*.

Conclusion

Alors que la conformation du 3-formyl pyrrole a fait l'objet de controverses, les études que nous avons effectuées à partir de calculs théoriques, de mesures de moments dipolaires, de l'utilisation du couplage stéréospécifique à travers cinq liaisons et des expériences de NOESY, montrent une convergence des résultats.

Le 2,5-diméthyl 3-formyl pyrrole (**1**) existe en solution de façon prépondérante sous la conformation 3*c* (NH, O *cis*). Le 2-formyl *N*-phényl pyrrole (**2**) présente une énergie mi-

Can. J. Chem. Downloaded from www.nrcresearchpress.com by 213.200.69.106 on 09/08/12
For personal use only.

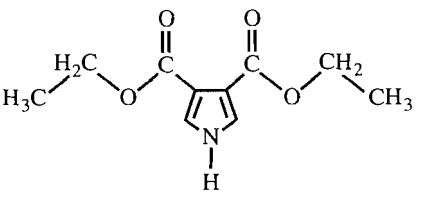

7a

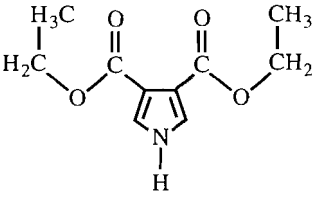

7b

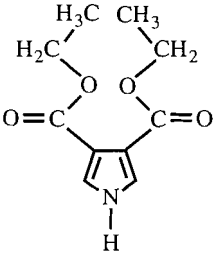

7c

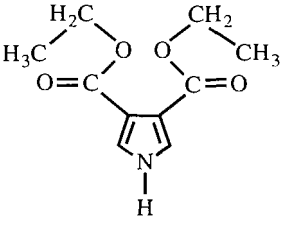

7d

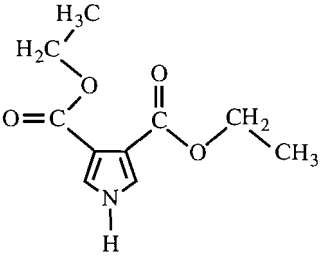

7e

nimale avec le phényle perpendicularie au plan du cycle. Dans le cas du 2-*tert*-butyliminométhyl pyrrole (**3***a*) et du 2-méthyliminométhyl *N*-phényl pyrrole (**3***b*), il existe un équilibre conformationnel entre les formes 2*c trans* et 2*t trans*. Le 3-méthyliminométhyl pyrrole (**4***a*) et le 3-isopropyliminométhyl pyrrole (**4***b*) existent majoritairement, respectivement sous les conformations 3*t trans* et 3*c trans*. Le 2,5-bis(méthyliminométhyl) pyrrole **5** est présent sous la conformation 2*c* 5*c trans*. Enfin, pour les composés **6** et **7** les conformations **6***d* et **7***a* sont privilégiées.

Il est à noter, qu'en aucun cas, en refroidissant les solutions jusqu'à −60°C, nous n'avons pu, par RMN ^{1}H, mettre en évidence une barrière à la rotation.

Remerciements

Nous remercions A. Colomer et G. Pelletier pour l'enregistrement respectifs des spectres IR et de RMN à 250 MHz.

1. V. N. Sheinker, A. D. Garnovskii et O. Osipov. Russ. Chem. Rev. (Engl. Transl.) **50**, 336 (1981) et références incluses.
2. S. Sternhell. Q. Rev. Chem. Soc. **23**, 236 (1969).
3. A. Marinangelli. Ann. Chim. (Rome), **44**, 219 (1954).
4. R. A. Jones et A. G. Moritz. Spectrochim. Acta, **21** 295 (1965).
5. R. W. Guy et R. A. Jones. Aust. J. Chem. **19**, 107 (1966).
6. M. Farnier et T. Drakenberg. J. Chem. Soc. Perkin Trans. 2, 333 (1975).
7. H. Lumbroso et G. C. Papalardo. J. Chim. Phys. **71**, 3 (1974).
8. K. Jao, A. L. Hinde et L. Radom. Nouv. J. Chem. **3**, 473 (1979).
9. I. G. John, G. L. Ritchie et L. Radom. J. Chem. Soc. Perkin Trans. 2, 1601 (1977).
10. C. Jaureguiberry, M. C. Fournie-Zaluski et B. Roques. Can. J. Chem. **51**, 165 (1973).
11. B. Roques, C. Jaureguiberry, M. C. Fournie-Zaluski et S. Combrisson. Tetrahedron Lett. 2693 (1971).
12. D. H. Bertin, M. Farnier et C. Liegeois. Bull. Soc. Chim. Fr. 2677 (1974).
13. F. A. Bottino, M. L. Longo, D. Sciotto et M. Torre. Can. J. Chem. **59**, 1205 (1981).
14. J. Kao et L. Radom. J. Am. Chem. Soc. **101**, 311 (1979).
15. D. J. Chadwick et I. A. Cliffe. J. Chem. Soc. Perkin Trans. 2, 737 (1980).
16. M. J. Dewar et W. Thiel. J. Am. Chem. Soc. **99**, 4899 (1977).
17. G. Elisa et D. Annamaria. Atti Accad. Sci. Ist. Bologna, **11**, 14 (1957); Chem. Abstr. **52**, 11818 (1958).
18. C. F. Candy, R. A. Jones et P. H. Wright. J. Chem. Soc. (C), 2563 (1970).
19. G. C. Van Stein, G. Van Koten, H. Passenier, O. Steinebach et K. Vrieze. Inorg. Chem. Acta, **89**, 79 (1984).
20. R. Miller et K. Olsson. Acta. Chem. Scand. Ser. B: **35**, 303 (1981).
21. A. M. Van Leusen, H. Siderius, B. E. Hoogenboom et D. Van Leusen. Tetrahedron Lett. 5337 (1972).
22. I. F. Halverstadt et W. D. Kumler. J. Am. Chem. Soc. **64**, 2888 (1942).
23. M. J. Dewar et W. Thiel. J. Am. Chem. Soc. **99**, 4907 (1977).

Can. J. Chem. Downloaded from www.nrcresearchpress.com by 213.200.69.106 on 09/08/12
For personal use only.

Preparation, characterization, and biologic evaluation of copper(II) – Schiff base complexes derived from anthranilic acid and aldoses

MOHAMMAD S. IQBAL
Pakistan Atomic Energy Commission, DNFM, P.O. Box 1114, Islamabad, Pakistan

SYED J. KHURSHID[1]
Nuclear Chemistry Division, Pakistan Institute of Nuclear Science and Technology, P.O. Nilore, Islamabad, Pakistan

AND

MOHAMMAD Z. IQBAL
Institute of Chemistry, University of the Punjab, Lahore, Pakistan

Received April 6, 1992[2]

MOHAMMAD S. IQBAL, SYED J. KHURSHID, and MOHAMMAD Z. IQBAL. Can. J. Chem. **71**, 629 (1993).

Cu(II) – Schiff base complexes containing anthranilic acid and aldoses (sugars) as part of the base were prepared and characterized by microanalytical, thermogravimetric, magnetic, and spectroscopic data. The complexes are four-coordinate, anhydrous, and ML_2 type. The electron paramagnetic resonance spectral lines exhibited rhombic distortion from axial symmetry in the square-planar Cu(II) complexes with $g_{\parallel} > g_{\perp} > g_e$. The complexes were found to be active against kaolin paw oedema and standard strains of *Escherichia coli*, *Staphylococcus aureus*, and *Pseudomonas aeruginosa*.

MOHAMMAD S. IQBAL, SYED J. KHURSHID et MOHAMMAD Z. IQBAL. Can. J. Chem. **71**, 629 (1993).

On a préparé des complexes du Cu(II)/bases de Schiff contenant de l'acide anthranilique et des aldoses (sucres) dans la base et on les a caractérisés par des méthodes microanalytique, thermogravimétrique, magnétique et spectroscopique. Les complexes sont tétracoordinés, anhydre et du type ML_2. Les raies des spectres de résonance paramagnétique électronique des complexes Cu(II) plan carrés présentent une distorsion rhombique par rapport à la symétrie axiale avec $g_{\parallel} > g_{\perp} > g_e$. On a trouvé que les complexes sont actifs contre l'oedème et certaines souches d'*Escherichia coli*, *Staphylococcus aureus* et *Pseudomonas aeruginosa*.

[Traduit par la rédaction]

Introduction

Schiff bases and transition metal – Schiff base complexes are important intermediates in certain biologic processes, such as non-enzymatically controlled transamination reactions (1). In these reactions amino acids lend their amino group for Schiff base formation whereas the carbonyl group can be provided by a host of carbonyl compounds, such as pyridoxal compounds, aldoses, and certain hormones, occurring naturally in biological systems. The chemistry and the biochemistry of Schiff bases and transition metal – Schiff base complexes derived from amino acids and pyridoxal compounds, and some other carbonyl compounds that do not occur in biological systems, have been extensively studied (2, 3). Although they occur abundantly in biological systems, no attempt has been made to study the possibility of Schiff base formation in vitro utilizing the carbonyl group of aldoses. However, Horecker *et al.* (see refs. 4–6 in ref. 4) suggest Schiff base formation, in vivo, between an aldose and a terminal amino group associated with an amino acid of an enzyme. In the present work we prepared and characterized some copper(II) – Schiff base complexes in which the Schiff bases were derived from anthranilic acid and naturally occurring sugars.

Since the claim (5) of enhanced anti-inflammatory (AI) activity of Cu(II) complexes of AI drugs, a variety of Cu(II) complexes of both non-AI and AI drugs have been prepared and studied for their AI activity (6–10). The present work includes a study of the effect of the complexes under investigation on kaolin paw oedema in rat. Taking into consideration the possible role of pathogens in rheumatic diseases (11, 12), the antibacterial activity of these complexes is also presented. The combination of the sugar components in these complexes is of significance because sugar containing substances have been used since ancient time for wound treatment (13–15) and in antimicrobial effects (16).

Experimental

Materials

L-Arabinose, D-xylose, D-glucose, and D-galactose were obtained from Sigma Chemical Co. and anthranilic acid and copper acetate dihydrate from E. Merck. The standard strains used for antibacterial activity were *Escherichia coli* (ATCC 25922), *Staphylococcus aureus* (ATCC 25923), and *Pseudomonas aeruginosa* (ATCC 27853).

Preparation of complexes

Anthralinic acid (0.1 mol) and the appropriate sugar (0.1 mol) were mixed together in ethanol (200 mL), and potassium hydroxide (0.1 mol) was added. The mixture was refluxed for 15 min. To the lemon-yellow solution thus obtained a solution of copper acetate dihydrate (0.05 mol in 50 mL ethanol) was added slowly and the reaction mixture was refluxed for a further 15 min. The resulting green precipitate was isolated by filtration, washed with ethanol and ether, and dried under vacuum. The complexes thus obtained are listed in Table 1.

Characterization

Microanalysis was carried out by the usual techniques. Copper was estimated by the Hitachi Z-8000 atomic absorption spectrophotometer. Molecular weights were determined mass spectrometrically. Thermal analysis was carried out on a Netzsch simultaneous thermal analyzer on TGA and DTA modes. Conductivity measurements were carried out using a Wescan 212 conductivity meter in *N*,*N*-dimethylformamide (DMF) at room temperature. Magnetic moments were determined by Gouy's

[1]Author to whom correspondence may be addressed.
[2]Revision received December 8, 1992.

Can. J. Chem. Downloaded from www.nrcresearchpress.com by 213.200.69.106 on 09/08/12
For personal use only.

TABLE 1. Microanalytical data of the complexes: found (calculated)[a]

Complex	C	H	N	Cu
1. Bis(*N*-L-arabinose-imine-anthranilate) Cu(II), (arab anth)$_2$Cu, ($C_{12}H_{14}NO_6$)$_2$Cu MW 600.006	47.88 (48.03)	4.80 (4.67)	4.73 (4.67)	10.61 (10.59)
2. Bis(*N*-D-xylose-imine-anthranilate) Cu(II), (xyl anth)$_2$Cu, ($C_{12}H_{14}NO_6$)$_2$Cu MW 600.006	47.98 (48.03)	4.88 (4.67)	4.45 (4.67)	10.56 (10.59)
3. Bis(*N*-D-glucose-imine-anthranilate) Cu(II), (glu anth)$_2$Cu, ($C_{13}H_{16}NO_7$)$_2$Cu MW 660.054	47.26 (47.30)	5.01 (4.85)	4.39 (4.24)	9.49 (9.63)
4. Bis(*N*-D-galactose-imine-anthranilate) Cu(II), (gal anth)$_2$Cu, ($C_{13}H_{16}NO_7$)$_2$Cu MW 660.054	47.44 (47.30)	5.00 (4.85)	4.41 (4.24)	9.58 (9.63)

[a]Abbreviations: arab = arabinose; xyl = xylose; glu = glucose; gal = galactose; anth = anthranilic acid.

TABLE 2. Observed infrared bands (cm^{-1}) and assignments

Complex	ν(OH)	ν(C=N)	ν(COO)	ν(COO)	δ(CO)	π(CO)	ν(MN)	ν(MO)
1. (arab anth)$_2$Cu	3405	1610	1540	1325	750	500	410	300
2. (xyl anth)$_2$Cu	3375	1620	1540	1325	750	500	410	320
3. (glu anth)$_2$Cu	3388	1618	1545	1325	755	525	425	340
4. (gal anth)$_2$Cu	3405	1618	1540	1325	720	550	420	340

technique and diamagnetic corrections were calculated from Pascal's constants (17). Infrared spectra were recorded on a Perkin–Elmer 882 IR spectrophotometer using KBr disc and Nujol mull techniques. Electronic absorption spectra were obtained with a Hitachi 220S spectrophotometer using DMF as solvent. Electron paramagnetic resonance (EPR) spectra were recorded in powder and solution (in DMF) form, both at room temperature, on a Jeol JES-FE 1XG machine, in the X-band, operating at a microwave frequency of 9.44 GHz. The g values were determined by use of the Kneubühl approximation (18). The spectra were calibrated using α,α-diphenyl-β-picrylhydrazyl radical (dpph, g = 2.0036) as a field marker.

Anti-inflammatory activity

Kaolin paw oedema was induced, according to a reported method (19), in male Wistar rats (90–100 g) in groups of five. The Cu(II) complexes under investigation were administered orally in 5% Mulgophen (GAF Co. Manchester) in distilled water (0.2 mL/100 g body weight) 1 h before the kaolin. The rats were dosed on a weight of drug (mg) per body weight (kg) of animal basis. Oedema was evaluated 4 h after the subplantar administration of kaolin in 0.9% w/v sodium chloride solution. Inhibition of oedema was evaluated by comparing the swelling obtained in treated animals with the controls, and was expressed as percentage inhibition. The statistical significance was evaluated by using the Student t-test.

Antibacterial activity

The antibacterial activity against the standard strains of *E. coli*, *S. aureus*, and *P. aeruginosa* of the complexes was determined using the plate method (20). The inhibitory zones were measured in mm.

Results and discussion

Characterization

Microanalytical data (Table 1) agree with a ML_2 composition of the complexes, where M = Cu(II) and L = the Schiff base ligand. Thermal analysis indicated the absence of any lattice or coordinated water. The molecular weights as determined mass spectrometrically also confirm the ML_2 composition. The infrared (IR) spectra of the complexes contained all the bands due to the ligands with additional bands indicative of the coordination of the ligands with copper through N and O. Some important bands along with their assignments are listed in Table 2. The assignments were made by comparison with related Schiff base complexes (21). It is seen that ν(C=N) frequencies are slightly higher due to coordination and lie in the 1610–1620 cm^{-1} range, which is in agreement with the literature values for such compounds (22). The C=N coordination was confirmed by the appearance of a new ν(M—N) mode around 420 cm^{-1}. In the complexes the ν(CO_2) were observed to be on the lower side as a result of coordination of the carboxylate ion.

Imine formation occurred when a sugar and anthranilic acid were mixed, and was indicated by a yellowing of the solution and development of an absorption band with a maximum at about 400 nm (23). The Schiff base ligands could not be isolated due to their instability. It is known that, normally, the Schiff bases obtained from aliphatic carbonyl compounds hydrolyze readily and are, therefore, not very stable; however, they can be isolated as metal chelates. On addition of the metal salt the yellow color was replaced by

Can. J. Chem. Downloaded from www.nrcresearchpress.com by 213.200.69.106 on 09/08/12
For personal use only.

TABLE 3. Electronic absorption spectra [nm (ε, mol^{-1} cm^2)] in DMF

Complex	Ligand bands	*d–d* bands
1. (arab anth)$_2$Cu	280(40 005), 370(7090), 410(1700)	650(566)
2. (xyl anth)$_2$Cu	280(40 006), 370(7003)	655(509)
3. (glu anth)$_2$Cu	280(40 006), 329(7100)	655(550)
4. (gal anth)$_2$Cu	280(40 003), 370(6881)	655(560)

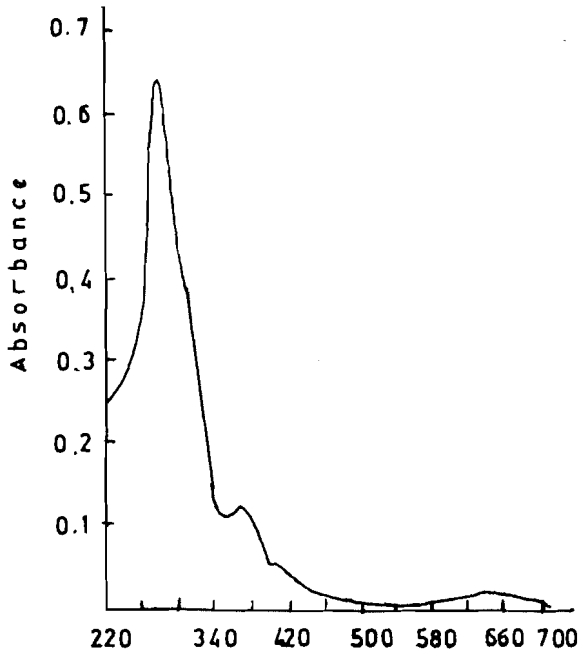

FIG. 1. Electronic absorption spectrum of (arab anth)$_2$Cu in DMF.

TABLE 4. Magnetic moments of the complexes

Complex	μ (BM)
1. (arab anth)$_2$Cu	1.92
2. (xyl anth)$_2$Cu	1.85
3. (glu anth)$_2$Cu	1.90
4. (gal anth)$_2$Cu	2.00

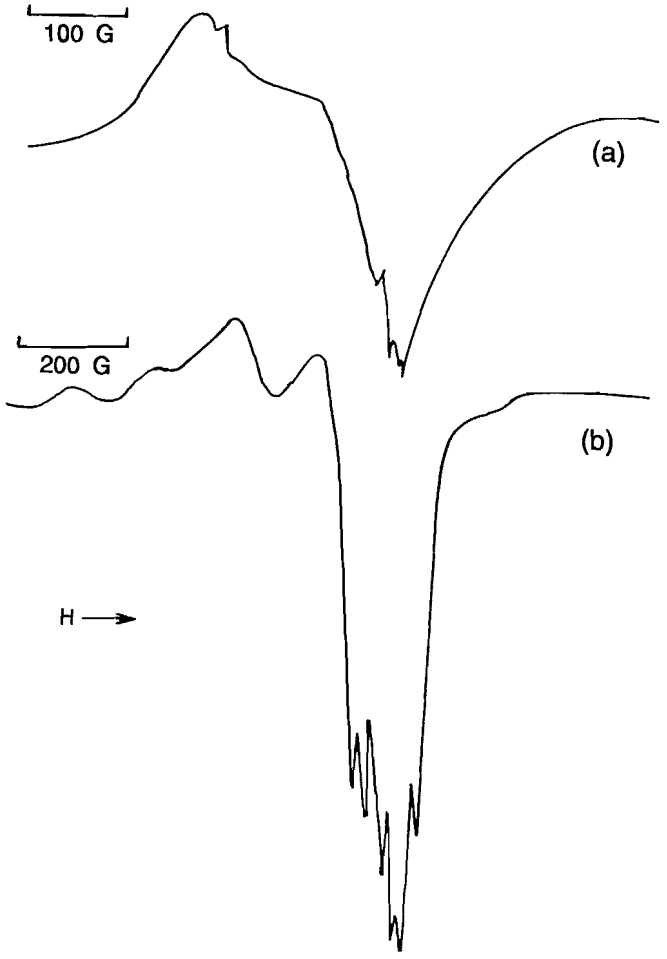

FIG. 2. EPR spectra of (arab anth)$_2$Cu: (a) powder; (b) in DMF.

a green color and complexation occurred. The electronic absorption maxima of the complexes under investigation are listed in Table 3. The representative spectrum of (arab anth)$_2$Cu is reproduced in Fig. 1. The intense band at 280 nm was assigned to a phenyl ring π–π* transition (24). The bands in the 329–370 nm range, by analogy with (Sal)(−)pn–Zn (25), were attributed to a π–π* transition originating in the -CH=N- chromophore, while the lower energy bands were due to *d–d* transitions. The electronic spectra of Cu(II) complexes are generally poor indicators of geometry. However, the values of extinction coefficient and position of the absorption bands of the Cu(II) complexes under investigation are consistent with a distorted square-planar environment (26).

The magnetic moments of the complexes (Table 4) are normal values as expected for mononuclear Cu(II) complexes. From the microanalytical and the spectroscopic data all the complexes reported in this work appear to be four-coordinate. The coordinating groups as indicated by the IR spectra are C=N and -COO^- present in the Schiff base ligands. Lower molar concentration values (15.23–17.19 ohm^{-1} mol^{-1} cm^2) were indicative of the nonelectrolytic nature of the complexes. Neutral four-coordinate Cu(II) complexes with chelating agents are usually planar.

The polycrystalline and solution EPR spectra of the (arab anth)$_2$Cu are shown in Fig. 2. The spectra produced by other complexes were similar and hence are not shown. There was general correspondence between the powder and solution spectra, however; the $g_\parallel$ region was well resolved in solution. The spectra exhibited rhombic distortion from axial symmetry in the square-planar geometry because of two different kinds of atoms (O and N) coordinating directly to the metal ion. The spectra were characteristic of magnetically dilute systems with Cu(II) ions in the $d_{x^2-y^2}$ ground state ($g_\parallel > g_\perp > g_e$ (Table 5)). Hyperfines due to nitrogen ($I = 1$)

Can. J. Chem. Downloaded from www.nrcresearchpress.com by 213.200.69.106 on 09/08/12
For personal use only.

TABLE 5. EPR parameters of the complexes

Complex	Solid	Solution		
	g_0[a]	$g_\parallel$[b]	$g_\perp$[b]	$\lvert A_\parallel(\mathrm{Cu})\rvert$[c]
1. (arab anth)$_2$Cu	2.17	2.256	2.028	16.00
2. (xyl anth)$_2$Cu	2.20	2.310	2.030	16.51
3. (glu anth)$_2$Cu	2.19	2.298	2.029	16.23
4. (gal anth)$_2$Cu	2.14	2.200	2.028	16.00

[a]±0.02.
[b]±0.001.
[c]$\times 10^3$ cm^{-1}, ±0.08.

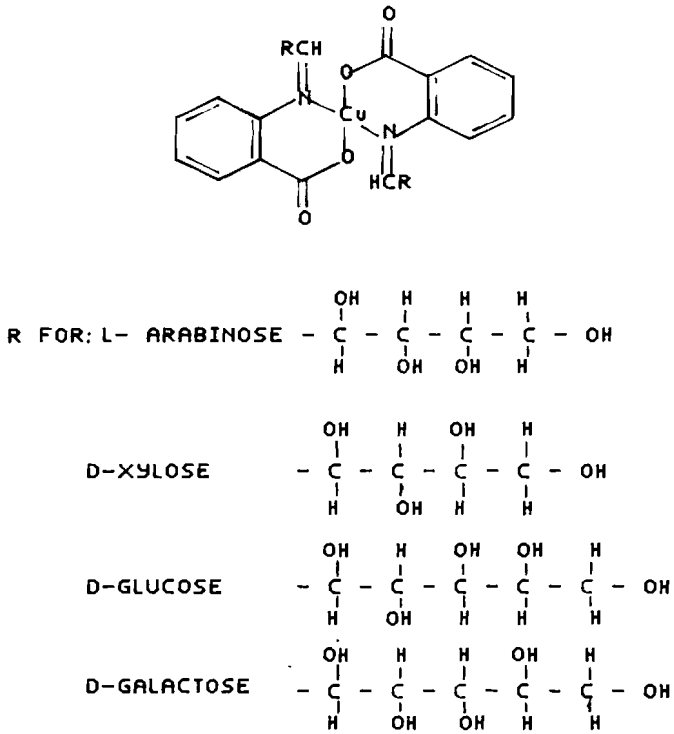

FIG. 3. Proposed structures of the complexes.

TABLE 6. AI effect of the complexes in kaolin paw oedema

Complex	Dose (mg/kg)	% Inhibition of odema	LD_{50} (mg/kg)
1. (arab anth)$_2$Cu	50	30[a]	1750
2. (xyl anth)$_2$Cu	50	25[a]	1750
3. (glu anth)$_2$Cu	50	28[a]	1800
4. (gal anth)$_2$Cu	50	25[a]	1700

[a]$p < 0.05$.

are visible on the main absorption line, $g_\perp$ (Fig. 2), confirming the coordination through N.

Sugars usually exhibit hemiacetal structure in solution, which results from cyclization of the carbonyl group. Apparently there is no free carbonyl group available. From the results obtained it appears that the hemiacetal linkage of the reducing sugars is labile and the carbonyl group becomes available for formation of the Schiff base. This phenomenon is not unusual as the reactivity of the carbonyl group in cyclic or acyclic form (which are in equilibrium) has been demonstrated in some other reactions as well (27). We have included two hexsoses and two pentoses in the preparation of the ligands because the hexsoses are by far the most abundant, while the pentoses are important components of nucleic acids and various polysaccharides.

The present study clearly indicates that the ligands form stable coordinate complexes with Cu(II) as evidenced by microanalytical, magnetic, and spectroscopic data. Unsuccessful attempts to isolate crystals suitable for X-ray studies prevented further structure elucidation. The structures of the complexes under investigation, proposed on the basis of the above experimental evidence, are shown in Fig. 3.

Anti-inflammatory activity

All of the complexes inhibited kaolin paw oedema (Table 6). They were found to be equipotent at the dose tested. The toxicity data (LD_{50}, Table 6) indicate that these compounds can become potential AI drugs because they possess comparable AI activity to that of Cu(II)-aspirinate and far less toxicity (ca. $LD_{50} = 760 \pm 100$ for Cu(II)-aspirinate (5). The low toxicity of these complexes can be attributed to greater biocompatibility of the Schiff base ligands and also to the presence of sugar as one of the components in the complexes.

Antibacterial activity

All the complexes under investigation were found to be active against the strains tested. The observed antibacterial activity of the complexes is of interest and supports the speculated role of pathogens in inflammatory processes, as previously indicated by the antibacterial activity of a variety of AI drugs including Cu(II) complexes (12).

1. E. E. Snell and D. E. Metzler. Pyridoxal catalysis, enzymes and model systems. Interscience, New York. 1968.
2. R. H. Holm, G. W. Everett, and A. Chakravarty. Prog. Inorg. Chem. **7**, 83 (1966).
3. G. N. Weinstein, M. J. O'Connor, and R. H. Holm. Inorg. Chem. **9**, 2104 (1970).
4. M. L. Wolform. Adv. Carbohydr. Chem. **10**, 170 (1955).
5. J. R. J. Sorenson. J. Med. Chem. **19**, 135 (1976).
6. G. E. Jackson, P. M. May, and D. H. Williams. J. Inorg. Nucl. Chem. **40**, 1189 (1978).
7. D. H. Brown, A. J. Lewis, W. E. Smith, and J. W. Teape. J. Med. Chem. **23**, 729 (1980).
8. J. R. J. Sorenson. Inflammatory diseases and copper. Humana Press, N.J. 1982.
9. R. Nagir and G. Mohan. J. Inorg. Biochem. **42**, 9 (1991).
10. S. Oga, S. F. Tanguchi, R. Najjar, and A. R. Souza. J. Inorg. Biochem. **41**, 45, (1991).
11. T. Pullar, J. A. Hunter, and H. A. Capell. Br. Med. J. **290**, 1535 (1985).
12. M. S. Iqbal, S. J. Khurshid, and M. Z. Iqbal. J. Pak. Med. Assoc. **40**, 221 (1990).
13. R. D. Forrest. J. R. Soc. Med. **75**, 268 (1982).
14. L. Herszage, J. R. Montenegro, and A. L. Joseph. Bol. Trab. Soc. Cir. Buenos Aires, **41**, 315 (1980).
15. J. L. Trouillet, J. Y. Fagoon, Y. Domart, J. Chastre, J. Pierre, and C. Gibert. Lancet, 180 (1985).
16. J. Chirife, L. Herszage, A. Joseph, and E. S. Kohn. Antimicrob. Agents Chemother. **23**, 766 (1983).
17. A. Earnshaw. Introduction to magnetochemistry. Academic Press, New York. 1968. p. 6.
18. F. K. Kneubühl. J. Chem. Phys. **33**, 1074 (1960).
19. A. J. Lewis, J. Cottney, and M. F. Sugrue. J. Pharm. Pharmacol. **27**, 375 (1975).
20. P. Gerhardt. *In* Manual of methods for general bacteriology.

Can. J. Chem. Downloaded from www.nrcresearchpress.com by 213.200.69.106 on 09/08/12
For personal use only.

Edited by R. N. Castello. American Society for Microbiology. 1981. pp. 65–208.
21. S. T. Chow, D. M. Jones, and C. A. MacAuliffe. Inorg. Chim. Acta, **22**, 1 (1977).
22. G. H. Rist, J. S. Hyde, and T. Vangard. Proc. Natl. Acad. Sci. U.S.A. **77**, 1339 (1977).
23. D. E. Metzler. J. Am. Chem. Soc. **91**, 5977 (1962).
24. B. Bosnich. J. Am. Chem. Soc. **90**, 627 (1968).
25. R. S. Dowing and F. L. Urbach. J. Am. Chem. Soc. **91**, 5977 (1966).
26. L. Sacconi and M. Ciampolini. J. Chem. Soc. 276 (1964).
27. F. Shafizada. Adv. Carbohydr. Chem. **13**, 9 (1958).

Can. J. Chem. Downloaded from www.nrcresearchpress.com by 213.200.69.106 on 09/08/12
For personal use only.

Ryanoids and related compounds. A total synthesis of 3-epiryanodine

LUC RUEST[1] AND PIERRE DESLONGCHAMPS

Laboratoire de synthèse organique, Département de chimie, Faculté des sciences, Université de Sherbrooke, Sherbrooke (Québec), Canada J1K 2R1

Received November 24, 1992

LUC RUEST and PIERRE DESLONGCHAMPS. Can. J. Chem. **71**, 634 (1993).

In the course of a preliminary investigation on the relationships between chemical structure of ryanoids and their affinity to the ryanodine (**1**) binding site, we have synthesized 3-epiryanodine (**13**) from anhydroryanodol (**4**), a key intermediate in our total synthesis of (+)-ryanodol (**2**).

LUC RUEST et PIERRE DESLONGCHAMPS. Can. J. Chem. **71**, 634 (1993).

Dans le cadre d'une étude préliminaire des relations structures chimiques – activité biologique des ryanoïdes et de leur affinité au site récepteur de la ryanodine (**1**), nous avons synthétisé la 3-épiryanodine (**13**) à partir de l'anhydroryanodol (**4**), un intermédiaire-clé de la synthèse totale du (+)-ryanodol (**2**).

Can. J. Chem. Downloaded from www.nrcresearchpress.com by 213.200.69.106 on 09/08/12
For personal use only.

Introduction

Ryanodine (**1**), a natural product isolated from *Ryania speciosa Vahl* (1), is the ester of α-pyrrole carboxylic acid and the complex diterpene (+)-ryanodol (**2**). It is an interesting and important calcium release channel modulator in mammalian muscle (2). Its chemical structure was elucidated several decades ago by Wiesner and co-workers (3). We completed a total synthesis of (+)-ryanodol (**2**) in 1979 (4) and have published a detailed report on that work (5–8).

Recently, we began to investigate the influence of chemical modifications of the ryanodine substituents on the biological activity (affinity to the [^{3}H]-ryanodine binding site) in a search to identify the structural features that are necessary to maintain biological activity. Several natural ryanoids isolated from the plant by us (9, 10) and others (11–16) have thus been examined (10, 17), as well as some of their derivatives (10, 12). In the course of this work we also carried out some chemical modifications on anhydroryanodine (**3**) and anhydroryanodol (**4**) obtained from natural source (3), which led to the synthesis of 3-epiryanodine (**13**). We wish now to report this work.

Results and discussion

It was shown earlier (12) that anhydroryanodine (**3**), easily obtained by dehydration of ryanodine (**1**) (3) (see Scheme 1) has a low affinity to the ryanodine binding site. To measure the importance of the hemiketalic hydroxyl at C15 for the affinity, we thought that the simple reduction of the lactone moiety of anhydroryanodine (**3**) to a hemiketal (see **5**) could afford an answer to the problem, especially if this modification results in a retrieved affinity.

Unfortunately, using the usual reducing agents, we were not successful in reducing the lactone moiety specifically. We noted, nevertheless, that treatment of either anhydroryanodine (**3**) (Scheme 1) or anhydroryanodol (**4**) with lithium in ammonia led to olefin **7** in moderate yields. A similar reductive cyclization had been previously used to synthesize ryanodol from 1,2-epoxyanhydroryanodol (**8**) (8) (Scheme 1). Formation of olefin **7** can formally be explained as follows: under treatment with lithium in ammonia, the lactone carbonyl group of either **3** or **4** would be reduced to the dianion **6** (X = OPyr or OH) (or a radical anion) making C15 nucleophilic enough to perform a transannular S_N2' displacement of the allylic substituent X at position 3, i.e., α-pyrrole carboxylate for anhydroryanodine (**3**) or simple hydroxyl group for anhydroryanodol (**4**). Analogous intramolecular cyclization by S_N' cleavage of allylic ether by enolate anion has recently been reported by Paquette and Schreiber (18, 19).

Introducing a double bond in ring A provided a possible entry to chemical modifications in that ring. Epoxidation of the C2—C3 double bond of olefin **7** (Scheme 2) with an excess of reagent led directly to epoxylactone **11** formed successively through the acid-catalyzed opening of unstable β-epoxide **9** to give, first, 3-epianhydroryanodol (**10**), followed by epoxidation of the newly formed 1,2-double bond to yield epoxide **11** bearing a β-hydroxyl group at position 3.

The reducing conditions previously discussed (Li/NH_3) (*vide supra*) were then applied to epoxide **11** and 3-epiryanodol (**12**) was obtained in good yield. This compound showed significant differences in its NMR data compared to ryanodol (**2**), especially noticeable upfield shifts for the HC3 (+0.34 ppm) and the H_AC14 (+0.53 ppm) signals, in concordance with their new magnetic environment. In addition, the structure of compound **12** was confirmed by monocrystal X-ray diffraction analysis (20) (Fig. 1).

Esterification of 3-epiryanodol (**12**) with α-pyrrole carboxylic acid following a known procedure (21) led to 3-epiryanodine (**13**) in good yield. This new 3-epimer of ryanodine was shown to have ~0.01 the affinity of ryanodine.[2] We reported earlier (8) our fruitless efforts to esterify ryanodol (**2**) to ryanodine (**1**): in the conditions just described, ryanodol (**2**) gave a modest yield of 10-O-α-pyrrolecarbonylryanodol (**14**). This compound, surprisingly, showed an interesting affinity to the binding site of ryanodine. The details of this preliminary observation will soon appear elsewhere.[2]

Conclusion

We have achieved a total synthesis of 3-epiryanodine (**13**) starting from anhydroryanodol (**4**). The global "epimerization" at position 3 was performed through transannular reactions typical of the ryanoid skeleton.

[1]Author to whom correspondence may be addressed.

[2]J. Sutko, P. Deslongchamps, and L. Ruest. Unpublished results.

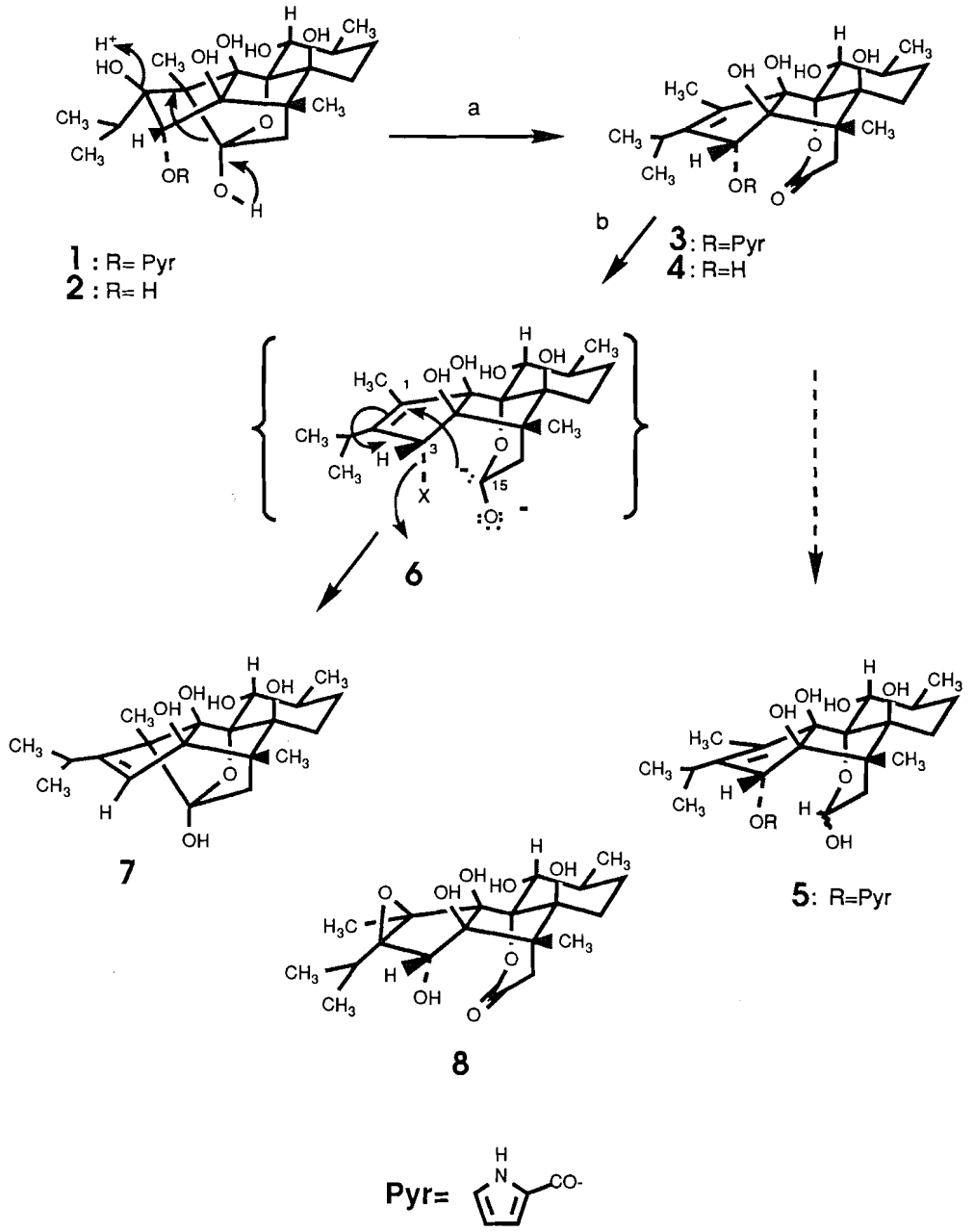

a: H_2SO_4, 2 N; b: Li, NH_3, THF, −78°C, 20–100 min

SCHEME 1

Experimental

Apparatus, materials, and methods

Melting points were determined on a Reichert hot stage apparatus and are uncorrected. Tetrahydrofuran was dried by distilling over sodium benzophenone ketyl. Dichloromethane, ethylene dichloride, and acetonitrile used for reactions were distilled over calcium hydride. All reactions were performed under nitrogen atmosphere. Analytical and preparative thin-layer chromatography were carried out on glass plates precoated with silica gel 60F-250 (Merck). Column chromatography was performed with Merck (200–400 mesh) silica gel. The infrared spectra (ir) were taken on a Perkin–Elmer 681 spectrophotometer. The ^1H nmr spectra were recorded on a Bruker WM-250 instrument (with CHD_2OD as internal standard centered at 3.30 ppm). The following abbreviations have been used: s, singlet; d, doublet; dd, doublet of doublets; t, triplet; m, multiplet; br, broad. Mass spectra and peak matching (Exact Mass) were recorded on a VG Micromass ZAB-2F spectrometer.

2,3-Dideoxy-2,3-didehydroryanodol (7)

(a) From anhydroryanodol (4) (Method A)

A solution of anhydroryanodol (**4**) (77 mg, 0.202 mmol) in anhydrous tetrahydrofuran (THF) (3 mL) was transferred to a cold (−78°C) blue mixture of lithium (~8 mg, 2.67 mmol) in ammonia (10 mL). The mixture was stirred for 1.5 h, then treated with solid ammonium chloride (~100 mg). The cold bath was removed and ammonia was allowed to escape with a nitrogen stream while raising the temperature to ~25°C. The mixture was then dissolved in water, neutralized (HCl, 1 N), and extracted with ethyl acetate. The crude product was purified by flash chromatography ($CHCl_3$:CH_3OH; 2–10%) to give olefin **7** (55 mg, 75%) together

Can. J. Chem. Downloaded from www.nrcresearchpress.com by 213.200.69.106 on 09/08/12
For personal use only.

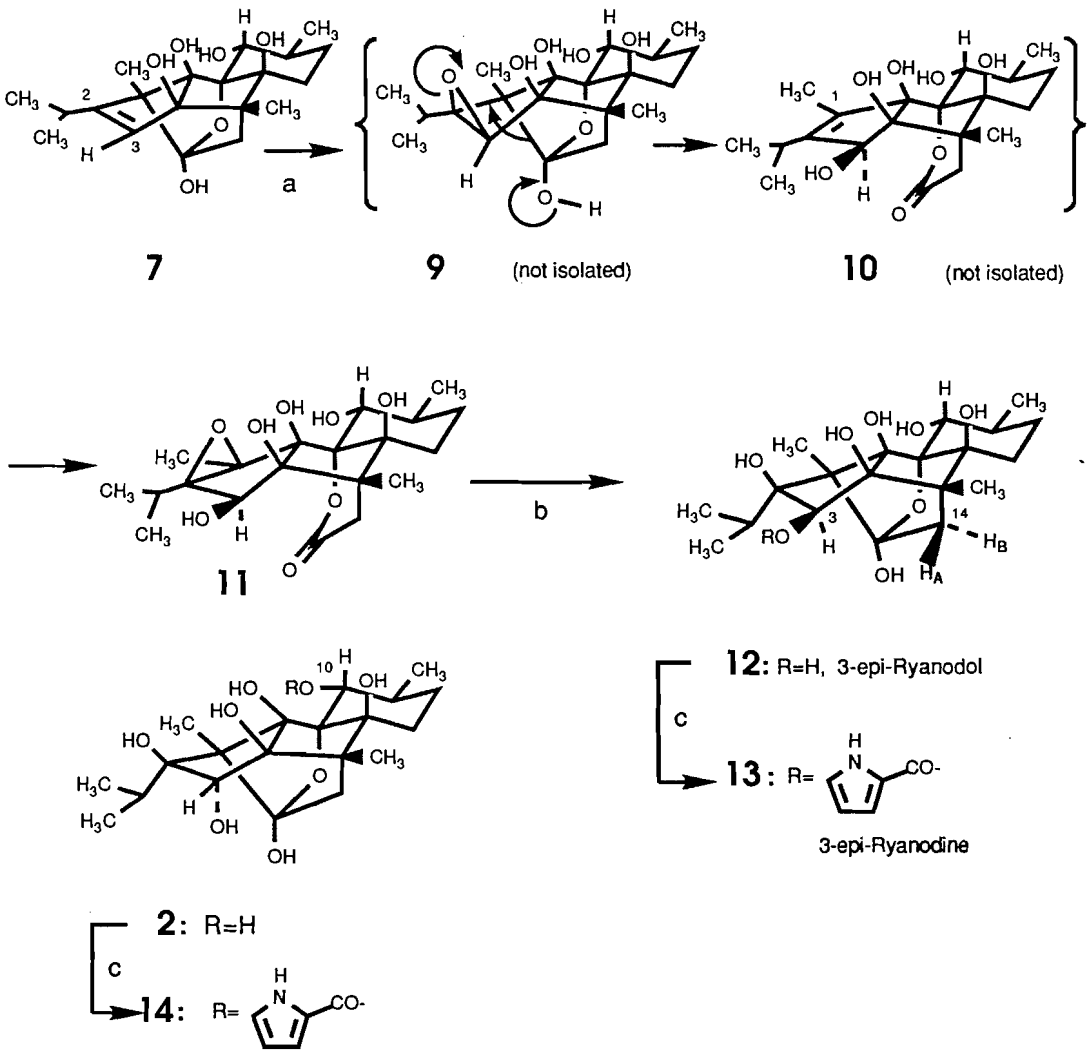

a: CF_3CO_3H, $NaHCO_3$, $(CH_2Cl)_2$, 25°C, 5 h; b: Li, NH_3, THF, −78°C, 20 min; c: pyrrole 2-carboxylic acid, DCC, DMAP, THF, CH_2Cl_2, 25°C, 24–60 h

SCHEME 2

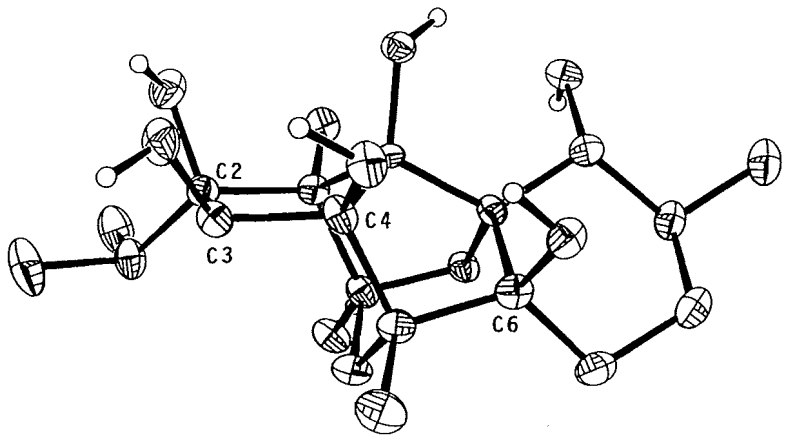

FIG. 1. ORTEP perspective view of crystalline **12**; 30% probability thermal ellipsoids are shown for the non-hydrogen atoms. For clarity, only hydroxyl hydrogen atoms are shown. Internal hydrogen bondings become evident between C2, C3, C4, and C6 hydroxyl groups.

Can. J. Chem. Downloaded from www.nrcresearchpress.com by 213.200.69.106 on 09/08/12
For personal use only.

Can. J. Chem. Downloaded from www.nrcresearchpress.com by 213.200.69.106 on 09/08/12
For personal use only.

with some starting material **4** (10 mg, 13%); mp 220–223°C (ether); ir (KBr, ν cm^{-1}): 3600–3350 (br); ^1H nmr (CD_3OD, δ ppm): 5.18 (1H, d, 1.3 Hz, HC3), 3.77 (1H, d, 10.2 Hz, HC10), 2.28 (1H, m, HC13), 2.20 (1H, m, HC9), 1.82 (1H, m), 1.80 (1H, d, 12.8 Hz, H_AC14), 1.70 (1H, d, 12.8 Hz, H_BC14), 1.50 (1H, m), 1.27 (2H, m), 1.15 (3H, s, CH_3C1), 1.09 (3H, d, 6.8 Hz, CH_3C9), 1.06 (3H, d, 6.8 Hz, CH_3C13), 1.00 (3H, d, 6.5 Hz, CH_3C13), 0.88 (3H, s, CH_3C5). Exact Mass calcd. for $C_{20}H_{30}O_6$: 366.2042 (M^+); found: 366.2035.

(b) From anhydroryanodine (3)

A solution of anhydroryanodine (**3**) (25 mg, 0.053 mmol) in dry THF (3 mL) was transferred into a cold (−78°C), blue mixture of lithium (~20 mg, large excess) in ammonia (~10 mL). The reaction mixture was quenched after 20 min by the addition of ammonium chloride. Extraction was performed as described above to furnish a colored crude product that was chromatographed to give olefin (**7**) (6 mg, 31%) and anhydroryanodol (**4**) (9 mg, 45%).

Epoxydation of olefin 7

A freshly prepared solution of trifluoroperacetic acid (0.9 M in $(CH_2Cl)_2$, 400 μL, 0.360 mM) was added to a cold solution (0°C) of olefin **7** (40 mg, 0.109 mmol) in a mixture of 1,2-dichloroethane (8 mL) and acetonitrile (2 mL) containing a suspension of $NaHCO_3$(120 mg). After 6 h of stirring at room temperature, the mixture was poured into a dilute solution of sodium thiosulfate (0.5 M) and extracted with ethyl acetate. Flash chromatography of the crude product ($CHCl_3$:CH_3OH; 2–10%) yielded crystalline 1,2-epoxy-3-epianhydroryanodol (**11**) (28 mg, 65%); mp 230–232°C (ether); ir ($CHCl_3$, ν cm^{-1}): 3600, 3420 (br), 1744, 1252; ^1H nmr (CD_3OD, δ ppm): 4.41 (1H, s, HC3), 4.04 (1H, d, 10.3 Hz, HC10), 2.74 (1H, d, 20.2 Hz, H_AC14), 2.63 (1H, d, 20.2 Hz, H_BC14), 1.68 (2H, m, HC9 and HC13), 1.55 (3H, s, CH_3C1), 1.6–1.45 (4H, m), 1.16 (3H, d, 7.0 Hz), 1.06 (3H, d, 6.3 Hz), 1.04 (3H, d, 7.0 Hz), 0.92 (3H, s, CH_3C5). Exact Mass calcd. for $C_{20}H_{30}O_8$ (M^+): 398.1941; found: 398.1936.

3-Epiryanodol (12) from epoxide 11

A solution of 1,2-epoxy-3-epianhydroryanodol (**11**) (33 mg, 0.083 mmol) in THF (2 mL) was transferred to a cold (−78°C), stirred, blue solution of lithium (15 mg) in ammonia (~10 mL). After 20 min, work-up procedure was done as described previously for the preparation of olefin **7** (Method A) (*vide supra*). Flash chromatography of the crude product (28 mg) ($CHCl_3$:CH_3OH, 9:1) gave crystalline material (27 mg, 81%) that was recrystallized (CH_2Cl_2–CH_3OH) to beautiful tetrahedral crystals suitable for monocrystal X-ray diffraction analysis; mp 310°C (dec.); ^1H nmr (CD_3OD, δ ppm): 3.80 (1H, d, 10.2 Hz, HC10), 3.74 (1H, s, HC3), 2.10 (1H, m, HC9), 2.05 (1H, m, HC13), 1.87 (1H, d, 14.0 Hz, H_AC14), 1.85 (1H, m), 1.66 (1H, d, 14.0 Hz, H_BC14), 1.52 (2H, m), 1.33 (3H, s, CH_3C1), 1.27 (1H, m), 1.04 (3H, d, 6.6 Hz, CH_3C13), 1.00 (3H, d, 6.4 Hz, CH_3C9), 0.97 (3H, d, 6.8 Hz, CH_3C13), 0.89 (3H, s, CH_3C5). Exact Mass calcd. for $C_{20}H_{32}O_8$ (M^+): 400.2097; found: 400.2102.

3-Epiryanodine (13)

To a solution of 3-epiryanodol (**12**) (18 mg, 0.045 mmol) in THF (3 mL) and dichloromethane (2 mL) was successively added α-pyrrole carboxylic acid (10 mg, 0.090 mmol), dimethylaminopyridine (DMAP) (2 mg), and a solution of dicyclohexylcarbodiimide (DCC) (18 mg, 0.09 mmol) in dichloromethane (1 mL). The mixture was stirred at room temperature for 60 h, then poured into aqueous sodium bicarbonate and extracted with ethyl acetate. The crude product was purified by thin-layer chromatography ($CHCl_3$:CH_3OH, 9:1) to yield 3-epiryanodine (**13**) (14 mg, 63%) together with unreacted starting material **12** (6 mg, 33%): mp 228–230°C (CH_2Cl_2–CH_3OH); ^1H nmr (CD_3OD, δ ppm): 6.98 (2H, m) and 6.21 (1H, dd, 3.6 and 2.6 Hz) (pyrrole ring hydrogens), 5.25 (1H, s, HC3), 3.78 (1H, d, 10.2 Hz, HC10), 2.05 (2H, m, HC9 and HC13), 1.96 (1H, d, 14.2 Hz, H_AC14), 1.82 (1H, d, 14.2 Hz, H_BC14), 1.81 (1H, m), 1.52 (2H, m), 1.40 (3H, s, CH_3C1), 1.27 (1H, m), 1.05 (3H, d, 6.6 Hz, CH_3C13), 1.03 (3H, s, CH_3C5), 1.00 (3H, d, 6.5 Hz, CH_3C9), 0.84 (3H, d, 6.8 Hz, CH_3C13). Exact Mass calcd. for $C_{25}H_{35}O_9N$ (M^+): 493.2312; found: 493.2297.

10-O-α-Pyrrolecarbonylryanodol (14)

In similar conditions just described (*vide supra*) for the esterification of 3-epiryanodol (**12**), a solution of ryanodol (**2**) (157 mg, 0.392 mmol) in THF (15 mL) and dichloromethane (5 mL) was treated with α-pyrrole carboxylic acid (157 mg, 1.414 mmol), dicyclohexylcarbodiimide (300 mg, 1.46 mmol), and DMAP (3 mg). After 24 h, the mixture was extracted and the crude product was purified by flash chromatography to give 10-*O*-α-pyrrolecarbonyl ryanodol (**14**) (36 mg, 18%) together with unreacted ryanodol (**2**) (110 mg, 70%); mp 187–189°C (CH_2Cl_2–CH_3OH); ^1H nmr (CD_3OD, δ ppm): 6.95, 6.90, and 6.18 (3 dd of 1H each for pyrrole hydrogens), 5.41 (1H, d, 10.4 Hz, HC10), 4.06 (1H, s, HC3), 2.56 (1H, d, 13.2 Hz, H_AC14), 2.15 (2H, m, HC13 and HC9), 1.78 (1H, d, 13.2 Hz, H_BC14), 1.62 (1H, m), 1.35 (2H, m), 1.24 (3H, s, CH_3C1), 1.13 (3H, s, CH_3C5), 1.08 (1H, m), 1.04 (3H, d, 6.8 Hz, CH_3C9), 0.95 (3H, d, 6.4 Hz, CH_3C13), 0.85 (3H, d, 6.5 Hz, CH_3C13). Exact Mass calcd. for $C_{25}H_{33}O_8N$ ($M^+ - H_2O$): 475.2206; found: 475.2201.

Acknowledgements

This research was supported partly by the Natural Sciences and Engineering Research Council of Canada (NSERCC) and by Glaxo Inc., NC 27709, U.S.A.

1. E. F. Rogers, F. R. Koniuszy, J. Shavel, and K. Folkers. J. Am. Chem. Soc. **70**, 3086 (1948).
2. D. J. Jenden and A. S. Fairhurst. Pharmacol. Rev. **21**, 1 (1969), and references therein; Z. J. Penefsky. Pfluegers Arch. 185 (1974); J. L. Sutko and J. L. Kenyon. J. Gen. Physiol. **82**, 385 (1983); M. R. Mitchell, T. Powell, D. A. Terrar, and V. W. Twist. Br. J. Pharmacol. **81**, 543 (1984).
3. (*a*) K. Wiesner. *In* Advances in organic chemistry. Vol. 8. *Edited by* E. C. Taylor. Wiley–Interscience Publishers, New York. 1972. p. 295; (*b*) R. B. Kelly, D. J. Whittingham, and K. Wiesner. Can. J. Chem. **29**, 905 (1951).
4. A. Bélanger, D. J. F. Berney, H.-J. Borschberg, R. Brousseau, A. Doutheau, R. Durand, H. Katayama, R. Lapalme, D. M. Leturc, C.-C. Liao, F. N. MacLachlan, J.-P. Maffrand, F. Marazza, R. Martino, C. Moreau, L. St-Laurent, R. Saintonge, P. Soucy, L. Ruest, and P. Deslongchamps. Can. J. Chem. **57**, 3348 (1979).
5. P. Deslongchamps, A. Bélanger, D. J. F. Berney, H.-J. Borschberg, R. Brousseau, A. Doutheau, R. Durand, H. Katayama, R. Lapalme, D. M. Leturc, C.-C. Liao, F. N. MacLachlan, J. P. Maffrand, F. Marazza, R. Martino, C. Moreau, L. Ruest, L. St-Laurent, R. Saintonge, and P. Soucy. Can. J. Chem. **68**, 115 (1990).
6. P. Deslongchamps, A. Bélanger, D. J. F. Berney, H.-J. Borschberg, R. Brousseau, A. Doutheau, R. Durand, H. Katayama, R. Lapalme, D. M. Leturc, C.-C. Liao, F. N. MacLachlan, J. P. Maffrand, F. Marazza, R. Martino, C. Moreau, L. Ruest, L. St-Laurent, R. Saintonge, and P. Soucy. Can. J. Chem. **68**, 127 (1990).
7. P. Deslongchamps, A. Bélanger, D. J. F. Berney, H.-J. Borschberg, R. Brousseau, A. Doutheau, R. Durand, H. Katayama, R. Lapalme, D. M. Leturc, C.-C. Liao, F. N. MacLachlan, J. P. Maffrand, F. Marazza, R. Martino, C. Moreau, L. Ruest, L. St-Laurent, R. Saintonge, and P. Soucy. Can. J. Chem. **68**, 153 (1990).
8. P. Deslongchamps, A. Bélanger, D. J. F. Berney, H.-J. Borschberg, R. Brousseau, A. Doutheau, R. Durand, H. Katayama, R. Lapalme, D. M. Leturc, C.-C. Liao, F. N. MacLachlan, J. P. Maffrand, F. Marazza, R. Martino, C. Moreau, L. Ruest, L. St-Laurent, R. Saintonge, and P. Soucy. Can. J. Chem. **68**, 186 (1990).

9. L. Ruest, D. R. Taylor, and P. Deslongchamps. Can. J. Chem. **63**, 2840 (1985).
10. P. Deslongchamps, L. Ruest, W. Welch, and J. Sutko. Biochemistry. Submitted.
11. A. L. Waterhouse, I. Holden, and J. E. Casida. J. Chem. Soc. Chem. Commun. 1265 (1984).
12. A. L. Waterhouse, I. N. Pessah, A. O. Francini, and J. E. Casida. J. Med. Chem. **30**, 710 (1987).
13. R. A. Humerickhouse, J. Paschal, T. Elvey, D. Berry, H. R. Besch, Jr. Pharmacologist, **31**, 185 (1989).
14. P. R. Jefferies, R. F. Toia, and J. E. Casida. J. Nat. Prod. **54**, 1147 (1991).
15. P. R. Jefferies, R. F. Toia, B. Brannigan, I. Pessah, and J. E. Casida. J. Agric. Food Chem. **40**, 142 (1992).
16. P. R. Jefferies, W. W. Lam, R. F. Toia, and J. E. Casida. J. Agric. Food Chem. **40**, 509 (1992).
17. J. L. Sutko, E. Robinson, F. A. Lattanzio, Jr., R. G. Schlatterer, P. Deslongchamps, and L. Ruest. *In* Transduction in biological systems. Chap. 31. Pharmacology of the ryania alkaloids: The ester A, a ryanodine analog that only increases sarcoplasmic reticulum calcium permeability. *Edited by* C. Hidalgo, J. Bacigalupo, E. Jaimovich, and J. Vergara. Plenum Publishing Corporation, New York. 1990. p. 465.
18. L. A. Paquette, J. Reagan, S. L. Schreiber, and C. A. Teleha. J. Am. Chem. Soc. **111**, 2331 (1989).
19. L. A. Paquette and Y. J. Shi. J. Am. Chem. Soc. **112**, 8478 (1990).
20. M. Drouin and A. Michel. Acta Crystallogr. In press.
21. B. Neises and W. Steglich. Angew. Chem. Int. Ed. Engl. **17**, 522 (1978).

Can. J. Chem. Downloaded from www.nrcresearchpress.com by 213.200.69.106 on 09/08/12
For personal use only.

^{1}H nuclear magnetic resonance and molecular orbital studies of the internal rotational potential and electron delocalization in triphenylphosphine

TED SCHAEFER,[1] RUDY SEBASTIAN, AND FRANK E. HRUSKA
Department of Chemistry, University of Manitoba, Winnipeg, Man., Canada R3T 2N2

Received September 15, 1992

TED SCHAEFER, RUDY SEBASTIAN, and FRANK E. HRUSKA. Can. J. Chem. **71**, 639 (1993).

The ^{1}H nuclear magnetic resonance spectral parameters are reported for triphenylphosphine as solutions in CS_2/C_6D_{12} and acetone-d_6 at 300 K. The internal rotational potential opposing torsion about the P—C bond is computed by AM1 and STO-3G MO methods. The computed potentials are used to calculate the average shielding of the *para* protons caused by the diamagnetic anisotropies of the neighbouring phenyl groups. The results are used to estimate the degree of electron delocalization from the lone pair on phosphorus. The extent of delocalization depends on the internal motions and comparisons are made with phenylphosphine. The maximum possible screening of the *para* protons in phenylphosphine is calculated as 0.19 ppm for a conformation in which the lone pair on phosphorus is oriented perpendicular to the aromatic plane. The intramolecular rotational potentials then yield 0.02_9 ppm as the shielding of the *para* protons in triphenylphosphine due to electron delocalization, just as found for the CS_2/C_6D_{12} solution after correction for diamagnetic anisotropy fields.

TED SCHAEFER, RUDY SEBASTIAN et FRANK E. HRUSKA. Can. J. Chem. **71**, 639 (1993).

On a déterminé les paramètres des spectres de résonance magnétique nucléaire du ^{1}H déterminés à 300 K pour des solutions de triphénylphosphine dans du CS_2/C_6D_{12} ou de l'acétone-d_6. Faisant appel à des méthodes AM1 et STO-3G, on a calculé le potentiel de la rotation interne qui s'oppose à la torsion autour de la liaison P—C. On a utilisé les potentiels ainsi évalués pour calculer le blindage moyen des protons en *para* provoqué par les anisotropies diamagnétiques des groupes phényles avoisinants. On utilise les résultats pour évaluer le degré de délocalisation électronique de la paire libre du phosphore. Le degré de délocalisation dépend des mouvements internes et on fait des comparaisons avec la phénylphosphine. On a évalué que le maximum de blindage des protons *para* de la phénylphosphine est égal à 0,19 ppm pour une conformation dans laquelle la paire d'électrons libres sur le phosphore est orientée perpendiculairement par rapport au plan du noyau aromatique. À cause de la délocalisation électronique, les potentiels de la rotation intramoléculaire ajoutent alors $0,02_9$ ppm au blindage des protons *para* de la triphénylphosphine, comme on l'a observé pour la solution dans le CS_2/C_6D_{12}, après correction pour les champs d'anisotropie diamagnétique.

[Traduit par la rédaction]

Introduction

Although triphenylphosphine (TPP) has been studied by a variety of physical techniques, the torsion about the P—C bonds has not been characterized. The dipole moment is insensitive to this torsion and also, apparently, to a large variation in the CPC angle (1). In the crystal the torsion angles about the three P—C bonds are unequal (2), probably best discussed as follows. With reference to **1**, it is convenient

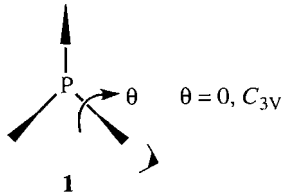

1

to define the torsion angle, θ, as zero for this conformation in which the C_3 axis lies in the phenyl planes. The other conformation of C_{3V} symmetry has θ as 90°. Intermediate chiral conformers with three equal θ values have C_3 symmetry. The conformer present in the crystal displays torsion angles of about 22°, 25°, and 54°, deviation from C_3 symmetry perhaps attributable to intermolecular forces (2).

However, the ^{31}P chemical shift tensor is axially symmetric in the solid, consistent with a large amplitude of motion of the phenyl groups about the P—C bonds (3); the inversion barrier is computed as 147 kJ/mol (4) and so inversional motions can be neglected at ambient temperatures. A large torsional amplitude implies a low barrier to rotation about the P—C bonds, consistent with ease of distortion of the molecular symmetry by packing forces in the crystal. Also implied is slight conjugation of the lone pair on phosphorus with the π electron system of the phenyl groups, consistent with P—C bond lengths of 1.83 Å, differing by only about 0.01 Å from the slightly longer P—C lengths in $P(CH_3)_3$ (2). A low degree of p...π conjugation in TPP is also indicated by its photoelectron spectrum (5), there being little apparent perturbation by the phosphorus atom of the π orbital energies of the phenyl groups.

The chemical shift of the *para* ^{13}C nucleus (C-4) is essentially the same as that in benzene (6), again consistent (7) with the absence of p–π conjugation in TPP. By way of contrast, the *para* proton (H-4) is relatively strongly shielded for solutions of TPP in benzene-d_6. δ_4 is 7.042 for a 55% w/w solution (8) and 6.926 for a 12% w/v solution (9), both at 305 K, whereas we measure δ_H as 7.153 for a 3 mol% solution of benzene in benzene-d_6 at 300 K. Of course, the benzene molecule is diamagnetically highly anisotropic and, on average, will pack about the phenyl groups of TPP so as to shield H-4; for example, a global minimum energy of −10 kJ/mol is computed for a T-arrangement of two benzene molecules, a C—H bond of one molecule lying along the C_6 axis of the other (10–12). Hence the intrinsic chemical shift of H-4 is unknown. Indeed, benzene solutions of TPP were used in the ^{1}H nmr studies because the solvent molecules, via their magnetic anisotropy, dispersed the proton shifts sufficiently to allow an analysis of the nmr spectrum.

[1]Author to whom correspondence may be addressed.

Can. J. Chem. Downloaded from www.nrcresearchpress.com by 88.255.202.194 on 09/08/12
For personal use only.

Can. J. Chem. Downloaded from www.nrcresearchpress.com by 88.255.202.194 on 09/08/12
For personal use only.

Returning to the conformational properties of TPP, both C_{3v} conformations are unstable because they entail large repulsions between the *ortho* hydrogen atoms of neighboring rings, which approach each other to within less than 1 Å in such conformations. Neither conformation will represent a global minimum in the torsional potential, written as a function of θ, even though a θ of 90° allows the maximum p...π interaction (the lone-pair orbital is roughly sp^2 hybridized, there being no direct relationship between the CPC bond angle and the hybridization state in such a description (13, 14)). Hence a collection of TPP molecules will represent, at a given instant, a mixture of nonchiral (C_{3v}) and chiral conformations, only some of the latter being characterized by three equal θ values (finite temperature). On average, however, as measured in solution by most physical methods, the conformation of TPP can be described in terms of a potential function hindering rotation about the P—C bond, having a minimum at $0° < \theta < 90°$. An approximation to this minimum is available from birefringence measurements on TPP in a benzene solution at 298 K, giving a value of 59 ± 4° (15). This number is at best a value of arc sin $\sqrt{\sin^2\theta}$ and, of course, does not define the depth of the minimum. It does raise the question as to which of the angles in the crystal are distorted by packing forces. The need for a potential was noted in a discussion of ^{13}C and ^{31}P spin-lattice relaxation times measured as a function of temperature for TPP in $CDCl_3$ solution (16). In its absence it could only be concluded that internal rotation was rather faster than rotation of the whole molecule. The latter rotation, treated as an activated process, was hindered by some 15 kJ/mol (16). While molecular mechanics calculations of the molecular geometry and the dipole moment of TPP agree well with experiment, the internal barrier has not been calculated, although such calculations yield good results for alkylphosphines (17).

The aim of the present work is threefold: first, to find the chemical shifts of the ring protons of TPP in nonpolar and polar solvents; second, to compute the potential hindering torsion of the phenyl groups; and, third, to use this potential to calculate the average shift of H-4 due to the magnetic anisotropies of the neighbouring rings. The chemical shift of H-4, corrected for the anisotropic fields and compared to the ^1H shielding of benzene in the same solvents, provides a measure of electron density at the *para* site or, at least, of p...π conjugation, in the manner usually employed (7, 18, 19) in such discussions.

Experimental

Dilute solutions of triphenylphosphine in CS_2/C_6D_{12}/TMS and acetone-d_6TMS solvent mixtures (see Table 1 for details) were filtered into 5-mm o.d. nmr sample tubes. The tubes were degassed by five cycles of the freeze–pump–thaw procedure and then flame-sealed to give symmetrical tops. The ^1H nmr free induction decays were acquired at a probe temperature of 300 K on a Bruker AM 300 spectrometer. Shimming of the magnetic field utilized the TMS response signal. Our standard procedures (20) yielded spectra in which line widths at half height were approximately 0.06 Hz, allowing the resolution of many peaks for this tightly coupled spin system.

Molecular orbital computations with the GAUSSIAN 86 algorithms (21) utilized geometry optimization procedures in the sense that the phenyl groups were constrained to be planar while all other bond angles and lengths were allowed to vary. With reference to **1**, the angle θ was increased in steps of 15° between 0 and 90° and, during the SCF cycles, the other phenyl groups were allowed to rotate. Because of the size of TPP, the computations included only the semiempirical AM1 procedure (22) and the ab initio STO-3G basis (23).

TABLE 1. The ^1H nmr spectral parameters for triphenylphosphine in CS_2/C_6D_{12} and $(CD_3)_2C{=}O$ solutions at 300 K

Parameter	Value	
	CS_2/C_6D_{12}[a]	$(CD_3)_2C{=}O$[b]
ν_2[c]	2155.095(3)[d]	2188.230(1)
ν_3	2155.907(3)	2204.190(2)
ν_4	2156.817(4)	2204.876(2)
$^3J_{23}$	7.672(5)	7.666(4)
$^3J_{34}$	7.411(5)	7.472(3)
$^4J_{26}$	1.669(7)	1.717(2)
$^4J_{24}$	1.285(4)	1.273(3)
$^4J_{35}$	1.383(6)	1.392(2)
$^5J_{25}$	0.664(2)	0.636(1)
^3J(H,P)	7.493(5)	7.656(3)
^4J(H,P)	1.449(5)	1.469(3)
^5J(H,P)	0.670(7)	0.726(4)
Calculated transitions	130	156
Assigned	75	156
Assigned	75	120
Peaks observed	54	94
Largest difference	0.019	0.017
Root-mean-square deviation	0.009	0.008

[a]As 3.0 mol% solution in CS_2 containing also 10.0 mol% of C_6D_{12} and 0.5 mol% of tetramethylsilane (TMS).
[b]As a 5.0 mol% solution in acetone-d_6, containing also 0.5 mol% of TMS.
[c]In Hz at 300.135 MHz to high frequency of internal TMS.
[d]Numbers in parentheses are standard deviations in the NUMARIT analyses.

Results and discussion

Spectral analyses

The analyses of the ^1H nmr spectra of TPP were aided by the knowledge of reasonably precise coupling constants for the spectra in benzene solutions (8, 9). The program NUMARIT (24), greatly modified by R. Sebastian, yielded the spectral parameters in Table 1. The relatively large standard deviations of some of the coupling constants, as large as 0.007 Hz for $^4J_{26}$ in CS_2/C_6D_{12}, are a consequence of the very small dispersion of the chemical shifts; the shift range is only 1.7 Hz for the nonpolar solution. The analyses are reliable, in our opinion. Thus, the iterated spectrum in acetone-d_6 solution has 156 transitions, some of which overlap, giving rise to 112 peaks; some are of very low intensity. The experimental spectrum has 94 "non-noise" peaks (significant intensities); of these, 91 were assigned, some to multiple transitions, giving rise to 120 assignments. If the total calculated intensity of the spectrum is 160.0, then the assigned intensity is 146.4, that is, over 91% of the intensity is assigned. The experimental and simulated spectra are congruent. Similar remarks apply to the analysis for the CS_2/C_6D_{12} solution.

The torsional potential

The θ dependence of the computed energies of TPP is presented in Table 2. The relative energies can be fitted to a series in $\sin^2(n\theta)$, resulting in eqs. [1] and [2] for the STO-3G

$$[1]\quad V(\theta)/\text{kJ mol}^{-1} = 1.18\sin^2\theta - 2.71\sin^2 2\theta + 0.18\sin^2 3\theta - 0.58\sin^2 4\theta$$

TABLE 2. Relative AM1 and STO-3G MO energies for P—C rotation in triphenylphosphine

Torsion angle/deg	Relative Energy/kJ mol^{-1}					
	AM1	φ_1	φ_2	STO-3G	φ_1	φ_2
0	0.00	54.8	35.1	0.00	63.7	43.6
15	−1.85	33.5	31.6	−1.13	57.1	45.6
28.3_6[a]	−2.58	28.3_6	28.3_6	—	—	—
30	−2.56	28.3	28.3	−1.87	48.6	46.6
42.5_0[a]	—	—	—	−2.06[b]	42.5_0	42.5_0
45	−1.81	26.8	24.6	−2.05	42.0	40.9
60	−0.79	26.0	23.0	−1.64	35.5	33.5
75	−0.42	27.2	24.2	0.19_5	27.4	15.9
90	0.25	22.3	25.5	1.22	4.5	−16.1

[a]At these values of θ, the other two torsion angles also have this value in the respective calculation. At other θ values, the torsion angles for the other phenyl groups, φ_1 and φ_2, are not equal to θ, naturally.
[b]The total energy is −1018.903 601 au.

[2] $V(\theta)/\text{kJ mol}^{-1} = 1.46 \sin^2\theta - 1.68 \sin^2 2\theta - 1.12 \sin^2 3\theta - 0.77 \sin^2 4\theta - 0.31 \sin^2 6\theta$

and AM1 data, respectively; the standard error of fit is 0.08 and 0.05 kJ/mol, respectively. The dominant term is the fourfold component[2] in $\sin^2 2\theta$.

The minima occur at 42.5° (STO-3G) and 28.4° (AM1) where all three torsion angles are equal (C_3 symmetry) but, at 300 K, the average values of θ are 42.0° (STO-3G) and 40.3° (AM1), suggesting perhaps that all of the angles in the crystal (see above) are significantly affected by the packing forces. The computed potentials indicate the ease with which the torsion angles can change. The AM1 energy for the conformation in the crystal is about 1.5 kJ/mol higher than that at the minimum.

Which of the two potentials is more realistic is difficult to assess. The STO-3G geometry near phosphorus for the conformation of lowest energy (Table 2) has the P—C length as 1.839 (1.828 ± 0.005) Å, the CPC angle as 101.2°(103.0 ± 0.2), and the two PCC angles as 124.9°(124.0 ± 0.4) and 117.3°(116.1 ± 0.4), the crystal (2) values being given in parentheses. The AM1 geometry is characterized by 1.751 Å, 103.2°, 124.7°, and 115.4° for these parameters. The rather short P—C length found by the semiempirical algorithm is its only apparent drawback. However, both potentials yield very similar averages in the computations below, no doubt because of their relatively shallow nature compared to thermal energies. Only if the intermolecular forces in solution were to alter the potentials dramatically, would these averages be altered significantly.

The magnetic anisotropy model

Computation of the anisotropic magnetic fields at H-2 or H-3 as a function of the internal rotational potentials is difficult because it depends on the torsional motion of the phenyl group carrying H-2 and H-3 as well as on the torsion of the group giving rise to the magnetic field. We have not solved this problem. However, the distance from H-4 to the centre of a neighbouring phenyl group is independent of the torsions about the P—c bonds. The average anisotropic field at H-4 from another phenyl group, given an internal rotational potential, is easily calculated as follows. It is convenient to define a coordinate system indicated by **2**. The origin, O, lies at the centre of the neighbouring phenyl group. The *z*-axis, the principal axis in the treatment of the neighbour anisotropic effect (25–27), is perpendicular to the page in **2** and the vector *r* lies in the plane of this phenyl group when θ′ is zero. Given that the diamagnetic anisotropy of the

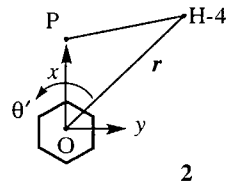

P-O, 3.2_2 Å
P-H4, 5.6_9 Å
∠CPC, 103°

2

phenyl group, $\Delta\chi = \chi_{11} - \chi_1$, is negative, and that the δ scale increases as the shielding decreases, one has eq. [3].

[3] $\Delta\delta_4 = -\Delta\chi(1 - 3\cos^2\phi)/3r^3$

Here φ is the angle between ***r*** and the *z* axis. A straightforward analysis then yields eq. [4],

[4] $\cos\phi = 0.77_6 \sin\theta'$

the coefficient depending on the angles and lengths given for **1**, as obtained from the crystal structure (2).

The calibration of eq. [3] depends on the anisotropic shift of the protons in benzene, most often taken as 1.50 ppm (27). For TPP it follows that $\Delta\delta_4 = 0.043\ \langle 1 - 3\cos^2\phi\rangle$, angular brackets indicating the expectation value determined by the torsional potential and the temperature.

The computations of the torsional potential, however, employed a different origin of the rotation angle, θ (see **1** and **2**). A simple projection into a plane perpendicular to the P—C bond demonstrates that the phase shift between θ in **1** and θ′ in **2** is very nearly 60°. Hence, write $\langle\sin^2\theta'\rangle = \langle\sin^2(\theta \pm 60)\rangle$, which, from eqs. [1] and [2], is 0.536 (AM1) and 0.521 (STO-3G) at 300 K. Consequently, eqs. [3] and [4] yield $\Delta\delta_4$ as 0.00_4 (AM1) and 0.00_7 (STO-3G) as the contributions from the magnetic anisotropy of the two neighbouring phenyl groups to the shielding of the *para* proton. The very small

[2]At first sight, the C_3 symmetry at phosphorus (ignoring the phenyl moieties) would suggest a significant threefold component, absent in eqs. [1] and [2]. While it is true that the energies for $0° \le \theta \le 60°$ are fit well by a potential containing threefold and sixfold components, the actual potential repeats at intervals of 180°.

Can. J. Chem. Downloaded from www.nrcresearchpress.com by 88.255.202.194 on 09/08/12
For personal use only.

magnitudes are a consequence of geometry and of the theoretical potentials.

Now, we measure δ_H for benzene in CS_2/C_6D_{12} as 7.218 at 300 K, to be compared with the δ_4 in TPP of 7.186. It appears that H-4 is shielded by 0.02_8 ppm due to electron delocalization from phosphorus. By way of comparison, δ_4 of phenylphosphine in C_6D_{12} is 7.078 (28) and δ_H of C_6H_6 in C_6D_{12} is 7.211, implying a $\Delta\delta_4$ of −0.133, presumably again due to p...π conjugation. The degree of conjugation depends on $\langle\sin^2\theta\rangle$, θ being the angle between the lone-pair direction and the phenyl plane.

Geometry-optimized computations give the internal barrier to rotation in phenylphosphine as eqs. [5] and [6].

[5] $V/\text{kJ mol}^{-1} = -4.72\sin^2\theta - 0.56\sin^2 2\theta + 0.04\sin^3 3\theta$ (STO-3G, standard error of 0.01 kJ/mol)

[6] $V/\text{kJ mol}^{-1} = -0.61\sin^2\theta - 0.42\sin^2 2\theta - 0.06\sin^2 3\theta$ (AM1, standard error <<0.01kJ/mol/mol)

It seems that, if the barrier is dominated by the p...π conjugation, then eq. [5] is the more reasonable, possibly because the P—C length is given satisfactorily by the STO-3G basis (see above for TPP), while the AM1 parameterization has this length rather too small.

At 300 K, the potential in eq. [5] yields $\langle\sin^2\theta\rangle$ as 0.70_3, so that the maximum $\Delta\delta_4$ is predicted[3] as $-0.133/0.70_3$ or −0.189. If this $\Delta\delta_4$ is apportioned equally among the three phenyl groups in TPP, then, for the *same* torsion potential as in phenylphosphine, $\Delta\delta_4$ is -0.06_3. But $\langle\sin^2\theta\rangle$ for TPP is 0.46 from eq. [1]. Therefore $\Delta\delta_4$ due to p...π conjugation for TPP is -0.02_9 ($\langle\sin^2\theta\rangle$ from the AM1 potential is 0.43).

This number agrees exactly with the corrected experimental value of -0.02_8 above. The small amount of shielding of H-4 in TPP due to p...π conjugation is therefore a consequence of two factors: the delocalization is shared by three phenyl groups that, due to geometry, are not oriented for optimal conjugation with the lone pair on phosphorus.

Turning to the δ_4 of 7.346 for the acetone-d_6 solution, compare it to the δ_H of 7.352 for benzene in acetone-d_6. The decreased screening of the benzene protons in acetone, relative to CS_2 solution, is understandable as a result of C^-—H^+ ... O=C interactions, the C—H bonds in benzene being polarized in the indicated manner (10–12, 30). The application of the small anisotropy shift computed for TPP above to δ_4 of TPP yields δ_4 equal to δ_H of benzene. In view of the other possible mechanisms possible in a polar solvent it is perhaps surprising at the near equivalence of these shifts. The present discussion ignores electric dipolar fields originating at phosphorus. Although the dipole moment of TPP is 1.40(3) D (1), the electronegativity of phosphorus is close to that of hydrogen. It may be that the dipole components are such that electric dipolar fields are small at the *para* position.

The coupling constants

The coupling parameters in Table 1 agree reasonably well with the earlier values (8, 9), which were necessarily of lower precision. The solvent dependences of ^nJ(H,H) are not peculiar to TPP, being similar to those found in this laboratory for a variety of benzene derivatives. For example, $^4J_{26}$ increases in the polar solvent, whereas $^4J_{24}$ decreases and $^4J_{35}$ is relatively unchanged, a generally applicable statement for monosubstituted benzene derivatives. The solvent dependences of ^nJ(H,P) in Table 1 are reminiscent of those for ^nJ(H,F) in fluorobenzene and its derivatives. For example, ^5J(H,F), while negative in 2-fluorobenzaldehyde (31), increases algebraically in passing from CS_2/C_6D_{12} to acetone-d_6 solution. Parenthetically, we find ^5J(H,P) in a TPP derivative to be negative for the benzene ring carrying the substituent. It is thought (8) that ^nJ(H,P) depends on the orientation of the lone pair relative to the phenyl plane. Hence the numbers in Table 1 imply that the internal motion about the P—C bonds is much the same in the two solvents, in line with the above discussion of the chemical shifts of H-4.

[3] $\Delta\delta_4$ is -0.62_5 for aniline in cyclohexane (19). The internal barrier to rotation about the C—N bond is relatively large, about 21 kJ/mol (29); hence this value of $\Delta\delta_4$ can be compared to the -0.18_9 for phenylphosphine. In other words if, for steric or other reasons, the lone pair on phosphorus is situated in a plane perpendicular to the benzene plane, then the degree of delocalization is about 30% effective relative to the amino group.

Acknowledgments

We thank the Natural Sciences and Engineering Research Council of Canada for a grant-in-aid of research.

1. M. P. Warchol, E. N. DiCarlo, C. A. Maryanoff, and K. Mislow. Tetrahedron Lett. 917 (1975).
2. J. J. Daly. J. Chem. Soc. 3799 (1964).
3. G. H. Penner and R. E. Wasylishen. Can. J. Chem. **67**, 1909 (1989).
4. C. A. Jolly, F. Chan, and D. S. Marynick. Chem. Phys. Lett. **174**, 320 (1990).
5. M. A. Winer, M. Lattman, and S. O. Grim. J. Org. Chem. **40**, 1292 (1975).
6. B. E. Mann. J. Chem. Soc. Perkin Trans. 2, 310 (1972).
7. E. Breitmaier and W. Voelter. Carbon-13 nmr spectroscopy. 3rd ed. VCH Publishers, New York. 1987. pp. 254–264.
8. S. Sorensen and H. J. Jakobsen. Acta Chem. Scand. Ser. A: **28**, 249 (1974).
9. L. Radics, E. Baitz-Gacs, and A. Neszmelyi. Org. Magn. Reson. **6**, 60 (1974).
10. S. K. Burley and G. A. Petsko. J. Am. Chem. Soc. **108**, 7995 (1986).
11. C. A. Hunter and J. K. M. Sanders. J. Am. Chem. Soc. **112**, 5525 (1990).
12. C. Seel and F. Vögtle. Angew. Chem. Int. Ed. Engl. **31**, 528 (1992).
13. E. Magnusson. Aust. J. Chem. **38**, 23 (1985); J. Am. Chem. Soc. **106**, 1177 (1984).
14. E. Shustorovich and P. A. Dobosh. J. Am. Chem. Soc. **101**, 4090 (1979).
15. M. J. Aroney, R. J. W. Le Fèvre, and J. D. Saxby. J. Chem. Soc. 1739 (1963).
16. M. I. M. Wazeer. Spectrochim. Acta, Part A: **45A**, 1257 (1989).
17. J. P. Bowen and N. L. Allinger. J. Org. Chem. **52**, 2937 (1987).

Can. J. Chem. Downloaded from www.nrcresearchpress.com by 88.255.202.194 on 09/08/12
For personal use only.

18. H. Günther. NMR spectroscopy. Wiley & Sons. New York. 1980. pp. 67–70.
19. H. Spiesecke and W. G. Schneider. J. Chem. Phys. **35**, 731 (1961).
20. T. Schaefer, R. Sebastian, and G. H. Penner. Can. J. Chem. **63**, 2597 (1985).
21. M. J. Frisch, J. S. Binkley, H. B. Schlegel, K. Raghavachari, C. F. Melius, R. L. Martin, J. J. P. Steward, F. W. Bobrowicz, C. F. Rohlfing, L. R. Kahn, D. J. Defrees, R. Seeger, R. A. Whiteside, D. J. Fox, E. F. Fluder, and J. A. Pople. Carnegie-Mellon Quantum Publishing Unit, Pittsburgh, Pa. 1984.
22. M. J. S. Dewar, E. J. Zoebisch, E. F. Healy, and J. J. P. Stewart. J. Am. Chem. Soc. **107**, 3902 (1985).
23. W. J. Hehre, R. Ditchfield, R. F. Stewart, and J. A. Pople. J. Chem. Phys. **52**, 2796 (1970).
24. J. S. Martin, A. R. Quirt, and K. E. Worvill. The NMR program library, Daresbury Laboratory, Daresbury, U.K.
25. H. M. McConnell. J. Chem. Phys. **27**, 226 (1957).
26. J. A. Pople. J. Chem. Phys. **24**, 111 (1956).
27. C. W. Haigh and R. B. Mallion. Prog. Nucl. Magn. Reson. Spectrosc. **13**, 303 (1980), and references therein.
28. W. J. E. Parr. J. Chem. Soc. Faraday Trans. 2, **74**, 933 (1978).
29. N. W. Larsen, E. L. Hansen, and F. M. Nicolaisen. Chem. Phys. Lett. **43**, 584 (1976).
30. M. Akiyama, Y. Shimizu, H. Itaya, and M. Kakihana. J. Phys. Chem. **93**, 2280 (1989).
31. T. Schaefer and C. S. Takeuchi. Can. J. Chem. **68**, 339 (1990).

Can. J. Chem. Downloaded from www.nrcresearchpress.com by 88.255.202.194 on 09/08/12
For personal use only.

High-resolution NMR spectroscopic analysis of the C-polysaccharide of *Streptococcus pneumoniae*[1]

MALGORZATA KULAKOWSKA, JEAN-ROBERT BRISSON, DOUGLAS W. GRIFFITH, N. MARTIN YOUNG, AND HAROLD J. JENNINGS[2]

Institute for Biological Sciences, National Research Council of Canada, Ottawa, Ont. Canada K1A 0R6

Received October 27, 1992

MALGORZATA KULAKOWSKA, JEAN-ROBERT BRISSON, DOUGLAS W. GRIFFITH, N. MARTIN YOUNG, and HAROLD J. JENNINGS. Can. J. Chem. **71**, 644 (1993).

The complete structure of the complex cell-wall C-polysaccharide from *Streptococcus pneumoniae* R36A was elucidated using a combination of high-resolution NMR spectroscopy and theoretical calculations. The C-polysaccharide is composed of the following repeating unit β-D-Glc*p*1→3-α-D-AAT*p*1→4-α-D-Gal*p*NAc1→3-β-D-Gal*p*NAc1→1-ribitol-5-phosphate where AAT is 2-acetamido-4-amino-2,4,6-trideoxygalactopyranoside. The C-polysaccharide contains two phosphorylcholine substituents per repeating unit, which are situated on O-6 of each of the two 2-acetamido-2-deoxygalactopyranose residues. The repeating units are linked through a diphosphate ester from ribitol to O-6 of the β-D-glucopyranosyl residue.

MALGORZATA KULAKOWSKA, JEAN-ROBERT BRISSON, DOUGLAS W. GRIFFITH, N. MARTIN YOUNG et HAROLD J. JENNINGS. Can. J. Chem. **71**, 644 (1993).

Faisant appel à une combinaison de RMN à haute résolution et de calculs théoriques, on a résolu la structure complète du C-polysaccharide complexe de la cellule de la paroi du *Streptococcus pneumoniae* R36A. Le C-polysaccharide est composé de l'unité répétitive suivante : β-D-Glc*p*1-β→3-α-D-AAT*p*1→4-α-D-Gal*p*NAc1→3-β-D-Gal*p*NAc1→1-ribitol-5-phosphate dans laquelle ATT est le 2-acétamido-4-amino-2,4,6-tridésoxygalactopyranoside. Le C-polysaccharide porte deux substituants phosphorylcholines par unité répétitive et elles sont situées sur le O-6 de chacun des deux résidus 2-acétamido-2-désoxygalactopyranose. Les unités répétitives sont liées par un ester diphosphate du ribitol au O-6 du résidu β-D-glucopyranosyle.

[Traduit par la rédaction]

Can. J. Chem. Downloaded from www.nrcresearchpress.com by 213.200.69.106 on 09/08/12
For personal use only.

Introduction

Streptococcus pneumoniae produce a complex species-specific antigenic polysaccharide (PnC), which was first described by Tillett and Francis (1). It is of interest as a common antigen of the various strains of pneumococci because, as a common antigen, it has the potential to be a simpler vaccine than the currently used complex mixture of type-specific polysaccharide (3). PnC contains phosphorylcholine (2) and this component is responsible for several properties of the polysaccharide. It is a major antigenic determinant (4), and the interactions of PnC with acute phase serum C-reactive protein (1) and with certain mouse myeloma proteins (5) are both due to phosphorylcholine (6, 7). PnC is attached to the cell-wall mucopeptide in the organism and mucopeptide fragments are often present in PnC preparations.

We previously published a structure for the C-polysaccharide based on methylation analysis and ^{13}C NMR spectroscopic studies (8); however, the more recent application of high-resolution NMR spectroscopic studies on PnC has revealed some minor discrepancies in the previously reported structure. Therefore, we wish now to report the revised structure of PnC based on these studies.

Experimental procedures

Growth of the organism and isolation of PnC

A frozen stock of *S. pneumoniae* R36A was used to inoculate 25 mL of sterile medium and the culture was incubated overnight at 37°C without shaking. The basal medium was Bacto Todd-Hewitt Broth (Difco No. 0492-01), which was supplemented with 0.1% (v/v) sodium bicarbonate and 1% D-glucose (50 mL of a sterile 20% (w/v) aqueous D-glucose solution added asceptically to the basal medium following autoclaving). The basal medium plus sodium bicarbonate was adjusted to pH 7.3 prior to autoclaving. The first culture was then used to inoculate 125 mL of medium and, following an additional overnight incubation, this was added to 600 mL of medium. Finally after overnight incubation, the 600 mL was used to inoculate the production flask (2500 mL of medium in a 4.0 L Erlenmeyer flask). The cultures were killed with formalin of a final concentration of 0.75% (v/v) and the cells were obtained by centrifugation.

The cells of *S. pneumoniae* R36A were extracted with trichloroacetic acid and the extract was fractionated as previously described (8). PnC was then purified from the above crude fraction by column chromatography by the method of Brundish and Baddiley (2), also as previously described by us (8). *N*-Acetylated PnC (PnCNAc) was produced by treating PnC with acetic anhydride in aqueous solution buffered with $NaHCO_3$. Oligosaccharide fragment III was obtained by periodate oxidation of PnCNAc as previously described (8) and was designated oligosaccharide III in this latter publication.

Nuclear magnetic resonance

All experiments were performed as described before by Baumann *et al.* (9) on a Bruker AMX spectrometer at 300 K using a 5-mm broadband probe with ^1H coil nearest the sample. The NMR samples consisted of 10–20 mg of each substance dissolved in 0.5 mL D_2O, at pH 7 using Na^+ counterions. Phosphoric acid (25%) was used as an external chemical shift reference for ^{31}P NMR (δ 0.00 ppm) and acetone was used as an internal chemical shift reference for ^1H NMR (δ 2.225 ppm) and for ^{13}C NMR (δ 31.07 ppm).

Calculations

The starting geometry for AAT*p* NAc (*N*-acetylated AAT*p*) and Gal*p*NAc was generated from the crystallographic data for the methyl glycoside of galactose (10). The coordinates of the methyl glycosides obtained by potential energy minimizations, using the molecular mechanics program MM2 (87) (QCPE) of Burket and Allinger (11), were then used in all calculations.

[1]NRCC No. 34321.

[2]Author to whom correspondence may be addressed.

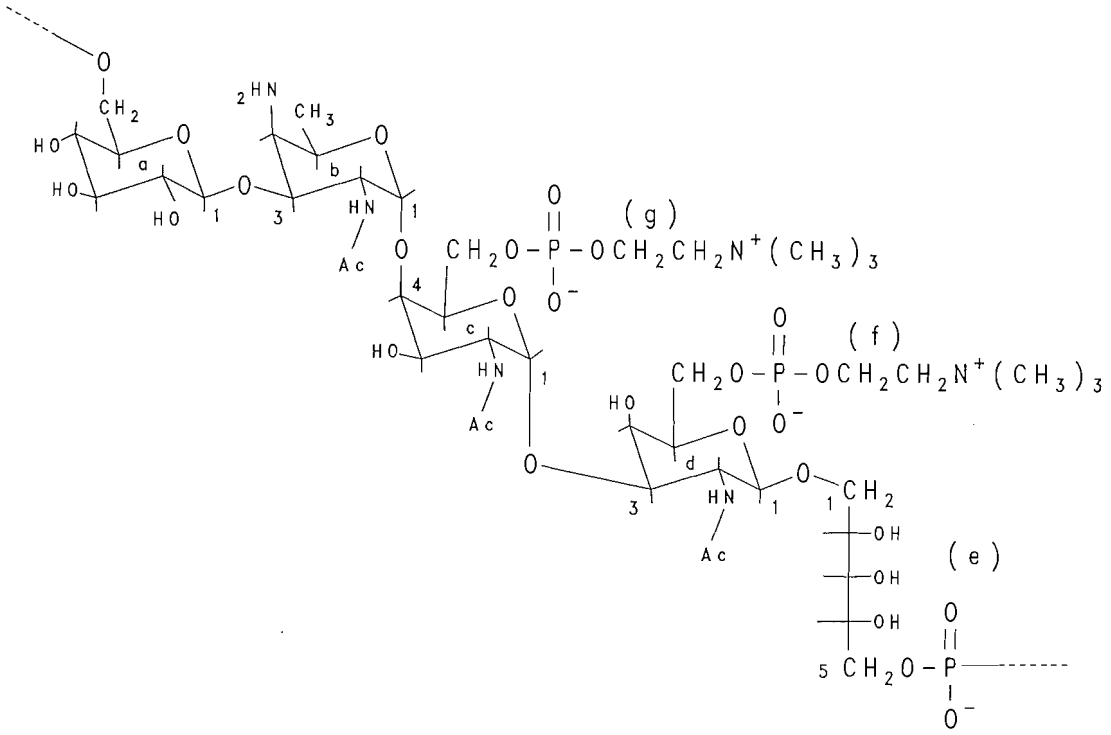

FIG. 1. Structure of the repeating unit of PnC.

The conformational analysis was evaluated using the PFOS potential designed by Tvaroska and Perez (12). Rotational barriers of 1.0 and 0.5 kcal/mol were used for ϕ and ψ, respectively. The linkage conformation for α-AAT*p*NAc-(1→4)-α-Gal*p*NAc (**b**–**c**) was defined by ϕ = (H1**b**—C1**b**—O1**b**—C4**c**) and ψ = (C1**b**—O1**b**—C4**c**—H4**c**). The glycosidic bridge angle C1**b**—O1**b**—C4**c** was set at 117°. Potential energy maps were calculated at 5° intervals for ϕ and ψ.

The truncated driven NOE was calculated using the complete relaxation matrix with the assumption of isotropic tumbling (13). The (ϕ,ψ) ensemble $\langle r^{-6}\rangle$ averaged NOE was calculated as described by Cumming and Carver (14). The rotational correlation time of 2 ns used in the NOE calculations was determined from a best fit of the experimental data to the calculated values for the intraresidue NOE's.

Results and discussion

Structure of PnC

The revised structure of PnC as determined by high-resolution NMR spectroscopy and theoretical calculations is shown in Fig. 1. The complete assignment of proton and carbon signals was carried out as described by Baumann *et al.* (9) and each spin system could be combined with one of the five sugar residues or one of two phosphorylcholine substituents in the repeating unit of PnC. The ^{1}H and ^{13}C NMR chemical shifts for the individual components of PnC together with their corresponding monosaccharides are given in Tables 1 and 2. The residues are labeled **a**–**e** in order of sequence, **g** and **f** being phosphorylcholine substituents. The high-resolution ^{1}H and ^{13}C NMR spectra are consistent with the same five sugar residues identified earlier (8) in the repeating unit of PnC, e.g., β-D-glucopyranose (a), 2-acetamido-4-amino-2,4,6-trideoxy-D-galactopyranose (b), 2-acetamido-2-deoxy-α-D-galactopyranose (c), 2-acetamido-β-D-galactopyranose (d), and ribitol-5-phosphate (e), except that both residues **c** and **d** were found to be *N*-acetylated. Previous studies (8) had identified two free amino functions on residues **b** and **d**, whereas in the revised structure of PnC only residue **b** was found to have a free amino group. This observation is also consistent with the identification of three distinct *N*-acetyl signals at 2.092, 2.083, and 2.050 ppm in the ^{1}H NMR spectrum of PnC (Table 1) and an additional *N*-acetyl signal in the ^{1}H NMR spectrum of PnCNAc and the oligosaccharide fragment (III) of PnCNAc (8) containing residues **b**, **c**, **d**, **g**, and **f** (Table 1).

After determination of all the residues and substituents of PnC, the revised structure was established with the help of other NMR methods. Although the sequence of sugars in the repeating unit of PnC had been well established by fragmentation techniques (8), it was further confirmed in 2D NOE studies. Interresidue NOE's were found for all linkages in PnC, and cross sections from the 2D NOE spectrum showing enhancements from the anomeric protons are shown in Fig. 2. The pattern of enhanced signals is entirely consistent with the sequence proposed for the repeating unit of PnC (Fig. 1), the only complexity being due to the overlap of the 1**d** and 5**b** signals.

The identification of two different phosphorylcholine substituents in PnC was not previously detected (8) in earlier ^{13}C NMR spectroscopic studies, where only one (**f**) was identified situated on O6 of **d**. The additional phosphorylcholine substituent was also identified in a ^{1}H–^{31}P correlated spectrum (HMQC) of PnC (Fig. 3), which showed the presence of three different diphosphate esters (^{31}P chemical shifts listed in Table 3) and their connectivities. Consistent with previous assignments (8) the phosphate diester linkage in PnC has connectivities to C5 of **e** and C6 of **a**, indicating linkages to O5 of **e** and O6 of **a**, and the phosphodiester group of one of the phosphorylcholine substituents (f) has connectivities to C6 of **d**, indicating a linkage to O6 of **d**. For the newly identified phosphorylcholine substituent the phos-

Can. J. Chem. Downloaded from www.nrcresearchpress.com by 213.200.69.106 on 09/08/12
For personal use only.

TABLE 1. Proton chemical shifts[a] of PnC, PnCNAc, and oligosaccharide fragment from PnCNAc

Compound	Unit	H1	H2	H3	H4	H5	H6
PnC[b]	A	4.619	3.31	3.50	3.54	3.55	4.11, 4.11
	B	4.918	4.31	4.17	3.44	4.58	1.202
	C	5.181	4.32	3.91	4.07	4.00	4.02, 3.99
	D	4.640	4.10	3.85	4.17	3.83	4.06, 4.06
	E	3.96, 3.86	3.99	3.76	3.88	4.04, 3.98	
	F	4.33	3.69	3.23			
	G	4.28	3.67	3.23			
PnCNAc[c]	A	4.554	3.27	3.48	3.52	3.50	4.12, 4.12
	B	4.927	4.34	4.27	4.43	4.60	1.039
	C	5.156	4.31	3.90	4.07	3.99	4.02, 3.99
	D	4.612	4.09	3.85	4.17	3.83	4.06, 4.06
	E	3.96, 3.86	3.98	3.76	3.85	4.06, 3.99	
	F	4.33	3.69	3.23			
	G	4.29	3.67	3.23			
III[d]	B	4.926	4.08	4.19	4.29	4.62	1.060
	C	5.139	4.33	3.90	4.06	4.00	4.02, 3.98
	D	4.599	4.09	3.85	4.17	3.82	4.05, 4.05
	E	3.94, 3.75	3.72				
	F	4.33	3.67	3.23			
	G	4.29	3.67	3.23			

[a]In ppm measured at 600 MHz in D_2O and at 300 K with internal acetone (2.225 ppm).
[b]NAc at 2.092, 2.083, and 2.050 ppm.
[c]NAc at 2.103, 2.097, 2.080, and 2.051 ppm.
[d]NAc at 2.108, 2.103, 2.074, and 2.046 ppm.

TABLE 2. Carbon-13 chemical shifts[a] of PnC, PnCNAc, and oligosaccharide fragment from PnCNAc

Compound	Unit	C1	C2	C3	C4	C5	C6
PnC[b]	A	104.81	73.79	76.37	69.68	75.22[e]	64.92[f]
	B	99.28	48.98	78.66	54.51	66.82	16.68
	C	94.19	50.26	67.74	77.17	71.64[e]	64.54[f]
	D	102.08	51.46	75.49	64.07	74.30[e]	65.33[f]
	E	71.46	71.35	72.23	71.46	67.46[f]	
	F	60.37[f]	66.82	54.82			
	G	60.30[f]	66.82	54.82			
PnCNAc[c]	A	104.12	73.78	76.26	69.48	75.45[e]	64.80[f]
	B	99.19	49.99	75.80	53.54	67.29	16.39
	C	94.21	50.19	67.67	77.04	71.46[e]	64.44[f]
	D	102.03	51.43	75.49	64.08	74.23[e]	65.26[f]
	E	71.46	71.22	72.20	71.46	67.42[f]	
	F	60.32[f]	66.78	54.82			
	G	60.32[f]	66.78	54.82			
III[d]	B	99.24	51.41	67.25	54.36	66.95	16.35
	C	94.14	50.20	67.79	77.32	71.71[e]	64.70[f]
	D	102.09	51.32	75.44	63.97	74.27[e]	65.24[f]
	E	72.08	61.45				
	F	61.81	60.33[f]	54.83[f]			
	G	61.81	60.30[f]	54.80[f]			

[a]In ppm measured at 600 MHz (^1H) in D_2O and at 300 K, with the methyl group of internal acetone set at 31.07 ppm.
[b]NAc at 23.23, 22.97, 22.86, 175.60, 175.46, 175.24 ppm.
[c]NAc at 23.21, 23.02, 22.86, 175.67, 175.53, 175.43, 175.15 ppm.
[d]NAc at 23.16, 22.89, 22.81, 22.71, 176.47, 175.58, 175.48, 175.09 ppm.
[e]$J(^{31}P-^{13}C)$ of 7–8 Hz.
[f]$J(^{31}P-^{13}C)$ of 3–5 Hz.

phate diester has connectivities to C6 of **c** as determined from the HMQC spectrum of PnC (Fig. 3), indicating that it is linked to O6 of **c**.

In previous studies on the structure of PnC (8), the absolute configuration of AAT was not assigned. However, more recently it has been shown that potential energy calculations can be used in combination with NMR to determine the absolute configuration of sugars, including AAT, while they

Can. J. Chem. Downloaded from www.nrcresearchpress.com by 213.200.69.106 on 09/08/12
For personal use only.

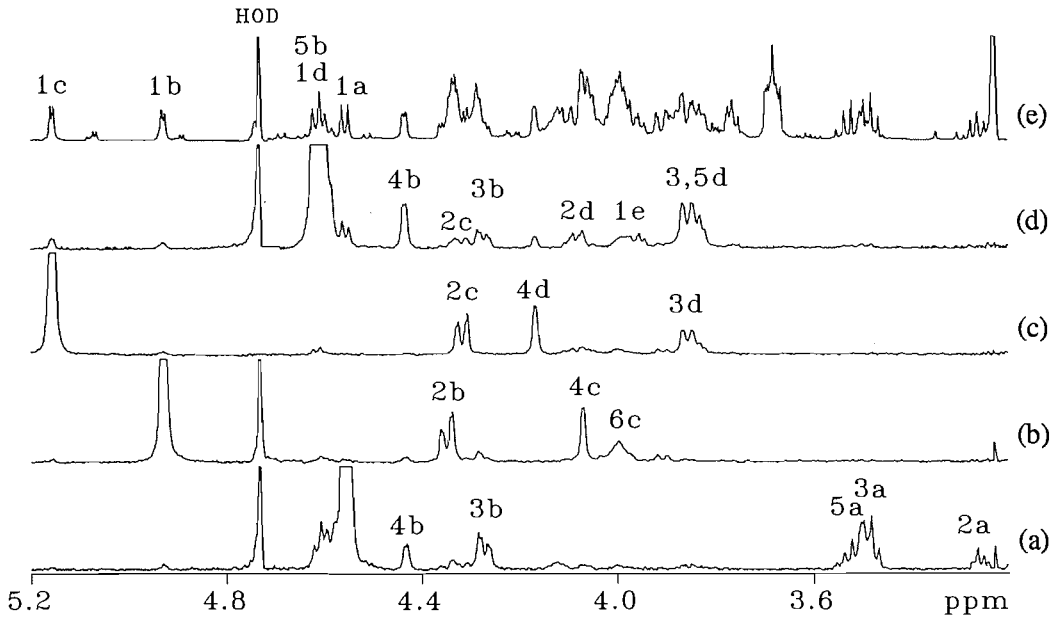

FIG. 2. Truncated driven NOE difference spectra for 400 ms irradiation of H1**a** (*a*), H1**b** (*b*), H1**c** (*c*), H1**d** and H5**b** (*d*) and the resolution enhanced partial ^{1}H spectrum (*e*) at 600 MHz for PnCNAc in D_2O at 300 K.

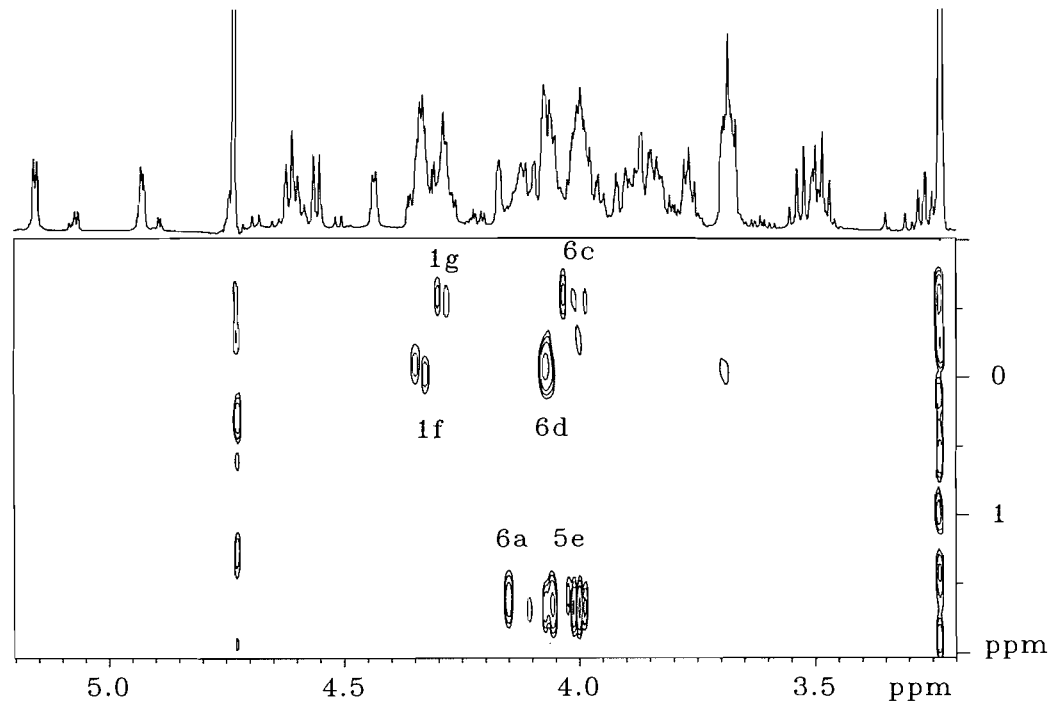

FIG. 3. Proton detected $^1H-^{31}P$ correlated spectrum (HMQC) of PnCNAc indicating the presence of three phosphorus atoms and the linkage sites.

are still components of the polysaccharide chain (9). The NOE, due to its sensitivity to interatomic proton distances, was also used to determine the absolute configuration of AAT (b) in PnCNAc. The (ϕ,ψ) potential energy contour map for α-D-AAT$_p$NAc-(1–4)-α-D-Gal$_p$NAc and α-L-AAT$_p$NAc-(1–4)-α-D-Gal$_p$NAc (Fig. 4) showed that the conformational space of each disaccharide was quite different. The calculated ensemble average NOE's for both disaccharides were also quite different (Table 4) and clearly indicated that AAT had the D configuration. Especially, the H1**b**–H6**c** and H5**b**–H2**c** NOE's were quite sensitive to the absolute configuration of AAT. In contrast, the calculated inter-residue NOE's for β-D-Glc$_p$-(1–3)-α-D-AAT$_p$NAc and β-D-Glc$_p$-(1–3)-α-L-AAT$_p$NAc where not very sensitive to the relative configuration of both sugars, since the potential energy surfaces for both disaccharides were similar (data not shown).

In a recent publication using mass spectrometric studies (15), Behr *et al.* proposed an identical structure to the one

Can. J. Chem. Downloaded from www.nrcresearchpress.com by 213.200.69.106 on 09/08/12
For personal use only.

TABLE 3. Phosphorus-31 chemical shifts[a] of PnC, PnCNAc, and oligosaccharide fragment from PnCNAc

Compound	E	F	G
PnC	1.42	−0.12	−0.60
PnCNAc	1.65	−0.07	−0.56
III		−0.14	−0.59

[a]In ppm measured at 600 MHz (^{1}H) in D_2O and at 300 K with external phosphoric acid (25%) as reference (0 ppm).

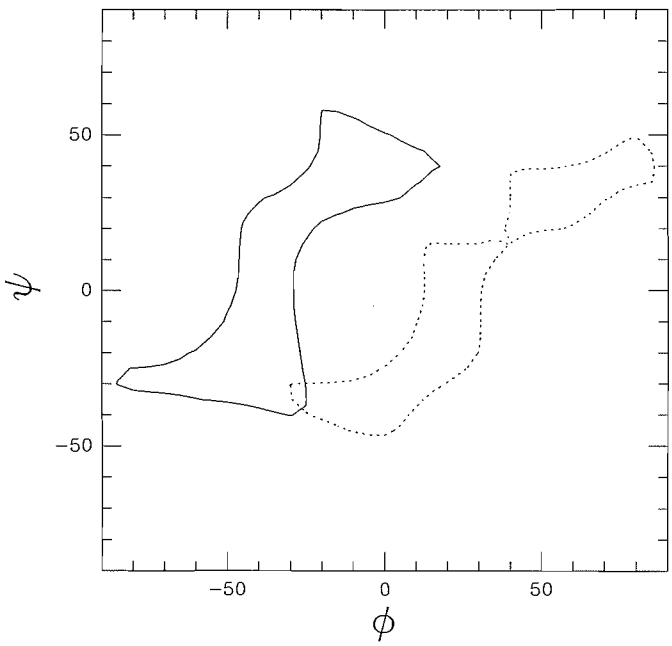

FIG. 4. (ϕ,ψ) potential energy contour map for disaccharide **b**–**c** showing the 10 kcal/mol level above the global minimum for α-D-AAT$_p$NAc-(1–4)-α-D-Gal$_p$NAc (solid line) and α-L-AAT$_p$NAc-(1–4)-α-D-Gal$_p$NAc (dotted line) with ϕ = (H1**b**—C1**b**—O1**b**—C4**c**) and ψ = (C1**b**—O1**b**—C4**c**—H4**c**).

shown in Fig. 1 for the repeating unit of the glycose chain of pneumococcal lipoteichoic acid. Therefore the structure of the glycose chains of pneumococcal cell wall teichoic acid and pneumococcal lipoteichoic acid are identical.

TABLE 4. Experimental NOE[a] for PnCNAc and Calculated (ϕ,ψ) ensemble $\langle r^{-6} \rangle$ averaged NOE for α-D-AAT$_p$NAc-(1–4)-α-D-Gal$_p$NAc (DD) and α-L-AAT$_p$NAc-(1–4)-α-D-Gal$_p$NAc (LD)

Irr.	Obsd.	Experimental	Calcd. (DD)	Calcd. (LD)
H1**b**	H1*b*	100	100	100
	H2*b*	23	18	18
	H3*c*	2	3	5
	H4*c*	15	23	32
	H6*c*	24	8–20[b]	1–3[b]
H5**b**	H5*b*	100	100	100
	H1*b*	1	2	2
	H3*b*	9	12	12
	H4*b*	15	15	15
	H6*b*	10	9	10
	H1*c*	2	1	<1
	H2*c*	7	4	<1

[a]Truncated driven NOE with 400 ms irradiation time with an estimated relative error of ±25%.
[b]The expected NOE range H6*R* and H6*S* for the three staggered rotamers of the hydroxymethyl group of unit **c** is shown.

1. W. S. Tillett and T. Francis. J. Exp. Med. **52**, 561 (1930).
2. D. E. Brundish and J. Baddiley. Biochem. J. **110**, 573 (1968).
3. D. E. Briles, C. Forman, and M. Crain. Infect. Immun. **60**, 1957 (1992).
4. M. Heidelberger, E. C. Gotschlich, and J. D. Higginbotham. Carbohydr. Res. **22**, 1 (1972).
5. M. Potter and M. A. Leon. Science (Washington, D.C.), **162**, 369 (1968).
6. M. A. Leon and N. M. Young. Biochemistry, **10**, 1424 (1971).
7. J. E. Volonakis and M. H. Kaplan. Proc. Soc. Exp. Biol. Med. **136**, 612 (1971).
8. H. J. Jennings, C. Lugowski, and N. M. Young. Biochemistry, **19**, 4712 (1980).
9. H. Baumann, A. O. Tzianabos. J.-R. Brisson, D. L. Kasper, and H. J. Jennings. Biochemistry, **31**, 4081 (1992).
10. S. Takagi and G. A. Jeffrey. Acta. Crystallogr. Sect. B: Struct. Crystallogr. Cryst. Chem. **B35**, 902 (1979).
11. V. Burket and N. L. Allinger. Molecular mechanics. ACS Monogr. **177**, American Chemical Society, Washington, D.C. 1982.
12. I. Tvaroska and S. Perez. Carbohydr. Res. **149**, 389 (1986).
13. D. Neuhaus and M. P. Williamson. The nuclear Overhauser effect in structural and conformational analysis. VCH Publishers, Inc., New York. 1989.
14. D. A. Cumming and J. P. Carver. Biochemistry, **26**, 6664 (1987).
15. T. Behr, W. Fischer, J. Peter-Katalinic, and H. Egge. Eur. J. Biochem. **207**, 1063 (1992).

Can. J. Chem. Downloaded from www.nrcresearchpress.com by 213.200.69.106 on 09/08/12
For personal use only.

A kinetic study on the reactivity of chromium(IV)

JOAQUIN F. PEREZ-BENITO AND CONCHITA ARIAS
Departamento de Quimica Fisica, Facultad de Quimica, Universidad de Barcelona, Marti i Franques, 1, 08028 Barcelona, Spain

Received November 24, 1992

JOAQUIN F. PEREZ-BENITO and CONCHITA ARIAS. Can. J. Chem. **71**, 649 (1993).

The inhibition effect of Mn^{2+} on the rates of the Cr(VI) oxidations of 13 different organic reductants (RH) in aqueous perchloric acid has been studied. The reductants were formaldehyde, formic acid, maleic acid, and 10 alcohols (8 primary and 2 secondary). The second-order rate constants decrease with increasing $[Mn^{2+}]$ according to the law

$$k_2 = a/(1 + b'\,[Mn^{2+}]/[RH]) + c$$

Parameter b' is interpreted as the ratio between the rate constants for the Cr(IV)–Mn^{2+} and Cr(IV)–RH reactions. Cr(IV) is reduced by Mn^{2+} (and also by Ce^{3+}) much faster than by organic reductants RH. The Cr(IV) oxidations of primary alcohols follow Taft's equation with a negative reaction constant ($\rho^* = -0.80 \pm 0.06$). The Cr(IV) present in aqueous perchloric acid is postulated as an oxo species (CrO^{2+}) capable of reacting by one-electron transfer with both Mn^{2+} and Ce^{3+}, and by hydride-ion transfer with organic reductants. Relevance of these results to the general mechanism for the Cr(VI) oxidations of organic substrates is discussed.

JOAQUIN F. PEREZ-BENITO et CONCHITA ARIAS. Can. J. Chem. **71**, 649 (1993).

On a étudié l'effet inhibiteur du Mn^{2+} sur les vitesses d'oxydations chromiques de 13 agents réducteurs organiques différents (RH), dans de l'acide perchlorique aqueux. Les agents réducteurs étudiés sont : le formaldéhyde, l'acide formique, l'acide maléique et 10 alcools (dont 8 primaires et 2 secondaires). Les constantes de vitesse du deuxième ordre diminuent avec une augmentation de $[Mn^{2+}]$ en suivant la loi suivante :

$$k_2 = a/(1 + b'[Mn^{2+}]/[RH]) + c.$$

On interprète le paramètre b' comme le rapport entre les constantes de vitesse des réactions avec Cr(IV)–Mn^{2+} et Cr(IV)–RH. Le Cr(IV) est réduit par le Mn^{2+} (ainsi que par Ce^{3+}) à une vitesse beaucoup plus grande que celle observée avec les agents réducteurs RH. Les oxydations des alcools primaires par le Cr(IV) suivent l'équation de Taft et la constante de la réaction est négative ($\rho^* = -0{,}80 \pm 0{,}06$). On fait l'hypothèse que le Cr(IV) présent dans l'acide perchlorique aqueux est sous la forme d'une espèce oxo (CrO^{2+}) capable de réagir par un transfert monoélectronique avec le Mn^{2+} ainsi qu'avec le Ce^{3+} et par un transfert d'hydrure avec les agents réducteurs organiques. On discute de l'importance de ces résultats pour le mécanisme général des oxydations des substrats organiques par le Cr(VI).

[Traduit par la rédaction]

Introduction

In a pioneering work, Westheimer (1) proposed two possible mechanisms for the chromium(VI) oxidations of organic substrates (RH). In one of them chromium(V) and chromium(IV) are involved as the only chromium intermediates (Mechanism I).

Mechanism I

$$\mathrm{Cr(VI)} \xrightarrow{\mathrm{RH}} \mathrm{Cr(IV)} \xrightarrow{\mathrm{Cr(VI)}} 2\mathrm{Cr(V)} \xrightarrow{\mathrm{RH}} 2\mathrm{Cr(III)}$$

Alternatively, the second mechanism also involves chromium(II) as an intermediate (Mechanism II).

Mechanism II

$$\mathrm{Cr(VI)} \xrightarrow{\mathrm{RH}} \mathrm{Cr(IV)} \xrightarrow{\mathrm{RH}} \mathrm{Cr(II)} \xrightarrow{\mathrm{Cr(VI)}} \mathrm{Cr(III)}$$

$$+\ \mathrm{Cr(V)} \xrightarrow{\mathrm{RH}} \mathrm{Cr(III)}$$

We can see that in both Westheimer's mechanisms the organic substrate behaves as a two-equivalent reducing agent throughout the reaction sequence. However, Rocek and coworkers (2) have proposed a third mechanism in which the organic substrate behaves as a two-equivalent reducing agent toward both chromium(VI) and chromium(V), and as a one-equivalent reducing agent toward chromium(IV) (Mechanism III).

Mechanism III

$$\mathrm{Cr(VI)} \xrightarrow{\mathrm{RH}} \mathrm{Cr(IV)} \xrightarrow{\mathrm{RH}} \mathrm{Cr(III)} + \mathrm{R}\cdot$$

$$\mathrm{Cr(VI)} \xrightarrow{\mathrm{R}\cdot} \mathrm{Cr(V)} \xrightarrow{\mathrm{RH}} \mathrm{Cr(III)}$$

Although Mechanism I has been preferred in the past, in recent years Mechanism III has been widely accepted as the correct mechanism for the chromium(VI) oxidations of many organic compounds (3*a*).

On the other hand, Mechanism II has been dismissed by most authors, largely because chromium(II) is such a powerful reducing agent that it is not considered a likely species in the system (4). Although Beattie and Haight (5) pointed out that Mechanism II had not been ruled out by any valid experiment or theoretical argument, neither was there evidence to support it.

However, in recent work Scott, Bakac, and Espenson have clearly demonstrated that chromium(IV) is actually reduced by methanol (6*a*) and other organic compounds (6*b*) to chromium(II) and not to chromium(III). Therefore, Mechanism II has to be considered as correct.

We now wish to report some experiments which, by an independent method, confirm the results found by those authors. Whereas they trapped chromium(II) with oxygen to form superoxochromium(III) ion (CrO_2^{2+}) and followed formation of the latter at 245 and 290 nm (6*b*), we have used the inhibitory effect that manganese(II) ion is known to exert

Can. J. Chem. Downloaded from www.nrcresearchpress.com by 213.200.69.106 on 09/08/12
For personal use only.

on the rates of the chromium(VI) oxidations of many organic compounds (7, 8). Mn(II) behaves as a trap for chromium(IV) (9),

[1] $Cr(IV) + Mn(II) \rightarrow Cr(III) + Mn(III)$

whereas the direct oxidation of manganese(II) ion by chromium(VI) is thermodynamically unfavorable (5). In this way, we have been able to study the reactivity of Cr(IV), which (as can be seen in Mechanisms I–III) is the key intermediate for selecting the correct mechanism.

Experimental section

The solvent water was purified by deionization followed by double distillation (the first time from a potassium permanganate solution). The acidity of the solutions was controlled with perchloric acid. The ionic strength of the solutions was kept constant with appropriate additions of sodium perchlorate.

The oxidant was chromium(VI) from commercially available potassium dichromate. The organic substrates acting as reductants were formaldehyde, formic acid, maleic acid, methanol, ethanol, 2-chloroethanol, 2-methoxyethanol, 2-ethoxyethanol, 1-propanol, 2-propanol, 1-butanol, benzyl alcohol, and 2,5-hexanediol. The reductants were in all cases in large excess with respect to chromium(VI).

The inhibitors were manganese(II) ion from commercial manganese(II) sulfate, and cerium(III) ion from commercial cerium(III) nitrate. They always were in very low concentration, so that the ionic strength of the solution was controlled by the total perchlorate concentration ($HClO_4$ + $NaClO_4$).

All of the reagents were used as purchased (analytical grade), except 2-propanol (reagent grade), which was used after distillation.

The reactions were followed by monitoring the chromium(VI) decay at 352 nm with a Varian Cary 219 UV–vis spectrophotometer. This instrument was equipped with a cell holder with capacity for five cuvettes (quartz, lightpath 1 cm) that was connected to an externally thermostated bath at 25.0°C.

The kinetic data were obtained by means of the initial-rates method. Since initial rates were found to be rather sensitive toward the room temperature (at which some manipulations at the beginning of the kinetic runs had to be necessarily done), the temperature of the laboratory was kept as close as possible to that of the runs (external temperature 25.0 ± 0.8°C). The kinetic data given in this work are the averages of two independent determinations for each rate constant. Reproducibility of those duplicate determinations was excellent (average standard deviation ±0.6% for 1700 kinetic runs).

Results

Although the reductants always were in large excess with respect to chromium(VI), the first-order rate plots (ln [Cr(VI)] vs. time) failed, in some of the cases, to yield straight lines. Actually, for four of the reductants (methanol, 2-chloroethanol, 2-methoxyethanol, and maleic acid) the reaction rate decreased more slowly than expected from the corresponding chromium(VI) decay. This behavior, typical of autocatalytic processes (10, 11), is probably due to overoxidation of the organic reaction products by chromium(VI) (2*b*). For the other nine reductants, however, the first-order rate plots were fairly linear.

As a consequence, the kinetic data were obtained by means of the initial-rates method. The initial reaction rate was directly proportional to the concentrations of both oxidant (initial) and reductant in all of the cases. The second-order rate constants were obtained from the initial rates (r_0) as indicated in eq. [2],

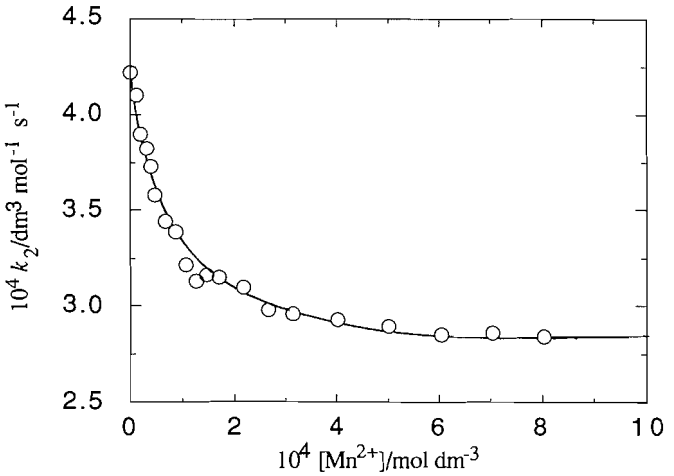

FIG. 1. Decrease of the second-order rate constant with the manganese(II) ion concentration for the oxidation of 2-ethoxyethanol (0.206 mol dm^{-3}) by chromium(VI) (8.74×10^{-4} mol dm^{-3}) in aqueous perchloric acid (0.366 mol dm^{-3}) at 25.0°C.

[2] $k_2 = r_0/[Cr(VI)]_0\,[RH]$

where [RH] denotes the concentration of organic substrate. For the nine reductants with linear first-order rate plots the rate constants obtained from those plots were in good agreement with those obtained from the initial rates (typical difference, ±2%).

In all of the cases studied by us, the reaction rate decreased when manganese(II) ion was added in low concentration to the solutions (Fig. 1). The decrease of the second-order rate constant with increasing manganese(II) ion concentration could always be fitted to functions of the type given in eq. [3] (12).

[3] $k_2 = a/(1 + b[Mn^{2+}]) + c$

Parameters *a*, *b*, and *c* were obtained in each case by a nonlinear least-squares fit.

The second-order rate constants corresponding to the noninhibited reactions were obtained from the sums $a + c$, and are given in Table 1. The ratios $(a + c)/c$ gave the values of the maximum inhibition attained in each case. Those ratios always were in the range 1–2, and they were fairly independent of the concentrations of both chromium(VI) and organic substrate, but decreased markedly as the perchloric acid concentration increased (Table 2).

The slopes of both the log *b* vs. log $[Cr(VI)]_0$ and log *b* vs. log. [RH] plots were obtained for nine different organic substrates and are given in Table 3. We can see that the slope of the log *b* vs. log $[Cr(VI)]_0$ plots ranged between −0.15 and +0.17, the average value being 0.00 ± 0.10, whereas the slope of the log *b* vs. log [RH] plots ranged between −1.19 and −0.88, the average value being −1.00 ± 0.10. Therefore, we can conclude that parameter *b* was in all cases roughly independent of the initial concentration oxidant, whereas it was inversely proportional to the reductant concentration. Hence, eq. [3] can be rewritten as

[4] $k_2 = a/(1 + b'\,[Mn^{2+}]/[RH]) + c$

Can. J. Chem. Downloaded from www.nrcresearchpress.com by 213.200.69.106 on 09/08/12
For personal use only.

Can. J. Chem. Downloaded from www.nrcresearchpress.com by 213.200.69.106 on 09/08/12
For personal use only.

TABLE 1. Values of the second-order rate constant for the oxidations of several reductants (RH) by chromium(VI) (8.74×10^{-4} mol dm^{-3}) in aqueous percloric acid (0.366 mol dm^{-3}) at 25.0°C in the absence of inhibitors

RH	$10^4 k_2$ (dm^3 mol^{-1} s^{-1})
Formic acid	0.529
2-Chloroethanol	0.567
Methanol	0.587
2-Methoxyethanol	1.40
2-Ethoxyethanol	4.22
2-Propanol	13.5
Ethanol	14.6
1-Propanol	14.8
1-Butanol	22.7
Maleic acid[a]	29.0
2,5-Hexanediol	39.7
Benzyl alcohol	177
Formaldehyde	250

[a][$HClO_4$] = 1.83 mol dm^{-3}.

TABLE 2. Dependence of the maximum inhibition ratio on the concentration of perchloric acid for inhibition by manganese(II) ion in the chromium(VI) oxidation of formic acid[a]

[$HClO_4$] (mol dm^{-3})	Ratio[b]
0.37	1.90
0.73	1.68
1.10	1.53
1.46	1.42
1.83	1.36

[a][Cr(VI)]$_0$ = 8.00×10^{-4} mol dm^{-3}, [HCO_2H] = 0.530 mol dm^{-3}, ionic strength = 1.83 mol dm^{-3} ($NaClO_4$), temperature 25.0°C.
[b]Calculated as $(a + c)/c$.

TABLE 3. Dependence of parameter b on the concentrations of both oxidant and reductant for inhibition by manganese(II) ion in the chromium(VI) oxidations of several reductants (RH) at 25.0°C

RH	Oxidant[a]	Reductant[b]
2-Propanol[c]	−0.15 ± 0.05	−0.88 ± 0.11
Ethanol[c]	−0.14 ± 0.02	−1.00 ± 0.08
Formic acid[d]	−0.03 ± 0.03	−0.91 ± 0.04
Maleic acid[e]	−0.01 ± 0.04	−0.92 ± 0.04
2,5-Hexanediol[c]	0.00 ± 0.04	−1.00 ± 0.09
Methanol[c]	0.02 ± 0.10	−1.19 ± 0.18
2-Methoxyethanol[c]	0.06 ± 0.07	−1.01 ± 0.04
Formaldehyde[f]	0.09 ± 0.03	−1.09 ± 0.09
1-Propanol[c]	0.17 ± 0.08	−1.01 ± 0.02

[a]Slopes from log b vs. log [Cr(VI)]$_0$ plots. Average slope: 0.00 ± 0.10.
[b]Slopes from log b vs. log [RH] plots. Average slope: −1.00 ± 0.10.
[c][$HClO_4$] = 0.366 mol dm^{-3}.
[d][$HClO_4$] = 0.731 mol dm^{-3}.
[e][$HClO_4$] = 1.83 mol dm^{-3}.
[f][$HClO_4$] = 0.146 mol dm^{-3}.

TABLE 4. Values of parameter b' for inhibition by manganese(II) ion in the oxidations of several reductants (RH) by chromium(VI) (8.74×10^{-4} mol dm^{-3}) in aqueous percloric acid (0.366 mol dm^{-3}) at 25.0°C

RH	$10^{-3}b'$	$b'_{2\text{-PrOH}}/b'_{RH}$[a]	$k_{RH}/k_{2\text{-PrOH}}$[b]
1-Propanol	0.98	10.1	—
1-Butanol	1.06	9.4	3.6
Formaldehyde	1.17	8.5	7.6
Ethanol	1.64	6.1	7.4
2-Ethoxyethanol	1.76	5.6	—
Benzyl alcohol	2.04	4.9	4.7
Methanol	2.08	4.8	4.4
2-Methoxyethanol	4.14	2.4	—
2,5-Hexanediol	4.98	2.0	—
2-Chloroethanol	8.90	1.1	—
Maleic acid[c]	9.48	1.0	—
2-Propanol	9.93	1.0	1.0
Formic acid	81.6	0.12	0.16

[a]Ratios between the values of parameter b' for 2-propanol and RH.
[b]Ratios between the values of the rate constants for the reactions of Cr(IV) with RH and 2-propanol given in ref. 6*b*.
[c][$HClO_4$] = 1.83 mol dm^{-3}.

where b' is a new, dimensionless parameter defined as $b' = b[RH]$.

The values of b' obtained for the organic substrates studied in this work are listed in Table 4. All these values are given for the same perchloric acid concentration (0.366 mol dm^{-3}) except for the case of maleic acid (1.83 mol dm^{-3}), since the latter was very unreactive toward chromium(VI) unless a high concentration of perchloric acid was used. It is interesting to notice that all the values given in Table 4 are much larger than unity (the lowest is around 10^3). Also, the value obtained for oxidation of formic acid was much higher than those obtained for the other organic substrates. In particular, b' for formic acid was around 70 times higher than the value for formaldehyde, which means that manganese(II) ion was a much more efficient inhibitor for the Cr(VI)–HCO_2H reaction than for the Cr(VI)–HCHO reaction.

It can be seen in Fig. 2 for inhibition by manganese(II) ion in the chromium(VI) oxidations of primary alcohols that, except for the case of benzyl alcohol, the logarithm of parameter b' gave a good linear correlation with Taft's polar substituent constant σ^* (13), and the associated slope was $\rho^* = -0.80 \pm 0.06$.

Parameter b' has also been represented against the second-order rate constant corresponding to the non-inhibited oxidation of each organic substrate by chromium(VI) in a double-logarithmic plot (Fig. 3). For six of the eight primary alcohols studied a good linear correlation was obtained, the only primary alcohols falling outside of the linear correlation being methanol and benzyl alcohol. It is interesting to notice that the point corresponding to the latter correlated well with those corresponding to the two secondary alcohols studied (2-propanol and 2,5-hexanediol).

Finally, since the cerium(III) ion is known to exert an inhibitory effect on the chromium(VI) oxidations of many organic compounds similar to that exerted by the manganese(II) ion (14), given that both ions reduce chromium(IV) to chromium(III), we performed some experiments in order to compare the inhibitory effects caused by the two ions on the

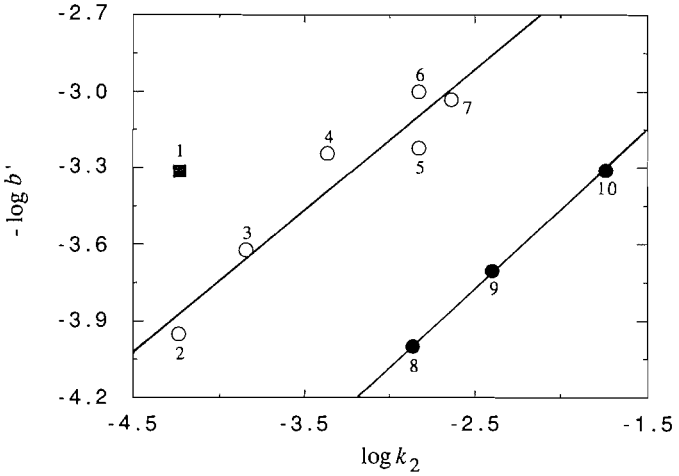

FIG. 2. Logarithm of parameter b' against Taft's polar substituent constant for inhibition by manganese(II) ion in the oxidations of primary alcohols by chromium(VI) (8.74×10^{-4} mol dm^{-3}) in aqueous perchloric acid (0.366 mol dm^{-3}) at 25.0°C. Alcohols: 2-chloroethanol (1), 2-methoxyethanol (2), methanol (3), ethanol (4), 1-propanol (5), 1-butanol (6), and benzyl alcohol (7). The value for methanol has been corrected with the statistical factor 3/2. The value for benzyl alcohol has been excluded from the fit. Reaction constant: $\rho^* = -0.80 \pm 0.06$.

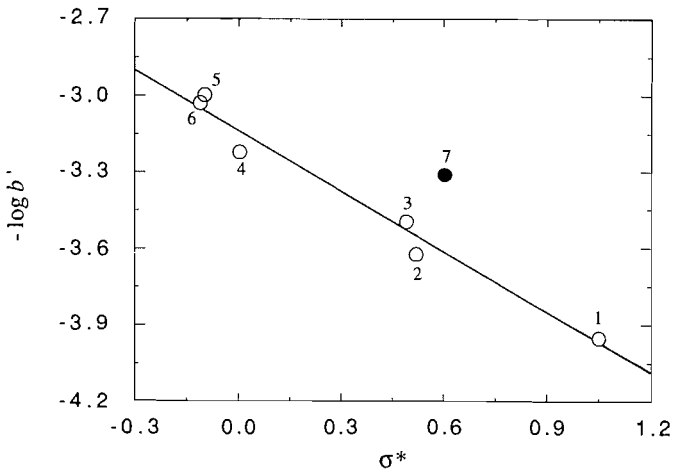

FIG. 3. Double-logarithmic plot of parameter b' for inhibition by manganese(II) ion against the second-order rate constant in the absence of inhibitor for the oxidations of both primary and secondary alcohols by chromium(VI) (8.74×10^{-4} mol dm^{-3}) in aqueous perchloric acid (0.366 mol dm^{-3}) at 25.0°C. Alcohols: methanol (1), 2-chloroethanol (2), 2-methoxyethanol (3), 2-ethoxyethanol (4), ethanol (5), 1-propanol (6), 1-butanol (7), 2-propanol (8), 2,5-hexanediol (9), and benzyl alcohol (10). Slopes: 0.56 ± 0.08 (points 2–7) and 0.61 ± 0.01 (points 8–10).

chromium(VI) oxidation of formic acid. The results indicated that the maximum inhibition attained by the manganese(II) ion was notably inferior to that attained by the cerium(III) ion, as shown by the corresponding $(a + c)/c$ ratios (1.64 for Mn^{2+} and 1.92 for Ce^{3+}). However, the asymptotic value of the second-order rate constant was reached earlier when the manganese(II) ion was the inhibitor, as reflected by the corresponding values of parameter b' (9.62×10^4 for Mn^{2+} and 6.47×10^4 for Ce^{3+}).

Discussion

Interpretation of parameter b'

By application of the steady-state approximation to the intermediate Cr(IV) in the case of Mechanism I, to both Cr(IV) and Cr(II) for Mechanism II, and to both Cr(IV) and R· for Mechanism III, it is easy to demonstrate that the expression obtained for parameter b in the case of Mechanism I is

$$[5] \quad b = k_{inh}/k_{ox}\,[Cr(VI)]_0$$

whereas for both Mechanisms II and III we obtain

$$[6] \quad b = k_{inh}/k_{red}\,[RH]$$

where k_{inh}, k_{ox}, and k_{red} are the rate constants for the reactions of the intermediate chromium(IV) with manganese(II) ion (inhibitor), chromium(VI) (oxidant), and the organic substrate (reductant), respectively (12).

We can see in Table 3 that parameter b is independent of the chromium(VI) initial concentration, but is inversely proportional to the concentration of organic substrate. Thus, we can conclude that the reduction of chromium(VI) by organic substrate does not take place via Mechanism I, since the intermediate chromium(IV) does not react with chromium(VI) but with the organic substrate instead, either in a two-equivalent reduction (Mechanism II) or in a one-equivalent reduction (Mechanism III).

Although the fact that chromium(IV) is not oxidized by chromium(VI) is consistent with considerations based on reduction potentials, as reported by Rahman and Rocek (2*d*), Ghosh and Gould (15) have reported that a complex of chromium(IV) with 2-ethyl-2-hydroxybutanoic acid is actually oxidized by chromium(VI). However, the reactivity of that complex might presumably be very different from that of the chromium(IV) species present in aqueous perchloric acid solution.

Since $b' = b[RH]$, from eq. [6], this yields the following expression for parameter b':

$$[7] \quad b' = k_{inh}/k_{red}$$

It can be seen in Fig. 2 that the negative logarithm of parameter b' for inhibition by manganese(II) ion in the chromium(VI) oxidations of primary alcohols decreases linearly with Taft's polar substituent constant σ^*. According to eq. [7], we can conclude that the logarithm of rate constant k_{red} decreases linearly with increasing σ^*, given that the logarithm of rate constant k_{inh} for the Cr(IV)–Mn^{2+} reaction affects the intercept but not the slope since it is a constant in the plot. Therefore, Fig. 2 must be interpreted as a Taft-like plot for the reactions between the intermediate chromium(IV) and primary alcohols. It can also be seen that the data for the chromium(IV) oxidation of benzyl alcohol do not correlate well with those for the other primary alcohols, which is possibly due to the fact that Taft's polar substituent constant σ^* does not take into account resonance effects.

Rahman and Rocek (2*c*) also studied the chromium(IV) – primary alcohols reactions; after Espenson's work (16), they proposed chromium(IV) as an intermediate in the reduction of chromium(VI) by vanadium(IV). The value of Taft's reaction constant determined in our work for the reactions between chromium(IV) and primary alcohols ($\rho^* = -0.80 \pm 0.06$, Fig. 2) agrees well with the one determined by Rahman

Can. J. Chem. Downloaded from www.nrcresearchpress.com by 213.200.69.106 on 09/08/12
For personal use only.

Can. J. Chem. Downloaded from www.nrcresearchpress.com by 213.200.69.106 on 09/08/12
For personal use only.

and Rocek (2*c*) for the same reactions ($\rho^* = -0.85$). This concordance is notable because the two values of the reaction constant were determined by two very different, indirect, methods. In both studies, what was determined was not the rate constant for each Cr(IV)–RH reaction but the value of its ratio with another rate constant.

In Table 4 the values of parameter b' obtained in this work for different reductants RH are compared with the rate constants obtained by Scott *et al.* (6*b*) for the Cr(IV)–RH reactions using a different method. To that end, both the b' and rate constant values are referred to a standard (2-propanol). We can see that, among the seven reductants common to both studies, the two sets of data are in good agreement in all but two cases, formic acid and 1-butanol (especially the latter). The values found in the two studies for the other five reductants (formaldehyde, ethanol, benzyl alcohol, methanol, and 2-propanol) have been combined to obtain the rate constant corresponding to the reaction between the intermediate chromium(IV) and manganese(II) ions (eq. [1]), yielding the value $k_{inh} = (1.19 \pm 0.15) \times 10^5$ dm^3 mol^{-1} s^{-1}.

Hydrogen-atom versus hydride-ion transfer

It can be seen in Table 4 that the values of parameter b' for inhibition by manganese(II) ion in the chromium(VI) oxidations of organic substrates are always much higher than unity (10^3 or higher). The value of b' determined for inhibition by cerium(III) ion in the chromium(VI) oxidation of formic acid was also of the same order of magnitude. We can then conclude that the reactions of the intermediate chromium(IV) with the inorganic ions acting as inhibitors (Mn^{2+} and Ce^{3+}) have rate constants at least 10^3-fold higher than the reactions of the same intermediate with organic substrates. This finding clearly suggests that the Cr(IV)–RH reactions involve cleavage of a C—H bond in the organic molecule by transfer of either a hydrogen atom (Mechanism III) or a hydride ion (Mechanism II) from the organic molecule to chromium(IV). Therefore, they are much slower than both the Cr(VI)–Mn^{2+} and Cr(IV)–Ce^{3+} one-electron transfer reactions, which do not involve bond cleavage (eq. [1]).

If hydrogen-atom transfer is accepted for the Cr(IV)–RH reactions, there would be a competition between bimolecular destruction (recombination or dismutation) of the free radicals R· and their oxidation by chromium(VI) (see Mechanism III). Since the oxidizing power of chromium(VI) is dramatically reduced by a decrease in the acidity of the medium (5), it follows that bimolecular destruction of free radicals should predominate at low perchloric acid concentrations.

In Mechanism III the free radicals are formed from the Cr(IV)–RH reaction, but the Cr(IV)–Mn(II) reaction (eq. [1]) does not yield free radicals. Hence, given that when enough Mn(II) is added free radicals are not formed, according to that mechanism it is precisely the elimination of the Cr(VI)–R· reaction by addition of manganese(II) ion to the reaction mixture that explains the inhibitory effect of the latter. As a result, in a situation where the free radicals were not consumed by chromium(VI) oxidation but instead by recombination of dismutation (at $[H^+] \cong 0$), no inhibition by manganese(II) ion would be expected, for recombination and dismutation of free radicals do not affect the rate of disappearance of chromium(VI). Therefore, if Mechanism III holds, the maximum inhibition ratio $(a + c)/c$ should decrease with decreasing acidity. However, we have seen in Table 2 that a decrease of the acidity of the medium actually led to an increase of that ratio.

Furthermore, Rahman and Rocek (2*c*,*d*), pointed out that an increase in the concentration of organic substrate would lead to an increase in the concentration of free radicals R·, and so also to an increase of the bimolecular destruction of free radicals relative to their oxidation by chromium(VI), since the rates of the R·–R· and Cr(VI)–R· reactions increase with the second and first powers of [R·], respectively. Therefore, if Mechanism III holds, a decrease of the maximum inhibition ratio with increasing concentration of organic substrate would be expected. However, we have found that $(a + c)/c$ is essentially independent of the RH concentration.

According to eq. [7], Fig. 3 is actually a representation of the Cr(IV)–RH reactivity against the corresponding Cr(VI)–RH reactivity, since the rate constant k_{inh} for the Cr(IV)–Mn(II) reaction is a constant in the plot, and the abscissa is the logarithm of the second-order rate constant for each Cr(VI)–RH reaction in the absence of inhibitor. We can see that in the case of primary alcohols the rate constants for the Cr(IV)–RH reactions correlate well with those corresponding to the Cr(VI)–RH reactions. Since it is widely accepted that the rate-determining redox step for the chromium(VI) oxidation of alcohols involves a two-equivalent reduction of the oxidizing agent (1, 2*d*), this finding seems to support that the redox step of the Cr(IV)–RH reactions also involves a two-equivalent reduction of chromium(IV).

However, the oxidations of both methanol and benzyl alcohol by chromium(IV) do not correlate well with those by chromium(VI), in contrast to the other primary alcohols. In the case of methanol, it should be noted that its reactivity toward chromium(VI) is known to be much lower than expected from polar substituent considerations (2*b*), but we can see in Fig. 2 that methanol correlates well with the other primary alcohols for their oxidation by chromium(IV), which explains the position of the point corresponding to methanol in Fig. 3 above the linear correlation observed for the other primary alcohols. Hence, the position of that point seems to be due to some specific effect in the Cr(VI)–CH_3OH reaction that is not present in the Cr(IV)–CH_3OH reaction.

We can also see in Fig. 3 that the point corresponding to benzyl alcohol is below the linear correlation found for primary alcohols, and that it seems to correlate well with the two secondary alcohols studied by us (2-propanol and 2,5-hexanediol). This fact is relevant to the hydrogen-atom versus hydride-ion transfer argument. If the redox step of the Cr(IV)–RH reactions takes place by hydrogen-atom transfer, one would expect the organic free radical formed by oxidation of benzyl alcohol to be highly stabilized by resonance. Moreover, the free radicals formed in the chromium(IV) oxidations of secondary alcohols should be more stable than those formed from primary alcohols (3*b*). Hence, in a representation of the reactivity toward chromium(IV) against the reactivity toward chromium(VI), the points corresponding to benzyl alcohol and secondary alcohols would all be expected to be above the linear correlation observed for primary alcohols, which is in open disagreement with the situation shown in Fig. 3.

Nevertheless, the positions of the points corresponding to both benzyl alcohol and the secondary alcohols in Fig. 3 require consideration. Actually, we believe that steric hindrance caused by the phenyl or alkyl groups might be a

Can. J. Chem. Downloaded from www.nrcresearchpress.com by 213.200.69.106 on 09/08/12
For personal use only.

plausible explanation for that low reactivity of chromium(IV) toward benzyl alcohol and secondary alcohols, respectively.

Since the first step in the oxidation of alcohols by chromium(VI) is the formation of the corresponding chromate(VI) esters (17, 18), and the esterification equilibrium constants can be assumed to be roughly independent of the molecular structure of the alcohol (19), steric hindrance caused by the structure of the alcohol is not expected to play an important role in the case of oxidation by chromium(VI). This is corroborated by the fact that we have found that the reactivity of 1-propanol toward chromium(VI) is only 1.10 times greater than that of 2-propanol (Table 1).

However, alcohols do not seem to form esters with chromium(IV). This hypothesis is based on the finding that chromium(VI) is 2400 times more reactive toward ethanol than toward diethyl ether (2*c*), whereas chromium(IV) is only 30 times more reactive toward the alcohol than toward the ether (2*c*) (20 times according to results of Scott *et al.* (6*b*)). Thus it seems that the presence of a hydroxyl group in the organic substrate to allow the formation of a chromate ester is essential in the case of chromium(VI) oxidation, but it is not so important in the case of chromium(IV) oxidation. In fact, steric hindrance might be a plausible explanation for the low Cr(IV)–$C_2H_5OC_2H_5$ reactivity as compared with that of Cr(IV)–C_2H_5OH.

Therefore, steric hindrance caused by the phenyl or alkyl groups might play an important role in the redox step of the oxidation of both benzyl alcohol and secondary alcohols by chromium(IV). Actually, we can see in Table 4 that parameter b' for 1-propanol is ca. 10 times lower than that for 2-propanol, which means that the reactivity of 1-propanol toward chromium(IV) is 10 times higher than that of 2-propanol, since the reactivity of RH toward Cr(IV) is inversely proportional to the corresponding value of parameter b' (eq. [7]). That big difference in reactivity contrasts with the small difference for the reactions of those substrates with chromium(VI).

The fact that the value of parameter b' corresponding to formic acid is ca. 70 times higher than that corresponding to formaldehyde (Table 4) can be taken as another proof supporting hydride-ion transfer. Effectively, the finding that the reactivity of formic acid toward chromium(IV) is much lower than the reactivities of the other 12 organic substrates studied by us (70 times lower than that of formaldehyde, for instance) might be due to the fact that, among the organic substrates given in Table 4, formic acid is the only one for which there would be two oxygen atoms attached to the carbon atom bearing the positive charge in the carbocation formed by hydride-ion transfer from the organic substrate to chromium(IV). As indicated in eq. [8], due to the lower electronegativity of the carbon atom with respect to that of oxygen, transfer of a C-H hydride ion is preferred to that of an O-H hydride ion.

$$[8] \quad Cr(IV) + HCO_2H \rightarrow Cr(II) + {}^{+}CO_2H$$

Formation of the stable oxidation product (carbon dioxide) would occur by proton transfer from the carbocation formed in eq. [8] to the solvent (3*c*). However, since the high electronegativity of the two oxygen atoms attached to the carbon atom bearing the positive charge will render that carbocation very unstable, the reactivity of formic acid toward chromium(IV) would be much lower than those of other organic substrates (Table 4).

It should be pointed out that carbocations are also formed in hydride-ion transfer from other organic compounds (such as alcohols) to chromium(IV). Since carbocations are known to initiate polymerization reactions (20), they might be responsible for the polymerization of acrylamide and acrylonitrile detected in the reaction of chromium(IV) with 2-propanol (2*d*), because, according to Scott's (6) results and our own, it seems that free radicals are not formed in that reaction. In the absence of easily polymerizable substrates, those carbocations would instead be stabilized by proton transfer to the solvent (3*c*).

Nature of the chromium(IV) species

There are some clues leading to elucidation of the nature of the chromium(IV) species present in aqueous perchloric acid. These are the following:

1. It cannot be chromium(IV) oxide, because, due to the high polarity of the Cr—O double bonds, the neutral CrO_2 molecules would have a high tendency to coagulate (as happens in the case of the MnO_2 molecule (21)), so that chromium(IV) would then be an insoluble, stable product instead of a soluble, unstable intermediate.

2. The tendency of chromium(VI) ($HCrO_4^-$ or H_2CrO_4) to form esters with alcohols and other organic compounds (17, 18), and also ester-like species with inorganic compounds (22), is well known. However, chromium(IV) does not seem to form esters with alcohols. This suggests that the chromium(IV) molecule does not contain any hydroxyl group. Hence, possible formulas corresponding to neutral molecules containing OH groups (such as H_2CrO_3) can be discarded. Therefore, the two arguments considered so far suggest that the chromium(IV) species is not a neutral molecule. It cannot be a hydroxyl-containing oxyanion (such as $HCrO_3^-$) either.

3. It is well known that protonation increases the oxidizing power of oxyanions dramatically. Thus permanganic acid is a much stronger oxidant than permanganate ion (23), and the oxidizing power of chromium(VI) is known to be enhanced by an increase of the acidity of the medium (5). However the oxidizing power of chromium(IV) does not seem to be much influenced by the acidity of the medium (2*c*), except when the reductant is a carboxylic acid (6*b*). This suggests that the chromium(IV) species does not show any tendency to take protons from the solution under acidic conditions and, therefore, is not an oxyanion. Hence, species such as CrO_3^{2-} (even if they do not contain any hydroxyl group) can also be discarded. Thus, the arguments considered so far lead to the conclusion that the chromium(IV) species is either Cr^{4+} or CrO^{2+}.

4. We have seen that the chromium(IV) species seems to present a strong tendency to withdraw a hydride ion from organic substrates RH. This is more consistent with an oxo species such as CrO^{2+} than with Cr^{4+}, since the high electronegativity of the oxygen atom of the former can easily explain the hydride-ion transfer process via the transition state $[Cr{=}O \cdots H \cdots R]^{2+}$.

Thus the results found in this work support the hypothesis that the chromium(IV) species present in aqueous perchloric acid solutions is actually CrO^{2+}, in agreement with the proposal of Scott *et al.* (6). This conclusion also agrees with the structure proposed by Ghosh and Gould (15) for the

bischelated complex formed in the stabilization of chromium(IV) by 2-ethyl-2-hydroxybutanoic acid (LigH), since it was assumed to be an oxo species featuring a $Cr^{IV}=O$ linkage. In fact, that complex would be easily formed as the neutral molecule resulting from the association of CrO^{2+} with two Lig^- (2-ethyl-2-hydroxybutanoate) ions, as indicated in eq. [9].

[9] $CrO^{2+} + 2LigH \rightarrow (Lig)_2Cr^{IV}=O + 2H^+$

Conclusions

These results suggest that the chromium(IV) present in aqueous perchloric acid solution is an oxo species (CrO^{2+}). It does not react with chromium(VI) (at least under the conditions of this work), but it reacts with reducing organic substrates by hydride-ion transfer, yielding chromium(II) and a carbocation that is stabilized by proton transfer to the solvent. It also reacts with the inorganic reductants, manganese(II) and cerium(III) ions, by one-electron transfer.

1. F. H. Westheimer. Chem. Rev. **45**, 419 (1949).
2. (*a*) J. Rocek and J. Krupicka. Collect. Czech. Chem. Commun. **23**, 2068 (1958); (*b*) J. Rocek. Collect. Czech. Chem. Commun. **25**, 1052 (1960); (*c*) M. Rahman and J. Rocek. J. Am. Chem. Soc. **93**, 5455 (1971); (*d*) J. Am. Chem. Soc. **93**, 5462 (1971); (*e*) J. Rocek and C. S. Ng. J. Org. Chem. **38**, 3348 (1973); (*f*) J. Am. Chem. Soc. **96**, 1522 (1974); (*g*) J. Am. Chem. Soc. **96**, 2840 (1974).
3. J. March. Advanced organic chemistry. Wiley, New York. 1985. (*a*) p. 630. (*b*) p. 164. (*c*) p. 150.
4. R. Stewart. Oxidation mechanisms. Benjamin, New York. 1964. p. 37.
5. J. K. Beattie and G. P. Haight. *In* Inorganic reaction mechanisms. Part II. *Edited by* J. O. Edwards. Wiley, New York. 1972. p. 93.
6. (*a*) S. L. Scott, A. Bakac, and J. H. Espenson. J. Am. Chem. Soc. **113**, 7787 (1991); (*b*) **114**, 4205 (1992).
7. K. B. Wiberg and T. Mill. J. Am. Chem. Soc. **80**, 3022 (1958).
8. B. M. Rao and R. P. Dhabre. Ann. Chim. (Rome), **73**, 565 (1983).
9. G. P. Haight, T. J. Huang, and B. Z. Shakhashiri. J. Inorg. Nucl. Chem. **33**, 2169 (1971).
10. F. Mata and J. F. Perez-Benito. J. Chem. Educ. **64**, 925 (1987).
11. J. F. Perez-Benito, C. Arias, and E. Brillas. An. Quim. **87**, 849 (1991).
12. J. F. Perez-Benito, C. Arias, and D. Lamrhari. J. Chem. Soc. Chem. Commun. 472 (1992).
13. R. W. Taft. *In* Steric effects in organic chemistry. *Edited by* M. S. Newman. Wiley, New York. 1956. p. 556.
14. A. C. Chatterji and S. K. Mukherjee. Z. Phys. Chem. (Leipzig), **210**, 255 (1959).
15. M. C. Ghosh and E. S. Gould. Inorg. Chem. **30**, 491 (1991).
16. J. H. Espenson. J. Am. Chem. Soc. **86**, 5101 (1964).
17. U. Klaning. Acta Chem. Scand. **11**, 1313 (1957).
18. K. B. Wiberg and H. Schäfer. J. Am. Chem. Soc. **91**, 927 (1969).
19. H. G. Kuivila and W. J. Becker. J. Am. Chem. Soc. **74**, 5329 (1952).
20. F. W. Billmeyer. Textbook of polymer science. Wiley, New York. 1984. p. 85.
21. F. Freeman. Rev. React. Species Chem. React. **1**, 179 (1976).
22. D. G. Lee and R. Stewart. J. Am. Chem. Soc. **86**, 3051 (1964).
23. N. A. Frigerio. J. Am. Chem. Soc. **91**, 6200 (1969).

Can. J. Chem. Downloaded from www.nrcresearchpress.com by 213.200.69.106 on 09/08/12
For personal use only.

An empirically corrected quantum mechanical potential energy curve of internal rotation of acryloyl fluoride, CH_2=CH-CF=O

GEORGE R. DE MARÉ[1] AND YURII N. PANCHENKO[2]

Laboratoire de chimie physique moléculaire, Faculté des sciences CP.160/09, Université Libre de Bruxelles, 50, Av. F. D. Roosevelt, B-1050 Brussels, Belgium

ALEXANDER V. ABRAMENKOV

Laboratory of Molecular Structure and Quantum Chemistry, Chair of Physical Chemistry, Department of Chemistry, Moscow State University, 119899, Moscow, Russian Federation

AND

CHARLES W. BOCK

Chemistry Department, Philadelphia College of Textiles and Science, Philadelphia, PA 19144, U.S.A.
and
American Research Institute, Materials Science Division, Suite 1212, Upper Darby, PA 19061, U.S.A.

Received November 3, 1992

GEORGE R. DE MARÉ, YURII N. PANCHENKO, ALEXANDER V. ABRAMENKOV, and CHARLES W. BOCK. Can. J. Chem. **71**, 656 (1993).

The geometrical parameters of acryloyl fluoride were optimized completely at the MP2/6-31G* computational level for 17 points on the internal rotation potential energy (IRPE) curve for rotation around the formal single carbon–carbon bond. The expansion coefficients of the reduced rotational constant function $F(\varphi)$ and the four, five, and six-term expansions of the IRPE function,

$$V(\varphi) = \sum_n 1/2\, V_n (1 - \cos n\varphi), \qquad \text{where } n = 1, 2, 3\ldots,$$

were obtained from these data. The theoretical IRPE functions were then refined using only the experimental torsional transition frequencies in both the *s-trans* and *s-cis* wells. The IRPE functions obtained are compared with those in the literature, calculated at lower levels of theory in both the rigid and nonrigid rotation approximations. The best representation of the refined IRPE function is given by the six-term expansion with $V_1 = 71.7$, $V_2 = 1944.8$, $V_3 = 113.0$, $V_4 = -122.8$, $V_5 = -8.7$, and $V_6 = 12.5$ cm^{-1}, respectively. From this IRPE function, one correctly predicts the *s-trans* conformer to be more stable with $\Delta H_0 = 168$ cm^{-1}. The barrier to rotation from the *s-trans* to the *s-cis* positions, $\Delta H^{\#}$, is 2048 cm^{-1} at 88° from the *s-trans* well. The advantages of using the nonrigid rotation approximation, based on high-quality quantum mechanical calculations that include correlation effects, to construct the effective IRPE function for molecules are emphasized.

GEORGE R. DE MARÉ, YURII N. PANCHENKO, ALEXANDER V. ABRAMENKOV et CHARLES W. BOCK. Can. J. Chem. **71**, 656 (1993).

On a optimisé complètement les paramètres géométriques du fluorure d'acryloyle au niveau de calcul MP2/6-31G* pour 17 points de la courbe d'énergie potentielle de rotation interne (EPRI) pour la rotation autour de la liaison carbone–carbone formellement simple. À l'aide de ces données, on a déduit les coefficients d'expansion de la fonction de la constante de rotation réduite, $F(\phi)$, ainsi que les expansions à quatre, cinq et six termes de la fonction d'EPRI,

$$V(\phi) = \sum_n 1/2\, V_n (1 - \cos n\phi), \qquad \text{où } n = 1, 2, 3\ldots,$$

On a alors affiné les fonctions théoriques de l'EPRI en utilisant seulement les fréquences experimentales des transitions de torsion des puits d'énergie des conformères *s-trans* et *s-cis*. On a comparé les fonctions théoriques de l'EPRI avec celles rapportées dans la littérature et calculées à des niveaux inférieurs de la théorie dans les approximations de rotation tant rigides que non rigides. La meilleure représentation de la fonction EPRI affinée est donnée par une expansion à six termes dans laquelle $V_1 = 71{,}7$, $V_2 = 1944{,}8$, $V_3 = 113{,}0$, $V_4 = -122{,}8$, $V_5 = -8{,}7$ et $V_6 = 12{,}5$ cm^{-1}. À partir de cette fonction d'EPRI, on peut prédire correctement que le conformère *s-trans* est le plus stable. $\Delta H_0 = 168$ cm^{-1}. La barrière à la rotation des positions *s-trans* à *s-cis*, $\Delta H^{\#}$, située à 88° du puits d'énergie du conformère *s-trans*, est égale à 2048 cm^{-1}. On met en évidence les avantages qu'il y a d'utiliser l'approximation non rigide de la rotation, basée sur des calculs de mécanique quantique d'excellent qualité qui incluent les effets de corrélation, pour construire une fonction d'EPRI efficace des molécules.

[Traduit par la rédaction]

Introduction

It is well established that the curve for internal rotation about the formal C—C single bond in acryloyl fluoride, CH_2=CH-CF=O (Fig. 1), has minima at the planar *s-trans* and *s-cis* structural points (see refs. 1–3, and references therein). This rotational curve was studied recently (1) using a technique that combines quantum mechanical calculations of the geometrical parameters (non-rigid rotation) with experimental data on the torsional transition frequencies and their overtones in both wells. This approach (4, 5), which is based on a one-dimensional model of internal rotation (6),

[1]Author to whom correspondence may be addressed.

[2]On leave from Laboratory of Molecular Spectroscopy, Chair of Physical Chemistry, Department of Chemistry, Moscow State University, 119899, Moscow, Russian Federation.

Can. J. Chem. Downloaded from www.nrcresearchpress.com by 88.255.202.194 on 09/08/12
For personal use only.

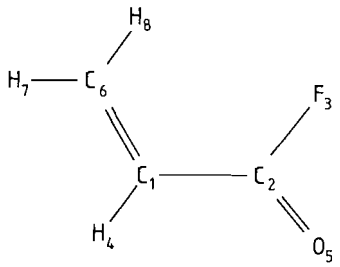

FIG. 1. Atom numbering used throughout the text.

makes it possible to obtain a physically meaningful picture of the nonrigid rotation, but still guarantees the necessary accuracy. It is important to note that this approach does *not* use the enthalpy difference (ΔH_0) between the rotational isomers in the refinement procedure for the theoretical curve since the experimental enthalpy differences are often determined with relatively low accuracy.

The difference in enthalpy between the two conformers of acryloyl fluoride is rather small and the populations of molecules in the two wells are quite similar (1–3). This is an unusual feature for structures with conjugated double bonds, for which the relative populations of molecules in the *cis* and *gauche* wells are usually low (see, for example, refs. 2, 4, 7–27, and references therein). Thus, in typical refinement procedures for conjugated molecules, one often has available only the frequencies of a few of the lowest torsional transitions. Recently it was demonstrated that in such a case (for example for glyoxal (26, 27)) the calculated energy difference between the minima depends on the computational level used to account for the molecular relaxation during the rotation. A marked improvement was obtained (26) in going from the Hartree–Fock model to a model based on second-order Møller–Plesset perturbation theory, which recovers a significant portion of the correlation energy for a given basis set. It is therefore desirable to update the effective curve for internal rotation of acryloyl fluoride using completely relaxed geometries at the MP2/6-31G* level. The ΔH_0 between the two stable rotamers, calculated from the final refined potential curve, should provide a better estimate of the "true experimental" value than previously obtained (1). We also consider the effects of truncating the internal rotational potential energy (IRPE) function expansion on the values of the coefficients and the values of ΔH_0. The *s-trans* and *s-cis* acryloyl fluoride rotamers provide an excellent opportunity for such an investigation, since a relatively large number of torsional transition frequencies are known for both potential wells (3).

Method

The theoretical IRPE function for rotation about the formal C—C single bond of acryloyl fluoride was obtained from MP2/6-31G* level optimizations at the *s-cis*, *s-trans*, and *transition state* (TS) critical points and at 14 additional points along the curve for which only the rotational angle (φ) was kept fixed ($\varphi = \phi - 180°$; where ϕ = the C=C—C=O dihedral angle). The optimizations were carried out using GAUSSIAN 90 (28) on the Cray Y-MP2E/116 computer of the ULB/VUB Computing Centre. The optimized geometrical parameters for the *s-trans* and *s-cis* planar forms are juxtaposed to the experimental microwave data (29, 30) and other theoretical structures (2, 3) in Table 1. The geometrical parameters from the 17 MP2/6-31G* points were used to calculate the reduced moments of inertia for constructing the reduced rotational constant function, $F(\varphi)$ (5) (see Table 2), and its Fourier expansion coefficients up to the ninth term. Including higher terms in this function does not affect the final results. Literature results (1, 3) are included in Table 2 for comparison purposes.

A least-squares procedure was used to fit the MP2/6-31G* IRPE curve of acryloyl fluoride to the function

$$V(\varphi) = \sum_n 1/2\, V_n\,(1 - \cos n\varphi), \qquad \text{where } n = 1, 2, 3\ldots,$$

truncated after the first four, five, six, seven, and eight terms, respectively. As observed previously for other conjugated molecules, and notably for the isoelectronic series butadiene, acrolein, and glyoxal (4, 7, 10, 13, 14, 16, 26, 27), truncation of the above series after six terms reproduces the theoretical IRPE curve satisfactorily; i.e., the standard deviation of the energies for the 17 theoretical points is only about 3 cm^{-1}. In contrast, the standard deviations for the four and five-term expansions are almost an order of magnitude larger, approximately 15 cm^{-1}.

The four, five, and six-term expansions of the theoretical IRPE function were refined by a least-squares method to obtain the best agreement between predicted torsional transition frequencies for both the *s-trans* and the *s-cis* conformers and the corresponding experimental values (3) (see Table 3). This procedure, implemented in the program of ref. 31, may cause some difficulties inherent in most inverse problems. Special measures, such as the SVD algorithm (32), were taken to avoid possible ill-conditioned sets of equations. The refined coefficients of the IRPE functions, as well as other results from the literature, are given in Table 4.

Discussion

The optimized MP2/6-31G* geometrical parameters for the *s-trans* and *s-cis* acryloyl fluoride conformers coincide reasonably well with the results of ref. 2 (obtained with an earlier version of the GAUSSIAN programs (see Table 1)). Small deviations in the extreme right digits of some parameter values are the result of rounding off or of small differences in the cutoff criteria for the optimizations.

The major variations observed in the geometrical parameters on going from the *s-trans* to the *s-cis* conformations of acryloyl fluoride are (1) the single C—C bond length at first increases up to $\varphi \cong 90°$, and then decreases, becoming essentially constant for $\varphi \geq 165°$ (see Fig. 2); (2) the O=C—C and C—C—H bond angles increase regularly; and (3) the C=C—C, F—C—C, and C=C—H_8 bond angles decrease regularly. The predicted variation of the single C—C bond length as a function of φ for optimizations at the RHF/6-31G* level (1) is also shown in Fig. 2. Including electron correlation markedly affects the slope of the curve, which is much less sharply peaked for the MP2/6-31G* optimizations. The shape of these curves is similar to that for many conjugated hydrocarbon compounds (for examples see refs. 10, 14, and 16) and also for substituted cyclopropanes, where the three-membered ring may be assimilated to a double bond (for example vinylcylopropane (35), isopropenylcyclopropane (36), and cyclopropanecarboxaldehyde (37). Note that the character of the slopes and of the variations of the analogous curves is different than that observed in the case of glyoxal (26). It is precisely these differences in the parameter dependencies that require one to take into account the relaxation of the geometry in such investigations. Note also that the presence of substituents and the asymmetrical structure of acryloyl fluoride (in comparison with such related compounds as buta-1,3-diene and oxalyl fluoride) result in some unexpected structural changes. For example, the C=C—C bond angle in acryloyl fluoride decreases on going

Can. J. Chem. Downloaded from www.nrcresearchpress.com by 88.255.202.194 on 09/08/12
For personal use only.

TABLE 1. Structural parameters and total energies of *s-trans* and *s-cis* acryloyl fluoride (angstroms, degrees, and atomic units)

	s-trans-CH_2=CH-CF=O							*s-cis*-CH_2=CH-CF=O					
			Calculation						Calculation				
	Exptl.		3-21G	6-31G	6-31G*	MP2/ 6-31G*	MP2/	Exptl.	3-21G	6-31G	6-31G*	MP2/ 6-31G*	MP2/
Parameter	ref. 29	ref. 30	ref. 3	ref. 2	ref. 3	ref. 2	6-31G* this work	ref. 29	ref. 3	ref. 2	ref. 3	ref. 2	6-31G* this work
r(C=O)	1.18	1.195	1.186	1.191	1.171	1.201	1.201	1.18	1.187	1.192	1.171	1.201	1.201
r(C—C)	1.49	1.470	1.463	1.461	1.475	1.470	1.470	1.48	1.464	1.468	1.477	1.474	1.474
r(C=C)	1.35	—	1.316	1.325	1.320	1.338	1.338	1.35	1.316	1.325	1.320	1.338	1.338
r(C—F)	1.35	1.350	1.360	1.376	1.325	1.366	1.367	1.35	1.355	1.373	1.323	1.365	1.364
r(C—H_7)	—	1.085	1.071	1.072	1.075	1.084	1.084	—	1.071	1.072	1.074	1.084	1.084
r(C—H_8)	—	1.085	1.071	1.071	1.074	1.083	1.083	—	1.073	1.073	1.074	1.085	1.085
r(C—H_4)	—	1.085	1.069	1.071	1.074	1.085	1.085	—	1.068	1.070	1.073	1.084	1.084
∠O=C—C	127.0	123.3	128.1	127.8	126.6	127.7	127.9	128.2	128.9	129.4	128.4	128.5	128.5
∠C=C—C	121.8	120.0	121.8	123.4	122.7	123.1	123.1	119.9	119.7	120.8	121.0	119.7	119.8
∠F—C—C	111.3	120.9	112.1	113.1	113.0	112.5	112.4	110.1	110.9	111.2	110.2	110.8	110.6
∠C=C—H_7	—	121.5	121.5	120.8	121.1	120.9	120.9	—	121.9	121.2	120.7	121.4	121.5
∠C=C—H_8	—	120.0	121.3	122.0	121.5	121.6	121.5	—	120.7	121.4	121.9	120.6	120.5
∠C—C—H_4	—	117.4	114.9	114.1	114.2	114.6	114.6	—	117.3	116.5	116.9	117.5	117.5
Energy[a]				−0.52413		−1.37966	−1.379655			−0.52373		−1.37922	−1.379225

[a]Add −289 atomic units to obtain the total energy.

TABLE 2. The Fourier expansion coefficients (cm^{-1}) of the reduced rotational constant function $F(\varphi)$ of acryloyl fluoride

Coefficient	Ref. 3[a]	RHF/6-31G*[b] (ref. 1)	MP2/6-31G* (this work)[b]
F_0	1.8981	1.8866	1.7956
F_1	−0.0078	−0.0077	−0.0039
F_2	0.0710	0.1349	0.1444
F_3	−0.0010	0.0177	0.0056
F_4	0.0038	0.0185	0.2306
F_5	−0.0001	−0.0029	0.0027
F_6	0.0002	−0.0023	0.0019
F_7	−0.0000	−0.0009	0.0002
F_8	−0.0000	0.0012	0.0000
F_9	—	0.0004	0.0000

[a]The authors state (*i*) that *ab initio* structural parameters were used (either 3-21G or 6-31G*, this is not specified) and (*ii*) "The effects of structural relaxation were included in the calculation of $F(\alpha)$." How these effects were included is apparently not mentioned in the paper.
[b]Refined potential, nonrigid rotation.

from the *s-trans* to the *s-cis* conformer whereas in buta-1,3-diene it is larger for the *gauche* than for the *s-trans* rotamer and is predicted to be even larger for the *s-cis* transition state (10, 14). An "inverse" behaviour is also observed for the F—C—C and C—C—H bond angles (see Table 1). Indeed, the central C—C—H bond angles in buta-1,3-diene are predicted to be smaller in the *gauche* than in the *s-trans* conformation (10, 14), whereas the C—C—F bond angle in the O=CF-CF=O molecule increases on going from the *s-trans* to *s-cis* conformer (2). It should be emphasized that all the predicted changes in the geometrical parameters on going from the planar *s-trans* to the planar *s-cis* acryloyl fluoride conformations are in good agreement with the observed experimental differences (29) (see Table 1). This gives weight to the predicted changes at intermediate angles. These peculiarities demonstrate the rough character of the rigid rotor approximation and emphasize again the importance of involving the dependence of the geometrical parameters on the rotational angle when constructing the effective IRPE function for a molecule. It is worth mentioning here that the values of the O=C—C and F—C—C bond angles, calculated from the moments of inertia reported in ref. 30, deviate considerably, from the present calculations and results of refs. 1, 2, and 29.

Including correlation effects in the optimizations at the MP2/6-31G* level produced marked differences in the Fourier expansion coefficients of the reduced rotational constant function, $F(\varphi)$, when compared with the corresponding coefficients calculated from theoretical geometrical parameters optimized at the RHF/6-31G* level (see Table 2). In fact, some higher coefficients are changed by an order of magnitude. The plots of the two functions are shown in Fig. 3.

The purely theoretical six-term MP2/6-31G* IRPE curve and the four-term and six-term experimentally refined IRPE curves are shown in Fig. 4. Comparison of these three curves reveals that the rotational barrier height computed at the MP2/6-31G* level is somewhat overestimated. This is most likely connected with the truncation of the basis set and the failure to pick up all the correlation energy at the MP2 level. However, comparing the theoretical and the six-term refined IRPE curves shows that the difference in ΔE is much less than the difference in the heights of the corresponding barriers to internal rotation ($\Delta H^{\#}$). This suggests that the possible errors in estimating ΔE (or ΔH_0) are apparently less than those incurred in estimating $\Delta H^{\#}$ when using this approach. In the case of the four-term refined IRPE function the deviation of ΔE from the theoretical curve is approximately the same as that between the corresponding barrier heights. Note, however, that, considering experimental accuracy, the standard deviations of the calculated torsional transition frequencies from the experimental values are

Can. J. Chem. Downloaded from www.nrcresearchpress.com by 88.255.202.194 on 09/08/12
For personal use only.

TABLE 3. The experimental (far IR) and calculated torsional transition frequencies of the *trans* and *cis* conformers of acryloyl fluoride (cm^{-1})

	trans-CH_2=CH-CF=O			*cis*-CH_2=CH-CF=O		
	Exptl.	Calcd. − Exptl.[a]		Exptl.	Calcd. − Exptl.[a]	
Transition	ref. 3	A	B	ref. 3	A	B
1–0	116.72	0.00	−0.24	101.37	0.07	−0.30
2–1	114.86	0.01	−0.02	100.15	−0.08	−0.04
3–2	113.06	−0.01	0.09	98.85	−0.06	0.20
4–3	111.26	0.00	0.16	97.59	−0.01	0.28
5–4	109.48	0.00	0.15	96.31	0.09	0.28
6–5	107.68	0.00	0.11	95.16	0.08	0.04
7–6	105.85	0.01	0.04	94.14	−0.09	−0.45
8–7	103.98	0.01	−0.07	—	—	—
9–8	102.08	−0.01	−0.22	—	—	—

[a]A and B are for deviations of the calculated frequencies from the experimental ones for the six- and the four-term refined IRPE functions, respectively.

TABLE 4. Internal rotation potential energy functions of acryloyl fluoride (cm^{-1})

	Rigid rotation			Non-rigid rotation			
				HF/6-31G*	MP2/6-31G*		
Coefficient	ref. 3	ref. 33	ref. 34	ref. 1	this work		
V_1	57	−108	0	171.5	314.2	276.0	71.7
V_2	1881	1859	1960	1883.7	1871.6	1871.9	1944.8
V_3	115	168	45	88.9	63.9	72.0	113.0
V_4	−129	−80	−75	−124.9	−81.2	−81.3	−122.8
V_5	−8	−16	—	−5.5	—	−1.6	−8.7
V_6	16	3	—	14.1	—	—	12.5
ΔH_0	(156)[a]	36	40	247	370	339	168
Barrier height, $\Delta H^{\#}$	1981	1897[b]	1980	2025	2061	2045	2048
Barrier position[c]	88	86	89	89	91	90	88

[a]Calculated using the above coefficients, i.e., ΔE (*cis-trans*) = $V_1 + V_3 + V_5$ = 164 cm^{-1} and $\Delta H_0 = \Delta E + 0.5\ (\omega_{cis} - \omega_{trans})$ = 156 cm^{-1}. The value of 79 ± 50 given in Table I of ref. 3 does not correspond to these coefficients.

[b]Calculated using the above coefficients.

[c]In degrees from the *s-trans* conformation, calculated using the appropriate coefficients; rounding off of the coefficients may affect the barrier position.

practically the same for both the four-term and the six-term IRPE functions (see Table 3). The same is true in the case of the five-term IRPE function. This implies that successfully fitting the calculated torsional transition frequencies to the experimental ones, while necessary, is not a sufficient condition to assume the accuracy of the IRPE function obtained.

It is important to stress that the value of ΔH_0 obtained from the six-term refined function is much lower than in the case of the analogous calculation starting from the RHF/6-31G* level calculation in ref. 1 (see Table 4). (Note that a value of ΔH_0 = 156 cm^{-1} can be deduced from the RHF/6-31G* torsional potential energy curve reported by Durig *et al.* (3).) The present value, 168 cm^{-1}, seems quite realistic when one considers the experimental data on the intensities of the IR bands of both conformers reported in refs. 3 and 38. It follows from these considerations that using only the first four terms in the potential energy expansion is insufficient to describe adequately the corresponding IRPE function. The effect of the quality of the quantum mechanical potential energy surface calculation was also demonstrated in the case of glyoxal (26), where starting with the theoretical MP2/6-31G* IRPE curve instead of the RHF/6-31G* curve significantly improved the agreement between the calculated and experimental values of ΔH_0. It should be mentioned that the measured value of ΔH_0 for glyoxal (39) is a relatively rare example of a high-quality experimental determination of an enthalpy change between rotational conformers of conjugated molecules.

Let us consider the problem of the number of terms used in the IRPE function expansion and the value of ΔH_0 from another point of view: the rigid rotor (RR) approximation method.

The RR approximation arises quite naturally from the purely empirical approach to constructing the IRPE curve in the framework of the one-dimensional model since there are

Can. J. Chem. Downloaded from www.nrcresearchpress.com by 88.255.202.194 on 09/08/12
For personal use only.

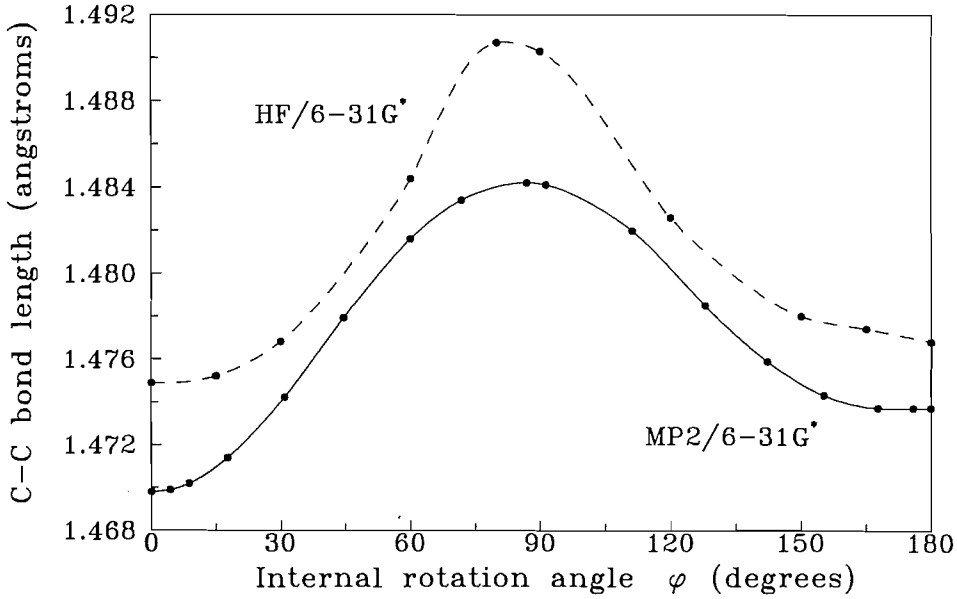

FIG. 2. The optimized single C—C bond length as a function of the internal rotation angle, φ, in acryloyl fluoride (*s-trans* corresponds to φ = zero degrees).

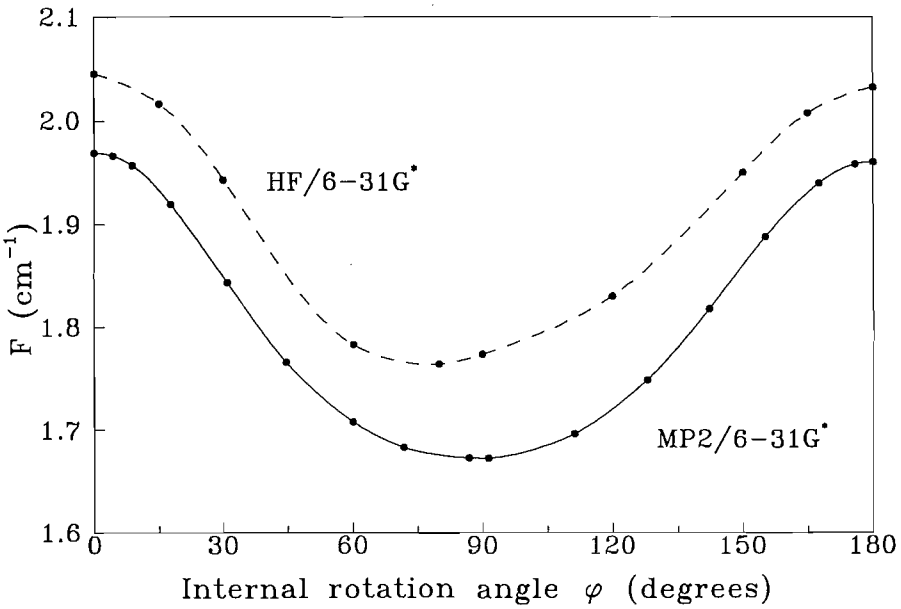

FIG. 3. Plots of the reduced rotational constant function F versus the internal rotational angle in acryloyl fluoride (*s-trans* corresponds to φ = zero degrees).

no experimental methods giving the necessary information about the change of the molecular geometrical parameters in the course of internal rotation. The rather rough character of the RR approximation does not prevent one from properly reproducing the torsional transition frequencies at the last step of iterative fitting of the initial IRPE curve to the experimental data. This may be explained by the fact that the potential function used in the one-dimensional model is, in reality, an effective potential including some terms from the kinetic energy operator (6). In the case of the RR approximation, neglecting the changes in the molecular moiety geometries means that the corresponding contributions are excluded from the kinetic energy and transferred into potential. In this case the solution of the inverse problem results in the correct description of the spectrum although the actual shape of the IRPE curve is, of course, disturbed. This brings about incorrect estimations of the ΔH_0 and $\Delta H^{\#}$ magnitudes and may even result in absolutely unrealistic values. Similar disturbances are especially noticeable when a small number of terms are used in the expansion of the IRPE function. Such a function cannot provide sufficient flexibility for adequate representation of the kinetic component of this pseudo-potential. To try to overcome these difficulties when using the RR approximation one involves the experimental value of ΔH_0 (and sometimes even $\Delta H^{\#}$) together with the torsional transition frequencies in the set of the experimental data from which the refinement of the initial theoretical IRPE curve is performed by the least-squares method.

Can. J. Chem. Downloaded from www.nrcresearchpress.com by 88.255.202.194 on 09/08/12
For personal use only.

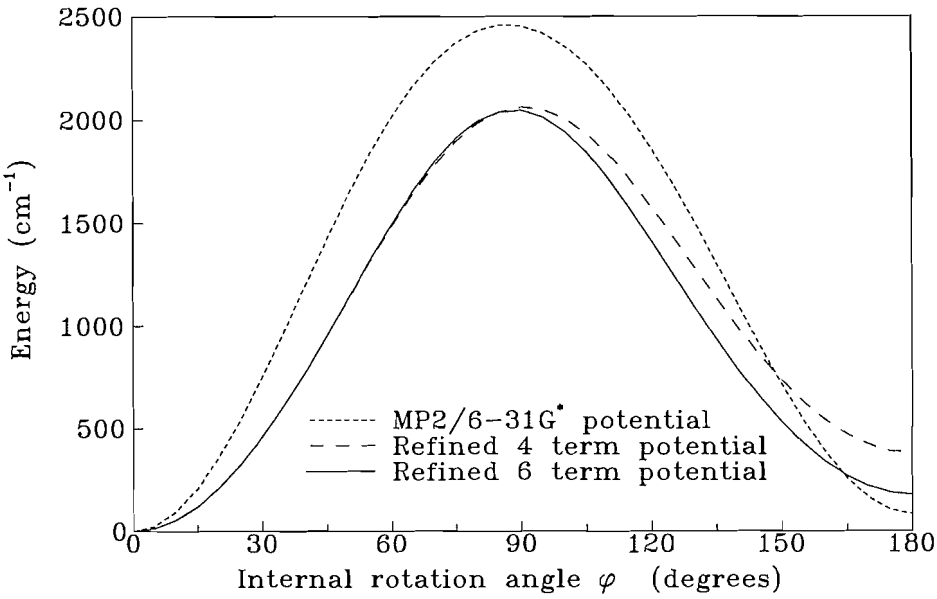

FIG. 4. The internal rotation potential energy curves for rotation about the single C—C bond in acryloyl fluoride (*s-trans* corresponds to φ = zero degrees).

TABLE 5. Experimental ΔH_0 and calculated *ab initio* ΔE values of the rotational isomers of acryloyl fluoride (cm^{-1})[a]

Experimental		Calculated	
Method (ref.)	ΔH_0	Theoretical level	ΔE
MW (25)	31 ± 35	HF/3-21G (3)	32
IR, Raman (24)	35 ± 5	HF/4-21G (43)	140
UV (34)	40 ± 30	HF/6-31G (2)	86
IR (40)	52 ± 35	HF/6-31G* (3)	79
IR (38)	88	MP2/6-31G* (2)	96
NMR (41)	88 ± 23	MP2/6-31G* (this work)	94[c]
NMR (42)	280 ± 87		
Raman (3)[b]	−93 ± 33		

[a]In the harmonic approximation $\Delta H_0 = \Delta E + 1/2(\omega_{cis} - \omega_{trans})$.
[b]From temperature studies of the Raman spectra of the gas the *cis* conformer was calculated to be more stable.
[c]The difference between the present result and that of ref. 2 is partially due to rounding off of the last digits.

Concerning the accuracy of experimental ΔH_0 values, acryloyl fluoride is a very instructive example. Indeed, the dispersion of the values measured using various experimental methods is large (see Table 5). There is even a negative experimental ΔH_0 value: measurements of the Raman band intensities as a function of temperature indicated that *s-cis* acryloyl fluoride is more stable than the *s-trans* conformer (3). Nevertheless, the authors of ref. 44 suggested using a mean value of the experimental ΔH_0 data in determining a IRPE function by the RR approximation method. Because of the negative value of ΔH_0 mentioned above, this approach seems to be especially unrealistic in the case of the CH_2=CH-CF=O molecule.

As mentioned above, using different numbers of terms in the IRPE function expansion showed that it is possible to approximate the theoretical potential curve satisfactorily only with a minimum of six terms. Also, discussion of the results of Table 4 revealed that use of the four-term IRPE function leads to an overestimated value of ΔH_0. The use of the experimental value of ΔH_0 in the least-squares fitting with the RR approximation probably alters the actual slope of the IRPE curve approximated by the four-term expansion which results in a loss of the physical meaning of the final IRPE function obtained. Therefore, in the case of more complicated molecular systems of low symmetry, such as the α,β-unsaturated carbonyl compounds, all the four-term IRPE functions that have been reported to date need to be recalculated without using the experimental value of ΔH_0, using a six-term IRPE expansion, and including data on molecular relaxation during rotation.

Nevertheless, it is necessary to mention the special role of the number of the available experimental torsional transition frequencies used in the inverse problem of refining the initial IRPE function. It is desirable that their number be sufficient to allow refinement of *all* the coefficients of the six-term IRPE function expansion. Otherwise only a certain number of these coefficients may be varied during the IRPE function refinement.

Can. J. Chem. Downloaded from www.nrcresearchpress.com by 88.255.202.194 on 09/08/12
For personal use only.

Can. J. Chem. Downloaded from www.nrcresearchpress.com by 88.255.202.194 on 09/08/12
For personal use only.

Conclusions

The considerations given above for the acryloyl fluoride molecule reveal that the use of a high quality theoretical *ab initio* IRPE curve (which necessarily implies accounting for molecular relaxation during rotation) as the initial IRPE function provides very important advantages in the course of determination of an effective IRPE function. They are the following:

1. Accurate prediction of the number of wells and barriers and their positions.
2. Construction of a correct reduced rotational constant function $F(\varphi)$.
3. Use of the six-term starting IRPE function.
4. The possibility of avoiding using the experimental ΔH_0 value in the corresponding inverse problem. This is very desirable because the accuracy of ΔH_0 measurements is usually quite low.
5. It permits one to obtain a *physically meaningful* effective IRPE function that not only reproduces the frequencies of the torsional transitions in all the wells, but also predicts the values of ΔH_0 and $\Delta H^{\#}$ with a certain degree of accuracy. The accuracy of such predictions is increased as the theoretical level of the initial *ab initio* curve is enhanced.

As pointed out by a referee, $\Delta H_0 = 168$ cm^{-1}, obtained using the refined six-term MP2/6-31G* IRPE and the zero-point energies for torsional transitions of the acryloyl fluoride rotamers, is "more than a factor of 2 larger than either the mean or the median experimental values." It is nevertheless smaller than the NMR result (42) (where solvent or aggregation effects may, however, be important). We feel that $\Delta H_0 = 168$ cm^{-1} for the acryloyl rotamers is credible. The overall picture points out the necessity for further experimental studies on the rotational isomerism of this molecule, preferably with very accurate far-IR intensity measurements by a method such as that recently reported by Hurtmans *et al.* (45).

Acknowledgement

The authors wish to thank Georges Destrée of the Université Libre de Bruxelles/Vrije Universiteit Brussel Computing Center for his assistance with GAUSSIAN 90.

1. Ch. W. Bock, A. V. Abramenkov, G. R. De Maré, and Yu. N. Panchenko. J. Comput. Chem. **13**, 718 (1992).
2. Ch. W. Bock, Yu. N. Panchenko, and S. V. Krasnoshchiokov. Chem. Phys. **147**, 65 (1990).
3. J. R. Durig, R. J. Berry, and P. Groner. J. Chem. Phys. **87**, 6303 (1987).
4. Yu. N. Panchenko, V. I. Pupyshev, A. V. Abramenkov, M. Traetteberg, and S. J. Cyvin. J. Mol. Struct. **130**, 355 (1985).
5. P. Gomez, M. Fernandez, and V. Botella. J. Mol. Struct. **122**, 317 (1985).
6. J. D. Lewis, T. B. Malloy, Jr., T. H. Chao, and J. Laane. J. Mol. Struct. **12**, 427 (1972).
7. G. R. De Maré. J. Mol. Struct. Theochem. **107**, 127 (1984).
8. G. R. De Maré. *In* Computational theoretical organic chemistry. *Edited by* I. G. Csizmadia and R. Daudel. NATO ASI Ser. C, **67**, 371 (1981).
9. Yu. N. Panchenko, A. V. Abramenkov, V. I. Mochalov, A. A. Zenkin, G. Keresztury, and G. Jalsovszky. J. Mol. Spectrosc. **99**, 288 (1983).
10. G. R. De Maré and D. Neisius. J. Mol. Struct. Theochem. **109**, 103 (1984).
11. M. Traetteberg, G. Poulen, S. J. Cyvin, Yu. N. Panchenko, and V. I. Mochalov. J. Mol. Struct. **116**, 141 (1984).
12. Ch. W. Bock, Yu. N. Panchenko, S. V. Krasnoshchiokov, and V. I. Pupyshev. J. Mol. Struct. **129**, 57 (1985).
13. G. R. De Maré. Can. J. Chem. **63**, 1672 (1985).
14. Yu. N. Panchenko, A. V. Abramenkov, and Ch. W. Bock. J. Mol. Struct. **140**, 87 (1986).
15. Ch. W. Bock, Yu. N. Panchenko, S. V. Krasnoshchiokov, and R. Aroca. J. Mol. Struct. **160**, 337 (1987).
16. G. R. De Maré, Yu. N. Panchenko, and A. V. Abramenkov. J. Mol. Struct. **160**, 327 (1987).
17. Yu. N. Panchenko, S. V. Krasnoshchiokov, and Ch. W. Bock. J. Comput. Chem. **9**, 443 (1988).
18. Ch. W. Bock, Yu. N. Panchenko, and S. V. Krasnoshchiokov. Chem. Phys. **125**, 63 (1988).
19. Ch. W. Bock and Yu. N. Panchenko. J. Mol. Struct. Theochem. **187**, 69 (1989).
20. Ch. W. Bock and Yu. N. Panchenko. J. Mol. Struct. **221**, 159 (1990).
21. Ch. W. Bock, Yu. N. Panchenko, and V. I. Pupyshev. J. Comput. Chem. **11**, 623 (1990).
22. K. W. Wiberg and R. E. Rosenberg. J. Am. Chem. Soc. **112**, 1509 (1990).
23. H. Guo and M. Karplus. J. Chem. Phys. **94**, 3679 (1991).
24. Yu. N. Panchenko and Ch. W. Bock. Struct. Chem. **3**, 27 (1992).
25. Yu. N. Panchenko, S. V. Krasnoshchiokov, P. George, and Ch. W. Bock. Struct. Chem. **3**, 15 (1992).
26. G. R. De Maré, Yu. N. Panchenko, and A. V. Abramenkov. J. Phys. Chem. **96**, 2111 (1992).
27. G. R. De Maré. J. Mol. Struct. Theochem. **253**, 199 (1992).
28. M. J. Frisch, M. Head-Gordon, G. W. Trucks, J. B. Foresman, H. B. Schlegel, K. Raghavachari, M. A. Robb, J. S. Binkley, C. Gonzalez, D. J. De Frees, D. J. Fox, R. A. Whiteside, R. Seeger, C. F. Melius, J. Baker, R. L. Martin, L. R. Kahn, J. J. P. Stewart, S. Topiol, and J. A. Pople. GAUSSIAN 90, Gaussian, Inc., Pittsburgh, Pa. 1990.
29. J. J. Keirns and R. F. Curl, Jr. J. Chem. Phys. **48**, 3773 (1968).
30. A. A. Zenkin, L. N. Margolin, Yu. A. Pentin, and V. I. Tyulin. J. Mol. Struct. **29**, 65 (1975).
31. I. A. Godunov, A. V. Abramenkov, and V. I. Tyulin. Zh. Strukt. Khim. **22**, 49 (1981) (Russian pagination).
32. S. Brodersen. J. Mol. Spectrosc. **142**, 122 (1990).
33. J. R. Durig, J. S. Church, and D. A. C. Compton, J. Chem. Phys. **71**, 1175 (1979).
34. L. A. Glebova, L. N. Margolin, Yu. A. Pentin, and V. I. Tyulin. Zh. Strukt. Khim. **17**, 703 (1976) (Russian pagination).
35. G. R. De Maré and M. R. Peterson, J. Mol. Struct. Theochem. **89**, 213 (1982).
36. G. R. De Maré. J. Mol. Struct. Theochem. **153**, 341 (1987).
37. G. R. De Maré and M. R. Peterson. J. Mol. Struct. Theochem. **104**, 115 (1983).
38. R. L. Redington. J. Chem. Phys. **62**, 4927 (1975).
39. K. W. Butz, J. R. Johnson, D. J. Krajnovich, and C. S. Parmenter. J. Chem. Phys. **86**, 5923 (1987).
40. G. L. Carlson, W. G. Fately and R. W. Witkowski. J. Am. Chem. Soc. **89**, 6437 (1967).
41. F. F. S. Lin and H. L. Servis. J. Am. Chem. Soc. **94**, 5794 (1972).
42. D. F. Koster. J. Am. Chem. Soc. **88**, 5067 (1966).
43. A. J. P. Devaquet, R. E. Townshend, and W. J. Hehre. J. Am. Chem. Soc. **98**, 4068 (1976).
44. V. I. Tyulin, L. A. Glebova, L. N. Margolin, and Yu. A. Pentin. Russ. J. Phys. Chem. **66**, 392 (1992) (Russian pagination).
45. D. Hurtmans, R. Pétrisse, D. Lemaître, C. Clerbaux, and J. Vander Auwera. EPA Newsl. **44**, 40 (1992).

Hydrogen isotopic exchange between D_2 and H_2O on alumina prepared by sputtering

FUMIO IOKA, TETSUO SAKKA, YUKIO OGATA,[1] AND MATAE IWASAKI
Institute of Atomic Energy, Kyoto University, Gokasho, Uji, Kyoto 611, Japan

Received August 4, 1992

FUMIO IOKA, TETSUO SAKKA, YUKIO OGATA, and MATAE IWASAKI. Can. J. Chem. **71**, 663 (1993).

Hydrogen isotopic exchange between D_2 and H_2O has been investigated on alumina prepared by sputtering at 803 K and at low pressures. The alumina is amorphous, consisting of aluminum with coordination numbers four, five, and six in the ratio 1:2:1 as determined by NMR. A kinetic model is proposed on the basis of the pressure dependence of the exchange rate and the heats of adsorption at adsorbed sites, evaluating by molecular orbital calculations. The adsorbed sites are assumed to be Lewis acid–base pairs composed of a coordinatively unsaturated aluminum and the adjacent unsaturated oxygen site. The site relating to the rate-determining step contains threefold aluminum, which is formed by unsaturation of fourfold aluminum at the surface. As a consequence, the exchange rate depends on the amount of fourfold aluminum when the alumina is heat treated and changes its phase.

FUMIO IOKA, TETSUO SAKKA, YUKIO OGATA et MATAE IWASAKI. Can. J. Chem. **71**, 663 (1993).

On a étudié l'échange isotopique d'hydrogène entre le D_2 et le H_2O, qui se produit sur de l'alumine préparée par bombardement à 803 K et à de basses pressions. L'alumine est amorphe et elle comporte de l'aluminium avec des indices de coordination de quatre, cinq et six dans un rapport de 1 : 2 : 1, tel que déterminé par RMN. On propose un modèle cinétique qui permet d'expliquer la relation entre la vitesse d'échange et les chaleurs d'adsorption évaluées par des calculs d'orbitales moléculaires. On fait l'hypothèse que les sites d'adsorption sont des paires d'acide et de base de Lewis formées d'un aluminium insaturé pentacoordiné et du site oxygéné insaturé adjacent. La site impliqué dans l'étape cinétiquement limitante contient trois fois plus d'aluminium et cette situation est le résultat d'une insaturation dans une quantité quatre fois plus grande d'aluminium à la surface. En conséquence, la vitesse d'échange dépend de la quantité d'aluminium présent en quantité quatre fois plus grande quand l'alumine est traitée par chauffage et qu'elle change de phase.

[Traduit par la rédaction]

Can. J. Chem. Downloaded from www.nrcresearchpress.com by 213.200.69.106 on 09/08/12
For personal use only.

Introduction

Catalytic behavior of supported platinum catalysts for hydrogen isotopic exchange has been extensively investigated in relation to the separation of deuterium and tritium (1). In practical processes operated in a gas–liquid system, the use of waterproofed platinum catalysts (2) is considered promising; otherwise the exchange rate becomes sluggish by the retardation of hydrogen transfer across condensed water over platinum (3, 4). Both platinum alone and mixtures of other components are used as catalytic particles. The second component promotes the dispersion of platinum and prevents sintering during heat treatment, realizing a large effective surface area. In addition, it often enhances the catalytic activity (5–7). Thus, the apparent catalytic activity of supported catalysts varies in both the physical and the chemical sense.

For the design of effective catalysts it is of importance to comprehend the catalytic activity of each single element. Along this line, some researchers have investigated the hydrogen isotopic exchange reaction between hydrogen and water vapor on unsupported platinum powder and plate (8, 9). The results showed that the reaction mechanism was equivalent to the mechanism proposed by Rolston and Goodale (3) for an alumina-supported platinum catalyst: the rate was controlled by an exchange step between hydrogen chemisorbed on the platinum and water physically adsorbed on the alumina. A pure platinum catalyst provides the two kinds of sites mentioned above (9). Such support materials as silica and graphite (8) do not exhibit any appreciable catalytic activity for hydrogen exchange, but some materials exhibit this activity, if used by themselves as catalyst. Of the latter, alumina shows activity at high temperatures (10, 11), and also shows catalytic activity for isomerization of alkenes, dehydration of alcohols, and other organic reactions (12).

We have studied the actual catalytic activity of platinum at low pressures of reactants where hindrance of the transport of gaseous reactants due to condensation of water at the surface could be avoided, and have obtained reasonable kinetic relationships for the isotopic exchange between D_2 and H_2O (9). In this paper, hydrogen isotopic exchange kinetics is investigated on a pure alumina surface at low pressures and high temperature. Alumina has been extensively employed not only as a catalyst support but also as an active catalyst. The activity is closely connected with the surface structure. Catalytic alumina has a γ or η form in the polymorphs and is generally prepared from amorphous alumina made by thermal decomposition of aluminum hydroxide or aluminum nitrate, or by anodization of aluminum. Sputtering offers another possibility for preparing amorphous alumina. The sputtering technique permits formation of an alumina layer with a large area. This study employs alumina prepared by sputtering. The kinetics is related to the surface states of alumina, particularly to the coordination states of the aluminum. A model for the hydrogen exchange, stressing the reaction sites, is proposed.

Experimental procedure

Preparation of alumina

For the isotopic exchange experiments and the X-ray diffraction, alumina was sputtered onto a silica glass substrate by an rf-diode glow discharge magnetron sputtering instrument (Shimadzu HSR-322S). An aluminum foil substrate was also employed when a considerable amount of the alumina sample was required for the characterization. An α-alumina target of purity 99.9999% was set

[1]Author to whom correspondence may be addressed.

Can. J. Chem. Downloaded from www.nrcresearchpress.com by 213.200.69.106 on 09/08/12
For personal use only.

under the substrate. Pressure and flow rate of argon discharge gas were adjusted to 0.01 Torr (1 Torr = 133.3 Pa) and 5 cm^3 min^{-1}, respectively. Temperature control of the substrate was not carried out. An rf power of 200 W was utilized and the average deposition rate was then 0.58 nm s^{-1}, measured by a quartz crystal microbalance, Inficon XTC.

Characteristics of the deposited alumina were evaluated by an X-ray diffractometer (XRD), Rigaku RAD-2C, equipped with an attachment for measurement of thin films where Cu-K_α was used and the θ angle was fixed at 2°, and by a thermal analysis unit, Rigaku SN 82151, with a temperature increase of 10 K min^{-1} for the DTA and TG measurements.

The coordination numbers of aluminum in powdered alumina samples were measured by a JEOL JNM-X400 NMR spectrometer. ^{27}Al NMR spectra were obtained at a resonance frequency of 104.17 MHz at 9.4 T with the magic angle spinning (MAS) technique at 7.0 kHz with a zirconia rotor. $\pi/18$ pulses of 0.5 μs were applied and the repetition time was 1 s. This short excitation pulse assures that the error is less than 5% in the central transition (13). Chemical shifts of ^{27}Al were recorded with respect to $AlCl_3 \cdot 6H_2O$. ^{27}Al CP/MAS NMR spectra were also measured by using alumina samples without heat treatment and with heat treatment at 1073 K under conditions satisfying the Hartman–Hahn condition (14). A contact time of 0.5 ms was employed and the repetition time was 3 s.

Kinetic measurements

Hydrogen exchange rates between D_2 and H_2O were measured at 803 K on alumina of surface area 35 cm^2, prepared by sputtering and positioned in a silica glass. The operating temperature was selected as a compromise between the sluggish exchange rate at low temperatures and avoidance of the phase transition of alumina during the kinetic runs at high temperatures. The progress of the exchange reaction was followed by monitoring the variation of the quantities of D_2, HD, and H_2 with a quadrupole mass spectrometer, Nichiden Anelva AQA-100MPX. The isotope effects on introducing the sample gas to the mass analyzing chamber and the ionic reactions in the chamber were taken into account and the readings were corrected. The other details of the experimental setup and procedures were as described previously (9).

Results

Characterization of sputtering alumina

Alumina prepared by sputtering was transparent and the surface was smooth. The weight loss of about 1% caused by dehydration was completed below 600 K in the TG curve measured under atmospheric conditions, as Peri and Hannan (15) observed that heating at 673 K removed all water molecules though surface hydroxyl groups still remained, and any significant weight changes were not observed above that temperature. This implies that the sputtered alumina satisfied its stoichiometry: there was no significant oxygen deficiency. In the DTA curve, two exothermic peaks appeared at 1170 K and 1460 K. The phase transition was followed by XRD using alumina samples treated at various temperatures. The alumina treated at lower than 1073 K was amorphous; γ-type appeared at 1173 K, then α-type coexisted at 1273 K, and finally the alumina was composed of only α-type at 1373 K. As a result, two peaks in the DTA curve are attributed to the transitions from amorphous to γ-type and from γ-type to α-type, respectively. It is to be noted that the transition temperature of amorphous to γ-type, 1170 K, is 200–400 K higher than other alumina obtained by conventional techniques such as thermal decomposition of aluminum hydroxide (970 K) (16) and anodization of aluminum (770 K) (17).

Figure 1 shows typical ^{27}Al MAS NMR spectra of heat-

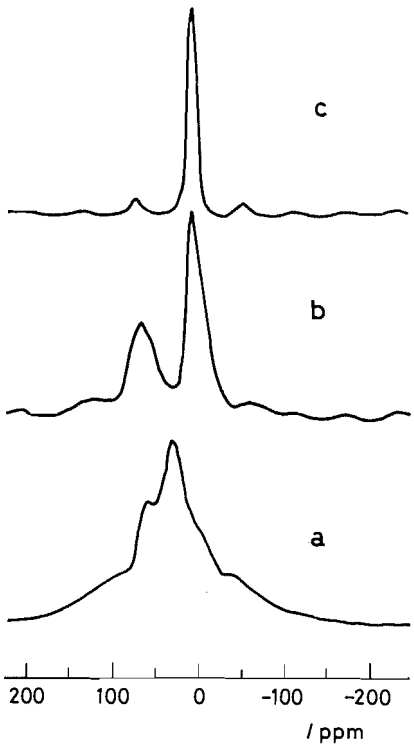

FIG. 1. Variation of ^{27}Al MAS NMR spectrum with heat treatment of alumina: (*a*) as prepared, (*b*) 1173 K, and (*c*) 1473 K. Resonance frequency = 104.17 MHz, excitation pulse = 0.5 μs, repetition time = 1 s, and number of scans = 256.

treated alumina. Three peaks were found in the spectra and the chemical shifts were about 5, 35, and 70 ppm, respectively. The chemical shifts of octahedrally (sixfold) and tetrahedrally (fourfold) coordinated aluminum are well established, appearing in the regions 0–20 ppm and 50–80 ppm (18), respectively. The other chemical shift around 30 ppm has been assigned to the fivefold coordination and it exists only in disordered materials (19). The observed spectra were resolved into three Gaussians to separate the coordinations, where the line width and intensity were adjusted to minimize the root-mean-square errors between the observed and the calculated spectra. The amounts of the different coordinations were evaluated from the area of each Gaussian. This procedure made a quantitative evaluation of the coordination states possible. Variations of the coordinations are shown in Fig. 2 as a function of the temperature of heat treatment. The ratio of the coordinations varied with the temperature. At temperatures lower than 1100 K, four-, five-, and sixfold coordinated aluminum existed in a ratio about 1:2:1. The fivefold coordination disappeared above 1150 K and the four and sixfold coordinations increased in the fractions, 35 and 65%, respectively. When the temperature was raised over 1400 K, the alumina consisted solely of the sixfold coordination. The transition temperatures correspond to the peak temperatures observed in the DTA curves. The structures tell us that α-alumina is composed of only sixfold coordinated aluminum and the coordination numbers of γ-alumina are four and six in the ratio 1:2, while the ratio of the coordinations in the amorphous alumina prepared by sputtering has been determined to be 1:2:1 in the present measurements.

^{27}Al CP/MAS NMR spectra with different heat treatments are shown in Fig. 3. The surface environment of alu-

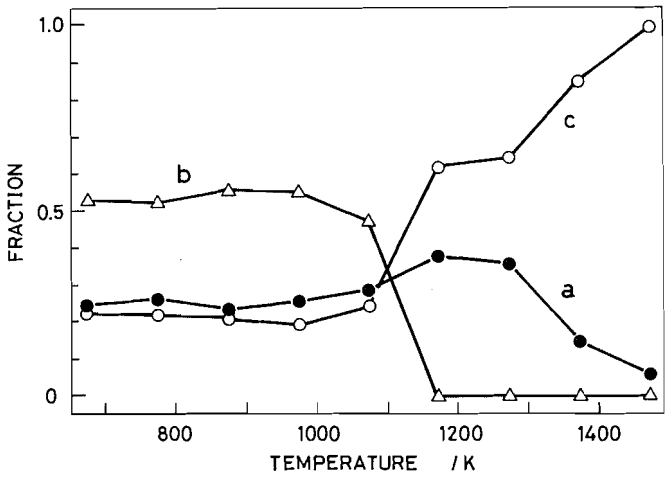

FIG. 2. Changes of coordination numbers of aluminum as a function of heat treatment temperature of alumina. Coordination numbers: (*a*) 4, (*b*) 5, and (*c*) 6.

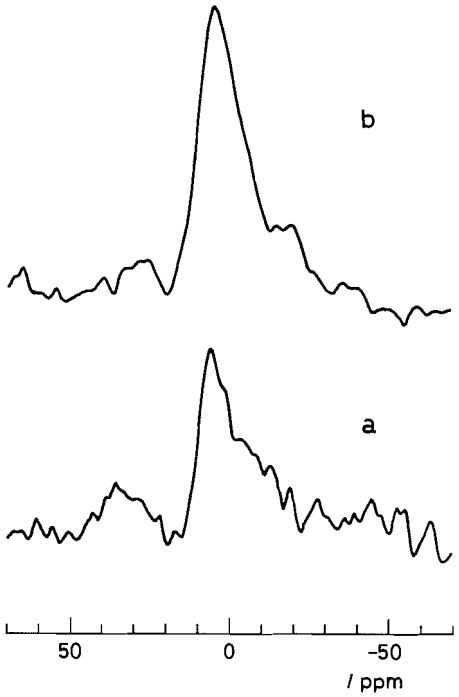

FIG. 3. ^{27}Al CP/MAS NMR spectra of alumina (*a*) without and (*b*) with heat treatment at 1073 K. Contact time = 0.5 ms, repetition time = 3 s, and number of scans > 21 000.

minum can be obtained by the cross polarization technique between ^{27}Al and ^{1}H (20) because the surface of alumina is covered with hydroxyl groups. Quantitative analysis of the peak strength is, however, difficult because the peak intensity depends on the separation between aluminum and proton and on the symmetry. Both samples should belong to the amorphous type according to the results from the bulk measurements, i.e., DTA and ^{27}Al MAS NMR, but the local environment of the surface exhibited different features. Two peaks, six- and fivefold coordinated aluminum, were observed at ca. 5 and 35 ppm, respectively, for the sample without heat treatment. However, the intensity of the fivefold was very weak relative to the sixfold coordination, in

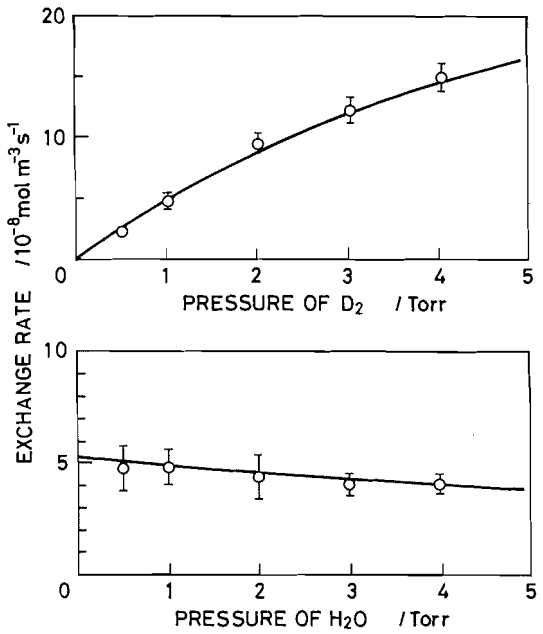

FIG. 4. Pressure dependence of hydrogen exchange rate with variation of deuterium and water pressures. Fixed gas pressure is 1 Torr in each case. Solid lines are regression curves according to eq. [7].

contrast to the bulk measurements where the ratio was ca. 2:1. Furthermore, the fourfold coordination was hardly observable in the spectrum. This low sensitivity is attributed to the unfavorable CP parameters caused by the geometry of the tetrahedral site and adsorbed hydroxyl groups on the site. It has been observed that substances composed of completely fourfold coordinated aluminum, such as lithium aluminum hydride and sodium magnesium aluminosilicate, give no significant signals in the CP/MAS NMR spectrum (20). Fivefold coordinated aluminum at the surface is formed by unsaturation of the sixfold coordination (12). Hydroxyl groups easily occupy the unsaturated sites exposed at the surface, resulting in the formation of the sixfold coordination and hence a decrease in the ratio of the fivefold coordination at the surface. Fivefold coordinated aluminum disappeared in the CP/MAS NMR spectrum when alumina was heat treated at 1073 K. This indicates that the transition from amorphous to γ starts at lower temperatures at the surface than in the bulk (see Fig. 2). Removal of water or hydroxyl from alumina might facilitate the transition since the desorption would be accompanied by some reorganization. This interpretation is in accordance with the fact that sputtered alumina has a higher transition temperature than alumina prepared by other techniques, as mentioned above, in which some amount of residual water or hydroxyl would exist.

Hydrogen isotopic exchange on alumina

Initial exchange reaction rates were determined by the decrease in D_2 in a reaction cell heated at 803 K by an electric furnace. The temperature fluctuation was within ±5 K. Variations of the exchange rates as a function of the pressures of D_2 and H_2O are shown in Fig. 4 where alumina as prepared was employed. The fixed gas pressure was set to 1 Torr. The D_2 pressure dependence was evaluated preliminarily by curve fitting with three types of functions (Fig.

Can. J. Chem. Downloaded from www.nrcresearchpress.com by 213.200.69.106 on 09/08/12
For personal use only.

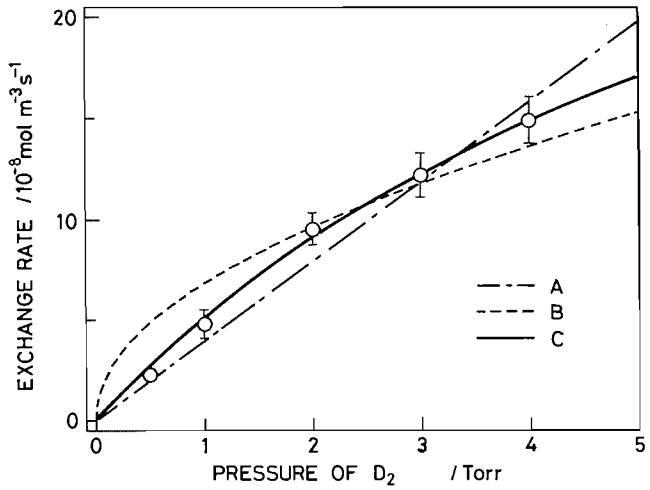

FIG. 5. Curve fitting for D_2 pressure dependence of the exchange rate. (*a*) $r = 4.0 \times 10^{-8} C_{D_2}$, (*b*) $r = 6.8 \times 10^{-8} C_{D_2}^{1/2}$, (*c*) $r = 5.8 \times 10^{-8} C_{D_2}/(1 + 0.14C_{D_2})$.

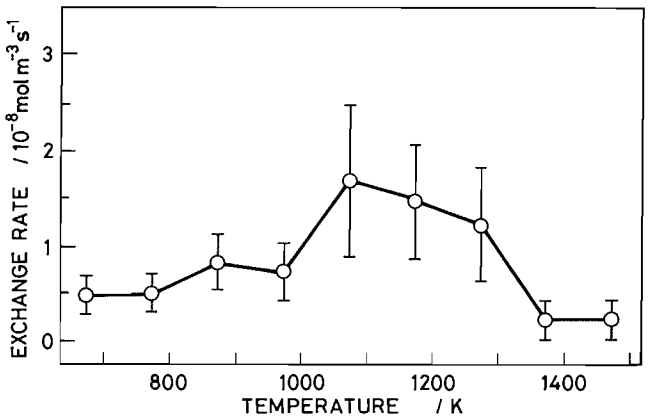

FIG. 6. Change of hydrogen exchange rate on alumina heat treated at various temperatures. Pressures of deuterium and water were 1 Torr. Vertical lines indicate the errors.

5). The exchange rate increased with increasing pressure of D_2 depending on the D_2 concentration rather than on the square root, and the fitting curve (*c*) satisfied the relation. It seems that the adsorption took place without dissociation. H_2O slightly inhibited the exchange rates, where it was not plausible to assume that condensation of water on the catalyst hindered transport of reactants or caused the inhibition because the experiments were performed under such low-pressure conditions. The possible reaction mechanism will be discussed later.

The exchange rate varied with temperature of heat treatment, as shown in Fig. 6. The quantitative reproducibility was poor in specimens separately prepared; however, each specimen showed a similar variation with the temperature and the results obtained by repeated measurements using a given specimen agreed satisfactorily. The error bars in the figure, which are large, indicate that the fluctuation originated from different specimens measured. The catalytic activity increased at 1073 K, then alumina lost its activity at the temperatures over 1373 K. The catalytic change is attributed to the phase transition of alumina: γ-alumina has the highest activity but the α surface does not exhibit an appreciable catalytic activity. It seems that the catalytic activity is responsible for the amount of fourfold coordinated aluminum, although the transition temperature shifted to somewhat low temperature compared to the NMR spectra because the surface could transform at low temperatures and the exchange rate depended on the surface state but not on the bulk state. The BET surface area of alumina as prepared and treated at 1273 K did not cause any significant difference, and it was ca. 2 $m^2 g^{-1}$ for both samples, which were prepared by collecting the deposit on aluminum foil and weighed 0.2–0.3 mg. Therefore, the difference in the exchange rates could not be caused by that of the actual surface area; Abbatista *et al.* reported that amorphous alumina prepared by the conventional method decreased the surface area and increased the catalytic activity by a factor of three in the dehydration reaction of methanol after the transition to γ-alumina by thermal treatment (21). It is to be noted that the surface area of γ-alumina thus prepared by sputtering and heat treatment is extraordinarily small compared to that of the usual active transition alumina, which has a surface area up to several hundred $m^2 g^{-1}$.

Discussion

The surface adsorptive states of hydrogen and water on alumina were investigated by molecular orbital (MO) calculations to clarify the states in the course of the exchange process. Aluminum at an alumina surface is bonded to unsaturated oxygen or hydroxyl groups, or is exposed as its bare state. Under ambient conditions, almost all of the bare and oxygen sites are covered by hydroxyl groups due to adsorption of water (22). The adsorption forms a bond and occupies the unsaturated sites, so that only a small amount of fivefold aluminum with unsaturated coordination was detected at the alumina surface in the CP/MAS NMR results. However, the hydroxyl groups are removed at high temperatures, e.g., evacuation at 800 K decreases the coverage of hydroxyl groups to 0.3 (23). Thus unsaturated oxygen and bare aluminum exist at the alumina surface at 803 K, which is the temperature at which the present kinetic experiments were conducted, and these sites function as Lewis acid and base providing adsorptive sites or catalytically active sites (12, 24). Adsorption of hydrogen on alumina has been considered to take place at the acid–base sites composed of coordinatively unsaturated aluminum and oxygen, on the basis of results of IR measurements (11) and quantum chemical calculations (24). So, *ab initio* MO calculations were conducted using small clusters, modeling alumina with three- and fivefold coordinated aluminum formed by unsaturation of the four- and sixfold coordinations, respectively; the Al—O network was terminated by hydrogen as $Al(OH)_3$ and $Al(OH)_5$. The model clusters employed are shown in Fig. 7 together with the optimized parameters. The calculations were carried out using the GAUSSIAN-82 program (26). The structures were optimized by using the 3-21G basis set with the gradient method. The angles of Al—O—H and O—Al—O were fixed and the separations of Al—O and O—H were optimized for the coordinatively unsaturated sites. In the case of the adsorbed states of hydrogen and water, the structures of the adsorbents kept their original coordinatively unsaturated structures, and separations between adsorbates and adsorbents and the related angles were optimized. No stable structure was obtained in hydrogen adsorption on alumina with fivefold coordinated aluminum.

Can. J. Chem. Downloaded from www.nrcresearchpress.com by 213.200.69.106 on 09/08/12
For personal use only.

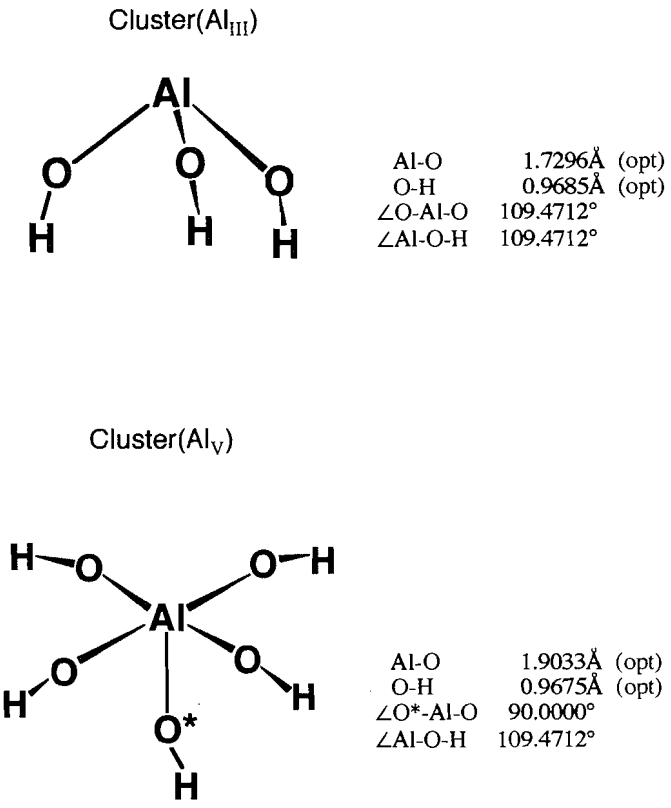

FIG. 7. Model clusters for alumina with coordinatively unsaturated aluminum.

TABLE 1. Calculated energy of clusters and heat of adsorption

Cluster	Energy (hartree)	Heat of adsorption (kJ mol^{-1}) Adsorbed site	Adsorbate D_2	Adsorbate H_2O
D_2	−75.5860	$Al(OH)_3$	127.3	302.7
H_2O	−1.1230	$Al(OH)_5$	—	83.2
$Al(OH)_3$	−465.7731			
$Al(OH)_5$	−615.6596			
D_2 on $Al(OH)_3$	−466.9446			
D_2 on $Al(OH)_5$[a]	—			
H_2O on $Al(OH)_3$	−541.4744			
H_2O on $Al(OH)_5$	−691.2773			

[a]Stable structure is not obtained.

These optimized geometries were used for single point calculations with the 3-21G basis set in order to obtain the total energy. The results and the resulting heats of adsorption are given in Table 1 for the respective cases. The heats of adsorption thus obtained may not be *quantitative* but the order of the values is plausible: H_2O at $Al(OH)_3$, D_2 at $Al(OH)_3$, and H_2O at $Al(OH)_5$. The experimental results of the exchange kinetics were strongly dependent on D_2 pressure as shown in Fig. 4, and the active site should be related to the fourfold coordinated aluminum judging from the results in Fig. 6. The adsorption site for D_2 must be the threefold coordinated site from the MO calculations because the adsorptive state at the fivefold coordination is unstable and a large portion of the fourfold coordinated

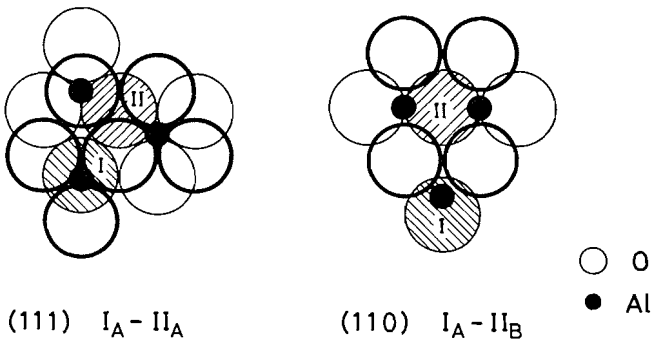

FIG. 8. Examples of the Lewis acid–base pair produced from adjacent aluminum sites. Circle with thin line denotes oxygen existing at the upper layer. OH is desorbed from the hatched I site and H is desorbed from the hatched II site; they becomes the acid and base sites, respectively.

TABLE 2. Net charge of adsorption for different adsorptive states

State X	X-OH	X-O	X-
I_A	−0.25	−1.25	+0.75
I_B	−0.5	−1.5	+0.5
II_A	+0.25	−0.75	+1.25 (+0.5 + 0.75)[a]
II_B	0.0	−1.0	+1.0 (+0.5 × 2)[a]
III	+0.5	−0.5	+1.5 (+0.5 × 3)[a]

[a]The values in parentheses are the net charges for the fragments.

aluminum would be unsaturated at a high temperature such as 803 K and would have the threefold coordination. Competitive adsorption of H_2O is also possible at the site and the heat of adsorption is greater than that of the D_2 adsorption, and hence the threefold aluminum site is in favor of the H_2O adsorption. H_2O can be adsorbed also at the fivefold site but the heat is small, i.e., the desorption is easy there.

Now we consider the adsorptive states. The (111), (110), and (100) planes are preferentially exposed at the surface of active transition alumina such as the γ- and η-types. Almost the whole surface was covered by adsorbed hydroxyl groups at room temperature and the states have been classified into five types (12, 27): I_A, I_B, II_A, II_B, and III, where the number denotes the number of aluminum atoms participating in the adsorption and subscripts A and B mean tetrahedral and octahedral aluminum atoms, respectively, with the exception of II_A, which is composed of a tetrahedral and an octahedral aluminum atom, and III, which contains three octahedral aluminum atoms, and each type has different vibrations of the O—H stretching. We assume that such sites exist also in amorphous alumina. As shown in the experimental results and the MO calculation, D_2 can be adsorbed only at the fourfold aluminum. The layers containing fourfold aluminum have sites where the different types adjoin each other as nearest neighbors: I_A–II_A on the (111) plane, and I_A–II_B on the (110) plane (Fig. 8). The other possible combination is II_B–III but it consists only of sixfold aluminum. The I_B site also exists due to the removal of aluminum ion from II_A or II_B. Since a large fraction of hydroxyl groups are removed as water from the surface at 803 K as mentioned before (23), OH is desorbed from I_A and H is desorbed from II_A or II_B on considering the values of the net electronic charge (12) given in Table 2, which can be a

Can. J. Chem. Downloaded from www.nrcresearchpress.com by 213.200.69.106 on 09/08/12
For personal use only.

measure for stability. The sites where the desorption occurs are indicated by hatching in Fig. 8. In consequence, Lewis acid–base pairs consisting of coordinatively unsaturated threefold aluminum and oxygen are produced (Fig. 8). It is expected that analogous pairs would exist also in the case of the amorphous state. These sites denoting A–B, where A means the Lewis acid site and consists of the threefold aluminum and B means the base site, can be an adsorption site for D_2. The exchange of hydrogen and the desorption should be rate-determining steps because of the D_2 dependence of the exchange kinetics.

A possible scheme for the exchange process is proposed as below.

$$[1]\quad \text{A–B} + \text{D}_2 \overset{K_1}{\rightleftarrows} \begin{matrix} \text{D} & \text{D} \\ | & | \\ \text{A–B} \end{matrix}$$

$$[2]\quad \begin{matrix} \text{D} & \text{D} \\ | & | \\ \text{A–B} \end{matrix} + \text{S–H} \overset{k}{\rightarrow} \text{DH} + \begin{matrix} \text{D} \\ | \\ \text{A–B} \end{matrix} + \text{S}$$

$$[3]\quad \text{S} + \text{H}_2\text{O} \overset{K_3}{\rightleftarrows} \text{S–H}_2\text{O}$$

$$[4]\quad \begin{matrix} \text{D} \\ | \\ \text{A–B} \end{matrix} + \text{S–H}_2\text{O} \overset{K_4}{\rightleftarrows} \text{DHO} + \text{A–B} + \text{S–H}$$

$$[5]\quad \text{A–B} + \text{H}_2\text{O} \overset{K_5}{\rightleftarrows} \begin{matrix} \text{OH} & \text{H} \\ | & | \\ \text{A–B} \end{matrix}$$

where k and K are rate constant and equilibrium constant, respectively. Although step [2] might be separated into a surface reaction and a desorption process of DH, both processes were combined above because the rate of desorption is usually not known separately (28); in step [4] this is also the case. D_2 is adsorbed at the Lewis acid–base site A–B containing unsaturated threefold aluminum and the adsorption would be dissociative because of its high heat of adsorption at the threefold aluminum, as can be seen in Table 1 (eq. [1]). At the A–B site, H_2O adsorption is also possible (eq. [5]); the adsorption competes with the adsorption of D_2 and the adsorptive state is stable because of the high value of the heat of adsorption. Then the adsorbed D_2 at A–B exchanges with H from S–H, producing DH and leaving D adsorbed at A–B and site S (eq. [3]). Here, the source supplying H denoted as S–H must be present at the start of the exchange process because sources formed by adsorption of H_2O should not participate in this rate-determining step; otherwise we should have observed a strong dependence of H_2O pressure on the exchange rate, but we could not. The S–H probably consists of the remaining hydroxyl groups on the alumina surface because a significant percentage of the surface would be still covered by hydroxyl groups under the present experimental conditions (23). The dehydrogenated site S adsorbs H_2O (eq. [3]). Although the site is simply denoted by S because we could not know the structural state, it is probable that the site is also composed of the Lewis acid–base pair consisting of fivefold aluminum sites, which is favorable for the adsorption of polar molecules such as water and the heat of adsorption is low. The two types of adsorption sites are regenerated by producing DHO and they recover their original states, A–B and S–H (eq. [4]).

On assuming that amounts of DH, H_2, DHO, and D_2O are small because the exchange rates were measured in the early stage, the rate equation becomes

$$[6]\quad r = \frac{kS_1^T S_2 K_1 C_{D_2}}{1 + K_1 C_{D_2} + K_5 C_{H_2O}}$$

where r is the hydrogen exchange rate, C denotes concentration, and S_1^T and S_2 are the total number of A–B sites and the number of S–H sites, respectively. S_2 may be constant at the initial stage of the exchange process because the S–H "site" is considered to include those sites adsorbing OH remaining at the surface. This equation was applied for the least-squares fitting of the experimental results, resulting in a satisfactory agreement with the experimental values as shown by the solid lines in Fig. 4, and the regression gave a relation:

$$[7]\quad r = \frac{6.09 \times 10^{-8} C_{D_2}}{1 + 0.150 C_{D_2} + 0.086 C_{H_2O}}$$

where the units of r and C are given by mol m^{-3} s^{-1} and Torr, respectively. Coefficients in the denominator are equivalent to the adsorption equilibrium constants for reactions [1] and [5]. The equilibrium equation can be expressed as follows (29),

$$[8]\quad K = \frac{C_a}{C_g C_s} = \frac{f_a}{f_g f_s} \exp\left(\frac{H_{ad}}{RT}\right)$$

where f is a partition function, subscripts a, g, s denote adsorbed species, reactant gas, and site, respectively, and H_{ad} is equal to the heat of adsorption where the sign is positive when the adsorptive process is exothermic. The partition function for the site may be taken as unity because it has little freedom of motion. The partition function for adsorbed species may also be negligible in terms of the translation and the rotation. On denoting translational, rotational, and vibrational terms by subscripts t, r, and v, respectively, the above equation is represented by

$$[9]\quad K = \frac{f_{a,v}}{f_{g,t} f_{g,r} f_{g,v}} \exp\left(\frac{H_{ad}}{RT}\right)$$

If the change in the fundamental vibrations due to adsorption is small and (or) the new modes to be created by adsorption have relatively high wavenumbers, say, higher than 1500 cm^{-1}, the ratio of the vibrational partition functions of gas and the adsorbed species can be taken as unity. Equation [9] is then reduced to an equation composed solely of the partition functions of translational and rotational contributions for gas. Using the values of the mass and the moment of inertia for D_2 and H_2O (30), and the values obtained for K_1 and K_5, the heats of adsorption can be estimated as 145 ± 3 kJ mol^{-1} for the adsorption of D_2 and 177 ± 7 kJ mol^{-1} for H_2O. The order of magnitude corresponds to the result obtained by MO calculations in the case of adsorption at the threefold aluminum site. The value for the water adsorption is equivalent to the result for a γ-alumina sample outgassed at 800 K, measured by means of a differential microcalorimeter by Hendriksen *et al.* (31). In the case of hydrogen adsorption on alumina, Senchenya and Kazanskii have given a value, 110 kJ mol^{-1}, which is close to the

Can. J. Chem. Downloaded from www.nrcresearchpress.com by 213.200.69.106 on 09/08/12
For personal use only.

present result, for the heat of adsorption at the threefold coordinatively unsaturated aluminum site (25).

Thus the proposed model can explain the experimental results: the strong dependence of the exchange rate on D_2 pressure, the inhibition caused by the presence of H_2O, and the function of the fourfold aluminum as the active site. The concentration dependence of the exchange rate appeared to be physisorptive as described in the results section, but the adsorption must be dissociative from the viewpoint of the heat of adsorption. The reason becomes clear on considering the model: a D_2 molecule is adsorbed dissociatively at a Lewis acid–base pair but the adsorbed D atoms do not work equally in the hydrogen exchange due to their different environments, and hence only a D atom adsorbed at the threefold aluminum is effective for the exchange in the rate-determining step (eq. [2]); accordingly, the exchange rate depends on D_2 concentration rather than on its square root. Phase transition by heat treatment affected the exchange rate at the alumina surface together with the change in the coordinated states. A threefold coordinatively unsaturated site, which represents a Lewis acid–base site for the rate-determining step, plays an important role in the hydrogen exchange process at high temperatures. Since unsaturated threefold aluminum is produced from the saturated fourfold state at the surface, the amount of fourfold aluminum in the bulk can be a measure of the amount of the threefold state at the surface, and the state enhances the exchange rate; consequently, the amount of fourfold aluminum was closely related to the exchange rate, as can be seen in Figs. 2 and 6.

In conclusion, the active site in the hydrogen exchange process on alumina between D_2 and H_2O is a Lewis acid–base pair containing coordinatively unsaturated threefold aluminum. A possible model for the exchange is proposed, based on the pressure dependence of the rate and the estimation of heats of adsorption. Although the model must be verified by further detailed energy calculations and others, at least it is assumed to be true that the active site is composed of the acid–base pair at which D_2 can be adsorbed since otherwise we cannot explain that the exchange rate depends on D_2 pressure rather than the square root of the pressure, which dependence has been observed for pure platinum (8, 9) and platinum–alumina catalysts (3).

Acknowledgments

The authors gratefully acknowledge that a part of this work was done under the Grant-in-Aid for Scientific Research, Contract No. 02 453 066 by the Ministry of Education, Science and Culture, Japan. We would like to thank K. Hotta for his technical efforts and the Data Processing Center of Kyoto University for providing the GAUSSIAN 82 program and for the use of the FACOM M780 computer system. We are also indebted to Prof. F. Horii for the NMR measurements and for useful discussions of the results and to Y. Suzuki, C. Uyemura & Co., for performing the thermal analyses.

1. R. Nakane, S. Isomura, and M. Shimizu (*Editors*). Separation of deuterium and tritium. Gakkai Shuppan Center, Tokyo. 1982.
2. W. H. Stevens. Can. Patent No. 907 292 (1972).
3. J. H. Rolston and J. W. Goodale. Can. J. Chem. **50**, 1900 (1972).
4. I. Iida, J. Kato, and K. Tamaru. Bull. Chem. Soc. Jpn. **49**, 3433 (1976).
5. N. H. Sagert and R. M. Pouteau. Can. J. Chem. **51**, 4031 (1973).
6. P. Margineanu and A. Olariu. J. Catal. **8**, 359 (1967).
7. N. H. Sagert, P. E. Shaw-Wood, and R. M. L. Pouteau. Can. J. Chem. **53**, 3257 (1975).
8. N. H. Sagert and R. M. L. Pouteau. Can. J. Chem. **50**, 3686 (1972); **52**, 2960 (1974).
9. S. Miyamoto, T. Sakka, and M. Iwasaki. Can. J. Chem. **67**, 857 (1989).
10. W. K. Hall and F. E. Lutinski, J. Catal. **2**, 518 (1963).
11. J. Carter, P. Lucchesi, P. Corneil, D. J. C. Yates, and J. H. Sinfelt. J. Phys. Chem. **69**, 3070 (1965).
12. H. Knoezinger and P. Ratnasamy. Catal. Rev. Sci. Eng. **17**, 31 (1978).
13. E. Lippmaa, A. Samoson, and M. Maegi. J. Am. Chem. Soc. **108**, 1730 (1986).
14. S. R. Hartman and E. L. Hahn. Phys. Rev. **128**, 2042 (1962).
15. J. B. Peri and R. B. Hannan. J. Phys. Chem. **64**, 1526 (1960).
16. T. Sato and F. Ozawa. Rep. Asahi Glass Found. Ind. Technol. **16**, 379 (1970).
17. H. Glassl, R. Kramer, and K. Hayek. J. Catal. **68**, 388 (1981).
18. D. Mueller, W. Gessner, H. J. Behrens, and G. Scheler. Chem. Phys. Lett. **79**, 59 (1981).
19. I. Farnan, R. Dupree, A. J. Forty, Y. S. Jeong, G. E. Thompson, and G. C. Wood. Philos. Mag. Lett. **59**, 189 (1989); Thin Solid Films. **173**, 209 (1989).
20. H. D. Morris and P. D. Ellis. J. Am. Chem. Soc. **111**, 6045 (1989).
21. F. Abbatista, S. Delmastro, G. Gozzelino, D. Mazza, M. Vallino, B. Busca, V. Lorenzelli, and G. Ramis. J. Catal. **117**, 42 (1989).
22. T. Seiyama. Metal oxides and their catalysis. Kodansha Scientific, Tokyo. 1978. p. 131.
23. J. B. Peri. J. Phys. Chem. **69**, 211 (1965).
24. L. H. Little. Infrared spectra of adsorbed species. Academic Press, London. 1966. Chap. 7.
25. I. N. Senchenya and V. B. Kazanski. Kinet. Katal. **29**, 1331 (1988).
26. J. S. Binkley, M. J. Frisch, D. J. DeFrees, K. Rahgavachari, R. A. Schlegel, E. M. Fluder, and J. A. Pople. GAUSSIAN 82. Department of Chemistry, Carnegie-Mellon University, Pittsburgh, Pa. 1982.
27. H. Knoezinger and B. Stuebner. J. Phys. Chem. **82**, 1526 (1978).
28. K. J. Laidler. Chemical kinetics. 3rd ed. Harper & Row, New York. 1987. p. 242.
29. S. Glasstone, K. J. Laidler, and H. Eyring. The theory of rate processes. McGraw–Hill, New York. 1941. Chap. 4.
30. W. S. Benedict, N. Gailar, and K. Plyler. J. Phys. Chem. **24**, 1139 (1956).
31. B. A. Hendriksen, D. R. Pearce, and R. Rudham. J. Catal. **24**, 82 (1972).

Can. J. Chem. Downloaded from www.nrcresearchpress.com by 213.200.69.106 on 09/08/12
For personal use only.

Micellar catalysis of organic reactions. Part 33.[1] Amide hydrolysis in neutral solution in the presence of a copper-containing micelle

TREVOR J. BROXTON[2]
Department of Chemistry, La Trobe University, Bundoora, Victoria, Australia 3083

AND

ROBIN A. COX
Department of Chemistry, University of Toronto, Toronto, Ont., Canada M5S 1A1

Received October 13, 1992

TREVOR J. BROXTON and ROBIN A. COX. Can. J. Chem. **71**, 670 (1993).

The hydrolysis of 5-nitro-2-(trifluoroacetylamino)benzoic acid (**1**) has been studied at pH 7 in water and in the presence of micelles of cetyltrimethylammonium bromide (ctab) and of copper-containing micelles formed from the reaction of *N,N,N'*-trimethyl-*N'*-hexadecylethylenediamine and cupric chloride. It has been found that the hydrolysis of **1** is inhibited by micelles of ctab but strongly catalysed by the copper-containing micelle at this pH. At a higher pH where the hydroxide ion reaction becomes important the reaction is catalysed by micelles of ctab as well, but the catalysis is stronger by the copper-containing micelle. The effect of added sodium chloride on the rate of reaction is shown to be larger for reaction in the presence of ctab than for reaction in the presence of the copper micelles. Also reported are the effects of the buffer concentration on the rate of reaction at various pH for both micelles. It is concluded that the mechanism of reaction in the copper-containing micelle involves a metal-bound hydroxyl rather than a free hydroxide ion loosely associated with the cationic micelle surface. It is interesting that the catalysis of this reaction by the copper-containing micelle is large enough to allow amide hydrolysis at a reasonable rate at neutral pH at ambient temperature.

TREVOR J. BROXTON et ROBIN A. COX. Can. J. Chem. **71**, 670 (1993).

On a étudié l'hydrolyse de l'acide 5-nitro-2-(trifluoroacétylamino)benzoïque (**1**) dans l'eau à un pH de 7 et en présence de micelles de bromure de cétyltriméthylammonium (bcta) ou de micelles contenant du cuivre formées par la réaction de la *N,N,N'*-triméthyl-*N'*-hexadécyléthylènediamine et le chlorure cuivrique. On a trouvé que l'hydrolyse de **1** est inhibée par la présence de micelles de bcta, mais que, à ce pH, elle est fortement catalysée par la micelle contenant le cuivre. À un pH plus élevé, quand la réaction de l'ion hydroxyde devient importante, la réaction est aussi catalysée par les micelles de bcta; toutefois, la catalyse est plus forte avec la micelle contenant le cuivre. On montre que l'addition de chlorure de sodium provoque un effet plus grand sur la réaction réalisée en présence de bcta que sur celle réalisée en présence de micelles de cuivre. On rapporte aussi les effets de la variation de la concentration du tampon sur les vitesses des réactions à divers pH, en présence des deux micelles. On en conclut que la mécanisme de la réaction avec la micelle contenant du cuivre implique un groupe hydroxyle lié au métal plutôt qu'un ion hydroxyde libre faiblement associé avec la surface micellaire cationique. Il est intéressant de réaliser que la catalyse de cette réaction par les micelles contenant le cuivre est suffisamment importante pour permettre l'hydrolyse de l'amide à une vitesse raisonnable, à un pH neutre, à la température ambiante.

[Traduit par la rédaction]

Introduction

The preparation and the catalytic activity of metallomicelles on various organic reactions is currently of interest. Menger *et al.* (1) have reported the preparation of the copper(II) complex of *N,N,N'*-trimethyl-*N'*-tetradecylethylenediamine and have studied its effect on the hydrolysis of phosphate esters. Tonellato and co-workers (2) have reported the preparation of metal chelating micelles containing copper(II) or zinc(II) and have studied their effect on the hydrolysis of *p*-nitrophenylpicolinate. Tonellato and co-workers (3) also reported the preparation of bolaform metallomicelles and studied their effect on the same reaction. Nolte and co-workers (4) have reported the preparation of vesicles containing metal ions including copper(II) and zinc(II). Engbersen and co-workers (5) have also reported the preparation of copper(II)- and zinc(II)-containing metallosurfactants and studied their effect on both carboxylic and phosphate ester hydrolysis.

Because of our interest in the kinetic and mechanistic effects of micelles on amide hydrolysis (6) and because of the reported (7) cleavage of *N*-terminal peptides by the complex $Co(trien)H_2O(OH)^{2+}$ we have studied the effect of the C_{16} analogue of the Menger metallomicelle on the hydrolysis of 5-nitro-(2-trifluoroacetylamino)benzoic acid (**1**).

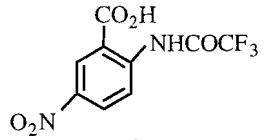

1

We have compared the effect of micelles of cetyltrimethylammonium bromide (ctab) and the copper-containing micelle on the hydrolysis of this amide. We report the effects of detergent concentration (Table 1), the pH (Table 2), the concentration of added salt (Table 3), and the buffer concentration (Table 4) on the rate of this amide hydrolysis in both micelles.

Results and discussion

N,N,N'-Trimethyl-*N'*-hexadecylethylenediamine was prepared from the reaction of *N,N,N'*-trimethylethylenediamine with 1-bromohexadecane in absolute ethanol. This

[1]Part 32: see ref. 17.
[2]Author to whom correspondence may be addressed.

Can. J. Chem. Downloaded from www.nrcresearchpress.com by 88.255.202.194 on 09/08/12
For personal use only.

Can. J. Chem. Downloaded from www.nrcresearchpress.com by 88.255.202.194 on 09/08/12
For personal use only.

TABLE 1. Effect of detergent concentration on the pseudo-first-order rate constants ($10^6 \times k_\psi$, s^{-1}) for the hydrolysis of **1** at pH 7 (1.14 mM free Tris/48.86 mM Tris H^+Cl^- buffer) in the presence of micelles at 31°C

[Detergent] mM	ctab	Cu micelle
0	11.2	11.2[a]
0.17	—	431
0.27	7.52	555
0.54	6.90	430
0.81	6.56	313
1.08	6.15	259
1.68	5.83	166
3.37	5.93	80.4
5.06	5.28	72
6.74	5.39	63.1

[a]At pH 7 in water containing 0.25 mM Cu^{2+} $10^6 \times k_\psi = 13.4\ s^{-1}$.

TABLE 2. The effect of pH on the pseudo-first-order rate constants ($10^6 \times k_\psi$, s^{-1}) for the hydrolysis of **1** in water and in the presence of micelles at 31°C

pH[a]	Water	ctab (1.7 mM)	Cu micelle (1.7 mM)
7	11.2	5.83	166
7.5	26.1	47.0	1090
8	57.0	336	—
8.5	194	3130	—
9	809	17200	—

[a]1.14 mM free Tris at pH 7, 3.23 mM free Tris at pH 7.5, 6.93 mM free Tris at pH 8, 11.8 mM free Tris at pH 8.5, 14.8 mM free Tris at pH 9. [Tris H^+Cl^-] = 50 − [free Tris] mM.

amine was then treated with anhydrous cupric chloride to give the copper-containing metallomicelle.

From Table 1 we see that at pH 7 the hydrolysis of **1** is inhibited by micelles of ctab but strongly catalysed (×50) by the copper-containing micelle. As the pH is increased (Table 2) the observed rate of hydrolysis increased in all systems. The reaction in ctab was actually catalysed at a pH of 7.5 or above and the magnitude of this catalysis increased as the pH was increased. We thus conclude that the water reaction at pH 7 is inhibited by micelles of ctab but that the hydroxide ion reaction at higher pH is catalysed. This effect was previously observed (8) for the hydrolysis of aspirin. In that case, however, the water reaction involved intramolecular general base catalysis by the ionized carboxylate group. Previous studies (9) of the hydrolysis of **1** in water provided no evidence of such intramolecular catalysis of this reaction. As is typical of amide hydrolysis, the reaction in water is slow at a neutral pH and a pH of at least 9 is required before hydrolysis is observed at a rate similar to that found in the copper micelle at a pH of 7. The magnitude of the catalysis of this hydrolysis by the copper-containing micelle at pH 7 is interesting in that it results in amide hydrolysis at a reasonable rate in neutral solution at ambient temperature. The

TABLE 3. Effect of added salt on the pseudo-first-order rate constants ($10^6 \times k_\psi$, s^{-1}) for the hydrolysis of **1** in the presence of micelles at 31°C

(*a*) In ctab 0.51 mM

[NaCl] (mM)	pH 7.5[a]	pH 8
0	44.5	293
1.77	38.3	251
3.53	35.9	226
5.30	—	212

(*b*) In Cu micelle 0.51 mM

[NaCl] (mM)	pH 7	pH 7.5
0	445	647
1.77	438	636
3.53	420	623
5.30	424	594

[a]1.14 mM free Tris at pH 7, 3.23 mM free Tris at pH 7.5, 6.93 mM free Tris at pH 8. [Tris H^+Cl^-] = 50 − [free Tris] mM.

half-life of this hydrolysis is 20–66 min, depending on the concentration of the copper-containing micelle. While the cleavage of N-terminal peptide bonds with the complex $Co(trien)H_2O(OH)^{2+}$ was also achieved at pH 7.5, a temperature of 65°C was necessary for that reaction (7).

Salt effects

The effect of added sodium chloride on the rate of hydrolysis of **1** (Table 3) is instructive. In ctab at pH 7.5 or 8, approximately 20% reduction in rate is seen on the addition of NaCl. This is consistent with a hydroxide ion reaction. The added chloride ions compete with hydroxide ions for sites on the micelle surface, as required by the pseudophase ion exchange (PPIE) kinetic model (10), resulting in a decrease in the observed rate. In the copper-containing micelle the effect of added chloride ions is much smaller (5–8%) and this indicates that ion exchange at the surface of this micelle is less important than in ctab. According to Menger *et al.* (1), either a hydroxyl chelated to the copper or a hydroxide ion loosely associated with the cationic micelle surface could be the catalytically active nucleophile in this type of micelle. The small effect of added chloride ions argues strongly in favour of the metal-bound hydroxyl. This metal-bound hydroxyl is most likely formed by the loss of a proton from a metal-bound water molecule. The pK_a of a copper-bound water molecule has been variously estimated (11) to be as high as 9 or to be as low as 6.8 (12) depending on the ligand attached to the copper ion and on the geometry of the complex. Menger *et al.* (1) found that in the presence of the copper-containing cationic micelle the hydrolysis rate of their phosphate ester was insensitive to pH between 6.0 and 8.3. They thus concluded that the copper-bound water molecule was completely ionized at pH = 6.0. We observe some variation in the rate of hydrolysis of **1** in the copper-containing micelle between pH 7 and pH 7.5, possibly due to the deprotonation of the metal-bound water molecule as the pH is increased within this range, and this indicates that the pK_a of a copper-bound water molecule in the presence of a

Can. J. Chem. Downloaded from www.nrcresearchpress.com by 88.255.202.194 on 09/08/12
For personal use only.

TABLE 4. Effect of Tris buffer concentration on the pseudo-first-order rate constants ($10^6 \times k_\psi$, s^{-1}) for the hydrolysis of **1** in the presence of micelles at 31°C

(*a*) In ctab 1.7 mM

[Free Tris] mM	pH 7.5[a]	pH 8.5
3.23	47	—
4.85	33.7	—
6.47	27.2	—
8.08	22.7	—
11.8	—	2930
17.6	—	2310
23.5	—	1880
29.4	—	1530

(*b*) In Cu micelle 0.51 mM

[Free Tris] mM	pH 7	pH 7.5
1.14	555	
1.71	547	
2.28	450	
2.85	385	
3.23	—	748
4.85	—	443
6.47	—	216
8.08	—	159

[a][Tris H^+Cl^-] = 50 − [free Tris] mM.

cationic micelle is somewhat higher than Menger suggests. Above a pH of 7.5 in the copper-containing micelle, precipitation of a pale blue material, presumably copper hydroxide, was observed.

Buffer effects

The effect on the rate of hydrolysis of **1**, of increasing the tris buffer concentration 2.5-fold in both ctab and in the copper-containing micelle, is given in Table 4. In ctab at both pH 7.5 and 8.5 such an increase in buffer concentration resulted in a decrease in rate of about 50% at either pH. This is probably due to the inhibitory effect of the added chloride ion component of the buffer on a reaction of hydroxide ion at the surface of the ctab micelle. In the presence of the copper-containing micelle the buffer effect was dependent on the pH, increasing at higher pH. At a higher pH the concentration of free Tris is higher than at a lower pH and it is possible that this is responsible for the inhibitory effect rather than the chloride ion. At pH 7 the rate decreased by about 30% as the buffer concentration was increased 2.5-fold while at pH 7.5 the decrease was 79%. It seems likely that this inhibition could be due to complexation of the free Tris buffer by the metal ion thus excluding water and, ultimately, the metal-bound hydroxyl group, which is the catalytically active species.

The optimum rate of hydrolysis of the amide in the presence of the copper-containing micelle was at 0.27 mM. Menger *et al.* (1) found that the critical micelle concentration (cmc) of their tetradecyl micelle was 0.18 mM. From conductance measurements as a function of detergent concentration we conclude that the cmc of the hexadecyl micelle in the absence of any additives is about 0.8 mM. An interesting observation in this case, however, was that whereas, for ctab solutions, the slope of the graph of conductance versus detergent concentration decreased above the cmc, for solutions of the copper-containing micelle, the slope increased above the cmc.

Further studies showed that the pH of the solution decreased as the detergent concentration was increased. The slope of the plot of pH versus the detergent concentration showed two linear sections with a clear break at 0.8 mM that we attribute to the cmc of this micelle. The pH at this concentration was 5.6. A probable reason for this break in the pH – detergent concentration plot is the increased acidity of the water bound to the copper atom once micelles are formed (1). This results in an increase in the amount of free protons in solution and, as a consequence, an increase in the conductivity above the cmc.

The optimum rate of amide hydrolysis in the copper micelle at 0.27 mM is not unreasonable because it has previously been shown that the cmc of ctab is reduced by additives. Although the normally accepted cmc of ctab in the absence of additives is 0.9 mM (13), previous kinetic studies (14) have indicated that the cmc of ctab in the presence of hydroxide ions and chlorodinitrobenzoate ions may be as low as 0.3 mM. Thus it is not unreasonable that the cmc of the copper micelle may also be reduced in the presence of substrate **1** and tris buffers. We find little difference in the rate of hydrolysis between 0.5 and 5.0 mM ctab. It therefore seems that the substrate is very efficiently solubilized by micelles. Furthermore, the rate in the absence of chloride ions at 0.51 mM ctab (Table 3) was 70% faster than that in water at pH 7.5 (Table 2) while at pH 8 the rate of hydrolysis was more than five times faster in ctab than in water (Tables 2 and 3). This also indicates the presence of micelles even at this low ctab concentration.

Experimental section

Materials

Compound **1** was available from previous work (9); ctab was commercially available (BDH) and was purified by the method of Mukerjee and Mysels (15). Distilled water was further purified by a Millipore system to achieve a resistivity of at least 10 MΩ cm^{-1}.

N,N,N'-Trimethyl-*N'*-hexadecylethylene diamine was prepared by the alkylation of *N,N,N'*-trimethylethylene diamine (6.0 g) with 1-bromohexadecane (7.0 g) in absolute ethanol (35 mL) at reflux for 10 min. The mixture was then cooled and NaOH (2.0 g) in water (2 mL) was added to neutralize the HCl produced. The resulting solution was then heated to reflux for 16 h. The product was cooled to room temperature, added to a mixture of 1-butanol (10 mL), benzene (10 mL), and water (50 mL), shaken, and allowed to separate. The organic layer was washed with a saturated salt solution, separated, dried ($MgSO_4$), and concentrated under vacuum. The product, a yellow semisolid, was distilled under reduced pressure (160°C at 0.05 Torr (1 Torr = 133.3 Pa)) to produce a light yellow solid, mp 30–35°C. The electrospray mass spectrum of this compound was recorded on a VG Bio-Q triple quadrupole mass spectrometer (VG Bio Tech, Altringham, Cheshire, U.K.) using a mobile phase of 50:50 aqueous methanol also containing 1% acetic acid, and had a principal ion at m/z 327 corresponding to the protonated amine.

The copper(II) complex of this amine was prepared by dissolving the amine (1.0 g) in absolute ethanol (10 mL) and adding the solution slowly to a solution of anhydrous $CuCl_2$ in absolute ethanol (15 mL) with stirring. The anhydrous $CuCl_2$ was prepared from the hydrated material by heating at 120°C for 16 h. After addition of the amine the mixture was stirred for 30 min at 0°C. The dark blue-

green precipitate was filtered at the pump, washed with ice-cold ethanol, and recrystallized from ethanol. Further purification was achieved by a second recrystallization, this time from acetonitrile, giving blue crystals, mp 99–101°C. Anal. calcd. for $C_{21}H_{46}N_2Cl_2Cu$: C 54.7, H 10.0, N 6.1%; found: C 54.7, H 9.8, N 6.2. The electrospray mass spectrum of this complex obtained under the above conditions had a principal ion at m/z corresponding to $Cu(L)OAc^+$ where L represents the diamine ligand. This m/z value was for the most intense peak in the isotopic mass cluster and the experimental distribution (100:29:53:15) agreed well with the calculated one (100:25:47:10).

Kinetics

A stock solution (0.01 M) of **1** was prepared in HPLC-grade acetonitrile. Stock solutions of ctab (20 mM) and the copper micelle (1.6 mM, 3 mM, and 10 mM) were prepared in purified water. Tris buffer solutions of pH 7, 7.5, 8, 8.5, and 9 were prepared as described in the Handbook of chemistry and physics (16). Kinetic solutions (6 mL) were made up by taking appropriate amounts of these stock solutions and water as required. Kinetic runs were initiated by the addition of substrate (20 μL) to the kinetic solutions that had been temperature equilibrated (to 31°C) in 1-cm cuvettes in the jacketed cell compartment of a Varian Associates 635 UV–VIS spectrophotometer. Reactions were followed by monitoring product formation at 375 nm. The UV–visible spectrum of the hydrolysis product from this reaction was identical to that of 2-amino-5-nitrobenzoic acid under these conditions.

Critical micelle concentration

The cmc was determined in neutral solution at 30.0°C, using a jacketed beaker containing purified water (30 mL) and a platinum electrode attached to an Activon PT1-10 conductivity meter. Aliquots (0.5 mL) of detergent solution (0.01 M) were added and the conductivity was measured as a function of detergent concentration.

pH

The pH of the detergent solutions as a function of detergent concentration was measured by a similar technique using a glass electrode and a Radiometer PHM 80 portable pH meter.

Can. J. Chem. Downloaded from www.nrcresearchpress.com by 88.255.202.194 on 09/08/12
For personal use only.

Acknowledgments

We are indebted to Dr. R. Colton for assistance in obtaining the electrospray mass spectra.

1. F. M. Menger, L. H. Gan, E. Johnson, and D. H. Durst. J. Am. Chem. Soc. **109**, 2800 (1987).
2. G. De Santi, P. Scrimin, and U. Tonellato. Tetrahedron Lett. 4791 (1990).
3. R. Fornasier, P. Scrimin, P. Tecilla, and U. Tonellato. J. Am. Chem. Soc. **111**, 224 (1989).
4. J. H. van Esch, A. L. H. Stols, and R. J. M. Nolte. J. Chem. Soc. Chem. Commun. 1658 (1990).
5. J. G. J. Weijnen, A. Koudijs, and J. F. J. Engbersen. J. Chem. Soc. Perkin Trans. 2, 1121 (1991).
6. T. J. Broxton and N. W. Duddy. Aust. J. Chem. **32**, 1717 (1979).
7. J. P. Collman and D. A. Buckingham. J. Am. Chem. Soc. **85**, 3039 (1963).
8. T. J. Broxton. Aust. J. Chem. **35**, 1357 (1982).
9. T. J. Broxton. Aust. J. Chem. **36**, 1885 (1983).
10. H. Al-Lohedan, C. A. Bunton, and L. S. Romsted. J. Phys. Chem. **85**, 2123 (1981).
11. J. W. Allison and R. J. Angelici. Inorg. Chem. **10**, 2233 (1971).
12. F. Basolo and R. G. Pearson. Mechanisms of inorganic reactions. 2nd ed. John Wiley & Sons Inc., New York. 1967.
13. C. Otero and E. Rodenas. J. Phys. Chem. **90**, 5771 (1986).
14. T. J. Broxton, J. R. Christie, and R. P.-T. Chung. J. Org. Chem. **53**, 3081 (1988).
15. P. Mukerjee and K. J. Mysels. J. Am. Chem. Soc. **77**, 2937 (1955).
16. R. C. Weast (*Editor*). Handbook of chemistry and physics. 57th ed. The Chemical Rubber Company, Cleveland, Ohio. 1976–1977. p. D 134.
17. T. J. Broxton. J. Org. Chem. **56**, 5958 (1991).

Chemical and electrochemical oxidation of phenothiazine

ALEXEI N. PANKRATOV,[1] INNA M. UCHAEVA, AND ALEXANDER N. STEPANOV
Department of Chemistry, N.G. Chernyshevskii Saratov State University, Saratov 410026, Russia

Received September 21, 1992

ALEXEI N. PANKRATOV, INNA M. UCHAEVA, and ALEXANDER N. STEPANOV. Can. J. Chem. **71**, 674 (1993)

The oxidation of phenothiazine in dilute solutions of sulphuric acid leads to the corresponding cation radical. Using a potentiometric technique, a pK_a value of 5.72 ± 0.05 was determined for phenothiazine. The kinetics has been studied and participation of both protonated and unprotonated oxidant in the oxidation reaction has been confirmed. Using a voltammetric technique with a rotating disk electrode, the anodic oxidation of phenothiazine was shown to be a one-electron diffusion-controlled process. A quantum chemical explanation was found for the direction of phenothiazine protonation and the absence of a dimerization stage of oxidation.

ALEXEI N. PANKRATOV, INNA M. UCHAEVA et ALEXANDER N. STEPANOV. Can. J. Chem. **71**, 674 (1993)

L'oxydation de la phénothiazine, en solutions diluées d'acide sulfurique, conduit au cation radical. Faisant appel à une technique potentiométrique, on a déterminé un pK_a de 5,72 ± 0,05 pour la phénothiazine. On a étudié la cinétique de la réaction et on a démontré que l'oxydant protoné aussi bien que le non protoné participent à la réaction d'oxydation. Faisant appel à la technique de voltampérométrie avec une électrode à disque tournant, on a démontré que l'oxydation anodique est une réaction impliquant un électron dans un processus contrôlé par la diffusion. On a expliqué la direction de la protonation de la phénothiazine et l'absence d'étape de dimérisation durant l'oxydation.

[Traduit par la rédaction]

Can. J. Chem. Downloaded from www.nrcresearchpress.com by 213.200.69.106 on 09/08/12
For personal use only.

Introduction

To contribute to the understanding of the mechanisms of oxidation of aromatic amino compounds, investigation of the oxidation reactions of substances containing the fragment Ar-N-Ar′ is of interest. Phenothiazine is representative of such compounds, derivatives of which have found application as photometric redox indicators in dilute solutions of acids (1).

Chemical (2–6) and electrochemical (7, 8) oxidation of phenothiazine has been studied in acidic media. Oxidation of phenothiazine in concentrated sulphuric acid leads via cation radical states to 3,10′-diphenothiazinyl and small quantities of 1,10′-diphenothiazinyl (2). 10-Acyl- and 10-alkylphenothiazines oxidized by HNO_3 and H_2O_2 yield the corresponding sulphoxides and sulphones (3). The reaction of phenothiazine with HNO_3 in the presence of $HClO_4$ results in the formation of 3-nitrophenothiazine-*S*-oxide (4–6). Electrooxidation of some phenothiazines in the chronopotentiometric mode has been studied using a tubular graphite electrode in sulphuric acid media; formation of cation radicals that are stable in acidic medium and unstable in neutral and weakly acidic solutions occurs (7). Some phenothiazine derivatives have been oxidized to sulphoxides in dilute sulphuric acid on a gold anode (8). Thus an investigation of the reactions of different oxidants with phenothiazine and a kinetic study of the homogeneous oxidation process of the substrate seem appropriate. Some additional information about anodic oxidation of phenothiazine may be obtained using a rotating disk electrode.

The aim of the present communication was spectrophotometric, voltammetric, and quantum chemical investigation of the reaction of phenothiazine oxidation in acidic media.

Experimental

Electronic spectra were obtained using a Specord M40 spectrophotometer. Kinetic measurements were carried out with a KFK-2 photoelectric colorimeter using a colour filter No. 5 (λ_{max} = 490 nm). For mixing the solutions, a Budarin vessel (9) was used. The time was measured with a chronometer, from the moment of mixing the solutions, which were thermostatted at 298 K and 315 K using a UT-10 thermostat. The reaction orders for the oxidation reaction of phenothiazine were established using the method of Neues and Ostwald (10). Reaction rate $V = dC_{PO_x}/dt$ (where C_{PO_x} is the concentration of coloured oxidation product of phenothiazine) was measured for reaction mixtures of phenothiazine and ammonium vanadate (concentrations of both substances varying between 2×10^{-5} and 1.4×10^{-4} M) and of phenothiazine (2×10^{-5}–1.4×10^{-4} M) and potassium dichromate (3.3×10^{-6}–2.3×10^{-5} M) in sulphuric acid (2.1×10^{-1}–3×10^{-1}M for vanadate, and 4.4×10^{-6}–8.8×10^{-2} M for dichromate oxidations). Linear dependence of V on concentrations of substrate and oxidant indicated a second-order reaction, first in phenothiazine and first in oxidant.

The value of pK_a for phenothiazine conjugate acid was determined by potentiometric titration using a pH-673.M pH-meter with a glass electrode and a saturated silver, silver chloride reference electrode (26.47 wt.% KCl) at 298 K. The ionic strength of the solution was maintained equal to 0.1 using potassium chloride.

A glassy-carbon rotating disk electrode with a surface area of 0.035 cm^2 was used together with a spiral platinum wire as an auxiliary electrode and a saturated silver, silver chloride electrode (26.47% KCl) as a reference electrode. The circular rotation rates (w) were 81.7; 117.3; 167.6; 209.4; 303.7 rps. Current–potential curves were recorded using a P-5848 potentiostat; the current was registered using an LKD-4 pen recorder. The potential sweep rate was 4 mV/s. To determine the number of electrons involved in the redox process, the method of Hitchman and Albery (11) was applied.

Quantum chemical calculations by the SCF MO LCAO method with CNDO/2, INDO approximations were carried out using the programs of the VIKING complex on a BESM-6 electronic computer (12), and by the Hückel MO method using the program (13) on a personal computer Elektronika D3-28.

Results and discussion

We have stated that a stable, coloured, oxidation product is formed during interaction of phenothiazine with various oxidants: $Ce(SO_4)_2$, NH_4VO_3, $K_2Cr_2O_7$, $KMnO_4$, $(NH_4)_2S_2O_8$, KIO_3, KIO_4, H_2O_2 in the medium of 6.55×10^{-4}–5.4 M sulphuric acid. Spectral curves in the electronic absorption

[1]Author to whom correspondence may be addressed.

Can. J. Chem. Downloaded from www.nrcresearchpress.com by 213.200.69.106 on 09/08/12
For personal use only.

spectra of oxidized forms of the substrate feature bands with λ_{max} = 436.0 and 516.5 nm. This allows one to conclude, in accordance with literature references (14–16), that the corresponding cation radical is the final product of oxidation in all the aforementioned cases.

At pH about 1–3 in the sulfuric acid solutions studied, phenothiazine is present in the solution prodominantly in the protonated form. This follows from the reported (17) pK_a values of between 4.5 and 7.8 for substituted phenothiazines. At ionic strength 0.1 we found, by potentiometric titration, the value of $pK_a = 5.72 \pm 0.05$. Using the Hückel MO LCAO method and parameters for thiazine (18), a pK_a value of 5.99 was obtained, in acceptable agreement with experimental results. The pK_a value found provides evidence for the protonation of the phenothiazine molecule at the nitrogen atom, which is given a quantum chemical explanation below.

The reaction kinetics of phenothiazine oxidation by ammonium vanadate and potassium dichromate was studied in the sulphuric acid medium. The reaction with both oxidizing agents was shown to be first order in substrate (phenothiazine) and first order in oxidant. Furthermore, the reaction rate depends upon the concentration of the acidic component.

For explanation of the latter, let us consider the following two reaction schemes of substrate with oxidant, assuming the participation of protonated phenothiazine PH^+ in the redox process.

1. The conjugate acid PH^+ reacts with unprotonated oxidant (VO_3^- or $Cr_2O_7^{2-}$):

[1] $PH^+ + Ox \rightarrow POx + Red$

where Ox is the oxidant, Red its reduced form, and POx the product of phenothiazine oxidation. Then the dependence of second-order rate constant k' on acidity would be as follows:

$$k' = \frac{k[H^+]}{K_a + [H^+]}$$

and at $[H^+] >> K_a$ (fulfilled at $pH < (pK_a - 2)$) this leads to the constant value $k' = k$.

2. The species PH^+ interacts with protonated oxidant. Since PH^+ predominates in solution at pH 1–3, no proton transfer occurs before reaction with Ox. If $V \sim [H^+]$ at pH 1–3, it means that another proton transfer occurs before the electron transfers. This may be protonation of the anions of the oxidants: pK_a values for HVO_3 and $HCr_2O_7^-$ are 3.8 and 0.7, respectively (19), and hence the sequence is

[2] $PH^+ \rightleftarrows P + H^+$

[3] $OxH^+ \rightleftarrows Ox + H^+$

[4] $PH^+ + OxH^+ \rightarrow POx + RedH^+$

Since $pH < (pK_a - 2)$, the role of equilibrium [2] is negligible and

$$k' = \frac{k[H^+]}{K_{OxH^+} + [H^+]}$$

where K_{OxH^+} is the equilibrium constant of process [3]. For potassium dichromate at $pH > 2$, $K_{OxH^+} >> [H^+]$ and, approximately,

[5] $k' = K[H^+]/K_{OxH^+}$

The values of $[H^+]$ for H_2SO_4 solutions were estimated assuming a complete first dissociation step and that, with regard to the second step, sulphuric acid is an electrolyte of middle strength: $K_2 = 1.15 \times 10^{-2}$ (20). If the molar concentration of sulphuric acid is C, then, considering the dissociation equilibrium of the HSO_4^- ion, one can obtain

$$[H^+] = 0.5\,(-K_2 + C + \sqrt{(K_2 + C)^2 + 4K_2C})$$

Our experiments have shown that the dependence k' vs. $[H^+]$ for dichromate oxidations within the range of H_2SO_4 concentrations 4.4×10^{-3}–2.2×10^{-2} M is linear, but the line does not pass through the origin and gives a positive intercept at the ordinate axis (Fig. 1). Under the conditions considered, obviously both processes [1] and [4] proceed in parallel. This is related to the existence of the oxidant in solutions at pH 1–3 in the two forms, Ox and OxH^+: at pH 1 the degree of protonation of dichromate anion is 0.334 and at pH 3 it is 0.005.

Additional evidence that the acid–base equilibrium affecting k' at pH 1–3 does not reflect biprotonation of P is the independence of $E_{1/2}$ from pH in the range studied (see below). The electrochemical process does not involve oxidant and hence is not affected by $[H^+]$.

On the basis of the dependence k' vs. $[H^+]$:

$$k' = k + \frac{k}{K_{OxH^+}}[H^+]$$

using the least-squares method, we have evaluated the rate constants k of reaction [1]: $(4.61 \pm 0.71) \times 10^4$ L mol^{-1} min^{-1} at 298 K and $(7.83 \pm 1.08) \times 10^4$ L mol^{-1} min^{-1} at 315 K (confidence intervals have been found for confidence probability 0.95 for three parallel measurements of each k value). An estimation of the activation energy for reaction [1] gives the value of 24.3 kJ mol^{-1}, which confirms the homolytic character of the process.

At H_2SO_4 concentrations exceeding 2.2×10^{-2} M the dependence k' vs. $[H^+]$ is no longer linear, since relationship [5] becomes inadequate. At $C_{H_2SO_4} < 4.4 \times 10^{-3}$ M, linearity of the function $k' = f([H^+])$ is also not observed; this may be related to deprotonation of the species PH^+ and $HCr_2O_7^-$.

To compare with the homogeneous oxidation, electrooxidation of 1 mM phenothiazine was investigated in sulphuric acid solutions containing 50% ethanol and using 0.3 M LiCl as supporting electrolyte. Using a glassy-carbon rotating disk electrode, an anodic wave was obtained with limiting current controlled by diffusion. This was proved by linear dependence of i_{lim} on $w^{1/2}$. The half-wave potential ($E_{1/2}$ = 0.51 V vs. saturated silver, silver chloride electrode in 26.47% KCl solution) is independent of the sulphuric acid concentration between 0.65 and 6.8 mM acid. Independence of $E_{1/2}$ from pH indicates that the species predominating in the bulk of solution undergoes electrooxidation. Because in all instances the conjugate base of a substrate is oxidized more readily than the acid, the observed independence also means that the dissociation of PH^+ under the conditions used is slow when compared with rate of oxidation. The number of oxidations on rotating disk electrodes accompanied by acid–base equilibria reported in the litera-

Can. J. Chem. Downloaded from www.nrcresearchpress.com by 213.200.69.106 on 09/08/12
For personal use only.

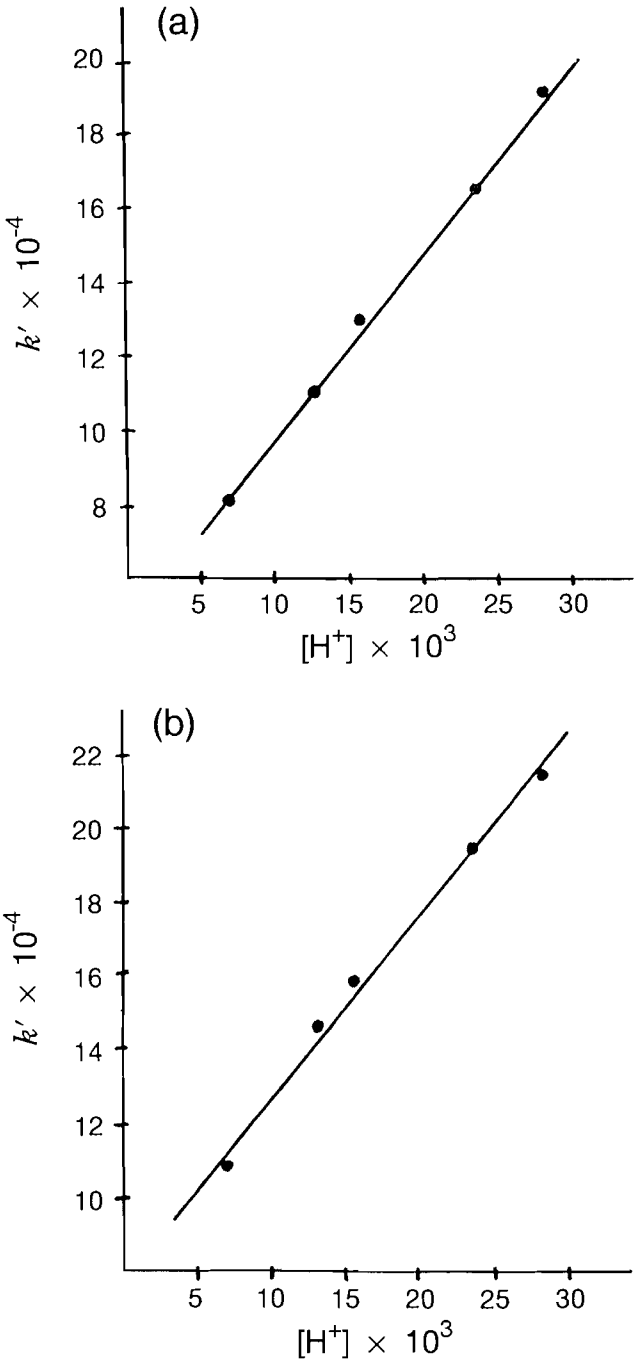

FIG. 1. Dependence of second-order rate constant k' (L mol^{-1} min^{-1}) of phenothiazine oxidation by potassium dichromate upon the hydronium ion concentration (mol L^{-1}) at temperatures (*a*) 298 K and (*b*) 315 K.

ture (21) is limited and hence no estimate of the rate of dissociation of PH^+ can be offered.

Decay curves of the limiting current with time at the potential 0.80 V vs. saturated silver, silver chloride electrode (26.47% KCl) were measured. A linear dependence of i_{lim} on $t^{1/2}$ (t is time) at the end part of the decay curve provides evidence for mixed control conditions of the anodic reaction in the corresponding time interval (22).

Using the method of Hitchman and Albery, we have found the diffusion coefficient of depolarizer to be 1.00×10^{-5} cm^2 s^{-1} in the medium 1.31×10^{-3} M H_2SO_4. Determination of the number of electrons (n) involved in the redox process gave the value $n = 0.91$, and the phenothiazine cation radical is formed.

A scheme of the both chemical (from the viewpoint of substrate behaviour) and electrochemical oxidation of phenothiazine may be represented as follows:

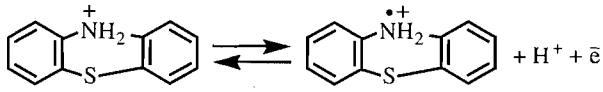

We have calculated the electronic structure of phenothiazine molecule and cation radical using the methods SCF MO LCAO, CNDO/2, and INDO. One should note the existence of negative charges at the nitrogen and sulphur atoms, as well as at carbon atoms in positions 1 and 3 of the molecule. According to the data of the CNDO/2 method, in the *sp* basis the aforementioned charge values are −0.184, −0.064, −0.040, and −0.014, respectively. Reactions of polar molecules with charged particles are known to be charge controlled (23). On the basis of charge control, electrophilic attack of the hydronium ion at the nitrogen atom during protonation of the phenothiazine molecule can be readily explained.

As has already been mentioned, the phenothiazine cation radical under certain conditions may undergo dimerization leading to the formation of 3,10′-diphenothiazinyl and a small amount of 1,10′-diphenothiazinyl (2). In the present work, the formation of diphenothiazinyls was not detected. At the same time, oxidational dimerization via the cation radical step under identical or similar conditions (oxidation by vanadate or dichromate in sulphuric acid medium) is characteristic for structurally similar diarylamines (24–26). Using the INDO method, we found spin density distribution in the cation radical. An excess of this spin density value features the following atoms: nitrogen (−0.468), sulphur (−0.323), carbon in positions 1 (−0.029) and 3 (−0.071) of the cycle. The most probable centre of recombination is the nitrogen atom. However, N,N-coupling is hindered by the lability of the N—N bond in acidic media (27, 28).

Also, S,S-coupling is impossible, since it would lead to the formation of an S—S bond between positively charged sulphur atoms. Dimerization of the C,S-type cannot be realized either: the formation of sulphonium salts is known to occur only in heterolytic alkylation (but not arylation) reactions of sulphides (29).

Coupling involving the C-3 and C-1 carbon atoms may occur, the latter to a lesser degree owing to both a lesser density of the uncoupled electron and the steric factor (which has been proved for diphenylamine derivatives (25)). From the viewpoint of spin density, the formation of 3,10′- and 1,10′-diphenothiazinyls as well as their relative quantities is explained.

At the same time, following from the present work and the previous data (7), oxidational dimerization for phenothiazine is characteristic to a lesser degree than for diarylamines, the reason being a smaller value of spin density at the nitrogen and C-3 atoms in the phenothiazine cation radical, as compared to the cation radicals of diphenylamines (30).

Acknowledgement

The authors would like to thank Dr. Alexander A. Kamnev for technical assistance.

1. E. Bishop (*Editor*). Indicators. Pergamon Press, Oxford. 1972.
2. Y. Tsujino. Nippon Kagaku Zasshi, **90**, 809 (1969).
3. H. Gilman and D. R. Nelson. J. Am. Chem. Soc. **75**, 5422 (1953).
4. A. S. Morkovnik, O. Yu. Okhlobystin, and E. Yu. Belinskii. Zh. Org. Khim. **15**, 1565 (1979).
5. A. S. Morkovnik, N. M. Dobaeva, and O. Yu. Okhlobystin. Khim. Geterotsikl. Soedin. 1214 (1981).
6. A. S. Morkovnik. Zh. Obshch. Khim. **52**, 1877 (1982).
7. R. Parkash, H. O. Gupta, and J. Dutt. J. Heyrovský Centennial Congr. Polarogr. organized jointly with 41st Meet. Int. Soc. Electrochem. Prague, Aug. 20–25, 1990: Proc. 1. Aug. 20–21. Prague. 1990. p. Tu-109.
8. P. Kabasakalian and J. McGlotten. Anal. Chem. **31**, 431 (1959).
9. K. B. Yatsimirskii. Kinetic methods of analysis (in Russian). Khimiya, Moscow. 1967.
10. E. T. Denisov. Kinetics of homogeneous chemical reactions (in Russian). Vysshaya Shkola, Moscow. 1988.
11. M. L. Hitchman and W. J. Albery. Electrochim. Acta, **17**, 787 (1972).
12. G. A. Shchembelov, Yu. A. Ustynyuk, V. M. Mamaev, S. Ya. Ishchenko, I. P. Gloriozov, V. B. Luzhkov, V. V. Orlov, B. Ya. Simkin, V. I. Pupyshev, and V. N. Burmistrov. Quantum chemical methods of calculation of molecules (in Russian). Khimiya, Moscow. 1980.
13. S. L. Shmakov, O. V. Sivanova, B. L. Faifel', and V. A. Sheenson. Manual for computer applications in practical laboratory work in the specialization Inorganic Chemistry (in Russian). Saratov University Press, Saratov. 1988.
14. P. Hanson and R. O. C. Norman. J. Chem. Soc. Perkin Trans. 2, 264 (1973).
15. A. S. Morkovnik, O. Yu. Okhlobystin, Z. S. Morkovnik, and E. Yu. Belinskii. Khim. Geterotsikl. Soedin. 1696 (1979).
16. K. Yoshida. Electrooxidation in organic chemistry. The role of cation radicals as synthetic intermediates. John Wiley and Sons, New York. 1984.
17. L. G. Chatten and L. E. Harris. Anal. Chem. **34**, 1495 (1962).
18. A. N. Pankratov and E. I. Grigor'eva. Zh. Anal. Khim. **45**, 2121 (1990).
19. A. Albert and E. P. Serjeant. Ionisation constants of acids and bases. Chapman and Hall, London. 1971.
20. Yu. Yu. Lur'ye. Handbook on analytical chemistry (in Russian). Khimiya, Moscow. 1989.
21. R. P. Bell. The proton in chemistry. Chapman and Hall, London. 1973.
22. K. J. Vetter. Elektrochemische Kinetik. Springer-Verlag, Berlin. 1961.
23. J. A. Pople and D. L. Beveridge. Approximate molecular orbital theory. McGraw–Hill, New York. 1970.
24. A. N. Pankrotov, V. I. Morozov, S. P. Mushtakova, and A. V. Il'yasov. Izv. AN SSSR Ser. Khim. 1483 (1984).
25. A. N. Pankratov, S. L. Shmakov, S. P. Mushtakova, and L. A. Gribov. Zh. Anal. Khim. **41**, 810 (1986).
26. A. N. Pankratov. Zh. Obshch. Khim. **58**, 2323 (1988).
27. R. Huisgen. Proc. Chem. Soc. 210 (1958).
28. G. S. Hammond, B. Seidel, and R. E. Pincock. J. Org. Chem. **28**, 3275 (1963).
29. J. D. Roberts and M. C. Kaserio. Basic principles of organic chemistry. Supplement. W. A. Benjamin, Inc., New York. 1964.
30. A. N. Pankratov, S. P. Mushtakova, and L. A. Gribov. Zh. Anal. Khim. **42**, 352 (1987).

Can. J. Chem. Downloaded from www.nrcresearchpress.com by 213.200.69.106 on 09/08/12
For personal use only.

A ^{13}C NMR spectroscopy study of the structure of N-H pyrazoles and indazoles

CONCEPCION LOPEZ AND ROSA MA. CLARAMUNT[1]

Departamento de Química Orgánica y Biología, Facultad de Ciencias, Universidad Nacional de Educación a Distancia, Senda del Rey s/n, E-28040 Madrid, Spain

SWIATOSLAW TROFIMENKO

Du Pont Polymers, Research and Development, Experimental Station, Wilmington, DE 19880-0302, U.S.A.

AND

JOSÉ ELGUERO

Instituto de Química Médica, Consejo Superior de Investigaciones Cientificas, Juan de la Cierva, 3, E-28006 Madrid, Spain

Received November 27, 1992

CONCEPCION LOPEZ, ROSA MA. CLARAMUNT, SWIATOSLAW TROFIMENKO, and JOSÉ ELGUERO. Can. J. Chem. **71**, 678 (1993).

The ^{13}C chemical shifts and some $^{1}H-^{13}C$ coupling constants of 23 pyrazoles and indazoles are reported and discussed. The spectra were recorded in $CDCl_3$ and in DMSO-d_6 solutions and, in several cases, also in the solid state (CP/MAS technique). These data allow us to determine the tautomerism of these compounds in the solid state (usually only one tautomer) and in solution. The position of the tautomeric equilibrium is related to the Hammett σ_m value of the 3(5)-substituent.

CONCEPCION LOPEZ, ROSA MA. CLARAMUNT, SWIATOSLAW TROFIMENKO et JOSÉ ELGUERO. Can. J. Chem. **71**, 678 (1993).

Les déplacements chimiques du carbone-13 et quelques constantes de couplage $^{1}H-^{13}C$ de 23 pyrazoles sont rapportées et discutées. Les spectres de RMN ont été déterminées en solution dans du $CDCl_3$ et DMSO-d_6 et, dans plusieurs cas, à l'état solide (technique CP/MAS). Ces données ont permis de determiner la position de l'équilibre tautomère à l'état solide (en général, un seul tautomère) et en solution. D'une façon qualitative, cette position est reliée au coefficient σ_m d'Hammett.

Can. J. Chem. Downloaded from www.nrcresearchpress.com by 213.200.69.106 on 09/08/12
For personal use only.

Introduction

The aim of this work is twofold: first, to report accurate and properly assigned ^{13}C chemical shifts and $^{1}H-^{13}C$ coupling constants of a set of N-H pyrazoles; second, to use these data to discuss the tautomeric structure of pyrazoles in solution and, in some cases, in the solid state.

Pyrazoles unsubstituted on nitrogen are important ligands in metallo-organic chemistry, either by themselves or as pyrazolate anions (1–3). Moreover, they can be transformed into tris-pyrazolylborates, one of the most used anionic ligand classes (4). In earlier work, only commercial or readily accessible pyrazoles were used but, lately, more complex pyrazoles have been introduced. This is a consequence of the search for more specific ligand properties towards the metal and, in particular, has led to a series of pyrazolylborates with substituents at positions 3 and 5 of different size and geometry (5–28).

Since NMR, and particularly ^{13}C NMR, is the method of choice to establish the structure of the resulting complexes in solution, a careful characterization of the pyrazolyl ligands is useful (in a subsequent work the corresponding borates will be reported[2]). With this purpose in mind, we report the study of the NMR spectroscopy of 32 N-H pyrazoles (including some indazoles), of which 23 have not been previously described and 9 are already known but are necessary for comparisons.

The formulae of these pyrazoles are represented in Scheme 1 (3(5)-aryl derivatives), Scheme 2 (3(5)-alkyl, 3(5)-alkyl-4-bromo, and 3,5-disubstituted derivatives), and Scheme 3 (bicyclic pyrazoles and indazoles).

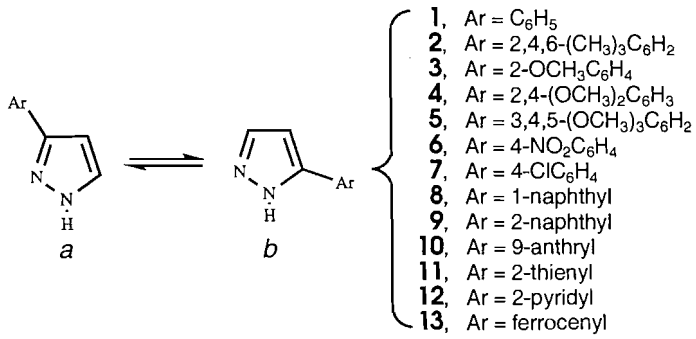

SCHEME 1

Results and discussion

Thanks to experience (29–31, 33–39), the assignment of pyrazole and indazole carbon chemical shifts has become routine. For this reason, the ^{1}H NMR study and the NOESY and HETCOR experiments used in some cases will not be reported. Also, most $^{1}H-^{13}C$ coupling constants of the substituents will be omitted for the sake of brevity. The data corresponding to compounds depicted in Schemes 1, 2, and 3 are given in Tables 1, 2, and 3, respectively.

The numbering of pyrazole carbons depends on the chosen tautomer, since the N-H is always N1. For instance, in tautomer **1***a*, C3 is the carbon bearing the phenyl substituent while in **1***b* it is a C-H. In the tables, when there is a letter, *a* or *b*, after the number, the chemical shifts refer to a particular tautomer and the numbering of carbons corre-

[1]Author to whom correspondence may be addressed.

[2]S. Trofimenko, R. M. Claramunt, C. Lopez, and J. Elguero. Unpublished results.

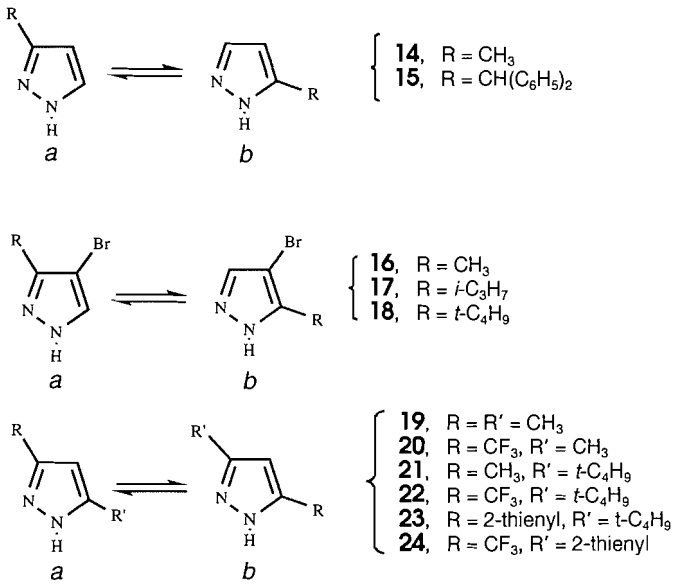

SCHEME 2

sponds to that tautomer. When there is no letter, the chemical shifts are those of the tautomeric mixture; in that case, the numbering *always* corresponds to tautomer *a*, without any implication concerning tautomerism. For instance, C3 in compounds **20**, **22**, and **24** (Table 2) is the carbon bearing a CF_3 substituent.

This problem does not arise for indazoles (Scheme 3) where the atom numbering is independent of tautomerism. In this case, *a* and *b* tautomers (compounds **30–32**) are called 1*H*- and 2*H*-indazoles, respectively.

Chemical shifts and coupling constants of pyrazole and indazole carbons

The chemical shifts of carbons C3 and C5 of Table 1 depend too much on the $a \rightleftharpoons b$ tautomerism and will be discussed later on. On the other hand, the chemical shift of C4 is, in a first approximation, the same for both tautomers but depends on the conformation of the 3-aryl residue. In "planar" compounds it appears at 102–103 ppm while in "twisted" ones the signal appears at 105.6 (**2**), 106.8 (**8**) (compare with 102.2 ppm for **9**), and 108.0 ppm in the "orthogonal" anthryl derivative **10**. Note that compounds **3**, **4**, and **12** behave like "planar" compounds, a fact that is related to their tautomerism. When X-ray diffraction data are available (30), the conformation of the aryl group deduced from ^{13}C CP/MAS is consistent with those found in the monocrystals.

The most remarkable observation in the bicyclic pyrazoles of Table 3 is the ring strain effect, common to pyrazoles **25** and **27**, that deshields C3 and C5. The chemical shifts of indazole **30** and benzo[*g*]indazole **31** show similar relationships as those in naphthalene/phenanthrene (40), except for carbon C7, which in the first case is deshielded by 2.4 ppm, and in the second by 9.1 ppm.

Since this paper concerns pyrazoles, only the ^1H-^{13}C coupling constants of annular carbons (C3, C4, and C5) are reported in Tables 1–3; they are consistent with previous values (35) and with those of the already known compounds, which we have included in the tables. There is much less information about ^{13}C–^{19}F coupling constants in pyrazoles (35); for this reason all of them have been included in the tables.

Chemical shifts and coupling constants of the substituents

The chemical shifts of the substituents and, especially, the carbon atom linked to the pyrazole ring depend on their position on the ring; they are more deshielded when they are at position 3 than when they are at position 5: CH_3 (13–14 vs. 10–10.5 ppm) (35), CF_3(121.5–122 vs. 119.5–120 ppm) (41, 42), C_6H_5, C_{ipso}(134.5–135 vs. 130–130.5 ppm) (35), and thienyl C2′ (136.5–137 vs. 130 ppm).

The methylene signals of the CH_2CH_2 bridge (compounds **28** and **29**, carbon atoms C7′ and C8′, Scheme 3) have chemical shifts consistent with the shielding effect of the pyrazole ring compared with the phenyl ring in *C*-methyl derivatives, 4-methylpyrazole (35) vs. toluene (40).

The $^1J(^{13}C–^{19}F) \sim 268$ Hz measured in the CF_3 substituents of compounds **20**, **22**, and **24** is reported here for the first time.

The use of ^{13}C NMR spectroscopy to study the annular tautomerism of pyrazoles and indazoles

In the solid state, only one pyrazole tautomer is observed (33). Exceptions are compound **26**[3] and compound **13** (Table 1, tautomers **13***a* and **13***b*). Compound **19** being symmetrical, tautomers **19***a* and **19***b* are identical.

The determination of the tautomer present in the solid state requires either the knowledge of "blocked" pyrazoles, i.e., those in which the N-H is replaced by an N-R (35), or the slowing down of prototropic exchange in order to observe the signals of both tautomers in solution (29, 30, 32, 43). Several examples of this last case are reported in the tables.

To illustrate the determination of the structure of the tautomer consider, for instance, the 3(5)-aryl derivatives of Table 1. The carbon bearing the aryl group appears at 149.7 ppm (C3) in tautomer **1***a* and at 141.1 (C5) in tautomer **1***b* (150.2 and 142.1 ppm in the case of tautomers **5***a* and **5***b*). Clearly the tautomer present in the solid state for pyrazole **4** is the **4***b* (C5 at 141.0 ppm) whereas for pyrazole **11** it is the **11***a* (C3 at 151.4 ppm). In Table 2, the pyrazoles whose methyl substituent resonates at 10 ppm are 5-methyl pyrazoles (**16***b*, **19**, **20***a*) whereas those with a methyl signal at 13 ppm are 3-methyl pyrazoles (**19**, **21***a*).

The knowledge of the chemical shifts of the tautomer present in the solid state allows us to determine, at least qualitatively, the tautomeric composition in solution. The results are collected in Table 4. More quantitative information is not available at this moment except for a few compounds.

The main conclusions of the Table 4 results are as follows:

1. Clearly, the tautomer present in the solid is also the major tautomer in solution. A possible exception is 3(5)-phenylpyrazole, which in solution is mainly (72%, Table 1) in the 3-phenyl form **1***a* whereas in the solid state it seems to be the 5-phenyl tautomer **1***b* (to be confirmed by crystallography[4]).

2. In the case of pyrazoles **3**, **4**, and **12**, the most abundant tautomers are **3***b*, **4***b*, and **12***a*. Only these tautomers can be "planar" as we have deduced above from the chemical shifts of C4.

[3]A. Martinez, J. Elguero, and A. Fruchier. Unpublished results.

[4]C. Lopez, R. M. Claramunt, and J. Elguero. Work in progress.

Can. J. Chem. Downloaded from www.nrcresearchpress.com by 213.200.69.106 on 09/08/12
For personal use only.

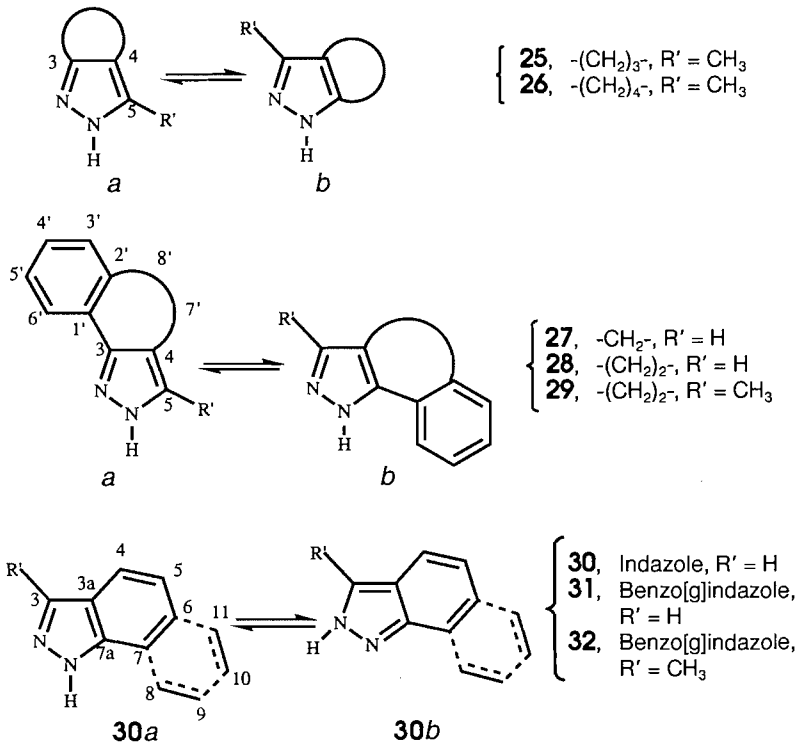

SCHEME 3

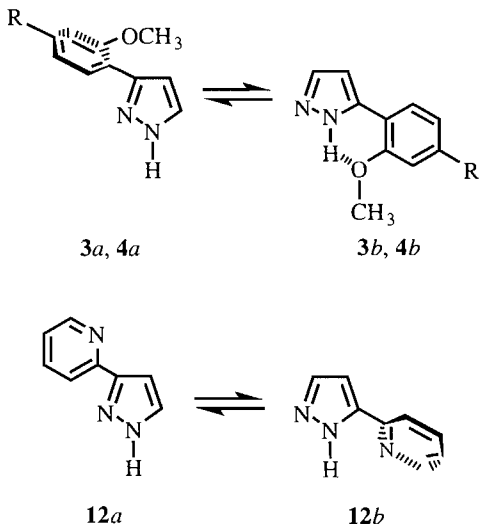

3. The ferrocenyl derivative **13** appears to be a mixture of both tautomers in the solid state. This was unexpected for a 3(5)-monosubstituted pyrazole (the only other example, **26**, is a 3,4,5-trisubstituted derivative). All attempts to obtain convenient crystals to determine the structure of pyrazole **13** by crystallography proved unsuccessful.

4. Together with the results reported earlier (33), we now have a large collection of data of the predominant (solution) or the only observed tautomer (solid state): (*i*) Substituents that prefer the position 3: CF_3 > Br > Ar(Het) (exception: *ortho*-methoxyphenyl). (*ii*) Substituents that prefer the position 5: *tert*-butyl > isopropyl > methyl. (*iii*) No preference: ferrocenyl.

Since the pK_a's of pyrazoles (44) follow a linear relationship with the σ_m of the substituent, and since tautomerism and pK_a are related (1), we find it interesting to report the literature values of σ_m for the above substituents (45): CF_3 (0.46) > Br (0.37) > 2-thienyl (0.09) > phenyl (0.05) > ferrocenyl (0.00) > $CHPh_2$ (−0.03) > Me (−0.06) > iPr (−0.08) > *t*Bu (−0.09). It can be observed that there is a clear relationship between σ_m and the tautomerism of pyrazoles: when σ_m is positive the substituent prefers the 3-position, when it is null (ferrocenyl) both tautomers have the same energy, and when σ_m is negative the substituent prefers the 5-position. The qualitative order is followed even in the two extreme groups.

In the gas phase (46) the phenyl substituent stabilizes the 3-substituted tautomer while the *tert*-butyl substituent stabilizes the 5-tautomer, in agreement with the findings in solution and in the solid state. However, since the intrinsic differences in the gas phase are quite small (46), formation of hydrogen bonds with the solvent in solution or with other molecules in the crystal could modify the tendency observed in the isolated molecule.

Conclusion

For a variety of substituents (alkyl, aryl, heteroaryl, trifluoromethyl) the possible isomers are characterized as tautomers *a* and *b*. A knowledge of the preferred tautomers has been gathered which can be relevant for the reactivity of these systems. Even in the case where no suitable crystals for X-ray crystallography can be obtained, high-resolution ^{13}C NMR spectroscopy provides a method for determining the structure of pyrazoles in the solid state.

Experimental

Synthesis

Of the 23 pyrazoles whose NMR spectroscopy is described here for the first time, some are new compounds[5] and the remaining ones

[5]S. Trofimenko. Unpublished results.

Can. J. Chem. Downloaded from www.nrcresearchpress.com by 213.200.69.106 on 09/08/12
For personal use only.

TABLE 1. Some ^{13}C chemical shifts and $^{1}H-^{13}C$ coupling constants of N-unsubstituted 3(5)-arylpyrazoles

Compound no.	Solvent	C3	C4	C5	Substituent
1*a*	[a]	149.7	101.1	134.5	C_{ipso}(Ph) = 134.5
1*b*	[a]	139.3	101.1	141.1	C_{ipso}(Ph) = 129.9
2	$CDCl_3$	143.98	105.55 ^1J = 175.9 ^2J = 10.0	135.73 ^1J = 186.5 ^2J = 6.6	Ar: 128.27(C1′), 137.72(C2′,C6′), 128.03(C3′,C5′) 137.94(C4′), 21.06(Me-4′), 20.21(Me-2′,Me-6′)
2*a*	DMSO-d_6	149.1(br)	104.92	132.5(br)	Ar: 128.4(C1′,br), 137.0(C2′,C3′), 127.89(C3′,C5′)
2*b*	DMSO-d_6	139.4(br)	104.92	139.4(br)	137.5(C4′), 20.66(Me-4′), 20.18(Me-2′,Me-6′, br)
2	DMSO-d_6[b]	143.60	105.15	134.72	Ar:129.02(C1′), 136.99(C2′,C6′), 127.96(C3′,C5′), 137.15(C4′), 20.69(Me-4′), 20.20(Me-2′,Me-6′)
3*b*[c]	$CDCl_3$	138.3 ^1J = 184.5 ^2J = 5.2	102.9 ^1J = 175.5 ^2J = 10.8	140.9 ^3J = 4.5	C_{ipso}(Ar) = 118.0
4	$CDCl_3$	140.95 ^2J = 5.9 ^3J = 5.9	101.95 ^1J = 175.1 ^2J = 6.3	138.35 ^1J = 184.3 ^2J = 6.2	Ar: 111.22(C1′), 156.90(C2′), 98.75(C3′), 160.49(C4′) 105.37(C5′), 128.70(C6′), 55.50(OMe-2′), 55.27(OMe-4′)
4	DMSO-d_6[d]	142.4	104.0	134.9	
	DMSO-d_6[b]	142.61	104.57	135.40	
4*b*	Solid	140.97	102.92	140.97	Ar: 110.92(C1′), 158.40(C2′), 96.38(C3′), 161.47(C4′) 110.92(C5′), 129.17(C6′), 56.63(OMe-2′), 54.97(OMe-4′)
5	$CDCl_3$	149.0	102.3 ^1J = 175.1 ^2J = 9.1	132.8 ^1J = 185.8 ^2J = 7.7	Ar: 127.8(C1′), 102.9(C2′,C6′), 153.3(C3′,C5′), 137.8(C4′), 60.7(OMe-4′), 55.9(OMe-3′,OMe-5′)
5*a*[e]	$CDCl_3$	150.3	102.3	130.0 ^1J = 185.6	C_{ipso}(Ar) = 129.8
5*b*[e]	$CDCl_3$	140.2 ^1J = 179.2	102.3	142.1	C_{ipso}(Ar) = 125.2
5	DMSO-d_6	150.6	102.6	130.2	
6	DMSO-d_6	148.1(br)	103.4 ^1J = 176.1 ^2J = 7.7	130.7(br) ^1J = 182.4	Ar: 140.2(br)(C1′), 125.8(C2′,C6′), 124.0(C3′,C5′), 146.3(C4′)
7	DMSO-d_6	149.0(br)	102.1 ^1J = 175.1 ^2J = 9.3	132.7(br)	Ar: 130.1(C1′), 126.8(C2′,C6′), 128.7(C3′,C5′), 131.8(C4′)
8	DMSO-d_6	~147(v br)	105.56 ^1J = 175.2 ^2J = 9.5	~131(v br)	Ar: 133.64, 130.75, 128.32, 128.06, 126.89, 126.39, 125.99, 125.92, 125.52
8	DMSO-d_6[b]	147.93	106.56	130.63	
9	DMSO-d_6	150.22	102.25 ^1J = 174.5	130.05	Ar: 133.35, 132.50, 131.54, 128.18, 127.98, 127.67, 126.36, 125.75, 124.03, 123.49
10	$CDCl_3$	144.37	108.01	133.01	Ar: 131.01, 130.95, 128.23, 127.75, 126.22, 125.74, 125.06
11	DMSO-d_6	145.77	101.80 ^1J = 175.3	130.01 ^1J = 188.8	Thienyl: 137.23(C2′), 127.65(C3′), 123.58(C4′), 124.47(C5′)
11*a*	Solid	151.36	102.27	136.65	Thienyl: 136.65(C2′), 129.89(C3′), 124.47(C4′), 124.47(C5′)
12	DMSO-d_6	151.13	103.25 ^1J = 175.9	129.29 ^1J = 182.9	Pyridyl: 152.40(C2′), 122.45(C3′), 136.75(C4′), 119.32(C5′), 149.23(C6′)
12*a*	Solid	152.28	105.26	128.22	Pyridyl: 152.28(C2′), 123.67(C3′), 136.66(C4′)
13	$CDCl_3$	N.o.[g]	~103(v br)	N.o.	Ferrocenyl: 69.51(5C), 68.63(2C), 66.67(2C)
13	DMSO-d_6	N.o.	101.79 ^1J = 174.6 ^2J = 9.5	N.o.	Ferrocenyl: ~77(1C,v br), 69.17(5C), 68.14(2C), 66.12(2C)
13	THF-d_8[f]	147.4(br)	103.5	135.5(br)	Ferrocenyl: 76.8, 69.8, 69.0, 67.0
13*a*	Solid	151.8	105.2	130.3	Ferrocenyl: 77.3, 70.4, 62.8
13*b*	Solid	140.0	102.2	142.3	Ferrocenyl: 77.3, 70.4, 62.8

[a]HMPT–acetone-d_6 at −20°C (72%(**1***a*), 28%(**1***b*)) (29,30).
[b]With a small amount of TFAA.
[c]Predominantly **3***b* (31).
[d]At 80°C.
[e]**5***a*(75%)–**5***b*(25%).
[f]Data (unassigned) from ref. 21.
[g]N.o., not observed.

Can. J. Chem. Downloaded from www.nrcresearchpress.com by 213.200.69.106 on 09/08/12
For personal use only.

TABLE 2. ^{13}C chemical shifts and $^{1}H-^{13}C$ and $^{13}C-^{19}F$ coupling constants of N-unsubstituted 3(5)-alkyl-, 3(5)-alkyl-4-bromo-, and 3(5)-alkyl(heteroaryl)-5(3)-methyl(trifluoromethyl)-pyrazoles

Compound no.	Solvent	C3	C4	C5	Substituent
14	$CDCl_3$	142.78	103.98 ^{1}J = 174.2 ^{2}J = 9.6 ^{3}J = 3.3	134.51 ^{1}J = 183.5 ^{2}J = 7.5	CH_3 = 11.58 ^{1}J = 127.7
14*a*	[a,b]	146.05	103.17	128.34	CH_3 = 13.68
14*b*	[a,b]	137.18	103.17	138.59	CH_3 = 10.55
15	$CDCl_3$	142.7	105.1 ^{1}J = 176.2 ^{2}J = 9.4 ^{3}J = 3.1	132.9 ^{1}J = 185.6 ^{2}J = 7.4	CH = 49.8, Ar: 150.8(C1'), 128.8(C2',C6'), 128.4(C3',C5'), 126.6(C4')
15	DMSO-d_6	143.6	104.2	N.o.	
16	DMSO-d_6[c]	140.8	92.2	134.7	CH_3 = 10.3
16*b*	Solid[c]	139.0	N.o.[h]	139.0	CH_3 = 10.4
17	$CDCl_3$	149.4	91.5 ^{2}J = 7.4 ^{3}J = 3.2	136.4 ^{1}J = 190.2	CH = 25.6, CH_3 = 21.3
17	DMSO-d_6[d]	150.0	90.7	135.0	
18	$CDCl_3$	149.6	90.4 ^{2}J = 7.4 ^{3}J = 3.2	138.8 ^{1}J = 190.2	$t$$C_4H_9$-3: C = 32.2, CH_3 = 28.5
18	DMSO-d_6[d]	151.5	89.9	136.4	
18*b*	Solid	140.6	N.o.	148.0	$t$$C_4H_9$-5: C = 32.3, CH_3 = 29.0
19	[a]	146.54	102.67	138.03	CH_3-3 = 13.84, CH_3-5 = 10.61
19	Solid[e]	147.5	104.8	139.3	CH_3-3 = 12.8, CH_3-5 = 10.5
20	DMSO-d_6[f]	141.6 $^{2}J_F$ = 36.7	102.1 $^{3}J_F$ = 2.2	140.6	CF_3-3 = 122.1, CH_3-5 = 10.0 $^{1}J_F$ = 267.6
20*a*	Solid	141.5	102.0	141.5	CF_3-3 = 121.8, CH_3-5 = 9.9
21	$CDCl_3$	144.5	100.7 ^{1}J = 171.7 ^{3}J = 3.2	157.3	CH_3-3 = 12.4, $^{t}C_4H_9$-5: C = 31.2, CH_3 = 30.3
21	DMSO-d_6[g]	N.o.	100.0	N.o.	
21	DMSO-d_6[c]	145.6	104.2	158.6	
21*a*	Solid	146.45	100.48	154.51	CH_3-3 = 13.87, $^{t}C_4H_9$-5: C and CH_3 = 30.92
22	DMSO-d_6	140.7 $^{2}J_F$ = 36.6	99.2 ^{1}J = 177.7	154.5	CF_3-3 = 122.05, $^{t}C_4H_9$-5: C = 31.8, CH_3 = 30.7 $^{1}J_F$ = 268.0
22*a*	Solid	142.4	99.7	156.4	CF_3-3 = 121.3, $^{t}C_4H_9$-5: C and CH_3 = 29.9
23	$CDCl_3$	145.7	98.6 ^{1}J = 174.0	155.3	$^{t}C_4H_9$-5: C = 31.1, CH_3 = 30.2, thienyl: 136.6(C2'), 127.2(C3'), 123.5(C4'), 124.0(C5')
23*a*	Solid	147.46	100.55	156.71	$^{t}C_4H_9$-5: C and CH_3 = 31.73, thienyl: 139.58(C2'), 125.82(C3',C4',C5')
24	DMSO-d_6	142.1 $^{2}J_F$ = 35.9	101.0 ^{1}J = 180.8	138.6(br)	CF_3-3 = 121.5 ($^{1}J_F$ = 268.1), thienyl-5: 129.9(C2'), 128.2(C3'), 125.9(C4'), 127.0(C5')
24*a*	Solid	142.0	N.o.	139.6	CF_3-3 = 121.6, thienyl-5: 128.8(C2'), 128.8(C3',C4',C5')

[a]HMPT at −20°C (32).
[b]**14***a*(46%) + **14***b*(54%) (32).
[c]Reference 33.
[d]With a small amount of TFAA.
[e]At −40°C (34) (**19***a* ≡ **19***b*).
[f]At 80°C.
[g]Reference 35.
[h]N.o., not observed.

are described in the following references: **6** (47), **7** (47), **11** (48), **12** (49), **13** (21), **17** (8), **21** (50), **24** (51), **28** (52), and **32** (53).

Spectroscopy. In solution

Proton noise-decoupled ^{13}C NMR spectra and gated decoupled ^{13}C NMR spectra were recorded at 50.32 MHz on a Bruker AC-200 instrument; all chemical shifts are expressed in ppm relative to tetramethyl-silane (TMS) and are given with a precision of ±0.01 ppm; the coupling constants are given with a precision of ±0.1 Hz.

Spectroscopy. Solid state NMR

The high-resolution solid state ^{13}C NMR spectra were obtained at room temperature on a Bruker AC-200 spectrometer working at 50.32 MHz under conditions of cross polarization (CP) and magic angle spinning (MAS) using a 7-mm Bruker DAB 7 probehead that achieves rotation frequencies of about 3.5–4.5 kHz. Samples were carefully packed in ZrO_2 rotors (approximately 200 mg of material). The standard CP/MAS pulse sequence was applied with a 7 μs $^{1}H-90°$ pulse width, 3–5 ms contact pulses, and 5 s repeti-

Can. J. Chem. Downloaded from www.nrcresearchpress.com by 213.200.69.106 on 09/08/12
For personal use only.

TABLE 3. Some ^{13}C chemical shifts and ^{1}H–^{13}C coupling constants of N-unsubstituted tricyclic pyrazoles (including indazoles)

Compound no.	Solvent	C3	C4	C5	Substituent
25	$CDCl_3$[a]	159.53 ^2J = 3.2(t)	122.56	133.62 ^2J = 6.5(q)	CH_3 = 10.40, CH_2 = 22.08(7′) ^1J = 127.8
26	$CDCl_3$[a]	143.32 ^2J = 3.4(t)	113.38	139.27 ^2J = 6.7(q)	CH_3 = 9.38, CH_2 = 18.83(7′), CH_2 = 21.06(8′) ^1J = 128.7
27	DMSO-d_6	157.29	123.08	124.13 ^1J = 186.1	CH_2 = 27.9(7′, ^1J = 131.6), Ar: 134.4(C1′) 148.3(C2′), 125.7(C3′,C4′), 125.7(C3′,C4′), 126.4(C5′), 119.0(C6′)
28	$CDCl_3$	145.81	115.84	128.04 ^1J = 184.4	CH_2 = 19.1(7′, ^1J = 131.0), 29.7(8′, ^1J = 130.5), Ar: 129.0(C1′), 136.7(C2′), 128.4(C3′), 127.4(C4′), 126.7(C5′), 121.95(C6′)
29	$CDCl_3$	145.90	113.43	137.55	CH_2 = 18.5(7′, ^1J = 131.5), 29.75(8′, ^1J = 130.3), Ar: 129.3(C1′), 136.45(C2′), 127.1(C3′), 128.2(C4′), 126.6(C5′), 122.1(C6′), CH_3 = 9.90(^1J = 127.8)
		C3	C3a	C7a	Other carbons
30	DMSO-d_6[b]	133.4 ^1J = 188.1 ^3J = 7.3(H_1) ^3J = 2.1(H_4)	122.8	139.9	120.4(C4), 120.1(C5), 125.8(C6), 110.0(C7)
31	DMSO-d_6	134.51 ^1J = 188.5	120.10	137.07	Ar: 119.3(C4), 121.9(C5), 131.8(C6), 119.1(C7), 121.6(C8), 126.3(C9,C10), 128.5(C11),
32	DMSO-d_6	142.08	118.10	137.71	Ar: 118.7(C4), 121.9(C5), 131.8(C6), 120.1(C7), 120.6(C8), 126.1(C9), 126.2(C10), 128.4(C11), CH_3 = 11.7(^1J = 127.0)

[a]Reference 36.
[b]References 37, 38.

TABLE 4. Annular tautomerism of N-H pyrazoles and indazoles (⊗, only this tautomer; ●, major tautomer; ○, minor tautomer; ◐, both tautomers present in equal or nearly equal proportions)

	Solid		Solution			Solid			Solution	
Compound	*a*	*b*	*a*	*b*	Compound	*a*		*b*	*a*	*b*
1		⊗	●	○	**17**			⊗	○	●
2	⊗		◐	◐	**18**			⊗	○	●
3		⊗	○	●	**19**	⊗	≡	⊗	◐	≡ ◐
4		⊗	○	●	**20**	⊗			●	○
5	⊗		●	○	**21**	⊗			●	○
6	⊗		●	○	**22**	⊗			●	○
7	⊗		●	○	**23**	⊗			●	○
8	⊗		●	○	**24**	⊗			●	○
9	⊗		●	○	**25**	⊗			●	○
10	⊗		●	○	**26**	⊗		⊗	◐	◐
11	⊗		●	○	**27**	⊗			●	○
12	⊗		●	○	**28**	—			◐	◐
13	⊗	⊗	◐	◐	**29**	—			◐	◐
14	Liquid		◐	◐	**30**	⊗			●	○
15	—		◐	◐	**31**	⊗			●	○
16		⊗	○	●	**32**	⊗			●	○

tion time, the spectral width being 20 000 Hz. All chemical shifts are given with respect to the spectrometer reference frequency, which was calibrated by the glycine signal at 176.1 ppm.

Acknowledgements

We thank Mrs. María José Retuerce, who kindly recorded the NMR spectra.

1. J. Elguero. *In* Comprehensive heterocyclic chemistry. Vol. 5. Pergamon Press, Oxford. 1984. p. 167.
2. S. Trofimenko. Prog. Inorg. Chem. **34**, 115 (1986).
3. E. C. Constable and P. J. Steel. Coord. Chem. Rev. **93**, 205 (1989).
4. K. Niedenzu and S. Trofimenko. Top. Curr. Chem. **131**, 1 (1986).
5. J. C. Calabrese, S. Trofimenko, and J. S. Thompson. J. Chem. Soc. Chem. Commun. 1122 (1986).
6. S. Trofimenko, J. C. Calabrese, and J. S. Thompson. Inorg. Chem. **26**, 1507 (1987).
7. N. Kitajima, K. Fujisawa, C. Fujimoto, and Y. Moro-oka. Chem. Lett. 421 (1989).

Can. J. Chem. Downloaded from www.nrcresearchpress.com by 213.200.69.106 on 09/08/12
For personal use only.

8. S. Trofimenko, J. C. Calabrese, P. J. Domaille, and J. S. Thompson. Inorg. Chem. **28**, 1091 (1989).
9. R. Han, A. Looney, and G. Parkin. J. Am. Chem. Soc. **111**, 7276 (1989).
10. A. H. Cowley, R. L. Geerts, C. M. Nunn, and S. Trofimenko. J. Organomet. Chem. **365**, 19 (1989).
11. R. Alsfasser, A. K. Powell, and H. Vahrenkamp. Angew. Chem. **102**, 939 (1990).
12. T. J. Desmond, F. J. Lalor, G. Ferguson, M. Parvez, and T. Wieckowski. Acta Crystallogr. Sect. C: Cryst. Struct. Commun. **C46**, 59 (1990).
13. J. W. Egan and K. H. Theopold. Acta Crystallogr. Sect. C: Cryst. Struct. Commun. **C46**, 1013 (1990).
14. I. B. Gorrell and G. Parkin. Inorg. Chem. **29**, 2452 (1990).
15. J. C. Calabrese, P. J. Domaille, J. S. Thompson, and S. Trofimenko. Inorg. Chem. **29**, 4429 (1990).
16. J. W. Egan, B. S. Haggerty, A. L. Rheingold, S. C. Senlinger, and K. H. Theopold. J. Am. Chem. Soc. **112**, 2445 (1990).
17. I. B. Gorrell, A. Looney, G. Parkin, and A. L. Rheingold. J. Am. Chem. Soc. **112**, 4068 (1990).
18. I. B. Gorrell, A. Looney, and G. Parkin. J. Chem. Soc. Chem. Commun. 220 (1990).
19. N. Kitajima, K. Fujisawa, T. Koda, S. Hikichi, and Y. Moro-oka. J. Chem. Soc. Chem. Commun. 1357 (1990).
20. M. Cano, J. V. Heras, S. Trofimenko, A. Monge, E. Gutierrez, C. J. Jones, and J. A. McCleverty. J. Chem. Soc. Dalton Trans. 3577 (1990).
21. K. Niedenzu, J. Serwatowski, and S. Trofimenko. Inorg. Chem. **30**, 524 (1991).
22. J. C. Calabrese, P. J. Domaille, S. Trofimenko, and G. J. Long. Inorg. Chem. **30**, 2795 (1991).
23. A. Looney, G. Parkin and A. L. Rheingold. Inorg. Chem. **30**, 3099 (1991).
24. R. Han and G. Parkin. J. Am. Chem. Soc. **113**, 9707 (1991).
25. R. Han, I. B. Gorrell, A. G. Looney, and G. Parkin. J. Chem. Soc. Chem. Commun. 717 (1991).
26. R. Han and G. Parkin. Organometallics, **10**, 1010 (1991).
27. R. Han and G. Parkin. J. Am. Chem. Soc. **114**, 748 (1992).
28. N. Kitajima, K. Fujisawa, C. Fujimoto, Y. Moro-oka, S. Hashimoto, T. Kitagawa, K. Toriumi, K. Tatsumi, and A. Nakamura. J. Am. Chem. Soc. **114**, 1277 (1992).
29. C. Cativiela, J. I. G. Laureiro, J. Elguero and E. Elguero. Gazz. Chim. Ital. **121**, 477 (1991).
30. F. Aguilar-Parrilla, C. Cativiela, M. D. D. de Villegas, J. Elguero, C. Foces-Foces, J. I. G. Laureiro, F. H. Cano, H. H. Limbach, J. A. S. Smith, and C. Toiron. J. Chem. Soc. Perkin Trans. 2, 1737 (1992).
31. J. Catalan, F. Fabero, R. M. Claramunt, M. D. Santa Maria, M. C. Foces-Foces, F. H. Cano, M. Martinez-Ripoll, J. Elguero, and R. Sastre. J. Am. Chem. Soc. **114**, 5039 (1992).
32. M. T. Chenon, C. Coupry, D. M. Grant, and R. J. Pugmire. J. Org. Chem. **42**, 659 (1977).
33. R. Faure, E. J. Vincent, A. Rousseau, R. M. Claramunt, and J. Elguero. Can. J. Chem. **66**, 1141 (1988).
34. A. Baldy, J. Elguero, R. Faure, M. Pierrot, and E. J. Vincent. J. Am. Chem. Soc. **107**, 5290 (1985).
35. M. Begtrup, G. Boyer, P. Cabildo, C. Cativiela, R. M. Claramunt, J. Elguero, J. I. G. Laureiro, C. Toiron, and P. Vedso. Magn. Reson. Chem. **31**, 107 (1993).
36. J. Elguero, A. Martinez, S. P. Singh, and D. Kumar. J. Heterocycl. Chem. **28**, 647 (1991).
37. P. Bouchet, A. Fruchier, G. Joncheray, and J. Elguero. Org. Magn. Reson. **9**, 716 (1977).
38. A. Fruchier and J. Elguero. Spectrosc. Lett. **12**, 809 (1979).
39. P. K. Byers, A. J. Canty, R. T. Honeyman, R. M. Claramunt, C. Lopez, J. L. Lavandera, and J. Elguero. Gazz. Chim. Ital. **122**, 341 (1992).
40. E. Breitmaier and W. Voelter. ^{13}C NMR spectroscopy. 2nd ed. Verlag Chemie, Weinheim. 1978. p. 188.
41. K. Burger, F. Hein, and O. Dengler. J. Fluorine Chem. **19**, 437 (1982).
42. S. P. Singh, D. Kumar, S. Kumar, and M. D. Threadgill. Indian J. Chem. **31B**, 233 (1992); S. P. Singh, D. Kumar, and J. K. Kapoor, J. Chem. Soc. Perkin Trans. 2. Submitted.
43. R. M. Claramunt, J. Elguero, C. Marzin and J. Seita. An. Quim. **75**, 701 (1979).
44. J. Elguero, E. Gonzalez, and R. Jacquier. Bull. Soc. Chim. Fr. 5009 (1968).
45. O. Exner. *In* Correlation analysis in chemistry. *Edited by* N. B. Chapman and J. Shorter. Plenum Press, New York. 1978. p. 439.
46. J. L. M. Abboud, P. Cabildo, T. Cañada, J. Catalan, R. M. Claramunt, J. L. G. de Paz, J. Elguero, H. Homan, R. Notario, C. Toiron, and G. I. Yranzo. J. Org. Chem. **57**, 3938 (1992).
47. M. R. Grimmett, K. H. R. Lim, and R. T. Weavers. Aust. J. Chem. **32**, 2203 (1979).
48. T. Tsuchiya, M. Enkaku, and H. Sawanishi. Chem. Pharm. Bull. **27**, 2188 (1979).
49. M. Tisler, B. Stanovnik and B. Vercek. Vestn. Slov. Kem. Drus. **27**, 65 (1980).
50. P. G. Dayton. C. R. Hebd. Seances Acad. Sci. **236**, 2515 (1953).
51. S. P. Singh, S. Sehgal, L. S. Tarar, and S. N. Dhawan. Indian J. Chem. **29B**, 310 (1990).
52. C. Ainsworth. J. Am. Chem. Soc. **79**, 5242 (1957).
53. H. Duewell and T. J. Haig. J. Chem. Soc. (C), 169 (1968).

Can. J. Chem. Downloaded from www.nrcresearchpress.com by 213.200.69.106 on 09/08/12
For personal use only.

An X-ray and conformational study of 5,7-dihydro-1,11-dimethyl-6*H*-dibenzo[*a*,*c*]cyclohepten-6-one and its methyl derivatives

ROBERT R. FRASER,[1] CORINNE BENSIMON, FANZUO KONG,[2] AND XINFU WU
Department of Chemistry, University of Ottawa, Ottawa, Ont., Canada K1N 6N5

Received July 15, 1992[3]

ROBERT R. FRASER, CORINNE BENSIMON, FANZUO KONG, and XINFU WU. Can. J. Chem. **71**, 685 (1993).

The crystal structures for the title compound **1** and its α-methyl derivatives **2–4** have been determined. Molecular mechanics calculations of the conformation of minimum energy for **1**, **3**, and **4** correspond closely to the symmetric structures observed in the crystal. For **2**, rotation at the CO—CH_2 bond by 24° produced an asymmetric conformation matching that seen in the solid state. The calculated changes in energy as a function of the torsional angle for **1** and **2** were compared with those for cyclohexanone and the axial conformer of the α-methyl derivative. The energy requirements for conformational change in the seven-membered ring were significantly greater than for the cyclohexane analogue. The calculated energy differences between diastereomeric methyl derivatives **2–4**, **6**, and **7** were in agreement with epimerization experiments. The distance of closest approach observed between a proton of the axial methyls of **2** and **3** and the distal benzene ring is smaller than expected on the basis of van der Waals' radii.

ROBERT R. FRASER, CORINNE BENSIMON, FANZUO KONG et XINFU WU. Can. J. Chem. **71**, 685 (1993).

On a déterminé les structures cristallines du composé **1** mentionné dans le titre et de ses dérivés α-méthylés, **2–4**. Des calculs de mécanique moléculaire de la conformation d'énergie minimale des composés **1**, **3** et **4** correspondent bien aux structures symétriques observées dans les cristaux. Pour le composé **2**, la rotation de 24° autour de la liaison CO—CH_2 provoque une conformation asymétrique qui correspond à celle observée à l'état solide. On a comparé les changements d'énergie en fonction de l'angle de torsion qui ont été calculés pour les composés **1** et **2** avec ceux de la cyclohexanone et du conformère axial de son dérivé α-méthylé. L'énergie requise pour effectuer le changement conformationnel dans le cycle à sept chaînons est beaucoup plus grand que celui nécessaire avec l'analogue de la série cyclohexanique. Les différences d'énergie calculées entre les dérivés méthylés diastéréoisomères **2–4**, **6** et **7** sont en accord avec ceux de données d'épimérisation. La distance la plus courte observée entre un proton des groupes méthyles axiaux des composés **2** et **3** et le noyau benzénique distal est plus courte que celle attendue sur la base des rayons de van der Waals.

[Traduit par la rédaction]

The bridged biaryl ketone, 5,7-dihydro-1,11-dimethyl-6*H*-dibenzo[*a*,*c*]cyclohepten-6-one, **1**, is a chiral derivative of biphenyl whose barrier to racemization was found to be 39 kcal/mol (1, 2). A C_2 axis passes through the central ring of **1** and along the C—O bond of the carbonyl group. As a consequence there are two possible orientations α to the carbonyl, either "axial" or "equatorial" on the basis of their similarity to the geometry at the α positions of cyclohexanone (see Fig. 1). The ring possesses a single rigid conformation, as indicated by molecular models and supported by its proton nmr spectra (2). We previously made use of **1** and its α-methyl derivatives in three separate studies of stereoselective reactions of the carbonyl group (3–5). In each case, **1** appeared to provide advantages over the more frequently used cyclohexanone and its derivatives. It is the aim of this paper to assess the relative merits of these two ketones as models for stereochemical studies.

Since the recognition of the fundamental effect of its chair conformation on reactivity (6), cyclohexane has played a central role in the development of the field of conformational analysis (7). The rigid[4] nature of its six-membered ring provided a skeleton on which the reactivity of pendant groups could be studied. The degree of rigidity of the ring was found to be high in mono- and disubstituted derivatives whose barriers to conformational change (8) were normally around 10 kcal/mol. Conformational homogeneity was achievable using a *tert*-butyl substituent whose energetic preference for the equatorial position was over 5 kcal/mol. Unfortunately the "rigidity" of the ketone derivative, cyclohexanone, is much less pronounced. The chair conformation of this ketone is only 3 kcal/mol more stable than its boat forms (8, 9). Consequently, the involvement of such less stable species in reaction pathways is of concern, though difficult to assess. This is one of several weaknesses that have been recognized in the use of cyclohexanone derivatives for conformational studies. Also of concern is the fact that a large anchoring group such as *tert*-butyl (10) or phenyl (11) changes the geometry of the ring significantly from that of cyclohexanone itself.

The relative lack of rigidity of cycloheptanes is well known. As discussed by Dunitz and Waser (12), a seven-membered ring has seven fixed bonds and seven fixed internal angles, leaving one torsional degree of freedom to permit flexibility. If one or more torsional constraints appear, the ring will become rigid. This has been proposed to be the case for ketone **1**. The only quantitative information regarding its rigidity is the very high barrier of 39 kcal/mol reported for the racemization of **1**. The major contribution to this barrier comes from the two *ortho* methyls, in whose absence the barrier falls to below 10 kcal/mol (13). Since the double bonds of the central ring are also fixed, the only possible mobile portions of the ring are the C—C single bonds that bridge the biphenyl moiety. We initially sought to probe the resistance of **1** to conformational change in a qualitative manner. We obtained X-ray data for crystalline samples of

[1]Author to whom correspondence may be addressed.
[2]Permanent address: Research Center for Eco-Environmental Sciences, Academia Sinica, P.O. Box 2871. Beijing, China.
[3]Revision received January 21, 1993.
[4]The term "rigid" is vague, implying that the molecule resides at the minimum of a potential energy well of unspecified depth or shape.

Can. J. Chem. Downloaded from www.nrcresearchpress.com by 213.200.69.106 on 09/08/12
For personal use only.

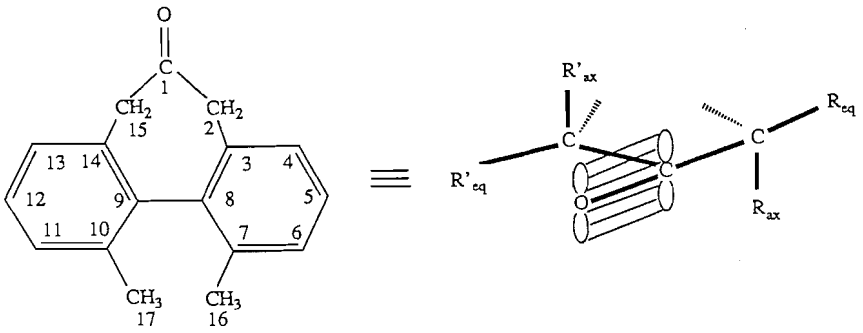

FIG. 1. The structure and three-dimensional representation for **1** and its derivatives **2–6**.

1 and three of its methyl derivatives, **2**, **3**, and **4**. Some variation in their conformations was observed. Molecular mechanics calculations were then carried out to assess the energy requirements of these conformational changes and, where possible, were compared with the available experimental data. The results provide evidence that **1** is of significantly greater rigidity than cyclohexanone.

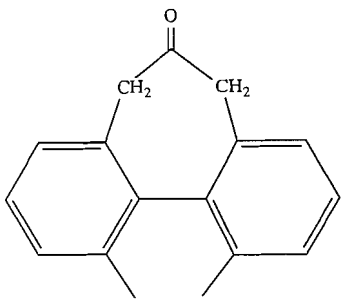

1

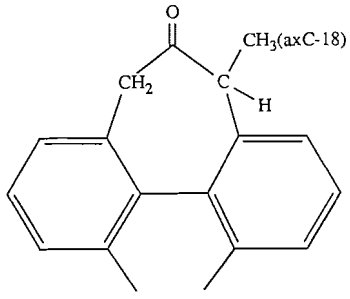

2

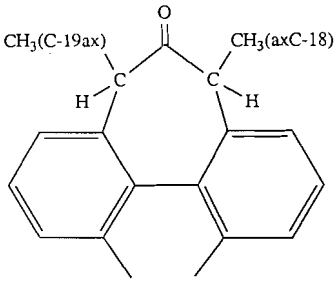

3

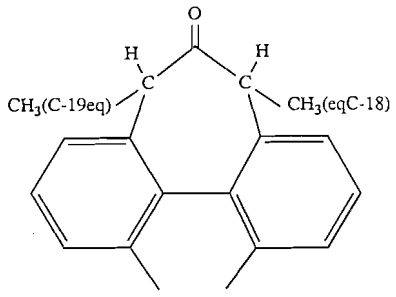

4

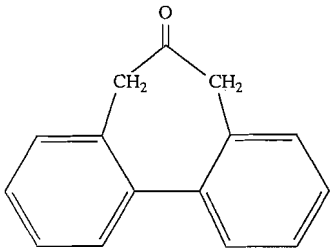

5

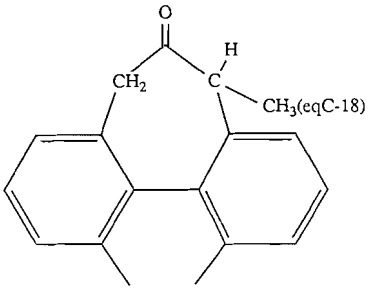

6

X-ray crystallographic analysis

A summary of the crystal data for compounds **1–4** appears in Table 1. The bond distances and bond angles are in the expected ranges. The most informative data come

Can. J. Chem. Downloaded from www.nrcresearchpress.com by 213.200.69.106 on 09/08/12
For personal use only.

TABLE 1. X-ray crystal data for compounds **1–4**

	1	**2**	**3**	**4**
Empirical formula	$C_{17}H_{16}O$	$C_{18}H_{18}O$	$C_{19}H_{20}O$	$C_{19}H_{20}O$
F.W.	236.31	250.34	264.36	264.36
Crystal dimensions (mm)	0.20 × 0.20 × 0.20	0.20 × 0.20 × 0.20	0.30 × 0.20 × 0.20	0.20 × 0.20 × 0.2
Space group	Monoclinic $C2/c$	Monoclinic $P2_1/c$	Monoclinic Cc	Monoclinic $P2_1/c$
Lattice parameters a(Å)	37.097 (8)[a]	8.175 (2)	8.146 (5)	8.565 (3)
b(Å)	10.104 (3)	15.238 (4)	27.536 (16)	13.664 (7)
c(Å)	10.328 (2)	22.177 (7)	7.199 (5)	13.313 (3)
β(°)	102.84 (1)	91.08 (3)	107.22 (4)	106.18 (2)
V (Å^3)	3774.6 (14)	2761.9 (14)	1542.6 (16)	1495.2 (12)
Z	12	8	4	4
D_c (g/cm^3)	1.248	1.204	1.138	1.174
No. of reflections measured	3337	4386	1236	2382
No. of unique reflections	3286	4068	1236	2218
No. of reflections with I_{net} > 2.5 $\sigma(I_{net})$	2281	2986	917	1318
For significant reflections R_f	0.056	0.082	0.051	0.061
R_w	0.031	0.039	0.022	0.073
For all reflections R_f	0.093	0.117	0.091	0.111
R_w	0.032	0.039	0.022	0.076
F(000)	1512.50	1072.35	567.93	611.93
In the last D-map				
the deepest hole (e/Å^3)	−0.500	−0.450	−0.160	−0.170
the highest peak (e/Å^3)	0.610	0.360	0.150	0.230
S	4.08	6.4	3.4	2.3

[a]Figures in parentheses refer to standard deviations.

TABLE 2. Torsional angles[a] (deg) obtained from the X-ray study

	1*a*	**1***b*	**2***a*	**2***b*	**3**	**4**
O—C1—C2—R_e	−29.8 (14)[b]	−12.3 (14)	42.3 (21)	49.2 (19)	−35.1 (28)	−7.6 (3)
O—C1—C2—R_a	81.3 (18)	97.4 (14)	−67.2 (5)	−67.8 (4)	88.7 (8)	104.4 (22)
O—C1—C15—R'_e	−2.0 (12)	−12.3 (14)	−11.4 (18)	−4.7 (2)	−24.5 (28)	−4.7 (4)
O—C1—C15—R'_a	118.5 (14)	97.4 (14)	−126.0 (19)	−127.5 (19)	87.7 (8)	109.3 (20)
O—C1—C2—C3	−153.8 (4)	−138.8 (3)	162.7 (6)	163.1 (6)	−139.5 (10)	−139.1 (6)
O—C1—C15—C14	−122.5 (4)	−138.8 (3)	116.8 (5)	117.4 (5)	−142.3 (10)	−136.4 (6)
C2—C1—C15—C14	55.6 (2)	41.2 (3)	−59.4 (3)	−61.5 (3)	35.8 (5)	42.1 (3)
C3—C2—C1—C15	28.1 (2)	41.2 (3)	−20.4 (3)	−18.5 (3)	42.5 (5)	42.4 (3)
C1—C2—C3—C4	112.6 (3)	109.9 (3)	−119.1 (5)	−120.9 (5)	109.1 (8)	107.7 (4)
C1—C15—C14—C13	104.8 (3)	109.9 (3)	−102.8 (15)	−103.0 (5)	112.7 (9)	105.6 (4)
C3—C8—C9—C14	56.5 (2)	56.8 (3)	−59.1 (4)	−57.9 (4)	55.3 (6)	61.4 (2)
C7—C8—C9—C10	61.3 (3)	59.7 (4)	−62.8 (4)	−61.4 (6)	64.6 (6)	58.6 (2)

[a]The relative sign is important with respect to the data for an individual structure.
[b]Standard deviations appear in parentheses.

from the torsional or dihedral angles given in Table 2. It is noteworthy that two crystallographically independent molecules were found in one unit cell for both **1** and **2**. The ORTEP plots for **1** appear in Fig. 2. Only one of these, **1***b*, was exactly symmetric about its C_2 axis as shown by the equal values for the torsional angles O—C1—C15—C14 and O—C1—C2—C3. The second structure, **1***a*, differs from the symmetric form primarily through rotation of about 15° about C1—C2 and C1—C15.[5] As seen in the representation in Fig. 3, the unit cell of **1** contains an aggregate of three antipodes. In this arrangement the central molecule would be expected to be symmetric, as in **1***b*, while the terminal members of the cell could adopt a structure reflecting their asymmetric environment. Since the cocrystallization of **1***a* with **1***b* suggests that their energies are similar, the observed distortion in **1***a* is an indication of some flexibility in **1**. In contrast, each of the structures **2***a* and **2***b* was distinctly asymmetric, possessing a further distortion relative to **1***a* of 8° rotation at each of the single bonds at C1. This undoubtedly occurs to lessen the repulsive interaction (vide infra) between the axial methyl and the π cloud of the distal benzene ring. These differences in rotation about the C1—C2 bond in **1***b*, **1***a* and the C1—C15 bond in **2***b* are illustrated by the stereochemical formulae in Fig. 4.

For **3** and **4**, the axis of symmetry is again in evidence, as indicated by the torsional angles about C1—C2 and C1—C15. Bond displacement from C_2 symmetry cannot relieve the strain in the diaxial dimethyl derivative **3**, as any rotation that diminishes one of the two axial methyl inter-

[5]These rotations are accompanied by smaller changes at the C2—C3 and C15—C14 bonds.

Can. J. Chem. Downloaded from www.nrcresearchpress.com by 213.200.69.106 on 09/08/12
For personal use only.

Can. J. Chem. Downloaded from www.nrcresearchpress.com by 213.200.69.106 on 09/08/12
For personal use only.

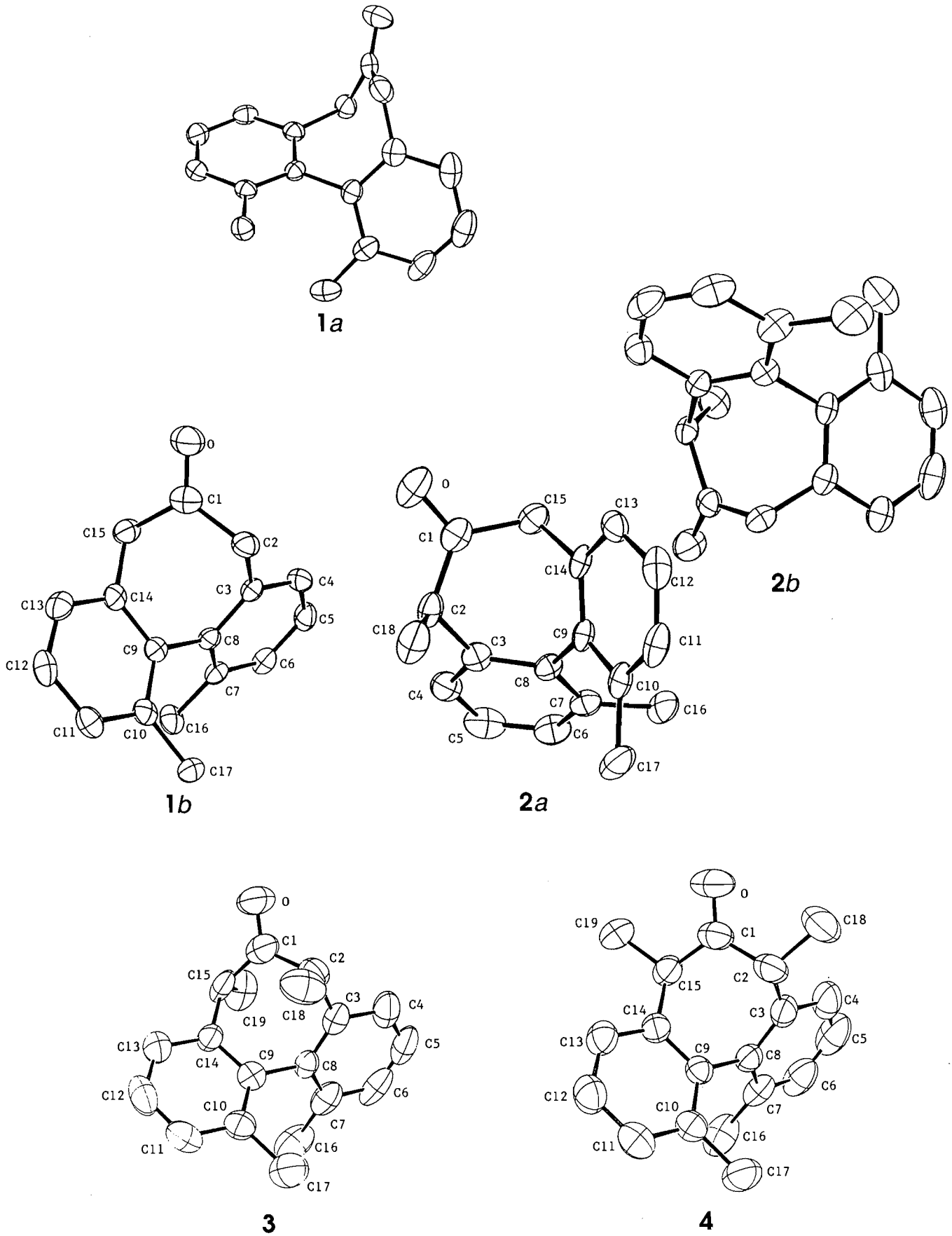

FIG. 2. The ORTEP plots for **1**–**4**.

Can. J. Chem. Downloaded from www.nrcresearchpress.com by 213.200.69.106 on 09/08/12
For personal use only.

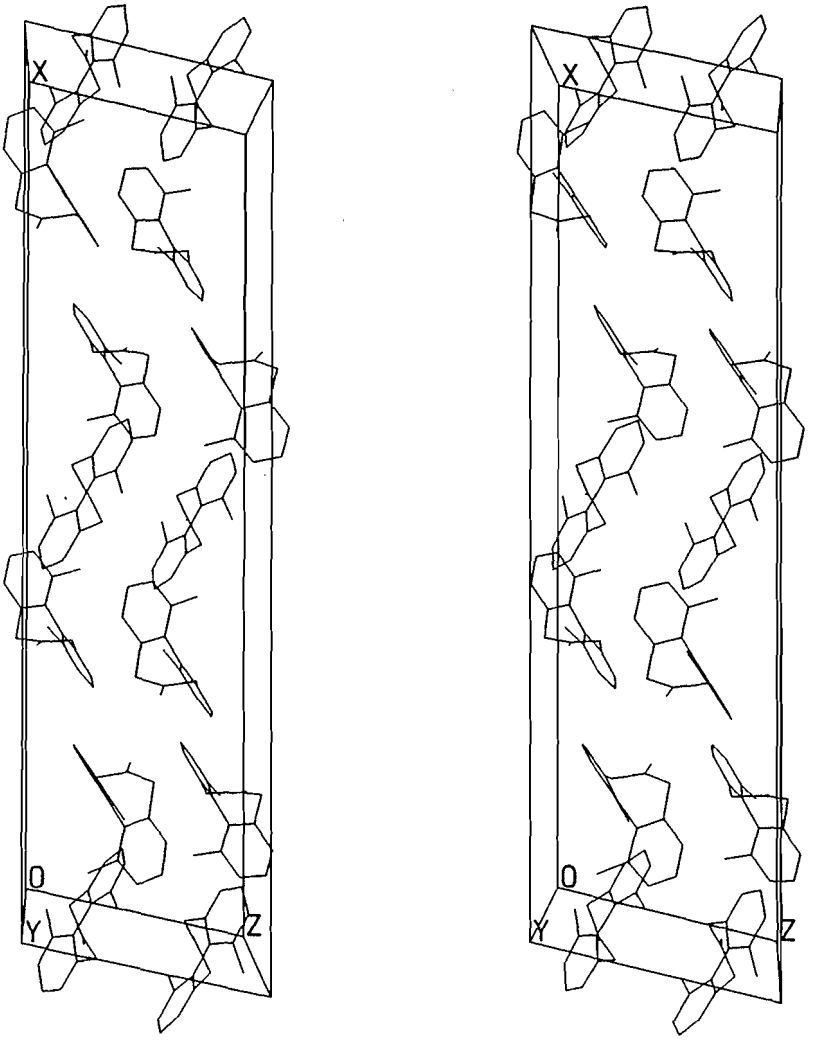

FIG. 3. A stereoview of the unit cell for **1**.

actions will increase the other. Partial relief appears to be achieved by angular distortion, i.e., an increase in the C3—C2—Me and C14—C15—Me bond angles. These angles are 117.4° and 115.2°, respectively, in **3** compared to the value of 111.3° found for C3—C2—Me in **2**. In the diequatorial dimethyl compound, both methyl groups are almost eclipsed with the adjacent carbonyl, each dihedral angle being 6°. This type of eclipsed conformation is energetically favored over the *anti*(axial-like) conformation in 2-butanone (9).

A feature common to all six structures for **1–4** is the value of 60° ± 4 for the dihedral angle between the two benzene rings. This increase in angle of about 8° over that reported (14) for the unsubstituted biaryl ketone **5** is clearly due to a repulsion between the two *ortho* methyls of **1**. Since this increase is limited by the three-carbon bridge, the two methyl groups are only 3.23 Å apart (average found for **1–4**), at which distance sufficient repulsion remains to produce a measurable distortion of each aromatic ring. These deviations from the planarity of the aromatic ring are listed in Table 3.

There is an additional important contribution available from the above data for **1** and its methyl derivatives. The axial methyl substituents in **2** and **3** are all periplanar with respect to the adjacent π orbital of the carbonyl group, as previously claimed (3–5). The methyl substituents in **4** are equatorial.

Conformational properties of **1** *and its derivatives as calculated by* MMX

Recently a new molecular mechanics program, MMX, has been developed (15).[6] It calculates strain energies using the MM2 method (16) and includes π-VESCF routines taken from MMPI (15). In view of the potential utility of this program for compounds containing aromatic rings, we wished to use the results of the crystallographic analyses as a test of the ability of MMX to calculate the conformational properties of **1–4**. Energy minimization provided the most stable conformation for **1**, having a C_2 axis of symmetry and corresponding closely to that of **1***b*, found in the crystal. For **2–4** we also calculated the most stable conformation as well as that most closely corresponding to each of the crystal forms. Table 4 lists the energies and torsional angles for all the

[6]PCMODEL Molecular Modeling Program, Serena Software. P.O. Box 3076, Bloomington IN 47402-3076, U.S.A.

Can. J. Chem. Downloaded from www.nrcresearchpress.com by 213.200.69.106 on 09/08/12
For personal use only.

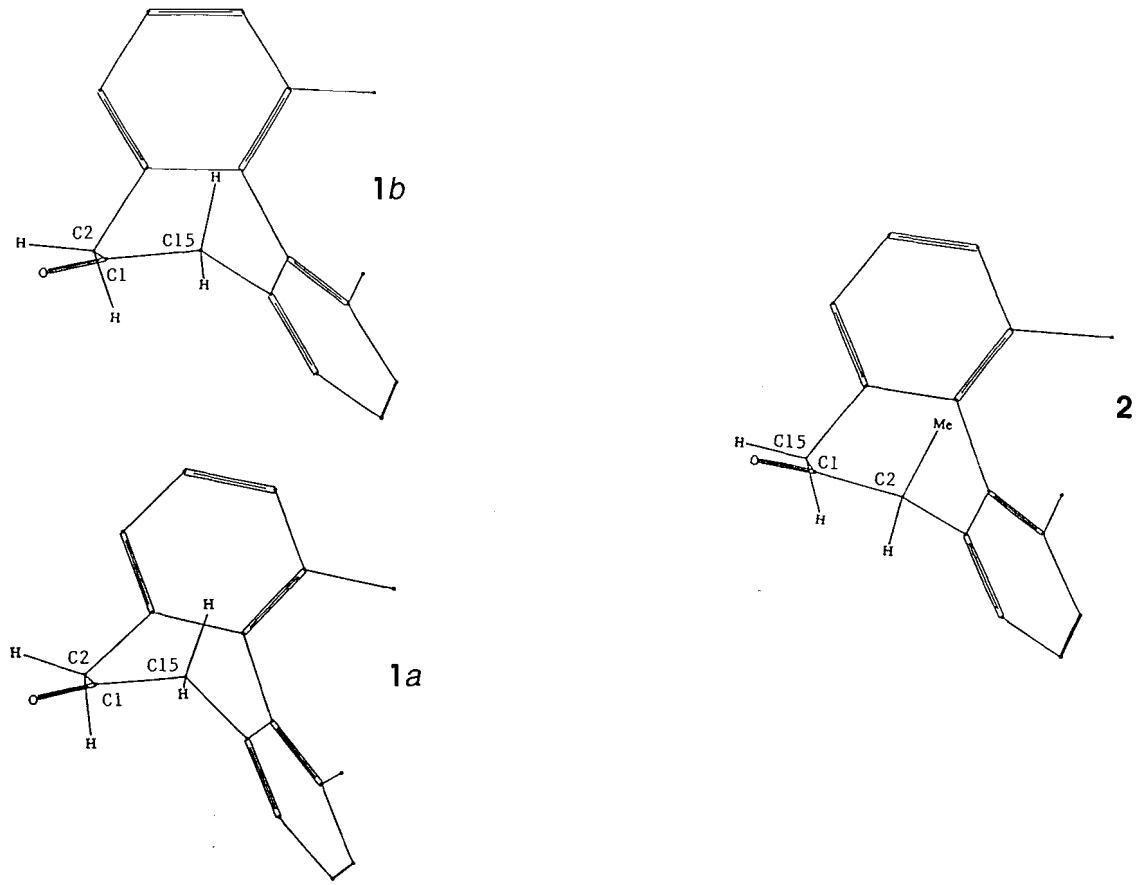

FIG. 4. Three-dimensional formulae for **1***b*, **1***a*, and **2**.

TABLE 3. Typical deviations (Å) of the benzene ring atoms from its mean plane

	C3	C4	C5	C6	C7	C8	C9	C10	C11	C12	C13	C14
1*a*	0.014	−0.005	−0.007	0.004	0.006	−0.014	0.027	−0.016	−0.006	0.020	−0.007	−0.017
1*b*	−0.007	−0.009	0.014	0.002	−0.017	0.017	0.019	−0.016	−0.001	0.012	−0.010	−0.006

TABLE 4. Calculated dihedral angles[a] (deg) for compounds 1–6.

Energy (kcal/mol):	**1** 25.7	**1′** 26.6	**2** 29.2	**2′** 29.2	**3** 33.4	**4** 31.4	**5** 22.8	**6** 28.6
O—C1—C2—R_e	15.8 (3.5)[b]	30.0 (0.2)[c]	39.3	47.0 (2.2)[d]	22.2 (12.9)[e]	7.6 (0.0)[f]	15.7	6.0
O—C1—C2—R_a	−100.5 (3.1)	−86.3 (5.0)	−75.0	−68.4 (0.6)	−91.8 (3.1)	−107.0 (2.6)	−100.2	−108.8
O—C1—C15—R'_e	15.4 (3.1)	1.0 (1.0)	2.2	−3.1 (1.6)	28.3 (3.8)	7.9 (3.2)	15.7	17.5
O—C1—C15—R'_a	−100.8 (3.4)	−114.7 (3.8)	−123.7	−120.6 (6.9)	−85.7 (2.0)	−106.7 (2.6)	−100.4	−98.7
O—C1—C2—C3	138.0 (0.8)	152.4 (1.4)	156.1	162.9 (0.2)	137.8 (1.7)	137.1 (2.0)	138.9	135.5
O—C1—C15—C14	138.4 (0.4)	124.6 (2.1)	123.7	117.9 (0.5)	144.5 (2.2)	137.4 (1.0)	138.7	140.1
C2—C1—C15—C14	−41.6 (0.4)	−52.2 (3.4)	−55.7	−60.3 (1.2)	−35.7 (0.1)	−42.6 (0.5)	−43.4	−40.0
C3—C2—C1—C15	−42.0 (0.8)	−30.7 (2.6)	−24.4	−18.9 (0.4)	−42.0 (0.5)	−42.9 (0.5)	−42.2	−44.5
C1—C2—C3—C4	−111.7 (1.8)	−116.2 (3.6)	−109.5	−124.0 (3.1)	118.9 (6.1)	−109.5 (1.8)	−112.1	−109.5
C1—C15—C14—C13	−111.5 (1.6)	−108.6 (3.8)	−111.9	−108.0 (5.0)	116.4 (7.3)	−109.4 (3.7)	−112.0	−111.9
C3—C8—C9—C14	−58.2 (1.4)	−58.3 (1.8)	−58.2	−58.4 (0.5)	−58.1 (2.8)	−59.2 (2.2)	−48.7	−58.8
C7—C8—C9—C10	−62.2 (2.5)	−62.2 (0.9)	−62.2	−62.2 (0.8)	−62.5 (2.1)	−63.6 (5.0)	−48.6	−63.0

[a]These data represent the minimum energy conformations for **1–6**. The data for **1′** and **2′** were calculated to reproduce the conformations observed for **1***a* and **2***b*.
[b]Difference with respect to **1***b*.
[c]Difference with respect to **1***a*.
[d]Difference with respect to **2***b*.
[e]Difference with respect to crystal structure **3**.
[f]Difference with respect to crystal structure **4**.

Can. J. Chem. Downloaded from www.nrcresearchpress.com by 213.200.69.106 on 09/08/12
For personal use only.

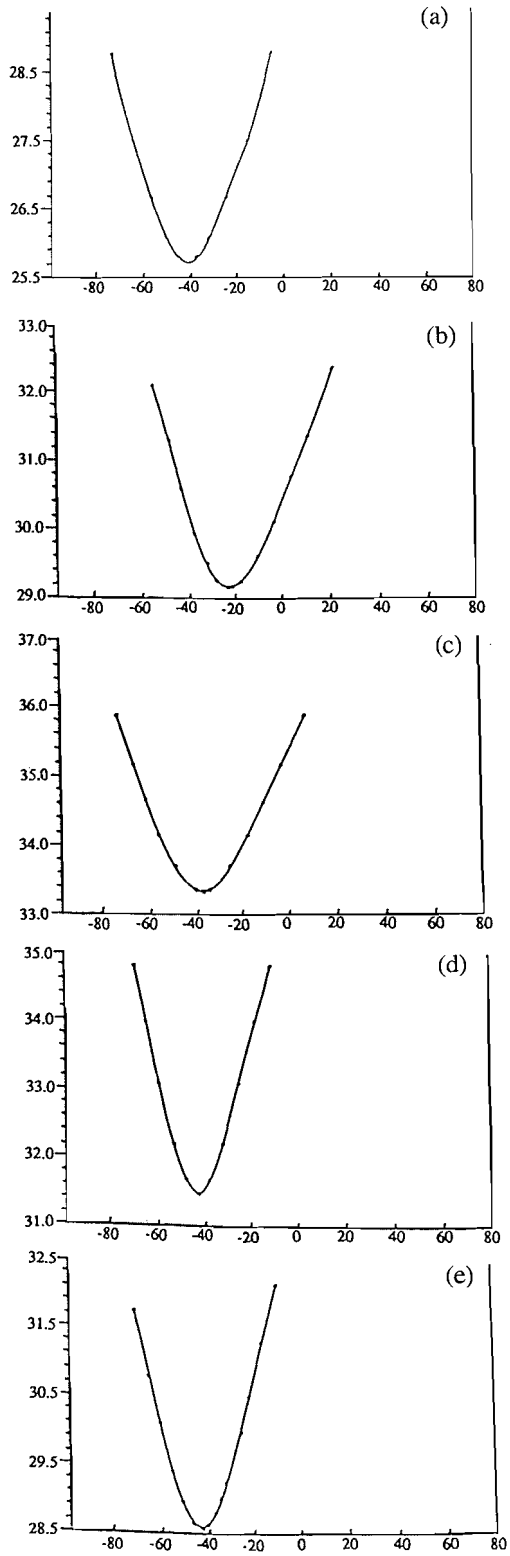

FIG. 5. A plot of energy (kcal/mol) versus the torsional angle (deg) at C15—C1—C2—C3 for **1**, **2**, **3**, **4**, and **6**(*a*–*e*).

minimum energy conformations as calculated by MMX. The difference between the calculated angles and the experimental angles in Table 1*a* appear in parentheses.

For **1**–**4** we calculated the variation in energy over a 40° range in the dihedral angle at C1—C2. For **1** the results are plotted in Fig. 5*a*. The curve shows the calculated energy difference between **1***a* and **1***b* to be 0.9 kcal/mol.[7] The calculated energy well is relatively shallow, thereby allowing some change in the conformation of **1** with a change in its position in the unit cell.

The two distinct structures found in the unit cell of **2** are both asymmetric. They have similar conformations in which the C15—C1—C2—C—3 torsional angle is increased 21° and 23° from that in **1***b*. The most stable conformation for **2** as calculated by MMX is similar to each of those found in the solid state. The energy dependence of **2** versus dihedral angle is plotted in Fig. 5*b*. The calculated energy change for conversion of the minimum energy form to either observed crystal conformation is only 0.1 kcal/mol, which accounts for the occurrence of two forms for **2** in the solid state.

The plots of energy versus dihedral angle for **3**, **4**, and **6** appear in Figs. 5*c*, 5*d*, and 5*e*. It is evident that the strain in **3** has caused it to be more flexible than either **4** or **6**.

In Table 4, agreement between the calculated and experimental dihedral angles about C1—C2 is within 1° for **1**, **2**, and **4** and within 3° for **1***a* and **3**. Larger differences are found for the angles involving a proton, presumably due to the less accurate experimental data. There are differences of over 5° in several of the angles involving carbons of the aromatic ring. The MMX calculations are apparently less accurate in this area, though the reason for this is not clear.

The van der Waals' radius of a benzene ring

In **2** and **3** the distance between the aromatic ring and the hydrogens of the axial methyl group could be determined from the crystallographic data. One of the methyl protons (H18A) of **2** was found to be very close to the distal ring, as indicated by the following spatial relations. The distances from H18A to C9, C10, and C14 were 2.56, 2.86, and 2.93 Å, respectively. Such proximity even after rotation by 24° is surprising. In **3** the distance between either of the axial methyl protons H18A and the carbons C9, C10, and C14 or H19A and C8, C7, and C3 of the distal benzene showed similar values. All these distances are summarized in Table 5 along with the data provided from the MMX calculations. For any of the axial methyls the distance of closest approach[8] is between 2.54 and 2.73 Å, which is significantly less than the estimated sum of the van der Waals' distances (3.05 Å) for a hydrogen and an aromatic ring (17). It appears that some strain has been relieved in **3** as reflected in a slightly larger internal angle for C3—C2—Me (vide supra). The data to be presented later for epimerization of **2** and **3** to the more stable equatorial isomers reveal much greater residual strain in **3**. Since the repulsive portion of a van der Waals' curve is steep, the above observed distance of approach (2.6 Å) very likely represents its min-

[7]This calculated difference does not include any effects of entropy. It is noteworthy that **1***a* is statistically favoured over **1***b* by the factor R ln 2, which reduces the free energy difference to 0.5 kcal/mol.

[8]This distance is normally considered to be the most reliable estimate for the sum of the van der Waals' radii for two contiguous atoms. Any example of distance less than the accepted minimum is then considered as evidence for the presence of a bonding interaction (16). In certain situations this distance may require a modification to include the effects of attractive intramolecular interactions (ref. 16, p. 41).

TABLE 5. Selected proton–carbon distances (Å) obtained from crystalline structure and calculated by MMX (in parentheses)

	1*a*	1*b*	2*a*	3	4
C2H—C9	2.80	2.78 (2.72)			2.58 (2.57)
—C14	2.95	2.84 (2.89)			2.66 (2.75)
—C8	2.77	2.80 (2.80)			2.66 (2.70)
C15H—C8	2.61	2.78 (2.72)			2.51 (2.57)
—C3	2.65	2.84 (2.89)			2.70 (2.75)
—C9	2.73	2.80 (2.80)			2.63 (2.70)
C18MeH(A)—C9			2.56 (2.61)	2.73 (2.55)	
—C10			2.86 (2.91)	2.93 (2.78)	
—C14			2.93 (2.94)	2.64 (2.80)	
C19MeH(A)—C8				2.54 (2.55)	
—C3				2.82 (2.78)	
—C7				2.86 (2.80)	

TABLE 6. The energies (kcal/mol) of diastereoisomers calculated by MMX and their energy differences determined by equilibration (in parentheses)

2	29.16	**3**	33.33
6	28.59	**7**	31.94
$\Delta E_{2,6}$	0.57 (1.2 ± 0.1)[a]	**4**	31.48
		$\Delta E_{3,4}$	1.9 (2.2 ± 0.4)[b]
		$\Delta E_{4,7}$	0.5 (0.90 ± 0.1)[b]

[a]Methanol used as the solvent.
[b]Tetrahedrofuran used as the solvent.

imum. Consequently, the presently accepted value for one half of the thickness of a benzene ring of 1.85 Å (17) appears to be too large when the approaching atom is hydrogen.[9] There are some recent data in support of this proposal. Ab initio calculations regarding the interaction of a proton of a water molecule in a vertical approach to the center of the benzene ring found the energy minimum at 2.5 Å. For the vertical approach of one benzene towards another the minimum occurred at 2.4 Å (18) although more recent theoretical estimates report this distance to be larger (19, 20). A recent X-ray study of an inclusion complex, in which an aromatic guest is oriented perpendicular to one aromatic ring of the host, measures the distance between the guest proton and the plane of the host ring to be 2.7 Å (21).

Comparison of conformational properties; MMX versus experiment

Although we were unable to obtain a crystalline sample of **6**, the monoequatorial epimer of **2**, we investigated its conformational properties by MMX. These are described through its torsional angles and energy profile given in Table 4 and Fig. 5*e*. The calculations indicate that the equatorial conformer is more stable than its epimer **2** by 0.6 kcal/mol. This energy difference, which is for the vapor phase, is in reasonable agreement with the experimental value of 1.2 kcal/mol measured in methanol (see Table 6).

Calculations have also been carried out for the α-axial, α-equatorial dimethyl derivative **7**. Table 5 reports its energy relative to **3** and **4** along with the experimental values obtained from the proportions measured at equilibrium in tetrahydrofuran. The close correspondence between the calculated energy differences and the experimental values provides support for the reliability of the energy data obtained from MMX.

Finally, calculation of the minimum energy structure for the ketone **5** yielded a value of 49° for the dihedral angle between the rings, similar to that calculated earlier by Mislow and co-workers (14).

*Comparison of **1** with cyclohexanone **8** for use as stereochemical models*

The most important property of a hydrocarbon skeleton when used to test stereoelectronic effects is its ability to provide derivatives of known fixed stereochemistry. This follows from the fact that the maximum observable magnitude of any identifiable effect is limited by the energy requirement for skeletal distortion. Figures 6*a* and *b* describe the energies required for ring distortion in **1** and **8**.[10] These show a significant difference. A 40° change in dihedral angle from its ground state requires 1.3 and 0.85 kcal/mol of energy for **1** and **8**, respectively. The curve for the methyl derivative **9** can be seen in Fig. 6*c* and indicates still greater flexibility. Thus all of these curves indicate the ring skeleton in **1** to be more rigid than that of cyclohexanone, yet possessing some degree of flexibility. In addition, **1** offers simpler spectral properties while **8** provides more easily accessible derivatives. The differing symmetry characteristics of the two cyclic ketones complement one another.

Conclusion

The crystal structures for **1–4** establish their ground state conformational properties. The axial methyl groups in **2** and **3** are oriented antiperiplanar to the distal lobe of the carbonyl, as was earlier claimed (3). MMX calculations provide a quantitative measure of the rigidity of the central ring. The calculated energy difference between epimers is supported by equilibration experiments. A comparison of the data for

[9]Errors in determining the position of the hydrogen preclude any quantitative estimate of this thickness.

[10]The barrier to ring inversion by MMX is seen to be 3.8 kcal/mol, in agreement with earlier calculations (9) and nmr measurements (22).

Can. J. Chem. Downloaded from www.nrcresearchpress.com by 213.200.69.106 on 09/08/12
For personal use only.

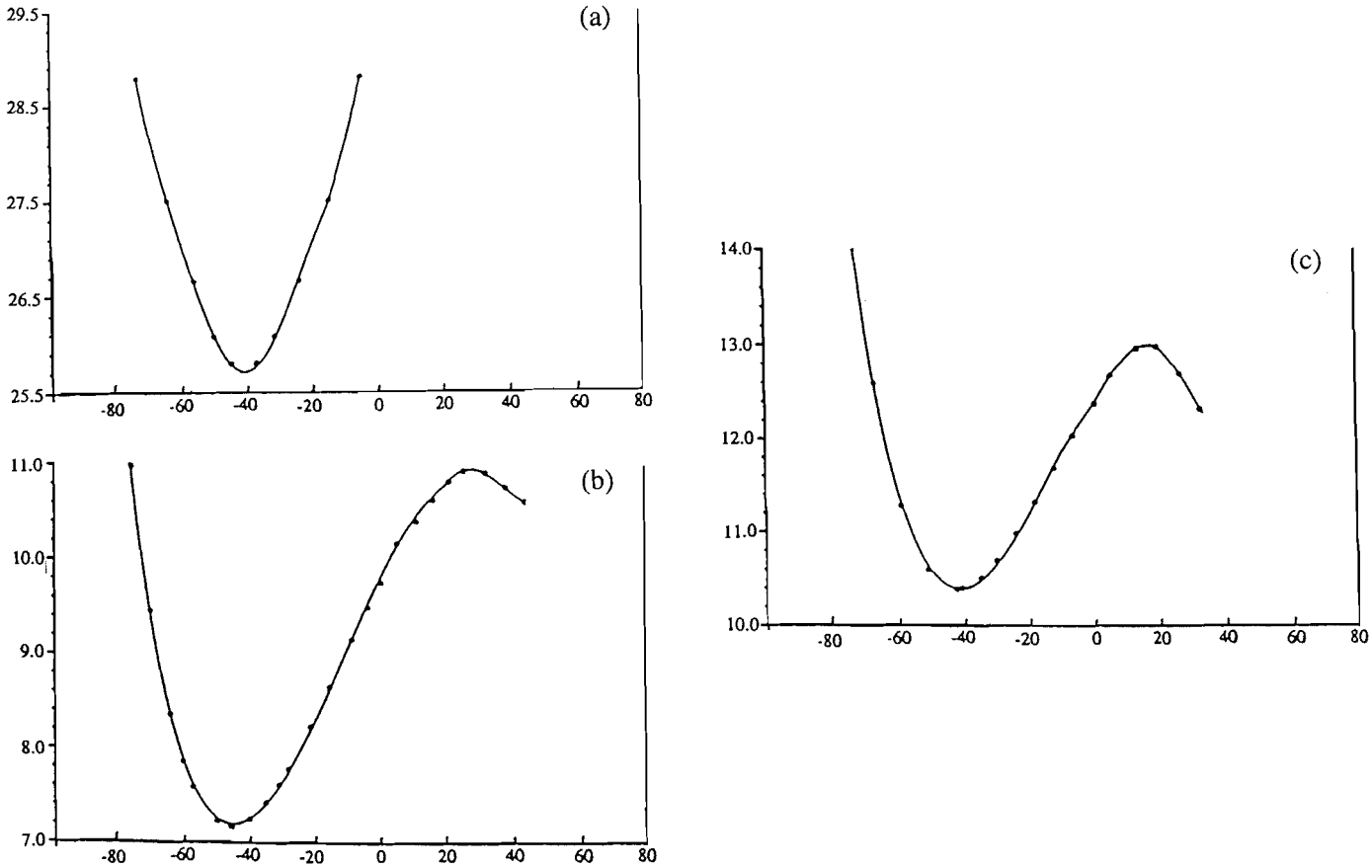

FIG. 6. A plot of energy (kcal/mol) versus the torsional angle (deg) for the biaryl ketone **1** (*a*), cyclohexanone **8** (*b*), and axial methyl cyclohexanone **9** (*c*).

TABLE 7. Selected bond lengths (Å)

	1*a*	**1***b*	**2***a*	**2***b*	**3**	**4**
C1—O1	1.210 (4)	1.242 (6)	1.218 (5)	1.223 (6)	1.212 (8)	1.203 (6)
C1—C2	1.519 (5)	1.536 (4)	1.502 (6)	1.506 (7)	1.555 (16)	1.522 (7)
C2—C3	1.507 (5)	1.502 (5)	1.504 (6)	1.516 (7)	1.502 (11)	1.515 (5)
C1—C15	1.515 (5)	1.536 (4)	1.533 (7)	1.520 (7)	1.529 (15)	1.532 (7)
C15—C14	1.515 (5)	1.502 (5)	1.490 (7)	1.533 (6)	1.498 (12)	1.528 (7)
C2—R_a			1.529 (7)	1.525 (7)	1.531 (13)	
C2—R_e						1.523 (7)
C15—R'_a					1.569 (13)	
C15—R'_e						1.531 (8)
C8—C9	1.502 (4)	1.501 (6)	1.521 (6)	1.504 (6)	1.483 (11)	1.486 (4)
C7—C16	1.516 (5)	1.509 (5)	1.528 (7)	1.526 (7)	1.543 (14)	1.517 (6)
C10—C17	1.501 (4)	1.509 (5)	1.498 (7)	1.503 (7)	1.516 (14)	1.499 (8)

1 and **8** indicates that the former possesses greater rigidity for use as a stereochemical model. Observations of the distance between protons of an axial methyl and the π cloud of the neighbouring aromatic ring suggest the currently accepted thickness of a benzene ring (17) is too large.

Experimental

Compound **1** was synthesized according to the literature (1). Recrystallization from ether–hexanes gave a suitable single crystal. Compounds **2**, **3**, and **4** were synthesized according to the reported method (4), and recrystallization from hexanes afforded suitable crystals for X-ray determination.

A summary of the crystal data for compounds **1–4** is given in Table 1.[11] Selected bond lengths and bond angles are given in

[11]Tables of all bond lengths, bond angles, atomic coordinates, mean plane data, anisotropic parameters, and structure factors for **1**, **2**, **3**, and **4** may be purchased from: The Depository of Unpublished Data, Document Delivery, CISTI, National Research Council Canada, Ottawa, Canada K1A 0S2.

Tables of bond lengths, bond angles, and atomic coordinates have also been deposited with the Cambridge Crystallographic Data Centre and can be obtained on request from The Director, Cambridge Crystallographic Data Centre, University Chemical Laboratory, 12 Union Road, Cambridge, CB2 1EZ, U.K.

Can. J. Chem. Downloaded from www.nrcresearchpress.com by 213.200.69.106 on 09/08/12
For personal use only.

TABLE 8. Selected bond angles (deg)

	1*a*	1*b*	2*a*	2*b*	3	4
C15—C1—C2	115.3 (3)	117.0 (4)	116.7 (4)	115.1 (4)	119.5 (7)	117.1 (4)
C15—C1—O1	123.2 (3)	121.5 (2)	121.9 (4)	120.7 (4)	119.5 (9)	121.3 (5)
C2—C1—O1	121.5 (3)	121.5 (2)	121.4 (4)	119.7 (4)	121.0 (9)	121.6 (5)
C1—C2—C3	114.8 (3)	111.3 (3)	115.7 (4)	115.1 (4)	111.2 (7)	110.6 (4)
C1—C2—R_a			112.1 (4)	110.6 (4)	110.8 (8)	
C1—C2—R_e						110.5 (5)
C3—C2—R_a			111.4 (4)	111.3 (4)	117.4 (8)	
C3—C2—R_e						117.2 (4)
C1—C15—C14	108.3 (3)	111.3 (3)	106.8 (4)	106.3 (4)	113.1 (8)	109.8 (4)
C1—C15—R'_a					109.7 (8)	
C1—C15—R'_e						110.2 (5)
C14—C15—R'_a					115.2 (8)	
C14—C15—R'_e						118.1 (6)

Tables 7 and 8, respectively. The diffraction intensities were collected on a Rigaku diffractometer at 295 K with MoKα radiation (λ = 0.7093 Å) using the θ/2θ scan technique with profile analysis (23). The standards were measured after every 150 reflections; no crystal decay was noticed. The space group was determined by systematic absence. Unit cell parameters were obtained by least-squares refinement of the setting angle for 25 reflections ($40° < 2\theta < 47°$ for **2**, **3**, **4** and $40° < 2\theta < 50°$ for **1**). Lorentz and polarization factors were applied but no corrections were made for absorption.

For compounds **1** and **4** all the hydrogens were found by difference Fourier map. For compounds **2** and **3**, most of the hydrogens were found by difference Fourier map and the rest were calculated. All the calculations were performed with the NRCVAX Crystal Structure Package (24).

Molecular mechanics calculations were performed using the MMX program embedded in the PCMODEL 4.1 (footnote 6) on an IBM-386. The dielectric constant used throughout the calculations was 1.50. Each calculated total energy consisted of stretching, bending, stretching–bending, torsional, van der Waals, and dipole–dipole contributions.

Equilibration of **2** and **6** was carried out by treating a 3 mg sample of either compound in THF (4 mL) with 3 mg of sodium methoxide at room temperature for 24 h. The mixture of **2** and **6** after neutralization and isolation was analysed by 300 MHz ^{1}H NMR. The integral ratio for the two well-resolved methyl doublets for **2** and **6** at δ 0.80 and 1.34, respectively, gave the value of 2.0 ± 0.1 for the equilibrium constant. The equilibrium distribution between **3**, **4**, and **7** was similarly determined. The results appear in Table 5.

Acknowledgment

We wish to thank the Natural Sciences and Engineering Research Council of Canada for their financial support.

1. K. Mislow, M. A. W. Glass, R. E. O'Brien, P. Rutkin, D. H. Steinberg, J. Weiss, and C. Djerassi. J. Am. Chem. Soc. **84**, 1455 (1962).
2. K. Mislow and A. J. Gordon. J. Am. Chem. Soc. **85**, 3521 (1963).
3. R. R. Fraser and P. J. Champagne. Can. J. Chem. **54**, 3809 (1976).
4. R. R. Fraser and M. Stanciulescu. J. Am. Chem. Soc. **109**, 1580 (1987).
5. R. R. Fraser, F. Kong, M. Stanciulescu, Y. Wu, and K. Houk. J. Org. Chem. Submitted.
6. D. H. R. Barton. Top. Stereochem. **6**, 1 (1971).
7. E. L. Eliel, N. L. Allinger, S. J. Angyal, and G. A. Morrison. Conformational analysis. Interscience, New York. 1967.
8. J. Sandstrom. Dynamic NMR spectroscopy. Academic Press, London. 1982.
9. N. L. Allinger, K. Chen, M. Rahman, and A. Pathiaseril. J. Am. Chem. Soc. **113**, 4505 (1991).
10. A. Lectard, A. Lichanot, F. Metras, J. Gaultier, and C. Houw. J. Mol. Struct. **34**, 113 (1976).
11. J. B. Lambert, R. E. Carhart, and P. W. R. Corfield. J. Am. Chem. Soc. **91**, 3567 (1969).
12. J. D. Dunitz and J. Waser. J. Am. Chem. Soc. **94**, 5645 (1972).
13. M. Oki, H. Iwamura, and G. Yamamoto. Bull. Chem. Soc. Jpn. **44**, 262 (1971).
14. M. A. W. Glass, K. Mislow, H. B. Hopps, E. Simon, and G. H. Wahl, Jr. J. Am. Chem. Soc. **86**, 1710 (1964).
15. J. J. Gajewski, K. E. Gilbert, and J. McKelvey. Adv. Mol. Model. **2**, 65 (1990).
16. U. Burkert and N. L. Allinger. Molecular mechanics. ACS Monograph 177. 1982.
17. J. D. Dunitz. X-ray analysis and the structure of organic molecules. Cornell University Press, Ithaca and London. 1979. p. 339.
18. G. Karlstrom, P. Linse, A. Wallqvist, and B. Jonsson. J. Am. Chem. Soc. **105**, 3777 (1983).
19. P. Linse. J. Am. Chem. Soc. **114**, 4366 (1992).
20. W. L. Jorgensen and D. L. Severance. J. Am. Chem. Soc. **112**, 4768 (1990).
21. J. E. Cochran, T. J. Parrott, B. J. Whitlock, and H. W. Whitlock. J. Am. Chem. Soc. **114**, 2270 (1992).
22. F. A. L. Anet, G. N. Chmurny, and J. Krane. J. Am. Chem. Soc. **95**, 4423 (1973).
23. D. F. Grant and E. J. Gabe. J. Appl. Crystallogr. **11**, 114 (1978).
24. E. J. Gabe, F. L. Lee, and Y. Lepage. J. Appl. Crystallogr. **22**, 284 (1989).

Can. J. Chem. Downloaded from www.nrcresearchpress.com by 213.200.69.106 on 09/08/12
For personal use only.

Transannular Diels–Alder reactions on 14-membered macrocyclic trienes. Part I: stereoselective syntheses of the macrocyclic trienes precursors

ALEXIS NDIBWAMI, SERGE LAMOTHE, DANIEL GUAY, RAYMOND PLANTE, PIERRE SOUCY, SOLO GOLDSTEIN, AND PIERRE DESLONGCHAMPS[1]

Laboratoire de synthèse organique, Département de chimie, Faculté des sciences, Université de Sherbrooke, Sherbrooke (Québec), Canada J1K 2R1

Received November 16, 1992

ALEXIS NDIBWAMI, SERGE LAMOTHE, DANIEL GUAY, RAYMOND PLANTE, PIERRE SOUCY, SOLO GOLDSTEIN, and PIERRE DESLONGCHAMPS. Can. J. Chem. **71**, 695 (1993).

Transannular Diels–Alder reactions on 14-membered macrocycles containing properly located diene and methyl-substituted dienophile units lead to A.B.C.[6.6.6] tricycles related to steroids. To study the influence of the olefin and diene geometry on the stereochemical outcome of the Diels–Alder reaction it was necessary to prepare macrocyclic trienes of well-defined stereochemistry. Eight different types of macrocyclic trienes might be obtained by the coupling of appropriate dienophiles and dienes, namely, TTC, TTT, TCC, TCT, CTC, CTT, CCC, and CCT. In this paper (first in a series of two), the synthesis of appropriately functionalized dienophile and diene synthons, as well as their coupling reaction affording macrocyclic triene precursors, is described.

ALEXIS NDIBWAMI, SERGE LAMOTHE, DANIEL GUAY, RAYMOND PLANTE, PIERRE SOUCY, SOLO GOLDSTEIN et PIERRE DESLONGCHAMPS. Can. J. Chem. **71**, 695 (1993).

Les macrocycles à 14 chaînons contenant en positions appropriées un diène et un diénophile portant un substituant méthyle, fournissent par une réaction de Diels–Alder transannulaire des tricycles A.B.C.[6.6.6] apparentés aux stéroïdes. Afin d'étudier l'influence de la géométrie du diène et du diénophile, il était nécessaire de préparer des triènes macrocycliques de stéréochimie bien définie. Huit types de ces triènes peuvent être obtenus par le couplage de différents diènes et diénophiles, à savoir TTC, TTT, TCC, TCT, CTC, CTT, CCC et CCT. Dans cet article (le premier dans une série de deux) on décrit la synthèse des synthons diène et diénophile fonctionnalisés de manière adéquate ainsi que leur réaction de couplage générant les précurseurs de triènes macrocycliques.

Can. J. Chem. Downloaded from www.nrcresearchpress.com by 213.200.69.106 on 09/08/12
For personal use only.

Among the various synthetic methods available for the construction of complex carbocyclic skeletons (1) the transannular Diels–Alder reaction on macrocycles developed in our laboratory shows enormous synthetic potential. As recently pointed out, this novel methodology allows a particularly easy, convergent, and predictable stereoselective entry to polycyclic structures related to steroids and terpenes (2).

The case of 14-membered macrocyclic trienes containing various geometrical isomers of the diene and methyl-substituted dienophile moieties was illustrated in our recent papers (3). As outlined below in a general manner (Scheme 1), these macrocycles leading to A.B.C.[6.6.6] tricycles related to steroids were obtained by the cyclization of appropriate acyclic trienes, which in turn were assembled from the different geometrical isomers of the diene and dienophile synthons using dimethyl malonate connectors.

To study the influence of olefin and diene geometry on the stereochemical outcome of the transannular Diels–Alder reaction, it was necessary to prepare the macrocyclic trienes from stereochemically well-defined acyclic precursors.

The geometry of the dienophile might be either *cis* (C) or *trans* (T), while the diene moiety might possess a *trans-trans* (TT), *trans-cis* (TC), *cis-trans* (CT), or *cis-cis* (CC) arrangement; coupling of the diene and dienophile synthons will therefore lead to eight possible macrocyclic trienes, namely, *trans-trans-cis* (TTC), TTT, TCC, TCT, CTC, CTT, CCC, and CCT, the three letters referring to unsaturations at C5, C3, and C11, respectively (cf. Scheme 1).

The synthesis of the appropriately functionalized dienophile and diene synthons as well as their coupling reaction leading to the corresponding macrocyclic triene precursors is described in the present paper.

[1]Author to whom correspondence may be addressed.

Synthesis of dienes

The preparation of the requisite dienes (all geometrical isomers) is outlined in Scheme 2. Syntheses were planned to place, at appropriate positions, a leaving group or precursors thereof to be used later in the coupling with the dienophile synthon.

Diene ester **2** (*trans-trans*) was prepared as previously described (4) starting with commercially available *cis*-2-butene-1,4-diol, which was monoprotected (5) and then oxidized with pyridinium chlorochromate to the corresponding *trans* aldehyde (6), which was further reacted with the anion derived from ethyl diisopropyl phosphonoacetate. The *trans-trans* geometry could be easily established by virtue of the coupling constant (J = 15.3 Hz) observed for the vinylic protons in the ^{1}H nmr spectrum of the compound (4). Reduction of the ester function using two equivalents of diisobutyl aluminium hydride (8) gave the corresponding alcohol **3**, in 96% yield, which was quantitatively[2] transformed into the *trans-trans* allylic chloride **4** (LiCl, CH_3SO_2Cl, *s*-collidine, DMF) (9). The above allylic chloride was employed as such for the subsequent steps.

The remaining dienes were also prepared from the same starting material (Scheme 2). Thus, Swern oxidation (10) of alcohol **1** at −78°C afforded *cis* aldehyde **5**, which was reacted in tetrahydrofuran (THF) at low temperature with the carbanion (NaH) derived from methyl bis(trifluoroethyl)-phosphonoacetate, a reagent known to produce selectively *Z*-unsaturated esters (11). In our case the reaction products, *cis-cis* diene ester **6** and *trans-cis* diene ester **7**, were obtained in a 85:15 ratio (68% overall yield from alcohol **1**). This selectivity did not change when either sodium hydride and a crown ether or potassium hexamethyldisilazide were

[2]Lower yields of **4** were obtained after attempted purification by chromatography due to decomposition.

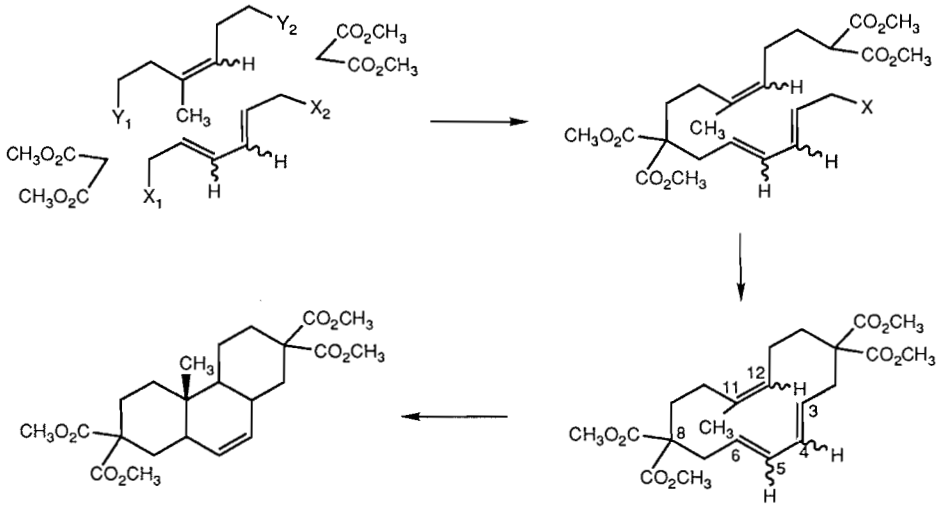

SCHEME 1

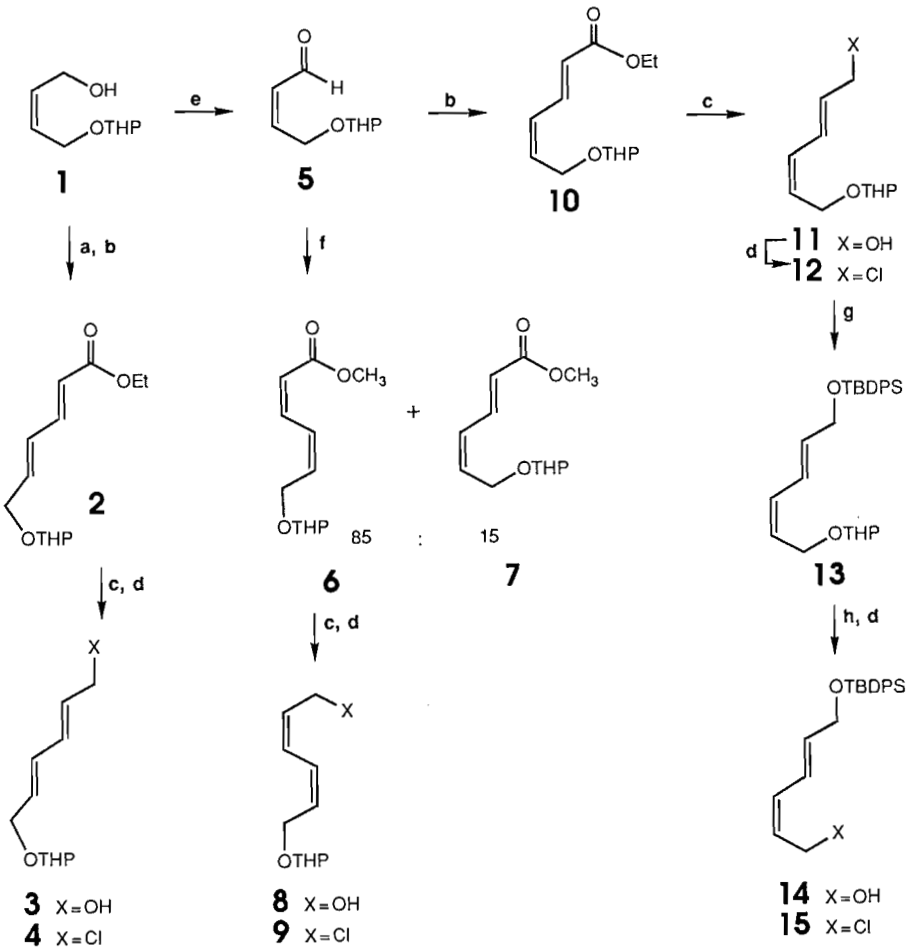

(a) PCC, CH_3CO_2Na, CH_2Cl_2, 0°C;
(b) NaH, THF, $((CH_3)_2CHO)_2POCH_2CO_2Et$;
(c) DIBAL-H, CH_2Cl_2, -78°C;
(d) LiCl, CH_3SO_2Cl, *s*-collidine, DMF;
(e) DMSO, $(COCl)_2$, CH_2Cl_2, -78°C;
(f) NaH, THF, $(CF_3CH_2O)_2POCH_2CO_2CH_3$, -78°C;
(g) *t*-Bu$(Ph)_2SiCl$, imidazole, DMF;
(h) 80% AcOH, 40°C.

SCHEME 2. Diene syntheses.

Can. J. Chem. Downloaded from www.nrcresearchpress.com by 213.200.69.106 on 09/08/12
For personal use only.

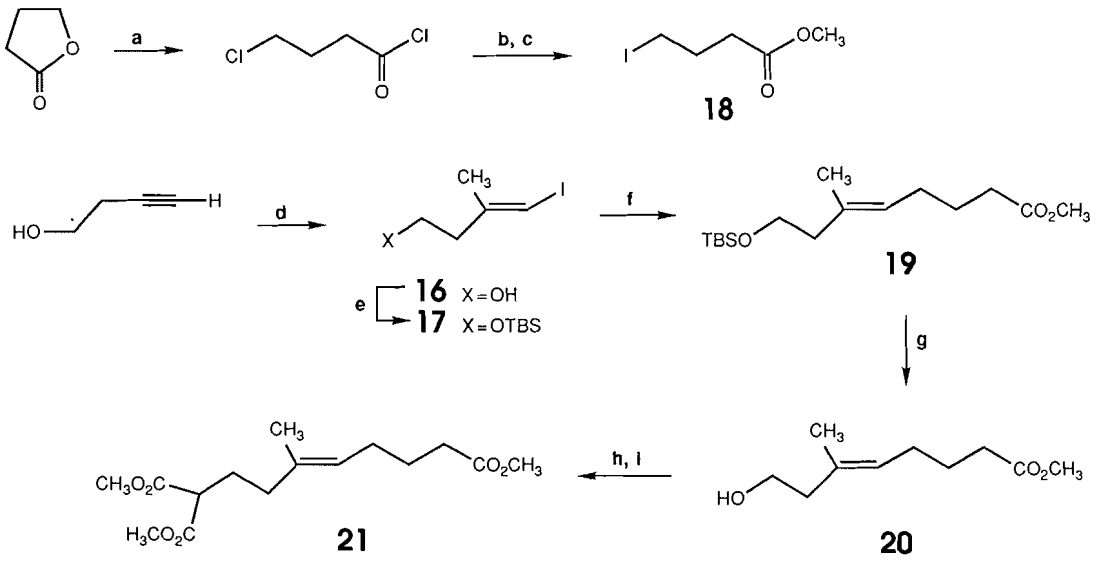

(a) $SOCl_2$, $ZnCl_2$, Δ;
(b) CH_3OH, pyridine, Δ;
(c) NaI, acetone, Δ;
(d) (i) $(CH_3)_3Al$, $Cl_2Zr(Cp)_2$, $(CH_2Cl)_2$, 0°C to r.t.; (ii) I_2/THF, -40°C to 0°C;
(e) *t*-$Bu(CH_3)_2SiCl$, Et_3N, DMAP, CH_2Cl_2, r.t.;
(f) (i) Zn(Cu), $C_6H_6/CH_3CON(CH_3)_2$, **18**, 60°C; (ii) $[(C_6H_5)_3P]_4Pd$, C_6H_6, **17**, 60°C;
(g) Bu_4NF, THF, r.t.;
(h) CH_3SO_2Cl, Et_3N, CH_2Cl_2, 0°C;
(i) NaH, $CH_2(CO_2CH_3)_2$, KI, DMF/THF, 95°C.

SCHEME 3. Preparation of *trans* dienophiles.

used to form the phosphonate anion (11). The above compounds were readily separated by column chromatography on silica gel and their ^1H nmr spectra were found to be consistent with the indicated structures. Diene ester **6** was transformed into alcohol **8** (76% crude) and then into allylic chloride **9** in the same manner as described for **3** and **4**.

On the other hand, an Emmons–Horner reaction performed on crude *cis* aldehyde **5** using the anion derived from ethyl diisopropylphosphonoacetate (12) led to protected *trans-cis* diene ester **10** in 68% overall yield from alcohol **1**, after flash chromatography on silica gel. The stereochemistry of the double bonds could be again secured via ^1H nmr spectra, which show coupling constants of 11.7 Hz and 15.3 Hz for the corresponding *cis* and *trans* vinylic protons. As before, reduction of the ester function led to allylic alcohol **11** in 91% yield after flash chromatography. This compound was then transformed, using the Collington Meyers protocol (9), into chlorodiene **12** (~100% crude yield).

Furthermore, protection of alcohol **11** (*tert*-butyldiphenyl silyl chloride, imidazole, dimethylformamide) (13) followed by selective cleavage of the tetrahydropyranyl ether (80% acetic acid) (14) afforded, after purification by flash chromatography, *cis-trans* diene alcohol **14** in 48% overall yield. The corresponding allylic chloride was obtained by the usual procedure, in 82% yield, after flash chromatography.

Thus all the desired diene isomers could be obtained from a common starting material using appropriate reagents and reaction conditions.

Synthesis of dienophiles

The synthesis of the *trans* dienophile building block **21** (Scheme 3) started with the preparation of the known vinyl iodide **16**, which was obtained in 92% crude yield by a zirconium-catalyzed carboalumination of homopropargyl alcohol followed by iodinolysis (15). The alcohol function was protected (16) to afford the silyl derivative **17** in 90% yield after flash chromatography. Palladium-catalyzed cross coupling (17*a*, *b*) with 3-carbomethoxypropylzinc iodide obtained from iodoester **18**[3] then afforded *trans* olefin **19**[4] in 75% yield after flash chromatography. Cleavage of the silyl ether (Bu_4NF, THF) afforded alcohol **20**, which was transformed into its mesylate (CH_3SO_2Cl, Et_3N, CH_2Cl_2), followed by displacement, in the presence of potassium iodide, with the anion derived from dimethyl malonate to afford triester **21** in 85% yield after flash chromatography.

The synthesis of the *cis*-dienophile building block **27** is outlined in Scheme 4. Thus, reduction of 3-methylanisole (Li/NH_3, EtOH) (18), at −78°C, led to **22** in 92% yield. Ozonolysis of **22** followed by reduction (O_3, $(CH_3)_2S$, CH_2Cl_2/CH_3OH; $NaBH_4$, EtOH) (19) afforded hydroxy ester **23** in about 50% yield. Protection of the alcohol function (20) gave silyl derivative **24** (96% after flash chromatography) whose ester function was then reduced to afford alcohol **25** ($LiAlH_4$, Et_2O, 97%). Crude alcohol **25** was transformed into its mesylate (99% yield), which was reacted without further purification with the anion derived from

[3]Iodo-ester **18** could be obtained on a large scale from the reaction of γ-butyrolactone with thionyl chloride in the presence of zinc chloride to afford 4-chlorobutyryl chloride, which was transformed into the corresponding methyl ester (pyridine, MeOH) (17*c*) and then to **18** (NaI, acetone, reflux) in 46% overall yield.

[4]About 5% of the corresponding *cis* isomer was detected by gas chromatography.

Can. J. Chem. Downloaded from www.nrcresearchpress.com by 213.200.69.106 on 09/08/12
For personal use only.

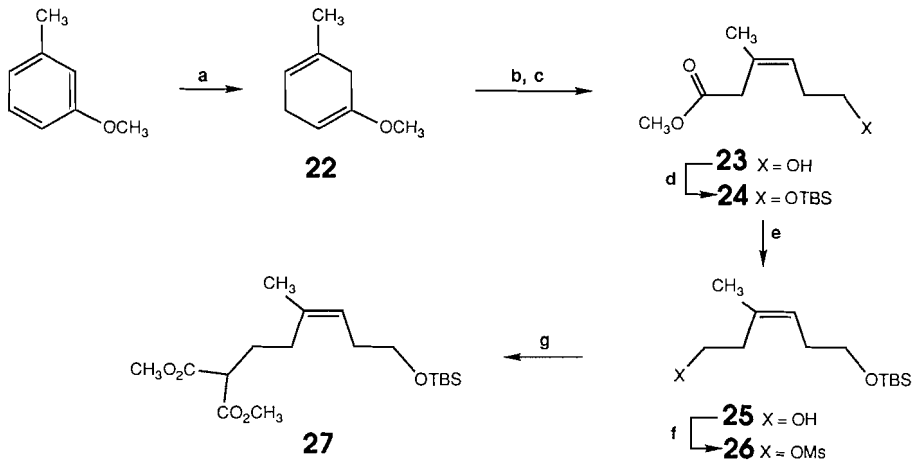

(a) Li, NH_3, EtOH, -78°C;
(b) O_3, CH_3OH/CH_2Cl_2 then $(CH_3)_2S$, -78°C;
(c) EtOH, $NaBH_4$, -78°C;
(d) *t*-Bu$(CH_3)_2$SiCl, Et_3N, DMAP, CH_2Cl_2, r.t.;
(e) $LiAlH_4$, ether;
(f) CH_3SO_2Cl, Et_3N, CH_2Cl_2;
(g) $CH_2(CO_2CH_3)_2$, NaH, KI, DMF-THF, 85°C.

SCHEME 4. Preparation of *cis* dienophile.

dimethyl malonate (*vide supra*) to afford *cis* dienophile **27** in 81% yield. Consistent with the olefin geometry, the methyl protons were observed in the ^1H nmr spectra as a singlet at 1.69 ppm in the case of **27** and as a doublet (J = 1.2 Hz) at 1.58 ppm in the case of **21**. The patterns observed for the vinylic proton in the two compounds are also in accord with the respective *cis* and *trans* stereochemistry (see experimental). Next, the assembling of acyclic trienes via coupling of the different diene and dienophile building blocks was undertaken.

Synthesis of acyclic trienes

TTC, CTC, TCC, and CCC trienes (Scheme 5)

Reaction of allylic chloride **4** with the anion derived from **27** (NaH, THF/DMF) occurred at room temperature to afford acyclic triene **28** in 80% yield. Selective cleavage of the silyl ether (Bu_4NF, THF) (20) led to alcohol **29** in 87% yield after chromatography. The introduction of a second malonate unit was performed starting with alcohol **29**, in the same manner as described for **27**, to obtain, after flash chromatography, tetraester **30** in 79% yield. Finally, cleavage of the tetrahydropyranyl ether (PPTS, CH_3OH) (21) at room temperature afforded the TTC triene **31** in 77% yield after chromatography.

Preparation of CTC trienes required the coupling of a *cis* olefin with a *cis-trans* diene. Thus, coupling of **27** with diene **15** by the above-mentioned procedure led to disilylated triene **32** (88% yield). Selective cleavage of the *tert*-butyldimethylsilyl ether (PPTS, iPrOH, 70°C) (22)[5] afforded the corresponding alcohol **33** in 90% yield. CTC triene **36** could then be obtained using our standard procedure involving mesylation, displacement with the anion derived from dimethyl malonate, and cleavage of the remaining silyl ether (~68% yield for the three steps). TCC triene **40** and CCC triene **44** were obtained in a similar manner, by first coupling olefin **27** with either diene **12** or diene **9**, respectively.

[5]Also, L. Ruest, unpublished results.

CTT, TCT, CCT, and TTT trienes (Scheme 6)

For this series of trienes, *trans* olefin **21** was employed in the coupling step. Thus, displacement of the allylic chloride in **15** by the usual method furnished triester **45** in 84% yield. The lithium-diisopropylamide-generated enolate of **45** (23) was then trapped with methyl chloroformate, giving **46** in 74% yield, which, following the usual deprotection procedure, afforded CTT triene **47** (72% yield).

TCT triene **48** was obtained in 77% yield by alkylation of the malonate anion derived from **21** with allylic chloride **12**. Generation of the second malonate unit as described above afforded **49** (42% yield), which led to TCT triene **50** by deprotection of the alcohol function. CCT triene **53** and TTT triene **56** were obtained in an analogous manner by first coupling **21** with either CC diene **9** or TT diene **4**, respectively.

To examine the influence of steric interactions due to one of the esters in position 8 (cf. Scheme 1) on the course of the Diels–Alder reaction of TCC and TCT macrocyclic trienes (see following paper in this series), it was necessary to prepare such compounds bearing only one ester in this position. Therefore, the corresponding acyclic triene precursors were synthesized along the lines depicted in Scheme 7.

Thus, diester **38** was decarbalkoxylated (NaCN, DMSO) (24), giving triene **57** in 81% yield after purification. Introduction of the malonate unit and deprotection of the alcohol were performed in the usual manner to afford TCC triester **59** in 67% overall yield (Scheme 7A).

TCT triene **62** was obtained by two alternative sequences, as follows. Decarbalkoxylation of **48** under the conditions described above provided **60** in 69% yield. Treatment of the enolate derived from this compound with methyl chloroformate provided triester **61** (44% yield) and tetraester **49** (53% yield). Separation of **61** by chromatography followed by removal of the alcohol protecting group afforded TCT triene **62** in 92% yield (Scheme 7B).

A more efficient way for the preparation of **61** (Scheme 7C) started from *trans* olefin **63***a* (prepared as outlined in

Can. J. Chem. Downloaded from www.nrcresearchpress.com by 213.200.69.106 on 09/08/12
For personal use only.

Can. J. Chem. Downloaded from www.nrcresearchpress.com by 213.200.69.106 on 09/08/12
For personal use only.

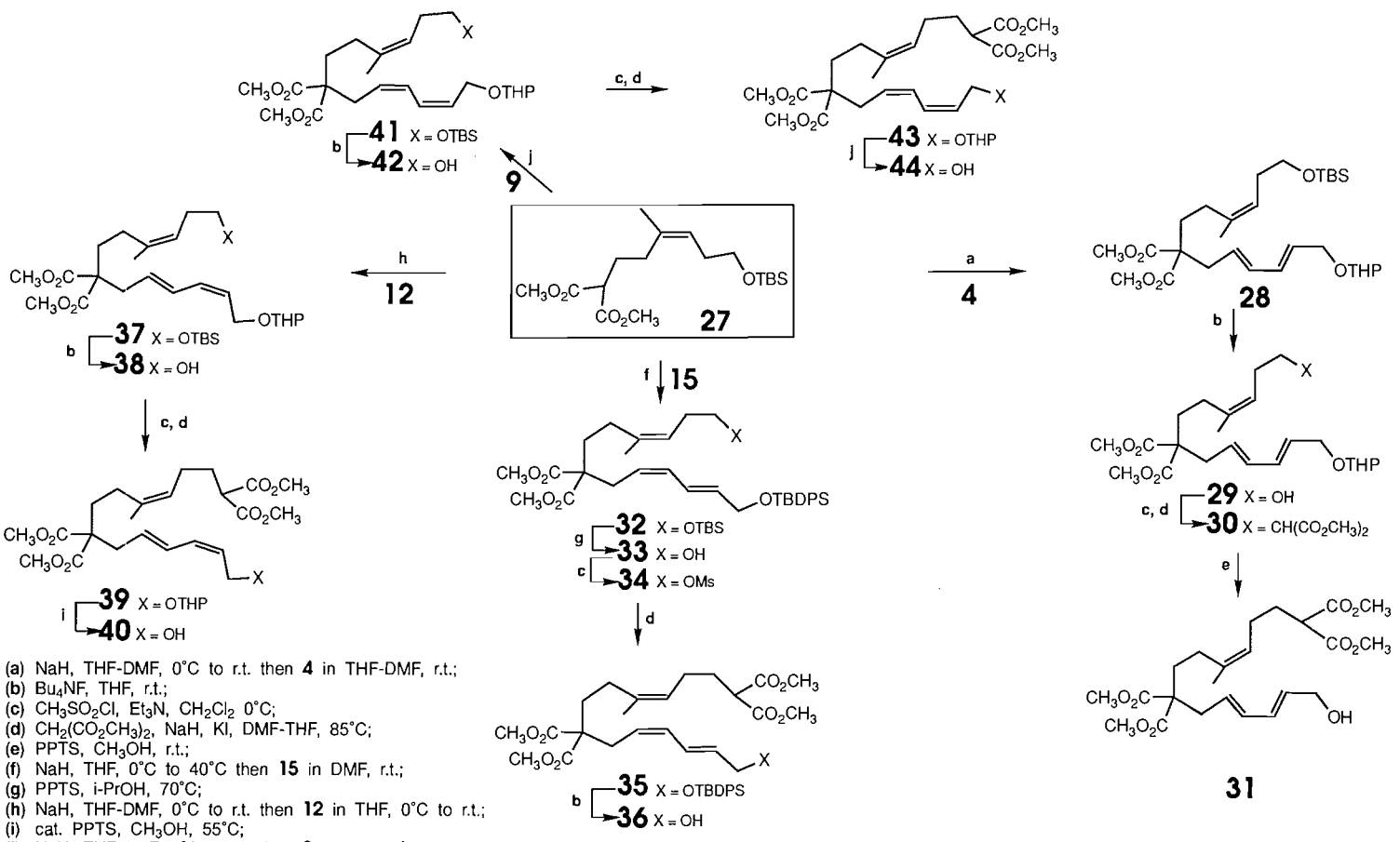

SCHEME 5. TTC, CTC, TCC, and CCC sequences.

Can. J. Chem. Downloaded from www.nrcresearchpress.com by 213.200.69.106 on 09/08/12
For personal use only.

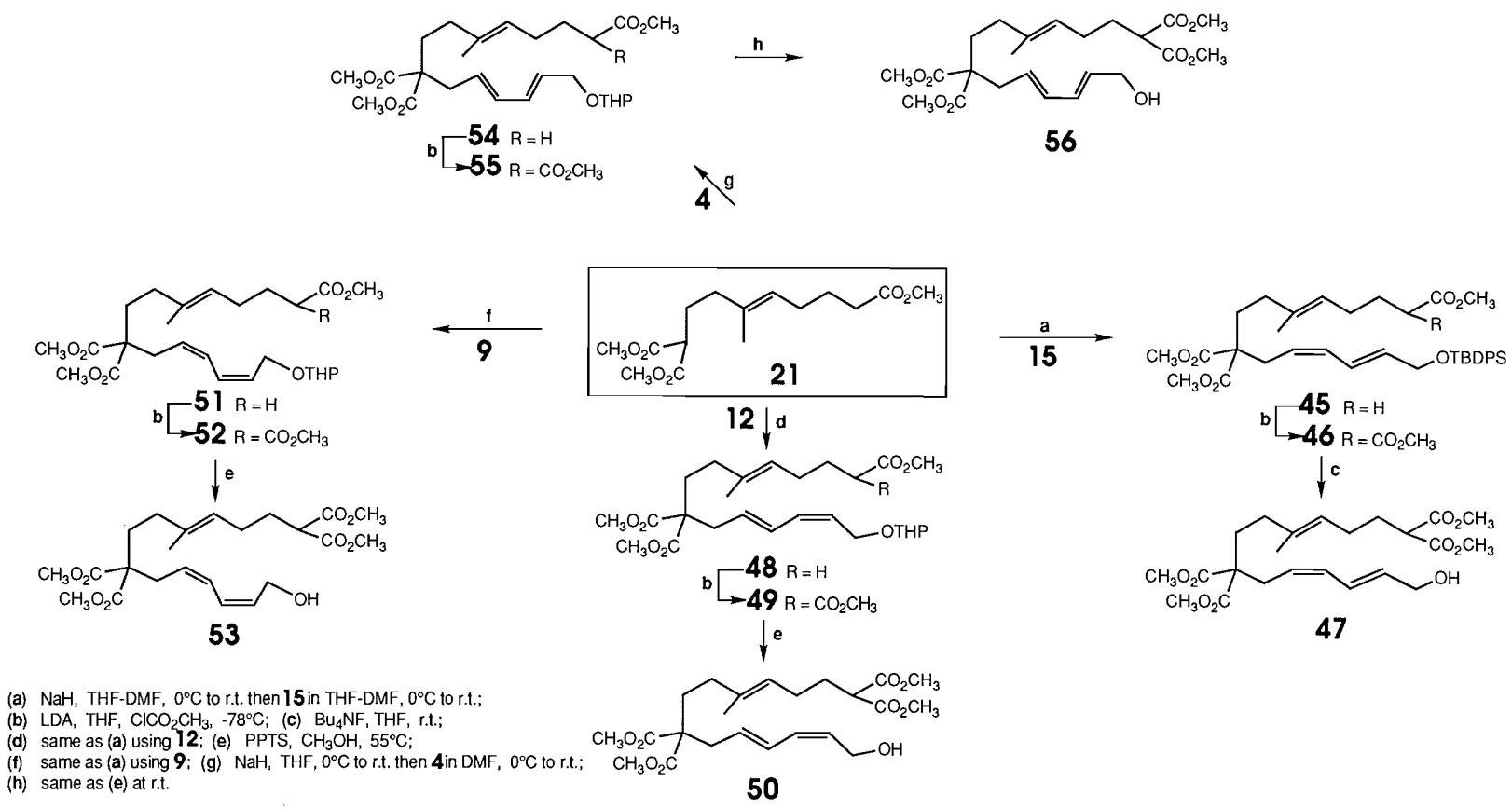

SCHEME 6. CTT, TCT, CCT, and TTT sequences.

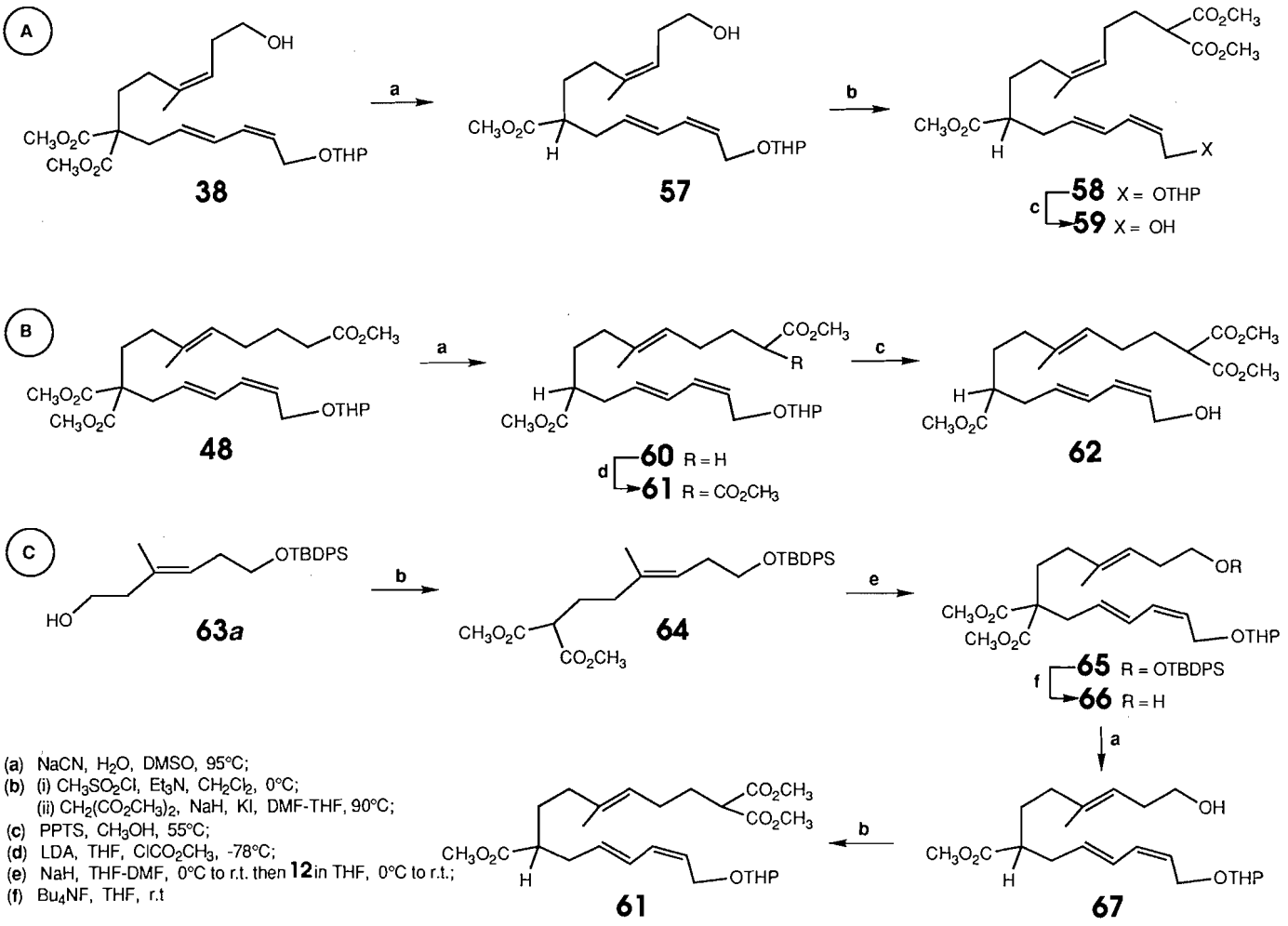

SCHEME 7. Decarboxylative TCC and TCT sequences.

Scheme 8). Mesylation followed by displacement with sodiomalonate furnished **64** in 85% yield after purification. Usual coupling with allylic chloride **12** (62% yield) followed by removal of the silyl group (92% yield) afforded diester **66**. Decarbalkoxylation led to monoester **67** (85% yield), which was then transformed into TCT triene **61** (77% yield) by the before-mentioned procedure.

In conclusion, this work outlines a highly convergent approach for the preparation of acyclic trienes containing a diene and a methyl-substituted dienophile moiety. All possible geometrical isomers could be easily obtained by the coupling of readily prepared and stereochemically defined olefins and dienes. Further elaboration of these compounds into A.B.C.[6.6.6] tricycles via the 14-membered macrocyclic trienes is described in the following paper of this issue.

Experimental

General

The ir spectra were taken on a Perkin–Elmer 681 spectrophotometer using chloroform ($CHCl_3$) or dichloromethane (CH_2Cl_2), or run as neat films on sodium chloride cells. Proton nmr spectra were recorded on a Bruker WP-80 or Bruker WM-250 instrument. The following abbreviations have been used: s, singlet; d, doublet; dd, doublet of doublets; dt, doublet of triplets; ddd, doublet of doublets of doublets; dddd, doublet of doublets of doublets of doublets; ddt, doublet of doublets of triplets; ddq: doublet of doublets of quartets; t, triplet; td: triplet of doublets; q, quartet; and m, multiplet. Chemical shifts are reported in δ values relative to chloroform as internal standard. Carbon nuclear magnetic resonance spectra were recorded on a Bruker WP-80 or Bruker WM-250 instrument (chloroform as internal standard). Mass spectra were obtained on a Micromass ZAB-2F instrument. Melting points were determined on a Büchi M-50 or on a Reichert apparatus and are uncorrected.

Unless otherwise specified all reactions were performed under an argon atmosphere and were monitored by thin-layer chromatography. For flash chromatography, silica gel Merck Kieselgel 60 (230–400 mesh, ASTM) was used. All solvents used in chromatography were distilled. Anhydrous solvents were obtained by standard means.

Dienes syntheses

trans,trans *Hydroxy diene 3*

DIBAL-H (30 mmol from a 1 M solution in cyclohexane) was slowly added at −78°C to a solution of hexadienoate **2** (see ref. 4) (3.34 g, 13.9 mmol) in dichloromethane. The mixture was stirred for 1.5 h at this temperature followed by addition of a saturated ammonium chloride solution (50 mL). Ether (25 mL) was added and the reaction mixture was allowed to reach room temperature. The aqueous layer was separated, extracted with ether, and then was acidified and reextracted with ether (2 × 40 mL). The organic phases were dried on magnesium sulfate, filtered, and evaporated. The crude product was purified by flash chromatography (40–

Can. J. Chem. Downloaded from www.nrcresearchpress.com by 213.200.69.106 on 09/08/12
For personal use only.

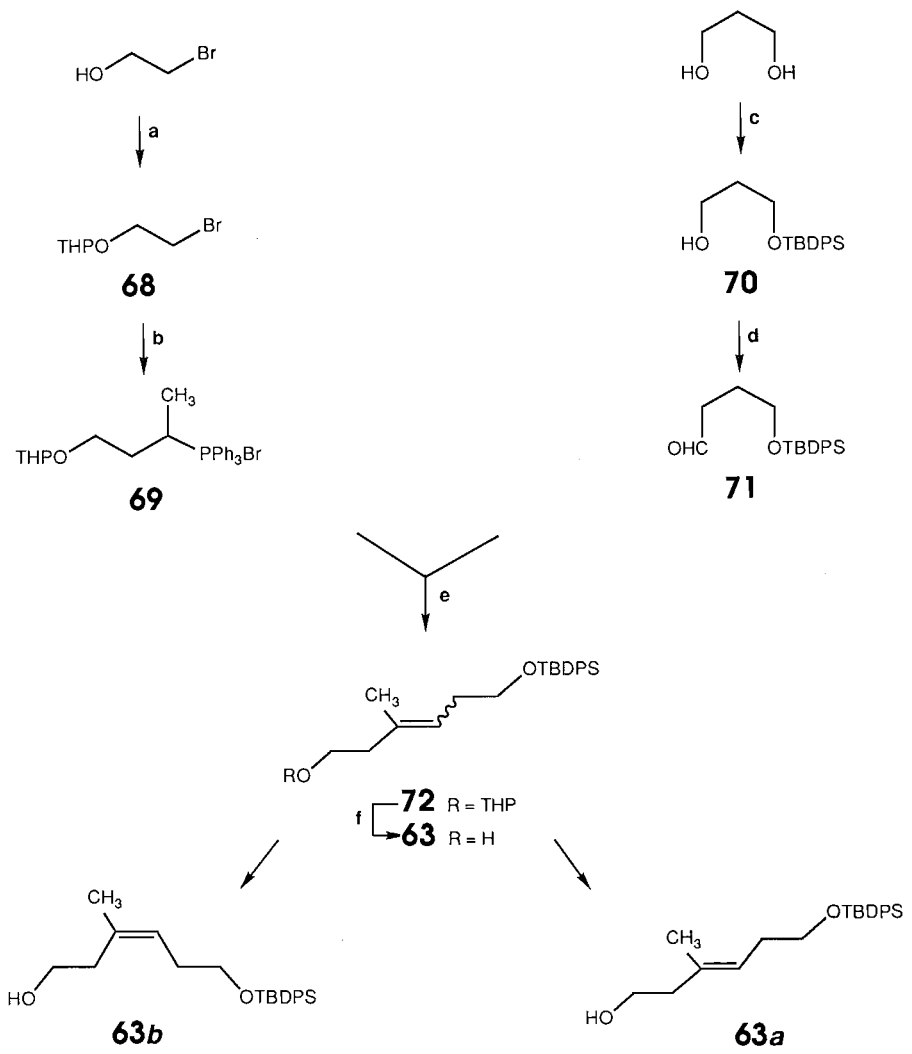

(a) PPTS, 3,4-DHP, CH_2Cl_2, r.t., 23 h;
(b) $C_2H_5P(Ph_3)Br$, $KN(TMS)_2$, THF, 0°C, 2 h;
(c) t-Bu$(Ph)_2SiCl$, imidazole, THF, r.t., 25 h;
(d) $(COCl)_2$, DMSO, CH_2Cl_2, -78°C, 1.75 h;
(e) **69**, n-BuLi, THF, 0°C, 4 h;
(f) PPTS, isopropanol, 75-80°C, 4 h.

SCHEME 8

60% EtOAc in hexane) affording 2.63 g (96%) of hydroxy diene **3**; ir ($CHCl_3$): 3400, 1100–1000 cm^{-1}; ^1H nmr (δ): 6.47–5.60 (4H, olefinic protons), 4.64 (1H, s, O-C*H*-O), 4.41–3.4 (6H, m, 3 × -CH_2-O), 2.0–1.4 (7H, m, O*H* and -$(CH_2)_3$-); ms *m/e*: 198 (M^+), 180 ($M^+ - H_2O$).

trans,trans *Allylic chloride 4*

To a solution of allylic alcohol **3** (360 mg, 1.8 mmol) in 5 mL of dimethylformamide, cooled to −10°C, were added lithium chloride (110 mg, 2.6 mmol), collidine (385 mL, 2.9 mmol), and methanesulfonyl chloride (210 mL, 2.7 mmol). The reaction mixture was stirred for 16 h while temperature changed from −10°C to 25°C. Ether (10 mL) and hexane (20 mL) were added followed by a 2% sodium bicarbonate solution (20 mL). The aqueous phase was extracted with a 1:1 mixture of ether and hexane (2 × 20 mL), and the combined organic layers were washed with water, dried ($MgSO_4$), and evaporated. The residue was rapidly purified by flash chromatography (10% EtOAc in hexane, containing 2% of triethylamine) giving 183 mg (46%) of **4**; ir ($CHCl_3$): 1100–1000 cm^{-1}; ^1H nmr ($CDCl_3$) δ: 6.5–5.5 (4H, m, olefinic protons), 4.64 (1H, s, O-C*H*-O), 4.5–3.3 (6H, m, -CH_2Cl and 2 × -CH_2-O), 2.0–1.3 (6H, m, -$(CH_2)_3$-).

(2Z,4Z)-Methyl 6-tetrahydropyranyloxy-2,4-hexadienoate (6)

A solution of anhydrous dimethyl sulfoxide (1 mL, 14 mmol) in dichloromethane (5 mL) was added dropwise, with stirring, to a solution of oxalyl chloride (1 mL, 11 mmol) in dichloromethane (20 mL) at −78°C. The mixture was stirred for an additional 10 min, then alcohol **1** (1.72 mg, 10 mmol) in dichloromethane (10 mL) was added over a period of 15 min using a syringe pump. The stirring was continued at −78°C, for 45 min. Diisopropylethylamine (8.7 mL, 50 mmol) was added and the mixture was warmed to −10°C. After addition of water (50 mL), the reaction mixture was extracted with ether. The organic layer was washed with brine, dried, and the solvent was evaporated. The resulting crude aldehyde **5** was used as such for the next step.

Can. J. Chem. Downloaded from www.nrcresearchpress.com by 213.200.69.106 on 09/08/12
For personal use only.

Can. J. Chem. Downloaded from www.nrcresearchpress.com by 213.200.69.106 on 09/08/12
For personal use only.

To a suspension of sodium hydride (60% in oil, 48 mg, 1.2 mmol) in tetrahydrofuran (5 mL) at 0°C was added a solution of methylbis(trifluoroethyl)phosphonoacetate (see ref. 11) (477 mg, 1.5 mmol) in tetrahydrofuran (2 mL). The mixture was stirred at 0°C for 30 min, then the temperature was lowered to −78°C and aldehyde **5** (about 1 mmol) in tetrahydrofuran (1 mL) was added dropwise. The reaction mixture was stirred for an additional 30 min. Saturated aqueous ammonium chloride solution was added and the resulting solution was extracted with ether. The organic layer was dried and the solvent evaporated. Chromatography on silica gel (0.5% acetone in dichloromethane) afforded *cis,cis* isomer **6** (124 mg) and *cis,trans* isomer **7** (21 mg) in 68% combined overall yield, from alcohol **1**; ir ($CHCl_3$):3010–2860, 1715, 1640, 1600, 1220, and 1030 cm^{-1}; ^1H nmr ($CDCl_3$) δ: 7.39 (1H, tq, J = 11.4 Hz, 1.3 Hz, -OCH_2CH=C*H*CH=CH-), 6.94 (1H, td, J = 11.7 Hz, 1.2 Hz, -OCH_2CH=CHC*H*=CH-), 5.99 (1H, dddd, J = 11.2 Hz, 7.2 Hz, 6.7 Hz, 1.4 Hz, -OCH_2CH=CHCH=CH-), 5.74 (1H, dd, J = 11.5 Hz, 1.2 Hz, -OCH_2CH=CHCH=C*H*-), 4.64 (1H, t, J = 3.9 Hz, -OCHO-), 4.43 (1H, ddd, J = 13.1 Hz, 6.2 Hz, 1.8 Hz, -OC*H*HCH=), 4.28 (1H, ddd, J = 13.6 Hz, 7.2 Hz, 1.6 Hz, -OCH*H*CH=), 3.86 (1H, m, -OCHO-C*H*H-), 3.73 (3H, s, -OCH_3), 3.52 (1H, m, -OCHO-CH*H*-), 1.87–1.47 (6H, m, -OCHO-CH_2-(CH_2)$_3$-).

(2Z,4Z)-6-Tetrahydropyranyloxy-2,4-hexadien-1-ol (8)

To a solution of ester **6** (124 mg, 0.55 mmol) in dichloromethane (3 mL) was added dropwise, at −78°C, a solution of DIBAL-H (1 M in cyclohexane, 1.4 mL, 1.4 mmol). The reaction mixture was stirred at −78°C for 3 h. Sodium sulfate decahydrate (500 mg) was added and the mixture was allowed to reach room temperature, then diluted with anhydrous acetone (5 mL). The solid was filtered off and washed several times with acetone. The solvents were evaporated, leaving alcohol **8** (82.4 mg, 76%); ir ($CHCl_3$): 3600, 3450, 3000–2850, and 1020 cm^{-1}; ^1H nmr ($CDCl_3$) δ: 6.38 (2H, m, -OCH_2CH=C*H*C*H*=C*H*CH_2OH), 5.70 (2H, m, -OCH_2CH=CHCH=C*H*CH_2OH), 4.64 (1H, t, J = 2.9 Hz, -OC*H*O-), 4.32 (3H, m, -OC*H*HCH=CHCH=CHCH_2OH), 4.21 (1H, ddd, J = 13.1 Hz, 7.2 Hz, 1.3 Hz, -OCH*H*CH=), 3.87 (1H, m, -OCHO-C*H*H-), 3.52 (1H, m, -OCHO-CH*H*-), 2.75 (1H, br, -CH_2OH), 1.86–1.47 (6H, m, -OCHO-CH_2-(CH_2)$_3$-); ^{13}C nmr ($CDCl_3$) δ: 131.44, 129.18, 125.48, 124.96 (C=C), 97.99 (-OCHO), 62.51, 62.21, 58.46 (-OCH_2-), 30.55, 25.37, 19.36 (-OCHO-CH_2-(CH_2)$_3$-); ms *m/e*: 113 (M^+ −C_5H_9O), 101 (M^+ −97), 95 (M^+ −$C_5H_{11}O_2$), 85 (M^+ −113). Exact Mass calcd. for M^+ −C_5H_9O: 113.0602; found: 113.0601 ± 0.0003.

Allylic chloride 9

To a solution of alcohol **8** (247 mg, 1.25 mmol) in dimethylformamide (5 mL) was rapidly added 212 mg (5 mmol) of lithium chloride. After complete dissolution, *s*-collidine (330 mL, 2.5 mmol) was added and the reaction mixture was stirred at room temperature for 5 min. The temperature was lowered to 0°C and methanesulfonyl chloride (194 mL, 2.5 mmol) was added dropwise. The reaction mixture was stirred at 0°C for 1 h, at room temperature for an additional hour, and was then poured in an ice–water mixture. Extraction with a 1:2 mixture of hexane and ether (3 × 50 mL) was followed by washing the combined organic layers with a saturated copper nitrate solution and drying over magnesium sulfate. The solvent was evaporated leaving 271 mg (~100%) crude chloride, which was used as such for the next step; ir ($CHCl_3$): 3000–2850, 1120, 1030 cm^{-1}; ^1H nmr ($CDCl_3$) δ: 6.43 (2H, m, (CH_2CH=C*H*C*H*=CHCH_2Cl), 5.75 (2H, m, -OCH_2CH=CHCH=C*H*CH_2Cl), 4.71 (1H, m, -OC*H*O-), 4.55–4.05 (4H, m, -OCH_2CH=CHCH=CHCH_2Cl), 4.00–3.72 (1H, m, -OCHO-C*H*H-), 3.65–3.35 (1H, m, O-CHO-CH*H*), 1.65 (6H, m, -OCHO-CH_2-(CH_2)$_3$-).

(2E,4Z)-Ethyl 6-tetrahydropyranyloxy-2,4 hexadienoate (10)

Ethyl diisopropylphosphonoacetate (3.78 g, 15 mmol; see ref. 12) in tetrahydrofuran (10 mL) was added at 0°C to a suspension of sodium hydride (60% in oil, 500 mg, 12 mmol) in tetrahydrofuran (50 mL). The solution was stirred for 20 min, then the temperature was lowered to −78°C. Aldehyde **5** (~10 mmol) in tetrahydrofuran (20 mL) was added over a period of 30 min using a syringe pump. The stirring was continued for an additional 30 min, then a saturated aqueous ammonium chloride solution (20 mL) was added, the mixture was extracted with ether, the organic layer dried, and the solvent was evaporated. Flash chromatography (30% EtOAc in hexane) gave diene **10** (1.64 g, 68% overall yield from alcohol **3**); ir ($CHCl_3$): 3000–2850, 1710, 1640, 1620, 1270, 1180, 1120, and 1030 cm^{-1}; ^1H nmr ($CDCl_3$) δ: 7.61 (1H, ddd, J = 15.3 Hz, 11.6 Hz, 1.0 Hz, -OCH_2CH=CHC*H*=CH-), 6.23 (1H, tm, J = 11.7 Hz, -OCH_2CH=C*H*CH=CH-), 5.96 (1H, m, -OCH_2CH=CHCH=CH-), 5.90 (1H, d, J = 15.3 Hz, -OCH_2CH=CHCH=C*H*-), 4.47 (1H, ddd, J = 15.2 Hz, 6.1 Hz, 1.6 Hz, =CHC*H*HOCHO-), 4.29 (1H, ddd, J = 15.0 Hz, 7.0 Hz, 1.6 Hz, =CHCH*H*OCHO-), 4.20 (2H, q, J = 7.1 Hz, -OCH_2CH_3), 3.87 (1H, m, -OCHO-C*H*H-), 3.65 (1H, m, -OCHO-CH*H*-), 1.90–1.50 (6H, m, -OCHO-CH_2-(CH_2)$_3$-), 1.29 (3H, t, J = 7.2 Hz, -OCH_2CH_3).

(2E,4Z)-6-Tetrahydropyranyloxy-2,4-hexadien-1-ol (11)

Diisobutylaluminium hydride (1 M in cyclohexane, 15 mL, 15 mmol) was added dropwise, at −78°C, to a solution of ester **10** (1.64 g, 6.8 mmol) in dichloromethane (50 mL). The solution was stirred for 2 h, then saturated aqueous ammonium chloride (30 mL) was added and the mixture was allowed to warm to room temperature. Ether (100 mL) was added and the solution was filtered on Celite. The aqueous layer was separated and extracted with ether (2 × 100 mL). The combined organic layers were washed with water, then dried, and the solvent was evaporated. Flash chromatography (40% ether in hexane) afforded allylic alcohol **11** (1.23 g, 91%); ir ($CHCl_3$): 3610, 3440, 3010–2850, and 1025 cm^{-1}; ^1H nmr ($CDCl_3$) δ: 6.56 (1H, ddq, J = 15.4 Hz, 11.4 Hz, 1.2 Hz, -OCH_2CH=CHC*H*=CHCH_2OH), 6.16 (1H, t, J = 11.0 Hz, -OCH_2CH=C*H*CH=CHCH_2OH), 5.85 (1H, dt, J = 15.2 Hz, 5.5 Hz, -OCH_2CH=CHCH=C*H*CH_2OH), 5.59 (1H, dt, J = 10.9 Hz, -OCH_2CH=CHCH=CHCH_2OH), 4.64 (1H, t, J = 2.9 Hz, -OC*H*O-), 4.36 (1H, ddd, J = 12.7 Hz, 6.3 Hz, 1.5 Hz, =CHC*H*H-OCHO), 4.23 (1H, ddd, J = 12.7 Hz, 6.53 Hz, 1.3 Hz, =CHCH*H*-OCHO), 4.21 (2H, dd, J = 5.2 Hz, 1.3 Hz, -CHCH_2OH), 3.88 (1H, m, -OCHO-C*H*H-), 3.53 (1H, m, OCHO-C*H*H-), 1.88–1.48 (6H, m, -OCHO-CH_2-(CH_2)$_3$-); ^{13}C nmr ($CDCl_3$) δ: 134.27, 130.77, 127.32, 125.65 (-*C*H=*C*H-), 97.74 (-O*C*HO-), 63.01, 62.69, 62.15 (-O*C*H_2-), 30.54, 25.38, 19.32 (-OCHO-CH_2-(*C*H_2)$_3$-); ms *m/e*: 183 (M^+ −15), 113 (M^+ −C_5H_9O), 101 (M^+ −97), 95 (M^+ −$C_5H_{11}O_2$), 85 (M^+ −113). Exact Mass calcd. for M^+ −C_5H_9O: 113.0602; found: 113.0604 ± 0.0003.

Allylic chloride 12

The same procedure as that used for the preparation of **9** was employed, starting with alcohol **11** (297 mg, 1.5 mmol). As before, the crude chloride (216 mg, ~100%) was used as such for the next step; ir ($CHCl_3$): 3010–2860, 1025 cm^{-1}; ^1H nmr ($CDCl_3$) δ: 6.80–5.10 (4H, m, olefinic protons), 4.65 (1H, m, -OCHO-), 4.40–4.05 (4H, m, -OCH_2CH=CHCH=CHCH_2Cl), 4.00–3.30 (2H, m, -OCHO-CH_2-), 1.90–1.40 (6H, m, -OCHOCH_2-(CH_2)$_3$-).

*(2Z,4E)-1-Tetrahydropyranyloxy-6-*tert*-butyldiphenylsilyloxy-2,4-hexadiene (13)*

tert-Butyldiphenylsilyl chloride (75.6 mg, 0.27 mmol) was added to a solution of alcohol **11** (49 mg, 0.25 mmol) and imidazole (37 mg, 0.55 mmol) in dimethylformamide (4 mL). The reaction mixture was stirred at room temperature for 9 h. Saturated aqueous ammonium chloride (5 mL) was added and the solution was extracted with a 1:1 mixture of ether and hexane. The organic layer was dried over magnesium sulfate and the solvent was evaporated. The crude product was used, as such for the next step; ir ($CHCl_3$): 2080, 3050, 3000–2860, and 1580 cm^{-1}; ^1H nmr ($CDCl_3$) δ: 7.85–7.30 (10 H, m, 2 × -C_6H_5), 7.10–5.40 (4H, m, olefinic protons), 4.70 (1H, m, -OC*H*O-), 4.40–4.10 (4H, m, -OCH_2CH=

Can. J. Chem. Downloaded from www.nrcresearchpress.com by 213.200.69.106 on 09/08/12
For personal use only.

CHCH=CHCH_2O-), 3.90–3.35 (2H, m, -OCHO-CH_2-), 1.80–1.40 (6H, m, -OCHO-CH$_2$-(CH_2)$_3$-), 1.10 (9H, s, *t*-Bu).

*(2Z,4E)-6-*tert*-Butyldiphenylsilyloxy-2,4-hexadien-1-ol (**14**)*

A solution of the diene **13** in 80% acetic acid (2.5 mL) was stirred at room temperature for 3 h, then was heated at 30°C–40°C for an additional 3 h. Saturated aqueous sodium bicarbonate was added and the solution was extracted with ether. The organic layer was dried and the ether was evaporated to give, after purification on silica gel (50% EtOAc in hexane), alcohol **14** (42 mg, 48% overall from alcohol **11**); ir ($CHCl_3$): 3610, 3440, 3080, 3050, 3010–2860, 1580, and 1110 cm^{-1}; ^{1}H nmr ($CDCl_3$) δ: 7.76–7.36 (10H, m, 2 × -C$_6$H$_5$), 6.77–5.44 (4H, m, olefinic protons), 4.30 (4H, m, -OCH_2CH=CHCH=CHCH_2O-), 1.44 (1H, br, -CH$_2$O*H*), 1.10 (9H, s, *t*-Bu).

*Allylic chloride **15***

Methanesulfonyl chloride (324 mg, 2.84 mmol) was added dropwise over a period of 5 min to a solution of alcohol **14** (950 mg, 2.70 mmol), lithium chloride (180 mg, 4.29 mmol), and *s*-collidine (359 mg, 2.97 mmol) in 30 mL of dimethylformamide at 0°C. The mixture was stirred at room temperature for 8 h, then was quenched with 300 mL of ice-water and extracted with a 2:1 mixture of ether and hexane (4 × 125 mL). The combined organic layers were washed with water (2 × 50 mL), then with a saturated aqueous copper nitrate solution (2 × 50 mL), and finally again with water (50 mL). Drying over magnesium sulfate followed by evaporation of the solvents and purification by column chromatography on silica gel (5% EtOAc in hexane), afforded pure chloride **15** (815 mg, 82%); ir ($CHCl_3$): 3015, 2960, 2935, and 2860 cm^{-1}; ^{1}H nmr ($CDCl_3$) δ: 7.68 and 7.40 (10H, 2m, -C$_6H_5$), 6.62 (1H, br dd, J = 14.8 and 11.4 Hz, -C*H*=CH-CH$_2$-O-), 6.18 (1H, t, J = 11.0 Hz, -C*H*=CH-CH$_2$-Cl), 5.89 (1H, dt, J = 15.0 and 4.6 Hz, =C*H*-CH$_2$-O-), 5.60 (1H, bq, J = 10.4 Hz, =C*H*-CH$_2$Cl), 4.30 (2H, d, J = 4.4 Hz, -CH_2-O-), 4.20 (2H, d, J = 8.1 Hz, -CH_2-Cl), 1.09 (9H, s, *t*-Bu).

Dienophile syntheses

*(3E)-4-Iodo-3-methyl-3-butene-1-ol (**16**)*

To a solution of trimethylaluminium (20.6 mL, 214.2 mmol) and bis(cyclopentadienyl)zirconium dichloride (5.21 g, 17.85 mmol; see ref. 15) in 1,2-dichloroethane (150 mL) at 0°C was added dropwise, over a period of 90 min, a solution of 3-butyn-1-ol (5.43 mL, 71.4 mmol) in 1,2-dichloroethane (36 mL). The mixture was stirred at room temperature for 14 h. The solution temperature was lowered to −40°C, and then a solution of iodine (22 g, 86 mmol) in tetrahydrofuran (70 mL) was added at a rate such as to maintain the mixture at a constant temperature of −30°C. The resulting solution was warmed to 0°C and saturated aqueous potassium carbonate (15 mL) was added over a period of 2 h. The product was extracted with a 2:1 mixture of hexane and ether (5 × 200 mL). The combined organic layers were dried on magnesium sulfate, and the solvent was evaporated to give iodo-alcohol **16** (13.98 g, 92%); ^{1}H nmr ($CDCl_3$) δ: 6.20 (1H, q, J = 0.8 Hz, -C=C(I)-*H*), 3.74 (2H, m, HOCH_2-), 2.48 (2H, td, J = 6.4 Hz, 0.8 Hz, -CH_2C=), 1.88 (3H, d, J = 0.8 Hz, CH_3-C=), 1.44 (1H, m, -CH$_2$O*H*).

*(3E)-4-Iodo-3-methyl-1-*tert*-butyldimethylsilyloxy-3-butene (**17**)*

To a solution of alcohol **16** (13.98 g, 66 mmol) in dichloromethane (300 mL) were added triethylamine (23 mL, 165 mmol), *tert*-butyldimethyl silyl chloride (12.06 g, 80 mmol), and 4-dimethylaminopyridine (1.2 g, 9.9 mmol). The resulting solution was stirred at room temperature for 3.5 h. Saturated aqueous ammonium chloride solution (100 mL) was added and the mixture was extracted with ether. The organic layer was dried and the solvent was evaporated. Flash chromatography on silica gel (hexane) afforded silyl ether **17** (21 g, 90% from 3-butyn-1-ol); ir ($CHCl_3$): 3000–2860, 1620, and 1100 cm^{-1}; ^{1}H nmr ($CDCl_3$) δ: 5.93 (1H, q, J = 1.1 Hz, C=C(I)-*H*), 3.68 (2H, t, J = 6.6 Hz, -OCH_2-), 2.41 (2H, td, J = 6.6 Hz, 0.9 Hz, -CH_2C=), 1.85 (3H, d, J = 1.1 Hz, CH$_3$-C=), 0.88 (9H, s, *t*-Bu), 0.00 (6H, s, -Si-(CH_3)$_2$).

*(5E)-Methyl 6-methyl-8-*tert*-butyldimethylsilyloxy-5-octenoate (**19**)*

To a suspension of Zn–Cu couple (5.13 g) in a 100:7 mixture of benzene and dimethylacetamide (100:7) (107 mL) was added methyl 4-iodobutyrate **18** (11.7 g, 51.3 mmol), and the mixture was stirred at room temperature for 1 h, then at 60°C for 3.5 h. A suspension of tetrakis(triphenylphosphine) palladium(0) (5 g, 4.34 mmol) in anhydrous benzene (35 mL) was added. The stirring was continued for 5 min, and vinylic iodide **17** (11.18 g, 34.3 mmol) in benzene (13 mL) was added. The reaction mixture was stirred at 60°C for 90 min, and was cooled to room temperature. The resulting suspension was diluted with ethyl acetate (185 mL), then filtered, and the solid washed with ethyl acetate. The solvent was evaporated, the residue was diluted again with ether, filtered, and the ether was evaporated. Flash chromatography on silica gel (4% EtOAc in hexane) gave alkene **19** (7.7 g, 75%); ir ($CHCl_3$): 2960–2860, 1735, 1250, and 1090 cm^{-1}; ^{1}H nmr ($CDCl_3$) δ: 5.13 (1H, tq, J = 7.2 Hz, 1.2 Hz, =C*H*-), 3.66 (3H, s, -OCH_3), 3.65 (2H, t, J = 7.0 Hz, -OCH_2-), 2.30 (2H, t, J = 7.4 Hz, -CH_2CO$_2$CH$_3$), 2.19 (2H, t, J = 7.1 Hz, -CH_2C-(CH$_3$)=CH-), 2.02 (2H, q, J = 7.3 Hz, -C=CHCH_2CH$_2$-), 1.69 (2H, dt, J = 7.3 Hz, 7.2 Hz, -C=CHCH$_2$CH_2CH$_2$-), 1.60 (3H, d, J = 1.0 Hz, CH_3-C=CH-), 0.88 (9H, s, *t*-Bu), 0.04 (6H, s, Si-(CH$_3$)$_2$).

*(5E)-Methyl 6-methyl-8-hydroxy-5-octenoate (**20**)*

Tetrabutylammonium fluoride (1 M in tetrahydrofuran, 5.8 mL, 5.8 mmol) was added to a solution of silyl ether **19** (864.7 mg, 2.88 mmol) in tetrahydrofuran (10 mL) at 0°C. The solution was stirred at room temperature for 4 h, and the solvent was evaporated. The residue was purified by chromatography on silica gel (40% EtOAc in hexane) to afford alcohol **20** (535 mg, 99%); ir ($CHCl_3$): 3500, 3000–2870, 1730, 1240, and 1050 cm^{-1}; ^{1}H nmr ($CDCl_3$) δ: 5.25 (1H, m, -C=C*H*-), 3.75 (3H, s, -OCH_3), 3.73 (2H, t, J = 6.5 Hz, HOCH_2-), 2.70–1.85 (9H, m, *H*OCH$_2$CH$_2$C-(CH$_3$)=CH(CH_2)$_3$-), 1.90 (3H, m, CH_3-C=CH-).

*(4E)-4-Methyl-1,1,8-trimethoxycarbonyl-4-octene (**21**)*

Methanesulfonyl chloride (268 μL, 3.45 mmol) was added dropwise to a solution of alcohol **20** (535 mg, 2.87 mmol) and triethylamine (0.6 mL, 4.3 mmol) in dichloromethane (10 mL). The reaction mixture was stirred at 0°C for 1 h, then the solution was poured into ice-cold water and extracted with dichloromethane. The organic layer was separated and dried. The solvent was evaporated and the residue (776.5 mg) (homogenous on thin-layer chromatography) was used as such for the next step.

Methyl malonate (1.64 mL, 14.35 mmol) was added dropwise to a suspension of sodium hydride (517.7 mg, 12.9 mmol) in a 1:1 mixture of dimethylformamide and tetrahydrofuran (30 mL) at 0°C. The mixture was stirred at 0°C for 30 min, then at room temperature for an additional 30 min. The above mesylate dissolved in tetrahydrofuran (5 mL) was then added, followed by a catalytic amount of potassium iodide (249 mg, 1.44 mmol). The reaction mixture was heated at 95°C (oil bath temperature) for 6 h, then was cooled to room temperature. Saturated aqueous ammonium chloride solution (15 mL) was added and the resulting solution was extracted with a 1:2 mixture of hexane and ether (3 × 100 mL). The combined organic layers were dried and the solvent was evaporated. The product was purified by chromatography on silica gel (25% EtOAc in hexane) yielding 742 mg (86%) of triester **21**; ir ($CHCl_3$): 3020–2840, 1740, and 1150 cm^{-1}; ^{1}H nmr ($CDCl_3$) δ: 5.10 (1H, tq, J = 7.2 Hz, 1.1 Hz, -C=C*H*-), 3.73 (6H, s, -CH(CO$_2$CH_3)$_2$), 3.66 (3H, s, CH$_2$CO$_2$CH_3), 3.33 (1H, m, -C*H*-(CO$_2$CH$_3$)$_2$), 2.29 (2H, t, J = 7.4 Hz, -CH_2CO$_2$CH$_3$), 2.00 (6H, m, -CH_2CH_2C(CH$_3$=CHCH$_2$-), 1.66 (2H, dt, J = 7.3 Hz, 7.2 Hz, -CH$_2$CH_2CH$_2$CO$_2$CH$_3$), 1.58 (3H, d, J = 1.2 Hz, CH_3-C=CH-); ^{13}C nmr ($CDCl_3$) δ: 174.06 (*C*O$_2$CH$_3$), 169.86 (-CH(*C*O$_2$-CH$_3$)$_2$), 134.38 (-*C*(CH$_3$)=CH-), 124.99 (-C(CH$_3$)=*C*H-), 52.31,

Can. J. Chem. Downloaded from www.nrcresearchpress.com by 213.200.69.106 on 09/08/12
For personal use only.

51.31, 50.92 (-CO_2CH_3, -$CH(CO_2CH_3)_2$), 37.06, 33.38 (-CH_2-$C(CH_3)$=$CHCH_2$-), 27.17, 26.97 ($(CH_3O_2C)_2CHCH_2$-, -CH_2CO_2-CH_3), 24.83 (-$CH_2CH_2CH_2CO_2CH_3$), 15.60 (CH_3-C=CH-); ms *m/e*: 300 (M^+). Exact Mass calcd: 300.1573; found: 300.1566 ± 0.0009.

Cyclohexadiene 22

Lithium (450 mg, 64 mmol) was added in small portions to a solution of *meta*-methylanisole (2.0 g, 16.3 mmol) and ethanol (12 mL) in liquid ammonia (60 mL) at −78°C. The mixture was stirred for 30 min and ammonium chloride (1.5 g) was then added in portions. The resulting mixture was warmed to room temperature and the ammonia was allowed to evaporate overnight. Water (10 mL) was added to the residue and the product was extracted with ether (3 × 20 mL). The combined organic layers were washed with water (5 mL), dried over potassium carbonate, and the solvent was evaporated. The crude material (1.86 g, 92%) was used without further purification; ir (CH_2Cl_2); 3000, 2825, 1695, 1665, and 1220 cm^{-1}; ^1H nmr ($CDCl_3$) δ: 5.43 (1H, m, CH_3-C=C*H*-), 4.64 (1H, m, CH_3-O-C=C*H*-), 3.56 (3H, s, CH_3-O-), 3.00–2.40 (4H, m, -CH_2-), 1.72 (3H, m, CH_3-CH=).

Hydroxy ester 23

Ozone was bubbled into a solution of cyclohexadiene **22** (6.10 g, 49.2 mmol) in 40 mL of methanol and 20 mL of dichloromethane at −78°C, until 95% of the starting material had disappeared (the reaction was monitored by gas chromatography). Excess ozone was removed by bubbling argon through the solution, followed by addition of dimethyl sulfide (3.97 g, 64 mmol). The mixture was stirred for 1 h at −78°C and was then slowly warmed up to room temperature. The solvents were evaporated, ethanol (60 mL) was added to the residue, and the solution was cooled to −78°C. Sodium borohydride (700 mg, 18.4 mmol) was added portionwise over a period of 30 min, the resulting mixture was stirred for an additional 15 min at −78°C, and was then allowed to warm up to room temperature. The solvent was evaporated, the residue was treated with 200 mL of a 10% hydrochloric acid solution, and the mixture was extracted with ether (4 × 200 mL). The combined organic layers were washed with a saturated sodium bicarbonate solution (2 × 50 mL) and dried over magnesium sulfate. The residue obtained after evaporation of the solvent was purified by column chromatography on silica gel (hexane: EtOAc: ether, 7:2:1) to afford 900 mg (12%) of pure **23** along with 3.4 g (44%) of the same material, which was analysed to be 90% pure; ir ($CHCl_3$): 3615, 3480, 3010, 2950, and 1730 cm^{-1}; ^1H nmr ($CDCl_3$) δ: 5.39 (1H, br t, *J* = 7.7 Hz, -C*H*=), 3.69 (3H, s, -CO_2CH_3), 3.64 (2H, m, -CH_2-OH), 3.10 (2H, s, -CH_2-CO_2CH_3), 2.29 (2H, br q, *J* = 6.7 Hz, -CH_2-CH_2-OH), 2.07 (1H, m, -O*H*), 1.78 (3H, q, *J* = 1.2 Hz, =C-CH_3).

Ester 24

To a solution of alcohol **23** (680 mg, 4.30 mmol) in 20 mL of dichloromethane at room temperature were added *tert*-butyldimethylsilyl chloride (805 mg, 5.37 mmol), triethylamine (868 mg, 8.59 mmol), and dimethylaminopyridine (10 mg, 0.08 mmol). The resulting mixture was stirred at room temperature overnight, after which time 30 mL of ether were added. The resulting precipitate was filtered off and the solvents were evaporated. Purification of the crude material by column chromatography on silica gel (3% acetone in hexane) afforded 1.12 g (96%) of ester **24**; ir ($CHCl_3$): 2950, 2930, 2860, 1730, and 840 cm^{-1}; ^1H nmr ($CDCl_3$) δ: 5.36 (1H, br t, *J* = 7.3 Hz, =C*H*-), 3.67 (3H, s, -CO_2CH_3), 3.59 (2H, t, *J* = 7.0 Hz, -CH_2-O-Si-), 3.06 (2H, s, -CH_2-CO_2CH_3), 2.24 (2H, br q, *J* = 7.1 Hz, -CH_2-CH_2-O-), 1.77 (3H, q, *J* = 1.3 Hz, CH_3-C=), 0.88 (9H, s, *t*-Bu), 0.04 (6H, s, -Si(CH_3)$_2$).

Alcohol 25

The ester **24** (5.30 g, 19.5 mmol) dissolved in 50 mL of ether was added dropwise, over a period of 10–15 min, to a suspension of lithium aluminum hydride (405 mg, 10.7 mmol) in ether (75 mL) at room temperature. The rate of addition was controlled in order to maintain gentle reflux of the solvent. The mixture was stirred for 1.5 h at room temperature and then sodium sulfate decahydrate (1.47 g, 4.57 mmol) was added portionwise. The resulting mixture was stirred for 1.5 h, the solid was decanted, and the solution was filtered through a pad of Celite covered with magnesium sulfate. The crude alcohol **25** (4.60 g, 97%) obtained after evaporation of the solvent was used for the next step without further purification; ir (neat): 3610, 3440, 2950, 2930, 2860, and 835 cm^{-1}; ^1H nmr ($CDCl_3$) δ: 5.30 (1H, br t, *J* = 7.0 Hz, =C*H*-), 3.65 (2H, q, *J* = 6.5 Hz, -CH_2-OH), 3.63 (2H, t, *J* = 7.0 Hz, -CH_2-O-Si-), 2.32 (2H, t, *J* = 6.5 Hz, -CH_2-CH_2-OH), 2.28 (2H, q, *J* = 7.0 Hz, -CH_2-CH_2-O-Si-), 2.08 (1H, t, *J* = 6.5 Hz, -O*H*), 1.74 (3H, q, *J* = 1.2 Hz, CH_3-C=), 0.88 (9H, s, *t*-Bu) 0.04 (6H, s, -Si(CH_3)$_2$).

Mesylate 26

To a solution of alcohol **25** (7.70 g, 31.5 mmol) and triethyl amine (4.77 g, 47.3 mmol) in 200 mL of dichloromethane was added dropwise, at 0°C, methanesulfonyl chloride (3.79 g, 33.1 mmol). The reaction mixture was stirred for 5 min and was then poured into ice-water (100 mL). The water layer was separated and extracted with dichloromethane (3 × 100 mL). The combined organic layers were washed with water (3 × 50 mL) and dried over magnesium sulfate. The crude mesylate **26** obtained after evaporation of solvent (10.1 g, 99%) was used as such for the next step; ir ($CHCl_3$): 2960, 2930, 2860, 1360, 1175, and 840 cm^{-1}; ^1H nmr ($CDCl_3$) δ: 5.34 (1H, t, *J* = 7.1 Hz, =C*H*-), 4.24 (2H, t, *J* = 7.2 Hz, -CH_2-O-S-), 3.60 (2H, t, *J* = 6.8 Hz, -CH_2-O-Si-), 2.98 (3H, s, CH_3-S-), 2.50 (2H, br t, *J* = 7.2 Hz, -CH_2-CH_2-O-S-), 2.23 (2H, br q, *J* = 6.8 Hz, -CH_2-CH_2-O-Si-), 1.75 (3H, q, *J* = 1.3 Hz, CH_3-C=), 0.89 (9H, s, *t*-Bu), 0.05 (6H, s, -Si(CH_3)$_2$).

Malonate 27

Dimethylmalonate (11.9 g, 90.1 mmol) was added dropwise to a suspension of sodium hydride (1.95 g, 81.2 mmol) in 300 mL of a 1:1 tetrahydrofuran and dimethylformamide mixture at 0°C. The mixture was warmed to room temperature and stirred until hydrogen evolution ceased. The crude mesylate **26** (5.80 g, 18.0 mmol) dissolved in 20 mL of the above solvent mixture was then added, followed by potassium iodide (149 mg, 0.9 mmol). The resulting reaction mixture was refluxed (oil bath temperature at 80–85°C) for 12 h. After cooling to room temperature, 50 mL of a saturated aqueous solution of ammonium chloride were slowly added, and the water layer was separated and extracted with a 2:1 ether and hexane mixture (3 × 150 mL). The combined organic layers were washed with water (2 × 50 mL) and dried over magnesium sulfate. Column chromatography on silica gel (5–20% EtOAc in hexane) afforded 5.20 g (81%) of **27**; ir ($CHCl_3$): 2950, 2930, 2860, 1730, and 840 cm^{-1}; ^1H nmr ($CDCl_3$) δ: 5.19 (1H, br t, *J* = 7.2 Hz, =C*H*-), 3.74 (6H, s, -(CO_2CH_3)$_2$), 3.56 (2H, t, *J* = 7.0 Hz, -CH_2-O-), 3.33 (1H, t, *J* = 7.0 Hz, -CH(CO_2CH_3)$_2$), 2.17 (2H, q, *J* = 7.2 Hz, =CH-CH_2-), 2.10–1.90 (4H, m, -(CH_2)-$CH(CO_2CH_3)_2$), 1.68 (3H, s, CH_3-C=), 0.88 (9H, s, *t*-Bu), 0.04 (6H, s, -Si(CH_3)$_2$); ms *m/e*: 301 (M^+ − $C(CH_3)_3$).

Alcohol 29

To a suspension of sodium hydride (121 mg, 5.05 mmol) in 5 mL of tetrahydrofuran and 5 mL of dimethylformamide at 0°C was added malonate **27** (1.50 g, 4.21 mmol) dissolved in 10 mL of tetrahydrofuran and 10 mL of dimethylformamide. The mixture was stirred for 15 min at 0°C and was then warmed to room temperature and stirred for another 15 min. Chloride **4** (1.00 g, 4.63 mmol) dissolved in 40 mL of tetrahydrofuran and 5 mL of dimethylformamide was added and the resulting mixture was stirred at room temperature for 22 h. A saturated aqueous solution of ammonium chloride (5 mL) was added, followed by 150 mL of water. The water layer was extracted with a 2:1 ether and hexane mixture (3 × 100 mL), and the combined organic layers were washed with water (50 mL) and with a saturated bicarbonate solution after which they were dried over magnesium sulfate. Evaporation of the solvents gave a crude oil that was purified by column chromatography on silica gel (10% EtOAc in hexane) to afford 1.24 g (80% based on 30% recovered malonate **27**) of silyl ether **28**.

Can. J. Chem. Downloaded from www.nrcresearchpress.com by 213.200.69.106 on 09/08/12
For personal use only.

The silyl ether **28** (1.12 g, 2.08 mmol) was dissolved in 35 mL of tetrahydrofuran at room temperature. To this solution was added tetrabutylammonium fluoride (1 M in tetrahydrofuran, 3.1 mL, 3.1 mmol) and the resulting mixture was stirred for 3 h, after which the solvent was evaporated. The crude product was purified by column chromatography on silica gel (25 to 50% EtOAc in hexane), to afford alcohol **29** (768 mg, 87%); ir ($CHCl_3$): 3610, 3005, 2950, 2870, and 1730 cm^{-1}; ^1H nmr ($CDCl_3$) δ: 6.17 (2H, m=C*H*-C*H*=), 5.72 (1H, dt, *J* = 14.6 and 6.2 Hz, =C*H*-CH_2-O-), 5.49 (1H, dt, *J* = 14.2 and 7.7 Hz, =C*H*-CH_2-$C(CO_2CH_3)_2$-), 5.12 (1H, tl, *J* = 7.3 Hz, =C*H*-CH_2-CH_2-O-), 4.63 (1H, t, *J* = 3.5 Hz, -O-C*H*-O-), 4.25 (1H, dd, *J* = 13.2 and 6.1 Hz, =CH-C*H*H-O-), 3.97 (1H, dd, *J* = 13.0 and 7.0 Hz, =CH-CH*H*-O-), 3.86 (1H, m, -O-C*H*H-CH_2-CH_2-), 3.73 (6H, s, -$(CO_2CH_3)_2$), 3.58 (2H, t, *J* = 6.5 Hz, -CH_2-OH), 3.54 (1H, m, -O-CH*H*-CH_2-CH_2-), 2.71 (2H, d, *J* = 7.7 Hz, -$(CO_2CH_3)_2$C-CH_2-CH=), 2.20 (2H, q, *J* = 6.5 Hz, -CH_2-CH_2-OH), 1.90 (4H, s, -CH_2-CH_2-$C(CH_3)$=), 1.69 (3H, d, *J* = 1.1 Hz, CH_3-C=), 1.95–1.45 (7H, m, -$(CH_2)_3$-CH_2-O- and -O*H*); ms *m/e*: 425 (M^+ +H), 407 (M^+ −OH). Exact Mass calcd. for $M^+ - C_5H_{10}O_2$: 322.1780; found: 322.1780 ± 0.009.

Tetraester 30

Using the procedure employed for the preparation of **26**, alcohol **29** (160 mg, 0.38 mmol) and triethylamine (58 mg, 0.57 mmol) in 5 mL of dichloromethane were treated with methanesulfonyl chloride (47 mg, 0.42 mmol) for 1.5 h. The crude mesylate was reacted according to the procedure employed for the synthesis of **27** using sodium hydride (41 mg, 1.71 mmol), dimethyl malonate (251 mg, 1.90 mmol), and potassium iodide (6.1 mg, 0.037 mmol) in 10 mL of a 1:1 tetrahydrofuran and dimethylformamide mixture for 20 h. The crude product was purified by column chromatography on silica gel (25% EtOAc in hexane) affording tetraester **30** (160 mg, 79% overall); ir ($CHCl_3$): 3025, 2955, and 1730 cm^{-1}; ^1H nmr ($CDCl_3$) δ: 6.17 (2H, m, =C*H*-C*H*=), 5.71 (1H, dt, *J* = 14.3 and 6.2 Hz, =C*H*-CH_2-O-), 5.49 (1H, dt, *J* = 14.3 and 7.2 Hz, -$(CO_2CH_3)_2$C-CH_2-C*H*=), 5.07 (1H, m, =C*H*-CH_2CH_2-), 4.63 (1H, t, *J* = 3.5 Hz, -O-C*H*-O-), 4.25 (1H, dd, *J* = 13.2 and 6.3 Hz, =CH-C*H*H-O-), 3.98 (1H, dd, *J* = 13.5 and 6.5 Hz, =CH-CH*H*-O-), 3.86 (1H, m, -O-C*H*H-CH_2-CH_2), 3.73 and 3.72 (12H, 2s, -CO_2CH_3), 3.52 (1H, m, -O-CH*H*-CH_2-CH_2-), 3.35 (1H, t, *J* = 7.1 Hz, -C*H*$(CO_2CH_3)_2$), 2.69 (2H, d, *J* = 7.9 Hz, -$(CO_2CH_3)_2$C-CH_2-CH=), 1.85 (4H, br s, -CH_2-CH_2-$C(CH_3)$=), 1.66 (3H, d, *J* = 1.1 Hz, CH_3-C=), 2.0–1.45 (10H, m, =CH-CH_2-CH_2 and -$(CH_2)_3$-CH_2-O-); ms *m/e*: 528 (M), 507 (M−OCH_3). Exact Mass calcd. for $M^+ - C_5H_{10}O_2$: 436.2097; found: 436.2095.

Alcohol 31

To a solution of tetraester **30** (150 mg, 0.28 mmol) in methanol (1.5 mL) was added pyridinium *p*-toluenesulfonate (17 mg, 0.068 mmol). The mixture was stirred at room temperature for 22 h. The solvent was evaporated and the residue was purified by column chromatography on silica gel (30% EtOAc in hexane) to yield 97 mg (77%) of alcohol **31**; ir ($CHCl_3$): 3610, 3020, 2955, and 1730 cm^{-1}; ^1H nmr ($CDCl_3$) δ: 6.17 (2H, m, =C*H*-C*H*=), 5.77 (1H, app. dt, *J* = 14.7 and 5.8 Hz, =C*H*-CH_2-O-), 5.49 (1H, app dt, *J* = 14.6 and 7.3 Hz, -$(CO_2CH_3)_2$C-CH_2-C*H*=), 5.06 (1H, m, =C*H*-CH_2-CH_2-), 4.16 (2H, br t, *J* = 4.8 Hz, -CH_2-OH), 3.72 (12H, s, -CO_2CH_3), 3.34 (1H, t, *J* = 7.3 Hz, -$CH(CO_2CH_3)_2$), 2.70 (2H, d, *J* = 7.7 Hz, -$(CO_2CH_3)_2$C-CH_2-CH=), 2.00–1.80 (4H, m, =CH-CH_2-CH_2-), 1.83 (4H, br s, -CH_2-CH_2-$C(CH_3)$=), 1.68 (1H, m, -O*H*), 1.65 (3H, d, *J* = 0.9 Hz, CH_3-C=); ms *m/e*: 454 (M^+), 436 (M^+ −H_2O). Exact Mass calcd: 454.2203; found: 454.2203 ± 0.0017.

Triene 32

To a suspension of sodium hydride (45 mg, 1.9 mmol) in 10 mL of tetrahydrofuran at 0°C was added malonate **27** (644 mg, 1.80 mmol) dissolved in 10 mL of tetrahydrofuran. The mixture was warmed to room temperature, stirred for 1 h, and then heated to 35–40°C for one more hour (or until hydrogen gas evolution ceased). Allylic chloride **15** (825 mg, 2.23 mmol) dissolved in 20 mL of dimethylformamide was added and the resulting mixture was stirred at room temperature for 15 h. The work-up of the reaction is identical with that used for **28**. After chromatography (5% EtOAc in hexane), 1.09 g (88%) of triene **32** was obtained; ir ($CHCl_3$): 2955, 2930, 2860, 1730, and 840 cm^{-1}; ^1H nmr ($CDCl_3$) δ: 7.68 and 7.40 (10H, 2m,-C_6H_5), 6.59 (1H, m, -C*H*=CH-CH_2-O-), 6.13 (1H, br t, *J* = 11.0 Hz, -$(CO_2CH_3)_2$C-CH_2-CH=C*H*-), 5.78 (1H, dt, *J* = 15.1 and 5.0 Hz, =C*H*-CH_2-O), 5.26 (1H, m, -$(CO_2CH_3)_2$C-CH_2-C*H*=), 5.13 (1H, m, =C*H*-CH_2-CH_2-O-), 4.26 (2H, br d, *J* = 4.9 Hz, =CH-CH_2-O-), 3.70 (6H, s, -$(CO_2CH_3)_2$), 3.54 (2H, t, *J* = 7.0 Hz, -CH_2-CH_2-O-), 2.82 (2H, d, *J* = 8.0 Hz, -$(CO_2CH_3)_2$C-CH_2-CH=), 2.14 (2H, br q, *J* = 7.1 Hz,-CH_2-CH_2-O-), 1.90 (4H, m, -CH_2-CH_2-$C(CH_3)$=), 1.66 (3H, d, *J* = 1.2 Hz, CH_3-C=), 1.07 (9H, s, t-*Bu*-Si$(C_6H_5)_2$), 0.88 (9H, s, t-*Bu*-Si$(CH_3)_2$), 0.03 (6H, s, -Si$(CH_3)_2$).

Alcohol 33

To a solution of disilyl ether **32** (1.05 g, 1.52 mmol) in 20 mL of isopropanol was added pyridinium *p*-toluenesulfonate (38 mg, 0.15 mmol). The mixture was stirred at 70°C for 17 h; then 50 mg of solid sodium carbonate was added and the solvent was evaporated under vacuum at 35°C. The residue was purified by column chromatography on silica gel (25% EtOAc in hexane) affording alcohol **33** (790 mg, 90%); ir ($CHCl_3$): 3620–3300, 3005, 2955, 2930, 2860, and 1730 cm^{-1}; ^1H nmr ($CDCl_3$) δ: 7.68 and 7.40 (10H, 2m, -C_6H_5), 6.61 (1H, ddq, *J* = 15.0, 11.2, and 1.1 Hz, -C*H*=CH-CH_2-O-), 6.14 (1H, br t, *J* = 11.1 Hz, -$(CO_2CH_3)_2$C-CH_2-CH=C*H*-), 5.80 (1H, dt, *J* = 15.0 and 4.9 Hz, =C*H*-CH_2-O-), 5.24 (1H, dt, *J* = 10.9 and 7.9 Hz, -$(CO_2CH_3)_2$C-CH_2-C*H*=), 5.14 (1H, tq, *J* = 7.4 and 1.4 Hz, -C*H*-CH_2-CH_2-O-), 4.27 (2H, dd, *J* = 4.9 and 1.3 Hz, =CH-CH_2-O-), 3.71 (6H, s, -$(CO_2CH_3)_2$), 3.57 (2H, br t, *J* = 6.4 Hz, -CH_2-CH_2-OH), 2.83 (2H, dd, *J* = 7.9 and 1.2 Hz, -$(CO_2CH_3)_2$C-CH_2-CH=), 2.19 (2H, qd, *J* = 6.6 and 1.1 Hz, -CH_2-CH_2-OH), 1.92 (4H, s, -CH_2-CH_2-$C(CH_3)$=), 1.69 (3H, q, *J* = 1.2 Hz, CH_3-C—), 1.48 (1H, m, -O*H*), 1.07 (9H, s, *t*-Bu); ms *m/e*: 578 (M^+), 521 (M^+ − *t*-Bu).

Mesylate 34

Using the procedure employed for the preparation of **26**, alcohol **33** (775 mg, 1.34 mmol) and triethylamine (202 mg, 2.00 mmol) in 25 mL of dichloromethane were treated with methanesulfonyl chloride (169 mg, 1.47 mmol) affording mesylate **34** (890 mg, > 100% crude); ir ($CHCl_3$): 2955, 2930, 2860, and 1730 cm^{-1}: ^1H nmr ($CDCl_3$) δ: 7.68 and 7.40 (10H, 2m, -C_6H_5), 6.61 (1H, br dd, *J* = 15.0 and 11.2 Hz, -C*H*=CH-CH_2-O-), 6.15 (1H, br t, *J* = 11.1 Hz, -$(CO_2CH_3)_2$C-CH_2-CH-C*H*-), 5.81 (1H, dt, *J* = 15.0 and 4.8 Hz, =C*H*-CH_2-O-), 5.24 (1H, m, -$(CO_2CH_3)_2$C-CH_2-C*H*=), 5.11 (1H, br t, *J* = 7.3 Hz, =C*H*-CH_2-CH_2-O-), 4.27 (2H, br d, *J* = 4.7 Hz, =CH-CH_2-O-), 4.14 (2H, t, *J* = 6.9 Hz, -CH_2-CH_2-O-), 3.72 (6H, s, -$(CO_2CH_3)_2$), 2.97 (3H, s, CH_3-S-), 2.82 (2H, dd, *J* = 7.9 and 1.2 Hz, -$(CO_2CH_3)_2$C-CH_2-CH=), 2.37 (2H, br q, *J* = 7.0 Hz, -CH_2-CH_2-O-), 1.90 (4H, s, -CH_2-CH_2-$C(CH_3)$=), 1.68 (3H, q, *J* = 1.2 Hz, CH_3-C=), 1.07 (9H, s, *t*-Bu).

Tetraester 35

Using the procedure employed for the preparation of **27**, sodium hydride (144 mg, 6.00 mmol) and dimethyl malonate (884 mg, 6.70 mmol) were reacted in 15 mL of tetrahydrofuran to which were then added mesylate **34** (880 mg, 1.34 mmol) and potassium iodide (22 mg, 0.13 mmol) dissolved in 15 mL of dimethylformamide. The mixture was heated for 16 h at 80°C affording tetraester **35** (761 mg, 82%); ir ($CHCl_3$): 3025, 2955, 2930, 2860, and 1730 cm^{-1}; ^1H nmr ($CDCl_3$) δ: 7.68 and 7.40 (10H, 2m, -C_6H_5), 6.60 (1H, m, -C*H*=CH-CH_2-O-), 6.13 (1H, br t, *J* = 11.1 Hz, -$(CO_2CH_3)_2$C-CH_2-CH=C*H*-), 5.26 (1H, m, -$(CO_2CH_3)_2$C-CH_2-C*H*=), 5.07 (1H, m, =C*H*-CH_2-CH_2-), 4.26 (2H, br d, *J* = 4.9 Hz, -CH_2-O-), 3.71 (12H, 2s, -$(CO_2CH_3)_2$-), 3.34 (1H, m, -C*H*$(CO_2CH_3)_2$), 2.81 (2H, br d, *J* = 7.9 Hz,

Can. J. Chem. Downloaded from www.nrcresearchpress.com by 213.200.69.106 on 09/08/12
For personal use only.

-(CO_2CH_3)$_2$C-CH_2-C*H*=), 3.02–2.78 (8H, m, -(CH_2)$_2$-C(CH_3)=CH(CH_2)$_2$-), 1.65 (3H, d, J = 1.2 Hz, CH_3-C=), 1.07 (9H, s, *t*-Bu).

Alcohol ***36***

Using the procedure employed for the preparation of **29**, silyl ether **35** (750 mg, 1.08 mmol) was treated with tetrabutylammonium fluoride (1 M in tetrahydrofuran, 1.18 mL, 1.18 mmol) in 25 mL of tetrahydrofuran to afford alcohol **36** (409 mg, 83%); ir ($CHCl_3$): 3600, 3520, 3020, 2950, and 1730 cm^{-1}; ^{1}H nmr ($CDCl_3$) δ: 6.56 (1H, ddq, J = 15.1, 11.1, and 1.2 Hz, -C*H*=CH-CH_2-O-), 6.13 (1H, br t, J = 11.1 Hz, -(CO_2CH_3)$_2$C-CH_2-CH=C*H*-), 5.87 (1H, dt, J = 15.1 and 5.5 Hz, =C*H*-CH_2-OH), 5.25 (1H, dt, J = 10.9 and 7.8 Hz, -(CO_2CH_3)$_2$C-CH_2-C*H*=), 5.06 (1H, m, =C*H*-CH_2-CH_2-), 4.22 (2H, br d, J = 5.1 Hz, -CH_2-OH), 3.73 and 3.72 (12H, 2s, -(CO_2CH_3)$_2$-), 3.34 (1H, t, J = 7.3 Hz, -C*H*(CO_2CH_3)$_2$), 2.82 (2H, dd, J = 7.9 and 1.5 Hz, -(CO_2CH_3)$_2$C-CH_2-CH=), 2.03–1.70 (9H, m, -(CH_2)$_2$-C(CH_3)=CH-(CH_2)$_2$- and -O*H*), 1.65 (3H, d, J = 1.2 Hz, CH_3-C=).

Triene ***37***

Malonate **27** (300 mg, 0.84 mmol) in tetrahydrofuran (3 mL) was added dropwise to a suspension of sodium hydride (24 mg, 1 mmol) in a 2:1 tetrahydrofuran and dimethylformamide mixture (15 mL) at 0°C. The suspension was stirred at 0°C for 20 min and then at room temperature for an additional 10 min. The temperature was again lowered to 0°C and allylic chloride **12** (216 mg, 1 mmol) in tetrahydrofuran (3 mL) was added. The reaction mixture was stirred at room temperature for 17 h. A saturated aqueous ammonium chloride solution (10 mL) was added and the product was extracted with a 3:2 ether and hexane mixture (3 × 100 mL). The combined organic layers were dried and the solvents were evaporated. Purification by chromatography on silica gel (10% EtOAc in hexane) gave triene **37** (402 mg, 89%); ir ($CHCl_3$): 3030–3010, 2960–2860, 1730, and 1075 cm^{-1}; ^{1}H nmr ($CDCl_3$) δ: 6.60–5.30 (4H, m, olefinic protons), 5.15 (1H, m, -C(CH_3)=C*H*-), 4.65 (1H, m, -OC*H*O-), 4.40–3.00 (6H, m, 3 × -CH_2O-), 3.73 (6H, s, 2 × -OCH_3), 2.72 (2H, d, J = 8.0 Hz, (CH_3O_2C)$_2$C-CH_2CH=), 2.15 (2H, q, J = 8.0 Hz, -C(CH_3)=CH-CH_2CH_2O-), 1.88 (4H, s, (CH_3O_2C)$_2$-CH_2-CH_2-C(CH_3)=), 1.65 (6H, m, -OCHO-CH_2-(CH_2)$_3$-), 0.88 (9H, s, *t*-Bu), 0.04 (6H, s, -Si(CH_3)$_2$).

Alcohol ***38***

To the silyl ether **37** (363 mg, 0.675 mmol) in tetrahydrofuran (5 mL) at 0°C, was added tetrabutylammonium fluoride (1 M in tetrahydrofuran, 1.25 mL, 1.25 mmol). The reaction mixture was stirred at room temperature for 4 h. The solvent was evaporated and the resulting residue was purified by chromatography on silica gel (30% EtOAc in hexane) to give alcohol **38** (277 mg, 97%); ir ($CHCl_3$): 3620, 3480, 3000–2870, 1730, and 1030 cm^{-1}; ^{1}H nmr ($CDCl_3$); δ: 6.44 (1H, ddd, J = 15.0 Hz, 11.7 Hz, 1.1 Hz, -OCH_2CH=CHC*H*=CH-), 6.09 (1H, tm, J = 11.8 Hz, -OCH_2-CH=C*H*CH=CH-), 5.54 (2H, m, -OCH_2C*H*=CHCH=C*H*-CH_2-), 5.13 (1H, td, J = 7.5 Hz, 1.4 Hz, -C(CH_3)=C*H*-), 4.63 (1H, t, J = 3.8 Hz, -OC*H*O-), 4.36 (1H, ddd, J = 13.8 Hz, 6.0 Hz, 1.6 Hz, -OCHO-C*H*HCH=), 4.15 (1H, ddd, J = 13.8 Hz, 7.3 Hz, 1.4 Hz, -OCHO-CH*H*CH=), 3.74 (1H, m, -C*H*H-OCHO-), 3.73 (6H, s, 2 × -OCH_3), 3.57 (3H, m, -CH*H*-OCHO, -CH_2OH), 2.74 (2H, d, J = 6.6 Hz, (CH_3O_2C)$_2$C-CH_2CH=), 2.21 (2H, qd, J = 6.3 Hz, 1.1 Hz, -C(CH_3)=CH-CH_2CH_2OH), 1.90 (4H, s, (CH_3O_2C)$_2$C-CH_2CH_2-C(CH_3)=CH-), 1.69 (3H, d, J = 1.3 Hz, -C(CH_3)=CH-), 1.75–1.50 (6H, m, -(CH_2)$_3$-CH_2-OCHO-).

Tetraester ***39***

Methanesulfonyl chloride (61 μL, 0.78 mmol) was added, dropwise, to a solution of alcohol **38** (277 mg, 0.653 mmol) and triethylamine (136 μL, 0.98 mmol) in dichloromethane (5 mL) at 0°C. The mixture was stirred at 0°C for 1 h and was then poured into ice-cold water. The product was extracted with dichloromethane (3 × 50 mL). The combined organic layers were washed with water, dried, and the solvent was evaporated. The resulting crude mesylate (310 mg) was used as such for the next step.

Methyl malonate (354 μL, 3.1 mmol) was added, dropwise, to a suspension of sodium hydride (67 mg, 2.79 mmol) in a 1:1 dimethylformamide and tetrahydrofuran mixture (8 mL) at 0°C. The mixture was stirred at 0°C for 20 min, and at room temperature for 10 min. The above mesylate in tetrahydrofuran (3 mL) was added, followed by a catalytic amount of potassium iodide (52 mg, 0.31 mmol). The reaction mixture was heated at 95°C for 4 h and was then cooled to room temperature. Saturated aqueous ammonium chloride solution was added and the product was extracted with a 2:1 ether and hexane mixture (3 × 50 mL). The combined organic layers were dried and the solvent was evaporated. Chromatography on silica gel (25% EtOAc in hexane) gave tetraester **39** (268 mg, 76% overall from the alcohol **38**); ir ($CHCl_3$): 3000–2850 and 1730 cm^{-1}; ^{1}H nmr ($CDCl_3$) δ: 6.60–5.30 (4H, m, olefinic protons), 5.10 (1H, m, -C(CH_3)=C*H*-), 4.65 (1H, m, -OC*H*O-), 4.40–3.25 (5H, m, -C*H*(CO_2CH_3)$_2$, -CH=CH-CH_2-OCHO-CH_2-), 2.70 (2H, d, J = 8.0 Hz, (CH_3O_2C)$_2$C-CH_2-CH=CH-), 2.10–1.30 (17H, m, -CH_2-CH_2-C(CH_3)=CH-CH_2-CH_2-, -OCHO-CH_2-(CH_2)$_3$-).

Alcohol ***40***

A catalytic amount of pyridinium *p*-toluenesulfonate (25 mg, 0.1 mmol) was added to the tetrahydropyranyloxy derivative **39** (268 mg, 0.5 mmol) in methanol (5 mL). The mixture was heated at 55°C for 3 h. The solvent was evaporated and the resulting residue was purified by chromatography on silica gel (40% EtOAc in hexane) to give alcohol **40** (216 mg, 96%)); ir ($CHCl_3$): 3600, 3500, 3020–2870, and 1730 cm^{-1}; ^{1}H nmr ($CDCl_3$) δ: 6.65–5.30 (4H, m, olefinic protons), 5.10 (1H, m, -C(CH_3)=C*H*-), 4.30 (2H, apparent d, J = 6.9 Hz, -CH=CH-CH_2OH), 3.75 (12H, s, 4 × -OCH_3), 3.45 (1H, t, J = 8.0 Hz, -C*H*(CO_2CH_3)$_2$), 2.72 (2H, d, J = 7.0 Hz, (CH_3O_2C)$_2$C-CH_2CH=CH-), 2.15–1.80 (8H, m, -CH_2-CH_2-C(CH_3)=CH-CH_2-CH_2-), 1.65 (3H, d, -C(CH_3)=CH-).

Triene ***41***

The procedure employed was identical with that described for the preparation of triene **37** except for using allylic chloride **9**; yield: 80%; ir ($CHCl_3$): 3010–2860, 1730, 1100, and 1030 cm^{-1}; ^{1}H nmr ($CDCl_3$) δ: 6.39 (2H, m, -OCH_2CH=C*HCH*=CH-), 5.66 (1H, m, -OCH_2C*H*=CHCH=CH-), 5.35 (1H, m, -OCH_2CH=CH-CH=C*H*-), 5.12 (1H, td, J = 7.2 Hz, 1.5 Hz, -C(CH_3)=C*H*-), 4.62 (1H, dd, J = 4.8 Hz, 3.0 Hz, -OC*H*O-), 4.34 (1H, ddd, J = 12.9 Hz, 6.2 Hz, 1.3 Hz, -OC*H*HCH=CH-), 4.19 (1H, ddd, J = 12.7 Hz, 7.0 Hz, 1.1 Hz, -OCH*H*CH=CH-), 3.86 (1H, m, -OCHO-C*H*H-), 3.71 (6H, s, 2 × -OCH_3), 3.55 (1H, t, J = 7.0 Hz, -CH_2-CH_2O-), 3.52 (1H, m, -OCHO-CH*H*-), 2.81 (2H, d, J = 7.3 Hz, (CH_3O_2C)$_2$C-CH_2CH=), 2.13 (2H, qd, J = 7.1 Hz, 1.2 Hz, -C(CH_3)=CH-CH_2CH_2O-), 1.89 (4H, m, (CH_3O_2C)$_2$C-C*H*CH_2-C(CH_3)=CH-), 1.85–1.48 (6H, m, -OCHO-CH_2-(CH_2)$_3$-), 1.66 (3H, d, J = 1.3 Hz, -C(CH_3)=CH-), 0.88 (9H, s, *t*-Bu), 0.03 (6H, s, -Si(CH_3)$_2$).

Alcohol ***42***

The same procedure as that described for the preparation of alcohol **38** was employed; yield: 92%; ir ($CHCl_3$): 3620, 3480, 3000–2860, 1730, 1220, and 1030 cm^{-1}; ^{1}H nmr ($CDCl_3$) δ: 6.40 (2H, m, -OCH_2CH=C*HCH*=CH-), 5.80–4.90 (3H, m, -OCH_2C*H*=CHCH=C*H*-, -C(CH_3)=C*H*-), 4.60 (1H, m, -OC*H*O-), 4.50–3.30 (6H, m, -CH_2OH, =CHCH_2OCHOCH_2-), 3.70 (6H, s, 2 × -OCH_3), 2.80 (2H, d, J = 8.0 Hz, (CH_3O_2C)$_2$C-CH_2-CH=), 2.15 (2H, m, =CHCH_2CH_2OH), 1.88 (4H, s, (CH_3O_2C)$_2$C-CH_2-CH_2C(CH_3)=CH-), 1.80 (1H, s, -CH_2O*H*), 1.70–1.40 (9H, m, -C(CH_3)=CH-, -OCHO-CH_2-(CH_2)$_3$-).

Tetraester ***43***

The procedure was identical with that described for the preparation of **39**; yield: 90% (overall from alcohol **42**); ir ($CHCl_3$): 3000–2840, 1730, 1230, 1200, and 1020 cm^{-1}; ^{1}H nmr ($CDCl_3$) δ: 6.40 (2H, m, -OCH_2CH=C*HCH*=CH-), 5.80–5.25 (2H, m, -OCH_2-

Can. J. Chem. Downloaded from www.nrcresearchpress.com by 213.200.69.106 on 09/08/12
For personal use only.

CH=CHCH=CH-), 5.04 (1H, m, -C(CH$_3$)=CH-), 4.60 (1H, m, -OCHO-), 4.25 (2H, m, -OCH$_2$CH=), 3.90–3.20 (3H, m, -OCHO-CH$_2$-, CH(CO$_2$CH$_3$)$_2$), 3.70 (12H, 2 × s, 4 × -OCH$_3$), 2.80 (2H, d, J = 7.2 Hz, (CH$_3$O$_2$C)$_2$CCH$_2$-CH=), 2.00–1.40 (17H, m, -CH$_2$CH$_2$-C(CH$_3$)=CHCH$_2$CH$_2$, -OCHO-CH$_2$-(CH$_2$)$_3$-).

Alcohol ***44***

The procedure described for the preparation of alcohol **40** was employed; yield: 92%; ir ($CHCl_3$): 3610, 3520, 3020–2840, 1730, 1440, 1200, and 1020 cm^{-1}; ^{1}H nmr ($CDCl_3$) δ: 6.38 (2H, m, HOCH$_2$CH=CHCH=CH-), 5.71 (1H, m, HOCH$_2$CH=CHCH=CH-), 5.36 (1H, m, HOCH$_2$CH=CHCH=CH-), 5.31 (1H, m, -C(CH$_3$)=CH-), 4.32 (2H, d, J = 6.7 Hz, HOCH$_2$CH=), 3.73 (12H, 2 × s, 4 × -OCH$_3$), 3.34 (1H, t, J = 7.2 Hz, -CH(CO$_2$CH$_3$)$_2$), 2.82 (2H, d, J = 7.5 Hz, (CO$_2$CH$_3$)$_2$C-CH$_2$-CH=), 1.99–1.67 (9H, m, -CH$_2$CH$_2$-C(CH$_3$)=CH-CH$_2$CH$_2$-, -CH$_2$OH), 1.65 (3H, s, -C(CH$_3$)=CH-).

Triester ***45***

Using previously described procedures (see the preparation of **28** for example), sodium hydride (46 mg, 1.92 mmol) was reacted with malonate **21** (520 mg, 1.73 mmol) followed by reaction with allylic chloride **15** (700 mg, 1.89 mmol), in 50 mL of a 1:1 tetrahydrofuran and dimethylformamide mixture, at room temperature for 8 h. The crude triester was purified by chromatography on silica gel (20% ether in hexane) yielding pure triester **45** (930 mg, 84%); ir (CH_2Cl_2): 2955, 2930, 2860, and 1730 cm^{-1}; ^{1}H nmr ($CDCl_3$) δ: 7.68 and 7.40 (10H, 2m, -C$_6$H$_5$), 6.59 (1H, br dd, J = 15.0 and 11.3 Hz, -CH=CH-CH$_2$-O-), 6.13 (1H, br t, J = 11.1 Hz, -(CO$_2$CH$_3$)$_2$C-CH$_2$-CH=CH-), 5.80 (1H, dt, J = 15.0 and 4.8 Hz, =CH-CH$_2$-O-), 5.24 (1H, dt, J = 10.9 and 8.0 Hz, -(CO$_2$CH$_3$)$_2$C-CH$_2$-CH=), 5.10 (1H, br t, J = 7.3 Hz, =CH-CH$_2$-CH$_2$-), 4.26 (2H, br d, J = 4.8 Hz, -CH$_2$-O-), 3.70 (6H, s, -(CO$_2$CH$_3$)$_2$-), 3.65 (3H, s, -CO$_2$CH$_3$), 2.80 (2H, br d, J = 8.0 Hz, -(CO$_2$CH$_3$)$_2$C-CH$_2$-CH=), 2.28 (2H, t, J = 7.5 Hz, -CH$_2$-CO$_2$-CH$_3$), 2.07–1.77 (6H, m, -(CH$_2$)$_2$-C(CH$_3$)=CH-CH$_2$-), 1.64 (2H, qn, J = 7.3 Hz, -CH$_2$-CH$_2$-CO$_2$CH$_3$), 1.56 (3H, d, J = 1.0 Hz, CH$_3$-C=), 1.07 (9H, s, *t*-Bu).

Tetraester ***46***

Stock solution of LDA. *n*-Butyllithium (1.55 M in hexane, 1.72 mL, 2.67 mmol) was added dropwise to a solution of diisopropylamine (289 mg, 2.86 mmol) in 4 mL of tetrahydrofuran at 0°C. The mixture was stirred at 0°C for 15 min.

Carbomethoxylation. To a solution of triester **45** (455 mg, 0.72 mmol) in 7 mL of tetrahydrofuran at −78°C was added 1.63 mL of the LDA stock solution (0.72 mmol). The mixture was stirred for 30 min and then methyl chloroformate (34 mg, 0.36 mmol) was added. After 20 min, a second aliquot of 815 μL (0.36 mmol) of the stock solution was added; the resulting mixture was stirred for 20 min after which time methyl chloroformate (20.4 mg, 0.22 mmol) was again added. The process was repeated twice, reducing the quantities by a twofold factor each time. After the last addition of methyl chloroformate the mixture was stirred for 5 min at −78°C and then 15 mL of a saturated aqueous ammonium chloride solution was added. The mixture was extracted with ether (3 × 20 mL), and the combined organic layers were washed with water (10 mL) and dried over magnesium sulfate. The solvent was evaporated, giving an oil that was purified by chromatography on silica gel (10–20% EtOAc in hexane) to afford tetraester **46** (365 mg, 74%); ir ($CHCl_3$): 3020, 2960, 2930, 2860, and 1730 cm^{-1}; ^{1}H nmr ($CDCl_3$) δ: 7.68 and 7.40 (10H, 2m, -C$_6$H$_5$), 6.59 (1H, br dd, J = 14.9 and 11.2 Hz, -CH=CH-CH$_2$-O-), 6.12 (1H, br t, J = 11.1 Hz, -(CO$_2$CH$_3$)$_2$C-CH$_2$-CH=CH-), 5.79 (1H, dt, J = 15.0 and 5.0 Hz, =CH-CH$_2$-O-), 5.23 (1H, dt, J = 10.9 and 8.9 Hz, -(CO$_2$CH$_3$)$_2$C-CH$_2$-CH=), 5.08 (1H, br t, J = 6.5 Hz, =CH-CH$_2$-CH$_2$-), 4.26 (2H, br d, J = 4.8 Hz, -CH$_2$-O), 3.72 and 3.69 (12H, 2s, -(CO$_2$CH$_3$)$_2$-), 3.35 (1H, t, J = 7.2 Hz, -CH(CO$_2$CH$_3$)$_2$), 2.79 (2H, br d, J = 7.9 Hz, -(CO$_2$CH$_3$)$_2$C-CH$_2$-CH=), 2.05–1.75 (8H, m, (-CH$_2$)$_2$-C(CH$_3$)=CH-(CH$_2$)$_2$-), 1.55 (3H, d, J = 1.1 Hz, CH$_3$-C=), 1.07 (9H, s, *t*-Bu).

Alcohol ***47***

Using the procedure employed for the preparation of **29**, silyl ether **46** (360 mg, 0.52 mmol) was treated with tetrabutylammonium fluoride (1 M in THF, 572 μL, 0.572 mmol) in 8 mL of tetrahydrofuran to afford alcohol **47** (170 mg, 72%); ir ($CHCl_3$): 3600, 3520, 3020, 2950, and 1730 cm^{-1}; ^{1}H nmr ($CDCl_3$) δ: 6.53 (1H, ddq, J = 15.1, 11.1, and 1.2 Hz, -CH=CH-CH$_2$-O-), 6.12 (1H, br t, J = 11.1 Hz, -(CO$_2$CH$_3$)$_2$C-CH$_2$-CH=CH-), 5.86 (1H, dt, J = 15.1 and 5.6 Hz, =CH-CH$_2$-O-), 5.26 (1H, dt, J = 10.9 and 7.9 Hz, -(CO$_2$CH$_3$)$_2$C-CH$_2$-CH=), 5.07 (1H, br t, J = 6.0 Hz, =CH-CH$_2$-CH$_2$-), 4.21 (2H, br d, J = 5.3 Hz, -CH$_2$-OH), 3.73 and 3.70 (12H, 2s, -(CO$_2$CH$_3$)$_2$-), 3.34 (1H, t, J = 7.2 Hz, -CH(CO$_2$CH$_3$)$_2$), 2.80 (2H, dd, J = 7.9 and 1.3 Hz, -(CO$_2$CH$_3$)$_2$C-CH$_2$-CH=), 2.05–1.75 (8H, m, -(CH$_2$)$_2$-C(CH$_3$)=CH-(CH$_2$)$_2$), 1.64 (1H, m, -OH), 1.55 (3H, d, J = 1.1 Hz, CH$_3$-C=).

Triester ***48***

Malonate **21** (1.205 g, 4 mmol) in tetrahydrofuran (5 mL) was added, dropwise, to a suspension of sodium hydride (125 mg, 5.2 mmol) in a 1:2 dimethylformamide and tetrahydrofuran mixture (90 mL) at 0°C. The reaction mixture was stirred at 0°C for 30 min and then at room temperature for an additional 30 min. The temperature was lowered to 0°C and the allylic chloride **12** (954 mg, 4.4 mmol) in tetrahydrofuran (5 mL) was added, followed by stirring at room temperature for 21 h. A saturated aqueous ammonium chloride solution (50 mL) was added and the resulting solution was extracted with a 3:2 ether and hexane mixture (5 × 100 mL). The combined organic layers were dried and the solvent was evaporated. Purification by chromatography on silica gel (15% EtOAc in hexane) gave the triene **48** (1.476 g, 77%); ir ($CHCl_3$): 3030–2860, 1730, 1440, 1230, 1200, and 1020 cm^{-1}; ^{1}H nmr ($CDCl_3$) δ: 6.37 (1H, ddd, J = 15.0 Hz, 11.8 Hz, 0.9 Hz, -OCH$_2$CH=CHCH=CH-), 6.08 (1H, t, J = 11.1 Hz, -OCH$_2$CH=CHCH=CH-), 5.51 (2H, m, -OCH$_2$CH=CHCH=CH-), 5.09 (1H, td, J = 6.7 Hz, 1.1 Hz, -C(CH$_3$)=CH-), 4.62 (1H, t, J = 2.9 Hz, -OCHO-), 4.32 (1H, ddd, J = 12.8 Hz, 6.2 Hz, 1.4 Hz, =CH-CHHO-), 4.16 (1H, ddd, J = 12.3 Hz, 7.4 Hz, 1.3 Hz, =CH-CHHO-), 3.87 (1H, m, -OCHO-CHH-), 3.71 (6H, s, -C(CO$_2$CH$_3$)$_2$), 3.66 (3H, s, -CH$_2$CO$_2$CH$_3$), 3.51 (1H, m, -OCHO-CHH-), 2.69 (2H, d, J = 6.7 Hz, (CH$_3$O$_2$C)$_2$C-CH$_2$CH=), 2.28 (2H, t, J = 7.5 Hz, -CH$_2$CO$_2$CH$_3$), 2.04–1.48 (17H, m, -CH$_2$CH$_2$C(CH$_3$)=CHCH$_2$CH$_2$-, -OCHO-CH$_2$-(CH$_2$)$_3$-).

Tetraester ***49***

Triester **48** (529 mg, 1.1 mmol) was reacted in tetrahydrofuran at −78°C with a total of 2.2 mmol lithium diisopropylamide (from a 0.635 M stock solution in tetrahydrofuran) and with a total of 1.1 mmol methyl chloroformate, using the same procedure as described for the preparation of **46**. Tetraester **49** (250 mg) was obtained in 42% yield after chromatography on silica gel (25% EtOAc in hexane); ir ($CHCl_3$): 3010–2840, 1730, 1440, 1220, and 1020 cm^{-1}; ^{1}H nmr ($CDCl_3$) δ: 6.38 (1H, ddd, J = 15.1 Hz, 11.1 Hz, 1.0 Hz, -OCH$_2$CH=CHCH=CH-), 6.08 (1H, t, J = 11.0 Hz, -OCH$_2$CH=CHCH=CH-), 5.51 (2H, m, -OCH$_2$CH=CHCH=CH-), 5.09 (1H, m, -C(CH$_3$=CH-), 4.63 (1H, m, -OCHO-), 4.25 (1H, ddd, J = 12.5 Hz, 6.2 Hz, 1.3 Hz, -OCHHCH=), 4.16 (1H, ddd, J = 12.8 Hz, 7.5 Hz, 1.3 Hz, -OCHHCH=), 3.84 (1H, m, -OCHO-CHH-), 3.73 (6H, s, 2 × -OCH$_3$), 3.71 (6H, s, 2 × -OCH$_3$), 3.51 (1H, m, -OCHO-CHH-), 3.36 (1H, t, J = 7.4 Hz, -CH(CO$_2$CH$_3$)$_2$), 2.70 (2H, d, J = 7.6 Hz, (CH$_3$O$_2$C)$_2$CCH$_2$CH=), 2.02–1.45 (17H, m, -CH$_2$CH$_2$C-(CH$_3$)=CH-CH$_2$CH$_2$-, -OCHO-CH$_2$-(CH$_2$)$_3$-); ms *m/e*: 538 (M$^+$).

Alcohol ***50***

To a solution of tetrahydropyranyloxy derivative **49** (242 mg, 0.45 mmol) in methanol (5 mL) was added pyridinium *p*-toluenesulfonate (22.5 mg, 0.1 mmol). The mixture was stirred at 55°C for 2 h. The methanol was evaporated, and the residue was purified by chromatography on silica gel (5% acetone in dichloromethane) to give alcohol **50** (197 mg, 97%); ir ($CHCl_3$): 3600, 3500, 3020–2840, 1730, 1440, and 1230 cm^{-1}; ^{1}H nmr ($CDCl_3$)

Can. J. Chem. Downloaded from www.nrcresearchpress.com by 213.200.69.106 on 09/08/12
For personal use only.

δ: 6.36 (1H, ddd, J = 15.0 Hz, 11.2 Hz, 1.2 Hz, $HOCH_2CH$=$CHCH$=CH-), 6.03 (1H, t, J = 11.3 Hz, $HOCH_2CH$=$CHCH$=CH-), 5.54 (2H, m, $HOCH_2CH$=$CHCH$=CH-), 5.08 (1H, td, J = 6.2 Hz, 1.2 Hz, -$C(CH_3)$=CH-), 4.28 (2H, d, J = 7.1 Hz, $HOCH_2$-), 3.73 (6H, s, 2 × -OCH_3), 3.72 (6H, s, 2 × -OCH_3), 3.35 (1H, t, J = 7.2 Hz, -$CH(CO_2CH_3)$), 2.70 (2H, d, J = 7.5 Hz, $(CH_3O_2C)_2C$-CH_2CH=), 2.04–1.81 (9H, m, -$CH_2CH_2C(CH_3)$=CH-CH_2CH_2-, -CH_2OH), 1.56 (3H, d, J = 1.1 Hz, -$C(CH_3)$=CH-).

Triester 51

The procedure described for the preparation of **48**, except for using allylic chloride **9**, led to triene **51** in 78% yield; ir ($CHCl_3$): 3000–2840, 1730, 1440, 1220, and 1020 cm^{-1}; ^1H nmr ($CDCl_3$) δ: 6.39 (2H, m, -OCH_2CH=$CHCH$=CH-), 5.66 (1H, m, -OCH_2-CH=$CHCH$-CH-), 5.36 (1H, m, -OCH_2CH=$CHCH$=CH-), 5.09 (1H, td, J = 7.1 Hz, 1.2 Hz, -$C(CH_3)$=CH-), 4.62 (1H, dd, J = 4.3 Hz, 4.1 Hz, -OCHO-), 4.38 (1H, ddd, J = 12.5 Hz, 5.3 Hz, 1.2 Hz, -OCHHCH=CH-), 4.21 (1H, ddd, J = 12.9 Hz, 6.5 Hz, 1.0 Hz, -OCHHCH=CH-), 3.86 (1H, m, -OCHO-CHH-), 3.70 (6H, s, 2 × -OCH_3), 3.66 (3H, s, -$CH_2CO_2CH_3$), 3.50 (1H, m, -OCHO-CHH-), 2.80 (2H, d, J = 7.4 Hz $(CH_3O_2C)_2C$-CH_2CH=), 2.28 (2H, t, J = 7.5 Hz, -$CH_2CH_2CO_2CH_3$), 2.04–1.42 (17H, m, -$CH_2CH_2C(CH_3)$=$CHCH_2CH_2$-, -OCHO-CH_2-$(CH_2)_3$-); ms m/e: 480 (M^+), 462 (M^+ − 18), 396 (M^+ − C_5H_9O), 378 (M^+ − $C_5H_{10}O_2$). Exact Mass calcd. for M^+ − $C_5H_{10}O_2$: 378.2042; found: 378.2042 ± 0.0011.

Tetraester 52

The same procedure as described for the preparation of **46** was employed, affording **52** in 44% yield; ir ($CHCl_3$): 3020–2840, 1730, 1435, 1200, and 1020 cm^{-1}; ^1H nmr ($CDCl_3$) δ: 6.39 (2H, m, -OCH_2CH=$CHCH$=CH-), 5.63 (1H, m, -OCH_2CH=$CHCH$=CH-), 5.35 (1H, m, -OCH_2CH=$CHCH$=CH-), 5.08 (1H, td, J = 7.5 Hz, 1.1 Hz, -$C(CH_3)$=CH-), 4.62 (1H, t, J = 3.0 Hz, -OCHO-), 4.35 (1H, dd, J = 13.9 Hz, 5.6 Hz, -OCHH-CH=), 4.19 (1H, dd, J = 12.9 Hz, 7.0 Hz, -OCHH-CH=), 3.86 (1H, m, -OCHO-CHH-), 3.73 (6H, s, 2 × -OCH_3), 3.70 (6H, s, 3 × -OCH_3), 3.49 (1H, m, -OCHO-CHH-), 3.35 (1H, t, J = 7.2 Hz, -$CH(CO_2CH_3)_2$), 2.80 (2H, d, J = 7.5 Hz, $(CH_3O_2C)_2C$-CH_2-CH=), 2.04–1.48 (14H, m, -CH_2CH_2-$C(CH_3)$=CH-CH_2CH_2-, -OCHO-$CH_2(CH_2)_3$-), 1.55 (3H, d, J = 0.9 Hz, $C(CH_3)$=CH-).

Alcohol 53

The procedure described for the preparation of **50** was employed, affording alcohol **53** in 93% yield; ir ($CHCl_3$): 3600, 3500, 3020–2840, 1730, 1440, and 1220 cm^{-1}; ^1H nmr ($CDCl_3$) δ: 6.35 (2H, m, $HOCH_2CH$=$CHCH$=CH-), 5.70 (1H, m, $HOCH_2CH$=$CHCH$=CH-), 5.35 (1H, m, $HOCH_2CH$=$CHCH$=CH-), 5.07 (1H, t, J = 7.5 Hz, -$C(CH_3)$=CH-), 4.32 (2H, d, J = 6.6 Hz, HOH_2CH=), 3.73 (6H, s, 2 × -OCH_3), 3.71 (6H, s, 2 × -OCH_3), 3.35 (1H, t, J = 7.2 Hz, -$CH(CO_2CH_3)_2$), 2.80 (2H, d, J = 7.6 Hz, $(CH_3O_2C)_2C$-CH_2CH=), 2.02–1.80 (8H, m, -CH_2CH_2-$C(CH_3)$=CH-CH_2CH_2-), 1.60 (1H, br s, $HOCH_2$-), 1.55 (3H, s, -$C(CH_3)$=CH-).

Triester 54

Using the procedure described for the preparation of **28**, sodium hydride (164 mg, 6.83 mmol) was reacted with malonate **21** (1.96 g, 6.53 mmol) in 75 mL of tetrahydrofuran to give the corresponding sodiomalonate, which was treated at room temperature for 11 h with allylic chloride **4** (1.90 g, 8.77 mmol) dissolved in 75 mL of dimethylformamide. The crude product was purified by column chromatography on silica gel (10% acetone in hexane) to give triester **54** (2.51 g, 80%); ir ($CHCl_3$): 3030, 3010, 2955, and 1730 cm^{-1}; ^1H nmr ($CDCl_3$) δ: 6.14 (2H, m, =CH-CH=), 5.70 (1H, dt, J = 14.3 and 6.4 Hz, =CH-CH_2-O-), 5.48 (1H, dt, J = 14.3 and 7.5 Hz, -$(CO_2CH_3)_2C$-CH_2CH=), 5.10 (1H, m, =CH-CH_2-CH_2-), 4.63 (1H, m, -O-CH-O-), 4.25 (1H, dd, J = 13.2 and 6.3 Hz, =CH-CHH-O-), 3.98 (1H, m, -CH-CHH-O-), 3.86 (1H, m, -O-CHH-CH_2-CH_2-), 3.71 and 3.66 (12H, 2s, -$(CO_2CH_3)_2$-), 3.51 (1H, m, -O-CHH-CH_2-CH_2-), 2.68 (2H, d, J = 7.7 Hz, -$(CO_2CH_3)_2C$-CH_2-CH=), 2.28 (2H, t, J = 7.5 Hz, -CH_2-CO_2CH_3), 2.07–1.45 (14H, m, -$(CH_2)_2$-$C(CH_3)$=CH-$(CH_2)_2$- and -$(CH_2)_3$-CH_2-O-), 1.56 (3H, d, J = 1.2 Hz, CH_3-C=).

Tetraester 55

To a solution of *n*-butyllithium (1.6 M in hexane, 1.77 mL, 2.84 mmol) in 7 mL of tetrahydrofuran at 0°C was added diisopropylamine (300 mg, 2.97 mmol) dissolved in 2 mL of tetrahydrofuran. The mixture was stirred at 0°C for 30 min and was then cooled to −78°C. Triester **54** (680 mg, 1.42 mmol) dissolved in 7 mL of tetrahydrofuran was added dropwise over a period of 10 min. The dark-red mixture was stirred at −78°C for 40 min and was transferred via canula to a solution of methyl chloroformate (1.34 g, 14.2 mmol) dissolved in 5 mL of tetrahydrofuran at −78°C. The solution was kept at −78°C for 35 min and was then quenched with a saturated aqueous solution of ammonium chloride (50 mL). The phases were separated and the aqueous layer was extracted with ether (3 × 30 mL). The combined organic layers were washed with water (20 mL) and brine (20 mL), and were dried over magnesium sulfate. The crude material obtained after evaporation of the solvents was purified by chromatography on silica gel (10% acetone in hexane) to afford tetraester **55** (454 mg, 60%); ir ($CHCl_3$): 3020, 2955, and 1730 cm^{-1}; ^1H nmr ($CDCl_3$) δ: 6.16 (2H, m, =CH-CH=), 5.70 (1H, dt, J = 14.5 and 6.2 Hz, =CH-CH_2-O-), 5.48 (1H, dt, J = 14.5 and 7.1 Hz, -$(CO_2CH_3)_2C$-CH_2-CH=), 5.08 (1H, m, =CH-CH_2-CH_2-), 4.63 (1H, m, -O-CH-O-), 4.25 (1H, dd, J = 12.9 and 5.5 Hz, -CH-CHH-O-), 3.98 (1H, dd, J = 12.9 and 6.7 Hz, =CH-CHH-O-), 3.86 (1H, m, -O-CHH-CH_2-CH_2-), 3.73 and 3.71 (12H, 2s, -$(CO_2CH_3)_2$-), 3.51 (1H, m, -O-CHH-CH_2-CH_2-), 3.36 (1H, t, J = 7.2 Hz, -$CH(CO_2CH_3)_2$), 2.68 (2H, d, J = 7.6 Hz, -$(CO_2CH_3)_2C$-CH_2-CH=), 2.09–1.45 (14H, m, -$(CH_2)_2$-$C(CH_3)$=CH-$(CH_2)_2$- and -$(CH_2)_3$-CH_2-O-), 1.55 (3H, d, J = 1.1 Hz, CH_3-C=).

Alcohol 56

Using the procedure described for the preparation of **31**, tetraester **55** (450 mg, 0.84 mmol) was treated with pyridinium *p*-toluenesulfonate (21 mg, 0.084 mmol) in 6 mL of methanol to afford alcohol **56** (288 mg, 76%); ir ($CHCl_3$): 3610, 3020, 2950, and 1728 cm^{-1}; ^1H nmr ($CDCl_3$) δ: 6.15 (2H, m, =CH-CH=), 5.76 (1H, dt, J = 14.9 and 5.7 Hz, =CH-CH_2-O-), 5.49 (1H, dt, J = 14.4 and 7.0 Hz, -$(CO_2CH_3)_2C$-CH_2-CH=), 5.08 (1H, m, =CH-CH_2-CH_2-), 4.16 (1H, br d, J = 5.8 Hz, -CH_2-O-), 3.73 and 3.71 (12H, 2s, -$(CO_2CH_3)_2$-), 3.35 (1H, t, J = 7.2 Hz, -CH-$(CO_2CH_3)_2$), 2.68 (2H, d, J = 7.6 Hz, -$(CO_2CH_3)_2C$-CH_2-CH=), 2.08–1.75 (8H, m, -$(CH_2)_2$-$C(CH_3)$=CH-$(CH_2)_2$-), 1.61 (1H, m, -OH), 1.55 (3H, d, J = 1.1 Hz, CH_3-C=).

Monoester 57

Sodium cyanide (49.7 mg, 1.01 mmol) and water (28 μL, 1.5 mmol) were added to a solution of the diester **38** (214 mg, 0.5 mmol) in dimethyl sulfoxide (8 mL). The mixture was heated at 95°C for 30 h and was then cooled to room temperature. The resulting solution was poured into ice-cold water, which was then saturated with sodium chloride and extracted with hexane (4 × 50 mL). The combined organic layers were dried and the solvent was evaporated. Purification by chromatography on silica gel (40% EtOAc in hexane) gave monoester **57** (149.8 mg, 81%); ir ($CHCl_3$): 3500, 3000–2840, 1730, 1440, and 1220 cm^{-1}; ^1H nmr ($CDCl_3$) δ: 6.36 (1H, ddq, J = 14.9 Hz, 11.1 Hz, 1.0 Hz, -OCH_2CH=$CHCH$=CH-), 6.09 (1H, tm, J = 11.2 Hz, -OCH_2CH=$CHCH$=CH-), 5.63 (1H, dt, J = 15.0 Hz, 7.2 Hz, -OCH_2CH=$CHCH$=CH-CH_2-), 5.49 (1H, dt, J = 10.9 Hz, 6.9 Hz, -OCH_2-CH=$CHCH$=CH-), 5.15 (1H, tq, J = 7.3 Hz, 0.9 Hz, -$C(CH_3)$=CH-), 4.64 (1H, apparent t, J = 3.1 Hz, -OCHO-), 4.34 (1H, dddd, J = 12.6 Hz, 4.9 Hz, 3.2 Hz, 1.3 Hz, -OCHO-CHH-CH=CH-), 4.17 (1H, dddd, J = 12.7 Hz, 7.5 Hz, 2.7 Hz, 1.3 Hz, -OCHO-CHH-CH=CH-), 3.88 (1H, m, -CHH-OCHO-), 3.67 (3H, s, -CO_2CH_3), 3.60 (2H, m, -CH_2OH), 3.51 (1H, m, -CHH-OCHO-), 2.45–2.19 (7H, m, =CH-CH_2CH-$(CO_2CH_3)CH_2CH_2C(CH_3)$=$CHCH_2$-), 2.03 (3H, m, -CH($CO_2$-

Can. J. Chem. Downloaded from www.nrcresearchpress.com by 213.200.69.106 on 09/08/12
For personal use only.

$CH_3)CH_2$-, -CH_2OH), 1.88–1.48 (6H, m, -$(CH_2)_3CH_2$-OCHO-), 1.69 (3H, d, J = 1.3 Hz, -C(CH_3)=CH-).

Triester ***58***

Methanesulfonyl chloride (40 μL, 0.51 mmol) was added, dropwise, to a solution of alcohol **57** (155 mg, 0.42 mmol) and triethylamine (89 μL, 0.64 mmol) in dichloromethane (5 mL). The reaction mixture was stirred at 0°C for 1 h, then was poured into ice-cold water and extracted with dichloromethane. The combined organic layers were dried and the solvent was evaporated to give a crude mesylate, which was used as such for the next step.

Methyl malonate (242 μL, 2.1 mmol) was added to a suspension of sodium hydride (45.7 mg, 1.9 mmol) in a 1:1 mixture of tetrahydrofuran and dimethylformamide at 0°C. The mixture was stirred at 0°C for 30 min, then at room temperature for 10 min. The above mesylate in tetrahydrofuran (2 mL), followed by a catalytic amount of potassium iodide (35.1 mg, 0.21 mmol), was then added. The reaction mixture was heated at 95°C for 4 h. The solution was cooled to room temperature, saturated aqueous ammonium chloride solution was added, and the resulting solution was extracted with a 2:1 ether and hexane mixture. The combined organic layers were dried and the solvent was evaporated to afford crude triester **58** (234 mg), which was used without purification for the next step.

Alcohol ***59***

Pyridinium *p*-toluenesulfonate (23 mg, 0.09 mmol) was added to a solution of the tetrahydropyranyloxy derivative **58** (233.6 mg, crude product of the preceding reaction) in methanol (5 mL). The mixture was heated at 95°C for 1.5 h, was then cooled to room temperature, and the solvent was evaporated. Purification by chromatography on silica gel (40% EtOAc in hexane) gave alcohol **59** (112 mg, 67% overall from **57**); ir ($CHCl_3$): 3600, 3480, 3020–2840, 1730, 1435, and 1220 cm^{-1}; ^1H nmr ($CDCl_3$) δ: 6.35 (1H, ddq, J = 15.0 Hz, 11.2 Hz, 1.1 Hz, -OCH_2CH=CHC*H*=$CHCH_2$-), 6.04 (1H, tm, J = 11.2 Hz, -OCH_2CH=C*H*CH=CH-), 5.65 (1H, dt, J = 15.0 Hz, 7.2 Hz, -OCH_2CH=CHCH=C*H*-CH_2-), 5.52 (1H, dt, J = 10.9 Hz, 6.9 Hz, -OCH_2C*H*=CHCH=CH-), 5.09 (1H, tm, J = 7.1 Hz, -C(CH_3)=C*H*-CH_2-), 4.29 (2H, dd, J = 6.6 Hz, 2.7 Hz, -O*C*H_2CH=), 3.73 (6H, s, -$CH(CO_2CH_3)_2$), 3.67 (3H, s, -$CH(CO_2CH_3)$-), 3.56 (1H, t, J = 7.2 Hz, -C*H*$(CO_2CH_3)_2$), 2.45–2.26 (5H, m, -$CHCH_2CH(CO_2CH_3)CH_2CH_2C(CH_3)$=$CHCH_2$-), 2.04–1.81 (7H, m, -$CH_2CH_2C(CH_3)$=$CHCH_2$-$CH_2$-, -CH=CH-$CH_2OH$), 1.65 (3H, d, J = 1.2 Hz, -C(CH_3)=CH-).

Diester ***60***

Sodium cyanide (22.5 mg, 0.46 mmol) and water (12 μL, 0.69 mmol) were added to a solution of triester **48** (110 mg, 0.23 mmol) in dimethyl sulfoxide (3 mL). The reaction mixture was heated at 95°C for 35 h and was then cooled to room temperature and poured into ice-cold water. The resulting solution was saturated with sodium chloride and extracted with hexane (3 × 100 mL). The organic layers were dried and the solvent was evaporated. Purification by chromatography on silica gel (15% EtOAc in hexane) gave diester **60** (67 mg, 69%); ir ($CHCl_3$): 3020–2850, 1730, 1440, 1210, and 1020 (cm^{-1}; ^1H nmr ($CDCl_3$) δ: 6.34 (1H, dd, J = 14.8 Hz, 11.1 Hz, OCH_2CH=CHC*H*=$CHCH_2$-), 6.08 (1H, t, J = 11.1 Hz, -OCH_2CH=C*H*CH=CH-CH_2-), 5.63 (1H, dt, J = 14.9 Hz, 7.0 Hz, -OCH_2CH=CHCH=C*H*CH_2-), 5.49 (1H, dt, J = 10.8 Hz, 6.8 Hz, -OCH_2C*H*=CHCH=$CHCH_2$-), 5.08 (1H, apparent t, J = 6.8 Hz, -C(CH_3)=C*H*CH_2-), 4.63 (1H, apparent t, J = 3.0 Hz, -OCHO-), 4.33 (1H, dd, J = 12.6 Hz, 6.6 Hz, -OCHO-C*H*HCH=), 4.17 (1H, dd, J = 12.6 Hz, 7.2 Hz, OCHO-CH*H*CH=), 3.88 (1H, m, -C*H*HOCHOCH_2-CH=), 3.66 (6H, s, 2 × -CO_2CH_3), 3.54 (1H, m, -CH*H*OCHO-CH_2CH=), 2.50–2.20 (3H, m, =$CHCH_2CH(CO_2CH_3)$-), 2.30 (2H, t, J = 7.5 Hz, -$CH_2CO_2CH_3$), 2.10–1.90 (4H, m, -CH_2C-(CH_3)=CHCH_2-), 1.88–1.40 (13H, m, -$CH_2CH_2C(CH_3)$=$CHCH_2$-$CH_2CH_2CO_2CH_3$, -$(CH_2)_3CH_2OCHO$-).

Triester ***61***

Method A. To a solution of diisopropylamine (20 μL, 0.146 mmol) in tetrahydrofuran (1 mL) at 0°C was added a solution of butyllithium (1.6 M in hexane, 87 μL, 0.14 mmol). The mixture was stirred at 0°C for 1 h, the temperature was lowered to −78°C, and then ester **60** (31 mg, 0.073 mmol) in tetrahydrofuran (0.5 mL) was added. The resulting solution was stirred at −78°C for 30 min, then excess methyl chloroformate (102 μL, 1.46 mmol) was added and stirring was continued for another 15 min. A saturated aqueous ammonium chloride solution (1 mL) was added and the solution was extracted with ether (3 × 10 mL). The organic layer was dried and the solvent was evaporated. Separation by chromatography on silica gel (25% EtOAc in hexane) gave triester **61** (15.6 mg, 44%) and tetraester **49** (21.8 mg, 53%).

Method B. Methyl malonate (285 μL, 2.5 mmol) was added to a suspension of sodium hydride (54 mg, 2.25 mmol) in a 1:1 dimethylformamide and tetrahydrofuran mixture (15 mL) at 0°C. The reaction mixture was stirred at 0°C for 20 min, then at room temperature for 30 min. The crude mesylate prepared from alcohol **67** (see below) (184 mg, 0.5 mmol, Et_3N, MsCl, 0°C) in tetrahydrofuran (5 mL) was added, followed by a catalytic amount of potassium iodide (42 mg, 0.25 mmol). The reaction mixture was heated at 95°C for 4 h. After cooling to room temperature, a saturated aqueous ammonium chloride solution was added and the product was extracted with a 2:1 ether and hexane mixture. The organic layer was dried and the solvent was evaporated. Purification by chromatography on silica gel (25% EtOAc in hexane) gave triester **61** (185 mg, 77% overall from alcohol **67**); ir ($CHCl_3$): 3040–2850, 1730, 1440, 1220, and 1020 cm^{-1}; ^1H nmr ($CDCl_3$) δ: 6.34 (1H, ddd, J = 15.0 Hz, 10.7 Hz, 1.0 Hz, -OCH_2CH=CHC*H*=$CHCH_2$-), 6.08 (1H, apparent t, J = 11.0 Hz, -OCH_2CH=C*H*CH=CH-), 5.63 (1H, dt, J = 14.9 Hz, 7.4 Hz, -OCH_2CH=CHCH=C*H*CH_2-), 5.48 (1H, dt, J = 10.7 Hz, 7.5 Hz, -OCH_2C*H*=CHCH=$CHCH_2$-), 5.07 (1H, tm, J = 7.5 Hz, 1.2 Hz, -C(CH_3)=C*H*-CH_2-), 4.64 (1H, apparent t, J = 3.1 Hz, -OCHO-), 4.35 (1H, dd, J = 12.5 Hz, 7.5 Hz, -OC*H*HCH=CH-), 4.18 (1H, dd, J = 12.5 Hz, 7.5 Hz, -OCH*H*CH=CH-), 3.90 (1H, m, -OCHO-C*H*H-), 3.73 (6H, s, -$CH(CO_2CH_3)_2$), 3.66 (3H, s, -$CH(CO_2CH_3)$-), 3.54 (1H, m, -OCHO-CH*H*-), 3.37 (1H, t, J = 7.5 Hz, -$CH_2CH(CO_2CH_3)_2$), 2.39 (5H, m, -CH=CH-$CH_2CH(CO_2CH_3)$-$(CH_2)_2C(CH_3)$=$CHCH_2$-), 1.94 (6H, m, -CH_2-$CH_2C(CH_3)$=$CHCH_2$-CH_2-), 1.90–1.45 (9H, m, -C(CH_3)=CH-, -OCHO-$CH_2(CH_2)_3$-); ms m/e: 480 (M^+).

Alcohol ***62***

Pyridinium *p*-toluenesulfonate (20 mg, 0.08 mmol) was added to a solution of tetrahydropyranyloxy derivative **61** (178 mg, 0.37 mmol) in methanol (5 mL). The mixture was heated at 55°C for 3 h and then the solvent was evaporated. Purification by chromatography on silica gel (10% acetone in dichloromethane) gave alcohol **62** (134 mg, 92%); ir ($CHCl_3$): 3600, 3500, 3020–2850, 1730, 1440, 1220, and 1170 cm^{-1}; ^1H nmr ($CDCl_3$) δ: 6.34 (1H, apparent ddd, J = 15.0 Hz, 11.3 Hz, 1.1 Hz, $HOCH_2CH$=CHC*H*=$CHCH_2$-), 6.04 (1H, apparent t, J = 10.9 Hz, $HOCH_2$-CH=C*H*CH=$CHCH_2$-), 5.63 (1H, dt, J = 15.1 Hz, 7.5 Hz, $HOCH_2CH$=CHCH=C*H*CH_2-), 5.53 (1H, dt, J = 10.8 Hz, 6.9 Hz, $HOCH_2$C*H*=CHCH=$CHCH_2$-), 5.07 (1H, tq, J = 7.5 Hz, 1.2 Hz, -C(CH_3)=C*H*-), 4.29 (2H, m, HOC*H*$_2$CH=), 3.73 (6H, s, -$CH(CO_2CH_3)_2$), 3.66 (3H, s, -$CH(CO_2CH_3)$-), 3.37 (1H, t, J = 7.3 Hz, -C*H*$(CO_2CH_3)_2$), 2.50–2.20 (3H, m, =$CHCH_2CH(CO_2CH_3)$-), 2.10–1.50 (9H, m, -$CH_2CH_2C(CH_3)$=$CHCH_2CH_2$-, -CH_2OH), 1.55 (3H, d, J = 0.9 Hz. -C(CH_3)=CH-).

Malonate ***64***

To a solution of alcohol ***63a*** (1.258 g, 3.145 mmol; see below) and triethylamine (658 mL, 4.72 mmol) in dichloromethane (40 mL) at 0°C was added, dropwise, methanesulfonyl chloride (294 μL, 3.8 mmol). The mixture was stirred at 0°C for 1 h and was then poured into ice-cold water and extracted with dichloromethane. The organic layer was washed with water and dried. Evaporation of the solvent gave a crude mesylate (1.5 g, ~99%), which was used as such for the next step.

Methyl malonate (1.8 mL, 15.7 mmol) was added, at 0°C, to a suspension of sodium hydride (341 mg, 14.2 mmol) in a 1:1 tet-

Can. J. Chem. Downloaded from www.nrcresearchpress.com by 213.200.69.106 on 09/08/12
For personal use only.

rahydrofuran and dimethylformamide mixture (40 mL). The mixture was stirred at 0°C for 30 min and then at room temperature for an additional 30 min. The above mesylate in tetrahydrofuran (5 mL) was added, followed by a catalytic amount of potassium iodide (269 mg, 1.6 mmol). The reaction mixture was heated at 95°C for 4 h. The resulting solution was cooled to room temperature, and saturated aqueous ammonium chloride solution (15 mL) was added. The solution was extracted with a 2:1 ether and hexane mixture (4 × 100 mL). The combined organic layers were dried and the solvent was evaporated. Purification by chromatography on silica gel (15% EtOAc in hexane) gave malonate **64** (1.42 g, 86% from alcohol **63**); ir ($CHCl_3$): 3080–3020, 3000–2860, 1730, and 1120 cm^{-1}; ^1H nmr ($CDCl_3$) δ: 7.67 and 7.39 (10 H, m, 2 × -C_6H_5), 5.13 (1H, t, J = 7.0 Hz, -C=CH-), 3.71 (6H, s, 2 × -OCH_3), 3.62 (2H, t, J = 7.0 Hz, -CH_2O-), 3.33 (1H, m, -C*H*(CO_2CH_3)$_2$), 2.25 (2H, q, J = 7.0 Hz, =CH-C*H*$_2$-CH_2O-), 1.99 (4H, m, -CH-C*H*$_2$C*H*$_2$-C=CH-), 1.55 (3H, s, CH_3-C-CH-), 1.04 (9H, s, *t*-Bu); ^{13}C nmr ($CDCl_3$) δ: 169.88 (C=O), 135.60 (C_3, aromatic ring), 135.26 (C_1, aromatic ring), 134.11 (-*C*(CH_3)=CH-), 129.52 (C_4, aromatic ring), 127.58 (C_2, aromatic ring), 122.10 (C=*C*H-), 63.64 (*C*H(CO_2CH_3)$_2$), 52.34 (-OCH_3), 51.03 (-CH_2O-), 37.15 (-*C*H$_2$-C(CH_3)=CH-), 31.58 (-C=CH-*C*H$_2$-), 27.03 ((CH_3O_2C)$_2$CH-*C*H$_2$-), 26.84 (-CH_3, *t*-Bu), 19.16 (-*C*(CH_3)$_3$), 15.82 (*C*H$_3$-C=CH-); ms *m/e*: 425 ($M^+ - C_4H_9$). Exact Mass calcd. for $M^+ - C_4H_9$: 425.1784; found; 425.1789 ± 0.0012.

Diester 65

The *trans* olefin **64** (1.36 g, 2.94 mmol) in tetrahydrofuran (5 mL) was added, dropwise, to a suspension of sodium hydride (82 mg, 3.4 mmol) in a 1:2 dimethylformamide and tetrahydrofuran mixture (100 mL) at 0°C. The reaction mixture was stirred at 0°C for 30 min, then at room temperature for an additional 30 min. The temperature was lowered to 0°C and allylic chloride **12** (760 mg) in tetrahydrofuran (5 mL) was added. The reaction mixture was stirred at room temperature for 24 h. A saturated aqueous ammonium chloride solution (40 mL) was added and the resulting solution was extracted with a 3:2 ether and hexane mixture. The organic layer was dried and the solvent was evaporated. Purification by chromatography on silica gel (10% EtOAc in hexane) gave triene **65** (1.2 g, 62%); ir ($CHCl_3$): 3080–3010, 2960, 2860, 1730, 1430, and 1110 cm^{-1}; ^1H nmr ($CDCl_3$) δ: 7.66 and 7.40 (10H, m, 2 × -C_6H_5), 6.37 (1H, dd, J = 15.0 Hz, 11.3 Hz, -OCH_2CH=CHC*H*=CH-), 6.06 (1H, t, J = 11.3 Hz, -OCH_2CH=C*H*CH=CH-), 5.50 (2H, m, -OCH_2C*H*=CHCH=C*H*-), 5.11 (1H, td, J = 7.5 Hz, 1.3 Hz, -C(CH_3)=C*H*-), 4.61 (1H, t, J = 3.8 Hz, -OCHO-), 4.30 (1H, ddd, J = 12.5 Hz, 5.0 Hz, 1.3 Hz, -OC*H*H-CH=), 4.13 (1H, ddd, J = 12.5 Hz, 6.5 Hz, 1.4 Hz, -OCH*H*-CH=), 3.86 (1H, m, -OCHO-C*H*H-), 3.69 (6H, s, 2 × -OCH_3), 3.61 (2H, t, J = 7.1 Hz, -C*H*$_2$OSi-), 3.50 (1H, m, -OCHO-CH*H*-), 2.69 (2H, d, J = 7.3 Hz, (CH_3O_2C)$_2$C-C*H*$_2$CH=), 2.24 (2H, q, J = 7.0 Hz, -CH-C*H*$_2$$CH_2O$;-), 1.97–1.41 (10H, m, -C*H*$_2$C*H*$_2$C(CH_3)=CH-, -OCHO-CH_2-(C*H*$_2$)$_3$-), 1.56 (3H, s, -C(C*H*$_3$)=CH-), 1.04 (9H, s, *t*-Bu).

Alcohol 66

Tetrabutylammonium fluoride (1 M in tetrahydrofuran, 3 mL, 3 mmol) was added to a solution of silyl ether **65** (990 mg, 1.5 mmol) in tetrahydrofuran (5 mL) at 0°C. The reaction mixture was stirred at room temperature for 4 h. Tetrahydrofuran was evaporated and the residue was purified by chromatography on silica gel (40% EtOAc in hexane) to give alcohol **66** (583 mg, 92%); ir ($CHCl_3$): 3620, 3460, 3040–2840, 1730, 1440, 1200, and 1040 cm^{-1}; ^1H nmr ($CDCl_3$) δ: 6.39 (1H, dd, J = 15.0 Hz, 11.4 Hz, -OCH_2CH=CHC*H*=CH-), 6.08 (1H, t, J = 11.3 Hz, -OCH_2CH=C*H*CH=CH-), 5.50 (2H, m, -OCH_2C*H*=CHCH=C*H*-), 5.15 (1H, t, J = 7.1 Hz, -C(CH_3)=C*H*-), 4.63 (1H, t, J = 3.2 Hz, -OCHO-), 4.35 (1H, ddd, J = 12.8 Hz, 6.4 Hz, 1.3 Hz, -OC*H*HCH=), 4.16 (1H, ddd, J = 12.2 Hz, 7.4 Hz, 1.2 Hz, -OCH*H*CH-), 3.87 (1H, m, -OCHO-C*H*H-), 3.71 (6H, s, 2 × -OCH_3), 3.62 (2H, m, -C*H*$_2$OH), 3.50 (1H, m, -OCHO-CH*H*-), 2.71 (2H, d, J = 7.4 Hz, (CH_3O_2C)C-C*H*$_2$CH=), 2.26 (2H, q, J = 6.8 Hz, =CH-C*H*$_2$$CH_2$OH), 2.02–1.80 (4H, m, -C*H*$_2$C*H*$_2$-C(CH_3)=CH-), 1.79–1.37 (7H, m, -OCHO-CH_2-(C*H*$_2$)$_3$-, -CH_2-OH), 1.61 (3H, s, -C(CH_3)=CH-).

Ester 67

Sodium cyanide (59 mg, 1.2 mmol) and water (33 μL, 1.8 mmol) were added to a solution of the diester **66** (257.5 mg, 0.6 mmol) in dimethyl sulfoxide (5 mL). The reaction mixture was heated at 95°C for 39 h, then cooled to room temperature. The solution was poured into ice-cold water, saturated with sodium chloride, and then extracted with hexane. The organic layer was dried and the solvent was evaporated. Purification by chromatography on silica gel (40% EtOAc in hexane) gave monoester **67** (187 mg, 85%); ir ($CHCl_3$): 3620, 3500, 3030–2850, 1730, 1450, and 1020 cm^{-1}; ^1H nmr ($CDCl_3$) δ: 6.34 (1H, ddd, J = 15.9 Hz, 11.0 Hz, 1.0 Hz, -OCH_2CH=CHC*H*=CH-), 6.08 (1H, t, J = 11.1 Hz, -OCH_2CH=C*H*CH=CH-), 5.62 (1H, dt, J = 15.0 Hz, 7.1 Hz, -OCH_2-CH=CHCH=C*H*-), 5.48 (1H, dt, J = 11.2 Hz, 7.2 Hz, -OCH_2C*H*=CHCH=CH-), 5.12 (1H, tq, J = 7.2 Hz, 1.2 Hz, -C(CH_3)=C*H*-), 4.63 (1H, t, J = 3.4 Hz, -OCHO-), 4.35 (1H, ddt, J = 12.6 Hz, 8.3 Hz, 2.3 Hz, =CH-C*H*H-OCHO-), 4.15 (1H, ddt, J = 12.5 Hz, 7.4 Hz, 2.3 Hz, -CHCH*H*-OCHO-), 3.88 (1H, m, -OCHO-C*H*H-), 3.66 (3H, s, -OCH_3), 3.62 (2H, m, -C*H*$_2$OH), 3.51 (1H, m, -OCHO-CH*H*-), 2.43–2.23 (5H, m, =CHC*H*$_2$-C*H*(CO_2CH_3)-CH_2CH_2C(CH_3)=CH-C*H*$_2$-), 2.00 (2H, t, J = 7.2 Hz, -C*H*$_2$C(CH_3)=CH-), 1.86–1.49 (9H, m, -CH(CO_2CH_3)-C*H*$_2$$CH_2$-, -$CH_2$O*H*, -OCHO-$CH_2$-(C*H*$_2$)$_3$-), 1.61 (3H, d, J = 0.8 Hz, -C(C*H*$_3$)=CH-).

2-(2-Bromoethoxy)tetrahydropyran (68)

To a solution of 2-bromoethanol (19.2 g, 154 mmol) in CH_2Cl_2 (200 mL) at 0°C under argon was added over 10 min, with stirring, pyridinium *p*-toluenesulfonate (387 mg, 1.5 mmol) followed by 3,4-dihydro-2*H*-pyran (210 mL, 230 mmol). The mixture was allowed to warm to room temperature, becoming increasingly dark purple in colour. After 2.3 h of total reaction time, a saturated sodium bicarbonate solution (120 mL) was added to produce a light brown-yellow coloured solution. The organic phase was separated and concentrated to an orange-brown crude oil (38.1 g) that was purified by distillation at 1.4 Torr (1 Torr = 133.3 Pa) (63–64°C) to afford 25.7 g (81%) of **68**, as a colourless oil; ir ($CHCl_3$): 2945–2850, 1125, and 1030 cm^{-1}; ^1H nmr ($CDCl_3$) δ: 4.67 (1H, t, J = 3.3 Hz, O-C*H*-O), 4.06–3.97 and 3.81–3.72 (2H, 2 dt, J = 11.2 Hz and 6.2 Hz, -CH_2-C*H*$_2$-OTHP), 3.93–3.84 and 3.56–3.48 (2H, 2m, -O-CHO-C*H*$_2$-), 3.53–3.48 (2H, m, Br-C*H*$_2$-CH_2-), 1.85–1.49 (6H, m, -O-CHO-CH_2-(C*H*$_2$)$_3$-).

4-Tetrahydropyranyloxybutyl-2-triphenylphosphonium bromide (69)

(Ethyl)triphenylphosphonium bromide (32.3 g, 87 mmol) was dried under high vacuum overnight at 115°C and was then suspended in THF (200 ml) at 0°C under argon with stirring. Potassium hexamethyldisilazane (174 mL, 87 mmol, 0.5 M in toluene) was added dropwise at 0°C over 50 min, producing a cherry-orange-coloured suspension that was stirred for an additional 0.5 h at 0°C. A solution of protected bromoethanol **68** (25.8 g, 125 mmol) in THF (70 mL) was then added dropwise at 0°C over 0.5 h. The red-orange mixture was warmed to room temperature and stirred for a total of 50 h, becoming successively orange, peach, orange-pink, and pink in colour. The thick, pink mixture was filtered on a Buchner funnel, leaving a white solid, and a rose-coloured filtrate that contained only impurities. The solid was repeatedly washed with tetrahydrofuran. The filtrate collection flask was changed and the solid was washed with dichloromethane until only solid, grey, KBr (10.1 g) remained in the funnel. The dichloromethane filtrate was concentrated to yield an off-white crude salt (40.8 g) that was recrystallized from a minimum volume of hot dichloromethane in hot hexane, to afford 38 g (88%) of **69** as fine clear snowflake crystals; yield: 38.0 g (88%); ir ($CHCl_3$): 3060–3010, 2950–2860, 1442, 1115, and 1038 cm^{-1}; ^1H nmr (250 MHz) ($CDCl_3$) δ: 8.01–7.62 (15H, 2m, P*Ph*$_3$), 5.27–5.13 and 5.08–4.87 (1H, 2m from diastereoisomers, -P-C*H*-CH_2), 4.63–4.61 and 4.59–

Can. J. Chem. Downloaded from www.nrcresearchpress.com by 213.200.69.106 on 09/08/12
For personal use only.

4.57 (1H, 2m from diastereoisomers, -O-C*H*-O-), 4.17–3.87 (2H, large m, -CH_2-CH_2-OTHP), 3.85–3.79 and 3.54–3.45 (2H, 2m, -CH-O-CH_2), 2.30–2.19 and 1.87–1.69 (2H, 2m, -CH-CH_2-CH_2-OTHP), 1.63–1.31 (6H, large m, -CH-O-CH_2-$(CH_2)_3$-), 1.43 (3H, dd, J_{HCCP} = 19.8 Hz and 7.1 Hz, -CH(CH_3)-).

1-tert-*Butyldiphenylsilyloxy propanol (**70**)*

A solution of 1,3-propanediol (20.0 g, 263 mmol) and imidazole (3.58 g, 52.6 mmol) in tetrahydrofuran (180 mL) was stirred under argon at room temperature. *tert*-Butylchlorodiphenylsilane (13.7 mL, 52.6 mmol) was added by syringe and the cloudy, white mixture was stirred for 25 h before being poured into a separatory funnel containing water (100 mL). The products were extracted into hexane (5 × 100 mL) and the combined organic layers were washed once with water (200 mL), then dried, filtered, and concentrated to give a crude, brown-tinged oil (17.41 g) that was purified by flash chromatography (10% EtOAc in hexane) to afford 15.86 g (96%) of a colourless oil; yield: 15.86 g; ir ($CHCl_3$): 3620, 3080–3020, 2960–2860, 1430, 1115, and 1068 cm^{-1}; ^1H nmr (80 MHz) ($CDCl_3$) δ (ppm): 7.66 and 7.46 (10H, m, Ph_2Si-), 3.88 (2H, t, J = 5.7 Hz, -CH_2-$OSiPh_2$), 3.86 (2H, q, J = 5.7 Hz, -CH_2-OH), 2.35 (1H, t, J = 5.4 Hz, -CH_2-O*H*), 1.98–1.52 (2H, m, -CH_2-CH_2-CH_2OH), 1.05 (9H, s, $(CH_3)_3$CSi-).

3-tert-*Butyldiphenylsilyloxy propanal (**71**)*

To a solution of oxalyl chloride (4.8 mL, 55.3 mmol) in dichloromethane (115 mL) at −78°C under argon was added with stirring over a period of 20 min freshly distilled dimethyl sulfoxide (7.9 mL, 110.6 mmol) in dichloromethane (25 mL). The mixture was stirred for 20 min before adding a solution of alcohol **70** (15.8 g, 50.3 mmol) in dichloromethane (50 mL) over a period of 25 min. The cloudy mixture was stirred for another 45 min at −78°C before triethylamine (35 mL) was added. The thick white mixture was then allowed to warm to room temperature over 1 h. Water (100 mL) was added to the yellow paste and the mixture was extracted with dichloromethane (3 × 100 mL). The combined organic layers were washed with water (2 × 50 mL) and brine (100 mL) before being dried, filtered, and concentrated to give a crude yellow oil (15.3 g) that was purified by flash chromatography (10% EtOAc in hexane) to afford 13.6 g (86%) of **71** as an off-white solid oil; ir ($CHCl_3$): 3080–3010, 2960–2860, 2740, 1728, 1430, 1115 cm^{-1}; ^1H nmr (80 MHz) ($CDCl_3$) δ: 9.83 (1H, t, J = 2.4 Hz, -CH_2-C*H*O), 7.81–7.35 (10H, m, Ph_2Si-), 4.03 (2H, t, J = 6.1 Hz, -CH_2-OSi), 2.61 (2H, dt, J = 5.6 and 2.8 Hz, -CH_2-CHO), 1.05 (9H, s, $(CH_3)_3$CSi-).

*(3*E *and 3*Z*)-3-Methyl-6-*tert-*butyldiphenylsilyloxy-1-tetrahydropyrannyloxy-3-hexene (**72**)*

The phosphorane salt **69** (25.9 g, 51.9 mmol), previously dried overnight under high vacuum at 110°C, was suspended in tetrahydrofuran (200 mL) at 0°C under argon with stirring. *n*-Butyllithium (29.7 mL, 47.6 mmol, 1.6 M in hexane) was added dropwise over 17 min, creating a deep-burgundy colour, and stirring was continued for an additional 40 min at 0°C. A solution of the aldehyde **71** (13.5 g, 43.3 mmol) in tetrahydrofuran (70 mL) was added dropwise over 35 min to the above ylide solution. With syringe washings, the total tetrahydrofuran volume was increased to approximately 350 mL. The mixture was stirred at 0°C for 3 h and then evaporated to a rust-coloured solid–oil combination. A 1:1 petroleum ether and hexane mixture was introduced to the flask and the contents were filtered over a Celite plug. Concentration of the filtrate yielded a crude yellow-coloured oil (15.2 g). The solid remaining in the funnel was dissolved in water, which was then extracted with ethyl ether (5 × 100 mL). The combined organic layers were dried, filtered, and concentrated to give a solid–oil (~8 g), which was washed carefully while filtering with ethyl ether. Concentration of the filtrate yielded a yellow-coloured solid–oil (~5 g), which was combined with the original crude material. Flash chromatography (4% EtOAc in hexane) gave 1.2 g (61%) of purified products as a mixture of *cis* and *trans* isomers (43:57 ratio by ^1H nmr); ir (neat): 3075, 2940 and 2860, 1430, 1115, 1036 cm^{-1}; ^1H nmr (250 MHz) ($CDCl_3$) δ (ppm): 7.70–7.62 and 7.48–7.33 (10H, 2m, Ph_2Si-), 5.23–5.15 (1H, m (2 tq), -CH_2-C*H*=C(CH_3)-), 4.58–4.53 (1H, m (2t), -O-C*H*-O-), 3.88–3.70 and 3.52–3.32 (4H, 2m, -O-CH-O-CH_2- and -CH_2-CH_2-OTHP), 3.63 and 3.62 (2H, 2t, J = 7.1, -CH_2-CH_2-OSi-), 2.34–2.19 (4H, m, -CH_2-CH=C(CH_3)-CH_2-), 1.89–1.30 (6H, large m, -O-CH-O-CH_2-$(CH_2)_3$-), 1.71 (3H, d, $J_{allylic}$ = 1.3 Hz, -HC=C(CH_3)-*cis*), 1.58 (3H, s, -HC=C(CH_3)-*trans*), 1.04 (9H, s, *t*-Bu).

*(3*E *and 3*Z*)-3-Methyl-6-*tert-*butyldiphenylsilyloxy-3-hexen-1-ol (**63**a) and (**63**b)*

A solution of the *cis* and *trans* isomers **72** (8.0 g, 17.7 mmol) in isopropanol (370 mL) was stirred under argon at room temperature. Pyridinium *p*-toluenesulfonate (800 mg, 3.2 mmol, 10% by weight of dienophile) was added and the mixture was heated to between 75°C and 80°C for 4 h. The mixture was cooled to room temperature and then partitioned between water and ethyl ether. The separated aqueous phase was extracted with additional aliquots of ethyl ether. The combined organic phases were dried, filtered, and concentrated to yield a yellow-coloured crude oil (6.7 g, 100% crude). The *cis–trans* mixture was separated by medium pressure chromatography (29–31 psi (1 psi = 6.89 kPa), 5% EtOAc in hexane) affording 355 mg of pure **63***b*, 522 mg of **63***a*, and 80 mg of a *cis–trans* mixture (1 g, loading).

cis *Isomer **63**b:* ir ($CHCl_3$): 3618, 3460, 3075–3055, 2960–2860, 1430, 1385, 1110, and 1055 cm^{-1}; ^1H nmr (250 MHz) ($CDCl_3$) δ: 7.72–7.63 and 7.46–7.34 (10H, 2m, Ph_2Si-), 5.30 (1H, br t, J = 7.0 Hz, $J_{allylic}$ = variable, -CH_2-C*H*=C(CH_3)-), 3.63 (2H, t, J = 6.7 Hz, -Si-O-CH_2-), 3.61 (2H, t, J = 6.4 Hz, -CH_2-CH_2-OH), 2.31 (2H, qd, ^3J = 6.8 Hz, J = 0.7, SiO-CH_2-CH_2-), 2.264 (2H, t, J = 6.4 Hz, =C(CH_3)-CH_2-), 1.723 (3H, d, J = 1.3 Hz, =C(CH_3)-CH_2-), 1.043 (9H, s, *t*-Bu).

trans *Isomer **63**a:* ir (neat): 3360, 3070–3045, 2925–2858, 1430 and 1385, 1110, 1050 cm^{-1}; ^1H nmr (250 MHz) ($CDCl_3$) δ (ppm): 7.69–7.62 and 7.45–7.26 (10H, 2m, Ph_2Si-), 5.25 (1H, apparent td, J = 7.3 Hz, $J_{allylic}$ = 1.3 Hz, -CH_2-C*H*=C(CH_3)-), 3.65 (2H, t, J = 6.8 Hz, -Si-O-CH_2-), 3.64 (2H, t, J = 6.2 Hz, -CH_2-CH_2-OH), 2.29 (2H, q, J = 6.9 Hz, -Si-O-CH_2-CH_2-), 2.24 (2H, t, J = 6.6 Hz, =C(CH_3)-CH_2-), 1.59 (3H, m, -C(CH_3)-CH_2-), 1.45 (1H, br s, -CH_2-O*H*), 1.04 (9H, s, *t*-Bu).

Acknowledgements

This research was supported by the Natural Sciences and Engineering Research Council of Canada (NSERCC, Ottawa) and by the "Ministère de l'Enseignement supérieur et de la Science (Fonds FCAR, Québec)."

1. (*a*) R. A. Micheli, Z. G. Hajos, N. Cohen, D. R. Parrish, L. A. Portland, W. Sciamanna, M. A. Scott, and P. A. Wherli. J. Org. Chem. **40**, 675 (1975); (*b*) W. S. Johnson, B. E. McCarry, R. L. Harkezich, and S. G. Boots. J. Am. Chem. Soc. **102**, 352 (1980); (*c*) A. G. Fallis. Can. J. Chem. **62**, 183 (1984), and references therein; (*d*) J.-F. Lavallée and P. Deslongchamps. Tetrahedron Lett. **29**, 6033 (1988), and references therein.
2. P. Deslongchamps. Aldrichimica Acta, **24**, 43 (1991).
3. S. Lamothe, A. Ndibwami, and P. Deslongchamps. Tetrahedron Lett. **29**, 1641 (1988), and references therein.
4. G. Bérubé and P. Deslongchamps. Can. J. Chem. **68**, 404 (1990).
5. D. Raederstorff, A. Y. L. Shu, J. E. Thompson, and C. Djerassi. J. Org. Chem. **52**, 2337 (1987).
6. E. J. Corey and I. W. Suggs. Tetrahedron Lett. **31**, 2647 (1975).
7. H. Nagaoka and Y. Kishi. Tetrahedron, **37**, 3873 (1981).
8. (*a*) K. E. Wilson, R. T. Seidner, and S. Masamune. J. Chem. Soc. Chem. Commun. 213 (1970); (*b*) T. R. Kelly and P. N. Kaul. J. Org. Chem. **48**, 2775 (1983).

9. E. W. Collington and A. I. Meyers. J. Org. Chem. **36**, 3044 (1971).
10. (*a*) P. A. Grieco, K. Yoshida, and Z. He. Tetrahedron Lett. **25**, 5715 (1984); (*b*) K. Omura and D. Swern. Tetrahedron, **34**, 1651 (1978); (*c*) A. J. Mancuso, S. L. Huang, and D. Swern. J. Org. Chem. **43**, 2480 (1978).
11. W. C. Still and C. Gennari. Tetrahedron Lett. 4405 (1983).
12. J. Boutagy and R. Thomas. Chem. Rev. **74**, 87 (1974).
13. S. Hanessian and P. Lavallée. Can. J. Chem. **53**, 2975 (1975).
14. K. K. Ogilvie, K. L. Sadana, E. E. Thompson, M. A. Quilliam, and J. B. Westmore. Tetrahedron Lett. 2861 (1974).
15. C. L. Rand, D. E. Van Horn, M. W. Moore, and E. Megishi. J. Org. Chem. **46**, 4093 (1981).
16. S. K. Chaudhary and O. Hernandez. Tetrahedron Lett. 99 (1979).
17. (*a*) Y. Tamaru, H. Ochidi, T. Nakamura, and Z. Yoshida. Tetrahedron Lett. **27**, 955 (1986); (*b*) J. K. Stille and J. H. Simpson. J. Am. Chem. Soc. **109**, 2138 (1987); (*c*) O. P. Goel and R. E. Seamans. Synthesis, 538 (1973).
18. G. L. Burge, D. J. Collins, and J. D. Reitze. Aust. J. Chem. **35**, 1913 (1982).
19. E. J. Corey, J. A. Katzenellenbogen, N. W. Gilman, S. A. Roman, and B. W. Erickson. J. Am. Chem. Soc. **90**, 5618 (1968).
20. E. J. Corey and A. Venkateswarlu. J. Am. Chem. Soc. **94**, 6190 (1972).
21. M. Miyashita, A. Yoshikoshi, and P. A. Grieco. J. Org. Chem. **42**, 3772 (1977).
22. C. Prakash, S. Saleh, and I. A. Blair. Tetrahedron Lett. **30**, 19 (1989).
23. R. J. Gregge, J. L. Herrmann, C. S. Lee, J. E. Richman, and R. H. Schlessinger. Tetrahedron Lett. 2425 (1973).
24. A. P. Krapcho and J. F. Weimaster. J. Org. Chem. **45**, 4105 (1980).

Can. J. Chem. Downloaded from www.nrcresearchpress.com by 213.200.69.106 on 09/08/12
For personal use only.

Transannular Diels–Alder reactions on 14-membered macrocyclic trienes. Part II: formation of macrocycles and thermal conversion into tricyclic systems

ALEXIS NDIBWAMI, SERGE LAMOTHE, PIERRE SOUCY, SOLO GOLDSTEIN, AND PIERRE DESLONGCHAMPS[1]

Laboratoire de synthèse organique, Département de chimie, Faculté des sciences, Université de Sherbrooke, Sherbrooke (Québec), Canada J1K 2R1

Received November 16, 1992

ALEXIS NDIBWAMI, SERGE LAMOTHE, PIERRE SOUCY, SOLO GOLDSTEIN, and PIERRE DESLONGCHAMPS. Can. J. Chem. **71**, 714 (1993).

In the preceding paper (Part I) we described the synthesis of eight isomeric acyclic trienes. These compounds could be transformed into the corresponding macrocyclic trienes, which were further converted into tricyclic A.B.C.[6.6.6] products by a thermal transannular Diels–Alder reaction. The experimental results of this study and their analysis are reported in the present paper. The comparison with theoretical predictions is also discussed.

ALEXIS NDIBWAMI, SERGE LAMOTHE, PIERRE SOUCY, SOLO GOLDSTEIN et PIERRE DESLONGCHAMPS. Can J. Chem. **71**, 714 (1993).

Dans l'article précédent (Partie I), nous avons décrit la synthèse de huit trièns acycliques isomères. Ces produits ont été transformés en trièns macrocycliques correspondants qui à leur tour fournissent des produits tricycliques A.B.C.[6.6.6] par une réaction de Diels–Alder transannulaire. Les résultats expérimentaux de ces travaux ainsi que leur analyse sont décrits dans l'article qui suit (Partie II). La comparaison avec les prédictions théoriques est également discutée.

Can. J. Chem. Downloaded from www.nrcresearchpress.com by 213.200.69.106 on 09/08/12
For personal use only.

We recently reported, in preliminary form (1, 2), a general study on the transannular Diels–Alder reaction[2] of 14-membered macrocyclic trienes having a methyl-substituted dienophile. In the preceding paper (4) (Part I) we reported in detail the synthesis of the eight isomeric acyclic triene precursors **1***a–h* (Scheme 1) that were necessary for this study. In this paper (Part II) we wish to report on the formation of the corresponding eight isomeric macrocycles **3***a–h* as well as their thermal conversion into tricyclic products **4***a–f* via the transannular Diels–Alder reaction.

Theoretical predictions on the outcome of transannular Diels–Alder reaction as a function of olefin geometry are first disclosed. The macrocyclization of the eight different acyclic trienes is then presented, followed by a report on the thermal transformation of the eight macrocyclic trienes to tricyclic products. A discussion of the results follows.

Predictions for the transannular Diels–Alder reaction (1)

We first examine the relationship between geometrical isomerism of the macrocyclic triene and stereochemistry in the resulting tricycle.

A diene can have four different configurations (TT (*trans-trans*), TC, CT, and CC) and the dienophile two (C or T). The corresponding macrocyclic trienes **3** can therefore have eight different configurations: *cis-trans-trans* **3***a* (CTT), **3***b* (TCT), **3***c* (CCT), **3***d* (TTT), **3***e* (CTC), **3***f* (TCC), **3***g* (CCC), and **3***h* (TTC). For example, a TC diene with a T dienophile corresponds to a TCT configuration, where the three letters refer to the unsaturations at C5, C3, and C11 respectively. Tricycles **4**, which have four chiral centers (C5 and C8–10, steroid numbering), can exist in eight different racemic diastereoisomeric configurations i.e., *cis-anti-cis* (CAC), *trans-syn-trans* (TST), etc. (Scheme 1).

On first analysis, each triene configuration can theoretically lead to two different tricyclic diastereoisomers (and their respective enantiomer). For example, triene **3***a* (CTT) can give either TAT or CAC tricycles. However, as indicated in Table 1, it can be predicted that several transannular Diels–Alder reactions cannot take place. This is because the Diels–Alder reaction must take place via a boat-like transition state, producing an A.B.C.[6.6.6] tricycle in which the middle ring must be in a boat conformation. Indeed, molecular models show that because of this restriction, which is stereoelectronic in nature, it is sterically impossible in some cases to reach the required transition state. For instance, due to steric reasons, a TAT tricycle cannot take a conformation with ring B in a boat form, and as a result it becomes impossible to produce this compound from **3***a* (CTT) and **3***b* (TCT) macrocyclic trienes.

On the other hand, there are tricycles that can take two such conformations and can thus be produced from two different trienes. This is the case for the CAC tricycle that can be formed from either a **3***a* (CTT) or a **3***b* (TCT) macrocyclic triene. There are other situations where the tricycle can take only one conformation with ring B in a boat form and, therefore, these tricycles can be produced from only one macrocyclic triene. For instance, a TSC tricycle can be produced from the **3***f* (TCC) but not from the **3***e* (CTC) macrocycle. Also, if the triene cannot take a conformation leading to a boat-like transition state as required for the transannular Diels–Alder reaction, then this reaction should not take place. This is the case for the **3***c* (CCT) macrocyclic triene.

In summary, the predictions for the eight triene configurations are the following: one triene, **3***c* (CCT), cannot undergo the transannular Diels–Alder, five trienes, **3***a* (CTT), **3***b* (TCT), **3***c* (CTC), **3***f* (TCC), and **3***g* (CCC), can give only one racemic diastereoisomer, and two trienes, **3***d* (TTT) and **3***h* (TTC), can theoretically lead to two racemic diastereoisomers. Only one (TAT) of the eight diastereoisomeric tricycles cannot be produced directly by a transannular Diels–Alder reaction. It is also interesting to mention that *syn* and *anti* tricyclic compounds are derived from *cis* and *trans* dienophiles, respectively.

The next stage in our investigation was to submit these predictions to experimental verification (2). The required four dienes and two dienophiles were synthesized and assembled

[1]Author to whom correspondence may be addressed.
[2]For recent review, see ref. 3.

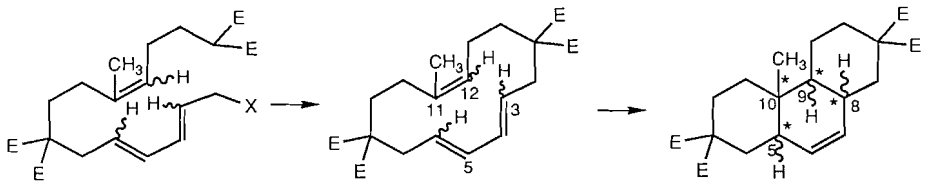

1*a* (CTT)	**2***a* (CTT)	**3***a* (CTT)	**4***a* (CAC)
1*b* (TCT)	**2***b* (TCT)	**3***b* (TCT)	**4***b* (TAC)
1*c* (CCT)	**2***c* (CCT)	**3***c* (CCT)	**4***c* (CAT)
1*d* (TTT)	**2***d* (TTT)	**3***d* (TTT)	**4***d* (CST)
1*e* (CTC)	**2***e* (CTC)	**3***e* (CTC)	**4***e* (TSC)
1*f* (TCC)	**2***f* (TCC)	**3***f* (TCC)	**4***f* (TST)
1*g* (CCC)	**2***g* (CCC)	**3***g* (CCC)	
1*h* (TTC)	**2***h* (TTC)	**3***h* (TTC)	
X = OH	X = Cl		

SCHEME 1

TABLE 1. Predictions for the transannular Diels–Alder reaction

Entry	Tricycles **4** stereochemistry		Triene **3** geometry		Tricycles **4** stereochemistry
1	TAT	←✕—	CTT	⟶	CAC
2	TAT	←✕—	TCT	⟶	CAC
3	TAC	←✕—	CCT	✕⟶	CAT
4	TAC	←—	TTT	⟶	CAT
5	TSC	←✕—	CTC	⟶	CST
6	TSC	←—	TCC	⟶	CST
7	TST	←✕—	CCC	⟶	CSC
8	TST	←—	TTC	⟶	CSC

using dimethyl malonate to produce the eight acyclic triene precursors as described in Part I.

Macrocyclization and transannular Diels–Alder reaction

The allylic alcohol triene precursors **1***a–h* were first converted into their corresponding allylic chlorides **2***a–h* using the method described by Collington and Meyers (5) (CH_3SO_2Cl, LiCl, collidine, DMF). Macrocyclization of allylic chlorides **2***a–h* was carried out (6) by slow addition under medium dilution conditions ((1–5) × 10^{-3} M) to a solution of cesium carbonate in tetrahydrofuran–dimethylformamide (1:1) at 80–85°C. The results obtained at the macrocyclization step and at the Diels–Alder stage are summarized in Table 2. The expected macrocycles were isolated in six cases (entries 1–3 and 5–7). These macrocycles, namely, **3***a* (CTT), **3***b* (TCT), **3***c* (CCT), **3***e* (CTC), **3***f* (TCC), and **3***g* (CCC), were found to be crystalline and the structures of three of them, **3***e* (CTC),[3] **3***a* (CTT),[3] and **3***b* (TCT),[4] were rigorously confirmed by X-ray diffraction analysis. In the remaining cases, **3***d* (TTT) and **3***h* (TTC), which have a TT diene, tricyclic compounds rather than the expected macrocycles were directly isolated, indicating that the Diels–Alder reactions took place at the macrocyclization temperature (~80°C). More precisely, the **3***d* (TTT) acyclic triene gave a 2:1 mixture of **4***b* (TAC) and **4***c* (CAT) tricycles in 65% yield, whereas the **3***h* (TTC) macrocylic triene gave the **4***f* (TST) tricycle (53%) along with a side product **5** (23%) (Scheme 2) having a 12-membered ring. Compound **5**, whose structure was established by X-ray analysis (7), is the result of an S_N2' macrocyclization of the TTC allylic chloride **2**.

The mild reaction conditions for the cycloaddition of the **3***d* (TTT) and **3***h* (TTC) macrocycles are explained by the fact that the TT diene can easily adopt the required *cisoid* conformation, which is devoid of steric repulsion. The other macrocycles had to be heated at high temperature (>300°C) in order to observe a complete thermal conversion, indicating that, as expected, there is severe steric hindrance that prevents the formation of the *cisoid* conformation when the diene has a CT or CC geometry.

The macrocyclization experiment on the TTC allylic chloride **2***h* was repeated at lower temperature (45°C), where it was found possible to isolate the corresponding **3***h* (TTC) macrocycle (26%) along with compound **5** as well as cyclic dimer **6** (11%). The TTC macrocycle was shown to undergo

[3]G. Boulay, M. Drouin, and A. Michel. Unpublished results.
[4]J. P. Springer, K. Hoogsteen, and A. Michel. Unpublished results.

Can. J. Chem. Downloaded from www.nrcresearchpress.com by 213.200.69.106 on 09/08/12
For personal use only.

TABLE 2. Macrocyclization and transannular Diels–Alder reaction

Entry	Macrocycle **3** geometry (yield)	Diels–Alder Temperature (°C)	Diels–Alder Time	Tricycle **4** (stereochemistry)	Ratio	Yield (%)
1	**3***a* (CTT) (87%)	300	1 h 45 min	**4***a* (CAC)	—	91
2	**3***b* (TCT) (46%)	350	1 h	**4***a* (CAC) + **13** + **15**	2:1:3	>90
3	**3***c* (CCT) (45%)	300	3 h	**4***a* (CAC) +**17** + **13** + **15**	1:4.6:1:2	>90
4	**3***d* (TTT) (not isolated)	80	—	**4***c* (CAT) + **4***b* (TAC)	1:2	65
5	**3***e* (CTC) (89%)	300	2 h 45 min	**4***d* (CST)	—	89
6	**3***f* (TCC) (86%)	300	2 h	**4***e* (TSC)	—	100
7	**3***g* (CCC) (78%)	365	30 min	**4***d* (CST) + **4***e* (TSC)	1:1	95
8	**3***h* (TTC) (not isolated)	80	—	**4***f* (TST) + **5**	2:1	53 + 23

a cycloaddition at 80°C, giving the TST tricycle in quantitative yield. On the other hand, the TTT allylic chloride **2***d* does not undergo macrocyclization at a temperature lower than 60°C, and at this temperature it leads directly to the same 2:1 mixture of TAC and CAT tricycles. Thus, macrocyclization of **2***d* (TTT) is more difficult than that of TTC macrocycles **3***h*, but it was not possible to verify the minimum temperature required for the cycloaddition reaction as it takes place readily at 60°C.

Macrocycles **3***a* (CTT), **3***e* (CTC), and **3***f* (TCC) (entries 1, 5, and 6), upon heating at 300°C, gave the predicted tricycles **4***a* (CAC), **4***d* (CST), and **4***e* (TSC), respectively. Upon heating at 350°C, the **3***b* (TCT) macrocycle (entry 2) gave, in addition to the predicted **4***a* (CAC) tricycle, two other products having structures **13** and **15** (Scheme 3) (see also footnote 8). As mentioned above, the **3***d* (TTT) macrocycle (entry 4) could not be isolated, since the result obtained indicates that it led to the predicted **4***b* (TAC) and **4***c* (CAT) tricycles. Also, the **3***h* (TTC) macrocycle (entry 8) gave the predicted **4***f* (TST) tricycle; however, none of the other predicted diastereoisomer, i.e., the CSC tricycle, was observed. Upon heating at 365°C, the **3***g* (CCC) macrocycle (entry 7) did not lead to the predicted CSC tricycle, but rather gave a 1:1 mixture of the **4***d* (CST) and **4***e* (TSC) tricycles. Finally, the **3***c* (CCT) macrocycle (entry 3), which was predicted not to produce a Diels–Alder adduct, upon heating at 365°C gave a mixture of four isomeric products. The major isomer was shown to have the bicyclic structure **17** (Scheme 4) by X-ray diffraction analysis.[5] The other three products were found to be identical to those obtained from the **3***b* (TCT) macrocycles, i.e., CAC tricycle **4***a* plus compounds **13** and **15** (see footnote 8). All thermal processes took place in high yield. The lower overall yield observed in the **3***d* (TTT) and **3***h* (TTC) series (entries 4 and 8) is mainly the result of a low yield at the macrocyclization step. The structures of the **4***e* (TSC)[4] and **4***f* (TST) (7) tricycles were established by X-ray analyses. The structure of the **4***a* (CAC) tricycle was rigorously established in a closely related series.[6] The structure of CAT tricycle **4***c* was elucidated by a chemical correlation. In another study,[7] a mixture of TAC and CAT tricycles **7***a* and **7***b* (Scheme 2), which contain only three ester functions, was obtained from the corresponding TTT macrocycle. The structure of TAC tricycle **7***a* was established by X-ray analysis[7] and the other isomer, CAT tricycle **7***b*, was converted (LDA, $ClCOOCH_3$) into CAT tricycle **4***c*.

Discussion

The **3***a* (CTT) and **3***b* (TCT) macrocycles, which are predicted to give the same **4***a* (CAC) tricycle, can be analyzed together (Scheme 3). Assuming that the Diels–Alder reaction takes place via a chair–boat–chair-like transition state, molecular models clearly indicate that the methyl group of the dienophile creates more steric hindrance in the CAC transition state resulting from TCT (cf. **10** → **11**) than in that resulting from CTT (cf. **8** → **9**). As a consequence, the reaction TCT → CAC, i.e., **10** → **11**, is not quantitative and the formation of side products **13** and **15** is observed. The formation of the a priori unexpected tricycle **15** from the TCT macrocycle **3***b* can be explained by the competing transannular ene reaction **12** → **13** producing a bicyclic intermediate that undergoes another transannular ene reaction to give the new CTT macrocyclic triene **14**. Compound **14** is then easily transformed into CAC tricycle **15**, because the Diels–Alder reaction is no longer sterically hindered by the presence of the methyl group. Interestingly, the sequence **12** → **13** → **14** is an oxido-reduction process in which the dienophile and the diene have been mutually interconverted.[8]

The results obtained from the CCT macrocycle **3***c*, which cannot undergo a direct Diels–Alder reaction, are examined next. The formation of the major product, bicyclo[8.4.0] system **17**, is readily rationalized via a transannular ene reaction as shown (**16**→ **17**) in Scheme 4. On the other hand, since we know that the TCT macrocycle **3***b* gives CAC tricycle **4***a* as well as **13** and **15** whereas the CTT macrocycle **3***a* gives only the CAC tricycle **4***a*, it is reasonable to as-

[5]A. Ndibwami, M. Drouin, and A. Michel. Unpublished results.

[6]In another study, it was shown that CTT macrocycle **3** having three ester functions gave the corresponding CAC tricycle whose structure was confirmed by X-ray analysis (8).

[7]M. Drouin, A. G. Michel, P. Soucy, and P. Deslongchamps. Unpublished results.

[8]The structure of CAC tricycle **15** was secured by X-ray analysis (9*b*). In another study,[9] it was observed that when TCT macrocycle contains an additional methyl group on the diene, i.e., **12** (H1 = CH_3), the formation of a CAC tricycle corresponding to **4** with an additional CH_3 at C8 is not observed because there are too many severe steric interactions in the corresponding transition state. Instead, the exclusive formation of CAC tricycle **15** (H1 = CH_3) occurs via the intermediate **13** (H1 = CH_3), which was characterized spectroscopically. The structure of CAC tricycle **15** (H1 = CH_3) was also firmly established by X-ray analysis (9*a*).

[9]A. Roughton and P. Deslongchamps. Unpublished results.

Can. J. Chem. Downloaded from www.nrcresearchpress.com by 213.200.69.106 on 09/08/12
For personal use only.

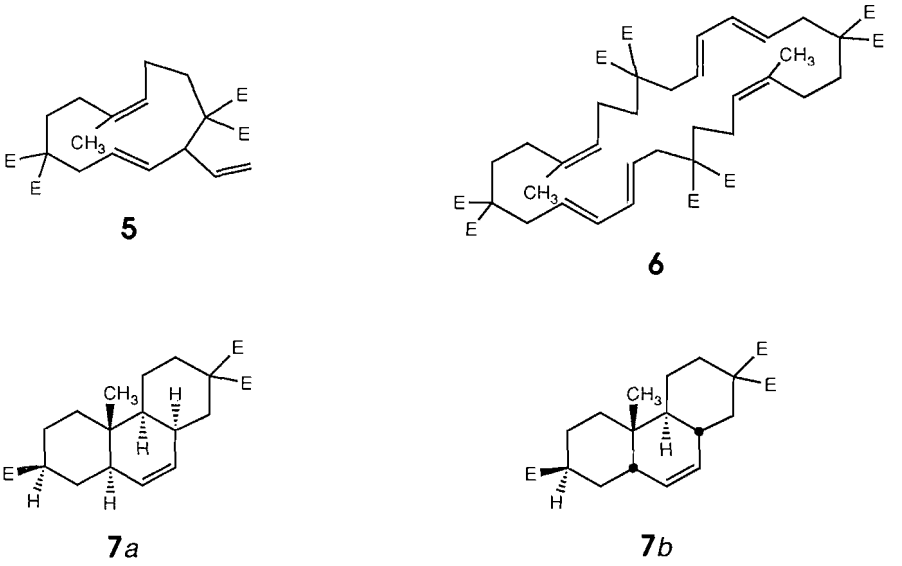

(E = $COOCH_3$)

SCHEME 2

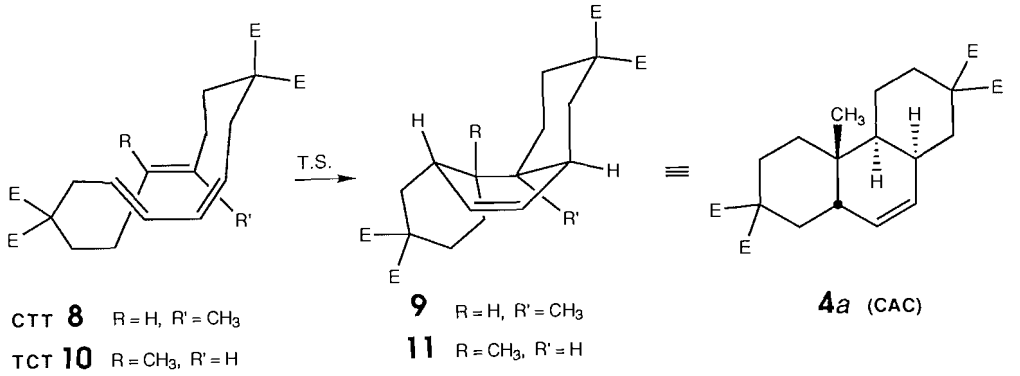

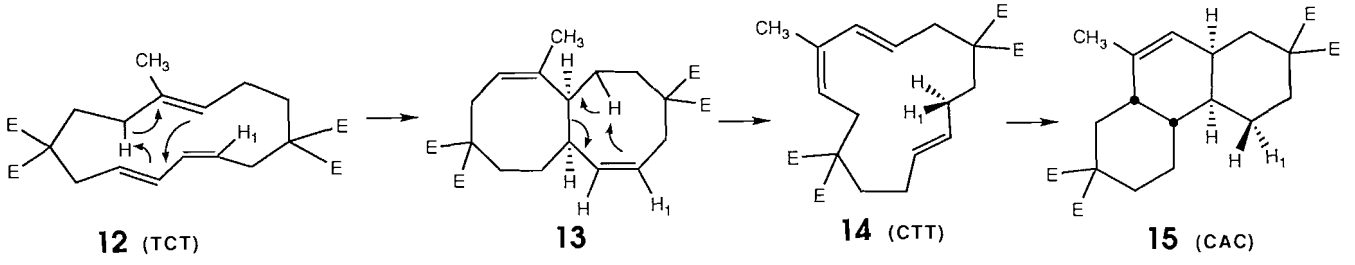

(E = $COOCH_3$)

SCHEME 3

sume that the CCT macrocycle **3***c* must have partly isomerized into a mixture of CTT and TCT macrocycles **3***a* and **3***b* in order to produce a mixture of CAC tricycle **4***a*, **13**, and **15** (but in a different ratio than that from TCT macrocycle **3***b*). The thermal isomerization of the CCT macrocycle **3***c* can be explained by two series of [1,5] hydride shifts. First, CCT macrocycle **3***c* can either produce CTT macrocycle **19** (cf. **18** → **19**) or TCT macrocycle **20** (cf. **18** → **20**). Then, the new CTT and TCT macrocycles **19** and **20** can be transformed into the known TCT and CTT macrocycles **3***b* and **3***a* by another [1,5] sigmatropic hydrogen migration. The mixture obtained, of TCT and CTT macrocycles **3***b* and **3***a*, is finally converted into a mixture of **4***a* (CAC), **13**, and **15** in a ratio different than that obtained from the TCT macrocycle **3***b*. It is interesting to note that intermediates **19** and **20** do not undergo a Diels–Alder reaction, probably because they would produce tricycles having an A.B.C.[5.6.7] ring structure. Such processes must be sterically disfavored due to the formation of the seven-membered ring.

The Diels–Alder reactions of the **3***e* (CTC) and **3***f* (TCC)

Can. J. Chem. Downloaded from www.nrcresearchpress.com by 213.200.69.106 on 09/08/12
For personal use only.

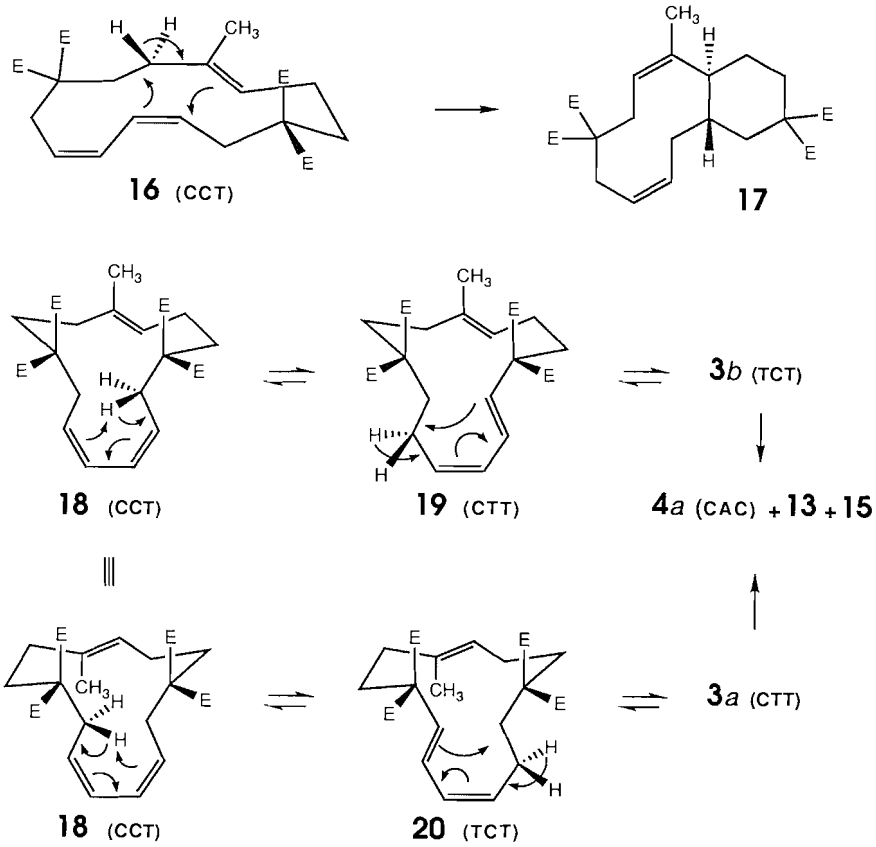

SCHEME 4

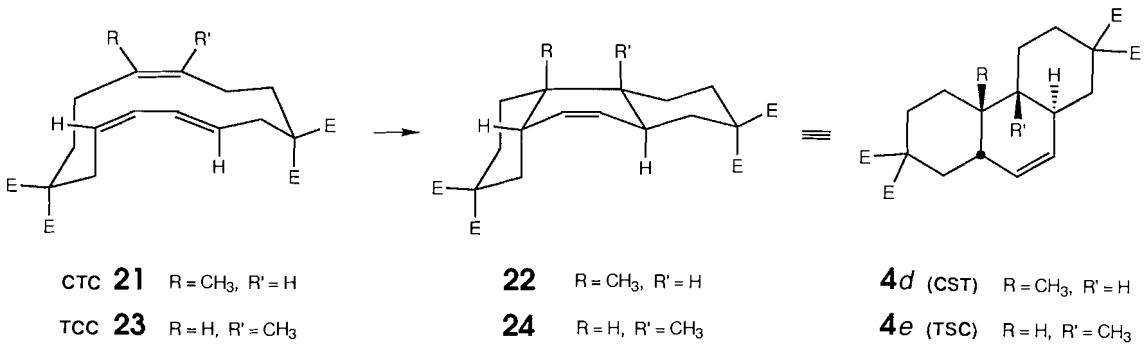

SCHEME 5

macrocycles yielding **4***d* (CST) and **4***f* (TSC) tricycles, respectively, are readily explained. Indeed, both processes (**21** → **22** and **23** → **24**) can take place via a chair–boat–chair-like transition state essentially devoid of severe steric repulsions, as indicated in Scheme 5.

The predicted formation of the CSC tricycle from the CCC macrocycle **3***g* did not occur because this process would have to take place via a very severely crowded transition state (cf. **25** → **26**, Scheme 6). This situation results from the fact that the *cis-cis* diene becomes sterically congested when it must take the *cisoid* geometry required for the Diels–Alder reaction. The formation of a 1:1 mixture of CST and TSC tricycles **4***d* and **4***e* suggests that rather than yielding the CSC tricycle, which is too costly energetically (cf. conformation **26**), CCC macrocycle **3***g* undergoes a thermal isomerization through sequential hydride shift (**27** → **28** → **21** or **29** → **30** → **23**) to give a mixture of CTC and TCC macrocycles **21** and **23**, which are then respectively converted into CST and TSC tricycles **4***d* and **4***e* as described in Scheme 5.

The selective formation of TST tricycle **4***d* from TTC

Can. J. Chem. Downloaded from www.nrcresearchpress.com by 213.200.69.106 on 09/08/12
For personal use only.

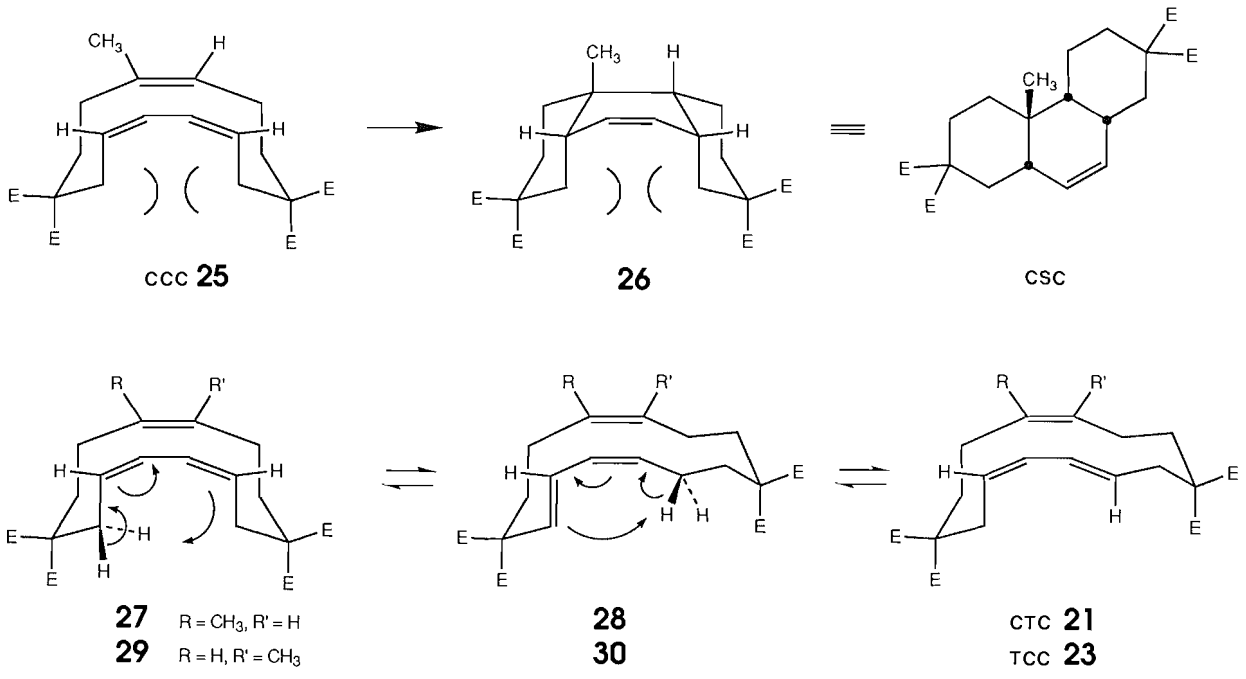

SCHEME 6

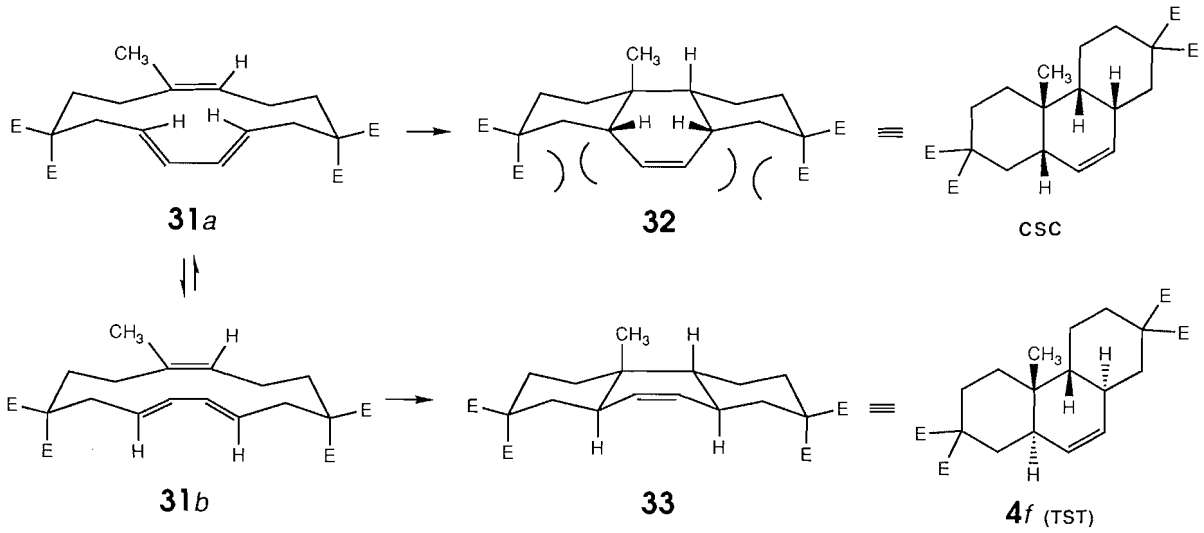

SCHEME 7

macrocycle **3***h* can be readily explained by considering the relative steric effect played by the ester function at the transition state level. TTC macrocycle **3***h* can either react via conformations **31***a* or **31***b* (Scheme 7) producing CSC and **4***f* (TST) tricycles in conformations **32** and **33**, respectively. Analysis of molecular models reveals that, in the chair–boat–chair transition state which leads to the CSC tricycle (**31***a* → **32**), there are two 1,3-diaxial-type steric interactions between each pseudo-axial ester function and a CH group of the olefin. There are no equivalent interactions in the competing transition state (**31***b* → **33**). This steric effect would therefore be the main discriminating factor favoring formation of a **4***f* (TST) tricycle.

It remains to explain the formation of TAC and CAT tricycles **4***b* and **4***c* from TTT macrocycle **3***d*. Assuming chair–boat–chair-like transition states, TTT macrocycle **3***d* was expected to react via conformations **34***a* and **34***b* (Scheme 8) to yield **4***c* (CAT) and **4***b* (TAC) tricycles, respectively. The two competing pathways can be best compared by examining their respective transition states (**34***a* → **35** and **34***b* → **36**). Examination of molecular models shows that structures **35** and **36** have identical conformations. Indeed if rings

Can. J. Chem. Downloaded from www.nrcresearchpress.com by 213.200.69.106 on 09/08/12
For personal use only.

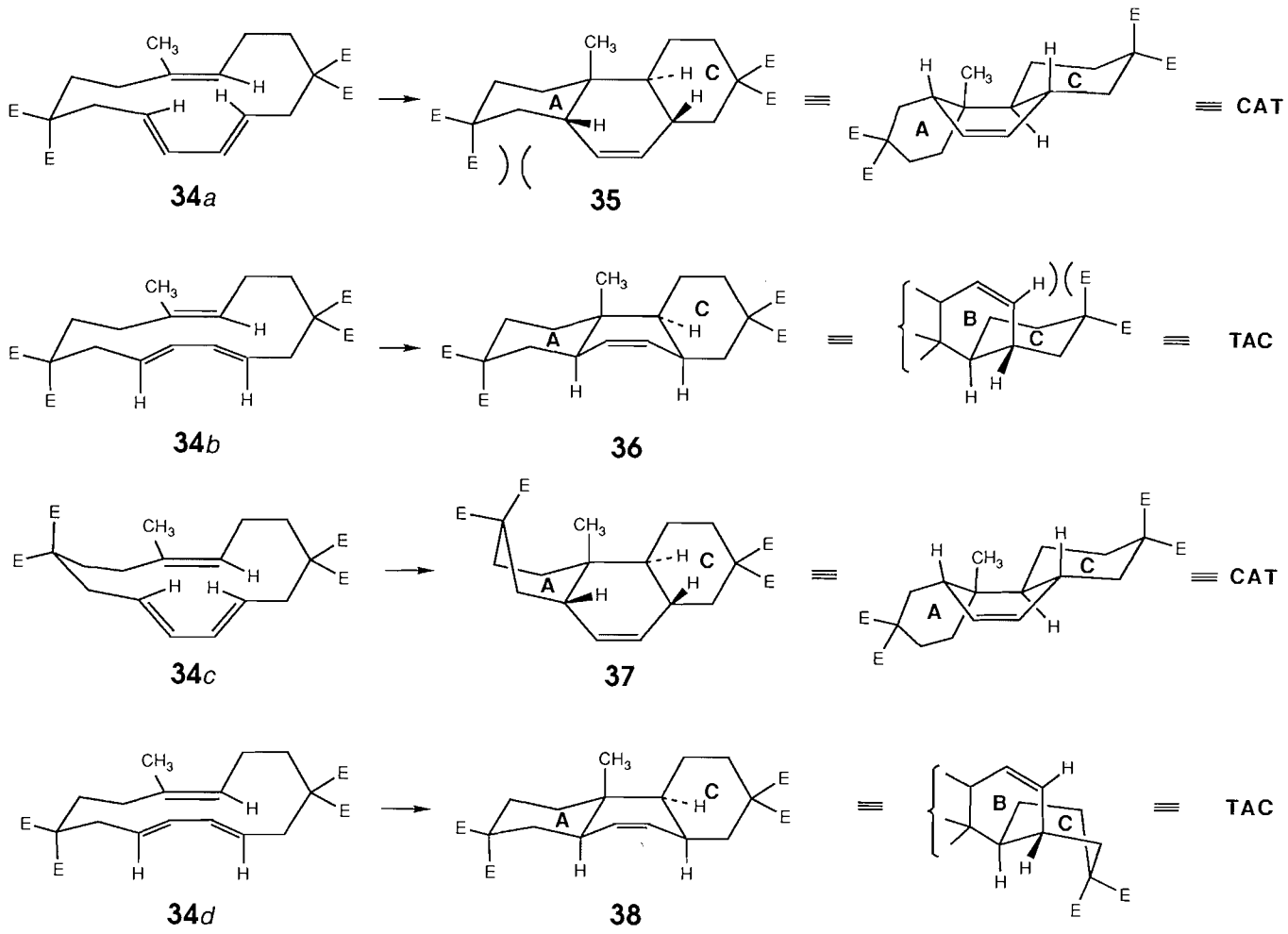

SCHEME 8

CBA of **36** are superposed on rings ABC of **35** the only difference resides in the location of the methyl group. The models also indicate that this group is sterically more crowded in **36** than in **35**. The difference does not appear to be very large, and a mixture is therefore expected; surprisingly, however, this analysis predicts a ratio with the CAT tricycle (**34***a* → **35**) predominating, in contradiction of the experimental ratio observed!

Since it does not appear possible to involve the influence of a stereoelectronic effect because the only substituent is a methyl group, this led us to assume that the formation of the **4***c* (CAT) and **4***b* (TAC) tricycles might take place via a boat–boat–chair rather than the normally more appealing chair–boat–chair transition state. In transition states **34***a* → **35** and **34***b* → **36**, there is a severe pseudo 1,3 diaxial steric interaction between one ester function and the olefinic CH group; this interaction occurs in ring A for CAT (cf. **35**) and in ring C for TAC (cf. **36**). These steric interactions can be eliminated if the formation of the **4***c* (CAT) and **4***b* (TAC) tricycles takes place, respectively, from boat–boat–chair or chair–boat–boat transition states **34***c* → **37** and **34***d* → **38** (Scheme 8). These two new transition states are quite appealing because the relative ratio of the **4***b* (TAC) and **4***c* (CAT) tricycles can be readily explained. Indeed, in **34***c* → **37**, the methyl group is in a boat-like conformation (cf. ring A in **37**), creating more steric hindrance than in **34***d* → **38** where the methyl group is in a chair-like conformation (cf. ring A in **38**). On that basis, transition state **34***d* → **38** is of lower energy than **34***c* → **37**, and this explains why the TAC tricycle is obtained as the major isomer. As bond formation is not yet completed at the transition state level, boat–boat–chair can easily compete on a steric basis with chair–boat–chair in order to avoid additional steric interactions occurring in the latter.[10]

In general, the results summarized in Table 2 confirm the predictions made in Table 1. The anomalous results observed (entries, 2, 7, and 8) are readily rationalized on the basis of a simple analysis at the transition state level. The global results demonstrate the power of the transannular Diels–Alder reaction on macrocyclic trienes for the construction of tricyclic compounds. Indeed, so far, six of the eight possible diastereoisomers can be obtained and the degree of stereochemical control is remarkable.

[10]An experimental demonstration that boat–boat–chair can compete with chair–boat–chair was later obtained in another study (C. Ouellet and P. Deslongchamps, unpublished results). This work has been summarized (cf. p. 53 and Scheme 17 in ref. 3).

Can. J. Chem. Downloaded from www.nrcresearchpress.com by 213.200.69.106 on 09/08/12
For personal use only.

Can. J. Chem. Downloaded from www.nrcresearchpress.com by 213.200.69.106 on 09/08/12
For personal use only.

These assumptions were also examined using Sybyl molecular modeling software. Thus the TTT macrocycle (*transoid* diene) was constructed by standard functions within Sybyl; a dynamic trajectory was then simulated (1 fs time step) at 500 K (temperature coupling factor 25 fs) during 10 ps. Conformers at each 100 fs were saved and minimized by Maximin. The assembly of 100 conformers thus generated was checked to remove duplicata and locate lowest energy conformers. Besides conformers with a *transoid* diene moiety (lowest in energy), four other minima (*cisoid* diene) were found within a 3 kcal range (Fig. 1).

The planes of the diene and dienophile moieties are perpendicular to the plane of the macrocycle, thus minimizing transannular nonbonded interactions (10) and placing the π systems in the plane of the ring. The distances between the extremities of the diene and dienophile are only 3–3.5 Å, with the olefin slightly twisted relative to the diene.

To mimic the situation in the transition state more closely, the torsion angle between the forming bonds and the torsion angle in the butadiene moiety were set at 0° as found by *ab initio* calculations for the transition state of butadiene and ethylene (11).

The distances between the termini of the dienophile and the diene were set to 3 Å and the structures obtained were minimized using these constraints,[11] leading to the geometries depicted in Fig. 2. Structures like A′ (chair–boat–chair) (cf. **34***b* → **36**) and B′ (chair–boat–boat) (cf. **34***d* → **38**) would generate the **4***b* (TAC) product while C′ (chair–boat–chair) (cf. **34***a* → **35**) and D′ (chair–boat–boat) (not shown) would produce the **4***c* (CAT) isomer.

Taking into account the early nature of the Diels–Alder transition state and the close similarity of the structures, one might expect to get a fair estimation of the product ratio from the relative energies of A′–D′. Indeed a Boltzmann distribution among the above four states indicated that the TTT macrocycle should lead to a product ratio **4***b* (TAC):**4***c* (CAT) of 2:1, in complete agreement with the experimental result (A′:B′:C′:D′ = 0.58:0.1:0.3:0). To investigate further possible transition states a structure with a boat–boat–chair arrangement (cf. **34***c* → **37**, Scheme 8) leading to CAT isomer **4***c* has been constructed:[13] the energy of the minimized structure was found to be 4 kcal higher than that of C′ (chair–boat–chair arrangement) thus indicating that this kind of transition state should be eliminated. Even if the boat–boat–chair state is considered instead of D′ (chair–boat–boat), which is about 2 kcal higher in energy, the Boltzmann distribution of the four states is still that indicated previously. Thus, the above calculations suggest that the TAC tricycle **4***b* would be obtained mainly via a chair–boat–boat transition state while the **4***c* (CAT) isomer would be obtained from a chair–boat–chair transition state, and this explains nicely the ratio of the obtained products.

[11]An accurate description of the transition state requires a higher level of theory. Very recently empirical force-field models for the transition states of intramolecular Diels–Alder reactions based upon *ab initio* transition structures have been described (12). Available software that uses the MMX[12] force field and allows a choice of bond orders between two atoms in the transition state did not lead in our case to results in agreement with experiment. This has been observed also for other examples (12).

[12]PC MODELS. Serena Software, P.O. Box 3076, Bloomington, IN 47402-3076, U.S.A.

[13]The corresponding conformers have not been detected by our short dynamic simulation; the structure was constructed from structure B′ by removing the methyl group and placing it at the other end of the olefin.

Conclusion

The work reported in the present paper further extends the scope of the transannular Diels–Alder reaction as a powerful synthetic strategy for the stereoselective preparation of A.B.C.[6.6.6] tricycles. It also answers questions about the factors governing the stereochemical outcome of the cycloaddition reaction and factors leading to competing chemical processes.

The knowledge of such factors stemming from a high degree of conformational restriction of macrocyclic trienes leads to predictable results in terms of stereochemistry, and therefore such an approach should be more advantageous than conventional intramolecular reactions. Moreover, transannular Diels–Alder reactions may be performed with nonactivated dienophiles and with *cis,trans* dienes, processes that are very rare in classical inter- and intramolecular cycloadditions. Also, all eight stereoisomers of the tricyclic products might be obtained by such a strategy whereas conventional cycloadditions usually afford one or two such stereoisomers.

Optimization of the developed schemes as well as applications of the described results to syntheses of natural products is underway in our laboratory.

Experimental

General

The ir spectra were taken on a Perkin–Elmer 681 spectrophotometer using chloroform ($CHCl_3$), dichloromethane (CH_2Cl_2), or run as neat films on sodium chloride cells. Proton nmr spectra were recorded on a Bruker WP-80 or Bruker WM-250 instrument. The following abbreviations have been used: s, singlet; d, doublet; dd, doublet of doublets; dt, doublet of triplets; ddd, doublet of doublets of doublets; dddd, doublet of doublets of doublets of doublets; ddt, doublet of doublets of triplets; ddq: doublet of doublets of quartets; t, triplet; td: triplet of doublets; q, quartet; and m, multiplet. Chemical shifts are reported in δ values relative to chloroform as internal standard. Carbon nuclear magnetic resonance spectra were recorded on a Bruker WP-80 or Bruker WM-250 instrument (chloroform as internal standard). Mass spectra were obtained on a Micromass ZAB-2F instrument. Melting points were determined on a Büchi M-50 or on a Reichert apparatus and are uncorrected.

Unless otherwise specified, all reactions were performed under an argon atmosphere and were monitered by thin-layer chromatography. For flash chromatography, silica gel Merck Kieselgel 60 (230–400 mesh, ASTM) was used. All solvents used in chromatography were distilled. Anhydrous solvents were obtained by standard means.

Macrocyclization

Allylic chloride **2**a *(CTT)*

To a solution of CTT alcohol **1***a* (160 mg, 0.35 mmol), lithium chloride (59 mg, 1.40 mmol), and *s*-collidine (68 mg, 0.56 mmol) in 5 mL of dimethylformamide at 0°C was added, dropwise, methanesulfonyl chloride (60 mg, 0.53 mmol). The mixture was then warmed up to room temperature and stirred for 3 h, and was then poured onto 25 mL of ice-water. After extraction with a 2:1 mixture of ether and hexane (3 × 20 mL) the combined organic layers were washed with water (10 mL), then with a saturated aqueous solution of copper nitrate (10 mL), again with water (10 mL), and were dried over magnesium sulfate. The crude product obtained after evaporation of the solvent was purified by column

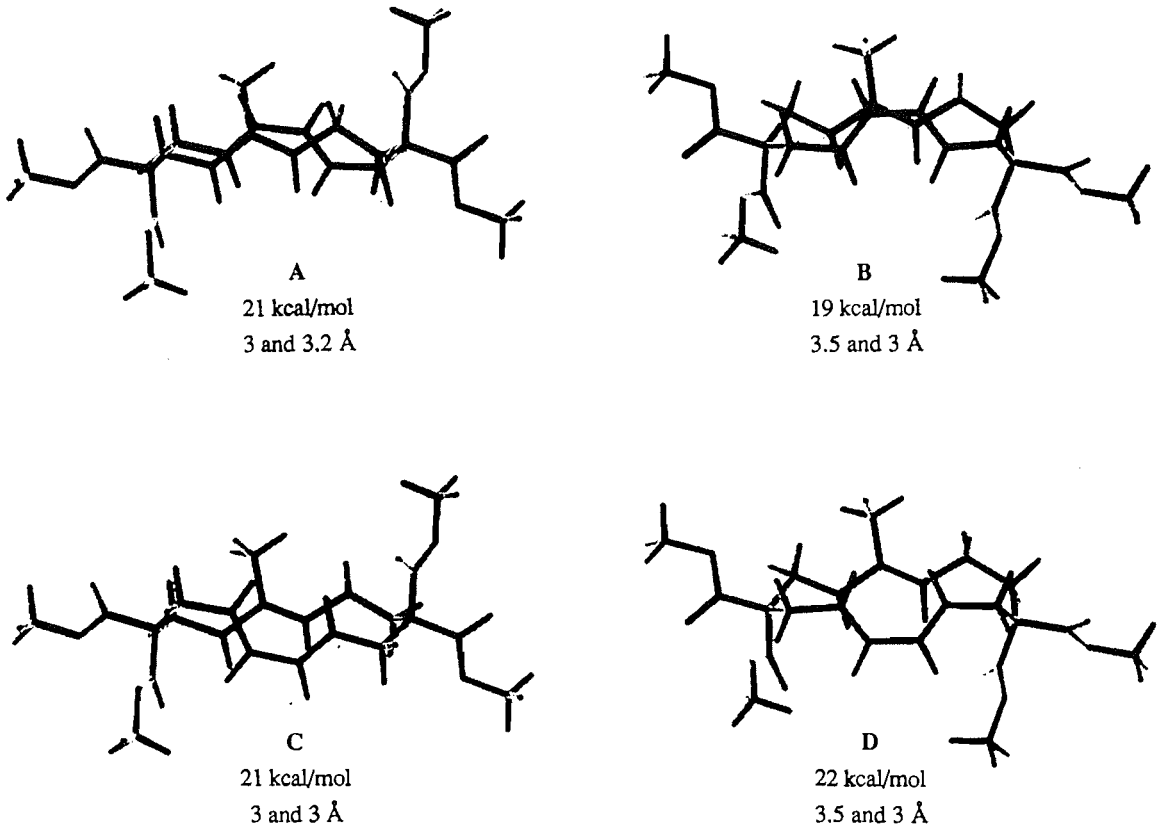

FIG. 1. Lowest energy conformers of TTT macrocycle (*cisoid* diene). Steric energies and distances between the diene and dienophile extremities.

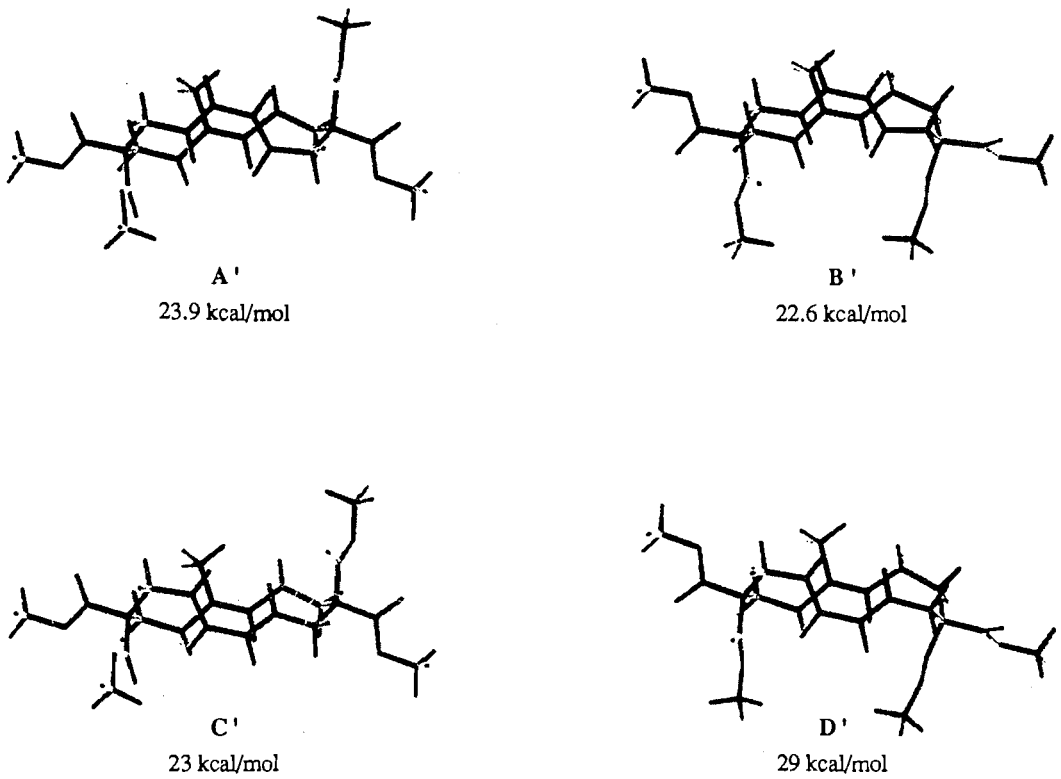

FIG. 2. Transition-state-like structures (steric energies).

Can. J. Chem. Downloaded from www.nrcresearchpress.com by 213.200.69.106 on 09/08/12
For personal use only.

Can. J. Chem. Downloaded from www.nrcresearchpress.com by 213.200.69.106 on 09/08/12
For personal use only.

chromatography on silica gel with 10% ethyl acetate in hexane to afford CTT chloride **2***a* (147 mg, 89%); ir ($CHCl_3$): 3015, 2950, and 1730 cm^{-1}; ^1H nmr ($CDCl_3$) δ: 6.57 (1H, ddq, J = 14.9, 11.1, and 1.1 Hz, -C*H*=CH-CH_2-Cl), 6.11 (1H, br t, J = 11.1 Hz, -$(CO_2CH_3)_2$C-CH_2CH=C*H*-), 5.83 (1H, dt, J = 14.9 and 7.3 Hz, =C*H*-CH_2-Cl), 5.36 (1H, dt, J = 11.0 and 7.8 Hz, -$(CO_2CH_3)_2$C-CH_2-C*H*=), 5.08 (1H, br t, J = 6.8 Hz, =C*H*-CH_2-CH_2-), 4.13 (2H, dd, J = 7.2 and 1.0 Hz, -CH_2-Cl), 3.73 and 3.71 (12H, 2s, -$(CO_2CH_3)_2$-), 3.35 (1H, t, J = 7.3 Hz, -C*H*$(CO_2CH_3)_2$), 2.80 (2H, dd, J = 8.0 and 1.4 Hz, -$(CO_2CH_3)_2$C-C*H*$_2$-CH=), 2.07–1.75 (8H, m, -$(CH_2)_2$-C(CH_3)=CH-$(CH_2)_2$-), 1.55 (3H, d, J = 1.2 Hz, C*H*$_3$-C=).

Allylic chloride **2**d *(TTT)*

To a solution of TTT alcohol **1***d* (101 mg, 0.22 mmol), lithium chloride (19 mg, 0.44 mmol), and *s*-collidine (40 mg, 0.33 mmol) in dimethylformamide (1 mL) at 0°C was added methanesulfonyl chloride (35 mg, 0.31 mmol). The mixture was warmed up to room temperature and stirred for 3 h. It was then poured into water (10 mL) and extracted with a mixture of ether and hexane (2:1) (3 × 10 mL). The combined organic layers were washed with water (5 mL), a saturated aqueous solution of copper nitrate (5 mL), and finally with brine (5 mL). The crude oil obtained after evaporation of the solvent was purified by column chromatography on silica gel using 20% ethyl acetate in hexane to give TTT chloride **2***a* (71 mg, 68%); ir ($CHCl_3$): 3020, 2955, 1740, and 1730 cm^{-1}; ^1H nmr ($CDCl_3$) δ: 6.23 (1H, dd, J = 14.8 and 10.5 Hz, =C*H*-CH=), 6.07 (1H, dd, J = 14.8 and 10.5 Hz, =CH-C*H*=), 5.71 (1H, dt, J = 14.7 and 7.2 Hz, =C*H*-CH_2-Cl), 5.56 (1H, dt, J = 14.8 and 7.4 Hz, -$(CO_2CH_3)_2$C-CH_2-C*H*=), 5.08 (1H, m, =C*H*-C*H*$_2$-CH_2), 4.07 (2H, d, J = 7.3 Hz, -C*H*$_2$-Cl), 3.72 and 3.71 (12H, 2s, -$(CO_2CH_3)_2$-), 3.35 (1H, t, J = 7.2 Hz, -C*H*$(CO_2CH_3)_2$), 2.68 (2H, d, J = 7.6 Hz -$(CO_2CH_3)_2$C-C*H*$_2$-CH=), 2.10–1.77 (8H, m, -$(CH_2)_2$-C(CH_3)=CH$(CH_2)_2$), 1.55 (3H, s, C*H*$_3$-C=); ms *m/e*: 441 ($M^+ - OCH_3$), 436 ($M^+ - HCl$). Exact Mass calcd.: 441.1680 ($M^+ - OCH_3$); found: 441.1674 ± 0.0013.

Macrocycle **3**a *(CTT)*

To a solution of cesium carbonate (103 mg, 0.32 mmol) in 4.5 mL of tetrahydrofuran and 3.5 mL of dimethylformamide at 85°C was added, over a period of 5 h, CTT chloride **2***a* (30 mg, 0.063 mmol) dissolved in 9 mL of a mixture of tetrahydrofuran and dimethylformamide (4:5). After the addition was completed, the mixture was stirred for an additional hour and, after cooling to room temperature, the carbonate was filtered off. The solvents were evaporated (0.5 Torr (1 Torr = 133.3 Pa), 45°C) and the residue was subjected to column chromatography purification using 10% ethyl acetate in hexane to afford CTT macrocycle **3***a* (24 mg, 87%), which could be recrystallized from ether (mp 143–153°C); ir ($CHCl_3$): 2955 and 1730 cm^{-1}; ^1H nmr ($CDCl_3$) δ: 6.13 (2H, m, =C*H*-C*H*=), 5.36–5.16 (2H, m, =C*H*-CH_2-CH_2- and -C*H*=CH-CH_2-), 5.01 (1H, br, q, J = 9.1 Hz, -CH_2=C*H*-), 3.74 and 3.73 (12H, 2s, -CO_2CH_3), 2.77 (2H, br, d, J = 6.8 Hz, -CH=CH-C*H*$_2$), 2.74 (2H, br, d, J = 8.4 Hz, -C*H*$_2$-CH=CH-), 2.05–1.74 (8H, m, -$(CH_2)_2$-C(CH_3)=CH-$(CH_2)_2$), 1.58 (3H, d, J = 1.1 Hz, C*H*$_3$-C=); ms *m/e*: 436 (M^+), 421 ($M^+ - CH_3$), 405 ($M^+ - OCH_3$). Exact Mass calcd.: 436.2097; found: 436.2095 ± 0.015.

Macrocycle **3**e *(CTC)*

CTC Allylic chloride **2***e* was obtained in 76% yield after chromatography (based on 10% recovered starting material), following the procedure described above; ir ($CHCl_3$): 3020, 2950, 1730 cm^{-1}; ^1H nmr ($CDCl_3$) δ: 6.58 (1H, ddm, J = 14.9 and 11.1 Hz, -C*H*=CH-CH_2-Cl), 6.12 (1H, bt, J = 11.3 Hz, -$(CO_2CH_3)_2$C-CH_2-CH=C*H*-), 5.83 (1H, dt, J = 14.9 and 7.2 C*H*, =C*H*-CH_2-Cl), 5.37 (1H, dt, J = 10.9 and 8.0 Hz, $(CO_2CH_3)_2$C-CH_2-C*H*=), 5.02 (1H, m, =C*H*-CH_2-CH_2), 4.13 (2H, dd, J = 7.2 and 1.0 Hz, -C*H*$_2$Cl), 3.73 and 3.72 (12H, 2s, 4 × -CO_2CH_3), 3.34 (1H, t, J = 7.2 Hz, -C*H*$(CO_2CH_3)_2$), 2.81 (2H, dd, J = 8.0 and 1.4 Hz, -$(CO_2CH_3)_2$C-C*H*$_2$-CH=), 2.03–1.75 (8H, m, -$(CH_2)_2$), 1.65 (3H, d, J = 1.2 Hz, C*H*$_3$-C=).

The above chloride (16 mg, 0.034 mmol) dissolved in 2 mL of a 1:1 tetrahydrofuran–dimethylformamide mixture was added, over 11 h, to a solution of cesium carbonate (55 mg, 0.17 mmol) in 5 mL of the same solvent mixture kept at 75°C. The reaction mixture was stirred for an additional 2 h at this temperature. After cooling to room temperature, the carbonate was filtered off and the solvents evaporated (0.5 Torr) to afford a crude oil that was subjected to purification by column chromatography on silica gel with 10–25% ethyl acetate in hexane, yielding CTC macrocycle **3***e* (12 mg, 81%), which could be recrystallized from dichloromethane–hexane (mp 210–220°C); ir ($CHCl_3$): 3020, 2950, and 1730 cm^{-1}; ^1H nmr ($CDCl_3$) δ: 6.57 (1H, br dd, J = 14.9 and 11.1 Hz, -C*H*=CH-CH_2-), 6.16 (1H, t, J = 11.1 Hz, -C*H*=CH-CH_2-), 5.43 (1H, dt, J = 15.0 and 8.0 Hz, -CH=C*H*-CH_2-), 5.13 (1H, m, =C*H*-CH_2-CH_2-), 4.98 (1H, dt, J = 10.8 and 8.8 Hz, -CH_2-C*H*=CH-), 3.75 and 3.74 (12H, 2s, -CO_2CH_3), 2.83 (2H, br d, J = 8.6 Hz, -C*H*$_2$-CH=CH-), 2.78 (2H, br d, J = 8.0 Hz, -C*H*$_2$-CH=CH-), 2.00–1.65 (8H, m, -$(CH_2)_2$-C(CH_3)=CH-$(CH_2)_2$), 1.75 (3H, d, J = 0.7 Hz, C*H*$_3$-C=); ms *m/e*: 436 (M^+), 421 ($M^+ - CH_3$), 405 ($M^+ - OCH_3$). Exact Mass calcd.: 436.2097; found: 436.2097 ± 0.0017.

Macrocycle **3**f *(TCC)*

Methanesulfonyl chloride (21 μL, 0.264 mmol) was added, dropwise, to a solution of TCC alcohol **1***f* (59.5 mg, 0.132 mmol), lithium chloride (22.3 mg, 0.530 mmol), and collidine (35 μL, 0.265 mmol) in dimethylformamide (1 mL) at 0°C. The mixture was stirred at 0°C for 1 h, then at room temperature for 2.5 h. The solution was poured into ice-cold water and extracted with ether–hexane (2:1). The organic layer was washed with saturated aqueous copper(II) nitrate solution, then with water. This organic layer was dried and the solvent was evaporated to give the TCC allylic chloride **2***f*, which was used as such for the macrocyclization step.

TCC chloride **2***f* in 5 mL of a 1:1 tetrahydrofuran–dimethylformamide mixture was added, over 15 h, using a syringe pump, to a suspension of cesium carbonate (215 mg, 0.66 mmol) in 21.4 mL of a 1:1 tetrahydrofuran–dimethylformamide mixture at 70°C. After the addition was finished, the stirring was continued at 70°C for 5 h. The resulting solution was cooled down to room temperature and excess cesium carbonate was removed by filtration.

Tetrahydrofuran was evaporated and dimethylformamide was distilled off under reduced pressure. The TCC macrocyclic triene **3***f* was purified by chromatography on silica gel using a 1:2:7 mixture of ethyl acetate – dichloromethane–hexane yielding 49 mg (86% overall yield). The product was recrystallized from dichloromethane–hexane (3:4) (mp 224–225°C); ir ($CHCl_3$): 3020–2840, 1730, 1450, and 1220 cm^{-1}; ^1H nmr ($CDCl_3$) δ: 6.57 (1H, ddd, J = 15.0, 11.3, 0.8 Hz, -CH_2CH=C*H*CH=CHCH_2-), 6.19 (1H, t, J = 11.1 Hz, -CH_2CH=CHC*H*=CHCH_2-), 5.37 (1H, dt, J = 14.8, 7.5 Hz, -CH_2C*H*=CHCH=CHCH_2-), 5.02 (2H, m, CH_2CH=CHCH=C*H*CH_2-, -C(CH_3)=CH-), 3.75, 3.73 (12H, 2 singlets, 4 × -CO_2CH_3), 2.81 (4H, m, J = 7.6 Hz, -C*H*$_2$-CH=CHCH=CHC*H*$_2$-), 1.90–1.70 (8H, m, -C*H*$_2$C*H*$_2$C(CH_3)=CH-C*H*$_2$C*H*$_2$-), 1.65 (3H, d, J = 1.0 Hz, -C(C*H*$_3$)=CH-); ms *m/e*: 436 (M^+). Exact Mass calcd.: 436.2097; found: 436.2095 ± 0.0013.

Macrocycle **3**b *(TCT)*

Following the previous procedure, 243 mg (0.535 mmol) of alcohol **2***b* (TCT) afforded 106.5 mg (46% yield; 1 × 10^{-3} M dilution conditions). The product could be recrystallized from methanol (mp 154–156°C); ir ($CHCl_3$): 3020–2850, 1730, 1435, and 1220 cm^{-1}; ^1H nmr ($CDCl_3$) δ: 6.26 (1H, ddd, J = 14.6, 11.1, 0.8 Hz, -CH_2CH=C*H*CH=CHCH_2-), 6.08 (1H, tm, J = 11.0 Hz, -CH_2CH=CHC*H*=CHCH_2-), 5.40 (1H, dt, J = 15.0, 7.9 Hz, -CH_2C*H*=CHCH=CHCH_2-), 5.18 (1H, tm, J = 6.5, 1.1 Hz, -C(CH_3)=C*H*-), 4.94 (1H, dt, J = 10.7, 7.8 Hz, -CH_2CH=CHCH=C*H*CH_2-), 3.74, 3.73 (12H, 2s, 4 × -CO_2CH_3), 2.85 (2H, dd, J = 7.4, 1.5 Hz, -CH=CHC*H*$_2$-), 2.74 (2H, d, J = 7.9 Hz,

Can. J. Chem. Downloaded from www.nrcresearchpress.com by 213.200.69.106 on 09/08/12
For personal use only.

-CH_2CH=CH-), 2.03–1.80 (8H, m, -CH_2CH_2C(CH_3)=CHCH_2-CH_2-), 1.58 (3H, br s, -C(CH_3)=CH-); ^{13}C nmr ($CDCl_3$) δ: 171.77, 171.70 (C=O), 133.84 (-C(CH_3)=CH-), 131.66, 131.16, 127.93, 124.66, 124.43 (=CH-), 58.43, 56.99 (-*C*(CO_2CH_3)$_2$), 52.42 (-OCH_3), 35.06, 31.32, 30.35, 30.23, 28.75, 23.23 (-CH_2-), 17.14 (-CH_3); ms *m/e*: 436 (M^+). Exact Mass calcd.: 436.2097; found: 436.2095 ± 0.0013.

Macrocycle **3**c *(CCT)*

Following the previous procedure starting with 58 mg (0.128 mmol) alcohol **2***c* (CCT), this macrocycle was obtained in 45% yield (1×10^{-3} M dilution conditions) and it was recrystallized from methanol (mp 158–159°C); ir ($CHCl_3$): 3020–2850, 1730, 1435, and 1200 cm^{-1}; ^{1}H nmr ($CDCl_3$) δ: 6.24 (2H, m, CH_2CH=*CHCH*=CHCH_2-), 5.25, 5.22 (2H, 2 × m, -CH_2*CH*=CH-CH=*CH*CH_2-), 5.09 (1H, tq, *J* = 6.6, 1.3 Hz, -C(CH_3)=CH-), 3.73 (12H, s, 4 × -CO_2CH_3), 2.77 (2H, dd, *J* = 7.4, 1.5 Hz, -CH_2CH=CHCH=CHCH_2-), 2.71 (2H, d, *J* = 8.0 Hz, -CH_2-CH=CHCH=CHCH_2-), 2.11–1.65 (8H, m, -CH_2CH_2C(CH_3)=CHCH_2CH_2-), 1.51(3H, bs, -C(*C*H_3)=CH-); ^{13}C nmr ($CDCl_3$) δ: 171.94, 171.82 (C=O), 134.37 (-*C*(CH_3)=CH-), 128.33, 127.20, 127.00, 125.83, 124.98 (=CH-), 58.04, 56.97 (-*C*(CO_2CH_3)$_2$), 52.51, 52.43 (-OCH_3), 32.59, 31.74, 31.35, 30.54, 28.90, 22.22 (-CH_2-), 16.13 (-CH_3); ms *m/e*: 436 (M^+). Exact Mass calcd.: 436.2097; found: 436.2095 ± 0.0013.

Macrocycle **3**g *(CCC)*

This macrocycle was obtained in 78% yield starting with 139 mg (0.306 mmol) of alcohol **2***g* (CCC) and using 1×10^{-3} M dilution conditions, as described above. The compound was recrystallized from methanol (mp 179–182°C); ir ($CHCl_3$): 3020–2840, 1730, 1450, and 1200 cm^{-1}; ^{1}H nmr ($CDCl_3$) δ: 6.48 (2H, m, -CH_2-CH=*CHCH*=CHCH_2-), 5.35 (2H, m, -CH_2*CH*=CHCH=*CH*-CH_2-), 5.12 (1H, m, -C(CH_3)=C*H*-), 3.76, 3.74 (12H, 2s, 4 × CO_2CH_3), 3.04 (1H, dd, *J* = 12.9, 6.5 Hz, -*CH*HCH=CH-CH=CHCH_2-), 2.99 (1H, dd, *J* = 12.9, 6.5 Hz, -CH*H*CH=CHCH=CHCH_2-), 2.64 (2H, dm, *J* = 15.3 Hz, -CH_2CH=CHCH=CHCH_2-), 2.20–1.50 (11H, m, -CH_2CH_2C(CH_3)=CH-CH_2CH_2-); ^{13}C nmr ($CDCl_3$) δ: 171.70, 171.55, 171.46 (C=O), 135.57 (-*C*(CH_3)=CH-), 127.76, 126.50, 126.33, 123.82 (-CH=), 56.97, 56.54 (-*C*(CO_2CH_3)$_2$), 52.58 (-OCH_3), 32.19, 30.53, 30.01 (-CH_2CH=), 26.06, 22.97 (-CH_2-), 22.07 (-CH_3); ms *m/e*: 436 (M^+). Exact Mass calcd.: 436.2097; found: 436.2095 ± 0.0013.

Tricycle **15**

This compound was obtained from the transannular Diels–Alder reaction of TCT macrocycle **3***b* (see Table 2) (mp 151–153°C) (recrystallized from methanol); ir ($CHCl_3$): 3030–2860, 1730, 1460, 1440, 1230 cm^{-1}; ^{1}H nmr (C_6D_6) δ: 5.22 (1H, dd, *J* = 4.5 Hz, -C(CH_3)=C*H*-), 3.41, 3.28, 3.27 (12H, 3s, 4 × CO_2CH_3), 2.67 (1H, dq, *J* = 13.6, 2.3 Hz), 2.48 (1H, dm, *J* = 13.6, 2.2 Hz), 2.31 (3H, m), 2.13 (1H, dt, *J* = 12.5, 4.0 Hz), 1.90–1.50 (8H, m), 1.63 (3H, app t, *J* = 1.3 Hz, -C(*C*H_3)=CH-), 1.33 (2H, m).

Transannular Diels–Alder reactions

Tricycle **4**a *(CAC)*

CTT Macrocycle **3***a* (8.2 mg, 0.019 mmol) dissolved in toluene (0.5 mL) was heated to 300°C in a quartz tube (sealed under vacuum) for 1 h 45 min. The crude mixture obtained after evaporation of the solvent was purified by column chromatography on silica gel with 30% ethyl acetate in hexane to yield CAC tricycle **4***a* (7.5 mg, 91%), which could be recrystallized from methanol (mp 161–162°C); ir ($CHCl_3$): 3030, 2960, and 1730 cm^{-1}; ^{1}H nmr ($CDCl_3$) δ: 5.26 (2H, br s, -*CH*=*CH*-), 3.68, 3.66, 3.65 (12H, 3s, -CO_2CH_3), 2.72–0.90 (15H, m, -C*H*- and -CH_2-), 1.00 (3H, s, CH_3-C); ms *m/e*: 436 (M^+), 421 ($M^+ - CH_3$), 405 ($M^+ - OCH_3$). Exact Mass calcd.: 436.2097; found: 436.2091 ± 0.0013.

Bicyclic compound **17**

This compound was obtained in 64% yield after chromatography by the transannular Diels–Alder reaction performed on CCT macrocycle **3***c* (see Table 2 for conditions) (mp 175–176°C) (recrystallized from methanol); ir ($CHCl_3$): 3020–2840, 1730, 1450, 1435, 1240, and 1200 cm^{-1}; ^{1}H nmr ($CDCl_3$) δ: 5.63 (1H, dddd, *J* = 13.7, 9.6, 4.3, 0.9 Hz, -CH_2*CH*=CHCH_2C(CO_2CH_3)$_2$-). 5.13 (1H, dddd, *J* = 12.9, 11.5, 7.4, 1.0 Hz, -CH_2CH=*CH*CH_2C-(CO_2CH_3)$_2$-), 4.83 (1H, dm, *J* = 9.3 Hz, -C(CH_3)=C*H*-), 3.77, 3.76, 3.71 (12H, 3s, 4 × -CO_2CH_3), 2.77 (2H, dd and ddd, *J* = 13.0, 7.2, 1.1 Hz, -C(CH_3)=CH*CH*HC(CO_2CH_3)$_2$*CH*HCH=CH-), 2.35 (5H, m, -*CH*C(CH_3)=CHCH*H*C(CO_2CH_3)$_2$-CH*H*CH=CH*CH*HCH-), 1.90–1.30 (7H, m, =CHCH*H*CH-CH_2C(CO_2CH_3)$_2$-CH_2CH_2-), 1.56 (3H, d, *J* = 1.1 Hz, -C(*C*H_3)=CH-); ^{13}C nmr ($CDCl_3$) δ: 172.75, 171.66, 171.54 (C=O), 141.32 (-*C*(CH_3)=CH-), 129.59, 125.74, 120.40 (-CH=), 57.22, 55.45 (*C*(CO_2-CH_3)$_2$), 52.55, 52.43 (-OCH_3), 40.57, 34.73 (-CH-), 35.19, 30.84, 29.98, 29.91, 29.85, 26.69 (-CH_2-), 18.89 (-CH_3); ms *m/e*: 436 (M^+). Exact Mass calcd.: 436.2097; found: 436.2095 ± 0.0013.

Tricycle **4**d *(CST)*

The transannular Diels–Alder reaction was performed as described before (see Table 2 for conditions) on CTC macrocycle **3***e* (7.0 mg, 0.016 mmol) affording 6.2 mg (89%) of CST tricycle **4***d* after chromatography on silica gel (25% ethyl acetate in hexane); ir $CHCl_3$): 3025, 2960, and 1732 cm^{-1}; ^{1}H nmr (C_6D_6) δ: 5.36 (2H, m, -*CH*=*CH*-), 3.33, 3.30, 3.27, and 3.26 (12H, 4s, -CO_2CH_3), 2.75–2.65 (2H, m, H_{eq}C12 and H_{eq}C14), 2.58 (1H, dd, *J* = 14.5 and 6.0 Hz, H_{ax}C4), 2.47 (1H, m, H_{eq}C2), 2.40 (1H, dt, *J* = 14.2 and 3.0 Hz, H_{eq}C4), 2.12 (1H, tm, *J* = 12.0 Hz, HC8), 1.98 (1H, tdd, *J* = 13.7, 4.0, and 0.5 Hz, H_{ax}C1), 1.92 (1H, m, HC5), 1.70 (1H, t, *J* = 12.9 Hz, H_{ax}C14), 1.64 (1H, dt, *J* = 13.2 and 4.1 Hz, H_{ax}C12), 1.57 (1H, td, *J* = 13.5 and 3.4 Hz, H_{ax} C2), 1.52 (1H, m, H_{eq}C11), 0.97 (1H, dt, *J* = 14.1 and 2.4 Hz, H_{eq}C2), 0.87 (1H, tm, *J* = 12.0 Hz, HC9), 0.76 (3H, s, -*CH*$_3$); ms *m/e*: 436 (M^+), 421 ($M^+ - CH_3$), 405 ($M^+ - 0CH_3$). Exact Mass calcd.: 436.2097; found: 436.2095 ± 0.0013.

Tricycle **4**e *(TSC)*

Using the previously described procedure (see Table 2 for conditions), TCC macrocyclic triene **3***f* (39 mg) in toluene (2.5 mL) afforded 39.5 mg (~100%) of TSC tricycle **4***e*, homogeneous by tlc and gc. The product was recrystallized from dichloromethane–hexane (mp 123–124°C); ir ($CHCl_3$): 3020–2860, 1725, 1450, 1435, and 1250 cm^{-1}; ^{1}H nmr ($CDCl_3$) δ: 5.33 (1H, ddd, *J* = 9.7, 3.4, 3.6 Hz, HC6), 5.21 (1H, ddd, *J* = 9.7, 2.6 Hz, HC7), 3.76, 3.69, 3.68, 3.67 (12H, 4s, 4 × -CO_2CH_3), 2.71 (1H, m, HC8), 2.49 (1H, dt, *J* = 13.5, 2.6 Hz, H_{eq}C14), 2.39 (1H, dt, *J* = 9.5, 3.2 Hz, H_{eq}C12), 2.30 (1H, m, *J* = 14.4 Hz, H_{eq}C2), 2.12 (1H, dd, *J* = 10.2, 2.3 Hz, H_{eq}C4), 2.06 (1H, dd, *J* = 14.4, 5.9 Hz, H_{ax}C14), 1.98 (1H, ddd, *J* = 13.6, 13.4, 4.7 Hz, H_{ax}C2), 1.85 (2H, m, HC5 and H_{ax}C4), 1.74 (1H, dddq, *J* = 13.1, 12.9, 4.6, 1.1 Hz, H_{ax}C1), 1.58 (1H, app dd, *J* = 11.9, 4.2 Hz, H_{eq}C11), 1.44 (2H, m, H_{ax}C11 and H_{ax}C12), 1.27 (1H, m, HC9), 1.07 (1H, dm, *J* = 13.7 Hz, H_{eq}C1), 0.87 (3H, s, -CH_3); ^{13}C nmr ($CDCl_3$) δ: 173.11, 172.72, 171.72, 171.29 (C=O), 129.70 (-*CH*=*CH*-), 55.53 (C10), 52.60 (-OCH_3), 51.95 (C3, C13), 44.16, 35.50, 35.19, 35.05, 32.63, 30.91, 26.70, 19.16 (-CH- and -CH_2), 17,72 (-CH_3); ms *m/e*: 436 (M^+). Exact Mass calcd.: 436.2097; found: 436.2095 ± 0.0013.

Tricycles **4**b *(TAC) and* **4**c *(CAT)*

To a solution of cesium carbonate (93 mg, 0.29 mmol) in 20 mL of tetrahydrofuran and 28 mL of dimethylformamide at 85°C was added, over a period of 16 h, TTT chloride **2***d* (27 mg, 0.057 mmol) dissolved in 8 mL of tetrahydrofuran. After the end of the addition, the mixture was stirred for an hour at 85°C and was then cooled down to room temperature. The carbonate was filtered and the solvents distilled off (45°C, 0.5 Torr). The residue was purified by column chromatography on silica gel using 15% ethyl acetate in hexane to yield a 2:1 unseparable mixture of tricycles **4***b* (TAC) and **4***c* (CAT) (16.1 mg, 65%); ir (CH_2Cl_2): 3055, 2955, and 1730 cm^{-1}; ^{1}H nmr ($CDCl_3$) δ: 5.62–5.52 (1H, m, -*CH*= (CAT)), 5.54 (1H, dm, *J* = 9.8 Hz, -*CH*= (TAC)), 5.38–5.30 (1H, m, -*CH*= (CAT)), 5.32 (1H, dm, *J* = 10.2 Hz, -*CH*= (TAC)), 3.73,

Can. J. Chem. Downloaded from www.nrcresearchpress.com by 213.200.69.106 on 09/08/12
For personal use only.

3.72, and 3.70 (12H, 3s, -CO_2CH_3 (TAC)), 3.74, 3.70, and 3.69 (12H, 3s, -CO_2CH_3 (CAT)), 2.65–0.80 (15H, m, -CH_2 and -CH- for both compounds), 0.83 (3H, s, CH_3-C (TAC)), 0.75 (3H, s, CH_3-C (CAT)).

Tricycle **4**c *(CAT) (from* 7b*)*

To a solution of diisopropylamine (30 mg, 41.7 μL, 0.297 mmol) in freshly distilled anhydrous tetrahydrofuran (0.5 mL) at 0°C was added *n*-butyllithium (1.6 M solution, 148.5 μL, 0.238 mmol). The mixture was stirred for 20 min at 0°C, and then was cooled to −78°C. A solution of triester **7***b* (30 mg, 0.0793 mmol) in anhydrous tetrahydrofuran (0.3 mL) was then added. The resulting mixture was allowed to warm to 0°C for 45 min, then cooled again to −78°C and dry methylchloroformate was added. The mixture was allowed to warm to 0°C and stirred for 2 h. The reaction mixture was diluted with dichloromethane and was washed successively with a dilute hydrochloric acid solution and water. Drying and removal of the solvent left a crude product that was purified by preparative chromatography on silica gel using 20% ethyl acetate in hexane as eluant to provide 13.3 mg (45%) of CAT tetraester **4***c* (mp 122–125°C); ir (CH_2Cl_2): 3055, 2950, 1730 cm^{-1}; ^1H nmr ($CDCl_3$) δ: 5.63–5.52 (2dd, 1H, J = 2.5, 10 Hz, HC6), 5.40–5.31 (br d, 1H, J = 9.8, 0.5 Hz, HC7), 3.75, 3.70, and 3.69 (3s, 12H, 4 × H_3COOC), 2.56–2.37 (m, 2H, H_{eq}C11 and H_{eq}C2), 2.36–2.23 (m, 1H, H_{eq}C14), 2.12–1.96 (m, 1H, HC5), 1.96–0.95 (m, 11H), 0.75 (s, 3H, H_3C); ms *m/e*: 436 (M^+).

Tricycle **4f** *(TST) and macrocycle* **5**

To a solution of TTC alcohol **1***h* (435 mg, 0.96 mmol), lithium chloride (84 mg, 2.0 mmol), and *s*-collidine (161 mg, 1.3 mmol) in 8 mL of dimethylformamide at 0°C was added methanesulfonyl chloride (140 mg, 1.2 mmol). The mixture was stirred at room temperature for 18 h and was poured into ice-water (40 mL). The water layer was extracted with a mixture of ether and hexane (2:1, 4 × 40 mL) and the combined organic layers were washed with water (20 mL) and with saturated copper nitrate solution (20 mL), and were dried over magnesium sulfate. The crude chloride **2***h* obtained after evaporation (435 mg, 0.92 mmol) was dissolved in 15 mL of tetrahydrofuran and was added over a period of 15 h with the help of a syringe pump to a suspension of cesium carbonate (1.63 g, 5.0 mmol) in 255 mL of tetrahydrofuran and 250 mL of dimethylformamide at 80°C. After the addition was completed, the mixture was stirred for 3 h and was cooled down to room temperature. The carbonate was filtered off and the solvents were evaporated (0.5 Torr). The crude material was purified by column chromatography on silica gel using 25% ethyl acetate in hexane to yield TST tricyle **4***e* (220 mg, 53% overall), which could be recrystallized from methanol (mp 116–118°C); ir (CH_2Cl_2): 3055, 2985, 2955, 1730 cm^{-1}; ^1H nmr ($CDCl_3$) δ: 5.59 (2H, m, -CH=CH-), 3.74, 3.73, 3.68, and 3.67 (12H, 4s, -CO_2CH_3), 2.60–0.75 (15H, m, -CH_2- and -CH-), 0.78(3H, s, -CH_3); ms *m/e*: 436 (M^+), 405 ($M^+ - OCH_3$). Exact Mass calcd.: 436.2097; found: 436.2095 ± 0.0013; and macrocycle **5** (93 mg, 23% overall), which could be recrystallized from ether (mp 143–144°C); ir (CH_2Cl_2): 3060, 2960, 1735 cm^{-1}; ^1H nmr ($CDCl_3$) δ: 6.01 (1H, br dd, J = 15.5 and 7.2 Hz, -CH_2-CH=CH-), 5.89 (1H, ddd, J = 18.2, 10.4, and 7.9 Hz, -CH=CH_2), 5.47 (1H, dt, J = 15.5 and 6.8 Hz, -CH_2-CH=CH-), 5.16 (1H, m, =CH-CH_2-CH_2-), 5.04 (1H, br d, J = 10.4 Hz, CH=CH_{cis}H), 5.00 (1H, br d, J = 18.1 Hz, -CH=CHH_{trans}), 3.74, 3.73, 3.72, and 3.64 (12H, s, 4 × -CO_2CH_3), 3.52 (1H, br t, J = 7.4 Hz, -CH-CH=CH_2), 2.94 (1H, ddd, J = 14.9, 6.4, and 1.5 Hz, -CHH-CH=CH-), 2.65 (1H, br dd, J = 14.9 and 7.7 Hz, CHH-CH=CH-), 2.25–1.90 and 1.80–1.50 (8H, 2 m, $(CH_2)_2$-C(CH_3)=CH-$(CH_2)_2$), 1.67 (3H, d, J = 1.2 Hz, CH_3-C=C). Exact Mass calcd.: 436.2097; found: 436.2095 ± 0.0013.

Macrocycle **3**h *(TTC) and dimer* **6**

Crude TTC allylic chloride **2***h* (47 mg, 0.09 mmol) (prepared as above) afforded, using the previous procedure (45°C, addition time 16 h) and after chromatography on silica gel (10–20% in hexane), TTC macrocycle **3***h* (11.5 mg, 26% contaminated with 15% **5**); ir ($CHCl_3$): 3025, 2955, and 1730 cm^{-1}; ^1H nmr ($CDCl_3$) δ: 6.30–6.10 (2H, m, =CH-CH=), 5.85–5.57 (2H, m, -CH=CH-CH=CH-), 4.99 (1H, m, =CH-CH_2-CH_2-), 3.74 and 3.72 (12H, 2s, -CO_2-CH_3), 2.69 and 2.65 (4H, 2d, J = 7.4 Hz, -CH_2CH-CH-CH=CH-CH_2-), 1.90–1.60 (8H, m, -CH_2-CH_2-C(CH_3)-CH-CH_2CH_2), 1.62 (3H, d, J = 1.3 Hz, CH_3-C=); and dimer **6** (4.7 mg, 11%) (mp 130–138°C); ir (CH_2Cl_2): 3055, 2955, and 1735 cm^{-1}; ^1H nmr ($CDCl_3$) δ: 6.15–5.95 (4H, m, =CH-CH=), 5.58–5.32 (4H, m, -CH=CH-CH=CH-), 5.02 (2H, m, =CH-CH_2-CH_2-), 3.72 and 3.68 (24H, 2s, -CO_2CH_3), 2.69 and 2.61 (8H, 2d, J = 7.5 and 7.7 Hz, -CH_2-CH=CH-), 2.00–1.60 (16H, m, -CH_2-CH_2-), 1.62 (6H, d, J = 1.0 Hz, CH_3-C=); ms *m/e*: 872 (M^+), 841 ($M^+ - OCH_3$). Exact Mass calcd.: 872.4194; found: 872.4200 ± 0.0026.

Acknowledgements

This research was supported by the Natural Sciences and Engineering Research Council of Canada (NSERCC, Ottawa) and by the "Ministère de l'Enseignement supérieur et de la Science (Fonds FCAR, Québec)." We also acknowledge the support of IBM Canada Ltd (Cooperative Project Program) and the Tripos Company that allowed us to use the Sybyl Software, as well as the contribution of Prof. A. Michel through helpful discussions.

1. S. Lamothe, A. Ndibwami, and P. Deslongchamps. Tetrahedron Lett. **29**, 1639 (1988).
2. S. Lamothe, A. Ndibwami, and P. Deslongchamps. Tetrahedron Lett. **29**, 1641 (1988).
3. P. Deslongchamps. Aldrichimica Acta, **24**, 43 (1991).
4. A. Ndibwami, S. Lamothe, P. Soucy, S. Goldstein, and P. Deslongchamps. Can. J. Chem. **71**, 695 (1993).
5. E. W. Collington and A. I. Meyers. J. Org. Chem. **36**, 3044 (1971).
6. (*a*) A. Marinier, K. Baettig, C. Dallaire, R. Pitteloud, and P. Deslongchamps. Can. J. Chem. **67**, 1609 (1989); (*b*) D. Brillon and P. Deslongchamps. Can. J. Chem. **65**, 56 (1987).
7. M. Drouin, S. Lamothe, and A. G. Michel. Acta Crystallogr. In press.
8. M. Drouin, A. G. Michel, P. Giguere, and P. Deslongchamps. Acta Crystallogr. Sect. C: Cryst. Struct. Commun. **C46**, 1882 (1990).
9. (*a*) A. G. Michel, M. Drouin, N. Michel-Dewez, A. Roughton, and P. Deslongchamps. Acta Crystallogr. Sect. C: Cryst. Struct. Commun. **C47**, 1032 (1991); (*b*) A. G. Michel, M. Drouin, P. Soucy, and P. Deslongchamps. Acta Crystallogr. Submitted.
10. W. C. Still and I. Galynker. Tetrahedron, **37**, 3981 (1981).
11. F. K. Brown and K. N. Houk. Tetrahedron Lett. **25**, 4609 (1984).
12. L. Raimondi, F. K. Brown, J. Gonzalez, and K. N. Houk. J. Am. Chem. Soc. **114**, 4796 (1992).

"A-frame" vs. "open-book" geometries in binuclear complexes bridged by diphosphines and mercaptothiazolinate ligands. Unusual examples involving a bridging bis(diphenylphosphino)ethane group

JIANLIANG XIAO AND MARTIN COWIE[1]

Department of Chemistry, The University of Alberta, Edmonton, Alta., Canada T6G 2G2

Received November 27, 1992

JIANLIANG XIAO and MARTIN COWIE. Can. J. Chem. **71**, 726 (1993).

Reaction of the tetracarbonyl species $[M(CO)_2(\mu\text{-mtz})]_2$ (M = Rh, Ir; mtz = 2-mercaptothiazolinate) with 1 equivalent of the diphosphines $(Ph_2P(CH_2)_nPPh_2$; n = 1 (dppm), 2 (dppe)) yields the compounds $[M_2(CO)_2(\mu\text{-L})(\mu\text{-mtz})_2]$ (M = Rh, L = dppm (**1**), dppe (**3**); M = Ir, L = dppm (**2**)), which readily undergo oxidative addition of iodine to give $[M_2I_2(CO)_2(\mu\text{-L})(\mu\text{-mtz})_2]$ (M = Rh, L = dppm (**4**), dppe (**6**); M = Ir, L = dppm (**5**)). When 2 equivalents of dppm are used, the A-frame compounds $[M_2(CO)_2(\eta^1\text{-mtz})(\mu\text{-mtz})(dppm)_2]$ (M = Rh (**7**), Ir (**8**)) are afforded. In solution the dangling mtz group of **7** undergoes exchange with both the free mtz anion and the bridging mtz ligand. Compounds **7** and **8** are also produced by treatment of *trans*-$[MCl(CO)(dppm)]_2$ (M = Rh, Ir) with 2 equivalents of the mtz anion. Reaction of these dppm-bridged dichloro species with 1 equivalent of the mtz anion yields $[M_2Cl(CO)_2(\mu\text{-mtz})(dppm)_2]$ (M = Rh (**9***a*), Ir (**10**)). Compound **9***a* undergoes reversible Cl^- dissociation to give $[Rh_2(CO)_2(\mu\text{-mtz})(dppm)_2][Cl]$ (**9***b*), which is also the stable form in the solid. Reaction of **9** with CO gives the carbonyl-bridged species $[Rh_2(CO)_2(\mu\text{-CO})(\mu\text{-mtz})(dppm)_2][Cl]$. The structures of **6** and **9***b* have been determined by X-ray crystallography. Compound **6** crystallizes in the triclinic space group $P\bar{1}$ with one-half equivalent of THF per asymmetric unit in a cell having a = 9.856(3) Å, b = 14.078(6) Å, c = 16.245(5) Å, α = 103.66(3)°, β = 93.21(3)°, γ = 92.91(3)°, V = 2182(1) Å^3, and Z = 2, and has refined to R = 0.045 and R_w = 0.057 on the basis of 433 parameters varied. Compound **9***b* crystallizes with one equivalent of CH_2Cl_2 in the monoclinic space group $P2_1/n$ with a = 11.400(1) Å, b = 21.944(2) Å, c = 22.134(1) Å, β = 92.494(7)°, V = 5532(1) Å^3, and Z = 4, and has refined to R = 0.062 and R_w = 0.082 on the basis of 613 parameters varied.

JIANLIANG XIAO et MARTIN COWIE. Can. J. Chem. **71**, 726 (1993).

La réaction des espèces tétracarbonylées $[M(CO)_2(\mu\text{-mtz})]_2$ (M = Rh, Ir; mtz = 2-mercaptothiazolinate) avec un équivalent de diphosphines $(Ph_2P(CH_2)_aPPh_2$; n = 1 (dppm), 2 (dppe)) fournit les composés $[M(CO)_2(\mu\text{-L})(\mu\text{-mtz})_2]$ (M = Rh, L = dppm (**1**), dppe (**3**); M = Ir, L = dppm (**2**)), qui subissent l'addition oxydative d'iode pour donner les $[M_2I_2(CO)_2(\mu\text{-L})(\mu\text{-mtz})_2]$ (M = RH, L = dppm (**4**), dppe (**6**); M = Ir, L = dppm (**5**)). Lorsqu'on utilise deux équivalents de dppm, on obtient les composés en forme de A, $[M_2(CO)_2(\eta^1\text{-mtz})(\mu\text{-mtz})_2(dppm)_2]$ (M = Rh (**7**) et Ir (**8**)). En solution, le groupe mtz pendant du produit **7** subit un échange avec l'anion mtz libre ainsi qu'avec le coordinat mtz agissant comme pont. On obtient aussi les composés **7** et **8** par traitement du *trans*-$[MCl(CO)dppm)]_2$ (M = Rh ou Ir) avec deux équivalents de l'anion mtz. Le réaction de ces espèces dichlorées comportant un pont dppm avec un équivalent de l'anion mtz fournit les espèces $M_2Cl(CO)_2(\mu\text{-mtz})(dppm)_2]$ (M = Rh (**9***a*), Ir (**10**)). Le composé **9***a* subit une dissociation réversible du Cl^- pour donner le $[Rh_2(CO)_2(\mu\text{-mtz})(dppm)_2][Cl]$ (**9***b*) qui est aussi la forme stable à l'état solide. La réaction du produit **9** avec du CO fournit des espèces comportant un pont carbonyle $[Rh_2(CO)_2(\mu\text{-CO}(\mu\text{-mtz})(dppm)_2][Cl]$. Les structures des composés **6** et **9***b* one été déterminées par diffractions des rayons X. Le composé **6** cristallise dans le groupe d'espace triclinique $P\bar{1}$, avec un demi équivalent de THF par unité asymétrique, avec a = 9,856(3), b = 14,078(6) et c = 16,245(5) Å, α = 103,66(3)°, β = 93,21(3)° et γ = 92,91(3)°, V = 2182(1) Å^3 et Z = 2; on a affiné sa structure jusqu'à des valeurs de R = 0,045 et R_w = 0,057 pour 433 paramètres. Le composé **9***b* cristallise avec un équivalent de CH_2Cl_2 dans le groupe d'espace monoclinique $P2_1/n$ avec a = 11,400(1), b = 21,944(2) et c = 22,134(1) Å, β = 92,494(7)°, V = 5532(1) Å^3 et Z = 4; on a affiné sa structure jusqu'à des valeurs de R = 0,062 et R_w = 0,082 pour 613 paramètres.

[Traduit par la rédaction]

Introduction

Binuclear complexes, in which the metals are held in close proximity, are of interest because of the possibility that the two metals may interact in a cooperative manner and in so doing may display chemistry unique from that displayed at a single metal (1). Two common classes of binuclear complexes involving Rh and Ir are those of the "A-frame" and related compounds (2) or of the "open-book" (3) complexes. In the former class the metals are bridged by two neutral diphosphine or related groups (most often dppm $(Ph_2PCH_2PPh_2)$), occupying a *trans* orientation at each metal, whereas in the latter class the only bridging groups are anionic and occupy *cis* positions at both metals, as shown below for **A** and **B**, respectively.

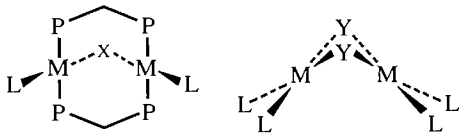

A **B**

In an effort to combine some of the features of both classes of binuclear species we set out to prepare open-book complexes that also contained bridging dppm groups. As a starting point we chose species related to the 2-mercaptothiazolinate-bridged complexes, $[M(CO)L(\mu\text{-mtz})]_2$ (M = Rh, Ir), since the dirhodium species, in which L = PMe_3, was shown to have a short metal–metal separation of ca. 3.05 Å (3*m*), comparable to the bite of dppm, suggesting that this group could be incorporated as an additional bridge in these complexes. Previous work had also shown that the mtz-

[1]Author to whom correspondence may be addressed.

Can. J. Chem. Downloaded from www.nrcresearchpress.com by 213.200.69.106 on 09/08/12
For personal use only.

Can. J. Chem. Downloaded from www.nrcresearchpress.com by 213.200.69.106 on 09/08/12
For personal use only.

bridged binuclear frameworks readily undergo fragmentation in reactions involving molecules such as H_2S and H_2.[2] It seemed likely that the incorporation of a bridging diphosphine group into these complexes would offer greater stability and may allow the isolation of open-book complexes in which one, or even both, bridging mercaptothiazolinate groups were terminally bound. Such "bridge-opened" species had been proposed as key intermediates in the activation of substrates by open-book binuclear complexes (4). We were also interested in the possibility of incorporating dppe ($Ph_2PCH_2CH_2PPh_2$) as a bridging group by utilizing an open-book complex in which the metals are constrained to be in close proximity. Complexes having this diphosphine as a bridging group are extremely rare (5) owing to the well-established propensity of this group to chelate (6). These and related studies are reported herein.

Experimental

All solvents were dried and distilled before use and were stored under dinitrogen. Reactions were carried out at room temperature by using standard Schlenk procedures. 2-Mercaptothiazoline (Hmtz) and bis(diphenylphosphino)methane (dppm) were purchased from Aldrich, bis(diphenylphosphino)ethane (dppe) was obtained from Strem Chemicals, hydrated iridium(III) chloride was obtained from Johnson–Matthey, and ^{13}CO (99%) was supplied by Isotec Inc. These and all other reagents were used as received. The compounds *trans*-$[MCl(CO)(dppm)]_2$ (M = Rh (7), Ir (8)), $[M(COD)(\mu\text{-mtz})]_2$ (M = Rh, Ir)(3*n*), and $[Rh(CO)_2(\mu\text{-mtz})]_2$ (3*m*) were prepared by the previously reported procedures.

The NMR spectra were recorded on a Bruker AM400 spectrometer at 400.1 MHz for ^1H, at 161.9 MHz for $^{31}P\{^1H\}$, and at 100.6 MHz for $^{13}C\{^1H\}$ spectra. The $^{13}C\{^1H, ^{31}P\}$ NMR spectra were obtained on a Bruker WH200 spectrometer operating at 50.32 MHz. Infrared spectra were performed on Nicolet 7199 or Mattson Polaris Fourier transform interferometers with use of Nujol mulls on KBr plates, or in solution in KCl cells with 0.5-mm window path lengths. Spectral data for all compounds are given in Table 1. Elemental analyses were performed by the microanalytical service within the department. Conductivity measurements were made on 1.0×10^{-3} M solutions with use of a Yellow Springs Instrument Co., model 31 conductivity bridge.

Preparation of compounds

(a) $[Rh_2(CO)_2(\mu\text{-mtz})_2(dppm)]$ (1)

To a THF solution of $[Rh(CO)_2(\mu\text{-mtz})]_2$, prepared by the addition of CO to a THF solution of $[Rh(COD)(\mu\text{-mtz})]_2$ (66.0 mg, 0.10 mmol, in 10 mL), was added 38.4 mg (0.10 mmol) of dppm in 5 mL of THF, causing an immediate colour change from wine red to dark purple. After stirring for 1 h, the volume was reduced to ca. 5 mL and 10 mL of hexane was slowly added to the solution, affording the compound as dark purple microcrystals (75% yield). Anal. calcd. for $Rh_2S_4P_2O_2N_2C_{33}H_{28}$: C 44.90, H 3.43, N 3.17; found: C 44.91, H 3.98, N 3.03.

(b) $[Ir_2(CO)_2(\mu\text{-mtz})_2(dppm)]$ (2)

The procedure was the same as for **1**, except that $[Ir(COD)(\mu\text{-mtz})]_2$ was used to prepare the tetracarbonyl precursor. The dark purple compound was only spectroscopically characterized due to its extreme air sensitivity.

(c) $[Rh_2(CO)_2(\mu\text{-mtz})_2(\mu\text{-dppe})]$ (3)

To a THF solution of $[Rh(CO)_2(\mu\text{-mtz})]_2$ (prepared from $[Rh(COD)(\mu\text{-mtz})]_2$ (66.0 mg, 0.10 mmol, in 10 mL of THF)) was slowly added 38.5 mg (0.097 mmol) of dppe in 5 mL of THF, causing an immediate colour change to deep red. The mixture was stirred for ca. 0.5 h and the volume was then reduced to ca. 2 mL followed by addition of hexane to give a red precipitate. This compound was extremely air sensitive, the solid instantly changing colour to brown upon exposure to air.

(d) $[Rh_2I_2(CO)_2(\mu\text{-mtz})_2(dppm)]\cdot 0.5$ THF (4)

To a THF solution of **1** (prepared from 66.0 mg (0.10 mmol) of $[Rh(COD)(\mu\text{-mtz})]_2$ (in 10 mL of THF)) was added 24.5 mg (0.097 mmol) of I_2 in 4 mL of THF, causing an immediate colour change from intense purple to dark red. After stirring for 1 h, the volume was reduced to ca. 2 mL, and addition of hexane precipitated a dark red solid (70% yield). Anal. calcd. for $Rh_2I_2S_4P_2O_{2.5}N_2C_{35}H_{32}$: C 35.84, H 2.93, N 2.39, I 21.65; found: C 35.61, H 2.85, N 2.31, I 21.80.

(e) $[Ir_2I_2(CO)_2(\mu\text{-mtz})_2(dppm)]$ (5)

To a THF solution of **2** (prepared by using $[Ir(COD)(\mu\text{-mtz})]_2$ (84.0 mg, 0.10 mmol, in 10 mL of THF)) was added 24.5 mg (0.097 mmol) of I_2 in 4 mL of THF, causing an immediate colour change to orange. The mixture was stirred for 0.5 h, after which reduction of the volume followed by addition of hexane precipitated an orange solid.

(f) $[Rh_2I_2(CO)_2(\mu\text{-mtz})_2(\mu\text{-dppe})]\cdot 0.5$ THF (6)

To a THF solution of **3** (prepared from 134.0 mg (0.20 mmol) of $[Rh(COD)(\mu\text{-mtz})]_2$) was added 51.0 mg of I_2 in 5 mL of THF; a deep purple solution was immediately formed. Reduction of the volume followed by addition of hexane yielded a dark red solid (70–75% yield). The solid was stored overnight under vacuum. Anal. calcd. for $Rh_2I_2S_4P_2O_{2.5}N_2C_{36}H_{36}$: C 36.44, H 3.06, N 2.36, I 21.39; found: C 36.80, H 3.18, N 2.29, I 22.66. The presence of THF was verified by NMR and the X-ray study (*vide infra*).

(g) $[Rh_2(mtz)(CO)_2(\mu\text{-mtz})(dppm)_2]\cdot CH_2Cl_2$ (7)

Method A. To a THF solution of $[Rh(CO)_2(\mu\text{-mtz})]_2$ (prepared from $[Rh(COD)(\mu\text{-mtz})]_2$ (132.0 mg, 0.2 mmol, in 20 mL)) was added 153.0 mg (0.40 mmol) of dppm, resulting in an immediate colour change to deep red. After stirring for 0.5 h, the volume was reduced to ca. 5 mL followed by precipitation with hexane. Compound **7** was crystallized from CH_2Cl_2–hexane. Anal. calcd. for $Rh_2Cl_2S_4P_4O_2N_2C_{59}H_{54}$: C 52.41, H 4.03, N 2.07, S 9.49; found: C 52.85, H 3.95, N 2.20, S 9.70.

Method B. A 110.0 mg (0.10 mmol) sample of *trans*-$[RhCl(CO)(dppm)]_2$ was suspended in 10 mL of THF, to which was added 28.4 mg (0.20 mmol) of sodium-2-mercaptothiazolinate in 5 mL of THF, causing a colour change to red within several min. After stirring for 5 h, the solvent was removed under vacuum. The red solid was redissolved in 10 mL of CH_2Cl_2. The solution was then filtered and concentrated to ca. 3 mL. Microcrystals were obtained upon addition of hexane (90% yield).

(h) $[Ir_2(mtz)(CO)_2(\mu\text{-mtz})(dppm)_2]$ (8)

To a slurry of *trans*-$[IrCl(CO)(dppm)]_2$ (220.0 mg, 0.17 mmol) in 10 mL of THF was added 49.0 mg (0.34 mmol) of sodium-2-mercaptothiazolinate in 5 mL of THF. The mixture was stirred overnight, during which time a red-orange solution was formed. Filtration followed by reduction in the volume of the solution and addition of hexane gave an orange solid (85–90% yield). Anal. calcd. for $Ir_2S_4P_4O_2N_2C_{58}H_{52}$: C 48.18, H 3.63, N 1.94; found: C 47.83, H 3.70, N 2.03.

(i) $[Rh_2(CO)_2(\mu\text{-mtz})(dppm)_2][Cl]\cdot CH_2Cl_2$ (9b)

The procedure was the same as for **7** in method B, except that 1 equivalent of sodium-2-mercaptothiazolinate was used. Red crystals of **9*b*** were obtained from CH_2Cl_2-hexame (87% yield). Conductivity measurements: $\Lambda = 29.8\ \Omega^{-1}\ cm^2\ mol^{-1}$ in CH_2Cl_2; $\Lambda = 71.6\ \Omega^{-1}\ cm^2\ mol^{-1}$ in CH_3NO_2. Anal. calcd. for $Rh_2Cl_3S_2P_4O_2NC_{56}H_{50}$: C 52.99, H 3.99, N 1.10; found: C 52.97, H 3.95, N 1.01.

(j) $[Rh_2(CO)_2(\mu\text{-mtz})(dppm)_2][PF_6]$ (9c)

To a CH_2Cl_2 solution of **9*b*** (118.0 mg, 0.10 mmol, in 10 mL) was added 1 equivalent of $AgPF_6$ (25.0 mg, 0.10 mmol, in 5 mL of CH_2Cl_2). After stirring for 0.5 h, the solution was filtered and the volume was then reduced to ca. 3 mL. Microcrystals were obtained upon addition of hexane (90% yield). Anal. calcd. for

[2] J. Xiao and M. Cowie, unpublished results.

TABLE 1. Spectroscopic data[a]

	IR, cm^{-1}		NMR[d]		
	Solid[b]	Solution[c]	$\delta(^{31}P\{^1H\})$[e]	$\delta(^{13}C\{^1H\})$[f]	$\delta(^1H)$[f]
$[Rh_2(CO)_2(dppm)$-$(\mu\text{-mtz})_2]$ (**1**)	1995 (vs), 1948 (vs)[g]		45.9 (dd, $^1J_{Rh-P}$ = 142.8 Hz, $^2J_{P-P}$ = 58.2 Hz), 30.8 (dd, $^1J_{Rh-P}$ = 153.4 Hz)		4.20 (m, 1H), 3.70 (m, 1H), 4.28 (m, 2H), 3.80 (m, 1H), 3.41 (m, 1H), 3.33 (m, 1H), 3.06 (m, 1H), 2.94 (m, 2H)
$[Ir_2(CO)_2(dppm)$-$(\mu\text{-mtz})_2]$ (**2**)	1962 (vs, br)		−5.7 (m), −2.8 (m)		5.20 (m, 1H), 4.18 (m, 1H), 4.38 (m, 1H), 3.55 (m, 2H), 3.40 (m, 2H), 3.20 (m, 1H), 2.20 (m, 1H), 2.00 (m, 1H)
$[Rh_2(CO)_2(dppe)$-$(\mu\text{-mtz})_2]$ (**3**)		1980 (st), 1960 (med)[g]	40.2 (dd, $^1J_{Rh-P}$ = 147.6 Hz, $^3J_{P-P}$ = 2.6 Hz), 39.1 (dd, $^1J_{Rh-P}$ = 157.8 Hz)		4.20 (m 1H), 3.73 (m, 1H), 2.37 (m, 1H), 1.80 (m, 1H), 4.16 (m, 1H), 3.34 (m, 1H), 3.23 (m, 1H), 3.10 (m, 2H), 2.98 (m, 1H), 2.70 (m, 1H), 2.32 (m, 1H)
$[Rh_2I_2(CO)_2(dppm)$-$(\mu\text{-mtz})_2]$ (**4**)	2059 (st) 2037 (med)	2062 (st), 2020 (med)	19.2 (m), 18.6 (m)	189.2 (dd, $^1J_{Rh-C}$ = 55.6 Hz, $^2J_{P-C}$ = 7.7 Hz), 186.0 (dd, $^1J_{Rh-C}$ = 56.6 Hz, $^2J_{P-C}$ = 7.7 Hz)	5.20 (m, 1H), 4.15 (m, 1H), 5.06 (m, 1H), 4.08 (m, 2H), 3.90 (m, 1H), 3.32 (m, 1H), 3.20 (m, 1H), 2.94 (m, 1H), 2.10 (m, 1H)
$[Ir_2I_2(CO)_2(dppm)$-$(\mu\text{-mtz})_2]$ (**5**)	2039 (vs), 2018 (med)	2034 (vs, br)	−26.1 (d, $^2J_{P-P}$ = 37.8 Hz), −21.5 (d)		4.98 (m, 1H), 4.01 (m, 1H), 4.52 (m, 1H), 3.89 (m, 2H), 3.80 (m, 1H), 3.34 (m, 1H), 3.10 (m, 1H), 2.87 (m, 1H), 2.02 (m, 1H)
$[Rh_2I_2(CO)_2(dppe)$-$(\mu\text{-mtz})_2]$ (**6**)	2062 (st), 2025 (med)	2062 (st), 2020 (med)	40.9 (d, $^1J_{Rh-P}$ = 109.2 Hz), 22.3 (d, $^1J_{Rh-P}$ = 110.0 Hz)		2.42 (m, 1H), 2.30 (m, 1H), 2.20 (m, 1H), 1.97 (m, 1H), 5.32 (m, 1H), 4.32 (m, 1H), 3.96 (m, 1H), 3.69 (m, 1H), 3.37 (m, 1H), 3.32 (m, 1H), 3.25 (m, 1H), 2.85 (m, 1H)
$[Rh_2(CO)_2(\eta^1\text{-mtz})$-$(\mu\text{-mtz})(dppm)_2]$ (**7**)[h]	1926 (st), 1825 (w, br)	2000 (vs), 1973 (st), 1936 (vs, br), 1820 (w, br)	31.4 (br), 24.5 (br)	205.3 (br), 195.0 (br)	4.32 (m, 4H), 3.78 (m, 2H), 3.15 (t, 2H), 2.70 (t, 2H), 1.83 (t, 2H)
$[Ir_2(CO)_2(\eta^1\text{-mtz})$-$(\mu\text{-mtz})(dppm)_2]$ (**8**)	1946 (w), 1896 (st)	1952 (st, br), 1893 (vs, br)	4.5 (m), −6.9 (m)	186.3 (t, $^2J_{P-C}$ = 14.6 Hz), 180.6 (br)	4.93 (m, 2H), 4.26 (m, 2H), 4.41 (t, 2H), 3.30 (t, 2H), 2.68 (t, 2H), 1.67 (t, 2H)
$[Rh_2(CO)_2(\mu\text{-mtz})$-$(dppm)_2][Cl]$ (**9***b*)	1988 (vs), 1953 (vs)	2001 (vs), 1970 (st, br)	30.1 (m), 20.6 (m)	194.4 (dt, $^1J_{Rh-C}$ = 67 Hz, $^2J_{P-C}$ = 12 Hz), 193.4 (dt, $^1J_{Rh-C}$ = 75 Hz, $^2J_{P-C}$ = 15 Hz)	3.94 (m, 2H), 3.84 (m, 2H), 2.39 (t, 2H), 1.46 (t, 2H)
$[Rh_2(CO)_2(\mu\text{-}$ $mtz)(dppm)_2]$-$[PF_6]$ (**9***c*)	1991 (vs), 1952 (vs)	2001 (vs), 1977 (st)	29.0 (m), 20.7 (m)		3.63 (m, 2H), 3.75 (m, 2H), 2.35 (t, 2H), 1.36 (t, 2H)
$[Ir_2Cl(CO)_2(\mu\text{-mtz})$-$(dppm)_2]$ (**10**)	1944 (st), 1893 (vs)	1960 (med), 1902 (vs)	5.4 (m), −5.8 (m)		4.88 (m, 2H), 4.18 (m, 2H), 2.56 (t, 2H), 1.98 (t, 2H)
$[Rh_2(CO)_2(\mu\text{-CO})$-$(\mu\text{-mtz})(dppm)_2]$ [Cl] (**11***a*)	1981 (st), 1958 (vs), 1797 (st)	1985 (vs, br), 1812 (st)	32.2 (m), 30.8 (m)		4.22 (m, 2H), 4.12 (m, 2H), 3.00 (t, 2H), 1.86 (t, 2H)

Can. J. Chem. Downloaded from www.nrcresearchpress.com by 213.200.69.106 on 09/08/12
For personal use only.

TABLE 1 (*concluded*)

	IR, cm^{-1}		NMR[d]		
	Solid[b]	Solution[c]	$\delta(^{31}P\{^1H\})$[e]	$\delta(^{13}C\{^1H\})$[f]	$\delta(^1H)$[f]
$[Rh_2(CO)_2(\mu\text{-}CO)(\mu\text{-}mtz)(dppm)_2][PF_6]$ (**11***b*)	1976 (vs, br), 1798 (st)	1987 (vs, br), 1813 (st)	32.4 (m), 30.9 (m)		4.25 (m, 2H), 3.95 (m, 2H), 3.02 (t, 2H), 1.88 (t, 2H)

[a]Abbreviations used: d = doublet, t = triplet, m = multiplet, dd = doublet of doublets, dt = doublet of triplets, br = broad, w = weak, med = mesium, st = strong, vs = very strong.
[b]Nujol mull.
[c]THF solution except compounds **7**, **9**, and **11**, CH_2Cl_2 solution.
[d]CD_2Cl_2 solution at 25°C, except compound **3**, in THF-d_8, and compounds **9***b*, *c*, at −80°C.
[e]Versus 85% H_3PO_4.
[f]Versus TMS.
[g]ν(CO).
[h]See text.

$Rh_2ClS_2P_5F_6O_2NC_{55}H_{48}$: C 49.69, H 3.65, N 1.05; found: C 49.56, H 3.64, N 1.14.

*(k) [$Ir_2Cl(CO)_2(\mu\text{-}mtz)(dppm)_2$] (**10**)*

The procedure was the same as for **8**, except that 1 equivalent of sodium-2-mercaptothiazolinate was used. Compound **10** was crystallized from THF–hexane. Anal. calcd. for $Ir_2ClS_2P_4O_2NC_{55}H_{48}$: C 48.47, H 3.56, N 1.03; found: C 48.63, H 3.90, N 0.91.

*(l) [$Rh_2(CO)_2(\mu\text{-}CO)(\mu\text{-}mtz)(dppm)_2$][Cl] (**11**a)*

A stream of CO was passed through a CH_2Cl_2 solution of **9**, causing an immediate colour change to orange accompanied by formation of an orange precipitate. Carbonyl loss from **11***a* occurred very rapidly under dinitrogen. Compound **11***a* was determined to be a 1:1 electrolyte in CH_3NO_2 (Λ = 74.0 Ω^{-1} cm^2 mol^{-1}).

*(m) [$Rh_2(CO)_2(\mu\text{-}CO)(\mu\text{-}mtz)(dppm)_2$][$PF_6$] (**11**b)*

The procedure was the same as for **11***a*, except that **9***c* was used. Carbonyl loss from **11***b* also occurred very readily.

X-ray data collection

*(a) [$Rh_2I_2(CO)_2(\mu\text{-}mtz)_2(dppe)$]·0.5 THF (**6**)*

Dark red crystals of **6** were grown by diffusion of hexane into a THF solution of the complex. Suitable crystals were mounted on glass fibres with use of epoxy cement. Data were collected on an Enraf–Nonius CAD4 diffractometer using MoKα radiation. Unit-cell parameters were obtained from a least-squares refinement of the setting angles of 25 reflections in the range $12.6 \leq 2\theta \leq 33.6°$. The automatic peak search and reflection indexing programs[3] generated a triclinic cell with the possible space groups of $P1$ or $P\bar{1}$. The space group $P\bar{1}$ was chosen, and later verified by the successful refinement of the structure.

Intensity data were collected at 22°C by using the $\theta/2\theta$ scan technique to a maximum $2\theta = 50°$. Backgrounds were scanned for 25% of the peak width on either side of the peak scan. Three reflections were chosen as intensity standards, being remeasured after every 120 min of X-ray exposure; no unusual variation in their intensities was evident. The data were processed in the usual manner with a value of 0.04 for p to downweigh intense reflections (9). Corrections for Lorenz and polarization effects and for absorption by using the method of Walker and Stuart were applied (10).

*(b) [$Rh_2(CO)_2(\mu\text{-}mtz)(dppm)_2$][Cl]·$CH_2Cl_2$ (**9**b)*

Red crystals of **9***b* were obtained by diffusion of hexane into a CH_2Cl_2 solution of the complex. Crystals were mounted and flame-sealed in glass capillaries under solvent vapour to minimize solvent loss. Data collection and derivation of unit-cell parameters proceeded in a manner similar to that above (the setting angles of 25 reflections were in the range $22.0° \leq 2\theta \leq 25.7°$). The monoclinic diffraction symmetry and systematic absences ($h0l$, $h + l$ = odd; $0k0$, k = odd) were consistent with the space group $P2_1/n$.

Intensity data were collected at 22°C with use of the $\theta/2\theta$ scan technique to a maximum $2\theta = 50.0°$. No unusual variation was found for the intensity standards. See Table 2 for pertinent crystal data and details of intensity collection for both **6** and **9***b*.

Structure solution and refinement

Both structures were solved in the respective space groups ($P\bar{1}$ for **6** and $P2_1/n$ for **9***b*) with use of standard Patterson and Fourier techniques. Full-matrix least-squares refinements proceeded so as to minimize the function $\Sigma w(|F_o| - |F_c|)^2$, where $w = 4F_o^2/\sigma^2(F_o^2)$. Atomic scattering factors and anomalous dispersion terms were taken from the usual tabulations, refs. 11–13. The positions of all hydrogen atoms in the complex were generated on the basis of the geometry of their attached carbon atom with C—H distances of 0.95 Å. Thermal parameters for the hydrogens were fixed at 1.2 times that of their attached carbon atom. The hydrogen atoms were included as fixed contributions in the least-squares calculations. The solvent atoms of complex **6** were input as a rigid half-occupancy five-carbon ring that most appropriately described the ring of poorly resolved, smeared-out electron density that appeared on Fourier maps. The occupancy of $\frac{1}{2}$ was established by ^1H NMR of the crystals and the thermal parameters of 12 $Å^2$ were arbitrarily selected since these atoms were not well behaved in refinement attempts; they were not refined in subsequent least-squares cycles, and their hydrogen atoms were not included. Due to the bad disorder of the THF molecule the carbon and oxygen atoms could not be distinguished so were all input as carbon atoms.

The final model for complex **6**, with 433 parameters varied, refined to $R = 0.045$ and $R_w = 0.057$. In the final difference Fourier map the 10 highest residuals had intensities of 0.8–1.1 e $Å^{-3}$ and were primarily located near the disordered solvent molecule. For compound **9***b* the final model, with 613 parameters varied, converged to $R = 0.062$ and $R_w = 0.082$. The 10 highest peaks (0.6–2.5 e $Å^{-3}$) were again located near the solvent molecule. There is apparently some slight disorder of the mtz^- ligand as seen by the larger thermal parameters of S(2) and C(7); however, this was not resolvable. The positional and thermal parameters for the non-hydrogen atoms, excluding the phenyl groups, of **6** are given in Table 3, and selected bond lengths and angles are given in Tables 5 and 6, respectively. For complex **9***b* the pertinent data are found in Tables 4, 7, and 8. Anisotropic thermal parameters, idealized hydrogen parameters, and bond lengths and angles within the phenyl

[3]Programs used were those of the Enraf–Nonius Structure Determination Package, in addition to local programs by R. G. Ball.

Can. J. Chem. Downloaded from www.nrcresearchpress.com by 213.200.69.106 on 09/08/12
For personal use only.

TABLE 2. Summary of crystal data and details of intensity collection

Compound	$[Rh_2I_2(CO)_2(\mu\text{-mtz})_2(dppe)]\cdot 0.5$ THF (**6**)	$[Rh_2(CO)_2(\mu\text{-mtz})(dppm)_2][Cl]\cdot CH_2Cl_2$ (**9***b*)
Formula	$C_{36}H_{36}I_2N_2O_{2.5}P_2Rh_2S_4$	$C_{56}H_{50}Cl_3NO_2P_4Rh_2S_2$
fw	1186.52	1269.22
Space group	$P\bar{1}$	$P2_1/n$
Temp, °C	22	22
Radiation (λ, Å)	Graphite-monochromated MoKα (0.71069)	
Cell parameters		
a, Å	9.856(3)	11.400(1)
b, Å	14.078(6)	21.944(2)
c, Å	16.245(5)	22.134(1)
α, deg	103.66(3)	
β, deg	93.21(3)	92.494(7)
γ, deg	92.91(3)	
V, Å^3	2182(3)	5532(1)
Z	2	4
ρ(calcd.), g/cm^3	1.806	1.524
No. of unique data collected	7606 (h, $\pm k$, $\pm l$)	9932 (h, k, $\pm l$)
No. of unique data used ($F_o^2 \geq 3\sigma(F_o^2)$)	5164	6170
Final no. of parameters refined	433	613
R	0.045	0.062
R_w	0.057	0.082

$R = \Sigma||F_o| - |F_c||/\Sigma|F_o|$.
$R_w = (\Sigma w(|F_o| - |F_c|)^2/\Sigma w|F_o|^2)^{1/2}$.

rings and solvent molecules for **6** and **9***b* are available as supplementary data.[4]

Discussion

Previous studies (3*m*,*n*) have shown that the 2-mercaptothiazolinate ion (mtz$^-$), diagrammed below, coordinates to two metal centres through the mercapto sulfur and the nitrogen atom. The complexes of Rh and Ir so-formed have

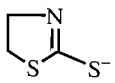

typical open-book structures. Although the tetracarbonyl species $[Rh(CO)_2(\mu\text{-mtz})]_2$ has been described (3*m*), the diiridium analogue $[Ir(CO)_2(\mu\text{-mtz})]_2$ was not previously reported. Both are prepared by the reaction of their cyclooctadiene precursors, $[M(COD)(\mu\text{-mtz})]_2$ (3*n*) with CO in THF. Neither species was isolated but each was reacted *in situ* with the appropriate phosphine to obtain the desired product. The IR spectrum of the diiridium tetracarbonyl precursor displays the expected carbonyl bands (2075, 2040, 2005, and 1990 cm^{-1}) typical of these open-book complexes (3*j*,*l*,*m*).

A series of mtz-bridged complexes of rhodium, containing monodentate tertiary phosphines such as PPh_3, has been described (3*m*); however, no complex involving this anionic bridging group and diphosphine ligands such as $Ph_2PCH_2PPh_2$ (dppm) has been reported. As was the case for monodentate phosphines, these tetracarbonyl species react readily with the diphosphine, dppm, yielding the dppm-bridged products, $[M_2(CO)_2(dppm)(\mu\text{-mtz})_2]$ (M = Rh(**1**), Ir(**2**)), as shown below. For the rhodium species **1** the two carbonyl stretches in the IR spectrum (1995, 1948 cm^{-1}) display a significantly larger separation than those of the PPh_3 analogue (1974, 1966 cm^{-1}). This is probably a consequence of the geometrical difference in these two species. In the PPh_3 adduct the phosphines have a *trans* disposition at the two metals and both carbonyl groups are opposite the nitrogen ends of the bridging mtz ligands (3*m*). In **1**

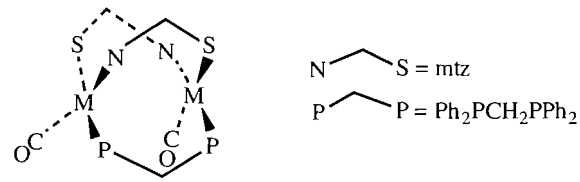

M = Rh (**1**); Ir (**2**)

and **2**, however, the bridging dppm group demands that the ends of the diphosphine group be mutually *cis*, so assuming a head-to-tail arrangement of mtz ligands, one carbonyl will be *trans* to nitrogen while the other is opposite sulfur. A head-to-tail arrangement, in which different ends of the two ligands are bound to each metal, is most often seen in binuclear complexes containing these anionic three-atom bridges (3*b*,*g*,*h*,*k*,*l*), although the head-to-head arrangement has also been reported (3*j*). The bifunctional nature of the mtz ligands in **1** gives rise to two chemically inequivalent phosphorus nuclei (also opposite either N or S) as shown in the $^{31}P\{^1H\}$ NMR spectrum, which displays two doublets of doublets at δ 30.8 ($^1J_{RhP}$ = 153.4 Hz, $^2J_{PP}$ = 58.2 Hz) and δ 45.9 ($^1J_{RhP}$ = 142.8 Hz). The geometry observed leads to the inequivalence of all 10 methylene protons associated with the dppm and mtz groups, although owing to overlap of two of these resonances in the ^1H NMR spectrum only nine are

[4]A complete set of data may be purchased from: The Depository of Unpublished Data, Document Delivery, CISTI, National Research Council Canada, Ottawa, Canada K1A 0S2.

Tables of hydrogen atom parameters and bond lengths and angles have also been deposited with the Cambridge Crystallographic Data Centre and can be obtained on request from The Director, Cambridge Crystallographic Data Centre, University of Chemical Laboratory, 12 Union Road, Cambridge CB2 1EZ, U.K.

Can. J. Chem. Downloaded from www.nrcresearchpress.com by 213.200.69.106 on 09/08/12
For personal use only.

TABLE 3. Positional and thermal parameters of the atoms of $[Rh_2I_2(CO)_2(\mu\text{-mtz})_2(\mu\text{-dppe})]\cdot 0.5THF$ (**6**)[a]

Atom	*x*	*y*	*z*	*B* (Å^2)
I(1)	0.05272(6)	0.27594(5)	0.49247(4)	4.10(2)
I(2)	−0.04596(6)	0.24254(5)	−0.02031(4)	4.23(2)
Rh(1)	0.06825(6)	0.26932(4)	0.32039(4)	2.32(1)
Rh(2)	0.04262(6)	0.26163(4)	0.14957(4)	2.29(1)
S(1)	0.1953(2)	0.4219(1)	0.3365(1)	2.84(5)
S(2)	0.1022(3)	0.5931(2)	0.2780(2)	4.78(7)
S(3)	−0.1984(2)	0.2637(2)	0.1703(2)	3.78(6)
S(4)	−0.3236(2)	0.4296(2)	0.2825(2)	6.28(9)
P(1)	0.2595(2)	0.1801(1)	0.3199(1)	2.66(5)
P(2)	0.2691(2)	0.2727(2)	0.1160(1)	2.57(5)
O(1)	−0.1215(7)	0.0878(5)	0.3003(5)	5.6(2)
O(2)	0.0142(7)	0.0441(4)	0.1132(4)	4.7(2)
N(1)	0.0546(6)	0.4152(4)	0.1872(4)	2.6(2)
N(2)	−0.1046(6)	0.3553(5)	0.3286(4)	2.9(2)
C(1)	−0.0503(9)	0.1557(7)	0.3056(5)	3.7(2)
C(2)	0.0287(8)	0.1269(6)	0.1274(5)	3.2(2)
C(3)	0.3543(7)	0.1630(5)	0.2250(5)	2.9(2)
C(4)	0.3891(7)	0.2584(5)	0.1999(5)	2.7(2)
C(5)	0.1107(8)	0.4653(6)	0.2574(5)	2.8(2)
C(6)	0.028(1)	0.5798(7)	0.1778(7)	6.4(4)
C(7)	−0.0102(9)	0.4758(6)	0.1396(6)	4.3(3)
C(8)	−0.1955(8)	0.3465(7)	0.2674(6)	3.7(2)
C(9)	−0.253(1)	0.4822(8)	0.3870(7)	5.6(3)
C(10)	−0.1238(9)	0.4393(7)	0.3977(6)	4.7(3)

[a]Numbers in parentheses are estimated standard deviations in the least significant digits in this and all subsequent tables. All atoms shown were refined anisotropically. Thermal parameters for the anisotropically refined atoms are given in the form of the equivalent isotropic displacement parameters defined as $4/3[a^2\beta_{11} + b^2\beta_{22} + c^2\beta_{33} + ab(\cos\gamma)\beta_{12} + ac(\cos\beta)\beta_{13} + bc(\cos\alpha)\beta_{23}]$. Atoms of solvent molecule of crystallization and of the phenyl carbons are given as supplementary material.

TABLE 4. Positional and thermal parameters of the atoms of $[Rh(CO)_2(\mu\text{-mtz})(dppm)_2][Cl]\cdot CH_2Cl_2$ (**9***b*)[a]

Atom	*x*	*y*	*z*	*B* (Å^2)
Rh(1)	0.11508(6)	0.25121(3)	0.15107(3)	2.51(2)
Rh(2)	0.25220(6)	0.36751(3)	0.16145(3)	2.50(2)
Cl(1)	0.5878(3)	0.1926(2)	0.9490(1)	7.5(1)
S(1)	0.3954(2)	0.2938(1)	0.1995(1)	3.23(6)
S(2)	0.4559(2)	0.1667(1)	0.2336(1)	4.76(8)
P(1)	0.0518(2)	0.2647(1)	0.2493(1)	2.98(6)
P(2)	0.2012(2)	0.3801(1)	0.2610(1)	2.66(5)
P(3)	0.1864(2)	0.2297(1)	0.0556(1)	2.71(6)
P(4)	0.3179(2)	0.3516(1)	0.0648(1)	2.81(6)
O(1)	−0.0506(6)	0.3452(3)	0.1024(3)	4.7(2)
O(2)	0.1887(7)	0.4958(3)	0.1332(4)	6.0(2)
N(1)	0.2497(6)	0.1963(3)	0.1889(3)	2.8(2)
C(1)	0.0109(8)	0.3065(5)	0.1202(4)	3.4(2)
C(2)	0.2069(9)	0.4453(5)	0.1430(4)	3.8(3)
C(3)	0.1582(7)	0.3078(4)	0.2947(4)	2.6(2)
C(4)	0.3241(7)	0.2710(4)	0.0448(3)	2.5(2)
C(5)	0.3502(8)	0.2193(4)	0.2039(4)	3.0(2)
C(6)	0.2485(9)	0.1298(5)	0.1976(4)	4.3(3)
C(7)	0.344(1)	0.1110(6)	0.2395(7)	7.4(4)

[a]See footnote of Table 3.

resolved (Table 1). The methylene resonances for the dppm group (δ 4.20, 3.70) were identified by the appropriate ^{31}P-decoupling experiments. The spectroscopic parameters for **2** are comparable to those of **1**, suggesting similar structures.

Although these species have been identified as open-book species having a bridging dppm group, they can also be viewed as A-frame complexes having the dppm and one of the mtz groups in mutually *trans* bridging positions and the other mtz group in the apical position opposite the carbon-

Can. J. Chem. Downloaded from www.nrcresearchpress.com by 213.200.69.106 on 09/08/12
For personal use only.

Can. J. Chem. Downloaded from www.nrcresearchpress.com by 213.200.69.106 on 09/08/12
For personal use only.

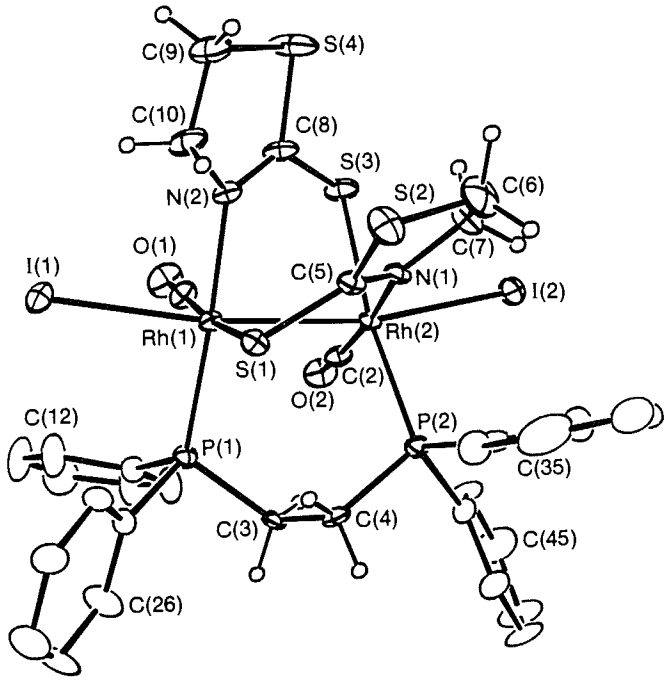

FIG. 1. A representation of $[Rh_2I_2(CO)_2(\mu\text{-mtz})_2(\mu\text{-dppe})]$ (**6**) showing the numbering scheme. Thermal ellipsoids are shown at the 20% probability level except for methylene hydrogens, which are artifically small. Phenyl hydrogens are not shown.

TABLE 5. Selected distances (Å) in $[Rh_2I_2(CO)_2(\mu\text{-dppe})(\mu\text{-mtz})_2]\cdot 0.5$ THF (**6**)

Rh(1)—Rh(2)	2.748 (1)	Rh(1)—I(1)	2.788 (1)
Rh(1)—S(1)	2.382 (2)	Rh(1)—P(1)	2.317 (2)
Rh(1)—N(2)	2.132 (5)	Rh(1)—C(1)	1.892 (7)
Rh(2)—I(2)	2.794 (1)	Rh(2)—S(3)	2.418 (2)
Rh(2)—P(2)	2.333 (2)	Rh(2)—N(1)	2.099 (5)
Rh(2)—C(2)	1.842 (7)	S(1)—C(5)	1.737 (6)
S(3)—C(8)	1.724 (7)	S(2)—C(5)	1.758 (6)
S(2)—C(6)	1.712 (8)	S(4)—C(8)	1.754 (7)
S(4)—C(9)	1.772 (8)	P(1)—C(3)	1.821 (6)
P(1)—C(11)	1.820 (7)	P(1)—C(21)	1.829 (6)
P(2)—C(4)	1.809 (6)	P(2)—C(31)	1.806 (7)
P(2)—C(41)	1.816 (7)	O(1)—C(1)	1.139 (8)
O(2)—C(2)	1.133 (7)	N(1)—C(5)	1.270 (7)
N(1)—C(7)	1.430 (8)	N(2)—C(8)	1.280 (8)
N(2)—C(10)	1.453 (8)	C(3)—C(4)	1.522 (8)
C(6)—C(7)	1.47 (1)	C(9)—C(10)	1.453 (9)

yls. In these compounds, with three similar bridging groups, the A-frame and open-book formulations are clearly two equivalent ways of categorizing the same structure.

Reaction of $[Rh(CO)_2(\mu\text{-mtz})]_2$ with 1 equivalent of dppe ($Ph_2PCH_2CH_2PPh_2$) yields $[Rh_2(CO)_2(\mu\text{-dppe})(\mu\text{-mtz})_2]$ (**3**), an unusual example of a dppe-bridged species, analogous to compounds **1** and **2**. This species is extremely air sensitive and was only characterized spectroscopically. Its IR spectrum shows two carbonyl stretches like those of the dppm analogue **1**, and its $^{31}P\{^1H\}$ NMR spectrum shows two resonances, at δ 39.1 ($^1J_{RhP}$ = 157.8 Hz, $^3J_{PP}$ = 2.6 Hz) and δ 40.2 ($^1J_{RhP}$ = 147.6 Hz). Although the 3-bond P–P coupling is much smaller than that observed in other dppe-bridged complexes such as $[WM(CO)_{10}(dppe)]$ (M = Cr, Mo, W), for which values of ca. 35 Hz are observed (14), it is comparable to the results obtained for $[Ru_4H_4(CO)_{10}(\mu\text{-dppe})]$, for which no P–P coupling was observed (15).

The ^1H NMR spectrum of **3** resembles those of **1** and **2**, suggesting a structure similar to the dppm analogues, as shown. The four resonances (δ 4.20, 3.73, 2.37, 1.80) assigned to the dppe methylene groups were identified by

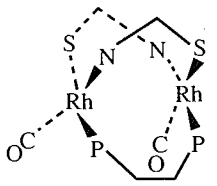

3

broad-band ^{31}P decoupling.

One of the unique reactivity patterns of binuclear compounds is the transannular oxidative-addition reaction, which results in a formal one-electron oxidation of each metal, often accompanied by metal–metal bond forming or breaking (*3a,e,i,l*). Although each of the monophosphine complexes $[M(CO)(PR_3)(\mu\text{-mtz})]_2$ (M = Rh; Ir; R = Ph, Me) gives mixtures of several species in the reactions with halogens (footnote 2), all three diphosphine-bridged species **1–3** readily undergo transannular oxidative addition of I_2 to cleanly yield the respective products **4–6**, diagrammed below. These three oxidized products are more stable than their M(+1) precursors, permitting the isolation of the dppe-bridged **6**, and allowing unambiguous confirmation of the bridging dppe group. In these three products the IR spectra show two carbonyl stretches, the frequencies of which have increased by ca. 70 cm^{-1} from those of the precursors, as expected for the oxidation of the metals from the +1 to the +2 oxidation state. The $^{31}P\{^1H\}$ NMR spectra for all three compounds are consis-

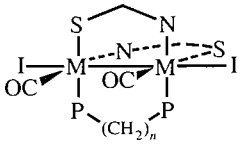

M = Rh, *n* = 1 (**4**); *n* = 2 (**6**)
= Ir, *n* = 1 (**5**)

tent with two chemically different phosphorous environments, one opposite sulfur and the other opposite nitrogen. For **4** the Rh–P and P–P couplings are not immediately obvious owing to the complexity of the spectrum; however, for **5** and **6** the $^{31}P\{^1H\}$ spectra are simple, both appearing as two sets of doublets, resulting from two-bond phosphorus–phosphorus coupling in **5** and one-bond rhodium–phosphorus coupling in **6**. No P–P coupling is resolved in the spectrum of **6**. Other spectral parameters, shown in Table 1, are in agreement with these structural formulations, which have been verified by the X-ray structure determination of **6**.

The structure of $[Rh_2I_2(CO)_2(\mu\text{-mtz})_2(\mu\text{-dppe})]$ (**6**) is shown in Fig. 1, and the associated structural parameters are summarized in Tables 5 and 6. This determination clearly confirms the binuclear, dppe-bridged structure, in which the two mtz ligands bridge in a head-to-tail arrangement. In this geometry the complex can again be viewed as an open-book complex bridged by dppe or it can be thought of as resembling an A-frame complex, except with rather substantial distortions resulting from the small bite of the mtz ligands combined with the wide bite of the dppe group. In this latter

TABLE 6. Selected angles (deg) in $[Rh_2I_2(CO)_2(\mu\text{-mtz})_2(\mu\text{-dppe})]\cdot 0.5$ THF (**6**)

I(1)—Rh(1)—Rh(2)	171.61 (2)	I(1)—Rh(1)—S(1)	97.51 (5)
I(1)—Rh(1)—P(1)	89.21 (5)	I(1)—Rh(1)—N(2)	87.8 (1)
I(1)—Rh(1)—C(1)	83.6 (2)	Rh(2)—Rh(1)—S(1)	86.73 (5)
Rh(2)—Rh(1)—P(1)	97.72 (5)	Rh(2)—Rh(1)—N(2)	85.4 (1)
Rh(2)—Rh(1)—C(1)	91.4 (2)	S(1)—Rh(1)—P(1)	94.29 (6)
S(1)—Rh(1)—N(2)	84.5 (1)	S(1)—Rh(1)—C(1)	173.5 (2)
P(1)—Rh(1)—N(2)	176.6 (1)	P(1)—Rh(1)—C(1)	92.1 (2)
N(2)—Rh(1)—C(1)	89.2 (3)	I(2)—Rh(2)—Rh(1)	166.88 (2)
I(2)—Rh(2)—S(3)	83.22 (6)	I(2)—Rh(2)—P(2)	90.54 (5)
I(2)—Rh(2)—N(1)	97.6 (1)	I(2)—Rh(2)—C(2)	87.3 (2)
Rh(1)—Rh(2)—S(3)	84.09 (6)	Rh(1)—Rh(2)—P(2)	102.38 (5)
Rh(1)—Rh(2)—N(1)	85.3 (1)	Rh(1)—Rh(2)—C(2)	89.3 (2)
S(3)—Rh(2)—P(2)	172.03 (7)	S(3)—Rh(2)—N(1)	88.3 (1)
S(3)—Rh(2)—C(2)	89.6 (2)	P(2)—Rh(2)—N(1)	87.6 (1)
P(2)—Rh(2)—C(2)	95.0 (2)	N(1)—Rh(2)—C(2)	174.3 (3)
Rh(1)—S(1)—C(5)	99.8 (2)	C(5)—S(2)—C(6)	89.2 (3)
Rh(2)—S(3)—C(8)	100.3 (2)	C(8)—S(4)—C(9)	90.1 (3)
Rh(1)—P(1)—C(3)	116.2 (2)	Rh(1)—P(1)—C(11)	113.8 (2)
Rh(1)—P(1)—C(21)	118.5 (2)	C(3)—P(1)—C(11)	103.7 (3)
C(3)—P(1)—C(21)	99.1 (3)	C(11)—P(1)—C(21)	103.4 (3)
Rh(2)—P(2)—C(4)	113.3 (2)	Rh(2)—P(2)—C(31)	112.1 (2)
Rh(2)—P(2)—C(41)	121.3 (2)	C(4)—P(2)—C(31)	107.3 (3)
C(4)—P(2)—C(41)	98.1 (3)	C(31)—P(2)—C(41)	103.1 (3)
Rh(2)—N(1)—C(5)	124.5 (4)	Rh(2)—N(1)—C(7)	123.6 (4)
C(5)—N(1)—C(7)	111.7 (5)	Rh(1)—N(2)—C(8)	123.0 (4)
Rh(1)—C(1)—O(1)	177.1 (6)	Rh(2)—C(2)—O(2)	177.0 (6)
P(1)—C(3)—C(4)	113.0 (4)	P(2)—C(4)—C(3)	110.1 (4)
S(1)—C(5)—S(2)	115.7 (3)	S(1)—C(5)—N(1)	127.4 (5)
S(2)—C(5)—N(1)	116.9 (5)	S(2)—C(6)—C(7)	109.8 (5)
N(1)—C(7)—C(6)	110.6 (6)	S(3)—C(8)—S(4)	117.5 (4)
S(3)—C(8)—N(2)	125.7 (5)	S(4)—C(8)—N(2)	116.8 (5)
S(4)—C(9)—C(10)	108.0 (5)	N(2)—C(10)—C(9)	112.5 (6)

formulation the dppe and mtz groups, which are mutually *trans*, take the positions occupied by dppm groups in the majority of A-frames, while the other mtz ligand occupies the apical site opposite the carbonyls. Both iodo ligands occupy the positions on each metal opposite the Rh—Rh bond, giving the metals octahedral geometries. The Rh—Rh separation of 2.748(1) Å is consistent with a single bond, as expected between the two Rh(II) centres. The octahedra are offset from each other in two ways. First they are inclined about the axial directions (parallel to the Rh–P vectors) by a dihedral angle of 16.4° owing to the differing bites of the mtz and dppe groups, as noted. These different bites are clearly seen in the N(2)–S(3) and P(1)–P(2) non-bonded separations of 2.685(6) and 3.841(3) Å, respectively. Second, the octahedra are staggered about the Rh—Rh bond by an average torsion angle of ca. 33°. Although this skewing may be required to minimize nonbonded contacts between the carbonyl groups, it is more likely necessary in order to accommodate the bridging dppe ligand. A similar twisting of the metal framework has been observed in dppe-bridged complexes of rhenium in which torsion angles up to 50° have been noted (16).

Most parameters within the complex are normal, therefore the Rh—P distances (2.317(2), 2.333(2) Å) are in good agreement, and resemble the analogous distances in dppm-bridged complexes. The Rh—S and Rh—N distances are also normal, except that the distances for atoms opposite dppe are longer than those opposite the carbonyls (Rh—S = 2.418(2), 2.382(2) Å; Rh—N = 2.132(5), 2.099(5) Å). This is the opposite of that observed in the related species $[Rh(CO)(PPh_3)(\mu\text{-SPh})]_2$, in which the Rh—S bonds opposite phosphorus were found to be shorter than those opposite CO (17).

Unlike diphosphine bridges, which are generally rather inert, the mercaptothiazolinate bridges are quite labile and are readily broken (footnote 2). It was therefore of interest to determine whether both mtz bridges would remain intact upon reaction with two equivalents of dppm. Given the overwhelming preference of dppm to bridge metals, and the unlikelihood that both dppm *and* both mtz ligands would simultaneously bridge, it was anticipated that one or both mtz ligands might move from their bridging sites. Treatment of $[M(CO)_2(\mu\text{-mtz})]_2$ (M = Rh, Ir) with two equivalents of dppm yields $[M_2(CO)_2(\eta^1\text{-mtz})(\mu\text{-mtz})(dppm)_2]$ (M = Rh(**7**), Ir(**8**)) as diagrammed below. The diiridium species **8** displays two signals in the $^{31}P\{^1H\}$ NMR spectrum, characteristic of an AA′BB′ spin system, and shows four resonances in the ^1H NMR spectrum for the mtz methylene hydrogens at δ 4.41, 3.30, 2.68, and 1.67, in addition to the dppm resonances. Based on a comparison with the resonances for the free mtz anion, at δ 4.0 and 3.6, the low-field resonances above are attributed to the dangling group, while the high-field pair are identified as those of the bridging group. The dangling mtz ligand, as shown, is proposed to coordinate through sulfur as has been suggested for closely related ligands in other complexes (*3h*, 18). In the IR spectrum of **8** the two carbonyl bands (1946, 1896 cm^{-1}) are consistent with terminally bound carbonyls, although the lower frequency stretch suggests that this may result from a weak semi-bridging interaction with the second metal, as is demonstrated for **7** (*vide infra*). The $^{13}C\{^1H\}$ NMR spectrum

Can. J. Chem. Downloaded from www.nrcresearchpress.com by 213.200.69.106 on 09/08/12
For personal use only.

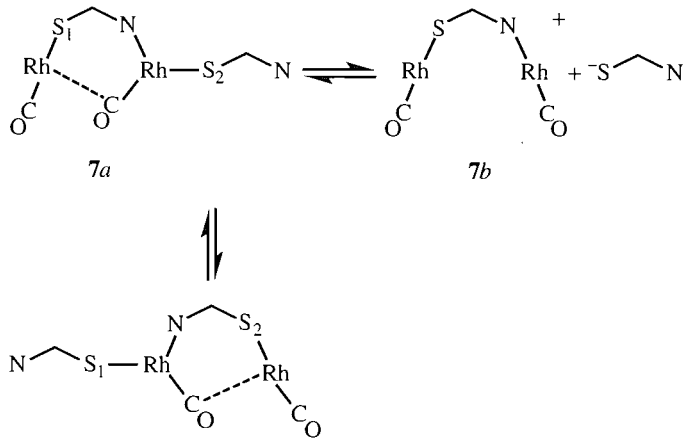

7*a* 7*b*

SCHEME 1

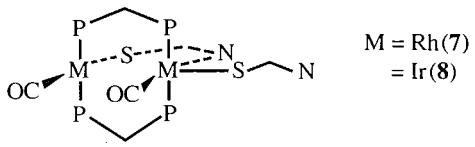

M = Rh(7)
= Ir(**8**)

displays two sharp triplets for the carbonyls at −70°C, the high-field one of which becomes broad and featureless at room temperature, without changing significantly in position. The reason for the broadening is not obvious.

In contrast to **8**, the NMR spectra of **7** show strong temperature dependence, and its solution IR spectrum is more complicated than expected for a dicarbonyl. In the solid the IR spectrum of **7** displays the two carbonyl bands expected at 1926 and 1825 cm^{-1}; again the low-frequency band is suggestive of a semibridging mode as shown for structure **7***a* in Scheme 1. However, in solution, four carbonyl stretches are observed. The lower frequency pair (1936, 1820 cm^{-1}), which are close to those of the solid, appear to correspond to **7***a* while those at 2000 and 1973 cm^{-1} appear to arise from the cationic species **7***b*, which results from mercaptothiazolinate ion dissociation. Addition of excess mtz^- (as the sodium salt) supports this proposed equilibrium, causing a decrease in the intensity of the two high-frequency bands and an increase in those ascribed to **7***a*. This equilibrium is also apparent in the NMR spectra. At ambient temperature the mtz protons appear in the ^1H NMR spectrum at δ 4.32, 3.15, 2.70, and 1.83. As excess mtz^- is added to a solution of **7**, the two low-field resonances increase in intensity and shift towards the resonances for free mtz^- (δ 4.0, 3.6). Not only does this behaviour support the previous assignment for the mtz proton resonances in **8**, it also supports the equilibrium between **7***a* and **7***b*. At −80°C resonances due to both **7***a* (δ 32.5, 26.5) and **7***b* (δ 29.5, 20.8) are observed in the $^{31}P\{^1H\}$ NMR spectrum, in an approximate 4:1 intensity ratio, respectively. This assignment is based on the close resemblance of the spectral parameters of the minor species (**7***b*) with those of the cationic species, $[Rh_2(CO)_2(\mu\text{-mtz})(dppm)_2][X]$ (X = Cl(**9***b*), PF_6(**9***c*)) (*vide infra*). In the $^{13}C\{^1H\}$ NMR spectrum of **7** at −80°C the resonance at δ 193.3 ($^1J_{RhC}$ = 74.6 Hz, $^2J_{PC}$ = 16 Hz) is assigned to the terminal carbonyl of **7***a* and the broad doublet at δ 211.8 is ascribed to the semibridging carbonyl of this species. Broadband ^{31}P decoupling experiments clearly show this semibridging interaction, as the ^{13}C resonance transforms from a broad doublet to a doublet of doublets with 67 Hz coupling to one rhodium and 13 Hz coupling to the other. The signals arising from the carbonyls of the minor species (**7***b*) are apparently obscured by the high-field ^{13}C resonance of **7***a*, as indicated by the broadness of the bottom part of the latter as well as by its integration. In the ^1H NMR spectrum at −80°C the appearance of a major and minor species in the appropriate ratio is also apparent, although a couple of the resonances for the major species shift substantially, and some of those for the minor species are obscured by other resonances. Selective homonuclear decoupling experiments at ambient temperature point to an additional fluxionality that occurs slowly on the NMR time scale. Irradiation of one of the methylene proton resonances of the bridging mtz group causes the other methylene resonance of this group to collapse to a singlet, as expected. However, unexpectedly this results in a significant decrease in the intensity of the corresponding methylene resonance of the dangling group. This observation of spin saturation transfer indicates a slow exchange of terminal and bridging mtz groups as diagrammed vertically in Scheme I. Attempts to increase the rate of terminal-bridging mtz exchange to achieve rapid interconversion, by raising the temperature, were unsuccessful since the compound decomposed at temperatures above ca. 45°C.

TABLE 7. Selected distances (Å) in $[Rh_2(CO)_2(\mu\text{-mtz})(dppm)_2]$-$[Cl]\cdot CH_2Cl_2$ (**9***b*)

Rh(1)—P(1)	2.339 (2)	Rh(1)—P(3)	2.346 (2)
Rh(1)—N(1)	2.097 (5)	Rh(1)—C(1)	1.811 (7)
Rh(2)—S(1)	2.422 (2)	Rh(2)—P(2)	2.320 (2)
Rh(2)—P(4)	2.324 (2)	Rh(2)—C(2)	1.824 (7)
S(1)—C(5)	1.719 (6)	S(2)—C(5)	1.775 (6)
S(2)—C(7)	1.78 (1)	P(1)—C(3)	1.809 (6)
P(1)—C(11)	1.801 (6)	P(1)—C(21)	1.838 (7)
P(2)—C(3)	1.829 (6)	P(2)—C(31)	1.836 (6)
P(2)—C(41)	1.826 (6)	P(3)—C(4)	1.838 (6)
P(3)—C(51)	1.820 (6)	P(3)—C(61)	1.840 (7)
P(4)—C(4)	1.824 (6)	P(4)—C(71)	1.848 (6)
P(4)—C(81)	1.837 (6)	O(1)—C(1)	1.159 (7)
O(2)—C(2)	1.147 (8)	N(1)—C(5)	1.283 (7)
N(1)—C(6)	1.472 (8)	C(6)—C(7)	1.46 (1)

Complexes containing two bridging dppm groups and a bridging mtz ligand can also be obtained by the reactions of *trans*-$[MCl(CO)(dppm)]_2$ (M = Rh, Ir) with sodium mercaptothiazolinate. When two equivalents of mtz^- are used, compounds **7** and **8** are obtained, as seen in the reactions of $[M(CO)_2(\mu\text{-mtz})]_2$ with two equivalents of dppm. When the above dppm-bridged dichloro complexes are reacted with only one equivalent of mtz^-, replacement of only one chloride ligand occurs, yielding $[M_2Cl(CO)_2(\mu\text{-mtz})(dppm)_2]$ (M = Rh(**9**), Ir(**10**)). The spectral parameters for **10** are closely comparable to those of **8**, apart from the absence of resonances for the dangling mtz group in the ^1H NMR spectrum, so this compound is assigned an analogous structure in which the dangling mtz group in **8** is replaced by a terminal chloro ligand in **10**.

Although **9** is shown above as having a coordinated chloro ligand, in solution it, like compound **7**, is better represented as an equilibrium mix of the neutral species **9***a* together with the cationic species **9***b*, resulting from chloride dissociation as shown in eq. [1]. This is clearly seen in the IR spectrum

Can. J. Chem. Downloaded from www.nrcresearchpress.com by 213.200.69.106 on 09/08/12
For personal use only.

TABLE 8. Selected angles (deg) in $[Rh_2(CO)_2(\mu\text{-mtz})(dppm)_2][Cl]\cdot CH_2Cl_2$ (**9***b*)

P(1)—Rh(1)—P(3)	174.96(6)	P(1)—Rh(1)—N(1)	87.3 (1)
P(1)—Rh(1)—C(1)	92.4 (2)	P(3)—Rh(1)—N(1)	88.1 (1)
P(3)—Rh(1)—C(1)	92.4 (2)	N(1)—Rh(1)—C(1)	172.9 (2)
S(1)—Rh(2)—P(2)	86.69 (6)	S(1)—Rh(2)—P(4)	88.86 (6)
S(1)—Rh(2)—C(2)	151.9 (2)	P(2)—Rh(2)—P(4)	175.27 (6)
P(2)—Rh(2)—C(2)	91.2 (2)	P(4)—Rh(2)—C(2)	92.0 (2)
Rh(2)—S(1)—C(5)	117.1 (2)	C(5)—S(2)—C(7)	89.7 (3)
Rh(1)—P(1)—C(3)	110.9 (2)	Rh(1)—P(1)—C(11)	120.9 (2)
Rh(1)—P(1)—C(21)	110.5 (2)	C(3)—P(1)—C(11)	107.2 (3)
C(3)—P(1)—C(21)	104.5 (3)	C(11)—P(1)—C(21)	101.3 (3)
Rh(2)—P(2)—C(3)	111.5 (2)	Rh(2)—P(2)—C(31)	113.3 (2)
Rh(2)—P(2)—C(41)	118.6 (2)	C(3)—P(2)—C(31)	103.7 (3)
C(3)—P(2)—C(41)	103.8 (3)	C(31)—P(2)—C(41)	104.4 (3)
Rh(1)—P(3)—C(4)	110.4 (2)	Rh(1)—P(3)—C(51)	117.8 (2)
Rh(1)—P(3)—C(61)	116.6 (2)	C(4)—P(3)—C(51)	107.0 (3)
C(4)—P(3)—C(61)	102.1 (3)	C(51)—P(3)—C(61)	101.3 (3)
Rh(2)—P(4)—C(4)	112.7 (2)	Rh(2)—P(4)—C(71)	112.9 (2)
Rh(2)—P(4)—C(81)	119.4 (2)	C(4)—P(4)—C(71)	102.5 (3)
C(4)—P(4)—C(81)	103.1 (3)	C(71)—P(4)—C(81)	104.4 (3)
Rh(1)—N(1)—C(5)	120.5 (4)	Rh(1)—N(1)—C(6)	127.7 (4)
C(5)—N(1)—C(6)	111.7 (5)	Rh(1)—C(1)—O(1)	174.9 (6)
Rh(2)—C(2)—O(2)	173.6 (6)	P(1)—C(3)—P(2)	114.3 (3)
P(3)—C(4)—P(4)	113.9 (3)	S(1)—C(5)—S(2)	116.1 (3)
S(1)—C(5)—N(1)	128.8 (5)	S(2)—C(5)—N(1)	115.1 (5)
N(1)—C(6)—C(7)	110.7 (6)	S(2)—C(7)—C(6)	106.1 (6)

Can. J. Chem. Downloaded from www.nrcresearchpress.com by 213.200.69.106 on 09/08/12
For personal use only.

[1] $[Rh_2Cl(CO)_2(\mu\text{-mtz})(dppm)_2]$ (**9***a*)

$$\rightleftharpoons [Rh_2(CO)_2(\mu\text{-mtz})(dppm)_2][Cl] \text{ (9}b\text{)}$$

in solution, which displays three carbonyl stretches at 2001, 1970, and 1933 cm^{-1}. The middle band is broad and apparently results from two overlapping bands, so the stretches due to **9***a* appear at 1970 and 1933 cm^{-1} whereas those of **9***b* appear at 2001 and 1970 cm^{-1}. Addition of $AgBF_4$ to solutions of **9** results in the disappearance of the 1933 cm^{-1} band and sharpening of the central band, and addition of sodium chloride causes these bands to reappear. In the solid state the two carbonyl bands observed (1988, 1953 cm^{-1}) are consistent with the ionic structure **9***b*, and this is confirmed by an X-ray structure determination of this species (*vide infra*).

As was noted for **7***a* and **7***b*, the exchange between **9***a* and **9***b* is fast on the NMR time scale. Thus at ambient temperature both the $^{31}P\{^1H\}$ and the $^{13}C\{^1H\}$ NMR spectra of the equilibrium mixture display two broad resonances, while the ^1H NMR spectrum shows only two triplets (δ 2.43, 1.85) for the mtz methylene protons. Lowering the temperature sharpens the signals in the $^{31}P\{^1H\}$ and $^{13}C\{^1H\}$ NMR spectra. However, in contrast to the equilibrium involving **7***a* and **7***b*, only one species is revealed at −80°C, the spectroscopic parameters of which closely resemble those of $[Rh_2(CO)_2(\mu\text{-mtz})(dppm)_2][PF_6]$ (**9***c*) obtained by reaction of **9** with $AgPF_6$. Therefore it is clear that lowering the temperature shifts the equilibrium in favor of **9***b*. At −80°C, the $^{31}P\{^1H\}$ NMR spectrum of **9***b* is as expected for an unsymmetric structure, and the $^{13}C\{^1H\}$ NMR spectrum reveals two doublets of triplets at δ 194.4 and 193.4, reminiscent of those of **7***b*. The mtz methylene hydrogens appear as triplets at δ 2.39 and 1.46.

Among the dppm-bridged binuclear compounds of group VIII metals, complexes **7–10** represent a new type of A-frames, in which the anionic capping ligand is bifunctional, binding to the two metals by different atom types, and because of this the two metal centres in these A-frames are electronically different, which could give rise to interesting reactivity patterns. The bifunctional feature of the apical mtz ligand also provides an easy access to coordinative unsaturation through cleavage from a metal of one of its ends, which is shown to be feasible by the dynamic behavior of **7**. Coordinative unsaturation induced by bridge opening has been proposed to be crucial in substrate activation by open-book compounds (4), as noted earlier. Related A-frame complexes of group VIII metals, in which the anionic apical ligands are those typically used as bridges in open-book compounds, have been reported recently (2*e*,*f*,*i*,*j*). However, these ligands, such as pyrazolyl groups, have the same atom type binding to each metal.

The structure of **9***b*, as the methylene chloride solvate, has been determined and a representation of the cation is shown in Fig. 2. This compound much more resembles conventional "A-frames" than does **6**, in that the *trans*-bridging groups are dppm with the anionic group (mtz^-) at the apex opposite the carbonyls. In fact the structure quite closely resembles that of $[Rh_2(CO)_2(\mu\text{-dmpz})(dppm)_2]^+$ (2*j*), (dmpz = 3,5-dimethylpyrazolate). The structure determination clearly shows that the chloride ion is not associated with the complex, and the closest contact between rhodium and this anion is 6.842(2) Å. Similarly the CH_2Cl_2 molecule is isolated from both the anion and the cation. Although the geometries about the Rh centres are essentially square planar, there are significant distortions from the idealized geometry. Therefore the N(1)—Rh(1)—C(1) angle is 172.9(2)° and the S(1)—Rh(2)—C(2) angle is 151.9(2)°, resulting from an apparent movement of C(1)O(1) towards Rh(2) and C(2)O(2) away from Rh(1). This distortion is accompanied by a Rh(1)—Rh(2) separation of 2.9957(7) Å, which is compressed slightly compared with the intraligand P–P nonbonded contacts of 3.056(2) and

Can. J. Chem. Downloaded from www.nrcresearchpress.com by 213.200.69.106 on 09/08/12
For personal use only.

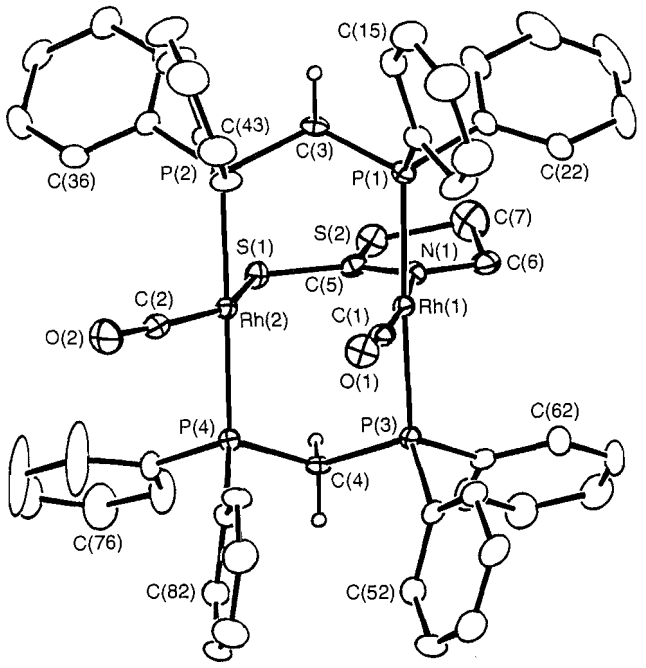

FIG. 2. A representation of the $[Rh_2(CO)_2(\mu\text{-mtz})(dppm)_2]^+$ cation of **9***a*. Thermal ellipsoids are as in Fig. 1.

3.068(2) Å, suggesting a possible weak interaction between the metals. We believe, however, that these distortions result from the packing. As can be seen in Fig. 2, phenyl rings 4 and 8 are aimed between the carbonyls and the short C(2)—H(42) and C(2)—H(86) contacts of 2.72 and 2.62 Å appear to distort this carbonyl from its idealized position. Similarly rings 1 and 5 appear to force C(1)O(1) towards Rh(2), giving a C(1)—H(12) contact of 2.56 Å. The contact between Rh(2) and C(1) (3.158(6) Å) appears to be too long to suggest even a weak semi-bridging interaction, and the IR spectra also do not argue in favor of such an interaction.

In conventional A-frames (2*a*–*c*) the capping ligand binds to both metals through a common atom, resulting in a substantial tilt of the two metal square planes by about 83°. In **9***b* (and in **6**) the capping mtz ligand binds through two well-separated donor atoms, opening up the A-frame and resulting in more closely parallel coordination planes at the metals (the dihedral angle is only 16(2)°). As such, the structure of **9***b* takes on a geometry similar to the face-to-face dimers such as *trans*-$[Rh_2Cl_2(CO)_2(dppm)_2]$ (19) and $[Rh_2(CNR)_4(dppm)_2]^{2+}$ (20, 21).

All other parameters within the complex are essentially as expected, comparing well with the appropriate parameters in **6**, so deserve no further comment.

The equilibrium mix of **9***a* and **9***b* reacts with CO to give $[Rh_2(CO)_2(\mu\text{-mtz})(\mu\text{-CO})(dppm)_2][Cl]$ (**11***a*), whereas **11***b*, having PF_6^- as the counterion, is obtained by the analogous reaction of **9***c*. Carbonyl loss from both species to give the starting complexes is very facile, occurring simply under an N_2 purge. The $^{31}P\{^1H\}$ NMR spectra of the two compounds are similar and appear as sharp AA'BB'XY spin patterns, consistent with the structure as shown. The infrared spectrum of **11***a* displays two terminal carbonyl stretches (1981, 1958 cm^{-1}), whereas for **11***b* only one stretch (1976 cm^{-1}) is revealed for the terminal carbonyls. However, the broadness of this stretch suggests that another band is beneath it. Both compounds display bridging carbonyl stretches at ca. 1797 cm^{-1} in the IR spectra. The CO stretches of **11***a*, *b* appear at significantly lower frequencies than those (2005–1860 cm^{-1}) observed for the closely related compounds, $[Rh_2(CO)_2(\mu\text{-X})(\mu\text{-CO})(dppm)_2][X]$ (X = Cl, Br, I) (19), suggesting that the mtz ligand is more electron releasing than the halides.

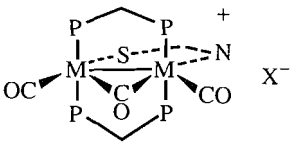

X = Cl(**11***a*); PF_6(**11***b*)

Summary

A series of binuclear complexes of Rh and Ir has been synthesized, in which the metals are bridged by both neutral diphosphine ligands (dppm and dppe) and anionic mercaptothiazolinate (mtz) groups. In the first class, $[M_2(CO)_2(\mu\text{-mtz})_2(\mu\text{-L})]$ (L = diphosphine), containing two anionic bridging groups, the complexes can be classified as having either "open-book" or "A-frame" geometries, and both descriptions appear to be equally valid. Two of these species, $[Rh_2(CO)_2(\mu\text{-mtz})_2(\mu\text{-dppe})]$ and $[Rh_2I_2(CO)_2(\mu\text{-mtz})_2(\mu\text{-dppe})]$, are unusual examples in which dppe functions as a *bridging* group. In the second class of compounds, $[M_2X(CO)_2(\mu\text{-mtz})(dppm)_2]$ (M = Rh, Ir; X = Cl, mtz), containing two bridging dppm groups, the ease of displacement of the anionic groups from a bridging site has been demonstrated. These species have only one mtz group bridging the metals and are best viewed as classical A-frame complexes. The additional anionic ligand (Cl^- or mtz^-) is terminally bound to one metal, and for M = Rh these terminal groups readily dissociate, yielding cationic complexes.

Although numerous open-book complexes containing phosphine ligands are known, the complexes $[M_2(CO)_2(\mu\text{-mtz})_2(\mu\text{-L})]$ are the first examples in which diphosphines have been incorporated as ligands together with a bifunctional ligand, binding through different atom types (S,N). It will be of interest to further explore the chemistry of these species. The complexes of the second class are interesting in that they contain a bifunctional apical ligand, the possible effects of which have been noted. It may be the bifunctionality of the mtz ligand that gives rise to the unusual dynamic behavior for the complex $[Rh_2(\eta^1\text{-mtz})(CO)_2(\mu\text{-mtz})(dppm)_2]$, as shown in Scheme 1.

Acknowledgments

We thank the Natural Sciences and Engineering Research Council of Canada (NSERC) and the University of Alberta for support of this work and NSERC for partial support of the diffractometer. We are grateful to Drs. Bernie Santarsiero and Bob McDonald of the X-ray Structure Determination Laboratory of this department for data collection on com-

pound **6**, and assistance in the final stages of refinement and data presentation.

1. (*a*) R. Poilblanc. Inorg. Chim. Acta, **62**, 75 (1982); (*b*) M. H. Chisholm. *In* Reactivity of metal–metal bonds. *Edited by* M. H. Chisholm. ACS Symp. Ser. **155**, 17 (1981); (*c*) E. L. Muetterties and J. Stein. Chem. Rev. **79**, 479 (1979).
2. (*a*) C. P. Kubiak and R. Eisenberg. Inorg. Chem. **19**, 2726 (1980); (*b*) C. P. Kubiak, C. Woodcock, and R. Eisenberg. Inorg. Chem. **19**, 2733 (1980); (*c*) M. Cowie and S. K. Dwight. Inorg. Chem. **18**, 2700 (1979); (*d*) B. A. Vaartstra, J. Xiao, J. A. Jenkins, R. Verhagen, and M. Cowie. Organometallics, **10**, 2708 (1991); (*e*) L. J. Tortorelli, C. Woods, and A. T. McPhail. Inorg. Chem. **29**, 2726 (1990); (*f*) C. Woods, L. J. Tortorelli, D. P. Rillema, J. L. E. Burn, and J. C. DePriest. Inorg. Chem. **28**, 1673 (1989); (*g*) B. A. Vaartstra and M. Cowie. Inorg. Chem. **28**, 3138 (1989); (*h*) J. A. Jenkins, J. P. Ennett, and M. Cowie. Organometallics, **7**, 1845 (1988); (*i*) D. Carmona, L. A. Oro, P. L. Pérez, A. Tiripicchio, and M. Tiripicchio-Camellini. J. Chem. Soc. Dalton Trans. 1427 (1989); (*j*) L. A. Oro, D. Carmona, P. L. Pérez, M. Esteban, A. Tiripicchio, and M. Tiripicchio-Camellini. J. Chem. Soc. Dalton Trans. 973 (1985); (*k*) B. R. Sutherland and M. Cowie. Organometallics, **4**, 1637 (1985); (*l*) R. J. Puddephatt. Chem. Soc. Rev. **12**, 98 (1983).
3. (*a*) M. T. Pinillos, A. Elduque, J. A. López, F. J. Lahoz, and L. A. Oro. J. Chem. Soc. Dalton Trans. 1391 (1991); (*b*) M. A. Ciriano, J. J. Pérez-Torrente, L. A. Oro, A. Tiripicchio, and M. Tiripicchio-Camellini. J. Chem. Soc. Dalton Trans. 255 (1991); (*c*) J. A. Bailey, S. L. Grundy, and S. R. Stobart. Organometallics, **9**, 536 (1990); (*d*) D. Carmona, F. J. Lahoz, L. A. Oro, J. Reyes, and M. P. Lamata. J. Chem. Soc. Dalton Trans. 3551 (1990); (*e*) M. T. Pinillos, A. Elduque, L. A. Oro, F. J. Lahoz, F. Bonati, A. Tiripicchio, and M. Tiripicchio-Camellini. J. Chem. Soc. Dalton Trans. 989 (1990); (*f*) G. S. Rodman and A. J. Bard. Inorg. Chem. **29**, 4699 (1990); (*g*) D. C. Boyd, R. Szalapski, and K. R. Mann. Organometallics, **8**, 790 (1989); (*h*) M. A. Ciriano, F. Viguri, J. J. Perez-Torrente, F. J. Lahoz, L. A. Oro, A. Tripicchio, and M. Tiripicchio-Camellini. J. Chem. Soc. Dalton Trans. 25 (1989); (*i*) R. B. Brost and S. R. Stobart. J. Chem. Soc. Chem. Commun. 498 (1989); (*j*) M. A. Ciriano, B. E. Villarroya, L. A. Oro, M. C. Apreda, C. Foces-Foces, and F. H. Cano. J. Organomet. Chem. **366**, 377 (1989); (*k*) G. S. Rodman and K. R. Mann. Inorg. Chem. **27**, 3338 (1988); (*l*) M. A. Ciriano, S. Sebastián, L. A. Oro, A. Tiripicchio, M. Tiripicchio-Camellini, and F. J. Lahoz. Angew. Chem. Int. Ed. Engl. **27**, 402 (1988); (*m*) M. Cowie and T. Sielisch. J. Organomet. Chem. **348**, 241 (1988); (*n*) T. Sielisch and M. Cowie. Organometallics, **7**, 707 (1988), and refs. therein.
4. (*a*) A. Dedieu, P. Escaffre, J. M. Frances, Ph. Kalck, and A. Thorez. Nouv. J. Chim. **10**, 631 (1986); (*b*) M. El Amane, R. Mathieu, and R. Poilblanc. Organometallics, **2**, 1618 (1983).
5. A. C. Price and R. A. Walton. Polyhedron, **6**, 729 (1987).
6. D. M. A. Minahan, W. E. Hill, and C. A. McAuliffe. Coord. Chem. Rev. **55**, 31 (1984).
7. J. T. Mague and J. P. Mitchener. Inorg. Chem. **8**, 199 (1969).
8. B. R. Sutherland and M. Cowie. Inorg. Chem. **23**, 2324 (1984).
9. R. J. Doedens and J. A. Ibers. Inorg. Chem. **6**, 204 (1967).
10. N. Walker and D. Stuart. Acta Crystallogr. Sect. A: Found. Crystallogr. **A39**, 158 (1983).
11. D. T. Cromer and J. T. Waber. International tables for crystallography. Vol. IV. Kynoch Press, Birmingham. 1974. Table 2.2A.
12. R. F. Stewart, E. R. Davidson, and W. T. Simpson. J. Chem. Phys. **42**, 3175 (1965).
13. D. T. Cromer and D. Liberman. J. Chem. Phys. **53**, 1891 (1970).
14. R. L. Keiter, S. L. Kaiser, N. P. Hansen, J. W. Brodack, and L. W. Cary. Inorg. Chem. **20**, 283 (1981).
15. M. R. Churchill, R. A. Lashewycz, J. R. Shapley, and S. I. Richter. Inorg. Chem. **19**, 1277 (1980).
16. (*a*) P. E. Fanwick, D. R. Root, and R. A. Walton. Inorg. Chem. **25**, 4832 (1986); (*b*) F. A. Cotton, G. G. Stanley, and R. A. Walton. Inorg. Chem. **17**, 2099 (1978).
17. J. J. Bonnet, Ph. Kalck, and R. Poilblanc. Inorg. Chem. **16**, 1514 (1977).
18. (*a*) E. S. Peterson, D. P. Bamcroft, D. Min, F. A. Cotton, and E. H. Abbott. Inorg. Chem. **29**, 229 (1990); (*b*) M. A. Ciriano, J. J. Perez-Torrente, F. Viguri, F. J. Lahoz, L. A. Oro, A. Tiripicchio, and M. Tiripicchio-Camellini. J. Chem. Soc. Dalton Trans. 1493 (1990).
19. M. Cowie and S. K. Dwight. Inorg. Chem. **19**, 2500 (1980).
20. A. L. Balch. J. Am. Chem. Soc. **98**, 8049 (1976).
21. J. T. Mague and S. H. DeVries. Inorg. Chem. **19**, 3743 (1980).

Can. J. Chem. Downloaded from www.nrcresearchpress.com by 213.200.69.106 on 09/08/12
For personal use only.

^{13}C and ^{1}H NMR investigation of pilocarpine hydrochloride in water solution

ELENA GAGGELLI, NICOLA GAGGELLI, GIANNI VALENSIN,[1] AND ANTONIO VIVI
Department of Chemistry, University of Siena, Pian dei Mantellini 44, Sienna 53100, Italy

Received April 27, 1992[2]

ELENA GAGGELLI, NICOLA GAGGELLI, GIANNI VALENSIN, and ANTONIO VIVI. Can. J. Chem. **71**, 738 (1993).

Dynamic and geometric features of pilocarpine in water solution were delineated by interpreting ^{13}C and ^{1}H NMR spin-lattice relaxation rates and nuclear Overhauser effects. The motional correlation time was evaluated at 53 ± 5 ps at 298 K. $^{1}H—^{1}H$ distances, as calculated from double-selective ^{1}H spin-lattice relaxation rates, and $^{13}C—^{1}H$ distances, as calculated from selective $^{13}C–\{^{1}H\}$ Overhauser effects, gave evidence of a *C*7 puckered conformation of the furanone ring and of an angle of ca. 50° between the two rings.

ELENA GAGGELLI, NICOLA GAGGELLI, GIANNI VALENSIN et ANTONIO VIVI. Can. J. Chem. **71**, 738 (1993).

En se basant sur les vitesses de relaxation spin-réseau et sur les effets nucléaires Overhauser des spectres RMN du ^{1}H et du ^{13}C de ses solutions aqueuses, on a pu déterminer les caractéristiques dynamiques et géométriques de la pilocarpine. On a évalué que, à 298 K, le temps de corrélation des mouvements est égal à 53 ± 3 ps. On a calculé les distances $^{1}H—^{1}H$ à partir des temps de relaxation spin-réseau du ^{1}H doublement sélectifs et les distances $^{13}C—^{1}H$ à partir d'effets Overhauser $^{13}C–\{^{1}H\}$ sélectifs; ces données suggèrent que le cycle furanone existe dans une conformation plissée et que l'angle entre les deux cycles est d'environ 50°.

[Traduit par la rédaction]

Introduction

Pilocarpine ((3*S*-*cis*)-3-ethyldihydro-4-[(1-methyl-1*H*-imidazol-5-yl)methyl]-2(3*H*)-furanone) (PLC) (Fig. 1) is the chief alkaloid obtained from the leaves of South American shrubs of the genus *Pilocarpus* (1). It is a cholinomimetic agent that acts mainly at muscarinic acetyl-choline receptors (mAChR) of autonomic effector cells, mediating a large diversity of neurophysiological actions in the central and peripheral nervous systems (2).

As a drug, PLC is valued as a topical miotic, in ophthalmic solution, in the treatment of glaucoma (3), although it has been shown that aqueous solutions are poorly stable at pH > 7, at elevated temperature (4), and in the presence of phosphate and carbonate buffers (5). Chemical, pharmaceutical, and spectroscopic properties of PLC have been summarized elsewhere (6).

An understanding of mechanisms responsible for binding of agonists and antagonists to mAChR is quite important for rational drug design. Since effector molecules are usually highly flexible, the basis for such drug design has to be sought in determining the conformation in the bound rather than in the free state. From this point of view NMR is the technique of choice as it has the potential of determining dynamic and geometric features in both states, provided the ligand exchanges between the two at a relatively fast rate. Another aspect is, moreover, relevant. In the free state flexible molecules are characterized by several conformations separated by relatively low energy barriers, whereas in the bound state it is commonly accepted that the same molecules exist in unique conformations. Consequently, binding interactions imply a process of conformational selection, the role of which has been neglected so far.

As a first step, NMR data are herein presented for pilocarpine in water solution at pH 5–6; conformational features are discussed in the light of reorientational dynamics, and the "preferred" structure in solution is determined. The structure detected by NMR is not, of course, a minimum energy conformation but, rather, a geometric arrangement arising by motional averaging of many low-energy conformations. The ^{1}H NMR data for PLC in water solution have been previously published (7).

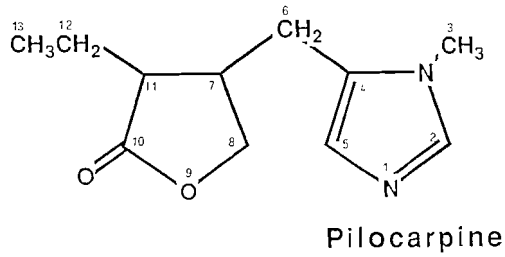

FIG. 1. Molecular formula of pilocarpine.

Experimental

Pilocarpine hydrochloride was purchased from Sigma Chemical Co. and used without further purification. Solutions were made in deuterium oxide 99.95% (Merck), adjusted in pH with either DCl or NaOD, and carefully deoxygenated by bubbling nitrogen gas.

NMR spectra were obtained on a Varian VXR 200 spectrometer operating at the controlled temperature of 300 ± 1 K. Spin-lattice relaxation rates were measured with inversion–recovery pulse sequences and calculated in the initial rate approximation. Selective and double-selective ^{1}H NMR spin-lattice relaxation rates were measured with inversion–recovery pulse sequences where the 180° inverting pulse was provided by a DANTE (8) or a double-DANTE pulse train (9). In either case the relaxation rate values were calculated from the initial slope of longitudinal magnetization recovery (10).

$^{13}C–\{^{1}H\}$ nuclear Overhauser effects (nOe) were measured with gated decoupling methods either in the noise-modulated or in the long-pulse mode to provide nonselective or selective presaturation, respectively (11).

Molecular modelling was achieved by using the molecular graphics package ChemX implemented on a Vax 750 computer connected to a digital VT 240 terminal (19).

Results and discussion

Geometric features can be obtained by relaxation rates or nuclear Overhauser effects. In both cases the relevant pa-

[1]Author to whom correspondence may be addressed.
[2]Revision received February 22, 1993.

Can. J. Chem. Downloaded from www.nrcresearchpress.com by 213.200.69.106 on 09/08/12
For personal use only.

Can. J. Chem. Downloaded from www.nrcresearchpress.com by 213.200.69.106 on 09/08/12
For personal use only.

TABLE 1. The 50.3 MHz ^{13}C NMR parameters for pilocarpine 20 mmol dm^{-3} in D_2O at pH = 5.5 and T = 300 K

Carbon	δ (ppm)	R_1 (s^{-1})	η_{obs} (η units)	R_1/n_H (s^{-1})
C2	116.9	1.08 ± 0.06	1.89	1.08
C4	132.7	0.03 ± 0.02	0.92	—
C5	135.4	1.10 ± 0.06	1.84	1.10
C6	20.7	2.18 ± 0.10	1.92	1.09
C7	36.2	1.14 ± 0.06	1.91	1.07
C8	71.3	2.24 ± 0.10	1.95	1.12
C10	182.4	0.02 ± 0.01	0.92	—
C11	44.6	1.07 ± 0.04	1.93	1.01
C12	17.9	1.53 ± 0.06	1.97	0.70
C13	11.4	0.41 ± 0.04	1.91	0.12
NMe	33.3	0.37 ± 0.03	1.57	0.07

rameter is the dipolar interaction energy between spin pairs, which depends upon the inverse of the sixth power of the internuclear distance and the correlation time of the reorientational motion undergone by the internuclear vector. Since the ^{13}C NMR spin-lattice relaxation rate or protonated carbons is mainly determined by the one-bond $^{13}C-^1H$ dipolar interaction, the usual approach consists of interpreting ^{13}C NMR rates in terms of reorientational dynamics and, thereafter, in interpreting single $^1H-^1H$ or $^{13}C-^1H$ dipolar interaction energies in terms of geometric parameters.

^{13}C NMR data are summarized in Table 1. The $^{13}C-\{^1H\}$ nuclear Overhauser effects (nOe) measured upon noise-modulated gated decoupling of all ^1H resonances were found, within the limits of experimental error, at the maximum value (η_{max} = 1.98) for all protonated carbons. The $^{13}C-^1H$ dipolar interaction was therefore considered as the dominant relaxation mechanism and spin-lattice relaxation rates (R_1) were interpreted by the dipolar interaction with the n_H protons attached at the distance r = 1.09 Å (12). The reorientational motional correlation times could consequently be evaluated by using the usual approach from the literature (13). It may be noticed that all protonated carbons, except the *N*-methyl and the ethyl, experience nearly the same dipolar relaxation energies, yielding a mean value of 53 ± 5 ps at 298 K for the correlation time. The ethyl chain carbons relax with features typical of segmental motion with shorter effective correlation times. As for the *N*-methyl, the fact that its normalized relaxation rate (R_1/n_H) is much slower than that

TABLE 2. The 200 MHz ^1H NMR parameters for pilocarpine 20 mmol dm^{-3} in D_2O at pH = 5.5 and T = 300 K

Proton	δ (ppm)	R_i^{nsel} (s^{-1})	R_i^{sel} (s^{-1})[a]	F	$R_i^{j,k}$ (s^{-1})[b]
H2	8.49	0.19 ± 0.01	0.16 ± 0.01	1.19 ± 0.14	
H5	7.17	0.28 ± 0.01	0.23 ± 0.01	1.22 ± 0.10	
H6a	2.74	1.39 ± 0.05			
H6b	2.51	1.45 ± 0.06	0.99 ± 0.03	1.46 ± 0.11	
H7	2.96	0.83 ± 0.03	0.61 ± 0.02	1.36 ± 0.10	0.67 ± 0.02 (H7–H11) 0.66 ± 0.02 (H7–H8a) 0.63 ± 0.02 (H7–H8b) 0.66 ± 0.02 (H7–H6a) 0.63 ± 0.02 (H7–H6b)
H8a	4.24	1.37 ± 0.05	0.93 ± 0.02	1.47 ± 0.09	1.38 ± 0.04 (H8a–H8b) 0.98 ± 0.03 (H8a–H7)
H8b	4.00	1.25 ± 0.04	0.86 ± 0.03	1.45 ± 0.10	1.29 ± 0.03 (H8b–H8a) 0.88 ± 0.02 (H8b–H7)
H11	2.78	0.88 ± 0.03			
H12a	1.62	1.29 ± 0.05	1.18 ± 0.04	1.09 ± 0.09	1.20 ± 0.02 H12a–H11
H12b	1.45	1.50 ± 0.05	1.23 ± 0.04	1.22 ± 0.08	1.24 ± 0.02 H12b–H11
H13	0.89	0.83 ± 0.03			
NMe	3.66	0.65 ± 0.03			

[a] R_i^{sel} is the spin-lattice relaxation rate measured for the *i*-proton after selective inversion of its longitudinal magnetization components.

[b] $R_i^{j,k}$ is the spin-lattice relaxation rate measured for the *i*-proton after double-selective inversion of longitudinal magnetization components of the *i*- and *k*-protons (the pair of excited protons is indicated in parentheses).

TABLE 3. Cross-relaxation rates (s^{-1}) (top number) and $^1H-^1H$ distances (Å) (bottom number) measured for pilocarpine in water solution

	H7	H8a	H8b	H11	H12a	H12b
H5	0.04					
	2.66					
H6a	0.05					
	2.55					
H6b	0.02					
	3.03					
H7		0.05		0.06		
		2.55		2.47		
H8a			0.45			
			1.77			
H8b	0.02					
	3.03					
H11					0.02	0.01
					2.57	3.07

TABLE 4. $^{13}C-\{^1H\}$ selective Overhauser effects (η units) (top number) and $^{13}C—^1H$ distances (Å)[a] (bottom number) for pilocarpine 20 mmol dm^{-3} in D_2O at pH = 5.5 and T = 300 K

Observed carbon	{H6a}	{H6b}
C7	0.07	0.07
	2.17	2.17
C8		0.01
		2.73
C11	0.02	0.03
	2.75	2.64
C12	0.03	0.02
	2.43	2.57
C13	0.12	
	2.38	

[a]Calculated from eq. [3] by taking r_{C7H6} = 2.17 Å as the reference distance.

of the ring carbons suggests that it is likely to behave as a free rotor.

An independent check of the value of the correlation time was obtained by measuring dipolar interaction energies between protons at fixed distance. This can be achieved either by detecting $^1H-\{^1H\}$ nuclear Overhauser effects (14) (which measure, for a proton pair, the ratio, σ/ρ, between the cross-dipolar and the direct dipolar spin-lattice relaxation rates) or, better, by measuring absolute values of σ from double-selective and single-selective proton spin-lattice relaxation rates ($\sigma_{ik} = R_i^{i,k} - R_i^{sel}$, where $R_i^{i,k}$ is the rate obtained upon double-selective excitation of Hi and Hk and R_i^{sel} is that obtained upon single-selective excitation of Hi) (15–18). In this last case problems arising from cross-saturation effects are avoided. When this method is applied to the two geminal H8 protons (Table 2) a mean value of 0.46 s^{-1} is obtained for the cross-relaxation rate, which is consistent with a motional correlation time of 50 ± 10 ps at 298 K.

As for the total ^1H NMR data, reported in Table 2, it is apparent that the relaxation mechanism is dominated by the $^1H-^1H$ dipole–dipole interactions, as verified by the fact that the ratio, F, between nonselective and single-selective spin-lattice relaxation rates ($F = R_i^{nsel}/R_i^{sel}$) is found at $F \sim 1.5$ for most protons (10). Lower F values for H2 and H5 are accounted for by dipolar interactions with nitrogens and those for H12a and H12b by imperfect selectivity of the excitation pulse. The cross-relaxation rate is the structure-sensitive parameter (15):

$$[1] \quad \sigma_{ik} = \frac{1}{10}\frac{\gamma^4 h^2}{r_{ik}^6}\left\{\frac{6\tau_c}{1+4\omega^2\tau_c^2} - \tau_c\right\}$$

where γ is the magnetogyric ratio, h is the reduced Planck constant ($= h/2\pi$), r_{ik} is the Hi—Hk internuclear distance, and τ_c is the motional correlation time for reorientational modulation of the Hi–Hk internuclear vector. Substitution of τ_c values from ^{13}C NMR relaxation analysis and application of eq. [1] allowed the calculation of some relevant distances, as reported in Table 3. The distances obtained gave evidence of a *C*7 puckered conformation of the furanone ring and of an angle of ca. 50° between the two rings.

Occurrence of such a "preferred" conformation was ratified by a second set of geometric information obtained by measuring $^{13}C-\{^1H\}$ nOe's upon selective presaturation of single proton resonances. Such an nOe is interpreted (11) by the equation:

$$[2] \quad \eta_i = f_{Ci}\{Hk\} = \frac{0.1}{R_{Ci}}\frac{\gamma_H^3\gamma_C h^2}{r_{CiHk}^6} f(\omega C, \omega H, \tau_c)$$

where R_{Ci} is the ^{13}C spin-lattice relaxation rate and f is a function of Larmor frequencies and motional correlation time. The simplest way of evaluating distances is to assume the same correlation time functions for nOe's generated on two different carbons, Ci and Cj, by presaturation of a given proton resonance, Hk, such that eq. [2] can be reduced to:

$$[3] \quad \frac{f_{Ci}\{Hk\}R_{Ci}}{f_{Cj}\{Hk\}R_{Cj}} = \left(\frac{r_{CjHk}}{r_{CiHk}}\right)^6$$

If one of the two distances is fixed and known or it can be measured in molecular models, the other can be evaluated. The measured nOe's and the evaluated proton–carbon distances are summarized in Table 4. Although the assumption of the same correlation time function may be not justified and, therefore, the calculated distances may not be very precise, what was observed upon selective saturation of one or the other of the two H6 methylene protons satisfactorily fits the conformation shown by ^1H NMR and also adds new information, such as some folding back of the ethyl chain. This last result was quite unexpected for a small flexible mole-

Can. J. Chem. Downloaded from www.nrcresearchpress.com by 213.200.69.106 on 09/08/12
For personal use only.

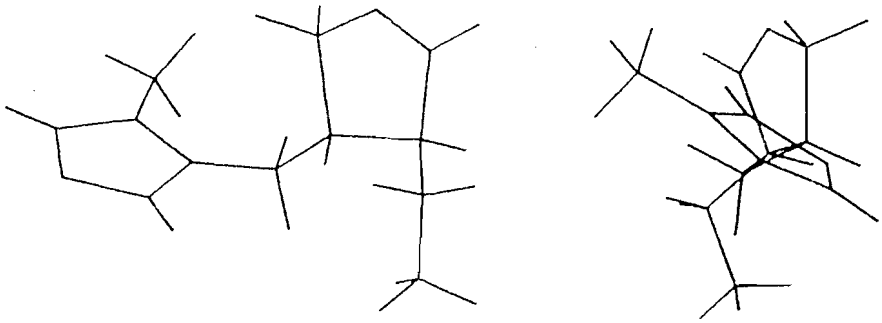

FIG. 2. Stereoviews of the molecular model (built with the aid of the ChemX package and using the NMR constraints) showing the relative angle between the furanone and the imidazole rings and the folding of the ethyl chain as delineated by conformational averaging of NMR parameters.

Can. J. Chem. Downloaded from www.nrcresearchpress.com by 213.200.69.106 on 09/08/12
For personal use only.

cule, but we believe that sufficient evidence was provided; the distance measured between the low-field methylene proton and the methyl carbon may be not very accurate, but no nOe would have been measured in the absence of chain folding.

All conformational features, as obtained by NMR, were used to build up the Dreiding model of the "preferred" structure of protonated pilocarpine in water solution. Such a structure is shown in Fig. 2 as stereo projections obtained with the ChemX software implemented on a graphics terminal. The conformation in solution proves different from that of pilocarpine-trichlorogermanate(II) hemihydrate in the solid state (20). In this last case an angle of 87.6° was evaluated between the two rings and the ethyl chain was not folded towards the imidazole ring.

1. A.R. Battersby and H.T. Hopenshaw. *In* The alkaloids. Vol. III. *Edited by* R.H. Manske and H.L. Holmes. Academic Press, New York. 1953. p. 201.
2. J.M. van Rossum, M.J.W.J. Cornelissen, C.T.P. De Groot, and J.A.T.M. Hurkman. Experientia. **16**, 373 (1960).
3. I.H. Leopold and E. Keates. Clin. Pharmacol. Ther. **6**, 262 (1965).
4. P.-H. Chung, T.-F. Chin, and J.L. Lach. J. Pharm. Sci. **59**, 1300 (1970).
5. G.A. Neville, F.B. Hassan, and I.C.P. Smith. Can. J. Chem. **54**, 2094 (1976).
6. A.A. Al-Badr and H.Y. Aboul-Enein. Anal. Profiles Drug Subst. **12**, 385 (1983).
7. L. Maat, J.A. Peters, and H.Y. Aboul-Enein. Magn. Reson. Chem. **22**, 454 (1984).
8. G.A. Morris and R. Freeman. J. Magn. Reson. **29**, 433 (1978).
9. H. Geen, X.-L. Wu, P. Xu, J. Friedrich, and R. Freeman. J. Magn. Reson. **81**, 646 (1989).
10. R. Freeman, H.D.W. Hill, B.L. Tomlinson, and L.D. Hall. J. Chem. Phys. **61**, 4466 (1974).
11. N. Niccolai, C. Rossi, V. Brizzi, and W.A. Gibbons. J. Am. Chem. Soc. **106**, 5732 (1984).
12. K. Dill and A. Allerhand. J. Am. Chem. Soc. **101**, 4376 (1979).
13. A. Allerhand, D. Doddrell, and R. Komoroski. J. Chem. Phys. **55**, 189 (1971).
14. J.H. Noggle and R.E. Schirmer. The nuclear Overhauser effect. Academic Press, New York. 1971.
15. L.D. Hall and H.D.W. Hill. J. Am. Chem. Soc. **98**, 1269 (1976).
16. G. Valensin, T. Kushnir, and G. Navon. J. Magn. Reson. **46**, 23 (1982).
17. E. Gaggelli, A. Maccotta, A. Scopa, and G. Valensin. Biophys. Chem. **32**, 297 (1988).
18. N. Marchettini, G. Valensin, and E. Gaggelli. Biophys. Chem. **36**, 65 (1990).
19. Chem-X: Molecular modelling system. Chemical Design Ltd., Oxford, U.K.
20. S. Fregerslev and S.E. Rasmussen. Acta Chem. Scand. **22**, 10 (1968).

Electrochemistry and spectroelectrochemistry of substituted tetrabenzotriazaporphine

YU-HONG TSE, ALOK GOEL, MOUGANG HU, A. B. P. LEVER,[1] AND C. C. LEZNOFF
Department of Chemistry, York University, North York, Ont., Canada M3J 1P3

AND

JOHAN E. VAN LIER
Medical Research Council (MRC) Group in the Radiation Sciences, Faculty of Medicine, University of Sherbrooke, Sherbrooke Que., Canada J1H 5N4

Received November 3, 1992

YU-HONG TSE, ALOK GOEL, MOUGANG HU, A. B. P. LEVER, C. C. LEZNOFF, and JOHAN E. VAN LIER. Can. J. Chem. **71**, 742 (1993).

The spectral and electrochemical properties of tetrabenzo[5,10,15]triazaporphine (TBTAP) and its magnesium derivatives having a long alkyl chain attached to the *meso* carbon have been studied. Both metal-free and metallated species show typical metal-free phthalocyanine-like spectra. Two reduction and two oxidation redox couples have been observed. The cation, anion, and dianion species of these porphyrin derivatives have been electrochemically generated and their electronic spectra are recorded.

YU-HONG TSE, ALOK GOEL, MOUGANG HU, A. B. P. LEVER, C. C. LEZNOFF et JOHAN E. VAN LIER. Can. J. Chem. **71**, 742 (1993).

On a étudié les propriétés spectrales et électrochimiques de la tétrabenzo[5,10,15]triazaporphine (TBTAP) portant une longue chaîne alkyle attaché au carbone *méso* et de ses dérivés contenant du magnésium. Les espèces tant métalliques que non métalliques présentent les spectres caractéristiques des composés ressemblant aux phtalocyanines non-métallisées. On a observé deux couples rédox de réduction et deux d'oxydation. Faisant appel à des méthodes électrochimiques, on a généré les espèces cationiques, anioniques et dianioniques de ces dérivés de la porphyrine et on a enregistré leurs spectres électroniques.

[Traduit par la rédaction]

Introduction

Tetrabenzo[5,10,15]triazaporphine (TBTAP) differs from phthalocyanine (Pc) by a methine group, instead of a nitrogen, at a *meso* position. These unsymmetrical porphyrin derivatives have received relatively less attention than related macrocyclic compounds. During the early development of phthalocyanine chemistry (1, 2) it was shown that reaction of methylmagnesium halide with phthalonitrile yields magnesium tetrabenzotriazaporphine (TBTAPMg). Recently, a variety of TBTAP derivatives (3), substituted at both benzo and *meso* positions, were prepared using a similar procedure. When substituted phthalonitriles are used, inseparable mixtures of regioisomers are obtained. However tetrabenzotriazaporphines derived from unsubstituted phthalonitrile and long-chain alkylmagnesium halide gave only one isomer, which was usually readily soluble in organic solvents. Variations in the alkyl chain length of the Grignard reagent can provide an interesting series of new TBTAP(C_n)M derivatives substituted at the *meso* position. ((C_n) designates the length of the alkyl chain at the *meso* position.) Unsymmetrical porphyrins have also been used in cancer photodynamic therapy (4). The TBTAP derivatives may provide higher stability and efficiency, in this application, than the generally less stable porphyrin nuclei.

This work reports the syntheses of a series of metal-free, TBTAP(C_n)H_2, and metallated, TBTAP(C_n)M, species with an alkyl chain at the *meso* position. The electrochemical and spectroelectrochemical properties of some of these derivatives will also be reported.

[1]Author to whom correspondence may be addressed.

Experimental

Materials

Tetrabutylammonium perchlorate (TBAP; Kodak) was recrystallized from absolute ethanol and dried in a vacuum oven at 50°C for 2 days. 1,2-Dichlorobenzene (DCB, Aldrich) and *N*,*N*-dimethylformamide (DMF; Aldrich) were used as supplied. Argon gas (Linde) was purified by passage through heated copper filings for electrochemical measurement. Matheson high-purity argon was used to maintain inert atmosphere conditions for syntheses.

Methods

Differential pulse voltammetry was performed with a Princeton Applied Research (PAR) model 174A polarographic analyzer. Cyclic voltammetry was performed with a Pine Instruments RDE-3 potentiostat, and rotating disk electrode studies with a Pine Instruments PIR rotator.

A conventional three-electrode cell was used in electrochemical experiments. A platinum (Pt) disk described by the cross-sectional area of a 27-gauge wire, sealed in glass, was used as the working electrode, a Pt wire as the counter electrode, and a AgCl/Ag wire as the quasi-reference electrode. Potentials were referenced internally to the ferricenium/ferrocene (Fc^+/Fc) couple. For the rotating disc study, a Pt disk with an area of 0.44 cm^2 was used as working electrode.

Electronic spectra were recorded with a Guided Wave Inc. model 100-20 optical waveguide spectrum analyser or a Cary model 2400 spectrometer. Spectroelectrochemical data were collected following a published design (5). Note that we used an internal AgCl/Ag electrode and that, in the thin-layer cell, the actual potential of the AgCl/Ag electrode may deviate slightly from its true thermodynamic value. Infrared (ir) spectra were recorded on a Pye Unicam SP1000 infrared spectrophotometer using KBr discs. Nuclear magnetic resonance (nmr) spectra were recorded on a Bruker AM300 nmr spectrometer. The observed splittings of the nmr signals are described as singlets(s), doublets(d), triplets(t), or multiplets(m). Mass spectra (ms) were recorded at 70 eV on a VG Micromass 16F mass spectrometer in the EI mode.

Can. J. Chem. Downloaded from www.nrcresearchpress.com by 213.200.69.106 on 09/08/12
For personal use only.

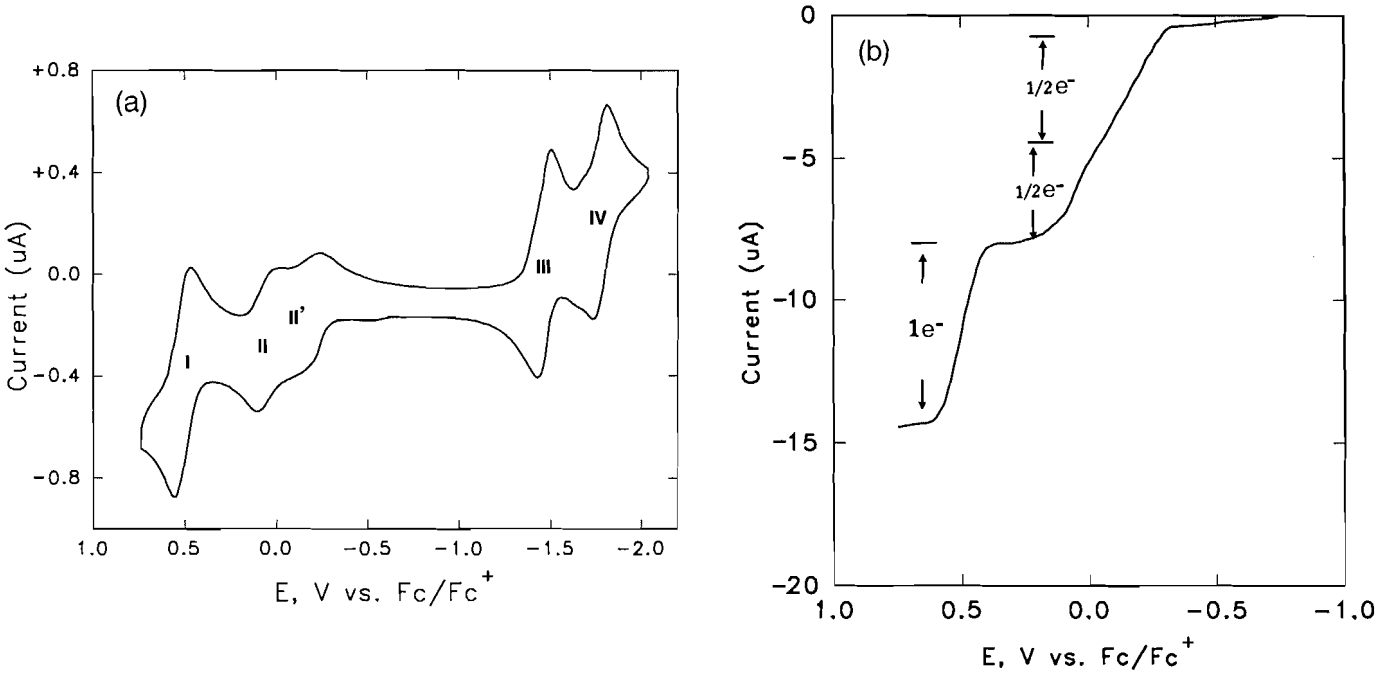

FIG. 1. (*a*) Cyclic voltammogram for *t*-NTNTAP(C_{15})H_2 (**14**) in DCB (0.15 M TBAP, Pt working electrode, scan rate 100 mV/s). (*b*) Rotating disc electrode (RDE) study for *t*-NTNTAP(C_{15})H_2 (**14**) in DCB (0.15 M TBAP, Pt disc working electrode, scan rate 10 mV/s, 400 rpm, [*t*-NTNTAP(C_{15})H_2] = 2×10^{-4} M).

Thin-layer chromatography (tlc) was performed using silica gel G as the adsorbent. Flash chromatography was performed using silica gel of particle size 20–45 μm. All reactions were stirred with a magnetic stirrer. Sublimations were generally carried out at 300°C and 0.005 Torr pressure (1 Torr = 133.3 Pa). Microanalyses were performed by Guelph Chemical Laboratories Ltd., Guelph, Ontario.

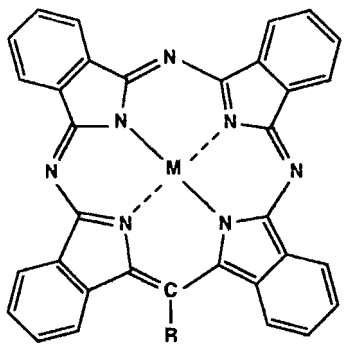

1 M = Mg, R = $(CH_2)_4CH_3$
2 M = H_2, R = $(CH_2)_4CH_3$
3 M = Zn, R = $(CH_2)_4CH_3$
4 M = Mg, R = $(CH_2)_8CH_3$
5 M = H_2, R = $(CH_2)_8CH_3$
6 M = Zn, R = $(CH_2)_8CH_3$
7 M = Mg, R = $(CH_2)_{12}CH_3$
8 M = H_2, R = $(CH_2)_{12}CH_3$
9 M = Zn, R = $(CH_2)_{12}CH_3$
10 M = Mg, R = $(CH_2)_{16}CH_3$
11 M = H_2, R = $(CH_2)_{16}CH_3$
12 M = Zn, R = $(CH_2)_{16}CH_3$

Syntheses

*(27-Pentyl-29*H*,31*H*-tetrabenzo[*b,g,l,q*][5,10,15]-triazaporphine) magnesium (**1**)*

Hexylmagnesium chloride (8.0 mL of 2 M solution in diethyl ether, 16 mmol) was added dropwise to a stirred suspension of phthalonitrile (2 g, 15.6 mmol) in dry diethyl ether (10 mL), under an argon atmosphere. The reaction mixture was stirred for 2 h at room temperature. During this time the reaction underwent a colour change from purple to reddish-brown. Ether was removed by passing a stream of argon through the reaction flask for 15 min to obtain a brown residue. This residue was dissolved in distilled quinoline (5 mL) and stirred at 185°C, under argon. After 2 h the reaction mixture underwent a colour change from reddish-brown to green, and tlc analysis (THF–hexane (1:4) as eluant) of this mixture showed the presence of a blue compound, a green compound, and a very mobile purple intermediate. After 24 h the purple intermediate had disappeared and the reaction mixture comprised mainly a blue and a green pigment. The reaction mixture was cooled to room temperature, passed through a silica gel column, and eluted with THF–hexane (1:9). This procedure removed an insoluble blue-black impurity and gave a green fraction. Evaporation of the solvent gave a green semisolid. A solution of this solid was loaded on a silica gel column (flash) and eluted with THF-hexane (1:9) to obtain a green and then a blue fraction. The blue fraction proved to be the magnesium phthalocyanine (by comparison of the uv/vis spectrum with that of an authentic sample). The green fraction was evaporated to obtain a green solid. A solution of this solid was loaded on a gel permeation column (Bio-beads, SX-2, 200–400 mesh) and eluted with THF. This procedure removed a residual trace of yellow impurity. Crystallization from ether–hexane (1:9) gave green needles. After sublimation, under reduced pressure, the sublimate was found to be pure **1** (TBTAP(C_5)Mg) (182 mg, 8% yield); uv/vis (THF) peak λ_{max} (nm) (log ε): 668(5.20), 647(5.00), 615(4,10), 593(4.21), 445(4.43), 400(4.70); ir (cm^{-1}): 2920, 2860, 1490, 1330, 1290, 1170, 1130, 1120, 1090, 720; ^1H nmr (pyridine-d_5) δ: 10.14(m, 2H), 9.80(m, 4H), 9.36(m, 2H), 8.20(m, 8H), 5.40(m, 2H),

Can. J. Chem. Downloaded from www.nrcresearchpress.com by 213.200.69.106 on 09/08/12
For personal use only.

Can. J. Chem. Downloaded from www.nrcresearchpress.com by 213.200.69.106 on 09/08/12
For personal use only.

TABLE 1. Half-wave potentials (V vs. Fc^+/Fc) of metal-free and metallated TBTAP(C_n) species

		I	II	II′	III	IV[a]
TBTAP(C_9)H_2[b] (**5**)	(i)[c]	0.79(ir)	0.41	0.24	−1.42	−1.78
	(ii)	0.76	0.33		−1.41	−1.86
TBTAP(C_{17})H_2[b] (**11**)	(i)	0.88(ir)	0.47	0.28	−1.36	−1.72
	(ii)	0.84	0.34		−1.37	−1.74
TBuTBTAP(C_{15})H_2[b] (**13**)	(i)	0.74(ir)	0.32	0.11	−1.49	−1.88
	(ii)	0.71	0.24		−1.51	−1.91
t-NTNTAP(C_{15})H_2[b] (**14**)	(i)	0.51	0.05	−0.21	−1.48	−1.78
	(ii)	0.46	0.01		−1.44	−1.75
TBTAP(C_9)Mg[d] (**4**)	(i)	0.64(ir)	0.14		−1.50	−2.03
	(ii)	0.58	0.12		−1.49	−2.03
TBTAP(C_{17})Mg[d] (**10**)	(i)	0.64(ir)	0.14		−1.48	−2.04
	(ii)	0.58	0.09		−1.48	−2.02

[a]See text for assignments. Potentials cited for irreversible processes are peak potentials.
[b]DCB, 0.15 M TBAP.
[c](i) cyclic voltammetry at 100 mV/s, (ii) differential pulse voltammetry at 2 mV/s, pulse amplitude 25 mV.
[d]DMF, 0.15 M TBAP.

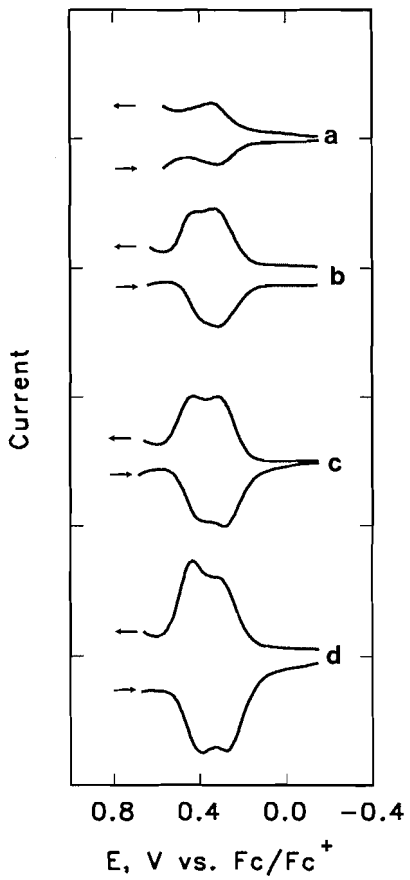

FIG. 2. Differential pulse voltammogram for TBTAP(C_9)H_2 in DCB (0.15 M TBAP, Pt electrode). a: 1.8×10^{-5} M; b: 6.1×10^{-5} M; c: 7.9×10^{-5} M; d: 1.8×10^{-4} M. Scan rate 2 mV/s, pulse amplitude 25 mV.

2.85(m, 2H), 2.10(m, 2H), 1.58(m, 2H), 1.01(t, J = 7.0 Hz, 3H) ppm; ms *m/z*: 605(M^+, 100), 548(55), 274(28). Anal. calcd. for $C_{38}H_{27}N_7Mg$: C 75.32, H 4.49, N 16.18; found: C 75.28, H 4.72, N 16.01.

27-Pentyl-29H,31H-tetrabenzo[b,g,l,q][5,10,15]-triazaporphine (2)

Species **1** (61 mg, 0.1 mmol) was dissolved in glacial acetic acid (10 mL), refluxed for 2 h, cooled to room temperature, and centrifuged to obtain a bluish-green precipitate. The precipitate was washed with water and then with methanol. Reprecipitation from a concentrated solution of toluene by methanol gave a bluish-green solid. Crystallization from toluene gave bluish-green needles (44 mg, 75% yield). Residual traces of impurities were sublimed off, under reduced pressure, to obtain a pure sample of **2** (TBTAP(C_5)H_2); uv/vis (THF) peak λ_{max} (nm) (log ε): 682(5.10), 642(4.89), 616(4.41), 589(3.79), 385(4.33); ir (cm^{-1}): 3440 (br, NH), 2920, 2860, 1500, 1470, 1440, 1340, 1320, 1130, 1120, 1100, 1030, 760, 720; ms *m/z*: 583(M^+, 100), 526(16). Anal. calcd. for $C_{38}H_{29}N_7$: C 78.19, H 5.01, N 16.80; found: C 78.00, H 4.77, N 16.60.

(27-Pentyl-29H,31H-tetrabenzo[b,g,l,q][5,10,15]-triazaporphine) zinc (3)

To a solution of **2** (29 mg, 0.05 mmol) in 5 mL of dry dimethylformamide(DMF)–toluene (1:1) was added anhydrous zinc acetate (92 mg, 0.5 mmol), and the mixture was refluxed for 20 h (under argon). The reaction mixture was cooled to room temperature and the solvent was evaporated to obtain a green solid. After washing with water and methanol, crystallization from ether gave crystals with a purple reflex. Impurities were removed by sublimation under reduced pressure, affording a residue of pure **3** (TBTAP(C_5)Zn) (26 mg, 80% yield) as microcrystals with a purple reflex; uv/vis (THF) peak λ_{max} (nm) (log ε): 668(5.13), 645(4.98), 615(4.22), 591(4.21), 443(4.01), 385(4.50); ir (cm^{-1}): 2920, 2860, 1490, 1410, 1330, 1290, 1170, 1130, 1120, 1100, 780, 720; ms *m/z*: 645 (M^+, 100), 588(39), 294(23). Anal. calcd. for $C_{38}H_{27}N_7Zn$: C 70.54, H 4.18, N 15.15; found: C 70.28, H 4.00, N 15.00.

(27-Nonyl-29H,31H-tetrabenzo[b,g,l,q][5,10,15]-triazaporphine) magnesium (4)

Decylmagnesium bromide (7.8 mL of 1 M solution in diethyl ether, 7.8 mmol) was added dropwise to a stirred suspension of phthalonitrile (1 g, 7.8 mmol) in dry diethyl ether (5 mL), under an argon atmosphere. The reaction mixture was stirred for 2 h at room temperature. During this time, the reaction underwent a colour change from purple to reddish-brown. Ether was removed by passing a stream of argon through the reaction flask for 15 min to obtain a brown residue that was dissolved in distilled quinoline (5 mL) and stirred at 120°C, under argon. After 2 h the reaction

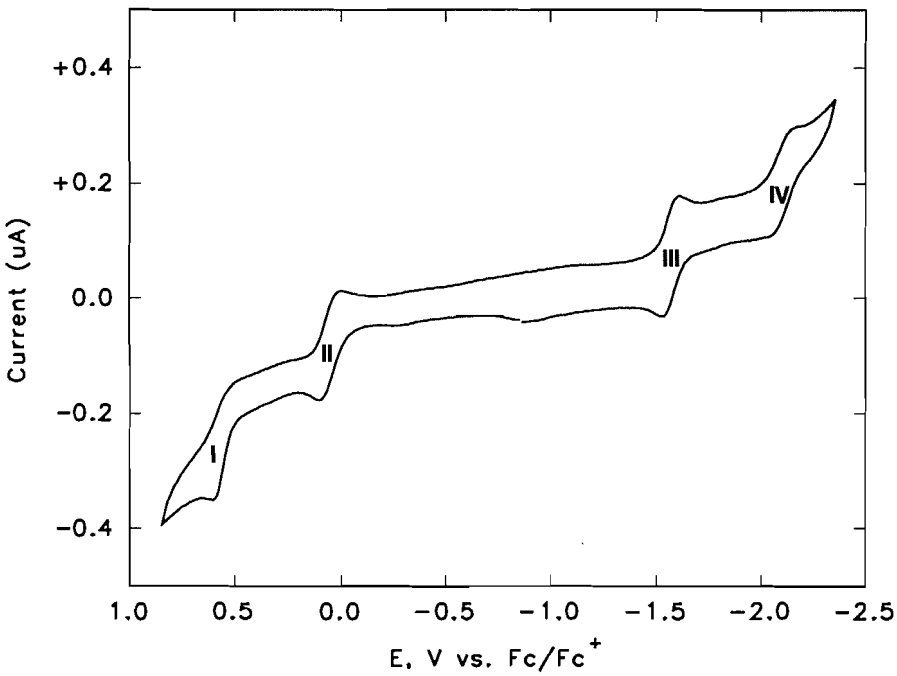

FIG. 3. Cyclic voltammogram for TBTAP(C_9)Mg in DMF (0.15 M TBAP, Pt working electrode, scan rate 100 mV/s).

mixture underwent a colour change from reddish-brown to green, and tlc analysis (pyridine–hexane (1:4) as eluant) of this mixture showed the presence of a blue compound, a green compound, and a very mobile purple intermediate. After 18 h the purple intermediate had disappeared and the reaction mixture comprised mainly a blue and a green pigment. The reaction mixture was cooled to room temperature, passed through a silica gel column, and eluted with ether–hexane (1:1). This procedure removed an insoluble blue-black impurity and gave a green fraction. Evaporation of the solvent gave a green semisolid. A solution of this solid was loaded on a silica gel column (flash) and eluted with pyridine–hexane (1:4) to obtain a green and then a blue fraction. The green fraction was evaporated to obtain a green solid. Crystallization from ether–hexane (1:9) gave pure **4** (TBTAP(C_9)Mg) as green needles (100 mg, 8% yield); uv/vis (THF) peak λ_{max} (nm) (log ε): 668(5.22), 647(5.06), 615(4.18), 593(4.25), 445(4.48), 400(4.74); ir (cm^{-1}): 2920, 2860, 1490, 1330, 1290, 1170, 1130, 1120, 1090, 720; ^{1}H nmr (pyridine-d_5) δ: 10.14 (m, 2H), 9.80 (m, 4H), 9.42 (d, J = 7.5 Hz, 2H), 8.22 (m, 8H), 5.46 (m, 2H), 2.92 (m, 2H), 2.22 (m, 2H), 1.62 (m, 2H), 1.60–1.20 (m, 8H), 0.91 (t, J = 7.0 Hz, 3H) ppm; ms *m/z*: 661 (M^+, 100), 548(41), 535(9).

*27-Nonyl-29*H,*31*H-*tetrabenzo*[b,g,l,q][*5,10,15*]-*triazaporphine (5)*

Species **4** (75 mg, 0.11 mmol) was dissolved in glacial acetic acid (10 mL), refluxed for 2 h, cooled to room temperature, and centrifuged to obtain a bluish-green precipitate. The precipitate was washed with water and then with methanol. Reprecipitation from a concentrated solution of toluene by methanol gave a bluish-green solid. Crystallization from toluene gave bluish-green needles (55 mg, 78% yield). Residual trace impurities were sublimed off, under reduced pressure, to obtain pure **5** (TBTAP(C_9)H_2); uv/vis (THF) peak λ_{max} (nm) (log ε): 682(5.13), 642(4.93), 616(4.40), 589(3.80), 385(4.38); ir (cm^{-1}): 3440 (br, NH), 2920, 2860, 1500, 1470, 1440, 1340, 1320, 1130, 1120, 1100, 1030, 760, 720; ms *m/z*: 639 (M^+, 80), 473 (38). Anal. calcd. for $C_{42}H_{37}N_7$: C 78.85, H 5.83, N 15.32; found: C 78.50, H 6.23, N 14.95.

*(27-Nonyl-29*H,*31*H-*tetrabenzo*[b,g,l,q][*5,10,15*]-*triazaporphine) zinc (6)*

To a solution of **5** (25.5 mg, 0.04 mmol) in 5 mL of dry dimethylformamide (DMF)–toluene (1:1) was added anhydrous zinc acetate (73.6 mg, 0.4 mmol), and the mixture was refluxed for 20 h (under argon). The reaction mixture was cooled to room temperature and the solvent was evaporated to obtain a green solid. After washing with water and methanol, crystallization from ether gave crystals with a purple reflex. Sublimation under reduced pressure afforded a sublimate of pure **6** (TBTAP(C_9)Zn) (24 mg, 85% yield) as microcrystals with a purple reflex; uv/vis (THF) peak λ_{max} (nm) (log ε): 668(5.15), 645(4.98), 615(4.23), 591(4.20), 443(3.98), 385(4.58); ir (cm^{-1}): 2920, 2860, 1490, 1410, 1330, 1290, 1170, 1130, 1120, 1100, 780, 720; ms *m/z*: 703(M^+, 71), 576(100), 471(34), 288(33).

*(27-Tridecyl-29*H,*31*H-*tetrabenzo*[b,g,l,q][*5,10,15*]-*triazaporphine) magnesium (7)*

Tetradecylmagnesium chloride (7.8 mL of 1 M solution in THF, 7.8 mmol) was added dropwise to a stirred suspension of phthalonitrile (1 g, 7.8 mmol) in freshly distilled THF (5 mL), under an argon atmosphere. The reaction mixture turned purple immediately. The reaction mixture was stirred for a further 2 h at room temperature. During this time, the reaction underwent a colour change from purple to reddish-brown. Tetrahydrofuran was removed by passing a stream of argon through the reaction flask for 15 min to obtain a dark brown residue, which was dissolved in distilled quinoline (3 mL) and the mixture stirred at 120°C, under an argon atmosphere. After 0.5 h the reaction mixture underwent a colour change from reddish-brown to dark green, and tlc analysis (pyridine–hexane (1:4) as eluant) of this mixture showed the presence of a blue compound, a green compound, and a purple intermediate. After 18 h the purple intermediate was still present. Hence, the temperature was raised to 180°C and the mixture was refluxed for a further 24 h. The reaction mixture was cooled to room temperature and loaded on a short silica gel column (flash). The column was eluted with pyridine–hexane (1:4) and a green fraction was collected. The solvent was evaporated to obtain a green oil. This oil was loaded on another silica gel column (flash) and again eluted with pyridine–hexane (1:4). This chromatographic procedure afforded separation of the required product from the phthalocyanine by-product. Reprecipitation from a concentrated solution of THF (1 mL) by methanol (9 mL) gave crude **7** (TBTAP(C_{13})Mg) (47 mg, 3% yield). After sublimation, under

Can. J. Chem. Downloaded from www.nrcresearchpress.com by 213.200.69.106 on 09/08/12
For personal use only.

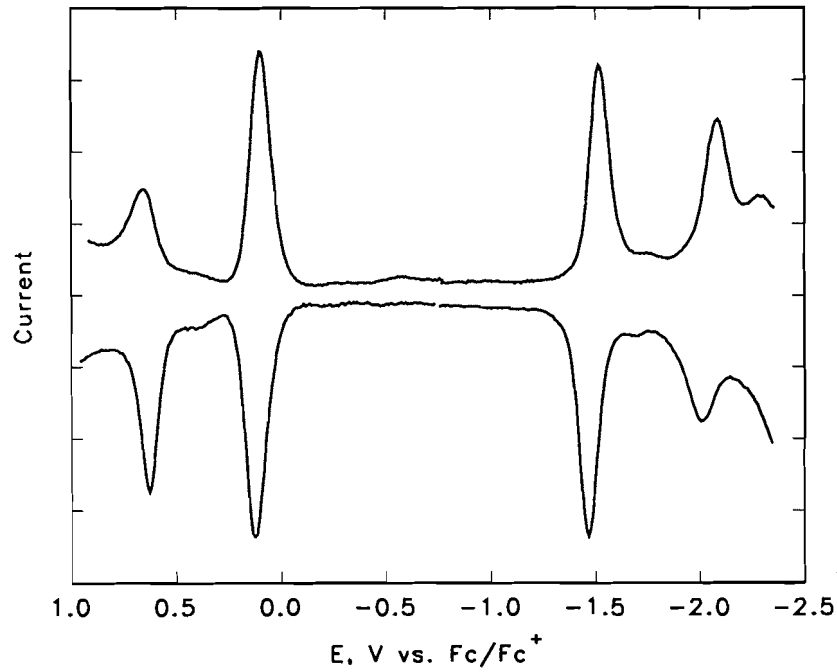

FIG. 4. Differential pulse voltammogram for TBTAP(C_9)Mg in DMF (0.15 M TBAP, Pt electrode). Scan rate 2 mV/s, pulse amplitude 25 mV.

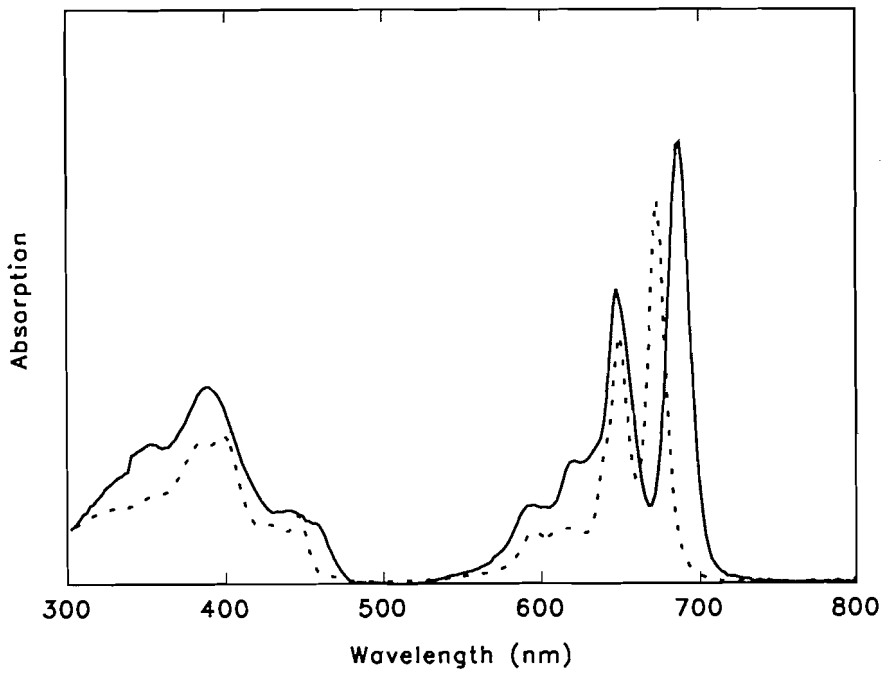

FIG. 5. Absorption spectra of TBTAP(-2)(C_9)H_2 (**5**) (solid line) in DCB and TBTAP(C_9)Mg (**4**) (dotted line) in DMF.

reduced pressure, the sublimate had a purple reflex and was found to be the pure **7**; uv/vis (THF) peak λ_{max} (nm) (log ε): 668(5.25), 647(5.03), 615(4.09), 593(4.20), 445(4.62), 400(4.74); ir (cm^{-1}): 2920, 2860, 1490, 1330, 1290, 1170, 1130, 1120, 1090, 720; ^{1}H nmr (pyridine-d_5) δ: 10.14 (m, 2H), 9.80 (m, 4H), 9.42 (d, J = 7.3 Hz, 2H), 8.22 (m, 8H), 5.46 (m, 2H), 2.92 (m, 2H), 2.22 (m, 2H), 1.64 (m, 2H), 1.42–1.25 (m, 16H), 0.91 (t, J = 7.0 Hz, 3H) ppm; ms m/z: 717(M^+, 100), 548(44), 535(18). Anal. calcd. for $C_{46}H_{43}N_7Mg$: C 76.93, H 6.03, N 13.65; found: C 76.74, H 6.22, N 13.44.

*27-Tridecyl-29*H*,31*H*-tetrabenzo[*b,g,l,q*]-[5,10,15]-triazaporphine (8)*

Species **7** (40 mg, 0.056 mmol) was dissolved in glacial acetic acid (5 mL), refluxed for 2 h, cooled to room temperature, and centrifuged to obtain a bluish-green precipitate. The precipitate was washed with water and then with methanol until the washings were colourless. Reprecipitation from a concentrated solution of toluene by methanol gave a bluish-green solid. Crystallization from toluene gave needles with a purple reflex (28 mg, 72% yield). After sublimation under reduced pressure, the residue was found to be

Can. J. Chem. Downloaded from www.nrcresearchpress.com by 213.200.69.106 on 09/08/12
For personal use only.

TABLE 2. Observed maxima in the absorption spectra of TBTAP(-2)(C_n) species[a]

Complex	λ_{max}(nm) (log ε)				
TBTAP(C_9)H_2 (**5**)[b]	687(4.81)	647(4.62)	621(4.21)	593(4.02)	388(4.48)
TBTAP(C_{17})H_2 (**11**)[b]	686(4.69)	647(4.49)	619(4.11)	593(3.90)	386(4.49)
TBTAP(C_9)Mg (**4**)[c]	672(5.13)	648(4.95)	619(4.28)	595(4.26)	399(4.73)
				355(4.48)	327(4.42)
TBuTBTAP(C_{15})H_2 (**13**)[b]	693(5.19)	653(4.99)	625(4.62)	598(4.42)	390(4.87)
t-NTNTAP(C_{15})H_2 (**14**)[b]	785(5.31)	753(5.10)	718(4.63)	683(4.56)	376(4.80)
TBTAP(C_{17})Mg (**10**)[c]	672(5.26)	648(5.05)	617(4.35)	595(4.32)	398(4.80)
				353(4.53)	327(4.46)

[a]The solvent was that used for the electrochemistry experiments and therefore contains 0.15 M TBAP.
[b]Solvent, DCB.
[c]Solvent, DMF.

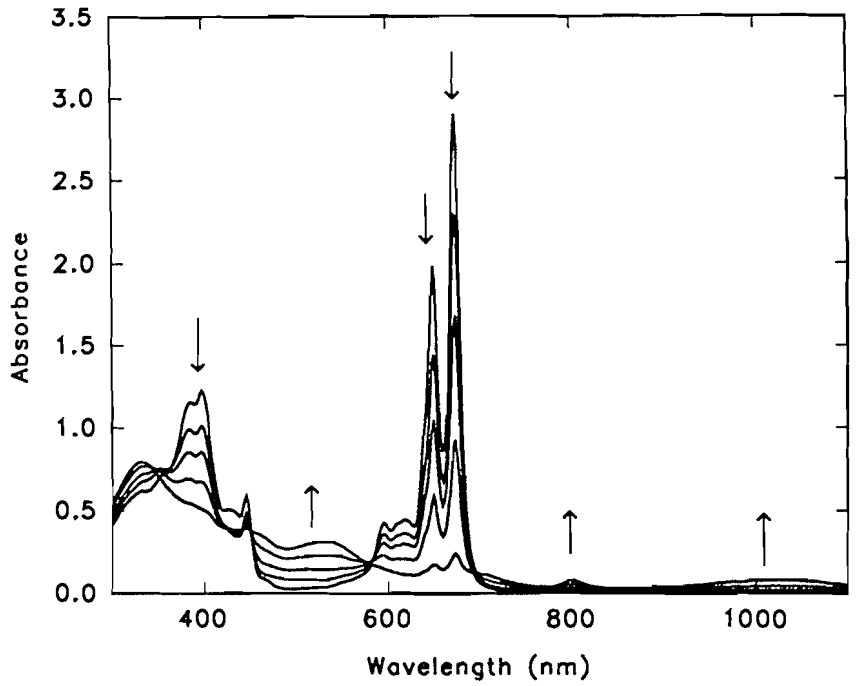

FIG. 6. Spectroscopic changes accompanying the controlled potential oxidation of TBTAP(-2)(C_9)Mg (**4**) (8.6×10^{-4} M) in DMF (0.15 M TBAP). The first (top) spectrum is the starting material, unpolarized. Successive spectra are equilibrium spectra obtained with the electrode polarized at 0.45, 0.50, 0.55, and 0.575 V vs. AgCl/Ag.

the pure **8** (TBTAP(C_{13})H_2); uv/vis (THF) peak λ_{max} (nm) (log ε): 682(5.15), 642(4.94), 616(4.45), 589(3.82), 385(4.47); ir (cm^{-1}): 3440 (bd, NH), 2920, 2860, 1500, 1470, 1440, 1340, 1320, 1130, 1120, 1100, 1030, 760, 720; ms *m/z*: 695 (M^+, 100), 526 (10). Anal. calcd. for $C_{46}H_{45}N_7$: C 79.39, H 6.52, N 14.09; found: C 79.42, H 6.34, N 14.39.

*(27-Tridecyl-29*H,*31*H-*tetrabenzo*[b,g,l,q]*[5,10,15]-triazaporphine) zinc (9)*

Anhydrous zinc acetate (73.6 mg, 0.4 mmol) was added to a solution of **8** (17.35 mg, 0.025 mmol) in 5 mL of dry DMF–toluene (1:1) and the mixture refluxed for 24 h (under argon). The reaction mixture was cooled to room temperature and the solvent evaporated to obtain a green solid. After washing with water and methanol, crystallization from ether gave dark blue crystals. After sublimation under reduced pressure, the residue was found to be the pure **9** (TBTAP(C_{13})Zn), (12 mg, 63% yield); uv/vis (THF) peak λ_{max} (nm) (log ε): 668(5.13), 645(5.00), 615(4.28), 591(4.25), 443(4.21), 385(4.63); ir (cm^{-1}): 2920, 2860, 1490, 1410, 1330, 1290, 1170, 1130, 1120, 1100, 780, 720; ms *m/z*: 758(M^+, 100), 588(41), 575(14), 294(14).

*(27-Heptadecyl-29*H,*31*H-*tetrabenzo*[b,g,l,q]*[5,10,15]-triazaporphine) magnesium (10)*

Octadecylmagnesium chloride (7.8 mL of 1 M solution in THF, 7.8 mmol) was added dropwise to a stirred suspension of phthalonitrile (1 g, 7.8 mmol) in freshly distilled THF (5 mL), under an argon atmosphere. The reaction mixture was stirred for 2 h at room temperature. Tetrahydrofuran was removed by passing a stream of argon through the reaction flask. Distilled quinoline (5 mL) was added and the mixture was stirred at 140°C, under argon, for 18 h. A tlc analysis (THF–hexane (1:1) as eluant) showed a very mobile green spot for the required product along with some brown impurities. The reaction mixture was cooled to room temperature, passed through a silica gel column, and eluted with THF–hexane (1:1). This procedure removed an insoluble blue-black impurity and gave a green fraction. A tlc analysis (pyridine–hexane (1:4) as eluant) of this fraction showed a green spot (R_f 0.9) for the required magnesium tetrabenzotriazaporphine and a blue spot (R_f 0.25) for the magnesium phthalocyanine by-product. The solvent was evaporated and the residue loaded onto a silica gel column (flash) and eluted with pyridine–hexane (1:9). This chro-

Can. J. Chem. Downloaded from www.nrcresearchpress.com by 213.200.69.106 on 09/08/12
For personal use only.

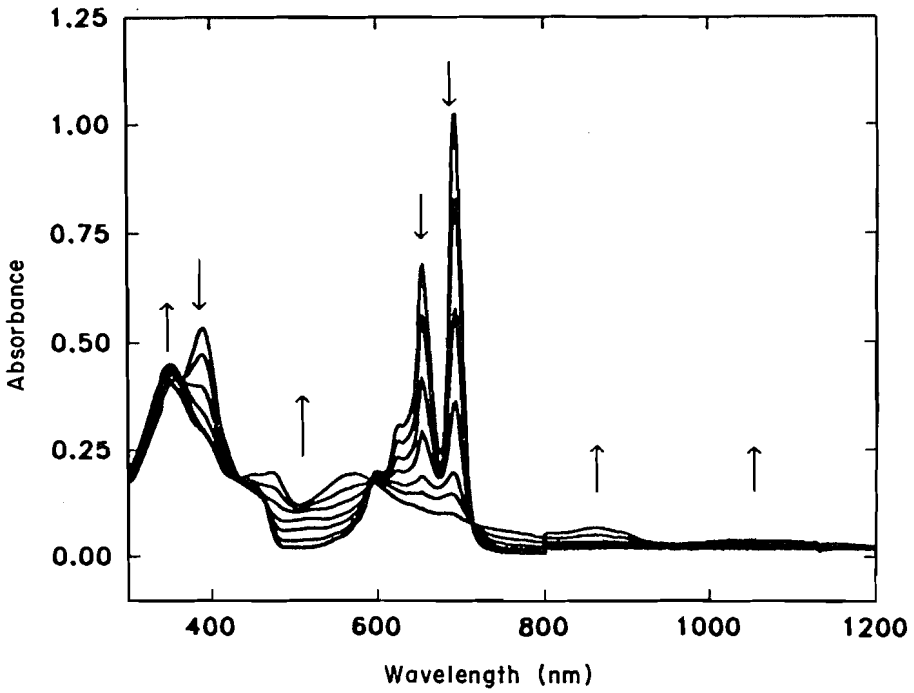

FIG. 7. Spectroscopic changes accompanying the controlled potential oxidation of TBuTBTAP(-2)(C_{15})H_2 (**13**) (2.7×10^{-4} M) in DCB (0.15 M TBAP). The first (top) spectrum is the starting material, unpolarized. Successive spectra are equilibrium spectra obtained with the electrode polarized at 0.575, 0.60, 0.625, 0.65, 0.675, and 0.70 V vs. AgCl/Ag (see experimental section for additional comment).

TABLE 3. Observed maxima in the absorption of [TBTAP(-1)(C_n)]$^+$ cations[a]

Complex	λ_{max}(nm)					
TBTAP(C_9)H_2 (**5**)[b]	1019	859	684	570	472	345
TBTAP(C_9)Mg (**4**)[c,d]	1023	800	678	530	449	330
TBuTBTAP(C_{15})H_2 (**13**)[b]	1070	856	683	558	470	342

[a]The solvent was that used for the electrochemistry experiments and therefore contains 0.15 M TBAP. The product is an equilibrium mixture of mononuclear and binuclear species; the extinction coefficients have therefore not been included.
[b]DCB.
[c]DMF.
[d]Incomplete oxidation of parent species.

matographic procedure afforded separation of the required **10** (TBTAP(C_{17})Mg) from the phthalocyanine by-product. Crystallization from THF–methanol (1:1) gave **10** as needles with a purple reflex (86 mg, 6% yield); uv/vis(THF) peak λ_{max} (nm) (log ε): 668(5.24), 647(5.06), 615(4.09), 593(4.20), 445(4.60), 400(4.71); ir (cm^{-1}): 2920, 2860, 1490, 1330, 1290, 1170, 1130, 1120, 1090, 720; ^{1}H nmr (pyridine-d_5) δ: 10.14(m, 2H), 9.8(m, 4H), 9.42(d, J = 7.9 Hz, 2H), 8.22(m, 2H), 5.46(m, 2H), 2.92(m, 2H), 2.21(m, 2H), 1.62(m, 2H), 1.42–1.23(m, 24H), 0.84(t, J = 7.0 Hz, 3H) ppm; ms m/z: 774(M^+, 100), 548(56), 535(20).

*27-Heptadecyl-29*H,*31*H-*tetrabenzo*[b,g,l,q][*5,10,15*]-*triazaporphine (**11**)*

Compound **10** (86 mg, 0.11 mmol) was dissolved in glacial acetic acid (5 mL), refluxed for 2 h, cooled to room temperature, and centrifuged to obtain a bluish-green precipitate. The precipitate was washed with water and then with methanol until the washings were colourless. Reprecipitation from a concentrated solution of toluene by methanol gave a bluish-green solid. Crystallization from toluene gave plates with a purple reflex (60 mg, 70% yield). After sublimation under reduced pressure, the residue was found to be the pure **11** (TBTAP(C_{17})H_2); uv/vis (THF) peak λ_{max} (nm) (log ε): 682(5.28), 642(5.09), 616(4.61), 589(3.71), 385(4.46); ir (cm^{-1}): 3260 (br, NH), 2920, 2860, 1500, 1470, 1440, 1340, 1320, 1130, 1120, 1100, 1030, 760, 720; ms m/z: 751(M^+, 100), 526(9).

*(27-Heptadecyl-29*H,*31*H-*tetrabenzo*[b,g,l,q][*5,10,15*]-*triazaporphine) zinc (**12**)*

To a solution of **11** (30 mg, 0.04 mmol) in 5 mL of dry DMF–toluene (1:1) was added anhydrous zinc acetate (73.6 mg, 0.4 mmol), and the mixture was refluxed for 24 h (under argon). The reaction mixture was cooled to room temperature and the solvent evaporated to obtain a green solid. After washing with water and methanol, crystallization from ether gave a bluish-green solid. Further purification by flash chromatography, using a solvent system of pyridine–hexane (1:9), and sublimation under reduced pressure gave a residue with a purple reflex. It was found to be the pure **12** (TBTAP(C_{17})Zn) (20 mg, 61% yield); uv/vis (THF) peak λ_{max} (nm) (log ε): 668(5.23), 645(5.05), 615(4.34), 591(4.29), 443(4.16), 385(4.66); ir (cm^{-1}): 2920, 2860, 1490, 1410, 1330, 1290, 1170, 1130, 1120, 1100, 780, 720; ms m/z: 814(M^+, 100),

Can. J. Chem. Downloaded from www.nrcresearchpress.com by 213.200.69.106 on 09/08/12
For personal use only.

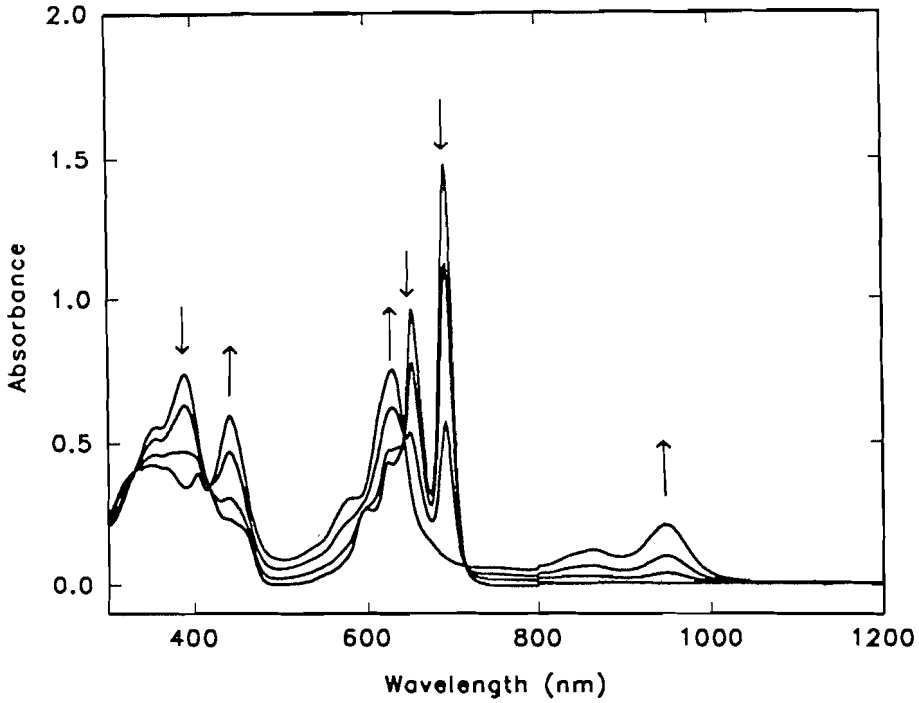

FIG. 8. Spectroscopic changes accompanying the controlled potential reduction of TBuTBTAP(-2)(C_{15})H_2 (**13**) (3.8 × 10^{-4} M) in DCB (0.15 M TBAP). The first (top) spectrum is the starting material, unpolarized. Successive spectra are equilibrium spectra obtained with the electrode polarized at −1.25, −1.275, and −1.30 V vs. AgCl/Ag.

TABLE 4. Observed maxima in the absorption spectra of TBTAP(C_n) anion radicals

Complex	λ_{max}(nm) (log ε)			
[TBTAP(-3)(C_9)H_2]$^-$ (5^-)[b]	948(4.38)	864(4.08)	630(4.90)	583(sh)
		442(4.83)	404(4.61)	351(4.61)
[TBTAP(-4)(C_9)H_2]$^{2-}$ (5^{2-})[b]	619(sh)	530(4.96)	338(4.55)	
[TBTAP(-3)(C_9)Mg]$^-$ (4^-)[c]	860(4.23)	754(3.89)	631(4.77)	534(sh)
	449(4.78)	401(4.46)	372(4.48)	319(4.41)
[TBuTBTAP(-3)(C_{15})H_2]$^-$ (13^-)[b]	943(4.51)	862(4.27)	630(5.06)	579(sh)
	443(4.96)	403(4.77)	348(4.81)	
[TBuTBTAP(-4)(C_{15})H_2]$^{2-}$ (13^{2-})[b]	623(sh)	528(5.16)	340(4.74)	

[a]The solvent was that used for the electrochemistry experiments and contains 0.15 M TBAP.
[b]DCB.
[c]DMF.

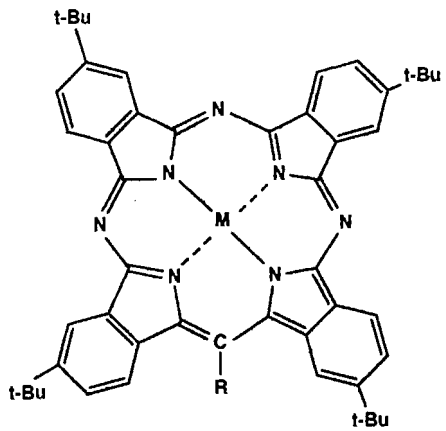

13 M = H_2, R = $(CH_2)_{14}CH_3$

589(47), 575(29), 294(21). Anal. calcd. for $C_{50}H_{51}H_{17}Zn$: C 73.65, H 6.30, N 12.02; found: C 73.60, H 6.43, N 12.55.

2,9,16,23-Tetrakis(2,2-dimethylethyl)-27-pentadecyl-29H,31H-tetrabenzo[b,g,l,q]*[5,10,15]triazaporphine (TBuTBTAP(C_{15})H_2) (**13**) and 2,11,20,29-tetrakis(2,2-dimethylethyl)-34-pentadecyl-37H,39H-tetranaphtho-[2,3-b:2',3'-g:2'',3''-1-2''',3'''-q]*[5,10,15]*triazaporphine (t-NTNTAP(C_{15})H_2) (**14**)* were synthesized as previously described (3).

Results and discussion

A. Syntheses

Reaction of phthalonitrile with a variety of Grignard reagents led to the formation of magnesium tetrabenzotriazaporphines, TBTAP(C_n)Mg, along with some magnesium phthalocyanine (MgPc) by-product. Magnesium tetrabenzotriazaporphines could be separated from the magnesium phthalocyanine by using flash chromatography. Sometimes

Can. J. Chem. Downloaded from www.nrcresearchpress.com by 213.200.69.106 on 09/08/12
For personal use only.

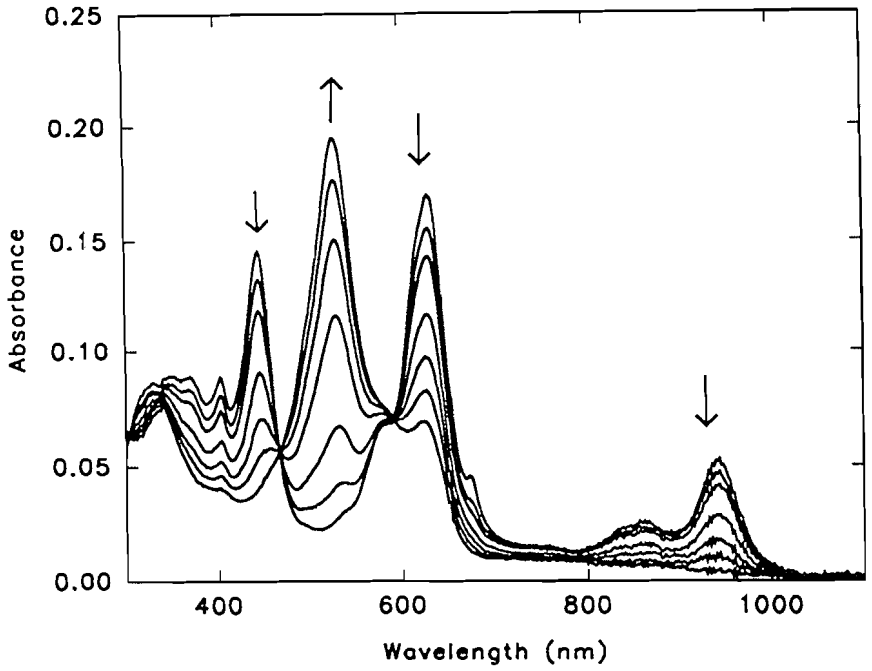

FIG. 9. Spectroscopic changes accompanying the controlled potential reduction of $[TBTAP(-3)(C_9)H_2]^-$ (5^-) (8.8×10^{-5} M) in DCB (0.15 M TBAP). These spectra were obtained as a series by polarizing the electrode from −1.30 to −1.45 V vs. AgCl/Ag in 0.025 V steps (see experimental section for further comment).

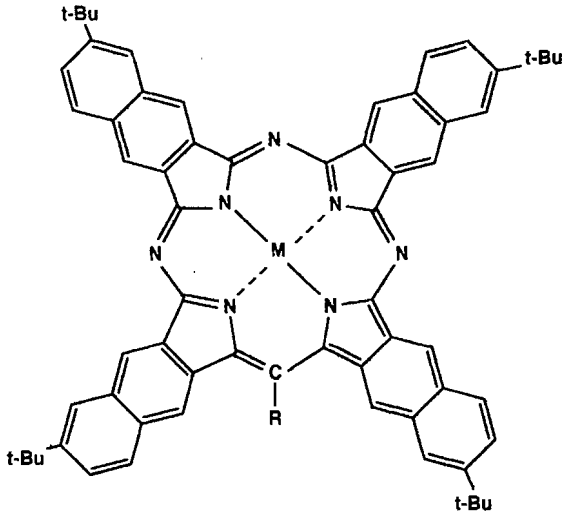

14 **M = H_2, R = $(CH_2)_{14}CH_3$**

it was necessary to filter the product mixture through a normal silica gel column to remove insoluble impurities, before performing the flash chromatography. Magnesium TBTAP species were further purified by crystallization from ether–hexane or tetrahydrofuran (THF)–methanol, and sublimation under reduced pressure. The sublimate was usually a brown impurity and the residue the required pure $TBTAP(C_n)Mg$.

Magnesium tetrabenzotriazaporphines could be demetallated by refluxing in glacial acetic acid. Metal-free tetrabenzotriazaporphines ($TBTAP(C_n)H_2$) were generally less soluble than the corresponding magnesium tetrabenzotriazaporphines. Metal-free tetrabenzotriazaporphines were purified by crystallization from toluene, followed by removal of impurities by sublimation, the residue after sublimation being the required $TBTAP(C_n)H_2$. Zinc tetrabenzotriazaporphines could be obtained from reaction of the corrresponding metal-free tetrabenzotriazaporphines and anhydrous zinc acetate.

B. Electronic structure of the TBTAP system

Simple PcM species have D_{4h} symmetry, while demetallation leads to the PcH_2 species of D_{2h} symmetry. However, in contrast, in the TBTAP species, the metallated complexes at best have twofold symmetry, while the free base species cannot exceed C_s; thus all orbital degeneracies are lifted, for both metallated and free base. The electronic structure of $TBTAPC_1Mg$ has been discussed by Solovev *et al.* (6) using Gouterman's four-orbital model. For the metal-free and main-group metal derivatives, the HOMO-1, HOMO, LUMO, and LUMO + 1 orbitals of the $TBTAP(C_n)$ system are $[b_1(\pi)]^2$, $[a_2(\pi)]^2$, $[b_2(\pi^*)]^0$, and $[b_1(\pi^*)]^0$, respectively (with electron occupations noted). Thus the overall electronic structure parallels that of metal-free phthalocyanine.

C. Electrochemistry

The electrochemical properties of phthalocyanine species are well known (7). The electrochemistry of these triazabenzporphine species was briefly studied to investigate how the replacement of one aza bridgehead by a long-chain-linked CH methine bridgehead influences these properties.

(i) $TBTAP(C_n)H_2$

Species **5**, $n = 9$, and **11**, $n = 17$, were chosen to study the effect of the length of the alkyl group in the *meso* position on the electrochemical properties of the unsubstituted benzo TBTAP derivatives. The electrochemistry of species **13** and **14**, $n = 15$, were investigated to monitor the effect of changing the substituents on the benzo position.

Oxidation and reduction of these compounds directly involve the triazaporphine ring system, since the metal centres

Can. J. Chem. Downloaded from www.nrcresearchpress.com by 213.200.69.106 on 09/08/12
For personal use only.

Can. J. Chem. Downloaded from www.nrcresearchpress.com by 213.200.69.106 on 09/08/12
For personal use only.

are not redox active. Cyclic voltammograms generally show (e.g., Fig. 1*a*) (Table 1) three waves (two reduction (**III,IV**), one oxidation (**I**); **III,IV** are reversible or quasi-reversible, **I** is usually irreversible) diffusion controlled with $i_c = i_a$, and $i \propto v^{1/2}$ (v = scan rate in cyclic voltammogram) and, in addition, two less well-defined and overlapping oxidation waves, **II** and **II′**. The rest potential lies between processes **II′** and **III**.

A rotating disc (RDE) analysis shows that the sum of the limiting current for waves **II** and **II′** corresponds to a one-electron transfer process (Fig. 1*b*) and is equal to the current for process **I**. Thus processes **II** and **II′** (combined) correspond with ring oxidation to the cation radical, $[TBTAP(-1)H_2]^+$/TBTAP(-2)H_2 (using previously defined nomenclature (8)). A differential pulse voltammetry study shows that the redox potentials for waves **II** and **II′** are concentration dependent. At very low concentration, only one differential pulse signal was observed at a potential close to that of wave **II′** (Table 1, Fig. 2). The concentration limit for observing one peak for species **5** and **13** is below 10^{-5} M, and is below 10^{-6} M for species **14**.

The dual wave arises from aggregation, a well-known phenomenon in phthalocyanine derivative chemistry (9). However Beer–Lambert plots for the parent **5** from 8.2×10^{-5} M to 6.6×10^{-7} M at 687 and 647 nm do not show any deviation from linearity, indicating that the parent unoxidized species is not aggregated. Therefore the oxidized species, $[TBTAP(-1)H_2]^+$, must aggregate according to:

$$[1] \quad [TBTAP(-1)H_2]^+ + TBTAP(-2)H_2 \; <= = => \{[TBTAP(-1)H_2]TBTAP(-2)H_2\}^+$$

Since it is apparently wave **II′** and not wave **II** which survives in very dilute solution, wave **II′** must correspond to oxidation of the mononuclear species, which then combines, as in eq. [1], to form a mixed valence species that then oxidizes at wave **II** to 2 $[TBTAP(-1)H_2]^+$ (but see below that this species is in equilibrium with a dipositively charged dimeric species). The equilibrium [1] becomes much less important at very low concentrations, as shown in Fig. 2, when only direct oxidation of TBTAP(-2)H_2 to $[TBTAP(-1)H_2]^+$ is observed. The formation of binuclear mixed-valence single-ring oxidized species such as that shown in eq. [1] is becoming fairly well known in phthalocyanine chemistry, especially with binuclear linked species (10–12), but is also purported to occur (13) during the oxidation of MgPc(-2), via $[MgPc(-1).MgPc(-2)]^+$, to $2[MgPc(-1)]^+$.

Wave **I** is assigned to oxidation to the dication radical, namely, process $[TBTAP(0)H_2]^{2+}/[TBTAP(-1)H_2]^+$. This redox couple is irreversible except for species **14**. Waves **III** and **IV** are quasi-reversible diffusion-controlled one-electron transfer processes assigned to the reduction processes TBTAP(-2)H_2/$[TBTAP(-3)H_2]^-$ and $[TBTAP(-3)H_2]^-$/$[TBTAP(-4)H_2]^{2-}$, respectively.

Increasing the alkyl chain from 9 to 17 carbon atoms in the *meso* position provides no significant change in the redox potential.

*(ii) TBTAP(C_n)Mg (species **4**, **10**)*

These magnesium species show voltammograms typical for MPc-like species with oxidation processes **II** and **I** to the ring-oxidized mono- and di-cation radical, respectively, and two reduction processes (**III**, **IV**) to the ring-reduced mono- and di-anion radical, respectively (Figs. 3, 4; Table 1). The forward and reverse differential pulse polarograms are especially well behaved (Fig. 4), showing the electrochemical reversibility of all the observed processes, with the exception of **I** (and possibly **IV**, see below).

(iii) Comparison with regular phthalocyanine species

Although the overall features in the electrochemical behaviour of the TBTAP species parallel those of the phthalocyanines very closely, the first and second reductions for TBTAP(C_n)H_2 are about 300 mV negative of those for regular metal-free phthalocyanine species such as metal-free tetraneopentoxyphthalocyanine (6, 14). This is due to the replacement of one electron-withdrawing bridgehead nitrogen link by the less-withdrawing methine link. Porphyrins are more difficult to reduce than the corresponding phthalocyanines and these TBTAP species obviously lie, in character, between the porphyrins and phthalocyanines.

The naphthalene-substituted species, **14**, is easier to oxidize and more difficult to reduce than the corresponding benzotriazaporphin, an observation consistent with previous phthalocyanine experience (7).

D. Electronic absorption

(i) TBTAP(C_n)H_2 and TBTAP(C_n)M

In the electronic spectroscopy of fourfold symmetry, D_{4h}, MPc(-2) species, π–π^* transitions from the two upper filled π orbitals (HOMO and HOMO-1) to the π^* LUMO orbital provide a strong band, usually in the range 620–720 nm, called the *Q* band, and a second band, in the range 320–420 nm, called the *B* band (or Soret). The *Q* band is usually associated with a weaker vibrational satellite to higher energy (near 600–620 nm) (15). In the metal-free species, of twofold symmetry, the *Q* band is split into two strong features, usually with at least two weaker vibrational satellites. Such a doubled *Q* band is expected, and observed, in these lower symmetry TBTAP(-2)(C_n)H_2 and TBTAP(-2)-(C_n)M species (Fig. 5). The data reported here (Table 2) correspond closely with those previously published for TBTAP(-2)H_2, TBTAP(-2)Mg, and TBTAP(-2)Zn (3, 5).

The *Q*-band splitting in the spectra of the TBTAP(-2)(C_n)M species is about 500 cm^{-1}, whereas it is about 900 cm^{-1} in the spectra of metal-free TBTAP(-2)(C_n)H_2, perhaps because of the lower symmetry of the latter. This *Q*-band splitting is substantially larger than that imposed on mixed benzo, naphthophthalocyanines where one or three benzene rings is replaced by a napthalene ring; such systems show splittings (16) of 225–250 cm^{-1}. Changing the length of the alkyl chain causes no significant shift or change in the relative intensities of either the *Q* or *B* bands, in the spectrum recorded in THF.

(ii) Spectroelectrochemistry

(a) Cation radicals, $(a_2)^1$, $^2A_2$: The spectroscopic changes accompanying the oxidation of TBTAP(C_9)Mg (**4**) and *t*-BuTBTAP(C_{15})H_2 (**13**) to their corresponding cation radicals are shown in Figs. 6 and 7. The resulting loss of *Q*-band intensity between 600 and 700 nm, and the growth of weaker and broader absorption near 550 and 850 nm, is typical of the formation of a phthalocyanine cation radical, Pc(-1), species (13, 17, 18) (Table 3). Indeed the spectra (13, 18) of ZnPc(-1) and MgPc(-1) species are dramatically similar to those spectra reported here, leaving no doubt that these species are cation radicals. The principal difference is that

Can. J. Chem. Downloaded from www.nrcresearchpress.com by 213.200.69.106 on 09/08/12
For personal use only.

the band near 850 nm, reputed to be the *Q* band for the monomeric cation radical (13), is relatively less strong, and is broader, than in the MPc(-1) species. The broadness may reflect incipient splitting in the lower symmetry of these species. The peak at 530–570 nm is a $\pi-\pi$ transition in the mononuclear species, similar to previous assignments of related species (13, 14, 18, 20, 21).

These species show isosbestic points upon reduction and may be oxidized back to the starting species with recovery of the initial spectrum; thus the spectroelectrochemistry is reversible with no significant decomposition.

The presence of a hole in the HOMO orbital frequently leads, in phthalocyanine chemistry, to some stabilization of a dimeric species (8, 10–12, 18, 19), which may be written for the TBTAP species as:

[2] $2[\text{TBTAP(-1)H}_2]^+ <= = => [\text{TBTAP(-1)H}_2]_2^{2+}$

Comparison of the electronic spectra of phthalocyanine and TBTAP cation radical spectra leads to the presumption that the peak at 1010–1080 nm arises from dimeric TBTAP radical cation species. Support for this conclusion arises from concentration-dependent studies that show, for TBTAP-$(C_{15})H_2$, that the intensity ratio for the peak at 1070 nm relative to that at 860 nm increases with increasing concentration, e.g., the ratio 1070/860 is 0.4 at 2.5×10^{-4} M, and 1.1 at 1×10^{-3} M TBTAP(-2)H_2.

(*b*) *Mono-anion radicals* $(a_2)^2(b_2)^1$, $^2B_2$: Figure 8 shows the spectroscopic changes during the reduction of **13** to its anion radical with related data for other species in Table 4. Isosbestic points again attest to good behaviour with no significant decomposition. The spectroscopic features are characteristic of Pc(-3) anion radicals (14, 16, 22–24). While MPc(-2) species yield a single *Q* band, $[\text{MPc(-3)}]^-$ species usually have a doubled band in the *Q* region. Conversely, these low-symmetry $[\text{TBTAP(-3)}(C_n)]^-$ species only exhibit a single band in the *Q* region (Fig. 8). A magnetic circular dichroism study of these and related systems provides an explanation of this apparent anomaly and will be published elsewhere.[2] Otherwise the spectra are characteristic of the mono-anion radical, especially with respect to the band near 440 nm and the double system (assigned as $\pi^*-\pi^*$) near 860 and 950 nm, which, however, is red shifted from the corresponding bands in the phthalocyanine series (14, 22–24).

(*c*) *Di-anion radicals* $(a_2)^2(b_2)^2$ $^1A_1$: The spectroscopic changes during the reduction of the mono-anion radical of **5** to its di-anion radical are shown in Fig. 9, with data for other di-anion radicals summarized in Table 4. The metal-free di-anion radical spectra show clean complete reduction with isosbestic points. However, some decomposition is noted during the reduction of the Mg species to the di-anion state. These spectroscopic data are characteristic for Pc(-4) species, especially the strong band near 530 nm (14); in this case, the number of strong features in the Pc(-4) and TBTAP(-4)(C_n) spectra and the overall shape of the band envelope are similar.

Summary

The spectroscopic and electrochemical properties of the triazaporphine species parallel very closely those for two-fold symmetry metallophthalocyanines. The presence of one methine linkage replacing an aza bridgehead does not, it appears, have a major effect upon the electronic properties of these phthalocyanine-like species save for removing all orbital degeneracies. Thus the wealth of understanding that has grown in the phthalocyanine field can be transferred with some confidence to the triazaporphines, subject only to the change in symmetry. These species do have some important properties, however, which make them very useful in the pursuit of molecular electronic applications, namely: (*i*) organic solvent soluble, single isomer, species can readily be synthesized; (*ii*) Langmuir–Blodgett films may readily be made from amphiphilic species constructed with long alkyl chains (25–27); (*iii*) the facile ability to modify the functional group attached to the methine linkage should provide for the synthesis of a wide range of strategically designed molecules.

Acknowledgement

We are indebted to the Natural Sciences and Engineering Research Council of Canada and to the Office of Naval Research (Washington) for financial support. We would like to thank Professor A. A. Vlcek for useful discussion during his visit to York University.

1. P. A. Barrett, R. P. Linstead, G. A. P. Tuey, and J. M. Robertson. J. Chem. Soc. 1809 (1939).
2. R. L. Wheeler, G. Nagasubramanian, A. J. Bard, L. A. Schectman, D. R. Dininny, and M. E. Kenney. J. Am. Chem. Soc. **106**, 7404 (1984).
3. C. C. Leznoff and N. B. McKeown. J. Org. Chem. **55**, 2186 (1990).
4. T. J. Dougherty, W. R. Potter, and K. R. Weishaupt. *In* Porphyrin localization and treatment of tumors. *Edited by* D. R. Doirin and C. J. Gomer. Alan R. Liss Inc., New York. 1984. p. 301; S. G. Brown, C. J. Tralau, P. D. Coleridge Smith, D. Akademir, and T. Weiman. J. Cancer, **54**, 43 (1986); I. Rosenthal, E. Ben-Hur, S. Greenberg, A. Conception-Lam, D. M. Drew, and C. C. Leznoff. Photochem. Photobiol. **46**, 959 (1987); I. Rosenthal and E. Ben-Hur. *In* Phthalocyanines; properties and applications. Vol. 1. *Edited by* C. C. Leznoff and A. B. P. Lever. VCH Publishers, New York. 1989. p. 393. J. E. Van Lier. Photodynamic therapy of neoplastic disease. Vol. 1. *Edited by* D. Kessel. CRC Press, Boca Raton, Fla. 1990. p. 279; T. J. Dougherty. Photochem. Photobiol. **45**, 897 (1987); B. W. Henderson and T. J. Dougherty. Photochem. Photobiol. **55**, 145 (1992).
5. M. Krejcik, M. Danek, and F. Hartl. J. Electroanal. Chem. **317**, 179, (1991).
6. K. N. Solovev, V. A. Mashenkov, and T. F. Kachura. Opt. Spectrosc. (Engl. Transl.) **27**, 24 (1969).
7. A. B. P. Lever. *In* Phthalocyanines; properties and applications. Vol. 3. *Edited by* C. C. Leznoff and A. B. P. Lever. VCH Publishers, New York. 1993. p. 1.
8. J. F. Myers, G. W. Rayner Canham, and A. B. P. Lever. Inorg. Chem. **14**, 461 (1975).
9. W. A. Nevin, W. Liu, and A. B. P. Lever. Can. J. Chem. **65**, 855 (1986); W. A. Nevin, W. Liu, M. Melnik, and A. B. P. Lever. J. Electroanal. Chem. **213**, 217 (1986); W. A. Nevin, W. Liu, S. Greenberg, M. R. Hempstead, S. M. Marcuccio, M. Melnik, C. C. Leznoff, and A. B. P. Lever. Inorg. Chem. **26**, 891 (1987); Z. A. Schelly, R. D. Farina, and E. M. Eyring. J. Phys. Chem. **74**, 616 (1970); K. Bernauer and S. Fallab. Helv. Chim. Acta, **44**, 1287 (1961); A. Giraudeau, A. Louati, M. Gross, J. J. Andre, J. Simon, C. H. Su, and K. M. Kadish. J. Am. Chem. Soc. **105**, 2917 (1983).
10. V. Manivannan, W. A. Nevin, C. C. Leznoff, and A. B. P. Lever. J. Coord. Chem. **19**, 139 (1988).

[2]N. Kobayashi, A. B. P. Lever, and M. J. Stillman. Manuscript in preparation.

11. N. Kobayashi, H. Lam, W. A. Nevin, P. Janda, C. C. Leznoff, and A. B. P. Lever. Inorg. Chem. **29**, 3415 (1990).
12. C. C. Leznoff, H. Lam, W. A. Nevin, N. Kobayashi, P. Janda, and A. B. P. Lever. Angew. Chem. Int. Ed. Engl. **26**, 1021 (1987).
13. E. Ough, E. Z. Gasyna, and M. J. Stillman. Inorg. Chem. **30**, 2301 (1991).
14. G. Fu, Y. S. Fu, K. Jayaraj, and A. B. P. Lever. Inorg. Chem. **29**, 4090 (1990).
15. M. J. Stillman. *In* Phthalocyanines; properties and applications. Vol. 1. *Edited by* C. C. Leznoff and A. B. P. Lever. VCH Publishers, New York. 1989. p. 133.
16. Y. Ikeda, H. Konami, M. Hatano, and K. Mochizuki. Chem. Lett. 763 (1992).
17. M. J. Stillman. *In* Phthalocyanines: properties and applications. Vol. 3. *Edited by* C. C. Leznoff and A. B. P. Lever. VCH Publishers, New York. 1993. p. 277.
18. T. Nyokong, T. Z. Gasyna, and M. J. Stillman. Inorg. Chem. **26**, 548 (1987).
19. H. Z. Homborg. Z. Anorg. Allg. Chem. **507**, 35 (1983).
20. W. A. Nevin, M. R. Hempstead, W. Liu, C. C. Leznoff, and A. B. P. Lever. Inorg. Chem. **26**, 570 (1987).
21. P. A. Bernstein and A. B. P. Lever. Inorg. Chem. **29**, 608 (1990).
22. P. C. Minor, M. Gouterman, and A. B. P. Lever. Inorg. Chem. **24**, 1894 (1985).
23. D. W. Clack and J. R. Yandle. Inorg. Chem. **11**, 1738 (1972).
24. J. Mack, S. Kirkby, E. A. Ough, and M. J. Stillman. Inorg. Chem. **31**, 1717 (1992).
25. S. Baker, M. C. Petty, G. G. Roberts, G. G. and M. V. Twigg. Thin Solid Films, **99**, 53 (1983); H. Fuchs, H. Ohst, and W. Prass. Adv. Mater. (Weinheim, Fed. Repub. Germany), **3**, 10 (1991); G. G. Roberts, M. C. Petty, S. Baker, M. T. Fowler, and N. J. Thomas. Thin Solid Films, **132**, 113 (1985); M. Sugi. J. Mol. Electron. **1**, 3 (1985); R. H. Tredhold. Rep. Prog. Phys. **50**, 1609 (1987).
26. Y. S. Fu and A. B. P. Lever. J. Phys. Chem. **95**, 6979 (1991).
27. M. J. Cook, N. B. McKeown, A. J. Thomson, K. J. Harrison, R. M. Richardson, A. N. Davies, and S. J. Roser. Chem. Mater. **1**, 287 (1989); J. R. Fryer, C. M. Mcconnell, R. A. Hann, B. L. Eyres, and S. K. Gupta. Philos. Mag. B: **61**, 843 (1990); S. Palacin, A. Ruaudel-Teixier, and A. Barraud. J. Phys. Chem. **93**, 7195 (1989).

Can. J. Chem. Downloaded from www.nrcresearchpress.com by 213.200.69.106 on 09/08/12
For personal use only.

Silylation de l'isoquinoléine : influence des conditions opératoires sur l'obtention de nouveaux hétérocycles siliciés

MICHELINE GRIGNON-DUBOIS[1] ET MICHELLE FIALEIX

Laboratoire de chimie organique et organométallique, Université Bordeaux I, 351, Cours de la Libération, 33405 Talence CEDEX, France

ET

JEAN-MICHEL LEGER

Laboratoire de chimie analytique, Université Bordeaux II, 3, Place de la Victoire, 33076 Bordeaux CEDEX, France

Reçu le 20 octobre 1992

MICHELINE GRIGNON-DUBOIS, MICHELLE FIALEIX et JEAN-MICHEL LEGER. Can. J. Chem. **71**, 754 (1993).

La silylation de l'isoquinoléine par les réactifs $Me_3SiCl/Li/THF$ ou $Me_3SiCl/Mg/THF$ a été étudié en détail. L'influence de la nature du métal utilisé et des conditions opératoires a été mise en évidence. Ces paramètres conditionnent l'orientation de la réaction et permettent l'accès à des produits de silylation originaux.

MICHELINE GRIGNON-DUBOIS, MICHELLE FIALEIX, and JEAN-MICHEL LEGER. Can. J. Chem. **71**, 754 (1993).

Silylation of isoquinoline with $Me_3SiCl/Li/THF$ or $Me_3SiCl/Mg/THF$ reagents has been studied. The choice of the metal and the experimental conditions govern the course of the silylation reaction and lead to new trimethylsilyl heterocyclic compounds.

Can. J. Chem. Downloaded from www.nrcresearchpress.com by 213.200.69.106 on 09/08/12
For personal use only.

Nous avons précédemment montré (1) que la silylation réductrice de la quinoléine par le système $Me_3SiCl/Li/THF$ permettait d'accéder à des hydroquinoléines polysiliciées originales. L'intérêt de ces composés pour des fonctionnalisations ultérieures justifiait d'étudier d'autres hétérocycles aromatiques. La première étape de ces réactions étant la silylation de l'atome d'azote, sa position dans le squelette devrait jouer un rôle important dans la réactivité. L'étude de l'isoquinoléine paraissait donc particulièrement intéressante; en particulier, la disilylation réductrice qui intervenait essentiellement en position 1,4 avec la quinoléine (1) ne pourra ici s'effectuer qu'en 1,2 ou, éventuellement, en 2,6.

Le seul dérivé silicié d'hydroisoquinoléine connu était le 2,2′-bis-triméthylsilyl-1,1′,2,2′-tétrahydro-1,1′biisoquinoléine isolé par Becker et Neumann (2) par silylation de l'isoquinoléine au moyen du bis-triméthylsilyl-mercure. Nous avons pour notre part utilisé les réactifs $Me_3SiCl/Li/THF$ et $Me_3SiCl/Mg/THF$. L'étude de la quinoléine (1) ayant montré l'importance des conditions expérimentales sur l'orientation de la réaction, nous avons examiné en détail le rôle de ces paramètres et plus particulièrement l'influence de la nature du métal, de la concentration des réactifs et de leur ordre d'introduction dans le milieu réactionnel.

Résultats et discussion

Silylation par $Me_3SiCl/Li/THF$

La réaction est effectuée à 0°C avec 2, 4 ou 6 équivalents d'agent silylant et poursuivie jusqu'à disparition du métal ou de l'isoquinoléine. Elle conduit à des produits siliciés différents, selon que Me_3SiCl ou l'hétérocycle sont additionnés au mélange des autres réactifs.

(a) Addition de Me_3SiCl

Ce procédé permet d'être toujours en défaut de Me_3SiCl. L'utilisation de 2 équivalents de lithium et 2 équivalents de Me_3SiCl conduit au mélange de deux composés originaux, **2** et **3** (schéma 1; tableau 1)) obtenus avec des rendements respectifs de 30 et 50%. Il n'y a pas formation de dérivés disiliciés. Quatre équivalents d'agent de silylation conduisent au même résultat; par contre, avec 6 équivalents, les composés **2** et **3** ne sont isolés qu'avec respectivement 13 et 33% de rendement à côté de résidu abondant provenant de la polymérisation de l'isoquinoléine.

Le *cis,cis-ortho,ortho*-(*N,N′*-bis-triméthylsilyl-2-aminoéthényl)-stilbène, **2**, qui résulte de l'ouverture du cycle azoté n'avait pas été précédemment décrit. Il est isolé du mélange par précipitation dans le cyclohexane. Les analyses physicochimiques habituelles (RMN, spectrométries de vibration et de masse) ne permettant pas d'élucider totalement sa structure, nous avons effectué une étude radiocristallographique (tableau 2). La figure **1** montre une vue spatiale de la molécule, qui est centrosymétrique. On constate que la gêne stérique introduite par les groupes silyles provoque une torsion de 5° au niveau de la double liaison énamine et une déformation plus importante (45°) entre le plan de cette double liaison et celui du noyau aromatique adjacent.

Le deuxième produit de la réaction est isolé par évaporation du filtrat et a été identifié au 2,2′-bis-triméthylsilyl-1,1′,2,2′-tétrahydro-1,1′-biisoquinoléine, **3**. Son état physique (huile jaune pâle) montre que nous n'avons pas obtenu le même stéréoisomère que Becker et Neumann, qui par action du bis-triméthylsilyl-mercure (2) isolait un solide (*F* 162–164°C) mais sans préciser sa stéréochimie. Afin d'élucider totalement la structure du composé **3**, nous l'avons mis à réagir avec le chlorure d'acétyle à 0°C; nous avons ainsi isolé le dimère *N*-acétylé correspondant **4**, sous la forme d'un solide blanc (rdt. 80%; *F* 196°C). Par action d'un mélange zinc – anhydride acétique sur l'isoquinoléine, A.T. Nielsen (3) avait obtenu le 2,2′-diacétyl-1,1′,2,2′-tétrahydro-1,1′-biisoquinoléine sous la forme d'un mélange des deux diastéréoisomères (rdt. 58%; *thréo/méso* 50 : 50). Le produit que nous isolons présente les mêmes caractéristiques que l'isomère *thréo* obtenu par Nielsen, qui attribue cette stéréochimie par corrélation chimique (3). Cependant les réactions mises en jeu s'effectuant à 118°C et ayant constaté pour notre part que cette température peut être suffisante pour en-

[1]Auteur à qui adresser toute correspondance.

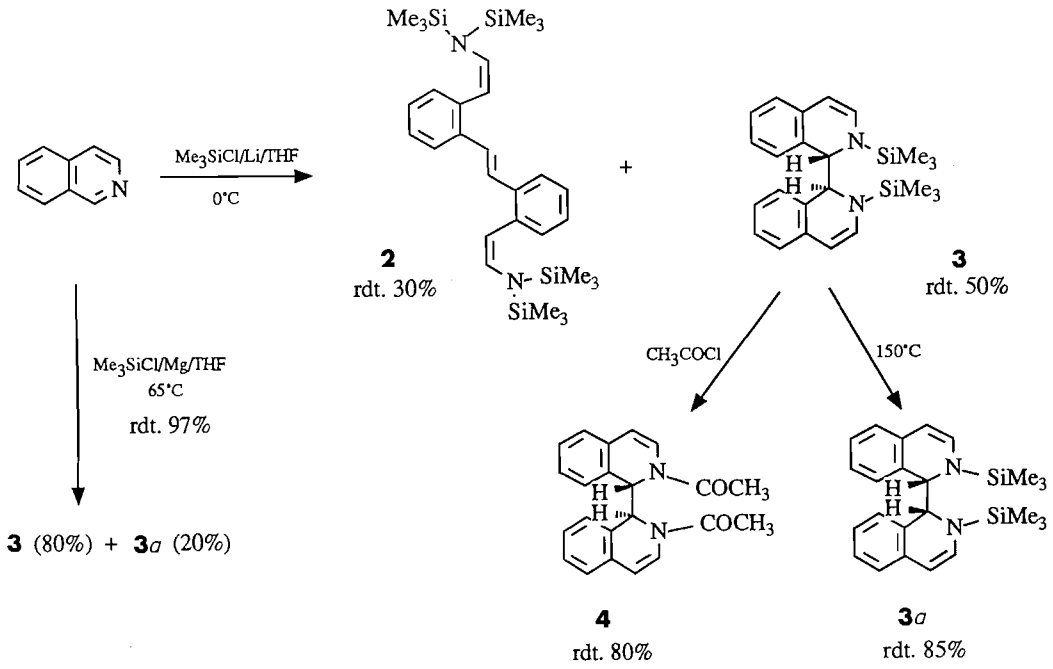

SCHÉMA 1. Silylation de l'isoquinoléine par $Me_3SiCl/Li/THF$ ou $Me_3SiCl/Mg/THF$.

TABLEAU 1. Influence des conditions opératoires sur l'orientation de la silylation

Conditions expérimentales	Produits formés, rdt. (%)							
	2	**3**	**3*a***	**5**	**6**[a]	**7**[a]	**8**[a]	**9**[a]
$Me_3SiCl/Li/THF$								
Add. Me_3SiCl	30	50	—	—	—	—	—	—
Add. isoquinoléine :								
2 équiv. Me_3SiCl	—	15	—	—	—	—	—	—
4 équiv. Me_3SiCl	—	—	—	4	6	10	25	9
6 équiv. Me_3SiCl	—	—	—	8	63	5	10	15
$Me_3SiCl/Mg/THF$								
4 h 65°C	—	78	19	—	—	—	—	—
20 h 65°C	—	68	29	—	—	—	—	—
$Me_3SiCl/Mg–Zn/THF$								
2,5 h 65°C	—	83	15	—	—	—	—	—

[a]Produits résultants de l'aromatisation de **I** et **II** : cf. fig. 4.

traîner une isomérisation partielle de ces dimères, nous avons effectué une analyse cristalline du dérivé **4** (fig. 2, tableau 2). Nous avons ainsi mis en évidence la géométrie *thréo* de l'enchaînement 1–1′, ce qui confirme les résultats de Nielsen et permet d'attribuer la même stéréochimie au composé **3**. Signalons que Kurkutova et al. (4) avaient rapporté une étude radiocristallographique d'un des deux isomères de **4**, mais sans préciser lequel et de manière très succincte. Le dimère *N*-silicié *thréo* **3** n'était pas connu. Par chauffage à 150°C sous atmosphère inerte, il conduit à l'isomère *méso*, **3*a*** (rdt. 85%), qui est cristallisé (*F* 160°C) et identique au dérivé isolé par Becker et Neumann (2) dont nous établissons ainsi la stéréochimie. La stéréosélectivité de la dimérisation, différente selon le réactif utilisé, est remarquable. Elle montre que le mécanisme intervenant avec le système $Me_3SiCl/Li/THF$ doit être plus complexe qu'une simple duplication radicalaire : les phénomènes de solvatation associés à des effets de sel pourraient jouer ici un rôle dans le déroulement de la réaction. L'isomérisation thermique de **3** en **3*a*** implique une scission homolytique de la liaison 4,4′ conduisant au radical correspondant ce qui est en accord avec les résultats décrits par Mitchell dans la série des 1,1′,2,2′-tétrahydrobipyridines (5). L'examen de modèles moléculaires montre que la forme *méso* est moins encombrée que la forme *thréo*; la facilité de cette isomérisation pourrait s'expliquer par la décompression stérique qui en résulte. Lorsque la thermolyse est conduite en présence d'air, on isole l'isoquinoléine (rdt. 80%) à côté d'un résidu noir.

(b) Addition de l'isoquinoléine

La réaction est conduite à 0°C pendant 3 h, temps nécessaire à la disparition du lithium engagé. Afin d'être toujours en excès d'agent silylant, l'isoquinoléine a été additionnée lentement au mélange $Me_3SiCl/Li/THF$ dont nous avons fait varier la concentration (2–6 équivalents par mole

Can. J. Chem. Downloaded from www.nrcresearchpress.com by 213.200.69.106 on 09/08/12
For personal use only.

TABLEAU 2. Données cristallographiques des composés **2**, **4**, **5**

Composé **2**		Composé **4**		Composé **5**	
Formule $(C_{15}H_{25}N_1Si_2)2$		Formule $(C_{22}H_{22}N_2O_2)$		Formule $(C_{24}H_{55}N_1Si_5)2$	
Masse molaire 551,20		Masse molaire 344,41		Masse molaire 875,36	
Symétrie triclinique		Symétrie monoclinique		Symétrie monoclinique	
Groupe spatial	$P\bar{1}$	Groupe spatial	$P2_{1/n}$	Groupe spatial	$P2_{1/n}$
a, Å(σ)	8,486(2)	a, Å(σ)	9,075(2)	a, Å(σ)	10,686(2)
b, Å(σ)	8,878(2)	b, Å(σ)	10,061(2)	b, Å(σ)	23,619(3)
c, Å(σ)	12,723(3)	c, Å(σ)	19,426(5)	c, Å(σ)	13,086(2)
α, °(σ)	68,07(1)	β, °(σ)	93,26(1)	β, °(σ)	105,93(1)
β, °(σ)	71,30(1)	V, Å^3	1770,8	V, Å^3	3176,0
γ, °(σ)	77,03(1)	Z	4	Z	2
V, Å^3	836,2	D_x, g cm^{-3}	1,29	D_x g cm^{-3}	0.92
Z	1	N° de reflexions mesurées	3002	N° de reflexions mesurées	5407
D_x, g cm^{-3}	1,09	N° de reflexions utilisées	1833	N° de reflexions utilisées	2467
N° de reflexions mesurées	2835	N° de paramètres affinés	315	N° de paramètres affinés	479
N° de reflexions utilisées	2059	R	0,061	R	0,096
N° de paramètres affinés	263	R_w	0,072	R_w	0,130
R	0,055	S	0,886	S	2,115
R_w	0,071	Δρ Max., e Å^{-3}	0,30	Δρ Max., e Å^{-3}	0,80
S	1,168	Δρ Min., e Å^{-3}	−0,29	Δρ Min., e Å^{-3}	−0,72
Δρ Max., e Å^{-3}	0,27				
Δρ Min., e Å^{-3}	−0,30				

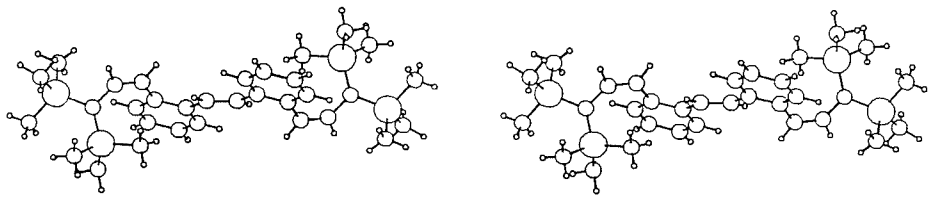

FIG. 1. Vue stéréoscopique du composé **2**.

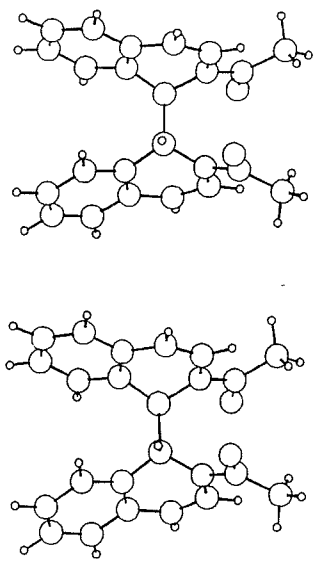

FIG. 2. Vue stéréoscopique du composé **4**.

d'isoquinoléine; tableau 1). Dans ces conditions, nous n'observons pas la formation du composé **2**. Avec 2 équivalents de réactif, la réaction est incomplète : 55% de l'isoquinoléine engagée est récupérée en fin de réaction et le composé **3** n'est isolé qu'avec 15% de rendement. Par contre, avec 4 ou 6 équivalents, la réaction est totale mais conduit à des mélanges réactionnels très instables qui se désilylent rapidement lorsqu'on les manipule. Leurs spectres de RMN ^{1}H montrent l'absence de protons aromatiques et un massif large et intense, constitué de plusieurs singulets indiscernables centrés vers 0,1 ppm. Ceci semble indiquer la présence de produits persiliciés, hypothèse en accord avec le fait qu'aucune trace de produits disiliciés n'est isolé lors des tentatives de distillation et que la masse du mélange réactionnel augmente avec la quantité de réactif (pour 1 g de substrat elle est respectivement de 1,8,3 ou 4,3 g pour 2, 4 ou 6 équiv.). L'addition de cyclohexane aux mélanges réactionnels isolés à partir de 4 ou 6 équivalents conduit à la précipitation d'un solide jaune pâle montrant cinq groupes $SiMe_3$ en RMN (^{1}H, ^{13}C). Une analyse radiocristallographique (fig. 3, tableau 2) a permis de l'identifier au diastéréoisomère *méso* du 2,2′,3,3′,5,5′,6,6′,7,7′-déca-triméthylsilyl-1,1′, 2,2′, 3,3′, 5,5′, 6,6′,7,7′-dodécahydro-1,1′-biisoquinoléine, **5**, qui doit résulter de la persilylation du dimère *N*-silicié **3***a* dans le milieu réactionnel. Les rendements sont respectivement de 4% (4 équiv.) et 8% (6 équiv.). La figure 3 montre que la molécule est centrosymétrique, chaque motif renfermant une structure diénique *transoïde* comparable à celle obtenue par persilylation de la quinoléine (1). Les calculs effectués à partir des coordonnées atomiques montrent que les doubles liaisons forment un angle de 19,6° et que tous les groupes silyles sont en *trans* les uns par rapport aux autres (positions équatoriales sur les sommets 3, 5 et 6 et axiales sur les sommets 2 et 7. Les liaisons

Can. J. Chem. Downloaded from www.nrcresearchpress.com by 213.200.69.106 on 09/08/12
For personal use only.

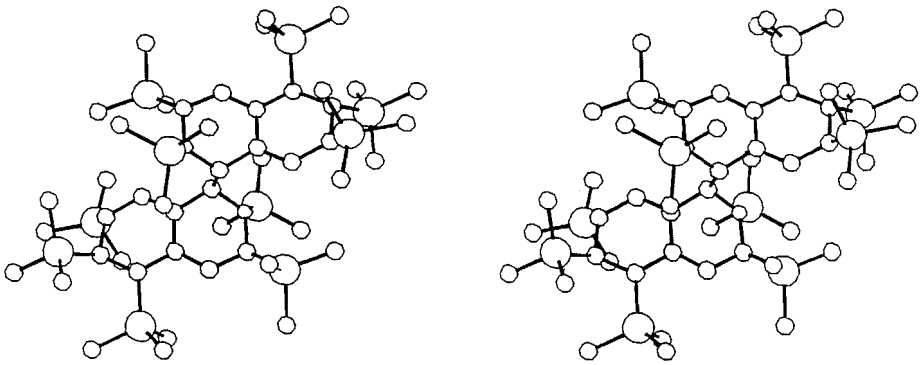

FIG. 3. Vue stéréoscopique du composé **5**.

C_6—Si et C_7—H sont pratiquement en position éclipsée (3°) de même que les liaisons C_7—Si et C_6—H (3°). À l'exception de l'angle dièdre entre les protons H_5 et H_6 qui est de 133°, tous les autres sont compris entre 44° et 109° ce qui rend compte des faibles couplages observés dans le spectre de RMN ^{1}H. Le composé **5** de stéréochimie *thréo* n'est pas observé. L'encombrement stérique, plus important dans le dimère monosilicié *thréo* **3** que dans le *méso* **3***a*, pourrait empêcher ici la polysilylation du cycle. Cependant, nous ne pouvons rejeter l'hypothèse de sa formation. En effet, nous avons constaté que le composé **3**, beaucoup moins stable que son isomère **3***a*, se désilyle en présence d'air pour conduire à l'isoquinoléine par scission de la liaison 1–1′. Il n'est donc pas exclu que le dimère pentasilicié *thréo* se forme également et évolue vers un monomère par aromatisation et perte partielle de silicium.

Les autres produits de la silylation n'ont pu être isolés par suite de leur fragilité. Toute tentative de purification par distillation ou par chromatographie liquide–liquide aboutit à leur désilylation partielle et à la formation de résidu. Le même phénomène intervient en solution, ce qui empêche leur analyse par RMN. Les mélanges réactionnels ont donc été abandonnés à l'air pendant 1 nuit puis chromatographiés sur silice afin d'isoler les produits d'aromatisation; ils ont été identifés aux composés **6–9** (fig. 4), obtenus avec des rendements variables selon la quantité d'agent de silylation mis en jeu (tableau 1) : avec 4 équiv., on isole le mélange suivant : **6** (rdt. 6%), **7** (rdt. 10%), **8** (rdt. 25%), **9** (rdt. 9%); avec 6 équiv., on isole : **6** (rdt. 63%), **7** (rdt. 5%), **8** (rdt. 10%), **9** (rdt. 5%). Dans ce dernier cas nous avons également séparé les constituants par distillation et obtenu : **6** (rdt. 70%), **7** (rdt. 5%), **9** (rdt. 11%).

Ces résultats montrent que **6** est toujours le produit majoritaire lorsqu'on travaille avec 6 équivalents de réactif. Les composés **6** et **8** présentent en RMN ^{1}H les signaux caractéristiques d'une 5,6,7,8-tétrahydroisoquinoléine : on note en particulier en RMN ^{1}H le couplage $^3J_{3,4}$ voisin de 5 Hz et un singulet attribuable au proton H-1 vers 8 ppm. Nous les avons identifié au 5,6,7-tris-triméthylsilyl-5,6,7,8-tétrahydroisoquinoléine, **6**, et au 6,7-bis-triméthylsilyl-5,6,7,8-tétrahydroisoquinoléine, **8**. Le composé **6** est constitué de deux isomères **6***a* et **6***b* dans les proportions 50 : 50. Les constantes de couplage $^3J(^1H,^1H)$ du cycle carboné ont été comparées à celles mesurées pour le 5,6,7-tris-triméthylsilyl-5,6,7,8-tétrahydroquinoléine, obtenu dans les mêmes conditions par aromatisation du 1,2,3,5,6,7-hexakis-triméthylsilyl-1,2,3,5,6,7-hexahydroquinoléine (1). Ces valeurs sont rassemblées dans le tableau 3. Nous y avons également inclus celles rapportées par Birkofer et Ramadan pour le 1,2,3,7-tétrakis-triméthylsilyl-1,2,3,7-tétrahydronaphtalène provenant de la silylation du naphthalène (6) ainsi que celles que nous avons mesurées pour le 1,1,3,5,6,7-hexakis-triméthylsilyl-1,4,5,6,7,8-hexahydronaphtalène, dont nous avons déterminé la géométrie par radiocristallographie (7*a*). La comparaison de ces valeurs montre que tous les composés, à l'exception de **6***a*, ont la même géométrie. Ceci permet d'attribuer sans ambiguïté à l'isomère **6***b*, la structure où les siliciums sont *trans*-diaxiaux sur les sommets 5 et 6 et *trans*-équatorial sur le sommet 7 avec un cycle en conformation bateau (fig. 5). Ces résultats confirment les structures que nous avions précédemment proposées dans le cas de la quinoléine (1) mais remettent en cause celle que Birkofer et Ramadan avaient avancée dans le cas du trisilyl-tétrahydronaphtalène (6). En ce qui concerne l'isomère **6***a*, la similitude des couplages $J_{7,8}$ et $J_{7,8}$, montre que le proton H-7 est sur la bissectrice de l'angle formé par les protons H-8 et H-8′ ce qui impose à Si-7 d'être axial. Les couplages $J_{5,6}$ et $J_{6,7}$, voisins de 3,5 Hz, sont compatibles avec des siliciums *trans*-diaxiaux sur un cycle demi-chaise (fig. 5). Ces conclusions sont en accord avec les études radiocristallines effectuées sur les produits polysiliciés obtenus par silylation réductrice du naphtalène (7*a*) et de benzènes monoalkylés (7*b*) : elles ont montré que la polysilylation des cycles aromatiques conduit à des composés tout-*trans* et la structure du dimère pentasilicié **5** que nous rapportons ici en est une nouvelle confirmation. De plus, des calculs MM2 effectués par Cartledge et coll. (8) dans la série des 1,2-bis-triméthylsilyl-cyclohexane et cyclohexène ont permis de montrer la plus grande stabilité des isomères *trans*-diaxiaux par rapport aux *trans*-diéquatoriaux.

Les composés **7** et **9** sont des isoquinoléines disiliciées. La présence dans les deux spectres de RMN ^{1}H d'un singulet vers 9 ppm montre que le carbone 1 n'est pas substitué. L'analyse des autres signaux nous a conduit à les identifier respectivement au 3,6-bis-triméthylsilyl-isoquinoléine, **7** et au 6,7-bis-triméthylsilyl-isoquinoléine, **9**. Cette attribution a été confirmée sur la base des déplacements chimiques du ^{13}C, qui ont été comparés aux valeurs calculés selon Ewing (9) pour tous les isomères théoriquement possibles. Notons que le composé **9** est toujours présent, quel que soit la quantité de réactif et la méthode de purification. Par contre, le composé **8**, auquel il s'apparente, n'est obtenu que lorsqu'on effectue une chromatographie sur silice. La forma-

Can. J. Chem. Downloaded from www.nrcresearchpress.com by 213.200.69.106 on 09/08/12
For personal use only.

Can. J. Chem. Downloaded from www.nrcresearchpress.com by 213.200.69.106 on 09/08/12
For personal use only.

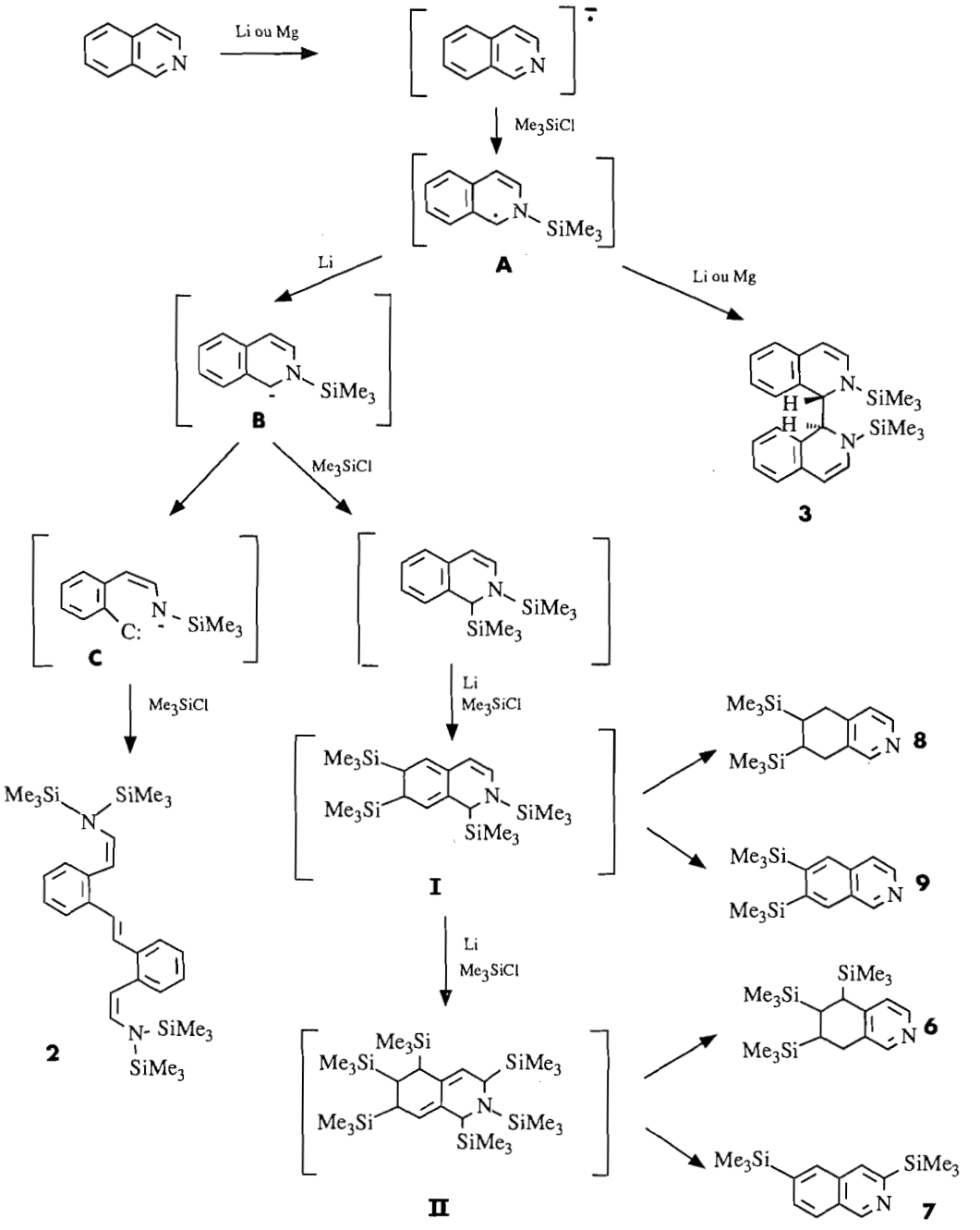

FIG. 4. Influence des conditions opératoires sur l'évolution de la silylation.

tion de ce dernier implique la fixation de deux atomes d'hydrogène, processus qui pourrait s'effectuer lors de la purification sur silice. Ceci est à rapprocher des résultats de Laguerre et al. (10) qui avaient obtenu le 6,7-bis(triméthylsilyl)-5,6,7,8-tétrahydronaphtalène à partir du 1,2,6,7-tétrakis(triméthylsilyl)-1,2,6,7-tétrahydronaphtalène.

Compte tenu de la structure de ces composés et des résultats précédemment observés à partir de la quinoléine, nous pensons que la polysilylation de l'isoquinoléine conduit au mélange des composés tétra- et hexasiliciés **I** et **II** (fig. 4), à côté du dimère pentasilicié **5**. Notons que certaines tentatives d'analyse RMN ^{1}H, effectuées sur les mélanges réactionnels débarrassés du dimère pentasilicié, ont montré la présence de quatre doublets d'égale intensité à 5,15 (1,7 Hz), 5,20 (1,7 Hz), 5,42 (1,5 Hz) et 5,51 ppm (1,5 Hz) compatibles avec un mélange de deux isomères hexasiliciés, ce qui confirmerait la filiation de **6** à **II**. Le composé **6** est toujours accompagné de 3,6-bis-triméthylsilyl-isoquinoléine, **7**, ce qui suggère qu'ils proviennent du même précurseur. Les composés **8** et **9** se formeraient à partir de **I**.

Silylation par $Me_3SiCl/Mg/THF$

Les premiers essais ont été conduits à température ambiante avec 1 équivalent de magnésium et 1,1 équivalent de Me_3SiCl. Après 48 h, la réaction étant toujours incomplète, nous avons opéré au reflux du THF. Dans ces conditions, l'isoquinoléine est entièrement consommée en 4 h pour conduire au mélange des deux dimères *N*-siliciés **3** et ***3a*** (rdt. : 97%; ***3/3a*** 80 : 20) (schéma 1). La prolongation du reflux à 20 h conduit au même rendement global, mais le rapport ***3/3a*** passe à 70 : 30. L'utilisation d'un excès de

TABLEAU 3. Caractéristiques RMN ^1H de poly-triméthylsilyl-polyhydro-isoquinoléines, quinoléine et naphtalènes

	δ (ppm)						*J* (Hz)				
	$SiMe_3$	H-5	H-6	H-7	H-8	H-8′	$J_{5,6}$	$J_{6,7}$	$J_{7,8}$	$J_{7,8'}$	$J_{8,8'}$
6a	−0,40 −0,07 +0,17	2,1	1,5	1,1	2,5	2,7	4,3	3,2	7,6	8,1	16,4
6b	−0,30 −0,13 0,0	2,2	1,3	0,8	2,2	2,4	—	9,0	13,6	4,8	14,6
5,6,7-TriSiMe$_3$ 5,6,7,8-tétrahydroquinoléine	−0,3 −0,14 0,0	2,2	1,3	1,0	2,4	2,7	—	9,1	14,2	4,6	14,5
5,6,7-TriSiMe$_3$ 5,6,7,8-tétrahydronaphtalène		2,3	1,4	1,0	2,3	2,6	—	8,5	13,0	5,0	14,0
1,1,3,5,6,7-HexaSiMe$_3$ 1,4,5,6,7,8-hexahydronaphthalène		1,6	1,2	0,8	1,8	1,9	1,0	10,6	12,8	4,3	14,8

réactif (4–6 équiv.) ne modifie pas ces résultats. Le magnésium n'est donc pas suffisamment réducteur pour permettre la polysilylation du squelette. L'adjonction de petite quantité de zinc (10% en poids par rapport au magnésium utilisé) ne modifie pas le cour de la réaction mais permet de diminuer le temps de chauffage (2,5 h au lieu de 4 h) conduisant ainsi à une meilleure stéréosélectivité puisque le rapport **3**/**3***a* atteint 85 : 15. Cette réaction constitue donc une bonne voie d'accès au dimère *thréo* qui n'était pas précédemment accessible. La stéréosélectivité de la réaction est remarquable et on peut raisonnablement penser que la formation de **3***a* résulte d'un début d'isomérisation au reflux du THF.

L'ensemble de ces résultats, associés à ceux précédemment obtenus à partir de la quinoléine (1) et ceux décrits dans le cas du naphtalène (10) montre l'importance de l'azote et de la position qu'il occupe dans la réactivité de ces squelettes. Ils mettent en outre en évidence le rôle du métal et des conditions opératoires. De plus, la position de l'atome d'azote, conditionnant le site de la première silylation, joue en rôle important tant au niveau de la structure des produits formés que de leur stabilité. Ainsi, avec l'isoquinoléine la réaction débute par le sommet 2 conduisant à un radical essentiellement localisé sur le sommet 1, position très favorable à une dimérisation ou à une ouverture du cycle azoté. Ceci explique que les conditions opératoires aient ici une influence beaucoup plus importante qu'avec la quinoléine et que nous n'ayons jamais observé la formation de dérivés résultant de la simple disilylation réductrice de l'isoquinoléine (fig. 4). Ainsi, avec le magnésium, métal faiblement réducteur comparé au lithium (11), la dimérisation à partir de **A**, beaucoup plus rapide que la capture d'un deuxième électron, s'effectue quantitativement. Le lithium, plus réducteur que le magnésium, permet un deuxième transfert d'électron conduisant à l'anion **B**. Cependant, lorsqu'on se trouve en défaut de Me_3SiCl (addition de Me_3SiCl au mélange des autres réactifs), la dimérisation intervient encore pour 50%. Elle est concurrencée par l'ouverture du cycle de **B** qui est plus rapide que la silylation du sommet 1; elle conduit à l'intermédiaire **C** de type ⟨⟨anio-carbénique⟩⟩ dont la duplication accompagnée de la silylation de l'atome d'azote rendent compte de l'obtention du composé **2**. Par contre, lorsqu'on est en excès de réactif (addition de l'isoquinoléine au mélange des autres réactifs), la polysilylation devient la réaction principale; l'utilisation de 6 équivalents d'agent de silylation permet alors de fixer six groupes triméthylsilyles sur le cycle azoté et la dimérisation n'intervient plus que pour 8% du substrat. L'influence de la position de l'atome d'azote se traduit par la facilité manifestée par l'isoquinoléine à conduire à des dimérisations par le sommet 1 et sa plus grande réactivité : ainsi le magnésium permet le silylation de l'isoquinoléine avec un rendement quantitatif, alors que, dans les mêmes conditions, le naphtalène ne réagit pas et la quinoléine conduit à un mélange inexploitable renfermant beaucoup de polymères.

Partie expérimentale

Caractéristiques physico-chimiques des produits siliciés obtenus

Les points de fusion ont été mesurés sur un appareil Mettler FP 61. Les analyses centésimales ont été effectuées au service central d'analyse du CNRS (F-69390 Vernaison). Les spectres de masse (SM) ont été enregistrés sur un appareil VG micromass 16 F (70 eV) et les spectres IR sur un spectromètre Perkin–Elmer 1420 ; tous les dérivés siliciès isolés présentent en IR des bandes de très forte intensité à 1250 et 850 cm^{-1} caractéristiques des groupes $SiMe_3$ et qui peuvent masquer le reste du spectre.[2] Les spectres de RMN du ^{13}C ont été enregistrés sur un appareil Bruker AC 250 fonctionnant à 62,9 MHz (C_6H_{12} réf. int. à 27,08 ppm) et ceux du ^{29}Si sur un appareil Bruker WH 500 fonctionnant à 99,32 MHz (TMS réf. int. à 0,0 ppm). Les spectres RMN ^1H ont été enregistrés sur les spectromètres Bruker AC 250 et Bruker WH 500 fonctionnant respectivement à 250 et 500 MHz (C_6H_{12} ref. int. à 1,4 ppm).

*Études radiocristallographiques des composés **2**, **4**, **5***

L'enregistrement des réflexions a été effectué sur un diffractomètre automatique CAD-4 Enraf–Nonuis en balayage $\omega/2\theta$ avec la radiation CuKα. Les détails expérimentaux sont rassemblés dans le tableau 2. Les mesures ont été corrigées des facteurs de Lorentz et polarisation. Les structures ont été résolues avec le programme MULTAN 80 (12). Les positions atomiques et les paramètres ther-

[2]Les caractéristiques physico-chimiques suivantes : spectres IR des composés **2** et **3**; spectre Raman du composé **2**; paramètres atomiques et écarts types des composés **2**, **4** et **5**, peuvent être achetés de : Dépôt des données non publiées, Service de fourniture de documents, ICIST, Conseil national de recherches Canada, Ottawa Canada K1A 0S2.

Les paramètres atomiques des composés **2**, **4** et **5** sont également disponibles au Cambridge Crystallographic Data Centre. On peut les obtenir en s'adressant au directeur, Cambridge Crystallographic Data Centre, University Chemical Laboratory, 12 Union Road, Cambridge CB2 1EZ, Royaume-Uni.

Can. J. Chem. Downloaded from www.nrcresearchpress.com by 213.200.69.106 on 09/08/12
For personal use only.

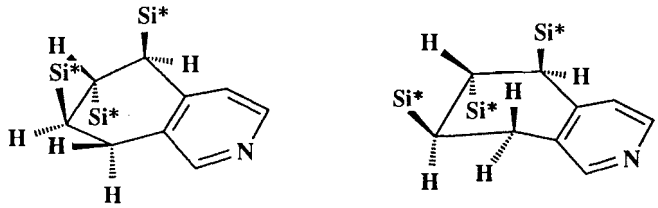

6*a* : Si-5 ax
Si-6 ax
Si-7 ax

6*b* : Si-5 ax
Si-6 ax
Si-7 eq

($Si^* = SiMe_3$)

FIG. 5. Géométrie des isomères **6***a* et **6***b*.

miques ont été affinés par moindres carrés avec la matrice diagonale.[2] Pour le dérivé **2**, le groupe d'espace centrosymétrique P_1 est nettement établi à partir des tests de centrosymétrie sur les facteurs de structure normalisés et conduit à $Z = 1$. La molécule est en position particulière sur le centre de symétrie. Pour le dérivé **5**, une variation significative et régulière des intensités de référence (environ 50% entre début et fin des mesures) a conduit à effectuer des corrections sur les mesures enregistrées. Le groupe spatial est $P2_1/n$ avec $Z = 2$; la molécule est en position particulière sur le centre de symétrie.

Le THF est distillé sur sodium et benzophénone afin d'enlever les traces d'eau et le Me_3SiCl sur Mg en poudre. Le lithium est préalablement granulé par fusion dans l'huile de vaseline puis lavé au THF. Le magnésium est utilisé en poudre. Les réactions sont conduites à la rampe à vide sous atmosphère d'argon.

Silylation par le système $Me_3SiCl/Li/THF$

Addition de MeSiCl

À une suspension de lithium finement granulé (0,28 g; 0,04 at.g) dans 150 mL de THF et 0,02 mol d'isoquinoléine (2,58 g) fraîchement distillée, on ajoute goutte à goutte 0,044 mol (4,75 g) de Me_3SiCl tout en maintenant la température entre 0 et 5°C. L'avancement de la réaction est suivi par CCM (SiO_2, hexane–EtOH 80 : 20). Au bout de 3 h, on note la disparition du produit de départ. Le THF est alors évaporé à la rampe à vide puis on ajoute 120 mL de cyclohexane, solvant dans lequel LiCl précipite, ce qui permet de l'éliminer par filtration. Le filtrat est ensuite évaporé et redissout dans 120 mL de cyclohexane afin d'éliminer les sels qui pourraient subsister. On obtient ainsi une huile jaune qui est redissoute dans 50 mL de cyclohexane et laissée au repos pendant 1 nuit. Dans ces conditions, le composé **2** précipite et est isolé par filtration à la rampe à vide (1,65 g; rdt. 30%). L'évaporation du filtrat conduit au composé **3**, isolé sous forme d'huile. Il est purifié par chromatographie sur silice (éluant : hexane–ether 80 : 20) (2 g; rdt. 50%). Il peut également être distillé, à condition toutefois d'opérer sous un vide inférieur à 0,01 Torr (1 Torr = 133.3 Pa). Dans le cas contraire, le chauffage entraîne l'isomérisation partielle de **3** en **3***a*.

cis,cis-ortho,ortho-(N,N'-*Bis-triméthylsilyl-2-aminoéthényl)-stilbène* (**2**) : rdt. 30%; *F* 158°C; IR (KBr cm^{-1}) : 1625, 1600, 1565; Raman (cm^{-1}) : 1629 (FFP), 1599 (FdP). RMN ^1H (500 MHz, $CDCl_3$) δ ppm : 0,09 (s, 18H, 4 $SiMe_3$), 6,03 (d, 1H, *J* 8,4 Hz), 6,17 (d, 1H, *J* 8,4 Hz), 7.18–7,21 (m, 2H), 7,20 (s, 1H), 7,56 (dd, 1H, *J* 6,9 et 1,9 Hz), 7,82 (dd, 1H, *J* 6,7 et 1.6 Hz). RMN ^{13}C ($CDCl_3$; 99,32 MHz) δ ppm : $SiMe_3$ à 2,0; 7 CH à 119,9, 126,4, 126,9, 127,1, 129,1, 130,3, 135,8; 2 C à 136,05 et 136,6. RMN ^{29}Si (C_6D_6, 200,132 MHz) δ ppm : 5,5. SM *m/e* (%) : 550 (26),478 (7), 477 (10), 390 (6), 202 (5), 176 (5), 175 (12), 174 (60), 172 (6), 130 (6), 74 (9), 73 (100), 59 (6), 45 (6), 28 (19). Anal. calc. pour $C_{30}H_{50}N_2Si_4$: C 65,38, H 9,15, N 5,08; trouvée : C 64,98, H 9,10, N 4,94.

2,2'- Bis-triméthylsilyl-1,1',2,2'- tétrahydro-1,1'- biisoquinoléine (**3**) : Eb 70°C/0,003 Torr; rdt. 50% par action du système $Me_3SiCl/Li/THF$ et 82% par action du système $Me_3SiCl/Mg/THF$. IR (NaCl, cm^{-1}) : 1610, 1560, 1490. RMN ^1H ($CDCl_3$, 250 MHz) δ ppm : 0,2(s, 9H), 4,4(s, 1H, H-1), 5,8(d, 1H, *J* 7,4 Hz), 5,9(d, 1H, *J* 7,4 Hz), 6,6–7,3(m, 4H). RMN ^{13}C ($CDCl_3$; 50,3 MHz) δ ppm : $SiMe_3$ à −0,27; 7 CH à 54,5, 105,5, 121,6, 123,9, 126,4, 127,4, 133,9; 2 C à 127,6 et 132,2. RMN ^{29}Si (C_6D_6, 99,32 MHz) δ ppm : 7,1.

2,2'- Bis- triméthylsilyl-1,1',2, 2'- tétrahydro-1,1'- biisoquinoléine (**3***a*) : il est obtenu par chauffage de l'isomère **3** (4,0 g; 0,02 mol) à 150°C pendant 3 h. La réaction est effectuée sans solvant sous atmosphère d'argon. Puis les cristaux obtenus sont rincés au cyclohexane afin d'éliminer les traces de l'isomère **3**.

3*a* : 3,5 g; rdt. 85%; *F* 163°C (hexane); IR (KBr, cm^{-1}) : 1608, 1560. RMN ^1H ($CDCl_3$, 500 MHz) δ ppm : −0,35 (s, 9H), 4,3 (s, 1H, H-1), 5,9 (d, 1H, H-4, $J_{4,3}$ 7,0 Hz), 6,4 (d, 1H, H-3, $J_{3,4}$ 7 Hz), 6,9 (d, 1H, *J* 7,3 Hz), 7,0 (dd, 1H, *J* 7,5 et 1,1 Hz), 7,1 (dt, 1H, *J* 7,3 et 1,3 Hz), 7,2 (dt, 1H, *J* 7,5 et 1,3 Hz). RMN ^{13}C (CD_2Cl_2 ; 50,3 MHz) δ ppm : $SiMe_3$ à −2,3; 7 CH à 53,6, 105,2, 121,9, 124,1, 126,6, 128,2, 128,9; 2 C à 128,4 et 132,7. RMN ^{29}Si (C_6D_6, 99,32 MHz) δ ppm : 9,9. SM *m/e* (%) : 203 (19), 202 (100, M/2), 129 (11), 73 (51). Anal. calc. pour $C_{24}H_{32}N_2Si_2$: C 71,23, H 7,97, N 6,92; trouvée : C 70,31, H 7,95, N 6,87.

Addition de l'isoquinoléine

À une suspension de lithium finement granulé (0,84 g; 0,12 at.g) dans 350 mL de THF et 0,12 mol (13 g) de Me_3SiCl fraîchement distillé, on ajoute goutte à goutte 0,02 mol (2,58 g) d'isoquinoléine de telle sorte que le température du milieu réactionnel soit maintenue entre 0 et 5°C. Les réactifs sont laissés en contact pendant 6 h puis le THF est évaporé à la rampe à vide et on effectue le traitement précédemment décrit. On isole ainsi une gomme orange (11,1 g) qui est redissoute dans 60 mL de cyclohexane afin de faire précipiter le composé **5**. Il est isolé, après 2 h de repos, par filtration (0,79 g; rdt. 8%). L'évaporation du filtrat conduit à une huile orangée très épaisse montrant plusieurs singulets indiscernables vers 0 ppm et l'absence de protons aromatiques en RMN ^1H. Elle est abandonnée à l'air pendant 1 nuit; une nouvelle analyse en RMN ^1H montre un éclatement des signaux centrés vers 0 ppm ainsi que l'apparition de plusieurs signaux entre 7 et 9,5 ppm. Le mélange est chromatographié sur silice (éluant : C_6H_{12}–Et_2O 70 : 30). On isole ainsi successivement les composés **7** (0,28 g; rdt. 5%), **6***a* (2,18 g; rdt. 31%), **6***b* (2,24 g; rdt. 32%), **9** (0,28 g; rdt. 5%) et **8** (0,57 g; rdt. 10%). Le mélange réactionnel a également été distillé à l'aide d'un four à boules. Dans ces conditions on isole les composés **7** (0,27 g; rdt. 5%), **6***a* (2,54 g; rdt. 36%), **6***b* (2,37 g; rdt. 34%) et **9** (0,28 g; rdt. 5%).

méso*2,2',3,3',5,5',6,6',7,7'-Décatriméthylsilyl-1,1',2,2',3,3', 5,5',6,6',7,7'-dodécahydro-1,1'-biisoquinoléine* (**5**) : rdt. 8%; *F* 198°C (Et_2O). RMN ^1H ($CDCl_3$, 500 MHz) δ ppm : −0,04(s, 9H), −0,01(s, 9H), 0,07(s, 9H), 0,14(s, 9H), 0,18(s, 9H), 1,3(dd, 1H, H-6, *J* 7,9 et 3,0 Hz), 1,8(signal large, 1H, H-7), 2,0(signal large, 1H, H-5), 3,3(dd, 1H, *J* 4,0 et 4,2 Hz), 5,4(d, 1*H*, *J* 5,3 Hz), 5,5(signal large, 1H). RMN ^{13}C ($CDCl_3$, 62,9 MHz) δ ppm : 5 $SiMe_3$ à −0,96, 0,2, 1,0, 1,2 et 1,95; 7 CH à 16,0, 25,1, 25,50, 49,0, 59,7, 121,2 124,7; 2 C à 129,0 et 147,1. SM *m/e* (%) : 494 (12; M/2), 350 (11), 348 (70), 275 (11), 203 (6), 202 (28), 186 (6), 147 (17), 133 (20), 132 (6), 117 (9), 84 (33), 83 (5), 81 (5), 75 (16), 74 (9), 73 (100), 69 (19), 9 (5), 57 (9), 56 (48), 55 (21), 45 (16), 43 (14), 42 (14), 39 (9), 29 (8), 28 (5), 27 (9). Anal. calc. pour $C_{48}H_{104}N_2Si_{10}$: C 58,22, H 10,59, N 2,83; trouvée : C 58,45, H 10,62, N 3,01.

5,6,7-Tris-triméthylsilyl-5,6,7,8-tétrahydro-isoquinoléine (**6**)

Isomère **6***a* : R_f 0,40 (SiO_2; C_6H_{12}–Et_2O 50 : 50). RMN ^1H ($CDCl_3$, 250 MHz) δ ppm : −0,4(s, 9H, $SiMe_3$), −0,07(s, 9H, $SiMe_3$), 0,17(s, 9H, $SiMe_3$), 1,1(dt, 1H, H-7, *J* 7,8 et 3,2 Hz), 1,5(dd, 1H, H-6, *J* 3,2 et 4,3 Hz), 2,1(d, 1H, H-5, *J* 4,3 Hz), 2,5(dd, 1H, H-8, *J* 16,4 et 7,6 Hz), 2,7(dd, 1H, H-8', *J* 16,4 et 8,1Hz), 6,9(d, 1H, H-4, *J* 4,8 Hz), 8,2(d, 1H, H-3, *J* 4,8 Hz), 8,3(s, 1H, H-1). RMN ^{13}C ($CDCl_3$, 62,9 MHz) δ ppm : 3 $SiMe_3$ à −2,5, 0,0 et 0,5; 6 CH à 22,0, 23,9, 29,8, 122,9, 146,7 et 147,3;

Can. J. Chem. Downloaded from www.nrcresearchpress.com by 213.200.69.106 on 09/08/12
For personal use only.

1 CH_2 à 28,7; 2 C à 137,8 et 148,1. Anal. calc. pour $C_{18}H_{35}NSi_3$: C 61,82, H 10,09, N 4,0; trouvée : C 62,03, H 10,11, N 4,06.

Isomère **6***b* : R_f 0,38 (SiO_2; C_6H_{12}–Et_2O 50 : 50). RMN ^1H ($CDCl_3$, 250 MHz) δ ppm : −0,30(s, 9H, $SiMe_3$), −0,13(s, 9H, $SiMe_3$), 0,0(s, 9H, $SiMe_3$), 0,8(ddd, 1H, H-7, *J* 9,0, 4,8 et 13,6 Hz), 1,3(d, 1H, H-6, *J* 9,0 Hz), 2,2(s, 1H, H-5), 2,2(dd, 1H, H-8, *J* 13,6 et 14,6 Hz), 2,4(dd, 1H, H-8′, *J* 14,6 et 4,8 Hz), 6,8(d, 1H, H-4, *J* 4,9 Hz), 8,0(s, 1H, H-1), 8,1(d, 1H, H-3, *J* 4,9 Hz). RMN ^{13}C ($CDCl_3$, 62,9 MHz) δ ppm : 3 $SiMe_3$ à −2,0, −1,8 et −1,3; 6 CH à 18,8, 20,5, 29,5, 121,7, 145,4 et 149,5; 1 CH_2 à 31,6; 2 C à 136,9 et 149,6. Anal. calc. pour $C_{18}N_{35}N\,Si_3$: C 61,82, H 10,09, N 4,06; trouvée : C 61,65, H 10,07, N 3,89.

3,6-Bis-triméthylsilyl-isoquinoléine (7) : R_f 0,31 (SiO_2; C_6H_{12}–Et_2O 70 : 30). RMN ^1H ($CDCl_3$, 250 MHz) δ ppm : 0,30(s, 9H, $SiMe_3$), 0,35(s, 9H, $SiMe_3$), 7,7(dd, 1H, H-8, *J* 1,0 et 8,1 Hz), 7,8(s, 1H, H-4), 7,87(d, 1H, H-7, *J* 8,1 Hz), 7,9(s, 1H, H-5), 9,3(s, 1H, H-1). RMN ^{13}C ($CDCl_3$, 62,9 MHz) δ ppm : 2 $SiMe_3$ à −1,3 et −0,9; 5 CH à 126,7, 126,8, 131,8, 132,5 et 152,7; 4 C à 128,3, 134,0, 144,4 et 159,9. Anal. calc. pour $C_{15}H_{23}NSi_2$: C 65,86, H 8,48, N 5,12; trouvée : C 65,69, H 8,53, N 5,21.

6,7-Bis-triméthylsilyl-5,6,7,8-tétrahydroisoquinoléine (8) : R_f 0,25 (SiO_2; C_6H_{12}–Et_2O 50 : 50). RMN ^1H ($CDCl_3$, 500 MHz) δ ppm : −0,14(s, 9H, $SiMe_3$), −0,11(s, 9H, $SiMe_3$), 1,20 et 1,24(2m, 2H, H-6 et H-7), 2,65 et 2,77(2m, 4H, H-5,5′ et H-8,8′), 7,0(d, 1H, H-4, *J* 4,9 Hz), 8,28(s, 1H, H-1), 8,32(d, 1H, H-3, *J* 4,9 Hz). RMN ^{13}C ($CDCl_3$, 62,9 MHz) δ ppm : 2 $SiMe_3$ superposés à −2,5; 2 CH_2 à 25,9 et 28,5; 5 CH à 19,7, 19,4, 122,5, 146,7 et 147,7; 2 C à 135,04 et 148,5. Anal. calc. pour $C_{15}H_{27}NSi_2$: C 64,90, H 9,81, N 5,05; trouvée : C 64,82, H 9,77, N 5,09.

6,7-Bis-triméthylsilyl-isoquinoléine (9) : R_f 0,30 (SiO_2; C_6H_{12}–Et_2O 50 : 50). RMN ^1H ($CDCl_3$, 250 MHz) δ ppm : 0,41(s, 9H, $SiMe_3$), 0,43(s, 9H, $SiMe_3$), 7,5(d, 1H, H-4, *J* 5,8 Hz), 8,1(s, 1H, H-5 ou H-8), 8,2(s, 1H, H-8 ou H-5), 8,5(d, 1H, H-3, *J* 5,8 Hz), 9,2(s, 1H, H-1). RMN ^{13}C ($CDCl_3$, 62,9 MHz) δ ppm : 2 $SiMe_3$ à 1,85 et 1,94; 5 CH à 120,1, 133,8, 134,7, 143,7 et 152,4; 4 C à 127,5, 134,5, 144,5 et 148,4. Anal. calc. pour $C_{15}H_{23}NSi_2$: C 65,86, H 8,48, N 5,12; trouvée : C 65,77, H 8,43, N 5,19.

Silylation par le système $Me_3SiCl/Mg/THF$

À une suspension de magnésium (0,84 g; 0,035 at.g) dans 120 mL de THF et 0,035 mol d'isoquinoléine (4,5 g) on additionne rapidement 0,038 mol de Me_3SiCl (4,1 g). Le mélange est ensuite porté au reflux pendant 4 h. Après évaporation du THF, on additionne 150 mL de cyclohexane et les sels de magnésium sont éliminés par filtration. Cette opération est répétée à nouveau puis le filtrat est évaporé. L'addition d'éthanol permet, en quelques minutes, de faire chuter le composé **3***a* qui est isolé par filtration (1,37 g; rdt. 19%). L'évaporation du filtrat conduit à **3** isolé sous forme d'huile (5,48 g; rdt. 77%). Ils sont identiques aux échantillons isolés par action du système $Me_3SiCl/Li/THF$ (addition de Me_3SiCl). L'addition de zinc en poudre (0,08 g) lors de la silylation permet de limiter la durée du chauffage à 2,5 h. Les rendements sont alors de 83% pour **3** et 14% pour **3***a*.

Acétylation

Le chlorure d'acétyle (0,044 mol; 3,45 g) préalablement distillé sur magnésium est additionné à 0,02 mol de **3** (8,08 g). Le mélange est agité à 0°C pendant 6 h, puis le solvant et l'excès de chlorure d'acétyle sont éliminés à l'évaporateur rotatif conduisant à un solide orangé (6,1 g) qui est recristallisé dans l'acétone. On isole ainsi **4** (5,5 g) qui présente les mêmes caractéristiques IR et RMN ^1H que le composé décrit par Nielsen (3).

2,2′-Diacétyl-1,1′,2,2′-tétrahydro-1,1′-biisoquinoléine (4) : rdt. 80%; *F* 195°C (acétone) (litt. (3) *F* 194–195°C). RMN ^{13}C ($CDCl_3$, 62,9 MHz) δ ppm : 1 CH_3 à 21,5; 6 CH à 52,5, 111,0, 124,2, 125,8, 128,0, 128,85; 2 C à 128,7 et 130,85; C=O à 169,1. SM *m/e* (%) : 172 (31), 130 (100), 73 (15), 43 (16), 28 (15). Anal. calc. pour $C_{22}H_{20}N_2O_2$: C 76,73, H 5,85, N 8,13, O 9,29; trouvée : C 76,80, H 5,87, N 8,09, O 9,19.

Remerciements

Ce travail a bénéficié d'une subvention des Laboratoires SARGET (Avenue J.F. Kennedy, BP 100, 33701 Mérignac Cédex) que nous remercions vivement en la personne de Monsieur C. Feniou.

1. M. Grignon-Dubois, M. Fialeix et B. Rezzonico. Can. J. Chem. **68**, 2153 (1990).
2. H.P. Becker et W.P. Neumann. J. Organomet. Chem. **37**, 57 (1972).
3. A.T. Nielsen, J. Org. Chem. **35**, 2498 (1970).
4. E.N. Kurkutova, O.I. Levina, T.F. Rau, E.A. Gladkikh et V.V. Ilyukhin. Sov. Phys. Crystallogr. (Engl. Transl.) **22**, 103 (1977).
5. T.N. Mitchell. J. Chem. Soc. Perkin Trans. 2, 1149 (1976).
6. L. Birkofer et N. Ramadan. Chem. Ber. **104**, 138 (1971).
7. (*a*) M. Grignon-Dubois, M. Laguerre, J-M. Leger et M. Saux. Résultats à paraître; (*b*) M. Laguerre et J-M. Leger. Tetrahedron, **42**, 669 (1986).
8. R.J. Unwalla, S. Profeta, Jr. et F. K. Cartledge. J. Org. Chem. **53**, 5658 (1988).
9. D.F. Ewing. Org. Magn. Reson. **12**, 499 (1979).
10. M. Laguerre, J. Dunogues et R. Calas. Tetrahedron Lett. **22**, 1227 (1981).
11. R. Calas, N. Duffaut, C. Biran, P. Bourgeois, F. Pisciotti et J. Dunogues. C. R. Acad. Sci. Fr. **267 C**, 1968 (1968); J. Dunogues, R. Calas, M. Boulourtchian, C. Biran et N. Duffaut. J. Organomet. Chem. **57**, 55 (1973); J. Dunogues, A. Ekouya, R. Calas et N. Duffaut. J. Organomet. Chem. **87**, 151 (1975).
12. P. Main, S.E. Hull, L. Lessinger, G. Germain, J.-P. Declercq et M.M. Woolfson. MULTAN 80, A system of computer programs for the automatic solution of crystal structures from X-ray diffraction data. Universités de Angleterre et York, Louvain, Belge. 1978.

Can. J. Chem. Downloaded from www.nrcresearchpress.com by 213.200.69.106 on 09/08/12
For personal use only.

Solution speciation in the aqueous Na(I)–EDTA and K(I)–EDTA systems

MIN CHEN and R. STEPHEN REID[1]
Department of Chemistry, University of Saskatchewan, Saskatoon, Sask., Canada S7N 0W0

Received October 28, 1992

MIN CHEN and R. STEPHEN REID. Can. J. Chem. **71**, 763 (1993).

Speciation in the aqueous sodium(I) – ethylenediaminetetraacetic acid and potassium(I) – ethylenediaminetetraacetic acid equilibrium systems was investigated by automated gravimetric potentiometric titration. It was found that in both cases, particularly below neutral pH values, speciation includes a previously uncharacterized diprotonated complex. All formation and acid dissociation constants were measured for the full systems. The validity of previous literature equilibrium constants, which are based on incomplete equilibrium models, is discussed.

MIN CHEN et R. STEPHEN REID. Can. J. Chem. **71**, 763 (1993).

Faisant appel à des titrages gravimétriques potentiométriques automatisés, on a étudié la spéciation des systèmes aqueux à l'équilibre des sels de sodium (ou de potassium) avec l'acide éthylènediaminetétraacétique. On a trouvé que, dans les deux cas, particulièrement à des pH inférieurs à ceux de la neutralité, la spéciation inclut un complexe diprotoné qui n'avait pas été caractérisé antérieurement. On a mesuré, pour tous les systèmes, toutes les constantes de formation et de dissociation. On discute de la validité des constantes d'équilibre rapportées antérieurement dans la littérature et basées sur des modèles d'équilibre incomplets.

[Traduit par la rédaction]

Can. J. Chem. Downloaded from www.nrcresearchpress.com by 213.200.69.106 on 09/08/12
For personal use only.

Introduction

Ethylenediaminetetraacetic acid (EDTA) is a widely used metal-ion complexing agent. It finds considerable use in complexation titrations (1), and as a metal-sequestering agent in many different applications — for instance, in the sequential extraction of metal ions from soil and sediment samples (2). The complexation of EDTA with a large variety of metal ions has been investigated, and the relevant complex formation constants measured. These data have been compiled and reviewed on several occasions (3–5).

While the EDTA complexes with sodium and potassium ions are weak compared to those formed with many other metal ions, the complexation of EDTA by these two metal ions may be important in certain situations. Firstly, many environmental water samples contain these ions at high concentration, especially estuarine (brackish) or marine samples. So also do many biological fluids. Secondly, these ions (as "inert salts") are often used to adjust ionic strength and maintain it at a more or less constant value during equilibrium studies.

The Na(I)–EDTA and K(I)–EDTA systems have been studied a number of times (6–10). Literature formation constant values for complexes of 1:1 stoichiometry are given in Tables 1 and 2. However, this does not completely characterize the speciation in these mixtures. Neutral EDTA can lose four hydrated protons in a series of "acid dissociations."[2] In addition, since the coordination number of the alkali metal ions is generally 4–6 (11), there is the possibility that some EDTA coordinating groups are not in fact coordinated to the metal ion, or coordinated only weakly, in the complex. If so, the complex could also display one or more acid dissociations. A few of the literature studies (7, 10) have recognized the possibility of one protonation; none, to our knowledge, of two. A reaction scheme, using our established convention of representing metal complexation horizontally and protonation vertically (12), is given in Fig. 1.

If all species existing in any multiequilibrium system are not accounted for in modelling that system, it is axiomatic that the apparent equilibrium constants resulting, and any prediction of speciation made from them, will be to some extent in error. The observed poor agreement between values from different laboratories for the same constants (Tables 1 and 2) underlines this possible complication. Further, while studying the Gd(III)–EDTA system in the presence of Na(I) and K(I) in this laboratory (13), it became obvious that corrections for complexation by these ions based on literature constants were in error.

We therefore decided to investigate the complexation of EDTA by Na(I) and K(I) in more detail, using potentiometric titrations implemented on our previously developed gravimetric equilibrium autotitrator (14). Following the recommendation of Anderegg (4), tetramethylammonium hydroxide (TMA-OH) was employed as a strong base for titrations. (Because of the low charge density of the TMA^+ ion, it was assumed that its strength of complexation to EDTA is negligible. We evaluate this assumption below.) Ionic strength was maintained close to 0.15 M, using tetramethylammonium chloride (TMA-Cl). In addition to being close to a physiological value, this value of ionic strength has the advantage that ionic activity coefficients vary only slightly with variations in ionic strength in this region.

Experimental

Reagents

All chemicals used were of analytical grade and were used without further purification except as noted below. All solutions were prepared using distilled, deionized water (Millipore). Where applicable, materials were dried for about 2 h at 110°C before use to remove surface moisture.

Titration apparatus and conditions

Titrations were performed using a microcomputer-controlled gravimetric autotitrator, which is described elsewhere (14). Five replicate titrations were normally performed, of the "combination" type, with a constant potential increment (typically 4 mV) between successive additions of titrant, defaulting to a minimum

[1]Author to whom correspondence may be addressed.

[2]Neutral EDTA can also gain two additional protons, but only under extremely acidic conditions.

TABLE 1. Literature formation constants of 1:1 Na(I)–EDTA complexes

Medium/ionic strength	Temperature, °C	$\log(K_f)^a$	Reference
0.1 M KCl	25	1.66	6
0.32 M CsCl	25	1.79	7
0.1 M TMA-Cl	25	1.82(1)[b]	8
1 M TMA-Cl	20	1.69(5)	9
0.1 M TMA-Cl	25	1.84(5)	10

[a]See Fig. 1 for definition.
[b]Standard deviation (in terms of least-significant digit) in parentheses, where given by authors.

TABLE 2. Literature formation constants of 1:1 K(I)–EDTA complexes

Medium/ionic strength	Temperature, °C	$\log(K_f)^a$	Reference
0.32 M CsCl	25	0.96	7
0.1 M TMA-Cl	25	0.55(6)[b]	8
1 M TMA-Cl	25	0.69(6)	8
0.1 M TMA-Cl	25	0.80(10)	10

[a]See Fig. 1 for definition.
[b]Standard deviation (in terms of least-significant digit) in parentheses, where given by authors.

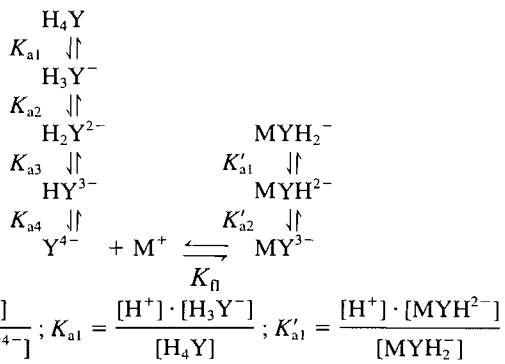

$$K_{fl} = \frac{[MY^{3-}]}{[M^+]\cdot[Y^{4-}]}\ ;\ K_{a1} = \frac{[H^+]\cdot[H_3Y^-]}{[H_4Y]}\ ;\ K'_{a1} = \frac{[H^+]\cdot[MYH^{2-}]}{[MYH_2^-]}$$

FIG. 1. Equilibrium scheme for the M(I)–EDTA system (M = K, Na), and definition of some typical equilibrium constants. Y^{4-} refers to fully deprotonated EDTA.

titrant addition of typically 0.0010 g in the region of the titration endpoint. Titrant solutions were degassed by the slow bubbling of argon gas through the solution for 10 min prior to titration. Titrant solutions were prepared under argon, using freshly boiled and cooled water, and dispensed from bottles equipped with soda-lime tubes, to prevent any carbonate contamination. Titrations were performed under an argon atmosphere at a temperature of 25 ± 1°C. A standard glass electrode/saturated calomel electrode setup was calibrated routinely using secondary standard buffers (BDH, nominal pH values 4.00, 7.00, and 10.00 ± 0.01), the exact pH values of which were established periodically by standardization against pH standard solutions prepared to NBS specifications (15).

Solutions for titrations

The ionic strength of all solutions was adjusted to approximately 0.15 M using TMA-Cl. A solution of TMA-OH of approximate concentration 0.02 M was standardized by titration against potassium hydrogen phthalate (KHP). An HCl solution of approximate concentration 0.006 M was standardized by titration against TMA-OH. Solutions of EDTA alone, and of approximate NaCl:EDTA ratios 4:1 and 20:1 and of KCl:EDTA 5:1 and 20:1, were prepared with an approximate concentration of EDTA of 0.001 M. This is close to the solubility of EDTA; in order to avoid any further dilution, 0.001 M EDTA was also added to the titrant (see above).

Data analysis

This was performed on a Dell System 310 80386 PC-standard microcomputer. A utility contained within SASKWATCH (the autotitrator software) automatically sets up titration data in suitable form for data analysis by the routine SUPERQUAD (16). Preliminary analysis and graphing was accomplished using Quattro Pro, Version 4.0 (Borland International).

Titrations performed

The exact shape of a potentiometric titration curve depends upon a large number of variables. These include the relative stoichiometry of the reactants (the concentrations initially added), the equilibrium constants, fundamental solution parameters (activity coefficients, the autolysis constant of water), and electrode parameters (slope and standard potential). Although in principle all these parameters could be determined in a single experiment, in practise this is not feasible. The optimal values for many of the parameters are strongly dependent upon each other, so large uncertainties result. A "divide and conquer" approach, involving sequential determination of parameters in systems of gradually increasing complexity, is preferable.

A summary of the titrations performed in the present study is given in Table 3. In the first set of titrations, the acidimetric standard KHP was titrated. The gravimetrically determined moles of KHP (T_{KHP}) and a literature value of the apparent molar ionic product of water (pK^c_w) were input to SUPERQUAD as constants. SUPERQUAD then refined estimates of the total moles of titratable proton (T_{H^+}), the concentration of the TMA-OH titrant (C_{OH^-}), $\log(K_a)$ for KHP, and (as for all titrations) the apparent electrode standard potential ($E^{0\prime}$). T_{H^+} was within experimental error of the value predicted from the mass of KHP used, confirming its purity. The value of pK^c_w was refined using a second set of titrations with an aqueous solution of HCl as titrand, determining also T_{H^+} for this solution. The third set of titrations assumed the values (determined in the first two sets) for pK^c_w and C_{OH^-}, and a gravimetrically derived value for the total moles of EDTA (T_{EDTA}). The values of the acid dissociation constants of free EDTA were refined, together with T_{H^+} (which again, on comparison with T_{EDTA}, confirmed the purity of the EDTA). Finally, in titrations of metal ion – EDTA mixtures, all values from previous titrations were assumed. T_{H^+}, T_M, and the log complex formation constants and the acid dissociation constants for metal-complexed EDTA were refined.

Results and discussion

Apparent molar ionic product of water (K^c_w)

This is defined as:

$$[1]\quad K^c_w = [H^+].[OH^-] = (a_H + .a_{OH^-})/(\gamma_M\cdot\gamma_{OH}) = K_W/(\gamma_M\cdot\gamma_{OH})$$

where K_w is the "true" or thermodynamic molar ionic product, a refers to activity, and γ to activity coefficient. The pK^c_w value yielded in this study is compared with literature values in Table 4. Agreement with the value of Anderegg in 0.1 M TMA-Cl is excellent (corrected using the Davies equation (19) to an ionic strength of 0.15 M, Anderegg's value is 13.92 ± 0.03). Furthermore, the value of mean activity coefficient obtained here (0.88) is in excellent agreement with the value estimated from electrode calibra-

Can. J. Chem. Downloaded from www.nrcresearchpress.com by 213.200.69.106 on 09/08/12
For personal use only.

TABLE 3. Summary of titrations performed, and refined (variable) and constant parameters. T refers to total moles of a substance, C to formal (added) concentration. See text for further definitions

Titrand	Variable parameters	Constant parameters
KHP	T_{H^+}, C_{OH^-}, $E^{0\prime}$, $\log(K_a)$	pK_w^c, T_{KHP}
HCl	T_{H^+}, $E^{0\prime}$, pK_w^c	C_{OH^-}
EDTA	T_{H^+}, $E^{0\prime}$, $\log(K_a)$	pK_w^c, T_{EDTA}, C_{OH^-}
EDTA + M[a]	T_{H^+}, T_M, $E^{0\prime}$, $\log(K_f)$, $\log(K_a')$	pK_w^c, T_{EDTA}, C_{OH^-}, $\log(K_a)$

[a]M = Na or K.

TABLE 4. Values of pK_w^c under various conditions

Medium/ionic strength	Temperature, °C	pK_w^c	Reference
0.1 M TMA-Cl	20	13.96(2)[a]	17
1 M TMA-Cl	20	14.11(2)	17
1 M KCl	20	13.96(2)	17
0.14 M KNO_3	25	13.753(2)	18
0.15 M TMA-Cl	25	13.89(1)	This work
0.15 M KNO_3	25	13.86(1)	This work

[a]Standard deviation (in terms of least-significant digit) in parentheses.

tion. (The standard potential of the electrode, E_0, obtained from calibration, and the apparent standard potential, E_0', obtained from the titration, are related by the expression:

$$[2] \quad E_0' = E_0 - S.\log\gamma$$

where S is the experimental "slope" of the electrode response, obtained from calibration. A value of $\gamma = 0.87 \pm 0.02$ was otained by this method.)

However, the present value of pK_w^c in TMA-Cl seems to compare only indifferently with that of Jameson and Wilson (18). The measurement was repeated in 0.1 M KNO_3 (see Table 3) to demonstrate that the identity of the electrolyte did not account for the discrepancy. Jameson and Wilson calculated pK_w^c based upon only 10 points on the titration curve, 5 each side of the titration endpoint. Simulation of this approach with our data showed that choice of the particular points used could significantly affect the value of pK_w^c obtained from the experimental data. The present value, based on the entire titration curve (60 or more points) was therefore considered more trustworthy and is used in further calculations below.

Acid dissociation constants of EDTA

These are shown in Table 5, together with some literature values. The fairly small differences observed can again be ascribed to variations in ionic strength, temperature, and possibly sophistication of data analysis.

Complex formation constants

A typical titration curve, for a titrand 0.001 M in EDTA and 0.004408 M in KCl, is shown in Fig. 2. Points represent experimental data; every second point is omitted for clarity. The line is calculated from the model of Fig. 1 using the mean equilibrium constants yielded by separately fitting the data from five replicate titrations to the model. Using SUPERQUAD, the experimental data were fitted to a series of multi-equilibrium models involving the successive addition of species MY^{3-}, MHY^{2-}, MH_2Y^-, and MH_3Y. SUPERQUAD has the ability to "reject" a species from a model if its inclusion seems unwarranted on statistical grounds. This occurred with the species MH_3Y. However, the other species were "retained" by SUPERQUAD and values of the relevant equilibrium constants with acceptable uncertainties were returned. Residuals decreased steadily as the first three species were added into the model. Residuals for the final model appeared randomly distributed and were well within those expected from experimental uncertainties. Results are given in Table 6.

The values of both formation constants are significantly larger than those previously reported, particularly in the potassium case (see Tables 1 and 2). This is because previous studies neglected the presence of the diprotonated complex MYH_2^-. To demonstrate this further, the portion of the present data in the pH range 7.5–11 was fitted to a model involving no diprotonated complex. The "$\log(K_f)$" values thus obtained were 0.57(2) and 1.75(1) for the K(I) and Na(I) cases, respectively, close to the corresponding values in Tables 1 and 2. However, even in this restricted pH region, there was some evidence (indifferent fit, trends in residuals) that the equilibrium model was incorrect. The importance of including the diprotonated complexes in an equilibrium model of these systems is therefore confirmed.

The pK_a' values are similar for the Na(I) and K(I) complexes, and similar also to pK_{a3} and pK_{a4} for free EDTA itself. Since these equilbria can be plausibly assumed to involve EDTA functional groups not involved in complexation, this is scarcely surprising. Which specific groups are involved cannot, of course, be determined by potentiometry, which can measure the overall status of protonation of a species, but gives no indication as to the site of protonation. We are currently studying the sites of protonation and metal-ion complexation in EDTA complexes by nuclear magnetic resonance spectroscopy.

Speciation in the Na(I)–EDTA and K(I)–EDTA equilibrium systems

The speciation in a 0.001 M EDTA/0.004 M Na^+ solution was calculated as a function of pH using a simple Turbo Pascal (Borland International) program, and is shown in Fig. 3. Figure 4 shows a similar plot for a 0.001 M EDTA/0.005 M K^+ solution. In both cases, maximal amounts of MH_2Y^- are observed in the pH range 4–5, and significant amounts up to and beyond neutrality. Obviously, any speciation calculations outside the fairly alkaline region

Can. J. Chem. Downloaded from www.nrcresearchpress.com by 213.200.69.106 on 09/08/12
For personal use only.

TABLE 5. Acid dissociation constants of EDTA in TMA-Cl

[TMA-Cl] M	Temperature, °C	pK_{a1}[a]	pK_{a2}	pK_{a3}	pK_{a4}	Reference
0.1	20	—	—	6.16	10.44	17
1	20	2.2	2.7	6.07	10.12	17
0.1	25	—	—	6.16(2)	10.39(7)	8
1	25	2.2(2)	2.8(1)	6.17(2)	10.25(7)	8
0.1	25	—	—	—	10.35	10
0.15	25	2.08(2)	2.83(1)	6.11(1)	10.35(1)	This work

[a]See Fig. 1 for definitions.
[b]Standard deviation (in terms of least-significant digit) in parentheses.

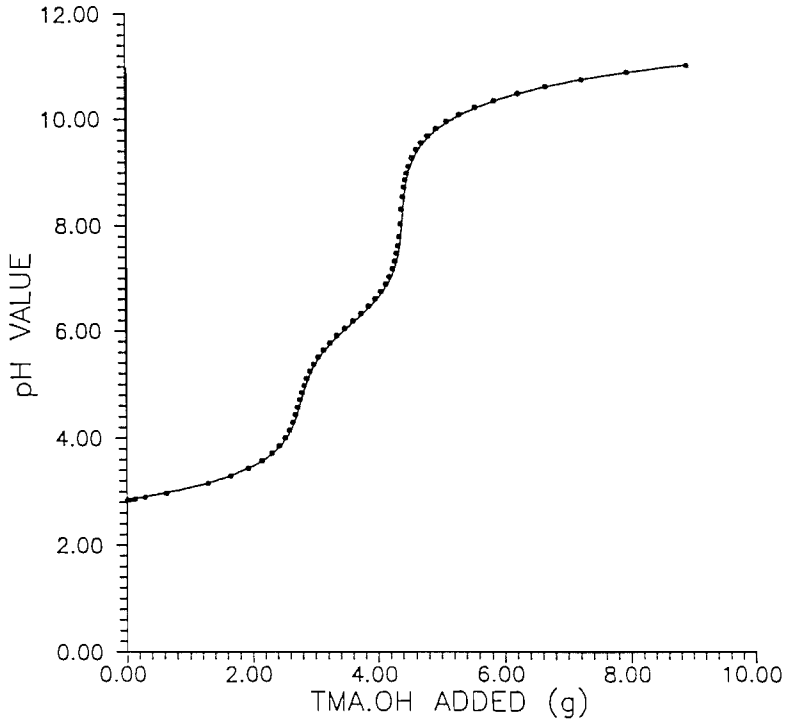

FIG. 2. Titration curve for 0.001 M EDTA + 0.004408 M KCl. See text for experimental conditions.

TABLE 6. Equilibrium constants determined in the Na(I)–EDTA and K(I)–EDTA systems[a]

Metal ion	$\log(K_f)$[b]	pK'_{a1}	pK'_{a2}
Na(I)	2.35(1)[c]	6.01(1)	10.09(1)
K(I)	1.60(2)	6.05(2)	10.32(2)

[a]For conditions see text.
[b]For definitions see Fig. 1.
[c]Standard deviation (in terms of least-significant digit) in parentheses.

will be in error if they neglect the diprotonated complexes.

In viewing a titration curve such as Fig. 2, the temptation to attempt to analyze the curve intuitively may prove irresistible. However, use of Fig. 4 to determine the species present at each stage in the titration shows the pitfalls in such an approach. Although Fig. 2 shows two apparent "breaks" and two "buffer regions," these are due to multiple changes in the solution speciation, not to the titration of any one species. In fact, the gross shape of the titration curve is determined mainly by the titration of free EDTA species, the more interesting chemistry described here being "hidden" in the exact shape of the curve.

Complexation of TMA^+ with EDTA?

No effects of changing TMA concentrations not readily ascribable to simple activity coefficient effects were observed. It can be concluded that if TMA–EDTA complex(es) form, it is to an extent negligible even by the standards of K^+ and Na^+.

Conclusions

This study has reexamined the Na(I)–EDTA and K(I)–EDTA equilibrium systems. It has been shown that a full description of speciation, particularly below pH 7, must include the presence of a diprotonated complex. All relevant formation and acid dissociation constants have been measured.

More generally, the study provides a cautionary tale. It suggests that other literature equilibrium studies, especially

Can. J. Chem. Downloaded from www.nrcresearchpress.com by 213.200.69.106 on 09/08/12
For personal use only.

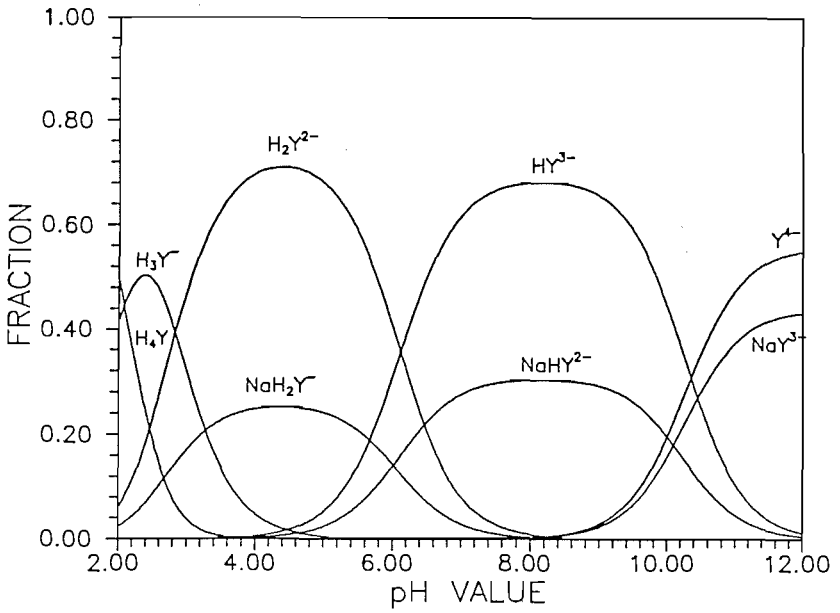

FIG. 3. Speciation of a Na(I)–EDTA solution as a function of pH. Calculated using the equilibrium constants in Table 6 and the model of Fig. 1, assuming a total EDTA concentration of 0.001 M and a total Na(I) concentration of 0.004 M. For definitions of species, see Fig. 1 and text.

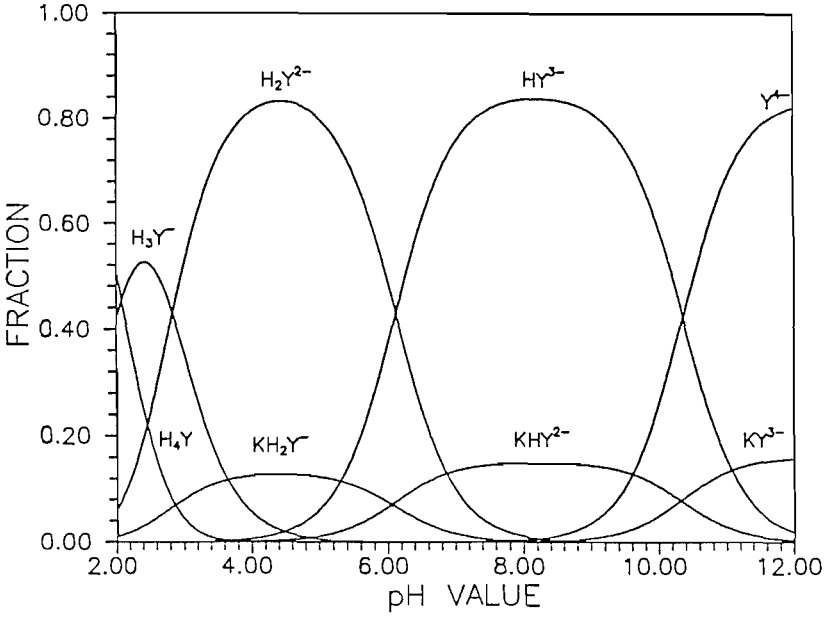

FIG. 4 Speciation of a K(I)–EDTA solution as a function of pH, assuming a total EDTA concentration of 0.001 M and a total K(I) concentration of 0.005 M. Other conditions as per Fig. 3.

older ones, may involve high-quality but small or incomplete data sets, and incomplete modelling. Ongoing pleas in the literature, for adequate documentation of experimental details when reporting equilibrium studies, should be heeded, to minimize such problems in the future.

Acknowledgements

Receipt of a University of Saskatchewan Graduate Scholarship by M.C., and of an Natural Sciences and Engineering Research Council of Canada Operating Grant by R.S.R., are gratefully acknowledged.

1. W.E. Harris and B. Kratochvil. *In* An introduction to chemical analysis. Saunders, Philadelphia. 1981. Chap. 7.
2. A.M Ure. Fresenius J. Anal. Chem. **337**, 577 (1990).
3. A.E. Martell and R.M. Smith. Critical stability constants. Vol. 1. Plenum Press, New York. 1974.
4. G. Anderegg. Critical survey of stability constants of EDTA complexes. No. 14 in IUPAC Chemical Data Series, Pergamon Press, Oxford. 1977.
5. A.E. Martell and R.M. Smith. Critical stability constants. Vol. 5. First Supplement. Plenum Press, New York. 1982.
6. G. Schwarzenbach and H. Ackerman. Helv. Chim. Acta, **30**, 1798 (1947).

Can. J. Chem. Downloaded from www.nrcresearchpress.com by 213.200.69.106 on 09/08/12
For personal use only.

7. J. Botts, A. Chasin, and H.L. Young. Biochemistry, **4**, 1788 (1965).
8. J.I. Waters and O.E. Shupp. J. Inorg. Nucl. Chem. **30**, 3359 (1968).
9. G. Anderegg. Z. Naturforsch. B: Anorg. Chem. Org. Chem. **31B**, 786 (1976).
10. P.G. Daniele, C. Rigano, and S. Dammartano. Anal. Chem. **57**, 2956 (1985).
11. T.P. Whaley. *In* Comprehensive inorganic chemistry. Vol. 1. *Edited by* J.C. Bailiar, Jr., H.R. Emeleus, R. Nyholm, and A.F. Trotman-Dickinson. Pergamon Press, Oxford. 1973. p. 527.
12. R.S. Reid and B. Podanyi. J. Inorg. Biochem. **32**, 183 (1988).
13. M. Chen and R.S. Reid. Inorg. Chem. Submitted.
14. R.S. Reid and M. Chen. Can. Res. **21**, 22 (1988).
15. R.G. Bates. Determination of pH: theory and practice. Wiley, New York. 1973. Chap. 2.
16. P. Gans, A. Sabatini, and A. Vacca. J. Chem. Soc. Dalton Trans. 1195 (1985).
17. G. Anderegg. Helv. Chim. Acta, **50**, 2333 (1967).
18. R.F. Jameson and M.F. Wilson. J. Chem. Soc. Dalton Trans. 2607 (1972).
19. C.W. Davies. J. Chem. Soc. 2093 (1938).

Can. J. Chem. Downloaded from www.nrcresearchpress.com by 213.200.69.106 on 09/08/12
For personal use only.

Determination of Al, P, and Si in fruit juices stored in glass and aluminized containers

K. SOLIMAN, L. ZIKOVSKY,[1] AND C. DALLAIRE[2]

Institut de génie énergétique, École polytechnique de Montréal, C.P. 6079, Succursale "A", Montréal (Québec), Canada H3C 3A7

Received April 10, 1992

K. SOLIMAN, L. ZIKOVSKY, and C. DALLAIRE. Can. J. Chem. **71**, 769 (1993).

The concentration of Al, P, and Si in 142 samples of five fruit juices, measured with neutron activation analysis and atomic absorption spectroscopy, varies from 0 to 1.44, 31 to 201, and 1.5 to 35 μg/mL, respectively. The mean concentration of Al in apple, grape, grapefruit, orange, and pineapple juices is 0.54, 0.94, 0.24, 0.29, and 0.62 μg/mL, respectively. The mean concentration of P in the same juices is 102, 115, 124, 127, and 76 μg/mL. The storage of juice in aluminized containers with internal plastic coating does not increase the concentration of Al in the juice.

K. SOLIMAN, L. ZIKOVSKY et C. DALLAIRE. Can. J. Chem. **71**, 769 (1993).

Les concentrations d'Al, de P et de Si, mesurées par activation neutronique et par absorption atomique, dans 142 échantillons de cinq types de jus de fruits varient de 0 à 1,44, 31 à 201 et 1.5 à 35 μg/mL respectivement. Les concentrations moyennes d'Al mesurées dans les jus de pomme, de raisin, de pamplemousse, d'orange et d'ananas sont égales à 0,54, 0,94, 0,24, 0,29 et 0,62 μg/mL respectivement. Les concentrations moyennes de P dans les mêmes jus sont égales à 102, 115, 124, 127 et 76 μg/mL respectivement. L'utilisation de récipients en carton aluminisé avec un revêtement interne en plastique n'augmente pas les teneurs en Al de ces jus.

Introduction

Aluminum is the third most common element and the most abundant metal. It has historically been regarded as nonessential and nontoxic. Recently there has been an increase in reports of aluminum toxicity from environmental exposure. Aluminum has been implicated in the pathogenesis of a number of clinical disorders ranging from cancer and renal osteodystrophy to Alzheimer's disease (1). Its toxicity towards the central nervous system has been demonstrated in several mammalian species (2). Despite all this, there are many researchers who believe that aluminum can safely be used with food, and that the correlation between Alzheimer's disease and Al is purely coincidental (3). Thus the question concerning the toxicity of aluminum remains quite controversial. The food industry is using aluminum-coated paper with internal plastic coating for some juice containers. This implies that aluminum could be leached out of the packing material by the juice. For this reason, neutron activation analysis and atomic absorption spectroscopy were used to measure the concentration of aluminum in juice stored in glass and aluminized containers, to see if there is any difference in the leaching behaviour of these containers.

Experimental procedure

The juices were bought from stores in Montreal while the fresh juices were prepared by hand extraction from fruits. Because aluminum is ubiquitous in our environment, all handling of samples was done in a clean room. No metal tools were used and, of course, no aluminum. The juice was transferred directly from its container to a plastic irradiation vial. Each sample was irradiated in a Slowpoke reactor for 200 s, at a flux of 10^{12} n cm^{-2} s^{-1}. The juice was then transferred into a new vial (in 60 s or less) and counted for 600 s. The γ-ray spectra were analyzed and the concentrations were calculated using the semi-absolute method (4). Phosphorus and silicon can interfere with the determination of aluminum and these elements were also measured in some samples. To determine phosphorus, the juices were irradiated for 15 min at a flux of 10^{12} n cm^{-2} s^{-1}, left to decay for 28 days, mixed with a liquid scintillator (Aquasol), and β-counted for 10 min with a Packard Tricarb analyzer. The silicon content was determined by atomic absorption spectroscopy.

Results and discussion

The aluminum concentration was determined using the following nuclear reaction: Al-27 (n, γ)Al-28. Unfortunately, Al-28 can also be produced from P or Si via the reactions: P-31(n,α)Al-28 and Si-28(n,p)Al-28. The results obtained for Al must be corrected for these nuclear interferences. In our case, the interference factor (5) for the first reaction is 690 and for the second 207. This means that 690 μg/mL of P or 209 μg/mL of Si would produce an apparent concentration of 1 μg/mL of aluminum. For this reason, some of the juices studied were also analyzed for P and Si. The concentrations found (Table 1) vary from 31 to 201 μg/mL for P and from 1.5 to 35 for Si. These data can be compared with values cited by Quaranta et al. (6) for fresh strawberries (P: 180 μg/mL; Si: 21 μg/mL). The mean concentration of P found in the juice was then divided by the interference factor for P (690), and subtracted from the apparent Al concentration.

For Si, the mean concentration is 11.5 μg/mL. Considering its interference factor of 207, its concentration to the activity of 28-Al is less than 0.06 μg/mL and was neglected.

The mean concentration of Al (corrected values) determined in the fruit juices studied is listed in Table 1. It varies from 0.17 to 1.3 μg/mL. These concentrations are low when compared with other elements.

To decide whether the difference of mean concentrations of juices packaged in different containers is statistically significant, the Student's *t*-test for small samples was used (7). The hypothesis that there is essentially no difference between the mean concentrations was tested at a 0.01 level of significance (t_{995}). The results obtained are listed in Table 2. There are five cases (out of 11 possibilities) where the difference between the aluminized and glass containers is sig-

[1]Author to whom correspondence may be addressed.
[2]Department de génie minéral.

Can. J. Chem. Downloaded from www.nrcresearchpress.com by 213.200.69.106 on 09/08/12
For personal use only.

TABLE 1. Concentration (in μg/mL) of Al, P, and Si in fruit juices stored in different containers

Juice	C-B	Al			P		Si
		n	*M*	SD	*M*	SD	*C*
Apple	A-1	11	0.32	0.23	106	5	1.5
Apple	A-2	6	0.38	0.12	104	5	—
Apple	A-3	8	1.05	0.05	111	4	4.2
Apple	G-1	11	0.51	0.14	89	3	1.8
Grapes	A-2	8	1.01	0.08	40	2	29
Grapes	F	6	0.59	0.15	195	3	—
Grapes	F	6	0.60	0.15	125	15	—
Grapes	G-6	10	1.30	0.09	101	2	5.5
Grapefruit	A-2	5	0.22	0.10	110	9	5.8
Grapefruit	F	6	0.19	0.04	132	2	—
Grapefruit	G-4	5	0.40	0.18	106	11	—
Grapefruit	G-5	6	0.17	0.07	148	5	2.5
Orange	A-2	9	0.31	0.19	100	10	7.1
Orange	A-5	7	0.22	0.04	155	3	—
Orange	F	6	0.26	0.21	170	12	—
Orange	G-4	5	0.39	0.06	82	3	2.5
Pineapple	A-2	7	0.30	0.17	39	3	—
Pineapple	A-3	7	0.44	0.06	87	2	—
Pineapple	A-5	6	1.28	0.13	78	4	35
Pineapple	G-2	7	0.55	0.10	100	3	32

C = Container: A = Aluminum, G = Glass, F = Fresh; B = Brand, *M* = Mean, SD = Standard deviation (n = 6, for P).

TABLE 2. Students t values of tests of significance for differences of means

Juice	C1-C2	t	t_{995}	DF
Apple	A1-A2	0.56	2.95	15
	A1-A3*	8.35	2.92	17
	A1-G1	2.23	2.84	20
	A2-A3*	13.18	3.06	12
	A2-G1	1.81	2.95	15
	A3-G1*	9.87	2.90	17
Grapes	A2-F*	6.24	3.06	12
	A2-F*	6.09	3.06	12
	A1-G6*	6.73	2.92	16
	F-F	0.11	3.17	10
	F-G6*	11.07	2.98	14
	F-G6*	10.91	2.98	14
Grapefruit	A2-F	0.61	3.25	9
	A2-G4	1.75	3.36	8
	A2-G5	0.88	3.25	9
	F-G4	2.51	3.25	9
	F-G5	0.55	3.10	10
	G4-G5	2.60	3.25	9
Orange	A2-A5	1.15	2.98	14
	A2-F	0.45	3.01	13
	A2-G4	0.85	3.06	12
	A5-F	0.45	3.11	11
	A5-G4*	5.37	3.17	10
	F-G4	1.21	3.25	9
Pineapple	A2-A3	1.90	3.06	12
	A2-A5*	10.60	3.11	11
	A2-G7*	3.10	3.06	12
	A3-A5*	14.07	3.11	11
	A3-G7	2.31	3.06	12
	A5-G7*	10.51	3.11	11

C1-C2: Container brand.
DF: Degrees of freedom.
*Indicates a significant difference.

nificant. But there are also four cases (from seven) where juices prepared by two different companies and packaged in aluminized containers have significantly different concentrations. There are also concentration differences between the fresh juice and the juice sold in a glass container (two cases out of five possibilities) or in an aluminized container (two cases out of five). Consequently, we conclude that the observed differences are due to the processing or the natural variation rather than to the effect of the container. The higher concentrations of Al in juices may be caused by contamination during preparation.

Finally, it is useful to estimate the potential intake of Al from juices with the amount ingested from all other sources. This amount has been estimated (8) to be 30–50 mg of aluminum per day. We have calculated the overall mean concentrations (and their standard deviations) of Al in the juices studied. They are equal to 0.55(0.32), 0.94(0.33), 0.24(0.13), 0.29(0.18), 0.62(0.39) for apple, grape, grapefruit, orange, and pineapple juice, respectively. If we assume the consumption of 1 litre of juice per day, based on our data, the daily intake of Al would vary from 0.24 to 0.94 mg. This amounts to 0.1–3% of the total intake. Consequently, the contribution of fruit juices to the total aluminum intake seems to be minor.

Conclusions

The concentration of aluminum in commercial fruit juices is low when compared with other elements (Ca,K,Na). The use of aluminized containers for the packaging of juices does not seem to increase the concentration of Al in the packaged juice. The concentration of Al in juice varies considerably, probably as a result of contamination during processing. Finally, aluminum from juice constitutes a minor contribution to the total daily intake of aluminum.

1. S. Krishnan. Can. Res. **21**, 33 (1988).
2. S.J. Karlik, G.L. EichHorn, and D.R.C. McLachlan. Neurotoxicology, **1**, 83 (1980).
3. W.O. Caster and M. Wang. Sci. Total Environ. **17**, 31 (1981).
4. C. Bergerioux, G. Kennedy, and L. Zikovsky. J. Radioanal. Chem. **50**, 229 (1978).
5. G. Kennedy, J.L. Galinier, and L. Zikovsky. Can. J. Chem. **64**, 790 (1986).
6. H.O. Quaranta, J.E. Eterovic, and J.L. Piccini. Appl. Radiat. Isot. **37**, 633 (1986).
7. M.R. Spiegel. Probability and statistics. McGraw-Hill, New York. 1975. pp. 215 and 346.
8. J.A. Bjorksten. Sci. Total Environ. **25**, 81 (1982).

Can. J. Chem. Downloaded from www.nrcresearchpress.com by 213.200.69.106 on 09/08/12
For personal use only.

Acid and oxidative dissolution of coprecipitated iron–chromium oxides

LUIS GARCÍA RODENAS, PEDRO J. MORANDO,[1] AND MIGUEL A. BLESA[1]

Departamento Química de Reactores, Comisión Nacional de Energía Atómica, Avda. del Libertador 8250, 1429-Buenos Aires, Argentina

AND

STELLA DUHALDE AND CELIA SARAGOVI

Departamento de Física, Comisión Nacional de Energía Atómica, Avda. del Libertador 8250, 1429-Buenos Aires, Argentina

Received July 31, 1992

Can. J. Chem. Downloaded from www.nrcresearchpress.com by 213.200.69.106 on 09/08/12
For personal use only.

LUIS GARCÍA RODENAS, PEDRO J. MORANDO, MIGUEL A. BLESA, STELLA DUHALDE, and CELIA SARAGOVI. Can. J. Chem. **71**, 771 (1993).

A mixed Fe,Cr oxide formed of maghemite and chromium hydrous oxide was prepared by oxidative precipitation at 90°C. Mineral acids dissolve the chromium phase very quickly, whereas iron dissolves slowly and independently; there is little mutual influence in the dissolution behaviour. Calcination of this oxide at 600°C yields a mixture of α-Fe_2O_3 and $Cr_{1.3}Fe_{0.7}O_3$ that leaches iron slowly upon acid attack. The reactivity of the oxide towards H^+ is largely determined by the degree of crosslinking of the Cr-containing phase. Oxidative attack (by $KBrO_3$) increases the rate of dissolution of both Cr and Fe, against simple expectations that Fe dissolution rates might be reduced. This effect is of importance in chemical cleaning and decontamination of stainless steels. This influence of acidity and $[BrO_3^-]$ are interpreted in terms of the formation of surface $\equiv$Cr(III)-O-Br(V) species that evolve to produce $Cr(VI)_{aq}$. These surface complexes form more readily than analogous solution species, making surface Cr(III) more readily oxidizable than aqueous (Cr(III).

LUIS GARCÍA RODENAS, PEDRO J. MORANDO, MIGUEL A. BLESA, STELLA DUHALDE et CELIA SARAGOVI. Can. J. Chem. **71**, 771 (1993).

On a préparé un oxyde mixte de Fe et de Cr par précipitation oxydante, à 90°C, de maghemite et d'oxyde de chrome hydraté. Les acides minéraux dissolvent la phase chromée très rapidement alors que le fer ne se dissout que lentement et d'une façon indépendante; il n'y a que peu d'interaction mutuelle sur le comportement de dissolution. La calcination de cet oxyde à 600°C fournit un mélange d'oxydes formé de α-Fe_2O_3 et de $Cr_{1.3}Fe_{0.7}O_3$ qui, sous l'influence d'acide, ne relargue le fer que lentement. La réactivité de l'oxyde vis-à-vis des H^+ est grandement déterminée par le degré de réticulation de la phase contenant du chrome. Alors qu'on s'attendait à ce que les vitesses de dissolution du Fe pourraient être réduites, une attaque oxydante (par du $KBrO_3$) augment la vitesse de dissolution du Cr ainsi que celle du Fe. Cet effet est important lors du nettoyage chimique et la décontamination des aciers inoxydables. On interprète l'influence de l'acidité et de la $[BrO_3^-]$ en fonction de la formation à la surface d'espèces $\equiv$Cr(III)-O-Br(V) qui évoluent pour conduire à des espèces $Cr(VI)_{aq}$. Ces complexes de surface se forment plus facilement que les espèces analogues en solution et rendent les espèces Cr(III) de surface plus susceptibles à l'oxydation que les espèces aqueuses correspondants.

[Traduit par la rédaction]

Introduction

Chemical dissolution of metal oxides is important in a wide variety of fields, ranging from materials science (1–3) to environmental science (4–6), and even including aspects of biochemistry such as the mobilization of iron in living organisms (7, 8). Two very important metal oxides are those of chromium(III) and iron(III); their dissolution behaviour has been amply studied by us and by others (9–16). Both oxides may dissolved by acid attack, although very drastic conditions are required in the case of α-Cr_2O_3 (G. B. Reartes, P. J. Morando, M. A. Blesa, P. Hewlett and E. Matijević, unpublished results). More importantly, both oxides are prone to redox dissolution; the chemical conditions conducive to fast dissolution of iron(III) oxides include the presence of reductants capable of reducing surface $\equiv$Fe(III) complexes, usually via inner sphere mechanisms (12). On the other hand, chromium(III) oxides are better dissolved by strong oxidants (17). Inspection of the corresponding Pourbaix diagrams are especially illustrative of these drastically differing behaviours (12).

Examples of cases in which dissolution of these oxides is important include the chemical cleaning of metal surfaces, microbiological corrosion, hydrometallurgy, corrosion of Fe- and Cr-based ceramic oxides, environmental fate, and availability of both metals in natural media, etc.

One important point that has not yet been addressed is the cross effects appearing in the dissolution behaviour when both oxides are present. This is a matter of importance both in the case of single-phase mixed oxides such as $FeCr_2O_4$ and in the case of complex mixtures of two or more phases containing either or both metal ions.

The first case, the dissolution of well-defined binary oxidic phases, has been conceptually analyzed by Valverde (18), who suggested that the overall behaviour may be determined either by the fast-dissolving metal oxide or by the more passive one. Current work in our laboratory is directed to the experimental study of the important iron chromite $FeCr_2O_4$ (L. García Rodenas, P. J. Morando, and M. A. Blesa, unpublished results).

The second case is of widespread occurrence in practice. Preferential leaching of minerals, behaviour of multiphase ceramic oxides, and the chemical cleaning of stainless steel surfaces are examples. Thus, oxide films grown or deposited onto stainless steels are complex mixtures of Cr(III) and Fe(III) oxides, as evidenced, e.g., by in-depth profiling studies using X-ray photoemission spectroscopy (XPS)

[1]Authors to whom correspondence may be addressed.

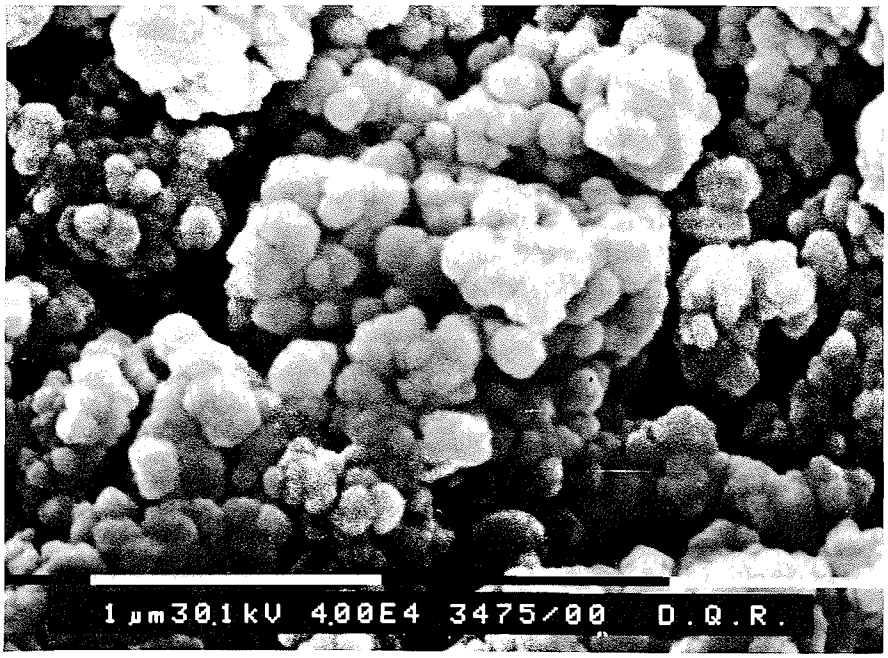

FIG. 1. Scanning electron micrograph (SEM) of the oxide A particles.

Can. J. Chem. Downloaded from www.nrcresearchpress.com by 213.200.69.106 on 09/08/12
For personal use only.

techniques (19, 20). It is therefore not surprising that the most efficient processes developed to clean stainless steel surfaces are composed of two stages, an oxidative one to attack chromium(III) (hydrous) oxides, and a reductive one to remove iron(III) (hydrous) oxides (21). In principle, the efficiency of the two-stage cleaning procedures may be interpreted simply in terms of noninteracting processes, the oxidative stage leaving the iron oxides practically unaffected, and the chromium oxide behaving as impervious to the reductive attack.

By contrast, in all analyses of the leaching of minerals, the importance of the evolution of surface area is stressed, and many types of complex behaviour are found in practice.

The purpose of this paper is to determine experimentally the degree of mutual influence evidenced in the dissolution behaviour of multiphase Cr,Fe oxides by studying the acid and the oxidative attack of coprecipitated Cr/Fe (hydrous) oxides. The acid attack is used here as an alternative to reductant attack; both procedures are efficient in dissolving iron oxides and ineffective in dissolving chromium from crystalline α-Cr_2O_3. The aggressiveness of acid toward chromium oxides is a sensitive measure of the degree of crosslinking, as demonstrated in this and a related paper (17). The degree of crosslinking is measured by the average coordination number of oxygen atoms; in a highly crystalline material such as α-Cr_2O_3 this number is four, and it decreases as the hydration/hydroxylation of the material increases (42). The study of the dissolution of mixed oxides by acids therefore provides a tool to explore the changes in their reactivity patterns as the chromium-containing phase becomes more crystalline.

Experimental

Materials

Two types of synthetic mixed oxides were used.

Oxide A was prepared by oxidative precipitation of 600 cm^3 of 0.155 M $FeSO_4$ and 0.065 M $Cr(NO_3)_3$ upon addition of 30 cm^3 NH_3 27 wt.%, in the presence of 0.2 M $NaNO_3$. The atomic ratio Fe/Cr = 2.6 in solution was chosen to adjust the ratio in the resulting solids; both ratios were similar. Precipitation was carried out at 90°C. This procedure differs in several aspects from that reported by Schwertmann and Cornell (22) to synthesize Cr-substituted goethites. The most important differences in our preparation are the stronger oxidizing conditions and the lower alkalinity that lead to a fast total oxidation of Fe(II), and to total precipitation of Cr(III). The scanning electron micrograph (SEM) observed in Fig. 1 was obtained using a Philips SEM 500 electron microscope and showed the presence of irregularly shaped polydisperse particles, without evidence for gel-like amorphous material. The oxidative procedure used here is known to yield crystalline product in short reaction times (23). X-ray diffraction (XRD) showed that the resulting solids were mixtures of maghemite (γ-Fe_2O_3) and chromium(III) (hydrous) oxide ($Cr(OH)_3 \cdot 3.3\ H_2O$). Using elementary analysis data for Fe and Cr (38.0 and 14.8 wt.% respectively), the solid is found to be composed of 54 wt.% γ-Fe_2O_3 and 46 wt.% $Cr(OH)_3 \cdot 3.3\ H_2O$. According to Schwertmann and Cornell (22), crystalline goethite particles incorporate up to 12% Cr (referred to total metal content, on an atomic basis) when synthesized from solutions containing Cr(III). If Cr-substitution in γ-Fe_2O_3 was also operative in our case, the actual composition of the mixture was somewhat different. For example, for a 12% substitution, the composition would be 61 wt.% $Fe_{1.8}Cr_{0.2}O_3$ and 39 wt.% $Cr(OH)_3 \cdot 3.3\ H_2O$. Our structural characterization and the results of the kinetic experiments are not sensitive enough to derive an experimental value for the degree of Cr-substitution in γ-Fe_2O_3. The BET specific surface area was 54 $m^2\ g^{-1}$.

Oxide B was obtained by calcining oxide A at 600°C during 45 min in a N_2 atmosphere. It was characterized by X-ray diffraction using a Philips X-ray generator PW 1130 and by Mössbauer spectroscopy. Mössbauer spectra were obtained in a transmission geometry with a source of ^{57}Co in Rh matrix and the measurements were carried out with the source at room temperature and the absorber, in powder form, at room temperature and liquid N_2 temperature. Mössbauer spectra were least-squares fitted employing pure Lorentzian shapes and constraining the peak intensities to

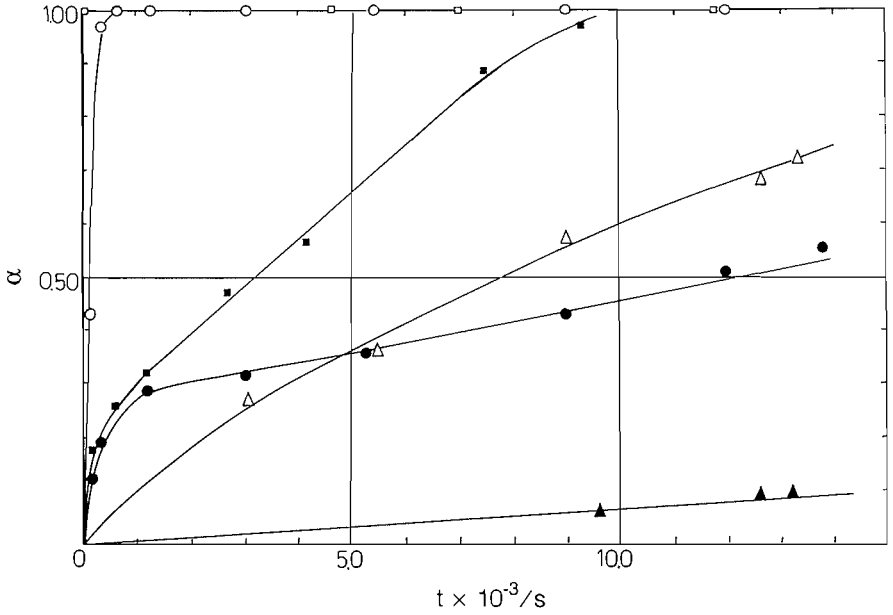

FIG. 2. Fraction (α) of dissolved Fe (full symbols) and Cr(III) (empty symbols) from oxide A vs. time at 65°C: ▲, △: 10^{-2}; ●, ○: 0.5; and ■, □: 2.5 mol dm^{-3} H_2SO_4.

TABLE 1. Initial chromium and iron dissolution rates for oxide A in sulfuric acid at 65°C

$[H_2SO_4]$ (M)	$R_0(\gamma\text{-}Fe_2O_3) \times 10^8$ (mol Fe m^{-2} s^{-1})	$R_0(Cr(OH)_3 \cdot 3.3\ H_2O) \times 10^7$ (mol Cr m^{-2} s^{-1})
10^{-2}	0.15	0.12
0.5	15.4	4.1
2.5	17.0	19.0

satisfy the 3:2:1 ratio in the case of sextets; the quality of each computer fit was checked by a χ^2 test. The results of the structural characterization are given below. The BET area decreased to 15 m^2 g^{-1} in the calcination procedure, and the assay of Cr (19.0 wt.%) and Fe (50.8 wt.%) indicated total dehydration while maintaining the same Fe:Cr ratio.

All reagents were analytical grade; water was bidistilled.

Procedure

Dissolution experiments of oxides A and B were performed in a magnetically stirred cylindrical beaker provided with a jacket connected to a thermostat. Temperature was controlled to 65.0 ± 0.1°C. In a typical experiment, oxide A or B (ca. 12 mg) was poured over 100 cm^3 of solution containing the appropriate oxidant and acid concentrations. Samples of 1 cm^3 were taken periodically with a syringe and filtered through a 0.45 μm cellulose acetate membrane. Care was taken to withdraw the samples under strong stirring to avoid changes in the surface area/volume ratio.

Cr(VI) and total Fe were measured spectrophotometrically using diphenylcarbazide (24) and thioglycolic acid (25), respectively. In the acid dissolution experiments, total Cr was measured by atomic absorption spectrometry (AAS) using a Varian AAR 5 spectrophotometer, to explore the possible presence of Cr(III).

Results and discussion

Oxide A dissolution

Figure 2 shows the fraction of dissolved iron and chromium α ($\alpha = w_0 - w/w_0$, where w is the mass of solid at time t and w_0 is the initial mass) as a function of time in 0.01, 0.5, and 2.5 M H_2SO_4 at 65°C. Chromium dissolves very quickly as chromium(III), whereas the dissolution of maghemite is slower. Table 1 shows the initial rates, $R_0 = (d\alpha/dt)_{t=0}$, for both metals. The iron dissolution rate can be compared with literature data. Sidhu *et al.* (26) reported an initial dissolution rate of maghemite in 0.5 M HCl of 4.98×10^{-10} mol Fe m^{-2} s^{-1} at 25°C and an activation energy of 84.9 kJ mol^{-1}. Extrapolation to 65°C yields $R_0 = 2.79 \times 10^{-8}$ mol Fe m^{-2} s^{-1}, i.e., a factor 5.5 lower than our result in 0.5 M H_2SO_4. Although a contribution to this difference produced by the change in acid (H_2SO_4 vs. HCl) cannot be totally ruled out, the most important factor is certainly the influence of the different preparative methods on the extent of defects associated to imperfect coordination polyhedra: Sidhu *et al.* (26) heated magnetite at 220°C for 3 h whereas our samples were precipitated at 90°C and not subjected to further heat treatment. As shown previously (27), important changes in reactivity are caused by annealing of coordination polyhedra defects.

Figure 3 shows the fraction of dissolved iron and chromium in an experiment with 2.5 M H_2SO_4 in the presence of 0.1 M $KBrO_3$ at 65°C. As expected, bromate does not noticeably influence the iron dissolution rates. Chromium dissolution rates are also not affected by bromate (cf. Figs. 2 and 3). The inset of Fig. 3 shows the data from two different experiments. In the first one, the evolution of Cr(III) and Cr(VI) concentration in the dissolution of oxide A in $KBrO_3$ (0.1 mol dm^{-3}) and H_2SO_4 (2.5 mol dm^{-3}) at 65°C was measured. In the second one, the oxidation of a solution of $Cr(NO_3)_3 \cdot 9H_2O$ was monitored. This solution contained an initial concentration of Cr(III) equal to the final concentration of total chromium in the first experiment. The curve obtained shows that the appearance rate of Cr(VI) coincides in both experiments and therefore demonstrates that chromium is dissolved essentially as Cr(III).

In the strong acidic medium chosen for this study, the hydrous chromium(III) oxide is highly reactive to acids, and each metal oxide behaves nearly independently.

Can. J. Chem. Downloaded from www.nrcresearchpress.com by 213.200.69.106 on 09/08/12
For personal use only.

Can. J. Chem. Downloaded from www.nrcresearchpress.com by 213.200.69.106 on 09/08/12
For personal use only.

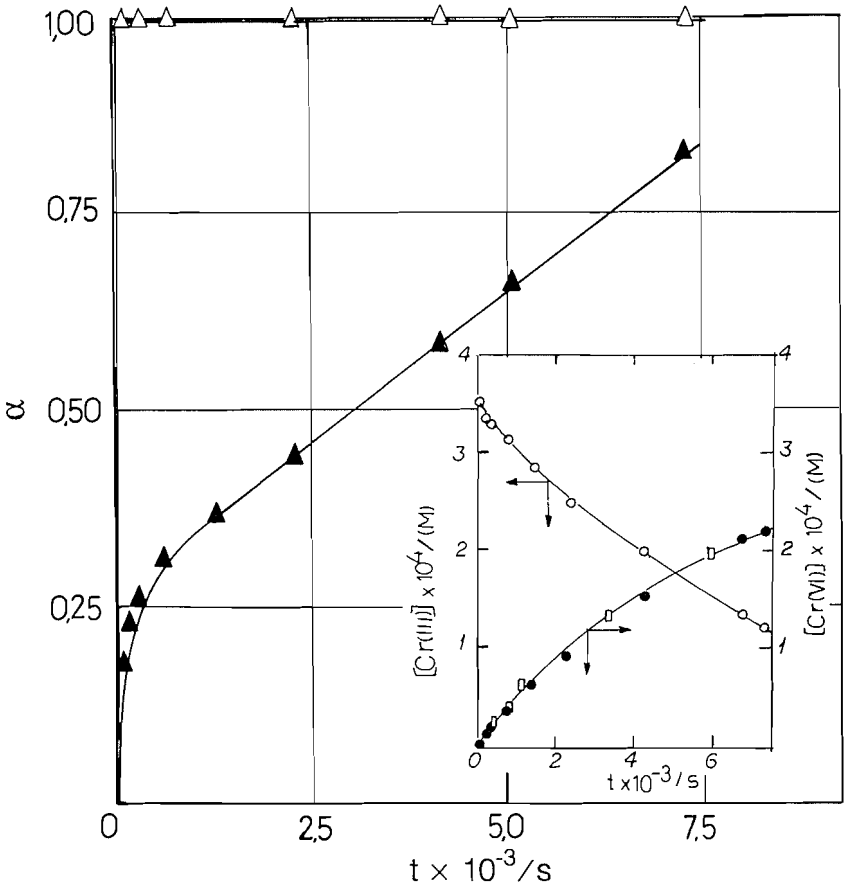

FIG. 3. ▲: fraction (α) of dissolved Fe, △: fraction of dissolved Cr from oxide A vs. time in 0.1 mol dm^{-3} $KBrO_3$ + 2.5 mol dm^{-3} H_2SO_4 at 65°C. Inset: evolution of Cr(III) and Cr(VI) in $[BrO_3^-]$ = 0.1 mol dm^{-3}, $[H_2SO_4]$ = 2.5 mol dm^{-3} at 65°C. ○ [Cr(III)] and ● [Cr(VI)] from dissolution of oxide A; □ [Cr(VI)] from 3.5 × 10^{-4} mol dm^{-3} Cr(III) solution (see text).

Oxide B characterization

To interpret the dissolution experiments, it was necessary to know in detail the nature of the phases present in oxide B. This was essentially achieved by using Mössbauer spectroscopy. Chemical analyses and XRD data could be interpreted as indicative of mixtures of $(Fe_xCr_{1-x})_2O_3$ and α-Fe_2O_3, but independent values of x and of the chromite:hematite ratio could not be derived from this information. Available ASTM diffraction pattern cards (28) suggested $Cr_{1.3}Fe_{0.7}O_3$ and α-Fe_2O_3. The relative amounts of these phases would be 43 and 57 wt.%, respectively, from the elementary Cr and Fe analysis data, but this interpretation required better substantiation.

Figure 4 shows a typical Mössbauer spectrum of oxide B. The fitting of the spectrum requires the inclusion of at least two sextets, and better fitting results are obtained if a third one is included.

Table 2 shows the parameters that best fit the observed three sextets. The H sextet parameters indicate the existence of hematite and the c_1 and c_2 sextet parameters correspond to those of the $(Fe_xCr_{1-x})_2O_3$ system (29). The linewidths of these two sextets are broad (0.6 mm s^{-1}) pointing to a distribution of similar Fe-ion environments, which is characteristic of Fe_2O_3–Cr_2O_3 solid solutions. It is possible to find the relative concentration of chromite and hematite using the corresponding area ratio (30). Using the fitted values, this ratio is 1:1.27 assuming equal f values for the hematite and chromite and the formula $Cr_{1.3}Fe_{0.7}O_3$ for this last component. This result is in reasonable agreement with those obtained from the stoichiometry 1:1.33. Moreover, the low values obtained for the c_1 and c_2 magnetic fields support the assigned x value for the iron content in the chromite. In addition to the magnetic signals, a significant contribution of a central doublet is apparent in Fig. 4; this disappears when the temperature is lowered, the associated Mössbauer signal probably merging with the magnetic signals.

Oxide B dissolution

At 65°C, 2.5 M H_2SO_4 does not attack chromium and dissolves iron only very slowly (α = 0.08 in 120 min). Assuming that the chromite is not attacked, the initial rate of dissolution of the purely ferric phase α-Fe_2O_3 is calculated to be R_0 = 7.66 × 10^{-8} mol Fe m^{-2} s^{-1}, i.e., ca. 2 times slower than that of γ-Fe_2O_3 in oxide A. Because of the lower reactivity of α-Fe_2O_3 compared to γ-Fe_2O_3 (31) and the decrease in surface area, the results do not indicate any special decrease in reactivity in iron oxides, although the initial rates measured in this work may reflect the contribution of the nonmagnetic phase responsible for the doublet in the Mössbauer spectrum. On the other hand, extensive cross-linking and dehydration of the Cr-containing phase brings about the drastic decrease observed in the rate of Cr dissolution. Over long periods, this effect should produce a passivation of iron, which can only be leached through the passive $Cr_{1.3}Fe_{0.7}O_3$ phase.

Figure 5 shows a typical α/t profile using 0.05 M $KBrO_3$

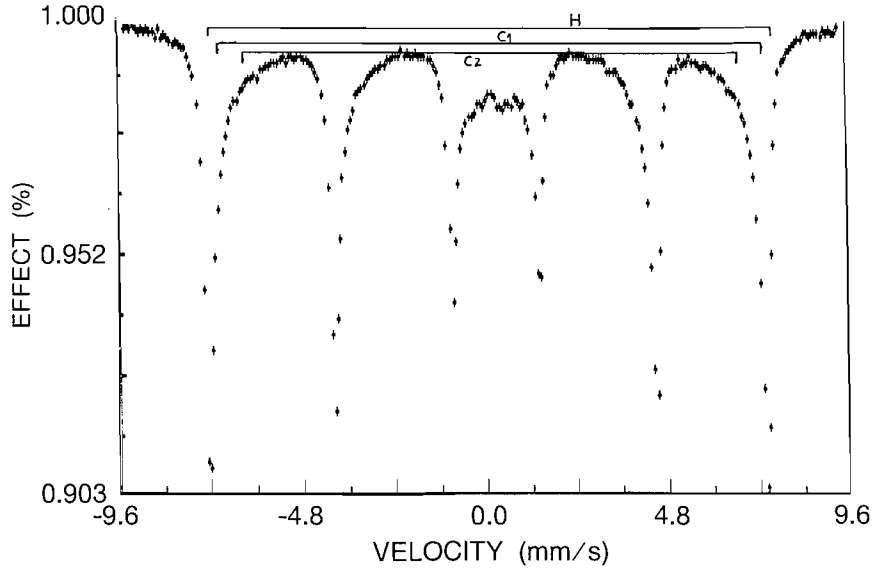

FIG. 4. Sample B: room temperature Mössbauer spectrum.

TABLE 2. Mössbauer parameters[a] at room temperature

	H_1(kOe)	IS_1[b] (mm s^{-1})	QS_1 (mm s^{-1})
H	516 ± 6	0.35 ± 0.02	0.20 ± 0.02
c_1	503 ± 8	0.35 ± 0.02	0.26 ± 0.03
c_2	450 ± 8	0.20 ± 0.03	0.16 ± 0.03

[a]H: Magnetic field; IS: isomer shift; QS: quadrupole splitting.
[b]The IS are referred to α-Fe metal at room temperature.

and the same acid concentration and temperature as above. In this case, iron is released from both phases, $Cr_{1.3}Fe_{0.7}O_3$ and α-Fe_2O_3. Assuming congruent dissolution for the first phase, Fig. 5 can be replotted showing the iron fraction released from each phase separately. The results are shown in Fig. 6 for different oxidant concentrations. Table 3 shows the R_0 values calculated for each phase from Fig. 6, on the assumption that the specific surface areas of both phases were equal.

Dependence of $R_0(Cr_{1.3}Fe_{0.7}O_3)$ *on oxidant concentration*

The $Cr_{1.3}Fe_{0.7}O_3$ phase dissolution rates are first order with respect to the oxidant concentration. The data in Table 3 yield

$$[1] \quad R_0(Cr_{1.3}Fe_{0.7}O_3) = k\,[BrO_3^-]$$

where $k = 1.28 \times 10^{-5}$ mol Cr m^{-2} s^{-1} M^{-1}.

The oxidative dissolution of α-Cr_2O_3 with $KBrO_3$ was studied recently (17). In agreement with the present results, it was found that α-Cr_2O_3 dissolution rates increase with increasing oxidant concentration. Small deviations from linearity, together with evidence from related Cr_2O_3 dissolution by other oxidants, lead us to postulate a Langmuir–Hinshelwood equation to describe the rate (17):

$$[2] \quad R_0 = \frac{R_{0\max}\,[BrO_3^-]}{1/K_s + [BrO_3^-]}$$

where K_s is the adsorption constant of BrO_3^- on the surface Cr(III) sites. K_s and $R_{0\max}$ values were 1.3 dm^3 mol^{-1} and 2.0×10^{-5} mol Cr m^{-2} s^{-1}, respectively. Our present data can be described by the same K_s value and can be fitted with a slightly lower $R_{0\max}$ value of 1.35×10^{-5} mol Cr m^{-2} s^{-1}.

Dependence of R_0 *(α-*Fe_2O_3*) on oxidant concentration*

In principle, it could be expected that the α-Fe_2O_3 dissolution would not be affected by the oxidant concentration.[2] However, the α-Fe_2O_3 dissolution rate increases with increasing BrO_3^- concentration. The data in Table 3 fitted by linear least squares yield

$$[3] \quad R_0(\alpha\text{-}Fe_2O_3) = k_1 + k_2\,[BrO_3^-]$$

where $k_1 = 1.11 \times 10^{-7}$ mol Fe m^{-2} s^{-1} and $k_2 = 4.80 \times 10^{-6}$ mol Fe m^{-2} s^{-1} M^{-1}. The influence of BrO_3^- on the rate of dissolution of α-Fe_2O_3 disappears when all $Cr_{1.3}Fe_{0.7}O_3$ has dissolved (see Fig. 6). It is concluded that eq. [3] represents the effective increase in the specific surface area of α-Fe_2O_3 brought about by the oxidative dissolution of the chromite. Thus, the presence of chromium phase makes the hematite also less reactive, passivation is only broken by oxidative attack, and iron oxide dissolution rates increase with increasing oxidant concentration. As an example of a practical consequence of this behaviour, it should be expected that the first stage of two-stage procedures to dissolve oxide films grown onto stainless steels (oxidative attack) may produce an important release of iron, especially in cases where acidic oxidants are used (32). Iron release is not necessarily restricted to the second, reducing/complexing, stage.

Dependence of R_0 *on acid concentration*

The dependences of the initial dissolution rates R_0 on the concentration of H_2SO_4, HNO_3, and $HClO_4$, at constant oxidant concentration ($[BrO_3^-]$ = 0.1 M) and temperature (65°C) are shown in Fig. 7 for both phases. A linear dependence is observed:

$$[4] \quad R = k_3[\text{acid}]$$

Table 4 shows the k_3 values for each phase in different

[2]As mentioned, these rates may include a contribution from the nonmagnetic phases that should also be insensitive to bromate concentration.

Can. J. Chem. Downloaded from www.nrcresearchpress.com by 213.200.69.106 on 09/08/12
For personal use only.

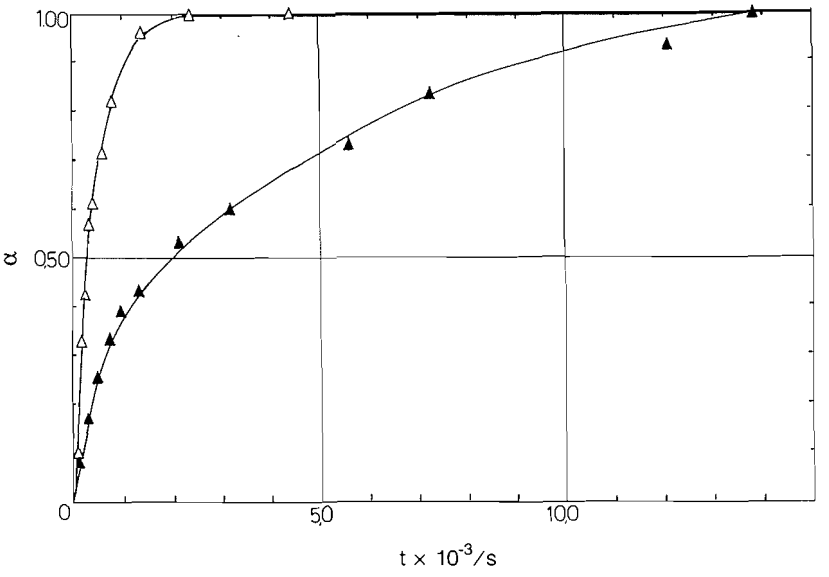

FIG. 5. ▲: fraction of dissolved Fe and △: fraction of dissolved Cr(VI) vs. time from oxide B at 65°C; $[BrO_3^-]$ = 0.05 mol dm^{-3}, $[H_2SO_4]$ = 2.5 mol dm^{-3}.

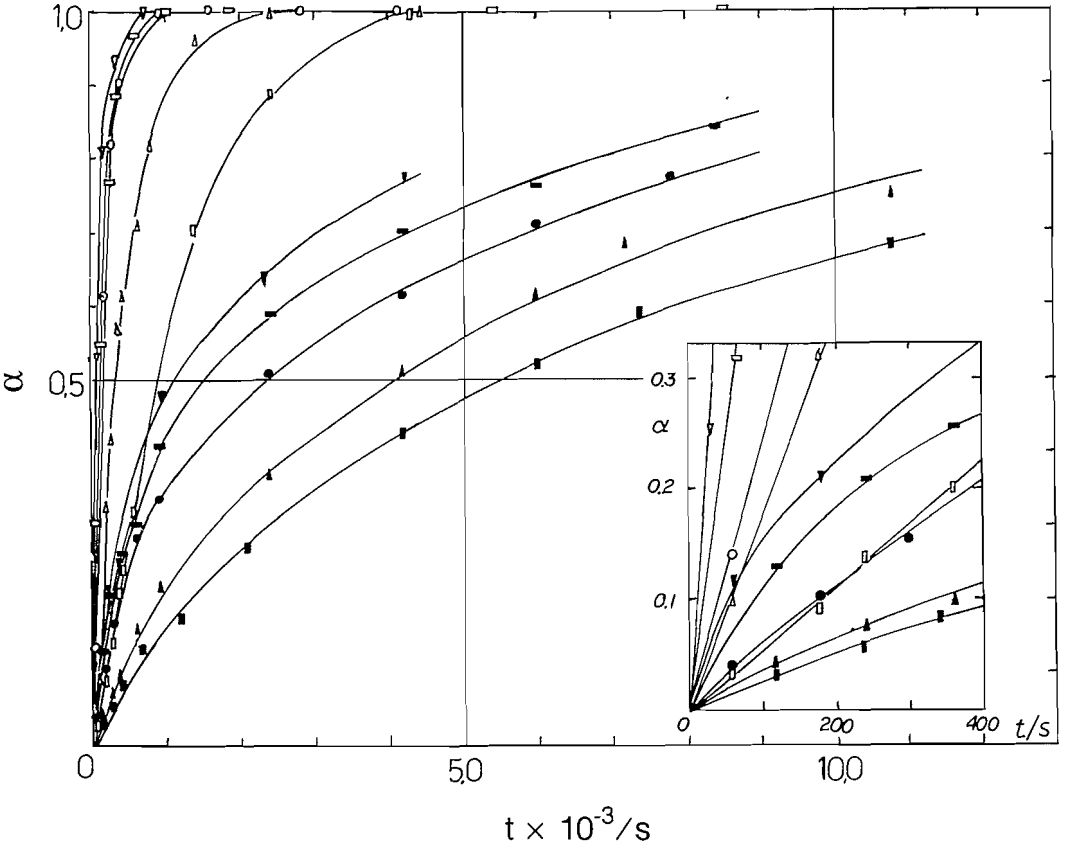

FIG. 6. Fraction (α) of dissolved Fe vs. time from α-Fe_2O_3 (full symbols) and $Cr_{1.3}Fe_{0.7}O_3$ (empty symbols) phases of oxide B for: ■, □: 0.02; ▲, △: 0.05; ●, ○: 0.1; ▬, ▭: 0.2 and ▼, ▽: 0.4 mol dm^{-3} $KBrO_3$. Inset: expanded plot for shorter reaction times.

mineral acids. Hematite dissolution is accelerated by a factor of ca. 3.6 when sulfuric acid is substituted for $HClO_4$ or HNO_3 of the same molar concentration. The main factor seems to be that HSO_4^- is as effective as H_3O^+ as an acid; in addition, these results are in line with the known influence of sulfate on acid dissolution, through the formation of surface ≡Fe(III)-SO_4^{2-} complexes (33). The possibility of dissociative chemisorption of HSO_4^- (M. A. Blesa, unpublished) is a related phenomenon with the same consequences. In the case of $Cr_{1.3}Fe_{0.7}O_3$ the increase of ca. 50% in the rate of dissolution when sulphuric is substituted for perchloric acid can again be attributed to the increased acidity of the medium. This conclusion is supported by complementary rate measurements in HNO_3 in the presence of

Can. J. Chem. Downloaded from www.nrcresearchpress.com by 213.200.69.106 on 09/08/12
For personal use only.

TABLE 3. Influence of oxidant concentration on the initial rate of dissolution from both phases of oxide B in [H_2SO_4] (2.5 mol dm^{-3}) at 65°C

[$KBrO_3$] (M)	$R_0(Cr_{1.3}Fe_{0.7}O_3) \times 10^6$ (mol Cr m^{-2} s^{-1})	$R_0(\alpha\text{-}Fe_2O_3) \times 10^7$ (mol Fe m^{-2} s^{-1})
0	0	0.77
0.02	0.34	1.96
0.05	0.91	3.76
0.1	1.31	6.40
0.2	2.56	10.4
0.4	4.95	16.7

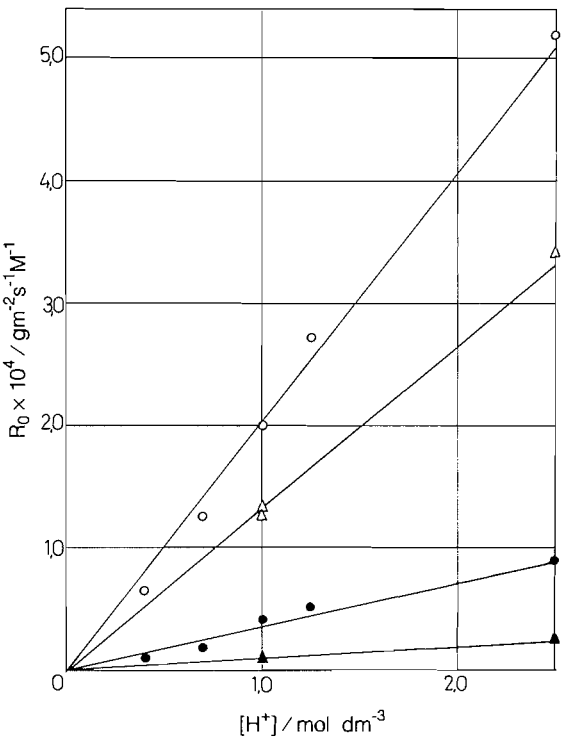

FIG. 7. Dependence of R_0 on acid concentration at 65°C; [BrO_3^-] (0.1 mol dm^{-3}) for α-Fe_2O_3 (full symbols) and $Cr_{1.3}Fe_{0.7}O_3$ phases (empty symbols) of oxide B: ●, ○: H_2SO_4 and ▲, △: HNO_3 = $HClO_4$.

TABLE 4. k_3 values from both phases of oxide B in different minerals acids at 65°C

Acid	$k_3(Cr_{1.3}Fe_{0.7}O_3) \times 10^7$ (mol m^{-2} s^{-1} M^{-1})	$k_3(\alpha\text{-}Fe_2O_3) \times 10^7$ (mol m^{-2} s^{-1} M^{-1})
H_2SO_4	5.62	1.23
HNO_3 = $HClO_4$	3.67	0.34

K_2SO_4: the rate of Cr dissolution is unaffected by the substitution of HSO_4^- for HNO_3, whereas the overall Fe dissolution rate is increased, probably due to the complexing effect on hematite.

Reactivity of chromium in the oxide B

The kinetics of Cr(III) surface oxidation by BrO_3^- were compared with those of the hydrated dissolved species $Cr(H_2O)_6^{3+}$. The amount of aqueous Cr(VI) formed by reaction with 0.1 M $KBrO_3$ from dissolved $Cr(NO_3)_3 \cdot 9\ H_2O$ and from an oxide B suspension, both with the same initial Cr(III) content, are plotted in Fig. 8. To compare R_{homog}/[Cr(III)] and R_{heter}/[active sites], the active sites concentration was calculated using eq. [5]:

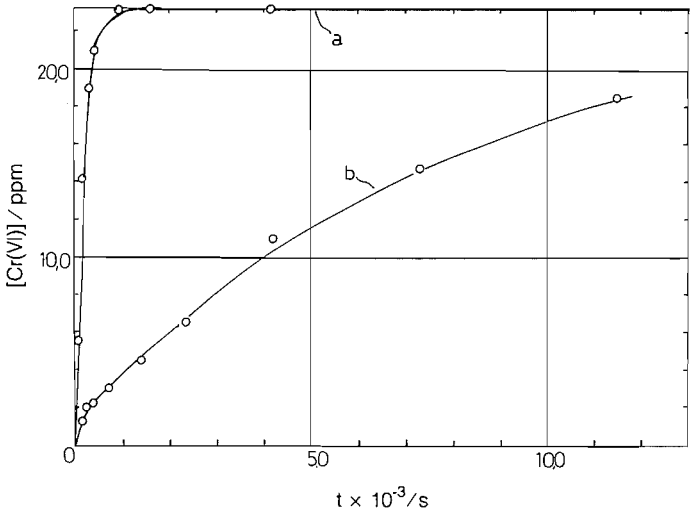

FIG. 8. (*a*) [Cr(VI)] from an oxide B suspension and (*b*) from $Cr(NO_3)_3 \cdot 9\ H_2O$ solution by reaction with 0.1 mol dm^{-3} $KBrO_3$, both with the same initial Cr(III) content (23.2 ppm).

$$[5] \quad [\text{active sites}] = N_s S_e w / V$$

where S_e = specific surface area. w = weight of chromite, and V = volume of solution. N_s, the number of active sites per unit area, was estimated to be ~5 sites nm^{-2}, or 8.30 μmol m^{-2} (the literature value for KF absorption on α-Fe_2O_3 (34) is 10 sites nm^{-2} and for EDTA adsorption on magnetite varies between 1.2 and 2.4 sites nm^{-2} depending on pH (35)).

The resulting ratios are (R_{heter}/[active sites]) = 3.6×10^2 dm^3 mol^{-1} s^{-1} and (R_{homog}/[Cr(III)]) = 1.7 dm^3 mol^{-1} s^{-1}. Surface Cr(III) in oxide B is oxidized ca. 2×10^2 times faster than the hydrated species $Cr(H_2O)_6^{3+}$. A probable rationale for this finding is provided by the surface complexation approach to describe dissolution kinetics (42). If the rate of substitution on BrO_3^- to form the precursor complex determines the rate, as found in homogeneous oxidations by BrO_3^- (36, 37), rate enhancement may be related to a higher rate of formation of interfacial ≡Cr(III)-O-BrO species as compared to aqueous Cr(III)-O-BrO. Whereas it is reasonable to assume that substitution on BrO_3^- controls the rate of homogeneous oxidation, a very substantial increase in this rate on the surface of the oxide may lead to a shift in rate control to subsequent steps involving the redox evolution of the surface complex and (or) phase transfer of Cr in higher oxidation states.

Metal oxide dissolution is in essence an electrochemical phenomenon. The kinetics of dissolution must therefore comply with the standard electrochemical formalisms, and the importance of the potential drop profile across the interface must be taken into account. Electrochemical descriptions of the dissolution of iron oxides and chromium oxides are available both from our previous work (17, 33) and from the work of other authors (38, 39). Two effects are incorporated in the influence of surface potential: (*a*) the influ-

Can. J. Chem. Downloaded from www.nrcresearchpress.com by 213.200.69.106 on 09/08/12
For personal use only.

ence on ionic adsorption; and (*b*) the influence on the kinetics of ionic phase transfer (Butler–Volmer kinetics). The surface complexation model in the simplest version used above neglects the second effect; this approximation is justified in cases in which the rate-determining step precedes the phase transfer step (for further discussion of this point see ref. 42). For oxides grown or deposited onto metals the electrochemical nature of the dissolution reaction results in further complications that obviously must be taken into account, especially in chemical cleaning applications. For instance, the underlying metal is not indifferent in the course of Fe_3O_4 dissolution from carbon steel films (40, 41).

Acknowledgements

To Lic. M. Tudino, Dto. Qca. Inorg. Anal. y Quím. Fís., Facultad de Ciencias Exactes y Naturales, University of Buenos Aires, for AAS facilities and to R. Rodano, Div. Estudios Especiales, Gerencia de Exploración, Comisión Nacional de Energía Atómica, for X-ray diffractograms. P.J.M. and M.A.B. are members of the Consejo Nacional de Investigaciones Científicas y Técnicas (CONICET). Partially supported by grant PID 30 31 800 90 from CONICET.

1. R. L. Segall, R. St. C. Smart, and P. S. Turner. *In* Surface and near-surface chemistry of oxide materials. *Edited by* J. Nowotny and L.-C. Dufour. Elsevier Science Publishers B.V., Amsterdam. 1988. p. 527.
2. I. H. Warren and E. Devuyst. Proc. Int. Symp. Hydrometallurgy, Chicago, Ill. Annu. Meeting A.I.M.E. 1973.
3. B. Terry. Hydrometallurgy, **11**, 315 (1983).
4. R. A. Berner. *In* Kinetics of geochemical processes, review in mineralogy. Vol. 8. *Edited by* A. C. Lasaga and R. J. Kirkpatrick. Mineral Soc. America, Washington, D.C. 1981. p. 117.
5. J. S. LaKind and A. T. Stone. Geochim. Cosmochim. Acta, **53**, 961 (1989).
6. B. Sulzberger, D. Suter, C. Siffert, S. Banwart, and W. Stumm. Marine Chem. **28**, 127 (1989).
7. W. Schneider. Chimia, **42**, 9 (1988).
8. P. Aisen and I. Listowsky. Annu. Rev. Biochem. **49**, 357 (1980).
9. M. G. Segal and R. M. Sellers. J. Chem Soc. Chem. Commun. 991 (1980).
10. E. C. Baumgartner, M. A. Blesa, and A. J. G. Maroto. J. Chem. Soc. Dalton Trans. 1694 (1982).
11. M. A. Blesa, H. A. Marinovich, A. J. G. Maroto, and E. C. Baumgartner. Inorg. Chem. **26**, 3713 (1987).
12. M. A. Blesa, A. E. Regazzoni, and A. J. G. Maroto. Mater. Sci. Forum, **29**, 31 (1988).
13. S. Banwart, S. Davies, and W. Stumm. Colloids Surf. **39**, 303 (1989).
14. M. dos Santos Afonso, P. J. Morando, M. A. Blesa, S. Banwart, and W. Stumm. J. Colloid Interface Sci. **138**, 74 (1990).
15. A. E. Regazzoni and M. A. Blesa. Langmuir, **7**, 473 (1991).
16. E. B. Borghi, P. J. Morando, and M. A. Blesa. Langmuir, **7**, 1652 (1991).
17. G. B. Reartes, P. J. Morando, M. A. Blesa, P. Hewlett, and E. Matijević. Chem. Mater. **3**, 1101 (1991).
18. N. Valverde. Ber. Bunsen-Ges. Phys. Chem. **81**, 380 (1977).
19. A. M. Olmedo. Ph.D. Thesis, University of Buenos Aires. 1990.
20. R. L. Tapping, P. D. Davidson, E. Mc Alpine, and H. Lister. Corros. Sci. **26**, 563 (1986).
21. M. A. Blesa, A. J. G. Maroto, and A. E. Regazzoni. Proc. Japan Atomic Industrial Forum. Int. Conf. Water Chemistry in Nuclear Power Plants, Fukui City, Japan. 1991.
22. U. Schwertmann, U. Gasser, and H. Sticher. Geochim. Cosmochim. Acta, **53**, 1293 (1989).
23. U. Schwertmann and R. M. Cornell. *In* Iron oxides in the laboratory. Preparation and characterization. VCH, Weinheim. 1991.
24. A. I. Vogel. *In* Química Analítica Cuantitativa. Vol. 2. *Edited by* Kapelusz. Buenos Aires. 1961. p. 911.
25. D. L. Leussing and L. Newman. J. Am. Chem. Soc. **78**, 552 (1956).
26. P. S. Sidhu, R. J. Gilkes, R. M. Cornell, A. M. Posner, and J. P. Quirk. Clays Clay Miner. **29**, 269 (1981).
27. M. dos Santos Afonso, C. Di. Risio, A. Roitberg, R. O. Marques, and M. A. Blesa. Radiat. Phys. Chem. **36**, 457 (1990).
28. Powder diffraction file. Alphabetical index. Inorganic phases. JCPDS International Centre for Diffraction Data, Pennsylvania. 1986.
29. D. Barb, O. Bunescu, M. Morariu, and M. Popescu. Rev. Roum. Phys. **26**, 417 (1981).
30. A. H. Muir, Jr. *In* Mössbauer effect methodology. Vol. 4. *Edited by* Irwin J. Gruverman. Plenum Press, New York. 1968.
31. M. I. Litter and M. A. Blesa. Can. J. Chem. **70**, 2502 (1992).
32. M. E. Pick. Proc. ANS–CNA Conf. Decontam. Nucl. Facil. Niagara Falls, Canada. 1982.
33. V. I. E. Bruyère and M. A. Blesa. J. Electroanal. Chem. Interfacial Electrochem. **182**, 141 (1985).
34. A. E. Regazzoni, M. A. Blesa, and A. J. G. Maroto. J. Colloid Interface Sci. **122**, 315 (1988).
35. M. A. Blesa, E. B. Boghi, A. J. G. Maroto, and A. E. Regazzoni. J. Colloid Interface Sci. **98**, 295 (1984).
36. J. P. Birk and S. G. Kozub. Inorg. Chem. **12**, 2460 (1973).
37. J. P. Birk. Inorg. Chem. **12**, 2468 (1973).
38. J. W. Diggle. *In* Oxides and oxide films. Vol. 2. *Edited by* J. W. Diggle. M. Dekker, New York. 1973. Chap. 3.
39. M. Seo, R. Furuichi, G. Okamoto, and G. Sato. Trans. Japan. Inst. Metals, **16**, 519 (1975).
40. D. W. Shoesmith, T. E. Rummery, Woon Lee, and D. G. Owen. Power Industrial Research, **1**, 43 (1981).
41. D. W. Shoesmith, Woon Lee, and D. G. Owen. Power Ind. Res. **1**, 253 (1981).
42. M. A. Blesa, P. J. Morando, and A. E. Regazzoni. *In* Chemical dissolution of metal oxides. CRC Press, Boca Raton, Fla. In press.

Can. J. Chem. Downloaded from www.nrcresearchpress.com by 213.200.69.106 on 09/08/12
For personal use only.

Fractionation of woodmeal by prehydrolysis and thermal organosolv. Alkaline depolymerization, chemical functionality, and molecular weight distribution of recovered lignins and their fractions

RONALD W. THRING[1] AND ESTEBAN CHORNET
Department of Chemical Engineering, University of Sherbrooke, Sherbrooke, Que., Canada J1K 2R1

AND

RALPH P. OVEREND
National Renewable Energy Laboratory, Golden, CO 80401 U.S.A.

Received October 13, 1992

Can. J. Chem. Downloaded from www.nrcresearchpress.com by 213.200.69.106 on 09/08/12
For personal use only.

RONALD W. THRING, ESTEBAN CHORNET, and RALPH P. OVEREND. Can. J. Chem. **71**, 779 (1993).

Thermal organosolv glycol lignins and their fractions have been characterized by means of elemental composition, molecular weight distribution, and ^1H and ^{13}C NMR spectroscopy. Fractionation of each lignin by sequential solvent extraction produced fractions of increasing molecular weight and polydispersity. Structures in the highest molecular weight fractions were found to be linked by a high proportion of β-*O*-4 type bonds, whilst the lowest molecular weight fractions consisted of a high content of saturated aliphatic side-chain structures. A noticeable difference in the content of carbohydrate contaminants in both starting lignins indicated the formation of relatively stable lignin–carbohydrate complexes, especially in the lignin recovered from pretreated wood. In addition, depolymerization of the lignins and their fractions to monomeric compounds was explored using alkaline hydrolytic and nitrobenzene oxidative routes. The highest molecular weight fractions from each lignin were identified as the best candidates for production of useful monomeric phenolic compounds.

RONALD W. THRING, ESTEBAN CHORNET et RALPH P. OVEREND. Can. J. Chem. **71**, 779 (1993).

En se basant sur la composition élémentaire, la distribution des poids moléculaires et la RMN du ^1H et du ^{13}C, on a caractérisé les lignines thermiques de l'organosolv glycol et leurs fractions. Le fractionnement de chaque lignine par extraction séquentielle par les solvants a fourni des fractions de poids moléculaires et de polydispersités croissants. On a trouvé que les structures des fractions de poids moléculaires les plus élevés sont liées en grande partie par des liaisons de type β-*O*-4 alors que celles des fractions de poids moléculaires plus faibles comportent de grandes quantités de chaînes latérales aliphatiques saturées. On a noté une différence notable dans le contenu en hydrates de carbone des deux lignines; elle indique qu'il y a formation de complexes lignine – hydrate de carbone relativement stables, particulièrement dans la lignine récupérée du bois prétraité. On a de plus examiné la dépolymérisation des lignines et de leurs fractions en composés monomères par hydrolyse alcaline et par oxydation avec du nitrobenzène. Pour la production de composés phénoliques monomères utiles, on a identifié que les fractions de poids moléculaires les plus élevés de chacune des lignines seraient les plus appropriées.

[Traduit par la rédaction]

Introduction

New developments in lignocellulosic fractionation technologies by aqueous-steam (1) and solvolytic treatments (2, 3) have demonstrated that clean, uncontaminated lignins with a low degree of polymerization can be obtained in significant yields.

Our laboratory has recently carried out a number of studies of the fractionation of lignocellulosics and succeeded in isolating one or more of the three constituent polymers in high yields by aqueous-steam (4, 5) and solvolysis treatments (6–9). To achieve the last objective, we have studied two strategies: (*a*) direct solvolysis using ethylene glycol, whereby the lignin and hemicelluloses are preferentially solubilized, leaving the cellulose virtually intact as a residue (6–9); (*b*) a sequential aqueous-steam and solvolytic treatment in which all three fractions are isolated in high yields from the same initial substrate (10, 11). The two strategies were applied to the prototype hardwood aspen poplar (*Populus deltoides*).

One of our goals is to deduce the structural changes induced in each polymer as a function of the conditions of fractionation of the wood. This information will provide the basis for further upgrading studies on each wood constituent to valuable products. In one study, using the direct solvolysis approach, we found a similarly produced lignin to be a potential source of monomeric compounds (7, 12). Fractionation of this lignin by sequential extraction with organic solvents demonstrated that it consisted of fractions of distinct molecular weight also showing structural differences (13).

The objectives of this paper then are twofold. The first objective is to elaborate on an earlier comparative study by us (9) on the properties of lignins (subsequently designated as thermal organosolv lignin (TOL) and thermal organosolv lignin from pretreated wood (PTOL), respectively) isolated by strategies (*a*) and (*b*) above. A detailed characterization study on the lignins and their fractions by elemental composition, molecular weight distribution, and ^1H and ^{13}C NMR spectroscopy is reported here. An assessment of the potential of the lignins and their fractions as a source for production of monomeric phenolic compounds is also presented. Alkaline hydrolysis and nitrobenzene oxidation were selected as the two modes of depolymerization due to their simplicity in experimental technique as well as the relatively small number of monomers produced in rather significant yields (i.e., high selectivity) when compared to other methods of lignin degradation (14).

[1]Author to whom correspondence may be addressed. Present address: Department of Chemical Engineering, University of New Brunswick, Fredericton, N.B., Canada E3B 5A3.

Can. J. Chem. Downloaded from www.nrcresearchpress.com by 213.200.69.106 on 09/08/12
For personal use only.

Experimental

Apparatus

Reactor

A 500-mL stainless steel autoclave equipped with a magnetic stirrer was used for the depolymerization experiments. Heating and cooling were provided by a preheated salt bath (for hydrolysis) or an oil bath (for oxidation) and a cold water bath, respectively, such that heating and quenching periods did not exceed 6 min each.

Gas chromatographs

A Hewlett–Packard 5890A gas chromatograph equipped with a DB-5 capillary column (0.25 mm i.d. and 60 m column length) was used for analyses of the ether solubles from the hydrolysis runs. The carrier gas was helium at 1.2 mL/min. A DB-1 wide-bore column (0.53 mm i.d. and 30 m length) was used for analyses of the ether solubles from the alkaline nitrobenzene oxidation runs.

Chemicals and reagents used were of pure or analytical grade. Samples for preparing standards for quantifying the monomers identified were purchased from Aldrich Chemicals Co. and Alfa Chemicals Co. (U.S.A.).

Materials and methods

Sample preparation

The isolated thermal organosolv lignins were fractionated into three fractions by successive extraction on 125-g dry samples with ethyl acetate followed by methanol (13). The detailed method of fractionation employed has already been presented (15). All samples were kept in a desiccator over Drierite until further use.

Analytical techniques

1. *Elemental composition*: Analyses were conducted in-house using a Perkin Elmer 240C instrument. Oxygen was determined by difference as (100 − C% − H% − N%).

2. *Sugar analyses*: The carbohydrate content was estimated from determination of the total amount of identifiable monosaccharides present according to the acid hydrolysis procedure (16).

3. *High-pressure solvent elution chromatography (HPSEC)*: Analyses by HPSEC were carried out by using a Varian model 5000 liquid chromatograph connected to an on-line computer via a Waters Maxima 820 data system. Two sets of two stainless steel columns connected in series were used; the columns (300 × 7.5 mm) were packed with PLgel spherical particles from Polymer Laboratories (UK). The first set consisted of 5-μm particles of 50 Å (column 1) and 500 Å (column 2) porosity. The second set consisted of 10-μm particles of 10^4 Å (column 1) and 10^5Å (column 2) porosity. Detection was made with a UV monitor at 254 nm. A constant flow rate through the system was maintained by a single piston, reciprocating pump. The following operating conditions were employed: eluent, degassed tetrahydrofuran (purged with N_2); flow rate, 1 mL/min; pressure, 7.0 MPa; temperature, 25°C; injection volume, 10 μL; sample concentration, 1 mg/mL.

4. *^1H and ^{13}C NMR*: Both NMR spectra were recorded on samples (ca. 800 mg/2 g of solvent) dissolved in DMSO-d_6. The instrument used was a Brüker 250 WM spectrometer. The carbon-13 spectra were recorded at a frequency of 62.9 MHz with broad band decoupling, in the Fourier transform mode, and without nuclear Overhauser effect (NOE). A pulse tip angle of 45° and a time delay of 16 s were used, and the transients were accumulated at a sweep width of 20 kHz with 6800 data points. The solvent was used as the reference.

5. *Acetylation*: Analyses by both HSPSEC and NMR methods were conducted on lignin samples that were acetylated using a previously described procedure (13).

Depolymerization

1. *Alkaline hydrolysis*: Lignins and fractions were each subjected to hydrolytic treatment in alkali media using a 500-mL top-stirred batch autoclave. Reaction conditions selected were those previously reported for producing the highest amount of identifiable monomeric compounds from a similarly produced lignin (7).

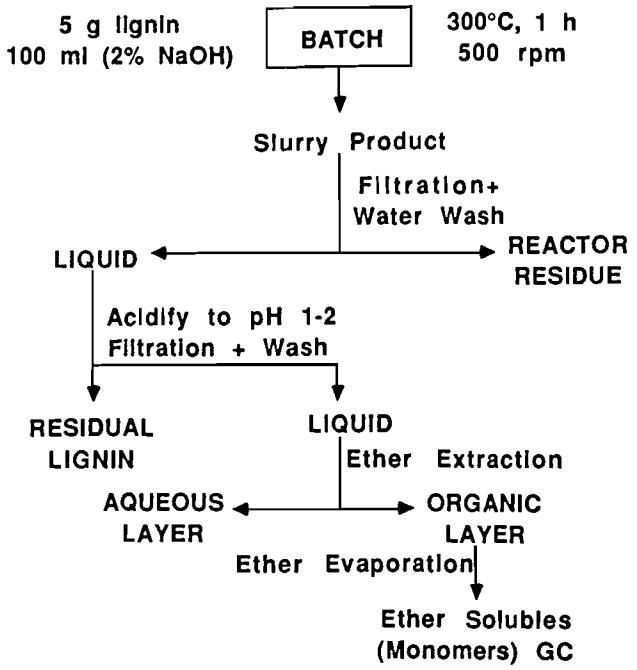

FIG. 1. Procedure for product work-up after alkaline hydrolysis of TOL and PTOL lignins and their fractions.

These conditions were 100 mL of 2% (w/w) sodium hydroxide solution, 5 g of sample, temperature of reaction 300°C (held for 1 h). Throughout the reaction period, the reactor contents were agitated at 500 rpm.

After the desired treatment, the reaction was quenched by immersing the reactor in a cold-water bath maintained with running water. The products were decanted and the reactor washed with water. The combined washings and product liquids were stored in 250-mL bottles at −18°C for subsequent analysis.

The procedure employed for product work-up is presented in Fig. 1.

2. *Nitrobenzene oxidation*: The experiments were conducted in the same autoclave as above. Amounts of initial sample and reactants used per run were as follows: 5 g of dry sample, 120 mL of 2 N sodium hydroxide solution, and 16 mL nitrobenzene. Reaction conditions were 180°C held for 1.5 h, 500 rpm agitation. The amounts of reactants used and the product separation methodology were based on the work of Pepper et al. (17).

After reaction, the combined washings and product liquids were stored in 250-mL bottles at −18°C prior to work-up by the following procedure. The solution was initially extracted (5×) with 100 mL of ether to remove the excess nitrobenzene. The aqueous layer was then acidified with 10% (v/v) hydrochloric acid to a pH of 1–1.5, filtered, and the filtrate extracted with ether until the last ether extract was judged to be colourless. The combined ether extracts were evaporated to constant weight under reduced pressure at room temperature, leaving an oily yellowish fraction as residue.

Product identification: A portion of the ether-soluble fraction was derivatized by the acetic anhydride – pyridine procedure and directly analysed by gas chromatography (18). Compounds were identified by comparing their peak retention times to those of authentic samples. Response factors were determined for each compound to be quantified and tests on a standard blend showed the deviation to be within 5% of the true value for the majority of compounds. Both GC columns were found to give similar response factors and errors, using 4-ethylresorcinol as the internal standard. The following oven program was found to produce good product separation for both columns: initial temperature, 65°C; rate,

TABLE 1. Elemental analyses (moisture, ash-free basis) of TOL and PTOL lignins and their fractions

	TOL				PTOL			
Fraction no.	C%	H%	N%	O%[a]	C%	H%	N%	O%
1	63.7	6.9	0.1	29.3	63.1	6.7	0.1	30.1
2	61.8	6.1	0.2	31.9	61.9	6.1	0.2	31.8
3	61.3	6.0	0.2	32.5	61.5	6.1	0.3	32.1
Initial lignin	61.8	6.3	0.2	31.7	61.4	5.9	0.2	32.5

[a]Determined by difference.

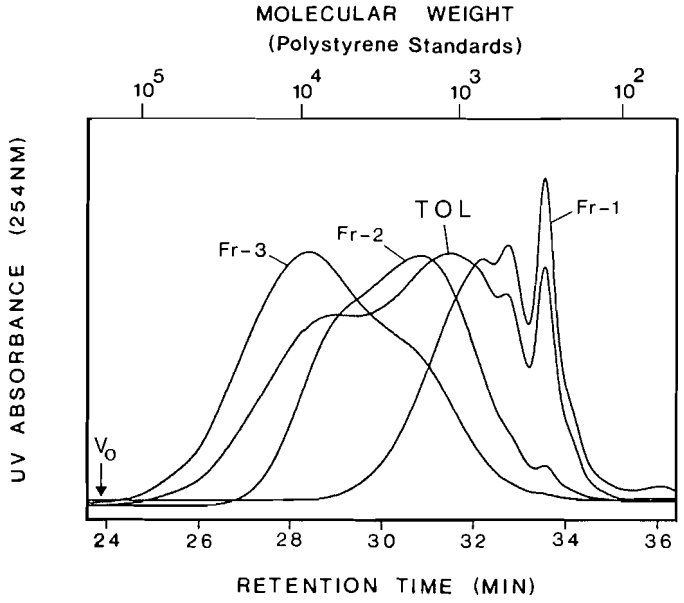

FIG. 2. Molecular weight distribution (polystyrene weight equivalent) of acetylated TOL lignin and its fractions.

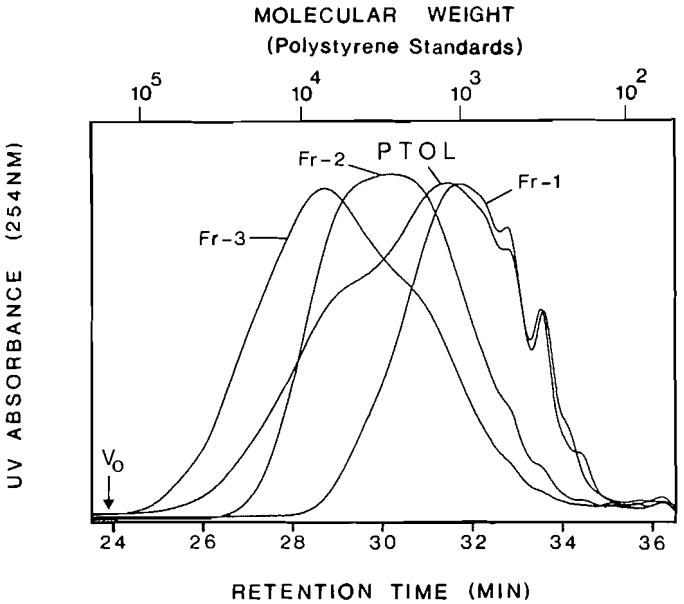

FIG. 3. Molecular weight distribution (polystyrene weight equivalent) of acetylated PTOL lignin and its fractions.

6°C/min; held constant at 140°C for 10 min; rate, 4°C/min; held constant at 220°C for 10 min; cool to 65°C.

Results and discussion

It should be pointed out here that a first characterization of the starting lignins via elemental composition, solvent fractionation, molecular weight distribution, and ^{13}C NMR has already been made in a related article (9). The data are only included here for ease of comparison with the corresponding fractions.

Elemental composition

The values of the carbon, hydrogen, nitrogen, and oxygen content listed in Table 1 are average values from duplicate analyses of the same sample. Both starting lignins have a comparable carbon content whose magnitude provides a first indication of their low degree of condensation and high purity (i.e., low in carbohydrate contaminants). The fractions (Fr) from both starting lignins each show a small increase in C content (and a decrease in O) with increase in fraction number. This trend has been attributed to differences in the proportions of syringyl to guaiacyl units in fractions from a similarly isolated lignin (13) (also see complementary data below). The same behaviour has also been reported for organosolv lignins extracted from cooking spruce chips at increasing times by the Organocell process (19). These authors attributed this trend to the presence of organic nonlignin substances, namely, extractives and sugar degradation products. Chua and Wayman (20), in their work on the characterization of autohydrolysis lignins, also reported the presence of nonlignin portions, and postulated that incorporation of hemicelluloses into the lignin may occur during autohydrolysis.

Carbohydrate content

The total amount of monosaccharides (five sugars) from the starting lignins TOL and PTOL was estimated to be 0.6 wt.% and 4.1 wt.%, respectively.

HPSEC

As seen in Figs. 2 and 3, both solvolysis lignins yield three fractions of increasing molecular weight when subjected to sequential solvent fractionation. The yields of these fractions have been presented and interpreted in a related article (9). Other important observations in the chromatograms of the two lignins and corresponding fractions are as follows. Both starting lignins exhibit multimodal distribution patterns, with TOL showing a larger low molecular weight peak, whose maximum corresponds to 300 g/gmol (polystyrene equivalent), than PTOL. This implies that TOL contains a high proportion of low molecular weight material. This is to be expected since it has been found that, under optimal conditions of operation of the aqueous-steam unit for recovery of the sugars from *Populus deltoides*, almost 20 wt.% of the protolignin in the wood is invariably removed with the hemicelluloses (4, 6). This lignin was extractable from the filtrate using ethyl acetate, suggesting that it is of low molecular weight. Fr-1 from PTOL exhibits more high molecular weight material than the corresponding fraction isolated from TOL.

Table 2 shows the weight and number average molecular weight values (polystyrene weight equivalent) M_w and M_n, respectively, and polydispersity M_w/M_n. The M_w and M_n values are slightly higher for TOL and PTOL lignin, suggesting that PTOL is more depolymerized to lower molec-

Can. J. Chem. Downloaded from www.nrcresearchpress.com by 213.200.69.106 on 09/08/12
For personal use only.

TABLE 2. Molecular weight averages and polydispersities of TOL and PTOL lignins and their fractions[a]

	TOL			PTOL		
Fraction no.	M_w	M_n	M_w/M_n	M_w	M_n	M_w/M_n
1	942	426	2.2	1214	586	2.1
2	2964	1233	2.4	3230	1234	2.6
3	8210	2486	3.3	7148	2062	3.5
Initial lignin	4285	833	5.1	3248	822	4.0

[a]Acetylated samples, M_w and M_n, are polystyrene weight equivalent values.

ular weight material during its isolation. The values for Fr-1 and Fr-2 from TOL are lower than the corresponding ones from PTOL, indicating that the latter contains more material of higher molecular weight in the low and medium molecular weight fractions than the former.

A steady increase is observed in both polydispersity and molecular weight for fractions from Fr-1 to Fr-3 from both lignins. This shows that Fr-1 contains materials of essentially similar molecular weight whereas Fr-3 comprises more of a mixture of medium and high molecular weight materials.

Alkaline hydrolysis

Among the advantages found in utilizing this method for depolymerizing lignin are that the yields of monomeric products can be significant and the spectrum of products as a whole is not extensive. The technique has been applied by a number of other workers (21–23). Depolymerization patterns of a glycol lignin similarly produced by alkaline hydrolysis have also been mapped by us (7) via the reaction ordinate, a severity parameter that combines the effects of temperature and time into a single variable. Optimum reaction conditions were determined for the production of important identifiable monomers, namely, catechol and its methyl and ethyl derivatives, which made up 9 wt.% of the initial lignin added to the reactor.

The same reaction conditions (see experimental section) were employed here. Table 3 shows the results for both lignins and their fractions. The low content of reactor residue from all the samples suggests that little or no recondensation of the lignin occurred due to cross-linking reactions between the lignin fragments during the alkaline treatment. The highest values were from the lowest molecular weight fraction, particularly Fr-1 from PTOL. This agrees with results from nitrobenzene oxidation (see below), which indicated that this fraction contains the highest amount of condensed structures, which are rather resistant to degradation. Also, the presence of nonlignin components or a stable lignin–carbohydrate complex (LCC) in this fraction, which are not only resistant to degradation by alkaline hydrolysis but are insoluble in the alkaline medium, may account for the high amount of reactor residue.

The total yield of catechols from each sample is approximately 7.5 wt.% of the initial sample, except from Fr-3 (PTOL). For the experimental conditions employed, this fraction produced the highest yield of catechols, namely, 9.06 wt.% of the initial sample, further revealing that it contains the highest amounts of guaiacyl and syringyl units, which would give rise to catechols upon demethoxylation and (or) demethylation during alkaline hydrolysis. Nitrobenzene oxidation and ^{13}C NMR (see below) have all demonstrated that indeed this particular fraction has the highest content of guaiacyl and, especially, syringyl units.

Alkaline nitrobenzene oxidation

This depolymerization technique has been widely used for characterizing protolignin in order to deduce its structural features as well as any changes in extracted lignins caused by the method of isolation (24–26). As has been demonstrated by Leopold (27) in studies on lignin model compounds, lower yields of aromatic aldehydes are obtained upon the alkaline nitrobenzene oxidation of condensed lignin structures (i.e., carbon-carbon linked). The method has been applied to isolated lignins to deduce their degree of condensation (25) and to compare the structural features of wood lignins in different wood species (17). We applied the method here to elucidate if significant structural differences exist between TOL and PTOL lignins as well as between their respective fractions.

The results are shown in Table 4. The yields of identifiable monomers suggest that moderate structural differences do exist between TOL and PTOL lignins. In particular, the lower yield of the total aromatic aldehydes in PTOL indicates that it is more condensed than TOL. The lower value of the syringaldehyde/vanillin (S/V) ratio in PTOL than in TOL strongly suggests that the lignin extracted during the aqueous-steam treatment was richer in syringyl than guaiacyl units. The same observation was reported by Wayman and Chua (25) in their work on the characterization of extracted autohydrolysis lignin from aspen wood.

Yields of 4-hydroxybenzaldehyde are seen to be the same from both starting lignins; they are highest in the lowest molecular weight fractions, particularly in Fr-1 from TOL, and decrease with increasing fraction number. On the other hand, the yield of 4-hydroxybenzoic acid from PTOL lignin is somewhat higher than that found in TOL lignin. For both lignins, the yield of this acid generally increases with increasing fraction number, and is lowest in Fr-1 from TOL lignin. The presence of 4-hydroxybenzoic acid structures in different tissues and lignins isolated from hardwoods was previously demonstrated by Venverloo (28). That work showed that higher yields of this acid are obtained during the alkaline hydrolysis of native lignin than for lignin isolated from the same wood species. Thus, in our work, the low yields of both aldehyde and acid obtained upon alkaline nitrobenzene oxidation of both TOL and PTOL lignins indicate that some of these compounds are split off during the isolation of the lignins. The loss is almost identical in both lignins.

The yields of aromatic aldehydes were lowest in Fr-1 from both lignins, and highest in Fr-3, suggesting that the latter contains the highest amount of uncondensed syringyl units. Fr-1 (PTOL), in particular, produced the lowest amount of aromatic aldehydes, indicating that it contains the highest amount of condensed structures, which makes it the least amenable to oxidative degradation to phenolic aldehydes.

By virtue of the high aromatic aldehyde content, which reflects their uncondensed nature, Fr-2 and Fr-3 in particular may be valuable as prepolymers in phenolic resin applications or as a source of chemicals via specific catalytic bond cleavage. Fr-1, on the other hand, due to its low molecular weight and high hydroxyl content (especially phenolic) (see ^{13}C NMR below) may prove useful in the adhesives area.

Can. J. Chem. Downloaded from www.nrcresearchpress.com by 213.200.69.106 on 09/08/12
For personal use only.

TABLE 3. Yields of products (% initial sample) from the alkaline hydrolysis of TOL and PTOL lignins and their fractions

	TOL				PTOL			
Reaction products	Initial lignin	Fr-1	Fr-2	Fr-3	Initial lignin	Fr-1	Fr-2	Fr-3
Reactor residue	1.44	1.61	0.35	1.40	1.52	3.28	0.37	1.36
Residual lignin	46.74	43.24	41.17	41.24	45.27	42.72	40.72	43.59
Ether solubles	21.01	27.47	22.05	22.62	17.68	23.39	22.06	19.76
Main monomers								
Phenol	0.43	0.31	0.44	0.37	0.76	0.62	0.59	0.48
Guaiacol	0.73	0.45	0.68	0.75	0.72	0.73	0.49	0.61
Catechol	4.96	5.51	5.25	5.89	5.75	5.46	5.23	4.79
4-Methylcatechol	1.58	1.55	1.88	2.35	1.56	1.80	1.87	1.80
4-Ethylcatechol	0.50	0.48	0.64	0.82	0.41	0.47	0.59	0.56
Total catechols	7.04	7.54	7.77	9.06	7.72	7.73	7.69	7.15
Total monomers	8.20	8.30	8.99	10.18	9.20	9.08	8.77	8.24

TABLE 4. Yields of identified monomeric products (% initial sample) from the alkaline nitrobenzene oxidation of TOL and PTOL lignins and their fractions

	TOL				PTOL			
Monomeric products	Initial lignin	Fr-1	Fr-2	Fr-3	Initial lignin	Fr-1	Fr-2	Fr-3
Phenol	0.29	0.40	0.34	0.30	0.33	0.43	0.51	0.36
Guaiacol	0.25	0.34	0.24	0.24	0.26	0.30	0.35	0.28
4-Hydroxybenzaldehyde	0.09	0.16	0.12	0.08	0.09	0.11	0.11	0.08
4-Hydroxybenzoic acid	0.65	0.54	1.06	0.96	0.88	0.68	0.84	0.85
Syringol	0.26	0.31	0.29	0.27	0.28	0.25	0.37	0.25
Vanillin (V)	6.44	6.13	6.81	8.25	5.41	4.91	7.66	7.85
Syringaldehyde (S)	12.64	9.66	15.68	17.40	9.60	6.19	15.16	15.13
S/V (g/g)	1.96	1.58	2.30	2.11	1.78	1.26	1.98	1.93
(S + V)	19.08	15.79	22.49	25.65	15.01	11.10	22.82	22.08
Ether solubles	53.33	44.13	60.76	60.85	51.37	42.36	58.69	54.13

Also, it was postulated by Wayman and Chua (25) that the obtention of low yields of aromatic aldehydes is due to the incorporation, by physical or chemical means during autohydrolysis, of nonlignin materials such as carbohydrate degradation products. As suggested by Klemola and Nyman (26), furfural and its precursors might react with lignin to form new carbon–carbon bonds, thus giving rise to a more condensed, stable material.

The data reported so far show that moderate differences exist between the monomers, isolated with slightly higher yields, produced from TOL than PTOL. The higher yields of 4-hydroxybenzaldehyde from the Fr-1 fractions than from the corresponding initial lignins suggest a higher content of 4-hydroxybenzoic acid residues in this fraction. Further evidence for this is the presence of a higher amount of aromatic hydroxyl groups in this fraction (see ^{13}C NMR below). In fact this fraction was previously reported to have the highest content of total hydroxyl (aromatic + aliphatic) groups (13). The syringyl/guaiacyl (S/V) ratio has been reported to be an important criterion for assessing the degree of condensation of a lignin (25). Syringol is excluded in the S/V calculation because it is not an aromatic aldehyde, and is produced only in trace quantities (unlike syringaldehyde and vanillin) during the alkaline nitrobenzene oxidation of lignin. From Table 4, no significant differences can be observed in the S/V ratios for Fr-2 and Fr-3 except that the values for TOL are slightly higher than those from PTOL. However, a clear distinction is seen when comparing the S/V values of the Fr-1 fractions to the others. The low values obtained in Fr-1 again confirm the high guaiacyl content, as was previously reported (13). The lowest value of Fr-1 (PTOL) suggests that pretreatment by autohydrolysis of the initial wood removed more syringyl than guaiacyl moieties from the lignin.

Nuclear magnetic resonance

^1H NMR

The proton NMR spectra of TOL and PTOL lignins and their fractions are shown in Figs. 4 and 5, respectively. The assignments of peaks recorded in Table 5 are in accordance with those of other workers (29–32).

From Fig. 4, the intensity of the signal of acetates due to aromatic hydroxyl protons decreases steadily from Fr-1 to Fr-3, suggesting a decrease in aromatic hydroxyl bearing units (e.g., catecholic) with increase in fraction number. The same trend is seen in the spectra of the PTOL fractions, as shown

Can. J. Chem. Downloaded from www.nrcresearchpress.com by 213.200.69.106 on 09/08/12
For personal use only.

Can. J. Chem. Downloaded from www.nrcresearchpress.com by 213.200.69.106 on 09/08/12
For personal use only.

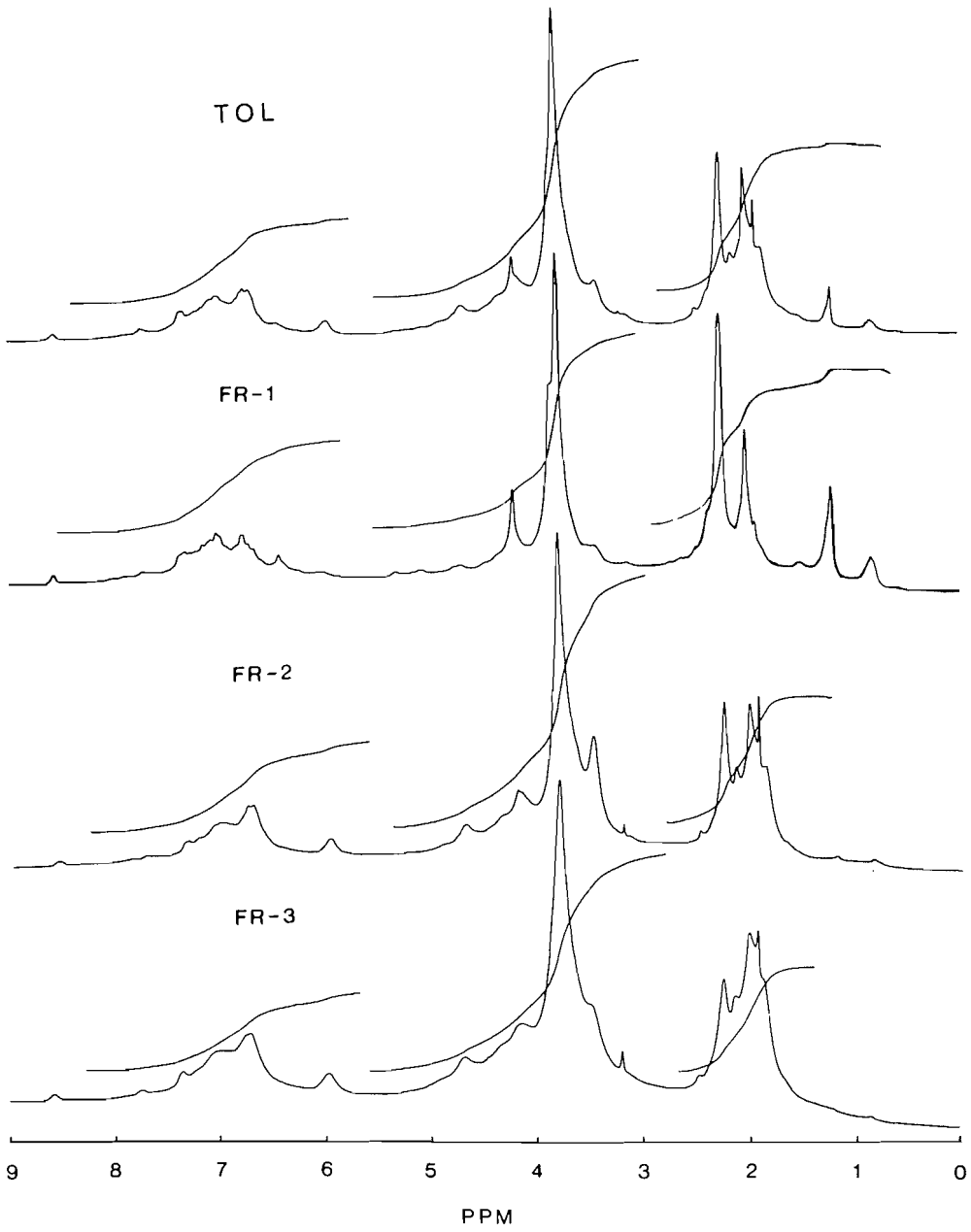

FIG. 4. ^{1}H NMR spectra of acetylated TOL lignin and its fractions; solvent, DMSO-d_6.

in Fig. 5. For both lignins, Fr-1 exhibits the highest intensity of signals at 4.2 ppm (H-α in β-*O*-4) and 0.9–1.3 ppm (methyl, methylene protons), which suggests that these fractions contain the most β-*O*-4 interlinkages and aliphatic saturated structures. The strong sharp signals at about 2 ppm and at 3.3 ppm are significant in the fractions from PTOL, and may also arise from carbohydrate contaminants (29, 33). As seen, the intensity of the sharp signal at 3.3 ppm increases steadily from Fr-1 to Fr-3 in PTOL, indicative of a possible increase in carbohydrate contamination from Fr-1 to Fr-3.

The signals in the 1.9–2.2 ppm region have also been attributed to protons on saturated or reduced side chains (34). The high intensity of these signals in this case would indicate that fractions from PTOL contain more structures whose side chains are saturated than the corresponding fractions from TOL. The intensity of signals between 4.2 and 6.4 ppm (due to protons attached to carbons involved in aryl ether bonds) in Fr-2 and Fr-3 from PTOL are lower in intensity than in the spectra of the corresponding fractions from TOL. This strongly supports the interpretation that more β-*O*-4 linkages have been cleaved during the isolation of PTOL than TOL. In particular, the intensity of the signal at 6.03 ppm (H-α in β-aryl ether bonds) is higher in Fr-2 and Fr-3, but is almost absent in Fr-1 of both lignins, suggesting that the former fractions contain more structures linked by β-aryl ether linkages than the latter. This is confirmed by the results from ^{13}C NMR below and nitrobenzene oxidation.

The spectra of Fr-1 from each lignin display a marked difference in the 6.4–8.0 ppm region (protons attached to aromatic carbons). This implies that the aromatic character of this fraction is distinct from that of the starting lignin and its higher fractions, whose spectra are more similar in appearance.

Can. J. Chem. Downloaded from www.nrcresearchpress.com by 213.200.69.106 on 09/08/12
For personal use only.

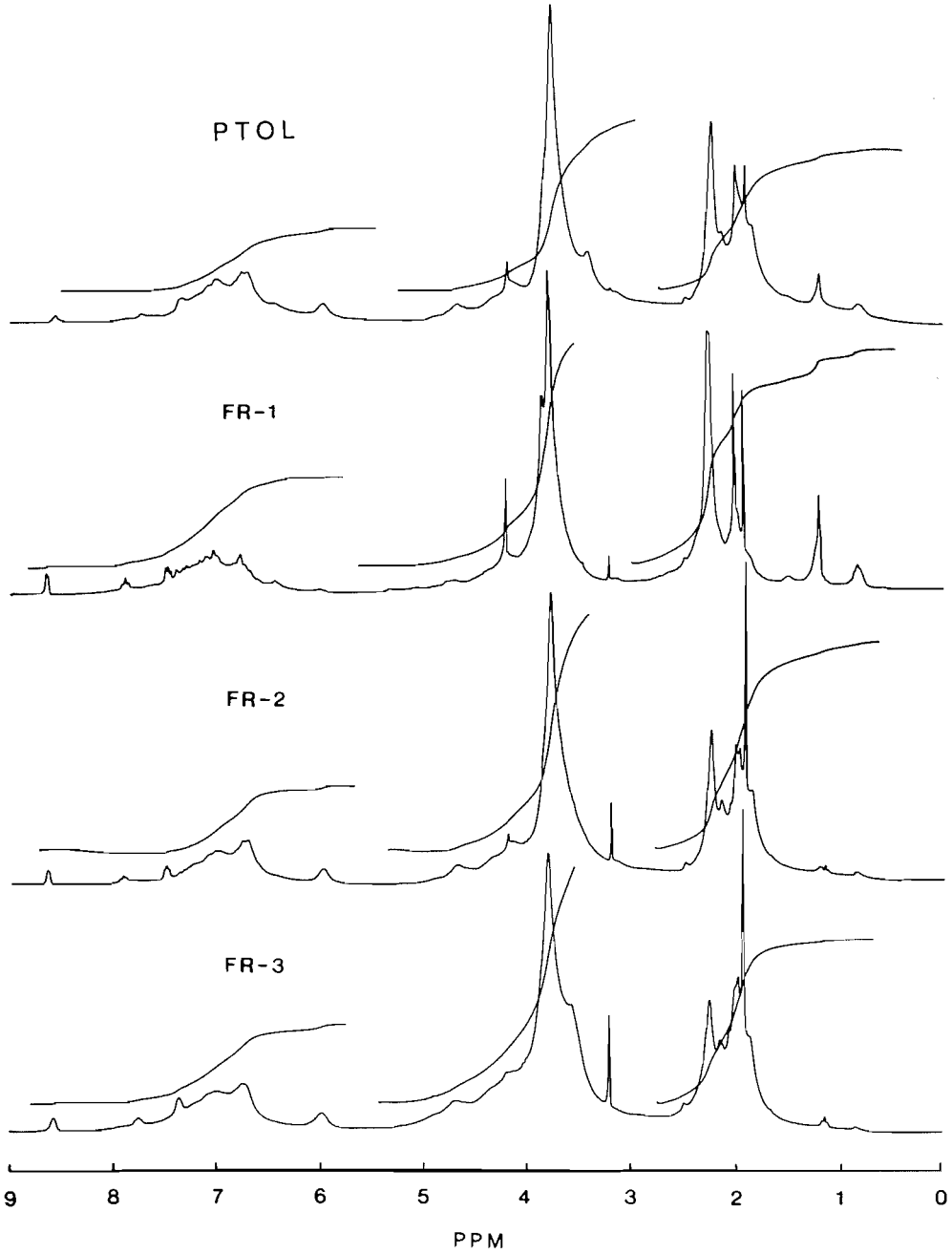

FIG. 5. ^{1}H NMR spectra of acetylated PTOL lignin and its fractions; solvent, DMSO-d_6.

TABLE 5. Assignments of signals in the ^{1}H NMR spectra of acetylated TOL and PTOL lignins and their fractions; solvent DMSO-d_6

Chemical shift (ppm)	Assignment
0–1.6	Hydrocarbon protons
1.6–2.2	H of aliphatic acetates/acetylated carbohydrates
2.2–3.0	H of aromatic acetates
3.0–4.2	H of methoxyl groups
4.2–6.4	Hα, Hβ, Hγ in β-*O*-4 structures
6.4–6.8	Aromatic protons in syringyl units
6.8–8.0	Aromatic protons in guaiacyl units
8.0–10.0	H of carboxylic acid groups

Can. J. Chem. Downloaded from www.nrcresearchpress.com by 213.200.69.106 on 09/08/12
For personal use only.

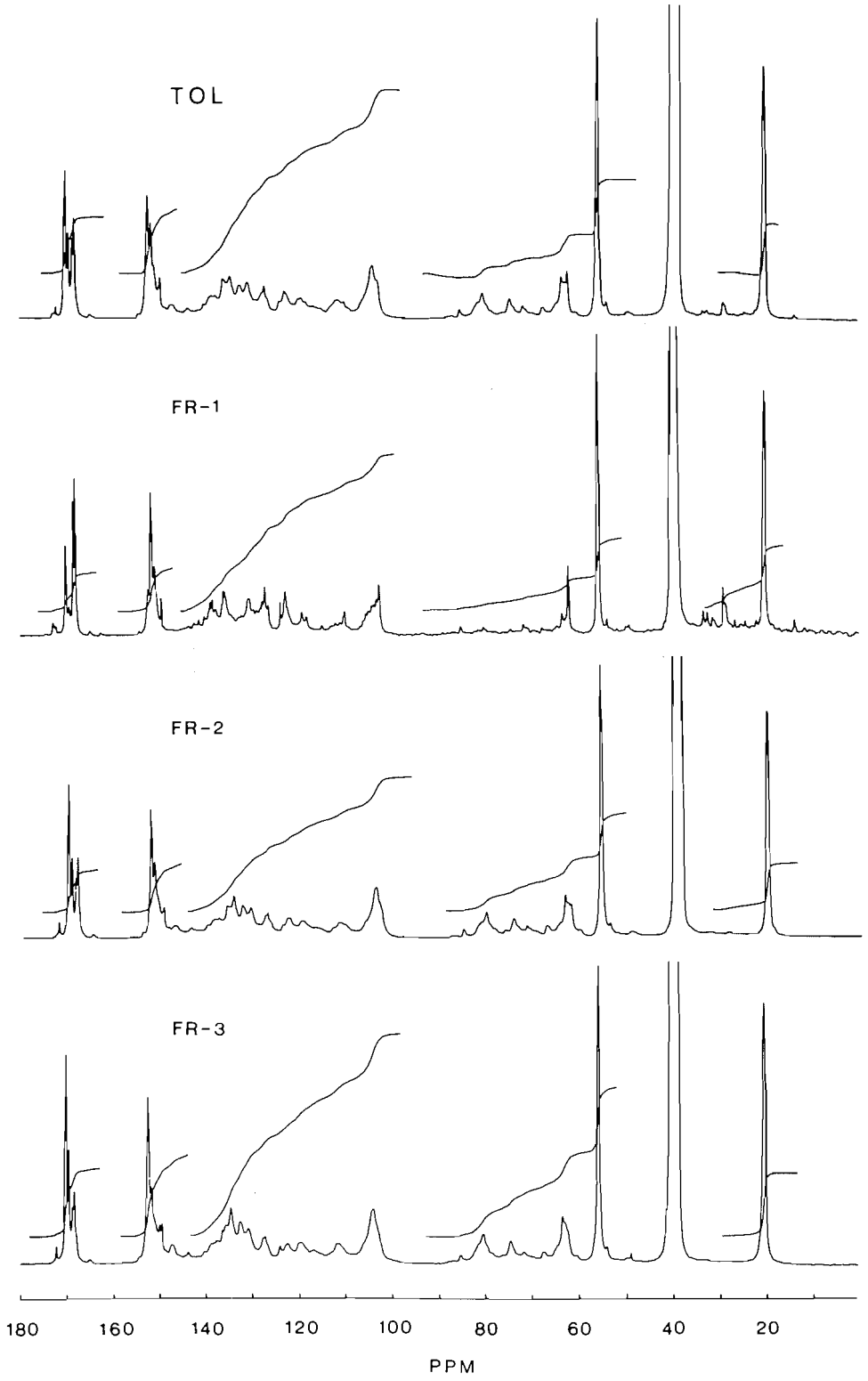

FIG. 6. ^{13}C NMR spectra of acetylated TOL lignin and its fractions; solvent, DMSO-d_6.

The signals between 8 and 9 ppm, assigned to protons of carboxylic acid groups, are more intense in PTOL and its fractions but are very weak in TOL and its corresponding fractions. This suggests that these groups are formed during the aqueous-steam pretreatment (also confirmed by ^{13}C NMR below).

^{13}C NMR

The ^{13}C NMR spectra of TOL and PTOL lignins and their corresponding fractions are shown in Figs. 6 and 7, respectively. The assignment of peaks can be found in other related work and in one of our articles (13).

As we shall see below, the major differences between

Can. J. Chem. Downloaded from www.nrcresearchpress.com by 213.200.69.106 on 09/08/12
For personal use only.

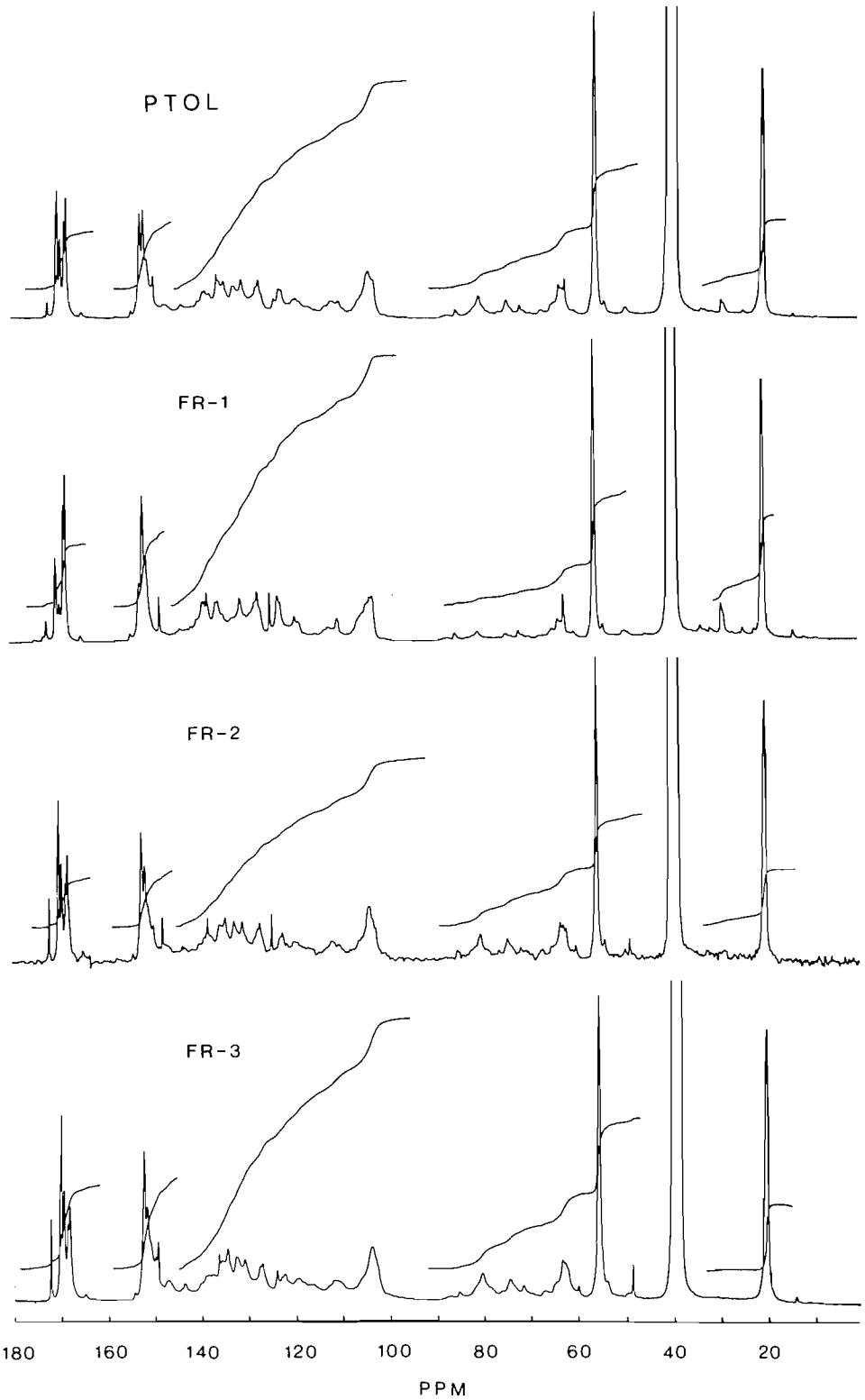

FIG. 7. ^{13}C NMR spectra of acetylated PTOL lignin and its fractions; solvent, DMSO-d_6.

spectra of the same fraction number may be related primarily to the method of isolation and the presence of contaminants in the starting lignins. The discussion will only focus on signals that reflect important structural differences between the two sets of spectra.

The carboxylic signal at 172 ppm increased in intensity with increasing fraction number for fractions in both sets of spectra, and was much more significant in the fractions from PTOL. This signal may be due to aliphatic esters, like the acetate or uronic esters in carbohydrate components (27). The data from sugar analysis also showed a higher content of carbohydrates in PTOL than in TOL. However, the results suggest that for practical purposes, the carbohydrate contamination in both starting lignins is negligibly low.

Can. J. Chem. Downloaded from www.nrcresearchpress.com by 213.200.69.106 on 09/08/12
For personal use only.

From the spectrum of TOL lignin, the intensity of the signal at 170 ppm (aliphatic hydroxyl groups) is higher than the one at 168 ppm (phenolic hydroxyl groups), suggesting that this lignin contains a higher content of aliphatic than phenolic hydroxyl groups. However, the intensity of these signals in the spectrum of PTOL lignin shows this lignin to have a higher phenolic than aliphatic hydroxyl content. As seen from the spectra of both starting lignins, PTOL lignin has a higher content of phenolic hydroxyl groups than TOL lignin. The variation of the signals due to hydroxyl groups in the fractions is similar in both sets of spectra. As seen, the intensity of the signals strongly suggests that the content of aliphatic hydroxyl groups increases whilst that of the aromatic hydroxyl groups decreases with increase in fraction number.

In the portion of the spectra attributed to aromatic carbons, signals at approximately 119 and 149 ppm (due to guaiacyl units) were more intense in Fr-1 from both lignins than in the other fractions. In particular, these signals had the highest intensity in Fr-1 (PTOL), indicating the guaiacyl moiety to be the most important in this fraction. In both lignins, the intensity of the signals around 85 and 65 ppm, attributed to β-*O*-4 structures, is much lower in Fr-1 than in the higher molecular weight fractions, where each signal has virtually the same intensity.

Thus, as demonstrated in this work, lignins can be recovered as a "clean" fraction from the lignocellulosic raw material. Subsequently, their conversion into basic oxychemicals can be readily accomplished via thermo-catalysis.

Conclusions

In this work, a detailed comparison was carried out on thermal organosolv lignins from untreated and aqueous-steam pretreated wood.

The data from alkaline hydrolysis showed that, under optimal conditions for production of catechols from a similarly produced thermal organosolv lignin, both lignins and their fractions produced approximately 7.5% catechols, except Fr-3 from TOL, from which 9% of the initial sample formed catechols.

Nitrobenzene oxidation revealed an increase in the ratio of syringyl to guaiacyl units from Fr-1 to Fr-3 in both lignins. This ratio was found to be generally higher in TOL and its fractions than in PTOL and its corresponding fractions. This finding was confirmed by NMR studies. The highest and lowest yields of total aromatic aldehydes were obtained from Fr-3 (TOL) and Fr-1 (PTOL), respectively. This is directly related to the amounts of uncondensed structures in these fractions. Proton and ^{13}C NMR revealed that these structures are linked by a high proportion of β-*O*-4 type bonds in Fr-3, but Fr-1 consists of a high content of structures with saturated aliphatic linkages. The potential of the former fraction as a source of phenolic monomeric compounds, when compared to its respective starting lignin and other fractions, has been demonstrated in this study.

Carbohydrate contamination of the lignins and isolated fractions was evident from ^{1}H and ^{13}C NMR, and from sugar analyses. Analysis by acid hydrolysis for monosaccharides in both starting lignins revealed 0.6 wt.% to be present in TOL and 4.1 wt.% in PTOL.

The evidence presented has unequivocally demonstrated that the differences in heterogeneity between TOL and PTOL lignins are primarily a consequence of the different routes employed in their isolation from the wood.

This work shows conclusively that isolated lignins obtained from the hardwood *Populus deltoides* via direct solvolysis using ethylene glycol and a sequential aqueous-steam followed by solvolysis treatment do not differ significantly in terms of their structural characteristics. However, noticeable differences in their content of carbohydrate contaminants suggest the formation of relatively stable lignin–carbohydrate complexes via possible covalent bonding in the lignin isolated from pretreated wood. Complementary evidence has been provided by spectral and lignin depolymerization methods.

Acknowledgements

We would like to thank the following members of our research group for their invaluable assistance: J. Bouchard and P.F. Vidal for helpful discussions; A. Roireau for recording the HPSEC spectra; M. Trottier for the elemental analyses; J. Lapointe for calibrating the DB-1 column for GC analyses. Thanks are also expressed to S. Bérubé (Department of Chemistry, University of Sherbrooke) for recording the NMR spectra. Financial assistance by the Natural Sciences and Engineering Research Council of Canada; Energy, Mines and Resources (Bioenergy Division) (Ottawa, Canada); and the Ministry of Education of Quebec (FCAR) is deeply appreciated.

1. E.A. Delong. Canadian Patent No. 1 096 374. 1981.
2. G.C. April, P.G. Nayak, P.L. Daley, F. Jabali, and J. Maraab. Report NSF/CPE-8304, NTISPB 85-180719, U.S. Dept. of Commerce, Springfield, Va. 1983.
3. J.H. Lora, C.F. Wu, E.K. Pye, and J.J. Balantinecz. *In* Lignin: properties and materials. ACS Symp. Ser. No. 397. *Edited by* W.G. Glasser and K.V. Sarkanen. American Chemical Society, Washington, D.C. 1989. pp. 312–323.
4. J. Bouchard, T.S. Nguyen, E. Chornet, and R.P. Overend. Biomass, **23**, 243 (1990).
5. J. Bouchard, T.S. Nguyen, E. Chornet, and R.P. Overend. Bioresour. Technol. **36**, 121 (1991).
6. C. Vanasse. Thèse de M.Sc.A., Dépt. de génie chimique, Université de Sherbrooke, Québec. 1986.
7. R.W. Thring, E. Chornet, R.P. Overend, and M. Heitz. *In* Lignin: properties and materials. ACS Symp. Ser. No. 397. *Edited by* W.G. Glasser and K.V. Sarkanen. American Chemical Society, Washington, D.C. 1989. pp. 228–244.
8. E. Chornet, C. Vanasse, and R.P. Overend. Entropie, No. 130/131, 89 (1986).
9. R.W. Thring, E. Chornet, and R.P. Overend. Can. J. Chem. Eng. **71**, 116 (1993).
10. R.W. Thring, E. Chornet, and R.P. Overend. 39th Canadian Chemical Engineering Conference, Hamilton, Ontario. October 1–4, 1989.
11. R.W. Thring, E. Chornet, and R.P. Overend. Biomass, **23**, 289 (1990).
12. R.W. Thring, E. Chornet, and R.P. Overend. Can. J. Chem. Eng. **71**, 107 (1993).
13. R.W. Thring, E. Chornet, and R.P. Overend. Ind. Eng. Chem. Res. **29**, 232 (1991).
14. H.L. Chum, D.K. Johnson, S. Black, M. Ratcliffe, and D.W. Goheen. *In* Advances in solar energy — An annual review of research and development. Vol. 4. *Edited by* K.W. Boer. Plenum Press, New York. 1988. pp. 91–171.
15. R.W. Thring, E. Chornet, P.F. Vidal, J. Bouchard, and R.P. Overend. Proceedings of the 5th International Symposium on Wood and Pulping Chemistry (TAPPI), North Carolina State University, Raleigh, N.C. May 1989.

16. J. Bouchard, N. Abatzoglou, E. Chornet, and R.P. Overend. Wood Sci. Technol. **23**, 343 (1989).
17. J.M. Pepper, M. Manolopoulo, and R. Burton. Can. J. Chem. **40**, 1976 (1962).
18. R.W. Thring, E. Chornet, and R.P. Overend. J. Chromatogr. **467**, 441 (1989).
19. A. Lindner and G. Wegener. J. Wood Chem. Technol. **8**, 323 (1988).
20. M.G.S. Chua and M. Wayman. Can. J. Chem. **57**, 1141 (1979).
21. J. Gierer, B. Lenz, I. Noren, and S. Soderberg. TAPPI J. **47**, 233 (1964).
22. I.T. Clark and J. Green. TAPPI J. **51**, 44 (1968).
23. T.P. Schultz. Ph.D. Thesis, North Carolina State University, Raleigh, N.C. 1981.
24. J.M. Pepper and M. Siddiquellah. Can. J. Chem. **39**, 1454 (1961).
25. M. Wayman and M.G.S. Chua. Can. J. Chem. **57**, 2599 (1979).
26. A. Klemola and G.A. Nyman. Paperi Puu, **48**, 595 (1966).
27. B. Leopold. Acta Chem. Scand. **4**, 1523 (1950).
28. C.J. Venverloo. Holzforschung, **25**, 18 (1971).
29. C. Lapierre, J.Y. Lallemand, and B. Monties. Holzforschung, **36**, 275 (1982).
30. K. Lundquist. Acta. Chem. Scand. **B33**, 27 (1979).
31. K. Lundquist. K. Acta. Chem. Scand. **B34**, 21 (1980).
32. B. Lenz. TAPPI J. **51**, 511 (1968).
33. B. Hortling, K. Poppius, and J. Sundquist. *In* Proceedings of the International Symposium on Wood and Pulping Chemistry (TAPPI), North Carolina State University, Raleigh, N.C. May 1989.
34. R.H. Marchessault, S. Coulombe, and H. Morikawa. Can. J. Chem. **60**, 2372 (1982).

Can. J. Chem. Downloaded from www.nrcresearchpress.com by 213.200.69.106 on 09/08/12
For personal use only.

Excess molar volumes and viscosities for the *n*-decane + 1-chlorodecane system at different temperatures

MERCEDES E. F. DE RUIZ HOLGADO, CECILIA R. DE SCHAEFER, FRANCO DAVOLIO, AND MIGUEL KATZ[1]

Cátedra de Fisicoquímica, Instituto de Ingeniería Química, Facultad de Ciencias Exactas y Tecnología, U.N. de Tucumán, Avda. Independencia 1800, S.M. de Tucumán (4000), R. Argentina

Received August 12, 1992

MERCEDES E. F. DE RUIZ HOLGADO, CECILIA R. DE SCHAEFER, FRANCO DAVOLIO, and MIGUEL KATZ. Can. J. Chem. **71**, 790 (1993).

Excess molar volumes, excess viscosities, and excess energies of activation for viscous flow have been determined for the *n*-decane + 1-chlorodecane system at different temperatures, over the whole concentration range. The Prigogine–Flory–Patterson model for solution thermodynamics has been used to calculate the excess molar volumes. Grunberg and Nissan, McAllister, Teja and Rice, and Schrodt and Akel models have been used to calculate viscosity coefficients and these were compared with experimental data for the mixtures.

MERCEDES E. F. DE RUIZ HOLGADO, CECILIA R. DE SCHAEFER, FRANCO DAVOLIO et MIGUEL KATZ. Can. J. Chem. **71**, 790 (1993).

Opérant à diverses températures et faisant varier la concentration sur l'ensemble des concentrations possibles, on a déterminé les excés de volumes molaires, de viscosités et d'énergies d'activation de l'écoulement visqueux du système *n*-décane + 1-chlorodécane. On a utilisé la modèle de Prigogine–Flory–Patterson de la thermodynamique des solutions pour calculer les excès de volume molaires. On a utilisé les modèles de Grunberg et Nissan, de McAllister, de Teja et Rice et de Schrodt et Akel pour calculer les coefficients de viscosité et on a comparé ces valeurs aux données expérimentales obtenues pour les mélanges.

[Traduit par la rédaction]

Can. J. Chem. Downloaded from www.nrcresearchpress.com by 213.200.69.106 on 09/08/12
For personal use only.

Introduction

Excess molar volumes (V^E) and excess viscosities (η^E) of binary mixtures have been extensively studied from both theoretical and experimental points of view (1, 2). This work reports V^E, η^E, and excess energies of activation for viscous flow (ΔG^{*E}) for *n*-decane + 1-chlorodecane mixtures at 293.15, 298.15, 303.15, and 308.15 K. An equation that reproduces the viscosity as a function of temperature and composition has been established for this system.

Information could be obtained concerning the interaction between the mixed chemical species. The V^E values were analyzed in terms of the Prigogine–Flory–Patterson model. The analysis shows the importance of the three contributions, ΔV_{int}, ΔV_{P*}, and ΔV_F, to V^E.

Excess viscosities and energies of activation for viscous flow were used to calculate some thermodynamic parameters of activation. Some existing equations that calculate viscosities, viz., those of Grunberg and Nissan (3), McAllister (4), Teja and Rice (5), and Schrodt and Akel (6), have been compared, and this last equation showed the best agreement with experimental data.

Experimental

The methods used in our laboratory have been described previously (1, 2). Densities were determined with an AP digital densimeter, model DMA 45. A thermostatically controlled bath (constant to ±0.01 K) was used. Calibration was carried out with air and doubly distilled water with an error of ±0.1 kg m^{-3}. All weighings were made on a Mettler H315 balance. Temperatures were read from calibrated thermometers.

Viscosities of the pure components and of the mixtures were determined with a Schott-Geräte AVS 300 viscosimeter. The Ubbelohde viscosimeter tubes were calibrated and the temperature were maintained to ±0.02 K with a Schott-Geräte CT 1450 temperature controller. The estimated error was ±0.005 mPa s.

n-Decane Fluka (puriss.) and 1-chlorodecane Schuchardt (puriss.) were distilled and only the middle fractions were collected. The binary mixtures were prepared by mixing weighed amounts of the pure liquids. Caution was taken to prevent evaporation.

Results and discussion

The experimental results for the pure components are reported in Table 1 together with literature values for comparison.

The excess molar volumes were calculated with the following equation:

$$[1] \quad V^E = x_1M_1(\rho^{-1} - \rho_1^{-1}) + x_2M_2(\rho^{-1} - \rho_2^{-1})$$

where x_1 and x_2 are the mole fractions of the components, M_1 and M_2 are the molecular weights of the components 1 and 2, and ρ, ρ_1, and ρ_2 are the densities of the solution and of the pure components.

Excess viscosities were calculated from:

$$[2] \quad \eta^E = \eta - \exp(x_1 \ln \eta_1 + x_2 \ln \eta_2)$$

where the additivity law in a logarithm form has been considered for the ideal mixture.

The excess free energies of activation for viscous flow were obtained from the following equation:

$$[3] \quad \Delta G^{*E} = RT(\ln \eta V - x_1 \ln \eta_1 V_1 - x_2 \ln \eta_2 V_2)$$

where V_1 and V_2 are the molar volumes of the components and V is the molar volume of the solution: $V = (x_1M_1 + x_2M_2)/\rho$.

Tables 2 and 3 show the experimental values of densities and viscosities at four different temperatures.

Each set of results was fitted with a Redlich–Kister equation of the type:

$$[4] \quad X^E = x_1(1 - x_1) \sum_{j=1}^{n} a_j(1 - 2x_1)^{j-1}$$

[1]Author to whom correspondence may be addressed.

TABLE 1. Densities and viscosities of the pure components

	293.15 K		298.15 K		303.15 K		308.15 K	
	Exp.	Lit.	Exp.	Lit.	Exp.	Lit.	Exp.	Lit.
				n-Decane				
Density, $\rho \times 10^{-3}$ (kg m^{-3})	0.7298	0.73012[a]	0.7264	0.7263[b]	0.7222	—	0.7187	—
Viscosity, η (mPa s)	0.927	0.9284[c]	0.870	0.8614[a]	0.814	—	0.759	—
				1-Chlorodecane				
Density, $\rho \times 10^{-3}$ (kg m^{-3})	0.8664	0.8705[c]	0.8624	—	0.8588	—	0.8551	—
Viscosity, η (mPa s)	1.944	—	1.787	—	1.630	—	1.471	—

[a]Reference 7.
[b]Reference 8.
[c]Reference 9.

TABLE 2. Experimental densities for the *n*-decane (1) + 1-chlorodecane (2) system

	$\rho \times 10^{-3}$ (kg m^{-3})			
x_1	293.15 K	298.15 K	303.15 K	308.15 K
0.1000	0.8531	0.8491	0.8456	0.8416
0.2004	0.8397	0.8357	0.8318	0.8281
0.2954	0.8269	0.8220	0.8190	0.8152
0.3988	0.8129	0.8090	0.8049	0.8012
0.4972	0.7995	0.7956	0.7915	0.7878
0.5930	0.7864	0.7826	0.7784	0.7747
0.6968	0.7721	0.7684	0.7642	0.7605
0.7947	0.7586	0.7550	0.7507	0.7471
0.8906	0.7452	0.7417	0.7375	0.7339

TABLE 3. Experimental viscosities for the *n*-decane (1) + 1-chlorodecane (2) system

	η (mPa s)			
x_1	293.15 K	298.15 K	303.15 K	308.15 K
0.1000	1.796	1.649	1.500	1.353
0.2004	1.660	1.523	1.388	1.250
0.2954	1.539	1.415	1.291	1.167
0.3988	1.419	1.307	1.196	1.084
0.4972	1.315	1.214	1.114	1.013
0.5930	1.225	1.133	1.042	0.951
0.6968	1.136	1.054	0.973	0.891
0.7947	1.063	0.990	0.917	0.844
0.8906	0.997	0.931	0.867	0.802

where X^E is V^E or η^E or ΔG^{*E}; a_j are the parameters obtained by a least-squares fitting procedure. In each case, the optimum number of coefficients are ascertained from an examination of the variation of the standard error σ estimated with n (calculated with a VAX 11/780 computer):

$$[5] \quad \sigma = [\Sigma (X^E_{obs} - X^E_{calc})^2/(n_{obs} - n)]^{1/2}$$

The values adopted for the coefficients a_j and the standard error estimates associated with the use of eq. [5] are summarized in Table 4.

The viscosity of liquids varies with temperature according to the classical Andrade equation:

$$[6] \quad \eta = A \exp(B/T)$$

where A and B are constants that depend on the nature of the liquids. The viscosity of liquid mixtures varies also with composition as:

$$[7] \quad \eta = f(T,x)$$

By using a multiple linear regression, an equation has been obtained which correlates T and x. For this system, the equation is

$$[8] \quad \ln \eta = -4.626 - 0.79\, x_1 + \frac{1549}{T} + 0.09\, x_1^3$$

with $\sigma = 0.02$, where x_1 is the mole fraction of *n*-decane. The standard deviation of the logarithm of the viscosity coefficients has the form of eq. [5].

Figures 1, 2, and 3 show the experimental values of V^E, η^E, and ΔG^{*E}, respectively. The continuous curves were calculated from eq. [4] using the adopted values for the coefficients.

This system shows positive values of V^E and negative values of η^E. Several effects may contribute to the values of V^E, such as breaking of liquid order on mixing, contribution due to the difference in size and shape of the components, difference in free volumes, and dipole–dipole interactions. The observed V^E is a resultant contribution of the above effects. The positive values of V^E indicate that the two former effects are dominant over the latter effects in this system (10, 11), implying that dispersion forces are dominant. The variation in the magnitude of V^E with increasing temperature is found to be small.

Generally, positive V^E corresponds to negative η^E, as in this case. The free energy ΔG^{*E} is considered a reliable means of detecting the interaction between molecules (12, 13). Positive values of ΔG^{*E} can be seen in binary systems where specific interactions between molecules take place. In this system, ΔG^{*E} is negative; thus we conclude again that dispersion forces are dominant.

Molar excess volume can be calculated from the Prigogine–Flory–Patterson (PFP) theory (14). The original Prigogine–Flory theory includes three contributions in order

Can. J. Chem. Downloaded from www.nrcresearchpress.com by 213.200.69.106 on 09/08/12
For personal use only.

TABLE 4. Coefficients of eq. [4] and standard deviations determined by the method of least squares for the *n*-decane (1) + 1-chlorodecane (2) system

	$V^E \times 10^6$ (m^3 mol^{-1})				η^E (mPa s)				ΔG^{*E} (J mol^{-1})			
	293.15 K	298.15 K	303.15 K	308.15 K	293.15 K	298.15 K	303.15 K	308.15 K	293.15 K	298.15 K	303.15 K	308.15 K
a_1	0.53	0.71	0.90	0.99	−0.120	−0.140	−0.161	−0.186	−221	−281	−348	−441
a_2	−0.04	−0.10	−0.10	−0.11	−0.005	−0.012	−0.017	−0.041	116	100	100	70
a_3	−0.16	−0.60	−0.30	−0.10	−0.050	−0.019	−0.009	−0.050	76	50	10	−70
a_4	0.10	0.40	0.20	0.30	—	−0.040	−0.088	−0.040	−91	−110	−180	−200
a_5	—	0.60	—	—	—	—	—	—	—	—	—	—
σ	0.005	0.006	0.006	0.005	0.0006	0.0003	0.0006	0.0008	1.1	1.2	1	1.6

TABLE 5. Equation of state parameters for the pure components at 298.15 K

	$\alpha \times 10^3$ (K^{-1})	$\kappa_T \times 10^7$ (kPa^{-1})	$V \times 10^6$ (m^3 mol^{-1})	$V^* \times 10^6$ (m^3 mol^{-1})	$P^* \times 10^6$ (J m^{-3})	T^* (K)	$\tilde{V}$	$\tilde{T}$
n-Decane	1.04[a]	10.94[a]	195.876	155.952	448	5114	1.2560	0.0583
1-Chlorodecane	0.874[b]	10.20[c]	202.220	165.577	381	3255	1.2213	0.0528

[a]Reference 19.
[b]From density measurements.
[c]Reference 20.

Can. J. Chem. Downloaded from www.nrcresearchpress.com by 213.200.69.106 on 09/08/12
For personal use only.

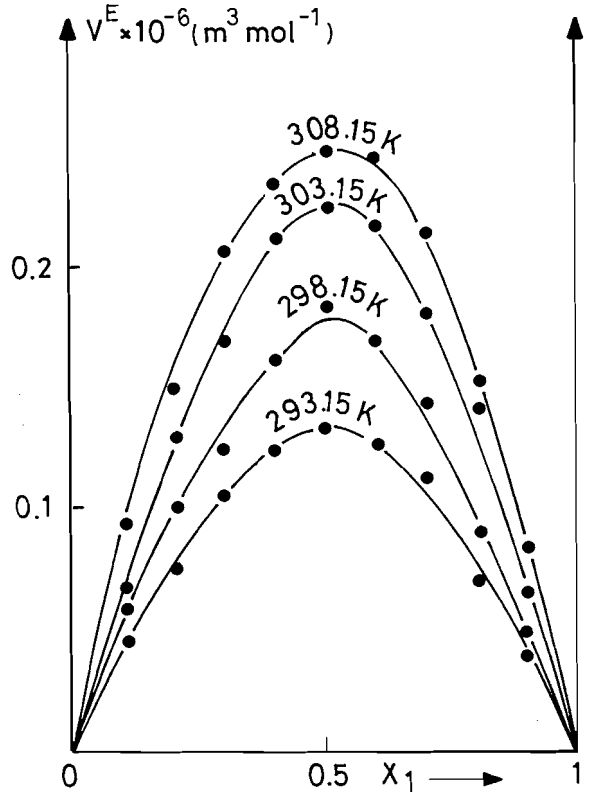

FIG. 1. Excess molar volumes for the *n*-decane (1) + 1-chlorodecane (2) system. Continuous curves were calculated from eq. [4].

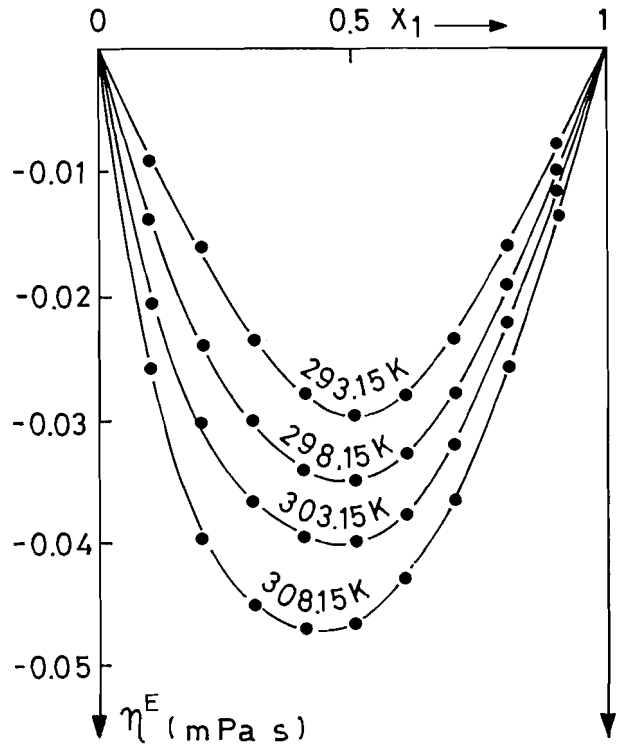

FIG. 2. Excess viscosities for the *n*-decane (1) + 1-chlorodecane (2) system. Continuous curves were calculated from eq. [4].

to explain the thermodynamic behavior of the liquid mixtures: an interactional contribution (ΔV_{int}), which is proportional to the interactional parameter X_{12}; the free volume contribution, which arises from the dependence of the reduced volume upon the reduced temperature as a result of the difference between the degree of expansion of the two components (ΔV_F); and the internal pressure contribution (ΔV_{P*}), which depends on both the difference of characteristic pressures and on the reduced volumes of the components.

Some new effects not treated in this theory have been discussed for molecules of different shape (15). The equation is

$$[9]\quad \frac{V^E}{x_1V_1^* + x_2V_2^*} = \frac{(\tilde{V}^{1/3} - 1)\tilde{V}^{2/3}}{(4/3)\tilde{V}^{-1/3} - 1}\psi_1\theta_2\frac{X_{12}}{P_1^*} - \frac{(\tilde{V}_1 - \tilde{V}_2)^2\left(\frac{14}{9}\tilde{V}^{-1/3} - 1\right)}{[(4/3)\tilde{V}^{-1/3} - 1\ \tilde{V}]}\psi_1\psi_2 + \frac{(\tilde{V}_1 - \tilde{V}_2)\,(P_1^* - P_2^*)}{\psi_1P_2^* + \psi_2P_1^*}\psi_1\psi_2$$
$$= \Delta V_{int} - \Delta V_F + \Delta V_{P^*}$$

where $\tilde{V}$ is the reduced volume, V^* is the characteristic volume, P^* is the characteristic pressure, ψ is the contact energy fraction, ϕ is the hard core volume fraction, and θ is the surface site fraction.

Heintz (16) introduced the so-called ERAS model, which combines the linear chain association model with Flory's equation of state theory. In this case, both components are not associated in the pure state and the chemical contribution is not taken into account.

The various parameters involved in eq. [9] for the pure components (with subscript) and the mixture (without subscripts) are obtained from Flory's theory (17) and are shown in Table 5.

The interactional contribution to V^E contains the interaction parameter X_{12}, which is usually calculated using experimental values of the excess enthalpy H^E. As no values of H^E are available for this system, X_{12} values were derived by fitting the theory to experimental values of V^E for this system.

The value of X_{12} obtained at 298.15 K is -0.316×10^{-6} J m^{-3} and, for equimolecular values, the three contributions are $\Delta V_{int} = -6.56 \times 10^{-5}$, $\Delta V_F = 4.26 \times 10^{-4}$, and $\Delta V_{P^*} = 1.40 \times 10^{-3}$ with a calculated $V^E = 0.143 \times 10^{-6}$ m^3 mol^{-1}.

An analysis of each of the three contributions to V^E shows that the interaction contribution is negative and small compared with the other two. The free volume contributions are positive and smaller than the internal pressure contribution. The total theoretical values are found to be in agreement with the experimental data, as shown in Fig. 4, with more error observed between x_1 0.4 and 0.6.

Different equations exist in the literature that can calculate viscosity coefficients for mixtures. Grunberg and Nissan (3) proposed an empirical equation to describe real mixtures:

$$[10]\quad \ln\eta = x_1\ln\eta_1 + x_2\ln\eta_2 + x_1x_2\delta$$

where δ reflects the nonideality of the system. The parameter δ has usually been regarded as an approximate measure of the strength of the interaction between the components. However, it has been shown that in certain cases it can also be correlated with the difference in molecular volumes of the components and with the entropy of mixing (10). The values obtained for δ at 298.15 K for the system are summarized in Table 6 together with the percent error.

The McAllister correlation (4) is based on a model proposed by Eyring *et al.* (18), which considers that interaction occurs between three bodies:

$$[11]\quad \ln\nu = x_1^3\ln\nu_1 + x_2^3\ln\nu_2 + x_1^3\ln M_1 + x_2^3\ln M_2 - \ln(x_1M_1 + x_2M_2) + 3x_1^2x_2\ln\left(2M_1 + \frac{M_2}{3}\right)$$
$$+ 3x_1x_2^2\ln\left(M_1 + \frac{2M_2}{3}\right) + 3x_1^2x_2\ln\nu_{12} + 3x_1x_2^2\ln\nu_{21}$$

where ν represents the kinematic viscosity (η/ρ) and ν_{12} and ν_{21} are the interaction parameters obtained by a least-squares method. Table 6 gives these values with their percent error.

We applied the corrresponding states method of Teja and Rice (5) to calculate viscosities of the mixtures. These authors proposed the relation:

$$[12]\quad \ln(\eta\xi) = \ln(\eta\xi)^{(r_1)} + \frac{\omega - \omega^{(r_1)}}{\omega^{(r_2)} - \omega^{(r_1)}}[\ln(\eta\xi)^{(r_2)} - \ln(\eta\xi)^{(r_1)}]$$

where (r_1) and (r_2) refer to the properties of two reference fluids (in this case, the pure components) and ω is the acentric factor.

The values of ξ from eq. [12] were obtained from:

$$[13]\quad \xi = V_c^{2/3}/(T_cM)^{1/2}$$

where V_c and T_c are the critical volume and temperature, respectively. For mixtures, the pseudo-critical properties V_{cm}, T_{cm}, and ω_m of hypothetical substances that replace the pure fluids are defined (22). Values of $(\eta\xi)^{(r_1)}$ and $(\eta\xi)^{(r_2)}$ at the same reduced temperature have been calculated with ψ values, indicated in Table 6.

Table 7 shows the parameters used for this application.

Following the model of Schrodt and Akel (6), which is based upon Eyring's concept of fluid viscosity, the equation applying to mixtures (22), is

$$[14]\quad \ln\eta = \ln\frac{hN_A}{V} + \Sigma\, x_i\ln\eta_i^0 + \Sigma\, x_i\ln\gamma_i^v$$

where $\eta_0^0 = \eta_iV_i/hN_A$, γ_i^v is the viscosity activity coefficient, and N_A is Avogadro's number.

Using a set of binary viscosity data, we found ΔG^{*E} values, and the viscosity activity coefficients were determined in this

Can. J. Chem. Downloaded from www.nrcresearchpress.com by 213.200.69.106 on 09/08/12
For personal use only.

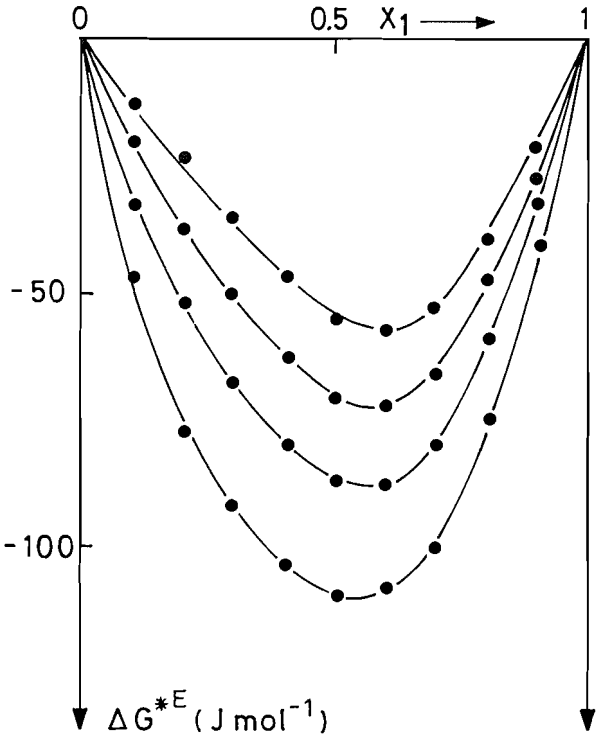

FIG. 3. Excess molar energies of activation for viscous flow for the *n*-decane (1) + 1-chlorodecane (2) system. Continuous curves were calculated from eq. [4].

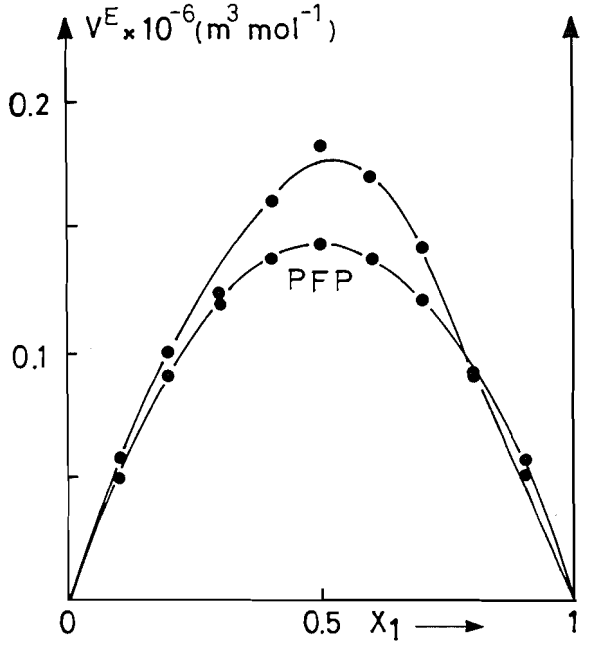

FIG 4. Experimental and calculated excess molar volumes for the *n*-decane (1) + 1-chlorodecane (2) system at 298.15 K.

TABLE 6. Parameters of eqs. [10], [11], [12], and [14] of the *n*-decane (1) + 1-chlorodecane (2) system at 298.15 K

[10]	$\delta = -0.1095$	AD = 0.21
[11]	$\nu_{12} = 0.612$; $\nu_{21} = 1.061$	AD = 0.11
[12]	$\psi = 1$	AD = 0.53
[14]	$\alpha = 0.30$; $\tau_{12} = -1.000$; $\tau_{21} = 1.2798$	AD = 0.09

TABLE 7. Parameters for the pure components

Substance	M (g mol^{-1})	$V_c \times 10^6$ (m^3)	T_c (K)	P_c (atm)	ω
n-Decane	142.284	603[a]	617.6[a]	20.89[a]	0.490[a]
1-Chloro-decane	176.76	639[a]	686.85[a]	20.59[a]	0.577[a]

[a]Reference 21.

case from equations like non-random two liquids' theory (NRTL) and related to $\Delta G^{*E}/RT$. The parameters of the NRTL equations are also given in Table 6 together with the percent error defined as:

$$[15] \quad AD = [\Sigma(\eta_{exp} - \eta_{calc})^2/n]^{1/2} \times 100$$

Various thermodynamic properties of activation for viscous flow have been determined using Eyring's equation (ref. 18); for example:

$$[16] \quad \ln \frac{vM}{hN_A} = -\frac{\Delta S^*}{R} + \frac{\Delta H^*}{RT}$$

Over a short range of temperatures, the molar enthalpy of activation ΔH^* and the molar entropy of activation ΔS^* are approximately constant. Using a least-squares method, the activation parameters ΔH^* and ΔS^* were obtained and ΔG^* was determined from the following equation:

$$[17] \quad \Delta G^* = \Delta H^* - T\Delta S^*$$

The values obtained for ΔG^* vary between 26 000 and 29 000 J mol^{-1}. They decrease with mole fraction of *n*-decane and increase with temperature. The values of ΔH^* at 298.15 K vary from 10 000 to 14 000 J mol^{-1} and ΔS^* varies from -49 to -55 J K^{-1} mol^{-1}.

Only 1-chlorodecane is a polar molecule and η^E is very small. This does not necessarily mean absence of interaction, but could imply that there is an interaction of the dipole–dipole induced type. Fort and Moore (11) and Nigam and Mahl (23) have reported that specific interactions are stronger in binary mixtures where η^E and δ are large and positive. In this system, both are negative and that means weak interactions. In regard to the values of ΔG^*, the sign and magnitude are governed by the corresponding values of ΔH^* and ΔS^* according eq. [17]. A negative ΔS^* indicates that the formation of an activated complex requires comparatively increased molecular order for an increase in its viscous flow.

From the different equations that calculate viscosities of mixtures, the Schrodt and Akel model shows the best agreement with experimental data, since it presents the smallest deviation when compared with the other relations.

Can. J. Chem. Downloaded from www.nrcresearchpress.com by 213.200.69.106 on 09/08/12
For personal use only.

Acknowledgments

The present work was financed by a research grant from the Consejo de Investigaciones Científicas y Técnicas and the Consejo de Investigaciones de la U.N. de Tucumán. We are grateful to Ing. Mario R. Cesca for aid in computer programming.

1. S. B. de Katz, G. C. Pedrosa, and M. Katz. Phys. Chem. Liq. **23**, 15 (1991).
2. I. L. Acevedo and M. Katz. J. Solution Chem. **19**, 1061 (1990).
3. L. Grunberg and A. N. Nissan. Nature, **164**, 799 (1949).
4. P. A. McAllister. AIChE J. **6**, 427 (1960).
5. A. S. Teja and P. Rice. Ind. Eng. Chem. Fundam. **20**, 77 (1981).
6. J. T. Schrodt and R. M. Akel. J. Chem. Eng. Data, **34**, 8 (1989).
7. J. A. Riddick, N. R. Bunger, and T. Sakano. Organic solvents. 4th ed. J. Wiley & Sons, New York. 1986.
8. T. Kasprzycka-Guttman and N. Wilczura. Thermochim. Acta, **159**, 1 (1990).
9. R. C. Weast (*Editor*). Handbook of chemistry and physics. 60th ed. C.R.C. Press, Boca Raton, Fla. 1979–1980.
10. M. G. Prolongo, R. M. Masegosa, I. M. Fuentes, and H. Horta. J. Phys. Chem. **88**, 2163 (1984).
11. R. J. Fort and T. E. Moore. Trans. Faraday Soc. **62**, 1112 (1962).
12. T. M. Reed and T. E. Taylor. J. Phys. Chem. **63**, 58 (1959).
13. R. Meyer, M. Meyer, J. Metzer, and A. Peneloux. J. Chim. Phys. **62**, 405 (1971).
14. P. Tancrede, P. Botoherl, P. de St. Romain, and D. Patterson. J. Chem. Soc. Faraday Trans. 2, **73**, 15 (1977).
15. P. de St. Romain, G. H. T. Van, and D. Patterson. J. Chem. Soc. Faraday Trans. 2, **75**, 1700 (1979).
16. A. Heintz. Ber. Bunsen-Ges. Phys. Chem. **89**, 172 (1985).
17. P. J. Flory, R. A. Orwoll, and A. Vrij. J. Am. Chem. Soc. **86**, 1507 (1964); **86**, 3515 (1964).
18. H. Eyring, E. E. Powell, and W. E. Rosenveare. Ind. Eng. Chem. **33**, 837 (1941).
19. A. D. Matilla, G. Tardajos, E. Junquera, and E. Aicart. J. Solution Chem. **20**, 805 (1991).
20. J. A. Salas, B. O'Donell, L. Scida, and M. Katz. Anal. Asoc. Quím. Argent. **76**, 427 (1988).
21. R. C. Reid, J. M. Prausnitz, and T. K. Sherwood. The properties of gases and liquids. 3rd ed. McGraw–Hill Book Co., New York. 1977.
22. I. L. Acevedo, E. L. Arancibia, and M. Katz. Thermochim. Acta, **195**, 129 (1992).
23. R. K. Nigam and B. S. Mahl. Ind. J. Chem. **9**, 1255 (1971).

Can. J. Chem. Downloaded from www.nrcresearchpress.com by 213.200.69.106 on 09/08/12
For personal use only.

The reactions of 4-hydroxymethylsydnones with alcohols and benzene

LING-LING TIEN AND SHAW-TAO LIN[1]
Department of Applied Chemistry, Providence University, Sha-Lu, Taichung Hsien, Taiwan, 433, Republic of China

AND

HSIEN-JU TIEN[1] AND GWO-MING FANG
Department of Chemistry, National Chung-Kung University, Tainan, Taiwan, 701, Republic of China

Received July 13, 1992[2]

LING-LING TIEN, SHAW-TAO LIN, HSIEN-JU TIEN, and GWO-MING FANG. Can. J. Chem. **71**, 796 (1993).

In the presence of a Lewis acid, 4-hydroxymethylsydnones undergo reaction with alcohols and benzene to form 4-alkoxysydnones **1***a*, bis(4-sydnonylmethyl) ethers **1***b*, or 4-benzylsydnones **1***d* depending upon the reaction conditions. At 0°C, compounds **1***a* and **1***b* are formed from compound **1** in benzene and alkyl alcohol, respectively. Compound **1***b* is converted to compound **1***d* at 40°C. When the reactions are carried out in a cosolvent of benzene and methyl alcohol at 40°C, compound **1***a* is obtained preferentially and followed by conversion to compound **1***d*. The α-sydnonylmethylene cation derived from either compound **1** or **1***a* is responsible for the formation of compound **1***d*.

LING-LING TIEN, SHAW-TAO LIN, HSIEN-JU TIEN et GWO-MING FANG. Can. J. Chem. **71**, 796 (1993).

Les 4-hydroxyméthylsydnones mises en présence d'un acide de Lewis réagissent avec les alcools et le benzène pour former, suivant les conditions de la réaction, les 4-alkoxysydnones (**1***a*), les éthers bis(4-sydnonylméthyle) (**1***b*) ou les 4-benzylsydnones (**1***d*). À 0°C, le composé **1** conduit aux composés **1***a* ou **1***b* suivant qu'il mis en présence d'alcool aliphatique ou de benzène. À 40°C, les composés **1***b* se transforment en produits **1***d*. Lorsqu'on réalise les réactions en présence d'un cosolvant de benzène et de méthanol, à 40°C, les composés **1***a* sont obtenus d'une façon préférentielle avant d'être transformés en composés **1***d*. Le cation α-sydnonylméthylène qui dérivé soit du composé **1** ou des composés **1***a* est responsable de la formation des composés **1***d*.

[Traduit par la rédaction]

The nature of the sydnone ring demonstrates the electron-withdrawing character on N(3) and electron-donating properties on C(4) (1). This dual character of the ring has been observed in the nitration of 3-(4′-alkylphenyl)sydnones and 3-benzylsydnone, resulting in the formation of 3-(4′-alkyl-3′-nitrophenyl)sydnone and 3-(3′-nitrobenzyl)sydnone, respectively (2). Electrophilic substitution, i.e., formylation and acetylation, takes place at the C(4) position (3). In the gas phase, the sydnonylmethylene cation has been generated from sydnonylmethanols and their derivatives (4). This fact suggested that the C(4) is also able to stabilize the methylene group (4). If the sydnonyl ring is able to stabilize the C(4)-methylene cation as in the benzylic system, the sydnonylmethanol will then be able to act as an electrophile in the presence of Lewis acid. In this work we study the reaction of sydnonylmethanol with benzene and (or) alcohol in the presence of either sulfuric acid or boron trifluoride to ascertain the properties of C(4) of the sydnonyl ring.

Results and discussion

The sydnone carbinols are highly soluble in chlorinated solvents. In chloroform or in the presence of strong acid, these compounds are less stable and tend to give highly colored solutions. The condensations between sydnonylmethanol and alkyl alcohol were carried out in methylene chloride solution because of these considerations of solubility and stability. At 40°C, using Lewis acids such as sulfuric acid, boron trifluoride, and trifluoroacetic acid, this leads to condensation products as shown in Table 1. The darkening of color reflects product yields, sulfuric acid being better than BF_3 and CF_3COOH. When CF_3COOH is used as a catalyst, longer reaction times (24 h) are required to obtain comparable yields (entry 3).

The steric factor of alkyl groups plays an insignificant role in the yields of **1***g*. Clean products obtained from the reaction

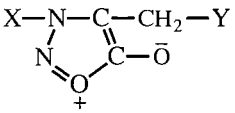

Y = OH
X: C_6H_5, **1**; 4-MeO-C_6H_4, **2**; 4-Me-C_6H_4, **3**; 4-Br-C_6H_4, **4**; 4-NO_2-C_6H_4, **5**; cyclo-C_6H_{11}, **6**

Y = OMe
X: C_6H_5, **1***a*; 4-MeO-C_6H_4, **2***a*; 4-Me-C_6H_4, **3***a*; 4-Br-C_6H_4, **4***a*; 4-NO_2-C_6H_4, **5***a*; cyclo-C_6H_{11}, **6***a*

Y = C_6H_5
X: C_6H_5, **1***d*; 4-MeO-C_6H_4, **2***d*; 4-Me-C_6H_4, **3***d*; 4-Br-C_6H_4, **4***d*; 4-NO_2-C_6H_4, **5***d*; cyclo-C_6H_{11}, **6***d*

X = C_6H_5
Y: OEt, **1***e*; OPr-*n*, **1***f*; OPr-i, **1***g*

of compound **1** and *n*-propanol in the presence of either H_2SO_4 or BF_3 indicate that there is no isomerization of the *n*-propyl group during the reaction (entries 6, 7). The formation of the ether product can occur by either an S_N1 or an S_N2 mechanism (5). However, the absence of rearranged product implies either that no carbocation is derived from *n*-propanol or that the Lewis acid reacts preferentially with sydnonylmethanol rather than with the alkyl alcohol.

Further inspection of the yields of the products obtained from different sydnones reflects the important role of substituents: electron-withdrawing groups destabilize the reaction center through the sydnonyl ring resulting in lower yields of products (entry 16).

The kinetic study on the rate of conversion to the corre-

[1]Authors to whom correspondence may be addressed.
[2]Revision received February 18, 1993.

Can. J. Chem. Downloaded from www.nrcresearchpress.com by 213.200.69.106 on 09/08/12
For personal use only.

TABLE 1. Reaction of sydnonylmethanol with alcohols in methylene chloride in the presence of Lewis acid catalyst[a]

Entry	Compound	Alcohol	Acid	Product	Yield (%)[b]
1	**1**	MeOH	S	**1***a*	82
2	**1**	MeOH	B	**1***a*	66
3	**1**	MeOH	C	**1***a*	70[c]
4	**1**	EtOH	S	**1***e*	88[d]
5	**1**	EtOH	B	**1***e*	65*d*
6	**1**	*n*-PrOH	S	**1***f*	68[d]
7	**1**	*n*-PrOH	B	**1***f*	51[d]
8	**1**	i-PrOH	S	**1***g*	70[d]
9	**1**	i-PrOH	B	**1***g*	50[d]
10	**2**	MeOH	S	**2***a*	85
11	**2**	MeOH	B	**2***a*	72
12	**3**	MeOH	S	**3***a*	83
13	**3**	MeOH	B	**3***a*	70
14	**4**	MeOH	S	**4***a*	54
15	**4**	MeOH	B	**4***a*	46
16	**5**	MeOH	S	**5***a*	51
17	**5**	MeOH	B	**5***a*	42
18	**6**	MeOH	S	**6***a*	58
19	**6**	MeOH	B	**6***a*	41

[a]Arylsydnonylmethanol(0.01 mol) in methylene chloride (50 mL) containing methanol (10 mL). Reaction period was 3 h at a temperature of 40°C. The yields are isolated yields. S: sulfuric acid; B: boron trifluoride: C: trifluoroacetic acid.
[b]Isolated yield.
[c]Time, 24 h.
[d]Reference 9.

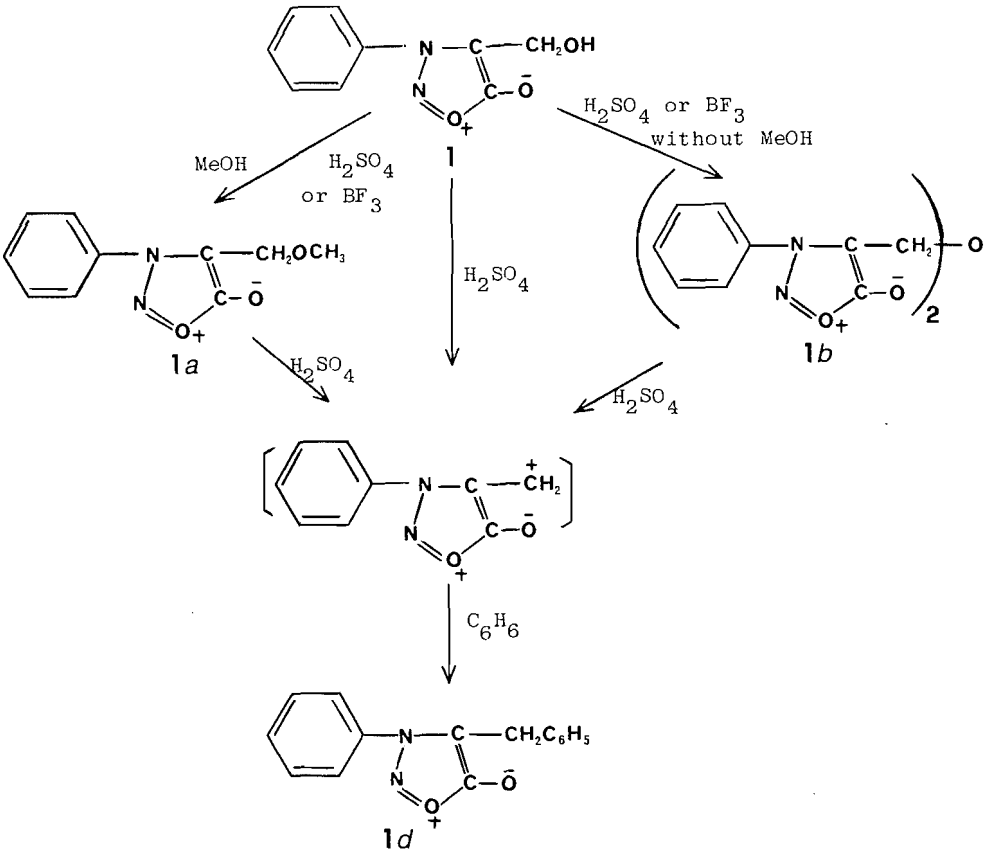

SCHEME 1

Can. J. Chem. Downloaded from www.nrcresearchpress.com by 213.200.69.106 on 09/08/12
For personal use only.

TABLE 2. Kinetics of the reaction of 3-arylsydnonylmethanol and methanol in methylene dichloride in the presence of sulfuric acid at 40°C[a]

Entry	Compound	σ	Rate(mol/h)	$\log(r_1/r_0)$
20	**2**	−0.27	0.051	0.048
21	**3**	−0.17	0.049	0.027
22	**1**	0	0.046	
23	**4**	0.23	0.042	−0.040
24	**5**	0.78	0.034	−0.131

[a]The rates were measured by ^{1}H NMR spectroscopy monitoring the decrease of the methylene signal for the first 30% conversion.

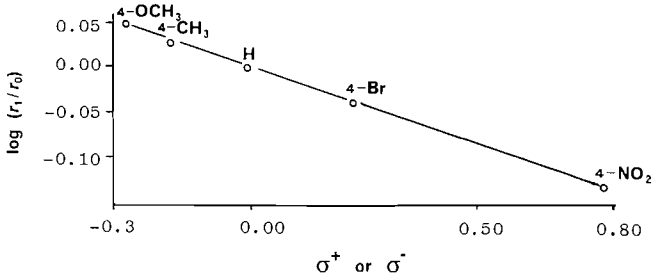

FIG. 1. The correlation between log (r_0/r_1) and the Hammett substituent constant (σ) for aryl-substituted 4-hydroxymethylsydnones.

sponding ethers was carried out at 40°C and monitored by ^{1}H NMR to the first 30% conversion (Table 2). The correlation between the substituent constant σ of the specific substituents on the phenyl ring and the conversion rate gives $\rho = -0.02$ with a correlation coefficiency of 0.956 (Fig. 1). The small and negative ρ value implies that the reaction center bearing the positive charge is influenced by the remote substituent. This ability of the sydnonyl ring to transmit the inductive effect has also been observed in the gas phase (4).

Boron trifluoride has been shown to be an effective catalyst for the reaction of benzyl alcohol and benzene to form diphenylmethane via a typical Friedel–Crafts reaction (5). However, BF_3 is not an ideal catalyst for the sydnone system. This might be due to the formation of a complex as is observed for γ-diketones (6), i.e., the BF_3 interacts with the oxygen atoms of hydroxyl groups as well as with the carbonyl of the sydnonyl ring.

To undergo electrophilic substitution, the sydnonylmethanol must be converted to its corresponding carbocation. In the presence of H_2SO_4, the reaction of the sydnonyl methanols and benzene at 40°C, either without solvent or in CH_3CN, CH_2Cl_2, leads to 3-aryl-4-benzylsydnones in good yields (Table 3). The variation of the yield as a function of the substituent on the phenyl ring reflects the reactivity of the corresponding cation. Bis-sydnonylmethyl ethers *b* are obtained from the same reactions at 0°C when H_2SO_4 or BF_3 is used. Also, the same results are obtained in the presence of BF_3 at 40°C (Scheme 1). The inability of BF_3 to catalyze the formation of compounds *d* may be due either to insufficient reactivity to form the carbocation or to the formation of stable complexes with boron fluoride as described above.

During the reaction, the sydnonylmethanol can be converted to either a carbocation or a protonated state. The carbocation reacts either with benzene or with methanol yielding a Friedel–Crafts product *d* or ether *a*, respectively. However, the protonated sydnonylmethanol may react only with alcohol, yielding an ether *a* rather than *d* as a final product. To differentiate whether carbocation or protonated sydnone is involved in this reaction system, compound **1** was dissolved in a mixture of equal amounts of benzene and methanol (1.0 mL: 1.0 mL) in the presence of H_2SO_4 as a catalyst. At 0°C, after a 3 h reaction period, only ether **1***a* was isolated. On the other hand, when the same reaction was carried out at 40°C, 4-benzylsydnone **1***d* was obtained as a major product (Table 4). We interpret these results as follows. At a lower temperature, the ether is produced via an S_N2 process, i.e., the methylene group of protonated sydnonylmethanol is attacked by methanol. At a higher temperature, the carbocation derived from sydnonylmethanol or ether **1***a* undergoes electrophilic substitution. The formation of carbocation could be caused by cleavage of ether *b*, methyl ether *a*, or derived from the precursor itself. To ascertain which of these three possible sources is involved in this system, the following experiments were carried out. The benzene-d_6 solution of methyl-d_3 ether in the presence of H_2SO_4 was monitored by ^{1}H NMR at 40°C by comparing the methylene signal of ether **1***a* (4.35 ppm) with that of the methylene of the benzyl ether **1***d* (3.85 ppm). The signal at 4.35 ppm completely disappeared within 2 h, suggesting that the methyl ether *a* is readily cleaved to generate cation *c* for further reaction. The same experiment was carried out with ether **1***b* instead of methyl ether **1***a*. The signal of the methylene group of ether **1***b* at 3.95 ppm completely disappeared after 5 h. Therefore, the formation of 4-benzylsydnone from ether *b* can be an alternative pathway. Even so, the above pathway is unlikely because of the insignificant amount of ether *b* that is formed in the presence of methanol.

Conclusion

In the presence of Lewis acids, sydnonylmethanols readily react with alcohols to produce the corresponding ether derivatives. Below room temperature, no Friedel–Crafts reaction is observed due to insufficient energy for the formation of the sydnonylmethyl cation intermediate. However, its formation at 40°C has been established from either sydnonylmethanols or methoxymethylsydnones. For aryl-substituted sydnones, the rate of electrophilic substitution is a function of the substituent; this fact implies the ability of the sydnonyl ring to transmit electron density from the aryl ring and the ability of the aryl substituent to stabilize the methylene cation in a manner similar to effects observed for the benzyl system. This observation is consistent with results obtained from mass spectroscopic studies (4).

Experimental

Melting points were measured on a Yanaco MP-J3 micro melting apparatus and are uncorrected. Infrared spectra were determined with a Perkin–Elmer model 457n grating infrared spectrophotometer using a potassium bromide pellet. Mass spectra were measured on a Jeol JMS DX-300 mass spectrometer using 70 eV ionization energy. NMR spectra were determined with a Bruker AC-250 FT-NMR by using $CDCl_3$ as a solvent and Si_4Me as an internal standard.

3-Aryl-4-hydroxymethylsydnones were prepared according to literature procedures (7, 8).

Can. J. Chem. Downloaded from www.nrcresearchpress.com by 213.200.69.106 on 09/08/12
For personal use only.

TABLE 3. The preparation of 3-aryl-4-benzylsydnones from the reaction of 3-arylsydnonylmethanol with benzene in the presence of Lewis acid[a]

Entry	Compound	Lewis acid	Temperature (°C)	Product (%)
25	**1**	S	40	**1***d*(72)
26	**1**	S	40	**1***d*(72)[b]
27	**1**	S	40	**1***d*(70)[c]
28	**1**	S	0	[d]
29	**1**	B	40	[d]
30	**2**	S	40	**2***d*(78)
31	**2**	S	0	[d]
32	**2**	B	40	[d]
33	**3**	S	40	**3***d*(74)
34	**4**	S	40	**4***d*(54)
35	**5**	S	40	**5***d*(50)
36	**6**	S	40	**6***d*(52)

[a]Arylsydnonylmethanol (0.44 mmol) in methylene chloride (5 mL) containing benzene (1 mL). The yields are isolated yields. S: sulfuric acid; B: boron trifluoride.
[b]No solvent was used.
[c]The solvent was acetone.
[d]Bis-sydnonylmethyl ether was obtained.

TABLE 4. Competitive reaction between benzene and methanol toward arylsydnonylmethanol in the presence of sulfuric acid or boron trifluoride[a]

				Products (%)[b]	
Entry	Compound	Lewis acid	Temperature (°C)	Ether	Benzyl
37	**1**	B	40	**1***a*(65)	—
38	**1**	S	40	**1***a*(32)	**1***d*(47)[c]
39	**2**	B	40	**2***a*(70)	—
40	**2**	B	40	**2***a*(68)	—
41	**2**	S	40	**2***a*(27)	**2***d*(55)
42	**2**	S	0	**2***a*(83)	—
43	**3**	B	40	**3***a*(69)	—
44	**3**	B	0	**3***a*(68)	—
45	**3**	S	40	**3***a*(23)	**3***d*(53)
40	**3**	S	0	**3***a*(78)	—
46	**4**	B	40	**4***a*(38)	—
47	**4**	S	40	**4***a*(28)	**4***d*(33)
48	**5**	B	40	**5***a*(35)	—
49	**5**	S	40	**5***a*(32)	**5***d*(20)
50	**6**	B	40	**6***a*(36)	—
51	**6**	S	40	**6***a*(42)	**6***d*(18)

[a]Arylsydnonylmethanol (0.01 mol) in a mixture of benzene and methanol (10 mL: 10 mL). Reaction time was 3 h.
[b]Ether: arylsydnonylmethyl methyl ether; benzyl: 3-aryl-4-benzylsydnone.
[c]The purity of the products isolated was determined by ^{1}H NMR. The ratio of two products was also obtained by NMR calculated from the areas of the methylene groups at 4.20 and 3.80 ppm, respectively.

Preparation of 3-aryl-4-alkoxylsydnones. Typical procedure

(*a*) To an ice-cooled and stirred solution of 4-(hydroxymethyl)-3-phenylsydnone (0.2 g, 1.04 mmol) in CH_2Cl_2 (5 mL) containing methanol (1 mL) was added concentrated H_2SO_4 (0.2 mL). After being stirred for 0.5 h, the solution was allowed to warm to 30°C, and was stirred for an additional 3 h. The resultant solution was poured into ice-cold sodium bicarbonate aqueous solution. Following filtration, the crude product was recrystallized from 95% ethanol yielding **1***a* as colorless needle crystals: 0.18 g (82% yield); mp 56°C.

The following compounds were obtained according to this procedure.

*3-(4-Methoxyphenyl)-4-methoxymethylsydnone(***2**a*):* mp 181–182°C; IR(KBr) $\nu_{C=O}$: 1744 cm^{-1}; NMR(DMSO-d_6) δ: 3.40(s, 3H, OCH_3), 3.98(s, 3H, OCH_3), 4.24(s, 2H, CH_2), 7.24(d, 2H, J = 9.1 Hz, aromatic), 7.91(d, 2H, J = 9.1 Hz, aromatic); MS, m/z(relative intensity): 236(M^+, 16), 178(100). Anal. calcd. for $C_{11}H_{12}N_2O_4$: C 55.93, H 5.08, N 11.86; found: C 55.82, H 5.09, N 11.83).

*3-(4-Nitrophenyl)-4-methoxymethylsydnone(***5**a*):* mp 116–117°C; IR(KBr) $\nu_{C=O}$: 1775 cm^{-1}; NMR (DMSO-d_6) δ: 3.45(s, 3H, OCH_3), 4.29(s, 2H, CH_2), 8.08(d, 2H, J = 9.0 Hz, aromatic), 8.83(d, 2H, J = 9.0 Hz, aromatic); MS, m/z(relative intensity): 251(M^+, 3), 45(100). Anal. calcd. for $C_{10}H_9N_3O_5$: C 47.81, H 3.59, N 16.73; found: C 47.77, H 3.68, N 16.78.

*3-(Cyclohexyl)-4-methoxymethylsydnone(***6**a*):* mp 95–96°C; IR(KBr) $\nu_{C=O}$: 1734 cm^{-1}; NMR (DMSO-d_6) δ: 1.37–1.62(m, 11H, C_6H_{11}), 3.94(s, 3H, OCH_3), 4.32(s, 2H, CH_2); MS, m/z(relative intensity): 212(M^+, 33), 83(100). Anal. calcd. for $C_{10}H_{16}N_2O_3$: C 56.60, H 7.55, N 13.20; found: C 56.39, H 7.51, N 13.21.

Can. J. Chem. Downloaded from www.nrcresearchpress.com by 213.200.69.106 on 09/08/12
For personal use only.

Can. J. Chem. Downloaded from www.nrcresearchpress.com by 213.200.69.106 on 09/08/12
For personal use only.

(*b*) This reaction was carried out by the same procedure as above, except that CH_2Cl_2 (5 mL) containing methanol (1 mL) and benzene (1 mL) was used instead of methanol and CH_2Cl_2 solution. After work-up, colorless needles of **1***a* were obtained; yield: 0.17 g (78%).

Preparation of 3-aryl-4-benzylsydnones. Typical procedure

(*a*) To an ice-cooled and stirred solution of 4-(hydroxymethyl)-3-(4-tolyl)sydnone (0.09 g, 0.44 mmol) in CH_2Cl_2 (5 mL) containing benzene (1 mL), was added concentrated H_2SO_4 (0.1 mL). After being stirred for 5 min, the solution was allowed to warm to 40°C, and stirred for an additional 3 h. During the reaction, the color of solution changed from light brown to deep green. This resultant solution was poured into ice-water yielding a glue-like precipitate. The crude solid product obtained upon treating with sodium bicarbonate solution was recrystallized from 95% ethanol, yielding **3***d* as colorless crystals (0.09 g, 72% yield); mp 97–98°C; IR(KBr) $\nu_{C=O}$: 1748 cm^{-1}; NMR(DMSO-d_6) δ: 2.42(s, 3H, CH_3), 3.79(s, 2H, CH_2), 6.99–7.60(m, 9H, aromatic); MS, *m/z* (relative intensity): 266(M^+, 16), 91(100). Anal. calcd. for $C_{16}H_{14}N_2O_2$: C 72.18, H 5.26, N 10.53; found: C 72.19, H 5.16, N 10.46.

The followwing compounds were obtained by this procedure:

*3-(Phenyl)-4-benzylsydnone(**1**d):* mp 99–100°C; IR(KBr) $\nu_{C=O}$: 1734 cm^{-1}; NMR(DMSO-d_6) δ: 3.80(s, 2H, CH_2), 6.94–7.25(m, 5H, aromatic), 7.74–7.83(m, 5H, aromatic); MS, *m/z*(relative intensity): 252(M^+, 11), 91(100) Anal. calcd. for $C_{15}H_{12}N_2O_2$: C 71.43, H 4.76, N 11.11; found: C 71.22, H 4.65, N 10.99.

*3-(4-Methoxyphenyl)-4-benzylsydnone(**2**d):* mp 175–176°C; IR-(KBr) $\nu_{C=O}$: 1744 cm^{-1}; NMR (DMSO-d_6) δ: 3.80(s, 2H, CH_2), 3.98(s, 3H, OCH_3), 6.95–7.59(m, 9H, aromatic); MS, *m/z*(relative intensity): 282(M^+, 21), 91(100). Anal. calcd. for $C_{16}H_{14}N_2O_2$: C 68.09, H 4.96, N 9.93; found: C 67.79, H 4.96, N 9.91.

*3-(4-Bromophenyl)-4-benzylsydnone(**4**d):* mp 197–199°C; IR-(KBr) $\nu_{C=O}$: 1740 cm^{-1}; NMR(DMSO-d_6) δ: 3.73(s, 2H, CH_2), 6.90–7.24(m, 5H, aromatic), 7.57–7.92(m, 5H, aromatic); MS, *m/z*(relative intensity): 330(M^+, 5), 91(100). Anal. calcd. for $C_{15}H_{11}N_2O_2Br$: C 54.50, H 3.32, N 8.46; found: C 54.21, H 3.25, N 8.34.

*3-(4-Nitrophenyl)-4-benzylsydnone(**5**d):* mp 110–112°C; IR(KBr) $\nu_{C=O}$: 1762 cm^{-1}; NMR(DMSO-d_6) δ: 3.83(s, 2H, CH_2), 6.98–7.36(m, 5H, aromatic), 8.08(d, 2H, J = 9.0 Hz, aromatic), 8.83(d, 2H, J = 9.0 Hz, aromatic); MS, *m/z*(relative intensity): 297(M^+, 4), 91(100). Anal. calcd. for $C_{15}H_{11}N_3O_4$: C 60.61, H 3.70, N 14.14; found: C 60.43, H 3.69, N 14.10.

*3-(Cyclohexyl)-4-benzylsydnone(**6**a):* mp 106–107°C; IR(KBr) $\nu_{C=O}$: 1722 cm^{-1}; NMR(DMSO-d_6) δ: 1.30–1.75(m, 11H, C_6H_{11}), 3.94(s, 2H, CH_2), 6.95–7.33(m, 5H, aromatic); MS, *m/z*(relative intensity): 258(M^+, 50), 83(100). Anal. calcd. for $C_{15}H_{18}N_2O_2$: C 69.74, H 6.98, N 10.84; found: C 69.52, H 6.90, N 10.79.

(*b*) The reaction was also carried out by the same procedure as above, except for the use of benzene instead of CH_2Cl_2 as solvent. After work-up, colorless crystals of **2***d* were obtained (0.10 g, 81% yield).

Competitive reaction between benzene and methanol with 3-phenyl-4-hydroxymethylsydnone in the presence of H_2SO_4

To an ice-cooled stirred solution of 4-(hydroxymethyl)-3-phenylsydnone (0.2 g, 1.04 mmol) in CH_2Cl_2 (5 mL) containing methanol (1 mL) and benzene (1 mL) was added concentrated H_2SO_4 (0.2 mL). After being stirred for 10 min, the solution was allowed to warm to 40°C, and was stirred for an additional 3 h. The reaction mixture was poured into ice-cold aqueous sodium bicarbonate solution; the precipitate was then collected and dried to give 0.19 g of product. The ratio of *a* to *d* was determined from the ^1H NMR spectra by measuring the areas of the methylene groups at 4.30 and 3.85 ppm, respectively.

Reaction between 3-phenyl-4-trideuteriomethoxymethylsydnone and deuteriobenzene in the presence of H_2SO_4

To an ice-cold solution of 3-phenyl-4-trideuteriomethoxymethylsydnone (0.005 g) in 0.5 mL C_6D_6 in a 5-mm NMR tube was added concentrated H_2SO_4 (ca. 1 μL). The mixture was monitored using NMR regularly at 40°C until the signal at 4.20 ppm disappeared (ca. 2 h).

Reaction of bis(3-phenylsydnonylmethyl) ether and benzene in the presence of H_2SO_4

To an ice-cold solution of bis(3-phenylsydnonylmethyl) ether (0.005 g) in 0.5 mL of C_6D_6 in a 5-mm NMR tube was added concentrated H_2SO_4 (ca. 1 μL). The mixture was monitored by using NMR regularly at 40°C to observe the changes of the proton signals at 3.95 and 3.80 ppm. No proton signal at 3.95 ppm was observed after 5 h.

Kinetic study of the reaction between 3-arylsydnonylmethanols and methanol in methylene chloride in the presence of H_2SO_4

To an ice-cold solution of 3-arylsydnonylmethanol (0.01 mmol) and methanol (2 μL, 0.05 mmol) in CD_2Cl_2 (0.3 mmol) was added concentrated H_2SO_4 (1 μL). The rate of conversion was determined by monitoring the relative intensities of the methylene absorption at 4.50 and 4.35 ppm, respectively, in the ^1H NMR spectra. The spectra were recorded at 10 min intervals. Rates were calculated on the basis of monitoring the reaction to 30% conversion.

Acknowledgment

Financial support by the National Science Council of the Republic of China is gratefully acknowledged.

1. H.J. Tien, T. Nonaka, T. Fuchigami, T. Sekine, and M. Ohta. Nippon Kagaku Kaishi, 1310 (1978); H.J. Tien and M.Y. Yeh. K'o Hsueh Fa Chan Yueh K'an, **14**, 1273 (1986).
2. P.M. Weintraub and R.E. Bambury. Tetrahedron Lett. 579 (1969).
3. H.J. Tien and M. Ohta. Bull. Chem. Soc. Jpn. **45**, 2944 (1972).
4. S.T. Lin and L.L. Tien. J. Chin. Chem. Soc. (Taipei), **37**, 95 (1990).
5. A.H. Blatt. Org. Synth. Coll. Vol. II, 234 (1955).
6. C.R. Hauser, F.W. Swamer, and J.T. Adams. Org. React. **8**, 98 (1954).
7. M.Y. Yeh and H.J. Tien. Ch'eng-kung Ta Hsueh Hsueh Pao, K'o Chi Pien, 23 (1979); Chem. Abstr. **92**, 181091y (1980).
8. M.Y. Yeh, H.J. Tien, and C.C. Au. Chemistry (Taipei), 5 (1981).
9. H.J. Tien, G.M. Fang, S.T. Lin, and L.L. Tien. J. Chin. Chem. Soc. (Taipei), **39**, 107 (1992).

Thallimetric oxidations Part VII: Titrimetric and spectrophotometric methods for the determination of hypophosphite and ternary mixtures of hypophosphite, phosphite, and oxalate

M.S. PRASADA RAO,[1] A. RAMA MOHAN RAO, KARRI V. RAMANA, and S.R. SAGI
Inorganic Chemistry Laboratories, Andhra University, Visakhapatnam 530 003, India

Received January 12, 1991[2]

M.S. PRASADA RAO, A. RAMA MOHAN RAO, KARRI V. RAMANA, and S.R. SAGI. Can. J. Chem. **71**, 801 (1993).

Titrimetric and spectrophotometric methods are developed for the estimation of hypophosphite (PO_2^{3-}) at mmol and micromol ranges, respectively. In these methods thallium(III) is used as an oxidant and the reduced thallium(I) is determined either oxidimetrically by potassium bromate in the titrimetric method or by measurement of the optical density of thallium(III) at 260 nm in the presence of 0.1 M NaCl and 1 M $HClO_4$ in the spectrophotometric method. Convenient methods are described for the determination of ternary mixtures of hypophosphite (PO_2^{3-}), phosphite (PO_3^{3-}), and oxalate ($C_2O_4^{2-}$). A method is also described for the estimation of thallium(III) using hypophosphite as reductant, and the method is applied to the determination of mixtures of thallium(I) and thallium(III).

M.S. PRASADA RAO, A. RAMA MOHAN RAO, KARRI V. RAMANA et S.R. SAGI. Can. J. Chem. **71**, 801 (1993).

On a mis au point méthodes titrimétriques et spectrophotométriques pour évaluer les concentrations d'hypophosphite (PO_2^{3-}) aux niveaux respectivement des mmol et de micromol. Dans ces méthodes, on utilise du thallium(III) comme oxydant et on détermine la concentration du thallium(I) produit soit d'une façon oxydimétrique, par le bromate de potassium dans la méthode titrimétrique, soit par la mesure de la densité optique du thallium(III), à 260 nm, en présence de NaCl 0,1 M et de $HClO_4$ 1 M, dans la méthode spectrophotométrique. On décrit des méthodes faciles pour la détermination d'ions hypophosphite (PO_2^{3-}), phosphite (PO_3^{3-}) et oxalate ($C_2O_4^{2-}$) dans des mélanges tertiaires. On décrit aussi une méthode de détermination de la concentration du thallium(III) qui fait appel à l'hypophosphite comme réducteur; on a appliqué la méthode à des mélanges de thallium(I) et de thallium(III).

[Traduit par la rédaction]

Introduction

Hypophosphite (PO_2^{3-}) is a powerful reducing agent. Hypophosphites act as inorganic anti-oxidants and are used as such, specifically for the prevention of oxidation of iodides and iron(II) compounds. Hypophosphite has been used in medicine as a source of phosphorus in tonics. It is used as an anti-oxidant in hydroiodic acid and ferrous iodide syrups and also as a pharmaceutical aid. In all these preparations there is a need to maintain specific concentrations of hypophosphite. A survey of the literature reveals that few redox methods are available for the estimation of hypophosphite. Komarowsky et al. (1) determined hypophosphite by oxidizing hypophosphite to phosphite by treating with excess chloramine-T in a sulphuric acid medium for 24 h at room temperature, followed by iodometric titration of its excess. Rupp and Kroll (2) determined hypophosphite by treatment with excess potassium bromate for 1 h at room temperature or by heating at 60°C for 30 min in a sulphuric acid medium, followed by iodometric titration of its excess. Bernhart (3) described a method in which hypophosphite is oxidized quantitatively to phosphate by cerium(IV) in sulphuric acid solution at room temperature within 2 h. The excess of cerium(IV) is determined by titration with iron(II) solution using ferroin as indicator. Boyer and Bauzil (4) described a method in which an excess of iodine slowly oxidizes hypophosphite to phosphate in bicarbonate solution. The excess iodine is then back-titrated with standard 0.1 N arsenite. Rao and Gowda (5) reported that hypophosphite is oxidized by vanadate in the presence of silver sulphate as catalyst after heating for 20 min in a boiling water bath. After cooling, the mixture is titrated with 0.05 N Mohr's salt in the presence of *N*-phenylanthranilic acid as indicator.

In all of these indirect methods, after a prolonged treatment with an excess of an oxidant, the unreacted excess oxidant is determined with a suitable reductant. Because there are virtually no methods available for the estimation of hypophosphite in the micromol range, there is a need for simple and direct methods for its estimation in this range. Thus, we examined the photochemical and thermal reaction between thallium(III) and hypophosphite in the presence of various catalysts. Based on this reaction, convenient photochemical and thermal methods were developed for the determination of hypophosphite in the mmol and micromol ranges.

It was suggested in the literature (6) that phosphite and oxalate are likely to occur along with hypophosphite and, whenever the purity of these samples have to be tested, tests for phosphite and oxalate should be carried out. Keeping this point in view, an attempt was made to analyse the hypophosphite, phosphite, and oxalate present in a mixture. Based on work done earlier on the thallium(III)–oxalate system (7) and the thallium(III)–phosphite system (8), and on the results of the present study, a convenient method is described for the analysis of ternary mixtures of hypophosphite, phosphite, and oxalate.

Experimental

Thallium(III) solutions in perchloric and sulphuric acids were prepared and standardized as reported earlier (9,10) and verified by other methods. An aqueous solution of sodium hypophosphite (May and Baker) was prepared and determined by cerimetry (3). All other reagents were of analytical reagent grade. Although the photochemical reactions described take place at a much faster rate under direct sunlight, all the work was done using a Phillips high-pressure mercury vapour lamp (200/250 V, 125 W) as the light source, as the direct sunlight is of variable intensity. The photochemical reactions were performed by exposing the solutions, in

[1]Author to whom correspondence may be addressed.
[2]Revision received July 6, 1992.

Can. J. Chem. Downloaded from www.nrcresearchpress.com by 213.200.69.106 on 09/08/12
For personal use only.

TABLE 1. Estimation of hypophosphite (titrimetric method)

Hypophosphite (mmol)					
Thermal			Photochemical		
Taken	Found	% Error	Taken	Found	% Error
0.010	0.010	Nil	0.010	0.010	Nil
0.020	0.020	Nil	0.015	0.015	Nil
0.030	0.030	Nil	0.025	0.025	Nil
0.040	0.040	Nil	0.040	0.040	Nil
0.050	0.049	2.0	0.055	0.055	Nil
0.060	0.061	1.67	0.070	0.069	1.42
0.070	0.070	Nil	0.085	0.084	1.25
0.080	0.081	1.25	0.090	0.090	Nil
0.090	0.090	Nil	0.095	0.095	Nil
0.100	0.100	Nil	0.100	0.101	1.0
Average[a] = 0.0806 mmol (0.080 mmol) RSD = 0.67%			Average[a] = 0.1006 mmol (0.100 mmol) RSD = 0.54%		

[a]Six determinations.

colourless uncovered glass containers, directly from the top at a constant distance of 15 cm from the light source.

A Shimadzu UV-260 recording spectrophotometer with silica cells of 1-cm path length was used for the absorbance measurements.

Recommended procedures for the estimation of hypophosphite

A. Titrimetric procedure (mmol range)

Thermal method. To an aliquot containing 0.01–0.1 mmol of hypophosphite in a 250-mL round-bottom flask add 20 mL of 5 M $HClO_4$ and 0.40 mmol of thallium(III), and dilute the mixture with water to 100 mL. Reflux for 60 min. Add 15 mL of concentrated hydrochloric acid and cool to 60°C. Add 0.1 mL of 0.1% methyl orange indicator and titrate the thallium(I) formed with 0.05 N potassium bromate (1.392 g/L) until the indicator becomes colourless. This method is also applicable in sulphuric acid medium.

Photochemical method. To an aliquot containing 0.01–0.1 mmol of hypophosphite in a 150-mL beaker add 20 mL of 5 M $HClO_4$, 0.20 mmol of bromide, and 0.40 mmol of thallium(III), and dilute the mixture with water to 100 mL. Stir the solution and expose it to the radiation from a high-pressure mercury vapour lamp for 5 h. Add 15 mL of concentrated hydrochloric acid, 0.1 mL of 0.1% methyl orange indicator, heat to 60°C, and titrate with 0.05 N potassium bromate (1.392 g/L) until the indicator becomes colourless. This method is also applicable in sulphuric acid medium. Although the method requires prolonged exposure to the mercury vapour lamp, it will be highly useful for the estimation of hypophosphite under conditions where heating has to be avoided.

The results (recovery data) presented in Table 1 show that both methods are quite satisfactory and accurate.

B. Spectrophotometric method (μmol range)

Preparation of Beer's Law calibration curve. Prepare six sample solutions by taking different amounts of hypophosphite (0.25, 0.50, 0.75, 1.00, 1.25, and 1.50 μmol) along with 6 mL of 1×10^{-3} M thallium(III) and 1.0 mL of 5 M perchloric acid. Reflux each solution for 60 min. For the photochemical method, instead of refluxing, expose a similar set of solutions to the radiation from a high-pressure mercury vapour lamp for 5 h in the presence of 3 μmol of sodium bromide as catalyst. Transfer the solutions to 25-mL volumetric flasks and add 2.00 mL of 11.6 M perchloric acid and 2.5 mL of 1.0 M sodium chloride. Dilute with water to produce standards 1A, 1B, 1C, 1D, 1E, and 1F. Prepare another solution in a 25-mL volumetric flask by mixing all the above solutions except hypophosphite. This provides solution II. Mix well and wait for 60 min. Measure the optical density of solution II six times, adjusting the spectrophotometer each time to read the optical density of each of the standards to read zero. A calibration curve is drawn by taking the hypophosphite concentration on the *x*-axis and the absorbance of the corresponding solution on the *y*-axis.

Thermal method. To an aliquot containing 0.5–1.25 μmol of hypophosphite add 1 mL of 5 M perchloric acid and 5 mL of 1×10^{-3} M thallium(III). Reflux for 60 min. Transfer the solution to a 25-mL volumetric flask, add 2.00 mL of 11.6 M perchloric acid and 2.5 mL of 1 M sodium chloride, and dilute with water to produce solution I. Prepare another solution in a 25-mL volumetric flask by mixing all the above solutions except hypophosphite. This provides solution II. Mix well and wait for 60 min, then adjust the spectrophotometer to read the optical density of solution I to zero and measure the optical density of solution II (which corresponds to the thallium(III) reacted). The concentration of thallium(III) thus reacted corresponds to the hypophosphite concentration, which can be read from the Beer's Law calibration curve.

Photochemical method. To an aliquot containing 0.5–1.25 μmol of hypophosphite add 1 mL of 5 M perchloric acid, 2.5 μmol of sodium bromide, and 5 mL of 1×10^{-3} M thallium(III), and expose the solution to the radiation from a high-pressure mercury vapour lamp for 5 h. Transfer the solution to a 25-mL volumetric flask, add 2.00 mL of 11.6 M perchloric acid and 2.5 mL of 1 M sodium chloride, and dilute with water to produce solution I. Adopting the same procedure, in the absence of hypophosphite prepare another solution and dilute with water to solution II. The amount of hypophosphite is computed as described before.

The results (recovery data) are presented in Table 2.

Recommended procedure for the titrimetric estimation of thallium(III) (mmol range)

Photochemical method

To an aliquot containing 0.05–0.20 mmol of thallium(III) in a 150-mL beaker add 20 mL of 5 M perchloric acid, 0.8 mmol of hypophosphite, and 0.05 mmol of bromide, and dilute the mixture with water to 100 mL. Stir the solution and expose it to the light from a high-pressure mercury vapour lamp for 10 min or add 0.4 mmol of chloride instead of 0.05 mmol of bromide and dilute the mixture with water to 100 mL. Stir the solution and expose it to the light from a high-pressure mercury vapour lamp for 30 min. Add 15 mL of concentrated hydrochloric acid and 0.1 mL of 0.1% methyl orange indicator, heat to 60°C and titrate the thallium(I) formed with 0.05 N potassium bromate until the indicator becomes colourless.

Can. J. Chem. Downloaded from www.nrcresearchpress.com by 213.200.69.106 on 09/08/12
For personal use only.

TABLE 2. Estimation of hypophosphite (spectrophotometric method)

Hypophosphite (μmol)					
Thermal			Photochemical		
Taken	Found	% Error	Taken	Found	% Error
0.500	0.505	1.0	0.500	0.500	Nil
0.600	0.600	Nil	0.550	0.554	0.72
0.700	0.702	0.28	0.650	0.648	0.30
0.800	0.798	0.25	0.800	0.801	0.125
0.900	0.900	Nil	0.850	0.850	Nil
1.000	1.001	0.10	0.900	0.903	0.33
1.110	1.110	Nil	0.950	0.947	0.31
1.125	1.124	0.08	1.000	1.000	Nil
1.250	1.250	Nil	1.125	1.125	Nil
Average[a] = 1.124 μmol (1.125 μmol) RSD = 0.06%			Average[a] = 0.9476 μmol (0.950 μmol) RSD = 0.09%		

[a]Six determinations.

TABLE 3. Estimation of thallium

Taken, mmol		Found, mmol	
Tl(III)	Tl(I)	Tl(III)	Tl(I)
0.150	0.150	0.150	0.150
0.100	0.200	0.100	0.200
0.250	0.250	0.250	0.250
0.300	—	0.300	—
0.350	—	0.349	—
0.400	—	0.400	—
0.450	0.500	0.451	0.500
0.500	—	0.500	—

Thermal method

To an aliquot containing 0.05–0.20 mmol of thallium(III) in a 150-mL beaker add 20 mL of 5 M perchloric acid (to maintain 1 M) and 0.8 mmol of hypophosphite, dilute the mixture to 100 mL, and heat on a boiling water bath for 5 min. The reduced thallium(I) is titrated with potassium bromate under the conditions already described.

Recommended procedure for the estimation of mixtures of thallium(I) and thallium(III)

Using the differential method, mixtures of thallium(I) and thallium(III) are also estimated. Take two identical aliquots of mixtures of thallium(I) (0.1–0.5 mmol) and thallium(III) (0.1–0.5 mmol). First estimate the thallium(I) directly by titrating the first sample bromatometrically using methyl orange as indicator. Reduce the second sample either thermally or photochemically as described earlier and titrate to find the total thallium. The difference between the two titres corresponds to the thallium(III) present in the mixture. The results (Table 3) show that thallium(III) can be determined satisfactorily either alone or in such mixtures. This method is also applicable in sulphuric acid medium.

Recommended procedure for the analysis of ternary mixtures of hypophosphite, phosphite, and oxalate

To an aliquot containing 0.01–0.05 mmol each of hypophosphite, phosphite, and oxalate in a 150-mL beaker, add 20 mL of 5 M perchloric acid and 0.4 mmol of thallium(III). Then add 0.2 mmol of sodium bromide and dilute the mixture with water to 100 mL. Stir the solution and expose to light from a high-pressure mercury vapour lamp for 5 h or, in the absence of sodium bromide, reflux for 60 min. Add 15 mL of concentrated hydrochloric acid and 0.1 mL of 0.1% methyl orange indicator, heat to 60°C, and titrate with 0.05 N potassium bromate (1.392 g/L) until the indicator becomes colourless. The titre corresponds to the amount of thallium(I) formed (*a* mmol) equivalent to the conversion of both hypophosphite and phosphite to phosphate and of oxalate to carbon dioxide.

To a second aliquot of the mixture in a 150-mL beaker add 0.4 mmol of thallium(III) and 4.0 mmol of chloride instead of bromide. Then add 20 mL of 5 M perchloric acid and dilute the mixture with water to 100 mL. Stir the solution and expose to light from a high-pressure mercury vapour lamp for 10 min. Repeat the same procedure; this titre corresponds to the thallium(I) formed (*b* mmol), which is equivalent to the oxalate present in the mixture.

To the third aliquot of the mixture in a 150-mL beaker add 0.1 mmol of chloramine-T and 10 mL of 5 M sulphuric acid. Keep the solution for 24 h at room temperature. The unreacted chloramine-T is determined iodometrically. The chloramine-T reacted (*c* mmol) corresponds to the amount of hypophosphite present in the mixture. The amount of phosphite corresponds to $a-(b + 2c)$ mmol.[3]

The conditions for analysis of the ternary mixtures are summarized in Table 4 and the results (recovery data) are presented in Table 5.

Interferences

Cd(II), Zn(II), Ru(III), Co(II), Ni(II), Hg(II), Al(III), Pb(II), NH_4^+, Na^+, K^+, Ca^{2+}, Ba^{2+}, SO_4^{2-}, CH_3COO^-, PO_4^{3-}, 2,2′-bipyridyl, and 1,10-phenanthraline do not interfere even if they are present in 100-fold excess over hypophosphite. Traces of oxalate and phosphite interfere by reducing thallium(III) to thallium(I). Arsenite interferes with the bromatometric titration method; Cu(II) up to 0.05 M does not interfere, but at high concentrations its colour interferes with detection of the end point in the bromatometric titration. Traces of chloride and higher concentrations of bromide retard the photochemical oxidation of hypophosphite. Optimum concentrations of chloride and bromide catalyse the photochemical reduction of thallium(III) with hypophosphite.

Results and discussion

Titrimetric procedure for the estimation of hypophosphite

Oxidation of hypophosphite with thallium(III) is slow but the reaction is catalysed in the presence of light. In addi-

[3]Twice the equivalent of thallium(I) will be formed during the conversion of hypophosphite to phosphate.

Can. J. Chem. Downloaded from www.nrcresearchpress.com by 213.200.69.106 on 09/08/12
For personal use only.

TABLE 4. Conditions for the analysis of ternary mixtures of hypophosphite, phosphite, and oxalate[a]

Composition of mixture (0.01–0.05 mmol each)	Tl(III) (mmol)	Chloramine (mmol)	Catalyst (mmol) Cl^-	Catalyst (mmol) Br^-	Time of exposure	Oxidations effected	Amount of Tl(I) formed/ mmol	Amount of chloramine reacted (mmol)
1.* PO_2^{3-} + PO_3^{3-} + $C_2O_4^{2-}$	0.4	—	—	0.2	5 h (photochemical)	PO_2^{3-} to PO_4^{3-}, PO_3^{3-} to PO_4^{3-}, and $C_2O_4^{2-}$ to $2CO_2$	*a*	—
	0.4	—	—	—	Reflux for 60 min (thermal)	PO_2^{3-} to PO_4^{3-}, PO_3^{3-} to PO_4^{3-}, and $C_2O_4^{2-}$ to $2CO_2$	*a*	—
2.* PO_2^{3-} + PO_3^{3-} + $C_2O_4^{2-}$	0.4	—	4.0	—	10 min (photochemical)	$C_2O_4^{2-}$ to $2CO_2$, PO_2^{3-} and PO_3^{3-} are unaffected	*b*	—
3.** PO_2^{3-} + PO_3^{3-} + $C_2O_4^{2-}$	—	0.1	—	—	24 h at room temperature	PO_2^{3-} to PO_3^{3-}, PO_3^{3-} and $C_2O_4^{2-}$ are unaffected	—	*c*

[a]Total volume of reaction mixture = 100 mL. Concentration of perchloric acid* = 1.0 M. Concentration of sulphuric acid** = 0.5 M. The thallium(I) formed is determined bromatometrically (11). Unreacted chloramine-T is determined iodometrically (1).

TABLE 5. Analysis of ternary mixtures (A + B + C) of hypophosphite, phosphite, and oxalate

A Amount of hypophosphite (mmol)		B Amount of phosphite (mmol)		C Amount of oxalate (mmol)	
Taken	Found	Taken	Found	Taken	Found
0.010_0	0.010_5	0.020_0	0.020_0	0.020_0	0.020_0
0.015_0	0.015_2	0.025_0	0.024_4	0.050_0	0.049_9
0.025_0	0.024_8	0.050_0	0.049_8	0.025_0	0.025_6
0.060_0	0.060_0	0.020_0	0.020_2	0.020_0	0.020_0
0.020_0	0.019_9	0.020_0	0.020_0	0.080_0	0.080_0
0.040_0	0.040_5	0.030_0	0.030_0	0.030_0	0.029_7
0.020_0	0.020_2	0.040_0	0.040_0	0.040_0	0.040_3
0.050_0	0.050_3	0.025_0	0.025_2	0.025_0	0.025_0
Average[a] = 0.0502 mmol (0.050_0 mmol) RSD = 0.28%		Average[a] = 0.04986 mmol (0.050_0 mmol) RSD = 0.17%		Average[a] = 0.04994 mmol (0.050_0 mmol) RSD = 0.22%	

[a]Six determinations.
Note: The subscript is not a significant figure.

tion, the reaction is considerably faster at elevated temperatures. Separate studies have shown that hypophosphite does not interfere in the titration of thallium(I) with bromate, using methyl orange as indicator. This reaction was therefore used to monitor the progress of all the reactions described in the investigation. The reactions were carried out in sulphuric and perchloric acid media.

As per the stoichiometry of the reaction, eq. [1], a minimum of two moles of thallium(III) per mole of hypophosphite is required for a quantitative oxidation.

$$[1] \quad PO_2^{3-} + 2Tl(III) + 2H_2O \rightarrow PO_4^{3-} + 2Tl(I) + 4H^+$$

The rate of the reaction is found to increase with an excess of thallium(III) up to a concentration four times that of hypophosphite. Any concentration ratio of thallium(III) to hypophosphite above 4:1 does not appear to further increase the rate of the reaction. In the case of the above reaction a positive acid effect was observed up to an acid concentration of 1.0 mol/L with respect to perchloric acid for both the photochemical and thermal reactions. During the kinetic investigations a negative hydrogen ion effect was reported for this reaction by Gupta and Gupta (12). However, they attributed this observation to medium effects. In the presence of chloride ion, a hydrogen ion effect similar to that observed in the present investigation was noticed by these workers (13). The acid effect can be explained by assuming Tl^{3+} rather than $Tl(OH)^{2+}$ to be the reactive species. At low acid concentrations both these species will be present in solution. However, because of the small hydrolysis constant of thallium(III), the concentration of $Tl(OH)^{2+}$ gradually decreases with an increase in acid concentration. At a particular acid concentration (about 1 M) all the thallium exists as Tl^{3+} and a further increase in acid concentration has no effect on the nature of the species, which explains initial catalysis and then the levelling effect observed at higher acid concentrations.

The hydrogen ion effect can also be linked with hypo-

Can. J. Chem. Downloaded from www.nrcresearchpress.com by 213.200.69.106 on 09/08/12
For personal use only.

phosphite. In aqueous solutions it will be present as $H_2PO_2^-$ and H_3PO_2. Increasing the hydrogen ion concentration will increase the concentration of H_3PO_2. Thus the hydrogen ion effect can be explained by assuming H_3PO_2 as the reactive species and limiting rates can be ascribed to the complete conversion of $H_2PO_2^-$ to H_3PO_2. Jenkins and Yost (14) studied the exchange of radioactive hydrogen between hypophosphorous acid and water. The rate law obtained by these investigators for the exchange reaction is identical with the rate law derived for the oxidation of hypophosphorous acid by a variety of oxidizing agents. Hence they suggested that the exchange and oxidation reactions take place by similar mechanisms and also that these mechanisms involve two tautomeric forms of hypophosphorous acid in aqueous solution. Further, the non-exchangeability of hypophosphite hydrogens in neutral solutions was established by Erlenmeyer et al. (15) and verified by Jenkins and Yost (14). The existence of a tautomeric equilibrium was confirmed (14) and the exchange reaction is represented as:

[2] 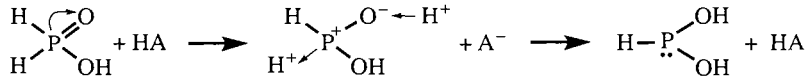

Active form

[3] 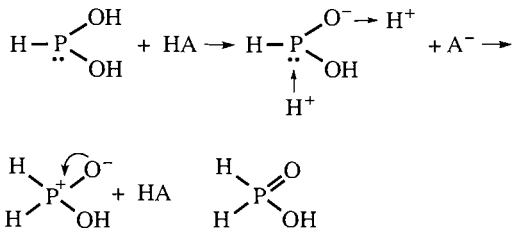

The formation of the active form of the tautomer (shown in eq. [2]) due to the exchange reaction is the active species in the reduction reaction. The exchange reaction is catalysed in the presence of mineral acid, the rate reaching a maximum at a certain acid concentration but showing a leveling effect at still higher values of acid. This might also be one of the reasons for the trend in acid effect observed in the present investigation.

The use of halides to catalyse thallimetric oxidations has been reported (7, 8, 10, 16–21). Hence the effect of bromide and chloride ions on the rate of this reaction was examined. The reaction between thallium(III) and bromide in different acid concentrations at high temperatures confirmed that bromide itself reduces thallium(III) to thallium(I) (22). Thus the effect of bromide ion on the thermal reaction between thallium(III) and hypophosphite could not be studied. The effect of bromide ion on the photochemical oxidation of hypophosphite by thallium(III) in varying concentration of perchloric acid was investigated and the results are shown in Fig. 1. From the data presented in the figure it is clear that photochemical oxidation is fastest when the ratio of thallium(III) to bromide is in the range 4:1–1:1. From the above data it is also clear that the acid effect follows the trend; that is, there is an initial increase in rate as acid concentration is increased, and after reaching a particular acid concentration the rate remains steady at all bromide ion concentrations.

So far, our studies have shown that the photochemical oxidation of hypophosphite to phosphate is complete in 10 h. Further, the effect of chloride on the photochemical and thermal oxidation of hypophosphite was investigated. In the presence of chloride ion the reaction is not complete in 10 h, and these investigations indicated a two-stage process for the oxidation of hypophosphite to phosphate via phosphite that can be represented by the following equations.

[1*a*] $PO_2^{3-} + Tl(III) + H_2O \rightarrow PO_3^{3-} + Tl(I) + 2H^+$

[1*b*] $PO_3^{3-} + Tl(III) + H_2O \rightarrow PO_4^{3-} + Tl(I) + 2H^+$

The first stage of the reaction, that is, the oxidation of hypophosphite to phosphite (eq. [1*a*]) is catalysed by chloride ions with a concentration of up to 50 times that of thallium(III). But the second stage of the reaction (eq. [1*b*]) is retarded in the presence of chloride ions. In the presence of still higher concentrations of chloride, more than 50 times that of thallium(III) (14), both stages of the reaction are retarded. For the reduction of thallium(III) in the presence of excess hypophosphite, only reaction [1*a*] occurs and hence the chloride catalyses throughout the progress of the reaction. The results of these investigations on the thermal oxidations show a trend similar to the results observed in photochemical reactions except for the fact that the thermal reaction is fast compared to the photochemical reaction (Tables 6 and 7).

Unlike chloride, however, which catalyses only the first stages of the photochemical and thermal reactions, bromide in low concentrations catalyses both stages of the photochemical oxidation. As already reported (23), the phosphorus nucleophiles are known to attack the halogen when the latter is bonded to an electron-withdrawing group. Hence, in this case, Cl^- or Br^- attached to Tl^{3+}, a highly positively charged metal ion, can be assumed to be attacked by the phosphorus nucleopile. Under these conditions the lower halo complexes (24) with high formation constants (13, 25) are likely to occur and probably can be active. Hence, these complexes can be considered attached to the active form of the hypophosphite, as proposed by Jenkins and Yost (14), through chloro or bromo bridges that facilitate the electron transfer. Hence, the probable structure of the activated complex may be represented as

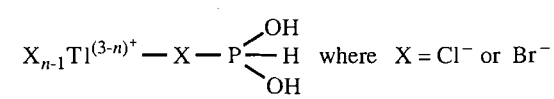

Can. J. Chem. Downloaded from www.nrcresearchpress.com by 213.200.69.106 on 09/08/12
For personal use only.

Can. J. Chem. Downloaded from www.nrcresearchpress.com by 213.200.69.106 on 09/08/12
For personal use only.

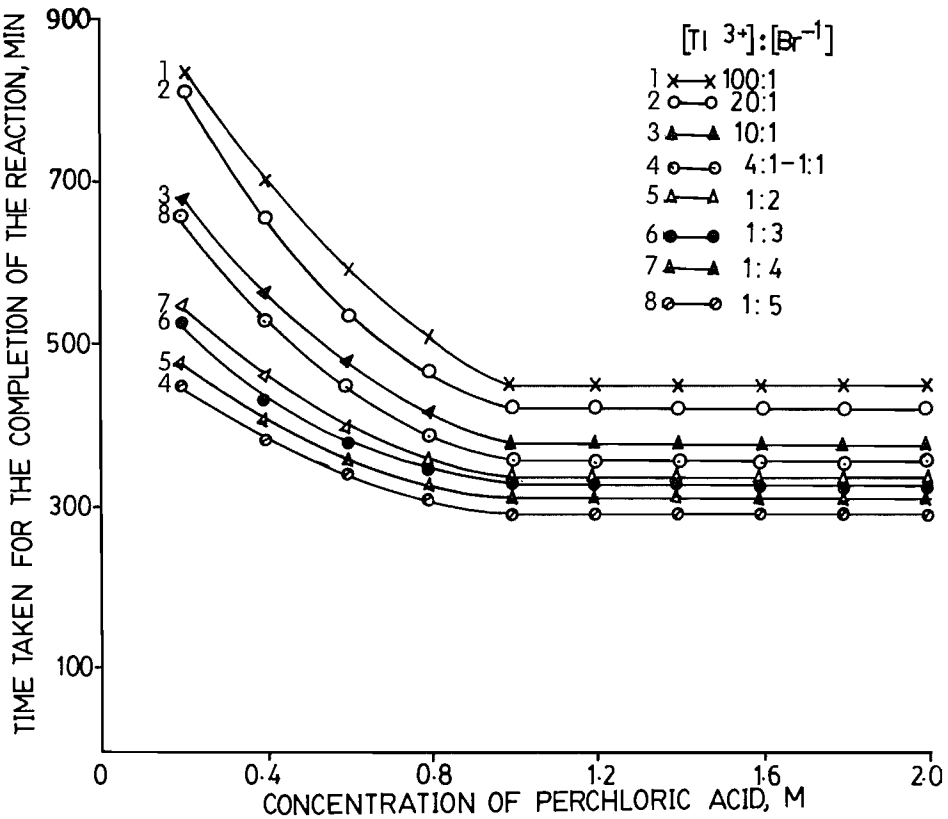

FIG. 1. Effect of $[H^+]$ and $[Br^-]$ on the rate of photochemical oxidation of hypophosphite by thallium(III). Volume of the reaction mixture = 100 mL; amount of thallium(III) = 0.1 mmol; amount of hypophosphite = 0.025 mmol.

However, in the case of Cl^-, the general mechanism proposed here holds good for the first stage of the reaction only.

Spectrophotometric method for the estimation of microquantities of hypophosphite

The absorption spectra (26) of thallium(I) and thallium(III) alone in a medium containing 1 M perchloric acid and 0.1 M hydrochloric acid show that thallium(III) absorbs at 260 nm (molar absorptivity $\epsilon = 9150$ L M^{-1} cm^{-1}) while thallium(I) has no absorbance at this wavelength. In this method an excess of thallium(III) is allowed to react with hypophosphite either photochemically (using bromide as a catalyst) or thermally. The optical density of thallium(III) at 260 nm in the presence of 0.1 M NaCl and 1 M $HClO_4$ is measured to determine the concentration of thallium(III) before and after reaction with hypophosphite. Thallium(I), hypophosphite, and the other reagents employed in this reaction have no absorbance at this wavelength and the thallium(III) chloro species obey Beer's Law. The amount of hypophosphite corresponds to the amount of thallium(III) reduced to thallium(I), which can be computed from the standard curve.

Estimation of thallium(III)

Further investigation of this reaction (eq. [1*a*]) led to the development of a procedure for estimation of thallium(III) that can be applied to the determination of mixtures of thallium(I) and thallium(III). Reduction of thallium(III) with hypophosphite is normally a slow reaction. At room temperature, reduction of thallium(III) with hypophosphite requires 72 h for completion of the reaction. However, in the presence of light the reaction is complete within 3 h. A minimum of one mole of hypophosphite is required per one mole of thallium(III) for a quantitative reduction as per eq. [1*a*].

It was found that four times the amount of hypophosphite to that of thallium(III) was necessary for a rapid reaction and that any ratio of hypophosphite to thallium(III) above 4:1 will not further alter the rate of the reaction. With the concentration of hypophosphite four times that of thallium(III), the effect of acid, chloride, and bromide concentrations on the speed of the reaction was studied in perchloric acid medium and the conditions optimized. Chloride catalyses the photochemical reduction of thallium(III) in the presence of excess hypophosphite as the oxidation of hypophosphite to phosphite is sufficient to bring about the quantitative reduction of thallium(III) to thallium(I). As already pointed out, this stage of the reaction is catalysed by chloride.

Analysis of ternary mixtures of PO_2^{3-}, PO_3^{3-}, and $C_2O_4^{2-}$

Based on the fact that the thallimetric oxidations of hypophosphite, phosphite, and oxalate proceed selectively, convenient methods can be developed for the determination of ternary mixtures of these anions. Chloride and bromide in small concentrations catalyse the photochemical oxidation of oxalate by thallium(III) (7). Bromide in small concentrations catalyses the photochemical oxidation of hypophosphite and phosphite (8) by thallium(III), while chloride in small concentrations inhibits the overall oxidations of hypophosphite and phosphite to phosphate.

TABLE 6. Effect of chloride ion concentration on the photochemical oxidation of hypophosphite by thallium(III)[a]

Amount of chloride taken (mmol)	Percentage of photochemical oxidation of hypophosphite				
	In 2 h	In 4 h	In 6 h	In 8 h	In 10 h
0.00	5.0	21.0	44.0	73.0	100.0
0.10	8.0	44.0	56.0	58.0	72.0
0.50	10.0	47.0	58.0	66.0	73.0
1.00	12.0	49.0	60.0	67.0	75.0
2.00	14.0	51.0	54.0	60.0	70.0
3.00	15.0	52.0	56.0	61.0	71.0
4.00	17.0	54.0	57.0	62.0	73.0
5.00	20.0	55.0	59.0	64.0	75.0
8.00	3.0	11.0	28.0	35.0	47.0
10.00	1.0	5.0	12.0	18.0	26.0

[a]Amount of hypophosphite = 0.025 mmol. Amount of thallium(III) = 0.100 mmol. Perchloric acid = 1 M. Total volume of the reaction mixture = 100 mL.

TABLE 7. Effect of chloride ion concentration on thermal oxidation of hypophosphite by thallium(III)

Amount of chloride taken (mmol)	Percentage of thermal oxidation of hypophosphite (reflux time in min)					
	10	20	30	40	50	60
0.00	23	45	60	74	88	100.00
0.10	45	50	59	70	80	90.0
0.50	47	50	58	66	74	88.0
1.00	48	51	57	64	70	85.0
2.00	49	52	56	64	70	85.0
3.00	50	51	55	61	64	84.0
4.00	52	52	54	59	62	79.0
5.00	54	53	54	57	62	78.0
7.00	19	24	33	40	52	61.0
8.00	16	19	25	34	45	54.0
10.0	11	17	22	27	36	50.0

[a]Amount of hypophosphite = 0.025 mmol. Amount of thallium(III) = 0.10 mmol. Perchloric acid = 1 M. Total volume of the reaction mixture = 100 mL.

Thallium(III) oxidizes oxalate, hypophosphite, and phosphite photochemically in the presence of sufficient bromide or at elevated temperatures. In the presence of a suitable concentration of chloride, oxalate is photochemically oxidized, leaving hypophosphite and phosphite unaltered. As reported earlier in this paper, even though the first phase of the reaction, that is, the oxidation of hypophosphite to phosphite by thallium(III), is catalysed by chloride, no noticeable change in the concentration of hypophosphite was observed during the exposure time of 10 min prescribed for the determination of the oxalate in the reaction mixture, under the experimental conditions (Tables 4 and 6). Therefore, if the reaction is carried out in the presence of chloride the result is the quantitative photochemical oxidation of oxalate only under the prescribed time of exposure. In both cases, the thallium(I) formed is determined bromatometrically. The first titre value corresponds to the total thallium(I) formed, corresponding to the conversion of hypophosphite and phosphite to phosphate and oxalate to carbon dioxide and water. The second titre value corresponds to the concentration of oxalate.

Hypophosphite alone can be determined by oxidizing it to phosphite (1) by treating with a known excess of chloramine-T in a sulphuric acid medium for 24 h at room temperature, leaving the original phosphite and oxalate unaltered. Excess chloramine-T is determined iodometrically. The amount of chloramine-T consumed corresponds to the hypophosphite present in the mixture. The concentration of phosphite can be computed from the above two titre values and the chloramine-T consumed.

Acknowledgement

One of the authors, Dr. A. Rama Mohana Rao, thanks the Council of Scientific and Industrial Research, New Delhi, India, for the award of a Senior Research Fellowship.

1. A.S. Komarowsky, W.F. Filonowa, and I.M. Korenman. Z. Anal. Chem. **96**, 321 (1934).
2. E. Rupp and A. Kroll. Arch. Pharm. **249**, 493 (1911).
3. D.N. Bernhart. Anal. Chem. **26**, 1798 (1954).
4. Boyer and J. Bauzil. Pharm. Chim. **18**, 321 (1918).
5. G.G. Rao and H.S. Gowda. Z. Anal. Chem. **146**, 167 (1955).
6. M.L. Schroff. Pharmaceutical chemistry. Part II. Inorganic. 1st ed. National Book Centre, Calcutta, India. 1969. p. 968.
7. S.R. Sagi, K.A. Rao, and M.S.P. Rao. Can. J. Chem. **61**, 2795 (1983).
8. M.S.P. Rao, A.R.M. Rao, K.V. Ramana, and S.R. Sagi. Talanta, **38**, 937 (1991).
9. S.R. Sagi and K.V. Ramana. Talanta, **16**, 1217 (1969).
10. S.R. Sagi, G.S.P. Raju, K.A. Rao, and M.S.P. Rao. Talanta, **29**, 413 (1982).
11. I.M. Kolthoff. Recl. Trav. Chim. Pays-Bas, **41**, 172 (1922).
12. K.S. Gupta and Y.K. Gupta. J. Chem. Soc. 256 (1970).
13. K.S. Gupta and Y.K. Gupta. Inorg. Chem. **13**, 851 (1974).
14. W.A. Jenkins and D.M. Yost. J. Inorg. Nucl. Chem. **11**, 297 (1959).
15. H. Erlenmeyer, W. Schoenauer, and G. Schwarzenbach. Helv. Chim. Acta, **20**, 726 (1937).
16. A.R.M. Rao, M.S.P. Rao, K.V. Ramana, and S.R. Sagi. Talanta, **36**, 686 (1989).
17. S.R. Sagi, K.A. Rao, and M.S.P. Rao. Talanta, **30**, 282 (1983).

Can. J. Chem. Downloaded from www.nrcresearchpress.com by 213.200.69.106 on 09/08/12
For personal use only.

18. S.R. Sagi, K.A. Rao, and M.S.P. Rao. Analyst, **109**, 53 (1984).
19. M.S.P. Rao, A.R.M. Rao, K.V. Ramana, and S.R. Sagi. Talanta, **37**, 753 (1990).
20. M.S.P. Rao and A.R.M. Rao. Anal. Chim. Acta, **242**, 229 (1991).
21. M.S.P. Rao and A.R.M. Rao. Anal. Chim. Acta, **257**, 159 (1992).
22. R. Kalavathi. M. Phil. Dissertation. Andhra University, Waltair (1989).
23. K.S. Gupta and Y.K. Gupta. Inorg. Chem. **14**, 2000 (1975).
24. T.G. Spiro. Inorg. Chem. **4**, 731 (1965).
25. L.G. Carpenter, M.H. Ford Smith, R.P. Bell, and R.W. Dodson. Discuss. Faraday Soc. **29**, 92 (1960).
26. L.B. Mønsted, O. Mønsted, and G. Nord. Trans. Faraday Soc. **66**, 936 (1970).

Can. J. Chem. Downloaded from www.nrcresearchpress.com by 213.200.69.106 on 09/08/12
For personal use only.

Electron paramagnetic resonance study of radicals derived from 2- and 3-fluoropropene

PETER SMITH,[1] CYNTHIA ANN HOUGUM, AND ART ARESH HOSSEINIAN
Paul M. Gross Chemical Laboratory, Duke University, Box 90346, Durham, NC 27708-0346, U.S.A.

Received November 25, 1992

PETER SMITH, CYNTHIA ANN HOUGUM, and ART ARESH HOSSEINIAN. Can. J. Chem. **71**, 809 (1993).

Using the $TiCl_3$–H_2O_2, –NH_2OH, –$Na_2S_2O_8$, and –H_2O_2/Na_2SO_3, continuous-flow, radical-generating methods at 25°C, we have successfully characterized by electron paramagnetic resonance spectroscopy radicals formed by the reaction of each of the substrates 2- and 3-fluoropropene with the radicals •OH, $•NH_3^+$, $•OSO_3^-$, and $•SO_3^-$, respectively. With 2- and 3-fluoropropene, respectively, the radicals identified were of general formula $CH_3(X)\dot{C}FCH_3$ and $CH_2(X)\dot{C}HCH_2F$ where -X is the added group, except that treatment of 3-fluoropropene with the $TiCl_3$–H_2O_2 reaction system also yielded $•CH_2CH(X)CH_2F$. The results obtained are discussed in terms of the effect of the presence of the fluorine substituent on both the apparent reactivity of the substrate molecules towards the radical-generating systems and the spectroscopic properties of the radicals observed.

PETER SMITH, CYNTHIA ANN HOUGUM et ART ARESH HOSSEINIAN. Can. J. Chem. **71**, 809 (1993).

Opérant à 25°C, utilisant des méthodes d'écoulement continue pour générer des radicaux à l'aide de $TiCl_3$–H_2O_2, –NH_2OH, –$Na_2S_2O_8$ et –H_2O_2/Na_2SO_3, et faisant appel à la résonance paramagnétique électronique, on a caractérisé les radicaux qui résultent de la réaction des 2- et 3-fluoropropènes avec respectivement les radicaux •OH, $•NH_3^+$, $•SO_3^-$ et $•SO_3^-$. Avec respectivement les 2- et 3-fluoropropènes, les radicaux identifiés étaient de la formule générale $CH_2(X)\dot{C}FCH_3$ et $CH_2(X)\dot{C}HCH_2F$ dans lesquels X est le groupe ajouté; toutefois, dans le cas du traitement du 3-fluoropropène avec le système réactionnel $TiCl_3$–H_2O_2, il y a aussi formation de $•CH_2CH(X)CH_2F$. On discute des résultats obtenus en fonction de l'effet de la présence du fluor sur la réactivité apparente du substrat pour les systèmes générant des radicaux ainsi que sur les propriétés spectrales des radicaux observés.

[Traduit par la rédaction]

Introduction

In our laboratory, there have been a number of electron paramagnetic resonance (epr) investigations of radicals formed from allyl alcohol, CH_2=$CHCH_2OH$, methallyl alcohol, CH_2=$C(CH_3)CH_2OH$, and related compounds using $TiCl_3$-based, continuous-flow, radical-generating methods (1–6). These previous investigations deal mainly with the addition of •OH and $•NH_3^+$ radicals to these compounds. The present study extends this earlier work to include the reactions of two fluorinated isomers, 3-fluoropropene, CH_2=$CHCH_2F$ (**1**), and 2-fluoropropene, CH_2=$CFCH_3$ (**2**), with not only •OH and $•NH_3^+$ radicals, but also the radical anions $•SO_3^-$ and $•OSO_3^-$. The species identified were addition radicals that, to our knowledge, have not been characterized before by epr.

Fluoropropenes are of interest because the fluorine substituent would be expected to affect the reactivity of these monomers towards attack by electrophilic radicals such as those generated by the $TiCl_3$-based reaction systems employed in our work (7–11). Moreover, the geometry and consequently the spectroscopic properties of the radical adduct formed would tend to be affected by the presence of the highly electronegative fluorine substituent (7–13). The results of this investigation are discussed in the light of these factors.

Experimental

The experimental arrangements and procedures were essentially as before (14) except that all measurements were taken using a Varian E-231 multipurpose single cavity. The field and *g*-value standard was potassium peroxylamine disulfonate (Alpha, 95%) (15, 16) in an aqueous solution saturated at room temperature with potassium carbonate (Fisher, anhydrous, ACS reagent), the temperature of the standard as used being 25.0 ± 1.0°C. Spectrum simulation was carried out on a VAX 8350 utilizing a program by Oehler and Janzen (17) and assuming the lineshape to be primarily Lorentzian (90%). Previous work in our laboratory has shown that variation of the lineshape made little difference in the appearance of simulated spectra (1). All spectra were recorded at 25.0 ± 1.0°C as the first derivative of the signal at a 100-kHz field-modulation frequency. The field-modulation amplitude was normally 0.050–1.0 G and all results refer to that range. Relative radical concentrations were estimated using the peak-height method and non-overlapping lines of equal peak-to-peak linewidth (ΔH_{pp}) (18, 19).

All radicals were observed using either a two- or a three-stream, rapid-mixing, continuous-flow epr system (14, 20, 21). The epr sample flow cells employed were of the aqueous, mix-and-flow type and were either of the Borg design (22), as before (14), or as supplied by Wilmad Glass Company, Inc. (Cat. no. WG-804-Q), both cells yielding indistinguishable results. The total flow rate was maintained at 2.9–4.7 mL s^{-1}, this being equally divided between the individual reaction streams, and the results obtained being independent of flow rate over this range. Where necessary, pH measurements on reaction mixtures were taken using a DigiSense pH meter and a Fisher electrode (Cat. no. 13-620-104).

The substrates, 3-fluoropropene, **1**, and 2-fluoropropene, **2**, both from PCR, were mixed in turn with titanous chloride (Fisher, 20%) and each of the following oxidizing agents: hydrogen peroxide (Fisher 30%, ACS reagent), hydroxylamine hydrochloride (Aldrich, 99%), and sodium persulfate (Aldrich, 98+%). In addition, as an extension of the $TiCl_3$–H_2O_2 radical-generating method, **1** and **2** were each examined using this method modified to include sodium sulfite (Fisher, ACS reagent, anhydrous, 98+%) by way of a third reaction stream. The remaining reagents employed were H_2SO_4 (Mallinckrodt, analytical reagent, 96.0%), NH_4OH (Mallinckrodt, analytical reagent, 29.8%), and disodium ethylenediamine tetraacetate (EDTA, Fisher, 95%).

When employing the $TiCl_3$–H_2O_2 radical-generating method (14), the reducing stream was 0.004–0.005 M in $TiCl_3$, the oxidizing

[1]Author to whom correspondence may be addressed.

Can. J. Chem. Downloaded from www.nrcresearchpress.com by 213.200.69.106 on 09/08/12
For personal use only.

TABLE 1. Electron paramagnetic resonance data[a] for radicals derived from CH_2=$CHCH_2F$

Radical	Coupling constants (G)[b,c] α-CH	β-CH_2X[d]	β-CH_2F	Other[e]	Δg[f]
3 $CH_2(OH)\dot{C}HCH_2F$	21.45(7)	23.86(5)	15.72(3)	86.91(4)	41(5)
4 $\cdot CH_2CH(OH)CH_2F$	22.09(4)[g]	24.47(4)[h]	—	4.94(3)	54(5)
5 $CH_2(NH_3^+)\dot{C}HCH_2F$	22.02(4)	21.92(5)	19.25(4)	69.01(5), 5.58(5)[i]	44(2)
6 $CH_2(OSO_3^-)\dot{C}HCH_2F$[j]	21.68(6)	20.22(2)	18.45(6)	73.17(7)	37(3)
7 $CH_2(SO_3^-)\dot{C}HCH_2F$[j]	21.57(4)	15.64(4)	19.48(6)	69.42(3)	59(4)

[a]At 25.0 ± 1.0°C and, unless stated otherwise, pH ca. 1.
[b]Unless indicated otherwise, all *a* values are for protons. All protons at a given designation are magnetically equivalent. Each number in parentheses is the standard deviation of the mean, σ_{n-1}, times 10^2 and the maximum error limit is approximately $\pm 2\sigma_{n-1}$, based on the reported error limits for the field standard (15).
[c]The ΔH_{pp} values were 0.4–0.5 G for **3**, **4**, **5**, and **7** and 0.5–1.0 G for **6**.
[d]-X is equal to -OH, $-NH_3^+$, $-OSO_3^-$, or $-SO_3^-$, respectively, for **3**, **5**, **6**, and **7**.
[e]a_F, unless stated otherwise.
[f]Δg value = (g − 2.00200) times 10^5, and each number in parentheses is σ_{n-1} times 10^5. The maximum error limits are $\pm(\sigma_{n-1} + 0.00005)$ based on the reported error limits of the field and g-value standard (15, 16).
[g]α-CH_2.
[h]β-CH(OH).
[i]a_N.
[j]pH 9.0 ± 0.1.

stream 0.10 M in H_2O_2, and both streams 0.10 M in H_2SO_4 and of equal concentration, within the range 0.015–0.020 M, in **1** or **2**, unless stated otherwise. When using the $TiCl_3$–NH_2OH method (14), the reaction conditions were as for the $TiCl_3$–H_2O_2 work except that the H_2O_2 in the oxidizing stream was replaced with 1.0 M NH_2OH•HCl. When employing the $TiCl_2$–$Na_2S_2O_8$ system, the reaction conditions employed first were as for the $TiCl_3$–H_2O_2 work, i.e., with the reaction mixture at pH ca. 1, except that the H_2O_2 in the oxidizing stream was replaced with 0.20 M $Na_2S_2O_8$. However, to improve the signal-to-noise (S/N) ratio of the spectra obtained using the $TiCl_3$–$Na_2S_2O_8$ system, data were also taken with the pH of the reaction mixture varied over the range 7–9 (23, 24). This was achieved by making the reducing stream 0.016 M in EDTA, and eliminating H_2SO_4 from and adding NH_4OH to both streams, the results being qualitatively indistinguishable over that pH range. All results quoted for use of this system refer to pH 9.0 ± 0.1. Moreover, to further improve the S/N ratio when examining **1**, the concentration of substrate was increased to 0.060–0.080 M.

When utilizing the $TiCl_3$–H_2O_2/Na_2SO_3 reaction system, the conditions when the reaction mixture was of pH ca. 1 were as for the $TiCl_3$–H_2O_2 work except that the concentration of H_2O_2 in the oxidizing stream was lowered to 0.050 M and a third reaction stream containing 0.20 M Na_2SO_3 was added, all three streams being of equal concentration, within the range 0.015–0.045 M, in **1** or *2*. The Na_2SO_3 stream joined the reducing stream by way of a Y-piece located about 10 cm upstream from the mixing chamber of the epr sample flow cell where the mixture encountered the H_2O_2 stream. As was the case for the $TiCl_3$–$Na_2S_2O_8$ work, this system was run with the pH of the reaction mixture ca. 1 and 7–9. The data over the pH range 7–9 were taken with the $TiCl_3$ stream 0.016 M in EDTA and with H_2SO_4 omitted from the $TiCl_3$ and H_2O_2 streams and replaced, in the case of the $TiCl_3$ stream, with NH_4OH, the results obtained when the pH was 7–9 being essentially the same and of higher S/N than when the pH was ca. 1. All the data referred to for this system are for pH 9.0 ± 0.1. In the reactions with both **1** and **2** there was a residual signal from the unreacted $\cdot SO_3^-$, g-value = 2.0030 (21), that was evident in all spectra.

Results and discussion

Tables 1 and 2, respectively, summarize the epr spectroscopic data obtained from the reaction of monomers **1** and **2** within the $TiCl_3$–H_2O_2, –NH_2OH, –$Na_2S_2O_8$, and –H_2O_2/Na_2SO_3 systems. In all cases the concentration of monomer was low enough that polymeric radicals were not observed (5, 6).

In general, our results are consistent with simple expectations based on the electronic and steric character of both the fluorinated monomers and the attacking radicals. However, it should be noted that the kinetic complexity of the radical-generating systems used (6, 23–27) prevents a detailed analysis of these factors here. Nevertheless, while bearing in mind these factors, it seems that the $TiCl_3$–H_2O_2 radical-generating system is more reactive towards **1** and **2** than the other systems.

3-Fluoropropene, 1

When examined using the $TiCl_3$–H_2O_2 system, **1** underwent head and tail hydroxyl-radical addition to yield $CH_2(OH)\dot{C}HCH_2F$, **3**, and $\cdot CH_2CH(OH)CH_2F$, **4**, respectively. The major product, **3**, corresponded to radical addition to the unhindered end of the double bond, which is also the site of highest electron density (11, 28), the value of the ratio [**3**]/[**4**] in the steady state being equal to 4, in qualitative agreement with the corresponding data from analogous studies of other allyl compounds (5, 6). Not surprisingly, in view of the electrophilicity of •OH (5, 6, 28) and the high electron-withdrawing ability, *-I*, of fluorine (11, 29), there was no evidence for the formation of the allylic radical, CH_2=$CH\dot{C}HF$. This result contrasts with the observation of the CH_2=$CH\dot{C}HOH$ radical in analogous $TiCl_3$–H_2O_2 studies of allyl alcohol, consistent with the lower inductive ability of -OH in comparison with -F (5, 6, 28).

When reacting **1** with $\cdot NH_3^+$, $\cdot SO_3^-$, and $\cdot OSO_3^-$, only the head-addition radical product was observed. The result when using the $TiCl_3$–NH_2OH system is consistent with the electrophilicity of $\cdot NH_3^+$ (28) and the well-known lower apparent reactivity of this radical-generating system, in comparison to that of the $TiCl_3$–H_2O_2 method (5, 14, 30).

Can. J. Chem. Downloaded from www.nrcresearchpress.com by 213.200.69.106 on 09/08/12
For personal use only.

TABLE 2. Electron paramagnetic resonance data[a] for radicals derived from CH_2—$CFCH_3$

Radical	Coupling constants (G)[b,c]			Δg[f]
	β-CH_3	β-CH_2X[d]	Other[e]	
8 $CH_2(OH)\dot{C}FCH_3$	22.53(7)	10.51(6)	58.18(5)	147(3)
9 $CH_2(NH_3^+)\dot{C}FCH_3$	22.81(7)	13.52(5)	59.17(7), 8.02(9)[g]	139(6)
10 $CH_2(OSO_3^-)\dot{C}FCH_3$[h]	22.97(5)	7.96(8)	56.92(5)	150(4)
11 $CH_2(SO_3^-)\dot{C}FCH_3$[h]	22.82(2)	11.46(2)	55.43(7)	159(3)

[a]See Table 1, footnote *a*.
[b]See Table 1, footnote *b*.
[c]The ΔH_{pp} values were 0.3–0.6 G for each of **8**–**11**.
[d]-X is -OH, $-NH_3^+$, $-OSO_3^-$, or $-SO_3^-$, respectively, for **8**, **9**, **10**, and **11**.
[e]See Table 1, footnote *e*.
[f]See Table 1, footnote *f*.
[g]See Table 1, footnote *i*.
[h]See Table 1, footnote *j*.

The apparent reactivity of the $TiCl_3$–H_2O_2/Na_2SO_3 and $-Na_2S_2O_8$ systems in comparison with the $TiCl_3$–H_2O_2 system does not appear to have been reported in the literature. Consequently, it should be noted that although evidence for a signal was obtained when employing the $TiCl_3$–$Na_2S_2O_8$ system with **1** at the same concentration as that used with the other systems, i.e., 0.015–0.020 M, it was only with a quadrupled concentration of **1** that an acceptable S/N ratio was obtained.

The presence of only head-addition radical products in the reactions of **1** with $\cdot OSO_3^-$ and $\cdot SO_3^-$ provides evidence for the electrophilicity of these two attacking radicals, which is consistent with the literature (28). Previous experimental work indicated that $\cdot OSO_3^-$ is more reactive than SO_3^- in regard to hydrogen-atom abstraction from alkanes, this difference in reactivity being plausibly explained as arising because the unpaired electron is centered on the oxygen in $\cdot OSO_3^-$ and on the sulfur in $\cdot SO_3^-$ (31–33). However, $\cdot OSO_3^-$ and $\cdot SO_3^-$ are found to show variable differences in apparent reactivity in regard to addition to monosubstituted ethylenes that can be attributed to steric and electrostatic effects arising from the nature of the substituent (23, 24, 31, 32). Thus, the strong electronegativity of the fluorine substituent in **1** could account for the apparent low reactivity of $\cdot OSO_3^-$ with **1** in comparison with that of $\cdot SO_3^-$.

In analyzing the spectroscopic data obtained for the various radical adducts of **1**, Table 1, with the general structure $CH_2(X)\dot{C}HCH_2F$ and X being the added group, the following observations should be drawn. The coupling constant for the α-CH protons, $a_{\alpha\text{-H}}$, is relatively constant, 21.7 ± 0.3 G. This is in keeping with previous findings in our laboratory (5, 6) for radicals of general structure $CH_2(X)\dot{C}HCH_2Z$, where X and Z are various substituents, and is to be expected as ρ_α^π, the π-electron unpaired spin density at the α-C, and the value of Q_α in the McConnell equation (34)

$$[1] \qquad a_{\alpha\text{-H}} = Q_{\alpha\text{-H}}\rho_\alpha^\pi$$

should be relatively insensitive to the identity of X or Z (35). Therefore, it follows that, for a given radical, any observed differences in the two β-CH_2 proton coupling constants may be largely attributed to conformational differences in the -CH_2X and the -CH_2F groups, as may the variation of these two β-CH_2 proton coupling constants and of the β-CH_2F fluorine coupling constant for the radicals **3** and **5**–**7**. Thus, the data in Table 1 suggest that for each $CH_2(X)\dot{C}HCH_2F$ radical, the -CH_2 (1:2:1)-proton coupling may be assigned by utilizing the reasonable assumption that $a_{\beta\text{-H}}(CH_2F)$ should depend on $a_{\beta\text{-F}}(CH_2F)$ in an inverse fashion, while $a_{\beta\text{-H}}(CH_2X)$ should vary with the identity of X, but not depend to any large extent on the value of $a_{\beta\text{-F}}(CH_2F)$. This approach is in accord with the McConnell equation (34), which, for the case of the β-CH_2F protons, has the form

$$[2] \qquad a_{\beta\text{-H}}(CH_2F) = 2\,Q_{\beta\text{-H}}(CCH_2F)\rho_\alpha^\pi\langle\cos^2\theta\rangle$$

where θ is the dihedral angle between the C_β—F bond and the $2p_z$-orbital at C_α and $\langle\cos^2\theta\rangle$ is the time-averaged value, analogous relationships holding for $a_{\beta\text{-F}}(CH_2F)$ and $a_{\beta\text{-H}}(CH_2X)$.

Hence, for a -CH_2F group, when θ is small, the resulting dihedral angles between the C_β—H bonds and the $2p_z$-orbital at C_α are large, causing the β-CH_2F proton and fluorine coupling constants to be inversely related. The assignment of the remaining β-CH_2 proton coupling to the β-CH_2X group is further confirmed by comparisons with data for analogous radicals (5, 6, 23, 24). The *g*-values found for **3** and **5**–**7** are also in good agreement with those seen previously in radicals of this type (5, 6, 23).

Only in the case of •OH addition to **1** was a tail-addition radical $\cdot CH_2CH(OH)CH_2F$, **4**, produced. The resulting couplings and *g*-value of **4** are in accord with those seen for other radicals of general structure $\cdot CH_2CH(OH)CH_2Y$ (5, 6).

2-Fluoropropene, 2

In the reaction of **2** within each of the $TiCl_3$-based radical-generating systems, only one radical adduct was observed, corresponding to addition to the sterically unhindered end or head end of the double bond, where the electron density is a maximum (11, 36). The presence of the fluorine substituent on the hindered end of the double bond deactivates that carbon, the *-I* effect predominating over the *+M* effect as evidenced by head addition of electrophilic radicals, such as •OH, $\cdot NH_3^+$, $\cdot SO_3^-$, and $\cdot OSO_3^-$. That **1** yielded **3** and **4** when treated in the $TiCl_3$–H_2O_2 system and **2** produced only $CH_2(OH)\dot{C}FCH_3$, **8**, suggests this differ-

Can. J. Chem. Downloaded from www.nrcresearchpress.com by 213.200.69.106 on 09/08/12
For personal use only.

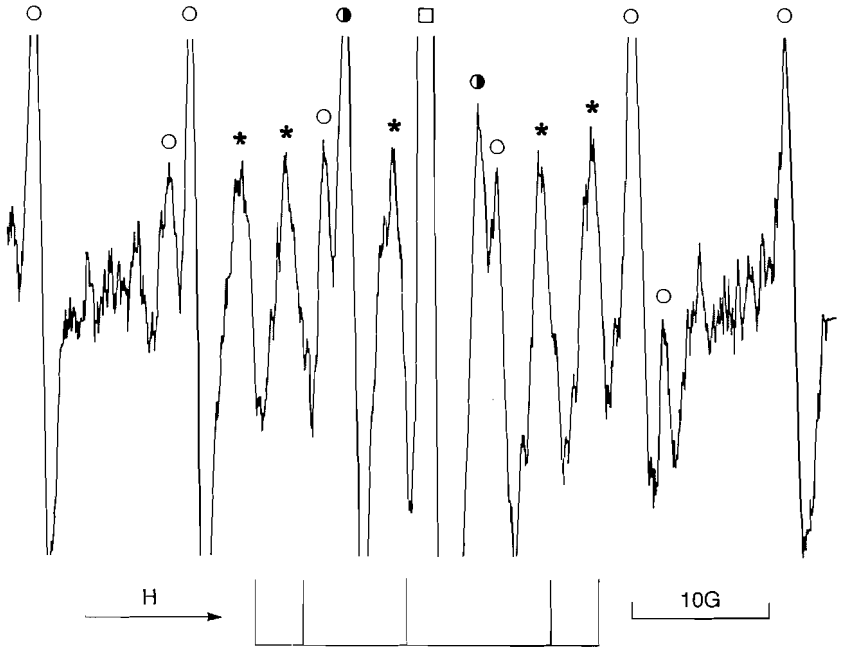

FIG. 1. The center of the epr absorption observed using the $TiCl_3$–H_2O_2/Na_2SO_3 system with **2**: [$TiCl_3$], 0.004 M, and [EDTA], 0.016 M, in the reducing stream, this containing enough NH_4OH so that the mixed reaction-mixture stream was of pH 9.0 ± 0.1; [H_2O_2], 0.050 M in the oxidizing stream; [Na_2SO_3], 0.20 M in the Na_2SO_3 stream; [**2**], 0.045 M in all three streams; total flow rate 2.9 mL s^{-1} equally divided between the three streams; modulation amplitude, 1.0 G; fieldscan rate, 12.5 G min^{-1}; time constant, 1.0 s; receiver gain, 4.0×10^4; microwave power, 20 mW. All the peaks expected in the first-order spectrum of **11** are identified by ○ or ◑, each of the latter representing two overlapping lines; the five peaks assigned to **12** are denoted by asterisks and the stick diagram; □ indicates the signal from $\cdot SO_3^-$. Apart from the uncertainty of the line structure for **12** about the spectrum center cited in the text, there is the possibility of the presence of low-intensity lines between the two outermost peaks of **11** in both the high- and the low-field regions shown in this figure.

ence in apparent monomer reactivity arises from electronic rather than steric interactions at the C-2 position in **1** and **2**, as we would expect the latter to be comparable in the two cases (36). This follows because -H and -F are roughly the same size and are clearly smaller than the similarly sized groups $-CH_3$ and $-CH_2F$ (36). Preferential head addition is seen in analogous studies of isopropenyl monomers that are deactivated or sterically hindered at one of the ethylene carbons (1, 2, 4–6, 37).

Most of the epr absorption produced by the reaction of **2** with $\cdot SO_3^-$ was readily assignable to the addition radical $CH_2(SO_3^-)\dot{C}FCH_3$, **11**. However, apart from this major component, the rest of the absorption, ca. 10% of the total signal, consisted of five lines, namely, a (1:1)-doublet of (1:1)-doublets with couplings of 3.6 G and 22.2 G and a *g*-value of ca. 2.0032, which, for the sake of discussion, we denote as arising from radical **12**. Close to the center of the four-line spectrum of **12** was one extra line 11.1 G upfield from the low-field wing peak with an intensity approximately equal to one of the other four; however, the observed intensity of this extra line and the apparent absence of any neighboring lines may be a result of overlap with those from **1** and $\cdot SO_3^-$. Figure 1 shows that part of the observed epr absorption is relevant to the discussion here. The two most plausible products would be the tail addition radical, $\cdot CH_2CF(SO_3^-)CH_3$, **13**, or the allylic hydrogen-abstraction product, $CH_2{=}CFCH_2\cdot$, **14**. The epr absorption found is inconsistent with that expected for **13**, which, for example, should have an α-CH_2 proton coupling similar in size to that in **4** and a β-CF fluorine coupling possibly as large as those present in **3** and **5–7**. Also, the isotropic epr spectrum of **14** has already been reported and is very different from the absorption we observed (8–10). It should also be noted the $TiCl_3$–H_2O_2/Na_2SO_3 radical-generating system is more complicated than the others used in this study because of the number of reactants present in the two-step method for $\cdot SO_3^-$ production.

In analyzing the spectroscopic data for **8–11** the following items should be noted. The *g*-values observed are in reasonable agreement with the literature for radicals of structure similar to **8–11** (13, 38). The β-CH_3 proton couplings are relatively constant, 22.8 ± 0.2 G, as are the α-CF fluorine couplings. Therefore, any differences in the β-CH_2X proton couplings must be largely the result of conformational preferences about the C_α—$C_\beta H_2X$ bond induced by the -X group. Moreover, the presence of the strongly electronegative fluorine on C_α may cause a lack of planarity about C_α compared to that expected in **3** and **5–7**, for example (9, 12). We would expect this lack of planarity to tend to hinder the rotation of the β-CH_2X group about the C_α—C_β bond in **8–1** relative to that occurring in **3** and **5–7**, respectively, this giving rise to smaller $a_{\beta\text{-H}}(CH_2X)$ values (9, 38, 39). This comparison of **8–11** with **3** and **5–7** rests on the previously mentioned assumption that -H and -F are roughly the same size and much less bulky than the similarly sized groups $-CH_2F$ and $-CH_3$ (37). This assumption implies quite reasonably that the non-planarity at C_α favors increased steric and polar interactions between the β-CH_2X and the α-$C(F)CH_3$ groups.

Can. J. Chem. Downloaded from www.nrcresearchpress.com by 213.200.69.106 on 09/08/12
For personal use only.

Acknowledgements

We thank the National Science Foundation and the North Carolina Board of Science and Technology for financial support.

1. W.H. Donovan. Ph.D. Dissertation, Duke University, Durham, N.C. 1988.
2. P. Smith and K.K. Karukstis. J. Magn. Reson. **46**, 200 (1982).
3. P. Smith, R.A. Kaba, L.M. Dominguez, and S.M. Denning. J. Phys. Chem. **81**, 162 (1977).
4. P. Smith, R.A. Kaba, and J.T. Pearson. J. Magn. Reson. **17**, 20 (1975).
5. P. Smith, R.A. Kaba, and P.B. Wood. J. Phys. Chem. **78**, 17 (1974).
6. P. Smith and P.B. Wood. Can. J. Chem. **45**, 649 (1967).
7. P. Smith, J.T. Pearson, and R.V. Tsina. Can. J. Chem. **44**, 753 (1966).
8. B.E. Smart, P.J. Krusic, P. Meakin, and R.C. Bingham. J. Am. Chem. Soc. **96**, 7382 (1974).
9. K.S. Chen, P.J. Krusic, and K.J. Kochi. J. Phys. Chem. **78**, 2030 (1974).
10. D.J. Edge and J.K. Kochi. J. Am. Chem. Soc. **94**, 6485 (1972).
11. W.E. Griffiths, G.F. Longster, J. Myatt, and P.F. Todd. J. Chem. Soc. (B), 530 (1967).
12. R.W. Fessenden and R.H. Schuler. J. Chem. Phys. **43**, 2704 (1965).
13. K.S. Chen and J.K. Kochi. Can. J. Chem. **52**. 3529 (1974).
14. P. Smith and W.H. Donovan. Can. J. Chem. **66**, 2304 (1988).
15. R.J. Faber and G.K. Fraenkel. J. Chem. Phys. **47**, 2462 (1967).
16. J.Q. Adams, S.W. Nicksic, and J.R. Thomas. J. Chem. Phys. **45**, 654 (1965).
17. U.M. Oehler and E.G. Janzen. Can. J. Chem. **60**, 1542 (1982).
18. P. Smith, J.T. Pearson, P.B. Wood, and T.C. Smith. J. Chem. Phys. **43**, 1535 (1965).
19. P. Smith, K.R. Maples, C.C. Devlin, and G. McCrohan. J. Magn. Reson. **67**, 539 (1986).
20. P. Smith and K.R. Maples. J. Magn. Reson. **65**, 491, (1985).
21. P. Smith, R.D. Stevens, and R.A. Kaba. J. Phys. Chem. **75**, 2048 (1971).
22. D.C. Borg. Nature, **201**, 1087 (1964).
23. R.O.C. Norman and P.M. Storey. J. Chem. Soc. (B), 1009 (1971).
24. R.O.C. Norman, P.M. Storey, and P.R. West. J. Chem. Soc. (B), 1087 (1970).
25. B.C. Gilbert, R.O.C. Norman, and R.C. Sealy. J. Chem. Soc. Perkin Trans. 2, 2174 (1973).
26. D. Meisel, G. Czapsi, and A. Samuni. J. Chem. Soc. Perkin Trans. 2, 1702 (1973).
27. D.J. Edge and R.O.C. Norman. J. Chem. Soc. (B), 182 (1969).
28. J. March. *In* Advanced organic chemistry. 3rd ed. Wiley–Interscience, New York. 1985. Chaps. 14 and 15.
29. W.T. Dixon, R.O.C. Norman, and A.L. Buley. J. Chem. Soc. 3625 (1964).
30. B. Rånby. Appl. Polym. Symp. **26**, 327 (1975).
31. T. Ozawa and T. Kwan. Polyhedron, **5**, 1531 (1986).
32. T. Ozawa and T. Kwan. Polyhedron, **4**, 1425 (1985).
33. T. Ozawa and T. Kwan. Polyhedron, **2**, 1019 (1983).
34. H.M. McConnell and D.B. Chesnut. J. Phys. Chem. **28**, 107 (1958).
35. H. Fischer. Z. Naturforsch. A: Astrophys. Phys. Phys. Chem. **20A**, 428 (1964).
36. L. Pauling. *In* The nature of the chemical bond. Cornell University Press, New York. 1945. p. 189.
37. B. Rånby and J.F. Rabek. *In* ESR spectroscopy in polymer research. Springer-Verlag, Berlin. 1977. Chap. 4.
38. K.S. Chen, P.J. Krusic, P. Meakin, and J.K. Kochi. J. Phys. Chem. **78**, 2014 (1974).
39. K.S. Chen and P.J. Krusic. Can. J. Chem. **52**, 3529 (1974).

Can. J. Chem. Downloaded from www.nrcresearchpress.com by 213.200.69.106 on 09/08/12
For personal use only.

1,2-Nucleophilic additions of organolithium reagents to chiral oxime ethers

R. KARL DIETER[1] AND RAVINDRA DATAR
Department of Chemistry, Clemson University, Clemson, SC 29634-1905, U.S.A.

Received January 3, 1993

R. KARL DIETER and RAVINDRA DATAR. Can. J. Chem. **71**, 814 (1993).

Chiral oxime ethers are readily prepared from chiral alkoxyamines derived from ephedrine and norephedrine. These chiral oxime ethers of isobutyraldehyde and benzaldehyde undergo 1,2-nucleophilic addition reactions with alkyllithium reagents (*n*-BuLi, PhLi and *n*-BuLi, *tert*-butyllithium, respectively) to afford the chiral alkoxyamines with a diastereomeric excess of 64–88%. Reduction of the alkoxyamines with $LiAlH_4$ gave the corresponding chiral amines. The diastereoselectivity of the reaction appears to directly mirror the *E*:*Z* ratio of the starting oxime ethers.

R. KARL DIETER et RAVINDRA DATAR. Can. J. Chem. **71**, 814 (1993).

On peut facilement préparer des éthers d'oxines chirales à partir des aldoximes chirales dérivées de l'éphédrine ou de la norephédrine. Ces éthers d'oximes chirales de l'isobutyraldéhyde ou du benzaldéhyde peuvent subir des réactions d'addition nucléophiles-1,2 avec des réactifs d'alkyllithium (respectivement *n*-BuLi, PhLi et *n*-BuLi, *tert*-butyllithium) pour conduire aux alkoxyamines chirales avec un excès diastéréoisomériques de 64–88%. La réduction des alkoxyamines avec du $LiAlH_4$ conduit aux amines chirales correspondantes. La diastéréosélectivité de la réaction semble être le reflet direct du rapport *E*:*Z* des éthers des oximes de départ.

[Traduit par la rédaction]

Can. J. Chem. Downloaded from www.nrcresearchpress.com by 213.200.69.106 on 09/08/12
For personal use only.

Although the enantioselective addition of organometallic reagents to aldehydes is a well-studied reaction (1), the corresponding 1,2-nucleophilic addition to imines (2) and their analogs (e.g., hydrazones and oximes) has only recently begun to receive comparable attention. This synthetic approach to chiral amines must contend both with the reduced electrophilicity of imines and their analogs and with the problem of C=N double bond geometry, which generally produces mixtures of *E* and *Z* stereoisomers. Enantioselective addition of organometallic reagents to chiral imines (3), hydrazones (4), oximes (5, 6), nitrones (7), and iminium ions (8) has been reported and promising studies involving addition of organometallic reagents to imines (9), oximes (10), and mixed benzotrazole aminals (11) in the presence of chiral catalysts have recently appeared. Some of these procedures, however, appear limited to aryl imines. The RAMP and SAMP hydrazones give good asymmetric induction upon reaction with organolithium (4*d*, *e*) and organocerium (4*a*–*c*) reagents. Reduction of the hydrazine N—N bond, however, requires strong reducing agents that may not be compatible with a wide range of functional groups, although improved procedures (4*f*) have been developed.

The N—O bond of alkoxy amines is much easier to reduce, but activated chiral oxime ethers are reported (5*b*, *c*) to give relatively modest optical yields upon reaction with organolithium reagents. Addition of organolithium reagents to unactivated oxime ethers has only recently been achieved (12) with the aid of $BF_3 \cdot Et_2O$. Utilization of chiral unactivated oxime ethers has been limited to reduction reactions with metal hydrides (6) and addition of allyl Grignard, lithium, and cerium reagents (5*a*) to chiral α-alkoxyoximes. Our recently reported procedure (13) for effecting regio- and stereoselective substitution of the benzylic hydroxyl group in ephedrine derivatives provides a facile synthetic route to chiral alkoxyamines. We have examined the reaction of chiral oxime ethers (prepared from the ephedrine-derived alkoxyamines) with organometallic reagents as a potentially viable route to chiral amines. Some qualitative insight into the relative reactivity of oxime ether *E* and *Z* geometrical isomers and their role in determining the diastereoselectivity of the reaction has been obtained.

Results

The chiral alkoxyamines **3** and **4** can be readily prepared from *N*-methylephedrine **1***a* and the known (14) norephedrine derivative **1***b*, respectively, in a stereo- and regiospecific manner (Scheme 1) (13). Treatment of **1***a*,*b* with methanesulfonyl chloride – triethylamine followed by addition of *N*-hydroxyphthalimide affords alkoxyimides **2***a*,*b*. Cleavage of the phthalimide with hydrazine gave the alkoxyamines **3** and **4** in excellent overall yield from ephedrine and norephedrine, respectively. Reaction of **3** and **4** with aldehydes in ethanol (eq. [1]) afforded the corresponding oxime ethers **5***a*–*c* and **6**, respectively, as mixtures of *E*:*Z* stereoisomers (Table 1, 94:6 to 63:37 ratios). The ratio of *E*:*Z* isomers was determined from ^1H NMR (15) integration ratios or ^{13}C NMR (16) peak height ratios. Comparison of *E*:*Z* ratios determined by both ^1H and ^{13}C NMR measurements provides an independent verification since values de-

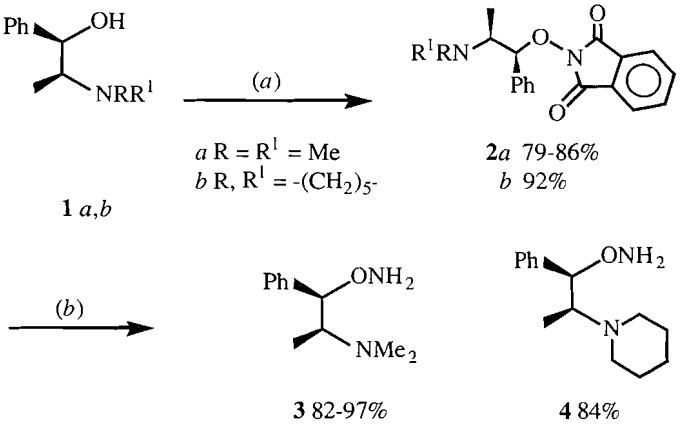

(a) *i*. MsCl, Et_3N, CH_2Cl_2, −78°C to room temperature. *ii*. *N*-Hydroxyphthalimide, Et_3N, reflux, 24 h. (b) H_2NNH_2, EtOH, reflux, 12 h

SCHEME 1

[1]Author to whom correspondence may be addressed.

TABLE 1. Preparation of chiral oxime ethers and determination of E:Z ratios

Oxime	Yield[c] (%)	E:Z[d]	^{1}H NMR[a] δH_A		^{13}C NMR[b] δC_α		δC_{imine}	
			E	Z	E	Z	E	Z
5*a*	93	63:37[e]	7.52	6.76	15.2	12.1	147.5	147.5
5*b*	96	92:8	7.38	6.50	29.2	25.2	156.4	157.5
5*c*	95	94:6[f]	8.21	—	132.2	—	149.1	146.1
6	100	87:13	7.35	6.50	20.2	19.8	156.3	157.5

[a]See ref. 15.
[b]See ref. 16.
[c]Yields are based upon crude product weights >95% homogeneous by ^{1}H NMR.
[d]Determined by ^{1}H NMR integrations or ^{13}C NMR peak height measurements.
[e]In two experiments, E:Z ratios of 38:62 and 47:53 were obtained when the oxime was prepared in pyridine as the solvent.
[f]The E:Z ratio could be determined from the benzylic (δ 5.54 Z, 5.50 E) and methyl (δ 1.17 Z, 1.09 E) proton absorptions.

TABLE 2. Effect of number of equivalents of ^{n}BuLi–$BF_3 \cdot Et_2O$ in addition reactions to chiral oxime ethers

Entry	Oxime ether *a*	Equiv.	Temperature (°C)	Time (h)	Product:oxime ether[a,b]
1	**5***a*	1.2	−78 to 0	2	78:22[c]
2		2	−78 to 0	—	55:45[d]
3		3	−78 to −50	5	100:0[d,e]
4	**5***b*	1.2	−78 to −80	5	48:52
5		2	−78 to −45	5	83:17
6		3	−78 to −50	5	100:0
7	**5***c*	1.2	−78 to 0	2	72:28
8		3	−78 to −50	8	100:0

[a]The crude reaction mixture was >90% homogeneous for oxime and addition product by ^{1}H NMR.
[b]Product to starting material mole ratios were determined by ^{1}H NMR integration ratios.
[c]In this experiment, the E:Z ratio of **5***a* was 38:62.
[d]In this experiment, the E:Z ratio of **5***a* was 63:37.
[e]THF was added as a cosolvent to facilitate solubility.

termined from ^{13}C NMR measurements may be inaccurate due to differential T_1 and nuclear Overhauser effects (16*a*). Formation of oxime ether **5***a* in pyridine gave predominantly the Z stereoisomer.

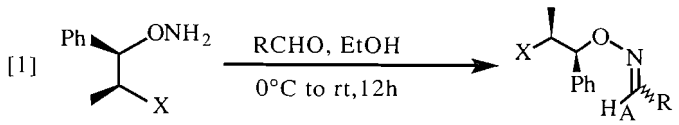

3 X = NMe_2

4 X = 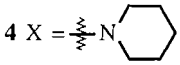

5 X = NMe_2 *a* R = Me; *b* R = ^{i}Pr; *c* R = Ph

6 X = 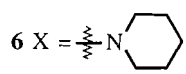 , R = ^{i}Pr

Oxime ethers **5***a* and **5***b* were treated with several organometallic reagents in an initial probe of oxime ether reactivity and reagent efficacy. The reagents PhMgCl ($PhCH_3$), PhMgBr–$ZnBr_2$ (THF), and PhLi (THF–$PhCH_3$) gave only recovered starting material while n-BuLi–$CeCl_3$ (THF) (4*a*–*c*) and PhMgBr–$LiClO_4$ (Et_2O) (17) gave a mixture of starting material and N-methylephedrine resulting from cleavage of the N—O bond. The cuprate reagent, n-Bu_2CuLi (THF), gave a complex mixture consisting chiefly of N-methylephedrine. Reaction of oxime ether **5***a* (63:37 E:Z mixture) with n-BuLi (THF, −78°C, 30 min) gave the addition product **7***a* (40%, 60:40 mixture of diastereomers), recovered Z-oxime ether **5***aZ* (22%), and N-methylephedrine (37%).

Examination of $BF_3 \cdot Et_2O$ as an additive (12) in the addition reactions of n-BuLi to oxime ethers **5***a*–*c* revealed that 3.0 equivalents of n-BuLi–$BF_3 \cdot Et_2O$ were required for complete disappearance of the starting oxime ethers (Table 2). In these experiments, the n-BuLi reagent was added dropwise to the toluene solution of the oxime and $BF_3 \cdot Et_2O$. The reactions of oxime ether **5***a* provided several interesting observations. First, oxime ether **5***a* rich in the Z isomer gave greater conversion to the addition product (Table 2, entry 1) with 1.2 equivalents of the reagents than the sample of **5***a* rich in the E isomer (Table 2, entry 2) gave with 2 equivalents of the reagents. Second, unreacted oxime ether **5***a* originally rich in the Z isomer displayed a 1:1 E:Z ratio

Can. J. Chem. Downloaded from www.nrcresearchpress.com by 213.200.69.106 on 09/08/12
For personal use only.

TABLE 3. Comparison of the *E*:*Z* ratios of the starting oxime ether **5***a* with the recovered oxime ether and diastereomeric ratio of addition product obtained upon reaction of **5***a* with *X* equivalents of ^{n}BuLi–$BF_3 \cdot Et_2O$

		E:*Z* ratio			
Entry	Equiv.	Oxime ether	Recovered oxime ether	Product:oxime ether[a]	Product diastereomeric ratio
1	1.2	38:62[b]	50:50	78:22	40:60
2	2	63:37	60:40	55:45	50:50
3	3	63:37	—	100:0	60:40

[a]Ratios were determined by ^{1}H NMR integration ratios.
[b]Obtained by preparation of oxime ether in pyridine.

after treatment with *n*-BuLi–$BF_3 \cdot Et_2O$ whereas unreacted oxime ether **5***a* originally rich in the *E* isomer displayed the same *E*:*Z* ratio after treatment with *n*-BuLi–$BF_3 \cdot Et_2O$ as it did before treatment (Table 3, entries 1, 2). Third, in the reactions of oxime ether **5***a* with *n*-BuLi–$BF_3 \cdot Et_2O$, the addition product diastereomeric ratios closely mirrored the original *E*:*Z* ratios of the starting oxime ether sample (Table 3, entries 1 and 3).

The yield of addition product **7***a* derived from **5***a* could be increased to 70% (Table 4, entry 1) by using 3 equivalents of an *n*-BuLi–$BF_3 \cdot Et_2O$ mixture (12) in toluene at −78 to −30°C. At higher reaction temperatures complex mixtures of products were obtained. Oxime ethers **5***b*,*c* similarly required 3.0 equivalents of *n*-BuLi–$BF_3 \cdot Et_2O$ for complete disappearance of starting oxime ether (Table 2) to give the addition products in yields of 90% and 72%, respectively (Table 4, entries 3 and 5).

The chiral oxime ether of acetaldehyde (**5***a*) gave a 20% diastereomeric excess (d.e.) with *n*-BuLi and 61% d.e. with the more sterically bulky *t*-BuLi (Table 4, entries 1 and 2). The addition of *tert*-butyllithium to **5***a* also afforded *N*-methylephedrine (19%) and unreacted oxime ether **5***a* recovered as the *Z* isomer. Similarly, good diastereoselectivities (64–88% d.e.) were obtained upon reaction of the isobutyraldehyde oxime ether **5***b* with PhLi or *n*-BuLi and the benzaldehyde oxime ether **5***c* with *n*-BuLi or *t*-BuLi (Table 4, entries 3–6). Chiral isobutyraldehyde oxime ether **6**, containing a piperidine ring in the chiral auxiliary, afforded a diminution in the enantioselectivity by approximately 25% (Table 4, entries 3, 4 vs. 7, 8). When these alkyllithium addition reactions were run on a large scale (>1.0 g) a precipitate was obtained upon warming the solution to −45 to −50°C, causing difficulty with the magnetic stirring bars. Running the reaction at −78°C, using a greater volume of $PhCH_3$ as solvent or dropwise addition of THF (approx. 1 mL THF/15 mL $PhCH_3$), resulted in dissolution of the precipitate and none of these modifications affected the observed diastereoselectivity.

The diastereomeric excess was determined directly by analysis of the ^{1}H or ^{13}C NMR spectra. The d.e. could be determined from both the ^{1}H and ^{13}C NMR spectra for alkoxyamines **7***b*, **8***a*,*b*, and **9***a* and only from the ^{13}C NMR spectra for **7***a* and **9***b*. The values determined from the ^{1}H and ^{13}C NMR spectra were generally in close agreement, differing by ±4.8%. To confirm the diastereoselectivity of these reactions and to assign the absolute configuration at the newly formed stereogenic center, alkoxyamines **8***a*,*b* and **9***a*,*b* were reduced to the amines **11***a*,*b* and **12***a*,*b* with $LiAlH_4$ (eq. [2]). In all cases, except the conversion of **8***b* to **11***b*, the enantiomeric excess determined by optical rotation on the free amine corresponded very closely to the highest value determined for the diastereomeric excess determined from the ^{1}H or ^{13}C NMR spectra (Table 4) of alkoxyamines **8** and **9**. Racemization appears to have occurred during the reduction of **8***b* to amine **11***b*.

Several organolithium reagents did not undergo 1,2-addition reactions to these chiral oxime ethers. Reaction of methyllithium with oxime ethers **5***b*,*c* gave only starting oxime ether while oxime ether **5***b* failed to react with 2-thienyllithium or 1-hexynyllithium (recovered oxime ether had the same *E*:*Z* ratio). Similarly, oxime ether **5***c* failed to react with the lithium derivative of methyldiphenylphosphine oxide

[2] 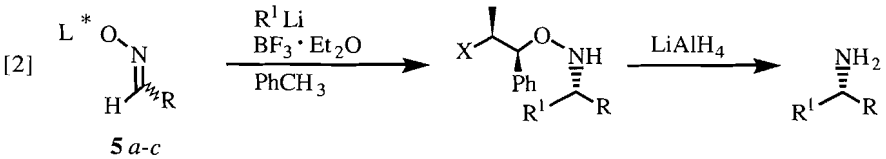

5 *a-c* **6**

X = NMe_2 **7***a* R^1 = ^{n}Bu; R = Me
b R^1 = ^{t}Bu; R = Me
8*a* R^1 = ^{n}Bu; R = ^{i}Pr **11***a*
b R^1 = Ph; R = ^{i}Pr **11***b*
9*a* R^1 = ^{n}Bu; R = Ph **12***a*
b R^1 = ^{t}Bu; R = Ph **12***b*

X = 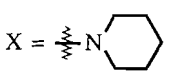 **10***a* R^1 = ^{n}Bu; R = ^{i}Pr
b R^1 = Ph; R = ^{i}Pr

Can. J. Chem. Downloaded from www.nrcresearchpress.com by 213.200.69.106 on 09/08/12
For personal use only.

TABLE 4. Diastereoselective formation of chiral alkoxyamines and conversion to chiral amines

Entry	Oxime ether	*E*:*Z* d.e.	R	R^{1}Li	Alkoxyamine	Yield[a] (%)	d.e.[b]	Amine	Yield[c] (%)	e.e.[d]	Configuration
1	**5***a*	26	Me	^{n}Bu	**7***a*	70	20				
2				^{t}Bu	**7***b*	61	64				
3	**5***b*	84	^{i}Pr	^{n}Bu	**8***a*	90	80	**11***a*	80[e]	85	*S*
4				Ph	**8***b*	70	64	**11***b*	56	12	*R*
5	**5***c*	88	Ph	^{n}Bu	**9***a*	72	78	**12***a*	46	81	*S*
6				^{t}Bu	**9***b*	71	88	**12***b*	49	90	*S*
7	6	74	^{i}Pr	^{n}Bu	**10***a*	70	60				
8				Ph	**10***b*	70	47				

[a]Yields are based upon isolated products purified by column chromatography (silica gel, MeOH).
[b]The diastereomeric excess was determined from ^{1}H NMR integration ratios and (or) ^{13}C NMR peak heights.
[c]Yields are based upon isolated products purified by distillation unless otherwise noted.
[d]The enantiomeric excess was determined from optical rotation measurements that were compared with reported values (see experimental section).
[e]The yield was determined from the crude weight and ^{1}H NMR integration ratios.

[3] 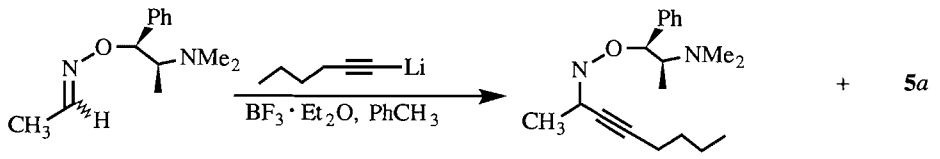

5*a*
63:37 *E*:*Z*
47:53 *E*:*Z*

13
37%
30%

63% *E* - isomer
47:23% *E*:*Z*

and gave recovered oxime ether with an unchanged *E*:*Z* ratio. Treatment of oxime ether **5***a*, however, with 1-hexynyllithium (eq. [3]) afforded the addition product **13** (37%) along with recovered oxime ether (63%) present as the *E* isomer. The addition product displayed a single set of adsorptions characteristic of a single diastereomer. In a second experiment, addition of 4 equivalents of 1-lithiohexyne–$BF_3 \cdot Et_2O$ to **5***a* (−78 to −60°C) existing as a 47:53 *E*:*Z* ratio yielded recovered oxime ether (47:23, *E*:*Z*) and addition product **13** (30%) as determined by ^{1}H NMR analysis.

Discussion

The alkoxyamines **8** and **9** could be reduced with lithium aluminium hydride in Et_2O at room temperature to afford the chiral amines **11** and **12**. Measurement of the optical rotations for the free amines and comparison with reported literature values (18) provided the enantiomeric excess for the method, which could be directly compared with the diastereomeric excess for the initial addition reaction as measured by ^{1}H and ^{13}C NMR spectroscopy. In all cases the two values were within ±5% except for the addition of phenyllithium to isobutyraldehyde oxime ether **5***b*, which gave 64% d.e. for the alkoxyamine and only 12% e.e. for the amine, indicative of racemization occurring during the $LiAlH_4$ reduction step. For this benzylic alkoxyamine, racemization may occur by initial β-elimination of a metal alkoxide followed by reduction of the achiral imine.

Although the diastereomeric excess appears, in general, to parallel the *E*:*Z* ratio of starting oxime ether (Table 4), the oxime ether of acetaldehyde (**5***a*, 63:37 *E*:*Z* ratio) gave a significantly better diastereoselectivity of 64% d.e. upon reaction with *tert*-butylithium–$BF_3 \cdot Et_2O$. This reaction, however, gave ephedrine (19%) from N—O bond cleavage and 6% recovered *Z*-oxime ether. If, for the sake of argument, it is assumed that the ephedrine arises from cleavage of the *Z* isomer, then the *E*:*Z* diastereomer ratio would be 84:16 (68% d.e.), which correlates nicely with the 64% d.e. observed in the addition reaction. However, reaction of **5***a* (63:37 *E*:*Z* ratio) with *n*-BuLi in THF in the absence of $BF_3 \cdot Et_2O$ gave addition product **7***a* (40% yield, 60:40 diastereomer ratio), ephedrine from N—O bond cleavage (37%), and recovered oxime ether (22%) existing as the *Z* isomer (i.e., **5***aZ*). These numbers suggest that the recovered *Z* isomer derives from the original *Z* isomer of the starting material, and the ephedrine now derives solely from the *E* isomer! The achievement of 40% addition in this reaction is in contrast to the general reluctance of alkyllithium reagents to add to oxime ethers in the absence of $BF_3 \cdot Et_2O$ (12), and the failure of alkyllithiums to add to oxime ethers in THF even in the presence of $BF_3 \cdot Et_2O$ as reported by Brooks and co-workers (12*b*). These data and the literature reports are internally consistent if it is assumed that complexes **14** and **15** are formed in THF in the absence of $BF_3 \cdot Et_2O$ and complexes **16** and **17** are formed with $BF_3 \cdot Et_2O$ in toluene. Complex **14** can fragment via a *syn* elimination to afford acetonitrile and ephedrine and complex **15** can undergo enolization to afford the *Z* enolate. In the presence of $BF_3 \cdot Et_2O$, complex **17** is expected to undergo both enolization and elimination (*anti* elimination) at a faster rate then complex **16**. Formation of complexes **14** and **15** followed by deprotonation is consistent with the formation of dipole-stabilized carbanions via complex-induced proximity effects (19) (CIPE). This interpretation is also consistent with the observation that deprotonation of oxime ethers occurs exclusively *syn* to the oxime ether oxygen atom (20). There are, however, other routes for cleavage of the N—O bond in these reactions. Addition of alkyllithium reagents to oxime ethers generates alkoxyamine nitrogen anions, which

Can. J. Chem. Downloaded from www.nrcresearchpress.com by 213.200.69.106 on 09/08/12
For personal use only.

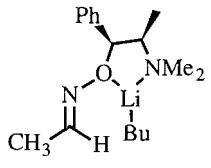

14

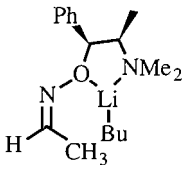

15

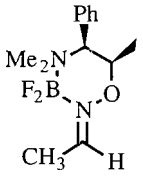

16

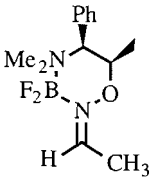

17

are known to undergo substitution reactions with alkyllithium reagents with displacement of the alkoxy group (21). Mechanisms involving a nitreneoid intermediate (12*a*) and direct S_N2 displacement of the alkoxy group by the alkyllithium reagent (21) have been proposed and evidence for both mechanistic pathways has been obtained. If N—O bond cleavage occurs from the nitrogen anion obtained upon addition of RLi to these chiral oxime ethers, the yield of ephedrine should not reflect the stereoelectronic and complex-induced proximity effects described above. Efforts to detect acetonitrile in the reaction of *t*-BuLi–$BF_3 \cdot Et_2O$ with **5***a* were unsuccessful and we are unable to draw a conclusion as to the probable reaction mechanism for the cleavage pathway.

From these observations, it appears that the addition reaction of organolithium reagents with these chiral oxime ethers is highly stereospecific with the diastereoselectivity largely reflecting the ratio of *E*:*Z* isomers undergoing the addition reaction. Direct experimental confirmation was provided by reaction of oxime ether **5***a* with *n*-butyllithium. Reaction of **5***a* existing as a 63:37 *E*:*Z* mixture gave a 60:40 mixture of two diastereomers, which was exactly reversed to a 40:60 ratio of the same two diastereomers when a 38:62 *E*:*Z* mixture of **5***a* was used (Table 3). The *E*:*Z* ratio of recovered unreacted oxime ether **5***a* (Table 3) appears to be a reflection of the relative reaction rates of the *E* and *Z* geometrical isomers and not a result of *E*/*Z* isomerization occurring under the reaction conditions. This view is consistent with the observation that oxime ethers **5***b*,*c* recovered after treatment with lithiomethyldiphenylphosphine oxide – $BF_3 \cdot Et_2O$ or 1-lithiohexyne–$BF_3 \cdot Et_2O$ (no reaction) displayed the same *E*:*Z* ratio as the starting oxime ethers.

The relative reactivity of the oxime ether *E* and *Z* isomers is indicated by several experimental results. Treatment of oxime ether **5***a*, rich in the *Z* isomer, with *n*-butyllithium gave a higher ratio of product to starting material (78:22) than **5***a* rich in the *E* isomer (55:45) even though a smaller quantity of *n*-BuLi–$BF_3 \cdot Et_2O$ was employed (1.2 vs. 2 equivalents). Since most of the oxime ethers that we examined existed largely in the *E* configuration, the failure of lithium acetylides and 2-thienyllithium to undergo reaction with these chiral oxime ethers may be a reflection of the relative reactivity of the oxime ether stereoisomers. This was confirmed by the successful addition of 1-lithiohexyne to **5***a* (63:37 *E*:*Z* ratio) to afford addition product **13** and unreacted recovered *E* oxime in a 37:63 ratio. Similarly, in a second experiment the *E*:*Z* ratio of recovered unreacted oxime ether **5***a* (47:23, *E*:*Z* ratio) and addition product **13** (30%) mirrored exactly the *E*:*Z* ratio (47:53) of the starting oxime ether sample. This observation also suggests that *E*:*Z* isomerization does not occur under these reaction conditions. Although the addition product could not be separated from the *E* oxime, a single diastereomer was observed for the addition product, providing additional evidence for the stereospecificity of the reaction.

Although the nature of the reagent in these reactions is unclear, the results are consistent with literature suggestions that alkyllithiums are stable and react slowly with $BF_3 \cdot Et_2O$ at low temperatures (e.g., −78°C) (22). From this perspective, the Lewis acid activates the oxime ether by complexation[2] to form **16** and **17**, which then undergo addition by the alkyllithium reagent. Three equivalents of RLi–$BF_3 \cdot Et_2O$ are required to compensate for competitive destruction of the alkyllithium reagent, which can occur by reaction with $BF_3 \cdot Et_2O$ to afford alkylidifluoroboranes, alkylfluoroborates, and tetralkylborates or by reaction with the aminoboron trifluoride salt formed in the addition reaction. The work of Ganem and co-workers (22*a*) suggests that the aminoboron trifluoride salts formed in the addition reaction may be more reactive with alkyllithium reagents then $BF_3 \cdot Et_2O$. The use of 3 equivalents of RLi/$BF_3 \cdot Et_2O$ ensures that addition of the alkyllithium reagent to the oxime ether will proceed to completion even in the presence of the competitive destruction of the alkyllithium reagent.

It appears, therefore, that very basic strongly nucleophilic reagents such as *n*-BuLi, PhLi, and *t*-BuLi add very readily to both the *E* and *Z* oxime ether geometrical isomers in the presence of $BF_3 \cdot Et_2O$, although the failure of MeLi to add seems surprising. Weaker bases and less nucleophilic species such as lithium acetylides appear to react only with the more reactive *Z* isomers. Recovery of the oxime ether *Z* stereoisomer in the reaction of **5***a* with *tert*-butyllithium suggests that α-deprotonation of the *Z* isomer forms an oxime ether enolate that is protected from further reaction and that affords the starting *Z* oxime ether upon workup. A similar result is obtained when **5***a* is reacted with *n*-BuLi in the absence of $BF_3 \cdot Et_2O$; the addition product reflects the ratio of *E* isomer, and unreacted oxime ether of *Z* configuration is recovered. This is consistent with the known regioselective deprotonation *syn* to the oxime hydroxyl or oxime ether oxygen (20).

The absolute configuration of the stereogenic center created in these reactions can be understood in terms of complexes **16** and **17**, which can exist in a chair-like conformation. The absolute configurations for the major enantiomers of amines **11***a*,*b* all arise from addition of the alkyllithium reagent to the bottom face of the chair conformation (i.e., **18**) of complex **16** formed from the *E* oxime (see eq. [4]). The *R* configuration observed for amine **11***b* is an artifact of the Cahn–Ingold–Prelog convention for determination of absolute configuration and not a result of the direction of attack. Attack from the bottom face of complex **17** arising from the *Z*

[2]In an NMR study of oxime hydrochlorides, the authors argue that protonation occurs on the nitrogen atom (23).

Can. J. Chem. Downloaded from www.nrcresearchpress.com by 213.200.69.106 on 09/08/12
For personal use only.

oxime affords the minor enantiomer. Molecular models suggest that the axial methyl substituent of the *N,N*-dimethyl group provides much of the steric hindrance required for the observed facial selectivity.

[4] 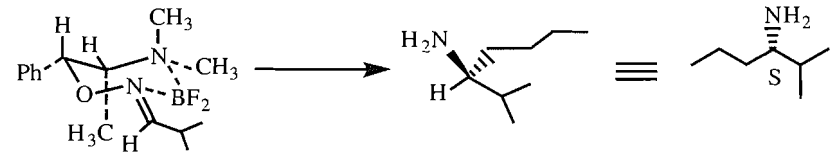

18

In summary, ephedrine or norephedrine can be readily converted into chiral alkoxyamines, which give chiral oxime ethers upon reaction with aldehydes. These chiral oxime ethers undergo 1,2-nucleophilic addition reactions with organolithium reagents in the presence of $BF_3 \cdot Et_2O$ to afford alkoxyamines, which can be reduced to chiral amines. The reaction appears to be highly stereospecific, with the diastereoselectivity of the addition reaction mirroring the initial *E*:*Z* geometry of the starting oxime ether.

Experimental

NMR spectra were recorded as $CDCl_3$ solutions on a Bruker AC-300 instrument. ^1H NMR chemical shifts are reported as δ values in parts per million (ppm) relative to tetramethylsilane (δ_{TMS} = 0.00 ppm) as an internal standard. The ^{13}C NMR chemical shifts are reported in ppm downfield from TMS and referenced with respect to internal $CDCl_3$ (δ_{CDCl_3} = 77.04 for the center line). Infrared spectra (IR) were recorded on a Nicolet 5 DX FT-IR spectrometer as neat samples (sodium chloride plates) unless otherwise noted. Mass spectral measurements were performed on a Hewelett–Packard 5840 or 5890 gas chromatography/mass spectrometer at 70 eV; mass data are tabulated as *m/z* and intensity is expressed as a percent of the base peak. Melting points were determined on a Haake Buchler melting point apparatus and are uncorrected. Elemental analyses were determined by Atlanta Microlab Inc., Atlanta, Ga. The optical rotation measurements were performed on a Horiba Sepa-200 polarimeter.

Tetrahydrofuran and diethyl ether were distilled from sodium benzophenone ketyl. Toluene was distilled from sodium. Commercially available ethanol, methanol, hexane, and methylene chloride were used without further purification. $BF_3 \cdot Et_2O$ was purified by distillation. Alkyllithium reagents were purchased from Aldrich Chemical Company. All the reactions were carried out under a nitrogen atmosphere.

(1R,2S)-O-(2-Dimethylamino-1-phenylethyl) hydroxylamine (3)

To a suspension of *N*-alkoxyphthalimide derivative (13) **2***a* (13.0 g, 40 mmol) in ethanol (120 mL), anhydrous hydrazine (2.0 mL, 63 mmol) was added. The mixture was heated under reflux for 12 h and then cooled to room temperature; the precipitate was filtered and the solvent from the filtrate was evaporated under vacuum. The filter cake from the filtration and the residue from the evaporation were mixed together and water (20 mL) and concentrated HCl (20 mL) were added to it. The resulting mixture was heated under reflux for 3 h. The resulting solid was filtered off. The pH of the filtrate was adjusted to 5 by adding solid NaOH. The resulting aqueous solution of the alkoxyaminehydrochloride was then washed with methylene chloride (20 mL) and the organic layer was discarded. The aqueous layer was diluted if necessary and solid Na_2CO_3 was added to it to adjust the pH to between 8 and 9. The alkaline aqueous layer was extracted with CH_2Cl_2 (4 × 20 mL), and the organic layer was washed with water, brine, and dried over $MgSO_4$. Evaporation of the solvent under reduced pressure provided crude alkoxyamine **3** (6.4 g, 82% yield) as a pale-yellow solid. A spectroscopically pure sample was obtained by crystallization from hexane; mp 81–83°C; IR (KBr): 3296 (w), 3233 (w), 3149 (w) cm^{-1}; ^1H NMR δ: 1.01 (d, *J* = 6.6 Hz, 3H), 2.32 (s, 6H), 2.64 (dq, *J* = 4.2 Hz, *J* = 6.9 Hz, 1H), 4.73 (d, *J* = 4.2 Hz, 1H), 5.22 (br s, 2H), 7.24–7.38 (m, 5H); ^{13}C NMR δ: 8.8, 41.9 (2C), 64.2, 87.7, 126.7 (2C), 127.3, 128.3 (2C), 141.1; mass spectrum *m/z* (intensity) CI: 195 (M + 1, 100); EI: 162 (M − ONH_2, 3.8), 72 ($CH_3CH{=}N^+Me_2$, 100).

*(1R,2S)-2-(1-Piperdino)-1-phenyl-1-*N*-phthalimidohydroxypropane (2b)*

The procedure reported by Dieter et al. (13) was used. To a CH_2Cl_2 solution of (1*R*,2*S*)-1-phenyl-2-piperidinopropanol **1***a* (4.38 g, 20 mmol) and triethyl amine (2.22 g, 22 mmol), cooled to −78°C, methanesulfonyl chloride (1.7 mL, 22 mmol) was added in a dropwise manner. The reaction was allowed to warm to room temperature and stirred at room temperature for 6 h. Additional triethyl amine (2.22 g, 22 mmol) and *N*-hydroxyphthalimide (6.525 g, 40 mmol was added as a solid) were added to the reaction mixture, which was heated under vigorous reflux for 16 h. The solvent was evaporated under reduced pressure and benzene (100 mL) and aqueous $NaHCO_3$ solution were added to the residue. The mixture was stirred until no solid remained and two clear phases were formed. The organic layer was washed with saturated aqueous $NaHCO_3$ solution until the red color of the organic phase disappeared. Further washing of the organic phase with water and brine followed by drying ($MgSO_4$) provided the crude product **2***b* (6.7 g, 92% yield), which was >95% homogenous by ^1H NMR and ^{13}C NMR and was used without further purification; ^1H NMR δ: 1.35 (d, *J* = 6.6 Hz, 3H), 1.34–1.40 (m, 6H), 2.53–2.59 (m, 4H), 2.98–3.06 (m, 1H), 5.52 (d, *J* = 6.3 Hz, 1H), 7.23–7.69 (m, 9H); ^{13}C NMR δ: 10.3, 24.7, 26.5 (2C), 50.2 (2C), 64.1, 89.6, 123.2 (2C), 127.7 (2C), 128.2 (2C), 128.3 (2C), 128.9, 134.1 (2C), 138.1, 163.6 (2C).

(1R,2S)-O-(1-(2-Piperidino)-1-phenylethyl)hydroxylamine (4)

The same procedure employed for the synthesis of **3** was used except for the change of substrate. *N*-Hydroxyphthalimide derivative **2***b* (6.7 g, 18.4 mmol) was treated with hydrazine (1.0 mL, 31.5 mmol). The crude alkoxyamine **4** (3.60 g, 84% yield) was >95% pure by ^1H and ^{13}C NMR. It was used in the subsequent reactions without further purification; ^1H NMR δ: 1.03 (d, *J* = 6.9 Hz, 3H), 1.39–1.50 (m, 6H), 2.54–2.67 (m, 5H), 4.74 (d, *J* = 4.2 Hz, 1H), 5.22 (s, 2H), 7.25–7.37 (m, 5H); ^{13}C NMR δ: 9.5, 24.7, 26.5 (2C), 50.7 (2C), 65.1, 87.7, 126.6 (2C), 127.1, 128.1 (2C), 141.4.

General procedure A: Synthesis of oxime ethers

To a round-bottom flask fitted with a nitrogen inlet were added alkoxyamine (**3** or **4**) (1 mmol) and absolute ethanol (10 mL). The resulting solution was cooled to 0°C and aldehyde (2 mmol, neat) was added to it in a dropwise manner. The reaction mixture was allowed to warm to room temperature while stirring was continued for 12 h. After evaporating ethanol in vacuo, CH_2Cl_2 (20 mL) was added to the residue. The organic layer was washed successively with water (2 × 20 mL), saturated $NaHCO_3$ solution (20 mL), water (2 × 20 mL), and brine (20 mL) and was then dried over $MgSO_4$. Evaporation of the solvent in vacuo afforded prod-

Can. J. Chem. Downloaded from www.nrcresearchpress.com by 213.200.69.106 on 09/08/12
For personal use only.

Can. J. Chem. Downloaded from www.nrcresearchpress.com by 213.200.69.106 on 09/08/12
For personal use only.

uct oxime ethers that were analyzed by ^1H and ^{13}C NMR spectroscopy.

*(1R,2S)-2-Dimethylamino-1-phenyl-1-[[ethylideneamino]oxy]propane (**5**a)*

General procedure A was followed. To an ethanol solution of alkoxyamine **3** (1.00 g, 5.15 mmol), cooled to 0°C, acetaldehyde (0.60 mL, 10.7 mmol) was added. The crude product **5***a* (1.06 g, 93% yield, *E*:*Z*/60:40) was >95% homogeneous by ^1H and ^{13}NMR. An analytically pure sample was obtained by column chromatography on silica gel (MeOH); IR: 3085 (w), 3064 (m), 3029 (m), 1679 (w), 899 (s) cm^{-1}; ^1H NMR (*E* isomer) δ: 1.03 (d, J = 6.9 Hz, 3H), 1.78 (d, J = 6.0 Hz, 3H), 2.36 (s, 6H), 2.74 (dq, J = 6.9 Hz, J = 3.3 Hz, 1H), 5.31 (d, J = 3.9 Hz, 1H), 7.19–7.34 (m, 5H), 7.52 (q, J = 6 Hz, 1H); ^1H NMR (*Z* isomer) δ: 1.07 (d, J = 6.9 Hz, 3H), 1.92 (d, J = 5.4 Hz, 3H), 2.37 (s, 6H), 2.83 (dq, J = 6.9 Hz, J = 3.3 Hz, 1H), 5.38 (d, J = 3.6 Hz, 1H), 6.76 (q, J = 5.4 Hz, 1H); ^{13}C NMR (*E* isomer) δ: 9.1, 15.2, 41.7, 64.4, 84.0, 126.6 (2C), 127.0, 128.0 (2C), 142.0, 147.3; ^{13}C NMR (*Z* isomer) δ: 8.9, 12.2, 41.4, 84.3, 126.3 (2C), 126.9; mass spectrum *m/z* (intensity) EI: 162 (M − ON=CHCH$_3$, 1.4), 72 ($CH_3CH{=}N^+Me_2$, 100). Anal. calcd. for $C_{13}H_{20}N_2O$: C 70.88, H 9.14; found: C 70.70, H 9.11.

*(1R,2S)-2-Dimethylamino-1-phenyl-1-[[[2-methylpropylidene]amino]oxy]propane (**5**b)*

General procedure A was followed. To an ethanol solution of alkoxyamine **3** (1.00 g, 5.15 mmol), cooled to 0°C, isobutyraldehyde (0.94 mL, 10.3 mmol) was added. The crude product **5***b* (1.22 g, 96% yield, *E*:*Z*/92.8) was >95% homogeneous by ^1H and ^{13}C NMR. An analytically pure sample was obtained by column chromatography on silica gel (MeOH); IR: 3085 (w), 3064 (w), 3029 (w), 1644 (w), 1454 (s), 913 (s) cm^{-1}; ^1H NMR (*E* isomer) δ: 0.92–0.97 (apparent t, m, 9H), 2.31 (s, 6H), 2.35 (oct, J = 6.9 Hz, 1H), 2.70 (dq, J = 6.9 Hz, J = 3.3 Hz, 1H), 5.24 (d, J = 3.6 Hz, 1H), 7.14–7.27 (m, 5H), 7.31 (d, J = 6.9 Hz, 1H); ^1H NMR (*Z* isomer) δ: 0.99–1.03 (apparent t, m, 9H), 2.32 (s, 6H), 2.80 (dq, J = 6.9 Hz, J = 3.3 Hz, 1H), 3.17 (oct, J = 6.9 Hz, 1H), 5.27 (d, J = 3.6 Hz, 1H), 6.40 (d, J = 6.9 Hz, 1H); ^{13}C NMR (*E* isomer) δ: 9.19, 20.16, 29.15, 41.75, 64.31, 83.76, 126.55 (2C), 126.67, 127.85 (2C), 141.85, 156.44; ^{13}C NMR (*Z* isomer) δ: 9.01, 19.69, 29.20, 41.45, 64.37, 84.49, 157.51; mass spectrum *m/z* (intensity) EI: 162 (M − ON=CH(i-Pr), 5.6), 72 ($CH_3CH{=}N^+Me_2$, 100). Anal. calcd. for $C_{15}H_{24}N_2O$: C 72.55, H 9.73; found: C 72.32, H 9.68.

*(1R,2S)-2-Dimethylamino-1-phenyl-1-[[[1-phenylmethylidene]amino]oxy]propane (**5**c)*

General procedure A was followed. To an ethanol solution of alkoxyamine **3** (2.04 g, 10.5 mmol), cooled to 0°C, benzaldehyde (1.60 mL, 15.8 mmol) was added. The crude product **5***c* (2.81 g, 95% yield, *E*:*Z*/90:10) was >95% homogeneous by ^1H and ^{13}C NMR. An analytically pure sample was obtained by column chromatography on silica gel (MeOH); IR: 3064 (m), 3029 (m), 1686 (w), 941 (s), cm^{-1}; ^1H NMR (*E* isomer) δ: 1.09 (d, J = 6.6 Hz, 3H), 2.40 (s, 6H), 2.80 (dq, J = 6.9 Hz, J = 3.3 Hz, 1H), 5.50 (d, J = 3.6 Hz, 1H), 7.22–7.53 (m, 10H), 8.21 (s, 1H); ^1H NMR (*Z* isomer) δ: 1.17 (d, J = 6.9 Hz, 3H), 5.54 (d, J = 3.6 Hz, 1H); ^{13}C NMR (*E* isomer) δ: 9.3, 41.8, 64.2, 85.2, 126.6 (2C), 126.9, 127.1 (2C), 128.0 (2C), 128.5 (2C), 129.7, 132.2, 141.9, 149.1; ^{13}C NMR (*Z* isomer) δ: 41.5, 86.5, 146.4; mass spectrum *m/z* (intensity) EI: 162 (M − ON=CHPh, 1.4), 77 (Ph^+, 12.9), 72 ($CH_3CH{=}N^+Me_2$, 100). Anal. calcd. for $C_{18}H_{22}N_2O$: C 76.57, H 7.85; found: C 76.37, H 7.86.

*(1R,2S)-2-(1-Piperidino)-1-phenyl-1-[[[2-methylpropylidene]amino]oxy]propane (**6**)*

General procedure A was used. The alkoxyamine **4** (2.3 g, 10.0 mmol) was treated with isobutylaldehyde (1.080 g, 15.0 mmol) in ethanol. The crude oxime ether **6** (2.88 g, 100% yield) was >95% homogeneous by ^1H and ^{13}C NMR and was used without purification; ^1H NMR (*E* isomer) δ: 0.98–1.10 (m, 9H), 1.39–1.53 (m, 6H), 2.44 (sept, J = 6.9 Hz, 1H), 2.57–2.81 (m, 5H), 5.31 (d, J = 3.6 Hz, 1H), 7.19–7.31 (m, 5H), 7.35 (d, J = 7 Hz, 1H); ^1H NMR (*Z* isomer) δ: 5.32 (d, J = 3.0 Hz, 1H), 6.50 (d, J = 7 Hz, 1H); ^{13}C NMR (*E* isomer) δ: 9.7, 20.2 (2C), 24.7, 26.4 (2C), 29.2, 50.5 (2C), 65.2, 83.8, 126.3, 126.4 (2C), 127.7 (2C), 142.4, 156.3; ^{13}C NMR (*Z* isomer) δ: 19.8, 157.5.

General procedure B: Addition of organolithium reagents to chiral oxime ethers

To a round-bottom flask fitted with a nitrogen inlet were added oxime ether (0.5 mmol) and toluene (5 mL). The resulting solution was cooled to −78°C and $BF_3 \cdot Et_2O$ (1.5 mmol, neat) was added to it. The alkyllithium reagent (1.5 mmol) was then added dropwise to the solution via syringe over 10 min. After the addition was complete the resulting clear, pale-yellow solution was stirred at −78°C for 1 h. The reaction was quenched by addition of water (0.5 mL). After evaporation of the solvent, the residue was taken up in CH_2Cl_2 (40 mL), washed successively with 15% NaOH (2 × 20 mL), water (2 × 20 mL), brine (20 mL), and then dried over $MgSO_4$. After filtration and solvent removal in vacuo, the resulting crude material was dissolved in hexane (20 mL), filtered through Celite, and concentrated in vacuo to afford product alkoxyamines that were analyzed by ^1H and ^{13}C NMR. Spectroscopically pure samples were obtained by column chromatography on silica gel (MeOH).

*(1R,2S)-N-[1-Phenyl-2-(dimethylamino)propyl]oxy]hexane-2-amine (**7**a)*

General procedure B was followed. To acetaldehyde oxime derivative **5***a* (0.110 g, 0.5 mmol), dissolved in toluene, $BF_3 \cdot Et_2O$ (0.18 mL, 1.5 mmol) and *n*-BuLi (0.63 mL, 2.4 M, 1.5 mmol) were added. Evaporation of the solvent gave product **7***a* (0.097 g, 70%), which was >95% homogeneous by ^1H and ^{13}C NMR spectroscopy; IR: 3296 (w, br) cm^{-1}; ^1H NMR (major diastereomer) δ: 0.83–0.96 (m, 3H), 0.97–1.16 (m, 6H), 1.18–1.30 (m, 6H), 2.30 (s, 6H), 2.70–2.74 (m, 1H), 2.97 (m, 1H), 4.73 (d, J = 5.1 Hz, 1H), 5.10 (s, 1H) 7.22–7.36 (m, 5H); ^1H NMR (minor diastereomer) δ: 4.74 (d, J = 4.8 Hz, 1H); ^{13}C NMR (major diastereoisomer) δ: 8.84, 14.04, 18.19, 22.85, 28.11, 33.88, 41.46 (2C), 55.92, 64.16, 85.67, 126.80 (2C), 127.02, 128.11 (2C), 142.17; ^{13}C NMR (minor diastereomer) δ: 14.00, 18.64, 22.78, 33.66, 64.06; mass spectrum (GC–MS): 162 (M − ONHCH(*n*-Bu)CH$_3$), 72 ($CH_3CH{=}N^+Me_2$).

*(1R,2S)-N-[1-Phenyl-2-(dimethylamino)propyl]oxy]-3-dimethyl-2-aminobutane (**7**b)*

General procedure B was followed. To acetaldehyde oxime derivative **5***a* (0.770 g, 3.5 mmol) dissolved in toluene were added $BF_3 \cdot Et_2O$ (1.28 mL, 10.5 mmol) and *t*-BuLi (7.0 mL, 1.5 M, 10.5 mmol). The crude material obtained (0.800 g) was purified by column chromatography on silica gel (MeOH) to obtain pure **7***b* (0.590 g, 61% yield); IR: 3212 (br) cm^{-1}; ^1H NMR (major diastereomer) δ: 0.84 (s, 9H), 1.04 (d, J = 7.0 Hz, 3H), 1.09 (d, J = 7.0 Hz, 3H), 2.30 (s, 6H), 2.69–2.75 (m, 2H), 4.73 (d, J = 4.8 Hz, 1H), 5.10 (br s, 1H), 7.23–7.34 (m, 5H); ^1H NMR (minor diastereomer) δ: 0.77 (s, 9H), 2.29 (s, 6H); ^{13}C NMR (major diastereomer) δ: 8.67, 14.14, 26.76 (3C), 33.34, 41.44 (2C), 63.81, 63.89, 84.86, 126.78 (2C), 126.89, 128.02 (2C), 142.33; ^{13}C NMR (minor diastereomer) δ: 8.96, 26.57, 33.15, 85.16, 126.33 (2C); mass spectrum *m/z* (intensity) EI: 162 (M − ONHCH(*t*-Bu)CH$_3$, 31), 72 ($CH_3CH{=}N^+Me_2$, 100).

*(1R,2S)-3-Amino-2-methyl-N-[1-phenyl-2-(dimethylamino)propyl]oxy]heptane (**8**a)*

General procedure B was followed. To isobutyraldehyde oxime derivative **5***b* (0.500 g, 2.0 mmol) dissolved in toluene, $BF_3 \cdot Et_2O$ (0.77 mL, 6.0 mmol) and *n*-BuLi (2.40 mL, 2.5 M, 6.0 mmol) were added. Evaporation of the solvent gave product **8***a* (0.541 g, 90% yield), which was >95% homogeneous by ^1H and ^{13}C NMR spectroscopy; IR: 3346 (br) cm^{-1}; ^1H NMR (major diastereomer) δ: 0.80 (d, J = 6.9 Hz, 2H), 0.86–0.88 (m, 6H), 1.05 (d, J = 6.8 Hz, 3H), 1.12–1.49 (m, 6H), 1.92 (oct, J = 7.5 Hz, 1H), 2.29

Can. J. Chem. Downloaded from www.nrcresearchpress.com by 213.200.69.106 on 09/08/12
For personal use only.

(s, 6H), 2.54–2.63 (m, 1H), 2.72 (pent, J = 7.8 Hz, 1H), 4.71 (d, J = 5.1 Hz, 1H), 5.30 (vbr s, 1H), 7.22–7.36 (m, 5H); ^{13}C NMR (major diastereomer) δ: 8.88, 14.10, 18.09, 19.16, 22.95, 27.95, 28.81, 29.01, 41.44 (2C), 64.00, 65.68, 85.33, 126.90 (2C), 127.03, 128.08 (2C), 142.37; ^{13}C NMR (minor diastereomer) δ: 85.53; mass spectrum (GC–MS): 162 (M − ONHCH(*n*-Bu)i-Pr), 72 ($CH_3CH{=}N^+Me_2$).

(1R,2S)-α-(1-Methylethyl)-N-*[1-phenyl-2-(dimethylamino)propyl]oxy]benzenemethanamine (**8**b)*

General procedure B was followed. To isobutyraldehyde oxime derivative **5***b* (0.500 g, 2.0 mmol) dissolved in toluene, $BF_3 \cdot Et_2O$ (0.73 mL, 6.0 mmol) and PhLi (3.35 mL, 1.8 M, 6.04 mmol) were added. The crude material obtained (0.690 g) was purified by column chromatography on silica gel (MeOH) to obtain spectroscopically pure **8***b* (0.46 g, 70% yield); IR: 3198 (br) cm^{-1}; ^{1}H NMR (major diastereomer) δ: 0.65 (d, J = 6.6 Hz, 3H), 0.73 (d, J = 6.6 Hz, 3H), 0.88 (d, J = 6.6 Hz, 3H), 1.80 (oct, J = 6.6 Hz, 1H), 1.95 (s, 6H), 2.49–2.58 (m, 1H), 3.71 (dd, J = 7.2 Hz, J = 3.6 Hz, 1H), 4.54 (d, J = 5.1 Hz, 1H), 5.57 (d, J = 3.6 Hz, 1H), 7.14–7.43 (m, 10H); ^{1}H NMR (minor diastereomer) δ: 2.23 (s, 6H), 4.74 (d, J = 5.6 Hz, 1H), 5.45 (d, J = 3.6 Hz, 1H); ^{13}C NMR (major diastereomer) δ: 8.64, 19.27, 20.13, 31.15, 40.80 (2C), 63.71, 71.59, 85.59, 126.80, 126.88, 126.94, 127.70, 128.07, 128.46, 141.88, 142.31; ^{13}C NMR (minor diastereomer) δ: 18.52, 30.50, 41.42, 70.85, 85.46; mass spectrum m/z (intensity) CI: 328 (M + 2, 20), 327 (M + 1, 100); EI: 162 (M − ONHCH(i-Pr)Ph, 20), 72 ($CH_3CH{=}N^+Me_2$, 100).

(1R,2S)-α-Butyl-N-*[1-phenyl-2-(dimethylamino)propyl]oxy]benzenemethanamine (**9**a)*

General procedure B was followed. To benzaldehyde oxime derivative **5***c* (1.00 g, 3.54 mmol) dissolved in toluene, $BF_3 \cdot Et_2O$ (1.30 mL, 10.6 mmol) and *n*-BuLi (4.24 mL, 2.5 M, 10.6 mmol) were added. The crude material obtained (1.010 g) was purified by column chromatography on silica gel (MeOH) to obtain spectroscopically pure **9***a* (0.870 g, 72% yield); IR: 3212 (br) cm^{-1}; ^{1}H NMR (major diastereomer) δ: 0.83 (t, J = 7.0 Hz, 3H), 0.98 (d, J = 6.8 Hz, 3H), 1.00–1.35 (m, 4H), 1.50–1.65 (m, 1H), 1.84–1.96 (m, 1H), 2.26 (s, 6H), 2.69 (dq, J = 6.4 Hz, J = 3.3 Hz, 1H), 3.94 (s, br, 1H), 4.76 (d, J = 5.2 Hz, 1H), 5.35 (s, br, 1H), 7.16–7.34 (m, 10H); ^{1}H NMR (minor diastereomer) δ: 1.97 (s, 6H), 4.54 (d, J = 5.2 Hz, 1H), ^{13}C NMR (major diastereomer) δ: 8.82, 13.96, 22.71, 28.27, 33.42, 41.49 (2C), 63.95, 65.59, 85.71, 126.87, 127.00, 127.23, 127.64, 128.04, 128.19, 141.78, 141.89; ^{13}C NMR (minor diastereomer) δ: 33.90, 40.87; mass spectrum m/z (intensity) CI: 342 (M + 2, 18.7), 341 (M + 1, 100), 162 (M − ONHCH(*n*-Bu)Ph, 55); EI: 341.3 (M + 1, 1.7), 162 (M − ONHCH(*n*-Bu)Ph, 6.7), 72 ($CH_3CH{=}N^+Me_2$, 100).

(1R,2S)-α-(1-Dimethylethyl)-N-*[1-phenyl-2-(dimethylamino)propyl]oxy]benzenemethanamine (**9**b)*

General procedure B was followed. To benzaldehyde oxime derivative **5***c* (1.00 g, 3.54 mmol) dissolved in toluene, $BF_3 \cdot Et_2O$ (1.30 mL, 10.6 mmol) and *t*-BuLi (7.0 mL, 1.5 M, 10.6 mmol) were added. The crude material obtained (1.220 g) was purified by column chromatography on silica gel (MeOH) to obtain spectroscopically homogeneous **9***b* (0.842 g, 71% yield); IR: 3219 (br) cm^{-1}; ^{1}H NMR (major diastereomer) δ: 0.81 (d, J = 6.0 Hz, 3H), 0.82 (s, 9H), 2.18 (s, 6H), 2.65 (dq, J = 6.4 Hz, J = 3.3 Hz, 1H), 3.80 (d, J = 7.5 Hz, 1H), 4.75 (d, J = 5.1 Hz, 1H), 5.70 (d, J = 9.0 Hz, 1H), 7.16–7.30 (m, 10H); ^{1}H NMR (minor diastereomer) δ: 0.80 (s, 9H), 2.22 (s, 6H); ^{13}C NMR (major diastereomer) δ: 8.41, 27.38 (3C), 34.05, 41.39 (2C), 63.57, 73.17, 84.61, 126.67, 127.04, 127.41, 128.00, 128.55, 140.82, 141.71; ^{13}C NMR (minor diastereomer) δ: 28.36; mass spectrum m/z (intensity) CI: 342 (M + 2, 16.6), 341 (M + 1, 100); EI: 162 (M − ONHCH(*t*-Bu)Ph, 48), 72 ($CH_3CH{=}N^+Me_2$, 100).

(1R,2S)-3-Amino-2-methyl-N-*[1-phenyl-2-(1-piperidino)propyl]oxy]heptane (**10**a)*

General procedure B was followed. To isobutyraldehyde oxime derivative **6** (0.144 g, 0.5 mmol) dissolved in toluene, $BF_3 \cdot Et_2O$ (0.183 mL, 1.5 mmol) and *n*-BuLi (0.6 mL, 2.5 M, 1.5 mmol) were added. The crude product **10***a* (0.187 g) was analyzed by ^{1}H and ^{13}C NMR. No attempts to purify the product were made; ^{1}H NMR δ: 0.80–0.95 (m, 9H), 1.06 (d, J = 6.6 Hz, 3H), 1.17–1.55 (m, 12H), 1.87–1.94 (m, 1H), 2.50–2.69 (m, 6H), 4.75 (d, J = 4.2 Hz, 1H), 5.31 (s, br, 1H), 7.14–7.33 (m, 5H); ^{13}C NMR (major diastereomer) δ: 9.74, 14.08, 18.19, 19.17, 22.94, 24.82, 26.54, 28.04, 28.85, 28.93, 50.58 (2C), 65.12, 65.63, 85.13, 126.73 (2C), 126.82, 127.83 (2C), 142.61; ^{13}C NMR (minor diastereomer) δ: 13.86, 19.01, 25.81, 85.71.

(1R,2S)-α-(1-Methylethyl)-N-*[1-phenyl-2-(1-piperidino)propyl]oxy]benzenemethanamine (**10**b)*

General procedure B was followed. To isobutyaldehyde oxime derivative **6** (0.144 g, 0.5 mmol) dissolved in toluene, $BF_3 \cdot Et_2O$ (0.183 mL, 1.5 mmol) and PhLi (0.83 mL, 1.8 M, 1.5 mmol) were added. The crude product **10***b* (0.173 g, 94% yield) was analyzed by ^{1}H and ^{13}C NMR. No attempt to purify the product was made; ^{1}H NMR (major diastereomer) δ: 0.65 (d, J = 6.9 Hz, 3H), 0.81 (d, J = 6.9 Hz, 3H), 0.88 (d, J = 6.9 Hz, 3H), 1.08–1.44 (m, 6H), 1.77 (oct, J = 6.9 Hz, 1H), 2.15–2.54 (m, 5H), 3.73 (d, J = 7.5 Hz, 1H), 4.70 (d, J = 4.2 Hz, 1H), 5.63 (s, br, 1H), 7.17–7.43 (m, 10H); ^{1}H NMR (minor diastereomer) δ: 0.74 (d, J = 6.9 Hz, 3H), 0.91 (d, J = 6.9 Hz, 3H), 0.96 (d, J = 6.9 Hz, 3H), 3.77 (d, J = 7.5 Hz, 1H), 4.84 (d, J = 4.2 Hz, 1H); ^{13}C NMR (major diastereomer) δ: 9.18, 19.28, 20.00, 24.23, 26.12, 26.41, 31.29, 49.33 (2C), 65.13, 71.53, 84.65, 126.56 (2C), 126.81 (2C), 127.75 (3C), 128.03 (2C), 128.19 (2C), 128.44, 141.97, 142.25; ^{13}C NMR (minor diastereomer) δ: 18.45, 30.47, 50.57, 64.97, 70.66, 85.03.

General procedure C: Reduction of alkoxyamines to amines

To the alkoxyamine **8**(*a*,*b*) and **9**(*a*,*b*) (2 mmol) dissolved in dry ether at room temperature, $LiAlH_4$ (3 mmol) was added in a portionwise manner. The reaction was allowed to stir at room temperature for 12 h. The reaction was then quenched by successive dropwise addition of water (0.1 mL), 15% NaOH (0.1 mL), and water (0.3 mL). The granular precipitate formed after stirring for 15 min was filtered off and the filtrate was dried over K_2CO_3. Ether was evaporated by warming the flask on a water bath. The amines **11**(*a*,*b*) and **12**(*a*,*b*) thus obtained were volatile. Careful distillation using a Kugelrohr apparatus provided the pure amines (yields were low because of the losses due to evaporation) as a distillate and *N*-methylephedrine **1***a* (quantitative yield) as a pot residue. The optical rotations of the amines were recorded immediately. All the amines gave satisfactory spectral data.

*(3S)-2-Methyl-3-heptanamine (**11**a)*

General procedure C was followed using **8***a* (1.00 g, 3.3 mmol) as the starting compound. The product amine **11***a* was purified by Kugelrohr distillation (80% yield, determined by ^{1}H NMR): bp 40°C (40 Torr; 1 Torr = 133.3 Pa); $[\alpha]_D^{24}$ − 17.18 (*c* 3.2, C_2H_5OH), *S*, 85% ee (lit. (18*a*) $[\alpha]_D^{24}$ +17.4 (*c* 3.3, C_2H_5OH), *R*, 86% ee); ^{1}H NMR δ: 0.86 (d, J = 6.9 Hz, 3H), 0.90 (d, J = 6.6 Hz, 3H), 0.84–0.93 (overlapping t, 3H), 1.14–1.20 (m, 8H), 1.58–1.60 (m, 1H), 2.48–2.49 (m, 1H); ^{13}C NMR δ: 14.10, 17.07, 19.27, 22.90, 28.87, 33.23, 34.45, 56.51.

*(1-R)-α-(1-Methylethyl)benzenemethanamine (**11**b)*

General procedure C was followed using **8***b* (0.624 g, 1.91 mmol) as the starting compound. The product amine **11***b* was purified by Kugelrohr distillation (0.156 g, 56% yield): bp 40–50°C (0.1 Torr); $[\alpha]_D^{24}$ +2.11 (*c* 2.0, C_2H_5OH), *R*, 12% ee (lit. (18*b*) $[\alpha]_D^{24}$ +13.0 (*c* 2.5, C_2H_5OH), *R*); ^{1}H NMR δ: 0.76 (d, J = 6.6 Hz, 3H), 0.97 (d, J = 6.6 Hz, 3 H), 1.52 (s, 2H), 1.82–1.86 (m, 1H), 3.59 (d, J = 7.2 Hz, 1H), 7.22–7.33 (m, 5H); ^{13}C NMR δ: 18.90, 19.80, 35.44, 62.47, 126.74, 127.00 (2C), 128.12 (2C), 145.49.

*(1-S)-α-Butyl benzenemethanamine (**12**a)*

General procedure C was followed using **9***a* (0.450 g, 1.32 mmol) as the starting compound. The product amine **12***a* was

purified by Kugelrohr distillation (0.100 g, 46% yield): bp 45°C (0.25 Torr); $[\alpha]_D^{24}$ −10.31 (*c* 3.2, $CHCl_3$), *S*, 81% ee (lit. (18*c*) $[\alpha]_D^{24}$ +11.7 (*c* 1.0, $CHCl_3$), *R*, 92% ee); ^{1}H NMR δ: 0.84–0.88 (m, 3H), 1.10–1.32 (m, 4H), 1.50–1.68 (m, 4H), 3.86 (t, *J* = 6.9 Hz, 1H), 7.25–7.32 (m, 5H); ^{13}C NMR δ: 14.00, 22.67, 28.77, 39.38, 56.29, 126.30 (2C), 126.83, 128.40 (2C), 146.84.

*(1S)-α-(1,1-Dimethylethyl)benzenemethanamine (**12**b)*

General procedure C was followed using **9***b* (0.700 g, 2.05 mmol) as the starting compound. The product amine **12***b* was purified by Kugelrohr distillation (0.165 g, 49% yield): bp 45°C (0.25 Torr); $[\alpha]_D^{24}$ −2.26 (*c* 5.3, CH_3OH), *S*, 90% ee (lit. (18*d*) $[\alpha]_D^{24}$ +2.5 (*c* 4.0, CH_3OH), *R*); ^{1}H NMR δ: 0.90 (s, 9H), 1.51 (s, 2H), 3.69 (s, 1H), 7.22–7.31 (m, 5H); ^{13}C NMR δ: 26.51 (3C), 35.00, 65.31, 126.71, 127.48 (2C), 128.23 (2C), 143.76.

*(1R,2S)-2-Amino-*N*-[1-phenyl-2-(dimethylamino)propyl]oxy]-3-octyne (**13**)*

To a solution of 1-hexyne (0.164 g, 2.0 mmol) in THF (2 mL) cooled to −30°C was added *n*-BuLi (0.83 mL, 2.4 M, 2.0 mmol) and the resulting solution was stirred for 45 min. In another flask, to a solution of acetaldehyde oxime ether derivative **5***a* (0.110 g, 0.5 mmol) in toluene (15 mL) cooled to −78°C was added boron trifluoride etherate (0.244 mL, 2.0 mmol, neat). The anion of 1-hexyne was then added to this flask in a dropwise manner via cannula over a period of 10 min. The reaction was allowed to warm to room temperature over 8 h before quenching with aqueous 15% NaOH solution. Toluene was then evaporated under vacuum and methylene chloride was added to the residue. The organic layer was washed with 15% NaOH, water, and brine. Drying the organic layer over $MgSO_4$ and filtration of the drying agent, followed by evaporation of the solvent, gave crude material (0.117 g) that was analyzed by ^{1}H and ^{13}C NMR. It was identified as a 60:40 mixture of *E* isomer of the starting oxime ether **5***a* and the product alkoxyamine in quantitative yield. Attempted purification of the crude material by column chromatography on silica gel (MeOH) did not result in separation of the product from starting oxime. Data from the crude sample for **13**: IR: 3310 (w, br), 3085 (w), 3064 (w), 2235 (w) cm^{-1}; ^{1}H NMR δ: 0.88 (t, *J* = 7.0 Hz, 3H), 1.06 (d, *J* = 6.6 Hz, 3H), 1.29 (d, *J* = 6.9 Hz, 3H), 1.36–1.46 (m, 4H), 2.11–2.16 (m, 2H), 2.32 (s, 6H), 2.69–2.76 (m, overlapping with starting oxime, 1H), 3.81–3.83 (m, 1H), 4.80 (d, *J* = 4.8 Hz, 1H), 5.19 (br s, 1H), 7.19–7.55 (m, overlapping with starting oxime 5H); ^{13}C NMR δ: 8.57, 13.53, 18.31, 19.83, 21.81, 30.73, 41.43 (2C), 48.02, 64.08, 80.24, 83.58, 85.55, 126.71 (2C), 126.99, 128.04 (2C), 141.85.

Acknowledgements

Support for this work by the National Science Foundation (NSF CHE-8614665) is gratefully acknowledged.

1. G. Solladie. *In* Asymmetric Synthesis. Vol. 2. *Edited by* J.D. Morrison. Academic Press, New York. 1983. Chap. 6. p. 157, and references cited therein.
2. For reviews on the addition of organometallic reagents to imines and imine derivatives see: (*a*) R.A. Volkmann. *In* Comprehensive organic synthesis. Vol. 1. *Edited by* B.M. Trost and I. Fleming. Pergamon Press, Oxford. 1991; *Edited by* S.L. Schreiber. p. 355. (*b*) E.F. Kleinman and R.A. Volkmann. *In* Comprehensive organic synthesis. Vol. 2. *Edited by* C.H. Heathcock. Pergamon Press, Oxford. 1991. p. 975.
3. For addition of organometallic reagents see: (*a*) H. Takahashi, Y. Suzuki, and H. Inagaki. Chem. Pharm. Bull. **30**, 3160 (1982); (*b*) Y. Suzuki and H. Takahashi. Chem. Pharm. Bull. **31**, 2895 (1983); (*c*) H. Takahashi, Y. Suzuki, and T. Hori. Chem. Pharm. Bull. **31**, 2183 (1983); (*d*) H. Takahashi, Y. Chida, T. Suzuki, S. Yanaura, Y. Suzuki, and C. Masuda. Chem. Pharm. Bull. **31**, 1659 (1983); (*e*) Y. Yamamoto, S. Nishii, K. Maruyama, T. Komatsu, W. Ito. J. Am. Chem. Soc. **108**, 7778 (1986); (*f*) C. Fuganti, P. Grasselli, and G. Pedrocchi-Fantoni. J. Org. Chem. **48**, 909 (1983); (*g*) P. Ermert, J. Meyer, C. Stucki, J. Schneebeli, and J.-P. Obrecht. Tetrahedron Lett. **29**, 1265 (1988); (*h*) H. Kunz and D. Schanzenbach. Angew. Chem. Int. Ed. Engl. **28**, 1068 (1989). For asymmetric reduction of imines see: (*i*) G.-J. Kang, W.R. Cullen, M.D. Fryzuk, B.R. James, and J.P. Kutney. J. Chem. Soc. Chem. Commun. 1466 (1988).
4. (*a*) S.E. Denmark, O. Nicaise, and J.P. Edwards. J. Org. Chem. **55**, 6219 (1990); (*b*) T. Weber, J.P. Edwards, and S.E. Denmark. Synlett, **1**, 20 (1989); (*c*) S.E. Denmark, T. Weber, and D.W. Piotrowski. J. Am. Chem. Soc. **109**, 2224 (1987); (*d*) D. Enders, H. Schubert, and C. Nubling. Angew. Chem. Int. Ed. Engl. **25**, 1109 (1986); (*e*) H. Takahashi, K. Tomita, and H. Noguchi. Chem. Pharm. Bull. **29**, 3387 (1981); (*f*) A. Alexakis, N. Lensen, J.-P. Tranchier, and P. Mangeney. J. Org. Chem. **57**, 4563 (1992).
5. For addition of organometallic reagents to chiral unactivated oximes see: (*a*) Y. Ukaji, K. Kume, T. Watai, and T. Fujisawa. Chem. Lett. 173 (1991). For addition to chiral glyoxylate oximes see: (*b*) T. Kolasa, S.K. Sharma, and M.J. Miller. Tetrahedron, **44**, 5431 (1988); (*c*) Y. Yamamoto and W. Ito. Tetrahedron, **44**, 5415 (1988).
6. For metal hydride reduction of chiral oximes see: (*a*) S. Itsuno, K. Tanaka, and K. Ito. Chem. Lett. 1133 (1986). (*b*) T. Mukaiyama, K. Yorozu, K. Kato, and T. Yamada. Chem. Lett. 181 (1992).
7. Z.-Y. Chang and R.M. Coates. J. Org. Chem. **55**, 3464 (1990).
8. R.P. Polniaszek and L.W. Dillard. Tetrahedron Lett. **31**, 797 (1990).
9. (*a*) K. Tomioka, I. Inoue, M. Shindo, and K. Koga. Tetrahedron Lett. **32**, 3095 (1991); (*b*) S. Itsuno, H. Yanaka, C. Hachisuka, and K. Ito. J. Chem. Soc. Perkin. Trans. 1, 1341 (1991); (*c*) K. Soai, T. Hatanaka, and T. Miyazawa. J. Chem. Soc. Chem. Commun. 1097 (1992).
10. For the use of chiral ligands and metal hydrides see: (*a*) S. Itsuno, Y. Sakurai, K. Shimizu, and K. Ito. J. Chem. Soc. Perkin. 1, 1548 (1989); (*b*) S.R. Landor, Y.M. Chan, O.O. Sonola, and A.R. Tatchell. J. Chem. Soc. Perkin. Trans. 1, 493 (1984); (*c*) S. Itsuno, M. Nakano, K. Miyazaki, H. Masuda, K. Ito, A. Hirao, and S. Nakahama. J. Chem. Soc. Perkin. Trans. 1, 2039 (1985).
11. A.R. Katritzky and P.A. Harris. Tetrahedron: Asymmetry, **3**, 437 (1992).
12. (*a*) H. Uno, T. Terakawa, and H. Suzuki. Synlett, 559 (1991); (*b*) K.E. Rodriques, A. Basha, J.B. Summers, and D.W. Brooks. Tetrahedron Lett. **29**, 3455 (1988).
13. R.K. Dieter, N. Deo, B. Lagu, and J.W. Dieter. J. Org. Chem. **57**, 1663 (1992).
14. K. Soai, S. Yokoyama, and T. Hayasaka. J. Org. Chem. **56**, 4264 (1991).
15. G.J. Karabatsos and N. Hsi. Tetrahedron, **23**, 1079 (1967).
16. (*a*) G.E. Hawkes, K. Herwig, and J.D. Roberts. J. Org. Chem. **39**, 1017 (1974); (*b*) J. Jirman, A. Lycka, and M. Ludwig. Collect. Czech. Chem. Commun. **55**, 136 (1990); (*c*) R. Fraser, R. Capoor, J.W. Bovenkamp, B.V. Lacroix, and J. Pagott. Can. J. Chem. **61**, 2616 (1983).
17. (*a*) M. Chastrette, R. Amouroux, and M. Subit. J. Organomet. Chem. **99**, C41 (1975); (*b*) J. Khazarian, S. Geribaldi, L. Ferrero, M. Rouillard, and M. Azzaro. J. Org. Chem. **43**, 1817 (1978).
18. (*a*) D. Enders, H. Schubert, and C. Nubling. Angew. Chem. Int. Ed. Engl. **25**, 1109 (1986); (*b*) O. Cervinka, V. Dudek, and L. Hub. Collect. Czech. Chem. Commun. **35**, 724 (1970); (*c*) M.-J. Wu and L.N. Pridgen. J. Org. Chem. **56**, 1340 (1991); (*d*) M.E. Warren, Jr. and H.E. Smith. J. Am. Chem. Soc. **87**, 1757 (1965).
19. (*a*) M. Al-Aseer, P. Beak, D. Hay, D.J. Kempf, S. Mills, and S.G. Smith. J. Am. Chem. Soc. **105**, 2080 (1983); (*b*) A.I.

Can. J. Chem. Downloaded from www.nrcresearchpress.com by 213.200.69.106 on 09/08/12
For personal use only.

Meyers, W.F. Rieker, and L.M. Fuentes. J. Am. Chem. Soc. **105**, 2082 (1983). For a review on CIPE see: (*c*) P. Beak, and A.I. Meyers. Acc. Chem. Res. **19**, 356 (1986).
20. (*a*) A. Hassner and F. Naumann. Chem. Ber. **121**, 1823 (1988); (*b*) S. Shatzmiller and B.-Z. Dolitzki. Liebigs Ann. Chem. 189 (1991); (*c*) T.A. Spencer and C.W. Leong. Tetrahedron Lett. 3889 (1975); (*d*) H.E. Ensley and R. Lohr. Tetrahedron Lett. 1415 (1978).
21. P. Beak, A. Basha, and B. Kokko. J. Am. Chem. Soc. **106**, 1511 (1984).
22. (*a*) M.J. Eis, J.E. Wrobel, and B. Ganem. J. Am. Chem. Soc. **106**, 3693 (1984); (*b*) M. Yamaguchi, Y. Nobayashi, and I. Hirao. Tetrahedron, **40**, 4261 (1984); (*c*) H.C. Brown, U.S. Racherla, and S.M. Singh. Tetrahedron Lett. **25**, 2411 (1984).
23. H. Saito, I. Terasawa, M. Ohno, and K. Nukada. J. Am. Chem. Soc. **91**, 6696 (1969).

Can. J. Chem. Downloaded from www.nrcresearchpress.com by 213.200.69.106 on 09/08/12
For personal use only.

Determination of aluminum in human cerebrospinal fluid through the electrochemical and spectroscopic properties of its complex formed with Solochrome Violet RS

KEITH E. JOHNSON[1]
Department of Chemistry, University of Regina, Regina, Sask., Canada S4S 0A2

AND

RONALD G. TREBLE
Laboratory and Disease Control Services Branch, Department of Health, Regina, Sask., Canada S4S 5W6

Received November 25, 1992

KEITH E. JOHNSON and RONALD G. TREBLE. Can. J. Chem. **71**, 824 (1993).

Aluminum present in pooled samples of cerebrospinal fluid is essentially uncomplexed since it may be determined by differential pulse polarography of the Al: Solochrome Violet RS (SVRS) complex. The aluminum may also be determined spectrophotometrically through its depression of the SVRS absorbance at 600 nm at pH 8.4. The Al:SVRS ratio in the complex is 1:2.

KEITH E. JOHNSON et RONALD G. TREBLE. Can. J. Chem. **71**, 824 (1993).

L'aluminium présent dans des échantillons regroupés de fluide cérébrospinal est essentiellement non complexé puisqu'il peut être déterminé par polarographie impulsionnelle différentielle du complexe Al : Solochrome Violet RS (SVRS). On peut aussi déterminer l'aluminium d'une façon spectrophotométrique par le biais de la diminution de l'absorption du SVRS à 600 nm, à un pH de 8,4. Le rapport de Al : SVRS dans le complexe est de 1 : 2.

[Traduit par la rédaction]

Can. J. Chem. Downloaded from www.nrcresearchpress.com by 213.200.69.106 on 09/08/12
For personal use only.

The role, if any, of aluminum in Alzheimer's disease has not been unequivocally settled. We reasoned that it would be useful to be able to determine low levels (<10 μg L^{-1}) of aluminum in cerebrospinal fluid (CSF), the medium that bathes the surfaces of the central nervous system. We have shown (1) that graphite furnace atomic absorption spectrophotometry (GFAAS) is a reliable and accurate method for determining total aluminum in this, and other, biological fluids from the level of μg L^{-1} up to hundreds of micrograms per litre. It is generally believed (2) that aluminum is toxic to plant and animal life when it is present as free aquo ionic complexes in solution; hence, the concern exists for the effect of acid rain on aluminum-containing rocks, sediments, and soils. Various methods seem feasible for the differentiation of free ionic from complexed aluminum, but we chose electroactivity as a measure of the ionic Al in water (2). This was accomplished by determining aluminum as its complex at pH 4.6 with the azo-dye Solochrome Violet RS (sodium 4-hydroxy-3-[(2-hydroxy-1-naphthalenyl)azo] benzene-sulfonate) by differential pulse polarography (DPP).

Normal CSF samples have a pH of ~7.4 but a variety of infectious samples obtained from the Regina General Hospital had pH values of 8 or more. The use of the above electrochemical method, therefore, implied its evaluation under alkaline conditions. This paper reports the results of this action and a spectrophotometric study of the Al^{3+} : SVRS system in both a simple bicarbonate buffer and in actual CSF media.

Experimental

(a) Differential pulse polarography

A Metrohm Polarecord 626 was employed with an E354 Metrohm Polarography stand utilizing a mercury electrode with an electronically controlled drop knocker. The auxiliary electrodes were platinum. The reference electrode was AgCl/Ag for the small cell (~3 mL working volume) used for CSF solutions. Deaeration of the surfactant CSF's required the use of a Nupro model "M" fine metering valve and a Varian 0–60 mL gas flow meter no. 29-000086-00. Operating conditions were: peak height, 2 nA mm^{-1}; scan rate, 5 mV s^{-1}; pulse amplitude, 50 mV; Hg drop rate, 1 drop s^{-1}; chart printout, 100 mV cm^{-1}; CSF deaeration rate, 43 mL min^{-1}.

SMI, Oxford, and Eppendorf pipets (10–200 μL) were used for the addition of SVRS and aluminum standards to CSF aliquots.

pH was measured with a Fisher ACUMET pH Meter, model 805 MP. All containers were of polypropylene or were plastic vacutainers. All vessels were rinsed thoroughly with deionized water prior to use.

(b) Spectrophotometry

A Hewlett Packard diode array UV–visible spectrometer, model no. 8452A, was employed. Solutions were prepared in new plastic vacutainers accommodating plastic stoppers.

(c) Reagents

UHP argon for deaeration was from Canadian Oxygen Limited. Aluminum stock solutions were prepared from $AlK(SO_4)_2 \cdot 12H_2O$ (BDH) and water was purified by reverse osmosis and ion exchange. Acetate (0.1 M) and bicarbonate (0.1 M) solutions were used for pH 4.6 and 8.4 buffers, respectively. Solochrome Violet RS (Lot no. KJ101187, INC Pharmaceuticals Inc.) was recrystallized twice from 50% aqueous ethanol and dried at 70–80°C for 8 h.

(d) Total aluminum analysis

Total aluminum in samples and reagents was determined by GFAAS (1).

Results and discussion

Differential pulse polarography

The CSF obtained was in the form of pooled samples (potentially infectious) and each pooled sample was first analyzed for total aluminum by GFAAS. The remainder of the sample was then analyzed by DPP using the method of standard additions. For each sample point the specimen was first decanted. SVRS and standard aluminum solution were

[1]Author to whom correspondence may be addressed.

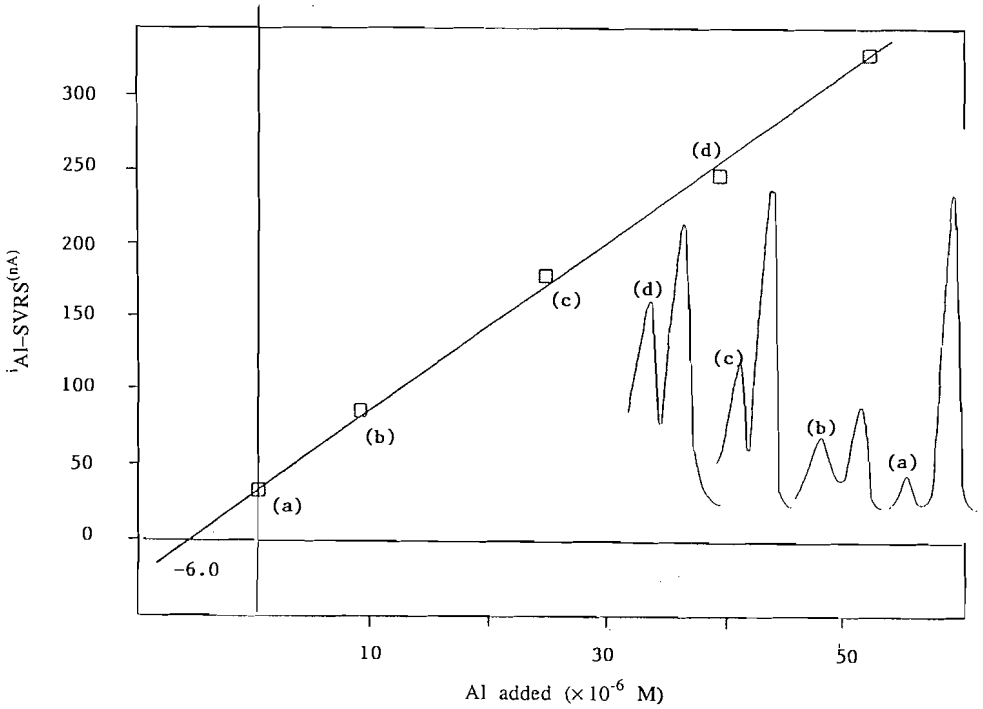

FIG. 1. Standard addition calibration curve for $i_{Al-SVRS}$(nA) vs. added Al concentration. Inset: form of differential pulse polarogram. Lettered peaks and points are corresponding $i_{Al-SVRS}$ values. Large unlettered peaks correspond to excess SVRS reduction.

TABLE 1. DPP analysis of unbuffered CSF pools for Al using standard additions

Parameter	Pool A	Pool B
Initial volume	6.5 mL	3.0 mL
Volume used for DPP	5.0 mL	1.9 mL
Initial pH	8.1	8.1
Final pH	9.1	8.8
SVRS potential	−0.56 V	−0.54 → − 0.55 V
Al-complex potential	−0.72 V	−0.72 → −0.79 V
Number of additions	3	4
Al found by GFAAS (10^6 × M)	3.76 ± 0.2	5.74 ± 0.3
Al found by DPP (10^6 × M)	3.8 ± 0.5	6.0 ± 0.6

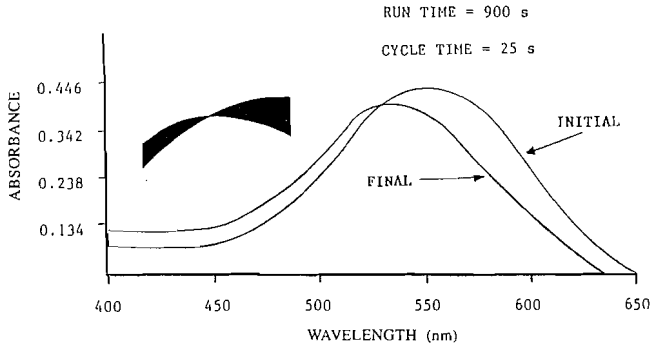

FIG. 2. The effect of additions of Al on the UV–visible spectrum of 2.0×10^{-5} M SVRS. pH = 8.4, temperature = 22°C. Inset: Isosbestic point region.

then added and the mixture heated to 70°C for 10 min, cooled, and then subjected to DPP. The results for two pools are summarized in Table 1. Figure 1 shows the standard addition calibration curve for determining Al in pool B with an indication of the form of the polarogram.

Thus, it appears that differential pulse polarography is applicable to the Al:SVRS system in alkaline media; indeed, attempts to acidify the CSF samples caused much frothing. Further, since the aluminum concentrations found by GFAAS and DPP are the same, we infer that any complexes formed between aluminum and the constituents of CSF are sufficiently weak that conversion to the Al:SVRS complex is complete; this conversion is complete for aluminum in some but not all natural water samples brought to a pH of 4.6.

UV–visible spectophotometry

The purified free SVRS dye showed an absorption maximum at 500 nm at pH = 4.6; Beer's law is obeyed over the range $(1.0–8.0) \times 10^{-5}$ M with $\varepsilon_{max} = 2.1 \times 10^4$ L mol^{-1} cm^{-1}, in agreement with the value of 2.2×10^4 L mol^{-1} cm^{-1} obtained by Coates and Rigg (3). λ_{max} was shifted to 554 nm at pH = 8.4 and ε_{max} had the value of 2.2×10^4 L mol^{-1} cm^{-1} for the range $(2.0–9.0) \times 10^{-5}$ M. Using pH = 8.4 data, the purity of the crude dye was found to be 54%.

The addition of aluminum solution to SVRS at pH 8.4 and a temperature of 22°C gives rise to the spectral changes shown in Fig. 2. After 900 s the spectrum is stable. Although we have an isosbestic point at 530 nm, there is no λ_{max} corresponding to the formation of the aluminum complex; instead, the most significant absorbance change is the decrease in intensity at 600 nm with the addition of aluminum. This decrease in absorbance was used to determine the stoichi-

Can. J. Chem. Downloaded from www.nrcresearchpress.com by 213.200.69.106 on 09/08/12
For personal use only.

Can. J. Chem. Downloaded from www.nrcresearchpress.com by 213.200.69.106 on 09/08/12
For personal use only.

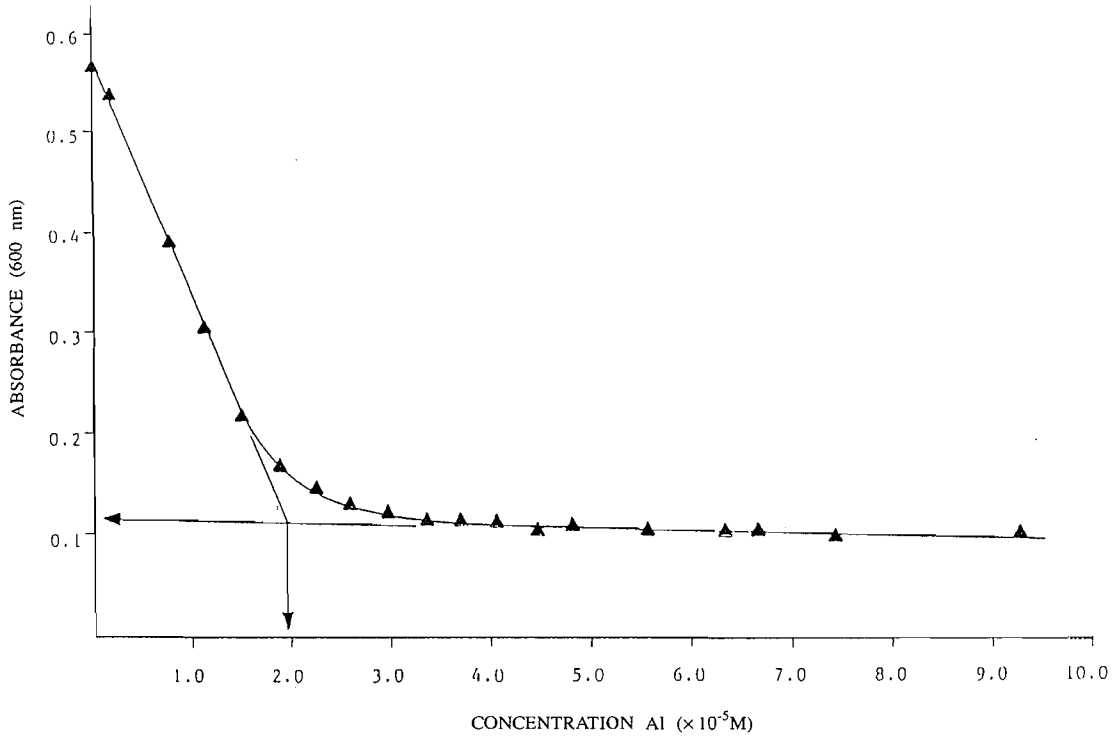

FIG. 3. Absorbance at 600 nm vs. concentration of Al added to 4.0×10^{-5} M SVRS. pH = 8.5, temperature = 22°C. Reaction time 17 h for each of the 19 separate sample solutions.

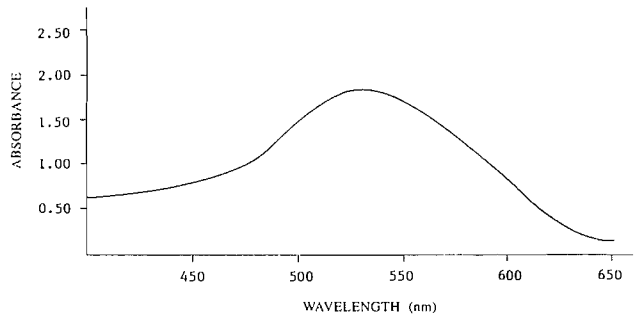

FIG. 4. UV–visible spectrum of a human CSF pool sample containing 7.40 μM Al and 90.9 μM SVRS.

TABLE 2. Spectrophotometry of human CSF containing Al

Solution	CSF vol. (mL)	Aqueous Al vol (μL)	10^5 Al in CSF (M)	$Abs_{600\,nm}$
1	0.50	0	0.74	0.787
2	0.48	20	2.06	0.639
3	0.47	30	2.72	0.550
4	0.46	40	3.38	0.486

SVRS concentration throughout = 9.09×10^{-5} M.
Reaction time = 15 min. Temperature ≈ 22°C. pH = 8.4.

ometry of the complex as depicted in Fig. 3: the formation of $Al(SVRS)_2$ is quite clear. ε_{600} was found to be 1.4×10^4 L mol^{-1} cm^{-1} for SVRS and 6.0×10^3 L mol^{-1} cm^{-1} for $Al(SVRS)_2$.

The spectrum of a CSF pool containing 7.40 μM aluminum (as determined by GFAAS) and 90.9 μM SVRS is shown in Fig. 4. It has essentially the same shape as that of the Al:SVRS system in a bicarbonate buffer (Fig. 3). To verify that the spectrophotometric determination of Al in CSF is possible using SVRS, several additions of standard Al and SVRS solutions were made to this solution (Table 2). A linear decrease of absorbance at 600 nm occurred. The change in predominant medium from $NaHCO_3$ solution to CSF led to ε_{600} values for SVRS and $Al(SVRS)_2$ of 9.6×10^3 and 7.6×10^3 L mol^{-1} cm^{-1}, respectively. Thus, in any actual Al determination it is more appropriate to make separate small additions of both the standard Al solution and CSF to the dye:buffer mixture.

Conclusions

The determination of aluminum in human cerebrospinal fluid is possible by both an electrochemical and a spectrophotometric method, certainly at the 50–100 μg L^{-1} level, although probably with greater sensitivity. Both methods employed the dye Solochrome Violet RS with measurement of (*a*) the differential pulse current of the aluminum complex and (*b*) the decrease in absorbance at 600 nm of the dye upon complexation. It appears that CSF does not contain strong complexing agents and any aluminum present therein would be potentially toxic if transferred to other parts of the body. It is planned to miniaturize the electrochemical operation and thus be able to measure aluminum in vitro or in vivo and correlate the results with clinical diagnoses on an individual basis.

1. K.E. Johnson and R.G. Treble. J. Clin. Lab. Anal. **6**, 264 (1992).
2. K.E. Johnson, A.K. Brichta, and K.L. Holter. Can. J. Chem. **66**, 139 (1988).
3. E. Coates and B. Riggs. Trans. Faraday Soc. **58**, 1 (1962).

The mechanism of stereoselectivity in the cycloaddition reactions of α-hydroxy-*ortho*-quinodimethanes with the fumarate of methyl lactate and mandelate

JAMES L. CHARLTON[1] AND SHAWN MADDAFORD
Department of Chemistry, University of Manitoba, Winnipeg, Man. Canada R3T 2N2

Received November 17, 1992

JAMES L. CHARLTON and SHAWN MADDAFORD. Can. J. Chem. **71**, 827 (1993).

The Diels–Alder cycloaddition reaction of the fumarate of methyl lactate or methyl mandelate with α-hydroxy-*ortho*-quinodimethane produces an unexpected *exo* product with very high asymmetric induction. Experiments and calculations have been carried out that show that the origin of the stereoselectivity in these reactions is related to hydrogen bonding between the α-hydroxy-*o*-quinodimethane and the lactate or mandelate group in the dienophile.

JAMES L. CHARLTON et SHAWN MADDAFORD. Can. J. Chem. **71**, 827 (1993).

La réaction de cycloaddition de Diels–Alder du fumarate du lactate de méthyle ou du mandélate de méthyle avec l'α-hydroxy-*ortho*-quinodiméthane conduit à un produit *exo* inattendu, avec une induction asymétrique très élevée. On a effectué des expériences et des calculs qui montrent que l'origine de la stéréosélectivité de ces réactions est reliée à la liaison hydrogène entre l'α-hydroxy-*ortho*-quinodiméthane et le groupe lactate ou mandélate du diénophile.

[Traduit par la rédaction]

Introduction

We recently published several accounts of the stereoselective and asymmetric Diels–Alder reactions of α-hydroxy-*ortho*-quinodimethanes (α-hydroxy-*o*-QDMs) with the fumarate of methyl lactate or methyl mandelate (1–5).

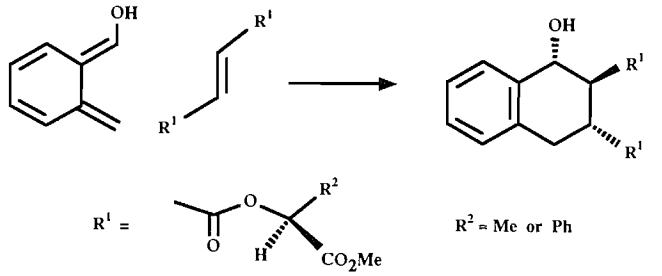

While these reactions are proving useful in asymmetric synthesis (1, 3, 6), a satisfactory explanation of the stereoselectivity observed has not yet been proposed. Such an explanation would have to account for both the absolute stereoselectivity and the unusual relative stereoselectivity observed. The relative stereoselectivity is unusual in that all previous accounts of Diels–Alder reactions of α-hydroxy or α-alkoxy-*o*-QDMs with dienophiles have shown that the reactions produce *cis*-1,2 adducts via *endo* transition states (**A**) (7–11). This is in contrast to the reactions of α-hydroxy-*o*-QDMs with the fumarates of lactate or mandelate, where predominantly *trans*-1,2 adducts are formed via *exo* transition states (**B**).

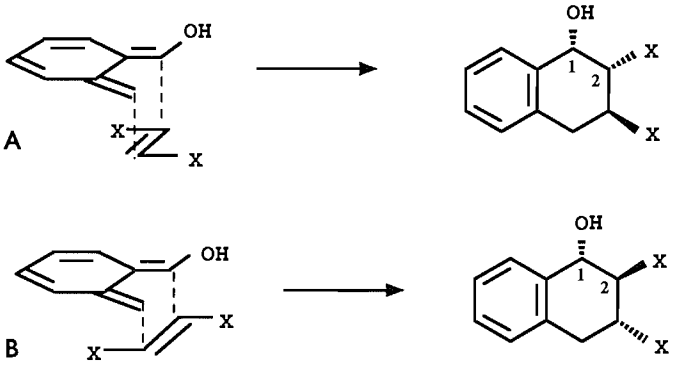

[1]Author to whom correspondence may be addressed.

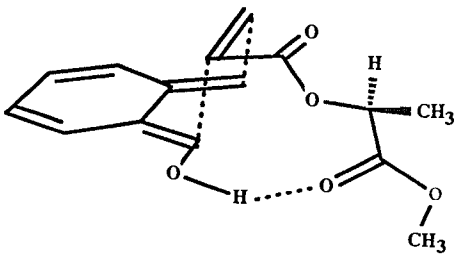

FIG. 1. Possible transition state for the Diels–Alder reaction of α-hydroxy-*o*-QDM with the acrylate of methyl (*S*)-lactate.

The *absolute* stereochemistry of the products is that produced from *exo* addition of the *o*-QDM to the *re* face of the fumarate of methyl (*S*)-lactate **1** (as in transition state **B**, see also Fig. 1). The observed addition to the *re* face of the dienophile is similar to results of previous Diels–Alder studies on this dienophile by Helmchem and co-workers (12, 13), who attributed this absolute stereoselectivity to steric blocking of the *si* face of the dienophile. While steric factors could be used to explain facial selectivity with respect to the dienophile when reaction occurs with an α-hydroxy-*o*-QDM, it would not explain the unusual preference for the *exo* transition state geometry **B**. It seemed possible, given the position of the hydroxyl group on the *o*-QDM, that hydrogen bonding between the hydroxyl group and the lactyl carbonyl might be responsible for this preferred *exo* reaction geometry as illustrated in Fig. 1.

Models show that a similar hydrogen-bonded transition state is sterically unlikely for the *endo* transition state. Although controlling stereoselectivity by such a long-range hydrogen bond may seem implausible, a similar type of nine-membered ring hydrogen bond has been found to be responsible for facial selectivity in the Diels–Alder reaction shown in Fig. 2 (14).

Even if one accepts the hypothesis of a hydrogen-bonded *exo* transition state for the reaction of the fumarate of methyl (*S*)-lactate with an α-hydroxy-*o*-QDM, it is not immediately obvious how the *S* chiral auxiliary directs addition to the *re* face of the dienophile (as is shown in Fig. 1). The steric crowding appears to be similar for both the *S* and *R* chiral

Can. J. Chem. Downloaded from www.nrcresearchpress.com by 213.200.69.106 on 09/08/12
For personal use only.

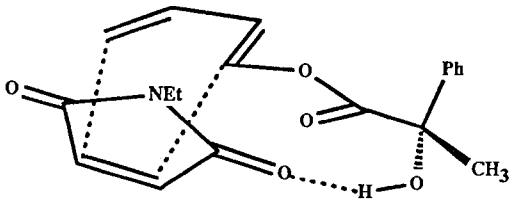

FIG. 2. Hydrogen bonding control of facial selectivity in Diels–Alder reaction (14).

auxiliaries when reaction occurs at the *re* face of the dienophile.

In an attempt to determine the mechanism of the stereoselectivity in the title reactions, we have studied the effect of variation in *o*-QDM structure, solvent, and dienophile structure. We have also carried out molecular orbital calculations (GAUSSIAN-86 AM1) on possible transition states for the reaction of the acrylate of methyl (*S*)-lactate with α-hydroxy-*o*-QDM.

Results and discussion

As a probe of structural effects on stereoselectivity we have studied the reactions of α-hydroxy-*o*-QDM **1** with several new dienophiles, **5**, **6**, **10**, and **11**, and the reactions of α-methoxy-*o*-QDM **2** with **7** and **10**. The stereoselectivity of these reactions was compared to the stereoselectivity of reactions previously reported.[2]

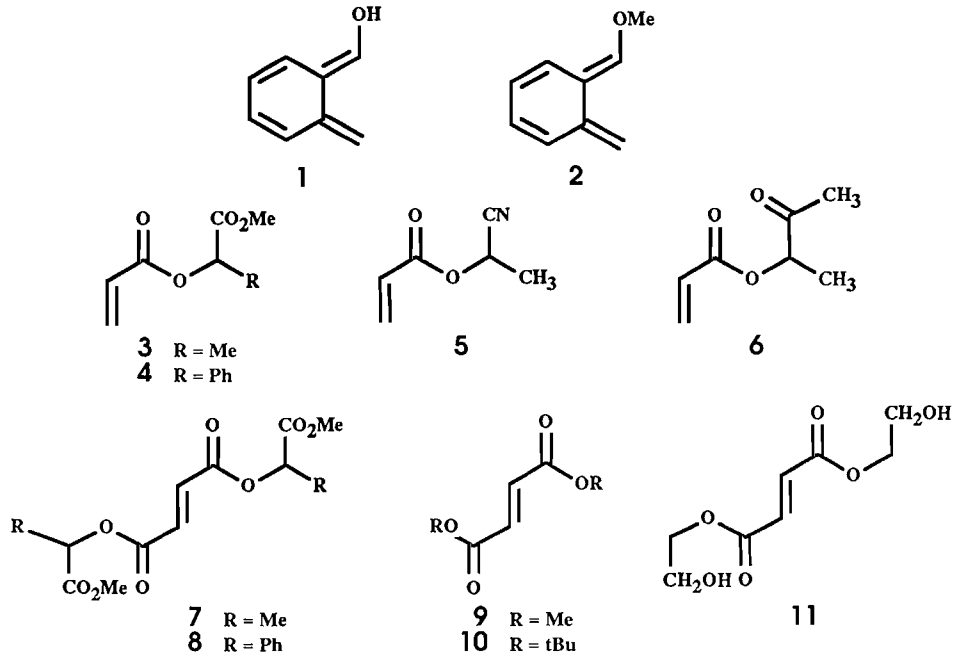

Dienophiles **5**, **6**, **10**, and **11** were all synthesized by an uncatalysed reaction of the acid chloride with an excess of the appropriate alcohol, followed by chromatography on silica gel.

o-QDMs **1** and **2** were generated by heating either benzocyclobutenol **12** (16) or 1-methoxybenzocyclobutene **13** (16) in toluene containing the dienophile and 4Å molecular sieves.

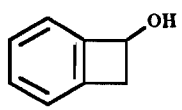

12

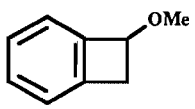

13

Cycloadducts were separated by flash chromatography on silica gel using ethyl acetate – hexanes as solvent. In some cases separation and characterization of all of the individual isomers was not possible. Determination of isomer ratios was carried out using either ^{1}H nmr (300 or 500 MHz) or hplc (ODS-2, methanol–water as eluent). The assignment of relative stereochemistry within the tetralin ring of the cycloadducts (*endo* vs. *exo*) was made using ^{1}H nmr. For all cycloadducts H1 appear between 4.6 and 5.2 ppm (in $CDCl_3$) and *endo* (*cis*-1,2) coupling constants, $J_{1,2}$, are 2–5 Hz, while *exo* (*trans*-1,2) coupling constants are 7–12 Hz (for previous examples see refs. 2–6, 17). The results of the product study are shown in Table 1.

In the case of cycloadducts from dienophiles **3–8**, there are four possible diastereomeric products (two *endo* and two *exo*) for each absolute configuration of the chiral center in the dienophile. These four possible diastereomers are illustrated in Fig. 3 for **1** reacting with the acrylate of methyl (*S*)-lactate, **3**.

As mentioned above, it has been shown that the major product from the reaction of **1** with **3** is the *exo-re* cycloadduct (4). The *exo-re* cycloadduct is also the major cycloadduct from the reaction of **1** with (*S*)-**4**, (*S*)-**7**, and (*S*)-**8** (2, 4). Racemic material was studied in the case of dienophiles **5** and **6** and, although the *endo* isomers could be distinguished from the *exo* isomers by ^{1}H nmr, no attempt was

[2]The preparation of dienophiles **3** and **7** is given in ref. 4 while that of **8** is given in ref. 1. The preparation of dienophile **4** is described by K.K.S. Koh (15).

Can. J. Chem. Downloaded from www.nrcresearchpress.com by 213.200.69.106 on 09/08/12
For personal use only.

TABLE 1. Diastereoselectivity of Diels–Alder reactions of *o*-QDMs **1** and **2**

o-QDM	Dienophile	Yield (%)	Facial selectivity[a]	endo; exo	Ref.
1	**3**	77	95:5 *exo*	*exo* only	5
1	**4**	56	>90:10 *exo*	>90% *exo*	2
1	**5**	58	33:17 *endo*, 34:16 *exo*	50:50	
1	**6**	45	—	*exo* only	
1	**7**	55	—	*exo* only	5
1	**8**	90	—	*exo* only	2
1	**9**	87	—	74:26	16
1	**10**	43	—	60:40	
1	**11**	22	—	20:80	
2	**7**	62	61:39 *endo*	*endo* only	
2	**9**	32	—	*endo* only	15
2	**10**	98	—	88:12	

[a]Ratio of *exo* and (or) *endo* diastereomers for cases in which the dienophile carries a chiral auxiliary.

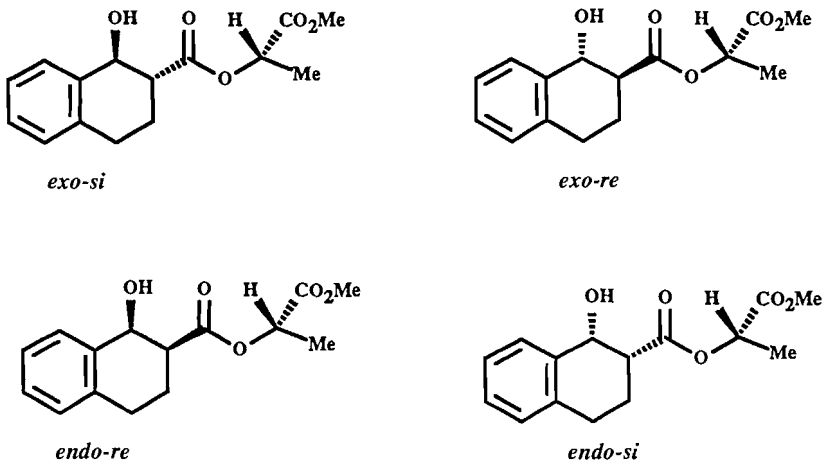

FIG. 3. Possible products from the reaction of α-hydroxy-*o*-QDM, **1**, with the acrylate of methyl (*S*)-lactate.

made to determine the configuration of the tetralin ring carbons relative to the center in the chiral auxiliary.

Reaction of **1** with dienophile **5** gave a mixture of four diastereomers as evidenced by the number of doublets in the H1 region of the ^{1}H spectrum. Correct elemental composition was confirmed by elemental analysis of the mixture. The ^{1}H nmr at 500 MHz in 20% $CDCl_3$ in deuterobenzene allowed integration of the four H1 signals of isomers *exo*-1, *exo*-2, *endo*-1, and *endo*-2, giving the ratio of 34:16:33:17, respectively (J = 9.1, 8.9, 3.25, and 3.45, respectively). The hplc separation of the mixture on ODS-2 using a methanol–water mixture as eluent resulted in the isolation of three of the four isomers (in order of elution, *exo*-1, *endo*-1, *endo*-2) and their individual ^{1}H nmr spectra are reported in the experimental.

Reaction of **1** with dienophile **6** gave only a single *exo* cycloadduct in 45% yield after chromatography. No signals consistent with other diastereomers could be observed in the nmr of the crude product.

The product mixture from dienophile **11** was more complicated. An ^{1}H nmr spectrum of the crude product mixture showed doublets at 5.43 (J = 5.17), 5.12 (J = 3.65), and 4.86 (J = 9.53) ppm ($CDCl_3$). Chromatography on silica gel resulted in the isolation and characterization of only one of the three compounds. Based on its ir spectrum (1788 cm^{-1}) and comparison of its ^{1}H nmr spectrum to that of a similar compound (4), it was assigned structure **14**.

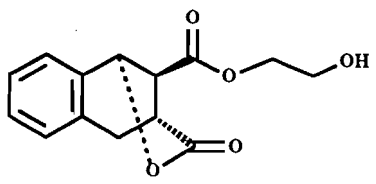

14

The doublet appearing at 5.43 ppm in the nmr spectrum of the crude product comes from compound **14** and the remaining two doublets at 5.13 and 4.86 ppm were tentatively assigned to the *endo* and *exo* cycloadducts, respectively, on the basis of the coupling constants. Presumably the *exo* cycloadduct readily closes to the lactone **14** as has been noted in similar cycloadducts (4). The *endo*/*exo* ratio given in Table 1 for dienophile **11** is calculated using the ratio of the nmr integration for the presumed *endo* doublet at 5.13 ppm to the sum of the other two doublets.

Dienophile **9** has been reported to give a mixture of *endo* (major) and *exo* (minor) isomers in good yield on reaction with *o*-QDM **1**, produced by irradiation of *o*-methylbenzaldehyde (18).

The reaction of di-*tert*-butyl fumarate, **10**, with **1** gave a mixture of the *endo* (major) and *exo* (minor) cycloadducts, which were separated by chromatography and characterized.

In the case of α-methoxy-*o*-QDM **2**, primarily *endo* prod-

Can. J. Chem. Downloaded from www.nrcresearchpress.com by 213.200.69.106 on 09/08/12
For personal use only.

Can. J. Chem. Downloaded from www.nrcresearchpress.com by 213.200.69.106 on 09/08/12
For personal use only.

ucts were formed with dienophiles **7**, **9**, and **10**. Reaction with **7** gave two diastereometric *endo* adducts, which were both isolated and characterized. Reaction with **9** was reported previously to give only an *endo* cycloadduct (32%) with no indication of the presence of other isomeric cycloadducts (18). Reaction of *o*-QDM **2** with di-*tert*-butyl fumarate **10** gave primarily an *endo* cycloadduct, which was isolated by chromatography and characterized. The ^{1}H nmr spectrum of the crude reaction mixture also exhibited a doublet at 4.74 ppm (J = 8.1), which was assumed to be the *exo* cycloadduct. The integration of this peak relative to that assigned to H1 of the *endo* cycloadduct (4.53 ppm, J = 3.39) gave the *endo/exo* ratio of 88:12 reported in Table 1.

From the above results a pattern of reactivity can be seen. Only *o*-QDM **1**, with an α-hydroxyl group, gives *exo* cycloadducts with high stereoselectivity. *o*-QDM **2**, with an α-methoxy group, gives primarily *endo* adducts. Steric bulk of the ester group in the dienophile makes little difference to the *endo/exo* ratio as evidenced by the comparison of dimethyl and di-*tert*-butyl fumarate, **9** and **11**. Only dienophiles with a strong hydrogen-bonding acceptor group give *exo* cycloadducts, with the exception of **5**.

All of the above facts suggest that a hydrogen-bonded transition state, perhaps similar to that depicted in Fig. 1, directs the *endo/exo* stereoselectivity of the cycloaddition reaction of **1** with dienophiles **3**, **4**, **6**, **7**, **8**, and **11**. In the case of dienophile **5**, it appears that the linear geometry of the nitrile function makes it sterically impossible for it to form a hydrogen bond to the hydroxyl group of the *o*-QDM. For dienophiles **9** and **10** and (or) reactions involving *o*-QDM **2**, the expected *endo* products are predominantly formed.

If the proposed hydrogen bonding theory is correct, it should be easily disrupted by solvent effects. Just such an effect was found for the reaction of *o*-QDM **1** with the fumarate of methyl (*S*)-lactate **7**. When **1** (from **12** at 100°C) was reacted with **7** in toluene containing 30% dimethyl sulfoxide (DMSO) by volume, a mixture of four products was formed. Their ratios, measured by hplc, were 9:15:34:42 (presumed *exo-si*, *exo-re*, *endo*-1, and *endo*-2 respectively. The *exo-re* isomer was identified by comparison to an authentic sample (4, 5). The two *endo* adducts were both separated and characterized, although it could not be determined which was the *endo-re* and which was the *endo-si* isomer. The remaining minor product could not be isolated in sufficient quantity for characterization but was assumed to be the remaining *exo-si* diastereomer. As expected, DMSO appears to interfere with the normal diastereoselectivity by hydrogen bonding to the hydroxyl group of the *o*-QDM, thereby preventing the formation of a hydrogen-bonded transition state similar to that illustrated in Fig. 1. This results in the formation of more *endo* products and a loss in asymmetric induction for both *endo* and *exo* products.

Molecular orbital calculations

If the hydrogen-bonded transition state shown in Fig. 1 is correct it must also be able to account for the high facial selectivity observed with respect to the dienophile. For example, the reaction of α-hydroxy-*o*-QDM **1** with the acrylate of methyl (*S*)-lactate **3** gives the *exo-re* cycloadduct with higher than 90% de. To test the validity of the model, molecular orbital calculations have been carried out on the *exo-re* transition state for the acrylate of both methyl (*S*)-lactate and methyl (*R*)-lactate. Such a calculation is equivalent to comparing the *exo-re*-(*S*) transition state to the *exo-si*-(*S*) transition state since *exo-si*-(*S*) is the mirror image of *exo-re*-(*R*). If the model is correct, the energy of the *exo-re*-(*S*) transition state should be lower than that of the *exo-re*-(*R*) (*exo-si*-(*S*)). By using geometry optimization it should also be possible to confirm that a hydrogen bond, similar to that depicted in Fig. 1, is possible for a conformationally relaxed transition state.

Molecular orbital calculations were carried out at the semiempirical level (AM1) with geometry optimization using the program GAUSSIAN-86 (19). To model the transition state the calculations were started at the cycloadduct stage with the saturated tetralin ring in a boat conformation, typical of the final state of Diels–Alder reactions. The lactyl side chain was twisted into a conformation for which hydrogen bonding to the OH group was possible. The initial atom coordinates for the starting structure were obtained from a model constructed, and conformationally relaxed (molecular mechanics minimization), using the computer program PC-MODEL (20).[3] The dienophile and diene were then iteratively separated by elongation of the 1,2 and 3,4 bonds until a separation (diene–dienophile) of 2.0 Å was reached, a distance close to the Diels–Alder reaction transition state (21). At each stage of the iterative dissociation of the adduct, the 1,2 and 3,4 bond lengths were fixed and the rest of the geometry optimized.

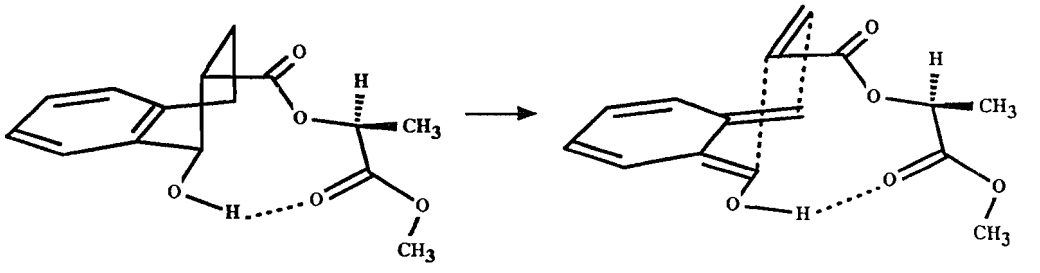

The calculations confirmed that it is possible to have a conformationally relaxed transition state with hydrogen bonding between the OH group and the lactyl carbonyl (2.14–2.31 Å). The calculations also showed that there are two low-energy conformations of the lactyl side chain that allow for hydrogen bonding and that these two conformations roughly correspond to the *s-cis* and the *s-trans* dienophile conformations. The *s-cis* conformation is shown in the diagram

[3]Calculations carried out on a Silicon Graphics IRIS 4D70/GT workstation.

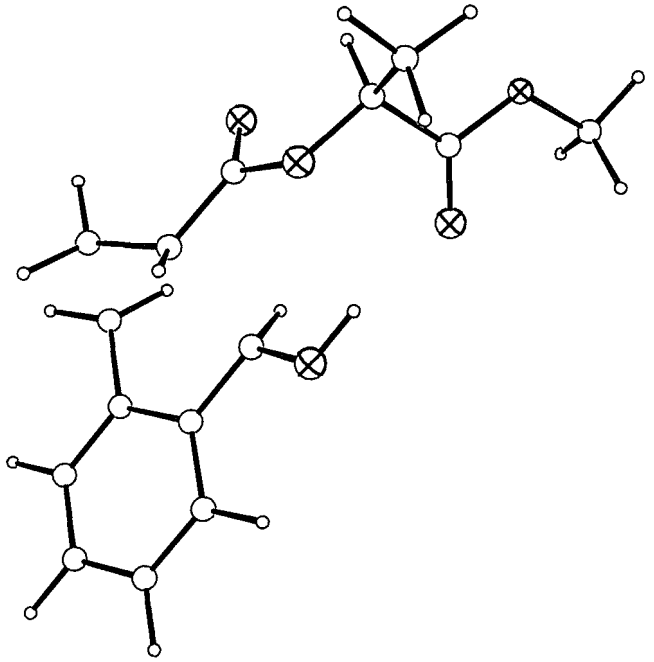

FIG. 4. An ORTEP diagram of the *exo-re-s-cis-S* transition state.

although calculations were carried out for both the *s-cis* and the *s-trans* conformations (for both the *R* and *S* dienophile). The relative energies of the *exo-re* transition state with the *s-cis-S*, *s-cis-R*, *s-trans-S*, and *s-trans-R* dienophile were found to be 0.0 (reference), 8.51, 10.6, and 5.79 kJ/mol, respectively. An ORTEP (22) plot of the conformationally minimized *exo-re-s-cis-S* transition state is shown in Fig. 4.

The calculations are consistent with the experimental results since the calculated lowest energy transition state, *exo-re-S*, leads to the observed product. It is interesting to note that the correct prediction of asymmetric induction can be achieved only if the dienophile is in the *s-cis* conformation.

It was hoped that the calculated optimized geometries of the *exo-re-S* and *exo-re-R* transition states would give some hint as to the mechanism of the asymmetric control exerted by the chiral auxiliary. However, there was very little difference in the geometries of the two diastereotopic transition states, indicating that the effect of the auxiliary on reaction diastereoselectivity is very subtle and not simply due to sterically induced changes in reaction geometry.

The calculations do confirm that a hydrogen-bonded transition state leading to the preferred product is structurally and energetically feasible. Large rate enhancements have been observed as a result of hydrogen bonding in other Diels–Alder reactions involving dienolic substrates such as 9-hydroxyanthracene (23). A similar rate enhancement in the reactions described here may explain the preference for the hydrogen-bonded transition state leading to the *exo* cycloadducts.

Experimental

The ^{1}H nmr spectra were recorded on a Bruker AM-300 or AMX-500 instrument using tetramethylsilane as internal standard. The ir spectra were recorded on a Perkin–Elmer 881 spectrometer. Aldrich silica gel (28,859-4) was used for all chromatography. Elemental analyses were performed by Guelph Chemical Laboratories Ltd., Guelph, Ontario. Exact Mass/mass spectra were obtained on an Analytical VG 7070E-HF instrument. Melting points were measured on a hot stage instrument and are uncorrected.

Acrylate of rac-*lactonitrile*, ***5***

Acryloyl chloride (5.9 g, 5.3 mL, 65 mmol) and lactonitrile (2.95 g, 3 mL, 37.8 mmol) were refluxed in methylene chloride (50 mL) over dry molecular sieves (6.7 g, 4 Å) for 68 h. The solution was filtered and the solvent evaporated, leaving a light yellow liquid. The liquid was fractionally distilled (bp 160°C, 1 atm (1 atm = 101.3 kPa)) to remove the lower boiling acryloyl chloride and methylene chloride. The distillate was chromatographed on silica gel (5% ethyl acetate/hexanes) to give a colourless liquid (1.4 g, 11.3 mmol, 30%): ir (CH_2Cl_2): 1739 cm^{-1}; ^{1}H nmr ($CDCl_3$) δ: 6.52 (dd, 1H, J = 1.29, 17.21), 6.15 (dd, 1H, J = 10.44, 17.14), 5.98 (dd, 1H, J = 1.29, 10.5), 5.47 (q, 1H, J = 6.9), 1.69 (d, 3H, J = 6.97); ^{13}C nmr ($CDCl_3$) δ: 164.06, 133.29, 126.64, 117.46, 57.39, 18.79; mass spectrum, ammonia ionization *m/e* (rel. %): 143 (M + NH_4^+, 11), 126 (M + H^+, 1.1), 99 (2.2), 72 (12), 70 (5), 55 (100), 46 (4). Exact Mass (EI) calcd. for $C_6H_7O_2N$: 125.0477; found: 125.0484.

Acrylate of rac-*3-hydroxy-2-butanone*, ***6***

Acryloyl chloride (5 mL, 61.5 mmol) and 3-hydroxy-2-butanone (5.46 g, 61.9 mmol) were refluxed in CH_2Cl_2 (5 mL) over dry molecular sieves (4 Å, 8 g) for 4 days. The solution was filtered and the solvent evaporated to leave an oil. The crude oil was chromatographed on silica (10% ethyl acetate/hexanes) to give a colourless oil (5.7 g, 66%): ir (CH_2Cl_2): 1730 cm^{-1}; ^{1}H nmr ($CDCl_3$) δ: 6.41 (dd, 1H, J = 1.35, 17.34), 6.13 (dd, 1H, J = 10.40, 17.33), 5.85 (dd, 1H, J = 1.36, 10.40), 5.09 (q, 1H, J = 7.05), 2.12 (s, 3H), 1.38 (d, 3H, J = 7.06); ^{13}C nmr ($CDCl_3$) δ: 205.61, 165.37, 131.90, 127.67, 75.07, 25.58, 16.02; mass spectrum *m/e* (rel. %): 142 (M^+, 0.4), 100 (1.8), 99 (7.7), 98 (13), 87 (2.4), 55 (100), 43 (36). Exact Mass calcd. for $C_7H_{10}O_3$: 142.0630; found: 142.0646.

*Di-*tert*-butyl fumarate*, ***10***

Fumaryl chloride (5.1 g, 0.033 mol) was dissolved in benzene (50 mL) and *tert*-butyl alcohol (15 mL, 4.8 mol-equiv.) was added at room temperature. Molecular sieves (5.01 g, 4 Å, flame-dried under nitrogen) were added and the solution refluxed for 38 h. The resulting solution was filtered through a short column of silica (EtOAc) and the filtrate washed with aqueous $NaHCO_3$ solution (5%, 3 × 20 mL). The solution was dried ($MgSO_4$) and evaporated, giving a yellow oil (2.99 g, 42%) that crystallized on standing. Flash chromatography on silica (eluent 20% ethyl acetate/hexanes) yielded a colourless solid (1.74 g, 24%) a sample of which was crystallized from ethyl acetate/hexanes; mp 62–63°C; ir (CH_2Cl_2): 1709 cm^{-1}; ^{1}H nmr (60 MHz, $CDCl_3$) δ: 6.73 (s, 2H), 1.53 (s, 18H); ^{13}C nmr (75.47 MHz, $CDCl_3$) δ: 164.38, 134.53, 81.64, 27.99; mass spectrum *m/e* (rel. %): 155 (15), 99 (53), 57 (100), 56 (30). Anal. calcd. for $C_{12}H_{20}O_4$: C 63.14, H 8.83; found: C 63.41, H 8.91.

Di-(2-hydroxyethyl) fumarate, ***11***

Fumaryl chloride (1 mL, 1.40 g, 9.16 mmol) and ethylene glycol (5.2 mL, 10 mol-equiv.) were stirred at 27°C for 24 h. The solution was diluted with water (25 mL) and extracted with EtOAc (3 × 25 mL). The organic phase was dried (Na_2SO_4) and the solvent evaporated, leaving a viscous oil (1.51 g). The oil was chromatographed on silica (80% ethyl acetate/hexanes) to give a semicrystalline product (1.01 g, 54%); mp 52–53°C; ir (CH_2Cl_2): 1728 cm^{-1}; ^{1}H nmr (300 MHz, $CDCl_3$) δ: 6.92 (s, 2H), 4.33 (m, 4H), 3.87 (m, 4H), 2.79 (bs, 2H); ^{13}C nmr (75.47 MHz, $CDCl_3$) δ: 165.06, 133.64, 66.87, 60.67; mass spectrum *m/e* (rel. %): 144 (15), 143 (100), 117 (12.5), 99 (65.9), 85 (23), 82 (26). 57 (29). Anal. calcd. for $C_8H_{12}O_6$: C 47.06, H 5.92; found: C 46.99, H 5.77.

Reactions of benzocyclobutenol ***12*** *with dienophiles* ***5***, ***6***, ***10***, *and* ***11***

Reaction of ***1*** *with* ***5***

Benzocyclobutenol (0.125 g, 1.04 mmol) and acrylate **5** (0.439 g, 3.51 mmol, 3.36 mol-equiv.) were refluxed in toluene

Can. J. Chem. Downloaded from www.nrcresearchpress.com by 213.200.69.106 on 09/08/12
For personal use only.

Can. J. Chem. Downloaded from www.nrcresearchpress.com by 213.200.69.106 on 09/08/12
For personal use only.

(anhydrous, 5 mL) in the presence of 4Å molecular sieves (0.92 g) under nitrogen for 11 h. The solution was filtered and the solvent removed in vacuo to leave a yellow oil (0.260 g). The oil was chromatographed on silica (20% ethyl acetate/hexanes) to give a colourless oil (148 mg, 58%), which on examination by ^{1}H nmr appeared to be a mixture of four diastereomers: ir (CH_2Cl_2): 3604, 2309, 1748, 1734 cm^{-1}. Anal. calcd. for $C_{14}H_{15}NO_3$: C 68.56, H 6.16, N 5.71; found: C 68.52, H 6.57, N 5.45. Three of the four isomers were isolated by hplc on ODS-2 using a methanol–water eluent (44:56 to 70:30 over 36 min) and their ^{1}H nmr and mass spectral data are given below in order of their elution.

exo-**1**: ^{1}H nmr ($CDCl_3$) δ: 7.59 (d, 1H, J = 9.4), 7.14–7.3 (m), 7.10 (m, 1H), 5.49 (q, 1H, J = 6.94), 5.09 (dd, 1H, J = 8.7, 6.6), 2.68–3.0 (m, 3H), 2.49 (d, 1H, J = 6.6), 2.89–2.2 (m, 1H), 2.03–1.88 (m, 1H, J = 6.0), 1.68 (d, 3H, J = 6.92); mass spectrum m/e (rel. %): 227 ($M^+ - H_2O$, 19), 191 (7), 173 (24), 145 (16), 129 (100), 81 (12), 69 (54).

endo-**1**: ^{1}H nmr ($CDCl_3$) δ: 7.41–7.38 (m, 1H), 7.26–7.10 (m, 3H), 5.51 (q, 1H, J = 6.90), 5.10 (bs, 1H), 3.00–2.75 (m, 3H), 2.46 (d, 1H, J = 5.9), 2.31–2.03 (m, 2H), 1.69 (d, 3H, J = 6.93); mass spectrum m/e (rel. %): 227 ($M^+ - H_2O$, 14), 191 (3.2), 173 (12), 145 (11), 130 (27), 129 (100), 128 (26.4), 119 (20), 115 (16), 91 (15).

endo-**2**: ^{1}H nmr ($CDCl_3$) δ: 7.41–7.38 (m, 1H), 7.27–7.22 (m, 2H), 7.17–7.14 (m, 1H), 5.52 (q, 1H, J = 6.97), 5.07 (d, 1H, J = 3.18), 3.12–2.75 (m, 3H), 2.29–2.10 (m, 2H), 1.71 (d, 3H, J = 6.98); mass spectrum m/e (rel. %): 227 ($M^+ - H_2O$, 21), 173 (8), 155 (2.9), 145 (8), 130 (39), 129 (100), 128 (34), 119 (20), 115 (16), 91 (13).

Reaction of ***1*** *with* ***6***

Benzocyclobutenol **12** (0.219 g, 1.82 mmol) and acrylate **6** (0.268 g, 1.89 mmol, 1.04 mol-equiv.) were refluxed in toluene (10 mL) in the presence of molecular sieves (4Å, 0.5 g) for 19 h. The solution was filtered through silica gel (EtOAc) and the solvent evaporated under reduced pressure to leave a yellow oil (0.471 g). The oil was chromatographed on silica (40% ethyl acetate/hexanes) and recrystallized from ethyl acetate/hexanes to give long, colorless crystals (0.215 g, 45%); mp 65–69°C; ir (CH_2Cl_2): 1721 cm^{-1}; ^{1}H nmr (300 MHz, $CDCl_3$) δ: 7.65 (d, 1H, $J_{8,7}$ = 7.19), 7.22 (m, 2H), 7.08 (d, 1H, $J_{5,6}$ = 7.06), 5.26 (q, 1H, J = 7.19), 4.98 (d, 1H, $J_{1,2}$ = 9.32), 3.68 (d, 1H, J = 2.82), 2.88–2.77 (m, 3H), 2.21 (s, 3H), 2.20–2.12 (m, 1H), 2.07–1.92 (m, 1H), 1.48 (d, 3H, J = 7.19); ^{13}C nmr (75.47 MHz, $CDCl_3$) δ: 205.88, 174.35, 137.44, 135.32, 128.22, 127.28, 126.93, 126.38, 75.23, 70.52, 48.77, 28.13, 25.68, 23.69, 15.80; mass spectrum m/e (rel. %): 244 (2.2), 191 (17), 173 (25), 157 (30), 146 (27), 129 (100), 105 (43), 91 (27). Exact Mass calcd. for $C_{15}H_{18}O_4$: 262.1205; found: 262.1203.

Reaction of ***1*** *with di-*tert*-butyl fumarate,* ***10***

Benzocyclobutenol (63.5 mg, 0.529 mmol) and di-*tert*-butyl fumarate (242 mg, 1.12 mmol, 2.12 mol-equiv.) were heated in toluene (5 mL) at 110°C in the presence of molecular sieves (1.0 g, 4 Å, dried under vacuum) for 19 h. The solution was filtered through a short silica gel column using EtOAc as eluent and the solvent evaporated to leave a yellow oil. An ^{1}H nmr spectrum (300 MHz) of this crude product exhibited two doublets at δ 4.88 (J = 8.88) and 5.03 (J = 3.57) in a ratio of 1.5:1 (*endo/exo*). The two isomers were separated by chromatography on silica (15% ethyl acetate/hexanes) in a combined yield of 45%.

exo Adduct: mp 91–92°C; ir (CH_2Cl_2): 1731 cm^{-1}; ^{1}H nmr ($CDCl_3$) δ: 7.65 (d, 1H, J = 7.2), 7.27–7.18 (m, 2H), 7.08 (d, 1H, J = 7.03), 4.88 (dd, 1H, J = 8.88, 5.6), 2.8–3.1 (m, 5H), 2.81 (d, 1H, J = 5.6), 1.50 (s, 9H), 1.46 (s, 9H); ^{13}C nmr ($CDCl_3$) δ: 172.90, 172.58, 137.20, 133.57, 128.00, 127.58, 126.78, 81.85, 81.05, 70.35, 51.58, 42.07, 31.74, 28.07, 28.01; mass spectrum m/e (rel. %): 257 (4.3), 218 (5.4), 189 (9.8), 172 (10), 129 (15), 97 (28), 83 (36), 69 (57), 57 (100). Anal. calcd. for $C_{20}H_{28}O_5$: C 68.94, H 8.10; found: C 68.62, H 8.10.

endo Adduct: mp 99–102°C; ir (CH_2Cl_2): 1733 cm^{-1}; ^{1}H nmr ($CDCl_3$) δ: 7.39–7.35 (m, 1H), 7.27–7.20 (m, 2H), 7.15–7.11 (m, 1H), 5.03 (dd, 1H, J = 4.63, 3.57), 3.23–3.12 (m, 2H), 2.99 (dd, 1H, J = 11.05, 3.57), 2.82 (dd, 1H, J = 18.10, 12.99), 2.17 (bd, 1H), 1.50 (s, 9H), 1.48 (s, 9H); ^{13}C nmr ($CDCl_3$) δ: 173.83, 171.78, 136.44, 134.19, 129.33, 128.60, 128.47, 126.74, 81.39, 80.68, 68.52, 48.87, 38.30, 31.99, 28.08; 28.01; mass spectrum m/e (rel. %): 236 (3.8) 235 (11), 217 (13), 189 (27), 173 (18), 172 (19), 145 (19), 129 (26), 69 (14), 57 (100). Anal. calcd. for $C_{20}H_{28}O_5$: C 68.94, H 8.10; found: C 68.98, H 8.23.

Reaction of ***1*** *with* ***11***

The fumarate of ethylene glycol (330 mg, 1.62 mmol) and benzocyclobutenol (214 mg, 1.78 mmol, 1.1 mol-equiv.) were refluxed in toluene (10 mL) in the presence of molecular sieves (4Å) for 18 h. The solution was filtered through a short column of sicila (eluent, ethyl acetate) and the solvent evaporated in vacuo. The ^{1}H nmr spectrum of the crude product revealed the presence of three doublets at δ 5.43 (J = 5.18), 5.12 (J = 3.65), and 4.86 (J = 9.53). The crude oil was chromatographed on silica (eluant 70% ethyl acetate/hexanes) to give only one pure fraction (93 mg, 22%); mp 114–115°C; ir (CH_2Cl_2): 3600, 1788, 1745 cm^{-1}; ^{1}H nmr ($CDCl_3$) δ: 7.35 (dd, 1H, J = 1.71, 7.3), 7.29–7.16 (m, 3H), 5.46 (d, 1H, J = 5.18), 4.18 (ddd, 1H, J = 3.08, 6.04, 9.13), 3.94 (m, 1H), 3.84 (t, 1H, J = 5.19), 3.51 (dd, 1H, J = 17.9, 5.28), 3.46 (bm, 2H), 3.35 (m, 1H, J = 1.14, 5.34), 3.09 (d, 1H, J = 17.9); ^{13}C nmr ($CDCl_3$) δ: 176.52, 167.37, 133.84, 126.80, 78.06, 66.38, 60.72, 47.64, 39.04, 27.32; mass spectrum m/e (rel. %): 262 (M^+, 7.0), 200 (12), 173 (5.7), 172 (8.2), 156 (5.9), 129 (100), 128 (77), 127 (16). Exact Mass calcd. for $C_{14}H_{14}O_5$: 262.0841; found: 262.0845.

Reactions of 1-methoxybenzocyclobutene ***13*** *with dienophiles* ***7*** *and* ***10***

Reaction of ***2*** *with* ***7***

The fumarate of methyl (*S*)-lactate, **7** (115 mg, 0.397 mmol), and 1-methoxybenzocyclobutene (66.6 mg, 0.496 mmol) were refluxed together in toluene (10 mL) for 3 days. The solution was filtered through a short column of silica gel (eluent EtOAc) and evaporated to leave a yellow oil (185 mg). The ^{1}H nmr spectrum exhibited two doublets at δ 4.75 (J = 2.96) and 4.56 (J = 3.33) in a ratio of 1.57:1; hplc (ODS-2, acetonitrile–water–methanol) exhibited two peaks in a ratio of 1.56:1. Chromatography of the crude oil on silica gel (eluent 5% EtOAC–benzene) gave adduct *endo*-**1** (62.6 mg) and adduct *endo*-**2** (27.1 mg) (combined yield 62%).

endo-**1**: ir (CH_2Cl_2): 1746 cm^{-1}; ^{1}H nmr ($CDCl_3$) δ: 7.18–7.32 (m, 4H), 5.24 (q, 1H, J = 7.04), 5.16 (q, 1H, J = 7.10), 4.68 (d, 1H, J = 3.00), 3.77 (s, 3H), 3.75 (s, 3H), 3.65 (m, 1H), 3.44 (dd, 1H, J = 7.04, 17.16), 3.34 (s, 3H), 3.17 (dd, 1H, J = 11.62, 3.00), 2.94 (dd, 1H, J = 10.94, 17.16), 1.54 (d, 3H, J = 7.11), 1.53 (d, 3H, J = 7.04); ^{13}C nmr ($CDCl_3$) δ: 174.85, 171.34, 171.24, 134.49, 133.13, 129.63, 129.14, 128.87, 125.66, 77.19, 68.65, 56.67, 52.24, 47.12, 36.24, 31.17, 17.20, 16.87; mass spectrum m/e (rel. %): 422 (M^+, 1.1), 359 (21), 258 (25), 187 (42), 186 (33), 185 (34), 159 (86), 155 (100), 128 (46). Exact Mass calcd. for $C_{21}H_{26}O_9$: 422.1577; found: 422.1582.

endo-**2**: ir (CH_2Cl_2): 1745 cm^{-1}; ^{1}H nmr ($CDCl_3$) δ: 7.19–7.35 (m, 4H), 5.26 (q, 1H, J = 7.02), 5.13 (q, 1H, J = 7.08), 4.66 (d, 1H, J = 3.31), 3.75 (s, 3H), 3.74 (s, 3H), 3.63–3.54 (m, 1H), 3.36–3.26 (m, 2H), 3.28 (s, 3H), 3.01 (dd, 1H, J = 10.49, 16.92), 1.55 (d, 3H, J = 7.04), 1.48 (d, 1H, J = 7.05); ^{13}C nmr ($CDCl_3$) δ: 173.52, 171.12, 170.96, 170.87, 134.60, 132.91, 129.63, 129.03, 128.89, 125.75, 77.43, 68.86, 68.64, 56.73, 52.26, 52.22, 47.04, 37.26, 52.22, 47.04, 37.10, 31.11, 17.05, 16.72; mass spectrum m/e (rel. %): 422 (M^+, 0.5), 359 (1.0), 258 (25), 187 (45), 186 (31), 185 (9) 155 (100), 128 (39). Exact Mass calcd. for $C_{21}H_{26}O_9$: 422.1577; found: 422.1559.

Reaction of **2** *with* **10**

Di-*tert*-butylfumarate (108 mg, 0.474 mmol) and 1-methoxybenzocyclobutene (111 mg, 0.825 mmol, 1.74 mol-equiv.) were heated in toluene (5 mL) at reflux for 16 h in the presence of molecular sieves (4Å, 0.19 g). The solution was filtered through a short silica gel column (eluent EtOAc) and the solvent evaporated at reduced pressure to leave a yellow oil. Further evaporation at 0.5 Torr (1 Torr = 133.3 Pa) for 4 h (20°C) left an oil (168 mg, 98%). The ^{1}H nmr spectrum of this crude product exhibited two doublets at δ 4.53 (J = 3.39) and 4.74 (J = 8.1) in the ratio of 7.7:1. Only the major cycloadduct could be characterized; ir (CH_2Cl_2): 1734 cm^{-1}, ^{1}H nmr ($CDCl_3$) δ: 7.28–7.13 (m, 4H), 4.53 (d, 1H, J = 3.39), 3.36–3.19 (m, 2H), 3.31 (s, 3H), 2.95 (dd, 1H, J = 11.29, 3.39), 2.28 (dd, 1H, J = 16.16, 10.4), 1.50 (s, 9H), 1.47 (s, 9H); ^{13}C nmr ($CDCl_3$) δ: 174.52, 171.17, 135.05, 133.69, 129.59, 128.92, 128.60, 125.58, 80.69, 80.24, 78.29, 56.99, 48.37, 38.01, 31.80, 28.11, 27.99; mass spectrum *m/e* (rel. %): 200 (62), 172 (35), 156 (24), 155 (32), 129 (80), 128 (100), 127 (58), 126 (20). Anal. calcd. for $C_{21}H_{30}O_5$: C 69.58, H 8.34; found: C 69.46, H 8.37.

Reaction of benzocyclobutenol **12** *with the fumarate of methyl (S-lactate* **7** *in DMSO/toluene*

Benzocyclobutenol (42 mg, 0.35 mmol) and fumarate **7** (83 mg, 0.29 mmol) were heated at 100°C in 30% DMSO–toluene (by volume, 10 mL), over molecular sieves (4Å, 300 mg), for 21 h. The solution was filtered through a short silica gel column (eluant EtOAc), diluted with benzene, and extracted with water. The organic fraction was dried ($MgSO_4$) and the solvent evaporated. Residual solvent was removed at high vacuum (0.5 Torr, 30°C) to leave an oil (109 mg, 72%). The major isomers were separated using reverse phase hplc (ODS-2, 53% water- 41% methanol: 6% acetonitrile increasing to 100% methanol). The identity of the fourth eluted peak was established as the *exo-re* adduct by comparison to an authentic sample (4,5). The two major adducts, eluting second and third, were isolated and characterized.

endo *Adduct 1:* ^{1}H nmr ($CDCl_3$) δ: 7.13–7.42 (m, 4H), 5.22 (q, 1H, J = 7.15), ca. 5.14 (m, 1H), 5.13 (q, 1H, J = 7.01), 3.78 (s, 3H), 3.75 (s, 3H), 3.63 (dt, 1H, J = 5.82, 11.6), 3.43 (d, 1H, J = 4.03), 3.19 (dd, 1H, J = 3.06, 11.54), 3.30 (dd, 1H, J = 11.7, 16.8), 2.96 (dd, 1H, J = 5.82, 16.82), 1.56 (d, 3H, J = 7.2), 1.52 (d, 3H, J = 7.1); mass spectrum *m/e* (rel. %): 408 (M^+, 0.34), 172 (19), 155 (50), 145 (38), 129 (100), 128 (64). Exact Mass calcd. for $C_{20}H_{18}O_9$: 408.1432; found: 408.1440.

endo *Adduct 2:* ^{1}H nmr ($CDCl_3$) δ: 7.45–7.40 (m, 1H), 7.27–7.24 (m, 2H), 7.14–7.20 (m, 1H), 5.35 (d, 1H, J = 3.49), 5.28 (q, 1H, J = 7.17), 5.17 (q, 1H, J = 7.1), 3.93 (bs, 1H), 3.80 (s, 3H), 3.77 (s, 3H), 3.48 (dt, 1H, J = 6.0, 12.3), 3.36 (dd, 1H, J = 6.0, 16.6), 3.22 (dd, 1H, J = 3.49, 11.7), 2.89 (dd, 1H, J = 12.3, 16.6), 1.57 (d, 3H, J = 7.2), 1.55 (d, 3H, J = 7.1); mass spectrum *m/e* (rel. %): 408 (M^+, 0.31), 287 (2.5), 276 (6), 258 (7), 173 (9), 172 (15), 155 (34), 129 (100), 128 (60), 127 (14). Exact Mass calcd. for $C_{20}H_{18}O_9$: 408.1432; found: 408.1434.

Can. J. Chem. Downloaded from www.nrcresearchpress.com by 213.200.69.106 on 09/08/12
For personal use only.

Acknowledgments

We gratefully acknowledge the financial support of this project by the Natural Sciences and Engineering Research Council of Canada. The technical assistance of Wayne Buchannon in recording mass spectra is also gratefully acknowledged.

1. J.L. Charlton and K. Koh. J. Org. Chem. **57**, 1514 (1992).
2. J.L. Charlton and K. Koh. Synlett, 333 (1990).
3. J.L. Charlton, G.L. Plourde, K. Koh, and A.S. Secco. Can. J. Chem. **68**, 2022 (1990).
4. J.L. Charlton, G.L. Plourde, K. Koh, and A.S. Secco. Can. J. Chem. **67**, 574 (1989).
5. J.L. Charlton, K. Koh, and G.L. Plourde. Tetrahedron Lett. **30**, 3279 (1989).
6. J.L. Charlton, K. Koh, and G.L. Plourde. Can. J. Chem. **68**, 2028 (1990).
7. J.L. Charlton and M.M. Alauddin. Tetrahedron, **43**, 2873 (1987), and references cited (1–13).
8. M. Pfau, J.E. Rowe, Jr., and N.D. Heindel. Tetrahedron, **34**, 3469 (1978).
9. P.G. Sammes. Tetrahedron, **32**, 405 (1976).
10. M.B. Glinski and T. Durst. Can. J. Chem. **61**, 573 (1983).
11. E. Block and R. Stevenson. J. Chem. Soc. Perkin Trans. 1, 308 (1973).
12. G. Helmchen, R. Karge, and J. Weetman. *In* Modern synthetic methods. Vol. 4. *Edited by* R. Scheffold. Springer-Verlag, New York. 1986. p. 261.
13. H. Hartmann, A.F.A. Hady, K. Sartor, J. Weetman, and G. Helmchen. Angew. Chem. Int. Ed. Engl. **26**, 1143 (1987).
14. R. Tripathy, P.J. Carrol, and E.R. Thornton. J. Am. Chem. Soc. **113**, 7630 (1991).
15. K.K.S. Koh. Ph.D. Thesis, University of Manitoba, Winnipeg. 1991.
16. W.A. Bubb and S. Sternhell. Aust. J. Chem. **29**, 1685 (1965).
17. T. Durst, E.C. Kozma, and J.L. Charlton. J. Org. Chem. **50**, 4829 (1985).
18. G.L. Plourde. Ph.D. Thesis, University of Manitoba, Winnipeg. 1990.
19. M.J. Frisch, J.S. Binkley, H.B. Schlegel, K. Raghavachari, C.F. Melius, R.L. Martin, J.J.P. Steward, F.W. Bobrowicz, C.J. Whiteside, D.J. Fox, E.M. Fluder, and J.A. Pople. Carnegie-Mellon Publishing Unit, Pittsburg, Pa. 1984.
20. PCMODEL v. 4.0, Serena Software, Box 3076, Bloomington, Ind. 1990.
21. R.J. Loncharich, F.K. Brown, and K.N. Houk. J. Org. Chem. **54**, 1129 (1989).
22. C.K. Johnson. ORTEP II: Report ORNL-TM-306-5138. Oak Ridge National Laboratory, Oak Ridge, Tenn. 1976.
23. M. Koerner and B. Rickborn. J. Org. Chem. **55**, 2662 (1990).

A new and simple spectrophotometric method for the determination of selenium in the presence of copper and tellurium

GÜLER SOMER[1] AND NURAY KUTAY
Department of Chemistry, Faculty of Science, Gazi University, 06500 Ankara, Turkey

Received February 22, 1991[2]

GÜLER SOMER and NURAY KUTAY. Can. J. Chem. **71**, 834 (1993).

Selenium in anodic slime is determined by using an indirect method. Selenite is reduced by ferrous iron, the ferric iron formed is complexed with KSCN, and the absorbance at 480 nm is measured. In this way selenium (10^{-3}–10^{-2} M) can be determined in the presence of copper and tellurium without any separation.

GÜLER SOMER et NURAY KUTAY. Can. J. Chem. **71**, 834 (1993).

Faisant appel à des méthodes indirectes, on peut déterminer la quantité de sélénium présente dans les boues anodiques. Le sélénite est réduit par l'ion ferreux; l'ion ferrique qui se forme est complexé par du KSCN et on mesure alors l'absorption à 480 nm. De cette façon, on peut déterminer des quantités de sélénium de l'ordre de 10^{-3}–10^{-2} M en présence de cuivre et de tellure sans séparation préalable.

[Traduit par la rédaction]

Can. J. Chem. Downloaded from www.nrcresearchpress.com by 213.200.69.106 on 09/08/12
For personal use only.

The most important source for selenium production is the anodic slime that is obtained during the electrolytic purification of copper. It is therefore important to determine the amount of selenium present in the anodic slime with a method that is simple and rapid. Anodic slime contains Se, Te, Cu, Au, Ag, Pb, As, and Sb. The level of selenium is between 8 and 20%, copper is between 20 and 40%, and tellurium is between 0.3 and 3%. In most selenium determination methods, copper seems to be the most serious interfering element due to its very similar redox properties. The aim of this work is to determine selenium in the presence of copper and tellurium without any separation. The quantity of selenium can be determined by titrimetric (1–3), spectrophotometric (4, 5), and gravimetric (6, 7) methods. Selenium in trace quantities is determined by Atomic Absorption Spectroscopy (AAS) (8), by polarography (9, 10), and by Anodic Stripping Voltammetry (ASV) (11, 12). In most of these methods separation of selenium is required.

We propose here a spectrophotometric method, in which selenium can be determined without any separation. Selenite is reduced by FeII. FeIII, the reaction product, is complexed by the addition of KSCN. The absorption of this complex is measured and the FeIII concentration is calculated. Since a stoichiometric amount of selenite has reacted, the amount of selenium is readily calculated.

Experimental

Reagents

All reagents used were analytical reagent grade. Triply distilled water was used for the preparation of all solutions and at all other stages of analysis.

FeII solution (0.1 M): Approximately 2.0 g $Fe(NH_4)_2SO_4$ is diluted to 100 mL with water that contains 40 mL of concentrated hydrochloric acid. Since this solution contains FeIII, it is reduced with $SnCl_2$ and the excess $SnCl_2$ is oxidized with $HgCl_2$. This solution is standardized with $K_2Cr_2O_7$ and stored under a nitrogen atmosphere to protect it from air oxidation.

Selenite solution (0.1 M): 0.547 g of SeO_2 is dissolved in 500 mL water.

FeIII solution (1.5×10^{-2} M): Approximately 0.32 g $FeCl_3 \cdot 6H_2O$ is diluted to 100.0 mL with water that contains 4.0 mL of HCl. This solution is standardized both with $KMnO_4$ and $K_2Cr_2O_7$ solutions.

Calibration curve

The molecular absorption spectrum of FeIII–thiocyanate has a maximum at 480 nm. FeIII solutions ($(0.67–1.40) \times 10^{-4}$ M) mixed with 100 times excess of KSCN show a linear relationship between concentration and absorbance.

In all absorption measurements, FeII solutions with KSCN were used as the blank.

Procedure

FeII solution, which is about 80–10 times more concentrated than that of the selenite, is added to the selenite solution. (For 1 mL of approximately 10^{-2} M SeO_3^{2-}, 8–10 mL of 0.1 M FeII solution is added.) The same volume of FeII solution is used as the reference. Both solutions are left to stand at room temperature for 15–20 min. Then measured volumes are taken, 2 M KSCN is added (the volumes are taken so that FeII/SCN concentration ratios are about 200), and absorbance is measured at 480 nm. Using the calibration curve for the FeIII–thiocyanate complex the amount of selenium in the sample can be calculated.

Solutions resembling anodic slime solutions were prepared (e.g., 10^{-2} M SeO_3^{2-}, 3×10^{-2} M Cu, and 5×10^{-3} M Te) and the recovery of selenite was determined. The results are given in Table 1. While the recovery for 10^{-2} M selenite solution was nearly 100%, it was reduced to 95% for 10^{-3} M solutions.

The same procedure has been applied for anodic slime after digestion. (This anodic slime contains 37% copper, 2% tellurium, and 4% lead.) For this purpose about 0.6 g of anodic slime was dissolved in an HCl + HNO_3 mixture (1).

The nitrous oxides were destroyed by adding urea. The solution was boiled and the reaction mixture was diluted to 100 mL with water. This solution did not show any absorbance at 480 nm after the addition of KSCN. For selenite determination, the above procedure was applied. The results obtained are in agreement with the results using different methods (Table 2) for the same anodic slime.

Results and discussion

When anodic slime is dissolved in a mixture of HCl + HNO_3, selenium and tellerium are present in the solution as selenite and tellurite. In this solution only selenite reacts with FeII, forming FeIII. Tellurite does not react. This reaction therefore can be used as a specific reaction for selenite determination. The FeIII concentration can be determined by the addition of KSCN and then by measuring the absorbance of the FeIII–SCN complex. The reaction between selenite and ferrous ion is an equilibrium reaction as given below:

[1] $SeO_3^{2-} + 4Fe^{2+} + 6H_3O^+ \rightleftharpoons Se + 4Fe^{3+} + 9H_2O$

[1]Author to whom correspondence may be addressed.
[2]Revision received November 2, 1992.

TABLE 1. Recovery of selenium from different solutions

Se_3^{2-} concentration (mol/L)	Concentration ratios $FeII/SeO_3^{2-}$	Concentration ratios $SCN^-/FeII$	Number of experiments	% Recovery of selenium[c]
10^{-2} [a]	80	200	6	101 ± 2
10^{-3} [b]	80	200	7	94 ± 0.7
10^{-3} [b]	160	200	3	95 ± 0,9

[a]FeII(8.0 mL 0.1 M) + SeO_3^{2-} (1.0 mL 10^{-2} M).
[b]FeII(1.0 mL 0.1 M) + SeO_3^{2-}(1.0 mL 10^{-3} M).
[c]90% confidence interval.

TABLE 2. Percentage of selenium in an anodic slime determined by four different methods

Method used	Weight percentage of selenium in slime
This work	10 ± 1
Volumetric (1)	10 ± 1
Polarographic (9)	10 ± 1
Spectrophotometric (13)	10 ± 1

To make use of the above reaction, certain variables that affect the reaction equilibrium must be investigated. For this purpose the effects of hydrogen ion concentration, FeII concentration, temperature, and time were investigated.

(a) Hydrogen ion concentration

The equilibrium constant is proportional to the sixth power of the hydrogen ion concentration. Therefore the FeII solution is prepared in concentrated HCl, so that the hydrogen ion concentration is 5 M. This acidity also inhibits the oxidation of the ferrous sulphate solution. H_2SO_4 could not be used because it decomposes KSCN, which is used for complexation of FeIII.

(b) FeII concentration

It was found experimentally that the FeII concentration must be 20–40 times larger than is stoichiometrically required. (For 1.0 mL of 10^{-3} M SeO_3^{2-}, 1.0 mL of 0.1 M FeII is enough.) Since FeII is oxidized by air during the reaction, use of higher concentrations of FeII should be avoided. As would be expecteed, large concentrations of FeIII favor the reverse reaction.

(c) Temperature

As was found in the previous experiment, for the reaction to be quantitative the FeII concentration had to be about 100 times higher than the selenite concentration. To check the temperature dependence, a mixture was prepared in which the FeII concentration was much less than it should be (5–10 times higher instead of 100 times). Under these conditions all the selenite cannot be reduced. When this solution was warmed up it showed higher absorbance values than the solution that was held at room temperature. This result may lead to the conclusion that the equilibrium was shifted to the right at higher temperatures. However, FeIII may be formed from two different reactions: either the above reaction (eq. [1]) is endothermic and more FeIII is formed by increasing the temperature, or FeII is oxidized by the air. To investigate the second possibility, an FeII solution with KSCN was warmed up in air; the colorless solution became red. It was concluded therefore that the oxidation of FeII by air increases with temperature. To eliminate the effect of the air oxidation of FeII, two reaction vessels containing the same amounts of FeII were prepared and SeO_3^{2-} solution was added to one vessel. Both solutions were kept at the same temperature for a certain time. Then KSCN was added and the absorbance of the selenite solution was measured using the FeII solution as the reference. This absorbance value must be proportional to the concentration of FeIII that is formed from the reaction of selenite with FeII. When the temperature was increased, the absorbance of the solution that contained selenite increased a little. The small increase of FeIII concentration with temperature tells us that selenite reduction is slightly endothermic. The larger temperature dependence of absorbance is because of the oxidation of FeII with air, and to eliminate it, this solution has to be used as the reference.

(d) Time

The FeIII concentration continued to increase for about 15 min after selenite and FeII were mixed. Therefore it was decided to wait 20 min for the completion of the reaction.

Conclusion

In nearly all selenium determination methods copper and tellurium seem to be the most serious interfering elements. They have to be separated either by precipitation or by exchange resins. The method suggested here is relatively simple and does not need expensive reagents or long and tedious separation procedures.

1. H. Aydin and G. Somer. Talanta, **36**, 723 (1989).
2. E.R. Caley and B. Henderson. Anal. Chem. **32**, 975 (1960).
3. R. Bye. Talanta, **30**, 993 (1983).
4. F.L. Chan and J.P. Ritey. Anal. Chim. Acta, **33**, 36 (1965).
5. E.P. Shkrobot and N.I. Shebarshina. Trudy Gintsvetmet, **28**, 18 (1968).
6. R. Williams and R. Haskett. Anal. Chem. **41**, 1138 (1969).
7. M. Tanoka. Bunseki Kagaku, **12**, 897 (1963).
8. R.E. Sturgeon, S.N. Willie, and S.S. Berman. Anal. Chem. **57**, 6 (1985).
9. E. Hasdemir and G. Somer. Analyst, **115**, 238 (1990).
10. R.S. Posey and R.W. Andrews. Anal. Chem. Acta, **124**, 107 (1981).
11. H. Aydin and G. Somer. Anal. Sci. **5**, 89 (1989).
12. T.W. Hamilton, J. Ellis, and T.M. Florence. Anal. Chim. Acta, **110**, 87 (1979).
13. G. Ekmekçi, M.S. Thesis. Gazi University, Ankara, Turkey. 1988.

Can. J. Chem. Downloaded from www.nrcresearchpress.com by 213.200.69.106 on 09/08/12
For personal use only.

The structures of dioxolan-2-ylium cations; carbon–oxygen bond distances in acetoxonium ions

RONALD F. CHILDS,[1] RICHARD M. ORGIAS, COLIN J.L. LOCK, AND MALIVAGANAM MAHENDRAN
Department of Chemistry, McMaster University, Hamilton, Ont., Canada L8S 4M1

Received November 2, 1992

RONALD F. CHILDS, RICHARD M. ORGIAS, COLIN J.L. LOCK, and MALIVAGANAM MAHENDRAN. Can. J. Chem. **71**, 836 (1993).

The X-ray structures of four dioxolan-2-ylium cations, 2-phenyl-1,3-dioxolan-2-ylium trifluoromethanesulfonate, **6**, and 2-(4-methoxyphenyl)-1,3-dioxolan-2-ylium, **7**, 2-(2,4-pentadienyl)-1,3-dioxolan-2-ylium, **8**, and 2-(4-methoxyphenyl)-4,4-dimethyl-1,3-dioxolan-2-ylium, **9**, hexafluoroantimonates, have been determined. Crystals of **6** are monoclinic, $C2/c$, a = 28.934(5), b = 6.022(2), c = 14.831(3) Å, β = 113.37(1)°, Z = 8; 1944 reflections were used to determine the structure; R = 0.0488, wR = 0.0477. Crystals of **7** are monoclinic, $P2_1/c$, a = 11.948(4), b = 10.686(3), c = 10.853(2) Å, β = 106.31(2)°, Z = 4; 2260 reflections were used to determine the structure; R = 0.0551, wR = 0.0807. Crystals of **8** are monoclinic, $P2_1/c$, a = 10.549(2), b = 10.457(3), c = 11.702(2) Å, β = 105.69(1)°, Z = 4; 2190 reflections were used to determine the structure; R = 0.0337, wR = 0.0299. Crystals of **9** are orthorhombic, $Pmnb$, a = 8.297(4), b = 15.269(3), c = 12.638(2) Å, Z = 4; 1736 reflections were used to determine the structure; R = 0.0796, wR = 0.0726. Intensities were measured on Syntex $P2_1$ or Nicolet P3 diffractometers at −65°C with use of Mo Kα radiation. These structures are discussed in terms of the conjugation and charge distribution in these cations. In each case the cations are almost planar with very small twist angles between the plane of the C(2) substituent and that of the dioxolanylium ring. Cation **8** is the first reported example of the structure determination of an acyclic, substituted dienyl carbenium ion. The unsaturated five-carbon chain in **8** has an all-*trans* conformation about all the C—C bonds, but, apart from the C(2)—C(1′) distance, none of the other bond distances differ significantly from those found in corresponding neutral systems. The C(2)—C(1′) distance in **7** is significantly shorter than that of **6**, suggesting enhanced conjugation of the aryl ring with the positive centre in the former cation. This suggestion is supported by the significant quinonoid-type distortion that is observed in the *p*-methoxyphenyl ring of **7**. Systematic variations in the O(1)—C(5)/O(3)—C(4) bond distances are examined and it is shown that alkyl substitution at C(4)/C(5) leads to a large increase in their lengths, suggesting that the presence of a significant fraction of the positive charge is located on C(4) and (or) C(5). Support for this suggestion is found in a large variety of previously reported spectroscopic and calorimetric measurements.

RONALD F. CHILDS, RICHARD M. ORGIAS, COLIN J.L. LOCK et MALIVAGANAM MAHENDRAN. Can. J. Chem. **71**, 836 (1993).

Faisant appel à la diffraction des rayons X, on a déterminé les structures de quatre cations dioxolan-2-ylium : le trifluorométhanesulfonate de 2-phényl-1,3-dioxolan-2-ylium (**6**) et les hexafluoroantimonates de 2-(4-méthoxyphényl)-1,3-dioxolan-2-ylium (**7**), de 2-(penta-2,4-diényl)-1,3-dioxolan-2-ylium (**8**) et de 2-(4-méthoxyphényl)-4,4-diméthyl-1,3-dioxolan-2-ylium (**9**). Les cristaux du produit **6** sont monocliniques, $C2/c$, avec a = 28,934(5), b = 6,022(2) et c = 14,831(3) Å, β = 113,37(1)°, Z = 8 et R = 0,0488 et R_w = 0,0477 pour 1944 réflexions. Les cristaux du produit **7** sont monocliniques, $P2_1/c$, avec a = 11,948(4), b = 10,686(3) et c = 10,853(2) Å, β = 106,31(2)°, Z = 4 et R = 0,0551 et R_w = 0,0807 pour 2260 réflexions. Les cristaux du produit **8** sont monocliniques, $P2_1/c$, avec a = 10,549(2), b = 10,457(3) et c = 11,702(2) Å, β = 105,69(1)°, Z = 4 et R = 0,0337 et R_w = 0,0299 pour 2190 réflexions. Les cristaux du composés **9** sont orthorhombiques, $Pmnb$, avec a = 8,297(4), b = 15,269(3) et c = 12,638(2) Å, Z = 4 et R = 0,0796 et R_w = 0,0726 pour 1736 réflexions. On a mesuré les intensités avec des diffractomètres Syntex $P2_1$ ou Nicolet P3, à −65°C, utilisant le rayonnement Mo Kα. On discute de ces structures en fonction de la conjugaison et de la distribution de charge dans ces cations. Dans chaque cas, les cations sont pratiquement plans; ils ne présentent que des faibles angles de déformation entre le plan du substituant en C(2) et celui du cycle dioxolanylium. Le cation **8** est le premier exemple d'un ion carbénium diényle substitué et acyclique dont la structure soit rapportée. La chaîne insaturée à cinq atomes de carbone du composé **8** est dans la conformation complètement *trans* autour de toutes les liaisons C—C; toutefois, la distance C(2)—C(1′) mise à part, aucune des longueurs des autres liaisons ne diffère d'une façon marquée des longueurs que l'on retrouve normalement dans les composés neutres correspondants. La longueur de la liaison C(2)—C(1′) observée dans le composé **7** est considérablement plus courte que celle observée dans le composé **6**; ce résultat suggère la présence, dans la premier cation, d'une plus grande conjugaison du cycle aryle avec le centre positif. Cette suggestion est supportée expérimentalement par la distorsion importante de type quinonoïde qui est observée dans le cycle *p*-méthoxyphényle du composé **7**. On a examiné les variations systématiques observées dans les longueurs des liaisons O(1)—C(5)/O(3)—C(4) et on montre que la substitution par un groupe alkyle en positions C(4)/C(5) conduit à une forte augmentation de leurs longueurs suggérant qu'une fraction de charge importante se trouve en C(4) et (ou) en C(5). On retrouve un support expérimental pour cette suggestion dans une grande variété de mesures spectroscopiques ou calorimétriques rapportées antérieurement.

[Traduit par la rédaction]

Introduction

Dioxolan-2-ylium cations are an important subset of the widely encountered dialkoxy/hydroxy-substituted carbenium ions (1).[2] Their existence as transient species (called acetoxonium ions) was first proposed by Winstein and Buckles in 1942 to account for the rate enhancements and stereoselectivities associated with the solvolysis of 2-acetoxy-3-bromobutanes and 1-acetoxy-2-bromocyclohexanes (2). The involvement of dioxolanylium cations in the reactions of systems such as acetylated carbohydrates was rapidly recognized (3). The transition from reactive intermediate to

[1]Author to whom correspondence may be addressed.

[2]For reviews on oxygen-substituted carbenium ions see ref. 1.

Can. J. Chem. Downloaded from www.nrcresearchpress.com by 213.200.69.106 on 09/08/12
For personal use only.

stable, characterizable carbocations was initiated in 1955 when Meerwein and colleagues first reported the isolation of a dioxolan-2-ylium salt (4). The ^{1}H NMR spectra of these ions were obtained by Winstein and co-workers in 1963 (5) and systematic NMR studies were reported by Hart and Tomalia in 1977 (6). Since this pioneering work, numerous studies of these cations have been reported and work still continues in order to understand the reactions and properties of these ions (7–10).[3]

Dioxolan-2-ylium cations are ambident and can undergo a variety of reactions with nucleophiles including addition to C(2) with the formation of cyclic products or addition to C(4)/C(5) with ring opening to form substituted esters (11). To understand these reactions it is important to know the structure of these cations and the way the structure varies as a function of substituent (12). The determination of the crystal structures of ions **1–5** has been reported (13–17) and the structure of the parent cation has been examined theoretically (18). In general, the five-membered ring of the dioxolan-2-ylium cation is planar, with relatively long O(3)—C(4)/O(1)—C(5) bonds. In the case of **3** and **4** the O(3)—C(4) bond distances are among the longest known C—O bonds (19).

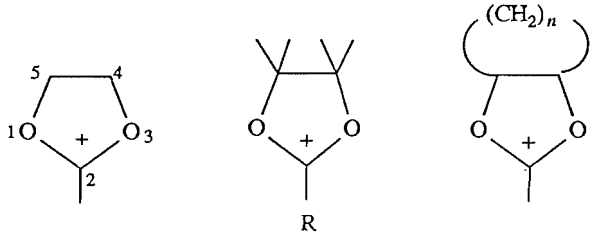

1 **2** R = Me **3** R = C_6H_5 **4** n = 3 **5** n = 4

The value in examining the crystal structures of a series of closely related molecules is well established (20). In this present context the O(3)—C(4) bond distance and the relationship of this length to the S_N1 reaction profile discussed by Edwards, Jones, and Kirby is of considerable interest (21). Unfortunately, the errors associated with the limited number of reported structures of dioxolan-2-ylium cations makes examination of systematic trends in these ions difficult. For this reason we have determined the structures of a further group of these cations in which substitution at C(4), C(5), and C(2) is varied. This present work, in conjunction with the previous reports, clearly demonstrates that systematic structural changes occur in these dioxolan-2-ylium cations as the substitution pattern is changed.

Results

The cations chosen for study in this work were **6–9**. The first three of these represent systems in which the substituent on C(2) is changed while the rest of the ring remains constant. In the last case, **9**, methyl groups are added to C(4) while keeping C(2) constant. The purpose of placing substituents at C(4) while leaving C(5) unsubstituted was to provide, in one cation, examples of two differently substituted O—C single bonds.

[3]For reviews on dioxolan-2-ylium cations see refs. 7 and 11.

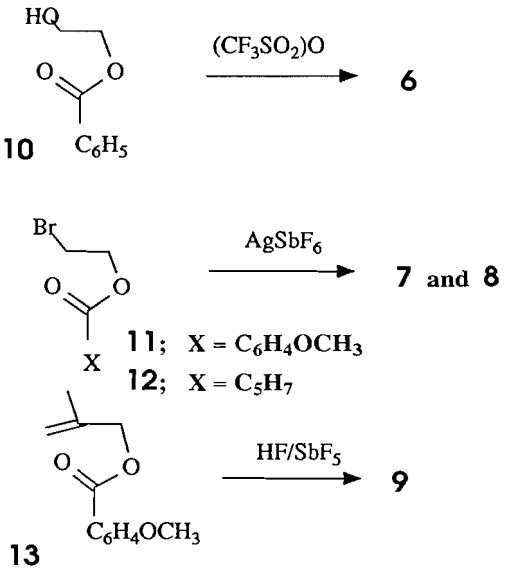

10 **6**

11; X = $C_6H_4OCH_3$

12; X = C_5H_7

13 **9**

SCHEME 1

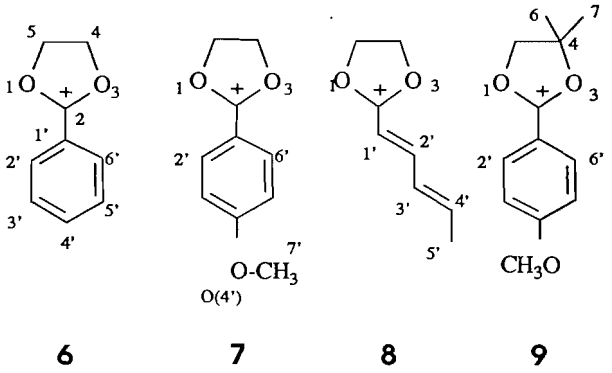

6 **7** **8** **9**

The cation **6** was prepared as its triflate salt by treatment of β-hydroxyethylbenzoate with triflic anhydride in CH_2Cl_2, Scheme 1. The procedure used to prepare **7** and **8** involved the treatment of β-bromoethyl or β-bromoisopropyl esters with $AgSbF_6$ in CH_2Cl_2, in a manner analogous to that used by Meerwein (4). After removal of the silver bromide, the cation salts were precipitated by the addition of anhydrous ether. In the case of **9**, the methallyl ester of *p*-methoxybenzoate was treated with HF/SbF_5 in CH_2Cl_2 (22, 23), Scheme 1. The salts were recrystallized from anhydrous CH_3CN/ether, **6–8**, or CH_2Cl_2/ether mixtures, **9**, to give single crystals suitable for X-ray diffraction. The cations were characterized by comparison of ^{1}H NMR spectra of solutions of the salts in CD_2Cl_2 with those previously reported (6). Cation **8**, a new material, had an NMR spectrum that was fully consistent with the assigned structure.

The structures of **6–9** were determined by X-ray diffraction. The crystals were mounted in Lindemann tubes in order to prevent contact with atmospheric moisture. Details of the structure solutions are given in Table 6, and the structures of the cations are shown in Figures 1–4. Atomic positional parameters are given in Tables 2–5. In the case of **7** the SbF_6^- group was disordered and two orientations of the counterion were assumed.

Discussion

The overall structures of **6–9** are similar to those previously reported for cations of this type (13–17). In each case

Can. J. Chem. Downloaded from www.nrcresearchpress.com by 213.200.69.106 on 09/08/12
For personal use only.

Can. J. Chem. Downloaded from www.nrcresearchpress.com by 213.200.69.106 on 09/08/12
For personal use only.

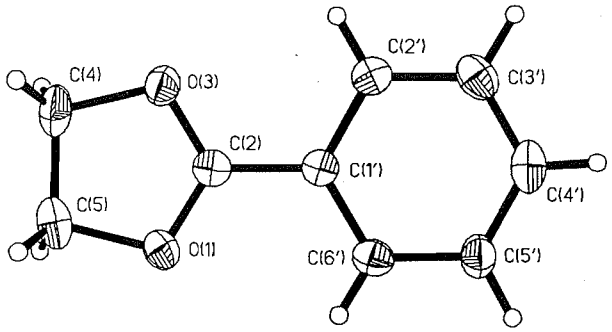

FIG. 1. Structure of the cation of **6**.

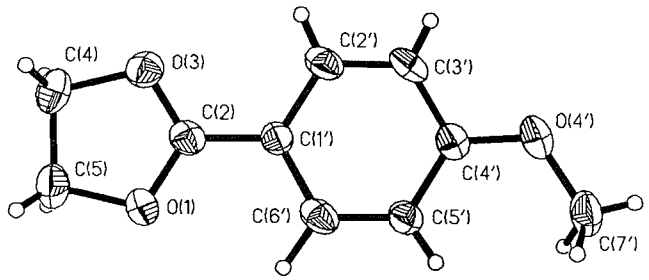

FIG. 2. Structure of the cation of **7**.

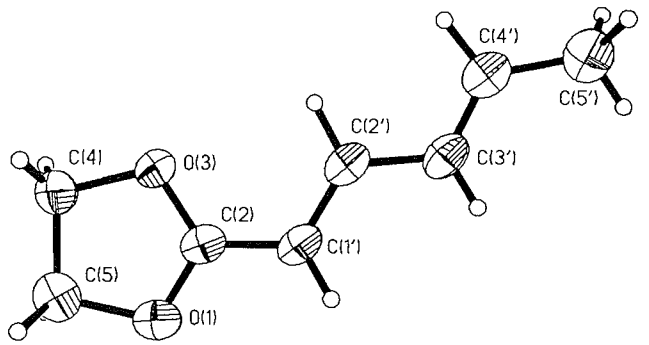

FIG. 3. Structure of the cation of **8**.

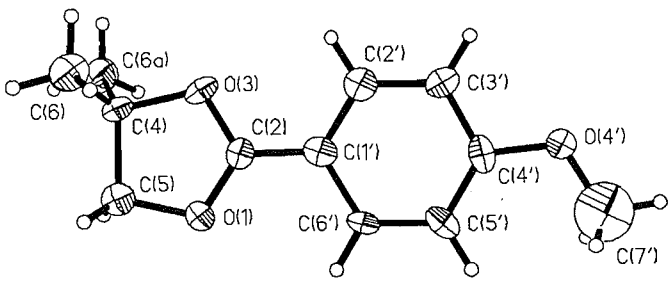

FIG. 4. Structure of the cation of **9**.

the 5-membered dioxolanylium rings are planar. The aryl rings in **6**, **7**, and **9** lie almost in the same plane as the atoms of the five-membered rings, being twisted from this plane by a small amount (see Table 7). The conformation of the aryl-substituted dioxolanylium cations found here supports one of the key structural assumptions made to account for the effect of a phenyl group on the hydrolysis of ortho esters (12, 24, 25). The anions have the expected structures, and bond lengths and angles are normal.

All intermolecular ion distances were equal to or greater than the sum of the van der Waals radii, except perhaps for the C(2)–anion distances. Each C(2) atom had an anion atom fairly close (O or F) on each side of the cation. Distances varied from 2.82 Å to 3.12 Å. While the shorter distances are less than the sum of the van der Waals radii for carbon and fluorine or oxygen (27), they may not be shorter than the distances involving C^+, for which we do not have a good van der Waals radius. Those atoms near C(2) are displaced away from C(1′) towards O(1) and (or) O(3), but not in a systematic manner. Ranges of angles are as follows: C(1′)—C(2)—X, 94.8°–107.9°; O(1)—C(2)—X, 79.5°–87.8°; O(3)—C(2)—X, 75.8°–99.6°. We do not think these distances and angles indicate any remarkable interactions, and are thus not important in the effects discussed hereafter.

The salt **8** is the first example of the structure determination of a cation with an acyclic polyenyl chain. As can be seen on inspection of Fig. 3, the dienyl chain in **8** exists in an *s-trans* conformation about both of the formal single bonds. The five carbon atoms of the chain lie in a plane, with the angle between this plane and that of the five-membered ring again being small (2.7°).

It is clear that the conformations adopted by all these cations are such that there can be effective conjugation between the substituent on C(2) and the charged system on the five-membered rings. Examination of the data given in Table 1 shows that this conjugation also results in relatively short C(2)—C(1′) bond distances in cations **6**–**9**. The average C(2)—C(1′) distance in the aryl-substituted cations **6**, **7**, and **9** is 1.42(1) Å, which is significantly less than the corresponding distance in aryl esters (1.487(12) Å) (difference 4.2σ where $\sigma = \sqrt{(\sigma_1^2 + \sigma_2^2)}$) (26). Previous analyses of the NMR spectra of these cations have shown that there is a transfer of charge onto the aryl rings of 2-substituted dioxolanylium cations (6, 7).

It is interesting that the C(2)—C(1′) bond distance in **7** is significantly shorter (difference 3.2σ) than the corresponding bond in **6**, suggesting that conjugation of the aryl ring with the cationic centre at C(2) is more important in the former ion. This is not unexpected given the presence of a methoxy group on C(4′) in **7** and the possibility of transfer of some of the charge to this function. Examination of the aryl-ring C—C bond distances in **7** (Table 1) is informative in that it is apparent that there is a considerable distortion of the C—C bond distances in the benzenoid ring. The C(2′)—C(3′) and C(5′)—C(6′) bond distances (mean 1.354(10) Å) are significantly shorter than the remainder of the aryl C—C bonds (mean 1.405(11) Å), indicating the presence of a "quinonoid" structure in the six-membered ring, Scheme 2. No significant differences are observed in the C(4′)—O(4′) bond lengths from those normally encountered with anisole derivatives (26). (In the case of **9** the errors associated with the structure determination make analysis of bond distances in the aryl rings difficult.) A quinonoid-type distortion of the C—C bond distances comparable to that found here in the aryl ring of **7** has recently been observed in other protonated *p*-methoxyphenylcarbonium ions (28). On the basis of INDO calculations and the NMR chemical shift correlations with σ observed by Hart and Tomalia (6), Pittman et al. (18) have suggested that this type of conjugative interaction of a

TABLE 1. Selected bond distances (Å) and angles (deg) for the cations

	Cation			
	6	**7**	**8**	**9**
O(1)—C(2)	1.281 (3)	1.292 (8)	1.288 (5)	1.30 (2)
C(2)—O(3)	1.282 (3)	1.294 (9)	1.290 (5)	1.29 (2)
O(3)—C(4)	1.472 (3)	1.475 (9)	1.469 (5)	1.51 (2)
C(4)—C(5)	1.505 (5)	1.504 (11)	1.515 (6)	1.58 (2)
C(5)—O(1)	1.480 (3)	1.468 (9)	1.472 (5)	1.46 (2)
C(4)—C(6)				1.52 (3)
C(2)—C(1′)	1.442 (3)	1.413 (9)	1.417 (5)	1.40 (2)
C(1′)—C(2′)	1.399 (4)	1.407 (12)	1.349 (6)	1.36 (2)
C(2′)—C(3′)	1.383 (4)	1.350 (10)	1.435 (5)	1.41 (2)
C(3′)—C(4′)	1.384 (4)	1.407 (11)	1.324 (6)	1.41 (2)
C(4′)—C(5′)	1.374 (4)	1.410 (11)	1.482 (6)	1.36 (2)
C(5′)—C(6′)	1.377 (4)	1.359 (10)		1.37 (2)
C(6′)—C(1′)	1.391 (4)	1.403 (12)		1.43 (2)
C(4′)—O(4′)		1.338 (8)		1.36 (2)
O(4′)—C(7′)		1.441 (11)		1.37 (2)
C(2)—O(1)—C(5)	108.1 (2)	109.2 (6)	108.7 (3)	112 (1)
O(1)—C(5)—C(4)	103.4 (2)	103.2 (6)	103.2 (3)	101 (1)
C(5)—C(4)—O(3)	103.1 (2)	103.5 (6)	103.0 (3)	102 (1)
C(4)—O(3)—C(2)	108.6 (2)	108.7 (6)	109.0 (3)	109 (1)
O(3)—C(2)—O(1)	116.8 (2)	115.3 (6)	115.9 (3)	115 (1)
C(5)—C(4)—C(6)				114 (2)
O(3)—C(4)—C(6)				105 (1)
C(6)—C(4)—C(6A)				114 (2)
O(1)—C(2)—C(1′)	121.1 (2)	122.3 (7)	121.5 (4)	125 (1)
O(3)—C(2)—C(1′)	122.1 (2)	122.4 (7)	122.6 (4)	120 (1)
C(2)—C(1′)—C(2′)	119.4 (2)	121.1 (7)	120.4 (4)	123 (1)
C(2)—C(1′)—C(6′)	120.0 (2)	119.3 (7)	—	119 (1)
C(6′)—C(1′)—C(2′)	120.6 (2)	119.6 (7)	—	118 (1)
C(1′)—C(2′)—C(3′)	118.8 (3)	120.2 (8)	125.3 (4)	122 (1)
C(2′)—C(3′)—C(4′)	120.2 (3)	120.7 (7)	121.4 (4)	117 (1)
C(3′)—C(4′)—C(5′)	121.0 (2)	118.8 (6)	127.3 (4)	122 (1)
C(4′)—C(5′)—C(6′)	119.9 (3)	120.6 (7)		120 (1)
C(5′)—C(6′)—C(1′)	119.7 (3)	119.9 (7)		121 (1)
C(3′)—C(4′)—O(4′)		116.7 (7)		112 (1)
C(5′)—C(4′)—O(4′)		124.5 (7)		127 (1)
C(4′)—O(4′)—C(7′)		120.1 (6)		115 (1)

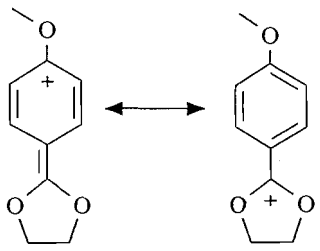

SCHEME 2

p-methoxyphenyl group with a dioxolanylium cation is relatively unimportant. The structural changes observed here would seem to be at odds with this suggestion.

It is instructive to examine the C—C bond distances in the pentadienyl fragment of **8** and compare them with what would be expected for an unsaturated ester, Scheme 3 (26). The only significant difference in distances between **8** and the corresponding neutral ester is for the C(2)—C(1′) bonds (difference 4.8σ). All of the other bond distances in the dienylic chain differ by less than 3σ from the corresponding bond lengths in the model. It is clear that there is a considerable degree of bond alternation in the unsaturated chain of **8** with a large fraction of the positive charge residing on the dioxolanylium ring. While the differences in individual bond distances in the unsaturated chain of **8** and the model are not significant, there does appear to be a consistent pattern to these differences that would suggest that the unsaturated chain in **8** is starting to exhibit changes in the various bond distances towards those expected for a simple pentadienyl cation. Thus the C(1′)—C(2′) formal double bond in the cation is longer than that of the model compound while both the C(2′)—C(3′) and C(4′)—C(5′) single-bond distances are shorter in the cation than those of the model. Comparison of the chemical shifts of the various protons of the pentadienyl chain as **8** is formed from its neutral precursor indicate that positive charge is being delocalized to some extent in this unsaturated substituent.

C—O bond distances

There are four C—O bonds in the five-membered ring of a dioxolan-2-ylium cation. In discussing the variations in the distances of these bonds it is useful to combine the results

Can. J. Chem. Downloaded from www.nrcresearchpress.com by 213.200.69.106 on 09/08/12
For personal use only.

Can. J. Chem. Downloaded from www.nrcresearchpress.com by 213.200.69.106 on 09/08/12
For personal use only.

TABLE 2. Atomic positional parameters ($\times 10^4$) and temperature factors ($Å^2 \times 10^3$) for **6**

Atom	x	y	z	U_{eq}[a]
S(1A)	900.4 (2)	7003 (1)	9515.4 (4)	22.5
O(1A)	440.9 (7)	5766 (3)	9191 (2)	44
O(2A)	1183.2 (7)	7020 (3)	10556 (1)	35.0
O(3A)	1200.6 (8)	6709 (4)	8950 (1)	41
C(1A)	682.2 (9)	9843 (5)	9255 (2)	26
F(1A)	1061.2 (6)	11265 (3)	9529 (1)	41.5
F(2A)	418.6 (6)	10162 (3)	8303 (1)	47.4
F(3A)	384.8 (7)	10383 (3)	9709 (1)	49.0
O(1)	3699.5 (6)	983 (3)	7857 (1)	23.4
C(2)	3605.6 (9)	9049 (4)	7467 (2)	20
O(3)	3985.9 (6)	7817 (3)	7578 (1)	26.3
C(4)	4449 (1)	9070 (6)	8135 (2)	34
C(5)	4253 (1)	11236 (5)	8347 (2)	31
C(1′)	3098.8 (9)	8284 (4)	6918 (2)	19.4
C(2′)	3021 (1)	6166 (4)	6496 (2)	24
C(3′)	2533 (1)	5469 (5)	5957 (2)	29
C(4′)	2132 (1)	6859 (5)	5837 (2)	31
C(5′)	2210 (1)	8941 (5)	6249 (2)	28
C(6′)	2693 (1)	9666 (5)	6793 (2)	24

[a]$U_{eq} = 1/3(U_{11} + U_{22} + U_{33} + 2U_{13} \cos \beta)$.

obtained here with the structures of **1**–**5** previously reported (13–17).

In all the dioxolan-2-ylium cations the O(1)—C(2) and O(3)—C(2) bonds are intermediate in length between those of C—O single and double bonds. The mean distance of these C—O bonds in cations **6**–**9** and **3** with an aryl or unsaturated substituent at C(2) is 1.291(2) Å.[4] Cations with an alkyl substituent at C(2) (**1**, **2**, **4**, and **5**) have significantly shorter O(1)—C(2)/O(3)—C(2) bonds (mean 1.261(5) Å, difference 5.2σ). The longer O(1)—C(2)/O(3)—C(2) mean bond distance in the aryl-substituted cations presumably reflects the delocalization of charge onto these unsaturated substituents with a resulting diminution of double-bond character in the C—O bonds, Scheme 2.[5] This structural difference in the alkyl- and aryl-substituted dioxolan-2-ylium ions is of interest in terms of the extensive discussion that has taken place over the relative stabilizing effects of methyl and phenyl substituents at C(2) in these cations (12, 22, 24, 25, 29, 30).

In contrast to the O(1)—C(2)/O(3)—C(2) bond lengths, the O(3)—C(4) and O(1)—C(5) distances in these dioxolan-2-ylium cations show no significant dependence on the nature of the substituent on C(2). Thus the lengths of these bonds in **6**, **7**, and **1**, where the C(2) substituent varies from phenyl, *p*-methoxyphenyl, to methyl, are not significantly different. The small chemical shift dependence observed for the C(4)/C(5) proton resonances as the C(2) substituent is varied is clearly not reflected in detectable changes in the lengths of the O(3)—C(4) and O(1)—C(5) bonds (6).

The O(3)—C(4) and O(1)—C(5) bond lengths in the dioxolan-2-ylium cations show a large dependence on the substituents on C(4)/C(5). The errors associated with the structure determination of cation **9** make it impossible to detect significant differences in the lengths of the individual O(3)—C(4) and O(1)—C(5) bonds in a single cation. The ions can be grouped according to the number of substituents at C(4) or C(5), however, and, when this is done, it is apparent that there is a consistent pattern to the various bond distances observed in these cations (see Table 8).

The O—CH_2 bond distances in these dioxolan-2-ylium

TABLE 3. Atomic positional parameters ($\times 10^4$) and temperature factors ($Å^2 \times 10^3$) for **7**

Atom	x	y	z	U_{eq}[a]
Sb	1676.1 (4)	−493.7 (4)	2461.2 (4)	27.3
F(1)	962 (4)	−2052 (4)	2399 (5)	46
F(2)	2367 (4)	1092 (4)	2502 (5)	49
F(3)	1347 (10)	−505 (8)	652 (9)	31
F(4)	2025 (9)	−523 (8)	4222 (9)	31
F(5)	165 (11)	167 (12)	1802 (13)	57
F(6)	3172 (10)	−1108 (11)	3033 (12)	55
F(11)	1787 (12)	−679 (11)	840 (12)	56
F(21)	1520 (13)	−265 (11)	4109 (12)	64
F(31)	3106 (8)	−1352 (9)	2491 (9)	40
F(41)	323 (9)	405 (8)	2353 (10)	41
O(1)	1035 (4)	1260 (5)	6282 (5)	40
C(2)	2129 (6)	1214 (6)	6339 (6)	29
O(3)	2443 (4)	1926 (5)	5531 (5)	34
C(4)	1406 (7)	2589 (7)	4741 (7)	39
C(5)	432 (7)	2095 (8)	5231 (8)	45
C(1′)	2923 (6)	429 (6)	7213 (7)	27
C(2′)	4105 (7)	378 (7)	7236 (8)	34
C(3′)	4847 (6)	−390 (7)	8066 (7)	34
C(4′)	4452 (6)	−1155 (7)	8913 (6)	30
C(5′)	3269 (6)	−1092 (7)	8895 (7)	32
C(6′)	2523 (6)	−306 (6)	8074 (8)	33
O(4′)	5242 (5)	−1907 (5)	9681 (5)	42
C(7′)	4902 (7)	−2737 (8)	10559 (8)	43

[a]$U_{eq} = 1/3(U_{11} + U_{22} + U_{33} + 2U_{13} \cos \beta)$.

TABLE 4. Atomic positional parameters ($\times 10^4$) and temperature factors ($Å^2 \times 10^3$) for **8**

Atom	x	y	z	U_{eq}[a]
Sb	1778.2 (2)	343.1 (2)	2448.0 (2)	30.6
F(1)	1672 (3)	501 (2)	834 (2)	63
F(2)	1831 (3)	221 (2)	4054 (2)	51
F(3)	1163 (2)	2020 (2)	2435 (2)	49
F(4)	46 (2)	−260 (2)	2042 (2)	59
F(5)	2351 (3)	−1349 (2)	2446 (2)	56
F(6)	3512 (2)	910 (3)	2844 (2)	63
O(1)	−2561 (3)	2172 (2)	4639 (2)	40
C(2)	−2306 (4)	1355 (4)	3908 (3)	34
O(3)	−1076 (2)	1183 (2)	3978 (2)	39
C(4)	−284 (4)	2025 (4)	4904 (4)	47
C(5)	−1310 (4)	2676 (4)	5392 (4)	45
C(1′)	−3323 (4)	685 (4)	3087 (3)	39
C(2′)	−3035 (3)	−128 (4)	2297 (3)	36
C(3′)	−3983 (4)	−816 (4)	1396 (3)	40
C(4′)	−3615 (4)	−1569 (4)	634 (3)	40
C(5′)	−4477 (5)	−2335 (5)	−335 (4)	53

[a]$U_{eq} = 1/3(U_{11} + U_{22} + U_{33} + 2U_{13} \cos \beta)$.

[4]The errors for mean bond lengths are given by $\sigma_D = \sqrt{\Sigma_n(D - d_n)^2/n(n-1)}$ where D is the mean bond distance of n independent variables.

[5]The relative order of the stabilizing ability of methyl and phenyl substituents on carbocations can change depending on the system in question, ref. 29. In the dioxolan-2-ylium cation the recent results of Kresge, Larsen, and co-workers establish that phenyl is a better charge-stabilizing group than methyl, ref. 30.

TABLE 5. Atomic positional parameters ($\times 10^4$) and temperature factors ($Å^2 \times 10^3$) for **9**

	x	y	z	U_{eq}[a] or U_{iso}*
Sb(1)	2500	2116 (1)	1292 (1)	33
F(1)	4081 (8)	1243 (4)	1337 (5)	53
F(2)	2500	2174 (7)	2766 (7)	61
F(3)	2500	2053 (7)	−186 (7)	56
F(4)	892 (9)	2999 (4)	1232 (5)	56
O(1)	2500	−1872 (6)	8851 (7)	33
C(2)	2500	−1027 (8)	8720 (10)	24
O(3)	2500	−570 (6)	9580 (7)	37
C(4)	2500	−1184 (9)	10516 (10)	35
C(5)	2500	−2114 (10)	9967 (11)	41
C(6)	4040 (13)	−978 (7)	11120 (7)	42
C(1′)	2500	−599 (9)	7738 (11)	34
C(2′)	2500	290 (10)	7647 (11)	35*
C(3′)	2500	713 (10)	6660 (11)	41
C(4′)	2500	178 (11)	5749 (12)	57
C(5′)	2500	−711 (10)	5818 (14)	61
C(6′)	2500	−1110 (9)	6786 (11)	46
O(4′)	2500	665 (9)	4851 (10)	27*
C(7′)	2500	189 (18)	3933 (19)	109*

[a] $U_{eq} = 1/3(U_{11} + U_{22} + U_{33})$.

cations are remarkably uniform. Within the structures determined here and that of **1**, there are some 10 examples of O(3)—C(4)/O(1)—C(5) bonds where C(4) or C(5) is a CH_2 group. The mean O—CH_2 bond distance of this group of cations is 1.474(2) Å. Directly comparable distances have been found for the O—CH_2 bond in other cations such as the 6-ethoxytetrahydropyrylium ions (31).

As alkyl substituents are joined to C(4) and (or) C(5) the O(3)—C(4) and (or) O(1)—C(5) bond distances are lengthened substantially from the 1.474(2) Å observed for the O—CH_2 cases. A significant increase in the mean O(3)—C(4)/O(1)—C(5) bond distance is observed as first one, then two, alkyl substituents are joined to C(3) or C(4) (see Table 8).

The O—C(alkyl) bond distances in alkyl esters form a good reference point for the O(3)—C(4) and O(1)—C(5) bonds in these dioxolanylium cations, and the relevant data taken from the extensive analysis of the bonding in esters undertaken by Allen and Kirby (32) are shown in Table 8. Two points stand out on comparison of the data given in this table. In the first place all the O(3)—C(4) and O(1)—C(5) bond distances in these cations are significantly longer than the corresponding O—C bonds in esters or, indeed, 1,3-dioxolans (32).[6] Comparable long O—C bonds have been observed with 6-ethoxytetrahydropyrylium cations (31).[7]

The second important aspect is the differing sensitivity

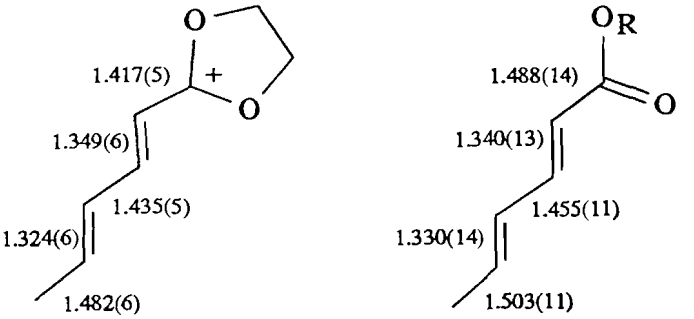

SCHEME 3

towards substitution at the alkyl carbon of the dioxolanylium cations, as compared to neutral esters. The length of an O—C bond is expected to increase as the number of alkyl substituents at the carbon is increased. This is well demonstrated by the data for esters shown in Table 8. The notable feature of the changes in bond distance of these cations is, however, that the magnitude of the increase is very much larger than that of the esters.

In a previous paper on the tetrahydropyrylium cations we suggested the long O–alkyl bonds coupled with the changes in bond angles at the alkyl carbons could be accounted for by an ionic contribution to this bond with positive charge residing on the alkyl carbon atom (31). The results of this present study of the C—O bond distances in dioxolanylium cations fully support this suggestion. As the alkyl group bonded to oxygen becomes more highly substituted and better able to support a positive charge, the longer is the O—C bond distance, Scheme 4.

It is not customary to draw the third structure shown in Scheme 4 when considering the resonance structures of an alkoxy- or, for that matter, a hydroxy-substituted carbenium ion and it is worth reviewing other lines of evidence that support its involvement. There is good evidence that this third structure is an important resonance contributor and that a considerable fraction of the positive charge resides on the alkyl carbon of dioxolanylium and other alkoxy-substituted carbenium ions. In the first place, the calculations of Pittman et al. (18) and the detailed ^{13}C NMR and ESCA spectroscopic studies of Paulsen and Dammeyer (16) indicate the presence of positive charge at C(4) and C(5) in dioxolan-2-ylium cations. The calorimetric studies of Larsen et al. are particularly compelling (22, 24). It was shown by these workers that methyl substitution at C(2) of a 2*H*-3,4-dihydrofuranylium cation leads to a 3.1 kcal mol^{-1} stabilization of the cation.[8] Indeed, it was noted by these workers that the effect of methyl substitution at C(2), the alkyl carbon, is almost as large as that of placing a methyl group at C(2) of a dioxolan-2-ylium cation! Larsen et al. also found that the relative heats of protonation of ethyl esters are significantly more exothermic than those of the corresponding methyl esters (24). Both of these calorimetric examples show that substitution at the alkyl carbon atom of an alkoxy carbenium ion leads to a significant thermodynamic stabilization of the cation. Further support for the involvement of the third structure in Scheme 4 can be found from values of the substituent constants of alkoxy groups. For example, σ^+ values

[6] In the dimer of 1,3-dioxolan the average C—O distance is 1.41 Å, ref. 33.

[7] The bond angle of the dioxolan-2-ylium cations is less definitive than that of the tetrahydropyrylium salts, presumably as a result of the constraints imposed by the five-membered rings and eclipsed methyl groups at C(4) and C(5) in the former cations. Again, however, the trend in cations **2** and **3** is for a flattening of C(4) and C(5) as the O(3)—C(4) and O(1)—C(5) bonds are lengthened (13, 14). The complexity of bond angle changes accompanying the lengthening of a C—O bond of esters has previously been noted by Edwards, Jones, and Kirby (21).

[8] The C(2) position of a dihydrofuranylium cation corresponds to C(4) or C(5) in a dioxolan-2-ylium ion.

Can. J. Chem. Downloaded from www.nrcresearchpress.com by 213.200.69.106 on 09/08/12
For personal use only.

TABLE 6. Crystal data

Compound name	2-Phenyl-1,3-dioxolan-2-ylium trifluoromethanesulfonate **6**	2-(4-Methoxyphenyl)-1,3-dioxolan-2-ylium hexafluoroantimonate **7**	2-(2,4-Pentadienyl)-1,3-dioxolan-2-ylium hexafluoroantimonate **8**	2-(4-Methoxyphenyl)-4,4-dimethyl-1,3-dioxolan-2-ylium hexafluoroantimonate **9**
Compound formula	$C_9H_9O_2^+CF_3SO_3^-$	$C_{10}H_{11}O_3^+SbF_6^-$	$C_8H_{11}O_2^+SbF_6^-$	$C_{12}H_{15}O_3^+SbF_6^-$
Formula weight	298.2	414.9	374.9	443.0
Crystal shape and size (mm)	Rectangular prism; 0.15 × 0.15 × 0.50	Rectangular prism; 0.30 × 0.30 × 0.50	Plates; 0.32 × 0.30 × 0.06	Cube, 0.30 × 0.30 × 0.30
Systematic absences	*hkl*, $h + k = 2n + 1$; *h*0*l*. *h*,*l* = $2n + 1$; 0*kl*, *k* = $2n + 1$; *hk*0, $h + k = 2n + 1$; *h*00, *h* = $2n + 1$; 00*l*, *l* = $2n + 1$	*h*0*l*, *l* = $2n + 1$; 0*k*0, *k* = $2n + 1$; 00*l*, *l* = $2n + 1$	*h*0*l*, *l* = $2n + 1$; 0*k*0, *k* = $2n + 1$; 00*l*, *l* = $2n + 1$ *h*00, *h* = $2n + 1$; 00*l*, *l* = $2n + 1$	*h*0*l*, *h* = $2n + 1$; 0*kl*, $k + l = 2n + 1$; 0*k*0, *k* = $2n + l$;
Space group	*C*2/*c* (No. 15)	$P2_1/c$ (No. 14)	$P2_1/c$ (No. 14)	*Pmnb*
Diffractometer	Syntex $P2_1$	Syntex $P2_1$	Nicolet P3	Syntex $P2_1$
Unit cell parameters (Å and deg)	*a* = 28.934(5), *b* = 6.022(2), *c* = 14.831(3) β = 113.37(1)	*a* = 11.948(4), *b* = 10.686(3), *c* = 10.853(2) β = 106.31(2)	*a* = 10.549(2), *b* = 10.457(3), *c* = 11.702(2) β = 105.69(1)	*a* = 8.297(4), *b* = 15.259(3), *c* = 12.638(2)
Volume (Å^3)	2372.5(9) *Z* = 8	1329.9(5) *Z* = 4	1242.7(5) *Z* = 4	1596.5 *Z* = 4
Temperature (K)	208	208	208	208
$Density_{calc}$, $Density_{obs}$ (g cm^{-3})	1.67, not measured	2.07, not measured	2.00, 2.0(1)	1.837, 1.8(2)
Linear absorption coefficient, cm^4	3.32	21.83	23.17	18.17
No. of reflections to determine cell, limits in θ	15, 20.5° < 2θ < 24.1°	15, 20.5° < 2θ < 27.9°	15, 21.1° < 2θ < 26.0°	15, 20.2° < 2θ < 28.0°
Reflections measured, max 2θ	$0 \le h \le 30$, $0 \le k \le 7$, $-17 \le l \le 17$, 50°	$0 \le h \le 13$, $0 \le k \le 12$, $-12 \le l \le 12$, 50°	$0 \le h \le 12$, $0 \le k \le 12$, $-13 \le l \le 13$, 50°	$0 \le h \le 8$, $0 \le k \le 19$, $0 \le l \le 16$, 50°
Standard reflections (esd %)	7 1 −8(1%) −2 0 8(2%)	1 0 6(2%) −2 −5 −2(1%)	−5 −2 0(1%) 0 −6 1(2%)	2 1 7(.3%) 3 4 6(.3%)
No. of reflections measured	2133	2468	2312	1884
R_{int}	0.0168	0.0175	0.0201	—
No. of unique reflections	2092	2350	2350	1736
No. of reflections used	1944	2260	2190	1736
No. of parameters	209	222	155	116
Final *R*, *wR*	0.0488, 0.0477	0.0551, 0.0807	0.0337, 0.0299	0.0796, 0.0726
Final/shift error max. (avg.)	0.171(0.042)	0.006(0.001)	0.007(0.002)	0.498(0.050)
Secondary extinction	0.00089	0.00546	0.00024	0.00020
Highest peak, lowest valley (Å^3)	0.38, −0.33	1.40, −2.39	0.60, −0.43	1.24, −1.19
Weighting	$w = ((\sigma_F)^2 + 0.000507F_o^2)^{-1}$	$w = ((\sigma_F)^2 + 0.00088F_o^2)^{-1}$	$w = ((\sigma_F)^2 + 0.000142F_o^2)^{-1}$	$w = ((\sigma_F)^2 + 0.00088F_o^2)^{-1}$
Error in an observation of unit weight, *S*	1.41	4.10	2.13	3.18
F(000)	1216	800	720	864

$R = \Sigma\|F_o| - |F_c\|/\Sigma|F_o|$.
$wR = \{\Sigma w(|F_o| - |F_c|)^2/\Sigma wF_o^2\}^{1/2}$.
$S = \{\Sigma w(|F_o| - |F_c|)^2/(n - m)\}^{1/2}$.
$\sigma_F = 1/2(k/\sqrt{LP})(\sigma_I/\sqrt{I})$.

TABLE 7. Dihedral angles between dioxolanylium ring and plane of C(2)-substituent

Cation	Dihedral angle (deg)
6	2.4
7	3.4
8	2.7
9	0.0

TABLE 8. O—C(alkyl) bond lengths

	Bond distance (Å)	
O—C bond type	Dioxolanylium ion	Ester
O—CR_3	1.525(5)	1.475(2)
O—CHR_2	1.491(5)	1.460(2)
O—CH_2R	1.474(2)	1.452(2)
O—CH_3	—	1.450(1)

Can. J. Chem. Downloaded from www.nrcresearchpress.com by 213.200.69.106 on 09/08/12
For personal use only.

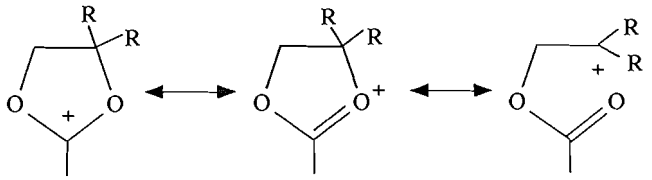

SCHEME 4

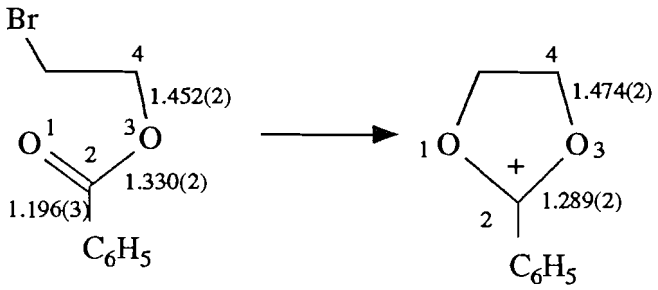

SCHEME 5

of alkoxy substituents become increasingly negative as the alkyl carbon becomes more substituted, indicating that the larger alkoxy groups are better able to stabilize a positive charge.[9] One also notes that the well-known facile cleavage of the O—C bond of *tert*-butyl esters and ethers under acid-catalyzed conditions is consistent with this picture of the charge distribution in alkoxy cations.

There is then a well-established and diverse body of evidence to indicate that a significant fraction of the positive charge resides on the alkyl carbon atom of an alkoxy-substituted carbenium ion. What this present work has done is show that the variations in spectroscopic, thermodynamic, and kinetic properties of these alkoxy cations can be related to systematic differences in their structures.

In conclusion, it is interesting to reflect on the relative importance of the first two resonance contributors shown in Scheme 4. One way of approaching this is to consider the O—C bond length changes that occur on the formation of a dioxolan-2-ylium cation, Scheme 5.

It can be seen from the data presented in Scheme 5 that the formation of the ring results not only in the elongation of the O(3)—C(4) bond discussed above, but also in a contraction of the O(3)—C(2) bond.[10] Thus the decrease in bond order of the O(3)—C(4) bond that results from this expansion is to some extent compensated for by an increase in that of the O(3)—C(2) bond. The question at issue is the degree of coupling of these changes and whether the sum of the bond valences of the two O(3)—C bonds remains close to 2, as in the starting ester, or is higher, indicating a significant involvement of the second resonance structure in Scheme 4. In principle this question could be examined by using the well-known bond distance/bond order relationship developed initially by Pauling (see ref. 35) or by seeking a correlation between the O(3)—C(2) and O(1)—C(2) bond distances on substitution at C(2) of this and related cations. The errors associated with some of these structures, however, do not permit these analyses to be carried out with any degree of confidence. When the structures of further series of alkoxy-substituted cations are determined it should be possible to address this question.

Experimental section

NMR spectra were obtained on Varian EM-390, and Bruker WM-250 and Bruker WM-500 spectrometers. All spectra were related to tetramethylsilane. Mass spectra were obtained on an VG-ZAB-E mass spectrometer operating at an ionization potential of 70 eV and a source temperature of 200°C.

Ether was freshly distilled from lithium aluminum hydride immediately before use. CH_2Cl_2 and CH_3CN were refluxed over phosphorus pentoxide and distilled under a nitrogen atmosphere. 2-Bromoethyl 4-methoxybenzoate, **11** (36), 2-bromopropyl 4-methoxybenzoate, **13** (37), and 2-methyl-2-propenyl 4-methoxybenzoate, **14** (38), were prepared by standard procedures. The structures of each of these materials were verified by NMR spectroscopy before use in the preparation of the cations.

2-Bromoethyl 2,4-pentadienoate, **14**, was prepared using the procedure of Rehberg (37). The properties of the ester are as follows: bp 78°C at 0.5 Torr (1 Torr = 133.3 Pa); ^{1}H NMR δ: 1.80 (3H, d, Me), 3.6 and 4.4 (each 2H, t, CH_2), 7.3 (6H, m, vinyl H); MS (*m/e*): M^+ obsd.: 217.9947; M^+ calcd.: 217.9942.

Preparation of cations

2-Phenyl-1,3-dioxolan-2-ylium trifluoromethanesulfonate, **6**, was prepared by reaction of **10** with triflic anhydride. The solid obtained was recrystallized from CH_3CN/ether mixtures at −15°C to give crystals suitable for X-ray diffraction studies.

2-(Methoxyphenyl)-1,3-dioxolan-2-ylium hexafluoroantimonate, 7, and 2-(2,4-pentadienyl)-1,3-dioxolan-2-ylium hexafluoroantimonate, **8**, were prepared from **11** and **12**, respectively, by use of the method of Meerwein (4). The products were recrystallized from CH_3CN/ether mixtures at −15°C to give crystalline samples suitable for X-ray diffraction studies. The ^{1}H NMR spectrum of **8** in CD_2Cl_2 consisted of peaks at δ 2.1 (3H, m, CH_3), 5.59 (4H, s, CH_2), 7.7–8.3 (4H, m, vinyl H).

2-(4-Methoxyphenyl)-4,4-dimethyl-1,3-dioxolan-2-ylium hexafluoroantimonate, **9**, was prepared by treating **14** (0.41 g) dissolved in CH_2Cl_2 (4 mL), contained in a Schlenck tube under N_2 and cooled to −78°C, with a cooled mixture of $HSbF_6$ (157 μL) in CH_2Cl_2 (2 mL). The tube and its contents were shaken vigorously and left at −78°C for 1.5 h. Dry ether (5 mL) was added to the solution, and the tube was tightly sealed and stored in a freezer at −15°C. Crystallization ensued to yield colourless rectangular prisms suitable for X-ray diffraction.

Structure determinations

All crystals studied were handled under a dry nitrogen atmosphere at all times. Crystals chosen for study were mounted in Lindemann glass capillary tubes. In all cases Buerger-type precession photographs were used to determine potential space groups and to establish approximate unit cell dimensions before the crystals were transferred to the diffractometer. X-ray studies were carried out on Syntex $P2_1$ or Nicolet automatic diffractometers equipped with low-temperature apparatus. All measurements were made at −65°C with graphite monochromated Mo Kα radiation (λ = 0.71069 Å). Unit cell parameters were determined from a least-squares fit of χ, φ, and θ for 15 reflections. Intensities were measured with θ–2θ scans, and were corrected for Lorentz-polarization effects. Standard reflections were measured every 100 reflections collected. Methods of intensity measurement and initial data treatment have been described previously (39, 40). Corrections were not made for absorption. This will make maximum errors in F_o of 0.6%, **6**; 7.5%, **7**; 12.8%, **8**; 11.6%, **9**. The structure of **6** was solved by direct methods and those of **7**, **8**, and **9** by the Patterson method. All other atoms were located from differ-

[9] σ^+ values of alkoxy groups are −OMe, −0.76; OEt, −0.81; OPr^i, −0.85; OH, −0.92, ref. 34. No value for OBu^t seems to be available.

[10] The bond distances of the ester are derived from the analysis of Allen and Kirby (19).

Can. J. Chem. Downloaded from www.nrcresearchpress.com by 213.200.69.106 on 09/08/12
For personal use only.

ence syntheses. Full-matrix least-squares calculations minimized $\Sigma w(|F_o| - |F_c|)^2$ and were terminated when Δ/σ_{max} was less than 0.1. In general non-hydrogen atoms were given anisotropic temperature factors, except for the disordered fluorine atoms in **7** and C(2′), O(4′), C(7′) in **9**, which went non-positive definite, if attempts were made to refine the atoms anisotropically. Although the standard reflections indicated that **9** was reasonably stable in the X-ray beam, the crystal was not particularly well formed. A refinement of the occupancies of the disordered fluorine positions in **7** (F(1), F(2), F(3), F(4), F(11), F(21), F(31), F(41)) showed that the values were close to 0.5, so the occupancies were fixed at this value. For **6** and **7**, hydrogen atoms were located and refined with isotropic temperature factors. For **8**, hydrogen atoms were refined for one cycle with isotropic temperature factors, when they were located, but were not refined further. Few hydrogen atoms could be located for **9** so they were placed in calculated positions and were not refined. For **6**, **7**, and **8**, the structures were refined with the use of SHELX (41) on a VAX 6800 computer and used reflections with $I > 0$. The structure of **9** was solved with use of SHELXTL PC (42) on a LASER 386 micro-computer and used all reflections. For this structure reflections with $3\sigma_I \geq I \geq -3\sigma_I$ were treated by the method of French and Wilson (43). Higher R values were observed for **7** and **9**. This was partly caused by crystal imperfection, but in the latter case a contributing factor was that all reflections were used for structure refinement. The major peaks and valleys in the final difference maps for **7**, **8**, and **9** were all near the Sb atom. Cell diagrams for **6**, **7**, and **8** were prepared with use of SNOOPI (44). Scattering factor curves were taken from the *International tables* (45) and anomalous dispersion corrections were made to the curves for O, F, S, and Sb (46). Details of data acquistion and structure refinement are given in Table 6. The atomic positional coordinates are given in Tables 2–5.[11]

Acknowledgement

This work was supported by a grant from the Natural Sciences and Engineering Research Council of Canada and by IBM through a collaborative project with McMaster University.

1. U. Pinder, J. Müller, C. Flo, and H. Witzel. Chem. Soc. Rev. **16**, 75 (1987); H. Perst. *In* Oxonium ions in organic chemistry. Academic Press, New York. 1971; *In* Carbonium ions. Vol. V. *Edited by* G.A. Olah and P.v.R. Schleyer. Interscience, New York. 1961. Chap. 34.
2. S. Winstein and R.E. Buckles. J. Am. Chem. Soc. **64**, 2780 (1942).
3. R.U. Lemieux. Adv. Carbohydr. Chem. **9**, 1 (1954). E. Pascu. Adv. Carbohydr. Chem. **1**, 77 (1945).
4. H. Meerwein. Angew. Chem. **67**, 374 (1955). H. Meerwein and K. Wunderlich. Angew. Chem. **69**, 481 (1957).
5. C.B. Anderson, E.C. Friedrich, and S. Winstein. Tetrahedron Lett. 2037 (1963).
6. H. Hart and D.A. Tomalia. Tetrahedron Lett. 3383 (1966); 1347 (1967); D.A. Tomalia and H. Hart. Tetrahedron Lett. 3389 (1866).
7. H. Paulsen. Pure Appl. Chem. **41**, 69 (1975).
8. B. Capon, M.I. Dosunmu, and M. de N. de M. Sanchez. Adv. Phys. Org. Chem. **21**, 37 (1985).
9. S. Steenken and R.A. McClelland. J. Am. Chem. Soc. **111**, 4967 (1989).
10. R.A. McClelland and S. Steenken. J. Am. Chem. Soc. **110**, 5860 (1988).
11. C.U. Pittman, Jr., S.P. McManus, and J.W. Larsen. Chem. Rev. **72**, 357 (1972).
12. Y. Chiang, A.J. Kresge, P. Salomaa, and C.I. Young. J. Am. Chem. Soc. **96**, 4494 (1974).
13. M.R. Caira and J.E. de Wet. Acta Crystallogr. Sect. B: Struct. Crystallogr. Cryst. Chem. **B37**, 709 (1981).
14. H. Paulsen and R. Dammeyer. Chem. Ber. **106**, 2324 (1973).
15. H. Paulsen and R. Dammeyer. Chem. Ber. **109**, 1837 (1976).
16. H. Paulsen and R. Dammeyer. Chem. Ber. **109**, 605 (1976).
17. H. Paulsen and E. Schüttpelz. Chem. Ber. **112**, 3214 (1979).
18. C.U. Pittman, Jr., T.B. Patterson, Jr., and L.D. Kispert. J. Org. Chem. **38**, 471 (1973).
19. F.H. Allen and A.J. Kirby. J. Am. Chem. Soc. **106**, 6197 (1984).
20. H.B. Bürgi and J.D. Dunitz. Acc. Chem. Res. **16**, 153 (1983); H.B. Bürgi, J.D. Dunitz, and E.J. Shefter. J. Am. Chem. Soc. **95**, 5065 (1973); Acta Crystallogr. Sect. B: Struct. Crystallogr. Cryst. Chem. **B30**, 1517 (1974).
21. M.R. Edwards, P.G. Jones, and A.J. Kirby. J. Am. Chem. Soc. **108**, 7067 (1986).
22. J.W. Larsen and S. Ewing. J. Am. Chem. Soc. **93**, 5107 (1971); J.W. Larsen, S. Ewing, and M. Wynn. Tetrahedron Lett. 539 (1970).
23. C.U. Pittman, Jr. and S.P. McManus. Tetrahedron Lett. 339 (1969).
24. J.W. Larsen, P.A. Bouis, and C.A. Riddle. J. Org. Chem. **45**, 4969 (1980).
25. G. Scorrano and V. Lucchini. J. Org. Chem. **44**, 1726 (1979).
26. F.H. Allen, O. Kennard, D. Watson, L. Brammer, A.G. Orpen, and R. Taylor. J. Chem. Soc. Perkin Trans. 2, S1 (1987).
27. A. Bondi. J. Chem. Phys. **68**, 441 (1964).
28. C. Bleasedale, W. Clegg, S.B. Ellwood, and B.T. Golding. Acta Crystallogr. Sect. C: Cryst. Struct. Commun. **C47**, 550 (1991).
29. E.M. Arnett and T.C. Hofelich. J. Am. Chem. Soc. **105**, 2889 (1983).
30. R.A. Burt, C.A. Chambers, Y. Chiang, C.S. Hillock, A.J. Kresge, and J.W. Larsen. J. Org. Chem. **49**, 2622 (1984).
31. R.F. Childs, M.D. Kostyk, C.J.L. Lock, and M. Mahendran. Can. J. Chem. **69**, 2024 (1991).
32. F.H. Allen and A.J. Kirby. J. Am. Chem. Soc. **106**, 6197 (1984).
33. S. Furberg and O. Hassel. Acta Chem. Scand. **4**, 1584 (1950).
34. K.V. Seshadri and R. Ganesan. Tetrahedron, **28**, 3827 (1972); O. Exner. Correlation analysis in organic chemistry. *Edited by* N.B. Chapman and J. Shorter. Plenum Press, New York. 1978. Chap. 10.
35. A.D. Brown. Struct. Bonding Cryst. **2**, 1 (1981).
36. A.H. Forde-Moore. Org. Synth. **30**, 11 (1950).
37. C.E. Rehberg. Org. Synth. Coll. Vol. **3**, 146 (1955).
38. E.S. Blake. U.S. Patent 3,378,578. Apr. 1968; Chem. Abstr. **69**, S1849 (1968).
39. B. Lippert, C.J.L. Lock, B. Rosenberg, and M. Zvagulis. Inorg. Chem. **16**, 1525 (1977).
40. R.P. Hughes, N. Krishnamachari, C.J.L. Lock, J. Powell, and G. Turner. Inorg. Chem. **16**, 314 (1977).
41. G.M. Sheldrick. SHELX. Program for crystal structure determination. University of Cambridge, England. 1976.

[11]Tables of anisotropic temperature factors, bond distances and angles for the anions, hydrogen atom positional parameters, F_o and F_c, best planes, dihedral angles and torsional angles, and figures showing the packing of the compounds in the unit cells have been deposited. They may be purchased from: The Depository of Unpublished Data, Document Delivery, CISTI, National Research Council Canada, Ottawa, Canada K1A 0S2.

Tables of hydrogen atom parameters, bond lengths and angles for the anions, and packing diagrams for the cells have also been deposited with the Cambridge Crystallographic Data Centre and can be obtained on request from The Director, Cambridge Crystallographic Data Centre, University Chemical Laboratory, 12 Union Road, Cambridge CB2 1EZ, U.K.

Can. J. Chem. Downloaded from www.nrcresearchpress.com by 213.200.69.106 on 09/08/12
For personal use only.

42. G.M. Sheldrick. SHELXTL-Plus. Release 4.21/V. Siemens Analytical Instruments, Inc., Madison, Wis. 1990.
43. S. French and K. Wilson. Acta Crystallogr. Sect. A: Cryst. Phys. Diffr. Theor. Gen. Crystallogr. **A34**, 517 (1978).
44. K. Davies. CHEMGRAF Suite: Program SNOOPI, Chemical Design Ltd., Oxford. 1983.
45. D.T. Cromer and J.T. Waber. International tables for X-ray crystallography. Vol. IV. *Edited by* J.A. Ibers and W.C. Hamilton. Kynoch Press, Birmingham. 1974. Table 2.2B, pp. 99–101.
46. D.T. Cromer and J.A. Ibers. International tables for X-ray crystallography. Vol. IV. *Edited by* J.A. Ibers and W.C. Hamilton. Kynoch Press, Birmingham. 1974. Table 2.3.1, pp. 149–150.

Can. J. Chem. Downloaded from www.nrcresearchpress.com by 213.200.69.106 on 09/08/12
For personal use only.

The photocycloaddition of dibenzoylmethanatoboron difluoride ($DBMBF_2$) with conjugated enones and en-esters

YUAN L. CHOW,[1] SHI-SEN WANG, AND XIAN-EN CHENG
Department of Chemistry, Simon Fraser University, Burnaby, B.C., Canada V5A 1S6

Received April 13, 1992

YUAN L. CHOW, SHI-SEN WANG, and XIAN-EN CHENG. Can. J. Chem. **71**, 846 (1993).

Dibenzoylmethanatoboron difluoride ($DBMBF_2$), the BF_2 complex of dibenzoylmethane, reacted from its singlet excited state with α,β-unsaturated ketones and esters to give 1,5-diketones by a [2+2] cycloaddition and ring-opening sequence in an analogous pathway to that observed in the photocycloaddition to olefins and dienes. The present photoreaction is unexpected since conjugated enones and en-esters are poor electron donors to comply with the previously proposed charge transfer requirement in $DBMBF_2$ photoreactions. The photocycloaddition to these substrates was highly regioselective and stereoselective, giving the head-to-head orientation, which could be enhanced by α-methyl substitution; β-methyl substitution increased the alternate head-to-tail orientation. The photolysis of a mixture of $DBMBF_2$ and a cyclic enone also caused the latter to dimerize to give head-to-head and head-to-tail dimers in significant yields. These photodimerizations were apparently caused by $DBMBF_2$ sensitization. The mechanism of the sensitization is discussed.

YUAN L. CHOW, SHI-SEN WANG et XIAN-EN CHENG. Can. J. Chem. **71**, 846 (1993).

Le difluorure de debenzoylméthanobore (BF_2DBM), le complexe du BF_3 avec le dibenzoylméthane, réagit avec les cétones et les esters α,β-insaturés par son état singulet et conduit à des 1,5-dicétones par une séquence d'une cycloaddition [2+2] et d'une ouverture de cycle semblable à celle observée lors de sa photocycloaddition sur des oléfines et des dienes. La photoréaction observée ici est inattendue puisque les énones et les esters conjugués sont des mauvais donneurs d'électrons qui ne peuvent que difficilement se plier aux exigences proposées antérieurement suggérant des transferts de charge pour les photoréactions impliquant le BF_2DBM. La photocycloaddition de ces substrats est hautement régiosélective et stéréosélective; elle conduit à une orientation tête-à-tête qui pourrait être améliorée par une substitution par un méthyle en α alors qu'une substitution par un méthyle en β augmente l'orientation tête-à-queue. La photolyse d'un mélange de BF_2DBM et d'une énone cyclique provoque une dimérisation de cette dernière conduisant à des dimères tête-à-tête et tête-à-queue avec des rendements significatifs. Ces photodimérisations sont apparemment causées par une sensibilisation par le BF_2DBM. On discute du mécanisme de sensibilisation.

[Traduit par la rédaction]

Introduction

A variety of β-diketones react readily from their enol form with BF_3 etherate to give the tetracoordinate boron difluoride complexes (1–10) that show greatly enhanced absorbance without noticeably shifting the maxima (7, 10, 11), and that also show reduction potentials lower by 0.2 volt than the parent β-diketones (2). Using dibenzoylmethanatoboron difluoride($DBMBF_2$) as a model compound, we have shown that it interacts with various olefins from the lowest singlet excited state through exciplexes possessing different extents of electron transfer (12–14). The interaction with electron-rich conjugated dienes approaches the diffusion-controlled rate (12) and generates olefin cation radicals that undergo the typical dimerization and rearrangement reported previously (14). On the other hand, those reactions with simple olefins are slower, leading to [2+2] cycloaddition to give **1**, and subsequent rearrangement–hydrolysis to 1,5-diketones **2** in high quantum yields as shown in Scheme 1 (13). Mechanistic studies on these photocycloadditions were also described recently (13).

While the role of electron transfer controlling the [2+2] photocycloaddition to olefins and dienes was being investigated, we discovered that $DBMBF_2$ also undergoes photocycloaddition with α,β-unsaturated ketones and esters. Since these conjugated carbonyl compounds are poor electron donors, the inevitable conclusion is that electron transfer probably exerts feeble control over the cycloaddition with enones. This observation suggests that the generally accepted concept of exciplexes based on charge (or electron) transfer (15, 16) is no longer adequate to explain the driving force of the [2+2] photocycloaddition of $DBMBF_2$. In anticipation of further mechanistic studies, we describe the preparative aspects of photocycloaddition to conjugated enones and enesters. As these reactions are analogous to the de Mayo reation (17) and comprise a broad spectrum of synthetically useful photolytic cyclobutane formations (18), and the quantum efficiency of the product formation ranges from good to excellent under defined conditions, they merit detailed studies. The synthetic utility of this reaction was considerably enhanced when it was discovered that the BF_2 complexes derived from alkyl β-diketones also undergo efficient photocycloadditions with benzene derivatives (14).

Results

The photocycloaddition of $DBMBF_2$ with en-esters **3***a*–**3***c* and enones **3***d*–**3***f* was carried out under similar conditions to those described for similar reactions with simple olefins (13). Generally, $DBMBF_2$ (0.05 M) and a substrate (0.5 M) in acetonitrile were irradiated in a Rayonet photoreactor equipped with RPR 3500 lamps. The progress of the photoreactions was monitored by GC and (or) TLC analysis showing the disappearance of $DBMBF_2$ and reaching the maximum of the product yield after 1 h for methyl methacrylate, after about 2 h for *trans*-3-penten-2-one, and after 4 h for vinylmethyl ketone. For acyclic substrates, the reactivity is in the decreasing order: methyl methacrylate (**3***b*) > mesityl oxide (**3***f*) > *trans*-3-penten-2-one (**3***e*) > vinylmethyl ketone (**3***d*) > ethyl acrylate (**3***a*) > ethyl crotonate (**3***c*). For facile visualization of the sequence of the photocycloaddition, the possible orientation and mode of ring

[1]Author to whom correspondence may be addressed.

Can. J. Chem. Downloaded from www.nrcresearchpress.com by 213.200.69.106 on 09/08/12
For personal use only.

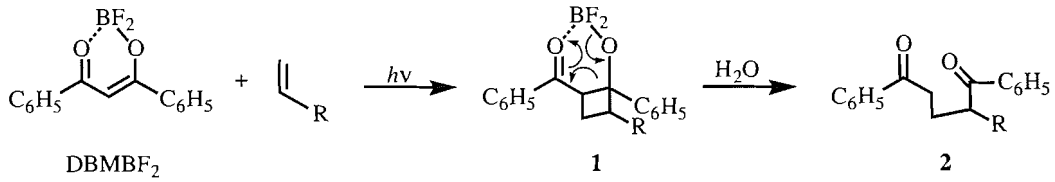

DBMBF$_2$ 1 2

SCHEME 1

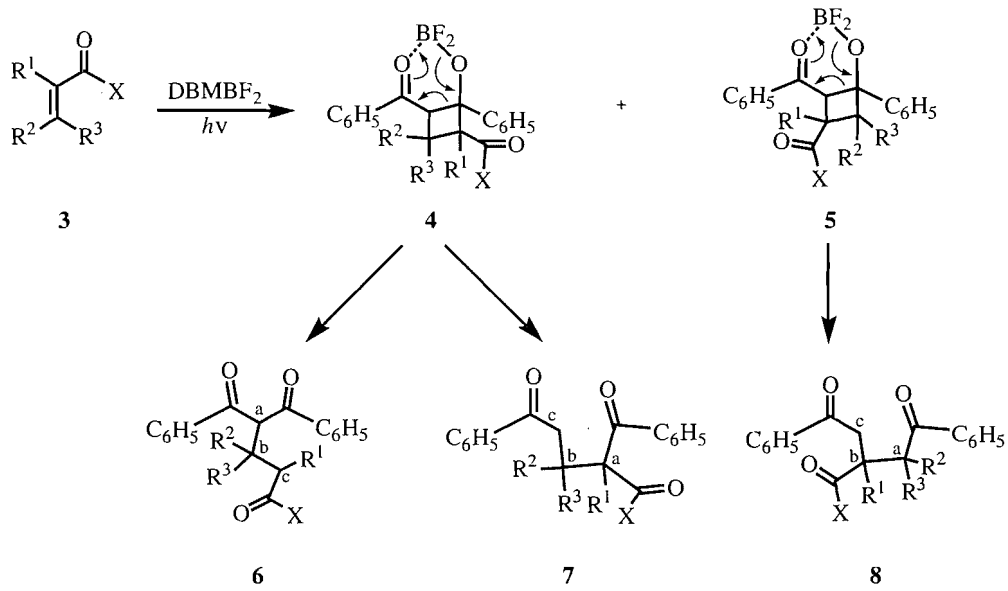

3 4 5

6 7 8

	R^1	R^2	R^3	X	Irradiation (h)	Products (yield %)	Quantum yield
3*a*	H	H	H	OEt	14	**7***a* (64%)	0.047
3*b*	CH_3	H	H	OCH_3	2	**7***b* (85%)	0.35
3*c*	H	CH_3	H	OEt	6	**7***c* (65%); **8***c* (16%)	0.027
3*d*	H	H	H	CH_3	7	**7***d* (43%); **6***d* (38%)	0.056
3*e*	H	CH_3	H	CH_3	5	**7***e* (34%); **6***e* (36%)	—
3*f*	H	CH_3	CH_3	CH_3	2	**7***f* (48%); **8***f* (3%) **9** (35%)	0.17

SCHEME 2

openings are shown in Scheme 2, which will be used for discussion later. The quantum yields were determined at [DBMBF$_2$] = 0.05 M and the concentration of substrates **3** at 0.5 M in acetonitrile (see Scheme 2). However, photolysis of dibenzoylmethane in the presence of one of these substrates failed to give the adducts.

The photolysis of DBMBF$_2$ in the presence of ethyl acrylate (**3***a*) and methyl methacrylate (**3***b*) gave one product in each case; **7***a* and **7***b* were isolated in excellent yields. These structures were shown to be **7**, which could be derived from the head-to-head (HH) adduct **4**, on the basis of the NMR coupling pattern of the methylene protons that exhibited magnetic non-equivalence of the geminate pairs. Compound **7***b*, which was isolated as a crystalline product, showed two groups of symmetrical multiplets at 2.48 and 2.98 ppm (2H each) that undoubtedly arose from the two adjacent groups of magnetically non-equivalent methylenes. It must be pointed out that if the product were **8***b*, the methylene protons should be a singlet. For **7***a*, the two corresponding methylene groups showed large geminal couplings owing to magnetic non-equivalence; even the CH_2 protons of the ethyl group are magnetically non-equivalent, showing two double quartets at 3.86 and 3.96 ppm. In addition, they show complimentary IR, ^{13}C NMR, and mass spectral data to support the proposed structures.

The photocycloaddition to ethyl *trans*-crotonate (**3***c*) gave a more complex product pattern than those shown above. It gave 16% of **8***c*, arising from alternative regioselective addition (head-to-tail, HT). The structural assignment was supported by appropriate spectral data in which neither methine proton was found below 4 ppm; i.e., none of them was connected directly to two neighboring carbonyl groups. Only one compound of **8***c* out of possible *threo* and *erythro* isomers was obtained, but its stereochemistry remained unknown. The major product was **7***c-erythro*; upon adsorption on silicic acid it slowly epimerized to give **7***c-threo*. By repeated preparative thin-layer chromatography both compounds could be isolated, but only as partially pure samples that were eventually used for spectroscopic examinations. The use of methyl *trans*-crotonate for photocycloaddition and similar chromatographic separation gave the corresponding *erythro* and *threo* samples. The NMR spectra of the dia-

Can. J. Chem. Downloaded from www.nrcresearchpress.com by 213.200.69.106 on 09/08/12
For personal use only.

Can. J. Chem. Downloaded from www.nrcresearchpress.com by 213.200.69.106 on 09/08/12
For personal use only.

stereoisomers of **7***c* show double doublets for the methylene protons at point c and a typical doublet at about the 4.5 ppm region for the methine proton at point a activated by two carbonyl groups. In agreement, the latter hydrogen was slowly exchanged in several days in $CDCl_3$-D_2O (1 drop) solution in the presence of a trace of pyridine. No other hydrogen was exchanged under the conditions. These data confirmed the structure but did not differentiate the stereochemistry. The assignment of *erythro* and *threo* configurations was derived from mechanistic consideration as discussed later.

The photocycloadditions of $DBMBF_2$ with vinylmethyl ketone (**3***d*) and *trans*-3-penten-2-one (**3***e*) were terminated on the consumption of $DBMBF_2$ and gave good yields of head-to-head adducts **7** and **6** as mixtures. However, photolysis of **7***d* and **7***e* in acetonitrile under similar irradiation conditions caused extensive decomposition without yielding **6***d* or **6***e*, respectively; such retroactive formations could be possible via a type II cyclobutane formation and the alternative ring opening. Owing to difficulties in obtaining pure **3***e* free of **3***f*, the photocycloaddition to **3***e* was plagued with unwanted side products; a detailed investigation was not continued. The structure of **6***d* was readily decided by well-defined ^1H NMR spectra; the lack of chiral centers gave a straightforward triplet, double triplet, and doublet for the proton at the points a, b, and c, respectively. For **7***d*, due to the presence of the chiral center at carbon a, the geminal protons in two methylene groups were magnetically nonequivalent, showing a big geminal coupling. The ^1H NMR spectra of **6***e* and **7***e* were more complex than those of **6***d* and **7***d*, but the chemical shifts for the methine proton vicinal to the two carbonyl groups were 5.74 and 4.66 ppm (both doublets), respectively, and very close to those corresponding doublets shown by **6***d* and **7***d* (5.57 and 4.42 ppm). In addition, **7***e* slowly epimerized in storage to give the other diastereoisomer in a similar pattern to that observed for **7***c*.

The photocycloaddition of $DBMBF_2$ in CH_3CN under nitrogen to mesityl oxide **3***f* showed a high quantum efficiency (ϕ = 0.17) to give **7***f* (48%) and furan **9** (35%), in addition to a small amount of **8***f* (3%) after 2 h irradiation. Extended irradiation beyond this point caused a slow decrease of **7***f* (to about 40% after 5 h, obviously arising from photodecomposition), and complete disappearance of **8***f* to give only **9**; the latter transformation was catalysed by a trace amount of HF generated in the system, but not due to irradiation. Because of its good quantum efficiency this reaction was used as a model to show the reaction profile. The photoreaction in CH_3CN under N_2 is shown in Fig. 1; under air, the formation rates slowed and caused slightly lower yields, but the general reaction pattern was not changed. In benzene and CH_2Cl_2 the photoreaction was faster, to reach the maximum amounts of **7***f* (31–35%) after 1.2–1.5 h irradiation; this decreased to 25% after 5 h; furan **9** gradually increased to 40–45% yields after 5 h irradiation. In tetrahydrofuran, the cyclization of **8***f* to **9** was slow, resulting in yields of 25 and 13%, respectively, in addition to 21% of **7***f* after irradiation for 5 h.

The furan **9** was readily identified from ^{13}C NMR spectra showing only one carbonyl carbon at 203.1 ppm and two α-carbons for a furan ring at 151.4 and 147.1 ppm (19). The IR absorption at 1673 cm^{-1} and the lack of alkyl hydrogens in ^1H NMR (except methyl singlets) support the furan structure derived from **8***f*. The structure of **8***f* was confirmed by the clearly defined ABX system in the ^1H NMR spectrum (see Table 1) and supported by pertinent IR and ^{13}C NMR data to show the presence of three carbonyl groups. An acid-catalysed cyclization of **8***f* to form furan **9** could be easily envisioned. The structure of **7***f* was readily concluded by an AB quartet and one hydrogen singlet (at 5.74 ppm) in the ^1H NMR spectrum in addition to the IR and ^{13}C NMR spectra. Although the chemical shift of the one-proton singlet is relatively deshielded, the compound is not **6***f* because of magnetic non-equivalence of the two *geminal* dimethyl groups, and also because of the mass spectral fragmentation patterns (see below). In some cases when the photoreaction was run in CH_3CN, an additional small GC peak (triketone **6***f*) was observed in a chromatographic fraction; the GC–MS of this extra peak showed the compound to possess, by either EI or CI modes, a strong fragment *m/e* 224 common to **6***d*, **6***e*, and **6***f*. This peak must arise from a McLafferty rearrangement in all compounds **6** to give a dibenzoylmethane cation radical, which was not present and could not be formed from any of the compounds **7** or **8**.

The photocycloaddition of $DBMBF_2$ to cyclic enones **10** in CH_3CN solution was relatively fast with 2-cyclooctenone (**10***i*), but became more inefficient with 2-cyclohexenone (**10***h*) and 2-cyclopentenone (**10***g*), in that order. The reactions afforded the dimers **12** as well as the cycloadducts **11** of these cyclic enones as shown by GC–MS analysis of the crude products. Under comparable conditions of

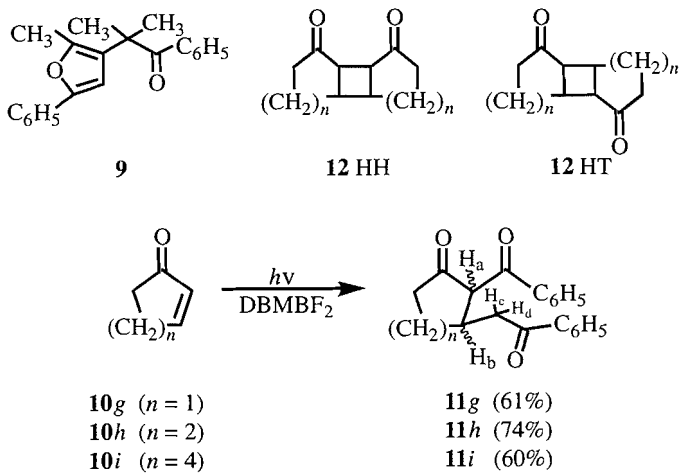

10*g* (*n* = 1) **11***g* (61%)
10*h* (*n* = 2) **11***h* (74%)
10*i* (*n* = 4) **11***i* (60%)

[$DBMBF_2$] = 0.05 M and [enone] = 0.5 M in CH_3CN, the mole ratio of dimers **12** to adducts **11** were 1:4 for **10***g*, 29:71 for **10***h*, and 74:26 for **10***i*. For each cyclic enone, the dimers were mixtures of four possible isomers, showing two major peaks in GC analysis; for the case **10***h*, two additional minor peaks close to the major ones were also detected. The dimers from **10***g* and **10***h* were also prepared by direct photolysis to give these major peaks (20, 21); one peak represented the head-to-tail cycloadduct and the other the head-to-head cycloadduct. The ratios of (head-to-head):(head-to-tail) from $DBMBF_2$ sensitization and direct photolysis were not significantly different; 66:34 against 63:37 for cyclohexenone (**10***h*), and 46:54 against 41:59 for cyclopentenone (**10***g*). However, direct irradiation of 2-cyclooctenone (**10***i*) in CH_3CN under comparable conditions gave an intractable complex mixture in which the reported (22) dimers were swamped by other products. As expected, the rates of dimer formation compared to those of cycload-

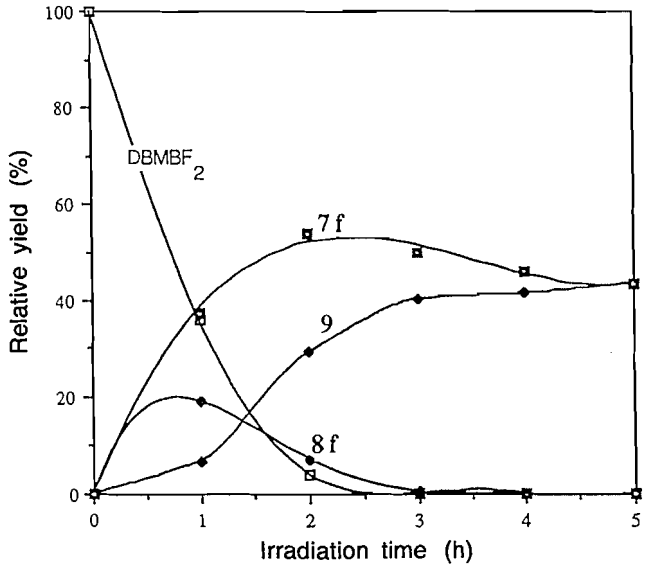

FIG. 1. The formation profile of the photoaddition of $DBMBF_2$ (0.05 M) with mesityl oxide (0.5 M) in CH_3CN; the yields were calculated against the internal standard.

ducts **11** rapidly increased with higher concentrations of cyclic enones **10** at a fixed concentration of [$DBMBF_2$]; for example, the percentage of **12** increased from 26 to 75% (of consumed **10***h*) when cyclohexenone **10***h* changed from 0.5 M to 3.0 M at [$DBMBF_2$] = 0.03 M.

In the photoreactions, only one cycloadduct was formed and isomerized to the other during isolation. The primary cycloadduct was the *cis* isomer of **11**, which was isomerized to *trans*-**11** during photolysis and isolation. In the $DBMBF_2$ photocycloaddition to 2-cyclohexenone **10***h*, GC and TLC analysis showed the formation of *cis*-**11***h*, which isomerized only slowly to form a trace of *trans*-**11***h*. The isomerization was rapid under alkaline conditions on addition of $NaHCO_3$ solution; the process afforded *trans*-**11***h*, which showed H_a at 4.51 ppm with J_{ab} = 9.2 Hz supporting the *trans* configuration. The remaining *cis*-**11***h* was isolated as a mixture, and showed the corresponding H_a chemical shift at 4.86 ppm with J_{ab} = 4.9 Hz. In the photocycloaddition to 2-cyclopentenone, the primary adduct isomerized more rapidly during photolysis, which showed slightly acidic conditions. As the photoreaction was slow, isomerized secondary product accumulated to be isolated as the major product, which showed H_a at 4.21 ppm with J_{ab}=10.0 Hz; this was assigned as *trans*-**11***g*. A small amount of the primary product (*cis*-**11***g*) was isolated as a mixture to give the chemical shift of H_a at 4.76 (d) with J_{ab} = 7.7 Hz. The coupling constants of the *cis*-**11***g* stereoisomer were very close to that of *cis*-1-benzoyl-2-phenacylcyclopentane (6.8 Hz) (14). On the other hand, J_{ab} of *trans*-**11***g* was close to that calculated for the corresponding *trans* isomer (11.9 Hz)(14). These agreements serve to support the stereochemical assignment for the two products.

The photocycloaddition of $DBMBF_2$ to 2-cyclooctenone was relatively fast, yielding, in addition to dimers **12***i*, only *cis*-**11***i*, but showed a trace of *trans*-**11***i* in the TLC analysis at the end of reaction (4 h). The addition of aqueous $NaHCO_3$ solution and work-up caused partial isomerization to *trans*-**11***i*. Both isomers were isolated by preparative TLC to give samples each contaminated by the other. In $CDCl_3$ solution, *cis*-**11***i* slowly transformed to *trans*-**11***i*, which showed H_a at 4.88 ppm (d) with J_{ab} = 11.0 Hz; the corresponding parameters for *cis*-**11***i* were H_a at 4.93 ppm (d) with J_{ab} = 3.6 Hz. The *J* values not only were close to the observed *J* value of 4.2 Hz for *trans*-1-benzoyl-2-phenacylcyclooctane, but also agreed well with the calculated values for the corresponding *cis* and *trans* isomers at 11.8 and 5.5 Hz respectively (14). In addition, all of these cycloadducts **11** exhibited the complementary IR and ^{13}C NMR data to show the presence of three carbonyl groups, and ^1H NMR signals of two double doublets for the magnetically nonequivalent geminal methylene group in the phenacyl moiety. It should be added that the chemical shifts of H_a were <5.00 ppm; this, combined with the observation of double doublets assigned to the methylene group of the phenacyl moiety, provided evidence to eliminate the structures corresponding to **6** and **8** for these cycloadducts.

Discussion

The product pattern of the $DBMBF_2$ photoadditions to α,β-unsaturated carbonyl compounds follows the basic pattern observed for similar photoadditions to simple olefins (14), but exhibits more complexity with respect to regioselectivity and side reactions owing to the presence of a carbonyl group. This is shown in the formation of compounds **8***c* and **8***f* arising from head-to-tail cycloadduct **5**, and the formation of **6***d*, **6***e*, and **6***f* arising from a side reaction. The photocycloaddition to cyclic enones is regioselective and stereoselective to give only one adduct, the *cis* adduct of **11**, which isomerizes through facile enolization to give the *trans* adduct of **11**. Though the proofs of the *cis–trans* configuration in **11***g* and **11***i* are not unequivocal, the pattern of the formation leaves no doubt that one compound is stereospecifically formed; in view of the fact that the cyclobutane intermediate **4** imposes a steric constraint, it is most likely that *cis* adducts of **11** are formed. In the case of the cycloaddition to 2-cyclohexenone, GC and TLC analysis at various intervals coupled with ^1H NMR analysis of stereochemistry confirm this sequence. As this reaction sequence is also followed in the cycloaddition to other cyclic olefins (14), the conclusion of a highly stereoselective $DBMBF_2$ cycloaddition is established. The allied cycloaddition to acyclic compounds **3** must be equally stereoselective. Although the *erythro* and *threo* configuration of **7***c* have not been experimentally proven, the pattern of the formation of the single product and the subsequent isomerization agree with the mechanistic conclusion. The primary cycloadduct from *trans*-crotonates must be an enantiomeric pair of (*RS–SR*) configuration, that is, **7***c-erythro*, which is isomerized to the *RR–SS* pair (**7***c-threo*). Owing to the slow but spontaneous epimerization at the doubly activated carbon centers in **6** and **7**, these products could not be obtained in a pure state; some elemental analyses have been carried out with mixtures of diastereoisomers.

The regioselectivity in the $DBMBF_2$ cycloaddition is clean with cyclic enones and is shown as head-to-head in our description. This regioselectivity also prevails with **3***a*, **3***b*, and **3***d* but starts to decline in the presence of a β-methyl substituent, as in **3***c*. With two β-methyl substituents, **3***f* gives substantial amounts of **8***f* in the final form of **9**; **8***e* is assumed to be formed from **3***e*, but this could not be substantiated due to experimental difficulties. It is clear that an α-methyl substitution enhances the head-to-head regiose-

Can. J. Chem. Downloaded from www.nrcresearchpress.com by 213.200.69.106 on 09/08/12
For personal use only.

TABLE 1. ^{1}H NMR parameters of the products

Compound	δ (ppm) and J (Hz)
6*d*[a,b]	1.54 (CH_3, s), 2.31 ($2H_c$, t), 2.04 ($2H_b$, td), 5.57 (H_a, t), 7.0–8.2 (10H, m). J_{ab} = 6.5, J_{bc} = 5.8
6*e*[a,b]	1.20 (CH_3, d), 1.59 (CH_3, s), 2.26 (H_c, dd), 2.70 ($H_{c'}$, dd), 3.26 (H_b, dddq), 5.74 (H_a, d), 6.94–8.20 (10H, m). J_{ab} = 6.7, $J_{cc'}$ = 18.0, J_{bc} = 6.3, $J_{bc'}$ = 6.0, $J_{a\,Me}$ = 6.9
7*a*[a]	0.81 (CH_3, t), 2.59 (H_b $H_{b'}$, m), 2.76 (H_c, ddd), 3.01 ($H_{c'}$, ddd), 3.86 and 3.96 (OCH_2, dq), 4.69 (H_a, dd), 7.0–8.25 (10H, m). J_{ab} = $J_{ab'}$ = 7.1, J_{cb} = $J_{c'b}$ = 6.1, $J_{b'c}$ = $J_{b'c'}$ = 6.8, $J_{cc'}$ = 18.0, J_{gem} = 10.5 and J_{vic} = 6.6 (for Et)
7*b*	1.60 (CH_3, s), 2.47 (H_b, $H_{b'}$, m), 2.98 (H_c, $H_{c'}$, m), 3.63 (CH_3, s), 7.30–8.0 (10H, m)
7*c-erythro*[b,c]	1.12 (CH_3, d), 1.15 (CH_3, t), 2.85 (H_c, dd), 3.13 (H_b, m), 3.35 ($H_{c'}$, dd), 4.13 (-OCH_2-, m),4.56 (H_a, d), 7.3–8.1 (10H, m). J_{ab} = 7.2, J_{cb} = 7.7, $J_{cc'}$ = 16.6, $J_{c'b}$ = 5.5, $J_{Me\,b}$ = 7.0
7*c-threo*[b,c]	1.07 (CH_3, d), 1.17 (CH_3, t), 2.96 (H_c, dd), 3.13 (H_b, m), 3.31 ($H_{c'}$, dd), 4.13 (-OCH_2-, m), 4.52 (H_a, d), 7.3–8.1 (10H, m). J_{ab} = 7.6, J_{cb} = 9.0, $J_{cc'}$ = 16.3, $J_{c'b}$ = 3.9, $J_{Me\,b}$ = 6.8
7*d*[a]	1.81 (CH_3, s), 2.37 (H_b, dddd), 2.44 ($H_{b'}$, dddd), 2.64 (H_c, ddd), 2.89 ($H_{c'}$, ddd), 4.42 (H_a, dd), 7.0–8.2 (10H, m). J_{ab} = $J_{ab'}$ = 6.8 $J_{cc'}$ = 18.1, J_{cb} = $J_{cb'}$ = 6.5, $J_{c'b}$ = 7.3, $J_{c'b'}$ = 6.8 $J_{bb'}$ = 16.8
7*e*[a,b]	1.07 (CH_3, d), 1.78 (CH_3, s), 2.57 (H_c,dd), 3.23 ($H_{c'}$dd), 3.25 (H_b, m), 4.66 (H_a,d), 6.95–8.25 (10H, m). J_{ab} = 7.3, $J_{cc'}$ = 13.9, J_{cb} = 6.6, $J_{c'b}$ = 5.0, $J_{b\,Me}$ = 6.9
7*f*[a]	1.25 (CH_3, d), 1.49 (CH_3, s), 1.84 (CH_3, s), 2.96 (H_c, d), 3.63 ($H_{c'}$,d), 5.74 (H_a, s), 7.0–8.3 (10H, m). $J_{cc'}$ = 17.8
8*c*[a]	1.00 (CH_3, t), 1.20 (CH_3, d), 3.13 (H_c, dd), 3.56 ($H_{c'}$, dd), 3.82 (H_a, m), 3.87 (H_b, m), 4.0 (-CH_2O-, m), 7.0–8.0 (10H, m). $J_{a\,Me}$ = 6.8, J_{cb} = 4.2, $J_{c'b}$ = 8.5, $J_{cc'}$ = 17.5, J_{ab} = 14.5
8*f*[a]	1.30 (CH_3, s), 1.32 (CH_3, s), 2.30 (CH_3, s), 2.98 (H_c, dd), 3.61 ($H_{c'}$, dd), 4.25 (H_b, dd), 7.0–8.0 (10H, m). $J_{cc'}$ = 17.7, J_{bc} = 10, $J_{bc'}$ = 2.86
9[a]	1.60 ($2CH_3$, s), 1.98 (CH_3, s), 6.66 (1H, s), 7.0–8.1 (10H, m)
trans-**11***g*[d]	2.36–2.69 (-CH_2- of ring, m), 3.07 (H_d, dd), 3.24 (H_c, d), 3.48 (H_b, m), 4.21 (H_a, d), 7.30–8.00 (10H, m). J_{ab} = 10.0, J_{cb} = 5.7, J_{cd} = 16.3, J_{bd} = 7.9
trans-**11***h*[d]	1.60–2.20 (-CH_2- of ring, m), 2.50 (H_f, m), 2.60 (H_e, m), 2.80 (H_d, dd), 3.10 (H_b, m), 3.15 (H_c, dd), 4.51 (H_a, d), 7.0–8.0 (10H, m). J_{ab} = 9.2, J_{cd} = 17.3, J_{cb} = 4.5, J_{db} = 8.1
trans-**11***i*[e]	1.30–2.00 (-CH_2- of ring, m), 2.37 (H_f, m), 2.75 (H_d, dd), 2.85 (H_e, m), 3.06 (H_c, dd), 3.44 (H_b, m), 4.88 (H_a, d), 7.0–8.0 (10H, m). J_{ab} = 11.0, J_{cb} = 3.3, J_{cd} = 15.8, J_{db} = 9.1
cis-**11***i*[f]	1.40–2.23 (-CH_2- of ring, m), 2.40 (H_f, m), 2.90 (H_e, m), 2.95 (H_d, dd), 3.25 (H_c, dd), 3.45 (H_b, m), 4.93 (H_a, d), 7.0–8.0 (10H, m). J_{ab} = 3.6, J_{cb} = 7.2, J_{cd} = 17.8, J_{db} = 6.2

[a]These spectra were taken in C_6D_6, but others were in $CDCl_3$.
[b]The sample was a mixture containing other isomers (diastereoisomers).
[c]This sample contains the ratio **7***c-erythro*:**7***c-threo* of 3:1 as calculated on the NMR signal of H_a.
[d]These samples contain *cis*-isomer (9–10%) as calculated on the NMR signal of H_a: its NMR parameters are *cis*-**11***g* doublet at 4.75 ppm, J_{ab} = 7.7 Hz, and *cis*-**11***h* doublet at 4.86 ppm, J_{ab} = 4.9 Hz.
[e]This sample contains a trace amount (<5%) of *cis*-**11***i*.
[f]This sample contains about 25% of *trans*-**11***i*.

lectivity **4**, while a β-methyl substitution does the opposite, facilitating the formation of **5**. At this stage the overall picture is too complex to rationalize the effects of a polar carbonyl group and a substituent toward the orientation. The answer appears to be hidden in the nature (polarity and (or) orbital interactions) of the exciplex formed from singlet excited $DBMBF_2$; this should be the direction of future efforts. The isolation of small amounts of **6** in the photocycloaddition to enones **3***d*–**3***f*, but not to en-esters **3***a*–**3***c*, must mean that the intermediate **4** (head-to-head adduct), can ring-open in the alternative mode to give **6***d*–**6***f* even if the BF_2 group still maintains the binding to the original benzoyl oxygen. This indicates that a carbonyl group is a better electron sink than an ester group.

During photoreaction, the formation of cyclic enone dimers **12** is unexpected and must mean sensitization of enones **10** through excitation transfer to generate *a reactive state*. Although enone **10***h* at 0.5 M also can dimerize under the photolytic conditions (20, 21), $DBMBF_2$ possesses a high molar extinction coeficient (ϵ = 40 000) and absorbs >99% of the light intensity at 350 nm at the concentrations used in the photoreactions. In view of the fact that the dimerization of **10***h* could be caused by triplet sensitization (naphthalene triplet, E_T = 61 kcal/mol), to give about the same HH:HT ratio (21) as that obtained in the $DBMBF_2$ photolysis, there is no doubt that the same reactive state of **10***h* has been obtained by sensitization. The $DBMBF_2$ triplet energy has been determined to be 62 kcal/mol (11). There is a train of critical studies reported from various groups claiming that these enones have different reactive states for various photoreactions (22–27). For **10***i*, it is most likely that ground state *trans*-2-cyclooctenone is generated from $DBMBF_2$ sensitization and undergoes dimerization in analogy to the results from direct excitation (22), though direct photolysis in CH_3CN gave a complex mixture in our hands without giving a clean dimer mixtures of **12***i* as obtained by $DBMBF_2$

Can. J. Chem. Downloaded from www.nrcresearchpress.com by 213.200.69.106 on 09/08/12
For personal use only.

TABLE 2. ^{13}C NMR parameters[a]

Compound	δ (ppm)
6*d*[b]	207.11, 196.06, 136.77, 133.28, 128.99, 128.87, 55.48, 40.47, 29.27, 23.57
6*e*[b]	207.00, 195.97 (2C), 137.64, 137.16, 133.35, 133.17, 128.96 (3C), 128.70, 59.99, 47.54, 30.55, 29.76, 17.78
7*a*[b]	198.61, 195.19, 169.90, 137.24, 136.75, 133.36, 132.87, 129.00, 128.85, 128.61, 128.22, 61.12, 53.15, 35.74, 23.65, 13.82
7*b*	198.95, 197.08, 174.46, 136.68, 135.31, 133.04, 132.84, 128.60, 128.55, 128.48, 128.02, 56.24, 52.49, 33.57, 30.82, 21.57
7*c-erythro*[b]	198.61, 194.82, 169.10, 137.53, 137.17, 133.29, 132.81, 128.96, 128.84, 128.62, 128.40, 60.95, 58.27, 43.26, 30.04, 17.30, 13.84
7*c-threo*[b]	198.34, 194.82, 169.28, 137.63, 137.25, 133.20, 132.73, 128.84, 128.77, 128.62, 128.40, 61.07, 58.42, 42.70, 30.48, 18.39, 13.84
7*d*[b,c]	202.74, 198.65, 196.61, 137.29, 137.02, 133.45, 132.84, 129.06 (2C), 128.95, 128.61, 61.60, 35.77, 28.10, 22.30
7*f*[b]	202.65, 199.90, 198.08, 139.05, 138.52, 133.24, 132.75, 128.97 (2C), 128.82, 128.58, 64.82, 47.59, 37.19, 30.86, 27.45, 26.46
8*c*[b]	201.11, 197.28, 173.42, 136.90, 136.68, 132.65, 132.51, 128.54, 128.40, 128.29, 128.04, 60.35, 43.47, 42.00, 38.56, 15.04, 13.77
8*f*[b]	209.01, 206.80, 197.71, 138.51, 136.62, 132.75, 130.60, 128.40, 128.11, 127.98, 127.73, 52.23, 48.95, 38.40, 32.48, 24.40, 22.85
9	203.10, 151.40, 147.10, 136.0, 130.70, 131.93, 129.40, 128.60, 128.0, 127.0, 123.28, 125.6, 104.5, 45.21, 27.30, 12.70
trans-**11***g*	211.72, 198.44, 195.04, 136.95, 136.66, 133.42, 133.28, 129.44, 128.66, 128.54, 128.08, 63.26, 42.61, 38.90, 36.48, 26.94
trans-**11***h*	207.81, 198.60, 197.71, 137.31, 136.81, 133.32, 133.26, 128.68, 128.66, 128.49, 128.17, 63.31, 42.67, 41.75, 37.35, 28.94, 24.48
trans-**11***i*	210.45, 199.10, 195.51, 136.95, 136.87, 133.69, 133.08, 128.87, 128.80, 128.59, 128.16, 66.87, 43.11, 40.26, 35.38, 32.08, 26.78, 26.48, 24.04
cis-**11***i*	212.20, 199.54, 198.11, 138.30, 136.91, 135.15, 133.03, 128.66, 128.53, 127.97, 127.87, 60.30, 41.91, 41.53, 33.62, 32.45, 27.83, 27.23, 23.82

[a]The same samples as cited in Table 1 were used for measurement.
[b]These spectra were taken in C_6D_6, but others in $CDCl_3$.
[c]One signal was buried in the solvent peaks.

sensitization. It is speculated that *trans*-2-cyclooctenone, being a twisted ground state molecule (22), has a long lifetime, and can be photolysed to give other products. For **10***h* and 4,4-dimethyl-2-cyclohexenone, a twisted (or relaxed) state, either on the ground (26) or an excited state energy surface (25), has been suggested to undergo dimerization, cycloaddition, and rearrangement (23–27). It is reported that 2-cyclopentenone undergoes photodimerization from some kind of triplet state as concluded from laser photolysis (24). Since **10***g* does not twist easily, its spectroscopic triplet state has a relatively long lifetime (24, 25), but it is doubtful that this is the reactive state. Our results show that these reactive states of cyclic enones can be reached by $DBMBF_2$ sensitization.

As the lowest spectroscopic singlet and triplet states of **10***g* and **10***h* are 80–83 and 74(π,π^*) kcal/mol (20), respectively, sensitization to these states by $DBMBF_2$ is not likely. If a sensitization to a non-spectroscopic triplet state (with $E_T < 62$ kcal/mol) is accepted, a number of mechanistic possibilities can be considered. First of all, the concept of a non-vertical energy transfer (21) can be invoked to account for these $DBMBF_2$ sensitizations, though this explanation is close to an exercise in frustration as many factors remain unknown. Secondly, Hammond's group (21) has reported that at higher concentrations of **10***h* (>0.01 M) the absorption spectra do not follow Beer's law, but show the molar extinction coefficient rising at about 0.01–0.1 M. We have observed that at [**10***h*] up to 0.5 M, the absorption can be red-shifted to show the cutoff of absorption at 380 nm. The absorption at these high wavelengths may be attributed to aggregates that undoubtedly can be sensitized to the excimer (of **10***h*) whose triplet energy must be lower than that of **10***h*; about 62 kcal/mol may be regarded as a reasonable triplet energy of the excimer that can transform to the dimer. The lack of phosphorescence from these cyclic enones prevents us from confirming this idea. However, the presence of molecular aggregate in the ground state of **10***h* has been shown to be questionable when the absorption spectra at 0.01–0.3 M were examined with 1-cm and 0.1-cm UV cells.[2] The absorbance follows Beer's law. The result reported by Hammond's group may have been caused by either a wide slit opening or stray light in their spectrophotometer.[2]

Thirdly, we may assume a kind of exciplex formation be-

[2]C. I. Johansson, Simon Fraser University, unpublished results.

Can. J. Chem. Downloaded from www.nrcresearchpress.com by 213.200.69.106 on 09/08/12
For personal use only.

TABLE 3. IR data[a]

Compound	ν (cm^{-1}) in neat film[a]
6*d*	3089, 2960, 1710, 1700, 1674, 1603, 1590, 1550, 1457, 1374, 1300, 1255, 1220, 1189, 1171, 1054, 1011, 946, 768, 702, 654, 611
6*e*	3076, 2980, 2948, 2892, 1715, 1700, 1673, 1602, 1587, 1454, 1360, 1270, 1208, 1189, 1009, 950, 768, 717, 702
7*a*	3080, 2998, 2954, 2921, 1740, 1690, 1605, 1589, 1457, 1377, 1270, 1230, 1165, 1030, 1011, 986, 760, 703
7*b*[b]	2990, 2940, 1730, 1683, 1596, 1579, 1450, 1369, 1296, 1269, 1240, 1267, 1198, 1175, 1102, 1005, 970, 753, 715, 700
7*c*	3060, 2980, 2940, 1725, 1682, 1597, 1582, 1466, 1450, 1363, 1320, 1220, 1186, 1103, 1036, 1006, 976, 760, 698
7*d*	3074, 2946, 1738, 1695, 1680, 1603, 1588, 1484, 1361, 1225, 1189, 1166, 1010, 981, 766, 740, 702
7*e*	3080, 2992, 2950, 2898, 1720, 1685, 1606, 1589, 1457, 1368, 1278, 1223, 1190, 1011, 993, 950, 768, 704
7*f*	3074, 2980, 2946, 1715, 1700, 1674, 1602, 1574, 1454, 1360, 1270, 1208, 1188, 1009, 950, 768, 717, 703, 672
8*c*	3060, 2980, 2940, 1722, 1682, 1597, 1580, 1451, 1365, 1305, 1268, 1265, 1185, 1035, 1004, 974, 764, 699
8*f*	3058, 2972, 2932, 1704, 1677, 1594, 1577, 1540, 1463, 1443, 1355, 1245, 1220, 1168, 971, 753, 700
9	3076, 2977, 2932, 1673, 1595, 1576, 1550, 1480, 1460, 1440, 1382, 1359, 1252, 1220, 1178, 1155, 1090, 974, 934, 804, 766, 727, 700, 670
trans-**11***g*[c]	3061, 2961, 2905, 1742, 1680, 1596, 1580, 1448, 1405, 1374, 1340, 1273, 1228, 1206, 1182, 1135, 1074, 1001, 915, 883, 843, 782, 754, 690
trans-**11***h*[c]	3061, 2941, 2868, 1711, 1681, 1597, 1581, 1507, 1480, 1448, 1408, 1352, 1289, 1241, 1181, 1160, 1110, 1076, 1048, 1001, 753, 690
trans-**11***i*[c]	3062, 2931, 2859, 1704, 1680, 1596, 1580, 1447, 1410, 1322, 1269, 1242, 1209, 1181, 1125, 1078, 1002, 971, 760, 690

[a]The same samples as cited in Table 1 were used for measurements.
[b]The sample was prepared as a KBr pellet for measurement.
[c]The samples were prepared as a liquid film on NaCl plate by evaporation of their $CDCl_3$ solution.

Can. J. Chem. Downloaded from www.nrcresearchpress.com by 213.200.69.106 on 09/08/12
For personal use only.

tween enone **10** and singlet excited state $DBMBF_2$ through a combined driving force of charge transfer and exciton resonance.[2] Such a singlet state exciplex may be transformed to a triplet state exciplex and finally dissociated to a *relaxed* triplet state of **10** and $DBMBF_2$. This idea may be regarded as an elaboration of the first non-vertical energy transfer. Whatever the explanation, it is in general agreement with the higher yield ratio of dimers **12** to cycloadducts **11** at higher concentrations of enones **10**; i.e., cycloadduct **11***h* is formed in much higher percentages at lower concentrations of **10***h*. Such a photodimerization is characteristic of a cyclic enone and has never been reported from acyclic α,β-unsaturated carbonyls **3***a*–**3***f*, which fact may also support the concept of strained twisted enone precursors (22); such precursors from **3***a*–**3***f* would be rapidly nullified by the rotation of the carbonyl group around the α C—CO bond. This study has clarified the product patterns and stereoselectivity of the photocycloaddition to α,β-unsaturated carbonyl compounds. We intend to investigate the reaction mechanism in the future.

Experimental section

Material and general conditions

Commercially available enones and en-esters were purified and their IR and NMR spectra were compared with the reported spectra for authenticity. The samples were distilled before use. 2-Cyclooctenone was prepared from cyclooctanone by the published procedure (28). $DBMBF_2$ (mp 192–194°C) was prepared in the previous experiment (13, 14). Other experimental conditions, analytical procedures, and instrumentations were the same as those reported in refs. 13 and 14.

Photocycloaddition to acyclic α,β-unsaturated carbonyl compounds

A CH_3CN solution (15 mL) containing $DBMBF_2$ (0.75 mmol, 0.05 M) and a freshly distilled enone (7.5 mmol, 0.5 M) was distributed in three Pyrex tubes (100 mm × 13 mm), and was purged using N_2. These tubes were irradiated with RPR 3500 Å lamps. The photolysate was analysed by GC and (or) TLC to show the formation of the products and the consumption of $DBMBF_2$. The photolysis was stopped after the disappearance of $DBMBF_2$. To the photolysate, a calculated amount of n-$C_{20}H_{42}$ (Internal standard) was added for GC analysis.

For work-up of the photolysate, ether (20 mL) was added and the total solution was washed with aqueous $NaHCO_3$ (10%) solution three times. The crude product was chromatographed on a silica gel column using hexane–CH_3CO_2Et eluent; this afforded fractions containing various proportions of products. Column chromatography or preparative thin-layer chromatography can be repeated with certain fractions to afford analytical samples. The spectral data of the products are given in Tables 1–4 and the elemental anlysis data in Table 5.

To acrylates

The adduct **7***a* was obtained as an oil from column chromatography, and was distilled. The adduct **7***b* was recrystallized from ethyl acetate – hexane to afford white crystals, mp 113.5–113.8°C. The percentage yields of the products from **3***a*, **3***b*, **3***d*, and **3***e* were those isolated, and others were from GC determinations.

To trans*-ethyl crotonate (***3***c)*

During photoaddition, TLC analysis on silica plates (Merck Kieselgel, 60 F254) showed two spots at R_f 0.13 and 0.082 (hex-

TABLE 4. GC–MS data

Compound	Mode	*m/e* (%)
6*d*	EI	294 (M^+, 4), 276 (22), 236 (45), 224 (46), 189 (68), 172 (18), 105 (100), 77 (74)
	CI	295 (M + 1, 100), 225 (25), 173 (14)
6*e*	EI	290 ($M^+ - H_2O$, 8), 250 (10), 224 (35), 203 (18), 186 (37), 171 (35), 105 (100), 77 (50)
	CI	309 (M + 1, 42), 225 (100)
7*a*	EI	324 (M^+, 3), 306 (3), 279 (25), 250 (21), 216 (8), 105 (100), 77 (32)
	CI	325 (M + 1, 100), 279 (21), 193 (20)
7*b*	EI	324 M^+, 1), 293 (1), 264 (45), 224 (51), 219 (24), 160 (10), 105 (B, 100), 77 (35)
	CI	326 (M + 2), 20), 325 (M+1, 100), 193 (70), 133 (57), 105 (53)
7*c*	EI	338 (M^+, 2), 320 (5), 305(3), 293 (55), 277 (14), 264 (31), 247 (26), 233 (59), 219 (67), 192 (21), 173 (10), 147 (6), 105 (100), 77 (33)
7*d*	EI	294 (M^+, 4), 276 (22), 251 (66), 234 (61), 189 (77), 105 (100), 77(60)
	CI	295 (M + 1, 100), 163 (75)
7*e*	EI	290 ($M^+ - H_2O$, 20), 265 (32), 203 (26), 189 (44), 162 (58), 105 (100), 77 (52)
	CI	309 (M + 1, 33), 163 (68), 147 (100)
7*f*	EI	304 ($M^+ - H_2O$, 4), 203 (22), 161 (25), 105 (100), 77 (62)
	CI	323 (M + 1, 20), 161 (100)
8*c*	CI	339 (M^+ 1, 15), 321, (M−18, 25), 293 (100), 161 (14), 159 (15), 135 (54), 121 (25), 107 (25), 105 (63)
8*f*	EI	322 (M^+, 2), 304 (M − 18, 2), 217 (8), 175 (11), 105 (B, 100), 77 (40)
	CI	323 (M + 1, 10), 305 (95), 177 (63), 175 (55), 149 (100), 147 (40)
9	EI	304 (M^+, 6), 199 (B, 100), 105 (20), 77 (25)
	CI	306 (M + 2, 21), 305 (M + 1, 100)
trans-**11***g*	EI	306 (M^+, 20), 288 (23), 260 (10), 201 (16), 186 (31), 185 (15), 105 (100), 77 (52)
trans-**11***h*	EI	320 (M^+, 4), 302 (50), 215 (32), 201 (35), 105 (100), 77 (40)
	CI	321 (M + 1, 100), 201 (70)
trans-**11***i*	EI	348 (M^+, 10), 330 (50), 320 (25), 302 (20), 243 (35), 229 (61), 201 (95), 120 (33), 105 (100), 77 (60)
cis-**11***i*	EI	348 (M^+, 10), 330 (48), 320 (23), 302 (17), 243 (54), 229 (46), 201 (90), 120 (30), 105 (100), 77 (50)

TABLE 5. Elemental analyses

Compound	Molecular formulae	%	C	H
7*b*[a,b]	$C_{20}H_{20}O_4$	Calcd.	74.07	6.17
		Found	74.07	6.18
7*c*	$C_{21}H_{22}O_4$	Calcd.	74.56	6.51
		Found	74.42	6.57
7*d*[a]	$C_{19}H_{18}O_3$	Calcd.	77.55	6.12
		Found	77.64	6.23
7*f*[a]	$C_{21}H_{22}O_3$	Calcd.	78.26	6.83
		Found	78.58	6.93
8*f*	$C_{21}H_{22}O_3$	Calcd.	78.26	6.83
		Found	77.99	6.86
9[a]	$C_{21}H_{20}O_2$	Calcd.	82.89	6.58
		Found	82.74	6.46
11*g*	$C_{20}H_{18}O_3$	Calcd.	78.43	5.88
		Found	78.30	6.02
11*h*	$C_{21}H_{20}O_3$	Calcd.	78.75	6.25
		Found	78.08	6.17

[a]These compounds were obtained as pure samples as shown by GC, others were mixtures as indicated in the footnotes to Table 1.

[b]Crystals were obtained from the recrystallization of ethyl acetate – hexane (1:8), mp 113.5–113.8°C.

ane:Et_2O = 6:1). During chromatography a new spot was developed at R_f 0.11 at the cost of the R_f 0.13 spot. Repeated column chromatography gave an analytical sample with the ratio of R_f 0.13:R_f 0.11 of 3:1, and another with R_f 0.11 as the major portion.

Photocycloaddition to cyclic enones

CH_3CN solutions containing $DBMBF_2$ (0.5 M) and a cyclic enone (0.1–0.07 M) were distributed in several tubes and photolysed similarly under N_2. During photolysis, GC analysis showed the formation of only one product from **10***h* and **10***i*, but the initial product from **10***g* isomerized to the second one in slow photolysis. When $DBMBF_2$ was consumed the photolysate was diluted with ether and washed with aqueous $NaHCO_3$ solution (10%). The crude product showed, by TLC analysis, that the secondary products increased considerably during $NaHCO_3$ solution washing, as well as in the subsequent column chromatography. Column chromatography of the crude products from **10***g* and **10***h* gave only the secondary product as the major product; the original product became the minor product.

The crude product from **10***i* showed two TLC spots with hexane:CH_3CO_2Et 5:1 at R_f 0.25 and R_f 0.31 for *cis*-**11***i* (the original compound formed) and *trans*-**11***i* (isomerized); the R_f 0.31 spot was faint at the end of the photolysis but became stronger after $NaHCO_3$ washings and kept growing during chromatography. This was treated with preparative thin-layer chromatography (Merck Kieselgel 60) to give a sample containing the ratio of *trans*-**11***i*:*cis*-**11***i* = 89:11; and another with a ratio of 25:75. In $CDCl_3$ solution the former sample changed to a ratio of *trans*-**11***i*:*cis*-**11***i* ≥ 95:5 in a few weeks and the latter sample to a ratio of 49:51.

Can. J. Chem. Downloaded from www.nrcresearchpress.com by 213.200.69.106 on 09/08/12
For personal use only.

Similarly, TLC analysis of photolysate 2-cyclohexenone (**10***h*) gave a strong spot at R_f 0.17 (for *cis*-**11***h*), but a barely noticeable one at R_f 0.13 (for *trans*-**11***h* with hexane:CH_2Cl_2:Et_2O = 3:0.8:0.2). After washing with aqueous $NaHCO_3$ solution, the TLC picture was completely reversed, giving a strong R_f 0.13 spot, with a weak R_f 0.17 spot. Column chromatography gave samples of *trans*-**11***h* contaminated with 5–10% of *cis*-**11***h*.

Acknowledgements

The authors are grateful for the generous financial support provided by the Natural Sciences and Engineering Research Council of Canada. We thank Mr. Carl Ingemar Johansson of this group for allowing us to cite the spectral study of 2-cyclohexenone before publication.[2]

1. N. M. D. Brown and P. Bladom. J. Chem. Soc. (A), 526 (1969).
2. L. H. Toporcer, R. E. Dessy, and I. E. Green. Inorg. Chem. **4**, 1649 (1965).
3. F. Umland, E. Hohaus, and K. Brodie. Chem. Ber. **106**, 2427 (1973).
4. H.-D. Ilge, D. Fabler, and H. Hartmann. Z. Chem. **24**, 218 (1984).
5. H.-D. Ilge, D. Fabler, and H. Hartmann. Z. Chem. **24**, 292 (1984).
6. H.-D. Ilge, E. Birckner, D. Fassler, M. V. Kozmenko, M. G. Kuz'min, and H. Hartmann. J. Photochem. **32**, 177 (1986).
7. H.-D. Ilge, E. Birckner, D. Fassler, M. V. Kozmenko, M. G. Kuz'min, and H. Hartmann. J. Photochem. **36**, 27 (1987).
8. V. E. Karasev and O. A. Korotkikh. Russ. J. Inorg. Chem. (Engl. Transl.), **30**, 1290 (1985).
9. V. E. Karasev and O. A. Korotkikh. Russ. J. Inorg. Chem. (Engl. Transl.), **31**, 493 (1986).
10. N. P. Shapkin, O. A. Korotkikh, and V. E. Karasev. Russ. J. Inorg. Chem. (Engl. Transl.), **30**, 1069 (1985).
11. Y. L. Chow, X. E. Cheng, and C. I. Johansson. J. Photochem. Photobiol. A: **51**, 247 (1990).
12. Y. L. Chow and X. E. Cheng. J. Chem. Soc. Chem. Commun. 1043 (1990).
13. Y. L. Chow and X. E. Cheng. Can. J. Chem. **69**, 1575 (1991).
14. (*a*) Y. L. Chow and X. E. Cheng. Can. J. Chem. **69**, 1331 (1991); (*b*) Y. L. Chow and X. X. Ouyang. Can. J. Chem. **69**, 423 (1991).
15. S. L. Mattes and S. Farid. Org. Photochem. **6**, 233 (1983).
16. (*a*) H. Knibbe, D. Rehm and A. Weller. Z. Phys. Chem. **56**, 95 (1967); (*b*) Ber. Bunsen-ges. Phys. Chem. **72**, 257 (1968); (*c*) D. Rehm and A. Weller. Isr. J. Chem. **8**, 259 (1970).
17. P. de Mayo. Acc. Chem. Res. **4**, 41 (1971).
18. (*a*) A. C. Weedon. *In* Synthetic organic photochemistry. *Edited by* W. M. Horspool. Plenum, New York. 1984. p. 61; (*b*) S. W. Baldwin. Org. Photochem. **5**, 123 (1981); (*c*) W. Oppolzer. Acc. Chem. Res. **15**, 135 (1982); (*d*) P. A. Wender. *In* Photochemistry in organic synthesis. *Edited by* J. D. Coyle. The Royal Society of Chemistry, London. 1986. Chap. 9.
19. R. M. Silverstein, G. C. Bassler and T. C. Morrill. Spectrometric identification of organic compounds. 5th ed. John Wiley, New York. 1991. Chaps. 1, 5.
20. P. J. Wagner and D. J. Bucheck. J. Am. Chem. Soc. **91**, 5090 (1969).
21. E. Y. Y. Lam, D. Valentine, and G. S. Hammond. J. Am. Chem. Soc. **39**, 3482 (1967).
22. P. E. Eaton and K. Lin. J. Am. Chem. Soc. **86**, 2087 (1964).
23. D. I. Schuster, M. M. Greenberg, I. M. Nunez, and P. C. Tucker, J. Org. Chem. **48**, 2615 (1983).
24. R. Bonneau. J. Am. Chem. Soc. **102**, 3816 (1980).
25. D. I. Schuster, R. Bonneau, D. A. Dunn, J. M. Rao, and J. Joussot-Dubien. J. Am. Chem. Soc. **106**, 2706 (1984).
26. D. I. Schuster, P. B. Brown, L. J. Capponi, C. A. Rhodes, J. C. Scaiano, P. C. Tucker, and D. Weir. J. Am. Chem. Soc. **109**, 2533 (1987).
27. D. I. Schuster, G. E. Heibel, P.B. Brown, N. J. Turro, and C. V. Kumar. J. Am. Chem. Soc. **110**, 8261 (1988).
28. E. N. Garbisch, Jr. J. Org. Chem. **30**, 2109 (1965).

Can. J. Chem. Downloaded from www.nrcresearchpress.com by 213.200.69.106 on 09/08/12
For personal use only.

2′-*O*-Methyl-*cis*-adenosine 3′,5′-cyclic methyl monophosphate, a new model system for cAMP. Aspects of structure and reactivity

NIEK L.H.L. BROEDERS,[1] ARTHUR P. VAN DER HEIDEN, AND LEO H. KOOLE[2]

Department of Organic Chemistry, Eindhoven University of Technology, P.O. Box 513, 5600 MB Eindhoven, The Netherlands

AND

JAN A. KANTERS AND ARIE SCHOUTEN

Department of Crystal and Structural Chemistry, Bijvoet Center for Biomolecular Research, University of Utrecht, Transitorium 3, Padualaan 8, 3584 CH Utrecht, The Netherlands

Received October 21, 1992

NIEK L.H.L. BROEDERS, ARTHUR P. VAN DER HEIDEN, LEO H. KOOLE, JAN A. KANTERS, and ARIE SCHOUTEN. Can. J. Chem. **71**, 855 (1993).

This study is focussed on 2′-*O*-methyl-*cis*-adenosine 3′,5′-cyclic methyl monophosphate (*cis*-**4**; *cis* describes the relationship between OMe (bound to phosphorus) and the adenine base), which is regarded a model for enzyme-bound cyclic adenosine monophosphate (cAMP). In this complex the negative phosphate charge is shielded in part via complexation with cationic sites on the enzyme surface. We report synthesis, crystal structure, solution conformation (400 MHz ^{1}H NMR), and kinetic-mechanistic aspects of the alkaline hydrolysis of *cis*-**4**. The methanol solvate of *cis*-**4** crystallizes in the orthorhombic space group $P2_12_12_1$ and the cell dimensions are a = 8.170(2) Å, b = 9.249(1) Å, c = 23.699(4) Å; V = 1788.5(6) Å^3; Z = 4 molecules per cell. Least-squares refinement converged at R = 0.062 for 2006 observed reflections. The adenine bases are linked via N6—H···N1 and N6—H···N7 hydrogen bonds in such a way that infinite one-dimensional chains are formed. This hydrogen bond scheme is very similar to that observed in the structure of 2′-deoxy-3′,5′-di-*O*-acetyl adenosine. An additional hydrogen bond is formed between methanol, incorporated in the crystal structure, and the adenine base. The conformational preferences of the *cis*-**4** dissolved in methanol have been determined with 400 MHz ^{1}H NMR. It is found that the conformations observed in the solid and solution states are practically the same. Hydrolysis of the title compound yields two acyclic phosphate diesters (a 3′- and a 5′-phosphate diester). The intermediates formed during the hydrolysis reaction are most likely five-coordinated phosphorus (P^V) compounds with a trigonal bipyramidal geometry and an equatorial-axial located 3′,5′-dioxaphosphorinane ring.

NIEK L.H.L. BROEDERS, ARTHUR P. VAN DER HEIDEN, LEO H. KOOLE, JAN A. KANTERS et ARIE SCHOUTEN. Can. J. Chem. **71**, 855 (1993).

La présente étude est orientée vers le monophosphate cyclique-3′,5′ de méthyle de la 2′-*O*-méthyl-*cis*-adénosine (*cis*-**4**; *cis* se réfère à la relation entre le OMe (lié au phosphore) et la base adénine) qui est considéré comme un modèle pour le monophosphate cyclique de l'adénosine liée à un enzyme (cAMP). Dans ce complexe, la charge négative du phosphate est masquée en partie par une complexation avec les sites cationiques sur la surface de l'enzyme. On rapporte la synthèse et des études sur la détermination de la structure, de la conformation en solution (400 MHz, RMN du ^{1}H) et des aspects cinétique-mécanisme de l'hydrolyse alcaline du produit *cis*-**4**. La produit de solvatation de *cis*-**4** avec du méthanol cristallise dans le groupe d'espace orthorhombique $P2_12_12_1$ avec a = 8,170(2), b = 9,249(1) et c = 23,669(4) Å, V = 1788,5(6) Å^3, Z = 4 molécules par maille élémentaire. La structure a été affinée par la méthode des moindres carrés jusqu'à une valeur finale de R = 0,062 pour 2006 réflexions observées. Les bases adénines sont liées par des liaisons hydrogénes N6—H···N1 et N6—H···N7 d'une façon telle qu'il y a formation de chaînes unidimensionnelles infinies. Cette arrangement par liaisons hydrogènes est très semblable à celui observé dans la structure de la 2'-désoxy-3′,5′-di-*O*-acétyl adénosine. Une liaison hydrogène additionnelle se forme avec le méthanol, incorporé dans la structure cristalline, et la base adénine. Faisant appel à la RMN du ^{1}H, à 400 MHz, on a déterminé les préférences conformationnelles du produit *cis*-**4** en solution dans le méthanol. On a trouvé que les conformations observées en phase solide et en solution sont les mêmes. L'hydrolyse du composé mentionné dans le titre fournit deux esters acycliques de l'acide phosphorique (un diester 3′- et un diester 5′-phosphate). Ces intermédiaires qui se forment durant la réaction d'hydrolyse sont probablement des composés pentacoordinés du phosphore (P^V) de géométrie bipyramidale trigonale et comportant un cycle dioxaphosphorinane attaché aux positions équatoriale/axiale-3′,5′.

[Traduit par la rédaction]

Introduction

Adenosine 3′,5′-cyclic monophosphate (cAMP; **A**) plays an important regulatory role in both eukaryotic and prokaryotic cells (1, 2). In eukaryotic cells the major receptor for cAMP is the regulatory subunit of cAMP-dependent protein kinase (3). Binding of cAMP to the regulatory subunit releases the catalytic subunit that is responsible for the phosphorylation leading to activation of certain key metabolic enzymes (4). In prokaryotic cells the catabolite gene

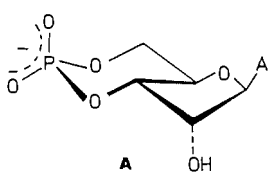

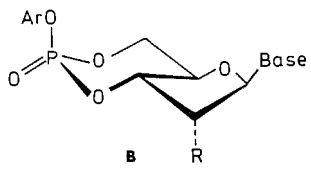

activator protein (CAP) senses the level of cAMP and regulates transcription from several operons in the presence of cAMP (5, 6). The enzymatic, hydrolytic ring-opening con-

[1]Author to whom correspondence may be addressed.

[2]Present address: Bioprime Research Institute, Section Bioorganic Chemistry, Limburg State University, P.O. Box 616, 6200 MD Maastricht, The Netherlands.

Can. J. Chem. Downloaded from www.nrcresearchpress.com by 213.200.69.106 on 09/08/12
For personal use only.

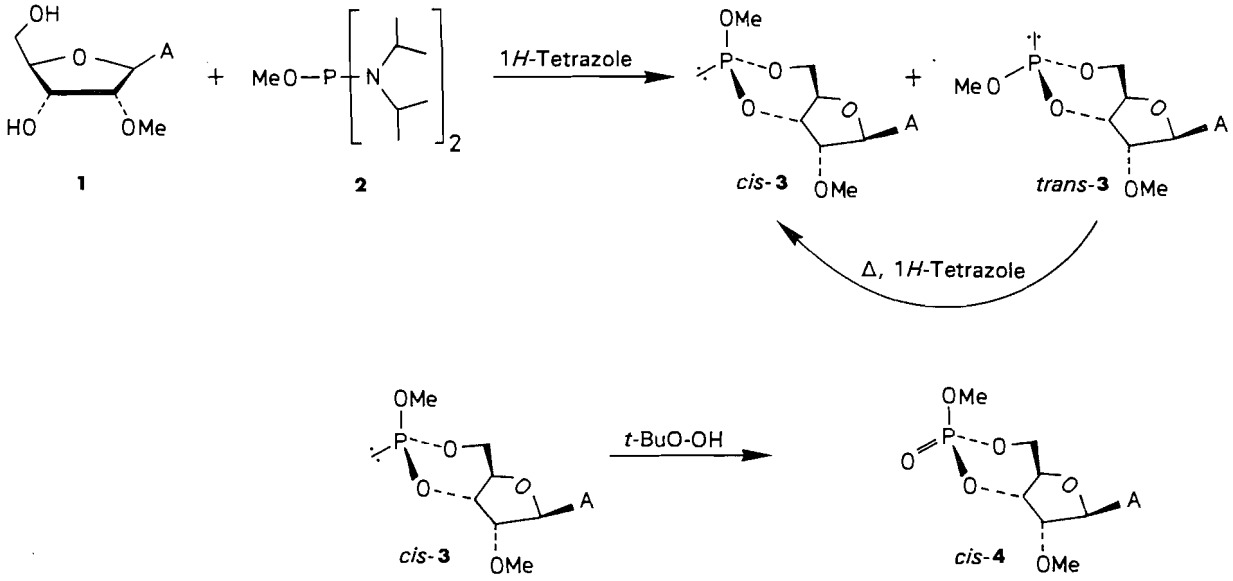

SCHEME 1

version of cAMP to 5′-adenosine monophosphate (5′-AMP) is accomplished by specific phosphodiesterases (7). A detailed understanding of the binding of cAMP to the active site of the enzyme is essential to understand the interaction of cAMP with protein kinases (in prokaryotic cells: CAP) or phosphodiesterases. X-ray studies of the cAMP binding domain of the crystal structure of the bacterial CAP dimer revealed that the interaction between cAMP and CAP is mainly based on ionic interactions and hydrogen bonds (8–10). Due to these ionic interactions the negative charge on the phosphoryl oxygen anions will be shielded. Because of the absence of negative charge, nucleophiles can attack phosphorus more readily. This means that the phosphorus atom has become more electrophilic due to the shielding of the negative charge.

Our interest is primarily focussed on the role of 3′,5′-linked phosphodiester in the mechanism of action of cAMP. Most likely a five-coordinated phosphorus (P^V) species is involved, either as an intermediate or as a transition state, in both the hydrolysis of cAMP to 5′AMP and the activation of protein kinases by cAMP (11). These ideas have prompted several groups, including ours, to investigate model systems for the proposed activated state of cAMP (12–16). Essentially, these models incorporate a stabilized five-coordinated phosphorus atom that is part of a 3′,5′-dioxaphosphorinane ring, which is *trans*-annelated with the ribose ring. These investigations support the idea that the 3′,5′-dioxaphosphorinane ring has access to both an equatorial–axial (e,a) *and* a diequatorial (e,e) orientation with respect to the trigonal bipyramidal (TBP) structure of the five-coordinated phosphorus. As an alternative approach, we have recently studied the alkaline hydrolysis of a set of cAMP models that feature a *cis*-aryl-3′,5′-cyclic phosphotriester structure (**B**) (17). These studies independently support the ideas that (*i*) hydrolysis proceeds via a five-coordinated phosphorus structure, and (*ii*) both (e,e) and (e,a) orientations of the 3′,5′-dioxaphosphorinane ring are feasible as long as five-coordination is present. In the course of these investigations we have synthesized and characterized 2′-*O*-methyl-*cis*-adenosine 3′,5′-cyclic methyl monophosphate (*cis*-**4**; *cis* describes the relationship between OMe (bound to P) and the A-base), which is the key compound of the present study. Compound *cis*-**4** features a methoxy group on the 2′-position of the ribose ring, as well as the adenine base, and can therefore be regarded as an improved model for the interaction between cAMP and an enzyme; this is compared with previous studies, which are mainly based on 2′-deoxy-3′,5′-cyclic phosphate derivatives from thymidine.

We report (*i*) the synthesis of *cis*-**4**, (*ii*) the crystal structure of *cis*-**4**, (*iii*) an NMR analysis of the conformational properties of *cis*-**4** in methanol, and (*iv*) observations concerning the alkaline hydrolysis of *cis*-**4** (i.e., kinetics and product distribution, and mechanistic aspects).

Experimental

Materials and chromatography

Merck silica gel 60 (particle size 0.063–0.200 mm) was used for column separations. Dry diethyl ether was obtained by storing diethyl ether, predried on calcium chloride, on sodium wire. Ethyl acetate was refluxed on calcium hydride prior to atmospheric distillation. Acetonitrile (DNA grade) was used as received. *tert*-Butyl hydroperoxide was used as a 80% (8.0 M) solution in di-*tert*-butyl hydroperoxide. 1*H*-Tetrazole was purified through sublimation. Reactions were routinely run at ambient temperature in an inert atmosphere of dry nitrogen or argon, unless otherwise noted.

NMR spectroscopy

^{1}H NMR spectra were recorded at 400.13 MHz on a Bruker AM 400 spectrometer. Tetramethylsilane (TMS) was used as the internal standard. ^{13}C and ^{31}P NMR were recorded at 100.62 and 162.98 MHz, respectively, on the same instrument. The ^{31}P NMR spectra were referenced against 85% H_3PO_4 as external standard.

*2′-O-Methyl-*cis*-adenosine 3′,5′-cyclic methyl monophosphite (*cis*-**3**)*

2′-*O*-Methyladenosine (2.25 g, 8.0 mmol) (23) and 1*H*-tetrazole (1.68 g, 24.0 mmol) were dissolved in 160 mL of acetonitrile. A solution of bis(*N*,*N*-diisopropylamino)methoxyphosphine (2.52 g, 9.6 mmol) in 10 mL of dichloromethane was added and the mixture was stirred for 20 h. ^{31}P NMR analysis indicated a *trans*-phosphite/*cis*-phosphite ratio of ca. 2:3 (δ (CH_3CN/CD_3CN 1:1 v/v): 129.7 ppm (*trans*), 123.5 ppm (*cis*)). To convert the *trans* epimer into the *cis* epimer, the temperature of the mixture was raised

Can. J. Chem. Downloaded from www.nrcresearchpress.com by 213.200.69.106 on 09/08/12
For personal use only.

Can. J. Chem. Downloaded from www.nrcresearchpress.com by 213.200.69.106 on 09/08/12
For personal use only.

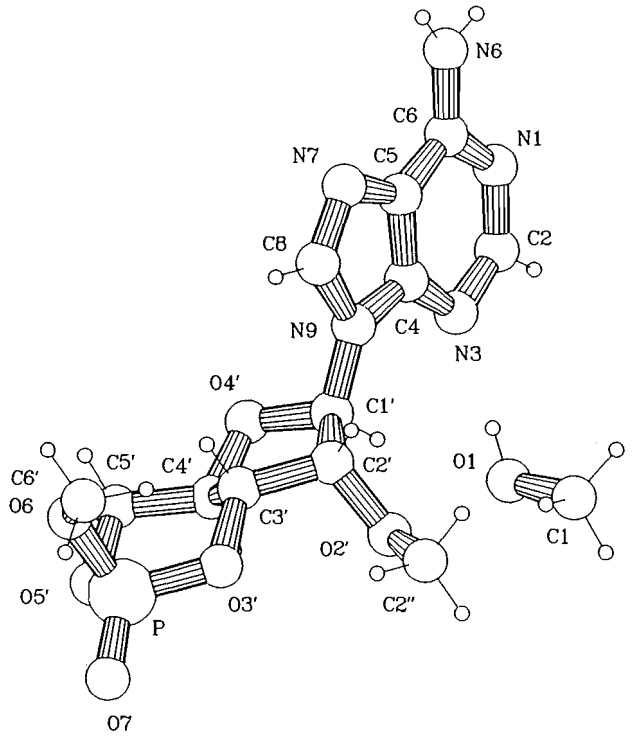

FIG. 1. Perspective view and atomic labelling of the title compound.

TABLE 1. Refined fractional coordinates of non-hydrogen atoms, and equivalent isotropic thermal parameters U_{eq} (Å^2); estimated standard deviations are given in parentheses

	x	*y*	*z*	U_{eq}[a]
P	0.0720(2)	0.5992(2)	0.20366(7)	0.0182(4)
O2′	0.3691(4)	0.5267(3)	0.3520(1)	0.027(1)
O3′	0.1366(5)	0.5706(4)	0.2654(2)	0.019(1)
O4′	0.4498(5)	0.8356(4)	0.2858(2)	0.020(1)
O5′	0.2172(5)	0.6712(4)	0.1690(2)	0.020(1)
O6	−0.0509(5)	0.7293(4)	0.2086(2)	0.024(1)
O7	0.0100(5)	0.4685(5)	0.1766(2)	0.024(1)
N1	0.7960(5)	1.0852(6)	0.4744(2)	0.020(2)
N3	0.7328(6)	0.8856(6)	0.4142(2)	0.022(2)
N6	0.6063(5)	1.2581(6)	0.5017(2)	0.023(2)
N7	0.3614(6)	1.0865(5)	0.4284(2)	0.019(2)
N9	0.4492(7)	0.8895(5)	0.3817(2)	0.018(1)
C2	0.8292(7)	0.9662(7)	0.4462(3)	0.023(2)
C4	0.5804(7)	0.9419(6)	0.4119(3)	0.018(2)
C5	0.5264(6)	1.0626(6)	0.4400(3)	0.018(2)
C6	0.6409(7)	1.1388(6)	0.4726(3)	0.019(2)
C8	0.3233(7)	0.9843(6)	0.3937(3)	0.021(2)
C1′	0.4502(7)	0.7768(6)	0.3412(3)	0.021(2)
C2′	0.3027(4)	0.6689(3)	0.3453(1)	0.021(2)
C3′	0.2249(6)	0.6909(6)	0.2892(3)	0.016(2)
C4′	0.3661(7)	0.7325(7)	0.2518(2)	0.020(2)
C5′	0.3123(7)	0.7881(6)	0.1950(3)	0.023(2)
C6′	−0.2017(7)	0.7086(7)	0.2411(3)	0.028(2)
C2″	0.2585(4)	0.4319(3)	0.3805(1)	0.033(3)
O1	0.8842(7)	0.6219(5)	0.3781(2)	0.051(2)
C1	0.8249(9)	0.5274(8)	0.4212(3)	0.059(3)

[a] U_{eq} = (1/3)(trace of orthogonalized U_{ij} tensor).

TABLE 2. Bond distances (Å)

Bond	Length	Bond	Length
P—O6	1.572(4)	N3—C4	1.351(8)
P—O7	1.459(5)	N6—C6	1.331(8)
P—O3′	1.576(5)	N7—C5	1.393(7)
P—O5′	1.589(5)	N7—C8	1.290(8)
O6—C6′	1.465(7)	N9—C4	1.377(8)
O4′—C1′	1.420(8)	N9—C8	1.381(7)
O4′—C4′	1.423(7)	N9—C1′	1.416(8)
O2′—C2′	1.432(4)	C4—C5	1.372(8)
O2′—C2″	1.428(4)	C5—C6	1.403(8)
O3′—C3′	1.441(7)	C1′—C2′	1.568(6)
O5′—C5′	1.467(7)	C2′—C3′	1.486(7)
N1—C2	1.315(8)	C3′—C4′	1.504(8)
N1—C6	1.361(7)	C4′—C5′	1.505(9)
N3—C2	1.323(8)	O1—C1	1.428(9)

to 40°C and maintained at this value for 90 h. ^{31}P NMR indicated complete conversion of the *trans* isomer. The solution was filtered and evaporated *in vacuo*. The solid was suspended in 50 mL of ethyl acetate and, after filtering, the filtrate was washed twice with a saturated sodium bicarbonate solution. The ethyl acetate layer was dried on magnesium sulfate. After filtering and evaporation of the filtrate, the residue was suspended in diethyl ether. After filtering, a white solid is obtained. Yield 0.92 g (39%). ^{31}P NMR (CD_3CN)δ: 123.5; ^{1}H NMR (CD_3CN)δ: 8.26 (1H, s, H8), 7.98 (1H, s, H2), 6.11 (2H, bs, NH_2), 5.95 (1H, bs, H1′), 4.90 (1H, ddd, H3′), 4.42 (1H, ddd, H5′), 4.34 (1H, bd, H2′), 4.28 (1H, ddd, H5″), 4.00 (1H, ddd, H4′), 3.59 (3H′s, d, OCH_3, $^3J_{POCH}$ = 12.0 Hz), 3.55 (3H′s, s, 2′-OCH_3); ^{13}C NMR (CD_3CN) δ: 157.0 (C4 or C6), 154.1 (C8), 150.3 (C6 or C4), 140.6 (C2), 121.0 (C5), 88.5 (C1′), 82.7 (C2′), 72.8 (C4′, $^3J_{POCC}$ = 7.2 Hz), 71.0 (C3′), 67.1 (C5′, $^2J_{POC}$ = 4.0 Hz), 59.5 (2′-OCH_3), 50.9 (OCH_3, $^2J_{POC}$ = 17.3 Hz).

*2′-O-Methyl-*cis*-adenosine 3′,5′-cyclic methyl monophosphate (*cis*-**4**)*

tert-Butyl hydroperoxide (0.15 mL, 1.2 mmol) was added to a solution of *cis*-**3** (100 mg, 0.29 mmol) in 3 mL of acetonitrile and the mixture was stirred for 15 h. After filtering, the filtrate was evaporated and dissolved in dichloromethane/methanol 95:5 (v/v). After addition of diethyl ether, a precipitate was formed, which was isolated by means of centrifugation. Afterwards, purification was obtained by means of column chromatography on a silica gel column with a gradient of methanol in acetonitrile (5 → 10 vol% methanol). Compound *cis*-**4** was obtained as a white solid. Recrystallization from methanol yielded colorless crystals. Yield 75 mg (72%). ^{31}P NMR (CD_3OD)δ: -3.00; ^{1}H NMR (CD_3OD) δ: 8.25 (2H′s, s, H8 and H2), 6.18 (1H, bs, H1′), 5.40 (1H, ddd, H3′), 4.66 (1H, ddd, H5″), 4.53 (1H, bd, H2′), 4.45 (1H, bt, H5′), 4.32 (1H, ddd, H4′), 3.94 (3H′s, d, OCH_3, $^3J_{POCH}$ = 11.2 Hz), 3.60 (3H′s, s, 2′-OCH_3); ^{13}C NMR (CD_3CN)δ: 157.4 (C4 or C6), 154.2 (C8), 150.2 (C6 or C4), 141.7 (C2), 120.7 (C5), 92.0 (C1′), 81.8 (C2′, $^3J_{POCC}$ = 7.6 Hz), 80.6 (C3′, $^2J_{POC}$ = 5.9 Hz), 72.1 (C4′, $^3J_{POCC}$ = 5.8 Hz), 71.3 (C5′, $^2J_{POC}$ = 8.9 Hz), 59.6 (2′-OCH_3), 55.1 (OCH_3, $^2J_{POC}$ = 6.0 Hz).

Hydrolysis of cis-**4**

cis-**4** (15 mg; 0.038 mmol) was transferred into a 5-mm NMR sample tube and dissolved in 360 μL of D_2O. After addition of 19 μL of a 2.00 M sodium hydroxide solution, initiating the hydrolysis, the solution turned yellowish. The reaction was monitored at 21°C by means of ^{31}P NMR: 8 FIDs were collected (time domain: 16K; size: 16K; sweep width: 4854 Hz) at distinct time intervals. The start of the 5th scan was chosen as the reaction time.

^{31}P NMR (D_2O) δ: 2.19 (5′-phosphate diester), 1.51 (3′-phosphate diester).[3]

Crystallographic measurements and structure resolution

$C_{12}H_{16}N_5O_6P \cdot CH_3OH$ fw = 389.30. Orthorhombic, a = 8.170(2) Å, b = 9.249(1) Å, c = 23.669(4) Å, V = 1788.5(6) Å^3, Z = 4, D_c = 1.446 g cm^{-3}, λ(MoKᾱ) = 0.71073 Å, t = 100 K, μ(MoKᾱ) = 2.1 cm^{-1}, F(000) = 816. Absent reflections: $h00$, h odd; $0k0$, k odd; and $00l$, l odd; space group $P2_12_12_1$ (D_2^4, No. 19).

A colorless crystal with dimensions (mm) 1.1 × 0.5 × 0.2 was used for data collection on an Enraf–Nonius CAD-4 diffractometer. Lattice parameters were determined from the setting angles of 25 reflections in the θ range 10.66°–19.20°. The intensities of 8388 reflections (2358 unique, R_{int} = 0.049) were collected at liquid nitrogen temperature (100 K) within the sphere of reflection limited by 2θ = 55° and $-10 \le h \le 0$, $-12 \le k \le 12$, and $-30 \le l \le 30$, using Zr-filtered MoKα radiation. The ω/2θ scan technique was applied with, Δω = (1.74 + 0.35 tan θ)°. The intensities of three standard reflections (024, 203 and 122) measured every hour showed an average deviation of less than 3% during the duration of the data collection. The intensities were corrected for Lorentz-polarization effects, but not for absorption. A total of 2006 reflections that satisfied the criterion $I \ge 2.5\sigma(I)$ were retained for the structure determination and refinement. σ(I) was derived from counting statistics. The structure was solved with the direct methods program of SHELXS86 (18), the coordinates of all non-hydrogen atoms being determined from an E-map. The hydrogen atoms were placed at idealized positions (C—H 1.00 Å) and refined riding on their bonded atoms, except those involved in hydrogen bonds. The three donor hydrogen atoms could be located in difference Fourier maps. As these atoms showed appreciable drifts upon refinement, they were fixed on the donor···acceptor vectors at 0.90 Å from the donor atoms, assuming linearity of the hydrogen bond. The overall isotropic thermal parameter of all hydrogen atoms refined to 0.056(5) Å^2. The absolute configuration was assigned in accordance with that reported for a number of nucleoside 3′,5′-cyclic monophosphates (see ref. 29 and Table 6). Anisotropic full-matrix least-squares refinement on F of 230 parameters converged at R = 0.062 and R_w = 0.043 with $w = 1/\sigma^2(F_o)$. The quantity minimized was $\Sigma\Delta F^2$, the goodness of fit, $s = [\Sigma w\Delta F^2/(m-n)]^{1/2}$, was 1.57 and the average and maximal shift-to-error ratio's 0.004 and 0.03, respectively. A final ΔF map showed maximal fluctuations of +0.65 and −0.42 e Å^{-3}, the positive maxima lying near the phosphorus atom. The scattering factors were those of Cromer and Mann (19) and anomalous dispersion terms from Cromer and Liberman (20). The least-squares refinement was performed with the SHELX76 program (21) and the program package EUCLID (22) was used for the calculations of geometries and preparation of illustrations. All calculations were done on an ULTRIX DECsystem-5000.

Results and discussion

Synthesis of cis-***4***

The preparation of *cis*-**4** is outlined in Scheme 1. 2′-*O*-Methyl adenosine (23) is brought into reaction with bis(*N*,*N*-diisopropylamino)methoxyphosphine and 1*H*-tetrazole as catalyst. This results in the formation of 2′-*O*-methyl-*cis*-adenosine 3′,5′-cyclic methyl monophosphite (*cis*-**3**) and its *trans* epimer in a ratio of ca. 3:2 (*cis*/*trans*). At elevated temperature and in the presence of 1*H*-tetrazole, the *trans* diastereoisomer completely inverts into the *cis* diastereoisomer. After evaporation of the volatiles of the reaction mixture, the residue is suspended in ethyl acetate and filtered. The filtrate is washed with a sodium bicarbonate solution. Evaporation of ethyl acetate, and suspension of the residue in diethyl ether, affords *cis*-**3** as a white solid (yield 39%). Oxidation of *cis*-**3**, using *tert*-butyl hydroperoxide as oxidation agent (24–26), yields pure crystalline *cis*-**4** (yield 72%) (see Scheme 1).

TABLE 3. Bond angles (°)

Bond	Angle	Bond	Angle
O6—P—O7	116.4(2)	N7—C5—C4	110.2(5)
O6—P—O3′	105.9(2)	N7—C5—C6	132.4(5)
O6—P—O5′	101.2(2)	C4—C5—C6	117.5(5)
O7—P—O3′	112.6(3)	N1—C6—N6	118.9(5)
O7—P—O5′	112.3(3)	N1—C6—C5	117.1(5)
O3′—P—O5′	107.4(2)	N6—C6—C5	124.0(5)
P—O6—C6′	118.4(4)	N7—C8—N9	114.6(5)
C1′—O4′—C4′	105.5(4)	O4′—C1′—N9	110.1(4)
C2′—O2′—C2″	112.1(3)	O4′—C1′—C2′	107.4(4)
P—O3′—C3′	113.6(4)	N9—C1′—C2′	115.0(5)
P—O5′—C5′	119.2(4)	O2′—C2′—C1′	107.5(3)
C2—N1—C6	118.7(5)	O2′—C2′—C3′	112.8(3)
C2—N3—C4	110.8(5)	C1′—C2′—C3′	100.7(4)
C5—N7—C8	104.0(5)	O3′—C3′—C2′	117.2(4)
C4—N9—C8	104.5(5)	O3′—C3′—C4′	110.6(5)
C4—N9—C1′	127.3(5)	C2′—C3′—C4′	103.5(4)
C8—N9—C1′	127.6(5)	O4′—C4′—C3′	102.0(4)
N1—C2—N3	129.7(5)	O4′—C4′—C5′	114.6(5)
N3—C4—N9	127.1(5)	C3′—C4′—C5′	112.9(5)
N3—C4—C5	126.2(6)	O5′—C5′—C4′	106.1(5)
N9—C4—C5	106.7(5)		

Crystal structure

The molecular structure of *cis*-**4** with its atomic numbering is shown in Fig. 1. The fractional coordinates, along with equivalent isotropic temperature factors, are summarized in Table 1. The bond distances and bond angles between non-hydrogen atoms are given in Tables 2 and 3, respectively. Table 4 contains only torsion angles involving the glycosidic link (C1′—N9), the ribose, and the six-membered dioxaphosphorinane ring. Table 5 lists the hydrogen-bond geometries (distances and bond angles). Calculated and observed structure factors, calculated hydrogen atom parameters, and anisotropic thermal parameters have been deposited as Tables S-1, S-2, and S-3, respectively.[4]

Conformation of the ribose ring

The ribose ring is found in the C3′-*endo* puckered form. The values for the phase angle of pseudorotation (P) and the puckering amplitude (ν_{max}), which can be calculated from the five ribose endocyclic torsion angles (ν_0 ... ν_4) (Table 4) using the pseudorotation concept (27), are 49.1° and 46.1°, respectively. From these values can be concluded that the structure of the ribose ring can best be described by a twist ($_4T^3$) conformation, which is characteristic for cyclic nucleotides (Table 6). From Table 6, showing the pseudoro-

[3]The assignment of the 3′- and 5′- phosphate diester lines in the ^{31}P NMR spectrum is based on a 2D ^{31}P–^{1}H correlation spectrum.

[4]These tables may be purchased from: The Depository of Unpublished Data, Document Delivery, CISTI, National Research Council Canada, Ottawa, Canada K1A OS2.

The calculated hydrogen atom parameters have also been deposited with the Cambridge Crystallographic Data Centre and can be obtained on request from The Director, Cambridge Crystallographic Data Centre, University Chemical Laboratory, 12 Union Road, Cambridge CB2 1EZ, U.K.

Can. J. Chem. Downloaded from www.nrcresearchpress.com by 213.200.69.106 on 09/08/12
For personal use only.

Can. J. Chem. Downloaded from www.nrcresearchpress.com by 213.200.69.106 on 09/08/12
For personal use only.

TABLE 4. Selected torsion angles (°) for non-hydrogen atoms

Bond	Torsion angle	Bond	Torsion angle
C4′—O4′—C1′—C2′(ν_0)	−23.9(5)	C8—N9—C1′—O4′	69.2(7)
O4′—C1′—C2′—C3′(ν_1)	−4.5(5)	C8—N9—C1′—C2′	−52.3(8)
C1′—C2′—C3′—C4′(ν_2)	29.4(5)	C4—N9—C1′—C2′	137.9(5)
C2′—C3′—C4′—O4′(ν_3)	−45.5(5)	N9—C1′—C2′—C3′	118.3(5)
C1′—O4′—C4′—C3′(ν_4)	42.5(5)	N9—C1′—C2′—O2′	−123.5(4)
C1′—O4′—C4′—C5′	164.8(5)	C4′—O4′—C1′—N9	−149.7(4)
O4′—C1′—C2′—O2′	113.7(4)	O6—P—O3′—C3′	−62.3(4)
O2′—C2′—C3′—C4′	−84.8(4)	O7—P—O3′—C3′	169.4(4)
O2′—C2′—C3′—O3′	37.1(5)	O5′—P—O3′—C3′	45.2(4)
C1′—C2′—C3′—O3′	151.4(4)	O6—P—O5′—C5′	65.7(4)
O3′—C3′—C4′—O4′	−171.8(4)	O7—P—O5′—C5′	−169.4(4)
C2′—C3′—C4′—C5′	−168.9(4)	O3′—P—O5′—C5′	−45.0(4)
O3′—C3′—C4′—C5′	64.7(6)	P—O3′—C3′—C4′	−56.6(5)
O4′—C4′—C5′—O5′	−175.2(4)	P—O3′—C3′—C2′	−174.8(3)
C3′—C4′—C5′—O5′	−59.0(6)	P—O5′—C5′—C4′	51.5(5)
C4—N9—C1′—O4′ (χ)	−100.7(6)		

TABLE 5. Hydrogen-bond geometries (distances in Å, angles in °)

Donor	Acceptor	D···A	D—H	H···A	D—H···A
O1—H3	N3	2.865(7)	0.90	1.965	180
N6—H1	N1*i*	2.974(6)	0.90	2.074	180
N6—H2	N7*ii*	3.024(7)	0.90	2.124	180

The symmetry operation is performed on the acceptor atom A: (*i*) $-\frac{1}{2}+x, 2\frac{1}{2}-y, 1-z$; (*ii*) $\frac{1}{2}+x, 2\frac{1}{2}-y, 1-z$.

TABLE 6. Pseudorotational parameters and some conformational properties of the ribose ring in 3′,5′-cyclic nucleotides[a]

	cis-**4**	**A**[b]	**B**	$\mathbf{C_A}$[c]	$\mathbf{C_B}$[c]	**D**	**E**	**F**	Mean value[d]
P(deg)	49.1	46.5	27.6	33	15	44.5	51.0	48.8	39(13)
ν_{max} (deg)	46.1	46.9	43.4	49	47	49.9	47.3	47.5	47(2)
Ribose pucker	$_4T^3$	$_4T^3$	$^3T_4$	$^3T_4$	$^3T_2$	$_4T^3$	$_4T^3$	$_4T^3$	—

[a]The estimated standard deviations are given in parentheses.
[b]Compound names and references: **A**: 5-iodo-2′-*cis*-deoxyuridine 3′,5′-cyclic methyl monophosphate (ref. 29); **B**: inosine 3′,5′-cyclic monophosphate (ref. 30); **C**: adenosine 3′,5′-cyclic monophosphate sodium salt (there are two molecules of the salt in the asymmetric unit ($\mathbf{C_A}$ and $\mathbf{C_B}$) (ref. 31); **D**: *cis*-adenosine 3′5′-cyclic ethyl monophosphate (ref. 32); **E**: 8-[(2-aminoethyl)amino]-adenosine cyclic 3′,5′-monophosphate tetrahydrate (ref. 33); **F**: 2′-acetyl-*cis*-uridine 3′,5′-cyclic benzyl monophosphate (ref. 34).
[c]Compound **C** remains in two different geometries.
[d]The mean values and standard deviations of the tabulated values.

TABLE 7. Torsion angles (°) of the 3′,5′-dioxaphosphorinane ring in 3′,5′-cyclic nucleotides[a]

	cis-**4**	**A**[b]	**B**	$\mathbf{C_A}$[c]	$\mathbf{C_B}$[c]	**D**	**E**	**F**	Mean value[d]
[P—O5′—C5′—C4′]	51.5(5)	52.1(8)	59.8(3)	57.2	56.6	50.9	60.5	53.9	55(4)
[O5′—C5′—C4′—C3′]	−59.0(6)	−66.0(10)	−64.5(3)	−61.1	−60.8	−59.3	−62.9	−58.9	−62(3)
[C5′—C4′—C3′—O3′]	64.7(6)	69.4(10)	69.1(3)	66.6	68.3	65.9	66.8	67.1	67(2)
[C4′—C3′—O3′—P]	−56.6(5)	−52.8(8)	−59.7(3)	−58.1	−61.9	−54.1	−60.0	−60.9	−58(3)
[C3′—O3′—P—O5′]	45.2(4)	36.1(7)	47.8(2)	46.0	48.9	39.7	50.1	49.3	45(5)
[O3′—P—O5′—C5′]	−45.0(4)	−37.4(9)	−51.0(2)	−49.0	−49.9	−40.3	−53.6	−49.1	−47(6)

[a]The estimated standard deviations are given in parentheses.
[b]Compound names and references: **A**: 5-iodo-2′-*cis*-deoxyuridine 3′,5′-cyclic methyl monophosphate (ref. 29); **B**: inosine 3′,5′-cyclic monophosphate (ref. 30); **C**: adenosine 3′,5′-cyclic monophosphate sodium salt (there are two molecules of the salt in the asymmetric unit ($\mathbf{C_A}$ and $\mathbf{C_B}$) (ref. 31); **D**: *cis*-adenosine 3′,5′-cyclic ethyl monophosphate (ref. 32); **E**: 8-[2-aminoethyl)amino]-adenosine cyclic 3′,5′-monophosphate tetrahydrate (ref. 33); **F**: 2′-acetyl-*cis*-uridine 3′,5′-cyclic benzyl monophosphate (ref. 34).
[c]Compound **C** remains in two different geometries.
[d]The mean values and standard deviations of the tabulated values.

Can. J. Chem. Downloaded from www.nrcresearchpress.com by 213.200.69.106 on 09/08/12
For personal use only.

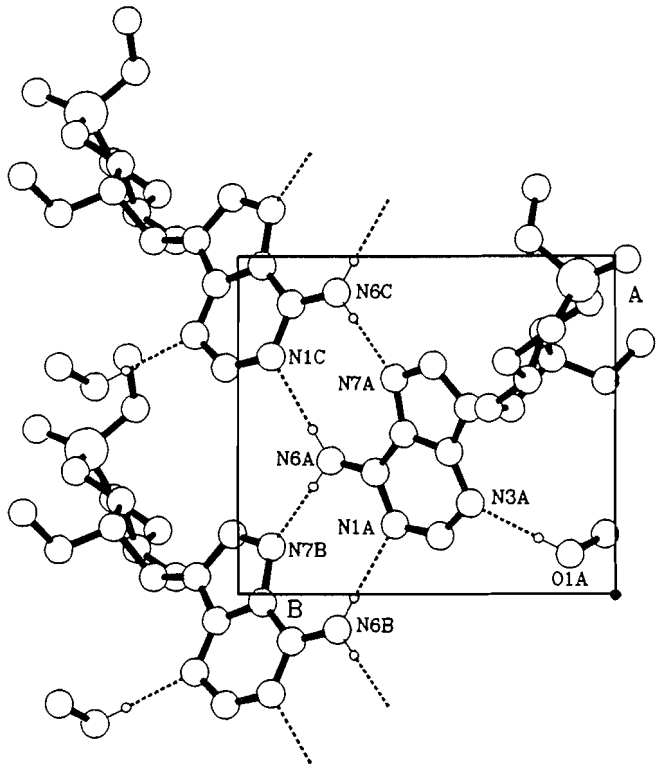

FIG. 2. Projection of a part of the structure down the *c* axis, showing the hydrogen-bonded chain in the *ab* plane. Hydrogen atoms not involved in hydrogen bonds have been omitted for clarity. The cell origin is indicated by the black dot. Molecule A is at $1 - x, -\frac{1}{2} + y, \frac{1}{2} - z$; molecule B is at $\frac{1}{2} - x, 2 - y, -\frac{1}{2} + z$; molecule C is at $1\frac{1}{2} - x, 2 - y, -\frac{1}{2} + z$;

tational parameters of several cyclic nucleotides, it can be observed that the values of phase angle and amplitude of pseudorotation (P and ν_{max}) vary within rather narrow ranges (P: 15°–51°; ν_{max}: 43°–50°). The pseudorotational parameters of the ribose ring in *cis*-**4** fit perfectly in the data ranges as shown in Table 6.

Conformation of the 3′,5′-dioxaphosphorinane ring

The 3′,5′-dioxaphosphorinane ring adopts a distorted chair conformation. To characterize this conformation we define three planes: plane 1 is the least-squares plane through the atoms O3′, O5′, C3′, and C5′ ($-0.411X + 0.286Y - 0.0091Z = 1$; $\sigma_{plane} = 0.016$ Å; X, Y, and Z are measured in angstroms along with the crystallographic a, b, and c axes); plane 2 is the plane through O3′, P, and O5′ ($-0.0512X + 0.0147Y + 0.0450Z = 1$); and plane 3 is the plane defined by the atoms C3′, C4′, and C5′ ($-0.00355X + 0.111Y + 0.0436Z = 1$). The dihedral angle between the planes 1 and 2 is 39.4°, whereas the dihedral angle between the planes 1 and 3 is 56.7°. This means that the ring resides in a distorted chair conformation in which P and C4′ are on opposite sides with respect to plane 1. The distances of the atoms P and C4′ to plane 1 are 0.59 and 0.69 Å, respectively. This leads to the conclusion that the P part is flattened in comparison with the C4′ part of the 3′,5′-dioxaphosphorinane ring. The distortion of the 3′,5′-dioxaphosphorinane ring can also be characterized by the significantly different values of the bond angles C3′—O3′—P (113.6°) and C5′—O5′—P (119.2°). The largest endocyclic torsion angle in the dioxaphosphorinane ring is found in the C3′—C4′ bond (C5′—C4′—C3′—O3′ = 64.7°), the *trans* junction with the ribose ring. The endocyclic P—O bonds show the smallest ring torsion angles (O3′—P—O5′—C5′ = −45.0°; C3′—O3′—P—O5′ = 45.2°) (Table 7). These values also demonstrate that the P part is flattened in comparison with the C4′ part of the six-membered ring. The values of the torsion angles of the 3′,5′-dioxaphosphorinane ring in *cis*-**4** shown in Table 7 fit perfectly within the data ranges defined by several 3′,5′-cyclic nucleotides (28–33).

TABLE 8. Proton–proton and proton-phosphorus coupling constants (in Hz) of *cis*-**4**, measured in methanol-d_4 at 20°C

Parameter	Value[a]	Parameter	Value[a]
$J_{H1'H2'}$	0.8	$J_{H4'H5''}$	4.7
$J_{H2'H3'}$	5.1	$J_{H5'H5''}$	−9.3
$J_{H3'H4'}$	9.8	$J_{H5'P}$	~0[b]
$J_{H3'P}$	1.4	$J_{H5''P}$	22.3
$J_{H4'H5'}$	10.6	J_{POMe}	11.2

[a]Estimated error ±0.1 Hz.
[b]Estimated error ±0.2 Hz.

Geometry and orientation of the base

The torsion angle χ(O4′—C1′—N9—C4) about the glycosidic bond is −100.7° and corresponds to the *anti* conformation. The values of the bond lengths and angles for the purine base are similar to those reported for the standard adenine ring (34). Largest deviations were found for the N1—C2 and N7—C8 bonds (bond lengths smaller than the standard values by 0.023 and 0.022 Å, respectively). The least-squares plane through the nine atoms of the purine base is $-0.255X - 0.559Y + 0.789Z = 1.610$; $\sigma_{plane} = 0.019$ Å; where X, Y, and Z are measured in angstroms along with the crystallographic a, b, and c axes. The dihedral angle between the planes of the pyrimidine and imidazole ring is 1.7°. The largest torsion angle in the adenine ring is found about the N3—C4 and N7—C8 bonds (C2—N3—C4—C5 = −2.4°; C5—N7—C8—N9 = 1.6°), resulting in a small deviation from planarity (Table 4).

Molecular packing and hydrogen bonding

In Fig. 2 is illustrated that each NH_2 group in *cis*-**4** is hydrogen bonded by two molecules. There is one hydrogen bond between N6 and N7 ($\frac{1}{2} + x, 2\frac{1}{2} - y, 1 - z$) and one between N6 and N1 ($-\frac{1}{2} + x, 2\frac{1}{2} - y, 1 - z$) (see Table 5). The hydrogen bond accepting molecules are one translation apart along the *a* axis, leading to a one-dimensional chain of hydrogen-bonded molecules. The direction of the one-dimensional chain is almost parallel to the *a* axis. The hydrogen bonds between the bases are very similar to those in 2′-deoxy-3′,5′-di-*O*-acetyl adenosine (35). An additional hydrogen bond is formed between the OH group of the methanol molecule, which is incorporated in the crystal structure, and the adenine base: O1—H3···N3.

Conformation in solution

The conformation of *cis*-**4** in methanol-d_4 was determined at room temperature with ^{1}H NMR at 400.13 MHz. The set of experimental coupling constants are summarized in Table 8.

Conformation of the ribose ring

The conformational analysis of the sugar ring of *cis*-**4** was performed with the PSEUROT program (36). The sets of vic-

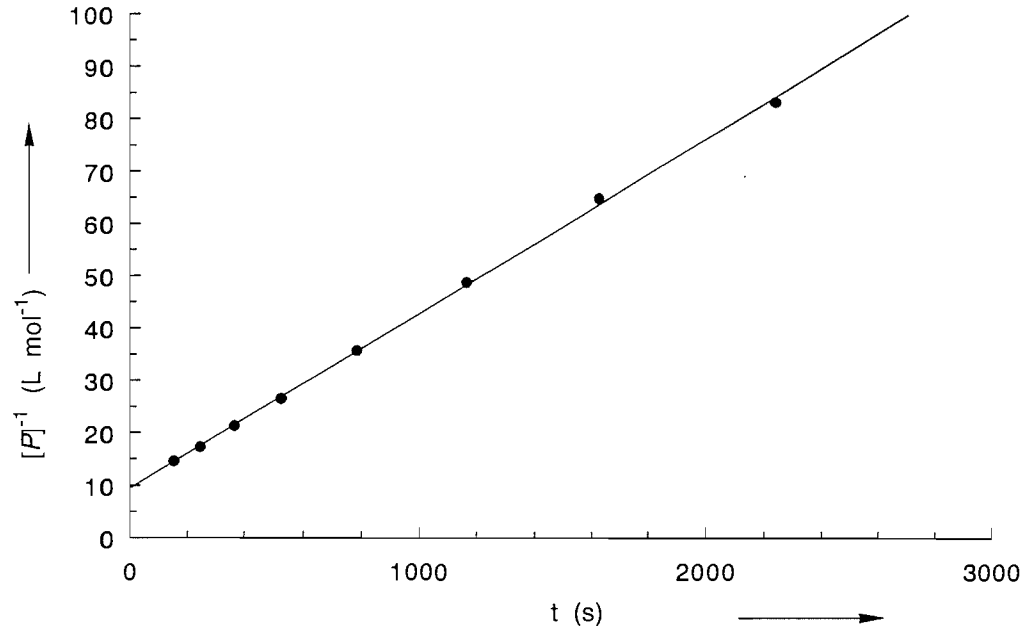

FIG. 3. Graphical presentation of the alkaline hydrolysis in D_2O of *cis*-**4** at 294 K, based on eq. [1]. Both initial concentrations of *cis*-**4** and hydroxide are 0.100 M. The values for k^{exp} and r are 0.0334 L. mol^{-1} s^{-1} and 0.999, respectively.

TABLE 9. Kinetic parameters for the hydrolysis of *cis*-**4** at 294 K

Compound	Initial concentrations (M)		Rate constant 10^3k^{exp}		Product distribution (%)		
	$10^2[P]_0$	$10^2[OH^-]_0$	(M^{-1} .s^{-1})	r^c	3′	5′	Cyclic
cis-**4**[a]	1.00	1.00	33	0.999	65	35	0
B[b] (R = OMe; B = adenine)	4.77	14.3	21	0.998	19	29	52

[a]Kinetics were performed in D_2O.
[b]Kinetics were performed in D_2O/1,4-dioxane-d_8 3:7 (v/v).
[c]Correlation coefficient.

inal H–H coupling constants ($J_{H(1')H(2')}$, $J_{H(2')H(3')}$, $J_{H(3')H(4')}$) measured for *cis*-**4** (Table 8) were used as input data. PSEUROT calculates the best-fit conformational parameters of two sugar structures (a North (C3′-*endo*) and a South (C2′-*endo*) conformation) participating in a rapid conformational equilibrium as well as the equilibrium composition. PSEUROT converged toward a single conformation (North), characterized by a phase angle (P) of 23.7° and a maximum puckering amplitude (ν_{max}) of 41.4°. The five endocyclic torsion angles ($\nu_0 \ldots \nu_4$) can be calculated from P and ν_{max} according to the formula: $\nu_j = \nu_{max} \cdot \cos(P + (j - 2) \cdot 144)$ (27), i.e., $\nu_0 = -4.1°$, $\nu_1 = -20.9°$, $\nu_2 = 37.9°$, $\nu_3 = -40.4°$, $\nu_4 = 27.5°$. From these results it can be derived that the structure of the ribose ring in *cis*-**4** resides in a twist ($^3T_4$) conformation, which is closely related to the $_4T^3$ conformation in the solid state.

Conformation of the 3′,5′-dioxaphosphorinane ring

The rigidity of the *trans*-annealed six-membered ring allows us to take only a few conformations into account: (*i*) a chair, (*ii*) two boat conformations (one with P and C4′ as prow and one with O5′ and C3′ as prow), or (*iii*) a twist-boat geometry. Discrimination between these geometries is based on the values of two H–P coupling constants ($^3J_{PH(5')}$ and $^3J_{PH(5'')}$, describing the conformation around the O5′—C5′ bond) and two H–H coupling constants ($^3J_{H(4')H(5')}$ and $^3J_{H(4')H(5'')}$, characterizing the conformation around the C4′—C5′ bond). Generally the H–P coupling constants of phosphates fit into classic Karplus type relations (37–39). From the work of Bentrude and co-workers (40) on cyclic phosphates a *trans* orientation of a P—O—C—H fragment corresponds to a $^3J_{POCH}$ value of ≈22.5 Hz, whereas a *gauche* conformation is related to a $^3J_{POCH}$ value of ≈1 Hz. From Table 8 we conclude that H5″ and P adopt a *trans* orientation (P—O—C—H5′ ≃ ±60°). These results are in agreement with the chair conformation. The boat geometry, in which O3′, O5′, C3′, and C5′ are approximately in the same plane while P and C4′ are both located on the *exo* side of this plane, would yield approximately identical values for $^3J_{PH(5')}$ and $^3J_{PH(5'')}$, whereas the twist-boat and the boat conformation, in which O5′ and C3′ are located on the *endo* side of the least-squares plane through P, C4′, C5′, and O3′, would correspond to a large value for $^3J_{POCH(5')}$ (≈20–23 Hz) and a small value for $^3J_{POCH(5'')}$.

A second clue for characterization of the geometry of the 3′,5′-dioxaphosphorinane ring is provided by the coupling constants $^3J_{H(4')H(5')}$ and $^3J_{H(4')H(5'')}$, from which the conformation around the C4′—C5′ (γ) bond can be deduced. By using the generalized Karplus equation of Altona and co-

Can. J. Chem. Downloaded from www.nrcresearchpress.com by 213.200.69.106 on 09/08/12
For personal use only.

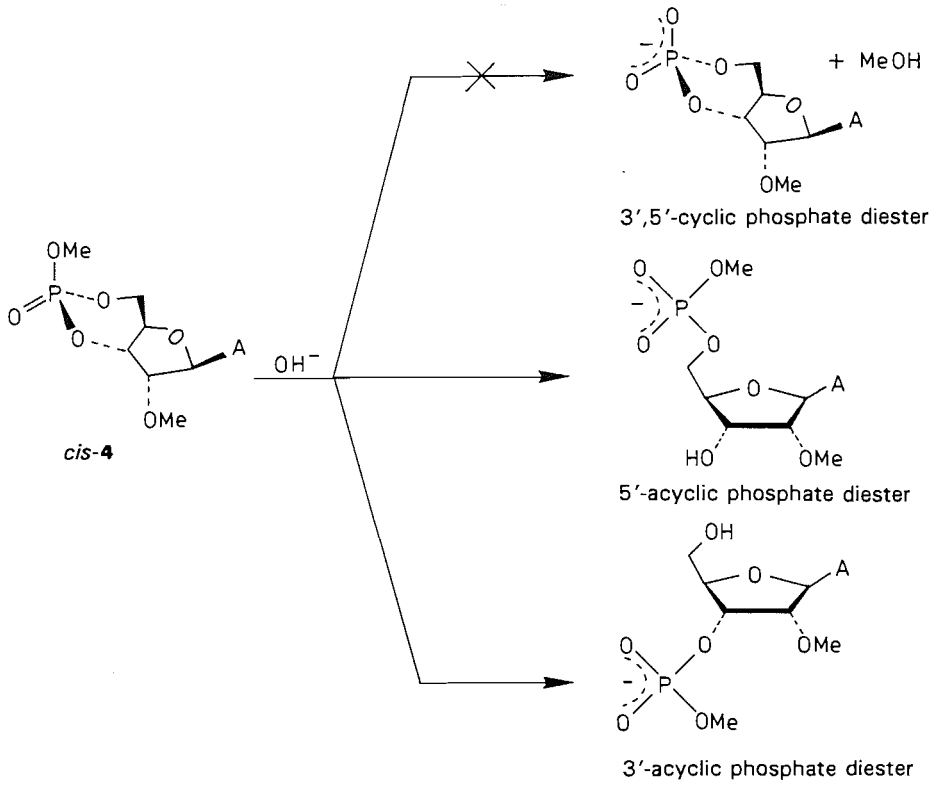

SCHEME 2

workers (41),[5] we calculated $^3J_{H(4')H(5')}$ and $^3J_{H(4')H(5'')}$ as a function of the torsion angle O5′—C5′—C4′—O4′ (see Fig. 2 in ref. 16). This graph indicates that the torsion angle adopts a value of approximately 180°, which is in agreement with the chair conformation of the six-membered ring.

Hydrolysis of cis-**4**

To obtain information about the mechanistic aspects of the alkaline hydrolysis of *cis*-**4** we investigated the kinetics and product distribution by means of ^{31}P NMR. The hydrolysis reaction was assumed to obey second-order kinetics (42, 43): first order in cyclic phosphate triester and first order in hydroxide. Using equivalent amounts of *cis*-**4** and OH^- the kinetic equation becomes:

$$[1] \quad \frac{1}{[P]} = k^{exp}t + \frac{1}{[P]_0}$$

with $[P]$ = concentration of *cis*-**4** at time $t = t$; $[P]_0$ = initial concentration of *cis*-**4**; k^{exp} = experimental second-order reaction rate constant.

Our data on the hydrolysis reaction of *cis*-**4** are visualized in Fig. 3; the linear relationship ($r = 0.999$) between $[P]^{-1}$ and t substantiates the assumption that the hydrolysis proceeds via a second-order reaction mechanism. In Table 9 and k^{exp} value is tabulated.

Two different acyclic products were formed: a 3′-phosphate diester and a 5′-phosphate diester (ratio 3′:5′ = 65:35) (see Scheme 2). Comparing the product distribution in the hydrolysis of *cis*-**4** with those of 2′-*O*-methyl-*cis*-adenosine 3′,5′-cyclic *phenyl* monophosphate (17) (Table 9), it is remarkable that during hydrolysis the latter compound affords 52% of 3′,5′-cyclic phosphate diester, whereas hydrolysis of *cis*-**4** yields no cyclic product at all. The reason for this difference may be found in the formation of different P^V-TBP intermediates during the hydrolysis reactions. The main difference between the P^V-TBPs is the location of the 3′,5′-dioxaphosphorinane ring: (e,e) or (e,a). Since phenoxide (pK_a (phenol) = 10.1) is a much better leaving group than the methoxide (pK_a (methanol) = 15.5), in the P^V-TBPs the phenoxy group is more axiophilic than the methoxy. Since expulsion of a ligand from the P^V-TBP only takes place on the axial site of the TBP, formation of the 3′,5′-cyclic phosphate can be expected during hydrolysis of 2′-*O*-methyl-*cis*-adenosine 3′,5′-cyclic *phenyl* monophosphate. Since methoxy has no axiophilic character, hydrolysis of *cis*-**4** yields no 3′,5′-cyclic phosphate at all; only acyclic phosphates are formed.

Conclusion

The molecular conformation of *cis*-**4** is not significantly different from the conformations of several cAMP analogs (28–33). The ribose ring of *cis*-**4** shows virtually the same configuration in the solid state and in solution. Comparison of the crystal structure of *cis*-**4** with a set of related systems (28–33) shows that the absence or presence of the substituent on C2′ is relatively unimportant.

[5]In this generalized equation, the standard Karplus relation is extended with a correction term which accounts for the influence of electronegative substituents on $^3J_{HH}$:

$$^3J_{HH} = 13.22\cos^2\phi - 0.99\cos\phi + \Sigma[0.87 - 2.46\cos^2(\xi_i\phi + 19.9|\Delta\chi_i|)]\Delta\chi_i$$

ϕ is the proton–proton torsion angle, $\Delta\chi_i$ is the difference in electronegativity between the substituent and hydrogen according to the electronegativity scale of Huggins, and ξ_i is a substituent orientation parameter.

Can. J. Chem. Downloaded from www.nrcresearchpress.com by 213.200.69.106 on 09/08/12
For personal use only.

Can. J. Chem. Downloaded from www.nrcresearchpress.com by 213.200.69.106 on 09/08/12
For personal use only.

Due to the *trans* fusion of the 3′,5′-dioxaphosphorinane ring to the five-membered ribose ring, the 3′,5′-dioxaphosphorinane ring of *cis*-**4** adopts a fixed distorted chair conformation in the solid state. In this distorted chair geometry the atoms O3′, O5′, C3′, and C5′ are located in approximately the same plane, whereas P and C4′ are situated on opposite sides of this plane. The P side of the six-membered ring is flattened in comparison with the C4′ side. This conformation resembles the distorted chair conformation found in the set of related systems mentioned above (28–33). With respect to the conformation of the 3′,5′-dioxaphosphorinane ring of *cis*-**4** in solution it must be mentioned that the available set of coupling constants do not allow us to discriminate between a chair conformation and a distorted chair conformation.

In the crystal structure the adenine ring is oriented in the *anti* conformation and the adenine bases are linked via N6—H1···N1 and N6—H2···N7 hydrogen bonds, in such a way that infinite one-dimensional chains are formed. This hydrogen bond scheme is very similar to that observed in the structure of 2′-deoxy-3′,5′-di-*O*-acetyl adenosine (35). An additional hydrogen bond is formed between the OH group of methanol and the adenine base.

Alkaline hydrolysis of *cis*-**4** yields two acyclic products: only 3′-phosphate diester and a 5′-phosphate diester. In comparison with the hydrolysis of 2′-*O*-methyl-*cis*-adenosine 3′,5′-cyclic phenyl monophosphate (17), no cyclic phosphate diester is formed. We conclude that hydrolysis of *cis*-**4** is "thermodynamically controlled," whereas hydrolysis of 2′-*O*-methyl-*cis*-adenosine 3′,5′-cyclic phenyl monophosphate (17) is more "kinetically controlled" due to the good leaving group character of phenoxide.

Acknowledgement

The authors thank Prof. Dr. E.W. Meijer for his critical view on the manuscript, and Mr. H. Eding and Mr. J.H. Damen for their assistance in the layout.

1. L. Stryer. *In* Biochemistry. Freeman and Co., San Francisco. 1980.
2. P. Greengard and G.A. Robinson, Sr. (*Editors*). Review series: Advances in cyclic nucleotide research. Vols. 11–17. Raven Press, New York. 1980–1986.
3. D.A. Walsh, J.P. Perkins, and E.G. Krebs. J. Biol. Chem. **243**, 3763 (1968).
4. S.S. Taylor, J.A. Buechler, and W. Yonemoto. Annu. Rev. Biochem. **59**, 971 (1990).
5. G. Zubay, D. Schwartz, and J. Beckwith. Proc. Natl. Acad. Sci. U.S.A. **66**, 104 (1970).
6. W.B. Anderson, R.L. Perlman, and I. Pastan. J. Biol. Chem. **247**, 2717 (1972).
7. J.A. Beavo. Adv. Second Messenger Phosphoprotein Res. **22**, 1 (1988).
8. I.T. Weber and T.A. Steitz. J. Mol. Biol. **198**, 311 (1987).
9. I.T. Weber, T.A. Steitz, J. Bubis, and S.S. Taylor. Biochemistry, **26**, 343 (1987).
10. M.C. Vaney, G.L. Gilliland, J.G. Harman, A. Peterkofsky, and I.T. Weber. Biochemistry, **28**, 4568 (1989).
11. P.J.J.M. van Ool and H.M. Buck. Eur. J. Biochem. **121**, 329 (1982).
12. T.K. Prakasha, R.O. Day, and R.R. Holmes. Inorg. Chem. **31**, 725 (1992).
13. T.K. Prakasha, R.O. Day, and R.R. Holmes. Inorg. Chem. **31**, 1913 (1992).
14. Y. Huang, A.M. Arif, and W.G. Bentrude. J. Am. Chem. Soc. **113**, 7800 (1991).
15. J.H. Yu, A.M. Arif, and W.G. Bentrude. J. Am. Chem. Soc. **112**, 7451 (1990).
16. N.L.H.L. Broeders, L.H. Koole, and H.M. Buck. J. Am. Chem. Soc. **112**, 7475 (1990).
17. N.L.H.L. Broeders, A.P. van der Heiden, I. Peeters, H.M. Janssen, and L.H. Koole. J. Am. Chem. Soc. **114**, 9624 (1992).
18. G.M. Sheldrick. SHELXS86. Program for the solution of crystal structures, University of Göttingen, Germany. 1986.
19. D.T. Cromer and J.B. Mann. Acta Crystallogr. Sect. A: Cryst. Phys. Diffr. Theor. Gen Crystallogr. **A24**, 321 (1968).
20. D.T. Cromer and D. Liberman. J. Chem. Phys. **53**, 1891 (1970).
21. G.M. Sheldrick. SHELX76. Program for crystal structure determination, University of Cambridge, England. 1976.
22. A.L. Spek. *In* The EUCLID package in computational crystallography. *Edited by* D. Sayre. Clarendon Press, Oxford. 1982. p. 528.
23. P.J.L.M. Quaedflieg, A.P. van der Heiden, L.H. Koole, A.J.J.M. Coenen, S. van der Wal, and E.M. Meijer. J. Org. Chem. **56**, 5846 (1991).
24. W.G. Bentrude, J.H. Hargis, and P.E. Rusek. Chem. Commun. 296 (1969).
25. W.G. Bentrude and J.H. Hargis. J. Am. Chem. Soc. **92**, 7136 (1970).
26. D.B. Denney and W.H. Hanifin, Jr. Tetrahedron Lett. 2177 (1963).
27. C. Altona and M. Sundaralingam. J. Am. Chem. Soc. **94**, 8205 (1972).
28. J. Béres, P. Sándor, A. Kálmán, T. Koritsánszky, and L. Ötvös. Tetrahedron **40**, 2405 (1984).
29. M. Sundaralingam, T.P. Haromy, and P. Pruisner. Acta Crystallogr. Sect. B: Struct. Crystallogr. Cryst. Chem. **B38**, 1536 (1982).
30. K.I. Varughese, C.T. Lu, and G. Kartha. J. Am. Chem. Soc. **104**, 3398 (1982).
31. F.A. Cotton, R.G. Gillen, R.N. Gohil, E.E. Hazen, Jr., C.R. Kirchner, J. Nagyvary, J.P. Rouse, A.G. Stanislowski, J.D. Stevens, and P.W. Tucker. Proc. Natl. Acad. Sci. U.S.A. **72**, 1335 (1975).
32. W.S. Sheldrick and E. Rieke. Acta crystallogr. Sect. B: Struct. Crystallogr. Cryst. Chem. **B34**, 2324 (1978).
33. W. Depmeier and J. Engels. Acta Crystallogr. Sect. B: Struct. Crystallogr. Cryst. Chem. **B33**, 2435 (1977).
34. R. Taylor and O. Kennard. J. Am. Chem. Soc. **104**, 3209 (1984).
35. L.H. Koole, H.M. Buck, J.A. Kanters, and A. Schouten. Can. J. Chem. **65**, 326 (1987).
36. F.A.A.M. de Leeuw and C. Altona. Quantum Chemistry Program Exchange 463; J. Chem. Soc. Perkin Trans. 2, 375 (1982).
37. P.P. Lankhorst, C.A.G. Haasnoot, C. Erkelens, and C. Altona. J. Biomol. Struct. Dyn. **1**, 1387 (1984).
38. W.G. Bentrude and W.N. Setzer. *In* ^{31}P NMR spectroscopy in stereochemical analysis: organic compounds and metal complexes. *Edited by* J.G. Verkade and L. Quin. VCH Publishers, Inc., Deerfield Beach, Fla. 1987. Chap. 11.
39. R.J.M. Hermans and H.M. Buck. J. Org. Chem. **52**, 5150 (1987).
40. K.A. Nelson, W.G. Bentrude, W.N. Setzer, and J.P. Hutchinsonn. J. Am. Chem. Soc. **109**, 4058 (1987).
41. C.A.G. Haasnoot, F.A.A.M. de Leeuw, and C. Altona. Tetrahedron, **36**, 2783 (1980).
42. A.J. Kirby and S. G. Warren. *In* The organic chemistry of phosphorus. *Edited by* C. Eaborn and N.B. Chapman. Elsevier, Amsterdam. 1967.
43. J.R. Cox and O.B. Ramsay. Chem. Rev. **64**, 317 (1964).

Formation of isomeric monohalo-*n*-alkanoic acids in the reactions of γ- and δ-*n*-alkanolactones with hydrogen halides

ALESSANDRO GRANATA AND ARTHUR S. PERLIN[1]
Department of Chemistry, McGill University, Montreal, Que., Canada H3A 2A7

Received December 18, 1992

ALESSANDRO GRANATA and ARTHUR S. PERLIN. Can. J. Chem. **71**, 864 (1993).

In 57% hydriodic acid or 48% hydrobromic acid, under reflux, *n*-alkanoic γ- or δ-lactones of from 5 to 18 carbon atoms undergo facile ring opening to monohalo-*n*-alkanoic acids. With both reagents the ratio of acid to lactone at equilibrium varies widely, ranging from about 1:3 for γ-valerolactone (C_5) to 3:1 or more for γ-octanolactone and the larger members of the series. Extensive scrambling of the halogen atoms accompanies the formation of the haloacids, whereby mixtures of monohalo isomers substituted at all positions from C-4 to the penultimate carbon are found. In an 18 h reaction with HBr, for example, γ-caprolactone was converted into a 1:3 mixture of 4- and 5-bromohexanoic acids, and γ-decanolactone into a 1:1.4:1.4:1.4:2.3:2.3 mixture of 4-, 5-, 6-, 7-, 8-, and 9-bromodecanoic acids. By contrast, the γ-lactones containing 14 or 16 carbon atoms gave only 10:1 mixtures of the 4- and 5-bromoacids, and at the level of 18 carbon atoms rearrangement was no longer evident; i.e., γ-octadecanolactone afforded only 4-bromooctadecanoic acid. Similar isomer distributions were obtained for the iodoacid homologs. Hydrochloric acid (37%) was far less effective in opening the lactone rings, and also in inducing rearrangement of the chlorine atoms introduced. Differences in entropy and in solvation appear to be the main factors contributing to the variations observed among isomeric lactones.

ALESSANDRO GRANATA et ARTHUR S. PERLIN. Can. J. Chem. **71**, 864 (1993).

Soumis à de l'acide iodhydrique à 57% ou à de l'acide bromhydrique à 48%, les γ- ou δ-lactones des acides *n*-alcanoïques comportant de 5 à 18 atomes de carbone donnent facilement lieu à une ouverture de cycle conduisant aux acides *n*-alcanoïques monohalogénés. Avec les deux réactifs, le rapport des concentrations d'acide et de lactone présentes à l'équilibre varie considérablement; il passe d'environ 1 : 3 pour la γ-valérolactone (C_5) à 3 : 1 ou plus pour la γ-octanolactone et les autres grands cycles de la série. La formation des haloacides s'accompagne de beaucoup de brouillage des halogènes; on retrouve des mélanges de dérivés monohalogénés dans lesquels les halogènes sont fixés sur chacun des carbones de l'acide, de la position 4 jusqu'à l'avant dernier carbone. Par example, lors d'une réaction de 18 h avec du HBr, la γ-caprolactone a été transformée en un mélange 1 : 3 des acides 4- et 5-bromohexanoïques alors que la γ-décanolactone est transformée en un mélange 1 : 1,4 : 1,4 : 1,4 : 2,3 : 2,3 des acides 4-, 5-, 6-, 7-, 8- et 9-bromodécanoïques. Par ailleurs, les γ-lactones contenant 14 ou 16 atomes de carbone ne donnent que des mélanges 10 : 1 des acides 4- ou 5-bromés alors que, au niveau de 18 atomes de carbone, on n'observe plus de transposition, c'est-à-dire que la γ-octadécanolactone ne fournit que de l'acide 4-bromoctanoïque. On a obtenu des distributions semblables avec analogues iodés. L'acide chlorhydrique (37%) est beaucoup moins efficace pour ouvrir les cycles des lactones et pour induire des transpositions des atomes de chlore introduits. Il semble que des différences d'entropie et de solvatation soient les principaux facteurs contribuant aux variations observées avec les lactones homologues.

[Traduit par la rédaction]

Introduction

In reactions with 57% hydriodic acid under reflux, aldonolactone derivatives of sugars are reduced to the corresponding γ-*n*-alkanolactones and (or) monoiodoalkanoic acids (1–3). The lactone–acid ratio at equilibrium varies widely (3) with the number of carbon atoms in these molecules. In 1–4 h reaction time, for example, D-erythrono-1,4-lactone afffords 3-iodobutanoic acid almost exclusively, whereas D-xylono-1,4-lactone gives a 4:1 mixture of γ-valerolactone and 4-iodopentanoic acid. Aldonolactones containing six to eight carbon atoms are converted into mixtures of γ-*n*-alkanolactone and iodoacid in which the latter becomes the preponderant product.

Another characteristic (3) of these reactions is a progression in the number of iodoacids produced, which is determined by chain length. Hence, 4-iodopentanoic acid (**2**) is the only five-carbon acid derivative obtained from γ-valerolactone (**1**), whereas there are two isomers (4- and 5-) of iodohexanoic acid, three isomeric (4-, 5-, and 6-) iodoheptanoic acids, and four (4-, 5-, 6-, and 7-) iodooctanoic acids. Moreover, the isomer substituted at the penultimate carbon is the major species in each mixture, e.g., 7-iodooctanoic acid (**4**) from γ-octanolactone (**3**).

These characteristics of lactone-ring opening by hydriodic acid have been demonstrated (3) not only for the aldonolactones but also, more simply, with the corresponding four- to eight-carbon γ-*n*-alkanolactones that are formed from them in the reduction reaction with hydriodic acid. The present study describes results obtained with homologous *n*-alkanolactones having from 8 to 18 carbon atoms, as well as a comparison between the action of hydriodic acid and those of hydrobromic and hydrochloric acids over the entire range of chain lengths.

Results and discussion

Lactone-ring opening by hydriodic and hydrobromic acids

As already noted for the reaction of hydriodic acid with γ-*n*-alkanolactones, the amount of iodoacid produced in 1 h relative to that of unreacted lactone increases sharply from a ratio of 0.4 for the 5-carbon compound through 10.1 for the 8-carbon member of the series (see Table 1). Data that have now been obtained for longer carbon chains are also presented in the table. The estimates of iodoacid:lactone ratios (A:L) are based on the relative intensities of ^{1}H nmr

[1]Author to whom correspondence may be addressed.

Can. J. Chem. Downloaded from www.nrcresearchpress.com by 213.200.69.106 on 09/08/12
For personal use only.

signals at δ ~4.2 and ~4.5, which are characteristic of methine protons deshielded by the α-iodine atom and the lactone-ring O atom, respectively. A high iodoacid content (ratio of 10) was again found for the product mixtures from the C_9 and C_{10} lactones, whereas the values were lower for the C_{11}(4.9) and C_{12}(2.3) homologues. These data are for a reaction time of 18 h, and as they were largely unchanged from results obtained with reaction periods of 4 h — which was true particularly for the series γ-valerolactone to γ-undecanolactone — it appeared that close to equilibrium conditions had been attained in most of the experiments (also see later).

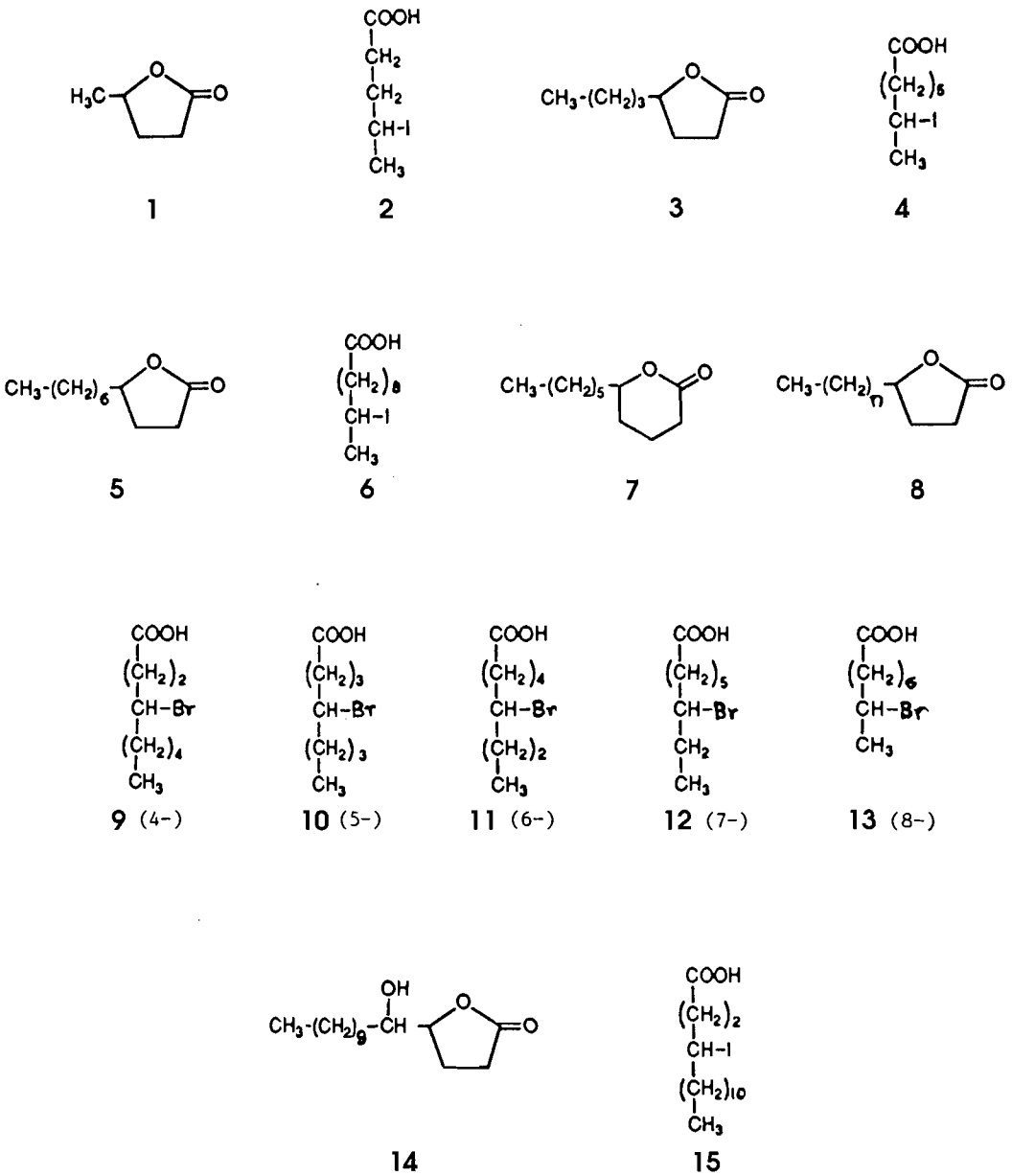

Overall, there is a progressive increase in sensitivity of the lactones towards ring-opening displacement by the halide, from the γ-butyrolactone structure to which a methyl group is appended (γ-*valero* (**1**)), to one in which the ring substituent is *n*-butyl. Then, there is relatively little difference through to an *n*-heptyl substituent. The *n*-dodecanolactone examined was the δ-form, which, at 18 h, yielded a 3:7 mixture of lactone and iodoacid. Although this result is entered with the γ-lactone data, its inclusion is justified by comparative experiments with γ- and δ-aldonolactones, and by the fact that δ-undecanolactone gave data (Table 1) closely similar to that of its γ-C_{11} counterpart.

In reactions with 57% hydrobromic acid under reflux, the γ-alkanolactones show characteristics broadly similar to those with hydriodic acid (Table 1), the product ratios again being based on integration of nmr spectra. Hydrobromic acid is noticeably less effective in the ring opening of the γ-valero- to γ-octanolactones, whereas its impact on the 9- to 16-carbon lactones is closer to, or surpasses, that of hydriodic acid.

Can. J. Chem. Downloaded from www.nrcresearchpress.com by 213.200.69.106 on 09/08/12
For personal use only.

TABLE 1. Molar ratio of haloacid produced (A) to alkanolactone remaining (L) in an 18 h reaction period with 57% hydriodic or 48% hydrobromic acid

Lactone	Hydrogen halide	A:L	Lactone	Hydrogen halide	A:L
γ-Valero-	HI	0.4	γ-Undecano-	HI	4.9
	HBr	0.2		HBr	13.3
γ-Capro-	HI	0.8	δ-Undecano-	HI	4.6[a]
	HBr	0.4		HBr	11.5[a]
γ-Heptano-	HI	5.6	δ-Dodecano-	HI	2.3[a]
	HBr	1.6		HBr	32.3[a]
γ-Octano-	HI	10.1	γ-Tetradecano-	HI	20.0
	HBr	2.4		HBr	1.9
γ-Nonano-	HI	10.1	γ-Hexadecano-	HI	2.3
	HBr	8.3		HBr	1.9
γ-Decano-	HI	10.1	γ-Octadecano	HI	4.3
	HBr	11.5		HBr	3.3

[a]Lactone (L) was the rearranged γ isomer.

*Formation of isomeric monohalo-*n*-alkanoic acids*

Not only do these reactions produce the isomer corresponding to the expected halide displacement in the opening of the γ-lactone ring, i.e., the 4-halo derivative, but additional species in which carbon atoms of the chain exocyclic to the ring become substituted. For example, γ-octanolactone was found to yield an approximately 1:1.5:1.5:2 mixture of 4-, 5-, 6-, and 7-iodooctanoic acids. It seems probable (3) that this extensive isomerization involves the formation of a series of homologous olefinic and cationic (or radical) intermediates that accommodate migration of the iodine atom, from C-4 initially, towards the methyl terminus. However, substitution by halogen proceeds only to the *penultimate* carbon, corresponding overall to Markownikow addition of hydriodic acid.

The iodination products of γ-nonoic, -decanoic, and -undecanoic lactones were found, analogously, to be mixtures of correspondingly more numerous species. For example, the ^{13}C nmr spectrum of the 18 h reaction product from the C_{11} lactone (**5**) accounted for at least 60 individual resonances, including a minimum of 6 carboxyl signals. The ^{1}H nmr evidence that one prominent component was the 10-iodo isomer (**6**) was a strong doublet (δ 1.95) attributable to the deshielded CH_3 group.

The δ-isomer of undecanolactone (**7**) was converted into a mixture of iodoacids closely similar to that described for the γ-lactone, by reaction with HI for 18 h (Table 1). At 1 h and 4 h, however, none of the δ-lactone was detectable, which showed that opening of the six-membered ring occurred rapidly and quantitatively. Subsequently, isomerization reactions afforded not only the same mixture of iodoacids as obtained from the γ-lactone in 18 h, but 18% of the latter lactone as well.

The ^{13}C nmr spectra of the bromo- and iodoalkanoic acids

The mixed populations of haloacids obtained from the reaction of hydrogen bromide with the longer-chain lactones were more easily characterized by ^{13}C nmr spectroscopy than were the iodoacids, because stronger deshielding by the bromine atoms causes the ^{13}C nuclei to which they are attached to resonate in a region (δ 50–60) well separated from those of the other carbons. This provided evidence of a self-consistent pattern of chemical shifts and intensities within the series as the number of isomers progressed from two (for caprolactone) to eight (for dodecanolactone). Representative is the spectrum of the mixture recovered from the reaction of nonanolactone (**8**, $n = 4$) (Fig. 1), in which five signals for bromine-substituted carbons, attributed to monobromoacids **9**–**13**, are evident (δ 52–60). Complementing these are the five carboxyl ^{13}C signals at δ ~ 180. Results are given in Table 2 for all of the products obtained in a reaction period of 18 h, which, for most of the lactones, appear to be close to equilibrium values. Among these data are found nearly constant chemical shift values attributable to C-4 (δ ~ 57), and also for the ω − 1 and ω − 2 carbons (δ ~ 52 and δ ~ 60), which, respectively, are the most and least strongly shielded within each group. In general, the values are listed in the order shown on the basis of known additivity relationships (e.g., see ref. 4), and because as additional isomers appear with a progressive increase in chain length, their ^{13}C-Br signals conform to a seemingly consistent pattern of chemical shifts. Nevertheless, the reliability of these latter assignments is of lesser importance in the overall analysis because, within each set, these isomers were formed in approximately equal proportions (Table 2).

Comparable ^{13}C data were not readily accessible for the alkyl carbons of the iodoacids, because of an overlap between the range of chemical shifts for the substituted and methylenic carbons, and attempts to differentiate between them (by means of DEPT experiments) were only partially successful. However, data for the carboxyl carbons provided evidence that the compositions of the mixtures of iodoacids were closely similar to those of the bromoacids.

To a substantial degree, the patterns of $^{13}C{=}O$ signals in the two series were duplicates, and matched the data in Table 2 for the methine carbons. For example, representative data for the iodoacids (Table 3) show that the products of the reaction of the C_7–C_{10} lactones with HI for 18 h gave three, four, five, and six $^{13}C{=}O$ peaks, respectively (see, e.g., Fig. 1). The latter accounted for both the same number of isomers and for ratios of similar magnitude (i.e., largely independent of differences in T_1 and nOe) as had been deduced from ^{13}C-Br signals (Table 1) for the corresponding bromoacids. Table 3 also shows that the location of a halogen atom on C-4, or C-5, through to C-9, makes for small incremental differences in the shielded state of a carboxyl carbon, so that it resonates furthest downfield (δ ~ 180)

Can. J. Chem. Downloaded from www.nrcresearchpress.com by 213.200.69.106 on 09/08/12
For personal use only.

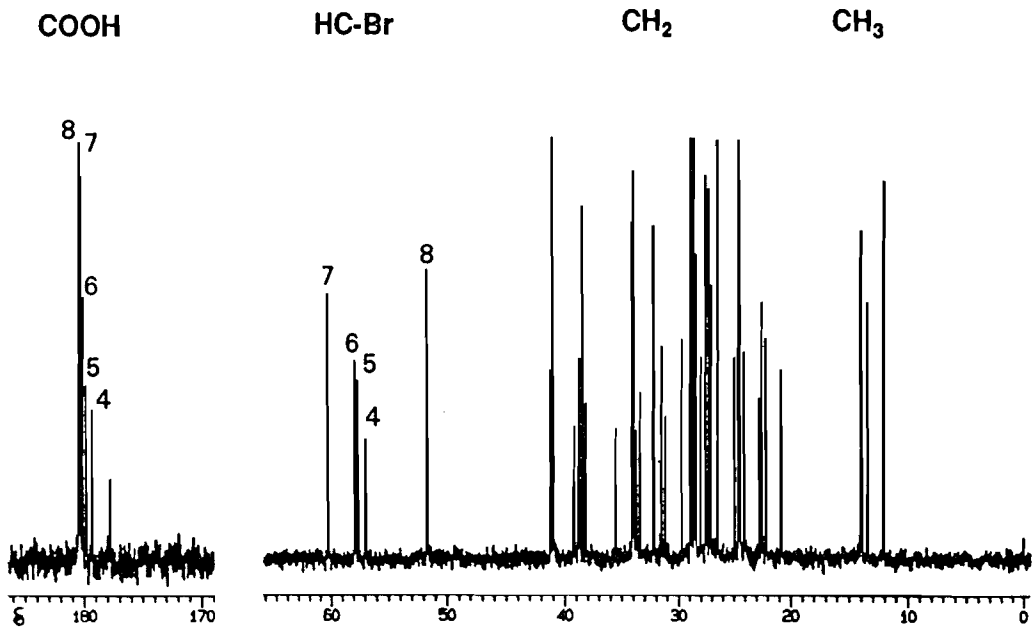

FIG. 1. The 67.8 MHz ^{13}C nmr spectrum of the mixture of monobromooctanoic acids isolated from the reaction of γ-nonanolactone with 48% hydrobromic acid under reflux for 18 h. The numbered signals in the region δ ~ 50–60 are those assigned to the individual isomers in which a bromine atom is attached to carbon-4, -5, -6, -7, or -8. Signals near δ 180, attributable to the carboxyl carbons of these monobromoacids, are designated accordingly. The minor signal at δ 177.8 is due to the C=O group of the unreacted lactone.

when the halogen is on the penultimate carbon (ω − 1), and at highest field (δ ~ 179) when it is on C-4. Although we are unable to assign the other individual peaks, which are due to C-5 through C-8, the consistency evident in the order of their occurrence as the length of the carbon chain is increased implies a simple linear progression of accompanying downfield shifts. It is also worth noting that the bromo acids gave $^{13}C{=}O$ results closely analogous to those in Table 3; this implies that the stronger deshielding effect by the bromine atom relative to the iodine atom, evident at the site of substitution, is not transmitted to the carboxyl carbons.

Limits to isomerization among longer-chain haloacids

Whereas the isomers substituted at the penultimate (ω − 1) carbon or its secondary neighbor (ω − 2) were the major products among the shorter-chain molecules, their percentages decreased as the number of carbon atoms reached 11 and 12 (Table 2). This suggested that factors controlling the migration of halogen atoms along the *n*-alkyl chains are subject to limiting conditions in the larger molecules.

In fact, a notable change in reaction characteristics was found with the C_{14} lactone, γ-tetradecanolactone (**8**, $n = 9$). Although 65% of this compound was converted into bromoacid (Table 1; more iodoacid was formed), little isomerization occurred (Table 2). By far the major product was the 4-isomer, and the only other species detected corresponded to about 10% of 5-bromotetradecanoic acid. However, the 18 h reaction had not reached equilibrium, as shown by the fact that a 65 h run resulted not only in a higher yield of bromoacid (A:L = 8:1), but also in the formation of a mixture of 9- and 10-isomers, all present in about the same proportion. By contrast, control experiments of 65 h with HBr for the C_{10} and C_{12} lactones gave essentially the same results as at 18 h, confirming that the data for them in Table 2 represent close to equilibrium conditions.

Among other reactions examined was that of a 15-carbon lactone, i.e., 5-hydroxy-γ-pentadecanolactone (**14**), with HI. By analogy with aldonolactones, it would be expected to undergo reduction and lactone-ring opening to yield 4-iodopentadecanoic acid (**15**), or more than one iodoacid if isomerization were to occur. In 18 h reaction time, according to the $^{13}COOH$ signals observed for the products isolated (Table 3), only four iodoacids had been formed. When the reaction time was increased to 36 h, the presence of two or three additional, more minor, species was detected. Consequently, the iodine atom introduced at C-4 during, or following, reduction of OH-5 of **14** was much more resistant to migration along the carbon chain than for lactones having 12 or fewer carbons.

It is worth noting that as an optically active form of **14** was available, it was used as an additional check on evidence that the products formed through hydriodic acid reduction and iodination undergo racemization. The mixture of iodoacids proved, in fact, to be optically inactive.

Supplementing the observation that the rate and (or) degree of isomerization of these haloacids becomes notably smaller when chain lengths reach a value of about 14 carbon atoms are the results obtained with the C_{16} and C_{18} lactones. That is, whereas they also undergo extensive lactone-to-acid interconversion (Table 1), it is not accompanied by appreciable isomerization. In addition to the 4-bromoacid (^{13}C-Br signal at δ 56.9, Table 2), γ-hexadecanolactone (**8**, $n = 11$) afforded a low yield of only one other isomer, likely the 5-bromide. In its reaction with HI, on the basis of the carboxyl ^{13}C data (Table 3), γ-hexadecanolactone gave four iodoacids; the isomer taken to be 4-iodohexadecanoic acid (δ 178.81) made up almost one-half of the mixture, whereas the 5-iodo isomer (δ 179.43) accounted for another one-quarter of the product.

Only a single product, likely 4-bromooctadecanoic acid, was produced in the 18 h reaction of γ-octadecanolactone (**8**, $n = 13$) with HBr (Table 2), and when the reaction time was increased to 65 h, only a trace proportion of a second species was detected.

Can. J. Chem. Downloaded from www.nrcresearchpress.com by 213.200.69.106 on 09/08/12
For personal use only.

Can. J. Chem. Downloaded from www.nrcresearchpress.com by 213.200.69.106 on 09/08/12
For personal use only.

TABLE 2. Molar ratios of the isomeric monobromoacids formed in 18 h by reaction of *n*-alkanolactones with 48% hydrobromic acid, and (in parentheses) chemical shifts of the corresponding halogen-substituted ^{13}C nuclei used for estimation of the ratios

	Position of bromine atom							
Lactone	4	5	6	7	8	9	10	11
C_6	1 (58.6)	3.2 (50.6)						
C_7	1 (57.0)	4.4 (59.4)	7.2 (51.3)					
C_8	1 (57.0)	1.6 (57.3)	2.4 (59.9)	2.8 (51.6)				
C_9	1 (56.9)	1.5 (57.5)	1.7 (57.8)	2.2 (60.2)	2.4 (51.7)			
C_{10}	1 (56.9)	1.4 (57.6)	1.4 (58.1)	1.4 (58.2)	2.3 (60.4)	2.3 (51.8)		
C_{11}	1 (56.9)	1.3 (57.5)	1.2 (58.1)	1.2 (58.3)	1.2 (58.5)	2.1 (60.5)	1.9 (51.8)	
C_{12}	1 (56.8)	1.4 (57.5)	1.7 (58.1)	1.5 (58.4)	1.9 (58.5)	1.9 (58.6)	2.6 (60.5)	2.2 (51.9)
C_{14}	1 (56.9)	0.1 (57.6)						
C_{16}	1 (56.9)	0.1 (57.6)						
C_{18}	1 (56.9)	<<0.1						

TABLE 3. ^{13}C Chemical shifts and relative peak intensities (in parentheses) for the carboxyl groups of isomeric monoiodoacids formed in 18 h by reaction of 47% hydriodic acid with *n*-alkanolactones, and the corresponding sites of iodination

	Position of iodine atom							
Lactone	11	10	9	8	7	6	5	4
C_6							179.10 (1)	178.41 (0.5)
C_7						179.66 (1)	179.50 (0.7)	178.90 (0.2)
C_8					180.19 (1)	180.00 (0.8)	179.69 (0.4)	179.02 (0.3)
C_9				180.52 (1)	180.42 (0.7)	180.23 (0.4)	179.91 (0.3)	179.27 (0.2)
C_{10}			180.57 (1)	180.52 (0.5)	180.40 (0.4)	180.21 (0.4)	179.90 (0.3)	179.27 (0.2)
$C_{11}(\gamma)$		180.61 (1)	180.58 (1)	180.51 (0.6)	180.42 (0.5)	180.21 (0.6)	—	179.40
$C_{11}(\delta)$		180.60 (1)	180.57 (0.8)	180.52 (0.5)	180.41 (0.5)	180.21 (0.5)	179.90 (0.4)	179.40 (0.3)
$C_{12}(\delta)$	180.62–180.60 (1)		180.5 (0.5)	180.50 (0.5)	180.40 (0.5)	180.19 (0.4)	179.98 (0.3)	179.50 (0.2)
C_{14}					180.31 (1)	180.08 (1.3)	179.77 (3.0)	179.95 (10.0)
C_{15}[a]					180.27 (1)	180.06 (2.2)	179.76 (4.6)	179.12 (3.4)
C_{16}					179.97 (1)	179.76 (1.5)	179.43 (1.9)	178.81 (3.7)
$C_{16}(HBr)$[b]							179.43 (1)	178.93 (9.1)

[a]5-Hydroxy derivative.
[b]Product of reaction with 48% hydrobromic acid.

Can. J. Chem. Downloaded from www.nrcresearchpress.com by 213.200.69.106 on 09/08/12
For personal use only.

Consequently, it is clear that the length of the carbon chain eventually introduces limits to the impetus for isomerization of the 4-haloalkanoic acid produced through lactone-ring opening. The presence of 14–16 carbon atoms in a molecule imposes a marked reduction in the rate of isomerization relative to 10–12 (or fewer) carbon atoms, whereas when the 4-haloacid contains 18 carbon atoms, it is a uniquely stable species within the series. This distinctiveness is emphasized by the fact that the 4-substituted isomer is the *least* populous (Tables 2 and 3) among the individual members of the C_6 to C_{12} mixtures of haloacids.

Sources of variations in haloacid composition

A number of possibilities have been considered to account for these marked variations in product composition among the equilibrated lactone–haloacid mixtures. In view of the large array of isomeric haloacids produced by the short-to-medium chain lactones (C_6 to C_{12}), we have surmised (3) that an increase in entropy will favor the occurrence of as many isomers as possible in each mixture, i.e., from the product monosubstituted on C-4, to that on the $\omega - 1$ carbon. This is consistent with the production of an overall lower yield of haloacid from the C_5 lactone, which yields only one isomer, than from, e.g., its C_9 homologue, which gives five isomers. Perhaps, however, such a factor decreases in importance as the carbon chain length reaches a level of 12 or more, because the ring opening of the lactones would then lead to increasing degrees of disorder associated with the release of increasingly more flexible alkyl chains. (Whether or not the reduction in entropy due to dimerization of the carboxylic acids would even out across the series is unclear.) As to enthalpy contributions, we are unaware of thermochemical data that may account for the observed differences in relative stability among individual isomers *within* each mixture, e.g., to account for the 1–2.3 difference found in the equilibrated populations of 4- and 9-bromodecanoic acids.

Among the longer-chain molecules, less effective solvation by the haloacid media also should be a factor. That the initial ring-opening step appears to occur with about equal facility for C_8 to C_{18} lactones (<30% of each lactone remains intact at 18 h, Table 1) is consistent with the fact that this step involves attack on the more hydrophilic site common to each of these molecules. However, solvation could be a limiting factor during the subsequent isomerization process, which may comprise (3) such steps as thermal elimination, protonation, and carbocation rearrangement,[2] because the longer the hydrocarbon chain of the 4-haloacid (or 5-, from a δ-lactone), the less effective its interaction with the hydrated hydrogen halide. Consequently, the marked decrease in the extent of isomerization of the haloacids having more than 12 carbon atoms may by analogy be related to well-known characteristics of long-chain *n*-alkyl derivatives that have a polar terminus, as found (7) in the formation of micelles or lipid bilayers.

[2]It is less likely that a free radical mechanism is involved, because no halogen atom is introduced at C-2, C-3, and CH_3, whereas these carbons are substituted, e.g., in the free radical chlorination of methyl heptanoate (5) (as kindly pointed out by a referee). Nevertheless, one analogy with the present data is the fact that the major product of this, and related, free radical halogenations (5, 6), is the isomer substituted at the penultimate position.

TABLE 4. Molar ratio of haloacid produced (A) to alkanolactone remaining (L) at different reaction periods with (ca. 37%) HCl

Lactone	Ratio acid/lactone 18 h	65 h
γ-Valerolactone	0.02	—
γ-Caprolactone	0.04	0.04
γ-Octanolactone	0.25	0.38
γ-Nonanolactone	0.38	—
γ-Decanolactone	0.16	0.17
γ-Undecanolactone	0.19	0.23
γ-Octadecanolactone	—	0.10

Reactions of lactones with 38% hydrochloric acid

In marked contrast to the facile conversion of *n*-alkano-γ- or δ-lactones into haloacids by HI or HBr, little reaction occurred under reflux in HCl (37%). As already described for reactions of the other haloacids, the extent of chloroacid formation was estimated by nmr spectroscopy from the relative intensities of the appropriate signals, i.e., those of ^{1}H-C-Cl and ^{1}H-C-O at δ 3.9 and 4.5, respectively (or the corresponding ^{13}C signals). Both γ-valerolactone and γ-caprolactone remained almost unaffected in the HCl solution (Table 4), although the longer-chain lactones gave appreciable yields of chloroacids. This difference parallels the increase in reactivity towards HI and HBr with respect to an increase in the length of the *n*-alkyl chain.

Some rearrangement was also observed, although relatively longer reaction times were required. For example, whereas the 18 h reaction product from γ-octanolactone exhibited mainly one signal (δ 62.80) attributable to ^{13}C-Cl, assumed to be that of C-4, several chloroacids were detected at 65 h. They were represented by peaks at δ 65.44, 63.22, 62.94, and 58.74, in a ratio of 1.1:1:1.2:1.5. By analogy with the other haloacids, the peaks are taken to be those of the 6-, 5-, 4-, and 7-chlorooctanoic acids, respectively, which shows that in this series also the penultimate carbon was the most highly substituted, despite the low overall level of chlorination. Supporting evidence was furnished by data for the carboxyl carbons, which have characteristics similar to those of the other haloacids. Referring again to the 65 h reaction product from γ-octanolactone, its ^{13}C spectrum contained peaks at δ 178.88, 178.67, 178.33, and 177.81, in a ratio of 1.7:1.5:1.2 (in addition to the much stronger lactone peak at δ 177.69) consistent with the presence of four isomeric chloroacids, among which the C-7 isomer was the major species.

Synthesis of-γ-tetra- and-γ-hexa-decanolactone

These syntheses involved the formation, initially, of the appropriate 4-keto-acid, by condensation of succinic anhydride with either decyl or dodecyl magnesium bromide in the presence of cadmium chloride (2, 8, 9). The ketone was reduced with borohydride to the 4-hydroxy-acid which, upon distillation, afforded the γ-lactone (**8**, $n = 9$, or **8**, $n = 11$).

Experimental

Nuclear magnetic resonance spectra were recorded with a Jeol CPF-270 spectrometer operating at 270 MHz for ^{1}H and 67.8 MHz for ^{13}C and (or) a Varian Unity 500 spectrometer operating at

Can. J. Chem. Downloaded from www.nrcresearchpress.com by 213.200.69.106 on 09/08/12
For personal use only.

500 MHz for ^1H and 125.7 MHz for ^{13}C. The solvent was $CDCl_3$ and chemical shifts are given with respect to TMS. Mass spectra were recorded with a double focusing Kratos MS25RFA mass spectrometer. Chemical ionization mass spectra were obtained with ammonia as the ionization reagent. Hydriodic acid (57%, <0.01% stabilizer) and hydrochloric acid (37%) were obtained from ACP Chemicals. Hydrobromic acid (48%) was obtained from Aldrich Chemical Co. The *n*-alkanolactones of from 8 to 12 carbon atoms were also obtained from Aldrich Chemical Co., whereas the C_{14}, C_{15}, C_{16}, and C_{18} lactones were prepared by slight modifications of established methods. The γ-tetradecanolactone and the γ-hexadecanolactone were obtained from the corresponding 4-ketoacids, whereas the C_{15} and the C_{18} lactones were synthesized by different routes. Representative examples of the lactone preparations and their reactions with haloacids are given below.

4-Keto-tetradecanoic acid

Cadmium chloride (3.27 g, 17.8 mM), previously dried at 120°C, was added to decylmagnesium bromide (Aldrich, 1 M solution in diethyl ether, 33 mL). The reaction mixture was heated to reflux under nitrogen for 45 m. Dry benzene (10 mL + 20 mL) was then added while the ether was distilled off, which was followed by a reflux period of 15 min. Succinic anhydride (3,0 g, 30 mM) was then added, the reaction mixture was heated under reflux for 4 h, and then stirred at room temperature for 18 h. The product, a dark brown paste, was poured onto 65 g of ice and the complex was decomposed with 1 N H_2SO_4. Ethyl ether (150 mL) was added, causing the solid to dissolve, the organic layer was separated, and the aqueous layer was washed with ether (2 × 100 mL). The combined ether fractions were washed with a saturated NaCl solution (2 × 50 mL) and water (50 mL), dried over anhydrous $MgSO_4$, and concentrated. A white solid was obtained, and was recrystallized from ether–hexane; yield 6.14 g (84%); mp 85–86°C; ^{13}C nmr (ppm): 209.1, 178.3, 42.8, 36.8, 31.9, 29.6, 29.4, 29.2, 27.7, 23.8, 22.7, 14.1; ms *m/z*: 242.1877 (M, $C_{14}H_{26}O_3$ = 242.1881). EI-mass spectrum *m/z*: 242, 169, 116, 111, 101, 98, 85, 71, 57, 51, 43. CI-mass spectrum (NH_3 induction) *m/z*: 260 [M + 18], 243 [M + 1], 242 [M].

4-Keto-hexadecanoic acid

The procedure and scale were as above, using dodecyl magnesium bromide (Aldrich). A portion of the crude product (8.1 g, 100%) was recrystallized from ether, mp 82–83°C (lit. (7) mp 91–92°C); ^{13}C nmr (ppm) 209.1, 178.8, 42.8, 36.8, 31.9, 29.7, 29.7, 29.5, 29.5, 29.4, 29.3, 29.2, 27.8, 23.8, 22.7, 14.1; ms *m/z*: 270.2194 (M − $C_{16}H_{30}O_3$ = 270.2181). EI-mass spectrum *m/z*: 270, 253, 197, 116, 111, 98, 85, 71. CI-mass spectrum (NH_3 induction) *m/z*: 288 [M + 18], 271 [M + 1], 253 [M − 17].

*γ-Tetradecanolactone (**8**, n = 9)*

The 4-keto-tetradecanoic acid (1.57 g, 6.5 mM) was stirred in EtOH (20 mL) at 5°C, while a solution of $NaBH_4$ (0.5 g, 13 mM) in 50 mL of 1 N NaOH was added dropwise. The reaction mixture was then stirred at room temperature for a further 3 h, acidified with dilute H_2SO_4, and extracted into CH_2Cl_2 (3 × 75 mL). The organic layer was washed with saturated NaCl solution (2 × 25 mL), dried over anhydrous $MgSO_4$, and concentrated. A white solid was obtained that, on distillation (150–155°C, 0.5 mM), afforded a colorless oil; yield 0.52 g (80%); ir (neat, cm^{-1}): 1773 (C=O); ^1H nmr: 4.5 (m 1H), 2.2–2.6 (m 3H), 1.5–2.0 (m 3H), 1.2–1.4 (s 16H), 0.8–0.10 (t, 3H); ms *m/z*: 226.1987 (M − $C_{14}H_{26}O_2$ = 226.1932); EI-mass spectrum *m/z*: 226, 208, 85, 69, 55. CI-mass spectrum (NH_3 induction) *m/z*: 244 [M + 18], 227 [M + 1].

*γ-Hexadecanolactone (**8**, n = 11)*

4-Keto-hexadecanoic acid was reduced by the same procedure as above. The product was a white solid; yield, 72.5%; mp 38°C (lit. (9) mp 40.7–41.3°C); ir (cm^{-1}): 1751 (C=O); ^1H nmr (ppm): 4.5 (m 1H), 3.45–3.6 (m 2H), 2.2–2.4 (m 1H), 1.5–2.00 (m 3H), 1.2–1.5 (s 20H), 0.8–0.9 (t 3H); ^{13}C nmr (ppm): 177.32, 81.08, 35.59, 31.91, 29.63, 29.53, 29.47, 29.35, 28.88, 28.02, 25.23, 22.68, 14.17; ms *m/z*: 254.2237 (M − $C_{16}H_{30}O_2$ = 254.2257). EI-mass spectrum *m/z*: 254, 236, 85. CI-mass spectrum (NH_3 induction) *m/z*: 272 [M + 18], 255 [M + 1].

*γ-Octadecanolactone (**8**, n = 13) (γ-stearic lactone)*

Prepared according to the method of Clutterbuck (10), the white solid was obtained in 25% yield, mp 45–47°C (lit. (8) mp 52–53°C; yield 30%); ir (film, cm^{-1}): 1751 (C=O), 1195; ^1H nmr: 4.4–4.6 (m 1H), 2.2–2.6 (m 6H), 1.4–1.8 (m 3H), 1.2–1.3 (s 24H), 0.0–0.9 (t 3H); ^{13}C nmr: 177.34, 81.08, 35.59, 31.93, 29.66, 29.53, 29.46, 29.35, 29.07, 28.88, 28.00, 25.23, 27.71, 22.70, 14.12; EI-mass spectrum *m/z*: 282 [M], 129, 97, 85 (major peak), 69, 60, 57, 43, 29.

*5-Hydroxy-γ-pentadecanolactone (**14**)*

This compound was prepared according to ref. 11, in an overall yield from glutamic acid of 43%. All of its spectra were in accord with those reported in ref. 11.

Reactions of the lactones with HI, HBr, and HCl

Representative are the following (the reactions were not protected against light or oxygen):

*Reaction of γ-undecanolactone (5-octyl-dihydro-2(3)-furanone) (**5**) with HI*

A solution of the lactone (0.40 g, 2.11 mM) in HI (57%, 5 mL), containing a suspension of red phosphorus (0.15 g), was heated under reflux for 18 h, and then cooled to room temperature. Saturated aqueous NaCl (5 mL) was added, followed by dichloromethane (50 mL), and the mixture was decolorized with concentrated sodium thiosulfate solution during the extraction. The organic layer was separated, washed with sodium chloride solution (2 × 5 mL), dried over anhydrous $MgSO_4$, and concentrated. A yellow oil was obtained, 0.65 g (95–99% yield), that according to ^1H and ^{13}C nmr spectra (see Tables 1–3) consisted of the lactone (9%) and a mixture of monoiodoundecanoic acids (91%).

*Reaction of γ-undecanolactone (**5**) with HBr*

A solution of the lactone (0.40 g, 2.11 mM) in HBr (48%, 5 mL) was heated under reflux for 18 h. The reaction mixture was worked up as above, with omission of the washing with thiosulfate. A yellow oil was obtained, 0.51 g (80% yield), that according to ^1H and ^{13}C nmr spectra (see Tables 1–3) consisted of the lactone (7%) and a mixture of monobromo-*n*-undecanoic acids (93%).

Reaction of γ-undecanolactone (5) with HCl

A solution of the lactone (0.38 g, 2.1 mM) in HCl (ca. 37%, 5 mL) was heated under reflux for 18 h, followed by work-up as above. A yellow oil was obtained, 0.48 g (99% yield), that according to ^1H and ^{13}C nmr spectra (see Table 4) consisted mostly of the lactone (84%) and a monochloroundecanoic acid (16%).

Estimation of product ratios

Ratios of haloacid produced to unreacted lactone (A:L) were estimated from the relative intensities of the ^1H nmr signals of the methine protons α to the halogen atom (δ ~ 4.2) and the lactone-ring oxygen (δ ~ 4.5), respectively. The ^{13}C nmr spectra were used to estimate ratios of the isomeric haloacids produced, based on the relative intensities of the resonances of the individual substituted carbons (H-^{13}C-X) and (or) of the individual carbonyl carbons. The ^{13}C data reported were obtained with a pulse angle of 40°, pulse delay of 0.80 s, and acquisition time of 1.0 s; comparative measurements of isomer ratios, based on the methine ^{13}C signals of the bromoacid mixture obtained from γ-undecanolactone, varied by a maximum of ~10% for pulse delays ranging from 0.80 to 2.0 s. (No allowance was made for possible variations in nOe values among the methine ^{13}C nuclei, or among the ^{13}CO nuclei.)

Gas–liquid chromatography, which was also examined as a means for product analysis in early experiments in this series (3), proved to be unsatisfactory because it was found that haloacid was readily reconverted into lactone within the chromatograph.

Acknowledgements

We express our thanks to the Natural Sciences and Engineering Research Council of Canada for valuable support, and to B. Lennox for helpful discussion.

1. H. Kiliani. Ber. Dtsch. Chem. Ges. **19**, 767 (1886); **19**, 1128 (1886).
2. A.S. Perlin and C.B. Purves. Can. J. Chem. **31**, 227 (1953).
3. Z. Liu, A. Granata, X. Shen, and A.S. Perlin. Can. J. Chem. **70**, 2081 (1992).
4. F.W. Wehrli, A.P. Marchand, and S. Wehrli. Interpretation of carbon-13 NMR spectra. 2nd ed. Heyden, London. 1983.
5. F. Minisci, G.P. Gardini, and F. Bertini. Can. J. Chem. **48**, 544 (1970).
6. D.D. Tanner and M.W. Mosher. Can. J. Chem. **47**, 715 (1969).
7. C. Tanford. The hydrophobic effect: formation of micelles and biological membranes. Krieger Publishing Co., Malabar, Fla. 1991.
8. F.S. Prout and J. Cason. J. Am. Chem. Soc. **66**, 47 (1944).
9. D.S. Houston. J. Am. Chem. Soc. **69**, 517 (1947).
10. P.W. Clutterbuck. J. Chem. Soc. 2330 (1924).
11. S. Iwaki, S. Marumo, T. Saito, M. Yamada, and K. Katagiri. J. Am. Chem. Soc. **96**, 7842 (1974).

Can. J. Chem. Downloaded from www.nrcresearchpress.com by 213.200.69.106 on 09/08/12
For personal use only.

What happens to formamide during C—N bond rotation? Atomic and molecular energetics and molecular reactivity as a function of internal rotation

KEITH E. LAIDIG[1]
College of Chemistry, University of California, Berkeley, CA 94720, U.S.A.

AND

LYNN M. CAMERON
Department of Chemistry, University of Victoria, Victoria, B.C., Canada V8W 3P6

Received December 21, 1992

KEITH E. LAIDIG and LYNN M. CAMERON. Can. J. Chem. **71**, 872 (1993).

We investigate the energetics of rotation about the C—N bond in formamide at the molecular and atomic levels using the HF/6-31G**//HF/6-31G** level of theory. At the molecular level, the barrier to rotation results from a decrease in overall attractive energies upon rotation away from the planar conformation, primarily due to the lengthening of the C—N bond. At the atomic level, the barrier is due to the loss in interatomic attraction between the nitrogen and its bonded neighbors. We investigate the susceptibility of formamide to electrophilic attack at nitrogen and oxygen as well as nucleophilic attack at carbonyl carbon as a function of C—N bond rotation using the Laplacian model of reactivity. The model predicts the susceptibility to nucleophilic attack at carbonyl carbon to reach a maximum with a O—C—N—H torsional angle of 60°. As a mimic of solvent fields, we investigate the effect of solvation upon these predictions with the application of homogeneous electric fields. This geometry–reactivity relationship is related to proposed models of activation in the enzymatic catalysis of peptides.

KEITH E. LAIDIG et LYNN M. CAMERON. Can. J. Chem. **71**, 872 (1993).

Opérant au niveau HF/6-31G**//HF/6-31G** de la théorie, on a examiné l'énergie de rotation autour de la liaison C—N du formamide aux niveaux moléculaire et atomique. Au niveau moléculaire, la barrière à la rotation est le résultat d'une diminution des énergies globales d'attraction sur la rotation provoquant une déviation par rapport à la conformation planaire et elle est due principalement à une augmentation de la longueur de la liaison C—N. Au niveau atomique, la barrière est due à une perte de l'attraction interatomique entre l'azote et les voisins qui lui sont liés. Faisant appel au modèle laplacien de la réactivité, on a examiné la susceptibilité du formamide aux attaques électrophiles sur l'azote et sur l'oxygène ainsi qu'aux attaques nucléophiles sur le carbone du carbonyle en fonction de la rotation autour de la liaison C—N. Le modèle prédit que la susceptibilité à une attaque nucléophile au niveau du carbone du carbonyle atteint son maximum lorsque l'angle de torsion du O—C—N—H est égal à 60°. Pour représenter les champs de solvant, on a étudié l'effet de la solvatation sur ces prédictions en appliquant des champs électriques homogènes. Cette relation géométrie–réactivité est reliée aux modèles proposés pour l'activation dans la catalyse enzymatique des peptides.

[Traduit par la rédaction]

Can. J. Chem. Downloaded from www.nrcresearchpress.com by 213.200.69.106 on 09/08/12
For personal use only.

Introduction

As an especially important model in the study of biological systems, there have been a number of investigations into the origin of the barrier to rotation in amides (1). The amide bond (or peptide bond) is the repeating structural unit linking amino acids together to form proteins and the hindered rotation about the C—N bond is responsible for the important secondary structure of polypeptides (2). Formamide is the smallest molecule incorporating this peptide bond and its barrier to rotation and its consequences will be the subject of this paper. We focus on the geometric changes and molecular and atomic energetics during the C—N bond rotation, and link these changes to the reactivity of the molecule.

The explanation for the hindered rotation most widely subscribed to invokes a resonance interaction that stabilizes the planar structure and delocalizes charge from the amide nitrogen to the carbonyl oxygen, schematically depicted in Fig. 1 (3). The contribution of the minor resonance structure on the right creates a double-bond-like character in the C—N interaction, hindering its rotation and inhibiting protonation at nitrogen. Recent studies brought this concept into question (1*a*) by comparing the distribution of electronic charge in the molecule predicted by the resonance model with that determined by theoretical calculation on the molecular and atomic levels, the latter by the application of the theory of atoms in molecules (4). This work and, subsequently, others (1*b*) demonstrated that the carbonyl group changes little during the process and that the dominant interaction is between the carbon and the nitrogen.[2]

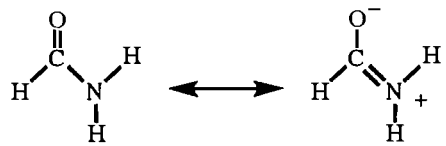

FIG. 1. A graphical depiction of the resonance interaction invoked as the explanation for the hindered rotation about the C—N bond in formamide. The formal charges suggested are the prediction of the resonance model as a result of delocalizing charge from the amide nitrogen to the carbonyl oxygen.

A recent theoretical investigation into the energetics of rotation and inversion processes demonstrated that the changes in the energetic contributions defined within the Hamiltonian could be readily reconciled with the geometric changes the molecule undergoes during these processes, thereby linking the geometrics and energetics in a dramati-

[1]Author to whom correspondence may be addressed.

[2]These conclusions have been contested recently (5*a*), but the arguments presented have been shown to be seriously flawed and without physical basis (5*b*).

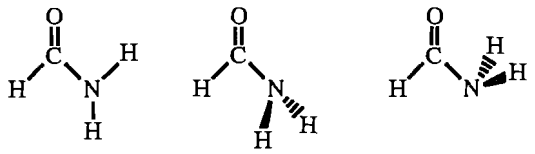

FIG. 2. A graphical depiction of the planar structure, **0**, and the two transition states, **TS(T)**, with its amide hydrogens *trans* to the carbonyl oxygen, and **TS(S)**, with its amide hydrogens *syn* to the carbonyl oxygen.

cally informative manner (6). The authors also briefly discussed the barrier to rotation in formamide, concluding that the molecule preferred the planar conformation as it was able to maximize the attractive energies despite larger repulsive energies. This peptide linkage and its hindered rotation are crucial to the conformational properties of biological systems. Given this, as well as its inherent interest, we have undertaken a detailed study of this rotational process using the same analytical approach, extending previous works by considering conformations throughout the rotation about the C—N bond at both the molecular and atomic levels.

We have employed the Laplacian model of chemical reactivity (7) to investigate the geometry–reactivity relationship during the C—N bond rotation in formamide. The oxygen of formamide is protonated in acidic solutions in favor of the nitrogen (8). Brown and co-workers extended this study to a range of amides in which the C—N bond is increasingly twisted and found that protonation at nitrogen became thermodynamically favored over protonation at oxygen (9). They also found that the C—N bond twisting increased the susceptibility of the carbonyl carbon to nucleophilic attack. We previously showed that the vulnerability to nucleophilic attack in formamide is correlated with the "holes" in the valence shell charge concentration (VSCC) of the carbonyl carbon (10). The rotation of the C—N bond from planarity pyramidalizes the carbon atom, enlarges the hole in the VSCC occupying the tetrahedral position, and leads to the enhanced reactivity of distorted amides. We have extended this to include study of both nucleophilic and electrophilic susceptibility during the bond rotation process. In addition, to mimic and investigate the effect of a solvent field, we have determined the nucleophilic susceptibility of each rotamer in the presence of homogeneous electric fields.

Methodology

We have considered a large number of conformers within the rotation process about the C—N bond in formamide. The planar conformation, **0**, and the two perpendicular transition states, one in which the amide hydrogens are *syn* to the carbonyl oxygen, **TS(S)**, and the other in which they are *trans* to it, **TS(T)** (see Fig. 2), were optimized using the constraint of C_S symmetry at the HF/6-31G** level of theory (11). Both transition states were characterized via the determination of the analytical second derivatives and were each found to possess one imaginary vibrational frequency, the normal coordinate of which would move the atoms towards **0**. The question of which is the transition state for the process under investigation is discussed below. We chose to use SCF procedures without the addition of electron correlation as the SCF wavefunctions generally obey the virial theorem (12) and the energetic contributions to the total energy are well defined.[3] Previous studies using MP2 correlation found barrier heights and conformations quite similar to those predicted here by the SCF procedures (*1b*). We performed multiconfiguration SCF (MCSCF) calculations using the 6-31G** basis with 4815 configurations for both **0** and **TS(T)**, and the resulting wavefunctions consisted of 99% of the ground state configuration in both cases. This demonstrates that this rotational process is primarily a ground state phenomenon and is well represented by our single-determinant SCF calculations. The conformers corresponding to the rotation about the C—N bond were also optimized using the HF/6-31G** basis, constraining only one O—C—N—H torsional angle and allowing all other internal coordinates to relax. In this manner, structures of C_1 symmetry, corresponding to points along the rotation coordinate, were calculated with torsional angles of 20°, 40°, 60°, 80°, and 100°, each referred to by its torsional angle, **20**, **40**, etc. The conformation in which the NH_2 group was held planar and made perpendicular to the carbonyl bond, **90P**, was also determined. The molecular calculations were done using the GAUSSIAN88 program suite (14). The MCSCF calculations were preformed with the GAMESS package (15). The HF/6-31G** wavefunction was used to determine the properties of the charge distribution and the atomic properties using the AIMPAC suite of programs (16).

We restricted ourselves to using energetic terms that are, in the absence of forces upon the nuclei or external fields, the only energetic quantities contained within the usual fixed nucleus Hamiltonian. We will group them into the attractive, or stabilizing, energies (V_a), the nuclear–electron attraction, and the repulsive, or destabilizing, energies (V_r), the sum of the electron–electron and nuclear–nuclear repulsions. These are related, by the viral theorem, to the total energy of the system (12). It should be remembered that the attractive energies are different in sign and that their components cancel one another in the sum to the total energy. In other words, given that the attractive energies are negative in sign, discussion of an increase in attractive energies implies a decrease in the absolute value and, similarly, an increase in the repulsive energies means an increase in its absolute value.

Molecular and atomic energetics

The total molecular energetics and their component parts are listed in Table 1, as are the relative values in comparison with the planar conformation, **0**. The total energy increases smoothly from the planar conformation to **TS(T)**, as do the torsion angles, Fig. 3. The energy change is initially quite small, being less than 1 kcal/mol to **20**, consistent with the very low vibrational frequency associated with out-of-plane torsion of NH_2. Our calculation predicts a frequency of 197.3 cm^{-1} at HF/6-31G**//HF/6-31G** for this mode. From **40** on to **100**, the energy decreases with roughly the same rate of change, a decrease of roughly 4.580 kcal/mol in the total energy for each 20°. From **100** on, the energy decreases much more slowly until **TS(T)** is reached, 18.665 kcal/mol above **0**. The conformation **90P** was pre-

[3]This is not necessarily the case with correlated methods. For example, there is no unique definition of a density matrix within the many-body perturbation series from which to calculate the molecular properties. See the appendix in ref. 13.

Can. J. Chem. Downloaded from www.nrcresearchpress.com by 213.200.69.106 on 09/08/12
For personal use only.

TABLE 1. Formamide molecular energetics and their components as well as the relative values in comparison to the planar conformation at HF/6-31G**//HF/6-31G**

	0[a]	20	40	60	80	100	TS(T)	TS(S)	90P
V_a[b]	−542.479	−542.276	−542.023	−541.390	−540.861	−540.430	−540.259	−540.486	−540.598
V_r	204.598	204.397	204.152	203.533	203.020	202.603	202.438	202.656	202.789
V	−337.881	−337.879	−337.871	−337.857	−337.840	−337.827	−337.822	−337.830	−337.809
E	−168.941	−168.940	−168.936	−168.928	−168.920	−168.914	−168.911	−168.915	−168.905
ΔE[c]	0.000	+0.521	+3.120	+7.579	+12.726	+16.852	+18.665	+15.973	+22.590
ΔE[d]	0.000	+0.001	+0.005	+0.012	+0.020	+0.027	+0.030	+0.026	+0.036
ΔV_a	0.000	+0.203	+0.456	+1.089	+1.618	+2.049	+2.220	+1.993	+1.881
ΔV_r	0.000	−0.201	−0.446	−1.065	−1.578	−1.996	−2.160	−1.942	−1.809
ΔV	0.000	+0.002	+0.010	+0.024	+0.040	+0.054	+0.060	+0.051	+0.072

[a]The conformers are listed by the O—C—N—H torsional angle.
[b]The energies listed are the total, E, the attractive, V_a, the repulsive, V_r, and total potential energies, V, for each conformer. They have been corrected for the virial defect and are listed in atomic units.
[c]The relative total energies are taken with respect to the planar conformation and are listed in kcal/mol.
[d]The relative energies are taken with respect to the planar conformation and are listed in atomic units.

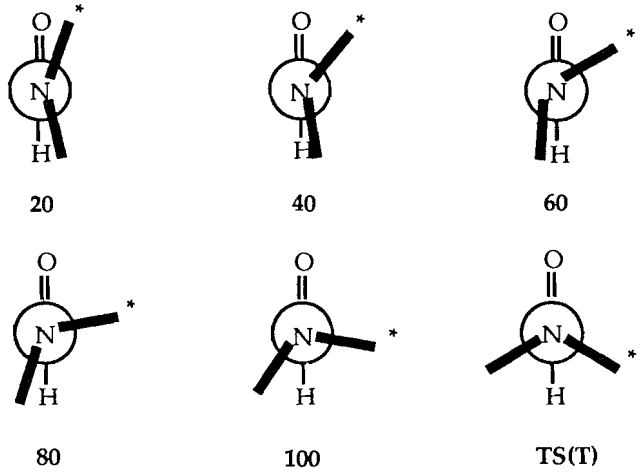

FIG. 3. The conformation rotamers during the C—N bond rotation, in which the N—H bonds are drawn with bold lines. The N—H that was constrained during the geometric relaxation is marked with an asterisk. The torsional angles are accurately depicted.

dicted to be 22.560 kcal/mol above the planar conformation and is not along the reaction coordinate.

The second transition state, **TS(S)**, is less destabilized than **TS(T)**, being 15.973 kcal/mol above **0**. This is the transition state used as the starting point of the potential energy surface walk of Wiberg and Breneman in their study of the rotation coordinate (1*b*). We were unsuccessful in our attempts to find **TS(S)** along the path of C—N rotation using the constrained approach discussed above. The change in O—C—N—H torsional angles in the coordinate walk of Wiberg and Breneman was not smoothly synchronous, having a large jump in one O—C—N—H torsion as the planar conformation was neared. The non-synchronicity of the internal coordinate change suggests that they are the result of a higher energy reaction coordinate and not the lowest energy pathway (17). Given the smooth synchronous change in internal coordinates and energies between **0** and **TS(T)**, we shall use it as the transition state in our C—N bond rotation study.

The geometric parameters change at rates in parallel with the changes in total energy, Table 2. As noted in other works, the C—O bond changes little along the reaction coordinate, shortening 0.014 Å by the transition state (1*a*). The C—N bond changes by five times as great an amount over the reaction coordinate, 0.073 Å, with a lengthening of roughly 0.015 Å per 20° C—N rotation, between **20** and **100**. Both N—H bonds lengthen slightly, as nitrogen pyramidalizes, while the C—H bond lengthens a similar amount. The bond angles involving N and H show the ever-increasing pyramidalization of N as the coordinate approaches the transition state.

As listed in Table 1, the energy changes can be broken into changes in the molecular attractive and repulsive potential energies, which, by virtue of the virial theorem, are related to the changes in the total energy. The energetic barrier to the C—N bond rotation is dominated by the decrease in attractive energy in the molecule. There is also a decrease in the repulsive energies of the system, but this is overcome by the loss in attraction and the system is destabilized. This loss in attraction is largely the result of the increase in the C—N interatomic distance with much smaller contribution from the increase in C—H and N—H distances. The decrease in the C—O bond length results in a gain in attractive energy during rotation, but as the C—O decrease is much smaller, so the attractive energy contributed is much smaller. Thus the barrier to rotation in formamide is the result of a loss in attractive energies due to the C—N bond lengthening during the process.

The atomic interactions are summarized in a quantitative manner by the properties of the charge density at the bond critical point between the two interacting atoms (18). The properties at the bond critical points between the pairs C—O and C—N are listed in Table 3. The C—N interaction decreases during the rotation, the magnitude of electronic charge dropping by roughly 10%. For C—O, the strength of interaction increases during rotation by roughly 2%. Both changes are in accord with expectations based upon the change in the bond lengths, the former bond lengthening by roughly five times the amount that the latter shortened. The large value of the charge density combined with the positive Laplacian at the bond critical point of C—O indicates an intermediate interaction. The depletion of charge in the interatomic region increases during the rotation, signalling the slowly increasing ionic character of the interaction. The negative

Can. J. Chem. Downloaded from www.nrcresearchpress.com by 213.200.69.106 on 09/08/12
For personal use only.

TABLE 2. Geometric parameters during C—N bond rotation[a]

	0[b]	20	40	60	80	100	TS(T)	TS(S)	90P
C—O	1.193	1.191	1.189	1.186	1.183	1.180	1.179	1.183	1.182
C—N	1.348	1.356	1.369	1.384	1.401	1.415	1.421	1.425	1.404
C—H	1.093	1.093	1.093	1.094	1.095	1.096	1.096	1.089	1.092
N—H[c]	0.994	0.996	0.998	1.000	1.002	1.004	1.003	1.004	0.991
N—H	0.991	0.994	0.997	0.999	1.001	1.003	1.003	1.004	0.991
O—C—N	124.887	124.804	123.691	124.413	123.929	123.451	123.251	125.018	124.527
O—C—H	122.362	122.238	122.831	121.259	120.768	120.487	120.320	121.410	119.941
H—C—N	112.750	112.883	113.196	113.908	114.964	115.939	116.429	113.572	115.532
C—N—H[c]	119.137	116.943	115.360	114.219	112.574	110.580	109.926	108.644	120.656
C—N—H	121.638	118.710	115.045	112.143	110.014	108.899	109.926	108.644	120.656
H—N—H	119.226	116.360	112.128	108.533	105.964	104.908	106.667	105.814	118.689
O—C—N—H[c]	0.000	20.000	40.000	60.000	80.000	100.000	121.438	58.290	90.000
O—C—N—H	180.000	167.809	172.967	184.009	197.932	214.772	236.562	301.710	270.000
H—C—O(—N)[d]	0.0	2.600	5.476	6.713	6.014	3.585	0.0	0.0	0.0

[a]The bond lengths are in angstroms and the bond angles and torsional angles are in degrees.
[b]The conformers are listed by O—C—N—H torsional angle, see text for definition.
[c]The hydrogen is fixed so as to define the O—C—N—H torsional angle.
[d]The pyramidalization of the carbonyl carbon is quantified by the angle between the C—H bond and the O—C—N plane.

TABLE 3. Bond critical point properties during C—N bond rotation[a]

	0	20	40	60	80	100	TS(T)	TS(S)	90P
C—O									
$\rho(r)$	0.434	0.432	0.436	0.437	0.438	0.434	0.440	0.436	0.436
$\nabla^2\rho(r)$	0.406	0.444	0.505	0.588	0.687	0.777	0.823	0.781	0.818
ε	0.085	0.088	0.096	0.108	0.124	0.139	0.146	0.122	0.152
C—N									
$\rho(r)$	0.333	0.332	0.328	0.323	0.317	0.312	0.309	0.308	0.309
$\nabla^2\rho(r)$	−0.775	−0.874	−0.991	−1.116	−1.222	−1.245	−1.228	−1.223	−1.180
ε	0.011	0.009	0.032	0.056	0.071	0.074	0.076	0.076	0.139

[a]These are the properties of the charge density at the (3,−1) critical point between the two atoms, listed in atomic units.

Laplacian at the C—N critical point signals a shared, or covalent, interaction. The decrease in the absolute value of this during the rotation process indicates an increase in the concentration of charge between the two atoms. As the ability of the increasingly pyramidal nitrogen to withdraw charge from carbon decreases, the interaction becomes more and more evenly shared between the two atoms. The shortening of the C—O bond length increases the dominance of the oxygen atom on the interaction, while the lengthening of the C—N bond results in a more evenly shared interaction between the two.

The theory of atoms in molecules predicts the properties of atoms in the same way as the properties for the entire molecule (4). The atomic energetics are listed in Table 4 for all the rotamers. To briefly review the atomic properties, discussed previously (*1a*), on going from **0** to **TS** the changes in the atomic energy and population are much smaller for oxygen than for either carbon or nitrogen. The nitrogen atom shows the largest changes between **0** and **TS(T)**, losing population (−0.261 e) and becoming destabilized (+158.133 kcal/mol) as it pyramidalizes. The carbon gains population (+0.200 e) and is stabilized by a comparable amount (−90.989 kcal/mol). In contrast, the oxygen is relatively unchanged, losing a small amount of charge (−0.075 e) and becoming slightly more stable (−3.138 kcal/mol). This transformation is predicted by a simple hybridization model; the pyramidalizing N atom is less electronegative (it has less "s character"), loses charge to all its bonded neighbors during rotation, and is destabilized because of this.

We can attribute the changes in molecular energetic contributions to the total energy to changes within individual atoms. The nitrogen atom's contribution to both the attractive and repulsive energy decreases in magnitude during the rotation. The decrease in the atomic attraction energy $V_a(N)$ is greater than the decrease in the atomic repulsion energy $V_r(N)$, thus the atom is destabilized. In contrast, the carbon atom is stabilized by a larger increase in $V_a(C)$ than in $V_r(C)$. The oxygen atom is stabilized by the slightly greater decrease in repulsion energy over the decrease in attractive energies. Overall, the destabilizing loss in attractive energies for the nitrogen atom dominates the other atomic energy changes and is the origin of the barrier to rotation in formamide.

The amount of the total atomic attraction energy coming from the attraction of the nucleus to the electronic charge within its own atomic basin, the atomic value of $V_{neo}(\Omega)$ is also listed in Table 4. This "self-stabilization" of the atom

Can. J. Chem. Downloaded from www.nrcresearchpress.com by 213.200.69.106 on 09/08/12
For personal use only.

TABLE 4. Formamide atomic values HF/6-31G**//HF/6-31G**[a]

	0[b]	20	40	60	80	100	TS(T)	TS(S)	90P
Oxygen									
$N(\Omega)$	9.393	9.387	9.378	9.362	9.344	9.327	9.318	9.343	9.321
$E(\Omega)$	−75.651	−75.652	−75.653	−75.655	−75.656	−75.656	−75.656	−75.661	−75.664
$V_{neo}(\Omega)$	−185.664	−185.639	−185.596	−185.527	−185.442	−185.362	−185.319	−185.422	−185.335
$V_a(\Omega)$	−233.002	−232.978	−232.943	−232.705	−232.523	−232.368	−232.287	−232.673	−232.305
$V_r(\Omega)$	81.699	81.673	81.636	81.395	81.212	81.056	80.976	81.351	80.977
$V(\Omega)$	−151.303	−151.304	−151.306	−151.310	−151.312	−151.311	−151.311	−151.322	−151.328
Nitrogen									
$N(\Omega)$	8.478	8.444	8.394	8.344	8.285	8.227	8.217	8.230	8.429
$E(\Omega)$	−55.233	−55.203	−55.159	−55.107	−55.049	−54.995	−54.981	−54.985	−55.107
$V_{neo}(\Omega)$	−135.745	−135.588	−135.360	−135.127	−134.487	−134.617	−134.576	−134.623	−135.467
$V_a(\Omega)$	−182.725	−182.201	−181.482	−180.542	−179.538	−178.583	−178.339	−178.242	−180.741
$V_r(\Omega)$	72.260	71.796	71.163	70.328	69.440	68.594	68.377	68.272	70.527
$V(\Omega)$	−110.465	−110.405	−110.319	−110.214	−110.098	−109.989	−109.962	−109.970	−110.214
Carbon									
$N(\Omega)$	4.022	4.038	4.064	4.098	4.148	4.202	4.222	4.243	4.143
$E(\Omega)$	−36.549	−36.563	−36.582	−36.607	−36.643	−36.681	−36.694	−36.714	−36.624
$V_{neo}(\Omega)$	−81.557	−81.631	−81.746	−81.896	−82.116	−82.358	−82.443	−82.544	−82.062
$V_a(\Omega)$	−109.557	−109.711	−109.946	−110.269	−110.754	−111.312	−111.501	−111.688	−110.533
$V_r(\Omega)$	36.460	36.586	36.782	37.054	37.468	37.950	38.112	38.260	37.285
$V(\Omega)$	−73.097	−73.125	−73.164	−73.214	−73.285	−73.362	−73.389	−73.428	−73.248
Formyl hydrogen									
$N(\Omega)$	1.035	1.034	1.032	1.036	1.037	1.037	1.038	1.005	1.025
$E(\Omega)$	−0.654	−0.653	−0.652	−0.655	−0.655	−0.655	−0.654	−0.644	−0.652
$V_{neo}(\Omega)$	−1.331	−1.329	−1.327	−1.331	−1.331	−1.330	−1.330	−1.307	−1.324
$V_a(\Omega)$	−8.470	−8.458	−8.433	−8.467	−8.460	−8.446	−8.434	−8.174	−8.337
$V_r(\Omega)$	7.162	7.151	7.129	7.158	7.151	7.137	7.126	6.886	7.033
$V(\Omega)$	−1.308	−1.307	−1.304	−1.309	−1.310	−1.309	−1.308	−1.288	−1.305
Hydrogen[c]									
$N(\Omega)$	0.528	0.538	0.549	0.560	0.574	0.591	0.603	0.591	0.540
$E(\Omega)$	−0.421	−0.427	−0.434	−0.440	−0.446	−0.455	−0.463	−0.456	−0.429
$V_{neo}(\Omega)$	−0.841	−0.852	−0.865	−0.876	−0.890	−0.907	−0.922	−0.908	−0.854
$V_a(\Omega)$	−4.370	−4.458	−4.544	−4.597	−4.672	−4.779	−4.851	−4.864	−4.342
$V_r(\Omega)$	3.527	3.604	3.676	3.718	3.780	3.869	3.925	3.953	3.484
$V(\Omega)$	−0.843	−0.854	−0.868	−0.879	−0.892	−0.910	−0.925	−0.911	−0.857
Hydrogen									
$N(\Omega)$	0.544	0.559	0.583	0.600	0.613	0.617	0.603	0.591	0.540
$E(\Omega)$	−0.433	−0.442	−0.455	−0.465	−0.472	−0.473	−0.463	−0.456	−0.429
$V_{neo}(\Omega)$	−0.862	−0.880	−0.906	−0.924	−0.938	−0.941	−0.922	−0.908	−0.854
$V_a(\Omega)$	−4.338	−4.472	−4.669	−4.810	−4.923	−4.959	−4.851	−4.864	−4.342
$V_r(\Omega)$	3.472	3.588	3.759	3.880	3.979	4.014	3.925	3.953	3.484
$V(\Omega)$	−0.866	−0.884	−0.911	−0.930	−0.944	−0.946	−0.925	−0.911	−0.857
Sum of atomic properties over atoms									
N	23.998	24.000	23.999	24.000	24.001	24.002	24.001	24.002	24.000
E	−168.941	−168.940	−168.936	−168.929	−168.920	−168.914	−168.910	−168.915	−168.904
V_{neo}	−406.000	−405.919	−405.800	−405.681	−405.203	−405.515	−405.512	−405.712	−405.897
V_a	−542.461	−542.278	−542.017	−541.391	−540.870	−540.447	−540.263	−540.504	−540.600
V_r	204.579	204.399	204.145	203.533	203.030	202.620	202.442	202.675	202.791
V	−337.882	−337.879	−337.872	−337.857	−337.841	−337.827	−337.821	−337.830	−337.809

[a]The values are atomic population, $N(\Omega)$; atomic energy, $E(\Omega)$; atomic nuclear–electron attraction energy from density within the atomic basin, $V_{neo}(\Omega)$; total nuclear–electron attraction, $V_a(\Omega)$; atomic repulsion energy, $V_r(\Omega)$; total atomic potential energy, $V(\Omega)$, where Ω represents the generic symbol for an atom. See the text for definitions. All values are in atomic units. The energetic terms have been corrected for virial defects.

[b]The molecules are listed according to O—C—N—H angle. See text for definition.

[c]The constrained hydrogen used to define the torsional angle.

Can. J. Chem. Downloaded from www.nrcresearchpress.com by 213.200.69.106 on 09/08/12
For personal use only.

TABLE 5. Properties of the VSCC of oxygen, nitrogen, and carbon during C—N bond rotation[a,b]

(*a*) Magnitudes of charge concentration at the maxima in the VSCC of nitrogen and oxygen

	0	**20**	**40**	**60**	**80**	**100**	**TS(T)**	**TS(S)**	**90P**	
N	−214.436[c]	−251.745	−268.955	−284.696	−303.932	−332.794	−332.100	−332.081	−262.426[d]	−264.311[d]
O[e]	−624.521	−629.388	−637.535	−651.228	−667.180	−682.463	−690.728	−677.012	−694.190	
O	−629.740	−634.458	−641.987	−652.704	−667.482	−682.157	−691.299	−681.466	−694.867	

(*b*) Magnitudes of charge depletion at the holes in the VSCC of carbon[f]

	0	**20**	**40**	**60**	**80**	**100**	**TS(T)**	**TS(S)**	**90P**
No electric field									
h_1	129.822	144.798	151.584	152.666	148.896	140.110	128.284	141.905	143.064
h_2	129.822	119.764	115.957	114.086	114.042	117.634	128.284	141.905	143.064
Electric field: −0.01 au along *Z* axis									
h_1	132.359	146.219	152.443	153.389	149.889	141.800	131.471	144.574	
h_2	127.338	116.068	111.523	109.147	108.949	112.956	125.104	139.241	
Electric field: +0.01 au along *Z* axis									
h_1	127.338	143.433	150.761	151.966	147.923	138.440	125.104	139.241	
h_2	132.359	123.476	120.394	119.019	119.128	122.305	131.471	144.574	

[a]All values are listed in units of 10^{-3} au.
[b]The O—C—N linkage remains roughly within the *XY* plane during the rotation process.
[c]The listed value is one of the two symmetrically related maxima in the VSCC of N, one on either side of the molecular plane.
[d]The two maxima on either side of the N VSCC are not equal, the first being *syn* to the O.
[e]This maxima is *syn* to the NH_2 group.
[f]The hole labeled "h_1" is *syn* to the "lone pair" in the VSCC of N.

can be used to determine if the change in attractive energy is due to inter- or intra-atom interaction. The loss in $V_{neo}(N)$ for nitrogen during rotation is 26.6% of the total loss in attractive energy, suggesting that the major portion of stabilization loss is due to a decrease in interatomic interaction. For carbon, the stabilization from $V_{neo}(C)$ is 45.6% of the total stabilization, gaining roughly half of its stabilization from the gain in charge within its basin. Similarly, the loss in attractive energies for the oxygen atom is due to a 48.3% loss of $V_{neo}(O)$. So, the rotational barrier is dominated by a loss of attractive energies between nitrogen and its bonded neighbors during its pyramidalization.

Molecular reactivity

The susceptibility of oxygen and nitrogen to electrophilic attack is predicted by the magnitude of the Laplacian at the nonbonded maxima in the VSCC of the two atoms (4). These entities are the physical manifestation of the chemical concept of "lone pairs" and their size and extent are the physical basis for the Lewis and VSEPR models of chemistry (19). The values of the charge concentration at the maxima in the VSCC of both oxygen and nitrogen are listed in Table 5 for each of the rotamers along the reaction coordinate. The nonbonded maximum in the VSCC of nitrogen steadily increases from the planar to the transition state, increasing the predicted susceptibility to electrophilic attack. The planar nitrogen has two symmetrically related maxima on either side of the molecular plane, but by **20** there is only one maximum, found roughly in the tetrahedral position. This charge concentration increases until a maximum is reached at **100** and then decreases slightly to **TS(T)**. The two nonbonded maxima in the VSCC of the oxygen both increase during the rotation from **0** to **TS(T)**. The nonbonded maximum *syn* to the NH_2 group starts out smaller than the *anti*, but as the C—N rotation reaches **80** the maxima values become nearly the same and remain similar until **TS(T)** is reached. The magnitude of the VSCC in nitrogen increases by 54.9% during the rotation while the oxygen VSCC increases by only 10%.

The susceptibility of the carbonyl carbon to nucleophilic attack is predicted by the magnitude of depletion of charge at the hole in the atom's VSCC. These are the regions of greatest *depletion of charge* in the VSCC about the carbon atom and thus the favored pathway for nucleophilic attack (4, 10). An important consequence of rotation is the slight pyramidalization of the carbonyl carbon away from the constrained N—H bond, O—C—N—(H) torsion angle in Table 2, reaching a maximum of 6.7° out of the O—C—N plane at **60**. We have depicted the minima of the VSCC of the carbonyl carbon in a plane orthogonal to the O—C—N plane in Fig. 4. The magnitude of charge depletion in the VSCC of the carbonyl carbon is also listed in Table 5 and graphed versus torsion angle in Fig. 5. As noted previously (10), the charge depletion in the VSCC *syn* to the nonbonded maximum on nitrogen (h_1) increases in parallel with the degree of pyramidalization of the carbonyl carbon, Table 2. Both reach a maximum near **60** (the change in the VSCC of carbon is depicted in Fig. 4*b*) and then decrease as the transition state is reached, with the depletion being less than in the planar structure. Similarly, the charge depletion *anti* to the nitrogen maximum and *syn* to the hydrogens of NH_2 (h_2) decreases to a minimum in the region of **60–80** and then increases. This model predicts that the susceptibility towards nucleophilic attack at carbonyl carbon, *syn* to the nitrogen "lone pair," reaches a maximum in the vicinity of **60** and then decreases as the C—N bond is rotated further.

Can. J. Chem. Downloaded from www.nrcresearchpress.com by 213.200.69.106 on 09/08/12
For personal use only.

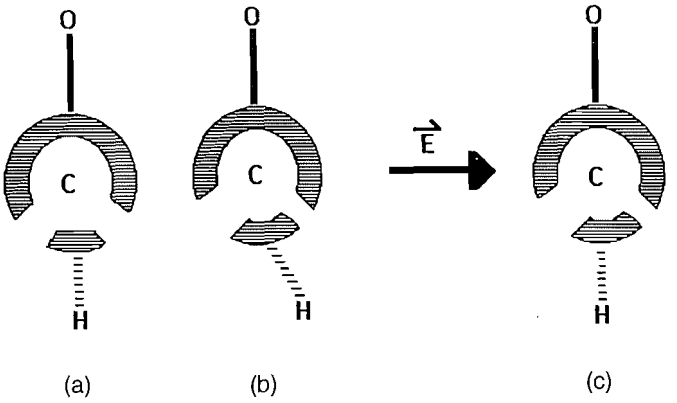

FIG. 4. A depiction of the VSCC (the dashed regions around C) of the carbonyl carbon in a plane perpendicular to the O—C—N plane and containing the holes in the valence shell. Figure 4*a* is the VSCC in the planar conformation, **0**; 4*b* depicts the reorganization of the VSCC of the carbonyl carbon after it has pyramidalized during C—N bond rotation; 4*c* depicts the reorganization of the VSCC under the influence of an electric field applied perpendicularly to the O—C—N plane. Notice that the internal fields (due to atomic motion) and the external fields yield the same changes within the VSCC.

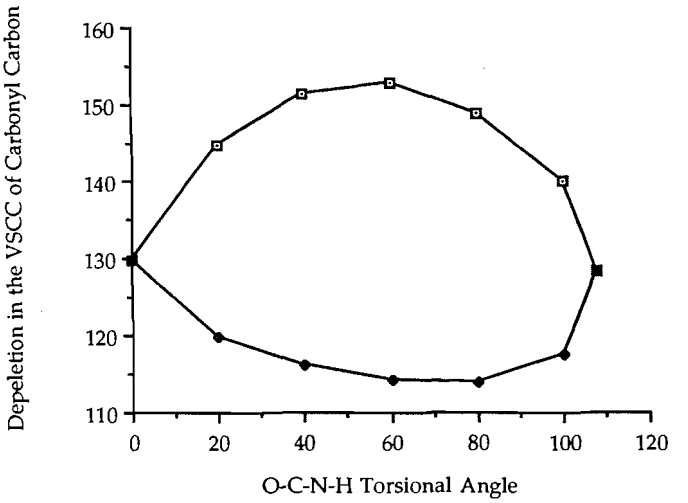

FIG. 5. This graph depicts the depletions in the VSCC of the carbonyl carbon as a function of torsion along the reaction coordinate; h_1, ⊡; h_2, ◆.

There has been some concern as to the stability of the predicted values of the Laplacian in the valence shell of carbonyl carbon to the effects of solvent or an approaching reacting molecule. To address this, we mimicked the effect of an external field upon these predictions by applying homogeneous electric fields to each rotamer along the reaction coordinate as a first-order approximation to the Onsager reaction field (20). The charge depletion at the holes in the resulting VSCC of the carbon are listed in Table 5. For the field orthogonal to the O—C—N plane, both positive and negative, the correlation between the pyramidalization of the carbonyl carbon and the charge depletion is kept. For example, the application of +0.01 au along the *Z* axis (roughly perpendicular to the molecular plane) results in a decrease in the charge depletion at the VSCC hole *syn* to the nitrogen maxima during the C—N bond rotation. This is the result of the reorganization of the valence shell of the carbonyl carbon under the influence of the electric field and is depicted in Fig. 4*c*, and demonstrates that the differences in the depletion on the two sides of the carbonyl carbon are physically significant and resistant to perturbation by external fields or reactant molecules. In addition, the systematic changes in the charge depletion when perturbed by applied electric fields show that the VSCC and its critical points respond in a physically reasonable manner.

Discussion

Proteases catabolize proteins by catalytic hydrolysis of the peptide bonds (21). One proposed mode for the activation of the peptide bond is the addition of strain and distortion to the peptide linkage at the protease active site (22). This mechanism is believed to involve either the distortion of the NH_2 away from planarity or the direct pyramidalization of carbonyl carbon by the nucleophilic characteristics of the active site. In both cases, the induced strain is proposed to raise the energy of the peptide linkage, effectively reducing the barrier to hydrolysis. Brown and co-workers synthesized a variety of distorted amides with fixed pyramidalization of nitrogen and studied their relative rates of hydrolysis in acidic media (9). These experiments reveal that the degree of nitrogen pyramidalization is directly related to the increasing N—C(O) bond length and that the more distorted the amide, the faster it is hydrolyzed. This distortion of the amide from its favored planar structure was proposed to result in an activation of the peptide bond, producing a system that is closer in energy to the hydrolysis transition state. Quite recently, Krug et al. undertook a detailed theoretical analysis of the acid, neutral, and base hydrolysis mechanisms of peptides (23). They concluded that the key feature of the hydrolysis mechanisms is the lengthening and weakening of the C—N bond, which follows the pyramidalization and (or) protonation of the amide nitrogen.

Our results strongly support these findings. We find that rotation about the C—N bond results in a weaker C—N interaction and, consequently, a longer bond. The increased C—N distance causes a large loss in the stabilizing attractive energy for the nitrogen atom. To maximize the self-stabilization within its own basin, nitrogen pyramidalizes, further decreasing its interaction with its bonded neighbors and increasing its susceptibility to electrophilic attack. Although the C atom gains charge during this process it pyramidalizes slightly to maximize its self-stabilization and minimize its interaction with nitrogen. The valence shell of carbon reorganizes during its pyramidalization, resulting in an increased depletion, or enlargement of the hole in the VSCC opposite the N—H bonds, and thus making it more susceptible to nucleophilic attack. This mode of activation or increased susceptibility may come about from either the rotation about the C—N bond or, more directly, from the pyramidalization of carbonyl carbon by the local environment.

Conclusion

We have presented a detailed energetic analysis of the barrier to rotation in formamide at both the molecular and atomic levels. The energetic barrier results from a loss of attractive energies, despite decreases in repulsive energies, due to the lengthening of the C—N bond as nitrogen py-

Can. J. Chem. Downloaded from www.nrcresearchpress.com by 213.200.69.106 on 09/08/12
For personal use only.

ramidalizes. At the atomic level, the destabilization is dominated by the loss in interatomic attraction between the nitrogen and its bonded neighbors. The pyramidalization of nitrogen decreases its effective electronegativity, allowing its bonded neighbors to withdraw charge from it. The energetic stabilization gained by pyramidalization of N is large and determines the lowest energy pathway away from the planar conformation towards the transition state during the C—N rotation. We have also investigated the relationship between the geometrical changes and molecular susceptibility to electrophilic and nucleophilic reactivity. We found that the susceptibility to nucleophilic attack reached a maximum at the structure **60** and then decreased on to the **TS(T)**. The quantitative predictions made by the Laplacian model of reactivity were shown to be robust in the face of applied electric fields and the magnitudes of the depletion in the VSCC of the carbonyl carbon changed in readily understood ways. Our results were shown to be consistent with proposed models of enzymatic hydrolysis in peptides in that distortion around the carbonyl leads to enhanced susceptibility. We also found that our observations agree with solvolytic studies of strained amides and theoretical investigations of hydrolysis mechanisms.

Acknowledgements

We acknowledge the financial support of the National Institutes of Health (NIH grant no. 850RR05651A) for computational facilities that were used for the MCSCF calculations (Berkeley) and thank Dr. P. Speers for carefully reviewing our manuscript. We also acknowledge the support of Professor A. Streitwieser at Berkeley (K.E.L.) and of Professor T. Fyles at Victoria (L.M.C.).

1. (*a*) K.B. Wiberg and K.E. Laidig. J. Am. Chem. Soc. **109**, 5935 (1987); (*b*) K.B. Wiberg and C. Breneman. J. Am. Chem. Soc. **114**, 831 (1992); (*c*) R.H. Flegg and R.D. Harcourt. J. Mol. Struct. (Theochem), **164**, 67 (1988); (*d*) T. Tsuzuki, and K. Tanabe. J. Chem. Soc. Perkin Trans. 2, **8**, 1255 (1991); (*e*) T. Kizaki, K. Morihasi, and O. Kikuchi. J. Mol. Struct. (Theochem), **45**, 265 (1988).
2. B. Robson and J. Garner. Introduction to proteins and protein engineering. Elsevier, New York. 1986.
3. G.W. Wheland. Resonance in organic chemistry. Wiley, New York. 1955.
4. (*a*) R.F.W. Bader. Atoms in molecules: a quantum theory. Oxford University Press, Oxford. 1990; (*b*) Chem. Rev. **91**, 893 (1991).
5. (*a*) C.L. Perrin. J. Am. Chem. Soc. **113**, 2865 (1991); (*b*) K.E. Laidig. J. Am. Chem. Soc. **114**, 7912 (1992).
6. R.F.W. Bader, J.R. Cheeseman, K.E. Laidig, K.B. Wiberg, and C. Breneman. J. Am. Chem. Soc. **112**, 6530 (1990).
7. R.F.W. Bader, P.J. MacDougall, and C.D.H. Lau. J. Am. Chem. Soc. **106**, 1594 (1984).
8. R.J. Gillespie and T. Birchall. Can. J. Chem. **41**, 149 (1963).
9. (*a*) Q.-P. Wang, A.J. Bennet, and R.S. Brown. Can. J. Chem. **68**, 1732 (1990); (*b*) A.J. Bennet, Q.-P. Wang, H. Slebocka-Tilk, V. Somayaji, and R.S. Brown. J. Am. Chem. Soc. **112**, 6383 (1990); (*c*) Q.-P. Wang, A.J. Bennet, R.S. Brown, and B.D. Santarsiero. J. Am. Chem. Soc. **113**, 5757 (1991).
10. K.E. Laidig and R.F.W. Bader. J. Am. Chem. Soc. **113**, 6312 (1991).
11. W.J. Hehre, R. Ditchfield, and J.A. Pople. J. Chem. Phys. **56**, 2257 (1972); P.C. Hariharan and J.A. Pople. Theor. Chim. Acta, **28**, 213 (1973).
12. J.C. Slater. J. Chem. Phys. **1**, 687 (1933).
13. S.L. Price, J.L. Andrews, C.W. Murray, and R.D. Amos. J. Am. Chem. Soc. **114**, 8268 (1992).
14. (*a*) M.J. Frisch, M. Head-Gordon, H.B. Schlegel, K. Raghavachari, J.S. Binkley, C. Gonzalez, D.J. DeFrees, D. Fox, R. Seeger, R. Whiteside, C.F. Melius, J. Baker, R. Martin, L.R. Kahn, J.J.P. Stewart, E.M. Fluder, S. Topiol, and J.A. Pople. GAUSSIAN88, Gaussian Inc., Pittsburgh, Pa. 1988.
15. M.W. Schmidt, J.A. Boatz, K.K. Baldridge, S. Koseki, M.S. Gordon, S.T. Elbert, and B. Lam. QCPE Bull. **7**, 115 (1987).
16. F.W. Biegler-König, R.F.W. Bader, and T.H. Tang. J. Comput. Chem. **3**, 317 (1982).
17. T.A. Halgren and W.N. Lipscomb. Chem. Phys. Lett. **49**, 225 (1977).
18. R.F.W. Bader and H. Essen. J. Chem. Phys. **80**, 1943 (1984).
19. J. Gillespie. The VSEPR model of molecular geometry. Allyn and Bacon, Boston. 1991.
20. L. Onsager. J. Am. Chem. Soc. **58**, 1486 (1936); M.A. Wong, K.B. Wiberg, and M.J. Frisch. J. Chem. Phys. **95**, 8991 (1991).
21. W.P. Jencks. Catalysis in chemistry and enzymology. McGraw–Hill, New York. 1969.
22. S. Blackburn. Enzyme structure and function. Marcel Dekker, New York. 1976. p. 169.
23. J.P. Krug, P.L.A. Popelier, and R.F.W. Bader. J. Phys. Chem. **96**, 7604 (1992).

Can. J. Chem. Downloaded from www.nrcresearchpress.com by 213.200.69.106 on 09/08/12
For personal use only.

Synthesis of diaminodideoxyalditol analogs of cisplatin as antitumor agents

S. HANESSIAN,[1] J.-Y. GAUTHIER, K. OKAMOTO, A.L. BEAUCHAMP, AND T. THEOPHANIDES
Department of Chemistry, Université de Montréal, Montréal (Québec), Canada H3C 3J7

Received November 27, 1992

S. HANESSIAN, J.-Y. GAUTHIER, K. OKAMOTO, A.L. BEAUCHAMP, and T. THEOPHANIDES. Can. J. Chem. **71**, 880 (1993).

Acyclic vicinal polyol complexes related to cisplatin were synthesized from D-mannitol by stereocontrolled manipulation of the hydroxy groups. Controlled cleavage of a 3,4-diazido hexitol gave the corresponding D-threitol and D-xylitol analogs, which were converted to their diamino platinum complexes. The antitumor activity of these compounds is reported.

S. HANESSIAN, J.-Y. GAUTHIER, K. OKAMOTO, A.L. BEAUCHAMP et T. THEOPHANIDES. Can. J. Chem. **71**, 880 (1993).

Des dérivés acycliques de diamino polyols vicinaux ont été synthétisés à partir du D-mannitol en utilisant des méthodes de transformations stéréocontrôlées. Le clivage sélectif du dérivé 3,4-diazido hexitol a donné les analogues correspondants du D-threitol et du D-xylitol. Les diamines ont été transformées en complexe de platine et l'activité antitumorale des complexes est rapportée.

Can. J. Chem. Downloaded from www.nrcresearchpress.com by 213.200.69.106 on 09/08/12
For personal use only.

Two decades after its discovery (1), *cis*-diammine dichloroplatinum(II) (cisplatin) and its structural variants (for recent reviews, see ref. 2) remain as one of the most widely used group of oncolytic drugs against a variety of cancers (3) (Fig. 1). To date, well over 1000 analogs of cisplatin have been synthesized and examined for antitumor activity, particularly against cancer of the testes, ovaries, bladder, head, and neck. Concurrently, the molecular mechanism of action of cisplatin has been the subject of intensive studies (4). The drug has been shown to bind covalently to chromosomal DNA in the cell nucleus, thus inhibiting replication (5). The site of most stable binding is at the N-7 position of guanine in the DNA, which results in the weakening of hydrogen bonding of the base pairs and the inevitable unwinding of the double helix (6).

In spite of its dramatic success in the treatment of certain types of cancer (7), cisplatin has a number of drawbacks that present difficulties in its continued use. Toxicity of several types (8), narrow range of activity, cross-resistance, and lack of solubility are among the more serious limitations. A number of derivatives in which the dichloro ligands have been changed to other anionic groups (e.g., 1,1-cyclobutanedicarboxylato (carboplatin)) (9) have shown reduced toxicity, presumably due to better pharmacokinetic properties. Several other second and third generation platinum complexes are known (2, 3).

We wish to report on the synthesis and antitumor properties of a series of stereochemically defined, novel platinum complexes derived from a diaminotetritol, -pentitol, and -hexitol, having the generalized structure shown in Fig. 1. After our work was completed a report of cisplatin analogs of 2,3-diamino-2,3-dideoxy-1,4-di-*O*-methyl-D- and -L-threitol was published by Haines *et al.* (10). Other examples of chiral or racemic diaminoalcohol complexes of platinum are found in the patent literature (11).

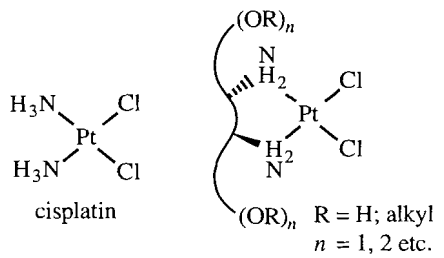

FIG. 1

The design of our alditol-derived platinum analogs took into consideration the distinctly superior activity of cisplatin compared to the *trans* isomer (1). Our synthetic plan took advantage of the C_2 symmetrical properties of D-mannitol and the possibility of preparing *trans*-oriented vicinal diaminodideoxy derivatives therefrom. As shown in Scheme 1, a double nucleophilic displacement of the crystalline dimesylate derivative **2**, employing tetra-*n*-butyl ammonium azide in toluene (12), gave the pivotal diazido derivative **3** as a syrup. The yield of **3** was lower when DMF or DMSO was used in the presence of sodium azide. Hydrolysis of the acetal functions led to the corresponding tetrol **4**, which was methylated in the usual way to give **5**. Hydrogenation of **4** and **5** individually, followed by treatment of the corresponding diamino derivatives with dipotassium tetrachloroplatinate, gave the crystalline complexes **6** and **7**, respectively. The double inversion of configuration in the displacement of **2** with azide ion was anticipated in the absence of neighboring group participation. The structure of **6** was unequivocally confirmed by single crystal X-ray analysis (see below).

With the availability of the diazidohexitol **4**, we could now address the problem of a single and double cleavage of the terminal vicinal glycol units in order to obtain four- and five-carbon diamino cisplatin polyols, respectively. The diazidohexitol **4**, when treated with 1 equivalent of sodium metaperiodate at 0°C, followed by reduction of the corresponding lactol, gave the diazidodideoxy-D-xylitol derivative **8** in good overall yield. Hydrogenation of **8** followed by formation of the platinum(II) complex gave **9** as bright yellow crystals.

Oxidation of **4** with 2 equivalents of sodium metaperiodate at 0°C, followed by reduction with sodium borohydride, gave the crystalline diazidodideoxy-D-threitol derivative **10**. Hydrogenation and treatment of the resulting diamino compound with dipotassium dichloroplatinate afforded the crystalline platinum(II) complex **11**. A number of other di-*O*-alkyl and mono-*O*-alkyl Pt(II) derivatives in this series were also prepared, and were obtained in crystal-

[1]Author to whom correspondence may be addressed.

Can. J. Chem. Downloaded from www.nrcresearchpress.com by 213.200.69.106 on 09/08/12
For personal use only.

line form. All the complexes described were water soluble at concentrations ranging from 4 to 10 mg/mL at 25°C. The interaction of several of the diaminopolyol platinum(II) complexes reported here with guanosine, 5′-GMP, and 3′-GMP has been studied by FT-IR and ^{1}H NMR spectroscopy (13).

X-ray crystallographic analysis of compound **6**

Compound **6** crystallized as yellow plates belonging to space group $C222_1$ (polymorph I). A small amount of another polymorph, II (space group $P2_12_12_1$), appeared as yellow needles upon recrystallization from water. The crystal data and refined coordinates are listed in Tables 1 and 2, respectively.

Both crystalline modifications contain the monomeric square-planar *cis*-$PtCl_2$(L–L) complex. Molecule *c* (polymorph II) is shown in Fig. 2. The Pt atom and the middle of the C(3c)—C(4c) bond lie on an approximate twofold axis bisecting the N—Pt—N and Cl—Pt—Cl angles. Coordination is very similar in the two independent types of molecules (*a* and *b*) in polymorph I (drawings in supplementary material), but in these cases the twofold axis is imposed by crystallographic symmetry. Individual distances and angles are provided as supplementary material.[2] The mean Pt—Cl and Pt—N distances (2.32 and 2.03 Å, respectively) compare well with those found in $PtCl_2N_2$ systems with related ligands. The "bite" of the diamine reduces the N—Pt—N angle to 83.8° with a concomitant increase of the Cl—Pt—Cl angle to 94.5°, as found in other diamines forming five-membered chelate rings (14). The puckered chelate ring has the δ conformation (N—C—C—N = 45–56°). The $PtCl_2N_2$ unit is planar with 1σ for molecules *a* and *c*. In molecule *b*, the atom-to-plane distance reaches 0.20(4) Å, the $PtCl_2$ plane being twisted by 9.2° about the twofold axis with respect to the PtN_2 plane. The three independent molecules adopt different conformations of their -CH(OH)-CH_2OH "arms". This likely results from molecular packing, which is largely controlled by hydrogen bonding between water, coordinated chloride, and ligand -OH and -NH_2 groups.

Antitumor activity

The hydroxy analogs **6**, **9**, and **11** showed significant in vitro activity against sensitive strains of L1210 leukemia and P388 with ID_{50} values ranging between 2 and 4.45 μg/mL (cisplatin showed 0.25 μmL) (15). In vivo tests (subcutaneous and intravenous) against PU-239 showed levels of activity approaching that of cisplatin. In vivo test results with M5076 sarcona were inferior to cisplatin.

The *O*-methyl analog **7**, as well as *O*-methyl analogs of **9** and **11** (16), also showed significant in vitro and in vivo antitumor activity against several tumor lines. In vitro tests against sensitive *and* resistant strains of L1210 leukemia showed ID_{50} values of 6–15 μg/mL). The same trend was observed in vivo with values of ID_{50} 13–30 μM for the *O*-methyl analogs with good resistant/sensitive ratios compared to cisplatin (0.8 sens. and 9.9 resist. μM). In vitro activity was demonstrated by **7** and related *O*-methyl analogs of **9** and **11** (15) against P388 (sensitive and resistant with values ranging from 15 to 28 μg/mL (compare cisplatin with 0.25–485 μg/mL). The ratio activity of the *O*-methyl analogs resistant and sensitive strains is an interesting observation that indicates a potential for better cross-resistance.

Although more detailed biological studies are still required, the promising antitumor activity exhibited by these stereochemically well-defined, novel platinum(II) complexes derived from diaminodideoxy alditols should open newer avenues to explore in this important area of cancer chemotherapy.

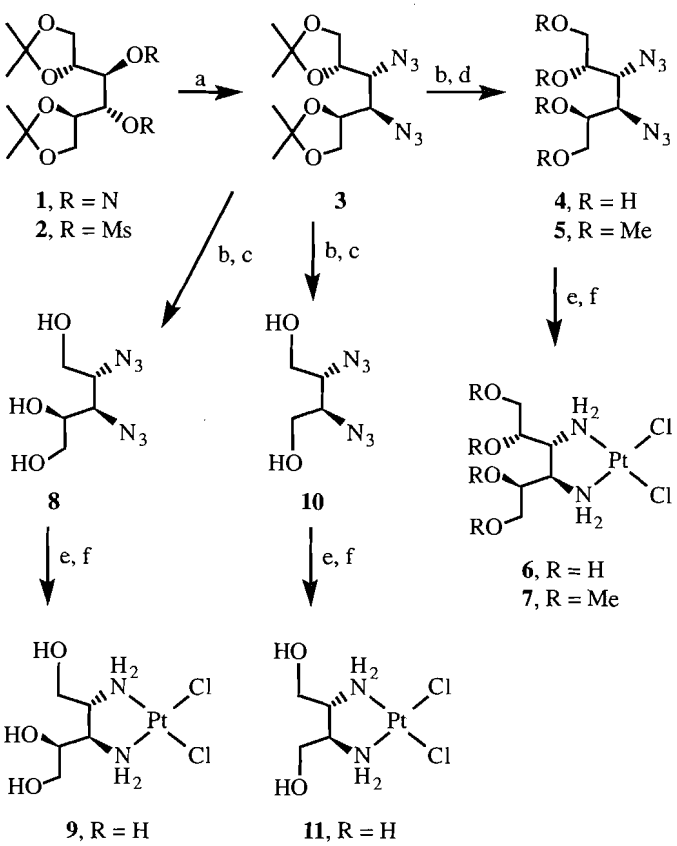

(a) NaN_3, Bu_4NCl, toluene, reflux; (b) AcOH, H_2O, 60°C, 1 h; (c) 1 equiv. $NaIO_4$, 0°C, 1.5 h and then $NaBH_4$; for **10**, 2 equiv. $NaIO_4$; (d) MeI, NaH, DMF; (e) Pd/C, H_2, MeOH; (f) K_2PtCl_4, H_2O

SCHEME 1

Experimental

Melting points (mp) were determined on a Fisher–Johns apparatus and they are uncorrected. Optical rotations were measured at 25°C using a Perkin–Elmer model 241 automatic polarimeter. Chromatography was done on silica gel (Merck) according to Still et al. (17). Combustion analyses were done at Guelph Laboratories, Ltd., Guelph, Ontario.

[2]Detailed crystallographic results (hydrogen coordinates, temperature factors, distances and angles, torsion angles, least-squares plane calculations, hydrogen-bond geometry, structure factors, and ORTEP drawings) (18 pages) may be purchased from: The Depository of Unpublished Data, Document Delivery, CISTI, National Research Council Canada, Ottawa, Canada K1A OS2.

Tables of hydrogen coordinates, distances and angles, and hydrogen-bond geometry, as well as ORTEP drawings, have also been deposited with the Cambridge Crystallographic Data Centre and can be obtained on request from The Director, Cambridge Crystallographic Data Centre, University Chemical Laboratory, 12 Union Road, Cambridge, CB2 1EZ, U.K.

Can. J. Chem. Downloaded from www.nrcresearchpress.com by 213.200.69.106 on 09/08/12
For personal use only.

TABLE 1. Crystal data and conditions for data collection

	Polymorph I	Polymorph II
Formula	$C_6H_{16}Cl_2PtN_2O_4 \cdot H_2O$	$C_6H_{16}Cl_2PtN_2O_4 \cdot H_2O$
Formula weight	464.22	464.22
Crystal system	Orthorhombic	Orthorhombic
Space group	$C222_1$	$P2_12_12_1$
a, Å	7.283(3)	6.720(9)
b, Å	25.949(7)	11.549(9)
c, Å	12.691(6)	15.371(9)
V, Å^3	2398.4	1192.9
D_{calc}, g cm^{-3}	2.571	2.585
Z	8	4
Radiation, λ (Å)	MoKα, 0.71069	MoKα, 0.71069
μ, cm^{-1}	122.9	123.5
Crystal size, mm	0.018 × 0.185 × 0.192	0.025 × 0.025 × 0.60
Transmission range	0.19–0.65	0.67–0.77
Scan type	ω/2θ	ω/2θ
Scan range Δω, deg	1.00 + 0.35 tan θ	1.00 + 0.35 tan θ
Scan speed, deg(ω) min^{-1}	1.0	1.0
2θ max, deg	50.0	50.0
No. unique reflections measured	1223 ($h + k = 2n$)	927
No. observed reflections	699	734
Rejection criterion, $I/\sigma(I) <$	3.0	3.0
T, K	298	298
R^a	0.039	0.023
$R_w{}^a$	0.044	0.028
Goodness-of-fit ratio, S	1.60	1.12

$^aR = \Sigma||F_o| - |F_c||/\Sigma|F_o|$, $R_w = [\Sigma w(|F_o| - |F_c|)^2/\Sigma w|F_o|^2]^{1/2}$.

*1,2:5,6-Di-*O*-isopropylidene-3,4-di-*O*-methanesulfonyl-*D*-mannitol (**2**)*

A solution of 1,2:5,6-di-*O*-isopropylidene-D-mannitol (25 g, 95 mmol) in dry methylene chloride (430 mL) and triethylamine (32 g, 0.3 mmol) was treated with methanesulfonyl chloride (26.6 g, 0.233 mmol) dropwise at 0°C under nitrogen atmosphere. After allowing the mixture to warm up to room temperature, it was washed abundantly with cold distilled water, and the organic phase was dried (sodium sulfate) and evaporated under vacuum. The resulting crude solid was recrystallized from a mixture of hot methanol and water to afford 34 g (85%) of long white needles, mp 142–143°C; $[\alpha]_D$ −5.3 (*c* 1, $CHCl_3$). Anal. calcd. for $C_{14}H_{26}O_{10}S_2$: C 40.19, H 6.22; found: C 40.11, H 6.02.

*3,4-Diazido-3,4-dideoxy-1,2:5,6-di-*O*-isopropylidene-*D*-iditol (**3**)*

To a solution of **2** (12 g, 28.7 mmol) in dry toluene (300 mL) was added sodium azide (50 g, 25 equiv.) and tetrabutylammonium chloride (25 g, 3 equiv.). The mixture was heated at reflux temperature under mechanical stirring for 16 h, poured into ice-water (500 mL), and extracted with ethyl acetate. The organic extract was washed with brine, dried over sodium sulfate, filtered, and evaporated. Chromatography of the residue on silica gel (40:2 toluene–acetone) afforded a pale yellow syrup (5.12 g, 57%), which when sublimed at 110°C (0.3 Torr; 1 Torr = 133.3 Pa) gave a low-melting crystalline product; $[\alpha]_D$ +130 (*c* 1, $CHCl_3$). Anal. calcd. for $C_{12}H_{20}N_6O_4$: C 46.15, H 6.41, N 26.92; found: C 45.92, H 6.22, N 26.86.

*3,4-Diazido-3,4-dideoxy-*D*-iditol (**4**)*

A solution **3** (1.32 g, 4.2 mmol) in a mixture of acetic acid (25 mL) and water (13 mL) was heated at 80°C for 75 min. Evaporation gave a dark-brown syrup that was dissolved in methanol and treated with activated charcoal. The pale yellow filtrate was evaporated to dryness to give a chromatographically homogeneous syrup (895 mg, 91%). A portion was crystallized from a mixture of ethyl acetate and hexanes, mp 87–88°C; $[\alpha]_D$ −124 (*c* 1, H_2O). Anal. calcd. for $C_6H_{12}N_6O_4$: C 31.03, H 5.20, N 36.19; found: C 31.21, H 5.13, N 35.94.

*3,4-Diazido-3,4-dideoxy-1,2:5,6-tetra-*O*-methyl-*D*-iditol (**5**)*

A solution of **4** (500 mg, 2.15 mmol) in dry *N*,*N*-dimethylformamide (7.5 mL) was transferred to a round-bottom flask containing sodium hydride (1.037 g, 20 equiv.) in dry *N*,*N*-dimethylformamide (5 mL) at 0°C under nitrogen atmosphere. Upon ceasing of the effervescence, methyl iodide (3.05 g, 10 equiv.) was added dropwise. The reaction mixture was then stirred at 0°C for 1 h, and neutralized with methanol followed by 1 N sulfuric acid. The mixture was evaporated, dissolved in chloroform (50 mL), and washed with distilled water and saturated sodium thiosulfate solution. The organic extract was dried (sodium sulfate) and evaporated under vacuum, and the resulting syrup chromatographed on silica gel (35:65 ethyl acetate – hexanes) to afford the pure product as a colorless syrup (554 mg, 89%); $[\alpha]_D$ 188 (*c* 1, $CHCl_3$).

*3,4-Diamino-3,4-dideoxy-*D*-iditol*

To a solution of **4** (406 mg, 1.75 mmol) in methanol (30 mL) and distilled water (5 mL) was added 10% palladium-on-charcoal (150 mg) suspended in water (5 mL). The mixture was hydrogenated under atmospheric pressure at room temperature for 12 h; the catalyst was then removed by filtration through Celite, washed with distilled water (~5 mL), and the filtrate was evaporated to dryness from absolute ethanol several times. A white solid was obtained (302 mg, 85%); recrystallization form hot ethanol – water afforded colorless needles, mp 160–161°C; $[\alpha]_D$ −104 (*c* 1, H_2O). Anal. calcd. for $C_6H_{16}N_2O_4$: C 40.00, H 8.89, N 15.56; found: C 39.87, H 8.66, N 15.01.

*(SP-4-2)-Dichloro(3,4-diamino-3,4-dideoxy-*D*-iditol-*N*,*N*′) platinum (**6**)*

The preceding diaminopolyol (487 mg, 2.7 mmol) in 2 mL of water was added to a solution containing K_2PtCl_4 (1.124 g, 2.7 mmol) in distilled water (12 mL). The mixture was stirred manually until it became homogeneous, and the solution was left standing in the dark. After 2 h bright yellow plates were obtained

Can. J. Chem. Downloaded from www.nrcresearchpress.com by 213.200.69.106 on 09/08/12
For personal use only.

TABLE 2. Atomic coordinates ($\times 10^3$, Pt $\times 10^5$, Cl $\times 10^4$) and equivalent isotropic temperature factors ($\times 10^3$)

	x	y	z	U_{eq}
Polymorph I				
Pt(1a)	0	−694(8)	25000	21
Pt(1b)	50000	205(6)	25000	21
Cl(1a)	647(21)	531(4)	3796(7)	32
Cl(1b)	4406(24)	−591(4)	1214(8)	41
O(1a)	249(3)	−210(1)	487(2)	33
O(1b)	110(3)	203(1)	113(2)	24
O(2a)	−90(3)	−161(1)	423(2)	33
O(2b)	502(4)	203(1)	144(1)	24
O(10a)	−364(4)	−217(1)	321(2)	62
N(3a)	59(6)	−65(1)	352(3)	34
N(3b)	424(6)	61(1)	152(3)	25
C(1a)	240(5)	−162(1)	434(2)	29
C(1b)	202(4)	165(1)	178(3)	31
C(2a)	71(5)	−159(1)	364(2)	12
C(2b)	391(5)	157(1)	140(3)	28
C(3a)	81(5)	−115(1)	291(2)	17
C(3b)	499(8)	111(1)	191(2)	19
Polymorph II				
Pt(1c)	20251(7)	23153(4)	225(5)	20
Cl(1c)	2038(6)	4324(3)	103(3)	33
Cl(2c)	2013(6)	2255(3)	−1490(2)	30
O(1c)	491(2)	90(1)	353(1)	41
O(2c)	1(2)	95(1)	264(1)	42
O(5c)	427(2)	−131(1)	91(1)	31
O(6c)	142(2)	−311(1)	78(1)	33
O(10c)	675(2)	−65(1)	233(1)	45
N(3c)	203(2)	217(1)	133(1)	30
N(4c)	207(2)	55(1)	6(1)	25
C(1c)	327(3)	150(1)	320(1)	33
C(2c)	212(3)	77(1)	256(1)	31
C(3c)	259(2)	100(1)	161(1)	25
C(4c)	160(2)	15(1)	98(1)	26
C(5c)	227(3)	−113(1)	113(1)	26
C(6c)	98(3)	−190(1)	59(1)	29

and the crystallization was allowed to continue until the original red color of the solution became yellow or orange-yellow. The crystals were filtered, washed with cold water (2–3 mL), and dried in the absence of light, to afford bright yellow crystals (565 mg), mp 226–229°C (gradual darkening at 190°C); $[\alpha]_D$ 6.3 (*c* 0.4, H_2O). Concentration of the mother liquors in vacuo (50°C) yielded a second crop of **6** (91 mg). Anal. calcd. for $C_6H_{16}N_2O_4PtCl_2 \cdot H_2O$: C 15.52, H 3.90, N 6.03, Cl 15.27; found: C 15.41, H 3.58, N 6.11, Cl 15.03.

The procedure described above yielded yellow plates belonging to space group $C222_1$. By recrystallization from water, the same crystalline phase was obtained as the major component, but the sample also contained a small amount of yellow needles, which were identified as a second crystalline modification of the same compound with space group $P2_12_12_1$. X-ray work was carried out on both polymorphs (see below).

*2,3-Diazido-2,3-dideoxy-D-threitol (**10**)*

To a solution of **4** (500 mg, 2.15 mmol) in distilled water (10 mL) was added solid sodium metaperiodate (925 mg, 4.32 mmol) portionwise at 0°C, in the absence of light. The mixture was stirred for 2 h, and sodium borohydride (0.9 g) was added. After 2 h at 0°C, the solution was acidified with 1 N sulfuric acid, decolorized with sodium thiosulfate, and evaporated under vacuum. The residue was dissolved in water (25 mL) and extracted with ethyl acetate (5 × 40 mL); the combined organic extracts were decolorized

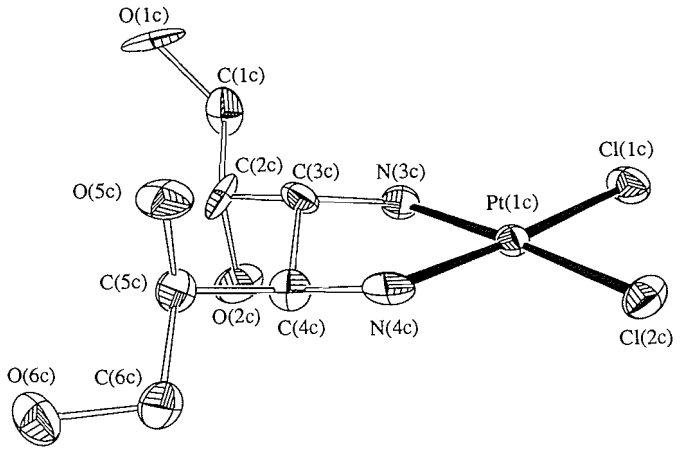

FIG. 2. ORTEP drawing of molecule *c* in polymorph II. Ellipsoids correspond to 50% probability. Hydrogens are omitted for simplicity. Drawings for the two independent molecules (*a* and *b*) of polymorph I are provided in the supplementary material.

with sodium thiosulfate, dried, and evaporated under vacuum to afford a colorless oil (390 mg, 95%). Thin-layer chromatography of the oil showed the presence of diol and triol in equal proportions. The product was recycled through the oxidative cleavage and the reduction as described above, and the reaction mixture was processed to afford the diol **10** in the form of white crystals. Recrystallization from chloroform–hexanes yielded 303 mg (82%) of product, mp 78–79°C; $[\alpha]_D$ +41.4 (*c* 0.5, MeOH). Anal. calcd. for $C_4H_8N_6O_2$: C 27.91, H 4.65, N 48.84; found: C 27.62, H 4.44, N 48.53.

2,3-Diamino-2,3-dideoxy-D-threitol

To a solution of the diazide **10** (487 mg, 2.83 mmol) in methanol – distilled water (1:1, 20 mL) was added palladium-on-charcoal (300 mg) suspended in methanol (5 mL). The mixture was hydrogenated under atmospheric pressure at room temperature for 12 h. The catalyst was then removed by filtration over Celite, and the filtrate was evaporated under vacuum. The residue was co-evaporated with ethanol to dryness to afford a colorless syrup (333 mg, 98% yield); $[\alpha]_D$ −151 (*c* 1, H_2O).

*(SP-4-2)-Dichloro(2,3-diamino-2,3-dideoxy-D-threitol-N,N′) platinum (**11**)*

The previous diamino derivative was dissolved in distilled water (0.7 mL) and added to a solution containing K_2PtCl_4 (1 equiv.) in distilled water (4.4 mL for 1 mmol). The mixture was stirred manually until it became homogeneous, and the solution was left standing in darkness. After 2 h, bright yellow crystals were formed. When the original red color of the solution became yellow or orange-yellow, the crystals were filtered, washed with cold water (1–2 mL), and dried under air suction in the absence of light for several hours, to afford bright yellow crystals (yield 60%), mp > 300°C; $[\alpha]_D$ −94 (*c* 0.083, H_2O). Anal. calcd. for $C_4H_{12}N_2O_2PtCl_2$: C 12.47; H 3.12, N 7.27, Cl 18.18; found: C 12.60, H 3.13, N 7.22, Cl 18.60.

*2,3-Diazido-2,3-dideoxy-D-xylitol (**8**)*

To a solution of **4** (1 g, 4.3 mmol) in distilled water (25 mL) was added sodium metaperiodate (920 mg) in distilled water (10 mL), portionwise at 0°C, and in the absence of light. The mixture was stirred 90 min at 0°C, then it was treated with sodium borohydride (1.75 g) in distilled water (20 mL). After 1 h, the reaction was acidified with 1 N sulfuric acid, decolorized with a few millilitres of saturated sodium thiosulfate, and evaporated under vacuum. The residue was dissolved in water (25 mL) and extracted with ethyl acetate (5 × 100 mL). The combined organic extract was decolorized with sodium thiosulfate, dried, and evaporated under vacuum

Can. J. Chem. Downloaded from www.nrcresearchpress.com by 213.200.69.106 on 09/08/12
For personal use only.

and the residue was chromatographed on silica gel (85:15 ethyl acetate – hexanes) to afford the triol **8** (577 mg; 66% yield); $[\alpha]_D$ −239 (*c* 1.35, CH_3OH).

2,3-Diamino-2,3 dideoxy-D-xylitol

To a solution of **8** (577 mg, 28 mmol) in methanol (25 mL) was added palladium-on-charcoal (300 mg) suspended in methanol–water (1:1, 5 mL). The mixture was hydrogenated at room temperature under atmospheric pressure for 12 h. The catalyst was removed by filtration through Celite, the filtrate was evaporated under vacuum, and the residue was coevaporated with ethanol to dryness to afford a colorless syrup (421 mg, yield 98%); $[\alpha]_D$ −200 (*c* 1, H_2O).

(SP-4-3)-Dichloro(2,3-diamino-2,3-dideoxy-D-xylitol-N,N′*) platinum (9)*

The above diamino derivative was dissolved in distilled water (1 mL), and added to a solution containing K_2PtCl_4 (1 equiv.) in distilled water (5 mL). The mixture was stirred manually until homogeneous, and was left standing in the dark. After 2 h, bright yellow plates were formed. When the original red color of the solution became yellow or orange-yellow, the crystals were filtered, washed with cold water, and dried, in the absence of light for several hours, to afford bright yellow crystals (yield 57%); mp 255°C (dec.); $[\alpha]_D$ −52 (*c* 0.27, H_2O). Anal. calcd. for $C_5H_{14}N_2O_3PtCl_2$: C 14.46, H 3.37, N 6.75, Cl 16.87; found: C 14.40, H 3.38, N 6.80, Cl 17.32.

(SP-4-2)-Dichloro(3,4-diamino-3,4-dideoxy-1,2,4,6-tetra-O-*methyl-D-iditol*-N,N′*) platinum (7)*

A solution of **5** (0.5 g) was hydrogenated as described above and the resulting diamino derivative was treated with K_2PtCl_4 as described for **6**. The title compound **7** was obtained as a crystalline product in 52% yield, mp 286–287°C (dec.); $[\alpha]_D$ −25.2 (*c* 0.33, H_2O). Anal. calcd. for $C_{10}H_{22}N_6O_4PtCl_2$: C 23.91, H 4.81, N 5.57, Cl 14.11; found: C 23.98, H 4.72, N 5.56, Cl 14.48.

X-ray data collection and structure determination

Crystal data are provided in Table 1. Starting cell parameters and space group were determined from precession and cone-axis photographs. For both polymorphs, the space group was uniquely defined from the systematic absences: *hkl*, $h + k \neq 2n$ and 00*l*, $l \neq 2n$ for $C222_1$ (polymorph I); *h*00, $h \neq 2n$; 0*k*0, $k \neq 2n$; 00*l*, $l \neq 2n$ for $P2_12_12_1$ (polymorph II).

The intensity data were collected on an Enraf–Nonius CAD-4 diffractometer with graphite-monochromatized MoKα radiation, following the procedure described elsewhere (18). The data were corrected for the effects of Lorentz, polarization, and absorption (Gaussian integration, grid 10 × 10 × 10).

For polymorph I, the Patterson synthesis provided relative positions for the Pt atoms, but there were eight nonequivalent ways of positioning this pattern with respect to the origin in the $C222_1$ unit cell and each of these starting models showed pseudosymmetry. The ΔF map phased on any of these models showed, around each Pt atom, eight peaks corresponding to two superimposed square-planar units in which the Cl and N corners could not be differentiated. A small number of starting points could be rejected because they generated abnormally short intermolecular contacts. The remaining models were systematically tested. By structure factor and ΔF map calculations, resolution could generally progress up to a certain point, where inconsistencies developed in the positions of the ligand free "arms". The correct model turned out to contain two nonequivalent sets of Pt atoms occupying twofold axes (independent *4b* equipoints). The known absolute configuration was imposed. Isotropic refinement of the non-hydrogen atoms using full-matrix least squares converged to $R = 0.096$. The hydrogens on C and N atoms were fixed at idealized positions (N—H = 0.87, C—H = 0.95 Å, $B_{iso} = 6.0$ Å^2). Their parameters were not refined, but the coordinates were recalculated after each cycle of refinement. The hydrogens of the hydroxyl groups and water molecule were not detected. Anisotropic refinement of the non-hydrogen atoms converged to $R = 0.039$ and $R_w = 0.044$. The goodness-of-fit ratio was 1.60. The final ΔF map showed maximum residuals of ±1.3 e Å^{-3} within 1 Å from Pt atoms. The general background was lower than ±0.5 e Å^{-3}.

For polymorph II, the Pt atoms occupying a general equipoint were located from the Patterson map. The remaining non-hydrogen atoms were then found from a ΔF map. The structure was refined by full-matrix least squares. Isotropic refinement converged to $R = 0.052$. Hydrogens were handled as above. Anisotropic refinement of the non-hydrogen atoms converged to $R = 0.023$ and $R_w = 0.028$. The goodness-of-fit ratio was 1.12. The final ΔF map showed a general background below ±0.3 e Å^{-3}, except for a few peaks of ±|0.3–0.6| e Å^{-3} near Pt or Cl.

The scattering curves used were those of Cromer and Waber (19), except for hydrogen (20). The anomalous dispersion terms of Pt and Cl were taken from Cromer (21). The programs used are listed elsewhere (22).

Acknowledgments

We are greatly indebted to Drs. W. R. Leopold, A. Kraker, and J. Hoeschele, Warner–Lambert Research Laboratories, Ann Arbor, Michigan, and the National Cancer Institute (NCI) (Washington) for conducting the in vitro and in vivo biological assays. We thank NCI (Canada), the Natural Sciences and Engineering Research Council of Canada (NSERCC), and le Fonds pour la formation de chercheurs et l'aide à la recherche (FCAR) for financial assistance. We acknowledge the participation of M. J. Olivier in the X-ray diffraction work.

1. B. Rosenberg, L. Van Camp, J.E. Trosko, and V.H. Mansour. Nature, 222 (1969).
2. J.C. Dabrowiak and W.T. Bradner. Prog. Med. Chem. **24**, 129 (1987); A. Pasini and F. Zunino. Angew. Chem. Int. Ed. Engl. **26**, 615 (1987); B. Lippert. Gazz. Chim. Ital. **118**, 163 (1988).
3. J.H. Krakoff. *In* Platinum and other metal coordination compounds in cancer chemotherapy: clinical applications of platinum complexes. *Edited by* M. Nicolini. M. Nijhoff Publishing, Boston, Mass. 1988. p. 351.
4. S.J. Lippard. Science, **218**, 1075 (1982); J.J. Roberts and M.P. Pera, Jr. *In* Molecular aspects of anticancer drug action. *Edited by* S. Neidle and M.J. Waring. MacMillan Press, London. 1983. p. 183.
5. J.J. Roberts and A.J. Thompson. Prog. Nucl. Acid. Biol. **22**, 71 (1979).
6. B. Lippert. J. Am. Chem. Soc. **103**, 5691 (1981).
7. P.J. Loehrer, Sr., S.D. Williams, and L.H. Einhorn. J. Natl. Cancer Inst. **80**, 1373 (1988).
8. I.H. Krakoff. Cancer Treat. Rep. **63**, 1523 (1979); J.B. Vermorken and H.M. Pinedos. Neth. J. Med. **25**, 270 (1982); D.D. Vonhoff, R. Schilsky, and C.M. Reichert. Cancer Treat. Rep. **63**, 1527 (1979).
9. A.H. Calvert, S.J. Harland, D.R. Newell, Z.H. Siddik, A.C. Jones, T.J. McElwain, S. Raju, E. Wiltshaw, J.E. Smith, J.M. Baker, M.J. Peckam, and K.R. Harrap. Cancer Chemother. Pharmacol. **9**, 140 (1982).
10. A.H. Haines, C. Morley, and B.A. Murrer. J. Med. Chem. **32**, 742 (1989).
11. A.R. Amundsen and E.W. Stern. Eur. Patent. 98,135 (1983); Chem. Abstr. **100**, 161788a (1984).
12. A. Brändstrom, B. Lamm, and I. Palmertz. Acta Chem. Scand. **28**, 699 (1974).
13. K. Okamoto, V. Benham, J.-Y. Gauthier, S. Hanessian, and T. Theophanides. Inorg. Chim. Acta, **123**, L1 (1986); K. Okamoto, M.T. Phan Viet, M. Polissiou, J.-Y. Gauthier, S. Hanessian, and T. Theophanides. Inorg. Chim. Acta, **123**, L3 (1986).
14. J. Wang, Y.L. Bennani, F. Bélanger-Gariépy, and S.

Hanessian. Acta Crystallogr. Sect. C: Cryst. Struct. Commun. **C47**, 1067 (1991); J.C.L. Lock and P. Pilon. Acta Crystallogr. Sect. B: Struct. Crystallogr. Cryst. Chem. **B37**, 45 (1981); T. Tsubomura, M. Ogawa, S. Yano, K. Kobayashi, T. Sakurai, and S. Yoshikawa. Inorg. Chem. **29**, 2622 (1990); R. Mélanson, C. de la Chevrotière, and F.D. Rochon. Acta Crystallogr. Sect. C: Cryst. Struct. Commun. **C43**, 57 (1987); J. Iball, M. MacDougall, and S. Scrimgeour. Acta Crystallogr. Sect. B: Struct. Crystallogr. Cryst. Chem. **B31**, 1672 (1975).

15. S. Hanessian and T. Theophanides. Can. Pat. No. 1,282,058. March 26, 1991.
16. S. Hanessian. Can. Pat. No. 1,265,811. February 13, 1990.
17. W.C. Still, M. Kahn, and A. Mitra. J. Org. Chem. **43**, 2923 (1978).
18. F. Bélanger-Gariépy and A.L. Beauchamp. J. Am. Chem. Soc. **102**, 3461 (1980).
19. D.T. Cromer and J.T. Waber. Acta Crystallogr. **18**, 104 (1965).
20. R.F. Stewart, E.R. Davidson, and W.T. Simpson. J. Chem. Phys. **42**, 3175 (1965).
21. D.T. Cromer. Acta Crystallogr. **18**, 17 (1965).
22. M. Authier-Martin and A.L. Beauchamp. Can. J. Chem. **55**, 1213 (1977).

Can. J. Chem. Downloaded from www.nrcresearchpress.com by 213.200.69.106 on 09/08/12
For personal use only.

Synthesis and biological evaluation of novel chiral non-racemic diaminoplatinum analogs based on a tetrahydropyran motif

STEPHEN HANESSIAN[1] AND JIANGUO WANG
Department of Chemistry, Université de Montréal, Montréal (Québec), Canada H3C 3J7

Received November 27, 1992

STEPHEN HANESSIAN and JIANGUO WANG. Can. J. Chem. **71**, 886 (1993).

Mono and dihydroxy diamino tetrahydropyran derivatives, readily available from L-arabinose, were prepared and converted into the corresponding diamino *cis*-platinum analogs. The presence of hydroxy groups imparts water solubility and enhanced antitumor activity.

STEPHEN HANESSIAN et JIANGUO WANG. Can. J. Chem. **71**, 886 (1993).

Des dérivés mono et dihydroxylé d'un diamino tétrahydropyran, aisément préparés à partir du L-arabinose, ont été synthétisés et convertis en complexes diamino *cis*-platines correspondants. La présence des groupes hydroxy augmente la solubilité de ces complexes tout en conservant leur activité antitumorale.

Can. J. Chem. Downloaded from www.nrcresearchpress.com by 213.200.69.106 on 09/08/12
For personal use only.

Introduction

In view of the clinical importance of the *trans*-1,2-diamino cyclohexane *cis*-platinum complex (DACH) (1), much effort has been expended in the synthesis of related cyclic analogs, particularly those incorporating polar functionality in order to maximize water solubility. A number of years ago, we initiated studies aimed at the synthesis of analogs of cisplatin that are derived from diamino dideoxy sugars. The antitumor activities of diaminodideoxyalditol platinumII derivatives are reported in the preceding paper (2). We now describe the synthesis and antitumor activity of a series of methyl 2,3-diamino-2,3-dideoxy-L-xylopyranosides, **2** and **3**, as well as that of 2,3-diamino-2,3-dideoxy-1,5-anhydro-L-xylitol **4**.

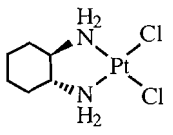

1

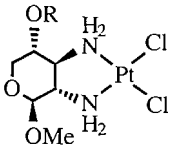

2, R=H; **3**, R= Me

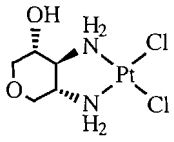

4

Results and discussion

Related derivatives prepared from other diamino sugars have recently been described in the literature (3). In designing these derivatives, particular attention was paid to the site and sense of chirality of the vicinal *trans* diamino groups, which were patterned after the biologically potent (*R*,*R*)-DACH derivative **1**. The presence of free hydroxy groups on the tetrahydropyran-type ring could not only increase water solubility, but also alter electrostatic stabilization due to the presence of polar groups. Moreover, the changes in the hydrophilic character of the complexes might lead to useful differences in their effective transport and distribution in plasma, and hence improve their chemotherapeutic index. Another reason for this investigation is that the stereochemistry of these complexes might have an effect on the antitumor activity. For example, the stereochemical features inherent in the chiral non-racemic analogs could change the selective interaction with certain receptors, membrane constituents, and the DNA helix itself. In patterning the new analogs after (*R*,*R*)-DACH, we chose vicinal diamines with a *trans* configuration, which is believed to be more active than the *cis* form. The disposition of hydroxy or methoxy groups was also fixed vis-a-vis the *trans* diamino function. Dichloride as well as cyclobutane-1,1-dicarboxylate ligands were used as the leaving group for some of the complexes. Since the bidentate ligand slows down the binding rates of the platinum complexes to components present in human plasma (4), these analogs may have a different physiological activity. The degree of hydrophilicity was expected to be controlled by the presence or absence of a hydroxy group at C-4 as in **2** and **3**, respectively, while the functional and stereochemical relevance of the anomeric methoxy group was to be evaluated by comparison to the anhydroalditol derivative **4**.

We chose L-arabinose as a starting material because it could be amenable to the chemical modifications we envisaged for the preparation of the *trans* diamino derivatives **2**, **3**, and **4**. Thus, the readily available epoxide **5** was transformed into the corresponding *O*-tetrahydropyranyl derivative **6**, obtained as a mixture of diasteroisomers (Scheme 1).

Ring opening of the epoxide **6** with azide ion using sodium azide and ammonium chloride in methoxyethanol (6) produced a separable 2:1 mixture of the 3-azido sugar derivative **7** and the diastereomeric OTHP derivatives corresponding to **8**. The $^4C_1$ and $^1C_4$ conformations of the pyranose rings in **7** and **8**, respectively, were confirmed by ^{1}H nmr spectroscopy. In the case of **8** the proton coupling constants ($J_{1,2}$ = 8 Hz, $J_{2,3}$ = 10 Hz, $J_{3,4}$ = 9 Hz) indicated that the hydrogens at C-1, C-2, C-3, and C-4 are in the *trans* axial orientation corresponding to a $^1C_4$ conformation. The ^{1}H nmr spectrum of isomer **7** could not be adequately analyzed because of the presence of diastereomers. However, after conversion to **9**, the coupling constants for the hydrogen atoms at C-1, C-2, C-3, and C-4 ($J_{1,2}$ = 3.5 Hz, $J_{2,3}$ = 10.5 Hz, $J_{3,4}$ = 3 Hz) indicated that the protons at C-1 and C-4 are in the equatorial position while the protons at C-2 and C-3 are in the axial position, which reflects a $^4C_1$ conformation. Interestingly, the two tetrahydropyranyl diastereomers of **9** could be separated by column chromatography. According to the Fürst–Plattner rule (7), the opening of conformationally biased epoxides such as **6***a* and **6***b* (Scheme 2), should proceed in a diaxial mode to afford **7** and **8**, respectively. The higher proportion of **7** than of **8** may be because the tetrahydropyranyloxy group in **6***b* is in a pseudoaxial position, which hinders the attack at the C-2

[1]Author to whom correspondence may be addressed.

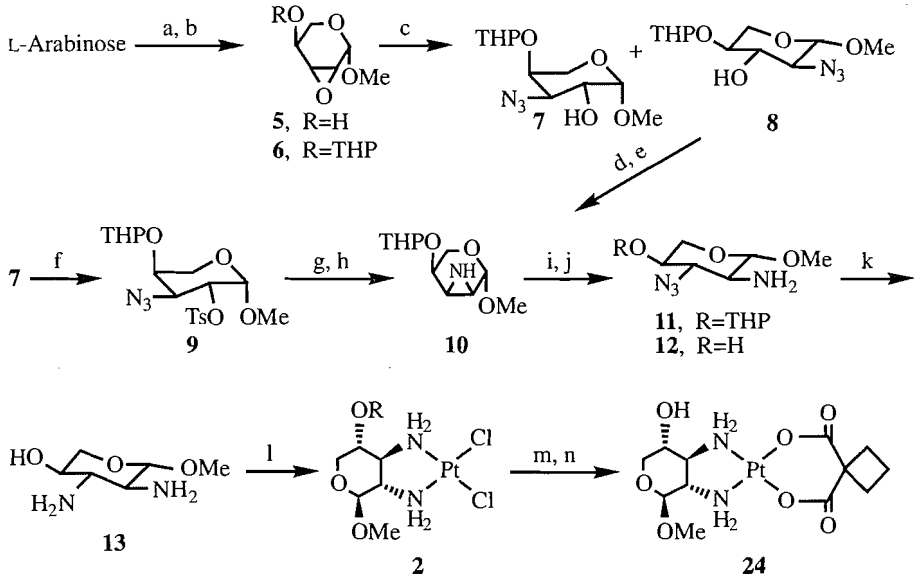

(*a*) Reference 5; (*b*) dihydropyran, PPTS, CH_2Cl_2, r.t., 1.5 h, 91%; (*c*) NaN_3, NH_4Cl, $CH_3OCH_2CH_2OH/H_2O$, 110°C, 5 h, 90%; (*d*) MsCl, pyr., r.t., 81%; (*e*) $NH_2NH_2 \cdot H_2O$, Ra-Ni, MeOH, reflux, 5 h, 97%; (*f*) TsCl, pyr., 40–50°C, 1 day, 82%; (*g*) $NH_2NH_2 \cdot H_2O$, Ra-Ni, MeOH, reflux 3 h, 97%; (*h*) $NaOAc \cdot 3H_2O$, DMF, 85°C, overnight, 95%; (*i*) NaN_3, NH_4Cl, $CH_3OCH_2CH_2OH/H_2O$, 110°C, 11 h, 80%; (*j*) PPTS, ethanol, 70°C, 1 day, 80%; (*k*) Pd/C (10%), H_2, 85%; (*l*) K_2PtCl_4, H_2O, r.t., 2 h, 44%; (*m*) $AgNO_3$, H_2O, r.t., 1 day; (*n*) dipotassium cyclobutane-1,1-dicarboxylate, H_2O, 3 days, 81%

SCHEME 1

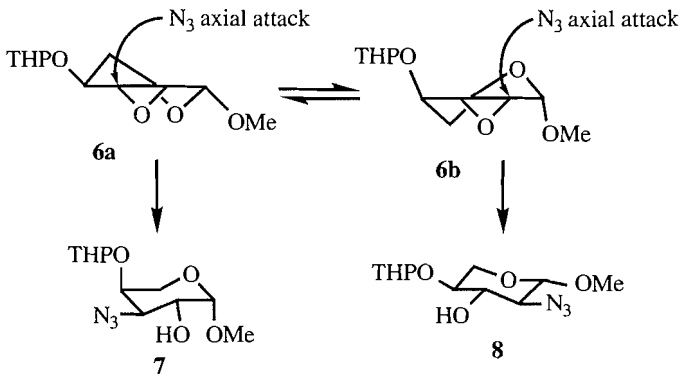

SCHEME 2

position due to nonbonded 1,3-diaxial interactions. *trans*-Diaxial opening of **6***a* is not impeded by neighboring groups, and could favor the formation of **7**, which also benefits from the axially orientated anomeric methoxy group (8).

Compounds **7** and **8** were individually manipulated and transformed into the same aziridine derivative **10** by different routes. Thus, mesylation of **8** followed by treatment with hydrazine monohydrate and Raney nickel (6) in methanol afforded the aziridine derivative **10** in excellent yield. Unfortunately, application of this method to the isomer **7** led to the reduced amine derivative, which did not undergo cyclization to the expected aziridine derivative **10**.

Therefore, an alternative two-step method (9) was used. Tosylation of **7** led to **9** in 82% yield. Reduction of the azido group with hydrazine hydrate in the presence of Raney nickel in refluxing methanol was followed by treatment of the resulting amino derivative with sodium acetate in DMF to effect the formation of the aziridine **10**. Unlike the epoxide analog **6**, opening of the aziridine ring in **10** with sodium azide proceeded in a site-selective manner to give the 3-azido derivative **11** as the major product, which could be isolated as diastereomeric OTHP ethers. In each of these, the molecule adopts a $^1C_4$ conformation, which was confirmed by ^1H nmr since the proton coupling constants ($J_{1,2}$ = 7.7 Hz, $J_{2,3}$ = 10.3 Hz, $J_{3,4}$ = 9.8 Hz, $J_{4,5ax}$ = 10.3 Hz) indicate that all the substituents are in the equatorial position. It is possible that under the slightly acidic conditions, the site-selective opening at C-3 is proceeding via the aziridinium ion. This type of activation may favor a diaxial opening to a greater extent than in the case of epoxide **6**.

When treated with acid, compound **11** led to the corresponding alcohol derivative **12**. Catalytic hydrogenation gave the crystalline diamino derivative **13**, which upon treatment with aqueous K_2PtCl_4 produced the desired complex **2**, as bright yellow crystals.

The methoxy series was prepared from the minor isomer **8** (Scheme 3). Thus, mesylation afforded **14**, which could be separated into two diastereomers. Selective cleavage of

Can. J. Chem. Downloaded from www.nrcresearchpress.com by 213.200.69.106 on 09/08/12
For personal use only.

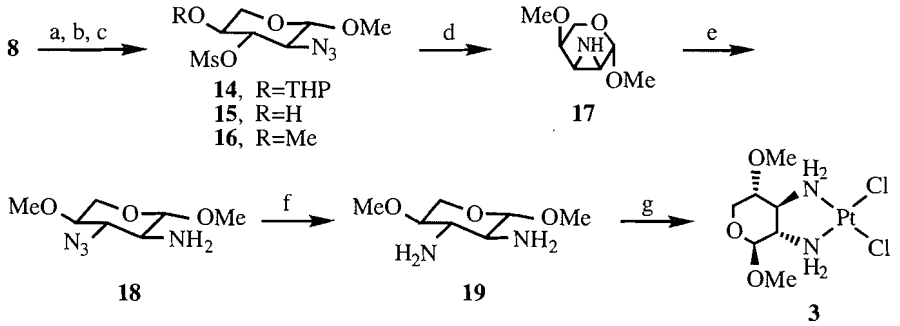

(a) MsCl, pyr., r.t., 1 day, 81%; (b) PPTS, EtOH, 55°C, 1 h, quant.; (c) MeI, Ag_2O, ether, reflux, 4 days, 90%; (d) $NH_2NH_2 \cdot H_2O$, Ra-Ni, MeOH, reflux, 5 h, 70%; (e) NaN_3, NH_4Cl, $CH_3OCH_2CH_2OH/H_2O$, 110°C, 17 h, 80%; (f) Pd/C (10%), H_2, $MeOH/H_2O$, r.t., 1 day, 94%; (g) K_2PtCl_4, H_2O, r.t., 4 h, 60%

SCHEME 3

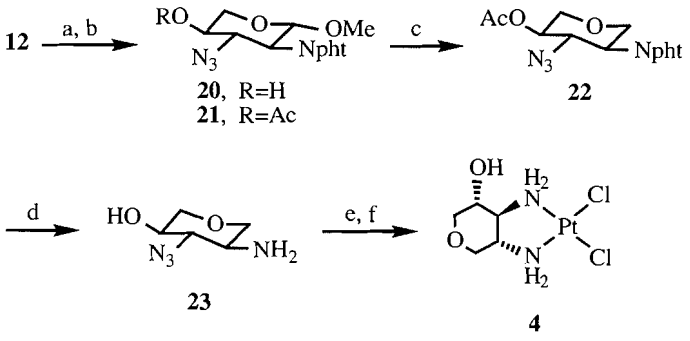

(a) *N*-(Ethoxycarbonyl)phthalimide, Et_3N, THF, 55°C, 1 day, 82%; (b) Ac_2O, EtOAc, DMAP, r.t., 30 min, 87%; (c) $Me_3SiOTfl$, $BF_3 \cdot Et_2O$, Et_3SiH, CH_2Cl_2, 0°C–r.t., 18 h, 73%; (d) $NH_2NH_2 \cdot H_2O$, 95% EtOH/THF, r.t., 19 h, 68%; (e) Pd/C (10%), H_2, MeOH, 90%; (f) K_2PtCl_4, H_2O, r.t., 3 h, 39%

SCHEME 4

the OTHP group in **14**, followed by methylation using a suspension of silver oxide in ether, gave **16**, which after treatment with hydrazine led to the aziridine derivative **17**. Ring opening with sodium azide led to **18**, which after catalytic hydrogenation gave the crystalline diamino derivative **19**. Finally, treatment with aqueous K_2PtCl_4 gave the intended platinum(II) complex **3**, which was isolated as bright yellow crystals.

The synthesis of the tetrahydropyran complex **4** from a common intermediate such as **12** presented logistical problems concerned with functional group compatibility. How could one reductively demethoxylate the anomeric position en route to the desired 1,5-anhydroalditol derivative? A method of choice involved treatment of a suitably N-protected derivative obtained from **12** with trimethylsilyl triflate and triethylsilane in the presence of a Lewis acid (10). However, previous studies showed that in the 2-*N*-acetylamino sugar series, the cleavage of the glycosidic carbon–oxygen bond did not take place under these conditions due to neighboring group participation (11).

After exploring a number of possibilities, the *N*-phthalimido derivative **20** proved to be the most compatible N-protective group (Scheme 4). Thus reductive demethoxylation of the corresponding acetate **21** afforded **22** without apparently affecting the azido or ester groups. Functional group manipulation led to the amino derivative **23**, which was hydrogenated, and then transformed into the platinum(II) complex **4** in the usual fashion.

In view of the known influence of the anionic counterparts of *cis*-platinum complexes of vicinal diamines on solubility and biological activity (12), we prepared the cyclobutane 1,1-dicarboxylate derivative **24** by adaptations of known procedures (ref. 13, Scheme 1). Thus, the complex **2** was transformed into the corresponding dinitrate and this was treated with dipotassium cyclobutane 1,1-dicarboxylate to give the corresponding crystalline complex **24**.

The structure of **24** was definitively ascertained by a single crystal X-ray diffraction determination on the dihydrate obtained by recrystallization in water. The ORTEP representation of one of two independent molecules is shown in Fig. 1. The structure of the second molecule (figure in the supplementary material)[2] is very similar. The coordination about Pt is roughly square-planar as expected, and the Pt—N and

[2]Detailed crystallographic results (ORTEP, drawing of molecule **2**, anisotropic temperature factors, hydrogen parameters, bond distances and angles, torsion angles, geometry of hydrogen bonds, least-squares plane calculations, and structure factors) (49 pages) may be purchased from: The Depository of Unpublished Data, Document Delivery, CISTI, National Research Council Canada, Ottawa, Canada K1A 0S2.

Tables of hydrogen parameters, bond distances and angles, and geometry of hydrogen bonds and the ORTEP view of molecule **2** have also been deposited with the Cambridge Crystallographic Data Centre and can be obtained on request from The Director, Cambridge Crystallographic Data Centre, University Chemical Laboratory, 12 Union Road, Cambridge, CB2 1EZ, U.K.

Can. J. Chem. Downloaded from www.nrcresearchpress.com by 213.200.69.106 on 09/08/12
For personal use only.

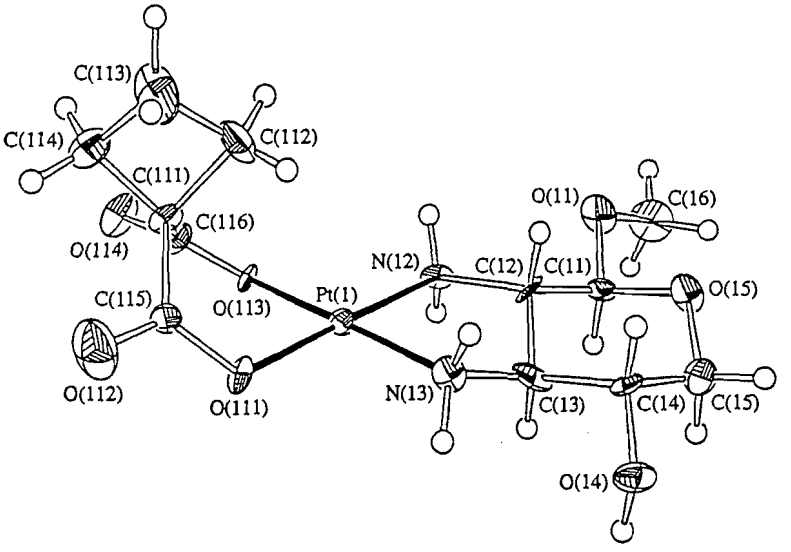

FIG. 1. ORTEP view showing the molecular conformation of compound **24**. Ellipsoids correspond to 40% probability. Hydrogens are shown as spheres of arbitrary size.

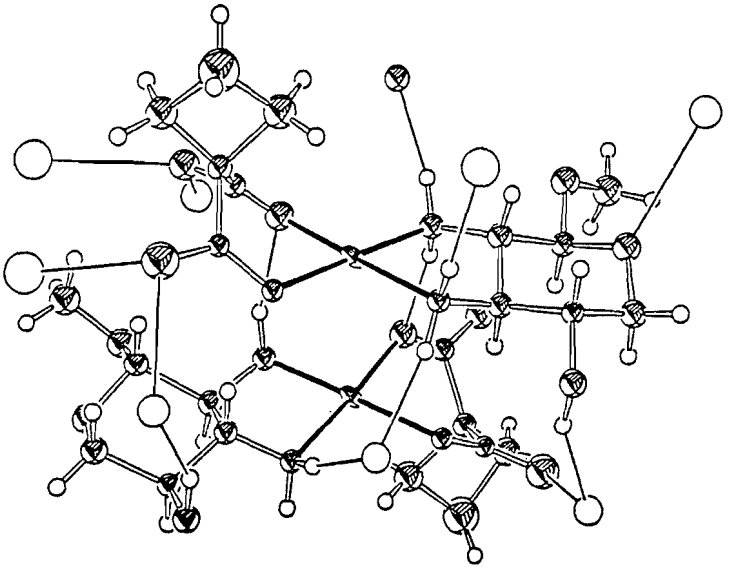

FIG. 2. View of the hydrogen-bonded dimeric unit including two independent complexes (Pt(1) above, Pt(2) below). Hydrogen bonding indicated by thin bonds. The water molecules are shown as undashed spheres without hydrogens.

Pt—O distances (mean 2.02 and 2.01 Å, respectively) are normal. The O—Pt—O angles (mean 89.3°) are close to ideality, but the "bite" of the diamine ligand imposes small N—Pt—N angles (mean 84.6°). The pyran ring is in the chair conformation, all the substituents on this ring are in a *trans* orientation relative to one another, and the coordinated dicarboxylate ligand is puckered, having the cyclobutane moiety significantly displaced above the coordination plane. The two types of molecules are packed as dimers in the crystal, with the square planes stacked to give a relatively short Pt—Pt distance of 3.33 Å (Fig. 2). The dimer is held together by a number of hydrogen bonds involving water molecules, the carboxylates, and the amino groups. Intermolecular hydrogen bonds are also found between the nitrogen atom of the amine group in one molecule and the oxygen atom of the carboxyl group in the other molecule.

Antitumor activity

Biological evaluation of the platinum complexes in vitro and in vivo gave interesting results. Compounds **2** (T/C 227, i.p. dose 25 mg/kg) and **4** (T/C > 236, i.p. dose 12.5 mg/kg) showed comparable activity to cisplatin (T/C > 236, i.p. dose 4 mg/kg) against P338 leukemia in vivo. The complex **3** (T/C 191, i.p. dose 25 mg/kg) was less active than the hydroxy analog **2**. Compound **24** (T/C 114, i.p. dose 25 mg/kg) showed much reduced activity in the same tests. In vivo testing against intraperitoneal L1210 implants showed that **2** (T/C 323, i.p. dose 50 mg/kg) was more active than **3** (T/C 218, i.p. dose 50 mg/kg). Cisplatin (i.p. dose 25 mg/kg) had an activity rating of T/C 323. The comparatively better in vitro activity of **2** over **3** was also evident when tested against strains of L1210, DDP5, P388, and their resistant lines, although DACH was considerably more ac-

Can. J. Chem. Downloaded from www.nrcresearchpress.com by 213.200.69.106 on 09/08/12
For personal use only.

Can. J. Chem. Downloaded from www.nrcresearchpress.com by 213.200.69.106 on 09/08/12
For personal use only.

tive. Compounds **2** and **3** had solubilities of 2 mg/mL and 1.5 mg/mL, respectively, in water. It is clear that the introduction of hydroxy groups in these analogs has a beneficial effect on the in vivo antitumor activity as well as on the water solubility of the complex.

Experimental

Melting points (mp) were determined on a Fisher–Johns melting point apparatus and are uncorrected. Optical rotations were measured at 25°C using a Perkin–Elmer automatic spectropolarimeter model 141. Proton magnetic resonance (^{1}H nmr) spectra were determined on either a 300 MHz Varian or a 400 MHz Bruker spectrometer in deuterated chloroform, methanol-d_4, dimethyl sulfoxide-d_6, or deuterium oxide (D_2O) with $CHCl_3$ (δ_{ppm} = 7.265), Me_4Si (δ_{ppm} = 0.00), or dioxane (δ_{ppm} = 67.40 for ^{13}C) as references. Coupling constants are expressed in hertz (Hz). The abbreviations used for the description of the peaks are as follows: s, singlet; d, doublet; dd, doublet of doublets; dt, doublet of triplets; ddd, doublet of doublet of doublets; t, triplet; q, quartet; m, multiplet; br, broad. The ^{13}C nmr spectra were recorded on a Varian VXR 300 at 75 MHz. Low-resolution mass spectra were determined on a VG Micro Mass 1212 mass spectrometer by using desorption chemical ionization (DCI), or by fast atom bombardment (FAB). High-resolution mass spectra were determined on a Kratos MS-50 TCTA mass spectrometer by using electron impact (EI) at 70 eV or by the fast atom bombardment (FAB) techniques. Infrared spectra (ir) were recorded on a Perkin–Elmer 781 infrared spectrophotometer. The spectra of solids were recorded as Nujol mulls or as concentrated solutions in carbon tetrachloride between sodium chloride plates. Liquid samples were determined as films between sodium chloride plates. Combustion analyses were performed by Guelph Laboratories Ltd, Guelph, Ont. Flash chromatography was done according to the procedure of Still *et al.* (14) using Kieselgel 60 silica gel.

Crystal data

$C_{12}H_{20}N_2O_7Pt \cdot 4.5H_2O$ fw = 580.45.

Monoclinic, *C*2, a = 13.233(6), b = 12.778(6), c = 23.305(7) Å, β = 96.96(3)°, V = 3912(3) Å^3, D_c = 1.971 g cm^{-3}, Z = 8, λ(MoKα) = 0.70930 Å, μ(MoKα) = 73.1 cm^{-1}, T = 220 K.

Data collection and structure determination

Cell dimensions and space group were obtained from precession and cone-axis photographs. The systematic absences (*hkl*, $h + k$ odd) were consistent with space groups *C*2, *Cm*, and *C*2/*m*, but the presence of the chiral ligand unambiguously identified *C*2. The specimen used for diffractometer work had the following dimensions (mm) between the indicated pairs of faces: 0.10 (001–00$\bar{1}$) × 0.25 ($1\bar{1}1$–$\bar{1}1\bar{1}$) × 0.37 (111–$\bar{1}\bar{1}\bar{1}$). Data collection was run as described in the previous paper (2). The whole sphere of data (13 625 reflections, $2\theta < 50°$) was collected. These data were corrected for absorption (Gaussian integration, grid 10 × 10 × 10, transmission range: 0.15–0.52). Equivalent reflections were averaged assuming symmetry 2 (R_{av} = 0.068), yielding 3595 unique *hkl* and *hkl* reflections (3167 with $I > 1.96\ \sigma I$ used to solve the structure) and 3260 Friedel equivalent reflections (2947 with $I > 1.96\ \sigma I$). The data were corrected for the effects of Lorentz and polarization.

The structure was solved by the direct methods of SHELX-86 (15), which provided coordinates for the two independent Pt atoms. All other calculations were done with the NRCVAX system (16). The remaining non-hydrogen atoms were located from ΔF maps. Anisotropic refinement of all non-hydrogen atoms was done on $|F_o|$ by full-matrix least squares. Ligand hydrogens were fixed at idealized positions (C(N)—H = 0.95 Å) with isotropic temperature factors adjusted in relation to the B_{eq} value of the attached atom. Water hydrogens were not visible in the ΔF map and were neglected. A secondary extinction coefficient was also refined (0.131 (17)). The final agreement factors were $R = \Sigma\|F_o| - |F_c\|/\Sigma|F_o| = 0.045$, $R_w = [\Sigma w\ (|F_o| - |F_c|)^2/\Sigma w|F_o|^2]^{1/2} = 0.049$ and the goodness-of-fit ratio was 2.94 for 480 parameters refined. The general background in the final ΔF map was below ±1.55 e/Å^3, except for nine peaks in the range ±|1.6–2.9|e/Å^3 within 1.2 Å from Pt. Friedel reflections were used to check the absolute configuration already known from the ligand chirality. Bijvoet analysis on the 100 most significant reflections rejected the other enantiomer whose probability is $<10^{-20}$. The refined coordinates are listed in Table 1.

*Methyl 2,3-anhydro-4-O-(2-tetrahydropyranyl)-β-L-lyxopyranoside (**6**)*

A solution of compound **5** (0.923 g, 6.32 mmol) and dihydropyran (3.0 mL, 32.9 mmol) in dry dichloromethane (50 mL) containing pyridinium *p*-toluenesulfonate (PPTS) (0.180 g, 0.720 mmol) was stirred for 1.5 h at room temperature. The solution was diluted with 50 mL ether, then washed with half-saturated NaCl (2 × 25 mL), dried (Na_2SO_4), and the solvent was evaporated to give a syrup that was applied to a silica gel column. Elution with ethyl acetate – hexanes (1:1) and concentration gave a mixture of the two isomers of the THP ether **6** (1.32 g, 91%) as a syrup; ^{1}H nmr (300 MHz, $CDCl_3$) δ: 1.51–1.92 (m, 12H), 3.46 (s, 3H, OCH_3), 3.47 (s, 3H, OCH_3), 3.30–3.66 (m, 8H), 3.80–4.05 (m, 6H), 4.74 (dd, 1H, J = 2.7 Hz, 5.0 Hz), 4.81 (dd, 1H, J = 2.8 Hz, 4.4 Hz), 4.95 (d, 2H, J = 3.0 Hz); ^{13}C nmr (75 MHz, $CDCl_3$) major isomer, δ: 19.70, 30.66, 50.83, 51.35, 55.53, 58.51, 63.03, 68.27, 94.66, 98.23; minor isomer, δ: 19.46, 25.17, 30.74, 50.31, 51.30, 55.58, 60.59, 62.68, 69.03, 94.75, 99.52; ms, *m/e*: 231 $(M + 1)^+$. Exact Mass calcd. for $C_{11}H_{18}O_5$: 230.1154; found: 230.1109.

*Methyl 3-azido-3-deoxy-4-O-(2-tetrahydropyranyl)-β-L-arabinopyranoside (**7**) and methyl 2-azido-2-deoxy-4-O-(2-tetrahydropyranyl)-β-L-xylopyranoside (**8**)*

To a solution of the epoxide **6** (26.4 g, 115 mmol) in 2-methoxyethanol–water (14:1, 1000 mL) was added sodium azide (30.0 g, 153 mmol) and ammonium chloride (12.3 g, 230 mmol). The mixture was heated at 110°C for 20 h, and evaporated to give a residue that was dissolved in dichloromethane. The solution was washed with water and the organic phase was dried ($MgSO_4$), then evaporated, to give a syrup that was applied to a silica gel column. Elution with ethyl acetate – hexanes (1:1) gave the two THP ether isomers of the 2-azido derivative, **8***a* and **8***b* (total 7.50 g, 24%), and an inseparable mixture of the two THP ether isomers of the 3-azido derivative **7** (14.8 g, 47.2%); **8***a*: $[\alpha]_D$ +11.9 (*c* 0.78, $CHCl_3$); ir ($CHCl_3$): 3380 (OH), 2110 (N_3) cm^{-1}; ^{1}H nmr (400 MHz, $CDCl_3$) δ: 1.5–1.8 (m, 6H, H-2′, 3′, 4′), 3.26 (dd, 1H, J = 8.7 Hz, 10.3 Hz, H-2), 3.26 (dd, 1H, J = 10.5 Hz, 11.5 Hz, H-5ax), 3.44 (m, 1H, H-3), 3.56 (s, 3H, OCH_3), 3.57–3.62 (m, 2H, H-4, H-5′ax), 3.96 (dd, 1H, J = 5.5 Hz, 11.5 Hz, H-5eq), 4.01–4.05 (m, 1H, H-5′eq), 4.13 (d, 1H, J = 8.1 Hz, H-1), 4.54 (m, 1H, H-1′eq), 5.01 (d, 1H, J = 0.7 Hz); ms, *m/e*: 274 $(M + 1)^+$; **8***b*: ir ($CHCl_3$): 3400 (br, OH), 2110 (N_3) cm^{-1}; ^{1}H nmr (400 MHz, $CDCl_3$) δ: 1.5–1.8 (m, 6H, H-2′, 3′, 4′), 2.76 (s, 1H, OH), 3.24 (dd, 1H, J = 10.2 Hz, 11.7 Hz, H-5ax), 3.28 (dd, 1H, J = 7.8 Hz, 9.8 Hz, H-2), 3.46 (m, 1H, H-3), 3.49–3.54 (m, 1H, H-5′ax), 3.55 (s, 3H, OCH_3), 3.63 (ddd, 1H, J = 5.4 Hz, 8.8 Hz, 10.2 Hz, H-4), 3.86 (m, 1H, H-5′eq), 4.15 (d, 1H, J = 7.8 Hz, H-1), 4.16 (dd, 1H, J = 5.4 Hz, 11.7 Hz, H-5eq), 4.75 (dd, 1H, J = 2.6 Hz, 5.4 Hz, H-1′); ms, *m/e*: 274 $(M + 1)^+$; ^{13}C nmr (75 MHz, $CDCl_3$) **8** (mixture of **8***a* and **8***b*), δ: 19.90, 20.53, 24.60, 24.95, 30.44, 31.02, 56.86, 56.96, 63.37, 63.84, 64.85, 64.95, 65.26, 65.48, 73.87, 73.39, 79.61, 100.90, 101.24, 103.10; **7**: ir ($CHCl_3$): 3450 (OH), 2105 (N_3) cm^{-1}; ^{1}H nmr (400 MHz, $CDCl_3$) δ: 1.52–1.95 (m, 6H, H-2′, 3′, 4′), 2.18 (m, 1H, OH), 3.45 (2 × 5, 3H, OCH_3), 3.40–4.09 (m, 7H, H-2, 3, 4, 5, 5′), 4.80–4.91 (m, 2H, H-1, 1′); ^{13}C nmr (75 MHz, $CDCl_3$) δ: 18.48, 19.21, 25.21, 25.24, 30.08, 30.66, 55.49, 55.53, 58.49, 61.10, 61.47, 61.68, 62.39, 62.47, 67.32, 67.65, 70.64, 75.79, 94.29, 99.26, 99.36, 101.08; ms, *m/e*: 274 $(M + 1)^+$.

Can. J. Chem. Downloaded from www.nrcresearchpress.com by 213.200.69.106 on 09/08/12
For personal use only.

TABLE 1. Final atomic coordinates and equivalent isotropic temperature factors

Atom	*x*	*y*	*z*	B_{iso}[a]
Pt(1)	0.40078(5)	0.00680	0.94856(3)	1.24(3)
Pt(2)	1.07639(5)	0.06794(7)	0.44431(3)	1.30(3)
O(11)	0.2012(10)	0.1607(10)	1.0886(7)	2.4(6)
O(14)	0.2659(9)	−0.2622(9)	1.0715(6)	2.0(6)
O(15)	0.1650(9)	−0.0087(10)	1.1122(6)	2.3(6)
O(111)	0.4620(9)	−0.0876(10)	0.8897(5)	1.5(6)
O(112)	0.5031(13)	−0.0975(12)	0.8019(8)	4.2(8)
O(113)	0.4695(9)	0.1295(10)	0.9191(5)	1.6(5)
O(114)	0.5172(11)	0.2143(10)	0.8427(7)	2.6(7)
O(21)	1.3258(10)	−0.0955(10)	0.5879(6)	2.1(6)
O(24)	1.2665(10)	0.3276(10)	0.5691(7)	2.4(6)
O(25)	1.3734(9)	0.0709(11)	0.6126(6)	2.2(5)
O(211)	0.9947(9)	0.1564(10)	0.3848(6)	2.0(6)
O(212)	0.9247(10)	0.1736(11)	0.2936(6)	2.5(7)
O(213)	0.9910(9)	−0.0585(10)	0.4139(6)	2.1(6)
O(214)	0.9120(11)	−0.1473(11)	0.3409(7)	3.3(7)
N(12)	0.3376(10)	0.0908(11)	1.0072(6)	1.3(6)
N(13)	0.3330(11)	−0.1183(11)	0.9833(7)	1.8(7)
N(22)	1.1593(12)	−0.0234(10)	0.5049(8)	2.0(7)
N(23)	1.1607(11)	0.1851(11)	0.4818(7)	1.7(7)
C(11)	0.2392(12)	0.0595(15)	1.0928(8)	1.7(8)
C(12)	0.2643(12)	0.0181(17)	1.0349(8)	1.7(8)
C(13)	0.3047(13)	−0.0893(15)	1.0405(9)	1.9(9)
C(14)	0.2279(13)	−0.1577(13)	1.0642(8)	1.2(7)
C(15)	0.1976(14)	−0.1170(16)	1.1184(10)	2.5(9)
C(16)	0.1929(17)	0.2079(15)	1.1428(11)	2.9(10)
C(21)	1.2883(13)	0.0024(18)	0.5926(8)	2.1(8)
C(22)	1.2421(12)	0.0406(12)	0.5332(8)	1.3(7)
C(23)	1.2090(14)	0.1534(14)	0.5399(9)	1.9(8)
C(24)	1.2976(14)	0.2200(15)	0.5619(9)	1.9(8)
C(25)	1.3442(16)	0.1774(16)	0.6177(10)	2.6(10)
C(26)	1.3501(18)	−0.1485(17)	0.6425(10)	3.1(10)
C(111)	0.4161(12)	0.0612(14)	0.8238(8)	1.5(7)
C(112)	0.2963(14)	0.0552(20)	0.8212(10)	3.2(11)
C(113)	0.2871(16)	0.0416(26)	0.7562(11)	5.1(17)
C(114)	0.3971(15)	0.0839(16)	0.7594(9)	2.5(9)
C(115)	0.4635(14)	−0.0466(15)	0.8385(9)	2.1(9)
C(116)	0.4719(14)	0.1416(19)	0.8643(10)	2.9(10)
C(211)	1.0020(13)	0.0084(16)	0.3174(8)	1.6(8)
C(212)	1.1197(15)	−0.0072(15)	0.3147(10)	2.5(9)
C(213)	1.0953(22)	−0.0646(27)	0.2558(16)	6.8(18)
C(214)	0.9821(17)	−0.0277(15)	0.2527(12)	3.3(11)
C(215)	0.9701(14)	0.1168(16)	0.3326(9)	2.2(8)
C(216)	0.9638(14)	−0.0730(17)	0.3612(10)	2.6(10)
W(1)	−0.0352(9)	0.0683(13)	1.0904(6)	2.8(7)
W(2)	0.4109(9)	−0.2850(10)	1.1713(7)	2.3(6)
W(3)	0.5000	−0.2767(15)	1.0000	2.0(9)
W(4)	1.0000	0.3340(19)	0.5000	3.9(12)
W(5)	0.1301(11)	−0.1335(13)	0.9170(8)	3.8(8)
W(6)	0.6603(13)	−0.0135(14)	0.7472(8)	5.2(10)
W(7)	1.3446(12)	0.2017(13)	0.4210(8)	3.8(8)
W(8)	1.1483(14)	0.3530(12)	0.6563(10)	5.5(11)
W(9)	1.5610(10)	−0.0036(12)	0.5815(8)	4.6(8)
W(10)	0.6231(14)	0.2032(12)	0.7418(8)	4.4(9)

[a] B_{iso} is the mean of the principal axes of the thermal ellipsoid.

*Methyl 2-azido-2-deoxy-3-*O*-methanesulphonyl-4-*O*-(2-tetrahydropyranyl)-β-L-xylopyranoside (**14**)*

To a cold solution of **8** (7.40 g, 27.1 mmol) and DMAP (catalytic amount) in pyridine (40 mL) was added dropwise a precooled (0°C) solution of methanesulphonyl chloride (6.5 mL, 84 mmol) in 40 mL pyridine, and the mixture was left at room temperature for 1 day. After hydrolysis of the excess of reagent, the solution was poured onto ice-water and extracted with chloroform. The extract was washed with cold hydrochloric acid (2%) and cold water, dried (Na_2SO_4), and evaporated to give a syrup. Flash column chromatography with ethyl acetate – hexane (1:3, then 1:1) gave the THP isomers **14***a* (4.09 g, 43%) and **14***b* (3.60 g, 38%); **14***a*: mp 89–91°C; $[\alpha]_D$ −26.9 (*c* 0.85, $CHCl_3$); ir ($CHCl_3$): 2110 (N_3), 1360, 1180 (S=O) cm^{-1}; ^1H nmr (400 MHz, $CDCl_3$) δ: 1.50–1.90 (m, 6H, H-2′, 3′, 4′), 3.14 (s, 3H, OSO_2CH_3), 3.26 (dd, 1H, J = 10.5 Hz, 11.8 Hz, H-5ax), 3.41 (dd, 1H, J = 7.8 Hz,

Can. J. Chem. Downloaded from www.nrcresearchpress.com by 213.200.69.106 on 09/08/12
For personal use only.

10.4 Hz, H-2), 3.52 (m, 1H, H-5′ax), 3.58 (s, 3H, OCH_3), 3.75 (ddd, 1H, J = 5.7 Hz, 9.2 Hz, 10.5 Hz, H-4), 3.82 (m, 1H, H-5′eq), 4.20 (d, 1H, J = 7.8 Hz, H-1), 4.23 (dd, 1H, J = 5.7 Hz, 11.8 Hz, H-5eq), 4.39 (dd, 1H, J = 9.2 Hz, 10.4 Hz, H-3), 4.73 (dd, 1H, J = 2.1 Hz, 5.1 Hz, H-1′); **14***b*: $[\alpha]_D$ +82.7° (*c* 1.8, $CHCl_3$); ir ($CHCl_3$): 2110 (N_3), 1360, 1180 (S=O) cm^{-1}; ^1H nmr (400 MHz, $CDCl_3$) δ: 1.50–1.90 (m, 6H, H-2′, 3′, 4′), 3.18 (dd, 1H, J = 10.3 Hz, 11.9 Hz, H-5ax), 3.20 (s, 3H, OSO_2CH_3), 3.44 (dd, 1H, J = 7.8 Hz, 10.3 Hz, H-2), 3.46 (m, 1H, H-5′ax), 3.58 (s, 3H, OCH_3), 3.99 (m, 1H, H-4), 4.03 (m, 1H, H-5′eq), 4.12 (dd, 1H, J = 5.2 Hz, 11.9 Hz, H-5eq), 4.22 (d, 1H, J = 7.8 Hz, H-1), 4.40 (t, 1H, J = 10.3 Hz, H-3), 4.68 (t, 1H, J = 3.3 Hz, H-1′); ms, *m/e*: 352 $(M + 1)^+$.

*Methyl 3-azido-3-deoxy-4-*O*-(2-tetrahydropyranyl)-2-*O*-tolylsulphonyl-β-*L*-arabinopyranoside (**9**)*

To a cold solution of the 3-azido derivative **7** (12.0 g, 44.0 mmol) in 90 mL of dry pyridine was added a catalytic amount of 4-dimethylaminopyridine, then, dropwise, a precooled (0°C) solution of tosyl chloride (8.60 g, 45.1 mmol) in 70 mL of dry pyridine at 5°C. The mixture was stirred at 40°C for 1 day, cold water (1 mL) was added to quench the reaction at 0°C, the resulting solution was poured onto 500 mL of ice-water, and then extracted with dichloromethane (4 × 150 mL). The combined extracts were washed with 1 N HCl, water, saturated $NaHCO_3$, water, and brine, dried (Na_2SO_4), and evaporated to give a syrup. Purification by flash chromatography, eluting with ethyl acetate – hexanes (2:3, then 3:1) gave a mixture of the THP ether isomers, **9***a* and **9***b* (15.4 g, 82%), which were difficult to separate on a large scale. However, the two isomers were partially separable by applying a small sample on a longer column; THP ether isomer **9***a*: $[\alpha]_D$ +70.0 (*c* 0.31, $CHCl_3$); ir ($CHCl_3$): 2100 (N_3) cm^{-1}; ^1H nmr (300 MHz, $CDCl_3$) δ: 1.50–1.90 (m, 6H, H-2′, 3′, 4′), 2.45 (s, 3H, $ArCH_3$), 3.35 (s, 3H, OCH_3), 3.51 (m, 1H, H-5′), 3.67 (dd, 1H, J = 3.2 Hz, 10.5 Hz, H-3), 3.72 (dd, 1H, J = 1.2 Hz, 12.4 Hz, H-5), 3.80 (dd, 1H, J = 2.0 Hz, 12.4 Hz, H-5), 3.90 (m, 1H, H-5′), 3.95 (m, 1H, H-4), 4.74 (t, 1H, J = 3.6 Hz, H-1′), 4.83 (dd, 1H, J = 3.5 Hz, 10.5 Hz, H-2), 4.91 (d, 1H, J = 3.5 Hz, H-1), 7.35 (m, 2H, ArH), 7.87 (m, 2H, ArH); ^{13}C nmr (75 MHz, $CDCl_3$) δ: 19.17, 21.55, 25.20, 30.44, 55.62, 58.14, 62.09, 62.47, 75.43, 76.09, 97.61, 101.15, 127.93, 129.67, 133.43, 144.99; THP ether isomer **9***b*: $[\alpha]_D$ +138.3 (*c* 0.12, $CHCl_3$); ir ($CHCl_3$): 2100 (N_3) cm^{-1}; ^1H nmr (300 MHz, $CDCl_3$) δ: 1.50–1.88 (m, 6H, H-2′, 3′, 4′), 2.45 (s, 3H, $ArCH_3$), 3.36 (s, 3H, OCH_3), 3.43–3.52 (m, 1H, H-5′), 3.61 (dd, 1H, J = 1.0 Hz, 13.0 Hz, H-5), 3.72 (dd, 1H, J = 2.0 Hz, 13.0 Hz, H-5), 3.74 (dd, 1H, J = 3.3 Hz, 10.4 Hz, H-3), 3.85–3.93 (m, 1H, H-5′), 4.10 (m, 1H, H-4), 4.79 (t, 1H, J = 3.2 Hz, H-1′), 4.86 (dd, 1H, J = 3.5 Hz, 10.4 Hz, H-2), 4.91 (d, 1H, J = 3.5 Hz, H-1), 7.36 (m, 2H, ArH), 7.88 (m, 2H, ArH); ^{13}C nmr (75 MHz, $CDCl_3$) δ: 18.53, 21.55, 25.18, 30.03, 55.68, 57.77, 58.00, 61.81, 71.18, 75.16, 94.31, 97.75, 127.96, 129.68, 133.50, 144.98.

*Methyl 2,3-dideoxy-2,3-epimino-4-*O*-(2-tetrahydropyranyl)-β-*L*-ribopyranoside (**10**)*

*Method A (from **9**)*

To a solution of **9** (14.0 g, 34.9 mmol) in 300 mL of DMF and distilled water (5:1) was added sodium acetate trihydrate (21.0 g, 154 mmol) and the mixture was heated to 85°C overnight with stirring. After removal of the solvent under reduced pressure, the residue was treated with acetone (50 mL) and the resulting white precipitate was filtered and washed with acetone. Evaporation of the filtrate gave crude product **10** (7.65 g, 95.6%) as a syrup that was used for next reaction without further purification. A small sample was applied to a silica gel column, eluting with dichloromethane/methanol (15:1) to give two tetrahydropyranyl isomers **10***a* and **10***b*.

*Method B (from **14**)*

Compound **14***a* (3.00 g, 8.55 mmol) in methanol (100 mL) was mixed with hydrazine monohydrate (99–100%) (4.6 mL, 82.5 mmol), Raney nickel (0.4 g) was added, and the mixture was heated to reflux until decomposition of the hydrazine was complete (monitored by tlc, approximately 5 h). The mixture was filtered and evaporated to a syrup that was applied to a silica gel column. Elution with ethyl acetate, then with ethyl acetate – methanol (10:1), gave compound **10***a* (1.90 g, 97%) as a syrup. **10***a*: $[\alpha]_D$ −80.5 (*c* 1.11, $CHCl_3$); ir ($CHCl_3$): 3300 (NH) cm^{-1}; ^1H nmr (400 MHz, $CDCl_3$) δ: 1.55–1.90 (m, 6H), 2.19 (br s, 1H), 2.48 (br s, 1H), 3.44 (s, 3H), 3.42–3.46 (m, 1H), 3.51–3.56 (m, 1H), 3.82–3.86 (m, 2H), 4.13 (m, 1H), 4.83 (s, 1H), 4.98 (m, 1H); ms, *m/e*: 230 $(M + 1)^+$. The THP ether isomer **10***b* was obtained from compound **14***b* following the same procedure as above; **10***b*: $[\alpha]_D$ +116.5 (*c* 0.81, $CHCl_3$); ir ($CHCl_3$): 3300 (NH) cm^{-1}; ^1H nmr (400 MHz, $CDCl_3$) δ: 1.50–1.95 (m, 6H), 2.19 (br s, 1H), 2.58 (br s, 1H), 3.40 (s, 1H), 3.42 (s, 3H), 3.55 (m, 1H), 3.78 (m, 1H), 3.98–4.06 (m, 2H), 4.77 (s, 1H), 4.80 (s, 1H); ms, *m/e*: 230 $(M + 1)^+$.

*Methyl 2-amino-3-azido-2,3-dideoxy-4-*O*-(2-tetrahydropyranyl)-β-*L*-xylopyranoside (**11**)*

A suspension of the aziridine derivative **10***a* (1.80 g, 7.86 mmol), sodium azide (2.00 g, 30.8 mmol), and ammonium chloride (0.85 g, 15.9 mmol) in 2-methoxyethanol (112 mL) and water (8 mL) was heated for 11 h at 110°C. The mixture was evaporated to dryness and the residue was extracted with dichloromethane (3 × 100 mL). The extract was washed with half-saturated $NaHCO_3$ (3 × 50 mL), dried (Na_2SO_4), and evaporated to give a yellow syrup that was applied to a silica gel column. Elution with dichloromethane–methanol (20:1) gave **11***a* (1.70 g, 80%) as a syrup; $[\alpha]_D$ −67.9 (*c* 0.99, $CHCl_3$); ir ($CHCl_3$): 3380, 3320 (NH), 2110 (N_3) cm^{-1}; ^1H nmr (400 MHz, $CDCl_3$) δ: 1.55–1.90 (m, 6H, H-2′, 3′, 4′), 2.60 (dd, 1H, J = 7.7 Hz, 10.3 Hz, H-2), 3.23 (dd, 1H, J = 10.3 Hz, 11.3 Hz, H-5ax), 3.30 (t, 1H, J = 10.3 Hz, H-3), 3.51 (s, 3H, OCH_3), 3.56–3.61 (m, 1H, H-5′ax), 3.89 (dt, 1H, J = 5.0 Hz, 10.3 Hz, H-4), 3.95 (m, 1H, H-5′eq), 4.06 (d, 1H, J = 7.7 Hz, H-1), 4.13 (dd, 1H, J = 5.0 Hz, 11.3 Hz, H-5eq), 4.78 (m, 1H, H-1′); ms, *m/e*: 273 $(M + 1)^+$. Exact Mass calcd. for $C_{11}H_{21}N_4O_4$ (M + H): 273.1564; found: 273.1608.

The mixture of THP isomers of **11** was obtained from crude **10** following the same procedure as that for the preparation of **11***a*; ^1H nmr (300 MHz, $CDCl_3$) δ: 1.48–1.85 (m, 12H, H-2′, 3′, 4′), 2.51 (dd, 1H, J = 7.7 Hz, 10.4 Hz, H-2), 2.56 (dd, 1H, J = 7.7 Hz, 10.4 Hz, H-2), 3.20 (dd, 1H, J = 10.4 Hz, 11.5 Hz, H-3), 3.24 (dd, 1H, J = 10.3 Hz, 11.6 Hz, H-3), 3.26–3.33 (m, 2H), 3.47, 3.48 (2 × 5, 6H, OCH_3), 3.49–3.63 (m, 3H), 3.81–3.91 (m, 3H), 4.00 (d, 1H, J = 7.7 Hz, H-1), 4.03 (d, 1H, J = 7.7 Hz, H-1), 4.09 (dd, 1H, J = 4.9 Hz, 11.4 Hz, H-5), 4.19 (dd, 1H, J = 5.3 Hz, 11.4 Hz, H-5), 4.72–4.76 (m, 2H, H-1′); ^{13}C nmr (75 MHz, $CDCl_3$) δ: 18.29, 19.52, 24.93, 30.05, 30.42, 55.00, 56.82, 61.69, 62.87, 63.88, 66.01, 67.53, 67.58, 71.12, 95.02, 101.27, 104.99, 105.26.

*Methyl 2-amino-3-azido-2,3-dideoxy-β-*L*-xylopyranoside (**12**)*

To a solution of THP ether **11** (32 mg, 0.12 mmol) in ethanol (1.5 mL) was added pyridinium *p*-toluenesulfonate (PPTS) (59 mg, 0.24 mmol). The solution was stirred for 1 day at 70°C, evaporated to dryness, and the residue was applied to a silica gel column. Elution with dichloromethane–methanol–triethylamine (100:10:1) followed by concentration gave compound **12** (18 mg, 80%) as white crystals; mp 141–143°C; $[\alpha]_D$ +20 (*c* 0.24, ethanol); ir ($CHCl_3$): 3360, 3300, 3150 (br), 2105 (N_3) cm^{-1}; ^1H nmr (300 MHz, methanol-d_4) δ: 2.39 (dd, 1H, J = 7.8 Hz, 10.5 Hz, H-2), 3.16 (dd, 1H, J = 9.2 Hz, 10.5 Hz, H-3), 3.26 (dd, 1H, J = 10.4 Hz, 11.4 Hz, H-5ax), 3.48 (s, 3H, OCH_3), 3.60 (ddd, 1H, J = 5.3 Hz, 9.2 Hz, 10.4 Hz, H-4), 3.91 (dd, 1H, J = 5.3 Hz, 11.4 Hz, H-5eq), 4.08 (d, 1H, J = 7.8 Hz, H-1); ^{13}C nmr (75 MHz, methanol-d_4) δ: 56.41, 57.29, 67.92, 70.41, 70.88, 106.34; ms, *m/e*: 189 $(M + 1)^+$. Anal. calcd for $C_6H_{12}N_4O_3$: C 38.29, H 6.43, N 29.77; found: C 38.18, H 6.28, N 29.26.

Can. J. Chem. Downloaded from www.nrcresearchpress.com by 213.200.69.106 on 09/08/12
For personal use only.

Methyl 2,3-diamino-2,3-dideoxy-β-L-xylopyranoside (13)

To a solution of the azide **12** (395 mg, 2.10 mmol) in methanol-distilled water (1:1, 18 mL) was added 10% palladium-on-activated charcoal (230 mg) suspended in methanol (5 mL). The mixture was hydrogenated under atmospheric pressure at room temperature for 24 h. The catalyst was then removed by filtration through Celite, and the filtrate was evaporated and co-evaporated with ethanol to dryness to give **13** (290 mg, 85%) as white crystals; mp 200–202°C (dec.); $[\alpha]_D$ +84.5 (*c* 0.33, methanol); ir (Nujol): 3380, 3330, 3280 (NH_2) cm^{-1}; ^1H nmr (400 MHz, methanol-d_4) δ: 2.41 (dd, 1H, *J* = 7.4 Hz, 9.8 Hz, H-2), 2.49 (t, 1H, *J* = 9.8 Hz, H-3), 3.23 (dd, 1H, *J* = 10.0 Hz, 11.2 Hz, H-5ax), 3.39 (m, 1H, H-4), 3.48 (s, 3H, OCH_3), 3.90 (dd, 1H, *J* = 4.8 Hz, 11.2 Hz, H-5eq), 4.07 (d, 1H, *J* = 7.4 Hz, H-1); ms, *m/e*: 163 $(M + 1)^+$. Exact Mass calcd. for $C_6H_{13}N_2O_2$ (−OH): 145.0978; found: 145.0978.

(SP-4-3)-Dichloro(methyl 2,3-diamino-2,3-dideoxy-β-L-xylopyranoside-N,N′) platinum (2)

A solution of the diamine **13** (218 mg, 1.00 mmol) in distilled water (0.9 mL) was added to a solution of K_2PtCl_4 (430 mg, 1.03 mmol) in distilled water (3.9 mL). The mixture was stirred manually until homogeneous, then left standing in the dark. After 2 h, crystallization began in the form of bright yellow plates. When the original red color of the solution became yellow or orange-yellow the crystals were filtered, washed with cold water (3 times), and dried under vacuum in the absence of light for several hours to afford bright yellow crystals of **2** (325 mg, 43.7%); mp 270°C (darkening), 305–310°C (dec.); $[\alpha]_D$ +144 (*c* 0.06, H_2O); ir (Nujol): 3390 (OH), 3280, 3250, 3200, 3120 (NH_2) cm^{-1}; ^1H nmr (300 MHz, DMSO-d_6) δ: 2.21 (m, 1H, H-2), 2.35 (m, 1H, H-3), 2.89 (dd, 1H, *J* = 10.1 Hz, 11.2 Hz, H-5ax), 3.33 (s, 3H, OCH_3), 3.48 (m, 1H, H-4), 3.64 (dd, 1H, *J* = 5.3 Hz, 11.2 Hz, H-5eq), 4.24 (d, 1H, *J* = 7.8 Hz, H-1), 5.14 (d, 1H, *J* = 4.5 Hz, OH), 5.25–5.55 (m, 4H, NH_2); ^{13}C nmr (75 MHz, DMSO-d_6) δ: 56.2, 66.8, 67.2, 69.5, 103.3; ms, *m/e*: 433 (M + 2), 432 (M + 1). Anal. calcd. for $C_6H_{14}Cl_2N_2O_3Pt$: C 16.83, H 3.30, N 6.54, Cl 16.56; found: C 16.83, H 3.31, N 6.39, Cl 16.85.

Methyl 2-azido-2-deoxy-3-O-methanesulphonyl-β-L-xylopyranoside (15)

(A): To a solution of THP ether **14***a* (0.960 g, 2.74 mmol) in ethanol (35 mL) was added pyridinium *p*-toluenesulfonate (PPTS) (0.100 g, 0.40 mmol). The solution was stirred for 7 h at 55°C, and then evaporated. The residue was applied to a silica gel column. Elution with hexanes – ethyl acetate (4:5, then 1:2) and then concentration gave **15** (0.730 g, quantitative) as white crystals.

(B): The compound **15** can be prepared from **14***b* following the same procedure that was used in (A); mp 111–111.5°C; $[\alpha]_D$ +27.0 (*c* 1.05, $CHCl_3$); ir ($CHCl_3$): 3520 (OH), 2120 (N_3), 1350, 1180 (S=O) cm^{-1}; ^1H nmr (400 MHz, $CDCl_3$) δ: 2.87 (d, 1H, *J* = 3.6 Hz, OH), 3.21 (s, 3H, SCH_3), 3.26 (dd, 1H, *J* = 10.4 Hz, 11.9 Hz, H-5ax), 3.44 (dd, 1H, *J* = 7.7 Hz, 9.7 Hz, H-2), 3.59 (3, 3H, OCH_3), 3.88 (m, 1H, H-4), 4.11 (dd, 1H, *J* = 5.7 Hz, 11.9 Hz, H-5eq), 4.22 (d, 1H, *J* = 7.7 Hz, H-1), 4.30 (t, 1H, *J* = 9.7 Hz, H-3); ^{13}C nmr (75 MHz, $CDCl_3$) δ: 38.63, 57.20, 63.21, 64.89, 68.15, 83.55, 103.35; ms, *m/e*: 268 $(M + 1)^+$.

Methyl 2-azido-2-deoxy-3-O-methanesulphonyl-4-O-methyl-β-L-xylopyranoside (16)

To a solution of compound **15** (2.48 g, 9.30 mmol) in dry ether (300 mL) was added iodomethane (2.3 mL, 37.0 mmol), followed by dry, finely divided, silver oxide (4.30 g, 18.5 mmol) in portions. The suspension was heated under reflux for 4 days. After cooling, the mixture was filtered, and then evaporated to a syrup that was applied to a silica gel column. Elution with ethyl acetate – hexanes (1:1) followed by concentration gave **16** (2.34 g, 89.6%) as a colorless syrup; $[\alpha]_D$ +34.4 (*c* 1.51, $CHCl_3$); ir ($CHCl_3$): 2110 (N_3), 1360, 1180 (S=O) cm^{-1}; ^1H nmr (400 MHz, $CDCl_3$) δ: 3.15 (s, 3H, SCH_3), 3.18 (dd, 1H, *J* = 10.2 Hz, 11.6 Hz, H-5ax), 3.41 (dd, 1H, *J* = 7.8 Hz, 10.2 Hz, H-2), 3.43 (ddd, 1H, *J* = 5.3 Hz, 9.2 Hz, 10.2 Hz, H-4), 3.48 (s, 3H, OCH_3), 3.58 (s, 3H, OCH_3), 4.16 (dd, 1H, *J* = 5.3 Hz, 11.6 Hz, H-5eq), 4.20 (d, 1H, *J* = 7.8 Hz, H-1), 4.33 (t, 1H, *J* = 9.7 Hz, H-3); ^{13}C nmr (75 MHz, $CDCl_3$) δ: 38.96, 57.22, 58.53, 62.75, 63.73, 77.07, 81.90, 103.51; ms, *m/e*: 282 $(M + 1)^+$.

Methyl 2,3-dideoxy-2,3-epimino-4-O-methyl-β-L-ribopyranoside (17)

Compound **16** (2.29 g, 8.15 mmol) in methanol (100 mL) was treated with hydrazine monohydrate (99–100%) (5.5 mL) and Raney nickel (0.3 g). The mixture was heated at reflux until decomposition of the hydrazine was complete (monitored by tlc, approximately 5 h), the suspension was filtered, and the filtrate was evaporated to a syrup that was applied to a silica gel column. Elution with dichloromethane–methanol (20:1), followed by concentration, gave the aziridine **17** (0.90 g, 70%) as a syrup; $[\alpha]_D$ −19.9 (*c* 1.18, $CHCl_3$); ir ($CHCl_3$): 3280 (NH) cm^{-1}; ^1H nmr (400 MHz, $CDCl_3$) δ: 2.20 (br s, 1H, H-2), 2.50 (br s, 1H, H-3), 3.43 (m, 1H, H-5ax), 3.44 (s, 3H, OCH_3), 3.46 (s, 3H, OCH_3), 3.60 (m, 1H, H-4), 3.77 (dd, 1H, *J* = 3.7 Hz, 12.5 Hz, H-5eq), 4.81 (s, 1H, H-1); ms, *m/e*: 160 $(M + 1)^+$.

Methyl 2-amino-3-azido-2,3-dideoxy-4-O-methyl-β-L-xylopyranoside (18)

A mixture of the aziridine **17** (0.840 g, 5.28 mmol), sodium azide (1.40 g, 21.4 mmol), and ammonium chloride (0.580 g, 10.8 mmol) in a mixture of 2-methoxyethanol (75 mL) and water (5.5 mL) was heated for 17 h at 110°C. The solution was evaporated directly to dryness and the residue was extracted with dichloromethane (4 × 25 mL). The extract was washed with half-saturated $NaHCO_3$ (3 × 25 mL), dried (Na_2SO_4), and evaporated to give a syrup that was applied to a silica gel column. Elution with dichloromethane–methanol (20:1) followed by concentration gave the azide **18** (0.850 g, 80%) as a syrup; $[\alpha]_D$ −5.2 (*c* 1.02, $CHCl_3$); ir ($CHCl_3$): 3380, 3300 (NH), 2100 (N_3) cm^{-1}; ^1H nmr (400 MHz, $CDCl_3$) δ: 2.56 (dd, 1H, *J* = 7.8 Hz, 10.3 Hz, H-2), 3.22 (dd, 1H, *J* = 10.1 Hz, 11.5 Hz, H-5ax), 3.24 (dd, 1H, *J* = 9.1 Hz, 10.3 Hz, H-3), 3.35 (ddd, 1H, *J* = 4.9 Hz, 9.3 Hz, 9.9 Hz, H-4), 3.50 (s, 3H, OCH_3), 3.51 (s, 3H, OCH_3), 4.03 (d, 1H, *J* = 7.6 Hz, H-1), 4.13 (dd, 1H, *J* = 4.9 Hz, 11.5 Hz, H-5eq); ^{13}C nmr (75 MHz, $CDCl_3$) δ: 55.11, 56.95, 58.32, 64.12, 67.47, 78.77, 105.33; ms, *m/e*: 203 $(M + 1)^+$.

Methyl 2,3-diamino-2,3-dideoxy-4-O-methyl-β-L-xylopyranoside (19)

To a solution of the azide **18** (0.770 g, 3.80 mmol) in methanol-distilled water (1:1) (30 mL) was added 10% palladium-on-charcoal (400 mg) suspended in methanol (8 mL). The mixture was hydrogenated under atmospheric pressure at room temperature for 24 h. The catalyst was then removed by filtration through Celite. Evaporation of the filtrate followed by co-evaporation with ethanol gave compound **19** (0.630 g, 94%) as white crystals; mp 60–62°C; $[\alpha]_D$ +101 (*c* 0.60, methanol); ir ($CHCl_3$): 3340, 3270 (NH) cm^{-1}; ^1H nmr (400 MHz, methanol-d_4) δ: 2.41 (dd, 1H, *J* = 7.2 Hz, 9.5 Hz, H-2), 2.54 (t, 1H, *J* = 9.0 Hz, H-3), 3.06 (ddd, 1H, *J* = 4.6 Hz, 8.5 Hz, 9.3 Hz, H-4), 3.22 (dd, 1H, *J* = 9.3 Hz, 11.3 Hz, H-5ax), 3.43 (s, 3H, OCH_3), 3.47 (s, 3H, OCH_3), 4.07 (d, 1H, *J* = 7.2 Hz, H-1), 4.12 (dd, 1H, *J* = 4.5 Hz, 11.3 Hz, H-5eq); ms, *m/e*: 177 $(M + 1)^+$.

(SP-4-3)-Dichloro(methyl 2,3-diamino-2,3-dideoxy-4-O-methyl-β-L-xylopyranoside-N,N′) platinum (3)

A solution of the diamine **19** (0.590 g, 3.35 mmol) in distilled water (2.4 mL) was added to a solution of K_2PtCl_4 (1.40 g, 3.37 mmol) in distilled water (15 mL). The mixture was stirred manually until homogeneous, and was left standing in the dark. After 4 h, crystallization began, forming bright yellow plates. When the original red color of the solution became yellow or orange-yellow, the crystals were filtered, washed with cold water (5 × 4 mL), and dried under vacuum in the absence of light for several hours to afford bright yellow crystals of complex **3** (0.890 g, 60%);

Can. J. Chem. Downloaded from www.nrcresearchpress.com by 213.200.69.106 on 09/08/12
For personal use only.

mp 295°C (darkening), 325–330°C (dec.); $[\alpha]_D$ +121 (*c* 0.11, H_2O); ir (Nujol): 3500, 3180, 3100 (NH) cm^{-1}; ^1H nmr (300 MHz, DMSO-d_6) δ: 2.29–2.33 (m, 1H, H-2), 2.48–2.55 (m, 1H, H-3), 2.90 (m, 1H, H-5ax), 3.23–3.41 (m, 1H, H-4), 3.30 (s, 3H, OCH_3), 3.33 (s, 3H, OCH_3), 3.90 (dd, 1H, *J* = 4.8 Hz, 11.1 Hz, H-5eq), 4.25 (d, 1H, *J* = 7.7 Hz, H-1), 5.41–5.64 (m, 4H, NH); ^{13}C nmr (75 MHz, DMSO-d_6) δ: 56.33, 58.07, 63.26, 64.55, 64.92, 78.81, 103.28. Anal. calcd. for $C_7H_{16}Cl_2N_2O_3Pt$: C 19.01, H 3.65, N 6.34, Cl 16.04; found: C 18.52, H 3.56, N 5.99, Cl 16.44.

*Methyl 3-azido-2,3-dideoxy-2-phthalimido-β-L-xylopyranoside (**20**)*

To a cold (ice-water bath) solution of *N*-(ethoxycarbonyl) phthalimide (2.16 g, 10.4 mmol) in 25 mL of dry THF was added dry triethylamine (2.0 mL, 14.3 mmol), then a solution of amine derivative **12** (1.63 g, 8.67 mmol) in 30 mL of dry THF. The mixture was stirred at room temperature overnight, then at 55°C for 1 day. After removal of the solvent under reduced pressure the residue was directly applied to a silica gel, column eluting with ethyl acetate – hexanes (1:1, then 5:1) to give **20** (2.25 g, 81.5%) as white crystals; mp 95–96°C; $[\alpha]_D$ +14.1 (*c* 0.96, $CHCl_3$); ir ($CHCl_3$): 3400 (br, OH), 3010, 2100 (N_3), 1775, 1710 (C=O) cm^{-1}; ^1H nmr (300 MHz, $CDCl_3$) δ: 2.82 (d, 1H, *J* = 4.0 Hz, OH), 3.40 (s, 3H, OCH_3), 3.49 (dd, 1H, *J* = 10.3 Hz, 11.5 Hz, H-5), 3.85 (dt, 1H, *J* = 5.3 Hz, 9.6 Hz, H-4), 4.02 (dd, 1H, *J* = 8.2 Hz, 11.4 Hz, H-2), 4.11 (dd, 1H, *J* = 5.3 Hz, 11.5 Hz, H-5), 4.30 (dd, 1H, *J* = 9.3 Hz, 11.4 Hz, H-3), 5.01 (d, 1H, *J* = 8.2 Hz, H-1), 7.75–7.78 (m, 2H, ArH), 7.88–7.90 (m, 2H, ArH); ^{13}C nmr (75 MHz, $CDCl_3$) δ: 53.93, 56.71, 63.48, 66.46, 70.39, 99.70, 123.58, 131.31, 134.27; ms, *m/e*: 319 $(M + 1)^+$.

*Methyl 4-O-acetyl-3-azido-2,3-dideoxy-2-phthalimido-β-L-xylopyranoside (**21**)*

To a cold solution of **20** (1.68 g, 5.28 mmol) in 20 mL of ethyl acetate was added 4-dimethylaminopyridine (DMAP) (0.968 g, 7.90 mmol), then acetic anhydride (1.53 mL, 15.9 mmol) at 0°C. The mixture was stirred at room temperature for 30 min, then cooled to 0°C again. The reaction was quenched by the addition of 2 mL of saturated ammonium chloride and the solution was washed with water, 1 N HCl, water, saturated $NaHCO_3$, water, and brine, then dried with anhydrous magnesium sulfate. Removal of the solvent gave a syrup that was purified by flash chromatography (ethyl acetate – hexanes 1:2, then 2:3) to afford **21** (1.66 g, 87.3%) as white crystals; mp 89–90°C, $[\alpha]_D$ −27.2 (*c* 0.50, $CHCl_3$); ir ($CHCl_3$): 2100 (N_3), 1775, 1750, 1710 (C=O) cm^{-1}; ^1H nmr (300 MHz, $CDCl_3$) δ: 2.12 (s, 3H, CH_3CO_2), 3.41 (s, 3H, OCH_3), 3.44 (dd, 1H, *J* = 9.9 Hz, 11.5 Hz, H-5), 4.07 (dd, 1H, *J* = 8.2 Hz, 11.5 Hz, H-2), 4.22 (dd, 1H, *J* = 5.5 Hz, 11.5 Hz, H-5), 4.51 (dd, 1H, *J* = 9.6 Hz, 11.5 Hz, H-3), 4.98 (ddd, 1H, *J* = 5.5 Hz, 9.6 Hz, 9.9 Hz, H-4), 5.01 (d, 1H, *J* = 8.2 Hz, H-1), 7.76 (m, 2H, ArH), 7.88–7.91 (m, 2H, ArH); ^{13}C nmr (75 MHz, $CDCl_3$) δ: 20.62, 53.71, 56.64, 60.15, 63.42, 71.27, 99.60, 123.59, 131.34, 134.27, 167.67, 169.59; ms, *m/e*: 360 $(M)^+$. Exact Mass calcd. for $C_{16}H_{16}N_4O_6$: 360.1071; found: 360.1070.

*4-O-Acetyl-1,5-anhydro-3-azido-2,3-dideoxy-2-phthalimido-L-xylitol (**22**)*

To a cold solution of **21** (0.500 g, 1.39 mmol) in 6 mL of dry dichloromethane was sequentially added triethylsilane (2.2 mL, 13.8 mmol), boron trifluoride etherate (0.20 mL, 1.63 mmol), and trimethylsilyl trifluoromethanesulfonate (1.34 mL, 6.93 mmol) at 0°C. The reaction mixture was allowed to warm to room temperature, and after 18 h it was diluted with 0.5 mL of methanol and stirred vigorously with solid $NaHCO_3$ (~1 g) for 2 h until pH 7, then filtered and evaporated to dryness. The residue was dissolved in water and extracted with dichloromethane three times. The organic extract was washed with saturated $NaHCO_3$, water, and brine, dried ($MgSO_4$), and evaporated to give a pale yellow residue. Purification by silica gel chromatography with ethyl acetate – hexanes (1:2, then 1:1) gave **22** (0.333 mg, 72%) as a syrup; $[\alpha]_D$ −58.2 (*c* 0.25, $CHCl_3$); ir ($CHCl_3$): 2100 (N_3), 1775, 1755, 1710 (C=O) cm^{-1}; ^1H nmr (300 MHz, $CDCl_3$) δ: 2.12 (s, 3H, CH_3CO_2), 3.33 (dd, 1H, *J* = 10.4 Hz, 11.0 Hz, H-5ax), 3.85 (ddd, 1H, *J* = 0.9 Hz, 5.2 Hz, 11.0 Hz, H-1eq), 3.97 (t, 1H, *J* = 11.0 Hz, H-1ax), 4.17 (ddd, 1H, *J* = 0.9 Hz, 5.3 Hz, 11.0 Hz, H-5eq), 4.28 (dt, 1H, *J* = 5.2 Hz, 11.0 Hz, H-2), 4.62 (dd, 1H, *J* = 9.7 Hz, 11.0 Hz, H-3), 4.96 (ddd, 1H, *J* = 5.2 Hz, 9.7 Hz, 10.4 Hz, H-4), 7.75–7.79 (m, 2H, ArH), 7.86–7.90 (m, 2H, ArH); ^{13}C nmr (75 MHz, $CDCl_3$) δ: 50.02, 60.86, 66.50, 67.61, 71.39, 77.09, 123.52, 123.60, 131.27, 134.23, 134.39, 169.80; ms *m/e*: 331 $(M+1)^+$. Exact Mass calcd. for $C_{15}H_{14}N_4O_5$: 330.0965; found: 330.0973.

*2-Amino-1,5-anhydro-3-azido-2,3-dideoxy-L-xylitol (**23**)*

To a solution of **22** (177 mg, 0.540 mmol) in 12 mL of 95% ethanol and THF (2:1) was added 1.3 mL of hydrazine monohydrate. The reaction mixture was stirred at room temperature for 19 h; the resulting white precipitate was filtered and washed with 95% ethanol a few times and the collected filtrate was then evaporated to dryness to give a residue that was purified by flash chromatography. Elution with dichloromethane–methanol (10:2) gave **23** (57 mg, 68%) as a syrup; ir ($CHCl_3$): 3350 (br), 2100 (N_3) cm^{-1}; ^1H nmr (300 MHz, $CDCl_3$) δ: 1.75 (br s, 3H, OH, NH_2), 2.89 (dt, 1H, *J* = 4.3 Hz, 8.4 Hz, H-2), 3.21 (dd, 1H, *J* = 8.6 Hz, 11.7 Hz, H-1ax), 3.24 (t, 1H, *J* = 8.4 Hz, H-3), 3.34 (dd, 1H, *J* = 8.4 Hz, 11.4 Hz, H-5ax), 3.67 (dt, 1H, *J* = 4.4 Hz, 8.4 Hz, H-4), 3.89 (ddd, 1H, *J* = 0.7 Hz, 4.3 Hz, 11.7 Hz, H-1eq), 3.94 (ddd, 1H, *J* = 0.7 Hz, 4.4 Hz, 11.4 Hz, H-5eq); ^1H nmr (300 MHz, D_2O) δ: 2.81 (dt, 1H, H-2), 3.22–3.34 (m, 3H, H-1, -3, -5), 3.72 (dt, 1H, H-4), 3.97 (dd, 1H, H-1eq), 4.02 (dd, 1H, H-5eq).

*(SP-4-3)-Dichloro (2,3-diamino-1,5-anhydro-2,3-dideoxy-L-xylitol-N,N′) platinum (**4**)*

The azide derivative **23** (57 mg, 0.36 mmol) was hydrogenated with palladium-on-activated carbon (10%) under an atmosphere of hydrogen in methanol to afford a white residue that was used for next reaction without further purification. The diamine derivative in distilled water (0.3 mL) was added to a solution of K_2PtCl_4 (140 mg, 0.34 mmol) in distilled water (1.5 mL). The mixture was stirred manually until homogeneous, and was left standing in the dark. After 30 min crystallization began, to give yellow plates. When the original red color of the solution became yellow or orange-yellow, the crystals were filtered, washed with cold water, and dried in a desiccator under vacuum, in the absence of light for several hours, to afford bright yellow crystals of **4** (50 mg, 39%); mp > 290°C (dec.); ir (Nujol): 3400 (br, OH), 3260, 3170, 3100 (NH) cm^{-1}; ^1H nmr (300 MHz, DMSO-d_6) δ: 2.12–2.25 (m, 1H, H-3), 2.25–2.42 (m, 1H, H-2), 2.67 (t, 1H, *J* = 10.4 Hz, Hax-5), 3.07 (t, 1H, *J* = 10.4 Hz, Hax-1), 3.35–3.49 (m, 1H, H-4), 3.54 (dd, 1H, *J* = 5.2 Hz, 10.5 Hz, Heq-5), 3.76 (dd, 1H, *J* = 4.5 Hz, 10.4 Hz, Heq-1), 5.09 (d, 1H, *J* = 4.6 Hz, OH), 5.18–5.25 (m, 1H, NH), 5.35–5.40 (m, 2H, NH_2), 5.56–5.60 (m, 1H, NH). Anal. calcd. for $C_5H_{12}N_2O_2Cl_2Pt \cdot 0.5H_2O$: C 14.75, H 3.22, N 6.88, Cl 17.41; found: C 14.64, H 2.96, N 6.64, Cl 17.55.

*(SP-4-3)-Cyclobutane-1,1-dicarboxylato (methyl 2,3-diamino-2,3-dideoxy-β-L-xylopyranoside-N,N′) platinum (**24**)*

To a suspension of platinum complex **2** (100 mg, 0.23 mmol) in 35 mL of deionized water was added a solution of silver nitrate (79 mg, 0.46 mmol) in 5 mL of deionized water. The yellow suspension was stirred vigorously in the dark at room temperature for 1 day. The resulting white precipitate was filtered through Celite and the filtrate was concentrated to ca 3 mL, then transferred into a solution of dipotassium cyclobutane-1,1-dicarboxylic acid (52 mg, 0.24 mmol) in 0.5 mL of deionized water. The mixture was stirred manually until homogeneous and was left standing in the dark, allowing for a slow evaporation to produce crystals after 3 days. A week later, the crystals were filtered and washed with deionized water, then dried over P_2O_5 under vacuum to afford the carboplatinum complex **24** (95 mg, 81%) as white crystals; $[\alpha]_D$ +135 (*c* 0.058, H_2O); ir (Nujol): 3400 (br, OH), 3220, 3120 (NH), 1640,

1615 (C=O) cm^{-1}; ^1H nmr (300 MHz, DMSO-d_6) δ: 1.59–1.69 (m, 2H, cyclobutane H-3), 2.04–2.17 (m, 1H, H-2), 2.18–2.31 (m, 1H, H-3), 2.62–2.78 (m, 4H, cyclobutane H-2), 2.90 (t, 1H, J = 10.8 Hz, Hax-5), 3.34 (s, 3H, OCH_3), 3.36–3.48 (m, 1H, H-4), 3.62 (dd, 1H, J = 5.2 Hz, 11.2 Hz, Heq-5), 4.19 (d, 1H, J = 7.8 Hz, H-1), 5.18 (d, 1H, J = 5.4 Hz, OH), 5.32–5.39 (m, 1H, NH), 5.52–5.59 (m, 1H, NH), 5.93–6.05 (m, 2H, NH_2); ^{13}C nmr (75 MHz, DMSO-d_6) δ: 15.09, 30.06, 30.38, 55.51, 56.32, 62.12, 66.00, 67.50, 69.38, 103.35, 177.38, 177.45; ms, *m/e*: 500 $(M + 1)^+$, 499 $(M)^+$, 498 $(M - 1)^+$. Exact Mass (FAB) calcd. for $C_{12}H_{20}N_2O_7Pt$: 499.0919; found: 499.0938.

Acknowledgments

We would like to acknowledge financial assistance from the Natural Sciences and Engineering Research Council of Canada (NSERCC) and le Fonds pour la formation des chercheurs et l'aide à la recherche (FCAR). We thank Parke-Davis/Warner Lambert, Ann Arbor, Michigan, and Drs. R. Leopold and J. Hoeschele for the biological tests. We thank Dr. Michel Simard for the crystallographic analyses and Professor André Beauchamp for assistance in the interpretation of the data.

1. M.J. Clear and J.D. Hoeschele. Bioinorg. Chem. **2**, 187 (1973); Y. Kidani, K. Inagaki, M. Iigo, A. Hoshi, and K. Kuretani. J. Med. Chem. **21**, 1315 (1978); L. S. Hollis, A.R. Amundsen, and E.W. Stern. J. Am. Chem. Soc. **107**, 274 (1985).
2. S. Hanessian, J.Y. Gauthier, K. Okamoto, A.L. Beauchamp, and T. Theophanides. Can. J. Chem. **71**, 880 (1993).
3. J.J. Hlavka, R.G. Child, and P. Bitha. U.S. Patent No. 4,587,331 (1986); Nippon Kayaku KK. Jpn. Patent No. 255943 (1983); T. Tsubomura, S. Yano, K. Kobayashi, T. Sakurai, and S. Yoshikawa. J. Chem. Soc. Chem. Commun. 459 (1986).
4. J.C. Dabrowiak and W.T. Bradner. Prog. Med. Chem. **24**, 129 (1987).
5. M.A. Oldham and J. Honeyman. J. Chem. Soc. 986 (1946); J. Honeyman. J. Chem. Soc. 990 (1946); S. Mukherjee and A.R. Todd. J. Chem. Soc. 969 (1947); Y.-L. Fu and M. Bobek. J. Org. Chem. **41**, 3831 (1976).
6. R.D. Guthrie and D. Murphy. J. Chem. Soc. 5288 (1963).
7. F.H. Newth. Q. Rev. Chem. Soc. **13**, 30 (1959).
8. R.F. Stoddart. Stereochemistry of carbohydrates. John Wiley & Sons Inc., New York. 1971, and references cited therein.
9. H. Hashimoto, K. Araki, Y. Saito, M. Kawa, and J. Yoshimura. Bull. Chem. Soc. Jpn. **59**, 3131 (1986); K. Araki, M. Kawa, Y. Saito, H. Hashimoto, and J. Yoshimura. Bull. Chem. Soc. Jpn. **59**, 3137 (1986).
10. D. Rolf and G.R. Gray. J. Am. Chem. Soc. **104**, 3539 (1982).
11. J.A. Bennek, M.J. Rice, and G.R. Gray. Carbohydr. Res. **157**, 125 (1986); J.-G. Jun and G.R. Gray. Carbohydr. Res. **163**, 247 (1987).
12. J.P. Macquet and J.L. Butour. JNCI, J. Natl. Cancer Inst. **70**, 899 (1983).
13. P. Schwartz, S.J. Meischen, G.R. Gale, L.M. Atkins, A.B. Smith, and E.M. Walker, Jr. Cancer Treat. Rep. **61**, 1519 (1977); B. Lippert, C.J.L. Lock, B. Rosenberg, and M. Zvagulis. Inorg. Chem. **16**, 1525 (1977); R.C. Harrison and C.A. McAuliffe. Inorg. Chim. Acta, **46**, L15 (1980); T. Totani, K. Aono, M. Komura, and Y. Adachi. Chem. Lett. 429 (1986).
14. W.C. Still, M. Kahn, and A. Mitra. J. Org. Chem. **43**, 2923 (1978).
15. G. Sheldrick. SHELXS-86. Crystallographic program system. Institute für Anorganische Chemie der Universität Gottingen, Germany. 1986.
16. E.J. Gabe, F.L. Lee, and Y. Le Page. The NRCVAX crystal structure system. *In* Crystallographic computing 3: data collection, structure determination, proteins, and databases. *Edited by* G.M. Sheldrick, C. Kruger, and R. Goddard. Clarendon Press, Oxford. 1985. pp. 167–174.

Can. J. Chem. Downloaded from www.nrcresearchpress.com by 213.200.69.106 on 09/08/12
For personal use only.

Design and synthesis of a cephalosporin–carboplatinum prodrug activatable by a β-lactamase

STEPHEN HANESSIAN[1] AND JIANGUO WANG
Department of Chemistry, Université de Montréal, Montréal (Québec), Canada H3C 3J7

Received November 27, 1992

STEPHEN HANESSIAN and JIANGUO WANG. Can. J. Chem. **71**, 896 (1993).

The design and syntheses of two cephalosporin–carboplatinum prodrugs that can be released by a β-lactamase are described. The hydrolysis of cephalosporins catalyzed by a β-lactamase with acetyl or DACCP as 3′-leaving groups is studied by ^{1}H nuclear magnetic resonance in deuterated buffer solutions. These notions provide a new approach to the use of platinum complexes for antitumor therapy.

STEPHEN HANESSIAN et JIANGUO WANG. Can. J. Chem. **71**, 896 (1993).

Deux agents antitumoraux du type «pro-drug» qui consistent en une unité cephalosporine et une unité de carboplatine ont été synthétisés. Les molécules ont le potentiel d'être hydrolyses par une β-lactamase qui libérerait l'agent antitumoral (DACCP). L'action enzymatique a été étudiée par la résonance magnétique nucléaire du proton.

Can. J. Chem. Downloaded from www.nrcresearchpress.com by 213.200.69.106 on 09/08/12
For personal use only.

Introduction

The development of chemotherapeutic agents for the treatment of neoplastic diseases has been an area of immense interest and importance during the last decades (1). The discovery of hybridoma technology (2) and the advent of monoclonal antibodies has also revolutionized many aspects of drug development (3). An obvious application has been in tumor immunotherapy (4), where monoclonal antibodies have been used as directed messengers through conjugation, delivery, and, ultimately, release of drugs at the tumor site.

There are, however, many problems remaining that have limited the more widespread use of this technique in clinical trials (5). Factors affecting the activity of immunotoxin conjugates include the number of target antigens on the cell surface (6), the route of entry into the cell by the conjugate (7), the limited numbers of drug molecules coupled to a single antibody (8), the heterogeneity of antigen expression (9), and maintaining the antigen recognition sites of the antibody after chemical conjugation to the drug. Most of the cytotoxic agents exert their activities once inside the cell, requiring that the monoclonal antibody carrier facilitate the delivery of the drug to its precise site of activity within the cell. Many monoclonal antibodies directed against tumor antigens are not effective in this regard (10).

An exciting development in this area of research has involved the conjugation of specific enzymes to monoclonal antibodies, and the enzymatic release of a drug at the tumor site. The advantage of this approach is that one can, in principle, deliver many drug molecules to the tumor site with each immunoconjugate molecule, and some of the limitations mentioned above could perhaps be overcome.

The mechanism by which most β-lactamases inactivate β-lactam antibiotics is through acylation of a serine residue at the active site of the enzyme (11). In the case of a cephalosporin, a potential leaving group (X) at the 3′-position is eliminated during the enzymatic reaction, which most probably proceeds in two steps (12).

In another context, the leaving group could be an antibacterial agent having a different mode of action than the cephalosporin. Thus, the enzymatic acylation of the cephalosporin moiety by a serine residue in endogenous proteins such as penicillin-binding proteins releases the antibacterial agent, hence the term dual action antibiotics (13).

Recently, the monoclonal antibody – enzyme conjugate technique has been applied to design the prodrugs related to vinca alkaloids (14), and to nitrogen mustards (15) using β-lactamases. The enzyme was obtained from *Enterobacter cloacae*, which offers a number of advantages (16), particularly in being tolerant of a wide variety of substituents at the 3′-position of cephalosporins.

As a general program aimed at the development of novel and effective *cis*-platinum analogs (17, 18), we have been investigating the prospects of applying the above-mentioned strategy to the design of a prodrug consisting of a cephalosporin–platinum complex. Figure 1 schematically illustrates the approach to cancer chemotherapy with a *cis*-platinum prodrug.

Results and discussion

We chose two platinum complexes, 4′-carboxyphthalato (1,2-cyclohexanediamine) platinum (DACCP), which is a potent antitumor agent (19), and a carboplatinum complex that contains a hydrophobic ester linking arm, as the releasable portion of the prodrug. The synthesis of the cephalosporin–DACCP prodrug **8** is illustrated in Scheme 1.

The synthesis started with the commercially available 7-aminocephalosporanic acid (7-ACA), which was converted to the known ester **2** (20). This was then coupled with trimellitic anhydride chloride to afford **3** as a mixture of Δ^2- and Δ^3-acyloxy methyl cephems (ratio 1.5:1). The Δ^2 isomer could be converted to the Δ^3 isomer via the sulfoxide **4**, a process that capitalizes on the fact that β,γ-unsaturated sulfoxides are thermodynamically more stable than the corresponding α,β-unsaturated sulfoxides (21). Reduction (22) of the Δ^3-cephem sulfoxide **4** by phosphorus trichloride gave Δ^3-cephem **5**. The diphenyl methyl ester was cleaved with trifluoroacetic acid (TFA) in the presence of anisole and the resulting carboxylic acid derivative **6** was subsequently converted into the monopotassium compound **7**. Complex formation with *trans*-1,2-diamino cyclohexane platinumII dinitrate (23) afforded the desired product **8** as a white amorphous powder, which was moderately soluble in DMSO and carbonate buffer (~2 mg/mL, pH 10), but very slightly soluble in water (<0.2 mg/mL).

[1]Author to whom correspondence may be addressed.

Can. J. Chem. Downloaded from www.nrcresearchpress.com by 213.200.69.106 on 09/08/12
For personal use only.

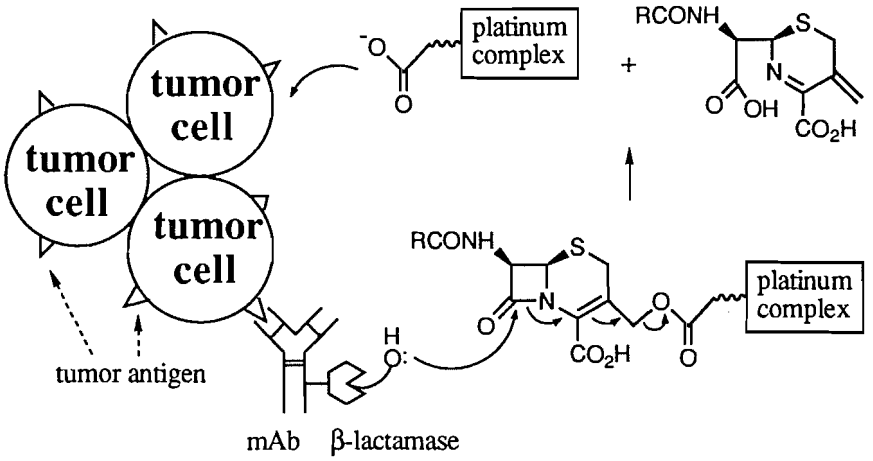

FIG. 1

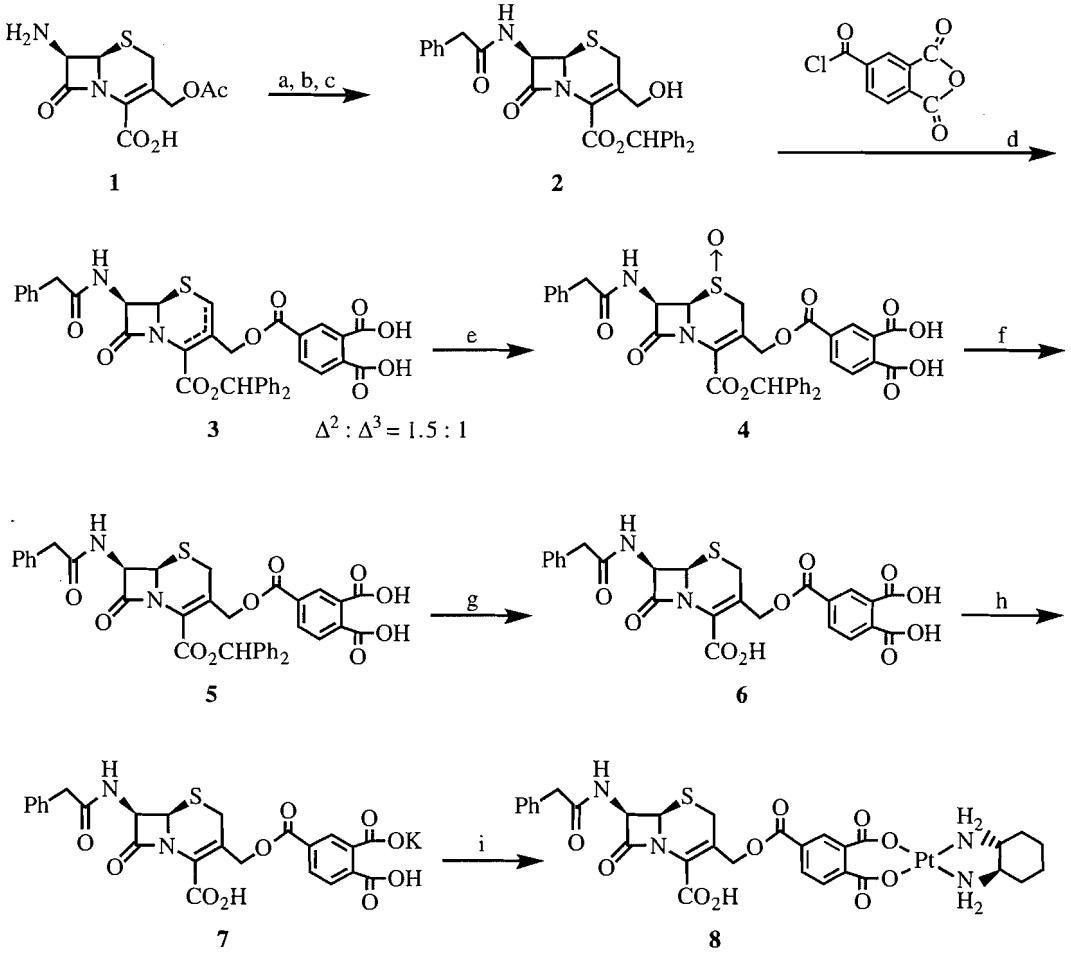

(a) aq NaOH, 0°C, 15 min; (b) $PhCH_2COCl$, acetone, 0°C, 1 h; (c) Ph_2CN_2, EtOAc, r.t., 2 h; (d) Et_3N, THF, 0°C, 1 h; (e) *m*-CPBA, EtOAc, 0°C, 3 h; (f) PCl_3, DMF, −25°C, 3 h; (g) TFA, anisole, CH_2Cl_2, 0°C, 2 h; (h) 0.1 N KOH; (i) dinitro(cyclohexane-1,2-diamine-*N*,*N*)platinum(II), H_2O, r.t., 3 h

SCHEME 1

We then turned our attention to the synthesis of a second type of cephalosporin – DACH platinum complex. Here, we chose to introduce a hydrophobic linker to provide some flexibility and "distance" between the *cis*-platinum component and the activatable units. The synthesis of the linker is illustrated in Scheme 2.

Alkylation of malonic acid diethyl ester with 8-bromo-1-octene gave compound **9**, which was then reduced to the diol **10** with lithium aluminum hydride. Tosylation of **10** in dichloromethane in the presence of triethylamine gave the ditosyl derivative **11**. The formation of the cyclobutane ring was carried out by treatment of malonic acid dibenzyl ester

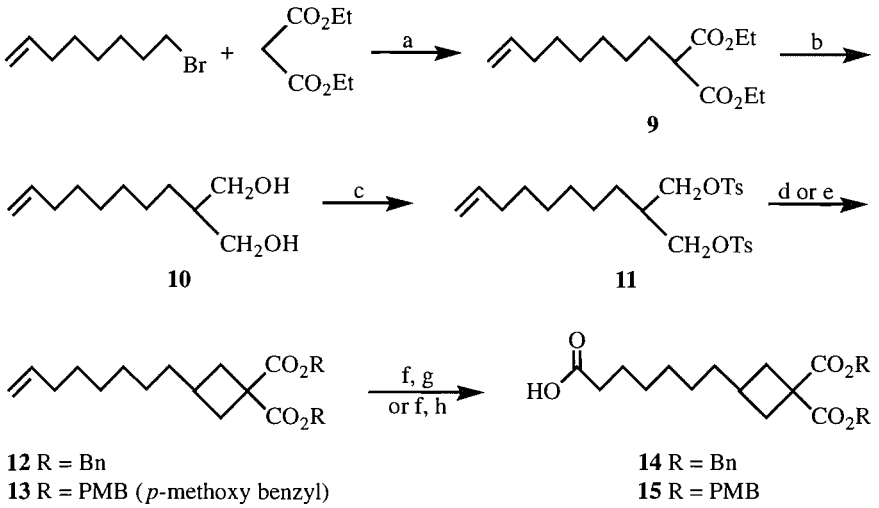

(a) NaH, THF, 55°C, 2 days; (b) LAH, THF, r.t., 30 min; (c) TsCl, Et_3N, CH_2Cl_2, r.t., 2 days; (d) dibenzyl malonate, $NaN(SiMe_3)_2$, dioxane, reflux, 1 day; (e) di-*p*-methoxybenzyl malonate, $NaN(SiMe_3)_2$, dioxane, reflux, 1 day; (f) O_3, CH_2Cl_2, −78°C, 5 h; (g) R=Bn: PDC, DMF, r.t., 14 h; (h) R=PMB: 2-methyl-2-butene, *t*-BuOH, $NaH_2PO_4 \cdot H_2O$, $NaClO_2$, r.t., 30 min.

SCHEME 2

and **11** with sodium bis(trimethylsilyl) amide in dioxane to give **12**, which was subsequently oxidized to the acid **14** in a two-step process. It is noteworthy that the normal conditions for malonate condensation (NaH, dioxane) (21) were not effective in the case of **11**. Unfortunately, after esterification of **14** with the Δ^3-cephem **2**, the dibenzyl ester of the resulting compound could not be cleaved by hydrogenation, and only several unidentified products were obtained. Other attempts at debenzylation either gave no reaction or complete degradation. We then decided to repeat the previous synthesis using the *p*-methoxybenzyl ester derivative (24) with *p*-methoxybenzyl chloride to give dimethoxybenzyl malonate. Condensation with ditosyl derivative **11** led to the cyclobutane compound **13**. Ozonolysis of **13** followed by oxidation with sodium chlorite in the presence of 2-methyl-2-butene and sodium dihydrogen phosphate (25) afforded the carboxylic acid **15** in good yield.

Esterification of **15** with **2** by using DCC and DMAP gave **16** as a mixture of two isomers (Δ^2:Δ^3 1.5:1) (Scheme 3). The Δ^2 isomer was converted to the Δ^3 isomer **18** by oxidation with *m*-CPBA and reduction with phosphorus trichloride via sulfoxide **17**. The protecting groups were cleaved with trifluoroacetic acid in the presence of anisole in one step to give tricarboxylic acid **19**. Treatment of this compound with 1 equivalent of aqueous 0.1 N potassium hydroxide solution at 5°C followed by lyophilization led to the desired monopotassium compound **20** and the Δ^2 isomer as a by-product. Finally, aqueous solutions of **20** and dinitrocyclohexane-1,2-diamine platinum(II) were mixed in an equimolar ratio to form the complex **21**, which was obtained as a white amorphous powder.

Model studies of enzymatic hydrolysis by ^1H nuclear magnetic resonance

Previous studies by Faraci and Pratt (12) showed that the enzymatic hydrolysis of cephaloridine and other cephem derivatives at pD 6.4 and pD 10.2 can be followed by ^1H nmr spectroscopy. Accordingly, a model study of the enzymatic hydrolysis was carried out utilizing 3-acetoxymethyl-7-phenylacetylamino cephem potassium salt **22** in phosphate buffer at pD 7 and in carbonate buffer at pD 10.1 (Scheme 4). In the presence of sufficient amounts of β-lactamase (EC 3.5.2.6, type III, from *Enterobacter cloacae*), the initial spectrum changed rapidly (<2 min) to that of the eliminated products (12, 26). Encouraged by, this we proceeded to test the enzymatic hydrolysis with the *cis*-platinum conjugate **8**.

Because of the poor solubility of complex **8** in neutral phosphate buffer solution, a carbonate buffer solution (pD 10.1) was used for the ^1H nmr study of β-lactamase catalyzed hydrolysis. In the presence of sufficient β-lactamase (from *E. cloacae*), the ^1H nmr spectrum of complex **8** changed rapidly to that of the eliminated compounds **23** and **25** (Scheme 5).

Figure 2 shows the ^1H nmr spectra of the cephalosporin–cisplatinum ester **8**, before and after treatment with the enzyme (A and B respectively). The product resulting from compound **22** is shown in C. It can be seen that B contains peaks from the products of enzymatic cleavage as expected. In a control experiment under the same conditions, **8** was stable to hydrolysis for over 2 h.

Conclusion

We have shown that carboplatinum prodrugs can be linked to a cephalosporin via an ester linkage as shown in structures **8** and **21**. The β-lactamase catalyzed hydrolysis of the cephalosporin derivative **8** with DACCP as the 3′-leaving group was studied by ^1H nmr in deuterated buffer solutions, showing that the carboplatinum subunit is indeed released as expected. These results could pave the way to further studies involving the effectiveness of monoclonal antibody – β-lactamase conjugates in releasing the platinum complexes in vivo and the obvious potential in tumor directed chemotherapy (27).

Can. J. Chem. Downloaded from www.nrcresearchpress.com by 213.200.69.106 on 09/08/12
For personal use only.

Can. J. Chem. Downloaded from www.nrcresearchpress.com by 213.200.69.106 on 09/08/12
For personal use only.

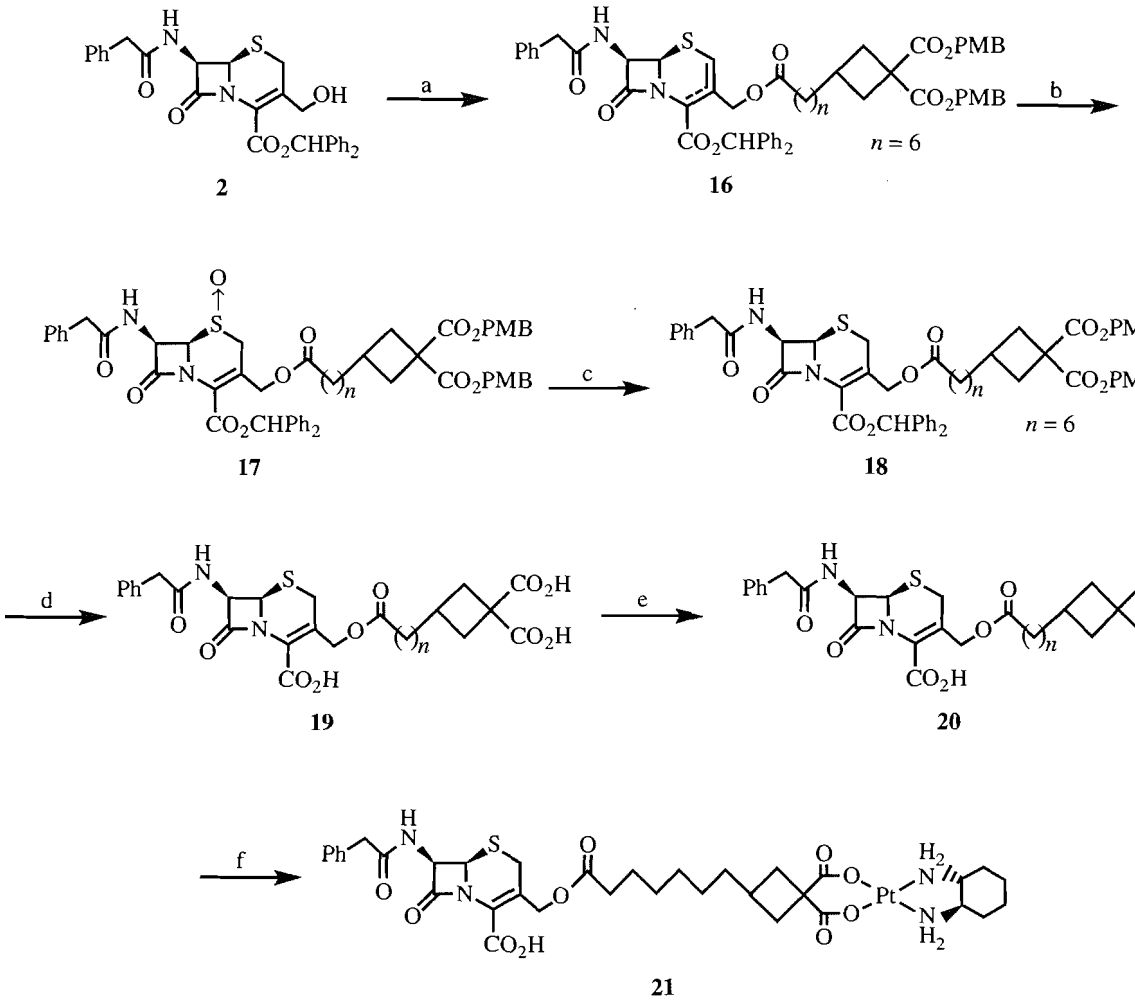

2 16 17 18 19 20 21

(*a*) **15**, DCC, DMAP, CH_2Cl_2, r.t., overnight; (*b*) *m*-CPBA, EtOAc, 0°C, 3 h; (*c*) PCl_3, DMF, −20°C, 1 h; (d) TFA, anisole, CH_2Cl_2, 0°C, 2 h; (e) 0.1 N KOH, H_2O, 0°C; (f) dinitro(cyclohexane-1,2-diamine-*N*,*N*′)platinum(II), H_2O, r.t., 3 h

SCHEME 3

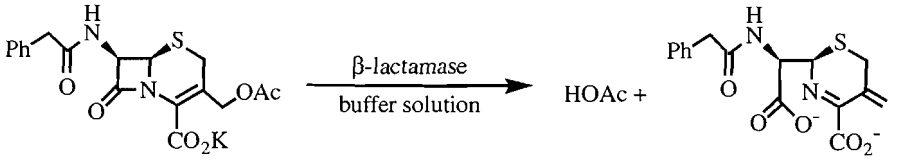

22 23

SCHEME 4

Experimental

Melting points (mp) were determined on a Buchi melting point apparatus and are uncorrected. Optical rotations were measured at 25°C using a Perkin–Elmer model 241 automatic polarimeter. Proton magnetic resonance (^{1}H nmr) spectra were determined on either a 300 MHz Varian or a 400 MHz Bruker spectrometer in deuterated chloroform, methanol-d_4, dimethyl sulfoxide-d_6, or deuterium oxide (D_2O) with $CHCl_3$ (δ_{ppm} = 7.265), Me_4Si (δ_{ppm} = 0.00), or dioxane (δ_{ppm} = 67.40 for ^{13}C) as references. Coupling constants are expressed in hertz (Hz). The abbreviations used for the description of the peaks are as follows: (s, singlet; d, doublet; dd, doublet of doublets; dt, doublet of triplets; ddd, doublet of doublet of doublets; t, triplet; q, quartet; m, multiplet; br, broad). The ^{13}C nmr spectra were recorded on a Varian VXR 300 at 75 MHz. Low-resolution mass spectra were determined on a VG Micro Mass 1212 mass spectrometer by using desorption chemical ionization (DCI), or by fast atom bombardment (FAB). High-resolution mass spectra were determined on a Kratos MS-50 TCTA mass spectrometer by using electron impact (EI) at 70 eV or by the fast atom bombardment (FAB) techniques. Infrared spectra (ir) were recorded on a Perkin–Elmer 781 infrared spectrophotometer. The spectra of solids were recorded as Nujol mulls. Liquid samples were determined as films between sodium chloride plates. Combustion analyses were performed by Guelph Laboratories Ltd., Guelph, Ontario.

Benzene-1,2,4-tricarboxylic acid 4-[[2R-(2α,6α,7β]-(2-benzhydryloxycarbonyl-8-oxo-7-phenylacetylamino-5-thia-1-azabicyclo[4.2.0]oct-3-en-3-yl)methyl] ester (Δ^2 isomer, 3a)

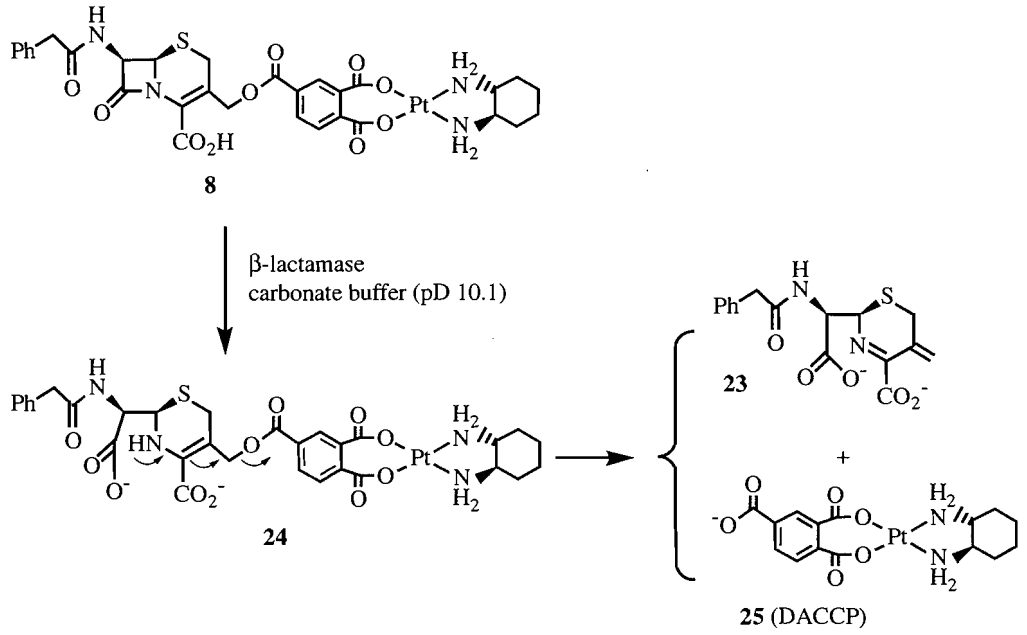

SCHEME 5

*and benzene-1,2,4-tricarboxylic acid 4-[(6*R-trans*)-(2-benzhydryloxycarbonyl-8-oxo-7-phenylacetylamino-5-thia-1-azabicyclo[4.2.0]oct-2-en-3-yl)methyl] ester (Δ³ isomer, 3*b*)*

To a cold (ice-water bath) solution of **2** (420 mg, 0.816 mmol) and DMAP (123 mg, 1.00 mmol) in 15 mL of dry THF was added a solution of trimellitic anhydride chloride (210 mg, 0.987 mmol) in 5 mL of dry THF. The mixture was stirred at that temperature for 30 min. After removing the solvent under vacuum, the residue was dissolved in 50 mL of ethyl acetate and acidified with 5% HCl. The ethyl acetate layer was washed with water and brine, dried ($MgSO_4$), and evaporated to give a slightly brown foam (560 mg, 99%). The crude product was purified by flash chromatography, eluting with ethyl acetate – hexanes (1:3) in the presence of 1% AcOH to give an inseparable mixture of the Δ^2 and Δ^3 isomers (ratio 1:1) of **3** as a foam; ir ($CHCl_3$): 3350, 1855, 1780 (C=O, β-lactam), 1730 (COOR), 1670 (CONH) cm^{-1}; ^1H nmr (300 MHz, $CDCl_3$) for Δ^3 isomer, δ: 3.42, 3.62 (ABq, 2H, J_{gem} = 18.7 Hz, SCH_2), 3.66 (m, 2H, $PhCH_2$), 5.00 (d, 1H, J = 4.9 Hz, H-6), 5.08, 5.34 (ABq, 2H, J_{gem} = 13.3 Hz, CH_2O), 5.91 (dd, 1H, J = 4.9 Hz, 9.1 Hz, H-7), 6.03 (d, 1H, J = 9.1 Hz, NH), 6.95 (s, 1H, $OCHPh_2$), 7.24–7.41 (m, 15H, PhH), 8.07 (d, 1H, J = 7.9 Hz, aromatic H-6), 8.45 (dd, 1H, J = 1.3 Hz, 7.9 Hz, aromatic H-5), 8.53 (s, 1H, aromatic H-3). For Δ^2 isomer, δ: 3.65 (m, 2H, $PhCH_2$), 4.84, 4.96 (ABq, 2H, J_{gem} = 12.6 Hz, OCH_2), 5.14 (d, 1H, J = 1.5 Hz, H-2), 5.20 (d, 1H, J = 3.9 Hz, H-6), 5.60 (dd, 1H, J = 3.9 Hz, 8.5 Hz, H-7), 6.18 (d, 1H, J = 8.5 Hz, NH), 6.58 (d, 1H, J = 1.5 Hz, H-4), 6.88 (s, 1H, $OCHPh_2$), 7.24–7.41 (m, 15H, PhH), 8.01 (d, 1H, J = 7.9 Hz, aromatic H-6), 8.37 (dd, 1H, J = 1.3 Hz, 7.9 Hz, aromatic H-5), 8.48 (s, 1H, aromatic H-3); ms (FAB), m/e: 729 $(M + Na)^+$, 707 $(M + 1)^+$.

*Benzene-1,2,4-tricarboxylic acid 4-[(6*R-trans*)-(2-benzhydryloxycarbonyl-5,8-dioxo-7-phenylacetylamino-5-thia-1-azabicyclo[4.2.0]oct-2-en-3-yl)methyl] ester (4)*

A solution of **3** (500 mg, 0.726 mmol) in 10 mL of ethyl acetate was cooled to 0°C and *m*-chloroperbenzoic acid (50–60%, 250 mg) in 5 mL of ethyl acetate was added dropwise. After stirring at this temperature for 3 h, the solution was diluted with 60 mL of ethyl acetate and washed with water and brine. The organic phase was dried ($MgSO_4$) and evaporated to give **4** (495 mg, 97%) as a pale yellow residue that was used for next reaction without further purification. However, a small sample was dissolved in a mixed solvent of dioxane (10 mL) and deionized water (1 mL) and stirred at room temperature for 15 min. The solvent was removed under vacuum and the residue was purified by flash chromatography, eluting with dichloromethane–methanol – acetic acid (90:10:1) to afford the pure product **4**; $[\alpha]_D$ +37 (*c* 0.57, methanol); ir ($CHCl_3$): 3300, 1850, 1800, 1780 (C=O, β-lactam), 1720 (COOR), 1710 (CONH) cm^{-1}; ^1H nmr (300 MHz, $CDCl_3$) δ: 3.29, 3.93 (ABq, 2H, J_{gem} = 18.8 Hz, SCH_2), 3.65 (s, 2H, $PhCH_2$), 4.53 (d, 1H, J = 4.1 Hz, H-6), 5.03, 5.53 (ABq, 2H, J_{gem} = 13.7 Hz, CH_2O), 6.11 (dd, 1H, J = 4.1 Hz, 9.6 Hz, H-7), 6.96 (s, 1H, $OCHPh_2$), 6.94 (d, 1H, J = 9.6 Hz, NH), 7.27 (m, 15H, PhH), 8.01 (d, 1H, J = 8.0 Hz, aromatic H-6), 8.40 (dd, 1H, J = 1.3 Hz, 7.9 Hz, aromatic H-5), 8.59 (s, 1H, aromatic H-3), 11.28 (br s, 2H, COOH); ^{13}C nmr (75 MHz, CD_3OD) δ: 43.22, 60.07, 65.48, 68.13, 81.40, 97.19, 122.15, 128.04, 128.11, 128.61, 128.98, 129.46, 129.52, 129.67, 130.30, 130.51, 131.07, 133.21, 133.82, 133.91, 135.42, 140.58, 161.35, 165.75, 168.20, 169.57, 170.60, 174.20; ms (FAB), m/e: 745 $(M + Na)^+$, 723 $(M + 1)^+$. Exact Mass calcd. for $C_{38}H_{30}N_2NaO_{11}S$: 745.1469; found: 745.1549.

*Benzene-1,2,4-tricarboxylic acid 4-[(6*R-trans*)-(2-benzhydryloxycarbonyl-8-oxo-7-phenylacetylamino-5-thia-1-azabicyclo[4.2.0]oct-2-en-3-yl)methyl] ester (5)*

Phosphorus trichloride (128 μL, 1.46 mmol) was added slowly to a solution of **4** (470 mg, 0.667 mmol) in 5 mL of dry DMF at −22°C. After stirring at a similar temperature for 3 h, the reaction mixture was poured onto 50 mL of ice-water. The precipitate was collected by filtration, washed with cold water, and dried over P_2O_5 under vacuum in a desiccator to afford **5** (430 mg, 93%) as a powder. The product could be purified by flash chromatography, eluting with ethyl acetate – hexanes (5:1, containing 1% acetic acid); $[\alpha]_D$ −9 (*c* 2.26, $CHCl_3$); ir ($CHCl_3$): 3290, 1850, 1780 (C=O, β-lactam), 1720 (COOR), 1670 (CONH) cm^{-1}; ^1H nmr (300 MHz, $CDCl_3$) δ: 3.41, 3.61 (ABq, 2H, J_{gem} = 18.5 Hz, SCH_2), 3.66 (d, 2H, J = 4.9 Hz, $PhCH_2$), 5.00 (d, 1H, J = 5.1 Hz, H-6), 5.08, 5.34 (ABq, 2H, J_{gem} = 13.2 Hz, CH_2O), 5.91 (dd, 1H, J = 5.1 Hz, 9.1 Hz, H-7), 6.28 (d, 1H, J = 9.1 Hz, NH), 6.95 (s, 1H, $OCHPh_2$), 7.22–7.45 (m, 15H, PhH), 8.06 (d, 1H, J = 7.7 Hz, aromatic H-6), 8.44 (dd, 1H, J = 1.3 Hz, 7.9 Hz, aromatic H-5), 8.53 (s, 1H, aromatic H-3); ^{13}C nmr (75 MHz, $CDCl_3$) δ: 26.42, 43.00, 57.22, 59.04, 64.08, 79.84, 126.07, 126.84, 126.91,

Can. J. Chem. Downloaded from www.nrcresearchpress.com by 213.200.69.106 on 09/08/12
For personal use only.

Can. J. Chem. Downloaded from www.nrcresearchpress.com by 213.200.69.106 on 09/08/12
For personal use only.

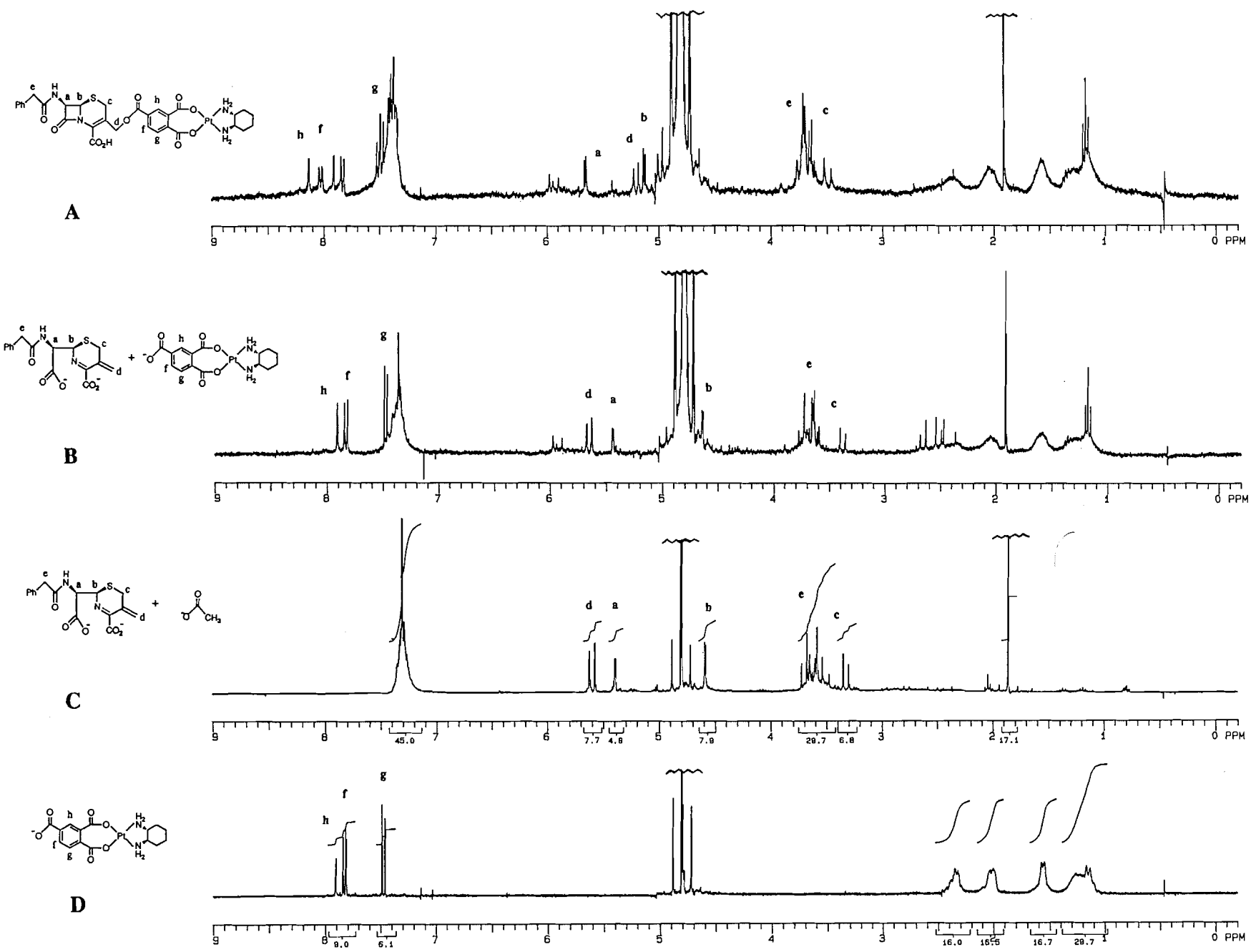

FIG. 2. The ^{1}H nmr spectra in deuterated buffer solution: (A) **8** in the absence of β-lactamase; (B) **8** in the presence of β-lactamase; (C) **22** in the presence of β-lactamase; (D) **25** (DACCP).

Can. J. Chem. Downloaded from www.nrcresearchpress.com by 213.200.69.106 on 09/08/12
For personal use only.

127.45, 127.59, 128.03, 128.11, 128.33, 128.44, 128.56, 128.94, 129.02, 129.33, 130.87, 131.40, 133.06, 133.45, 137.33, 138.43, 138.74, 138.86, 160.52, 164.18, 164.77, 167.68, 169.70, 171.66; ms (FAB), *m/e*: 729 $(M + Na)^+$, 707 $(M + 1)^+$. Exact Mass calcd. for $C_{38}H_{30}N_2NaO_{10}S$: 729.1520; found: 729.1599.

*Benzene-1,2,4-tricarboxylic acid 4-[(6*R-trans*)-(2-carboxy-8-oxo-7-phenylacetylamino-5-thia-1-azabicyclo[4.2.0]oct-2-en-3-yl)methyl] ester (**6**)*

Trifluoroacetic acid (1.5 mL, 19.5 mmol) was added dropwise to a solution of compound **5** (565 mg, 0.800 mmol) in anisole (0.52 mL, 4.80 mmol) and dichloromethane (12 mL) at 0°C (ice-water bath), and the mixture was stirred at a similar temperature for 2 h. After removal of the solvent under vacuum the residue was treated with 3 mL of ether and the resulting white precipitate was filtered and washed with ether (5 × 3 mL). This was dried under reduced pressure in a desiccator to give product **6** (410 mg, 95%) as white powder. The compound was used for the next reaction without further purification; $[\alpha]_D$ +25 (c 0.45, DMF); ir (Nujol): 3500–2500 (br, COOH, NH), 1780 (C=O, β-lactam), 1725 (COOR), 1660 (CONH) cm^{-1}; ^1H nmr (300 MHz, methanol-d_4–D_2O 1:1) δ: 3.49, 3.71 (ABq, 2H, J_{gem} = 18.0 Hz, SCH_2), 3.60 (m, 2H, $PhCH_2$), 5.07, 5.29 (ABq, 2H, J_{gem} = 12.5 Hz, $COOCH_2$), 5.08 (d, 1H, J = 4.6 Hz, H-6), 5.65 (d, 1H, J = 4.6 Hz, H-7), 7.22–7.35 (m, 5H, PhH), 7.75–8.42 (m, 3H, aromatic H); ms (FAB), *m/e*: 563 $(M + Na)^+$, 541 $(M + 1)^+$.

*Potassium benzene-1,2,4-tricarboxylic acid 4-[(6*R-trans*)-(2-carboxy-8-oxo-7-phenylacetylamino-5-thia-1-azabicyclo[4.2.0]oct-2-en-3-yl)methyl] ester (**7**)*

To a suspension of tricarboxylic acid **6** (100 mg, 0.185 mmol) in 10 mL of deionized water was slowly added 0.105 N aqueous potassium hydroxide (1.8 mL, 0.189 mmol) at 0°C, at which point the pH value was 6–7. The mixture was stirred at this temperature until most of the suspension had dissolved (pH ~4). The insoluble residue was filtered and the filtrate was lyophilized to give monopotassium salt **7** (102 mg, 95%) as a white powder; $[\alpha]_D$ +83 (*c* 0.9, H_2O); ^1H nmr (300 MHz, D_2O) δ: 3.50, 3.74 (ABq, 2H, J_{gem} = 17.9 Hz, SCH_2), 3.68, 3.74 (ABq, 2H, J_{gem} = 7 Hz, $PhCH_2$), 4.99, 5.20 (ABq, 2H, J_{gem} = 12.5 Hz, $COOCH_2$), 5.13 (d, 1H, J = 4.6 Hz, H-6), 5.67 (d, 1H, J = 4.6 Hz, H-7), 7.35–7.42 (m, 5H, PhH), 7.53 (d, 1H, J = 8.1 Hz, aromatic H-5), 8.05 (dd, 1H, J = 1.6 Hz, 8.1 Hz, aromatic H-6), 8.16 (d, 1H, J = 1.6 Hz, aromatic H-2).

*(SP-4-2)-Dichloro[(1*R,2R*)-cyclohexane-1,2-diamine*-N,N′*] platinum*

A quantity of (1*R*,2*R*)-(−)-1,2-cyclohexanediamine (28) (0.923 g, 8.08 mmol), was dissolved in 8 mL of deionized water at room temperature, and the solution was then added to a solution of K_2PtCl_4 in 40 mL of deionized water. The red colored solution was stirred manually, and was left standing in the dark until the color became yellow or orange yellow. The resulting yellow precipitate was filtered, washed with deionized water 5 times, and dried over P_2O_5 in the absence of light under vacuum to give the platinum complex (2.71 g, 88.2%) as bright yellow crystals: $[\alpha]_D$ +85.3 (*c* 0.66, DMF); ir (Nujol): 3270, 3180, 3100 (NH) cm^{-1}; ^1H nmr (300 MHz, DMSO-d_6) δ: 0.86–1.01 (m, 2H, CH_2), 1.14–1.21 (m, 2H, CH_2), 1.40–1.42 (m, 2H, CH_2), 1.80–1.84 (m, 2H, CH_2), 2.07–2.10 (m, 2H, H-1, -2), 5.00–5.06 (m, 2H, NH), 5.54–5.57 (m, 2H, NH); ^{13}C nmr (75 MHz, DMSO-d_6) δ: 24.19, 31.39, 62.77.

*(SP-4-2)-Dinitro [(1*R,2R*)-cyclohexane-1,2-diamine*-N,N′*] platinum*

To a suspension of the above complex (150 mg, 0.395 mmol) in 50 mL of deionized water was added a solution of silver nitrate (132 mg, 0.777 mmol) in 3 mL of deionized water. The yellow suspension was stirred vigorously in the dark at room temperature for 1 day. The resulting white suspension was filtered with the aid of Celite and the filtrate was concentrated to 12.5 mL. The colorless solution of the platinum complex (0.0315 mmol/mL) was used directly for the next reaction. A small sample was lyophilized to dryness to afford a white powder: $[\alpha]_D$ + 64 (*c* 1.00, H_2O); ir (Nujol): 3240, 3205, 3140 (NH_2) cm^{-1}; ^1H nmr (300 MHz, D_2O) δ: 1.14–1.36 (m, 4H, H-4, -5), 1.58–1.61 (m, 2H, H-3, -6), 2.02–2.08 (m, 2H, H-3, -6), 2.35–2.42 (m, 2H, H-1, -2).

*(SP-4-2)-[4-[(6*R-trans*)-(2-Carboxy-8-oxo-7-phenylacetylamino-5-thia-1-azabicyclo[4.2.0]oct-2-en-3-yl)methoxycarbonyl] benzene-1,2-dicarboxylato][(1*R,2R*)-cyclohexane-1,2-diamine*-N,N′*] platinum (**8**)*

(SP-4-2)-Dinitro (1,2-cyclohexanediamine *N,N′*) platinum (76 mg, 0.176 mmol) was dissolved in 7 mL of deionized water and traces of insoluble material were removed by centrifugation. The supernatant was transferred into a 20-mL vial, and a solution of potassium salt **7** (102 mg, 0.176 mmol) in 3 mL of deionized water was added. The mixture was stirred at room temperature in the dark for 3 h, and the resulting precipitate was filtered, washed with deionized water, and dried over P_2O_5 under vacuum to give the platinum complex **8** (115 mg, 76%) as white powder: $[\alpha]_D$ +60 (*c* 0.33, DMSO); ir (Nujol): 3500–2500 (br, COOH, NH), 2400, 2290, 1780 (C=O, β-lactam), 1720 (COOR), 1640 (CONH) cm^{-1}; ^1H nmr (300 MHz, deuterated carbonate buffer, pD 10.1) δ: 1.09–1.36 (br m, 4H, cyclohexane CH_2), 1.53–1.62 (br m, 2H, cyclohexane CH_2), 1.90–2.07 (br m, 2H, cyclohexane CH_2), 2.38 (br m, 2H, cyclohexane H-1, -2), 3.49, 3.74 (ABq, 2H, J_{gem} = 17.5 Hz, SCH_2), 3.61–3.76 (m, 2H, $PhCH_2$), 4.98, 5.20 (ABq, 2H, J_{gem} = 12.3 Hz, $COOCH_2$), 5.13 (d, 1H, J = 4.6 Hz, H-6), 5.66 (d, 1H, J = 4.6 Hz, H-7), 7.32–7.45 (m, 5H, PhH), 7.51 (d, 1H, J = 8 Hz, aromatic H-5), 8.03 (dd, 1H, J = 1.5 Hz, 7.9 Hz, aromatic H-6), 8.13 (d, 1H, J = 1.4 Hz, aromatic H-2); ms (FAB), *m/e*: 847 $(M)^+$. Anal. calcd. for $C_{31}H_{32}N_4O_{10}PtS \cdot 4H_2O$: C 40.48, H 4.38, N 6.09; found: C 40.62, H 4.21, N 6.24.

*Malonic acid bis(*p*-methoxybenzyl) ester*

A mixture of dipotassium malonate (8.00 g, 45.0 mmol), *p*-methoxybenzyl chloride (13.0 mL, 2.1 equiv.), and dry DMF (160 mL) was stirred at 60 °C for 2 days and then diluted with 700 mL of ether, washed with water, 10% HCl, water, saturated $NaHCO_3$ solution, water, and brine. The organic phase was dried (Na_2SO_4) and evaporated to give a syrup that was purified by flash column chromatography, eluting with ethyl acetate – hexanes (1:3, then 1:1) to give the ester (7.20 g, 47%) as a colorless syrup that was crystallized at 0°C in a refrigerator; mp 28–29°C; ir ($CHCl_3$): 1745, 1730 (C=O) cm^{-1}; ^1H nmr (300 MHz, $CDCl_3$) δ: 3.44 (s, 2H, H-2), 3.82 (s, 6H, OCH_3), 5.11 (s, 4H, $PhCH_2O$), 6.89 (m, 4H, aromatic H), 7.28 (m, 4H, aromatic H); ^{13}C nmr (75 MHz, $CDCl_3$) δ: 41.50, 55.12, 66.96, 113.79, 127.16, 130.06, 159.59, 166.24; ms (FAB), *m/e*: 345 $(M + 1)^+$, 344 $(M)^+$. Exact Mass calcd. for $C_{19}H_{20}O_6$: 344.1260; found: 344.1226.

*2-(Oct-7-enyl)malonic acid diethyl ester (**9**)*

Sodium hydride (1.07 g, 27.0 mmol) was washed with dry THF twice and then suspended in 60 mL of dry THF. Diethyl malonate (4.2 mL, 27.0 mmol) was added dropwise at −20°C. The resulting clear solution was stirred for 5 min before adding 8-bromo-1-octene (2.9 mL, 17 mmol). The reaction was stirred at 55–60°C for 2 days and quenched with ethanol. After addition of ether (350 mL), the resulting white precipitate was filtered, the filtrate was washed with cold water, brine, and dried (Na_2SO_4). Evaporation of the solvent gave a oil that was purified by a flash column (ethyl acetate – hexanes 1:6, then 1:4) to give product **9** (4.50 g, 99%) as a colorless oil; ^1H nmr (300 MHz, $CDCl_3$) δ: 1.27 (t, 6H, J = 7.1 Hz, CH_3), 1.26–1.40 (m, 8H, H-4, -5, -6, -7), 1.88 (m, 2H, H-3), 2.03 (m, 2H, H-8), 3.31 (t, 1H, J = 7.6 Hz, H-2), 4.19 (q, 4H, J = 7.1 Hz, $COOCH_2$), 4.91–5.02 (m, 2H, CH_2=), 5.80 (ddt, 1H, J = 6.8 Hz, 10.5 Hz, 17.3 Hz, C=CH).

*2-(Oct-7-enyl)propane-1,3-diol (**10**)*

To a cold (ice-water bath) solution of **9** (4.50 g, 16.6 mmol) in 100 mL of dry ether was added dropwise lithium aluminum hydride (1 M in THF solution, 34 mL, 34 mmol). After addition was

Can. J. Chem. Downloaded from www.nrcresearchpress.com by 213.200.69.106 on 09/08/12
For personal use only.

complete the mixture was stirred at room temperature for 30 min. The reaction was quenched by slow addition of water at 0°C until effervescence stopped. The mixture was neutralized with 6 N HCL (~25 mL), saturated with solid NaCl, and then extracted with ether (3 × 60 mL). The combined extract was washed with saturated $NaHCO_3$ solution and brine, dried (Na_2SO_4), and evaporated to afford **10** (3.01 g, 98%) as a syrup that was used directly for the next reaction; ir ($CHCl_3$): 3350 (br, OH) cm^{-1}; ^1H nmr (300 MHz, $CDCl_3$) δ: 1.19–1.41 (m, 10H, H-3, -4, -5, -6, -7), 1.71–1.82 (m, 1H, H-2), 2.00–2.07 (m, 2H H-8), 2.56 (s, 2H, OH), 3.65 (dd, 2H, J = 7.6 Hz, 10.7 Hz, H-1), 3.81 (dd, 2H, J = 3.8 Hz, 10.7 Hz, H-1), 4.95–5.03 (m, 2H, CH_2=), 5.81 (ddt, 1H, J = 6.7 Hz, 10.2 Hz, 17.1 Hz, C=CH-).

*2-(Oct-7-enyl)propane-1,3-diol di-*p*-toluenesulfonate (**11**)*

To a cold (ice-water bath) solution of **10** (162 mg, 0.870 mmol), triethylamine (0.44 mL, 3.1 mmol), and a catalytic amount of DMAP in 5 mL of dry dichloromethane was added slowly a solution of tosyl chloride (500 mg, 2.60 mmol) in 5 mL of dichloromethane. After stirring at room temperature for 2 days, the reaction was quenched by the addition of cold water (0.5 mL) at 0°C. The organic phase was dried over Na_2SO_4 and evaporated to give a syrup that was purified by flash chromatography on silica gel (ethyl acetate – hexanes 1:5, then 1:3, then 1:1) to give pure compound **11** (350 mg, 81%) as a syrup that crystallized on standing in a refrigerator; mp 49–50°C; ir ($CHCl_3$): 1640, 1600, 1465, 1360, 1190, 1175, 1095, 970, 815, 665 cm^{-1}; ^1H nmr (300 MHz, $CDCl_3$) δ: 1.11–1.34 (m, 10H, H-3, -4, -5, -6, -7), 1.92–2.04 (m, 3H, H-2, -8), 2.46 (s, 6H, $ArCH_3$), 3.94 (dq, 4H, J = 4.6 Hz, 6.1 Hz, 9.9 Hz, CH_2OSO_2), 4.91–5.02 (m, 2H, CH_2=), 5.79 (ddt, 1H, J = 6.7 Hz, 10.2 Hz, 17.1 Hz, C=CH-), 7.33–7.36 (m, 4H, ArH), 7.72–7.76 (m, 4H, ArH); ^{13}C nmr (75 MHz, $CDCl_3$) δ: 21.46, 26.01, 26.61, 28.50, 28.57, 29.05, 33.48, 37.71, 68.56, 114.12, 127.67, 129.75, 132.23, 138.72, 144.85.

*3-(Oct-7-enyl) cyclobutane-1,1-dicarboxylic acid bis(*p*-methoxybenzyl) ester (**13**)*

To a cold solution of dimethoxybenzyl malonate (5.10 g, 14.8 mmol) in 100 mL of dry dioxane was added dropwise 15 mL of sodium bis(trimethylsilyl)amide (1 M in THF) at 0°C. The solution was stirred at this temperature for 5 min, at which point a solution of the ditosyl derivative **11** (7.35 g, 14.9 mmol) in 100 mL of dry dioxane was slowly added, followed by 15 mL of sodium bis(trimethylsilyl)amide THF solution. The reaction mixture was stirred at 12°C for 15 min, then heated to reflux for 16 h, diluted with 700 mL of ether, washed with 1 N HCl, water, saturated $NaHCO_3$, water, and brine, dried with anhydrous sodium sulfate, and evaporated to give a syrup. Purification by flash chromatography (ethyl acetate – hexanes 1:5, then 1:2) afforded the cyclobutane derivative **13** (3.80 g, 52%) as a colorless syrup; ir ($CHCl_3$): 1725 (C=O) cm^{-1}; ^1H nmr (300 MHz, $CDCl_3$) δ: 1.15–1.40 (m, 10H, H-1′, -2′, -3′, -4′, -5′), 1.99–2.12 (m, 2H, H-6′), 2.15–2.19 (m, 2H, H-2, -4), 2.31 (m, 1H, H-3), 2.57–2.64 (m, 2H, H-2, -4), 3.80 (s, 6H, $PhOCH_3$), 4.91–5.03 (m, 2H, C=CH_2), 5.04 (s, 2H, $PhCH_2O$), 5.07 (s, 2H, $PhCH_2O$), 5.81 (ddt, 1H, J = 6.8 Hz, 10.3 Hz, 17.0 Hz, C=CH-), 6.81–6.87 (m, 4H, aromatic H), 7.16–7.27 (m, 4H, aromatic H); ^{13}C nmr (75 MHz, $CDCl_3$) δ: 26.53, 28.71, 28.92, 29.15, 29.52, 33.63, 34.70, 36.31, 49.55, 55.08, 66.62, 66.75, 113.67, 114.02, 127.59, 129.70, 139.01, 159.39, 171.45, 171.78; ms, *m/e*: 494 $(M)^+$. Exact Mass calcd. for $C_{30}H_{38}O_6$: 494.2669; found: 494.2676.

*3-(6-Carboxyhexyl) cyclobutane-1,1-dicarboxylic acid bis(*p*-methoxybenzyl) ester (**15**)*

A solution of compound **13** (0.500 g, 1.01 mmol) in 15 mL of dry dichloromethane was cooled to −78°C, and ozone was bubbled into it over 1 h at this temperature. After passing argon through the solution for 30 min, 0.4 mL of dimethyl sulfide was added, followed by 0.5 mL of triethylamine. The solution was stirred for 10 min, and warmed to 0°C for 1 h until almost all of the ozonide disappeared (monitored by tlc). The reaction mixture was diluted with 50 mL of dichloromethane and washed with saturated $NaHCO_3$, water, and brine. The organic phase was dried (Na_2SO_4) and evaporated to dryness to give the aldehyde. The crude aldehyde was dissolved in 20 mL of *tert*-butyl alcohol and 5 mL of 2-methyl-2-butene, then a solution of sodium chlorite (0.810 g, 8.96 mmol) and sodium dihydrogenphosphate hydrate (0.940 g, 6.81 mmol) in 8 mL of deionized water was added dropwise over a 15 min period. The yellow mixture was stirred at room temperature for 30 min. After removal of the volatile components under vacuum, the yellow liquid residue was extracted with 20 mL of ether. The aqueous phase was acidified to pH 3 with 6 N HCl and extracted with ether (2 × 10 mL). The combined ether extracts were washed with water and brine, dried ($MgSO_4$), and evaporated to give a syrup that was purified by flash chromatography on a silica gel column, eluting with ethyl acetate – hexanes (1:3, then 1:2) in the presence of 0.5% acetic acid to give carboxylic acid **15** (0.405 g, 79%, two steps from olefin **13**) as white crystals; mp 56–57°C; ir ($CHCl_3$): 3400–2500 (br, COOH), 1725, 1705 (C=O) cm^{-1}; ^1H nmr (300 MHz, $CDCl_3$) δ: 1.16–1.38 (m, 8H, H-1′, -2′, -3′, -4′), 1.58–1.63 (m, 2H, H-5′), 2.10–2.19 (m, 2H, H-2, -4), 2.33 (t, 2H, J = 7.4 Hz, H-6′), 2.20–2.35 (m, 1H, H-3), 2.57–2.64 (m, 2H, H-2, -4), 3.80 (s, 6H, $PhOCH_3$), 5.05 (d, 4H, J = 9.2 Hz, OCH_2Ph), 6.81–6.86 (m, 4H, aromatic H), 7.16–7.27 (m, 4H, aromatic H); ^{13}C nmr (75 MHz, $CDCl_3$) δ: 24.42, 26.35, 28.81, 28.89, 29.45, 33.84, 34.65, 36.20, 49.53, 55.05, 66.63, 66.74, 113.66, 127.56, 129.68, 159.37, 171.42, 171.74, 179.80; ms (FAB), *m/e*: 535 $(M + Na)^+$, 513 $(M + 1)^+$. Exact Mass calcd. for $C_{29}H_{36}NaO_8$: 535.2309; found: 535.2248.

*[2R-(2α,6α,7β)-3-[[6-(2-Benzhydryloxycarbonyl-8-oxo-7-phenylacetylamino-5-thia-1-azabicyclo[4.2.0]oct-3-en-3-yl)methoxycarbonyl]hexyl]cyclobutane-1,1-dicarboxylic acid bis(*p*-methoxybenzyl) ester (Δ^2 isomer, **16**a) and (6*R*-trans)-3-[[6-(2-Benzhydryloxycarbonyl-8-oxo-7-phenylacetylamino-5-thia-1-azabicyclo[4.2.0]oct-2-en-3-yl)methoxycarbonyl]hexyl]cyclobutane-1,1-dicarboxylic acid bis(*p*-methoxybenzyl) ester (Δ^3 isomer, **16**b)*

To a cold (ice-water bath) solution of **15** (350 mg, 0.683 mmol) in 50 mL of dry dichloromethane was added DCC (210 mg, 1.02 mmol), DMAP (20 mg), and then a solution of **2** (420 mg, 0.816 mmol) in 150 mL of dry dichloromethane. The mixture was stirred at room temperature overnight, and washed with water, 10% HCl, water, saturated $NaHCO_3$ solution, water, and brine. The organic layer was dried (Na_2SO_4) and evaporated to give a residue that was applied to a column of flash silica gel. Elution with ethyl acetate – hexanes (2:1) gave an inseparable mixture of the Δ^2 and the Δ^3 isomers (ratio 3:2) of **16** (532 mg, 64.6%); For Δ^2 isomer, ir ($CHCl_3$): 3320 (NH), 1780 (C=O, β-lactam), 1730 (COOR), 1680 (CONH) cm^{-1}; ^1H nmr (300 MHz, $CDCl_3$) δ: 1.15–1.58 (m, 10H, aliphatic CH_2), 2.13–2.34 (m, 5H, CH_2COOR, cyclobutane-CH_2, CH), 2.59–2.66 (m, 2H, cyclobutane-CH_2), 3.64 (ABq, 2H, J = 16.0 Hz, $PhCH_2CON$), 3.80 (s, 6H, $PhOCH_3$), 4.53, 4.59 (ABq, 2H, J_{gem} = 12.8 Hz, 3′-CH_2OCOR), 5.07 (d, 4H, J = 8.9 Hz, $COOCH_2Ph$), 5.09 (s, 1H, H-2), 5.19 (d, 1H, J = 4.0 Hz, H-6), 5.62 (dd, 1H, J = 4.0 Hz, 8.7 Hz, H-7), 6.35 (d, 1H, J = 8.7 Hz, CONH), 6.38 (d, 1H, J = 1.7 Hz, H-4), 6.82–6.87 (m, 4H, PMB-aromatic H), 6.89 (s, 1H, $COOCHPh_2$), 7.16–7.22 (m, 4H, PMB-aromatic H), 7.25–7.44 (m, 15H, aromatic H); ^{13}C nmr (75 MHz, $CDCl_3$) δ: 24.48, 26.35, 28.84, 29.43, 33.70, 34.64, 36.19, 43.08, 49.50, 50.13, 53.26, 55.04, 60.15, 65.14, 66.61, 66.73, 78.99, 113.66, 119.12, 121.66, 126.58–129.66 (multiple peaks), 133.49, 138.74, 159.37, 164.11, 165.81, 170.84, 171.37, 171.69, 172.92; ms (FAB), *m/e*: 1031 $(M + Na)^+$, 1009 $(M + 1)^+$. Exact Mass calcd. for $C_{58}H_{61}N_2O_{12}S$: 1009.3947; found: 1009.3824. For Δ^3 isomer, all the data, see **18**.

*(6R-trans-3-[[6-(2-Benzhydryloxycarbonyl-5,8-dioxo-7-phenylacetylamino-5-thia-1-azabicyclo[4.2.0]oct-2-en-3-yl)-methoxycarbonyl]hexyl]cyclobutane-1,1-dicarboxylic acid bis(*p*-methoxybenzyl) ester (**17**)*

Can. J. Chem. Downloaded from www.nrcresearchpress.com by 213.200.69.106 on 09/08/12
For personal use only.

A solution of **16** (230 mg, 0.228 mmol) in 25 mL of ethyl acetate was cooled to 0°C and a solution of *m*-chloroperbenzoic acid (50–60%, 88 mg) in 10 mL of ethyl acetate was added dropwise. After stirring at that temperature for 3 h, the solution was diluted with 50 mL of ethyl acetate and washed with saturated $NaHCO_3$ solution, brine, and dried ($MgSO_4$). The solvent was evaporated to give a syrup that was purified by flash chromatography. Elution with ethyl acetate and hexane (1:1, then 3:1) gave a colorless syrup **17** (180 mg, 77%) that crystallized on standing in a refrigerator; $[\alpha]_D$ + 18.9 (*c* 1.35, $CHCl_3$); mp 123–124 °C; ir ($CHCl_3$): 3280 (NH), 1795 (C=O, β-lactam), 1730 (COOR), 1690 (CONH) cm^{-1}; ^1H nmr (300 MHz, $CDCl_3$) δ: 1.14–1.58 (m, 10H, aliphatic CH_2), 2.15 (m, 2H, cyclobutane-CH_2), 2.25 (t, 2H, J = 7.6 Hz, CH_2COOR), 2.30 (m, 1H, cyclobutane-CH), 2.61 (m, 2H, cyclobutane-CH_2), 3.17, 3.78 (ABq, 2H, J_{gem} = 19.0 Hz, SCH_2), 3.61, 3.68 (ABq, 2H, J_{gem} = 5.6 Hz, $PhCH_2CON$), 3.81 (2 × s, 6H, $PhOCH_3$), 4.45 (dd, 1H, J = 1.5 Hz, 4.8 Hz, H-6), 4.37, 5.29 (ABq, 2H, J_{gem} = 14.3 Hz, 3′-CH_2OCOR), 5.06 (d, 4H, J = 9.5 Hz, $COOCH_2Ph$), 6.10 (dd, 1H, J = 4.8 Hz, 9.9 Hz, H-7), 6.76 (d, 1H, J = 9.9 Hz, CONH), 6.82–6.87 (m, 4H, PMB-aromatic H), 6.95 (s, 1H, $COOCHPh_2$), 7.17–7.20 (m, 4H, PMB-aromatic H), 7.27–7.48 (m, 15H, aromatic H); ^{13}C nmr (75 MHz, $CDCl_3$) δ: 24.55, 26.37, 28.86, 29.46, 33.73, 34.68, 36.18, 43.26, 45.64, 49.54, 55.11, 58.91, 62.99, 66.62, 66.68, 66.80, 80.21, 113.70, 121.34, 125.01, 126.94, 127.42, 127.48, 127.56, 128.05, 128.10, 128.37, 128.48, 128.92, 129.24, 129.71, 133.46, 138.75, 138.85, 159.43, 159.50, 163.97, 171.11, 171.43, 171.74, 172.98; ms (FAB), *m/e*: 1047 $(M + Na)^+$, 1025 $(M + 1)^+$.

*(6*R-trans*)-3-[[6-(2-Benzhydryloxycarbonyl-8-oxo-7-phenylacetylamino-5-thia-1-azabicyclo[4.2.0]oct-2-en-3-yl)methoxycarbonyl]hexyl]cyclobutane-1,1-dicarboxylic acid bis(*p*-methoxybenzyl) ester (**18**)*

Phosphorus trichloride (12 μL, 0.138 mmol) was added to a solution of **17** (70 mg, 0.068 mmol) in 1.5 mL of dry DMF at −22°C. After stirring at this temperature for 1 h, the slightly red solution was diluted with 20 mL of ether, and washed with cold water (2 × 5 mL) and brine. The organic phase was dried ($MgSO_4$) and evaporated to give a syrup that was purified by flash chromatography. Elution with ethyl acetate – hexanes (1:3, then 1:2) afforded the desired product **18** (66.5 mg, 96%) as a colorless syrup; $[\alpha]_D$ −1.2 (*c* 3.05, $CHCl_3$); ir ($CHCl_3$): 3320 (NH), 1790 (C=O, β-lactam), 1730 (COOR), 1680 (CONH) cm^{-1}; ^1H nmr (300 MHz, $CDCl_3$) δ: 1.16–1.59 (m, 10H, aliphatic CH_2), 2.17 (m, 2H, cyclobutane-CH_2), 2.25 (t, 2H, J = 7.6 Hz, CH_2COOR), 2.32 (m, 1H, cyclobutane-CH), 2.62 (m, 2H, cyclobutane-CH_2), 3.31, 3.50 (ABq, 2H, J_{gem} = 18.7 Hz, SCH_2), 3.61, 3.68 (ABq, 2H, J_{gem} = 16.0 Hz, $PhCH_2CON$), 3.81 (s, 6H, $PhOCH_3$), 4.79, 5.04 (ABq, 2H, J_{gem} = 13.7 Hz, 3′-CH_2OCOR), 4.95 (d, 1H, J = 4.8 Hz, H-6), 5.07 (d, 4H, J = 8.9 Hz, $COOCH_2Ph$), 5.88 (dd, 1H, J = 4.8 Hz, 9.1 Hz, H-7), 6.28 (d, 1H, J = 9.1 Hz, CONH), 6.84 (m, 4H, PMB-aromatic H), 6.94 (s, 1H, $COOCHPh_2$), 7.19 (m, 4H, PMB-aromatic H), 7.26–7.45 (m, 15H, aromatic H); ^{13}C nmr (75 MHz, $CDCl_3$) δ: 24.55, 26.22, 26.37, 28.87, 29.44, 33.73, 34.65, 39.19, 43.11, 49.50, 55.07, 57.15, 58.90, 62.63, 66.65, 66.77, 79.58, 113.66, 125.22, 126.86, 126.97, 127.48, 127.95, 128.04, 128.28, 128.40, 129.02, 129.31, 129.69, 133.47, 138.82, 138.99, 159.37, 160.42, 164.64, 171.01, 171.41, 171.72, 173.03; ms (FAB), *m/e*: 1031 $(M + Na)^+$, 1009 $(M + 1)^+$.

*(6*R-trans*)-3-[[6-(2-Carboxy-8-oxo-7-phenylacetylamino-5-thia-1-azabicyclo[4.2.0]oct-2-en-3-yl)methoxycarbonyl]hexyl]cyclobutane-1,1-dicarboxylic acid (**19**)*

Trifluoroacetic acid (0.95 mL, 12.3 mmol) was added dropwise to a solution of compound **18** (250 mg, 0.248 mmol) in anisole (0.40 mL, 3.68 mmol) and dichloromethane (6 mL) with cooling (ice-water bath) and the mixture was stirred at that temperature for 2 h. After removal of the volatile components, the residue was washed with dichloromethane and ether to give white powder **19**, which was used immediately for the next reaction without purification.

*(6*R-trans*-3-[[6-(2-Carboxy-8-oxo-7-phenylacetylamino-5-thia-1-azabicyclo[4.2.0]oct-2-en-3-yl)methoxycarbonyl]hexyl]cyclobutane-1,1-dicarboxylic acid potassium salt (**20**)*

To a mixture of compound **19** (0.25 mmol), ethyl acetate (3 mL), and deionized water (10 mL) was slowly added 0.105 N aqueous potassium hydroxide (2.4 mL, 0.25 mmol) at 0°C. The aqueous solution was then separated and washed with ether twice before lyophilizing to give a white powder **20** (80 mg). The organic phase was treated with 0.105 N KOH aqueous solution until pH 6.5. The aqueous layer was separated and washed with ether twice, then lyophilized to yield a further 58 mg of white powder **20**, bringing the total yield to 138 mg (87%, two steps from **18**); ^1H nmr showed that this powder was a mixture of the Δ^2 and Δ^3 (ratio 1:1.4) isomers; ^1H nmr (300 MHz, D_2O) δ: 1.24–1.68 (m, 20H, aliphatic CH_2), 2.08–2.17 (m, 4H, cyclobutane-CH_2), 2.24–2.38 (m, 2H, cyclobutane-CH), 2.46 (t, 4H, J = 7.4 Hz, CH_2COOR), 2.52–2.59 (m, 4H, cyclobutane-CH_2), 3.39, 3.66 (ABq, 2H, J_{gem} = 17.9 Hz, Δ^3-SCH_2), 3.76 (m, 4H, $PhCH_2$), 4.73, 4.89 (ABq, 2H, J_{gem} = 9.1 Hz, Δ^2-3′-CH_2O), 4.79, 4.98 (ABq, 2H, J_{gem} = 12.5 Hz, Δ^3-3′-CH_2O), 4.86 (d, 1H, J = 1.1 Hz, Δ^2-H-2), 5.15 (d, 1H, J = 4.7 Hz, Δ^2-H-6), 5.35 (d, 1H, J = 3.8 Hz, Δ^3-H-6), 5.47 (d, 1H, J = 3.8 Hz, Δ^3-H-7), 5.70 (d, 1H, J = 4.7 Hz, Δ^2-H-7), 6.52 (s, 1H, Δ^2-H-4), 7.41–7.51 (m, 10H, ArH).

*(SP-4-2)-[4-[(6*R-trans*)-(2-Carboxy-8-oxo-7-phenylacetylamino-5-thia-1-azabicyclo[4.2.0]oct-2-en-3-yl)methoxycarbonyl]hexyl]cyclobutane-1,1-dicarboxylato][(1*R,2R*)-cyclohexane-1,2-diamine-*N,N′*] platinum (**21**)*

(SP-4-2)-Dinitro (1,2-cyclohexanediamine-*N,N′*) platinum (16 mg, 0.036 mmol) was dissolved in 1 mL of deionized water and the trace of insoluble residue was removed by centrifugation. The supernatant was transferred into a 20-mL vial, then a solution of potassium salt **20** (23 mg, 0.036 mmol) in 1 mL of deionized water was added. The mixture was stirred at room temperature in darkness for 3 h and the resulting precipitate was filtered and washed with deionized water, then dried over P_2O_5 under vacuum to give the platinum complex **21** (21 mg, 64%) as a white powder; $[\alpha]_D$ +122 (*c* 0.50, DMSO); ^1H nmr (300 MHz, DMSO-d_6) δ: 1.00–1.50 (m, 16H, hexanyl H-1, -2, -3, -4, -5, cyclohexanyl H-4, -5, Hax-3, -6), 1.88–2.02 (m, 4H, cyclobutane H-2, -4, cyclohexanyl Heq-3, -6), 2.12–2.55 (m, 7H, cyclobutane H-2, -3, -4, hexanyl H-6, cyclohexanyl H-1, -2), 3.3–3.7 (m, 4H, $PhCH_2$, SCH_2), 4.55–6.45 (m, 8H, H-6, H-7, RCO_2CH_2, NH_2), 7.2–7.35 (m, 5H, ArH). Anal. calcd. for $C_{35}H_{46}N_4O_{10}PtS \cdot 3H_2O$: C 43.61, H 5.44, N 5.81; found: C 43.82, H 5.29, N 5.56.

*3-Acetoxymethyl-8-oxo-7-phenylacetylamino-5-thia-1-azabicyclo[4.2.0]oct-2-ene-2-carboxylic acid potassium salt (**22**)*

To a suspension of 7-aminocephalosporanic acid (7-ACA) (1.20 g, 4.40 mmol) in 40 mL of mixed solvent (acetone–water 1:1) was carefully added $NaHCO_3$ (0.930 g, 11.0 mmol) with cooling (ice-water bath). After the addition was complete, the mixture was warmed to room temperature and stirred until the suspended solid had dissolved in the solvent. The reaction mixture was cooled (0°C) again and a solution of phenyl acetyl chloride (0.87 mL, 6.6 mmol) in 20 mL of acetone was slowly added. Stirring was continued at room temperature overnight. After removal of the solvent, the residue was overlaid with ethyl acetate and acidified with 1 N HCl. The separated aqueous phase was extracted with ethyl acetate three times and the combined extracts were washed with cold water and brine, dried with anhydrous sodium sulfate, and evaporated to give the crude phenylacetylaminocephalosporanic acid. To the residue, dissolved in 150 mL of ethyl acetate, was added, with manual stirring, potassium 2-ethyl hexanoate (0.5 M solution in ethyl acetate) (8.8 mL, 4.4 mmol). The resulting precipitate was filtered and washed with ethyl acetate, then dried under vacuum to afford the desired product **22** (1.56 g, 83%) as yellow crystals; ^1H nmr (300 MHz, deuterated carbonate buffer, pD 10.1) δ: 2.09 (s, 3H, CH_3), 3.34, 3.60 (ABq, 2H, J_{gem} =

17.9 Hz, SCH_2), 3.65, 3.72 (ABq, 2H, J_{gem} = 14.9 Hz, $PhCH_2$), 4.69, 4.86 (ABq, 2H, J_{gem} = 12.7 Hz, CO_2CH_2), 5.07 (d, 1H, J = 4.7 Hz, H-6), 5.62 (d, 1H, J = 4.7 Hz, H-7), 7.32–7.43 (m, 5H, ArH); ^{13}C nmr (75 MHz, D_2O) δ: 18.68, 23.80, 40.37, 55.70, 57.56, 62.53, 114.52, 125.80, 127.31, 127.60, 129.84, 133.01, 163.13, 166.84, 172.40, 173.45; ms (FAB), *m/e*: 428 $(M)^+$. Exact Mass calcd. for $C_{18}H_{17}KN_2O_6S$: 428.0445; found: 428.0468.

Preparation of 0.2 M phosphate buffer (pD 7.2)

A solution containing Na_2HPO_4 (204.5 mg, 1.44 mmol) and $NaH_2PO_4 \cdot 2H_2O$ (87.4 mg, 0.56 mmol) in 2 mL of deuterated water was lyophilized to dryness and the resulting white crystalline residue was dissolved in 10 mL of deuterated water.

Preparation of 0.25 M carbonate buffer (pD 10.1)

A solution containing Na_2CO_3 (159 mg, 1.50 mmol) and $NaHCO_3$ (84 mg, 1.00 mmol) in 2 mL of deuterated water was lyophilized to dryness and the resulting white residue was dissolved in 10 mL of deuterated water.

Preparation of β-lactamase buffer solution

The commercially available (Sigma Chemical Co.) penicillinase (EC 3.5.2.6) type III, from *Enterobacter cloacae* (67 units/mg protein for cepholoridine) was used as hydrolytic enzyme. To the original vial containing 0.15 mg (~10 units) protein was added 0.6 mL of deuterated phosphate buffer (pD 7.2, 0.2 M). The solution (10 units/0.6 mL) was kept in 0–5°C and was used for nmr studies. One unit will hydrolyze 1.0 μmol of cephaloridine per minute at pH 7.0 at 25°C.

Enzymatic hydrolysis of **22** *in 0.2 M phosphate buffer (pD 7.2)—(^1H nmr study)*

Potassium cephalosporinate **22** (5 mg, 11.6 μmol) was dissolved in 0.2 M deuterated sodium phosphate buffer (0.6 mL, pD 7.2) at 20°C. The ^1H nmr spectrum was taken at this temperature and then 0.2 mL (3.3 units) of β-lactamase buffer solution was added. The ^1H nmr spectrum at 20°C was taken immediately; ^1H nmr (300 MHz, deuterated phosphate buffer, pD 7.2) δ: 1.88 (s, 3H, CH_3), 3.35, 3.72 (ABq, 2H, J_{gem} = 14.7 Hz, SCH_2), 3.59, 3.65 (ABq, 2H, J_{gem} = 14.8 Hz, $PhCH_2$), 4.61 (d, 1H, J = 3.0 Hz, H-6), 5.41 (d, 1H, J = 3.0 Hz, H-7), 5.60 (s, 1H, C=CH_2), 5.65 (s, 1H, C=CH_2), 7.27–7.40 (m, 5H, PhH).

Enzymatic hydrolysis of **22** *in 0.25 M carbonate buffer (pD 10.1)—(^1H nmr study)*

Potassium cephalosporinate **22** (5 mg, 11.6 μmol) was dissolved in 0.25 M deuterated sodium carbonate buffer (0.6 mL, pD 10.1) at 20°C. The ^1H nmr spectrum was taken immediately and, subsequently, after 40 min. Then 0.2 mL (3.3 units) of β-lactamase buffer solution was added and the ^1H NMR spectrum was taken immediately (Fig. 2 **C**).

Enzymatic hydrolysis of **8** *in 0.25 M carbonate buffer (pD10.1)—(^1H nmr study)*

A suspension containing 10 mg of platinum complex **8** was stirred in 0.8 mL of deuterated carbonate buffer (pD 10.1) at 0–5°C for 30 min and the mixture was centrifuged. The supernatant was lyophilized and the resulting white powder was dissolved in 0.6 mL of D_2O. The ^1H nmr spectrum was taken immediately (Fig. 2 **A**). To this sample was added 0.1 ml (5 units) of β-lactamase buffer solution. The ^1H nmr was taken immediately at room temperature (Fig. 2 **B**): ^1H nmr (300 MHz, deuterated carbonate buffer, pD 10.1) δ: 1.1–1.4 (br m, 4H, cyclohexane-CH_2), 1.53–1.68 (br m, 2H, cyclohexane-CH_2), 1.95–2.14 (br m, 2H, cyclohexane-CH_2), 2.35 (br m, 2H, cyclohexane-H-1,2), 7.48 (d, 1H, J = 7.8 Hz, aromatic H-5), 7.83 (dd, 1H, J = 1.6 Hz, 7.8 Hz, aromatic H-6), 7.91 (d, 1H, J = 1.5 Hz, aromatic H-2); and 3.93, 3.75 (ABq, 2H, J_{gem} = 14.8 Hz, SCH_2), 3.60–3.71 (m, 2H, $PhCH_2$), 4.64 (d, 1H, J = 3.0 Hz, H-6), 5.44 (d, 1H, J = 3.0 Hz, H-7), 5.63 (s, 1H, C=CH_2), 5.68 (s, 1H, C=CH_2), 7.30–7.42 (m, 5H, ArH).

Acknowledgment

We would like to acknowledge the financial assistance of the Natural Sciences and Engineering Research Council of Canada (NSERCC) and la Fonds pour la formation de chercheurs et l'aide à la recherche (FCAR–Québec).

1. R.K. Johnson and R.P. Hertzberg. Annu. Rev. Med. Chem. **25**, 129 (1990), and references therein.
2. G. Kohler and C. Milstein. Nature, 256, 495 (1975); Hybridoma technology in the biosciences and medicine. *Edited by* Plenum Press, New York, London. 1985.
3. G.A. Koppel. Bioconjugate Chem. **1**, 13 (1990); Monoclonal antibodies in cancer, contemporary biomedicine. *Edited by* S. Sell and R. Eeisfeld. Humana, Clifton, N.J. 1985. pp. 1–485; G. Kohler. Angew. Chem. Int. Ed. Engl. **24**, 827 (1985); D.E. Yelton and M. Scharff. Annu. Rev. Biochem. **50**, 657 (1981).
4. P.D. Senter, P.M. Wallace, H.P. Svensson, V.M. Vrudhula, D.E. Kerr, I. Hellerström, and K.E. Hellerström. Bioconjugate Chem. **4**, 3 (1993); D.R. Lovett, D.A. Scheinberg, and A.N. Houghton. Cancer chemotherapy and biological response modifiers annual 12. *Edited by* H.M. Pinedo, D.L. Longo, and B.A. Chabner. Elsevier Science Publishers B.V., Amsterdam. 1991. p. 147; R.W. Baldwin, V.S. Byers, and M.V. Pimm. Cancer chemotherapy and biological response modifiers annual 10. *Edited by* H.M. Pinedo, D.L. Longo, and B.A. Chabner. Elsevier Science Publishers B.V., Amsterdam. 1988. p. 397; R.W. Baldwin and V.S. Byers. Cancer chemotherapy and biological response modifiers annual 9. *Edited by* H.M. Pinedo, D.L. Longo, and B.A. Chabner. Elsevier Science Publishers B.V., Amsterdam. 1987. p. 409; P.D. Senter, M.G. Saulnier, G.J. Schreibeg, D.L. Hirschberg, J.P. Brown, I. Hellström, and K.E. Hellström. Proc. Natl. Acad. Sci. U.S.A. **85**, 4842 (1988).
5. E.D. Blumenthal, R.M. Sharkey, and D.M. Goldenberg. Adv. Drug Delivery Rev. **4**, 279 (1990).
6. P.M. Capone, L.D. Papsidero, and T.M. Chu. J. Natl. Cancer Inst. **72**, 673 (1984).
7. R.K. Jain. J. Natl. Cancer Inst. **81**, 570 (1989).
8. J.J. Dimaggio, D.A. Scheinberg, and A.N. Houghton. Cancer chemotherapy and biological response modifiers annual 11. *Edited by* H.M. Pinedo, B.A. Chabner, and D.L. Longo. Elsevier Science Publishers B.V., Amsterdam. 1990. p. 177.
9. M.F.A. Woodruff. Br. J. Cancer **47**, 589 (1983); P.H. Hand, M. Nuti, D. Colcher, and J. Schlom. Cancer Res. **43**, 728 (1983).
10. E.S. Vitetta, R.J. Fulton, R.D. May, M. Till, and J.W. Uhr. Science, **238**, 1098 (1987).
11. A.L. Fink. Pharm. Res. **2**, 55 (1985); D.J. Waxman and J.L. Strominger. J. Biol. Chem. **255**, 3964 (1980).
12. W.S. Faraci and R.F. Pratt. J. Am. Chem. Soc. **106**, 1489 (1984); D.B. Boyd. J. Org. Chem. **50**, 886 (1985); M.I. Page and P. Proctor. J. Am. Chem. Soc. **106**, 3820 (1984); E.J.J. Grabowski, A.W. Douglas, and G.B. Smith. J. Am. Chem. Soc. **107**, 267 (1985); R.F. Pratt and W.S. Faraci. J. Am. Chem. Soc. **108**, 5328 (1986).
13. S. Mobashery, S.A. Lemer, and M. Johnston. J. Am. Chem. Soc. **108**, 1685 (1986); D.B. Boyd and W.H.W. Lunn. J. Med. Chem. **22**, 778 (1979); H.A. Albrecht, G. Beskid, J.G. Christenson, J.W. Durkin, V. Fallat, N.H. Georgopapadakou, D.D. Keith, F.M. Konzelmann, E.R. Lipschitz, D.H. McGarry, J. Siebelist, C.C. Wei, M. Weigele, and R. Yang. J. Med. Chem. **33**, 669 (1991).
14. T.A. Shepherd, L.N. Jungheim, D.L. Meyer, and J.J. Starling. Bioorg. Med. Chem. Lett. **1**, 21 (1991); L.N. Jungheim, T.A. Shepherd, and D.L. Meyer. J. Org. Chem. **57**, 2334 (1992).
15. R.P. Alexander, N.R.A. Beeley, M. O'Driscoll, F.P.O'Neill,

Can. J. Chem. Downloaded from www.nrcresearchpress.com by 213.200.69.106 on 09/08/12
For personal use only.

T.A. Millican, A.J. Pratt, and F.W. Willenbrock. Tetrahedron Lett. **32**, 3269 (1991); H.P. Svensson, J.F. Kadow, V.M. Vrudhula, P.M. Wallace, and P.D. Senter. Bioconjugate Chem. **3**, 176 (1992).
16. D.L. Meyer, L.N. Jungheim, S.D. Mikolajczyk, T.A. Shepherd, J.J. Starling, and C.N. Ahlem. Bioconjugate Chem. **3**, 42 (1992).
17. S. Hanessian, J.Y. Gauthier, K. Okamoto, T. Theophanides, and A. Beauchamp. Can. J. Chem. **71**, 880 (1993).
18. S. Hanessian and J. Wang. Can. J. Chem. **71**, 886 (1993).
19. D.P. Kelsen, H. Scher, N. Alcock, B. Leyland-Jones, A. Donner, L. Williams, G. Greene, J.H. Burchenal, G. Tan, F.S. Philips, and C.W. Young. Cancer Res. **42**, 4831 (1982).
20. T. Takaya, H. Takasugi, T. Murakawa, and H. Nakano. J. Antibiot. **34**, 1300 (1981).
21. D.E. O' Oconner and W.I. Lyness. J. Am. Chem. Soc. **86**, 3840 (1964).
22. G.V. Kaiser, R.D.G. Cooper, R.E. Koehler, C.F. Murphy, J.A. Webber, I.G. Wright, and E.M. Van Heyningen. J. Org. Chem. **35**, 2430 (1970).
23. G.R. Gale, A.B. Smith, and P. Schwartz. J. Clin. Hematol. Oncol. **9**, 217 (1979).
24. F.H.C. Stewart. Aust. J. Chem. **21**, 2543 (1968).
25. B.S. Bal, W.E. Childers, Jr., and H.W. Pinnick. Tetrahedron, **37**, 2091 (1981).
26. J.M.T. Hamilton-Miller, G.G.F. Newton, and E.P. Abraham. Biochem. J. **116**, 371 (1970); J.M.T. Hamilton-Miller, E. Richards, and E.P. Abraham. Biochem. J. **116**, 385 (1970).
27. R.A. Reisfeld. *In* Molecular probes: technology and medical applications. *Edited by* A. Albertini et al. Raven Press, New York (1989); K.E. Hellström and I. Hellström. *In* Molecular probes: technology and medical applications. *Edited by* A. Albertini et al. Raven Press, New York. 1989 p. 191; M. Wilchek. New Methods Drug Res. **2**, 175 (1988).
28. F. Galsbøl, P. Steenbøl, and B. Søndergaard Sørensen. Acta Chem. Scand. **26**, 3605 (1972).

Can. J. Chem. Downloaded from www.nrcresearchpress.com by 213.200.69.106 on 09/08/12
For personal use only.

Substituent effects of rate constants for thermal [4π + 2π] cycloreversion of spiro-fused β-lactam oxadiazolines

MICHEL ZOGHBI AND JOHN WARKENTIN[1]
Department of Chemistry, McMaster University, Hamilton, Ont., Canada L8S 4M1

Received November 6, 1992

MICHEL ZOGHBI and JOHN WARKENTIN. Can. J. Chem. **71**, 907 (1993).

Twelve Δ^3-1,3,4-oxadiazolines in which C-2 is also C-4 of a β-lactam moiety (spiro-fused β-lactam oxadiazoline system) were thermolyzed as solutions in benzene. Substituents in the β-lactam portion affect the rate constant for thermal decomposition of the oxadiazolines to N_2, acetone, and a β-lactam-4-ylidene. The total spread of first-order rate constants at 100°C was 47-fold and the average value was 6.7×10^{-4} s^{-1}. A phenyl substituent at N-1 or at C-3 was found to be rate enhancing, relative to methyl. At C-3, H and Cl were also rate enhancing, relative to methyl. The data are interpreted in terms of the differential effects of substituents on the stabilities of the ground states, and on the stabilities of corresponding transition states for concerted, suprafacial, [4π + 2π] cycloreversion. The first products, presumably formed irreversibly, are N_2 and a carbonyl ylide. The latter subsequently fragments to form acetone (quantitative) and a β-lactam-4-ylidene.

MICHEL ZOGHBI et JOHN WARKENTIN. Can. J. Chem. **71**, 907 (1993).

Douze Δ^3-1,3,4-oxadiazolines dans lesquelles le C-2 fait partie d'une β-lactame (système oxadiazoline avec fusion spiro sur une β-lactame) en solution dans le benzène ont été soumises à une thermolyse. Les substituants de la portion β-lactame affectent le constante de vitesse de la décomposition thermique des oxadiazolines en N_2, acétone et β-lactam-4-ylidène. À 100°C, le rapport des vitesses de réaction du premier ordre de la réaction la plus rapide et de la réaction la plus lente est égal à 47; la valeur moyenne est égale à $6{,}7 \times 10^{-4}$ s^{-1}. On a trouvé que la présence d'un groupe phényle en positions N-1 ou C-3 augmente la vitesse par rapport à celle d'un méthyle. Par rapport au méthyle en C-3, le H et le Cl augmentent aussi la vitesse de réaction. On interprète les données en fonction d'effets différentiels des substituants sur les stabilités des états fondamentaux et sur les stabilités des états de transition correspondants des cycloréversions [4π + 2π] suprafacialles concertées. Les premiers produits, qui se forment vraisemblablement d'une manière irréversible, sont le N_2 et l'ylure de carbonyle. Ce dernier se fragmente ultérieurement pour former de l'acétone (rendement quantitatif) et une β-lactam-4-ylidène.

[Traduit par la rédaction]

Can. J. Chem. Downloaded from www.nrcresearchpress.com by 213.200.69.106 on 09/08/12
For personal use only.

Introduction

Pericyclic processes[2] constitute an important mechanistic class of chemical reactions. Such processes are very useful for the construction of new ring systems from precursors with fewer rings (associative pericyclic reactions), and for generating the products of the reverse, dissociative reactions (Scheme 1). Probably the most familiar examples are the Diels–Alder and retro Diels–Alder reactions.

From a mechanistic perspective, either the forward or the reverse reaction could be selected for study because the transition structures are independent of the direction of approach to them. In practice such a choice may not be available if one of the reactions of Scheme 1 is inaccessible experimentally. Cycloadditions of 4π systems to N_2, for example, are not known. Therefore the mechanisms of pericyclic reactions involving N_2 as one component must be inferred from studies of the dissociative process, which is very well known.[3]

Thermal cycloreversions of Δ^3-1,3,4-oxadiazolines (**1**) lead to carbonyl ylide intermediates (**2**) that are known to undergo a variety of intramolecular and intermolecular reactions, including electrocyclizations (2) to oxiranes (**3**), 1,4-sigmatropic rearrangements to enol ethers (**4**) (3), cycloadditions to dipolarophiles (4), and fragmentations to carbenes and carbonyl compounds (4*b*–*d*, 5), Scheme 2.

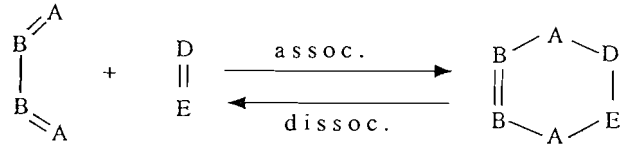

SCHEME 1

Fragmentations of carbonyl ylides have assumed increased importance with the discovery that they can be unidirectional, as in the cases of 2,2-dialkoxyoxadiazolines (**5**) (6) and spiro-fused β-lactam oxadiazolines (**8**) (5*b*), which afford dialkoxycarbenes (**7**) and β-lactam-4-ylidenes (**10**), respectively, Scheme 3.

In this paper we report the effects of substituents (R^2–R^3) on the rates of thermolysis of spiro-fused β-lactam oxadiazolines (**8**) to form carbonyl ylides (**9**) and N_2.

Methods and results

Spiro-fused β-lactam oxadiazolines **8** were prepared by [2π + 2π] cycloaddition[4] of 2-imino-Δ^3-1,3,4-oxadiazolines (**11**) to ketenes (**12**) generated, in situ, from appropriate acid chlorides and triethylamine[5] (eq. [1]). Thermolyses were carried out in sealed NMR tubes immersed in a constant temperature oil bath. A tube was removed periodically

[1]Author to whom correspondence may be addressed.

[2]A pericyclic reaction is a concerted reaction that occurs through a cyclic transition state.

[3]The facile thermal cycloreversion of Δ^3-1,3,4-thiadiazolines to N_2 and thiocarbonyl ylides, for example (1).

[4]Although the result is readily accounted for in terms of [2π + 2π] cycloaddition, the actual mechanism is still a controversial subject (7).

[5]Details of the syntheses, including isomer ratios and spectra, are in the accompanying paper (8).

Can. J. Chem. Downloaded from www.nrcresearchpress.com by 213.200.69.106 on 09/08/12
For personal use only.

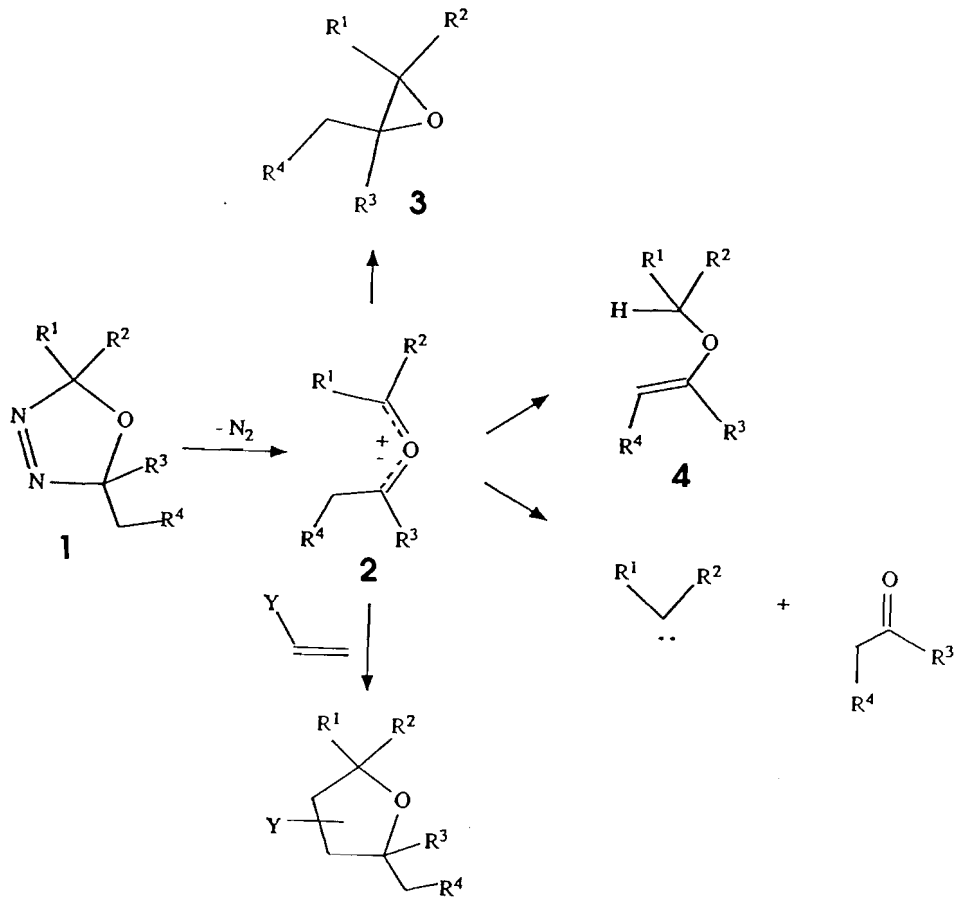

SCHEME 2

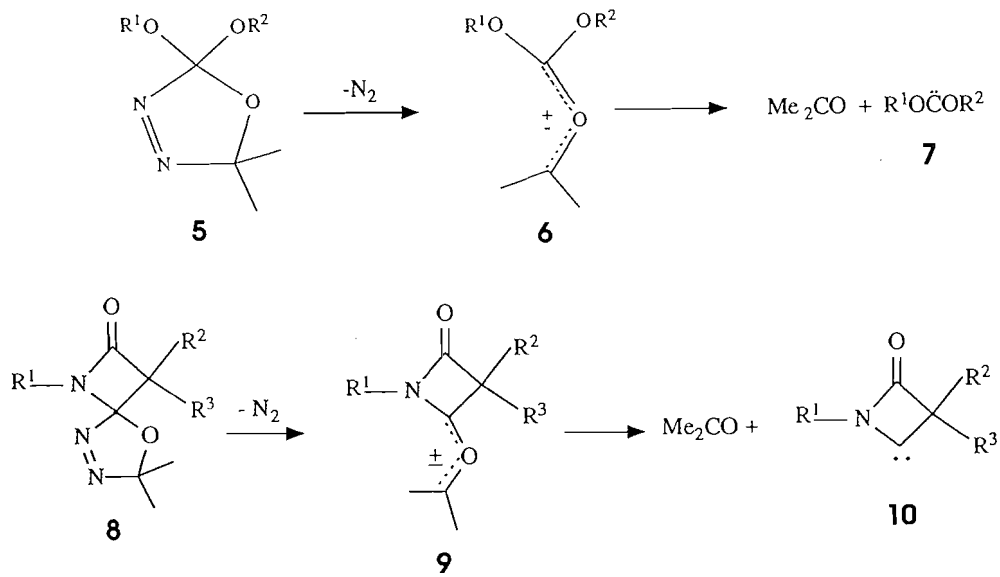

SCHEME 3

and chilled quickly to room temperature for integration of the ^{1}H NMR spectrum. Disappearance of the signals from the methyl groups at C-5 of the oxadiazoline ring, and appearance of the methyl signal of acetone were convenient for monitoring progress of the thermolyses. Reactions were followed to 75% or more of completion. Fits to the first-order rate law gave correlation coefficients ranging from 0.983 to 0.999. Even at high conversions, there was no evidence for consumption of acetone because the yields of acetone, by ^{1}H NMR spectroscopy, were at least 95%. The fates of the β-lactam-4-ylidenes (**10**) in benzene were not determined. Some of their chemistry, including reactions with hydrox-

[1] 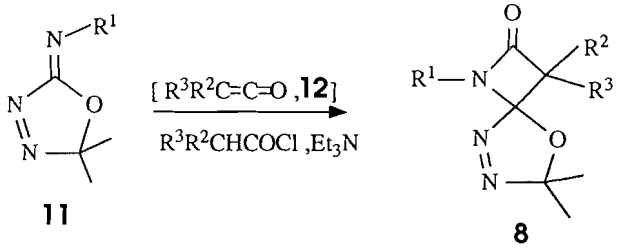

8*a*: $R^1 = R^2 = R^3 = Ph$; *b*: $R^1 = PhCH_2$, $R^2 = R^3 = Ph$; *c*: $R^1 = Me$, $R^2 = R^3 = Ph$; *d*: $R^1 = Ph$, $R^2 = R^3 = Me$; *e*: $R^1 = R^2 = R^3 = Me$; *f*: $R^1 = Ph$, $R^2 = OPh$, $R^3 = H$; *g*: $R^1 = Ph$, $R^2 = H$, $R^3 = OPh$; *h*: $R^1 = p\text{-}CH_3OC_6H_4$, $R^2 = OPh$, $R^3 = H$; *i*: $R^1 = Ph$, $R^2 = N_3$, $R^3 = H$; *j*: $R^1 = p\text{-}MeOC_6H_4$, $R^2 = R^3 = Cl$; *k*: $R^1 = Ph$, $R^2 = Me$, $R^3 = OPh$; *l*: $R^1 = Ph$, $R^2 = OPh$, $R^3 = Me$

ylic compounds and with alkynes, has been described (5*b*, 9).

Discussion

The overall mechanism of thermal decomposition of Δ^3-1,3,4-oxadiazolines bearing a heteroatom substituent at C-2 is quite well established. In the first step, N_2 is lost to afford a carbonyl ylide intermediate (4). Evidence for the latter includes trapping of ylide intermediates from 2-alkoxy- and 2,2-dialkoxy-Δ^3-1,3,4-oxadiazolines (4*b*–*d*, 6). For the family **8**, evidence for a discrete carbonyl ylide intermediate is less direct, as bimolecular trapping reactions failed. However, in the case of **13**, a minor product isolated was **14**, which is most easily accounted for in terms of a 1,4-sigmatropic rearrangement of a carbonyl ylide intermediate (Scheme 4). It is most likely then that a carbonyl ylide intermediate is a feature common to the thermolyses of such oxadiazolines, and that the lifetimes of those ylides are sensitive to structural features within them.

There is general agreement that the mechanism of thermal cycloreversion of Δ^3-1,3,4-oxadiazolines involves concerted cleavage of both C—N bonds and disrotatory motion of the end carbons of the developing carbonyl ylide fragment. If that ylide is symmetrically substituted, the cycloreversion is more likely to be synchronous than if it is not. Although transition states involving very asynchronous bond cleavages, with or without charge separation (modelled with **15**, and **16**), can be imagined, it is unlikely that iminium ion character in an amide (**15**) or homoenolate character in a β-lactam system (**16**) would be very significant, especially

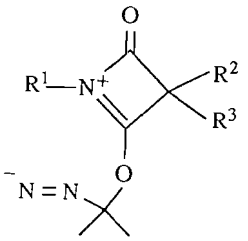

15

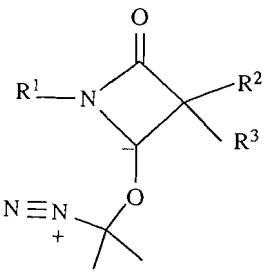

16

in benzene solvent. On the other hand, **16** is the more likely model for the *sense* of non-synchrony, if any, of the cycloreversions of **8** because the strain associated with introduction of double-bond character into the lactam ring is avoided and yet some relief of steric crowding is gained.

In addition to the question of non-synchronous but concerted cycloreversion and the consequent substituent effects on developing radical (or charged) sites at the transition state, there is the usual concern about the magnitude of substituent effects on the ground state energies. That these are not negligible is clear from the fact that pairs of diastereomers (**8***k* and **8***l*; **8***f* and **8***g*) that lead to enantiomeric carbonyl ylides differ in reactivity by factors of 1.5–5.4. At 100°C, those rate factors correspond to differences of 0.30 and 1.3 kcal mol^{-1}, respectively, in E_a. The ground state free energy difference ΔG (**8***f*–**8***g*), from equilibration of **8***f* and **8***g* with fluoride ion in THF at room temperature, is 0.8 kcal mol^{-1}, more than half as large as the difference (1.3 kcal mol^{-1}) between the activation energies for their decompositions. Therefore, if diastereomers of **8** have significantly different ground state free energies, it is likely that other **8** will show significant effects of both ground state and transition state free energy differences in their thermolysis kinetics. As a result, small rate factors in the family **8** must be interpreted with caution. The following analysis is subject to that caveat.

Taking **8***e* ($R^1 = R^2 = R^3 = R^4 = CH_3$) as reference (rel. rate = 1.0) is convenient because all of the other **8** decompose faster. The largest rate enhancement factors are 39, 47, 39, and 29 for thermolysis of **8***j*, **8***f*, **8***i*, and **8***h*, respectively (Table 1). They have, in common, an aryl group as R^1 (p-C_6H_4OMe or Ph) and the effect of p-anisyl relative to phenyl is small (<2), as judged from comparison of **8***h* with **8***f*. Three (**8***f*, **8***h*, **8***i*) also have, in common, H as R^2 or R^3. We suggest that two factors, electron withdrawal by substituents R^2 and (or) R^3 as well as low steric hinderance, are responsible for the high reactivities of **8***j*, **8***f*, **8***i*, and **8***h*. The former presumably operates by stabilizing the transition state for nitrogen loss (modelled with the carbonyl ylide) in which negative charge begins to build up at the ylide termini (Scheme 5). The latter should be important in permitting relatively facile cycloreversion to the "*exo*" ylide (Scheme 5).[6] In an all-planar geometry, the *endo* ylide has a large eclipsing interaction (R^1 against CH_3) whereas the *exo* ylide has CH_3 lying in the "dihedral gap" (large for small rings) between R^2 and R^3. With the more realistic assumption that neither ylide is all-planar at the energy minimum, the argument is similar. An *endo* ylide has to twist substantially to reduce eclipsing interactions whereas an *exo* ylide bearing H as R^2 or R^3 can relieve nonbonded interactions between CH_3 and the large group (R^3 or R^2) by allowing H to eclipse

[6]The *exo* and *endo* configurations are assigned on the basis of the higher priority of N over C.

Can. J. Chem. Downloaded from www.nrcresearchpress.com by 213.200.69.106 on 09/08/12
For personal use only.

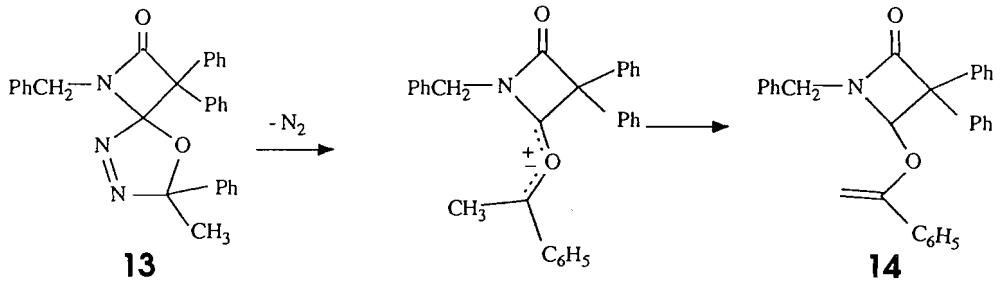

SCHEME 4

TABLE 1. Rate constants for thermolysis of **8** in benzene at 100°C

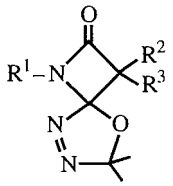

(R^2 *trans* to oxadiazoline oxygen)

8

	R^1	R^2	R^3	k, s^{-1}	k_{rel}
8*a*	Ph	Ph	Ph	2.8×10^{-4}	7.4
8*b*	$PhCH_2$	Ph	Ph	1.1×10^{-4}	2.9
8*c*	Me	Ph	Ph	1.2×10^{-4}	3.2
8*d*	Ph	Me	Me	0.99×10^{-4}	2.6
8*e*	Me	Me	Me	3.8×10^{-5}	1.0
8*f*	Ph	PhO	H	1.8×10^{-3}	47
8*g*	Ph	H	PhO	3.3×10^{-4}	8.7
8*h*	*p*-C_6H_4OMe	PhO	H	1.1×10^{-3}	29
8*i*	Ph	N_3	H	1.5×10^{-3}	39
8*j*	*p*-C_6H_4OMe	Cl	Cl	1.5×10^{-3}	39
8*k*	Ph	Me	PhO	4.8×10^{-4}	13
8*l*	Ph	OPh	Me	7.2×10^{-4}	19

CH_3 more strongly. Although the steric effect is probably important, **8***j* decomposes quickly without that advantage, pointing to an electronic effect of electron-withdrawing chlorine substituents. The phenoxy substituent is rate enhancing also (**8***l*, rel. rate 19 vs. **8***d*, rel. rate 2.6), and about equal to azido (**8***f* vs. **8***i*) in that respect, both presumably because of their inductive, electron-withdrawing effects. Finally, the influence of phenyls (**8***c* vs. **8***e*) as R^2 and R^3 can be seen in the same light. Although the rate enhancement is only 3.2-fold for two phenyls over two methyls, it is qualitatively in keeping with the small electronegativity difference between the sp^2 and sp^3 carbons. As expected on the basis of the picture that has been developed above, a phenyl group as R^1 should also be rate enhancing, and this was found: **8***d* vs. **8***e*, 2.6-fold; **8***a* vs. **8***b*, **8***c* (2.5, 2.3-fold). Moreover, a phenyl substituent in the oxadiazoline ring is strongly rate enhancing.[7]

The different reactivities of diastereomers (**8***f* and **8***g*; **8***k* and **8***l*) are more difficult to explain. Although ylides from diastereomeric oxadiazolines must be identical in energy, the transition states leading to those ylides are still diastereomers, and ground state energy differences could either be diminished or intensified at those transition states, depending on the details of the molecular reorganization that is involved.

In each of the diastereomeric pairs, the faster rate is that for thermolysis of the *trans* isomer, which, for the case of the **8***f*, **8***g* pair, is the less stable thermodynamically (by 0.8 kcal mol^{-1}) as shown by equilibration of **8***f* with **8***g* by fluoride ion.[5] The ground state energy difference is unlikely to be of steric origin; if anything, the *cis* isomer is more hindered. Therefore, we propose that the *trans* isomer is destabilized by a dipole–dipole repulsion between the azo and phenoxy groups. As the transition state is approached, the spiro carbon becomes less positive, either because cycloreversion is non-synchronous in the sense of **16** or because both C-2 and C-5 of the oxadiazoline ring have begun to accumulate some of the negative charge of the ylide product. The maximum rate enhancement from the dipole repulsion feature cannot be calculated because the equilibrium constant (**8***f* ⇄ **8***g*) was determined at room temperature in tetrahydrofuran whereas the rates were measured in benzene at 100°C. For the **8***k*, **8***l* pair we assume that the *cis* isomer is again the more stable but the energy difference must be smaller, leading to a rate factor of only 1.5.

That the C—N (azo) bond is polar is evident from the fact that thermolysis rate constants of *cis* azo compounds, in which the bond dipoles are additive, decrease with increasing solvent polarity (10). That feature can best be explained (10) in terms of greater solvation of the ground states of *cis* azo compounds than that of the transition states for thermolysis. Even when the azo group is in conjugation with a carbonyl group its net effect is electron withdrawal, as illustrated with the carbonyl group stretching frequencies of γ-lactone **17** (1750 cm^{-1}) and the diaza analogue **18** (1835 cm^{-1}) (11).

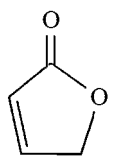

17

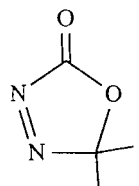

18

In summary, concerted cycloreversion of **8** probably occurs through a transition state with carbonyl ylide character significantly developed. The ylide-like transition state has negative charge distributed over C-2 and C-5 of the fragmenting oxadiazoline, as opposed to positive charge at those

[7]Separation of the diastereomers of **13** was not achieved and only a crude estimate of the effect of a phenyl substituent, in the oxadiazoline ring, was possible. The rate constants for **13** at 50°C, and for **8***b* at 100°C, are similar.

Can. J. Chem. Downloaded from www.nrcresearchpress.com by 213.200.69.106 on 09/08/12
For personal use only.

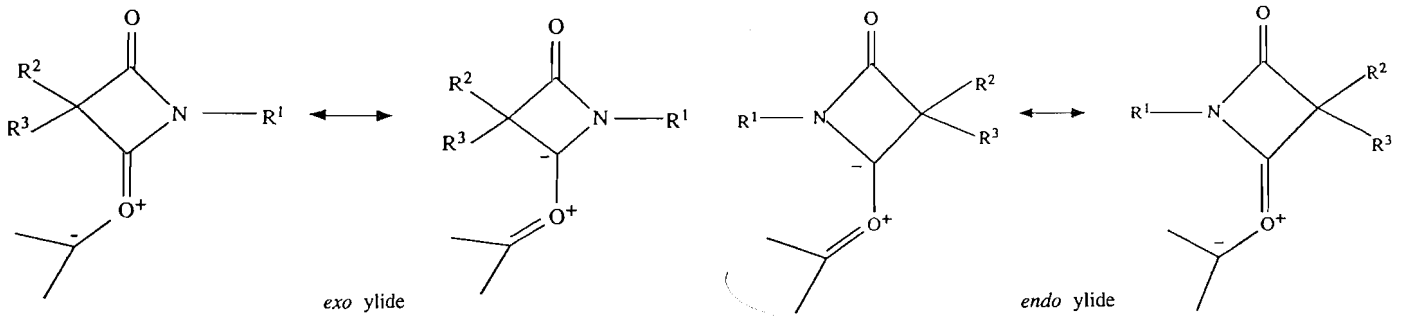

SCHEME 5

sites in the ground state. Moreover, steric interactions between *endo* substituents of the ylide are partly developed at the transition state. The observed substituent effects on thermolysis rate constants can be rationalized in terms of relief of ground state dipole–dipole repulsions, inductive effects of electron-withdrawing groups, and the low steric requirement of H.

Experimental

Thermolyses were carried out in medium-walled NMR tubes with solutions of **8** (25 mg, ca. 0.1 mmol) in C_6D_6 (0.5 mL) containing toluene (ca. 0.05 mmol). The solutions were degassed by means of three freeze–pump–thaw cycles at 10^{-2} Torr (1 Torr = 133.3 Pa) before the tubes were flame sealed, and transferred to a constant temperature bath at 100°C.

Tubes were removed from time to time, and chilled quickly to approximately room temperature with ice water. Integration of the oxadiazoline methyl signals against the methyl signal of the toluene reference afforded values of the concentrations of remaining oxadiazoline. The decompositions of **8** were followed through two to four half-lives. There was no difference, outside of experimental error, between rate constants from reactions followed for one half-life and those from the same reaction followed for four half-lives. Time outside the 100°C bath was not counted and time in the bath was not corrected for the warm-up period following insertion of a sample at room temperature. Standard first-order plots (typically six data points for two to four half-lives) gave the rate constants in Table 1. From the reproducibility of rate constants from duplicate runs conducted a day or more apart, those rate constants are associated with errors less than ±5% of the values quoted.

1. J. Buter, S. Wassenaar, and R.M. Kellogg. J. Org. Chem. **37**, 4045 (1972).
2. (*a*) K.N. Houk, N.G. Rondan, C. Santiago, C.J. Gallo, R.W. Gandour, and G.W. Griffin. J. Am. Chem. Soc. **102**, 1504 (1980); (*b*) P. Rajagopalan and B.G. Advani. Tetrahedron Lett. 2689 (1967); (*c*) R.W. Hoffmann and H.L. Luthardt. Chem. Ber. **101**, 3861 (1968); (*d*) M. Békhazi and J. Warkentin. J. Am. Chem. Soc. **103**, 2473 (1981); (*e*) M. Hamagushi and T. Ibata. Tetrahedron Lett. 4475 (1974); (*f*) D. Seyferth, W. Tronich, W.E. Smith, and S.P. Hopper. J. Organomet. Chem. **67**, 341 (1974), (*g*) P.C. Wong, D. Griller, and J.C. Scaiano. J. Am. Chem. Soc. **104**, 5106 (1982).
3. (*a*) N. Shimizu and P.D. Bartlett. J. Am. Chem. Soc. **100**, 4260 (1978); (*b*) A.P. Hitchcock, S. Zweep, T. Steel, M. Békhazi, and J. Warkentin. Can. J. Chem. **60**, 2914 (1982); (*c*) M.W. Majchrzak and J. Warkentin. Can. J. Chem. **67**, 1752 (1989); (*d*) Can. J. Chem. **68**, 795 (1990).
4. (*a*) R. Huisgen. Angew. Chem. Int. Ed. Engl. **17**, 572 (1977); (*b*) M. Békhazi and J. Warkentin. J. Am. Chem. Soc. **105**, 1289 (1983); (*c*) Can. J. Chem. **61**, 619 (1983); (*d*) M. Békhazi, P.A. Risbood, and J. Warkentin. J. Am. Chem. Soc. **105**, 5675 (1983).
5. (*a*) T. Wong, J. Warkentin, and J.K. Terlouw. Int. J. Mass Spectrom. Ion Processes, **115**, 33 (1992); (*b*) M. Zoghbi and J. Warkentin. J. Org. Chem. **56**, 3214 (1991).
6. M. El-Saidi, K. Kassam, D. Pole, T. Tadey, and J. Warkentin. J. Am. Chem. Soc. **114**, 8751 (1992).
7. L.S. Hegedus, J. Montgomery, Y. Narukawa, and D.C. Snustad. J. Am. Chem. Soc. **113**, 5784 (1991), and references therein.
8. M. Zoghbi and J. Warkentin. Can. J. Chem. **71**, 912 (1993).
9. M. Zoghbi and J. Warkentin. Can. J. Chem. **70**, 2967 (1992).
10. A. Schulz and C. Rüchardt. Tetrahedron Lett. 3893 (1976).
11. (*a*) P.R. West and J. Warkentin. J. Org. Chem. **33**, 2089 (1968); (*b*) S.L. Lee, G.B. Gubelt, A.M. Cameron, and J. Warkentin. Chem. Commun. 1074 (1970); (*c*) S.L. Lee, A.M. Cameron, and J. Warkentin. Can. J. Chem. **50**, 2326 (1972); (*d*) P. Knittel, S.L. Lee, and J. Warkentin. Can. J. Chem. **50**, 3248 (1972).

Can. J. Chem. Downloaded from www.nrcresearchpress.com by 213.200.69.106 on 09/08/12
For personal use only.

Spiro-fused β-lactam oxadiazolines by formal [2+2] cycloaddition of 2-imino-Δ^3-1,3,4-oxadiazolines to ketenes

MICHEL ZOGHBI AND JOHN WARKENTIN[1]
Department of Chemistry, McMaster University, Hamilton, Ont., Canada L8S 4M1

Received February 16, 1993

MICHEL ZOGHBI and JOHN WARKENTIN. Can. J. Chem. **71**, 912 (1993).

Sixteen spiro-fused β-lactam oxadiazolines were prepared by treatment of 2-imino-Δ^3-1,3,4-oxadiazolines with carboxylic acid chlorides in the presence of triethylamine. Two others were prepared by methylation of β-lactam oxadiazoline anion equivalents with methyl iodide. Isomer ratios, spectra, stereochemistry, and relative thermodynamic stabilities of a pair of diastereomeric β-lactam oxadiazolines are reported. Three cases of failure of the approach are noted, to define some of the limitations. The oxadiazolines are known to undergo thermolysis, in solution, to afford N_2, a ketone, and a β-lactam-4-ylidene. Phenyl substitution at C5 of the oxadiazoline ring serves to decrease the thermolysis temperature by about 50°C but it also leads to the onset of a side reaction that lowers the yield of ylidene. This observation indicates a limitation of the oxadiazoline approach to the generation of β-lactam-4-ylidenes.

MICHEL ZOGHBI et JOHN WARKENTIN. Can. J. Chem. **71**, 912 (1993).

Par traitement de 2-imino-Δ^3-1,3,4-oxadiazolines appropriées par des chlorures d'acides en présence de triéthylamine, on a préparé 16 β-lactames oxadiazolines à fusion spiro. On en a préparé deux autres par méthylation des équivalents de l'anion de la β-lactame oxadiazoline par l'iodure de méthyle. On rapporte les rapports d'isomères, les spectres, la stéréochimie et les stabilités thermodynamiques relatives d'une paire de β-lactames oxadiazolines diastéréoisomères. On note trois cas d'échecs de l'approche; ils permettent de définir ses limitations. Il est connu que les oxadiazolines subissent une thermolyse en solution pour donner de l'azote, une cétone et un β-lactam-4-ylidène. La présence d'un substituant phényle en position C5 diminue la température de thermolyse par environ 50°C; toutefois, cette substitution provoque une réaction secondaire qui diminue le rendement en ylidène. Cette observation suggère une limitation à l'approche des oxadiazolines pour générer les β-lactam-4-ylidènes.

[Traduit par la rédaction]

Introduction

The overall reaction of imines with acid chlorides in the presence of a base is one that affords β-lactams. Although the mechanism of the reaction is not well understood,[2] and the rationales for any stereoselectivity are therefore on a tenuous footing, there is no doubt that the reaction is very useful for the construction of the β-lactam ring system.

Following the discovery that 2-alkoxy-Δ^3-1,3,4-oxadiazolines (**1***a*) undergo thermolysis to carbonyl ylides that, in turn, fragment to carbonyl compounds and carbenes (5), we recognized that it might be possible to construct analogous N-substituted oxadiazolines (**1***b*) as potential sources of aminocarbenes (Scheme 1). Moreover, those aminocarbenes might be β-lactam-4-ylidenes if it were possible to synthesize the family of compounds **4** (Scheme 2). One approach to such compounds (**4**) is the [2+2] cycloaddition of ketenes (or ketene equivalents) to 2-imino-Δ^3-1,3,4-oxadiazolines (**3**), Scheme 2.

In this paper we report the synthesis of 18 members of the family **4**, 1,7,8-triaza-5-oxa-2-oxospiro[3,4]oct-7-enes, which we refer to as β-lactam oxadiazolines.[3] Most of them were made by the general approach of Scheme 2 but two were prepared by methylation of a 3-lithio analogue of **4**. Some aspects of stereochemistry, relative thermodynamic stabilities of isomers, as well as effects of a phenyl substituent at C6 on kinetic stability and on the distribution among thermolysis products are reported also.

Methods, results, and discussion

2-Imino-Δ^3-1,3,4-oxadiazolines (**3**) were prepared by oxidative cyclization of semicarbazones (**2**) of ketones as described in the literature (7), reaction [1]. Although two of them had been reported earlier (7*b*, 7*d*), Table 1 lists them also in order to provide all of the diagnostic ^{13}C NMR spectroscopic data in one place. In each case only a single isomer of **3** was obtained and the *Z* configuration shown was assumed by analogy to structures assigned on the basis of single crystal X-ray diffraction (7*a*, 8). Their ^{13}C NMR spectra (C2: δ = 159.0–163.6; C5: δ = 120.2–126.2) identify them as 2-imino-Δ^3-1,3,4-oxadiazolines, given the method of preparation and those X-ray structures.

[1] $R^4R^5C{=}NNHCONHR^1$ (**2**) $\xrightarrow[\text{or } MnO_2]{Pb(OAc)_4}$ (**3**)

Synthesis of a β-lactam oxadiazoline (**4**), Table 2, was accomplished by addition of the acid chloride to a solution of **3** and triethylamine. That mode of mixing of the reagents is believed to result in the formation of a ketene intermediate (9) while the other mode, addition of amine to a solution of acid chloride and imine, is generally assumed to lead to an acyliminium ion intermediate (9).

Attack of the iminooxadiazoline on the ketene should occur preferentially from the less-hindered face of the carbonyl π-bond (Scheme 3) leading to dipolar intermediate **5***a*. The latter, by conrotatory closure (1) would afford that β-lactam oxadiazoline having the larger group (L in Scheme 3) *trans* to the oxadiazoline oxygen. Rotation about the N=C bond

[1]Author to whom correspondence may be addressed.

[2]The literature on this subject, the Staudinger reaction (1), is too extensive to be surveyed here. For recent articles and reviews that include the mechanistic aspects, see refs. 2–4.

[3]A preliminary report of some of this work has been published as a communication (6).

Can. J. Chem. Downloaded from www.nrcresearchpress.com by 213.200.69.106 on 09/08/12
For personal use only.

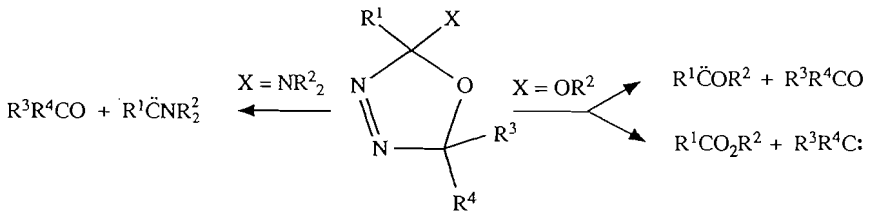

1a : X=OR2

1b : X=NR2 2

SCHEME 1

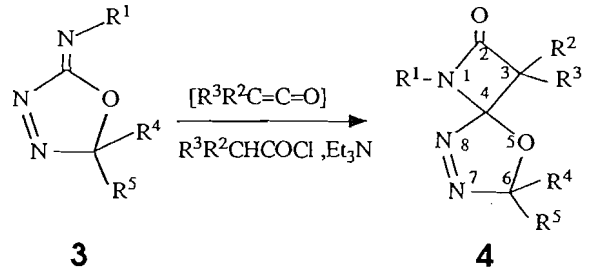

3 4

SCHEME 2

of **5***a* would convert it into **6***a* (not illustrated), which is simply the intermediate expected had the imine been of *E* rather than *Z* configuration. Such rotation is thought to be relatively facile in intermediates derived from imidates (10) because of the lower NC bond order (>N=COR ↔ >N—C=OR) in an imidate-derived intermediate. Although **3** are formally imidates, the azo group is powerfully electron withdrawing and modifies their properties.

Diastereoisomerism in the cycloadducts (Scheme 2) could arise from use of an unsymmetric ketene ($R^2 \neq R^3$) and a symmetric imine, because two stereocenters (C3, C4) are generated by cycloaddition, or from use of a symmetric ketene and an imine with a stereocenter. The potential for three stereocenters in the product(s) of cycloaddition was avoided in this study.

Diastereoisomeric products of cycloaddition were observed in some cases (**4***p* and **4***q*, **4***s* and isomer) but not in others (**4***g*, **4***i*, **4***j*), raising the interesting question of whether thermodynamics or kinetics is product controlling. The mechanism of Scheme 3 predicts kinetic control, and support for that mechanism came from the finding that the cycloaddition is under kinetic control. β-Lactam oxadiazoline **4***g*, formed as the exclusive product, was equilibrated with its *cis* isomer (**4***h*) upon treatment with fluoride ion in tetrahydrofuran. At equilibrium (25°C) the composition was **4***g*: **4***h* = 1:4.2. Examination of models suggests that the *trans* isomer is slightly less hindered than the *cis* isomer, although in both isomers the C6 methyl groups are far from the phenoxy substituent at C3. Consequently, the *trans* to *cis* isomerization is unlikely to be driven by steric hindrance. We propose, therefore, that there is a destabilizing dipole–dipole interaction in the *trans* isomer (**4***g*), from eclipsing of the C3-O and the C4-N(azo) dipoles that exceeds the corresponding interaction between the C3-O and C4-O bond dipoles in the *cis* isomer. A measure of the electron-withdrawing effect of the azo group is the σ-constant of the *p*-phenylazo substituent (0.34) (11). The value for the phenyl group (0.05) is small enough to suggest that alkylazo substituents will have σ_p-constants near 0.3, placing them between Cl and CO_2R in inductive electron-withdrawing power. A second indicator of the strong electron-withdrawing character of the azo group is the fact that α,β-diaza-α,β-unsaturated γ-lactones (Δ^3-1,3,4-oxadiazoline-2-ones) have CO stretching frequencies in the infrared near 1835 cm^{-1}, compared to 1750 cm^{-1} in α,β-unsaturated γ-lactones (7*c*, 7*d*, 12).

The assignment of stereochemistry to **4***p* and **4***q* rests on good analogy. Although the cycloaddition afforded both, the major isomer **4***p* was assigned the *trans* geometry, because **4***g* was the *only* product of cycloaddition of phenoxyketene to **3** (R^1=Ph, R^4=R^5=Me), and because the molecular structure of **4***g*, including the *trans* stereochemistry, rests firmly on X-ray crystallography.[4] Similarly, the azido compound **4***j* is most likely to be the *trans* isomer, as assigned. For the products of methylation (**4***m* and **4***n*) of a lithio lactam oxadiazoline, the assignment of stereochemistry could not be based on the same analogy, and the spectroscopic data did not afford any guidance for assignment of stereochemistry to those two compounds. However, the rate constant for thermolysis of **4***p* (*trans*) is about 5-fold larger than that for its *cis* diastereomer **4***q*. On that basis, **4***m* is *trans* and **4***n* is *cis*, because the former decomposes 1.5 times as fast as the latter, in benzene at 100°C (13*a*). Although those assignments are the most likely, a rate factor of 1.5 is not compelling evidence.

Iminooxadiazoline **3***g* is clearly a special case, in that it reacted, with 2:1 stoichiometry, with diphenylketene to afford **4***r*. The order of incorporation, whether **3***g* acts first as a nucleophile to acylate itself at the imino nitrogen, and the product then reacts as an imidate, or whether cycloaddition precedes N-acylation, is not clear.[5]

While it is evident, from the variety of substituents represented in Table 2, that many other spiro-β-lactam oxadiazolines should be accessible, there are limitations to the approach. Thus, attempts to add dimethylketene (from isobutyryl chloride) to **3***c* failed. Similarly, treatment of either **3***a* or **3***c* with phenylacetyl chloride – triethylamine failed to produce the corresponding β-lactam oxadiazolines. In each case of failure, most of the iminooxadiazoline was recovered.

Apart from the question of access to starting materials, potential users of a β-lactam-4-ylidene are interested in the

[4]C. Frampton, M. Zoghbi, and J. Warkentin, unpublished work.

[5]In anticipation of 1:1 stoichiometry, the reaction was conducted with one equivalent of diphenylacetyl chloride. Optimization of the yield through use of other ratios has not been attempted.

Can. J. Chem. Downloaded from www.nrcresearchpress.com by 213.200.69.106 on 09/08/12
For personal use only.

Can. J. Chem. Downloaded from www.nrcresearchpress.com by 213.200.69.106 on 09/08/12
For personal use only.

TABLE 1. ^{13}C NMR data for iminooxadiazolines, **3***a*–**3***f*

Compound	^{13}C NMR (50.3 MHz, $CDCl_3$) δ			
	C2	C5	C5-CH_3	Other
3*a*, R^1 = Ph $R^4 = R^5$ = Me	159.58	122.54	23.59	124.61, 126.64 128.88, 142.99
3*b*, R^1 = *p*-C_6H_4OMe $R^4 = R^5$ = Me	158.99	122.11	23.66	114.01, 126.90 135.62, 158.43
3*c*, R^1 = CH_2Ph $R^4 = R^5$ = Me	162.70	120.70	23.32	52.04, 126.78 127.46, 128.23, 138.52
3*d*, $R^1 = R^4 = R^5$ = Me	163.63	120.20	23.46	35.30
3*e*, R^1 = CH_2Ph R^4 = Me, R^5 = Ph	162.66	121.66	24.69	52.07 (CH_2)
3*f*, R^1 = CH_2Ph R^4, R^5 = 2-adamantylidene	162.14	126.19	—	26.12, 26.81, 27.19 34.01, 34.41, 36.02 36.58, 36.94, 37.09 38.99, 46.73, 52.09
3*g*, R^1 = H $R^4 = R^5$ = Me	^1H NMR spectrum in text; ^{13}C NMR spectrum not taken			

TABLE 2. ^{13}C NMR data for ring atoms and carbonyl stretching frequencies of spiro-β-lactam oxadiazolines **4**[a]

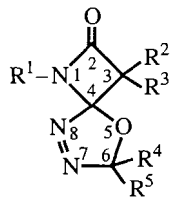

4

	^{13}C NMR (50 MHz, $CDCl_3$) δ				
	C2	C3	C4	C6	IR (cm^{-1})
$R^1 = R^2 = R^3$ = Ph, **4***a*	166.80	76.13	125.17	122.61	1770(KBr)
R^1 = $PhCH_2$, $R^2 = R^3$ = Ph, **4***b*	168.53	76.03	124.82	122.31	1770(KBr)
R^1 = Me, $R^2 = R^3$ = Ph, **4***c*	168.18	75.99	124.58	122.22	1782(KBr)
R^1 = Ph, $R^2 = R^3$ = Me, **4***d*	170.61	60.81	124.93	121.19	1758(KBr)
$R^1 = R^2 = R^3$ = Me, **4***e*	172.57	60.72	124.91	120.63	1779(KBr)
R^1 = $PhCH_2$, $R^2 = R^3$ = Ph, **4***f*	168.81	43.05	123.09	115.00	1772(KBr)
R^1 = Ph, R^2 = OPh, R^3 = H, **4***g*	162.13	88.21	129.66	122.85	1792(KBr)
R^1 = Ph, R^2 = H, R^3 = OPh, **4***h*	162.48	84.20	122.57	122.37	1785(film)
R^1 = *p*-C_6H_4OMe, R^2 = OPh, R^3 = H, **4***i*	162.41	87.68	125.30	122.39	1784(KBr)
R^1 = Ph, R^2 = N_3, R^3 = H, **4***j*	160.13	73.93	129.22	121.09	1778(KBr)
R^1 = *p*-C_6H_4OMe, $R^2 = R^3$ = Cl, **4***k*	159.07	86.03	124.94	121.65	1810(film)
R^1 = *p*-C_6H_4OMe, $R^2 = R^3$ = Me, **4***l*	170.65	60.36	125.08	120.95	1770(KBr)
R^1 = Ph, R^2 = OPh, R^3 = Me, **4***m*[b]	165.55	92.86	123.66	129.94	1777(film)
R^1 = Ph, R^2 = Me, R^3 = OPh, **4***n*[b]	165.33	93.50	123.73	122.04	1780(film)
R^1 = $PhCH_2$, $R^2 = R^3$ = Ph, **4***o*[a]	[c]	[c]	[c]	[c]	1775(film)
R^1 = Ph, R^2 = OMe, R^3 = H, **4***p*[b]	162.99	91.65	122.45	121.72	1782(KBr)
R^1 = Ph, R^2 = H, R^3 = OMe, **4***q*[b]	163.78	87.59	121.92	114.39	1780(film)
R^1 = Ph_2CHCO, $R^2 = R^3$ = Ph, **4***r*	166.06	75.59	127.69[d]	127.86[d]	1808(KBr)

[a]Substituent R^2 is *trans* to oxadiazoline oxygen. Substituents R^4 and R^5 are CH_3 except in the case of **4***f*, where R^4, R^5 = 2-adamantylidene, and **4***o*, where R^4 = Me, R^5 = Ph (mixture of diastereomers).
[b]The assignments of R^2 and R^3 may be reversed.
[c]Not assigned; mixture of diastereomers. ^1H NMR spectrum in text.
[d]These assignments may be reversed.

choice of available conditions for releasing the carbene. The C6 phenyl isomers **4***o* were prepared with the expectation that the phenyl group would enhance the rate constant for 1,3-dipolar cycloreversion to the carbonyl ylide, eq. [2]. As anticipated, thermolysis of **4***o* (unseparated diastereomers) was faster, with $t_{1/2}$ (50°C, major isomer) ≃90 min and $t_{1/2}$ (50°C, minor isomer) ≃2 × 10^2 min, compared to $t_{1/2}$ (100°C, **4***b*) = 115 min, all in benzene. A 50°C reduction of the

[2]

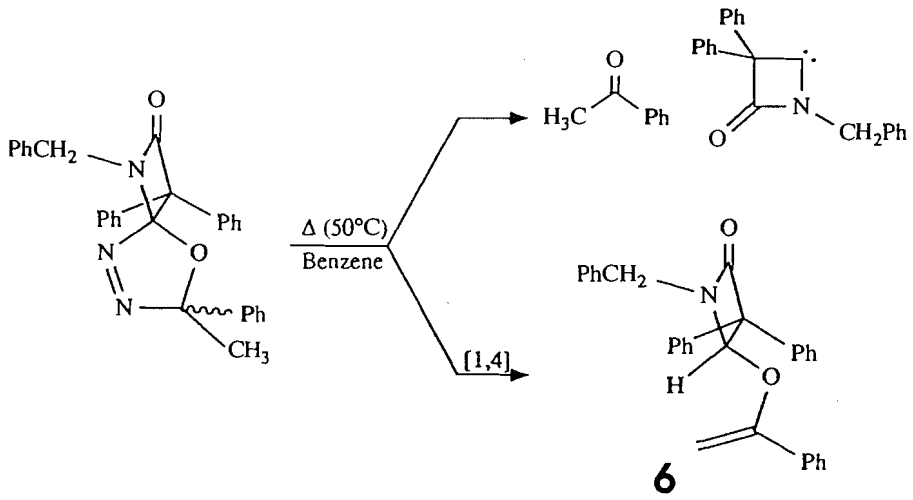

reaction temperature could be very significant for those ylidene reactions having negative $\Delta S^{\neq}$ values. The rate enhancement by phenyl comes at a small cost. Ylide fragmentation, apparently quantitative (NMR spectroscopy) for other **4**, constitutes about 76% of the fate of **4***o*.[6] The competition must be from 1,4-sigmatropic rearrangement of the carbonyl ylide, to form **6** (eq. [2]), as indicated by the vinyl and methine proton signals, in the ^{1}H NMR spectrum, that are characteristic of such products (13*b*).

Experimental

Materials

The 4-substituted semicarbazones (**2**) required for the preparation of 2-imino-Δ^3-1,3,4-oxadiazolines **3***a*–**3***c* (Table 1) were prepared by the method of Borsche (14) or by treating the appropriate ketone (R^4R^5CO) with a 4-substituted semicarbazide. Acetone-4-methylsemicarbazone was prepared from methylisocyanate, hydrazine, and acetone following Vogelsang's procedure (15). Acid chlorides required for ketenes, or ketene equivalents, were purchased from Aldrich Chemical Co., except for diphenylacetyl chloride and azidoacetyl chloride. The former was prepared as described below, and the latter was synthesized from ethyl chloroacetate by the method of Bertho and Maier (16). Arylimino oxadiazolines (7) and alkylamino oxadiazolines (7) were prepared by known methods.

2-Imino-5,5-dimethyl-Δ^3-1,3,4-oxadiazoline (**3***g*, R^1 = H, R^3 = R^4 = Me) was prepared as follows (17). To acetone semicarbazone (3.45 g, 0.030 mol) in ice-cold methylene chloride, with dry N_2 bubbling through, was added 30 g of K_2CO_3. Vigorous stirring was started and lead tetraacetate (30.0 g, 0.007 mol) was added. After 30 min an aqueous solution of potassium carbonate (200 mL of 50% solution) was added. A brown sludge was removed by filtration of the entire mixture through a bed of Celite. The organic layer was separated and washed twice with ice-cold aqueous potassium carbonate before it was dried over magnesium sulfate. Evaporation of the solvent left a clear, colourless oil that soon solidified to a white solid (75% yield), mp 56–57°C; IR(CCl_4) ν: 3340, 1705, 1530 cm^{-1}; ^{1}H NMR (90 MHz, CCl_4) δ: 1.60 (s, 6H), 7.70 (s, br, 1H). Anal. calcd. for $C_4H_7N_3O$: C 42.47, H 6.19, N 37.16; found: C 42.30, H 6.27, N 36.98.

Diphenylacetyl chloride.

A mixture of diphenylacetic acid (21.2 g, 0.10 mol) and thionyl chloride (17.8 g, 0.15 mol) was heated on a steam bath for 1 h. The excess $SOCl_2$ was removed under vacuum and the residue was recrystallized from petroleum ether to afford 20.8 g (90%) of the title compound, mp 55–57°C (lit. (18) mp 51–53°C).

General procedure for [2 + 2] cycloaddition to form spiro β-lactam oxadiazolines (4)

The acid chloride (3.0 mmol) in dry methylene chloride (10 mL) was added, drop by drop, to a stirring solution of the iminooxadiazoline (2.5 mmol), triethylamine (6.0 mmol), and methylene chloride (20 mL) under N_2 at ca. −23°C. When addition was complete the cooling bath was removed, and stirring was continued overnight. The reaction solution was then washed with saturated sodium bicarbonate solution and with brine. Aqueous layers were rewashed twice with methylene chloride. The combined organic layers were dried ($MgSO_4$) and filtered. Removal of the solvent afforded the β-lactam oxadiazolines in nearly pure form. Purification was by centrifugal chromatography (Chromatotron, 2-mm plates) with diethyl ether in hexanes (1:4) as eluent. Structures were anchored, through spectroscopic data, to two molecular structures determined by single crystal X-ray diffraction.

*1,7,8-Triaza-6,6-dimethyl-5-oxa-2-oxo-1,3,3-triphenylspiro[3.4]oct-7-ene, 4*a

White solid, in 90% yield; mp 154°C; IR (KBr) ν: 1770 (C=O), 1595 (N=N) cm^{-1}; ^{1}H NMR (500 MHz, $CDCl_3$) δ: 1.38 (s, 3H), 1.39 (s, 3H), 7.10–7.50 (m, 15H); ^{13}C NMR (125.8 MHz, $CDCl_3$) δ: 24.30, 24.40, 76.13 (C3), 122.61 (C6), 123.27 (Ar), 125.17 (C4), 127.57, 128.02, 128.33, 128.42, 128.69, 128.75, 129.39 (7 CH, aryl), 133.38, 134.64 (2 Cl, aryl), 166.80 (CO); MS (ei) *m/z*: 355 ($M^+ - N_2$, 1%), 269 ($M^+ - N_2 - C_3H_6O$, 68%), 236 ($M^+ - N_2$ − PhNCO, 7%), 194 (Ph_2CCO, 60%), 119 (PhNCO, 35%), 165 (9-fluorenyl, 100%); MS (ci, NH_3) *m/z*: 384 (M^+ + H, 100%); structure confirmed by single crystal X-ray diffraction (6, 13*a*).

*1,7,8-Triaza-1-benzyl-6,6-dimethyl-5-oxa-2-oxo-3,3-diphenylspiro[3.4]oct-7-ene, 4*b

White solid, 80% yield; mp 101–102°C; IR (KBr) ν: 1770 (C=O), 1600 (N=N) cm^{-1}; ^{1}H NMR (500 MHz, $CDCl_3$) δ: 1.35 (s, 3H), 1.45 (s, 3H), 4.53 (d, J = 15 Hz, 1H), 4.66 (d, J = 15 Hz, 1H), 7.20–7.55 (m, 15H); ^{13}C NMR (125.8 MHz, $CDCl_3$) δ: 24.32, 24.67, 76.03 (C3), 122.31 (C6), 124.82 (C4), 127.65, 127.80, 128.00, 128.36, 128.41, 128.60, 128.73 (7 CH, aryl), 135.13, 135.36, 136.81 (3 Cl, aryl), 168.53 (CO); MS (ei) *m/z*: 397 (M^+, 3%), 341 ($M^+ - N_2 - CO$, 11%), 265 (9%), 236 (18%), 194 (Ph_2CCO, 100%), 165 (9-fluorenyl, 83%), 132 (30%), 91 ($PhCH_2$, 87%); MS (ci, NH_3) *m/z*: 415 ($(M + NH_4)^+$, 28%), 398 (M^+ + H, 100%), 360 (11%), 345 (27%), 302 (71%), 267 (20%), 206 (32%), 194 (Ph_2CCO, 17%), 167 (43%), 108 (15%), 99 (40%).

[6]It is unlikely that the diastereomers of **4***o* lead to the same mixture of products. Their separation has not yet been achieved and they must therefore be treated as a collective.

Can. J. Chem. Downloaded from www.nrcresearchpress.com by 213.200.69.106 on 09/08/12
For personal use only.

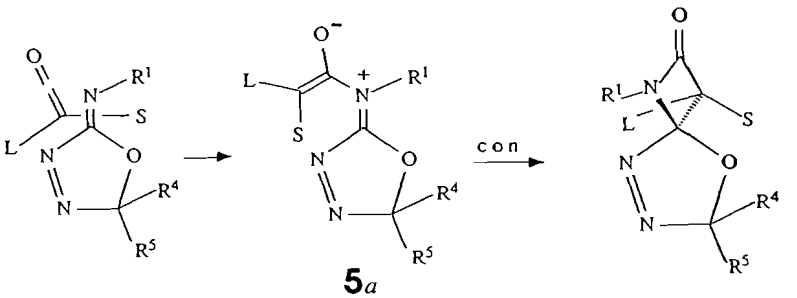

5*a*

(L = larger, S = smaller)

SCHEME 3

1,7,8-Triaza-1,6,6-trimethyl-5-oxa-2-oxo-3,3-diphenylspiro[3.4]oct-7-ene, **4**c

The starting material, 5,5-dimethyl-2-(methylimino)-Δ^3-1,3,4-oxadiazoline was contaminated with its hydrolysis product, 5,5-dimethyl-2-oxo-Δ^3-1,3,4-oxadiazoline, from which it could not be separated. The quantity of acid chloride was calculated on the basis of imine content (ca. 57%) and the yield was based on imine. Compound **4***c* was obtained in 65% yield as a white solid; mp 138–139°C; IR (KBr) *v*: 1782 (C=O), 1595 (N=N) cm^{-1}; ^1H NMR (200 MHz, $CDCl_3$) δ: 1.56 (s, 3H), 1.60 (s, 3H), 2.73 (s, 3H), 7.34 (s, br, 10H); ^{13}C NMR (125.8 MHz, $CDCl_3$) δ: 24.30, 24.36, 25.32, 75.99 (C3), 122.22 (C6), 124.58 (C4), 127.82, 127.88, 127.94, 128.28, 128.34, 128.41, 128.51, 128.63 (8 CH, aryl), 135.28, 136.77 (2 C1, aryl), 168.18 (CO); MS (ei) *m/z*: 293 ($M^+ - N_2$, 3%), 236 ($M^+ - N_2$ – MeNCO, 33%), 221 (5%), 207 (47%), 194 (Ph_2CCO, 41%), 193 (19%), 165 (9-fluorenyl, 100%), 133 (13%), 119 (10%); MS (ci, NH_3) *m/z*: 339 ($(M + NH_4)^+$, 54%), 322 (M^+ + H, 100%), 226 (12%) 208 (8%), 167 (10%).

1,7,8-Triaza-3,3,6,6-tetramethyl-5-oxa-2-oxo-1-phenylspiro[3.4]oct-7-ene, **4**d

White solid, 60% yield; mp 99–100°C; IR (KBr) *v*: 1758 (C=O), 1590 (N=N cm^{-1}); ^1H NMR (200 MHz, $CDCl_3$) δ: 1.32 (s, 3H), 1.43 (s, 3H), 1.46 (s, 3H), 1.66 (s, 3H), 6.95–7.40 (m, 5H); ^{13}C NMR (125.8 MHz, $CDCl_3$) δ: 17.20, 18.76, 23.76, 25.93, 60.81 (C3), 121.19 (C6), 124.93 (C4), 120.48, 126.22, 129.31, (3 CH, aryl), 134.84 (N-C1, aryl), 170.61 (CO); MS (ei) *m/z*: 203 ($M^+ - N_2$ – CO, 3%), 145 (203 – C_3H_6O, 100%), 130 (20%), 104 (10%), 77 (20%); MS (ci, NH_3) *m/z*: 277 ($(M + NH_4)^+$, 12%), 260 (M^+ + H, 100%), 232 (13%), 203 (10%), 145 (85%).

1,7,8-Triaza-1,3,3,6,6-pentamethyl-5-oxa-2-oxospiro[3.4]oct-7-ene, **4**e

White solid, in 60% yield based on starting imine content (see **4***c* above); mp 87–88°C; IR (KBr) *v*: 1779 (C=O), 1568 (N=N) cm^{-1}; ^1H NMR (200 MHz, $CDCl_3$) δ: 1.21 (s, 3H), 1.35 (s, 3H), 1.47 (s, 3H), 1.64 (s, 3H), 2.63 (s, 3H); ^{13}C NMR (125.8 MHz, $CDCl_3$) δ: 17.06, 18.59, 23.98 (NCH_3), 24.98, 25.48, 60.72 (C3), 120.63 (C6), 124.91 (C4), 172.57 (CO); MS (ei) *m/z*: 169 ($M^+ - N_2$, 2%), 141 ($M^+ - N_2$ – CO, 7%), 83 (100%), 68 (32%); MS (ci, NH_3) *m/z*: 215 ($(M + NH_4)^+$, 6%), 198 (M^+ + H, 100%), 170 (5%), 83 (45%).

6,6-Adamantylidene-1,7,8-triaza-1-benzyl-5-oxa-2-oxo-3,3-diphenylspiro[3.4]oct-7-ene, **4**f

White solid, 46% yield; mp 159–160°C; IR (KBr) *v*: 1772 (C=O), 1595 (N=N) cm^{-1}; ^1H NMR (200 MHz, $CDCl_3$) δ: 1.28–2.07 (m, 12H), 2.52 (m, 2H), 4.04 (d, J = 16.2 Hz, 1H), 4.64 (d, J = 16.2 Hz, 1H), 7.26–7.36 (m, 15H); ^{13}C NMR (50.3 MHz, $CDCl_3$) δ: 26.30 (−ve), 27.15 (−ve), 33.57 (+ve), 33.81 (+ve), 34.89 (+ve), 35.12 (+ve), 36.93 (+ve), 37.55 (−ve), 37.78 (−ve), 43.05 (C3), 115.00 (C6), 123.09 (C4), 127.51, 127.60, 128.08, 128.19, 128.29, 128.41, 128.53 (7 CH, aryl), 134.98, 135.57, 136.84 (3 C1, aryl), 168.61 (CO); MS (ei) *m/z*: 488 (M^+ – H, 13%), 356 ($M^+ - PhCH_2NCO$, 6%), 284 (23%), 194 (Ph_2CCO, 100%), 166 (22%), 150 (36%), 134 (60%), 91 (20%); MS (ci, CH_4) *m/z*: 490 (M^+ + H, 10%), 328 ($M^+ - N_2 - PhCH_2NCO$, 8%), 298 (12%), 255 (11%), 194 (Ph_2CCO, 100%), 150 (36%), 134 (16%), 91 (10%).

trans-*1,7,8-Triaza-6,6-dimethyl-5-oxa-2-oxo-1-phenyl-3-phenoxyspiro[3.4]oct-7-ene,* **4**g

White solid, 98%, one diastereomer; mp 95–96°C; IR (KBr) *v*: 1792 (C=O), 1594 (N=N) cm^{-1}; ^1H NMR (200 MHz, $CDCl_3$) δ: 1.48 (s, 3H), 1.56 (s, 3H), 5.49 (s, 1H), 7.00–7.40 (m, 10H); ^{13}C NMR (125.8 MHz, $CDCl_3$) δ: 23.93, 24.35, 88.21 (C3), 122.85 (C6), 129.66 (C4), 116.14, 121.91, 123.13, 127.33, 129.30 (5 CH, aryl), 133.24 (N-C1, aryl), 156.99 (O-C1, aryl), 162.13 (CO); MS (ei) *m/z*: 267 ($M^+ - N_2$ – CO, 4%), 209 (267 – C_3H_6O, 87%), 180 (76%), 134 (20%), 105 (70%), 77 (100%); MS (ci, CH_4) *m/z*): 324 (M^+ + H, 10%), 254 (9%), 230 (40%), 209 (100%), 180 (42%), 132 (46%), 104 (24%), 71 (75%); structure confirmed by single crystal X-ray diffraction.

trans-*1,7,8-Triaza-1-[4-methoxyphenyl]-6,6-dimethyl-5-oxa-2-oxo-3-phenoxyspiro[3.4]oct-7-ene,* **4**i

Pale yellow solid, 88%; mp 97–98°C; IR (KBr) *v*: 1784 (C=O), 1590 (N=N) cm^{-1}; ^1H NMR (200 MHz, $CDCl_3$) δ: 1.42 (s, 3H), 1.51 (s, 3H), 3.79 (s, 3H), 5.50 (s, 1H), 6.84–7.30 (m, 9H); ^{13}C NMR (50.3 MHz, $CDCl_3$) δ: 24.35 (2C), 55.45, 87.68 (C3), 122.39 (C6), 125.30 (C4), 114.57, 115.93, 123.00, 125.18, 129.66 (5CH, aryl), 156.99 (O-C1 or O-C4, aryl), 159.09 (O-C4 or O-C1, aryl), 162.41 (CO); MS (ei) *m/z*: 325 ($M^+ - N_2$, 5%), 283 ($M^+ - Me_2CN_2$, 11%), 239 (8%), 227 (13%), 221 (48%), 210 (14%), 176 (7%), 149 (41%), 134 (86%), 123 (23%), 94 (17%), 72 (100%); MS (ci, CH_4) *m/z*: 354 (M^+ + H, 4%), 340 (13%), 284 (25%), 256 (17%), 222 (100%), 190 (11%), 162 (33%), 134 (11%), 95 (7%), 72 (12%).

trans-*1,7,8-Triaza-3-azido-6,6-dimethyl-5-oxa-2-oxo-1-phenylspiro[3.4]oct-7-ene,* **4**j

Azidoacetyl chloride (1.06 mmol) in dry methylene chloride (3 mL) was added over a period of 1 h, by means of a syringe pump, to a stirring solution of 5,5-dimethyl-2-phenylimino-Δ^3-1,3,4-oxadiazoline (1.06 mmol) and triethylamine (1.06 mmol) in methylene chloride (6.5 mL). The latter solution was under N_2 and it was kept at 0–5°C. When addition was complete the cooling bath was removed but stirring was continued overnight. The solvent was removed and the crude, brown, oily residue was triturated twice with ether. Evaporation of the ether left an orange oil that was chromatographed (Chromatotron, 2-mm silica plate) with ethyl acetate in hexane (1:5) as eluent. The major, first fraction was starting material followed by the title compound as a white solid, 20% yield; mp 99–100°C; IR (KBr) *v*: 2110 (N_3), 1778 (C=O), 1595 (N=N) cm^{-1}; ^1H NMR (200 MHz, $CDCl_3$) δ: 1.54 (s, 3H), 1.67 (s, 3H), 4.65 (s, 1H) 7.10–7.45 (m, 5H); ^{13}C NMR (50.3 MHz, $CDCl_3$) δ: 23.53, 24.69, 73.93 (C3), 121.09 (C9), 129.22 (C4), 120.83, 127.16, 129.33 (3 CH, aryl), 133.41 (N-C1, aryl), 160.13 (CO), signal at 123.14 ascribed to impurity; MS (ei) *m/z*: 244 ($M^+ - N_2$, trace), 176 (3%), 161 (12%), 146 (11%), 130

Can. J. Chem. Downloaded from www.nrcresearchpress.com by 213.200.69.106 on 09/08/12
For personal use only.

Can. J. Chem. Downloaded from www.nrcresearchpress.com by 213.200.69.106 on 09/08/12
For personal use only.

(28%), 119 (PhNCO, 33%), 103 (100%), 91 (14%), 77 (22%); MS (ci, NH_3) *m/z*: 290 (($M^+ + NH_4$) 100%), 273 (7%), 230 (11%), 217 (25%), 161 (8%), 119 (10%), 99 (13%). The *trans* geometry was assigned on the basis of analogy.

1,7,8-Triaza-3,3-dichloro-1-[4-methoxyphenyl]-6,6-dimethyl-5-oxa-2-oxospiro[3.4]oct-7-ene, **4**k

Yellow oil, 75% yield; IR (film) *v*: 1810 (C=O), 1610 (N=N) cm^{-1}; ^1H NMR (200 MHz, $CDCl_3$) δ: 1.60 (s, 3H), 1.67 (s, 3H), 3.78 (s, 3H), 7.01 (AA′ BB′ pattern, 4H); ^{13}C NMR (50.3 MHz, $CDCl_3$) δ: 23.43, 25.18, 55.44, 86.03, (C3), 121.65 (C6), 124.94 (C4), 114.65, 123.44 (2 CH, aryl), 124.71 (N-Cl, aryl), 158.29 (O-C4, aryl), 159.07 (CO); MS (ei) *m/z*: 301 ($M^+ - N_2$, 10%), 303 (6%), 273 (7%), 238 (15%), 215 (21%), 168 (22%), 149 ($MeOC_6H_4NCO$, 100%), 134 (38%), 106 (18%), 92 (14%), 78 (16%), 63 (12%); MS (ci, NH_3) *m/z*: 347 (($M^+ + NH_4$), 100%), 351 (11%), 349 (60%), 303 (12%) 301 (17%), 270 (16%) 268 (49%), 238 (14%), 216 (30%), 174 (8%), 149 (12%), 123 (8%).

1,7,8-Triaza-1-[4-methoxyphenyl]-3,3,6,6-tetramethyl-5-oxa-2-oxospiro[3,4]oct-7-ene, **4**l

White solid, 92% yield; mp 89–90°C; IR (KBr) v: 1770 (C=O), 1583 (N=N) cm^{-1}; ^1H NMR (200 MHz, $CDCl_3$) δ: 1.32 (s, 3H), 1.44 (s, 3H), 1.46 (s, 3H), 1.54 (s, 3H), 3.77 (s, 3H), 7.00 (AA^1BB^1 pattern, 4H); ^{13}C NMR (50.3 MHz, $CDCl_3$) δ: 17.03, 18.55, 23.89, 25.58, 55.39, 60.36 (C3), 120.95 (C6), 125.08 (C4), 114.33, 123.50 (2CH, aryl), 126.84 (N-Cl, aryl), 158.08 (O-C4, aryl) 170.65 (CO); MS (ei) *m/z*: 261 ($M^+ - N_2$, 16%), 246 (12%), 191 (50%), 175 (20%), 163 (25%), 149 ($MeOC_6H_4NCO$, 59%), 133 (38%), 106 (11%), 92 (18%), 70 (42%); MS (ci, CH_4) *m/z*: 290 (M^+ + H, 28%), 281 (21%), 248 (20%), 220 (100%), 192 (21%), 175 (27%), 149 (14%), 71 (15%).

1,7,8-Triaza-1-benzyl-6-methyl-5-oxa-2-oxo-3,3,6-triphenylspiro[3.4]oct-7-ene, **4**o

Viscous oil, 60%, diastereomers in ratio 1:1.5, partially converted to acetophenone during attempted chromatography on silica; IR (film) *v*: 1775 (C=O), 1660 (N=N) cm^{-1}; ^1H NMR (200 MHz, $CDCl_3$) major isomer, δ: 1.77 (s, CH_3), 3.91 (d, J = 16 Hz, CH_2), 4.03 (d, J = 16 Hz, CH_2); minor isomer, δ: 1.63(s, CH_3), 4.32(d, J = 16 Hz, CH_2), 4.65 (d, J = 16 Hz, CH_2), other signals overlapping; MS (ei) *m/z* 312 ($M^+ - N_2 - PhCH_2NCO$, 6%), 284 (13%), 194 (Ph_2CCO, 11%), 165 ($C_{13}H_9^+$, 27%), 91 ($PhCH_2^+$, 100%); MS (ci, NH_3) *m/z*: 432 ($M^+ - N_2$ + 1, 100%), 312 (31%), 138 (40%).

1,7,8-Triaza-6,6-dimethyl-5-oxa-2-oxo-1-diphenylacetyl-3,3-diphenylspiro[3.4]oct-7-ene, **4**r

White solid, 38% yield; mp 135–136°C; IR (KBr) *v*: 1808 (C=O, lactam) 1730 (C=O, amide), 1600 (N=N) cm^{-1}; ^1H NMR (200 MHz, $CDCl_3$) δ: 1.47 (s, 3H), 1.76 (s, 3H), 5.97 (s, 1 H), 6.85–7.30 (m, 20 H); ^{13}C NMR (50.3 M Hz, $CDCl_3$) δ: 22.48 (CH_3), 22.95 (CH_3), 58.21 (Ph_2CHCO), 75.59 (C3), 127.69 (C6 or C4), 127.86 (C4 or C6), 127.96, 128.21, 128.28, 128.36, 128.55, 128.76, 128.84, 129.05, 129.34, 129.50 (10 CH, aryl), 135.56 (Cl, aryl), 137.08 (C1, aryl), 137.24 (2 C1, aryl), 166.06 (CO, lactam), 169.46 (CO, amide); MS (ei) *m/z*: 501 (M^+, 1%) 307 ($M^+ - Ph_2CCO$, trace), 237 (3%) 194 (Ph_2CCO, 50%), 167 (Ph_2CH, 100%), 139 (6%); MS (ci, NH_3) *m/z*: 519 (($M + NH_4$),$^+$ 20%), 502 (M^+ + 1, 1%), 449 (12%), 310 (7%), 265 (30%), 237 (16%), 212 (22%), 167 (100%), 99 (11%).

Synthesis of **4**p *and* **4**q

The general procedure described above gave, from 5,5-dimethyl-2-phenylimino-Δ^3-1,3,4-oxadiazoline and methoxyacetyl chloride, a mixture of **4***p* and **4***q*, formed in low yield, and oxadiazoline starting material. Attempts to separate the excess starting material from the products by chromatography were not successful. However, trituration of the crude material with hexane removed most of the more soluble iminooxadiazoline. The hexane insoluble residue was then chromatographed (Chromatoton, 2-mm silica plate) using ether (20%) in hexane to afford starting material followed by **4***q* (the minor β-lactam) and by **4***p*.

trans-*1,7,8-Triaza-3-methoxy-6,6-dimethyl-5-oxa-2-oxo-1-phenylspiro[3.4] oct-7-ene,* **4**p

White solid, 18% yield; mp 70°C; IR (KBr) *v*: 1782 (C=O), 1592 (N=N) cm^{-1}; ^1H NMR (200 MHz, $CDCl_3$) δ: 1.54 (s, 3H), 1.62 (s, 3H), 3.63 (s, 3H), 4.79 (s, 1H), 7.17–7.32 (m, 5H); ^{13}C NMR (50.3 MHz, $CDCl_3$) δ: 23.57, 24.55, 58.76, 91.65 (C3), 121.72 (C6), 122.45 (C4), 120.64, 126.66, 129.11 (3 CH, aryl), 133.59 (N-C1, aryl), 162.99 (CO); MS (ei) *m/z*: 147 (41%), 132 (13%), 104 (55%), 77 (100%); MS (ci, NH_3) *m/z*: 262 (M^+ + H, 2%), 234 (11%), 148 (100%), 94 (10%).

cis-*1,7,8-Triaza-3-methoxy-6,6-dimethyl-5-oxa-2-oxo-1-phenylspiro[3.4]oct-7-ene,* **4**q

Colourless, viscous oil, ca. 2% yield; IR (film) *v*: 1780 (C=O) cm^{-1}; ^1H NMR (200 MHz, $CDCl_3$) δ: 1.56 (s, 3H), 1.66 (s, 3H), 3.68 (s, 3H), 5.05 (s, 1H), 7.19–7.34 (m, 5H); ^{13}C NMR (50.3 MHz, $CDCl_3$) δ: 23.84, 25.14, 58.47, 87.59 (C3), 114.39 (C6), 121.92 (C4), 120.30, 126.68, 129.29 (3 CH, aryl), 133.99 (N-C1, aryl), 163.78 (CO); MS (ei) *m/z*: 147 (43%), 132 (12%), 104 (57%), 77 (100%); MS (ci, NH_3) *m/z*: 262 (M^+ + H, 5%), 234 (9%), 148 (100%), 94 (10%).

Isomerization of **4**g *to* cis-*1,7,8-triaza-6,6-dimethyl-5-oxa-2-oxo-1-phenyl-3-phenoxyspiro[3.4]oct-7-ene,* **4**h

Treatment of **4***g* (1.3 mmol) with tetra-*n*-butylammonium fluoride (2 mmol) in anhydrous THF (2 mL) at room temperature for 5 h was followed by evaporation of the solvent, addition of CH_2Cl_2 (4 mL) and 0.1 M HCl (2 mL). The aqueous layer was extracted three more times with CH_2Cl_2. The combined organic extract was washed with aqueous bicarbonate and with brine before being dried over $MgSO_4$. Evaporation of the solvent left **4***h* as a viscous yellow oil; IR (film) *v*: 1785 (C=O), 1595 (N=N) cm^{-1}; ^1H NMR (200 MHz, $CDCl_3$) δ: 1.38 (s, 3H), 1.56 (s, 3H), 5.79 (s, 1H) 6.96–7.40 (m, 10H); ^{13}C NMR (50.3 MHz, $CDCl_3$) δ: 24.08, 24.35, 84.20 (C3), 122.37 (C6), 122.57 (C4), 115.50, 121.14. 123.00, 127.14, 129.36, 129.75 (6 CH, aryl), 133.51 (N-C1, aryl) 156.75 (OC1, aryl), 162.48 (CO); MS (ei) *m/z*: 209 (95%), 180 (100%), 132 (18%), 105 (33%), 77 (34%); MS (ci, NH_3) *m/z*: 341 (($M + NH_4$)$^+$, 50%), 326 (7%), 308 (11%), 210 (100%), 180 (32%), 118 (11%).

Synthesis of **4**m *and* **4**n *by methylation of* **4**g

The procedure used is based on that reported by Durst et al. (19). A solution of LDA in THF was prepared as follows. A dry 25-mL round-bottom flask, equipped with a magnetic stirring bar, was flushed with dry N_2 through a septum. Dry THF (9 mL) was introduced from a syringe followed by dry diisopropylamine (2.3 mmol, 0.32 mL). The flask was cooled with ice and *n*-butyllithium (2.3 mmol, as a solution in hexane[7]) was added drop by drop from a syringe. That solution was used after 15 min following completion of the addition.

The solution of LDA (2.3 mmol, calcd.) was added, *via cannula*, to a stirring solution of β-lactam oxadiazoline **4***g* (2 mmol) in dry THF (125 mL) at −78°C. The colour changed from yellow to orange and, after 10 min, to red. After 15 min iodomethane (0.85 g, 6 mmol) was added and the resulting mixture was stirred, at −78°C and under dry N_2, for 2 h before it was allowed to warm to room temperature over a period of 3 h. Dilute HCl (100 mL of 10%) was added followed by extraction (3×) with methylene chloride. The combined organic layer was washed with brine and dried over $MgSO_4$. Evaporation of the solvent left a brown slurry that was chromatographed (Chromatotron, 2-mm silica plate) with ether (25%) in hexane. The first fraction was **4***m*, followed by **4***n* and by starting material (**4***g*) in 12% yield.

trans-*1,7,8-Triaza-3,6,6-trimethyl-5-oxa-2-oxo-3-phenoxy-1-phenylspiro[3.4]oct-7-ene,* **4**m

Thick yellow oil, 3.4% yield; IR (film) *v*: 1777 (C=O) cm^{-1}; ^1H NMR (200 MHz, $CDCl_3$) δ: 1.62 (s, 3H), 1.70 (s, 3H), 1.73

[7]Concentration determined by titration with diphenylacetic acid.

(s, 3H), 7.05–7.37 (m, 10H); ^{13}C NMR (50.3 MHz, $CDCl_3$) δ: 15.53, 23.58, 25.44, 92.86 (C3), 121.94 (C6), 123.66 (C4), 120.19, 120.46, 126.58, 129.25, 129.33 (5 CH, aryl), 134.12 (N-C1, aryl), 154.35 (O-C1, aryl), 165.55 (CO); MS (ei) *m/z*: 309 ($M^+ - N_2$, trace), 223 (32%), 180 (58%), 149 (11%), 130 (10%), 105 (48%), 77 (100%); MS (ci, NH_3) *m/z*: 310 ($M^+ - N_2 + H$, 3%), 224 (100%), 180 (12%), 147 (5%), 94 (6%).

cis-*1,7,8-Triaza-3,6,6-trimethyl-5-oxa-2-oxo-3-phenoxy-1-phenylspiro[3.4]-oct-7-ene*, ***4n***

Yellow oil, 26% yield; IR (film) *v*: 1780 (C=O), 1595 (N=N) cm^{-1}; ^{1}H NMR (200 MHz, $CDCl_3$) δ: 1.56 (s, 3H), 1.59 (s, 3H), 1.67 (s, 3H), 7.04–7.33 (m, 10H); ^{13}C NMR (50.3 MHz, $CDCl_3$) δ: 15.77, 23.36, 25.05, 93.50 (C3), 122.04 (C6), 123.73 (C4), 120.38, 120.82, 123.44, 126.70, 129.05, 129.09 (6 CH, aryl), 133.51 (N-C1, aryl), 154.11 (O-C1, aryl), 165.33 (CO); MS (ei) *m/z*: 224 (20%), 180 (30%), 130 (10%), 105 (28%), 88 (11%), 86 (63%), 84 (100%), 77 (49%); MS (ci, NH_3) *m/z*: 355 ($(M + NH_4)^+$, 2%), 310 ($M^+ - N_2$, 16%), 224 (100%), 210 (11%), 180 (10%), 147 (12%), 105 (6%).

Acknowledgements

Financial assistance from the Natural Sciences and Engineering Research Council of Canada (NSERC) is gratefully acknowledged.

1. H. Staudinger. Liebigs Ann. Chem. **51**, 356 (1907).
2. (*a*) L.S. Hegedus, J. Montgomery, Y. Narukawa, and D.C. Shustad. J. Am. Chem. Soc. **113**, 5784 (1991); (*b*) R.D.G. Cooper, B.W. Daugherty, and D.B. Boyd. Pure Appl. Chem. **59**, 485 (1987).
3. (*a*) D.E. Davis and R.C. Storr. *In* Comprehensive heterocyclic chemistry. Vol. 7. *Edited by* W. Lwowski. Pergamon Press, Oxford. 1984. p. 237; (*b*) G.A. Koppel. *In* Heterocyclic compounds. *Edited by* A. Hassner. Wiley–Interscience, New York. 1983. p. 219.
4. K.S. Holden. *In* Chemistry and biology of β-laactam antibiotics. Vol. 2. *Edited by* R.B. Morin and M. Gorman. Academic Press, New York. 1982. p. 99.
5. (*a*) M. Békhazi and J. Warkentin. J. Am. Chem. Soc. **105**, 1289 (1983); (*b*) Can. J. Chem. **61**, 619 (1983); (*c*) M. Békhazi, P.A. Risbood, and J. Warkentin. J. Am. Chem. Soc. **105**, 5675 (1983); (*d*) D. Keus, M. Kaminski, and J. Warkentin. J. Org. Chem. **49**, 493 (1984).
6. M. Zoghbi and J. Warkentin, J. Org. Chem. **56**, 3214 (1991).
7. (*a*) A.R. Katritzky, H.M. Faid-Allah, H. Aghabozorg, and G.J. Palenik. Chem. Scri. **23**, 123 (1984); (*b*) A.M. Cameron, P.R. West, and J. Warkentin. J. Org. Chem. **34**, 3230 (1969); (*c*) S.L. Lee, G.B. Gubelt, A.M. Cameron, and J. Warkentin. Chem. Commun. 1074 (1970); (*d*) S.L. Lee, A.M. Cameron, and J. Warkentin. Can. J. Chem. **50**, 2326 (1972).
8. (*a*) A. Prakash, C. Calvo, A.M. Cameron, and J. Warkentin. J. Cryst. Mol. Struct. **3**, 71 (1973); (*b*) R. Faggiani, M. Kaminski, C.J.L. Lock, and J. Warkentin. Can. J. Chem. **65**, 1154 (1987).
9. F. Duran and L. Ghosez. Tetrahedron Lett. 2633 (1974).
10. (*a*) M. Cardellini, F. Claudi, and F.M. Morracci. Synthesis, 1070 (1984); (*b*) I. Antonini, M. Cardellini, F. Claudi, and F.M. Morracci. Synthesis, 379 (1986).
11. J. March. Advanced organic chemistry. 4th ed. Wiley–Interscience, New York. p. 280.
12. P. Knittel, S.L. Lee, and J. Warkentin. Can. J. Chem. **50**, 3248 (1972).
13. (*a*) M. Zoghbi and J. Warkentin. Can. J. Chem. 71, 907 (1993); (*b*) A.P. Hitchcock, S. Zweep, T. Steel, M. Békhazi, and J. Warkentin. Can. J. Chem. **60**, 2914 (1982).
14. W. Borsche. Chem. Ber. **38**, 831 (1905).
15. C. Vogelsang. Recl. Trav. Chim. Pays-Bas, **62**, 5 (1943).
16. A. Bertho and J. Maier. Liebigs Ann. Chem. **498**, 52 (1932).
17. P. Knittel. Ph.D. Thesis, McMaster University, 1975.
18. E.C. Taylor, A. McKillop, and G.H. Hawks. Org. Synth. Coll. Vol. 6. *Edited by* W.E. Noland. Wiley, New York. 1988. p. 549.
19. T. Durst, M.K. Sharma, E.J. Gabe, and F.L. Lee. J. Org. Chem. **55**, 5525 (1990).

Can. J. Chem. Downloaded from www.nrcresearchpress.com by 213.200.69.106 on 09/08/12
For personal use only.

Structural studies of organoboron compounds LVIII.[1] 4-(1′-azoniabicyclo[2.2.2]-octanyl)-2,2-diphenyl-2-borata-1,3-dioxa-1,2,3,4-tetrahydronaphthalene

WOLFGANG KLIEGEL AND KLAUS DRÜCKLER

Institut für Pharmazeutische Chemie der Technischen Universität Braunschweig, Beethovenstrasse 55, 3300 Braunschweig, Germany

AND

STEVEN J. RETTIG AND JAMES TROTTER[2]

Department of Chemistry, University of British Columbia, 2036 Main Mall, Vancouver, B.C., Canada V6T 1Z1

Received November 24, 1992

WOLFGANG KLIEGEL, KLAUS DRÜCKLER, STEVEN J. RETTIG, and JAMES TROTTER. Can. J. Chem. **71**, 919 (1993).

Two synthetic routes leading to 4-(1′-azoniabicyclo[2.2.2]octanyl)-2,2-diphenyl-2-borata-1,3-dioxa-1,2,3,4-tetrahydronaphthalene, **5**, are described. Crystals of the product are orthorhombic, a = 18.099(2), b = 9.729(2), c = 12.113(2) Å, Z = 4, space group $Pca2_1$. The structure was solved by direct methods and was refined by full-matrix least-squares procedures to R = 0.034 and R_w = 0.037 for 1421 reflections with $I \geq 3\sigma(F^2)$. Compound **5** represents the first structurally characterized crystalline adduct of a trialkylamine to a carbonyl compound in which the newly formed C—N bond is acyclic. The adduct is stabilized by the neighboring Lewis acid diphenylboryloxyaryl moiety. Bond distances involving the boron atom ((aryl)O—B = 1.515(4), (alkyl)O—B = 1.508(4), and C(phenyl)—B = 1.613(5) and 1.623(5) Å) represent relatively strong overall binding of the *O,O*-chelating ligand to the diphenylboron moiety.

WOLFGANG KLIEGEL, KLAUS DRÜCKLER, STEVEN J. RETTIG et JAMES TROTTER. Can. J. Chem. **71**, 919 (1993).

On décrit deux voies de synthèse du 4-(1′-azoniabicyclo[2.2.2]octanyl)-2,2-diphényl-2-borata-1,3-dioxa-1,2,3,4-tétrahydronaphtalène (**5**) dont les cristaux sont orthorhombiques, groupe d'espace $Pca2_1$, avec a = 18,099(2), b = 9,729(2) et c = 12,113(2) Å et Z = 4. On a résolu la structure par des méthodes directes et on l'a affinée par la méthodes des moindres carrés (matrice complète) jusqu'à des valeurs de R = 0,034 et R_w = 0,037 pour 1421 réflexions avec $I \geq 3\sigma(F^2)$. Le composé **5** est le premier adduit cristallin d'une trialkylamine et d'un composé carbonylé avec liaison C—N acyclique à être caractérisé. L'adduit est stabilisé par la portion acide de Lewis diphénylboryloxyaryle adjacente. Les longueurs des liaisons impliquant le bore ((aryl)O—B = 1,515(4), (alkyl)O—B = 1,508(4) et C(phényl)—B = 1,613(5) et 1,623(5) Å) correspondent à des liaisons globales relativement fortes du ligand *O,O*-coordinant avec la portion diphénylbore.

[Traduit par la rédaction]

Introduction

The reaction product of salicylaldehyde **1** and the anhydride of diphenylborinic acid has been described in the literature (1) as an intramolecular O→B coordinated 2-diphenylboryloxybenzaldehyde **2**. The chelate structure **2** was established by an X-ray crystallographic analysis (2). It was of great interest to us to determine whether a strong nucleophile like a tertiary amine could compete with the carbonyl group as a Lewis base, breaking the chelate ring to form an open-chain N→B adduct **3**, or if the electron withdrawal from the carbonyl carbon atom would allow the addition of the nucleophile R_3N to the carbonyl group to give the zwitterionic adduct **5**. A similar structure, **6**, has been postulated for an intermediate borate complex in a reversible reaction during the boronic acid-catalyzed hydrolysis of an *N*-salicylidene amino acid (3). The importance of zwitterionic intermediates in the understanding of catalytic reactions in general (4) and enzyme-catalyzed reactions (3, 4) in particular, as well as our interest in the structure and function of stable *B,N*-betaines (5, 6), has motivated us to establish unambiguously the structure **5**. The nucleophilic addition of the amine at the carbonyl group to form the *O,N*-acetal moiety in **5** resembles the addition of a hydroxylamine at the salicylaldehyde carbonyl group leading to the product **7**, the structure of which has been established by an X-ray crystallographic analysis (7). Moreover, a complex like **5** would represent a stabilized derivative of the labile zwitterionic primary adduct **4** of an amine to salicylaldehyde. Such an adduct, **4**, corresponds directly to the proposed (8) mode of interaction between (tertiary) amines and the enol tautomers of β-dicarbonyl compounds, the latter being functionally related to salicylaldehyde.

Quinuclidine (1-azabicyclo[2.2.2]octane) was chosen as a suitable trialkylamine having a relatively low degree of steric hindrance and was reacted both directly with the diphenylboron chelate **2** and in an alternative three-component condensation with salicylaldehyde **1** and oxybis(diphenylborane). The latter reaction could involve either **2** or **4** as an intermediate. Both reactions produced colorless crystals having the same melting point and identical infrared spectra. The absence of a C=O absorption in the solid state (KBr pellet) infrared spectrum and the elemental composition strongly support the expected structure **5**. The ^{1}H nmr spectrum (DMSO-d_6 solution), however, shows two separate signals for the aldehyde methine proton, one at δ = 5.72 ppm (typical for an N—CH—O acetal grouping) and another one at 10.25 ppm (typical for an aldehyde (CH=O group), the two peaks comprising 88% and 12%, respectively, of the total peak area. A rearrangement by intramolecular exchange of the Lewis bases at the diphenylboryloxy moiety (**5** ⇔ **3**) does not seem very likely since the ^{1}H nmr spectrum also displays a peak corresponding to a phenolic OH proton at 10.94 ppm with 12% of the total peak area for one proton. This would indicate a partial hydrolysis (by solvent water) resulting in the liberation of salicylaldehyde **1**. An X-ray crystallographic analysis was undertaken in order to establish the structure of the crystalline addition product.

[1]Previous paper in this series: ref. 19.

[2]Author to whom correspondence may be addressed.

Can. J. Chem. Downloaded from www.nrcresearchpress.com by 213.200.69.106 on 09/08/12
For personal use only.

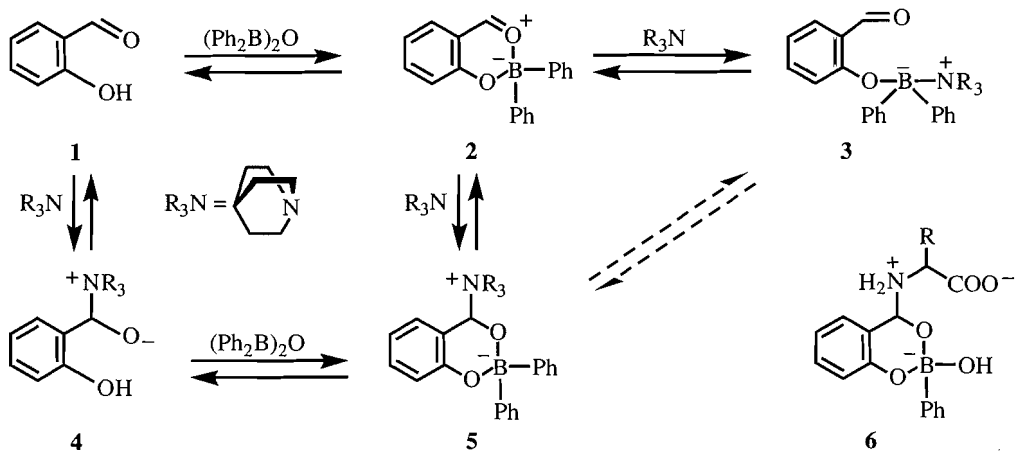

TABLE 1. Final atomic coordinates (fractional) and B_{eq} (Å^2)[a]

Atom	x	y	z	B_{eq}
O(1)	0.1960(1)	0.6962(2)	0.3425	4.0(1)
O(2)	0.1627(1)	0.6053(2)	0.1609(3)	4.0(1)
N(1)	0.2729(1)	0.4817(3)	0.1251(3)	3.9(1)
C(1)	0.2572(2)	0.7560(3)	0.2997(4)	4.1(2)
C(2)	0.2985(2)	0.8471(4)	0.3639(4)	5.1(2)
C(3)	0.3575(2)	0.9155(4)	0.3154(6)	6.4(3)
C(4)	0.3739(2)	0.8962(5)	0.2052(6)	6.7(3)
C(5)	0.3343(2)	0.8053(4)	0.1433(4)	5.6(2)
C(6)	0.2762(2)	0.7309(4)	0.1908(4)	4.3(2)
C(7)	0.2330(2)	0.6272(3)	0.1251(4)	4.2(2)
C(8)	0.2779(2)	0.4220(4)	0.2379(4)	4.6(2)
C(9)	0.3108(3)	0.2778(4)	0.2329(5)	7.2(3)
C(10)	0.3319(2)	0.2421(4)	0.1162(5)	5.7(2)
C(11)	0.3858(2)	0.3495(5)	0.0762(5)	7.6(3)
C(12)	0.3494(2)	0.4914(4)	0.0780(4)	6.1(2)
C(13)	0.2284(2)	0.3878(4)	0.0535(4)	5.5(2)
C(14)	0.2639(3)	0.2444(4)	0.0455(5)	6.7(3)
C(15)	0.1108(2)	0.8408(4)	0.2202(4)	4.0(2)
C(16)	0.0782(2)	0.8655(4)	0.1187(4)	5.4(2)
C(17)	0.0551(3)	0.9963(6)	0.0871(5)	7.0(3)
C(18)	0.0642(3)	1.1047(5)	0.1574(6)	7.3(3)
C(19)	0.0959(2)	1.0840(4)	0.2596(6)	7.2(3)
C(20)	0.1184(2)	0.9543(4)	0.2894(4)	5.5(2)
C(21)	0.0661(2)	0.6042(3)	0.3116(3)	3.4(1)
C(22)	0.0432(2)	0.4754(4)	0.2765(4)	5.0(2)
C(23)	−0.0159(2)	0.4066(4)	0.3226(4)	5.6(2)
C(24)	−0.0539(2)	0.4626(5)	0.4082(4)	5.4(2)
C(25)	−0.0329(2)	0.5897(5)	0.4443(4)	6.0(2)
C(26)	0.0253(2)	0.6596(4)	0.3974(4)	5.0(2)
B(1)	0.1345(2)	0.6869(4)	0.2580(4)	3.6(2)

[a]$B_{eq} = (8/3)\pi^2\Sigma\Sigma U_{ij} a_i^* a_j^* (a_i \cdot a_j)$.

TABLE 2. Bond lengths (Å) with estimated standard deviations

Atom	Atom	Distance	Atom	Atom	Distance
O(1)	C(1)	1.355(4)	C(10)	C(14)	1.500(6)
O(1)	B(1)	1.515(4)	C(11)	C(12)	1.530(5)
O(2)	C(7)	1.362(4)	C(13)	C(14)	1.540(5)
O(2)	B(1)	1.508(4)	C(15)	C(16)	1.385(5)
N(1)	C(1)	1.590(4)	C(15)	C(20)	1.393(5)
N(1)	C(8)	1.488(4)	C(15)	B(1)	1.623(5)
N(1)	C(12)	1.501(4)	C(16)	C(17)	1.394(6)
N(1)	C(13)	1.495(5)	C(17)	C(18)	1.366(8)
C(1)	C(2)	1.395(5)	C(18)	C(19)	1.380(8)
C(1)	C(6)	1.385(6)	C(19)	C(20)	1.374(6)
C(2)	C(3)	1.390(6)	C(21)	C(22)	1.387(5)
C(3)	C(4)	1.380(7)	C(21)	C(26)	1.384(5)
C(4)	C(5)	1.364(7)	C(21)	B(1)	1.613(5)
C(5)	C(6)	1.399(5)	C(22)	C(23)	1.380(5)
C(6)	C(7)	1.504(5)	C(23)	C(24)	1.357(6)
C(8)	C(9)	1.525(5)	C(24)	C(25)	1.366(5)
C(9)	C(10)	1.505(7)	C(25)	C(26)	1.377(5)
C(10)	C(11)	1.509(6)			

Experimental

4-(1'-Azoniabicyclo[2.2.2]octanyl)-2,2-diphenyl-2-borata-1,3-dioxa-1,2,3,4-tetrahydronaphthalene, 5 (R_3N = quinuclidine)

Method A

2-Diphenylboryloxybenzaldehyde[3] (1) (0.57 g, 2 mmol) is dissolved in 150 mL of dry diethyl ether, heating slightly. After the addition of a solution of quinuclidine (0.22 g, 2 mmol) in 10 mL of diethyl ether, crystallization starts spontaneously. One hour later the crystalline precipitate is filtered off and washed with diethyl ether. Yield: 0.67 g (85%). The same procedure, using absolute benzene (50 mL and 5 mL, respectively) as reaction medium yields 0.61 g (77%).

Method B

Oxybis(diphenylborane) (0.87 g, 2.5 mmol) is dissolved in 30 mL of absolute benzene and mixed with a solution of quinuclidine (0.56 g, 5 mmol) in 10 mL of absolute benzene with stirring. Turbidity develops, but disappears after the addition of salicylaldehyde (0.61 g, 5 mmol). After 1 h crystallization commences and is complete after about 6 h at room temperature. The crystals are filtered off and washed with diethyl ether. The colorless needles are analytically pure. Yield: 1.73 g (87%); mp 184–185°C (dec.).

Infrared (KBr): 1605, 1580 cm^{-1}. ^{1}H nmr (DMSO-d_6/TMS) δ (ppm): 1.51–1.98 (m, H—C(CH$_2$)$_3$), 2.96–3.23 (m, N(CH$_2$)$_3$), 5.72 (s, 88% of 1H, N—CH—O), 6.62–7.70 (m, 14 aromatic H), 10.25 (s, 12% of 1H, CH=O), 10.94 (s, 12% of 1H, OH). Anal. calcd. for $C_{26}H_{28}BNO_2$: C 78.60, H 7.10, B 2.72, N 3.53; found: C 78.56, H 7.16, B 2.75, N 3.47%. Crystals suitable for X-ray analysis were selected from the batch of crystals obtained from the benzene solution method B).

X-ray crystallographic analysis of 5 (R_3N = quinuclidine)

A crystal ca. 0.05 × 0.10 × 0.35 mm is size was mounted on a glass fiber. Unit-cell parameters were refined by least squares on

[3]Alternative nomenclature: (salicylaldehydato)diphenylboron (2); or systematically: 2,2-diphenyl-2-borata-1,3-dioxa-1,2-dihydronaphthalene.

Can. J. Chem. Downloaded from www.nrcresearchpress.com by 213.200.69.106 on 09/08/12
For personal use only.

TABLE 3. Bond angles (deg) with estimated standard deviations

Atom	Atom	Atom	Angle	Atom	Atom	Atom	Angle
C(1)	O(1)	B(1)	111.6(3)	C(10)	C(11)	C(12)	110.0(3)
C(7)	O(2)	B(1)	118.8(3)	N(1)	C(12)	C(11)	110.2(3)
C(7)	N(1)	C(8)	112.1(3)	N(1)	C(13)	C(14)	111.4(3)
C(7)	N(1)	C(12)	111.3(3)	C(10)	C(14)	C(13)	108.7(4)
C(7)	N(1)	C(13)	107.4(3)	C(16)	C(15)	C(20)	116.0(4)
C(8)	N(1)	C(12)	108.5(3)	C(16)	C(15)	B(1)	121.5(3)
C(8)	N(1)	C(13)	109.1(3)	C(20)	C(15)	B(1)	122.4(3)
C(12)	N(1)	C(13)	108.4(3)	C(15)	C(16)	C(17)	122.0(4)
O(1)	C(1)	C(2)	119.8(4)	C(16)	C(17)	C(18)	119.8(5)
O(1)	C(1)	C(6)	119.5(3)	C(17)	C(18)	C(19)	119.8(4)
C(2)	C(1)	C(6)	120.6(3)	C(18)	C(19)	C(20)	119.5(5)
C(1)	C(2)	C(3)	118.7(5)	C(15)	C(20)	C(19)	122.8(5)
C(2)	C(3)	C(4)	120.6(4)	C(22)	C(21)	C(26)	115.0(3)
C(3)	C(4)	C(5)	120.4(4)	C(22)	C(21)	B(1)	123.9(3)
C(4)	C(5)	C(6)	120.3(5)	C(26)	C(21)	B(1)	121.1(3)
C(1)	C(6)	C(5)	119.1(4)	C(21)	C(22)	C(23)	123.1(4)
C(1)	C(6)	C(7)	119.5(3)	C(22)	C(23)	C(24)	120.5(3)
C(5)	C(6)	C(7)	121.3(4)	C(23)	C(24)	C(25)	117.9(4)
O(2)	C(7)	N(1)	106.6(2)	C(24)	C(25)	C(26)	121.9(4)
O(2)	C(7)	C(6)	115.0(3)	C(21)	C(26)	C(25)	121.7(4)
N(1)	C(7)	C(6)	111.2(3)	O(1)	B(1)	O(2)	108.0(3)
N(1)	C(8)	C(9)	110.2(3)	O(1)	B(1)	C(15)	109.3(3)
C(8)	C(9)	C(10)	110.4(3)	O(1)	B(1)	C(21)	108.7(3)
C(9)	C(10)	C(11)	107.8(4)	O(2)	B(1)	C(15)	110.8(3)
C(9)	C(10)	C(14)	108.9(4)	O(2)	B(1)	C(21)	108.1(3)
C(11)	C(10)	C(14)	109.7(4)	C(15)	B(1)	C(21)	111.8(3)

TABLE 4. Intra-annular torsion angles (deg) with estimated standard deviations in parentheses

Atoms	Value (deg)
O(2)—B(1)—O(1)—C(1)	58.5(3)
B(1)—O(1)—C(1)—C(6)	−36.3(4)
O(1)—C(1)—C(6)—C(7)	−5.9(5)
C(1)—C(6)—C(7)—O(2)	24.7(4)
C(6)—C(7)—O(2)—B(1)	1.6(4)
C(7)—O(2)—B(1)—O(1)	−40.9(4)

setting angles for 25 reflections (2θ = 37.2–64.7°) measured on a diffractometer with Cu-K_α radiation (λ = 1.54178 Å). Crystal data at 21°C are as follows:

$C_{26}H_{28}BNO_2$ f.w. = 397.32

Orthorhombic, a = 18.099(2), b = 9.729(2), c = 12.113(2) Å, V = 2132.7(5) Å^3, Z = 4, ρ_c = 1.237 Mg m^{-3}, $F(000)$ = 848, μ(Cu-K_α) = 5.62 cm^{-1}. Absent reflections: $0kl$, l odd, and $h0l$, h odd, space group $Pca2_1$ (No. 29) from structure analysis.

Intensities were measured with graphite-monochromated Cu-K_α radiation on a Rigaku AFC6S diffractometer. An ω–2θ scan at 32° min^{-1} over a range of (0.94 + 0.20 tan θ)° in ω (with up to 8 rescans, background/scan time ratio = 0.5) was employed. Data were measured to 2θ = 155°. The intensities of three check reflections, measured every 200 reflections throughout the data collection, showed only small random variations. After data reduction,[4] decay and empirical absorption corrections (based on azimuthal scans for three reflections) were applied. Transmission factors range from 0.96 to 1.00. Intensities were measured for 2305 independent reflections of which 1421 had intensities greater than or equal to $3\sigma(F^2)$ above background where $\sigma^2(F^2) = [S^2(C + 4B) + (0.02F^2)^2]/\mathrm{Lp}^2$ (S = scan speed, C = scan count, B = total background count, and Lp = Lorentz-polarization factor) and were employed in the solution and refinement of the structure.

The systematic absences are consistent with the space groups $Pcam$ and $Pca2_1$. The structure was solved by direct methods, the analysis being initiated (and successfully completed) in the non-centrosymmetric space group $Pca2_1$ on the basis of the E-statistics and structural considerations. With four molecules in the unit cell, an ordered structure in the centrosymmetric space group $Pcam$ is ruled out since the molecule cannot possess mirror symmetry. The non-hydrogen atoms were refined with anisotropic thermal parameters and the hydrogen atoms were fixed in calculated positions (C—H = 0.98 Å, $B_H = 1.2B_{\text{bonded atom}}$). A correction for secondary extinction was applied, the final value of the extinction coefficient being 2.42 × 10^{-6}. Scattering factors for all atoms and anomalous dispersion corrections for the non-hydrogen atoms were taken from ref. 9. The weighting scheme $w = 4F_o^2/\sigma^2(F_o^2)$ gave uniform average values of $w(|F_o| - |F_c|)^2$ over ranges of both $|F_o|$ and sin θ/λ and was employed in the final stages of full-matrix least-squares refinement of 271 variables. Reflections with $I < 3\sigma(F^2)$ were not included in the refinement. Convergence was reached at R = 0.034 and R_w = 0.037 for 1421 reflections with $I \geq 3\sigma(F^2)$. Possible minor librational disorder of the C(15)—C(20) phenyl ring and minor rotational disordering of the quinuclidine moiety about the C(7)—N(1) bond or conformational flipping of the N(1)—C—C—C(10) fragment is noted. No attempt was made to model this minor disorder, but metrical parameters involving these regions of the molecule may be affected. A parallel refinement of the structure having the opposite polarity resulted in slightly higher residuals, the R and R_w ratios being 1.006 and 1.003, respectively. The function minimized was $\Sigma w(|F_o| - |F_c|)^2$, $R = \Sigma||F_o| - |F_c||/\Sigma|F_o|$, $R_w = (\Sigma w(|F_o| - |F_c|)^2/\Sigma w|F_o|^2)^{1/2}$.

[4] TEXSAN/TEXRAY structure analysis package, which includes versions of the following: MITHRIL, integrated direct methods, by C.J. Gilmore; DIRDIF, direct methods for difference structures, by P.T. Beurskens; ORFLS, full-matrix least squares, and ORFFE, function and errors, by W.R. Busing, K.O. Martin, and H.A. Levy, ORTEP II, illustrations, by C.K. Johnson.

Can. J. Chem. Downloaded from www.nrcresearchpress.com by 213.200.69.106 on 09/08/12
For personal use only.

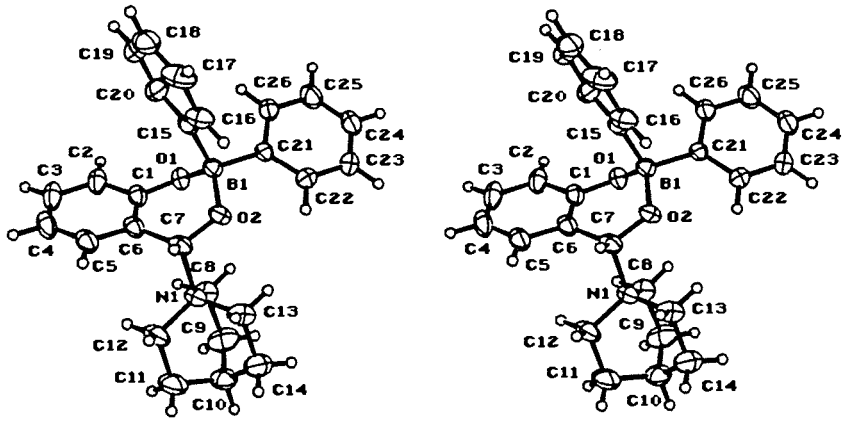

FIG. 1. Stereoview of **5** (R_3N = quinuclidine); 33% probability thermal ellipsoids are shown for the non-hydrogen atoms.

On the final cycle of refinement the maximum parameter shift corresponded to 0.01σ. The mean error in an observation of unit weight was 1.55. The final difference map showed maximum fluctuations of -0.10 to $+0.11$ e Å^{-3}. The final positional and (equivalent) isotropic thermal parameters for the non-hydrogen atoms appear in Table 1. Bond lengths, bond angles, and intra-annular torsion angles are given in Tables 2–4, respectively. Hydrogen atom parameters, anisotropic thermal parameters, torsion angles, intermolecular contacts, least-squares planes, and structure factors have been deposited.[5]

Results and discussion

The X-ray analysis confirms structure **5** for the crystalline compound. This is, to the best of our knowledge, the first structurally characterized crystalline open-chain[6] adduct of a trialkylamine to a carbonyl compound, stabilized by the neighboring Lewis acid diphenylboryloxyaryl moiety. Open-chain adducts of pyridine to carbonyl compounds, stabilized by trifluoroborane, have been predicted and calculated (by semi-empirical MNDO procedures) but could not be isolated (10). An $SbCl_5$-stabilized adduct of 4-*tert*-butylpyridine and 4-methoxybenzaldehyde, however, could be crystallized and has been characterized by an X-ray crystallographic analysis (10).

Stabilized adducts having the amine nitrogen inserted into a ring system along with the carbonyl carbon atom are already known and have been analyzed by single crystal X-ray analysis. Examples of this type of adduct include the phenylboronate-stabilized cyclic adduct **7** (7), the diphenylborinate-stabilized amine-aldehyde adducts like **8** (11), and others (6, 12, 13). The crystal structure of an intramolecular tertiary amine-aldehyde adduct **9**, stabilized by 3,5-dinitrobenzoic acid, has recently been published (14).

The carbonyl C=O double bond of salicylaldehyde **1** is lengthened to 1.261(4) Å in the diphenylborinate **2** and by an additional 0.1 Å in the quinuclidine adduct **5** (C(7)—O(2) = 1.362(4) Å). The C(7)—O(2) bond in **5**, however, still retains some double-bond character, the π-bond order being estimated at about 0.3 from plots of bond length vs. CO π-bond order (15). Similar carbonyl C=O bond lengths have been reported for the intramolecularly stabilized pyridine-formaldehyde adduct **8** (11) (1.363(4) Å) and for the cyclic intramolecular adduct **9** (14) (1.366(3) Å). The C—O bond in the *O,N*-acetal group of **7** (7) (1.378(2) Å) is significantly longer than that in **5**.

The N—C bond lengths in **5** and **7** follow the reverse of the trend noted for the C(7)—O bonds: that in **5** (N(1)—C(7) = 1.590(4) Å) is significantly longer than the corresponding bond in **7** (7) (1.565(2) Å) and marginally longer than the N—C bond of the *O,N*-acetal (semi-aminal) group of **9** (14) (1.581(4) Å). All of these N—C distances are unusually long, especially those in **5** and **9**, which exhibit N—C bond distances normally associated with sterically hindered systems such as the bulky substituted *O,N*-acetal moiety of the stabilized cyclic acetone adduct **10** (13) (1.584(3) Å). The

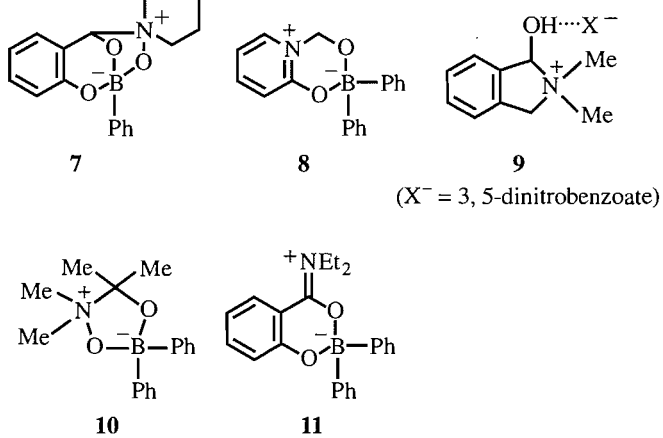

7 **8** **9**

(X^- = 3, 5-dinitrobenzoate)

10 **11**

relatively weak N(1)—C(7) bond in **5** could explain the solvolytic lability of the compound which can be observed in the solutions used for the nmr experiments (see above).

The increase of electron density at the carbonyl oxygen atom, caused by the addition of quinuclidine to salicylaldehyde **1** or to its diphenylboron complex **2**, is made evident by the shortening of the B—O(2) bond in **2** (1.569(4) Å) to 1.508(4) Å for the corresponding B(1)—O(2) bond in **5**.

[5]Supplementary material mentioned in the text may be purchased from: The Depository of Unpublished Data, Document Delivery, CISTI, National Research Council Canada, Ottawa, Canada K1A 0R6.

Tables of hydrogen atom coordinates and bond lengths and angles involving hydrogen atoms have also been deposited with the Cambridge Crystallographic Data Centre and can be obtained on request from The Director, Cambridge Crystallographic Data Centre, University Chemical Laboratory, 12 Union Road, Cambridge CB2 1EZ, U.K.

[6]In the sense that the newly formed C—N bond is acyclic.

Can. J. Chem. Downloaded from www.nrcresearchpress.com by 213.200.69.106 on 09/08/12
For personal use only.

The overall binding strength of the *O,O*-chelating ligand with respect to the diphenylboron moiety, defined as (mean C—B)/(mean O—B), ranges from 1.039 to 1.088 (mean 1.058) for "Ph_2BO_2" compounds having six-membered chelate rings (16). The value calculated for **5**, 1.070, represents relatively strong binding, while that for compound **2**, 1.044, indicates weak binding. In general, complexes of the diphenylborenium moiety, which behaves like a pseudo-metal cation, will undergo ligand exchange reactions if the difference in the overall binding strengths of the ligands is large enough. In view of the substantial difference between the binding parameters for **2** and **5**, it is not surprising that the latter can be synthesized directly from the salicylaldehyde complex.

The overall geometry of the molecule **5** displays a distorted "half-boat" arrangement of the six-membered boron chelate ring, with the fused benzene ring coplanar with the approximately planar O(1)—C(1)—C(6)—C(7) ring segment. The quinuclidine and one of the *B*-phenyl substituents are in axial positions. The axial B(1)—C(15) bond to the *B*-phenyl group (1.623(5) Å) is somewhat longer than the equatorial B(1)—C(21) bond (1.613(5) Å). Comparable differences between (pseudo-)axial and (pseudo-)equatorial B—C(aryl) bonds have been noted for a number of other diphenylboron chelates (17, 18, and references therein).

A *B,N*-betaine of type **5** can be considered, in a sense, as being a reduced form of the *B,N*-betaine **11**, both carrying the formal positive charge outside of the boron chelate ring in trialkyammonium and dialkyliminium groups, respectively. The structure of **11**, a diphenylboron chelate of *N,N*-diethylsalicylamide, has also been established by an X-ray crystallographic analysis (18). As can be expected from the different functionalities of the N—C—O moieties in the two compounds, the most drastic geometrical differences are found there: the N—C and C—O bonds in compound **11** both display partial double bond character and are thus substantially shorter than the corresponding bonds in **5**. The general geometry of the benzo-fused boron chelate rings is very similar in the two compounds.

The polar, but not chiral, crystal structure is built up from pairs of enantiomers (generated by the chiral carbon atom C(7) — the *S* isomer is depicted in Fig. 1). All intermolecular distances correspond to normal van der Waals interactions.

Acknowledgements

We thank the Natural Sciences and Engineering Research Council of Canada and the Fonds der Chemischen Industrie, Frankfurt am Main, for financial support.

1. (*a*) F. Umland and C. Schleyerbach. Angew. Chem. **77**, 426 (1965); (*b*) I. Bally, A. Arsene, M. Bacescu-Roman, and A.T. Balaban. Tetrahedron Lett. 3929 (1965).
2. S.J. Rettig and J. Trotter. Can. J. Chem. **54**, 1168 (1976).
3. G. Rao and M. Phillip. J. Org. Chem. **56**, 1505 (1991).
4. W.P. Jencks. Catalysis in chemistry and enzymology. McGraw–Hill, New York. 1969.
5. W. Kliegel. Organomet. Chem. Rev. Sect. A: **8**, 153 (1972).
6. W. Kliegel, S.J. Rettig, and J. Trotter. Can. J. Chem. **66**, 377 (1988).
7. W. Kliegel, H.-W. Motzkus, K. Drückler, S.J. Rettig, and J. Trotter. Can. J. Chem. **68,** 64 (1990).
8. (*a*) A. Gazit and Z. Rappoport. J. Chem. Soc. Perkin Trans. 1, 2863 (1984); (*b*) J. Emsley, N.J. Freeman, R.J. Parker, and R.E. Overill. J. Chem. Soc. Perkin Trans. 2, 1479 (1986).
9. International tables for X-ray crystallography. Vol. IV. Kynoch Press, Birmingham (present distributor: Kluwer Academic Publishers, Dordrecht, The Netherlands). 1974. pp. 99–102 and 149.
10. E. Anders, F. Markus, H. Meske, J. Tropsch, and G. Maas. Chem. Ber. **120,** 735 (1987).
11. W. Kliegel, H.-W. Motzkus, D. Nanninga, S.J. Rettig, and J. Trotter. Can. J. Chem. **64**, 507 (1986).
12. S.J. Rettig, J. Trotter, and W. Kliegel. Can. J. Chem. **52**, 2531 (1974).
13. W. Kliegel, H.-W. Motzkus, S.J. Rettig, and J. Trotter. Can. J. Chem. **62**, 838 (1984).
14. J.D. Carroll II, P.R. Jones, and R.G. Ball. J. Org. Chem. **56,** 4208 (1991).
15. G. Häfelinger. Chem. Ber. **103**, 2922 (1970).
16. W.R. Cullen, S.J. Rettig, J. Trotter, and E. B. Wickenheiser. Can. J. Chem. **66**, 2007 (1988), and references therein.
17. E. Ebeling, W. Kliegel, S.J. Rettig, and J. Trotter. Can. J. Chem. **67**, 933 (1989).
18. W. Kliegel, M. Tajerbashi, S.J. Rettig, and J. Trotter. Can. J. Chem. **67**, 1636 (1989).
19. E. Ahlenstiel, W. Kliegel, S.J. Rettig, and J. Trotter. Can. J. Chem. **71**, 263 (1993).

Can. J. Chem. Downloaded from www.nrcresearchpress.com by 213.200.69.106 on 09/08/12
For personal use only.

The volumetric and thermochemical properties of L-ascorbic acid in water at 288.15, 298.15, and 308.15 K

ANDREW W. HAKIN,[1] SUSAN A.M. MUDRACK, AND COLIN L. BESWICK
Department of Chemistry, University of Lethbridge, 4401 University Drive, Lethbridge, Alta., Canada T1K 3M4

Received November 30, 1992

ANDREW W. HAKIN, SUSAN A.M. MUDRACK, and COLIN L. BESWICK. Can. J. Chem. **71**, 925 (1993).

Measurements have been made at 288.15, 298.15, and 308.15 K with a flow microcalorimeter and densimeter to obtain heat capacities and densities for L-ascorbic acid and sodium chloride in water. These data are reported in terms of apparent molar volumes ($V_{\phi,2}$) and apparent molar heat capacities ($C_{p,\phi,2}$). The volume of ionization (ΔV^0) and heat capacity of ionization (ΔC_p^0) for the acid at 298.15 K have been calculated using a method that does not require volumetric and thermochemical data for the sodium salts of the acid. Details of our methodology are presented.

ANDREW W. HAKIN, SUSAN A.M. MUDRACK et COLIN L. BESWICK. Can. J. Chem. **71**, 925 (1993).

Dans le but de déterminer les capacités calorifiques et les densités de l'acide L-ascorbique et du chlorure de sodium dans l'eau, on a effectué des mesures à 288,15, à 298,15 et à 308,15 K à l'aide du microcalorimétre à écoulement et d'un densimètre. On rapporte ces données en fonction des volumes molaires apparents ($V_{\phi,2}$) et des capacités calorifiques molaires apparentes ($C_{p,\phi,2}$). Faisant appel à une méthode qui ne nécessite pas d'avoir des données volumétriques ou thermodynamiques pour les sels de sodium de l'acide, on a calculé le volume d'ionisation (ΔV^0) et la capacité calorifique d'ionisation (ΔC_p^0) de l'acide à 298,15 K. On présente de détails de notre méthodologie.

[Traduit par la rédaction]

Introduction

Equilibrium constants for ionization of most organic acids that are important in biochemistry, marine chemistry, and analytical chemistry are available. For some of these acids we also have values of the enthalpy of ionization, ΔH^0, (either from calorimetry or d ln K/dT) and thence values of the entropy of ionization, ΔS^0 (1–3). There are, however, relatively few ΔC_p^0 and ΔV^0 values for ionization of organic acids in aqueous solution (4).

The research described here was intended to provide ΔC_p^0 and ΔV^0 for ionization of L-ascorbic (vitamin C) at 298.15 K. Because of the ease of oxidation of aqueous solutions of the sodium salt of L-ascorbic acid we have also focussed on development and application of methodology that can minimize such chemical problems, with the expectation that our method will also be applicable to other aqueous acid systems.

Experimental

L-Ascorbic acid (99+%) was obtained from Aldrich Chemical Company. The purity of the compound was determined by titration with potassium bromate and was found to be greater than 99.5%. Sodium chloride 99.99% was obtained from Aldrich Chemical Company and was used without further purification. Samples of the acid and NaCl were dried and stored over phosphorus pentoxide in a vacuum oven set at 50°C. All solutions were prepared by weight with bi-distilled, degassed water. New solutions of the acid were prepared daily.

Densities were measured relative to water with a vibrating tube flow densimeter (5) (Sodev O2D). The densimeter is connected to a programmable circulating thermostat and has a working temperature range of 0–75°C with a thermal stability of ±0.001°C. This experimental apparatus routinely measures densities with part per million precision.

Calibration constants for the densimeter at 288.15, 298.15, and 308.15 K were calculated from the measured time periods of vibration and the densities of dry nitrogen gas and water (6). Calibration constants were determined prior to and following each series of experiments.

Volumetric heat capacities were measured relative to water using a Picker flow microcalorimeter (7). Automated data collection is achieved by interfacing one component of the system, a Hewlett–Packard HP-3456A digital voltmeter, via an IOtech Personal488 PC/IEEE 488 controller, to a 386SX 16-MHz IBM-clone computer. A BASIC program controls data collection and storage and directs data to a commercial data visualization package for interpretation and the calculation of volumetric heat capacities.

An inherent problem of Picker flow microcalorimeters is that they generally suffer from small heat leaks (8). These heat leaks are greatly reduced by evacuating the chamber that houses the calorimetric cells to a vacuum of approximately 1.5×10^{-6} mbar (1 bar = 100 kPa). A 1-in. stainless steel vacuum line incorporating a Leybold D4A backing pump and an Edwards EO 50/60 air-cooled diffusion pump was constructed for this purpose. The calorimeter was connected to the vacuum line with a Cajon O-ring fitting. Small residual heat leaks are easily corrected for by a heat loss correction factor (9). This factor is determined periodically by measuring the specific heat capacities of aqueous sodium chloride solutions at the temperature of interest.

Results and discussion

Apparent molar volumes, $V_{\phi,2}$, were calculated from measured density data using the equation

$$[1] \qquad V_{\phi,2} = \left[\frac{M}{\rho}\right] - \left[\frac{\rho - \rho_1^0}{m\,\rho\,\rho_1^0}\right]$$

where m is the molality of the solution, M is the molecular weight of the solute, ρ_1^0 is the density of pure water, and ρ is the density of the solution under study.

The specific heat capacities of our solutions were calculated using eq. [2]

$$[2] \qquad C_{p,\phi,2} = Mc_p + \frac{(c_p - c_{p,1}^0)}{m}$$

where c_p is the specific heat capacity of the solution, and $c_{p,1}^0$ is the specific heat capacity of pure water.

Estimated uncertainties in apparent molar volumes, $\delta V_{\phi,2}$

[1]Author to whom correspondence may be addressed.

Can. J. Chem. Downloaded from www.nrcresearchpress.com by 213.200.69.106 on 09/08/12
For personal use only.

Can. J. Chem. Downloaded from www.nrcresearchpress.com by 213.200.69.106 on 09/08/12
For personal use only.

TABLE 1. Comparison of experimental standard state volumes, V_2^0, and heat capacities, $C_{p,2}^0$, with literature data as a function of temperature for aqueous sodium chloride solutions

T (K)	V_2^0 (cm^3 mol^{-1})	$C_{p,2}^0$ (J K^{-1} mol^{-1})
288.15	15.69 15.60,[a] 15.58,[b] 15.62,[c] 15.55,[d] 15.63,[e], 15.43[f]	−108.85 −107.5[d]
298.15	16.62 16.62,[a] 16.62[b], 16.61,[c] 16.62,[d] 16.62,[e] 16.65[g]	−85.25 −84.3,[h] −84.6[i]
308.15	17.32 17.22,[a] 17.28,[b] 17.16,[c] 17.30[d]	−70.81 −66.4[d]

[a]Reference 13.
[b]Reference 14.
[c]Reference 15.
[d]Reference 16.
[e]Reference 17.
[f]Reference 18.
[g]Reference 19.
[h]Reference 20.
[i]Reference 21.

TABLE 2.(*a*) Densities, ρ, apparent molar volumes, $V_{\phi,2}$, and apparent molar heat capacities, $C_{p,\phi,2}$, of L-ascorbic acid in water at 288.15 K[a]

m (mol kg^{-1})	ρ (g cm^{-3})	$V_{\phi,2}$ (cm^3 mol^{-1})	$C_{p,\phi,2}$ (J K^{-1} mol^{-1})
0.0997	1.00616	104.67(0.05)	280.12
0.1713	1.01112	104.71(0.03)	287.98
0.2645	1.01746	104.81(0.02)	288.85
0.3679	1.02434	104.90(0.01)	291.08
0.5486	1.03598	105.06(0.01)	293.44
0.5892	1.03854	105.07(0.01)	294.90
0.7055	1.04575	105.13(0.01)	296.36
0.9257	1.05886	105.31(0.01)	298.29
0.1113	1.02854	104.58(0.04)	282.90
0.2263	1.03026	104.80(0.02)	284.96
0.3013	1.04156	104.80(0.02)	286.49
0.5093	1.06415	105.00(0.01)	292.29
0.6275	1.04095	105.05(0.01)	293.04
0.6722	1.04371	105.11(0.01)	293.29
0.7845	1.05054	105.18(0.00)	294.39
0.7462	1.04823	105.14(0.01)	294.18
1.0108	1.06384	105.29(0.01)	296.87

[a]Estimated uncertainties for $V_{\phi,2}$ appear in parentheses.

were calculated using the equation reported by Hedwig (10), eq. [3], and appear in parentheses in Tables 2*a*, *b*, and *c*.

$$[3] \qquad \delta V_{\phi,2} = -\left[M + \frac{1000}{m}\right]\frac{\delta\rho}{\rho^2}$$

The uncertainty in solution density, δρ, was estimated to be 5×10^{-6} g cm^{-3}. The utility of eq. [3] is limited since it assumes that contributions to $\delta V_{\phi,2}$ arising from uncertainties in solution concentrations are negligible. Uncertainties in calculated $C_{p,\phi,2}$ data arise primarily from two sources (11): errors in experimental molalities, and errors associated with the measurement of the displacements of the heat capacity curves. In agreement with ref. 11 we estimate the total errors observed in $C_{p,\phi,2}$ data to be in the range ±1–4 J K^{-1} mol^{-1} for solutions more concentrated than 0.03 mol kg^{-1} rising to ±9 J K^{-1} mol^{-1} for solutions with a molality of 0.01 mol kg^{-1}. Estimated uncertainties in $V_{\phi,2}$ and $C_{p,\phi,2}$ show large increases at low concentrations. This trend emphasizes the problems associated with the collection of $V_{\phi,2}$ and $C_{p,\phi,2}$ data at low concentrations.

Apparent molar properties of completely dissociated electrolytes are well represented by extended Debye–Hückel equations of the form

$$[4] \qquad Y_{\phi,2} = Y_2^0 + \omega A_Y I^{0.5} + B_Y I + C_Y I^{1.5}$$

where Y represents the extensive thermodynamic property of interest, Y_2^0 is the standard state (infinite dilution) property, I is the ionic strength, and ω is the valence factor. Debye–Hückel limiting slopes (A_Y) have been compiled for various temperatures by Ananthaswamy and Atkinson (12).

Densities and heat capacities of aqueous sodium chloride solutions, in the concentration range 0.050–1.000 mol kg^{-1}, were measured at 288.15, 298.15, and 308.15 K to assess the accuracy of our experimental apparatus and to evaluate the relevant heat loss correction factors for our calorimeter.

Standard state volumes and heat capacities for the sodium chloride solutions were calculated using a least-squares fit of the relevant version of eq. [4] to our experimental data. Table 1 compares our values of V_2^0 and $C_{p,2}^0$ to values reported in the literature (13–21).

The densities, apparent molar volumes, and apparent molar heat capacities of our aqueous L-ascorbic acid solutions at 288.15, 298.15, and 308.15 K are reported in Tables 2*a*, *b*, and *c*. Trends observed in $V_{\phi,2}$ and $C_{p,\phi,2}$ as a function of concentration are reported as Figs. 1 and 2, respectively.

The partial dissociation of L-ascorbic acid in aqueous solution prevents us from modelling our apparent molar data with either Debye–Hückel type or non-electrolyte type equations. Rather, we must develop a methodology for combining these two types of equations. The formalism described by Harned and Owen (22) provides a good starting point in this development.

To a first approximation the apparent molar volume of a partly dissociated acid in aqueous solution can be represented by eq. [5].

$$[5] \qquad V_{\phi,2} = \alpha V_{\phi,2,i} + (1 - \alpha)V_{\phi,2,u}$$

This equation defines two contributions to the observed apparent molar volumes of the aqueous acid solutions: one represents the ionic species present in solution, $V_{\phi,2,i}$; and the other the undissociated acid, $V_{\phi,2,u}$. α represents the degree of dissociation of the acid. The difference between the ionic and the undissociated acid contributions to the apparent molar volume, $\Delta V_{\phi,2}$, is defined by eq. [6].

$$[6] \qquad \Delta V_{\phi,2} = V_{\phi,2,i} - V_{\phi,2,u}$$

Using eq. [6], eq. [5] can be rewritten in the form

$$[7] \qquad V_{\phi,2,u} = V_{\phi,2} - \alpha\Delta V_{\phi,2}$$

When the standard state volumes for the ionic species, V_i^0, and the undissociated species, V_u^0, are used in eq. [6] the re-

TABLE 2.(*b*) Densities, ρ, apparent molar volumes, $V_{\phi,2}$, and apparent molar heat capacities, $C_{p,\phi,2}$, of L-ascorbic acid in water at 298.15 K[a]

m (mol kg^{-1})	ρ (g cm^{-3})	$V_{\phi,2}$ (cm^3 mol^{-1})	$C_{p,\phi,2}$ (J K^{-1} mol^{-1})
0.0302	0.99917	105.77(0.17)	—
0.0453	1.00022	105.79(0.11)	—
0.0645	1.00155	105.91(0.08)	—
0.0727	1.00212	105.93(0.07)	—
0.0878	1.00316	105.97(0.06)	—
0.1222	1.00551	106.08(0.04)	—
0.1506	1.00744	106.13(0.03)	—
0.1510	1.00744	106.30(0.03)	310.80
0.2636	1.01495	106.43(0.02)	312.32
0.3646	1.02153	106.49(0.01)	313.40
0.5074	1.03058	106.57(0.01)	313.97
0.7192	1.04350	106.70(0.01)	316.74
0.8557	1.05156	106.73(0.01)	317.47
0.9718	1.05818	106.82(0.01)	318.48
1.2313	1.07246	106.94(0.00)	319.45
1.4816	1.08563	106.99(0.00)	319.47
0.0138	0.99803	105.13(0.36)	307.98
0.0205	0.99849	105.42(0.25)	307.08
0.0262	0.99889	105.41(0.19)	308.37
0.0360	0.99958	105.58(0.14)	310.94
0.0589	1.00117	105.72(0.09)	307.05
0.0927	1.00351	105.79(0.05)	308.63
0.1271	1.00587	105.86(0.04)	311.06
0.1767	1.00924	105.95(0.03)	310.52

[a]Estimated uncertainties for $V_{\phi,2}$ appear in parentheses.

TABLE 2.(*c*) Densities, ρ, apparent molar volumes, $V_{\phi,2}$, and apparent molar heat capacities, $C_{p,\phi,2}$, of L-ascorbic acid in water at 308.15 K[a]

m (mol kg^{-1})	ρ (g cm^{-3})	$V_{\phi,2}$ (cm^3 mol^{-1})	$C_{p,\phi,2}$ (J K^{-1} mol^{-1})
0.1173	1.00204	107.24(0.04)	324.60
0.1608	1.00494	107.37(0.03)	328.31
0.2862	1.01317	107.45(0.02)	326.06
0.4463	1.02334	107.56(0.01)	328.99
0.6560	1.03615	107.64(0.01)	330.37
0.7950	1.04434	107.69(0.01)	331.29
0.6032	1.03299	107.61(0.01)	330.26
0.2199	1.00886	107.37(0.02)	325.20
1.0197	1.05710	107.76(0.00)	331.66
0.0379	0.99665	107.00(0.13)	—
0.0498	0.99747	107.00(0.10)	—
0.0536	0.99773	107.09(0.09)	—
0.0565	0.99792	107.11(0.09)	—
0.0716	0.99895	107.15(0.07)	—
0.0756	0.99923	107.14(0.07)	—
0.0813	0.99961	107.17(0.06)	—
0.0868	1.00000	107.15(0.06)	—
0.2485	1.01075	107.28(0.02)	—
0.2528	1.01103	107.29(0.02)	—
0.4780	1.02535	107.48(0.01)	—
0.5086	1.02724	107.50(0.01)	—
0.7164	1.03979	107.60(0.01)	—
0.7373	1.04099	107.64(0.01)	—
0.9033	1.05061	107.67(0.01)	—
1.0008	1.05610	107.69(0.00)	—

[a]Estimated uncertainties for $V_{\phi,2}$ appear in parentheses.

sulting equation, eq. [8], defines the volume of ionization of the acid, ΔV^0.

$$[8] \quad \Delta V^0 = V_i^0 - V_u^0$$

The first acid dissociation constant of L-ascorbic acid is reported to be $pK_1 = 4.10$. This value was obtained by Karrer, Schwarzenbach, and Schopp (23) using a hydrogen electrode at a temperature of 24°C. Dissociation constants for the acid at 25°C have been measured; however, they generally refer to solutions maintained at some fixed ionic strength (24). pK_2 of L-ascorbic acid is large enough that A^{2-} ions are not present to any significant concentration in acidic solutions, or even in slightly alkaline solutions.

Values of α at 298.15 K were calculated using an iterative procedure. An initial estimate of α was fed into the Davies equation (25), eq. [9], to produce an estimate of the activity coefficient, γ. The computed value of γ was in turn entered into eq. [10] to produce a new estimate of α. This successive approximation procedure was repeated until consistent values of α and γ were obtained.

$$[9] \quad \log \gamma = \frac{-A|z^+z^-|\sqrt{\alpha m}}{1 + \sqrt{\alpha m}} + 0.1|z^+z^-|\alpha m$$

$$[10] \quad K = \frac{\alpha^2\gamma^2 m}{(1 - \alpha)}$$

The Debye–Hückel constant, A, used in eq. [9] is the one reported by Robinson and Stokes (25) ($A = 0.5115$ at 298.15 K). This constant differs by a factor of 2.303 from the one reported by Ananthaswamy and Atkinson (12). The value of K used in eq. [10] was calculated from the pK_1 reported in ref. 23.

The apparent molar volumes of the ionic species, $V_{2,\phi,i}$, present in solution can be represented by a Debye–Hückel type equation.

$$[11] \quad V_{\phi,2,i} = V_i^0 + A_v\omega^{1.5}\alpha^{0.5}m^{0.5} + B_i\omega\alpha m$$

In a similar fashion the apparent molar volumes of the undissociated acid, $V_{\phi,2,u}$, can be modelled by eq. [12].

$$[12] \quad V_{\phi,2,u} = V_u^0 + B_u(1 - \alpha)m$$

Combining eqs. [11] and [12] with eq. [5] gives:

$$[13] \quad V_{\phi,2} = \alpha V_i^0 + A_v\omega^{1.5}\alpha^{1.5}m^{0.5} + B_i\omega\alpha^2 m + B_u(1 - \alpha)^2 m + (1 - \alpha)V_u^0$$

The terms $A_v\omega^{1.5}\alpha^{1.5}m^{0.5}$ and $B_i\omega\alpha^2 m$ are calculated to make only a very small contribution to $V_{\phi,2}$. Therefore, the apparent molar volumes of our L-ascorbic solutions can be modelled by the three-term equation

$$[14] \quad V_{\phi,2} = \alpha V_i^0 + (1 - \alpha)V_u^0 + B_u(1 - \alpha)^2 m$$

where V_i^0, V_u^0, and B_u are constants that can be calculated using a multiple regression fitting procedure. Our values of these constants, their standard errors, and the correlation coefficient of the fit are reported for the L-ascorbic acid system at 298.15 K in Table 3. The reported estimate of V_u^0 is in fair agreement with the extrapolated value of 105.17 cm^3 mol^{-1} obtained by Manzurola and Apelblat (26). Equation [8] yields $\Delta V^0 = -17.99 \pm 1.97$ cm^3 mol^{-1}. The reported

Can. J. Chem. Downloaded from www.nrcresearchpress.com by 213.200.69.106 on 09/08/12
For personal use only.

Can. J. Chem. Downloaded from www.nrcresearchpress.com by 213.200.69.106 on 09/08/12
For personal use only.

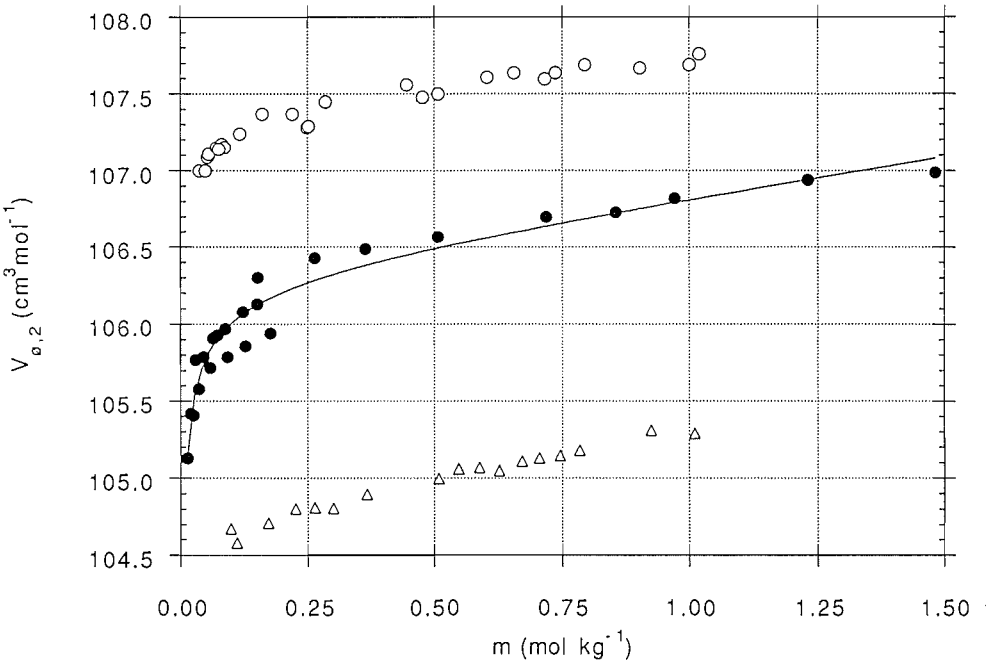

FIG. 1. Experimental apparent molar volumes, $V_{\phi,2}$, of aqueous L-ascorbic acid solutions as a function of concentration and temperature (○ = 308.15 K, ● = 298.15 K, Δ = 288.15 K). The least-squares fit of eq. [14] to our 298.15 K experimental data is shown as a solid curve.

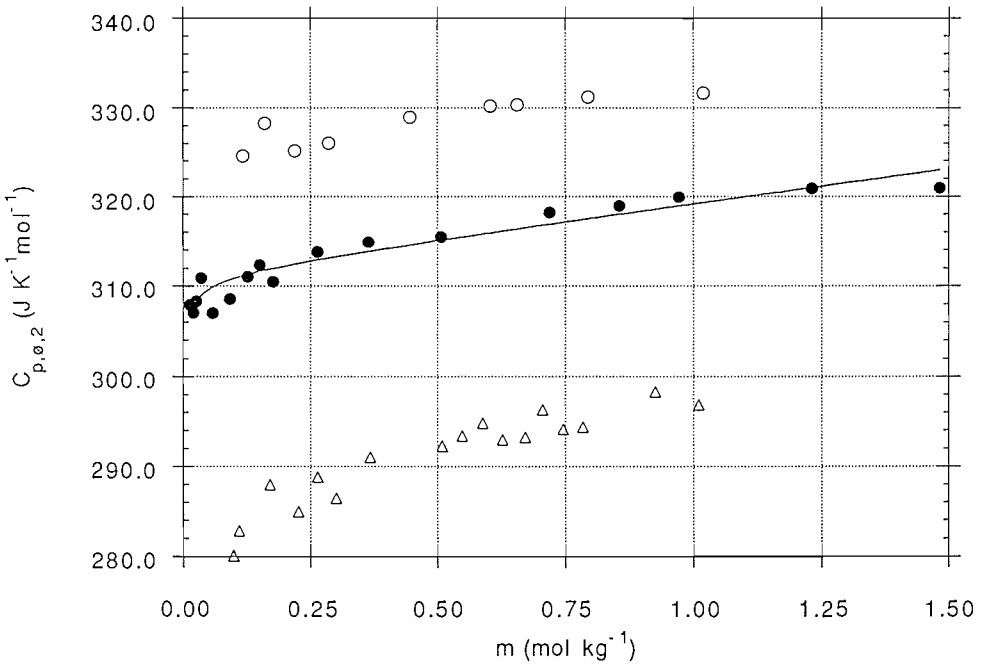

FIG. 2. The apparent molar heat capacities, $C_{p,\phi,2}$, of aqueous L-ascorbic acid solutions as a function of concentration and temperature (○ = 308.15 K, ● = 298.15 K, Δ = 288.15 K). The least-squares fit of the heat capacity form of eq. [14] to our 298.15 K experimental data is shown as a solid curve.

uncertainty in this number comes directly from the standard errors calculated in our fitting procedure.

This method of calculating ΔV^0 is particularly attractive for the L-ascorbic acid system. The usual route of obtaining volumes of ionization for weak acids requires accurate apparent molar volume data for the relevant sodium salt(s) of the acid (1, 27, 28). Solutions of sodium ascorbate in water are known to be very rapidly oxidized when exposed to the air. Accurate density and volume data for these systems are therefore very difficult to obtain.

To assess the validity of our methodology, eq. [14] was also fitted to apparent molar volume data for aqueous formic acid (27) and acetic acid (2, 27). Our calculated volumes of ionization obtained, ΔV^0 (formic acid) = -8.98 ± 0.16 cm^3 mol^{-1} and ΔV^0 (acetic acid) = -11.17 ± 1.25 cm^3 mol^{-1}, are in good agreement with the values of -8.43 and

TABLE 3. Calculated coefficients for eq. [14] for L-ascorbic acid in water at 298.15 K

	Value	Standard error on value
V_i^0 (cm^3 mol^{-1})	88.50	1.88
V_u^0 (cm^3 mol^{-1})	106.49	0.08
B_u (cm^3 kg mol^{-2})	0.5077	0.0868
Correlation coefficient	0.9754	

-11.50 cm^3 mol^{-1} previously reported in the literature (27). The latter values required apparent molar volume data for aqueous solutions of sodium formate and sodium acetate in their calculation.

Analysis of the experimental apparent molar heat capacity data for our acid system requires that we consider the contribution made by "relaxation" effects. These effects account for the temperature-dependent state of the equilibrium and related thermal effects (1). Relaxational contributions are defined by the expression $\Delta H(d\alpha/dT)$. Calculation of $(d\alpha/dT)$ requires equilibrium constants at several temperatures. These data are not available for the L-ascorbic acid system. We have therefore calculated a value of -74.97 ± 27 J K^{-1} mol^{-1} for ΔC_p^0 using the approach described earlier for volumes and the assumption that the relaxational contributions to our apparent molar heat capacity data are negligible. The uncertainty reported in this number comes from the standard errors calculated in our fitting procedure.

To obtain reliable estimates of V_i^0 and $C_{p,i}^0$ from eq. [14] it is necessary to obtain apparent molar volume and apparent molar heat capacity data at low concentrations, i.e., concentrations at which α rapidly increases. As previously noted, uncertainties in $V_{\phi,2}$, and $C_{p,\phi,2}$ increase with decreasing solution concentration. Precise apparent molar volume and apparent molar heat capacity data for the L-ascorbic acid system are therefore difficult to obtain in the low-concentration region. From this standpoint our fitting procedures were limited to using $V_{\phi,2}$ and $C_{p,\phi,2}$ data for solutions with concentrations greater than 0.01 mol kg^{-1}.

A lack of literature values for the first dissociation constant of L-ascorbic acid as a function of temperature has prevented our calculation of ΔC_p^0 and ΔV^0 for this system at temperatures other than 298.15 K. However, we are currently applying our methodology to other aqueous organic systems for which the temperature dependences of the acid dissociation constants are well documented. These studies will provide volumes and heat capacities of ionization as a function of temperature. There are very few systems for which these data are reported in the literature and even fewer systems for which these data are available at temperatures removed from 298.15 K.

Can. J. Chem. Downloaded from www.nrcresearchpress.com by 213.200.69.106 on 09/08/12
For personal use only.

Acknowledgments

The authors are grateful to the Natural Sciences and Engineering Research Council of Canada (NSERC) for operating support and to the University of Lethbridge for equipment funding. C.L.B. is grateful to NSERC for the award of an Undergraduate Student Research Award. In addition A.W.H. would like to thank David Daisley and Luis Delgado for providing assistance with the setup and modification of the Picker flow microcalorimeter.

1. J.W. Larson, K.G. Zeeb, and L.G. Hepler. Can. J. Chem. **60**, 2141 (1982).
2. G.C. Allred and E.M. Woolley. J. Chem. Thermodyn. **13**, 155 (1981).
3. E.M. Woolley and L.G. Hepler. Can. J. Chem. **55**, 158 (1977).
4. D. Smith-Magowan and R.N. Goldberg. A bibliography of sources of experimental data leading to thermal properties of binary aqueous electrolyte solutions. NBS Spec. Publ. (U.S.), 537 (1979).
5. P. Picker, E. Tremblay, and C. Jolicoeur. J. Solution Chem. **3**, 377 (1974).
6. G.S. Kell. J. Chem. Eng. Data, **12**, 66 (1967).
7. P. Picker, P.-A. Leduc, P.R. Philip, and J.E. Desnoyers. J. Chem. Thermodyn. **3**, 631 (1971).
8. J.K. Hovey. Ph.D. Thesis, University of Alberta (1988).
9. J.E. Desnoyers, C. DeVisser, G. Perron, and P. Picker. J. Solution Chem. **5**, 605 (1976).
10. G.R. Hedwig. J. Solution Chem. **17**, 383 (1988).
11. P.P. Saluja, R.J. Lemire, and J.C. LeBlanc. J. Chem. Thermodyn. **24**, 181 (1992).
12. J. Ananthaswamy and G. Atkinson. J. Chem. Eng. Data, **29**, 81 (1984).
13. A. Lo Surdo, E.M. Alzola, and F.J. Millero. J. Chem. Thermodyn. **14**, 649 (1982).
14. F.J. Millero. J. Phys. Chem. **74**, 356 (1970).
15. L.A. Dunn. Trans. Faraday Soc. **64**, 2961 (1968).
16. G. Perron, J.-L. Fortier, and J.E. Desnoyers. J. Chem. Thermodyn. **7**, 1177 (1975).
17. G. Dessauges, N. Miljevic, and W.A. Van Hook. J. Phys. Chem. **84**, 2587 (1980).
18. C.-T. Chen, R.T. Emmett, and F.J. Millero. J. Chem. Eng. Data, **22**, 201 (1977).
19. F. Vaslow. J. Phys. Chem. **70**, 2286 (1966).
20. I.O. Olofsson. J. Chem. Thermodyn. **11**, 1005 (1979).
21. P.P. Singh, E.M. Woolley, K.G. McCurdy, and L.G. Hepler. Can. J. Chem. **54**, 3315 (1976).
22. H.S. Harned and B.B. Owen. The physical chemistry of electrolytic solutions. 3rd ed. Reinhold Publishing Corp., New York. 1958.
23. P. Karrer, G. Schwarzenbach, and K. Schopp. Helv. Chem. Acta, **16**, 302 (1933).
24. O. Wahlberg and P. Ulmgren. Acta Chem. Scand. **21**, 2759 (1967).
25. R.A. Robinson and R.H. Stokes. Electrolyte solutions. 2nd ed. revised. Butterworths, London. 1965.
26. E. Manzurola and A. Apelblat. J. Chem. Thermodyn. **21**, 1005 (1989).
27. E.J. King. J. Phys. Chem. **73**, 1220 (1969).
28. H. Høiland. J. Chem. Soc. Faraday Trans. 1, **70**, 797 (1970).

Reactions of catecholborane with iridium complexes: molecular structure of *trans*-IrHCl(CO)(Bcat)$(PPh_3)_2$[1]

STEPHEN A. WESTCOTT AND TODD B. MARDER[2]
Department of Chemistry, University of Waterloo, Waterloo, Ont., Canada N2L 3G1

AND

R. THOMAS BAKER[2] AND JOSEPH C. CALABRESE
Central Research and Development, Science and Engineering Laboratories, E. I. du Pont de Nemours and Co., Experimental Station, Wilmington, DE 19880-0328, U.S.A.

Received December 8, 1992

STEPHEN A. WESTCOTT, TODD B. MARDER, R. THOMAS BAKER, and JOSEPH C. CALABRESE. Can. J. Chem. **71**, 930 (1993).

Reactions of certain iridium complexes with catecholborane (HBcat) gave boron-substituent redistribution products ($[Bcat_2]^-$, B_2cat_3) with concomitant formation of a complex mixture of iridium hydrides. While "$IrCl(PPh_3)(COE)_n$" generated in situ from $[Ir(\mu\text{-}Cl)(COE)_2]_2$ (COE = cyclooctene) (**2**) plus 2 equivalents of PPh_3 also promoted HBcat degradation, this catalyst system was extremely active and selective for alkene hydroborations. Oxidative addition of HBcat to the metal centre can be the sole reaction pathway, however, with iridium complexes containing electron-rich phosphines. The unsaturated boryl complex $IrHCl(Bcat)(PPr^i_3)_2$ was prepared and isolated in high yield from reaction of HBcat with **2** in the presence of four equivalents of PPr^i_3. Ancillary carbonyl ligands also appear to facilitate oxidative addition of HBcat to an iridium centre. Addition of HBcat to *trans*-$IrCl(CO)(PPh_3)_2$ gives the first structurally characterized metal-carbonyl boryl complex *trans*-$IrHCl(CO)(Bcat)(PPh_3)_2$ (**7**). Colourless crystals of **7** are triclinic, $P\bar{1}$ (No. 2) with two molecules per unit cell of dimensions a = 12.223(2) Å, b = 12.684(2) Å, c = 14.652(1) Å, α = 70.81(1)°, β = 72.47(1)°, and γ = 71.92(1)°.

STEPHEN A. WESTCOTT, TODD B. MARDER, R. THOMAS BAKER et JOSEPH C. CALABRESE. Can. J. Chem. **71**, 930 (1993).

Les réactions de certains complexes d'iridium avec le catécholborane (HBcat) conduisent à des produits de redistribution des substituants du bore ($[Bcat_2]^-$, B_2cat_3) avec la formation concomitante d'un mélange complexe d'hydrures d'iridium. Alors que le «$IrCl(PPh_3)(COE)_n$», généré in situ à partir du $[Ir(\mu\text{-}Cl)(COE)_2]_2$ (COE = cyclooctène) (**2**) et de deux équivalents de PPh_3, provoque aussi la dégradation du HBcat, ce système catalytique est extrêmement actif et sélectif pour les hydroborations d'alcènes. Toutefois, l'addition oxydante du HBcat sur un centre métallique peut n'être que la seule voie réactionnelle avec des complexes d'iridium contenant des phosphines riches en électrons. On a préparé le complexe boryle insaturé, $IrHCl(Bcat)(PPr^i_3)_2$, et on l'a isolé par réaction du HBcat avec le composé **2** en présence de quatre équivalents de PPr^i_3 avec un excellent rendement. Les ligands carbonyles ancillaires semblent rendre l'addition oxydante du HBcat sur un centre iridium plus facile. L'addition du HBcat sur le *trans*-$IrCl(CO)(PPh_3)_2$ conduit au premier complexe boryle métal-carbonyle caractérisé, le *trans*-$IrHCl(CO)(Bcat)(PPh_3)_2$ (**7**), qui se présente sous forme de cristaux incolores tricliniques, $P\bar{1}$ (No. 2), avec deux molécules par motif constitutif, a = 12,223(2), b = 12,684(2) et c = 14,652(1) Å, α = 70,81(1)°, β = 72,47(1)° et γ = 71,92(1)°.

[Traduit par la rédaction]

Introduction

There has been considerable recent interest in metal-catalyzed hydroboration of alkenes (for leading references, see ref. 1), owing largely to rate enhancements observed for less reactive boron reagents, such as catecholborane, HBcat (cat = 1,2-$O_2C_6H_4$) (2), as well as regio-, chemo-, and stereoselectivities that are complementary to or improved with respect to conventional procedures. While much effort has focussed on rhodium(I) complexes to catalyze such transformations (1, 3), recent work has demonstrated that analogous iridium compounds are also active catalyst precursors (4–7). Indeed, Sneddon and co-workers reported initially that complexes $[IrCl_2(\eta^5\text{-}C_5Me_5)]_2$ (**1**) (4) and *trans*-$IrCl(CO)(PPh_3)_2$ (5) catalyze the B-H addition of polyhedral boranes to alkynes to give a variety of alkenylboranes. Evans and Fu subsequently employed $[Ir(COD)(py)(PCy_3)]PF_6$ (COD = η^4-1,5-cyclooctadiene; py = pyridine) as a catalyst precursor for amide-directed hydroborations of alkenes using HBcat (6). In general, selectivities were higher using this iridium catalyst precursor than those observed with similar rhodium complexes. As part of our investigation into metal-catalyzed hydroborations of alkenes (1*h*, 3, 8), we examined the stoichiometric reactivity and catalytic activity of a number of iridium complexes with HBcat using multinuclear NMR spectroscopy, and we report herein our initial findings.

Results and discussion

Reactions of iridium complexes with HBcat

Initial work focussed on reactions of HBcat with iridium complexes that do not contain basic phosphine ligands. Addition of HBcat to a solution of $[IrCl_2(\eta^5\text{-}C_5Me_5)]_2$ (**1**) (9) in THF gave a complex mixture of iridium-hydride complexes. It was reported previously that reduction of dichloride **1** affords a number of binuclear μ-hydride complexes (10). While the observation of $[Bcat_2]^-$ (generated via the metal-mediated degradation of HBcat (11, 12)) in these solutions suggests that cationic iridium species are generated, we cannot rule out the possibility of zwitterionic compounds. The versatile $[Bcat_2]^-$ anion can coordinate to a metal centre in an η^6 fashion via one of its arene rings (1*h*, 8*b*).

[1]Contribution No. 6415 from Central Research and Development, Science and Engineering Laboratories, E. I. du Pont de Nemours and Co., Experimental Station, Wilmington, Del.

[2]Authors to whom correspondence may be addressed.

Can. J. Chem. Downloaded from www.nrcresearchpress.com by 213.200.69.106 on 09/08/12
For personal use only.

Can. J. Chem. Downloaded from www.nrcresearchpress.com by 213.200.69.106 on 09/08/12
For personal use only.

Iridium hydrides were observed from reactions of HBcat with phosphine-free complexes $[Ir(\mu\text{-}Cl)(COE)_2]_2$ (**2**) (COE = η^2-cyclooctene) and $[Ir(\mu\text{-}Cl)(COD)]_2$ (**3**) as well. Interestingly, resonances corresponding to COD ligands in the ^1H NMR spectrum of the latter were notably absent. The lack of B-C resonances in the ^{11}B NMR spectra (13) suggests that the COD ligands are being hydrogenated and not hydroborated. Indeed, the major boron-containing species was degradation product B_2cat_3 (11, 12).

Not all products arising from reactions with these three phosphine ligand-free iridium complexes were identified, as HBcat degradation was extensive and invariably led to Ir metal.

In contrast, only one new phosphinoiridium complex was observed (by ^{31}P NMR spectroscopy) from the reaction of monophosphine-containing $[Ir(COD)(py)(PCy_3)]^+[OTf]^-$ (**4**) (14) with excess HBcat. Although no resonance corresponding to an iridium hydride was observed in the ^1H NMR spectra, the COD ligand appears to have been hydrogenated. Unfortunately, characterization of the products derived from this reaction was complicated by further HBcat degradation where even $[OTf]^-$ (1*h*) and pyridine[3] were susceptible to attack by boron species in solution. That **4** promoted HBcat degradation is somewhat surprising as this cationic iridium species is a highly active and selective catalyst precursor for amide-directed hydroborations (6).

The ubiquity of rhodium complexes containing PPh_3 in catalyzed hydroborations (1) prompted us to investigate the analogous PPh_3 chemistry with iridium. Addition of HBcat to a THF solution of "$IrCl(PPh_3)(COE)_n$", generated in situ from **2** and PPh_3,[4] gave a complex mixture of phosphinoiridium products where most of the HBcat had been converted to B_2cat_3. This result was not unexpected as addition of PPh_3 to **2** affords several Ir(III) complexes arising from *ortho*-metalation of one of the phenyl rings in PPh_3 to the metal centre (16).

Similar product distributions were observed in analogous reactions with "$IrCl(PPh_3)_2$". Reactions carried out in CH_2Cl_2 gave fewer products, however, with dihydride *mer-cis*-$IrH_2Cl(PPh_3)_3$ (**5**) (17) being the major phosphine-containing product (ca. 45% by ^{31}P NMR spectroscopy). Formation of this complex parallels an earlier observation (3, 8*b*) that addition of HBcat to Wilkinson's catalyst, $RhCl(PPh_3)_3$, gave oxidative addition product $RhHCl(Bcat)(PPh_3)_2$ (18) along with varying amounts of dihydride *mer-cis*-$RhH_2Cl(PPh_3)_3$.

It is interesting to note that an ancillary CO ligand can facilitate the oxidative addition of HBcat to a metal centre. Thus, the saturated iridium boryl complex *trans*-$IrHCl(CO)(Bcat)(PPh_3)_2$ (**7**) was prepared (eq. [1]) in high yield from reaction of HBcat with Vaska's complex *trans*-$IrCl(CO)(PPh_3)_2$ (**6**) (19).

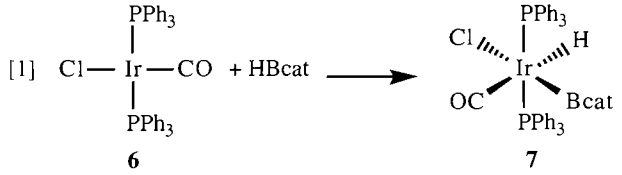

[3]P. Nguyen, S.A. Westcott, T.B. Marder, and R.T. Baker. Unpublished results.

[4]Similar in situ alkene hydrogenation catalysts formed from $[Ir(\mu\text{-}Cl)(COE)_2]_2/PR_3$ with P:Ir < 2.5 were reported previously (15).

TABLE 1. Summary of X-ray diffraction data for *trans*-$IrHCl(CO)(Bcat)(PPh_3)_2$ (**7**)

Parameter	Value
Formula	$IrCl_3P_2O_3C_{44}BH_{37}$
fw	985.09
Crystal system	Triclinic
a, Å	12.223(2)
b, Å	12.684(2)
c, Å	14.652(1)
α, deg	70.81(1)
β, deg	72.47(1)
γ, deg	71.92(1)
V, Å^3	1988.6
Z	2
ρ_{calcd}, g cm^{-3}	1.645
Space group	$P\bar{1}$ (No. 2)
Crystal dimensions, mm	0.46 × 0.40 × 0.45
Temperature, °C	−70
Radiation	MoKα
μ, cm^{-1}	36.65
Data collection method	ω
Max. 2θ, deg	48.0
Scan speed, deg min^{-1}	1.70–10.10
Scan width, deg	1.20–1.90 ω
Total no. of observations	6421
No. of unique data ($I > 3\sigma(I)$)	5478
Final no. of variables	635
Final Δ/σ	0.07
Max. residual density, e Å^{-3}	0.58
R^a	0.020
$R_w{}^b$	0.027
GOF^c	1.30

$^a\Sigma||F_o| - |F_c||/\Sigma|F_o|$.
$^b[\Sigma w(|F_o| - |F_c|)^2/\Sigma wF_o{}^2]^{1/2}$.
$^c[\Sigma w(|F_o| - |F_c|)^2/(NO - NV)]^{1/2}$.

Although CO inhibits orthometalation of the PPh_3 ligands and, hence, provides a coordination site required for oxidative addition of HBcat, the electron-withdrawing nature of this π acid is expected to destabilize the resulting M—B bonds. Indeed, a recent report showed that addition of HBcat to the osmium carbonyl $Os_3(\mu\text{-}H)_2(CO)_{10}$ affords $Os_3(\mu\text{-}H)_3(CO)_9(\mu_3\text{-}COBcat)$, where the boron is bound to the electron-rich oxygen of the unique carbonyl group (20).

Although a number of metal boryl complexes containing ancillary CO ligands were reported over 20 years ago, characterization of these compounds is based solely upon their melting points, IR, and ^{11}B NMR spectra (for a review, see ref. 21). As a result, the exact structure of these compounds remains uncertain. Complex **7**, on the other hand, represents the first example of a metal-carbonyl boryl compound to be characterized fully by IR, multinuclear NMR spectroscopy, and single crystal X-ray diffraction. A summary of the crystallographic data and parameters for data collection is presented in Table 1, selected bond distances and angles are given in Table 2, and final atomic coordinates are given in Table 3. The molecular structure of **7** consists of an octahedral arrangement of ligands with *trans* phosphine ligands and the catecholatoboryl group *trans* to chloride (Fig. 1). The hydride ligand is *cis* to the boryl group with an H—Ir—B angle of 78(1)°, and the boryl ligand plane is oriented parallel to the Ir—H—B plane. Interestingly, there is no close contact between the boron atom and the car-

TABLE 2. Selected bond distances (Å) and angles (°) for *trans*-IrHCl(CO)(Bcat)(PPh_3)$_2$ (**7**)

Bond	Distance	Bonds	Angle
Ir(1)—Cl(1)	2.518 (1)	Cl(1)—Ir(1)—P(1)	89.27 (4)
Ir(1)—P(1)	2.330 (1)	Cl(1)—Ir(1)—P(2)	87.15 (4)
Ir(1)—P(2)	2.335 (1)	Cl(1)—Ir(1)—C(1)	101.8 (1)
Ir(1)—C(1)	1.932 (4)	Cl(1)—Ir(1)—B(1)	167.8 (1)
Ir(1)—B(1)	2.045 (5)	Cl(1)—Ir(1)—H(1)	90 (1)
Ir(1)—H(1)	1.696 (43)	P(1)—Ir(1)—P(2)	173.21 (5)
Cl(3)—C(71)	1.767 (6)	P(1)—Ir(1)—C(1)	93.2 (1)
Cl(4)—C(71)	1.749 (6)	P(2)—Ir(1)—C(1)	93.2 (1)
P(1)—C(11)	1.835 (4)	P(1)—Ir(1)—B(1)	92.7 (1)
P(1)—C(21)	1.827 (4)	P(2)—Ir(1)—B(1)	89.6 (1)
P(1)—C(31)	1.825 (4)	P(1)—Ir(1)—H(1)	86 (1)
P(2)—C(41)	1.832 (4)	P(2)—Ir(1)—H(1)	88 (1)
P(2)—C(51)	1.828 (4)	C(1)—Ir(1)—B(1)	90.1 (2)
P(2)—C(61)	1.820 (4)	C(1)—Ir(1)—H(1)	168 (1)
O(1)—C(1)	1.134 (5)	B(1)—Ir(1)—H(1)	78 (1)
O(2)—C(2)	1.395 (5)	Ir(1)—P(1)—C(11)	114.3 (1)
O(3)—C(3)	1.386 (5)	Ir(1)—P(1)—C(21)	116.9 (1)
O(2)—B(1)	1.379 (6)	Ir(1)—P(1)—C(31)	113.7 (1)
O(3)—B(1)	1.422 (5)	Ir(1)—P(2)—C(41)	112.7 (1)
C(2)—C(3)	1.374 (6)	Ir(1)—P(2)—C(51)	114.5 (1)
C(2)—C(7)	1.369 (6)	Ir(1)—P(2)—C(61)	116.7 (1)
C(3)—C(4)	1.370 (6)	C(11)—P(1)—C(21)	101.6 (2)
C(4)—C(5)	1.390 (7)	C(11)—P(1)—C(31)	104.7 (2)
C(5)—C(6)	1.371 (7)	C(21)—P(1)—C(31)	104.1 (2)
C(6)—C(7)	1.395 (7)	C(41)—P(2)—C(51)	104.1 (2)
		C(41)—P(2)—C(61)	104.8 (2)
		C(51)—P(2)—C(61)	102.6 (2)
		C(2)—O(2)—B(1)	106.6 (3)
		C(3)—O(3)—B(1)	105.5 (3)
		Ir(1)—C(1)—O(1)	170.9 (4)
		Cl(3)—C(71)—Cl(4)	111.2 (3)
		Cl(3)—C(71)—H(71)	112 (4)
		Cl(3)—C(71)—H(71′)	106 (5)
		Cl(4)—C(71)—H(71)	106 (4)
		Cl(4)—C(71)—H(71′)	110 (5)
		Ir(1)—B(1)—O(2)	126.4 (3)
		Ir(1)—B(1)—O(3)	124.0 (3)
		O(2)—B(1)—O(3)	109.4 (3)

Can. J. Chem. Downloaded from www.nrcresearchpress.com by 213.200.69.106 on 09/08/12
For personal use only.

bonyl group (C—Ir—B = 90.1(2)°). The iridium–boron bond distance of 2.045(5) Å is consistent with other M—B σ bonds (7, 8, 22). For comparison, the Ir—B bond in *mer*-IrHCl(Bcat)(PMe_3)$_3$ is 2.023(10) Å (7). The oxidative addition of a B—H bond in B_5H_9 or the B—Br bond in 1- or 2-BrB_5H_8 to *trans*-IrCl(CO)(PMe_3)$_2$ was reported by Davison and co-workers (22*a*). From the former reaction, the colourless complex 2-[IrClH(CO)(PMe_3)$_2$]B_5H_8 was isolated. The ^{1}H and ^{31}P NMR and IR spectra of this species (22*a*) are similar to those for **7**. The molecular structure of 2-[$IrBr_2$(CO)(PMe_3)$_2$]B_5H_8 was determined (22) and the Ir—B bond distance was found to be 2.07(1) Å.

In contrast to reactions employing PPh_3, addition of HBcat to "IrCl(PPr^i_3)$_2$" (eq. [2]) gave the unsaturated hydrido-boryl complex IrHCl(Bcat)(PPr^i_3)$_2$ (**8**) in high yield with minimal HBcat degradation. The molecular structure of the rhodium analogue was reported recently (8*b*) and consists of a distorted trigonal-bipyramidal Rh(III) centre with apical PPr^i_3 ligands. Spectroscopic data for **8** are consistent with this structure. Likewise, by analogy with the PMe_3 analog (7), saturated iridium boryl *mer*-IrHCl(Bcat)(PEt_3)$_3$ (**10**) was prepared readily (eq. [3]) by addition of one equivalent of HBcat to a toluene solution of IrCl(PEt_3)$_3$ (**9**) (23).

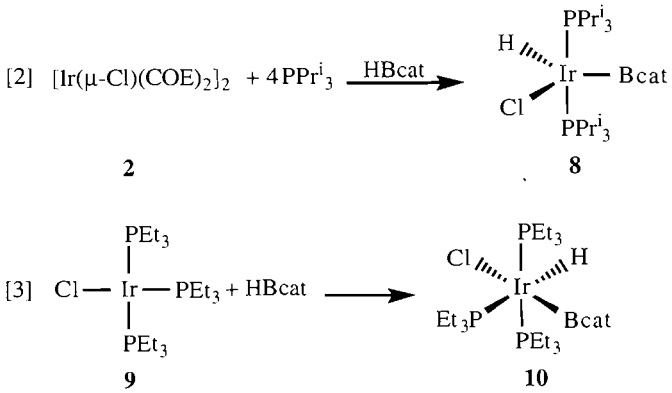

In summary, stoichiometric reactions of HBcat with certain iridium complexes result in the degradation of HBcat. Oxidative addition to a basic metal centre can be the sole reaction pathway with iridium complexes containing basic

Can. J. Chem. Downloaded from www.nrcresearchpress.com by 213.200.69.106 on 09/08/12
For personal use only.

.LE 3. Fractional coordinates ($\times 10^4$) and isotropic thermal parameters (Å $\times$ 1000)

Atom	x	y	z	B_{iso}
Ir(1)	4393.3(1)	6916.1(1)	6903.3(1)	1.2(1)
Cl(1)	4685.5(9)	4974.8(8)	6639.1(8)	2.1(1)
Cl(3)	5453(1)	7583(1)	91(1)	4.5(1)
Cl(4)	4015(2)	8633(1)	1683(1)	5.7(1)
P(1)	6396.3(9)	6496.9(8)	6879.1(8)	1.4(1)
P(2)	2376.0(9)	7142.0(8)	7084.2(7)	1.4(1)
O(1)	4669(3)	8553(3)	4827(2)	3.3(1)
O(2)	3745(3)	8341(2)	8407(2)	2.1(1)
O(3)	3938(3)	9469(2)	6814(2)	2.1(1)
C(1)	4581(4)	7875(4)	5560(3)	2.0(1)
C(2)	3431(4)	9493(3)	8419(3)	2.1(1)
C(3)	3546(4)	10165(3)	7461(3)	2.0(1)
C(4)	3249(4)	11340(4)	7241(4)	2.9(2)
C(5)	2825(5)	11820(4)	8044(4)	3.3(2)
C(6)	2727(5)	11148(4)	9000(4)	3.2(2)
C(7)	3031(5)	9951(4)	9219(4)	2.9(2)
C(11)	7377(3)	6347(3)	5681(3)	1.6(1)
C(12)	7038(4)	5964(3)	5041(3)	2.0(1)
C(13)	7799(4)	5814(4)	4152(3)	2.3(2)
C(14)	8899(4)	6035(4)	3901(4)	2.8(2)
C(15)	9250(4)	6405(4)	4536(4)	3.1(2)
C(16)	8496(4)	6560(4)	5418(3)	2.3(2)
C(21)	6917(3)	7558(3)	7127(3)	1.7(1)
C(22)	6753(4)	8664(4)	6508(4)	2.6(2)
C(23)	7208(4)	9481(4)	6625(4)	3.3(2)
C(24)	7821(4)	9192(4)	7355(4)	3.0(2)
C(25)	7976(4)	8112(4)	7976(4)	3.0(2)
C(26)	7526(4)	7287(4)	7859(3)	2.3(2)
C(31)	6896(3)	5158(3)	7767(3)	1.6(1)
C(32)	7801(4)	4275(4)	7456(3)	2.1(1)
C(33)	8177(4)	3277(4)	8157(4)	2.8(2)
C(34)	7673(4)	3150(4)	9143(4)	2.7(2)
C(35)	6780(4)	4016(4)	9459(3)	2.7(2)
C(36)	6381(4)	5021(4)	8768(3)	2.3(1)
C(41)	1965(3)	7480(3)	5899(3)	1.6(1)
C(42)	2749(4)	6973(4)	5161(3)	1.8(1)
C(43)	2492(4)	7241(4)	4242(3)	2.3(2)
C(44)	1447(4)	8001(4)	4057(3)	2.5(2)
C(45)	648(4)	8479(4)	4785(4)	2.7(2)
C(46)	900(4)	8221(4)	5706(3)	2.3(1)
C(51)	1429(3)	8310(3)	7633(3)	1.7(1)
C(52)	1377(4)	9453(4)	7101(3)	2.2(1)
C(53)	726(4)	10332(4)	7542(4)	2.9(2)
C(54)	125(4)	10093(5)	8512(4)	3.3(2)
C(55)	160(4)	8973(5)	9051(4)	3.1(2)
C(56)	821(4)	8079(4)	8622(3)	2.5(2)
C(61)	1757(4)	5922(3)	7862(3)	1.7(1)
C(62)	2287(4)	5108(4)	8610(3)	2.2(1)
C(63)	1753(5)	4234(4)	9236(4)	2.8(2)
C(64)	706(4)	4160(4)	9125(4)	3.1(2)
C(65)	180(4)	4941(4)	8392(4)	2.7(2)
C(66)	695(4)	5829(4)	7761(4)	2.4(2)
C(71)	4902(6)	7361(5)	1384(4)	3.9(2)
B(1)	4028(4)	8326(4)	7425(4)	1.8(2)
H(1)	4206(37)	6326(36)	8143(32)	2.5(9)
H(4)	3309(39)	11798(39)	6596(36)	2.7(10)
H(5)	2537(42)	12644(44)	7946(36)	3.5(11)
H(6)	2408(43)	11455(42)	9564(38)	3.5(11)
H(7)	2929(40)	9558(39)	9838(36)	2.5(10)
H(12)	6247(42)	5794(39)	5255(35)	3.0(10)
H(13)	7579(43)	5513(41)	3783(38)	3.3(11)
H(14)	9418(42)	5905(39)	3342(37)	3.1(11)
H(15)	10014(45)	6552(41)	4374(37)	3.6(11)

TABLE 3 (*concluded*)

Atom	x	y	z	B_{iso}
H(16)	8694(38)	6820(37)	5846(33)	2.3(10)
H(22)	6327(38)	8885(36)	6060(33)	2.0(9)
H(23)	7098(49)	10228(51)	6193(43)	5.1(14)
H(24)	8205(40)	9693(39)	7426(34)	2.8(10)
H(25)	8403(45)	7900(43)	8438(39)	3.7(12)
H(26)	7626(34)	6587(36)	8268(31)	1.4(8)
H(32)	8190(32)	4354(30)	6789(29)	0.6(7)
H(33)	8795(39)	2658(38)	7927(33)	2.6(10)
H(34)	7905(37)	2498(38)	9607(33)	2.0(9)
H(35)	6351(41)	3949(40)	10160(38)	3.3(11)
H(36)	5744(38)	5648(37)	9005(31)	2.2(9)
H(42)	3482(39)	6460(36)	5276(32)	2.2(9)
H(43)	2975(40)	6939(37)	3750(35)	2.5(10)
H(44)	1254(40)	8192(38)	3427(36)	2.8(10)
H(45)	−32(43)	8955(40)	4660(36)	3.1(11)
H(46)	329(41)	8579(39)	6185(36)	3.0(10)
H(52)	1810(39)	9625(37)	6459(35)	2.3(10)
H(53)	744(40)	11069(42)	7146(35)	3.0(11)
H(54)	−330(50)	10728(49)	8817(43)	5.3(14)
H(55)	−232(43)	8809(40)	9687(38)	3.0(11)
H(56)	862(40)	7287(41)	9041(36)	3.0(10)
H(62)	3038(40)	5144(36)	8619(33)	2.4(10)
H(63)	2121(41)	3732(40)	9744(36)	2.9(10)
H(64)	357(43)	3454(43)	9594(37)	3.9(12)
H(65)	−525(45)	4918(42)	8271(37)	3.7(12)
H(66)	315(47)	6340(46)	7275(41)	4.3(13)
H(71)	5536(55)	7115(51)	1733(46)	5.7(16)
H(71′)	4459(65)	6805(66)	1579(58)	9.1(23)

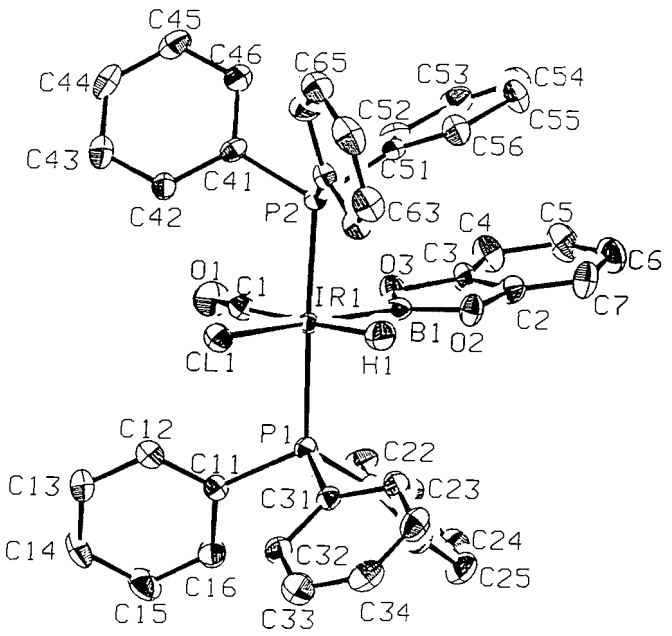

FIG. 1. The ORTEP diagram of the molecular structure of **7**. Hydrogen atoms other than the iridium-hydride ligand have been omitted for clarity.

phosphine ligands that stabilize the resulting boryl compounds.

Iridium-catalyzed hydroborations

Initial work focussed on iridium-catalyzed hydroborations of 1-octene, as addition of HBcat to this substrate in the

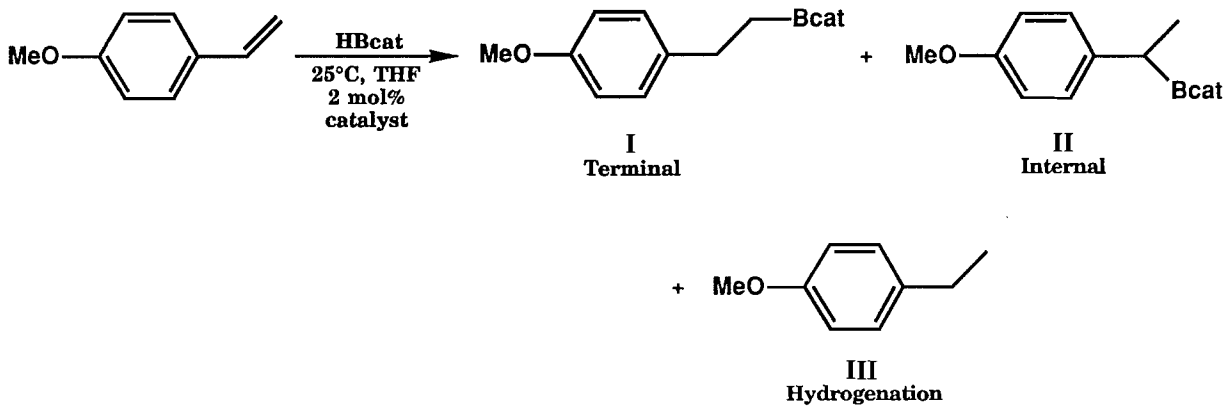

SCHEME 1

TABLE 4. Catalytic hydroboration of 4-vinylanisole[a]

Catalyst[a]	%I	%II	%III	Time (h)
$[IrCl_2(\eta^5\text{-}C_5Me_5)]_2$ (**1**)	98	—	2	0.5
$[Ir(\mu\text{-}Cl)(COE)_2]_2$ (**2**)	75	20	5	0.5
2/2 PPh_3	98	—	2	0.5
2/4 PPh_3	80	15	5	0.5
$[Ir(\mu\text{-}Cl)(COD)]_2$ (**3**)	75	15	10	0.5
$[Ir(COD)(py)(PCy_3)][OTf]$(**4**)	70	20	10	1.0
trans-$IrCl(CO)(PPh_3)_2$ (**6**)	—	—	—	5
$IrHCl(Bcat)(PPr^i_3)_2$ (**8**)	—	—	—	5
$IrCl(PEt_3)_3$ (**9**)	—	—	—	5

[a]All reactions were carried out in THF at room temperature in the presence of 2 mol% catalyst. Alkene:catecholborane:catalyst = 1.0:1.2:0.02. Product distributions determined by ^{13}C and ^1H NMR.

absence of a catalyst precursor occurs only at elevated temperatures (ca. 100°C). In all cases, we observed predominant formation of the terminal alkylboronate ester $CH_3(CH_2)_7Bcat$ (2) along with ca. 5% octane, arising from alkene hydrogenation. Stereochemical assignment of products is based upon ^1H, ^{11}B, and ^{13}C NMR spectroscopic data (1*h*). In contrast to its rhodium analogue (1*a*), hydroborations using either *trans*-$IrCl(CO)(PPh_3)_2$ (**6**) or isolated *trans*-$IrHCl(CO)(Bcat)(PPh_3)_2$ (**7**) proceeded only under photolytic conditions (see Experimental section). Initial loss of CO would provide the vacant coordination site at the metal centre required for catalysis (24). Complexes **6** and **7**, however, failed to catalyze the addition of HBcat to the more sterically hindered 4-vinylanisole (4-$MeOC_6H_4CH{=}CH_2$). Similarly, basic iridium complexes $IrHCl(Bcat)(PPr^i_3)_2$ (**8**) and $IrCl(PEt_3)_3$ (**9**) failed to hydroborate 4-vinylanisole.

Although complexes $[Ir(\mu\text{-}Cl)(COD)]_2$ (**3**) and $[Ir(COD)(py)(PCy_3)]^+[OTf]^-$ (**4**) catalyzed the hydroboration of 4-vinylanisole with moderate regiocontrol in favour of terminal alkylboronate ester **I** (Table 4), significant amounts (up to 10%) of hydrogenation product were also formed. More remarkable, however, is that reactions using $[IrCl_2(\eta^5\text{-}C_5Me_5)]_2$ (**1**) and "$IrCl(PPh_3)(COE)_n$" gave exclusive formation of terminal hydroboration product **I** with minimal hydrogenation. This is somewhat surprising as reactions in the absence of substrate promoted the rapid degradation of HBcat. It is plausible, therefore, that catalysis with these iridium precursors does not proceed via conventional pathways that invoke initial oxidative addition of HBcat to the metal centre (1*a*).

Hydroborations of 4-vinylanisole have been well studied and, depending on the catalyst precursor employed, can lead to exclusive formation of internal alkylboronate ester **II** (1*h*). We have found that use of iridium complexes **1** and "$IrCl(PPh_3)(COE)_n$", however, provide selective formation of terminal isomer **I**. Similar product distribution ranges have also been observed for hydroborations of 2-phenylpropene $Ph(Me)C{=}CH_2$, with certain Rh complexes giving as high as 95% selectivity to the internal product $Ph(Me)_2$-CBcat. Product distributions for hydroborations using **1** were complicated by formation of vinylboronate esters (arising presumably via dehydrogenative borylation). Analogous reactions employing "$IrCl(PPh_3)COE)_n$" afforded the corresponding terminal hydroboration product $Ph(Me)CHCH_2Bcat$ in excellent yield (98%) (8*d*). In summary, product distributions in hydroborations of vinylarenes can thus be tuned by judicious choice of catalyst precursor.

Conclusion

While oxidative addition of HBcat to several iridium complexes gave the expected iridium boryl compounds ($Ir\text{-}BR_2$), these species were ineffective as catalyst precursors for hydroborations of vinylarenes. In contrast, although "$IrCl(PPh_3)(COE)_n$" promoted HBcat degradation in the absence of substrate, this catalyst precursor is extremely active and selective for alkene hydroborations. Further work with this unique catalyst system is currently in progress.

Experimental section

General procedures

NMR spectra were recorded on General Electric QM-300 (^1H at 300 MHz, ^{13}C at 75.4 MHz, ^{31}P at 121 MHz) or Nicolet NMC (^{11}B at 96 MHz) instruments in THF-d_8 (tetrahydrofuran) unless stated otherwise. ^1H chemical shifts are reported in ppm relative to external TMS and referenced to residual protons in THF-d_8; coupling constants are in Hz. Multiplicities are reported as (br) broad, (ov) overlapping, (s) singlet, (d) doublet, (t) triplet, (q) quartet, and (m) multiplet. ^{11}B and ^{31}P chemical shifts are reported in ppm relative to the external standards $F_3B \cdot OEt_2$, and 85% H_3PO_4, respectively. THF and toluene were freshly distilled from sodium benzophenone ketyl. Catecholborane (Aldrich Chemical Co.) was distilled under reduced pressure. Alkenes were purchased from commercial suppliers and used as received. $[IrCl_2(\eta^5\text{-}C_5Me_5)]_2$ (25), $[Ir(\mu\text{-}Cl)(COE)_2]_2$ (26), $[Ir(\mu\text{-}Cl)(COD)]_2$ (27), $[Ir(COD)(py)(PCy_3)][OTf]$ (14), *trans*-$IrCl(CO)(PPh_3)_2$ (20), and $IrCl(PEt_3)_3$ (23) were prepared by established methods. Reagent purity was ascertained by ^1H NMR spectroscopy.

Can. J. Chem. Downloaded from www.nrcresearchpress.com by 213.200.69.106 on 09/08/12
For personal use only.

Can. J. Chem. Downloaded from www.nrcresearchpress.com by 213.200.69.106 on 09/08/12
For personal use only.

Reaction of HBcat with [$IrCl_2(\eta^5$-$C_5Me_5)]_2$ (1)

A solution of HBcat (36 mg, 0.3 mmol) in 1 mL of THF-d_8 was added dropwise to a suspension of **1** (40 mg, 0.05 mmol) in 1 mL of THF-d_8. Upon stirring for 0.5 h the resulting mixture became yellow in colour and was characterized spectroscopically by ^{1}H and ^{11}B NMR. Selected NMR spectroscopic data (in THF-d_8): $^{11}B\{^1H\}\delta$: 6.7 (s, minor), 14.9 (s, $[Bcat_2]^-$), 18.9 (br, B_2cat_3), 23.5 (s, HBcat), 24.4 (br s), 35.3 (br); $^1H\delta$: −17.44 (s, Ir-H), −16.40 (s, Ir-H), −14.39 (s, Ir-H, major), −12.49 (s, Ir-H), 1.76 (s, CH_3), 2.00 (s, CH_3, major), 2.07 (s, CH_3), 2.29 (s, CH_3), 6.6–7.1 (ov m, Bcat).

Reaction of HBcat with $[Ir(\mu\text{-}Cl)(COE)_2]_2$ (2)

A solution of HBcat (36 mg, 0.3 mmol) in 1 mL of THF-d_8 was added dropwise to a solution of $[Ir(\mu\text{-}Cl)(COE)_2]_2$ (45 mg, 0.05 mmol) in 1 mL of THF-d_8. Upon stirring for 0.5 h the resulting mixture became black in colour and was characterized spectroscopically by ^{1}H and ^{11}B NMR. Selected NMR spectroscopic data (in THF-d_8): $^{11}B\{^1H\}\delta$: 17.2 (br, minor), 19.5 (br, B_2cat_3); $^1H\delta$: −9.72 (s, Ir-H), −8.36 (s, Ir-H), −7.88 (s, Ir-H), −7.46 (s, Ir-H), −7.41 (s, Ir-H, major), −7.35 (s, Ir-H), −7.16 (s, Ir-H), 1.50 (s), 1.74 (br), 2.14 (br), 2.38 (br, minor), 4.83 (d, J = 9 Hz, minor), 5.55 (br, minor), 6.8–7.1 (ov m, Bcat).

Reaction of HBcat with $[Ir(\mu\text{-}Cl)(COE)_2]_2$/2 PPh_3

A solution of HBcat (36 mg, 0.3 mmol) in 1 mL of THF-d_8 was added dropwise to a premixed solution of $[Ir(\mu\text{-}Cl)(COE)_2]_2$ (45 mg, 0.05 mmol) and PPh_3 (26 mg, 0.1 mmol) in 1 mL of THF-d_8. Upon stirring for 0.5 h the resulting mixture became dark red in colour and was characterized spectroscopically by ^{1}H, ^{11}B, and ^{31}P NMR. Selected NMR spectroscopic data (in THF-d_8): $^{31}P\{^1H\}\delta$: −3.7 (br, minor), 15.8 (br), 22.1 (br), 24.3 (br), 31.2 (s), 33.3 (s), 34.6 (s, major); $^{11}B\{^1H\}\delta$: 17.7 (br, minor), 21.3 (br, B_2cat_3); $^1H\delta$: −19.93 (t, J_{HP} = 13 Hz, Ir-H), −18.86 (t, J_{HP} = 14 Hz, Ir-H), −17.90 (br, Ir-H), −8.84 (s, Ir-H), −8.63 (s, Ir-H), −8.31 (s, Ir-H), −7.39 (s, Ir-H), 1.51 (s), 1.55 (s), 2.14 (s), 5.59 (t, J = 5 Hz, minor) 6.6–7.7 (ov m, Bcat and PPh_3).

Reaction of HBcat with $[Ir(\mu\text{-}Cl)(COE)_2]_2$/4 PPh_3

A solution of HBcat (36 mg, 0.3 mmol) in 1 mL of THF-d_8 was added dropwise to a premixed solution of $[Ir(\mu\text{-}Cl)(COE)_2]_2$ (45 mg, 0.05 mmol) and PPh_3 (52 mg, 0.1 mmol) in 1 mL of THF-d_8. Upon stirring for 0.5 h the resulting mixture became light yellow in colour and was characterized spectroscopically by ^{1}H, ^{11}B, and ^{31}P NMR. Selected NMR spectroscopic data (in THF-d_8): $^{31}P\{^1H\}\delta$: −2.3 (br t, major), 7.3 (d, J_{PP} = 21 Hz, major), 11.9 (s), 15.5 (s, major), 18.8 (s), 22.2 (s), 25.5 (s), 26.2 (s, major); $^{11}B\{^1H\}\delta$: 16.4 (br, minor), 22.3 (br, B_2cat_3); $^1H\delta$: −21.20 (d, J_{HP} = 13 Hz, Ir-H, minor), −20.82 (t, J_{HP} = 14 Hz, Ir-H, minor) −12.44 (ov m, Ir-H, minor), −11.34 (complex d t, $J_{HPtrans}$ = 134 Hz, J_{HPcis} = 21 Hz, Ir-H, major), −8.0 (br, Ir-H, major), −7.97 to −7.11 (several s, Ir-H), 1.51 (s, major), 1.55 (s), 2.14 (s), 5.60 (t, J = 5 Hz, minor), 6.4–7.8 (ov m, Bcat and PPh_3). Selected NMR spectroscopic data for reactions carried out in CD_2Cl_2: $^{31}P\{^1H\}\delta$: 0.6 (t, J_{PP} = 13 Hz, **5**), 10.5 (d, J_{PP} = 13 Hz, **5**), 11.9 (s), 29.0 (s), 37.7 (s); $^{11}B\{^1H\}\delta$: 25.8 (br), 17.2 (br); $^1H\delta$: −20.78 (q, J_{HP} = 14 Hz, Ir-H, **5**), −19.04 (t, J_{HP} = 14 Hz), −10.62 (d t, $J_{HPtrans}$ = 130 Hz, J_{HPcis} = 20 Hz, Ir-H, **5**), 1.55 (s), 1.59 (s), 2.12 (s), 6.6--7.8 (ov m, Ph and Bcat).

Reaction of HBcat with $[Ir(\mu\text{-}Cl)(COD)]_2$ (3)

A solution of HBcat (36 mg, 0.3 mmol) in 1 mL of THF-d_8 was added dropwise to a solution of $[Ir(\mu\text{-}Cl)(COD)]_2$ (34 mg, 0.05 mmol) in 1 mL of THF-d_8. Upon stirring for 0.5 h the resulting mixture became light yellow in colour and was characterized spectroscopically by ^{1}H and ^{11}B NMR. Selected NMR spectroscopic data (in THF-d_8): $^{11}B\{^1H\}\delta$: 17.1 (br, minor), 22.9 (br, B_2cat_3); $^1H\delta$: 0.88 (d, J = 15 Hz, minor), 1.54 (s, major), 1.60 (s, minor), 2.14 (s), 6.8–7.1 (ov m, Bcat). The ^{1}H NMR spectra recorded after several hours are more complicated, however, as many iridium-hydride resonances are observed.

Reaction of HBcat with $[Ir(COD)(py)(PCy_3)]^+[OTf]^-$ (4)

A solution of HBcat (18 mg, 0.15 mmol) in 1 mL of CD_2Cl_2 was added dropwise to a solution of $[Ir(COD)(py)(PCy_3)]^+[OTf]^-$ (41 mg, 0.05 mmol) in 1 mL of CD_2Cl_2. Upon stirring for 0.5 h, the resulting mixture became light yellow in colour and was characterized spectroscopically by ^{1}H, ^{11}B, and ^{11}P NMR. Selected NMR spectroscopic data (in CD_2Cl_2): $^{31}P\{^1H\}\delta$: 53.4 (br); $^{11}B\{^1H\}\delta$: 9.0 (s), 22.2 (br, B_2cat_3), 30.5 (br); $^1H\delta$: 0.78–0.96 (ov m), 1.23 (s, major), 1.29 (br), 1.53 (br), 2.09 (br), 6.5–6.8 (ov m, Bcat), 7.53 (t, J = 6 Hz), 7.99 (ov m), 8.56 (d, J = 6 Hz). Reactions carried out in THF-d_8 or CD_2Cl_2 eventually became viscous.

Preparation of trans-*$IrHCl(CO)(Bcat)(PPh_3)_2$ (7)*

A solution of HBcat (36 mg, 0.3 mmol) in 5 mL of CH_2Cl_2 was added dropwise to a solution of *trans*-$IrCl(CO)(PPh_3)_2$ (**6**) (156 mg, 0.2 mmol) in 10 mL of CH_2Cl_2. After stirring for 1 h, the solvent was removed in vacuo and the colourless residue was triturated with Et_2O, filtered, and dried in vacuo to yield 157 mg (87%) of complex **7**. Complex **7** was characterized spectroscopically by ^{1}H, ^{11}B, and ^{31}P NMR. NMR spectroscopic data (in CD_2Cl_2): $^{31}P\{^1H\}\delta$: 7.9 (s); $^{11}B\{^1H\}\delta$: 30.8 (br), $^1H\delta$: −6.03 (t, J_{HP} = 17 Hz, 1H, Ir-H), 7.2–7.8 (ov m, 34H, Bcat and PPh_3); IR (CH_2Cl_2)ν_{IrH} = 2007, ν_{CO} = 2118 cm^{-1}. Solutions of **7** in CH_2Cl_2 decomposed eventually (days) to regenerate **6** along with concomitant formation of B_2cat_3 and presumably either H_2 or BH_3 (3).

Preparation of $IrHCl(Bcat)(PPr^i_3)_2$ (8)

A solution of PPr^i_3 (64 mg, 0.4 mmol) in 10 mL of toluene was added dropwise to a solution of $[Ir(\mu\text{-}Cl)(COE)_2]_2$ (89 mg, 0.1 mmol) in 10 mL of toluene. To this was added dropwise a solution of HBcat (36 mg, 0.3 mmol) in 5 mL of toluene. After stirring for 1 h, the solvent was removed in vacuo and the yellow residue was triturated with Et_2O, filtered, and dried in vacuo to yield 58 mg (93%) of complex **8**. Complex **8** was characterized spectroscopically by ^{1}H, ^{11}B, and ^{31}P NMR. NMR spectroscopic data (in THF-d_8): $^{31}P\{^1H\}\delta$: 46.9 (s); $^{11}B\{^1H\}\delta$: 40.1 (br); $^1H\delta$: −22.73 (t, J_{HP} = 7 Hz, 1H, Ir-H), 1.24 (dd, $^3J_{HH}$ = $^3J_{HP}$ = 7 Hz, 36H, PCHCH_3), 2.70 (d sept, $^3J_{HH}$ = $^3J_{HP}$ = 7 Hz, 6H, PCHCH$_3$), 6.80 (br, 2H, Bcat), 6.93 (br, 2H, Bcat).

Reaction of HBcat with $IrCl(PEt_3)_3$ (9)

A solution of HBcat (18 mg, 0.15 mmol) in 1 mL of CD_2CL_2 was added dropwise to a solution of $IrCl(PEt_3)_3$ (55 mg, 0.1 mmol) in 1 mL of CD_2Cl_2. Upon stirring for 0.5 h, the resulting mixture became light yellow in colour and was characterized spectroscopically by ^{1}H, ^{11}B, and ^{31}P NMR. NMR spectroscopic data (in CD_2Cl_2): $^{31}P\{^1H\}\delta$: −20.4 (t, J_{PP} = 6 Hz, **10**), −8.1 (d, J_{PP} = 6 Hz, **10**); $^{11}B\{^1H\}\delta$: 12.2 (s), 23.9 (br, B_2cat_3), 33.5 (br, **10**); $^1H\delta$: −10.84 (d t, $J_{HPtrans}$ = 131 Hz, J_{HPcis} = 20 Hz, 1H, Ir-H, **10**), 1.04 (d t, $^3J_{HP}$ = $^3J_{HH}$ = 7 Hz, 27H, PCH_2CH_3), 1.83 (dq, $^2J_{HP}$ = 14 Hz, $^3J_{HH}$ = 7 Hz, 18H, PCH_2CH$_3$), 6.8–7.0 (ov m, Bcat). Reaction mixtures decomposed rapidly to give a variety of new phosphinoiridium hydride complexes. Similar product distributions were observed for reactions carried out in toluene-d_8.

General procedure for the catalyzed hydroboration of alkenes

All reactions were carried out under an atmosphere of dry nitrogen using a continuous purge glovebox (Vacuum Atmospheres). Catecholborane (250 mg, 2.1 mmol), in 1 mL of THF-d_8, was added dropwise to a mixture of the alkene (2.0 mmol) and catalyst (0.04 mmol) in 1 mL of THF-d_8. Identical results were obtained if the alkene was added to a mixture of catecholborane and catalyst. The resulting solutions were stirred for 30 min and then analyzed by high-field ^{1}H, ^{13}C, and ^{11}B NMR spectroscopy (*1h*).

Catalyzed hydroborations using photolysis

For reactions using *trans*-$IrCl(CO)(PPh_3)_2$ (**6**), photochemical experiments were carried out in a sealed 5-mm NMR tube with a water-filtered 450-W medium-pressure Hg lamp. Saturated boryl complex **7** was the only phosphinoiridium complex present in solution, at detectable levels, upon completion of photolysis.

Molecular structure determination

Crystals of **7** · CH_2Cl_2 suitable for X-ray diffraction studies were obtained from CH_2Cl_2. Data were collected at low temperature on

an Enraf–Nonius CAD4 diffractometer using graphite-monochromated MoKα radiation (λ = 0.71069 Å) and ω scan methods. Standard reflection intensities were monitored periodically with little variation observed over the collection period. Azimuthal scans showed 15.3% variation in intensity and the data were corrected for absorption (DIFABS). The structure was solved by direct methods (SHELXS) (28). Refinement was performed using full-matrix least squares on F with anisotropic thermal parameters for all non-hydrogen atoms (29). The asymmetric unit consists of one Ir complex and one molecule of solvent in general positions. While other hydrogen atoms were idealized and refined, the hydride was taken from a difference map and refined. The function minimized was $\Sigma w(|F_o| - |F_c|)^2$ with the weights, w, assigned as $[\sigma^2(I) + 0.0009I^2]^{-1/2}$. The atomic scattering factors were taken from the *International tables for x-ray crystallography*, Vol. IV (30). Details of the crystal structure determination including complete tables of coordinates, bond distances and angles, anisotropic thermal parameters, calculated and observed structure factors, and alternative ORTEP views of compound **7** have been deposited.[5]

Acknowledgements

We thank Nancy J. Herling, Steve A. Hill, John Nguyen, and Fred Davidson for expert technical assistance. T.B.M. acknowledges support from the Petroleum Research Fund, administered by the American Chemical Society, and from the Natural Sciences and Engineering Research Council of Canada.

1. (*a*) D. Männig and H. Nöth. Angew. Chem. Int. Ed. Engl. **24**, 878 (1985); (*b*) K. Burgess and M.J. Ohlmeyer. Chem. Rev. **91**, 1179 (1991); (*c*) D.A. Evans, G.C. Fu, and A.H. Hoveyda. J. Am. Chem. Soc. **114**, 6671 (1992); (*d*) M. Satoh, N. Miyaura, and A. Suzuki. Tetrahedron Lett. **31**, 231 (1990); (*e*) J.M. Brown and G.C. Lloyd-Jones. Tetrahedron: Asymmetry, **1**, 869 (1990); (*f*) T. Hayashi, Y. Matsumoto, and Y. Ito. Tetrahedron: Asymmetry, **2**, 601 (1991); (*g*) J. Zhang, B. Lou, G. Guo, and L. Dai. J. Org. Chem. **56**, 1670 (1991); (*h*) S.A. Westcott, H.P. Blom, T.B. Marder, and R.T. Baker. J. Am. Chem. Soc. **114**, 8863 (1992); (*i*) P. Kocienski, K. Jarowicki, and S. Marczak. Synthesis, 1191 (1991).
2. A. Pelter, K. Smith, and H.C. Brown. *In* Borane reagents. Academic Press, New York. 1988.
3. K. Burgess, W.A. van der Donk, S.A. Westcott, T.B. Marder, R.T. Baker, and J.C. Calabrese. J. Am. Chem. Soc. **114**, 9350 (1992).
4. M.G.L. Mirabelli and L.G. Sneddon. J. Am. Chem. Soc. **110**, 449 (1988).
5. (*a*) R. Wilczynski and L.G. Sneddon. J. Am. Chem. Soc. **102**, 2857 (1980); (*b*) Inorg. Chem. **20**, 3955 (1981).
6. D.A. Evans and G.C. Fu. J. Am. Chem. Soc. **113**, 4042 (1991).
7. J.R. Knorr and J.S. Merola. Organometallics, **9**, 3008 (1990).
8. (*a*) R.T. Baker, D.W. Ovenall, J.C. Calabrese, S.A. Westcott, N.J. Taylor, I.D. Williams, and T.B. Marder. J. Am. Chem. Soc. **112**, 9399 (1990); (*b*) S.A. Westcott, N.J. Taylor, T.B. Marder, R.T. Baker, N.L. Jones, and J.C. Calabrese. J. Chem. Soc. Chem. Commun. 304 (1991); (*c*) R.T. Baker, J.C. Calabrese, S.A. Westcott, P. Nguyen, and T.B. Marder. J. Am. Chem. Soc. In press; (*d*) S.A. Westcott, T.B. Marder, and R.T. Baker. Organometallics, **12**, 975 (1993).
9. P.M. Maitlis. Acc. Chem. Res. **11**, 301 (1978).
10. (*a*) C. White, A.J. Oliver, and P.M. Maitlis. J. Chem. Soc. Dalton Trans. 1901 (1973); (*b*) D.S. Gill and P.M. Maitlis. J. Organomet. Chem. **87**, 359 (1975).
11. D. Männig and H. Nöth. J. Chem. Soc. Dalton Trans. 1689 (1985).
12. S.A. Westcott, H.P. Blom, T.B. Marder, R.T. Baker, and J.C. Calabrese. Inorg. Chem. **32**, 2175 (1993).
13. H. Nöth and B. Wrackmeyer. *In* Nuclear magnetic resonance spectroscopy of boron compounds. Springer-Verlag, Berlin. 1978.
14. R.H. Crabtree and M.W. Davis. J. Org. Chem. **51**, 2655 (1986), and references therein.
15. (*a*) A. van der Ent and T.C. van Soest. J. Chem. Soc. Chem. Commun. 225 (1970); (*b*) H. van Gaal, H.G.A.M. Cuppers, and A. van der Ent. J. Chem. Soc. Chem. Commun. 1694 (1970).
16. M.A. Bennett and D.L. Milner. J. Am. Chem. Soc. **91**, 6983 (1969).
17. R.C. Taylor, J.F. Young, and G. Wilkinson. Inorg. Chem. **5**, 20 (1966).
18. H. Kono, K. Ito, and Y. Nagai. Chem. Lett. 1095 (1975).
19. L. Vaska and J.W. DiLuzio. J. Am. Chem. Soc. **83**, 2784 (1961).
20. D.P. Workman and S.G. Shore. *In* Electron deficient boron and carbon clusters. *Edited by* G.A. Olah, K. Wade, and R.E. Williams. Wiley–Interscience, New York. 1991.
21. G. Schmid. Angew. Chem. Int. Ed. Engl. **9**, 819 (1970).
22. (*a*) M.R. Churchill, J.J. Hackbarth, A. Davison, D.D. Traficante, and S.S. Wreford, J. Am. Chem. Soc. **96**, 4041 (1974); (*b*) M.R. Churchill and J.J. Hackbarth. Inorg. Chem. **14**, 2047 (1975).
23. A.L. Casalnuovo, J.C. Calabrese, and D. Milstein. J. Am. Chem. Soc. **110**, 6738 (1988).
24. G.W. Parshall. *In* Homogeneous catalysis: the applications and chemistry of catalysis by soluble transition metal complexes. Wiley–Interscience, New York. 1980.
25. R.G. Ball, W.A.G. Graham, D.M. Heinekey, J.K. Hoyano, A.D. McMaster, B.M. Mattson, and S.T. Michel. Inorg. Chem. **29**, 2023 (1990).
26. A. van der Ent and A.L. Onderdelinden. Inorg. Synth. **28**, 90 (1990).
27. S.D. Robinson and B.L. Shaw. J. Chem. Soc. (A), 4997 (1965).
28. G.M. Sheldrick. SHELX. University of Gottingen, Federal Republic of Germany. 1986.
29. D.T. Cromer and J.A. Ibers. *In* International tables for X-ray crystallography. Vol. IV. Kynoch Press, Birmingham. 1974. Table 2.3.2.
30. D.T. Cromer and J.T. Waber. *In* International table for X-ray crystallography. Vol. IV. Kynoch Press, Birmingham. 1974. Table 2.2B.

[5]A complete set of data may be purchased from: The Depository of Unpublished Data, Document Delivery, CISTI, National Research Council Canada, Ottawa, Canada K1A 0S2.

Tables of coordinates, bond distances and angles, and alternate ORTEP views of **7** have also been deposited with the Cambridge Crystallographic Data Centre and can be obtained on request from The Director, Cambridge Crystallographic Data Centre, University Chemical Laboratory, 12 Union Road, Cambridge, CB2 1EZ, U.K.

Can. J. Chem. Downloaded from www.nrcresearchpress.com by 213.200.69.106 on 09/08/12
For personal use only.

Calorimetric investigation of complex formation in the aqueous Fe(III)–citrate system

QIYUAN CHEN,[1] XIN ZHANG,[2] CHING-HSIEN WU,[3] AND LOREN G. HEPLER
Department of Chemistry, University of Alberta, Edmonton, Alta., Canada T6G 2G2

Received September 14, 1992

QIYUAN CHEN, XIN ZHANG, CHING-HSIEN WU, and LOREN G. HEPLER. Can. J. Chem. **71**, 937 (1993).

We have made calorimetric measurements of thermal effects associated with adding NaOH(aq) or HCl(aq) to aqueous solutions (pH = 1.623) of ferric chloride + sodium citrate. Combination of these measured heats with concentrations of various species calculated from stoichiometric compositions and previously known K and ΔH values leads to ΔH values for four aqueous Fe(III)–citrate complexes. Further combination of ΔG^0 values from equilibrium constants with our ΔH values leads to ΔS^0 values, which are discussed in relation to conventional ideas about relationships between entropy and solute–water interactions.

QIYUAN CHEN, XIN ZHANG, CHIEN-HSIEN WU et LOREN G. HEPLER. Can. J. Chem. **71**, 937 (1993).

On a effectué des mesures calorimétriques des effets thermiques associés à l'addition de NaOH(aq) ou HCl(aq) à des solutions aqueuses (pH = 1,623) de chlorure ferrique + citrate de sodium. Une combinaison de ces chaleurs mesurées avec les concentrations des diverses espèces calculées à partir des compositions stoechiométriques et de valeurs déjà connues de K et de ΔH fournit les valeurs de ΔH pour quatre complexes aqueux de Fe(III)–citrate. Une autre combinaison des valeurs de ΔG^0 obtenues à partir de constantes d'équilibre avec les valeurs de ΔH fournit les valeurs de ΔS^0 dont on discute en fonction des idées conventionnelles concernant les relations entre l'entropie et les interactions soluté–eau.

[Traduit par la rédaction]

Introduction

Complexes of citric acid or citrate ions with various metal ions in aqueous solution are important in such fields as food chemistry and biochemistry. Stability constants are known for several metal ion – citrate complexes, but we do not know of any calorimetric investigations of any of these systems. In this paper we report the results of our calorimetric measurements on the aqueous iron(III)–citrate system.

Background information required for our investigations is as follows.

Bates and Pinching (1) carried out a thorough electrochemical investigation of aqueous citric acid, leading to standard state (infinite dilution) equilibrium constants for all three ionizations over the temperature range 0–50°C and thence to values for the enthalpies of all three ionization steps. We also have equilibrium constants (0.1 M KNO_3 solution) from Field et al. (2). Although the equilibrium constants from Bates and Pinching (1) are more accurate than the values from Field et al. (2), we choose to use these latter values as good averages for dilute solutions for which we do not have activity coefficients. These equilibrium constant values, along with enthalpies from Bates and Pinching (1), are listed in Table 1 with equations for the reactions to which they apply.

Field et al. (2) reported equilibrium constants for the Fe(III) – citric acid system, as summarized in Table 1. The species that Field et al. represented by $FeLH_{-1}^-$ is represented in Table 1 by $FeOHL^-(aq)$, which we[4] consider to be more realistic.

In addition to the equilibrium constants from Field et al. (1), we have an estimated constant (K_9, in Table 1) for $FeL_2^{3-}(aq)$ that Martin (3) provided in his useful review and analysis of citrate binding by Al^{3+} and Fe^{3+}.

In strongly acidic solutions in which there are no complexing species, Fe(III) is present as $Fe^{3+}(aq)$. As the pH increases, species such as $FeOH^{2+}(aq)$ become important. We used equilibrium constants tabulated by Martell and Smith (4) and Smith and Martell (5) and as calculated from $\Delta_f G^0$ values from the National Bureau of Standards (6) to establish that the only iron-hydroxy species in solution that should be considered in analyzing the results of our experiments is $FeOH^{2+}(aq)$. $Fe(OH)_3(ppct)$ occurs only at higher pH than in our calorimetric measurements.

The equilibrium constant and the enthalpy for $H^+(aq) + OH^-(aq) = H_2O(liq)$ from a critical review (7) are listed in Table 1.

In Fig. 1 we show a distribution diagram for the various iron species present in solutions having total iron and citrate concentrations in the same range as used in our calorimetric experiments.

Experimental

Certified ACS ferric chloride hexahydrate, $FeCl_3 \cdot 6H_2O$, was obtained from Fisher Scientific Co. Reagent grade (99.0% minimum assay) sodium citrate dihydrate, $Na_3C_6H_5O_7 \cdot 2H_2O$, was from Caledon Laboratories Ltd.

Sodium hydroxide solution was standardized by titration against potassium acid phthalate, and hydrochloric acid solution was standardized by titration with the previously standardized sodium hydroxide solution.

A stock solution for subsequent calorimetric measurements was prepared by dissolving ferric chloride hexahydrate in hydrochloric acid solution; this solution was then standardized by titration with aqueous EDTA. A known amount of sodium citrate dihydrate was then added to this acidic ferric chloride solution, followed by dilution with distilled water and hydrochloric acid to yield a final stock solution having pH = 1.623 and concentrations of Fe(III) and citric acid equal to 9.971×10^{-4} mol/L and 9.965×10^{-3} mol/L, respectively.

All pH measurements were made with an Accumet pH meter

[1]Visiting Professor from the Department of Chemistry, Central-South University of Technology, Changsha, Hunan 410083, People's Republic of China.

[2]Present address: Department of Chemistry, Simon Fraser University, Burnaby, B.C., Canada V5A 1S6.

[3]Visiting Professor from LaGuardia College, 31-10 Thomson Avenue, Long Island City, NY 11101, U.S.A.

[4]X. Zhang, C.-H. Wu, Q. Chen, and L.G. Hepler. To be published.

Can. J. Chem. Downloaded from www.nrcresearchpress.com by 213.200.69.106 on 09/08/12
For personal use only.

TABLE 1. Equilibrium constants and already known enthalpies of reaction[a]

$H^+(aq) + L^{3-}(aq) = HL^{2-}(aq)$	$K_1 = 5.0 \times 10^5$	$\Delta H_1 = 3.36$ kJ mol^{-1}
$2H^+(aq) + L^{3-}(aq) = H_2L^-(aq)$	$K_2 = 1.1 \times 10^{10}$	$\Delta H_2 = 0.92$ kJ mol^{-1}
$3H^+(aq) + L^{3-}(aq) = H_3L(aq)$	$K_3 = 7.4 \times 10^{12}$	$\Delta H_3 = -3.25$ kJ mol^{-1}
$H^+(aq) + OH^-(aq) = H_2O(liq)$	$K_4 = 1.0 \times 10^{14}$	$\Delta H_4 = -55.82$ kJ mol^{-1}
$Fe^{3+}(aq) + H_2O(liq) =$ $FeOH^{2+}(aq) + H^+(aq)$	$K_5 = 6.5 \times 10^{-3}$	$\Delta H_5 = 44$ kJ mol^{-1}
$Fe^{3+}(aq) + L^{3-}(aq) = FeL(aq)$	$K_6 = 1.5 \times 10^{11}$	
$Fe^{3+}(aq) + H^+(aq) + L^{3-}(aq) =$ $FeHL^+(aq)$	$K_7 = 2.3 \times 10^{12}$	
$Fe^{3+}(aq) + L^{3-}(aq) + H_2O(liq) =$ $FeOHL^-(aq) + H^+(aq)$	$K_8 = 3.1 \times 10^8$	
$Fe^{3+}(aq) + 2L^{3-}(aq) = FeL_2^{3-}(aq)$	$K_9 = 1.5 \times 10^{18}$	

[a]These equilibrium constants and molar enthalpies are from refs. 1, 2, 3, and 7 as discussed in the text.

Can. J. Chem. Downloaded from www.nrcresearchpress.com by 213.200.69.106 on 09/08/12
For personal use only.

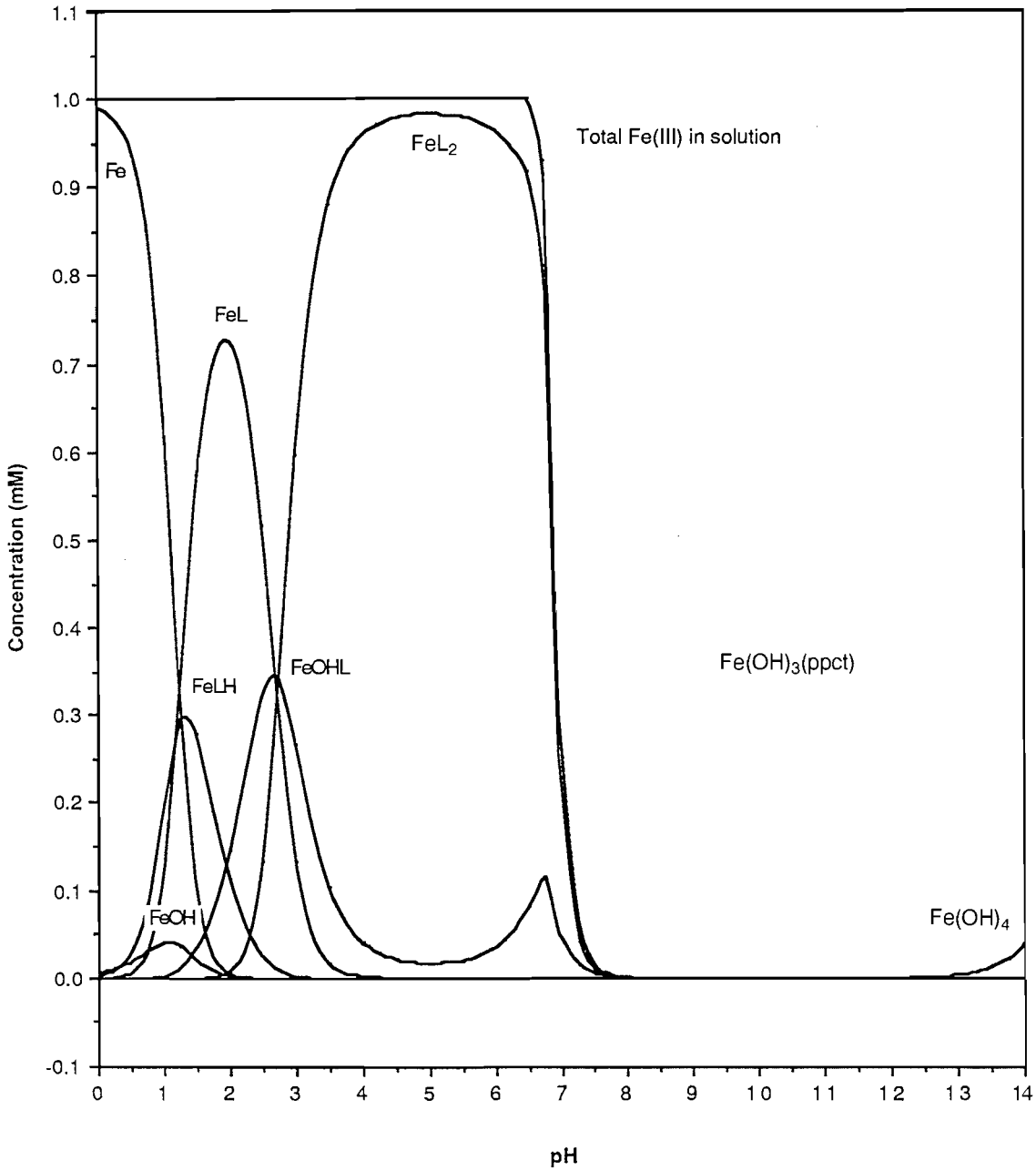

FIG. 1. Equilibrium concentrations of iron species (charges not shown) in a solution with Σ[Fe(III)] = 1 mM = 1×10^{-3} mol/L and Σ[citrate] = 10 mM = 1×10^{-2} mol/L.

Can. J. Chem. Downloaded from www.nrcresearchpress.com by 213.200.69.106 on 09/08/12
For personal use only.

(with combination pH-reference electrode from Orion Research Inc.), calibrated with standard buffer solutions from Fisher Scientific Co.

Our homemade solution calorimeter consisted of a glass Dewar vessel (360 cm^3 capacity) suspended in a brass can that was immersed in a constant temperature bath maintained at 25.00 ± 0.02°C, held constant to ±0.001°C during each measurement. Temperature changes in the calorimeter were measured with a thermistor (YSI 44005) combined with a current comparator resistance bridge (Guildline 9975). The calorimeter was calibrated electrically for each enthalpy measurement. We checked the accuracy of our calorimeter by way of test measurements of the enthalpy of solution of KCl(cr) in distilled water, the enthalpy of solution of 4-aminopyridine(cr) in excess aqueous perchloric acid, the enthalpy of solution of THAM(cr) in excess aqueous hydrochloric acid, and the enthalpy of neutralization of THAM(aq) by excess hydrochloric acid. Results of these measurements are in good agreement with "best" results from the literature (6, 8–13), as will be discussed elsewhere,[5] where we also provide a more detailed description of the calorimeter. Another test was provided by calculating the enthalpy of neutralization of OH^-(aq) by H^+(aq) as described in the fourth paragraph below.

Before carrying out calorimetric measurements as described below, we did "beaker experiments" in which we added known amounts of HCl or NaOH to known amounts of stock solution and measured the resulting pH. Amounts of NaOH and HCl for subsequent calorimetric measurements were chosen to produce changes in pH that would lead to appropriate changes in fractions of Fe(III) in various complexes.

Our experimental procedure for calorimetric measurements began with filling the calorimeter with a known amount of stock solution containing 9.971×10^{-4} mol/L Fe(III) and 9.965×10^{-3} mol/L citric acid at pH = 1.623. A glass ampoule containing a known amount of stock HCl or NaOH solution was attached to the end of the calorimeter's stirrer. The calorimeter and surrounding can were then immersed in the constant temperature bath. After the temperature–time drift became nearly constant, the calorimeter was calibrated electrically, followed by breaking the glass ampoule to permit the HCl or NaOH solution to mix with the acidic Fe(III) citric acid solution in the calorimeter, followed by another electrical calibration.

"Blank" calorimetric experiments were carried out to evaluate the total thermal effect associated with breaking the glass ampoules plus adding HCl(aq) or NaOH(aq) to aqueous HCl with initial pH = 1.623 (no Fe(III) or citric acid present). Amounts of HCl or NaOH were chosen so that the final pH of a solution would closely approximate that of a final solution resulting from adding HCl(aq) or NaOH(aq) to a stock solution containing Fe(III) and citric acid at initial pH = 1.623. In this way we obtained the heats that we represent later by q_{blank}.

In each of the blank experiments involving NaOH(aq) there was excess acid in the calorimeter so that the amount of reaction was determined by the number of moles of OH^-(aq) in the ampoule. Results of these measurements permitted calculation of the enthalpy of reaction of OH^-(aq) with H^+(aq) as follows. For this calculation we attributed the entire measured thermal effect (q) to the chemical reaction (neglecting the small contribution of bulb-breaking) and then obtained the ΔH as q/n, where n represents the number of moles of OH^-(aq) in the ampoule. In this way we found $\Delta H = -55.9 \pm 0.2$ kJ/mol as compared with a better standard value (8) of $\Delta H^0 = -55.815$ kJ/mol. Our ΔH, which refers to actual concentrations in our calorimeter rather than extrapolated to infinite dilution, is less accurate than the standard value because of our neglect of the *small* thermal effect of bulb-breaking and also because our measurements were done with excess H^+(aq) rather than excess OH^-(aq) to minimize complications due to small amounts of carbonate or silicate impurity in the NaOH(aq) solution.

[5]C. Dobrogowska and L.G. Hepler. To be published.

TABLE 2. Results of calorimetric measurements of thermal effects of adding NaOH(aq) or HCl(aq) to stock solution with initial pH = 1.623, total Fe(III) concentration = 9.971×10^{-4} mol/L, and total citrate concentration = 9.965×10^{-3} mol/L

Expt. no.	pH (final)	q_r (J)[a]	q_c (J)[b]
1	1.978	0.42	−0.35
2	4.811	37.32	23.00
3	2.804	−4.90	−9.89
4	0.980	11.83	12.80

[a]q_r is the total measured heat minus the "blank" heat, as described in the text.

[b]q_c is the heat associated with Fe(III)–citrate complexes, obtained as q_r minus contributions from reactions for which ΔH values are already known, as described in the text.

Results and calculations

Results of calorimetric measurements of thermal effects associated with adding HCl(aq) or NaOH(aq) to acidic solutions of Fe(III) and citric acid are summarized in Table 2. The "reaction heats" labelled q_r are calculated from the total measured heats q_m and the blank heats of combined bulb-breaking and mixing of the solution in the ampoule with the solution in the calorimeter (pH = 1.623, no Fe(III) or citric acid) according to

$$[1] \quad q_r = q_m - q_{blank}$$

We emphasize here that q_{blank} values are for amounts of NaOH(aq) or HCl(aq) that yield the same pH change in blank experiments as observed in the corresponding "reaction" experiment with a solution containing Fe(III) and citric acid.

Some of the heat represented by q_r is due to reactions for which we have equilibrium constants *and* ΔH^0 values (K_i and ΔH_i^0, i = 1 through 5 in Table 1). Knowledge of amount and stoichiometric composition of the original solution, initial pH = 1.623, amount of added HCl or NaOH, pH of final solution, and equilibrium constants listed in Table 1 permits calculation of the number of moles of various species in the final solution and number of moles of various species in the initial solution. All of these values permit us to calculate a "known" contribution q_{known} to q_r as

$$[2] \quad q_{known} = \Sigma(\Delta n_i)\Delta H_i^0$$

in which each Δn_i represents the change in number of moles of some species (as shown in Table 3) and each ΔH_i^0 represents the molar enthalpy of a corresponding reaction (as shown in Table 1). Next, we calculate the total heat q_c due to iron–citrate complexes as

$$[3] \quad q_c = q_r - q_{known}$$

This q_c is attributed to reactions involving Fe(III) and citric acid for which we have K_j values (j = 6 through 9 in Table 1).

Each of the calorimetric measurements for which results are summarized in Table 2 involved different concentrations of the four Fe(III) – citric acid species represented in Table 1 by FeL(aq), $FeHL^+$(aq), $FeOHL^-$(aq), and

TABLE 3. Changes in number of moles (Δn) of various species in calorimetric measurements in which NaOH(aq) or HCl(aq) was added to stock solution (see Table 2 for description of solution and calorimetric results)

	Δn for species below							
Expt. no.	$FeOH^{2+}$	H_3L	H_2L^-	HL^{2-}	FeL	$FeHL^+$	$FeOHL^-$	FeL_2^{3-}
1	-2.94×10^{-6}	-1.92×10^{-4}	1.73×10^{-4}	1.09×10^{-6}	2.40×10^{-5}	-3.43×10^{-5}	2.42×10^{-5}	1.78×10^{-6}
2	-4.11×10^{-6}	-2.59×10^{-3}	4.14×10^{-4}	1.65×10^{-3}	-1.97×10^{-4}	-7.28×10^{-5}	-1.10×10^{-5}	3.00×10^{-4}
3	-3.83×10^{-6}	-1.21×10^{-3}	1.05×10^{-3}	3.32×10^{-5}	-1.09×10^{-4}	-6.62×10^{-5}	8.02×10^{-5}	1.13×10^{-4}
4	7.38×10^{-6}	2.82×10^{-4}	-1.10×10^{-4}	-2.56×10^{-7}	-1.43×10^{-4}	-1.46×10^{-5}	-1.39×10^{-5}	-1.49×10^{-7}

TABLE 4. Changes of thermodynamic properties of reactions in iron(III)–citrate system

Reaction	ΔG^0 (kJ mol^{-1})	ΔH^0 (kJ mol^{-1})	ΔS^0 (J K^{-1} mol^{-1})
$Fe^{3+}(aq) + L^{3-}(aq) = FeL(aq)$	−63.8	−29 ± 3	117 ± 15
$Fe^{3+}(aq) + 2L^{3-}(aq) = FeL_2^{3-}(aq)$	−104	−18 ± 6	289 ± 15
$Fe^{3+}(aq) + H^+(aq) + L^{3-}(aq) = FeHL^+(aq)$	−70.6	−260 ± 10	−636 ± 40
$Fe^{3+}(aq) + L^{3-}(aq) + H_2O(liq) = FeOHL^-(aq) + H^+(aq)$	−48.5	−350 ± 10	−1012 ± 40

$FeL_2^{3-}(aq)$. It is therefore possible to write four simultaneous equations of the form

[4] $q_c = \Sigma(\Delta n_j)\Delta H_j$

in which each Δn_j represents the change in number of moles of one of the four iron–citrate complexes and each ΔH_j represents the molar enthalpy of forming that complex from $Fe^{3+}(aq)$ and $L^{3-}(aq)$ as represented by reaction equations in Tables 1 and 4. Solving these four simultaneous equations leads to the values for ΔH_j that are listed in Table 4. Combination of these ΔH values with the free energies calculated from $\Delta G^0 = -RT \ln K$ leads to the ΔS^0 values that are also listed in Table 4.

Uncertainties in our reported results are estimated as follows. First, it should be recognized that the K's (no activity coefficients) from Field et al. (2) are average values for specified "dilute" solutions. Because our "dilute" solutions had ionic strengths similar to those of the solutions investigated by Field et al. (2), it is a reasonable approximation to use their reported K values without activity coefficients in calculating the concentrations of various species. The ΔH_i^0 values used in eq. [2] appear to be quite accurate for $i = 1$ through 4 (see Table 1), but less accurate for $i = 5$, which makes only a small contribution to q_{known}. But it should be recognized that each of these ΔH_i^0 values refers to the infinite dilution state rather than to the "dilute" solutions of our experiments. Finally, it should be noted that each calorimetric experiment involved non-negligible changes (more than 5%) in concentrations of at least three different iron citrate species, making it necessary to solve simultaneous equations to obtain desired ΔH values for four different reactions, rather than the more accurate procedure of obtaining each ΔH of reaction separately from measured heats obtained from experiments involving only one dominant reaction. It is on the basis of all of these contributions to uncertainties that we have estimated the ±values shown in Table 4.

One way to make a tentative assessment of the reliability of thermodynamic properties associated with chemical reactions is to consider whether reported ΔS^0 values are "reasonable" in relation to ΔS^0 values for "similar" reactions, which also involves our ideas about the molecules and ions in our chemical systems.

We begin by noting that ΔS^0 values are negative for reactions of type

[5] $A(g) + B(g) = AB(g)$

in which there is a net decrease in number of molecules as the reaction proceeds from left to right. It is known from statistical mechanics that this overall loss of standard state entropy can be attributed to the loss of translational entropy that comes directly from the decreasing number of molecules. If this were the only factor to be considered, we would expect all of the ΔS^0 values in Table 4 to be negative.

For reactions in aqueous solution, however, it is necessary to consider the hydration of the solute species. We know in a general way that decreasing the absolute value of the charge on an ion results in an increase in entropy, which we attribute to a decrease in hydration or, expressed differently, release of (possibly only partly) bound water molecules to the bulk water. To illustrate this point we write

[6] $A(H_2O)_a + B(H_2O)_b = AB(H_2O)_c + (a + b - c)H_2O$

If $(a + b - c)$ is larger than unity, we have a net increase of "independent" particles as reaction proceeds from left to right, and we expect that ΔS^0 will be positive.

On the basis of the reasoning above and ΔS^0 values calculated (using properties reported in refs. 6 and 14) for reactions in which there is a net decrease in total charge and also a decrease in number of solute species, we expect that all of the ΔS^0 values in Table 4 should be positive. The reported ΔS^0 values for formation of FeL(aq) and $FeL_2^{3-}(aq)$ are positive, in accord with this expectation, but the two following ΔS^0 values are large and *negative*.

On the basis of the reasoning and observations summarized above, we suggest the following alternatives. (*i*) The

Can. J. Chem. Downloaded from www.nrcresearchpress.com by 213.200.69.106 on 09/08/12
For personal use only.

qualitative reasoning above is seriously inadequate for species such as $FeHL^+(aq)$ and $FeOHL^-(aq)$. (*ii*) The iron–citrate system is more complex than indicated by the reported (2) equilibrium constants, which means that more or different equilibria must be considered. Here we are attributing the "unreasonable" ΔS^0 values to partially inadequate analysis of the electrochemical and spectrophotometric data by Field et al. (2), followed by our similarly inadequate analysis of our calorimetric data. (*iii*) Field et al. (2) or we have made substantial experimental errors.

It is our opinion that (*ii*) above is more likely than either (*i*) or (*iii*).

Acknowledgements

We thank the Natural Sciences and Engineering Research Council of Canada for financial support and also thank Grace Liu for her help with some of the experimental work.

1. R.G. Bates and G.D. Pinching. J. Am. Chem. Soc. **71**, 1274 (1949).
2. T.B. Field, J.L. McCourt, and W.A.E. McBryde. Can. J. Chem. **52**, 3119 (1974).
3. R.B. Martin. J. Inorg. Biochem. **28**, 181 (1986).
4. A.E. Martell and R.M. Smith. Critical stability constants. Vol. 5. Plenum Press, New York. 1982.
5. R.M. Smith and A.E. Martell. Critical stability constants. Vol. 4. Plenum Press, New York. 1976.
6. D.D. Wagman, W.H. Evans, V.B. Parker, R.H. Schumm, I. Halow, S.M. Bailey, K.L. Churney, and R.L. Nuttall. J. Phys. Chem. Ref. Data, **11**, Suppl. No. 2, 1 (1982).
7. G. Olofsson and L.G. Hepler. J. Solution Chem. **4**, 127 (1975).
8. T.E. Burchfield and L.G. Hepler. J. Chem. Thermodyn. **13**, 513 (1981).
9. M.J. Akello, M.I. Paz-Andrade, and G. Pilcher. J. Chem. Thermodyn. **15**, 949 (1983).
10. J.O. Hill, G. Ojelund, and I. Wadso. J. Chem. Thermodyn. **1**, 111, (1969).
11. L.D. Hansen and E.A. Lewis. J. Chem. Thermodyn. **3**, 35 (1971).
12. A.P. Brunetti, E.J. Prosen, and R.N. Goldberg. J. Res. Natl. Bur. Stand. Sect. A: **77A**, 599 (1973).
13. R.B. Ahmad, J.O. Hill, and R.J. Magee. Thermochim. Acta, **71**, 25 (1983).
14. J.J. Christensen and R.M. Izatt. Handbook of metal ligand heats and related thermodynamic quantities. Marcel Dekker, Inc., New York. 1970.

Can. J. Chem. Downloaded from www.nrcresearchpress.com by 213.200.69.106 on 09/08/12
For personal use only.

Photodimerization of α,ω-diarylbutadienes. I. Crystal and molecular structures of *trans,trans*-1-(2′-methoxyphenyl)-4-(4′-nitrophenyl)-1,3-butadiene and its photodimer

MARIO V. CAPPARELLI[1] AND PENELOPE W. CODDING

Departments of Chemistry and of Pharmacology and Therapeutics, University of Calgary, Calgary, Alta., Canada T2N 1N4

Received February 1, 1993

MARIO V. CAPPARELLI and PENELOPE W. CODDING. Can. J. Chem. **71**, 942 (1993).

X-ray crystallographic studies showed that orange crystals of the title diarylbutadiene **1** undergo a topochemically controlled [2+2] photocycloaddition when exposed to visible light to produce the cyclobutane dimer **2**, which is yellow. The conformation of molecule **1** is planar with a maximum deviation from an all-atom mean plane, including substituents, of ≤ 0.28 Å. The crystal structure of **1** displays pairs of molecules packed in a head-to-tail arrangement across inversion centers that allows π orbital overlap between nearest neighbor butadiene double bonds. Intermolecular distances and angles between these photoreactive atoms are C···C, 3.517(2) Å and C—C···C, 92.0(2)°; and the dihedral angle between the plane of the four photoreactive atoms and the plane of the butadiene in one molecule is 72.9°. Molecule **2** lies on a crystallographic inversion centre, which constrains the cyclobutane ring to absolute planarity with C—C distances of 1.558(2) and 1.569(2) Å and C—C—C angle of 90.61(1)°. The dihedral angles between the cyclobutane ring and the two phenyl rings are 81.2° for the *p*-nitrophenyl and 54.0° for the *o*-methoxyphenyl. From the crystal structures of **1** and **2**, the displacement of each of the four photoreactive atoms during the solid-state dimerization can be estimated to be ca. 1.00 Å. Crystals of **1** are orthorhombic, *Pbca*, a = 7.471(1), b = 14.283(1), c = 25.940(1) Å, Z = 8, and those of **2** are monoclinic, $P2_1/c$, a = 11.5396(5), b = 16.129(1), c = 7.9035(3) Å, β = 90.264(3)°, Z = 4. Both structures were solved by direct methods and refined to final values of R = 0.0481 and 0.0512 using 2788 and 2333 observed ($I > 3\sigma(I)$) reflections, for **1** and **2**, respectively.

MARIO V. CAPPARELLI et PENELOPE W. CODDING. Can. J. Chem. **71**, 942 (1993).

Des études cristallographiques ont montré que lorsqu'on soumet les cristaux orange du diarylbutadiène **1** mentionné dans le titre à de la lumière visible, ils subissent une photocycloaddition [2+2] topochimiquement contrôlée qui conduit au cyclobutane dimère **2** qui est jaune. La conformation de la molécule **1** est plane et la déviation maximale du plan moyen des tous les atomes, y compris les substituants, est ≤ 0,28 Å. La structure cristalline du composé **1** présente des paires de molécules placées dans un arrangement tête à queue à travers les centres d'inversion ce qui permet un recouvrement d'orbitales π entre les doubles liaisons voisines les plus près du cyclobutadiène. Les distances intermoléculaires et les angles entres ces atomes photoréactifs sont C···C, 3,517(2) Å et C—C···C, 92,0(2)°; l'angle dièdre entre le plan des quatre atomes photoréactifs et le plan du butadiène d'une molécule est de 72,9°. La molécule **2** se trouve au centre d'inversion cristallographique, ce qui force le cyclobutane à exister sous une forme absolument plane avec des distances C—C de 1,558(2) et 1,569(2) Å et un angle C—C—C de 90,6(1)°. Les angles dièdres entre le cyclobutane et les deux noyaux phényles sont respectivement de 81,2° pour le *p*-nitrophényle et 54,0° pour le *o*-méthoxyphényle. Sur la base des structures des composés **1** et **2**, on peut évaluer que le déplacement de chacun des quatre atomes photoréactifs durant la dimérisation à l'état solide est d'environ 1,00 Å. Les cristaux du composé **1** sont orthorhombiques, *Pbca*, a = 7,471(1), b = 14,283(1) et c = 25,940(1) Å, Z = 8 alors que ceux du composé **2** sont monocliniques, $P2_1/c$, avec a = 11,5396(5), b = 16,129(1) et c = 7,9035(3) Å, β = 90,264(3)° et Z = 4. On a résolu les deux structures par des méthodes directes et on les a affinées jusqu'à des valeurs finales de R de 0,0481 et 0,0512 pour 2788 et 2333 réflexions observées ($I > 3\sigma(I)$) avec **1** et **2** respectivement.

[Traduit par la rédaction]

Introduction

Organic compounds are of interest as potential nonlinear optical (NLO) materials because they form molecular crystals (1, 2) in which individual molecules retain their identities to a much larger degree than in inorganic crystals. Accordingly, molecular polarizability and hyperpolarizability are exhibited as macroscopic crystal properties provided that the hyperpolarizable molecules crystallize in polar space groups (3). NLO effects arise from the polarization induced in a molecule by an electric field. Organic molecules with extensive conjugated systems and charge asymmetry may be suitable materials for second-order NLO properties, especially the α,ω-diarylpolyenes, D-(CH=CH)$_n$-A, with appropriate aromatic ring substituents to make the aryl groups efficient donors (D) and acceptors (A) (4).

As a part of a project aimed at the structural characterization of potential NLO organic compounds and the preparation of useful NLO crystals, the α,ω-diarylbutadienes were investigated. Here we present the crystal structure of *trans,trans*-1-(2′-methoxyphenyl)-4-(4′-nitrophenyl)-1,3-butadiene, **1**. All of the crystalline forms of this compound that we obtained were centrosymmetric and, therefore, unsuitable for NLO applications. During this study we observed that the orange crystals of **1** were sensitive to visible light and reacted to produce a yellow compound, which we characterized. The instability of compound **1** in the solid state suggests that butadiene-based NLO materials will frequently be unsuitable for the manufacture of electronic devices. The photoproduct crystal structure is also reported; it is a dimer of **1**: *r*-1, *t*-3-di(2′-methoxyphenyl)-*c*-2, *t*-4-di(4′-

[1]Present address: Escuela de Química, Universidad Central de Venezuela, Apartado 47102, Caracas 1041-A, Venezuela.

Can. J. Chem. Downloaded from www.nrcresearchpress.com by 213.200.69.106 on 09/08/12
For personal use only.

Can. J. Chem. Downloaded from www.nrcresearchpress.com by 213.200.69.106 on 09/08/12
For personal use only.

Can. J. Chem. Downloaded from www.nrcresearchpress.com by 213.200.69.106 on 09/08/12
For personal use only.

nitro-*trans*-styryl)cyclobutane, **2**. The possibility of solid-state photodimerization of **1** is also discussed in terms of its crystal packing.

Experimental

Under ordinary room lighting, evaporation of a toluene solution of the original sample of **1** (supplied by Dr. C.W. Spangler, Northern Illinois University) resulted in crystals of both compounds, easily recognizable by their colors. Those of **2** were needles, too thin for single-crystal X-ray work, and were separated manually under the microscope and dissolved in acetone. Slow evaporation of this solution produced needles thick enough to be cut into suitable X-ray specimens.

Unit cell and intensity measurements were carried out on an Enraf–Nonius CAD4 diffractometer, using Ni-filtered CuKα radiation (λ = 1.54178 Å). Measurements for **1** were made at low temperature, to prevent or slow down crystal deterioration. Crystal data, intensity data collection parameters, and final refinement results are summarized in Table 1. Unit cell parameters were obtained from least-squares fit of the setting angles of 22/25 (for **1**/**2**, respectively) automatically centered reflections with θ values in the ranges 13.0–51.5°/24.2–44.6° (for **1**/**2**). Both space groups were uniquely determined by the systematic absences. Intensity data were measured using ω/2θ scan modes with variable scan speeds to a maximum θ = 75° for four octants/one quadrant (for **1**/**2**). Three standard reflections were monitored every 2000 s of exposure time. Those of **2** showed no significant variation in their intensities, but for **1** the values displayed a significant and apparently random fluctuation. To overcome this problem we measured each independent reflection in four different octants. This behavior was attributed mainly to ice formation on the crystal (although some degree of crystal deterioration cannot be ruled out) and was reflected in the relatively large values of R_{int} and S. The data were scaled using the check reflections and corrected by Lorentz and polarization effects.

The structures were solved by direct methods and refined by full-matrix least squares using anisotropic thermal parameters for the non-hydrogen atoms. Hydrogen atoms were initially placed at calculated positions and then allowed to refine with isotropic temperature factors. Weighting schemes were applied during the last cycles of refinement, and for **2** an empirical extinction correction was also made. No absorption corrections were applied. The calculations were done using the SHELXS86 (5), SHELX76 (6), and XANADU (7) programs, and programs ORTEPII (8) and PLUTO (9) were used for drawings. Complex neutral-atom scattering factors from the *International tables for crystallography* (10) were employed.

The final fractional coordinates and equivalent isotropic temperature factors of the non-H atoms were listed in Table 2. The bond lengths, bond angles, and torsion angles are given in Table 3.[2] The molecular structures and atomic labeling schemes are shown in Figs. 1 and 2. The labeling scheme identifies three separate regions in these molecules: the donor region which has the suffix "d", the acceptor region which has the suffix "a", and the chain region which has the suffix "c"; hence, the atoms in the butadiene chain are C1c, C2c, C3c, and C4c.

[2]Tables of anisotropic temperature factors for the non-hydrogen atoms, positional and isotropic thermal parameters for hydrogen atoms, and observed and calculated structure factors for compounds **1** and **2** were deposited as supplementary material and may be purchased from: The Depository of Unpublished Data, Document Delivery, CISTI, National Research Council Canada, Ottawa, Canada K1A 0S2.

Tables of hydrogen positional parameters for **1** and **2** have also been deposited with the Cambridge Crystallographic Data Centre and can be obtained on request from The Director, Cambridge Crystallographic Data Centre, University Chemical Laboratory, 12 Union Road, Cambridge, CB2 1EZ, U.K.

Results

Molecular geometry of the monomer (1)

The regular hexagonal geometry of six-membered aromatic rings is modified when hydrogen atoms are substituted by other functional groups (11–13). Accordingly, in both of the phenyl rings of **1** the bonds adjacent to the butadiene chain are significantly longer than the rest, while the endocyclic angles at C(1) are significantly smaller than 120° and those at C(2) and C(6) are widened. Although these are the types of deformations expected for an electron-releasing substituent at C(1a) and C(1d) (11, 14), substitution of hydrogen by carbon (which would have the same electronegativity as the ring) would also produce a narrowing to 117.5–118.0°, as found in **1** (12). The widening at C(2d) is smaller than that at the other three *ortho* positions due to the presence of the methoxy substituent, which normally produces a small decrease (ca. 0.1–0.2°) in the corresponding endocyclic angle (12, 15). The endocyclic angle at C(4a) shows a significant widening because of the electron-withdrawing character of the NO_2 group (15); its value is identical to the average of 122.1° obtained from structural studies of many *para*-substituted nitrobenzenes (11, 12).

The chain has a *trans,trans* configuration and a clear pattern of alternative longer and shorter bonds; as usual in conjugated systems, the single C—C bonds (C1d—C1c, C2c—C3c, and C4c—C1a) show partial double-bond character (16, 17). The central single bond is slightly shorter than the outer ones, but in contrast to *trans,trans*-1-(2′,6′-dichlorophenyl)-4-phenyl-1,3-butadiene (18), the difference is not significant. To minimize the H···H intramolecular repulsions, the chain adopts a "stretched" distortion so that all of the C—C—C angles in the chain are significantly larger than 120°. As in other all-*trans*-α,ω-diphenylpolyenes (16), the wider angles are those at the ends of the chain (at C(1c) and C(4c)), and correspond to the closer H···H contacts: H(2c)···H(6d), 2.23 Å; H(3c)···H(6a), 2.19 Å.

The molecule is planar, which maximizes the overlap of the atomic π orbitals and, therefore, the delocalization of the π system. The maximum deviation from the all-atom mean plane (r.m.s.d. = 0.105 Å, including substituents) is 0.28 Å for O(9a); the rest of the atoms are within 0.16 Å of the plane. The dihedral angles between the mean planes of the three moieties are 4.7° (donor/chain) and 4.2° (chain/acceptor).

Molecular geometry of the dimer (2)

In general, the pattern of bond lengths and angles in the phenyl rings of **2** is similar to that observed in **1**. Owing to the lower precision in the determination, the effects of the substituents on the ring geometry are less clear.

The pattern of bond lengths and angles in the C(2c)—C(3c)=C(4c)—C(1a) fragment is similar to that observed in **1**, but in **2** the putative single bond C(2c)—C(3c) is significantly longer than C(4c)—C(1a) due to the absence of conjugation. In comparison with the structure of **1**, the change from sp^2 to sp^3 hybridization in C(1c) and C(2c) is reflected in the C(1d)—C(1c) and C(1c)—C(2c) bond lengths, and in the angles at C(1c) and C(2c). The C(1d)—C(1c) and C(2c)—C(3c) distances are in good agreement with the av-

TABLE 1. Crystal data, intensity data collection parameters and final refinement results for compounds **1** and **2**

	1	**2**
Crystal data		
Formula	$C_{17}H_{15}NO_3$	$(C_{17}H_{15}NO_3)_2$
MW	281.31	562.62
Crystals	Orange elongated prisms	Yellow needles
Specimen size (mm)	0.38 × 0.44 × 0.48	0.12 × 0.28 × 0.34
T (K)	168	291
a (Å)	7.471(1)	11.5396(5)
b (Å)	14.283(1)	16.129(1)
c (Å)	25.940(1)	7.9035(3)
β (°)	90	90.264(3)
V (Å^3)	2768.1(7)	1471.0(2)
Crystal system	Orthorhombic	Monoclinic
Space group	*Pbca*	$P2_1/c$
Z	8	4
D_c(g/cm^3)	1.350	1.270
F(000)	1184	592
μ(Cu-Kα) (cm^{-1})	7.2	6.8
Data collection		
h, k, l range	−9/9, −17/17, 0/32	−14/14, 0/20, 0/9
No. refl. measured	13166	3630
No. refl. unique	2851	3021
No. refl. obsd. [$I > 3\sigma(I)$]	2788	2333
R_{int}	0.0338	0.0146
Refinement		
a in $w = [\sigma^2(F_o) + aF_o^2]^{-1}$	0.001	0.0065
Ext. corr. (g)		0.016(2)
R	0.0481	0.0512
wR	0.0709	0.0706
g.o.f. (S)	2.73	1.01
No. param. refined	250	251
Δ/σ max.	0.089	0.022
ρ_r min., max. (e/Å^3)	−0.35, 0.17	−0.19, 0.18

erage values of 1.504(1) and 1.499(3) Å found for these types of exocyclic bonds in substituted cyclobutanes (19).

The molecule lies at a crystallographic center of symmetry, which constrains the four-membered ring to absolute planarity. The substituents are in a *cis-trans-cis-trans* disposition with respect to the cyclobutane plane. The bond lengths and angles in the ring are within the range of values observed in other substituted cyclobutanes (17, 20). The two independent C—C distances are significantly different; the longest bond is found between the atoms attached to the *cis* substituents (C1c—C2c′) and is due to steric repulsions. The bulk of the substituents in **2** causes the difference between the long and short cyclobutane bond distances to be somewhat larger, Δ = 0.011 Å, than the difference between average bond lengths compiled for planar 1,2-substituted cyclobutanes, Δ = 0.007 Å (20).

The dihedral angles between the mean planes of the cyclobutane and the phenyl rings are 81.2° (acceptor/chain) and 54.0° (donor/chain).

Discussion

Crystal packing and photodimerization

In the crystal structure of **1** the molecules are arranged in an α-type packing mode (24), with a separation between the photoreactive atoms C(1c)···C(2c)′ of 3.517(2) Å, and an angle C(2c)—C(1c)···C(2c)′ of 92.0(2)°. The solid-state photochemical behavior of **1** is totally consistent with its crystal packing, which also explains why only one of the two double bonds of the chain is involved in the reaction and only one product, rather than a mixture of products, is formed. (Crystals of a similar α,ω-diarylbutadiene that crystallizes in a different space group are light stable.) The centrosymmetric molecular structure of **2** is also in agreement with the crystal packing of **1**, in which the reaction partners are arranged in a head-to-tail fashion across inversion centers. Hence, the solid-state reactivity of **1** is a typical example of a well-known type of topochemically controlled [2+2] photocycloaddition (2*c*, 21). The geometrical parameters θ_1, θ_2, θ_3, and d, defined by Venkatesan and Ramamurthy (22*a*) (see also refs. 22*b* or 22*c* for figures defining the d parameter) to measure the degree of overlap between the π orbitals of the reactive double bonds, have values of 0.0°, 92.0°, 72.9°, and 1.03 Å, which equal or are close to the ideal values of 0°, 90°, 90°, and 0.0 Å.

The differences between some of the molecular and crystal parameters of **1** and **2** are listed in Table 4. To calculate these values, two different ways of forming the dimer are considered: *path A* — the bonds formed during the reaction

Can. J. Chem. Downloaded from www.nrcresearchpress.com by 213.200.69.106 on 09/08/12
For personal use only.

Can. J. Chem. Downloaded from www.nrcresearchpress.com by 213.200.69.106 on 09/08/12
For personal use only.

TABLE 2

(*a*) Fractional coordinate ($\times 10^5$) and equivalent isotropic thermal parameters[a] ($Å^2 \times 10^4$) for compound **1**

Atom	*x*	*y*	*z*	U_{eq}
C(1d)	71494(17)	−15266(8)	47166(5)	345(6)
C(2d)	80054(17)	−15103(8)	42307(5)	356(6)
C(3d)	81078(18)	−23152(9)	39307(5)	406(7)
C(4d)	73336(19)	−31428(9)	41056(6)	422(7)
C(5d)	64306(18)	−31666(9)	45723(6)	422(7)
C(6d)	63485(18)	−23650(9)	48735(5)	379(7)
O(7d)	87032(15)	−6667(6)	40873(4)	444(6)
C(8d)	92582(20)	−5587(10)	35653(5)	424(7)
C(1c)	71218(19)	−6786(8)	50290(5)	377(7)
C(2c)	64711(17)	−5806(8)	55063(5)	348(6)
C(3c)	65256(17)	3042(8)	57791(5)	355(6)
C(4c)	58834(16)	4331(8)	62560(5)	347(6)
C(1a)	59632(15)	13044(8)	65475(4)	313(6)
C(2a)	53312(17)	13071(8)	70598(5)	354(6)
C(3a)	54148(18)	21036(9)	73611(5)	363(6)
C(4a)	61333(16)	29108(8)	71497(4)	333(6)
C(5a)	67446(18)	29466(8)	66422(5)	361(6)
C(6a)	66424(18)	21452(9)	63473(5)	361(6)
N(7a)	63076(16)	37470(7)	74722(4)	388(6)
O(8a)	68570(19)	44699(7)	72783(5)	568(7)
O(9a)	58730(21)	36840(8)	79284(4)	600(7)

(*b*) Fractional coordinates ($\times 10^4$) and equivalent isotropic thermal parameters[a] ($Å^2 \times 10^4$) for compound **2**

Atom	*x*	*y*	*z*	U_{eq}
C(1d)	5227(1)	−672(1)	2701(2)	495(8)
C(2d)	6171(2)	−624(1)	3821(2)	557(9)
C(3d)	6307(2)	−1198(1)	5111(3)	665(12)
C(4d)	5500(2)	−1829(1)	5310(3)	718(12)
C(5d)	4575(2)	−1889(1)	4223(3)	728(13)
C(6d)	4451(2)	−1315(1)	2920(3)	614(11)
O(7d)	6915(1)	17(1)	3533(2)	712(9)
C(8d)	7799(3)	165(2)	4741(4)	840(16)
C(1c)	5107(1)	−6(1)	1383(2)	475(8)
C(2c)	4044(1)	0(1)	161(2)	472(8)
C(3c)	3274(1)	732(1)	415(2)	490(8)
C(4c)	2159(1)	689(1)	782(2)	515(9)
C(1a)	1409(1)	1388(1)	1241(2)	522(9)
C(2a)	244(2)	1247(2)	1603(3)	694(12)
C(3a)	−473(2)	1903(2)	2066(3)	795(14)
C(4a)	−21(2)	2688(1)	2182(3)	693(12)
C(5a)	1123(2)	2850(1)	1850(3)	702(13)
C(6a)	1827(2)	2200(1)	1389(3)	623(10)
N(7a)	−780(2)	3380(2)	2680(3)	949(16)
O(8a)	−1729(2)	3213(2)	3218(4)	1376(20)
O(9a)	−402(2)	4084(2)	2549(3)	1222(18)

[a]Equivalent isotropic thermal parameters are: $U_{eq} = (1/3)\ \Sigma_i\Sigma_j U_{ij}\mathbf{a}_i{}^*\mathbf{a}_j{}^*\mathbf{a}_i\mathbf{a}_j$.

are between C(1c)—C(2c)′ and C(1c)′—C(2c), in the numbering scheme of Fig. 3(*a*), or *path B* — the bonds formed in the dimerization are between C(1c)—C(2c) and C(1c)′—C(2c)′. The nature and size of the atomic movements accompanying the solid-state [2+2] photocycloaddition can be envisaged from Fig. 3(*b*), which gives a pictorial representation of path A, based on the molecular structure of **2**. The main differences in bond lengths and angles are due to the change of hybridization at the reacting atoms. There are also significant variations in several torsion angles. The modification in the torsion angle about C(1d)—C(1c) is dictated by the change from trigonal to tetrahedral geometry at the reacting atoms, whereas the variations in the other torsion angles are determined by nonbonded interactions, after the constraints imposed by conjugation are removed. Since the configuration about C(1c)—C(2c) is *trans* in the monomer and is *trans* about C(1c)—C(2c) and C(1c)′—C(2c)′ in the dimer, the dimerization probably occurs

TABLE 3

(*a*) Geometric data for compound **1**

Bond lengths (Å)

C(2d)—C(1d)	1.414(2)	C(4c)—C(3c)	1.340(2)
C(6d)—C(1d)	1.399(2)	C(1a)—C(4c)	1.457(2)
C(1c)—C(1d)	1.457(2)	C(2a)—C(1a)	1.410(2)
C(3d)—C(2d)	1.390(2)	C(6a)—C(1a)	1.403(2)
O(7d)—C(2d)	1.365(1)	C(3a)—C(2a)	1.382(2)
C(4d)—C(3d)	1.392(2)	C(4a)—C(3a)	1.385(2)
C(5d)—C(4d)	1.386(2)	C(5a)—C(4a)	1.394(2)
C(6d)—C(5d)	1.387(2)	N(7a)—C(4a)	1.464(1)
C(8d)—O(7d)	1.424(2)	C(6a)—C(5a)	1.379(2)
C(2c)—C(1c)	1.337(2)	O(8a)—N(7a)	1.220(1)
C(3c)—C(2c)	1.449(2)	O(9a)—N(7a)	1.230(2)

Bond angles (°)

C(6d)—C(1d)—C(2d)	117.8(1)	C(1a)—C(4c)—C(3c)	125.6(1)
C(1c)—C(1d)—C(2d)	119.2(1)	C(2a)—C(1a)—C(4c)	118.5(1)
C(1c)—C(1d)—C(6d)	122.9(1)	C(6a)—C(1a)—C(4c)	123.6(1)
C(3d)—C(2d)—C(1d)	120.7(1)	C(6a)—C(1a)—C(2a)	117.9(1)
O(7d)—C(2d)—C(1d)	115.5(1)	C(3a)—C(2a)—C(1a)	121.3(1)
O(7d)—C(2d)—C(3d)	123.8(1)	C(4a)—C(3a)—C(2a)	118.6(1)
C(4d)—C(3d)—C(2d)	119.8(1)	C(5a)—C(4a)—C(3a)	122.1(1)
C(5d)—C(4d)—C(3d)	120.5(1)	N(7a)—C(4a)—C(3a)	119.2(1)
C(6d)—C(5d)—C(4d)	119.5(1)	N(7a)—C(4a)—C(5a)	118.7(1)
C(5d)—C(6d)—C(1d)	121.6(1)	C(6a)—C(5a)—C(4a)	118.4(1)
C(8d)—O(7d)—C(2d)	117.8(1)	C(5a)—C(6a)—C(1a)	121.7(1)
C(2c)—C(1c)—C(1d)	127.4(1)	O(8a)—N(7a)—C(4a)	119.0(1)
C(3c)—C(2c)—C(1c)	122.2(1)	O(9a)—N(7a)—C(4a)	117.8(1)
C(4c)—C(3c)—C(2c)	124.1(1)	O(9a)—N(7a)—O(8a)	123.2(1)

Selected torsion angles (°)

C(2d)—C(1d)—C(1c)—C(2c)	−175.8(2)
C(6d)—C(1d)—C(1c)—C(2c)	4.7(2)
C(1d)—C(1c)—C(2c)—C(3c)	179.7(2)
C(1c)—C(2c)—C(3c)—C(4c)	179.7(2)
C(2c)—C(3c)—C(4c)—C(1a)	178.1(2)
C(3c)—C(4c)—C(1a)—C(2a)	−175.8(2)
C(3c)—C(4c)—C(1a)—C(6a)	4.0(2)

(*b*) Geometric data for compound **2**

Bond lengths (Å)

C(2d)—C(1d)	1.403(3)	C(4c)—C(3c)	1.322(2)
C(6d)—C(1d)	1.380(3)	C(1a)—C(4c)	1.467(2)
C(1c)—C(1d)	1.503(2)	C(2a)—C(1a)	1.394(2)
C(3d)—C(2d)	1.386(3)	C(6a)—C(1a)	1.401(3)
O(7d)—C(2d)	1.363(3)	C(3a)—C(2a)	1.393(3)
C(4d)—C(3d)	1.389(4)	C(4a)—C(3a)	1.372(4)
C(5d)—C(4d)	1.371(4)	C(5a)—C(4a)	1.372(3)
C(6d)—C(5d)	1.393(3)	N(7a)—C(4a)	1.472(3)
C(8d)—O(7d)	1.415(3)	C(6a)—C(5a)	1.376(3)
C(2c)—C(1c)	1.558(2)	O(8a)—N(7a)	1.207(3)
C(1c)—C(2c)′	1.569(2)	O(9a)—N(7a)	1.222(3)
C(3c)—C(2c)	1.492(2)		

Bond angles (°)

C(6d)—C(1d)—C(2d)	117.7(2)	C(3c)—C(2c)—C(1c)′	118.3(1)
C(1c)—C(1d)—C(2d)	117.8(2)	C(4c)—C(3c)—C(2c)	124.7(2)
C(1c)—C(1d)—C(6d)	124.5(2)	C(1a)—C(4c)—C(3c)	126.2(2)
C(3d)—C(2d)—C(1d)	120.8(2)	C(2a)—C(1a)—C(4c)	119.8(2)
O(7d)—C(2d)—C(1d)	115.1(2)	C(6a)—C(1a)—C(4c)	122.4(2)
O(7d)—C(2d)—C(3d)	124.1(2)	C(6a)—C(1a)—C(2a)	117.8(2)
C(4d)—C(3d)—C(2d)	120.0(2)	C(3a)—C(2a)—C(1a)	120.4(2)
C(5d)—C(4d)—C(3d)	120.1(2)	C(4a)—C(3a)—C(2a)	119.5(2)

Can. J. Chem. Downloaded from www.nrcresearchpress.com by 213.200.69.106 on 09/08/12
For personal use only.

TABLE 3 (*concluded*)

C(6d)—C(5d)—C(4d)	119.5(2)	C(5a)—C(4a)—C(3a)	121.9(2)
C(5d)—C(6d)—C(1d)	121.9(2)	N(7a)—C(4a)—C(3a)	119.4(2)
C(8d)—O(7d)—C(2d)	117.9(2)	N(7a)—C(4a)—C(5a)	118.7(2)
C(2c)—C(1c)—C(1d)	120.2(1)	C(6a)—C(5a)—C(4a)	118.4(2)
C(2c)′—C(1c)—C(1d)	119.2(1)	C(5a)—C(6a)—C(1a)	122.0(2)
C(2c)′—C(1c)—C(2c)	90.6(1)	O(8a)—N(7a)—C(4a)	117.9(3)
C(1c)—C(2c)—C(1c)′	89.4(1)	O(9a)—N(7a)—C(4a)	118.0(2)
C(3c)—C(2c)—C(1c)	112.9(1)	O(9a)—N(7a)—O(8a)	124.1(3)

Selected torsion angles (°)

C(2d)—C(1d)—C(1c)—C(2c)	−177.0(3)
C(2d)—C(1d)—C(1c)—C(2c)′	73.2(3)
C(6d)—C(1d)—C(1c)—C(2c)	0.9(3)
C(6d)—C(1d)—C(1c)—C(2c)′	−109.0(3)
C(1d)—C(1c)—C(2c)—C(1c)′	−124.8(2)
C(1d)—C(1c)—C(2c)—C(3c)	114.5(2)
C(2c)′—C(1c)—C(2c)—C(3c)	−120.7(2)
C(1d)—C(1c)—C(2c)′—C(1c)′	125.6(2)
C(2c)—C(1c)—C(2c)′—C(3c)′	−115.9(2)
C(1d)—C(1c)—C(2c)′—C(3c)′	9.8(2)
C(1c)—C(2c)—C(3c)—C(4c)	−122.5(3)
C(1c)′—C(2c)—C(3c)—C(4c)	135.1(3)
C(2c)—C(3c)—C(4c)—C(1a)	172.1(3)
C(3c)—C(4c)—C(1a)—C(2a)	−179.7(3)
C(3a)—C(4c)—C(1a)—C(6a)	−1.9(3)

"Symmetry code for primed atoms: $1 - x, -y, -z$.

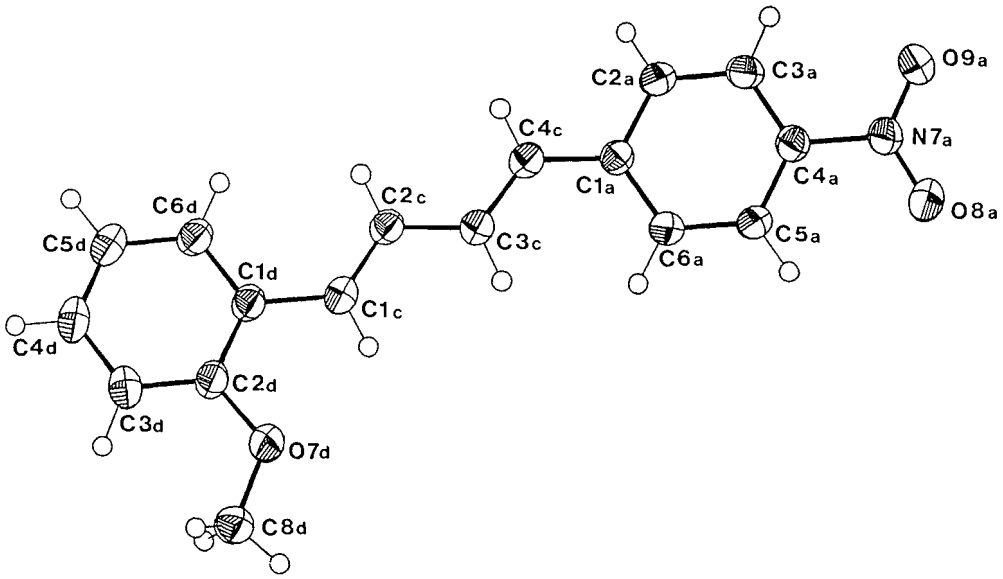

FIG. 1. Structure of **1** showing the thermal ellipsoids drawn at 50% probability and the atomic numbering scheme.

via path A and, therefore, the pair of bonds formed during the reaction are C(1c)—C(2c)′ and C(1c)′—C(2c), which have *cis* configurations about them. Further support for path A is given in Table 4 where it is shown that path A requires the smaller adjustment in key torsion angles in the transformation from the structure found in crystals of **1** to the structure found in crystals of **2**.

If both the postulate of minimum amount of atomic movement (23) is obeyed and the center of symmetry is conserved during the reaction, the photochemically active atoms, C(1c) and C(2c), and their centrosymmetrically related partners, must move within the plane defined by themselves and the inversion center, hereinafter called the *reference plane*. Then, during the reaction each of these four atoms, C(1c), C(2c), C(1)′, and C(2c)′, would move less than 1.00 Å, for either path A or B. However, the assumptions made above should be regarded only as approximate idealizations; indeed, incomplete X-ray studies of partially photolyzed crystals of related butadienes (in this laboratory) and other photochemical reactions (24) have shown small but significant departures from coplanarity in the reacting atoms of the intermediate photoproducts. Also, Craig and coworkers (25) have proposed that, in some cases, eximers could be formed as a result of the asymmetrical excitation

Can. J. Chem. Downloaded from www.nrcresearchpress.com by 213.200.69.106 on 09/08/12
For personal use only.

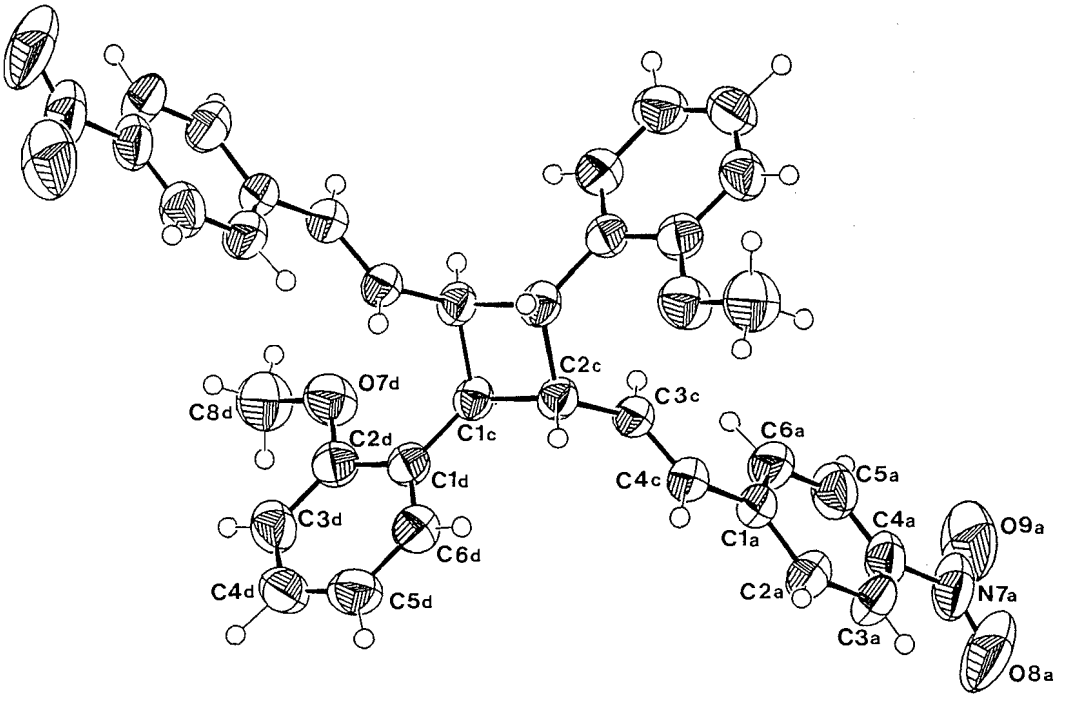

FIG. 2. Structure of **2** showing the thermal ellipsoids drawn at 50% probability and the atomic numbering scheme.

TABLE 4. Differences between key geometric features of compounds **1** and **2**. The columns give differences for compound **2** − compound **1** for each of reaction paths A and B (see text). Unlisted bond distances differed by ≤ |0.022 Å|, bond angles by ≤ |1.6°|, and torsion angles by ≤ |6.0°|

Feature	Path A [**2** − **1**]	Path B [**2** − **1**]
C(1c)—C(1d)	0.046 Å	0.046 Å
C(2c)—C(1c)	0.221 Å	0.232 Å
C(3c)—C(2c)	0.043 Å	0.043 Å
C(2c)—C(1c)—C(1d)	−7.2°	−8.2°
C(3c)—C(2c)—C(1c)	−9.5°	−3.9°
C(2d)—C(1d)—C(1c)—C(2c)	−1.2°	−111.0°
C(6d)—C(1d)—C(1c)—C(2c)	−3.8°	−113.7°
C(1d)—C(1c)—C(2c)—C(3c)	−65.2°	−169.4°
C(1c)—C(2c)—C(3c)—C(4c)	57.8°	−44.1°

of the ground-state equilibrium structures. Therefore, the displacements shown in Table 4 should be considered as the lower limits of atomic movement, rather than their actual values.

In the crystal structure of **1**, the *reference plane* (as defined above) is nearly parallel to the (110) plane, and in the crystal structure of **2** it is almost exactly parallel to (010): dihedral angles: 15.1° and 0.5°, respectively. The maximum deviation of any atom from the *reference plane* is approximately the same in both molecules, viz, 6.77 Å for O(8a) in **1** and 6.60 Å for O(9a) in **2**. Accordingly, the translations along [110] in **1** and along [010] in **2** also have similar values: 16.119 and 16.129 Å, respectively. A number of topotactic (single-crystal to single-crystal) photodimerizations (21*e*, 26) and other organic reactions (27) have been reported. In spite of the axial relationship indicated above, in the present case there is no topotaxy, probably because the changes in some molecular parameters, especially torsion angles, are too large. Examination of crystals of **1** under an optical microscope, over several days at room temperature, revealed progressive disruption of the crystal lattice, as shown by a slow development of cracks and an increasing opacity of the specimens.

In both crystals the packing is entirely due to van der Waals forces. The molecular volume in the crystals of **2** is larger by 21.6 $Å^3$, a difference that is mostly due to less efficient packing, owing to the molecular shape of this compound, rather than to the difference in the temperature of the structure determinations. The packing effect is partially overcome by shorter distances between the atoms C(1c)···C(2c)′ and C(1c)′···C(2c) in the dimer.

Conclusions

Molecules of the potential NLO material, **1**, are found to be unstable to exposure to light in the solid state. Formation of the dimer in crystals of **1** can be accomplished by atomic movements of approximately 1.0 Å to form **2**, a cyclobutane constrained by a centre of symmetry in the ring. The molecules of **1** display a planar structure in the solid state, indicating the existence of an extended π electronic system; thus, the molecular conformation and polar nature of **1** meet the molecular requirements for second-order NLO applications. Unfortunately, all known crystalline forms of **1** are centrosymmetric and can not have NLO properties. In addition, crystals of **1** are photoreactive; yet, suitable NLO materials must have an extraordinary stability with respect to high-intensity light sources. Nevertheless, the photodimerization that **1** undergoes appears to be a crystal lattice-controlled reaction leaving open the possibility that

Can. J. Chem. Downloaded from www.nrcresearchpress.com by 213.200.69.106 on 09/08/12
For personal use only.

Can. J. Chem. Downloaded from www.nrcresearchpress.com by 213.200.69.106 on 09/08/12
For personal use only.

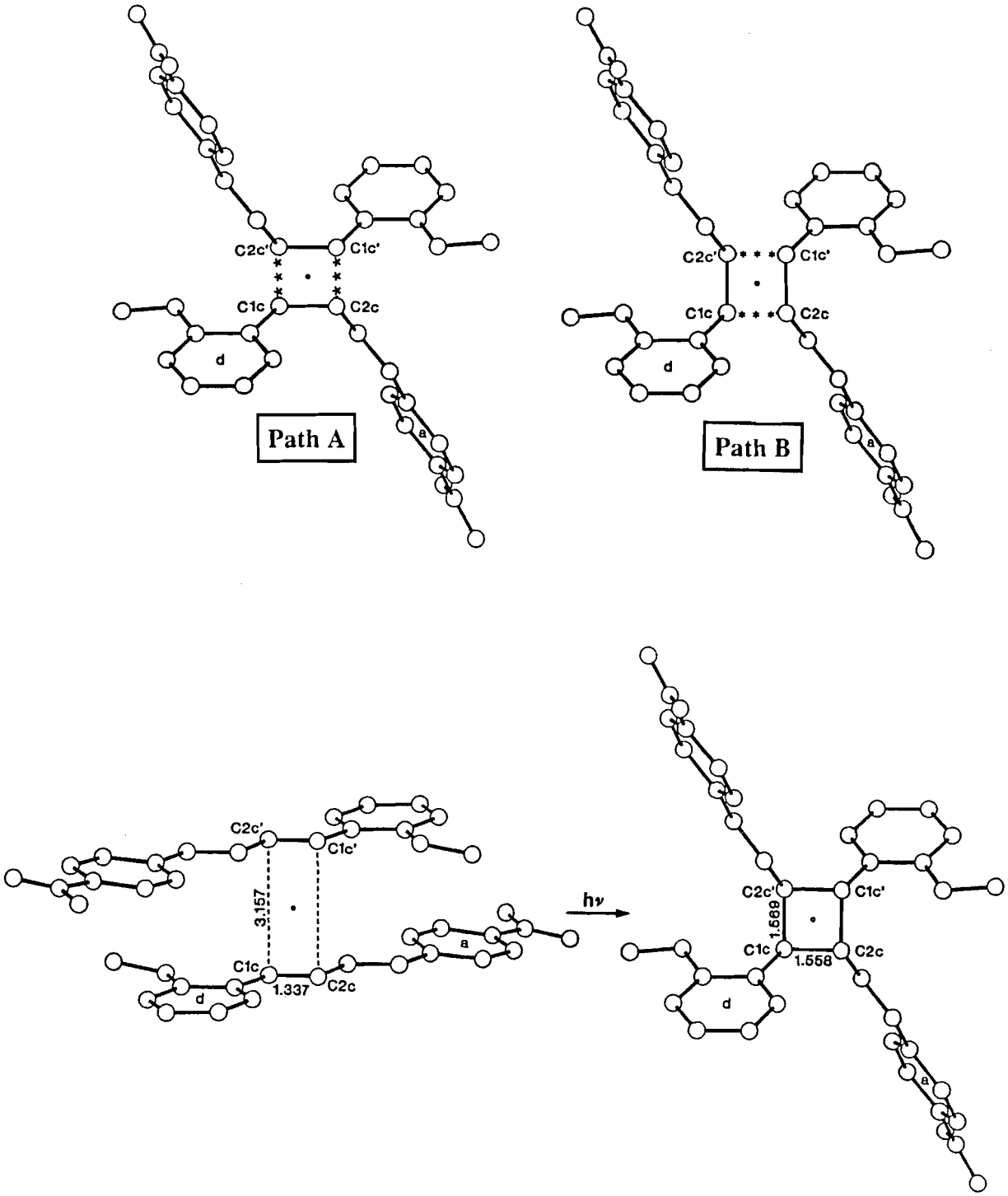

FIG. 3. Schematic representation of two dimerization pathways A and B, based on the crystal structure of the dimer, **2**. The arrows show the putative bond formation in the dimerization reaction.

appropriate "crystal engineering" (21*a*) could produce a noncentrosymmetric and light-stable crystal form.

Acknowledgments

This work was supported by an Natural Sciences and Engineering Council of Canada grant to P.W.C. The authors thank Dr. Charles W. Spangler of Northern Illinois University for the sample of compound **1**.

1. D.J. Williams (*Editor*). Nonlinear properties of organic and polymeric materials. ACS Symp. Ser. No. 233, American Chemical Society, Washington D.C. 1983; D.J. Williams. Angew. Chem. Int. Ed. Engl. **23**, 690 (1984); D.S. Chemla and J. Zyss (*Editors*). Nonlinear optical properties of organic molecules and crystals. Vols. I and II. Academic Press, Orlando, Fla. 1987; R.A. Hann and D. Bloor (*Editors*). Organic materials for nonlinear optics. RSC Special Publication No. 69, Royal Society of Chemistry, London. 1989; P.N. Paras

and D.J. Williams. Introduction to nonlinear optical effects in molecules and polymers. Wiley, New York. 1990; R.T. Bailey, F.R. Cruickshank, P.Pavlides, D. Pugh, and J.N. Sherwood. J. Phys. D: Appl. Phys. **24**, 135 (1991); R.T. Bailey, F.R. Cruickshank, D. Pugh, and J.N. Sherwood. Acta Crystallogr. Sect. A: Found. Crystallogr. **A47**, 145 (1991).
2. (*a*) A.I. Kitaigorodsky. Molecular crystals and molecules. Academic Press, New York. 1973; (*b*) E.A. Silinsh. Organic molecular crystals. Springer-Verlag, Berlin. 1980; (*c*) J.D. Wright. Molecular crystals. Cambridge University Press, Cambridge. 1987.
3. D.Y. Curtin and I.C. Paul. Chem. Rev. **81**, 525 (1981).
4. A. Dulcic, C. Flytzanis, C.L. Tang, D. Pépin, M. Fétizon, and Y. Hoppilliard. J. Chem. Phys. **74**, 1559 (1981); J.S. Horwitz, T. Itoh, B.E. Kohler, and C.W. Spangler. J. Chem. Phys. **87**, 2433 (1987); C.T. Lin, H.W. Guan, R.K. McCoy, and C.W. Spangler. J. Phys. Chem. **93**, 39 (1989); L.-T. Cheng, W. Tam, S.R. Marder, A.E. Stiegman, G. Rikken, and C.W. Spangler. J. Phys. Chem. **95**, 10643 (1991); B.E. Kohler, C.W. Spangler, and C. Westerfield. J. Chem. Phys. **94**, 908 (1991).
5. G.M. Sheldrick. SHELXS86. Program for the solution of crystal structures. University of Göttingen, Germany. 1986.
6. G.M. Sheldrick. SHELX76. Program for crystal structure determination. University of Cambridge, U.K. 1976.
7. P. Roberts and G.M. Sheldrick. XANADU. Program for torsion-angle, mean-plane and librational-correction calculations. University of Cambridge, U.K. 1975.
8. C.K. Johnson. ORTEPII. Report ORNL-5138, Oak Ridge National Laboratory, Oak Ridge, Tenn. 1976.
9. W.D.S. Motherwell and W. Clegg. PLUTO. Program for plotting molecular and crystal structures. University of Cambridge, U.K. 1978.
10. International tables for X-ray crystallography. Vol. IV. Kynoch Press, Birmingham. 1974. pp. 99–101.
11. A Domenicano, A. Vaciago, and C.A. Coulson. Acta Crystallogr. Sect. B: Struct. Crystallogr. Cryst. Chem. **B31**, 221 (1975).
12. A. Domenicano, P. Mazzeo, and A. Vaciago. Tetrahedron Lett. 1029 (1976).
13. R. Norrestam and L. Schepper. Acta Chem. Scand. **A35**, 91 (1981).
14. A. Domenicano and A. Vaciago. Acta Crystallogr. Sect. B: Struct. Crystallogr. Cryst. Chem. **B35**, 1382 (1979).
15. A. Domenicano and P. Murray-Rust. Tetrahedron Lett. 2283 (1979).
16. T. Hall, S.M. Bachrach, C.W. Spangler, L.S. Sapochak, C.T. Lin, H.W. Guan, and R.D. Rogers. Acta Crystallogr. Sect. C: Cryst. Struct. Commun. **C45**, 1541 (1989).
17. F.H.Allen, O. Kennard, D.G. Watson, L. Brammer, A.G. Orpen, and R. Taylor. J. Chem. Soc. Perkin Trans. 2, S1 (1987).
18. D. Rabinovich and Z. Shakked. Acta Crystallogr. Sect. B: Struct. Crystallogr. Cryst. Chem. **B31**, 819 (1975).
19. F.H. Allen. Acta Crystallogr. Sect. B: Struct. Sci. **B40**, 64 (1984).
20. F.A. Cotton and B.A. Frenz. Tetrahedron, **30**, 1587 (1974).
21. (*a*) G.M.J. Schmidt. Pure Appl. Chem. **27**, 647 (1971); (*b*) M.D. Cohen and B.S. Green. Chem. Br. **9**, 490 (1973); (*c*) M.D. Cohen. Angew. Chem. Int. Ed. Engl. **14**, 386 (1975); (*d*) M. Hasegawa. Chem. Rev. **83**, 507 (1983); (*e*) V. Ramamurthy and K. Venkatesan. Chem. Rev. **87**, 433 (1987).
22. (*a*) K. Gnanaguru, N. Ramasubba, K. Venkatesan, and V. Ramamurthy. J. Org. Chem. **50**, 2337 (1985); (*b*) P. Venugopalan and K. Venkatesan. Acta Crystallogr. Sect. B: Struct. Sci. **B46**, 826 (1990); (*c*) Bull. Chem. Soc. Jpn. **63**, 2368 (1990).
23. M.D. Cohen and G.M.J. Schmidt. J. Chem. Soc. (B), 1996 (1964).
24. H. Nakanishi, W. Jones, J.M. Thomas, M.B. Hursthouse, and M. Motevalli. J. Phys. Chem. **85**, 3636 (1981); C.E. Pfluger and R.L. Ostrander. Photochem. Photobiol. **49**, 375 (1989).
25. M.A. Collins and D.P. Craig. Chem. Phys. **54**, 305 (1981); D.P. Craig and C.P. Mallet. Chem. Phys. **65**, 129 (1982); K. Norris, P. Gray, D.P. Craig, C.P. Mallet, and B.R. Markey. Chem. Phys. **79**, 9 (1983); D.P. Craig; R.N. Lindsay, and C.P. Mallet. Chem. Phys. **88**, 187 (1984).
26. A. Gavezzotti and M. Simonetta. Chem. Rev. **82**, 1 (1982).
27. Y. Ohasi. Acc. Chem. Res. **21**, 268 (1988); A. Uchida and J.D. Dunitz. Acta Crystallogr. Sect. B: Struct. Sci. **B46**, 45 (1990).

Can. J. Chem. Downloaded from www.nrcresearchpress.com by 213.200.69.106 on 09/08/12
For personal use only.

cis-Cyclohexano-9-crown-3 ether. Solid state and low-temperature solution stereochemistry as determined by X-ray crystallography and nuclear magnetic resonance spectroscopy

G.W. BUCHANAN,[1] A.B. DRIEGA, A. MOGHIMI, C. BENSIMON, AND K. BOURQUE

Ottawa–Carleton Chemistry Institute, Department of Chemistry, Carleton University, Ottawa, Ont., Canada K1S 5B6

Received January 13, 1993

G.W. BUCHANAN, A.B. DRIEGA, A. MOGHIMI, C. BENSIMON, and K. BOURQUE. Can. J. Chem. **71**, 951 (1993).

The X-ray crystal structure of the title material has been determined at −130°C. Low-temperature $^1H^1H$ COSY, $^{13}C^1H$ HETCOR, and DEPT ^{13}C NMR spectra have been recorded, which permit unambiguous assignments of all carbon resonances when ring inversion is slow on the NMR timescale. The limiting low-temperature solution phase ^{13}C spectrum has many common features with the solid phase ^{13}C CPMAS spectrum recorded at 300 K. Spectra for the 7,10-tetradeuterio derivative have also been obtained and substituent influences on ^{13}C shieldings are discussed in detail.

G.W. BUCHANAN, A.B. DRIEGA, A. MOGHIMI, C. BENSIMON et K. BOURQUE. Can. J. Chem. **71**, 951 (1993).

Opérant à −130°C, on a déterminé la structure cristalline du composé mentionné dans le titre. On a aussi enregistré les spectres RMN du ^{13}C à basse température, en modes $^1H^1H$ COSY, $^{13}C^1H$ HETCOR et DEPT; ces données permettent de faire une attribution non-ambiguë des résonances de tous les carbones lorsque l'inversion de cycle est lente à l'échelle de temps de la RMN. Le spectre du ^{13}C de la solution à la basse température limite présente plusieurs caractéristiques communes au spectre ^{13}C en CPMAS de la phase solide, déterminé à 300 K. On a aussi déterminé le spectre RMN du dérivé 7,10-dideutéré et on discute en détail des influences des substituants sur les blindages du ^{13}C.

[Traduit par la rédaction]

Can. J. Chem. Downloaded from www.nrcresearchpress.com by 213.200.69.106 on 09/08/12
For personal use only.

Introduction

Stereochemical influences on NMR parameters in substituted cyclohexanes are most properly examined by recording spectra under low-temperature conditions where ring inversion is slow on the NMR timescale. Early definitive work in this area with respect to ^{13}C NMR was carried out using monosubstituted compounds (1–4). Consequently, axial and equatorial α, β, γ, and δ substituent effects have now been delineated for a wide variety of monosubstituted cyclohexane derivatives (1–7).

For molecules containing more than a single substituent, the problems of resonance assignment at low temperature can be significant. Herein we report the use of low-temperature homo- and heteronuclear COSY spectra, combined with the results of DEPT spectra, for the unambiguous assignment of cyclohexyl carbon resonances in *cis*-cyclohexyl-9-crown-3 ether **1**. A reversal of the normal β effect of axial vs. equatorial oxygen in *mono*substituted compounds has been found and is attributed to the dominance of the γ-*gauche* shielding effect of axial oxygen on the carbon that is β to equatorial oxygen in this *cis*-1,2-disubstituted compound.

For assignment of oxygenated methylene carbons, the results of deuterium incorporation and an inverse detected ^3J HETCOR experiment at low temperature were used.

A comparison has been made between the limiting low-temperature solution ^{13}C spectrum and that obtained in the solid phase at ambient temperature. The X-ray crystal structure has been determined and some of the stereochemical shielding trends are discussed in terms of torsional angle influences.

Results and discussion

The ORTEP diagram and numbering scheme for *cis*-cyclohexano-9-crown-3 ether **1** is shown in Fig. 1. Solution ^{13}C NMR spectra at 300 and 173 K are in Fig. 2, while low-temperature $^1H^{13}C$ HETCOR and $^1H^1H$ COSY spectra are shown in Figs. 3 and 4, respectively. The solid phase ^{13}C spectrum is presented in Fig. 5. Table 1 contains bond lengths and bond angles while torsional angles are collected in Table 2. Crystallographic data are listed in Table 3 and atomic parameters in Table 4. In Table 5 are presented the ^{13}C NMR data.[2]

(i) X-ray crystal structure

At −130°C, the nine-membered ring conformation of **1** exhibits O—C—C—O bond angles involving C7, C8, C9, and C10, which are *gauche* (67.4 and 78.0°, respectively) in accord with the expected geometry for these units in larger crown-type systems (8, 9). The O1—C1—C2—O2 angle of 58.9° is consistent with that expected in a *cis*-1,2-disubstituted cyclohexane. The X-ray crystal structure of 1,4,7-trioxanane (9-crown-3 ether, **2**, mp 0°C) is unknown. However, molecular mechanics calculations of its preferred conformations have been carried out (9) and low-temperature NMR and IR studies (10) of its solution and solid phase stereochemistries performed. The low-temperature ^{13}C NMR spectrum (10) shows six lines, consistent with a single asymmetric conformation for **2**. The present X-ray data for **1** also indicate an asymmetric nine-membered ring conformation, with the overall geometry similar to that of the calculated "*f*" conformation of **2** (9). This asymmetric "*f*" conformation was calculated to be the second lowest energy form of **2**, with steric energy only 0.83 kcal/mol above the minimum. Detailed comparisons of the X-ray data for **1** and the "*f*" conformation of **2** are presented below. To compare the two geometries, it should be noted that the mirror image of the calculated conformation (9) was refined in our X-ray structure and a transformation of ref. 9 atom numbers to the present numbering scheme is needed (i.e., C6 → C1, C7 → C2, O8 → O2, etc).

[1]Author to whom correspondence may be addressed.

[2]Tables of torsion angles for all atoms, anisotropic temperature factors, and structure factors have been deposited as supplementary data and may be purchased from: The Depository of Unpublished Data, Document Delivery, CISTI, National Research Council Canada, Ottawa, Canada K1A 0S2.

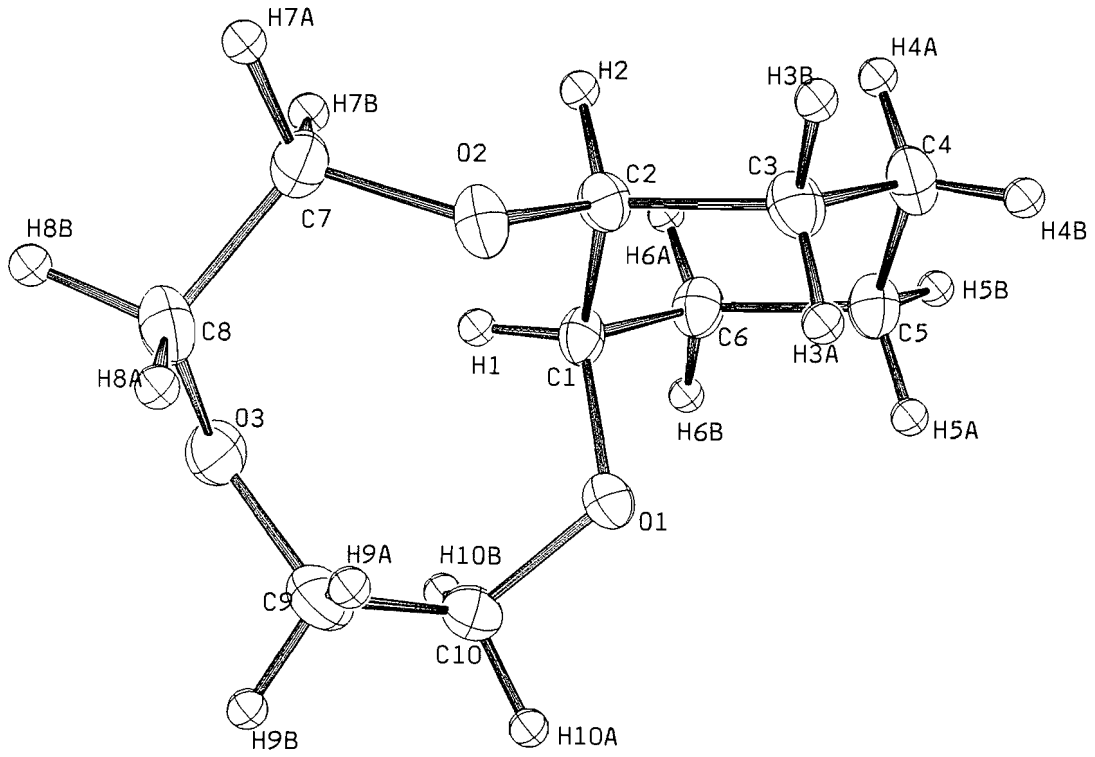

FIG. 1. The ORTEP plot for **1**.

Torsional network	θ° obsd. (**1**)	θ° calcd. ("*f*" conformation of **2** (9))
O1—C1—C2—O2	−58.9	63
C1—C2—O2—C7	−76.8	76
C2—O2—C7—C8	120.3	−116
O2—C7—C8—O3	−67.4	61
C7—C8—O3—C9	96.1	−95
C8—O3—C9—C10	−127.7	137
O3—C9—C10—O1	78.0	−78
C9—C10—O1—C1	−78.0	72
C10—O1—C1—C2	122.1	−120

Clearly, there is very good agreement between these two conformations, with the largest difference between calculated and observed torsional angles being 9.3°.

(ii) Solution NMR spectra

The five ^{13}C resonances observed for **1** at 300 K (Fig. 2) are consistent with rapid conformational interconversion on the NMR timescale at this temperature for both the six- and the nine-membered rings. The close correspondence between the solid phase ^{13}C spectrum and the solution ^{13}C spectrum at 173 K suggests that the "*f*" conformation is highly preferred in the nine-membered ring of **1** at 173 K. Minor amounts of other conformations may be present at higher temperatures but are not detectable at lower temperatures, where conformational interconversion is slow on the NMR timescale, due to ground state free energy differences that probably exceed 4 kJ/mol.

At 173 K, the two positive signals in the DEPT 135 spectrum arise from CH carbons, while the remaining eight negative lines are due to CH_2 sites. The CH resonance at 82.20 ppm can be assigned with confidence to C2, the carbon bearing equatorial oxygen, by analogy with well-established stereochemical trends (5, 11, 12). Its counterpart, the C1 site bearing axial oxygen, is shielded by 6.50 ppm and appears at 75.70 ppm.

In the low-temperature heteronuclear $^1H^{13}C$ COSY spectrum (Fig. 3), the methine protons attached to C1 and C2 are clearly visible and appear at ca. 4.30 and 3.20 ppm, respectively. There is a reverse correlation between ^{13}C and ^1H steric shifts here, since the deshielded C2 carbon is bonded to the most shielded proton while the shielded C1 carbon is bonded to the most deshielded proton.

With these proton assignments in hand, it is then possible to use the $^1H^1H$ COSY spectrum (Fig. 4) to assign protons on C3 and C6, respectively. Accordingly, the most deshielded proton on nonoxygenated carbon, appearing at ca. 1.85 ppm, must be bonded to C6, since it correlates to the ^1H resonance for the C1 proton at 4.30 ppm. Similarly, the C3 protons must appear near 1.65 ppm, since they correlate to the C2 resonance at 3.20 ppm. From the heteronuclear COSY spectrum, it then follows that C6 resonates at 30.07 ppm and C3 at 27.87 ppm. Finally, C5, being γ-*gauche* to the axial oxygen on C1, appears at 19.39 ppm and is shielded by 5.31 ppm relative to C4, which is γ-*trans* to the equatorial oxygen on C2.

The α and γ shielding trends at C1,2 and C4,5, respectively, are consistent with expectations based on α and γ substituent effects in related monosubstituted molecules (3, 5, 11); however, the β substituent effects on C3 and C6 are not. Indeed in **1**, C3, the carbon β to equatorial oxygen, is shielded by 2.20 ppm relative to C6. For a series of 23 monosubstituted cyclohexanes (5), it has been found that, with the exception of the $N(CH_3)_2$ group, carbons β to equatorial substituents are *deshielded* relative to their counterparts, which are β to axial functions.

Can. J. Chem. Downloaded from www.nrcresearchpress.com by 213.200.69.106 on 09/08/12
For personal use only.

TABLE 1

(*a*) Atomic bond distances in angstroms

O1—C1	1.435(3)	C5—C6	1.536(4)
O1—C10	1.435(3)	C5—H5A	0.999(24)
O2—C2	1.428(3)	C5—H5B	1.003(22)
O2—C7	1.442(3)	C6—H6A	0.93(3)
O3—C8	1.434(3)	C6—H6B	1.057(24)
O3—C9	1.421(3)	C7—C8	1.533(4)
C1—C2	1.518(4)	C7—H7A	1.129(22)
C1—C6	1.517(4)	C7—H7B	0.994(23)
C1—H1	0.937(23)	C8—H8A	1.024(23)
C2—C3	1.529(4)	C8—H8B	1.102(23)
C2—H2	1.014(22)	C9—C10	1.506(4)
C3—C4	1.527(4)	C9—H9A	0.96(3)
C3—H3A	1.010(25)	C9—H9B	1.02(3)
C3—H3B	1.051(20)	C10—H10A	1.03(3)
C4—C5	1.519(4)	C10—H10B	1.15(3)
C4—H4A	0.93(3)		
C4—H4B	0.93(3)		

(*b*) Atomic bond angles in degrees

C1—O1—C10	115.34(20)	C1—C6—C5	111.84(23)
C2—O2—C7	113.94(19)	C1—C6—H6A	103.9(14)
C8—O3—C9	115.66(21)	C1—C6—H6B	110.2(12)
O1—C1—C2	109.02(21)	C5—C6—H6A	113.2(14)
O1—C1—C6	109.51(21)	C5—C6—H6B	107.2(12)
O1—C1—H1	110.7(14)	H6A—C6—H6B	110.5(19)
C2—C1—C6	110.30(21)	O2—C7—C8	110.71(22)
C2—C1—H1	108.6(14)	O2—C7—H7A	110.2(11)
C6—C1—H1	108.7(14)	O2—C7—H7B	109.2(12)
O2—C2—C1	112.57(20)	C8—C7—H7A	109.2(11)
O2—C2—C3	107.63(20)	C8—C7—H7B	114.2(12)
O2—C2—H2	109.4(12)	H7A—C7—H7B	104.3(17)
C1—C2—C3	110.60(22)	O3—C8—C7	112.20(22)
C1—C2—H2	105.5(12)	O3—C8—H8A	109.9(13)
C3—C2—H2	111.2(11)	O3—C8—H8B	111.8(11)
C2—C3—C4	109.85(22)	C7—C8—H8A	111.2(12)
C2—C3—H3A	110.1(13)	C7—C8—H8B	105.0(11)
C2—C3—H3B	108.5(10)	H8A—C8—H8B	106.5(17)
C4—C3—H3A	111.7(13)	O3—C9—C10	112.63(24)
C4—C3—H3B	112.4(10)	O3—C9—H9A	106.6(15)
H3A—C3—H3B	104.1(16)	O3—C9—H9B	109.7(15)
C3—C4—C5	112.12(23)	C10—C9—H9A	113.4(14)
C3—C4—H4A	102.9(14)	C10—C9—H9B	108.2(15)
C3—C4—H4B	104.6(16)	H9A—C9—H9B	106.0(20)
C5—C4—H4B	107.9(14)	O1—C10—C9	114.00(23)
C5—C4—H4B	107.8(16)	O1—C10—H10A	102.4(12)
H4A—C4—H4B	121.5(20)	O1—C10—H10B	105.1(12)
C4—C5—C6	110.87(23)	C9—C10—H10A	111.5(13)
C4—C5—H5A	111.01(13)	C9—C10—H10B	115.3(12)
C4—C5—H5B	114.2(11)	H10A—C10—H10B	107.5(18)
C6—C5—H5A	110.0(12)		
C6—C5—H5B	108.9(11)		
H5A—C5—H5B	101.6(17)		

It is important to note for **1** and indeed for all *cis*-1,2-disubstituted cases, however, that C3 is γ-*gauche* to the axial oxygen on C1 and thus may experience a shielding γ effect that overrides the β deshielding from the equatorial O at C2.

One can test this hypothesis semi-quantitatively by considering the known β deshielding effect of 2.17 ppm in the equatorial conformation of methoxycyclohexane (3, 5) and the observed γ-*gauche* shielding effect of 5.31 ppm in **1** due to the axial oxygen. On this basis, one would predict that C3 would be shielded relative to C6 in **1** by 5.31 − 2.17 = 3.14 ppm, a result that is within 1 ppm of that observed. These unambiguous findings for the shifts of C3 vs. C6 in this *cis*-1,2-disubstituted crown ether suggest that earlier tentative assignments for the corresponding carbons in *cis*-1,2-dicyclohexano-14-crown-4 ethers (13) at low temperature should be reversed, while those made for *cis*-dicyclohexano-18-crown-6 systems (14) are correct.

Regarding ^{13}C assignments for the methylene carbons C8,9

Can. J. Chem. Downloaded from www.nrcresearchpress.com by 213.200.69.106 on 09/08/12
For personal use only.

Can. J. Chem. Downloaded from www.nrcresearchpress.com by 213.200.69.106 on 09/08/12
For personal use only.

TABLE 2. Torsion angles for non-H atoms

C10—O1—C1—C2	122.1(2)
C7—O2—C2—C1	−76.8(2)
C9—O3—C8—C7	96.1(2)
O1—C1—C2—O2	−58.9(2)
C6—C1—C2—C3	−58.8(2)
C2—C1—C6—C5	56.3(2)
O2—C2—C3—C4	−178.3(3)
C3—C4—C5—C6	53.7(2)
O2—C7—C8—O3	−67.4(2)
C10—O1—C1—C6	−117.1(2)
C1—O1—C10—C9	−78.0(2)
C7—O2—C2—C3	161.1(3)
C2—O2—C7—C8	120.3(3)
C8—O3—C9—C10	−127.7(3)
O1—C1—C2—C3	61.5(2)
C6—C1—C2—O2	−179.2(3)
O1—C1—C6—C5	−63.6(2)
C1—C2—C3—C4	58.4(2)
C2—C3—C4—C5	−56.2(2)
C4—C5—C6—C1	−53.7(2)
O3—C9—C10—O1	78.0(2)

TABLE 3. Crystallographic data

Formula	$C_{10}H_{18}O_3$
fw	186.25
Crystal system	Monoclinic
Space group	$P2_1/a$
a, Å	8.6768(13)
b, Å	7.3553(20)
c, Å	15.6677(20)
V, Å^3	986.3(3)
Z (molecules/cell)	4
D_c, g/cm^3	1.254
Crystal dimensions, mm^3	0.20 × 0.20 × 0.20
Radiation (λ, Å)	MoKα (0.70932)
Octants measured	h(−10 to +10), k(0 to +8), l(0 to +18).
Max 2θ	49.9
Temperature	−130°C
No. of unique reflections	1741
No. of observed reflections	1871
$I\sigma/I$ ratio	0.177
R_f	0.051
R_w	0.039
Goodness-of-fit	10.29

TABLE 4. Atomic parameters x, y, z and B_{iso} (ESDs refer to the last digit printed)

	x	y	z	B_{iso}[a]
O1	0.17241(19)	0.59535(23)	0.21880(10)	1.97(8)
O2	0.22742(19)	0.22035(23)	0.26015(10)	1.81(8)
O3	0.05931(20)	0.29485(23)	0.08329(10)	2.04(8)
C1	0.0663 (3)	0.4938 (4)	0.26153(17)	1.60(11)
C2	0.1550 (3)	0.3408 (4)	0.31308(16)	1.55(11)
C3	0.2832 (3)	0.4172 (4)	0.38248(17)	1.80(12)
C4	0.2114 (4)	0.5430 (4)	0.44281(18)	2.06(14)
C5	0.1168 (3)	0.6952 (4)	0.39396(18)	2.00(12)
C6	−0.0061 (3)	0.6188 (4)	0.32106(17)	1.89(12)
C7	0.1207 (3)	0.0949 (4)	0.21044(17)	2.01(13)
C8	0.1231 (4)	0.1224 (4)	0.11371(17)	2.16(13)
C9	0.1698 (4)	0.4361 (4)	0.08002(18)	2.37(14)
C10	0.1318 (4)	0.6055 (4)	0.12637(17)	2.27(13)
H1	−0.014 (3)	0.443 (3)	0.2211 (14)	1.9 (6)
H2	0.0740 (25)	0.272 (3)	0.3400 (12)	1.4 (5)
H3A	0.365 (3)	0.482 (3)	0.3545 (14)	2.7 (6)
H3B	0.3440 (22)	0.308 (3)	0.4155 (11)	0.5 (5)
H4A	0.143 (3)	0.467 (3)	0.4653 (15)	2.0 (6)
H4B	0.296 (3)	0.595 (3)	0.4779 (16)	3.8 (7)
H5A	0.186 (3)	0.783 (3)	0.3697 (13)	2.1 (6)
H5B	0.0636 (24)	0.777 (3)	0.4314 (12)	1.1 (5)
H6A	−0.080 (3)	0.546 (3)	0.3412 (15)	2.5 (7)
H6B	−0.060 (3)	0.731 (3)	0.2859 (13)	2.4 (6)
H7A	0.155 (3)	−0.050 (3)	0.2287 (13)	2.4 (6)
H7B	0.016 (3)	0.109 (3)	0.2271 (13)	1.4 (5)
H8A	0.234 (3)	0.109 (3)	0.1000 (13)	1.7 (5)
H8B	0.055 (3)	0.008 (3)	0.0814 (14)	2.1 (5)
H9A	0.270 (3)	0.386 (3)	0.1025 (15)	2.4 (6)
H9B	0.173 (3)	0.469 (4)	0.0174 (18)	4.8 (8)
H10A	0.196 (3)	0.714 (3)	0.1117 (13)	2.6 (6)
H10B	0.003 (3)	0.648 (3)	0.1136 (15)	3.7 (7)

[a] B_{iso} is the mean of the principal axes of the thermal ellipsoid.

Can. J. Chem. Downloaded from www.nrcresearchpress.com by 213.200.69.106 on 09/08/12
For personal use only.

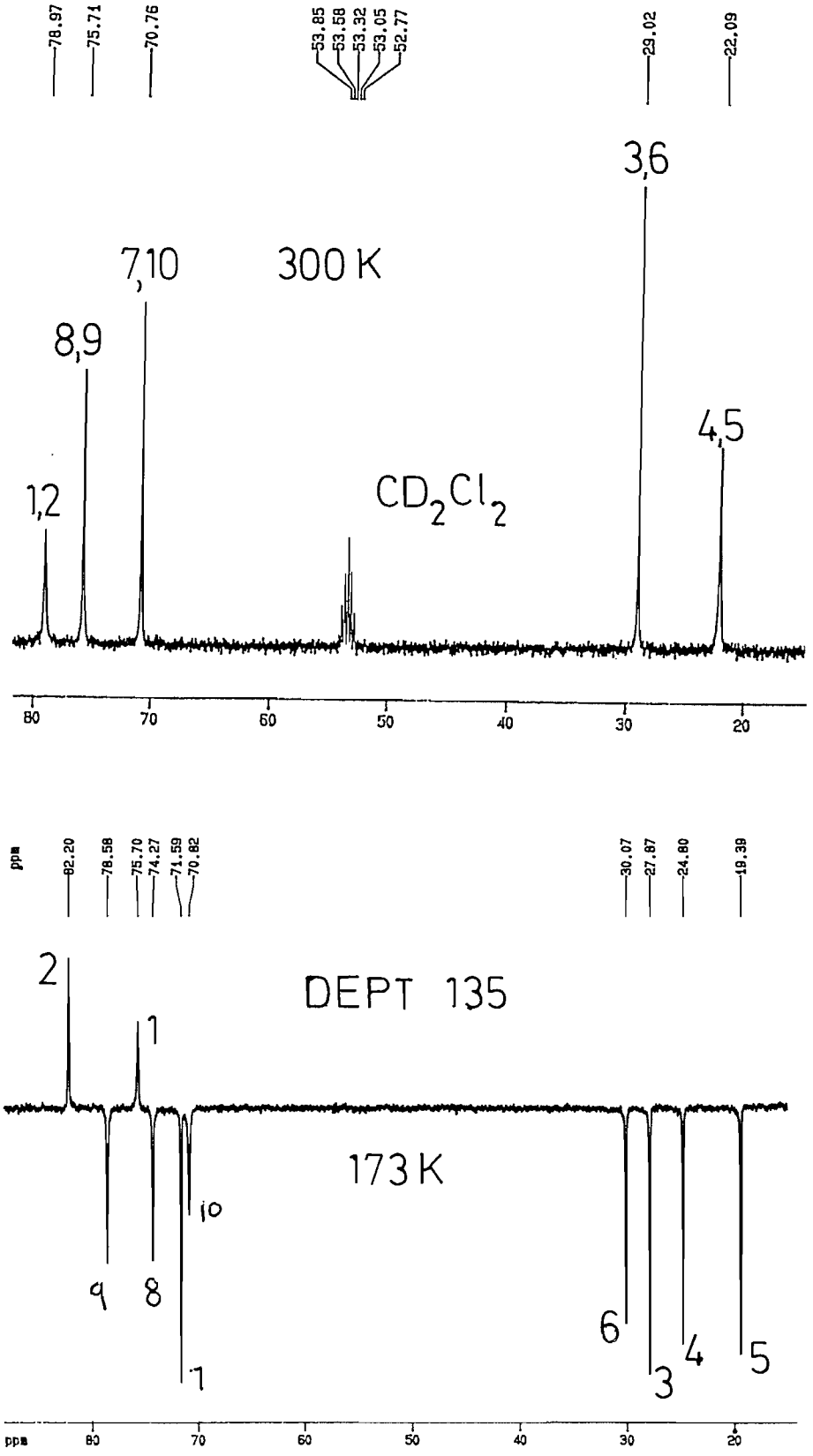

FIG. 2. Upper trace: 100 MHz ^{13}C NMR spectrum of **1** at 300 K. Lower trace: 100 MHz DEPT 135 ^{13}C NMR spectrum of **1** at 173 K.

Can. J. Chem. Downloaded from www.nrcresearchpress.com by 213.200.69.106 on 09/08/12
For personal use only.

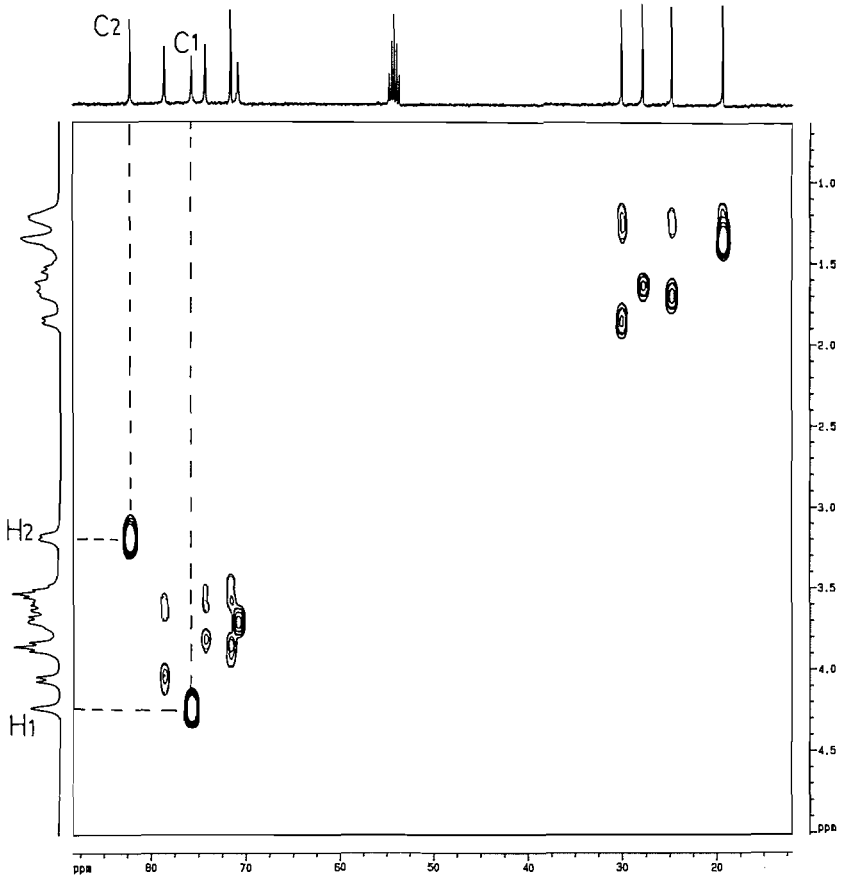

FIG. 3. ^1H ^{13}C HETCOR spectrum of **1** at 173 K.

TABLE 5. ^{13}C Chemical shifts (δ_C from TMS $\mp$ 0.1)

	Solution[a] (300 K)	Solution[a] (173 K)	Solid
C1	79.0	75.7	76.1
C2	79.0	82.2	82.0
C3	29.0	27.9	28.5
C4	22.1	24.8	26.0
C5	22.1	19.4	19.8
C6	29.0	30.1	28.5
C7	70.8	71.6	71.2
C8	75.7	74.3	75.0
C9	75.7	78.6	78.4
C10	70.8	70.8	71.2

[a]0.1 M in CD_2Cl_2.

vs. C7,10 of the nine-membered ring of **1**, the synthesis of the 7,10-d_4 derivative has permitted attribution of the resonance at 70.76 ppm in the 300 K spectrum to C7,10. At 173 K, the chemical shift difference between C7 and C10 is only 0.77 ppm (i.e., 71.59 vs. 70.82). In contrast, the shift difference bteween C8 and C9 at 173 K is 4.31 ppm.

In the solid phase ^{13}C spectra (Fig. 5), the observed chemical shifts are within 1.5 ppm of those found in CD_2Cl_2 solution at 173 K. The dipolar dephased spectrum of the 7,10-d_4 derivative clearly shows that the C7,10 sites are the most shielded of the oxygenated carbons and that the chemical shift difference between these sites is less than 1 ppm. The shift difference between C8 and C9 is 3.8 ppm in the solid phase spectrum and 4.3 ppm in solution at 173 K. It is of interest to note that in *benzo*-9-crown-3, the chemical shift difference between C7 and C10 is 7.7 ppm, while that between C8 and C9 is 2.8 ppm.[3]

Distinction between C7 and C10 was obtained via an inverse detected ^3J HETCOR experiment at low temperature. The ^{13}C resonance for C1 at 75.7 ppm shows a correlation to the ^1H resonance at 3.7 ppm. From the ^1J HETCOR spectrum these H's are bonded to the ^{13}C at 70.8 ppm. Hence C10 must resonate at 70.8. From the COSY, one then can get the connectivity to the H9 protons and subsequently, from the ^1J HETCOR, it is clear that C9 resonates at 78.6.

The 4.3 ppm deshielding of C9 relative to C8 is most likely due to a combination of two factors. Initially, it was calculated (16) that expansion of the O—C—C—O angle in ethylene glycol from 67° to 78° will deshield the carbon by ca. 1 ppm. Hence the O3—C8—C7—O2 angle of −67.4° is expected to result in some shielding of C8 relative to C9, since the O3—C9—C10—O1 angle is 78.0°.

Also there is a substantial difference between the C7—**C8**—O3—C9 torsion angle (96.1°) and the value of 127.7° for the C10—**C9**—O3—C8 unit. Recent *ab initio* ^{13}C calculations from these laboratories (16) for ethylmethyl ether indicate such an expansion should deshield C9 by ca. 2 ppm.

With more sophisticated computing methods, it is hoped that reliable *ab initio* ^{13}C calculations for a more complex molecule such as **1** will soon be available. Coupled with

[3]G.W. Buchanan, A.B. Driega, A. Moghimi, C. Bensimon, R.A. Kirby, and T.D. Bouman. Manuscript in preparation.

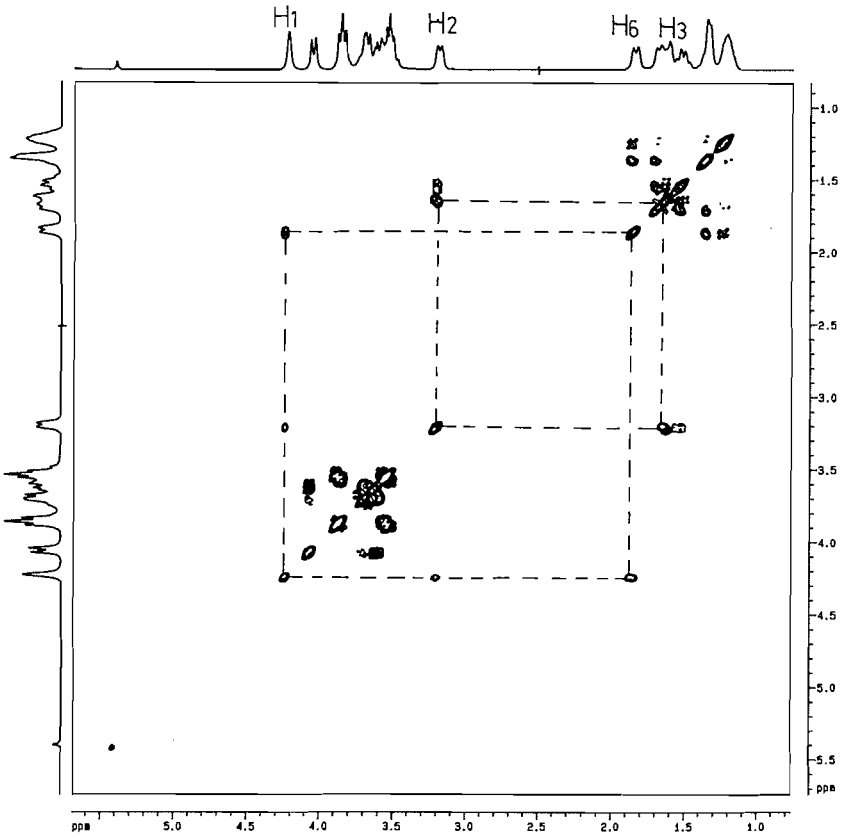

FIG. 4. The 400 MHz COSY 45 spectrum of **1** at 174 K.

single crystal chemical shift anisotropy data, the underlying features governing stereochemically dependent ^{13}C shifts will no doubt be delineated in the near future.

Experimental

(i) Materials

Diglycolic acid methyl ester

Diglycolic acid (Aldrich) (17.4 g, 0.13 mol) was dissolved in 100 mL of anhydrous methanol, and thionyl chloride (22 mL, 0.30 mol) was added dropwise with cooling and stirring over a period of 10 min. Stirring was continued for 30 min and the excess methanol was then removed by rotary evaporation. The resulting viscous liquid turned to a semi-solid upon standing (yield = 20.9 g, 98%). ^{13}C NMR ($CDCl_3$) δ_C = 170.2, 68.1, and 52.5. This crude material was used for the next step without further purification.

Diethylene glycol-d_4

$LiAlD_4$ (18.2 g, 0.12 mol) was added with stirring to a 1.5 L round-bottom three-necked flask, equipped with condensor and dropping funnel, containing 800 mL of dry THF under a nitrogen atmosphere. The flask was cooled in an ice–salt bath and dimethyl diglycolate (18.2 g, 0.11 mol) dissolved in 20 mL of dry THF was added with stirring over a period of 45 min. Two additional 50 mL aliquots of dry THF were added to reduce the viscosity and the reaction mixture was allowed to warm to 40°C with stirring for an additional 30 min. The excess $LiAlD_4$ was destroyed by dropwise addition of 3 mL water, and dilute H_2SO_4 (30 mL, 20%) was added with stirring to break down the alkoxide complex. The aqueous layer was separated and washed with additional THF (3 × 100 mL). Solvent was removed from the combined organics by rotary evaporation. The crude product was dissolved in water (100 mL) and washed with 20 mL of CH_2Cl_2. Water was removed by evaporation under vacuum (3 h), with occasional gentle warming, to yield 11.9 g (95%) diethylene glycol-d_4. ^{13}C NMR ($CDCl_3$) δ_C = 72.0, 60.6 (quintet).

1,5-Dichloro-3-oxapentane-d_4

Thionyl chloride (18.3 mL, 0.25 mol) was added dropwise over a period of 30 min, with stirring, to cooled diethylene glycol-d_4 (12.1 g, 0.11 mol) under nitrogen. The mixture was refluxed for 24 h and excess thionyl chloride was removed at reduced pressure. The residue was poured onto ice (15 g) and then washed with CH_2Cl_2 (3 × 50 mL). The combined extracts were washed with saturated $NaHCO_3$ (2 × 10 mL), saturated NaCl (20 mL), and water (2 × 20 mL), and dried over anhydrous Na_2SO_4. The solvent was removed by evaporation at reduced pressure to yield 12.3 g (76%) 1,5-dichloro-3-oxapentane-d_4. ^{13}C NMR ($CDCl_3$) δ_C = 71.1, 42.1 (quintet).

Benzo-9-crown-3-d_4

A 2-L round-bottom flask was charged with catechol (16.3 g, 0.148 mol), water (1700 mL), and LiOH (12.4 g, 0.296 mol), and the mixture was stirred for 5 min. To this was added dropwise 1,5-dichloro-3-oxapentane-d_4 (21.7 g, 0.148 mol) and the reaction mixture was refluxed for 86 h. Upon cooling, the mixture was acidified to pH 2 by addition of dilute H_2SO_4 and was extracted with CH_2Cl_2 (3 × 100 mL). After washing with 5% NaOH (3 × 100 mL), saturated NaCl (100 mL), and water, the extracts were dried over anhydrous Na_2SO_4. After solvent removal, the resulting reddish slurry was purified by column chromatography on silica gel (grade 60, 230–400 mesh). Elution with 1:1 CH_2Cl_2:diethyl ether yielded, in the initial fractions, 10.0 g (33%) benzo-9-crown-3-d_4, mp 69–71°C (lit. (15) mp (for protio analog) 67–69°C). Later fractions contained 1.0 g (1.6%) dibenzo-18-crown-6-d_8, mp 162–164°C (lit. (15) mp (for protio analog) 164–165°C).

cis-*Cyclohexyl-9-crown-3-*d_4

Benzo-9-crown-3-d_4 (1.0 g, 0.004 mol), in methanol (40 mL) containing 5% Rh on alumina catalyst and 0.5 mL acetic acid, was

Can. J. Chem. Downloaded from www.nrcresearchpress.com by 213.200.69.106 on 09/08/12
For personal use only.

Can. J. Chem. Downloaded from www.nrcresearchpress.com by 213.200.69.106 on 09/08/12
For personal use only.

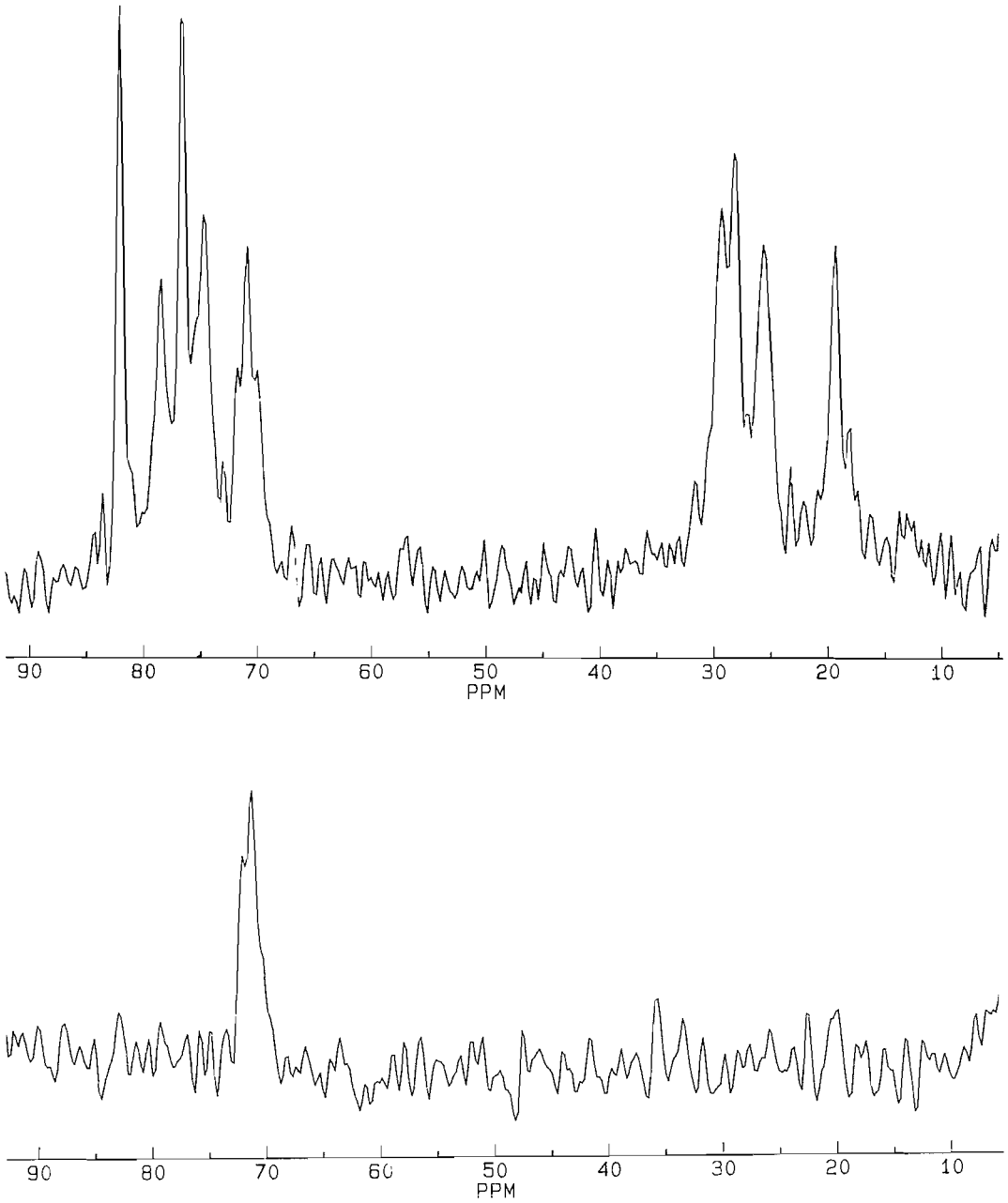

FIG. 5. Upper trace: 45.3 MHz ^{13}C CPMAS spectrum of **1**-C7,C10-d_4 at 300 K. Lower trace: same as upper except dipolar dephased.

hydrogenated for 6 h at 40°C and 5 atm (1 atm = 101.3 kPa) pressure using an American Instrument Co. high-pressure apparatus. After removal of the catalyst by filtration and solvent evaporation, the crude product was dissolved in 100 mL CH_2Cl_2 and washed with saturated NaCl and water. After drying over anhydrous Na_2SO_4, the solvent was removed to yield a viscous oil. Subsequent crystallization from *n*-hexane yielded 0.8 g (80%) of *cis*-cyclohexyl-9-crown-3-d_4, mp 41–42.5°C.

(ii) Spectra

Solution NMR spectra

All spectra were recorded using a Bruker AMX-400 spectrometer equipped with a 5-mm inverse probe and an Aspect X32 computer. An Aspect 3000 processing controller was employed and all standard microprograms used are in the Bruker Software Library.

The $^1H^1H$ COSY experiments were run using N-type phase cycling with a 45° mixing pulse. The free induction decays were acquired over 1024 data points for each of the 256 values of the evolution time, with a digital resolution of 5 Hz/point. The raw data were zero filled in F1 prior to transformation using the qsine window function for both F1 and F2. The matrix was symmetrized about the diagonal.

For the $^1H^{13}C$ HETCOR experiments, the free induction decays were typically acquired over 1024 data points for each of the 512 values of the evolution time, with a digital resolution of ca. 8 Hz/point in F2 and 4 Hz/point in F1. The raw data were zero filled in F1 prior to transformation using the qsine window function for both F1 and F2. The proton relaxation delays were set to 1 s. For one-bond couplings, delays were chosen to emphasize couplings of 135–140 Hz, while for the long-range HETCOR experiment, delays were set to correspond to couplings of 6 Hz.

For the DEPT 135 experiment, 32K data points were used with a digital resolution of 0.8 Hz/point. Proton relaxation delays were set to 1.0 s.

Solid phase ^{13}C spectra

The ^{13}C CPMAS spectra were recorded at 45.3 MHz using a Bruker CXP-180 spectrometer and techniques described previously (16). For the dipolar dephased spectra, the ^{1}H decoupler was gated off for a period of 40 μs during the delay before the ^{13}C acquisition.

(iii) X-ray crystallographic measurements and structure solution

A summary of the crystallographic data is given in Table 3. Diffration intensities were collected on a Rigaku diffractomer using MoKα radiation at −130°C. The θ/2θ scan technique with profile analysis (17) was employed. The space group was determined by systematic absences. Unit cell parameters were obtained by refinement of the setting angles of 24 reflections with 2θ values in the range of 30–49.9°C. Lorentz and polarization factors were applied but no correction for absorption was made. The structure was solved by direct methods plus Fourier maps and was refined by full-matrix least-squares analysis with weights based on counting statistics. Non-H atoms were refined anisotropically and H atoms were refined isotropically. All calculations were performed using the NRC VAX Crystal Structure programs (18). Anisotropic thermal parameters are available as supplementary data.

Acknowledgements

G.W.B. thanks the Natural Sciences and Engineering Research Council of Canada (NSERC) for continued support via an operating grant.

1. F.A.L. Anet, C.H. Bradley, and G.W. Buchanan. J. Am. Chem. Soc. **93**, 258 (1971).
2. H.-J. Schneider. J. Am. Chem. Soc. **94**, 3636 (1972).
3. H.-J. Schneider and V. Hoppen. Tetrahedron Lett. 579 (1974).
4. H. Booth and J.R. Everett. J. Chem. Soc. Chem. Commun. 278 (1976).
5. H.-J. Schneider and V. Hoppen. J. Org. Chem. **43**, 3866 (1978).
6. G.W. Buchanan. Can. J. Chem. **60**, 2908 (1982).
7. G.W. Buchanan, S.H. Preusser, and V.L. Webb. Can. J. Chem. **62**, 1308 (1984).
8. A.C. Coxon, D.A. Laidler, R.B. Pettman, and J.F. Stoddart. J. Am. Chem. Soc. **100**, 8260 (1978).
9. M.J. Bovill, D.J. Chadwick, and I.O. Sutherland. J. Chem. Soc. Perkin Trans. 2, 1529 (1980).
10. G. Borgen, J. Dale, F.A.L. Anet, and J. Krane. J. Chem. Soc. Chem. Commun. 243, (1974).
11. N.K. Wilson and J.B. Stothers. Top. Stereochem. **8**, 1 (1973).
12. G.W. Buchanan, R.A. Kirby, and J.P. Charland. J. Am. Chem. Soc. **110**, 2477 (1988).
13. G.W. Buchanan and R.A. Kirby. Tetrahedron Lett. **28**, 1507 (1987).
14. G.W. Buchanan, K. Bourque, J.W. Bovenkamp, and A. Rodrigue. Can. J. Chem. **63**, 2747 (1985).
15. C.J. Pedersen. J. Am. Chem. Soc. **89**, 7017 (1967).
16. G.W. Buchanan, A. Rodrigue, C. Bensimon, and C.I. Ratcliffe. Can. J. Chem. **70**, 1033 (1992).
17. D.F. Grant and E.J. Gabe. J. Appl. Crystallogr. **11**, 114 (1978).
18. E.J. Gabe, F.L. Lee, and Y. LePage. J. Appl. Crystallogr. **22**, 384 (1989).

Can. J. Chem. Downloaded from www.nrcresearchpress.com by 213.200.69.106 on 09/08/12
For personal use only.

Large perturbations of long-range $^nJ(^1H,^1H)$ and $^nJ(^1H,^{19}F)$ by the intramolecular hydrogen bonds in 2-mercaptobenzaldehyde, salicylaldehyde, and some derivatives. Reference structures for intramolecular hydrogen bonds

TED SCHAEFER,[1] RUDY SEBASTIAN, DAVID M. MCKINNON, PERRY W. SPEVACK, KERRY J. COX, AND CRAIG S. TAKEUCHI

Department of Chemistry, University of Manitoba, Winnipeg, Man., Canada R3T 2N2

Received December 22, 1992

TED SCHAEFER, RUDY SEBASTIAN, DAVID M. MCKINNON, PERRY W. SPEVACK, KERRY J. COX, and CRAIG S. TAKEUCKI. Can. J. Chem. **71**, 960 (1993).

Precise ^1H nuclear magnetic resonance spectral parameters are reported for salicyladehyde and its 3-fluoro and 5-fluoro derivatives in nonpolar solutions. Such data are also given for the 2-mercapto, 2-methylthio, and 2-methoxy derivatives of benzaldehyde. Comparison of the long-range coupling constants in the various compounds and their conformers shows a large perturbation of their magnitudes by hydrogen bond formation. For the salicylaldehyde system, the perturbation is particularly large for couplings involving the aldehyde proton and protons or fluorine nuclei placed *ortho* to the hydroxyl group. For example, ^5J_t (F, CHO) is reduced by about 50%. The perturbation, as expected, is much smaller for coupling constants of nuclei remote from the site of the hydrogen bond. In 2-mercaptobenzaldehyde the long-range coupling constants are also sensitive to hydrogen bond formation, those involving the sulfhydryl proton markedly so compared to the hydroxyl proton in salicylaldehyde. The strength of the C=O···H—S bond is discussed. It is argued that the reference conformer for the mercapto compound in such a discussion is less easily defined than for salicylaldehyde because C=O···S are similar to O=C—H···S energies. The experimental data for the CCl_4 solutions imply a free energy of formation of the C=O···H—S bond of 4.8(5) kJ/mol at 300 K. Molecular orbital computations on the four planar conformers of each salicylaldehyde and 2-mercaptobenzaldehyde with the 6-31 G**(5D) basis are reported. For salicylaldehyde, the O=C—H···O—H arrangement is taken as the reference conformer, with a computed energy of 25.7 kJ/mol relative to the hydrogen-bonded structure. For 2-mercaptobenzaldehyde, the H—C=O···S—H and O=C—H···S—H conformers are calculated to be isoenergetic, at 5.1 kJ/mol relative to the hydrogen-bonded conformer. Hence either arrangement serves as a reference structure in computations of the strength of the hydrogen bond. The computations are consistent with the experimental results for solutions of the molecules under discussion. An appendix gives the computed geometries of the eight planar conformers, as well as some atomic charges, allowing a rationalization of the relative energies of the conformers.

TED SCHAEFER, RUDY SEBASTIAN, DAVID M. MCKINNON, PERRY W. SPEVACK, KERRY J. COX et CRAIG S. TAKEUCHI. Can. J. Chem. **71**, 960 (1993).

On a déterminé des paramètres précis de résonance magnétique nucléaire du ^1H pour le salicylaldéhyde et ses dérivés 3-fluoro et 5-fluoro, en solutions non-polaires. On rapporte aussi des données semblables pour les dérivés 2-mercapto, 2-méthylthio et 2-méthoxy du benzaldéhyde. Une comparaison des constantes de couplage à longue distance dans les divers composés et dans leurs conformères indique que les ponts hydrogènes provoquent de grandes perturbations dans leurs amplitudes. Pour le système du salicylaldéhyde, la perturbation est particulièrement importante pour les couplages impliquant le proton de l'aldéhyde et les protons ou les noyaux de fluor placés en position *ortho* par rapport au groupe hydroxyle. Par example, la valeur de ^5J_t (F, CHO) est réduite de moitié. Comme on peut s'y attendre, la perturbation est plus faible pour les constantes de couplage des noyaux éloignés du site de la liaison hydrogène. Dans le 2-mercaptobenzaldéhyde, les constantes de couplage à longue distance sont aussi sensibles à la formation de liaisons hydrogènes, celles impliquant le proton sulfhydrile étant particulièrement influencées en comparaison avec celles du proton hydroxylique du salicylaldéhyde. On discute de la force de la liaison C=O···H—S. On suggère que le conformère de référence du composé mercapto est plus difficile à définir que celui du salicylaldéhyde parce que les énergies de des structures C=O···S et de O=C—H···S sont semblables. Les données expérimentales pour des solutions de CCl_4 impliquent que l'énergie libre de formation de la liaison C=O···H—S est de 4,8(5) kJ/mol à 300 K. On rapporte les résultats de calculs d'orbitales moléculaires effectués sur quatre conformères plans du salicylaldéhyde ainsi que du 2-mercaptobenzaldéhyde au niveau 6-31G G**(5D). Pour le salicylaldéhyde, l'arrangement O=C—H···O—H est pris comme conformère de référence et son énergie calculée est de 25,7 kJ/mol par rapport à celle de la structure comportant une liaison hydrogène. Pour le 2-mercaptobenzaldéhyde, on a calculé que les conformères H—C=O···S—H et O=C—H···S—H sont isoénergétiques, à 5,1 kJ/mol par rapport au conformère avec une liaison hydrogène. Les deux arrangements peuvent donc servir de structure de référence lors des calculs de la force de la liaison hydrogène. Les calculs sont en accord avec les résultats expérimentaux pour les solutions des molécules examinées. Un appendice donne les géométries calculées pour les huit conformères plans ainsi que quelques charges atomiques; elles permettent une rationalisation des énergies relatives des conformères.

[Traduit par la rédaction]

Introduction

The purposes of this report are three. The first is a demonstration that the intramolecular hydrogen bond in salicylaldehyde and some of its derivatives is associated with a large perturbation of the stereospecific long-range spin–spin coupling constants between the formyl proton and the ring protons or fluorine nuclei. The second purpose is the measurement of long-range coupling constants for 2-mercaptobenzaldehyde in order to assess the strength of the putative intramolecular hydrogen bond. The third purpose is to

[1]Author to whom correspondence may be addressed.

Can. J. Chem. Downloaded from www.nrcresearchpress.com by 213.200.69.106 on 09/08/12
For personal use only.

TABLE 1. The ^{1}H nmr spectral parameters of 2-methoxy- and 2-hydroxybenzaldehyde at 300 K

Parameter	2-OCH_3[a]	2-OH[b]	Parameter	2-OCH_3	2-OH
ν_X[c]	1162.000	3274.100	$^{5,6}J_{4X}$	0.090	0.487(2)
ν(CHO)	3106.171	2956.383	$^{5,6}J_{6X}$	0.001	0.060
ν_3	2069.844	2076.054	$^{6,7}J_{5X}$	0.001	0.045(2)[f]
ν_4	2298.948	2234.132	^4J(6, CHO)	−0.134	−0.130
ν_5	2074.056	2079.014	^5J(3, CHO)	−0.006	0.633(2)
ν_6	2302.598	2241.924	^5J(5, CHO)	0.859	−0.036(2)[f]
$^3J_{34}$	8.339	8.425(2)[d]	^6J(4, CHO)	0.000	0.010(2)[f]
$^3J_{45}$	7.306	7.256(2)	J(X, CHO)	0.001	0.008(2)[g]
$^3J_{56}$	7.648	7.704(2)	Calcd. transitions	661	228
$^4J_{35}$	0.932	1.035(2)	Peaks observed	99	120
$^4J_{46}$	1.870	1.744	Assigned trans.	362	194
$^5J_{36}$	0.434	0.466(2)	Largest difference	0.017	0.014
$^{4,5}J_{3X}$[e]	−0.338	−0.010(2)[f]	Root-mean-square deviation	0.006	0.006

[a]4.0 mol% in CS_2, containing also 10.0 mol% of C_6D_{12} and 0.5 mol% of TMS.
[b]~1 mol% in CCl_4 with C_6D_{12} and TMS as in footnote *a*.
[c]To high frequency of internal TMS at a transmitter frequency of 300.135$_2$ MHz.
[d]The standard deviations are less than or equal to 0.001 Hz except as indicated.
[e]X stands for methyl or hydroxyl protons, as appropriate; thus $^5J_{3X} \equiv {}^5J$(3, OCH_3) and $^4J_{3X} \equiv {}^4J$(3, OH).
[f]These signs and magnitudes, not previously determined (1), appear to be as given on the basis off the iterative procedure and of simulations with three other sign combinations.
[g]The sign is very likely positive and the magnitude, based on various simulations, is 0.015 ± 0.005 Hz.

provide some experimental and theoretical data relevant to the question of reference structures, those with respect to which the strengths of the H—C=O···H—O and H—C=O···H—S bonds should be computed. Reference structures are the subject of recent discussions (1–3).

Accordingly, precise analyses of the ^{1}H nmr spectra are reported for salicylaldehyde, its 3-fluoro and 5-fluoro derivatives, as well as for 2-methoxybenzaldehyde and 2-mercaptobenzaldehyde, all as solutions in nonpolar solvents. Together with previous precise spectral data for benzaldehyde and some of its derivatives, the present results are used to show that ^5J(H-3, CHO) is reduced by about 25% on formation of the H—C=O···H—O or H—C=O···H—S bonds and that ^5J(F-3, CHO) decreases by about 50%. The changes in the corresponding coupling constants for H-5 and F-5 are much smaller. Other perturbations involve the sulfhydryl proton, which couples not only to the aldehydic proton in 2-mercaptobenzaldehyde but also to H-6 in a manner implying the loss of stereospecificity of ^5J(H, SH).

The combined experimental and molecular orbital computational results suggest that the intramolecular hydrogen bond formed by the S—H group is about one-fifth as strong as that formed by the O—H group. Furthermore, these data imply that the O=C—H···O—H arrangement is the proper reference for the computation of the energy of the hydrogen bond in salicylaldehyde, whereas for the sulfur compound either structure, H—C=O···S—H or O=C—H···S—H, can play that role.

Experimental

The 2-mercaptobenzaldehyde was made from salicylaldehyde, following the procedure (4) for a synthesis of 2-mercapto-3-methoxybenzaldehyde, except that *N*,*N*-diethylthiocarbamoyl chloride was substituted for *N*,*N*-dimethylthiocarbamoyl chloride. The product was contaminated with some 2-hydroxybenzaldehyde. However, a dilute solution of the mixture in CCl_4/C_6D_{12}/TMS gave excellent ^{1}H nmr spectra, eventually yielding the spectral parameters for both compounds. The 5-fluorosalicylaldehyde was prepared from 4-fluorophenol via a modified Reimer–Tiemann reaction. The yield was very low; from 4.3 g of 4-fluorophenol only enough of the purified white crystalline product was obtained for the preparation of a ca. 1 mol% solution in 0.5 mL of the CCl_4/C_6D_{12}/TMS solvent mixture. The other compounds under investigation were of commercial origin. In each case, the solution of the compound was filtered into a 5-mm o.d. nmr sample tube and degassed by four to five cycles of the freeze–pump–thaw procedure. The tube was flame-sealed to give a reasonably symmetric top.

The ^{1}H nmr spectra were acquired on an AM 300 Bruker spectrometer at a probe temperature of 300 K. Acquisition times were not less than 40 s for the free induction decays, the final manual shimming having been done on the TMS response. The spectral windows ensured a digital resolution of at least 0.012 Hz/point. Zero-filling helped further to define line shapes. Judicious amounts of Lorentzian and Gaussian multiplication before Fourier transformation gave some resolution enhancement.

^{1}H{^{1}H} experiments (5) on 5-fluorosalicylaldehyde gave the signs of ^6J(OH), F) and ^5J(CHO, F) relative to the known signs of other coupling constants. Similar experiments yielded the relative signs of ^4J(H-3, SH), ^5J(CHO, SH), and ^5J(H-6, SH) for 2-mercaptobenzaldehyde. Other signs were either known or came from the iterative analyses and simulations of the second-order spectra (see tables).

AM1 (6), STO-3G (7), and 6-31G** (5D) (8) MO computations of the four planar conformers of each of 2-hydroxy and 2-mercaptobenzaldehyde employed the program GAUSSIAN 86 (9). Within the constraint of planarity all bond angles and lengths were optimized. The 6-31G** (5D) basis is recommended for computations in which hydrogen is involved in bridging interactions.

Results and discussion

Spectral analyses

The spectra were analyzed with the program NUMARIT (10), substantially modified by R. Sebastian. Tables 1–3 contain the ensuing chemical shifts and coupling constants. Figure 1 illustrates the determination of the sign of ^5J(SH, CHO) in 2-mercaptobenzaldehyde; it also demonstrates the resolution attainable in the spectra of the molecules under discussion.

Can. J. Chem. Downloaded from www.nrcresearchpress.com by 213.200.69.106 on 09/08/12
For personal use only.

TABLE 2. The ^{1}H nmr spectral parameters of 2-hydroxy-3-fluoro- and 2-hydroxy-5-fluorobenzaldehyde at 300 K

Parameter	3-F[a]	5-F[b]	Parameter	3-F	5-F
ν(CHO)[c]	2959.942(1)[e]	2947.012(1)	^5J(4, OH)	0.515	0.443
ν(OH)	3257.233[e]	3208.059(1)	^5J(6, OH)	0.000	0.079
ν_3	7666.062(1)[d]	2074.446(1)	^6J(5, OH)	0.001	−0.321[f]
ν_4	2165.604(1)	2159.624(1)	^4J(6, CHO)	−0.119	−0.092
ν_5	2070.083(1)	—	^5J(3, CHO)	1.892	0.647
ν_6	2187.791(1)	2149.646(1)	^5J(5, CHO)	0.001	−0.224[f]
$^3J_{34}$	10.488	9.123	^6J(4, CHO)	0.000	—
$^3J_{45}$	8.042	7.787(3)	^5J(OH, CHO)	0.000	—
$^3J_{56}$	7.799	7.431	Calcd. transitions	192	170
$^4J_{35}$	4.087	4.123	Peaks observed	73	67
$^4J_{46}$	1.559	3.116	Assigned trans.	162	159
$^5J_{36}$	−1.184	0.402	Largest difference	0.023	0.019
^4J(3, OH)	−0.740	—	Root-mean-square deviation	0.007	0.007

[a]3.8 mol% in CS_2, containing also 10.0 mol% of C_6D_{12}, 0.5 mol% of TMS and 0.25 mol% of C_6F_6.
[b]~1 mol% in CCl_4, with C_6D_{12}, TMS, and C_6F_6 as in footnote *a*.
[c]In Hz at 300.135$_2$ MHz to high frequency of internal TMS.
[d]In Hz at 282.363 MHz to high frequency of internal C_6F_6.
[e]Unless otherwise stated, the standard deviations are 0.002 Hz.
[f]Signs determined by irradiation experiments.

TABLE 3. The ^{1}H nmr spectral parameters of 2-mercapto and 2-methylthiobenzaldehyde in CCl_4 solution

Parameter	2-SCH$_3$[a]	2-SH[b]	Parameter	2-SCH$_3$	2-SH
ν_X	245.025(3)[c]	1865.1[d]	$^{5,6}J_{4X}$	—[f]	0.188
ν(CHO)	1026.722(2)	2995.188[e]	$^{5,6}J_{6X}$	—[f]	0.259
ν_3	727.620(3)	2175.227	$^{6,7}J_{5X}$	—[f]	−0.029[h]
ν_4	743.104(3)	2193.800	^4J(6, CHO)	−0.175(3)	−0.260
ν_5	702.149(3)	2163.320	^5J(3, CHO)	0.335(4)	0.579
ν_6	773.884(2)	2289.459	^5J(5, CHO)	0.486(3)	0.073[h]
$^3J_{34}$	8.026(4)	7.950	^6J(4, CHO)	−0.032(4)	−0.010[h]
$^3J_{45}$	7.323(4)	7.325	J(X, CHO)	—	0.135[g]
$^3J_{56}$	7.674(4)	7.702	Calcd. transitions	84	168
$^4J_{35}$	1.078(3)	1.118	Peaks observed	63	124
$^4J_{46}$	1.614(4)	1.570	Assigned trans.	80	146
$^5J_{36}$	0.476(4)	0.485	Largest difference	—	0.006
$^{4,5}J_{3X}$	−0.341(2)	0.216[g]	Root-mean-square deviation	0.008	0.003

[a]4 mol% at 305 K and 100.001 MHz (15).
[b]~2 mol% at 300 K, containing also 10.0 mol% of C_6D_{12} and 0.5 mol% of TMS.
[c]In Hz at 100.00 MHz to high frequency of internal TMS.
[d]In Hz at 300.135$_2$ MHz to high frequency of internal TMS.
[e]The standard deviations are all 0.001 Hz.
[f]These are present, but the most reliable iterative analysis was done under conditions where the methyl protons were decoupled.
[g]Signs from ^{1}H{^{1}H} experiments.
[h]Simulations with other sign combinations indicate these signs.

^5J(H, CHO) in salicylaldehyde

In benzaldehyde, ^5J(H, CHO) is 0.431(2) Hz for a CS_2/C_6D_{12} solution (11), an average of ^5J(H-3, CHO) ≡ ^5J_t and

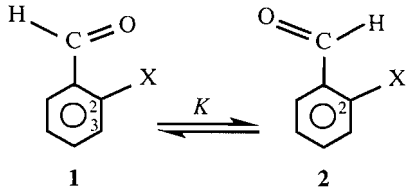

1 2

^5J(H-5, CHO) ≡ ^5J_c in **1** (X = H). It is assumed that ^5J_c effectively vanishes (12, 13) and therefore that ^5J(H, CHO) is a good indicator of the equilibrium between **1** and **2** (X ≠ H). A recent study of the solvent and temperature dependence of ^5J(H, CHO) for X = Cl in acetone-d_6 and CD_3CN solutions (13) suggests a small solvent perturbation, <0.01 Hz, of this coupling constant but that the ratio of ^5J(H-3, CHO) to ^5J(H-5, CHO) is a reliable measure of K.

Turning to X = OCH_3 (Table 1), the analysis gives ^5J(H-5, CHO) as 0.859(1) Hz, twice the magnitude of ^5J(H, CHO) in benzaldehyde, to within experimental error, and indicating that K is very large at 300 K. ^5J(H-3, CHO), however, is −0.006(1) Hz, according to the least-squares iterative analytical procedures; this coupling constant is not observable as a splitting in the spectrum. In any event, the sum of

Can. J. Chem. Downloaded from www.nrcresearchpress.com by 213.200.69.106 on 09/08/12
For personal use only.

Can. J. Chem. Downloaded from www.nrcresearchpress.com by 213.200.69.106 on 09/08/12
For personal use only.

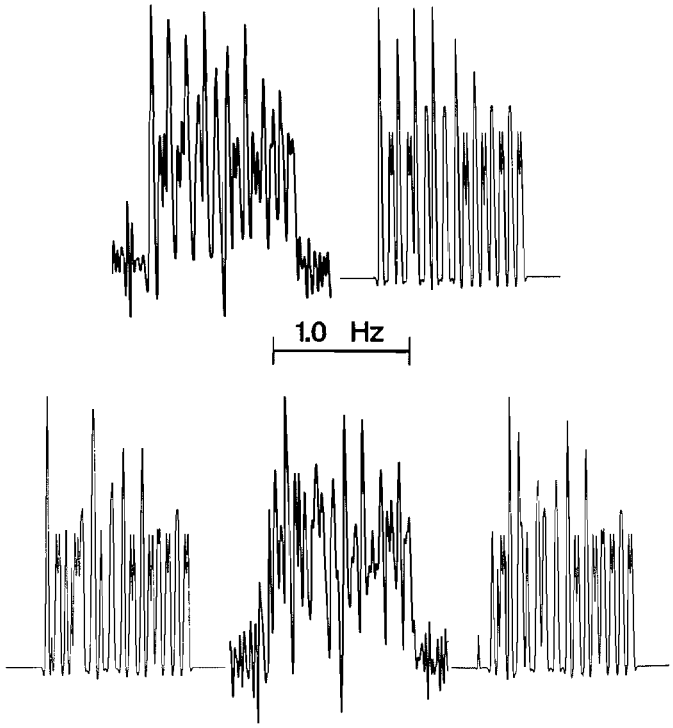

FIG. 1. The top of the figure displays the aldehydic ^{1}H nmr spectrum of a ca. 1 mol% solution of 2-mercaptobenzaldehyde in CCl_4 solution at 300 K. The span of the spectrum is just over 1 Hz. To resolve some of the small displayed splittings, whose magnitude is <0.03 Hz, a small amount of a Gaussian function is applied to the summed free induction decays. The computed spectrum takes this enhancement into account and uses the spectral parameters in Table 3. At the bottom and centre of the figure the aldehydic multiplet is shown under conditions in which the peak at highest frequency for H-6 is very weakly perturbed with a second radiofrequency field. The computed spectrum on the left assumes that ^5J(SH, CHO) < 0, that on the right, ^5J(SH, CHO) > 0. It is somewhat difficult to match exactly the amplitudes of the second field in the experimental and theoretical spectra. Yet it is clear that ^5J(SH, CHO) > 0, as confirmed by further experiments.

the two coupling constants is perturbed by not more than 0.01 Hz by the methoxy substituent.

Now, in salicylaldehyde only the hydrogen-bonded structure, **3**, need be considered at 300 K. ^5J(H-3, CHO) is

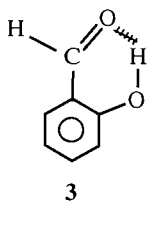

3

0.633(2) Hz, a reduction of about 25% from the expected ^5J_t value. Furthermore, ^5J(H-5, CHO) is −0.036(2) Hz, so that the sum of the two ^5J values, at 0.597(4) Hz, is only 70% of the sum in 2-methoxybenzaldehyde. Of course, the orientation of the formyl group in **3** is opposite to that in the main conformer, **2**, of the 2-methoxy derivative but it may be noted that in acetone-d_6 solutions the sums are 0.117(1) + 0.733(1) or 0.850(2) Hz for X = F at 300 K (12) and 0.062 + 0.808 or 0.870(1) Hz for X = Cl at 292 K (13). The finite ^5J(H-3, CHO) values are associated with significant populations of **1**, analogous to **3**, and their sums with ^5J(H-5, CHO) are consistent with a strong perturbation of ^5J(H-3, CHO) by the hydrogen bond in **3**, as distinct from a perturbation by an electronegative substituent, Cl, F, or OCH_3 placed *ortho* to the formyl group.

^{5}J(F, CHO) in 3- and 5-fluorosalicylaldehydes

^5J(F-3, CHO) is 1.892(2) Hz while ^5J(F-5, CHO) is −0.224(2) Hz in these fluorosalicylaldehydes (Table 2). By way of contrast, ^5J(F, CHO) in 3-fluorobenzaldehyde has a value of 1.889(1) Hz in a CS_2/C_6D_{12} solution at 300 K (12). ^5J(H-5, CHO) for this compound indicates an *O-cis* fractional population of 0.538(4). On this basis, write $^5J_c(0.46_2) + {}^5J_t(0.53_8) = 1.889$ Hz, where ^5J_t corresponds to an all-*trans* arrangement of the bonds between ^{1}H and ^{19}F. Now, if ^5J_c is taken as −0.224(2) Hz, the value for 5-fluorosalicylaldehyde, then ^5J_t becomes 3.70 Hz. These values of ^5J_c and ^5J_t predict ^5J(F, CHO) in 3,5-difluorobenzaldehyde to be 1.74 Hz, whereas it has been measured as 1.722(2) Hz for a CS_2/C_6D_{12} solution in this laboratory. These comparisons suggest a minor perturbation of ^5J(F-5, CHO) by the intramolecular hydrogen bond but that ^5J(F-3, CHO) is reduced by very nearly 50%. If ^5J_c vanishes in the absence of the hydrogen bond, that is, ^5J(F, CHO) in 5-fluorosalicylaldehyde is a consequence of a perturbation by the hydrogen bond, then ^5J_t becomes 3.51 Hz as deduced from the data for 3-fluorobenzaldehyde, but 3.44 Hz using ^5J(F, CHO) for the 3,5-difluoro derivative. In any event, ^5J(F-3, CHO) in 3-fluorosalicylaldehyde is reduced by at least 45% from the value anticipated in the absence of the hydrogen bond.[2]

Confirmation that it is the hydrogen bond, and not substitution by an electronegative group, which causes the large reduction in ^5J(F-3, CHO), comes from our analyses of the ^{1}H nmr and ^{19}F nmr spectra of 2,3-difluorobenzaldehyde in CS_2/C_6D_{12} and acetone-d_6 solutions. ^5J(H-5, CHO) is 0.845(2) Hz for the nonpolar solution, consistent with the essential absence of the *O-cis* conformer (see discussion of 2-fluorobenzaldehyde above). In the polar solution, ^5J(H-5, CHO) is 0.715(1) Hz, implying that the fractional population of the polar *O-cis* conformer is now 0.15. But ^5J(F-3, CHO) is 0.510(2) Hz in this solution, so that ^5J_t(F-3, CHO) is predicted as 0.51/0.15 or 3.4 Hz, very close to the unperturbed magnitude under discussion above and certainly far from the 1.9 Hz occurring in 3-fluorosalicylaldehyde.

^{5}J(H, CHO) in 2-mercapto and 2-thiomethylbenzaldehyde

For the 2-thiomethyl compound, ^5J(H-3, CHO) and ^5J(H-5, CHO) are 0.335(4) and 0.486(3) Hz, respectively. Their sum, 0.821(7) Hz, is consistent with a small perturbation of ^5J(H, CHO) by the substituent, while the individual values are discussed further below in connection with reference structures for intramolecular hydrogen bond computations. Turning to the 2-mercapto derivative, the strong perturbation of ^5J(H, CHO) is clear from the 0.579(1) Hz for ^5J(H-3,

[2]Our INDO MO FPT (14) computations give ^5J_t and ^5J_c as 3.67 and −0.26 Hz, respectively. for 3-fluorobenzaldehyde and 3.54 Hz for ^5J(F, CHO) in 3-fluorosalicylaldehyde. Analogous results come from CNDO/2 or INDO MO FPT calculations of ^5J(H, CHO) in benzaldehyde and salicylaldehyde. Thus, the stereospecificities of ^5J(F, CHO) and ^5J(H, CHO) are semiquantitatively reproduced, but the perturbations by the intramolecular hydrogen bonds are not.

Can. J. Chem. Downloaded from www.nrcresearchpress.com by 213.200.69.106 on 09/08/12
For personal use only.

CHO). This number is taken as strong evidence for the presence of an intramolecular C=O···H—S bond, not previously investigated. A naive approach takes the ratio of the two ^5J(H, CHO) values, 0.579 and 0.073 Hz, and deduces that 5.2 kJ/mol is the free energy difference at 300 K favoring the intramolecular hydrogen bond; naive because ^5J(H, CHO) is perturbed by the hydrogen bond and also because **4** and **5** are probably of similar stability, as judged by

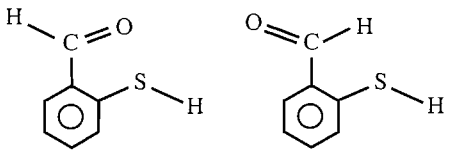

4 **5**

the conformational properties of 2-thiomethylbenzaldehyde for which the ratio of **1** to **2** is 41 to 59 at 305 K (15). A better approximation to the free energy difference is obtained by the recognition that, in **4** and **5**, ^5J(H, CHO) behaves "normally," so that it is effectively zero in **4** and 0.85(1) Hz in **5**. If $p_1 = 0.69p_5$, as for the thiomethyl derivative, and $p_5 = 0.073/0.85(1)$, the population of the intramolecularly hydrogen-bonded conformer follows as 0.86. Hence the free energy difference is 4.4(1) kJ/mol, suggesting a relatively weak hydrogen bond. These matters are discussed further below.

Perturbations of J*(H, SH) and* J*(H, OH)*

The most remarkable perturbations of the coupling constants involving the hydroxyl or sulfhydryl protons, caused by the intramolecular hydrogen bond, are those of $^{4,5}J$(H, SH). First, ^5J(H-4, SH), at 0.188 Hz, and ^5J(H-6, SH), at 0.259 Hz, have lost their stereospecificity. For example, the assumption that such coupling constants involving the protons placed *meta* to the SH group are large for the all-*trans* arrangement of the intervening bonds and very small or negligible for the other, gives 45 ± 5% for the Cl···H—S conformer of 2,4-dichlorothiophenol in CCl_4 solution (16), in close agreement with the equilibrium deduced from the dipole moment (17). In sharp contrast, ^5J(H-6, SH) > ^5J(H-4, SH) for 2-mercaptobenzaldehyde, which, however, exists as the intramolecularly hydrogen-bonded conformer to the extent of at least 85%. ^5J(H, SH) is thought to consist of a stereospecific σ electron component, just like ^5J(H, CHO), and a component dependent on a σ–π interaction mechanism proportional to $\sin^2\theta$, where θ is the angle by which the S—H bond twists out of the aromatic plane (18). It is unlikely that the average value of $\sin^2\theta$ in the hydrogen-bonded conformer is significant. In 2-mercaptobenzaldehyde, ^6J(H-5, SH) is −0.029(1) Hz while ^6J(H, SH) at θ = 90° lies near −1.0 Hz in thiophenol and some of its derivatives (19, 20). Consequently, the perturbation of ^5J(H, SH) by the formation of the intramolecular hydrogen bond must occur by another mechanism. Other peculiarities are represented by the presence of ^5J(SH, CHO), at 0.135(1) Hz, and ^4J(H-3, SH), which is 0.216(1) Hz. The latter is normally negative (19–21) and dominated by a σ–π electron mechanism.

Compared to $^{4,5}J$(H, OH) in phenol (22), and some derivatives (23), formation of the hydrogen bond in salicylaldehyde causes a relatively small perturbation of the coupling constants of the hydroxyl proton. Thus, while ^5J(H-6, OH) is 0.060(1) Hz, its magnitude is considerably smaller than the 0.487(2) Hz measured for ^5J(H-4, OH); the stereospecificity of ^5J(H, OH) is largely retained. Again, ^5J(OH, CHO) is indicated as 0.008(2) Hz by the spectral analysis, but is hardly significant. Yet, it is known that compression of the H—C=O···H—O bond in salicylaldehyde derivatives (1) can lead to a ^5J(OH, CHO) as large as that reported here for 2-mercaptobenzaldehyde.

Consideration of all the coupling data in Tables 1–3 leads to the tentative conclusion that the perturbations of the coupling constants involving the formyl proton have a different origin than those involving the hydroxyl or sulfhydryl protons. While our extensive CNDO/2 and INDO MO FPT computations do not account for the perturbations and are not reported here (but see footnote 2 for an example of such computations), a rationalization of the perturbations is attempted next.

An attempted rationalization of the large perturbation of J

The high polarity of the carbonyl bond is attested by extensive molecular orbital calculations. The role of oxygen is to polarize the bond, leading to a severely electron-deficient carbon atom (24). The valence bond structure, **A**, emphasizes this polarity and can be used to rationalize certain peculiarities (11) of ^nJ(H, CHO). This structure has been

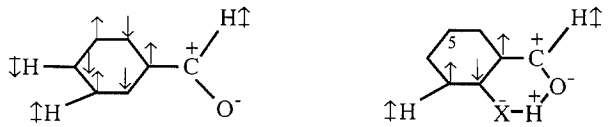

A **B**

invoked to rationalize the positive values of ^6J(H, CHO) in some 3,5-disubstituted benzaldehydes, in which ^6J(H, CHO) can be as large as 0.1 Hz (11). If the formation of the intramolecular hydrogen bond serves mainly to further stabilize the ionic structure, as in **B**, then a negative π-electron contribution[3] to ^5J(H, CHO) is implied (arrows indicate π-electron spin polarization, crossed arrows the spin state of protons). The consequence is a reduction in the magnitude of ^5J(H, CHO). Of course, the degrees of spin polarization in the coupling pathways leading to H-5 and H-3 need not be equal, so that the −0.04 Hz measured for ^5J(H-5, CHO) in salicylaldehyde is qualitatively consistent with the negative π coupling contribution.

Alternatively, structure **C** may play a role in the spin polarization of the π electrons; an electron has been moved

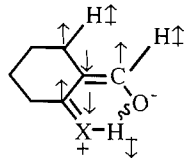

C

from the sulfur or oxygen orbitals to the previously electron-deficient carbon atom of the carbonyl group. The spin polarization implied by **C** accounts for the signs of ^5J(H-6, XH), ^5J(CHO, SH), and perhaps for the enhanced ^4J(H-6, CHO) in 2-mercaptobenzaldehyde. However, **C** must be more important for the sulfur than for the oxygen com-

[3]In benzaldehyde itself, ^5J(H, CHO) is an almost purely σ-electron coupling interaction in the sense that no $^6J(CH_3, CHO)$ is detectable in 3,5-dimethylbenzaldehyde, for example (11).

TABLE 4. Molecular orbital results for the conformational energies of 2-hydroxybenzaldehyde and 2-mercaptobenzaldehyde

	Relative energy (kJ/mol)					
	AMI[a]		STO-3G		6-31G**(5D)	
Conformer	OH	SH	OH	SH	OH	SH
C=O···H—X	0.00	0.00	0.00[b]	0.00[c]	0.00[d]	0.00[e]
C=O···X—H	23.47	21.08	27.00	−1.34	43.67	5.07
C—H···X—H	9.59	0.91	19.14	−1.98	25.69	5.08
C—H···H—X	16.21	8.37	31.51	11.84	37.79	14.03

[a]Heats of formation relative to the intramolecularly hydrogen bonded conformer.
[b]The total energy is −412.969 925 au.
[c]The total energy is −732.298 761 au.
[d]The total energy is −418.312 785 au.
[e]The total energy is −740.947 351 au.

pound, intuitively an unlikely situation even if such structures need not play an important thermodynamic role. Furthermore, the sign of ^4J(H-3, SH) is not accounted for by **C**.

The present discussion illustrates that the formation of the intramolecular hydrogen bond perturbs the spin–spin coupling mechanisms for the nuclei in the hydrogen-bonded moieties in a subtle way, not yet understood. Indeed, the weaker hydrogen bond causes the larger perturbations, that is, for the sulfhydryl proton. It is also true, however, that the S—H moiety is much more polarizable than the hydroxyl group (see Appendix).

The reference conformations for the intramolecular hydrogen bonds

(i) Salicylaldehyde

Computations on salicylaldehyde have taken different conformations with respect to which the energy of the hydrogen bond is assessed. An early computation (25*a*) uses **6**, whereas another (1) prefers **7**. The most recent molecular

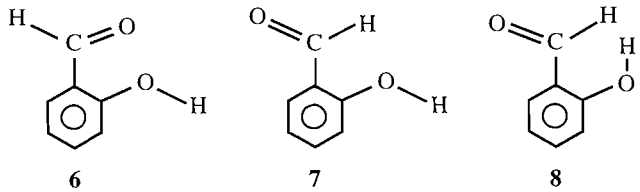

6 **7** **8**

orbital calculation (2) employs a 6-31G basis and argues that **6** represents the correct reference for the estimation of the strength of the intramolecular hydrogen bond. The hydrogen bond energy then becomes 49.8 kJ/mol and is thought to be overestimated by not more than 6.3 kJ/mol (basis set limitations); **8** is computed as 36.8 kJ/mol less stable than the hydrogen-bonded conformer. The conformation **7** is not discussed.

In Table 4, the three computational approaches agree qualitatively among each other, and also with the 6-31G basis (2), as to the relative stabilities of **6** and **8**. As might be expected from the interatomic distances and (or) bond polarities in **6–8**, it is **7** which is by far the most stable; the larger basis set, 6-31G** (5D), has its energy as 25.7 kJ/mol relative to the hydrogen-bonded conformer. While differences in zero-point energies together with corrections for finite temperatures will alter the enthalpy differences at ambient temperature by perhaps 5%, in our opinion **7** is the proper reference conformation for the hydrogen bond in salicylaldehyde. The high energy computed for **6** agrees qualitatively with the absence of the corresponding conformer of 2-methoxybenzaldehyde in the nonpolar solution.[4] The relative 6-31G** (5D) energies of **7** and the hydrogen-bonded conformer agree best with the energy of the hydrogen bond deduced from the torsional frequency of the hydroxyl group and the hydroxyl proton chemical shift (26). These deductions, however, are extrapolated from calculations (27) of the change in the shielding of the hydroxyl proton caused by electric fields present in the intermolecular hydrogen bond formed by phenol.

(ii) 2-Mercaptobenzaldehyde

The experimental results show that when the in-plane S—R group is turned away from the formyl substituent, as in 2-thiomethylbenzaldehyde, the H—C=O···SR and O=C—H···SR interactions are of very similar energy. These results imply two possible reference structures for 2-mercaptobenzaldehyde. This implication is borne out by the 6-31G** (5D) computations in Table 4. Structures of the type H—C=O···S—H, **4**, and O=C—H···S—H, **5**, are calculated to be 5.07 and 5.08 kJ/mol more energetic, respectively, than that of type H—C=O···H—S. The O=C—H···H—S interaction is most unstable, at 14.03 kJ/mol. The AM1 and STO-3G MO energies are included in Table 4 for comparison, but are here considered as inadequate indicators of the relative conformational stabilities.

The combined fractional population of **4** and **5** was experimentally deduced above as 0.14 at 300 K in CCl_4 solution, corresponding to a free energy difference of 4.4 kJ/mol in favor of the hydrogen-bonded conformer. To a first approximation the 6-31G** (5D) energies are consistent with experiment. A rigorous comparison would require the computation of not only zero-point energy and entropy differences between conformers but also the solvent stabilization of the various conformers.

The contrast between the C=O···S—H and C=O···O—H interactions is striking.[5] Partly, at least, it has

[4]In a rare gas matrix at 12 K, salicylaldehyde photolyzes to **7** (25*b*).

[5]The question of appropriate reference structures in the computation of the strength of intramolecular hydrogen bonds has recently been discussed for a thioxoketone and its thienol tautomer (3).

Can. J. Chem. Downloaded from www.nrcresearchpress.com by 213.200.69.106 on 09/08/12
For personal use only.

Can. J. Chem. Downloaded from www.nrcresearchpress.com by 213.200.69.106 on 09/08/12
For personal use only.

to do with the relatively high polarizability of sulfur, discussable in the guise of the the directional character of the mainly 3*p* orbital on sulfur (19, 28). Thus, structural data for crystals show that electrophilic moieties prefer the 3*p* direction at divalent sulfur, whereas nucleophilic groups tend to approach sulfur in the R—S—R^1 plane (29). Application to the present intramolecular case suggests that **4** is relatively stable because the 3*p* orbital on sulfur is oriented approximately perpendicular to the molecular plane; further, that a twist of the S—H group out of the molecular plane with a concomitant twist of the 3*p* orbital into that plane will destabilize **4**, as is indeed the result in 2-*S*-*tert*-butylbenzaldehyde (30). In consequence, the reference structure for an intramolecular hydrogen bond formed by the S—H group depends on the orientation of the orbitals on sulfur. For example, the intramolecular hydrogen bond in 2-mercaptophenol stabilizes the structure in which the S—H bond lies in a plane perpendicular to the rest of the molecule (19). The reference structure is surely not the one in which the O—H group is rotated away by 180° from the other substituent, leaving the 3*p* orbital in the molecular plane. This structure entails 3*p* · · · O—H repulsions which are not relevant to the strength of the O—H · · · S interaction. The reference structure is the more stable of the planar H—S · · · O—H or S—H · · · O—H structures.

Acknowledgments

The financial assistance of the Natural Sciences and Engineering Research Council of Canada is gratefully acknowledged.

1. T. Schaefer, R. Sebastian, R. Laatikainen, and S.R. Salman. Can. J. Chem. **62**, 326 (1984).
2. P. George, C.W. Bock, and M. Trachtman. J. Mol. Struct. (Theochem), **133**, 11 (1985).
3. J.S. Craw and G.D. Bacskay. J. Chem. Soc. Faraday Trans. **88**, 2315 (1992).
4. L.K.A. Rahman and R.M. Scrowston. J. Chem. Soc. Perkin Trans. 1, 2973 (1983).
5. R. Freeman and W.A. Anderson. J. Chem. Phys. **37**, 2053 (1962).
6. M.J.S. Dewar, E.J. Zoebisch, E.F. Healy, and J.J.P. Stewart. J. Am. Chem. Soc. **107**, 3902 (1985).
7. W.J. Hehre, R. Ditchfield, R.F. Stewart, and J.A. Pople. J. Chem. Phys. **52**, 2769 (1970).
8. P.C. Hariharan and J.A. Pople. Chem. Phys. Lett. **66**, 217 (1972).
9. M.J. Frisch, J.S. Binkley, H.B. Schlegel, K. Raghavachari, C.F. Melius, F.L. Martin, J.J.P. Steward, F.W. Bobrowicz, D.F. Rohlfing, L.R. Kahn, D.J. DeFrees, R. Seeger, R.A. Whiteside, K.J. Fox, E.M. Fluder, and J.A. Pople. Carnegie-Mellon Quantum Publishing Unit, Pittsburgh, Pa. 1984.
10. J.S. Martin, A.R. Quirt, and K.E. Worvill. The NMR program library. Daresbury Laboratory, Daresbury, U.K.
11. T. Schaefer and C.S. Takeuchi. Can. J. Chem. **67**, 827 (1989).
12. T. Schaefer and C.S. Takeuchi. Can. J. Chem. **68**, 339 (1990).
13. R. Laatikainen, K. Tuppurainen, Y. Hiltunen, and S. Lötjönen. Magn. Reson. Chem. **28**, 939 (1990).
14. J.A. Pople, J.W. McIver, Jr., and N.S. Ostlund. J. Chem. Phys. **49**, 2960 (1968); **49**, 2965 (1968).
15. T. Schaefer and R. Sebastian. Can. J. Chem. **61**, 26 (1983).
16. T. Schaefer and W.J.E. Parr. Can. J. Chem. **57**, 1421 (1979).
17. H. Lumbroso, J. Curé, and C.G. Andrieu. J. Mol. Struct. **43**, 87 (1987).
18. T. Schaefer, T.A. Wildman, and R. Sebastian. Can. J. Chem. **60**, 1924 (1982).
19. T. Schaefer, T.A. Wildman, and S.R. Salman. J. Am. Chem. Soc. **102**, 107 (1980).
20. T. Schaefer and T.A. Wildman. Chem. Phys. Lett. **80**, 280 (1981).
21. W.J.E. Parr and T. Schaefer. J. Magn. Reson. **25**, 171 (1977).
22. T. Schaefer, J.B. Rowbotham, and K. Chum. Can. J. Chem. **54**, 3666 (1976).
23. J.B. Rowbotham, M. Smith, and T. Schaefer. Can. J. Chem. **53**, 986 (1975).
24. K.B. Wiberg, C.M. Hadad, P.R. Rablen, and J. Cioslowski. J. Am. Chem. Soc. **114**, 8644 (1992).
25. (*a*) S.W. Dietrich, E.C. Jorgensen, P.A. Kollman, and S. Rothenberg. J. Am. Chem. Soc. **98**, 8310 (1976); (*b*) M.A. Morgan, E. Orton, and G.C. Pimentel. J. Phys. Chem. **94**, 7927 (1990).
26. T. Schaefer. J. Phys. Chem. **79**, 1888 (1975).
27. I. Gränacher. Helv. Phys. Acta, **34**, 272 (1961).
28. T. Schaefer, S.R. Salman, T.A. Wildman, and P.D. Clark. Can. J. Chem. **60**, 342 (1982).
29. T.N. Guro Row and R. Parthasarathy. J. Am. Chem. Soc. **103**, 477 (1981).
30. T. Schaefer, G.H. Penner, K.J. Davie, and R. Sebastian. Can. J. Chem. **63**, 777 (1985).

Appendix

The 6-31G**(5D) geometries of the four planar conformers of salicylaldehyde and 2-mercaptobenzaldehyde are reproduced in Scheme 1. Bond lengths are given in Ångstroms and bond angles in degrees.

Differences in these quantities exist between the conformers, of course, but are hardly large enough to explain the large perturbations of the coupling constants caused by the intramolecular hydrogen bonds. However, certain regularities related to the hydrogen bond strengths are apparent. For example, the relatively strong cross conjugation of the hydroxyl and formyl substituents, indicated by resonance structure **D**, is reflected in the C—C bond lengths

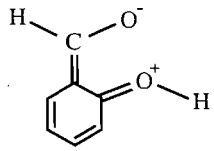

D

within the aromatic ring. These bond length variations are enhanced somewhat in the hydrogen-bonded conformer and, in addition, the C—C(HO) bond shortens by as much as 0.02 Å, as does the C—OH bond. In contrast, the changes in bond lengths are much smaller on formation of the hydrogen bond in 2-mercaptobenzaldehyde; the C—CHO length shortens by rather less than 0.01 Å. The relatively weak intramolecular hydrogen bond in the sulfur compound is also consistent with the exocyclic bond angles computed for the two compounds. Compare, for example, the angles defining the interior of the six-membered, hydrogen-bonded exocycle in the two compounds.

The computed Mulliken atomic charges in Scheme 2 provide a zero-order interpretation of the relative conformer energies given in Table 4. Thus, the instability of the C=O · · · O—H arrangement can be assigned to the electrostatic repulsion between the large negative charges on the two oxygen atoms. When distances between charges, as given in Scheme 1, are also considered, the order of stability of the four planar conformers of salicylaldehyde is seen

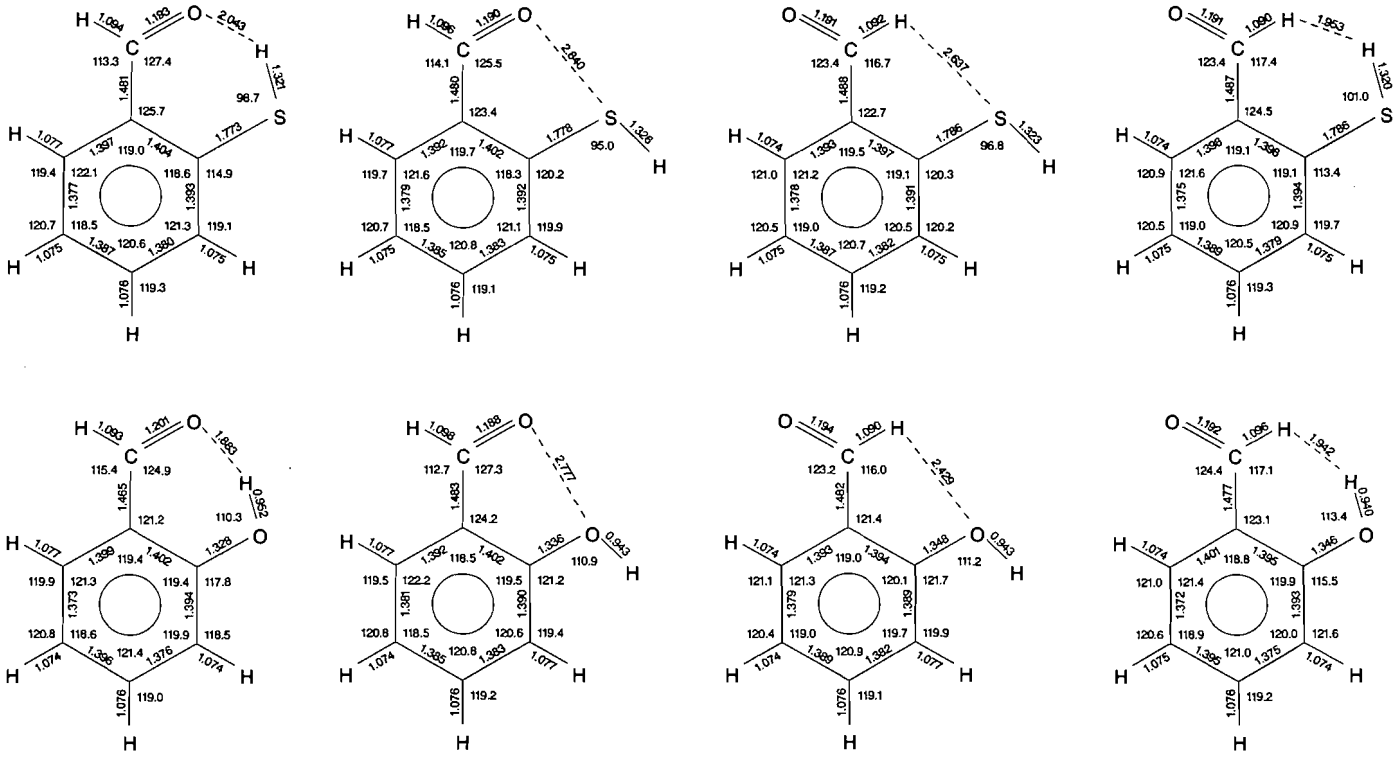

SCHEME 1

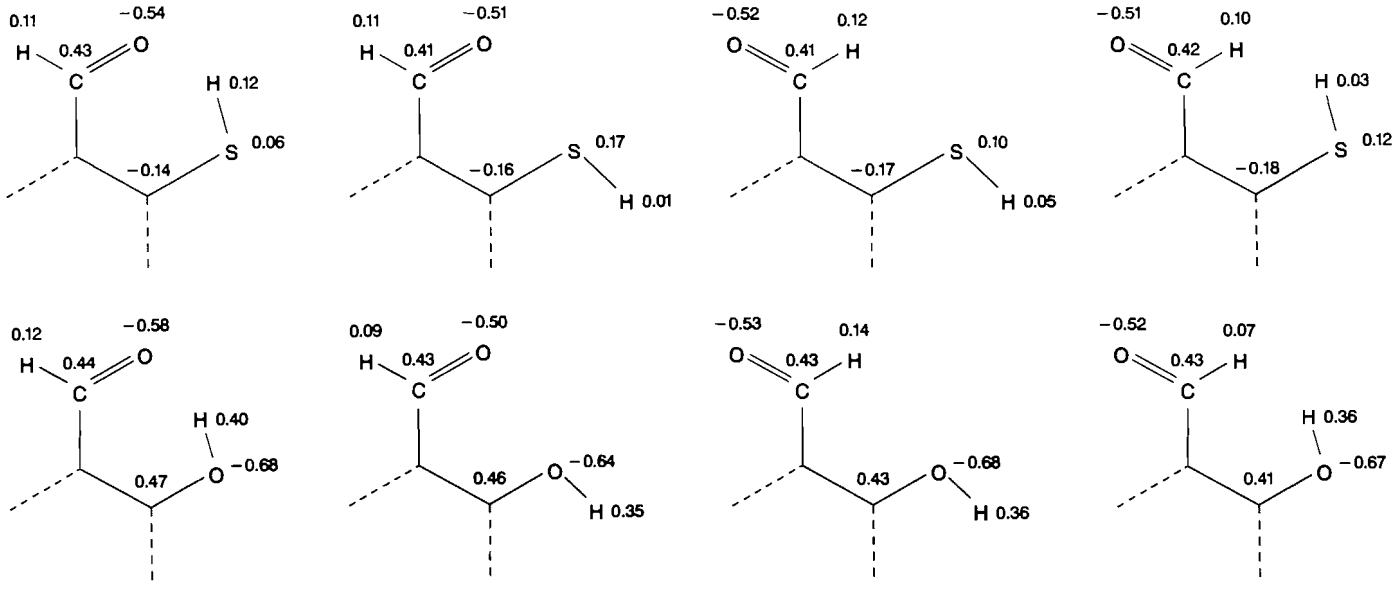

SCHEME 2

to be reasonable. Furthermore, note that formation of the hydrogen bond is calculated to further polarize the C=O and O—H bonds.

This enhanced polarization on hydrogen bond formation is less striking for the C=O bond in 2-mercaptobenzaldehyde, but is remarkably large for the S—H bond. On comparison of the C=O···H—S and C=O···S—H conformers, one notes an increase of 0.11 (electron units) in the positive charge, from 0.01 to 0.12, on the hydrogen atom. While both atoms in the S—H bond carry positive charge, the relative magnitudes of these charges are reversed by the formation of the hydrogen bond. The positive charge on the sulfur atom also rationalizes the small energy differences between these two conformers. Finally, the smaller magnitudes of the charges on the atoms of the S—H bond, compared to those for the O—H bond, are consistent with, first, the weaker hydrogen bond in the sulfur compound and, second, the much smaller energy differences (Table 4) between the conformers of this compound as compared to those between salicylaldehyde conformers.

Can. J. Chem. Downloaded from www.nrcresearchpress.com by 213.200.69.106 on 09/08/12
For personal use only.

Pattern recognition for screening of crude oils using multivariate circular profiles

EDWARD P.C. LAI,[1] RÉGI D. GIROUX, NAILIN CHEN, AND RUNDE GUO

Centre for Analytical and Environmental Chemistry, Ottawa–Carleton Chemistry Institute, Department of Chemistry, Carleton University, Ottawa, Ont., Canada K1S 5B6

Received November 20, 1992

EDWARD P.C. LAI, RÉGI D. GIROUX, NAILIN CHEN, and RUNDE GUO. Can. J. Chem. **71**, 968 (1993).

An appropriate pattern recognition method has been designed to visually discriminate between crude oils belonging to different geographic origins. Each oil is represented by a circular profile that consists of parameter axes that radiate from the centre like spokes on a wheel. One objective of this approach is to provide an optimum set of axes that will best differentiate one circular profile from another. Several parameters were considered for evaluating the oils: photoacoustic spectroscopy (PAS), carbon-13 nuclear magnetic resonance (^{13}C NMR, for $\%C_A$ = aromatic carbon content), high-performance liquid chromatography (HPLC, for unsaturated, aromatic, and polar compounds), initial boiling point (IBP), American Petroleum Institute (API) gravity, and ultraviolet–visible spectrophotometry (for λ_{max} = maximum absorption wavelength and ϵ_{max} = maximum molar absorptivity). By computerized statistical evaluation, the selected parameters are PAS and HPLC for unsaturated, aromatic, and polar compounds.

EDWARD P.C. LAI, RÉGI D. GIROUX, NAILIN CHEN et RUNDE GUO. Can. J. Chem. **71**, 968 (1993).

On a mis au point une méthode appropriée de reconnaissance des formes qui permet de distinguer visuellement entre des huiles brutes d'origines différentes. Chaque huile est représentée par une profil circulaire comportant des paramètres axiaux qui s'écartent du centre comme les rayons d'une roue. L'objectif de cette approche est de fournir un ensemble optimal de paramètres axiaux qui permettra de distinguer un profil circulaire d'un autre. On a considéré plusieurs paramètres pour évaluer les huiles : la spectroscopie photoacoustique (SPA), la résonance magnétique nucléaire du carbone-13 (RMN du ^{13}C, pour le $\%C_A$ = concentration de carbone aromatique), la chromatographie liquide à haute performance (CLHP, pour les composés insaturés, aromatiques et polaires), le point d'ébullition initial (PEI), la densité de l'Institut Américain des Pétroles (API) et la spectrophotométrie ultraviolette–visible (pour le λ_{max} = longueur d'onde d'absorption maximale et le ϵ_{max} = absorbance molaire maximale). Sur la base d'une évaluation statistique par ordinateur, les paramètres choisis sont la SPA et la CLHP pour les composés insaturés, aromatiques et polaires.

[Traduit par la rédaction]

Introduction

Crude oil or petroleum is a complex mixture that consists of many hundreds of different hydrocarbons plus traces of impurities. The hydrocarbons present in crude oil can be divided into three main groups: (*a*) paraffins (or alkanes), which are straight or branched hydrocarbon chains of general formula C_nH_{2n+2}; (*b*) naphthenes (or cycloalkanes), which are saturated ring structures of general formula C_nH_{2n}; (*c*) aromatics, which are hydrocarbons containing one or more benzene rings (C_6H_6). In addition, there is a fourth type, olefins (or unsaturates), which is formed during processing by the dehydrogenation of paraffins and naphthenes (1). Crude oil also contains small quantities of non-hydrocarbon impurities (oxygen, sulfur, nitrogen, and metals), which are generally present as components of complex molecules predominantly hydrocarbon in character. The complexity of the mixture has been shown by a partial analysis of a crude oil: 37 individual hydrocarbons were isolated from about 16.5% of the total mass of the oil (2). Since crude oil is a very complex mixture, no single measurement can be used for identification purposes. Refinery laboratories are equipped with capillary gas chromatographs and other sophisticated instruments to perform very detailed analyses of the crude oils their plants process. For less critical end uses, however, relatively simple analytical tests are run on the crude and the results of these are used with empirical correlations to evaluate the crude oils as feedstocks for the particular refinery (1). Alternatively, before making a preliminary purchase or environmental decision, some easily measured parameters are needed to give a rough indication of the relative proportions of the different components present and some idea of the physical and optical properties of the crude oil.

A great deal of effort has been devoted to the characterization and classification of petroleum samples. The most reliable methods used more than one analytical technique of data collection and then combined the results into a prediction. A wide variety of methods have been suggested for interpreting the data collected, ranging from visual analysis to sophisticated statistical or pattern recognition methods. Curtis first used pattern recognition techniques for typing and identification of oil spills (3). Clark and Jurs employed pattern recognition methods, based on 13 descriptors characterizing their gas chromatograms, to classify crude oils (4). Application of pattern recognition techniques to petroleum pollution research was first undertaken by Duewer et al. (5). Kwan and Clark also successfully assessed oil contamination in the marine environment by pattern recognition analysis of the paraffinic hydrocarbon content of mussels (6).

The subject of pattern recognition involves any attempt at developing descriptions (or models) of phenomena that in some way mimic human thinking. This includes research in the areas of artificial intelligence, interactive graphic computers, computer aided design, psychological and biological pattern recognition, and a variety of others. Computerized pattern recognition would seem to be the best solution for qualitative identification in screening analysis. A computer using artificial intelligence methods can rapidly search large amounts of multivariate data for obscure relationships between, for example, structure and activity (7). Given a spectrum of an unknown to interpret, each pattern recognition procedure attempts to answer a simple question: does the

[1]Author to whom correspondence may be addressed.

Can. J. Chem. Downloaded from www.nrcresearchpress.com by 213.200.69.106 on 09/08/12
For personal use only.

Can. J. Chem. Downloaded from www.nrcresearchpress.com by 213.200.69.106 on 09/08/12
For personal use only.

unknown compound belong to any of the structural classes X_1, X_2, . . ., X_n? To answer this question, previous work must have been performed to parameterize the spectrum such that each of these n structural classes can possibly be identified. In most cases this preliminary step draws upon a database of known spectra representing each of the structural classes. Work is then performed to discover the parameters that will provide the desired discrimination. The manner in which this task is accomplished distinguishes one pattern recognition technique from another. In each case, the process is completed with the calculation of n mathematical constructs (functions, vectors, etc.) that define the region of the plotted space occupied by spectra of each of the structural classes. The pattern recognition approach to automated spectral interpretation effectively distills information from the database into a form (the chosen parameters and the calculated mathematical constructs) that subsequently can be used independently. It defines screening tools that make no effort to identify the specific structure involved and merely try to suggest structural elements that the unknown may contain. A major advantage is that no a priori assumptions are made regarding the spectral information used to distinguish a structural class.

The principal component analysis is often used as a method of reducing the dimensionality of a data set; it can project data from higher dimensional space onto two dimensions for display. A p-dimensional plot was studied as a pattern recognition approach to represent two groups of infrared spectra (8). A set of carboxylic acid spectra was represented as circles, and the spectra of a set of substituted benzenes were depicted as squares. Each spectrum was reduced to a point with p coordinates (i.e., the absorbance in each of p-specific frequency windows; $p = 3$). If the frequency windows had been chosen such that carboxylic acid spectra yielded different absorbance values than the spectra of substituted benzenes, the p-dimensional plot would reveal a grouping of the spectra according to their respective structural classes. In this way, the chosen dimensions were said to discriminate the spectra of carboxylic acids from those of substituted benzenes. Similar pattern recognition was used to develop a potential method involving high-resolution pyrolysis (Py) and gas chromatography (GC) for the detection of carriers of the cystic fibrosis gene (9). The analyses were directed towards three specific goals: (*a*) finding discriminants that could separate the 72 heterozygote pyrochromatograms from the 72 normal pyrochromatograms on the basis of chemical differences between the two groups; (*b*) studying the structure of the Py/GC data to seek obscure relationships with mapping-and-display and clustering methods; and (*c*) developing the ability to predict class membership of unknowns. One of their ways of looking at the confounding eigenvector projections of the data was to plot the 144 pyrochromatograms in a two-dimensional map using the first two principal components derived from their n-dimensional data. Although this pattern recognition approach of discriminating between groups showed some order of discrimination, the boundaries that divide the groupings were not evident. The presentation of results was difficult to follow because much of the useful information employed for coming to such final classifications could not be readily retrieved.

In 1988, Rose-Pehrsson et al. evaluated an array of surface acoustic wave sensors as a monitor for the detection of hazardous vapours at sub-part-per-million concentrations (10). Each sensor was coated with a sorbent material selected to contribute unique chemical information. Bar graphs were first used to display the relative response patterns of eight coatings to nine test vapours and their binary mixtures. A hierarchical cluster analysis routine, using the Euclidean distance metric and flexible fusion, was then employed for the clustering of mixtures. The y axis of the resulting dendogram compared the responses of the coatings to the vapours. Coatings that were fused together by horizontal lines lower on the y scale were similar, while coatings fused at a higher level were different. Finally, visual display of the large data matrix of coating responses to the vapours and mixtures was simplified through the use of circular profiles. A circular profile consisted of pattern vectors that were drawn as axes radiating from a centre like spokes on a wheel. The length of each axis depended on the response of one sensor to a vapour. The open ends of adjacent axes were next connected by lines to form a polygonal figure.

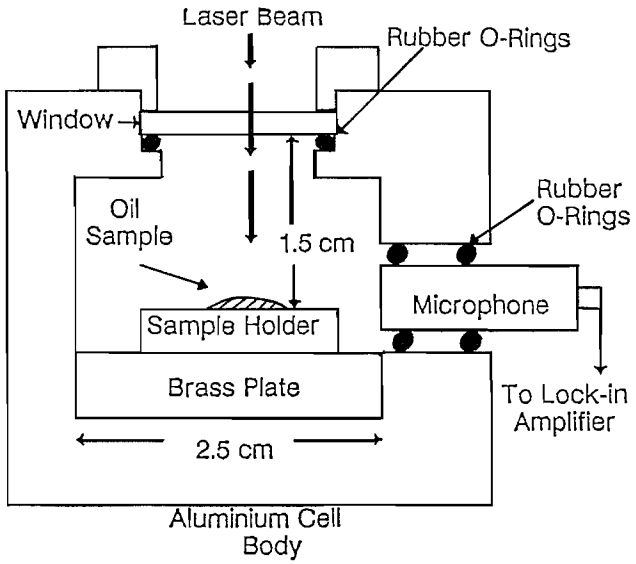

FIG. 1. Photoacoustic cell.

The present work was aimed at discriminating one crude oil from another using circular profiles as the pattern recognition method of choice. Several parameters were considered for constructing the circular profiles of crude oils. They were photoacoustic spectroscopy (PAS), carbon-13 nuclear magnetic resonance (^{13}C NMR, for $\%C_A$ = aromatic carbon content), high-performance liquid chromatography (HPLC, for unsaturated, aromatic, and polar compounds), initial boiling point (IBP), American Petroleum Institution (API) gravity, and UV–visible spectrophotometry (for λ_{max} = maximum absorption wavelength and ϵ_{max} = maximum molar absorptivity).

Experimental

Photoacoustic spectroscopy

A schematic diagram of the photoacoustic cell is shown in Fig. 1. A crude oil sample (60 μL in volume) was deposited on a sample holder made of grey rubber (13 mm diameter, 3 mm height) so as to form a 5 mm diameter oil drop. The loaded sample holder was

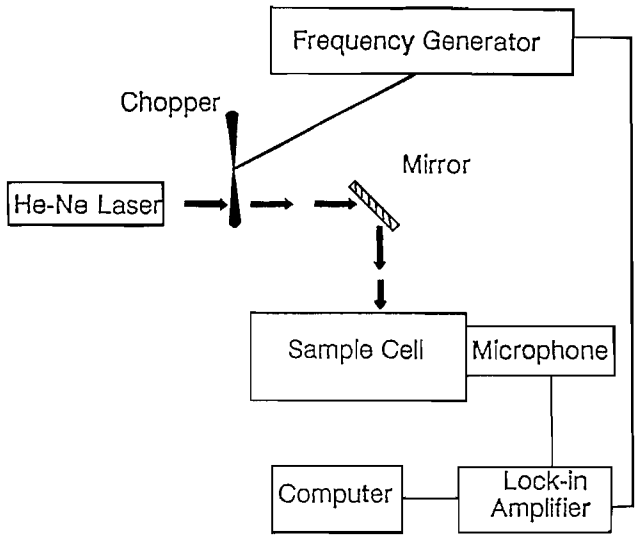

FIG. 2. Experimental setup for PAS measurements.

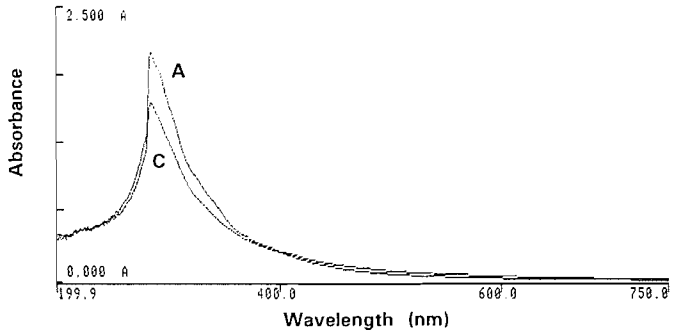

FIG. 3. UV–visible absorption spectra of crude oils A and C (0.1% by weight in toluene), which are dark brown in color.

TABLE 1. PAS signals (mean ± standard deviation, n = 6) for crude oils A–G and Castrol XRL 10W-30 motor oil

Crude oil	PAS signals (μV)		
	Top layer	Reference	Bottom layer
A	28.3 ± 1.0	43.1 ± 1.9	29.0 ± 0.8
B	24.7 ± 0.9	43.2 ± 1.2	24.6 ± 0.7
C	41.3 ± 0.9	42.5 ± 1.4	
D	37.6 ± 1.6	43.4 ± 1.6	
E	44.6 ± 0.5	43.3 ± 1.3	
F	48.5 ± 1.0	44.2 ± 0.9	
G	44.2 ± 0.4	44.2 ± 0.6	
Castrol XRL	0.0 ± 0.0	44.7 ± 0.1	

placed in the acoustically closed cell (2.5 cm inside diameter, 1.5 cm depth), sitting in a constant position relative to a sensitive microphone (Olympus Optical ME6, Tokyo, Japan). PAS measurements of the crude oil were attained by setting up the cell in the experimental arrangement shown in Fig. 2. A He-Ne laser beam (Spectra-Physics 157-1, 632.8 nm, 17 mW, 1.5-mm spot size), mechanically chopped at 32 Hz for optimum experimental photoacoustic signal-to-noise (considering the f^{-1} dependence of the PAS signal amplitude, signal saturation effects, the microphone transfer function, acoustic resonance of the sample cell, and the characteristics of background noise), was directed down onto the cell. Absorption of laser light by the sample generated a photoacoustic signal, which was detected by the microphone. The microphone output voltage was processed by a lock-in amplifier (Stanford Research Systems 510, Sunnyvale, Calif.). A special computer program (Stanford Research Systems 565) calculated and optimized the phase angle for the measurement of the signal amplitude. The PAS system was initially calibrated by using neutral density filters of known optical densities in the incident light path. A plot of PAS signal amplitude for a piece of black rubber (13 mm diameter, 3 mm height) versus laser power (from 3 mW to 18 mW) verified the linearity of the system response. PAS signals were then recorded for the seven crude oils under investigation.

The reduced crude oils were obtained from Imperial Oil Enterprises Ltd. (Sarnia, Ont.). Crude oils A and B are originally from Nigeria and Saudi Arabia, while oils C–G are from Venezuela. A Pasteur pipette was used to collect the oil samples from their glass containers. For oils A and B, samples were taken from the top and bottom layers of the bulk. Each sample measurement was repeated six times to determine its reproducibility. As for crude oils C, D, E, F, and G, measurements were repeated six times for the top layers only. New Castrol XRL 10W-30 motor oil was also measured to serve as a blank, while the piece of black rubber was used as a reference for normalization of the signals from the seven crude oils.

UV–visible spectrophotometry

Crude oils A–G were weighed out directly in volumetric flasks and dissolved in chloroform to give concentrations on the order of 10.0 ± 0.2 μg/mL. From a UV–visible spectrophotometer (Perkin–Elmer Lambda 4B, Norwalk, Conn.), the maximum absorption wavelength (λ_{max}) and maximum molar absorptivity (ϵ_{max}) of each oil solution were measured.

HPLC

Hydrocarbon class fractionation of crude oils was achieved with HPLC (11). The crude oils were dissolved in chloroform and ultrasonicated for 3 min to prepare 5.0 mg/mL sample solutions. Separations into unsaturated, aromatic, and polar compounds were performed on a Whatman Partisil-10 PAC column (Maidstone, England) using a Perkin–Elmer Series 4 liquid chromatograph and a Dionex VDM-1 variable-wavelength absorption detector (Sunnyvale, Calif.) operating at 254 nm. Retention data of model compounds were first produced to calibrate the retention characteristics of the HPLC system. With 5%:95% chloroform:heptane as the mobile phase at a flow rate of 2.0 mL/min, unsaturated compounds eluted first, followed by an envelope of aromatics. Polars were retained on the column but could be stripped by backflushing the system with 95%:5% chloroform:heptane at 8 min after the aromatics had eluted. Before the next sample was injected, the column was equilibrated with 5%:95% chloroform:heptane over 3 min or more to allow the absorbance baseline to return to zero.

^{13}C NMR

Quantitative ^{13}C NMR analysis of the crude oils was performed in the Department of Chemistry, Carleton University, according to previously reported procedures (11–14). Samples were prepared in the following ratio: 2 mL of crude oil, 1 mL of $CDCl_3$ containing 1% TMS, and 50 mg of paramagnetic chromium(acetylacetonate)$_3$ to serve as a relaxation agent. All spectra were obtained on a Varian Gemini spectrometer (Mississauga, Ont.) operating at 200 MHz in the pulse Fourier transform mode. A pulse width of 90° was used and free induction decay (FID) data were acquired over 1.023 s after each pulse. Full proton spin decoupling was gated off during the delay between pulses of 10 s. As many as 1000 scans were accumulated in the 10–60 ppm and 120–160 ppm characteristic shift ranges and integrated three times. After result averaging, the 120–160 ppm integral was expressed as a percentage of the total integral to yield a value of $\%C_A$ (aromatic carbon content).

Other parameters

The other two parameters used in the present pattern recognition study, IBP and API gravity (=141.5/specific gravity at

Can. J. Chem. Downloaded from www.nrcresearchpress.com by 213.200.69.106 on 09/08/12
For personal use only.

TABLE 2. Vector matrices for crude oils A–G

U = PAS (in μV)
NMR (%C_A)
HPLC (unsaturated, in arbitrary units × 10^6)
HPLC (aromatic, in arbitrary units × 10^6)
HPLC (polar, in arbitrary units × 10^6)
IBP (in °C)
API gravity (°)
UV–visible (λ_{max} − 200, in nm)[a]
UV–visible (ϵ_{max}, in L g^{-1} cm^{-1})

	A	B	C	D	E	F	G
PAS	28.3	24.7	41.2	37.6	44.0	48.5	44.2
NMR	20.0	20.0	23.0	21.0	22.0	22.0	21.0
$HPLC_u$	33.5	49.6	38.9	32.5	37.7	41.0	32.1
$HPLC_a$	84.5	26.0	20.2	22.7	21.0	18.8	21.9
$HPLC_p$	39.6	23.5	35.3	30.4	45.8	40.2	32.8
IBP	32.0	32.0	31.0	27.0	26.0	26.0	28.0
API	30.2	34.0	30.7	30.8	27.7	26.7	27.4
UV_λ	39.8	41.2	41.2	41.8	41.0	43.0	40.8
UV_ϵ	49.8	46.1	33.2	31.9	31.7	33.2	34.0

[a]The λ_{max} values have been subtracted by 200 to obtain differential values from a reference wavelength.

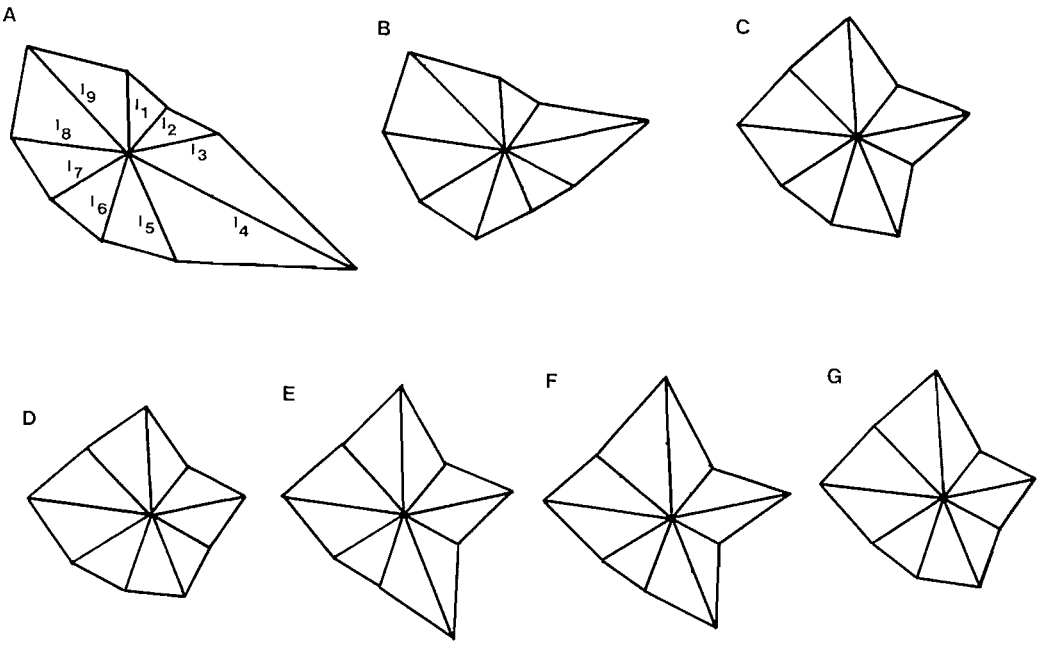

FIG. 4. Nine-parameter circular profiles for crude oils A–G. See Table 3 for the new designations I1–I9.

TABLE 3. Standard deviations of the nine parameters as analyzed by SPSS individually

Variable	Parameter	Mean	Stan. Dev.	%RSD
I1	PAS	38.36	8.81	22.97
I2	NMR (%C_A)	21.29	1.11	5.21
I3	HPLC (unsaturated)	37.91	6.19	16.33
I4	HPLC (aromatic)	30.74	23.81	77.46
I5	HPLC (polar)	35.40	7.33	20.71
I6	IBP	28.86	2.73	9.46
I7	API gravity	29.64	2.56	8.64
I8	UV–visible (λ_{max})	41.26	0.98	2.38
I9	UV–visible (ϵ_{max})	37.13	7.51	20.23

60°F − 131.5) of the total crude, were supplied with the crude oils by Imperial Oil Enterprises.

Results and discussion

Photoacoustic spectroscopy

Photoacoustic spectroscopy offers a simple and fast screening analysis of crude oils. This method is based on the formation of acoustic waves from a sample under irradiation by modulated light (15). After absorption of radiation, nonradiative relaxations are responsible for heating the sample. Part of the thermal energy is transferred through the sample surface to the gas (e.g., air) contacting the sample. Periodic heating of the gas causes variation in its pressure,

Can. J. Chem. Downloaded from www.nrcresearchpress.com by 213.200.69.106 on 09/08/12
For personal use only.

TABLE 4. Correlation matrix among I1–I9

	I1	I2	I3	I4	I5	I6	I7	I8	I9
I1	1.00	0.769*	−0.341	−0.578	0.556	−0.811*	−0.865*	0.550	−0.872*[a,b]
I2		1.00	−0.056	−0.577	0.464	−0.423	−0.450	0.442	−0.775*
I3			1.00	−0.276	−0.370	0.310	0.410	0.299	0.287
I4				1.00	0.179	0.552	0.171	−0.688	0.791*
I5					1.00	−0.468	−0.744	−0.030	−0.284
I6						1.00	0.750	−0.607	0.801*
I7							1.00	−0.273	0.565
I8								1.00	−0.581
I9									1.00

[a]The minus sign means that the two parameters involved are inversely correlated.
[b]The asterisk indicates that a correlation exists between the two parameters involved (with a 5% probability that such correlation occurs by chance).

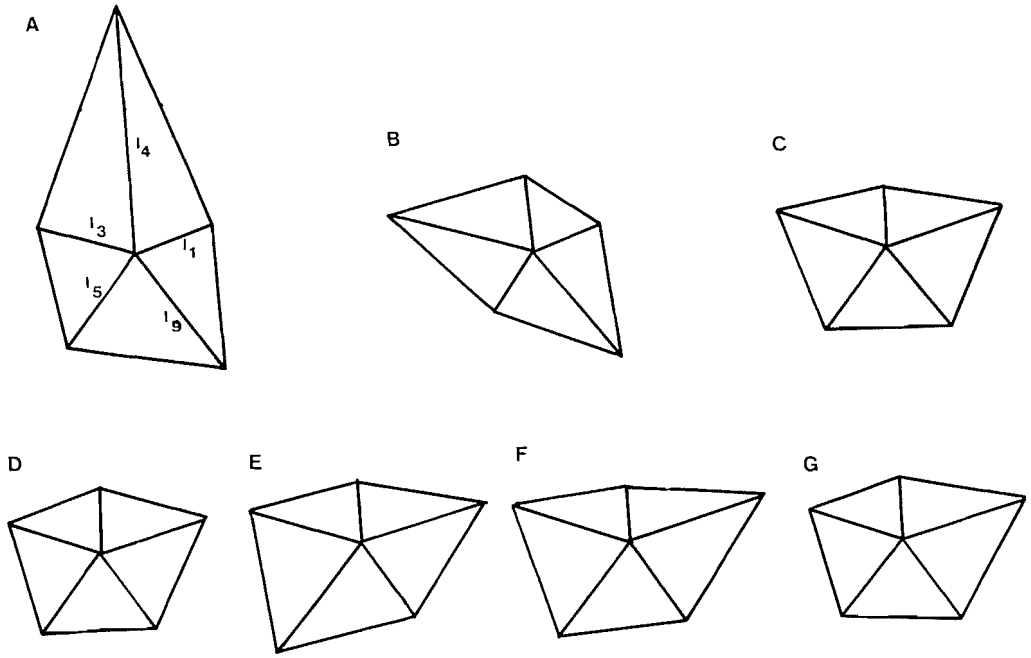

FIG. 5. Five-parameter circular profiles for crude oils A–G, using only I1, I3, I4, I5, and I9.

which is detected by a sensitive microphone to produce a voltage signal. A PAS spectrum may be obtained by recording the microphone signal as a function of the incident wavelength. The characteristic feature of PAS compared to conventional absorption spectrophotometry is that the PAS signal depends on both the optical properties and the thermoelastic parameters of the sample. The sample thickness contributing to surface heating and thermal gas oscillations is given by $L = 2(\pi\alpha/f)^{1/2}$, where f is the modulation (or chopping) frequency and α is the sample's thermal diffusivity (e.g., $\alpha = 9.1 \times 10^{-4}$ cm^2 s^{-1} for *n*-octane). Since the modulation frequency was set at 32 Hz for optimum signal-to-noise, the sample thickness contributing to surface heating was $L = 2(3.1416 \times 9.1 \times 10^{-4}\ \text{cm}^2\ \text{s}^{-1}/32\ \text{Hz})^{1/2} = 0.2$ mm. Therefore only a small oil drop (60 μL in volume, 5 mm in diameter) was required to obtain a good PAS signal for reproducible measurement.

Crude oils vary in color from light yellow, green, red, brown, to black (16). The darker browns and blacks are caused by the asphaltic-resinous material in the crude oil. The majority of the colors are due to molecules with aromatic character that have large π-electron systems, such as found in the condensed ring compounds or the polyunsaturated alkanes with aromatic groups attached where the π electrons are conjugated. The extent of the conjugation affects the color and, as the size of the conjugated electron system grows, the color of the compound moves from the ultraviolet, eventually extending into the visible spectrum (see Fig. 3). In this work, PAS measurements were made at a wavelength of 632.8 nm, which is in a region of weak optical absorption by the oils, to prevent signal saturation (17) without the need for sample dilutions. In accordance with the theory of photoacoustics, the onset of signal saturation occurs at an absorption coefficient of $\beta_{onset} = (\pi f/\alpha)^{1/2} \approx 3 \times 10^2$ cm^{-1} under the given experimental conditions (18). As long as the absorption coefficients of the crude oils at 632.8 nm fall below this value, no signal saturation would occur and the linear dynamic range (i.e., discriminating power) of PAS would be maximized.

The results of PAS measurements on crude oils A–G and Castrol XRL 10W-30 motor oil are shown in Table 1. After each oil was measured, a reference signal was obtained from

Can. J. Chem. Downloaded from www.nrcresearchpress.com by 213.200.69.106 on 09/08/12
For personal use only.

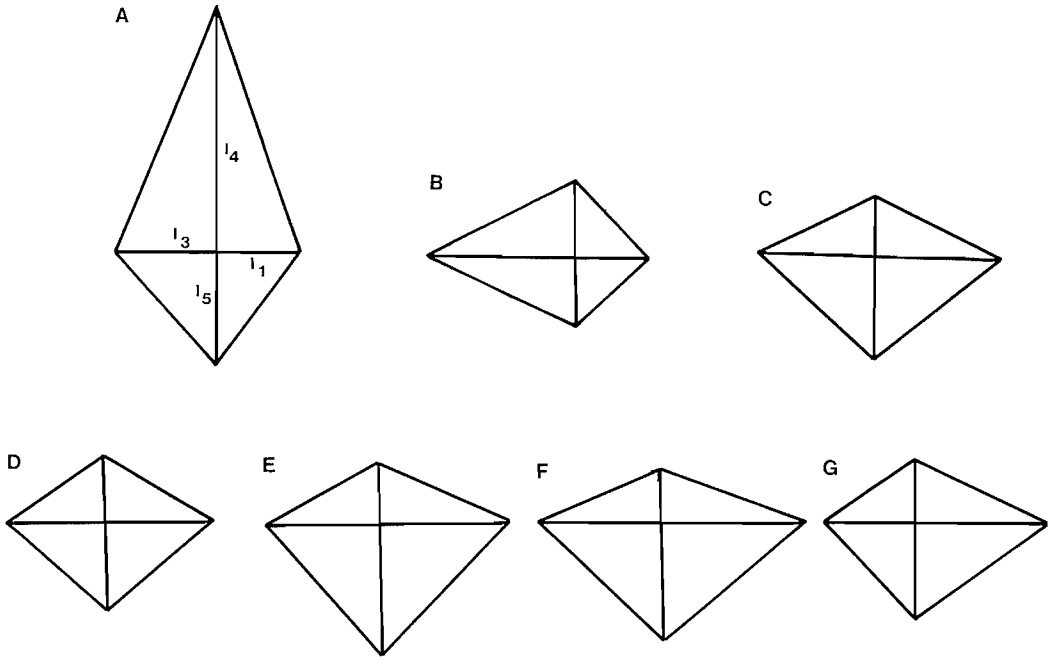

FIG. 6. Four-parameter circular profiles for crude oils A–G, using only I1, I3, I4, and I5.

Can. J. Chem. Downloaded from www.nrcresearchpress.com by 213.200.69.106 on 09/08/12
For personal use only.

a piece of black rubber to check if the PAS sensitivity remained constant. Firstly, the negligible PAS signal amplitude obtained for new Castrol XRL motor oil indicated that no laser energy was absorbed by the sample holder under the clear oil, in accordance with the contribution of the sample thickness to surface heating discussed above. Measurements were next obtained for both the top and bottom layers of oils A and B, in order to determine if oxidation of the top layers had occurred over a storage period of 2 years in capped containers. A Student's *t*-test was conducted to compare the PAS signal amplitudes for the top and bottom layers of each oil. The result showed that the two layers were significantly different only at the 50% confidence level for oil A and below 50% for oil B. This suggested that there was no significant difference in PAS signals between the top and bottom layers of either oil. Consequently, PAS measurements of the bottom layers were discontinued for the other crude oils. As shown in Table 1, the dissimilar PAS signals (mean ± standard deviations, $n = 6$) for the seven crude oils clearly demonstrate that PAS is a sensitive method that is capable of differentiating one crude oil from another. It was therefore used as one of the nine parameters in the pattern recognition analysis as described in detail below.

Pattern recognition

The nine parameters employed for pattern recognition analysis were PAS, ^{13}C NMR (for $\%C_A$), HPLC (for unsaturated, aromatic and polar compounds), IBP, API gravity, and UV–visible spectrophotometry (for λ_{max} and ϵ_{max}). The HPLC and λ_{max} data for each oil were scaled down to the order of 10^2, to compensate the effect of differing measurement magnitudes and to allow easy comparison with the other data. The scaled data may now be considered as the elements of a vector matrix $\boldsymbol{U}$ as illustrated in Table 2. Figure 4 shows the corresponding nine-parameter circular profiles for the crude oils. Each circular profile is constructed by drawing nine axes from a central point. Each axis represents the measurement of one parameter, although it does not include any information about experimental errors or measurement uncertainties for the sake of clarity in visual characterization. The order of the nine measured parameters in the circular profile follows the order of parameter placement in the vector matrix $\boldsymbol{U}$ given in Table 2, with the PAS measurement starting as the upper vertical line in the 12 o'clock position and the other measurements following a clockwise direction. The angle between each pair of adjacent axes is equal to 360° divided by the number of parameters. Thus far, both the selection of the nine parameters and the order of their arrangement in the circular profile are arbitrary. Nevertheless, these circular profiles show clearly both dissimilarities and similarities that exist among the seven crude oils. Although the nine-parameter circular profiles were satisfactory as discrimination patterns for the crude oils, the determination of nine parameters for each oil was time consuming, costly, and probably redundant in chemical information. Therefore a more concise circular profile should be derived by removing all those parameters that either are not very sensitive to different crude oils or can be expressed as a linear combination of the other parameters.

The most appropriate and effective technique for qualitative identification of the best parameters is computerized statistical evaluation. By using the Statistical Program of the Social Science (SPSS) at Carleton University on a UNIX system, relative standard deviations (%RSD), a matrix of correlation coefficients, and a multiple linear regression analysis were obtained for the nine parameter values. Table 3 shows the new designations and the standard deviation results from the SPSS analysis of the nine parameters individually. To construct a circular profile or any recognition pattern that discriminates between different oils, the selected parameters should ideally have the largest %RSD's. A large %RSD indicates that the parameter is sensitive to the different oils as the magnitudes of the measurements vary significantly. According to Table 3, I4 had the largest %RSD, followed by I1, I5, K9, and I3. It is notable that I2, I6, I7,

Can. J. Chem. Downloaded from www.nrcresearchpress.com by 213.200.69.106 on 09/08/12
For personal use only.

and I8 had relatively low %RSD's, which indicated that these four parameters were not sensitive to the different oils and were therefore reasonable candidates to be removed from the nine-parameter circular profiles. Since I8 had the lowest %RSD, it could be rejected immediately.

Further rejection of parameters could be achieved by statistical considerations of linear dependency. Table 4 shows a matrix of correlation coefficients for the nine parameters, which investigates the interdependence of the measurements. Values greater than ± 0.750 are considered highly correlated and are denoted by an asterisk to indicate that the two parameters being compared are linearly dependent on one another. In terms of pattern recognition, this signifies similarity as opposed to dissimilarities. If a parameter is dependent on or is a linear combination of other parameters, its use in pattern recognition is no longer important as it will only reflect similarities in the circular profiles. It can be seen in Table 4 that a high degree of correlation existed between I1 and I2, I1 and I6, I1 and I7, as well as I1 and I9. The parameters I2, I6, and I7 were therefore linearly related to I1 and were rejected from the circular profiles. As a result, a five-parameter circular profile was left behind, consisting only of I1, I3, I4, I5, and I8. In constructing the five-parameter circular profiles shown in Fig. 5, the order of parameter arrangement in the clockwise direction followed a decreasing value of the parameter's %RSD (see Table 3). I4 had the largest %RSD and was therefore drawn as the upper vertical line (in the 12 o'clock position). Next, I1 had the second largest %RSD and was drawn to the right of I4, and so on.

As an additional observation from Table 4, I9 seemed to be highly correlated to as many as four other parameters. From a computerized least-squares multiple linear regression analysis, I9 was found to be 88.4% expressable in terms of I1 and I4 with a 1.4% probability that such correlation occurred by chance. The linear combination expression was

$$I9 = 53.31 - 0.53\,I1 + 0.14\,I4$$

Consequently, I9 was later removed from the five-parameter circular profiles. Figure 6 shows the new four-parameter circular profiles for crude oils A–G. These simple four-parameter circular profiles still retain the capability for computerized discrimination among the seven crude oils (which cannot be actually identified by visual inspection because of the similarity in their dark brown colors). No two oil types are without distinguishable qualities, and subtle differences among the oils are qualitatively enhanced when the four parameters combine to obtain an overview of every circular profile. Note that the reduced set of four selected parameters (I1 = PAS, I3 = HPLC for unsaturated compounds, I4 = HPLC for aromatic compounds, and I5 = HPLC for polar compounds) were established for the crude oils presented here; they are not invariant if either different or additional oil types are studied. Although a computerized analysis greatly reduces the number of parameters for use in a circular profile, the final desired number will always be a personal choice. Usually a greater number of oil-sensitive parameters will give a better (or more accurate) pattern recognition. However, due to the time requirements and cost of multiple analyses, an optimum number of parameters must be reached in order to ensure the effectiveness of screening analysis (by visual evaluation of patterns) without producing redundant analytical information. Further reduction from four parameters to three was not considered because the next questionable parameter, I3, was actually generated simultaneously with I4 and I5 in one single HPLC determination.

Conclusion

Pattern recognition in the form of multivariate circular profiles has been shown to be an effective method for the screening analysis of crude oils. Circular profiles constructed from four statistically selected parameters could successfully discriminate between the seven crude oils (A from Nigeria, B from Saudi Arabia, and C–G from Venezuela). Computerized statistical analysis really makes this pattern recognition an effective technique for chemical characterization and classification. In order of decreasing sensitivity to oil differences, HPLC (for aromatic compounds), PAS, HPLC (for polar compounds), and HPLC (for unsaturated compounds) represent the best of the nine parameters studied in differentiating the crude oils. Particularly, PAS is now established as a useful technique that facilitates the fast screening analysis of crude oils. It does not require the preparation of sample solutions; the measurement can be made directly on neat oils in less than 5 min, each on a separate disposable sample holder. Since the PAS signal is apparently a function of so many undefined (and undefinable) variables, no special efforts were made to relate the signal to the other parameters. Although this work demonstrates the usefulness of circular profiles as applied to a small number of samples only, the method could serve as a powerful tool in reducing massive amounts of data to meaningful analytical information. Finally, further development of this work would include selective OH^- chemical ionization mass spectrometry to provide positive identification of the geographical area of origin and to possibly identify the individual oil fields (19).

Acknowledgements

This work was funded by the Natural Sciences and Engineering Research Council of Canada. A GR-5 grant from the Faculty of Graduate Studies and Research, Carleton University, is gratefully acknowledged. The authors thank Gerry Buchanan and Keith Bourque for performing the NMR analysis.

1. J.H. Gary and G.E. Handwerk. Petroleum refining, technology and economics. Marcel Dekker, New York. 1984. pp. 17–20.
2. S.W. Bennett. Principles of chemical processes. Open University Press, Great Britain. 1975. pp. 25–28.
3. M.L. Curtis. Use of pattern recognition techniques for typing and identification of oil spills. NTIS Acc. No. ADA 043802. 1977.
4. H.A. Clark and P.C. Jurs. Anal. Chem. **51**, 616 (1979).
5. D.L. Duewer, B.R. Kowalski, and T.F. Schatzki. Anal. Chem. **47**, 1573 (1975).
6. P.W. Kwan and R.C. Clark, Jr. Anal. Chim. Acta, **133**, 151 (1981).
7. A. Byers and W. Persone. Anal. Chem. **55**, 615 (1983).
8. G.W. Small. Anal. Chem. **59**, 535 (1987).
9. J.A. Pino. Anal. Chem. **57**, 295 (1984).
10. S.L. Rose-Pehrsson, J.W. Grate, D.S. Ballantine, Jr., and P.C. Jurs. Anal. Chem. **60**, 2801 (1988).

11. R. Miller. Anal. Chem. **54**, 1742 (1982).
12. J.N. Shoolery and W.L. Budde. Anal. Chem. **48**, 1458 (1976).
13. S. Gillet, P. Rubini, J.J. Delpuech, J.C. Escalier, and P. Valentin. Fuel, **60**, 221 (1981).
14. M. Bouquet and A. Bailleul. *In* Petroanalysis '81. *Edited by* G.B. Crump. John Wiley & Sons, New York. 1982. pp. 394–408.
15. V.P. Zharov and V.S. Letokhov. Laser optoacoustic spectroscopy. Springer-Verlag, Berlin. 1985. pp. 65–70.
16. R.R.F. Kinghorn. An introduction to the physics and chemistry of petroleum. John Wiley & Sons, New York. 1983. p. 108.
17. J.F. McClelland and R.N. Kniseley. Appl. Phys. Lett. **28**, 467 (1976).
18. A. Rosencwaig. Photoacoustics and photoacoustic spectroscopy. John Wiley & Sons, New York. 1980. p. 96.
19. P. Burke, K.R. Jennings, R.P. Morgan, and C.A. Gilchrist. Anal. Chem. **54**, 1304 (1982).

Can. J. Chem. Downloaded from www.nrcresearchpress.com by 213.200.69.106 on 09/08/12
For personal use only.

Oxidation of bis(1,4,7-triazacyclononane)nickel(II) by the peroxodisulphate anion in aqueous and binary aqueous media

ROBERT I. HAINES,[1] LORI BUTT, MURRAY K. PARK, AND DEBBIE WHEELER
Chemistry Department, Sir Wilfred Grenfell College, Memorial University of Newfoundland, Corner Brook, Nfld., Canada A2H 6P9

Received December 23, 1992

ROBERT I. HAINES, LORI BUTT, MURRAY K. PARK, and DEBBIE WHEELER. Can. J. Chem. **71**, 976 (1993).

The kinetics of oxidation of bis(1,4,7-triazacyclononane)nickel(II), $[Ni(tacn)_2]^{2+}$, by the peroxodisulphate anion has been studied in water as a function of $S_2O_8^{2-}$ concentration and temperature. The reaction is first order in both the nickel(II) complex and $S_2O_8^{2-}$, with a second-order rate constant of 1.13 mol dm^{-3} s^{-1} at 298 K. The activation energy for the reaction is 38.3 ± 1.8 kJ mol^{-1}. The reaction was also studied at 298 K in a series of mixed aqueous solvents. Rate retardation relative to water was observed in all solvent mixtures studied. Correlation of the solvent effects on the kinetics of reaction has been made with the free energy of transfer of the initial state and the transition state.

ROBERT I. HAINES, LORI BUTT, MURRAY K. PARK et DEBBIE WHEELER. Can. J. Chem. **71**, 976 (1993).

On a étudié la cinétique de l'oxydation du bis(1,4,7-triazacyclononane)nickel(II), $[Ni(tacn)_2]^{2+}$, par l'anion peroxodisulfate en solution aqueuse et en fonction de la concentration de $S_2O_8^{2-}$ et de la température. La réaction est du premier ordre tant en complexe de nickel(II) qu'en $S_2O_8^{2-}$ et, à 298 K, la constante de vitesse de la réaction du deuxième ordre est égale à 1,13 mol dm^{-3} s^{-1}. L'énergie d'activation de la réaction est de 38,3 ± 1,8 kJ mol^{-1}. On a aussi étudié la réaction à 298 K dans divers solvants aqueux mixtes. On a observé que toutes ces réactions sont plus lentes que celles réalisées dans l'eau. On a effectué une corrélation des effets de solvant sur la cinétique de la réaction avec l'énergie libre de transfert de l'état initial et de l'état de transition.

[Traduit par le rédaction]

Introduction

Over the past several years, there has been interest in the kinetics of redox reactions involving the peroxodisulphate anion, $S_2O_8^{2-}$, and transition metal complexes (1). Several of these studies examine the effects of added organic solvents on reaction rates (2) and explain the findings in terms of initial state (I.S.) versus transition state (T.S.) solvation. Changes in solvation of the initial state on going from water to binary aqueous mixtures, $\delta_m\mu^0$(I.S.), are estimated from solubilities of salts of the individual reactant species in the respective solvent mixtures. From these solubility measurements, transfer chemical potentials of the salts from water into the binary aqueous mixtures are calculated. Transfer chemical potentials of the single ions, $\delta_m\mu^0(X^{n\pm})$, of the reactants are estimated by subtraction of internally consistent literature values of the transfer function of the appropriate counterions. Finally, $\delta_m\mu^0$(I.S.) is obtained as the algebraic sum of $\delta_m\mu^0(X^{n\pm})$ of the reactants.

The activation free energy of transfer of the transition state, $\delta_m\Delta G^{\ddagger}$, from water into mixed solvents is calculated from reaction rates in the appropriate media, using the relationship:

$$[1] \quad \delta_m\Delta G^{\ddagger} = -RT\ln(k_{mixture}/k_{water})$$

where k_{water} is the rate constant for reaction in aqueous solution and $k_{mixture}$ is that for the appropriate binary aqueous mixture. Comparisons of the kinetic and thermodynamic transfer functions have been used to gain insight into the mechanisms of inorganic reactions, and the role of solvation therein. This approach has been reviewed (3).

We recently investigated the oxidation of nickel(II) tetraazamacrocycles by $S_2O_8^{2-}$, with a view to applying the I.S. versus T.S. solvation approach to solvant effects on the system (4). For these reactions, however, marked ion pairing between the reactants was kinetically observable, where electron transfer occurred within the solvent cage of the ion pair. The extent of ion pairing appeared to be independent of substituents on the ligands, suggesting close approach of the peroxodisulphate ion to the nickel centre along the axial direction.

To test whether the square-planar geometry of the nickel(II) tetraazamacrocycles lends special stability to the ion pairs, we have chosen to study the peroxodisulphate oxidation of the substitutionally inert, octahedral nickel(II) complex $[Ni(tacn)_2]^{2+}$ (where tacn = 1,4,7-triazacyclononane) (5).

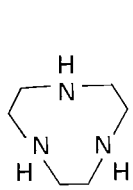

tacn

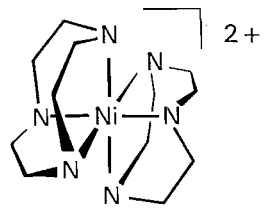

$[Ni(tacn)_2]^{2+}$

The $[Ni(tacn)_2]^{2+}$ ion is known to be stable in aqueous acidic solutions for relatively long periods (6). The tervalent product, $[Ni(tacn)_2]^{3+}$ has been well characterized (7) and many kinetic studies have shown the Ni(II) complex to be smoothly oxidized to the 3+ state by a variety of oxidants via outer-sphere mechanisms (8).

This paper presents a mechanistic study of the $S_2O_8^{2-}$ oxidation of $[Ni(tacn)_2]^{2+}$ as a function of temperature and solvent composition, with a view to interpreting the mechanism in terms of the solvation properties of the participating species.

Experimental

Materials

The title nickel(II) complex was prepared as the perchlorate salt according to the literature (9) and recrystallized from water prior

[1]Author to whom correspondence may be addressed.

Can. J. Chem. Downloaded from www.nrcresearchpress.com by 213.200.69.106 on 09/08/12
For personal use only.

TABLE 1. Observed first-order rate constants, $k_{obs}(s^{-1})$, for the oxidation of $[Ni(tacn)_2]^{2+}$ as a function of $[S_2O_8^{2-}]$ and temperature (ionic strength = 1.00 mol dm^{-3})

	$10^3[S_2O_8^{2-}]$ (mol dm^{-3})					
	2.00	4.00	6.00	8.00	10.0	
Temperature (K)	$10^3 \times k_{obs}(s^{-1})$					k_2(mol dm^{-3} s^{-1})
298.0	2.28	4.49	6.89	9.02	11.3	1.13 ± 0.01
300.7	2.33	5.50	7.30	10.6	12.5	1.27 ± 0.04
304.7	2.98	6.65	9.94	12.4	16.6	1.64 ± 0.05
309.3	4.11	8.29	11.5	15.5	20.5	2.00 ± 0.05
314.3	5.02	10.0	14.3	20.0	24.0	2.41 ± 0.04
319.6	6.85	12.6	20.1	25.8	33.0	3.28 ± 0.05

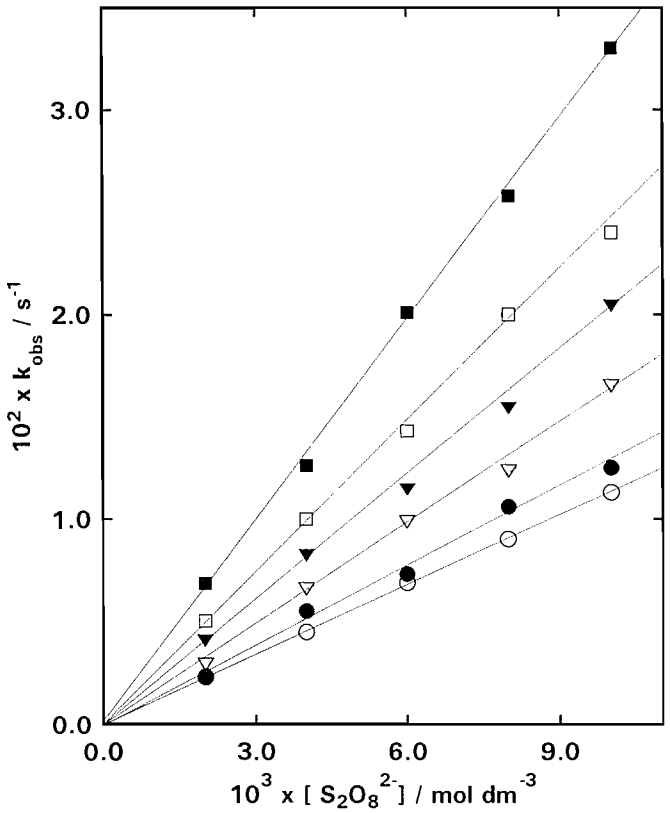

FIG. 1. Dependence of observed first-order rate constants on peroxodisulphate concentration for oxidation of the $[Ni(tacn)_2]^{2+}$ cation at various temperatures (○ = 298.0 K; ● = 300.7 K; ∇ = 304.7 K; ▼ = 309.3 K; □ = 314.3 K; ■ = 319.6 K).

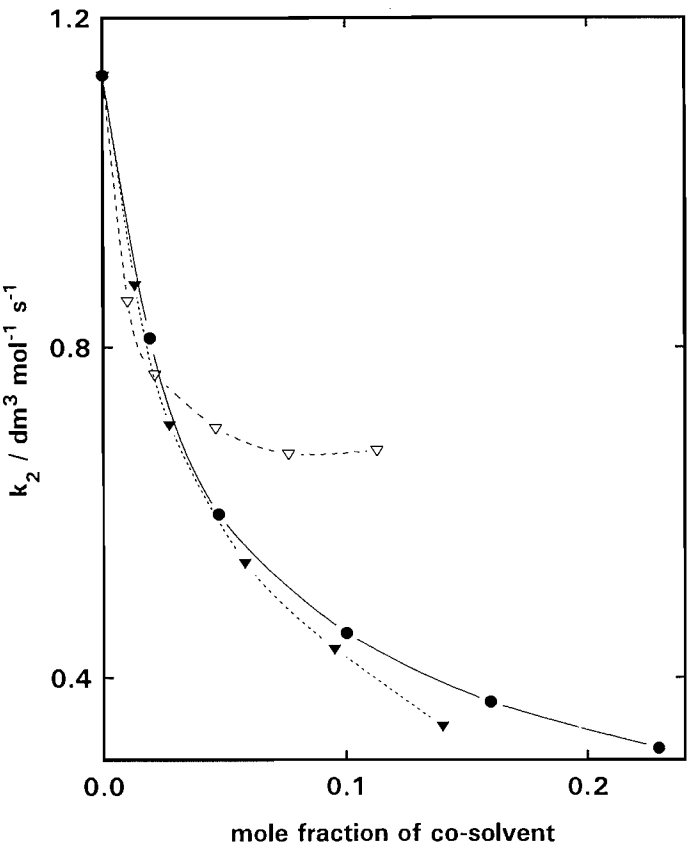

FIG. 2. Variation of second-order rate constants, k_2 (mol dm^{-3} s^{-1}) with mole fraction of added methanol (●), *tert*-butyl alcohol (∇) and acetone (▼), at 298 K.

to use. (**Warning!** Transition metal complex perchlorates are violently heat- and shock-sensitive in the dry state). **Handle with caution!**) The macrocyclic ligand was synthesized by a modified literature procedure (10). AnalaR grade potassium peroxodisulphate (BDH) was first washed several times with distilled water, then recrystallized four times from cold water, rinsed with ice-water, and dried over P_4O_{10} in vacuo. This procedure has been found necessary to obtain reproducible, clean kinetics. Lithium perchlorate was prepared by neutralization of perchloric acid with lithium carbonate and was recrystallized three times from water. All other reagents and solvents were of AnalaR grade and were used without further purification. All solutions were prepared using double-distilled, deionized water.

Stock solutions of perchloric acid were analyzed by titration against primary standards. Lithium perchlorate solutions, used as supporting electrolyte, were analyzed by conversion to the corresponding acid using Dowex ion exchange resin, then titrated as above.

Kinetics

Kinetics were performed under pseudo-first-order conditions, using an excess of peroxodisulphate. The concentration of $[Ni(tacn)_2]^{2+}$ used was 1.0×10^{-4} mol L^{-1}. Absorbance changes with time were measured using 1-cm pathlength quartz cells in the thermostatted cell compartment of a Beckman DU-65 recording spectrophotometer. Data were collected using Beckman Datacapture software on a Wise AT-compatible microcomputer. First-order rate constants, k_{obs}, were calculated from the slopes of linear regres-

Can. J. Chem. Downloaded from www.nrcresearchpress.com by 213.200.69.106 on 09/08/12
For personal use only.

TABLE 2. Observed first-order rate constants, $k_{obs}(s^{-1})$, for the oxidation of $[Ni(tacn)_2]^{2+}$ in binary aqueous mixtures at 298 K

Solvent		$10^3 \times [S_2O_8^{2-}]$ (mol dm^{-3}) 2.00	4.00	6.00	8.00	10.0	k_2(mol dm^{-3} s^{-1})
Water		2.28	4.49	6.89	9.02	11.3	1.13 ± 0.01
5%	Methanol		3.16	4.88	6.45	8.04	0.811 ± 0.012
10%			2.45	3.56	4.86	6.00	0.598 ± 0.013
20%			1.86	2.71	3.69	4.56	0.454 ± 0.009
30%			1.55	2.25	2.98	3.77	0.370 ± 0.007
40%			1.30	1.98	2.53	3.21	0.314 ± 0.009
5%	*tert*-Butyl alcohol		3.40	5.20	6.81	8.57	0.856 ± 0.012
10%			3.19	4.69	6.26	7.78	0.767 ± 0.005
20%			2.89	4.40	5.78	7.24	0.702 ± 0.008
30%			2.78	4.21	5.60	6.79	0.671 ± 0.020
40%			2.72	3.99	5.42	6.74	0.675 ± 0.010
5%	Acetone		3.38	5.23	6.85	8.68	0.876 ± 0.016
10%			2.80	4.16	5.64	7.01	0.706 ± 0.008
20%			2.06	3.12	4.26	5.27	0.539 ± 0.008
30%			1.79	2.60	3.52	4.38	0.435 ± 0.007
40%			1.35	1.98	2.74	3.37	0.341 ± 0.009

Can. J. Chem. Downloaded from www.nrcresearchpress.com by 213.200.69.106 on 09/08/12
For personal use only.

sion plots of $\ln(A_\infty - A_t)$ versus time. Reported values of k_{obs} are the means of at least three measurements; the relative standard deviations for all reported values were within 1%. Ionic strength was kept constant at 1.00 mol dm^{-3} for the temperature dependence studies in aqueous solution, using lithium perchlorate – perchloric acid mixtures. For the kinetic studies in binary aqueous mixtures, ionic strength was maintained at 0.100 mol dm^{-3} using lithium perchlorate – perchloric acid. This value was used to avoid precipitation of potassium perchlorate, whose solubility decreases with increasing mole fraction of organic cosolvent. All solvent mixtures used were made up as percent by volume. Absorbance measurements for all kinetics were made at 370 nm.

Solubilities

Saturated solutions of the complexes were prepared by addition of an excess of the solid complex to stoppered flasks, each containing the appropriate solvent mixture. The flasks were stored in a water bath, thermostatted at 298.0 ± 0.1 K, and were agitated periodically. The solutions were centrifuged and aliquots were removed daily for analysis, until constant values were obtained.

UV–visible spectroscopy was used to analyze the solutions for the perchlorate salt of the complex, using the band of 510 nm (ε_{510} = 6.13 ± 0.08). The molar absorptivity of this band was determined by correlating absorbances of a series of solutions of the nickel(II) complex with nickel concentrations, measured by atomic absorption spectrometry. Visible spectra were measured using 1-cm pathlength quartz cells in the thermostatted cell compartment of a Beckman DU 65 recording spectrophotometer.

Results

The title reaction produced a green solution with a UV–visible spectrum characteristic of the nickel(III) complex. Stoichiometric titrations showed a nickel(II) complex to $S_2O_8^{2-}$ ratio of 2:1 for all solvent mixtures studied, within 2%. The overall reaction is described by:

$$[2] \quad 2[Ni(tacn)_2]^{2+} + S_2O_8^{2-} \rightarrow 2[Ni(tacn)_2]^{3+} + 2SO_4^{2-}$$

Excellent first-order kinetics for product formation were observed over at least four half-lives for all solvent mixtures studied, with no discernible interference by SO_4^{-} radicals (11). Addition of allyl acetate as a radical scavenger (12) to the system had no effect on reaction rates. This indicates that the election transfer reaction is not occurring via an SO_4^{-} radical pathway.

Observed first-order rate constants for oxidation of the nickel(II) complex in water, as a function of temperature and peroxodisulphate concentration, are listed in Table 1. Figure 1 depicts the plots of k_{obs} versus $[S_2O_8^{2-}]$, showing the reaction to be first order in peroxodisulphate concentration.

The reaction rate was found to be independent of $[H^+]$ between 0.010 and 0.20 mol dm^{-3}, giving overall a relatively simple second-order rate law:

$$[3] \quad \text{Rate} = +\tfrac{1}{2}\, d[Ni(tacn)_2^{3+}]/dt = k_3[Ni(tacn)_2^{2+}][S_2O_8^{2-}]$$

Values for the second-order rate constant, k_2 were calculated using a least-squares fit of the k_{obs} versus $[S_2O_8^{2-}]$ data and are included in Table 1. From the temperature dependence, an activation energy of 38.3 ± 1.8 kJ mol^{-1} was determined. The activation enthalpy and entropy of the reaction were calculated to be 35.8 ± 1.8 kJ mol^{-1} and −109 ± 6 J K^{-1} mol^{-1}, respectively.

Table 2 lists the observed pseudo-first-order and derived second-order rate constants for the title reaction in a series of binary aqueous solvent mixtures. Trends in reaction rate with mole fraction of added cosolvent (Fig. 2) show retardation with increasing organic component.

The oxidation of $[Ni(tacn)_2]^{2+}$ by $S_2O_8^{2-}$ is several orders of magnitude faster than the oxidation of organic solvents such as alcohols (13, 14), and acetone (15). Thus possible side reactions of the oxidant with added cosolvents may be discounted in the present system.

Table 3 lists the solubilities of $[Ni(tacn)_2](ClO_4)_2$ in water and in a series of binary aqueous mixtures, at 298 K. Although there is little variation in solubility with solvent composition for the aqueous methanol mixtures, the solubility increases dramatically with increasing acetone concentration.

TABLE 3. Solubility data for $[Ni(tacn)_2](ClO_4)_2$ in water and in binary aqueous mixtures, together with corresponding transfer chemical potentials of the salt, at 298 K

% Cosolvent by volume	Mole fraction	Solubility (mol dm^{-3})	$\delta_m\mu^0([Ni(tacn)_2](ClO_4)_2)$ (kJ mol^{-1})
0	0	0.0322	0
Methanol cosolvent			
10	0.042	0.0295	0.67
20	0.100	0.0317	0.12
30	0.160	0.0324	−0.03
40	0.229	0.0362	−0.86
tert-Butyl alcohol cosolvent			
10	0.021	0.0323	−0.03
20	0.046	0.0342	−0.44
30	0.076	0.0343	−0.47
40	0.113	0.0344	−0.50
Acetone cosolvent			
10	0.027	0.0366	−0.94
20	0.058	0.0616	−4.8
30	0.095	0.0903	−7.6
40	0.140	0.152	−12

Discussion

Mechanism

Redox reactions involving metal ions or organic reductants and peroxodisulphate characteristically proceed via rate-determining fission of the peroxo bond (1), a step that may be assisted by the presence of a metal ion. A common mechanistic scheme for the oxidation of a cationic complex $[ML]^{n+}$ by $S_2O_8^{2-}$ may be described by eqs. [4–6]:

$$[4] \quad [ML]^{n+} + S_2O_8^{2-} \overset{K_{ip}}{\rightleftharpoons} \underbrace{\{ML^{n+}, S_2O_8^{2-}\}}_{\text{ion pair}}$$

$$[5] \quad \{ML^{n+}, S_2O_8^{2-}\} \xrightarrow{k_5} [ML]^{(n+1)+} + SO_4^{-} + SO_4^{2-}$$

$$[6] \quad [ML]^{n+} + SO_4^{-} \xrightarrow{\text{fast}} [ML]^{(n+1)+} + SO_4^{2-}$$

The rate law derived from this scheme is:

$$[7] \quad \text{Rate} = \{2k_5K_{ip}/(1 + K_{ip}[S_2O_8^{2-}])\}[S_2O_8^{2-}][ML^{n+}]$$

Such a rate law is expected to show curvature in the dependence of the observed first-order rate constant on peroxodisulphate concentration, if the ion-pairing constant is sufficiently large.

In the present system, where ML^{n+} represents $[Ni(tacn)_2]^{2+}$, no curvature in the k_{obs} versus $[S_2O_8^{2-}]$ plots was seen. This suggests that the ion-pairing constant is small and the approximation $(1 + K_{ip}[S_2O_8^{2-}]) \approx 1$ is valid over the range of oxidant concentrations used. Hence the rate law simplifies to:

$$[8] \quad \text{Rate} = k_{obs}[Ni(tacn)_2^{2+}] = 2k_5K_{ip}[S_2O_8^{2-}][Ni(tacn)_2^{2+}]$$

This contrasts with previous findings for oxidation of nickel(II) tetraazamacrocycles, where significant curvature in plots of the type shown in Fig. 1 led to kinetically determined ion-pairing constants of about 20 (4). For the $[Ni(tacn)_2]/S_2O_8^{2-}$ system, close approach of the anion to the nickel(II) centre is not possible, due to steric hindrance by the tacn ligands. Hence it is quite reasonable to presume that K_{ip} for this system would be considerably less than for the nickel(II) tetraazamacrocycles. Ion pairing between the reactants in the present study cannot be discounted, however, and the observed second-order rate constant must be considered as a composite term, where:

$$[9] \quad k_{obs}/[S_2O_8^{2-}] = 2k_5K_{ip}$$

Since the ion-pairing term appears to be relatively small, an activation entropy and enthalpy for the bimolecular rate-determining step has been calculated. The values obtained are compared in Table 4 with published activation parameters for reactions involving peroxodisulphate and transition metal complexes, as well as silver(I). It is apparent from these data that $[Ni(tacn)_2]^{2+}$ behaves similarly to other cationic complexes in its reaction with $S_2O_8^{2-}$. The activation enthalpy is significantly lower than that for thermal dissociation of the oxidant (22), suggesting cation(complex)-assisted peroxo-bond elongation in the transition state. The activation entropies are consistently large and negative for the reactions of the cationic complexes. Entropy values become less negative with decreasing positive charge on the complex. The activation parameters for the $[Co(cydta)]^{2-}/S_2O_8^{2-}$ system are anomalous, and clearly indicate a different mechanism. The enthalpy corresponds to that for thermal decomposition of $S_2O_8^{2-}$ into SO_4^{-} radicals (22).

Solvent effects

For reactions occurring in mixed aqueous solvents, the activation free energy of transfer, $\delta_m\Delta G^{\ddagger}$, measures the change in activation energy for the reaction as one changes the medium from water to the appropriate binary aqueous mixture. Table 5 lists the calculated values of $\delta_m\Delta G^{\ddagger}$ (according to eq. [1]) for a series of solvent mixtures. It is clear

Can. J. Chem. Downloaded from www.nrcresearchpress.com by 213.200.69.106 on 09/08/12
For personal use only.

TABLE 4. Comparison of activation parameters for reactions between peroxodisulphate and a range of transition metal complexes[a]

Metal complex	$\Delta H^{\ddagger}$(kJ mol^{-1})	$\Delta S^{\ddagger}$(J K^{-1} mol^{-1})	Reference
$[Ni(tacn)_2]^{2+}$	35.8 ± 1.3	−109 ± 6	This work
$[Fe(phen)_3]^{2+}$	54	−80	16
$[Fe(bipy)_3]^{2+}$	41	−117	16
$[Fe(terpy)_2]^{2+}$	42	−100	16
cis-$[CoCl(en)_2NCS]^{+}$	45.5	−129	17
$[CoCyS(en)_2]^{+}$	32.1 ± 1.5	−116 ± 3	18
Ag^{+}	38.5	−125	19
$[Co(en)_2SCH_2COO]^{+}$	36.3 ± 1.8	−91 ± 5	18
[Co(nta)]	65	−99	20
$[Co(ida)]^{2-}$	87	−32	20
$[Co(cydta)]^{2-}$	136 ± 9	+119 ± 10	20
$[Co(II)edta]^{2-}$	100	−50	21

[a]phen = 1,10-phenanthroline; bipy = 2,2′-bipyridyl; terpy = 2,2′,6′,2″-terpyridyl; en = 1,2-diaminoethane; cytda^{4-} = *trans*-1,2-diaminocyclohexane-*N*,*N*,*N*′,*N*′-tetraacetate; nta^{3-} = nitrilotriacetate; ida^{2-} = iminodiacetate.

TABLE 5. Transfer functions for reactants and transition state in binary aqueous mixtures, at 298 K

Cosolvent	Mole fraction	$\delta_m\mu^0(S_2O_8^{2-})$ (kJ mol^{-1})	$\delta_m\mu^0([Ni(tacn)_2^{2+}])$ (kJ mol^{-1})	$\delta_m\mu^0$(I.S.) (kJ mol^{-1})	$\delta_m\Delta G^{\ddagger}([Ni(tacn)_2^{2+}])$ (kJ mol^{-1})
Methanol	0.019				0.82
	0.042	0.4	0.7	1.1	1.6
	0.100	0.9	0	0.9	2.5
	0.160	1.4	0	1.4	2.8
	0.229	3.0	−0.7	2.3	3.2
tert-Butyl	0.010				0.69
alcohol	0.021	0.4	−0.2	0.2	0.96
	0.046	2.0	−1.8	0.2	1.2
	0.076	6.1	−3.9	2.2	1.3
	0.113	10.2	−6.5	3.7	1.3
Acetone	0.013				0.63
	0.027	2.3	−1.7	0.6	1.2
	0.058	5.2	−6.6	−1.4	1.8
	0.095	9.7	−10.8	−1.1	2.4
	0.140	13.9	−16.3	−2.4	3.0

that $\delta_m\Delta G^{\ddagger}$ increases as we go to more organic-rich solvent mixtures (more hydrophobic). This could be due to either (*a*) a stabilization of the initial state (reactants) or (*b*) destabilization of the transition state (or some combination of these), as the solvent composition is varied. To determine which case obtains, it is necessary to estimate the change in solvation of the initial state with solvent composition.

Table 5 presents single-ion transfer chemical potentials of the $[Ni(tacn)_2]^{2+}$ and $S_2O_8^{2-}$ ions in solvent mixtures corresponding to those of kinetic studies. The values for the nickel(II) complex cation were calculated from solubilities of the perchlorate salt in those solvents, using the relationship:

$$[10] \quad \delta_m\mu^0(MX_2) = 3RT \ln(S_w/S_x)$$

where MX_2 represents a 1:2 electrolyte, whose solubility is S_w in water and S_x in a mixture with mole fraction of cosolvent equal to x. As described in the Introduction, the single-ion transfer functions for the nickel(II) complex cation were obtained by subtraction of $2\delta_m\mu^0(ClO_4^-)$ from those of the salt. Values for $\delta_m\mu^0(S_2O_8^{2-})$ from water into aqueous methanol (23), *tert*-butyl alcohol (24) and acetone (25), and corresponding values for the perchlorate ion (26, 27) were taken from the literature. The extrathermodynamic assumption $\delta_m\mu^0(Ph_4As^+ \text{ or } Ph_4P^+) = \delta_m\mu^0(BPh_4^-)$ (TATB/TPTB) was used to arrive at the single-ion values throughout this work. Algebraic combination of these parameters gives $\delta_m\mu^0$(I.S.) from water into the mixed solvents. Figure 3 compares the single-ion transfer parameters of the reactants with $\delta_m\mu^0$(I.S.) and $\delta_m\Delta G^{\ddagger}$.

The transfer potential of $[Ni(tacn)_2]^{2+}$ into aqueous methanol mixtures is quite small, but the trend in the initial state transfer potential is one of destabilization with increasing mole fraction (Fig. 3(*a*)). In both aqueous *tert*-butyl alcohol and aqueous acetone mixtures (Fig. 3(*b*,*c*), there is a marked stabilization of the nickel(II) complex cation with increasing amount of cosolvent, which compensates for the destabilization of the hydrophilic peroxodisulphate anion. Thus, although there are significant changes in solvation of the individual reactant ions on changing solvent composition, the strongly hydrophobic periphery of the tacn ligands results in a stabilization, in spite of the 2+ charge on the complex ion.

Can. J. Chem. Downloaded from www.nrcresearchpress.com by 213.200.69.106 on 09/08/12
For personal use only.

Can. J. Chem. Downloaded from www.nrcresearchpress.com by 213.200.69.106 on 09/08/12
For personal use only.

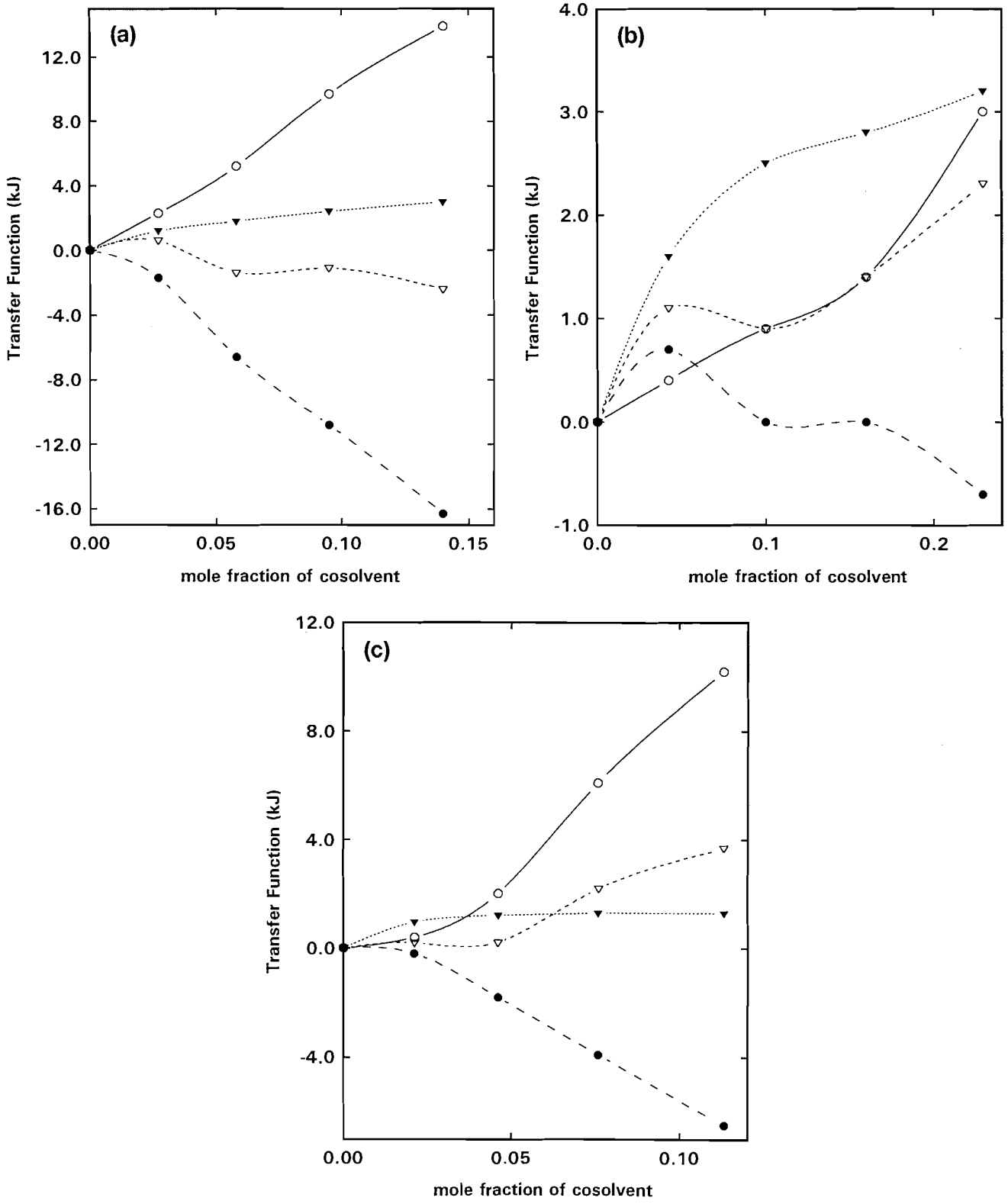

FIG. 3. Comparison of the transfer chemical potentials of $[Ni(tacn)_2]^{2+}$ (●), $S_2O_8^{2-}$ (○), and $\delta_m\mu^0$(I.S.) (▽) with the activation free energy of transfer, $\delta_m\Delta G^{\ddagger}$ (▼) from water into the following binary aqueous mixtures: (a) methanol–water; (b) *tert*-butyl alcohol water; (c) acetone–water (temperature 298 K).

Hence there is only a relatively small change in the initial state solvation with solvent composition.

There is a similar small change in the free energy of transfer of the transition state into these binary aqueous mixtures. In the transition state, ion pairing of the reactants is envisaged. One might expect a significant stabilization of such an ion pair in binary aqueous mixtures, because of charge neutralization. However, the periphery of the ion pair

should maintain hydrophobic character at the tacn side, and hydrophilic character at the peroxodisulphate side. As noted earlier, due to the substitutional inertness of the octahedral nickel(II) complex cation, approach of the $S_2O_8^{2-}$ anion to the inner sphere of the nickel complex is not possible. Even in the highest mole fractions of cosolvents, no ion pairing was kinetically observable, lending further support to the view that charge neutralization in an intimate ion pair is not a dominant feature.

The general observation of decreasing reaction rate with increasing mole fraction of organic cosolvent in the present system agrees with other studies of solvent effects on the oxidation of transition metal complexes by the peroxodisulphate anion (24, 28, 29). In those studies, ion pairing was not kinetically observable, due to expected lower ion-pairing constants between the anionic oxidant and singly charged metal complexes.

Acknowledgements

We are indebted to the Natural Sciences and Engineering Research Council of Canada (NSERC) for financial support. M.K.P. is grateful to NSERC for the award of an undergraduate summer research grant (USRA). We are grateful to Sir Wilfred Grenfell College for the award of the Principal's Research Grant. Thanks go to Dr. M. Mackay for atomic absorption measurements.

1. D.A. House. Chem. Rev. **62**, 185 (1962).
2. H. Eiberberger, S. Steenken, P. O'Neill, and D. Schulte-Frohlinde. J. Phys. Chem. **82**, 749 (1978).
3. M.J. Blandamer and J. Burgess. Coord. Chem. Rev. **31**, 93 (1980).
4. R.I. Haines and S.J. Northcott. Can. J. Chem. **70**, 2785 (1992).
5. R. Stranger, S.C. Wallis, L.R. Graham, C.H.L. Kennard, and K.A. Byriel. J. Chem. Soc. Dalton Trans. 2971 (1992).
6. R.O.C. Norman, P.M. Storey, and P.R. West. J. Chem. Soc. (B), 1087 (1978).
7. W.C. Vasudeva. J. Chem. Soc. Perkin Trans. 2, 697 (1975); M.E. Snook and G.A. Hamilton. J. Am. Chem. Soc. **97**, 1603 (1975).
8. M. Kimura, T. Akazome, K. Takenaka, and A. Kobayashi. Bull. Chem. Soc. Jpn. **53**, 1271 (1980).
9. K.A. Kumar, P. Sivawaroop, K.J. Rao, and P.V.K. Rao. Transition Met. Chem. (London), **12**, 441 (1987).
10. S. Fronaeus and C.O. Ostman. Acta Chem. Scand. **9**, 902 (1955); **22**, 2827 (1968).
11. D.H. Irvine. J. Chem. Soc. 2977 (1969); D. Benson. *In* Mechanisms of inorganic reactions in solution, an introduction. McGraw-Hill, London. 1968. Chap. 5.
12. I.M. Kolthoff, E.J. Meehan, and E.M. Carr. J. Am. Chem. Soc. **75**, 1439 (1953); D.L. Ball, M.M. Crutchfield, and J.O. Edwards. J. Org. Chem. **25**, 1599 (1960).
13. A.R. Gallopo and J.O. Edwards. J. Org. Chem. **36**, 4089 (1971).
14. W.C. Vasudeva and S. Wasif. J. Chem. Soc. (B), 960 (1970).
15. S.C. Agarwal, SMT P.L. Agarwal, V.B. Agarwal, and V. Dwivedi. Rev. Roum. Chim. **27**, 265 (1982).
16. J. Burgess and R.H. Prince. J. Chem. Soc. (A), 1772 (1966).
17. V. Holba, O. Grancicova, and P. Paulenova. Transition Met. Chem. (London), **12**, 121 (1987).
18. O. Volarova, J. Benko, and I. Matejekova, Collect. Czech. Chem. Commun. **51**, 1049 (1986).
19. G.D. Menghani and G.V. Bakore. Z. Phys. Chem. Neue Folge, **61**, 220 (1968).
20. P. Banerjee and P.M. Pujari. Z. Anorg. Allg. Chem. **473**, 224 (1981).
21. K. Ohashi, M. Matsuzawa, E. Hamaro, and K. Yamamoto. Bull. Chem. Soc. Jpn. **49**, 2440 (1976).
22. I.M. Kolthoff and I.K. Miller. J. Am. Chem. Soc. **73**, 3055 (1951); M. Kimura, T. Akazome, K. Takenaka, and A. Kobayashi. Bull. Chem. Soc. Jpn. **53**, 1271 (1980).
23. M.H. Abraham, T. Hill, H.C. Ling, R.A. Schultz, and R.A.C. Watt. J. Chem. Soc. Faraday Trans. 1, **80**, 489 (1984).
24. J. Juillard and C. Tissier. Electrochim. Acta, **27**, 123 (1982); J. Juillard, C. Tissier, J. Baraczynska, J. Mokrzan, and S. Taniewska-Osinska. J. Chem. Soc. Faraday Trans. 1, **81**, 3081 (1985).
25. J. Burgess and Ezz-Eldin A. Abu-Gharib. J. Chem. Res. (S), 8 (1985).
26. O. Volarova and J. Benko. J. Chem. Soc. Dalton Trans. 2359 (1983).
27. D. Bax, C.L. DeLigny, and A.G. Remijnse. Recl. Trav. Chim. Pays-Bas, **91**, 1225 (1972).
28. V. Holba, J. Benko, O. Grancicova, and O. Volarova. Transition Met. Chem. (London), **10**, 84 (1985).
29. J. Burgess, O. Volarova, and J. Benko. Transition Met. Chem. (London), **12**, 238 (1987).

Can. J. Chem. Downloaded from www.nrcresearchpress.com by 213.200.69.106 on 09/08/12
For personal use only.

A new annulation method. Total syntheses of the sesquiterpenoids (±)-chiloscyphone and (±)-6-*epi*-chiloscyphone

EDWARD PIERS[1] AND HOI LUN ALLAN TSE
Department of Chemistry, University of British Columbia, 2036 Main Mall, University Campus, Vancouver, B.C., Canada V6T 1Z1

Received February 12, 1993

EDWARD PIERS and HOI LUN ALLAN TSE. Can. J. Chem. **71**, 983 (1993).

The efficacy of a new annulation method, developed for the construction of functionalized bicyclic compounds, is illustrated by conversion of the β-keto esters **18** and **19** into the bicyclo[4.3.0]non-1-enes **33** and **34**, respectively, and by transformation of 2-methoxycarbonylcyclopentanone (**20**) into the bicyclo[4.3.0]non-6-ene **38** and the bicyclo[5.3.0]dec-7-enes **48** and **51**. Application of the method to total syntheses of the structurally unusual sesquiterpenoids (±)-chiloscyphone (**16**) and (±)-6-*epi*-chiloscyphone (**17**) is described.

EDWARD PIERS et HOI LUN ALLAN TSE. Can. J. Chem. **71**, 983 (1993).

On met en évidence l'efficacité d'une nouvelle methode d'annellation, développée pour la construction de composés bicycliques fonctionnalisés, en effectuant la conversion des β-céto esters **18** et **19** en bicyclo[4.3.0]non-1-ènes, **33** et **34** respectivement, ainis que la transformation de la 2-méthoxycarbonylcyclopentanone (**20**) en bicyclo[4.3.0]non-6-ène (**38**) et en bicyclo[5.3.0]déc-7-ènes, **48** et **51**. On décrit l'application de la méthode à la synthèse totale des sesquiterpénoïdes de structures inhabituelles, (±)-chiloscyphone (**16**) et (±)-6-*épi*-chiloscyphone (**17**).

[Traduit par la rédaction]

Introduction

The discovery and development of new annulation methods for the construction of functionalized carbocycles continues to be of importance in synthetic organic chemistry. In fact, such processes often play key roles in the total synthesis of natural products. Since the discovery of the Robinson annulation method more than 50 years ago (1), many different, synthetically effective six-membered ring annulation processes have been developed (1, 2). More recently, primarily in connection with research programs aimed at achieving total syntheses of natural products, operationally diverse annulation methods leading to functionalized carbocycles of various ring sizes have been described (3).

Recent reports from this laboratory have described in detail three annulation sequences that can be represented in general terms by the theoretical combination of the synthon **1** (a = acceptor center, d = donor center, see ref. 4) with each of the synthons **2**–**4** to produce methylenecyclopentane (**5**) (5), (*Z*)-ethylidenecyclopentane (**6**) (6), and methylenecyclohexane (**7**) (7) annulation products, respectively. In these processes, α,β-unsaturated ketones of general structure **8** serve as synthetic equivalents to the substrate synthon **1**, while structurally interesting bifunctional organocopper(I) species derived from the chloro trimethylstannanes **9**–**11** function as effective equivalents to the reagent synthons **2**–**4**.

We report in this paper the details of a new annulation method (8) that, although also based primarily on organotin chemistry, is quite different from those represented by the conversion of **8** into **5**–**7**. This method can be represented in general terms by the (theoretical) combination of the donor–donor synthon **12** (R = CO_2Me or a group derived therefrom) with an acceptor–acceptor synthon **13**, to form bicyclic substances of general structure **14**. In practice, cyclic β-trimethylstannyl α,β-unsaturated esters **15** and 1,ω-dihaloalkanes serve as synthetic equivalents to the synthons **12** and **13**, respectively. As described below, this method has successfully led to five-, six-, and seven-membered ring annulations. Furthermore, the method has been applied to the total syntheses of the sesquiterpenoid (±)-chiloscyphone (**16**) and of its C-6 epimer **17**.

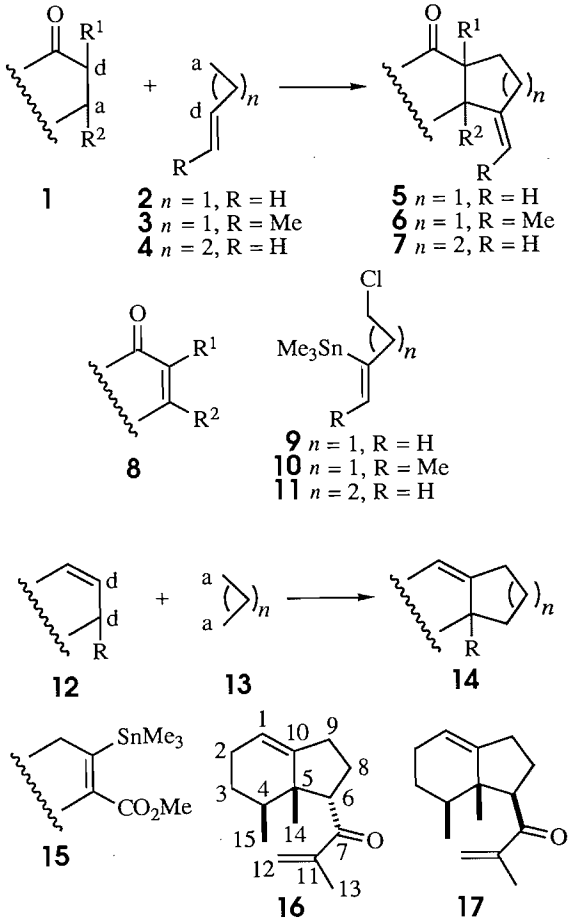

[1]Author to whom correspondence may be addressed.

Can. J. Chem. Downloaded from www.nrcresearchpress.com by 213.200.69.106 on 09/08/12
For personal use only.

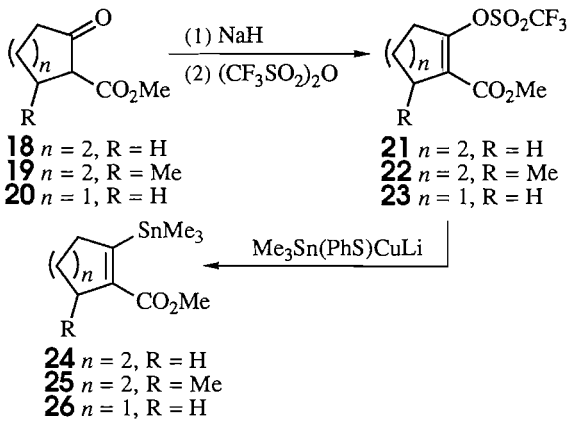

18 n = 2, R = H
19 n = 2, R = Me
20 n = 1, R = H
21 n = 2, R = H
22 n = 2, R = Me
23 n = 1, R = H
24 n = 2, R = H
25 n = 2, R = Me
26 n = 1, R = H

SCHEME 1

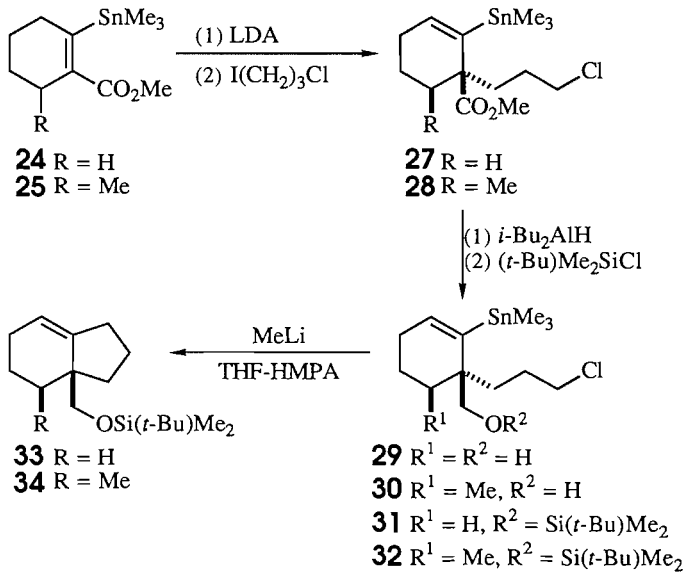

24 R = H
25 R = Me
27 R = H
28 R = Me
33 R = H
34 R = Me
29 $R^1 = R^2$ = H
30 R^1 = Me, R^2 = H
31 R^1 = H, R^2 = Si(t-Bu)Me_2
32 R^1 = Me, R^2 = Si(t-Bu)Me_2

SCHEME 2

Results and discussion

(a) Preparation of the cyclic β-trimethylstannyl α,β-unsaturated esters 24–26

The β-trimethylstannyl α,β-unsaturated esters **24–26** that were employed in this study were conveniently prepared from the corresponding 2-methoxycarbonylcycloalkanones **18–20**, as shown in Scheme 1. Thus, sequential treatment of 2-methoxycarbonylcyclohexanone (**18**) (9) with sodium hydride and trifluoromethanesulfonic anhydride in diethyl ether at 0°C gave, in 79% yield, the enol trifluoromethanesulfonate **21**. In similar fashion, the β-keto esters **19**[2] and **20** were converted efficiently into substances **22** and **23**, respectively.

Replacement of the trifluoromethanesulfonyloxy group present in each of compounds **21–23** by a trimethylstannyl function was accomplished by reaction of these materials with lithium (phenylthio)(trimethylstannyl)cuprate (12) in THF containing a small amount of hexamethylphosphoramide (HMPA). These reactions were clean and efficient and the ^{1}H nmr spectrum of each of the products **24–26** exhibited the expected nine-proton signal (δ 0.16) due to the trimethylstannyl moiety.

(b) Annulation reactions involving substrates 24–26

The efficient conversions of the cyclohexenecarboxylates **24** and **25** into the functionalized bicyclo[4.3.0]nonenes **33** and **34** are summarized in Scheme 2. Treatment of **24** with lithium diisopropylamide (LDA) (1.5 equiv.) in THF containing HMPA (3 equiv.), followed by addition of 1-chloro-3-iodopropane, provided the expected alkylation product **27** (78%). Similarly, **28** was obtained in 89% yield from **25**. As expected (13), the latter alkylation process was completely stereoselective, with the alkylating reagent approaching the substrate enolate anion from the side of the molecule opposite to the secondary methyl group.

Reduction of each of the esters **27** and **28** with diisobutylaluminum hydride in diethyl ether afforded the alcohols **29** and **30**. Treatment of the latter substances with *tert*-butyldimethylsilyl chloride – imidazole in *N*,*N*-dimethylformamide provided, in excellent overall yields, the functionalized cyclohexenes **31** and **32**.

Completion of the five-membered ring annulation sequences required alkyllithium-mediated transmetallation of the trimethylstannyl function in **31** and **32**, followed by intramolecular displacement of chloride ion by the resultant vinyllithium center. When **31** was treated with methyllithium in THF under different reaction conditions (e.g., 1.3 equiv. MeLi, −78°C, 3 h; 4 equiv. MeLi, −78°C, 4.5 h), no reaction occurred. In each case, starting material was recovered in high yield. Even when **31** was treated with a large excess (~20 equiv.) of methyllithium in THF at −20°C for 7 h, the material isolated from the reaction mixture consisted mainly of **31** (~75%) accompanied by a minor amount (~25%) of the desired product **33**. Clearly and, perhaps not surprisingly (14), the transmetallation of the (sterically hindered) trimethylstannyl function in **31** with methyllithium is, at least in THF, a very sluggish process.

It is known (14) that the rate of tin–lithium exchange reactions can be increased by use of solvents that coordinate with metal cations more efficiently than THF. Indeed, when a solution of **31** in THF containing 3 equiv. of HMPA was treated with methyllithium (−20°C, 30 min), 6-(*tert*-butyldimethylsiloxymethyl)bicyclo[4.3.0]non-1-ene (**33**) was obtained in 92% yield. In similar fashion, the substrate **32** was transformed into the bicyclic alkene **34** (94%). Thus, under appropriate conditions, the five-membered ring annulations are clean and efficient.

A successful six-membered annulation of the cyclopentenecarboxylate **26** is shown in Scheme 3. Alkylation (LDA, THF–HMPA) of **26** with 1,4-dibromobutane gave (72%) the β,γ-unsaturated ester **35**, which was cleanly reduced to the alcohol **36**. Treatment of **36** with *tert*-butyldimethylsilyl trifluoromethanesulfonate and 2,6-lutidine[3] in dichloromethane (15) gave the required silyl ether **37**.

Reaction (−20°C, 30 min) of **37** with methyllithium in THF–HMPA provided a mixture of the desired bicyclic alkene **38** and the monocyclic diene **39**, in a ratio of ~6:1 (analysis by glc). Column chromatography of this mixture

[2]2-Methoxycarbonyl-3-methylcyclohexanone (**19**) was prepared by reaction of 2-methoxycarbonyl-2-cyclohexen-1-one (10) with lithium (phenylthio)(methyl)cuprate (11) in tetrahydrofuran (THF) – diethyl ether (see Experimental).

[3]Reaction of **36** with (t-Bu)Me_2SiCl–imidazole in *N*,*N*-dimethylformamide gave a mixture of **36** and the corresponding chloride in a ratio of ~1:1. Use of (t-Bu)$Me_2SiOSO_2CF_3$ precluded the possibility of the unwanted side reaction.

Can. J. Chem. Downloaded from www.nrcresearchpress.com by 213.200.69.106 on 09/08/12
For personal use only.

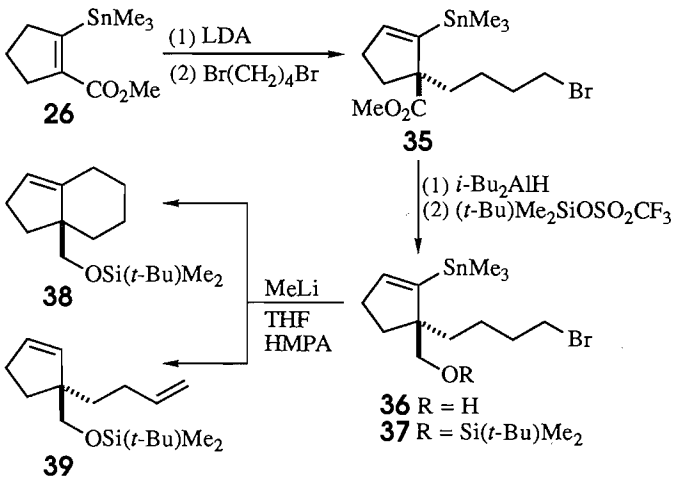

SCHEME 3

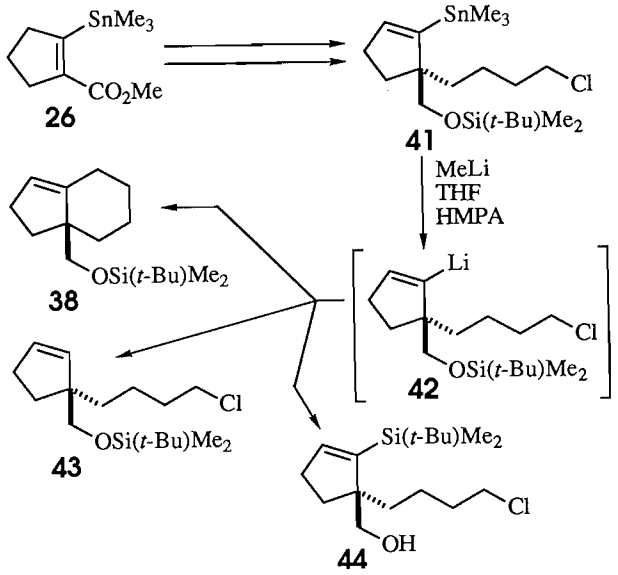

SCHEME 4

on silver nitrate impregnated silica gel produced **38** and **39** in isolated yields of 61 and 7%, respectively.

It seems likely that the diene **39** is formed from the same intermediate that gives rise to the bicyclic substance **38**. Thus, cyclization of the vinyllithium species **40** (formed by transmetallation of **37**) would afford **38**. On the other hand, an intramolecular elimination process via a six-centered transition state (see **40**, eq. [1]) would produce **39**. Fortunately, of these two competitive processes, the cyclization reaction predominates.

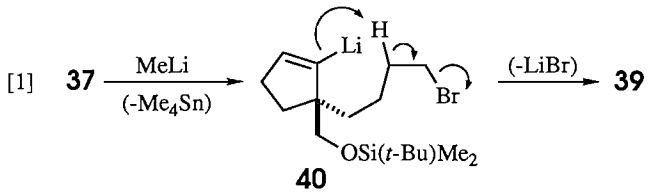

It is interesting to note that an earlier attempt to produce the annulation product **38** from the chloride **41** (Scheme 4) did not give satisfactory results. Alkylation of **26** with

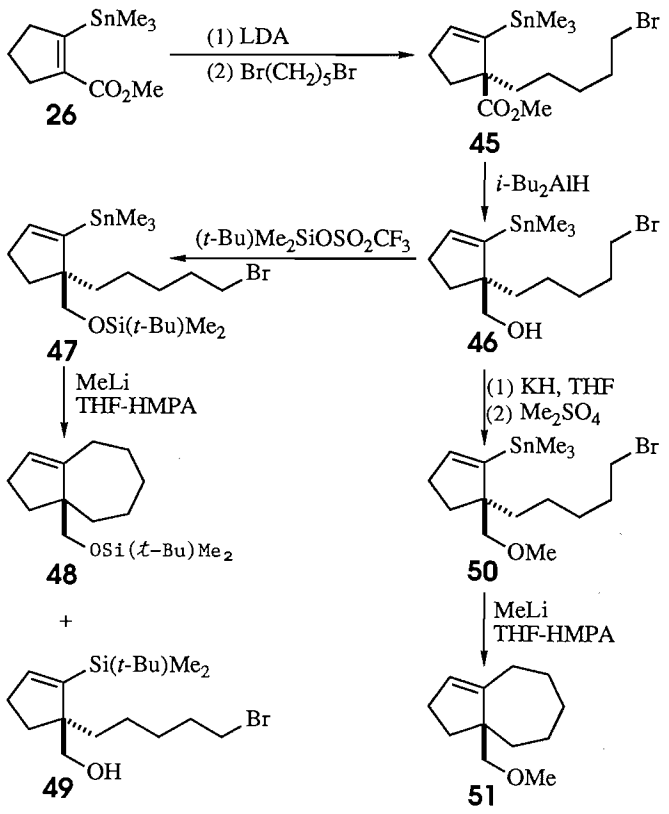

SCHEME 5

1-bromo-4-chlorobutane, followed by functional group manipulations identical with those described earlier (Scheme 2), gave the chloride **41**. Treatment of the latter substance with methyllithium in THF–HMPA under conditions identical with those used for the chlorides **31** and **32** (Scheme 2) gave three products. Two of these were formed in minor amounts (~10% in each case) and, on the basis of spectral data, were shown to be the (desired) annulation product **38** and the substance **43** resulting from transmetallation–protonation (Scheme 4). Interestingly, the major product **44** (~75%) proved to be that resulting from transfer of the *tert*-butyldimethylsilyl group from oxygen to carbon. Thus, the competition between ring closure of the intermediate vinyllithium species **42** (cyclic six-centered transition state, chloride ion as leaving group) and silyl group transfer (cyclic five-centered transition state) favored the latter process. Fortunately, this unsatisfactory result could be largely overcome by changing the leaving group from chloride to bromide (vide supra).

Use of the cyclopentenecarboxylate **26** as a substrate for seven-membered ring annulations is summarized in Scheme 5. Alkylation of **26** with 1,5-dibromopentane and reduction of the ester function of the resultant product **45** provided, efficiently, the alcohol **46**, which was readily transformed into the silyl ether **47**. When **47** was allowed to react with methylithium in THF–HMPA, two products were obtained in yields of 35 and 17%. These substances were accompanied by a considerable amount of intractable material. Spectral data showed that the major isolated material was the bicyclo[5.3.0]oct-7-ene **48**, while the minor substance was the silyl-transfer product **49**. Thus, in this case, with bro-

Can. J. Chem. Downloaded from www.nrcresearchpress.com by 213.200.69.106 on 09/08/12
For personal use only.

Can. J. Chem. Downloaded from www.nrcresearchpress.com by 213.200.69.106 on 09/08/12
For personal use only.

mide ion as the leaving group, the rate of ring closure (cyclic seven-membered transition state) is about twice that of migration of the (*t*-Bu)Me_2Si function from oxygen to carbon via a cyclic five-membered transition state.

Reaction of the alcohol **46** with potassium hydride – dimethyl sulfate afforded the methyl ether **50** in 84% yield. Treatment of this material with methyllithium in THF–HMPA provided one major product, the bicyclic olefinic ether **51**, accompanied by traces of unidentified side products and some intractable material. The fact that the isolated yield (54%) of the annulation product **51** was modest was probably due, at least in part, to the volatility of this substance.

The results of this brief study, as summarized above, showed that the originally envisaged annulation processes, as generalized by **12** + **13** → **14**, are viable synthetic operations. The overall method, which has led to the production of five-, six-, and seven-membered rings, should find use for the preparation of functionalized carbocyclic systems. An application of this chemistry in natural product synthesis is presented in the next section of this paper.

*(c) Total syntheses of (±)-chiloscyphone (**16**) and (±)-6-epi-chiloscyphone (**17**)*

The sesquiterpenoid (−)-chiloscyphone, the main constitutent of the essential oil of the liverwort *Chiloscyphus polyanthus* (L.) Corda, was first isolated by Hayashi et al. (16) and was later proposed (17, 18) to possess the constitution and absolute configuration shown in **52**. However, a subsequent synthesis of racemic **52** by Gras (19) revealed that the original structural proposals (16–18) were incorrect. In 1982, Connolly et al. (20) showed that (−)-chiloscyphone possesses the constitution and *relative* stereostructure depicted in formula **53**. Later, based on synthetic work and circular dichroism studies, Tori et al. (21) concluded that **53** also represents the correct absolute configuration of this natural product. This deduction also turned out to be incorrect and the fact that (−)-chiloscyphone possesses the constitution and absolute configuration shown in formula **16** was finally determined by an X-ray crystallographic study (22).

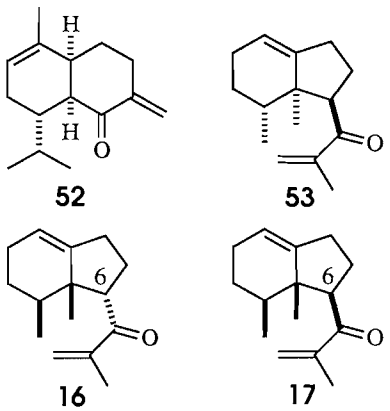

52 **53** **16** **17**

In the paragraphs that follow, we give an account of the use of the new annulation method described previously (vide supra) for total syntheses of (±)-chiloscyphone (**16**) and its C-6 epimer **17**.[4]

The route envisaged for the synthesis of (±)-**16** involved initially the alkylation of the β-trimethylstannyl α,β-unsaturated ester **25** with a 1,3-dihalo-1-alkoxypropane. The alkylating agent employed for this purpose was 1,3-dichloro-1-(2-trimethylsilylethoxy)propane (**55**), which was readily prepared (24) by treatment of acrolein (**54**) with 2-(trimethylsilyl)ethanol and dry hydrogen chloride (eq. [2]).

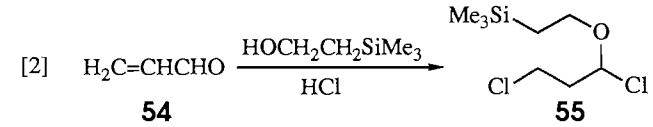

54 **55**

The C-1 chloride of **55** would be expected to be more easily displaced by a nucleophile than the C-3 chloride. Therefore, alkylation of the enolate anion of **25** with **55** should produce a product that contains an oxygen function on the carbon that would (eventually) become C-6 of (±)-**16**. This function would have to be used as a handle for the introduction of the carbonyl-containing side chain present in the natural product.

Treatment of the lithium enolate of **25** with the dichloride **55** provided a mixture of products that contained two major substances, **56** and **57**,[5] along with a number of very minor, unidentified side products (Scheme 6). Although flash chromatography (25) of this mixture on silica gel provided pure **56** (41%), the epimeric compound **57** could not be obtained free of minor contaminants. However, treatment of the mixture containing (mainly) **57** with diisobutylaluminum hydride, followed by silylation (15) of the resultant alcohol **66** and product purification (flash chromatography, distillation), gave the pure diether **67** (9% overall yield from **25**). Cyclization (MeLi, THF–HMPA) of **67** afforded the bicyclic alkene **68** (78%).

The three-step transformation of pure **56** into the functionalized bicyclo[4.3.0]non-1-ene **60** (Scheme 6) was achieved cleanly and efficiently (58% overall yield).

Chemoselective cleavage of the *tert*-butyldimethylsilyl ether function of **60** was easily accomplished by treatment of this substance with tetra-*n*-butylammonium fluoride in THF. Oxidation of the resultant primary alcohol **61** with pyridinium chlorochromate (PCC) gave the aldehyde **62**. Treatment of the corresponding hydrazone with sodium methoxide in diethylene glycol at 210°C provided the desired deoxygenated compound **63** (71% from **60**). In similar fashion, the diether **68** (epimer of **60**) could be converted, via the intermediates **69** and **70**, into the bicyclic ether **71** (56% overall yield).

The configurational assignments with respect to intermediates **63** and **71** require comment. As mentioned previously, alkylation of the enolate anion of **25** would undoubtedly occur, for steric reasons, from the face of the enolate opposite the adjacent secondary methyl group (13). Consequently, the relative configurations of C-5 and C-6 in substances **63** and **71** could be assigned with confidence. On the other hand, data derived from the ^1H nmr spectra of **63** and **71** allowed assignment of the C-7 configurations. In what appears to be the most stable conformation of compound **63**, the dihedral angle between H_A and H_C is close to 90° and, therefore, a very weak coupling between these two protons would be expected. In fact, in the ^1H nmr spectrum of **63** H_A gives rise to a doublet at δ 3.47, with a coupling constant (presumably J_{AB}) of 4 Hz.

[4]For other synthetic work related to chiloscyphone, see refs. 21 and 23.

[5]The relative configurations of these substances were subsequently assigned by use of ^1H nmr spectral data derived from the bicyclic intermediates **63** and **71**, respectively (vide infra).

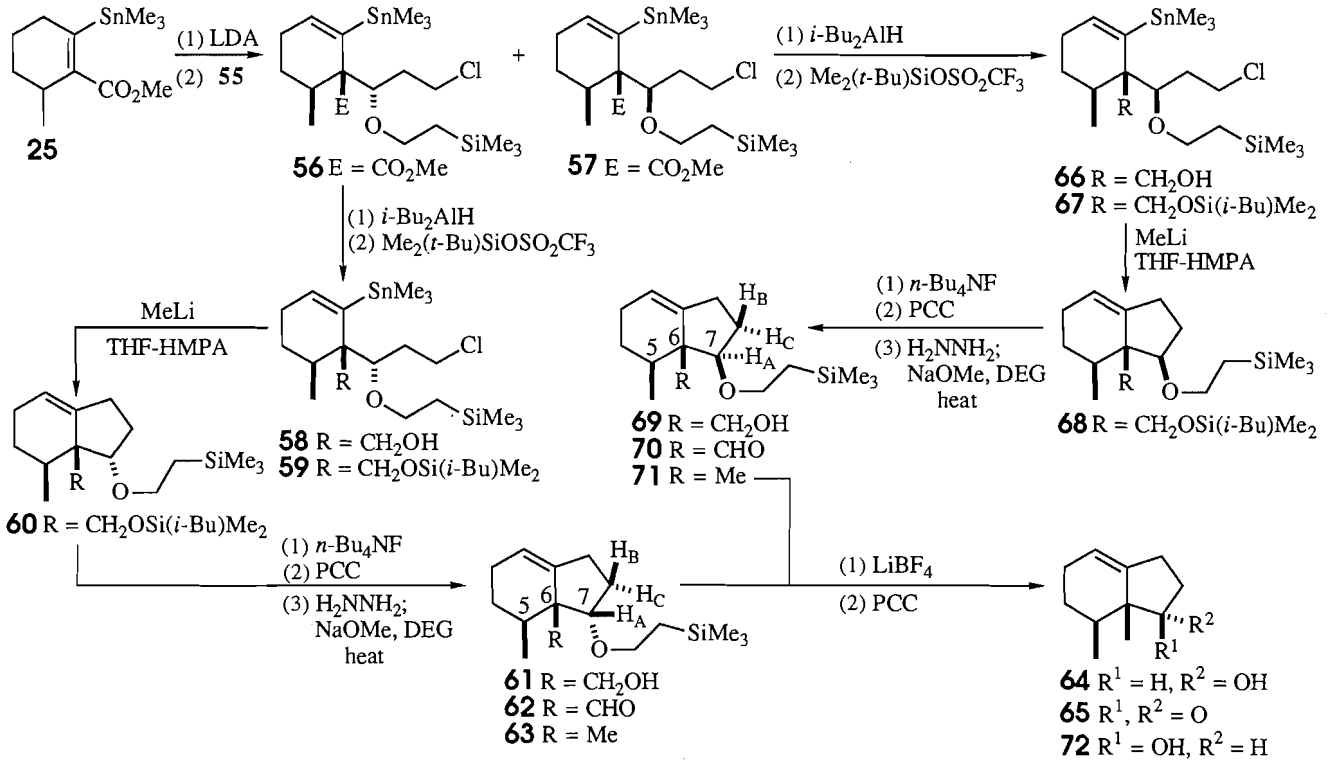

SCHEME 6

$Ph_3P{=}CHOMe$ **73**

$[Ph_2P\text{-}\bar{C}H\text{-}OMe]Li^+$ **74**

$[Me_3Si\text{-}\bar{C}H\text{-}Cl]Li^+$ **75**

$[Me_3Si\text{-}\bar{C}H\text{-}OMe]Li^+$ **76**

$[(EtO)_2P(O)\text{-}\bar{C}H\text{-}OCH_2CH_2OMe]Li^+$ **77**

CHART 1

In the case of compound **71**, molecular models indicate that, in the most stable conformation of this substance, the dihedral angles between H_A and H_B and between H_A and H_C are approximately 150° and 30°, respectively. Therefore, the magnitudes of J_{AB} and J_{AC} would be expected to be quite similar. In the ^1H nmr spectrum of **71**, the signal due to H_A appears as a triplet (J = 9 Hz) at δ 3.25.

Attempts to convert the ether **63** into the secondary alcohol **64** initially proved to be problematic. However, it was eventually found that the desired transformation could be achieved efficiently by use of lithium tetrafluoroborate.[6] Thus, treatment of **63** with a 1:1 mixture of boron trifluoride etherate and lithium fluoride in acetonitrile at room temperature afforded the alcohol **64** in 87% yield. Oxidation of the latter substance with PCC produced the ketone **65** (83%).

Lithium tetrafluoroborate mediated cleavage of the ether linkage of compound **71**, followed by oxidation of the resultant alcohol **72**, also produced, in 74% overall yield, the ketone **65**.[7]

The homologation of the ketone **65** was not straightforward. The carbonyl group in this substance is sterically quite hindered and, therefore, the 1,2-addition of nucleophiles to this function would be expected to be sluggish. Indeed, the failure to obtain the desired adducts from treatment of **65** with a variety of nucleophilic reagents (vide infra) was, no doubt, due to the fact that, in these cases, proton transfer (enolate anion formation) takes place in preference to addition.

Treatment of **65** with (methoxymethylene)triphenylphosphorane (**73**) (Chart 1) in THF (25°C) or dimethyl sulfoxide (70°C) (27) gave back only starting material. Similarly, reaction of **65** with each of the reagents **74** (28), **75** (29), and **76** (30) under conditions similar to those prescribed in the literature produced, in each case, little or no desired product. Upon work-up, each reaction mixture yielded primarily the starting material **65**.

Kluge and Cloudsdale (31) have reported that the reagent **77** (Chart 1) undergoes efficient 1,2-addition to readily enolizable ketones at low temperatures. Reaction of **65** with **77** (5 equiv.) in THF at −98°C did provide the desired 1,2-addition adduct, but the yield was low (less than 30%). In addition, approximately 40% of **65** was recovered.

A report by Conia and Limasett (32) has disclosed that methylenation of hindered ketones can be accomplished efficiently by treatment of the substrate with $Ph_3P{=}CH_2$ derived from reaction of $(Ph_3PMe)Br$ with sodium *tert*-amylate.

[6]This reagent has been used effectively for the conversion of 2-(trimethylsilyl)ethyl glycosides into the parent carbohydrates (26). We are grateful to Professor Lipshutz for suggesting this reagent to us.

[7]Obviously, the ketone **65** could have been derived from the *mixture* of **56** and **57** via a *single* synthetic sequence. However, in the interest of spectrally characterizing all of the synthetic intermediates involved, compounds **56** and **57** were each converted into **65** via separate synthetic pathways (Scheme 6).

Can. J. Chem. Downloaded from www.nrcresearchpress.com by 213.200.69.106 on 09/08/12
For personal use only.

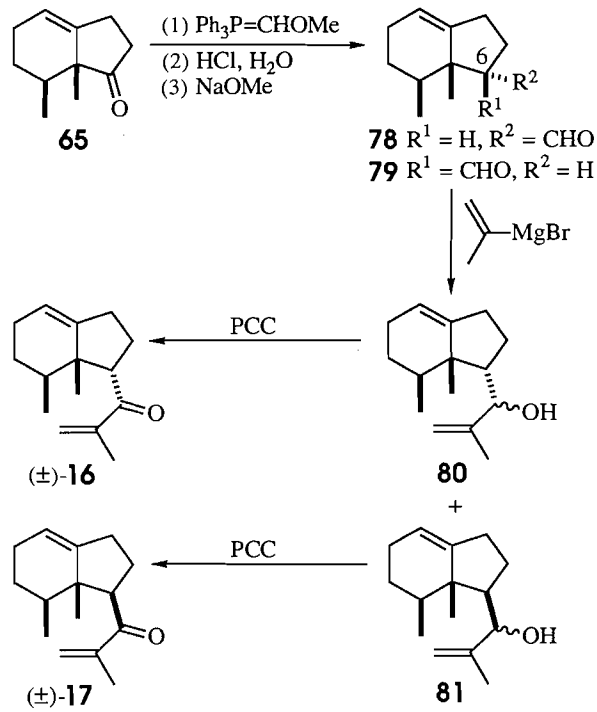

SCHEME 7

This method proved to be reasonably effective for the homologation of **65**. Thus, reaction of **65** with (methoxymethylene)triphenylphosphorane (**73**), prepared by reaction of $(Ph_3PCH_2OMe)Cl$ with $NaOC(Et)Me_2$ in benzene, followed by acid hydrolysis of the resultant mixture of enol ethers, gave a mixture of the two aldehydes **78** and **79** in ratio of ~1:4 (analysis by glc) (Scheme 7). The overall yield of this two-step process was 43%.

Base-catalyzed equilibration of the mixture of epimers **78** and **79** with sodium methoxide in methanol produced a 1:1 mixture of the two substances. Further treatment of this mixture with sodium methoxide and prolonged reaction times did not alter the product ratio. Thus, somewhat surprisingly, **78** and **79** do not differ in stability. Consequently, the expectation that, in the envisaged synthesis of (±)-chiloscyphone (**16**), the configuration at C-6 (chiloscyphone numbering system) could be controlled by thermodynamically controlled equilibration of **78** and **79** proved to be faulty.

Unfortunately, the aldehydes **78** and **79** could not be separated by chromatography on silica gel. However, the mixture of alcohols **80** and **81** derived from reaction of **78** and **79** with isopropenylmagnesium bromide were separable by flash chromatography (25) and were obtained in isolated yields of 33 and 42%, respectively.

Oxidation of **80** with PCC provided (±)-chiloscyphone (**16**), a colorless oil, in 59% yield. Similarly, racemic 6-*epi*-chiloscyphone (**17**) was obtained by oxidation of **81**.

Although we were not able to procure an authentic sample of (−)-**16**, the spectral data derived from our synthetic material agreed very well with those reported for natural (−)-**16** (18) and synthetic (±)-**16** (23). On the other hand, the ^{1}H nmr spectrum of (±)-6-*epi*-chiloscyphone (**17**), although similar, is clearly distinguishable from that of racemic **16**.

Experimental

General information

Distillation temperatures (short-path Kugelrohr distillations) are uncorrected. Proton nuclear magnetic resonance (^{1}H nmr) spectra were taken on $CDCl_3$ solutions. Signal positions (δ values) were measured relative to the Me_4Si resonance (internal standard) or the $CHCl_3$ signal (δ 7.25). The tin–proton coupling constants (J_{Sn-H}) are given as an average of the ^{117}Sn and ^{119}Sn values. For compounds containing the Me_3Sn function, high-resolution mass spectrometric measurements are based on ^{120}Sn and were measured on the (M^+ − Me) peak (33). Gas–liquid chromatographic (glc) analyses were performed on Hewlett-Packard models 5880 or 5890 gas chromatographs equipped with flame ionization detectors and 25 m × 0.21 mm fused silica columns coated with cross-linked SE-54. Thin-layer chromatography (tlc) analyses were carried out on commercial aluminum-backed silica gel plates (E. Merck, Type 5554). Conventional chromatography was done with 70–230 mesh silica gel (E. Merck), while flash chromatography was carried out with 230–400 mesh silica gel as described by Still et al. (25).

Note. All reactions were carried out under an atmosphere of dry argon in glassware that had been flame-dried under an argon flow.

Note. All compounds for which exact masses (high-resolution mass spectrometry) are reported gave clean ^{1}H nmr spectra and were homogeneous by glc and tlc analyses.

2-Methoxycarbonyl-3-methylcyclohexanone (19)

To a cold (−20°C), stirred solution of lithium (phenylthio)-(methyl)cuprate (11) (44.7 mmol) in a mixture of dry THF (140 mL) and dry Et_2O (32 mL) was added a solution of 4.92 g (31.9 mmol) of 2-methoxycarbonyl-2-cyclohexen-1-one (10) in 10 mL of dry THF and the reaction mixture was stirred at −20°C for 1 h. Saturated aqueous ammonium chloride (30 mL) and petroleum ether (200 mL) were added, the mixture was allowed to warm to room temperature, and stirring was continued until a clear, colorless organic layer was formed. The mixture was filtered to remove the solid material, the filtrate was washed with water and brine, and was then dried ($MgSO_4$). Removal of the solvent and distillation (80–90°C/0.1 Torr; 1 Torr = 133.3 Pa) of the residue provided 4.47 g (82%) of **19**, which, in $CDCl_3$ solution, consisted of a mixture of **19** and the corresponding enol tautomer (ratio approximately 2:1, respectively). The colorless oil exhibited ir (neat): 3450, 1735, 1700 cm^{-1}; ^{1}H nmr (80 MHz) δ: 1.03, 1.07 (d, d, 3H total, J = 6 Hz in each case), 1.25–2.90 (diffuse m, 7H), 3.05 (d, 0.7 H, J = 11 Hz), 3.75 (s, 3H), 12.26 (s, 0.3 H). Exact Mass calcd. for $C_9H_{14}O_3$: 170.0942; found: 170.0942.

Methyl 2-(trifluoromethanesulfonyloxy)-1-cyclohexene-carboxylate (21)

To a cold (0°C), stirred suspension of NaH (92 mg, 3.85 mmol) in 12 mL of dry Et_2O was added slowly a solution of 2-methoxycarbonylcyclohexanone (**18**) (9) (0.5 g, 3.2 mmol) in 3 mL of dry Et_2O. After the mixture had been stirred at 0°C for 10 min, trifluoromethanesulfonic anhydride (403 mg, 3.85 mmol) was added and stirring was continued at 0°C for 1 h. Saturated aqueous ammonium chloride (2 mL) and Et_2O (15 mL) were added and the resultant mixture was stirred at 25°C for 5 min. The phases were separated and the organic layer was washed (water, brine), dried ($MgSO_4$), and concentrated. Distillation (80–90°C/0.1 Torr) of the residual oil gave 732 mg (79%) of **21**, a colorless oil that displayed ir (neat): 1710, 1650, 1420, 1210 cm^{-1}; ^{1}H nmr (80 MHz) δ: 1.50–1.95 (m, 4H), 2.15–2.60 (m, 4H), 4.76 (s, 3H). Exact Mass calcd. for $C_9H_{11}F_3O_5S$: 288.0279; found: 288.0281.

Methyl 6-methyl-2-(trifluoromethanesulfonyloxy)-1-cyclohexene-carboxylate (22)

This material was prepared from 2-methoxycarbonyl-3-methylcyclohexanone (**19**) via a procedure identical with that described above. From 1.59 g (9.34 mmol) of **19** there was obtained 2.58 g (91%) of **22** (distillation temperature 90–100°C/0.1 Torr), a col-

Can. J. Chem. Downloaded from www.nrcresearchpress.com by 213.200.69.106 on 09/08/12
For personal use only.

Can. J. Chem. Downloaded from www.nrcresearchpress.com by 213.200.69.106 on 09/08/12
For personal use only.

orless oil that exhibited ir (neat): 1710, 1420, 1210 cm^{-1}; ^1H nmr (80 MHz) δ: 1.01 (d, 3H, J = 7 Hz), 1.40–2.00 (m, 4H), 2.25–2.50 (m, 2H), 2.90 (m, 1H), 3.80 (s, 3H). Exact Mass calcd. for $C_{10}H_{13}F_3O_5S$: 302.0437; found: 302.0437.

Methyl 2-(trifluoromethanesulfonyloxy)-1-cyclopentene-carboxylate (23)

This material was prepared from 2-methoxycarbonylcyclopentanone (**20**) via a procedure identical with that described above, except that the work-up procedure was changed as follows. The reaction mixture was diluted with Et_2O (10 mL) and then was filtered through a short column of Florisil (elution with Et_2O). The combined eluate was concentrated and the residue was distilled (70–80°C/0.1 Torr) to provide, from 0.5 g (3.52 mmol) of **20**, 714 mg (74%) of **23** as a colorless oil that displayed ir (neat): 1720, 1660, 1420, 1210 cm^{-1}; ^1H nmr (80 MHz) δ: 1.90–2.25 (m, 2H), 2.55–2.90 (m, 4H), 3.80 (s, 3H). Exact Mass calcd. for $C_8H_9F_3O_5S$: 274.0123; found: 274.0119.

Methyl 2-(trimethylstannyl)-1-cyclohexenecarboxylate (24)

To a cold (−20°C), stirred solution of lithium (phenylthio)-(trimethylstannyl)cuprate (12) (13.8 mmol) in 40 mL of dry THF was added a solution of the enol triflate **21** (2.65 g, 9.2 mmol) in 5 mL of dry THF. After the mixture had been stirred at −20°C for 1 h, dry HMPA (27.6 mmol) was added, the mixture was allowed to warm to 0°C, and was then stirred for an additional 1 h. Saturated aqueous ammonium chloride (25 mL) and a 3:7 mixture of Et_2O – petroleum ether (200 mL) were added and the mixture was stirred until the organic layer was colorless. The mixture was filtered to remove the solid material. The filtrate was washed (saturated aqueous copper(II) sulfate, water, brine), dried ($MgSO_4$), and concentrated. Flash chromatography (1:4 benzene – petroleum ether) of the residue on silica gel, followed by distillation (85–95°C/0.1 Torr) of the oil thus obtained, gave 2.1 g (75%) of **24** as a colorless oil that exhibited ir (neat): 1690, 1250, 770 cm^{-1}; ^1H nmr (270 MHz) δ: 0.16 (s, 9H, $^2J_{Sn-H}$ = 54 Hz), 1.65 (m, 4H), 2.42 (m, 4H), 3.77 (s, 3H). Exact Mass calcd. for $C_{10}H_{17}O_2Sn$ (M^+−Me): 289.0250; found: 289.0250.

Methyl 6-methyl-2-(trimethylstannyl)-1-cyclohexenecarboxylate (25)

This material was prepared from the enol triflate **22** via a procedure very similar to that described above. Flash chromatography (3:17 benzene – petroleum ether) of the crude product obtained from 2.58 g (8.55 mmol) of **22**, followed by distillation (90–100°C/0.1 Torr) of the oil thus obtained, provided 2.43 g (89%) of **25** as a colorless oil that exhibited ir (neat): 1690, 1250, 770 cm^{-1}; ^1H nmr (80 MHz) δ: 0.16 (s, 9H, $^2J_{Sn-H}$ = 54 Hz), 1.10 (d, 3H, J = 7 Hz), 1.62 (m, 4H), 2.40 (m, 2H), 2.80 (m, 1H), 3.78 (m, 3H). Exact Mass calcd. for $C_{11}H_{19}O_2Sn$ (M^+−Me): 303.0407; found: 303.0406.

Methyl 2-(trimethylstannyl)-1-cyclopentenecarboxylate (26)

The enol triflate **23** (2.5 g, 9.12 mmol) was converted into **26** via a procedure very similar to that described above. Purification of the crude product by flash chromatography (3:7 benzene – petroleum ether) and distillation (70–80°C/0.1 Torr) afforded 2.05 g (78%) of **26** as a colorless oil that showed ir (neat): 1700, 1260, 770 cm^{-1}; ^1H nmr (80 MHz) δ: 0.16 (s, 9H, $^2J_{Sn-H}$ = 54 Hz), 1.94 (m, 2H), 2.63 (m, 4H), 3.71 (s, 3H). Exact Mass calcd. for $C_9H_{15}O_2Sn$ (M^+−Me): 275.0094; found: 275.0092.

Methyl 1-(3-chloropropyl)-2-(trimethylstannyl)-2-cyclohexene-carboxylate (27)

To a cold (−48°C), stirred solution of LDA (3.7 mmol) and HMPA (7.4 mmol) in 7 mL of dry THF was added a solution of the ester **24** (746 mg, 2.48 mmol) in 3 mL of dry THF. After the mixture had been stirred at −48°C for 40 min, 1-chloro-3-iodopropane (1.01 g, 4.94 mmol) was added and the resultant solution was stirred at −48°C for 40 min. Saturated aqueous ammonium chloride (~1 mL) was added, the mixture was allowed to warm to room temperature, and was then diluted with 100 mL of Et_2O. The resultant mixture was washed (saturated aqueous copper(II) sulfate, water, brine), dried ($MgSO_4$), and concentrated. Flash chromatography (6:94 Et_2O – petroleum ether) of the residual material, followed by distillation (125–135°C/0.1 Torr) of the oil thus obtained, gave 728 mg (78%) of **27** as a colorless oil that displayed ir (neat): 1710, 1440, 770 cm^{-1}; ^1H nmr (80 MHz) δ: 0.15 (s, 9H, $^2J_{Sn-H}$ = 52 Hz), 1.50–1.90 (m, 6H), 1.95–2.25 (m, 4H), 3.50 (m, 2H), 3.68 (s, 3H), 5.98 (t, 1H, J = 4 Hz). Exact Mass calcd. for $C_{13}H_{22}{}^{35}ClO_2Sn$ (M^+−Me): 365.0331; found: 365.0321.

Methyl cis-1-(3-chloropropyl)-6-methyl-2-(trimethylstannyl)-2-cyclohexenecarboxylate (28)

This material was obtained from the ester **25** via a procedure very similar to that described above. Flash chromatography (2:3 benzene – petroleum ether) of the crude product derived from 500 mg (1.38 mmol) of **25**, followed by distillation (135–145°C/0.1 Torr) of the resultant oil, provided 551 mg (89%) of **28** as a colorless oil that showed ir (neat): 1710, 1210, 770 cm^{-1}; ^1H nmr (270 MHz) δ: 0.15 (s, 9H, $^2J_{Sn-H}$ = 52 Hz), 0.92 (d, 3H, J = 6 Hz), 3.53 (m, 2H), 3.69 (s, 3H), 6.03 (t, 1H, J = 4 Hz). Exact Mass calcd. for $C_{14}H_{24}{}^{35}ClO_2Sn$ (M^+−Me): 379.0486; found: 379.0485.

Methyl 1-(4-bromobutyl)-2-(trimethylstannyl)-2-cyclopentene-carboxylate (35)

To a cold (−48°C), stirred solution of LDA (3.63 mmol) and HMPA (7.26 mmol) in 20 mL of dry THF was added a solution of the ester **26** (700 mg, 2.42 mmol) in 3 mL of dry THF. After the solution had been stirred at −48°C for 40 min, it was cooled to −78°C and 1,4-dibromobutane (7.85 g, 36.3 mmol) was added. The mixture was stirred at −78°C for 10 min and at −48°C for 40 min. Saturated aqueous ammonium chloride (~1 mL) was added and the mixture was allowed to warm to room temperature. Diethyl ether (150 mL) was added and the mixture was washed (saturated aqueous copper(II) sulfate, water, brine), dried ($MgSO_4$), and concentrated. Most of the excess 1,4-dibromobutane was removed by careful distillation (125–130°C/30 Torr), the residue was subjected to flash chromatography (7:93 Et_2O – petroleum ether), and the oil thus obtained was distilled (120–130°C/0.1 Torr) to give 792 mg (72%) of **35** as a colorless oil, which exhibited ir (neat): 1710, 1160, 770 cm^{-1}; ^1H nmr (80 MHz) δ: 0.13 (s, 9H, $^2J_{Sn-H}$ = 54 Hz), 1.10–1.53 (m, 3H), 1.60–2.05 (m, 4H), 3.40 (t, 2H, J = 7 Hz), 3.68 (s, 3H), 6.00 (t, 1H, J = 4 Hz). Exact Mass calcd. for $C_{13}H_{22}{}^{79}BrO_2Sn$ (M^+−Me): 408.9787; found: 408.9796.

Methyl 1-(5-bromopentyl)-2-(trimethylstannyl)-2-cyclopentene-carboxylate (45)

Alkylation of the ester **26** (300 mg, 1.04 mmol) with 1,5-dibromopentane was accomplished via a procedure very similar to that described above. Removal of excess 1,5-dibromopentane from the crude product by distillation (55–65°C/0.1 Torr), flash chromatography (7:93 Et_2O – petroleum ether) of the residual material, and distillation (150–160°C/0.1 Torr) of the oil thus obtained afforded 330 mg (72%) of **45** as a colorless oil that displayed ir (neat): 1710, 1220, 770 cm^{-1}; ^1H nmr (80 MHz) δ: 0.14 (s, 9H, $^2J_{Sn-H}$ = 54 Hz), 1.00–1.65 (m, 5H), 1.66–2.15 (m, 4H), 2.17–2.70 (m, 3H), 3.40 (t, 2H, J = 7 Hz), 3.65 (s, 3H), 5.98 (t, 1H, J = 4 Hz). Exact Mass calcd. for $C_{14}H_{24}{}^{79}BrO_2Sn$ (M^+−Me): 422.9982; found: 422.9980.

3-(3-Chloropropyl)-3-(hydroxymethyl)-2-(trimethylstannyl)-cyclohexene (29)

To a cold (−20°C), stirred solution of the ester **27** (500 mg, 1.32 mmol) in 10 mL of dry Et_2O was added slowly a solution of i-Bu_2AlH (3.3 mL, 3.3 mmol) in hexanes and the mixture was stirred at −20°C for 1 h. Saturated aqueous ammonium chloride (2 mL) and petroleum ether (30 mL) were added, the mixture was allowed to warm to room temperature, and stirring was continued until the organic phase was clear and precipitation of the aluminum salts was complete. The mixture was filtered through a short column of Florisil (elution with Et_2O). Concentration of the fil-

Can. J. Chem. Downloaded from www.nrcresearchpress.com by 213.200.69.106 on 09/08/12
For personal use only.

trate, followed by distillation (125–135°C/0.1 Torr) of the crude product, afforded 419 mg (90%) of the alcohol **29** as a colorless oil that showed ir (neat): 3350, 1030, 770 cm^{-1}; ^1H nmr (80 MHz) δ: 0.17 (s, 9H, $^2J_{Sn-H}$ = 52 Hz), 1.30 (m, 1H, exchanged with D_2O), 1.45–1.75 (m, 8H), 1.80–2.20 (m, 2H), 3.30–3.62 (m, 4H), 6.08 (t, 1H, J = 4 Hz). Exact Mass calcd. for $C_{12}H_{22}{}^{35}ClOSn$ (M^+−Me): 337.0382; found: 337.0382.

cis-*3-(3-Chloropropyl)-3-(hydroxymethyl)-4-methyl-2-(trimethylstannyl)cyclohexene (**30**)*

Reduction of the ester **28** was accomplished via a procedure very similar to that described above, except that the reaction was carried out at 0°C for 2 h. Distillation (125–135°C/0.1 Torr) of the crude product derived from 95 mg (0.24 mmol) of **28** produced 76 mg (86%) of **30** as a colorless oil that displayed ir (neat): 3400, 1030, 770 cm^{-1}; ^1H nmr (80 MHz) δ: 0.19 (s, 9H, $^2J_{Sn-H}$ = 52 Hz), 1.00 (d, 3H, J = 6 Hz), 1.25 (m, 2H), 1.40–1.88 (m, 6H), 1.92–2.25 (m, 2H), 3.15–3.78 (m, 4H), 6.18 (t, 1H, J = 4 Hz). Exact Mass calcd. for $C_{13}H_{24}{}^{35}ClOSn$ (M^+−Me): 351.0538; found: 351.0538.

*3-(4-Bromobutyl)-3-(hydroxymethyl)-2-(trimethylstannyl)-cyclopentene (**36**)*

Reduction of the ester **35** (792 mg, 1.87 mmol) as described above, followed by distillation (135–145°C/0.1 Torr) of the crude product, provided 792 mg (98%) of **36** as a colorless oil that exhibited ir (neat): 3400, 1020, 770 cm^{-1}; ^1H nmr (80 MHz) δ: 0.17 (s, 9H, $^2J_{Sn-H}$ = 54 Hz), 1.13–1.50 (m, 5H), 1.60–2.05 (m, 4H), 2.30–2.55 (m, 2H), 3.30–3.55 (m, 4H), 6.03 (t, 1H, J = 4 Hz). Exact Mass calcd. for $C_{12}H_{22}{}^{81}BrOSn$ (M^+−Me): 382.9857; found: 283.9851.

*3-(5-Bromopentyl)-3-(hydroxymethyl)-2-(trimethylstannyl)-cyclopentene (**46**)*

Distillation (150–160°C/0.1 Torr) of the crude product obtained by reduction (see procedure above) of the ester **45** (313 mg, 0.17 mmol) afforded 277 mg (94%) of the alcohol **46**, a colorless oil that exhibited ir (neat): 3400, 1020, 770 cm^{-1}; ^1H nmr (80 MHz) δ: 0.13 (s, 9H, $^2J_{Sn-H}$ = 54 Hz), 1.03–1.60 (m, 7H), 1.61–2.08 (m, 4H), 2.23–2.63 (m, 2H), 3.25–3.55 (m, 4H), 6.00 (t, 1H, J = 4 Hz). Exact Mass calcd. for $C_{13}H_{24}{}^{79}BrOSn$ (M^+−Me): 395.0007; found: 395.0004.

*3-(3-Chloropropyl)-3-(*tert*-butyldimethylsiloxymethyl)-2-(trimethylstannyl)cyclohexene (**31**)*

A solution of the alcohol **29** (419 mg, 1.19 mmol), imidazole (325 mg, 4.76 mmol), and *tert*-butyldimethylsilyl chloride (360 mg, 2.38 mmol) in 2 mL of dry *N*,*N*-dimethylformamide was stirred at room temperature for 17 h. The mixture was treated with Et_2O (35 mL) and the resultant solution was washed (water, brine), dried ($MgSO_4$), and concentrated. Distillation (135–145°C/0.1 Torr) of the crude product gave 520 mg (94%) of the silyl ether **31**, a colorless oil that displayed ir (neat): 1460, 1260, 1080, 850, 770 cm^{-1}; ^1H nmr (80 MHz) δ: 0.06 (s, 6H), 0.15 (s, 9H, $^2J_{Sn-H}$ = 52 Hz), 0.92 (s, 9H), 1.35–1.75 (m, 8H), 1.90–2.23 (m, 2H), 3.30–3.63 (m, 4H), 5.96 (t, 1H, J = 4 Hz). Exact Mass calcd. for $C_{18}H_{36}{}^{35}ClOSiSn$ (M^+−Me): 451.1246; found: 451.1247.

cis-*3-(3-Chloropropyl)-3-(*tert*-butyldimethylsiloxymethyl)-4-methyl-2-(trimethylstannyl)cyclohexene (**32**)*

Conversion of the alcohol **30** (400 mg, 1.09 mmol) into the ether **32** was accomplished via a procedure very similar to that described above. Distillation (135–145°C/0.1 Torr) of the crude product gave 495 mg (94%) of **32** as a colorless oil that showed ir (neat): 1460, 1260, 1090, 850, 770 cm^{-1}; ^1H nmr (400 MHz) δ: 0.03, 0.04 (s, s, 3H each), 0.14 (s, 9H, $^2J_{Sn-H}$ = 52 Hz), 0.90 (s, 9H), 0.96 (d, 3H, J = 6 Hz), 1.25 (m, 1H), 1.54 (m, 1H), 1.65 (m, 2H), 1.71–1.83 (m, 3H), 2.07 (m, 2H), 3.44 (s, 2H), 3.50 (m, 2H), 5.94 (t, 1H, J = 4 Hz). Exact Mass calcd. for $C_{19}H_{38}{}^{35}ClOSiSn$ (M^+−Me): 465.1402; found: 465.1404.

*3-(4-Bromobutyl)-3-(*tert*-butyldimethylsiloxymethyl)-2-(trimethylstannyl)cyclopentene (**37**)*

A solution of the alcohol **36** (150 mg, 0.38 mmol), 2,6-lutidine (130 mg, 1.03 mmol), and *tert*-butyldimethylsilyl trifluoromethanesulfonate (152 mg, 0.76 mmol) in dry CH_2Cl_2 (1.0 mL) was stirred at 25°C for 30 min. Water (1 mL) and CH_2Cl_2 (25 mL) were added and the mixture was stirred for 5 min. This mixture was washed with water and brine, dried ($MgSO_4$), and concentrated. The residual material was passed through a short column of silica gel (elution with CH_2Cl_2). Removal of the solvent from the eluate, followed by distillation (125–135°C/0.1 Torr) of the residual oil, provided 178 mg (92%) of the silyl ether **37**, a colorless oil that displayed ir (neat): 1460, 1260, 850, 770 cm^{-1}; ^1H nmr (80 MHz) δ: 0.03 (s, 6H), 0.13 (s, 9H, $^2J_{Sn-H}$ = 54 Hz), 0.88 (s, 9H), 1.15–2.03 (diffuse m, 8H), 2.20–2.53 (m, 2H), 3.25–3.55 (m, 4H), 5.88 (t, 1H, J = 4 Hz). Exact Mass calcd. for $C_{18}H_{36}{}^{79}BrOSiSn$ (M^+−Me): 495.0740; found: 495.0751.

*3-(5-Bromopentyl)-3-(*tert*-butyldimethylsiloxymethyl)-2-(trimethylstannyl)cyclopentene (**47**)*

Conversion of the alcohol **46** (70 mg, 0.17 mmol) into the silyl ether **47** was carried out via a procedure very similar to that described above (preparation of **37**). Distillation (125–135°C/0.1 Torr) of the crude product gave 81 mg (90%) of **47**, a colorless oil that exhibited ir (neat): 1460, 1260, 850, 770 cm^{-1}; ^1H nmr (80 MHz) δ: 0.05 (s, 6H), 0.15 (s, 9H, $^2J_{Sn-H}$ = 54 Hz) 0.91 (s, 9H), 1.05–2.13 (diffuse m, 10H), 2.18–2.55 (m, 2H), 3.30–3.58 (m, 4H), 5.90 (t, 1H, J = 4 Hz). Exact Mass calcd. for $C_{19}H_{38}{}^{79}BrOSiSn$ (M^+−Me): 509.0897; found: 509.0901.

*3-(5-Bromopentyl)-3-(methoxymethyl)-2-(trimethylstannyl)-cyclopentene (**50**)*

To a stirred suspension (room temperature) of KH (80 mg, 2.0 mmol) in dry THF (1 mL) was added, sequentially, a solution of the alcohol **46** (328 mg, 0.8 mmol) in dry THF (2 mL) and dimethyl sulfate (544 mg, 4.0 mmol). After the mixture had been refluxed for 7.5 h, it was cooled and poured slowly into 10 mL of aqueous ammonium hydroxide (1.0 M). The resultant mixture was extracted with Et_2O (2 × 10 mL). The combined extracts were washed with water and brine, dried ($MgSO_4$), and concentrated. Flash chromatography (1:4 CH_2Cl_2 – petroleum ether) of the crude product, followed by distillation (125–135°C/0.1 Torr) of the material thus obtained, produced 283 mg (84%) of the ether **50**, a colorless oil that showed ir (neat): 1450, 1100, 770 cm^{-1}; ^1H nmr (80 MHz) δ: 0.10 (s, 9H, $^2J_{Sn-H}$ = 54 Hz), 1.13–2.05 (diffuse m, 10H), 2.23–2.50 (m, 2H), 3.00–3.50 (m, 4H), 3.18 (s, 3H), 5.88 (t, 1H, J = 4 Hz). Exact Mass calcd. for $C_{14}H_{26}{}^{79}BrOSn$ (M^+−Me): 409.0162; found: 409.0157.

*General procedure for the transmetallation–cyclization of the vinylstannane halides **31**, **32**, **36**, **47**, and **50***

To a cold (−20°C), stirred solution of the vinylstannane (1 equiv.) in the specified volume of dry THF was added, sequentially, HMPA (3 equiv.) and a solution of MeLi (1.5 equiv.) in Et_2O. After the mixture had been stirred at −20°C for 30 min, saturated aqueous NH_4Cl (~1 mL) was added and the resultant mixture was allowed to warm to room temperature. Diethyl ether was added and the mixture was washed sequentially with water, saturated aqueous $CuSO_4$, and water. The organic solution was dried ($MgSO_4$) and concentrated. The crude product was purified by column chromatography and (or) by distillation.

*6-(*tert*-Butyldimethylsiloxymethyl)bicyclo[4.3.0]non-1-ene (**33**)*

Distillation (85–95°C/0.1 Torr) of the crude product derived from transmetallation–cyclization of the vinylstannane chloride **31** (50 mg, 0.11 mmol; 1 mL of dry THF) provided 26.5 mg (92%) of the bicyclic alkene **33**, a colorless oil that showed ir (neat): 1460, 1250, 1090, 1070, 850 cm^{-1}; ^1H nmr (80 MHz) δ: 0.05 (s, 6H), 0.93 (s, 9H), 0.70–1.30 (m, 2H), 1.43–1.88 (m, 4H), 1.88–2.45 (m, 6H), 3.25, 3.44 (d, d, 1H each, J = 10 Hz in each case), 5.45 (m, 1H). Exact Mass calcd. for $C_{12}H_{21}OSi$ (M^+−*t*-Bu): 209.1362; found: 209.1360.

Can. J. Chem. Downloaded from www.nrcresearchpress.com by 213.200.69.106 on 09/08/12
For personal use only.

*cis-5-Methyl-6-(*tert*-butyldimethylsiloxymethyl)bicyclo[4.3.0]non-1-ene (**34**)*

Distillation (85–95°C/0.1 Torr) of the crude product obtained from transmetallation–cyclization of the vinylstannane chloride **32** (50 mg, 0.10 mmol; 1 mL of dry THF) gave 28 mg (94%) of the bicyclic alkene **34**, a colorless oil that exhibited ir (neat): 1460, 1250, 1090, 840 cm^{-1}; ^1H nmr (400 MHz) δ: 0.00 (s, 6H), 0.87 (s, 9H), 0.99 (d, 3H, J = 6 Hz), 1.13 (m, 1H), 1.31 (m, 1H), 1.45 (m, 1H), 1.55–1.70 (m, 3H), 1.98–2.13 (m, 3H), 2.20 (m, 1H), 2.39 (m, 1H), 3.31, 3.47 (d, d, 1H each, J = 10 Hz in each case), 5.40 (m, 1H). Exact Mass calcd. for $C_{13}H_{23}OSi$ (M^+-t-Bu): 223.1513; found: 223.1522.

*1-(*tert*-Butyldimethylsiloxymethyl)bicyclo[4.3.0]non-6-ene (**38**) and 3-(3-butenyl)-3-(*tert*-butyldimethylsiloxymethyl)-cyclopentene (**39**)*

The crude product obtained from transmetallation–cyclization of the vinylstannane bromide **37** (195 mg, 0.38 mmol; 3 mL of dry THF) consisted of two compounds Column chromatography of this mixture on silver nitrate impregnated silica gel (1:4 $AgNO_3$ – silica gel, elution with 1:19 Et_2O – petroleum ether), followed by distillation (90–100°C/0.1 Torr) of each of the oils thus obtained, gave 64.4 mg (61%) of the bicyclic alkene **38** (the chromatographically less polar product and 7.7 mg (7%) of the diene **39**.

Compound **38** exhibited ir (neat): 1460, 1260, 1100, 850 cm^{-1}; ^1H nmr (80 MHz) δ: 0.05 (s, 6H), 0.92 (s, 9H), 1.00–1.68 (m, 6H), 1.95–2.45 (m, 6H), 3.35, 3.60 (d, d, 1H each, J = 10 Hz in each case), 5.30 (m, 1H). Exact Mass calcd. for $C_{12}H_{21}OSi$ (M^+-t-Bu): 209.1362; found: 209.1360.

The diene **39** displayed ir (neat): 1630, 1250, 1100, 840 cm^{-1}; ^1H nmr (80 MHz) δ: 0.00 (s, 6H), 0.87 (s, 9H), 1.36–1.68 (m, 4H), 1.80–2.50 (diffuse m, 4H), 3.38 (s, 2H), 4.80–5.15 (m, 2H), 5.38–5.60 (m, 1H), 5.60–5.90 (m, 2H). Exact Mass calcd. for $C_{12}H_{21}OSi$ (M^+-t-Bu): 209.1362; found: 209.1361.

*1-(*tert*-Butyldimethylsiloxymethyl)bicyclo[5.3.0]dec-7-ene (**48**) and 2-(*tert*-butyldimethylsilyl)-3-(5-bromopentyl)-3-(hydroxymethyl)cyclopentene (**49**)*

The mixture of two products obtained from transmetallation of the vinylstannane bromide **47** (76 mg, 0.15 mmol; 2 mL of dry THF) was subjected to column chromatography on silica gel. Sequential elution with heptane and 3:7 Et_2O – petroleum ether, followed by distillation (95–105°C/0.1 Torr; 110–120°C/0.1 Torr) of the two oils thus obtained, gave 14 mg (35%) of the bicyclic alkene **48** and 9 mg (17%) of the alkene alcohol **49**, respectively.

Compound **48** displayed ir (neat): 1450, 1250, 1100, 850 cm^{-1}; ^1H nmr (80 MHz) δ: 0.02 (s, 6H), 0.91 (s, 9H), 1.00–2.60 (diffuse m, 14H), 3.38 (br s, 2H), 5.40 (m, 1H). Exact Mass calcd. for $C_{13}H_{23}OSi$ (M^+-t-Bu): 223.1518; found: 223.1524.

Compound **49** exhibited ir (neat): 3370, 1460, 1260, 1020, 840 cm^{-1}; ^1H nmr (80 MHz) δ: 0.13 (s, 6H), 0.93 (s, 9H), 1.10–2.10 (diffuse m, 11H), 2.20–2.60 (m, 2H), 3.25–3.60 (m, 4H), 6.28 (t, 1H, J = 4 Hz). Exact Mass calcd. for $C_{13}H_{24}{}^{79}BrOSi$ (M^+-t-Bu): 303.0780; found: 303.0783.

*1-(Methoxymethyl)bicyclo[5.3.0]dec-7-ene (**51**)*

The crude product derived from transmetallation–cyclization of the vinylstannane bromide **50** (61 mg, 0.14 mmol; 2 mL of dry THF) was subjected to flash chromatography on silica gel (elution with 1:6 CH_2Cl_2 – petroleum ether). Distillation (105–110°C/0.1 Torr) of the oil thus obtained provided 14 mg (54%) of the bicyclic alkene **51**, a colorless oil that showed ir (neat): 1440, 1110 cm^{-1}; ^1H nmr (80 MHz) δ: 1.00–2.51 (diffuse m, 14H), 3.15 (br s, 2H), 3.30 (s, 3H), 5.43 (m, 1H). Exact Mass calcd. for $C_{12}H_{20}O$: 180:1514; found 180.1517.

*1,3-Dichloro-1-(2-trimethylsilylethoxy)propane (**55**)*

Dry hydrogen chloride was passed into a well-stirred, cold (−10°C) mixture of 2-(trimethylsilyl)ethanol (9.3 g, 78.8 mmol) and acrolein (4.4 g, 78.8 mmol) until the required amount (5.8 g, 158 mmol) had been added. The mixture was diluted with dry CH_2Cl_2 (35 mL) and was then dried ($MgSO_4$). Removal of the solvent, followed by distillation (90–100°C/0.1 Torr) of the resultant oil, gave 14.1 g (78%) of **55** as a colorless oil, which exhibited ir (neat): 1250, 1120, 840 cm^{-1}; ^1H nmr (80 MHz) δ: 0.06 (s, 9H), 1.00 (m, 2H), 2.45 (m, 2H), 3.50–4.10 (m, 4H), 5.80 (t, 1H, J = 5 Hz). Exact Mass calcd. for $C_6H_{14}{}^{35}ClOSi$ ($M^+-CH_2CH_2{}^{35}Cl$): 165.0502; found: 165.0504.

*Preparation of compounds **56** and **67***

To a cold (0°C), stirred solution of LDA (1.04 mmol) in 11 mL of dry THF was added 2.08 mmol of HMPA and the solution was cooled to −48°C. A solution of the enoate **25** (220 mg, 0.69 mmol) in 2 mL of dry THF was added. After the solution had been stirred at −48°C for 40 min, it was cooled to −78°C and the dichloro ether **55** (318 mg, 1.39 mmol) was added. The mixture was stirred at −78°C for 40 min. Saturated aqueous NH_4Cl (2 mL) was added, the mixture was allowed to warm to 25°C, was diluted with water (35 mL), and was then extracted with Et_2O (3 × 35 mL). The combined extracts were washed successively with saturated aqueous $CuSO_4$, water, and brine, and were then dried ($MgSO_4$) and concentrated. Analysis (tlc) of the crude product indicated the presence of the epimeric products **56** (major) and **57** (minor), along with a number of minor components. Flash chromatography (1:9 Et_2O – petroleum ether) of the mixture provided two main fractions. Distillation (150–160°C/0.1 Torr) of the more polar fraction (one spot by tlc) afforded 145 mg (41%) of the ester **56**, a colorless oil that displayed ir (neat): 1725, 1250, 1070, 840, 770 cm^{-1}; ^1H nmr (400 MHz) δ: 0.00 (s, 9H), 0.12 (s, 9H, $^2J_{Sn-H}$ = 54 Hz), 0.90 (dd, 2H, J = 9.5, 8.0 Hz), 0.96 (d, 3H, J = 7 Hz), 1.60 (m, 1H), 1.72 (m, 1H), 1.90–2.16 (m, 5H), 3.48 (m, 1H), 3.56–3.76 (m, 3H), 3.66 (s, 3H), 3.86 (dd, 1H, J = 10, 3 Hz), 5.97 (t, 1H, J = 4 Hz). Exact Mass calcd. for $C_{19}H_{36}{}^{35}ClO_3SiSn$ (M^+ − Me): 495.1144; found: 495.1138.

Analysis (tlc) of the less polar fraction indicated that it contained primarily the ester **57**, along with minor side products. Distillation (150–160°C/0.1 Torr) of this material provided 54 mg of a colorless oil. Attempts to obtain, efficiently, pure **57** from this mixture were fruitless. Therefore, a solution of this material (54 mg) in a 2 mL of dry Et_2O was treated with a solution of i-Bu_2AlH in hexanes (0.63 mL, 0.63 mmol) and the solution was stirred at 25°C for 3 h. Saturated aqueous NH_4Cl (0.5 mL) and petroleum ether (7 mL) were added; the mixture was stirred until precipitation of the aluminum salts was complete and was then filtered through a plug of sand. The filtrate was dried ($MgSO_4$) and concentrated. Distillation (150–160°C/0.1 Torr) of the remaining material gave 36.5 mg of a colorless oil. A solution of this material in 1 mL of dry CH_2Cl_2 at 25°C was treated with 2,6-lutidine (24 mg, 0.22 mmol) and t-$BuMe_2SiOSO_2CF_3$ (37 mg, 0.14 mmol) and the mixture was stirred for 30 min. Saturated aqueous $NaHCO_3$ (0.5 mL) and Et_2O (12 mL) were added. The mixture was washed with water and brine and was then dried ($MgSO_4$) and concentrated. Flash chromatography (petroleum ether), followed by distillation (160–170°C/0.1 Torr) of the material thus obtained, provided 39 mg (9% overall yield from the enone **25**) of compound **67**, a colorless oil that showed ir (neat): 1470, 1260, 1080, 850, 770 cm^{-1}; ^1H nmr (400 MHz) δ: 0.02 (s, 9H), 0.05 (s, 9H, $^2J_{Sn-H}$ = 52 Hz), 0.06, 0.08 (s, s, 3H each), 0.91 (s, 9H), 1.02 (d, 3H, J = 7 Hz), 0.91–1.09 (m, 2H), 1.48 (m, 1H), 1.56–1.70 (m, 2H), 1.72–1.81 (m, 1H), 1.92–2.01 (m, 1H), 2.11 (m, 2H), 3.55 (m, 1H), 3.58 (s, 2H), 3.67 (m, 2H), 3.75–3.85 (m, 1H), 4.01 (dd, 1H, J = 9.5, 3.5 Hz), 6.04 (t, 1H, J = 4 Hz). Exact Mass calcd. for $C_{24}H_{50}{}^{35}ClO_2Si_2Sn$ (M^+ − Me): 581.2060; found: 581.2065.

*Preparation of the silyl ether **59***

To a stirred solution of the ester **56** (145 mg, 0.28 mmol) in 3 mL of dry Et_2O at 25°C was added a solution of i-Bu_2AlH in hexanes (1.7 mL, 1.7 mmol). After the mixture had been stirred for 3 h, saturated aqueous NH_4Cl (1 mL) and petroleum ether (10 mL) were added and stirring was continued until precipitation of the aluminum salts was complete. The mixture was filtered

Can. J. Chem. Downloaded from www.nrcresearchpress.com by 213.200.69.106 on 09/08/12
For personal use only.

through a plug of sand and the filtrate was dried ($MgSO_4$) and concentrated. Distillation (150–160°C/0.1 Torr) of the remaining liquid gave 109 mg (81%) of the alcohol **58**, a colorless oil that exhibited one spot by tlc analysis and exhibited the expected spectral data.

A stirred solution of this material (109 mg) in 1.5 mL of dry CH_2Cl_2 at 25°C was treated with 2,6-lutidine (69 mg, 0.54 mmol) and *t*-$BuMe_2SiOSO_2CF_3$ (108 mg, 0.41 mmol). After the solution had been stirred for 30 min, saturated aqueous $NaHCO_3$ (0.5 mL) and Et_2O (12 mL) were added and the resultant mixture was washed with water and brine and was then dried ($MgSO_4$) and concentrated. Flash chromatography (1:19 CH_2Cl_2 – petroleum ether), followed by distillation (160–170°C/0.1 Torr) of the resultant liquid, afforded 115 mg (68% from the ester **56**) of the silyl ether **59**, a colorless oil that exhibited ir (neat): 1250, 1070, 840, 770, cm^{-1}; ^1H nmr (400 MHz) δ: 0.02 (s, 9H), 0.04, 0.06 (s, s, 3H each), 0.16 (s, 9H, $^2J_{Sn-H}$ = 52 Hz), 0.89 (s, 9H), 0.90–1.00 (m, 2H) 1.04 (d, 3H, *J* = 7 Hz), 1.60 (m, 2H), 1.92 (m, 1H), 1.99 (m, 2H), 2.06 (m, 2H), 3.39 (d, 1H, *J* = 9.5 Hz), 3.43–3.64 (m, 4H), 3.68 (m, 1H), 4.03 (d, 1H, *J* = 9.5 Hz), 5.92 (t, 1H, *J* = 4 Hz). Exact Mass calcd. for $C_{24}H_{50}{}^{35}ClO_2Si_2Sn$ (M^+-Me): 581.2060; found: 581.2075.

*Preparation of the bicyclic diethers **60** and **68***

These substances were derived from transmetallation–cyclization of the vinylstannane halides **59** and **67**, via a procedure identical with that described earlier (vide supra).

Flash chromatography (1:9 CH_2Cl_2 – petroleum ether) of the crude product derived from transmetallation–cyclization of **59** (3.14 g, 5.73 mmol; 20 mL of dry THF), followed by distillation (130–140°C/0.1 Torr) of the liquid thus obtained, provided 1.94 g (86%) of the bicyclic diether **60**, a colorless oil that displayed ir (neat): 1460, 1250, 1090, 850 cm^{-1}; ^1H nmr (400 MHz) δ: −0.01 (s, 9H), 0.01, 0.02 (s, s, 3H each), 0.89 (s, 9H), 0.88–0.95 (m, 2H), 0.98 (d, 3H, *J* = 7 Hz), 1.52 (m, 1H), 1.79 (m, 2H), 1.92–2.13 (m, 4H), 2.36 (m, 2H), 3.20, 3.57 (d, d, 1H each, *J* = 10 Hz in each case), 3.37, 3.61 (m, m, 1H each), 3.94 (d, 1H, *J* = 4 Hz), 5.47 (m, 1H). Exact Mass calcd. for $C_{18}H_{35}O_2Si_2$ (M^+-t-Bu): 339.2176; found: 339.2169.

Flash chromatography (petroleum ether) of the crude product derived from transmetallation–cyclization of **67** (1.20 g, 2.02 mmol; 10 mL of dry THF), followed by distillation (130–140°C/0.1 Torr) of the liquid thus obtained, gave 623 mg (78%) of the bicyclic diether **68**, a colorless oil that showed ir (neat): 1460, 1250, 1100, 860, 780 cm^{-1}; ^1H nmr (400 MHz) δ: −0.01, 0.01 (s, s, 3H each), 0.02 (s, 9H), 0.86 (s, 9H), 0.90 (m, 2H), 1.07 (d, 3H, *J* = 7 Hz), 1.38 (m, 2H), 1.56–1.67 (m, 1H), 1.78–1.91 (m, 1H), 2.02 (m, 3H), 2.06–2.17 (m, 1H), 2.45–2.56 (m, 1H), 3.31–3.45 (m, 2H), 3.57 (m, 1H), 3.73, 3.75 (d, d, 1H each, *J* = 10.5 Hz in each case), 5.47 (m, 1H). Exact Mass calcd. for $C_{18}H_{35}O_2Si_2$ (M^+-t-Bu): 339.2176; found: 319.2188.

*Preparation of the alcohol ethers **61** and **69***

A solution of *n*-Bu_4NF (1.93 g, 7.37 mmol) and the diether **60** (1.95 g, 4.91 mmol) in 11 mL of dry THF was stirred at room temperature for 18 h. The mixture was diluted with Et_2O (50 mL), was washed with water and brine, and was then dried ($MgSO_4$) and concentrated. Removal of volatile material (0.1 Torr, room temperature), followed by distillation (105–115°C/0.1 Torr) of the remaining liquid, afforded 1.34 g (96%) of the alcohol **61**, a colorless oil that exhibited ir (neat): 3400, 1250, 1100, 850 cm^{-1}; ^1H nmr (400 MHz) δ: 0.00 (s, 9H), 0.90 (m, 2H), 1.00 (d, 3H, *J* = 7 Hz), 1.17 (dd, 1H, *J* = 8, 4 Hz, exchanged with D_2O), 1.55 (m, 1H), 1.65 (m, 1H), 1.76–1.96 (m, 2H), 1.98–2.17 (m, 3H), 2.40 (m, 2H), 3.38 (m, 2H, simplified on addition of D_2O), 3.50 (dd, 1H, *J* = 12, 8 Hz, collapsed to a d (*J* = 12 Hz) on addition of D_2O), 3.62 (m, 1H), 3.67 (d, 1H, *J* = 4 Hz), 5.68 (m, 1H). Exact Mass calcd. for $C_{16}H_{28}OSi$ (M^+-H_2O): 264.1910; found: 264.1910.

In very similar fashion, distillation (105–115°C/0.1 Torr) of the crude product obtained from the diether **68** (623 mg, 1.57 mmol; 5 mL of dry THF) gave 381 mg (86%) of the alcohol **69**, a colorless oil that displayed ir (neat): 3450, 1250, 840 cm^{-1}; ^1H nmr (400 MHz) δ: 0.03 (s, 9H), 0.97 (m, 2H), 1.25 (d, 3H, *J* = 7 Hz), 1.41–1.57 (m, 2H), 1.63 (m, 1H), 1.79 (m, 1H), 2.01–2.21 (m, 4H), 2.44–2.58 (m, 1H), 3.25 (dd, 1H, *J* = 8, 4 Hz, exchanged with D_2O), 3.45 (m, 1H), 3.65 (m, 2H), 3.72 (dd, 1H, *J* = 12, 8 Hz, collapsed to a d (*J* = 12 Hz) on addition of D_2O), 3.79 (dd, 1H, *J* = 12, 4 Hz, collapsed to a d (*J* = 12 Hz) on addition of D_2O), 5.45 (m, 1H). Exact Mass calcd. for $C_{16}H_{28}OSi$ (M^+-H_2O): 264.1910; found: 264.1920.

*Preparation of the aldehydes **62** and **70***

To a stirred solution of the alcohol **61** (330 mg, 1.06 mmol) in 18 mL of dry CH_2Cl_2 was added solid pyridinium chlorochromate (573 mg, 2.66 mmol). The resultant mixture was stirred at 25°C for 1 h. Dry Et_2O (70 mL) was added; the mixture was stirred for 15 min and was then filtered through a short column of neutral alumina (elution with Et_2O). The filtrate was concentrated and the crude product was passed through a short column of silica gel (elution with 1:1 CH_2Cl_2 – petroleum ether). Concentration of the eluate and distillation (95–105°C/0.1 Torr) of the remaining liquid gave 263 mg (88%) of the aldehyde **62**, a colorless oil that exhibited ir (neat): 1710, 1250, 840 cm^{-1}; ^1H nmr (300 MHz) δ: 0.00 (s, 9H), 0.91 (m, 2H), 0.99 (d, 3H, *J* = 7 Hz), 1.62–1.82 (m, 4H), 2.10–2.30 (m, 4H), 2.30–2.45 (m, 1H), 3.40, 3.64 (m, m, 1H each), 4.18 (d, 1H, *J* = 4.5 Hz), 5.72 (m, 1H), 9.76 (s, 1H).

Similarly, distillation (95–100°C/0.1 Torr) of the crude product derived from oxidation of the alcohol **69** (200 mg, 0.71 mmol) with pyridinium chlorochromate afforded 166 mg (83%) of the aldehyde **70**, a colorless oil that exhibited ir (neat): 1710, 1250, 860 cm^{-1}; ^1H nmr (270 MHz) δ: 0,00 (s, 9H), 0.93 (m, 2H), 1.31 (d, 3H, *J* = 7 Hz), 1.38–1.68 (m, 4H), 1.95–2.24 (m, 4H), 2.36–2.54 (m, 1H), 3.49 (m, 1H), 3.57–3.72 (m, 2H), 5.59 (m, 2H), 9.92 (s, 1H).

*Preparation of the alkene ethers **63** and **71***

A stirred solution of the aldehyde **62** (260 mg, 0.03 mmol) and anhydrous hydrazine (600 mg, 18.6 mmol) in 3 mL of MeOH was refluxed for 1 h. The solvent was removed under reduced pressure and the residual material was diluted with benzene. The benzene was removed under reduced pressure. This procedure was repeated. The residual material was placed under vacuum (0.1 Torr, 25°C) to remove last traces of solvent. The resultant viscous oil was dissolved in 2 mL of dry diethylene glycol containing 150 mg (2.78 mmol) of dry sodium methoxide and the mixture was heated at 210°C for 1.8 h. After the mixture had been cooled to 25°C, it was diluted with water (25 mL) and was then extracted with Et_2O (3 × 20 mL). The combined extracts were washed with water and brine, and were then dried ($MgSO_4$) and concentrated. Flash chromatography (1:4 CH_2Cl_2 – petroleum ether) of the crude product and distillation (90–100°C/0.1 Torr) of the liquid thus obtained provided 210 mg (84%) of the alkene ether **63**, a colorless oil that displayed ir (neat): 1250, 1100, 840 cm^{-1}; ^1H nmr (400 MHz) δ: −0.01 (s, 9H), 0.78 (s, 3H), 0.87 (d, 3H, *J* = 7 Hz), 0.90 (m, 2H), 1.35–1.50 (m, 2H), 1.71–1.91 (m, 2H), 1.93–2.15 (m, 3H), 2.25–2.50 (m, 2H), 3.35, 3.60 (m, m, 1H each), 3.47 (d, 1H, *J* = 4 Hz), 5.38 (m, 1H). Exact Mass calcd. for $C_{16}H_{30}OSi$: 266.2066; found: 266.2062.

In a very similar fashion, flash chromatography (1:9 CH_2Cl_2 – petroleum ether) of the crude product obtained from the aldehyde **70** (159 mg, 0.57 mmol), followed by distillation (105–110°C/0.1 Torr) of the liquid thus obtained, produced 118 mg (78%) of the alkene ether **71**, a colorless oil that showed ir (neat): 1250, 1110, 840 cm^{-1}; ^1H nmr (270 MHz) δ: 0.00 (s, 9H), 0.82 (s, 3H), 0.90 (m, 2H), 0.99 (d, 3H, *J* = 7 Hz), 1.37 (m, 3H), 1.43–1.60 (m, 1H), 1.90–2.13 (m, 4H), 2.35–2.52 (m, 1H), 3.25 (t, 1H, *J* = 9 Hz), 3.42, 3.57 (m, m, 1H each), 5.28 (m, 1H). Exact Mass calcd. for $C_{16}H_{30}OSi$: 266.2066; found: 266.2068.

*Preparation of the alkene alcohols **64** and **72***

To a stirred suspension of dry LiF (360 mg, 13.8 mmol) in 7 mL of dry MeCN was added $BF_3 \cdot Et_2O$ (1.96 g, 13.8 mmol). The

Can. J. Chem. Downloaded from www.nrcresearchpress.com by 213.200.69.106 on 09/08/12
For personal use only.

mixture was stirred at 25°C for 5 min and then a solution of the alkene ether **63** (368 mg, 1.38 mmol) in 2 mL of dry CH_2Cl_2 was added. Stirring (25°C) was continued for 2.5 h. Saturated aqueous $NaHCO_3$ (2 mL) and water (25 mL) were added and the mixture was extracted with Et_2O (3 × 35 mL). The combined extracts were washed with water and brine and were then dried ($MgSO_4$) and concentrated. Distillation (85–95°C/0.1 Torr) of the residual liquid provided 200 mg (87%) of the alcohol **64**, a colorless oil that displayed ir (neat): 3350, 1460, 1070, 970 cm^{-1}; ^1H nmr (400 MHz) δ: 0.80 (s, 3H), 0.93 (d, 3H, J = 7 Hz), 1.26 (m, 1H), 1.40–1.56 (m, 2H), 1.64 (m, 1H), 1.85 (m, 1H), 1.95–2.16 (m, 3H), 2.31–2.53 (m, 2H), 3.92 (d, 1H, J = 4 Hz), 5.49 (m, 1H). Exact Mass calcd. for $C_{11}H_{18}O$: 166.1357; found: 166.1356.

Similarly, cleavage of the ether **71** (116 mg, 0.44 mmol) with $LiF–BF_3 \cdot Et_2O$, followed by flash chromatography (3:7 Et_2O – petroleum ether) and distillation (95–100°C/0.1 Torr) of the crude product, produced 68 mg (93%) of the alcohol **72**. This colorless oil exhibited ir (neat): 3350, 1460, 1430, 1080 cm^{-1}; ^1H nmr (270 MHz) δ: 0.86 (s, 3H), 1.02 (d, 3H, J = 7 Hz), 1.33–1.50 (m, 4H), 1.55 (m, 1H), 1.95–2.20 (m, 4H), 2.36–2.52 (m, 1H), 3.73 (t, 1H, J = 9 Hz), 5.33 (m, 1H). Exact Mass calcd. for $C_{11}H_{18}O$: 166.1357; found: 166.1361.

*Preparation of the ketone **65** from the alcohols **64** and **72***

A mixture of the alcohol **64** (125 mg, 0.75 mmol) and pyridinium chlorochromate (325 mg, 1.51 mmol) in 7 mL of dry CH_2Cl_2 was stirred at 25°C for 1 h. Dry Et_2O was added and stirring was continued for 15 min. The mixture was filtered through a plug of neutral alumina (elution with Et_2O) and the filtrate was concentrated. Flash chromatography (1:2 CH_2Cl_2 – petroleum ether) of the residual material, followed by distillation (85–90°C/0.1 Torr) of the liquid thus obtained, provided 102 mg (83%) of the ketone **65**, a colorless oil that exhibited ir (neat): 1735, 1460, 1030 cm^{-1}; ^1H nmr (270 MHz) δ: 1.02 (s, 3H), 1.14 (d, 3H, J = 7 Hz), 1.35–1.64 (m, 3H), 2.05 (m, 2H), 2.10–2.25 (m, 1H), 2.40–2.52 (m, 2H), 2.56–2.71 (m, 1H), 5.55 (m, 1H). Exact Mass calcd. for $C_{11}H_{16}O$: 164.1200; found: 164.1200.

Oxidation of the alcohol **72** (65 mg, 0.39 mmol) via a procedure identical with that described above gave 51 mg (80%) of the ketone **65**, which displayed spectra identical with those summarized above.

*(±)-Chiloscyphone (**16**) and (±)-6-*epi*-chiloscyphone(**17**)*

To a stirred mixture of $(Ph_3PCH_2OMe)Cl$ (732 mg, 2.14 mmol) and dry benzene (4 mL) was added a solution of $NaOC(Et)Me_2$ in benzene (1.78 mL, 2.14 mmol) and the resultant dark-red solution was stirred at 25°C for 10 min. A solution of the ketone **65** (50 mg, 0.31 mmol) in 1 mL of dry benzene was added and the mixture was stirred at 25°C for 1.5 h. Water (0.5 mL) was added dropwise and the resultant yellow suspension was filtered through a plug of silica gel (elution with Et_2O). The filtrate was concentrated and a solution of the residue in THF (2.5 mL) containing 1 M hydrochloric acid (1 mL) was stirred at 25°C for 34 h. Et_2O (25 mL) was added, and the mixture was washed sequentially with saturated aqueous $NaHCO_3$, water, and brine and was then dried ($MgSO_4$) and concentrated. Flash chromatography (1:2 CH_2Cl_2 – petroleum ether) of the residual material produced 24 mg (43%) of a mixture of the aldehydes **78** and **79** (ratio 1:4, analysis by glc). A solution of this mixture in dry MeOH (1 mL) containing 21 mg (0.39 mmol) of NaOMe was stirred at 25°C for 1 h. Analysis (glc) of an aliquot showed that the aldehydes **78** and **79** were present in a ratio of 1:1. Addition of additional amounts of NaOMe and use of longer reaction times did not alter this ratio. Saturated aqueous NH_4Cl (10 mL) was added and the mixture was extracted with Et_2O (3 × 8 mL). The combined extracts were washed (water and brine), dried, and concentrated. The crude product was filtered through a short column of silica gel (elution with 1:2 CH_2Cl_2 – petroleum ether), thus affording 21 mg of a 1:1 mixture of the aldehydes **78** and **79** (ir (neat): 2710, 1720, 1460, 1380 cm^{-1}. Exact Mass calcd. for $C_{12}H_{18}O$: 178.1358; found: 178.1361).

A solution of this mixture and isopropenylmagnesium bromide (0.48 mmol) in 1.3 mL of dry THF was stirred at 25°C for 1 h. Saturated aqueous NH_4Cl (1.5 mL) and water (10 mL) were added and the mixture was extracted with Et_2O (3 × 10 mL). The combined extracts were washed (water, brine), dried ($MgSO_4$), and concentrated. Flash chromatography (1:9 Et_2O – petroleum ether) of the residual material (1:1 mixture of the alcohols **80** and **81**, analysis by glc) gave 8.7 mg (13% from the ketone **65**) of the less polar alcohol **80** and 11.1 mg (17% from the ketone **65**) of the more polar alcohol **81**. The ir spectrum of each of these alcohols showed absorptions at 3450, 1640, and 900 cm^{-1}.

A mixture of the less polar alcohol **80** (8.7 mg), dry CH_2Cl_2 (1 mL), and pyridinium chlorochromate (17 mg) was stirred at 25°C for 2.25 h. Dry Et_2O (7 mL) was added, the mixture was stirred for 15 min, and was then filtered through a plug of neutral alumina (elution Et_2O). The filtrate was concentrated. Column chromatography (1:4 CH_2Cl_2 – petroleum ether) of the crude product, followed by distillation (85–95°C/0.1 Torr) of the liquid thus obtained, provided 5 mg (7.5% from the ketone **65**) of (±)-chiloscyphone (**16**), a colorless oil that exhibited ir (neat): 1670, 1630, 1450, 1370, 1080 cm^{-1}; ^1H nmr (400 MHz) δ: 0.85 (d, 3H, J = 6 Hz), 0.97 (s, 3H), 1.33–1.46 (m, 3H), 1.64–1.76 (m, 1H), 1.85 (br s, 3H), 1.90–2.02 (m, 2H), 2.02–2.15 (m, 1H), 2.53 (m, 2H), 3.58 (dd, 1H, J = 8, 1.3 Hz), 5.41 (m, 1H), 5.73, 5.94 (s, s, 1H each). Exact Mass calcd. for $C_{15}H_{22}O$: 218.1670; found: 218.1671.

Oxidation of the more polar alcohol **81** (11.1 mg) was effected via a procedure identical with that described above. Column chromatography (1:19 Et_2O – petroleum ether) of the crude product and distillation (80–90°C/0.1 Torr) of the liquid thus obtained provided 4 mg (6% from the ketone **65**) of (±)-6-*epi*-chiloscyphone (**17**), a colorless oil that displayed ir (neat): 1670, 1630, 1460, 1390, 1090 cm^{-1}; ^1H nmr (270 MHz) δ: 0.72 (d, 3H, J = 6 Hz), 0.90 (s, 3H), 1.43 (m, 3H), 1.70–1.85 (m, 1H), 1.91 (br s, 3H), 1.95–2.08 (m, 3H), 2.12–2.32 (m, 1H), 2.48–2.65 (m, 1H), 3.18 (dd, 1H, J = 12, 8 Hz), 5.30 (m, 1H), 5.72, 5.97 (s, s, 1H each). Exact Mass calcd. for $C_{15}H_{22}O$: 218.1670; found: 218.1670.

Acknowledgement

We are indebted to the Natural Sciences and Engineering Research Council of Canada for financial support.

1. R.E. Gawley. Synthesis, 777 (1976).
2. M.E. Jung. Tetrahedron, **32**, 3 (1976).
3. B.M. Trost. Tetrahedron, **3**, 2615 (1977); W. Oppolzer and V. Snieckus. Angew. Chem. Int. Ed. Engl. **17**, 476 (1978); L.A. Paquette. Top. Curr. Chem. **79**, 41 (1979); **119**, 1 (1984); R. Noyori. Acc. Chem. Res. **12**, 61 (1979); B.M. Trost. Acc. Chem. Res. **13**, 385 (1980); M. Demuth and K. Schaffner. Angew. Chem. Int. Ed. Engl. **21**, 820 (1982); T. Hudlicky, T.M. Kutchan, and S.M. Naqvi. Org. React. **33**, 247 (1985); G.H. Posner. Chem. Rev. **86**, 831 (1986); T.A. Blumenkopf and L.E. Overman. Chem. Rev. **86**, 857 (1986); L.A. Paquette and A.M. Doherty. Polyquinane chemistry. Reactivity and structure concepts in organic chemistry. Vol. 26. Springer-Verlag, Berlin. 1987; B.M. Trost. Pure Appl. Chem. **60**, 1615 (1988); T. Hudlicky and J.D. Price. Chem. Rev. **89**, 1467 (1989); J.-E. Bäckvall. New J. Chem. **14**, 447 (1990); N.E. Schore. Org. React. **40**, 1 (1991); C.P. Jasperse, D.P. Curran, and T.L. Fevig. Chem. Rev. **91**, 1237 (1991); T. Hudlicky, R. Fan, J.W. Reed, and K.G. Gadamasetti. Org. React. **41**, 1 (1992).
4. D. Seebach. Angew. Chem. Int. Ed. Engl. **18**, 239 (1979).
5. E. Piers and V. Karunaratne. Tetrahedron, **45**, 1089 (1989); Can. J. Chem. **67**, 160 (1989); E. Piers and J. Renaud. Synthesis, 74 (1992).
6. E. Piers and A.V. Gavai. J. Org. Chem. **55**, 2380 (1990).
7. E. Piers, B.W.A. Yeung, and S.J. Rettig. Tetrahedron, **43**, 5521 (1987); E. Piers, B.W.A. Yeung, and F.F. Fleming. Can. J. Chem. **71** 280 (1993).

8. E. Piers and H.L.A. Tse. Tetrahedron Lett. **25**, 3155 (1984).
9. L. Ruest, G. Blouin, and P. Deslongchamps. Synth. Commun. **6**, 169 (1976).
10. H.J. Reich, J.M. Renga, and I.L. Reich. J. Am. Chem. Soc. **97**, 5434 (1975); D. Liotta, C. Barmun, R. Puleo, G. Zima, C. Bayer, and H.S. Kezar III. J. Org. Chem. **46**, 2920 (1981).
11. G.H. Posner, C.E. Whitten, and J.J. Sterling. J. Am. Chem. Soc. **95**, 7788 (1973); G.H. Posner, D.J. Brunelle, and L. Sinoway. Synthesis, 662 (1974).
12. E. Piers, H.E. Morton, and J.M. Chong. Can. J. Chem. **65**, 78 (1987).
13. T. Ibuka, K. Hayashi, H. Minikata, and Y. Inubushi. Tetrahedron Lett. 159 (1979).
14. J.S. Sawyer, T.S. Macdonald, and G.J. McGarvey. J. Am. Chem. Soc. **106**, 3376 (1984).
15. E.J. Corey, H. Cho, C. Rücker, and D.H. Hua. Tetrahedron Lett. **22**, 3455 (1981).
16. S. Hayashi, A. Matsuo, and T. Matsuura. Tetrahedron Lett. 1599 (1969).
17. A. Matsuo and S. Hayashi. Tetrahedron Lett. 1289 (1970).
18. A. Matsuo. Tetrahedron, **28**, 1203 (1972).
19. J.-L. Gras. J. Org. Chem. **46**, 3738 (1981).
20. J.D. Connolly, L.J. Harrison, and D.S. Rycroft. J. Chem. Soc. Chem. Commun. 1236 (1982).
21. M. Tori, T. Hasebe, and Y. Asakawa. Chem. Lett. 2059 (1988); J. Chem. Soc. Perkin Trans. 1, 1552 (1989); Bull. Chem. Soc. Jpn. **63**, 1706 (1990).
22. M. Tori, T. Hasebe, Y. Asakawa, K. Ogawa, and S. Yoshimura. Bull. Chem. Soc. Jpn. **64**, 2303 (1991).
23. K.-G. Gerling and H. Wolf. Tetrahedron Lett. **26**, 1293 (1985).
24. L. Wartski. Bull. Soc. Chim. Fr. 3066 (1965).
25. W.C. Still, M. Kahn, and A. Mitra. J. Org. Chem. **43**, 2923 (1978).
26. B.H. Lipshutz, J.J. Pegram, and M.C. Morey. Tetrahedron Lett. **22**, 4603 (1981).
27. S. Danishefsky, N. Nagaswa, and N. Wong. J. Org. Chem. **40**, 1989 (1975).
28. E.J. Corey and M.A. Tius. Tetrahedron Lett. **21**, 3535 (1980).
29. C. Burford, F. Cooke, E. Ehlinger, and P. Magnus. J. Am. Chem. Soc. **99**, 4536 (1977).
30. P. Magnus and G. Roy. Organometallics, **1**, 533 (1982).
31. A.F. Kluge and I.S. Cloudsdale. J. Org. Chem. **44**, 4847 (1979).
32. J.-M. Conia and J.-C. Limasset. Bull. Soc. Chim. Fr. 1936 (1967).
33. J. Occolowitz. Tetrahedron Lett. 5291 (1966); H.G. Kuivila, K.-H. Tsai, and D.G.I. Kingston. J. Organomet. Chem. **23**, 129 (1970).

Can. J. Chem. Downloaded from www.nrcresearchpress.com by 213.200.69.106 on 09/08/12
For personal use only.

Tandem Wessely oxidation and intramolecular Diels–Alder reactions. IV. The synthesis of (±)-coronafacic acid[1]

PETER YATES,[2] N.K. BHAMARE, THIERRY GRANGER, AND T.S. MACAS
Lash Miller Chemical Laboratories, University of Toronto, Toronto, Ont., Canada M5S 1A1

Received August 26, 1992[3]

PETER YATES, N.K. BHAMARE, THIERRY GRANGER, and T.S. MACAS. Can. J. Chem. **71**, 995 (1993).

Ethyl *E*-5-(4-ethyl-2-hydroxyphenyl)-2-pentenoate (**7**), prepared in four steps from *m*-ethylphenol (**9**), was converted via Wessely oxidation with lead tetraacetate followed by intramolecular Diels–Alder reaction in boiling xylene to ethyl 1-acetyloxy-6-ethyl-2,3,3a,4,5,7a-hexahydro-8-oxo-1,5-methano-1*H*-indene-*anti*-4-carboxylate (**16**). Hydrogenation of **16** followed by mild hydrolysis gave ethyl 6-ethyloctahydro-1-hydroxy-8-oxo-1,5-methano-1*H*-indene-*anti*-4-carboxylate (**24**), which on oxidation with periodate gave 4-(ethoxycarbonyl)-6-ethyloctahydro-1-oxo-1*H*-indene-5-carboxylic acid (**26**). Oxidative decarboxylation of this gave a mixture of ethyl 6-ethyl-2,3,3a,6,7,7a-hexahydro-1-oxo-1*H*-indene-4-carboxylate (**31**) and ethyl 6-ethyl-2,3,3a,4,7,7a-hexahydro-1-oxo-1*H*-indene-4-carboxylate (**32**); the latter was converted to the former by ethanolic sodium ethoxide. Hydrolysis of **31** with hot hydrochloric acid gave (±)-coronafacic acid (**4**).

PETER YATES, N.K. BHAMARE, THIERRY GRANGER et T.S. MACAS. Can. J. Chem. **71**, 995 (1993).

Le *E*-5-(4-éthyl)-2-hydroxyphényl)-2-pentanoate d'éthyle (**7**), préparé en quatre étapes à partir du *m*-éthylphénol (**9**), a été soumis à une oxydation de Wessely suivie d'une réaction intramoléculaire de Diels–Alder dans le xylène bouillant pour fournir du 1-acétyloxy-6-éthyl-2,3,3a,4,5,7a-hexahydro-8-oxo-1,5-méthano-1*H*-indène-*anti*-4-carboxylate d'éthyle (**16**). L'hydrogénation de **16**, suivie d'une hydrolyse douce, conduit au 6-éthyloctahydro-1-hydroxy-8-oxo-1,5-méthano-1*H*-indène-*anti*-4-carboxylate d'éthyle (**24**) qui, par oxydation à l'aide de periodate, conduit à l'acide 4-(éthoxycarbonyl)-6-éthyloctahydro-1-oxo-1,5-méthano-1*H*-indène-*anti*-carboxylique (**26**). Une décarboxylation oxydante de ce produit conduit à un mélange de 6-éthyl-2,3,3a,6,7,7a-hexahydro-1-oxo-1*H*-indène-4-carboxylate d'éthyle (**31**) et de 6-éthyl-2,3,3a,4,7,7a-hexahydro-1-oxo-1*H*-indène-4-carboxylate d'éthyle (**32**); sous l'action de l'éthylate de sodium dans l'éthanol, le composé **32** se transforme en composé **31**. L'hydrolyse du composé **31** par de l'acide chlorhydrique chaud fournit l'acide (±)-coronafacique (**4**).

[Traduit par la rédaction]

It has been shown previously (1) that a tandem Wessely oxidation – intramolecular Diels–Alder reaction sequence can be used to synthesize isotwistenones of type **3** from *o*-(3-alkenyl)phenols (**1**) via 6-acetyloxy-6-(3-alkenyl)-2,4-cyclohexadien-1-ones (**2**) (Scheme 1). Although the overall yields are sometimes modest, this is offset by the brevity of this pathway for the synthesis of bridged tricyclic ketones from aromatic precursors. Furthermore, this method, unlike some others involving intramolecular Diels–Alder reactions (cf., for example, ref. 2) results in the concomitant introduction of an oxygen function adjacent to the ketonic group. Hydrolysis of the acetyloxy group gives an α-ketol, which can serve two useful synthetic purposes. First, it constitutes a route to tricyclic α-ketols related to natural products (cf. ref. 3). Second, it provides a site for highly selective oxidative cleavage of the tricyclic compound to a *cis*-fused bicyclic keto acid that can be used for further synthetic elaboration, as is the case in the present work, which concerns the synthesis of (±)-coronafacic acid (**4**).

Coronafacic acid is the acid obtained on hydrolysis of the phytotoxic amide, coronatine (**5**), which is produced by bacteria of several *Pseudomonas* species and causes chocolate spot disease in Italian rye grass and outgrowths on potato tuber tissues (4). Coronafacic acid itself has also been isolated directly from the culture broths in some cases (4, 5). The absolute stereochemistry of coronafacic acid as determined by X-ray crystallography and ORD measurements is that shown in **4** (6). It should be pointed out, however, that this does not rigorously establish the stereochemistry of the corresponding moiety in coronatine since equilibration of configuration at C-6 and C-7a can occur and, in fact, both *cis*- and *trans*-fused forms of **4** are obtained in its hydrolysis (5).[4]

Several syntheses of coronafacic acid have been reported previously. Ichihara et al. have described two syntheses, one involving an intermolecular and the other an intramolecular Diels–Alder reaction (7), and Jung and co-workers reported three syntheses, one involving an anionic oxy-Cope rearrangement and the others intramolecular Diels–Alder reactions (8). Liu and Llinas-Brunet effected a synthesis utilizing an intermolecular Diels–Alder reaction (9). Other syntheses of coronafacic acid have been reported by Tsuji (10) and by Ohira and co-workers (11). Its biosynthesis has been investigated by Parry and Mafoti (12).

Our own synthesis was based on the premise that an appropriately substituted isotwistene derivative of type **3**, after hydrolysis to the corresponding α-ketol, could be oxidatively cleaved by periodate to give a *cis*-fused oxohexahydroindenecarboxylic acid of type **6** that could be converted to coronafacic acid. The Wessely substrate chosen for this purpose was the phenol **7**.[5] This was prepared from

[1]For the previous paper in this series, see ref. 1*a*.

[2]EDITOR'S NOTE: We wish to acknowledge with grateful thanks the many years of service that Professor Peter Yates devoted to chemistry in Canada. We also remember with gratitude his contributions, as an editor and author, to the Canadian Journal of Chemistry. Professor Yates passed away on November 16, 1992, and we dedicate this paper to his memory.

[3]Revision received April 2, 1993.

[4]The term "coronafacic acid" is now used to denote the *cis* form.

[5]All compounds prepared in the present investigation were achiral or racemic; the latter are represented by a single enantiomer without implication of absolute configuration.

Can. J. Chem. Downloaded from www.nrcresearchpress.com by 213.200.69.106 on 09/08/12
For personal use only.

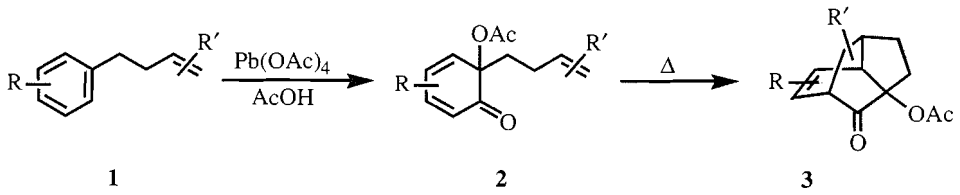

1 2 3

SCHEME 1

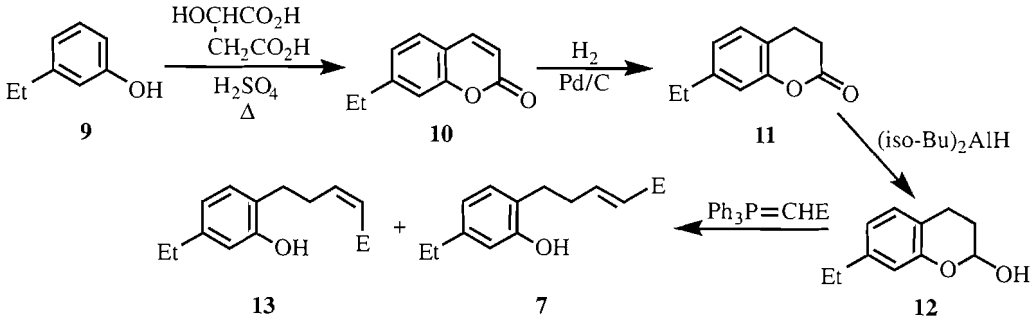

9 10 11 12 13 7

(E = CO_2Et)

SCHEME 2

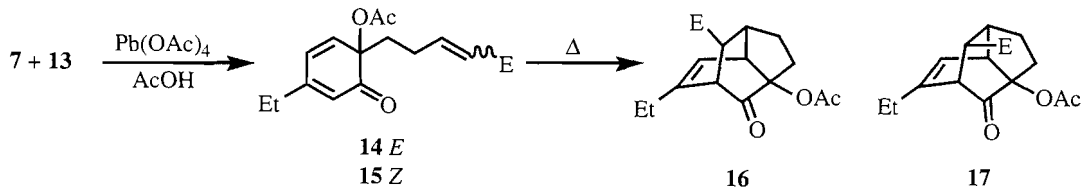

14 *E*
15 *Z*
16 17

(E = CO_2Et)

SCHEME 3

m-ethylphenol (**9**) by the route shown in Scheme 2, which follows closely the route we used previously for the synthesis of the corresponding methyl-substituted compound **8** (1). The structures of the intermediates **10–12** and of **7** were established by their elemental composition and their ir and ^{1}H and ^{13}C nmr spectra, which, *mutatis mutandis*, resembled those of analogous compounds prepared previously (1, 13) (see experimental section). The Wittig reaction of **12** with (ethoxycarbonyl)triphenylphosphorane gave the *E* isomer **7** as the major product accompanied by a small amount of the *Z* isomer **13** (<5%, as shown by ^{1}H nmr spectroscopy).

The mixture of **7** and **13** was subjected to Wessely oxidation with lead tetraacetate in acetic acid to give a mixture of the cyclohexadienones **14** and **15**, whose spectra corresponded with those of analogous compounds obtained previously. This mixture was not purified, but heated in dilute solution in boiling xylenes to effect an intramolecular Diels–Alder reaction. The product was a mixture of the epimeric isotwistenones **16** and **17** (ca. 20:1) (Scheme 3), which could be separated by column chromatography. The structure of the major product **16** was again established by comparison of its spectra with those of **18** and **19** and other close analogues (1, 13). This comparison shows that, as in the earlier cases, the Diels–Alder product is the quasi *ortho* regioisomer **16**, rather than the quasi *meta* regioisomer **20** (14). The minor product **17** was not fully characterized, but its spectra leave little doubt that it is the C-8 epimer of **16**.

Compound **16** was hydrolyzed with aqueous barium hydroxide to the α-ketol **21** and the corresponding carboxylic acid. It had originally been planned to cleave **21** by sodium periodate or lead tetraacetate oxidation. However, model studies with the α-ketol **19** showed that complex mixtures were formed that contained little if any of the desired keto acid **22** (13). Since it is known that β,γ-unsaturated acids are susceptible to ready oxidation (15), and since it was planned to saturate the ethylenic double bond of the oxidation product, the order of the reduction and hydrolysis steps was reversed (Scheme 4). Hydrogenation of **16** gave the dihydro product **23**. The relative configuration at C-6 was not determined but is likely to be *exo* since this stereochemistry would be expected to arise by addition of hydrogen from the less hindered side of the ethylenic double bond. Hydrolysis of **23** gave the α-ketol **24** together with the corresponding carboxylic acid **25**, which could be esterified to give **24**. Treatment of **24** with aqueous sodium periodate gave the desired oxidative cleavage product **26**. Analogous hydrogenation and hydrolysis reactions converted **17**, the C-4 epimer of **16**, via **27** to products considered to be **28** and **29**, the C-4 epimers of **24** and **25**, respectively (Scheme 5). These were not fully characterized because of the small amounts available and their irrelevance to the main synthetic scheme. Interestingly, attempted oxidative cleavage of **28** with aqueous sodium periodate left it unchanged, presumably because steric in-

Can. J. Chem. Downloaded from www.nrcresearchpress.com by 213.200.69.106 on 09/08/12
For personal use only.

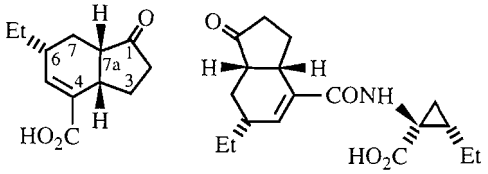

4

5

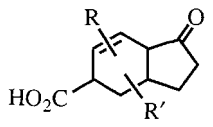

6

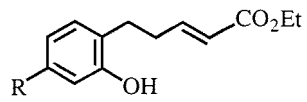

7 R = Et
8 R = Me

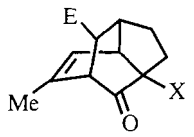

18 X = OAc
19 X = OH

(E = CO_2Et)

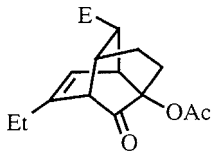

20

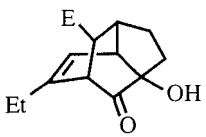

21

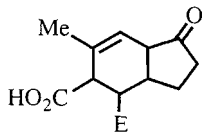

22

teractions in the transition states for either *endo* or *exo* attack by periodate inhibit the formation of **30**.

Oxidative decarboxylation of **26** with lead tetraacetate and cupric acetate monohydrate in pyridine gave a 1:2 mixture of the Δ^4 and Δ^5 isomers **31** and **32** (Scheme 6). Treatment of this mixture with ethanolic sodium ethoxide converted **32** to **31**. The preparation of **31** by another route has been reported previously (9). The assignment of stereochemistry is ambiguous because of the possibility of inversion at C-6 and C-7a under the basic reaction conditions. Fortunately this ambiguity is of no consequence since it is known that hydrolysis of **31** or the corresponding methyl ester with hot aqueous acid results in equilibration at C-6 and C-7a and the formation of coronafacic acid (**4**). In our case, hydrolysis of **31** with hot 30% hydrochloric acid gave a mixture that after several recrystallizations afforded pure coronafacic acid, mp 122–123°C, undepressed on admixture with an authentic sample of (±)-coronafacic acid, whose spectra were identical with those of the authentic sample.[6]

Synthetic yields were good to excellent throughout. The sequence of central interest, Wessely oxidation – intramolecular Diels–Alder reaction, converted **7** to **16** in 71% yield. The yield for each step of the sequence (hydrogenation, hydrolysis, periodate cleavage) that converted **16** to **26** was 94% or higher. The remaining steps from **26** to **4** (oxidative decarboxylation and hydrolysis) proceeded with excellent conversion (each about 88%), but the total synthetic yield can only be estimated (60%) because at each step equilibration of isomers was required to maximize yields. The conversion of **7** to coronafacic acid was thus carried out with a yield of about 28%, confirming the value of the Wessely oxidation – Diels–Alder reaction sequence for the synthesis of natural products. It is perhaps ironic that although, in general, the method provides a high degree of stereochemical control in the synthesis of tricyclic and derived bicyclic systems, this selectivity was not invoked in the present case because of the special circumstance that the relative configuration of coronafacic acid is achievable under equilibrium-controlled conditions. However, this does not detract from the potential of this method for the synthesis of *cis*-fused bicyclic systems.[7]

Experimental

Melting points were determined on a Fisher–Johns apparatus and are uncorrected. Infrared (ir) spectra were recorded in $CHCl_3$ solution; peaks are strong unless indicated to be medium (m) or weak (w). ^1H and ^{13}C nuclear magnetic resonance (nmr) spectra were recorded in $CDCl_3$ solution unless otherwise specified. Signal multiplicities (s,d,t,q) and parities (e,o) for the latter are based on SFORD and APT spectra, respectively. Solutions in organic solvents were dried over anhydrous $MgSO_4$ and the solvents were evaporated with a rotary evaporator at water aspirator pressure.

*7-Ethylcoumarin (**10**)*

m-Ethylphenol (**9**) (61.10 g, 0.500 mol) and concentrated sulfuric acid (125 mL) were heated with stirring in an oil bath at 110–112°C and treated over a 9 h period with six portions (each ca. 6 g) of malic acid (73.8 g, 0.55 mol); thereafter the amounts of malic acid added were doubled. The reaction mixture was stirred at the same temperature for a further 15 h and then cooled in an ice bath. The rapidly stirred reaction mixture was treated slowly with water (50 mL) with stirring over a period of 1 h and then poured slowly into a mixture of ethyl acetate (500 mL) and ice (1 L). The organic layer was separated and the aqueous layer was washed with ethyl acetate (2 × 200 mL). The combined organic solutions were washed with saturated aqueous $NaHCO_3$ (4 × 200 mL) and saturated brine (200 mL), dried, and evaporated to give a yellow liquid that solidified on standing overnight. The solid was recrystallized from carbon tetrachloride to give **10** (70.55 g, 0.405 mol, 81%), mp 41–42°C; ir ν_{max}: 1733, 1631 (m) cm^{-1}; ^1H nmr δ: 1.27 (t, J = 9 Hz, 3H), 2.72 (q, J = 9 Hz, 2H), 6.29 (d, J = 9.2 Hz, 1H), 7.05 (m, 2H), 7.36 (d, J = 7 Hz, 1H), 7.65 (d, J = 9.5 Hz, 1H); ^{13}C nmr δ: 160.9 (s)), 154.3 (s), 149.3 (s), 143.4 (d), 127.8 (d), 124.4 (d), 116.7 (s), 115.7 (d), 115.4 (d), 29.0 (t), 15.1 (q); ms m/z: 174 (100%). Anal. calcd. for $C_{11}H_{10}O_2$: C 75.84, H 5.79; found: C 75.86, H 5.81.

*7-Ethyl-3,4-dihydrocoumarin (**11**)*

7-Ethylcoumarin (**10**) (10.09 g, 57.0 mmol) was dissolved in ethyl acetate (250 mL) and 10% Pd/C (0.5 g) was added. The mixture was shaken in a Parr hydrogenation apparatus with hydrogen at 3 atm (1 atm = 101.3 kPa) for 10 h, after which no further uptake of hydrogen could be observed. The mixture was filtered and the filtrate was evaporated to give **11** as a colorless liquid

[6]We are most grateful to Professors A. Ichihara (Hokkaido University), M.E. Jung (University of California, Los Angeles), and H.-J. Liu (University of Alberta) for authentic samples and (or) spectra of (±)-coronafacic acid.

[7]For a preliminary account of this work, see ref. 16.

Can. J. Chem. Downloaded from www.nrcresearchpress.com by 213.200.69.106 on 09/08/12
For personal use only.

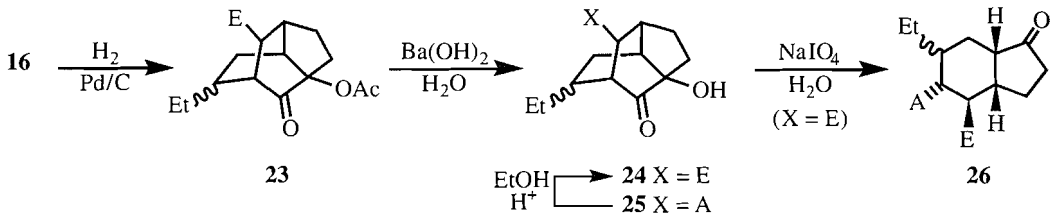

(E = CO_2Et , A = CO_2H)

SCHEME 4

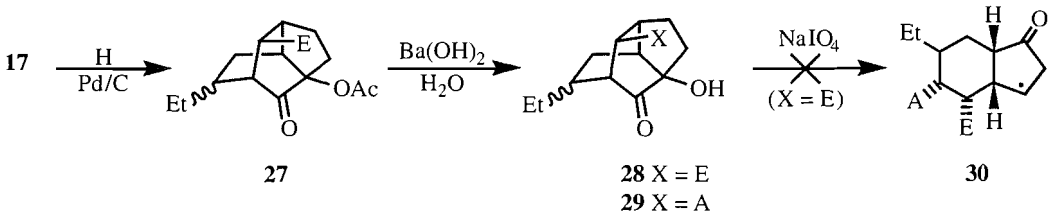

(E = CO_2Et , A = CO_2H)

SCHEME 5

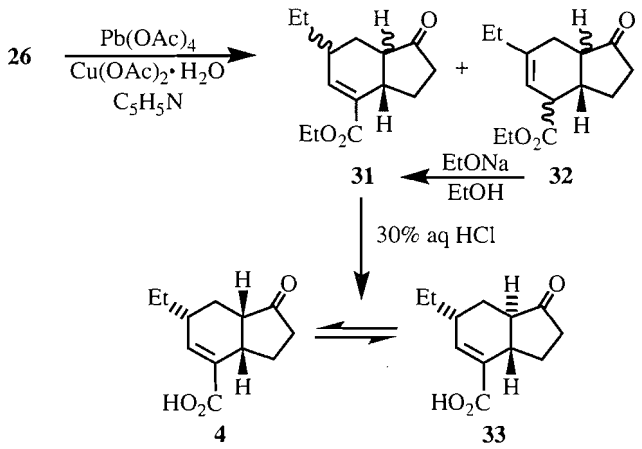

SCHEME 6

(10.0 g, 56.0 mmol, 98%): bp 103–105°C/0.25 Torr (1 Torr = 133.3 Pa); ir ν_{max}: 1761 cm^{-1}; ^1H nmr δ: 1.21 (t, J = 7 Hz, 3H), 2.4–3.1 (m, 6H), 6.7–7.2 (m, 3H); ^{13}C nmr δ: 168.5 (s), 152.1 (s), 144.8 (s), 127.9 (d), 123.9 (d), 119.9 (s), 116.0 (d), 29.3 (t), 23.4 (t), 15.4 (q); ms m/z: 176 (53%). Anal. calcd. for $C_{11}H_{14}O_2$: C 74.97, H 6.86; found: C 74.88, H 6.87.

*7-Ethyl-2-chromanol (**12**)*

7-Ethyl-3,4-dihydrocoumarin (**11**) (13.8 g, 77.4 mmol) in dry toluene (250 mL) was cooled to −78°C and treated over a 2 h period with diisobutylaluminum hydride (25% in toluene; 55.6 mL, 82 mmol). After a further 2 h water (100 mL) was added at −78°C, and the reaction mixture was allowed to warm to room temperature. After standing for 2 h it was filtered through Celite. The Celite was washed with ether (100 mL) and the aqueous layer of the filtrate was extracted with ether (3 × 250 mL). The combined organic solutions were washed with water (200 mL) and saturated brine (100 mL), dried, and evaporated to give a pale yellow liquid (13.2 g), which was distilled (bp 132–133°C/0.25 Torr) to give **12** as a clear, colorless liquid (12.8 g, 72.0 mmol, 93%) that crystallized upon standing: mp 46–47°C; ir ν_{max}: 3484, 3311 cm^{-1}; ^1H nmr δ: 1.17 (t, J = 7 Hz, 3H), 1.7–2.1 (m, 2H) 2.3–3.0 (m, 4H), 3.80 (bs, 1H), 5.47 (t, 1H), 6.5–7.0 (m, 3H); ^{13}C nmr δ: 152.8 (s), 143.9 (s), 129.1 (d), 120.6 (d), 119.2 (s), 116.1 (d), 92.3 (d), 28.6 (t), 27.4 (t), 20.2 (t), 15.5 (q); ms m/z: 178 (31%). Anal. calcd. for $C_{11}H_{14}O_2$: C 74.13, H 7.92; found: C 74.10, H 7.95.

Ethyl E- *and* Z-*5-(4-ethyl-2-hydroxyphenyl)-2-pentenoate (**7** and **13**)*

7-Ethyl-2-chromanol (**12**) (10.7 g, 60.1 mmol) in dry benzene (100 mL) was treated with (carboethoxymethylene)triphenylphosphorane (21.0 g, 62.1 mmol) in dry benzene (100 mL) over a period of 3 h. The solution was stirred for a further 24 h and the solvent was evaporated to give a viscous, pale yellow oil containing a mixture of **7**, **13**, and triphenylphosphine oxide, which was flash chromatographed on a silica column (hexane – ethyl acetate, 9:1) to give a mixture of **7** and **13** as a pale yellow oil (13.3 g, 53.5 mmol, 89%); tlc and ^1H nmr spectroscopy showed that the *Z* isomer **13** was a minor component (<5%). Compound **7** has ir ν_{max}: 1721, 1669 (m) cm^{-1}; ^1H nmr δ: 1.19 (t, J = 7 Hz, 3H), 1.27 (t, J = 8 Hz, 3H), 2.3–2.9 (m, 6H), 4.14 (q, J = 8 Hz, 2H), 5.84 (dt, J = 16 Hz, J = 1.5 Hz, 1H), 5.85 (br s, 1H), 6.5–7.1 (m, 3H); ^{13}C nmr δ: 167.4 (s), 153.9 (s), 149.5 (d), 143.9 (s), 130.0 (d), 124.5 (s), 121.5 (d), 120.1 (d), 115.0 (d), 60.4 (t), 32.6 (t), 28.6

Can. J. Chem. Downloaded from www.nrcresearchpress.com by 213.200.69.106 on 09/08/12
For personal use only.

Can. J. Chem. Downloaded from www.nrcresearchpress.com by 213.200.69.106 on 09/08/12
For personal use only.

(t), 14.3 (q); ms *m/z*: 248 (52%). Anal. calcd. for $C_{15}H_{20}O_3$: C 72.55, H 8.12; found: C 72.62, H 7.98.

*Ethyl 1-acetyloxy-6-ethyl-2,3,3a,4,5,7a-hexahydro-8-oxo-1,5-methano-1*H*-indene*-anti- *and* syn-*4-carboxylate (**16** and **17**)*

A solution of the mixture of isomeric phenols **7** and **13** (20:1; 12.4 g, 50 mmol) in acetic acid (50 mL) was added with stirring over a 3 h period to an ice-cold solution of lead tetraacetate (44.3 g, 100 mmol) in acetic acid (25 mL), and the reaction mixture was stirred for a further 6 h. The acetic acid was evaporated, the residue was extracted with ether (4 × 100 mL), and the extracts were washed with saturated aqueous $NaHCO_3$ (3 × 100 mL) and saturated brine (100 mL). The ethereal solution was dried and the ether was evaporated to give a pale yellow, viscous oil that was flash chromatographed on silica (hexane – ethyl acetate, 88:12) to give **14** containing a small amount of **15** as a viscous, yellow oil (11.03 g, 36 mmol, 72%); ir ν_{max}: 1751, 1715, 1672 (w) cm^{-1}; ^1H nmr δ: 1.0–1.4 (m, 6H), 1.6–2.6 (m, 9H), 4.15 (q, J = 7 Hz, 3H), 6.10 (dd, J = 12 Hz, 2H), 6.25 (d, J = 1.5, 1H), 6.75 (d, J = 16 Hz, 1H), 6.85 (d, J = 16 Hz, 1H).

The mixture of compounds **14** and **15** (10.7 g, 35.0 mmol) was dissolved in freshly distilled xylenes (1 L) and the solution was added dropwise over a 6 h period to boiling xylenes (500 mL). The reaction mixture was boiled under reflux for a further 6 h, the xylenes were evaporated, and the products were chromatographed on a silica column (hexane – ethyl acetate, 9:1) to give a mixture of **16** and **17** as a viscous, yellow oil that was further purified by distillation (bp 94–98°C/0.3 Torr), giving **16** as a colorless oil (9.53 g, 33 mmol, 89%); ir ν_{max}: 1754, 1733 cm^{-1}; ^1H nmr δ: 1.01 (t, J = 8 Hz, 3H), 1.25 (t, J = 7 Hz, 3H), 1.7–2.7 (m, 8H), 2.02 (s, 3H), 3.40 (m, 2H), 4.09 (q, J = 7 Hz, 2H), 5.78 (m, 1H); ^{13}C nmr δ: 205.6 (s), 171.8 (s), 169.7 (s), 141.4 (s), 122.9 (d), 84.0 (s), 61.1 (t), 54.3 (d), 46.9 (d), 46.0 (d), 39.7 (d), 30.5 (t), 28.6 (t), 27.4 (t), 21.6 (q), 14.2 (q), 11.2 (q); ms *m/z*: 306 (18%). Anal. calcd. for $C_{17}H_{22}O_5$: C 66.65, H 7.24; found: C 66.80, H 7.34.

The *syn* isomer **17** (0.215 g, 0.75 mmol, 2%) was isolated from the mixture of **16** and **17** on the same column with 85:15 hexane – ethyl acetate; ir ν_{max}: 1751, 1739 cm^{-1}; ^1H nmr δ: 1.15 (t, J = 7 Hz, 3H), 1.85–3.0 (m, 8H), 3.18 (br s, 1H), 3.7 (m, 1H), 4.15 (q, J = 7 Hz, 2H), 5.76 (m, 1H).

*Ethyl 6-ethyl-2,3,3a,4,5,7a-hexahydro-1-hydroxy-8-oxo-1,5-methano-1*H*-indene*-anti-*4-carboxylate (**21**) and the corresponding carboxylic acid*

A solution of **16** (0.918 g, 3.0 mmol) in ethanol (30 mL) was added dropwise over a period of 1 h to an ice-cold solution of $Ba(OH)_2 \cdot 8H_2O$ (0.413 g, 1.5 mmol) in ethanol (15 mL). After a further 4 h of stirring at room temperature, ethanol was evaporated and the residue was acidified with dilute hydrochloric acid and extracted with ether (3 × 50 mL). The extracts were washed with saturated aqueous $NaHCO_3$ (3 × 20 mL) and the ether was evaporated to give **21** as an oil (0.554 g, 2.1 mmol, 70%); ir ν_{max}: 1730 cm^{-1}; ^1H nmr δ: 1.00 (t, J = 8 Hz, 3H), 1.26 (t, J = 7 Hz, 3H), 1.7–3.2 (m, 9H), 3.18 (br, s, 1H, absent after D_2O treatment), 3.43 (m, 1H), 4.10 (q, J = 7 Hz, 2H), 5.86 (m, 1H); ^{13}C nmr δ: 212.0 (s), 172.1 (s), 140.8 (s), 124.3 (d), 79.0 (s), 61.1 (t), 53.7 (d), 48.3 (d), 47.3 (d), 40.0 (d), 33.3 (t), 28.6 (t), 27.4 (t), 14.2 (q), 11.3 (q); ms *m/z*: 264 (5%). Exact Mass calcd. for $C_{15}H_{20}O_4$: 264.1361; found: 264.1365.

The $NaHCO_3$ washings were acidified with dilute hydrochloric acid and extracted with ether (3 × 20 mL). Evaporation of the ether gave the carboxylic acid corresponding to the ester **21** as a viscous yellow oil (0.155 g, 0.66 mmol, 22%); ir ν_{max}: 3367 (br), 1727 cm^{-1}; ^1H nmr δ: 1.05 (t, J = 7 Hz, 3H), 1.75–3.2 (m, 9H), 3.45 (m, 1H), 5.9 (m, 1H).

*Ethyl 1-acetyloxy-6-ethyloctahydro-8-oxo-1,5-methano-1*H*-indene*-anti-*4-carboxylate (**23**)*

To compound **16** (9.18 g, 30 mmol) in ethyl acetate (250 mL) was added 10% Pd/C (0.5 g) and the mixture was hydrogenated at 1 atm until uptake of hydrogen ceased. The reaction mixture was filtered and evaporated to give a colorless oil that on standing gave crystalline **23** (8.98 g, 29 mmol, 97%), mp 67–68°C; ir ν_{max}: 1761, 1730 cm^{-1}; ^1H nmr δ: 0.86 (t, J = 6 Hz, 3H), 0.9–3.0 (m ,13H), 1.25 (t, J = 7 Hz, 3H), 2.07 (s, 3H), 4.17 (q, J = 7 Hz, 2H); ^{13}C nmr δ: 209.8 (s), 172.8 (s), 169.9 (s), 89.7 (s), 61.1 (t), 48.3 (d), 45.2 (d), 43.1 (d), 36.5 (d), 30.4 (t), 29.8 (t), 28.7 (t), 21.7 (t), 14.3 (q), 11.4 (q); ms *m/z*: 308 (29%). Anal. calcd. for $C_{17}H_{24}O_5$: C 66.23, 1H 7.83; found: C 66.20, H 7.91.

Ethyl 6-ethyloctahydro-1-hydroxy-8-oxo-1,5-methano-1-H-*indene*-anti-*4-carboxylate (**24**) and 6-ethyloctahydro-1-hydroxy-8-oxo-1,5-methano-1*H*-indene*-anti-*4-carboxylic acid (**25**)*

Compound **23** (7.70 g, 250 mmol) was dissolved in ethanol (300 mL) and the solution was added dropwise over a period of 3 h to an ice-cold solution of $Ba(OH)_2 \cdot 8H_2O$ (3.94 g, 12.5 mmol) in ethanol (150 mL). After further stirring at room temperature for 8 h, the ethanol was evaporated, and the residue was acidified with dilute hydrochloric acid and extracted with ether (3 × 200 mL). The combined extracts were washed with saturated aqueous $NaHCO_3$ (3 × 50 mL) and saturated brine (50 mL) and evaporated to give a colorless oil that solidified on standing at room temperature to give **24** (6.18 g, 23.23 mmol, 93%), mp 71–72°C; ir ν_{max}: 3521, 1733, 1709 cm^{-1}; ^1H nmr δ: 0.84 (t, J = 7 Hz, 3H), 1.21 (t, J = 7 Hz, 3H), 1.1–1.2 (m, 2H), 1.40 (dt, J = 14 Hz, J = 4 Hz, 1H), 1.7–2.0 (m, 5H), 2.20 (quintet, J = 3 Hz, 1H), 2.45 (d, J = 3 Hz, 1H), 2.75 (quintet, J = 5 Hz, 1H), 2.95 (d, J = 10 Hz, 1H), 3.10 (s, 1H; absent after D_2O treatment), 4.1 (m, 2H); ^{13}C nmr δ: 217.8 (s), 210.8 (s), 173.8 (s), 84.0 (s), 61.0 (s), 47.0 (d), 43.0 (d), 35.5 (d), 29.2 (s), 23.9 (d), 14.3 (q), 11.6 (q); ms *m/z*: 266 (22%). Anal. calcd. for $C_{13}H_{22}O_4$: C 67.67, H 8.27; found: C 67.55, H 8.35.

The combined $NaHCO_3$ washings were acidified with dilute hydrochloric acid and extracted with ether (3 × 50 mL), and the combined extracts were washed with water (3 × 50 mL). Evaporation gave a colorless, thick oil (80 mg, 0.33 mmol, 1.35%) that was crystallized from chloroform to give **25**, mp 166–167°C; ir ν_{max}: 3390 (br), 1730, 1709 cm^{-1}; ^1H nmr δ: 0.85 (t, J = 7 Hz, 3H) 1.15 (q, J = 7 Hz, 2H) 1.35 (dt, J = 14 Hz, J = 3 Hz, 2H), 1.7–2.15 (m, 5H), 2.23 (q, J = 3 Hz, 1H), 2.55 (q, J = 3 Hz, 1H), 2.68 (q, J = 3 Hz, 1H), 2.9 (br s, 1H); ^1H nmr δ(acetone-d_6): 0.83 (t, J = 7 Hz, 3H), 1.16 (quintet, J = 7 Hz, 2H), 1.26–1.44 (m, 4H), 1.66–2.15 (m, 7H), 2.48–2.59 (m, 2H), 2.79–2.89 (br s, 1H); ^{13}C nmr δ(acetone-d_6): 206.8 (e), 174.9 (e), 72.0 (o), 49.4 (o), 46.3 (o), 37.9 (o), 36.5 (o), 35.4 (o), 31.0 (e), 30.20 (e), 28.8 (e), 24.0 (e), 11.7 (o); ms *m/z*: 238 (31%).

*Esterification of **25**. Formation of **24***

Esterification of **25** (70 mg, 0.28 mmol) in refluxing ethanol (25 mL) and a catalytic amount of concentrated sulfuric acid for 3 h and chromatography of the product on silica gave **24** (50 mg, 0.19 mmol, 58%) and an oily mixture of **24** and a second product (10 mg), whose ^1H nmr spectrum showed the signals of **24** together with signals at δ 6.58 and 6.85.

*4-(Ethoxycarbonyl)-6-ethyloctahydro-1-oxo-1*H*-indene-5-carboxylic acid (**26**)*

Compound **24** (3.80 g, 14.3 mmol) was shaken with aqueous sodium periodate (0.21 M; 500 mL) until solution was effected. After 4 h of stirring at room temperature a solid began to deposit. After 8 h of stirring the reaction mixture was filtered to give a white powder (2.8 g) that was crystallized from 2-propanol–hexane to give **26**, mp 151–152°C. A further amount of product was obtained by extraction of the filtrate with ether (3 × 50 mL). The ethereal extracts were extracted with saturated aqueous $NaHCO_3$ (3 × 15 mL) and the $NaHCO_3$ extracts were acidified with dilute hydrochloric acid and extracted with ether (3 × 30 mL). The ether was evaporated to give **26** (total yield 3.77 g, 13.4 mmol, 94%); ir ν_{max}: 3450 (br), 1730, 1701 cm^{-1}; ^1H nmr δ: 0.93 (m, 3H), 1.26 (t, J = 7 Hz, 3H), 0.9–3.0 (m, 13H), 4.22 (q, J = 7 Hz, 2H), 8.44 (br s, 1H, absent after D_2O treatment); ^{13}C nmr δ: 219.8 (e), 180.3 (e), 175.5 (e), 61.2 (e), 48.2 (o), 47.8 (o), 40.7 (o), 39.4 (e), 36.8

Can. J. Chem. Downloaded from www.nrcresearchpress.com by 213.200.69.106 on 09/08/12
For personal use only.

(o), 34.7 (o), 24.2 (e), 23.8 (e), 21.5 (e), 14.3 (o), 12.2 (o); ms *m/z*: 282 (26%). Anal. calcd. for $C_{15}H_{22}O_5$: C 63.81, H 7.85; found: C 63.97, H 7.98.

*Ethyl 1-acetyloxy-6-ethyloctahydro-8-oxo-1,5-methano-1*H-*indene*-syn-*indene-4-carboxylate (27)*

Compound **17** (0.184 g, 0.6 mmol) with Pd/C (20 mg) in ethyl acetate (30 mL) was hydrogenated at 1 atm until there was no further uptake of hydrogen. The catalyst was filtered and the filtrate was evaporated to give **27** as a colorless oil (0.150 g, 0.49 mmol, 81.5%); ir ν_{max}: 1767, 1736 cm^{-1}; ^1H nmr δ: 1.23 (t, J = 7 Hz, 3H), 1.4–3.0 (m, 10H), 2.05 (s, 3H), 3.41 (m, 1H), 4.10 (q, J = 7 Hz, 2H).

Ethyl 6-ethyloctahydro-1-hydroxy-8-oxo-1,5-methano-1-H-*indene*-syn-*4-carboxylate (28) and 1-hydroxy-6-ethyloctahydro-8-oxo-1,5-methano-1*H-*indene*-syn-*4-carboxylic acid (29)*

A solution of **27** (123 mg, 0.4 mmol) in ethanol (30 mL) was added dropwise over a period of 30 min to a stirred ice-cooled solution of $Ba(OH)_2 \cdot 8H_2O$ (63 mg, 0.2 mmol) in ethanol (15 mL). After further stirring at room temperature for 6 h, the ethanol was evaporated and the residue was acidified with dilute hydrochloric acid, and extracted with ether (3 × 20 mL). The combined extracts were washed with saturated aqueous $NaHCO_3$ (2 × 10 mL). Evaporation of the ether gave **28** as a colorless oil (50 mg, 0.19 mmol, 48%); ir ν_{max}: 3450 (br), 1736 cm^{-1}; ^1H nmr δ: 0.79 (t, J = 7 Hz, 3H), 1.15 (t, J = 7 Hz, 3H), 1.28–1.4 (dt, J = 14 Hz, J = 3 Hz, 2H), 1.05–1.2 (m, 2H), 1.65–1.95 (m, 4H), 2.15 (quintet, J = 3 Hz, 1H), 2.40 (d, J = 3 Hz, 1H), 2.70 (quintet, J = 6 Hz, 1H), 2.90 (d, J = 12 Hz, 1H), 3.25 (br s, 1H; absent after D_2O treatment), 4.05 (m, 2H).

The $NaHCO_3$ washings were acidified with dilute hydrochloric acid and extracted with ether (3 × 10 mL). Evaporation of the ether gave **29** (30 mg, 0.125 mmol, 36%).

Esterification of 29. Formation of 28

To a solution of **29** (30 mg, 0.125 mmol) in ethanol (20 mL) was added 3 drops of concentrated sulfuric acid and the solution was boiled under reflux under argon for 3 h. Ethanol was evaporated and the residue was diluted with water and extracted with ether (2 × 10 mL). The extracts were washed with saturated aqueous $NaHCO_3$ (10 mL) and the ether was evaporated to give an oil (20 mg), whose ^1H nmr spectrum corresponded with that of **28** with additional signals at δ 6.8 (d, J = 8 Hz), 6.95 (d, J = 8 Hz).

Treatment of 28 with aqueous sodium periodate

Compound **28** (40 mg, 0.15 mmol) was treated with 0.21 M aqueous sodium periodate (100 mL) for 8 h. The ethanol was evaporated and the residue was acidified with dilute hydrochcloric acid and extracted with ether (3 × 20 mL). The extracts were washed with aqueous $NaHCO_3$ (2 × 10 mL). Evaporation of the ether returned **28** as an oil (30 mg, 0.11 mmol, 75%). The $NaHCO_3$ washings were acidified with dilute hydrochloric acid and extracted with ether (3 × 10 mL). Evaporation of the ether gave an oil (3 mg, 0.01 mmol, 7%), whose spectra resembled those of compound **26**. Three further treatments with 0.21 M aqueous sodium periodate failed to give any further quantity of **26**, and **28** was recovered in every case. It is therefore concluded that the small amount of **26** arose from **24** present as a contaminant in **28**.

*Ethyl 6-ethyl-2,3,3a,6,7,7a-hexaahydro- and 6-ethyl-2,3,3a,4,7,7a-hexahydro-1-oxo-1*H-*indene-4-carboxylate (31 and 32)*

A solution of **36** (1.04 g, 3.7 mmol) in dry benzene (250 mL) was degassed by passing argon through it for 30 min and was stirred at room temperature in a flask covered with aluminum foil. Lead tetraacetate (3.10 g, 7.0 mmol) and $Cu(OAc)_2 \cdot H_2O$ (0.2 g, 1 mmol) were added, followed by dropwise addition, with a syringe, of dry pyridine (5 mL) over a period of 15 min. The resulting solution was stirred at room temperature for 1 h and boiled under reflux for 3 h. The benzene layer was decanted after the mixture had cooled to room temperature and the sticky residue was extracted with ether (2 × 50 mL). The combined benzene and ether extracts were washed with saturated aqueous $NaHCO_3$ (2 × 50 mL), cold dilute hydrochloric acid (3 × 50 mL), and saturated brine (100 mL). The solution was dried and the solvents were evaporated to give a 1:2 mixture of **31** and **32** as a yellow oil (0.766 mg, 3.25 mmol, 88%); ir ν_{max}: 1736, 1721, 1656 (w) cm^{-1}; ^1H nmr δ: 0.8–1.4 (m, 6H), 1.65–3.0 (m, 11H), 4–4.4 (m, 2H), 5.39 (br s, 0.7H), 7.0 (d, J = 12 Hz, 0.3H).

Conversion of 32 to 31

A solution of the mixture of **31** and **32** (708 mg, 3 mmol) in dry ethanol (50 mL) was treated at ice temperature over a period of 15 min with ethanolic sodium ethoxide (1.43 g, 21 mmol), freshly prepared from sodium (483 mg) and dry ethanol (7 mL). The mixture was stirred at room temperature under argon for 48 h. The ethanol was evaporated; the residue was acidified with cold dilute sulfuric acid, and extracted with ether (4 × 50 mL). The extracts were washed with saturated aqueous $NaHCO_3$ (3 × 50 mL) and saturated brine (50 mL), dried, and evaporated to give **31** as a colorless oil (645 mg, 27.3 mmol, 91%); ir ν_{max}: 1736, 1715, 1645 (w) cm^{-1}; ^1H nmr δ: 0.8–1.1 (m, 3H), 1.2–1.4 (m, 3H), 1.45–2.8 (m, 9H), 3.1 (quintet, 1H), 3.3 (br s, 1H), 4.2 (m, 2H), 6.95 (m, 1H); ^{13}C nmr δ: 220.6 (e), 167.3 (e), 144.6 (o), 131.2 (e), 61.4 (e), 46.6 (o), 37.8 (e), 34.7 (o), 29.1 (o), 28.0 (e), 27.5 (e), 26.1 (e), 14.4 (o), 11.2 (o).

Coronafacic acid (4)

A mixture of **31** (50 mg, 0.21 mmol) and 30% hydrochloric acid (10 mL) was boiled under reflux for 3 h. The solution was extracted with ether (3 × 25 mL) and the ethereal extracts were extracted with saturated aqueous $NaHCO_3$ (3 × 20 mL). The $NaHCO_3$ extracts were acidified with 6 N sulfuric acid and extracted with ether (3 × 25 mL). These ethereal extracts were washed with water (2 × 20 mL), dried, and evaporated to give a mixture of **4** and **33** as a solid (38 mg, 18 mmol, 87%). Three crystallizations of this mixture from carbon tetrachloride gave samples of **4** of increasing purity (mp 114–117°C, 116–118°C, and 120–121°C); a final recrystallization from diisopropyl ether (11) gave pure (±)-coronafacic acid, mp 122–123°C, undepressed on admixture with an authentic sample of (±)-coronafacic acid (see footnote 7); ir ν_{max}: 3480 (br), 1736, 1715, 1645 (w) cm^{-1}; ^1H nmr δ: 0.97 (t, J = 7 Hz, 3H), 1.0–1.1 (m, 1H), 1.4–1.6 (m, 3H), 1.8–1.9 (m, 1H), 2.2–2.4 (m, 4H), 2.6 (m, 1H), 3.1 (m, 1H), 7.1 (m, 1H), 10.2 (v br s, 1H); ^{13}C nmr δ: 220.3 (e), 172.1 (e), 146.9 (o), 130.0 (e), 46.6 (o), 38.2 (e), 37.9 (o), 36.0 (o), 28.1 (e), 27.7 (e), 25.7 (e), 11.2 (o).

Acknowledgements

We thank the Natural Sciences and Engineering Research Council of Canada for financial support of this work, and S. McLean for assistance with the manuscript.

1. (*a*) P. Yates and T.S. Macas. Can. J. Chem. **66**, 1 (1988); (*b*) T.S. Macas and P. Yates. Tetrahedron Lett. **24**, 147 (1983).
2. H. Greuter, G. Frater, and H. Schmid. Helv. Chim. Acta, **55**, 526 (1972); H. Greuter and H. Schmid. Helv. Chim. Acta, **55**, 2382 (1972).
3. N.K. Bhamare, T. Granger, C.R. John, and P. Yates. Tetrahedron Lett. **32**, 4439 (1991).
4. K. Nishiyama, R. Sakai, A. Ezuka, A. Ichihara, K. Shiraishi, M. Ogasawa, H. Sato, and S. Sakamura. Ann. Phytopathol. Soc. Jpn. **42**, 613 (1976); K. Nishiyama, R. Sakai, A. Ezuka, A. Ichihara, K. Shiraishi, and K. Sakamura. Ann. Phytopathol. Soc. Jpn. **43**, 219 (1977).
5. R.E. Mitchell. Phytochemistry, **23**, 791 (1984); **24**, 1485 (1985).
6. A. Ichihara, K. Shiraishi, H. Sato, S. Sakamura, K. Nishiyama, R. Sakai, A. Furusaki, and T. Matsumoto. J. Am. Chem. Soc. **99**, 636 (1977); A. Ichihara, K. Shiraishi, S.

Sakamura, K. Nishiyama, and R. Sakai. Tetrahedron Lett. 269 (1977).
7. A. Ichihara, R. Kimura, K. Moriyasu, and S. Samakura. Tetrahedron Lett. 4331 (1977); A. Ichihara, R. Kimura, S. Yamada, and S. Samakura. J. Am. Chem. Soc. **102**, 6353 (1980).
8. M.E. Jung and J.P. Hudspeth. J. Am. Chem. Soc. **100**, 4309 (1978); **102**, 2463 (1980); M.E. Jung and K.M. Helweg. Tetrahedron Lett. **22**, 2735 (1981).
9. H.-J. Liu and M. Llinas-Brunet. Can. J. Chem. **62**, 1747 (1984).
10. J. Tsuji. Pure Appl. Chem. **53**, 2371 (1981).
11. N. Nakayama, S. Ohira, Y. Okamura, and S. Soga. Chem. Lett. 731 (1981); N. Nakayama and S. Ohira. Agric. Biol. Chem. **47**, 1689 (1983); S. Ohira. Bull. Chem. Soc. Jpn. **57**, 1902 (1984).
12. R.J. Parry and R. Mafoti. J. Am. Chem. Soc. **108**, 4681 (1986).
13. T.S. Macas. Ph.D. Thesis, University of Toronto. 1984.
14. G. Brieger and J.N. Bennett. Chem. Rev. **80**, 63 (1980).
15. E.J. Boorman and R.P. Linstead. J. Chem. Soc. 258 (1935).
16. N.K. Bhamare, T. Granger, T.S. Macas, and P. Yates. J. Chem. Soc. Chem. Commun. 739 (1990).

Can. J. Chem. Downloaded from www.nrcresearchpress.com by 213.200.69.106 on 09/08/12
For personal use only.

Ternary complexes of copper(II) and their use in the spectrophotometric determination of copper in alloys and rocks

ABD-ELHAFEEZ E. ALI

Chemistry Department, Faculty of Science at Sohag, Assiut University, Egypt

Received January 21, 1992[1]

ABD-ELHAFEEZ E. ALI. Can. J. Chem. **71**, 1002 (1993).

Some intensely coloured Cu(II)–L_1–2′,7′-dichlorofluorescein ternary complexes were studied. The absorbance characteristics for these ternary complexes were determined. The molar ratio for these complexes is $Cu:L_1:L_2 = 1:2:1$ and the formula $[Cu(L_1)_2]^{2+} \cdot [Cl_2FlCOO^-]^-$ is proposed. The effect of substituent groups of the L_1 and L_2 ligands on the complexing activity with copper(II) was studied. The interference of some cations and anions in the determination of the Cu(II) by the developed methods was examined. Highly sensitive and selective methods are proposed for the spectrophotometric determination of copper(II) in limestone and copper alloys.

ABD-ELHAFEEZ E. ALI. Can. J. Chem. **71**, 1002 (1993).

On a étudié quelques complexes tertiaires extrêmement colorés de Cu(II)–L_1–2′,7′-dichlorofluorescéine. On a déterminé les caractéristiques d'absorbance de ces complexes. On suggère que le rapport molaire dans ces complexes est $Cu : Li_1 : L_2 = 1 : 2 : 1$ et que la formule est $[Cu(L_1)_2]^{2+} \cdot [Cl_2FlCOO^-]^-$. On a étudié l'effet des substituants des ligands L_1 et L_2 sur propriétés complexantes avec le cuivre(II). On a évalué les interférences de quelques cations et de quelques anions sur la détermination du Cu(II) par les méthodes développées. On propose des méthodes extrêmement sensibles et sélectives pour la détermination spectrophotométrique du cuivre(II) dans le calcaire et les alliages de cuivre.

[Traduit par la rédaction]

Can. J. Chem. Downloaded from www.nrcresearchpress.com by 213.200.69.106 on 09/08/12
For personal use only.

Several authors have studied the reactions of Cu(I) with most of the phenanthroline derivatives (1–4), but the reaction of these ligands with Cu(II) has not been reported before in the literature. The spectrophotometric determination of copper has been the subject of several studies (5–14).

This work is devoted to the study of the reactions between copper(II), phenanthroline and its derivatives, and fluorescein (FlCOOH) or 2′,7′-dichlorofluorescein (Cl_2FlCOOH). These coloured complexes were used to develop selective and highly sensitive methods for the spectrophotometric determination of copper(II) in some of its alloys and in limestone.

Experimental

Reagents

All reagents used were of AR grade unless otherwise stated. Doubly distilled water was used throughout. The copper(II) solution was standardized by EDTA titration. Ethanolic stock solutions (10^{-3} to 5×10^{-3} M) of the L_1 and L_2 ligands were prepared. The anions (citrate, tartrate, chloride, carbonate, bicarbonate, phosphate, sulphide, nitrate, and sulphate) were used in the form of their sodium or potassium salts, while the cations (Fe(III), Sn(II), Cr(III), Al(III), Zn(II), Cd(II), Co(II), Ni(II), Bi(III), Hg(II), Mn(II), Ga(III), In(III), Y(III), and alkali and alkaline-earth metals) were taken as chloride, sulphate, or nitrate. Ammonium acetate was used as a buffer solution. The pH values were adjusted using solutions of hydrochloric acid and sodium hydroxide.

Apparatus

Absorption spectra were recorded using a CECIL recorder spectrophotometer model 599. An Orien Research model 601/digital Ionlyzer pH meter standardized with buffer solution at pH 4.0 and 9.15 was used for all pH measurements.

Results and discussion

1,10-Phenanthroline and its derivatives are interesting complexing agents for Cu(I) (1–4), but no information has been reported about coloured complexes for these reagents with Cu(II). This is probably because Cu(I) has chromophoric properties and so the *d* electrons of the Cu(I) atoms form a close conjugation chain with the system of the phenanthroline rings, but Cu(II) does not. No reactions take place between Cu(II) and pyridine, bipyridyl, or terpyridyl, and the secondary ligands studied (FlCOOH and Cl_2FlCOOH). From slightly basic medium, deep red and violet coloured Cu(II)–L_1–L_2 ternary complexes have been extracted by chloroform. (L_1 represents 1,10-phenanthroline (phen.), 2,9-dimethyl-1,10-phenanthroline (neocup.), 4,7-diphenyl-1,10-phenanthroline (bathophen.), and 2,3,8,9-dibenzo-4,7-diphenyl-5,6-dilydro-1,10-phenanthroline (cuprotest.) and L_2 is 2′,7′-dichlorofluorescein.) The possibility of extracting these ternary complexes from slightly alkaline medium into various organic solvents such as carbon tetrachloride, benzene, chloroform, cyclohexane, isoamyl alcohol, and ether was studied. From the analytical point of view, the extraction solvent should completely extract the ternary complex but not the ligands. These conditions were fulfilled only by chloroform.

Optimum conditions, spectra, and stoichiometry of the complexes

A study of the absorbance of the Cu(II) ternary complexes extracted from aqueous media over a range of pH indicates that the absorbance value of the extract at its maximum absorption (530 nm) is independent of pH over the range 6.4–9.6. Waiting times of shaking for 8 and 10 min were selected as optimal values for the quantitative extraction of the ternary complex by chloroform. Absorption spectra of the extracted Cu(II) ternary complexes and the ligands in chloroform were recorded from 400 to 600 nm. Figure 1 shows the spectra of the extracted Cu(II)–cuprotest.–Cl_2FlCOOH complex and the ligands in chloroform. The spectra of the ternary complexes examined are of similar nature. The spectrum in Fig. 1 displays a shoulder at 502 nm followed by a band with a sharp peak at 530 nm. The spectra of the extracted ligands (L_1 and L_2) in chloroform exhibit practically no absorption from 400 to 600 nm, hence no spectral interference from the reagent blanks with the

[1]Revision received July 16, 1992.

Can. J. Chem. Downloaded from www.nrcresearchpress.com by 213.200.69.106 on 09/08/12
For personal use only.

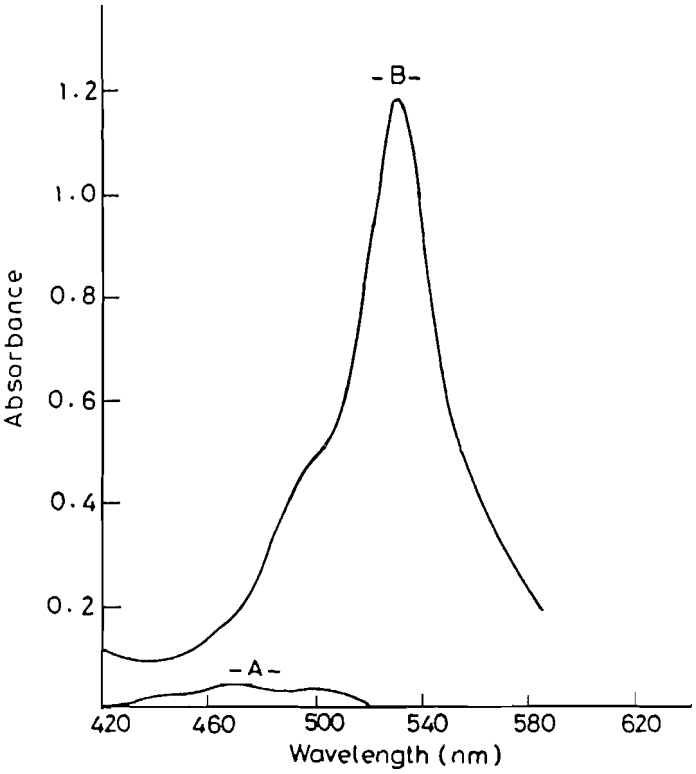

FIG. 1. Absorption spectra of the extracted 2,7-dichlorofluorescein (A) and its ternary complex with copper(II) and cuprotest. in $CHCl_3$ (B) (10^{-4} M) (spectrum of the extract of cuprotest. in $CHCl_3$ exhibits no absorption from 420 to 600 nm).

ternary complexes is expected (Fig. 1). The absorbance characteristics of the examined complexes were determined and the results are shown in Table 1. This table also contains the specific absorptivities of the complexes (15).

Molar ratios of the constituents of the ternary complexes were determined using two methods, that developed by Asmus (16) and the method of Koch and Ackerman (17). The former method is well known and the latter involves plotting $\log A_x/(A_0 - A_x)$ versus $\log Cl_2$, where A_0 is the absorbance of the ternary complex and A_x is the absorbance in the presence of different concentrations of L_2. This graph was linear and its slope was close to 1, indicating the number of the molecules of L_2 in the complex. Both methods showed that the composition of the complex was 1:2:1 and the formula $[Cu(L_1)_2]^{2+} \cdot [Cl_2FlCOO^-]^-$ is proposed. Thus, the suggested mechanism for this reaction can be represented as follows:

(*a*) Formation of colourless cationic complex

[1] $Cu^{2+} + 2L_1 \rightleftharpoons [Cu(L_1)_2]^{2+}$

(*b*) Formation of coloured ternary complex

[2] $[Cu(L_1)_2]^{2+} + Cl_2FlCOOH \rightleftharpoons [Cu(L_1)_2]^{2+} \cdot [Cl_2FlCOO^-]^- + H^+$

The coupling of chelate rings (eq. [1]) is across the two nitrogen atoms of L_1. Equation [2] shows the dependence of the formation of the ternary complex on the pH of the aqueous medium.

Influence of the substituents of the ligands on their complexing activity with Cu^{2+}

No reaction takes place between Cu^{2+}, the applied primary ligands, and fluorescein (FlCOOH), while Cl_2FlCOOH forms an intensely coloured ternary complex with Cu^{2+} and L_1. There is no doubt about a connection between the two chlorine atoms of Cl_2FlCOOH and its action in forming intensely coloured ternary complexes. This is due to the net effect of the electron-withdrawing inductive influence and the electron-donating mesomeric influence of its two chlorine atoms on its carboxylic group, which in turn increases the dissociation constant of Cl_2FlCOOH in comparison to FlCOOH; hence its ionizable hydrogen atom is more easily detached than that from FlCOOH. Thus, in the case of Cl_2FlCOOH, formation of the coloured complexes proceeds according to eq. [2].

It is clear also that a certain role is played by the type and position of substituents in the L_1 molecule. No coloured $CuL_1 \cdot Cl_2$FlCOOH complexes are formed by using pyridine, bipyridyl, terpyridyl, and bathocuproine. The ϵ of the coloured complexes formed decreases in the order: Cu–bathophen.–L_2 >> Cu–phen.–L_2 > Cu–cuprotest.–L_2 > Cu–neocup.–L_2 (Table 1). It is clear that the electron-donating effect of the two methyl groups in neocup. hinders the formation of the coloured ternary copper complex. On the contrary, the two phenyl groups are in the *para* position with respect to the two nitrogen atoms of the bathophen. molecule and this assists the quantitative formation of the coloured ternary complex that shows the highest molar absorptivity (Table 1).

Calibration, precision, interferences, and application

Beer's law is obeyed over the range 0.03–3.0 μg mL^{-1} Cu(II) for complexes 1 and 3, 6.5–60.0 μg mL^{-1} Cu(II) for 2, and 0.3–9.5 μg mL Cu(II) for 4 (see Table 1). Complex 2 is of little practical importance, since it has the lowest sensitivity in comparison to complexes 1, 3, and 4 (Table 1). The molar absorptivities are presented in Table 1. Bathophen. + Cl_2FlCOOH has the highest sensitivity and cuprotest. + Cl_2FlCOOH is the most selective for the spectrophotometric determination. They were used for the analysis of the copper in pure solutions and in its alloys, respectively (Tables 2–4).

The evaluation of the determination of trace amounts of Cu(II) at three concentration levels (2, 3, and 4 μg mL^{-1}) shows good precision and accuracy (Table 2).

With a view to applying cuprotest. and Cl_2FlCOOH for practical purposes, the effects of various cations, especially those accompanying copper in alloys such as zinc, tin, and nickel in brass, bronze, and cupronickel, were examined. Mn(II), Co(II), and Cd(II) can be tolerated at a 20:1 w/w ratio to copper(II) (4 μg mL^{-1}) and Al(III), Cr(III), and Fe(III) at a 30:1 ratio. Bi(III), Ga(III), Y(III), and In(III) give a +4.4% error at a 50-fold ratio to 4.0 μg mL^{-1} Cu(II). Acetate, citrate, oxalate, and tartrate do not interfere. The effects on the determination of copper of alkali, alkaline-earth metals, CO_3^{2-}, HCO_3^-, Cl^-, SO_4^{2-}, NO_3^-, and PO_4^{3-} as common ions and Zn(II), Fe(III), Mn(II) as trace constituents in sedimentary rocks, in addition to Ni(II), Zn(II), and Sn(II) as main components in copper alloys, were examined. The results of the interference studies are given in Table 3.

The results of the studies of the interferences given in

TABLE 1. Absorbance characteristics of the copper(II) ternary complexes studied

No.	Complex	λ_{max} (nm)	$\epsilon \times 10^{-4}$ (L mol^{-1} cm^{-1})	VBL[a] (μg mL^{-1} (Cu))	a[b]	S[c] (%)
1	$[Cu(phen.)_2]^{2+} \cdot [Cl_2FlCOO^-]^-$	530	9.45	0.03–3.0	1.0	1.32
2	$[Cu(neocup.)_2]^{2+} \cdot [Cl_2FlCOO^-]^-$	528	0.75	6.5–60	0.12	1.7
3	$[Cu(bothaphen.)_2]^{2+} \cdot [Cl_2FlCOO]^-$	528	50.3	0.03–3.0	7.92	1.06
4	$[Cu(cuprotest.)_2]^{2+} \cdot [Cl_2FlCOO^-]^-$	530	1.25	0.3–9.5	0.2	0.95

[a]Validity of Beer's law.
[b]Specific absorptivity.
[c]Standard deviation for five determinations.

TABLE 2. Statistical evaluation of results for the determination of copper(II) using bathophen. + Cl_2Fl-COOH

Copper (μg mL^{-1})		
Added	Found[a]	Error (%)
2.0	2.01	+0.5
3.0	3.03	+1.0
4.0	4.03	+0.75

[a]Average of five determinations.

TABLE 3. Effect of diverse ions on the determination of 4.0 μg mL^{-1} copper(II)

Foreign ion	Amount of foreign ion added (μg mL^{-1})	Cu(II) found[a] (μg mL^{-1})	Error (%)
Na^+	1000.0	4.0	0.0
K^+	1000.0	4.0	0.0
Ca^{2+}	1000.0	4.06	+1.5
Mg^{2+}	1000.0	4.05	+1.25
Zn^{2+}	40.0	4.08	+2.0
Ni^{2+}	40.0	4.1	+2.5
Tin(II)	40.0	4.08	+2.0
CO_3^{2-}	50.0	4.05	+1.25
HCO_3^-	500.0	4.02	+0.5
Cl^-	2000.0	4.0	0.0
NO_3^-	2000.0	4.0	0.0
SO_4^{2-}	1000.0	4.02	+0.5
PO_4^{3-}	1000.0	4.05	+1.25

[a]Average of three determinations.

TABLE 4. Results for determination of copper in bronze (A) and in limestone (B)

Foreign ion (μg mL^{-1})	Copper(II) (μg mL^{-1}) Taken	Found	Relative error
	A		
Sn(II), 2.0	6.0	6.07	+1.17
	B		
Ca, 1000.0	6.0	6.03	+0.5

Table 3 indicate that the proposed method is suitable for the determination of microamounts of copper(II) in sedimentary rocks and in cupronickels, brasses, and bronzes with the systems $Cu_{100-x}M_x$, where M = zinc, nickel, or tin and $0 \leq x \leq 90$.

Recommended procedure for determination of copper(II) in sedimentary rocks and alloys

An accurately measured amount of the sample can be dissolved in concentrated HCl or concentrated HNO_3 or in a mixture of the two acids. The acidic solution of the sample is neutralized with concentrated ammonia solution, diluted with redistilled water to a definite volume, and the copper(II) is determined by the method outlined below. The interferences of the common ions in the Cu(II) samples were studied by a preparation of synthetic mixtures of a composition corresponding to the samples.

A buffered 1.0 mL (2 μg mL^{-1} Cu) of the sample is placed in a separatory funnel, diluted to about 10 mL with redistilled water, and mixed with about 10 mL of chloroform containing about 2 mL each of solutions of $Cl_2FlCOOH$ and cuprotest. (5×10^{-3} M). The mixture is shaken and, after separation of the phases, the organic layer is transferred into a 10-mL standard flask and the volume is brought up to the mark with chloroform. The absorbance of the coloured ternary copper complex is measured at its maximum absorption against a reagent blank prepared in the same way and the concentration of the copper in the sample is determined by the standard method.

The precision and accuracy of the cuprotest. and $Cl_2FlCOOH$ method for the determination of copper(II) in bronzes and limestone were verified for synthetic samples containing 6.0 μg mL^{-1} of Cu(II) in the presence of 2.0 μg mL^{-1} Sn(II) and 1000.0 μg mL^{-1} Ca^{2+}, respectively, and the results are presented in Table 4.

The results indicate an average recovery of 101.71 (with mean relative error +1.17) and 100.5 (with mean relative error +0.5) for the spectrophotometric determination of the copper(II) in bronze and limestone, respectively, using cuprotest. and 2′,7′-dichlorofluorescein (Table 4).

Other well-known reagents have been proposed for the spectrophotometric determination of copper (Table 5) but most of them are less sensitive than the proposed methods. The proposed method (No. 13, Table 5 and No. 3, Table 1) is 50–100 times more sensitive than the well-known diethyl dithiocarbamate and hydroxyquinoline methods and about 20 times more sensitive than such recent methods as Nos. 10 and 11 (Table 5).

Cuprotest. and 2′,7′-dichlorofluorescein have advan-

Can. J. Chem. Downloaded from www.nrcresearchpress.com by 213.200.69.106 on 09/08/12
For personal use only.

TABLE 5. Comparison with other reagents used for the spectrophotometric determination of copper

No.	Reagent	Optimum pH	λ_{max} (nm)	$\epsilon \times 10^4$ (L mol^{-1} cm^{-1})	Ref.
1	Ammonia	NH_3, 3 N	620	0.012	5
2	Diethyl dithiocarbamate	9–9.2	440	1.2	5
3	Hydroxyquinoline	2.7–14	410	0.52	5
4	Neocuproine	2–9	455	0.79	18
5	TAR	2.7–3.4	560	1.9	19
6	$NH_2OH \cdot HCl$		560	0.79	20
7	Ferrozine	7	470	0.432	21
8	2-Hydroxyacetophenoneoxime	5.5	355	0.34	22
9	5,7-Dibromo-8-hydroxyquinoline	—	420	6.3	23
10	Chlorophosphonazo	—	604	2.54	24
11	Picramin RG	—	550	2.1	25
12	Cuprotest. + $Cl_2FlCOOH$	6.5–9.4	530	1.25	This work
13	Bathophen. + $Cl_2FlCOOH$	6.5–9.4	528	50.3	This work

tages for the spectrophotometric microdetermination of copper in bronzes and limestone. Moreover, the study of the interference of zinc and nickel in the determination of Cu(II) by cuprotest. and $Cl_2FlCOOH$ (Table 3) showed that this method can be applied to the determination of Cu(II) in brasses and cupronickels. Bathophen. and 2′,7′-dichlorofluorescein are not suitable for the determination of copper(II) in these substances, but can be applied as a highly sensitive method for the determination of copper(II) in the presence of alkali and alkaline-earth metals.

1. P. Gruzenskey. Monatsh. Chem. (Wien), **83**, 54 (1952).
2. G.F. Smith and D.H. Wilkins. Anal. Chem. **25**, 510 (1953).
3. G.F. Smith. Anal. Chem. **24**, 371 (1952).
4. E. Uhlemann. J. Prakt. Chem. **30**, 273 (1965).
5. Z. Marczonka. Separation and spectrophotometric determination of elements. Horwood, Chichester. 1986.
6. H. Bade. Z. Anal. Chem. **144**, 165 (1955).
7. E. Uhlemann. J. Prakt. Chem. **30**, 27 (1965).
8. Z. Kowalska. Chem. Anal. **16**, 197 (1971).
9. L.A. Albota. Z. Anal. **29**, 590 (1974).
10. K. Isugai. Bunseki Kagaku, **24**, 418 (1975).
11. J.M. Grana-Molares. Acta Quim. Compostelana, **2**, 4 (1978).
12. K. Fasihuddin. Indian J. Chem. Sect. A, 609 (1980).
13. S. Sundstrand. Acta Chem. Scand. **37**, 795 (1983).
14. S. Hoshi, S. Inoue, and M. Motsubara. Bunseki Kagaku, **34**, 549 (1985).
15. Z. Marczenka and R. Labniki. Talanta, **35**, 1001 (1988).
16. E. Asmus. Anal. Chem. **61**, 178 (1960).
17. S. Koch and G. Ackermann. Z. Chem. **15**, 364 (1975).
18. G.F. Smith. Anal. Chem. **24**, 371 (1952).
19. L. Sommer. Talanta, **13**, 667 (1966).
20. F. Buhl. Chem. Anal. (Warsaw), **19**, 361 (1974).
21. S.K. Kunda. Anal. Chem. **46**, 1605 (1974).
22. T. Reddy. Curr. Sci. **48**, 439 (1979).
23. C. Sanchez and T.L. Polo. An. Univ. Murica. Cienc. **43**, 269 (1984).
24. Y. Zhang. Yejin Fenxi, **9**, 22 (1989).
25. G. Li and R. Huang. Yanski Kuangwu Ji Ceshi, **8**, 99 (1989).

Can. J. Chem. Downloaded from www.nrcresearchpress.com by 213.200.69.106 on 09/08/12
For personal use only.

Proton nuclear magnetic resonance studies of nucleosides: hindered internal rotation in *N*-dimethylaminomethylene derivatives of adenosine, guanosine, and cytidine

EMMANUEL YAW OSEI-TWUM

Research Institute, King Fahd University of Petroleum and Minerals, Dhahran 31261, Saudi Arabia

Received March 9, 1993

EMMANUEL YAW OSEI-TWUM. Can. J. Chem. **71**, 1006 (1993).

Studies of the internal rotation about the C—N bond of the dimethylaminomethylene (DMAM) group of DMAM-adenosine, **1**, DMAM-guanosine, **2**, and DMAM-cytidine, **3**, was determined by high-resolution ^{1}H NMR spectroscopy. Arrhenius plots ($\ln k = \ln A - E_a/RT$) were used to determine the barriers to internal rotation, E_a, of the compounds. They were found to be 58.0 ± 2.4 kJ mol^{-1}, 71.2 ± 1.4 kJ mol^{-1}, and 62.8 ± 2.4 kJ mol^{-1} for **1**, **2**, and **3**, respectively. At the same time the coalescence temperatures, t_c, for the compounds were determined and found to be 93.5°C for **1**, 124.7°C for **2**, and 119.6°C for **3** in DMSO. In D_2O, compound **1** was found to have a t_c of 104.5°C. The compound decomposed so rapidly at this temperature that the barrier to internal rotation could not be determined. The results indicate that the oxo function in the nucleobase has a considerable effect on the barrier to internal rotation and coalescence temperature.

EMMANUEL YAW OSEI-TWUM. Can. J. Chem. **71**, 1006 (1993).

Faisant appel à la RMN du ^{1}H, on a réalisé des études sur la rotation interne de la liaison C—N du groupe diméthylaminométhylène (DMAM) de la DMAM-adénosine (**1**), de la DMAM-guanosine (**2**) et de la DMAM-cytidine (**3**). On a utilisé des courbes d'Arrhénius ($\ln k = \ln A - E_a/RT$) pour déterminer les barrières à la rotation interne, E_a, de ces composés. On a trouvé qu'elles étaient respectivement de 58,0 ± 2,4, 71,2 ± 1,4 et 62,8 ± 2,4 kJ mol^{-1} pour les composés **1**, **2** et **3**. On a aussi déterminé les températures de coalescence, t_c, de ces composés et on a trouvé qu'elles étaient respectivement de 93,5, 124,7 et 119,6°C pour les composés **1**, **2** et **3**. Pour le composé **1** dans le D_2O, on a trouvé que la t_c est de 104,5°C. À cette température, le composé se décompose tellement rapidement que l'on n'a pas pu déterminer sa barrière à la rotation interne. Les résultats indiquent que la fonction oxo de la nucléobase possède un effet important sur la barrière à la rotation interne ainsi que sur la température de coalescence.

[Traduit par la rédaction]

Introduction

N-Dimethylaminomethylene derivatives of purine and pyrimidine nucleosides similar to those shown in Scheme 1 were first reported by Zemlicka (1). They have since found uses in nucleic acid chemistry. Their use as protecting group in the synthesis of nucleoside analogs, nucleotides, and oligonucleotides has been reported (2–7). Their spectroscopic properties (8) and chromatographic and mass spectral characteristics (9, 10) have also been studied. The investigation of analogs of DMAM-adenosine as probes for the study of chemical determinants of bending in DNA fragments were recently reported (11).

The barriers to internal rotation about the exocyclic C—N bond in cytosine derivatives and other pyrimidines, as well as in adenine derivatives, have been studied using proton and ^{13}C NMR spectroscopy (12–19). There is, so far, no report on the barrier to internal rotation about the terminal C—N bond of the dimethylaminomethylene derivatives of these nucleosides or their corresponding nucleobases even though the methyl groups have been reported as a doublet in the ^{1}H NMR spectra of the adenosine and cytidine compounds (2*b*, 5, 6), indicating that they are nonequivalent.

This study is an attempt to determine the coalescence temperatures as well as the barriers to internal rotation about the exocyclic C—N bond of these derivatives. In these compounds, the terminal *N*-dimethylamino group is linked to the ring of the base through an exocyclic C—N double bond. Unlike the parent compounds, and their corresponding *N*-dimethylamino derivatives, all three derivatives have one more contributing structure to the resonance hybrid (Scheme 2). The compounds are, therefore, expected to have higher coalescence temperatures, t_c, and higher barriers to internal rotation than the *N*-dimethylamino derivatives of the parent compounds.

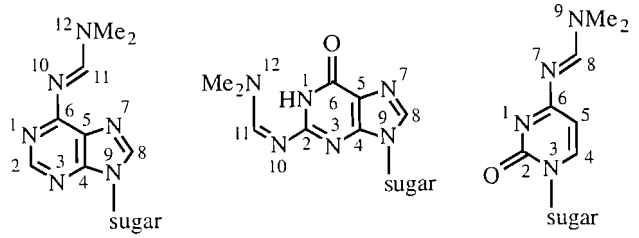

SCHEME 1

TABLE 1. FAB+ mass spectral data of nucleosides and derivatives

Compound	$[M + H]^+$	$[BH + H]^+$
Adenosine	268	136
1	323	191
Guanosine	284	152
2	339	207
Cytidine	244	112
3	299	167

Methods, results, and discussion

Dimethylaminomethylene nucleosides

The nucleosides containing the amino function reacted readily with excess dimethylformamide dimethyl acetal at room temperature. This was followed by treatment with excess water to provide the dimethylaminomethylene deriva-

Can. J. Chem. Downloaded from www.nrcresearchpress.com by 213.200.69.106 on 09/08/12
For personal use only.

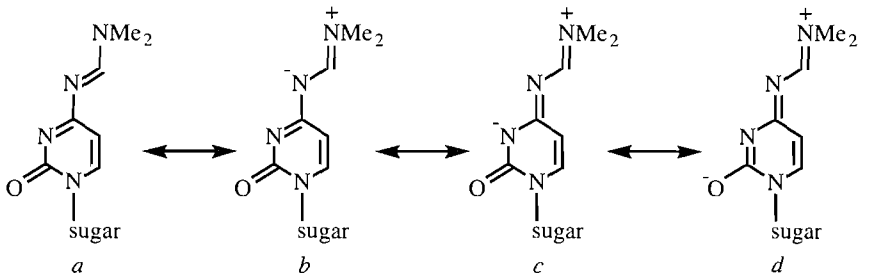

SCHEME 2. Resonance structures of DMAM–cytidine (**3**).

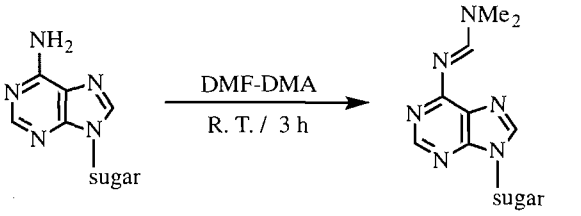

SCHEME 3

tives. The reaction of the DMF–DMA with ribonucleosides is known to result in the formation of 2′,3′-*O*-dimethylaminomethylene derivatives (2*a*). The 2′,3′-*O*-DMAM group is readily hydrolysed in H_2O. The reaction is illustrated in Scheme 3. At higher temperatures (60°C and above), the guanine nucleoside was observed to be slowly methylated at N1. However, the reaction did not prove to be quantitative, thus the more selective low-temperature reaction was chosen.

Formation of the derivatives was confirmed by positive fast atom bombardment (FAB+) mass spectrometry and NMR. Table 1 gives the pseudo-molecular ions of the starting nucleosides (and ions of their respective bases) and those of the derivatives.

Nuclear magnetic resonance

The ^{1}H NMR spectra of the compounds indicated the nonequivalence of the methyl groups. Figure 1 shows the ^{1}H NMR spectrum of DMAM-adenosine with the methyl signals at 3.15 and 3.21 ppm.

The rate constants, k, for the exchange of the methyl groups were determined at temperatures at and above the coalescence. The rate constants for DMAM-adenosine are given in Table 2. Using these values in the Arrhenius plots, the barriers to internal rotation were obtained for compounds **1**, **2**, and **3**. The values are given in Table 3. Figure 2 shows the Arrhenius plot for DMAM-adenosine.

The presence of one more contributing structure to the resonance hybrid (structure *b* in Scheme 2), as a result of the extended conjugation in the nucleobase, appears to be of considerable importance to the double bond character of the terminal C—N bond in these compounds. The energy of activation for **1**, 58.0 kJ/mol, is found to be higher than those for the dimethylamino adenine derivatives, 49.4 (19) and 51.0 (20) kJ/mol.

Compounds **2** and **3** have barriers (71.2 and 62.8 kJ/mol, respectively) that are comparable to the barriers for dimethylamino cytosine derivatives (12, 16, 19). They are, however, higher than those of *N*,*N*-dimethylamino pyrimidines, 38–59 kJ/mol (14). These results indicate that the oxo function has considerable influence on the barrier to internal rotation of these compounds. Like the cytosine derivatives, their barriers to internal rotation are lower than those of the amides; the activation energy for dimethylformamide (DMF) is reported to be 85.77 kJ/mol (21). This is probably due to the amidine, rather than the amido, character of the compounds.

The coalescence temperatures for all three compounds are much higher than those reported for the *N*,*N*-dimethylamino-adenine and -cytosine derivatives. The maximum reported for any of these derivatives is 37°C (12, 16). The high coalescence temperatures of the compounds under study can be accounted for in terms of the extended conjugation in the nucleobases and of the solvent effect. This extended conjugation would lead to a further restriction in the rotation of the C—N bond. The solvent has been shown to have an effect on the coalescence temperature (16). The t_c for DMF in $CDCl_3$ is reported to be 120°C. To find out whether there is any solvent effect on the t_c, a 0.1 M solution of DMF in DMSO-d_6 was studied over a temperature range of 80°C to 150°C. The methyl signals of DMF were observed to coalesce at about 145°C. This was helpful in removing any doubts that the methyl signals of the compounds could be those of DMF since this solvent could not be completely removed after the reaction.

N-Dimethylaminomethylene-adenosine was also studied in D_2O. The coalescence temperature was found to be approximately 104.5°C in D_2O. This higher t_c in D_2O may be explained in terms of a hydrogen-bonding interaction between the solvent and the substrate molecules. The barrier to internal rotation was not determined in this solvent due to a rapid hydrolysis of the compound at this high temperature.

The rapid hydrolysis is also observed for all the compounds in DMSO-d_6 at a much higher temperature (above 100°C). Studies showed that **3** rapidly formed the starting nucleoside and *N*,*N*-dimethylformamide at about 140°C. When a drier solvent was used, the compound, which was studied up to 150°C, was found to be quite stable even at the highest temperature. The compounds are known to decompose in both acidic and basic solutions and should therefore be handled with care in aqueous solutions.

In several cases the DMAM function has been used as protecting group in the synthesis of nucleosides, nucleotides, and oligonucleotides. In at least one case (22), the biological activity of derivatives of guanosine 3′,5′-cyclic phosphate was studied. In such studies a question that may be asked is whether the effect of the internal rotation of the exocyclic C—N bond would lead to unexpected results. This

Can. J. Chem. Downloaded from www.nrcresearchpress.com by 213.200.69.106 on 09/08/12
For personal use only.

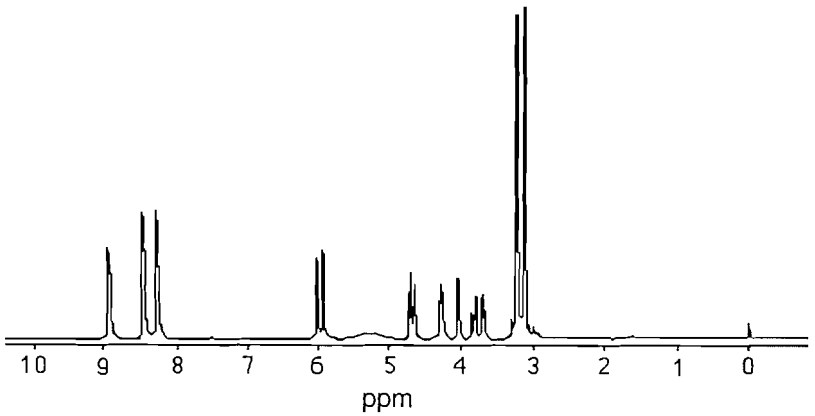

FIG. 1. Proton NMR spectrum of 40 mM DMAM-adenosine in DMSO-d_6 at 26°C.

TABLE 2. Rate constants for methyl exchange of DMAM-adenosine at and above coalescence

	T, K						
	367.15	371.15	375.15	379.15	383.15	388.15	393.15
$\Delta\nu$, Hz	14.61	10.71	7.80	6.17	4.67	3.90	3.02
k, s^{-1}	32.46	41.87	52.45	62.58	78.54	91.74	115.51

TABLE 3. Coalescence temperatures and energies of activation for compounds **1**, **2**, and **3** in DMSO-d_6

Compound	t_c, °C	E_a, kJ/mol
1	93.8	58.0 ± 2.4
2	124.7	71.2 ± 1.4
3	119.6	62.8 ± 2.4

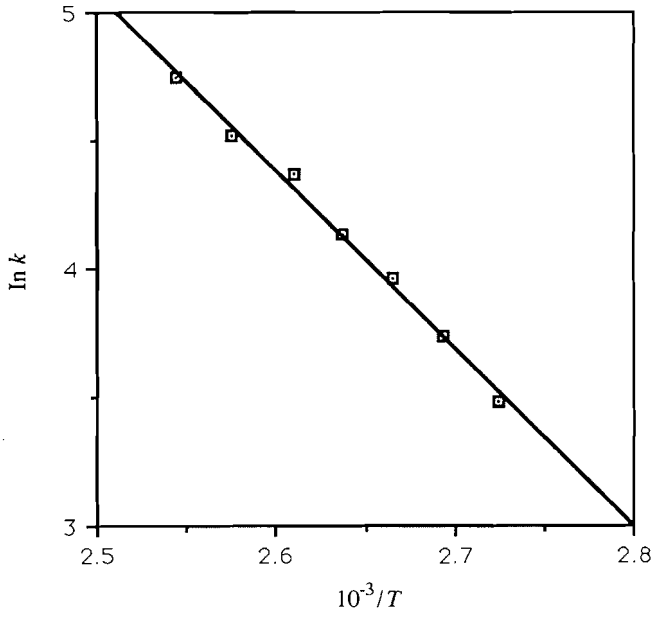

FIG. 2. Arrhenius plot of ln k vs. $1/T$ for DMAM-adenosine.

study indicates that the t_c's of these compounds are so high that in biological systems the methyl groups would remain nonequivalent and the effect of the rotation of the C—N bond will not be observed.

Experimental

The identity of each derivative was confirmed by positive fast atom bombardment (FAB+) mass spectrometry. The FAB mass spectra were obtained on a triple-sector (EBE) JMS-HX100 mass spectrometer (JEOL, Tokyo, Japan) equipped with a saddle field neutral beam gun. Xenon fast atoms were used to bombard the sample, dissolved in glycerol, on a stainless steel probe. The probe was introduced into a EI-FAB source. The accelerating voltage was 5 kV.

Proton and ^{13}C NMR spectra were obtained with a JNM-GX270 spectrometer (JEOL, Tokyo, Japan) using a 90 degree pulse and a pulse delay of 1 s. Tetramethylsilane was used as internal reference for both ^1H and ^{13}C spectra. For the determination of t_c and E_a, the ^1H NMR spectra were obtained as a function of temperature. The probe temperature was set electronically and the difference in temperature between the sample and the thermocouple corrected for with the temperature compensation feature of the spectrometer. Measurements were taken between 30 and 150°C. The probe was tuned at each temperature to correct for drifts in the field with temperature changes. The results were, however, obtained without correcting for shifts in chemical shifts with respect to temperature changes.

The coalescence temperatures were estimated by plotting the chemical shift differences of the methyl groups as a function of temperature and using a third-order polynomial for curve-fitting. They were then accurately determined by spectral acquisition at temperatures close to the estimated values.

Synthesis of dimethylaminomethylene nucleosides

Synthesis of the dimethylaminomethylene derivatives of nucleosides has been described elsewhere (9, 10). Briefly, the compounds were prepared by allowing a mixture of 0.1 mmol of the

Can. J. Chem. Downloaded from www.nrcresearchpress.com by 213.200.69.106 on 09/08/12
For personal use only.

nucleoside and 1 mmol of dimethylformamide dimethylacetal (DMF–DMA) to stand in 1 mL dry DMF at room temperature for 3 h (see Scheme 3). Water (100-fold) was added and the sample was evaporated to dryness under a steam of nitrogen. The sample was then taken up in either deuterated dimethyl sulfoxide (DMSO-d_6) or deuterium oxide (D_2O) for NMR analysis.

N-*Dimethylaminomethylene adenosine (1):* ^{1}H NMR δ: 3.15 (s, 3, first CH_3 of =CHN(CH_3)$_2$), 3.21 (s, 3, second CH_3 of =CHN(CH_3)$_2$), 3.67 (m, 2, H5′), 4.01 (m, 1, H4′), 4.21 (br, 1, H3′), 4.67 (t, 1, H2′), 5.31 (br, 3, OH), 5.99 (d, 1, H1′, $J_{1',2'}$ = 5.50 Hz), 8.44 (s, 1, H8), 8.52 (s, 1, H2), 8.94 (s, 1, C*H* of =CHN(CH$_3$)$_2$); ^{13}C NMR δ: 30.81 (first *C*H$_3$ of =CHN(CH$_3$)$_2$), 34.60 (second *C*H$_3$ of =CHN(CH$_3$)$_2$), 61.66 (C5′), 70.66 (C3′), 73.61 (C2′), 85.89 (C4′), 87.89 (C1′), 125.87 (C5), 141.67 (C8), 151.22 (*C*H of =CHN(CH$_3$)$_2$), 151.84 (C4), 158.15 (C2), 159.37 (C6).

N-*Dimethylaminomethylene guanosine (2):* ^{1}H NMR δ: 3.04 (s, 3, first CH_3 of =CHN(CH_3)$_2$), 3.16 (s, 3, second CH_3 of =CHN(CH_3)$_2$), 3.56 (m, 2, H5′), 3.90 (m, 1, H4′), 4.12 (s, 1, H3′), 4.52 (t, 1, H2′), 5.20 (br, 3, OH), 5.91 (d, 1, H1′, $J_{1',2'}$ = 5.49 Hz), 8.05 (s, 1, H8), 8.54 (s, 1, H2), 8.63 (s, 1, C*H* of =CHN(CH$_3$)$_2$). ^{13}C NMR δ: 34.64 (*C*H$_3$ of =CHN(CH$_3$)$_2$), 40.66 (second *C*H$_3$ of =CHN(CH$_3$)$_2$), 61.50 (C5′) 70.46 (C3′), 73.79 (C2′), 85.42 (C4′), 86.70 (C1′), 119.76 (C5), 136.95 (C8), 149.98 (*C*H of =CHN(CH$_3$)$_2$), 157.26 (C4), 157.57 (C2), 157.94 (C6).

N-*Dimethylaminomethylene cytidine (3):* ^{1}H NMR δ: 3.04 (s, 3, first CH_3 of =CHN(CH_3)$_2$), 3.17 (s, 3, second CH_3 of =CHN(CH_3)$_2$), 3.57 (m, 2, H5′), 3.85 (m, 1, H4′), 3.96 (s, 1, H3′), 5.1 (br, 3, OH), 5.45 (t, 1, H2′), 5.98 (d, 1, H1′, $J_{1',2'}$ = 7.33 Hz), 8.09 (s, 1, H4), 8.11 (s, 1, H5), 8.64 (s, 1, C*H* of =CHN(CH$_3$)$_2$). ^{13}C NMR δ: 34.81 (first *C*H$_3$ of =CHN(CH$_3$)$_2$), 40.88 (second *C*H$_3$ of =CHN(CH$_3$)$_2$), 60.27 (C5′), 69.07 (C3′), 74.37 (C2′), 84.08 (C4′), 89.65 (C1′), 101.47 (C5), 142.54 (C4), 155.36 (*C*H of =CHN(CH$_3$)$_2$), 157.90 (C6), 171.13 (C2).

Acknowledgements

This project was supported financially by the Research Institute, King Fahd University of Petroleum and Minerals. I would like to thank Dr. H. Perzanowski for all his helpful hints and suggestions.

1. J. Zemlicka. Collect. Czech. Chem. Commun. **28**, 1060 (1963).
2. (*a*) J. Zemlicka, S. Chladek, A. Holy, and J. Smrt. Collect. Czech. Chem. Commun. **31**, 3198 (1966); (*b*) S. Chladek and J. Zemlicka. J. Org. Chem. **39**, 2187 (1974).
3. K. Minamoto, Y. Fujiki, N. Shiomi, Y. Uda, and T. Sasaki. J. Chem. Soc. Perkin Trans. 1, 2337 (1985).
4. J. Kimura, H. Kobayashi, O. Miyahara, and O. Mitsunobu. Bull. Chem. Soc. Jpn. **59**, 869 (1986).
5. J. Castro-Pichel, M.T. Garcia-Lopez, and F.G. De las Heras. Tetrahedron, **43**, 383 (1987).
6. V.J. Davisson, D.R. Davis, V.M. Dixit, and C.D. Poulter. J. Org. Chem. **52**, 1794 (1987).
7. M.D. Hagen and S. Chladek. J. Org. Chem. **54**, 3189 (1989).
8. J. Zemlicka and H.L. Chung. J. Heterocycl. Chem. **14**, 135 (1977).
9. M.A. Quilliam and E.Y. Osei-Twum. Abstr. 28th Annu. Conf. Mass Spectrom. Allied Topics, New York. May 1980.
10. E.Y. Osei-Twum, O.A. Mamer, M.A. Quilliam, and R. Gergely. Nucleosides Nucleotides, **9**, 369 (1990).
11. F. Seela, H. Rosemeyer, H. Berg, W. Bourgeois, T. Grein, U. Bindig, R. Gumbiowski, and S. Fischer. Abstr. Int. Symp. on the Analysis of Nucleosides, Nucleotides and Oligonucleotide Compounds, University of Antwerp. September 1989.
12. R.R. Shoup, H.T. Miles, and E.D. Becker. J. Phys. Chem. **76**, 64 (1972).
13. A.R. Katritzky and G.J.T. Tiddy. Org. Magn. Reson. **1**, 57 (1969).
14. J. Riand, M.-T. Chenon, and N. Lumbroso-Bader. J. Chem. Soc. Perkin Trans. 2, 1248 (1979).
15. J. Almog, A.Y. Meyer, and H. Shanan-Atidi. J. Chem. Soc. Perkin Trans. 2, 451 (1972).
16. R.R. Shoup, E.D. Becker, and M.L. McNeel. J. Phys. Chem. **76**, 71 (1972).
17. J. Riand, M.-T. Chenon, and N. Lumbroso-Bader. Can. J. Chem. **58**, 466 (1980).
18. T.P. Pitner, H. Sternglanz, C.E. Bugg, and J.D. Glickson. J. Am. Chem. Soc. **97**, 885 (1975).
19. D.M.G. Martin and C.B. Reese. Chem. Commun. 1275 (1967).
20. Z. Neiman and F. Bergmann. Chem. Commun. 1002 (1968).
21. M. Rabinowitz and A. Pines. J. Am. Chem. Soc. **91**, 1585 (1969).
22. H.Y. Cai and L.H. Zhang. Yaoxue Xuebao, **24**, 726 (1989); Chem. Abstr. **112**, 198953k (1990).

Can. J. Chem. Downloaded from www.nrcresearchpress.com by 213.200.69.106 on 09/08/12
For personal use only.

On the mechanism of Wittig reactions with cyclic anhydrides. II.

MARGARET M. KAYSER[1], KRISTA L. HATT, AND HESHUI YU
Department of Chemistry, University of New Brunswick, P.O. Box 5050, Saint John, N.B., Canada E2L 4L5

AND

DONALD L. HOOPER
Department of Chemistry, Dalhousie University, Halifax, N.S., Canada B3H 4J3

Received August 27, 1992

MARGARET M. KAYSER, KRISTA L. HATT, HESHUI YU, and DONALD L. HOOPER. Can. J. Chem. **71**, 1010 (1993).

A study by NMR spectroscopic methods and trapping experiments of the mechanism of Wittig reactions between stabilized phosphoranes and unsymmetrically substituted cyclic anhydrides suggests that two reactions are involved: (1) a low-energy, reversible formation of acyclic adducts; and (2) a higher energy "Wittig olefination" reaction leading to enol-lactones. The latter, more selective, transformation requires a more highly organized transition state in which π-stacking and stabilizing complexations are important factors.

MARGARET M. KAYSER, KRISTA L. HATT, HESHUI YU et DONALD L. HOOPER. Can. J. Chem. **71**, 1010 (1993).

Une étude par des méthodes de RMN et des expériences de piégeage réalisées en vue d'élucider le mécanisme des réactions de Wittig entre des phosphoranes stabilisés et des anhydrides cycliques substitués d'une façon non symétrique suggèrent que deux réactions sont impliquées : (1) une formation réversible, de faible énergie, d'adduits acycliques et (2) une réaction d'oléfination de Wittig, d'énergie élevée, conduisant à des énol-lactones. Cette dernière réaction, une transformation plus sélective, fait appel à un état de transition très organisé dans lequel un empilement π et des complexations stabilisantes sont des facteurs importants.

[Traduit par la rédaction]

Can. J. Chem. Downloaded from www.nrcresearchpress.com by 213.200.69.106 on 09/08/12
For personal use only.

Introduction

The condensation of stabilized phosphoranes with substituted cyclic anhydrides provides an excellent route to the corresponding enol-lactones (1–5). However, for several anhydrides studied, regioselectivity of the enol-lactones produced could not be reliably predicted on the basis of steric or electronic effects of the substituents (1–3). This was particularly evident in phthalic anhydrides with oxygen-containing groups (-OCH_3 or -NO_2) in position 3, where regioselectivity projections based on the electronic and (or) steric effects did not correspond to the experimental results (1).

Initially, we suggested that the unexpectedly high proportion of enol-lactones resulting from condensation at the carbonyl group adjacent to the oxygen-bearing substituents might be due to the stabilizing complexation between the electron deficient phosphorus atom of the ylide and the oxygen atom of the substituent (1–3). Our more recent studies of the mechanism showed that condensations of cyclic anhydrides with stabilized phosphoranes lead, in a low-energy, reversible process, to acyclic adduct(s). The enol-lactones are subsequently formed via a higher energy irreversible transformation (6). Taking into account a facile reversibility of acyclic adduct(s) formation, it was not possible to determine if the initial addition products are converted to enol-lactones, or if there exists an alternate, higher energy, pathway leading directly from cyclic anhydrides to enol-lactones. In view of these developments the role of neighbouring substituents on stabilization or destabilization of the transition state and hence on the regioselectivity of these reactions needed to be reinvestigated and refined.

The condensations of 3-methoxyphthalic and 3-nitrophthalic anhydrides, as well as several substituted maleic and succinic anhydrides, with stabilized ylides **1** and **8** were followed by ^1H and ^{31}P NMR. The reversibility of the initial condensation step was confirmed for several reactions of phthalic, maleic, and succinic anhydrides. Experiments designed to trap intermediates were carried out, and the trapped regioisomers were identified. This paper describes the above study and discusses mechanistic implications of the results obtained.

Results and discussion

The general approach used is illustrated by the extensively investigated reactions of methyl(triphenylphosphoranylidene)acetate **1** with 3-methoxyphthalic anhydride **2** and 3-nitrophthalic anhydride **5**. The outlines for the reactions are illustrated in Scheme 1 and Scheme 3, respectively.

The effects of 3-methoxy and 3-nitro substituents on the rate of enol-lactone formation

The room temperature (25°C) condensation of 3-methoxyphthalic anhydride **2** with ylide **1**, monitored by ^1H NMR, showed that the reaction is 50% complete in approximately 25 min (Table 1). Under the same conditions condensation of 3-nitrophthalic anhydride **5** with ylide **1** does not progress beyond the formation of acyclic intermediates, and the conversion to enol-lactones is observed only on heating above 50°C (Fig. 1). This experiment did not provide an explanation for the sluggish formation of enol-lactones; which might be caused (*a*) by a slower conversion of the 3-nitrophthalic anhydride to enol-lactones, or (*b*) by a greater stability of the acyclic products. The results obtained so far suggested that, in order to understand the mechanism of the formation of enol-lactones, it is necessary to establish the role played in these reactions by the acyclic intermediates.

Reactions with methyl(triphenylphosphoranylidene)acetate

1. Acyclic intermediates: formation, stability and identity

3-Methoxyphthalic anhydride

During the room temperature condensation of anhydride **2** with ylide **1**, there was no significant buildup of adducts

[1]Author to whom correspondence may be addressed.

TABLE 1. Room temperature (25°C) reaction of 3-methoxyphthalic anhydride with ylide **1** monitored by ^{1}H NMR.

Time (min)	Ylide CH_3O (ppm)	%	Intermediates CH_3O (ppm)	%	Products CH_3O (ppm)	%
2	3.50	72	3.00	14	4.00 br 3.80 br	14
8	3.50	68	3.00	8	4.00 br 3.80 br	24
15	3.50	60	3.00	7	4.00 br 3.80 br	33
20	3.50	54	3.00	3	4.00 br 3.80 br	43
25	3.50	47	3.00	Trace	4.00 br 3.80 br	53
32	3.50	30	3.00	Trace	4.00 br 3.80 br	70
55	3.50	28	3.00	Trace	4.00 br 3.80 br	72
85	3.50	24	3.00	Trace	4.00 br 3.80 br	76
100	3.50	21	3.00	Trace	4.00 br 3.80 br	78
Next day	—	—	—	—	4.02 αZ 3.80 βE 3.83 βZ 3.93 αE	50 32 12 6

Can. J. Chem. Downloaded from www.nrcresearchpress.com by 213.200.69.106 on 09/08/12
For personal use only.

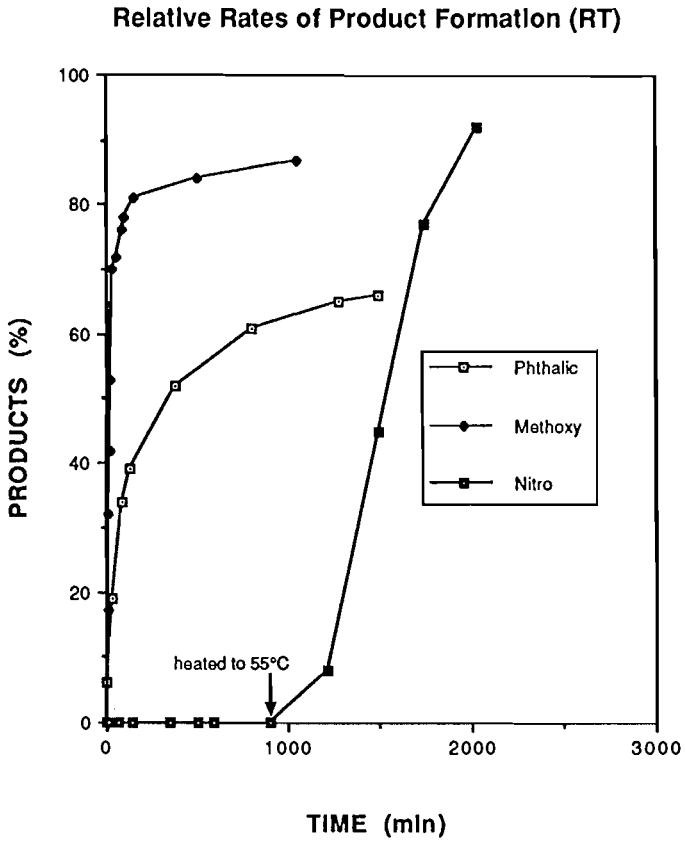

FIG. 1. The relative rates of enol-lactone formation in the reactions of 3-methoxy, 3-nitro, and unsubstituted phthalic anhydrides with ylide **1** at room temperature.

2α and **2**β at any time. The spectrum recorded immediately upon mixing showed that the reaction mixture was composed of 72% ylide (3.50 ppm), 14% acyclic intermediate (3.00 ppm, only one broad signal was observable), and 14% enol-lactone products, (Table 1). As the reaction progressed the proportion of the intermediate dropped rapidly, accompanied by a simultaneous increase in the quantity of the enol-lactones. After 20 min only a trace amount of an intermediate was observable in the ^{1}H NMR spectrum, and this situation persisted until all the remaining ylide was converted into products. The relative proportions of the four products were established from the integration of their methoxy and vinylic proton signals (1).

When the same reaction was initiated at −35°C (Scheme 1), two signals for the acyclic intermediates appeared immediately and, as enol-lactones did not form at low temperature, an important accumulation (>50%) of the intermediates was observed below 10°C (Table 2). As the reaction progressed the initial ratio of the two intermediates (3:7 recorded at −35°C) changed with the rising temperature until at 5°C the minor intermediate was visible only as a shoulder on the major methoxy signal (Table 2).

Our interpretation of these results is as follows: immediately upon mixing of the 3-methoxyphthalic anhydride **2** with ylide **1** at −35°C, the condensation occurs at both carbonyl groups, with the α-carbonyl adduct being produced in excess. As the temperature is raised stepwise, the α/β ratio increases slowly, indicating the shift toward the more stable adduct. The P–O affinity may be a key factor in stabilization of the **2**α adduct, as illustrated in Fig. 2*a*. When the reaction temperature reaches the point where the formation of enol-lactone can occur, the **4**α and **4**β enol-lactones appear.

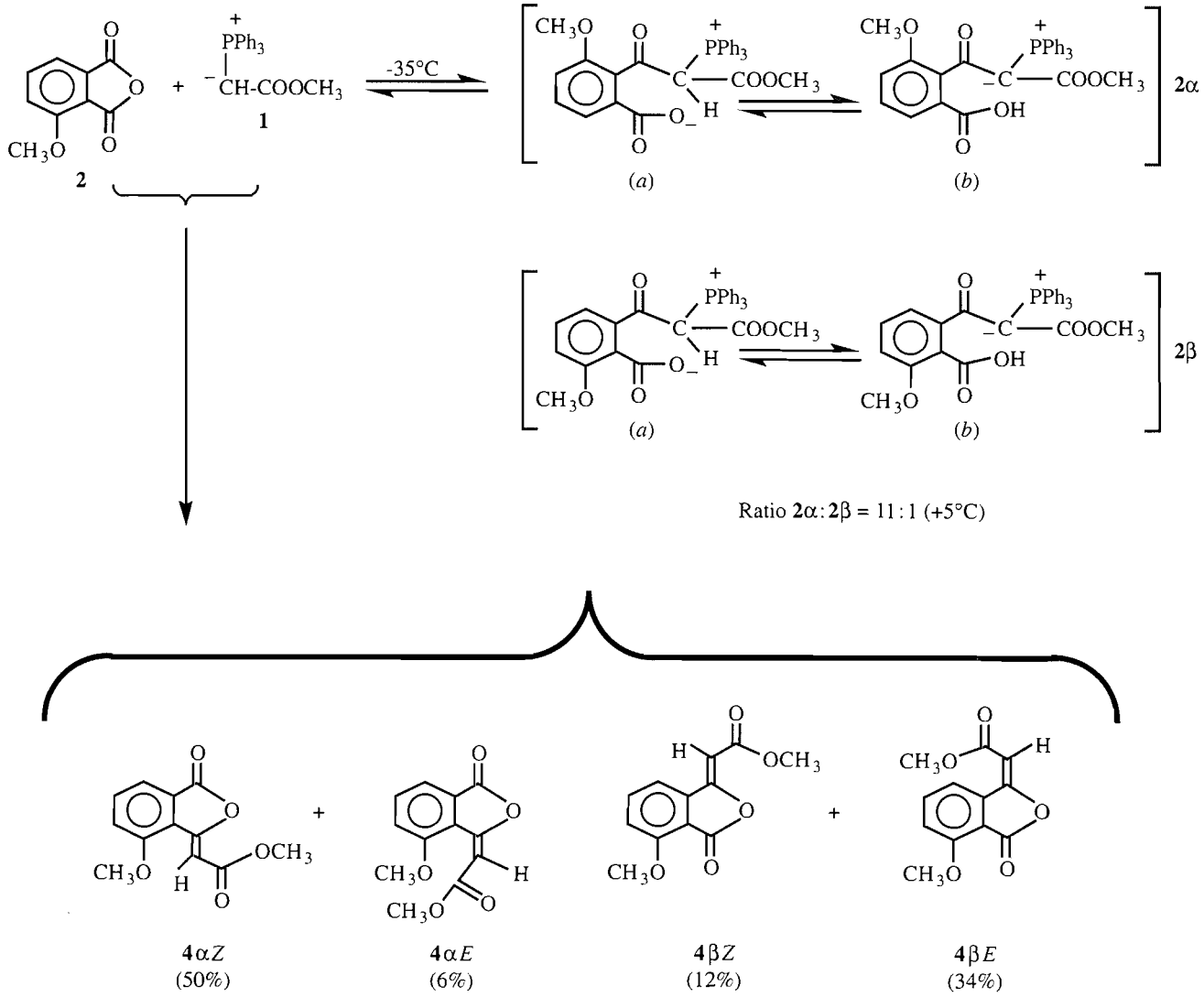

SCHEME 1

The slightly higher proportion of the **4α** enol-lactone produced corroborates the previously postulated π-stacked transition state (1), incorporating a stabilizing complexation between the 3-methoxy substituent and an electron-deficient phosphorus atom as illustrated in Fig. 3 (1). Such complexation justifies, at least in part, the formation of electronically and sterically unfavourable **4α** regioisomers (7). It is important to note that the product ratio (**4α**:**4β**) does not reflect the ratio of isomeric acyclic intermediates (**2α**:**2β**) at the temperature at which the enol-lactones appear (Scheme 1). These results put in question the role of acyclic adducts as true intermediates in the transformation of cyclic anhydrides to enol-lactones.

The proportion of esters **3α** and **3β** trapped with CH_2N_2 did not correspond to the ratio of the acyclic adducts **2α** and **2β** any more than did the ratio of enol-lactones. Treatment of the reaction mixture with CH_2N_2 at the time of the maximum buildup of the intermediates (5°C) when the ratio of **2α**:**2β** was approximately 11:1, gave a 5:3 mixture of **3α** and **3β** (Scheme 2). Subsequent trapping experiments carried out at various temperatures between −5°C and 15°C consistently produced significant quantities of **3β** (35–45%), showing that the initial addition of the ylide to the anhydride is an equilibrium and that the reaction with CH_2N_2 is faster with the **3β** intermediate.

The structural identities of the two isomeric acyclic adducts were established from their spectral data and were confirmed by the X-ray crystal structure obtained for the minor **3β** isomer.[2]

The reversibility of the condensation of ylide **1** with 3-methoxyphthalic anhydride was verified by the following experiment. The low temperature condensation reaction monitored by ^1H NMR was allowed to proceed until 50% of the ylide was converted into acyclic intermediates, at which point freshly distilled benzaldehyde was added to the reaction solution. The signals of both the ylide and the intermediate slowly disappeared and the only observable product, besides the recovered anhydride, was methyl cinnamate.

[2]F. Rochon, M.M. Kayser, Unpublished results.

Can. J. Chem. Downloaded from www.nrcresearchpress.com by 213.200.69.106 on 09/08/12
For personal use only.

TABLE 2. Low temperature reaction of 3-methoxyphthalic anhydride with ylide **1** monitored by ^1H NMR.

Temperature (°C)	Time (min)	Ylide CH_3O (ppm)	%	Intermediates CH_3O (ppm)	%	Products CH_3O (ppm)	%
−35	0	3.60					
		3.34					
−32	15	3.53	90	3.00 α	7	—	
				3.05 β	3		
−20	30	3.52	84	2.99 α	11	—	
				3.07 β	5		
−10	60	3.52	75	3.00 α	19	—	
				3.07 β	6		
−5	90	3.51	69	3.00 α	25	—	
				3.05 β	6		
−5	100	3.51	62	3.01 α	31	—	
				3.05 β	7		
+5	120	3.51	53	3.01 α	43	—	
				sh β	4		
+12	135	3.50	50	3.02 α	46	—	
				sh β	4		
+27	165	3.50	49	3.00 α	27	3.80 β*E*	12
				sh β		3.99 α*Z*	12
+27	180	3.51	21	3.00 br	16	3.80 β*E*	22
						3.99 α*Z*	29
						3.83 β*Z*	9
						3.92 α*E*	3

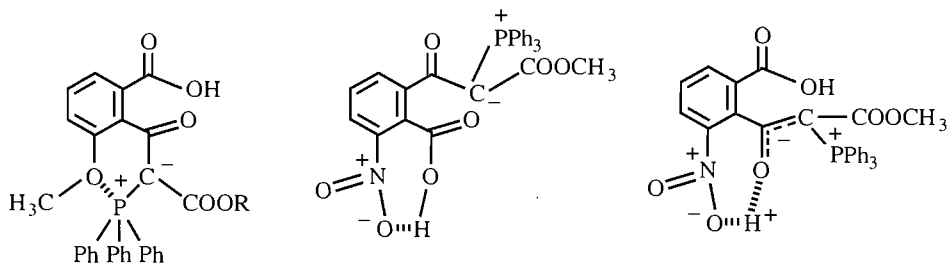

(*a*) (*b*) (*c*)

FIG. 2. Proposed stabilization of the acyclic adducts by strong P–O complexation in **2**α (*a*) and by H-bonding in compounds **5**β (*b*) and **5**α (*c*). The stabilizing H-bonding for the isomeric adduct **2**β, similar to that depicted in (*b*), should be considerably weakened by the competing conjugation of the electron pair from the oxygen atom with the electron-poor aromatic ring.

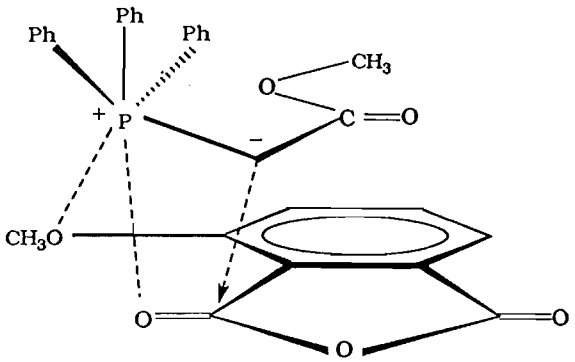

FIG. 3. The proposed stabilization of the transition state by complexation of the 3methoxy substituent with an electron-deficient phosphorus of the ylide.

3-Nitrophthalic anhydride

The reaction of ylide **1** with 3-nitrophthalic anhydride **5**, both freshly crystallized (Scheme 3), yielded the acyclic intermediates very rapidly at room temperature (25°C). The subsequent transformation to enol-lactones required a longer reaction time and a considerably higher temperature (above 50°C) in order to occur. Thus, at room temperature there was a large buildup of acyclic intermediates **5**α and **5**β in the ratio 1:8, which remained relatively unchanged until the reaction mixture was heated above 50°C (Table 3). It appears, therefore, that the presence of an electron-withdrawing 3-nitro substituent does not reduce the rate of formation of acyclic adducts; it does, however, affect the step leading to enol-lactones.

During the low temperature study, a bright yellow colour developed immediately upon mixing at −40°C, and the

Can. J. Chem. Downloaded from www.nrcresearchpress.com by 213.200.69.106 on 09/08/12
For personal use only.

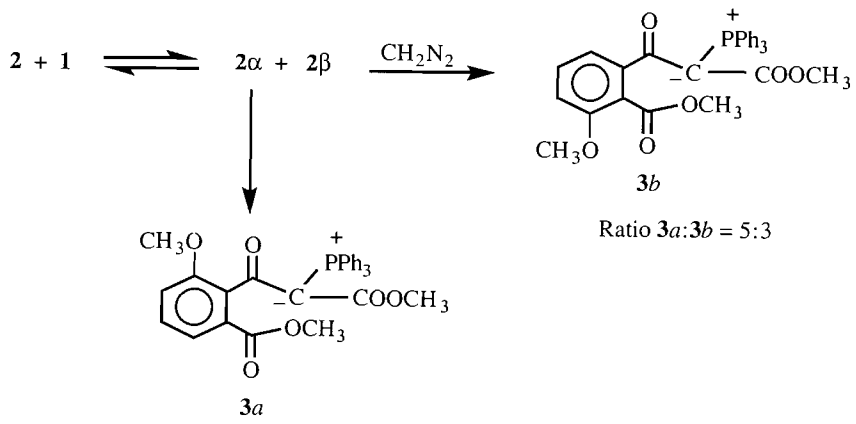

SCHEME 2

spectrum recorded within 10 min showed that the reaction mixture was composed of the ylide (25%) and two acyclic adducts (75%) in the ratio 5α:5β = 1:4 (Table 4). As the temperature was raised, a little more of the anhydride **5** was converted into acyclic intermediates, but the ratio α/β changed only slightly until about 50°C, when the relative proportion of 5α was further reduced and enol-lactones started to appear.[3]

It may be concluded that the higher stability of the 5β is enhanced by internal H-bonding of the *ortho* acid group with the substituent. Such intramolecular H-bonding, between the acid functionality and a highly negative oxygen atom of the nitro substituent, illustrated in Fig. 2*b*, should be especially strong. It would be expected to delay recyclization of the 5β acyclic adduct and consequently interfere with the formation of enol-lactones.

While the 5β adduct is the major regioisomer, the formation of enol-lactones favours the α-condensation. It may be that the stabilizing complexation with an oxygen-bearing nitro group, as shown in Fig. 4, lends a slight bias in favour of the α carbonyl group. It should be added, however, that in this case the α attack is also promoted by electronic effects, while being opposed by steric effects of the substituent (7).

Trapping of the intermediates with CH_2N_2, at 15°C, gave a high percentage (above 80%) of 7β, (identified from its ^{13}C and ^1H NMR spectra) compared with less than 20% of the 7α isomer. These values reflect almost exactly the ratio of the two intermediates 5α and 5β at the time of trapping, suggesting that the reaction with diazomethane is faster than retro-condensation (Scheme 4).

The reversibility of the formation of 5α and 5β was confirmed independently. Thus, upon mixing freshly crystallized ylide **1** and sublimed 3-nitrophthalic anhydride **5** at room temperature, a strong (65%) signal for the 5β appeared immediately. After 30 min at 25°C the bright yellow equilibrated reaction mixture consisted of approximately 80% intermediate (3.00 ppm) and 20% ylide **1** and conjugate acid **1***a* exchanging pair (broadened signal at 3.58 ppm). When freshly distilled benzaldehyde was added, the colour disappeared instantaneously, and so did the intermediate and the remaining ylide; the only signals observable were those for *trans*-methyl cinnamate and a small peak (<10%) for the methoxy group of the conjugate acid $Ph_3PCH_2COOCH_3Br$ **1***a* at 3.61 ppm.

Reactions with carboethoxyethylidene triphenylphosphorane ***8***.

To assess the importance of the stabilization of the acyclic adducts through proton exchange and H-bonding, we followed condensations of anhydrides **2** and **5** with carboethoxyethylidene triphenylphosphorane **8**, an ylide that does not possess an exchangeable hydrogen atom. Both reactions gave enol-lactones rapidly at room temperature. Interestingly, the reaction with 3-nitrophthalic anhydride was considerably faster than that with 3-methoxyphthalic anhydride. In the former case, the ^1H NMR spectrum recorded immediately on mixing of the reagents showed that the reaction was already completed and only the signals for enol-lactone and triphenylphosphine oxide were observable. In the latter case, the disappearance of **8** could be monitored for about an hour, with the last traces of the ylide still detectable a few hours later (Scheme 5).

The two reactions were entirely regio- and stereoselective, leading in both cases to a single enol-lactone in 100% yield based on ^1H NMR evidence. However, while the reaction of **8** with 3-methoxyphthalic anhydride gave selectively the 9α*E* enol-lactone, the reaction with 3-nitrophthalic anhydride produced exclusively the 10β*E* product. Similarly, 100% β selectivity was also observed in the reaction of 3-nitrophthalic anhydride with the fluorinated ylide $Ph_3PC(F)COOEt$ **11**. The only product isolated from this condensation showed a highly deshielded doublet at 9.7 ppm, characteristic of the aromatic proton *ortho* to the ylidene substituent in phthalic *E* enol-lactones (1).

A study of the condensation of ylide **8** with unsubstituted phthalic anhydride, reported previously (6), implied that an unstable intermediate formed during the reaction is in rapid equilibrium with the starting materials and cannot be observed by ^1H NMR as a distinct species even at low (−40°C) temperature. Its fleeting existence can be deduced from the

[3]Interestingly, when the same reaction was carried out with 3-nitrophthalic anhydride contaminated with 3-nitrophthalic acid, the two acyclic adducts 5α and 5β were present in a 1:1 ratio. The conversion to enol-lactones was very slow even above 55°C. It appears that an excess of acidic protons in the reaction mixture stabilizes 5α, possibly by an internal H-bonding (Fig. 2*c*), thus leading to its accumulation. Under these circumstances both regioisomers are slow to recyclize and formation of enol-lactones is further delayed.

Can. J. Chem. Downloaded from www.nrcresearchpress.com by 213.200.69.106 on 09/08/12
For personal use only.

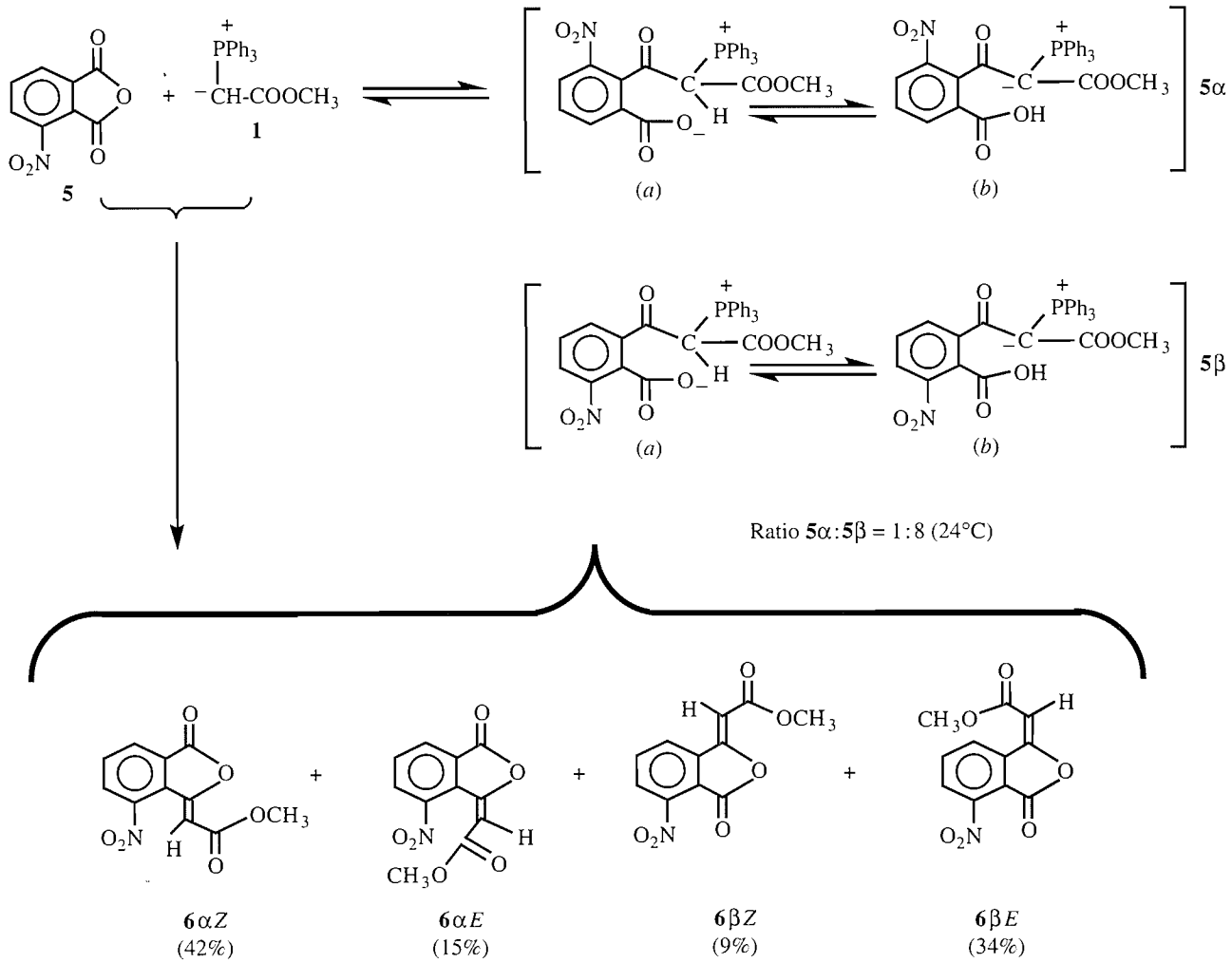

SCHEME 3

broadening of the methyl and methylene (CH_3CH_2O-) proton signals and a transient broad peak in the ^{31}P NMR spectrum. The situation is very similar in the corresponding reactions of **8** with the 3-substituted phthalic anhydrides. Here also, we were unable to trap any intermediates, and consequently regioselectivity of the initial attack (if distinct from the regioselectivity of enol-lactone products) cannot be determined.

The lack of success in trapping acyclic compounds during the reactions with ylide **8**, suggests that, if they do form at all (as appears to be the case judging by the broadening of the ^{31}P signal), they are highly unstable species in rapid equilibrium with the starting materials. In view of this, we may conclude that proton exchange within the **2**α,**2**β and **5**α,**5**β pairs contributes significantly to the stability of the adducts. The internal H-bonding, and complexations of electron-deficient phosphorus with substituent (vide supra) provide additional stabilization for these adducts.

Other interesting observations, which were not apparent from the reactions with ylide **1**, came to light and are summarized as follows:

1. The generation of highly stabilized acyclic adducts obscures the reaction leading to enol-lactones. When this effect is abstracted, it becomes possible to see that an electron-withdrawing nitro substituent accelerates (as might be expected) the rate of an ylide's attack compared to the rate of attack of the same ylide on an anhydride substituted with an electron-donating methoxy group. Hence, the sluggish formation of enol-lactones during the condensation of **1** with **5**, compared to the condensation of **1** with **2** (Fig. 1), can be linked to a higher stability of the acyclic compounds **5**α and **5**β.

2. The formation of acyclic products is a reversible process, with an equilibrium lying to the left when unstable, readily recyclable, adducts are produced (as in the reaction of ylide **8** with phthalic anhydride), or far to the right, when highly stabilized, not readily recyclable, products are formed (ylide **1** with **5**). This conclusion is supported by an earlier observation (8) that unsubstituted glutaric anhydride reacts with stabilized ylides to give a stable acyclic intermediate, but is converted to enol-lactones only with difficulty (several days of heating), while 2,2-*gem*-disubstituted glutaric anhydride, which recyclizes readily due to the Thorpe–Ingold

Can. J. Chem. Downloaded from www.nrcresearchpress.com by 213.200.69.106 on 09/08/12
For personal use only.

TABLE 3. Reaction of 3-nitrophthalic anhydride with ylide **1** monitored by ^{1}H NMR

Temperature (°C)	Time (min)	Ylide CH_3O (ppm)	%	Intermediates CH_3O (ppm)	%	Products CH_3O (ppm)	%
24	30	3.48	6	2.96 β	84		
				3.05 α	10		
40	60	3.48	5	2.96 β	89		
				3.05 α	6		
45	75	3.48	6	2.96 β	85	3.82 β*E*	2
				3.04 α	7	sh α*Z*	
						3.76 α*E*	
50	105	3.47	5	2.96 β	79	3.82 β*E*	10
				3.03 α	6	sh α*Z*	
						3.76 α*E*	
55	120	3.48	10	2.96 β	67	3.83 β*E*	5
				3.03 α	7	3.82 α*Z*	7
						3.76 α*E*	4
65	195	3.48	7	2.96 β	38	3.83 β*E*	15
				3.03 br	3	3.82 α*Z*	23
						3.80 β*Z*	1
						3.75 α*E*	12
65	270	3.55	4	2.96 β	18	3.83 β*E*	22
				3.05 br	1	3.82 α*Z*	35
						3.80 β*Z*	4
						3.75 α*E*	16

TABLE 4. Low temperature reaction of 3-nitrophthalic anhydride with ylide **1** monitored by ^{1}H NMR

Temperature (°C)	Time (min)	Ylide CH_3O (ppm)	%	Intermediate α CH_3O (ppm)	%	Intermediate β CH_3O (ppm)	%	Products CH_3O (ppm)	%
−40	15	3.43	25	3.02	14	2.93	61	—	
−25	30	3.44	24	3.03	14	2.94	62	—	
−15	50	3.47	23	3.04	14	2.94	63	—	
−5	75	3.49	20	3.05	15	2.95	65	—	
+6	95	3.52	20	3.05	12	2.95	68	—	
+17	115	3.52	20	3.05	12	2.95	68	—	
+55	325	3.55	6	3.05	3	2.95	36	3.82 α*Z*	25
								3.83 β*E*	18
								3.77 α*E*	10
								3.80 β*Z*	2

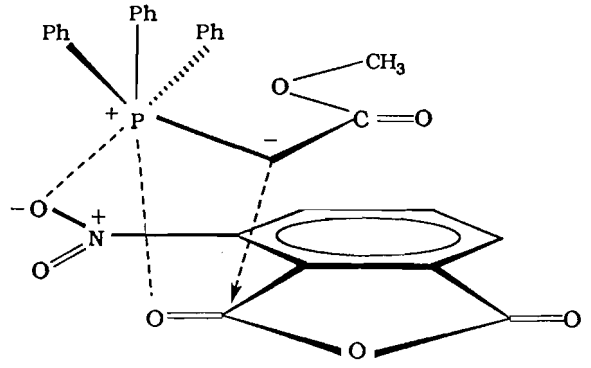

FIG. 4. A possible stabilizing complexation between the electron-rich oxygen atom of the 3-nitro substituent and an electron-deficient phosphorus of the ylide.

gem-dialkyl effect (9), produces enol-lactones considerably more rapidly.

Furthermore, in the reactions of 3-methoxy- and 3-nitrophthalic anhydrides with ylide **1**, the proportions of acyclic adducts were found to be different from the proportions of enol-lactones formed. These results suggest that two different reactions with different regioselectivity patterns are involved: the lower energy reversible condensation, leading to acyclic intermediates, and the higher energy irreversible formation of enol-lactones. To verify the above conclusions, we investigated the reactions of several substituted maleic and succinic anhydrides with stabilized ylides, following methodology employed in the study of 3-substituted phthalic anhydrides. The results, summarized in Table 5, show that in the majority of cases studied the ratios of enol-lactones obtained bear no relationship to the regioselectivity

Can. J. Chem. Downloaded from www.nrcresearchpress.com by 213.200.69.106 on 09/08/12
For personal use only.

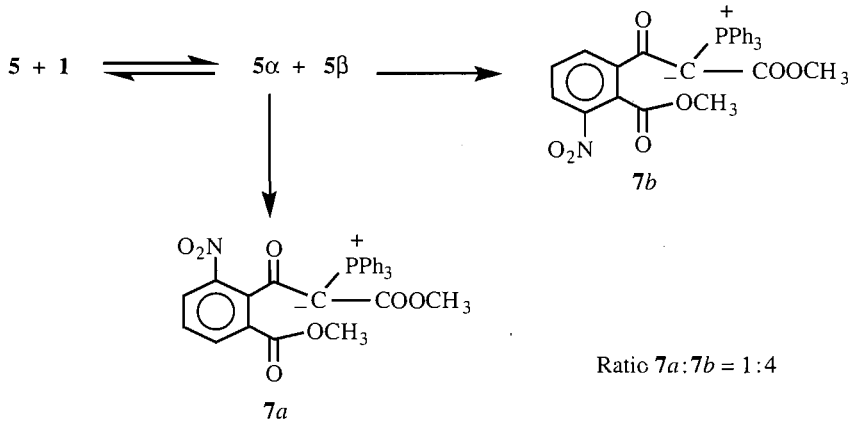

SCHEME 4

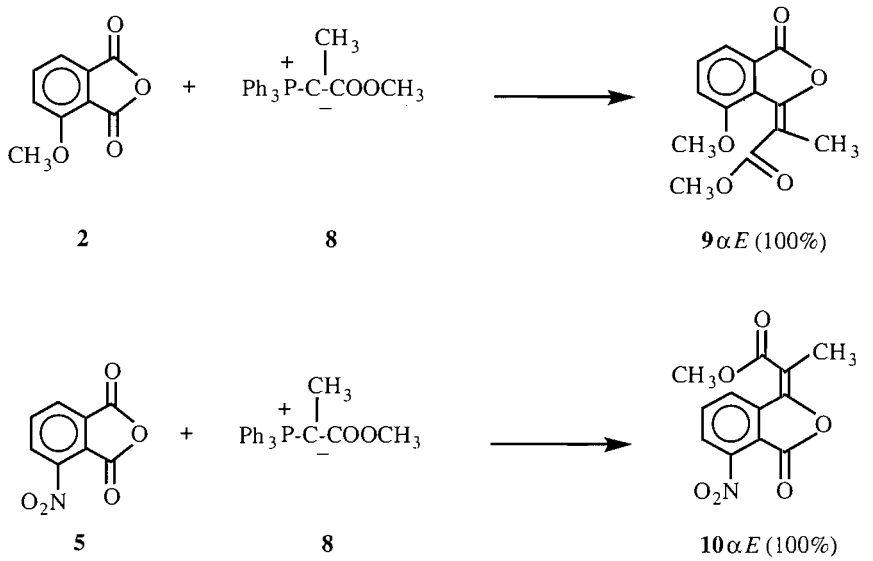

SCHEME 5

of the formation of acyclic adducts. It is most clearly evident in the reactions of ylide **1** with phenylmaleic, methoxymethylmaleic, and methoxysuccinic anhydrides where two acyclic adducts are formed at low temperatures, while the corresponding enol-lactones are produced in very high yields with 100% regioselectivity for α or β carbonyl groups depending on the substrate (1, 2, 3, 10).

The mechanisms of reactions of stabilized ylides with cyclic anhydrides have been the subject of much speculation and several reaction pathways have been proposed (1–4, 11–14). The data obtained in this study indicate that the formation of acyclic intermediate(s) is a reversible process, with an apparently quite low energy transition state. To obtain an acyclic adduct nucleophilic addition must proceed via a tetrahedral intermediate (15); in other words it must involve an unstable betaine intermediate or betaine-like transition state. The formation of acyclic products is clearly sterically dependent, as illustrated by regioselective formation of β adducts in 2,2-dimethyl- and 2,2-diphenylsuccinic anhydrides (Table 5). However, when steric congestion is not very severe, as is the case in planar maleic anhydrides or in mono substituted succinic anhydrides, the addition occurs at both carbonyl groups. The electronic/complexation effects of the substituents appear to have limited effect on the course of these reactions.

The formation of enol-lactones appears to follow a different route involving a more organized, higher energy, transition state. We suppose that this is a pathway entailing an oxaphosphetane intermediate or an "oxaphosphetane-like" transition state, thus corresponding to an extensively investigated mechanism of reactions of nonstabilized and semi-stabilized ylides with aldehydes and ketones (16–18). The principal difference between Wittig reactions with aldehydes and ketones and Wittig reactions with cyclic anhydrides lies in the fact that in the former, "salt-free," condensations, the betaine intermediates do not appear to play a role; betaine has never been trapped or detected (16–18) and, according to the calculations (19, 20), it should be a higher energy species than oxaphosphetane. In the latter case, presence of an excellent leaving group at the carbonyl centre obviously lowers the energy of the betaine-like transition state and provides a low-energy alternate pathway to acyclic addition products. The enol-lactones, therefore, are not formed unless the formation of acyclic adducts is reversible. The irreversible formation of such adducts, observed in reactions of stabilized ylides with acyclic anhydrides and acid halides

Can. J. Chem. Downloaded from www.nrcresearchpress.com by 213.200.69.106 on 09/08/12
For personal use only.

TABLE 5. Formation of acyclic adducts and enol - lactones

Anhydride	Acyclic adducts	Temperature	Reversibility	Enol - lactone αE	αZ	βE	βZ	Yield (%)
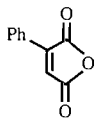	**2**	−30	Yes	—	—	100	—	86
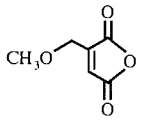	**2**	−20	[b]	—	—	100	—	60 90[a]
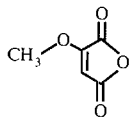	**1**	−30	[b]	28	72	—	—	96
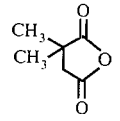	**1β**	+20	Yes	—	—	100	—	88
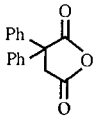	**1β**	+20	Yes	—	—	100	—	90
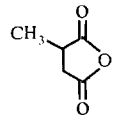	**2**	−20	[b]	43	14	43	—	67
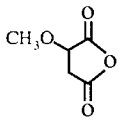	**2**	−30	Yes	100	—	—	—	71 96[a]

[a]NMR analyzed.
[b]Not studied.

(11), is probably responsible for the fact that these compounds do not give olefination products.

The higher energy, but also more highly organized, transition state leading to enol-lactones explains adequately the regio- and stereoselectivity observed in reactions of stabilized ylides with cyclic anhydrides. It is in agreement with Chopard's explanation of high *E*-selectivity observed in the reactions of stabilized ylides with phthalic anhydrides (12) and our justification of regioselectivity observed in 2-methoxymaleic (3), 2-methoxysuccinic (2), and 3-methoxy- and 3-nitrophthalic anhydrides (1).

The reaction of stabilized ylides with cyclic anhydrides can be described in kinetic terms as follows. Compounds A and B are rapidly and reversibly converted to an adduct AB; a product P is formed at a relatively slow rate. In such cases, unfortunately, there is no observable kinetic difference between the mechanism in which P is formed by the first-order rearrangement of AB, and one in which it is formed by a second-order reaction of A with B in which AB is not an intermediate, as shown in reactions 11 and 12 of ref. 21.

$$A + B \leftrightharpoons AB \rightarrow P \quad (11)$$

and

$$P \leftarrow A + B \rightleftharpoons AB \quad (12)$$

Although it is not possible to distinguish between these two possibilities on the basis of their kinetics, we interpret the observed results on the premise that the formation of acyclic "intermediates" and the formation of enol-lactones are two independent reactions, which proceed to different products via different reaction pathways (equation 12). The low-energy, reversible formation of acyclic adducts is in evidence when stabilized acyclic compounds can be produced. One can imagine that, at the limit, when the acyclic products are particularly stable or difficult to recyclize (six(or more)-member cyclic anhydrides) or the reagent ylide is too reactive to be displaced, the reaction becomes irreversible and consequently the corresponding enol-lactones are not produced. The alternate route, shown in equation 11, requires evocation of a betaine intermediate or a betaine-like transition state during the recyclization process. The subsequent

Can. J. Chem. Downloaded from www.nrcresearchpress.com by 213.200.69.106 on 09/08/12
For personal use only.

Can. J. Chem. Downloaded from www.nrcresearchpress.com by 213.200.69.106 on 09/08/12
For personal use only.

reorganization of that betaine via higher energy oxaphosphetane would then lead to enol-lactone. The betaine (or oxaphosphetane) in that case would be a common intermediate for the formation of acyclic adducts and enol-lactones. Considering the difference in regioselectivity of these two products, we consider the "two independent reactions scenario" illustrated by equation 12 more plausible (Scheme 6).[4]

Conclusion

In this paper we have described the study of condensations of stabilized ylides with substituted cyclic anhydrides. Based on these results, as well as the results of several prior investigations, we conclude that the reactions of stabilized ylides with cyclic anhydrides give acyclic addition products via a low-energy, reversible pathway, probably involving a betaine-like transition state, while the enol-lactones (the "Wittig" products) are formed through a higher energy route, most likely involving a highly organized transition state and possibly an unstable oxaphosphetane intermediate.

In five-member cyclic anhydrides, the stability of acyclic intermediates can vary from a transient species, rapidly equilibrating with the starting materials, through adducts stabilized by internal proton exchange readily observable in low-temperature, NMR to intramolecularly H-bonded compounds stable up to 45–50°C. Intermediates that can form strong intramolecular H-bonds, or are otherwise stabilized, are slow to recyclize and consequently are slow to form Wittig products.

In general, the stabilizing complexation between an electron-deficient phosphorus atom of the ylide and an electron-rich oxygen atom of a strategically located substituent on the anhydride ring has a controlling effect on the regioselectivity of the formation of enol-lactones.

Experimental

Melting points were determined on a Fisher–Johns melting point apparatus and are uncorrected. Infrared spectra were obtained on a Perkin–Elmer 297 infrared spectrophotometer. Nuclear magnetic resonance spectra were recorded on the Varian XL-200 spectrometer and on the Nicolet 360 NB spectrometer of the Atlantic Regional Magnetic Resonance Centre. All spectra were in $CDCl_3$ solutions unless otherwise specified, with TMS as internal reference (^1H and ^{13}C) or 85% H_3PO_4 as external standard (^{31}P). Temperature control was by the usual Nicolet method. Calibration of the thermocouple showed an estimated error of less than 1° in the temperature range used. Mass spectra were obtained on a Kratos MS 550 TC mass spectrometer. Gas chromatography analyses were carried out with a Shimadzu GC 9A chromatograph, using 5% OV101 on Supelcoport 100–120 mesh column. Chromatographic separations were performed on a Chromatotron 7924T radial thin-layer chromatograph.

General procedures

*Room temperature reactions of anhydrides **2** and **5** monitored by ^1H NMR*

An ylide (0.3 mmol) was dissolved in $CDCl_3$ (3 mL) and the spectrum was recorded. An anhydride (0.3 mmol) suspended in 0.5 mL $CDCl_3$ was added to the ylide. The mixture was shaken and the spectrum was recorded immediately. The composition of the reaction mixture was determined from integration of ^1H NMR spectra taken at regular intervals. After the reaction was completed, the enol-lactone products were separated from the triphenylphosphine oxide by chromatography on silica gel. The product distribution was compared with that obtained in the condensation reactions carried out in refluxing THF (1).

Low-temperature reactions were run on the same scale as described above. General procedures for low-temperature condensations and for reactions carried out under anhydrous conditions are described in previous papers (12, 13).

*Trapping of 3-methoxyphthalic anhydride **2** + ylide **1** with CH_2N_2*

3-Methoxyphthalic anhydride **2** (200 mg, 1.12 mmol) suspended in 10 mL of $CHCl_3$ was cooled to −5°C. Ylide **1** (375 mg, 1.12 mmol) dissolved in 10 mL of $CHCl_3$ and precooled to −5°C was added to the anhydride at −5°C and this temperature was maintained for 1, 5, 30, and 150 min. After the appropriate time, the reaction was quenched with a slight excess of diazomethane and left overnight before removing the ether. The ^1H NMR spectrum of the crude reaction mixture was recorded. In all cases studied the intermediates formed were trapped in ratios ranging from 5:3 to 5:4. Sometimes small quantities of the enol-lactones were also produced. The isomers formed were difficult to separate, and several chromatographic runs were required to obtain pure samples for ^1H NMR and mass spectra. The ^{13}C NMR spectra were run on mixtures of the two isomers and consequently the peak assignments reported here are tentative. The isomers were separated by repeated chromatography on silica gel. The minor, **3β**, isomer was eluted first with $CHCl_3$ (+ 0.8% MeOH) and was recrystallized from methanol to give white crystals melting at 199–203°C. 1-Methoxycarbonyl-2-(3′,2′-methoxycarbonylmethoxyphenyl)-2-oxoethylidenetriphenylphosphorane, **3β**: ^1H NMR δ: 3.11 (s, 3H, OCH_3), 3.70 (s, 3H, OCH_3), 3.81 (s, 3H, OCH_3), 6.91 (d, 1H), 7.15 (d, 1H), 7.34 (t, 1H), 7.44–7.98 (15 aromatic protons); ^{13}C NMR δ: 49.71, 51.67, 56.11, 72.10 (J_{PC} = 127 Hz), (overlapping aromatic carbons), 144.7 (J_{PC} = 8 Hz), 156.43, 166.75, 167.6 (J_{PC} = 5 Hz), 191.32(d); *m/z*: M^+ 526, 467($M^+ - COOCH_3$), 277(100), 248 ($M^+ - Ph_3POH$), 217, 77, 55. The major, **3α**, isomer was eluted second with $CHCl_3$ (+ 2% MeOH) and was recrystallized from methanol to give white crystals with melting point 224–226°C. 1-Methoxycarbonyl-2-(2′,3′-methoxycarbonylmethoxyphenyl)-2-oxoethylidenetriphenylphosphorane, **3α** : ^1H NMR δ: 3.01 (s, 3H, OCH_3), 3.74 (s, 3H, OCH_3), 3.85 (s, 3H, OCH_3), 7.05 (d, 1H), 7.25–7.96 (15 aromatic protons); ^{13}C NMR δ: 49.43, 51.87, 55.96, 70.9 (J_{PC} = 127 Hz) (overlapping aromatic carbons), 155.49 (J_{PC} = 4 Hz), 167.30, 167.60 (d), 189.77 (J_{PC} = 4 Hz); *m/z*: 525 ($M^+ - 1$), 494 ($M^+ - CH_3OH$), 466 ($M^+ - COOCH_3$), 276 (100), 261, 247, 77, 55. Overall yield of the two intermediates was 62%. These phosphoranes were completely unreactive towards benzaldehyde. Even after 24 h refluxing in toluene, no product was observed and the two intermediates were recovered unchanged.

*Trapping of 3-nitrophthalic anhydride **5** + ylide **1** with CH_2N_2*

3-Nitrophthalic anhydride **5** (196 mg, 1.0 mmol), recrystallized from $CHCl_3$ and suspended in 5 mL of $CHCl_3$, was added to the solution of methyl(triphenylphosphoranylidene)acetate **1** (339 mg, 1.0 mmol) in 5 mL of $CHCl_3$ at room temperature. A bright yellow solution was formed immediately upon mixing. The reaction was left 10 min before quenching with a slight excess of diazomethane (0.2 M in Et_2O, 6 mL). After standing overnight in the fumehood the solvent was evaporated and the ^1H NMR spectrum of the crude product (73%, 431 mg) was recorded. The mixture contained two isomers in the ratio 85:15. The major isomer **7β** was crystallized from ethanol to give a yellow compound, approximately 90% pure. After several crystallizations a pure sample of the major isomer was obtained. We were unable to get an equally pure sample of the minor isomer. 1-Methoxycarbonyl-2-(2′,3′-methoxycarbonylnitrophenyl)-2-oxoethylidenetriphenylphosphorane, **7β**: mp 165–167°C; ^1H NMR δ: 2.97 (s, 3H, OCH_3), 3.78 (s, 3H, OCH_3), 8.16–7.39 (m, 18H, aromatic protons); ^{13}C NMR δ:

[4]The referees for this paper indicated that the possibility of a common intermediate (betaine or oxaphosphetane) for the two reactions cannot be entirely rejected.

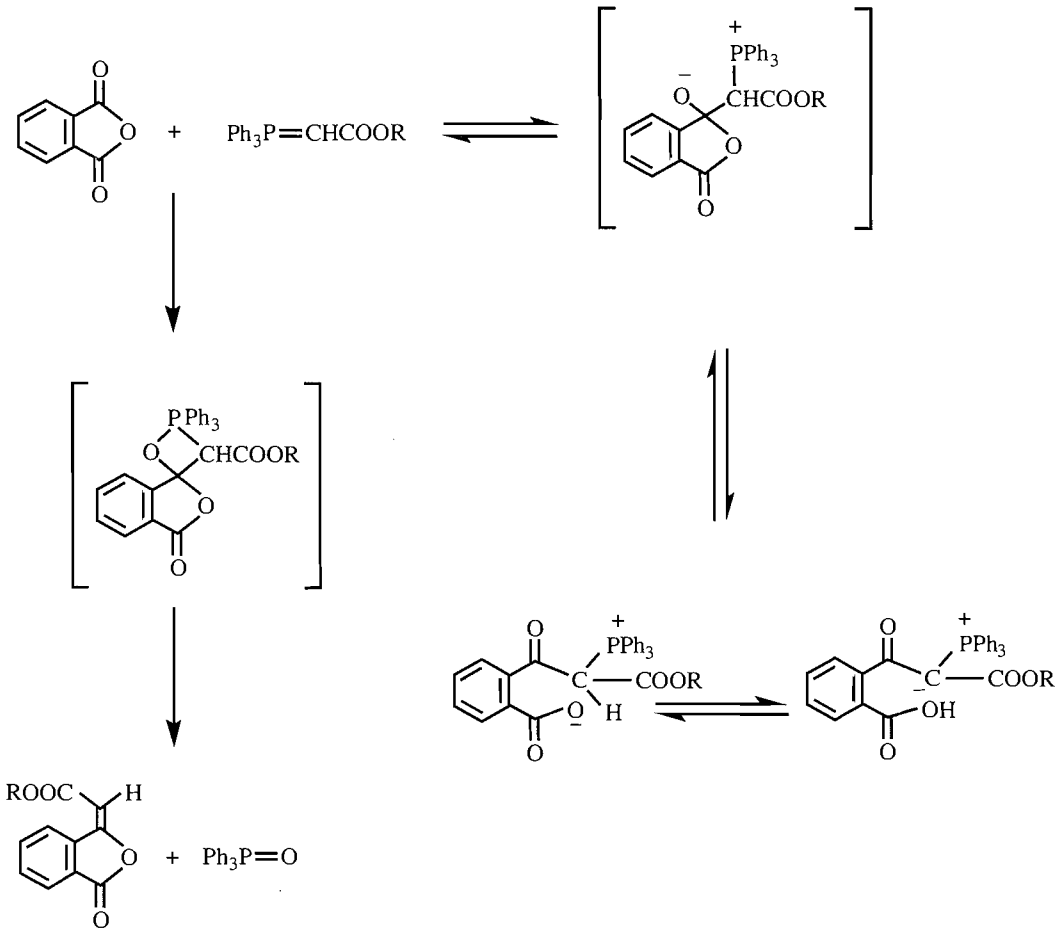

SCHEME 6

49.55, 52.35, 71 (J_{PC} = 125 Hz), 124.7–134.6 (overlapping aromatic carbons), 141.75 (J_{PC} = 8 Hz), 147.02, 165.63 (J_{PC} = 4.8 Hz), 167.96, 186.29; ^{31}P NMR δ: 16.08; *m/z*: 541 (M^+), 510 (M^+-OCH_3), 482 ($M^+-COOCH_3$), 349 (100), 277, 263. Exact Mass calculated for $C_{30}H_{24}NO_7P$: 541.12904; found: 541.1345. Minor isomer 1-methoxycarbonyl-2-(3′,2′-methoxycarbonylnitrophenyl)-2-oxoethylidenetriphenylphosphorane, **7**α: ^{1}H NMR δ: 3.07 (s, 3H, OCH_3), 3.73 (s, 3H, OCH_3), 8.16–7.39 (aromatic protons); ^{31}P NMR δ: 16.84.

*Reversibility study for the reaction of 3-nitrophthalic anhydride **5** with ylide **1***

3-Nitrophthalic anhydride **5** (63 mg, 0.31 mmol) suspended in 5 mL $CDCl_3$ and methyl(triphenylphosphoranylidene)acetate **1** (112 mg, 0.32 mmol) dissolved in 5 mL $CDCl_3$ were mixed at room temperature to give a bright yellow solution. The reaction was monitored by ^{1}H NMR until most of the ylide was converted into acyclic intermediates, at which point a slight excess of benzaldehyde was added to the reaction mixture. The disappearance of the intermediates could be easily followed by NMR. Overnight the solution turned colourless and the ^{1}H NMR showed the formation of methyl cinnamate. Under the reaction conditions described no enol-lactone products were formed. The products, methyl cinnamate and triphenylphosphine oxide were separated by chromatography. *trans*-Methylcinnamate was eluted with ether/petroleum ether (10:90) followed by triphenylphosphine oxide with 100% ether. Yield: triphenylphosphine oxide 69% (60 mg) and *trans*-methylcinnamate 88% (45 mg).

*Reversibility study for the reaction of 3-methoxyphthalic anhydride **2** with ylide **1***

3-Methoxyphthalic anhydride **2** (56 mg, 0.32 mmol) suspended in $CDCl_3$ (5 mL) and ylide **1** (112 mg, 0.32 mmol) dissolved in $CDCl_3$ (5 mL) were pre-cooled and mixed at −30°C. The temperature was raised slowly, over the period of 2.5 h, to 0–5°C. At that point 50% of the ylide was converted into the acyclic intermediates, but no enol-lactones could be detected by ^{1}H NMR. Freshly distilled benzaldehyde (34 mg, 0.32 mmol) dissolved in a few drops of $CDCl_3$ was added and the reaction mixture was allowed to warm to room temperature over 30 min. The ^{1}H NMR spectrum showed that the only products present were methyl cinnamate, 3-methoxyphthalic anhydride, and triphenylphosphine oxide. Chromatographic separation gave methyl cinnamate, triphenylphosphine oxide, and 3-methoxyphthalic acid, the result of the hydrolysis of the corresponding anhydride.

*Reaction of 3-methoxyphthalic anhydride **2** with carboethoxyethylidene triphenylphosphorane **8***

The ^{1}H NMR monitored reaction was carried out as described in the general procedure. On a slightly larger scale, ylide **8** (200 mg, 0.55 mmol) and 3-methoxyphthalic anhydride **2** (98 mg, 0.55 mmol) were dissolved in dry $CHCl_3$ (10 mL) and stirred at room temperature overnight under N_2. The solvent was removed under vacuum and the residue was separated by chromatography on silica gel with 20% acetone – 80% petroleum ether to give **9**α*E* (119 mg, 88%) and triphenylphosphine oxide. The enol-lactone **9**α*E*: mp 110–111°C. IR ($CHCl_3$) ν_{max}: 1775, 1700 cm^{-1}; ^{1}H NMR δ: 1.33 (t, 3H, CH_3CH_2), 2.20 (s, 3H), 3.97 (s, 3H, OCH_3), 4.30 (q, 2H,CH_3CH_2), 6.95 (d, 1H, aromatic), 7.59 (t, 1H, aromatic), 8.01 (d, 1H, aromatic); ^{13}C NMR δ: 14.21, 29.71, 56.20, 61.35, 112.94, 115.35, 117.79, 132.76, 136.94, 139.00, 149.59, 158.77, 163.83, 168.17; *m/z*: 262 (M^+), 217 ($M^+-OCH_2CH_3$), 189 ($M^+-COOCH_2CH_3$), 149 (100). Exact Mass calcd. for $C_{14}H_{14}O_5$: 262.08412; found: 262.0824.

Can. J. Chem. Downloaded from www.nrcresearchpress.com by 213.200.69.106 on 09/08/12
For personal use only.

Reaction of 3-nitrophthalic anhydride **5** *with carboethoxyethylidene triphenylphosphorane* **8**

The ^{1}H NMR monitored reaction was was carried out as described in the general procedure. On a slightly larger scale, ylide **8** (200 mg, 0.55 mmol) and 3-nitrophthalic anhydride **5** (107 mg, 0.55 mmol) were dissolved in dry $CHCl_3$ (10 mL) and stirred at room temperature overnight, under N_2. The solvent was removed under vacuum and the residue was separated by chromatography on silica gel with 20% acetone – 80% petroleum ether to give **10**β*E* (80%) and triphenylphosphine oxide. The enol-lactone **10**β*E*: mp 95–97°C. IR ($CHCl_3$) ν_{max}: 1795, 1710 cm^{-1}; ^{1}H NMR δ: 1.36 (t, 3H, CH_3CH_2), 2.30 (s, 3H), 4.35 (q, 2H, CH_3CH_2), 7.96 (m, 2H, aromatic), 8.95 (dd, 1H, J = 7.5, 3.0 Hz); ^{13}C NMR δ: 14.18, 29.72, 61.88, 115.99, 125.54, 128.17, 130.47, 135.62, 138.99, 146.68, 149.05, 166.78 ; *m/z*: 277 (M^+), 232 (M^+-COOH), 162 (100). Exact Mass calcd. for $C_{13}H_{11}O_5N$: 277.05863; found: 277.05830.

Acknowledgement

We would like to thank the Atlantic Regional Magnetic Resonance Centre for recording the NMR spectra and the Natural Sciences and Engineering Council of Canada for financial support.

1. L. Breau and M.M. Kayser. Can. J. Chem. **67**, 569 (1989).
2. M.M. Kayser and L. Breau. Can. J. Chem. **67**, 1401 (1989).
3. M.M. Kayser and L. Breau. Tetrahedron Lett. **29**, 6203 (1988).
4. A. Allahdad and D.W. Knight. J. Chem. Soc. Perkin Trans. 1, 1855 (1982).
5. J. Buck, N.G. Clemo and G. Pattenden. J. Chem. Soc. Perkin Trans. 1, 2399 (1985); D.W. Knight and G. Pattenden. J. Chem. Soc. Perkin Trans. 1, 62, 70, 84 (1979); G. Pattenden. Fortsch. Chem. Org. Naturst. **35**, 133 (1978); A.P. Gara, R.A. Massy-Westropp, and G.D. Reynolds. Tetrahedron Lett. **48**, 4171 (1969).
6. M.M. Kayser, K.L. Hatt, and D.L. Hooper. Can. J. Chem. **70**, 1985 (1992).
7. M.M. Kayser and O. Eisenstein. Can. J. Chem. **59**, 2457 (1981); M.M. Kayser and G. Wipff. Can. J. Chem. **60**, 1192 (1982).
8. A.D. Abell, I.R. Doyle, and R.A. Massy-Westropp. Aust. J. Chem. **35**, 2277 (1982).
9. N.L. Allinger and V. Zalkow. J. Org. Chem. **25**, 701 (1960).
10. H. Yu, Ph.D. Thesis, University of New Brunswick. 1993.
11. A.D. Abell, J.O. Trent, and B.I. Whittington. J. Org. Chem. **54**, 2762 (1989), and references cited therin.
12. P.A. Chopard, R.F. Hudson, and R.J.G. Searle. Tetrahedron Lett. 2357 (1965).
13. A.D. Abell and R.A. Massy-Westropp. Aust. J. Chem. **35**, 2077 (1982).
14. A.D. Abell and J.O. Trent. J. Chem. Soc. Chem. Commun. 409 (1989).
15. H.B. Bürgi, J.D. Dunitz, J.M. Lehn, and G. Wipff. Tetrahedron, **30**, 1563 (1974).
16. E. Vedejs and T.J. Fleck. J. Am. Chem. Soc. **111**, 5861 (1989).
17. E. Vedejs and C.F. Marth. J. Am. Chem. Soc. **112**, 3905 (1990).
18. B.E. Maryanoff and A.B. Reitz. Chem. Rev. **89**, 683 (1989).
19. R. Holler and H. Lischka. J. Am. Chem. Soc. **102**, 4632 (1980).
20. F. Volatron and O. Eisenstein. J. Am. Chem. Soc. **109**, 1 (1987); **106**, 6117 (1984).
21. L.P. Hammett. Physical organic chemistry. McGraw–Hill, New York. 1970. pp. 85–88.

Can. J. Chem. Downloaded from www.nrcresearchpress.com by 213.200.69.106 on 09/08/12
For personal use only.

The acyloin reaction using tethered diesters

TIM S. DAYNARD, PAUL S. EBY, AND JOHN H. HUTCHINSON[1]

Merck Frosst Centre for Therapeutic Research, P.O. Box 1005, Pointe Claire – Dorval, Que., Canada H9R 4P8

Received January 20, 1993

TIM S. DAYNARD, PAUL S. EBY, and JOHN H. HUTCHINSON. Can. J. Chem. **71**, 1022 (1993).

A study of the intramolecular acyloin condensation using diesters tethered by their alkoxide groups was undertaken. The goal was to provide a method for optimizing the yield of mixed acyloin products from the reaction of two different esters by utilizing tethered dissimilar esters as substrates. The results of the study show that the yield of the acyloin condensation is dependant on the tether length. Tethers of 8 and 14 carbons in length give yields comparable to those obtained from an intermolecular control reaction while shorter tethers give reduced yields of product. However, the use of mixed tethered diesters and a crossover experiment between two different tethered substrates provides a statistical distribution of products. These observations have been interpreted as resulting from a fragmentation of the initially formed radical anion intermediate that destroys the tethered nature of the substrate(s).

TIM S. DAYNARD, PAUL S. EBY et JOHN H. HUTCHINSON. Can. J. Chem. **71**, 1022 (1993).

On a entrepris une étude de la condensation intramoléculaire aux acyloïnes impliquant des diesters reliés par leurs groupes alcoolates. Le but du travail était de développer une méthode permettant d'optimiser le rendement en acyloïnes mixtes par réaction de deux esters différents reliés entre eux. Les résultats de l'étude montrent que le rendement de la condensation aux acyloïnes dépend de la longueur de la jonction. Des jonctions de 8 et 14 carbones conduisent à des rendements qui sont comparables à ceux obtenus avec des réactions sous contrôle intermoléculaire; des jonctions plus courtes conduisent à des rendements plus faibles. Toutefois, l'utilisation de diesters mixtes reliés et une expérience d'échange entre deux substrats différents reliés fournissent des distributions statistiques de produits. On interprète ces observations en fonction d'une fragmentation de l'intermédiaire anion radicalaire formé initialement qui provoque une destruction de la jonction du (ou des) substrat(s).

[Traduit par la rédaction]

Can. J. Chem. Downloaded from www.nrcresearchpress.com by 213.200.69.106 on 09/08/12
For personal use only.

The acyloin condensation is the reductive coupling of two esters (eq. [1]) and it is a powerful method of carbon–carbon bond formation resulting in the formation of an α-hydroxyketone **1** (1). This reaction is particularly useful in the case of diesters **2** where an intramolecular cyclization yields a cyclic acyloin product (eq. [2]) (1*a*, 2). With the introduction of chlorotrimethylsilane (TMSCl) as an alkoxide scavenger, the usefulness of this methodology has been extended considerably (3). Yields are increased and in some cases (e.g., the formation of four-membered rings) no product is formed at all in the absence of TMSCl (4, 5).

This procedure is limited, however, when two dissimilar esters are used, eq. [3]. Here four products are formed, in statistical yields, resulting from the random intermolecular reaction of both esters and thus the maximum yield of the desired products (**3** and **3′**) is only 50%. The separation of such a mixture is difficult and adds to the undesirability of the method. As a consequence, there are only a few reports of the mixed acyloin reaction in the literature (6).

An interesting possibility for improving the yield of the mixed acyloin products **3** and **3′** involves the use of tethered unsymmetrical diester substrates **4**. This approach relies on an intramolecular cyclization of a substrate in which two different esters are tethered via the alkoxide portions, as in eq. [4], to yield the mixed acyloins **3** and **3′** as the predominant products.

In this paper we will present the first data on the use of tethered esters as substrates in the acyloin reaction. In particular, we will focus on determining the optimum chain length for the tether (carried out on a series of symmetrical diesters) and the extension of this to unsymmetrical diesters. Lastly, these results and their implications on the currently accepted mechanisms will be discussed.

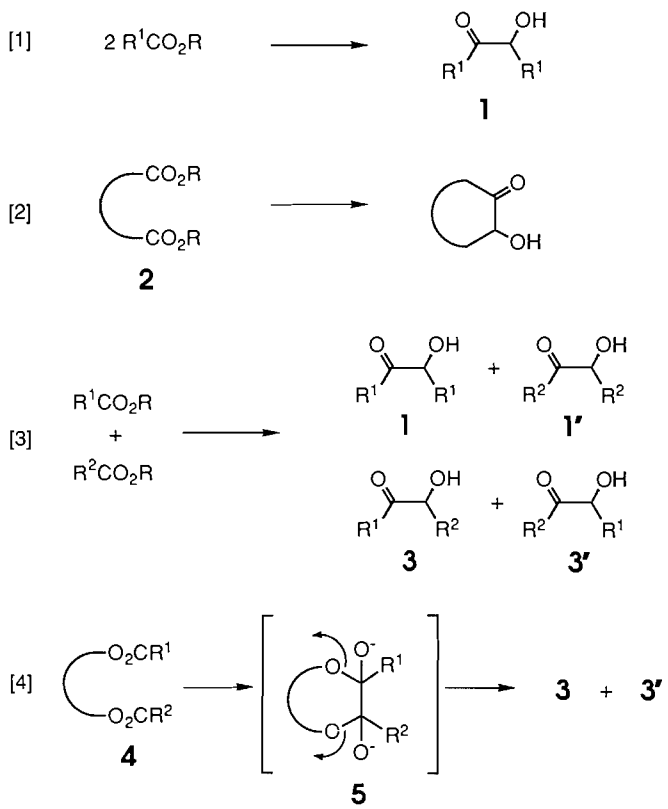

Results

We chose to study a series of tethered bis-hexanoyl esters as substrates in the acyloin condensation to determine which

[1]Author to whom correspondence may be addressed. Present address: Merck and Co. Inc., P.O. Box 4, WP44-J100, West Point, PA 19486, U.S.A.

TABLE 1. Effect of tether on the acyloin condensation

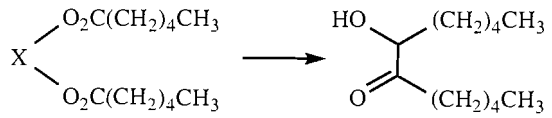

6 **7** capronoin

Compound	X	Intermediate ring size	% Yield of capronoin, **7**
Methyl hexanoate		Intermolecular	68
6*a*	$(iPr)_2Si$	5	5
6*b*	$(CH_2)_2$	6	22
6*c*	$(CH_2)_3$	7	20
6*d*	$(CH_2)_5$	9	42
6*e*	$(CH_2)_8$	12	76
6*f*	$(CH_2)_{14}$	18	73
6*g*	Triethylene glycol derivative	12	5

TABLE 2. The mixed acyloin reaction with tethered esters

Starting material(s)	% Yield of acyloin products	
	7	**11** + **12**
Methyl hexanoate and *n*-butyl acetate	20	38
8	20	37
9	20	34
8 (high dilution)	16	25
6*e* and **13**	17	40

tether afforded the product (capronoin, **7**) in the highest yield. Substrates **6***b–g* were prepared from hexanoyl chloride, the appropriate diol, and Et_3N in dichloromethane. In addition, a compound with a silicon tether (**6***a*) was prepared from diisopropyldichlorosilane, hexanoic acid, and Et_3N in dichloromethane. The results of the condensations with the tethered substrates are given in Table 1. For comparison (and to confirm our methodology), the intermolecular reaction between methyl hexanoate was carried out using fine sodium sand in refluxing toluene under nitrogen and **7** was then isolated in 68% yield. A similar yield (80%) was reported for this reaction when it was carried out in refluxing xylene (7). All the remaining condensation reactions were performed in the presence of TMSCl (8).

The reaction of the diisopropylsilyl tethered derivative **6***a* produced a complex mixture of nonpolar by-products with only a trace amount of the product **7** (5%) isolable. When ethylene glycol (**6***b*) or 1,3-propanediol (**6***c*) was used the yields, although improved, were still disappointing at only 20%. Increasing the tether length to $n = 5$, 8, and 14 gave increased yields of 42, 76, and 73% respectively. The yields for the 8- and 14-carbon tethered substrates are roughly the same as for the control intermolecular reaction. This requires ring sizes of 12 and 18 for the intermediate produced via an intramolecular process (**5**, eq. [4]). Such rings are readily formed in the cyclic acyloin reaction (cf. eq. [2]), with reported yields of 76 and 96% for the 12- and 18-membered tethers, respectively (1*a*).

A 10-membered tether, prepared from triethylene glycol, was also tested (compound **6***g*). It was hoped that the ether oxygens could act as a template to coordinate Na^+ and that, in addition, the transannular interaction would be reduced, thereby permitting high yields of the intramolecular acyloin product. This was not the case and again the yield was low with a considerable amount of nonpolar by-products being formed.

Since both the 8- and 14-carbon tethered esters gave results comparable to the intermolecular case we were confident that the tether was not impeding the reaction. However, the result gave no indication whether the product resulted from *intra-* or *inter*-molecular reactions. To determine this, we prepared two hexanoyl-acetyl diesters joined by either an 8-carbon (**8**) or a 14-carbon (**9**) chain. The substrates were prepared in two steps by sequential esterification of the diol using the previously described conditions. The diesters were then reacted under the normal acyloin reaction conditions and the results are listed in Table 2.

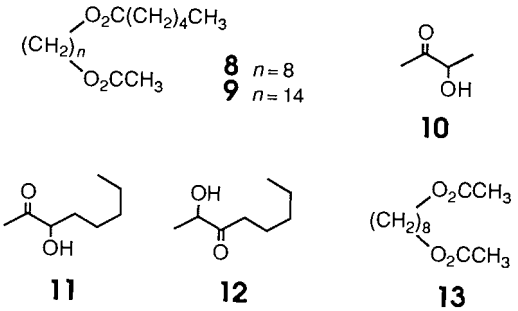

8 $n=8$
9 $n=14$

10 **11** **12** **13**

Included in Table 2 are the results for the untethered intermolecular reaction between methyl hexanoate and butyl acetate. A total yield of 38% of the combined unsymmetrical acyloin products **11** and **12** was obtained in addition to 20% of capronoin **7**. The other symmetrical product, acetoin (3-hydroxy-2-butanone, **10**), was lost during the aqueous work-up. However, the ratio of the unsymmetrical acyloin to capronoin is 2:1, indicating that a statistical product distribution was obtained. Virtually identical yields and therefore product distributions were obtained when both the 8- and 14-carbon tethered substrates were reacted (**8** and **9**, respectively). Even at very high dilution (slow addition of the

Can. J. Chem. Downloaded from www.nrcresearchpress.com by 213.200.69.106 on 09/08/12
For personal use only.

diester over 6 h to give a final concentration of 0.04 M, conditions that should promote an intramolecular reaction) the ratio of the unsymmetric to symmetric products isolated was close to 2:1. The yields in this case were slightly reduced due to the prolonged reaction time.

To confirm if an intermolecular reaction is indeed taking place, a crossover experiment was performed between the bis-hexanoyl ester of 1,8-octanediol **6***e* and the corresponding bis-acetate **13** (Table 2). Equimolar amounts of both bis-esters were reacted under the usual conditions and, after work-up and chromatography, the mixed acyloin products **11** and **12** were isolated in 40% combined yield. Capronoin was obtained in 17% yield.

These results indicate that the tethered systems are reacting in an intermolecular sense and that the tether is not conferring any advantage upon the system. Thus the *intra*-molecular acyloin reaction fails in the case where the two esters are tethered via the alkoxide groups. In addition, for short tethers the yields are low.

Discussion

The results obtained for the crossover experiment and the reaction of the mixed tethered diesters (**8** and **9**, Table 2) indicate that the reaction is proceeding via an intermolecular process. One possibility for this apparent lack of intramolecular reactivity could be because the conformation required for an intramolecular reaction is not readily accessible. Therefore the reaction proceeds more rapidly with a second molecule in an intermolecular sense. However, the results obtained using the cyclic acyloin reaction with diesters (eq. [2]) show that ring sizes from 4 to over 30 are formed in high yield without the need for high-dilution conditions (1*a*). Even the highly strained 4-, 8-, 9-, and 10-membered rings are readily prepared and they are obviously the product of highly strained intermediates. For the 8-carbon tethered systems (**6***e* and **8**) an intramolecular reaction would proceed via a 12-membered ring while the 14-carbon tether present in **6***f* and **9** would give rise to an 18-membered ring intermediate (**5**, eq. [4]). Both ring sizes are large and therefore should have no steric or strain impediment to their formation, especially when considered in context of the cyclic acyloin results.

Furthermore, if the bimolecular process is rapid and is competing with the unimolecular route, a high dilution experiment should increase the amount of product formed in an intramolecular sense. This is not the case; the high-dilution experiment yields a statistical distribution of products (Table 2).

Additionally, if an intermolecular acyloin condensation is occurring between two diester molecules, perhaps one would expect the yields from each tethered substrate (**6***a–g*) to be similar since the probability of an intermolecular collision and reaction is the same in each case. This is not the observed result. We feel that the results obtained are not consistent with a purely bimolecular acyloin condensation between two diester molecules.

To understand these results, we have reexamined the proposed mechanisms for the reaction. The mechanism of the acyloin condensation has not been conclusively elucidated and in fact much speculation regarding the nature of the intermediates exists. The situation is complicated further by the fact that acyloin condensations may be carried out using different metals (e.g., Na, K, or Na–K couples) on a

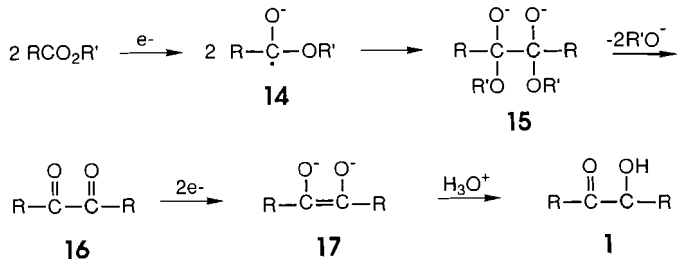

SCHEME 1

variety of substrates (e.g., esters, anhydrides, and acid chlorides) in solvents such as toluene, diethyl ether, and liquid NH_3. Each set of conditions may favour a particular mode of reactivity, giving rise to the acyloin, as well as by-products, in varying amounts (9).

The most commonly reported mechanism and the one most often described in undergraduate texts (for example, ref. 10) is shown in Scheme 1. This has been disputed (11) and is almost certainly not the complete mechanism. Bloomfield, Owsley et al. propose an alternative mechanism (12), which is given in Scheme 2. Both mechanisms, however, require that the reacting carbonyl carbons be joined (C—C bond in **15**, Scheme 1, and C—O—C bridge in **18**, Scheme 2) prior to expulsion of the alkoxide groups, i.e., the tether would bring the reaching centres together and then be expelled. This would favour an intramolecular process, which seems to be in disagreement with our results.

In addition, both mechanisms commence with a single electron transfer to one ester group to form a radical anion **14**. The fate of **14** is worth considering (Scheme 3) for it has been proposed that such radical anions may decompose to afford an alkoxide and an acyl radical **24** (13). The acyl radical could then decarbonylate to give CO and an alkyl radical. Alternatively the radical anion can fragment to generate a carboxylate anion and an alkyl radical. The combination of radical intermediates could then give rise to nonpolar products such as RH, RCOR, and RR. Indeed such products have been observed (especially in the case where the alkyl radical formed is particularly stable, as for benzyl (14) and allylic (13) radicals) and this explanation has been used to account for them. A more detailed discussion of the proposed mechanisms in Schemes 1 and 3 for the acyloin condensation in conjunction with TMSCl is given by Ruhlmann (3*b*).

This is not the only way to account for the observed by-products. Bloomfield and Owsley suggest that fragmentation of the radical intermediate **19** can account for the radical products observed. Also, fragmentation of the anion **20** could, they suggest, result in anion formation, which would be particularly favourable with tertiary, benzylic, and allylic systems (12). Thus, in some cases, free radicals may not be involved other than as very transient radical anion intermediates.

The results obtained from our experiments with tethered diesters would be consistent with a fragmentation process in which the tether is somehow cleaved, thus allowing randomization of the ester groups. An obvious candidate for fragmentation (and one that was previously proposed to explain by-product formation (13)) is the radical anion **14**. The radical anion **14** would not be particularly stable, especially in refluxing toluene (or even refluxing xylene). Parentheti-

Can. J. Chem. Downloaded from www.nrcresearchpress.com by 213.200.69.106 on 09/08/12
For personal use only.

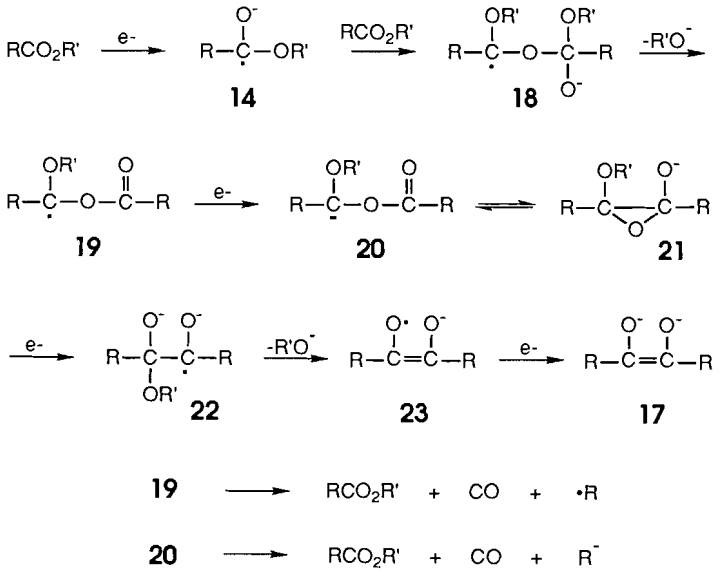

SCHEME 2

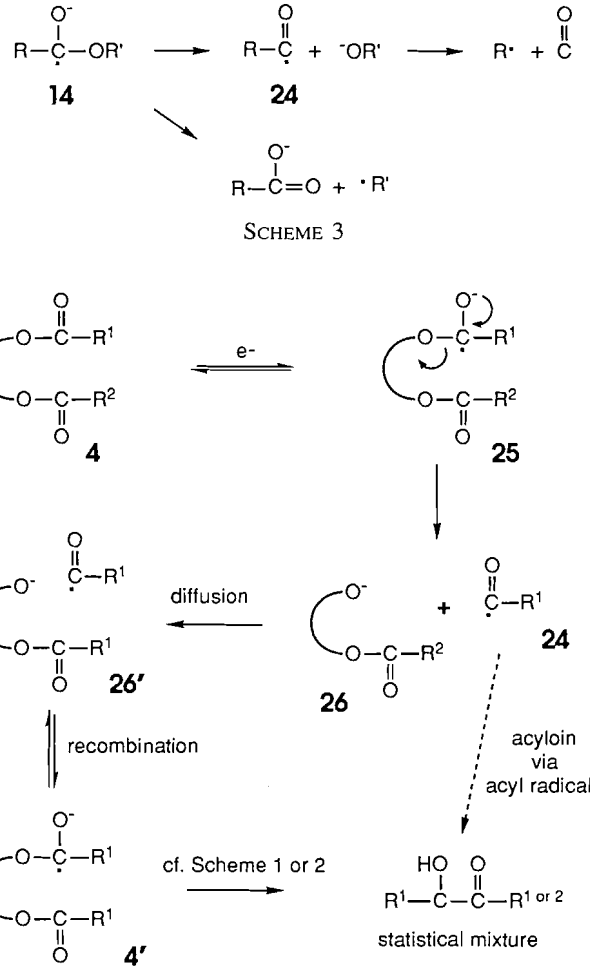

SCHEME 3

SCHEME 4

cally, the fragmentation of intermediates **19** or **20** (Scheme 2) would lead to loss of CO and destruction of the starting material and would not explain the results. We propose, therefore, that the fragmentation of **14** does indeed occur. Furthermore, the fragmentation must occur early in the reaction sequence *prior* to the joining of the two carbonyl carbons and the fragmentation must be rapid since a long-lived intermediate would allow an intramolecular reaction to occur.

Scheme 4 outlines a possible mechanism to explain the observed results. Electron transfer to the diester **4** produces the radical anion **25**; this then fragments to afford an acyl radical **24** and an alkoxide **26**. Diffusion and recombination with other fragments (e.g., **26'**) would lead to complete randomization of the substrate(s). If this fragmentation step is rapid and reversible, the reaction could proceed as previously proposed. Alternatively, if the acyl radical and the alkoxide do not recombine or if the recombination is slow in comparison to reaction of the alkoxide with chlorotrimethylsilane, the acyloin mechanism must proceed via an acyl radical. The radical anion **14** (Schemes 1 and 2) could not, therefore, be involved as the key reacting intermediate for C—C bond formation in this case.

This proposed mechanism could provide an explanation for the reduced yields observed in those substrates linked by short tethering units (Scheme 5).[2] In these cases, an equilibrium between the open chain and the cyclic form of the intermediate alkoxides could slow down or impede the recombination step thus giving rise to by-products resulting from decomposition of the acyl radical. Such an equilibrium may favor a cyclic intermediate in the case of short tethers (n = 0, 1, 3) while favoring the open chain form in the case of longer tethering units ($n > 5$). In the case of the triethylene glycol tether, chelation of the alkoxide intermediate by sodium (**27**) would result in a decrease in the rate of recombination with the acyl radical. Again, this would lead to an increase in the amount of by-products arising from further reaction of the acyl radical. Finally, fragmentation ofl the silicon-tethered substrate would produce a silyloxide **28**, which may eliminate RCO_2^- and further decompose to produce polymers and side products before it can recombine.

[2]We thank one of the reviewers for helpful comments regarding this point.

Can. J. Chem. Downloaded from www.nrcresearchpress.com by 213.200.69.106 on 09/08/12
For personal use only.

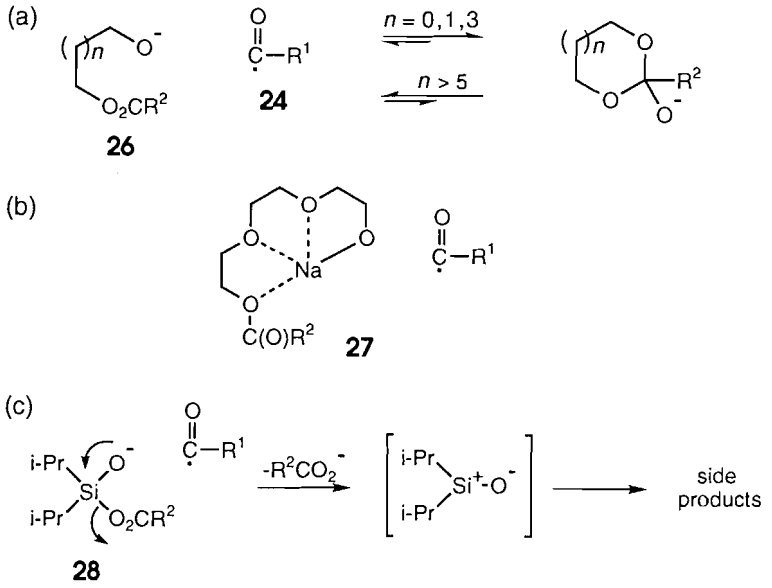

SCHEME 5

Thus, the mechanistic proposals described herein can account for the observation that tethered substrates react in an intermolecular sense and that the decreased yields observed for some substrates may be the result of sequestering the alkoxide (by formation of cyclic intermediates, chelates, or decomposition; Scheme 5).

Conclusion

In conclusion, the reaction of diesters tethered via their alkoxide portions has been shown to produce a statistical distribution of products. This is true for mixed diester substrates and for the crossover experiment involving two different symmetrical diesters. A bimolecular reaction between two substrate molecules appears unlikely since there appears to be little hindrance to an intramolecular process due to the large ring sizes that would be involved. Also there is the analogy with the cyclic acyloin condensation condensation in which highly strained cyclic intermediates are formed. It seems reasonable to account for the observed results by proposing that the first-formed radical anion intermediate **14** can fragment, thus destroying the tethered nature of the substrate. Our experiments do not, however, allow us to determine whether the acyloin condensation is then occurring by random recombination of the acyl radical and the alkoxide to regenerate a radical anion or if an acyl radical is a key intermediate in this process.

Experimental section

Proton nuclear magnetic resonance spectra were obtained on a Bruker AM250 or AM300 spectrometer and proton shifts are relative to tetramethylsilane (TMS) as internal standard. Melting points were measured on an Electrothermal IA 9100 melting point apparatus in open capillary tubes and are uncorrected. Infrared spectra were obtained using a Perkin–Elmer 681 spectrophotometer. Elemental analyses were carried out by Oneida Research Services, Inc., Whiteboro, N.Y., and high-resolution mass spectra were obtained from McGill University Biomedical Mass Spectrometry Unit, Montreal. Dichloromethane and toluene were freshly distilled from CaH_2 under a nitrogen atmosphere prior to use. TMSCl was distilled under nitrogen. $MgSO_4$ was used to dry all worked-up reactions and all NMR samples were run using $CDCl_3$ as solvent. Starting materials were obtained from Aldrich Chemical Company, Inc.

Diisopropylsilyl dihexanoate, ***6****a*

To a solution of dichlorodiisopropylsilane (2.5 g, 13.5 mmol) and Et_3N (3.76 mL, 27 mmol) in CH_2Cl_2 (55 mL) at 0°C under nitrogen was slowly added hexanoic acid (3.39 mL, 27 mmol). A white precipitate formed immediately. After 1 h, the solvent was removed, hexane was added, and the mixture was filtered through Celite. Evaporation of the solvent provided ***6a*** (4.5 g, 96% yield) as a pale yellow oil, which was used without further purification. IR (film): 2960, 2880, 1735, 1465, 1170, 885 cm^{-1}; ^1H NMR δ: 0.89 (6H, bt), 1.08 (12H, d, J = 8.1 Hz), 1.2–1.4 (10H, m), 1.62 (4H, m), 2.37 (4H, t, J = 7.7 Hz).

1,2-Ethanediol dihexanoate, ***6****b*

To a solution of ethanediol (520 mg, 8.4 mmol), pyridine (3.39 mL, 42 mmol), and DMAP (25 mg) in CH_2Cl_2 (30 mL) at 0°C was added dropwise hexanoyl chloride (2.75 mL, 18.5 mmol) in CH_2Cl_2 (10 mL). After 3 h the mixture was poured into 1 N HCl, extracted (3X) with CH_2Cl_2, washed with saturated $NaHCO_3$–brine solution, dried, and evaporated. The residue (2.79 g) was purified by column chromatography on silica gel (eluting with hexane–EtOAc 10:1) to afford the diester ***6b*** (2.10 g, 97% yield) as a colourless oil. IR (film): 2960, 2930, 2870, 1740, 1160 cm^{-1}; ^1H NMR δ: 0.89 (6H, bt), 1.3 (8H, m), 1.62 (4H, m), 2.32 (4H, t, J = 7.7 Hz), 4.28 (4H, s); MS (CI (CH_4)) m/z: 259 (MH^+,4), 241 (1), 143 (100), 99 (11). Anal. calcd. for $C_{14}H_{26}O_4$: C 65.09, H 10.14; found: C 65.28, H 10.17.

The following compounds were prepared using the procedure described above:

1,3-Propanediol dihexanoate, ***6****c*

Using 1,3-propanediol (912 mg) there was obtained 2.93 g (90%) of ***6c*** as a colourless oil. IR (film): 2960, 2935, 2870, 1740, 1170 cm^{-1}; ^1H NMR δ: 0.89 (6H, bt), 1.3 (8H, m), 1.61 (4H, m), 1.95 (2H, pentet, J = 6.5 Hz), 2.29 (4H, t, J = 7.7 Hz), 4.15 (4H, t, J = 6.5 Hz); MS (CI (CH_4)) m/z: 329 (MH^+, 17), 157 (100). Anal. calcd. for $C_{15}H_{28}O_4$: C 66.14, H 10.36; found: C 66.31, H 10.08.

1,5-Pentanediol dihexanoate, ***6****d*

Using 1,5-pentanediol (624 mg) there was obtained 1.72 g (96%) of ***6d*** as a colourless oil. IR (film): 2955, 2930, 2860, 1740, 1170 cm^{-1}; ^1H NMR δ: 0.88 (6H, bt), 1.2–1.5 (10H, m), 1.5–1.7 (8H, m), 2.29 (4H, t, J = 7.8 Hz), 4.06 (4H, t, J = 6.4 Hz); MS

Can. J. Chem. Downloaded from www.nrcresearchpress.com by 213.200.69.106 on 09/08/12
For personal use only.

Can. J. Chem. Downloaded from www.nrcresearchpress.com by 213.200.69.106 on 09/08/12
For personal use only.

(CI (CH_4)) *m/z*: 301 (MH^+, 76), 300 (1.3), 203 (4.9), 186 (14), 185 (100), 184 (4). Anal. calcd. for $C_{17}H_{32}O_4$: C 67.96, H 10.74; found: C 68.12, H 11.13.

*1,8-Octanediol dihexanoate, **6**e*

Using 1,8-octanediol (1.23 g) there was obtained 2.63 g (92%) of ***6e*** as a colourless oil. IR (film): 2930, 2860, 1735, 1170 cm^{-1}; ^1H NMR δ: 0.89 (6H, bt), 1.32 (16H, m), 1.55–1.70 (8H, m), 2.29 (4H, t, J = 7.5 Hz), 4.05 (4H, t, J = 6.7 Hz). Exact Mass calcd. for $C_{20}H_{38}O_4 + H^+$: 343.2848; found: 343.2848. Anal. calcd. for $C_{20}H_{38}O_4$: C 70.13, H 11.18; found: C 70.38, H 11.06.

*1,14-Tetradecanediol dihexanoate, **6**f*

Using 1,14-tetradecanediol (2.28 g) there was obtained 2.73 g (65%) of ***6f*** as a waxy solid, mp 27–29°C. IR (film): 2940, 2850, 1735, 1460, 1170 cm^{-1}; ^1H NMR δ: 0.89 (6H, bt), 1.2–1.4 (28H, m), 1.5–1.7 (8H, m), 2.29 (4H, t, J = 7.4 Hz), 4.05 (4H, t, J = 6.7 Hz). Exact Mass calcd. for $C_{26}H_{50}O_4 + H^+$: 427.3787; found: 427.3786. Anal. calcd. for $C_{26}H_{50}O_4$: C 73.19, H 11.81; found: C 73.16, H 11.78.

*Triethylene glycol dihexanoate, **6**g*

Using triethylene glycol (1.26 g) there was obtained 2.76 g (96%) of ***6g*** as a colourless oil. IR (film): 2960, 2930, 1735, 1170 cm^{-1}; ^1H NMR δ: 0.89 (6H, bt), 1.2–1.4 (8H, m), 1.5–1.7 (4H, m), 2.32 (4H, t, J = 7.7 Hz), 3.65 (4H, s), 3.70 (4H, m), 4.23 (4H, m). Exact Mass calcd. for $C_{18}H_{34}O_6 + NH_4^+$: 364.2699; found: 364.2698. Anal. calcd. for $C_{18}H_{34}O_6$: C 62.40, H 9.89; found: C 61.92, H 10.01.

*8-Acetoxy-1-octanyl hexanoate, **8***

Step 1. 8-Hydroxy-1-octanyl hexanoate

To a solution of 1,8-octanediol (6.14 g, 42 mmol), pyridine (11.3 mL, 140 mmol), and DMAP (100 mg) in DMF (200 mL) at 0°C was added hexanoyl chloride (4.17 mL, 28 mmol) dropwise. The mixture was stirred for 2 h at room temperature then poured onto 1 N HCl, and extracted (3X) with EtOAc. The organic layers were combined, washed with water, then with saturated $NaHCO_3$–brine solution, dried, and evaporated. Chromatography of the residue (silica gel; hexane–EtOAc 2:1) afforded 8-hydroxy-1-octanyl hexanoate (4.3 g, 63%) as an oil. IR (film): 3400 (br), 2930, 2850, 1735, 1170 cm^{-1}; ^1H NMR δ: 0.89 (3H, bt), 1.2–1.4 (12H, m), 1.5–1.7 (6H, m), 2.29 (2H, t, J = 7.5 Hz), 3.64 (2H, t, J = 6.6 Hz), 4.05 (2H, t, J = 6.6- Hz); MS (CI (CH_4)) *m/z*: 245 (MH^+, 100), 227 (2), 129 (10), 117 (8), 111 (16), 99 (9).

*Step 2. 8-Acetoxy-1-octanyl hexanoate, **8***

To a solution of the hydroxyester from Step 1 (2.1 g, 8.6 mmol), pyridine (3.47 mL, 43 mmol), and DMAP (50 mg) in CH_2Cl_2 (80 mL) at 0°C was added acetyl chloride (732 μL, 10.3 mmol) dropwise. After 30 min at room temperature the mixture was poured into 1 N HCl, extracted (3X) with EtOAc, washed with water, and then with saturated $NaHCO_3$/brine solution. The organic layer was dried, filtered, and evaporated to give an oil, which was chromatographed on silica gel (hexane–EtOAc 5:1) to afford **8** (2.37 g, 96%) as an oil. IR (film): 2935, 2860, 1740, 1240, 1170 cm^{-1}; ^1H NMR δ: 0.89 (3H, bt), 1.2–1.3 (12H, m), 1.5–1.6 (6H, m), 2.05 (3H, s), 2.29 (2H, t, J = 7.5- Hz), 4.05 (2 overlapping triplets, 2H each, J = 6.5 Hz and 6.5 Hz). Exact Mass calcd. for $C_{16}H_{30}O_4 + H^+$: 287.2222; found: 287.2222. Anal. calcd. for $C_{16}H_{30}O_4$: C 67.10, H 10.56; found: C 66.97, H 10.45.

*14-Acetoxy-1-tetradecanyl hexanoate, **9***

Following the procedures described for the preparation of 8-acetoxy-1-octanyl hexanoate, **8**, 1,14-tetradecanediol was initially converted into 14-hydroxy-1-tetradecanyl hexanoate (48%), mp 40–42.5°C. IR (KBr): 3450 (br), 2920, 2850, 1740, 1465, 1170 cm^{-1}; ^1H NMR δ: 0.89 (3H, bt), 1.2–1.4 (30H, m), 1.5–1.7 (6H, m), 2.29 (2H, t, J = 7.8 Hz), 3.63 (2H, t, J = 6.7 Hz), 4.06 (2H, t, J = 6.4 Hz); MS (CI (CH_4)) *m/z*: 329 (MH^+, 100), 311 (1), 111 (4), 99 (7).

Subsequent reaction with acetyl chloride provided the title compound 14-acetoxy-1-tetradecanyl hexanoate, **9**, as an oil (82%). IR (film): 2920, 2850, 1735, 1235, 1170 cm^{-1}; ^1H NMR δ: 0.89 (3H, bt), 1.2–1.4 (24H, m), 1.5–1.7 (6H, m), 2.04 (3H, s), 2.28 (2H, t, J = 7.7 Hz), 4.04 (2 overlapping triplets, 2H each, J = 6.4 Hz and 6.4 Hz). Exact Mass calcd. for $C_{22}H_{42}O_4 + H^+$: 371.3161; found: 371.3162.

*Preparation of capronoin, **7***

Method A. Intermolecular acyloin condensation of methyl hexanoate

Sodium metal (0.38 g, 16.5 mmol) and toluene (40 mL) were heated to reflux with vigorous mechanical stirring until the sodium formed a fine sand. To this was added methyl hexanoate (1.03 g, 7.95 mmol) in toluene (20 mL) dropwise over 45 min. Stirring was continued for a further 1.5 h, the solution was cooled, and MeOH (5 mL) added. The mixture was poured into water–EtOAc and acidified with 3 N HCl. Extraction with EtOAc followed by washing with water, then with saturated $NaHCO_3$–brine solution, drying, and evaporation provided 861 mg of a yellow oil. Purification by column chromatography on silica gel (hexane–EtOAc 10:1, then 5:1) afforded capronoin **7** (540 mg, 68%) as an oil. IR (film): 3490 (br), 2960, 2935, 2880, 2860, 1725, 1470 cm^{-1}; ^1H NMR δ: 0.89 (6H, bt), 1.2–1.4 (8H, m), 1.4–1.9 (6H, m), 2.45 (2H, m), 3.50 (1H, d, J = 4.8 Hz; exchangeable with D_2O), 4.16 (1H, m). Exact Mass calcd. for $C_{12}H_{24}O_2 + H^+$: 201.1855; found: 201.1854.

*Method B. intramolecular acyloin condensation of 1,8-octanediol dihexanoate, **6**e*

Sodium metal (0.92 g, 40 mmol) and toluene (27 mL) were stirred vigorously at reflux using a mechanical stirrer until the sodium formed a fine sand. To this was added the diester ***6e*** (2.74 g, 8 mmol) and TMSCl (5.28 mL, 41.6 mmol) in toluene (10 mL) dropwise over 30 min. After a further hour the solution was cooled and MeOH (5 mL) was added, followed by 1 N HCl. The mixture was extracted with EtOAc, washed with saturated $NaHCO_3$–brine solution, then with water, dried, and evaporated to give an oil (2.2 g). Purification on silica gel eluting with hexane–EtOAc 12:1, then 3:1, afforded capronoin **7** (1.21 g, 76%).

The following tethered diesters were reacted using the procedure described in Method B to yield capronoin **7**:

1. Diisopropylsilyl dihexanoate ***6a*** (1.3 g, 3.8 mmol) yielded capronoin **7** (36 mg, 5%).
2. 1,2-Ethanediol dihexanoate ***6b*** (1.03 g, 4 mmol) yielded capronoin **7** (173 mg, 22%).
3. 1,3-Propanediol dihexanoate ***6c*** (1.04 g, 3.8 mmol) yielded capronoin **7** (149 mg, 20%).
4. 1,5-Pentanediol dihexanoate ***6d*** (500 mg, 1.7 mmol) yielded capronoin **7** (144 mg, 42%).
5. 1,14-Tetradecanediol dihexanoate ***6f*** (2.5 g, 5.9 mmol) yielded capronoin **7** (866 mg, 73%).
6. Triethylene glycol dihexanoate ***6g*** (1.38 g, 4 mmol) yielded capronoin **7** (40 mg, 5%).

*Preparation of acyloins **11** and **12**: intermolecular reaction between methyl hexanoate and* n*-butyl acetate*

A mixture of sodium metal (1.04 g, 45 mmol) and toluene (30 mL) was heated at reflux with vigorous mechanical stirring until the sodium formed a fine sand. To this was added methyl hexanoate (1.17 g, 9 mmol), *n*-butyl acetate (1.05 g, 9 mmol), and TMSCl (5.94 mL, 46.8 mmol) in toluene (4 mL) dropwise over 30 min. The mixture was worked up as previously described to afford 1.6 g of an oil. Column chromatography on silica gel (hexane–EtOAc 12:1, then 3:1) afforded capronoin **7** (388 mg, 20%) and a 1:1 mixture of mixed acyloin products **11** and **12** (492 mg, 38% combined yield) as a colourless oil. IR (film): 3460 (br), 2960, 2930, 2860, 1715 cm^{-1}; ^1H NMR (mixture of isomers) δ: 0.89 (3H, bt), 1.2–1.9 (7H, m), 1.38 (1.5H, d, J = 7.1 Hz), 2.20 (1.5H, s), 2.45 (1H, m), 3.46 (0.5H, d, J = 4.6 Hz), 3.57 (0.5H, d, J = 4.7 Hz), 4.2 (1H, m). Anal. calcd. for $C_8H_{16}O_2$: C 66.63, H 11.18; found: C 66.72, H 11.21.

The following reactions were performed using the procedure described above:

1. 8-Acetoxy-1-octanyl hexanoate **8** (2.29 g) afforded capronoin **7** (320 mg, 20%) and a 1:1 mixture of **11** and **12** (424 mg, 37%).

2. 14-Acetoxy-1-tetradecanyl hexanoate **9** (1.27 g) afforded capronoin **7** (132 mg, 20%) and a 1:1 mixture of **11** and **12** (167 mg, 34%).

3. 1,8-Octanediol dihexanoate **6***e* (1.15 g, 3.3 mmol) and 1,8-octanediol diacetate **13** (0.77 g, 3.3 mmol) afforded capronoin **7** (228 mg, 17%) and a 1:1 mixture of **11** and **12** (387 mg, 40%).

*Preparation of acyloins **11** and **12**. High-dilution experiment*

To 90 mL of toluene was added sodium metal (460 mg, 20 mmol) and this was stirred vigorously with a mechanical stirrer at reflux until the sodium formed a fine sand. The diester **8** (1.16 g, 4.05 mmol) and TMSCl (2.64 mL, 20.8 mmol) in toluene (10 mL) were added dropwise over 6 h and reflux, then continued for a further hour. The mixture was worked up and purified as previously described to yield capronoin **7** (133 mg, 16%) and a 1:1 mixture of **11** and **12** (154 mg, 26%).

1. J.J. Bloomfield, D.C. Owsley, and J.M. Nelke. Org. React. (NY), **32**, 259 (1976); (*b*) S.M. McElvain. Org. React. (NY), **4**, 256 (1948).
2. K.T. Finley. Chem. Rev. **64**, 573 (1964).
3. (*a*) U. Schrapler and K. Ruhlmann. Chem. Ber. **97**, 1383 (1964); (*b*) K. Ruhlmann. Synthesis, 236 (1971).
4. J.J. Bloomfield. Tetrahedron Lett. 587 (1968).
5. J.J. Bloomfield. Tetrahedron Lett. 591 (1968).
6. (*a*) J.W. Lynn and J. English, Jr. J. Am. Chem. Soc. **73**, 4284 (1951); (*b*) D.E. Ames, G. Hall, and B.T. Warren. J. Chem. Soc. C, 2617 (1968); (*c*) P. Baudart. Bull. Soc. Chim. Fr. **13**, 87 (1946).
7. V.L. Hansley. J. Am. Chem. Soc. **57**, 2303 (1935).
8. J.J. Bloomfield and J.M. Nelke. Org. Synth. Coll. Vol. **6**, 167 (1988).
9. A.G.M. Barrett, C.R.A. Godfrey, D.M. Hollinshead, P.A. Prokopiou, D.H.R. Barton, R.B. Boar, L. Joukhadar, J.F. McGhie, and S.C. Misra. J. Chem. Soc. Perkin Trans. 1, 1501 (1981).
10. J. March. *In* Advanced organic chemistry. John Wiley and Sons, New York. 1985.
11. K. Ruhlmann, B. Fichte, T. Kiriakidis, C. Michael, G. Michael, and E. Grundemann. J. Organomet. Chem. **34**, 41 (1972).
12. J.J. Bloomfield, D.C. Owsley, C. Ainsworth, and R.E. Robertson. J. Org. Chem. **40**, 393 (1975).
13. E. Van Heyningen. J. Am. Chem. Soc. **77**, 4016 (1955).
14. E. Van Heyningen. J. Am. Chem. Soc. **74**, 4861 (1952).

Can. J. Chem. Downloaded from www.nrcresearchpress.com by 213.200.69.106 on 09/08/12
For personal use only.

Functionalization of spirocyclopentadienes using organomolybdenum reagents: approaches to the synthesis of (±)-silphinene[1]

DEREK J. NORRIS, JOHN F. CORRIGAN, YAN SUN, NICHOLAS J. TAYLOR, AND SCOTT COLLINS[2]
Department of Chemistry, University of Waterloo, Waterloo, Ont., Canada N2L 3G1

Received February 14, 1993

DEREK J. NORRIS, JOHN F. CORRIGAN, YAN SUN, NICHOLAS J. TAYLOR, and SCOTT COLLINS. Can. J. Chem. **71**, 1029 (1993).

(η^5-Indenyl)molybdenum dicarbonyl complexes of 1,3-dienes, including spirocyclopentadienes, can be cleanly prepared from stoichiometric amounts of 1,3-dienes and [(η^5-indenyl)$Mo(CO)_2(CH_3CN)_2$][BF_4] (**1**) in dichloromethane solution. Nucleophilic addition of lithium dimethylcuprate to the complexed diene occurs in the expected manner to provide η^3-allylmolybdenum complexes in high yield. Applications of this chemistry towards the synthesis of (±)-silphinene are described. The allylmolybdenum complexes [(η^5-C_9H_7)(η^3-$C_{10}H_{15}$)$Mo(CO)_2$] (**8**) and [(η^5-C_9H_7)(η^3-$C_{15}H_{23}$)$Mo(CO)_2$] (**33**) were structurally characterized by X-ray crystallography. Compound **8**: space group $P2_1/n$ with a = 9.393(1) Å, b = 10.469(2) Å, c = 17.704(2) Å, β = 91.05(1)°, Z = 4, and V = 1770.5(4) Å^3. Compound **33**: space group $P2_1/c$ with a = 17.616(4) Å, b = 7.688(2) Å, c = 15.873(2) Å, β = 90.12(2)°, Z = 4, and V = 2149.7(6) Å^3.

DEREK J. NORRIS, JOHN F. CORRIGAN, YAN SUN, NICHOLAS J. TAYLOR et SCOTT J. COLLINS. Can. J. Chem. **71**, 1029 (1993).

Utilisant des quantités stoechiométriques de 1,3-dièns et de [(η^5-indényl)$Mo(CO)_2(CH_3CN)_2$] [BF_4] (**1**) en solution dans le dichlorométhane, on a préparé proprement des complexes (η^5-indényl)molybdène dicarbonyle de 1,3-dièns comprenant des spirocyclopentadièns. L'addition nucléophile de diméthylcuprate de lithium sur le dièn complexé se fait d'une façon attendue et fournit des complexes η^3-allylmolybdène avec des rendements élevés. On décrit l'application de cette chimie à la synthèse du (±)-silphinène. On a caractérisé les complexes allylmolybdène [(η^3-C_9H_7)(η^3-$C_{10}H_{15}$)$Mo(CO)_2$] (**8**) et [(η^5-C_9H_7) (η^3-$C_{15}H_{23}$)$Mo(CO)_2$] (**33**) par diffraction des rayons X. Composé **8** : groupe d'espace $P2_1/n$, avec a = 9,393(1), b = 10,469(2) et c = 17,704(2) Å, β = 91,05(1)°, Z = 4 et V = 1770,5(4) Å^3. Composé **33** : groupe d'espace $P2_1/n$, avec a = 17,616(4), b = 7,688(2) et c = 15,873(2) Å, β = 90,12(2)°, Z = 4 et V = 2149,7(6) Å^3.

[Traduit par la rédaction]

Introduction

The addition of nucleophiles to dienes coordinated to a transition metal centre occurs with predictable regio- and stereochemistry (for reviews, see ref. 1). These features have been exploited in organic synthesis in which η^4-cyclohexa- and cycloheptadiene complexes of a cationic $CpMo(CO)_2$ moiety have figured prominently (see, inter alia, ref. 2). The usual synthetic route to such complexes involves hydride abstraction from (η^3-allyl)$CpMo(CO)_2$ complexes (e.g., using [Ph_3C][BF_4]), the latter compounds being prepared via a two-step route from $Mo(CO)_6$ and an allyl halide (3). It is less well appreciated that diene complexes of the (η^5-indenyl)-molybdenum dicarbonyl moiety can be directly prepared from an appropriate cationic molybdenum complex (e.g., **1**, eq. [1]) and an excess of a 1,3-diene (4). This latter approach is an attractive one in synthesis, provided that the 1,3-diene is readily available *or*, more importantly, can be used in stoichiometric amounts.

In this paper we disclose that direct functionalization of 1,3-dienes in the latter manner is efficient.

Nucleophilic additions of carbanions to diene complexes of molybdenum can be accomplished with a variety of reagents (2–4); in the absence of any electronic bias, nucleophilic attack occurs at the least-substituted terminus of the diene (4*f*) and in cyclic dienes *exo* to the metal centre (e.g., eq. [2]) (1–4).

While the chemistry of cyclohexa- and cycloheptadiene complexes of molybdenum has been extensively developed by others (2, 4), very little, if any, work has been reported for cyclopentadiene complexes. We envisaged that if aromatization of cyclopentadienes could be prevented on complexation to molybdenum, some useful chemistry for functionalization of five-membered rings might ensue. In practice, this proved possible by direct complexation of spirocyclopentadienes; we illustrate the potential of this methodology in an attempted synthesis of (±)-silphinene (for some previous syntheses of this compound, see ref. 5).

Results and discussion

Direct complexation of 1,3-dienes to molybdenum

The direct reaction of 1,3-cyclohexadiene (15 equiv.) with [(η^5-indenyl)$Mo(CO)_2(CH_3CN)_2$][BF_4] (**1**) was previously reported by Green et al. (4*h*) and provided cyclohexadiene complex **2** in 50% yield. We repeated this reaction and obtained complex **2** in slightly higher yield (63%, Scheme 1). When only 1 equivalent of diene was employed the yield was only slightly diminished (61%).

Direct stoichiometric complexation of spirocyclopentadienes **3** and **4** to cationic precursor **1** was also successful and provided access to cyclopentadiene complexes **5** and **6** in 82 and 65% yield, respectively (Scheme 1). Thus, it appears that stoichiometric complexation of dienes using complex **1** is reasonably general and affords diene complexes in one step in good to excellent yields.

While complex **2** underwent efficient reaction with MeMgBr in THF to provide the expected allylmolybdenum product **7** (4), the analogous reactions of diene complexes **5** and **6** were complicated by the concomitant formation of inseparable molybdenum-containing by-products.[3] However, the use of Me_2CuLi in THF provided access to allyl

[1]Abstracted in part from the M.Sc. thesis of Derek J. Norris, University of Waterloo, September 1992.

[2]Author to whom correspondence may be addressed.

Can. J. Chem. Downloaded from www.nrcresearchpress.com by 213.200.69.106 on 09/08/12
For personal use only.

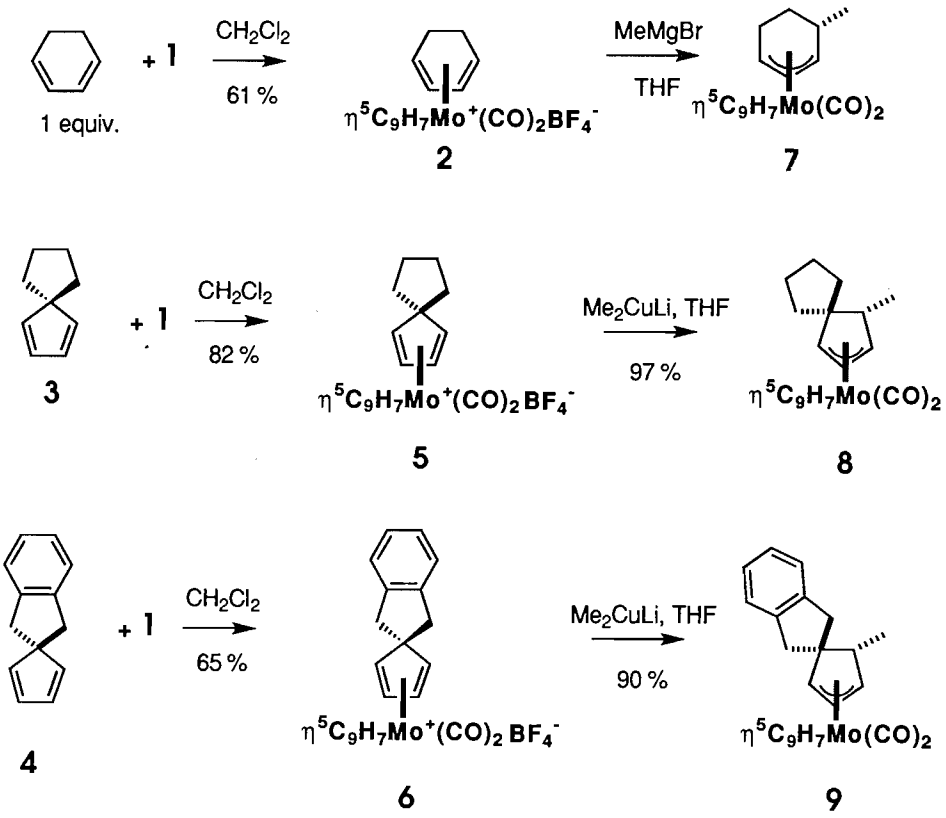

SCHEME 1

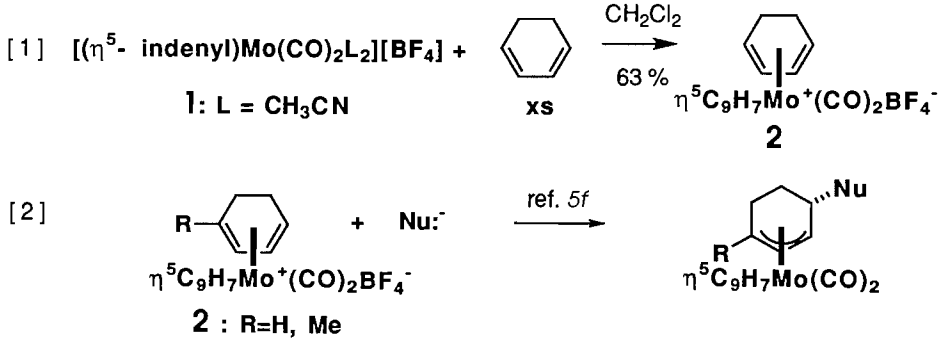

complexes **8** and **9** in excellent yield (Scheme 1). An X-ray structure of complex **8** confirmed that the methyl group of the cuprate was delivered to the diene in the expected fashion: *exo* to the metal and at the diene terminus (Fig. 1; Tables 1–3).

Having established that direct complexation of spirocyclopentadienes to molybdenum and subsequent delivery of a nucleophile could be accomplished in an efficient manner, we decided to investigate whether this methodology could be exploited in synthesis.

Approaches to the synthesis of silphinene. Synthetic analysis

We selected as our target (±)-silphinene (**11**), a natural product that has been prepared by a number of other groups (5). We envisaged that tricyclic spirocyclopentadiene **10** (Scheme 2) might serve as a precursor to **11** via stereoselective complexation with **1**, regioselective nucleophilic addition of Me_2CuLi to the derived diene molybdenum complex **12** at C-4 to provide **13**, followed by, for example, reductive decomplexation of molybdenum via the cationic nitrosyl complex **14** (3).

We recognized that there were several obstacles inherent in this synthetic approach. Complexation would have to occur on the *endo* face of diene **10** in order for subsequent *exo* delivery of the methyl group to occur in the nucleophilic addition step. We had hoped that the presence of the 9-methyl group might sterically block the *exo* face of diene **10**, thus preventing the favoured *exo* approach of reagents to the bicyclo[3.3.0]octadiene ring system inherent in this intermediate. We also envisaged that this same methyl group might direct nucleophilic attack towards C-4 (by sterically blocking C-1) of the complexed diene, and exert a similar effect on the reduction of nitrosyl complex **14**.

[3]Although we do not have conclusive evidence for the structure of these by-products, they are allylmolybdenum complexes that appear to result from a *reduction* of the diene complex at C-1.

Can. J. Chem. Downloaded from www.nrcresearchpress.com by 213.200.69.106 on 09/08/12
For personal use only.

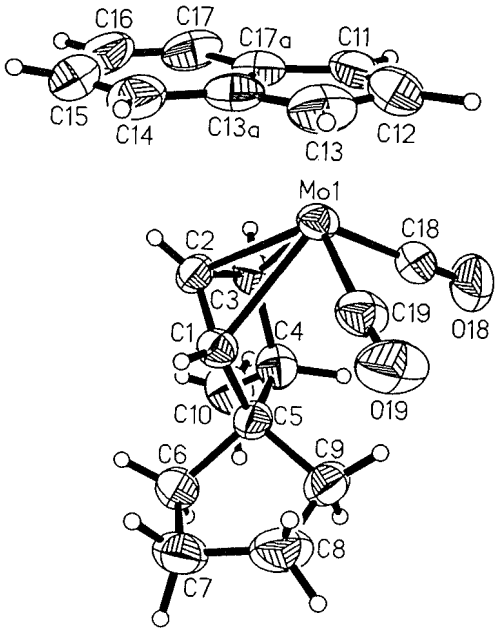

FIG. 1. Molecular structure of allylmolybdenum complex **8** with 30% thermal probability ellipsoids depicted. For selected bond lengths and angles, see Table 2.

As detailed below, although selective *endo* complexation of diene **10** proved possible, we have been unable to transform the diene complex **12** to the desired allyl complex **13**.

*Preparation of tricyclic diene **10***

Tricyclic diene **10** was prepared from cyclopentadiene and 3-hydroxy-2,2-dimethylpropanal as illustrated in Scheme 3. Condensation of this aldehyde with cyclopentadiene under the conditions developed by Stone and Little (6) provided fulvene **15** in 40–50% yield. The low yields obtained are a reflection of competing retro-aldol reaction of the aldehyde; 6-isopropylfulvene was also obtained as a major by-product. Reduction of the exocyclic double bond of **15** ($LiAlH_4$), followed by Swern oxidation (7) of alcohol **16** and subsequent intramolecular cyclization of aldehyde **17**, provided volatile, bicyclic, fulvene **18** in 50% overall yield. Nucleophilic addition of the dianion derived from 3-chloropropanol (8) to the exocyclic double bond of **18** and oxidation of the derived alcohol **19** (TPAP, NMO, 4A sieves) (9) provided aldehyde **20** in 35% yield from **18**.[4] Addition of excess MeMgBr to **20** provided a ~1:1 mixture of diastereomeric alcohols (**21**) in quantitative yield; these were converted to the target compound **10** and its C-9 epimer **23** (1:1.2) via base-mediated cyclization of the derived tosylates (56% combined yield from **20**). Dienes **10** and **23** could be separated by flash chromatography on silica gel impregnated with $AgNO_3$. Under these conditions, compound **10** undergoes preferential decomposition and was obtained in 55% yield from the crude mixture.

Assignment of stereochemistry to compounds **10** and **23** proved to be somewhat problematic. The ^1H NMR spectra of these compounds were very similar, the only significant differences were that the signal due to H1 in **10** was shifted 0.2 ppm to lower field when compared with **23** and the signal due to H5a in **10** was also shifted to lower field by the same amount (Scheme 3). Difference NOE spectra of both **10** and **23** were recorded while irradiating the signal due to H1 in each case. In the former case, the signal due to the C-9 methyl group exhibited slight enhancement, whereas in the latter case the signal due to H9 was subject to enhancement. While these results are consistent with the structures assigned to these dienes, unambiguous confirmation of stereochemistry at C-9 was based on an X-ray crystal structure of an organomolybdenum complex derived from **23** (vide infra).

*Complexation of dienes **10** and **23***

Attempted complexation of dienes **10** and **23** using cationic precursor **1** under the conditions previously developed was completely unsuccessful; starting materials were recovered even after extended reaction times. We reasoned that complexation of these dienes to the molybdenum centre was energetically much less favourable than for the model systems studied earlier, possibly due to steric hindrance.

However, it did prove possible to prepare molybdenum complexes of these dienes by generation of the unligated cationic (η^5-indenyl)$Mo(CO)_2$ moiety (by treatment of the dimer [(η^5-indenyl)$Mo(CO)_2$]$_2$ with $AgBF_4$, ref. 4) in the presence of an equimolar amount of diene **10** or **23** in CH_2Cl_2 solution (Scheme 4). Under these conditions, compound **10** provided a 2:1 mixture of two stereoisomeric complexes **12** and **24** in a combined yield of 71% whereas diene **23** provided epimeric complexes **25** and **26** in about the same ratio and in a combined yield of 85%.

At this point it was not clear whether complexation of **10** (or **23**) had occurred predominantly in the desired fashion (i.e., on the *endo* face of the diene). For comparison purposes, 9-normethyl diene **28** (prepared from alcohol **19** — see experimental section) was also complexed to molybdenum in the same fashion and complexes **29** and **30** were obtained in a 1:2 ratio. Complexes **12**, **25**, and **29** were structurally analogous, based on a comparison of their ^1H NMR spectra, as were their diastereomers **24**, **26**, and **30**. In particular, the signals due to the olefinic protons of the coordinated diene in the former series of complexes were at consistently higher field than for the latter series (see experimental section).

We had expected that diene **28** would undergo selective *exo* complexation in the usual fashion, as the steric impediment of the C-9 methyl group present in **10** (or **23**) had been removed. We therefore concluded that the *major* isomer produced in this case (**30**) was *exo* and by analogy so were the *minor* isomers (**24** and **26**) produced via complexation of **10** or **23**.

Nucleophilic additions to organomolybdenum complexes

Additional support for this conclusion was based on the reactions of the 1:2 mixture of diene complexes **29** and **30** with Me_2CuLi. Under the usual conditions (THF, −20°C) a *single* allylmolybdenum complex **31** was obtained in 57% yield and diene **28** was also produced in 30% yield (Scheme 4). The regiochemistry of methyl addition was readily established; only two allyl proton signals were observed in the ^1H NMR spectrum of **31**, a result that is only compatible with nucleophilic attack at C-1 in complexes **29** and (or) **30**.

A similar result was obtained in the less coordinating sol-

[4]Other oxidation methods (e.g., PCC; Swern) were uniformly unsuccessful in providing aldehyde **20**.

Can. J. Chem. Downloaded from www.nrcresearchpress.com by 213.200.69.106 on 09/08/12
For personal use only.

TABLE 1. Selected crystallographic and refinement data for compounds **8** and **33**[18]

	Compound **8**	Compound **33**
Empirical formula	$C_{21}H_{22}MoO_2$	$C_{26}H_{30}MoO_2$
Color	Yellow	Yellow
Habit	Plate fragment	Needle prism fragment
Crystal dimensions (mm)	0.48 × 0.47 × 0.52	0.62 × 0.08 × 0.22
Crystal Forms	(100), (001), (010)	{010}, {100}, {102}
Space group	$P2_1/n$	$P2_1/c$
a (Å)	9.393 (1)	17.616 (4)
b (Å)	10.649 (2)	7.688 (2)
c (Å)	17.704 (2)	15.873 (2)
β (°)	91.05 (1)	90.12 (2)
V (Å^3)	1770.5 (4)	2149.7 (6)
Z	4	4
ρ_{calc} (g cm^{-3})	1.509	1.454
Absorption coefficient (cm^{-1})	7.31	6.29
2θ range (°)	4.0–50.0	4.0–50.0
Scan type	ω	ω
Scan range (ω)	1.40°	1.30°
Independent reflections	3124	3801
Observed reflections ($F > 6.0\ \sigma(F)$)	2760	3082
R	0.0236	0.0245
R_w	0.0409	0.0270
GOF	1.05	1.99

TABLE 2. Atomic coordinates (× 10^4) and equivalent isotropic displacement coefficients (Å^2 × 10^3) for compound **8**

Atom	x	y	z	U_{eq}[a]
Mo(1)	554.2 (2)	918.0 (2)	2434.1 (1)	35.61 (9)
O(18)	−328 (3)	−1474 (2)	3271 (1)	74.7 (8)
O(19)	2451 (2)	1493 (3)	3833 (1)	79.1 (9)
C(1)	−574 (2)	2551 (2)	3115 (2)	36.9 (7)
C(2)	−1209 (2)	2240 (2)	2414 (1)	39.5 (7)
C(3)	−1922 (3)	1099 (2)	2523 (2)	43.1 (8)
C(4)	−2460 (3)	1063 (2)	3335 (2)	45.9 (8)
C(5)	−1540 (2)	2062 (2)	3746 (1)	38.9 (7)
C(6)	−2331 (3)	3232 (3)	4060 (2)	48.9 (8)
C(7)	−1247 (4)	3872 (3)	4595 (2)	63 (1)
C(8)	−241 (4)	2819 (4)	4858 (2)	75 (1)
C(9)	−795 (3)	1625 (3)	4476 (2)	56.2 (9)
C(10)	−4073 (3)	1303 (4)	3327 (2)	60 (1)
C(11)	1025 (3)	−237 (3)	1341 (2)	57.4 (9)
C(12)	2318 (3)	−65 (3)	1750 (2)	65 (1)
C(13)	2469 (3)	1214 (4)	1760 (2)	63 (1)
C(13A)	1591 (3)	1865 (3)	1324 (1)	49.5 (8)
C(14)	1406 (4)	3144 (3)	1133 (2)	66 (1)
C(15)	263 (5)	3470 (3)	702 (2)	82 (2)
C(16)	−740 (4)	2561 (4)	437 (2)	77 (1)
C(17)	−606 (3)	1335 (4)	615 (2)	61 (1)
C(17A)	573 (3)	950 (2)	1066 (1)	46.5 (8)
C(18)	−52 (3)	−571 (3)	2972 (1)	48.4 (8)
C(19)	1701 (3)	1292 (3)	3331 (2)	51.4 (8)

[a]Equivalent isotropic U defined as one third of the trace of the orthogonalized U_{ij} tensor.

vent, diethyl ether; complex **31** was obtained in 60% yield along with 36% of diene **28**. Reaction of **29** and **30** with MeMgBr (obtained from Aldrich Chemical Co. as a solution in ether) in CH_2Cl_2 solution at −78°C also led to the same product distribution (63% **31**; 33% **28**). Based on these results, it seemed clear that the major, *exo*, complex **30** was undergoing nucleophilic addition in the normal fashion (i.e., addition of Me_2CuLi *anti* to the metal and at the least substituted, terminal, position of the diene) to give complex **31** whereas the minor *endo* isomer **29** was undergoing selective decomplexation to **28** under these conditions.

Support for this hypothesis was based on the following observation: addition of a slight excess of THF-d_8 (i.e., ~2 equiv.) to a solution of complexes **29** and **30** in CD_2Cl_2 at room temperature led to selective destruction of the former complex as revealed by ^{1}H NMR spectroscopy of the

Can. J. Chem. Downloaded from www.nrcresearchpress.com by 213.200.69.106 on 09/08/12
For personal use only.

TABLE 3. Selected bond lengths and angles for compound **8**[a]

Bond	Length[b]	Bonds	Angle[b]
Mo—C(1)	2.376 (2)	C(1)—Mo—C(2)	35.7 (1)
Mo—C(2)	2.174 (2)	C(1)—Mo—C(3)	56.8 (1)
Mo—C(3)	2.342 (2)	C(2)—Mo—C(3)	35.9 (1)
Mo—C(11)	2.343 (3)	C(18)—Mo—C(19)	86.0 (1)
Mo—C(12)	2.320 (3)	C(5)—C(1)—C(2)	108.3 (2)
Mo—C(13)	2.341 (3)	C(1)—C(2)—C(3)	106.1 (2)
Mo—C(13a)	2.430 (2)	C(2)—C(3)—C(4)	108.5 (2)
Mo—C(17a)	2.424 (2)	O(18)—C(18)—Mo	177.5 (2)
Mo—C(18)	1.940 (3)	O(19)—C(19)—Mo	175.7 (2)
Mo—C(19)	1.943 (3)		
C(1)—C(2)	1.407 (3)		
C(2)—C(3)	1.403 (3)		

[a]For the numbering scheme employed please consult Fig. 1.
[b]Bond lengths (Å) and angles (deg) with estimated standard deviations in parentheses.

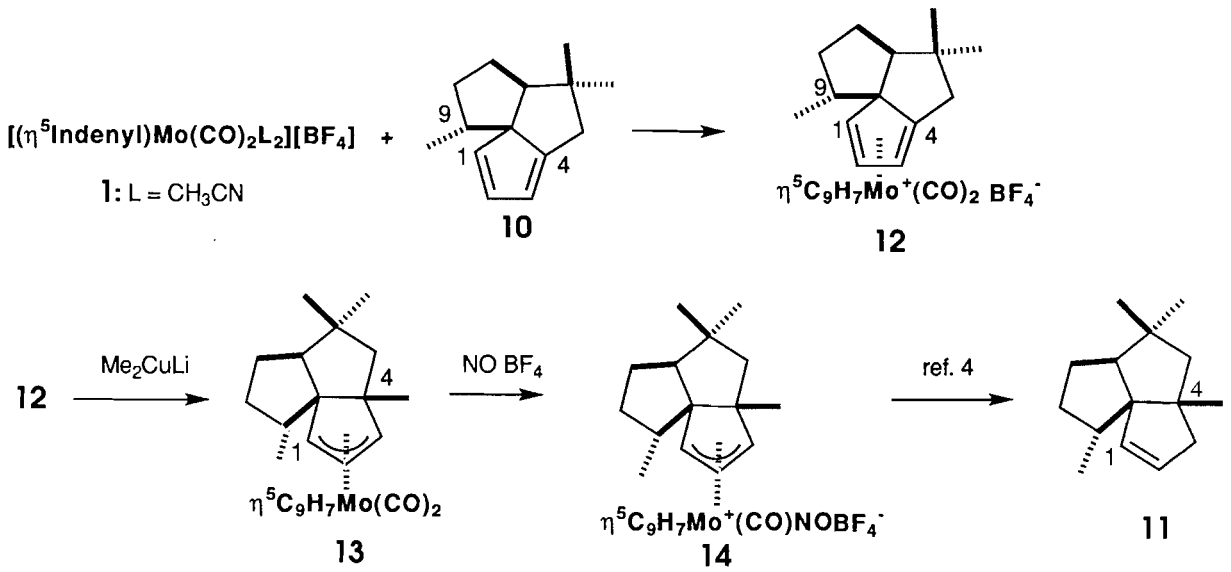

SCHEME 2

mixture. Although free diene **28** was not detected under these conditions, further addition of THF-d_8 led to decomposition of **30** as well and to formation of **28**. It thus appears that donor solvents will displace **28** from the molybdenum centre in complexes **29** and **30** with the former isomer being exceptionally labile towards nucleophilic substitution.[5]

Similar behaviour was observed when complexes **12** and **24** or **25** and **26** were treated with Me_2CuLi in diethyl ether (or MeMgBr in CH_2Cl_2). In the former case, allylmolybdenum complex **32** (structurally analogous to **31** based on spectroscopic data) was produced in 21% yield with diene **10** being produced in 44% yield, whereas in the latter case complex **33** was produced in 21% yield with diene **23** being recovered in 76% yield (Scheme 4). It thus appears that the desired transformation of **12** to silphinene (Scheme 2) is precluded by the unexpected lability of these complexes to donor solvents.

The structure of complex **33** could be confirmed by X-ray crystallography as suitable single crystals of this compound could be obtained by evaporation of a hexane solution (Fig. 2; Tables 1, 4, and 5). As the molecular structure depicted in Fig. 2 reveals, the molybdenum is coordinated to the *exo* face of the tricyclic framework, nucleophilic attack of Me_2CuLi has occurred *anti* to the metal centre at Cl, and the stereochemistry at C-9 is epimeric to that required for the synthesis of silphinene.

From this structure, it is clear that **33** is derived from diene complex **26**, the minor isomer produced on complexation of diene **23**. Hence, the stereochemistry of dienes **10** and **23** could be firmly established. The structural assignments of the other organometallic complexes prepared are based on the similarity in their spectral characteristics and the arguments presented above.

It should be noted that although the geometry about the allyl group of complex **33** does not differ much from that observed in compound **8** (compare Table 2 with Table 5), there is a distinct departure from linearity at the C(24) carbonyl carbon in complex **33** (see Fig. 2 and Table 5; Mo—C(24)—O(24) = 172.8 (2)°) that is not evident at either of the carbonyl groups in the structure of **8**. This bending may

[5]Nucleophilic displacement of the indenylmolybdenum moiety from unhindered diene complexes using strong donor ligands (e.g., bipy, dppe) has been reported (4*a*,*c*).

Can. J. Chem. Downloaded from www.nrcresearchpress.com by 213.200.69.106 on 09/08/12
For personal use only.

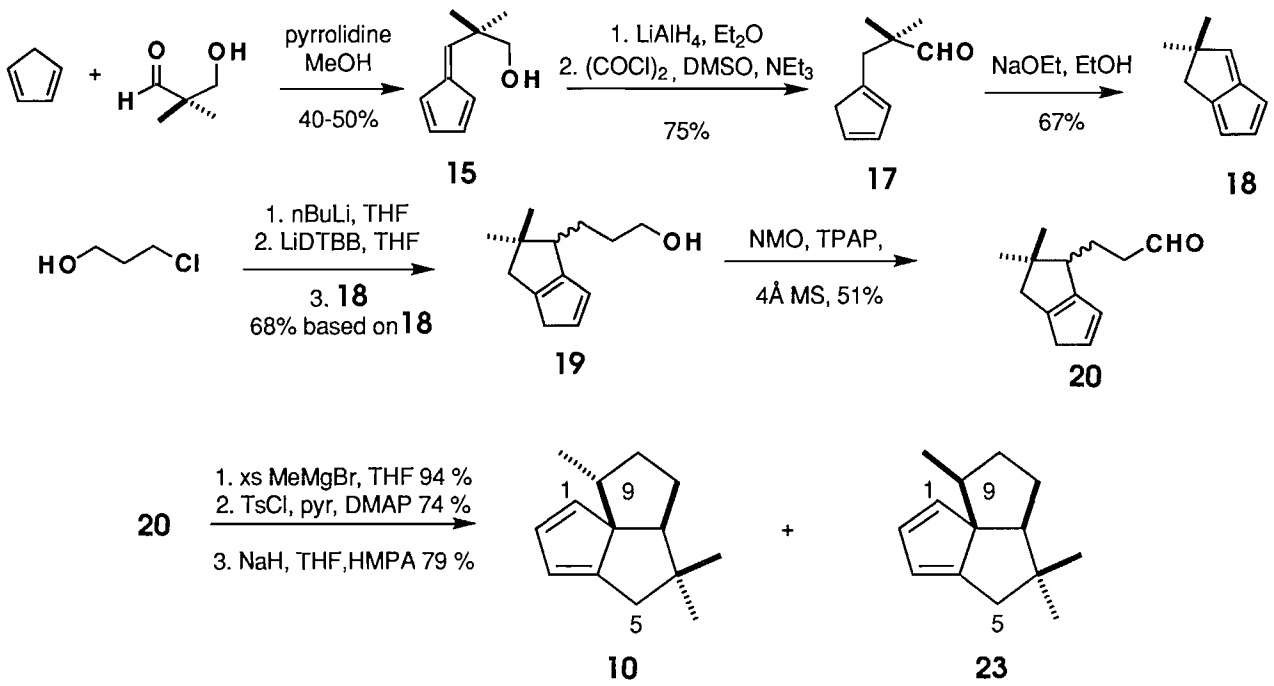

SCHEME 3

be due to steric repulsion between O(24) and the C(15) methyl group; short intramolecular contacts of 2.58 and 3.146(4) Å are observed between O(24) and H(15Y) and O(24) and C(15), respectively. The latter contact is well below the sum of the van der Waals radii for oxygen and a methyl group (3.40 Å).

Conclusions

Efficient and direct functionalization of spirocyclopentadienes is possible using indenylmolybdenum complex **1** or other precursors of the cationic indenylmolybdenum dicarbonyl moiety. Subsequent nucleophilic additions to these diene complexes can be an efficient process and provide a protocol for stereoselective alkylation of five-membered rings. Application of this methodology to the total synthesis of (±)-silphinene was prevented because of the unexpected lability of advanced intermediate **12** towards donor solvents required for the nucleophilic addition process. However, stereoselective complexation of diene **10** on the *endo* face of this compound proved possible. It is conceivable that sterically more hindered analogs of complex **1** (e.g., $[Cp^*Mo(CO)_2(CH_3CN)_2]$ $[BF_4]$ (ref. 10)) may enhance the stereoselectivity of diene complexation and hinder nucleophilic attack at the metal centre, a process that likely accounts for the lability of diene complexes such as **12**.

Experimental section

All reactions involving air- or moisture-sensitive reagents or compounds were performed under an atmosphere of dry N_2 or Ar using oven- or flame-dried glassware. Air- or moisture-sensitive compounds were stored in a Braun glove box under N_2 and weighed out as required. All solvents and reagents were obtained from commercial sources and purified as required. Diethyl ether, tetrahydrofuran, hexanes, and dimethoxyethane (DME) were distilled under N_2 from sodium and benzophenone. Dichloromethane, triethylamine, hexamethylphosphoramide (HMPA), pyrrolidine, acetonitrile, and dimethyl sulphoxide (DMSO) were distilled under N_2 (or in vacuo) from CaH_2. Cyclopentadiene was obtained by thermal cracking of dicyclopentadiene.

Molybdenum complex **1** was prepared from $[(h^5\text{-indenyl})\text{-}Mo(CO)_2]_2$ as described in the literature (4*g*). The latter dimeric complex was prepared from indene and $Mo(CO)_6$ as described in the literature (11). Spirocyclopentadiene **3** was prepared from cyclopentadiene and 1,4-dibromobutane with a slight modification of the literature conditions (12).

Reactions were monitored using thin-layer chromatography (TLC) performed on commercial, silica-coated, aluminum plates (silica gel 60, F254) purchased from E. Merck Co. Flash column chromatography was performed on silica gel 60 (230–400 mesh) supplied by E. Merck Co.

Boiling and melting points recorded are uncorrected. Elemental analyses were performed by M-H-W Laboratories (Phoenix, Ariz.). Low- and high-resolution mass spectra were performed on a Kratos MS-890 instrument at the University of Guelph. Infrared spectra (IR) were recorded on a Bomem MB-100 spectrophotometer. ^1H NMR and ^{13}C NMR spectra were obtained using either a Bruker AM-250 or AC-200 spectrometer; ^1H NMR chemical shifts are referenced with respect to residual undeuterated solvent while ^{13}C NMR shifts are referenced with respect to deuterated solvent.

*Indan-2-spiro-(cyclopenta-2',4'-diene) **4***

To a suspension of sodium hydride (3.3 g, 138 mmol) in 50 mL of THF at −30°C was added a solution of cyclopentadiene (2.8 g, 39 mmol) and α,α'-dibromo-*ortho*-xylene (10 g, 38 mmol) in 25 mL of THF via addition funnel over a period of 6 h. The reaction mixture was stirred for an additional 20 h at room temperature and then quenched with water. The reaction mixture was diluted with Et_2O and the organic phase was washed with water and brine and dried over $MgSO_4$. The organic phase was filtered, concentrated in vacuo, and dissolved in hexane. To remove uncyclized impurities, BuLi (17 mL, 2.5 M in hexanes, 42 mmol) was added to the hexane solution and the salts that formed from these compounds were filtered off under nitrogen. The filtrate was quenched with water and worked up as usual. The solid residue was sublimed (60–65°C, 0.1 Torr) (1 Torr = 133.3 Pa) to give **4** (0.96 g, 15%); melting point 70–71°C. ^1H NMR (250 MHz, $CDCl_3$) δ: 7.2–7.1 (m, 4H), 6.3 (m, 2H, AA'), 6.2 (m, 2H, BB'), 2.99 (s, 4H).

Can. J. Chem. Downloaded from www.nrcresearchpress.com by 213.200.69.106 on 09/08/12
For personal use only.

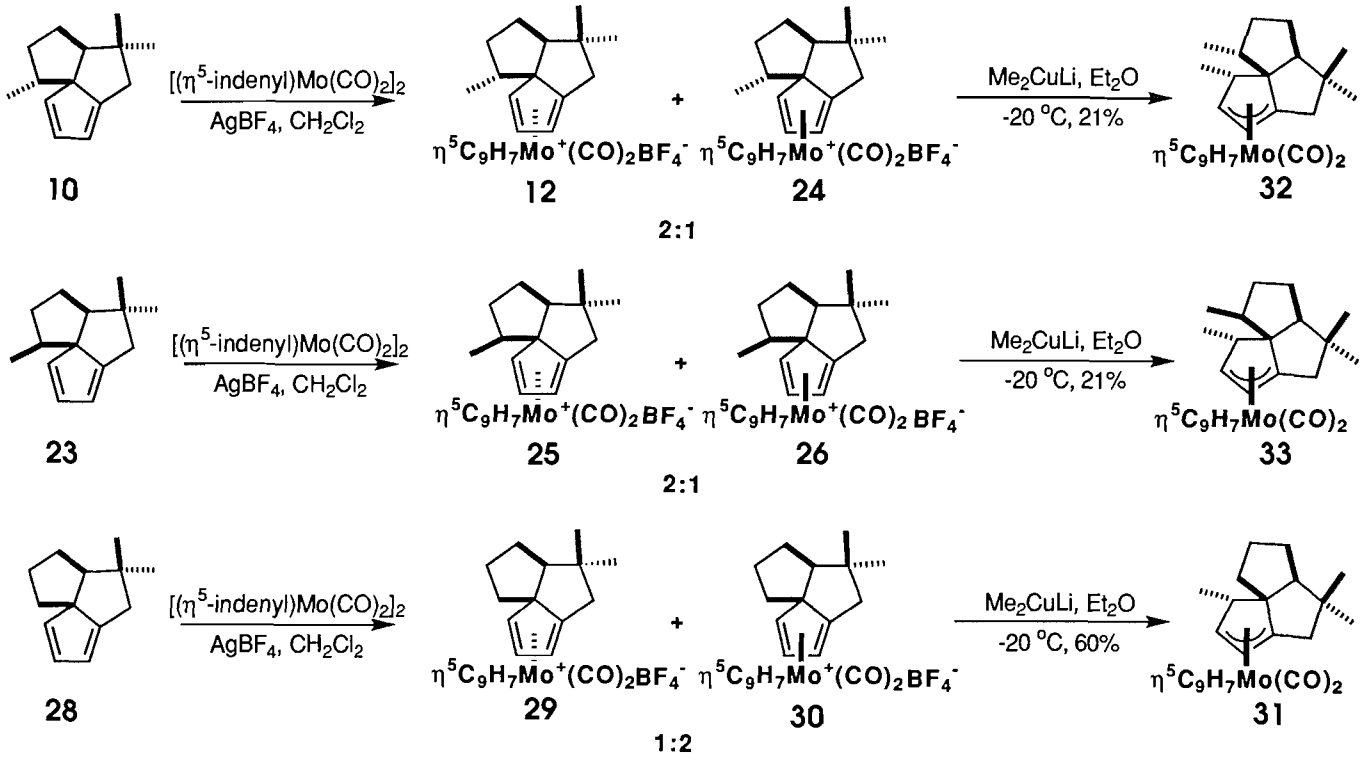

SCHEME 4

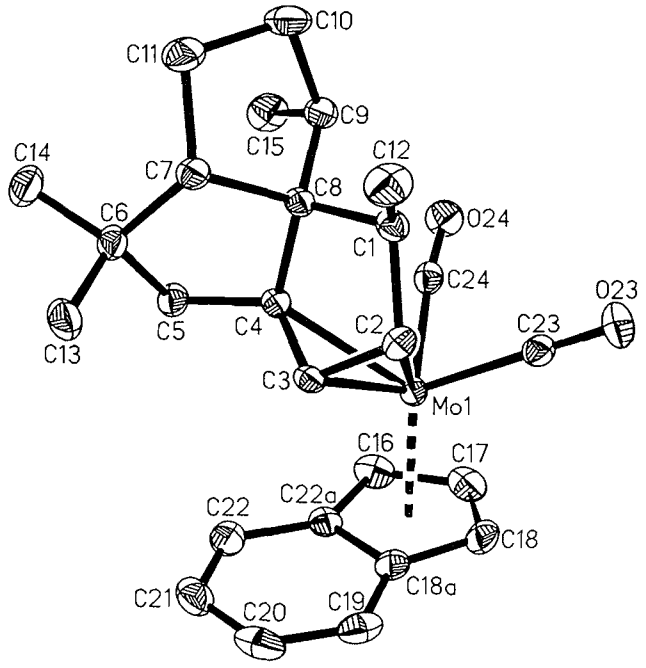

FIG. 2. Molecular structure of allylmolybdenum complex **33** with 30% thermal probability ellipsoids depicted; H-atoms have been removed for clarity. For selected bond lengths and angles see Table 5.

^{13}C NMR (62.5 MHz, $CDCl_3$) δ: 143.5, 143.2, 128.8, 126.3, 124.5, 64.0, 37.6. MS *m/z*: 168 (M^+). Anal. calcd. for $C_{13}H_{12}$: C 92.81, H 7.19; found: C 92.78, H 7.38.

Preparation of diene complex 5

To a solution of spirodiene **3** (1.2 g, 2.6 mmol) in 25 mL CH_2Cl_2 was added complex **1** (330 mg, 2.7 mmol) in 5 mL of CH_2Cl_2. The reaction was stirred for 10 h and then filtered. Et_2O (50 mL) was added to precipitate complex **5**, which was collected by filtration, rinsed with 2 × 10 mL of Et_2O, and dried in vacuo (1.0 g, 82%). IR (CH_2Cl_2): 2022, 1966 cm^{-1}. ^{1}H NMR (200 MHz, $CDCl_3$) δ: 7.79 (m, 2H, AA′), 7.41 (m, 2H, BB′), 6.40 (d, 2H, *J* = 2.9 Hz), 5.73 (t, 1H, *J* = 2.9 Hz, coupled to 6.40), 5.41 (t, 2H, *J* = 2.9 Hz), 4.85 (t, 2H, *J* = 2.9 Hz, coupled to 5.41), 1.86 (t, 2H, *J* = 7.1 Hz), 1.61 (m, 2H), 1.48 (m, 2H), 1.14 (t, 2H, *J* = 7.0 Hz). ^{13}C NMR (50 MHz, $CDCl_3$) δ: 227.2, 129.9, 125.6, 112.0, 95.6, 93.0, 92.2, 85.1, 71.4, 51.7, 36.9, 24.7, 24.6. Anal. calcd. for $C_{20}H_{19}BF_4MoO_2$: C 50.67, H 4.04; found: C 50.17, H 4.20.

Preparation of diene complex 6

Complex **6** was obtained in 65% yield (202 mg) from **1** (260 mg, 0.59 mmol) and diene **4** (100 mg, 0.59 mmol) using the same procedure as that described for the preparation of complex **5**. IR (CH_2Cl_2): 2025, 1970 cm^{-1}. ^{1}H NMR (200 MHz, $CDCl_3$) δ: 7.78 (m, 2H, AA′), 7.42 (m, 2H, BB′), 7.11 (m, 3H), 6.92 (br d, 1H, *J* = 5.7 Hz), 6.41 (d, 2H, *J* = 2.9 Hz), 5.77 (t, 1H, *J* = 2.9 Hz, coupled to 6.41), 5.46 (t, 2H, *J* = 2.9 Hz), 4.88 (t, 2H, *J* = 2.9 Hz, coupled to 5.46), 3.17 (s, 2H), 2.49 (s, 2H). ^{13}C NMR (50 MHz, CD_2Cl_2) δ: 226.4, 139.8, 139.2, 130.8, 127.6, 127.4, 125.8, 124.7, 112.1, 93.8, 93.1, 92.2, 85.4, 71.6, 57.0, 44.0. Anal. calcd. for $C_{24}H_{19}BF_4MoO_2$: C 54.96, H 3.65; found: C 54.82, H 3.85.

Preparation of allylmolybdenum complex 8

To a suspension of complex **5** (1.0 g, 2.1 mmol) in 40 mL of THF was added lithium dimethyl cuprate (21 mmol) prepared in THF from CuI (21 mmol) and MeLi (21 mL, 2.0 M in ether) at −20°C. The reaction was stirred for 1 h and quenched with a pH 8 mixture of aqueous NH_4Cl and NH_3. Hexane (30 mL) was added to the reaction mixture and the organic phase was syringed onto a small plug of silica gel and flushed with hexane into a round-bottom flask that was purged with N_2. The solvent was removed in vacuo to give **8** (770 mg, 91%). IR (CH_2Cl_2): 1936, 1856 cm^{-1}. ^{1}H NMR (200 MHz, $CDCl_3$) δ: 7.1–6.9 (m, 4H), 5.89 (m, 1H), 5.80 (m, 1H), 5.62 (t, 1H, *J* = 2.9 Hz), 3.58 (dd, 1H, *J* = 3.1 Hz, *J* = 3.9 Hz), 2.84 (t, 1H, *J* = 3.4 Hz), 1.6–1.2 (overlapping m,

Can. J. Chem. Downloaded from www.nrcresearchpress.com by 213.200.69.106 on 09/08/12
For personal use only.

Can. J. Chem. Downloaded from www.nrcresearchpress.com by 213.200.69.106 on 09/08/12
For personal use only.

TABLE 4. Atomic coordinates ($\times 10^4$) and equivalent isotropic displacement coefficients ($Å^2 \times 10^3$) for compound **33**

Atom	x	y	z	U_{eq}[a]
Mo(1)	1335.9 (1)	1381.0 (1)	3226.1 (1)	27.72 (7)
O(23)	882 (1)	882 (3)	1355 (1)	56.2 (9)
O(24)	1427 (1)	5184 (3)	2616 (1)	49.5 (8)
C(1)	2792 (2)	906 (4)	1982 (2)	32 (1)
C(2)	2261 (2)	−268 (4)	2487 (2)	32 (1)
C(3)	2409 (2)	−19 (4)	3350 (2)	28 (1)
C(4)	2670 (1)	1712 (3)	3458 (2)	27 (1)
C(5)	3121 (2)	2246 (5)	4222 (2)	36 (1)
C(6)	3949 (2)	1744 (4)	3969 (2)	36 (1)
C(7)	3958 (2)	1765 (4)	2972 (2)	33 (1)
C(8)	3127 (2)	2164 (4)	2667 (2)	29 (1)
C(9)	3181 (2)	4058 (4)	2348 (2)	38 (1)
C(10)	3951 (2)	4057 (5)	1893 (3)	53 (1)
C(11)	4477 (2)	3068 (5)	2507 (2)	52 (1)
C(12)	3355 (2)	−197 (6)	1470 (2)	52 (1)
C(13)	4113 (2)	−113 (5)	4267 (2)	48 (1)
C(14)	4531 (2)	2943 (6)	4392 (3)	52 (1)
C(15)	3174 (2)	5479 (5)	3010 (3)	52 (1)
C(16)	641 (2)	2232 (5)	4413 (2)	45 (1)
C(17)	128 (2)	1762 (6)	3770 (2)	51 (1)
C(18)	200 (2)	6 (5)	3592 (2)	47 (1)
C(18A)	732 (2)	−715 (4)	4163 (2)	37 (1)
C(19)	1007 (2)	−2433 (5)	4301 (2)	48 (1)
C(20)	1517 (3)	−2707 (5)	4925 (3)	55 (1)
C(21)	1787 (2)	−1337 (6)	5432 (2)	53 (1)
C(22)	1546 (2)	309 (5)	5321 (2)	45 (1)
C(22A)	1010 (2)	673 (4)	4678 (2)	34 (1)
C(23)	1060 (2)	1048 (4)	2055 (2)	36 (1)
C(24)	1445 (2)	3752 (4)	2850 (2)	34 (1)

[a]Equivalent isotropic U defined as one third of the trace of the orthogonalized U_{ij} tensor.

TABLE 5. Selected bond lengths and angles for compound **33**[a]

Bond	Length[b]	Bonds	Angle[b]
Mo—C(2)	2.376 (3)	C(2)—Mo—C(3)	35.6 (1)
Mo—C(3)	2.184 (3)	C(2)—Mo—C(4)	57.2 (1)
Mo—C(4)	2.391 (3)	C(3)—Mo—C(4)	35.7 (1)
Mo—C(16)	2.342 (4)	C(23)—Mo—C(24)	81.5 (1)
Mo—C(17)	2.317 (3)	C(1)—C(2)—C(3)	108.5 (2)
Mo—C(18)	2.338 (3)	C(2)—C(3)—C(4)	107.7 (2)
Mo—C(18a)	2.438 (3)	C(3)—C(4)—C(8)	106.6 (2)
Mo—C(22a)	2.437 (3)	O(23)—C(23)—Mo	178.3 (3)
Mo—C(23)	1.937 (3)	O(24)—C(24)—Mo	172.8 (2)
Mo—C(24)	1.927 (3)		
C(2)—C(3)	1.407 (4)		
C(3)—C(4)	1.418 (4)		

[a]For the numbering scheme employed please consult Fig. 2.
[b]Bond lengths (Å) and angles (deg) with estimated standard deviations in parentheses.

total 9H), 0.85 (d, 3H, J = 7.02 Hz), 0.05 (t, 1H, J = 4.0 Hz). ^{13}C NMR (50 MHz, $CDCl_3$) δ: 238.3, 235.7, 124.7, 124.2, 123.5, 122.6, 111.7, 109.8, 88.8, 81.2, 80.0, 78.9, 77.9, 70.47, 59.0, 46.6, 39.4, 37.7, 24.0, 23.7, 21.5. MS m/z: 404 (M^+). Anal. calcd. for $C_{21}H_{22}MoO_2$: C 62.69, H 5.59; found: C 62.60, H 5.41. Single crystals suitable for X-ray diffraction studies were grown by slow evaporation of a hexane solution.

X-ray structure determination of complex 8

A yellow plate fragment of dimensions 0.48 × 0.47 × 0.52 mm, corresponding to the forms (100), (001), and (010), respectively, and glued to a glass fiber using epoxy resin was mounted on a Siemens R3m/v diffractometer. The unit cell parameters were determined and refined from a set of 25 general reflections ($24.5 < 2\theta < 30.5°$) well distributed in reciprocal space.

Intensity data were collected with graphite monochromated MoKα radiation at 295 K by employing the ω-scan technique over a 2θ range of 4.0–50.0° with variable scan speeds (2.93–29.30° min^{-1}). Background measurements using the stationary crystal, stationary counter method were made at the beginning and end of each scan, each for 25% of the total scan time. Two standard reflections were measured after every 100 reflections and showed no significant loss in intensity during data acquisition.

Intensities were corrected for Lorentz and polarization effects.

Can. J. Chem. Downloaded from www.nrcresearchpress.com by 213.200.69.106 on 09/08/12
For personal use only.

A face-indexed numerical method was employed to correct for adsorption effects. Of the 3124 independent reflections collected, 2760 were considered observed ($F > 6.0\ \sigma(F)$) and were used in the structure solution and refinement. The minimum and maximum transmission factors through the crystal were calculated to be 0.6891 and 0.7437.

The structure was solved by Patterson and Fourier methods and refined by full-matrix least-squares techniques using the Siemens SHELXTL PLUS software. Anisotropic refinement of all non-hydrogen atoms revealed the positions of all the hydrogens atoms from a difference map. In the final cycles of refinement, the hydrogen atoms were refined isotropically in their found positions with the exception of one H atom on the indenyl ligand (H(16)), which was unstable during refinement and was therefore constrained at its calculated position.

Scattering factors for non-hydrogen atoms were taken from the *International tables* (13*a*) while the data of Stewart et al. were used for hydrogen atoms (13*b*). Selected details of the crystallographic data, data collection, and final refinement appear in Table 1, atomic coordinates and isotropic thermal parameters appear in Table 2, while selected bond lengths and angles appear in Table 3. Full details of the structure determination have been deposited.[6]

Preparation of complex ***9***

Complex **9** was obtained in 97% yield (640 mg) from **6** (766 mg, 1.47 mmol) using the same procedure as that described for the preparation of complex **8**. IR (CH_2Cl_2): 1938, 1859 cm^{-1}. ^1H NMR (200 MHz, $CDCl_3$) δ: 7.1–6.9 (m, 8H), 5.91 (m, 1H), 5.82 (m, 1H), 5.64 (t, 1H, J = 2.9 Hz), 3.67 (t, 1H, J = 3.4 Hz), 3.1 (d, 1H, A of AX spin system, J = 15.6 Hz), 2.92 (t, 1H, J = 3.4 Hz), 2.73 (d, 1H, B of BC spin system, J = 15.5 Hz), 2.62 (d, 1H, C of BC spin system, J = 15.5 Hz), 2.2 (d, 1H, J = 15.6 Hz, X of AX spin system), 1.67 (q, 1H, J = 6.9 Hz), 0.75 (d, 3H, J = 6.9 Hz), 0.08 (t, 1H, 3.4 Hz). ^{13}C NMR (50 MHz, $CDCl_3$) δ: 238.0, 235.8, 143.2, 143.1, 125.9, 125.8, 124.9, 124.2, 124.1, 123.7, 123.2, 122.7, 111.8, 109.9, 88.7, 81.3, 80.2, 78.3, 77.3, 70.8, 60.4, 48.0, 45.2, 21.7. HRMS calculated for $C_{25}H_{22}{}^{92}MoO_2$: 446.0682$_7$; found (EI): 446.06557.

6-(2-Hydroxy-1,1-dimethylethyl)fulvene ***15***

To a solution of 2,2-dimethyl-3-hydroxy propionaldehyde (3.2 g, 31 mmol) and cyclopentadiene (5.2 g, 78 mmol) in 30 mL of methanol was added pyrrolidine (3.5 mL, 42 mmol). The reaction was stirred for 24 h at 25°C and another 5.2 g of cyclopentadiene and 3.5 mL of pyrrolidine were added. The reaction was allowed to stir for another 24 h and acetic acid (2.5 g, 42 mmol) was then added. The mixture was diluted with water and extracted with 50 mL Et_2O. The aqueous phase was washed with 2 × 50 mL Et_2O. The combined organic extracts were washed with water, saturated Na_2CO_3, and brine, and dried over $MgSO_4$. The mixture was filtered and the solvent removed in vacuo. The crude reaction mixture was purified by column chromatography, eluting first with hexane, then with 20% Et_2O – hexane to provide fulvene **15** (2.3 g, 50%). IR (neat): 3347, 3071, 2957, 2869, 1634, 1468, 1379 cm^{-1}. ^1H NMR (200 MHz, $CDCl_3$) δ: 6.62 (t, 2H, J = 1.5 Hz), 6.40 (m, 2H), 6.16 (m, 1H), 3.57 (d, 2H, J = 6.6 Hz, collapsed to singlet with D_2O wash), 1.49 (t, 1H, J = 6.6 Hz, exchanges with D_2O), 1.3 (s, 6H). ^{13}C NMR (50 MHz, $CDCl_3$) δ: 149.3, 144.9, 134.9, 129.1, 128.2, 119.8, 72.0, 41.2, 25.7. MS m/z: 150 (M^+). Anal. calcd. for $C_{10}H_{14}O$: C 79.96, H 9.39; found: C 79.86, H 9.22.

2,2-Dimethyl-3-cyclopentadienyl-1-propanol ***16***

To a solution of fulvene **15** (1.01 g, 6.7 mmol) in 50 mL dry Et_2O at 0°C was added slowly $LiAlH_4$ (254 mg, 6.7 mmol) via a solid addition funnel. The reaction was warmed to room temperature and after 1 h was cooled to 0°C; water (250 μL), 15% NaOH (250 μL), and water (250 μL) were added sequentially dropwise via syringe with vigorous stirring. The mixture was diluted with Et_2O and filtered through a pad of Celite, washing with an additional 2 × 50 mL of Et_2O. The filtrate was concentrated in vacuo and distilled (bulb to bulb, 60–65°C, 0.1 Torr) to provide the title compound (1.02 g, 100%). IR (neat): 3365, 3061, 2916, 1604, 1468, 1368 cm^{-1}. ^1H NMR (200 MHz, $CDCl_3$) δ: 6.4–6.0 (m, 3H), 3.3 (d, 2H, J = 6.4 Hz, collapses to singlet with D_2O wash), 2.93 (m, 2H), 2.34 (br s) and 2.30 (br s, combined 2H), 1.3 (t, 1H, J = 6.4 Hz, exchanges with D_2O), 0.87 (s, 6H). ^{13}C NMR (50 MHz, $CDCl_3$) δ: 146.0, 143.7, 136.39, 132.7, 132.3, 131.0, 129.7, 129.4, 71.4, 45.7, 41.1, 39.2, 38.6, 36.1, 35.9, 24.2, 24.1. MS m/z: 152 (M^+). Anal. calcd. for $C_{10}H_{16}O$: C 78.90, H 10.59; found: C 78.74, H 10.80.

2,2-Dimethyl-3-cyclopentadienyl propionaldehyde ***17***

To a solution of oxalyl chloride (2.8 g, 22 mmol) in 20 mL of CH_2Cl_2 at −55°C was added DMSO (3.5 g, 45 mmol), slowly via syringe. A bubbler was used to release pressure. After 5 min, alcohol **16** (1.7 g, 12 mmol) in 20 mL of CH_2Cl_2 was added. The reaction was stirred for 2 h at −55°C, and then treated with Et_3N (9.1 g, 90 mmol). The mixture was brought to room temperature and excess water and Et_2O were added. The aqueous phase was washed with 2 × 20 mL of Et_2O. The combined organic extracts were washed with 2 × 50 mL of 1 M AcOH, water, saturated Na_2CO_3, and brine, and dried over $MgSO_4$. The solvent was removed in vacuo at 0°C and the crude material was subjected to column chromatography (hexanes). Bulb-to-bulb distillation (40–45°C, 0.1 Torr) provided compound **17** (1.3 g, 75%). IR (neat): 3059, 2928, 2703, 1728, 1462, 1367, 1100, 1028 cm^{-1}. ^1H NMR (200 MHz, $CDCl_3$) δ: 9.56 (s, 1H), 6.4–6.0 (m, 3H), 2.96 (br s) and 2.84 (br s, combined 2H), 2.62 (br s) and 2.56 (br s, combined 2H), 1.07 (s, 6H). ^{13}C NMR (50 MHz, $CDCl_3$) δ: 206.2, 142.0, 138.4, 135.6, 133.6, 132.2, 131.7, 130.6, 130.3, 62.1, 49.2, 45.0, 41.4, 37.4, 21.73, 21.6. MS m/z: 150 (M^+). Anal. calcd. for $C_{10}H_{14}O$: C 79.96, H 9.39; found: C 79.76, H 9.42.

7,7-Dimethylbicyclo[3.3.0]octa-1.3.5-triene ***18***

To 500 mL of 0.35 M sodium ethoxide in EtOH was added aldehyde **17** (10.5 g, 70 mmol) in 400 mL of EtOH over a period of 8 h. The reaction was stirred for an additional 2 h, then diluted with excess water and extracted with 4 × 100 mL of pentane. The combined organic extracts were washed with water (2 × 400 mL) and brine, and then dried over $MgSO_4$. The solvent was removed in vacuo at −10°C. Bulb-to-bulb distillation (25°C, 0.1 Torr) provided fulvene **18** (6.2 g, 67%). IR (neat): 3100, 3074, 3036, 2958, 2864, 1631, 1590, 1481, 1318, 1247, 1150 cm^{-1}. ^1H NMR (200 MHz, $CDCl_3$) δ: 6.80 (dd, 1H, J = 1.91 Hz, J = 5.11 Hz, coupled to 5.86 and 6.10), 6.53 (br d, 1H, J = 1.58 Hz, coupled to 5.86), 6.10 (dd, 1H, J = 0.68 Hz, J = 5.11 Hz, coupled to 5.86 and 6.80), 5.86 (m, 1H), 2.5 (d, 2H, J = 1.98 Hz, coupled to 5.86), 1.28 (s, 6H). ^{13}C NMR (62.5 MHz, $CDCl_3$) δ: 151.6, 150.5, 150.0, 141.8, 115.4, 112.5, 54.7, 39.6, 28.2. MS m/z: 132 (M^+). Anal. calcd. for $C_{10}H_{12}$: C 90.85, H 9.15; found: C 90.68, H 9.24.

6-(3-Hydroxypropyl)-7,7-dimethylbicyclo[3.3.0]-octa-(2–3),(1–5)-diene ***19***

To a solution of 3-chloro-1-propanol (2.97 mL, 35.6 mmol) in 25 mL of THF at −78°C was added a solution of *n*-BuLi (14.8 mL, 2.5 M in hexanes, 37.0 mmol). The mixture was stirred for 0.5 h.

[6]Complete sets of tables of crystallographic and refinement data, atomic coordinates and isotropic thermal parameters, bond lengths, bond angles, anisotropic thermal parameters, H-atom coordinates and isotropic thermal parameters, and structure factors for both compound **8** and **33** may be purchased from: The Depository of Unpublished Data, Document Delivery, CISTI, National Research Council Canada, Ottawa, Canada K1A 0S2.

Tables of crystallographic and refinement data, atomic coordinates, bond lengths and angles, and H-atom coordinates have also been deposited with the Cambridge Crystallographic Data Centre and can be obtained on request from The Director, Cambridge Crystallographic Data Centre, University Chemical Laboratory, 12 Union Road, Cambridge, CB2 IEZ, U.K.

Can. J. Chem. Downloaded from www.nrcresearchpress.com by 213.200.69.106 on 09/08/12
For personal use only.

To this solution was added the dark green-blue radical anion of 4,4′-di-*tert*-butylbiphenyl formed from reacting 4,4′-di-*tert*-butylbiphenyl (19.1 g, 72 mmol) and lithium metal (493 mg, 71 mmol) in 100 mL of THF at −5°C under an Ar atmosphere. The reaction was stirred for 10 min and fulvene **18** (1.8 g, 13.6 mmol) in 15 mL of THF was added. The reaction was stirred for 1 h, then warmed to room temperature. The reaction was quenched with water and diluted with Et_2O. The aqueous phase was washed with 2 × 20 mL of Et_2O and the combined organic extracts were washed with water and brine, and dried over $MgSO_4$. The solvent was removed in vacuo and the crude material was subjected to column chromatography, eluting first with hexane followed by 20% Et_2O – hexane to give **19** (1.8 g, 68%). IR (neat): 3332, 3072, 2909, 1615, 1457, 1379, 1364, 1057 cm^{-1}. ^1H NMR (200 MHz, $CDCl_3$) δ: 5.87 (m, 1H), 5.8 (m, 1H), 3.7 (q, 2H, J = 6.4 Hz, collapses to triplet with D_2O wash), 3.24–3.19 (m, 2H), 2.30–2.22 (m, 3H), 2.0–1.80 (m, 1H), 1.77–1.45 (m, 2H), 1.43–1.30 (m, 2H), 1.1 (s, 3H), 0.86 (s, 3H). ^{13}C NMR (50 MHz, $CDCl_3$) δ: 156.6, 151.7, 151.1, 146.9, 134.3, 133.9, 130.5, 130.1, 120.0, 119.6, 63.3, 63.2, 52.7, 51.3, 49.2, 48.0, 47.4, 46.1, 44.7, 43.8, 40.9, 38.2, 37.8, 32.1, 31.9, 29.9, 28.2, 26.4, 24.9, 24.7, 23.1. MS *m/z*: 192 (M^+). Anal. calcd. for $C_{13}H_{20}O$: C 81.20, H 10.48; found: C 81.42, H 10.68.

6-(3-p-Toluenesulphonyloxypropyl)-7,7-dimethylbicyclo-[3,3,0]octa-(2–3),(1–5)-diene ***27***

To a solution of alcohol **19** (1.0 g, 5.2 mmol), pyridine (1.3 mL, 15.6 mmol), and catalytic DMAP (61 mg, 0.5 mmol) in 10 mL of CH_2Cl_2, was added *p*-toluenesulphonyl chloride (1.5 g, 7.8 mmol) in small portions over a period of 2 h at 5°C. The reaction was warmed to room temperature and stirred for 2.5 h, at which time it was poured into ice water and diluted with Et_2O. The organic phase was washed with 1 M AcOH, water, saturated Na_2CO_3, and brine, and dried over $MgSO_4$. The mixture was filtered and the solvent removed in vacuo. The crude material was subjected to column chromatography, eluting with 5% Et_2O – hexane to yield **27** (1.3 g, 70%) and unreacted **19** (18%). IR (neat): 3066, 2927, 1598, 1457, 1362, 1180, 1098, 962, 929 cm^{-1}. ^1H NMR (200 MHz, $CDCl_3$) δ: 7.6 (d, 2H, J = 8.3 Hz), 7.3 (d, 2H, J = 8.3 Hz), 5.74 (m, 2H), 4.03 (t, 2H, J = 6.4 Hz), 3.14–3.12 (m, 2H), 2.4 (s, 3H), 2.20–2.05 (m, 3H), 2.00–1.85 (m, 1H), 1.76–1.61 (m, 1H), 1.50–1.37 (m, 1H), 1.25–1.10 (m, 1H), 0.99 (s, 3H), 0.77 (s, 3H). A satisfactory analysis of this compound was not obtained due to its thermal instability at room temperature, it was converted directly to tricyclic diene **28**.

6,6-Dimethyltricyclo[6.3.0.07.8]undeca-1,3-diene ***28***

To a solution of HMPA (550 μL, 3.16 mmol) and NaH (160 mg, 6.7 mmol) in 13 mL of THF was added **27** (1.0 g, 2.9 mmol) in 7 mL of THF. The reaction was stirred for 4 h with 5 min periods of sonication every 20 min. The reaction was quenched with water at 0°C and diluted with pentane. The organic phase was washed with saturated copper sulfate, water, and brine, and dried with $MgSO_4$. The mixture was filtered and the solvent removed in vacuo at 0°C. The crude mixture was subjected to column chromatography eluting with pentane to provide **28** (400 mg, 79%). IR (neat): 3082, 3061, 3022, 2948, 2862, 1613, 1524, 1455, 1381, 1363 cm^{-1}. ^1H NMR (200 MHz, $CDCl_3$) δ: 6.17 (d, 1H, J = 5.1 Hz), 6.08 (dd, 1H, J = 5.1 Hz, J = 1.6 Hz), 5.84 (br s, 1H), 2.30 (br d, 1H, long range coupled to 5.84, J = 12.8 Hz, A of AB spin system), 1.91 (d, 1H, J = 12.8 Hz, B of AB spin system), 1.81–1.60 (m, 7H), 1.01 (s, 3H), 0.72 (s, 3H). ^{13}C NMR (50 MHz, $CDCl_3$) δ: 161.9, 143.6, 129.8, 121.7, 72.3, 52.2, 47.8, 41.3, 33.6, 31.8, 31.4, 27.6, 25.4. MS *m/z*: 174 (M^+). Anal. calcd. for $C_{13}H_{18}$: C 89.58, H 10.42; found: C 89.51, H 10.59.

6-(2-Formylethyl)-7,7-dimethylbicyclo[3.3.0]octa-(2–3),(1–5)-diene ***20***

To a mixture of alcohol **19** (1.1 g, 5.7 mmol), powdered 4 Å molecular sieves (15 g), and 4-methylmorpholine-*N*-oxide (1.2 g, 10.2 mmol) in 30 mL of CH_2Cl_2 was added tetrapropylammonium perruthenate (TPAP, 108 mg, 0.31 mmol) in small portions. The reaction was stirred at room temperature until all of **19** was consumed as judged by TLC. The reaction was then poured directly onto a small plug of silica gel and eluted with CH_2Cl_2. The solvent was removed in vacuo and the crude material subjected to bulb-to-bulb distillation (60–65°C, 0.1 Torr), providing aldehyde **20** (554 mg, 51%). IR (neat): 3068, 2952, 2867, 2717, 1726, 1447, 1382, 1365, 1261, 1057 cm^{-1}. ^1H NMR (200 MHz, $CDCl_3$) δ: 9.81 (t, 1H, J = 1.6 Hz), 5.83 (m, 2H), 3.2 (m, 2H), 2.82–2.50 (m, 3H), 2.30–2.18 (m, 2H), 2.00–1.81 (m, 1H), 1.63–1.49 (m, 1H), 1.1 (s, 3H), 0.92 (s, 3H). ^{13}C NMR (50 MHz, $CDCl_3$) δ: 202.0, 156.0, 151.0, 134.5, 134.4, 129.0, 120.4, 120.0, 119.6, 58.2, 52.0, 48.6, 47.4, 46.1, 44.3, 43.6, 42.9, 40.4, 37.9, 29.9, 28.3, 24.6, 23.0, 21.0. MS *m/z*: 190 (M^+). Anal. calcd. for $C_{13}H_{18}O$: C 82.05, H 9.54; found: C 81.87, H 9.34.

[R,R] and [R,S] 6-(3-Hydroxybutyl)-7,7-dimethylbicyclo[3.3.0]octa-(2–3),(1–5)-diene ***21***

To a solution of MeMgBr (18.1 mmol) in 20 mL of THF at −25°C was added aldehyde **20** (862 mg, 4.53 mmol) in 20 mL of THF. The reaction was stirred for 15 min, then quenched with water and extracted with Et_2O. The aqueous phase was extracted 2 × 20 mL of Et_2O and the combined organic extracts were washed with water, brine, and dried over $MgSO_4$. The mixture was filtered and the filtrate concentrated in vacuo. The crude material was subjected to column chromatography eluting with 20% Et_2O – hexane to provided alcohols **21** (877 mg, 94%). IR (neat): 3345, 3073, 2913, 1458, 1373, 1115 cm^{-1}. ^1H NMR (200 MHz, $CDCl_3$) δ: 5.85 (m, 2H), 3.90–3.75 (m, 1H), 3.2 (m, 2H), 2.35–2.20 (m, 3H), 1.84–1.40 (m, 4H), 1.2 (several overlapping doublets, total 3H), 1.1 (s, 3H), 0.86 (s, 3H). ^{13}C NMR (50 MHz, $CDCl_3$) δ: 157.2, 157.1, 151.7, 146.7, 134.1, 130.0, 119.9, 119.5, 68.2, 67.9, 57.7, 49.3, 49.2, 47.3, 46.0, 43.6, 40.8, 38.3, 38.2, 28.0, 25.0, 24.8, 24.5, 23.3, 23.2, 22.9, 18.0. MS *m/z*: 206 (M^+). High-resolution mass spectrum calcd. for $C_{14}H_{22}O$: 206.16705; found: 206.16620.

*[R,R] and [R,S] 6-(3-*p*-Toluenesulphonyloxybutyl)-7,7-dimethylbicyclo[3.3.0]octa-(2–3),(1–5)-diene* ***22***

Compounds **22** were obtained in 74% yield (1.1 g), from **21** (880 mg, 4.3 mmol) using the same procedure described in the synthesis of **27**. IR (neat): 3066, 2960, 2869, 1601, 1465, 1366, 1184, 1101 cm^{-1}. ^1H NMR (200 MHz, $CDCl_3$) δ: 7.8 (d, 2H, J = 8.3 Hz), 7.3 (d, 2H, J = 8.3 Hz), 5.78 (m, 1H), 5.70 (m, 1H), 4.70–4.60 (m, 1H), 3.16 (m, 2H), 2.43 (s, 3H), 2.20–2.10 (m, 3H), 2.0–1.1 (m, 4H), 1.32 (two overlapping d, total 3H, in a 1.1:1 ratio, J = 6.2 Hz, coupled to 4.62), 1.0 (s, 3H), 0.74 (s, 3H). A satisfactory elemental analysis of these compounds could not be obtained and they were generally converted to dienes **10** and **23** without purification.

rac-*[7S,8R,9R]-6,9,9Trimethyltricyclo[6.3.0.0^{7,8}]undeca-1,3-diene* ***10*** *and* rac-*[7S,8R,9S]-6,9,9-trimethyltricyclo-[6.3.0.0^{7,8}]undeca-1,3-diene* ***23***

A 1:1 isometric mixture of **10** and **23** was obtained in 79% yield (445 mg total wt.) from **22** (1.1 g, 3 mmol) using the same procedure described for the preparation of compound **28**. The two isomers were separated by column chromatography on $AgNO_3$-impregnated silica gel, eluting with pentane, to provide **23** (221 mg) and **10** (112 mg). The $AgNO_3$-impregnated silica gel was prepared by stirring 200 g silica gel with 400 mL of 20% aqueous $AgNO_3$, filtering, washing with THF, and drying in vacuo.

Data for **10**: IR (neat): 3082, 3061, 3024, 2950, 2866, 1612, 1525, 1454, 1383, 1363 cm^{-1}. ^1H NMR (200 MHz, $CDCl_3$) δ: 6.26 (d, 1H, J = 5.1 Hz), 6.15 (dd, 1H, J = 5.1 Hz, J = 1.5 Hz), 5.89 (br s, 1H), 2.47 (br d, 1H, J = 13.0 Hz, A of AB spin system, long range coupled to 5.89), 2.1 (m, 1H, coupled to 0.72), 1.93 (d, 1H, J = 13.0 Hz, B of AB spin system), 1.94–1.60 (m, 4H), 1.46–1.34 (m, 1H), 1.03 (s, 3H), 0.73 (s, 3H), 0.72 (d, 3H, J = 6.7 Hz). ^{13}C NMR (62.5 MHz, $CDCl_3$) δ: 160.2, 140.5, 131.2, 122.4, 75.6, 53.1, 47.3, 41.7, 39.7, 36.7, 31.8, 27.9, 26.3, 15.4.

Can. J. Chem. Downloaded from www.nrcresearchpress.com by 213.200.69.106 on 09/08/12
For personal use only.

MS *m/z*: 188 (M^+). Anal. calcd. for $C_{14}H_{20}$: C 89.29, H 10.71; found: C 89.07, H 10.98.

Data for **23**: IR (neat): 3082, 3061, 3024, 2950, 2866, 1612, 1525, 1454, 1383, 1363 cm^{-1}. ^1H NMR (250 MHz, $CDCl_3$) δ: 6.13 (dd, 1H, J = 5.0 Hz, J = 1.7 Hz), 6.06 (d, 1H, J = 5.0 Hz), 5.89 (br s, 1H), 2.28 (br d, 1H, J = 12.6 Hz, A of AB spin system, long range coupled to 5.89), 2.1 (m, 1H, coupled to 0.71), 1.91 (d, 1H, J = 12.6 Hz, B of AB spin system), 1.98–1.76 (m, 3H), 1.68–1.11 (m, 2H), 1.03 (s, 3H), 0.74 (s, 3H), 0.71 (d, 3H, J = 6.5 Hz). ^{13}C NMR (62.5 MHz, $CDCl_3$) δ: 159.7, 142.7, 130.7, 123.7, 75.1, 52.4, 48.3, 43.7, 41.0, 34.9, 32.2, 30.1, 25.2, 13.0. MS *m/z*: 188 (M^+). Anal. calcd. for $C_{14}H_{20}$: C 89.29, H 10.71; found: C 89.10, H 10.86.

Preparation of endo- *and* exo-*diene complexes* ***29*** *and* ***30***

To a solution of [(η^5-indenyl)$Mo(CO)_2]_2$ (369 mg, 0.69 mmol) and diene **28** (240 mg, 1.377 mmol) in 16 mL of CH_2Cl_2 was added $AgBF_4$ (269 mg, 1.38 mmol) via a solid addition funnel. The reaction was stirred for 2 h, then filtered. The product was precipitated out in pure form by the addition of 30 mL of Et_2O. The product was filtered and dried in vacuo to yield an isomeric mixture of **29** and **30** in a 1:2 ratio (538 mg, 74%). IR (CH_2Cl_2): 2011, 1952 cm^{-1}. ^1H NMR **29** (200 MHz, $CDCl_3$) δ: 7.75 (m, 2H, total), 7.45 (m, 2H, total), 6.35 (m, 2H), 5.69 (t, 1H, J = 2.9 Hz), 5.09 (m, 1H), 4.20 (m, 2H, two overlapping signals), 2.65 (d, 1H, J = 20 Hz, A of AB spin system), 2.22 (d, 1H, J = 20 Hz, B of AB spin system), 1.88–1.44 (m, 7H, total), 1.25 (s, 3H), 1.07 (s, 3H). ^1H NMR **30** (200 MHz, $CDCl_3$) δ: 7.75 (m, 2H, total), 7.45 (m, 2H, total), 6.41 (d, 2H, J = 2.8 Hz), 5.65 (t, 1H, J = 2.8 Hz), 5.6 (m, 1H), 5.03 (m, 1H), 4.94 (m, 1H), 2.20 (d, 1H, J = 12.2 Hz, A of AB spin system), 1.85 (d, 1H, J = 12.2 Hz, B of AB spin system), 1.88–1.44 (m, 7H, total), 1.07 (s, 3H), 1.00 (s, 3H). ^{13}C NMR (50 MHz, $CDCl_3$) δ: 230.5, 229.0, 227.7, 224.0, 154.7, 130.2, 130.1, 129.9, 126.0, 125.9, 124.2, 113.8, 112.3, 112.1, 110.9, 109.4, 105.1, 104.9, 104.5, 95.2, 91.1, 84.9, 80.5, 68.0, 57.0, 52.5, 48.4, 41.9, 40.5, 38.9, 37.3, 32.2, 31.8, 28.9, 28.6, 26.8, 26.1, 25.9, 25.7. Anal. calcd. for $C_{24}H_{25}BF_4MoO_2$: C 54.57, H 4.77; found: C 54.11, H 4.87.

Preparation of endo- *and* exo-*diene complexes* ***12*** *and* ***24***

An isomeric mixture of **12** and **24** was obtained in a 2:1 ratio (180 mg, 71% crude yield) from **10** (88 mg, 0.47 mmol) using the same procedure described in the previous experiment except that the complexes were not precipitated out of solution with ether, this caused partial decomposition of these materials. IR (CH_2Cl_2): 2022, 1958 cm^{-1}. ^1H NMR **12** (250 MHz, $CDCl_3$) δ: 7.76–7.71 (m, 2H), 7.54–7.33 (m, 2H), 6.39 (br s, 1H), 6.32 (br s, 1H), 5.64 (m, 1H), 4.88 (br s, 1H, coupled to 4.21 and 3.91), 4.21 (br s, 1H), 3.91 (m, 1H), 2.63 (d, 1H, J = 20.6 Hz, A of AB), 2.47 (br d, 1H, J = 7.0 Hz), 2.24 (d, 1H, J = 20.6 Hz, B of AB), 1.9–1.2 (m, 7H, total), 1.25 (s, 3H), 1.02 (s, 3H), 0.80 (d, 3H, J = 6.4 Hz). ^1H NMR **24** (250 MHz, $CDCl_3$) δ: 7.76–7.71 (m, 2H), 7.54–7.33 (m, 2H), 6.42 (br s, 1H), 6.35 (br s, 1H), 5.95 (m, 1H, coupled to 5.00 and 4.81), 5.64 (m, 1H), 5.00 (br s, 1H), 4.81 (m, 1H), 2.07 (d, 1H, J = 11.6 Hz), 1.9–1.2 (m, 7H, total), 1.15 (s, 3H), 1.14 (d, 3H, J = 6.7 Hz), 1.02 (s, 3H). A satisfactory analysis could not be obtained because of the lability of these compounds in solvents used for their recrystallization.

Preparation of endo- *and* exo-*diene complexes* ***25*** *and* ***26***

An isomeric mixture of **25** and **26** was obtained in a 2:1 ratio (230 mg, 85% crude yield) from **23** (94 mg, 0.5 mmol). IR (CH_2Cl_2): 2019, 1958 cm^{-1}. ^1H NMR **25** (200 MHz, $CDCl_3$) δ: 7.85 (m, 1H), 7.68 (m, 1H), 7.46 (m, 2H), 6.34 (m, 1H), 6.26 (m, 1H), 5.75 (t, 1H, J = 3.0 Hz), 5.43 (m, 1H, coupled to 4.18 and 3.82), 4.18 (br s, 1H), 3.82 (m, 1H), 2.45 (d, 1H, J = 6.5 Hz, A of AB), 2.05 (d, 1H, J = 6.5 Hz, B of AB), 1.7 (m, 7H, total), 1.37 (s, 3H), 1.05 (s, 3H), 0.76 (d, 3H, J = 7.0 Hz). ^1H NMR **26** (200 MHz, $CDCl_3$) δ: 7.85 (m, 1H), 7.68 (m, 1H), 7.46 (m, 2H), 6.44 (m, 1H), 6.31 (m, 1H), 5.70 (t, 1H, J = 2.9 Hz), 5.64 (m, 1H, coupled to 5.19 and 4.57), 5.19 (dd, 1H, J = 2.2 Hz, J = 3.8 Hz), 4.57 (t, 1H, J = 2.2 Hz), 2.37–2.28 (m, 1H), 2.15 (d, 1H, J = 8.6 Hz), 1.1 (s, 3H), 1.05 (s, 3H), 1.04 (d, 3H, J = 5.6 Hz). A satisfactory analysis could not be obtained because of the lability of these compounds in solvents used for their recrystallization.

Preparation of allylmolybdenum complex ***31***

To a suspension of **29** and **30** (101 mg, 0.19 mmol) in 4 mL of Et_2O at −20°C was added Me_2CuLi (1.0 mmol). The reaction was stirred for 1 h, then quenched with a pH 8 solution of NH_4Cl and aqueous NH_3. Hexane (5 mL) was added and the organic phase syringed onto a small plug of silica gel and flushed, under N_2, with hexane into a round-bottom flask that was previously purged with N_2. The solvent was removed in vacuo and the crude material subjected to column chromatography, eluting with hexane under N_2. Recovered diene **28** (11 mg, 33%) eluted first and removal of the solvent from a second yellow fraction provided **31** (52 mg, 60%). IR (CH_2Cl_2): 1930, 1853 cm^{-1}. ^1H NMR (250 MHz, $CDCl_3$) δ: 7.15–6.93 (m, 4H), 5.88 (m, 1H), 5.78 (m, 1H), 5.67 (t, 1H, J = 2.9 Hz), 2.72 (d, 1H, J = 3.8 Hz), 2.10 (d, 1H, J = 12.6 Hz, A of AB spin system), 1.66 (q, 1H, J = 7.1 Hz), 1.60–1.32 (m, 5H), 1.23 (d, 1H, J = 12.6 Hz, B of AB spin system), 1.00 (s, 3H), 0.98 (s, 3H), 0.88 (d, 3H, J = 7.1 Hz), 0.76–0.70 (m, 1H), −0.08 (d, 1H, J = 3.8 Hz). ^{13}C NMR (62.5 MHz, $CDCl_3$) δ: 237.4, 234.9, 124.7, 124.6, 123.0, 122.4, 112.1, 109.5, 93.2, 89.1, 81.3, 79.8, 77.3, 69.9, 68.9, 53.5, 49.4, 43.8, 40.0, 39.5, 32.0, 29.1, 27.2, 26.9, 23.2. MS *m/z*: 458 (M^+). Anal. calcd. for $C_{25}H_{28}MoO_2$: C 65.79, H 6.18; found: C 65.39, H 6.28.

Preparation of allylmolybdenum complex ***32***

η^3-Allyl complex **32** was obtained in 21% yield (14 mg) from **12** and **24** (77 mg, 0.14 mmol), using the same procedure described for the preparation of **31**. Compound **10** (11.8 mg, 44%) was also recovered. IR (CH_2Cl_2): 1929, 1854 cm^{-1}. ^1H NMR (250 MHz, $CDCl_3$) δ: 7.14–6.95 (m, 4H), 5.88 (m, 1H), 5.80 (m, 1H), 5.68 (t, 1H, J = 2.9 Hz), 2.77 (d, 1H, J = 3.8 Hz), 2.12 (d, 1H, J = 12.7 Hz, A of AB spin system), 2.01 (q, 1H, J = 7.1 Hz), 1.87 (m, 1H), 1.69 (m, 1H), 1.5 (m, 3H), 1.16 (d, 1H, J = 12.7 Hz, B of AB spin system), 1.05 (m, 1H), 0.98 (s, 3H), 0.96 (s, 3H), 0.88 (d, 3H, J = 7.1 Hz), 0.66 (d, 3H, J = 6.6 Hz), −0.24 (d, 1H, J = 3.8 Hz). ^{13}C NMR (62.5 MHz, $CDCl_3$) δ: 235.7, 235.5, 124.8, 124.6, 123.1, 122.5, 112.5, 109.4, 104.3, 90.1, 89.2, 82.5, 80.15, 70.8, 70.2, 58.6, 43.8, 40.4, 39.2, 37.1, 37.0, 32.9, 28.0, 24.4, 21.1, 17.5. MS *m/z*: 472 (M^+). Anal. calcd. for $C_{26}H_{30}MoO_2$: C 66.38, H 6.43; found: C 65.95, H 6.61.

Preparation of allylmolybdenum complex ***33***

η^3-Allyl complex **33** was obtained in 22% yield (14 mg) from **25** and **26** (75 mg, 0.138 mmol), using the same procedure as for **31**. Also recovered was diene **23** (19.8 mg, 76%). IR (CH_2Cl_2): 1933, 1854 cm^{-1}. ^1H NMR (250 MHz, $CDCl_3$) δ: 7.17–6.93 (m, 4H), 5.79 (m, 1H), 5.77 (m, 1H), 5.69 (t, 1H, J = 2.9 Hz), 2.85 (d, 1H, J = 3.8 Hz), 2.14 (d, 1H, J = 12.5 Hz), 1.67 (q, 1H, J = 7.0 Hz), 1.62–1.26 (m, 5H), 1.16–1.07 (m, 2H), 1.04 (s, 3H), 0.98 (s, 3H), 0.90 (d, 3H, J = 7.1 Hz), 0.89 (d, 3H, J = 7.0 Hz), −0.06 (d, 1H, J = 3.8 Hz). MS *m/z*: 472 (M^+). Anal. calcd. for $C_{26}H_{30}MoO_2$: C 66.38, H 6.43; found: C 66.31, H 6.49. Crystals suitable for X-ray diffraction studies were grown by slow evaporation from a hexane solution.

X-ray structure determination of complex ***33***

A needle fragment of dimensions 0.62 × 0.08 × 0.11 mm, corresponding to the forms {010}, {100}, and {102}, respectively, and glued to a glass fiber using epoxy resin was mounted on a Siemens R3m/v diffractometer. The unit cell parameters were determined and refined from a set of 25 general reflections ($20.0 < 2\theta < 30.0°$) well distributed in reciprocal space.

Intensity data were collected with graphite monochromated MoKα radiation at 292 K by employing the ω-scan technique over a 2θ range of 4.0–50.0° with variable scan speeds (2.93–29.30° min^{-1}) and a 1.30° scan width. Background measurements using the stationary crystal, stationary counter method were made

at the beginning and end of each scan, each for 25% of the total scan time. Two standard reflections were measured after every 100 reflections and showed no significant loss in intensity during data acquisition.

Intensities were corrected for Lorentz and polarization effects. A face-indexed numerical method was employed to correct for adsorption effects. Of the 3801 independent reflections collected, 3082 were considered observed ($F > 6.0\ \sigma(F)$) and were used in the structure solution and refinement. The minimum and maximum transmission factors through the crystal were calculated to be 0.8531 and 0.9531.

The structure was solved by Patterson and Fourier methods and refined by full-matrix least-squares techniques using the Siemens SHELXTL PLUS software. Anisotropic refinement of all non-hydrogen atoms revealed the positions of all the hydrogens atoms from a difference map. In the final cycles of refinement, the hydrogen atoms were refined isotropically in their found positions.

Scattering factors for non-hydrogen atoms were taken from the *International tables* (13*a*) while the data of Stewart et al. were used for hydrogen atoms (13*b*). Selected details of the crystallographic data, data collection, and final refinement appear in Table 1, atomic coordinates and isotropic thermal parameters appear in Table 4, while selected bond lengths and angles appear in Table 5. Full details of the structure determination have been deposited (see footnote 6).

Acknowledgements

The authors would like to thank the Natural Sciences and Engineering Research Council of Canada for financial support of this work.

1. (*a*) S.L. Blystone. Chem. Rev. **89**, 1663 (1989); (*b*) S.G. Davies, M.L.H. Green, and D.M.P. Mingos. Tetrahedron, **34**, 3047 (1978).
2. (*a*) A.J. Pearson, S. Mallik, A.A. Pinkerton, J.P. Adams, and S. Zheng. J. Org. Chem. **57**, 2910 (1992); (*b*) A.J. Pearson and K. Chang. J. Chem. Soc. Chem. Commun. 394 (1991); (*c*) A.J. Pearson and K. Srinivasan. J. Chem. Soc. Chem. Commun. 392 (1991); (*d*) A.J. Pearson, S. Mallik, R. Mortezaei, M.W.D. Perry, R.J. Shively, Jr., W.J. Youngs. J. Am. Chem. Soc. **112**, 8034 (1990); (*e*) A.J. Pearson. Synlett, **1**, 10 (1990); (*f*) A.J. Pearson and V.D. Khetani. J. Am. Chem. Soc. **111**, 6778 (1989); (*g*) A.J. Pearson, S.L. Blystone, H. Narr, A.A. Pinkerton, B.A. Roden, and J. Yoon. J. Am. Chem. Soc. **111**, 134 (1989); (*h*) A.J. Pearson, M.N.I. Khan, J.C. Clardy, and H. Cun-Heng. J. Am. Chem. Soc. **107**, 2748 (1985); (*i*) A.J. Pearson and M.N.I. Khan. J. Org. Chem. **50**, 2587 (1985); (*j*) J. Am. Chem. Soc. **106**, 1872 (1984), (*k*) Tetrahedron Lett. **25**, 3507 (1984).
3. J.W. Faller, H.H. Murray, D.L. White, and K.H. Chao. Organometallics, **2**, 400 (1983).
4. (*a*) S.A. Benyunes and M. Green. J. Organomet. Chem. **390**, C32 (1990); (*b*) J.S. Baxter, M. Green, and T.V. Lee. J. Chem. Soc. Chem. Commun. 1595 (1989); (*c*) M. Green, S. Greenfield, M.J. Grimshire, M. Kersting, A.G. Orpen, and R.A. Rodrigues. J. Chem. Soc. Chem. Commun. **97** (1987); (*d*) M. Green, S. Greenfield, and M. Kerting. J. Chem. Soc. Chem. Commun. **18** (1985); (*e*) M. Bottrill, and M. Green. J. Chem. Soc. Dalton Trans. 2365 (1977); (*f*) M.L.H. Green, L.C. Mitchard, and W.E. Silverthorn. J. Chem. Soc. Dalton Trans. 1952 (1973).
5. (*a*) J.K. Dickson and B. Fraser-Reid. J. Chem. Soc. Chem. Commun. 1440 (1990); (*b*) Y. Shizuri, M. Ohkubo, and S. Yamamura. Tetrahedron Lett. **30**, 3797 (1989); (*c*) M. Frank-Neumann, M. Miesch, and E. Lacroix. Tetrahedron Lett. **30**, 3533 (1989); (*d*) Y.K. Rao, and M. Nagarajan. Tetrahedron Lett. **29**, 107 (1988); (*e*) M.T. Crimmons and S.W. Mascarella. J. Am. Chem. Soc. **108**, 3435 (1986); (*f*) D.D. Sternbach, J.W. Hughes, D.F. Burdi, and B.A. Banks. J. Am. Chem. Soc. **107**, 2149 (1985); (*g*) P.A. Wender and R.J. Ternansky. Tetrahedron Lett. **26**, 2625 (1985); (*h*) L.A. Paquette and A. Leone-Bay. J. Am. Chem. Soc. **105**, 7352 (1983); (*i*) T. Tsunoda, M. Kodama, and S. Ito. Tetrahedron Lett. **24**, 83 (1983).
6. K.J. Stone and R.D. Little, J. Org. Chem. **49**, 1849 (1984).
7. A.J. Mancuso, S.-L. Huang, and D. Swern. J. Org. Chem. **43**, 2480 (1978).
8. P.K. Freeman and L.L. Hutchison. Tetrahedron Lett. 1849 (1976).
9. W.P. Griffith, S.V. Ley, G.P. Whitcombe, and A.D. White. J. Chem. Soc. Chem. Commun. 1625 (1987).
10. S.A. Beyunes, A. Binelli, M. Green, and M.J. Grimshire, J. Chem. Soc. Dalton Trans. 895 (1991), and references therein.
11. M.A. Greaney, J.S. Merola, and T.R. Halbert. Organometallics, **4**, 2057 (1985), and references therein.
12. C.F. Wilcox and R.R. Craig. J. Am. Chem. Soc. **83**, 3866 (1961).
13. (*a*) International tables for X-ray crystallography. Kynoch Press, Birmingham. Vol. **4**. 1974; (*b*) R.F. Stewart, E.R. Davidson, and W.T. Simpson. J. Chem. Phys. **42**, 3175 (1965).

Can. J. Chem. Downloaded from www.nrcresearchpress.com by 213.200.69.106 on 09/08/12
For personal use only.

Étude par spectrophotométrie UV d'aldéhydes et d'amides parahydroxycinnamiques. Comparaison de leurs capacités complexantes vis à vis de $ZnBr_2$

HUBERT DURAN, ELISABETH DURAN, LILIANE GORRICHON[1] ET MARCEL PERRY

Synthèse et physicochimie organique, Unité de recherche associée au Centre national de la recherche scientifique, n° 471, Université Paul Sabatier, 118 route de Narbonne, 31062 Toulouse CEDEX, France

Reçu le 15 décembre 1992

HUBERT DURAN, ELISABETH DURAN, LILIANE GORRICHON et MARCEL PERRY. Can. J. Chem. **71**, 1041 (1993).

La capacité complexante des sels de zinc vis à vis des cinnamaldéhydes et des *N*-pyridyl cinnamides a été envisagée pour modéliser le site actif de la cinnamyl alcool déshydrogénase (CAD), un enzyme à zinc intervenant dans la lignification. Les parahydroxycinnamaldéhydes **4***a*–**6***a* sont des substrats spécifiques de cet enzyme alors que les cinnamides ont été synthétisés comme des ligands bidentés du zinc présentant une activité inhibitrice vis à vis de la CAD. L'interaction C=O...Zn est étudiée par des méthodes UV. Les constantes de stabilité sont faibles avec les aldéhydes (K = 3–16 L mol^{-1}) et (2–12) × 10^3 plus fortes avec les cinnamides correspondants, l'aminopyridine participant à la complexation. La stoechiométrie des complexes est ML (M : sel, L : ligand) avec les aldéhydes monosubstitués, et M_2L avec **5***a* ou **6***a*, correspondant à une seconde complexation par «effet catéchol». Avec les *N*-pyridylcinnamides la stoechiométrie des complexes est ML ou ML_2. Un fort effet bathochrome est observé, plus important pour les aldéhydes que pour les amides (conjugaison croisée); et une corrélation existe entre la bande d'absorption UV des ligands et de leurs complexes de zinc.

HUBERT DURAN, ELISABETH DURAN, LILIANE GORRICHON, and MARCEL PERRY. Can. J. Chem. **71**, 1041 (1993).

The ability of zinc salts to be complexed by cinnamaldehydes and *N*-pyridyl cinnamides has been investigated for modeling the active site of cinnamyl alcohol dehydrogenase (CAD), a zinc enzyme involved in the lignification process. Parahydroxycinnamaldehydes **4***a*–**6***a* are specific substrates of the enzyme while cinnamides were synthesized as bidendate ligands towards zinc, and present inhibitory effects toward CAD. The interaction C=O...Zn was studied by UV methods and was observed in each example; the complexation constants are rather low with aldehydes (K = 3–16 L mol^{-1}) and of the order (2–12) × 10^3 stronger with the corresponding cinnamides, due to the aminopyridine moiety participation. The stoichiometry of the complexes was found to be ML (M: salt, L: ligand) with monosubstituted aldehydes and M_2L with **5***a* or **6***a*, which was attributed to an additional complexation caused by the catechol effect. With the *N*-pyridylamides the complexation occurs according to a 1:1 (ML) or 1:2 (ML_2) stoichiometry. Strong bathochromic effects were also observed; they are more important with the aldehydes than with the amides (cross conjugation). Bathochromic effects due to the substitution of the aromatic ring are shown by a relationship between the ligands and their zinc complexes.

Can. J. Chem. Downloaded from www.nrcresearchpress.com by 213.200.69.106 on 09/08/12
For personal use only.

La complexation de composés cinnamiques et leur photoisomérisation en présence d'acides de Lewis ont fait l'objet d'études physicochimiques approfondies (1–5). En comparaison la complexation de composés cinnamiques polyphénoliques a été assez peu étudiée malgré l'importance de ces composés dans la constitution de polymères naturels tels que les tannins ou les lignines (6, 7).

Nous nous sommes intéressés à la complexation par les sels de zinc des cinnamaldéhydes **1***a*–**6***a*, et des *N*-pyridylcinnamides **1***b*–**6***b*.

Ces composés interviennent comme substrats (aldéhydes

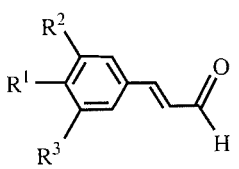

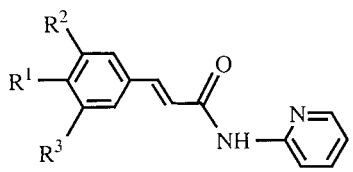

	R^1	R^2	R^3	
1*a*	H	H	H	**1***b*
2*a*	H	OMe	H	**2***b*
3*a*	OMe	H	H	**3***b*
4*a*	OH	H	H	**4***b*
5*a*	OH	OMe	H	**5***b*
6*a*	OH	OMe	OMe	**6***b*

4*a*–**6***a*) (8, 9) ou inhibiteurs (10) (amide **5***b*) d'une déshydrogénase à zinc, l'alcool cinnamylique déshydrogénase (CAD) qui catalyse la dernière étape de la biosynthèse des monomères des lignines. Le zinc en activant la fonction aldéhyde du substrat favorise sa réduction par le cofacteur NADPH dans le site actif de l'enzyme. Les amides ont été synthétisés pour leur capacité à complexer le zinc de l'enzyme cible et pour leur analogie de structure avec les substrats aldéhydes, ce qui devait assurer leur reconnaissance et leur transport au site actif de l'enzyme. La comparaison des propriétés complexantes entre aldéhydes et amides peut permettre d'éclairer le rôle d'un ligand bidenté du type *N*-2-pyridylcinnamides dans la complexation du zinc et dans l'inhibition enzymatique observée avec ce type de composé (10). Dans cette modélisation nous nous sommes particulièrement intéressés à l'interaction entre le carbonyle des ligands et les sels de zinc.

Le rôle catalytique du zinc est connu pour de nombreux enzymes comme les alcools déshydrogénases (11). La structure du site actif autour de l'ion zinc dans l'alcool déshydrogénase de foie de cheval (LADH) est tétraèdrique, comme dans la plupart des métalloenzymes à zinc. L'ion zinc du site actif de cette déshydrogénase est coordiné à deux thiolates de résidus de cystéine, à un groupe imidazole de l'histidine et à une molécule d'eau comme quatrième ligand (12). L'alcool cinnamylique déshydrogénase (CAD) ne peut être obtenu en quantité suffisante pour l'étude directe des

1. Auteur à qui adresser toute correspondance.

Can. J. Chem. Downloaded from www.nrcresearchpress.com by 213.200.69.106 on 09/08/12
For personal use only.

interactions entre enzyme et substrats (13). Les halogénures de zinc ont été largement utilisés comme modèle du site actif de l'alcool déshydrogénase (LADH), des similitudes spectroscopiques ayant été observées entre les complexes métalliques en solvant aprotique et le complexe LADH–substrat (14, 15). La complexation des substrats par les sels de zinc s'est avérée une modélisation acceptable de ces interactions au niveau du site actif de la protéine. Nous avons pris des conditions voisines de celles décrites dans les exemples avec la LADH et avons préféré le bromure de zinc au chlorure en raison de la meilleure solubilité dans les solvants aprotiques; de plus, il est moins hygroscopique. Les complexations ont été réalisées dans un solvant anhydre, sous atmosphère inerte pour éviter l'hydratation de la fonction carbonyle complexée à l'ion zinc (16). Les aldéhydes constituant des ligands peu favorables à la complexation, nous avons choisi le diéthyléther comme solvant car étant faiblement polaire et peu solvatant de manière à faciliter la comparaison entre aldéhydes et *N*-pyridylamides. L'étude présentée permet aussi d'examiner l'influence du degré de substitution du noyau aromatique et la participation de groupements phénol et (ou) méthoxyle à la complexation, en particulier pour les composés di- ou tri-substitués **5** et **6**. Les études de complexation des amides monosubstitués ayant déjà été réalisées (17), nous rapportons ici les résultats relatifs aux aldéhydes **1***a*–**6***a* et aux amides **5***b* et **6***b*, ainsi que la comparaison des données obtenues entre les deux séries.

Résultats

Propriétés spectrales UV

1. Aldéhydes ***1***a–***6***a *(tableau 1)*

Nous examinons l'absorption du chromophore correspondant à la transition $\pi \rightarrow \pi^*$ de ces composés. La longueur d'onde d'absorption des ligands est modifiée par la nature et la position des substituants fixés sur le noyau aromatique ($\Delta\lambda = \lambda_X^L(\text{ligand}) - \lambda_H^L(\text{cinnamaldéhyde})$) (1). La présence en *para* d'un substituant sur le noyau aromatique des aldéhydes induit un effet bathochrome de 32 nm pour un méthoxyle et de 34 nm pour un hydroxyle, alors que le méthoxyle en *méta* n'apporte aucune modification lorsqu'il est seul. Dans le cas des composés di- et tri-substitués possédant un hydroxyle en *para* et un ou deux méthoxyles en *méta* cet effet bathochrome augmente : 49 nm pour **5***a*, 57 nm pour **6***a* (tableau 1). Cet effet peut être expliqué par la présence d'une liaison hydrogène intramoléculaire qui renforce le caractère donneur du groupe hydroxyle en *para*. Cette hypothèse est confortée par les observations des spectres IR des composés **4***a* et **5***a*, montrant une fréquence $\nu_{\text{OH libre}}$ pour le *para* coumaraldéhyde **4***a* (**4***a* ν_{OH} = 3602 cm^{-1} dans CCl_4 M/400) et une fréquence $\nu_{\text{OH associé}}$ par liaison hydrogène intramoléculaire pour **5***a* (**5***a* ν_{OH} = 3546 cm^{-1} dans CCl_4 M/400) en accord avec des données de la littérature pour une liaison hydrogène entre les hydroxyles d'orthodiphénols (18, 19).

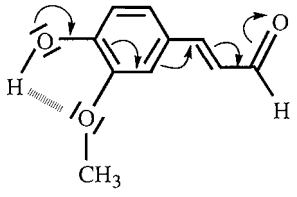

5*a*

Pour les amides correspondants on observe un phénomène similaire à celui des aldéhydes, seul l'effet bathochrome observé est plus faible : 49 nm pour **5***a* alors qu'il est de 33 nm pour **5***b*; la présence du groupe pyridyle induit une conjugaison croisée qui diminue l'effet bathochrome.

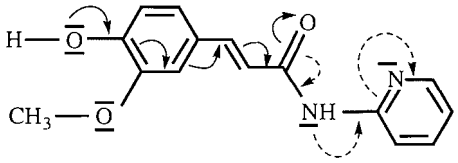

5*b*

2. Complexes des aldéhydes ***1***a–***6***a

Nous avons montré dans le cas des cinnamides **1***b*–**4***b* que l'addition d'acides de Lewis entraînait la formation de complexes faisant intervenir la fonction *N*-pyridylamide et le sel de zinc, complexes de stoechiométrie ML (**1***b*, **2***b*) ou ML et ML_2 (**3***b*, **4***b*). Ces résultats ont été confirmés par la caractérisation à l'échelle macroscopique de ces complexes (17).

Dans le cas des aldéhydes l'étude par spectrophotométrie UV fait aussi apparaître une forte perturbation de la transition $\pi \rightarrow \pi^*$ des aldédydes en présence de $ZnBr_2$; la complexation induit un effet bathochrome important par rapport au ligand (de 36 nm pour la complexation de **1***a* à 58 nm pour **6***a*).

La présence de substituants hydroxyle ou (et) méthoxyle sur le noyau aromatique renforce aussi cet effet bathochrome; on passe d'un λ_{max} de 315 nm pour le complexe Zn(II)–cinnamaldéhyde **1***a* à des valeurs de 357, 376 et 394 nm pour Zn(II)–*p*-coumaraldéhydes **4***a*, Zn(II)–coniferaldéhyde **5***a* et Zn(II)–sinapaldéhyde **6***a* (tableau 1).

Constantes de stabilité

Si l'on examine les ligands **1**–**6**, quatre cas sont à considérer : (*i*) les aldéhydes monosubstitués **1***a*–**4***a*; (*ii*) les *N*-2-pyridylamides monosubstitués **1***b*–**4***b* antérieurement décrits (17)–(20) (*iii*) les aldéhydes di- ou tri-substitués **5***a* et **6***a*; (*iv*) les amides di- ou tri-substitués **5***b*–**6***b*. Les fonctions susceptibles de participer à la complexation sont la fonction aldéhyde (ligand monodenté), les fonctions adjacentes sur le noyau aromatique OH, OMe par «effet catéchol» et la fonction *N*-pyridylamide (ligand bidenté).

1. Aldéhydes monosubstitués ***1***a–***4***a

R = H, *m*OMe, *p*OMe, *p*OH

Quand à une solution de ligand **1***a*–**4***a* on ajoute une solution de sel de zinc, une décroissance graduelle de ε_L et une augmentation de ε_C de l'absorption maximum du complexe (λ_{max}) sont observées. La présence d'un point isosbestique dans ces spectres (fig. 1) indique que le système contient deux chromophores en interconversion, le ligand libre et le complexe ligand – sel de zinc.

La courbe de variation $D_{exp} = f(\rho)$ (fig. 2) où ρ est le rapport de concentration en acide de Lewis sur la concentration en ligand (ρ = [$ZnBr_2$]/[L]) montre que la formation du complexe cinnamaldéhyde monosubstitué – bromure de zinc est en accord avec un mécanisme en une étape, avec une

TABLEAU 1. Effet de substitution sur le λ_{max} (nm) des aldéhydes et des amides *p*-hydroxycinnamiques et les complexes de zinc(II)

	H	*m*-OMe	*p*-OMe	*p*-OH	*p*-OH, *m*-OMe	*p*-OH, 2*m*-OMe
Composé n° :	**1***a* **1***b*	**2***a* **2***b*	**3***a* **3***b*	**4***a* **4***b*	**5***a* **5***b*	**6***a* **6***b*
$\lambda^{L}_{xa\,max}$	279	279	311	313	328	336
$\lambda^{L}_{xb\,max}$	295	294	314	318	328	332
$\lambda^{C}_{xa\,max}$	315	308	355	357	376	394
$\lambda^{C}_{xb\,max}$	312	311	343	336	367	372
$\lambda_{isos.a\,max}$[a]	292	290	327	328	343–345	333–356
$\lambda_{isos.b\,max}$	303	303	326–331	331–331	345–352	352–358
$\Delta\lambda = \lambda^{L}_{xa} - \lambda^{L}_{1a}$	—	0	32	34	49	57
$\Delta\lambda = \lambda^{L}_{xb} - \lambda^{L}_{1b}$	—	−1	19	23	33	37
$\Delta\lambda = \lambda^{C}_{xa} - \lambda^{C}_{1a}$	—	−7	40	42	61	79
$\Delta\lambda = \lambda^{C}_{xb} - \lambda^{C}_{1b}$	—	−1	31	24	45	60
$\Delta\lambda = \lambda^{C}_{xa} - \lambda^{L}_{xa}$	36	29	44	44	48	58
$\Delta\lambda = \lambda^{C}_{xb} - \lambda^{L}_{xb}$	17	17	29	18	39	40

[a] λ_{isos} : longueur d'onde du point isosbestique.

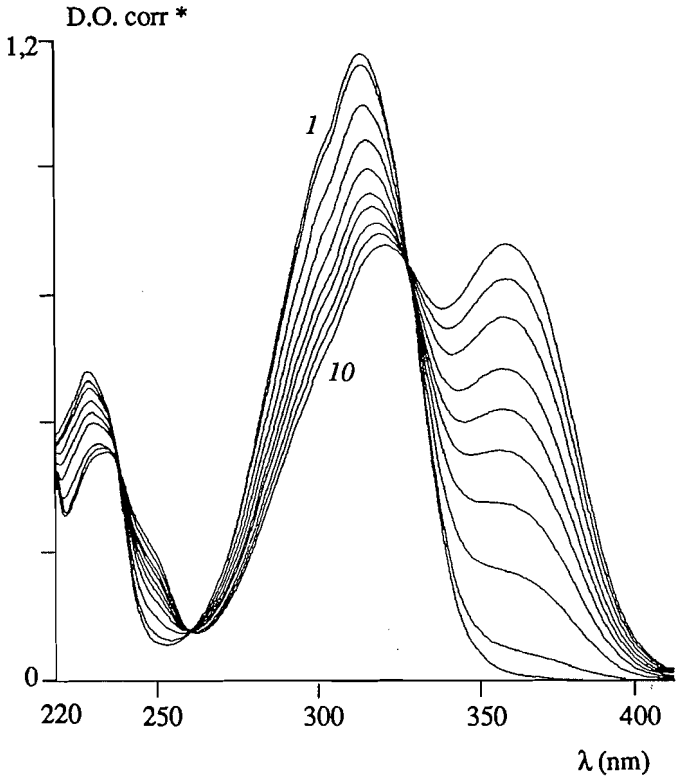

FIG. 1. Complexation du *p*-hydroxycoumaraldéhyde **4***a* par addition de $ZnBr_2$ dans le diéthyléther à 25°C. *D.O.$_{corr.}$ = densité optique corrigée du facteur de dilution.

stoechiométrie 1/1 entre l'ion métal et le ligand : M + L ⇌ ML (fig. 2).

La relation $D_{exp} = f(\rho)$ appliquée dans le cas du modèle (M + L ⇌ ML) est vérifiée à deux longueurs d'onde d'absorption maximum, pour la disparition du ligand (λ^{L}_{max}) et la formation du complexe (λ^{C}_{max}). Il n'y a pas de variation signi-

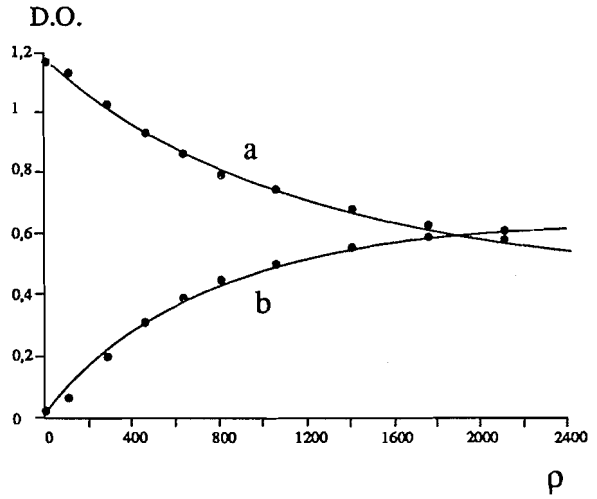

FIG. 2. Graphe $D = f(\rho)$ du complexe *para*-coumaraldéhyde **4***a* avec l'ion zinc(II); tracé (*a*) à la longueur d'onde d'absorption du ligand, tracé (*b*) à la longueur d'onde d'absorption du complexe (points : valeurs expérimentales, courbe : $D_{calc.}$ pour M + L ⇌ ML).

ficative de la constante de stabilité observée pour les deux longueurs d'onde (tableau 2).

Les résultats mathématiques montrent que la complexation des ligands **1***a*–**4***a* avec le bromure de zinc est effectivement en accord avec une stoechiométrie 1/1; la complexation de ces aldéhydes avec le bromure de zinc s'effectue par la fonction carbonyle mais les constantes de stabilité de ces complexes sont faibles. Les substituants *para*-hydroxyles, donneurs par effet mésomère, induisent un grand changement dans la structure électronique du ligand lors de la complexation avec le bromure de zinc, avec des plus fortes valeurs de K (15,9 L mol^{-1}) pour le coumaraldéhyde **4***a* que pour les composés **1***a* et **2***a*.

Can. J. Chem. Downloaded from www.nrcresearchpress.com by 213.200.69.106 on 09/08/12
For personal use only.

TABLEAU 2. Constantes de stabilité des complexes aldéhydes ou amides cinnamiques avec $ZnBr_2$

	λ	K(L mol^{-1}) C=O...Zn <	$\frac{K_{x_a}}{K_{x_b}} \times 10^{3a}$	a, K_1M_2L b, K_2ML_2	Q	Re
1*a*	280	3,2		—	$5,3 \times 10^{-4}$	0,008
	315	3,2	1,7		$8,2 \times 10^{-5}$	0,017
1*b*	295	5 500		—	$2,28 \times 10^{-4}$	0,006
2*a*	278	3,2		—	$1,6 \times 10^{-4}$	0,006
	308	3,6	~2,7		$6,6 \times 10^{-4}$	0,006
2*b*	294	9 300		—	$8,27 \times 10^{-6}$	0,001
3*a*	312	10,5		—	$9,1 \times 10^{-4}$	0,010
	355	11,7	1,8		$1,6 \times 10^{-4}$	0,007
3*b*	314	20 000		22 000	$9,82 \times 10^{-4}$	0,007
4*a*	313	15,9		—	$6,2 \times 10^{-4}$	0,010
	355	13,3	5,1		$1,6 \times 10^{-4}$	0,007
4*b*	318	72 000		22 000	$9,38 \times 10^{-4}$	0,009
5*a*	376	13,6	8,1	750	$2,2 \times 10^{-5}$	0,003
5*b*	328	$1,1 \times 10^5$		$1,25 \times 10^5$	$1,08 \times 10^{-5}$	0,011
6*a*	394	8,9	12,2	750	$4,45 \times 10^{-5}$	0,019
6*b*	332	$1,09 \times 10^5$		$1,7 \times 10^5$	$4,3 \times 10^{-5}$	0,003

$^a\frac{K_{x_a}}{K_{x_b}} = \frac{\text{constante de stabilité de l'aldéhyde } x_a}{\text{constante de stabilité de l'amide } x_b}$.

Can. J. Chem. Downloaded from www.nrcresearchpress.com by 213.200.69.106 on 09/08/12
For personal use only.

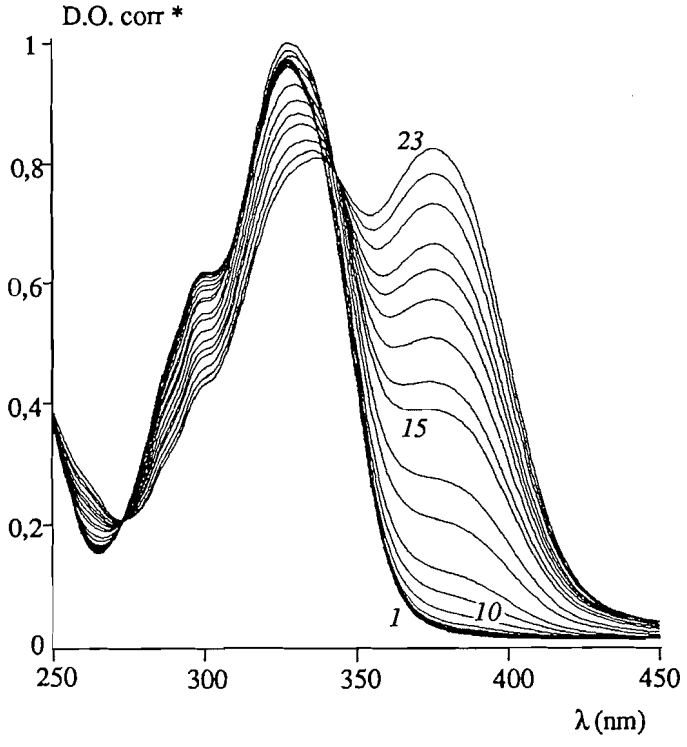

FIG. 3. Complexation du coniferaldéhyde **5***a* par addition de $ZnBr_2$ dans le diéthyléther à 25°C. *D.O.$_{corr.}$ = densité optique corrigée du facteur de dilution.

2. Aldéhydes di- et tri-substitués **5**a *et* **6**a

Ces composés présentent deux sites de complexation possibles et peuvent complexer les sels de zinc par l'oxygène du carbonyle et par les fonctions OH et OMe adjacentes sur le noyau aromatique. Lors de l'addition du bromure de zinc deux phases successives sont observées avec les composés **5***a* et **6***a*. Quand des faibles concentrations en sel métallique sont additionnées à une solution de ligand libre ($\rho < 150$) un faible effet bathochrome (2–3 nm) et une augmentation de ε_{max} sont observés. Pour les faibles valeurs de ρ les courbes présentent un premier point isosbestique (fig. 3, spectre 1–9). Si on continue l'addition de $ZnBr_2$, les complexes intermédiaires **5′** et **6′** disparaissent et une seconde bande d'absorption correspondant à la formation des complexes **5***a* et **6***a* apparaît (tableau 1).

La présence d'un point isosbestique à 345 nm (ou 356 nm) indique que seul un complexe intermédiaire **5′** (ou **6′**) intervient dans la formation des complexes finaux C5 (ou C6). Pour les ligands **5***a* et **6***a* la complexation de l'oxygène du carbonyle avec le bromure de zinc est donnée par la constante K_2 qui est du même ordre de grandeur que pour les aldéhydes monosubstitués **3***a* et **4***a*. La complexation de l'oxygène du carbonyle affecte la transition $\pi \rightarrow \pi^*$ du système conjugué, alors que par «l'effet catéchol» il se forme le complexe intermédiaire (λ_{max} **5′** = 330 nm; λ_{max} **6′** = 338 nm).

À titre de comparaison nous avons étudié dans des conditions identiques l'eugénol **7**. La complexation de **7** ne peut intervenir que par «effet catéchol», par l'intermédiaire des

Can. J. Chem. Downloaded from www.nrcresearchpress.com by 213.200.69.106 on 09/08/12
For personal use only.

hydroxyle et méthoxyle adjacents sur le noyau aromatique. L'addition d'un acide de Lewis ($ZnBr_2$) produit un effet bathochrome de 2 nm et une augmentation de ε_{max}. Ces observations sont identiques à celles observées précédemment pour les composés **5***a* et **6***a*.

Ces résultats confortent l'hypothèse retenue pour la complexation du coniferaldéhyde **5***a* et du sinapaldéhyde **6***a*. Il y a dès l'addition de $ZnBr_2$ complexation du sel par «effet catéchol» (entraînant un effet bathochrome de 2 nm), puis la complexation du carbonyle par le zinc intervient sur ce premier intermédiaire pour conduire à une stoechiométrie M_2L. C'est la constante K_2, représentative de la force de l'interaction C=O...Zn, qui nous intéresse dans le cadre de la modélisation du site enzymatique. Les valeurs obtenues sont respectivement de 13,6 et 8,9 L mol^{-1} pour **5***a* et **6***a* du même ordre de grandeur que celles obtenues pour la complexation du *p*-coumaraldéhyde **4***a* (K = 15,9 L mol^{-1}) ou du paraméthoxycinnamaldéhyde **3***a* (K = 11,7 L mol^{-1}).

3. Amides di- et tri-substitués **5**b *et* **6**b

La complexation des deux composés **5***b* et **6***b* peut faire intervenir deux types de ligands bidentés : les oxygènes des fonctions fixées sur le noyau aromatique (effet catéchol), et la fonction *N*-pyridylamide. Les spectres de complexation des phénolamides **5***b* et **6***b* présentent deux points isosbestiques (tableau 2); il existe un équilibre entre au moins deux complexes dont l'un est «intermédiaire». Les équilibres qui font intervenir trois espèces (L, ML, ML_2 ou M_2L) sont examinés :

$$[1]\quad L + M \rightleftharpoons ML \underset{+M}{\rightleftharpoons} M_2L$$

$$[2]\quad L + M \rightleftharpoons ML \underset{+L}{\rightleftharpoons} ML_2$$

De ces deux équilibres, la meilleure solution mathématique correspond à l'équilibre [2] qui fait intervenir la forme ML_2. Cette forme est majoritaire pour les faibles valeurs de ρ (ρ = [ZnBr2]/[L]) et peut être associée au complexe intermédiaire absorbant à 346 nm pour **5***b* et 351 nm pour **6***b*. Les constantes d'équilibre trouvées pour ces phénolamides sont élevées (équation [2] : $K_1 = 1{,}1 \times 10^5$ L mol^{-1} et $K_2 = 1{,}23 \times 10^5$ L mol^{-1} pour **5***b*).

Alors que pour les aldéhydes cinnamiques **5***a* et **6***a* possédant un site catéchol et un carbonyle, on observe une complexation de type M_2L faisant intervenir les deux sites de complexation, pour les amides cinnamiques équivalents **5***b* et **6***b*, seul le site amidopyridine complexe le bromure de zinc pour donner des stoechiométries de type ML ou ML_2. Ces résultats sont corroborés par la synthèse des complexes de zinc dont l'analyse élémentaire est en accord avec ces propositions (voir partie expérimentale). On retrouve à ce niveau des résultats analogues à ceux obtenus antérieurement pour la complexation des amides *para* hydroxylés et *para* méthoxylés (11).

L'ensemble des valeurs des constantes de complexation pour **1***a*–**6***a* et **1***b*–**6***b* et des longueurs d'onde d'absorption maximum sont rassemblés dans le tableau 2.

Discussion

Si nous considérons l'ordre de grandeur des constantes de stabilité déterminées pour les différents complexes issus des aldéhydes **1***a*–**6***a* et des amides **1***b*–**6***b* nous observons que :

une seule fonction OH ou OMe n'est pas suffisante pour observer des complexes avec $ZnBr_2$;

la fonction carbonyle des aldéhydes cinnamiques complexe le zinc avec des constantes faibles de 3,2–15,9 L mol^{-1}; il est donc impossible d'isoler ces complexes, le phénomène n'étant mis en évidence qu'en déplaçant l'équilibre à l'aide d'un large excès de sels de zinc;

la complexation par «effet catéchol» lorsqu'elle peut avoir lieu est plus forte que la complexation par le carbonyle de l'aldéhyde ($K \sim 750/3{,}2$–$15{,}9$ L mol^{-1} respectivement);

enfin, la complexation par «effet catéchol» n'intervient pas avec les *N*-pyridylcinnamides, la fonction amide constituant dans ce cas un bien meilleur ligand bidenté pour conduire à des complexes ML ou (et) ML_2 ($K \sim 5 \times 10^3$–$1{,}1 \times 10^5$ L mol^{-1}).

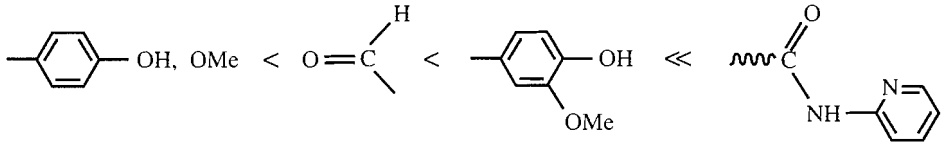

K : – 3,2–15,9 ~750 5 x 10^3–1,1 x10^5

Les effets bathochromes dus à la substitution du noyau aromatique sont importants pour les ligands et plus marqués encore pour les complexes.

Nous avons rapporté les valeurs des λ_{max} des complexes en fonction des λ_{max} des ligands libres (fig. 4). Pour les amides nous obtenons de bonnes corrélations aussi bien pour les complexes de type ML que ML_2, ce qui a posteriori confirme la stoechiométrie des complexes déduite des calculs mathématiques. La pente de la droite de corrélation avec les complexes ML_2 (courbe C) est très inférieure à celle obtenue avec les complexes ML (courbe B) (C : pente = 1,04, N = 6, cc = 0,99 (ML_2); B : pente = 1,63, N = 5, cc = 0,999 (ML)); les effets électroattracteurs du zinc sont diminués car ils sont partagés entre les deux groupements carbonyle conjugués. De même, la pente de la droite de corrélation pour les complexes ML pour les amides est inférieure à celle observée avec les aldéhydes (courbe A) (p = 1,34, cc = 0,99, N = 5); la double liaison carbonyle peut être conjuguée avec le motif aminopyridine ou avec le motif aromatique. La linéarité de la relation λ_{max} des complexes = $f(\lambda_{max}$ des ligands libres) pour ces trois séries de complexes met en évidence que la bande d'absorption des ligands libres et des complexes sont de même nature et correspondent à la transition $\pi \rightarrow \pi^*$ modifiée par la complexation.

Si nous examinons ces résultats du point de vue de la modélisation de l'interaction Zn–substrat au niveau du site actif de l'enzyme cible, la cinnamylalcool déshydrogénase,

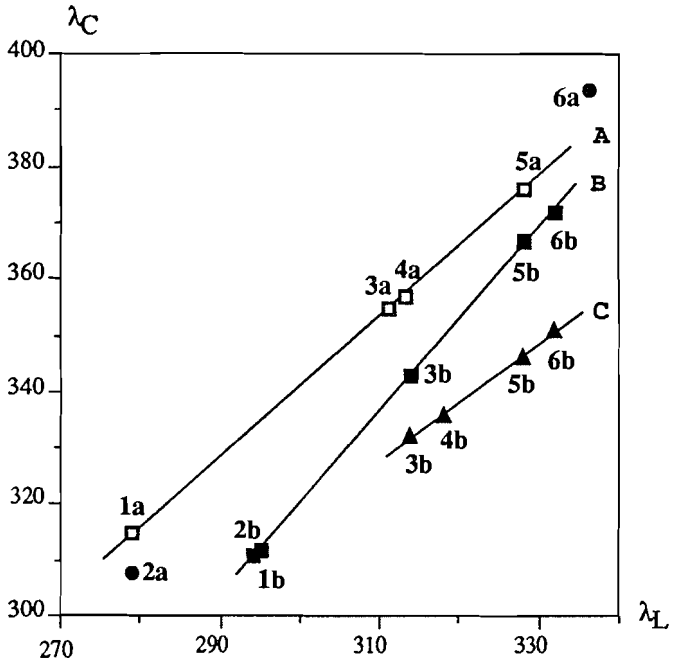

FIG. 4. Effet des substituants sur les longueurs d'onde d'absorption maximum des complexes aldéhydes ou amides cinnamiques – sels de zinc en fonction des longueurs d'onde d'absorption maximum des aldéhydes ou amides libres. □, ● : Complexe C=O....Zn avec les aldéhydes; ■ : complexe C=O....Zn avec les amides; ▲ : complexe C=O....Zn....O=C avec les amides.

nous sommes amenés à comparer les valeurs des constantes de stabilité pour les complexes de type ML entre CHO....Zn dans les aldéhydes et *N*-pyridyl C=O....Zn dans les amides. Ces valeurs varient sensiblement entre les aldéhydes eux-mêmes. Le cinnamaldéhyde qui n'est pas un substrat naturel de l'enzyme présente des constantes de stabilité quatre à cinq fois plus faibles que celles des aldéhydes substrats parahydroxylés **4***a*–**6***a*. Le paracoumaraldéhyde **4***a* et le coniferaldéhyde **5***a* qui ont la meilleure affinité pour l'enzyme (7), présentent les valeurs de constantes de stabilité les plus élevées dans la série. Néanmoins, ces résultats doivent être examinés avec précaution et ces valeurs de constantes restent en valeur absolue très faibles de 2 à 12 × 10^3 fois inférieures à celles obtenues pour les complexes issus des amides correspondants.

En conclusion, ces observations peuvent être mises en parallèle avec nos hypothèses de travail; les amides ont été initialement synthétisés pour leur aptitude à complexer le zinc de l'enzyme cible et pour leur analogie de structure avec les substrats aldéhydes, ce qui devait assurer leur reconnaissance et leur transport au site actif de l'enzyme. Les résultats de l'étude de complexation au niveau de l'interaction C=O...Zn d'une part, les propriétés inhibitrices vis à vis de la CAD observées d'autre part avec l'amide **5***b*, confortent dans une certaine mesure les deux termes de l'hypothèse.

En effet, l'étude physicochimique de la complexation des aldéhydes et des amides cinnamiques nous a permis de préciser ou de confirmer les points suivants :

1. Les aldéhydes **1***a*–**4***a* non substitués et substitués par un méthoxyle ou un hydroxyle se complexent avec le bromure de zinc par l'oxygène du carbonyle avec une faible constante de complexation et une stoechiométrie 1/1.

2. Les aldéhydes **5***a* et **6***a* se complexent par les fonctions OH et OCH_3 portées par le noyau phényle (K_1 = 750 L mol^{-1}) et par l'oxygène de la fonction carbonyle avec une constante faible (**5***a* K_2 = 13,6 L mol^{-1}, **6***a* K_2 = 8,9 L mol^{-1}), selon une stoechiométrie M_2L. Les effets bathochromes dus à la complexation sont de 48 et 58 nm, ce qui suggère la participation d'une forme quinonique (21).

3. Les phénolamides complexent fortement le zinc par l'intermédiaire de la fonction amido-pyridine K = 11 × 10^4 L mol^{-1}. Ces amides ont des constantes de complexation 2 à 12 × 10^3 fois plus grandes que les aldéhydes substrats **4***a*–**6***a*. Ces données sont cohérentes avec l'activité biologique de ces composés qui sont des inhibiteurs de l'enzyme cible (10).

Partie expérimentale

Matériel

Les aldéhydes et les amides cinnamiques ont été préparés à partir des acides cinnamiques correspondant en les activant par le chlorure de *N*,*N*-diméthyl-chloroéthylèniminium, en les réduisant en aldéhydes par l'hydrure de lithium et de tritertbutoxyaluminium, en les condensant avec l'amidure de l'aminopyridine pour les amides selon les conditions précédemment décrites (22–24). Le bromure de zinc (Aldrich) est séché à 150°C sous une pression de 10^{-2} mbar pendant 4 h (1 bar = 100 kPa). Le diéthyléther est distillé sur sodium. Les spectres infrarouges sont enregistrés sur un appareil Perkin–Elmer, modèle 783. Les spectres ultraviolets sont enregistrés à l'abri de la lumière du jour pour éviter une irradiation UV des ligands, et sous une atmosphère inerte afin de prévenir l'hydratation des sels de zinc.

Conditions de l'étude UV

Les ligands aldéhydes et amides sont préparés à une concentration de 4 × 10^{-5} mol L^{-1} dans le diéthyléther anhydre auxquels sont ajoutés à la seringue une solution de $ZnBr_2$ dans le diéthyléther (7,4 × 10^{-3} mol L^{-1} dans Et_2O), la solution est homogénéisée, puis le spectre UV est enregistré. Le rapport ρ est défini comme étant [M]/[L] (M = $ZnBr_2$, L = Ligand).

Les spectres enregistrés sont ceux d'une solution (V = 3 cm^3) d'aldéhydes de molarité donnée à laquelle sont ajoutés des volumes connus (v cm^3) de solution de bromure de zinc. Pour l'étude de la complexation, la densité optique expérimentale est corrigée d'un facteur de dilution ($V + v/V$) afin de se retrouver à molarité constante en aldéhyde :

$$\text{D.O.}_{\text{corr.}} = \left(\frac{V+v}{V}\right) \times \text{D.O.}_{\text{exp.}}$$

Les constantes de stabilité des complexes et leurs coefficients d'extinction molaire sont déterminés selon la méthode de Shapiro et Johnston (25) décrite dans la note concernant les amides monosubstitués (17).

Les constantes de stabilité K, K_1, K_2 sont données en fonction de x, y (qui sont les concentrations molaires respectives de ML et M_2L en équilibre) et de m_0 et l_0 (les concentrations initiales de $ZnBr_2$ et du ligand). Le coefficient de reliabilité est donné par

$$\text{Re} = \left[\frac{\sum_{i=1}^{p} (A_{i\,\text{exp}} - A_{i\,\text{calc}})^2}{\sum_{i=1}^{p} A_{i\,\text{exp}}^2}\right]^{1/2}$$

et l'erreur quadratique :

$$Q = \sum_{i=1}^{p} (A_{i\text{exp}}^2 - A_{i\,\text{calc}})^2$$

Can. J. Chem. Downloaded from www.nrcresearchpress.com by 213.200.69.106 on 09/08/12
For personal use only.

TABLEAU 3. Analyse élémentaire des complexes des amides **5***b* en **6***b* avec $ZnBr_2$

Stoechiométrie			Analyse élémentaire % calc.		% trouvé
5*b*	ML	C	36,36	C	36,42
		H	2,85	H	2,89
		N	5,65	N	5,80
	ML_2	C	47,06	C	46,29
		H	3,69	H	3,80
		N	7,32	N	7,27
	ML	C	36,57	C	36,52
		H	3,07	H	3,07
6*b*		N	5,33	N	5,31
	ML_2	C	46,54	C	48,25
		H	3,91	H	4,08
		N	6,78	N	6,99

Préparation des complexes des amides **5**b *et* **6**b

Les synthèses des complexes des amides **5***b* et **6***b* sont réalisées selon la méthode précédemment décrite (17).

Dans la méthode A on introduit le sel de zinc selon une stoechiométrie 1 : 1; dans la méthode B on introduit un excès de sel de zinc.

Les analyses élémentaires sont données dans le tableau 3.

Étude de la complexation de l'eugénol **7**

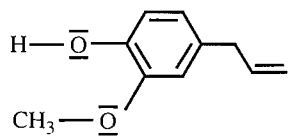

La complexation de l'eugénol est étudiée dans les conditions décrites dans la note sur les amides (17).

À une solution d'eugénol sont ajoutés des incréments de bromure de zinc en solution dans le diéthyléther. En faisant varier le rapport sel sur ligand on observe la formation d'un complexe absorbant à 284 nm alors que l'eugénol **7** absorbe dans le diéthyléther à 282 nm; on note également un point isosbestique à 270 nm. Eugénol **7** : λ_{max} (nm) = 282, ε_{max} = 3 200 L mol^{-1} cm^{-1}. Complexe eugénol **7** – $ZnBr_2$: λ_{max} (nm) = 284, ε_{max} = 3 700 L mol^{-1} cm^{-1}. La constante de complexation K calculée selon le modèle M + L $\rightleftharpoons$ ML est de 58 L mol^{-1} (Q = 2,8 × 10^{-5}, Re = 0,005).

1. F.D. Lewis, J.D. Oxman, L.L. Gibson, H.L. Hampsch et S.L. Quillen. J. Am. Chem. Soc. **108**, 3005 (1986).
2. F.D. Lewis, D.K. Howard, S.V. Barancyk et J.D. Oxman. J. Am. Chem. Soc. **108**, 3016 (1986).
3. F.D. Lewis, S.L. Quillen, P.D. Hale et J.D. Oxman. J. Am. Chem. Soc. **110**, 1261 (1988).
4. F.D. Lewis, J.E. Elbert, A.L. Upthagrove et P.D. Hale. J. Am. Chem. Soc. **110**, 5191 (1988).
5. F.D. Lewis, J.E. Elbert, A.L. Upthagrove et P.D. Hale. J. Org. Chem. **56**, 553 (1991).
6. K.V. Sarkanen et H.L. Hergert. *Dans* Lignins: occurrence, formation, structure and reactions. *Editeurs* : K.V. Sarkanen et S. Ludwig. Wiley, New York. 1971. p. 43.
7. T. Higuchi. Biosynthesis and biodegradation of wood components. Academic, New York. 1985.
8. G.G. Gross, J. Stöeckigt, R.L. Mansell et M.H. Zenk. FEBS Lett. **31**, 283 (1973).
9. D. Wijrambik et H. Grisebach. Eur. J. Biochem. **59**, 9 (1975).
10. A.M. Boudet et C. Grand. BCPC Monogr. **36**, 67 (1987).
11. M.F. Dunn, J.F. Biellmann et G. Branlant. Biochemistry, **14**, 4345 (1975).
12. B. Kaptein, G. Barf, R.M. Kellog et F. Van Bolhuis. J. Org. Chem. **55**, 1890 (1990).
13. F. Sarni, C. Grand et A.M. Boudet. Eur. J. Biochem. **139**, 259 (1984).
14. C.T. Angelis, M.F. Dunn, D.C. Muchmore et R.M. Wing. Biochemistry, **16**, 2922 (1977).
15. P.W. Jagodzinski et W.L. Petitcolas. J. Am. Chem. Soc. **103**, 234 (1981).
16. D.J. Creighton, J. Hajdu et D.S. Sigman. J. Am. Chem. Soc. **98**, 4619 (1976).
17. H. Duran, E. Duran, L. Gorrichon et M. Perry. J. Phys. Org. Chem. **6**, 15 (1993).
18. E. Duran. Thèse 3ème cycle, Toulouse III (1985).
19. M. Avram et G.H.D. Mateescu. Spectroscopie infra-rouge. Dunod, Paris. 1970. p. 374.
20. A. Bouayad, N. Bitit, E. Deydier, M.J. Menu, M. Dartiguenave, Y. Dartiguenave, H. Duran, L. Gorrichon, M. Simard et A.L. Beauchamp. Inorg. Chim. Acta, **190**, 79 (1991).
21. A. Zanarotti. Tetrahedron Lett. **23**, 3815 (1982).
22. E. Duran, L. Gorrichon, L. Cazaux et P. Tisnes. Tetrahedron Lett. **25**, 2755 (1984).
23. H. Duran, E. Duran, M. Ben Bakkar, L. Gorrichon et C. Grand. Bull. Soc. Chim. Fr. 672 (1987).
24. E. Duran, H. Duran et L. Gorrichon. Holzforschung **46**, 21, 1992.
25. B.L. Shapiro et M.D. Johnston. J. Am. Chem. Soc. **94**, 8185 (1972).

Can. J. Chem. Downloaded from www.nrcresearchpress.com by 213.200.69.106 on 09/08/12
For personal use only.

Dissociation constants of some alkanolamines

S. XU, F.D. OTTO, AND A.E. MATHER[1]

Department of Chemical Engineering, University of Alberta, Edmonton, Alta., Canada T6G 2G6

Received April 7, 1992[2]

S. XU, F.D. OTTO, and A.E. MATHER. Can. J. Chem. **71**, 1048 (1993).

The dissociation constants of piperidine (PD), 1-piperidineethanol (1-PE), *N*-methylmorpholine (MML), 4-(2-hydroxyethyl)morpholine (4-EML), and tropine (TP) have been determined at 15.0, 25.0, 35.0, 45.0, and 60.0°C. The standard state enthalpy changes of the dissociation reaction for these amines have been obtained from the dependence of the dissociation constants upon temperature.

S. XU, F.D. OTTO et A.E. MATHER. Can. J. Chem. **71**, 1048 (1993).

On a déterminé, à des températures de 15,0, 25,0, 35,0, 45,0 et 60,0°C, les constantes de dissociation de la pipéridine (PD), de la pipéridineéthanol-1 (PE-1), de la *N*-methylmorpholine (MML), de la (hydroxy-2-éthyl)-4-morpholine (EML-4) et de la tropine (TP). L'influence de la température sur les constantes de dissociation permet d'obtenir les changements d'enthalpie de l'état standard des réactions de dissociation de ces amines.

[Traduit par la rédaction]

Can. J. Chem. Downloaded from www.nrcresearchpress.com by 213.200.69.106 on 09/08/12
For personal use only.

Introduction

Aqueous alkanolamine solutions are widely used for the removal of acid gases such as H_2S, COS, and CO_2 from gaseous streams. It has been found that the dissociation constant of the alkanolamine is one of the very important factors in the selection of an amine solution or in the elucidation of a kinetic mechanism of absorption of the acid gas in the amine solution. A knowledge of the acid–base properties of these amine solvents plays an important role in our understanding of the relationships between molecular structures, chemical-physical properties of individual atoms or groups of atoms within molecules, and liquid–gas equilibrium constants or reaction rate constants.

The dissociation constants for some conventional alkanolamines were presented by Perrin (1), and more recently by other authors (2–6), at several temperatures and various ionic concentrations. Also, Antelo et al. (7) studied the influence of the ionic composition of the medium on the dissociation constants of some conventional amines. Nevertheless, the dissociation constants of less common alkanolamines are still unavailable. The purpose of the present investigation is to provide dissociation constants for some of these alkanolamines at several temperatures.

Experimental section

Analytical grade piperidine (PD), 1-piperidineethanol (1-PE), and 4-(2-hydroxyethyl)morpholine (4-EML), all with purities of ≥99%, were supplied by Aldrich Chemical (Milwaukee, Wis.). As analyzed by gas chromatography, the purity of the tropine (TP, Aldrich Chemical) was higher than 98% and the rest was water. *N*-Methylmorpholine (MML) with a purity of 99% was provided by Alfa Division of Ventron Chemicals Company. These chemicals were used as received.

The accuracy of the buffer solutions used to calibrate the pH meter was ±0.01 and ±0.02, respectively, at 25°C for pH 4.00, 7.00, and 10.00. The titration acid was 0.1000 ± 0.005 M hydrochloric acid. These chemicals were provided by the Fisher Scientific Company. All solutions were prepared using reverse osmosis water, which was made by passing triple-distilled water through anion exchange, cation exchange, activated carbon, and a 0.45-μm cartridge. The conductivity of the reverse osmosis water was higher than 0.06 μS cm^{-1}. The nitrogen used for blanketting the titration of the dissociation constant was supplied by Union Carbide Canada. It had a purity of 99.99% without any oxygen.

TABLE 1. Values of pK_a for several alkanolamines

Amine	Temperature (°C) 15.0	25.0	35.0	45.0	60.0	Reference
PD	11.443	11.123	10.818	10.526	10.19[a]	Perrin (1)
PD	11.44	11.16	10.81	10.53	10.18	This work
2-PE	10.47	10.14	9.82	9.52	9.16	Xu et al. (6)
1-PE	9.85	9.63	9.41	9.22	8.84	This work
MML	7.62	7.40	7.28	7.16	6.94	This work
4-EML	7.20	7.01	6.88	6.67	6.56	This work
TP	10.80	10.48	10.23	10.04	9.72	This work

[a]At 59.6°C.

The dissociation constants of the amine solvent were determined by potentiometric titration with standard hydrochloric acid in a special jacketted beaker that could be kept at a constant temperature within ±0.05°C. The solutions used in this experiment were protected by high-purity nitrogen. The pH meter, a model 520 digital pH/ion meter made by the Fisher Scientific Company, was read directly with an accuracy of ±0.002 pH and a reproducibility of ±0.001 pH. The pH meter, combined with glass and reference electrodes, was calibrated by the buffer solutions in the range of pH 4–10 before determination of the dissociation constant. After the dilute amine solutions were prepared, they were stripped by nitrogen to remove trace amount of gases such as oxygen. The solutions were then stored under a nitrogen atmosphere.

The pK_a values of the amines were directly calculated from the titration curve of the pair of pH values and acid volume titrated. The activities of the species in the solution were corrected by the activity coefficients obtained from the Debye–Hückel equation. Further detailed information about the experimental procedure is provided by Xu et al. (6).

Results and discussion

The values of pK_a for several uncommon amines measured in this work are listed in Table 1. Since the operating temperature is limited by the standard buffer solutions, the dissociation constants of the amines were determined in the temperature range from 15.0 to 60.0°C. Comparing the pK_a values of PD measured in this work with these of Perrin (1), the accuracy of this experiment is within ±0.02 pK_a.

Table 1 shows that the values of pK_a for PD are the high-

[1]Author to whom correspondence may be addressed.

[2]Revision received April 23, 1993.

Can. J. Chem. Downloaded from www.nrcresearchpress.com by 213.200.69.106 on 09/08/12
For personal use only.

est among those measured. In the family of piperidines, the value of pK_a may depend on the number of hydroxyethyl groups attached to the nitrogen atom or on the position of the hydroxyethyl group in the cyclic system. For example, the dissociation value of 2-PE, in which the hydroxyethyl group is connected at the α position of the cyclic system, is higher than that of PD; the dissociation constant of 1-PE is the highest in the family of piperidines in that its hydroxyethyl group is directly attached to the nitrogen atom. This characteristic is similar to that of conventional alkanolamines, in that the value of pK_a of a secondary amine is larger than that of a tertiary amine, and also the value of a sterically hindered amine is larger than that of a tertiary amine. It is interesting that although both morpholine and piperidine are secondary amines, and have almost the same molecular structures, their dissociation constants are very different, with pK_a values of 8.33 (1) and 11.44, respectively, at 25°C. This may be due to the effects of an oxygen atom connected to the naphthenic ring group, since a pair of isolated electrons of the nitrogen atom in morpholine are attracted to the oxygen atom so that the electronegativity of morpholine increases, and its ability to combine with the H^+ ion in water decreases. Furthermore, comparing the values of pK_a in the family of morpholines, the value of pK_a of morpholine, 8.33, is larger than that of *N*-ethylmorpholine, 7.67 (1), and larger than that of *N*-methylmorpholine, 7.40, and that of 4-EML, 7.01, at 25°C. It can readily be seen that the value of pK_a is also affected by the length of the carbon chain and the atoms attached to the chain. The higher the electronegativity of the atom in this compound, the lower the pK_a value of the compound. 4-EML, therefore, has the lowest pK_a value in Table 1. Although TP is one of the tertiary amines, its pK_a is higher than that of other tertiary amines as a result of its special molecular structure.

According to the experimental data, the values of pK_a for these alkanolamines can be correlated by the following equation:

$$[1] \quad pK_a = C_1 + \frac{C_2}{T}$$

where T is in K. The parameters in the equation for the alkanolamines are given in Table 2. The standard state enthalpy change (ΔH^0) of the reaction of amine dissociated in water can be calculated from the van't Hoff equation. Based on the experimental work, the standard state enthalpy changes (ΔH^0) of the amines decreases with the decrease in pK_a of the amine except for the sterically hindered amine 2-PE. The standard state enthalpy change (ΔH^0) of the sterically hindered amine, 2-PE, is the highest among those amines tested, which means that the pK_a value of 2-PE is sensitive to the temperature change. Also, the standard state enthalpy change of 2-amino-2-methyl-1-propanol (AMP), one of the primary sterically hindered amines, has the highest standard state enthalpy change of conventional amines (6).

TABLE 2. The parameters of eq. [1] and the standard enthalpy changes of alkanolamines

Amine	Parameter C_1	Parameter C_2	ΔH^0 kJ/mol	δ (%)[a]	Reference
PD	1.9557	2734.71	52.3	0.18	This work
2-PE	0.7050	2811.37	53.8	0.26	Xu *et al.* (6)
1-PE	2.4678	2134.60	40.9	0.15	This work
MML	2.8087	1378.20	26.4	0.21	This work
4-EML	2.5615	1332.31	25.5	0.21	This work
TP	2.9334	2257.45	43.2	0.12	This work

[a] $\delta = \frac{100\%}{n} \sum_{i=1}^{n} \left| \frac{pK_{a\,calc.} - pK_{a\,exp.}}{pK_{a\,exp.}} \right|_i$.

	Amine abbreviations	CA Registry No.	Structure
4-EML	4-(2-Hydroxyethyl)morpholine	[622-40-2]	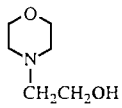
MM1	N-Methylmorpholine	[109-02-4]	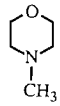
PD	Piperidine	[110-89-4]	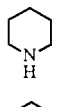
1-PE	1-Piperidineethanol	[3040-44-6]	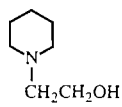
2-PE	2-Piperidineethanol	[1484-84-0]	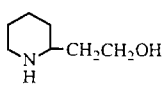
TP	Tropine	[120-29-6]	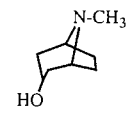

Acknowledgement

Financial support was provided by the Natural Sciences and Engineering Research Council of Canada (NSERC) Strategic Grant No. 100777.

1. D.D. Perrin. Dissociation constants of organic bases in aqueous solution. Butterworths, London. 1965. Nos. 967, 1440, 1454, and 1459.
2. K. Schwabe, W. Graichen, and D. Spiethoff. Z. Phys. Chem. (N. F.), **20**, 68, (1959).
3. P.M. Blauwhoff and M. Bos. J. Chem. Eng. Data, **26**, 7, (1981).
4. J.-H. Kim, C. Dobrogowska, and L.G. Hepler. Can. J. Chem. **65**, 1726 (1987).
5. R.J. Littel, M. Bos, and G.L. Knoop. J. Chem. Eng. Data, **35**, 276 (1990).
6. S. Xu, Y.-W. Wang, F.D. Otto, and A.E. Mather. J. Chem. Eng. Data, **37**, 407 (1992).
7. J.M. Antelo, F. Arce, J. Casado, M. Sastre, and A. Varela. J. Chem. Eng. Data, **29**, 10 (1984).

Can. J. Chem. Downloaded from www.nrcresearchpress.com by 213.200.69.106 on 09/08/12
For personal use only.

Coordination-induced keto–enol tautomerization in the formation of Ni^{2+} and Cu^{2+} complexes of a fluorinated keto-diol[1]

JAGADESE J. VITTAL AND CHRISTOPHER J. WILLIS[2]
Department of Chemistry, University of Western Ontario, London, Ont., Canada N6A 5B7

Received February 2, 1993

JAGADESE J. VITTAL and CHRISTOPHER J. WILLIS. Can. J. Chem. **71**, 1051 (1993).

The fluorinated keto-diol $(CF_3)_2C(OH)CH_2C(=O)CH_2C(CF_3)_2OH$ forms stable, neutral, 1:1 complexes of Ni^{2+} (**6***a*) and Cu^{2+} (**6***b*) with tetramethylethylenediamine (TMED) as coligand. The structure of each complex has been determined crystallographically; they are isomorphous and isostructural, monoclinic with space group *Cc* (No. 9). Complex **6***a*, $C_{15}H_{20}F_{12}N_2NiO_3$, has a = 11.495(2), b = 15.516(2), c = 12.323(2) Å, β = 99.88(1)°, V = 2165.4(6) Å^3, Z = 4. Complex **6***b*, $C_{15}H_{20}CuF_{12}N_2O_3$, has a = 11.603(2) b = 15.661(2), c = 12.276(2) Å, β = 99.75(2)°, V = 2198.5(6) Å^3, Z = 4. In each, the metal is in square-planar geometry bonded to two alkoxide groups and two N atoms of TMED. A previous assignment of a zwitterionic structure to these complexes has been shown to be incorrect. Instead, the ligand is coordinated as the di-ionized enol tautomer $(CF_3)_2C(-O^-)CH_2C(-O^-)=CHC(CF_3)_2OH$, the C=C double bond being external to the six-membered chelate ring. The remaining OH group of the ligand forms part of a second six-membered ring held together by hydrogen bonding.

JAGADESE J. VITTAL et CHRISTOPHER J. WILLIS. Can. J. Chem. **71**, 1051 (1993).

Le céto-diol fluoré $(CF_3)_2C(OH)CH_2C(=O)CH_2C(CF_3)_2OH$ forme des complexes stables, neutres, 1 : 1 de Ni^{2+} (**6***a*) et de Cu^{2+} (**6***b*) avec la tétraméthyléthylènediamine comme coligand. On a déterminé la structure de chaque complexe par cristallographie; ils sont isomorphes et isostructuraux et appartiennent au groupe d'espace monoclinique *Cc* (No. 9). Les paramètres du complexe **6***a*, $C_{15}H_{20}F_{12}N_2NiO_3$, sont a = 11,495(2), b = 15.516(2), c = 12,323(2) Å, β = 99,88(1)°, V = 2165,4(6) Å^3, Z = 4. Les paramètres du complexe **6***b*, $C_{15}H_{20}CuF_{12}N_2O_3$ sont a = 11,603(2), b = 15.661(2), c = 12,276(2) Å, β = 97,75(2)°, V = 2198,5(6) Å^3, Z = 4. Dans chacun de ces complexes, le métal a une géométrie carré-plan lié à deux groupes alcoolates et à deux atomes d'azote de la TMED. On démontre que la structure de zwittérion proposée antérieurement pour ces complexes est incorrecte. Le ligand est plutôt coordonné sous forme de tautomére énol diionisé, $(CF_3)_2C(-O^-)CH_2C(-O^-)=CHC(CF_3)_2OH$ avec la double liaison C=C à l'extérieur du cycle chélaté à six chaînons. Le groupe OH restant appartient à un second cycle à six chaînons, le tout étant maintenu ensemble par des liaisons hydrogènes.

[Traduit par la rédaction]

Introduction

Coordination to a metal ion of a ketone function in the form of its ionized enol tautomer is a familiar process. Complexes are frequently stabilized by delocalization in a chelate ring, of which the β-diketone systems are the most common. Stabilization may also occur through conjugation of the C=C bond in the enol with a C=N bond in a Schiff-base type of ligand. For example, it has long been known that β-diketones will condense with diamines in the presence of Ni^{2+} (1, 2) or Cu^{2+} (3, 4) to give neutral complexes of tetradentate, dinegative, ligands of the type $[R\text{-}C(\text{-}O^-)=CHC(R)=N\text{-}CH_2\text{-}]_2$. Additional conjugation may be present if R is phenyl.

It is unusual for an alkoxide to form by the coordination of an enolate in the absence of such interaction of the C=C bond with other bonds in the ligand molecule, but in this paper we describe the structures of stable complexes of Ni^{2+} and Cu^{2+} formed in this way. In each case, a six-membered chelate ring is formed by bonding to the enolate and to a highly fluorinated alkoxide, but the C=C bond is external to this ring.

The ready formation of alkoxides of transition metals by the coordination of fluorinated alkoxide ions is well established (5). Stability is considerably enhanced by chelation, and the highly fluorinated diol perfluoropinacol, $HOC(CF_3)_2C(CF_3)_2OH$, in its di-ionized, bidentate, form, is particularly suitable for the preparation of complexes of a variety of metals (5–7).

Thermal reaction of acetone with hexafluoroacetone gives both a 1:1 and a 1:2 adduct: the keto-alcohol $CH_3COCH_2C(CF_3)_2OH$, **1**, and the keto-diol 1,1,1,7,7,7-hexafluoro-2,6-bis(trifluoromethyl)-4-heptanone-2,6-diol $(CF_3)_2C(OH)CH_2COCH_2C(CF_3)_2OH$, **2** (8, 9). A recent structural study on the latter shows intramolecular hydrogen bonding between the carbonyl oxygen atom and both OH groups, forming two six-membered rings (10):

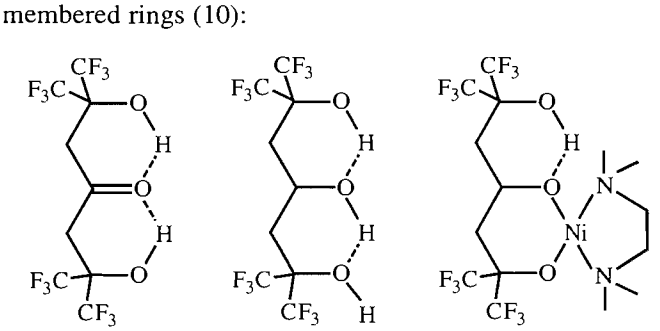

2 **3** **4**

Reduction of the keto-diol **2** gives the fluorinated triol **3**, which, in the di-ionized form, acts as a bidentate ligand to Ni^{2+}, giving the complex **4** in which the metal is four-coordinate (9). The failure of **3** to coordinate as a tridentate ligand is presumably due to steric constraints and the stability of the remaining H-bonded ring in **4**.

[1]Presented in part at the 76th Conference of the Canadian Society for Chemistry, Sherbrooke, Quebec, June 1993.

[2]Author to whom correspondence may be addressed.

Can. J. Chem. Downloaded from www.nrcresearchpress.com by 213.200.69.106 on 09/08/12
For personal use only.

Can. J. Chem. Downloaded from www.nrcresearchpress.com by 213.200.69.106 on 09/08/12
For personal use only.

TABLE 1. Crystal data and experimental details

		Compound **6***a*	Compound **6***b*
Compound, formula		$C_{15}H_{20}N_2F_{12}O_3Ni_1$	$C_{15}H_{20}N_2F_{12}O_3Cu_1$
Formula weight		563.03	567.87
Crystal system, space group		Monoclinic, *Cc* (No. 9)	
Cell dimensions	*a* =	11.495(2) Å	11.603(2) Å
	b =	15.516(2) Å	15.661(2) Å
	c =	12.323(2) Å	12.276(2) Å
	β =	99.88(1)°	99.75(2)°
	Z =	4	4
Cell volume (Å^3)		2165.4(6)	2198.5(6)
Density, g cm^{-3}, obsd., calcd.		1.73(3), 1.727	1.73(3), 1.719
F(000)		1138.2	1143.8
Diffractometer, monochromator		Enraf–Nonius CAD4F; graphite	
Radiation, wavelength (Å)		MoKα, 0.71073	
Absorption coeff. (cm^{-1})		10.2	11.1
No. of observations ($I \geq 2.5\sigma(I)$)		1758	1689
No. of variables		220	219
Final model; R_f and R_w		0.058, 0.031	0.067, 0.042
GOF		2.21	2.74

$R_f = \Sigma||F_o| - |F_c||/\Sigma|F_o|$.
$R_w = [\Sigma w(|F_o| - |F_c|)^2/\Sigma w|F_o|^2]^{1/2}$.
GOF = $\Sigma w(|F_o| - |F_c|)^2$/(no. of reflections − no. of parameters)$^{1/2}$.

Carbonyl oxygen is not a strong donor, and we had difficulty in preparing stable complexes of the ionized keto-alcohol **1**. Only with a tridentate macrocyclic amine as coligand was it possible to isolate a cationic complex in which **1** had chelated to five-coordinate Ni^{2+} (9). It was therefore surprising that the di-ionized keto-diol **2** was found to give stable, neutral, complexes with both Ni^{2+} and Cu^{2+}. Tetramethylethylenediamine (TMED) was used as coligand, and visible spectra showed the metal to be four-coordinate. Because of the geometry of the ligand **2**, it was considered very unlikely that the two fluorinated alkoxides could chelate to the same metal atom, and structure **5**, with a separation of formal charge, was therefore assigned. The C=O stretching frequency of the ligand was apparently reduced by ~50 cm^{-1} in each of the complexes, consistent with coordination of the ketone group. However, an alternate model in which ligand **2** bridged between two metal centres could not be ruled out.

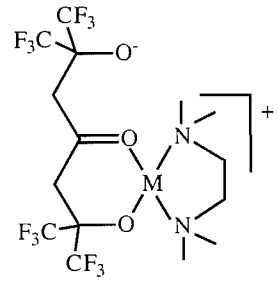

5

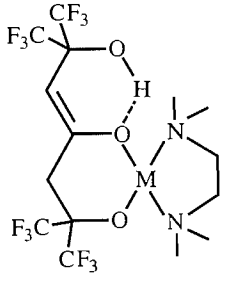

6*a*, M = Ni^{2+}; **6***b*, M = Cu^{2+}

To clarify the structures of these complexes, we have now undertaken an X-ray crystal structure determination of the Ni^{2+} and Cu^{2+} derivatives. It shows that our earlier assignment of type **5** structures was incorrect. Instead, ligand **2** has undergone keto–enol tautomerization on coordination, giving an unsaturated triol, and the bonding system in each complex is as shown at **6**.

Experimental

X-ray structure determination

Compounds **6***a* and **6***b* were prepared as previously reported (9). Single crystals were obtained by diffusion of pentane into a solution of the complex in dichloromethane at 5°C. The two compounds were examined by similar experimental procedures, as given below, and were subsequently found to be isomorphous and isostructural.

Densities were measured by the neutral buoyancy method in mixtures of dibromoethane and carbon tetrachloride. Crystals were mounted on glass fibres using epoxy resin in air. Data collection was carried out on an Enraf–Nonius CAD4F diffractometer using monochromated MoKα radiation at 23°C. Photo and automatic indexing routines, followed by least-squares fits of 21 accurately centered reflections ($12.1 \leq 2\theta \leq 14.3°$ for **6***a* and **6***b*), gave cell constants and an orientation matrix (11). Intensity data were recorded in ω–2θ mode, at variable scan speeds (0.915–4.12 deg min^{-1}) and a scan width of 0.8 + 0.35 tan θ, with a maximum time per datum of 60 s. Static background measurements were made at the end points of the width 0.9 + 0.35 tan θ. Three standard reflections were monitored every 120 min.

In all, 3325 ($-14 \leq h \leq 14$, $-1 \leq k \leq 20$, $-16 \leq l \leq 1$) and 2642 ($-15 \leq h \leq 0$, $0 \leq k \leq 20$, $-15 \leq l \leq 15$) reflections for **6***a* and **6***b*, respectively, were measured in the 2θ range 0–55°. The NRCVAX crystal structure programs (12) running on a SUN 3/80 workstation were used to process the data. Gaussian absorption corrections were applied. The cell parameters and the systematic absences (13) were consistent with either space group *Cc* (No. 9) or space group *C*2/*c* (No. 15). The *N*(*z*) statistics (14) strongly indicated the noncentrosymmetric space group. In addition, the expected molecular structure for $Z = 4$ did not possess 1 or 2-fold symmetry and hence the space group *C*2/*c* was not considered further. Successful structure solution and refinement confirmed the choice of the space group. Refinements were by full-matrix least-squares techniques on *F*. The metal, fluorine, and all the methyl carbon atoms were assigned anisotropic thermal parameters and were refined in the least-squares cycles. All the hydrogen atoms were located successfully by difference Fourier. The isotropic thermal parameters for **6***a* and the positional parameters for the enolic H atoms in **6***a* and **6***b* were refined. The isotropic temperature factor was fixed at $U = 0.05$ for the enolic H atom in **6***b*. All

TABLE 2. Atomic positional and thermal parameters

Atom	x	y	z	B_{iso}[a]
		Compound **6a**		
Ni	0.0000	0.90461(7)	0.0000	2.91(5)
F(1)	−0.0310(6)	1.0968(5)	−0.2088(5)	6.7(4)
F(2)	0.0169(6)	1.2149(4)	−0.1220(6)	8.3(5)
F(3)	−0.1517(5)	1.1550(5)	−0.1178(6)	7.9(4)
F(4)	0.0569(6)	1.0927(5)	0.1807(5)	6.3(4)
F(5)	−0.0783(6)	1.1779(4)	0.0974(6)	7.5(4)
F(6)	0.1064(6)	1.2039(4)	0.0979(6)	7.9(4)
F(7)	0.4759(6)	0.9907(5)	0.3926(5)	6.7(4)
F(8)	0.4791(6)	1.0997(5)	0.2870(5)	6.4(4)
F(9)	0.3197(5)	1.0664(4)	0.3425(5)	7.0(4)
F(10)	0.5537(7)	0.8894(5)	0.2518(6)	8.3(4)
F(11)	0.5588(6)	0.9937(5)	0.1405(6)	6.5(4)
F(12)	0.4546(6)	0.8823(4)	0.0884(5)	7.2(4)
N(1)	−0.1607(7)	0.8717(6)	−0.0564(7)	4.3(2)
N(2)	0.0463(6)	0.7830(5)	0.0023(6)	3.6(2)
O(1)	−0.0525(5)	1.0158(4)	−0.0053(5)	3.8(1)
O(2)	0.1536(5)	0.9306(4)	0.0764(5)	3.2(1)
O(3)	0.3138(6)	0.9064(5)	0.2449(5)	4.6(2)
C(1)	−0.1602(13)	0.7744(10)	−0.0786(13)	9.5(4)
C(2)	−0.0632(13)	0.7367(8)	−0.0374(11)	7.5(4)
C(3)	−0.2394(9)	0.8912(9)	0.0184(9)	7.8(8)
C(4)	−0.2034(10)	0.9099(9)	−0.1641(9)	7.2(7)
C(5)	0.0895(11)	0.7516(6)	0.1132(9)	6.8(8)
C(6)	0.1336(9)	0.7708(6)	−0.0669(9)	5.7(6)
C(7)	0.0190(8)	1.0853(6)	−0.0151(8)	3.3(2)
C(8)	0.1448(7)	1.0605(5)	−0.0318(7)	3.1(2)
C(9)	0.2047(7)	1.0031(5)	0.0547(7)	2.4(2)
C(10)	0.3099(7)	1.0278(6)	0.1159(7)	3.3(2)
C(11)	0.3778(7)	0.9752(6)	0.2085(7)	3.2(2)
C(12)	−0.0362(11)	1.1370(8)	−0.1160(10)	5.0(3)
C(13)	0.0259(11)	1.1416(8)	0.0868(11)	5.4(3)
C(14)	0.4119(11)	1.0332(8)	0.3099(10)	4.9(3)
C(15)	0.4862(10)	0.9339(8)	0.1743(9)	4.6(3)
		Compound **6b**		
Cu	0.0000	0.09495(8)	0.0000	3.15(6)
F(1)	0.0236(8)	−0.0973(8)	0.2200(7)	8.8(7)
F(2)	−0.0207(9)	−0.2151(5)	0.1286(8)	8.7(6)
F(3)	0.1470(7)	−0.1580(6)	0.1344(8)	8.2(6)
F(4)	−0.0438(8)	−0.0911(6)	−0.1725(7)	6.4(5)
F(5)	0.0892(9)	−0.1758(6)	−0.0830(8)	8.5(6)
F(6)	−0.0990(9)	−0.2015(5)	−0.0919(7)	7.7(6)
F(7)	−0.4673(9)	0.0078(7)	−0.3900(8)	7.2(5)
F(8)	−0.4722(8)	−0.1029(6)	−0.2847(8)	6.9(6)
F(9)	−0.3150(7)	−0.0663(5)	−0.3402(6)	6.9(5)
F(10)	−0.5485(9)	0.1088(7)	−0.2474(8)	8.4(6)
F(11)	−0.5510(7)	0.0021(6)	−0.1347(8)	7.1(6)
F(12)	−0.4505(7)	0.1171(5)	−0.0842(7)	7.5(6)
N(1)	0.1720(9)	0.1349(8)	0.0567(9)	4.7(3)
N(2)	−0.0454(8)	0.2230(6)	0.0088(8)	3.5(2)
O(1)	0.0556(7)	−0.0174(5)	0.0245(7)	4.2(2)
O(2)	−0.1514(7)	0.0687(5)	−0.0722(6)	3.4(2)
O(3)	−0.3108(7)	0.0910(6)	−0.2433(7)	4.3(2)
C(1)	0.1668(15)	0.2362(12)	0.0524(14)	7.8(5)
C(2)	0.0689(16)	0.2663(11)	0.0631(13)	6.6(5)
C(3)	0.2499(12)	0.1049(15)	−0.0185(14)	10.6(1)
C(4)	0.2072(12)	0.1016(13)	0.1673(15)	7.5(1)
C(5)	−0.0815(15)	0.2513(9)	−0.1024(11)	6.6(1)
C(6)	−0.1338(13)	0.2283(8)	0.0769(13)	5.6(8)
C(7)	−0.0145(11)	−0.0868(8)	0.0239(10)	3.8(3)
C(8)	−0.1442(10)	−0.0634(7)	0.0390(9)	3.1(2)
C(9)	−0.2027(9)	−0.0066(7)	−0.0540(9)	2.7(2)
C(10)	−0.3032(9)	−0.0325(7)	−0.1118(9)	2.9(2)
C(11)	−0.3738(10)	0.0235(8)	−0.2067(10)	3.3(3)
C(12)	0.0338(16)	−0.1405(12)	0.1291(15)	5.9(4)
C(13)	−0.0219(14)	−0.1370(11)	−0.0861(13)	5.1(4)
C(14)	−0.4070(13)	−0.0340(10)	−0.3107(12)	4.5(3)
C(15)	−0.4849(13)	0.0624(10)	−0.1706(13)	4.7(3)

[a] B_{iso} for non-H atom is the mean of the principal axes of the thermal ellipsoid.

other hydrogen atoms were placed in ideal positions (C—H = 1.08 Å) and their thermal parameters were assigned to ride 10% more on the attached carbon atoms.

Crystal **6**a

The dark red data crystal (dimensions 0.13 × 0.15 × 0.31 mm) has six faces, with indices {110}, (10-2), and (-10-2). The distances between the faces were measured under a filar microscope for absorption; transmission factors range from 0.8432 to 0.8817. The equivalent reflections were averaged to give 2665 unique reflections. Full-matrix least-squares refinement of 220 variables and 1758 observations with $I \geq 2.5\sigma(I)$ converged at $R_f = 0.058$, $R_w = 0.031$, and GOF, $S = 2.21$, using a weighting scheme based on counting statistics. In the final difference Fourier synthesis, the electron density ranged from 0.67 to −0.46 e A^{-3}. The maximum shift/σ ratio was 0.037. The inverted model converged at $R_f = 0.060$ and $R_w = 0.033$.

Crystal **6**b

The dark pink data crystal (with dimensions 0.14 × 0.14 × 0.41 mm) had seven faces. The face indices were {110}, (-111), (-1-11), and (-10-2). The transmission factors ranged from 0.7635 to 0.8591. The atomic coordinates of **6***a* were used for the initial least-squares refinement of **6***b*. Full-matrix least-squares refinement of 219 variables and 1689 observations with $I \geq 2.5\sigma(I)$ converged at $R_f = 0.067$, $R_w = 0.042$, and GOF = 2.79, using a weighting scheme based on counting statistics. The inverted model also converged at $R_f = 0.067$, $R_w = 0.042$, and GOF = 2.74. Between these two models the latter (inverted model) was preferred over the other since the esd's were slightly better and variations in C—F distances and F—C—F angles were smaller. In the final difference Fourier synthesis, the electron density ranged from 0.56 to −0.45 e A^{-3}. The maximum shift/σ ratio was 0.074.

The experimental details, crystal data, and positional and thermal (B_{iso}) parameters for **6***a* and **6***b* are given in Tables 1 and 2, respectively, while selected bond distances and bond angles are given in Table 3. Tables of anisotropic thermal parameters, hydrogen atom parameters, weighted least-squares planes, selected torsion angles, and structure factors for both compounds are available as supplementary material.[3]

Structure description and comparison

ORTEP views of the complexes **6***a* and **6***b*, showing the atom numbering scheme, are shown as Figs. 1 and 2, respectively. Each complex consists of discrete molecular units in which coordination to the metal occurs from one fluorinated alkoxide and from the central oxygen atom on the ligand, O(2), giving a six-membered

[3]These tables may be purchased from: The Depository of Unpublished Data, Document Delivery, CISTI, National Research Council Canada, Ottawa, Canada K1A0S2.

Tables of hydrogen atom parameters have also been deposited with the Cambridge Crystallographic Data Centre and are available on request from The Director, Cambridge Crystallographic Data Centre, University Chemical Laboratory, 12 Union Road, Cambridge, CB2 1EZ, U.K.

Can. J. Chem. Downloaded from www.nrcresearchpress.com by 213.200.69.106 on 09/08/12
For personal use only.

Can. J. Chem. Downloaded from www.nrcresearchpress.com by 213.200.69.106 on 09/08/12
For personal use only.

TABLE 3. Selected bond distances (Å) and bond angles (°) for **6***a* and **6***b*.

Bond(s)	M	
	Ni (**6***a*)	Cu (**6***b*)
M—N(1)	1.928(8)	2.095(11)
M—N(2)	1.960(7)	2.080(9)
M—O(1)	1.825(6)	1.881(8)
M—O(2)	1.897(6)	1.874(8)
N(1)—C(1)	1.535(18)	1.588(22)
N(1)—C(3)	1.430(14)	1.474(20)
N(1)—C(4)	1.459(14)	1.447(22)
N(2)—C(2)	1.459(16)	1.537(20)
N(2)—C(5)	1.456(13)	1.429(16)
N(2)—C(6)	1.437(12)	1.432(16)
O(1)—C(7)	1.374(11)	1.357(15)
O(2)—C(9)	1.317(10)	1.357(13)
O(3)—C(11)	1.413(11)	1.402(14)
C(1)—C(2)	1.284(20)	1.257(26)
C(7)—C(8)	1.544(12)	1.589(17)
C(7)—C(12)	1.523(16)	1.563(23)
C(7)—C(13)	1.521(16)	1.552(20)
C(8)—C(9)	1.467(11)	1.514(15)
C(9)—C(10)	1.365(11)	1.322(15)
C(10)—C(11)	1.507(12)	1.573(16)
C(11)—C(14)	1.535(15)	1.557(19)
C(11)—C(15)	1.524(14)	1.556(19)
O(2)—H(3)	1.87(8)	1.55(11)
O(3)—H(3)	0.89(9)	1.11(11)
N(1)—M—N(2)	89.5(3)	86.0(4)
N(1)—M—O(1)	87.0(3)	86.8(4)
N(1)—M—O(2)	171.3(3)	170.6(4)
N(2)—M—O(1)	176.5(3)	167.5(4)
N(2)—M—O(2)	88.3(3)	90.6(4)
O(1)—M—O(2)	95.2(3)	98.0(3)
M—N(1)—C(1)	107.0(7)	105.0(8)
M—N(1)—C(3)	112.6(6)	110.3(9)
M—N(1)—C(4)	111.8(7)	107.8(9)
C(1)—N(1)—C(3)	110.2(10)	108.8(13)
C(1)—N(1)—C(4)	104.4(9)	113.3(12)
C(3)—N(1)—C(4)	110.4(9)	111.5(12)
M—N(2)—C(2)	104.6(6)	103.9(8)
M—N(2)—C(5)	112.5(6)	106.6(8)
M—N(2)—C(6)	109.5(6)	107.4(7)
C(2)—N(2)—C(5)	106.6(8)	111.7(11)
C(2)—N(2)—C(6)	112.7(9)	111.8(11)
C(5)—N(2)—C(6)	110.7(8)	114.6(11)
M—O(1)—C(7)	123.1(5)	124.0(8)
M—O(2)—C(9)	119.4(5)	121.0(7)
N(1)—C(1)—C(2)	114.0(12)	113.6(15)
N(2)—C(2)—C(1)	123.3(12)	121.2(16)
O(1)—C(7)—C(8)	113.8(7)	113.2(10)
O(1)—C(7)—C(12)	108.3(8)	107.2(12)
O(1)—C(7)—C(13)	109.0(8)	110.7(10)
C(8)—C(7)—C(12)	106.9(8)	104.0(11)
C(8)—C(7)—C(13)	109.6(8)	107.7(11)
C(12)—C(7)—C(13)	109.1(9)	114.0(12)
C(7)—C(8)—C(9)	112.9(7)	111.1(9)
O(2)—C(9)—C(8)	119.7(7)	118.8(9)
O(2)—C(9)—C(10)	120.7(7)	123.4(10)
C(8)—C(9)—C(10)	119.5(7)	117.8(10)
C(9)—C(10)—C(11)	124.1(8)	121.9(10)
O(3)—C(11)—C(10)	114.8(7)	115.0(9)
O(3)—C(11)—C(14)	105.0(8)	104.1(10)
O(3)—C(11)—C(15)	105.3(8)	107.4(10)
C(10)—C(11)—C(14)	109.0(8)	108.0(10)
C(10)—C(11)—C(15)	111.2(7)	111.1(10)
C(14)—C(11)—C(15)	111.4(8)	111.0(11)
C(9)—O(2)—H(3)	94.9(28)	100.1(37)
C(11)—O(3)—H(3)	103.3(58)	103.2(51)
O(2)—H(3)—O(3)	132.2(74)	150.8(84)

chelate ring. Geometry at the metal is slightly distorted square-planar for each metal. In **6***a*, bond angles at Ni total 361° and the metal is 0.070(4) Å out of the least-squares plane of the four coordinated atoms; corresponding figures for **6***b* are 360° and 0.018(5) Å. The chelate ring is in a distorted "boat" conformation.

Metal–oxygen bond lengths are in the range usually found for fluorinated alkoxides of these metals (5) and for β-diketone complexes. Carbon–oxygen bond lengths in the chelate rings are in the range 1.32–1.37 Å; as usual, these are shorter than the C—O bonds found in unfluorinated alkoxides. However, C(1)—O(2) is 1.317(10) in **6***a* and 1.357(13) in **6***b*, in each case significantly longer than the value of 1.202(6) Å found for the double bond in the uncoordinated ligand **2** (10). At the same time, the C(9)—C(10) bond length shortens from an average of 1.51(2) Å in the ligand to 1.365(11) and 1.322(15) Å on complex formation. Bond angles at C(10), within the hydrogen-bonded ring, were 124.1(8)° and 121.9(10)°, consistent with sp^2 hybridization. These data support the bonding of the enol tautomer in each complex.

Confirmation of this comes from the detection of the migrated proton in a hydrogen-bonded ring in each complex, the dimensions being very similar to those found in the parent ligand (10).

Discussion

The revision of the structures of **6***a* and **6***b* explains why ligand **2** complexes more readily than the keto-alcohol **1**, in which keto–enol tautomerization stabilized by hydrogen bonding is not possible. It is clear that our previous interpretation of the infrared spectrum of the complexes was incorrect. The C=O vibration, found at 1730 cm^{-1} in free ligand **2**, is replaced by absorptions at 1650 and 1646 cm^{-1} in **6***a* and **6***b*, respectively, and these must be assigned to the C=C bonds present in the complexes, rather than to coordination-shifted carbonyl absorptions.

Since the electronic structure of the complexes would be very similar if the C=C bond were in the ring containing the metal ion (that is, running between C(8) and C(9)), we assume steric factors are responsible for it appearing in the H-bonded ring. The preference of each metal ion for square-planar coordination imposes greater restraints on the conformation of that chelate ring than the requirements of the less rigid ring containing the loosely bonded hydrogen atom.

This result confirms the importance of hydrogen bonding in highly fluorinated alcohols and demonstrates the surprising ease with which di-alkoxides of such highly oxophilic metals as nickel and copper may be formed from ketone functions in ligands of suitable geometry.

Acknowledgements

We thank the Natural Sciences and Engineering Research Council of Canada for financial support of this work and Dr. N.C. Payne for providing X-ray and computing facilities.

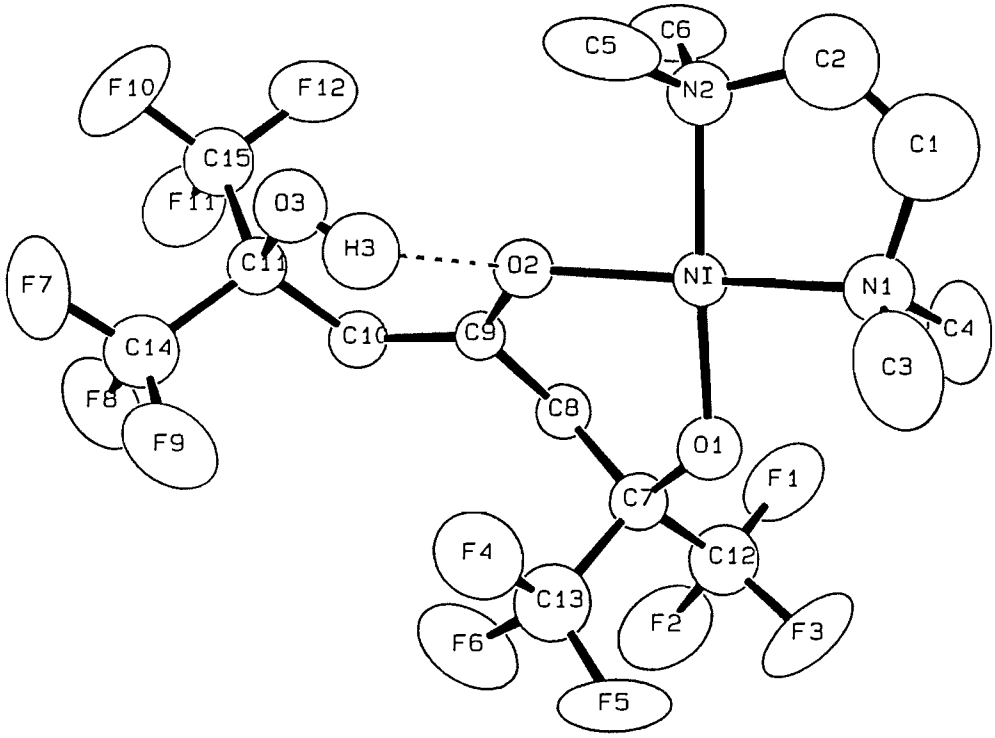

FIG. 1. ORTEP view of compound **6*a***, showing the atom numbering scheme (50% thermal ellipsoids). For clarity, the hydrogens attached to carbon atoms are omitted.

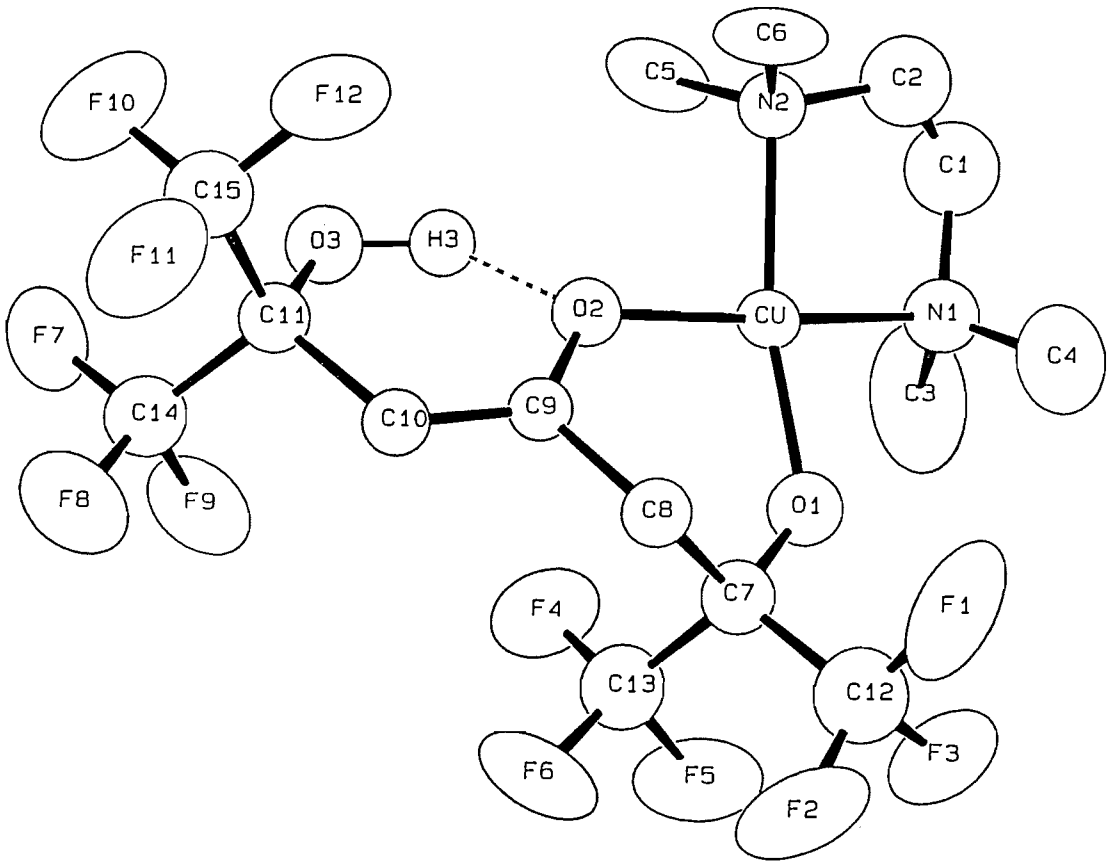

FIG. 2. ORTEP view of compound **6*b***, showing the atom numbering scheme (50% thermal ellipsoids).

Can. J. Chem. Downloaded from www.nrcresearchpress.com by 213.200.69.106 on 09/08/12
For personal use only.

1. P.J. McCarthy, R.J. Kovey, K. Ueno, and A.E. Martell. J. Am. Chem. Soc. **77**, 5820 (1955).
2. S.Z. Haider, M.S. Khan, A. Hashem, H. Riffel, and H. Hess. Cryst. Struct. Commun. **11**, 1269 (1982).
3. D. Hall, A.D. Rae, and T.N. Waters. J. Chem. Soc. 5897 (1963).
4. G.R. Clark, D. Hall, and T.N. Waters. J. Chem. Soc. (A), 223 (1968).
5. C.J. Willis. Coord. Chem. Rev. **88**, 133 (1988), and references therein.
6. W.S. Cripps and C.J. Willis. Can. J. Chem. **53**, 817 (1975).
7. R.T. Boeré and C.J. Willis. Inorg. Chem. **24**, 1059 (1985).
8. L.A. Simonyan, N.P. Gambaryan, and I.L. Knunyants. Zh. Vses. Khim. Ova. im D.I. Mendeleeva, **11**, 467 (1966); Chem. Abstr. **65**, 18489c (1966).
9. S.J. Loeb, J.W.L. Martin, and C.J. Willis. Can. J. Chem. **56**, 2369 (1978).
10. J.J. Vittal and C.J. Willis. Acta Crystallogr. Sect. C: Cryst. Struct. Commun. **C49**, 310 (1993).
11. CAD4 diffractometer manual. Enraf-Nonius, Delft, The Netherlands. 1988.
12. E.J. Gabe, Y. Le Page, J-P. Charland, and F.C. Lee. J. Appl. Crystallogr. **22**, 384 (1989).
13. International tables for X-ray crystallography. Vol. A. D. Reidel Publishing Co., Boston. 1983.
14. E.R. Howells, D.C. Phillips, and D. Rogers. Acta Crystallogr. **3**, 10 (1950).

Can. J. Chem. Downloaded from www.nrcresearchpress.com by 213.200.69.106 on 09/08/12
For personal use only.

Synthesis and characterization of 2,2-diphenyl-1-(5-acetonyl-2,4,6-trinitro-1,3-cyclohexadienyl)hydrazine, $C_{21}H_{19}N_5O_7$

DONNA L. DRAPER, RICHARD J. BARTON, AND BEVERLY E. ROBERTSON
Department of Chemistry, University of Regina, Regina, Sask., Canada S4S 0A2

AND

BARBARA R. NELSON AND JOHN A. WEIL[1]
Department of Chemistry, University of Saskatchewan, Saskatoon, Sask., Canada S7N 0W0

Received December 22, 1992

DONNA L. DRAPER, RICHARD J. BARTON, BEVERLY E. ROBERTSON, BARBARA R. NELSON, and JOHN A. WEIL. Can. J. Chem. **71**, 1057 (1993).

The reaction of 2,2-diphenyl-1-(2,4,6-trinitrophenyl)hydrazine with the enolate of acetone, followed by acidification, yields the title compound 2,2-diphenyl-1-(5-acetonyl-2,4,6-trinitro-1,3-cyclohexadienyl)hydrazine, $C_{21}H_{19}N_5O_7$. The identity of the latter was confirmed by a combination of mass spectrometry, FTIR, elemental analysis, and ^{1}H NMR. Crystals were grown from dichloromethane – 95% ethanol and the structure was determined by X-ray diffraction. Crystals are monoclinic, $P2_1/c$, a = 9.254(3), b = 13.531(3), c = 17.39(5) Å, β = 106.18(2)° at 225 K. R = 0.073, R_w = 0.038 for reflections with $I > 2\sigma(I)$. The Zachariasen extinction factor, g, refined to 18(3) × 10^{-4}. The cyclohexadiene ring is puckered with a primarily *twist-boat* conformation. Atoms C(1) to C(3), C(6), the nitro group on C(2), and the hydrazine moiety (N(8)—N(7)—H(7) attached to C(1)) all lie close to a common plane. The planes of the two phenyl rings, the acetonyl substituent, and the C(6) nitro group are each roughly perpendicular to this plane. The C(5) acetonyl and C(6) nitro groups are *trans* to each other.

DONNA L. DRAPER, RICHARD J. BARTON, BEVERLY E. ROBERTSON, BARBARA R. NELSON et JOHN A. WEIL. Can. J. Chem. **71**, 1057 (1993).

La réaction de la 2,2-diphényl-1-(2,4,6-trinitrophényl)hydrazine avec l'énolate de l'acétone, suivie par une acidification, conduit au composé mentionné dans le titre, la 2,2-diphényl-1-(5-acétonyl-2,4,6-trinitro-1,3-cyclohexadiényl)hydrazine, $C_{21}H_{19}N_5O_7$. L'identité de ce dernier a été confirmée par une combinaison de spectrométrie de masse, d'IR par TF, d'analyse élémentaire et de RMN du ^{1}H. On a obtenu les cristaux à partir d'une solution dichlorométhane – éthanol à 95% et on a déterminé la structure par diffraction des rayons X. Les cristaux sont monocliniques, $P2_1/c$, a = 9,254(3), b = 13,531(3) et c = 17,39(5) Å, β = 106,18(2)°, à 225 K. R = 0,073 et R_w = 0,038 pour les réflexions avec $I > 2\sigma I$. Le facteur d'extinction, g, s'affine à 18(3) × 10^{-4}. Le noyau cyclohexadiéne existe principalement sous une conformation *bateau déformé*. Les atomes C(1) à C(3), C(6), le groupe nitro attaché au C(2) et la portion hydrazine (N(8)—N(7)—H(7) attachée au C(1)) se retrouvent tous dans un plan commun. Les plans des deux noyaux phényles, du substituant acétonyle et du groupe nitro en C(6) sont chacun approximativement perpendiculaires à ce plan. Les groupes acétonyle en C(5) et nitro en C(6) sont *trans* l'un par rapport à l'autre.

[Traduit par la rédaction]

Introduction

It has long been known (1) that 2,4,6-trinitrobenzene (TNB) and its 1-X-substituted derivatives (1-X-TNB) react with the enolate carbanions of ketones, aldehydes, keto esters, and amides to form stable covalently bonded σ adducts. In the literature these adducts are often referred to as σ complexes or Meisenheimer complexes. A typical TNB–carbonyl σ adduct is represented by **1**.

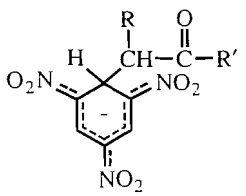

1

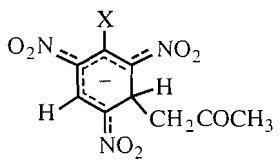

2

The presence of strong electron-withdrawing groups (NO_2) reduces the electron density of the aromatic ring. This not only facilitates the approach of the carbanion, but also stabilizes the negative charge of the σ adduct by conjugative withdrawal of the electron density into the nitro groups.

The formation of the σ adduct is characterized by the two-step process in which the enolate is generated in a pre-equilibrium step (eq. [1]) by reaction of an α-hydrogen-containing carbonyl compound with a base B^- prior to the rate-determining addition of the enolate to the TNB ring (eq. [2]). While enolates are potentially bidentate (addition to C or to O), in all the systems studied only carbon-bonded adducts were observed.

In the case of 1-X-TNBs there are two potential addition sites: C(1) to form the 1,1 adduct (*ipso*) and C(3) (or C(5)) to form the 1,3 adduct. Enolate attack at C(3) is the kinetically favored reaction because these carbons are less sterically hindered than C(1) with its X substituent. It is the 1,3 adduct that is formed when enolates are reacted with 1-X-TNBs.

In the synthesis of 2,2-diphenyl-1-(5-acetonyl-2,4,6-trinitro-1,3-cyclohexadienyl)hydrazine (**A**), the title compound, the 1-X-TNB species 2,2-diphenyl-1-(2,4,6-trinitrophenyl)-hydrazine (**D**) was reacted with the acetone enolate. Similar reactions of other 1-X-TNBs with the acetone enolate are described in the literature. These include X = OPh, Cl, OCH_3, SO_3Na, CH_3, COOH, SCH_3, and $COOCH_3$ (2–4). In all these reactions the product is the 1,3 adduct **2**.

[1]Author to whom correspondence may be addressed.

Can. J. Chem. Downloaded from www.nrcresearchpress.com by 213.200.69.106 on 09/08/12
For personal use only.

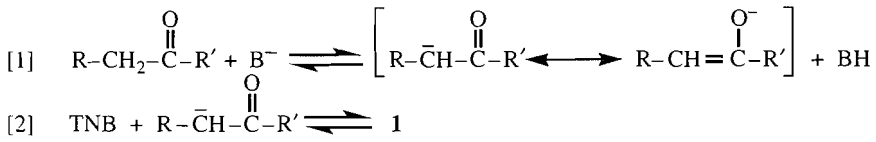

[2] TNB + R–$\bar{C}$H–C(=O)–R′ ⇌ **1**

However, the product from the reaction of **D** with the acetone enolate is not the 1,3 adduct (i.e., which is not observed to exist as a stable species) but rather $\mathbf{A}^-$ (eq. [5]), the product of conjugate addition (Michael reaction) (5). Equations [3–7] give the proposed reaction paths for the formation of **A** from **D** and are divided into three separate steps: (*a*) formation of the acetone enolate, (*b*) formation of the conjugate base of **A**, and (*c*) protonation of the conjugate base of **A**. The enolate is formed in step *a* by adding a non-nucleophilic base (e.g., K_2CO_3, triethylamine, *N*,*N*-dimethyl-4-aminopyridine, or lithium diisopropylamide (LDA)) to acetone (eq. [3]). The amount of enolate formed in this step depends on the pK_a of the base: <1% using K_2CO_3 with a pK_a = 10.3, and ~100% using LDA with pK_a = 37.

Because **D** contains an acidic proton, there are two electrophilic species in solution that potentially can react with the enolate to give $\mathbf{A}^-$. These are **D** and its conjugate base $\mathbf{D}^-$. (The potassium salt $K^+\mathbf{D}^-$ has been characterized (6).) A reaction path for each of these species is given in step *b*. If the enolate attacks $\mathbf{D}^-$, the formation of $\mathbf{A}^-$ would most likely proceed via Path I (eq. [4] and [5]). If the enolate attacks **D**, Path II (eq. [6]) would probably be followed. In step *c*, $\mathbf{A}^-$ is protonated using acetic acid or HCl to form **A**, the title compound. Further studies of this reaction are in progress.[2]

The present paper gives the X-ray crystallographic structure of **A** along with supporting spectroscopic data from proton nuclear magnetic resonance, infrared, and mass spectroscopy, and elemental analysis.

(a) Formation of the acetone enolate

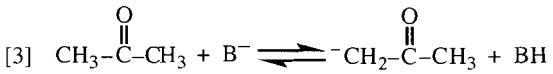

[3] $CH_3–C(=O)–CH_3 + B^- \rightleftharpoons {}^-CH_2–C(=O)–CH_3 + BH$

(b) Formation of the conjugate base of **A**

Path I

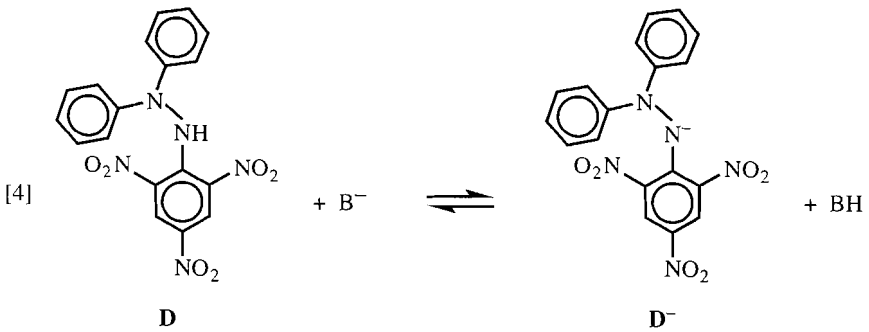

[4] **D** + B^- ⇌ $\mathbf{D}^-$ + BH

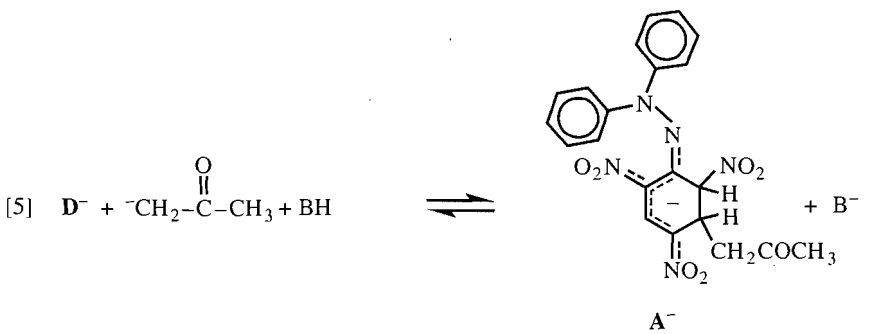

[5] $\mathbf{D}^-$ + ${}^-CH_2–C(=O)–CH_3$ + BH ⇌ $\mathbf{A}^-$ + B^-

Path II

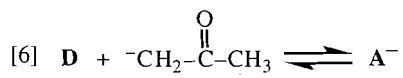

[6] **D** + ${}^-CH_2–C(=O)–CH_3$ ⇌ $\mathbf{A}^-$

[2] B.R. Nelson, J.A. Weil, and P.J. Smith. To be published.

Can. J. Chem. Downloaded from www.nrcresearchpress.com by 213.200.69.106 on 09/08/12
For personal use only.

(c) Protonation of the conjugate base of A

[7] $\mathbf{A}^- + H^+ \rightleftharpoons$

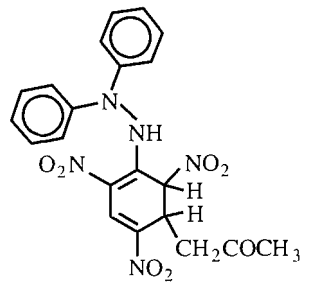

A

TABLE 1. ^{1}H NMR data for the salt K^+ $\mathbf{A}^-$ in acetone-d_6 at 294 K

Proton[a]	Chemical shift (ppm)	Protons	*J* (Hz)
H(3)	8.22	—	
H(5)	4.56	H(5)–H(6)	2.0
		H(5)–H(512)	3.0
		H(5)–H(511)	10.7
H(6)	5.27	H(6)–H(5)	2.0
H(512)	2.93	H(512)–H(5)	3.0
		H(512)–H(511)	18.0
H(511)	2.51	H(511)–H(5)	10.7
		H(511)–H(512)	18.0
H(53*i*)[b]	2.22	—	—

[a]See Fig. 1 for labels.
[b]*i* = 1,2,3.
Probable errors are: chemical shift, ±0.02 ppm; *J*, ±0.2 Hz.

TABLE 2. ^{1}H NMR data for **A** in chloroform-*d* at 294 K

Proton[a]	Chemical shift (ppm)	Protons	*J* (Hz)
H(3)	8.36	—	—
H(5)	4.58	H(5)–H(6)	1.9
		H(5)–H(512)	2.9
		H(5)–H(511)	10.7
H(6)	6.40	H(6)–H(5)	1.9
H(512)	2.77	H(512)–H(5)	2.9
		H(512)–H(511)	18.8
H(511)	2.34	H(511)–H(5)	10.7
		H(511)–H(512)	18.8
H(53*i*)[b]	1.86	—	—
H(7)	11.73	—	—

[a]See Fig. 1 for labels.
[b]*i* = 1,2,3.
Probable errors are: chemical shift, ±0.02 ppm; *J*, ±0.2 Hz.

Experimental

Crystal data

$C_{21}H_{19}N_5O_7$ Molar mass = 453.41 g mol^{-1}
Monoclinic, $P2_1/c$, a = 9.254(3), b = 13.531(3), c = 17.391(5) Å, β = 106.18(2)°, T = 225 K, V = 2091(1) Å^3, Z = 4, D_x = 1.413 g cm^{-3}, μ(MoKα) = 1.41 cm^{-1}, F_{000} = 944, λ(MoKα$_1$) = 0.70926 Å.

A was prepared by reacting 1.0 g (0.0025 mol) of **D**, 1.10 g (0.015 mol) of finely ground anhydrous potassium carbonate, and 15 mL of glass-distilled reagent-grade acetone (dried over molecular sieves) at reflux temperature for 48 h. The mixture was then filtered to remove any unreacted potassium carbonate, and the filtrate evaporated to dryness at 40°C on a rotary evaporator. The crude residue was washed with four 30-mL portions of distilled water. After each washing the dark red-brown solution was decanted into a filter and allowed to drip into a stirred solution of 30 mL of glacial acetic acid and 15 mL of 30% hydrogen peroxide. **A** precipitated as a dark orange solid. The solid was filtered and washed 4 times with a minimum of 95% ethanol, and crystallized from dichloromethane – 95% ethanol to yield 0.27 g (20%) of pure product, mp, 150–153°C (dec.).

TABLE 3. Atom coordinates and equivalent isotropic temperature factors (× 10^2) (Å^2) for the non-hydrogen atoms; with esd values in parentheses

Atom	*x*	*y*	*z*	U_{eq}[a]
C(1)	0.4415(2)	0.3117(1)	0.1245(1)	2.4
C(2)	0.3151(2)	0.2924(1)	0.0620(1)	2.7
C(3)	0.2248(2)	0.3721(1)	0.0181(1)	2.8
C(4)	0.2353(2)	0.4620(1)	0.0498(1)	2.7
C(5)	0.3283(2)	0.4811(1)	0.1338(1)	2.6
C(6)	0.4695(2)	0.4182(1)	0.1502(1)	2.5
C(11)	0.6482(2)	0.2931(1)	0.3010(1)	3.2
C(12)	0.5324(2)	0.2495(2)	0.3240(1)	4.0
C(13)	0.5116(3)	0.2738(2)	0.3976(1)	5.3
C(14)	0.6021(3)	0.3418(2)	0.4461(2)	5.9
C(15)	0.7171(3)	0.3847(2)	0.4234(1)	5.9
C(16)	0.7413(3)	0.3616(2)	0.3499(1)	4.5
C(21)	0.8080(2)	0.2394(1)	0.2145(1)	3.0
C(22)	0.8356(2)	0.2432(2)	0.1399(1)	3.8
C(23)	0.9695(2)	0.2094(2)	0.1305(1)	4.6
C(24)	1.0783(2)	0.1712(2)	0.1943(1)	4.8
C(25)	1.0517(2)	0.1680(2)	0.2681(2)	4.9
C(26)	0.9192(2)	0.2016(2)	0.2795(1)	4.0
C(51)	0.2391(2)	0.4555(2)	0.1937(1)	3.1
C(52)	0.3054(2)	0.4941(1)	0.2764(1)	3.4
C(53)	0.2281(3)	0.4685(2)	0.3379(1)	5.2
N(2)	0.2768(2)	0.1951(1)	0.0325(1)	3.2
N(4)	0.1529(2)	0.5426(1)	0.0046(1)	3.0
N(6)	0.5750(2)	0.4622(1)	0.1058(1)	3.3
N(7)	0.5418(2)	0.2453(1)	0.1638(1)	2.8
N(8)	0.6703(2)	0.2761(1)	0.2234(1)	3.0
O(21)	0.3576(2)	0.1260(1)	0.0652(1)	4.8
O(22)	0.1641(2)	0.1835(1)	−0.0243(1)	4.9
O(41)	0.1549(2)	0.6224(1)	0.0388(1)	4.2
O(42)	0.0842(1)	0.5289(1)	−0.0661(1)	4.0
O(52)	0.4177(2)	0.5463(1)	0.2916(1)	4.6
O(61)	0.6327(2)	0.5408(1)	0.1304(1)	5.6
O(62)	0.5921(1)	0.4187(1)	0.0484(1)	4.0

[a]$U_{eq} = \frac{1}{3}\Sigma_i\Sigma_j U_{ij} a_i^* a_j^* \mathbf{a}_i \cdot \mathbf{a}_j$.

Proton nuclear magnetic resonance spectra of **A** at 294 K were run on a Bruker AM300 spectrometer with TMS as the internal standard. Tables 1 and 2 give the chemical shifts and coupling constants for the salt $K^+\mathbf{A}^-$ and for **A** respectively.

A high-resolution positive-ion fast atom bombardment (FAB) mass spectrum of **A** was run on a VG Analytical 70-250 SEQ hybrid mass spectrometer. The largest mass-to-charge ratio found was 454.1370. This corresponds to the ratio for the protonated **A** cation with a molar mass M + 1, calculated to be 454.1363.

The Fourier-transform infrared spectrum of **A** showed carbonyl stretching at 1711 cm^{-1} and aliphatic C—H stretching at 2900–3000 cm^{-1}, confirming the presence of the acetonyl group.

Elemental analysis of carbon, hydrogen, and nitrogen gave C 55.79%, H 4.24%, N 15.15%, and O 24.82% (by difference). The calculated values are C 55.61%, H 4.23%, N 15.45%, and O 24.71%.

A crystal with dimensions 0.56 × 0.40 × 0.18 mm was selected for X-ray study.

Can. J. Chem. Downloaded from www.nrcresearchpress.com by 213.200.69.106 on 09/08/12
For personal use only.

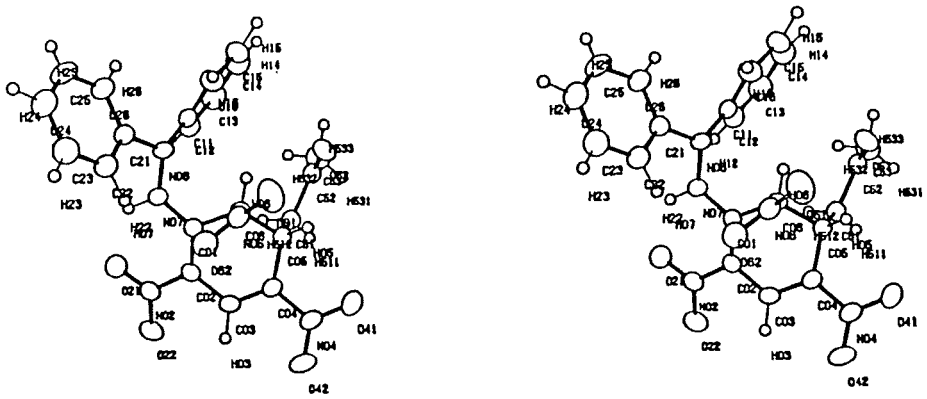

FIG. 1. Stereoscopic view of the **A** molecule.

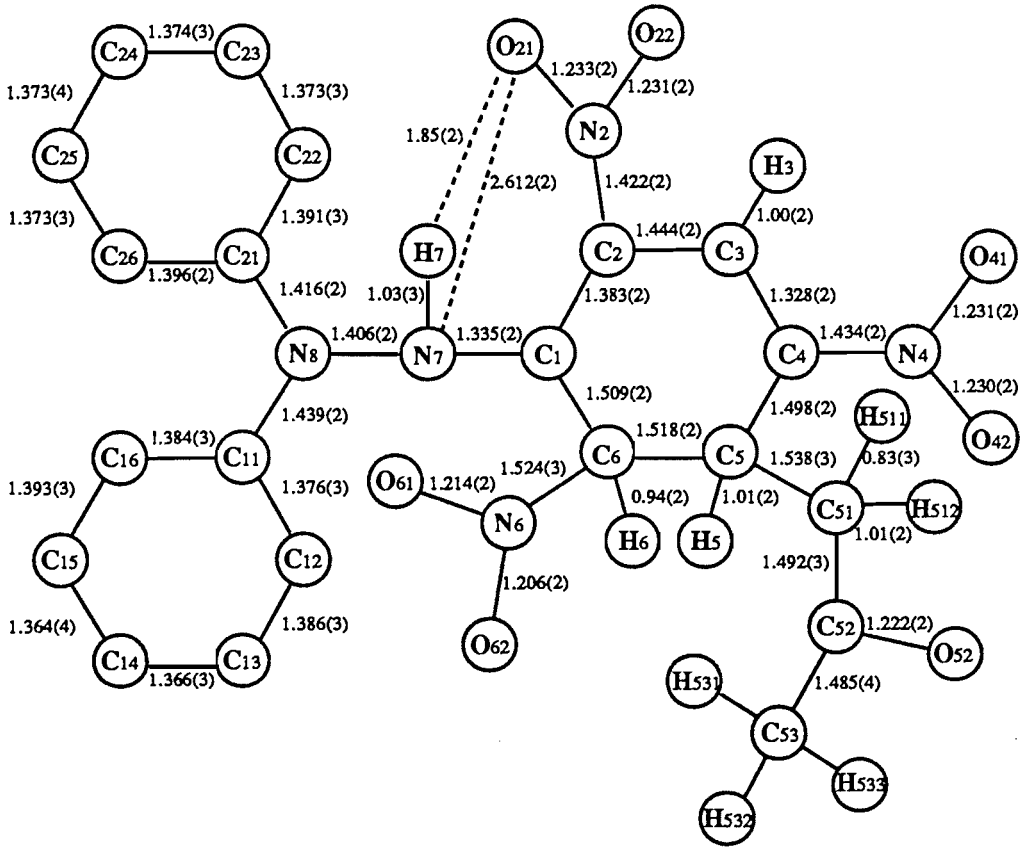

FIG. 2. Atom labels and bond lengths with esd values for **A**.

The space group was determined to be $P2_1/c$ from precession photographs. The lattice constants were determined by a least-squares fit to the positions of 28 reflections in the range $22° \leq 2\theta \leq 49°$. Intensity data for 3684 reflections were collected on a modified Picker four-circle diffractometer with graphite-monochromated radiation in the range $3 \leq 2\theta \leq 50°$, using MoKα radiation and the θ–2θ scan mode. Three reference reflections were measured after each group of 47 reflections. Their intensities did not change significantly. The 3035 reflections with $I/\sigma(I) \geq 2.0$, where $\sigma(I)$ is based on the machine-instability factor and counting statistics, were used in the refinement.

The intensities were corrected for Lorentz and polarization effects, but no corrections were made for absorption or anomalous dispersion. The structure was solved by direct methods and refined by least squares using the XTAL crystallographic system of programs (7). Weights were calculated as $\sigma^{-2}(F)$, where $\sigma(F)$ and $|F|$ are calculated from $\sigma(I)$ and I using Baysian statistics. Refinement at this stage, with anisotropic temperature factors applied to the non-hydrogen atoms and isotropic temperature factors applied to the hydrogen atoms, led to unacceptably high values of wR. (0.18). An isotropic extinction parameter was then refined according to the method of Zachariasen (8) and wR was reduced to 0.045 and the extinction parameter g refined to $41(7) \times 10^{-4}$. The weighting scheme was then modified to remove dependence of the average value of $w\Delta^2$ ($\Delta = |F_o| - |F_c|$) on $|F_o|$ and $\sin\theta/\lambda$ (9). The value of g was reduced to $18(3) \times 10^{-4}$ by further refinement, and R_w was reduced to 0.038.

The final value of the unweighted R factor was 0.073. The average and maximum shift/error ratio were 2×10^{-3} and 5×10^{-2}, respectively. The residual electron densities in the final difference maps were bounded by 0.53 and -0.68 e Å^{-3}.

The extinction coefficient $18(3) \times 10^{-4}$ is unusually large for an

Can. J. Chem. Downloaded from www.nrcresearchpress.com by 213.200.69.106 on 09/08/12
For personal use only.

Can. J. Chem. Downloaded from www.nrcresearchpress.com by 213.200.69.106 on 09/08/12
For personal use only.

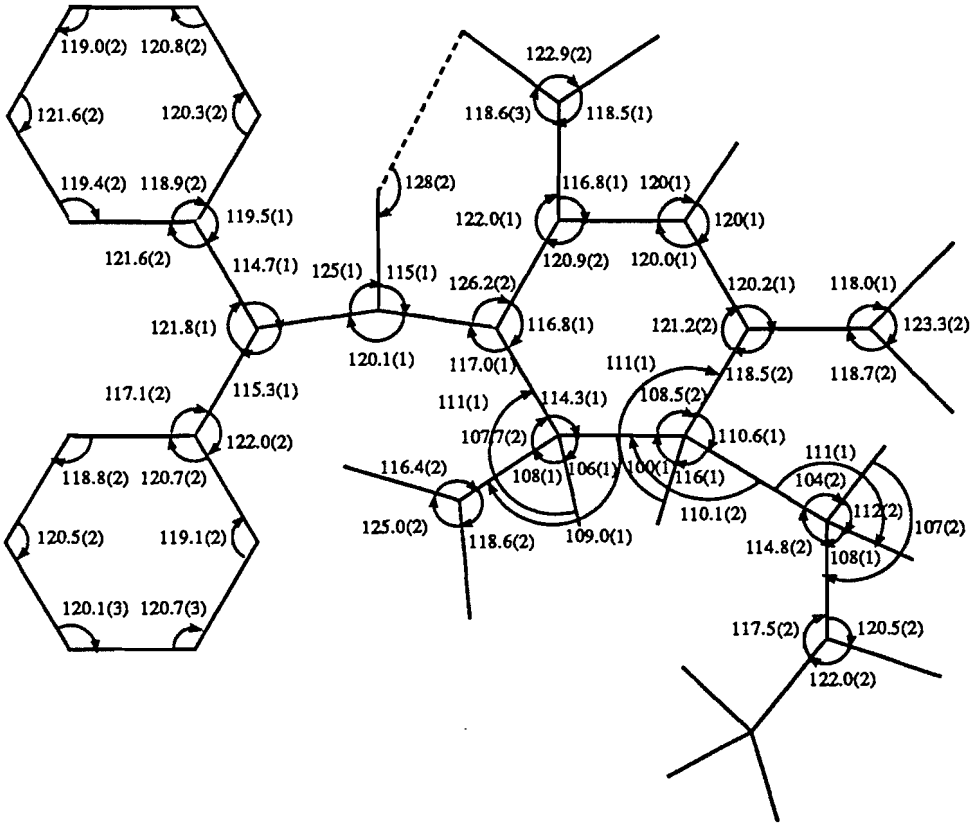

FIG. 3. Bond angles with esd values for **A**.

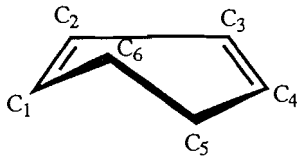

FIG. 4. Puckering of the cyclohexadiene ring.

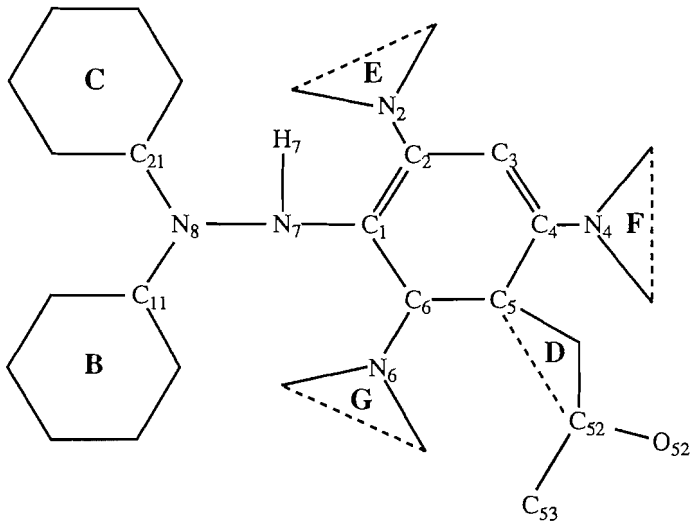

FIG. 5. Designation of the molecular planes of **A**.

organic crystal. Furthermore, its value is strongly dependent on the least-squares weighting scheme. Weight modification has the effect of decreasing the influence on least-squares refinement of reflections affected by larger random or systematic error relative to those less affected. These results imply that the true variance of the strong reflections was more severely underestimated by the unmodified weights than were the variances of the weaker reflections, and (or) that the model for the effects of secondary extinction is not adequate and systematic error associated with secondary extinction remains after corrections based on the Zachariasen model had been applied.

Results and discussion

The atom coordinates[3] and equivalent isotropic temperature factors for the non-hydrogen atoms are listed in Table 3 and a stereoscopic view of the **A** molecule is given in Fig. 1. The atom-numbering scheme and bond lengths are shown in Fig. 2, and the bond angles in Fig. 3.

The puckering of the cyclohexadiene ring was analyzed

[3]Lists of structure factor amplitudes, anisotropic thermal parameters, hydrogen atom parameters, bond lengths to hydrogen atoms, and least-squares planes may be purchased from: The Depository of Unpublished Data, Document Delivery, CISTI, National Research Council Canada, Ottawa, Canada, KIA 0S2.

Tables of hydrogen atom parameters and bond lengths to hydrogen atoms have also been deposited with the Cambridge Crystallographic Data Centre and can be obtained on request from The Director, Cambridge Crystallographic Data Centre, University Chemical Laboratory, 12 Union Road, Cambridge, CB2 1EZ, U.K.

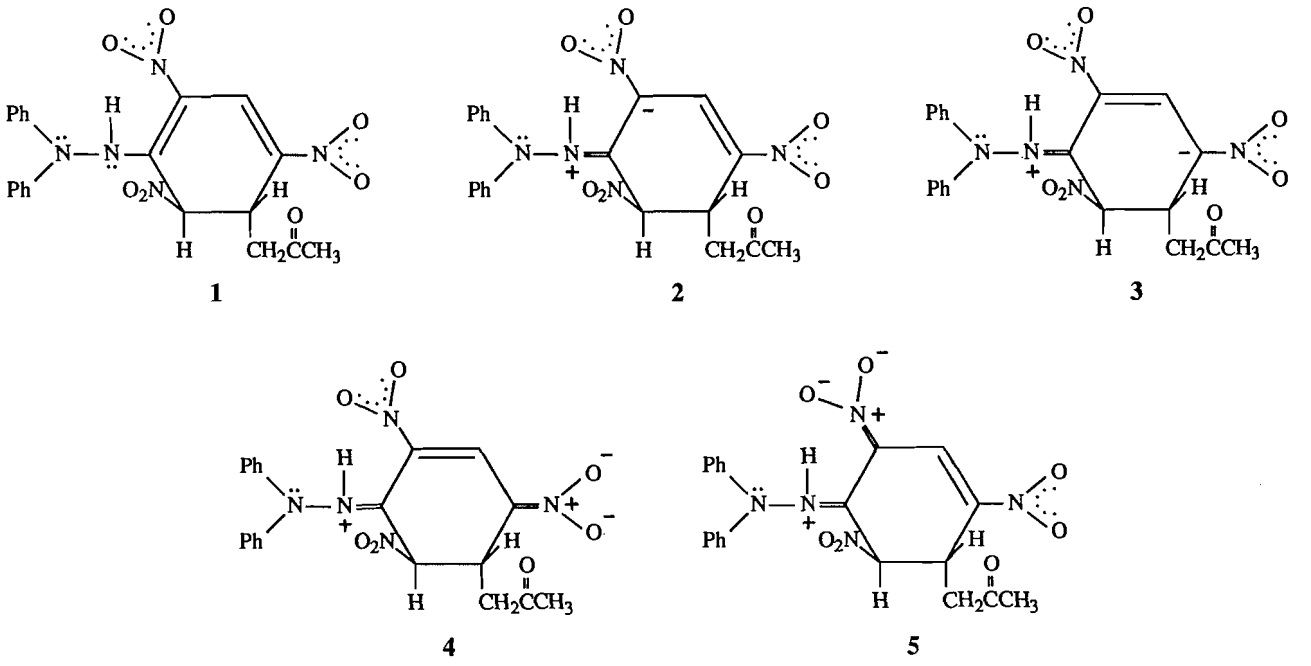

FIG. 6. Important canonical structures of the cyclohexadienyl ring thought to contribute to the ground state of **A**.

TABLE 4. Dihedral angles (deg) between planes

Planes	Angle
AB	91.44(6)
AC	102.86(6)
AD	83.49(10)
AE	1.28(12)
AF	26.00(8)
AG	87.07(19)
BD	12.75(14)
BC	66.29(8)

TABLE 5. Selected torsional angles (deg)

Atoms	Angle
C(6)—C(1)—C(2)—C(3)	6.8
C(1)—C(2)—C(3)—C(4)	−19.0
C(2)—C(3)—C(4)—C(5)	−5.9
C(3)—C(4)—C(5)—C(6)	37.9
C(4)—C(5)—C(6)—C(1)	−47.3
C(5)—C(6)—C(1)—C(2)	27.6
C(2)—C(1)—N(7)—N(8)	−3.7(2)
C(1)—N(7)—N(8)—C(11)	82.5(2)
C(1)—N(7)—N(8)—C(21)	51.5(2)
C(4)—C(5)—C(51)—C(52)	14.2(2)

by the method of Cremer and Pople (10). The puckering amplitude Q is 0.437. The pseudo-rotation angles are φ = 259.4° and θ = 67.9°, defined with respect to C(1). These parameters imply significant puckering with a conformation which is primarily *twist-boat*, as shown in Fig. 4.

Figure 5 indicates the definitions of various planes of molecular groups. Selected dihedral and torsional angles are listed in Tables 4 and 5.

In Fig. 5, atoms C(1) to C(3), C(6), the nitro group on C(2), and the hydrazine moiety N(8)—N(7)—H(7) lie close to the common plane A fitted to their positions by least squares. The two planes, B and C, fitted to the two phenyl rings, and the planes D and G, fitted to the acetone substituent and the C(6) nitro group, respectively, are all roughly perpendicular to plane A. Intramolecular hydrogen bonding[4] between H(7) and O(21) forces the C(2) nitro group to be coplanar with C(1) to C(3). This allows the N(2) p orbital containing the nonbonding electron pair to be parallel to (and overlapping) the p orbitals of C(1) and C(2), enabling the lone pair to participate in the π-electron system. That such participation occurs is indicated by the shortened length of the C(2)—N(2) bond: 1.422(2) Å in **A** versus 1.475(10) Å in nitromethane (11). Similar shortening is observed in the **D** molecule (12).

The C(5) acetonyl and the C(6) nitro groups are *trans* to each other and their conformation is axial with respect to the ring, allowing maximum separation and thus minimum steric interference with each other. The C(6) nitro group is also oriented so that its plane, G, is approximately parallel with plane B of the C(11) phenyl group. Thus steric interactions between these two groups are minimized. The acetonyl group projects outward from the ring, with plane D perpendicular to plane A. This conformation minimizes any interactions with the cylochexadiene ring system.

To minimize steric interactions between the two phenyl substituents, planes B and C are oriented 66° with respect to each other. This angle is 20° larger than that in D (12) and is assumed to be caused by the twisting of the C(11)–C(16) phenyl ring (plane B) to minimize steric interactions with the axial nitro group (plane G).

Various important canonical structures contributing to the

[4]The infrared spectrum of **A** shows N—H to be hydrogen bonded.

Can. J. Chem. Downloaded from www.nrcresearchpress.com by 213.200.69.106 on 09/08/12
For personal use only.

spatially averaged geometric configuration of the trinitrocyclohexadiene ring are shown in Fig. 6. The 0.055(3) Å shortening of C(3)—C(4) compared to C(1)—C(2) is contributed by some combination of structures **2** and **5**. The length of C(3)—C(4), 1.328(2) Å, is consistent with the double bond in cyclohexa-1,3-diene (1.332 Å) (13). C(2)—C(3) is slightly shorter than the typical Csp^2—Csp^2 single bond (1.455 Å) in conjugated aliphatic systems (13) with this shortening contributed by structures **3** and **4**. Due to interactions of the nitrogen lone-pair electrons with the π system of the cyclohexadiene ring, the C(2)—N(2) and C(4)—N(4) bonds are considerably shorter than the C—N bond (1.475 Å) in nitromethane (11). Structures **4** and **5** contribute to this shortening. C(6)—N(6), however, is much longer than the nitromethane C—N bond and is very close to that (1.533 Å) observed in compounds with a nitro group on a tertiary carbon (13).

Due to the intramolecular hydrogen bond and the resulting coplanarity of the σ-bond system of the N(7) atoms with that portion of the trinitro ring system in plane A, the N(7) *p* orbital containing lone-pair electrons is parallel to (and overlapping) the C(1)—C(2) π system, allowing participation of the lone-pair electrons. This results in a shortening of the C(1)—N(7) bond to a length similar to that of the C(3)—N(2) bond (1.329 Å) found in pyrazole (13). Canonical structures **2**–**5** illustrate this participation. The C(1)—N(7) bond in **D** is similarly shortened but is slightly longer (1.348(7) and 1.355(6) Å) than in **A**.

Like the N(7) atom, N(8) is also sp^2 hybridized (with some sp^3 character), which allows it to remain in plane A. This minimizes the steric interactions between the two phenyl groups at one end of the hydrazine linkage and the cyclohexadiene ring at the other. The N—N bond is similar in length to that of **D** (1.381(5) and 1.400(5) Å).

The C—O (1.222(2) Å) and the Csp^3—Csp^2 (1.485(4) Å) bonds in the acetonyl group are slightly shorter than those found in aliphatic linear unsubstituted ketones (13).

Acknowledgements

The authors thank the Natural Sciences and Engineering Research Council of Canada for operating grants to J.A.W., and the University of Regina for computer time.

1. E. Buncel, M.R. Crampton, M.J. Strauss, and F. Terrier. *In* Electron deficient aromatic- and heteroaromatic-base interactions. Elsevier, Amsterdam, The Netherlands. 1984.
2. M. Kimura. Pharm. Bull. **3**, 75 (1955).
3. M. Kimura, N. Obi, and M. Kawazoi. Chem. Pharm. Bull. **20**, 452 (1972).
4. A. Ya. Kaminskii, S.S. Gitis, Yu. D. Grudtsyn, L.I. Khabarova, E.G. Kaminskaya, and V. Sh. Golubchik. Zh. Org. Khim. **10**, 1205 (1974).
5. F.A. Carey and R.J. Sundberg. Advanced organic chemistry. Part B. Plenum, New York. 1990.
6. R. Gopal, B.E. Robertson, and J.A. Weil. Can. J. Chem. **61**, 2735 (1983).
7. J.M. Stewart and S.R. Hall. The XTAL system of crystallographic programs: user's manual. 2nd ed. TR 1364.1. Computer Science Center, University of Maryland, College Park, Md. 1985.
8. W.H. Zachariasen. Acta Crystallogr. **23**, 558 (1967).
9. H. Wang and B.E. Robertson. Structure and statistics in crystallography. *Edited by* A.J.C. Wilson. Adenine, Guilderland, N.Y. 1985. pp. 125–136.
10. D. Cremer and J.A. Pople. J. Am. Chem. Soc. **97**, 1354 (1975).
11. International tables for X-ray crystallography. Vol. 3. Kynoch, Birmingham, U.K. 1968.
12. H. Wang, R.J. Barton, B.E. Robertson, and J.A. Weil. J. Inclusion Phenom. Mol. Recognit. Chem. **10**, 203 (1991).
13. F.H. Allen, O. Kennard, D.G. Watson, L. Brammer, A.G. Orpen, and R. Taylor, J. Chem. Soc. Perkin Trans. 2, S1 (1987).

Can. J. Chem. Downloaded from www.nrcresearchpress.com by 213.200.69.106 on 09/08/12
For personal use only.

A comprehensive thermodynamic investigation of water–ethanolamine mixtures at 10, 25, and 40°C

MONIQUE PAGÉ
Institut Français du Pétrole, 1 et 4 avenue de Bois Préau, BP 311, 92506 Rueil-Malmaison CEDEX, France

JEAN-YVES HUOT
Centre de technologie Noranda, 240 Hymus, Pointe-Claire (Québec), Canada H9R 1G5

AND

CARMEL JOLICOEUR[1]
Departement de chimie, Université de Sherbrooke, Sherbrooke (Québec), Canada J1K 2R1

Received December 22, 1992

Can. J. Chem. Downloaded from www.nrcresearchpress.com by 213.200.69.106 on 09/08/12
For personal use only.

MONIQUE PAGÉ, JEAN-YVES HUOT, and CARMEL JOLICOEUR. Can. J. Chem. **71**, 1064 (1993).

The density, isobaric specific heat capacity, and isentropic compressibility of water–ethanolamine (W–EA) mixtures have been measured at three temperatures (10, 25, and 40°C) over the entire composition range. The results were used to calculate various thermodynamic excess functions of these mixtures, namely: the excess molar volume (V^E_m), excess molar isentropic and isothermal compressibilities ($\kappa^E_{S,m}$, $\kappa^E_{T,m}$), excess molar isobaric and isochoric heat capacities ($C^E_{p,m}$, $C^E_{V,m}$), and excess molar isobaric expansion $(\partial V^E_m/\partial T)_p$. The corresponding partial molar quantities for ethanolamine in the mixtures were also computed. These excess and partial molar quantities were compared with those observed earlier in the water – ethylene glycol (W–EG) (1) and in the water–2-methoxyethanol (W–ME) (2) mixtures. The similarities and differences in the properties of these systems are interpreted on the basis of the specific molecular features of the cosolvents and the concepts of cooperative fluctuations and hydrogen-bonding connectivity in liquid water and dilute aqueous solutions.

MONIQUE PAGÉ, JEAN-YVES HUOT et CARMEL JOLICOEUR. Can. J. Chem. **71**, 1064 (1993).

On a mesuré la densité, la capacité calorifique spécifique isobare et la compressibilité isentropique des mélanges eau–éthanolamine (W–EA) à trois températures (10, 25 et 40°C) et pour le domaine de composition. On a utilisé les résultats pour calculer les différentes fonctions thermodynamiques d'excès de ces mélanges et, en particulier : le volume molaire d'excès (V^E_m), la compressibilité isothermique et isentropique molaires d'excès ($\kappa^E_{S,m}$,$\kappa^E_{T,m}$), les capacités calorifiques isochore et isobare molaires d'excès ($C^E_{p,m}$,$C^E_{V,m}$) et l'expansion isobare molaire d'excès $(\partial V^E_m/\partial T)_p$. On a également calculé les quantités molaires partielles d'éthanolamine dans ces mélanges. On a comparé les quantités molaires en excès et les quantités molaires partielles avec celles observées antérieurement dans des mélanges d'eau–éthylèneglycol (W–EG) (1) et d'eau–méthoxy-2-méthanol (W–ME) (2). On interprète les similitudes et les différences dans les propriétés de ces systèmes sur la base des caractéristiques moléculaires spécifiques des cosolvants et des concepts de fluctuations coopératives et de connectivité des liaisons hydrogènes dans l'eau liquide et dans les solutions aqueuses diluées.

[Traduit par la rédaction]

Introduction

As part of an ongoing program in studies of molecular interactions in aqueous–organic mixtures, we are pursuing detailed thermodynamic investigations on selected water–cosolvent systems (1, 2). The cosolvents studied were chosen from among those that, in some of their physicochemical or molecular properties, may be considered as "analogues" of liquid water. Such solvents would be characterized typically by low molecular weights (small sizes), multiple polar groups, and a propensity towards extensive three-dimensional hydrogen bonding; H_2O_2, hydrazine, and ethylene glycol would be choice examples of these cosolvents (3). The solvents investigated in our work were also selected with reference to their industrial applications and their overall interest as mixed aqueous–organic solvent systems.

The main theme of this work is the study of excess thermodynamic functions corresponding to first, second, and third derivatives (with respect to P or T) of the Gibbs free energy of the water–cosolvent mixtures. It has now been amply shown (4, 5) that, while the first derivative properties (V, H, S) can reveal some of the peculiarities of aqueous solutions, the singularities of water and dilute aqueous systems are best evidenced in second or higher derivative functions (e.g., κ, α, C_p, $\partial\kappa/\partial T$, . . ., etc.); the latter are directly related to the thermodynamic fluctuations in the system and are highly discriminant towards low-energy interactions and the extent of their cooperativity.

In previous reports (1, 2), we presented thermodynamic data for the water – ethylene glycol (W–EG) and water–methoxyethanol (W–ME) systems. The thermodynamic excess functions in both systems could be qualitatively interpreted in accordance with a scheme proposed earlier by Lumry et al. (5). In the latter, the water–cosolvent composition scale was subdivided into three regions in which the following effects were assigned as predominant: (*i*) $0 < x_2 \leq 0.1$: the cosolvent disrupts the cooperative fluctuation units of liquid water; (*ii*) $0.1 < x_2 \leq 0.3$: the cosolvent eliminates the extensive hydrogen-bonding connectivity between water molecules; (*iii*) $x_2 \geq 0.3$: progressive replacement of water–cosolvent interactions by cosolvent–cosolvent interactions.

In addition, comparing the data for the W–ME and W–EG systems, sharp differences were noted in the composition range $0 < x_2 \leq 0.1$, particularly with second derivative partial molar properties of the cosolvent. Differences in C_p, and C_V due to the greater hydrophobic character of ME relative

[1]Author to whom correspondence may be addressed.

Can. J. Chem. Downloaded from www.nrcresearchpress.com by 213.200.69.106 on 09/08/12
For personal use only.

to EG were found to be parallel to those observed upon decreasing the temperature of water, but this observation did not extend to compressibilities (κ), and thermal expansion coefficients ($(\partial V/\partial T)_p$). This suggests that enthalpy and entropy fluctuations in aqueous solutions are affected similarly by hydrophobic hydration and by lowering the temperature, while fluctuations involving volume changes behave rather differently. In other words, in the water-rich region, there was little correlation between energy and volume fluctuations (as measured by $(\partial V/\partial T)_p$) in W–EG and W–ME mixtures.

In this report, we present detailed thermodynamic data for mixtures of water with ethanolamine (W–EA). This cosolvent was selected according to the criteria mentioned above, i.e., extensive H-bonding and high cohesive energy. It is further interesting since it should allow simple visualization of differences in the hydration of the R-NH_2 and R-OH groups by direct comparison of the properties of the W–EA and W–EG mixtures. Finally, the broad use of EA as a solvent, or as an organic base in many aqueous industrial formulations, should gain from improved knowledge of the thermodynamic properties of water–ethanolamine mixtures.

Experimental

Ethanolamine (H_2N-CH_2-CH_2-OH) was purchased from Fluka (stated purity >99.7 mol%) and was used without further purification. The residual water content was determined by Karl Fisher titration. All solutions were prepared by mass using deionized (Millipore ion exchange, MilliQ system) distilled water.

Solution densities (ρ) and isobaric volumic heat capacities (c_p^v) were measured independently using a flow densimeter and a flow microcalorimeter following methods described in details by Picker et al. (6, 7). The detection limits of the instruments used were respectively $\pm 2 \times 10^{-6}$ g cm^{-3} and $\pm 1 \times 10^{-5}$ J K^{-1} cm^{-3}. The temperature of the instruments was regulated to ± 0.001°C with a SODEV Programmable Circulating Thermostat (8).

The differential C_p measurements on W–EA solutions were carried out relative to water for dilute solutions ($x < 0.4$), and relative to pure ethanolamine for more concentrated solutions. Power losses were accounted for through proper calibration, and care was exercised to insure that mixing effects at the moving boundary between solvent and solution did not introduce significant artifacts. The isobaric specific heat capacities (c_p) were calculated from isobaric volumic heat capacities (c_p^v) and the measured densities as:

$$[1] \quad c_p = c_p^v/\rho$$

The densities and isobaric specific heat capacities are reported in Table 1.

The isentropic compressibility values (κ_S) were obtained from speed-of-sound measurements at atmospheric pressure using a Nusonic instrument (Mapco, model 6105) (9). The working cell (20 cm^3) was thermostated to ± 0.001°C and connected to a 250-cm^3 reservoir; the latter served as a closed transfer and mass-dilution vessel for incremental composition changes. The cell constants were determined through calibration with degassed deionized water in the temperature range 9–42°C using values from Del Grosso and Mader (10). The reproducibility of the speed-of-sound measurements was usually 0.02 m s^{-1}. The experimental results are given in Table 2.

The apparent molar volumes ($V_{2,\phi}$), apparent molar isobaric heat capacities ($C_{p,2,\phi}$), and apparent molar isentropic compressibilities $k_{S,2,\phi}$ were obtained according to the following relations (11):

$$[2] \quad V_{2,\phi} = M/\rho - [1000(\rho - \rho^*)/m\rho\rho^*]$$

$$[3] \quad C_{p,2,\phi} = Mc_p + [1000(c_p - c_p^*)/m]$$

$$[4] \quad k_{S,2,\phi} = \kappa_S V_{2,\phi} + [1000(\kappa_S - \kappa_S^*)/m\rho\rho^*]$$

where m is the molality of the solution, ρ and ρ^*, c_p and c_p^* and κ_S and κ_S^* represent the densities, the isobaric specific heat capacities, and the isentropic compressibilities for the solution and solvent respectively (1).

The molar excess thermodynamic functions (X_m^E) of the mixtures were calculated from

$$[5] \quad X_m^E = X_m - X_m^{id}$$

where X_m is the measured molar property for the solvent mixture, and X_m^{id} is the ideal value of this property; the latter is calculated as (except for the Gibbs energy and the entropy):

$$[6] \quad X_m^{id} = xX_m^*(\text{EA}) + (1 - x)X_m^*(H_2O)$$

where X_m^* denotes the molar properties of the pure components.

The partial molar quantities were calculated from the corresponding apparent molar quantities using the following relation:

$$[7] \quad X_2 = X_{2,\phi} + x(1 - x)\,[\partial X_{2,\phi}/\partial(1 - x)]_{T,p}$$

The values of the partial derivatives were obtained through spline function fitting procedures on the $X_{2,\phi}$ vs. X curve.

To facilitate interpretation and comparison with related systems, a number of other functions (excess or partial molar) were also calculated, namely isochoric heat capacities and isothermal compressibilities. The molar isochoric heat capacity ($C_{\tilde{V},m}^*$) of a pure liquid can be obtained from:

$$[8] \quad C_{\tilde{V},m}^* = C_{p,m}^* - T[\partial V_m^*/\partial T)_p]^2/10k_{T,m}^*$$

where $k_{T,m}^*$ is the molar isothermal compressibility of the liquid. The latter is obtained from the molar isentropic compressibilities ($k_{S,m}^*$) as:

$$[9] \quad k_{T,m}^* = k_{S,m}^* + T(\partial V_m^*/\partial T)_p^2/10C_{p,m}^*$$

Relations similar to eqs. [9] and [10] were applied to the properties of the solvent mixtures to calculate the molar excess functions ($C_{V,m}^E$) and ($k_{T,m}^E$). The corresponding partial molar properties were also computed using the expressions (12):

$$[10] \quad k_{T,2} = k_{S,2} - [TV_m\alpha/\kappa_T][2(\partial V_m/\partial T)_p - (V_m\alpha C_{p,2}/C_{p,m})]$$

$$[11] \quad C_{V,2} = C_{p,2} - (T\alpha/\kappa_T)[2(\partial V_2/\partial T)_p - (\alpha k_{T,2}/\kappa_T)]$$

where α is the thermal expansibility coefficient.

Finally, the internal pressure (p_i) and cohesive energy density ($\Delta U_m/V_m$) of the mixtures were also calculated as:

$$[12] \quad p_i = T\alpha/10\kappa_T$$

and

$$[13] \quad \Delta U_m/V_m = (\Delta_{vap}H_m - RT)/V_m$$

For a mixture, the enthalpy of vaporization ($\Delta_{vap}H_m$) is given by

$$[14] \quad \Delta_{vap}H_m = \Sigma_i\, x_i\Delta_{vap}H_{m,i} - \Delta H_m^E$$

Results and discussion

The experimental results for the water–ethanolamine (W–EA) mixtures are collected in Tables 1 and 2, which report the solution properties, ρ, c_p, and κ_S and the derived apparent molar quantities $V_{2,\phi}$, $C_{p,2,\phi}$, $k_{S,2,\phi}$ for ethanolamine. In the following sections, we will illustrate the total molar excess functions X_m^E of these mixtures and the partial molar quantities (X_2) of the ethanolamine cosolvent. In line with the theme of this and previous studies, we will emphasize differences in the composition dependence of the various (T, P) derivatives of the Gibbs excess energy. We will also attempt to underline differences in the trends observed in these derivatives when comparing the data for W–EA, W–

TABLE 1. Densities, apparent molar volumes, isobaric specific heat capacities, and apparent molar heat capacities as a function of the mole fraction of EA in W–EA mixtures at 10, 25, and 40°C

x_{EA}	ρ (g cm^{-3})	$V_{2,\Phi}$ (cm^3 mol^{-1})	c_p (J K^{-1} g^{-1})	$C_{p,2,\Phi}$ (J K^{-1} mol^{-1})
		10°C		
0	0.99970	—	4.1922	—
0.00242	1.00286	58.61	4.1675	178.4
0.00367	1.00302	58.64	4.1626	180.1
0.00449	1.00316	58.48	4.1593	180.6
0.01255	1.00154	58.39	4.1365	173.7
0.01908	1.00248	58.36	4.1079	172.8
0.06878	1.01006	57.97	3.8912	164.3
0.09592	1.01411	57.82	3.7840	161.8
0.13186	1.01878	57.74	—	—
0.14241	1.02032	57.67	—	—
0.19593	1.02655	57.57	3.4643	157.8
0.24599	1.03065	57.61	3.3420	157.2
0.34934	1.03542	57.84	3.1591	158.3
0.47253	1.03633	58.23	3.0303	161.7
0.50112	1.03624	58.32	2.9940	161.4
0.53966	1.03576	58.44	2.9535	161.4
0.58879	1.03483	58.60	2.9349	163.5
0.68657	1.03375	58.75	2.9160	165.0
0.69358	1.03225	58.93	2.8988	166.2
0.78295	1.02963	59.18	2.8768	169.2
0.84269	1.02797	59.33	2.8499	169.6
0.91793	1.02664	59.46	2.8261	170.4
1	1.02632	59.52	2.7562	168.4
		25°C		
0	0.99704	—	4.1796	—
0.00138	0.99989	59.33	—	—
0.00242	1.00002	59.15	—	—
0.00367	1.00011	59.38	4.1533	193.4
0.00449	1.00021	59.26	4.1503	192.3
0.01255	0.99839	59.08	—	—
0.01908	0.99914	59.06	4.1098	186.6
0.06878	1.00524	58.74	3.9385	181.8
0.09592	1.00853	58.61	3.8493	179.1
0.19593	1.01858	58.39	3.5787	174.2
0.28890	1.02399	58.48	3.3667	169.6
0.39459	1.02612	58.74	3.1867	167.6
0.50112	1.02564	59.05	3.1052	170.4
0.50547	1.02541	59.08	—	—
0.51143	1.02530	59.10	—	—
0.53966	1.02478	59.19	—	—
0.58879	1.02371	59.34	3.0479	171.9
0.63657	1.02256	59.48	—	—
0.69358	1.02095	59.64	—	—
0.74584	1.01924	59.80	2.9653	173.7
0.79125	1.01801	59.91	—	—
0.88072	1.01551	60.11	—	—
0.89221	1.01244	60.13	—	—
0.95393	1.01346	60.26	—	—
0.99695	1.01239	60.34	2.8388	172.7
1	1.01239	60.34	2.8332	173.1
		40°C		
0	0.99222	—	4.1786	—
0.00118	0.99501	60.51	—	—
0.00191	0.99507	60.29	4.1585	198.3
0.00317	—	—	4.1546	197.6
0.00396	0.99523	60.10	4.1530	201.8
0.02973	0.99513	59.65	4.0902	197.8
0.07265	0.99943	59.45	3.9699	194.5

Can. J. Chem. Downloaded from www.nrcresearchpress.com by 213.200.69.106 on 09/08/12
For personal use only.

TABLE 1 (*concluded*)

x_{EA}	ρ (g cm^{-3})	$V_{2,\Phi}$ (cm^3 mol^{-1})	c_p (J K^{-1} g^{-1})	$C_{p,2,\Phi}$ (J K^{-1} mol^{-1})
0.09560	1.00167	59.36	3.9075	192.5
0.14919	1.00642	59.23	3.7801	190.0
0.19357	1.00963	59.20	3.6785	187.2
0.24494	1.01238	59.22	3.5755	184.9
0.29264	1.01404	59.29	3.5216	186.5
0.34041	1.01495	59.40	3.4393	184.3
0.34397	1.01498	59.41	3.4461	185.3
0.54217	1.01312	59.98	3.2075	181.2
0.69452	1.00891	60.41	3.1085	181.4
0.78398	1.00580	60.66	3.0470	180.5
0.88999	1.00259	60.88	3.0059	181.0
0.99325	0.99981	61.10	2.9608	180.9
1	—	61.08	2.9552	180.5

ME, and W–EG mixtures, in relation to the molecular features of the cosolvents.

Several thermodynamic quantities measured on neat EA, or EA infinitely diluted in water, are collected in Tables 3 and 4 and compared with available literature data (13–18). The agreement between the data reported here and previous results is satisfactory except for $C^0_{p,2}$ of EA in water. In this case, the discrepancy is greater than the combined experimental uncertainties and may originate in protonation effects; the relative importance of the latter increases at high dilution, and this will affect the infinite extrapolated dilution value (in the present work, the protonation of EA in water was repressed using 0.06 M NaOH, instead of water, for measurements in dilute solutions).

Bulk properties of the W–EA mixtures

The cohesive energy density ($\Delta U_m/V_m$) and the internal pressure ($p_i = -(\partial U_m/\partial V_m)_T$) of the W–EA mixtures (19) are plotted in Fig. 1 as function of the EA mole fraction (x_2); the dotted curves illustrate the corresponding properties in the W–EG system (1). From comparisons of the properties of numerous solvents, it was concluded earlier (19) that p_i reflects mostly molecular interactions other than hydrogen bonding (dispersion, dipolar, and multipolar interactions). Since the cohesive energy density reflects the summation of all types of interaction energies, the difference ($\Delta U_m/V_m - p_i$) should emphasize the hydrogen-bonding contribution to the internal energy of the liquid.

Comparing the data for the W–EA and W–EG mixtures, both the internal pressures and cohesive energy densities (per unit volume) are found strikingly similar in these two systems. From the relative p_i values, the non H-bonding energy contribution in pure EA would be slightly higher (10–20%) than in EG.[3] Hence, from the relative cohesive energy densities, and the reasoning outlined above, the H-bonding contribution should be lower in EA than in EG. On the other hand, comparing the W–EA results with corresponding data for the W–ME system (not shown, ref. 2) reveals marked differences, namely, lower p_i values (in cosolvent-rich compositions) and much lower cohesive energy densities over all mixture compositions. Consequently, from these macroscopic measures of molecular interactions in the W–EA and W–EG systems, one would expect their thermodynamic excess functions to be qualitatively and quantitatively similar, though both sharply contrasting with those of the W–ME mixtures.

Molar excess functions (X^E_m)

The Gibbs excess energy (ΔG^E_m) of the W–EA mixtures at 25°C is shown as a function of composition in Fig. 2. The first temperature derivatives (ΔS^E_m, ΔH^E_m) of ΔG^E_m are also reported in Fig. 2 and the pressure derivative (ΔV^E_m) is shown in Fig. 3. All of the X^E_m vs. x_2 curves are negative and very nearly symmetrical (i.e., minima in all curves at x_2 = 0.4–0.5), more so than in W–EG mixtures. All excess functions are more negative in W–EA mixtures than in W–EG or W–ME mixtures (the latter were, however, highly skewed towards the water-rich compositions (2)). Comparing the data for these three systems further shows that the enthalpy–entropy compensation is less important in the W–EA system than in the other two. Typically, at the minimum on the curves, ($\Delta G^E_m/T\Delta S^E_m$) ≃ 0.5 in W–EA, ≃0.15 in W–EG, and ≃0.4 in W–ME. Considering the preceding comments on the similarity of internal pressures and cohesive energies, the relative magnitudes of the excess functions in W–EA vs. W–EG mixtures are surprising. The large negative ΔG^E_m in W–EA mixtures must be due to exothermic interactions between W and EA molecules. Indeed, the standard hydration enthalpy of an aliphatic -NH_2 group is approximately 3 kJ mol^{-1} more exothermic than that of an -OH group (21). This interpretation is also supported by the observation of less negative ΔG^E_m values in aqueous mixtures of *N*-methyl-2-aminoethanol and *N*,*N*-dimethyl-2-aminoethanol (14).

The V^E_m values of the W–EA mixtures exhibit a composition dependence very similar to the G^E_m values. As noted earlier, the minimum V^E_m is approximately twofold more negative for EA than for EG, and the V^E_m vs. x_2 curve is very nearly symmetrical ($x_{2,min}$ = 0.48). These observations further point to strong W–EA interactions, which must be attributed to the NH_2 . . . water interactions. Overall, from the shapes of the H^E_m (or TS^E_m) and V^E_m curves, it is apparent that the consequences of molecular interactions on the enthalpy (or entropy) and on the packing density (free volume) are better correlated in the W–EA system than in the W–EG (1) or the W–ME (2) systems.

The molar excess isothermal compressibilities ($k^E_{T,m}$) of W–EA mixtures are plotted in Fig. 4 and again compared

[3]Calculated from eqs. [12]–[14] and data from refs. 14 and 20.

Can. J. Chem. Downloaded from www.nrcresearchpress.com by 213.200.69.106 on 09/08/12
For personal use only.

Can. J. Chem. Downloaded from www.nrcresearchpress.com by 213.200.69.106 on 09/08/12
For personal use only.

TABLE 2. Adiabatic compression coefficients and apparent molar adiabatic compressions as a function of the mole fraction of EA in W–EA mixtures at 10, 25, and 40°C

x_{EA}	$10^5\ \kappa_S$ (bar^{-1})[a]	$10^4\ k_{S,2,\Phi}$ ($cm^3\ bar^{-1}\ mol^{-1}$)
	10°C	
0	4.7809	—
0.0025	4.6334	—
0.0057	4.6797	−4.08
0.0121	4.5719	−4.10
0.0170	4.4964	−3.54
0.0211	4.4344	−3.29
0.0505	4.0403	−1.81
0.0840	3.6976	−0.02
0.1202	3.4150	1.62
0.1560	3.2082	3.12
0.2070	3.0088	5.08
0.2840	2.7703	6.84
0.3738	2.7040	9.51
0.5130	2.7230	12.36
0.5748	2.7520	13.40
0.6556	2.7955	14.55
0.7440	2.8484	15.62
0.8293	2.9001	16.49
0.9181	2.9533	17.26
	25°C	
0	4.5247	—
0.0076	4.3970	7.21
0.0225	4.2357	5.87
0.0316	4.1458	5.90
0.0594	3.8943	6.03
0.1256	3.4782	7.69
0.1256	3.4699	7.56
0.3528	3.0050	12.74
0.4423	3.0120	14.37
0.5594	3.0675	16.15
0.6638	3.1327	17.42
0.7440	3.1175	17.79
0.7692	3.2011	18.46
0.7754	3.0258	17.35
0.7943	3.0173	17.39
0.8229	3.0676	17.85
0.8485	3.2516	19.13
0.8618	3.1314	18.42
0.8671	3.0953	18.21
	40°C	
0	4.4239	—
0.0076	4.2546	11.76
0.0225	4.1298	10.17
0.0316	4.0653	10.41
0.0594	3.8748	10.40
0.1256	3.5371	11.12
0.3528	3.1786	15.10
0.4423	3.1976	16.51
0.5594	3.2668	18.10
0.6638	3.3448	19.28
0.7440	3.3405	19.62
0.7692	3.4178	20.23
0.7754	3.2345	19.04
0.7943	3.2151	18.99
0.8229	3.2438	19.29
0.8485	3.4786	20.89
0.8618	3.3367	20.02
0.8671	3.2928	19.76

[a]1 bar = 100 kPa.

with the corresponding values for W–EG mixtures (molar excess isentropic compressibilities $k^E_{S,m}$ lead to very similar curves). The shapes and relative magnitudes of the $k^E_{T,m}$ curves in Fig. 4 are closely related to the V^E_m curves (Fig. 3). Hence, the pressure dependence of the excess volume, $k^E_{T,m}$, which reflects the magnitude of density fluctuations, does not appear to be very sensitive towards specific hydration effects involving EA or EG molecules. It is also interesting to note that $k^E_{T,m}$ values in the W–ME mixtures (not shown) are twice as negative as in the W–EA mixtures; this is likely a consequence of the high molar compressibility of the ME cosolvent.

The molar excess isobaric ($C^E_{p,m}$) and isochoric ($C^E_{V,m}$) heat capacities of W–EA mixtures are illustrated in Fig. 5 with reference to data for the W–EG mixtures. As found earlier for the latter (1), the composition dependence of $C^E_{p,m}$ (EA) exhibits a maximum at $x_2 \approx 0.2$, the amplitude of which is three times lower than that for the W–EG system. For the W–EA system, however, both $C^E_{p,m}$ and $C^E_{V,m}$ vs. x_2 curves exhibit a "W" shape (22). Similar features were observed in several nonaqueous solvent mixtures and were interpreted as partly due to cooperative molecular arrangements induced in the mixtures. Such a composition dependence of $C^E_{p,m}$ contrasts rather sharply with that observed with hydrophobic cosolvents, where a marked positive contribution is found in the water-rich compositions.

Finally, the molar excess isobaric expansions $(\partial V^E_m/\partial T)_p$ for W–EA and W–EG systems are compared in Fig. 6. The variations as a function of x_2 are sharply different in these systems; although $(\partial V^E_m/\partial T)_p$ is positive over the whole mole fraction range for the W–EG system, there is a sign change at $X \approx 0.2$ in W–EA mixtures.

The molar excess functions (X^E_m) examined above provide a useful representation of the non-ideality of mixtures for the various properties considered. However, as noted earlier (1, 5), their interpretation is difficult due to variations in the properties of the neat liquids (with T or P). Partial molar quantities are better suited for comparisons among the properties of different aqueous mixtures, particularly near the ends of the composition scale.

Partial molar thermodynamic properties of EA in W–EA mixtures

The partial molar volume (V_2) of EA in W–EA mixtures is illustrated in Fig. 7 as a function of x_2 at 10, 25, and 40°C. As with EG, V_2(EA) exhibits a sharp decrease and a minimum at low x_2 value. These features are often found in aqueous organic mixtures (23–28), and are especially pronounced for hydrophobic cosolvents (26, 29, 30).

It is most unlikely, however, that the enhanced minima in the V_2 vs. x_2 curve found with the W–EA system, relative to the W–EG mixtures, are due to the greater hydrophobic character of EA. There is no indication of this in the excess properties examined above; moreover, the x_2 value at the minimum V_2 would be expected to be lowest for the more hydrophobic cosolvent (26, 29, 30), in contrast to the situation depicted in Fig. 7.

The second derivative partial molar properties ($k_{T,2}$, $C_{p,2}$, $C_{V,2}$, and $(\partial V_2/\partial T)_p$) are reported in Figs. 8–11 as functions of x_2. As noted before, these properties are directly related to thermodynamic fluctuations (more precisely to changes in the latter induced by incremental changes in composition). There is, however, no simple formalism that allows

TABLE 3. Density, ρ*, specific isobaric heat capacity, c_p^*, and isentropic compressibility coefficient, k_S^*, of ethanolamine at 25°C

ρ* (g cm^3)		c_p^* (J g^{-1} K^{-1})		10^5 k_S^* (bar^{-1})	
This work	Lit.	This work	Lit.	This work	Lit.
1.01239	1.01186[a] 1.01130[b] 1.0127[c]	2.8332	—	4.0865	3.87[a]

[a]Reference 13.
[b]Reference 14.
[c]Reference 15.

TABLE 4. Partial molar volume, V_2°, isobaric heat capacity, $C_{p,2}^\circ$, and isentropic compressibility, $k_{S,2}^\circ$, of ethanolamine at infinite dilution at 25°C

V_2° (cm^3 mol^{-1})		$C_{p,2}^\circ$ (J K^{-1} mol^{-1})		$k_{S,2}^\circ$ (cm^3 bar^{-1} mol^{-1})	
This work	Lit.	This work	Lit.	This work	Lit.
59.78	59.25[a]	193	176[b]	5.7	6.4[c]

[a]Reference 16.
[b]Reference 17.
[c]Reference 18.

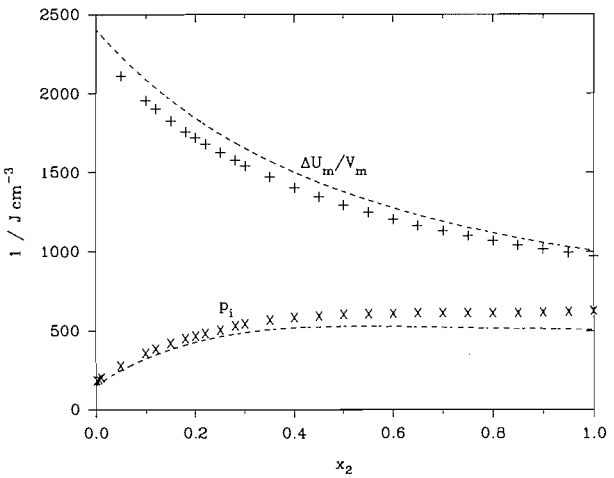

FIG. 1. Cohesive energy densities, $\Delta U_m/V_m$, and internal pressures, p_i, of W–EA (+, X) and W–EG (dotted lines) mixtures at 25°C.

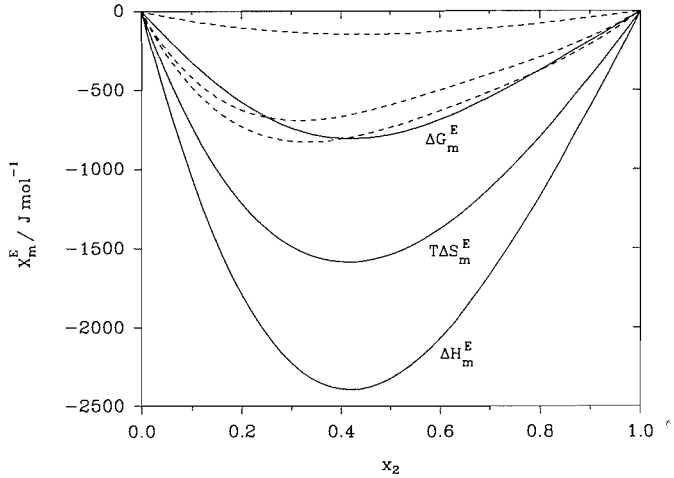

FIG. 2. Molar excess thermodynamic properties, G_m^E, H_m^E, and $T\Delta S_m^E$ for W–EA (full lines) and W–EG (dotted lines) mixtures at 25°C.

the separation of partial molar quantities into contributions originating from the solute or the solvent; hence, the distinction between effects due to water–water, water–cosolvent, and cosolvent–cosolvent interactions can only be inferred by varying the nature of the cosolvent and its concentration.

A cursory examination of the data in Figs. 8–11 reveals a remarkable similarity in the second derivative partial molar properties in these aqueous mixtures, particularly $k_{T,2}$ and $C_{V,2}$; the latter, respectively, reflect the fluctuations in density and internal energy. With the other partial molar quantities ($C_{V,2}$ and $(\partial V_2/\partial T)_p$) some differences are noted, but these can be seen to originate largely in the properties of the pure EA and EG (as suggested in the discussion of molar excess functions).

The variation in $C_{p,2}$ with x_2 at low x_2 values is less pronounced in the W–EA data than in the W–EG data. This tends to confirm that the hydrophobic character of the EA molecule is lower than that of the EG molecule. On the other hand, the higher value of the partial molar expansibility $(\partial V_2/\partial T)_p$ indicates better correlation between energy and volume fluctuations, except in the water-rich compositions ($x < 0.1$), i.e., low values of $(\partial V/\partial T)_p$ are typical of water and dilute aqueous solutions.

From this overview of partial molar quantities in W–EA and W–EG mixtures, two significant features are readily apparent. First, the second derivative properties are not dominated by the important differences in the first derivative properties of the W–EA and W–EG mixtures, i.e., marked differences in the heat of mixing of EA and EG with water, or in the heat of hydration of the -NH_2 and -OH groups, do not overwhelm the composition dependence of

Can. J. Chem. Downloaded from www.nrcresearchpress.com by 213.200.69.106 on 09/08/12
For personal use only.

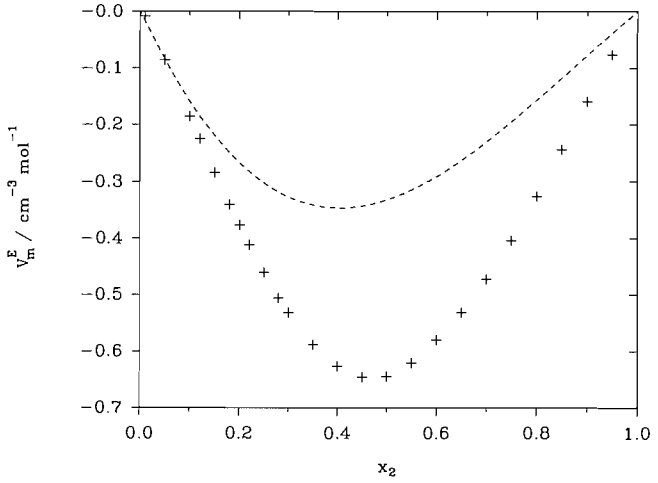

FIG. 3. Molar excess volumes, V_m^E, for W–EA (+) and W–EG (dotted line) mixtures at 25°C.

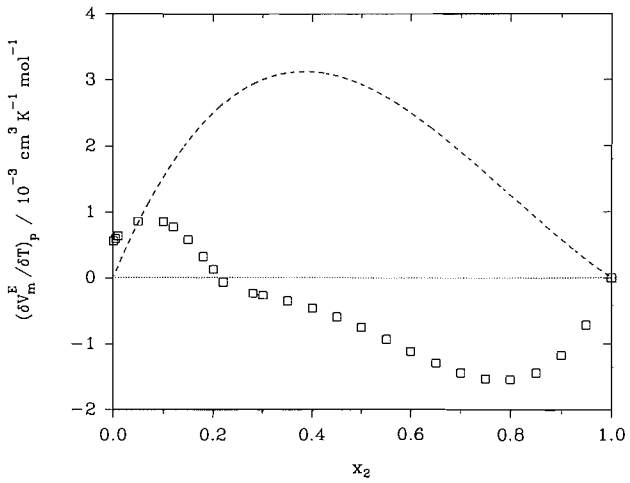

FIG. 6. Molar excess expansion, $(\partial V_m^E/\partial T)_p$, for W–EA (□) and W–EG (dotted line) mixtures at 25°C.

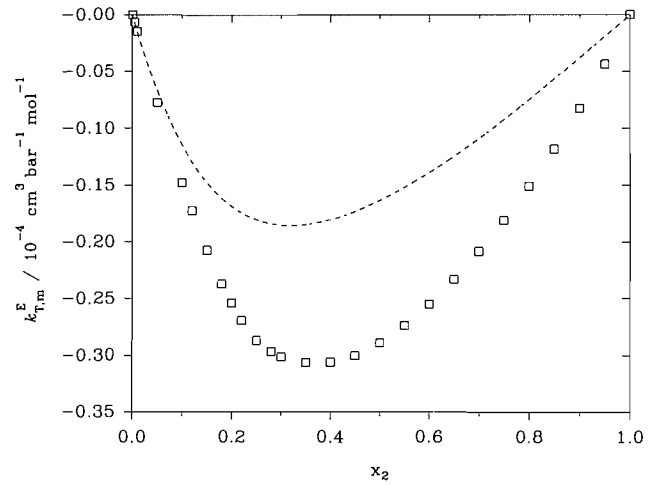

FIG. 4. Molar excess isothermal compressibilities, $k_{T,m}^E$, for W–EA (□) and W–EG (dotted line) mixtures at 25°C.

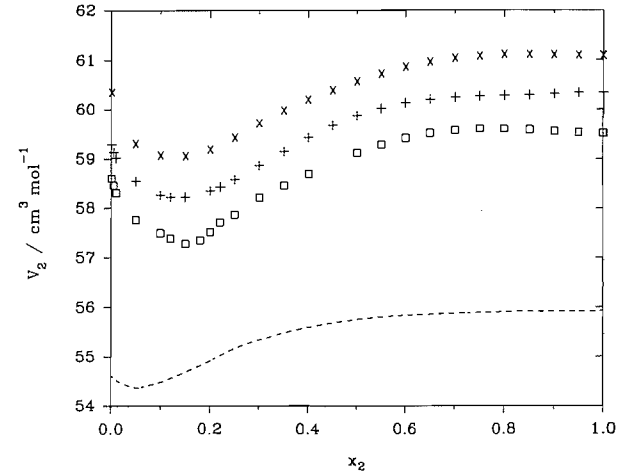

FIG. 7. Partial molar volumes, V_2, of EA in W–EA mixtures at 10°C (□), 25°C (+), and 40°C (X); dotted line: V_2 of EG in W–EG mixtures at 25°C.

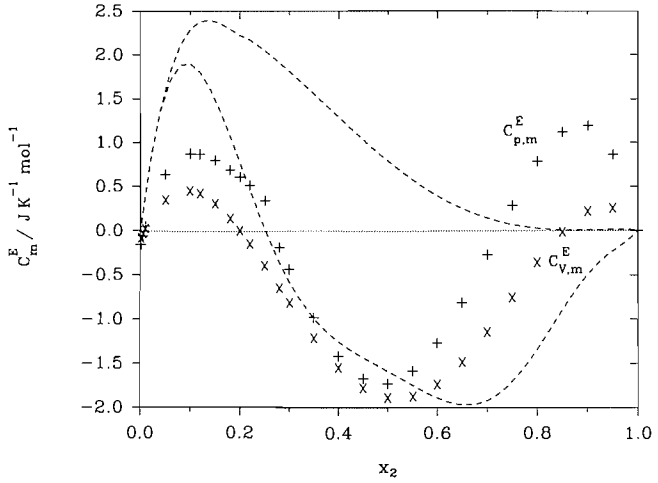

FIG. 5. Molar excess isobaric and isochoric heat capacities, $C_{p,m}^E$ and $C_{V,m}^E$, for W–EA (+, X) and W–EG (dotted lines) mixtures at 25°C.

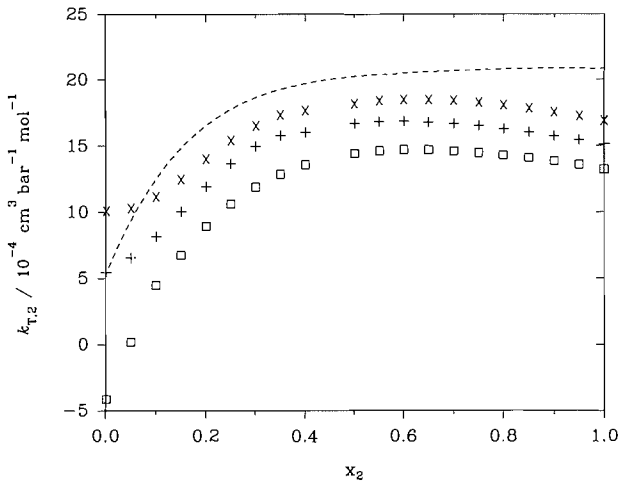

FIG. 8. Partial molar isothermal compressibilities, $k_{T,2}$, of EA in W–EA mixtures at 10°C (□), 25°C (+), and 40°C (X); dotted line: $k_{T,2}$ of EG in W–EG mixtures at 25°C.

Can. J. Chem. Downloaded from www.nrcresearchpress.com by 213.200.69.106 on 09/08/12
For personal use only.

Can. J. Chem. Downloaded from www.nrcresearchpress.com by 213.200.69.106 on 09/08/12
For personal use only.

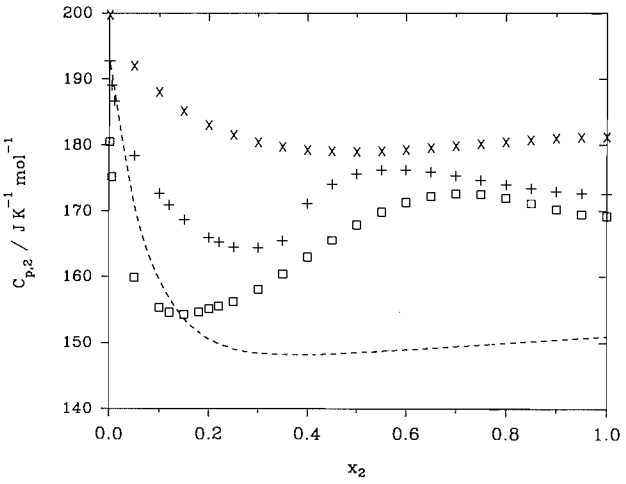

FIG. 9. Partial molar isobaric heat capacities, $C_{p,2}$, of EA in W–EA mixtures at 10°C (□), 25°C (+), and 40°C (X); dotted line: $C_{p,2}$ of EG in W–EG mixtures at 25°C.

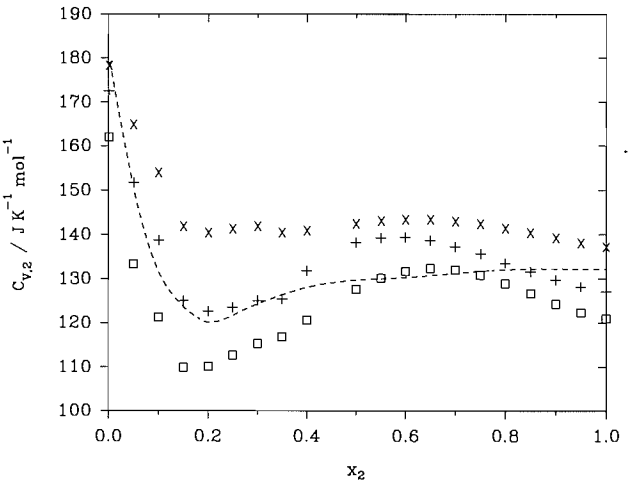

FIG. 10. Partial molar isochoric heat capacities, $C_{V,2}$, of EA in W–EA mixtures at 10°C (□), 25°C (+), and 40°C (X); dotted line: $C_{V,2}$ of EG in W–EG mixtures at 25°C.

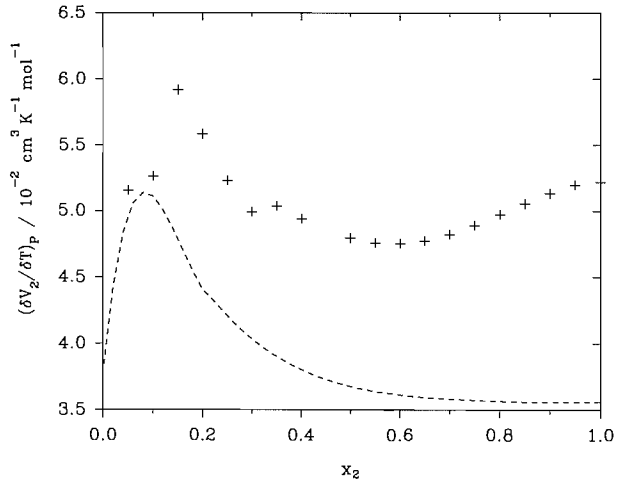

FIG. 11. Partial molar expansions, $(\partial V_2/\partial T)_p$, of EA (+) in W–EA mixtures at 25°C; dotted line: $(\partial V_2/\partial T)_p$ of EA in W–EG mixtures at 25°C.

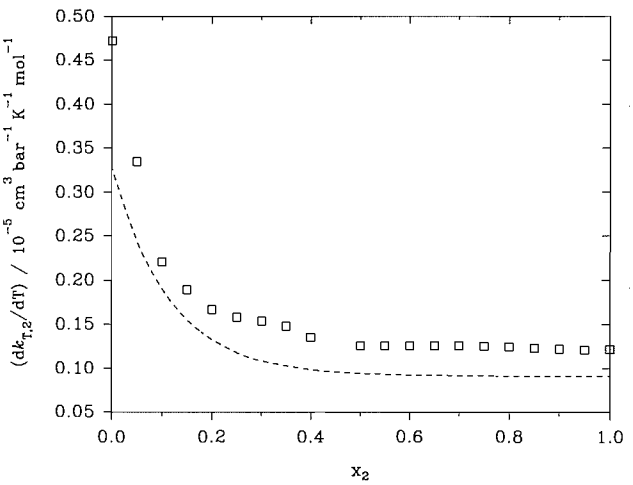

FIG. 12. Temperature coefficients of partial molar isothermal compressibilities, $\partial k_{T,2}/\partial T$, at 25°C of EA (□) in W–EA mixtures and of EG (dotted line) in W–EG mixtures.

the second derivative partial molar quantities. Indeed, the latter are more responsive towards the weak molecular interactions that are responsible for thermodynamic fluctuations.

Second, in view of the similarity of the second derivative functions in W–EA and W–EG mixtures, the separation of the composition range into three regions proposed earlier for W–EG mixtures (1) and other systems (5) would obviously be applicable to the W–EA mixture. In the $0 < x \leq 0.1$ region (corresponding to loss of cooperative fluctuations in liquid water), changes in quantities such as $k_{T,2}$ (Fig. 8) and $C_{p,2}$ (Fig. 9) with x_2 are less abrupt with EA than with EG. This would be consistent with the lower hydrophobic character of EA. In the $x > 0.3$ region, some of the second derivative properties of the W–EA system exhibit greater variations than those of the W–EG system; this could be understood from a larger variety of interactions possible between W and EA molecules, due to the presence of two different functional groups on the EA molecule, i.e., providing additional states that can contribute to thermodynamic fluctuations (increasing the width, or second moment, of the distribution functions representing these states). However, these effects are mostly apparent in the correlation between the energy and the volume fluctuations, such as in the volume expansion contribution to $C_{p,2}$, i.e., $(C_{p,2} - C_{V,2})$, or in $(\partial V_2/\partial T)_p$, which are of course related quantities (eq. [11]).

The third derivative partial molar quantities $(\partial k_{T,2}/\partial T)$ and $(\partial C_{p,2}/\partial T)$ were also calculated and are illustrated in Figs. 12 and 13; again, comparing EA and EG (the corresponding thermal expansion function $(\partial^2 V_2/\partial T^2)_p$ exhibits uncertainties too large for useful comparison). While the second derivatives are related to the magnitude of the H, S, or V fluctuations (second moment, or the width of the distribution function for the states involved), the third derivatives reflect the skewness (third moment) of these distribution functions. The quantitative similarity in the functions plotted in Figs. 12 and 13 for W–EA and W–EG mixtures is remarkable, given the important differences noted earlier in the first derivative molar excess functions H^E_m, TS^E_m, and V^E_m. The slightly larger values in the third derivative properties of EA compared to EG again appear consistent with a broader range of molecular interactions in W–EA, as com-

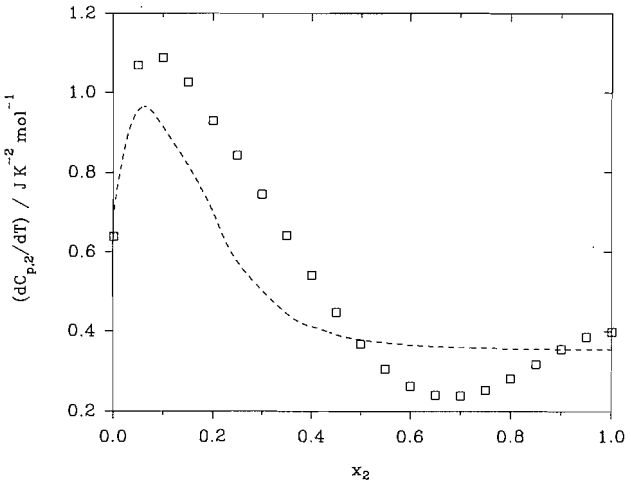

FIG. 13. Temperature coefficients of partial molar isobaric heat capacities, $\partial C_{p,2}/\partial T$, at 25°C of EA (□) in W–EA mixtures and of EG (dotted line) in W–EG mixtures.

pared to W–EG, due to the asymmetry of the EA molecules. From the data reported earlier on the W–ME system (2), it can be calculated that the third derivative quantities of a more hydrophobic cosolvent (methoxyethanol compared to ethylene glycol) are markedly different from those reported here for the hydrophilic, or weakly hydrophobic, EA and EG. From the observations presented here, the third derivative functions would seem to provide a clean distinction between hydrophobic and hydrophilic cosolvents, especially in water-rich systems.

Conclusion

The comprehensive thermodynamic investigation of the water–ethanolamine system, and a comparison of the results with similar data for water – ethylene glycol (1) and water–methoxyethanol (2), reveals important similarities and differences. While the various molar excess functions (X^E_m) in the three systems exhibit common qualitative features, major quantitative differences are found, even when comparing the two most hydrophilic solvents (EG and EA), which also have comparable molecular sizes and two hydrogen-bonding groups.

In comparisons involving the partial molar quantities of the cosolvent (X_2), it is further confirmed that the hydrophobic hydration effects in W–ME mixtures (2) are best distinguished from those in W–EA or W–EG mixtures through the second derivative properties (reflecting the width, or second moment, of the state distribution functions). On the other hand, comparisons between corresponding quantities in the W–EG and W–EA system show very similar second derivative properties; they further show a high degree of similarity between third derivative functions. This is quite remarkable considering the chemical differences in the EA and EG molecules, but lends additional support to the concept proposed earlier by Lumry et al. (5) as summarized in the introduction.

Can. J. Chem. Downloaded from www.nrcresearchpress.com by 213.200.69.106 on 09/08/12
For personal use only.

Acknowledgements

The authors gratefully acknowledge financial support from the Natural Sciences and Engineering Research Council of Canada and the ministère de l'Éducation du Québec. The assistance of Marc-André Simard and Jeffrey Sharman in data treatment and computations is also acknowledged with pleasure.

1. J.-Y. Huot, E. Battistel, R. Lumry, G. Villeneuve, J.-F. Lavallée, A. Anusiem, and C. Jolicoeur. J. Solution Chem. **17**, 601 (1988).
2. M. Pagé, J.-Y. Huot, and C. Jolicoeur. J. Chem. Thermodyn. **25**, 139 (1993).
3. M. Oguni and C.A. Angell. J. Chem. Phys. **73**, 1948 (1980); M. Allen, D.F. Evans, and R. Lumry. J. Solution Chem. **14**, 549 (1985); D. Mirejovsky and E.M. Arnett. J. Am. Chem. Soc. **105**, 1112 (1983).
4. R. Lumry and S. Rajender. Biopolymers, **9**, 1125 (1970).
5. R. Lumry, E. Battistel, and C. Jolicoeur. Faraday Symp. Chem. Soc. **17**, 93 (1982).
6. P. Picker, E. Tremblay, and C. Jolicoeur. J. Solution Chem. **3**, 377 (1969).
7. P. Picker, P.A. Leduc, P.R. Philip, and J.E. Desnoyers. J. Chem. Thermodyn. **3**, 631 (1971).
8. P. Picker, C. Jolicoeur, and J.E. Desnoyers. J. Chem. Educ. **45**, 614 (1968).
9. R. Garnsey, R.J. Boe, R. Mahoney, and T.A. Litovitz. J. Chem. Phys. **50**, 5222 (1969).
10. V.A. Del Grosso and C.W. Mader. J. Acoust. Soc. Am. **52**, 1442 (1972).
11. C. Jolicoeur. Methods Biochem. Anal. **27**, 172 (1981).
12. J.C.R. Reis. J. Chem. Soc. Faraday Trans. 2, **78**, 1595 (1982).
13. V.N. Kartsev, M.N. Rodnikova, V.V. Tsepulin, K.T. Dudnikova, and V.G. Markowa. Zh. Fiz. Khim. **27**, 187 (1986).
14. H. Touhara, S. Okazaki, F. Okini, H. Tanaka, K. Ikari, and K. Nakanishi. J. Chem. Thermodyn. **14**, 145 (1982).
15. F. Murrieta-Guevara and A.T. Rodriguez. J. Chem. Eng. Data, **29**, 204 (1984).
16. S. Cabani, V. Mollica, L. Lepori, and S.T. Lobo. J. Phys. Chem. **81**, 987 (1977).
17. S. Cabani, S.T. Lobo, and E. Matteoli. J. Solution Chem. **8**, 5 (1979).
18. S. Cabani, E. Matteoli, and M.R. Tinè. Z. Physik. Chem. Neue Folge, **137**, 23 (1983).
19. M.R.J. Dack. Aust. J. Chem. **28**, 1643 (1975).
20. A.F.M. Barton. Handbook of solubility parameters and other cohesion parameters. CRC Press Inc., Boca Raton, Fla. 1985.
21. S. Cabani, P. Gianni, V. Mollica, and L. Lepori. J. Solution Chem. **10**, 563 (1981).
22. J.P.E. Grolier and G. Benson. Can. J. Chem. **62**, 949 (1984).
23. M. Morenas and G. Douheret. Thermochem. Acta **25**, 217 (1978).
24. A. Ray and G. Nemethy. J. Chem. Eng. Data **18**, 309 (1978).
25. G.C. Benson and O. Kiyohara. J. Solution Chem. **9**, 791 (1980).
26. C. de Visser, G. Perron, and J.E. Desnoyers. Can. J. Chem. **55**, 856 (1977).
27. K. Nakanishi, N. Kato, and M. Maruyama. J. Phys. Chem. **71**, 814 (1967).
28. G.C. Benson, P.J. D'Arcy, and O. Kiyohara. J. Solution Chem. **9**, 931 (1980).
29. C. Jolicoeur and G. Lacroix. Can. J. Chem. **54**, 624 (1976).
30. G. Roux, D. Roberts, G. Perron, and J.E. Desnoyers. J. Solution Chem. **9**, 629 (1980).

Investigation of the mechanism of alkyl radical elimination from ionised pentenyl methyl and hexenyl methyl ethers by analysis of the collision-induced dissociation mass spectra of $C_4H_7O^+$ and $C_5H_9O^+$ ions

ANDREW D. WRIGHT AND RICHARD D. BOWEN[1]
Department of Chemistry, University of Warwick, Coventry, CV4 7AL, U.K.

Received February 15, 1993

ANDREW D. WRIGHT and RICHARD D. BOWEN. Can. J. Chem. **71**, 1073 (1993).

Collision-induced dissociation (CID) mass spectra are reported for $C_4H_7O^+$ and $C_5H_9O^+$ ions generated by loss of an alkyl radical from 11 isomers of $C_5H_9OCH_3^{+\bullet}$ and 8 isomers of $C_6H_{11}OCH_3^{+\bullet}$ produced by ionisation of alkenyl methyl ethers derived from stable alkenols. The oxonium product ions have acyclic structures ($CH_2{=}CHCH{=}O^+CH_3$ for $C_4H_7O^+$; $CH_2{=}CH(CH_3)C{=}O^+CH_3$, $CH_3CH{=}CHCH{=}O^+CH_3$, or $CH_2{=}(CH_3)CCH{=}O^+CH_3$ in the case of $C_5H_9O^+$). Elimination of a methyl radical does not always occur by simple α-cleavage. Expulsion of an alkyl substituent attached to a carbon atom at either end of the C=C double bond also takes place readily; this process sometimes competes with or pre-empts α-cleavage, as is shown by ^{2}H-labelling experiments. Plausible mechanisms for this σ′-cleavage are considered. A route involving a 1,2-H shift to the radical centre of a distonic ion, followed by γ-cleavage of the resultant ionised enol ether, is shown to provide the most accurate unifying description of this unusual fragmentation. The mechanistic significance of this interpretation of the σ′-cleavage is discussed by analysing the reverse reaction (addition of an alkyl radical to a methyl cationated enal) in frontier molecular orbital terms. A comparison is made between the mechanisms by which an alkyl radical is lost from ionised alkenyl methyl ethers by σ′-cleavage and the parallel process starting from ionised carboxylic acids or isomeric distonic ions derived from these $C_nH_{2n+1}CO_2H^{+\bullet}$ species. Both classes of fragmentation are best understood to occur via γ-cleavage of a distonic ion of general structure $R^1CH_2CH{\cdot}C^+(X)OR^2$ (R^1 = alkyl; X = OH, R^2 = H; or X = H, R^2 = CH_3), thus yielding $(R^1)\cdot$ and $CH_2{=}CHC^+(X)OR^2$.

ANDREW D. WRIGHT et RICHARD D. BOWEN. Can. J. Chem. **71**, 1073 (1993).

Nous reportons ici les spectres CID (Collision-Induced Dissociation) des ions $C_4H_7O^+$ and $C_5H_9O^+$ générés par perte d'un radical alkyle à partir de 11 isomères de $C_5H_9OCH_3^{+\bullet}$ et 8 isomères de $C_6H_{11}OCH_3^{+\bullet}$. Ces isomères de départ sont produits lors de l'ionisation d'éthers stables de méthyle et de pentène, et de méthyle et d'hexène. Les ions fragments oxoniums produits ont des structures acycliques ($CH_2{=}CHCH{=}O^+CH_3$ pour $C_4H_7O^+$; $CH_2{=}CH(CH_3)C{=}O^+CH_3$, $CH_3CH{=}CHCH{=}O^+CH_3$ ou $CH_2{=}(CH_3)CCH{=}O^+CH_3$ dans le cas de $C_5H_9O^+$. D'aprés les spectres CID, il apparait que l'élimination du radical méthyle ne se produit pas toujours par simple rupture α. De même, l'expulsion du substituant alkyle attaché à un atome de carbone, à un bout ou à l'autre de la double liaison, est aussi observé. Ce processus entre parfois en compétition ou même devance la rupture du type α, comme le montre les expériences de marquage par ^{2}H. Nous avons considéré les mécanismes possibles de cette rupture σ′ et, en particulier, un chemin réactionnel impliquant un déplacement 1,2 d'hydrogène vers le centre radicalaire de l'ion distonique, suivi d'une rupture du type γ de l'éther d'énol ionisé qui en résulte, semble donner une description globale et précise de ce type inhabituel de fragmentation. La signification mécanistique de cette rupture σ′ est interprétée par l'analyse de la réaction inverse (d'addition d'un radical alkyle à un ‹‹cation ène aldéhydique de méthyle›› en termes de frontières d'orbitales moléculaires. Une comparaison est faite entre les mécanismes par lesquels un radical alkyle est perdu à partir d'éthers de méthyle et d'alcènes par rupture σ′ et le processus parallèle commençant par des acides carboxyliques ionisés ou des ions isomères distoniques dérivés des espèces $C_nH_{2n+1}CO_2H^{+\bullet}$. Les deux types de fragmentation sont bien connues pour donner lieu, par l'intermédiaire d'une rupture γ, à un ion distonique de structure générale $R'CH_2CH{\cdot}C^+(X)OR^2$ (R' = alkyl; X = OH, R^2 = H; ou X = H, R^2 = CH_3) et donc conduisent à la production de $(R')\cdot$ et $CH_2{=}CHC^+(X)OR^2$.

A. Introduction

The chemistry of many $C_nH_{2n}O^{+\bullet}$ species in the gas phase is well documented (for an overview, see ref. 1). Until very recently, however, relatively little attention (2–4) had been given to $C_nH_{2n}O^{+\bullet}$ ions generated from alkenyl methyl ethers. A survey (5) of the mass spectra of these $C_mH_{2m-1}OCH_3$ compounds revealed that alkyl radical loss often dominates the fragmentation of the corresponding radical cations, especially when $m \geq 4$. More detailed investigations of the reactions of $C_3H_5OCH_3^{+\bullet}$ and $C_4H_7OCH_3^{+\bullet}$ species formed from alkenyl methyl ethers showed that several routes operate for alkyl radical expulsion (6, 7). At least some of these processes involve rearrangement to distonic (8) ions (9) (DIs, which are structures that have the notional charge and radical sites localised on different "heavy" atoms, typically separated by one or more sp^3 carbon atoms).

The principal objective of the research reported in this paper is to delineate the mechanism(s) for alkyl radical elimination from $C_mH_{2m-1}OCH_3^{+\bullet}$ species (m = 5, 6). The chemistry of these radical cations is of interest in its own right. In addition, extrapolation of the trends observed for $C_5H_9OCH_3^{+\bullet}$ and $C_6H_{11}OCH_3^{+\bullet}$ should permit the reactions of homologous and analogous systems to be understood or even predicted, thus enhancing the analytical value of mass spectrometry.

A subsidiary aim is to study the nature of the isomerisation steps involving the radical centre of DIs. Several of the routes for alkyl radical loss from ionised alkenyl methyl ethers cannot be formulated in terms of direct fragmentation of the original structure (5–7, 10, 11). In particular, two key rearrangement processes are found that involve the radical site of a DI. The former is a formal 1,2$^+$-CH-OCH$_3$ shift to the radical centre of a β-DI (i.e., one in which the charge and radical sites are separated by a single sp^3 carbon atom). Thus, $CH_3{\cdot}CHCH_2{}^+CHOCH_3$ is isomerised to CH_3-$(CH_2{\cdot})CH^+CHOCH_3$ (i.e., $\cdot CH_2(CH_3)CH^+CHOCH_3$) by this

[1]Author to whom correspondence may be addressed.

Can. J. Chem. Downloaded from www.nrcresearchpress.com by 213.200.69.106 on 09/08/12
For personal use only.

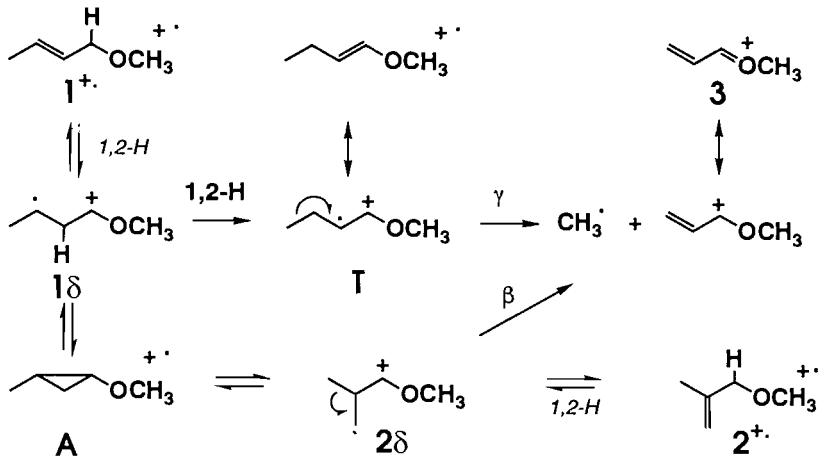

SCHEME 1

"carbene" rearrangement. This step can be conveniently visualised to occur via an ionised methoxycyclopropane (i.e., $CH_3{\cdot}CHCH_2{}^+CHOCH_3 \rightleftharpoons CH_3\overline{CHCH_2}CHOCH_3{}^{+\cdot} \rightleftharpoons CH_3(CH_2{\cdot})CH^+CHOCH_3$), but the cyclic species may merely represent the transition state for this isomerisation, rather than a genuine intermediate. The second type of rearrangement is a 1,2-H shift to the radical centre; this step converts a β-DI into an α-DI (e.g., $CH_3{\cdot}CHCH_2{}^+CHOCH_3 \rightarrow CH_3CH_2{\cdot}$-$CH^+CHOCH_3 \leftrightarrow CH_3CH_2CH{=}CHOCH_3{}^{+\cdot}$). These α-DIs, in which the charge and radical sites are localised on adjacent carbon atoms, are actually representations of ionised methyl enol ethers. Preliminary results on the fragmentation of $C_5H_9OCH_3{}^{+\cdot}$ and $C_6H_{11}OCH_3{}^{+\cdot}$ species reveal that α-DIs are probably the reacting configuration for alkyl radical expulsion from at least some of these radical cations (11). Consequently, the 1,2-H shift converting a β- into an α-DI promises to be of crucial significance in the reactions of $C_5H_9OCH_3{}^{+\cdot}$ and $C_6H_{11}OCH_3{}^{+\cdot}$ ions.

In the wider context, rearrangements in which ionised substituted cyclopropanes can be considered to play an important part have previously been postulated in other systems, including ionised alkenols (1, 12–14) and carboxylic acids (15–18). In the case of the latter class of compounds, a 1,2-H shift converting a β-DI into an α isomer was also observed (16–18). Indeed, compelling evidence was presented to show that alkyl radical loss always occurs from metastable $C_nH_{2n+1}CO_2H^{+\cdot}$ species via eventual isomerisation to an α-DI (here an ionised, 1,1-enediol), followed by C—C bond fission to give a protonated acrylic acid (18). A comparison between the "free-radical" chemistry of the $C_nH_{2n-1}OCH_3{}^{+\cdot}$ and $C_nH_{2n+1}CO_2H^{+\cdot}$ systems should, therefore, be informative.

B. Summary of the routes for alkyl radical loss from $C_3H_5OCH_3{}^{+\cdot}$ and $C_4H_7OCH_3{}^{+\cdot}$ species

The parent ionised ether, $CH_2{=}CHCH_2OCH_3{}^{+\cdot}$, loses a methyl group containing the carbon of the original methoxy group (6). This fragmentation, which is characterised by an extremely large and relatively specific kinetic energy (KE) release, is atypical of alkyl radical elimination from ionised alkenyl methyl ethers. The KE release ($T_{1/2}$) estimated from the width at half-height of the associated dish-topped metastable peak is 42 kJ mol^{-1} (6), indicating that this fragmentation takes place with a substantial reverse critical (19) energy. Only one of the higher homologues behaves in a remotely similar fashion: a minor component (~6%) of methyl loss from $CH_2{=}CH(CH_3)CHOCH_3{}^{+\cdot}$ occurs with a large KE release, as is shown by the dish-topped peak ($T_{1/2}$ = 50 kJ mol^{-1}) for $^{13}CH_3{\cdot}$ expulsion from $CH_2{=}CH(CH_3)CHO$-$^{13}CH_3{}^{+\cdot}$ (7). All other alkyl radical losses, including the bulk of methyl elimination ($CH_3{\cdot}$) from $CH_2{=}CH(CH_3)CHO$-$^{13}CH_3{}^{+\cdot}$, yield quite narrow Gaussian metastable peaks, with $T_{1/2}$ values typically in the range 1.5–2.5 kJ mol^{-1} (7).[2] Moreover, the O-alkyl group is not expelled. Thus, $CH_3CH{=}CHCH_2OCD_3{}^{+\cdot}$, $CH_2{=}(CH_3)CCH_2OCD_3{}^{+\cdot}$, $CH_3CH{=}CH$-$(CH_3)CHOCD_3{}^{+\cdot}$, and $CH_2{=}(CH_3)C(CH_3)CHOCD_3{}^{+\cdot}$ all lose only $CH_3{\cdot}$ in methyl radical elimination. Consequently, alkyl radical expulsion from ionised alkenyl methyl ethers derived from allylic alcohols containing four or more carbon atoms typically involves only the atoms of the alkenyl group. Moreover, the $T_{1/2}$ values suggest that this fragmentation usually does not ential a large reverse critical energy.

Many ionised ethers formed from secondary or tertiary allylic alcohols readily lose an α-alkyl group. The obvious explanation for this fragmentation is α-cleavage, eq. [1], but there is clear evidence (7, 10, 11) that this process is not always the simple σ-cleavage that it appears to be at first glance, especially when a methyl group is expelled. Fur-

[1] 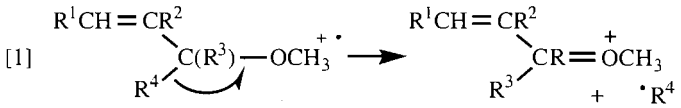

R^1, R^2, R^3, R^4, = H, alkyl

thermore, alkyl groups attached to either of the carbon atoms joined by the double bond are also eliminated with great facility (5, 7, 10, 11). This σ′-cleavage, which sometimes competes with the apparently more favourable α-cleavage alternative (10), can be explained in terms of rearrangements involving DIs and ionised methoxycyclopropanes (5, 7, 10, 11).

C. Mechanisms for σ′-cleavage

The two most plausible mechanisms for the σ′-cleavage are illustrated in Scheme 1 for the archetypical $C_4H_7OCH_3{}^{+\cdot}$

[2]R.D. Bowen, A.W. Colburn and P.J. Derrick. Unpublished results.

Can. J. Chem. Downloaded from www.nrcresearchpress.com by 213.200.69.106 on 09/08/12
For personal use only.

species, $CH_3CH{=}CHCH_2OCH_3^{+\cdot}$, $\mathbf{1}^{+\cdot}$, and $CH_2{=}(CH_3)CCH_2OCH_3^{+\cdot}$, $\mathbf{2}^{+\cdot}$. Interconversion of $\mathbf{1}^{+\cdot}$ and $\mathbf{2}^{+\cdot}$ is possible via isomerisation to the corresponding DIs, **1**δ and **2**δ, respectively; **1**δ and **2**δ then interconvert by ring closure to **A**. Loss of the methyl group originally attached to the double bond is possible by direct β-cleavage of **2**δ. Alternatively, a 1,2-H shift to the radical site of **1**δ affords the ionised enol ether, **T**, which then expels a methyl group by undergoing γ-cleavage. The crucial step in the second route is probably **1**δ → **T**; such 1,2-H shifts involving radical centres normally occur less rapidly than the analogous processes at cationic sites (20–22). Consequently, it is likely that **1**δ → **T** is the slow and rate-limiting step in this mechanism for $CH_3\cdot$ expulsion from $\mathbf{1}^{+\cdot}$ and $\mathbf{2}^{+\cdot}$. This view is consistent with earlier work on the related radical cations formed from ionised carboxylic acids. A 1,2-H shift to the radical centre of a β-DI certainly takes place in many of these systems (e.g., $CH_3CH\cdot(CH_3)CHC^+(OH)_2 \rightarrow CH_3CH_2(CH_3)C\cdot C^+(OH)_2$) (16–18). Moreover, these 1,2-H shifts were generally found to occur more slowly than the corresponding 1,2-$^+C(OH)_2$ shifts (this step is analogous to that (**1**δ ⇌ **A** ⇌ **2**δ) by which $\mathbf{1}^{+\cdot}$ and $\mathbf{2}^{+\cdot}$ are proposed to interconvert) (18).

A variation of the mechanism involving eventual γ-cleavage can be put forward in which the ionised enol ether is formed directly from the ionised alkenyl methyl ether via a 1,3-H shift (e.g., $\mathbf{1}^{+\cdot} \rightarrow$ **T**, Scheme 1). This change does not affect the predictions made for the structure of the product ion generated by eventual γ-cleavage of $C_5H_9OCH_3^{+\cdot}$ and $C_6H_{11}OCH_3^{+\cdot}$ species. However, three factors militate against the occurrence of the 1,3-H shift. Firstly, such processes involve significant and sometimes very substantial additional energy barriers, even in open-shell systems. These barriers may arise from the unfavourable orbital symmetry entailed in suprafacial concerted 1,3-H shifts (23, 24). Secondly, 1,3-H shifts of this type involve additional energetic and (or) geometric constraints that do not apply to consec-

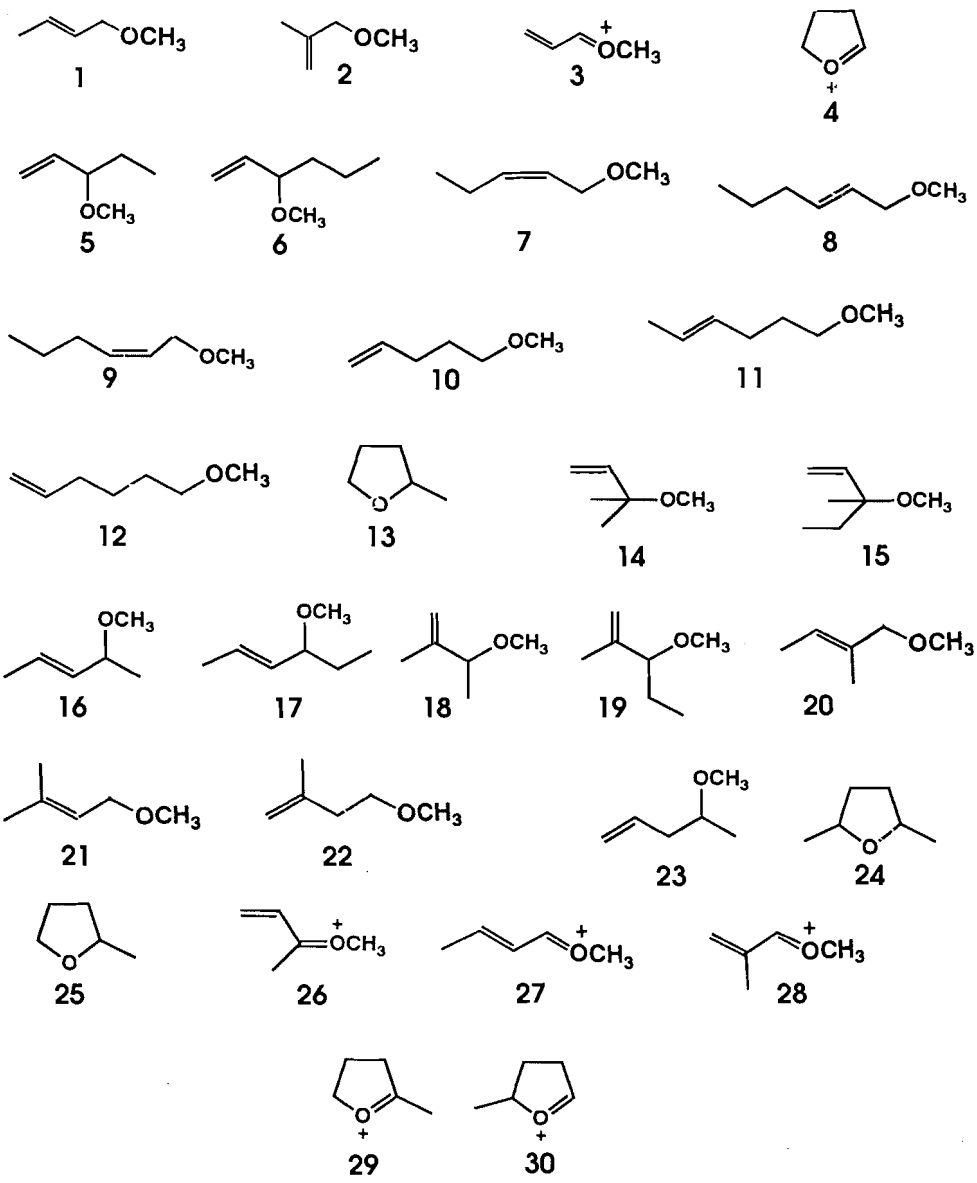

Structures of precursors and product ions relevant to the tables

Can. J. Chem. Downloaded from www.nrcresearchpress.com by 213.200.69.106 on 09/08/12
For personal use only.

Can. J. Chem. Downloaded from www.nrcresearchpress.com by 213.200.69.106 on 09/08/12
For personal use only.

utive 1,2-H shifts. This conclusion applies regardless of whether the shifts are considered to terminate at a cationic or a radical centre. In the former case (a 1,3-H shift to the cationic site in $CH_3CH^+CH{\cdot}CH_2OCH_3$, if $\mathbf{1}^{+\cdot}$ is depicted in this way), studies on $CH_3CH_2CH_2CH^+—OCH_3$ reveal that the corresponding process forming $CH_3CH^+CH_2CH_2OCH_3$ cannot take place at, or close to, the thermochemical threshold (25). In the latter case (a 1,3-H shift to the radical centre in $CH_3CH{\cdot}CH^+CH_2OCH_3$, if $\mathbf{1}^{+\cdot}$ is represented in this fashion), earlier work reveals no precedent whatever for a 1,3-H shift to a radical site (18), though 1,4- and 1,5-H shifts are known to be facile and 1,2-H shifts certainly occur in some circumstances. Thirdly, it will be shown in the subsequent discussion (Sect. E.2(*a*)) that the mechanism involving 1,2-H shifts can be logically extended to explain alkyl radical loss via eventual δ-cleavage of several $C_5H_9OCH_3^{+\cdot}$ and $C_6H_{11}OCH_3^{+\cdot}$ species. No such extension of the mechanism involving the 1,3-H shift is possible. Therefore, the formulation involving consecutive 1,2-H shifts offers a more general and unifying description of γ- and δ-cleavage.

In the schemes in this paper, 1,2 shifts to radical centres are shown in bold type, to distinguish them from the corresponding shifts to cationic sites, which are shown in italic type. Many of the steps (but probably not the 1,2-H shifts to a radical site) depicted in the schemes are likely to be at least partially reversible, especially at low internal energies; these steps are represented by equilibrium arrows.

In the parent $C_4H_7OCH_3^{+\cdot}$ system, the alternative descriptions of the σ′-cleavage cannot be distinguished by investigating the structure of the $C_4H_7O^+$ product ion because both routes result in formation of the same product ion, $CH_2=CHCH=O^+CH_3$, **3**. However, for the higher homologues $C_5H_9OCH_3^{+\cdot}$ and $C_6H_{11}OCH_3^{+\cdot}$, the processes corresponding to β-cleavage of **2**δ and γ-cleavage of **T** sometimes lead to isomeric products that can be differentiated by analysis of their collision-induced dissociation (CID) spectra (11). This paper presents an analysis of the CID mass spectra of $C_4H_7O^+$ and $C_5H_9O^+$ ions generated by electron ionisation and subsequent alkyl radical elimination from numerous isomers of $C_5H_9OCH_3$ and $C_6H_{11}OCH_3$ derived from stable alkenols.

D. Structure of the $C_4H_7O^+$ product ions

Table 1 gives the CID spectra of $C_4H_7O^+$ ions formed from eight isomers of $C_5H_9OCH_3^{+\cdot}$ and $C_6H_{11}OCH_3^{+\cdot}$. All the ions have closely similar spectra. Consequently, it is logical to conclude that the same product ion, **3**, is produced by alkyl radical expulsion from these ionised ethers. In contrast, the CID spectrum of the cyclic oxonium ion, $\overline{CH_2CH_2CH_2CH=O}^+$, **4**, ($[M - H]^+$ generated by ionisation and methyl radical loss from $\overline{CH_2CH_2CH_2CH(CH_3)O}$, **13**) is clearly distinct from that of **3**. There are three major differences between the spectra of **3** and **4**. First, the spectrum of **3** shows appreciable peaks at *m/z* 56 and 55 (corresponding to loss of $CH_3{\cdot}$ and CH_4, respectively). Secondly, the base peak in the spectrum of **4** is at *m/z* 43; the analogous peak in the spectrum of **3** is merely of minor importance (RI = 6–8%). Finally, the signals at *m/z* 41 (corresponding to $CH_2=O$ elimination), 39, 29, 27, and 15 are substantially enhanced in the spectrum of **3**.

The formation of **3**, instead of **4** (which is actually thermodynamically more stable than **3** by approximately 50 kJ mol^{-1} (26)) is intelligible on the basis of the following mechanisms.

D.1. Ethers of allylic alcohols

*(a) Loss of an α-substituent (**5**$^{+\cdot}$ and **6**$^{+\cdot}$)*

A simple cleavage (eq. [2]) rationalises this fragmentation for relatively fast dissociations. However, other processes

[2] 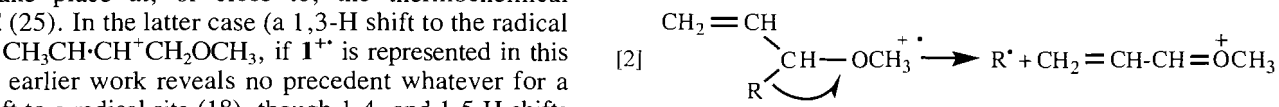

involving hydrogen exchange may compete with direct cleavage when ions of longer lifetimes and lower average internal energies dissociate. This caveat applies particularly when a methyl radical is expelled. Thus, the lower homologue $CH_2=CH(CD_3)CHOCH_3^{+\cdot}$ loses not only $CD_3{\cdot}$ (direct α-cleavage) but also $CHD_2{\cdot}$, $CH_2D{\cdot}$, and even a little $CH_3{\cdot}$ (7).

There is an interesting correlation in this respect with alkyl radical loss from α-DIs formed from ionised carboxylic acids, in which the leaving group ability (LGA) of a methyl group (0.022) was found to be grossly inferior to that (1.000) defined for an ethyl group (18). The comparatively poor LGA associated with the methyl group apparently persists in the α-cleavage of ionised alkenyl methyl ethers via eq. [2], thus permitting hydrogen exchange to compete with methyl radical elimination.

*(b) Loss of a γ-substituent (**7**$^{+\cdot}$, **8**$^{+\cdot}$, and **9**$^{+\cdot}$)*

Isomerisation via the appropriate DIs (and, possibly, ionised alkylmethoxycyclopropane) explains this reaction, as illustrated in Scheme 2 for $\mathbf{7}^{+\cdot}$. Details of the final step (γ-cleavage (7δ → **U** → products) or β-cleavage via **B**) cannot be elucidated since both possibilities lead to the same products.

*D.2. Ethers of non-allylic alcohols (**10**$^{+\cdot}$, **11**$^{+\cdot}$ and **12**$^{+\cdot}$)*

A combination of 1,4-, 1.5-, and 1,6-H shifts, followed by eventual γ-cleavage of an ionised enol ether, provides a logical explanation for the formation of **3** from these ionised ethers. Thus, a 1,4-H shift coupled with a 1,4-H shift leads from $\mathbf{11}^{+\cdot}$ to **V** which then expels $C_3H_7{\cdot}$, Scheme 3. Similarly, a 1,6-H shift and subsequent 1,4-H shift in $\mathbf{12}^{+\cdot}$ gives **V**. Other combinations of H shifts are also possible. It is significant that none of these ionised ethers fragments to give **4**; in contrast, ionised homoallyl methyl ether does yield **4** by loss of $CH_3{\cdot}$ (7). Unfortunately, the abundance of $C_4H_7O^+$ ions in the conventional mass spectra of $C_5H_9OCH_3^{+\cdot}$ and $C_6H_{11}OCH_3^{+\cdot}$ species derived from homoallylic alcohols is insufficient to allow reliable CID spectra to be recorded.

E. Structure of the $C_5H_9O^+$ product ions

Table 2 contains the CID spectra of $C_5H_9O^+$ ions generated from 16 isomers of $C_5H_9OCH_3^{+\cdot}$ and $C_6H_{11}OCH_3^{+\cdot}$. Four types of spectra are found. The first three classes comprise spectra that are attributable to a single product ion ($CH_2=CH(CH_3)C=O^+CH_3$, **26**, $CH_3CH=CHCH=O^+CH_3$, **27**, and $CH_2=(CH_3)CCH=O^+CH_3$, **28**, respectively). The fourth category consists of spectra that are a combination of the spectrum of **26** with that of **27** or **28**. As was the case with the homologous $C_4H_7O^+$ ions, there is no evidence for formation of cyclic oxonium ions ($\overline{CH_2CH_2CH_2(CH_3)C=O}^+$, **29**, or $CH_3\overline{CHCH_2CH_2CH=O}^+$,

TABLE 1. CID mass spectra of $C_4H_7O^+$ ions[a]

	Origin of ion								
m/z	$[M - C_2H_5]^+$ from **5**	$[M - C_3H_7]^+$ from **6**	$[M - C_2H_5]^+$ from **7**	$[M - C_3H_7]^+$ from **8**	$[M - C_3H_7]^+$ from **9**	$[M - C_2H_5]^+$ from **10**	$[M - C_3H_7]^+$ from **11**	$[M - C_3H_7]^+$ from **12**	$[M - H]^+$ from **13**[b]
70	1	2	2	2	1		1		3
69	8	9	8	8	8	7	3	8	2
56	14	15	16	15	15	16	17	18	
55	26	27	26	26	25	24	24	30	
53	4	5	4	4	4	3	1	3	
45	6	7	6	6	6	6	4	6	
43	6	7	7	6	7	7	8	7	100
42	16	18	16	15	15	16	15	19	20
41	100	100	100	100	100	100	100	100	31
40	11	13	12	12	12	13	14	13	2
39	68	72	69	68	69	68	68	75	32
38	16	18	17	17	16	18	13	17	5
37	6	7	6	7	7	6	7	6	2
31	5	5	6	6	5	3	3	5	1
29	44	47	45	45	45	44	43	48	20
28	14	16	16	15	15	15	14	18	4
27	60	67	62	64	63	64	63	66	30
26	16	18	17	17	17	18	16	20	6
25	2	2	2	2	2	1		2	
15	23	26	26	25	27	26	23	26	5
14	2	4	3	3	3	2	3	3	1

[a]Intensities were normalised to a value of 100 units for the most intense fragment ion peak.
[b]Essentially identical to the spectrum of $[M - CH_3]^+$ generated from **25**.

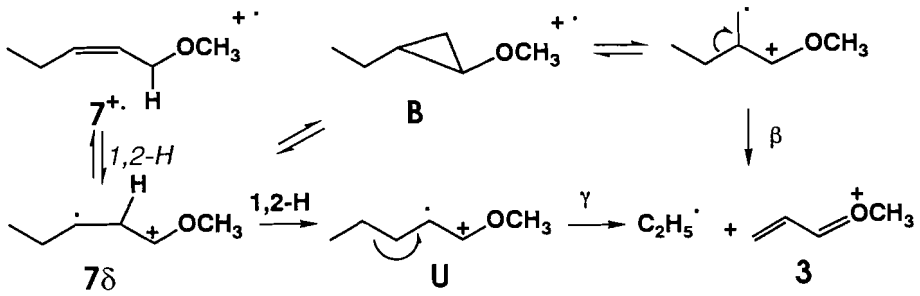

SCHEME 2

30). The CID spectra of the cyclic oxonium ions differ markedly from those of their acyclic conjugated isomers. Thus, the spectrum of **29** shows distinctive signals at *m/z* 67 and 57 (corresponding to CO elimination, as is also observed for the lower homologue, **4**); in addition, the peaks at *m/z* 29 and 27 are noticeably enhanced. Similarly, the spectrum of **30** is dominated in a unique way by the intense peak at *m/z* 43.

The following mechanisms explain the formation of **26**, **27**, and **28** from the ionised alkenyl methyl ethers.

E.1. Loss of an entire alkyl substituent

(a) Ethers of allylic alcohols

*(i) α-Cleavage (**14**$^{+\cdot}$, **15**$^{+\cdot}$, **17**$^{+\cdot}$, and **19**$^{+\cdot}$).* This mechanism provides an adequate interpretation for the dissociation of ethers derived from tertiary alcohols, or for elimination of an α-ethyl group from ionised ethers derived from secondary allylic alcohols. This route for loss of $CH_3\cdot$ and $C_2H_5\cdot$ from **14**$^{+\cdot}$ and **15**$^{+\cdot}$, respectively, leads to **26**, eq. [3]. Similarly, expulsion of $C_2H_5\cdot$ from **17**$^{+\cdot}$ and **19**$^{+\cdot}$ affords **27** and **28**, respectively, eqs. [4] and [5].

*(ii) α- and σ′-Cleavage (**16**$^{+\cdot}$ and **18**$^{+\cdot}$).* In contrast, elimination of a methyl group from the ionised secondary ethers, **16**$^{+\cdot}$ and **18**$^{+\cdot}$, in which there is both an α- and either a γ- or β-methyl substituent, is not so simple. Both **16**-*1,1,1-D_3*$^{+\cdot}$ and **18**-*1,1,1-D_3*$^{+\cdot}$ expel $CH_3\cdot$ as well as the expected $CD_3\cdot$, even in fast dissociations occurring in the ion source (5). Moreover, $CH_3\cdot$ loss from these species increases in importance as the internal energy of the fragmenting ions decreases. Indeed, $CD_3\cdot$ loss is practically pre-empted by $CH_3\cdot$ elimination for these metastable $C_6H_9D_3O^{+\cdot}$ ions, which expel 93–95% $CH_3\cdot$ and only 5–7% $CD_3\cdot$, with no contribution from $CH_2D\cdot$ or $CHD_2\cdot$ loss. Both $CH_3\cdot$ and $CD_3\cdot$ expulsion give rise to relatively narrow Gaussian metastable peaks ($T_{1/2}$ = 1.7 kJ mol^{-1}, in each case) (footnote 2). These comparatively small KE releases are consistent with dissociation of the reacting configuration by C—C cleavage without a sizeable reverse critical energy. The analogous $C_5H_9OCD_3^{+\cdot}$ radical cations eliminate only $CH_3\cdot$ over a range of internal energies, so precluding any explanation of the unexpected $CH_3\cdot$ loss from **16**-*1,1,1-D_3*$^{+\cdot}$ and **18**-*1,1,1-D_3*$^{+\cdot}$ based on fission of the *O*-methyl bond (5).

The CID spectra of the $[M - CD_3]^+$ ions formed from **16**-

Can. J. Chem. Downloaded from www.nrcresearchpress.com by 213.200.69.106 on 09/08/12
For personal use only.

Can. J. Chem. Downloaded from www.nrcresearchpress.com by 213.200.69.106 on 09/08/12
For personal use only.

TABLE 2. CID mass

m/z	$[M - CH_3]^+$ from **14**	$[M - C_2H_5]^+$ from **15**[c]	$[M - CH_3]^+$ from **16**	$[M - C_2H_5]^+$ from **17**	$[M - CD_3]^+$ from **16**-*1,1,1-D*$_3$	$[M - CH_3]^+$ from **18**	$[M - C_2H_5]^+$ from **19**[c]	$[M - CD_3]^+$ from **18**-*1,1,1-D*$_3$
83	7	7	4	1		5	5	
70	6	5	5	6	4	4	5	3
69	5	3	27	57	43	15	24	23
68			1	3	1			
67								
59							1	
58								
57	2	1	2	1	2	2	3	2
56	3	2	1	2		2	5	2
55	100	100	100	76	84	100	100	100
54	18	18	13	9	7	12	6	3
53	23	23	42	59	60	27	27	31
52	5	4	4	4	2	3	3	2
51	8	7	8	9	8	6	6	5
50	5	4	6	6	5	5	4	3
45	10	10	28	42	42	16	15	20
43	83	84	43	5	8	46	12	10
42	10	10	13	16	12	10	10	8
41	14	14	33	55	50	33	56	52
40	2	2	4	7	7	4	7	5
39	42	38	69	100	100	62	87	88
38	4	4	6	10	10	6	8	8
37	1	1	2	3	3	1	3	3
33			2	4	3			
31	1	2	2	3	1	1	2	
29[b]	14	13	30	44	43	28	43	43
28	9	9	10	11	10	8	10	9
27	42	42	40	42	45	35	29	32
26	7	7	7	8	9	6	5	6
15	14	13	15	17	16	13	14	11
14	1	1		1		1		
55/69	20	33	3.7	1.8	2.3	6.7	4.2	4.3
55/53	4.3	4.3	2.4	1.3	1.5	3.7	3.7	3.2
69/43	0.06	0.04	0.6	11	5	0.3	2.0	2.3
43/39	2.0	2.2	0.6	0.05	0.08	0.7	0.14	0.11
Assigned structure	**26**	**26**	**26/27**	**27**	**27**	**26/28**	**28**	**28**

[a]See footnote to Table 1.
[b]This peak was a doublet (HCO^+ and $C_2H_5^+$); the quoted intensity is the sum of the individual components.
[c]Apart from complications caused by contributions from the dissociation of ions that have not been energised by collision, these spectra are in excellent

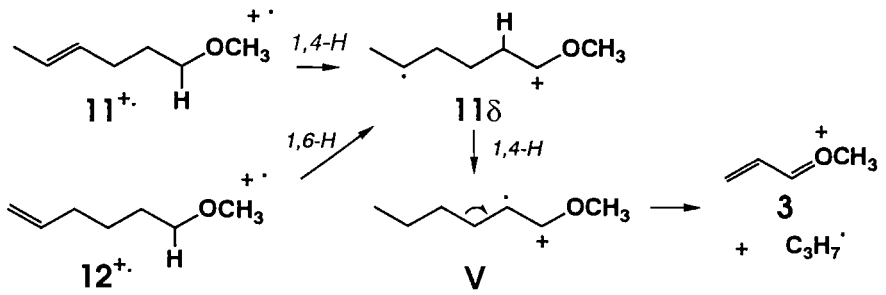

SCHEME 3

1,1,1-D$_3$$^{+\cdot}$ and **18**-*1,1,1-D*$_3$$^{+\cdot}$ resemble those of **27** and **28** generated from **17** and **19**, respectively. This component of methyl radical loss is, therefore, satisfactorily interpreted in terms of α-cleavage.

On the other hand, the $[M - CH_3]^+$ ions generated from **16**-*1,1,1-D*$_3$$^{+\cdot}$ and **18**-*1,1,1-D*$_3$$^{+\cdot}$ show CID spectra that are essentially identical to that of $CH_2{=}CH(CD_3)C{=}O^+CH_3$ ($[M - CD_3]^+$ in the ordinary mass spectrum of $CH_2{=}CH\text{-}(CD_3)_2COCH_3$), Table 3. This component of methyl radical elimination is, consequently, an example of the σ′-cleav-

spectra of $C_5H_9O^+$ ions[a]

Origin of ion									
$[M - CH_3]^+$ from **20**	$[M - CH_3]^+$ from **21**	$[M - CH_3]^+$ from **22**	$[M - CH_3]^+$ from **23**	$[M - CH_3]^+$ from **7**	$[M - C_2H_5]^+$ from **8**	$[M - C_2H_5]^+$ from **9**	$[M - C_2H_5]$ from **12**	$[M - CH_3]^+$ from **24**	$[M - H]^+$ from **25**
4	2	1	3	6	4	3	7	8	2
5	7	4	2	3	5	2	4	2	
23	53	43	23	19	26	24	19	5	1
	3	1				1		1	
							1	42	3
		1			1	1	3		
			7		1	1			
2	2	2	4	2	3	4	5	68	4
2	1	2	1	2	4	3	7	15	1
100	84	70	100	100	100	100	100	42	5
6	9	5	8	5	4	6	5	2	
36	61	49	49	27	33	24	24	8	3
3	4	3	2		2	2	1	1	
7	9	6	8	4	6	5	5	3	
4	6	4	3	4	3	2	6	2	
23	43	39	32	21	17	19	17	3	
17	8	26	20	14	11	11	24	63	100
9	15	14	10	5	8	10	16	21	9
45	54	61	47	45	51	47	64	83	9
5	8	7	7	4	6	4	11	7	1
78	100	100	71	77	74	79	86	69	
7	9	9	6	5	7	7	5	7	
2	3		1	2	1	1	2	2	
2	4	3	3			1	2		
2	3	2	2	3	1	2	1	5	1
36	43	38	38	30	40	41	46	100	9
9	11	6	11	10	10	9	9	11	
29	43	45	33	31	30	29	22	60	11
6	9	10	5	3	6	3	5	11	3
13	18	17	13	11	13	15	16	10	4
1	1	1							
4.3	1.9	2.3	4.3	5.3	3.8	4.2	5.3	8.4	5
2.8	1.4	1.4	2.0	3.7	3.0	4.2	4.2	5	1.6
1.6	7	1.6	1.2	1.4	2.3	2.2	0.8	0.08	0.01
0.22	0.08	0.26	0.28	0.18	0.14	0.14	0.28	0.91	>200
28	**27**	**27**	**26/28**(?)	**28**	**28**	**28**	**28**(?)	**29**	**30**

qualitative agreement with those reported in ref. 2.

age. The σ′-cleavage is evidently very facile, since it competes effectively with an apparently favourable α-cleavage that leads to a conjugated secondary oxonium ion (**27** or **28**). The main factor promoting σ′-cleavage is that it affords a tertiary conjugated oxonium ion (**26**-*1,1,1-D*$_3$), which should be even more stable than **27** or **28**. Accurate thermochemical data for **26**, **27**, and **28** are not yet available. Fortunately, however, reliable enthalpies of formation are accessible for the analogous oxonium ions $CH_2{=}CH(CH_3)C{=}OH^+$, $CH_3{-}CH{=}CHCH{=}OH^+$, and $CH_2{=}(CH_3)CCH{=}OH^+$ from the proton affinities of the corresponding C_4H_6O carbonyl compounds. These ΔH_f values (567, 603, and 607 kJ mol^{-1}, respectively (27)) reveal that the tertiary oxonium ion analogous to **26** is 35–40 kJ mol^{-1} more stable than the secondary oxonium ions corresponding to **27** and **28**. A parallel trend should operate in the energetics of **26**, **27**, and **28**; therefore, it is likely that **26** will be approximately 35–40 kJ mol^{-1} lower in energy than **27** or **28**. This difference in the stability of the product ions formed by the α- and σ′-cleavage processes is amply sufficient to allow the latter fragmentation to compete, even though it must entail more rearrangement than simple α-cleavage.

The ionised alkenols $CH_3CH{=}CH(CD_3)CHOH^{+\cdot}$ and $CH_2{=}(CH_3)C(CD_3)CHOH^{+\cdot}$ corresponding to **16**-*1,1,1-D*$_3^{+\cdot}$ and **18**-*1,1,1-D*$_3^{+\cdot}$ also show a tendency to undergo $CH_3{\cdot}$ loss via σ′-cleavage (1, 10). However, the situation is complicated for the ionised alkenols by the additional possibility that ketonisation may precede methyl radical expulsion.

Again, it is impossible to distinguish between β-cleavage (via rearrangement of **16**-*1,1,1-D*$_3^{+\cdot}$ and **18**-*1,1,1-D*$_3^{+\cdot}$ to **18**δ-*1,1,1-D*$_3^{+\cdot}$) and γ-cleavage (via a 1,2-H-shift in **16**δ-*1,1,1-D*$_3^{+\cdot}$, followed by fragmentation of **W**-*1,1,1-D*$_3^{+\cdot}$), Scheme 4. Both these routes yield **26**-*1,1,1-D*$_3^{+\cdot}$ as the product ion.

The CID spectra of the $[M - CH_3]^+$ ions formed from the unlabelled ethers **16** and **18** correspond to a combination of

Can. J. Chem. Downloaded from www.nrcresearchpress.com by 213.200.69.106 on 09/08/12
For personal use only.

TABLE 3. CID mass spectra of $C_5H_6D_3O^+$ ions[a]

	Origin of ion		
m/z	$[M - CH_3]^+$ from **16**-*1,1,1-D*$_3$	$[M - CH_3]^+$ from **18**-*1,1,1-D*$_3$	$[M - CD_3]^+$ from **14**-*1,1,1,1',1',1'-D*$_6$
86	4	4	6
73	3	3	4
69	2	2	2
59	<1	<1	2
58	76	76	71
57	14	14	15
56	11	11	13
55	47	48	47
54	2	2	3
53	3	3	5
52	2	1	3
51	<1	<1	2
46	100	100	100
45	16	18	18
44	11	11	12
43	7	7	8
42	3	4	5
41	22	22	21
40	18	19	19
39	9	8	9
38	<1	<1	2
32	1	1	3
31	10	10	12
30	10	10	12
29	19	20	21
28	12	12	14
27	31	32	35
26	4	3	6
18	8	8	11

[a]See footnote to Table 1.

the CID spectrum of **26** with an approximately equal pro-

[3] 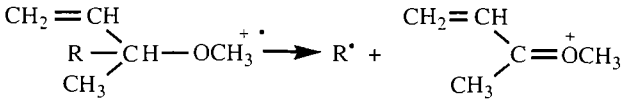

14$^{+\bullet}$, R = CH_3
15$^{+\bullet}$, R = C_2H_5

26

[4] 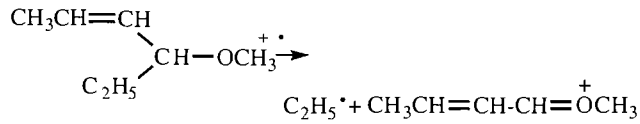

27

[5] 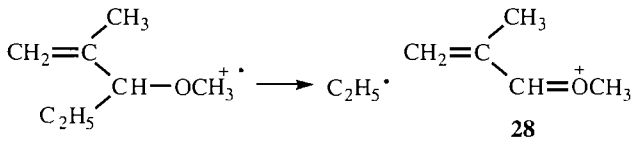

28

portion of those of **27** and **28**, respectively. These data are further evidence that rapid elimination of $CH_3\cdot$ from **16**$^{+\bullet}$ and **18**$^{+\bullet}$ occurs by α- and σ′-cleavages in comparable amounts. However, the fact that the CID spectra of $[M - CH_3]^+$ formed from **16**$^{+\bullet}$ and **18**$^{+\bullet}$ are significantly different indicates that the steps by which **16**$^{+\bullet}$ and **18**$^{+\bullet}$ interconvert do not take place rapidly and reversibly before $CH_3\cdot$ loss at high internal energies.

It is intriguing to note that σ′-cleavage becomes important only when the substituent that must be expelled by α-cleavage is a methyl group (i.e., for **16**$^{+\bullet}$ and **18**$^{+\bullet}$). Methyl loss via σ′-cleavage competes only very poorly with elimination of the α-ethyl substituent in the higher homologues **17**$^{+\bullet}$ and **19**$^{+\bullet}$ (5). This contrast probably reflects the much greater LGA (18) of $C_2H_5\cdot$ compared to $CH_3\cdot$ (see also section D.1(*a*)).

A final point concerns the abundance of the signals at *m/z* 69 (CH_4 expulsion) in the CID spectra of **26**, **27**, and **28**. The tertiary ion, **26**, shows only a weak peak, but **27** and **28** show intense and moderate signals, respectively. This trend suggests that CH_4 loss is preferentially associated with the $CH{=}O^+CH_3$ entity, which is present in **27** and **28**, but not in **26**.

*(iii) σ′-Cleavage (**20**$^{+\bullet}$ and **21**$^{+\bullet}$).* The CID spectra show that $CH_3\cdot$ elimination from **20**$^{+\bullet}$ and **21**$^{+\bullet}$ yields **28** and **27**, respectively. This behaviour is consistent with the mechanism involving a 1,2-H shift to the radical centre of the appropriate DI, followed by γ-cleavage (**20**$^{+\bullet}$ → **20**δ → **X** → $CH_3\cdot$ + **28**; **21**$^{+\bullet}$ → **21**δ → **Y** → $CH_3\cdot$ + **27**, respectively, Scheme 5). On the other hand, the observed specificity of methyl loss from **20**$^{+\bullet}$ and **21**$^{+\bullet}$ is the reverse of that which would be anticipated on the basis of β-cleavage of the relevant DI (**20**$^{+\bullet}$ → **20**δ → $CH_3\cdot$ + **27**; **21**$^{+\bullet}$ → **21**δ → **D** → **21**δ′

Can. J. Chem. Downloaded from www.nrcresearchpress.com by 213.200.69.106 on 09/08/12
For personal use only.

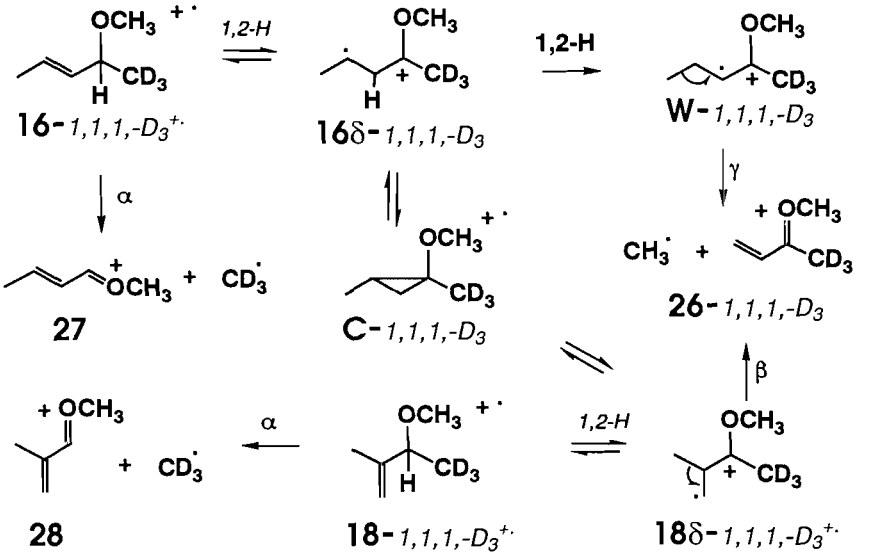

SCHEME 4

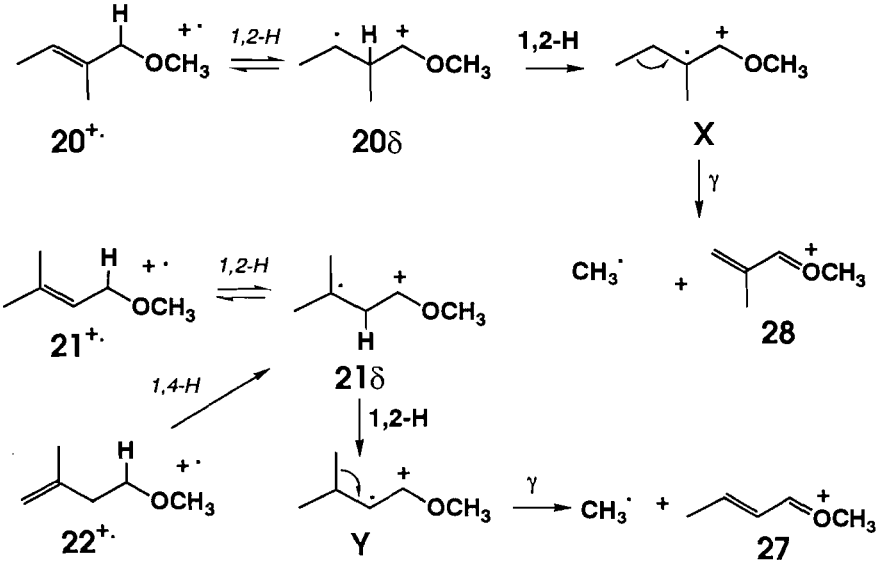

SCHEME 5

→ CH_3· + **28**, respectively, Scheme 6). Therefore, in these cases at least, the mechanism involving β-cleavage cannot account for σ′-cleavage.

This observation indicates that the reverse reaction, addition of CH_3· to the C=C double bond of a methyl-cationated enal, occurs more readily via a conjugate mechanism, e.g., eq. [6], than by simple attachment to the β-carbon, e.g., eq. [7]. Precisely parallel behaviour has been reported (16–18) in the fragmentation of β-DIs derived from ionised carboxylic acids. The reverse reaction (in this case, addition of CH_3· to protonated crotonic or methacrylic acid ($CH_3CH{=}CHC^+(OH)_2$ or $CH_2{=}(CH_3)CHC^+(OH)_2$, respectively)) occurs by attachment to the γ-carbon. In both systems, the preference shown in the reverse reaction for binding to the γ-carbon, via conjugate addition of CH_3· to a protonated acrylic acid or a methyl-cationated enal, can be understood qualitatively in terms of the nucleophilic (28, 29) properties of radicals.

Further light is shed on this site selectivity by considering the interactions that take place between the singly occupied molecular orbital (SOMO) of the radical and lowest unoccupied molecular orbital (LUMO) of the methyl-cationated enal. According to frontier orbital theory (FOT) (30), such SOMO–LUMO interactions are especially important in reactions involving radicals that have a high-energy SOMO; CH_3· falls into this category (31). The LUMO of the cationated enal should approximately resemble that of allyl cation; in other words, the electron density should be greater on the terminal carbon atoms (the γ and α positions) than on the central carbon atom (the β position). Therefore, the initial interaction that leads to binding of CH_3· to the γ-carbon atom of the cationated enal is more favourable than that leading to binding to the β-carbon atom.

The energy barrier towards a 1,2-H shift to the radical site of the DIs such as **20**δ must be less than that for β-cleavage. If this were not so, **20**δ would fragment via β-cleavage

Can. J. Chem. Downloaded from www.nrcresearchpress.com by 213.200.69.106 on 09/08/12
For personal use only.

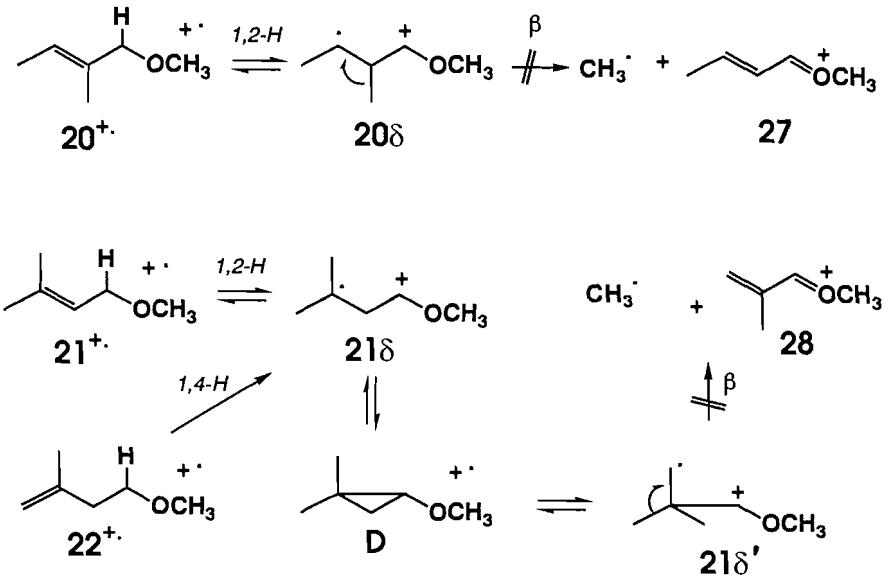

SCHEME 6

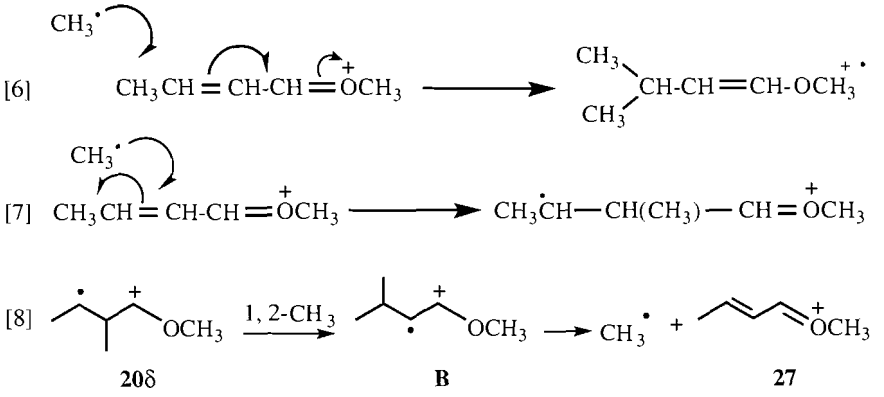

(**20**δ → CH_3· + **27**) instead of undergoing a 1,2-H shift and subsequent γ-cleavage (**20**δ → **X** → CH_3· + **28**). As mentioned previously, 1,2-H shifts to radical centres are less facile than those to cationic sites because they have additional critical energies (16–18, 20–22). Consequently, the energy barrier towards β-cleavage (and, by microscopic reversibility, that for addition of CH_3· to the β-carbon of a methyl-cationated enal) must be quite large.

A second significant conclusion concerns the relative ease of 1,2-H and 1,2-CH_3 shifts to radical centres. A 1,2-CH_3 shift, followed by γ-cleavage, would lead to the same product ion (**27**) as that formed by direct β-cleavage, e.g., eq. [8]. This is contrary to the observed specificity shown in the fragmentation of **20**$^{+\cdot}$. Indeed, there is no evidence that any of the ionised ethers studied in this work dissociate via steps involving 1,2-alkyl shifts to the radical centre of a DI. Therefore, 1,2-H shifts occur more readily than 1,2-alkyl shifts to radical sites, at least in these systems. Similar conclusions were reached in the earlier investigation of the reactions of DIs derived from ionised carboxylic acids. Whereas 1,2-H shifts to radical centres were definitely observed, no example of a comparable 1,2-alkyl shift was uncovered (16–18).

*(b) Ethers of non-allylic alcohols (**22**$^{+\cdot}$ and **23**$^{+\cdot}$)*

In the case of **22**$^{+\cdot}$, the structure of the $C_4H_7O^+$ product ion appears to be **27**. The mechanism of Scheme 5 explains this result (a 1,4-H shift converts **22**$^{+\cdot}$ into **21**δ, which then rearranges to **Y** prior to methyl radical elimination). In contrast, the mechanism involving β-cleavage (**22**$^{+\cdot}$ → **21**δ → **D** → **21**δ' → CH_3· + **28**, Scheme 6) predicts formation of the wrong product ion. Therefore, the behaviour of **22**$^{+\cdot}$ offers further evidence that the σ'-cleavage is more accurately described in terms of 1,2-H shifts and γ-cleavage than by β-fission.

The fragmentation of **22**$^{+\cdot}$ differs conspicuously from that of the lower homologue, $CH_2{=}CHCH_2CH_2OCH_3^{+\cdot}$, which expels CH_3· with production of a cyclic oxonium ion, $\overline{CH_2CH_2CH_2CH{=}O}^+$ (7). A similar route does not operate for CH_3· loss from **22**$^{+\cdot}$, since the CID spectra of the resultant ion is obviously distinct from those of $CH_3\overline{CHCH_2CH_2CH{=}O}^+$ and $\overline{CH_2CH_2CH_2(CH_3)C{=}O}^+$.

The $[M - CH_3]^+$ signal in the conventional mass spectrum of **23** is only weak (5). The CID spectrum of this ion resembles that of **28**. However, the resemblance is not conclusively close. In addition, the CID spectrum of $[M - CH_3]^+$ formed from **23** shows many features that are found in the

Can. J. Chem. Downloaded from www.nrcresearchpress.com by 213.200.69.106 on 09/08/12
For personal use only.

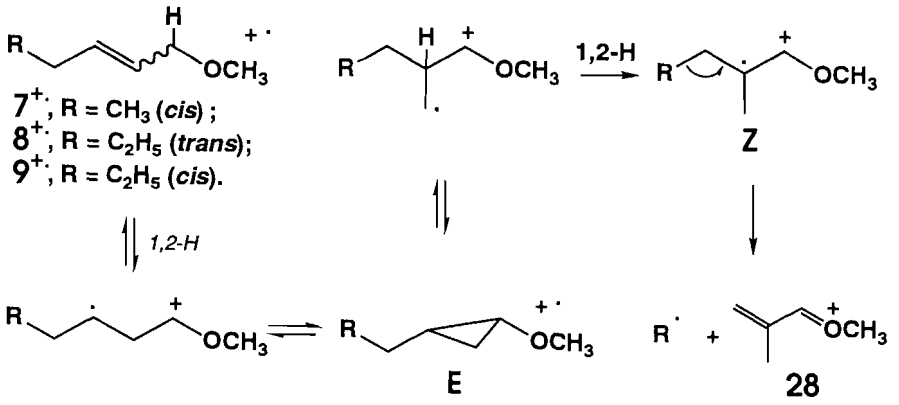

SCHEME 7

spectrum of the $C_4H_7O^+$ ion generated by methyl expulsion from $\mathbf{16}^{+\cdot}$. The latter spectrum corresponds to a combination of those of **26** and **27**, as is discussed above (Sect. E.1(*a*)(*ii*)). In view of these uncertainties, no definite mechanistic conclusions are possible. Formation of a mixture of **26** and **27**, after isomerisation of $\mathbf{23}^{+\cdot}$ to $\mathbf{16}^{+\cdot}$ via a series of hydrogen shifts, is perhaps the most likely possibility.

E.2. Loss of an alkyl group smaller than an intact β- or γ-substituent

(a) Ethers of allylic alcohols ($7^{+\cdot}$, $8^{+\cdot}$, and $9^{+\cdot}$)

This peculiar reaction corresponds to formal δ-cleavage; it is important for ionised ethers of primary allylic alcohols in which there is an ethyl or larger alkyl substituent on the γ-carbon atom. Thus, loss of R· occurs from $RCH_2CH{=}CHCH_2OCH_3^{+\cdot}$. It is favoured at lower internal energies (12 eV, as opposed to 70 eV ionising electron energies (5)), and it competes effectively with loss of the entire γ-substituent in the dissociation of metastable ions. For example, metastable $\mathbf{7}^{+\cdot}$ expels C_2H_5· (σ′-cleavage) and CH_3· (δ-cleavage) in comparable quantities (29 and 47%, respectively). Metastable $\mathbf{5}^{+\cdot}$ behaves similarly (footnote 2), as would be expected given the ease of interconversion of these species via DIs and ionised ethylmethoxycyclopropane, $C_2H_5\overline{CHCH_2}\overline{CHOCH_3}^{+\cdot}$. However, at higher internal energies, CH_3· expulsion from $\mathbf{5}^{+\cdot}$ is of negligible significance because it is pre-empted by α-cleavage (C_2H_5· loss) (5).

The CID spectra establish that CH_3· loss from $\mathbf{7}^{+\cdot}$ and C_2H_5· elimination from $\mathbf{8}^{+\cdot}$ or $\mathbf{9}^{+\cdot}$ yield **28** as the product ion. The formation of a branched oxonium ion, rather than the linear species, **27**, is at first sight surprising since $\mathbf{7}^{+\cdot}$, $\mathbf{8}^{+\cdot}$, and $\mathbf{9}^{+\cdot}$ all contain unbranched alkenyl chains with a terminal methoxy group. Nevertheless, a mechanism involving DIs, ionised ethylmethoxycyclopropane, a 1,2-H shift, and eventual γ-cleavage explains this process, Scheme 7.

The success of Scheme 7 in interpreting this reaction is further evidence that the σ′-cleavage proceeds via a 1,2-H shift to the radical site of a DI followed by γ-cleavage of the appropriate ionised enol ether. No mechanism involving β-cleavage can account for this process.

The occurrence of δ-cleavage of $\mathbf{7}^{+\cdot}$, $\mathbf{8}^{+\cdot}$, and $\mathbf{9}^{+\cdot}$, together with the apparent ease of interconversion of metastable $\mathbf{7}^{+\cdot}$ and $\mathbf{5}^{+\cdot}$ via DIs and ionised ethylmethoxycyclopropane, suggests strongly that the skeletal rearrangement corresponding to a 1,2-$^+$CHOCH$_3$ shift has a lower critical energy than the 1,2-H shift to the radical site of the appropriate DI. If this were not so, a 1,2-H shift to the radical centre in the DI ($RCH_2CH{\cdot}CH_2CH^+OCH_3$) formed from $\mathbf{7}^{+\cdot}$, $\mathbf{8}^{+\cdot}$, and $\mathbf{9}^{+\cdot}$ would preempt isomerisation via **E**; the resultant ionised enol ether ($RCH_2CH_2CH{\cdot}CH^+OCH_3$) would then expel RCH_2· via γ-cleavage, thus circumventing R· loss. For similar reasons, it is difficult to account for CH_3· elimination from metastable $\mathbf{5}^{+\cdot}$ unless the skeletal rearrangement occurs more readily than α-cleavage at low internal energies. It has already been shown that the 1,2-H shift to the radical site of the DIs has a smaller critical energy than β-cleavage. Consequently, the order of increasing critical energy for the isomerisation and dissociation steps in the fragmentation of $C_mH_{2m-1}OCH_3^{+\cdot}$ species is 1,2-$^+$CHOCH$_3$ rearrangement < 1,2-H shift to a radical centre < β-cleavage. The same trend was found in the decomposition of radical cations formed from $RCO_2H^{+\cdot}$ species (16–18).

However, one difference between the chemistry of the $C_mH_{2m-1}OCH_3^{+\cdot}$ and $RCO_2H^{+\cdot}$ radical cations becomes apparent at this point. Loss of C_2H_5· from $\mathbf{8}^{+\cdot}$ and $\mathbf{9}^{+\cdot}$ is interpreted in Scheme 7 as occurring after a 1,2-H shift to a radical centre. In the $RCO_2H^{+\cdot}$ system, radical losses after such 1,2-H shifts were confined to cases in which CH_3· was expelled (16–18).

(b) Ethers of non-allylic alcohols ($12^{+\cdot}$)

Only weak $[M - C_2H_5]^+$ signals are present in the normal mass spectra of most linear isomers of $C_6H_{11}OCH_3$ derived from non-allylic primary alcohols (5). In the case of **12**, the $C_5H_9O^+$ signal is sufficiently strong to permit a reliable CID spectrum to be recorded. This spectrum indicates that the structure of the product ion is predominantly **28**. A similar conclusion was reached in an earlier combined CID and labelling study of the mechanism of C_2H_5· elimination from $\mathbf{12}^{+\cdot}$ (4). In view of this detailed investigation, which showed that $\mathbf{12}^{+\cdot}$ expels C_2H_5· by at least two routes, no further mechanistic analysis is attempted.

Other types of isomerisation of these $C_mH_{2m-1}OCH_3^{+\cdot}$ radical cations could, in principle, intervene. For example, a facile 1,5-H shift in $\mathbf{11}^{+\cdot}$ would afford the γ-DI $CH_3CH_2{\cdot}CHCH_2CH_2CH^+OCH_3$. Many γ-DIs readily undergo skeletal rearrangement (32, 33) via steps that can be understood in terms of formation of an ion-neutral complex (INC (34–37). This isomerisation is sometimes referred to as a 1,2-[enol olefin] shift. In this case, cleavage of the bond connecting the α- and β-carbons gives the INC [CH_3CH_2-$CH{=}CH_2$ $CH_2{=}CHOCH_3^{+\cdot}$]. Recombination of the components via addition of the 1-butene to ionised methyl vinyl

Can. J. Chem. Downloaded from www.nrcresearchpress.com by 213.200.69.106 on 09/08/12
For personal use only.

Can. J. Chem. Downloaded from www.nrcresearchpress.com by 213.200.69.106 on 09/08/12
For personal use only.

ether with the opposite regiospecificity to that of the step forming the INC could then give access to $CH_3CH_2(CH_2\cdot)$-$CHCH_2CH^+OCH_3$. An α-DI, $CH_3CH_2(CH_3)CH\cdot CH_2{}^+OCH_3$, may then be formed via further hydrogen shifts. This α-DI could then expel either $C_2H_5\cdot$ or $CH_3\cdot$, via γ-cleavage, with production of a stable conjugated oxonium ion $RCH{=}CHCH{=}O^+CH_3$ (R = CH_3 or C_2H_5, respectively). Unfortunately, the abundances of the $[M - CH_3]^+$ and $[M - C_2H_5]^+$ ions in the conventional spectrum of **11** are too low to permit reliable CID spectra to be measured. Therefore, the extent to which these rearrangements actually occur cannot be elucidated from the current data. However, the absence of appreciable $[M - CH_3]^+$ and $[M - C_2H_5]^+$ signals in the spectrum of **11** suggests that these processes compete only poorly with that resulting in $C_3H_7\cdot$ loss (Sect. D.2), at least at high internal energies.

Conclusions

Elimination of an alkyl radical from ionised pentenyl and hexenyl methyl ethers takes place via several distinct routes. All these routes result in formation of acyclic conjugated oxonium ions. For ionised ethers of tertiary allylic alcohols, loss of an α-alkyl substituent occurs readily by direct cleavage. Similarly, ionised secondary ethers also appear to fragment via α-cleavage provided an ethyl or larger radical is expelled. The corresponding species containing an α-methyl substituent dissociate via two mechanisms, involving loss of the α-methyl group (α-cleavage) and expulsion of a methyl group attached to the double bond (σ′-cleavage). This σ′-cleavage is favoured at low internal energies. Ionised ethers of primary allylic alcohols also undergo σ′-cleavage; in addition, these ions decompose via formal δ-cleavage if the alkenyl chain is sufficiently long. A mechanism in which a 1,2-H shift to the radical site of a DI leads to an ionised enol ether that then fragments via γ-cleavage provides a satisfactory unifying explanation for the σ′- and δ-cleavage processes. Dissociation is evidently specifically associated with γ-cleavage of the ionised enol ether in which the formal cationic and radical sites are located on adjacent carbon atoms, one of which carries the methoxy group. This mechanism can be extended to explain the elimination of an alkyl radical from ionised ethers derived from certain non-allylic alcohols.

The preference for dissociation via γ-cleavage reveals that the reverse process, conjugate addition of an alkyl radical to a methyl-cationated enal, occurs more readily than addition to the β-carbon atom. This phenomenon is an illustration of the nucleophilic properties associated with alkyl radicals having a high-energy SOMO.

In general, the isomerisation process corresponding to a 1,2-$^+CHOCH_3$ shift in the DI $R^1CH\cdot CHR^2CH^+OCH_3$ (i.e., leading to $R^2CH\cdot CHR^1CH^+OCH_3$, via $R^1\overline{CHCHR^2}CHO$-$CH_3{}^{+\cdot}$) has a lower critical energy than a 1,2-H shift to the same radical centre to yield $R^1CH_2\cdot CR^2CH^+OCH_3$. Both these processes require less energy than β-cleavage of either DI to give, respectively, $R^2CH{=}CHCH{=}O^+CH_3 + \cdot R^1$ or $R^1CH{=}CHCH{=}O^+CH_3 + \cdot R^2$.

The unusual 1,2-H shifts to the radical site take place more readily than the analogous 1,2-alkyl shifts in these systems. In contrast to 1,2-H shifts, which play an important part in the chemistry of these $C_nH_{2n}O^{+\cdot}$ species, there is no evidence for the occurrence of 1,2-alkyl shifts to the radical centre.

The reactions of the DIs generated from these $C_mH_{2m-1}OCH_3{}^{+\cdot}$ species show many similarities to those of DIs formed from $RCO_2H^{+\cdot}$. In particular, both classes of radical cations expel an alkyl radical via γ-cleavage; moreover, 1,2-H shifts to radical centres are observed, and isomerisation steps involving 1,2-$^+CHOCH_3$ or 1,2-$^+C(OH)_2$ shifts take place. The relative ease of several key steps follows the same trend for both types of DIs (1,2-$^+CHOCH_3$ or 1,2-$^+C(OH_2)$ shifts occur more readily than 1,2-H shifts to radical sites, which are more facile than β-cleavage). Furthermore, certain apparently plausible steps (e.g., 1,2-alkyl shifts to a radical centre) are not observed in the dissociation of either kind of DI. These common features reflect the reactivity of free radicals that is manifested in the chemistry of these DIs.

Experimental

The ethers required in this work were prepared from the corresponding alkenols by condensation of a suspension of the appropriate sodium alkoxide in triglyme (triethyleneglycol dimethyl ether $CH_3O(CH_2CH_2O)_3CH_3$) with a slight deficiency (0.8 equivalents of iodomethane). The general procedure for this process has been published (5); further details are available on request. The unlabelled alkenols were commercial samples of high purity. The ^2H-labelled alkenols were synthesised by the following conventional routes: $CH_3CH{=}CH(CD_3)CHOH$ and $CH_2{=}(CH_3)C(CD_3)CHOH$ were made by addition of 0.8 equivalents of the appropriate enals ($CH_3CH{=}CHCHO$ and $CH_2{=}(CH_3)CCHO$, respectively) to an ethereal solution of CD_3MgI at −78°C; $CH_2{=}CH(CD_3)_2COH$ was made by addition of 0.8 equivalents of $(CD_3)_2CO$ to a solution of $CH_2{=}CHMgBr$ in tetrahydrofuran at 30–40°C. No impurities could be detected by mass spectrometry or ^1H NMR in any of the alkenyl methyl ethers used in this work.

The CID spectra were measured on a Kratos Analytical Concept II HH four-sector mass spectrometer (EBEB geometry). The collision cell was floated at 4 kV above ground potential; the collision gas was helium, and the precursor ion beam was attenuated to 70% of its initial intensity. The data quoted in Tables 1–3 are integrated spectra, compiled from 15 individual scans. These spectra are essentially free from contributions arising from the dissociation of ions that have not been energised by collision.

Acknowledgements

Financial support of this work from the Science and Engineering Research Council (S.E.R.C.) (including the award of an Advanced Fellowship to R.D.B.), the British Mass Spectrometry Society (funds for purchasing alkenols and labelled starting materials), and the Leverhulme Trust (Research Fellowship and Grant to R.D.B.) is gratefully acknowledged. Special thanks are due to Mrs. Margaret Hill for her care in preparing and revising the typescript.

1. G. Bouchoux. Mass Spectrom. Rev. **7**, 1 (1988); **7**, 203 (1988).
2. G. Bouchoux, Y. Hoppilliard, and P. Jaudon. Org. Mass. Spectrom. **22**, 98 (1987).
3. G. Bouchoux, F. Djazi, Y. Hoppilliard, P. Jaudon, and N. Nouts. Org. Mass Spectrom. **22**, 33 (1988).
4. T.A. Molenaar-Langeveld, R.H. Fokkens, and N.M.M. Nibbering. Org. Mass Spectrom. **23**, 364 (1988).
5. R.D. Bowen, A.D. Wright, S.R. Thomas, K.R. Jennings, and A. Maccoll. Org. Mass Spectrom. **26**, 421 (1991).
6. R.D. Bowen, A.D. Wright, and P.J. Derrick. Org. Mass Spectrom. **27**, 905 (1992).

7. R.D. Bowen, A.D. Wright, A.W. Colburn, and P.J. Derrick. Int. J. Mass Spectrom. Ion Processes, **116**, 193 (1992).
8. B.F. Yates, W.J. Bouma, and L. Radom. J. Am. Chem. Soc. **106**, 5808 (1984).
9. S. Hammerum. Mass Spectrom. Rev. **7**, 123 (1988).
10. R.D. Bowen and A.D. Wright. J. Chem. Soc. Chem. Commun. 1055 (1991).
11. R.D. Bowen and A.D. Wright. J. Chem. Soc. Chem. Commun. 96 (1992).
12. D.J. McAdoo, C.E. Hudson, and D.N. Witiak. Org. Mass Spectrom. **14**, 350 (1979).
13. D.J. McAdoo and C.E. Hudson. Org. Mass Spectrom. **18**, 466 (1983).
14. R.D. Bowen and A.G. Harrison. J. Chem. Soc. Perkin Trans. 2, 1483 (1989).
15. H.E. Audier and G. Sozzi. Org. Mass Spectrom. **19**, 150 (1983); see also references therein.
16. T. Weiske and H. Schwarz. Chem. Ber. **116**, 323 (1983).
17. T. Weiske, H. Halim, and H. Schwarz. Chem. Ber. **118**, 495 (1985).
18. T. Weiske and H. Schwarz. Tetrahedron, **42**, 6245 (1986).
19. A. Maccoll. Org. Mass Spectrom. **15**, 105 (1980).
20. H. Schwarz, T. Weiske, K. Levsen, A. Maquestiau, and R. Flammang. Int. J. Mass Spectrom. Ion Phys. **45**, 367 (1982).
21. S. Hammerum. Acta Chem. Scand. Ser. B, **38**, 707 (1984).
22. C.E. Hudson and D.J. McAdoo. Tetrahedron, **46**, 331 (1990); see also references cited therein.
23. D.H. Williams and G. Hvistendahl. J. Am. Chem. Soc. **96**, 6753 (1974); **96**, 6755 (1974); G. Hvistendahl and D.H. Williams. J. Chem. Soc. Perkin Trans. 2, 991 (1975); J. Am. Chem. Soc. **97**, 3097 (1975).
24. R.B. Woodward and R. Hoffmann. Angew. Chem. Int. Ed. Engl. **8**, 781 (1969).
25. R.D. Bowen, A.W. Colburn, and P.J. Derrick. J. Chem. Soc. Chem. Commun. 1274 (1989).
26. G. Bouchoux, Y. Hoppilliard, R. Houriet, and E. Rolli. Org. Mass Spectrom. **21**, 209 (1986).
27. S.G. Lias, J.F. Liebman, and R.D. Levin. J. Phys. Chem. Ref. Data, **13**, 693 (1984).
28. D.C. Nonhebel, J.M. Tedder, and J.C. Walton. Radicals. Cambridge University Press, Cambridge. 1979.
29. A.L.J. Beckwith. Tetrahedron, **37**, 3073 (1981).
30. K. Fukui. Acc. Chem. Res. **4**, 57 (1971).
31. I. Fleming. Frontier orbitals and organic chemical reactions. Wiley and Sons, London. 1976; see especially pp. 115–116 and 182–186.
32. G. Bouchoux, J. Tortajada, J. Dagaut, and J. Fillaux. Org. Mass Spectrom. **22**, 451 (1987).
33. G. Bouchox, F. Bidault, F. Djazi, B. Nicod, and J. Tortajada. Org. Mass Spectrom. **22**, 748 (1987).
34. T.H. Morton. Tetrahedron, **38**, 3195 (1982).
35. D.J. McAdoo. Mass Spectrom. Rev. **7**, 363 (1988).
36. R.D. Bowen. Acc. Chem. Res. **24**, 364 (1991).
37. P. Longevialle. Mass Spectrom. Rev. **11**, 157 (1992).

Can. J. Chem. Downloaded from www.nrcresearchpress.com by 213.200.69.106 on 09/08/12
For personal use only.

Coordination chemistry of thioether–pyridazine macrocycles. III. Synthetic, structural, and spectroscopic studies of Cu(II), Cu(II)Cu(I), and Cu(I) complexes of a hexathiapyridazinophane macrocyclic ligand

LIQIN CHEN, LAURENCE K. THOMPSON,[1] AND JOHN N. BRIDSON

Department of Chemistry, Memorial University of Newfoundland, St. John's, Nfld., Canada A1B 3X7

Received February 1, 1993

LIQIN CHEN, LAURENCE K. THOMPSON, and JOHN N. BRIDSON. Can. J. Chem. **71**, 1086 (1993).

The preparation and properties of the thioether–pyridazine macrocycle (L4; $C_{16}H_{20}S_6N_4$) containing two pyridazine subunits, and its Cu(II), Cu(II)Cu(I), and Cu(I) complexes are described. The ligand is characterized by ^1H nuclear magnetic resonance and mass spectrometry, and the complexes by infrared, eleetronic spectra, and magnetism, and in some cases by X-ray crystallography. The complex $[Cu_2(L4)Cl_4]_x$ (**1**) crystallized in the triclinic system, space group $P\bar{1}$ with a = 8.6204(8) Å, b = 9.850(1) Å, c = 8.348(1) Å, α = 111.46(1)°, β = 102.50(1)°, γ = 71.818(9)°, V = 622.6(1) Å^3, and Z = 1 (R = 0.043, R_w = 0.042 for 1312 reflections). Two monodentate pyridazine rings in the same ligand bind to one *trans* square-planar copper centre (CuN_2Cl_2) with two sulfurs from each ligand binding to another *trans* square-planar copper centre (CuS_2Cl_2) to form a polynuclear chain. The complex $[Cu(L4)Cl_2]$ (**3**) crystallized in the triclinic system, space group $P\bar{1}$, with a = 11.001(1) Å, b = 12.888(2) Å, c = 8.704(1) Å, α = 102.89(1)°, β = 103.36(1)°, γ = 75.84(1)°, V = 1145.8(3) Å^3, and Z = 2 (R = 0.056, R_w = 0.044 for 2059 reflections). A *trans* square-planar structure (CuN_2Cl_2) exists for **3** with monodentate pyridazines. $[Cu(L4)(NO_3)_2]$ (**4**) crystallized in the orthorhombic system, space group $P2_12_12_1$, with a = 15.148(2) Å, b = 15.562(3) Å, c = 11.064(1) Å, V = 2608.2(7) Å^3, and Z = 4 (R = 0.039, R_w = 0.034 for 1864 reflections). Two monodentate pyridazine rings and two bidentate nitrates bind to a pseudo-octahedral copper(II) centre.

LIQIN CHEN, LAURENCE K. THOMPSON et JOHN N. BRIDSON. Can. J. Chem. **71**, 1086 (1993).

On décrit la préparation et les propriétés du macrocycle thioéther-pyridazine (L4; $C_{16}H_{20}S_6N_4$) contenant deux sous-unités pyridazinesainsi que celles de ses complexes avec le Cu(II), le Cu(II)Cu(I) et le Cu(I). On a caractérisé le ligand par RMN du ^1H et par spectrométrie de masse et les complexes par spectroscopies infrarouge et électronique ainsi que par magnétisme et, dans certains cas, par diffraction des rayons X. Le complexe $[Cu_2(L4)Cl_4]_x$ (**1**) cristallise dans le système triclinique, groupe d'espace $P\bar{1}$, avec a = 8,6204(8), b = 9,850(1) et c = 8,348(1) Å, α = 111,46(1)°, β = 102,50(1)° et γ = 71,818(9)°, V = 622,6(1) Å^3 et Z = 1 (R = 0,043 et R_w = 0,042 pour 1312 réflexions). Deux noyaux pyridazines monodentates du même ligand se lient à un centre cuivre plan-carré *trans* (CuN_2Cl_2) alors que deux atomes de soufre de chaque ligand se lient à un autre centre cuivre plan-carré *trans* (CuS_2Cl_2) pour former une chaîne polynucléaire. Le complexe $[Cu_2(L4)Cl_2]$ (**3**) cristallise dans le système triclinique, groupe d'espace $P\bar{1}$, avec a = 11,001(1), b = 12,888(2) et c = 8,704(1) Å, α = 102,89(1)°, β = 103,36(1)° et γ = 75,84(1)°, V = 1145,8(3) Å^3 et Z = 2 (R = 0,056 et R_w = 0,044 pour 2059 réflexions). Il existe une structure (CuN_2Cl_2) plan-carré *trans* pour **3** avec pyridazines monodentates. Le $[Cu(L4)(NO_3)_2]$ (**4**) cristallise dans le système orthorhombique, groupe d'espace $P2_12_12_1$, avec a = 15,148(2), b = 15,562(3) et c = 11,064(1) Å, V = 2608,2(7) Å^3 et Z = 4 (R = 0,039 et R_w = 0,034 pour 1864 réflexions). Deux noyaux pyridazines monodentates et deux nitrates bidentates se lient à un centre cuivrique pseudo-tétraédrique.

[Traduit par la rédaction]

Introduction

The recent development of the coordination chemistry of thioethers has been stimulated by the discovery of thioether coordination to copper in the blue copper proteins (1). Metal ligation through sulfur donor centres has been considered to contribute not only to anomalously high redox potentials of these proteins but also to their exceptionally rapid electron transfer reactions. As a result, the current literature on copper complexes reveals many studies on thioether ligands, including homoleptic macrocyclic thioethers (2–12), open chain polythioethers (13), chelating ligands with built in thioether and azole functions (14), and macrocyclic thioethers with benzene, pyridine, furan, and thiophene heterocyclic subunits (15–20).

Our interest in mixed sulfur-nitrogen ligands involving thioether and diazine ligands stems from our earlier studies on open-chain tetradentate (N_4) thioether–pyridazine ligands (21–27), which involved non-coordinating thioether linkages and formed binuclear copper(II) complexes with, in some cases, positive (0 → +0.5 V vs. SCE) reduction potentials. The combination of pyridazine and thioether groups, suitably disposed for simultaneous coordination, might be expected to produce binuclear copper(II) complexes with more positive reduction potentials. However, our initial studies in this area, which have involved the syntheses and structural and spectroscopic studies of a series of copper(II), copper(I), and silver(I) complexes of thioether–pyridazine macrocycles containing one, two, and three pyridazine subunits (L3, L2, L1, Fig. 1) (28, 29), have shown that, so far, simultaneous intraligand NS coordination does not occur. The present paper describes the copper coordination chemistry of the 2:2 macrocyclic ligand L4 (Fig. 1), which involves 1,4,7-trithiaheptyl linkages between the pyridazine subunits. In one case the ligand acts as an N_2S_2 donor, but in a polymeric arrangement.

Experimental section

Commercially available reagents (Aldrich) were used without further purification. Infrared spectra were recorded using a Mattson Polaris FT instrument and electronic spectra with a Cary 5E spectrometer. Mass spectra were obtained using a VG Micromass 7070 HS spectrometer and nmr spectra using a GE 300 MHz instrument. X-ray diffraction data were collected using a Rigaku AFC6S

[1]Author to whom correspondence should be addressed.

Can. J. Chem. Downloaded from www.nrcresearchpress.com by 213.200.69.106 on 09/08/12
For personal use only.

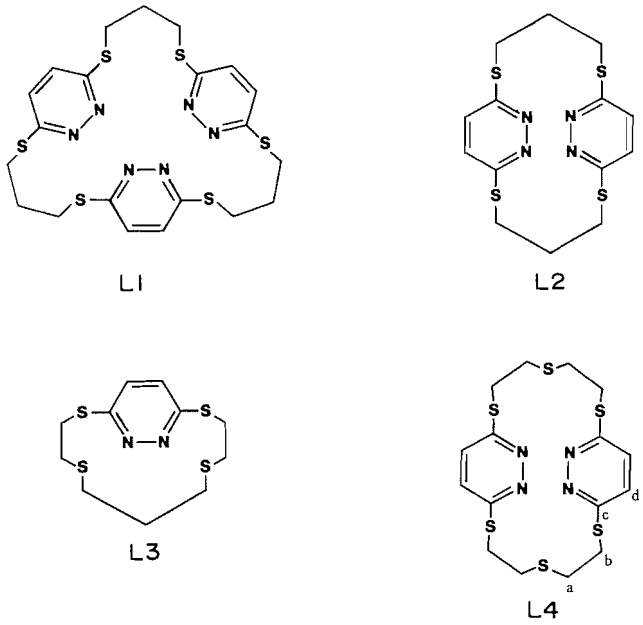

FIG. 1. Structural representation of the ligands L1, L2, L3, L4.

instrument and room temperature magnetic susceptibility data were measured by the Faraday method using a Cahn 7600 magnetic susceptibility system. Elemental analyses were performed by Canadian Microanalytical Service, Delta, B.C., Canada.

Synthesis of ligand and complexes

Safety note

Perchlorate salts of metal complexes with organic ligands are potentially explosive. Only small amounts of material should be prepared and these should be handled with caution. The complex described in this report has, so far, been found to be safe when used in small quantities.

L4

2-Mercaptoethyl sulfide (8.56 g, 50.0 mmol) was added to anhydrous ethanol (100 mL) in which sodium metal (2.30 g, 100.0 mmol) had been dissolved, and the resulting solution was stirred for 30 min. 3,6-Dichloropyridazine (7.68 g, 50.0 mmol) was then dissolved in anhydrous ethanol (100 mL) and both solutions were added dropwise simultaneously to anhydrous ethanol (500 mL) using pressure-equalizing funnels, over a period of 6 h during which time a white precipitate formed. The mixture was stirred overnight and then filtered. The white solid was washed with ethanol and deionized water, dried in vacuo, and recrystallized from $CHCl_3$ and then $MeNO_2$ to give white crystals. Yield 4.2 g.

The solvent of the original filtrate was removed using a rotary evaporator, the residue extracted with $CHCl_3$ and the extract washed several times with deionized water and dried over anhydrous Na_2SO_4. The concentrated extract was chromatographed on silica gel, eluted with $CHCl_3$, and the volume of the eluate reduced to a few mL on a rotary evaporator; white crystals were obtained (0.5 g). These two parts of the product have the same melting point 217–219°C (total yield 40.4%). Mass spectrum, major mass peaks (*m/e* (relative intensity)): 460(1) P, 401(22), 374(11), 231(47), 144(32), 87(100). ^1H nmr (Fig. 1) ($CDCl_3$/TMS) (δ ppm (relative intensity)): 3.07(8) (triplet, CH_2(a)), 3.62(8) (triplet, CH_2(b)), 7.04(4) (singlet, pyridazine (H_d)). ^{13}C nmr ($CDCl_3$/TMS) (δ ppm) 29.7 (C_a), 30.1 (C_b), 125.5 (C_d), 158.0 (C_c).

$[Cu_2(L4)Cl_4]_x$ (1)

Method A

To a solution of $CuCl_2 \cdot 2H_2O$ (85 mg, 0.50 mmol) in 20 mL CH_3CN was added a solution of L4 (92 mg, 0.20 mmol) in 20 mL $CHCl_3$. The resulting dark green solution was filtered and allowed to stand at room temperature overnight. Dark brown crystals formed which were filtered, washed with CH_3CN, and dried in air. Yield 125 mg (78%). Anal. calcd. for $[C_{16}H_{20}N_4S_6Cl_4Cu_2] \cdot 0.5CHCl_3$: C 25.11, H 2.62, N 7.10; found: C 24.75, H 2.70, N 7.27.

Method B

Cu powder (190 mg, 3.0 mmol) was added to a solution of $CuCl_2 \cdot 2H_2O$ (51 mg, 0.30 mmol) in CH_3CN (20 mL). The mixture was stirred for 6 h under N_2 and the resulting colourless solution filtered into a solution of L4 (92 mg, 0.20 mmol) in $CHCl_3$ (20 mL). The yellow solution was exposed to air for a couple of weeks and brown crystals formed. Yield 75 mg (52%). Suitable crystals were chosen for x-ray diffraction.

$[Cu_2(L4)Br_3]$ (2) was prepared in a similar manner by reaction of L4 with $CuBr_2$ following method A and was obtained as reddish brown crystals. Yield 110 mg (67%). Anal. calcd. for $[C_{16}H_{20}N_4S_6Cu_2Br_3]$: C 23.22, H 2.44, N 6.77; found: C 23.66, H 2.66, N 6.94.

$[Cu(L4)Cl_2]$ (3)

$CuCl_2 \cdot 2H_2O$ (34 mg, 0.20 mmol) was dissolved in CH_3CN (20 mL) and added to a solution of L4 (92 mg, 0.20 mmol) in $CHCl_3$ (20 mL). The resulting green solution was filtered and allowed to stand at room temperature overnight. Bright green crystals formed, which were filtered off, washed with CH_3CN and $CHCl_3$, and air dried. Yield 85 mg (71%). Anal. calcd. for $[C_{16}H_{20}N_4S_6Cl_2Cu]$: C 32.29, H 3.39, N 9.41; found: C 32.08, H 3.44, N 9.38.

$[Cu(L4)(NO_3)_2]$ (4)

A solution of L4 (55 mg, 0.12 mmol) in $CHCl_3$ (20 mL) was added to a solution of $Cu(NO_3)_2 \cdot 3H_2O$ (97 mg, 0.40 mmol) in CH_3CN (20 mL). The resulting solution was filtered and then refluxed for 2 h to form a dark green solution. The solution was allowed to stand at room temperature overnight. Bluish green crystals formed which were filtered, washed with CH_3CN, and dried in air. Yield 46 mg (59%). Anal. calcd. for $[C_{16}H_{20}N_4S_6Cu(NO_3)_2]$: C 29.64, H 3.11, N 12.96; found: C 29.75, H 3.13, N 13.13.

$Cu(L4)(ClO_4) \cdot H_2O$ (5)

A solution of L4 (46 mg, 0.10 mmol) in $CHCl_3$ (20 mL) was added to solution of $Cu(ClO_4)_2 \cdot 6H_2O$ (85 mg, 0.23 mmol) in CH_3CN (20 mL). The resulting deep green solution was filtered and allowed to stand at room temperature. The colour of the solution began to change from deep green to green to yellow and finally pale yellow crystals formed overnight. These crystals were filtered, washed with CH_3CN and $CHCl_3$ and dried in air. Yield 56 mg (86%). Anal. calcd. for $[C_{16}H_{20}N_4S_6Cu]$ $(ClO_4) \cdot H_2O$: C 29.95, H 3.46, N 8.73; found: C 29.93, H 3.45, N 8.65. **5** was also prepared by direct reaction of Cu(I) perchlorate and L4 in CH_3CN/$CHCl_3$.

$[Cu(L4)Cl] \cdot 0.5H_2O$ (6) and $[Cu(L4)Br] \cdot 0.5CHCl_3$ (7)

Cu powder (190 mg, 3.0 mmol) was added to a solution of $CuCl_2 \cdot 2H_2O$ (51 mg, 0.30 mmol) in CH_3CN (20 mL). The mixture was stirred for 6 h under N_2 and the resulting colourless solution filtered into a solution of L4 (92 mg, 0.20 mmol) in $CHCl_3$ (20 mL) under a nitrogen atmosphere. The pale yellow solution was left at room temperature overnight and pale yellow crystals formed. Yield 84 mg (74%). Anal. calcd. for $[C_{16}H_{20}N_4S_6CuCl] \cdot 0.5H_2O$: C 33.79, H 3.72, N 9.85; found: C 33.68, H 3.57, N 9.63. $[Cu(L4)Br] \cdot 0.5CHCl_3$ (**7**) was prepared similarly by using $CuBr_2$ and obtained as pale yellow crystals. Yield 105 mg (75%). Anal. calcd. for $[C_{16}H_{20}N_4S_6CuBr] \cdot 0.5CHCl_3$: C 29.85, H 3.11, N 8.44; found: C 29.80, H 3.12, N 8.44.

X-ray crystallographic analysis of $[Cu_2(L4)Cl_4]_x$ (1)

The diffraction intensities of a brown regular polyhedron crystal of $[Cu_2(L4)Cl_4]_x$ (**1**) of approximate dimensions 0.300 × 0.200 × 0.150 mm were collected using a Rigaku AFC6S diffractometer with graphite monochromatized CuKα radiation. Cell constants and the orientation matrix were obtained by a least-squares refinement using the setting angles of 20 carefully centred reflec-

Can. J. Chem. Downloaded from www.nrcresearchpress.com by 213.200.69.106 on 09/08/12
For personal use only.

Can. J. Chem. Downloaded from www.nrcresearchpress.com by 213.200.69.106 on 09/08/12
For personal use only.

TABLE 1. Summary of crystal data, intensity collection, and structure refinement for **1**, **3**, and **4**

Parameter	Value		
	$[Cu_2(L4)Cl_4]_x$ (**1**)	$[Cu(L4)Cl_2]$ (**3**)	$[Cu(L4)(NO_3)_2]$ (**4**)
Formula	$C_{16}H_{20}N_4S_6Cu_2Cl_4$	$C_{16}H_{20}N_4S_6CuCl_2$	$C_{16}H_{20}N_6S_6CuO_6$
Crystal colour (habit)	Brown (regular polyhedron)	Pale green (rhombic plates)	Deep green (polyhedron)
Formula weight	729.62	595.17	648.28
Crystal system	Triclinic	Triclinic	Orthorhombic
Space group	$P\bar{1}$ (No. 2)	$P\bar{1}$ (No. 2)	$P2_12_12_1$ (No. 19)
a (Å)	8.6204(8)	11.001(1)	15.148(2)
b (Å)	9.850(1)	12.888(2)	15.562(3)
c (Å)	8.348(1)	8.704(1)	11.064(1)
α (deg)	111.46(1)	102.89(1)	—
β (deg)	102.50(1)	103.36(1)	—
γ (deg)	71.818(9)	75.84(1)	—
Volume (Å^3)	622.6(1)	1145.8(3)	2608.2(7)
Density calcd. (g cm^{-3})	1.946	1.725	1.651
Z	1	2	4
Absorption coefficient μ (cm^{-1})	109.49	17.29	13.43
Radiation, λ (Å)	CuKα, 1.54178	MoKα, 0.71069	MoKα, 0.71069
Temperature (°C)	25	26	25
F_{000}	366	606	1324
Scan rate (deg min^{-1})	8.0 (ω scan)	8.0 (ω scan)	32.0 (ω scan)
$2\theta_{max}$ (deg)	120.1	50.0	50.0
Data collected	1989	4273	2622
Number of unique data ($I > 3.00\sigma(I)$)	1312	2059	1864
No. of variables	179	262	317
Goodness of fit	1.93	1.96	1.48
R	0.043	0.056	0.039
R_w	0.042	0.044	0.034

TABLE 2. Positional parameters and B(eq) values (esd's) for $[Cu_2L_4Cl_4]_x$ (**1**)

Atom	x	y	z	B(eq)
Cu(1)	1/2	1/2	1/2	1.83(7)
Cu(2)	1/2	0	1.0000	2.74(8)
Cl(1)	0.4140(2)	0.3158(2)	0.2753(3)	3.1(1)
Cl(2)	0.7685(2)	−0.0336(2)	1.0717(3)	2.9(1)
S(1)	0.7750(3)	0.1597(2)	0.5620(3)	3.4(1)
S(2)	0.0638(3)	0.4753(2)	0.8171(3)	2.9(1)
S(3)	0.5220(2)	0.0950(2)	0.7736(3)	2.53(9)
N(1)	0.7259(7)	0.3923(7)	0.4475(8)	1.9(3)
N(2)	0.7601(7)	0.4734(7)	0.3651(8)	2.3(3)
C(1)	0.8259(8)	0.2647(8)	0.461(1)	2.1(3)
C(2)	0.973(1)	0.207(1)	0.383(1)	2.8(4)
C(3)	1.010(1)	0.286(1)	0.301(1)	2.5(4)
C(4)	0.8964(9)	0.4215(9)	0.294(1)	2.1(3)
C(5)	0.269(1)	0.359(1)	0.862(1)	2.8(4)
C(6)	0.326(1)	0.220(1)	0.715(1)	2.9(4)
C(7)	0.656(1)	0.221(1)	0.864(1)	3.1(4)
C(8)	0.672(1)	0.298(1)	0.742(1)	2.9(4)

tions in the range $19.96 < 2\theta < 52.33°$. Based on a statistical analysis of the intensity distribution, and the successful solution and refinement of the structure, the space group was determined to be $P\bar{1}$. Machine and data collection parameters and crystal data are given in Table 1. The data were collected at 25 ± 1°C using ω–2θ scan technique to a maximum 2θ value of 120.1°. Omega scans of several intense reflections, made prior to data collection, had an average width at half-height of 0.30° with a take-off angle of 6.0°. Scans of (1.68 + 0.30 tan θ)° were made at a speed of 8.0°/min (in ω). The weak reflections ($I < 10.0\sigma(I)$) were rescanned (maximum of two rescans) and the counts were accumulated to assure good counting statistics. The ratio of peak counting time to background counting time was 2:1.

A total of 1989 reflections were collected. The intensities of three representative reflections, which were measured after every 150 reflections remained constant throughout data collection (no decay correction applied). An empirical absorption correction was applied, using the program DIFABS (30), which resulted in transmission factors ranging from 0.40 to 1.00. The data were corrected for Lorentz and polarization effects.

The structure was solved by direct methods (31, 32). The non hydrogen atoms were refined anisotropically. The final cycle of full-matrix least-squares refinement was based on 1312 observed reflections ($I > 3.00\sigma(I)$) and 179 variable parameteers and converged with unweighted and weighted agreement factors of $R = \Sigma\|F_o| - |F_c\|/\Sigma|F_o| = 0.043$ and $R_w = [(\Sigma w(|F_o| - |F_c|)^2/\Sigma w F_o^2)]^{1/2} = 0.042$. The standard deviation of an observation of unit weight was 1.93. The weighting scheme was based on counting statistics and included a factor ($p = 0.01$) to down weight the intense reflections. Plots of $\Sigma w(|F_o| - |F_c|)^2$ versus $|F_o|$, reflection order in data collection, $\sin\theta/\lambda$, and various classes of indices showed no unusual trends. The maximum and minimum peaks on the final difference Fourier map corresponded to 0.65 and −0.49 electrons/Å^3, respectively, and have no chemical significance. Neutral atom scattering factors (33) and anomalous dispersion terms (34, 35) were taken from the usual sources. All calculations were performed using the TEXSAN (36) crystallographic software package using a VAX 3100 workstation. Hydrogen atoms were located in a difference map but not refined. Thermal parameters were set at 1.2 times the isotropic thermal parameter of the bonded C atoms.

Atomic positional parameters are given in Table 2 and selected bonded distances and angles are given in Table 5. Thermal parameters (Table S-1), hydrogen atom parameters (Table S-2), a full

Can. J. Chem. Downloaded from www.nrcresearchpress.com by 213.200.69.106 on 09/08/12
For personal use only.

TABLE 3. Positional parameters and B(eq) values (esd's) for [Cu(L4)Cl_2] (**3**)

Atom	x	y	z	B(eq)
Cu(1)	0.7599(1)	0.2114(1)	0.2878(1)	2.95(6)
Cl(1)	0.8037(2)	0.0420(2)	0.3465(3)	3.7(1)
Cl(2)	0.7125(3)	0.3806(2)	0.2251(3)	5.0(2)
S(1)	1.0684(3)	0.2015(3)	0.1912(3)	4.8(2)
S(2)	0.6211(3)	0.0545(2)	−0.3178(3)	4.0(1)
S(3)	0.3285(3)	0.1847(2)	−0.0127(4)	4.7(2)
S(4)	0.4779(3)	0.2295(2)	0.3588(3)	4.1(1)
S(5)	0.8907(3)	0.4143(2)	0.8887(3)	4.1(1)
S(6)	1.1786(2)	0.3580(2)	0.5764(3)	3.8(1)
N(1)	0.8322(7)	0.1571(6)	0.0903(8)	2.9(4)
N(2)	0.7349(7)	0.1230(6)	−0.0216(8)	3.0(4)
N(3)	0.7003(7)	0.2770(6)	0.4936(8)	2.8(4)
N(4)	0.7939(7)	0.3140(6)	0.6056(8)	2.9(4)
C(1)	0.9424(8)	0.1556(7)	0.053(1)	2.8(5)
C(2)	0.9617(8)	0.1193(8)	−0.106(1)	2.8(5)
C(3)	0.8638(9)	0.0899(7)	−0.220(1)	2.7(5)
C(4)	0.7472(8)	0.0944(7)	−0.173(1)	2.5(4)
C(5)	0.501(1)	0.068(1)	−0.190(1)	5.8(7)
C(6)	0.443(1)	0.180(1)	−0.142(2)	6.8(8)
C(7)	0.336(2)	0.316(1)	0.109(2)	12(1)
C(8)	0.402(1)	0.339(1)	0.269(2)	9(1)
C(9)	0.5816(9)	0.2951(8)	0.515(1)	2.7(5)
C(10)	0.550(1)	0.3558(8)	0.659(1)	3.8(5)
C(11)	0.642(1)	0.3930(8)	0.775(1)	3.3(5)
C(12)	0.7673(9)	0.3692(7)	0.744(1)	2.9(5)
C(13)	1.0271(9)	0.3594(8)	0.793(1)	3.7(5)
C(14)	1.0378(9)	0.4186(7)	0.667(1)	3.4(5)
C(15)	1.1617(8)	0.2191(8)	0.509(1)	3.4(5)
C(16)	1.0417(9)	0.2000(8)	0.387(1)	3.4(5)

listing of bond distances and angles (Table S-3), and observed and calculated structure factors (10$|F_o|$ and 10$|F_c|$) (Table S-4) are deposited as supplementary material.[2]

*X-ray crystallographic analysis of [Cu(L4)Cl_2] (**3**)*

The diffraction intensities of a pale green rhombic platelike crystal of **3** of approximate dimensions 0.300 × 0.300 × 0.070 mm were collected in a manner similar to **1**. Crystal data, intensity collection, and refinement details are given in Table 1. Atomic positional parameters are given in Table 3 and selected bond distances and angles are given in Table 6. Thermal parameters (Table S-5), hydrogen atom positional parameters (Table S-6), a full listing of bond distances and angles (Table S-7), and observed and calculated structure factors (10$|F_o|$ and 10$|F_c|$) Table (S-8) are deposited as supplementary material.[2]

*X-ray crystallographic analysis of [Cu(L4) (NO_3)$_2$] (**4**)*

The diffraction intensities of a deep green polyhedral crystal of **4** of approximate dimensions 0.400 × 0.350 × 0.200 mm were collected in a manner similar to **1**. Crystal data, intensity collection, and refinement details are summarized in Table 1. Atomic positional parameters are given in Table 4 and selected bond distances and angles are given in Table 7. Thermal parameters

[2]A complete set of data may be purchased from: The Depository of Unpublished Data, Document Delivery, CISTI, National Research Council Canada, Ottawa, Canada K1A OS2.

Table S-3 (bond distances and angles for [Cu_2(L4)Cl_4]$_x$), Table S-7 (bond distances and angles for [CuCL4)Cl_2], and Table S-11 (bond distances and angles for [Cu(L4)(NO_3)$_2$] have also been deposited with the Cambridge Crystallographic Data Centre and can be obtained on request from The Director, Cambridge Crystallographic Data Centre, University Chemical Laboratory, 12 Union Road, Cambridge. CB2 1EZ, U.K.

TABLE 4. Positional parameters and B(eq) values (esd's) for [Cu(L4)(NO_3)$_2$] (**4**)

Atom	x	y	z	B(eq)
Cu(1)	0.97755(6)	0.22979(6)	0.35919(8)	2.46(4)
S(1)	1.1526(2)	0.3480(2)	0.3981(2)	4.6(1)
S(2)	0.9312(2)	0.3908(2)	−0.0663(2)	5.9(2)
S(3)	0.6821(2)	0.2525(2)	−0.0089(3)	6.7(2)
S(4)	0.7763(1)	0.1991(1)	0.2699(2)	4.3(1)
S(5)	0.8610(2)	0.4848(2)	0.6374(3)	4.9(1)
S(6)	1.1469(2)	0.5251(2)	0.6003(2)	5.4(1)
O(1)	0.9278(4)	0.1407(3)	0.4707(5)	3.4(3)
O(2)	1.0133(4)	0.2182(4)	0.5836(5)	4.8(3)
O(3)	0.9526(5)	0.1031(5)	0.6540(6)	8.1(5)
O(4)	1.0831(3)	0.1558(3)	0.3356(5)	3.6(3)
O(5)	0.9843(5)	0.1126(4)	0.2102(5)	4.8(3)
O(6)	1.1080(5)	0.0419(4)	0.2292(7)	7.1(5)
N(1)	1.0231(4)	0.3212(4)	0.2497(5)	2.8(3)
N(2)	0.9710(4)	0.3253(4)	0.1504(6)	3.2(3)
N(3)	0.8728(4)	0.3014(4)	0.3963(6)	2.5(3)
N(4)	0.8957(4)	0.3632(4)	0.4742(6)	2.8(3)
N(5)	0.9648(5)	0.1548(5)	0.5739(7)	3.8(4)
N(6)	1.0589(5)	0.1005(5)	0.2550(7)	4.1(4)
C(1)	1.0923(5)	0.3707(5)	0.2663(7)	3.0(4)
C(2)	1.1133(6)	0.4352(5)	0.1800(8)	3.4(4)
C(3)	1.0626(5)	0.4405(5)	0.0805(7)	3.2(4)
C(4)	0.9907(5)	0.3838(5)	0.0679(7)	3.4(4)
C(5)	0.8468(8)	0.3009(7)	−0.052(1)	7.1(7)
C(6)	0.7705(9)	0.3397(8)	−0.004(1)	8.8(9)
C(7)	0.6343(6)	0.2677(6)	0.137(1)	5.5(5)
C(8)	0.6614(5)	0.2010(6)	0.2314(8)	4.2(5)
C(9)	0.7896(4)	0.2871(4)	0.3656(7)	2.7(3)
C(10)	0.7232(5)	0.3389(5)	0.4151(8)	3.9(4)
C(11)	0.7439(5)	0.3998(5)	0.4969(8)	3.6(4)
C(12)	0.8332(5)	0.4104(5)	0.5251(7)	2.8(4)
C(13)	0.989(1)	0.4697(6)	0.645(1)	10.5(9)
C(14)	1.013(1)	0.5266(6)	0.5648(9)	8.3(7)
C(15)	1.1888(6)	0.5214(6)	0.4495(8)	4.1(5)
C(16)	1.2287(5)	0.4361(6)	0.4106(8)	3.8(4)

TABLE 5. Selected bond distances (Å) and angles (deg) for [Cu_2(L4)Cl_4]$_x$ (**1**)

Bond	Distance (Å)
Cu(1)—Cl(1)	2.260(2)
Cu(1)—N(1)	1.962(6)
Cu(2)—Cl(2)	2.212(2)
Cu(2)—S(3)	2.458(2)
Bond	**Angle (deg)**
Cl(1)—Cu(1)—Cl(1)	180.00
Cl(1)—Cu(1)—N(1)	88.1(2)
Cl(1)—Cu(1)—N(1)	91.9(2)
Cl(1)—Cu(1)—N(1)	91.9(2)
Cl(1)—Cu(1)—N(1)	88.1(2)
N(1)—Cu(1)—N(1)	180.00
Cl(2)—Cu(2)—Cl(2)	180.00
Cl(2)—Cu(2)—S(3)	88.49(7)
Cl(2)—Cu(2)—S(3)	91.51(7)
Cl(2)—Cu(2)—S(3)	91.51(7)
Cl(2)—Cu(2)—S(3)	88.49(7)
S(3)—Cu(2)—S(3)	180.00

TABLE 6. Selected bond distances (Å) and angles (deg) for $[Cu(L4)Cl_2]$ (**3**)

Bond	Distance (Å)
Cu(1)—Cl(1)	2.264(3)
Cu(1)—Cl(2)	2.274(3)
Cu(1)—N(1)	1.974(7)
Cu(1)—N(3)	1.987(7)
Cu(1)—O(5)	2.461(6)
Cu(1)—O(2)	2.547(6)

Bonds	Angle (deg)
Cl(1)—Cu(1)—Cl(2)	178.8(1)
Cl(1)—Cu(1)—N(1)	91.7(2)
Cl(1)—Cu(1)—N(3)	91.8(2)
Cl(2)—Cu(1)—N(1)	88.0(2)
Cl(2)—Cu(1)—N(3)	88.5(2)
N(1)—Cu(1)—N(3)	173.8(3)

(Table S-9), hydrogen atom parameters (Table S-10), a full listing of bond distances and angles (Table S-11), and observed and calculated structure factors (Table S-12) are deposited as supplementary material.[2]

Results and discussion

The synthesis of L4 was achieved in moderately high yield by a traditional high dilution cyclization reaction and no trace of any 11-membered macrocycle containing one pyridazine subunit and 33-membered macrocycle containing three pyridazine subunits was detected. The 1:2 and 1:1 complexes of L4 with $CuCl_2$ were prepared by controlling the molar ratio of ligand and copper salt. It is of interest to note that complex **1** can be synthesized from either copper(I) or copper(II) starting materials. Synthesis from copper(I) chloride clearly would require a source of adventitious chloride, which may result from disproportionation of the excess copper(I) chloride present. Moreover, since both copper(I) chloride and bromide complexes are readily prepared, and quite stable, it is perhaps not surprising that a mixed oxidation state complex (**2**) can be synthesized. Presumably the synthesis of **2** was accompanied by some ligand hydrolysis to provide a source of reducing thiol, as would also be the case for **5**. However, in both syntheses no such byproducts were isolated. The complexes did not dissolve appreciably in any solvent and were studied exclusively in the solid state.

Description of the structures of $[Cu_2(L4)Cl_4]_x$ (1), $[Cu(L4)Cl_2]$ (3), and $[Cu(L4)(NO_3)_2]$ (4)

The structure of a fragment of $[Cu_2(L4)Cl_4]_x$ (**1**), which includes the two different copper centres, is illustrated in Fig. 2*a*. The overall structure is that on an infinite, single stranded polymer with the macrocyclic ligand behaving in a tetradentate fashion, binding a *trans* square-planar copper(II) centre inside the macrocyclic cavity via two separate pyridazine nitrogens, and linking external *trans* square-planar copper(II) centres by exocyclic sulfur atoms (Fig. 2*b*). Unlike the situation in $[Cu(L2)Cl_2]$ (28), where, as a result of the smaller macrocyclic ring the square-planar CuN_2Cl_2 centre effectively exists outside the macrocyclic cavity, in **1** Cu(1) is bound within the macrocyclic cavity. Furthermore, opposite, rather than adjacent, pyradazine nitrogens are bound to the copper centre in **1**. The two copper(II) centres are very close to being exactly square-planar with angles around Cu(1)

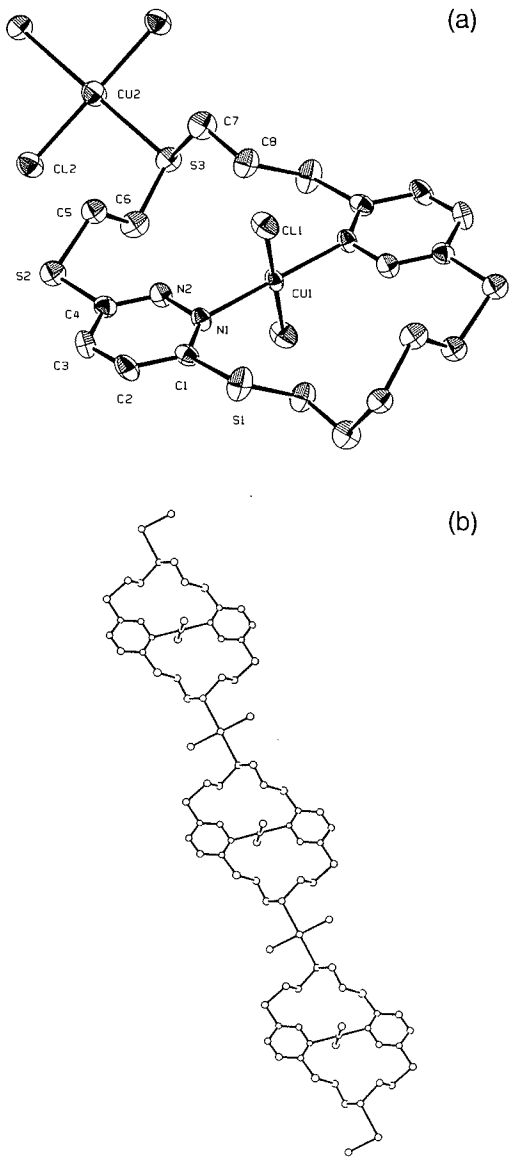

FIG. 2. (*a*) Molecular structure of $[Cu_2(L4)Cl_4]_x$ (**1**) (40% probability thermal ellipsoids) showing a single dinuclear fragment. (*b*) Structural representation of $[Cu_2(L4)Cl_4]_x$ (**1**) illustrating the single stranded polymer.

in the range 88.1–91.9°, and around Cu(2) in the range 88.4–91.6°, and copper–nitrogen, copper–sulfur, and copper–chlorine distances are normal for systems of this sort. The *endo / exo* coordination of L4 in **1** is reminiscent of the bonding of L1 in the complex $[Cu_3(L1)_2Cl_6]$ (28), in which two square-planar copper(II) centres are bound "internally," one within each ligand via two independent pyridazine nitrogens, and the third pyridazine in each ligand is bound to a third square-planar copper(II) centre. However, for the first time, the ligand L4 exhibits the desired mixed N / S coordination mode, but unfortunately it occurs in an intermolecular, rather than an intramolecular fashion.

The structure of $[Cu(L4)Cl_2]$ (**3**) is illustrated in Fig. 3 and consists of an almost square-planar *trans* copper(II) center bound by two opposite pyridazine nitrogens, one from each pyridazine ring and two chlorines. The coordination sphere is similar to one of the copper centers in **1**. The copper–nitrogen and copper–chlorine distances are slightly different

Can. J. Chem. Downloaded from www.nrcresearchpress.com by 213.200.69.106 on 09/08/12
For personal use only.

TABLE 7. Selected bond distances (Å) and angles (deg) for [Cu(L4) $(NO_3)_2$] (**4**)

Bond	Distance (Å)
Cu(1)—O(1)	2.003(5)
Cu(1)—O(2)	2.547(6)
Cu(1)—O(4)	1.987(5)
Cu(1)—O(5)	2.461(6)
Cu(1)—N(1)	1.992(6)
Cu(1)—N(3)	1.982(6)

Bonds	Angle (deg)	Bonds	Angle (deg)
O(1)—Cu(1)—O(4)	89.0(2)	O(1)—Cu(1)—N(1)	177.8(3)
O(1)—Cu(1)—N(3)	87.7(2)	O(4)—Cu(1)—N(1)	93.2(2)
O(4)—Cu(1)—N(3)	175.5(2)	N(1)—Cu(1)—N(3)	90.1(2)
N(3)—Cu(1)—O(5)	126.1(2)	N(3)—Cu(1)—O(2)	90.4(2)
N(3)—Cu(1)—N(2)	80.9(2)	O(4)—Cu(1)—O(5)	56.6(2)
O(4)—Cu(1)—O(2)	85.2(2)	O(4)—Cu(1)—N(2)	103.4(2)
N(1)—Cu(1)—O(5)	96.2(2)	N(1)—Cu(1)—O(2)	124.7(2)
N(1)—Cu(1)—N(2)	27.8(2)	O(1)—Cu(1)—O(5)	85.1(2)
O(1)—Cu(1)—O(2)	55.3(2)	O(1)—Cu(1)—N(2)	151.4(2)
O(5)—Cu(1)—O(2)	126.3(2)	O(5)—Cu(1)—N(2)	80.8(2)
O(2)—Cu(1)—N(2)	149.9(2)		

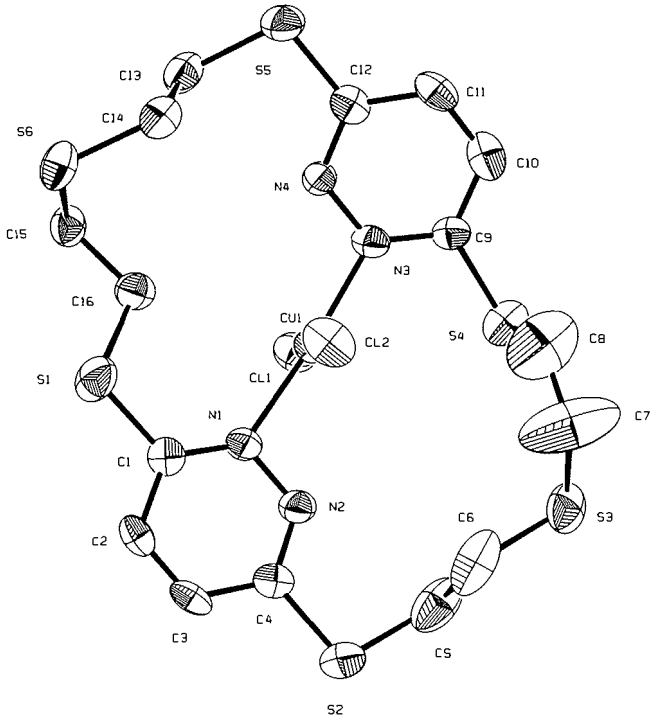

FIG. 3. Molecular structure of [Cu(L4)Cl_2] (**3**) (40% probability thermal ellipsoids).

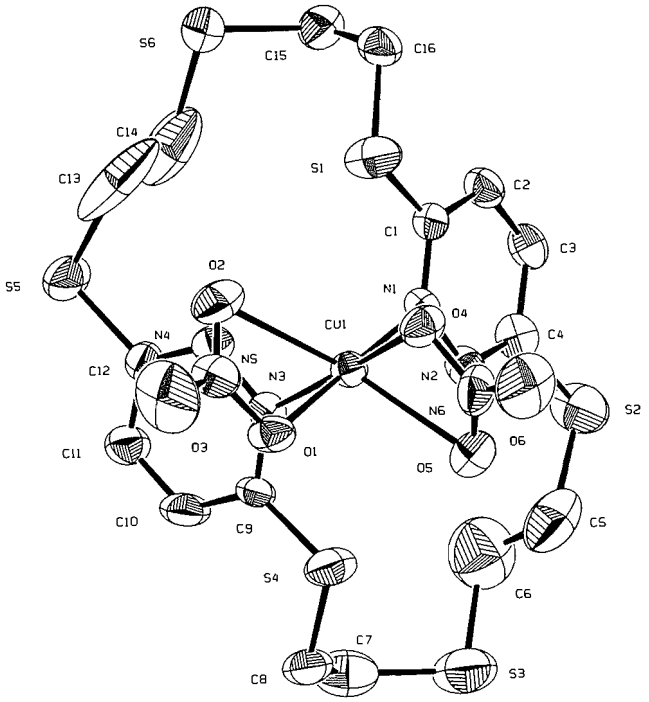

FIG. 4. Molecular structure of [Cu(L4) $(NO_3)_2$] (**4**) (40 % probability thermal ellipsoids).

from those in **1** but still in the normal range for ligands of this sort. The angles around the copper fall in the range 88.1–91.9°, comparing very closely with those in **1**.

The structure of [Cu(L4) $(NO_3)_2$] (**4**) is illustrated in Fig. 4 and consists of a highly distorted *cis*-octahedral copper(II) center bound by two opposite *cis*-pyridazine nitrogens, one from each pyridazine ring and two bidentate nitrates. Two copper–oxygen distances (1.980(12), 1.933(12) Å) and the short copper–nitrogen distances (1.992(6), 1.982(6) Å) are normal, but two of the in-plane angles are significantly different from 90° (N(3)—Cu(1)—N(2) 80.9(2)°, O(4)—Cu(1)—N(1) 93.2(2)° to imply a distorted structure. Two copper–oxygen distances (Cu(1)—O(5) 2.461(6) Å, Cu(1)—O(2) 2.547(6) Å) are quite long, but still within a reasonable bonding distance. When bonding to a single metal atom a nitrate group may behave as a monodentate ligand or a symmetrical or unsymmetrical bidentate ligand. It is suggested (37) that a nitrate is to be considered a bidentate ligand if the difference in the two closest metal–oxygen distances is less than 0.7 Å. In **4** the difference between the distances of Cu—O(5) and Cu—O(1) is 0.567 Å and the difference between Cu—O(5) and Cu—O(4) is 0.474 Å. It

Can. J. Chem. Downloaded from www.nrcresearchpress.com by 213.200.69.106 on 09/08/12
For personal use only.

TABLE 8. Spectral and magnetic data

Compound	Colour	IR(cm^{-1})	μ_{eff} (RT) BM	UV/VIS (cm^{-1})
$[Cu_2(L4)Cl_4]_x$ (**1**)	Brown	1572 (νCN), 306, 295 (νCu—Cl),	1.84	19600 14300
$[Cu_2(L4)Br_3]$ (**2**)	Reddish brown	1600, 1560 (νCN), 267 (νCu—Br)	1.78	18500 10800
$[Cu(L4)Cl_2]$ (**3**)	Green	1559 (νCN), 308, 298 (νCu—Cl),	1.80	13300
$[Cu(L4)(NO_3)_2]$ (**4**)	Deep green	1568 (νCN), 1758, 1753, 1721, 1709 ($\nu_1 + \nu_4$ NO_3^-), 323, 3304 (νCu—O)	1.76	17400 14300
$Cu(L4)ClO_4 \cdot H_2O$ (**5**)	Yellow	3523 (νH_2O), 1600, 1557 (νCN), 1096 (νClO_4^-)	—	—
$Cu(L4)Cl \cdot 0.5H_2O$ (**6**)	Yellow	3450 (νH_2O), 1568 (νCN)	—	—
$Cu(L4)Br \cdot 0.5CHCl_3$ (**7**)	Yellow	1570 (νCN)	—	—

[a]Mull transmittance.

is clear that from the structural information the nitrates are bidentate, and the copper centre is best regarded as a highly distorted *cis*-octahedral species.

Spectroscopy and magnetism

The ligand L4 has a simple infrared spectrum with a sharp νCN band at 1580 cm^{-1}. This band shifts 8–23 cm^{-1} to lower energy in all the complexes (Table 8), suggesting the coordination of pyridazine rings (28, 29). With ligands L1 and L2 sulfur coordination was accompanied by a small shift in this band to higher energy (1–2 cm^{-1}), while for nitrogen coordination shifts to lower energy were observed (−5 to −11 cm^{-1}) (28). The shifts to lower energy for **1**, **3**, and **4** are clear cut because X-ray data confirm pyridazine nitrogen coordination. For complex **2** two νCN bands are, in fact, observed at 1600 and 1560 cm^{-1}, suggesting the presence of two different pyridazine rings. The higher energy band is assigned to an uncoordinated pyridazine ring, in keeping with similar observations for L1 and L2 (28). Complex **2** is clearly a Cu(II) / Cu(I) species and, because of its lack of solubility, is likely to have a polymeric structure similar to **1**. Low energy *d–d* absorption also suggests sulfur coordination. The copper(II) site probably lies within the macrocyclic ring and involves a four-coordinate $CuNSBr_2$ chromophore, with one pyridazine nitrogen and one sulfur adjacent to a pyridazine involved in bonding to copper. A reasonable suggestion for the copper(I) site would be a CuS_2Br species bridging the macrocyclic rings and bound in an exocyclic fashion by each NS_3 ring.

The copper(I) perchlorate complex (**5**) has two prominent νCN bands at 1600 and 1557 cm^{-1}, suggesting the presence of both coordinated and uncoordinated pyridazine. A strong band at 1096 cm^{-1} indicates ionic perchlorate. It is suggested that structurally **5** involves a mixed NS donor set, possibly $CuNS_2$, but the coordination number and molecular nature of the complex must await a structural determination. The overall infrared spectra of **6** and **7** are very similar, suggesting comparable structures, which are likely to be polymeric and similar to **1**. The presence of only one νCN band at lower energy, in each case, suggests coordination of both pyridazine rings. Structurally the most reasonable suggestion for **6** and **7** involves a three-coordinate CuN_2X and an external CuS_2X species (X = Cl, Br) in a polymeric arrangement similar to **1**.

In the far infrared region, the Cu—N (pyridazine) stretching vibrations would be expected at quite low energy (38), but because of complexities in the spectra an unequivocal assignment of this band could not be made. Absorptions in **1** at 306 and 295 cm^{-1} can be associated with two different *trans* dichloro-copper(II) species. Complex **3** exhibits one strong band at 308 cm^{-1}, also consistent with a similar *trans* chromophore. A strong absorption at 239 cm^{-1} for the copper bromide complex **2** is assigned to Cu—Br stretch. In **4** there are two strong bands at 304 and 323 cm^{-1}, which are associated with Cu—O (NO_3^-) stretch. The ($\nu_1 + \nu_4$) nitrate combination bands of **4** are observed at 1758, 1753, 1721, 1709 cm^{-1} (39), and are associated with two different coordinated nitrates. The separation of each pair of bands is usually a reasonable indication of the bonding mode of such a group (39) and differences of 37 and 44 cm^{-1} are large enough to suggest a bidentate role for two different coordinated nitrates. In this case, X-ray data formally define the coordinated nitrates in a bidentate mode. For each nitrate, therefore, one oxygen is strongly coordinated, and one weakly coordinated.

Room temperature magnetic moments for compounds 1–4 (Table 8) all exceed the spin-only value for a one-unpaired electron system and suggest the presence of dilute copper(II) centers in all cases, with no spin exchange. The large distances separating the copper(II) centres in **1**, and the lack of appropriate magnetically active bridging groups would suggest the absence of any spin–spin interactions in this system. The normal value for **2** confirms the presence of just one paramagnetic copper(II) centre. Solid state, mull transmittance, electronic spectra for **1**–**3** are characterized by the presence of one major visible *d–d* absorption (Table 8). The *d–d* absorption energy of the chloro-complexes is comparable, as would be expected, but the very low energy band observed for **2** is consistent with copper(II) centres bound to N, S, and Br donors. The higher energy absorption for **4** is in agreement with the six-coordinate structure and mixed CuN_2O_4 chromophore. Other bands at higher energy observed for **1** and **2** (19600, 18500 cm^{-1}, respectively) are consistent with halogen-to-copper charge transfer.

Acknowledgement

We thank the Natural Sciences and Engineering Research Council of Canada for financial support for this study.

1. P.M. Colman, H.C. Freeman, J.M. Guss, M. Murata, V.A. Norris, J.A.M. Ramshaw, and M.P. Venkatappa. Nature, **272**, 319 (1978).
2. J.M. Guss and H.C. Freeman. J. Mol. Biol. **169**, 521 (1983).

Can. J. Chem. Downloaded from www.nrcresearchpress.com by 213.200.69.106 on 09/08/12
For personal use only.

3. E.T. Adman and L.H. Jensen. Isr. J. Chem. **21**, 8 (1981).
4. G.E. Norris, B.F. Anderson, and E.N. Baker. J. Am. Chem. Soc. **108**, 2784 (1986).
5. K.W. Penfield, A.W. Gewirth, and E.I. Solomon. J. Am. Chem. Soc. **107**, 4519 (1985).
6. H.J. Prochaska, W.F. Schwindinger, M. Schwartz, M.J. Burk, E. Berneducii, R.A. Lalancette, J.A. Potenza, and H.J. Schugar. J. Am. Chem. Soc. **103**, 3446 (1981).
7. J. Van Rijn, W.L. Driessen, J. Reedijk, and J-M. Lehn. Inorg. Chem. **23**, 3584 (1984).
8. J.V. Dagdigian, V. McKee, and C.A. Reed. Inorg. Chem. **21**, 1332 (1982).
9. S.C. Rawle, G.A. Admans, and S.R. Cooper. J. Chem. Soc. Dalton Trans. 93 (1988).
10. P.J.M.W.L. Birker, J. Helder, G. Henkel, B. Krebs, and J. Reedijk. Inorg. Chem. **21**, 357 (1982).
11. M.J. Schilstra, P.J.M.W.L. Birker, G.C. Verschoor, and J. Reedijk. Inorg. Chem. **21**, 2637 (1982).
12. N. Aoi, G.E. Matsubayashi, and T.J. Tanaka. J. Chem. Soc. Dalton Trans. 1059 (1983).
13. L.L. Diaddario, E.R. Dockal, M.D. Glick, L.A. Ochrymowycz, and D.B. Rorabacher. Inorg. Chem. **24**, 356 (1985).
14. E. Bouwman, W.L. Driessen, and J. Reedijk. Coord. Chem. Rev. **104**, 145 (1990).
15. D.B. Groot and S.J. Loeb. Inorg. Chem. **28**, 3573 (1989).
16. G.G. Newkome, J.D. Saver, J.M. Roper, and D.C. Hager. Chem. Rev. **77**, 513 (1977).
17. N. Atkinson, A.J. Blake, M.G.B. Drew, G. Forsyth, A.J. Lavery, G. Reid, and M. Schröder. J. Chem. Soc. Chem. Commun. 984 (1989).
18. A.J. Blake, G. Reid, and M. Schröder. J. Chem. Soc. Dalton Trans. 615 (1991).
19. C.R. Lucas, S. Liu, and M.J. Newlands. Can. J. Chem. **67**, 639 (1989).
20. C.R. Lucas, S. Liu, and L.K. Thompson. Inorg. Chem. **29**, 85 (1990).
21. S.K. Mandal, L.K. Thompson, E.J. Gabe, J-P. Charland, and F.L. Lee. Inorg. Chem. **27**, 855 (1988).
22. S.K. Mandal, L.K. Thompson, F.L. Lee, and J-P. Charland. Inorg. Chem. **26**, 2384 (1987).
23. L.K. Thompson, S.K. Mandal, J-P. Charland, and E.J. Gabe. Can. J. Chem. **66**, 348 (1988).
24. L.K. Thompson, S.K. Mandal, L. Rosenberg, F.L. Lee, and E.J. Gabe. Inorg. Chim. Acta, **133**, 81 (1987).
25. T.C. Woon, R. McDonald, S.K. Mandal, L.K. Thompson, S.P. Connors, and A.W. Addison. J. Chem. Soc. Dalton Trans. 2381 (1986).
26. S.K. Mandal, L.K. Thompson, M.J. Newlands, F.L. Lee, Y. Lepage, J-P. Charland, and E.J. Gabe. Inorg. Chim. Acta, **122**, 199 (1986).
27. L. Chen, L.K. Thompson, and J.N. Bridson. Inorg. Chem. To be published.
28. L. Chen, L.K. Thompson, and J.N. Bridson. Can. J. Chem. **70**, 1886 (1992).
29. L. Chen, L.K. Thompson, and J.N. Bridson. Can. J. Chem. **70**, 2709 (1992).
30. N. Walker and D. Stuart. Acta Crystallogr. **A39**, 158 (1983).
31. C.J. Gilmore. J. Appl. Crystallogr. **17**, 42 (1984).
32. P.T. Beurskens. Dirdif: Technical Report 1984 / 1, Crystallography Laboratory, Toernooiveld, 6525 Ed Nijimegen, Netherlands.
33. D.T. Cromer and J.T. Waber. International tables for X-ray crystallography. Vol. IV. The Kynoch Press, Birmingham, U.K. 1974. Table 2.2A.
34. J.A. Ibers and W.C. Hamilton. Acta Crystallogr. **17**, 781 (1974).
35. D.T. Cromer. International tables for X-ray crystallography. Vol. IV. The Kynoch Press, Birmingham, U.K. 1974. Table 2.3.1.
36. Texsan — Texray structure analysis package. Molecular Structure Corporation, 1985.
37. C.E. Addison, N. Logan, S.C. Wallwork, and C.D. Garner. Q. Rev. Chem. Soc. **25**, 289 (1971).
38. J.R. Ferraro. Low frequency vibrations of inorganic and coordination compounds. Plenum, New York. 1971.
39. A.B.P. Lever, E. Mantovani, and B.S. Ramaswamy. Can. J. Chem. **49**, 1957 (1971).

Can. J. Chem. Downloaded from www.nrcresearchpress.com by 213.200.69.106 on 09/08/12
For personal use only.

2-Carbomethoxy-1,3-butadiene: an electronically activated diene in [4 + 2] cycloadditions with electron-deficient dienophiles

CLAUDE SPINO[1] AND JASON CRAWFORD
University of Victoria, Chemistry Department, P.O. Box 3055, Victoria, B.C., Canada V8W 3P6

Received December 10, 1992

CLAUDE SPINO and JASON CRAWFORD. Can. J. Chem. **71**, 1094 (1993).

Cross Diels–Alder reactions between 2-carbomethoxy-1,3-butadiene **1** and electron-rich dienes were carried out. It was found that diene **1** had a higher reactivity than even the well-known Danishefsky diene in its Diels–Alder cycloaddition with electron-deficient dienophiles. In addition, (*Z*)-1-methylthio-3-carbomethoxy-1,3-butadiene **11** was found to have a higher reactivity than (*Z*)-1-methylthio-1,3-butadiene and (*Z*)-2-carbomethoxy-1,3-hexadiene, while both (*E*)- and (*Z*)-1,2-(bis)-carbomethoxy-1,3-butadiene **14** reacted efficiently with maleic anhydride to give the corresponding cycloadduct **15**.

CLAUDE SPINO et JASON CRAWFORD. Can. J. Chem. **71**, 1094 (1993).

Nous avons effectué des réactions de Diels–Alder croisées entre le 2-carbomethoxy-1,3-butadiene **1** et des dienes riches en électrons. Les résultats obtenus indiquent que **1** est plus réactif que le diène de Danishefsky, dans les cycloadditions avec des dièenophiles pauvres en électrons. De plus, le (*Z*)-1-methylthio-3-carbomethoxy-1,3-butadiene **11** a montré une plus grande réactivité que le (*Z*)-1-methylthio-1,3-butadiene et (*Z*)-2-carbomethoxy-1,3-hexadiene tandis que le (*E*)- et (*Z*)-1,2-(bis)-carbomethoxy-1,3-butadiene **14** ont réagi avec l'anhydride maléique pour donner le produit de cycloaddition **15**.

Can. J. Chem. Downloaded from www.nrcresearchpress.com by 213.200.69.106 on 09/08/12
For personal use only.

The facile dimerization of 2-carbomethoxy-1,3-butadiene **1** to give dimethyl mikanecate **4** has been known for some time (Scheme 1) (1, 2). Although the unusual ease with which this [4+2] cycloaddition takes place has been noted, a rationalization of this phenomenon has yet to be offered. A recent communication by Jung and Zimmerman provided the first kinetic data on this dimerization (3). They proposed that the high dienophilic character of the C1—C2 bond in **1** and the possibility that **1** may be more stable in its *E*-(*s-cis*) conformation could be major factors in accelerating this Diels–Alder reaction. We provide evidence herein that another electronic factor plays a significant role in the rate acceleration of this dimerization and that in fact **1** should be regarded as an electronically activated diene.

A 96% yield of dimer **4** was obtained by heating sulfolene **2** at 110°C (Scheme 1, method A) (1*a*) or by treating allylic bromide **3** with base at 25°C (Method B) (1*b*). However, in the presence of the electron-rich diene **5***a* (Y = Me) (4) and the very reactive diene **5***b* (Y = OMe) (4*b*), either method led to a mixture of dimer **4** and cross cycloadduct **6** (Table 1). In most cases, the dimerization product prevailed unless a large excess of the electron-rich diene was used. Note that the lower temperature seems to favor dimerization over cross-cycloaddition (entries 3, 4, 5, and 8). These results indicate that diene **1**, as a dienophile, cycloadds more rapidly to itself, an electron-deficient diene, than it does to the electron-rich dienes **5***a* and **5***b*. Note that the reactivity of diene **1** is underestimated here since diene **1** is generated slowly (3–4 h) and must be at low concentration relative to the other diene.

We ruled out the possibility of a local concentration effect, where molecules of diene **1** would dimerize faster because they were generated in proximity to one another, by stirring 1 equivalent each of sulfolene **2** and diene **5***b* with excess methyl acrylate (10 equiv.) in refluxing toluene (Scheme 2). After 4 h, diene **1** had reacted completely to give **7** and Danishefsky's diene **5***b* had reacted to the extent of 93% to give adduct **8** (gc analysis). Also detected were **6***b* (<5%) and **4** (traces). Control experiments in which each diene was reacted separately with excess methyl acrylate confirmed that diene **1** reacted more rapidly with methyl acrylate than did Danishefsky's diene **5***b*. We believe that diene **1** reacted as soon as it was generated since it (or dimer **4**) was not detected in significant amount throughout the reaction (the extrusion of SO_2 in **2** takes ~4 h). The reaction of **3** and **5***b* with methyl acrylate (10 equiv.) at 25°C following method B gave mostly dimer **4** (73%), adduct **7** (8%), and **6***b* (7%) (yields based on **3**). Diene **5***b* did not react at all with methyl acrylate under those conditions. The ethyl ester analog of **1** reacts as a dienophile with cyclopentadiene (excess) at 25°C in quantitative yield (5). As a diene, **1** is more reactive than **5***b* toward both methyl acrylate and itself. It also appears to be less reactive than cyclopentadiene. As a dienophile, **1** is more reactive than methyl acrylate towards both itself and **5***b*. We believe that this increased dienophilicity is due to a strong polarization of the C1—C2 double bond in **1**, as suggested by Jung and Zimmerman (3).

The regiochemistry of the dimer **4** (>97%) cannot be accounted for by any reasonable ionic pathway. Also, we repeated the dimerization of **1** from **2** or **3** and its cycloaddition with methyl acrylate in the absence of light and in the presence of 2,6-di-*tert*-butylphenol or hydroquinone with no effect on the rate of reaction. The above reactions thus appear to be proceeding via a normal thermal [4+2] cycloaddition mechanism.

We then prepared compounds **11** and **14** to examine the effect of an electron-donating or -withdrawing group at an end position on the reactivity of diene **1** (Schemes 3 and 4). Dihydrothiophene **9** was prepared from methyl acrylate following the method of Belleau and co-workers (6*a*). After

[1]Author to whom correspondence may be addressed.

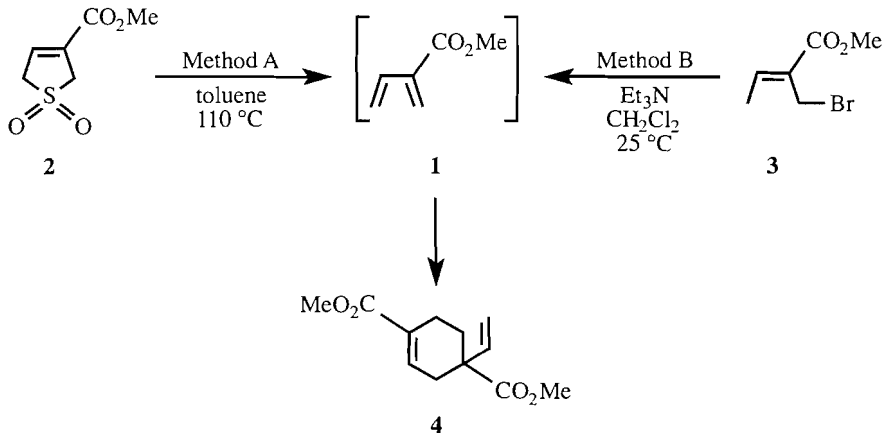

SCHEME 1

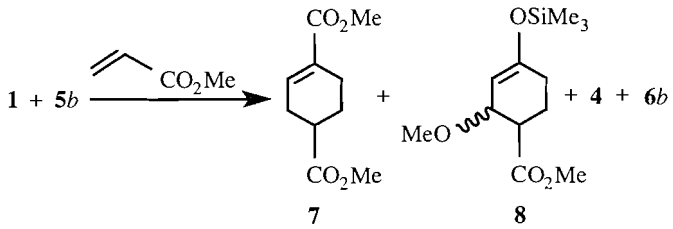

SCHEME 2

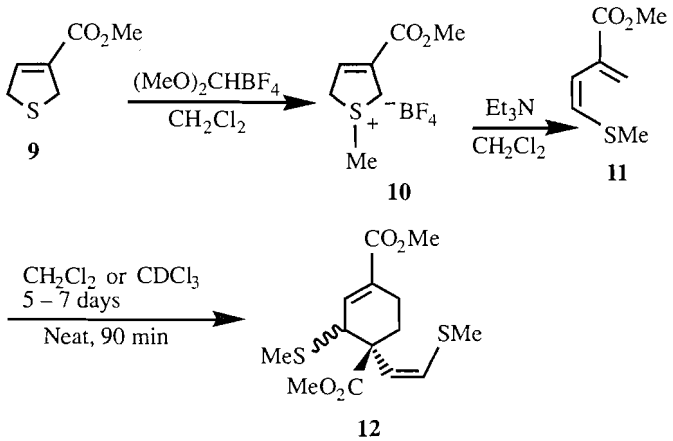

SCHEME 3

methylation with Borch's salt (7), the resulting sulfonium salt **10** underwent an elimination reaction with triethylamine at 25°C to yield the (*Z*)-enethiol ether **11**. Upon standing at 25°C in solvent, **11** dimerized to give a 9:1 mixture of stereoisomeric **12** in 5–7 days. However, when concentrated, **11** dimerized in 90 min in 89% yield. The ^{1}H nmr spectra of both isomers of **12** were consistent with (*Z*)-enethiol ether structures, indicative of a concerted cycloaddition mechanism. The slower dimerization of **11** compared to **1** is probably due to the severe steric interactions in the former when it adopts a *cisoid* conformation. Clearly the 2-carbomethoxy group activates **11** toward dimerization since the known (*Z*)-1-methylthio-1,3-butadiene does not undergo Diels–Alder reactions (8). However, the sulfur also plays an activating role since the carbon analog of **11**, (*Z*)-1-ethyl-2-carbomethoxy-1,3-butadiene, does not dimerize readily (9).

Finally, the dianion of sulfolene **2** was acylated with methyl chloroformate to give a 78% yield of **13** (10). Upon heating in toluene for 12 h, **13** underwent a sigmatropic elimination of SO_2 to afford the stable, but volatile, diene **14** as a 1:1 mixture of *E* and *Z* isomers. Heating **13** for 12 h in toluene containing maleic anhydride gave 87% of two isomeric cycloadducts **15** in a near 1:1 ratio, along with a small amount of unreacted (*E*)-**14**. Compound **15** undergoes a retro-Diels–Alder reaction upon chromatography on silica gel, to give back **14** and maleic anhydride. The ease of cycloaddition of **14**, especially the *E* isomer, with maleic anhydride is noteworthy. Studies to better assess the reactivities of **11** and **14** are underway and will be reported in a more detailed article in due course.

The above results cannot be reconciled with Frontier Molecular Orbital (FMO) theory arguments (11). Indeed, the HOMO of dienes like **1** have been shown to be of lower energy than that of 1,3-butadiene itself by approximately 0.2 eV (12). The results from the cross-cycloaddition experiments between **1** and Danishefsky's diene indicate that the high dienophilic character of **1** is not the sole factor in accelerating its dimerization and therefore the high eneophilic character of **1** must also play a role. Butadienes with other electron-withdrawing groups at C2 have also been shown to dimerize readily (6, 13) and it is likely that they, and dienes **11** and **14**, are all activated in a similar way. Importantly, studies on the dimerization of 2-cyano-1,3-butadiene and its cycloaddition reactions with electron-deficient dienophiles indicate that it has a comparable reactivity to **1** (13). 2-Cyano-1,3-butadiene is more stable in its (*Z*)-(*s-trans*) conformation relative to less eneophilic dienes such as 2,3-dimethyl-1,3-butadiene.[2] This suggests that it, and diene **1**, owe their eneophilicity to a factor other than an enhanced population of the *s-cis* conformation.

We therefore conclude that an electronic factor is activating *diene* **1** with respect to thermal [4 + 2] cycloadditions

[2]The ethyl ester analog of **1** dimerizes (90% yield) when generated in the presence of an excess of 2,3-dimethyl-1,3-butadiene (see ref. 5). Molecular Mechanics calculations using CSC Chem 3D plus™ software showed that while diene **1** was found to have a preferred (*E*)-(*s*)-*cis* conformation approximately 1.5 kcal/mol lowest in energy, 2-cyano-1,3-butadiene and 2,3-dimethyl-1,3-butadiene were more stable in their (*s*)-*trans* conformation by about 1 kcal/mol and 0.4 kcal/mol, respectively.

Can. J. Chem. Downloaded from www.nrcresearchpress.com by 213.200.69.106 on 09/08/12
For personal use only.

TABLE 1. Cross Diels–Alder reaction between diene **1** and electron-rich dienes

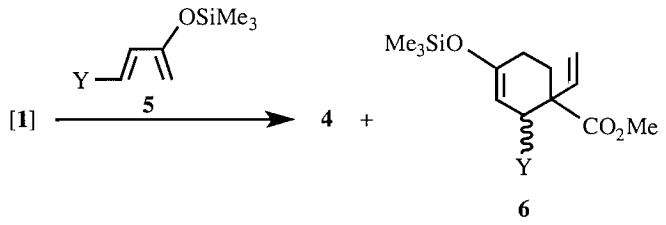

Entry	Y	Diene (Equiv.)[a]	Method[b]	Ratio **4**:**6**[c]	Combined yield of adducts (%)[d]
1	Me	**5***a* (1)	A	2:1[e]	95
2	Me	**5***a* (5)	A	1:4[e]	95
3	Me	**5***a* (1)	B	9:1[f]	94
4	Me	**5***a* (5)	B	3:1[f]	93
5	Me	**5***a* (>5)	B[g]	2:1[f]	98
6	OMe	**5***b* (1)	A	1:2[e]	89
7	OMe	**5***b* (5)	A	1:9[f]	80
8	OMe	**5***b* (1)	B	3:1[f]	80

[a]Molar equivalents with respect to **2** or **3**.
[b]Method A: toluene, reflux; method B: Et_3N, CH_2Cl_2, r.t.
[c]Adducts **6***a* and **6***b* were isolated as the hydrolyzed product after chromatography on silica gel.
[d]Isolated yields based on **2** or **3** after chromatography.
[e]Ratios of isolated adducts.
[f]Ratios determined by ^1H nmr integrations of crude mixture.
[g]Slow addition of **3** over 12 h.

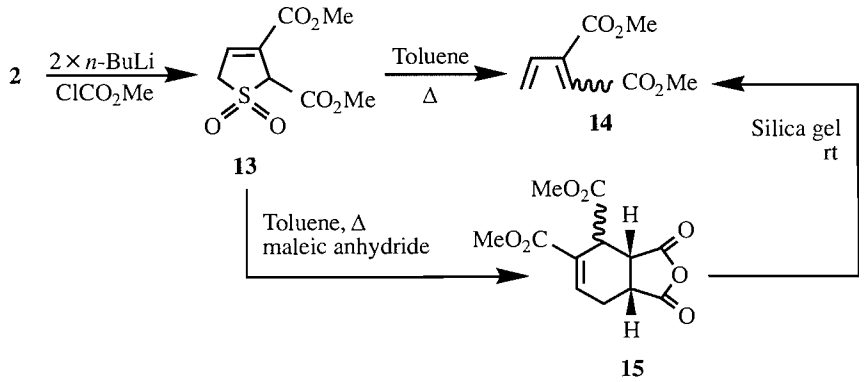

SCHEME 4

with electron-deficient dienophiles. Although we cannot draw conclusions, from our present studies, about the nature of this electronic effect, one possibility is that the cycloadditions of **1** with dienophiles proceed via a transition state (TS) having a high double-bond character between C2 and C3, such as was calculated for the reaction of butadiene with ethylene by Hehre and co-workers (14*a*) and Bach *et al.* (14*b*). Such a transition state could be stabilized due to conjugation with the ester group at C2. It is conceivable that the activation energy of such cycloadditions (from a cross-conjugated six-atom π-system in the starting diene to a conjugated four-atom π-system in the TS) may be lower than that of other cycloadditions involving dienes without a C2-conjugating group or other stabilizing effects (from a conjugated four-atom π-system in the starting diene to a non-conjugated two-atom π-system in the TS).

In any case, we have provided evidence that an electronic factor, at present unknown, is responsible for the activation of 2-carbomethoxy-1,3-butadiene. We believe that the above results could have far-reaching consequences for the theoretical aspect of the Diels–Alder reaction. We are initiating ab initio calculations of dienes like **1**, as well as extending the present studies to include other dienes, to gain a better understanding of the fundamental principles underlying their reactivity.

Acknowledgements

We thank the Natural Sciences and Engineering Research Council of Canada and the University of Victoria for the financial support of this work.

1. (*a*) J.M. McIntosh and R.A. Sieler. J. Org. Chem. **43**, 4431 (1978); (*b*) H.M.R. Hoffmann and J. Rabe. Angew. Chem. Int. Ed. Engl. **22**, 795 (1983).

Can. J. Chem. Downloaded from www.nrcresearchpress.com by 213.200.69.106 on 09/08/12
For personal use only.

2. W. Poly, D. Schomburg, and H.M.R. Hoffmann. J. Org. Chem. **53**, 3701 (1987); L.K. Sydnes, L. Skattebøl, C.B. Chapleo, D.G. Leppard, K.L. Svanholt, and A.S. Dreiding. Helv. Chim. Acta, **58**, 2061 (1975); O. Goldberg and A.S. Dreiding. Helv. Chim. Acta, **59**, 1904 (1976); A.I.D. Alanine, C.W.G. Fishwick, A.D. Jones, and M.B. Mitchell. Tetrahedron Lett. **30**, 5653 (1989).
3. M.E. Jung and C.N. Zimmerman. J. Am. Chem. Soc. **113**, 7813 (1991).
4. (*a*) H-J. Liu, T.K. Ngooi, and E.N.C. Browne. Can. J. Chem. **66**, 3143 (1988); (*b*) S. Danishefsky and T. Kitahara. J. Am. Chem. Soc. **96**, 7807 (1974).
5. D. Martina and F. Brion. Tetrahedron Lett. **23**, 865 (1982).
6. (*a*) J.F. Honek, M.L. Mancini, and B. Belleau. Synth. Commun. **14**, 483 (1984); (*b*) M. Franck-Neumann, D. Martina, and M.-P. Heitz. J. Organomet. Chem. **301**, 61 (1986); T.-s. Chou and S.-C. Hung. J. Org. Chem. **53**, 3020 (1988); (*c*) M. Franck-Neumann, D. Martina, and F. Brion. Angew. Chem. Int. Ed. Engl. **20**, 864 (1981).
7. R.F. Borch. J. Org. Chem. **34**, 627 (1969).
8. R.L. Crumbie and D.D. Ridley. Aust. J. Chem. **34**, 1017 (1981).
9. H. Düttmann and P. Weyertahl. Chem. Ber. **112**, 3480 (1979).
10. T.-s. Chou, C.-Y. Tsai, and L.-J. Huang. J. Org. Chem. **55**, 5410 (1990).
11. I. Fleming. *In* Frontier orbitals and organic chemical reactions. Wiley & Sons, New York. 1976. p. 110 and references therein.
12. K.N. Houk. J. Am. Chem. Soc. **95**, 4092 (1973).
13. P.G. Baraldi, A. Barco, S. Benetti, S. Manfredini, G.P. Pollini, D. Simoni, and V. Zanirato. Tetrahedron, **44**, 6451 (1988).
14. (*a*) R.E. Townshend, G. Ramunni, G. Segal, W.J. Hehre, and L. Salem. J. Am. Chem. Soc. **98**, 2190 (1976); (*b*) R.D. Bach, J.J.W. McDouall, H.B. Schlegel, and G.J. Wolber. J. Org. Chem. **54**, 2931 (1989).

Can. J. Chem. Downloaded from www.nrcresearchpress.com by 213.200.69.106 on 09/08/12
For personal use only.

^{13}C magnetic resonance studies. 144.[1] An examination of β-enolization in the bicyclo[3.3.1]- and [3.2.2]nonan-2-one system

DAVID J. MUIR AND J.B. STOTHERS
Department of Chemistry, University of Western Ontario, London, Ont., Canada N6A 5B7

Received February 8, 1993

DAVID J. MUIR and J.B. STOTHERS. Can. J. Chem. **71**, 1099 (1993).

While 3,3-dimethylbicyclo[3.3.1]nonan-2-one (**5**) is stable under strongly basic conditions (*t*-BuO$^-$/*t*-BuOH/185°C), its isomer, 3,3-dimethylbicyclo[3.2.2]nonan-2-one (**6**), is slowly transformed to **5**. Similarly, 3,3-dimethylbicyclo-[3.2.2]non-6-en-2-one (**8***b*) rearranges to a [3.3.1] isomer but the latter is not stable. Experiments with 3,3-dimethylbicyclo[3.3.1]non-6-en-2-one (**7**) revealed that it is converted to five compounds, none of which is **8***b*. The major product, 8,8-dimethylbicyclo[4.3.0]non-1$^{(6)}$-en-7-one (**11**) arises from β-enolate rearrangement. Enone **11** undergoes slow reduction to *cis*- and *trans*-8,8-dimethylbicyclo[4.3.0]nonan-7-one, presumably by single electron transfer. Experiments with **11** alone showed that β-enolate rearrangement of **7** → **11** is unidirectional. Haller–Bauer cleavage to acidic products occurs as a minor process in the reactions of the unsaturated ketones. The structures of the products were established primarily from their ^{1}H and ^{13}C magnetic resonance spectra.

DAVID J. MUIR et J.B. STOTHERS. Can. J. Chem. **71**, 1099 (1993).

Alors que la diméthyl-3,3-bicyclo[3.3.1]nonanone-2 (**5**) est stable dans des conditions fortement basiques (*t*-BuO$^-$/*t*-BuOH/185°C), son isomère la diméthyl-3,3-bicyclo[3.2.2]nonanone-2 (**6**) se transforme lentement en diméthyl-3,3-bicyclo[3.3.1]nonanone-2 (**5**). De la même façon, la diméthyl 3,3-bicyclo[3.2.2]nonèn-6-one-2 (**8***b*) se transpose en un isomère [3.3.1] instable. Des expériences révèlent que la diméthyl-3,3-bicyclo[3.3.1]nonèn-6-one-2 (**7**) se transforme en cinq composés parmi lesquels on ne retrouve pas le composé **8***b*. Le produit majoritaire, la diméthyl-8,8-bicyclo[4.3.0]nonèn-1$^{(6)}$-one-7 (**11**) provient d'une transposition β-énolate. L'énone **11** subit une lente réduction en *cis*- et *trans*-diméthyl-8,8-bicyclo[4.3.0]nonanone **7** probablement par simple transfert d'électron. Des expériences réalisées avec le composé **11** uniquement révèlent que la transposition β-énolate **7** → **11** est unidirectionnelle. Le clivage Haller–Bauer en produits acides intervient comme un processus mineur dans les réactions des cétones insaturées. On a établi la structure des produits principalement à partir de leurs spectres de résonnance magnétique nucléaire du ^{1}H et du ^{13}C.

[Traduit par la rédaction]

Introduction

The discovery of the homoenolization process by Nickon and Lambert, who found that 3,3-dimethylbicyclo[2.2.1]-heptan-2-one (camphenilone) is racemized by treatment with strong base at elevated temperatures, *t*-BuO$^-$/*t*-BuOH/185°C (1), revealed that proton abstraction occurred from sites more than one bond from the carbonyl group. Their finding led to studies of several related polycyclic ketones of which the majority were found to exhibit abstraction from β-carbons, or β-enolization (2), with a few examples of γ-enolate formation (3). More recently, some examples of β-enolization in acyclic (4) and monocyclic systems (5) have been described. With few exceptions (6), α-enolization has been blocked in these homoenolizable ketones by α-methyl substitution or structurally such that only anti-Bredt α-enolates could form.

The β-enolization process may be viewed as the formation of a cyclopropoxide anion, e.g., **A** in Scheme 1, whose fate is governed by the regioselectivity of its subsequent protonation, via path *a* to return to the initial ketone or path *b* to form an isomeric ketone. The regioselectivity of the process has attracted some interest because of the potential utility for new synthetic approaches to carbon skeletons not readily accessible by other routes. Sequences in which a β-enolate rearrangement is a key step have been developed for linear and angular triquinanes (7) and a [3.3.3]propellane.[2] Since paths *a* and *b* may proceed with either retention or inversion of configuration, the stereoselectivity of protonation has mechanistic interest and may be established by isotopic labelling experiments.

The regio- and stereoselectivity of β-enolization has been examined in detail for several saturated bicyclic ketones. For example, the [2.2.2] and [3.2.1] ketones, **1** and **2**, are slowly equilibrated under the usual homoenolization conditions (8) while **3** rearranges slowly but irreversibly to **4** (9). It was also found that, under these conditions, Δ^5-**1** rearranged >100 times faster than **1** to a mixture of Δ^2- and Δ^3-**2**, with the equilibrium more strongly biased toward the [3.2.1] skeleton (10). Each of these reactions proceeds cleanly with little evidence of other products. In contrast, Δ^6-**3** is transformed to a mixture of six products, none of which is an unsaturated ketone (11). As an extension of these studies of simple bicyclic systems, we have examined the behavior of the related [3.3.1] and [3.2.2] ketones, **5**, **6**, **7**, and **8***b*, under typical homoenolization conditions. We wish to present the results of these experiments in this paper.

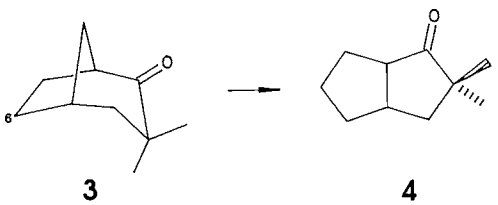

3 **4**

Results and discussion

Ketone **5** (12) was obtained by methylation (MeI/$NaNH_2$/Et_2O) of bicyclo[3.3.1]nonan-2-one prepared from cyclohexanone by the four-step sequence described by Inouye et al. (13). Following our standard methods (14), **5** was dissolved in anhydrous *t*-BuO$^-$/*t*-BuOH (1.00 M) to furnish a solution 0.25 M in **5**. Aliquots of this solution were rapidly transferred to glass tubes under nitrogen, degassed, and sealed

[1]For Part 143, see ref. 5.

[2]H.A. Patel, J.B. Stothers, and S.E. Thomas. Paper in preparation.

Can. J. Chem. Downloaded from www.nrcresearchpress.com by 213.200.69.106 on 09/08/12
For personal use only.

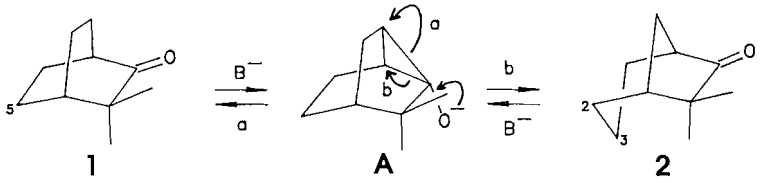

SCHEME 1

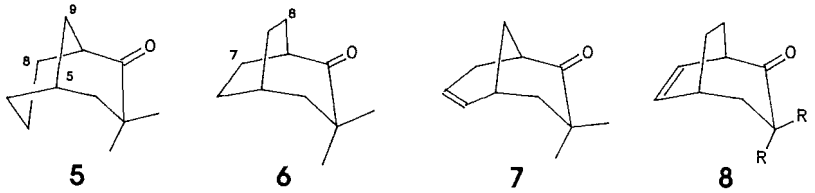

a R = H
b R = Me

under vacuum. After heating at 185°C in an oil-bath for various times (24, 48, 112, 240 h), the tubes were cooled and the neutral product isolated by pentane extraction. The alkaline washings were acidified and extracted with ether to isolate any acidic product but none was found even after 240 h at 185°C. In all cases, **5** was the only component detected (glc and ^{13}Cmr) in the neutral fractions and was recovered in >85% yields.

Under the same reaction conditions, however, **6** was found to rearrange slowly to **5**. Neutral fractions (>85% yields) containing 56:44, 42:58, and 35:65 mixtures of **6**:**5** were isolated after 96, 192, and 240 h, respectively, with no evidence of acidic products. Ketone **6** was prepared by catalytic hydrogenation of **8***b*, obtained by α,α-dimethylation of **8***a*, which was generated by ring expansion of bicyclo[2.2.2]octenone as described in an earlier report (15).

Ketones **5** and **6** are, in principle, interconvertible through the β-enolate **9**, which can be generated by abstraction of a proton from C-8 in **5** and C-7 or -8 in **6**. Subsequent cleavage via paths *a* or *b* would led to **5** or **6**, respectively. The results above showed that **9**, or an equivalent species, is formed from **6**, but there was no evidence that **9** is generated from **5**.

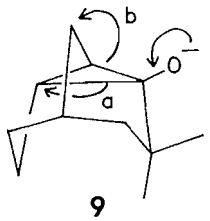

To examine this point, **5** was treated with *t*-BuO$^-$/*t*-BuOD at 185°C for various times and the ^{2}H content of the recovered **5**-d_x samples was assayed by mass spectrometry and ^{2}Hmr. The ^{2}H spectra of samples collected after treatment for 3, 6, 12, and 24 h in the deuterated base contained only two signals indicating that exchange occurred at C-1 (δ 2.38) and the *exo*-methyl site (δ 1.13). Earlier work (16) had shown that bridgehead exchange occurs under milder conditions (101°C in NaOMe/MeOD) and the methyl assignment followed from previous studies, which established that *exo*-methyl exchange is significantly faster than that at *endo*-methyl sites

TABLE 1. Deuterium incorporation in **5** at 185°C

Time (h)	Atoms D/molecule[b]	% Exchange/hydrogen[a] H-1	*exo*-Methyl
3	1.12	0.89	0.08
6	1.33	0.90	0.14
12	1.67	0.90	0.25
24	2.20	0.88	0.44

[a]Assayed by ^{2}Hmr (±2%).
[b]Determined by mass spectrometry.

in many related systems (2). From the proton spectrum of **5**, we can be certain that signals from other deuterated sites in **5**-d_x would not be obscured by the observed signals. The incorporation data are listed in Table 1. There was no evidence of proton abstraction from C-8 in **5**; thus, it must be a very slow process if, in fact, **9** is formed from **5**. An upper limit for a rate constant for C-8 exchange can be estimated to be ca. 10^{-7} s, which is an order of magnitude less than the observed rate for the **6** → **5** rearrangement. It may be noted that the ^{13}C spectra of the **5**-d_x samples confirm the ^{13}C assignments reported by Yamada et al. (12), since bridgehead (C-1) deuteration produced ^{2}H-induced isotope shifts of 125 and 111 ppb for the methylene signals at δ_C 29.5 (C-9) and 32.5 (C-8).

The fate of **7** under the homoenolization conditions was then examined. This ketone was prepared from bicyclo[3.3.1]nona-2,6-dione (17) through the sequence described by Bishop et al. (18), but using a modified procedure for ketalization of the dione (19). A series of runs (6, 12, 24, 48, and 72 h) gave neutral fractions (72–76% yields), containing five components after the longer reaction times, while small amounts of a single acidic component were obtained; the acid fraction represented 12% of the product after 72 h.

The ^{13}C spectra of the neutral products, isolated after 3 and 6 h, revealed two neutral components, in addition to **7**. Both were ketones and the more abundant contained a disubstituted double bond. Although attempts to isolate pure samples of this new ketone by column chromatography were unsuccessful, its ^{13}C shieldings strongly support structure **10**,

Can. J. Chem. Downloaded from www.nrcresearchpress.com by 213.200.69.106 on 09/08/12
For personal use only.

TABLE 2. ^{13}C shielding data[a] for **7**, **8***b*, and **10**

Compound	C-1	C-2	C-3	C-4	C-5	C-6	C-7	C-8	C-9	Me
7	42.4	221.6	42.8	43.9	29.4	126.5	132.1	32.0	29.2	30.2 30.5
10	47.0	215.4	42.7	45.5	25.8	33.6	131.0	126.8	29.0	30.2 32.2
8*b*	50.1	213.2	45.9	44.5	32.6	136.7	127.7	26.7	23.4	30.5 32.5

[a]In ppm from TMS in $CDCl_3$ solutions.

the Δ^7-isomer of **7**. The data are listed in Table 2 with those for **7** and **8***b*. The specific assignments for **7** followed from the results of $^1H\{^1H\}$ and $^{13}C\{^1H\}$ correlation spectra; the long-range $^{13}C\{^1H\}$ interactions of the methyl protons were found using the FLOCK sequence (20). For **10** and **7**, the shielding differences for the carbonyl and methine carbons are entirely consistent with isomerization of **7** to its Δ^7 isomer. The −6.2 ppm shift of the carbonyl signal in **10** relative to **7** is indicative of a homoconjugative interaction in a β,γ-enone (21) and the +4.6 and −3.6 ppm shifts for C-1 and -5, respectively, are as expected for this change in the position of the double bond. Since the allylic protons in **7** are the most acidic, equilibration of **7** and **10** may be anticipated under the strongly basic conditions and, in fact, the relative proportion of **7** and **10** was 3:2 in all of the neutral product mixtures.

The third ketone detected in the products from the shorter reaction times was readily isolated from the neutral mixture by chromatography on alumina. Its ^{13}Cmr spectrum contained signals for a tetrasubstituted double bond, δ_C 136.0 and 170.3, and a carbonyl carbon, δ_C 213.3, as well as those for five methylene carbons and a pair of equivalent methyl groups. The absence of methine signals clearly showed that a major skeletal change had occurred and the data indicated that this compound was **11**. The ^{13}C spectrum was the same as that of an authentic sample, prepared by 2,2-dimethylation of 4,5,6,7-tetrahydrindan-1-one (22); thus, the structural assignment was confirmed.

In the product mixtures from runs longer than a few hours, the presence of two additional compounds was apparent from glc analysis and ^{13}Cmr. Flash chromatography furnished a sample containing ca. 80% of these compounds and ca. 20% of a mixture of **7** and **10**. The ^{13}Cmr spectrum showed that these are ketones, δ_C 222.4 and 224.4, containing no olefinic carbons. There were signals for two methyl, five methylene, two methine, and one quaternary carbon for each of the two compounds. Identical sets of signals were found in the ^{13}C spectrum of the product from tetra-*n*-propylammonium per-ruthenate (TPAP) oxidation (23) of the alcohol mixture obtained by reduction of authentic **11** with lithium in liquid ammonia (24). Thus, these are the *cis* and *trans* isomers **12***b*. Specific ^{13}C assignments for the skeletal carbons of each isomer were made by comparison of the observed shieldings with the data for the parent ketones **12***a* (25). The ^{13}C data are collected in Table 3 from which it is evident that the methyl substituents have little effect on the shieldings of the methylene carbons in the six-membered ring. The synthetic sample was a 60:40 mixture of *cis*- and *trans*-**12***b*, while a 52:48 mixture was isolated from the runs with **7**.

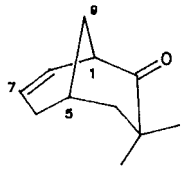

10

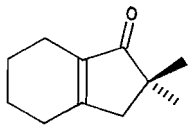

11

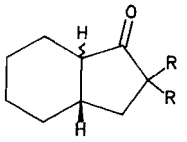

12

a R = H
b R = Me

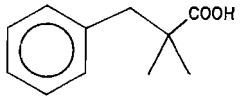

13

The acidic fraction contained a single carboxylic acid that exhibited a remarkably simple ^1Hmr spectrum having two singlets in the high-field region, δ 1.23 (6H) and 2.92 (2H), accompanied by low-field absorption, 7.15–7.35 ppm (5H), characteristic of a phenyl group. The ir, ms, and ^1H and ^{13}Cmr data indicated that the acid was **13** and this assignment was confirmed by the synthesis of an authentic sample from hydrocinnamic acid.

The compositions of the products isolated from the experiments with **7** are listed in Table 4 as a function of time. Although **8***b* was not detected in the neutral mixtures from the runs with **7**, its behavior under homoenolization conditions was of interest. A series of experiments showed that **8***b* is transformed slowly to **7** and, thence, to its rearrangement products. The compositions of the neutral products isolated in 72–80% yields are collected in Table 5. The acidic fractions, constituting <5% of the product after the longer reaction times, contained a single component, **13**. It may be noted that the ratio of **7** to **10** was 3:2, as in the product mixtures from **7** itself.

A series of runs with **11** was also carried out and the results clearly showed that the major mode of reaction involved reduction to *cis*- and *trans*-**12***b* in *t*-BuO^-/*t*-BuOH at 185°C, together with a minor process leading to a relatively small acidic fraction. Both glc analysis and ^{13}Cmr showed that the neutral fractions contained only **11** and the **12***b* isomers; there was no evidence of the presence of **7** and (or) **10**. The product compositions after various reaction times are listed in Table 6.

The generation of the neutral product mixtures found for the unsaturated ketones may be interpreted as outlined in Scheme 2. Irreversible rearrangement of the [3.2.2] ketone

Can. J. Chem. Downloaded from www.nrcresearchpress.com by 213.200.69.106 on 09/08/12
For personal use only.

TABLE 3. ^{13}C shielding data[a] for **12***a*[b] and *b*

Compound	C-1	C-2	C-3	C-4	C-5	C-6	C-7	C-8	C-9	Me
cis-**12***a*	36.0	28.0	23.9	22.7	22.4	49.3	219.5	34.6	25.5	
cis-**12***b*	32.5	28.1	23.0	23.8	22.5	48.0	224.4	44.2	40.7	26.5 27.2
trans-**12***a*	43.1	32.4	25.7	25.4	24.8	55.3	217.7	36.8	27.5	
trans-**12***b*	39.7	32.7	26.1	25.8	25.4	55.0	222.4	44.9	43.9	24.7 26.3

[a]In ppm from TMS in $CDCl_3$ solutions.
[b]Data from ref. 25.

TABLE 4. Composition[a] of the product mixtures from homoenolization of **7** (*t*-BuO^-/*t*-BuOH/185°C)

				12*b*		
Time (h)	**7**	**10**	**11**	*cis*	*trans*	**13**
6	37	24	12	–	–	5
12	20	14	26	7	6	6
24	13	9	33	11	10	8
48	6	4	34	15	14	8
72	<2	<1	31	21	20	12

[a]Ratios of the neutral products (>70% yields) estimated by ^{13}Cnmr.

TABLE 5. Composition[a] of the neutral product from homoenolization of **8***b* (*t*-BuO^-/*t*-BuOH/185°C)

					12*b*	
Time (h)	**8***b*	7	**10**	**11**	*cis*	*trans*
12	56	9	6	4	–	–
24	47	13	8	9	<2	<1
48	27	11	8	22	6	5
96	15	8	5	27	13	12
144	7	4	3	26	17	16

[a]Estimated by ^{13}Cnmr as percentage of isolated material (>70% yields).

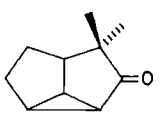

19

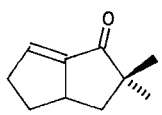

20

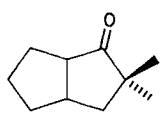

21

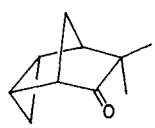

22

for ketones **19** (3) and **20** (11). It is interesting that the reduction of **20** (→ **21**) is faster than that observed for either **11** or **19** under these conditions. Both **11** and **19** (generated by γ-enolate rearrangement of **22**) are the primary rearrangement products whose concentrations increase in the early stages of reaction, before passing through a maximum and then decreasing as these are slowly consumed by reduction. In contrast, no unsaturated ketones were found as products from homoenolization of Δ^6-**3**, although **20**, or an isomeric enone, must be an intermediate in the generation of **21**, which is the major product from Δ^6-**3**.

In all experiments **13** was the only acidic product, presumably arising by dehydrogenation of **23**, or a double bond isomer. Haller–Bauer cleavage of **10**, after addition of *tert*-butoxide anion to the carbonyl carbon, would generate **23** (R = *tert*-butyl), a cyclohexenyl analog of **13**, as outlined in Scheme 3. Migration of the double bond in **23** should occur readily under these strongly basic conditions because of the acidity of the allylic protons; this is analogous to the observed equilibration of **7** and **10**. It is conceivable that hydride transfer to **11** from an intermediate cyclohexenyl anion could occur, thereby generating a cyclohexadienyl analog of **13**. Allylic proton abstraction from the latter species and subsequent hydride loss would lead to the formation of **13**.

In summary, the saturated [3.3.1] ketone **5** shows no tendency to rearrange to the [4.3.0] ring skeleton. Its unsaturated analog **10** undergoes this transformation, but, under the homoenolization conditions, the olefinic bond in the initial **8***b* via β-enolate **14**, or an equivalent species, affords **7**, which would be expected to equilibrate rapidly with **10** through a common allylic anion. Proton abstraction from C-9 in **10** could lead to the formation of β-enolate **15**, or an equivalent intermediate, which undergoes unidirectional cleavage to the [4.3.0] skeleton. This rearrangement is strictly analogous to that of **3** → **4** (9) but is significantly faster. The **3** → **4** conversion exhibited a half-life of ca. 60 h while more than 50% of the **7**:**10** mixture is consumed in less than 12 h (Table 4). While formation of an isomeric β-enolate from **7** may be envisaged, we suggest that this is less likely since **5** is stable under these conditions. In any event, it is clear that the incorporation of a double bond in the [3.3.1] skeleton enhances β-enolate formation. An analogous enhancement for **1** and **2** was noted in the Introduction. In principle, γ,δ-enone **16** or the β,γ isomer would be the initial product(s) from cleavage of **15** and, under the basic conditions, can be expected to isomerize rapidly. Only α,β-enone **11** was identified among the products, but traces of other isomers may have escaped detection.

The formation of the saturated ketone **12***b* clearly shows that **11** undergoes slow reduction. We propose that single electron transfer from the *tert*-butoxide anion to the carbonyl carbon of **11** to generate ketyl **17** or homolysis of the addition product **18** are the most probable intermediates in this process. Similar reduction processes have been observed

Can. J. Chem. Downloaded from www.nrcresearchpress.com by 213.200.69.106 on 09/08/12
For personal use only.

TABLE 6. Composition[a] of the product mixtures from **11** after treatment with *t*-BuO^-/*t*-BuOH at 185°C

		12*b*		
Time (h)	**11**	*cis*	*trans*	**13**
3	71	11	10	–
12	63	17	15	–
24	41	20	18	5
48	31	25	23	10
96	19	28	26	15

[a]Ratios of neutral components estimated by ^{13}Cmr.

rearrangement product **11** is subsequently reduced to furnish the saturated [4.3.0] system as the end product.

Experimental

Boiling points and melting points are uncorrected. Gas–liquid chromatography (glc) was done with Varian 940 or 3300 instruments using 1/8-in. columns of OV-101 (10 ft, 1.5% and 6 ft, 5%, respectively) on Chromosorb G. Tetrahydrofuran (THF) and ether were dried over sodium/benzophenone and freshly distilled before use.

Infrared spectra were recorded with a Bruker/IBM FTIR instrument. Mass spectral data were obtained with a Finigan MAT 8230 spectrometer at 70 eV for routine spectra and 20 eV for precise mass measurements. The nmr spectra were recorded with Varian Gemini-200, XL-200, or XL-300 instruments, with digital resolution of 0.1 (^{1}H) and 0.6 Hz (^{13}C). The protonation level for each carbon signal was found from APT or DEPT spectra. Assignments for the sp^3 carbon signals were aided by $^{13}C\{^1H\}$ correlations. Comparisons of the intensities of clearly resolved signals (CH_3 vs. CH_3 and CH_2 vs. CH_2) permitted estimation of the compositions of some product mixtures. The HETCOR sequence of the Varian software with 2048 × 512 data point matrices was used to show one-bond interactions and the FLOCK sequence (20) to identify longer range interactions. The HOMCOR sequence of the Varian software was used to record $^1H\{^1H\}$ COSY-45 spectra with 1024 × 1024 data matrices.

Materials

The parent ketones required to prepare the reactants for these experiments were obtained by published procedures. The four-step sequence from cyclohexanone employed by Inouye et al. (13) gave bicyclo[3.3.1]nonan-2-one, which was methylated in 67% yield, as described below, to furnish **5** (12). Bicyclo[3.3.1]nona-2,6-dione was obtained from Meerwein's ester as reported by Lightner et al. (17) and monoketalized, as described by Momose et al. (19). Then, with minor modifications, the sequence employed by Bishop et al. (18) was followed. The carbonyl group was reduced and the hydroxyketal treated with *p*-toluenesulfonyl chloride. Elimination of the tosyl group by refluxing in pyridine and deketalization with *p*-TsOH furnished bicyclo[3.3.1]non-6-en-2-one. Ring expansion of bicyclo[2.2.2]otenone by ketonization of its cyclopropanated silyl enol ether gave bicyclo[3.2.2]non-6-en-2-one (**8***a*) (15).

General procedure for the α,α-dimethylation of the bicyclic ketones

To a stirred suspension of freshly powdered $NaNH_2$ (30 mmol) in dry ether (5 mL) was added a solution of the ketone (5 mmol) in dry ether (5 mL) and the mixture heated under reflux for 2 h with vigorous stirring. The mixture was cooled and methyl iodide (30 mmol) was added slowly before the mixture was refluxed for 16 h, at which time a second addition of methyl iodide (10 mmol) was made. After a reflux period of 3 h, the mixture was cooled to 0°C and the excess $NaNH_2$ destroyed by the addition of cold water (20 mL). The ether layer was separated and the aqueous phase extracted with ether (2 × 25 mL). The combined extracts were washed with brine before drying over anhydrous $MgSO_4$. Evaporation of the solvent afforded the desired dimethylated ketone. The purification method, yield, and physical data for each product are listed below.

3,3-Dimethylbicyclo[3.3.1]non-6-en-2-one (7): isolated in 85% yield by flash chromatography (fc) with hexane as eluent; ir (liquid film): 1700 m^{-1}; ^{13}Cmr ($CDCl_3$) see Table 2; ^{1}Hmr ($CDCl_3$) δ: 1.11 (s, 3H, Me), 1.08 (s, 3H, Me), 1.77 ("dt," 1H, J = 13.8, 2.5 Hz, *endo*-H-4), 1.84 (dd, 1H, J = 5.3, 13.8 Hz, *exo*-H-4), 1.90 (bd, 1H, J = 12 Hz, *anti*-H-9), 2.00 (bd, 1H, J = 12 Hz, *syn*-H-9), 2.12 (bd, 1H, J = 18 Hz, *endo*-H-6), 2.34 (bd, 1H, J = 18 Hz, *exo*-H-6), 2.45 (m, 1H, H-5), 2.65 (m, 1H, H-1), 5.64 (m, 1H, H-7), 5.78 (m, 1H, H-8). Exact Mass calcd. for $C_{11}H_{16}O$: 164.1202; found: 164.1203.

3,3-Dimethylbicyclo[3.2.2]non-6-en-2-one (8b): isolated in 73% yield by fc (hexane – ethyl acetate, 95:5) and slowly crystallized on standing to a waxy solid that sublimed readily at room temperature to provide an analytical sample; mp 38–39°C; ir ($CHCl_3$): 1694 cm^{-1}; ^{13}Cmr ($CDCl_3$): see Table 2; ^{1}Hmr ($CDCl_3$) δ: 1.14 (s, 3H, Me), 1.16 (s, 3H, Me), 1.6–1.95 (m, 6H), 2.64 (m, 1H, H-5), 3.17 (m, 1H, H-1), 6.0 (bdd, 1H, J = 7, 8 Hz, H-6), 6.35 (bt, 1H, J = 8 Hz, H-7). Exact Mass calcd. for $C_{11}H_{16}O$: 164.1202; found: 164.1200.

3,3-Dimethylbicyclo[3.2.2]nonan-2-one (6)

To a solution of **8***b* (254 mg) in ethyl acetate (10 mL) was added palladium on activated carbon catalyst (10% Pd, 70 mg) and the mixture placed in a Parr hydrogenation bottle. Then the bottle was filled to 58 psi (1 psi = 6.9 kPa) with hydrogen before shaking for 30 min at room temperature. The mixture was filtered and the solvent evaporated to furnish **6** quantitatively; ir (liquid film): 1692 cm^{-1}; ^{13}Cmr ($CDCl_3$) δ_C: 30.8 $(CH_3)_2$, 21.8 (2), 24.8 (2), 45.1, (5 × CH_2), 29.4, 46.6 (2 × CH), 45.0 (quat C), 220.1 (C=O); ^{1}Hmr ($CDCl_3$) δ: 1.18 (s, 6H, Me_2), 1.6–1.8 (m, 8H), 2.17 (m, 1H, H-5), 2.58 (m, 1H, H-1). Exact Mass calcd. for $C_{11}H_{18}O$: 166.1358; found: 166.1360.

For the homoenolization experiments, samples were chromatographed over silica before use.

8,8-Dimethylbicyclo[4.3.0]non-1(6)-en-7-one (11)

To diisopropylamine (0.6 mL) in 12 mL of THF at −60°C was added *n*-butyllithium (1.5 mL, 2.5 M in hexane) and the mixture stirred for 10 min. Then, 4,5,6,7-tetrahydrohydrindan-1-one (360 mg) (22) was added and the mixture stirred for 10 min before methyl iodide (0.5 mL) was added and stirring was continued for 15 min. The mixture was then poured into 1 M HCl solution (25 mL) and the product was isolated by ether extraction. After a second methylation cycle, the product was purified by column chromatography on silica to give **11** (390 mg, 89% yield); ir (liq. film) 1649, 1698 cm^{-1}; ^{13}Cmr ($CDCl_3$) δ_C: 25.3 $(CH_3)_2$, 20.2, 21.8, 22.3, 28.4, 47.2 (5 × CH_2), 43.2 (quat C), 135.9, 170.2 (C=C), 213.2 (C=O); ^{1}Hmr ($CDCl_3$) δ: 1.06 (s, 6H, $(CH_3)_2$), 1.55–1.75 (m, 4H), 2.03–2.13 (m, 2H), 2.22–2.28 (m, 2H), 2.29–2.34 (m, 2H, H-9). Exact Mass calcd. for $C_{11}H_{16}O$: 164.1202; found: 164.1200. This compound was identical to one of the products from the homoenolization experiments with **7**.

cis- *and* trans-*8,8-Dimethylbicyclo[4.3.0]nonan-7-one (12*b*)*

Following the procedure of House et al. (24), a solution of enone **11** (35 mg) in THF (2 mL), containing *tert*-butyl alcohol (40 μL), was added to a cold (−78°C) solution of lithium (6 mg) in ammonia (4 mL). After the addition, the cold-bath was removed and the mixture allowed to reflux for 2 h. The reaction was quenched by the addition of water (2 mL) and the ammonia was allowed to evaporate before water (10 mL) and ether (10 mL) were added. The organic layer was separated and the aqueous phase extracted twice with Et_2O (10 mL). The solvent was evaporated and the residual oil (34 mg) was oxidized directly by the addition of *N*-methylmorpholino-*N*-oxide (35 mg) in CH_2Cl_2 (10 mL) with

Can. J. Chem. Downloaded from www.nrcresearchpress.com by 213.200.69.106 on 09/08/12
For personal use only.

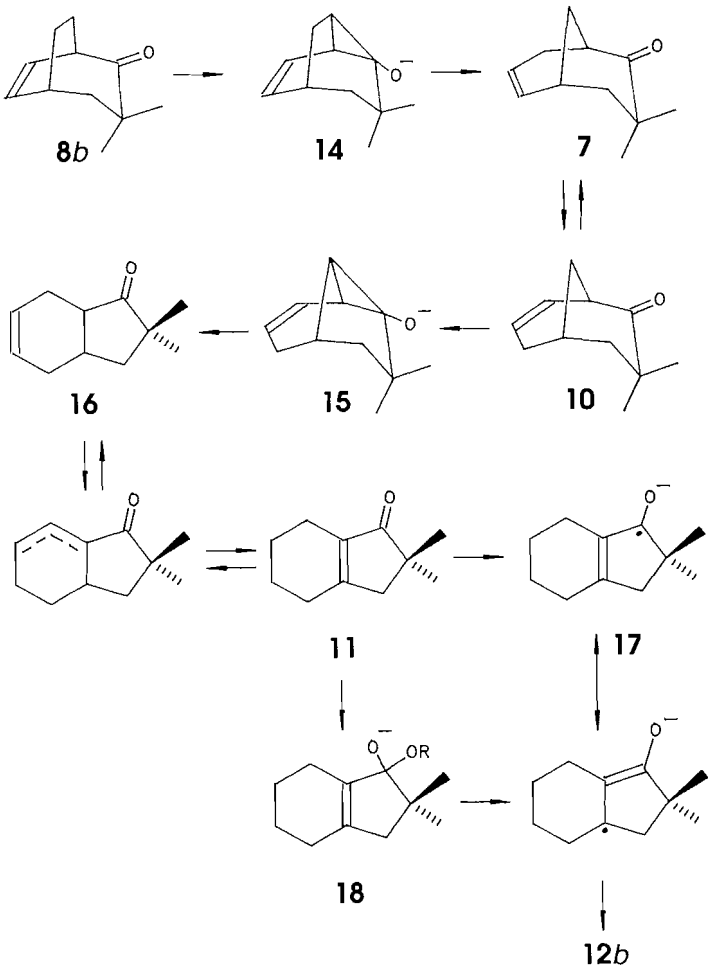

SCHEME 2

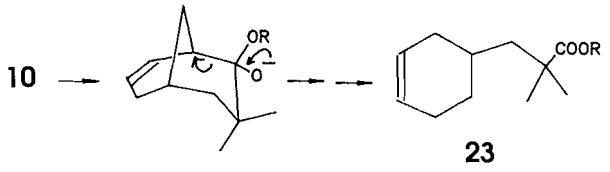

SCHEME 3

1 mg of tetra-*n*-propyl ammonium per-ruthenate (23). This reaction mixture was allowed to stand for 0.5 h before dilution with 20 mL of CH_2Cl_2. The solution was washed with 15 mL of each of saturated aqueous Na_2SO_3, brine, saturated aqueous $CuSO_4$, and brine before drying over anhydrous $MgSO_4$. Evaporation of the solvent left an oil (28 mg, 79% overall yield), which by ^{13}Cmr and glc was a 60:40 mixture of the desired *cis*- and *trans*-**12***b*; ir (liquid film): 1738 cm^{-1}; ^{13}Cmr ($CDCl_3$): see Table 3. Exact Mass calcd. for $C_{11}H_{18}O$: 166.1358; found: 166.1366 (*cis* isomer), 166.1353 (*trans* isomer); these data were obtained by gc/ms using a 30-m capillary column coated with DB-5.

2,2-Dimethyl-3-phenylpropanoic acid (13)

Methyl hydrocinnamate (500 mg) was methylated as described above for **11** (diisopropylamine (0.5 mL), THF (12 mL), n-BuLi (1.8 mL, 2.5 M in hexane), methyl iodide (0.5 mL). After a second methylation cycle, the methyl ester of **13** (550 mg, 94% crude yield) was isolated. The crude ester (37 mg) was heated in 3 M NaOH solution at 80°C for 5 h. The reaction mixture was extracted with ether (2 × 50 mL) and the aqueous phase acidified to pH 2 before extraction with ether (3 × 50 mL). After drying over $MgSO_4$, the solvent was removed to yield **13** (28 mg, 82%) with the following properties: ir (liquid film): 2400–3400, 1701 cm^{-1}; ^{13}Cmr ($CDCl_3$) δ_C: 24.7 (2 × CH_3), 45.9 (CH_2), 43.5 (quat C), 126.6, 128.1 (2), 130.3 (2) (5 × aryl CH), 137.6 (aryl C), 184.5 (COOH); ^{1}Hmr ($CDCl_3$) δ: 1.23 (s, 6H, Me_2), 2.92 (s, 2H, H-3), 7.15–7.35 (m, 5H, aryl H). Exact Mass calcd. for $C_{11}H_{14}O_2$: 178.0994; found: 178.0996.

Acknowledgements

We are grateful for the continued financial support of the Natural Sciences and Engineering Research Council of Canada. We wish to acknowledge the technical assistance of Ruben L. Boles and to thank Professor E.W. Warnhoff for helpful discussion.

1. A. Nickon and J.L. Lambert. J. Am. Chem. Soc. **84**, 4604 (1962); **88**, 1905 (1966).
2. N.H. Werstiuk. Tetrahedron, **39**, 205 (1983).
3. A.K. Cheng, A.K. Ghosh, and J.B. Stothers. Can. J. Chem. **62**, 1385 (1984), and references therein.
4. R.A. Dyllick-Brenzinger, V. Patel, M.B. Rampersad, J.B. Stothers, and S.E. Thomas. Can. J. Chem. **68**, 1106 (1990).
5. W. Sifton, J.B. Stothers, and S.E. Thomas. Can. J. Chem. **70**, 1274 (1992).
6. A. Nickon, J.L. Lambert, J.E. Oliver, D.F. Covey, and J. Morgan. J. Am. Chem. Soc. **98**, 2593 (1976).
7. (*a*) J.L. Jurlina, H.A. Patel, and J.B. Stothers. Can. J. Chem.

Can. J. Chem. Downloaded from www.nrcresearchpress.com by 213.200.69.106 on 09/08/12
For personal use only.

62, 1159 (1984); (*b*) B.A. Dawson, A.K. Ghosh, J.L. Jurlina, A.J. Ragauskas, and J.B. Stothers. Can. J. Chem. **62**, 2521 (1984).
8. A.K. Cheng, J.B. Stothers, and C.T. Tan. Can. J. Chem. **55**, 447 (1977).
9. A.L. Johnson, N.O. Petersen, M.B. Rampersad, and J.B. Stothers. Can. J. Chem. **52**, 4143 (1974).
10. A.K. Cheng and J.B. Stothers. Can. J. Chem. **56**, 1342 (1978).
11. G.A. Antoniadis, M.T.M. Clements, S. Pieris, and J.B. Stothers. Can. J. Chem. **65**, 1557 (1987).
12. K. Yamada, S. Manabe, Y. Kyotani, M. Suzuki, and Y. Hirata. Bull. Chem. Soc. Jpn. **52**, 186 (1979).
13. Y. Inouye, T. Kojima, J. Owada, and H. Kakisawa. Bull. Chem. Soc. Jpn. **60**, 4369 (1987), and references therein.
14. A.L. Johnson, J.B. Stothers, and C.T. Tan. Can. J. Chem. **55**, 212, (1975).
15. V. Patel, A.J. Ragauskas, and J.B. Stothers. Can. J. Chem. **64**, 1440 (1986).
16. E.N. Marvell, G.J. Gleicher, D. Sturmer, and K. Salisbury. J. Org. Chem. **33**, 3393 (1968).
17. D.A. Lightner, T.C. Chang, D.T. Hefelfinger, D.E. Jackman, W.M.D. Wijekoon, and J.W. Givens. J. Am. Chem. Soc. **107**, 7499 (1985).
18. R. Bishop, W. Parker, and J.R. Stevenson. J. Chem. Soc. Perkin Trans. 1, 565 (1981).
19. T. Momose, E. Yoshizawa, and O. Muraoko. Synth. Commun. **15**, 17 (1985).
20. W.F. Reynolds, S. McLean, M. Perpick-Dumont, and R.A. Enriquez. Magn. Reson. Chem. **27**, 162 (1989).
21. J.B. Stothers, J.R. Swenson, and C.T. Tan. Can. J. Chem. **53**, 581 (1975).
22. H.O. House and G.H. Rasmusson. J. Org. Chem. **28**, 31 (1963).
23. W.P. Griffith, S.V. Ley, G.P. Whitcombe, and A.D. White. J. Chem. Soc. Chem. Commun. 1625 (1987).
24. H.O. House, R.W. Giese, K. Kronberger, J.P. Kaplan, and J.F. Simeone. J. Am. Chem. Soc. **92**, 2800 (1970).
25. F. Fringuelli, F. Pizzo, A. Taticchi, T.D.J. Halls, and E. Wenkert. J. Org. Chem. **47**, 5056 (1982).

Can. J. Chem. Downloaded from www.nrcresearchpress.com by 213.200.69.106 on 09/08/12
For personal use only.

Studies on nitracrine and its nitro isomers devoted to tautomeric phenomena, structural and physicochemical features, as well as surrounding electrostatic potential

JANUSZ RAK AND JERZY BŁAŻEJOWSKI[1]
University of Gdańsk, Department of Chemistry, 80-952 Gdańsk, Poland

AND

RANDY J. ZAUHAR
Biotechnology Institute, The Pennsylvania State University, 519 Wartik Laboratory, University Park, PA 16802, U.S.A.

Received July 1, 1992[2]

JANUSZ RAK, JERZY BŁAŻEJOWSKI, and RANDY J. ZAUHAR. Can. J. Chem. **71**, 1106 (1993).

Relative stabilities and features of tautomers of *N*,*N*-dimethyl-*N'*-(1-nitro-9-acridinyl)-1,3-propanediamine (known as nitracrine by the World Health Organization (WHO) or as Ledakrin in Poland), which exhibits antitumour activity, and its three nitro isomers were examined by AM1 and, in some cases, by PM3 and ab initio (STO-3G) methods. The lowest energy form of three compounds was always an imino tautomer, while the energy of the amino tautomers was a few kcal mol^{-1} higher and that of the *aci* forms (in the case of the 2- and 4-nitro isomers) was more than 25 kcal mol^{-1} higher. Each tautomer can further exist in several structural forms (conformers or stereoisomers). In some of them internal hydrogen bonding interactions are feasible. The barriers to rotation of the -NHR group, as well as to inversion of the -NHR group (in amino tautomers of nitracrine and its 2-nitro isomer) and of the whole molecule (in the case of non-planar imino structures), were also evaluated, as were enthalpies of formation (total energies), entropies, free energies, dipole moments, and energies of HOMO and LUMO orbitals. Molecular electrostatic potential maps reveal that only in nitracrine are both $-NO_2$ and -NHR groups surrounded by a negative electrostatic potential, whereas in other isomers the -NHR fragment is surrounded by a positive electrostatic potential while the $-NO_2$ group remains in the region of a negative electrostatic potential. The possible influence of physicochemical features on the biological activity of the molecules is also considered.

JANUSZ RAK, JERZY BŁAŻEJOWSKI et RANDY J. ZAUHAR. Can. J. Chem. **71**, 1106 (1993).

Faisant appel à des méthodes AM1 et, dans quelques cas, à des méthodes PM3 et ab initio (STO-3G), on a étudié les stabilités relatives et les caractéristiques des tautomères de la *N*,*N*-diméthyl-*N'*-(1-nitro-9-acridinyl)-propane-1,3-diamine (nitracrine — OMS ou Ledakrin en Pologne), qui présente une activité antitumorale, et trois de ses isomères nitrés. Dans ces composés, la forme d'énergie minimale est toujours un tautomère imino. L'énergie des tautomères amino est toujours quelques kcal mol^{-1} plus élevée alors que celle des formes *aci* (dans les cas des isomères 2- et 4-nitro) est plus de 25 kcal mol^{-1} plus élevée. Chaque tautomère peut ensuite exister sous plusieurs formes structuralement différentes (conformères ou stéréoisomères). Dans quelques-unes d'entre elles, il est possible d'avoir des liaisons hydrogènes internes. On a aussi évalué les barrières à la rotation interne du groupe -NHR et à l'inversion du groupe -NHR (dans les tautomères animés de la nitracrine et de son isomère 2-nitro) et de la molécule complète (dans le cas des structures imino non-planaires) ainsi que les enthalpies de formation (énergies totales), les entropies, les énergies libres, les moments dipolaires et les énergies des orbitales moléculaires OH et BV. Les cartes de potentiel électrostatique moléculaire révèlent que seule la nitracrine contient des groupes $-NO_2$ et -NHR entourés par un potentiel électrostatique négatif; dans les autres isomères, le fragment -NHR se trouve dans la région d'un potentiel électrostatique positif alors que le fragment $-NO_2$ demeure dans la région d'un potentiel électrostatique négatif. On considère aussi la possibilité d'une influence des caractéristiques physicochimiques sur l'activité biologique des molécules.

[Traduit par la rédaction]

Introduction

Nitracrine, i.e., *N*,*N*-dimethyl-*N'*-(1-nitro-9-acridinyl)-1,3-propanediamine, belongs to the family of 9-acridinamine derivatives which have been intensively investigated over the last few decades by Ledóchowski and others, from the point of view of their utility as anticancer agents (1). Of several hundred compounds synthesized, only nitracrine was found to exhibit antitumour activity and has been successfully used as a drug in Poland (1–3). Recent work has also shown the compound to have a range of other biological activities (4, 5). Efforts devoted to syntheses have been accompanied by complementary studies of the structure (6–10), properties (1, 11–14), and mechanism of the biological action (1, 4, 5, 15–25) of nitracrine and other compounds. X-ray analyses revealed that the monohydriodide of nitracrine, in which protonation takes place at N(36), crystallizes into the imino form (**1**), a characteristic of which is that H(25) migrates from exocyclic to endocyclic nitrogen. In this structure, moreover, the central ring system is folded at an angle along the C(9)...N(10) axis and the nitro group is tilted with a torsion angle of ca. 60° to atoms in the acridine ring (1, 6, 7). On the other hand, the 2-nitro isomer exists as a planar amino tautomer (**2**), with coplanarity between the acridine nucleus and the nitro group (8, 9). Since only nitracrine exhibits enhanced antineoplastic activity and its 2-nitro isomer does not (1, 15, 16), it would suggest that the imino tautomeric structure, which in the case of nitracrine could be forced by steric overcrowding, is the one responsible for its unique biological properties (10). The prototropic tautomerism whose consequence is the transformation between amino and imino structures is a general phenomenon characteristic of 9-acri-

[1]Author to whom correspondence may be addressed.
[2]Revision received March 24, 1993.

Can. J. Chem. Downloaded from www.nrcresearchpress.com by 213.200.69.106 on 09/08/12
For personal use only.

Can. J. Chem. Downloaded from www.nrcresearchpress.com by 213.200.69.106 on 09/08/12
For personal use only.

dinamines (5, 9, 10, 26–29). We have studied this problem in the case of 9-acridinamine (30), as well as for both neutral nitracrine and its isomers (31, 32) and protonated forms of the compounds (32, 33), employing UV absorption (31–33) and luminescence (32, 33) techniques, as well as theoretical methods (30, 31). This work is devoted to detailed studies on the structural features, behaviour, and physicochemical properties of nitracrine and its nitro isomers, with regard to tautomeric phenomena, employing AM1, PM3, and ab initio (STO-3G) methods. The electrostatic potential around the molecules was also analyzed to show sites of potential specific interactions and to facilitate insight into the origin of these interactions, as well as into the nature of metabolic transformations.

Molecular orbital calculations have proved useful in studies of tautomeric phenomena (34–36). The systems investigated were relatively large; therefore we chose the semiempirical AM1 method, which has recently been used very successfully when examining structure, energetics, and properties of various tautomeric forms (36–39). It also correctly reproduced tautomeric equilibria in several systems (36, 37, 40, 41). Selected structures primarily optimized with AM1 were subsequently reexamined on the level of PM3 and ab initio (STO-3G) methods.

Methods

MO calculations

The molecules were modelled using SYBYL Molecular Modelling Software, Version 5.2 (provided by TRIPOS Associates, Inc.). Their geometries were then optimized, by minimizing the energy with respect to all internal coordinates (without any symmetry constraint), employing the semiempirical AM1 method (42) (incorporated in MOPAC, version 6.0 (43)) (the calculations were carried out using the "precise" option to provide the strictest convergence criterion (44)). Selected structures thus established were subsequently reoptimized employing PM3 (45) (incorporated in MOPAC) and ab initio (considering all electrons) STO-3G (46, 47) (incorporated in HONDO (48), version 8.1) methods. The rotation of the -NHR fragment around the C(9)—N(23) bond in the amino tautomer of nitracrine and its 2-nitro isomer was examined by maintaining the dihedral angle C(14)C(9)N(23)C(24), describing the position of the -NHR group relative to the acridine moiety, at a certain value and completely optimizing the remaining structural parameters of the molecules. The geometries and energies of molecules in the transition state for the rotation or inversion were studied combining the following three procedures: *saddle point* geometry estimation (49), gradient minimization at the *saddle point* (NLLSQ (43)), and evaluation of the force constants (43), and always afforded a single negative frequency for the molecule in the transition state. The MOPAC and HONDO routines were used to evaluate heats of formation (total energies), entropies, dipole moments, and energies of HOMO and LUMO orbitals (all thermochemical quantities refer to 298 K).

Molecular electrostatic potential (MEP)

The most "accurate" value of the electrostatic potential around a molecule is presumably obtained by applying the SCF procedure to the electronic wave function and combining the result with the core potential. However, at distances greater than 4 Å (sometimes even at 2–3 Å) it is very well represented by a point charge potential (50–52). In this latter case MEP (V_i) at a given site i around the molecule is given by the formula:

$$[1] \quad V_i = \frac{1}{4\pi\epsilon_0} \sum_{j=1}^{n} \frac{q_j}{r_{ij}}$$

where ϵ_0 is the permittivity of free space, q_j represents the net charge at atom j of the molecule, r_{ij} is the distance between atom j and site i, and n denotes the number of atoms in the molecule (51, 52). If point charge q_i is present at site i, the energy of electrostatic interaction between this charge and a molecule is equal to q_iV_i. Three-dimensional (3-D) MEP maps show equipotential surfaces that correspond to an electrostatic interaction energy of $|2|$ kcal mol^{-1} for a unit positive test charge. The two-dimensional (2-D) MEP maps, corresponding to the mean plane of the molecules, present lines that are sets of points of constant values of electrostatic energy. For V_i calculations, generally, net atomic charges corresponding to the lowest energy structures obtained from optimization with AM1 were used (Table 5 in the Supplementary material; see footnote 3).

It was proved that charges obtained by other semiempirical quantum chemistry methods (INDO, CNDO, MNDO) afforded MEP almost identical to that mentioned above. Moreover, it is shown for one chosen molecule that MEP obtained from AM1 atomic point charges corresponds quite well to MEP calculated from ab initio Mulliken point charges, as well as atom-centered charges obtained by fitting them, in a least-squares sense, to the electrostatic potential resulting from the electronic wavefunctions, relevant to the points on the van der Waals type surfaces around molecules (for the latter purpose the ESP routine, incorporated in MOPAC 6.0, was applied).

The calculations were done on Hewlett–Packard model 730 and VAX model 3600 computers.

Results and discussion

Geometry of isolated molecules

Nitracrine and its 3-nitro isomer can potentially exist in two tautomeric forms, amino and imino (e.g., **2** and **1**), whereas 2-nitro and 4-nitro isomers can also exist in a third *aci* form (e.g., **3**) (31). All the molecules investigated are asymmetrical. Thus, several conformers or stereoisomers can usually be considered for a given tautomeric form. They result from various possible arrangements of the -NHR and -NO_2 groups on the acridine skeleton, which may itself be expected to be nearly planar in amino and *aci*, and nonplanar in imino, tautomers. The alkyl chain can admit open

[3]Supplementary material available: Tables 3 and 4 in which are compared Z matrices of nitracrine (imino tautomer) and its 2-nitro isomer (amino tautomer), respectively, resulting from the AM1 geometry optimization with those obtained from the crystallographic data; Table 5 in which the AM1 net atomic charges for the lowest energy amino and imino structures are presented. These tables may be purchased from: The Depository of Unpublished Data, Document Delivery, CISTI, National Research Council Canada, Ottawa, Canada K1A 0S2.

Tables of bond lengths and angles (Tables 3 and 4) have also been deposited with the Cambridge Crystallographic Data Centre and can be obtained on request from The Director, Cambridge Crystallographic Data Centre, University Chemical Laboratory, 12 Union Road, Cambridge, CB2 1EZ, U.K.

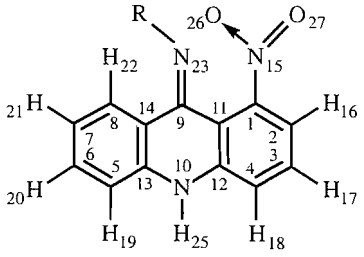

1

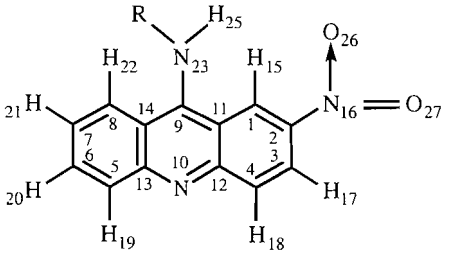

2

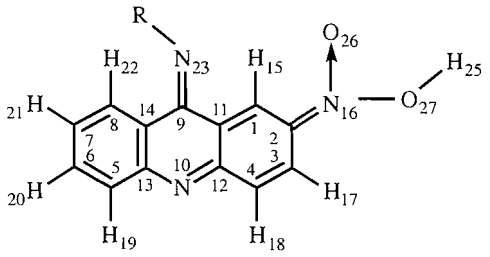

3

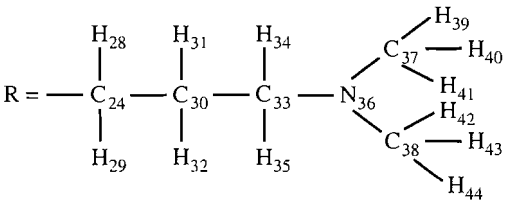

Can. J. Chem. Downloaded from www.nrcresearchpress.com by 213.200.69.106 on 09/08/12
For personal use only.

conformation (type A; Figs. 1–5 and Table 1) or a conformation in which H(25) and N(36) are involved in the internal hydrogen bond (type AH). It appears suitable to consider only two types of the former conformation, which result from the rotation of the whole open chain around the N(23)—C(24) bond. When the internal H-bond appears in the -NHR group, it is worthwhile also considering two types that differ in the arrangement of the six-membered ring system formed relative to the acridine moiety and that can be transformed into each other by rotating the whole chain again around the N(23)—C(24) bond. The -NHR fragment can be located either perpendicular to the acridine ring, in two positions with a lone electron pair at the nitrogen atom directed either towards or away from the ring with the attached nitro group, or in the plane of the acridine moiety, allowing this group to again assume two arrangements relative to the nitro group. The analysis regarding rotation of the -NHR fragment revealed that it is worthwhile considering eight various amino conformers for each isomer (four of type A and four of type AH). The number of structures considered in the case of each imino tautomer was always four and resulted from the nonplanarity of the central ring system and mutual arrangement of H(25) and the substituent at N(23) relative to the nitro group. However, only two boundary structures appear to be stable. In the case of the *aci* tautomer of 2-nitro and 4-nitro isomers the number of structures originally created was eight, considering possible arrangements of the -NHR group relative to the *aci*-nitro group. In this case it appears worthwhile to consider only four structures for the 2-nitro isomer and six for the 4-nitro isomer (since in the latter case the *aci*-nitro group can be additionally engaged in the hydrogen-bonding interactions with the endocyclic nitrogen). Finally, two *aci*-anion structures were considered for each isomer mentioned, since these species were previously found in strongly alkaline media. Altogether, the 54 structures seem to represent the most probable conformers and (or) stereoisomers of various possible forms of the compounds studied. These are listed in Table 1 and some of them are shown in Figs. 1–5. The total number of structures subjected to geometry optimization was over 100.

Quantum chemistry methods predict an almost planar acridine skeleton in amino tautomers, particularly if the alkyl chain admits open conformation (Table 2). In all imino tautomers the central ring system is folded along the C(9)...N(10) axis, and the whole skeleton is nonplanar. In *aci* and *aci*-anion forms of C-264 and C-265 the central ring system shows less deviation from planarity than in the case of the corresponding imino structures. Generally speaking, C-283 seems to have the most deformed skeleton among the molecules studied.

The nitro group is almost planar to the neighbouring benzene ring in all forms of C-264 and C-257, also the nitro group in the imino and *aci* tautomers of C-265 is only slightly distorted from planarity with the acridine moiety. Remarkable distortion from such planarity is seen in all forms of C-283, as well as in the amino and *aci*-anion forms of C-265, although the $-NO_2$ group is more twisted in the C-283 than in the C-265 forms. Distortion of C-283 from planarity and deformation of the whole molecule is mostly due to steric overcrowding and interaction of the electronegative $-NO_2$ group with negatively charged nitrogen(s) of the -NHR fragment situated near each other in *peri* positions (for charge distribution see Table 5 in the Supplementary material). In C-265 the steric effect may be expected to be less essential. The lone electron pair at N(10), being in a *peri* position relative to the nitro group, however, causes a strong electrostatic repulsive interaction whose consequence is the distortion of this group from planarity with the acridine moiety in the amino and *aci*-anion forms.

The AM1 method predicted that the most stable form of 9-acridinamine should be one with the amino group planar to the aromatic ring (30). If the -NHR fragment were situated to enable the strongest conjugation between the lone electron pair at N(23) and the acridine aromatic system, the C(11)C(9)N(23)C(24) angle would be equal to ca. 30°. Because of steric hindrances in nitracrine and its isomers caused by the substituent at N(23), the amino group is always twisted against the acridine nucleus (Table 2).

The substituent at N(23) of the imino and *aci* tautomers is always directed away from the concave side of the acri-

dine nucleus folding, and hydrogen (25), in the imino forms, lies on the line connecting C(9) and N(10).

To learn how far structures obtained by AM1 optimization correspond to crystal phase structures, we compared appropriate *Z* matrices for the C-283 (imino form) and C-264 (amino form) molecules (Tables 3 and 4 in the Supplementary material). For this comparison the theoretically derived structures that seemed to be closest to the solid phase struc-

TABLE 1. Physicochemical characteristics of *N*,*N*-dimethyl-*N'*-(1-nitro-9-acridinyl)-1,3-propanediamine and its nitro isomers

Compound				Physicochemical characteristics[a]						
Isomer	Symbol	Tautomer	Type of structure[b]	ΔH_f^c (kcal mol^{-1})	S (cal mol^{-1} K)$^{-1}$	ΔG_f (kcal mol^{-1})	μ^d (D)	LUMO (eV)	HOMO (eV)	Fig. no.
1-Nitro (nitracrine)	C-283	Amino[e]	A1	89.9	160.5	42.1	2.92	−1.562	−8.800	1
				58.9	159.2*	11.4*	3.34*	−1.796*	−8.928*	
				(−1047.4361)**			2.31**			
			A3	90.9	161.2	42.8	3.32	−1.618	−8.905	5
			A2[f]	91.6	157.6	44.7	1.73	−1.493	−8.559	5
				64.5*	161.6*	16.3*	2.91*	−1.797*	−8.758*	
				(−1047.4369)**			0.43**			
			A4[f]	91.7	163.0	43.1	2.51	−1.526	−9.613	5
		Amino[g]	AH4	89.2	154.8	43.0	3.95	−1.406	−8.511	1
			AH1[h]	90.7	154.2	44.7	3.80	−1.172	−8.555	5
				64.0*	157.2*	17.1*	3.80*	−1.578*	−8.304*	
				(−1047.4306)**			2.38**			
			AH3[h]	91.2	153.2	45.5	2.05	−1.368	−8.232	5
			AH2	91.8	156.2	45.3	4.63	−1.306	−8.211	5
		Imino	I1	85.5	157.3	38.6	5.86	−0.838	−8.694	1
				50.1*	156.6*	3.4*	5.77*	−0.967*	−8.755*	
				(−1047.4438)**			4.76**			
			I2	89.4	155.9	42.9	6.26	−1.128	−8.724	6
2-Nitro	C-264	Amino[e]	A1	83.1	163.6	34.3	6.36	−1.602	−8.637	2
				50.8*	160.6*	3.0*	6.46*	−1.819*	−8.768*	
				(−1047.4474)**			4.89**			
			A2	83.5			6.61	−1.647	−8.651	5
			A3	83.9	161.1	35.9	5.74	−1.616	−8.644	5
			A4	84.5			6.97	−1.641	−8.634	5
		Amino[g]	AH1	81.7	153.2	36.1	6.61	−1.406	−8.359	2
				51.0*	157.4*	4.1*	6.18*	−1.672*	−8.510*	
				(−1047.4488)**			5.18**			
			AH2	82.4			7.99	−1.371	−8.302	5
			AH3	82.5	155.4	36.2	5.73	−1.557	−8.620	5
			AH4	82.7			7.03	−1.433	−8.386	5
		Imino	I1	80.0	158.7	32.7	7.60	−1.004	−8.795	2
				45.7**	158.3*	−1.5*	7.48*	−1.083*	−8.851*	
				(−1047.4522)**			5.95**			
			I2	80.0			5.80	−1.143	−8.798	5
		aci	AC1	110.7	159.4	63.2	3.49	−1.803	−8.357	2
			AC2	110.8			2.73	−1.746	−8.277	5
			AC3	111.0			1.04	−1.728	−8.265	5
			AC4	111.1			2.83	−1.819	−8.359	5
		aci-Anion	ACA1	33.4	155.7	−13.0		2.482	−4.246	5
			ACA2	35.2				2.532	−4.183	5
3-Nitro	C-257	Amino[e]	A1	84.8	163.9	36.0	8.44	−1.635	−8.697	3
			A2	85.0			8.35	−1.644	−8.689	
			A3	85.8	162.0	37.5	7.35	−1.548	−8.697	
			A4	86.1			8.09	−1.655	−8.687	
		Amino[g]	AH1	84.7	158.6	37.4	9.03	−1.409	−8.322	3
			AH4	84.7			9.51	−1.547	−8.627	
			AH2	84.8			9.61	−1.409	−8.320	
			AH3	84.8	158.1	37.6	8.36	−1.522	−8.628	
		Imino	I1	81.7	159.1	34.3	6.43	−1.202	−8.754	3
			I2	82.5			3.16	−1.338	−8.721	

Can. J. Chem. Downloaded from www.nrcresearchpress.com by 213.200.69.106 on 09/08/12
For personal use only.

TABLE 1 (*concluded*)

Compound				Physicochemical characteristics[a]						
Isomer	Symbol	Tautomer	Type of structure[b]	ΔH_f[c] (kcal mol^{-1})	S (cal mol^{-1} K)$^{-1}$	ΔG_f (kcal mol^{-1})	μ[d] (D)	LUMO (eV)	HOMO (eV)	Fig. no.
4-Nitro	C-265	Amino[e]	A1	87.0	163.6	38.2	8.66	−1.552	−8.663	4
			A2	87.3	164.4	38.3	8.94	−1.558	−8.636	
			A3	87.9	161.9	39.7	7.82	−1.562	−8.661	
			A4	88.3			8.06	−1.567	−8.636	
		Amino[g]	AH2	86.7	159.3	39.2	9.87	−1.319	−8.288	4
			AH1	86.9	158.7	39.6	9.96	−1.305	−8.289	
			AH4	86.9			9.69	−1.459	−8.591	
			AH3	87.1			9.52	−1.466	−8.586	
		Imino	I1	79.2	159.4	31.7	5.00	−1.108	−8.678	4
			I2	79.9			3.45	−1.223	−8.687	
		aci	AC1	111.7	158.5	64.5	1.57	−1.615	−8.362	4
			AC4	111.9	159.7	64.3	4.35	−1.598	−8.289	
			AC2	112.0			1.14	−1.561	−8.216	
			AC3	112.2			2.52	−1.615	−8.301	
			AC3(1)	112.2			3.45	−1.788	−8.294	5
			AC1(1)	112.4			2.18	−1.809	−8.371	5
		aci-Anion	ACA1	40.8	156.3	−5.8		2.663	−4.073	
			ACA2	41.2				2.724	−4.032	

[a]Values not marked result from the AM1, whereas those with one asterisk are from the PM3, and those with two asterisks from the ab initio (STO-3G) calculations.
[b]Assumed following energy sequence of AM1 structures for C-264.
[c]The ab initio method provides, instead of ΔH_f, total energies, which are shown in parentheses in atomic units (1 au = 627.7 kcal mol^{-1}).
[d]1 D = 3.33564 × 10^{-30} C m.
[e]Conformers with the open alkyl chain.
[f]Conformers with the internal H(25)···O(26) hydrogen bond.
[g]Conformers with the internal H(25)···N(36) hydrogen bond.
[h]C-283 conformers with bifurcated hydrogen bond.

tures were chosen. Bond lengths are usually shorter in the crystal phase than those predicted for isolated molecules. Bond angles and dihedral angles are comparable for isolated molecules and for those forming a lattice, except for the parts concerning the arrangement and structure of the alkyl substituent. For the C-283 imino tautomer the AM1 method predicts a completely extended conformation of the alkyl chain, whereas in the crystal phase the chain is folded, adopting the most favourable structure for the crystal packing (1, 6, 7, 53). In the case of the C-264 amino tautomer, formation of the internal hydrogen bond forces almost the same configuration of the whole -NHR fragment in both the isolated molecule and the crystal phase, except for its arrangement relative to the acridine nucleus. The lowest energy conformation of the isolated molecule is such that the amino group is almost perpendicular to the acridine moiety, and the lone electron pair at N(23) is directed towards the nitro group (Figs. 1–5), whereas in the crystal phase, packing of the molecules produces a conformation in which the N(23)C(24)C(30)C(33)N(36)H(25) ring is situated almost in the plane of the acridine nucleus, thus creating the minimal volume for the whole molecule (8, 53). In this latter structure the lone electron pair at N(23) is directed away from the nitro group. Despite the differences mentioned, comparison reveals that the AM1 method provides correct structural information for the compounds studied.

A similar conclusion arises from comparison of PM3 and STO-3G optimized geometries with those for the crystal phase.

Intramolecular hydrogen bonding interactions

The presence of proton donor (=NH, -OH) and proton acceptor (≡N, -NO_2) sites in the molecules creates an opportunity for the formation of internal hydrogen bonds.

A hydrogen bond involving H(25) and N(36) occurs in the C-264 amino tautomer, forming the crystalline phase (8). Such a hydrogen bond is possible in the case of all amino tautomers and requires a particular arrangement of the alkyl substituent. The distances between the atoms forming this bond are rather typical for weak hydrogen-bond-type interactions (Table 2). The structures with the alkyl chain involved in the internal hydrogen bond usually exhibit lower enthalpies of formation than the relevant open chain conformations (this is not actually seen in the case of C-283) (Table 1). The former are, therefore, more stable from the energetic point of view. On the other hand, the entropy factor acts in favour of open chain structures. The result is that free energies (ΔG_f) exhibit a reverse tendency in comparison with that observed for ΔH_f values, i.e., they are lower for the open chain structures. Differences in ΔH_f and ΔG_f values for various A and AH type structures of a given isomer are, however, rather small, which means that all of these structures may be expected.

Quantum chemistry methods also predict the existence of a hydrogen bond between H(25) and one of the oxygen atoms of the nitro group. Such a hydrogen bond has been considered in 1-nitro-9-acridinamine (29). The H(25)···O(26) bond appears in both structures of nitracrine having an open alkyl chain, and in those in which a bifurcated hydrogen bond is

Can. J. Chem. Downloaded from www.nrcresearchpress.com by 213.200.69.106 on 09/08/12
For personal use only.

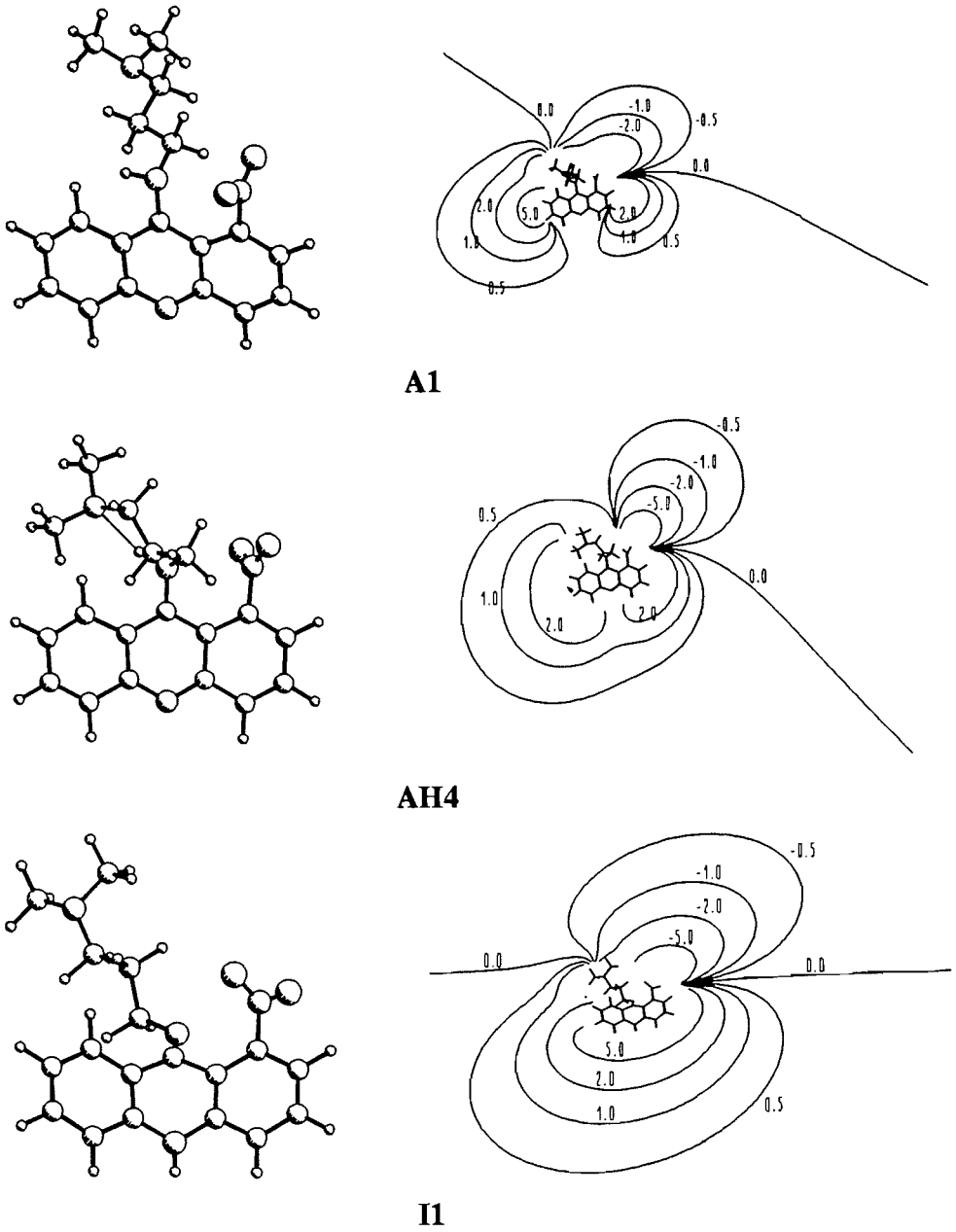

FIG. 1. AM1 geometry of the lowest energy tautomeric forms of nitracrine (thin line indicates hydrogen bond) together with the 2-D maps of MEP.

formed (Figs. 1 and 5). The H(25)···O(26) distance (Table 2) is fairly characteristic for weak hydrogen-bonding interactions. Moreover, the thermochemical characteristics (ΔH_f, ΔG_f) (Table 1) do not favour structures for which this bond is predicted.

An intramolecular hydrogen bond is further predicted in the imino tautomer of C-265 between H(25) attached to the endocyclic nitrogen and one of the oxygen atoms of the nitro group (Fig. 4). Its existence accounts for the relatively strong energy stabilization of the imino structures of C-265 (Table 1). Furthermore, this bond presumably causes the nitro group in the imino form to be much less distorted from planarity with the aromatic system than that in the amino forms of C-265 (Table 2).

Lastly, the intramolecular hydrogen bonds may occur within the *aci*-nitro group in *aci* tautomers of C-264 and C-265 (Figs. 2, 4, and 5) and also between the endocyclic nitrogen and hydrogen of the *aci*-nitro group in C-265 (Fig. 1). Since the energetic factor excludes the existence of molecules in *aci* forms we did not consider further details concerning these latter hydrogen-bonding interactions.

The AM1 method, primarily employed in this work, has been used with success in several hydrogen-bonding studies (42, 54, 55), although it often underestimates hydrogen-bonding interactions (39, 42, 56). It may be, therefore, that all hydrogen bonds discussed above are in reality thermodynamically more stable. This seems to be confirmed by the results of the ab initio (STO-3G) calculations (Table 1).

Structural transformations

The spatial arrangement of atoms is undoubtedly an important factor accounting for the biological activity of molecules. Knowledge of the lowest energy structures may be

Can. J. Chem. Downloaded from www.nrcresearchpress.com by 213.200.69.106 on 09/08/12
For personal use only.

Can. J. Chem. Downloaded from www.nrcresearchpress.com by 213.200.69.106 on 09/08/12
For personal use only.

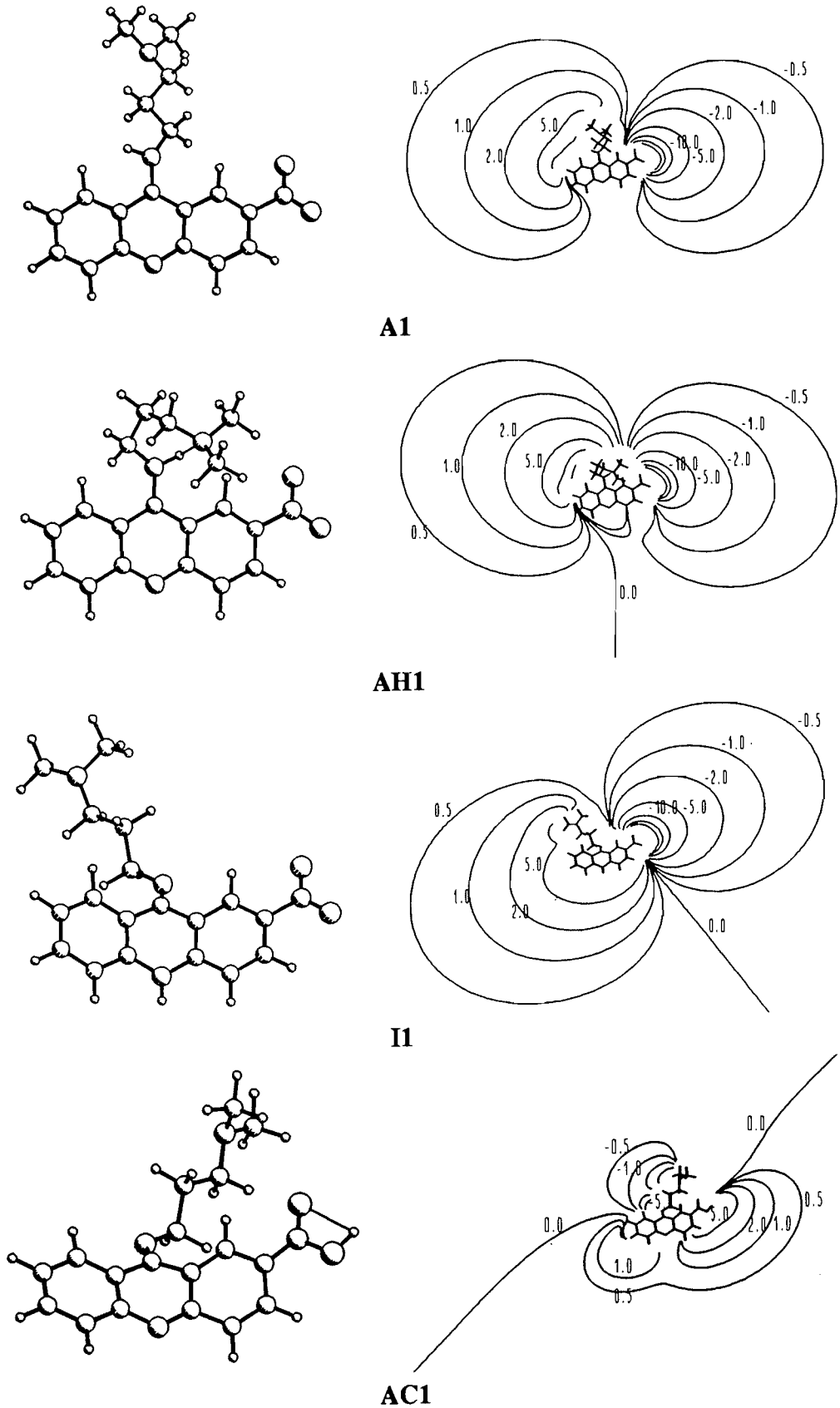

FIG. 2. AM1 geometry of the lowest energy tautomeric forms of C-264 (thin line indicates hydrogen bond) together with the 2-D maps of MEP.

Can. J. Chem. Downloaded from www.nrcresearchpress.com by 213.200.69.106 on 09/08/12
For personal use only.

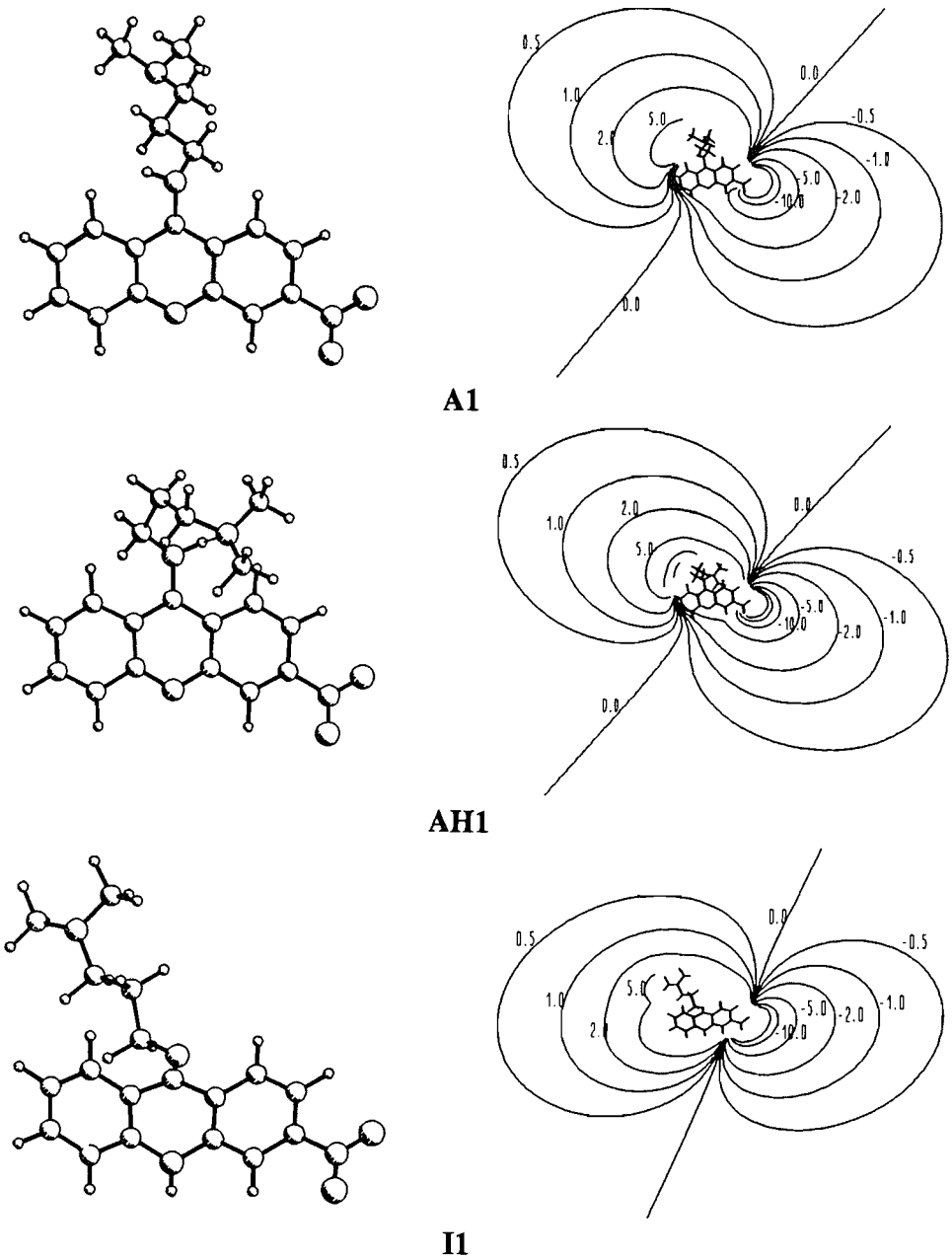

FIG. 3. AM1 geometry of the lowest energy tautomeric forms of C-257 (thin line indicates hydrogen bond) together with the 2-D maps of MEP.

insufficient if the possibility of them being transformed to somewhat higher energy stable states (corresponding to local minima) exists. Information in Table 1 reveals that such structures can actually occur. Various states can first of all be achieved as a result of rotation of the -NHR fragment, in amino tautomers, and inversion of the whole molecule, in the case of imino tautomers.

The energy changes upon rotation of the -NHR group in C-283 and C-264 are shown in Figs. 6 and 7. Rotation of the -NHR fragment is always accompanied by inversion at N(23), in both nitracrine and C-264 and, in addition, by rotation around the N(23)—C(24) bond in the case of C-264. The highest barrier to rotation of the -NHR group in C-264, determined by AM1, is equal to 5.6 kcal mol^{-1} and is most probably a consequence of the loss of conjugation between the lone electron pair at N(23) and the acridine aromatic system rather than a steric effect (30). In the case of nitracrine the highest energy barrier is equal to 10.7 kcal mol^{-1} and corresponds to the situation in which the -NHR fragment passes the nitro group. In such an arrangement strong repulsive interactions must occur between the two groups mentioned. The energy barrier to the rotation in C-283 seems to be too high to be overcome at room temperature. It may, therefore, be expected that the -NHR fragment in nitracrine undergoes only rocking movements, whereas in C-264 it may also rotate under certain conditions. Inversion at N(23), which sometimes accompanies rotation of the whole -NHR group, requires the overcoming of much lower barriers. Structures of C-283 and C-264 shown as examples in Fig. 8 correspond to the *saddle points* for the above pro-

Can. J. Chem. Downloaded from www.nrcresearchpress.com by 213.200.69.106 on 09/08/12
For personal use only.

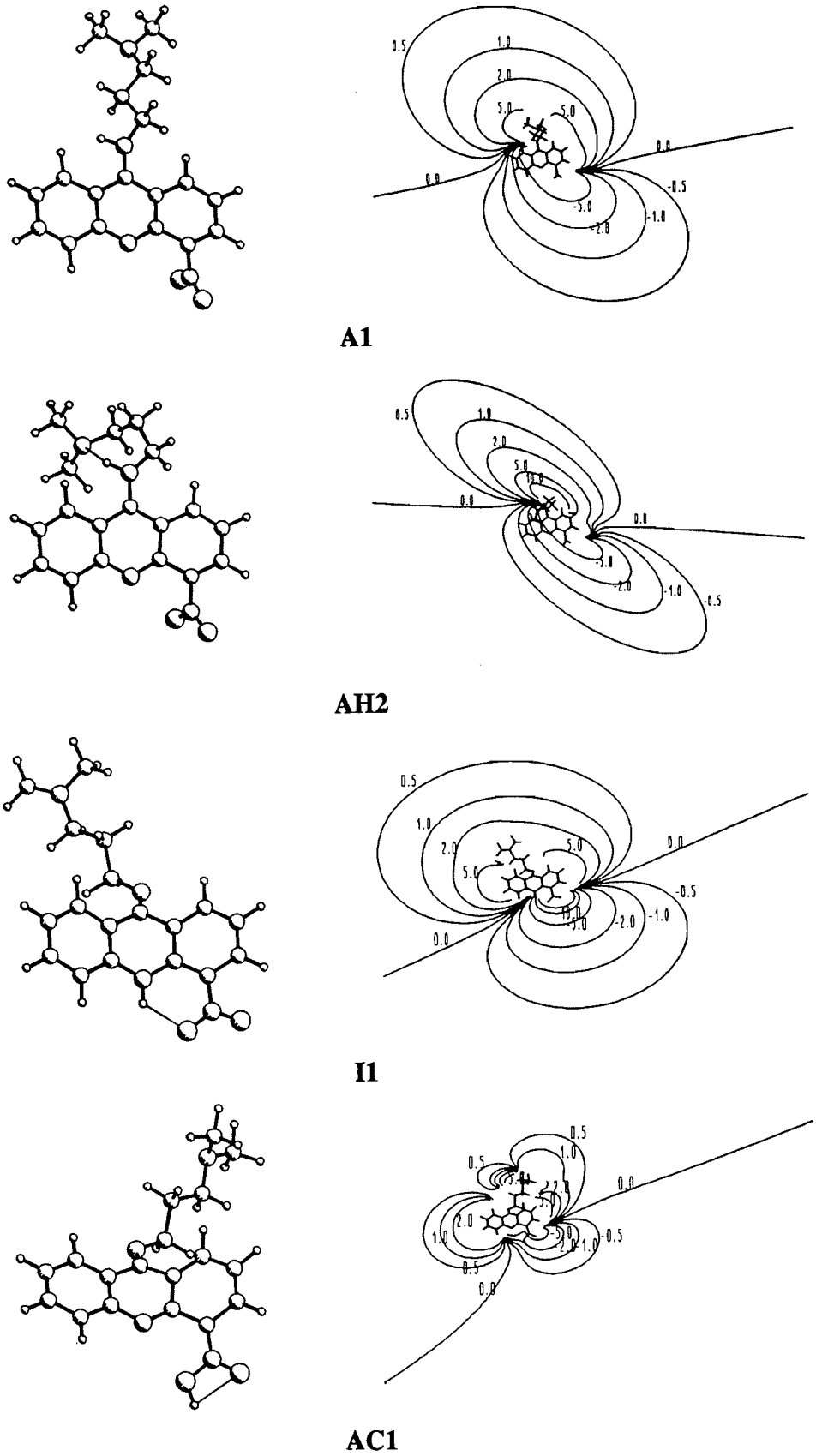

FIG. 4. AM1 geometry of the lowest energy tautomeric forms of C-265 (thin line indicates hydrogen bond) together with the 2-D maps of MEP.

Can. J. Chem. Downloaded from www.nrcresearchpress.com by 213.200.69.106 on 09/08/12
For personal use only.

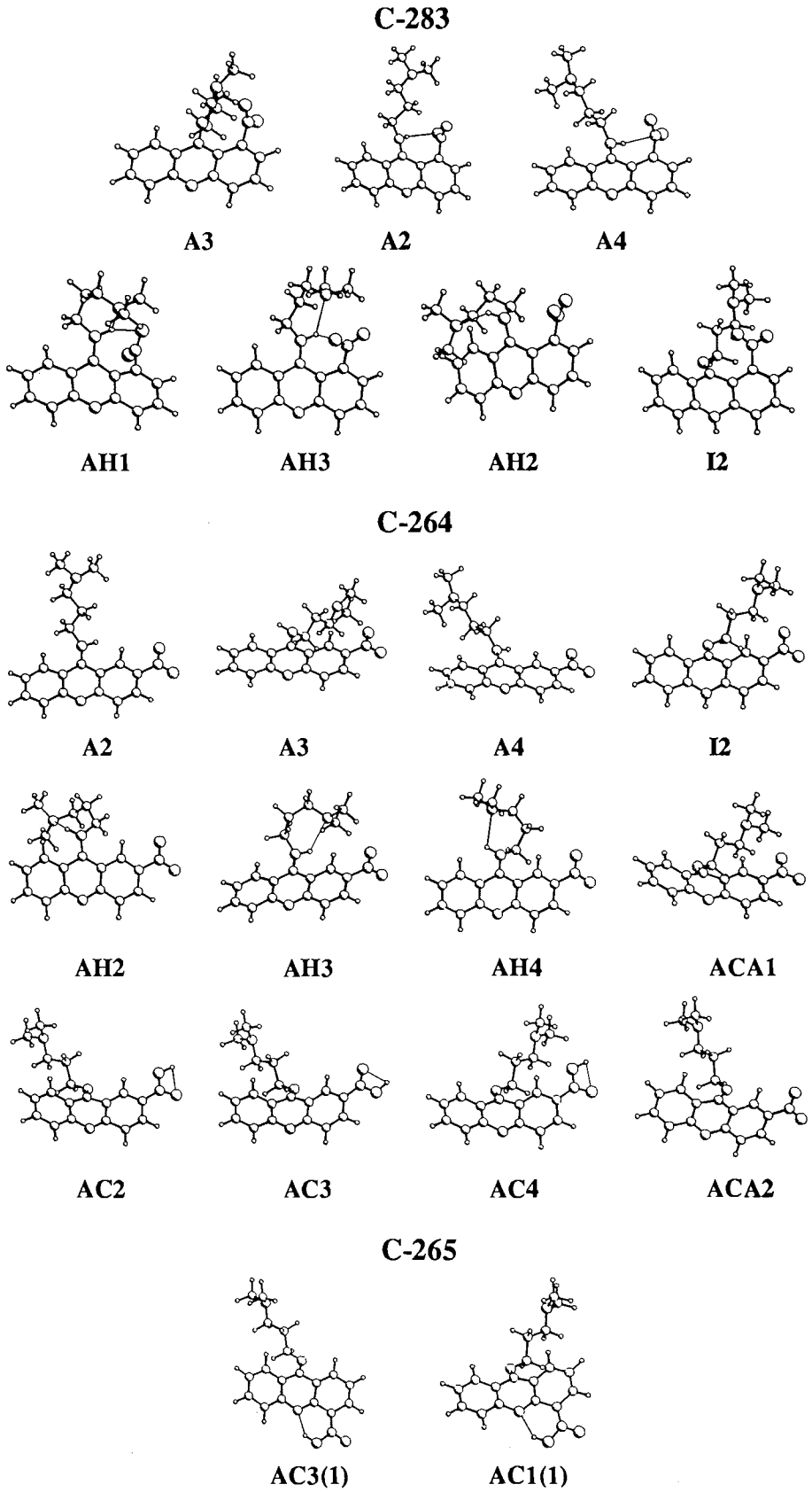

FIG. 5. AM1 geometries of C-283, C-264, and C-265 molecules (thin line indicates hydrogen bond) corresponding to local minima and representing types of structures (except for those shown in Figs. 1–4).

TABLE 2. Calculated geometric parameters

Compound (Table 1)			Bond length			Bond order		
Symbol	Tautomer	Type of structure	C(9)—N(23)	N(10)—C(12)	C—NO_2	C(9)—N(23)	N(10)—C(12)	C—NO_2
					C(1)—N(15)			C(1)—N(15)
C-283	Amino	A1	1.415	1.351	1.501	1.04	1.40	0.83
			1.450*	1.358*	1.510*	1.02*	1.40*	0.88*
			1.449**	1.356**	1.518**	1.01**	1.38**	0.84**
		A4	1.395	1.348	1.497	1.09	1.41	0.83
	Amino	AH4	1.403	1.349	1.500	1.08	1.40	0.83
		AH1	1.369	1.350	1.501	1.22	1.40	0.82
			1.418*	1.357*	1.506*	1.14*	1.39*	0.88*
			1.402**	1.355**	1.519**	1.14**	1.38**	0.83**
	Imino	I1	1.290	1.401	1.497	1.86	1.06	0.84
			1.295*	1.433*	1.508*	1.88*	1.06*	0.88*
			1.281**	1.430**	1.512**	1.88**	1.03**	0.85**
					C(2)—N(16)			C(2)—N(16)
C-264	Amino	A1	1.394	1.348	1.483	1.11	1.41	0.86
			1.435*	1.356*	1.495*	1.09*	1.40*	0.91*
			1.430**	1.355**	1.505**	1.06**	1.39**	0.86**
	Amino	AH1	1.384	1.347	1.481	1.16	1.41	0.87
			1.423*	1.354*	1.492*	1.12*	1.41*	0.91*
			1.425**	1.355**	1.504**	1.09**	1.38**	0.86**
	Imino	I1	1.291	1.390	1.481	1.86	1.10	0.87
			1.296*	1.421*	1.492*	1.88*	1.10*	0.91*
			1.283**	1.423**	1.503**	1.87**	1.04**	0.86**
	aci	AC1	1.293	1.307	1.359	1.85	1.76	1.39
	aci-Anion	ACA1	1.302	1.335	1.451	1.78	1.51	0.95
					C(3)—N(17)			C(3)—N(17)
C-257	Amino	A1	1.406	1.353	1.489	1.07	1.38	0.85
	Amino	AH1	1.390	1.353	1.489	1.14	1.38	0.85
	Imino	I1	1.292	1.402	1.490	1.86	1.06	0.85
					C(4)—N(18)			C(4)—N(18)
C-265	Amino	A1	1.405	1.349	1.494	1.08	1.40	0.84
		A2	1.404	1.348	1.494	1.08	1.41	0.84
	Amino	AH2	1.387	1.345	1.492	1.15	1.40	0.84
		AH1	1.388	1.348	1.494	1.15	1.42	0.85
	Imino	I1	1.292	1.382	1.479	1.85	1.14	0.88
	aci	AC1	1.293	1.307	1.362	1.85	1.75	1.38
	aci-Anion	ACA1	1.302	1.337	1.470	1.77	1.49	0.90

[a]Values not marked correspond to AM1, whereas those with one asterisk correspond to PM3, and those with two asterisks correspond to ab initio [b]H(25)···O(27) distance.

cess and to energy barriers of 1.2 and 0.3 kcal mol^{-1}, respectively.

In imino structures in which a double C(9)—N(23) bond hinders the rotation of the =NR group, the molecular transformation can be the inversion of the whole molecule towards its mirror image. In the case of inversion of two I1 type structures, chosen as examples, the barriers for the process are equal to 5.8 and 3.0 kcal mol^{-1}, respectively (the corresponding transition state structures are shown in Fig. 8). In this tautomeric form nitracrine also undergoes a structural transformation more difficult than the 2-nitro isomer does.

Physicochemical characteristics

Comparison of heats of formation predicted by AM1 and PM3, as well as STO-3G energies, indicates that imino tautomers should, at least in the gaseous phase, be favoured energetically before the relevant amino forms (Table 1). The differences between AM1 values of ΔH_f or ΔG_f for amino and imino forms decrease in the order: C-265 > C-283 > C-264 > C-257, which implies that in compounds in which, either as a result of steric overcrowding (C-283) or because of *peri* interactions (C-283 and C-265), the nitro group is markedly distorted from planarity to the acridine aromatic system, the imino forms should predominate. Characteristic of *aci* tautomers of C-264 and C-265 are the fairly high values of ΔH_f, and the existence of both compounds in these forms seems highly unlikely. The equilibrium constants calculated using AM1 values for the lowest energy structures (with the open alkyl chain in the case of amino forms) (Table 1), $K = c_{amino}/c_{imino}$, are equal to 0.0028, 0.0682, 0.0614, and 1.7×10^{-5}, for C-283, C-264, C-257, and C-265, respectively. One can expect, therefore, that the compounds should be present mainly in imino form in the gaseous phase. This may, however, change in the liquid or solid phases, where equilibrium between these two tautomeric forms may be strongly influenced by solute–solvent

Can. J. Chem. Downloaded from www.nrcresearchpress.com by 213.200.69.106 on 09/08/12
For personal use only.

(bond lengths in Å, angles in deg)[a]

Dihedral angle				Distance	
C(12)N(10)C(13)C(14)	C(12)C(11)C(9)C(14)	C(11)C(9)N(23)C(24)	NO_2 torsion	H(25)...N(36)	H(25)...O(26)
			C(11)C(1)N(15)O(26)		
3.12	5.62	83.48	83.39		
4.48*	9.97*	85.05*	76.31*		
2.89**	4.60**	83.02**	75.89**		
4.52	8.36	−116.32	73.18		
5.87	11.73	68.33	70.92	2.55	
−8.22	−23.26	−166.74	95.50	2.58	2.19
−9.07*	−21.71*	−156.88*	115.53*	2.59*	2.63*
−8.96**	−15.25**	−151.63**	74.29**	2.90**	1.71**
26.64	33.22	174.01	53.81		
31.36*	32.87*	173.72*	63.37*		
30.77**	33.93**	172.37**	49.64**		
			C(1)C(2)N(16)O(26)		
2.71	4.81	55.14	−2.67		
0.80*	1.46*	63.80*	−11.67*		
2.89**	4.31**	57.47**	−2.85**		
0.04	−3.20	−141.82	4.63	2.63	
−0.65*	−2.52*	−167.94*	−4.0*	2.63*	
−1.54**	−5.41**	−145.11**	4.32**	2.14**	
21.31	28.31	174.07	1.90		
28.15*	29.09*	174.11*	7.36*		
27.66**	29.18**	172.81**	2.22**		
9.24	29.29	0.83	0.20		2.15
8.11	24.00	1.28	−1.06		
			C(2)C(3)N(17)O(26)		
2.04	3.01	65.21	−0.37		
−0.77	−5.13	−141.02	0.83	2.64	
25.10	28.73	173.71	−0.54		
			C(3)C(4)N(18)O(26)		
2.01	3.86	64.40	51.76		
0.48	0.50	−121.35	53.57		
−1.24	−4.80	−142.53	54.46	2.64	
4.89	11.47	39.56	49.81	2.63	
19.89	29.68	174.38	3.13		2.05[b]
9.46	32.21	1.70	2.04		2.13
8.47	26.95	2.47	30.86		

(STO-3G) geometries.

interactions (35) or by the energetics of crystal formation. This conclusion is supported by the results of several of our earlier studies (31–33, 57). As regards the solid phase, it is worth remembering that C-283 actually crystallizes in the most stable imino form (6), whereas crystals of C-264 contain molecules of the less stable amino tautomeric form, in which the alkyl substituent is organized in a conformation with an internal hydrogen bond (8). It may, therefore, be that the energy required by the C-264 molecule to change its conformation from imino to amino is provided by the excess energy evolved upon the formation of the crystal. Moreover, the entropy factor prefers the formation of crystals from units containing an internal hydrogen bond. *aci* Tautomers in anionic form are characterized by relatively low ΔH_f values. The existence of such a form has actually been confirmed only in the case of the 2-nitro isomer (31).

Dipole moment values (μ) for amino tautomers generally increase in the sequence of 1- to 4-nitro isomers, whereas they decrease in the same order for imino tautomers (Table 1). Relatively low values of μ are predicted for all forms of C-283. Thus, both amino and imino structures of nitracrine seem to be the least polar of the compounds studied. It may be expected that the polarity of molecules strongly affects solute–solvent interactions and also tautomeric equilibria. Some aspects of this problem were discussed by us earlier (31, 32, 57).

According to Koopman's theorem (58), the energies of the lowest unoccupied (LUMO) and highest occupied (HOMO) molecular orbitals, multiplied by −1, can be regarded, in the first approximation, as the electron affinity and ionization potential of a molecule, respectively (59, 60). Furthermore, these quantities can be related to the reductive and oxidative capability of a molecule (30, 61, 62). Thus, the lower the energy of HOMO, the higher the oxidation potential, and the lower the energy of LUMO, the lower the reduction po-

Can. J. Chem. Downloaded from www.nrcresearchpress.com by 213.200.69.106 on 09/08/12
For personal use only.

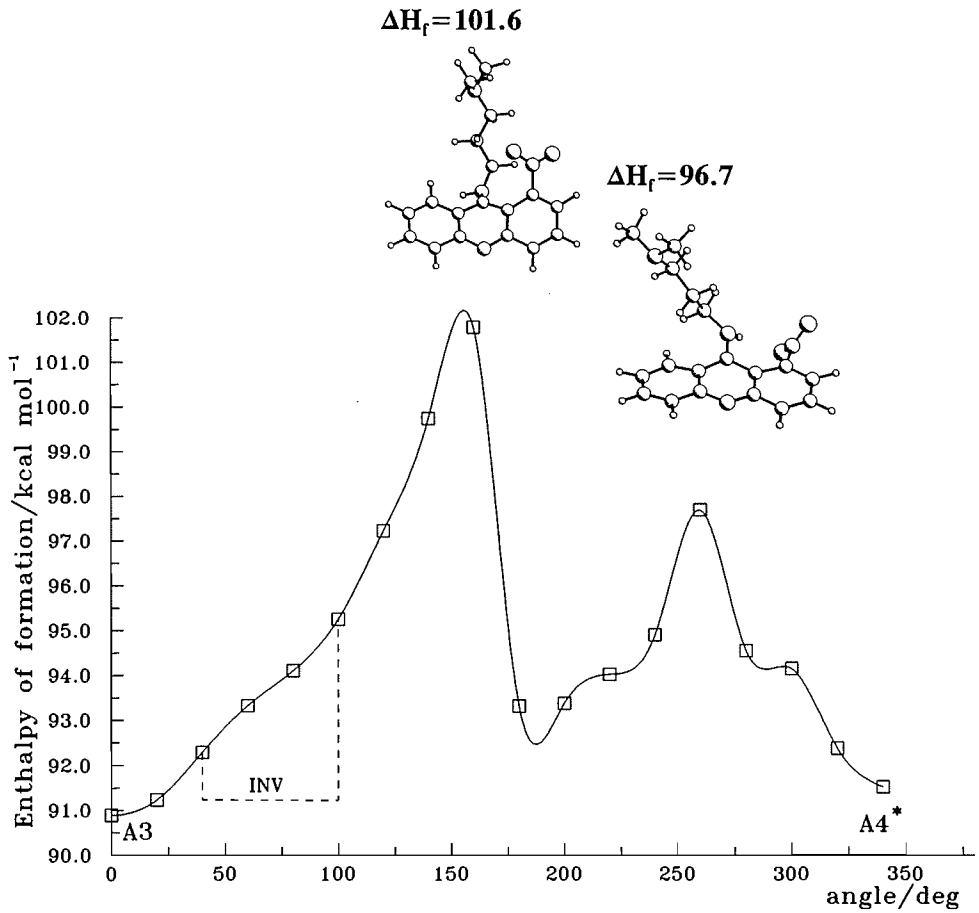

FIG. 6. Enthalpy determined by AM1 versus C(14)C(9)N(23)C(24) angle upon rotation of the -NHR group in nitracrine. A3 denotes structures shown in Fig. 5, whereas A4* structure is mirror image of A4; INV indicates the range of the angle in which rotation of the -NHR fragment against the acridine moiety is accompanied by inversion at N(23).

Can. J. Chem. Downloaded from www.nrcresearchpress.com by 213.200.69.106 on 09/08/12
For personal use only.

tential of a molecule. According to the AM1 data the LUMO energies of imino tautomers are higher than those characterizing the relevant amino forms (Table 1). This means that the reduction of the imino tautomers should proceed with more difficulty than that of the amino forms. On the other hand, theory does not generally differentiate the reductive capability of nitracrine and its isomers, which corresponds quite well to the experimentally obtained values (the half-wave potentials, in V, are equal to 0.60 and 0.56, 0.74 and 0.58, 0.65 and 0.58, 0.65 and 0.56, for C-283, C-264, C-257, and C-265, respectively (1, 11, 12)). The above-mentioned findings do not seem to indicate that nitracrine undergoes reduction more easily than any of its nitro isomers, as has been suggested by some authors (11, 12).

The problem discussed may have some significance in understanding differences in the biological activity of nitracrine and its isomers, which is connected with the fact that a reduced form of nitracrine occurs at site -NO_2 as a result of metabolic transformations (5, 20). Such a metabolite has not been found, so far, in the case of the remaining nitro isomers of C-283. The question, therefore, is why only nitracrine undergoes reduction and its isomers do not, especially since theory and experiment predict fairly similar electrochemical behaviour for all the compounds studied. It is probable that factors other than physicochemical control the process.

Electrostatic potential around isolated molecules

Maps of the molecular electrostatic potential (MEP) were obtained by employing eq. [1] and using net atomic point charges. It is shown in Fig. 9 that such maps resulting from various charge distributions correspond to each other reasonably well.

The two- (2-D) (Figs. 1–4), as well as three-dimensional (3-D) (Fig. 10) MEP maps reveal that, essentially, two zones of the potential appear around all the noncharged molecules. The negative region is always in the neighbourhood of the nitro group. Thus, in changing the position of this group from 1 to 4 the negative pole migrates from one to another side of a molecule. Simultaneously, the positive pole moves in the opposite direction. The -NHR group in the amino tautomer of C-283 appears in the region of a negative electrostatic potential. In the imino tautomer of nitracrine the alkyl chain remains on the boundary of the two opposite potentials. In C-264, C-257, and C-265, the -NHR fragment is always surrounded by a zone of positive electrostatic potential.

Conclusions

The theoretical studies revealed that nitracrine has a chance to exist in a fairly rigid structure due to the immediate engagement of both -NHR and -NO_2 fragments in hydrogen bonds. Furthermore the presence, in *peri* positions, of two

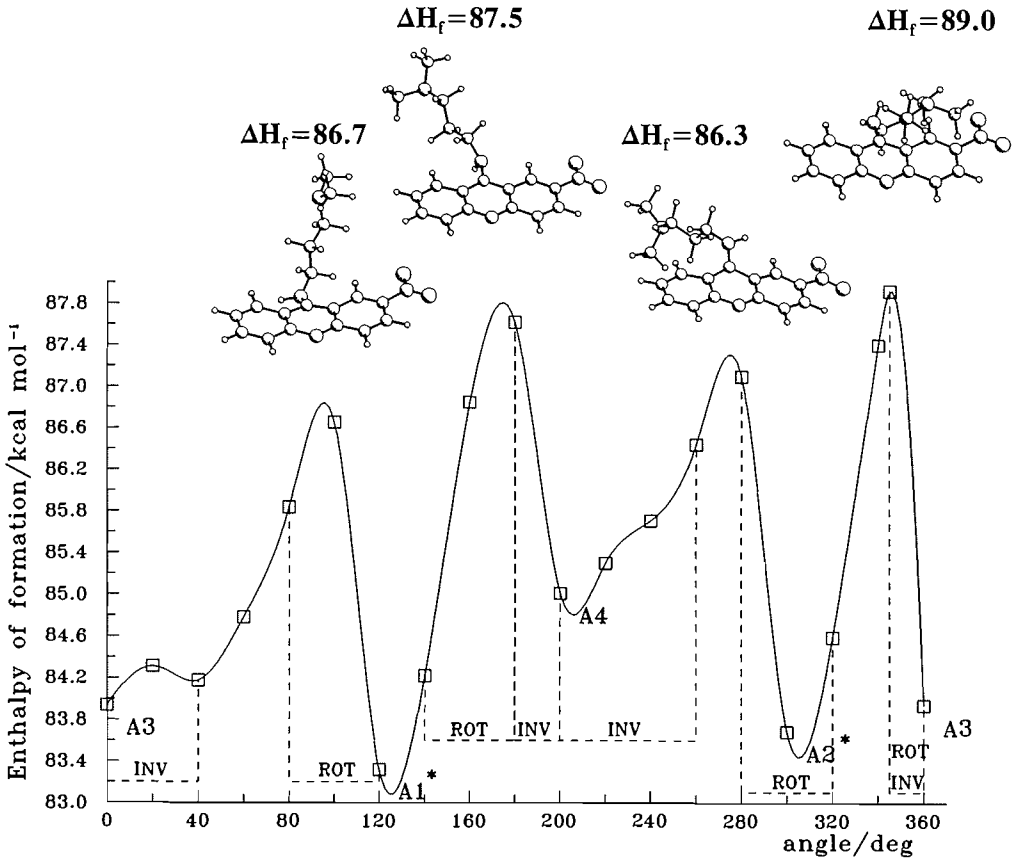

FIG. 7. Enthalpy determined by AM1 versus C(14)C(9)N(23)C(24) angle upon rotation of the -NHR fragment in C-264. A3 and A4 denote structures demonstrated in Fig. 5, whereas A1* and A2* structures are the mirror images of A1 and A2; INV and ROT indicate the range of the angle in which rotation of the -NHR fragment against the acridine moiety is accompanied by inversion at N(23) and rotation around the N(23)—C(24) bond, respectively.

voluminous and polar groups causes tremendous distortion from planarity of the whole acridine skeleton and practical loss of conjugation between these groups and the aromatic system. In consequence, nitracrine is less susceptible to any molecular transformations, e.g., those accompanying rotation of the -NHR fragment and inversion of the whole skeleton. These features undoubtedly distinguish nitracrine and can be significant for its unique behaviour.

Further, perhaps, even more distinct differences are revealed on examining electrostatic potential maps. Nitracrine is the only one of the compounds studied in which both -NHR and -NO_2 groups remain in the zone of the same negative potential. At the same time the zone of an opposite electrostatic potential surrounds the endocyclic nitrogen atom. This creates very convenient conditions for participation in intermolecular interactions. These interactions include, first and foremost, solute–solvent interactions, as well as those leading to the formation of associates. The distribution of the electrostatic potential around molecules may also play a role in molecular recognition, as well as in interactions with receptors and other macromolecules in living organisms (53, 63). If these interactions included the cross-linking of DNA, the endocyclic nitrogen would be one bonding centre and the nitrogen at the end of the alkyl substituent another bonding centre. Such a convenient distribution of the electrostatic potential does not exist in any other nitro isomer of nitracrine.

As mentioned earlier, certain findings indicate that nitra-

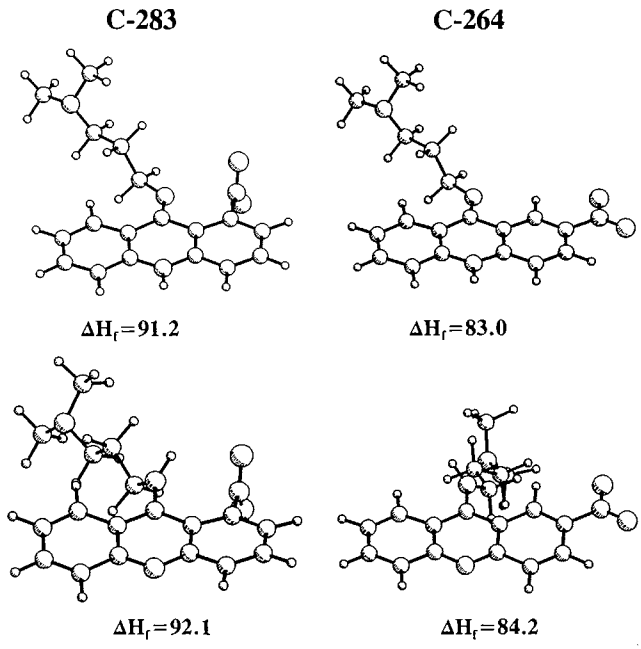

FIG. 8. The transition state structures predicted by AM1 for inversion of the I1 type molecules towards their mirror images (upper graphs) and for inversion of the A3 type molecules at N(23) (lower graphs) (ΔH_f in kcal mol^{-1}).

Can. J. Chem. Downloaded from www.nrcresearchpress.com by 213.200.69.106 on 09/08/12
For personal use only.

Can. J. Chem. Downloaded from www.nrcresearchpress.com by 213.200.69.106 on 09/08/12
For personal use only.

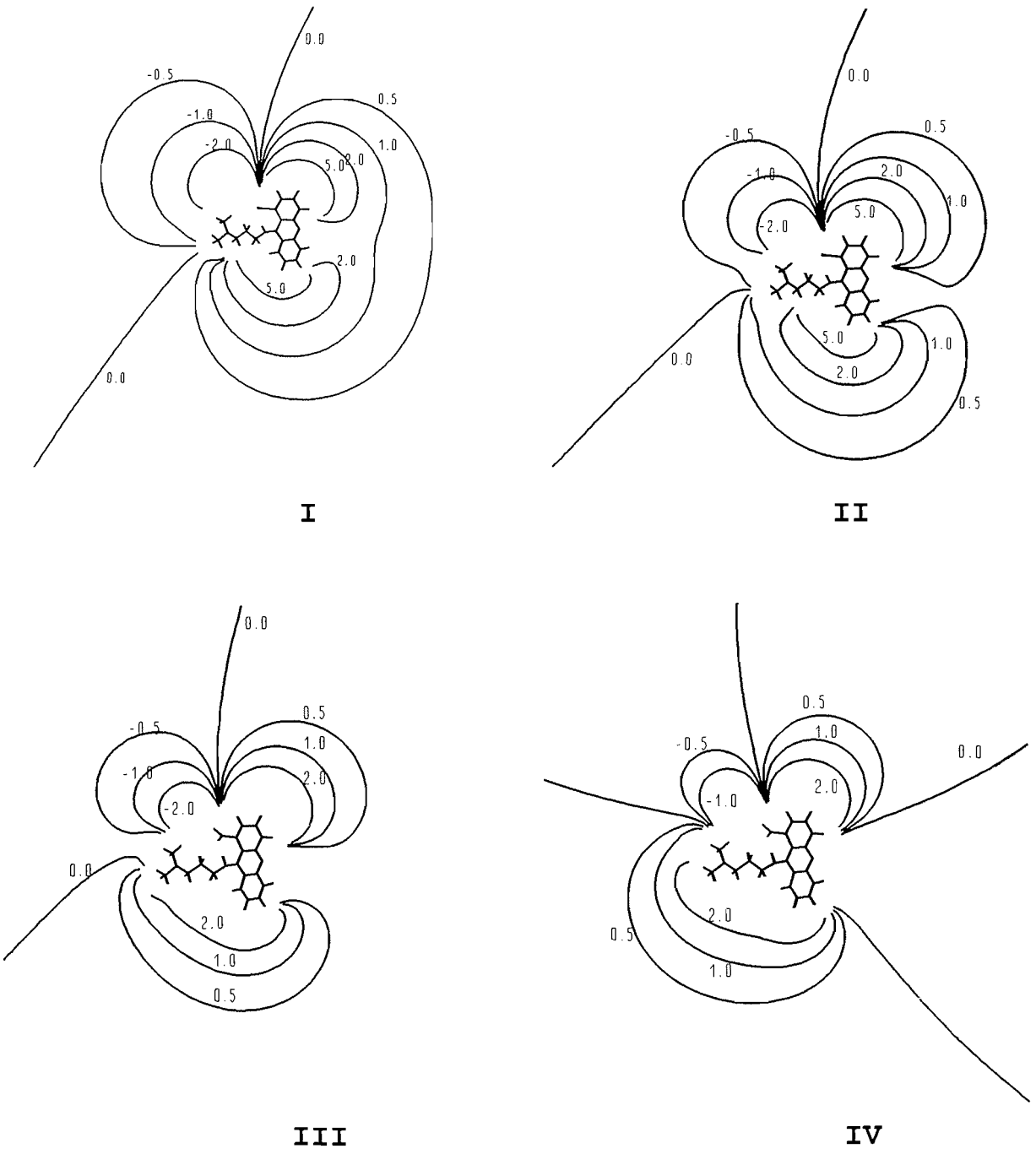

FIG. 9. 2-D MEP maps relevant to the A2 structure of nitracrine obtained using AM1 net atomic charges (I), charges fitted to the potential calculated from the AM1 wavefunction (II), Mulliken net atomic charges from the ab initio (STO-3G) calculations (III), and charges fitted to the potential calculated from the ab initio (STO-3G) wavefunction (IV).

crine undergoes reductive metabolism in which the $-NO_2$ group is changed to -NHOH (5, 20). The AM1 method predicts that all the compounds studied exhibit comparable capability to undergo reduction (reflected by energies of LUMO). It might, therefore be, that the presence of both -NHR and $-NO_2$ groups in close proximity, and in the region of a negative electrostatic potential, facilitates reduction. This would be so if the positive interaction region of an enzyme were matched with the negative region of nitracrine.

The role played by prototropic tautomerism in the biological activity of the compounds studied is rather difficult to answer. Both energy and free energy data indicate that nitracrine and its nitro isomers should exist predominantly in the imino tautomeric form (contrary to 9-acridinamine where the amino form is thermodynamically favoured (30)). However, differences in ΔH_f and ΔG_f are not too high, which implies that molecules can exist equally well, in both above forms, in equilibrium. This was fully confirmed by examining absorption and emission spectra (31, 32, 57). Recently Boyd and Denny (10), using high-resolution proton magnetic resonance spectroscopy, deduced that under certain conditions (similar to physiological conditions) nitracrine and the 4-nitro isomer exist in the imino configuration

Can. J. Chem. Downloaded from www.nrcresearchpress.com by 213.200.69.106 on 09/08/12
For personal use only.

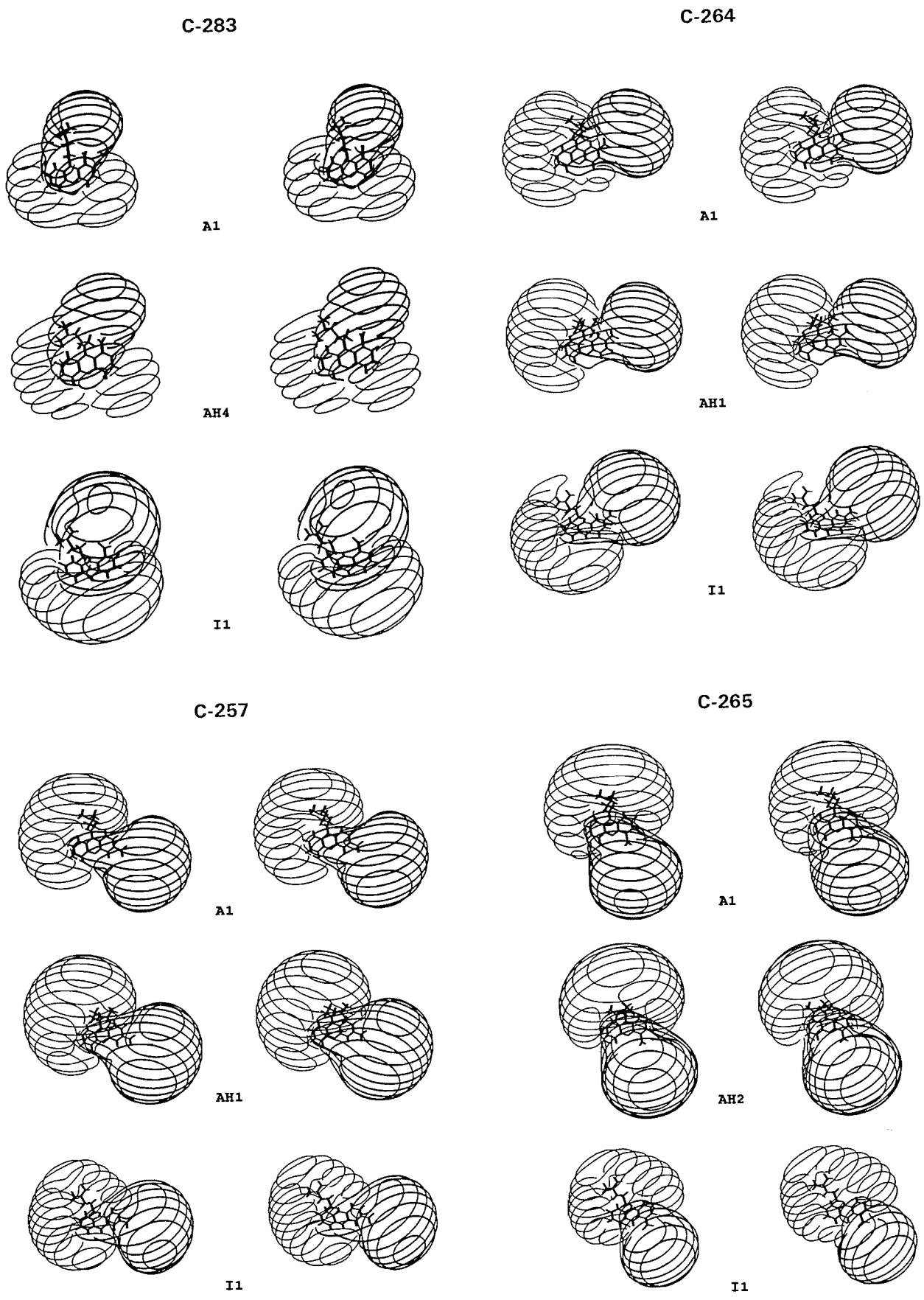

FIG. 10. The stereoviews of the 3-dimensional (3-D) maps of the molecular electrostatic potential resulting from AM1 net atomic charges (thin lines indicate a positive zone and thick lines a negative zone).

while the 2- and 3-nitro isomers exist in the amino structure. Our data thus show only qualitative correlation with those of Boyd and Denny. Nevertheless, both demonstrate that imino configuration may be a key factor in biological activity of molecules. To support this, the biological activity of the 4-nitro isomer has also recently been revealed (refs. cited in ref. 10).

Acknowledgments

We would like to thank Dr. A. Liwo for permitting us to use the program for calculations and drawing the molecular electrostatic potential maps. This work was supported by the Polish State Committee for Scientific Research (KBN) under grants DS/5-300-7-016-1 and BW/5-300-4-067-1.

1. "Ledakrin". Mater. Med. Pol. (Engl. Ed.) **8**, 237 (1976).
2. A. Ledóchowski and B. Stefanska. Rocz. Chem. **40**, 301 (1966).
3. C. Radzikowski, A. Ledóchowski, M. Hrabowska, B. Stefanska, B. Horowska, J. Konopa, E. Jereczek-Morawska, and M. Urbanska. Arch. Immunol. Ther. Exp. **17**, 99 (1969).
4. P.B. Roberts, R.F. Anderson, and W.R. Wilson. Int. J. Radiat. Biol. **51**, 641 (1987).
5. W.R. Wilson, L.H. Thompson, R.F. Anderson, and W.A. Denny. J. Med. Chem. **32**, 31 (1989).
6. Z. Dauter, M. Bogucka-Ledóchowska, A. Hempel, A. Ledóchowski, and Z. Kosturkiewicz. Rocz. Chem. **50**, 1573 (1976).
7. A. Hempel, S.E. Hull, M. Bogucka-Ledóchowska, and A. Dauter. Acta Crystallogr. Sect. B: Struct. Crystallogr. Cryst. Chem. **B35**, 474 (1979).
8. A. Hempel, S.E. Hull, Z. Dauter, M. Bogucka-Ledóchowska, and A. Konitz. Acta Crystallogr. Sect. B: Struct. Crystallogr. Cryst. Chem. **B35**, 477 (1979).
9. J.J. Stezowski, P. Kollat, M. Bogucka-Ledóchowska, and J.P. Glusker, J. Am. Chem. Soc. **107**, 2067 (1985).
10. M. Boyd and W.A. Denny. J. Med. Chem. **33**, 2656 (1990).
11. J. Chodkowski, W. Kiwak, and E. Walczak. Rocz. Chem. **44**, 1603 (1970).
12. J. Chodkowski and W. Kiwak. Rocz. Chem. **47**, 157 (1973).
13. J. Biedrzycki, J. Błażejowski, A. Ledóchowski, and J. Szychlinski. Rocz. Chem. **51**, 379 (1977).
14. J. Biedrzycki, J. Błażejowski, J. Szychlinski, and A. Ledóchowski. Z. Naturforsch. A: Phys. Phys. Chem. Kosmophys. **39a**, 195 (1984).
15. M. Gniazdowski, J. Filipski, and M. Chorazy, Antibiotics (N.Y.) **5**, 275 (1979).
16. K. Pawlak, A. Matuszkiewicz, J.W. Pawlak, and J. Konopa. Chem.-Biol. Interact. **43**, 131 (1983); **43**, 151 (1983); **43**, 175 (1983).
17. J.M. Woynarowski, A. Bartoszek, and J. Konopa. Chem.-Biol. Interact. **49**, 311 (1984).
18. K. Pawlak, J.W. Pawlak, and J. Konopa. Cancer. Res. **44**, 4289 (1984).
19. J.M. Woynarowski and A. Bartoszek. Biochim. Biophys. Acta, **825**, 244 (1985).
20. W.R. Wilson, W.A. Denny, G.M. Stewart, A. Fenn, and J.C. Probert. Int. J. Radiat. Oncol. Biol. Phys. **12**, 1235 (1986).
21. A. Bartoszek and J. Konopa. Biochem. Pharmacol. **36**, 4169 (1987).
22. L.R. Ferguson, A.M. Roberton, and P.M. Turner. Mutagenesis, **2**, 253 (1987).
23. Z. Mazerska, M. Cholody, J. Lukowicz, B. Wysocka-Skrzela, and A. Ledóchowski. Arzneim.-Forsch. **37**, 1276 (1987).
24. A. Bartoszek and J. Konopa. Biochem. Pharmacol. **36**, 4169 (1987).
25. L.R. Ferguson and P. Van Zijl. Mutat. Res. **204**, 655 (1988).
26. R.M. Acheson, M.L. Burstall, C.W. Jefford, and B.F. Sansom. J. Chem. Soc. 3742 (1954).
27. A.K. Sukhomlina. Zh. Obshch. Khim. **28**, 1038 (1958).
28. A.C. Capomacchia, J. Casper, and S.G. Schulman. J. Pharm. Sci. **63**, 1272 (1974).
29. V.B. Pett, M. Rossi, J.P. Glusker, J.J. Stezowski, and M. Bogucka-Ledóchowska. Bioorg. Chem. **11**, 443 (1982).
30. J. Rak, J. Błażejowski, and R.J. Zauhar. J. Org. Chem. **57**, 372 (1992).
31. A. Tempczyk, J. Rak, and J. Błażejowski. J. Chem. Soc. Perkin Trans. 2, 1501 (1990).
32. J. Rak, J. Błażejowski, K. Nowaczyk, and A. Kawski. J. Photochem. Photobiol. A: **61**, 343 (1991).
33. J. Rak, K. Nowaczyk, J. Błażejowski, and A. Kawski. J. Fluoresc. **1**, 57 (1991).
34. J.S. Kwiatkowski, T.J. Zielinski, and R. Rein. Adv. Quantum Chem. **18**, 85 (1986).
35. A. Les and L. Adamowicz. J. Phys. Chem. **99**, 7201 (1990).
36. W.M.F. Fabian. J. Phys. Org. Chem. **3**, 332 (1990).
37. M.M. Karelson, A.R. Katritzky, M. Szafran, and M.C. Zerner. J. Org. Chem. **54**, 6030 (1989).
38. M.N. Eberlin, Y. Takahata, and C. Kascheres. THEOCHEM, **66**, 143 (1990).
39. G. Buemi. J. Chem. Soc. Faraday Trans. **86**, 2813 (1990).
40. A.R. Katritzky and M.M. Karelson. J. Am. Chem. Soc. **86**, 2813 (1991).
41. G.A. Worth, P.M. King, and W.G. Richards. Biochim. Biophys. Acta, **993**, 134 (1989).
42. M.J.S. Dewar, E.G. Zoebisch, E.F. Healy, and J.J.P. Stewart. J. Am. Chem. Soc. **107**, 3902 (1985).
43. J.J.P. Stewart. J. Comput.-Aided Mol. Des. **4**, 1 (1990).
44. D.R. Boyd, D.W. Smith, J.J.P. Stewart, and E. Wimmer. J. Comput. Chem. **9**, 387 (1988).
45. J.J.P. Stewart. J. Comput. Chem. **10**, 209 (1989); **10**, 221 (1989).
46. W.J. Hehre, R.F. Stewart, and J.A. Pople. J. Chem. Phys. **51**, 2657 (1969).
47. J.A. Pople. Acc. Chem. Res. **3**, 217 (1970).
48. M. Dupuis. *In* MOTECC-89 (Modern Techniques in Computational Chemistry). *Edited by* S. Chin, E. Clementi, G. Corongiu, M. Dupuis, D. Frye, D. Logan, A. Mohanty, and V. Sonnad. IBM Corp., Kingston, N.Y. 1990. pp. 215–330.
49. M.J.S. Dewar, E.F. Healy, and J.J.P. Stewart. J. Chem. Soc. Faraday Trans. 2, **80**, 227 (1984).
50. U.C. Singh and P.A. Kollman. J. Comput. Chem. **5**, 129 (1984).
51. A. Liwo, A. Tempczyk, and Z. Grzonka. J. Comput.-Aided Mol. Des. **3**, 261 (1989).
52. C.A. Reynolds, J.W. Essex, and W.G. Richards. J. Am. Chem. Soc. **114**, 9075 (1992).
53. P. Murray-Rust. *In* Molecular structure and biological activity. *Edited by* J.F. Griftin and W.L. Duax. Elsevier Biomedical, New York. 1982. p. 117.
54. L.K. Vinson and J.J. Dannenberg, J. Am. Chem. Soc. **111**, 2777 (1989).
55. S. Galeva, J.M. Lluch, A. Oliva, and J. Bertan. THEOCHEM, **40**, 101 (1988).
56. W.M.F. Fabian. THEOCHEM, **206**, 295 (1990).
57. J. Rak and J. Błażejowski. Spectrochim. Acta, Part A: **A48**, 771 (1992).
58. T. Koopmans. Physica, **1**, 104 (1934).
59. N.S. Hush and J.A. Pople. Trans. Faraday. Soc. **51**, 600 (1955).
60. C.C.J. Roothaan. Rev. Mod. Phys. **23**, 61 (1951).
61. B.J. Tabner and J.R. Yandle. J. Chem. Soc. 381 (1968).
62. V. Podany, A. Vachalkova, S. Miertus, and L. Bahna. Neoplasma, **22**, 469 (1975).
63. D. Hadzi, J. Koller, M. Hodoscek, and D. Kocjan. Modelling of structure and properties of molecules. *Edited by* Z.B. Maksic. Ellis Harwood Ltd., London. 1987. p. 286.

Can. J. Chem. Downloaded from www.nrcresearchpress.com by 213.200.69.106 on 09/08/12
For personal use only.

Anomalous stabilizing and destabilizing effects in some cyclic π-electron systems

PETER POLITZER,[1] M. EDWARD GRICE, JANE S. MURRAY, AND JORGE M. SEMINARIO
Department of Chemistry, University of New Orleans, New Orleans, LA 70148, U.S.A.

Received March 19, 1993

PETER POLITZER, M. EDWARD GRICE, JANE S. MURRAY, and JORGE M. SEMINARIO. Can. J. Chem. **71**, 1123 (1993).

Ab initio computational studies have been carried out for three molecules that are commonly classed as antiaromatic: cyclobutadiene (**1**), 1,3-diazacyclobutadiene (**7**), and 1,4-dihydropyrazine (**6**). Their dinitro and diamino derivatives were also investigated. Stabilizing or destabilizing energetic effects were quantified by means of the isodesmic reaction procedure at the MP2/6-31G*//HF/3-21G level, and calculated molecular electrostatic potentials (HF/STO-5G//HF/3-21G) were used as a probe of electron delocalization. Our results do not show extensive delocalization in the π systems of any one of the three parent molecules. The destabilization found for **1** and **7** is attributed primarily to strain and to repulsion between the localized π electrons in the C=C and C=N bonds, respectively. However, **6** is significantly stabilized, presumably due to limited delocalization of the nitrogen lone pairs. NH_2 groups are highly stabilizing, apparently because of lone pair delocalization. NO_2 is neither uniformly stabilizing nor destabilizing.

PETER POLITZER, M. EDWARD GRICE, JANE S. MURRAY et JORGE M. SEMINARIO. Can. J. Chem. **71**, 1123 (1993).

On a étudié au moyen de calculs *ab initio* trois molécules qui sont communément classées comme des antiaromatiques : le cyclobutadiène (**1**), le diaza-1,3-cyclobutadiène (**7**) et la dihydro-1,4-pyrazine (**6**). On a également étudié leurs dérivés dinitro et diamino. On a quantifié les effets énergétiques stabilisants ou déstabilisants en faisant appel au procédé de la réaction isodesmique au niveau MP2/6-31G*//HF/3-21G, et on a utilisé les potentiels électrostatiques moléculaires calculés, (HF/STO-5G//HF/3-21G) comme preuve de la délocalisation de l'électron. Nos résultats ne révèlent pas une forte délocalisation dans le système π des trois molécules apparentées. La déstabilisation trouvée pour les composés **1** et **7** est attribuée principalement à la contrainte et à la répulsion existante entre les électrons π localisés des liaisons C=C et C=N respectivement. Cependant le composé **6** est stabilisé de façon significative, probablement à cause de la délocalisation limitée du doublet libre de l'azote. Les groupes NH_2 sont fortement stabilisés, apparemment à cause de la délocalisation du doublet libre. Le NO_2 n'est ni uniformément stabilisé ni déstabilisé.

[Traduit par la rédaction]

Introduction

A monocyclic fully conjugated (closed loop) planar π-electron system may be either aromatic or antiaromatic depending upon whether it is stabilized or would be destabilized, respectively, by π-electron delocalization (1–4). Simple molecular orbital considerations for planar rings have led to the generalizations that aromaticity is associated with the presence of $(4n + 2)$ π electrons ($n = 0, 1, 2, 3, \ldots$) and antiaromaticity with $4n$ ($n = 1, 2, 3, \ldots$) (3–5). An interesting example of the latter is the highly unstable cyclobutadiene molecule (**1**), which has four π electrons. By analogy to benzene, one might anticipate a square, resonance-stabilized structure, **2**; however, it is well established both experimentally (6–8) and computationally (9–11) that cyclobutadiene is a rectangular diene, **1**. As March has pointed out, ". . . simple cyclobutadienes, which could easily adopt a square planar shape if that would result in aromatic stabilization, do not in fact do so and are not aromatic" (ref. 3, p. 52).

1 **2** **3**

Antiaromatic destabilization does not necessarily preclude the existence of cyclic systems that formally have $4n$ π electrons, and many such compounds have been prepared and characterized (2–4, 12, 13). Structural factors can play an important role; cyclooctatetraene (**3**), a stable compound that has eight π electrons, is considered to be neither aromatic nor antiaromatic, because it has a highly puckered tub-shaped conformation that impedes π delocalization (3).

Very recently, the synthesis of the dihydrodiimidazopyrazines **4** and **5** has been reported (14); these are derivatives of 1,4-dihydropyrazine, **6**. If the lone pair electrons on the nitrogens of **6** are assumed to be of π-type, then this molecule has eight conjugated π electrons and satisfies the $4n$ rule. Indeed **6** is normally classed as antiaromatic (13, 15–17), which would then formally apply to **4** and **5** as well.

Our objective in this project has been to examine computationally any anomalous energetic features of **1** and **6**, and how these are affected by two significantly different substituents, NO_2 and NH_2. We also include 1,3-diazacyclobutadiene, **7**, in this analysis, since we and others have shown that ring nitrogens tend to stabilize both strained and unstrained molecules (18–20). If the lone pairs of the nitrogens in **7** are primarily in the ring plane, as in pyridine for example, then **7** has four π electrons and is formally antiaromatic. An unavoidable problem in trying to assess such energetic effects as aromatic stabilization, antiaromatic destabilization, strain, etc., is that these are not rigorously defined; they depend upon the choice of reference systems. Our approach has been to apply the widely used isodesmic reaction method (21, 22), and to refer the system of interest to the smallest possible molecules having the same types of bonds. Thus the anomalous energy associated with **8**, for example, is obtained by computing ΔE for eq. [1]:

[1]Author to whom correspondence may be addressed.

Can. J. Chem. Downloaded from www.nrcresearchpress.com by 213.200.69.106 on 09/08/12
For personal use only.

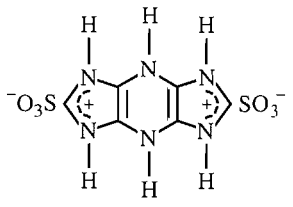

4

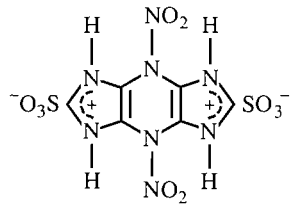

5

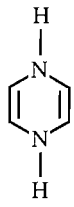

6

7

[1] $4H_3C-NH_2 + 2H_2C = CH_2 + 2H_2N-NO_2 \longrightarrow$ 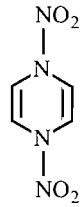 $+ 4CH_4 + 4NH_3$

8

If the bonds in **8** were energetically unchanged from the corresponding ones on the left side of eq. [1], then ΔE would be zero. $\Delta E < 0$ would indicate that stabilizing factors are associated with **8**; $\Delta E > 0$ would imply destabilization. It should be noted that this procedure gives the net result of *all* stabilizing and destabilizing contributions; thus one cannot separate, for example, the effects of antiaromaticity and strain.

Methods

Optimized geometries were computed with GAUSSIAN 92 (23) at the *ab initio* HF/3-21G level for **1**, **6**, and **7**, and for their NH_2 and NO_2 derivatives, **8**–**13**. The corresponding MP2/6-31G* energies were used to determine the isodesmic ΔE values for these molecules, using reactions analogous to eq. [1]. The energies of the reference systems were also obtained by MP2/6-31G*//HF/3-21G calculations.

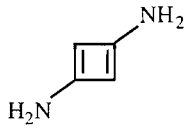

9

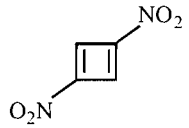

10

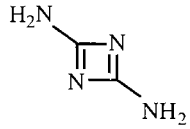

11

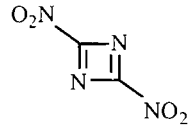

12

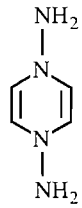

13

As part of our analysis, we calculated the electrostatic potential, $V(\boldsymbol{r})$, that is created in the space around each molecule by its nuclei and electrons. This is given rigorously by eq. [2]:

$$[2] \quad V(\boldsymbol{r}) = \sum_A \frac{Z_A}{|\boldsymbol{R}_A - \boldsymbol{r}|} - \int \frac{\rho(\boldsymbol{r}')d\boldsymbol{r}'}{|\boldsymbol{r}' - \boldsymbol{r}|}$$

Z_A is the charge on nucleus A, located at $\boldsymbol{R}_A$, and $\rho(\boldsymbol{r})$ is the electronic density, which we obtain from the molecular wave function. $V(\boldsymbol{r})$ is a real physical property, which can be determined experimentally as well as computationally (24), and is now widely used in interpreting and predicting reactive behavior (25). In the present work, however, we have used it as a sensitive probe of electron delocalization. We computed $V(\boldsymbol{r})$ for **1** and **6**–**13** at the HF/STO-5G//HF/3-21G level, which we have found, in extensive applications, to be effective for this property (25).

Results

Our calculated isodesmic energies are listed in Table 1, along with key optimized bond lengths and also the most negative values, V_{min}, of the electrostatic potentials associated with these molecules. All of the four-membered-ring systems were found to be essentially planar, as also was **8**. Since the 3-21G basis set sometimes overestimates amine bond angles (26), and thus may erroneously predict planarity (27), we repeated the optimization of **9** at the HF/6-31G* level and verified that it is planar.

The nonplanarity of **6** is due primarily to the pyramidal configurations of the two amine nitrogens, which give rise to two possible conformers, **6***a* and **6***b*, which we find to have the same HF/3-21G energy. In **6***a* and **6***b*, the N—N—H angles are in the range 142°–144°. In both conformers, there is also a slight puckering of the six-membered ring; the dihedral angle around the N—N axis is 7.2° in **6***a* and 1.2° in **6***b*. The greater degree of puckering in **6***a* may reflect an effort to minimize the repulsion between the nitrogen lone pairs.

The other nonplanar molecule is **13**, in which both the ring and the amine nitrogens have pyramidal configurations. An interesting feature of **13** is that it does not possess a plane of symmetry passing through the four nitrogens; instead, the amine groups are rotated so that there are dihedral angles of 83.5° involving each pair of bonded nitrogens and their respective lone pairs. These angles are very similar to the corresponding ones in 1,1-dimethylhydrazine, $(H_3C)_2N-NH_2$, which we found earlier to be 82.0° (28). (The locations of

Can. J. Chem. Downloaded from www.nrcresearchpress.com by 213.200.69.106 on 09/08/12
For personal use only.

TABLE 1. Computed properties

	Molecule	$\Delta E_{isodesmic}$, MP2/6-31G*//HF/3-21G, kcal/mol	Bond length, Å	V_{min}, HF/STO-5G//HF/3-21G, kcal/mol
1		+53.0	C—C: 1.602 C=C: 1.323	−13.1[a]
10	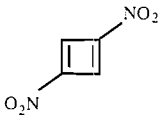	+46.5	C—C: 1.564 C=C: 1.322 C—N: 1.388 N—O: 1.247, 1.248	−48.2,[b] −33.2[b] −48.2,[b] −32.1[b]
9	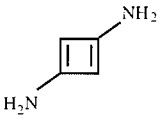	+18.2	C—C: 1.525 C=C: 1.377 C—N: 1.325	−41.1[c] −23.6[d]
12	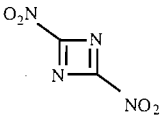	+41.1	C—N: 1.562 C=N: 1.261 C—NO_2: 1.411 N—O: 1.237, 1.238	−27.4[e] −34.8,[b] −27.0[b] −34.7,[b] −27.4[b]
7		+32.5	C—N: 1.577 C=N: 1.274	−73.0[e]
11	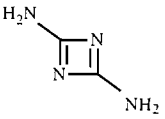	−39.0	C—N: 1.405 C=N: 1.406 C—NH_2: 1.297	−109.6[e] −5.2[d]
8	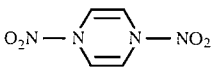	−25.5	C=C: 1.314 C—N: 1.413 N—O: 1.253 N—N: 1.351	−48.7,[b] −26.8[b]
6	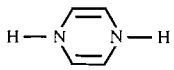	−39.6	C=C: 1.317 C—N: 1.424	−70.6[f] −10.8,[g] −19.0[h]
13	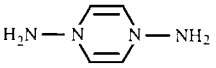	−124.2	C=C: 1.319 C—N: 1.423 N—N: 1.443	−90.5[i] −67.7[f]

[a]Above and below C=C double bonds.
[b]Nitro group oxygens.
[c]Above and below unsubstituted carbons.
[d]Above and below amine nitrogens.
[e]Aza nitrogens, in molecular plane.
[f]Lone pairs of ring nitrogens.
[g]Above C=C double bonds, same side of ring as hydrogens.
[h]Below C=C double bonds, side away from hydrogens.
[i]Lone pairs of amine nitrogens.

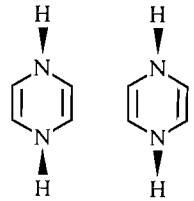

6a **6b**

the most negative electrostatic potentials associated with the lone pairs, V_{min}, were used in determining these dihedral angles (28).)

Within each subgroup in Table 1, the molecules are listed in order of decreasing isodesmic ΔE values. As anticipated, both **1** and **7** show considerable destabilization, although it is less in the case of **7**. On the other hand, the ΔE for **6** indicates stabilization, despite its normally being considered to be antiaromatic (13, 15–17). The introduction of NH_2 groups has a pronounced stabilizing effect in each instance, whereas NO_2 stabilizes **1**, but destabilizes **6** and **7**.

Discussion

The diene nature of cyclobutadiene, **1**, is emphasized by

Can. J. Chem. Downloaded from www.nrcresearchpress.com by 213.200.69.106 on 09/08/12
For personal use only.

Can. J. Chem. Downloaded from www.nrcresearchpress.com by 213.200.69.106 on 09/08/12
For personal use only.

its computed electrostatic potential, which shows a V_{min} of −13.1 kcal/mol above and below the C=C double bonds (Table 1); this is the same as was found for ethylene (29). The isodesmic ΔE of **1** presumably reflects both antiaromaticity and strain; its large positive magnitude, +53.0 kcal/mol, is fully consistent with the antiaromaticity contribution having been estimated as being larger than 12–16 kcal/mol (30) and the strain energy as at least 35 kcal/mol (31).

If antiaromatic destabilization is regarded as being associated with π delocalization (1–4), then a question arises as to the physical basis for the "antiaromatic" destabilizing energy of **1**, in view of the evidence that its π electrons are quite localized. We suggest that this may reflect, at least in part, the repulsive interaction between these π electrons, which are forced by the molecular framework to be in relatively close proximity, approximately one C—C bond length apart. The same reasoning may explain why this C—C bond is unusually long, by approximately 0.06 Å. By this interpretation, it is the π *localization,* rather than delocalization, that involves instability. The same explanation may apply to **7**, except that some of the C=N π charge may have been attracted to the nitrogens, making the repulsive interaction weaker.

Table 1 shows that both NO_2 and NH_2 substituents stabilize cyclobutadiene, especially the latter. They achieve this, however, in opposite ways. The NO_2 group is strongly electron withdrawing, through both induction and resonance; contributions from structures such as **10***b* can be anticipated. Indeed the C—N distances in **10** are 0.1 Å shorter than in nitromethane, for example (22), and there is no longer a negative electrostatic potential above the C=C bonds (Table 1). It had earlier been proposed that the withdrawal of electronic charge from cyclobutadiene has a stabilizing effect (30), and this is exactly what our results show.

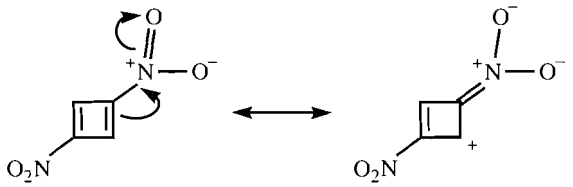

10*a* **10***b*

The reverse happens in the case of **9**. There is extensive resonance donation of charge by the amine groups to the ring, as shown below; the C—N bonds in **9** are fully 0.14 Å shorter than in methylamine (22), and the V_{min} of the nitrogen lone pairs is only −23.6 kcal/mol (Table 1), which is a relatively weak lone pair potential for nitrogen. To put this in perspective, V_{min} is −109 kcal/mol for NH_3 in its pyramidal conformation and −60 kcal/mol when it is planar (32); for methylamine, V_{min} = −105 kcal/mol (33). Most striking, however, are the strong negative potentials near the unsubstituted carbons, −41.1 kcal/mol. These are even more negative than the V_{min} of fluorine in hydrogen fluoride, −32 kcal/mol,[2] and attest to the importance of the contributions of structures like **9***b*. This delocalization of electronic charge into the ring is presumably the reason for the marked stabilizing effect of the NH_2 group. The unsubstituted carbons in **9** should be quite favorable sites for electrophilic attack.

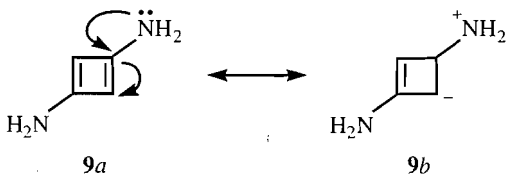

9*a* **9***b*

This is seen again, even more dramatically, in comparing **7** and **11**. Whereas the bond lengths in **7** clearly distinguish between C—N single and double bonds, the distinction is absent in **11**, apparently due to resonance such as is depicted below. Consistent with this picture, the lone pair

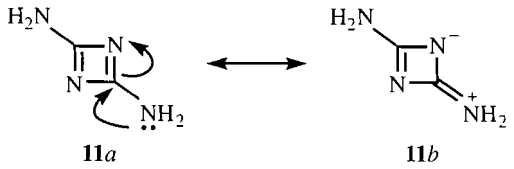

11*a* **11***b*

V_{min} of the ring nitrogens changes from −73.0 kcal/mol in **7** to a very highly negative −109.6 kcal/mol in **11**; the latter is similar to ammonia (see above) and is much more negative than pyridine, −92.9 kcal/mol (34). Thus the ring nitrogens in **11** can be anticipated to have very significant basic character, which is consistent with its structural similarity to guanidine, $(H_2N)_2C{=}NH$. The stabilization brought about by the NH_2 groups amounts to +32.5 − (−39.0) = 71.5 kcal/mol in **11**, compared to +53.0 − 18.2 = 34.8 kcal/mol in **9**.

The dinitro derivative **12** presents a rather complicated situation, in which it is difficult to evaluate all of the possible factors. The ring nitrogens are also electron attracting (34, 35), as well as the NO_2 groups; thus they are both competing for the polarizable electronic charge. Neither is as negative as it would be in the absence of the other; this can be seen by comparing the V_{min} of the ring nitrogens in **7** and **12**, and the V_{min} of the nitro group oxygens in **12** and **10**, as well as the C—NO_2 and N—O bond lengths in **12** and **10**, which show that the former has less resonance of the type depicted in structure **10***b*. Thus the withdrawal of charge from the ring through which the NO_2 groups stabilize **10** relative to **1** apparently does not occur to the same extent in **12**, and the net result is that the latter is actually destabilized by 8.6 kcal/mol relative to **7**.

Like the other parent molecules, **1** and **7**, 1,4-dihydropyrazine, **6**, clearly is a diene; this is confirmed by the C=C distances and the V_{min} associated with these bonds (Table 1). It is interesting that the diene character of **6** is maintained even when its nitrogens are forced to be planar, which should promote π delocalization; the planar conformation of **6**, which is 7.0 kcal/mol higher in energy than the pyramidal (at the MP2/6-31G*//HF/3-21G level), the lengths of the C=C bonds are 1.318 Å and their V_{min} are −21.4 and −21.6 kcal/mol. There is evidently no driving force for extensive π delocalization of these lone pairs.

In contrast to **1** and **7**, **6** has a negative isodesmic energy, which indicates a stabilizing effect. We suggest that this may reflect, in part, some degree of delocalization of the nitrogen lone pairs. (The nitrogens in **6** are not responsible for its

[2]T. Brinck. Private communication.

entire stabilization, since we found an isodesmic ΔE of −24.0 kcal/mol for the hydrocarbon analog of **6**, 1,4-cyclohexadiene.) The presence of NO_2 groups in **8** decreases the stabilization of the system, perhaps because the electron-withdrawing power of the NO_2 groups diminishes the extent of delocalization of the lone pairs to the ring.

While the introduction of NH_2 substituents leads to a very large stabilizing isodesmic ΔE for **13**, it does not appear that this can be attributed to delocalization of π charge into the ring, as in **9** and **11**. Such an interpretation would be inconsistent with the strongly negative lone pair V_{min} of the pyramidal NH_2 groups (Table 1) and their being rotated around the N—N bonds, as mentioned above. While the rotations around the N—N bonds and also the lengths of these bonds are reminiscent of 1,1-dimethylhydrazine, $(H_3C)_2N—NH_2$ (28), the V_{min} of the nitrogens are even more negative in the latter: −88.2 and −97.5 kcal/mol, compared to −67.7 and −90.5 kcal/mol, respectively, in **13**. This suggest that there does occur some significant delocalization in **13**, involving the lone pairs of both types of nitrogens, analogous to what was proposed above for **6**. This would help to explain the large stabilizing isodesmic ΔE that we obtain for **13**.

Summary

Our computed structures show that neither cyclobutadiene, **1**, nor 1,3-diazacyclobutadiene, **7**, avails itself of the opportunity for π delocalization in analogy to its six-membered cyclic counterpart, benzene or pyrazine. Instead their π electrons are highly localized in the C=C and C=N double bonds, and it is to the repulsion between these electrons that we attribute a major portion of the "antiaromatic" destabilization of these molecules.

1,4-Dihydropyrazine, **6**, is also a diene, and has pyramidal nitrogens in its most stable conformation; we believe that some delocalization of the nitrogen lone pairs occurs, and is partially responsible for **6** being significantly stabilized. Even when **6** is forced into a planar conformation, which should promote cyclic π delocalization, this option is not followed.

Amine substituents have highly stabilizing effects in all three cases investigated: **9**, **11**, and **13**. This appears to be due to delocalization of the amine lone pairs in each instance. It is more difficult to generalize about the effects of nitro groups, which are neither uniformly stabilizing nor destabilizing.

Acknowledgements

We greatly appreciate very helpful discussions with Dr. J.H. Boyer and Dr. J.W. Timberlake, and the support provided by the Office of Naval Research, contract no. N00014-91-J-0457.

1. R. Breslow and E. Mohacsi. J. Am. Chem. Soc. **85**, 431 (1963).
2. R. Breslow. Acc. Chem. Res. **6**, 393 (1973).
3. J. March. Advanced organic chemistry. 3rd ed. Wiley–Interscience, New York. 1985. Chap. 2.
4. T.H. Lowry and K.S. Richardson. Mechanism and theory in organic chemistry. 3rd ed. Harper Collins, 1987. Chap. 1.
5. E. Hückel. Z. Phys. **70**, 204 (1931); **76**, 628 (1932).
6. H. Kollmar and V. Staemmler. J. Am. Chem. Soc. **100**, 4304 (1978).
7. S. Masamune, F.A. Souto-Bachiller, T. Machiguchi, and J.E. Bertie. J. Am. Chem. Soc. **100**, 4889 (1978).
8. D.W. Whitman and B.K. Carpenter. J. Am. Chem. Soc. **102**, 4272 (1980), and references cited.
9. H. Kollmar and V. Staemmler. J. Am. Chem. Soc. **99**, 3583 (1977).
10. W.T. Borden, E.R. Davidson, and P. Hart. J. Am. Chem. Soc. **100**, 388 (1978).
11. J.A. Jafri and M.D. Newton. J. Am. Chem. Soc. **100**, 5012 (1978).
12. T.L. Amyes, J.P. Richard, and M. Novak. J. Am. Chem. Soc. **114**, 8032 (1992).
13. W. Kaim. Angew. Chem. Int. Ed. Engl. **20**, 599 (1981).
14. M. Vedachalam and J.H. Boyer. Heteroat. Chem. **4**, 85 (1993).
15. A. Streitwieser, Jr. Molecular orbital theory for organic chemists. Wiley, New York. 1961. Chap. 10.
16. W. Kaim. Angew. Chem. Int. Ed. Engl. **20**, 600 (1981).
17. A.E.A. Porter. In Comprehensive heterocyclic chemistry. Vol. 3. Part 2B. *Edited by* A.R. Katritzky. Pergamon Press, New York. 1984. Chap. 2.14.
18. J.S. Murray, P.C. Redfern, J.M. Seminario, and P. Politzer. J. Phys. Chem. **94**, 2320 (1990).
19. J.S. Murray, J.M. Seminario, P. Lane, and P. Politzer. J. Mol. Struct. (Theochem), **207**, 193 (1990).
20. I. Alkorta, J. Elguero, I. Rozas, and A.T. Balaban. J. Mol. Struct (Theochem), **208**, 63 (1990).
21. W.J. Hehre, R. Ditchfield, L. Radom, and J.A. Pople. J. Am. Chem. Soc. **92**, 4796 (1970).
22. W.J. Hehre, L. Radom, P.v.R. Schleyer, and J.A. Pople. Ab initio molecular orbital theory. Wiley, New York. 1986.
23. GAUSSIAN 92, Revision C, M.J. Frisch, G.W. Trucks, M. Head-Gordon, P.M.W. Gill, M.W. Wong, J.B. Foresman, B.G. Johnson, H.B. Schlegel, M.A. Robb, E.S. Replogle, R. Gomperts, J.L. Andres, K. Raghavachari, J.S. Binkley, C. Gonzalez, R.L. Martin, D.J. Fox, D.J. Defrees, J. Baker, J.J.P. Stewart, and J.A. Pople. Gaussian, Inc., Pittsburgh, Pa. 1992.
24. P. Politzer and D.G. Truhlar (*Editors*). Chemical applications of atomic and molecular electrostatic potentials. Plenum Press, New York. 1981.
25. P. Politzer and J.S. Murray. *In* Review in computational chemistry. *Edited by* K.B. Lipkowitz and D.B. Boyd. VCH Publishers, New York. 1991. Chap. 7.
26. J.E. Boggs nd Z. Niu. J. Comput. Chem. **6**, 46 (1985).
27. J.P. Ritchie. J. Am. Chem. Soc. **107**, 1829 (1985); **111**, 2517 (1989).
28. J.S. Murray, N. Sukumar, S. Ranganathan, and P. Politzer. Int. J. Quantum Chem. **37**, 611 (1990).
29. P. Politzer and W.L. Hedges. Int. J. Quantum Chem. Quantum Biol. Symp. **9**, 307 (1982).
30. R. Breslow, D.R. Murayama, S.-I. Murahashi, and R. Grubbs. J. Am. Chem. Soc. **95**, 6688 (1973).
31. A. Greenberg and J.F. Liebman. Strained organic molecules. Academic Press, New York. 1978. Chap. 3.
32. J.S. Murray and P. Politzer. Chem. Phys. Lett. **136**, 283 (1987).
33. J.S. Murray and P. Politzer. Chem. Lett. **152**, 364 (1988).
34. J.S. Murray, J.M. Seminario, and P. Politzer. J. Mol. Struct. (Theochem), **187**, 95 (1989).
35. P. Politzer, J.S. Murray, J.M. Seminario, and R.S. Miller. J. Mol. Struct. (Theochem), **262**, 155 (1992).

Can. J. Chem. Downloaded from www.nrcresearchpress.com by 213.200.69.106 on 09/08/12
For personal use only.

Nouveaux alcaloïdes isoquinoléiques isolés d'une Lauraceae bolivienne : *Aniba canelilla* H.B.K.

JEAN-MICHEL OGER, AGNÈS FARDEAU, PASCAL RICHOMME ET HÉLÈNE GUINAUDEAU[1]

Centre d'études des plantes médicinales, Unité de formation et de recherche des Sciences médicales et pharmaceutiques, 16 Bd. Daviers, 49045 Angers CEDEX, France

ET

ALAIN FOURNET

Office de la recherche scientifique et technique d'outre-mer — Institut bolivien de biologie d'altitude CP 824, La Paz, Bolivie[2]

Reçu le 16 décembre 1992

JEAN-MICHEL OGER, AGNÈS FARDEAU, PASCAL RICHOMME, HÉLÈNE GUINAUDEAU et ALAIN FOURNET. Can. J. Chem. **71**, 1128 (1993).

Une série de 11 alcaloïdes, dérivés d'un nouveau type de benzyltétrahydroisoquinoléine de substitution originale, a été isolée de l'écorce de tronc d' *Aniba canelilla* H.B.K. (Lauraceae). L'examen de ces composés, par plusieurs techniques spectroscopiques de résonance magnétique nucléaire (^{1}H, ^{13}C, nOe différence, COSY H–H et C–H, COLOC) a permis d'identifier : quatre benzylisoquinoléines monosubstituées sur le cycle C par un hydroxyle en position 11, la (−)-norcanelilline **2**, la (+)-canelilline **3**, l'anicanine **4** et la canelillinoxine **5**; deux tétrahydroprotoberbérines monosubstituées sur le cycle D en position 9, la (−)-anibacanine **6** et la (+)-manibacanine **8**; deux tétrahydroprotoberbérines monosubstituées sur le cycle D en position 11, la (−)-pseudoanibacanine **7** et la (+)-pseudomanibacanine **9**; et trois protoberbérines de la même série que les précédentes avec un substituant méthylique en position 8α ou 8β, la (−)-α-8-méthylpseudoanibacanine **10**, la (−)-β-8-méthylpseudoanibacanine **11** et la (−)-α-8-méthylanibacanine **12**. L'examen de l'ensemble des alcaloïdes isolés permet d'envisager chez *A. canelilla* l'existence de deux systèmes enzymatiques distincts, l'un permettant la bioconversion des alcaloïdes de type réticuline et coclaurine en proaporphines et aporphines classiques, l'autre conduisant à la biogenèse des protoberberines de type anibacanine et psuedoanibacanine à partir des benzyltétrahydroisoquinoléines de type canelilline.

JEAN-MICHEL OGER, AGNÈS FARDEAU, PASCAL RICHOMME, HÉLÈNE GUINAUDEAU, and ALAIN FOURNET. Can. J. Chem. **71**, 1128 (1993).

Eleven benzyltetrahydroisoquinoline alkaloids, with an original substitution pattern, were isolated from the stem bark of *Aniba canelilla* H.B.K. (Lauraceae). Structural studies of these compounds including ^{1}H, ^{13}C, nOe difference, COSY H–H and C–H, and COLOC nuclear magnetic resonance spectroscopy led to the identification of four benzylisoquinolines, monosubstituted on ring C with an hydroxyl at C-11, (−)-norcanelilline **2**, (+)-canelilline **3**, anicanine **4**, and canelillinoxine **5**; two tetrahydroprotoberberines monosubstituted on ring D at C-9, (−)-anibacanine **6** and (+)-manibacanine **8**; two tetrahydroprotoberberines monosubstituted on ring D at C-11, (−)-pseudoanibacanine **7** and (+)-pseudomanibacanine **9**; and three protoberberines with the same substitution pattern on rings A and D with a methyl substituent at the 8α or 8β position, (−)-α-8-methylpseudoanibacanine **10**, (−)-β-8-methylpseudoanibacanine **11**, and (−)-α-8-methylanibacanine **12**. An examination of all isolated alkaloids suggests the existence of two enzymatic systems in *A. canelilla*. In the first enzymatic system, reticuline- and coclaurine-type alkaloids are involved in the bioconversion of classical proaporphine and aporphine alkaloids. In the second system, canelilline-type alkaloids are intermediate in biosynthesis of anibacanine and pseudoanibacanine protoberberine alkaloids.

Introduction

Poursuivant l'étude des drogues végétales à activité antiparasitaire (1, 2), nous nous sommes intéressés à l'étude des constituants alcoloïdiques d'une Lauracée bolivienne, *Aniba canelilla* H.B.K. Cette espèce arborescente, originaire des régions tropicales de la Bolivie, possède un bois apprécié localement pour sa résistance aux attaques parasitaires ainsi que pour sa dureté.

Le genre *Aniba*, largement répandu en Amérique du Sud, comprend 41 espèces répertoriées. Ces espèces sont classées en plusieurs groupes et sous-groupes en fonction de l'anatomie des anthères et de l'épiderme inférieur des feuilles.

Aniba canelilla et *A. ferrea*, deux espèces du groupe des *Macroporantherae* (3) se différencient des autres espèces d'*Aniba* par l'histologie de leur tronc qui se rapproche de celle du genre *Licaria*.

Un examen préliminaire de la fraction basique des écorces de tronc a permis l'isolement et l'identification de la (+)-noranicanine **1** (4). L'originalité de cette benzyltétrahydroisoquinoléine réside dans la présence d'un cycle C monosubstitué en *meta*. La structure inédite de ce nouvel alcaloïde, confirmée par synthèse totale, permet d'envisager l'existence d'une nouvelle série de dérivés isoquinoléiques.

La poursuite de l'étude de contenu alcaloïdique des écorces de tronc d'*A. canelilla* a conduit à l'identification de 20 alcaloïdes dont 11 sont apparentés à la noranicanine **1**. Les neuf composés connus sont cinq benzyltétrahydroisoquinoléines ((+)-réticuline, (−)-coclaurine, (+)-*N*-méthylcoclaurine, armépavine et (−)-norjuziphine), une proaporphine ((−)-glaziovine) et trois aporphines ((+)-apoglaziovine, (+)-norisocorydine et (+)-isoboldine). Ils ont été identifiés par comparaison de leurs données spectrales avec celles décrites dans la bibliographie et, quand cela a été possible, avec un échantillon authentique.

1. Auteur auquel adresser toute correspondance.

2. Adresse actuelle : Laboratoire de pharmacognosie, Laboratoire associé au CNRS, Faculté de pharmacie, rue J.B. Clément, 92296 Châtenay-Malabry CEDEX, France.

Can. J. Chem. Downloaded from www.nrcresearchpress.com by 213.200.69.106 on 09/08/12
For personal use only.

Can. J. Chem. Downloaded from www.nrcresearchpress.com by 213.200.69.106 on 09/08/12
For personal use only.

Résultats et discussion

La (−)-norcanelilline **2**, de formule brute $C_{17}H_{19}NO_3$, présente un spectre de masse, obtenu par ionisation chimique (NH_3), avec un ion M+1 à *m/z* 286 et un fragment intense à *m/z* 178. Le spectre de masse en impact électronique présente un pic moléculaire très faible (0,15%) et le pic de base à *m/z* 178 dû à la rupture de la liaison benzylique. La masse de ce fragment indique la présence d'un noyau isoquinoléique disubstitué par un hydroxyle et un méthoxyle et porteur d'une fonction amine secondaire, le singulet de trois protons caractéristique d'une fonction *N*- méthyle étant absent du spectre de rmn ^1H (cf. tableau 1). La présence d'un fragment à *m/z* 107 suggère l'existence d'un groupement benzylique monohydroxylé. La séquence de substitution des noyaux aromatiques, comme dans le cas de la noranicanine **1**, est aisément déduite de l'étude des principaux signaux du spectre de rmn ^1H. En effet le spectre de rmn du proton de la norcanelliline **2** présente de grandes similitudes avec celui de la noranicanine **1**, en particulier en ce qui concerne les signaux dûs aux protons du

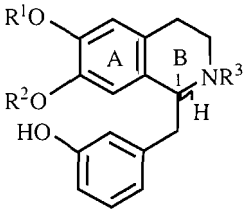

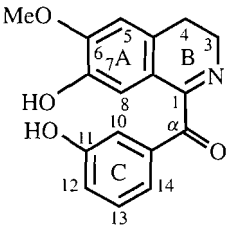

1 $R^1 = R^2 = Me$, $R^3 = H$, *1R*
2 $R^1 = Me$, $R^2 = R^3 = H$, *1S*
3 $R^1 = R^3 = Me$, $R^2 = H$, *1S*
4 $R^1 = R^2 = R^3 = H$

5

noyau benzylique (pseudotriplet dû au proton en 13 à δ 7,14 ppm), ainsi que la position dans les champs faibles du signal donné par le proton en 1. La présence d'un seul singulet de trois protons à δ 3,82 ppm confirme le type de substitution du cycle. A. Le singulet dû au proton en 8 (δ 6,77 ppm) étant déplacé vers les champs faibles, la fonction hydroxyle doit être portée par le carbone 7 alors que le groupe méthoxyle doit être en 6. Les positions des substituants du cycle A sont confirmées par deux expériences de type COSY C–H et COLOC. La première attribue les déplacements chimiques des protons et des carbones directement liés (cf. tableaux 1 et 2), et la seconde met notamment en évidence des corrélations ^3J entre : le carbone 1 à 56,4 ppm et le proton à 6,77 ppm (H-8); les protons du méthoxyle à 3,82 ppm et le carbone qui le porte à 145,7 ppm; ce même carbone et le proton à 6,77 ppm (H-8). Ces données permettent de positionner sans ambiguïté le méthoxyle en 6 et donc l'hydroxyle en 7. La (−)-norcanelilline correspond donc à la 1-(3′-hydroxybenzyl)-6-méthoxy-7-hydroxy-1,2,3,4,-tétrahydroisoquinoléine. L'identité des données spectrales de la norcanelilline et du composé **2** obtenu par synthèse totale confirme cette structure (5).

L'attribution complète du spectre de rmn ^{13}C (cf. tableau 2) a été déduite d'une expérience de type DEPT et des expériences de corrélation carbone–proton à deux dimensions précédemment citées.

L'enregistrement de la courbe de dichroïsme circulaire de la noranicanine **1** (4) nous ayant montré que les règles empiriques énoncées par Leet et al. (6) semblaient respectées dans cette nouvelle série de benzyltétrahydroisoquinoléines, nous proposons une configuration 1-*S* de la (−)-norcanelilline sur la base de la mesure de son pouvoir rotatoire.

La (+)-canelilline **3** de formule brute $C_{18}H_{21}NO_3$ présente un spectre de masse très voisin de celui de la (−)-norcanelilline **2** avec un pic moléculaire, supérieur de 14 uma, très faible à *m/z* 299 (0,06%) et un pic de base à *m/z* 192, également supérieur de 14 uma, accompagné des ions caractéristiques d'un noyau tétrahydroisoquinoléique à *m/z* 177 et 162 (7).

La présence d'un pic à *m/z* 107 est compatible avec l'existence d'un noyau benzylique monosubstitué par un hydroxyle. Le spectre de rmn ^1H (cf. tableau 1) de la (+)-canelilline **3** met en évidence la présence d'une fonction *N*-méthyle (δ 2,47 ppm) et d'un méthoxyle (δ 3,84 ppm). Les protons aromatiques résonnent à δ 6,55 (H-5), 6,61 ppm (H-10), H-12 et H-14) et à δ 7,08 ppm (pseudotriplet, intégrant pour un proton, caractéristique du proton en 13). Un singulet d'un proton à δ 6,35 ppm correspond au proton en 8, son déplacement chimique caractéristique indique que le carbone 7 est porteur d'une fonction hydroxyle.

Le pouvoir rotatoire positif ($[\alpha]_D$ +43) suggère une configuration absolue 1-*S*.

L'ensemble des attributions des résonances du spectre de rmn ^{13}C (cf. tableau 2) a été réalisé par analyse du spectre GASPE et par corrélation directe hétéronucléaire.

La dernière benzyltétrahydroisoquinoléine isolée au cours de ce travail est l'anicanine **4** de formule brute $C_{19}H_{23}NO_3$. Présent à l'état de trace, cet alcaloïde n'a été isolé qu'en mélange avec l'armépavine dans une proportion de 1 : 2. Le spectre de masse du mélange (ic) ne permet pas de déceler la présence de deux composés, en effet les deux alcaloïdes sont de même nature et ne diffèrent que par la place de l'hydroxyle sur le cycle C. Les ions fragments observés, de mêmes masses, ne peuvent donc différer que par leur abondance relative. Les pics les plus importants sont observés à *m/z* 314 (100%) correspondant à l'ion M+1, et à *m/z* 206 (40%). La masse de ce dernier ion indique que les deux alcaloïdes sont porteurs sur le noyau isoquinoléique d'une fonction *N*-méthyle et de deux méthoxyles. La présence d'un pic de faible intensité à *m/z* 107 (3%) permet de déduire la monosubstitution du cycle C, dans les deux molécules, par un hydroxyle phénolique.

Les signaux dûs aux deux alcaloïdes sont observables sur le spectre de rmn du proton. Les données spectrales (rmn ^1H, spectrométrie de masse) de l'alcaloïde en mélange avec l'armépavine sont en tous points identiques à ceux d'un échantillon d'anicanine **4** obtenu par hémisynthèse (voir partie expérimentale).

Le quatrième alcaloïde nouveau décrit dans ce travail est un dérivé phénolique benzylisoquinoléique oxydé et a été nommé la canelillinoxine **5**. La formule brute $C_{17}H_{15}NO_4$ est déduite du spectre de masse qui présente un pic moléculaire à *m/z* 297 (32%) et un pic de base à *m/z* 269 (M − 28) flanqué d'un pic important à *m/z* 268 (90%) (M − 29) qui correspond à la perte d'un groupement C=O; un ion à *m/z* 121 est dû à une fragmentation entre le carbone 1 et le carbone α et correspond à la partie oxybenzylique de la molécule, indiquant la monosubstitution par une fonction hydroxyle du noyau benzénique. Le spectre infrarouge

Can. J. Chem. Downloaded from www.nrcresearchpress.com by 213.200.69.106 on 09/08/12
For personal use only.

TABLEAU 1. Données spectrales de rmn ^{1}H des composés **2**–**5**[a]

H n°	**2**[b,c]	**3**[b,d]	**4**[b,e]	**5**[b,e]
1	4,05 dd $J_{1-\alpha_1}$ = 3,0 $J_{1-\alpha_2}$ = 10,0	3,77 t $J_{1-\alpha}$ = 6,0	4,00 dd $J_{1-\alpha_1}$ = 4,0 $J_{1-\alpha_2}$ = 9,0	
3α	2,75 m*	2,83 m*	3,00 m*	3,85 t
3β	3,16 m*	3,21 m*	3,40 m*	J_{3-4} = 7,5
4α	2,75 m	2,61 m°	2,74 m°	2,79 t
4β	2,75 m	2,83 m°	3,00 m°	J_{4-3} = 7,5
5	6,54 s	6,55 s	6,57 s	6,72 s
8	6,77 s	6,35 s	5,86 s	6,92 s
α_1	3,16 m′	3,08 dd′ J_{gem} = 14,0	3,40 m′	
α_2	2,75 m′	2,83 m′	2,74 m′	
10	6,70 m	6,61 m	6,83 s él	7,38 s él
12	6,70 m	6,61 m	6,72 d él	7,01 d él
13	7,14 dd J_{12-13} = 7,5 J_{13-14} = 7,5	7,08 dd J_{12-13} = 8,0 J_{13-14} = 8,0	7,05 dd J_{12-13} = 8,0 J_{13-14} = 8,0	7,28 dd J_{12-13} = 8,0 J_{13-14} = 8,0
14	6,70 m	6,61 m	6,46 d	7,51 d
2-NMe		2,47 s	2,56 s	
6-OMe	3,82 s	3,84 s	3,83 s	3,95 s
7-OMe			3,46 s	

[a]Les déplacements chimiques avec le même exposant sont interchangeables.
[b]$CDCl_3$.
[c]300 MHz.
[d]360 MHz.
[e]270 MHz.

TABLEAU 2. Données spectrales de rmn ^{13}C des composés **2**–**4**[a]

C n°	**2**[b,c]	**3**[b,d]	**4**[b,c]
1	56,4	64,4	64,6
2-NMe		42,0	41,0
3	40,3	46,3	45,4
4	28,7	24,4	23,4
4a	125,9	124,7	123,3
5	111,2	110,6	111,0
6	145,7	145,3	147,9
7	143,9	143,4	146,6
8	112,3	113,4*	111,0
8a	129,8	129,6	126,1
α	41,7	41,5	41,3
9	139,5	141,2	139,8
10	116,1	116,3	116,6
11	157,4	156,1	156,9
12	114,5	113,7*	113,9
13	130,0	129,3	129,4
14	120,4	121,5	121,7
6-OMe	55,8	55,8	55,8
7-OMe			55,4

[a]Les déplacements chimiques avec le même exposant sont interchangeables.
[b]$CDCl_3$.
[c]67 MHz.
[d]50 MHz.

présente une bande à 1670 cm^{-1} caractéristique d'une céto-imine (8). La présence, sur le spectre de rmn ^{1}H (cf. tableau 1), de deux pseudotriplets de deux protons chacuns à 2,79 et 3,85 ppm (J = 7,5 Hz) indique la nature dihydroisoquinoléique de la molécule; le déplacement vers les champs faibles du deuxième triplet est caractéristique de la présence de la céto-imine (8). Dans la région des protons aromatiques, deux singulets (δ 6,72 ppm et 6,92 ppm) sont dûs aux protons en 5 et 8 respectivement. La multiplicité des quatre autres signaux (δ 7,01 ppm d élargi, δ 7,28 ppm dd, δ 7,51 ppm d et δ 7,38 ppm s élargi) indique que le cycle C porte l'hydroxyle phénolique en position *meta* de la liaison benzylique comme pour les alcaloïdes **1**, **2**, **3**, et **4**. Le déplacement vers les champs faibles du signal du proton en 8 (δ 6,92 ppm, s) ainsi que de celui donné par le proton en 14 (δ 7,51 ppm, d) est dû également à la présence de la céto-imine. La canelillinoxine **5** est donc un dérivé oxydé de la (−)-norcanelilline **2**.

Les sept alcaloïdes suivants appartiennent tous au groupe des protoberbérines.

L'alcaloïde **6**, la (−)-anibacanine, et l'alcaloïde **7**, la (−)-pseudoanibacanine, possèdent la même formule brute, $C_{18}H_{19}NO_3$, déduite de leur spectre de masse. Dans les deux cas, on observe un pic moléculaire important à m/z 297 et le pic de base à m/z 178, accompagné d'un pic intense à m/z 176, résultant de la rupture des liaisons benzyliques du noyau C par un mécanisme de type rétro Diels–Alder. Ces deux derniers fragments sont indicatifs de la substitution de la partie tétrahydroisoquinoléique des deux molécules par une fonction hydroxyle et une fonction méthoxyle. La présence d'un ion de masse m/z 120 dans les deux spectres suggère une monosubstitution du cycle D par un hydroxyle phénolique.

Le spectre de rmn du proton des deux molécules (cf. tableau 3) présente les caractéristiques générales des tétrahydroprotoberbérines, en particulier les deux doublets de un proton (J_{gem} = 15,5 Hz) dûs au groupement

TABLEAU 3. Données spectrales de rmn ^{1}H des composés **6–11**[a]

H n°	**6**[b,d]	**7**[b,d]	**8**[b,d]	**9**[b,d]	**10**[b,d]	**10**[c,d]	**11**[b,d]	**11**[c,d]	**12**[b,d]	**12**[c,d]
1	6,83 s	6,80 s	6,74 s	6,72 s	6,77 s	6,70 s	6,82s	6,77 s	6,79 s	6,70 s
4	6,60 s	6,57 s	6,62 s	6,60 s	6,57 s	6,67 s	6,60 s	6,69 s	6,59 s	6,68 s
5α	2,66 m	2,60 m	3,18 m	3,12 m	2,83 m	2,80 m	2,43 m	2,66 m	3,03 m	2,80 m
5β	3,16 m	3,14 m	2,67 m	2,62 m	2,83 m	2,80 m	3,06 m	2,93 m	3,03 m	2,80 m
6α	2,66 m	2,60 m	3,18 m	3,12 m	2,83 m	2,80 m	2,78 m	2,32 m	3,03 m	2,80 m°
6β	3,16 m	3,14 m	2,67 m	2,62 m	2,83 m	2,80 m	3,38 m	3,37 m	3,03 m	2,96 m°
8α	3,49 d	3,61 d	4,21 d	3,94 d			3,69 m	3,57 m		
	J_{gem} 15,5	J_{gem} 14,5	J_{gem} 15,5	J_{gem} 15,5			J_{8-8Me} 6,5	J_{8-8Me} 6,0		
8β	4,19 d	3,93 d	3,51 d	3,63 d	4,11 q	4,04 q			4,35 q	4,21 q
					J_{8-8Me} 7,0	J_{8-8Me} 6,5			J_{8-8Me} 6,5	J_{8-8Me} 6,5
9		6,90 d		6,91 d	6,91 d	6,94 d	7,07 d	7,06 d		
		J_{9-10} 8,0		J_{9-10} 8,0	J_{9-10} 8,5	J_{9-10} 8,5	J_{9-10} 8,5	J_{9-10} 8,5		
10	6,57 d	6,67 dd	6,57 d	6,66 dd	6,59 d él	6,59 dd	6,69 dd	6,65 dd	6,54 d	6,63 d
	J_{10-11} 8,0	J_{10-12} 2,0	J_{10-11} 8,0	J_{10-12} 2,5		J_{10-12} 2,5	J_{10-12} 2,5	J_{10-12} 2,0	J_{10-11} 8,0	J_{10-11} 8,0
11	7,03 dd		7,02 dd						7,02 dd	6,99 dd
	J_{11-12} 8,0		J_{11-12} 8,0						J_{11-12} 8,0	J_{11-12} 8,0
12	6,75 d	6,62 d	6,76 d	6,64 d	6,42 s él	6,51 d	6,58 d	6,58 d	6,70 d	6,62 d
13α	3,29 dd	3,14 m	2,90 dd	2,83 dd	2,83 m	3,02 dd	3,06 m	3,15 dd	3,13 dd	3,10 dd
	$J_{13\alpha-14}$ 3,5	$J_{13\alpha-14}$ 3,5	$J_{13\alpha-14}$ 11,0	$J_{13\alpha-14}$ 10,5	$J_{13\alpha-14}$ 4,5	$J_{13\alpha-14}$ 4,0		$J_{13\alpha-14}$ 3,0	$J_{13\alpha-14}$ 4,5	$J_{13\alpha-14}$ 4,5
	J_{gem} 16,0	J_{gem} 15,5	J_{gem} 16,0	J_{gem} 16,0		J_{gem} 16,5		J_{gem} 16,0	J_{gem} 16,0	J_{gem} 16,0
13β	2,87 dd	2,79 dd	3,31 dd	3,23 dd	2,83 m	2,59 dd	2,78 m	2,66 m	2,79 dd	2,63 dd
	$J_{13\beta-14}$ 11,0	$J_{13\beta-14}$ 11,5	$J_{13\beta-14}$ 4,0	$J_{13\beta-14}$ 4,0	$J_{13\beta-14}$ 11,0	$J_{13\beta-14}$ 11,0			$J_{13\beta-14}$ 11,0	$J_{13\beta-14}$ 11,0
14	3,58 dd	3,53 dd	3,63 dd	3,57 dd	4,15 dd	4,12 dd	3,69 m	3,57 m	4,23 dd	4,19 dd
2-OMe			3,87 s°	3,85 s°						
3-OMe	3,88 s	3,84 s	3,89 s°	3,88 s°	3,84 s	3,81 s	3,87 s	3,83 s	3,87 s	3,82 s
8α-Me					1,34 d	1,29 d			1,39 d	1,31 d
8β-Me							1,52 d	1,44 d		

[a]Les déplacements chimiques avec le même exposant sont interchangeables.
[b]$CDCl_3$.
[c]CD_3CN.
[d]270 MHz.

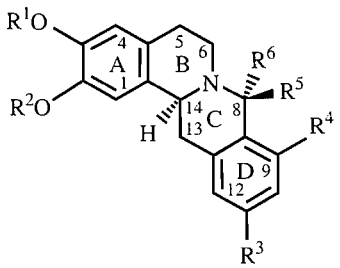

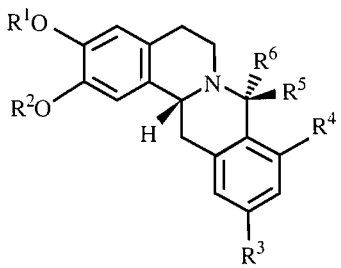

6 R^1 = Me, $R^2 = R^3 = R^5 = R^6$ = H, R^4 = OH
7 R^1 = Me, $R^2 = R^4 = R^5 = R^6$ = H, R^3 = OH
10 $R^1 = R^6$ = Me, $R^2 = R^4 = R^5$ = H, R^3 = OH
11 $R^1 = R^5$ = Me, $R^2 = R^6 = R^4$ = H, R^3 = OH
12 $R^1 = R^6$ = Me, $R^2 = R^5 = R^3$ = H, R^4 = OH

8 $R^1 = R^2$ = Me, $R^3 = R^5 = R^6$ = H, R^4 = OH
9 $R^1 = R^2$ = Me, $R^4 = R^5 = R^6$ = H, R^3 = OH

méthylénique en 8. Les déplacements chimiques de ces protons à δ 3,49 et 4,19 ppm dans le cas de la (−)-anibacanine **6** indiquent une substitution du carbone 9; ceux à δ 3,61 et 3,93 ppm dans le cas de la (−)-pseudoanibacanine **7** suggèrent la non substitution de ce même carbone (9, 10). Le groupement méthoxyle résonne dans des champs équivalents pour les deux alcaloïdes, vers 3,8 ppm. Les déplacements chimiques des protons en 1 et en 4 sont proches sur les deux spectres à δ ~6,8 ppm et ~6,6 ppm respectivement. La différence de 0,23 ppm entre ces deux déplacements chimiques permet de placer le groupement méthoxyle en 3 et l'hydroxyle phénolique en 2 (10). Ces éléments sont confirmés par une expérience de type COSY retardée qui, dans un premier temps, permet d'identifier des couplages benzyliques d'une part entre les signaux des proton en 4 et en 5 et d'autre part entre le singulet aromatique du proton en 1 et le doublet dédoublé du proton en 14. La corrélation longue-distance observée entre le singulet de 3 protons (OCH_3) vers 3,8 ppm et celui vers 6,6 ppm autorise alors la localisation définitive de l'hydroxyle en position 2 et du méthoxyle en position 3 sur le cycle A. Les deux spectres diffèrent par la position des signaux dûs aux protons du cycle D ce qui confirme la position différente de l'hydroxyle phénolique sur ce cycle.

Le spectre de rmn ^{1}H de la (−)-anibacanine **6** présente à δ 6,57 ppm et 6,75 ppm deux doublets (J = 8,0 Hz) et un

Can. J. Chem. Downloaded from www.nrcresearchpress.com by 213.200.69.106 on 09/08/12
For personal use only.

Can. J. Chem. Downloaded from www.nrcresearchpress.com by 213.200.69.106 on 09/08/12
For personal use only.

TABLEAU 4. Données spectrales de rmn ^{13}C des composés **6–12**[a]

C n°	**6**[b,f]	**7**[c,g]	**8**[d,g]	**9**[c,g]	**10**[e,g]	**11**[e,g]	**12**[e,g]
1	111,5	111,7	111,3″	111,0″	113,2	112,7	113,1
2	144,0	144,2	147,5*	147,0	145,1	145,0	145,1
3	145,7	145,4	147,4*	147,0	146,5	146,5	146,4
4	110,8	110,8	108,5″	108,3″	112,4	112,1	112,4
4a	125,1	125,7	126,7	126,4*	126,8	127,1	126,6
5	28,1	29,0	28,9	28,7	30,1	30,3	30,0
6	51,3	51,6	51,4	51,1	48,0	48,3	47,8
8	53,3	58,1	53,5	57,9	59,4	60,0″	55,5
8a	120,9	125,2	121,7	124,8*	132,5	132,0*	121,1
9	152,9	127,0	152,0	126,7	128,8	128,5	153,8
10	111,6	113,7	112,2″	113,5	114,1	114,3	112,9
11	126,6	155,8	126,8	155,9	155,7	155,5	127,5
12	119,5	115,1	120,9	114,8	115,3	115,1	121,1
12a	135,2	135,5	136,2	135,1	136,1	137,1	136,3
13	35,8	36,8	36,7	36,6	36,7	37,9	36,0
14	58,7	59,4	59,0	59,2	50,7	59,5″	50,6
14a	129,4	130,4	129,4	129,6	132,5	131,9*	132,7
2-OMe			56,0°	55,7°			
3-OMe	55,5	55,8	55,8°	55,4°	56,2	55,8	56,5
8-Me					18,1	22,5	14,9

[a]Les déplacements chimiques avec de même exposant sont interchangeables.
[b]$CDCl_3$ + MeOD.
[c]$CDCl_3$ + C_5D_5N.
[d]$CDCl_3$.
[e]CD_3CN.
[f]125 MHz.
[g]67 MHz.

pseudotriplet à δ 7,03 ppm (J = 8,0 Hz) ce qui indique que l'hydroxyle phénolique est porté par le carbone 9 ou 12.

L'analyse des résultats d'une expérience rmn de type nOe (voir partie expérimentale) met en évidence en particulier une proximité spatiale du proton en 12 (δ 6,75 ppm) et d'un des protons en 13 (δ 3,29 ppm), ce qui est en faveur de la substitution du carbone 9 par l'hydroxyle phénolique comme l'indique la position des signaux des protons méthylèniques en 8. La confirmation de cette substitution est apportée par l'analyse de la corrélation hétéronucléaire C–H longue distance (COLOC) qui met en évidence un couplage ^3J entre le carbone 13 (δ 35,8 ppm) et le proton en 12 (δ 6,75 ppm). Les attributions précises des signaux du spectre de rmn ^1H relatives aux protons 5, 6, 8 et 13 de cette tétrahydroprotoberbérine **6** et des composés **7**, **8**, **9**, **10**, **11**, **12** ci-après décrits, ont été réalisées sur la base de la mesure de leurs déplacements chimiques et constantes de couplage, conformément aux travaux publiés par Tourwé et al. (11).

L'attribution complète des signaux de rmn ^{13}C (cf. tableau 4) a été réalisée à l'aide des spectres de corrélation hétéronucléaire directe et longue distance.

En ce qui concerne la (−)-pseudoanibacanine **7**, les protons du cycle D résonnent sous forme d'un systéme ABX à 6,90 (d, J_o = 8,0 Hz), 6,67 (dd, J_o = 8,0 Hz; J_m = 2,0 Hz) et 6,62 (d, J_m = 2,0 Hz). L'hydroxyle phénolique est porté par le carbone 10 ou par le carbone 11. L'expérience de corrélation homonucléaire longue distance (réalisée dans $CDCl_3$–C_5D_5N) montre un couplage entre les deux protons méthyléniques en 8 et le proton en 9 (δ 6,90 ppm) ainsi qu'entre les protons méthylèniques en 13 et le proton en 12 (δ 6,62 ppm); ces résultats permettent de placer l'hydroxyle en position 11.

L'attribution complète des signaux de rmn ^{13}C (cf. tableau 4) a été réalisée à l'aide des spectres de corrélation C–H directe en longue distance.

La configuration absolue des protoberbérines pouvant, selon la règle empirique énoncée par Kametani et Ihara (12), être reliée au signe du pouvoir rotatoire de la molécule, nous proposons la configuration absolue 14-*S* pour la (−)-anibacanine **6** et la (−)-pseudoanibacanine **7**.

Les deux tétrahydroprotoberbérines suivantes, la (+)-manibacanine **8** et la (+)-pseudomanibacanine **9**, présentent des caractéristiques spectrales très proches de celles des deux alcaloïdes précédents. En effet, les spectres de masse de **8** et de **9** présentent un ion moléculaire à m/z 311, supérieur de 14 uma à ceux des composés **6** et **7**, correspondant à la formule brute $C_{19}H_{21}NO_3$. Le pic de base à m/z 190 accompagné d'un pic important à m/z 192 est également de 14 uma supérieur au pic correspondant observé pour la (−)-anibacanine **6** et la (−)-pseudoanibacanine **7**, le pic à m/z 120 étant également présent. Ces valeurs suggèrent la présence de deux méthoxyles au lieu d'un hydroxyle et d'un méthoxyle sur la partie isoquinoléique des deux composés, la substitution du cycle D restant inchangée. Cette hypothèse est confirmée, d'une part par la présence de deux signaux correspondant à deux méthoxyles sur le spectra de rmn du proton (cf. tableau 3) des deux alcaloïdes, et d'autre part par la différence des déplacements chimiques (Δδ) des protons en 1 et 4 qui est ici de 0,12 ppm (valeur caractéristique d'une telle substitution (9)). Les autres signaux ne sont pas modifiés. Le pouvoir rotatoire de ces deux alcaloïdes étant positif, la (+)-manibacanine **8** et la (+)-pseudomanibacanine **9** possèderaient une configuration 14 *R* (12).

Les trois dernières tétrahydroprotoberbérines isolées sont des dérivés, méthylés en 8, de la (−)-anibacanine **6** et de la (−)-pseudoanibacanine **7**.

Can. J. Chem. Downloaded from www.nrcresearchpress.com by 213.200.69.106 on 09/08/12
For personal use only.

Les spectres de masse des trois nouveaux composés **10**, **11** et **12** présentent un schéma de fragmentation similaire. Le pic moléculaire à *m/z* 311 est de faible intensité. Le pic de base à *m/z* 296 correspond à la perte d'un groupement méthyle. Les deux autres fragments de fréquence non négligeable à *m/z* 178 et à *m/z* 134, observables sur le spectre, résultent de la rupture des liaisons benzyliques et correspondent au fragment isoquinoléique de la molécule pour le premier, et à la partie benzylique de la molécule portant le groupement méthyle du carbone 8 pour le deuxième. L'ensemble de ces fragmentations montre que ces trois alcaloïdes portent le même type de substitution que les alcaloïdes **6** et **7**.

Les spectres de rmn du proton de la (−)-α-8-méthylpseudoanibacanine **10** et de la (−)-β-8-méthylpseudoanibacanine **11** (cf. tableau 3) sont semblables, dans la région des protons aromatiques et des méthoxyles, au spectre de la (−)-pseudoanibacanine **7**. De plus, un doublet de trois protons (δ ~1,4 ppm, *J* ~6,5 Hz) est attribuable à un groupement méthyle placé en 8 ou en 13. La présence d'un quadruplet (*J* ~6,5 Hz) correspondant à un proton géminé au groupement méthyle est observable à des champs différents sur les spectres de **10** (δ 4,11 ppm) et de **11** (δ 3,69 ppm) ce qui suggère que le groupement méthyle est porté par le carbone 8 dans des configurations différentes.

Afin d'obtenir une meilleure résolution des signaux donnés par les protons aliphatiques, le spectre de rmn ^{1}H a également été enregistré dans l'acétonitrile deutérié (cf. tableau 3). Les protons portés par les carbones 13 et 14 apparaissent, dans ce cas, sous forme de trois doublets dédoublés à δ 3,02 ppm ($J_{13\alpha,14}$ 4,0 Hz J_{gem} 16,5 Hz) et à δ 2,59 ppm ($J_{13\beta,14}$ 11,0 Hz, J_{gem} 16,5 Hz) pour les protons en 13 et à δ 4,12 ppm ($J_{13,14}$ 4,0 et 11,0 Hz) pour le proton en 14 sur le spectre de la (−)-α-8-méthylpseudoanibacanine **10**; les signaux dûs à ces protons sont plus difficilement observables sur le spectre de la (−)-β-8-méthylpseudoanibacanine **11** étant donné la superposition de ces signaux avec ceux donnés d'une part par le proton en 8 et par les protons en 5 et 6 d'autre part. Seul le doublet dédoublé dû à un des protons en 13 est clairement visible à δ 3,15 ppm ($J_{13\alpha,14}$ 3,0 Hz, J_{gem} 16,0 Hz), alors que le signal donné par le proton en 14 se superpose partiellement au signal du proton geminé au groupement méthyle en 8 à δ 3,57 ppm.

Le déplacement chimique vers les champs faibles du proton en 8 ainsi que du proton 14 dans le cas de la (−)-α-8-méthylpseudoanibacanine **10** est indicatif d'une relation *trans* de ces deux protons (13). Dans le cas de la (−)-β-8-methylpseudoanibacanine **11** ces mêmes protons résonnent à des champs plus forts indiquant une relation *cis*. Cette configuration respectivement *trans* pour le composé **10** et *cis* pour le composé **11** peut également être déduite de l'examen du spectre de rmn ^{13}C (cf. tableau 4) de chacun des deux alcaloïdes. En effet, les deux spectres diffèrent essentiellement par le déplacement chimique du carbone 14 ainsi que par celui de groupement méthyle. Il est connu que dans le cas d'une configuration *trans* ces deux carbones résonnent dans des champs légèrement plus élevés (δ 50,7 et 18,1 respectivement pour le composé **10**) que dans le cas d'une configuration *cis* (δ 59,5 et 22,5 respectivement pour le composé **11**) (13). En effet cette différence de déplacement chimique est liée au type de jonction des deux cycles du noyau quinolizidine, dans le cas du composé **10** la jonction est *cis*, alors qu'elle est *trans* dans le cas de **11** (13).

Étant donné que le pouvoir rotatoire des deux composés **10** et **11** est négatif la configuration du carbone 14 serait *S*. En effet, la synthèse des énantiomères de la *O*-méthylcorytenchirine et de la corydalydine a montré que seule la configuration du carbone 14 a une influence sur le signe du pouvoir rotatoire (14).

Les protons en 8 et en 14 de la (−)-α-8-méthylpseudoanibacanine **10** étant en relation *trans*, la configuration en 8 doit être *R*. Par contre cette relation étant *cis* dans le cas de la (−)-β-8-méthylpseudoanibacanine **11**, la configuration du carbone 8 doit être *S*.

Le spectre de rmn du proton de la (−)-α-8-méthylanibacanine **12** (cf. tableau 3), troisième tétrahydroprotoberbérine méthylée sur le carbone 8, présente un ensemble de signaux dûs aux protons aromatiques similaire à celui observé sur le spectre de la (−)-anibacanine **6**, permettant ainsi de placer l'hydroxyle phénolique du cycle D en 9. Le groupement méthyle et le proton geminé résonnent, comme dans le cas de la (−)-α-8-méthylpseudoanibacanine **10** sous forme respectivement d'un doublet à δ 1,39 ppm et d'un quadruplet à δ 4,35 ppm (*J* = 6,5 Hz). La position de ce dernier signal, la présence du doublet dédoublé dû au proton en 14 (δ 4,23 ppm $J_{13,14}$ 4,5 et 11,0 Hz), ainsi que le pouvoir rotatoire négatif, suggèrent une configuration absolue 8*R*, 14*S* pour le composé **12**. Le groupement méthyl est donc en position α.

À la suite de l'isolement de l'ensemble de ces alcaloïdes plusieurs remarques doivent être faites.

Il est tout d'abord intéressant de noter que les benzyltétrahydroisoquinoléines originales présenteraient les deux configurations possibles au niveau du carbone 1. La noranicanine **1** est de configuration 1-*R* alors que la norcanelilline **2** et son dérivé *N*-méthylé, la canelilline **3**, seraient de configuration 1-*S*.

Alors qu'une proaporphine et des aporphines dérivant des benzyltétrahydroisoquinoléines de substitution classique comme la coclaurine et la réticuline ont été isolées, aucune tétrahydroprotoberbérine tétrasubstituée (2,3,9,10 ou 2,3,10,11) n'a été isolée. Par contre, il est raisonnable de penser que les tétrahydroprotoberbérines décrites dans ce travail dérivent biogénétiquement de la (+)-noranicanine **1** (pour la (+)-manibacanine **8** et la (+)-pseudomanibacanine **9**) ou de la (−)-norcanelilline **2** (pour la (−)-anibacanine **6** et la (−)-pseudoanibacanine **7**).

L'hypothèse de la présence de deux systèmes enzymatiques différents dans *A. canelilla* peut donc être envisagée. Le premier transformant coclaurine, réticuline et leurs dérivés en aporphines, le second utilisant anicanine et canelilline comme substrat pur la biogenèse des protoberbérines (schéma 1).

Partie expérimentale

Appareillage

Les spectres uv ont été effectués sur un spectrophotomètre Hitachi U-2000. Les spectres ir ont été enregistrés sur un spectrophotomètre Perkin Elmer 580. Les pouvoirs rotatoires ont été mesurés à la longueur d'onde de la raie *D* du sodium à l'aide d'un polarimètre Schmidt–Haensch Polartronic I. Les spectres de rmn ont été effectués dans différents solvants deutériés à l'aide des spectromètres suivants : Jeol GSX 270 WB (270 MHz), Bruker AMWB 300 (300 MHz), Bruker AMWB 500 (500 MHz), Bruker AC 200 (200 MHz) et Bruker WB 360 (360 MHz).

Matériel végétal

Les écorces de tronc d'*Aniba canelilla* ont été récoltées à Fatima de Chimanes (Département du Beni, Bolivie) en 1988. Un

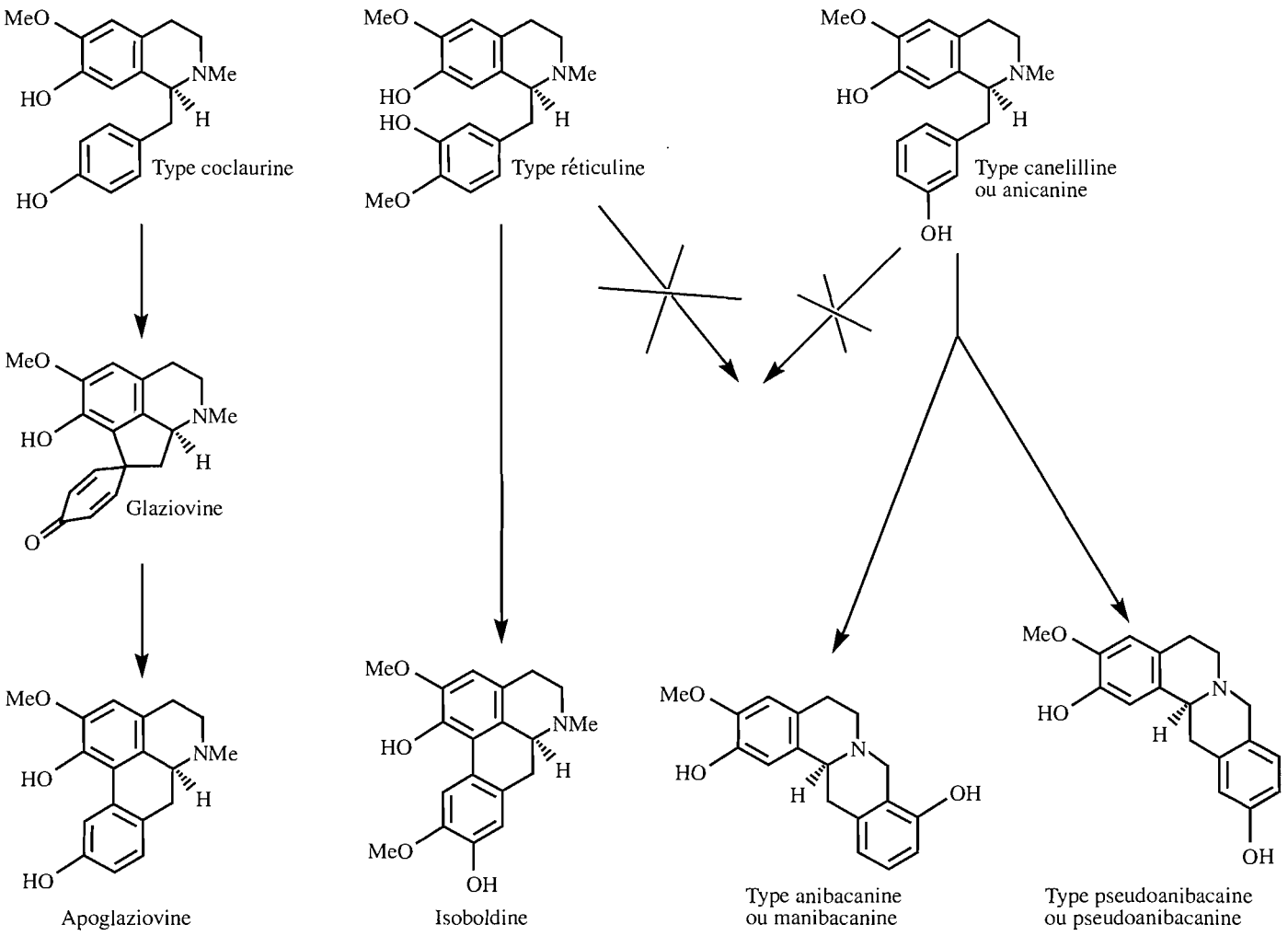

SCHÉMA 1. Hypothèse de biogenèse des alcaloïdes isoquinoléïques chez *Aniba canelilla*.

échantillon d'herbier est déposé à l'Herbier National de Bolivie à la Paz sous la référence A.F. 855.

Extraction et isolement des alcaloïdes

La drogue pulvérisée (3370 g) a été épuisée par l'hexane en milieu neutre dans un extracteur de type Soxhlet. Après élimination du solvant sous pression réduite un résidu de 58,8 g a été obtenu. Après alcalinisation par l'ammoniaque (15%), la poudre végétale a ensuite été extraite par le chloroforme dans un apareil de type Soxhlet. L'extrait brut résultant de l'évaporation partielle sous pression réduite du chloroforme a été épuisé par une solution aqueuse acide (HCl 4%). Après alcalinisation des eaux acides, les alcaloïdes ont été réextraits par le chloroforme. L'élimination du solvant sous pression réduite conduit à 34 g d'alcaloïdes. Le fractionnement des alcaloïdes totaux est réalisé sur colonnes de silice (Merck 0,040–0,063 mm) moyenne pression et ouverte, du chloroforme progressivement enrichi par du méthanol étant utilisé comme éluant. La purification des différents constituants est obtenue par ccm préparative ou par cristallisation. Ont ainsi été obtenus : (+)-réticuline (5231 mg), (−)-coclaurine (2245 mg), (+)-*N*-méthylcoclaurine (5131 mg), (−)-norjuziphine (20 mg), (−)-glaziovine (20 mg), (+)-apoglaziovine (10 mg), (+)-norisocorydine (175 mg) et (+)-isoboldine (1054 mg), (+)-noranicanine **1** (12 mg), (−)-norcanelilline **2** (373 mg), (+)-canelilline **3** (30 mg), anicanine **4** (1 mg), canelillinoxine **5** (4,5 mg), (−)-anibacanine **6** (1886 mg), (−)-pseudoanibacanine **7** (2505 mg), (+)-manibacanine **8** (5 mg), (+)-pseudomanibacanine **9** (2 mg), (−)-α-8-méthylpseudoanibacanine **10** (539 mg), (−)-β-8-méthylpseudoanibacanine **11** (40 mg), (−)-α-8-méthylanibacanine **12** (47 mg).

(−)-Norcanelilline **2**: $C_{17}H_{19}NO_3$; $[\alpha]_D$ −18 (*c* 1, $CHCl_3$); uv λ_{max} (MeOH) nm (log ε) : 226 épaulement (4,11), 283 (3,78); ir ν_{max} cm^{-1} (KBr) : 3290, 3230, 1610, 1595; rmn ^1H (cf. tableau 1); rmn ^{13}C (cf. tableau 2); smie (70 eV) *m/z* : 285 (M^+, 0,15%), 282 (5%), 179 (14%), 178 (100%), 163 (20%), 107 (3%); smic (NH_3). *m/z* : 286 ($[MH]^+$, 100%), 179 (8%), 178 (39%), 163 (8%), 107 (3%).

(+)-Canelilline **3** : $C_{18}H_{21}NO_3$; $[\alpha]_D$ +43 (*c* 0,5, MeOH); uv λ_{max} (MeOH) nm (log ε) : 223 épaulement (4,05), 281 (3,79); rmn ^1H (cf. tableau 1); rmn ^{13}C (cf. tableau 2); smie (70 eV) *m/z* : 299 (M^+, 0,06%), 193 (19%), 192 (100%), 177 (21%), 107 (3%).

Anicanine **4** : $C_{19}H_{23}NO_3$; uv λ_{max} (MeOH) nm (log ε) : 222 épaulement (4,10), 281 (3,64); rmn ^1H (cf. tableau 1); rmn ^{13}C (cf. tableau 2); smic (NH_3) *m/z* : 314 ($[MH]^+$, 100%), 206 (47%), 107 (1%).

La *N*-méthylation de la 1-(3′-benzyloxybenzyl)-6,7-diméthoxy-1,2,3,4-tétrahydroisoquinoléine (4) est réalisée par réaction avec l'aldéhyde formique en solution dans un mélange (1 : 1) de méthanol et de dichlorométhane; après refroidissement à −5°C du mélange réactionnel, l'intermédiaire iminium est réduit en amine. La débenzylation de cette amine par chauffage à 100°C dans un mélange (1 : 1) d'acide acétique et d'acide chlorhydrique conduit à l'anicanine **4**.

Canelillinoxine **5** : $C_{17}H_{15}NO_4$; uv λ_{max} (MeOH) nm (log ε) : 265 (3,78), 324 (3,58); ir ν_{max} (KBr) : 3350–3200, 1670, 1610 cm^{-1}; rmn ^1H (cf. tableau 1); smie *m/z* : 297 (M^+, 32%), 269 (100%), 268 (90%), 254 (7%), 253 (15%), 121 (47%), 93 (17%).

Can. J. Chem. Downloaded from www.nrcresearchpress.com by 213.200.69.106 on 09/08/12
For personal use only.

(−)-Anibacanine **6** : $C_{18}H_{19}NO_3$; $[\alpha]_D$ −129 (*c* 0,3, $CHCl_3$); uv λ_{max} (MeOH) nm (log ε) : 224 (4,46), 281 (4,05); rmn ^1H (cf. tableau 3); principaux effets Overhauser nucléaires (500 MHz, $CDCl_3$ + MeOD) : {H-1} : H-14 (3%), H-13α (5%); {3-OMe} : H-4 (4%); {H-4} : 3-OMe (11%), H-5α (3%); {H-5α} : H-4 (6%); {H-8α} : H-8β (7%), H-14 (2%); {H-8β} - H-8α (8%); {H-10} : H-11 (10%); {H-11} : H-10 (14%), H-12 (9%); {H-12} : H-11 (11%), H-13α (2%); {H-13α} : H-1 (5%), H-12 (2%), H-13β (8%); {H-13β} : H-13α (10%); {H-14} : H-1 (3%), H-8α (3%); rmn ^{13}C (cf. tableau 4); smie (70 eV) *m/z* : 297 (M^+, 93%), 296 (92%), 294 (12%), 282 (15%), 178 (100%), 177 (30%), 176 (96%), 163 (22%), 162 (11%), 135 (10%), 121 (16%), 120 (33%), 92 (28%), 91 (63%), 65 (13%), 57 (10%), 43 (15%), 28 (21%).

(−)-Pseudoanibacanine **7** : $C_{18}H_{19}NO_3$; $[\alpha]_D$ −31 (*c* 2, MeOH); uv λ_{max} (MeOH) nm (log ε) : 225 épaulement (3,98), 287 (3,76); rmn ^1H (cf. tableau 3); rmn ^{13}C (cf. tableau 4); smie *m/z* : 297 (M^+, 94%), 296 (87%), 294 (11%) 282 (18%), 179 (11%), 178 (100%), 177 (34), 176 (96), 163 (23), 162 (11), 121 (22), 120 (60); smic (NH_3) *m/z* : 298 ($[MH]^+$, 1,6%), 297 (11%), 296 (11%), 179 (11%), 178 (100%), 177 (34%), 176 (89%), 163 (19%), 121 (18%), 120 (45%), 91 (12%).

(+)-Manibacanine **8** : $C_{19}H_{21}NO_3$; $[\alpha]_D$ +176 (*c* 0,34, MeOH); uv λ_{max} (MeOH) nm (log ε) : 226 épaulement (4,28), 281 (3,86); rmn ^1H (cf. tableau 3); rmn ^{13}C (cf. tableau 4); smie *m/z* : 311 (M^+, 90%), 310 (85%), 296 (20%), 294 (19%), 193 (16%), 192 (96%), 191 (20%), 190 (100%), 176 (23%), 156 (11%), 127 (11%), 120 (36%), 83 (18%), 73 (12%), 71 (21%), 59 (14%), 57 (34%), 56 (25%), 55 (12%), 43 (20%).

(+)-Pseudomanibacanine **9** : $C_{19}H_{21}NO_3$; $[\alpha]_D$ +182 (*c* 0,22, MeOH); uv λ_{max} (MeOH) nm (log ε) : 227 épaulement (4,36), 282 (4,04); rmn ^1H (cf. tableau 3); rmn ^{13}C (cf. tableau 4); smie *m/z* : 311 (M^+, 73%), 310 (70%), 296 (10%), 193 (10%), 192 (66%), 191 (26%), 190 (100%), 176 (11%), 121 (10%), 120 (27%), 57 (14%), 56 (25%), 55 (12%), 43 (20%).

(−)-α-8-Méthylpseudoanibacanine **10** : $C_{19}H_{21}NO_3$; $[\alpha]_D$ −61 (*c* 1,1, MeOH); uv λ_{max} (MeOH) nm (log ε) : 224 épaulement (4,03), 286 (3,71); rmn ^1H (cf. tableau 3); rmn ^{13}C (cf. tableau 4); smie *m/z* : 311 (M^+, 14%), 310 (9%), 297 (19%), 296 (100%), 178 (52%), 134 (26%), 133 (10%), 28 (27%), 18 (38%).

(−)-β-8-Méthylpseudoanibacanine **11** : $C_{19}H_{21}NO_3$; $[\alpha]_D$ −62 (*c* 0,3, MeOH); uv λ_{max} (MeOH) nm (log ε) : 228 épaulement (3,91), 287 (3,68); rmn ^1H (cf. tableau 3); rmn ^{13}C (cf. tableau 4); smie *m/z* : 311 (M^+, 11%), 310 (10%), 297 (20%), 296 (100%), 294 (11%), 281 (10%), 178 (47%), 176 (10%), 134 (25%), 133 (13%), 129 (9%), 73 (23%), 69 (16%), 68 (23%), 67 (21%), 60 (10%), 57 (24%), 56 (13%), 55 (46%), 45 (9%), 44 (10%), 43 (37%), 42 (22%), 41 (56%), 39 (22%), 36 (22%), 32 (22%), 31 (28%), 30 (11%), 29 (30%), 28 (44%), 27 (21%), 18 (37%), 15 (15%).

(−)-α-8-Méthylanibacanine **12** : $C_{19}H_{21}NO_3$; $[\alpha]_D$ −60 (*c* 0,7, MeOH); uv λ_{max} (MeOH) nm (log ε) : 225 (398), 281 (3,61); rmn ^1H (cf. tableau 3); rmn ^{13}C (cf. tableau 4); smie *m/z* : 311 (M^+, 5%), 310 (6%), 297 (15%), 296 (100%), 178 (40%), 176 (15%), 134 (10%).

Remerciements

J.-M. Oger remercie le Conseil Général du Maine et Loire pour son soutien financier.

1. A. Fournet, B. Vagneur, P. Richomme et J. Bruneton. Can. J. Chem. **67**, 2116 (1989).
2. P. Richomme, M.-C. Godet, F. Foussard, L. Toupet, T. Sévenet et J. Bruneton. Planta Med. **57**, 552 (1991).
3. A.J.G.H. Kostermans. Recl. Trav. Bot. Néerl. **35**, 834 (1938).
4. J.-M. Oger, O. Duval, P. Richomme, J. Bruneton et H. Guinaudeau. Heterocycles, **24**, 17 (1992).
5. A. Benosman, J.-M. Oger, O. Duval et P. Richomme. C.R. Acad. Sci. Paris, Sér. II, **316**, 465 (1993).
6. J.E. Leet, S.F. Hussein, R.D. Minard et M. Shamma. Heterocycles, **19**, 2355 (1982).
7. A. Patra, C.T. Montgomery, A.J. Freyer, H. Guinaudeau, M. Shamma, B. Tantisewie et K. Pharadai. Phytochemistry, **26**, 547 (1987).
8. M.H.A. Zarga, G.A. Miana et M. Shamma. Heterocycles, **18**, 63 (1982).
9. N. Ruangrungsii, G.L. Lange et M. Lee. J. Nat. Prod. **49**, 253 (1986).
10. M. Shamma. *Dans* The isoquinoline alkaloids. *Editeurs* : A.T. Blomquist et H. Wasserman. Academic Press, New York. 1972. pp. 292–293.
11. D. Tourwé, G. Van Binst et T. Kametani. Org. Magn. Reson. **9**, 341 (1977).
12. T. Kametani et M. Ihara. J. Chem. Soc. (C), 1305 (1968).
13. T. Kametani, A. Ujiie, M. Ihara, K. Fukumoto et S.-T. Lu. J. Chem. Soc. Perkin Trans. 1, 1218 (1976).
14. H. Bruderer, J. Metzger et A. Brossi. Helv. Chim. Acta, **58**, 1719 (1975).

Can. J. Chem. Downloaded from www.nrcresearchpress.com by 213.200.69.106 on 09/08/12
For personal use only.

Electroréduction de dérivés dinitrés aromatiques. III. Rôle du sulfate de titanyle comme médiateur redox

ANNE-MARIE MARTRE

Laboratoire d'électrochimie organique, Université Blaise Pascal, Unité de recherche associée n° 434 du Centre national de la recherche scientifique, Thermodynamique et électrochimie en solution, 24 Avenue des Landais, 63177 Aubière CEDEX, France

VIRGINIA DANCIU

Universitatea "Babes-Bolyai," Facultatea de Chimie si Chimie Industrialà, Laboratorul de Electrochimie, Str. Arany Janos, nr. 11, 3400 CLUJ-NAPOCA, Romania

ET

GUY MOUSSET[1]

Laboratoire d'électrochimie organique, Université Blaise Pascal, Unité de recherche associée n° 434 du Centre national de la recherche scientifique, Thermodynamique et électrochimie en solution, 24 Avenue des Landais, 63177 Aubière CEDEX, France

Reçu le 22 décembre 1992

ANNE-MARIE MARTRE, VIRGINIA DANCIU et GUY MOUSSET. Can. J. Chem. **71**, 1136 (1993).

Une étude électrochimique du sulfate de titanyle utilisé en tant que médiateur redox de la réduction du 4,4′-dinitrodibenzyle est réalisée par polarographie et voltammétrie cyclique en milieu H_2SO_4 5 N/EtOH 50:50. Le rôle de Ti^{3+} électrogénéré intervenant comme réducteur chimique de ce substrat est également défini. Les résultats obtenus ont permis de dégager les conditions les plus favorables pour la réalisation de synthèses plus sélectives. Ainsi, lors d'électrolyses à potentiel constant en présence de $TiOSO_4$, le dérivé diaminé est obtenu très pur avec un rendement de 93% alors qu'il est de 75% sans médiateur. La réduction chimique en phase homogène du 4,4′-dinitrodibenzyle par Ti^{3+} préalablement électrogénéré est particulièrement sélective. La valeur du rapport des concentrations Ti^{3+}/dérivé dinitré conditionne la nature des produits formés. Le 4-amino-4′-nitrodibenzyle a été synthétisé avec un rendement de 70% dans le cas d'un rapport 6:1. Ses propriétés électrochimiques et spectrales sont définies. Pour des rapports supérieurs, la quantité de dérivé monoaminé diminue tandis que celle du diaminodibenzyle augmente jusqu'à atteindre 100%. Une comparaison est faite avec trois autres dérivés, les 1,5- et 1,8-dinitronaphtalènes et le 2,2′-dinitrodiphényle. Dans les mêmes conditions, le 1-amino-8-nitronaphtalène n'est pas détecté tandis que le 1-amino-5-nitronaphtalène et le 2-amino-2′-nitrodiphényle sont obtenus avec des pourcentages de 49% et 25%.

ANNE-MARIE MARTRE, VIRGINIA DANCIU, and GUY MOUSSET. Can. J. Chem. **71**, 1136 (1993).

The electrochemical behavior of titanium oxysulfate, used as a redox mediator in the reduction of 4,4′-dinitrodibenzyl, is studied in a 5 N H_2SO_4/EtOH 50:50 medium. The role played by electrogenerated Ti^{3+} ions in the chemical reduction of nitro groups is also defined. The results obtained allow the determination of the most suitable conditions leading to selective syntheses. Macroscale electrolyses at a constant potential in the presence of $TiOSO_4$ give 4,4′-diaminodibenzyl with a great purity and a higher yield (93%) than without mediator (75%). The homogeneous chemical reduction of 4,4′-dinitrodibenzyl by first electrogenerating the Ti^{3+} ions, then adding the organic substrate, is particularly selective. The nature of the reduction products depends on the [Ti^{3+}]/[dinitro derivative] ratio. The 4-amino-4′-nitrodibenzyl is synthesized in a 70% yield for a 6:1 ratio whereas the amount of diamino derivative increases and can constitute the sole reduction product for higher ratios. A comparison is made with 1,5- and 1,8-dinitronaphthalenes and 2,2′-dinitrodiphenyl. Using a 6:1 ratio, 1-amino-8-nitronaphthalene is not obtained while 45% of 1-amino-5-nitronaphthalene and 25% of 2-amino-2′-nitrodiphenyl are formed by reduction of the corresponding dinitro derivatives.

Introduction

Dans le cadre d'une étude générale concernant l'électroréduction de dérivés dinitrés aromatiques, un travail récent dans notre laboratoire a porté sur l'étude analytique de la réduction du 4,4′-dinitrodibenzyle (DNDB) en milieux aprotique ou hydroalcoolique en fonction du pH (1) ainsi qu'en présence de tensio-actifs (2). Ce dernier cas nous a permis de montrer l'importance des phénomènes d'adsorption à la surface de l'électrode.

La réduction électrochimique de dinitroarènes a fait l'objet de travaux antérieurs mentionnant tous la complexité des mécanismes et le grand nombre de produits susceptibles de se former (3–15). Afin d'améliorer la sélectivité de la réaction et plus particulièrement en vue d'obtenir des composés monoaminés, nous nous sommes intéressés à la réduction électrochimique ou chimique du 4,4′-dinitrodibenzyle et à titre de comparaison à celle de trois autres dérivés dinitrés, les 1,8- et 1,5-dinitronaphtalènes et le 2,2′-dinitrodiphényle en présence d'un médiateur.

Une première partie, à caractère analytique, a pour but de mieux connaître le rôle du sulfate de titanyle ($TiOSO_4$) choisi comme médiateur redox Ti^{3+}/Ti^{4+}. Ce dernier a été employé antérieurement pour la synthèse du 1,8-diaminonaphtalène (16). Nous avons envisagé la réduction de $TiOSO_4$ et celle du DNDB d'abord séparément puis en mélange et enfin l'examen, en fonction du temps, de l'évolution du DNDB en présence de l'ion Ti^{3+} électrogénéré.

L'étude a été faite dans les conditions de milieu identiques à celles des électrolyses à potentiel constant en vue de la synthèse d'amines, c'est-à-dire principalement H_2SO_4 5 N/EtOH (50:50) à 60°C. Les milieux $HClO_4$/EtOH et H_2SO_4

1. Auteur auquel la correspondance doit être adressée.

Can. J. Chem. Downloaded from www.nrcresearchpress.com by 213.200.69.106 on 09/08/12
For personal use only.

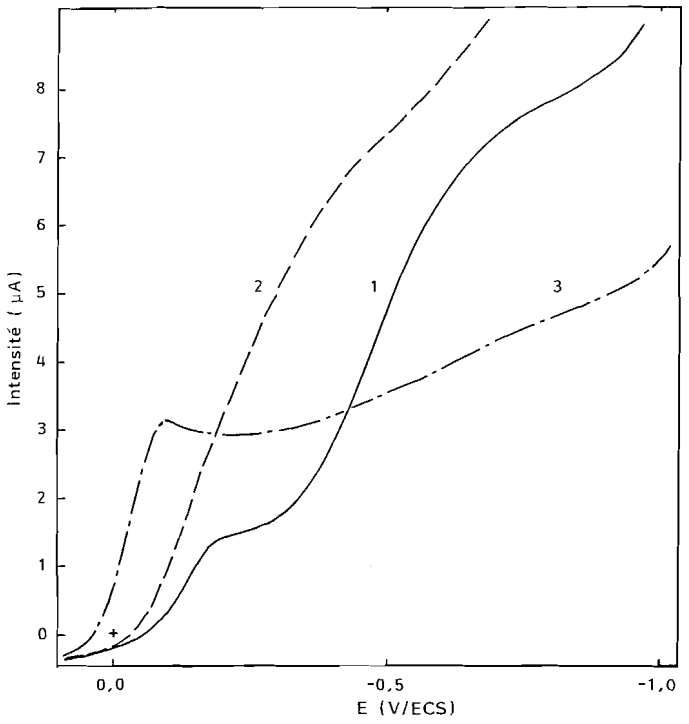

FIG. 1. Polarogrammes de réduction à 60°C. (1) $TiOSO_4$ ($3{,}3 \times 10^{-3}$ M) en milieu H_2SO_4(5 N)/EtOH 50 : 50; (2) $TiOSO_4$ ($3{,}3 \times 10^{-3}$ M) en milieu H_2SO_4(5 N); (3) DNDB (1×10^{-4} M) en milieu H_2SO_4(5 N)/EtOH 50 : 50.

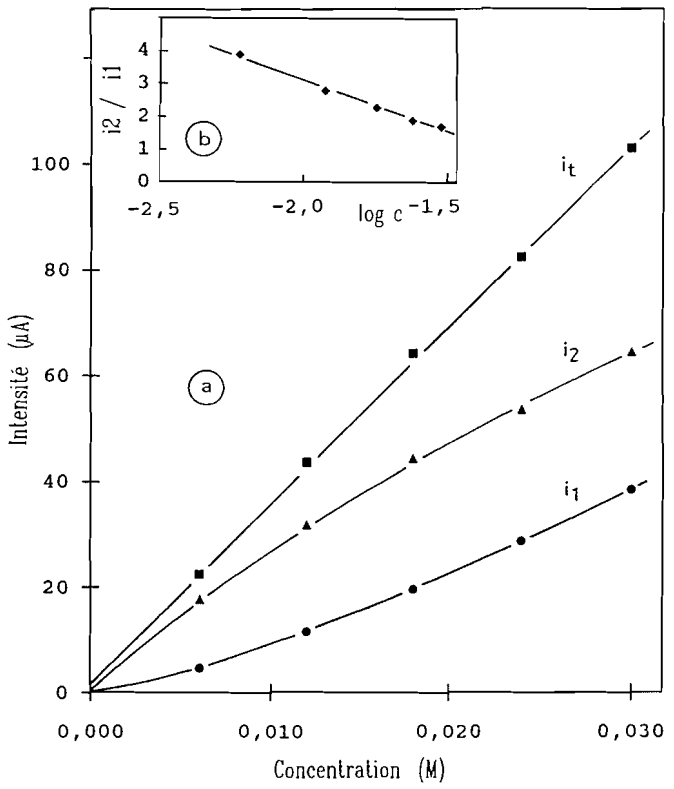

FIG. 2. (*a*) Variations des intensités des vagues de réduction de $TiOSO_4$ en fonction de la concentration. (*b*) Variation du rapport des intensités des deux vagues en fonction du logarithme de la concentration.

sans alcool ont été parfois utilisés à des fins d'interprétation.

Seule l'électrode de mercure permet une étude analytique satisfaisante, la limite cathodique est à environ −1,0 V. Les électrodes solides ne sont pas adaptées : en voltammétrie cyclique, sur électrodes de platine et de monel, la limite d'électro-inactivité de l'électrolyte se situe vers −0,35 V. Sur carbone vitreux, le domaine de potentiel est un peu plus étendu et atteint −0,60, −0,70 V mais ne permet pas d'observer la réduction de $TiOSO_4$.

Une deuxième partie est consacrée à la réalisation d'électrolyses mixtes des dérivés dinitrés en présence de sel de titane ou à des réductions chimiques par l'intermédiaire de Ti(III) électrogénéré par réduction préalable de $TiOSO_4$. Dans chacun des cas, nous examinons l'influence de la quantité de médiateur par rapport à celle de dérivé dinitré sur la nature et les proportions des produits de synthèse.

Comportement électrochimique du sulfate de titanyle, médiateur de réduction du 4,4′-dinitrodibenzyle

Réduction électrochimique du sulfate de titanyle

Polarographie

En milieu H_2SO_4 5 N/EtOH 50:50, le sulfate de titanyle ne se solubilise pas instantanément : la solution est laiteuse à la température ambiante, elle devient limpide et incolore à 60°C.

La réduction polarographique s'effectue en deux étapes d'importances inégales (fig. 1, courbe 1). La hauteur de la première vague est pratiquement indépendante de la pression de mercure, ce qui est caractéristique d'une vague cinétique. L'évolution de l'intensité du courant de diffusion de chacune des vagues (i_1 ou i_2) n'est pas proportionnelle à la concentration mais le rapport i_2/i_1 est une fonction linéaire du logarithme de ce paramètre (fig. 2, *a* et *b*). Seule, la somme des intensités, $(i_1 + i_2)$ est proportionnelle à la concentration et à la racine carrée de la hauteur de la colonne de mercure.

L'analyse logarithmique de la première vague (fig. 3, courbe 1) est une droite dont la pente de 60 mV par unité logarithmique indique un système réversible, $E_{1/2} = -0{,}122$ V ($[TiOSO_4] = 3{,}3 \times 10^{-3}$ M). Celle de la deuxième vague (fig. 3, courbe 2), formée de trois segments de pentes différentes, traduit le caractère complexe de cette étape. Le potentiel est −0,480 V lorsque $i = i_d/2$.

L'addition d'un tensio-actif, le BRIJ 35 (polyoxyéthylène dodécyl éther $C_{12}H_{25}(OCH_2CH_2)_{23}OH$), même en faible quantité, provoque la disparition presque totale de la première étape après une évolution de son potentiel vers les valeurs moins négatives et un déplacement de celui de la deuxième vers des valeurs plus négatives, l'intensité de cette vague devenant en fin d'évolution égale à la somme des deux présentes sans tensio-actif.

En milieu H_2SO_4 5 N sans alcool, on observe une seule vague de réduction située à des potentiels moins négatifs que les deux précédentes (fig. 1, courbe 2). Son intensité est proportionnelle à la concentration de $TiOSO_4$. L'analyse logarithmique (fig. 3, courbe 3) fait apparaître deux cinétiques successives, la deuxième étant beaucoup plus lente que la première. À mi-hauteur de la vague, $E = -0{,}220$ V. Par additions progressives d'alcool, on constate la scission progressive de la vague initiale obtenue en absence d'alcool avec formation d'une deuxième étape à des potentiels plus négatifs

Can. J. Chem. Downloaded from www.nrcresearchpress.com by 213.200.69.106 on 09/08/12
For personal use only.

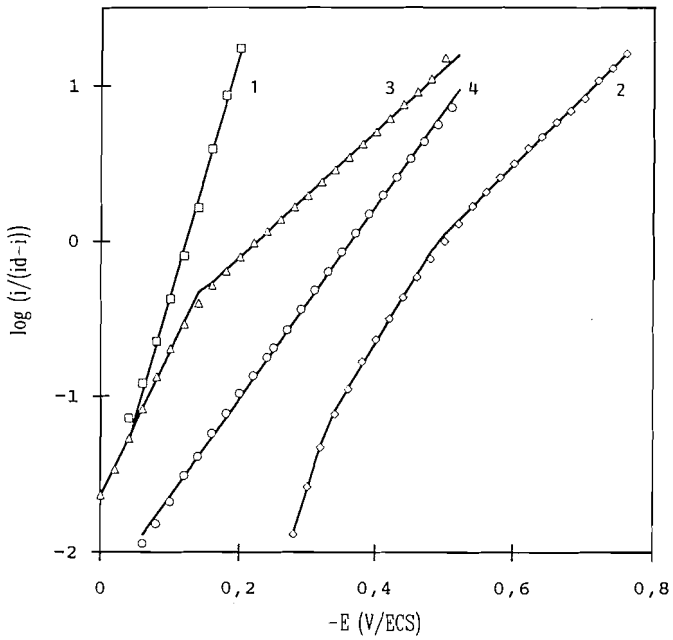

FIG. 3. Analyse logarithmique des vagues polarographiques de $TiOSO_4$ dans différents milieux à 60°C. (1) et (2) H_2SO_4(5 N)/EtOH 50 : 50 (1ère et 2e étape); (3) H_2SO_4(5 N); (4) $HClO_4$(5 N)/EtOH 50 : 50.

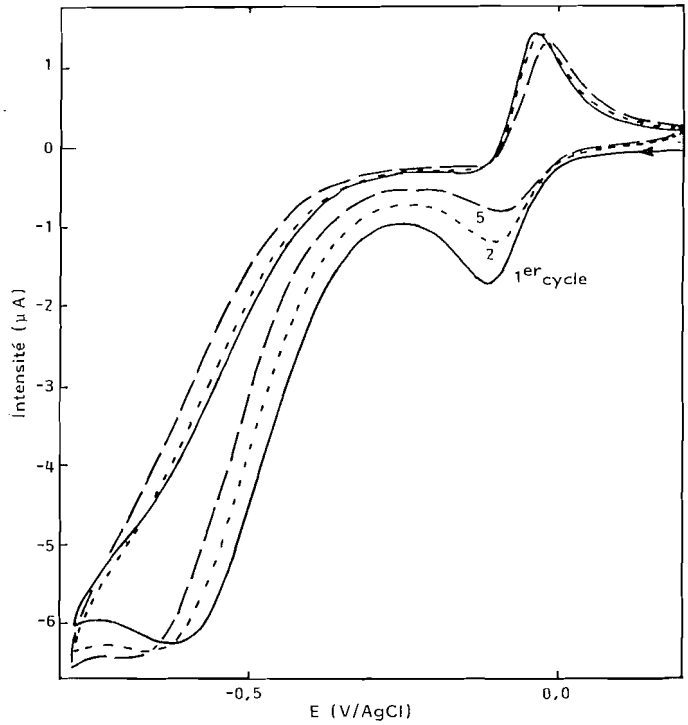

FIG. 4. Voltammogrammes de réduction sur électrode de mercure de $TiOSO_4$ ($5{,}6 \times 10^{-3}$ M) en milieu H_2SO_4(5 N)/EtOH 50 : 50 à 60°C. Cycles successifs : 1er, 2e et 5e cycles à v = 0,05 V s^{-1}.

et la diminution régulière de l'intensité de la première étape, ce qui correspond au passage de la courbe 2 à la courbe 1 sur la fig. 1.

En milieu $HClO_4$ 5N/EtOH, 50 : 50 (acide non complexant), on obtient une vague unique pour laquelle $\log(i/(i_d - i))$ varie linéairement en fonction du potentiel (fig. 3, courbe 4), avec une pente de 160 mV (vague irréversible, $E_{1/2} = -0{,}360$ V).

Voltammétrie cyclique

La réduction de $TiOSO_4$, sur électrode stationnaire de mercure (fig. 4), est également observée en deux étapes comme en polarographie tandis que la réoxydation au balayage retour a lieu en une étape unique dont l'intensité dépend du temps de balayage. Les potentiels des deux pics cathodiques et du pic anodique sont respectivement :

$$E_{Pc}(1) = -0{,}140 \text{ V} \quad E_{Pc}(2) = -0{,}50 \text{ V}$$

$$E_{Pa} = -0{,}06 \text{ V(Ag/AgCl)}$$

$$(v = 0{,}1 \text{ V s}^{-1},\ c = 2 \times 10^{-3} \text{ M})$$

Dans les mêmes conditions de vitesse et de domaine de balayage, jusqu'à −0,90 V, seule l'intensité du pic de réoxydation est proportionnelle à la concentration en $TiOSO_4$ (cette proportionnalité a été mesurée entre 5×10^{-4} et 8×10^{-3} M). Lorsque la vitesse de balayage est plus grande, l'intensité du pic de réoxydation (i_a) augmente proportionnellement plus que celles des pics de réduction, ce qui est également caractéristique d'une étape cinétique mais elle est linéaire en fonction de la racine carrée de la vitesse.

Au cours de plusieurs cycles successifs sur un même échantillon, l'intensité du premier pic diminue tandis que celle du deuxième augmente (fig. 4). Cette diminution est d'autant plus sensible que la vitesse de balayage est plus lente : à v = 10 mV s^{-1}, le premier pic a pratiquement disparu dès le deuxième balayage en tension. Le pic de réoxydation est peu modifié. Lors de la succession des cycles, on note également une évolution des potentiels de réduction : celui de la première étape se déplace vers des valeurs moins négatives et celui de la deuxième vers des valeurs plus négatives. Le potentiel du pic de réoxydation évolue vers des valeurs moins négatives.

De même qu'en polarographie, l'addition de BRIJ 35 entraîne la disparition du premier pic de réduction et le déplacement du deuxième vers des potentiels plus négatifs avec une augmentation de son intensité. Le pic anodique est déplacé vers les potentiels moins négatifs.

En absence d'alcool, la réduction en milieu H_2SO_4 a lieu en une seule étape quasi-réversible. Pour une vitesse de balayage v = 0,1 V s^{-1}, les potentiels des pics cathodique et anodique sont respectivement $E_{Pc} = -0{,}25$ V et $E_{Pa} = -0{,}025$ V (Ag/AgCl) (système lent). La réduction en milieu $HClO_4$/EtOH est irréversible, $E_{Pc} = -0{,}60$ V.

Déterminations coulométriques

Des coulométries et macroélectrolyses à potentiel contrôlé à −0,60 V, sur nappe de mercure, ont permis de déterminer que la quantité totale d'électricité mise en jeu est de 1 F mol^{-1}. Au cours des électrolyses, la solution prend une coloration bleu–violet clair, caractéristique des sels de Ti(III).

Discussion

Les premières études de la réduction électrochimique des sels de titane ont été effectuées principalement en milieux aqueux acides (17–25). Elles ont montré que la nature de l'acide et sa concentration sont des facteurs importants dans l'évolution des polarogrammes. La complexation de Ti(IV) avec les anions a été mise en évidence. En milieu acide sul-

Can. J. Chem. Downloaded from www.nrcresearchpress.com by 213.200.69.106 on 09/08/12
For personal use only.

furique, l'équilibre suivant a été proposé (21*a*) en présence d'ions H^+ et d'ions SO_4^{2-} :

$$TiO^{2+} \xrightleftharpoons{H^+} \underset{\text{instable}}{[Ti(OH)]^{3+}} \xrightleftharpoons{SO_4^{2-}} [Ti(OH)(SO_4)_n]^{(3-2n)+}$$

(A) (B)

$$\xrightleftharpoons{H^+} [Ti(OH_2)(SO_4)_n]^{(4-2n)+}$$

(C)

L'espèce A existe en solutions très diluées tandis que la formation de l'espèce C est obtenue pour des plus fortes concentrations en ions H^+ et sulfate. Cette dernière est la plus facilement réductible et sa réduction est réversible. L'espèce B existe aux concentrations intermédiaires. Elle a été plus particulièrement mise en évidence en milieu H_2SO_4 4 M (21). En milieu H_2SO_4 2 M/EtOH (1 : 3), d'autres auteurs (26) ont observé la réduction polarographique de Ti(IV) en deux étapes ayant sensiblement la même importance aux potentiels respectifs ($E_{1/2}$) de −0,18 et −0,43 V(ECS) pour une concentration en substrat de 5×10^{-4} M. Nos résultats montrent que l'importance relative des deux étapes dépend à la fois de la proportion acide/alcool et de la concentration en substrat (figures 1 et 2).

En milieu H_2SO_4/EtOH, la présence d'une étape cinétique et l'évolution de son intensité en fonction de la quantité d'alcool en solution prouve la participation de ce dernier (S) dans la formation de deux espèces électroactives (Ox_1) et (Ox_2) réduites à des potentiels différents :

$$A + S \rightleftarrows Ox_1$$

$$Ox_1 \underset{k_2}{\overset{k_1}{\rightleftarrows}} Ox_2$$

Il est connu que Ti(IV) peut complexer les alcools et former ainsi des espèces souvent utilisées en chimie organique dans la réalisation de réactions d'oxydation (27). Nous pouvons admettre l'établissement d'un équilibre comparable à celui proposé en milieu aqueux mais faisant intervenir les espèces $[Ti(HOR)(SO_4)_n]^{(4-2n)+}$ et $[Ti(OR)(SO_4)_n]^{(3-2n)+}$ avec R = C_2H_5, la présence d'alcool ou d'alcoolate dans les complexes entraînant de plus une meilleure séparation des vagues. L'hypothèse de différentes valeurs de *n* s'accorde avec l'existence de plusieurs segments dans l'analyse logarithmique de la deuxième étape. Il est à noter que nous avons observé un comportement électrochimique identique à celui de $TiOSO_4$ avec $Ti(SO_4)_2$ et $TiCl_4$,THF qui, en solution, doivent évoluer vers les mêmes espèces.

Lors d'additions de BRIJ 35, tensio-actif fortement adsorbable à la surface de l'électrode de mercure, la suppression progressive de la première étape et le déplacement de la seconde vers des potentiels plus négatifs traduit l'existence, à l'interface électrode–solution, d'une couche de tensio-actif qui rend la réduction des diverses espèces plus difficile. Il a été également noté que l'éthanol en forte concentration peut entraîner, par formation d'une couche adsorbée, le dédoublement de certaines étapes complexes (28). De même, on peut penser que la diminution de la première étape lors de cycles successifs est la conséquence d'une forte adsorption d'espèces réduites contenant ou non des molécules d'alcool. Une vitesse de balayage lente favorisera l'établissement de l'équilibre d'adsorption entraînant ainsi une diminution plus importante de la première étape à partir du deuxième cycle.

Réduction électrochimique du DNDB en absence de $TiOSO_4$

En milieu H_2SO_4/EtOH 50 : 50, la solubilité du DNDB à 60°C est limitée à environ 5×10^{-4} M. Le polarogramme présente deux vagues successives mettant en jeu respectivement huit et quatre électrons par molécule (fig. 1, courbe 3). La première possède un maximum d'adsorption et son potentiel de demi-vague $E_{1/2}$ est de l'ordre de −0,020 V. La deuxième étape est très étalée en potentiel ce qui ne permet pas une détermination précise de $E_{1/2}$.

En voltammétrie cyclique, quelle que soit la concentration, la première étape cathodique est toujours composée de deux pics rapprochés dont le potentiel est compris entre 0 et −0,05 V (Ag/AgCl). La deuxième étape, lente, est peu importante. On peut situer le potentiel de pic au voisinage de −0,75 V. Au balayage retour, aucun pic n'est observé.

Les mécanismes de réduction qui sont les mêmes qu'en milieu acide tamponné ont été donnés dans une étude antérieure (1). Globalement, la première étape conduit à la dihydroxylamine avec mise en jeu de huit électrons et huit protons :

La seconde correspond au passage de la dihydroxylamine à la diamine par échange de quatre électrons et quatre protons :

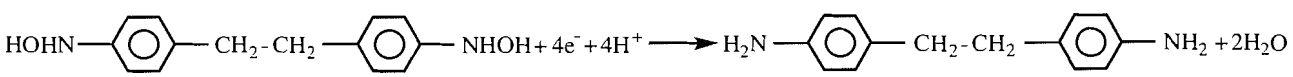

Comportement électrochimique du mélange $TiOSO_4$ + DNDB

Dans le cas d'additions de DNDB à une solution de $TiOSO_4$ ou inversement dans celui d'additions de $TiOSO_4$ à une solution de DNDB, la polarographie ne permet plus de séparer assez nettement les différents transferts électroniques et n'apporte pas d'informations supplémentaires exploitables ce qui nous a conduit à utiliser de préférence la voltammétrie cyclique.

Nous avons étudié plus particulièrement l'effet du DNDB sur les voltammogrammes de $TiOSO_4$ (fig. 5). Lors d'additions successives de DNDB, le pic complexe (à 0, −0,050 V) de la première étape de sa réduction précède toujours celui de $TiOSO_4$ et les secondes étapes de réduction des deux composés sont superposées. Au balayage retour, le pic d'oxydation de Ti(III) diminue notablement et parfois disparaît.

Dans les conditions de concentrations pour lesquelles le

Can. J. Chem. Downloaded from www.nrcresearchpress.com by 213.200.69.106 on 09/08/12
For personal use only.

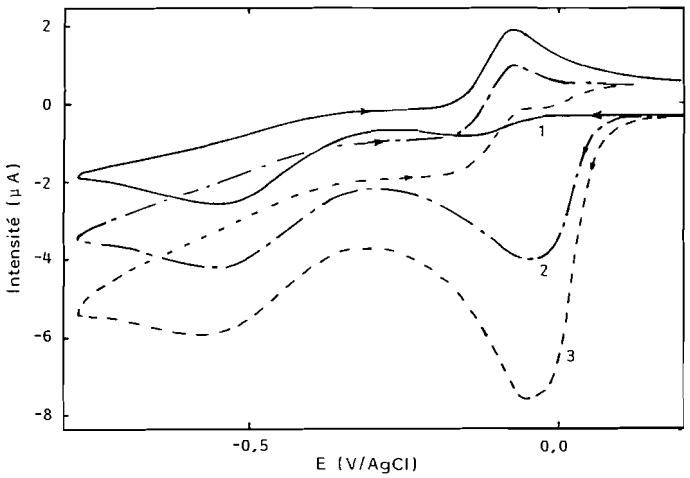

FIG. 5. Voltammogrammes de mélanges $TiOSO_4$ + DNDB sur électrode de mercure $v = 0{,}2$ V s^{-1}. (1) $TiOSO_4$ $1{,}2 \times 10^{-3}$ M; (2) = (1) + DNDB 10^{-4} M; (3) = (1) + DNDB 2×10^{-4} M.

DNDB est soluble, on note des comportements spécifiques en fonction de la vitesse de balayage en tension. Aux faibles vitesses, $v \leq 50$ mV s^{-1}, l'intensité relative de la deuxième étape cathodique a une croissance plus rapide que celle qui résulterait de la seule augmentation de la concentration en DNDB et son potentiel est légèrement déplacé vers des valeurs plus négatives. Au balayage retour, le pic anodique devient de plus en plus petit jusqu'à disparaître des voltammogrammes. À $v = 200$ mV s^{-1} (fig. 5), l'intensité du deuxième pic cathodique n'augmente pas en proportion de la quantité de DNDB ajouté et son potentiel reste constant tandis qu'au balayage retour, le pic anodique diminue également mais sans disparaître. Ainsi, le rapport des intensités des deux pics de réduction (i_2/i_1) est d'autant plus grand que la vitesse est plus petite.

L'ensemble de ces résultats montre que parallèlement à la réduction électrochimique du DNDB, une réaction chimique peut avoir lieu en solution entre le DNDB et le Ti(III) généré à la première étape; elle redonne du Ti(IV) et produit l'hydroxylamine. Si cette réaction chimique a lieu (balayage lent), du Ti(IV) et une quantité additionnelle d'hydroxylamine sont formés au voisinage de l'électrode, ce qui cause une augmentation du courant i_2. Le Ti(III) généré par réduction de Ti(IV) au deuxième pic est consommé par le DNDB, d'où, au balayage retour, la diminution du pic d'oxydation et même sa disparition si le balayage est suffisamment lent et la concentration de DNDB assez élevée. Si la réaction chimique n'a pas lieu (balayage rapide), l'hydroxylamine produite par réduction électrochimique à la première étape est réduite en amine au niveau du deuxième pic. L'intensité du pic d'oxydation correspond alors à la quantité de Ti(IV) généré aux premier et deuxième pics.

Réduction chimique du DNDB par Ti(III) électrogénéré

Le DNDB est ajouté à une solution de Ti(III) obtenu par réduction électrochimique de $TiOSO_4$ et l'évolution de la solution en fonction du temps est suivie par voltammétrie cyclique pour différentes concentrations des deux substrats.

La figure 6 représente l'évolution du mélange Ti(III)/DNDB dans un rapport 12 : 1 ($2{,}4 \times 10^{-3}$ M/2×10^{-4} M) nécessaire à la transformation complète du dérivé dinitré en dérivé diaminé (DADB) :

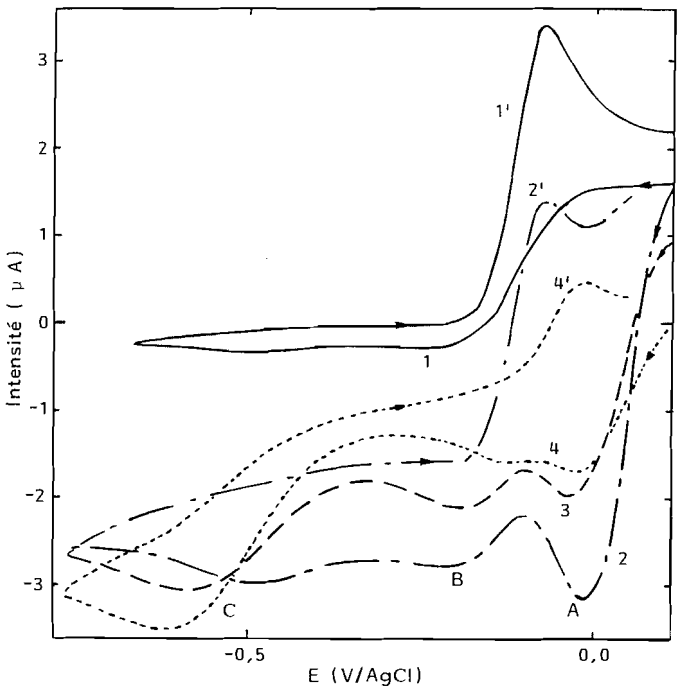

FIG. 6. Evolution en fonction du temps des voltammogrammes du mélange Ti(III)/DNDB 12 : 1. (1) Ti(III) $2{,}4 \times 10^{-3}$ M; (2) = (1) + DNDB 2×10^{-4} M; (3) = (2) après 8 min; (4) = (2) après 40 min. (Le balayage retour de la courbe 3 n'est pas représenté pour faciliter la lecture de l'ensemble.)

$$\text{DNDB} + 12\ \text{Ti(III)} + 12\ \text{H}^+ \rightarrow \text{DADB} + 12\ \text{Ti(IV)} + 4\ \text{H}_2\text{O}$$

La courbe 1 est le voltammogramme de Ti(III) avant l'introduction du produit organique. Au potentiel de départ du balayage (+0,150 V), on note la valeur positive de l'intensité par suite de l'oxydation de Ti(III) à la surface de l'électrode. Au cours d'un balayage aller (en direction des potentiels négatifs), ce courant s'annule au-delà de −0,150 V ce qui indique que Ti(IV) formé est, dans ces conditions, sous la forme la plus facilement réductible (comparaison des figures 4 et 6). En balayage retour, on reconnaît le pic unique de réoxydation de Ti(III).

Après additions de DNDB (courbes 2 à 4), la valeur de l'intensité au potentiel initial diminue de plus en plus en fonction du temps jusqu'à devenir nulle. Au balayage aller, le premier pic cathodique de la courbe 2 correspond à la réduction du DNDB. Sa diminution en fonction du temps est due à la réduction chimique progressive du substrat organique par Ti(III) en solution. L'effet médiateur du couple redox Ti(III)/Ti(IV) se traduit sur les voltammogrammes par l'apparition puis l'augmentation du pic C et la décroissance du pic de réoxydation.

La même expérience a été réalisée avec un rapport Ti(III)/DNDB de 6 : 1 en conservant la concentration en DNDB égale à 2×10^{-4} M. Des observations analogues aux précédentes peuvent être faites mais après un temps de réaction de 40 min, la voltammétrie de contrôle montre que le premier pic de réduction conserve une intensité plus importante que lorsque le rapport est 12 : 1. Le potentiel de ce pic étant celui de la réduction des groupement NO_2, la seule voltammétrie ne permet pas de dire s'il s'agit de la réduction

Can. J. Chem. Downloaded from www.nrcresearchpress.com by 213.200.69.106 on 09/08/12
For personal use only.

Can. J. Chem. Downloaded from www.nrcresearchpress.com by 213.200.69.106 on 09/08/12
For personal use only.

d'une quantité plus importante de DNDB non réduit ou s'il y a également en solution d'autres espèces nitrées résultant d'une réduction partielle du DNDB initial. Les électrolyses à potentiel constant, analysées dans la seconde partie, qui ont permis d'identifier les produits de réduction et de déterminer leurs pourcentages, ont confirmé cette dernière hypothèse et permettent d'attribuer ce pic principalement à la réduction du 4-amino-4′-nitrodibenzyle.

Sélectivité de l'ion Ti(III) électrogénéré dans la réduction de dérivés dinitrés aromatiques

L'utilisation de médiateurs est très développée dans les procédés d'électrosynthèses et plusieurs mises au point récentes ont présenté et comparé les principaux procédés d'électrolyses indirectes (29–31). Dans le cas de la réduction de dérivés nitrés par des médiateurs redox inorganiques, les composés du titane ont déjà été utilisés soit sous forme de chlorure (32–34) ou de sulfate (35–37) en solution dans les acides correspondants, soit sous forme d'oxyde déposé sur des électrodes de titane (38–41). En présence de $Ti(SO_4)_2$, la réduction électrochimique de dérivés dinitrés tels que le *m*-dinitrobenzène, le 2,4-dinitrotoluène, le 2,4-dinitrophénol et l'acide 4,4′-dinitrostylbène-2,2′-disulphonique que nous n'avons pas abordée dans ce travail a conduit aux diamines (35).

La très faible solubilité en milieu aqueux et même en milieu hydroalcoolique des dérivés dinitrés et spécialement du DNDB nous a orienté vers leur réduction par l'intermédiaire d'un médiateur. Nous avons pu constater en effet une accélération de la réaction en raison de la possibilité de formation d'un complexe plus soluble de type nitronate (33) ou du rôle de «transporteur d'électrons» du médiateur (16, 35, 36). De plus, le choix de paramètres tels que la nature et la concentration de ce dernier, la température, offre une meilleure sélectivité pour la réaction.

Les cinétiques de réduction du DNDB sur cathodes de plomb, étain et cuivre ainsi qu'en présence de sels d'étain ont été étudiées antérieurement et ont conduit à la détermination de la constante de vitesse et de l'énergie d'activation de l'électroréduction potentiostatique et galvanostatique du DNDB en milieu hydroalcoolique (42–44).

Dans cette partie, nous nous intéressons plus spécialement à la réduction mixte DNDB – sel de titane en milieu H_2SO_4 5N/EtOH 50 : 50 à 60°C et à des fins de comparaison, à celles des trois autres dérivés dinitrés, les 1,5- et 1,8-dinitronaphtalènes (1,5-DNN et 1,8-DNN) et le 2,2′-dinitrodiphényle (2,2′-DNDP), dans les mêmes conditions expérimentales.

Tout d'abord, nous avons vérifié que ces composés avaient des comportements polarographiques similaires. Comme il a été signalé dans la partie analytique pour le DNDB, seule la première étape qui conduit à la dihydroxylamine en mettant en jeu globalement huit électrons et huit protons est bien définie. Les potentiels $E_{1/2}$ sont donnés dans le Tableau 1.

Les synthèses ont été réalisées selon deux procédés :

(*i*) Le premier est une électrolyse à potentiel constant pour laquelle le substrat organique et le sulfate de titanyle sont mis simultanément en solution dans l'électrolyte. La valeur du potentiel imposé est comprise entre −0,50 et −0,60 V suivant les composés. L'électrolyse est arrêtée lorsque la quantité d'électricité qui a traversé la cellule correspond au moins au nombre théorique de coulombs nécessaire à la réduction du dérivé dinitré en son homologue diaminé. La réduction simultanée de Ti(IV) rend la valeur imprécise. En fin d'électrolyse, la solution est pratiquement incolore ou très légèrement colorée par la présence de Ti(III).

TABLEAU 1. Potentiels de la première étape de réduction de dérivés dinitrés en milieu H_2SO_4/EtOH 50 : 50 à 60°C

Composés	DNDB	1,5-DNN	1,8-DNN	2,2′-DNDP
$E_{1/2}$ (V/ECS)	−0,020	+0,015	−0,010	−0,115

(*ii*) Le second procédé est une réduction chimique du substrat organique par l'ion Ti^{3+} électrogénéré. Il se déroule en deux temps : la première phase est donc la réduction électrochimique à potentiel constant (E = −0,60 V) de $TiOSO_4$ seul en solution. Lorsque cette réduction est achevée, le dérivé nitré, mis en solution dans quelques millilitres de DMF pour favoriser sa dissolution, est introduit immédiatement dans la cellule en évitant toute entrée d'air. Les mêmes conditions de température et d'agitation sont maintenues. La réaction est considérée comme terminée lorsque la solution de couleur bleu–violet est redevenue incolore, ce qui demande 1–2 h.

Electrolyses mixtes dinitroarènes – sulfate de titanyle
Electrolyse du DNDB

La concentration en DNDB a été fixée pour toutes les expériences à 10^{-3} M. En absence de médiateur, la réduction électrochimique au potentiel E = −0,60 V a un rendement faradique de 90% par rapport à la réduction en diamine. L'analyse chromatographique des produits de réduction indique l'obtention de 75% de DADB, 1% de DNDB non réduit, 13% de divers sous-produits non identifiés. Deux pics très rapprochés de pourcentages respectifs 2 et 9% précèdent celui du DADB. L'analyse par spectrométrie de masse couplée à la chromatographie en phase vapeur a mis en évidence deux composés de masses molaires M = 213 et M = 214 dont la fragmentation principale fournit respectivement les ions à m/z = 106 et m/z = 107.

Ces résultats sont compatibles avec les formules

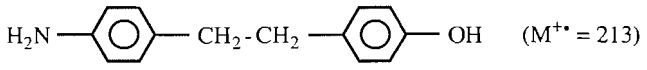

et

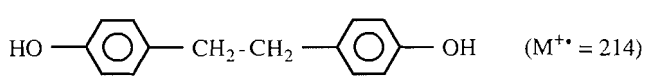

Une coupure benzylique donne les fragments

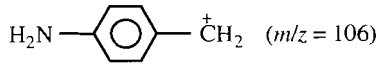

et

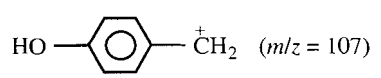

La formation de ces deux produits peut être expliquée par une décomposition des hydroxylamines en milieu fortement acide :

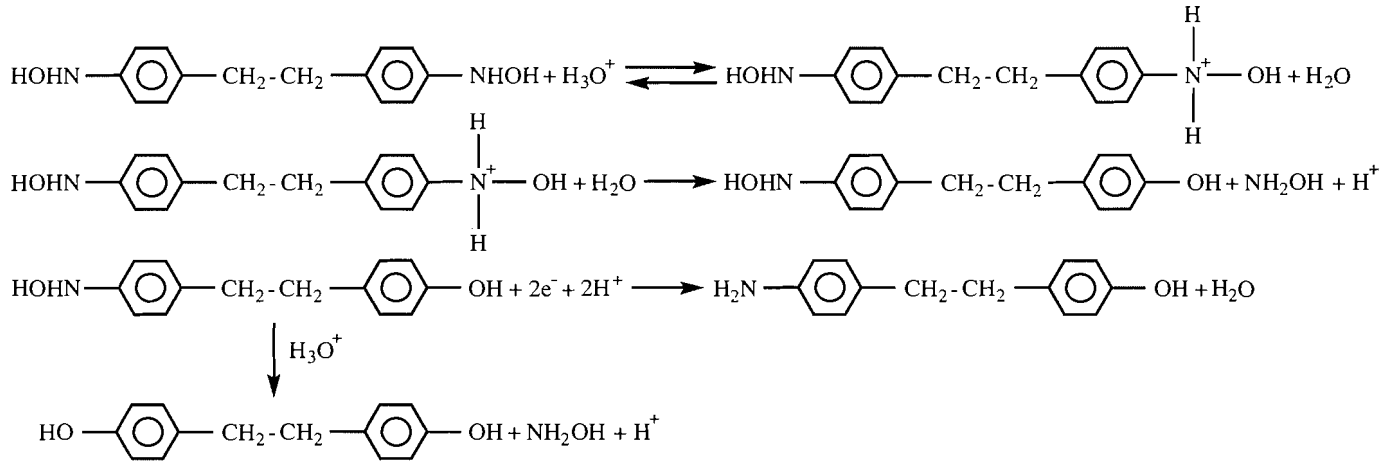

On ne peut cependant exclure un mécanisme impliquant la formation intermédiaire d'une structure de type quinone-imine plus facilement réduite que la molécule de départ :

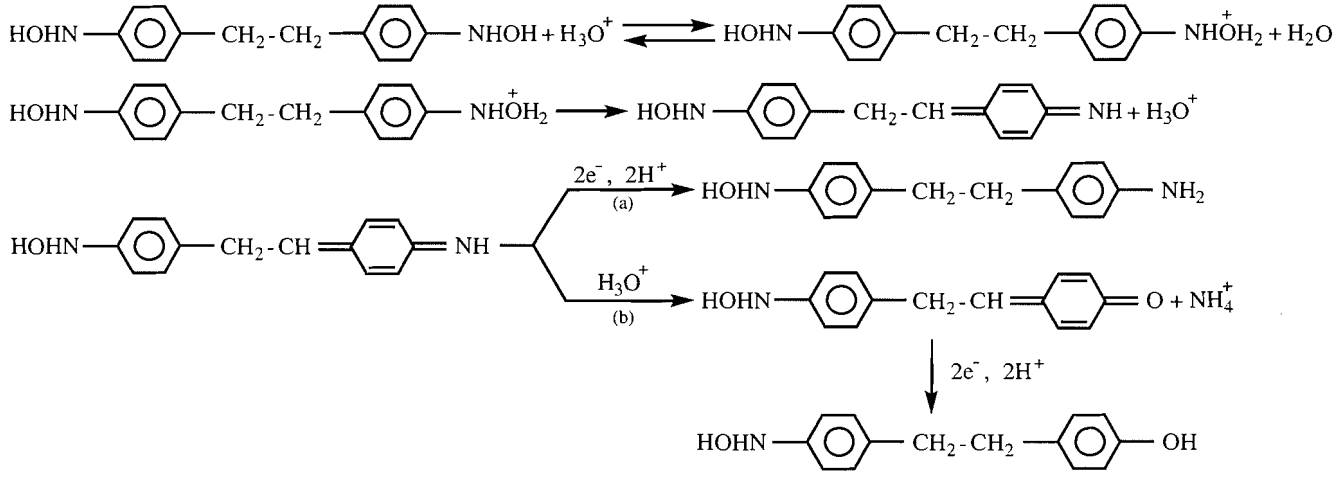

En présence de $TiOSO_4$, plusieurs essais ont été réalisés avec des concentrations croissantes de médiateur afin de déterminer la quantité minimale de ce dernier nécessaire à l'obtention du meilleur rendement possible en diamine.

1. Une concentration de $0,5 \times 10^{-3}$ M modifie peu les résultats obtenus sans médiateur. Dans ces conditions, la réduction fournit 76% de DADB avec des traces des produits de décomposition.

2. Pour une concentration de 2×10^{-3} M, le pourcentage de DADB est de 92% et celui du produit de départ de 3%. Dans ce cas, il est intéressant de noter la suppression des composés secondaires hydroxylés, ce qui permet d'isoler le DADB très pur.

3. Une quantité plus importante de $TiOSO_4$ (6×10^{-3} M) n'a plus d'influence significative sur les résultats, ce qui confirme son rôle de médiateur : l'ion Ti^{4+} régénéré après échange électronique avec le dérivé nitré est à nouveau réduit en Ti^{3+} au potentiel imposé pour l'électrolyse mais le processus catalytique est limité par la cinétique de la réaction chimique.

Electrolyses des 1,5-DNN, 1,8-DNN et 2,2'-DNDP

La réduction électrochimique des autres dérivés dinitrés a été réalisée pour une concentration en substrat organique de 2×10^{-3} M et une concentration en $TiOSO_4$ de 6×10^{-3} M.

La réduction du 1,5-DNN conduit à un bon rendement en 1,5-DAN (93%) et à des traces de produit de départ non réduit. Les résultats sont comparables à ceux obtenus avec le DNDB.

Le cas du 1,8-DNN est beaucoup plus complexe. Seulement 5 à 6% de 1,8-DAN et plusieurs sous-produits dont la formation est vraisemblablement favorisée par la proximité des deux groupements fonctionnels sur les noyaux aromatiques ont été analysés par chromatographie. Nos résultats sont en accord avec ceux cités par d'autres auteurs (7, 10 et réf. citées). Il est connu (6, 9) que par transposition de Gatterman, les hydroxylamines peuvent conduire à des composés hydroxylés ou éthoxylés dans l'éthanol. L'analyse des spectres de masse pourrait faire envisager la formation minoritaire de tels produits mais dans cette étude, nous n'avons pas chercher à les identifier de manière plus précise.

Dans le cas du 2,2'-DNDP, trois produits de réduction ont été détectés par les différentes méthodes d'analyse parmi lesquels le dérivé diaminé est en quantité prépondérante (68%). La benzo[*c*]cinnoline (14%) a également été caractérisée. Sa formation, signalée par d'autres auteurs (3, 8 et réf. citées), résulte d'une suite de réactions faisant intervenir le 2-nitroso-2'-hydroxylamino biphényle. Pour le troisième produit, la spectrométrie de masse permet d'envisager, suivant le même mécanisme que celui développé précédemment pour le DNDB, l'obtention du 2-nitroso-2'-hydroxy biphényle

Can. J. Chem. Downloaded from www.nrcresearchpress.com by 213.200.69.106 on 09/08/12
For personal use only.

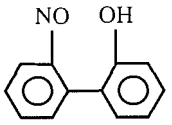

m/z = 199 ($M^{\bullet+}$); 182 (M – OH); 169 (M – NO)

Réductions chimiques par Ti^{3+} électrogénéré

Réduction du DNDB

Les premiers essais ont été réalisés avec une quantité de Ti^{3+} correspondant à 12 équivalents de DNDB (transformation en diamine) dont la concentration est toujours 10^{-3} M.

Les diverses techniques de chromatographie ont mis en évidence trois produits sans autres impuretés dans les proportions respectives 39, 8 et 53%. Il s'agit du DADB, du DNDB non réduit et d'un nouveau composé. D'autres techniques (RMN, IR, spectrométrie de masse) ont permis de caractériser ce dernier comme étant le 4-amino-4′-nitrodibenzyle (ANDB). Ce composé n'a pas été obtenu électrochimiquement sinon à l'état de traces, ni à notre connaissance par d'autres modes de synthèse.

Nous avons alors examiné l'influence du rapport Ti^{3+}/DNDB sur les réactions. Un excès de réactif conduit au DADB seul avec un très bon rendement. En abaissant la proportion de Ti^{3+}, la formation de ANDB est favorisée. C'est le rapport 6 : 1 qui semble le meilleur et il est possible, dans ce cas, d'isoler 70% de ANDB. Pour un rapport inférieur, une quantité plus importante de DNDB n'est pas réduite ce qui diminue le rendement.

Le tableau 2 présente l'évolution des pourcentages des différents produits de réduction avec la quantité de Ti^{3+} mise en jeu.

TABLEAU 2. Pourcentages des produits de la réduction chimique du DNDB en fonction de la quantité de Ti^{3+}

Ti^{3+}/DNDB	DADB (%)	ANDB (%)	DNDB (%)
24 : 1	98	0	2
12 : 1	39	53	8
6 : 1	19	69	10

Des mesures complémentaires ont permis de vérifier ou de définir les caractéristiques électrochimiques et spectrales de l'ANDB. Nous avons comparé son comportement à celui du DNDB. En milieu H_2SO_4 5 N/EtOH à 60°C, le potentiel de pic de la première étape en voltammétrie cyclique est −0,110 V (Ag/AgCl) (v = 0,1 V s^{-1}), soit légèrement plus négatif que celui du DNDB. En milieu diméthylformamide (DMF), dans lequel les mécanismes des dérivés nitrés sont bien connus, les deux étapes classiques, dans un rapport 1 : 3, sont observées aux potentiels $E_{1/2}(1)$ = −0,680 V et $E_{1/2}(2)$ = −1,77 V (Ag/AgI/(I^-)). Les valeurs citées pour le DNDB étaient $E_{1/2}(1)$ = −0,625 V et $E_{1/2}(2)$ = −1,76 V (1). La formation du radical anion, à la première étape de réduction en milieu DMF, a été mise en évidence par spectrométrie de RPE (fig. 7). Sa structure fine est identique à celle du radical anion du DNDB (1) et les constantes de couplage (en mT) sont respectivement : a(N) = 0,953; $a(H_o)$ = 0,313; $a(H_m)$ = 0,107; $a(H_{CH_2})$ = 0,267.

Réduction des 1,5-DNN, 1,8-DNN et 2,2′-DNDP

Afin de connaître si ce procédé de synthèse de produits monoaminés s'appliquait, dans les mêmes conditions, à d'autres composés, nous avons étendu notre recherche aux trois dérivés dinitrés (1,5-DNN, 1,8-DNN et 2,2′-DNDP). Des études antérieures ont montré que des réductions chimiques dans différents milieux permettent d'obtenir ou non des dérivés nitroaminés (45–54).

Comme dans le cas du DNDB, la concentration en substrat organique est toujours de 10^{-3} M et deux concentrations en $TiOSO_4$ préalablement réduit ont été utilisées correspondant aux rapports 12 : 1 et 6 : 1 nécessaires à la transformation théorique en diamine et en monoamine. Les tableaux 3, 4 et 5 résument, pour chaque dérivé, les pourcentages respectifs de produits diaminé, amino-nitré et non réduit obtenus.

TABLEAU 3. Pourcentages des produits de la réduction chimique du 1,5-DNN en fonction de la quantité de Ti^{3+}

Ti^{3+}/1,5-DNN	1,5-DAN (%)	1,5-ANN (%)	1,5-DNN (%)
12 : 1	74	20	5
6 : 1	17	49	32

TABLEAU 4. Pourcentages des produits de la réduction chimique du 1,8-DNN en fonction de la quantité de Ti^{3+}

Ti^{3+}/1,8-DNN	1,8-DAN (%)	1,8-ANN (%)	1,8-DNN (%)
12 : 1	40	0	Traces
6 : 1	5	0	58

TABLEAU 5. Pourcentages des produits de la réduction chimique du 2,2′-DNDP en fonction de la quantité de Ti^{3+}

Ti^{3+}/2,2′-DNDP	2,2′-DNDP (%)	2,2′-ANDP (%)	2,2′-DNDP (%)
12 : 1	92	6	2
6 : 1	36	25	39

Les données de ces tableaux entraînent plusieurs remarques : la réduction chimique par Ti(III) du 1,5-DNN et celle du 2,2′-DNDP conduisent essentiellement à deux composés : les dérivés diaminé et nitroaminé avec une augmentation sensible de ce dernier lorsque le rapport passe de 12 : 1 à 6 : 1 mais au détriment du rendement de la réaction car une quantité importante de dérivé dinitré n'est plus réduite. On peut également noter que la benzo[*c*]cinnoline n'est pas formée par ce procédé.

Comme par réduction électrochimique, la 1,8-DNN ne donne pas de résultats très satisfaisants dans ces conditions expérimentales. S'il est possible d'obtenir 40% de 1,8-DAN avec le rapport 12 : 1, les analyses n'ont pas mis en évidence le dérivé monoaminé mais l'obtention de sous-produits probablement instables déjà signalés précédemment. Une grande quantité de produit de départ non réduit se retrouve en fin de réaction dès que ce rapport diminue.

Can. J. Chem. Downloaded from www.nrcresearchpress.com by 213.200.69.106 on 09/08/12
For personal use only.

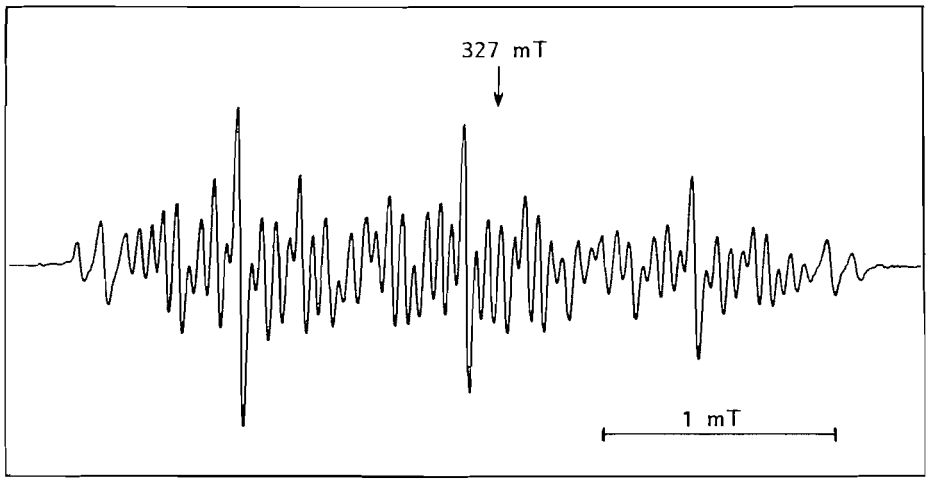

FIG. 7. Spectre de RPE du radical anion du 4-amino 4′-nitrodibenzyle en milieu DMF. Electrolyse à courant constant (80 μA).

Conclusion

L'étude analytique de la réduction électrochimique de $TiOSO_4$ a permis de définir le rôle de médiateur du couple redox Ti^{3+}/Ti^{4+} dans la réduction du DNDB en milieu hydroalcoolique à forte teneur en alcool.

Dans la réduction électrochimique du DNDB, la présence de ce médiateur améliore le rendement en diamine qui peut être obtenue particulièrement pure en raison de la disparition des produits secondaires qui se forment lors de la réduction sans médiateur. Cependant, cette méthode ne permet pas, à cause de la proximité des potentiels de réduction des deux groupements NO_2, l'obtention du dérivé monoaminé. Par contre, la réduction chimique par l'ion Ti^{3+} préalablement électrogénéré est sélective. Selon la valeur du rapport des concentrations Ti^{3+}/DNDB, les dérivés diaminé ou monoaminé peuvent être préparés. C'est une méthode qui s'avère être bien adaptée à la synthèse du 4-amino-4′-nitrodibenzyle.

Les résultats obtenus par ces mêmes procédés avec le 1,5-DNN, le 1,8-DNN et le 2,2′-DNDP montrent l'influence de la position des groupements fonctionnels sur les cycles aromatiques, leur distance plus ou moins grande pouvant modifier la nature et la quantité des produits formés.

Nous avons pu constater que le matériau d'électrode et la nature du médiateur interviennent également sur les mécanismes de réduction. Une étude est en cours sur ce sujet.

Partie expérimentale

Solvants et produits

L'eau des différentes solutions est de l'eau distillée et l'alcool de l'éthanol. Les acides sulfurique et perchlorique sont des produits Prolabo de qualité RP Normapur pour analyses et Normapur 70–72%.

Le sel de titane est un produit commercial Aldrich de formule $TiOSO_4$, x H_2SO_4, x H_2O. Sa composition a été déterminée par thermogravimétrie et dosage acide–base. La valeur de x a été trouvée égale à 0,95. La masse molaire correspondante est M = 270. Dans ce texte, il est écrit en abrégé $TiOSO_4$. D'autres composés du titane comme le sulfate de titane Prolabo ou le complexe tétrachlorure de titane – tétrahydrofuranne Fluka ont également été expérimentés.

Le 4,4′-dinitrodibenzyle est un produit industriel recristallisé trois fois dans le toluène. Les autres dérivés dinitrés sont des produits commerciaux : 1,5-dinitronaphtalène et 1,8-dinitronaphtalène (Aldrich) et 2,2′-dinitrodiphényle (EGA-Chemie). Les composés diaminés commerciaux : 4,4′-diaminodibenzyle, 1,5-diaminonaphtalène et 1,8-diaminonaphtalène (Aldrich) ainsi que la benzo[*c*]cinnoline (EGA-Chimie) ont permis de confirmer l'identification des produits de réduction. Le 2,2′-diaminodiphényle et le 2-amino-2′-nitrodiphényle ont été préparés antérieurement (3, 45–47, 50, 55). La synthèse et les caractéristiques spectroscopiques du 1-amino-5-nitronaphtalène sont également citées dans la littérature (51, 56). (Les abréviations DN.., DA.. et AN.. désignent respectivement les dérivés dinitrés, diaminés et amino-nitrés.)

Instrumentation électrochimique

Les principales techniques électrochimiques analytiques utilisées dans ce travail sont la polarographie et la voltammétrie cyclique à balayage linéaire en tension sur électrode de mercure. Les ensembles expérimentaux ont déjà fait l'objet de descriptions détaillées de notre part (1). Les tensions sont indiquées comme précédemment soit par rapport à l'électrode de référence au calomel saturé (ECS), soit en voltammétrie (électrode PAR 303) par rapport à l'électrode Ag/AgCl qui diffère de 20 mV de la précédente. Les cellules électrochimiques, à doubles parois, sont thermostatées par circulation d'eau à 60°C. Un réfrigérant fixé sur le couvercle réduit l'effet d'évaporation de l'alcool. Avant chaque expérience, les solutions sont toujours soigneusement désaérées par un courant d'argon. Une légère surpression de ce gaz est ensuite maintenue dans la cellule.

Le dispositif des électrolyses préparatives comprend un potentiostat Tacussel PRT 100-1X couplé à un intégrateur IG5-N et à un ampèremètre enregistreur qui permet de suivre l'évolution de l'intensité en fonction du temps. La cellule à trois compartiments est placée dans un bain-marie à 60°C. La cathode est une nappe de mercure de 72 mm de diamètre, l'anode une plaque de plomb et l'électrode de référence l'électrode ECS.

Extraction des produits de réduction

Après l'électrolyse, le catholyte est concentré puis neutralisé par une solution de soude jusqu'à pH basique. Les produits sont extraits à l'éther et la solution éthérée, après séchage sur $MgSO_4$, est évaporée sous vide.

Séparation des produits de réduction

Les produits sont isolés par chromatographie sur colonne de silice Kieselgel 60 Merck (granulométrie 0,063–0,200 mm). L'éluant toluène–acétone (80 : 20 v/v) qui permet une bonne solubilisation et la séparation des composés a dû être remplacé par le mélange toluène–méthanol (90 : 10 v/v) car l'acétone réagit sur les fonctions amines et forme les imines correspondantes détectées par chromatographie en phase vapeur et confirmées par les analyses de spectrométrie de masse.

Can. J. Chem. Downloaded from www.nrcresearchpress.com by 213.200.69.106 on 09/08/12
For personal use only.

Can. J. Chem. Downloaded from www.nrcresearchpress.com by 213.200.69.106 on 09/08/12
For personal use only.

Techniques de caractérisation des produits de réduction

Les techniques sont principalement les suivantes :

Chromatographie en phase vapeur (CPV)

Le chromatographe Shimatzu est équipé d'une colonne capillaire Méthylsilicone DB1 (J & W Scientific) de 30 m × 0,25 mm. La température du détecteur (FID) et de l'injecteur est de 300°C, celle du four est gérée par une programmation de température (palier à 100°C pendant 1 min, puis chauffage de 100 à 290°C à 5°C min^{-1} et palier pendant 20 min à 290°C). Le gaz vecteur est l'hélium (1,5 bar en entrée de colonne) (1 bar = 100 kPa).

Chromatographie sur couche mince (CCM)

Sur des plaques de silice Kieselgel 60, l'éluant est un mélange toluène–acétone ou toluène–méthanol dans un rapport volumique de 80 : 20 ou 90 : 10. Les plaques sont révélées par irradiation ultraviolette (λ = 250 nm).

Spectrométrie de masse

Les analyses par spectrométrie de masse (impact électronique) couplée à la chromatographie en phase gazeuse ont été faites par le Service Central d'Analyse du CNRS.

Spectrométrie de RMN ^1H

Les produits sont mis en solution dans $CDCl_3$. Le spectromètre est un appareil Bruker MSL 300.

Spectroscopie IR

Les échantillons, sous forme de pastilles avec KBr (1/100 mg), sont traités sur un appareil Nicolet FT-IR.

Spectrométrie de RPE

Le spectre est enregistré sur un appareil Bruker ER 200 D dans les conditions décrites précédemment (1).

Caractéristiques des produits de réduction

DADB

Cristaux beige-nacré; F = 134°C. Spectre IR : ν_{NH_2} = 3435 et 3350 cm^{-1}, ν_{arom} = 1620 et 1510 cm^{-1}. Spectre de RMN ^1H δ(ppm) : 2,75 (s,4H,CH_2), 3,6 (s,4H,NH_2), 6,65 (d,4H,arom), 7,0 (d,4H,arom). Spectre de masse : m/z = 212 ($M^{\cdot+}$);

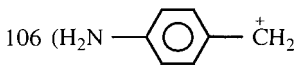

106 (H_2N — C$_6$H$_4$ — CH_2^+).

ANDB

Cristaux orange; F = 132°C. Spectre IR : ν_{NH_2} = 3451 et 3375 cm^{-1}, ν_{NO_2} = 1515 et 1340 cm^{-1}, ν_{arom} = 1630 et 1505 cm^{-1}. Spectre de RMN ^1H δ(ppm) : 2,8–2,95 (m,2H,CH_2), 2,95–3,1 (m,2H,CH_2), 3,0–5,0 (étalé,2H,NH_2), 6.75 (d,2H,arom), 6.95 (d,2H,arom), 7,3 (d,2H,arom), 8,15 (d,2H, arom). Spectre de masse : m/z = 242 ($M^{\cdot+}$); 106 (H_2N — C$_6$H$_4$ — CH_2^+).

Produit auxiliaire obtenu en présence d'acétone :

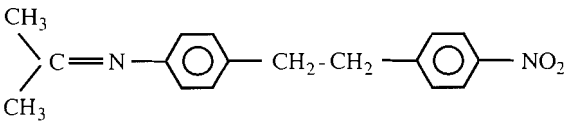

Spectre de masse : m/z = 282 ($M^{\cdot+}$);

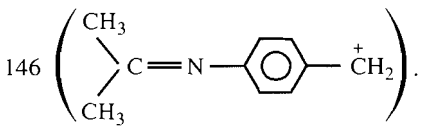

146 ($(CH_3)_2C{=}N$ — C$_6$H$_4$ — CH_2^+).

1,5-DAN

Spectre de RMN ^1H δ(ppm) : 4,15 (s,4H,NH_2), 6,7–6,8 (m,2H,arom), 7,2–7,3 (m,4H,arom).

1,5-ANN

Specte de RMN ^1H δ(ppm) : 4,3 (s,2H,NH_2), 6,9 (d,1H,arom), 7,45–7,6 (m,2H,arom), 7,9 (d,1H,arom), 8,1 (d,2H,arom). Spectre de masse : m/z = 188 ($M^{\cdot+}$); 158 (M − NO); 142 (M − NO_2).

1,8-DAN

Spectre de RMN ^1H δ(ppm) : 4,5 (s,4H,NH_2), 6,6 (d,2H,arom), 7,1–7,3 (m,4H,arom). Spectre de masse : m/z = 158 ($M^{\cdot+}$); 141 (M − NH_3); 130 (M − HCN − H).

2,2'-DADP

Spectre de RMN ^1H δ(ppm) : 3,6 (s,4H,NH_2), 6,75–6,9 (m,4H,arom). 7,1–7,25 (m,4H,arom). Spectre de masse : m/z = 184 ($M^{\cdot+}$); 167 (M − NH_3).

2,2'-ANDP

Spectre de RMN ^1H δ(ppm) : 3,3 (s,2H,NH_2), 6,7–6,9 (m,2H,arom), 7,0 (d,1H,arom), 7,1–7,3 (m,1H,arom), 7,4–7,6 (m,2H,arom), 7,6–7,8 (m,1H,arom), 8,0 (d,1H,arom). Spectre de masse : m/z = 214 ($M^{\cdot+}$); 197 (M − OH); 180 (benzo[*c*]cinnoline); 167 (M − HNO_2).

Benzo[c]cinnoline

Spectre de RMN ^1H δ(ppm) : 7,8–8,0 (m,4H,arom), 8,5–8,6 (m,2H,arom), 8,7–8,8 (m,2H,arom). Spectre de masse : m/z = 180 ($M^{\cdot+}$); 152 (M − N_2).

1. V. Danciu, A.M. Martre, P. Pouillen et G. Mousset. Electrochim. Acta, **37**, 1993 (1992).
2. V. Danciu, A.M. Martre, P. Pouillen et G. Mousset. Electrochim. Acta, **37**, 2001 (1992).
3. S.D. Ross, G.J. Kahan et W.A. Leach. J. Am. Chem. Soc. **74**, 4122 (1952).
4. R.N. Boyd et A.A. Reidlinger. J. Electrochem. Soc. **107**, 611 (1960).
5. A. Tallec. C.R. Acad. Sci. **260**, 3418 (1965); **261**. 2915 (1965).
6. A. Tallec et M.J. Gueguen. C.R. Acad. Sci. **262**, 484 (1966); **262**, 1688 (1966).
7. M. Jubault et E. Raoult. C.R. Acad. Sci. **268**, 2046 (1969).
8. E. Laviron et T. Lewandowska. Bull. Soc. Chim. Fr. 3177 (1970).
9. M. Jubault et D. Peltier. Bull. Soc. Chim. Fr. 1544 (1972); 1551 (1972).
10. D. Bernard, Y. Mugnier, G. Tainturier et E. Laviron. Bull. Soc. Chim. Fr. 2364 (1975).
11. A. Darchen et C. Moinet. (*a*) J. Chem. Soc. Chem. Commun. 487 (1976); (*b*) J. Electroanal. Chem. **68**, 173 (1976); **78**, 81 (1977).
12. R. Voigtlander, J. Hlavaty, J. Volke et V. Bakos. Collect. Czech. Chem. Commun. **48**, 364 (1983).
13. F. Taha, H.A. El Shayeb, A.A. Abd El Gaber et A.M. El Roudi. Bull. Soc. Chim. Belg. **95**, 229 (1986).
14. E. Laviron et L. Roullier. J. Electroanal. Chem. **288**, 165 (1990).
15. E. Laviron, R. Meunier-Prest, A. Vallat, L. Roullier et R. Lacasse. J. Electroanal. Chem. **341**, 227 (1992).
16. J. Chaussard, R. Rouget et M. Tassin. J. Appl. Electrochem. **16**, 803 (1986).
17. P. Pascal. *Dans* Nouveau traité de chimie minérale. Vol. IX. Masson et Cie, Paris. 1963. pp. 179–180.
18. A. Blazek et J. Koryta. Collect. Czech. Chem. Commun. **18**, 326 (1953).
19. J.J. Lingane and J.H. Kennedy. Anal. Chim. Acta, **15**, 294 (1956).
20. D.K. Banerjee, C.C. Blidke and F.D. Miller. Anal. Chem. **31**, 1836 (1959).
21. G.M. Habashy. (*a*) Collect. Czech. Chem. Commun. **25**, 3166 (1960); (*b*) J. Electroanal. Chem. **8**, 237 (1964).
22. J.M. Saveant et E. Vianello. Electrochim. Acta, **10**, 905 (1965).

23. E.G. Chikryzova et N. Van Nam. Zh. Obshch. Khim. **44**, 1331 (1974).
24. D.I. Kurbatov et G.A. Nikitina. Elektrokhimiya, **12**, 102 (1976).
25. L.M. Maluka, Y.I. Tur'yan et T.G. Tsyupko. J. Gen. Chem. USSR, **61**, 2223 (1991).
26. G. Donoso, I. Chadwick et M.A. Santa Ana. Anal. Chim. Acta, **77**, 1 (1975).
27. S.S. Woodard, M.G. Finn et K.B. Sharpless. J. Am. Chem. Soc. **113**, 106 (1991).
28. M. Person. Bull. Soc. Chim. Fr. 1832 (1966).
29. H. Wendt. Electrochim. Acta, **29**, 1513 (1984).
30. J. Simonet et G. Le Guillanton. Bull. Soc. Chim. Fr. 180 (1985).
31. A. Savall. L'Actualité Chimique n° 1, 35 (1992).
32. S.A. Newton, F.J. Stubbs et C. Hinshelwood. J. Chem. Soc. 3384 (1953).
33. J.E. McMurry. Acc. Chem. Res. **7**, 281 (1974).
34. O. Christofis, J.J. Habeeb, R.S. Steevensz et D.G. Tuck. Can. J. Chem. **56**, 2269 (1978).
35. M. Noel, P.N. Anantharaman et H.V.K. Udupa. J. Appl. Electrochem. **12**, 291 (1982).
36. Y.M. Kargin, B.V. Mel'nikov, Y.A. Lisitsyn et G.A. Kamlova. J. Gen. Chem. USSR, **58**, 2320 (1988).
37. P. Thirunavukkarasu, S. Thangavelu et K.S. Udupa. Bull. Electrochem. **4**, 245 (1988).
38. F. Beck et W. Gabriel. Angew. Chem. Int. Ed. Engl. **24**, 771 (1985).
39. D. Vasudevan, S. Chellammal et P.N. Anantharaman. J. Appl. Electrochem. **21**, 839 (1991).
40. C. Ravichandran, D. Vasudevan et P.N. Anantharaman. J. Appl. Electrochem. **22**, 179 (1992).
41. C. Ravichandran, D. Vasudevan, S. Thangavelu et P.N. Anantharaman. J. Appl. Electrochem. **22**, 1087 (1992).
42. L. Oniciu, I.A. Silberg, V. Danciu, M. Olea et S. Bran. 36th Meeting of International Society of Electrochemistry, Salamanca, Spain (1985).
43. V. Danciu, I.A. Silberg, O.H. Oprea et L.A. Oniciu. Rom RO 94157 (Cl C 07C87/14) 30/07/88, Appl. 122483, 07/03/86.
44. L. Oniciu, M. Olea et V. Danciu. Rev. Chim. (Bucharest), **41**, 779 (1990).
45. G.M. Badger et W.F.H. Sasse. J. Chem. Soc. 4 (1957).
46. J.P. Idoux. J. Chem. Soc. C, 435 (1970).
47. E. Ibuki, S. Ozasa et H. Kitamura. Nippon Kagaku Zasshi, **92**, 361 (1971); Chem Abstr. **76**, 24816r (1972).
48. V. Kalyanaraman et M.V. George. J. Org. Chem. **38**, 507 (1973).
49. T. Hirashima et O. Manabe. Nippon Kagaku Kaishi, 1223 (1975); Chem Abstr. **83**, 131252v (1975).
50. M.O. Terpko et R.F. Heck. J. Org. Chem. **45**, 4992 (1980).
51. N.R. Ayyangar, U.R. Kalkote et A.G. Lugade. Bull. Chem. Soc. Jpn. **56**, 3159 (1983).
52. I.M. Al-Daher et B. Kratochvil. (*a*) Can. J. Chem. **59**, 3346 (1981); (*b*) Talanta, **33**, 751 (1986).
53. Z. Hou, Y. Fujiwara et H. Taniguchi. J. Org. Chem. **53**, 3118 (1988).
54. K. Ohe, S. Uemura, N. Sugita, H. Masuda et T. Taga. J. Org. Chem. **54**, 4169 (1989).
55. E.F.M. Stephenson. J. Chem. Soc. 2354 (1954).
56. C.J. Pouchert. *Dans* The Aldrich Library of Infrared Spectra. Édition III. 1981. p. 843C.

Can. J. Chem. Downloaded from www.nrcresearchpress.com by 213.200.69.106 on 09/08/12
For personal use only.

Helianthoside from *Heliaster helianthus*, an asterosaponin with a C3′-sulphated pyranose

M. Jesus Vazquez, Emilio Quiñoa, and Ricardo Riguera[1]
Departamento de Química Orgánica, Universidad de Santiago de Compostela, 15706 Santiago de Compostela, Spain

AND

Aurelio San Martin
Departamento de Química, Universidad de Chile, Santiago, Chile

Received January 7, 1993

M. Jesus Vazquez, Emilio Quiñoa, Ricardo Riguera, and Aurelio San Martin. Can. J. Chem. **71**, 1147 (1993).

A new asterosaponin, named helianthoside (**1**), has been isolated from the butanolic extract of the starfish *Heliaster helianthus* and its structure established on the basis of extensive spectroscopic experiments and chemical correlations. Helianthoside is the first asterosaponin with a C3′-sulphated xylopyranose. The absolute stereochemistry at C24 was determined by the Trost–Mosher method.

M. Jesus Vazquez, Emilio Quiñoa, Ricardo Riguera et Aurelio San Martin. Can. J. Chem. **71**, 1147 (1993).

On a isolé une nouvelle astérosaponine dénommée hélianthoside (**1**) à partir d'un extrait d'étoile de mer, *Heliaster helianthus*, dans le butanol et on a établi sa structure à partir de nombreuses expériences spectroscopiques et des corrélations chimiques. L'hélianthoside est la première astérosaponine avec une xylopyranose sulfatée en C3′. On a déterminé la stéréochimie absolue en C24 par la méthode de Trost–Mosher.

[Traduit par la rédaction]

Introduction

Asterosaponins are a well-established class of marine metabolites with complex structures that can be classified in two major groups: (*i*) those characterized by a $\Delta^{9(11)}$-3β,6α-diol steroidal aglycone with an oligosaccharide moiety attached at C6 and a sulphate residue at C3 and (*ii*) those derived from a polyhydroxysteroidal aglycone. The latter occur in minute amounts and are generally based on a cholestane skeleton with a varying degree of hydroxylation involving carbons C4, C5, C6, C7, C8, C12, C14, C15, and C16, with a carbohydrate portion featuring one or two sugar units attached to C3 and (or) to the side chain. In the latter case, a number of variants have been described which differ in the exact location of the sulphate groups on the aglycone or sugar component. Recently, a very small number of polyhydroxysteroid saponins have been isolated from other marine organisms such as sponges (1) and tunicates (2).

As part of our work on marine organisms, we describe in this paper the structure of a novel sulphated monoglycosidic polyhydroxysteroid (**1**, Fig. 1) that we have isolated from the starfish *Heliaster helianthus* and named helianthoside. Complete structural analysis and signal assignment are based on extensive 1D and 2D nmr experiments, FAB mass spectral data, and selective hydrolysis and methylation. Use of the Trost–Mosher (3) method showed an *S* absolute configuration at the stereogenic centre C24.

An isomer of helianthoside, compound **2**, was also isolated. This compound was previously reported by Kitagawa and Kobayashi in *Pisaster ochraceus* (4).

Results and discussion

Starfish collected at Valparaiso, Chile, were extracted with methanol, and the extract was washed with solvents of successively lower polarity. The defatted methanol extract was partitioned into a mixture of *n*-butanol and water, and the polar material was recovered from the butanolic extract by successive chromatography on Amberlite XAD-2 and Sephadex LH-20, droplet countercurrent chromatography (dccc), and reversed-phase hplc, giving the polyhydroxysteroid saponins **1** (12 mg, $[\alpha]_D^{20}$ −15.3) and **2** (17 mg, $[\alpha]_D^{20}$ +90.4).

The positive ion FAB mass spectrum of **1** showed the molecular species $[(M + Na)]^+$ at *m/z* 709 and $[(M + K)]^+$ at *m/z* 725, with the molecular weight M, of 686 amu, corresponding to the monosodium salt formula $C_{32}H_{56}NaO_{12}S$. The peak observed at *m/z* 589 indicated the loss of a sodium sulphate group to leave $[(M + Na) - NaHSO_4]^+$. The fragments corresponding to the cleavage of the sugar (Fig. 1) were observed at *m/z* 307 $[C_9H_{16}NaO_8S]^+$ and 263 $[C_6H_9NaO_8S]^+$. Solvolysis of **1** in dioxane–pyridine afforded the desulphated derivative **1***a*, which under FAB (positive ion mode) produced the species $[(M + Na)]^+$ at *m/z* 607 and $[(M + Na) - C_5H_9O_5]^+$ at *m/z* 458, due to the loss of a pentose.

The negative FAB mass spectrum of **1** corroborated the above results, giving a molecular anion species $[(M - H)]^-$ at *m/z* 663, where the molecular weight M is 664 amu, corresponding to the molecular formula $C_{32}H_{57}O_{12}S$.

After acid hydrolysis and derivatization as an alditol acetate, gc–ms showed the sugar component to be xylose.

The ^{1}H nmr spectrum of **1** (see Tables 2 and 3) contains signals for two quaternary methyls at δ_H 1.08 and 1.13 and three secondary methyls at δ_H 0.98 (d, J = 5.96 Hz), 1.08 (d, J = 6.16 Hz), and 1.15 (d, J = 4.79 Hz) that are characteristic of steroidal aglycones, and for a number of methine protons geminal to oxygen in the region 5.25–3.50 ppm. It also showed one β-anomeric proton at 4.97 ppm (d, J = 7.50 Hz).

The ^{13}C and DEPT data of **1** (Table 1), recorded in pyridine-d_5, showed peaks for 32 carbons. The aglycone part featured three quaternary carbons, nine methylenes, nine methines, and five methyl groups. There were signals at δ_C 76.0, 74.8, 68.4, 64.9, and 85.1 ppm for five carbons bonded to oxygen. The chemical shift of the peak at 85.1 ppm suggests a side-chain carbon bound to a sulphate or sugar unit.

[1]Author to whom correspondence may be addressed.

Can. J. Chem. Downloaded from www.nrcresearchpress.com by 213.200.69.106 on 09/08/12
For personal use only.

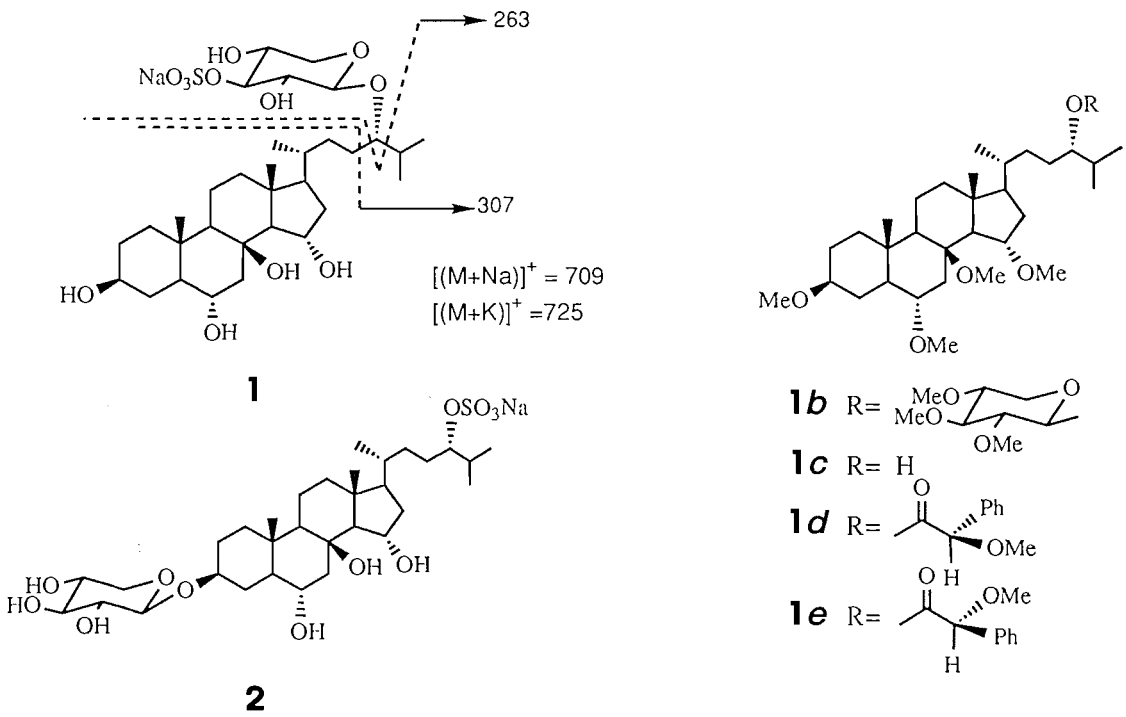

FIG. 1

The sugar part presented signals at 101.5 ppm for the anomeric carbon and at 66.2 ppm for the C5′ methylene group of a pentose; the remaining carbons were unambiguously identified on the basis of selective 1D TOCSY (5) and HMQC (6) experiments.

The above data coincide almost perfectly with those reported by Minale and co-workers (7) for compound **2**. Accordingly, we centered our subsequent efforts on identifying the exact location of the sulphate and the sugar. The location of the sulphate group at C3′ of the xylose was deduced by comparison of the ^{13}C chemical shifts for C2′, C3′ and C4′ in **1** with those of the desulphated compound **1***a* obtained by solvolysis (see Table 1); while the C3′ signals of **1** and **1***a* are practically the same, the C2′ and C4′ signals exhibit the expected β effect (+2 ppm) (7).

Further structural information on **1** was obtained in a series of 2D experiments performed using the inverse probehead technique (AMX 500). HMQC allowed the complete correlation of all the carbon and proton signals; RELAYED H,C-COSY (8) provided information on the connectivity of the molecule and the location of the oxygenated carbons at C3, C6, C15, and C24. The equatorial orientation of the hydroxyl groups at C3, C6, and C15 followed from their observed *J* values.

The glycoside bond was located at C24 by HMBC (9), which among other relevant correlations (Table 3) showed those between the anomeric carbon C1′ on the one hand and H24, the $H_2$5′ pair ($^3J_{CH}$ correlation), and H2′ ($^2J_{CH}$) in the other. HMBC also showed that xylose was present as a pyranose and not as a furanose; correlations between C4′ and H3′ and $H_2$5′ were found, but not between C4′ and H1′.

In keeping with the above conclusions, when the desulphated derivate **1***a* was subjected to exhaustive methylation it yielded a permethylated derivative containing seven methoxy groups, **1***b*, which under acid conditions yielded 3β,6α,8β,15α-tetramethoxy-5α-cholestan-24-ol (**1***c*). Furthermore, nmr data showed **2** to have the same aglycone as **1**.

The above findings show compound **1** to be 24-*O*-(β-xylopyranosyl)-5α-cholestane-3β,6α,8β,15α,24-pentaol 3′-*O*-sulphate.

Comparison with ^{13}C nmr data of known steroids suggests that the absolute configuration at C24 is *S*. We nevertheless decided to prove this by applying the Mosher–Trost nmr method to C24 of **1***c* (see ref. 10 for a recent example). We accordingly prepared the (+)-(*R*)-MPA (MPA = α-methoxyphenylacetic acid) and (−)-(*S*)-MPA esters, **1***d* and **1***e*, respectively. The ^1H nmr spectrum of **1***d* showed among other shifts the 6H doublet for the isopropyl methyl protons at δ_H 0.91, while in **1***e* they resonated at δ_H 0.84 and 0.86. The isopropyl group of **1***d* therefore lies on the same side as the phenyl group of the mandelate, which proves **1** and **2** to be 24*S*.

Of the 100 or so polyhydroxysteroid saponins isolated so far from echinoderms and other families, only 12 compounds with a sulphated sugar are known, all with the sugar attached to the side chain. *Dermasterias imbricata* (11) and *Patiria miniata* (12) afford disaccharides with sulphate groups on C3′ and C5′ of a furanose directly bound to the side chain, while the sulphate is located at C4′ of a pyranose in *Coscinasterias tenuspina* (13), *Astropecten scoparius* (14), and *Pisaster brevispinus* (15), at C6′ of a pyranose in *Pisaster ochraceus* (4) and *Pycnopodia helianthoides* (16), and on a furanose in *Patiria miniata* at C2′, in *Oreaster reticuiatus* (17) at C3′, and in *Astropecten scoparius*, *Asterina pectinifera* (18), and *Patiria pectinifera* (19) all at C5′. Helianthoside (**1**) is thus the first reported asterosaponin with a C3′-sulphated pyranose.

The presence in the same starfish of isomeric saponins such as **1** and **2** is not infrequent. *Pycnopodia helianthoides* af-

Can. J. Chem. Downloaded from www.nrcresearchpress.com by 213.200.69.106 on 09/08/12
For personal use only.

Can. J. Chem. Downloaded from www.nrcresearchpress.com by 213.200.69.106 on 09/08/12
For personal use only.

TABLE 1. The ^{13}C nmr chemical shifts of **1**, **1***a*, and **2** in C_5D_5N (298 K)

C[a]	DEPT	δ_C (**1**)	Δ_C (**1***a*)	δ_C (**2**)[b]
1	CH_2	37.4	39.4	38.2
2	CH_2	28.1	32.0	28.9
3	CH	76.0	76.8	78.2
4	CH_2	27.8	30.3	28.2
5	CH	53.5	53.7	52.0
6	CH_2	64.9	66.8	66.2
7	CH_2	51.1	51.3	49.3
8	C	74.8	75.8	74.8
9	CH	55.4	57.1	55.7
10	CH	36.0	35.9	36.6
11	CH_2	17.7	19.3	18.5
12	CH_2	45.3	42.3	41.4
13	C	47.9	45.1	44.0
14	CH	64.1	67.2	65.7
15	CH	68.4	69.3	68.6
16	CH_2	45.2	42.6	40.5
17	CH	54.9	55.5	54.1
18	CH_3	14.2	15.9	14.9
19	CH_3	13.0	14.6	13.7
20	CH	37.4	37.6	34.7
21	CH_3	17.6	20.1	18.2
22	CH_2	34.1	34.4	30.6
23	CH_2	26.5	29.3	27.1
24	CH	85.1	78.8	83.5
25	CH	29.9	33.2	30.3
26	CH_3	17.5	17.8	17.5
27	CH_3	16.8	19.3	18.3
1′	CH	101.5	103.4	102.2
2′	CH	73.2	75.5	74.1
3′	CH	78.9	78.8	77.1
4′	CH	69.3	71.6	70.3
5′	CH_2	66.2	67.5	66.1

[a]Assignments confirmed by HMBC.
[b]For nmr data taken in CD_3OD see ref. 4.

fords two saponins with identical aglycone and sugar in which the sugar and the sulphate group are respectively located at C24 and C3 in one, and at C3 and C24 in the other. *Asterias amurensis* (20) has two saponins with the same aglycone and sugar, and with a sulphate group placed either at C4′ or at C15. The fact that isomeric compounds like **1** and **2** with very similar ^{13}C nmr data are found in the same starfish is interesting from a biogenetical point of view and underlines the importance of chemical correlations in the correct structural analysis of asterosaponins.

We found in our study none of the known saponins recently reported (21) to have been isolated from *Heliaster helianthus*.

Experimental

General

Optical rotation was measured in MeOH in a Perkin–Elmer 141 polarimeter using a sodium lamp operating at 589 nm. One-dimensional nmr spectra were recorded in C_5D_5N at 298 K, ^{13}C nmr and DEPT spectra on a Bruker WM-250 spectrometer at 250 and 60.13 MHz, selective 1D TOCSY spectra on a Bruker AMX-400 spectrometer, and a proton spectrum on a Bruker AMX-500 at 500.14 MHz. The hplc was performed with a Waters model 6000A apparatus equipped with an R401 differential refractometer; dccc was carried out with an Eyela model 300-S apparatus equipped with 300 tubes. Fast atom bombardment mass (FAB ms) spectra were obtained on a Kratos MS50 mass spectrometer with a Kratos FAB source of 2–8 kV Xe atoms; samples were dissolved in a 1:1 glycerol–thioglycerol matrix with NaCl and KCl as additives for positive ion mode, and in a glycerol matrix for negative ion mode. Electronic impact mass (EI ms) spectra were obtained on a Hewlett–Packard 5988 A mass spectrometer, bombarding with electrons of 70 eV energy. The gc–ms analyses were carried out with a 5890 gas chromatograph and a Supelco SP™-2330 capillary column (15 m, i.d. 0.25 mm, film thickness 0.20 μm, carrier gas He 1 mL/min, 240°C), with T_1 = 80°C maintained for 2 min, then 2°C/min up to 100°C, 30°C/min up to 170°C, and 4°C/min up to 240°C, maintained for 10 min; for detection a Hewlett–Packard mass spectrometer was used. All solvents were dried and distilled under argon.

Two-dimensional nmr experiments

All two-dimensional nmr measurements were performed on a Bruker AMX-500 spectrometer with a Bruker X-32 computer running the UXNMR software package. Inverse ^1H–^{13}C correlation experiments with ^1H–^1H RELAYS (sl = 19 ms) were performed in phase sensitive mode (tppi) using the BMLTP sequence for mixing; the spectral widths (t_2) were 3012.05 and 45.52 Hz; 1024 experiments of 96 scans each (relaxation delay 1 s, mixing time 3.8 ms) were acquired in 2 K data points and subjected to QSINE transformation. The two-dimensional ^1H–^{13}C heteronuclear shift correlation (HMQC) spectra (512 × 2K) for directly bonded protons and carbons were obtained by accumulating 48 scans per t_1, with a relaxation delay of 1 s and J_{CH} = 130 Hz. The two-dimensional ^1H–^{13}C heteronuclear shift correlation (HMBC) spectrum (1024 × 2K) of helianthoside was obtained by accumulating 128 scans per t_1; the relaxation delay was 1.5 s and the value of J_{CH} selected was 9 Hz. The data were zero-filled to 1024 in F_1 and subjected to a QSINE transformation.

Extraction and isolation

The starfish *Heliaster helianthus* (3 kg) was collected by hand in December 1990 from intertidal rocks at Valparaiso (Chile) and was immediately freeze-dried. The specimens were identified by Dr. Cecilia Osorio, University of Chile. A voucher is deposited at the Facultad de Ciencias, University of Chile, Santiago. The remaining freeze-dried starfish (1.2 kg) were homogenized in methanol (four times) and the extract was evaporated to dryness under reduced pressure. The dry extract was dissolved in 70:30 MeOH–H_2O, defatted with CH_2Cl_2 (2 × 600 mL), and partitioned between *n*-BuOH and H_2O (4 × 400 mL). The *n*-BuOH extract (3.8 g) was concentrated and passed through a column of Amberlite XAD-2, which was first washed with water (3 L) and then eluted with MeOH (4 L). The methanol eluates were dried under reduced pressure at room temperature to give 1.5 g of a glassy material, which when chromatographed on Sephadex LH-20 (flow rate 60 mL/h) with methanol as eluant and tlc monitoring (silica gel, 12:3:5 *n*-BuOH/AcOH/H_2O) gave three main fractions. The second fraction (700 mg) was subjected to dccc (ascending mode, 7:13:8 $CHCl_3$/MeOH/H_2O, flow rate 12 mL/h), giving four fractions. The second fraction was subjected to repetitive reversed phase hplc on a 30 cm × 19 mm i.d. C_{18} μ-Bondapack column, eluting with 70:30 MeOH/H_2O; it afforded 17 mg of pure **2** (retention time 4.08 min). The third dccc fraction was subjected to hplc as before, eluting with 60:40 MeOH/H_2O; it gave 12 mg of pure helianthoside (**1**), retention time 6.30 min.

Helianthoside (**1**): $C_{32}H_{57}NaO_8S$; $[\alpha]_D^{20}$ −15.3, MeOH (1.70 mg/mL); mp 210–212°C; ^1H nmr: see Tables 1 and 2, ^{13}C nmr: see Table 3, FAB-ms (positive ion mode; *m/z* %): 709 ($[(M + Na)]^+$, 70), 589 ($[(M + Na) - NaHSO_4]^+$, 41), 307 ($[C_9H_{16}NaO_8S]^+$, 64), 285 ($[C_9H_{17}O_8S]^+$, 100), and 263 ($[C_6H_9NaO_8S]^+$, 58). FAB ms (negative ion mode, *m/z* %): 663 ($[(M - H)]^-$, 100); no further fragments were observed.

Compound **2**: $C_{32}H_{57}NaO_8S$; $[\alpha]_D^{20}$ +90.4, MeOH (1.15 mg/mL); mp 206–208°C; ^1H nmr (C_5D_5N) δ_H: 0.88 (d, 3H, J = 13 Hz, 21-Me), 0.10 (d, 3H, J = 13 Hz, 27-Me), 1.04 (d, 3H, J =

TABLE 2. The ^{1}H nmr and 2D correlation data of the aglycone part of **1**

Proton[a]	δ_H,[b] mult.	J (Hz)	$^2J_{CH}$	$^3J_{CH}$
H1a	1.08 dd			
H1e	1.79 ddd	10.00, 13.24		C3
H2a	1.86 ddd	2.50, 11.70		
H2e	2.12 t			
H3	4.06 m			
H4a	1.68 q		C5, C3	
H4e	3.22 dd	2.50, 11.50		
H5	1.44 ddd		C6	C1, C19
H6	4.30 ddd	5.00, 10.70, 12.50		
H7a	2.15 t		C5, C6	
H7e	3.38 dd	4.00, 13.50	C5, C6, C8	C9
H9	1.04 dd			C19
H11a	1.54 dd			
H11e	1.96 t			
H12a	1.22 dd			C14
H12e	1.96 t			C9, C14
H14	1.65 d		C13, C15	C16, C17, C18
H15	4.72 ddd	4.00, 6.00		
H16pa	2.25 ddd			C20
H16pe	2.05 dd			C20
H17	1.54 dd		C13, C16, C20	C18
$H_3$18	1.30 s		C17	C13, C14, C16
$H_3$19	1.24 s		C10	C1, C5, C9
H20	1.50 m			
$H_3$21	0.98 d	5.96	C17, C20	C22
$H_2$22	1.38 ddd, 1.90 dd			
$H_2$23	1.96, 2.08 dd			
H24	4.78 ddd	3.50, 9.75		C26, C27
H25	2.31 m		C24, C26, C27	
$H_3$26	1.08 d	6.16	C25	C24, C27
$H_3$27	1.15 d	4.79	C25	C24, C26

[a]a = axial, e = equatorial.
[b]Assignment confirmed by HMQC and RELAYED H, C-COSY.

TABLE 3. The ^{1}H nmr and 2D nmr correlation data of the xylopyranosyl[a] moiety of **1**

		Long-range correlations		
Proton	δ_H,[b] mult., J (Hz)	$^2J_{CH}$	$^3J_{CH}$	nOe's
H24	4.78, ddd, 3.5 9.8		C1′, C26, C27	
H1′	4.95, d, 7.5	C2′	C3′, C5′	H3′, H5α′
H2′	4.02, t, 8.5	C1′, C3′		H4′, H5β′
H3′	4.14, t, 9.5	C2′	C4′, C5′	H1′, H5α′
H4′	4.24, ddd, 5.0 10.0	C3′, C5′		H2′, H5β′
H5α′	4.35, dd, 5.0 11.5	C4′	C1′, C3′	H4′, H5α′
H5β′	3.64, t, 10.0	C4′	C1′, C3′	H1′, H3′, H5β′

[a]In pyridine-d_5.
[b]From HMQC.

13 Hz, 26-Me), 1.06 (s, 3H, 18-Me), 1.11 (s, 3H, 19-Me), 1.44 (dd, 1H, H-17), 1.57 (d, 1H, J = 10 Hz, H-1 eq), 2.02 (ddd, 1H, J = 4 and 11 Hz, H-2 eq), 2.94 (dd, 1H, J = 5 and 14 Hz, H-4 eq), 3.12 (dd, 1H, J = 8 and 17 Hz, H-7 eq), 3.75 (dd, 1H, J = 1 and 10 Hz, H-5′ eq), 3.88 (t, 1H, J = 16 Hz, H-2′), 3.91 (m, 1H, H-3 ax), 4.07 (t, 1H, J = 17 Hz, H-3′), 4.10 (dd, 1H, J = 5.5 and 11 Hz, H-4′), 4.14 (ddd, 1H, J = 2, 9, and 18 Hz, H-6 ax), 4.24 (dd, 1H, J = 10 and 13 Hz, H-5′ ax), 4.62 (dd, 1H, J = 10 and 12 Hz, H-15 pax), 4.67 (ddd, 1H, J = 7 and 9 Hz, H-24), 4.85 (d, 1H, J = 15 Hz, H-1′); for nmr data taken in CD_3OD, see ref. 4; ^{13}C nmr: see Table 3. FAB-ms (positive ion mode; m/z %): 725 ($[(M - H + 2Na)]^+$, 25), 709 ($[(M + Na)]^+$, 100), 589 ($[(M + Na) - NaHSO_4]^+$, 80), 559 ($[(M + Na) - C_5H_{10}O_5]^+$, 30).

Solvolysis of helianthoside (1)

A solution of compound **1** (10 mg) in a mixture of dioxane (1 mL) and pyridine (1 mL) was heated at 120°C overnight in a stoppered reaction vial. After the solution had cooled, the solvents were removed under reduced pressure and the residue was partitioned between water (3 mL) and *n*-BuOH (2 mL). The extraction was repeated three times and the combined organic extracts were washed with water and evaporated to dryness under reduced pressure. The residue was purified by hplc on a 30 cm × 19 mm i.d. C_{18} μ-Bondapack column, eluting with 70:30 MeOH/H_2O, to give one major compound (7 mg, retention time 16.35 min), identified as 24-*O*-(β-D-xylopyranosyl)-5α-cholestane-3β,6α,8β,15α,24-pentaol (**1***a*).

Can. J. Chem. Downloaded from www.nrcresearchpress.com by 213.200.69.106 on 09/08/12
For personal use only.

Can. J. Chem. Downloaded from www.nrcresearchpress.com by 213.200.69.106 on 09/08/12
For personal use only.

Compound **1**a: $C_{32}H_{58}O_8$; ^{1}H nmr (C_5D_5N) δ_H: 0.98 (d, 3H, J = 13 Hz, 21-Me), 1.10 (d, 3H, J = 13 Hz, 27-Me), 1.14 (d, 3H, J = 13 Hz, 26-Me), 1.26 (s, 3H, 18-Me), 1.32 (s, 3H, 19-Me), 3.22 (dd, 1H, H-4 eq), 3.42 (dd, 1H, J = 6 and 18 Hz, H-7 eq), 3.65 (t, 1H, J = 17 Hz, H-5′ eq), 3.88 (t, 1H, J = 16 Hz, H-2′), 3.91 (m, 1H, H-3 ax), 4.20 (dd, 1H, H-4′), 4.17 (t, 1H, J = 15 Hz, H-3′), 4.37 (t, 1H, J = 10, H-5′ ax), 4.95 (d, 1H, J = 15 Hz, H-1′); ^{13}C nmr: see Table 1. FAB-ms (negative ion mode; m/z %): 569 ([(M − H)]$^-$, 100), 419 ([(M − H) − $C_5H_{10}O_5$]$^-$, 70).

Methylation of compound **1**a *and hydrolysis of* **1**b

A solution of **1***a* (2 mg) in anhydrous dimethyl formamide (1 mL) was stirred with NaH at 60°C for 2 h under an Ar atmosphere. The mixture was treated with CH_3I (0.25 mL) under ice cooling and was stirred at room temperature for a further 12 h in the dark. The reaction mixture was then poured into ice-water and extracted with $CHCl_3$ (3 × 2 mL). The $CHCl_3$ extract was washed with saturated aqueous NaCl solution, and then dried over $MgSO_4$ and concentrated under reduced pressure to give the permethylated compound **1***b* as an oily residue.

Compound **1**b: $C_{39}H_{72}O_8$; ^{1}H nmr (CCl_3D) δ_H: 0.89 (d, 3H, J = 14 Hz, 21-Me), 0.92 (d, 6H, J = 13 Hz, 26-Me and 27-Me), 1.25 (s, 3H, 18-Me), 1.30 (s, 3H, 19-Me), 3.33, 3.34, 3.46, 3.58, 3.59, 3.60, 3.61 (s, 21H, OMe). EI-ms (m/z %): 668 ([M]$^+$, 40), 466 ([M − $C_8H_{16}O_5$]$^+$, 70).

A solution of the permethylated compound **1***b* in anhydrous MeOH (1 mL) and CH_2Cl_2 (1 mL) with *p*-toluenesulphonic acid (cat.) was stirred at 35°C for 24 h. After cooling, it was neutralized with KH_2PO_4 and extracted with $CHCl_3$ (3 × 2 mL). The $CHCl_3$ extract was washed with saturated aqueous NaCl solution, dried over $MgSO_4$, and concentrated to dryness under reduced pressure. The residue was purified by hplc on a 25 cm × 10 mm i.d. Spherisorb column, eluting with 75:25 AcOEt–hexane, to give two major peaks: 1 mg of **1***c* (retention time 4.3 min) and 1 mg of tetra-*O*-methylxylpyranose (**1***f*, retention time 6.8 min).

Compound **1**c: $C_{31}H_{56}O_5$; ^{1}H nmr (CCl_3D) δ_H: 0.89 (d, 3H, J = 14 Hz, 21-Me), 0.92 (d, 6H, J = 13 Hz, 26-Me and 27-Me), 1.25 (s, 3H, 18-Me), 1.30 (s, 3H, 19-Me), 3.33, 3.46, 3.59, 3.61 (s, 12H, OMe). EI-ms (m/z %): 372 ([M]$^+$, 60).

Preparation of the partially methylated alditol acetates of **1**f

The sugar was dissolved in MeOH (1 mL), $NaBH_4$ (1 mg) was added, and the mixture was stirred at room temperature for 2 h. After addition of AcOH to eliminate excess $NaBH_4$, the mixture was concentrated to dryness under reduced pressure and the resulting alditol was acetylated with Ac_2O–pyridine (1:1, 1 mL) by refluxing overnight. The solution was washed with saturated aqueous $CuSO_4$ solution and extracted with CH_2Cl_2. The alditol acetate was identified as 5-*O*-acetyl-1,2,3,4-tetra-*O*-methylxylitol by gc–ms.

Compound **1**d, *the (+)-(*R*)-MPA ester of* **1**c

To 0.4 mg of **1***c* dissolved in dry methylene dichloride (1 mL) were added 0.2 mg of (+)-(*R*)-MPA, excess DCC, and a catalytic amount of dimethylaminopyridine. The mixture was stirred at room temperature for 24 h and washed with saturated aqueous $NaHCO_3$ solution (2 × 2 mL) and 1 N HCl (2 × 2 mL). The organic layer was washed with brine, dried over $MgSO_4$, and concentrated under reduced pressure. The residue was purified on a silica gel column (9 cm × 0.3 cm), eluting with hexane and increasing amounts of AcOEt, to give the (+)-(*R*)-MPA ester of **1***c*.

Compound **1**d: $C_{40}H_{64}O_7$; ^{1}H nmr (CCl_3D) δ_H: 0.89 (d, 3H, J = 14 Hz, 21-Me), 0.91 (d, 6H, J = 13 Hz, 26-Me and 27-Me), 1.25 (s, 3H, 18-Me), 1.30 (s, 3H, 19-Me), 3.33, 3.46, 3.52, 3.59, 3.61 (s, 15H, OMe).

Compound **1**e, *the (−)-(*S*)-MPA ester of* **1**c

As above, but using the (−)-(*S*)-acid instead of the (+)-(*R*)-acid to obtain the (−)-(*S*)-MPA ester of **1***c*.

Compound **1**e: $C_{40}H_{64}O_7$; ^{1}H nmr (CCl_3D) δ_H: 0.84 (d, 3H, J = 13 Hz, 26-Me), 0.86 (d, 3H, J = 13 Hz, 27-Me), 0.89 (d, 3H, J = 14 Hz, 21-Me), 1.25 (s, 3H, 18-Me), 1.30 (s, 3H, 19-Me), 3.33, 3.46, 3.52, 3.59, 3.61 (s, 15H, OMe).

Acknowledgements

This work was supported by the Xunta de Galicia (XUGA 20906B91 and XUGA 20904A90) and the Comisión Interministerial de Ciencia y Tecnología (CICYT) (SAF 92-1023). M. J. V. acknowledges a fellowship from the Xunta de Galicia. We are grateful to Dr. Domingo Domínguez and Bruker (Wiesembourg) for the nmr experiments.

1. M. Valeria D'Auria, L. Gómez Paloma, L. Minale, and R. Riccio. Tetrahedron, **48**, 491 (1992).
2. J.M. Wasylyk, G.E. Martin, A.J. Weinheimer, and M. Alam. J. Nat. Prod. **52**, 391 (1989).
3. J.A. Dale and H.S. Mosher. J. Am. Chem. Soc. **95**, 512 (1973).
4. I. Kitagawa and M. Kobayashi. Chem. Pharm. Bull. **26**, 1864 (1978).
5. A. Bax and D.G. Davis. J. Magn. Reson. **65**, 355 (1985).
6. A. Bax and S. Subramanian. J. Magn. Reson. **67**, 565 (1986).
7. M. Valeria D'Auria, R. Riccio, E. Uriarte, L. Minale, J. Tanaka, and T. Higa. J. Org. Chem. **54**, 243 (1989).
8. A. Bax and M.F. Summers. J. Magn. Reson. **68**, 2093 (1986).
9. G. Wagner. J. Magn. Reson. **55**, 151 (1983).
10. J. Rodríguez, R. Riguera, and C. Debitus. J. Org. Chem. **57**, 4624 (1992).
11. I. Bruno, L. Minale, and R. Riccio. J. Nat. Prod. **53**, 366 (1990).
12. M. Valeria D'Auria, M. Iorizzi, L. Minale, R. Riccio, and E. Uriarte. J. Nat. Prod. **53**, 94 (1990).
13. R. Riccio, M. Iorizzi, and L. Minale. Bull. Soc. Chim. Belg. **95**, 869 (1986).
14. M. Iorizzi, L. Minale, R. Riccio, and H. Kamiya. J. Nat. Prod. **53**, 1000 (1990).
15. F. Zollo, E. Finamore, R. Riccio, and L. Minale. J. Nat. Prod. **52**, 693 (1989).
16. I. Bruno, L. Minale, and R. Riccio. J. Nat. Prod. **52**, 1022 (1989).
17. R. Segura de Correa, R. Riccio, L. Minale, and C. Duque. J. Nat. Prod. **48**, 751 (1985).
18. R. Riccio, L. Minale, S. Bano, N. Bano, and V.U. Ahmad. Gazz. Chim. Ital. **117**, 755 (1987).
19. A.A. Kicha, A.I. Kalinovsky, E.V. Levina, A.A. Stonik, and G. Elyakov. Tetrahedron Lett. **24**, 3893 (1983).
20. R. Riccio, M. Iorizzi, L. Minale, Y. Oshima, and T. Yasumoto. J. Chem. Soc. Perkin Trans. 1, 1337 (1988).
21. C. Neira, M. Silva, M. Iorizzi, and L. Minale. Bol. Soc. Chil. Quím. **37**, 142 (1992).

Stereocontrolled construction of 1,7-dimethyl A.B.C.[6.6.6] tricycles. Part I. Transannular Diels–Alder reactions of 14-membered macrocycles containing *trans*-dienophiles

YAO-CHANG XU, ANDREW L. ROUGHTON, RAYMOND PLANTE, SOLO GOLDSTEIN, AND PIERRE DESLONGCHAMPS[1]

Laboratoire de synthèse organique, Département de chimie, Faculté des sciences, Université de Sherbrooke, Sherbrooke (Québec), Canada J1K 2R1

Received February 18, 1992

YAO-CHANG XU, ANDREW L. ROUGHTON, RAYMOND PLANTE, SOLO GOLDSTEIN, and PIERRE DESLONGCHAMPS. Can. J. Chem. **71**, 1152 (1993).

Transannular Diels–Alder reactions of 14-membered macrocyclic trienes possessing a methyl substituent on both the diene and dienophile moiety have been investigated. Macrocyclic structures **1***a*, **1***b*, and **1***c* having *cis-trans-trans* (CTT), *trans-cis-trans* (TCT), and *trans-trans-trans* (TTT) geometries could be stereoselectively constructed by coupling appropriately functionalized dienes **5** and dienophile **4** following an intramolecular displacement of an allylic halide by the anion of an appropriately located dimethyl malonate unit. The transannular Diels–Alder reaction performed on **1***a* led to a mixture of four major tricyclic products, including **34** possessing the unexpected *trans-anti-cis* (TAC) stereochemistry. When heated at 300°C, macrocycle **1***b* underwent an unique conversion via an ene–retroene, Diels–Alder process, producing the unexpected tricycle **41** (racemic form) containing five contiguous chiral centers. A rationale for the above experimental facts is presented. In contrast to the previous results, the transannular Diels–Alder reaction of macrocycle **1***c* was straightforward, producing a 95% isolated yield of *trans-anti-cis* (TAC) tricycle **34**. This investigation demonstrates a general methodology for the stereocontrolled synthesis of 1,2-dimethyl A.B.C[6.6.6] tricyclic compounds, which are potential precursors to polycyclic natural products such as steroids and terpenes.

YAO-CHANG XU, ANDREW L. ROUGHTON, RAYMOND PLANTE, SOLO GOLDSTEIN et PIERRE DESLONGCHAMPS. Can. J. Chem. **71**, 1152 (1993).

La réaction de Diels–Alder transannulaire macrocycles à 14 chaînons contenant un diène et un diénophile substitués par un radical méthyl est décrite. Les macrocycles **1***a*, **1***b* et **1***c* de géométrie *cis-trans-trans* (CTT), *trans-cis-trans* (TCT), et *trans-trans-trans* (TTT) ont été préparés de manière stéréosélective par le couplage des diènes **5** et du diénophile **4** suivi par un déplacement intramoléculaire d'un halogénure allylique par l'anion d'une unité malonate. Le macrocycle **1***a* fournit par une réaction de Diels–Alder transannulaire un mélange de quatre produits tricycliques dont **34**, produit inattendu, de stéréochimie *trans-anti-cis* (TAC). Par chauffage à 300°C le macrocycle **1***b* subit une transformation unique par une suite de réactions ène–rétroène, Diels–Alder conduisant au tricycle inattendu **41** (forme racémique) qui possède cinq centres chiraux contigus. Une rationalisation de ces faits expérimentaux est proposée. Contrairement aux résultats précédents, la réaction Diels–Alder transannulaire effectuée sur le macrocycle **1***c* donna comme attendu le tricycle *trans-anti-cis* (TAC) **34** avec un rendement de 95% en produit isolé. Dès lors cette étude démontre une méthodologie générale permettant de synthétiser de manière stéréocontrôlée des structures tricycliques 1,2-diméthyl A.B.C.[6.6.6], précurseurs potentiels de produits naturels tels les stéroïdes et les terpènes.

Can. J. Chem. Downloaded from www.nrcresearchpress.com by 213.200.69.106 on 09/08/12
For personal use only.

Introduction

Recent research in our laboratories has centered on the development of general methodologies that can be used to prepare polycyclic compounds in a stereocontrolled manner (1, 2). Our approach, illustrated in Scheme 1, makes use of the transannular Diels–Alder reaction on macrocyclic trienes like **1** to give A.B.C.[6.6.6] tricyclic compounds such as **2**. The [4+2] cycloaddition adducts **2**, which possess four newly created chiral centers as well as different substituents and functional groups on the three fused six-membered rings, are potential precursors to polycyclic natural products such as steroids and terpenes (3).

Our earlier studies (4) involving the syntheses of carbon macrocycles having various ring size (10–14 carbons) by base-assisted intramolecular displacement reaction laid the foundation for the development of this new methodology. Having successfully constructed the necessary macrocyclic triene, the first transannular Diels–Alder reaction of 13-membered macrocycles was found to produce B.C.D.[6.6.5] tricyclic compounds (2*f–j*). Further investigations of the transannular Diels–Alder cycloaddition in 14-membered macrocycles such as **1** with no methyl (2*d*, *e*) or with one methyl substituent (2*a*, *b*) showed them to be very promising for the construction of A.B.C.[6.6.6] tricyclic compounds. In both cases, racemic tricyclic products could be obtained in good yields and excellent stereoselectivities of the four contiguous asymmetric centers. In the course of our study, a total synthesis of a steroid derivative using the transannular Diels–Alder approach was reported by Takahashi et al. (5).

In this article, we would like to report further investigations (1) of the transannular Diels–Alder reaction in a 14-membered macrocycle system containing a methyl substituent on both the diene and dienophile moiety. As indicated in Scheme 1, the cycloaddition in macrocycle **1** would lead to the formation of 1,7-dimethyl tricyclic product **2**. The skeleton of such a tricyclic system having two methyl groups, on C(1) and C(7), is a common constituent of many natural diterpene and triterpene products. This study can therefore lead to the development of new strategies for the synthesis of some of these polycyclic natural products.

Methods and discussion

Our general approach towards the tricyclic compounds bearing two methyl groups at C(1) and C(7) positions is

[1]Author to whom correspondence may be addressed.

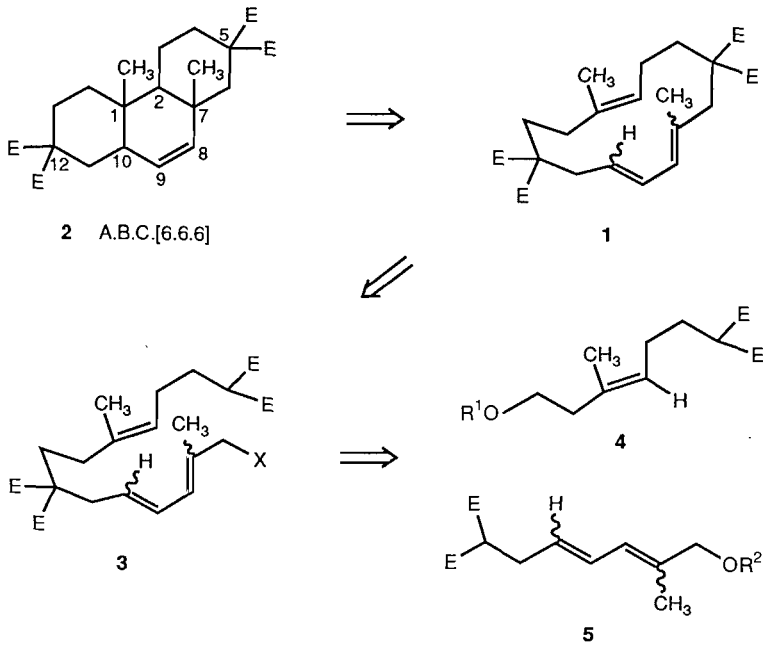

(E = $COOCH_3$)

SCHEME 1

outlined in Scheme 1. The target product **2** could be obtained by the transannular [4+2] cycloaddition in 14-membered macrocycle **1**, which, in turn, could be easily prepared from acyclic triene **3** via an intramolecular displacement of the allylic halide by base-generated dimethyl malonate anion. Triene **3** having different olefin geometries could be derived from the coupling reaction of appropriately functionalized dienes **5** and *E*-dienophile **4**.

Synthesis of E-*dienophile 4*

The basic strategy for the preparation of this trisubstituted olefin is based on the palladium-catalyzed coupling reaction of 2-carbomethoxypropyl zinc iodide **10** (6) and vinyl iodide **11** (7) as depicted in Scheme 2.

The preparation of zinc iodide **10** was readily achieved starting from commercially available γ-butyrolactone **6**. Methanolysis (methanol–pyridine) of acyl chloride **7**, which was obtained from **6** by reaction with thionyl chloride in the presence of zinc chloride (8), provided methyl 4-chlorobutyrate **8**. A halide exchange reaction on **8** (potassium iodide in acetone) gave the corresponding alkyl iodide **9**, which was treated with metal zinc at 60°C to give the desired product **10**.

The preparation of vinyl iodide **11** was realized stereoselectively starting from 4-butynol using Negishi's procedures (7) followed by silylation (9) of the primary alcohol. The coupling reaction of **11** and **10** provided *E*-dienophile **12**, no *Z* isomer being observed by nmr spectroscopy. The desired malonate **4** was obtained by treatment of **12** with lithium diisopropylamide followed by the addition off methyl chloroformate (10).

Syntheses of dienes 5

The syntheses of 2-methyl-substituted 2,4-diene **5***a* (*Z-E*), **5***b* (*E-Z*), and **5***c* (*E-E*) are outlined in Scheme 3 starting from the commercially available *Z*-2-butene-1,4-diol **13**. Swern oxidation of the monoprotected diol **14** (11) led to the α,β-unsaturated aldehyde **15***a* with the *Z*-olefin geometry retained (12). The selective *E* olefination of the aldehyde was performed via a Wittig–Horner–Emmons reaction with ethyldiisopropyl-2-phosphonopropionate and sodium hydride to provide the *Z-E* diene **16***a* (13), which was subsequently converted to the allylic alcohol **17***a* by diisobutylaluminium hydride (DIBAL-H) reduction. The desired allylic chloride **5***a* was finally obtained from **17***a* via Meyers' procedures (lithium chloride, methanesulfonyl chloride, and *s*-collidine in dimethylformamide (DMF) (14)).

Oxidation of mono-protected diol **14** with pyridinium chlorochromate at room temperature yielded the thermodynamically stable *E*-unsaturated aldehyde **15***b* (15), isomer of **15***a*. Condensation of **15***b* with ethyl bis(trifluoroethyl)-2-phosphonopropinate following Still's procedure (16) gave stereoselectively *E-Z* diene ester **16***b*, which was then reduced to alcohol **17***b* by diisobutylaluminium hydride. Protection of the allylic alcohol with *tert*-butyldiphenylchlorosilane in the presence of triethylamine (17) resulted in the formation of silyl ether **18***b*. Treatment of **18***b* with pyridinium *p*-toluenesulfonate in isopropanol selectively removed the tetrahydropyranyl ether to produce allylic alcohol **19***b*,[2] which was converted to allylic chloride **5***b* by the use of the previously mentioned Meyers' method (14).

Similarly, treatment of **15***b* with Wittig reagent derived from ethydiisopropyl-2-phosphonopropionate afforded the *E-E* diene ester **16***c* (13). This stereoselective *E*-olefination reaction from **15***b* to **16***c* could also be realized in good yield by commercially available triethyl-2-phosphonopropionate and sodium hydride. Diisobutylaluminium hydride reduc-

[2]L. Ruest, S. Lamothe, and P. Deslongchamps. Unpublished results.

Can. J. Chem. Downloaded from www.nrcresearchpress.com by 213.200.69.106 on 09/08/12
For personal use only.

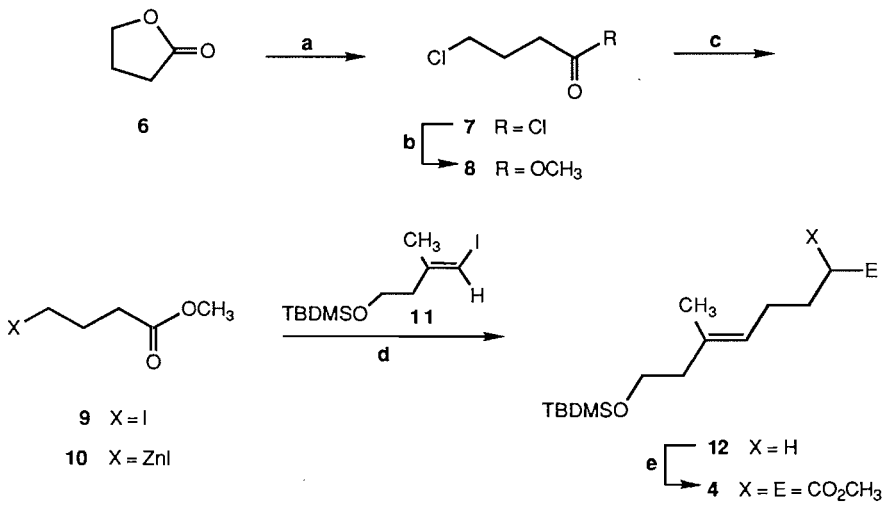

(a) $SOCl_2$, $ZnCl_2$, 55°C, 22 h, 65%;

(b) CH_3OH, Pyridine, 0°C to r.t., 18 h, 77%;

(c) NaI, acetone, reflux, 42 h, 78%;

(d) Zn-Cu, **9**, benzene/DMF, 25°C, 1 h, 60°C, 3 h; then $Pd(PPh_3)_4$, **13**, 60°C, 1 h, 65%;

(e) LDA, -78°C, 0.5 h; then $ClCO_2CH_3$, 67%.

SCHEME 2

tion of **16***c* followed by protection of the resulting allylic alcohol with *tert*-butyldiphenylchlorosilane (17) yielded diene diether **18***c*. Selective removal of the tetrahydropyranyl ether was realized by the previously mentioned method[2] to afford allylic alcohol **19***c*, which was then converted to allylic chloride **5***c* having the *E-E* diene geometry (14).

Preparations of macrocycles 1

The precursors of macrocycles **1***b* (*trans-cis-trans*, TCT) and **1***c* (*trans-trans-trans*, TTT), namely acyclic trienes **22***b* and **22***c*, are readily synthesized by coupling the appropriately functionalized basic building blocks, dienes **5***b* and **5***c*, with dienophile **4**. Thus, deprotection of *E*-dienophile **4** with tetrabutylammonium fluoride (18) provided alcohol **20**, which was subsequently transformed into the methanesulfonate ester **21** with methanesulfonyl chloride and triethylamine (Scheme 4). The coupling reactions were performed by treatment of dienophile **21** with sodium hydride to form the sodium enolate, followed by addition of dienes **5***b* and **5***c* to produce alkylated products **22***b* and **22***c*, respectively, in good yields (19). Introduction of the second malonate connector into the acyclic trienes was accomplished by displacement of the methanesulfonate ester group of trienes **22***b* and **22***c* with the sodium salt of dimethyl malonate in the presence of potassium iodide. The cleavage of the silyl ether protecting group of trienes **23***b* and **23***c* was effected with *n*-Bu_4NF in good yields (18). The resulting allylic alcohol **24***b* was then transformed into the corresponding allylic chloride **25***b* by Meyers' procedure (14), while the allylic alcohol **24***c* was converted to the allylic bromide **25***c* using carbon tetrabromide and triphenylphosphine in dichloromethane (20). A slight decomposition was observed when allylic halides **25***b* and **25***c* were submitted to purification by flash chromatography. This problem, however, could be avoided if the crude allylic halides were filtered through a short-path silica gel column and used for the next reaction immediately without purification by chromatography.

Having built the requisite carbon chain and appropriate functional groups at each end, acyclic trienes **25***b* and **25***c* were ready for the construction of 14-membered macrocycles. The macrocyclizations were performed by slow addition of a solution of allylic chloride **25***b* or allylic bromide **25***c* in tetrahydrofuran to a stirred suspension of cesium carbonate in a mixture of DMF and THF at about 80°C under dilution conditions so as to avoid dimerization (2). Macrocyclic products **1***b* (TCT) and **1***c* (TTT) were respectively obtained in good yields, as white solids, via an intramolecular displacement of allylic halides by base-generated dimethyl malonate anion. Small quantities (≤10%) of the corresponding macrocyclic dimers **26***b* and **26***c* were also isolated. The structures of macrocycles **1***b* and **1***c* were established by spectroscopic characterization including carbon-13 and proton nmr, infrared, and mass spectra. The conservation of the double bond geometries in the cyclization has been clearly established by comparing the proton nmr data of the cyclic products with those of their acyclic triene precursor. Furthermore, the structure of macrocycle **1***b* was confirmed by X-ray analysis (21).

The isolation of the stable 14-membered macrocycle **1***c* having *trans-trans-trans* (TTT) olefin geometries should be noted because previous attempts to isolate such macrocycles had failed due to the facile transannular Diels–Alder reaction under the cyclization conditions (2*b*, 2*e*). The introduction of a methyl substituent on the diene as in **1***c* considerably lowers its reactivity in the transannular Diels–Alder reaction. This is indeed true since the Diels–Alder reaction of **1***c* requires temperatures as high as 250°C (vide infra).

Can. J. Chem. Downloaded from www.nrcresearchpress.com by 213.200.69.106 on 09/08/12
For personal use only.

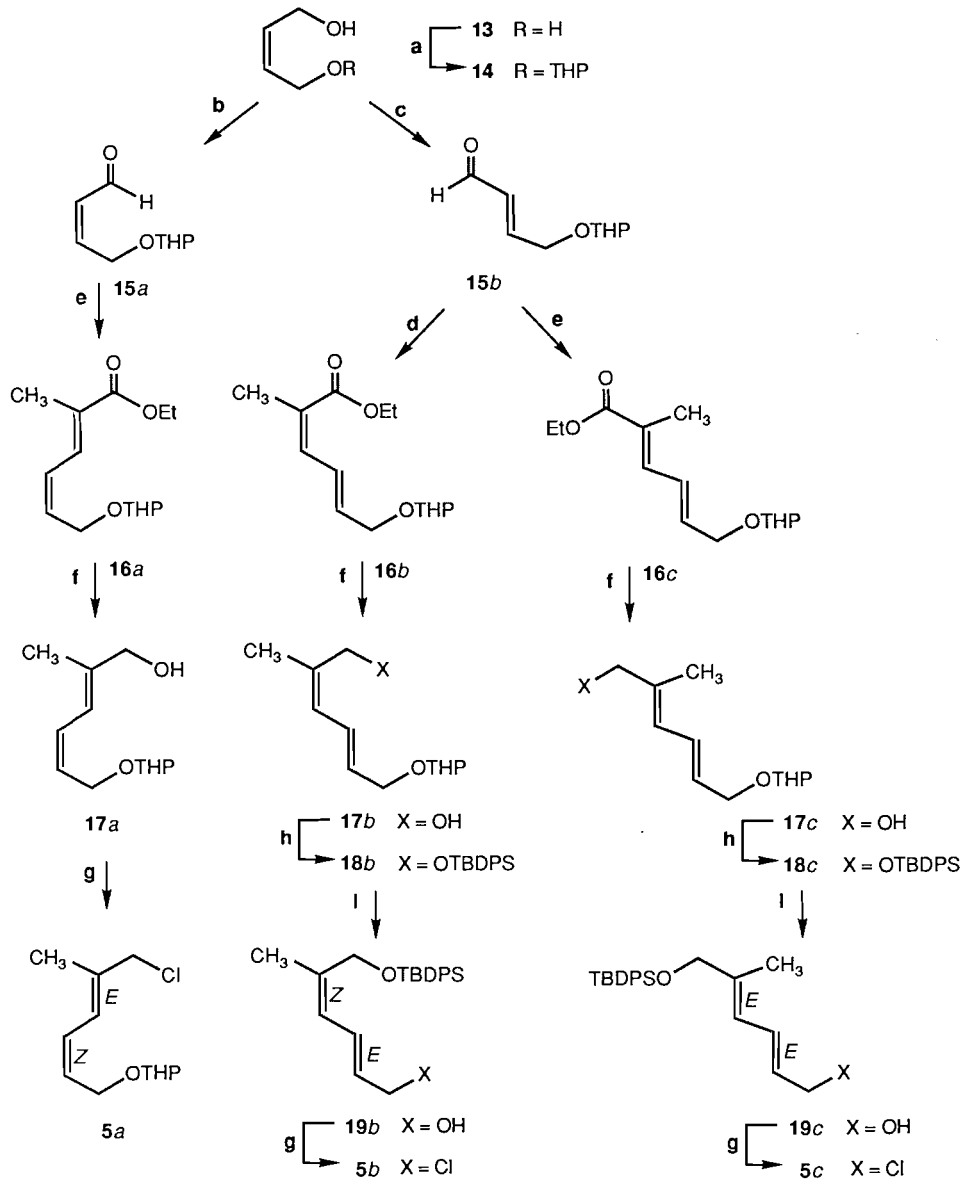

(a) 3,4-Dihydro-2H-pyran, PTSA, CH_2Cl_2, THF, 0°C;
(b) $(COCl)_2$, DMSO, iPr_2NEt, CH_2Cl_2, -60°C;
(c) PCC, NaOAc, Molecular sieves, CH_2Cl_2, 0°C to r.t.;
(d) $(CF_3CH_2O)_2POCH(CH_3)CO_2Et$, 18-crown-6-ether, $KN(TMS)_2$, tol., THF, -78°C;
(e) $iPrO_2POCH(CH_3)CO_2Et$, NaH, THF, -78°C;
(f) DIBAL, CH_2Cl_2, -78°C;
(g) LiCl, *s*-collidine, MsCl, DMF, 0°C to r.t.;
(h) *t*-$BuPh_2SiCl$, imidazole, THF, r.t.;
(i) PPTS, iPrOH, 75°C.

SCHEME 3

It should be also noted that in the case of TTT acyclic triene **25***c*, the allylic bromide was employed for macrocyclization instead of the allylic chloride, which was used extensively in our previous studies (2). As presented in Scheme 5, our original plan to synthesize *trans-trans-trans* macrocycle **1***c* was based on the cyclization of allylic chloride triene **27** (X = Cl). Such an approach was expected to be advantageous due to the reduced steric interactions (methyl group remote from the reaction site) for the cyclization process. However, no macrocyclic product **1***c* could be obtained after several attempts employing the usual cyclization conditions; only decomposition of starting material **27** was observed under various conditions of temperature and reaction time. This failure in transforming acyclic triene **27** to **1***c* prompted us to use the corresponding acyclic triene bromide **27** (X = Br), which is expected to be more reactive than the chloride. Macrocyclization of **27** (X = Br) under the same conditions provided a 24% yield of macrocycle **1***c*. Attempts to increase the yield failed, and we found that allylic bromide **27** decomposed quickly under the cyclization conditions. The instability of such a compound could be rationalized by the fact that **27** (X = Br) can easily form a stable

Can. J. Chem. Downloaded from www.nrcresearchpress.com by 213.200.69.106 on 09/08/12
For personal use only.

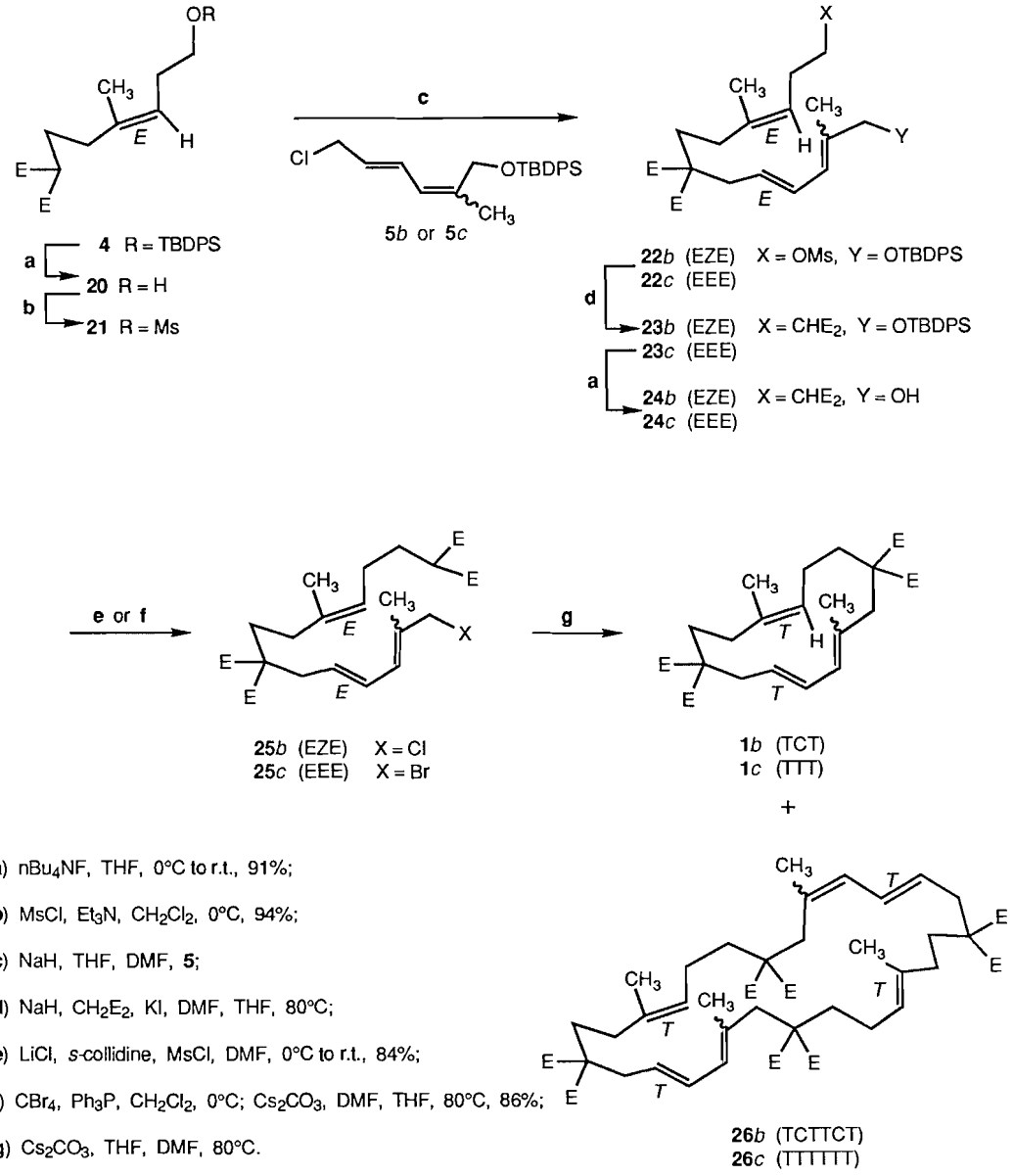

SCHEME 4

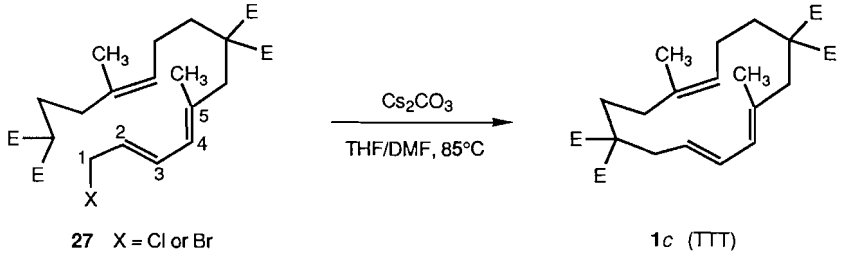

SCHEME 5

allylic carbocation, which is further stabilized by the presence of the methyl group. To circumvent this problem, our original plan was modified so that the cyclization would take place on the side of the diene bearing the methyl group as indicated by structure **25***c*, since we anticipated that **25***c* would be more stable than **27**. Indeed, the allylic bromide **25***c* was found to be stable even under flash chromatographic conditions and it cyclized efficiently to give **1***c* in 73% yield along with 5% of the dimer **26***c*.

The preparation of macrocycle **1***a* having the *cis-trans-*

Can. J. Chem. Downloaded from www.nrcresearchpress.com by 213.200.69.106 on 09/08/12
For personal use only.

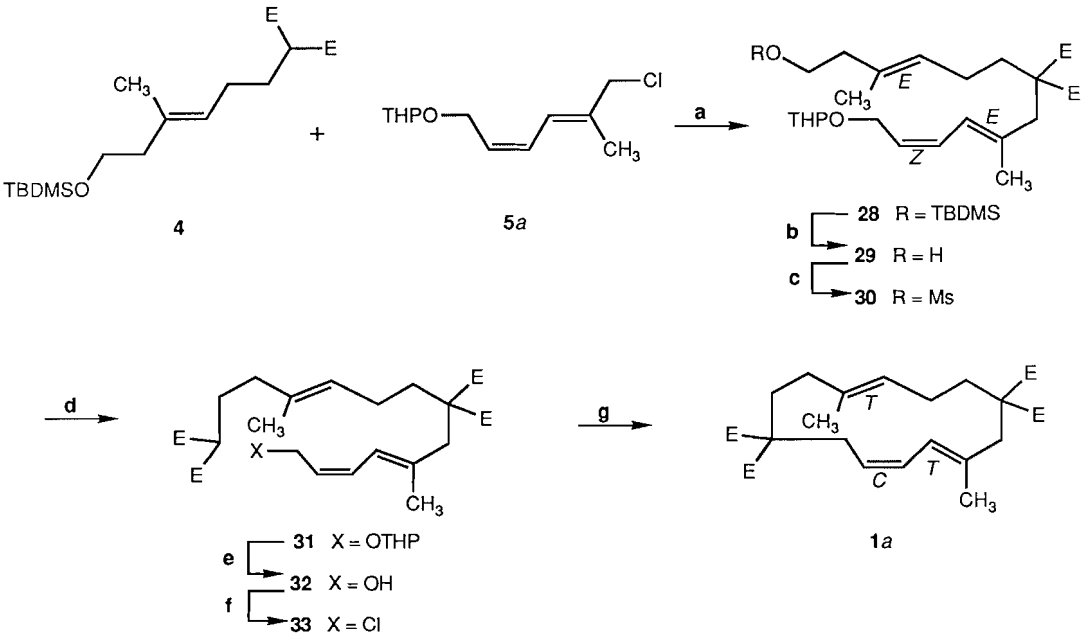

(a) NaH, THF, DMF, 61%;

(b) nBu_4NF, THF, 0°C to r.t., 81%;

(c) MsCl, Et_3N, CH_2Cl_2, 0°C, 98%;

(d) NaH, CH_2E_2, KI, DMF, THF, 80°C, 72%;

(e) PPTS, CH_3OH, 70°C, 97%;

(f) LiCl, MsCl, *s*-collidine, DMF, 0°C to r.t.;

(g) Cs_2CO_3, DMF, THF, 70°C.

SCHEME 6

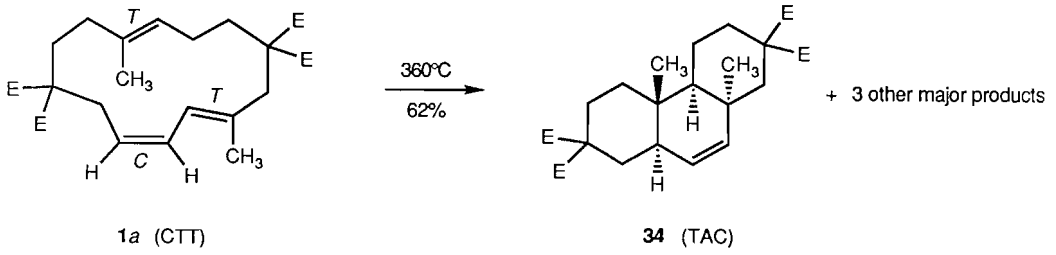

SCHEME 7

trans (CTT) geometry was accomplished following the procedures described in Scheme 6. The coupling reaction of diene **5***a* with dienophile **4** was conducted in the presence of sodium hydride to provide *Z-E-E* acyclic triene **28** (19), which was then converted to the methanesulfonate ester **30** by desilylation (n-Bu_4NF (18)) following mesylation of the resulting alcohol **29** (MsCl and Et_3N). After replacement of the mesylate group by dimethylmalonate, the resulting triene **31** was hydrolyzed to the allylic alcohol **32** (11), which was subsequently converted to the allylic chloride **33** (14). The cyclization step was then conducted in a similar fashion as described before to provide macrocycle **1***a* (CTT) as a crystalline solid. Again, the structure of **1***a* was established by spectroscopic data (nmr, ir, ms).

Synthesis of tricycles, Transannular Diels–Alder reaction

1. From CTT macrocycle ***1****a*

The transannular Diels–Alder reaction of CTT **1***a* was carried out by thermolysis in a sealed quartz tube at 360°C for 80 min to yield a mixture of four major products (Scheme 7). Each compound contributed between 10 and 19% to the total crude reaction mixture as determined by vapour phase chromatography (vpc). Thin-layer chromatography of the crude reaction mixture also revealed the presence of several other minor products. The identification and characterization of the major products was attempted, but failed due to the difficulty in isolating each compound in a pure state. The presence of tricycle **34** having the *trans-anti-cis* (TAC) stereochemistry was, however, demonstrated by comparing

Can. J. Chem. Downloaded from www.nrcresearchpress.com by 213.200.69.106 on 09/08/12
For personal use only.

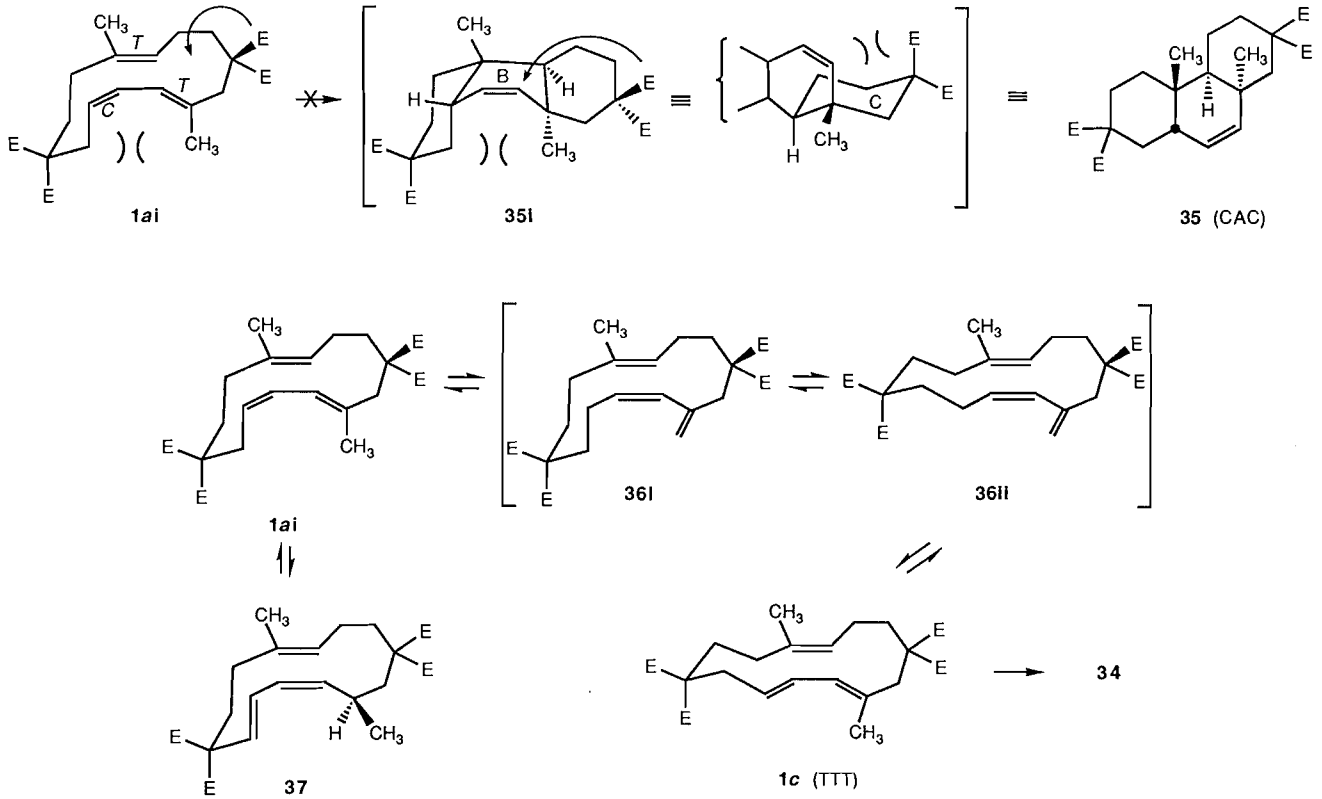

SCHEME 8

the products of the reaction mixture with an authentic sample of **34** prepared by the Diels–Alder reaction of TTT macrocycle **1***c* (vide infra, cf. Scheme 10).

The formation of this complex mixture of tricyclic products can be explained in the following way. In principle, a macrocyclic triene can yield two different diastereoisomers. However, and as previously discussed (2*a*), there are cases where one of the expected diastereoisomers cannot be formed because of a conformational restriction imposed by the fact that the Diels–Alder reaction must take place via a boat transition state. As shown in Scheme 8, the CTT macrocyclic triene **1***a* is expected to produce only the CAC tricycle **35** via the chair–boat–chair conformation **35***i*. Examination of molecular models reveals however that this process is, sterically, extremely crowded: the *cisoid* conformation **1***ai* of the diene that is required for the Diels–Alder reaction is severely hindered sterically due to the presence of the methyl group on the diene, and also due to steric repulsion between one of the ester functions and the diene moiety (Scheme 8); these effects are best seen in the conformation **35***i* of the Diels–Alder product **35** from which the CAC tricycle should be produced: one methyl group in the boat ring B is very severely hindered, and the β-ester function in ring C is in a 1,3 diaxial disposition relative to the olefin of ring B. These severe steric interactions will raise considerably the energy of this process and will allow competing processes to take place.

The unexpected formation of the TAC tricycle **34** as well as the formation of the other major products may be explained in the following way. CTT tricycle **1***a* in conformation **1***ai* can undergo a 1,5 sigmatropic hydrogen migration to give **36** in conformation **36***i*. This new macrocyclic triene can then undergo another 1,5 sigmatropic hydrogen migration via conformation **36***ii* to give TTT macrocyclic triene **1***c*, which can then give the TAC tricycle **34** (vide infra). The other tricyclic products may come from the [4+2] cycloaddition of **36** or via other unknown side reactions. For instance, CTT macrocycle **1***ai* could undergo another 1,5 sigmatropic hydrogen migration to give the isomeric macrocycle **37**, which can also produce tricycles via the transannular Diels–Alder reaction. It should be pointed out that the 1,5 sigmatropic hydrogen migration in a macrocyclic triene followed by a [4+2] cycloaddition process has already been previously observed in our laboratory (2*f*).

*2. From TCT macrocycle 1*b

The transannular Diels–Alder reaction of TCT macrocycle **1***b* was carried out at 300°C in a fashion similar to that described for **1***a*, and the interpretation of the results is presented in Scheme 9. To our surprise, a totally unexpected tricyclic product **41** having a methyl-substituted olefin was isolated in 66% yield. The presence of the methyl group on the double bond in ring B and of the secondary methyl group in ring C was shown by proton nmr, the former one being a singlet at 1.62 ppm and the latter a doublet at 0.92 ppm. The presence of only one rather than two vinyl protons further indicated that the tricycle did not have an expected structure. The overall structure and relative stereochemistry of tricycle **41** was established unambiguously by X-ray analysis (21). It is interesting to note that this compound exists in the solid state in conformation **41***ii* in which the secondary methyl group in ring C is axially oriented.

We previously predicted (2*a*) that 14-membered macrocyclic trienes having a *trans-cis-trans* geometry should give only one tricycle having the *cis-anti-cis* (CAC) stereochem-

Can. J. Chem. Downloaded from www.nrcresearchpress.com by 213.200.69.106 on 09/08/12
For personal use only.

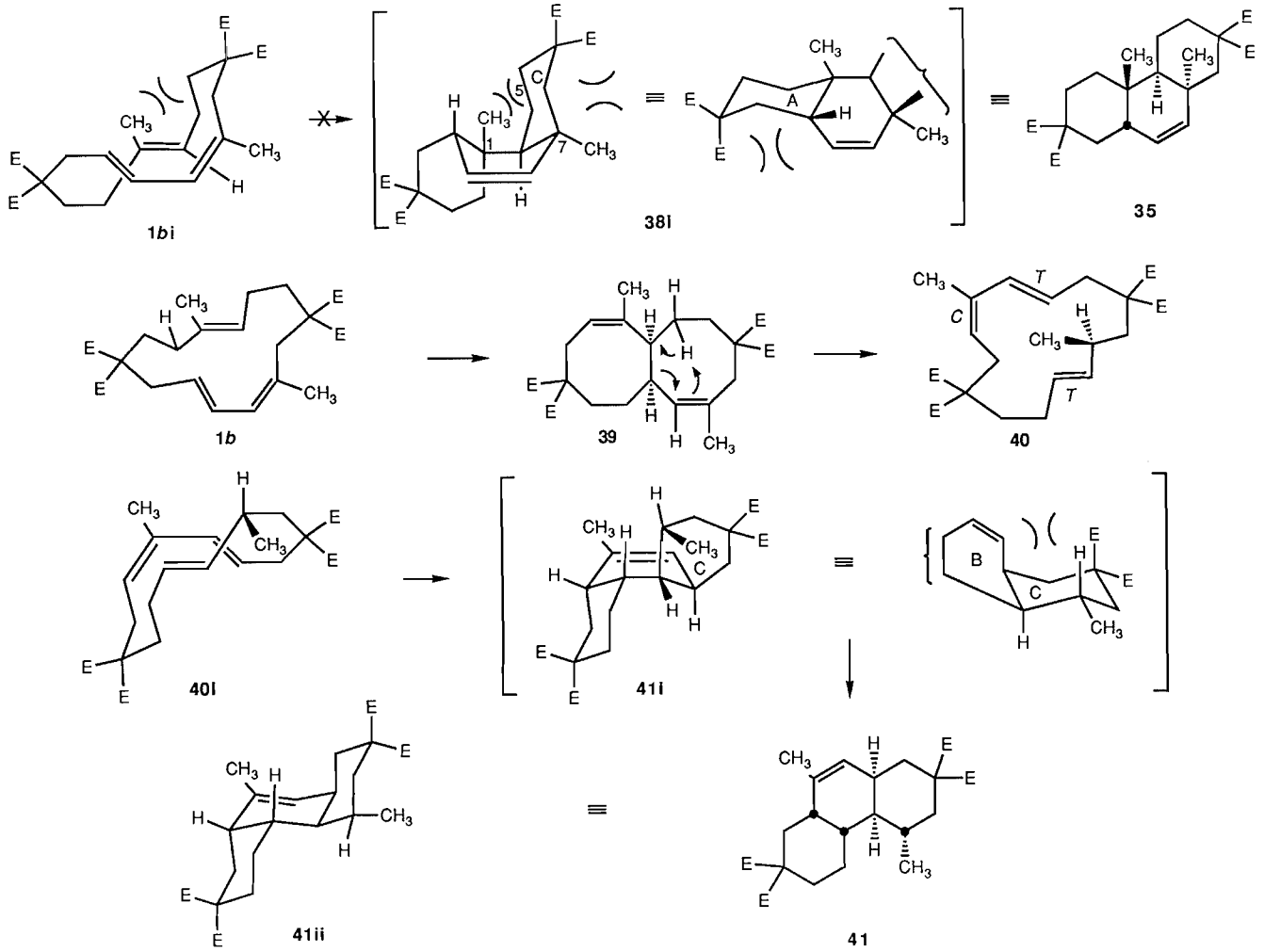

SCHEME 9

istry. It was therefore expected that the TCT macrocycle **1***b* would give the CAC tricycle **35** via conformation **1***bi*. Examination of this process in more detail reveals, however, that it must have a relatively high activation energy due to severe steric interactions caused by the presence of the methyl groups and the ester functions. This can best be seen in conformation **38***i*: the methyl group at C1 is sterically hindered by ring C while the other one at C7 is experiencing a 1,3 diaxial steric interaction with one of the esters of ring C. There is also a 1,3 diaxial steric interaction between the axial ester function in ring A and the olefin of ring B. It is therefore not surprising that macrocycle **1***b* underwent other reactions having a lower activation energy.

The formation of the CAC tricycle **41** having a methyl-substituted olefin can be rationalized by a transannular ene, a retroene, and finally a transannular Diels–Alder reaction as presented in Scheme 9. Thus, the transannular ene reaction would transform macrocycle **1***b* into the *cis*-bicyclic intermediate **39** having two eight-membered rings. This would then be followed by a retroene reaction from **39** to produce the macrocyclic triene **40**. This overall transformation is the equivalent of an oxidation–reduction process whereby the diene and dienophile have been interchanged. The new CTT macrocycle **40** can now easily undergo a transannular Diels–Alder reaction because both methyl groups are no longer located on carbon atoms directly involved in bond formation and therefore are almost completely devoid of severe steric repulsion during this process. Indeed, compound **40** would react via conformation **40***i*, which will produce tricycle **41** in conformation **41***i* having ring B in a boat form and an equatorially oriented secondary methyl group in ring C. In **41***i*, there is only one 1,3 diaxial interaction between an ester function in ring C and the olefin of ring B. Conformation **41***i*, once produced, would then revert to the more stable chair–half-chair–chair conformation **41***ii* having the secondary methyl group axially oriented as shown by X-ray crystallography.

The above interpretation is also in accord with previous studies on less substituted TCT macrocyclic trienes. Indeed, we found (2*e*) that when the TCT macrocyclic trienes bear no methyl groups on the diene and the dienophile, only the theoretically expected CAC tricycle corresponding to **35** (CH_3 = H) was obtained. This is of course not surprising as all the undesired steric effects that unduly raised the transition state energy in **38***i* have now been removed. On the other hand, we also observed (2*b*, 23) that when there is no substituent on the diene and only one methyl group on the dienophile, an intermediate situation occurs. In these cases two processes occur: one equivalent to **1***b* → **35** (40%) and the second equivalent to **1***b* → **41** (60%). In the dimethyl case, the process **1***b* → **35** does not take place because there is

Can. J. Chem. Downloaded from www.nrcresearchpress.com by 213.200.69.106 on 09/08/12
For personal use only.

TABLE 1. Chemical shifts of the methyl and olefin protons change on heating macrocycle **1***b* at 300°C

Entry[a]	Time (h)	Distinguishing ^{1}H nmr characteristics
1	0	5.92–6.11 (2H, m, olefin) 5.17 (1H, dt, olefin) 5.09 (1H, br t, olefin) 1.62 (3H, s, methyl) 1.57 (3H, s, methyl)
2	0.5	5.48 (1H, t, olefin) 4.93 (1H, d, olefin) 1.77 (3H, s, methyl) 1.47 (3H, s, methyl)
3	2	5.19 (1H, s, olefin) 1.62 (3H, d, methyl) 0.92 (3H, d, methyl)

[a]Entries 1 and 3 correspond to the NMR chemical shifts of **1***b* and **41**.

additional steric hindrance that further increases its energy barrier.

Our overall interpretation was further confirmed by detecting the presence of bicyclic intermediate **39** at shorter reaction time in a proton nmr monitored experiment. The intermediate **39** could not, however, be obtained pure by chromatography. Table 1 lists the chemical shifts for the characteristic olefin and methyl protons, which changed with time upon heating the macrocycle **1***b* at 300°C. The proton nmr data in entry 2 of Table 1 were obtained by subtracting the ^{1}H nmr data of both starting material **1***b* (entry 1) and product **41** (entry 3) from that of the reaction mixture after 0.5 h at 300°C. This set of ^{1}H nmr data in entry 2 is in full agreement with the proposed bicyclic structure **39**. The failure to isolate or even detect the TCT macrocyclic intermediate **40** can be explained by its higher reactivity in leading to tricycle **41** at 300°C via the transannular Diels–Alder reaction. In fact a macrocyclic TCT system similar to intermediate **40** was found to undergo a transannular Diels–Alder reaction at 250°C (*2e*).

The observation of this unique conversion, namely, **1***b* → **39** → **40** → **41** is mechanistically very interesting, since it is the first example of larger ring transformations through a transannular ene–retroene, Diels–Alder process, leading stereoselectively to a racemic tricyclic product **41** containing five contiguous chiral centers.

3. From TTT macrocycle **1***c*

In contrast to the previous results of CTT and TCT macrocycles, the transannular Diels–Alder reaction of TTT macrocycle **1***c* turned out to be straightforward. As illustrated in Scheme 10, thermolysis of **1***c* in toluene at 200°C for 18 h provided a 95% isolated yield of tricyclic compound **34** having the *trans-anti-cis* (TAC) stereochemistry, which was firmly established by X-ray analysis (22).

Theoretically, it is expected that the transannular Diels–Alder reaction of a 14-membered TTT macrocycle triene will produce a mixture of two tricycles having the TAC and CAT stereochemistry (*2a*). This was indeed observed in the case of a TTT macrocycle having a methyl group on the dienophile, which gave a 2:1 mixture of TAC and CAT tricycles (*2b*). In the present case, the TAC tricycle is formed exclusively and this result can be easily understood by examining the steric effects involved at the transition level of the two competing processes.

Tricycle TAC **34** and CAT **42** will be formed in conformations **34***i* and **42***i*, respectively, via the Diels–Alder reaction of macrocyclic triene **1***c* reacting in conformations **1***ci* and **1***cii*. Again, steric effects are best analyzed in the conformation in which the reaction products are formed. In stereoisomer **34***i*, there is a 1,3 diaxial steric interaction between the β-ester of ring C and the olefin of ring B. In stereoisomer **42***i*, there are two major steric interactions. The first one is essentially identical to that found in **34***i* (a 1,3 diaxial interaction between the α-ester of ring A and the olefin of ring B). The second one is the result of a 1,3 diaxial interaction between the methyl group at C7 and the β-ester in ring C, expected to be at least 2.5 kcal/mol. On that basis, one should anticipate the exclusive formation of TAC tricycle **34**, in agreement with the experimental result.

We also used molecular modeling to examine these assumptions. We recently (23) described a study of a 14-membered TTT macrocyclic triene, like **1***c* but lacking the methyl substituent of the diene moiety, using the Sybyl software.[3] The transition states of the chair–boat–chair (CBC) and chair–boat–boat (CBB) leading to the corresponding TAC and CAT macrocycles were mimicked and a Boltzman distribution based on their steric energies gave a calculated TAC:CAT ratio in complete agreement with the experimental results. As mentioned above, since the only difference between the two cases is a methyl substituent on the diene moiety, we reasoned that appropriate modifications might produce a fair description of transition structures for the present case as well. Thus the previously obtained transition state mimics (24) were modified by addition of a methyl substituent on the diene (a model of **1***c*), followed by a systematic conformational analysis (10° step) using the Search algorithm within Sybyl. The torsion angle between the forming bonds and the torsion angle in the butadiene moiety were kept at 0° as found by ad initio calculations for the transition state of butadiene and ethylene (24). Distances between the termini of the dienophile and the diene were left at 3 Å as in our previous study and the lowest energy conformers obtained in each case were minimized using the above-mentioned constraints. The four structures thus obtained and their respective steric energies are shown in Fig. 1. The lowest energy structures **A** (chair–boat–chair) and **B** (chair–boat–boat) would produce TAC tricycle **34** while the structures **C** and **D**, which are quite a bit higher in energy, would produce CAT tricycle **42**. A Boltzman distribution at 473 K of these four transition-state-like structures could lead to a product ratio TAC:CAT of 99:1, in excellent agreement with the experimental result.

Finally, as mentioned above, the Diels–Alder reaction of TTT macrocycle **1***c* requires a temperature of 250°C whereas that of the corresponding TTT macrocycle having no substituents on the diene takes place at ≤80°C (*2b*, *2d*). This is readily explained by the fact that when the methyl-substituted *trans-trans* diene takes the required *cisoid* conformation to undergo the cycloaddition, there is an additional severe steric repulsion between the methyl group and the diene moiety (cf. **1***ci*).

In résumé, CTT and TCT macrocycles **1***a* and **1***b* failed

[3]Sybyl 5.5 Tripos Associates, 1699 S. Hanley Road, Suite 303, St. Louis, MO 63144, U.S.A.

Can. J. Chem. Downloaded from www.nrcresearchpress.com by 213.200.69.106 on 09/08/12
For personal use only.

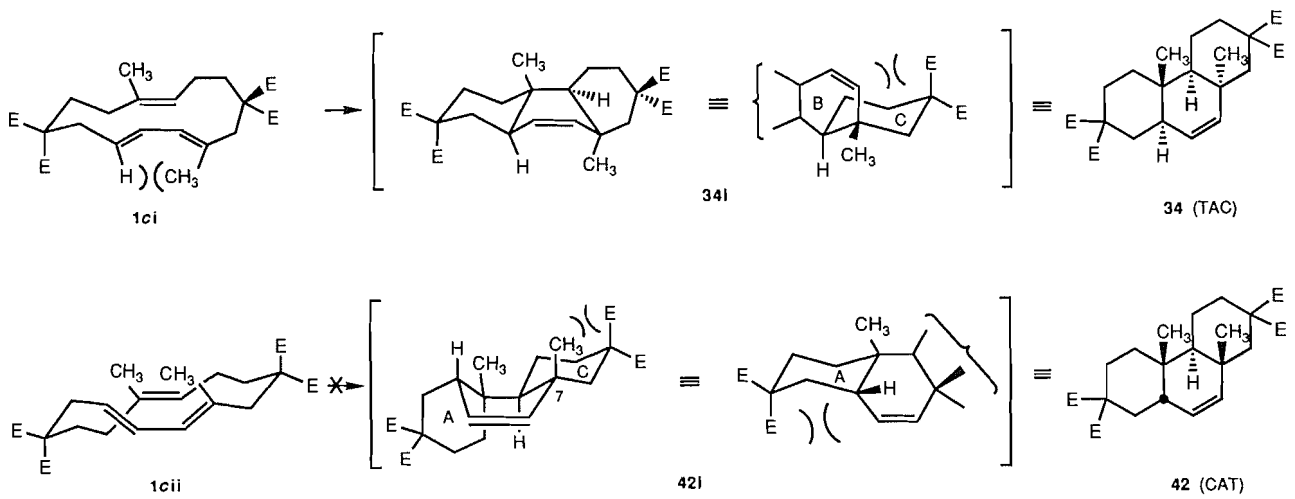

SCHEME 10

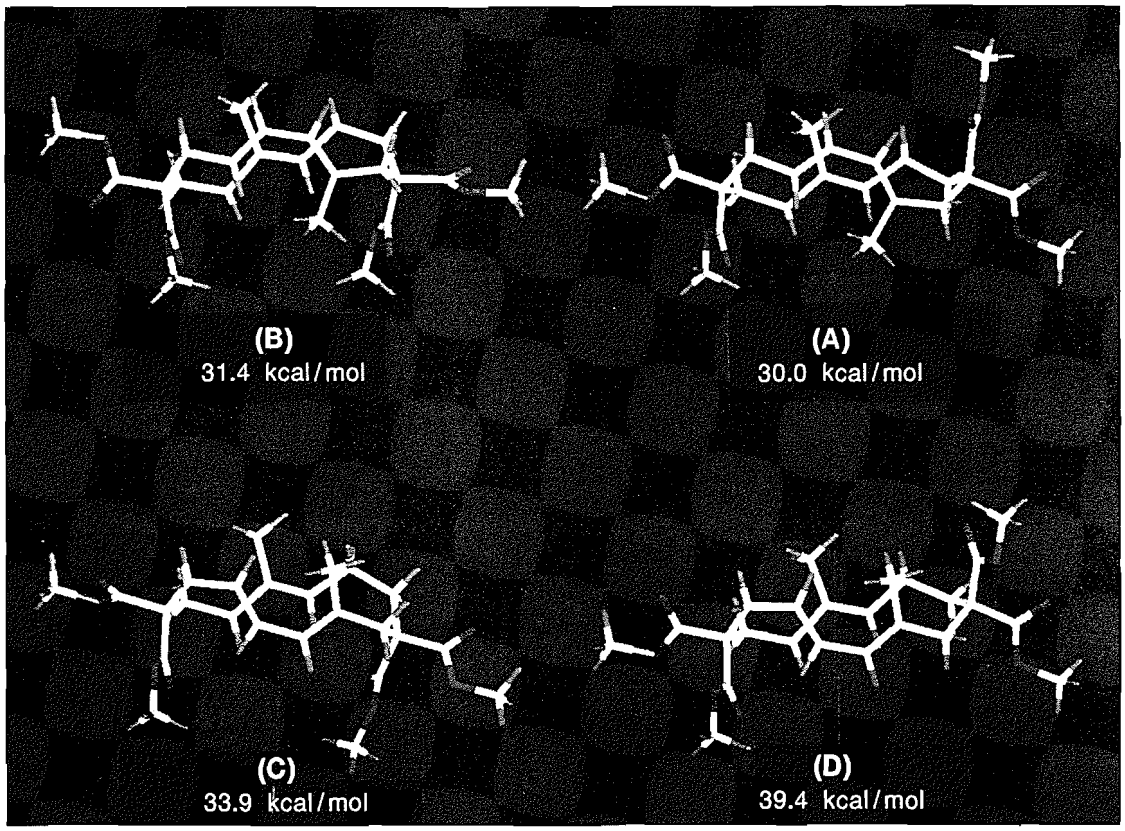

FIG. 1. Geometries and energies of transition state mimics.

to give the predicted CAC tricycle **35** because of severe steric hindrance at the transition level of the transannular Diels–Alder reaction. Macrocycle **1***a* gave a mixture of TAC tricycle **34** plus three unidentified isomers. The formation of **34** from macrocycle **1***a* can be explained by the isomerization of **1***a* into TTT macrocycle **1***c* via two consecutive 1,5 sigmatropic hydrogen migrations. The specific formation of tricycle **41** from macrocycle **1***b* took place via the intermediate formation of bicycle **39** via an ene–retroene process. Finally, TTT macrocycle **1***c* gave only TAC tricycle **34**; none of the other predicted CAT tricycle **42** was observed, a result which is explained on the basis of relative steric hindrance at the Diels–Alder transition state level.

In conclusion, this investigation has demonstrated a general methodology for the stereocontrolled synthesis of 1,7-dimethyl A.B.C.[6.6.6] tricyclic compounds. The macrocyclic trienes were constructed in good yields using an intramolecular displacement of allylic halides by a malonate anion in the acyclic triene precursors, which were assembled by coupling the diene and dienophile moieties. The

Can. J. Chem. Downloaded from www.nrcresearchpress.com by 213.200.69.106 on 09/08/12
For personal use only.

formation of unexpected tricycles from the CTT and TCT macrocycles has provided interesting information on competing transannular processes. The transannular Diels–Alder reaction of the TTT macrocycle stereoselectively produced a TAC tricyclic compound in excellent yield. This synthetic route could prove useful for the synthesis of suvanine (25), and kaurane and atisane diterpenes (26), which have the TAC stereochemistry with substituents at positions 8 and 10. The synthesis of these polycyclic natural products is currently under investigation.

Experimental

General

The ir spectra were taken on a Perkin–Elmer 681 spectrophotometer. Proton nmr spectra were recorded on a Bruker WP-80 or Bruker WM-250 instrument. The following abbreviations were used: s, singlet; d, doublet; dd, doublet of doublets; dt, doublet of triplets; ddd, doublet of doublets of doublets; ddt, doublet of doublets of triplets; t, triplets; q, quartet, and m, multiplet. Chemical shifts are reported in δ values relative to tetramethylsilane or chloroform as internal standard. Carbon nuclear magnetic resonance spectra were recorded on a Bruker WP-80 or Bruker WM-250 instrument (chloroform as internal standard). Mass spectra were obtained on a Micromass ZAB-2F instrument. Melting points were determined on a Büchi M-50 or on a Reichert apparatus and are uncorrected.

Thin-layer chromatography was performed using silica gel 60 F-250. For flash chromatography, Merck Kieselgel 60 (230–400 mesh A.S.T.M.) was used. All solvents used in chromatography were distilled. Unless otherwise noted, starting materials and reactants were obtained commercially and were used as such or purified by standard means. All solvents and reactants purified and dried were stored under argon.

Anhydrous reactions were performed under an inert atmosphere of argon. Organic solutions were dried over magnesium sulfate, and were evaporated on a rotatory evaporator and under reduced pressure.

4-Chlorobutyryl chloride 7

To a stirred mixture containing thionyl chloride (32.8 g, 19.9 mL, 0.28 mmol) and anhydrous zinc chloride (1.5 g, 11 mmol) at room temperature was rapidly added γ-butyrolactone **6** (21.6 g, 0.25 mol). The resulting mixture was then heated at 55°C for 22 h. The crude mixture was purified by distillation under reduced pressure to give **7** as a colorless oil (23.0 g, 65%). Boiling point: 51–59°C (5.0 Torr; 1 Torr = 133.3 Pa) (lit. (8) bp 69–74°C (14 Torr).

Methyl 4-chlorobutyrate 8

To a solution of pyridine (12.9 g, 13.2 mL, 0.136 mol) in methanol (6.53 g, 8.3 mL, 0.200 mol) was added, in dropwise fashion at 0°C, 4-chlorobutyryl chloride **7** (23.0 g, 0.163 mol). The mixture was then stirred at 25°C for 18 h following addition of precooled sulfuric acid (11.0 N, 55%, 75 mL). The mixture was extracted with diethyl ether (3 × 50 mL). The combined organic phases were washed with water and dried over Na_2SO_4. After filtration, the solvents were removed under reduced pressure and the residue was purified by vacuum distillation to provide methyl 4-chlorobutyrate **8** (17.1 g, 77%) as a colorless oil. Boiling point: 27–29°C (0.7 Torr) (lit. (8) bp 50–52°C (2–3 Torr); ir (neat): 2950, 1730, 1440, 1368, 1215 cm^{-1}; ^1H nmr ($CDCl_3$) δ: 2.10 (tt, 2H, J = 7.2 Hz, 6.3 Hz, $-CH_2CH_2CH_2-$), 2.51 (t, 2H, J = 7.2 Hz, $-CH_2COOCH_3$), 3.60 (t, 2H, J = 6.3 Hz, $-CH_2Cl$), 3.69 (s, 3H, $-COOCH_3$).

Methyl 4-iodobutyrate 9

Methyl 4-chlorobutyrate **8** (8.96 g, 65.5 mmol) in 65 mL of acetone was then heated to reflux for 42 h in the presence of sodium iodide (11.7 g, 78.6 mmol). The solution was cooled and filtered and the solvent was then evaporated. The residue was dissolved in 100 mL of diethyl ether, washed with aqueous sodium thiosulfate solution (5%), and then with saturated sodium chloride solution. The organic phase was dried over $MgSO_4$, filtered, and evaporated. The oily residue was purified by distillation under reduced pressure to give **9** (11.6 g, 77.5%) as a colorless oil. Compound **9** decomposes slowly even at −20°C under argon atmosphere. Boiling point 53–54°C (0.7 Torr), 50–52°C (0.35 Torr); ir (neat): 2940, 1735, 1435, 1365, 1200, 1120, 1018 cm^{-1}.

Methyl (E)-3-methyl-1-tert-butyldimethylsilyloxy-3-octenoate 12

To a flask containing the Zn–Cu couple (4.17 g, 63.9 mmol) under an argon atmosphere was added a solution of methyl 4-iodobutyrate **9** (9.51 g, 41.7 mmol) in a mixture of benzene and DMF (32 mL/5.6 mL). The resulting mixture was stirred at 25°C for 1 h and at 60°C for 3 h. A suspension of tetrakis(triphenylphosphine)palladium(0) (4.06 g, 3.53 mmol) in 28 mL of benzene was introduced by cannula and the mixture was stirred at 60°C for 5 min. Vinyl iodide **11** (9.06 g, 27.8 mmol) in 11 mL of benzene was added and the resulting mixture was stirred at 60°C for another hour. The reaction was stopped by addition of 150 mL ethyl acetate followed by filtration to remove the Zn–Cu. The orange filtrate was kept in a refrigerator overnight and the volatiles were then removed by evaporation. After addition of 50 mL ethyl acetate, the mixture was filtered again. The red solid was washed with 100 mL ethyl acetate and the filtrate was concentrated under reduced pressure to give a crude oily residue, which was passed through a short-path silica gel using hexane – ethyl acetate (10:1) as eluant. The oil obtained after evaporation was purified by flash chromatography with a mixture of hexane and ethyl acetate (20:1) as eluant to give compound **12** (5.38 g, 64.5%); ir (neat): 2950, 2920, 2860, 1740, 1435, 1252, 1100, 835 cm^{-1}; ^1H nmr ($CDCl_3$) δ: 0.04 (s, 6H, t-Bu-$(CH_3)_2Si$-), 0.89 (s, 9H, $(CH_3)_3CSi(CH_3)_2$)), 1.60 (d, 3H, J = 1.0 Hz, CH_3-C=C-), 1.66 (tt, 2H, J = 7.5 Hz, 7.6 Hz, $-CH_2CH_2CH_2COOCH_3$), 2.01 (dt, 2H, J = 6.2 Hz, 7.5 Hz, $-CH_2CH_2CH_2COOCH_3$), 2.19 (t, 2H, J = 7.1 Hz, $-OCH_2CH_2C$=C-), 2.30 (t, 2H, J = 7.6 Hz, $-CH_2COOCH_3$), 3.65 (t, 2H, J = 7.1 Hz, $-OCH_2CH_2$-), 3.66 (s, 3H, $-COOCH_3$), 5.14 (m, 1H, -C=CH-); ^{13}C nmr ($CDCl_3$) δ: 16.2, 18.1, 24.8, 25.8, 27.1, 33.3, 43.0, 51.1, 62.2, 125.1, 133.2, 173.9; ms m/e: 243 ($M^+ - C_4H_9$). Exact Mass ($M - C_4H_9$) calcd.: 243.1416; found: 243.1416.

Methyl (E)-3-octenoate 4

To a solution of the methyl ester **12** (1.00 g, 3.3 mmol) in 20 mL of THF was added, at −78°C under an argon atmosphere, a solution of lithium diisopropylamide (3.3 mmol) in THF. After stirring the mixture at −78°C for 30 min, methyl chloroformate (256 μL, 312 mg, 3.3 mmol) was introduced dropwise by syringe. The reaction was quenched with 50 mL of saturated ammonium chloride solution and extracted with a solvent mixture of hexane and ether (1:2). The organic phase was washed with water, dried over $MgSO_4$, filtered, and then concentrated under reduced pressure. The crude residue was purified by flash chromatography with a 20:1 mixture of hexane and ethyl acetate as eluant to give product **4** (792 mg, 67%) as a clear oil; ir (neat): 1740, 1435, 1255, 1150, 1100, 840 cm^{-1}; ^1H nmr ($CDCl_3$) δ: 0.04 (s, 6H, t-Bu-$CH_3)_2Si$-), 0.88 (s, 9H, $(CH_3)_3CSi(CH_3)_2$), 1.59 (s, 3H, CH_3-C=C-), 1.92–2.04 (m, 4H, $-CH_2CH_2CH(COOCH_3)_2$), 2.19 (t, 2H, J = 7.1 Hz, $-OCH_2CH_2C$=CH-), 3.38 (t, 1H, J = 7.2 Hz, $-CH(COOCH_3)_2$), 3.65 (t, 2H, J = 7.1 Hz, $-OCH_2CH_2$-), 3.73 (s, 6H, $-CH(COOCH_3)_2$), 5.11 (t, 1H, J = 6.2 Hz, CH_3C=CH-); ms m/e: 301 ($M^+ - C_4H_9$). Exact Mass ($M - C_4H_9$) calcd.: 301.1471; found: 301.1460.

2-Butene-1-ol 14

(Z)-2-Butene-1,4-diol **13** (49.5 mL, 52.9 g, 0.60 mol) and 3,4-dihydro-2H-pyran (54.7 mL, 50.5 g, 0.60 mol) were dissolved in 200 mL of CH_2Cl_2 and 500 mL of THF at 0°C. To this solution was then added p-toluenesulfonic acid monohydrate (2.65 g, 14 mmol) and the resulting mixture was stirred at 0°C for 2 h and at 20°C for

Can. J. Chem. Downloaded from www.nrcresearchpress.com by 213.200.69.106 on 09/08/12
For personal use only.

Can. J. Chem. Downloaded from www.nrcresearchpress.com by 213.200.69.106 on 09/08/12
For personal use only.

20 min. Solid sodium bicarbonate (2.35 g, 28 mmol) was added and the solution was stirred for 5 min. After filtration, the solvents were removed and the crude oil obtained was purified by flash chromatography with a 9:1 mixture of CH_2Cl_2 and acetone as eluant to provide monoprotected alcohol **14** (50.7 g, 49.1%) as an oil; ir (CH_2Cl_2): 3600, 3620–3300, 2940, 1200, 1120, 1024 cm^{-1}; ^1H nmr ($CDCl_3$) δ: 1.43–1.88 (m, 6H, -(CH_2)$_3$$CH_2$O-), 2.04 (t, 1H, J = 2.5 Hz, -CH_2O*H*), 3.49–3.58 and 3.81–3.90 (2m, 2H, -CH_2CH_2O-), 4.10–4.32 (m, 4H, -CH_2CH=CH-CH_2-), 4.69 (t, 1H, J = 3.0 Hz, -OC*H*O-), 5.66–5.77 and 5.81–5.92 (2m, 2H, -C*H*=C*H*-); ^{13}C nmr ($CDCl_3$) δ: 18.9, 25.1, 30.2, 57.8, 61.8, 62.2, 97.4, 127.3, 132.2; ms *m/e*: 155 (M^+ − OH). Exact Mass (M^+ − OH) calcd.: 155.1072; found: 155.1075.

(Z,E)-Diene ester ***16****a*

To a stirred solution of oxalyl chloride (5.0 mL, 55 mmol) in 125 mL of CH_2Cl_2 was added, at between −50 and −60°C, a solution of DMSO (8.5 mL, 110 mmol) in 25 mL of CH_2Cl_2. After stirring the mixture for 2 min, alcohol **14** (8.61 g, 50 mmol) in 50 mL of CH_2Cl_2 was introduced over a 5 min period. The stirring was continued for an additional 45 min following addition of diisopropylethylamine (43.5 mL, 250 mmol). After 5 min, the reaction mixture was allowed to warm to −10°C. The oxidation was stopped by addition of water (125 mL). The aqueous phase was extracted with CH_2Cl_2 (2 × 180 mL) and the combined organic phases were washed with saturated NaCl solution (200 mL), dried over $MgSO_4$, filtered, and evaporated. The oil, which contained *cis*-α,β-unsaturated aldehyde **15***a*, was used for the next reaction without further purification.

To a stirred suspension of NaH (2.47 g, 60% in oil, 62 mmol) in 100 mL of THF was rapidly added, at 0°C under an argon atmosphere, a solution of ethyldiisopropyl-2-phosphonopropinate (16.5 g, 62 mmol) in 60 mL of THF. Once the evolution of hydrogen gas ended, the solution was cooled to −78°C. Crude aldehyde **15***a* in 15 mL of THF was introduced and the resulting mixture was stirred at −78°C for 30 min and at 0°C for 15 min. The reaction was stopped by addition of saturated ammonium chloride (100 mL) and diethyl ether (150 mL). The aqueous phase was extracted with diethyl ether. The combined organic phases were washed with brine, dried over $MgSO_4$, and then filtered. After removal of volatiles, the oily residue was purified by flash chromatography using a 7:2 mixture of hexane and ethyl acetate to provide **16***a* (6.63 g, 52% for two steps) as an oil; ir (neat): 2940, 2870, 1710, 1633, 1600, 1245, 1201, 1025, 905, 870 cm^{-1}; ^1H nmr ($CDCl_3$) δ: 1.29 (t, 3H, J = 7.5 Hz, CH_3CH_2O-), 1.49–1.88 (m, 6H, -(CH_2)$_3$$CH_2$O-), 1.94 (d, 3H, J = 1.0 Hz, CH_3C=CH-), 3.49–3.58 and 3.84–3.94 (2m, 2H, -CH_2CH_2O-), 4.22 (q, 2H, J = 7.5 Hz, CH_3CH_2O-), 4.31 and 4.49 (2ddd, 2H, J = 14 Hz, 1.0 Hz, 6.2 Hz, -CH_2OTHP), 4.66 (t, 1H, J = 2.5 Hz, -OC*H*O-), 5.93 (dt, 1H, J = 11.2 Hz, 6.2 Hz, -OCH_2CH=CH-), 6.43 (ddt, 1H, J = 11.2 Hz, 11.0 Hz, 1.0 Hz, -OCH_2CH=C*H*CH-), 6.48 (dq, 1H, J = 11.0 Hz, 1.0 Hz, -OCH_2CH=C*H*=C-CH_3); ^{13}C nmr ($CDCl_3$) δ: 12.1, 14.1, 19.1, 25.2, 30.4, 60.3, 61.9, 63.0, 98.0, 125.4, 128.7, 131.9, 134.1.

Allylic alcohol ***17****a*

General procedure A

To a stirred solution of ester **16***a* (6.44 g, 25 mmol) in 450 mL of CH_2Cl_2 was added, over a period of 15 min at −78°C under an argon atmosphere, a solution of diisobutylaluminum hydride (1 M, 55 mL, 55 mmol). After 30 min, 16 g of solid $Na_2SO_4 \cdot 10$ H_2O was added. The reaction mixture was allowed to warm to room temperature following addition of 200 mL acetone. The reaction mixture was stirred for an additional hour, the solids were removed by filtration, and the filtrate was evaporated to dryness. The crude residue was purified by flash chromatography using a 7:3 mixture of hexane and ethyl acetate to provide alcohol **17***a* (3.48 g, 66%) as an oil; ir (neat): 3600–3100, 2940, 2860, 1655, 1200, 1020, 902, 868 cm^{-1}; ^1H nmr ($CDCl_3$) δ: 1.49–1.77 (m, 7H, -(CH_3)$_3$$CH_2$O- and -$CH_2$O*H*), 1.79 (s, 3H, CH_3C=CH-), 3.49–3.58 and 3.86–3.95 (2m, 2H, -OCH_2CH_2O-), 4.11 (s, 2H, -CH_2OH), 4.21–4.46 (m, 2H, -CH_2OTHP), 4.67 (t, 1H, J = 2.5 Hz, -OC*H*O-), 5.59–5.69 (m, 1H, -CH_2CH=CH(CH=C-)), 6.32–6.47 (m, 2H, -CH_2CH=C*H*C*H*=C-); ^{13}C nmr ($CDCl_3$) δ: 13.6, 19.1, 25.2, 30.4, 61.9, 62.6, 67.7, 97.5, 118.6, 126.3, 126.6, 139.3.

Allylic chloride ***5****a*

General procedure B

To a solution containing alcohol **17***a* (467 mg, 2.2 mmol) vacuum dried (heat-gun), lithium chloride (374 mg, 8.8 mmol), and *s*-collidine (0.58 mL, 532 mg, 4.4 mmol) in 12 mL of DMF was added, dropwise at 0°C under an argon atmosphere, methanesulfonyl chloride (0.34 mL, 504 mg, 4.4 mmol). The resulting mixture was stirred at 0°C for 1 h and then at 25°C for an additional hour. The reaction mixture was poured into 10 mL of ice water, and extracted with a 2:1 mixture of diethyl ether and hexane (3 × 25 mL). The combined organic phases were washed successively with precooled, saturated $Cu(NO_3)_2$ solution and water. After drying over $MgSO_4$, the mixture was filtered through a short-path column containing silica gel and Celite on top. After removal of the solvents, allylic chloride **5***a* was obtained (504 mg, 99%) as an oil that was used for the next reaction without further purification and characterization.

(E)-α,β-Unsaturated aldehyde ***15****b*

To a solution of alcohol **14** (10.0 g, 58 mmol) and sodium acetate (14.4 g, 170 mmol) in 250 mL of CH_2Cl_2 over type 4Å molecular sieves (20 g) was added, portionwise at 0°C under an argon atmosphere, pyridinium chlorochromate (18.9 g, 87 mmol). The reaction mixture was then stirred at room temperature until disappearance of starting material, monitored by tlc. A solution of hexane and diethyl ether (500 mL, 1:1) was added, and the resulting mixture was filtered until colorless (three filtrations) using a Büchner funnel containing Celite, silica gel, and sodium sulfate (after the second filtration, the filtrate was treated with activated carbon for a few minutes). The solvents were removed by evaporation, and the crude residue was purified by flash chromatography using a 1:1 mixture of hexane and diethyl ether to afford aldehyde **15***b* (5.44 g, 55%) as a clear oil; ir (CH_2Cl_2): 2943, 1690, 1120, 1040 cm^{-1}; ^1H nmr ($CDCl_3$) δ: 1.51–1.82 (m, 6H, -(CH_2)$_3$$CH_2$O), 3.50–3.56 and 3.77–3.88 (2m, 2H, -CH_2CH_2O-), 4.20–4.57 (m, 2H, -OCH_2CH=CH-), 4.68 (t, 1H, J = 2.5 Hz, -OC*H*O-), 6.38 (ddt, 1H, J = 16.0 Hz, 8.7 Hz, 2.5 Hz, -CH_2CH=C*H*CHO), 6.87 (dt, 1H, J = 16.0 Hz, 3.0 Hz, -CH_2CH=CHCHO), 9.58 (d, 1H, J = 8.7 Hz, CH=CHC*H*O); ^{13}C nmr ($CDCl_3$) δ: 18.9, 25.1, 30.1, 61.9, 65.3, 98.2, 131.3, 153.2, 193.1; ms *m/e*: 169 (M^+ − H). Exact Mass (M − H) calcd.: 169.0865; found: 169.0865.

(E,Z)-Diene ester ***16****b*

To a stirred solution of ethyl bis(trifluoroethyl)-2-phosphonopropionate (10.0 g, 29.0 mmol) and 18-crown-6 ether (38.0 g, 144.0 mmol) in 450 mL of THF was added at −78°C under argon a solution of potassium bis(trimethylsilyl)amide (0.657 M, 44 mL, 28.9 mmol) in toluene. The mixture was stirred for 5 min at −78°C before the *trans*-aldehyde **15***b* (4.9 g, 29.0 mmol) dissolved in 50 mL of THF was introduced by cannula over a period of 30 min. The cloudy mixture was stirred at −78°C for 1 h and then slowly allowed to warm to room temperature. A saturated ammonium chloride solution (300 mL) was added and the products were extracted with ether (3 × 150 mL). The combined organic phases were dried, filtered, and concentrated to a yellow oil that was purified by flash chromatography using a 9:1 mixture of hexane and ethyl acetate to furnish ester **18***b* (6.5 g, 88%) as a colorless oil; ir ($CHCl_3$): 3000–2850, 1700, 1640, 1605, 1452, 1375, 1218, 1167, 1118, 1022 cm^{-1}; ^1H nmr ($CDCl_3$) δ: 7.29 (ddt, 1H, J = 15.4 Hz, 11.2 Hz, 1.6 Hz, THPOCH$_2$-CH=C*H*-), 6.42 (d, 1H, J = 11.2 Hz, -CH=CH-C*H*=C-), 5.95 (dt, 1H, J = 15.4 Hz, 6.0 Hz, THPO-CH$_2$-C*H*=CH-), 4.65 (t, 1H, J = 3.4 Hz, -OC*H*O-), 4.34 and 4.08 (2dd, 2H, J = 13.6 Hz, 5.8 Hz,

Can. J. Chem. Downloaded from www.nrcresearchpress.com by 213.200.69.106 on 09/08/12
For personal use only.

THPOCH_2CH=), 4.22 (q, 2H, J = 7.1 Hz, OCH_2CH$_3$), 3.92–3.82 and 3.56–3.47 (2m, 2H, OCHOCH_2), 1.96 (s, 3H, -CH=C(CH_3), 1.88–1.49 (m, 6H, -OCH$_2$(CH_2)$_3$-), 1.32 (t, 3H, J = 7.1 Hz, -CH$_2$CH_3); ms m/e: 254 (M^+), 153 (M^+ − OTHP).

Allylic alcohol ***17***b

The reaction was carried out according to the previously described general procedure A. Thus, the reaction of ethyl ester **16***b* (6.5 g, 25.6 mmol) with diisobutylaluminum hydride (1.0 M, 56.4 mL, 56.4 mmol) and $Na_2SO_4 \cdot 10\ H_2O$ (16.2 g, 50.3 mmol) furnished alcohol **17***b* (5.3 g, 98%) as a colorless oil; ir (neat): 3410, 2940–2865, 1450, 1125, 1025 cm^{-1}; ^{1}H nmr ($CDCl_3$) δ: 6.55 (dd, 1H, J = 15.0 Hz, 11.0 Hz, THPOCH$_2$CH=C*H*-), 5.96 (d, 1H, J = 11.2 Hz, -C*H*=C(CH$_3$)-), 5.74 (dt, 1H, J = 15.0 Hz, 6.2 Hz, THPOCH$_2$-C*H*=CH-), 4.65 (t, 1H, J = 3.5 Hz, -O-C*H*-O-), 4.32–4.24 and 4.06–3.98 (2dd, 2H, J = 13.0 Hz, 6.9 Hz, THPO-CH_2CH=), 4.25 (d, 2H, J = 5.8 Hz, =C(CH$_3$)CH_2OH), 3.92–3.83 and 3.55–3.47 (2m, 2H, -OCHOCH_2-), 1.88 (s, 3H, =C(CH_3)-), 1.86–1.49 (m, 6H, -OCH$_2$(CH_2)$_3$-), 1.35 (t, 1H, J = 5.9 Hz, -CH$_2$O*H*).

Diene diether ***18***b

General procedure C

To a stirred solution of alcohol **17***b* (1.9 g, 9.0 mmol) and imidazole (1.4 g, 20.5 mmol) in 80 mL of THF was added dropwise over 5 min under argon, and at room temperature, *tert*-butylchlorodiphenylsilane (2.8 mL, 10.7 mmol). After stirring the cloudy white suspension for 1 h, a saturated ammonium chloride solution (50 mL) was added. The reaction mixture was extracted with a 2:1 mixture of hexane and ether (3 × 50 mL). The combined organic phases were washed with water, dried over $MgSO_4$, filtered, and concentrated to a crude residue that was purified by flash chromatography using a 98:2 mixture of hexane and ethyl acetate as eluant to afford **18***b* (4.0 g, 98%) as a colorless oil; ir ($CHCl_3$): 3075–3010, 2940, 2860, 1430, 1365, 1115, 1078, 1025 cm^{-1}; ^{1}H nmr ($CDCl_3$) δ: 7.72–7.62 and 7.44–7.36 (2m, 10H, *Ph*$_2$Si-), 6.26 (dd, 1H, J = 14.8 Hz, 10.2 Hz, THPOCH$_2$CH=C*H*-), 5.87 (d, 1H, J = 11.8 Hz, -C*H*=C(CH$_3$)-), 5.64 (dt, 1H, J = 14.7 Hz, 6.4 Hz, THPOCH$_2$-C*H*=), 4.60 (t, 1H, J = 3.6 Hz, -OC*H*O-), 4.29 (s, 2H, =C(CH$_3$)CH_2OSi-), 4.18 and 3.91 (2dd, 2H, J = 12.5 Hz, 6.6 Hz, THPOCH_2-), 3.88–3.80 and 3.53–3.44 (2m, 2H, -O-CH_2-), 1.89 (s, 3H, -CH=C(CH_3)-), 1.88–1.43 (m, 6H, -O-CH$_2$(CH_2)$_3$-), 1.05 (s, 9H, -(CH_3)$_3$C).

Diene alcohol ***19***b

General procedure D

To a stirred solution of diene diether **18***b* (4.0 g, 8.9 mmol) in 180 mL of isopropanol was added, under argon at room temperature, pyridinium *p*-toluenesulfonate (400 mg). The resulting mixture was heated at 75°C for 3 h. After adding 100 mL of a saturated $NaHCO_3$ solution, the mixture was extracted with ether (4 × 100 mL). The combined organic phases were washed with brine, dried over $MgSO_4$, filtered, and concentrated to a crude oil that was purified by flash chromatography using a 4:1 mixture of hexane and ethyl acetate as eluant to afford **19***b* (2.8 g, 85%) as a colorless oil; ir (neat): 3340, 3070–3000, 2930, 2858, 1470, 1430, 1112, 1070, 1000 cm^{-1}; ^{1}H nmr ($CDCl_3$) δ: 7.71–7.67 and 7.44–7.35 (2m, 10H, Ph_2Si=), 6.16 (dd, 1H, J = 14.9 Hz, 11.0 Hz, -CH=C*H*-), 5.84 (d, 1H, J = 11.8 Hz, =CH-C*H*=C(CH$_3$)-), 5.66 (dt, 1H, J = 15.0 Hz, 5.9 Hz, HOCH$_2$C*H*=), 4.30 (s, 2H, -CH_2OSi-), 4.05 (t, 2H, J = 6.0 Hz, HOCH_2-CH=), 1.90 (s, 3H, =C(CH_3)-), 1.13 (t, 1H, J = 6.0 Hz, *H*OCH$_2$-), 1.05 (s, 9H, -(CH_3)$_3$C); ms m/e: 366 (M^+), 335 (M^+ − OCH$_3$), 309 (M^+ − C_4H_9).

Allylic chloride ***5***b

The reaction was carried out according to the general procedure B described before. Thus, the reaction of alcohol **19***b* (180 mg, 0.49 mmol), lithium chloride (63 mg, 1.5 mmol), *s*-collidine (97 μL, 0.74 mmol), and methanesulfonyl chloride (57 μL, 0.74 mmol) in 2 mL of DMF afforded the allylic chloride **5***b* (188 mg, 99%) as an oil, which was used immediately in the coupling reaction without further purification and characterization.

(E,E)-Diene ester ***16***c

To a stirred suspension of NaH (1.48 g, 60% in oil, 37 mmol) in 60 mL of THF was rapidly added at 0°C under argon a solution of ethyl diisopropyl-2-phosphonopropionate (9.86 g, 37 mmol) in 35 mL of THF. Once the evolution of hydrogen gas ended, the solution was cooled to −78°C. Aldehyde **15***b* (5.2 g, 30 mmol) in 10 mL of THF was introduced and the resulting mixture was stirred at −78°C for 1.5 h and then at 0°C for 30 min. The reaction was stopped by addition of saturated ammonium chloride solution (75 mL) and ether (125 mL). The aqueous phase was extracted with ether (3 × 100 mL). The combined organic phases were washed with brine, dried, filtered, and evaporated to a crude residue that was purified by flash chromatography using a 7:3 mixture of hexane and ethyl acetate to furnish ester **16***c* (6.28 g, 82%) as a colorless oil; ir (CH_2Cl_2): 2940, 1700, 1644, 1610, 1230, 1038, 1025, 922 cm^{-1}; ^{1}H nmr ($CDCl_3$) δ: 1.30 (t, 3H, J = 7.5 Hz, CH_3CH$_2$O-), 1.51–1.84 (m, 6H, (CH_2)$_3$CH_2O-), 1.94 (d, 3H, J = 1.0 Hz, CH_3C=CH-), 3.48–3.57 and 3.83–3.92 (2m, 2H, -OCH_2CH$_2$-), 4.21 (q, 2H, J = 7.5 Hz, -OCH_2CH$_3$), 4.37–4.41 (m, 2H, -OCH_2CH=CH), 4.66 (t, 1H, J = 2.5 Hz, -OC*H*O-), 6.13 (dt, 1H, J = 15.3 Hz, 5.6 Hz, -OCH$_2$C*H*=CH-), 6.59 (ddt, 1H, J = 15.3 Hz, 1.6 Hz, 11.5 Hz, -OCH$_2$CH=C*H*CH=), 7.18 (d, 1H, J = 11.5 Hz, =CHC*H*=CCH$_3$); ^{13}C nmr ($CDCl_3$) δ: 12.4, 14.1, 19.2, 25.2, 30.4, 60.3, 61.9, 66.7, 97.8, 126.7, 127.3, 136.9, 137.1, 168.1; ms m/e: 254 (M^+). Exact Mass (M^+) calcd.: 254.1518; found: 254.1513.

Allylic alcohol ***17***c

The reduction was carried out according to the general procedure A described before. Thus, the reaction of ester **16***c* (6.08 g, 24 mmol) with diisobutylaluminum hydride (1 M in dichloromethane, 53 mL, 53 mmol) and $Na_2SO_4 \cdot 10\ H_2O$ (15 g, 46.6 mmol) in 450 mL of CH_2Cl_2 afforded alcohol **17***c* (4.43 g, 87%) as a colorless oil; ir (CH_2Cl_2): 3620, 1200, 1075, 1035, 1020 cm^{-1}; ^{1}H nmr ($CDCl_3$) δ: 1.35 (t, 1H, J = 5.0 Hz, -CH$_2$O*H*), 1.47–1.90 (m, 6H, (CH_2)$_3$CH$_2$O-), 1.79 (s, 3H, CH_3-), 3.48–3.57 and 3.84–3.94 (2m, 2H, -CH$_2$CH_2O-), 4.01–4.34 (m, 4H, -CH_2OH and CH_2OTHP), 4.66 (t, 1H, J = 2.5 Hz, -OC*H*O-), 5.80 (dt, 1H, J = 15.0 Hz, 5.0 Hz, -CH$_2$C*H*=CHCH=C), 6.09 (d, 1H, J = 11.0 Hz, -CH$_2$CH=CHC*H*=C), 6.51 (ddt, 1H, J = 15.0 Hz, 11.0 Hz, 1.0 Hz, -CH$_2$CH=C*H*CH=C); ^{13}C nmr ($CDCl_3$) δ: 13.8, 19.1, 25.2, 30.4, 61.9, 67.4, 67.6, 97.5, 123.5, 128.4, 128.7, 137.9; ms m/e: 212 (M^+). Exact Mass (M^+) calcd. 212.1412; found: 212.1410.

Diene diether ***18***c

The reaction was carried out according to the previously described general procedure C. Thus, the reaction of alcohol **17***c* (1.137 g, 5.36 mmol), imidazole (0.833 g, 12.24 mmol), and *tert*-butylchlorodiphenylsilane (1.64 mL, 1.73 g, 6.31 mmol) in 32 mL of THF afforded diene diether **18***c* (2.29 g, 95%) as a colorless oil; ir (neat): 3080–3010, 2945, 2860, 1450, 1360, 1120–1000 cm^{-1}; ^{1}H nmr ($CDCl_3$) δ: 1.06 (s, 9H, -(CH_3)$_3$C), 1.47–1.95 (m, 6H, -(CH_2)$_3$CH$_2$O-), 1.71 (s, 3H, -CH_3), 3.48–3.57 and 3.84–3.94 (2m, 2H, -CH$_2$CH_2O-), 4.00–4.10 and 4.30–4.39 (2m, 2H, -CH_2OTHP), 4.10 (s, 2H, -CH_2OSi-), 4.68 (t, 1H, J = 2.8 Hz, -OC*H*O-), 5.77 (dt, 1H, J = 15.0 Hz, 6.4 Hz, OCH$_2$C*H*=CHCH=C), 6.21 (d, 1H, J = 11.2 Hz, -CH=CHC*H*=C), 6.54 (dd, 1H, J = 15.1 Hz, 11.2 Hz, -CH$_2$CH=C*H*CH=C), 7.35–7.48 and 7.65–7.72 (2m, 10H, Ph_2Si-).

Diene alcohol ***19***c

The reaction was carried out according to the previously described general procedure D. Thus, the reaction of diene diether **18***c* (734.4 mg, 1.63 mmol) with pyridinium *p*-toluenesulfonate (73.4 mg) in 20 mL of isopropanol provided allylic alcohol **19***c* (484.9 mg, 81%) as a colorless oil; ir (neat): 3340, 3050, 2940, 2860, 1470, 1430, 1370, 1110, 1070 cm^{-1}; ^{1}H nmr ($CDCl_3$) δ:

Can. J. Chem. Downloaded from www.nrcresearchpress.com by 213.200.69.106 on 09/08/12
For personal use only.

1.07 (s, 9H, -(CH_3)$_3$C), 1.32 (t, 1H, J = 5.9 Hz, -CH_2OH), 1.72 (s, 3H, -CH_3), 4.20 (s, 2H, -CH_2OSi-), 4.23 (t, 2H, J = 5.7 Hz, HOCH_2CH=), 5.83 (dt, 1H, J = 15.0 Hz, 6.1 Hz, HOCH_2CH=CH-), 6.20 (d, 1H, J = 11.2 Hz, -CH=CHCH=C), 6.53 (dd, 1H, J = 15.1 Hz, 11.1 Hz, -CH=CHCH=C), 7.30–7.48 and 7.65–7.71 (2m, 10H, Ph_2Si-).

Allylic chloride **5**c

The reaction was carried out according to the general procedure B as described before. Thus, alcohol **19***c* (1.096 g, 2.99 mmol) reacted with lithium chloride (0.507 g, 11.97 mmol), *s*-collidine (0.79 mL, 0.724 g, 5.98 mmol), and methanesulfonyl chloride (0.46 mL, 0.681 g, 5.98 mmol) in 19 mL of DMF to give **5***c* (1.109 g, 96%) as a yellowish oil; ^{1}H nmr ($CDCl_3$) δ: 1.26 (s, 9H, -(CH_3)$_3$C), 1.71 (s, 3H, -CH_3), 4.11 (s, 2H, -CH_2OSi-), 4.18 (d, 2H, J = 6.9 Hz, ClCH_2CH=), 5.78 (dt, 1H, J = 14.8 Hz, 7.3 Hz, -CH_2CH=CH-), 6.21 (d, 1H, J = 10.0 Hz, -CH=CHCH=C-), 6.57 (dd, 1H, J = 14.8 Hz, 11.2 Hz, -CH=CHCH=C), 7.35–7.48 and 7.65–7.75 (2m, 10H, Ph_2Si-).

Alcohol **20**

General procedure E

To a stirred solution of silyl ether **4** (490.5 mg, 1.37 mmol) in 12 mL of THF was added dropwise over 12 min at 0°C under argon a solution of tetrabutylammonium fluoride (1.5 mL, 1 M, 1.5 mmol) in THF. The resulting mixture was stirred at 0°C for 10 min and then at room temperature for 2.5 h. The solvent was removed by evaporation and the resulting yellow residue was purified by flash chromatography using a 7:3 mixture of hexane and ethyl acetate as eluant to afford colorless oil **20** (305.4 mg, 91%); ir (neat): 3420, 2955, 2880, 1740, 1437, 1380, 1240, 1155, 1050 cm^{-1}; ^{1}H nmr ($CDCl_3$) δ: 1.64 (s, 3H, =C-CH_3), 2.10–2.00 (m, 4H, =C(CH_3)-CH_2CH_2-), 2.28 (q, 2H, J = 7.0 Hz, HOCH_2CH_2=CH), 3.34 (t, 1H, J = 7.0 Hz, -CH_2CH(CO_2CH_3)$_2$), 3.63 (m, 2H, HOCH_2CH_2-), 3.73 (s, 6H, CH(CO_2CH_3)$_2$), 5.16 (t, 1H, J = 7.0 Hz, -CH=C(CH_3)-); ms m/e: 244 (M^+), 213 (M^+ − OCH_3).

Methanesulfonate ester **21**

General procedure F

To a stirred solution of the alcohol **20** (277 mg, 1.1 mmol) and triethylamine (0.24 mL, 1.7 mmol) in 16 mL of CH_2Cl_2 was added, dropwise over 5 min at 0°C under argon, methanesulfonyl chloride (0.10 mL, 1.3 mmol). The mixture was stirred at 0°C for 1 h and then poured into 80 mL of H_2O. The aqueous layer was extracted with CH_2Cl_2 (4 × 50 mL) and the combined organic phases were washed with water, dried over $MgSO_4$, filtered, and concentrated to a crude residue that was purified by flash chromatography using a 3:1 mixture of hexane and ethyl acetate to provide **21** (346 mg, 94%) as a colorless oil; ir (neat): 2950, 2850, 1730, 1440, 1358, 1230, 1172 cm^{-1}; ^{1}H nmr ($CDCl_3$) δ: 1.64 (d, 3H, J = 1.1 Hz, =C(CH_3)-), 2.03–2.00 (m, 4H, -C(CH_3)CH_2CH_2-), 2.46 (q, 2H, J = 7.0 Hz, MsOCH_2CH_2-), 3.00 (s, 3H, -SO_2CH_3), 3.33 (m, 1H, -CH(CO_2CH_3)$_2$), 3.74 (s, 6H, -(CO_2CH_3)$_2$), 4.18 (t, 2H, J = 6.9 Hz, MsOCH_2CH_2-), 5.13 (t, 1H, J = 6.0 Hz, -CH=C(CH_3)-); ms m/e: 322 (M^+), 290 (M^+ − CH_3OH).

Triene **22**b

General procedure G

To a stirred suspension of NaH (46 mg, 60%, 1.2 mmol) in 6 mL of THF was added dropwise at 0°C under argon a solution of the mesylate **21** (340 mg, 1.1 mmol) in 6 mL of THF. The mixture was slowly warmed to room temperature and stirred for 45 min. After cooling again to 0°C, a solution of the crude allylic chloride **5***b* (540 mg, 1.4 mmol) in 6 mL of DMF was added dropwise over 15 min. The resulting mixture was stirred at room temperature for 36 h before it was poured into 60 mL of saturated ammonium chloride solution. The aqueous phase was extracted with a 2:1 mixture of ether and hexane (5 × 40 mL). The combined organic phases were washed with water, 5% $NaHCO_3$ solution, and brine, then dried, filtered, and concentrated. The thick yellow residue was purified by flash chromatography using a 5:1 mixture of hexane and ethyl acetate to give triene **22***b* (355 mg, 50%) along with both starting materials **21** and **5***b* in about 10% each. Compound **22***b*: ir (neat); 3070–3000, 2950, 2860, 1740, 1430, 1360, 1178, 1112 cm^{-1}; ^{1}H nmr ($CDCl_3$) δ: 1.05 (s, 9H, -(CH_3)$_3$C), 1.58 (d, 3H, J = 0.9 Hz, -CH_2CH_2C(CH_3)=), 1.80–1.95 (m, 7H, (CO_2CH_3)$_2$CRCH_2CH_2- and =CH-CH=C(CH_3)-), 2.41 (q, 2H, J = 7.0 Hz, -CH_2CH_2OMs), 2.59 (d, 2H, J = 7.5 Hz, (CO_2CH_3)$_2$CRCH_2-CH=), 2.98 (s, 3H, -SO_2CH_3), 3.67 (s, 6H, (CO_2CH_3)$_2$), 4.14 (t, 2H, J = 7.0 Hz, -CH_2OMs), 4.25 (s, 2H, -CH_2OSi-), 5.08 (t, 1H, J = 7.3 Hz, -C(CH_3)=CHCH_2-), 5.32 (dt, 1H, J = 14.8 Hz, 7.4 Hz, -CH_2CH=CH-), 5.80 (d, 1H, J = 11.0 Hz, =CHCH=C(CH_3)-), 6.08 (dd, 1H, J = 14.8 Hz, 11.0 Hz, -CH_2CH=CH-), 7.35–7.48 and 7.65–7.71 (2m, 10H, Ph_2Si-); ms m/e: 670 (M^+), 631 (M^+ − C_4H_9).

Triene **22**c

The reaction was carried in a similar fashion as described in the general procedure G. Thus, the reaction of dienophile **21** (201.1 mg, 0.62 mmol) with NaH (29.0 mg, 60%, 0.73 mmol) and diene **5***c* (310.0 mg, 0.81 mmol) in a mixture of DMF and THF (1:1, 6 mL) afforded triene **22***c* (289.6 mg, 70%) and recovered starting material **21** (35.4 mg, 18%). Compound **22***c*: ir (neat): 3020, 2940, 2850, 1740, 1430, 1350, 1170, 1110 cm^{-1}; ^{1}H nmr ($CDCl_3$) δ: 1.06 (s, 9H, -(CH_3)$_3$C), 1.64 (s, 3H, =CCH_3),1.68 (s, 3H, =CCH_3), 1.84–2.00 (m, 4H, C(CO_2CH_3)$_2$CH_2CH_2-), 2.45 (q, 2H, J = 7.2 Hz, -CH_2CH_2OMs), 2.72 (d, 2H, J = 7.5 Hz, -CH_2CH=CH-), 2.99 (s, 3H, -SO_2CH_3), 3.73 (s, 6H, C(CO_2CH_3)$_2$), 4.07 (s, 2H, -CH_2OSi-), 4.17 (t, 2H, J = 7.0 Hz, -CH_2OMs), 5.13 (t, 1H, J = 7.4 Hz, -(CH_3)C=CHCH_2-), 5.42 (dt, 1H, J = 14.8 Hz, 7.4 Hz, -CH_2CH=CHCH=C), 6.07 (d, 1H, J = 11.5 Hz, -CH=CHCH=C), 6.33 (dd, 1H, J = 14.7 Hz, 10.8 Hz, -CH=CHCH=C), 7.34–7.47 and 7.64–7.71 (2m, 10H, Ph_2Si-).

Tetraester **23**b

General procedure H

To a stirred suspension of NaH (84 mg, 60% in oil, 2.1 mmol) in a mixture of DMF and THF (1:1, 6 mL), dimethyl malonate (0.27 mL, 2.3 mmol) was added dropwise at 0°C under argon. After stirring the mixture at 0°C for 45 min, a solution of triene **22***b* (311 mg, 0.46 mmol) in a mixture of DMF and THF (1:1, 6 mL) was introduced by syringe, followed by addition of potassium iodide (7.6 mg, 46 mmol). The resulting mixture was heated at 80°C for 18 h before it was poured into 60 mL of H_2O. The mixture was extracted with CH_2Cl_2 (3 × 40 mL) and ether (3 × 40 mL). The combined organic phases were washed with H_2O, dried over $MgSO_4$, filtered, and concentrated to a crude residue that was purified by flash chromatography using a mixture of hexane and ethyl acetate (85:15) to afford **23***b* (235 mg, 72%) as a colorless oil; ir (neat): 3070–3000, 2955, 2860, 1735, 1435, 1200, 1110 cm^{-1}; ^{1}H nmr ($CDCl_3$) δ: 1.05 (s, 9H, -(CH_3)$_3$C), 1.52 (d, 3H, =C(CH_3)-CH_2CH_2), 1.85–2.00 (m, 11H, -CH_2CH_2CH=C(CH_3)CH_2CH_2-, and SiOCH_2-C(CH_3)=), 2.58 (d, 2H, J = 7.3 Hz, =CHCH_2CR(CO_2CH_3)$_2$), 3.24–3.40 (m, 1H, -CH-(CO_2CH_3)$_2$), 3.66–3.75 (3s, 12H, 4 × -OCH_3), 4.25 (s, 2H, -CH_2OSi-), 4.95–5.50 (m, 2H, -CH_2CH= and MsOCH_2CH_2-CH=), 5.70–6.25 (m, 2H, -C(CH_3)=CHCH=), 7.38–7.75 (m, 10H, Ph_2Si-).

Tetraester **23**c

The reaction was prepared as described in the general procedure H. Thus, the reaction of dimethyl malonate (0.25 mL, 2.15 mmol) with NaH (77.4 mg, 60%, 1.94 mmol) and triene **22***c* (289.6 mg, 0.43 mmol) in the presence of KI (7.1 mg, 43 mmol) yielded the tetraester **23***c* (273.3 mg, 90%); ^{1}H nmr ($CDCl_3$) δ: 1.05 (s, 9H, -(CH_3)$_3$C), 1.56 (s, 3H, =CCH_3), 1.67 (s, 3H, =CCH_3), 1.80–2.05 (m, 8H, -CH_2CH_2CH=C(CH_3)CH_2CH_2-), 2.71 (d, 2H, J = 7.5 Hz, -CH_2CH=CH-), 3.35 (m, 1H, -CH(CO_2CH_3)$_2$), 3.72

Can. J. Chem. Downloaded from www.nrcresearchpress.com by 213.200.69.106 on 09/08/12
For personal use only.

and 3.75 (2s, 12H, 4 × -OCH_3), 4.06 (s, 2H, -CH_2OSi-), 5.11 (t, 1H, J = 7.0 Hz, -(CH$_3$)C=CHCH$_2$-), 5.43 (dt, 1H, J = 15.0 Hz, 7.0 Hz, -CH=CHCH=CH-), 6.07 (d, 1H, J = 11.0 Hz, -CH=CHCH=C), 6.33 (dd, 1H, J = 15.0 Hz, 11.0 Hz, -CH=CHCH=C-), 7.30–7.47 and 7.63–7.70 (2m, 10H, Ph_2Si-).

Allylic alcohol ***24****b*

The reaction was performed in a similar fashion as described in the general procedure E. Thus, the silyl ether **23***b* (231 mg, 0.33 mmol) was treated with tetrabutylammonium fluoride (1.0 M in THF, 0.49 mL, 0.49 mmol) in 3 mL of THF to give the alcohol **24***b* (110 mg, 72%) as a colorless oil; ir (neat): 3500, 2950, 2860, 1735, 1438, 1200 cm^{-1}; ^{1}H nmr (CDCl$_3$) δ: 1.38 (t, 1H, J = 5.0 Hz, -CH$_2$OH), 1.56 (s, 3H, -CH$_2$CCCH_3)=), 1.85 (s, 3H, =CHCH=C(CH_3)-), 1.87–2.04 (m, 8H, -CH_2CH_2CH=C(CH$_3$)-CH_2CH_2-), 2.69 (d, 2H, J = 7.6 Hz, -CH_2CR(CO$_2$CH$_3$)$_2$), 3.35 (t, 1H, J = 7.1 Hz, -CH(CO$_2$CH$_3$)$_2$), 3.72 and 3.73 (2s, 12H, 4 × -OCH_3), 4.22 (d, 2H, J = 4.8 Hz, HOCH_2-), 5.09 (t, 1H, J = 7.0 Hz, -CH$_2$CH=), 5.42 (dt, 1H, J = 14.9 Hz, 7.5 Hz, -CH=CHCH=C-), 5.89 (d, 1H, J = 11.4 Hz, -CH=CHCH=C-), 6.36 (dd, 1H, J = 14.9 Hz, 11.1 Hz, CH=CHCH=C-); ms m/e: 468 (M$^+$), 450 (M$^+$ − H$_2$O).

Allylic alcohol ***24****c*

The reaction was carried out as described in the general procedure E. Thus, the silyl ether **23***c* (273.3 mg, 0.39 mmol) was treated with tetrabutylammonium fluoride (1.0 M in THF, 0.7 mL, 0.70 mmol) in 6 mL of THF to furnish the alcohol **24***c* (174.0 mg, 95%) as a colorless oil; ir (neat): 3520, 2950, 2850, 1735, 1435, 1200 cm^{-1}; ^{1}H nmr (CDCl$_3$) δ: 1.42 (t, 1H, J = 5.8 Hz, -CH$_2$OH), 1.56 (s, 3H, =CCH_3), 1.76 (s, 3H, =CCH_3), 1.80–2.08 (m, 8H, -CH_2CH_2CH=C(CH$_3$)CH_2CH_2-), 2.72 (d, 2H, J = 7.6 Hz, -CH_2CH=CHCH=C), 3.35 (t, 1H, J = 7.1 Hz, -CH(CO$_2$CH$_3$)), 3.72 and 3.73 (2s, 12H, 4 × -OCH_3), 4.05 (d, 2H, J = 5.9 Hz, -CH_2OH), 5.09 (t, 1H, J = 7.0 Hz, CH$_2$CH=CCCH$_3$-), 5.48 (dt, 1H, J = 14.9 Hz, 7.6 Hz, -CH=CHCH=C-), 6.01 (d, 1H, J = 10.4 Hz, -CH=CHCH=C-), 6.32 (dd, 1H, J = 14.9 Hz, 10.8 Hz, -CH=CHCH=C-).

Allylic chloride ***25****b*

The reaction was carried out as described in the general procedure B. Thus, treatment of allylic alcohol **24***b* (58.8 mg, 0.13 mmol) with lithium chloride (21.2 mg, 0.50 mmol), *s*-collidine (66.3 μL), and methanesulfonyl chloride (39 μL, 0.50 mmol) in DMF provided the allylic chloride **25***b* (51.0 mg, 84%) as a colorless oil that was used immediately in the next cyclization step without further purification and characterization.

Allylic bromide ***25****c*

To a stirred solution of the allylic alcohol **24***c* (22.0 mg, 47 μmol) and CBr$_4$ (19.4 mg, 58 μmol) in 0.6 mL of CH$_2$Cl$_2$ was added, dropwise at 0°C under argon, a solution of PPh$_3$ (17.3 mg, 66 μmol) in 0.4 mL of CH$_2$Cl$_2$. The resulting mixture was allowed to warm to room temperature and then stirred for about 2 h until the starting material **24***c* was consumed. After the solvent was evaporated, the crude residue was purified by flash chromatography using a 5:1 mixture of hexane and ethyl acetate to give allylic bromide **25***c* (21.4 mg, 40 μmol, 86%) as an oil that was used immediately in the next cyclization step without further purification and characterization.

TTC macrocycle ***1****b*

General procedure I

To a stirred suspension of Cs$_2$CO$_3$ (161.0 mg, 0.493 mmol) in a mixture of DMF and THF (1:1, 20 mL) was slowly added, at 70°C under argon by automatic syringe pump over a period of 12 h, a solution of allylic chloride **25***b* (51.3 mg, 0.105 mmol) in a mixture of DMF and THF (1:1, 15 mL). After the addition was completed, the stirring was continued for 9 h longer at 70°C. The solid was removed by filtration, and the filtrate was concentrated. The crude residue thus obtained was purified by flash chromatography using a 9:1 mixture of hexane and ethyl acetate to give two products, which were further purified by recrystallization from a minimum amount of CH$_2$Cl$_2$ in hexane to afford macrocyclic monomer **1***b* (34.0 mg, 72%) and macrocyclic dimer **26***b* (10 mg, 11%).

Compound ***1****b*: mp 140–143°C; ir (CHCl$_3$): 3020, 2945, 2850, 1727, 1435, 1225 cm^{-1}; ^{1}H nmr (CDCl$_3$) δ: 1.57 (s, 3H, -CH$_2$CH$_2$C(CH_3)=), 1.62 (s, 3H, =CHCH=C(CH_3)-), 1.80–1.91 and 1.97–2.08 (2m, 8H, -CH_2CH_2C(CH$_3$)=CHCH_2CH_2-), 2.67 (d, 2H, J = 7.7 Hz, =CH-CH_2CR(CO$_2$CH$_3$)$_2$), 2.90 (s, 2H, =C(CH$_3$)CH_2CR(CO$_2$CH$_3$)$_2$), 3.72 (s, 12H, 4 × -OCH_3), 5.07 (t, 1H, J = 5.0 Hz, -CH$_2$CH=C(CH$_3$), 5.17 (dt, 1H, J = 14.1 Hz, 7.2 Hz, -CH$_2$CH=CH-), 5.92–6.11 (m, 2H, -CH=CHCH=C(CH$_3$)-); ms m/e: 450 (M$^+$). Exact Mass (M$^+$) calcd.: 450.2253; found: 450.2246. Compound **1***b* was further characterized by X-ray crystallography.

Compound ***26****b*: mp 183–185°C; ir (neat): 3020, 2955, 2858, 1728, 1438, 1220 cm^{-1}; ^{1}H nmr (CDCl$_3$) δ: 1.52 (s, 6H, -CH$_2$CH$_2$C(CH_3)-), 1.59 (s, 6H, =CHCH=C(CH_3)-), 1.76–1.95 (m, 16H, -CH_2CH_2C(CH$_3$)CHCH_2CH_2-), 2.70 (d, 4H, J = 7.4 Hz, =CHCH_2CR(CO$_2$CH$_3$)$_2$), 2.89 (s, 4H, =C(CH$_3$)CH_2-CR(CO$_2$CH$_3$)$_2$), 3.71 (s, 24H, 8 × -OCH_3), 5.02 (m, 2H, -CH$_2$CH=C(CH$_3$)-), 5.34 (dt, 2H, J = 14.9 Hz, 7.4 Hz, -CH$_2$CH=CH-), 5.91 (d, 2H, J = 10.9 Hz, -CH=CHCH=C-), 6.31 (dd, 2H, J = 14.7 Hz, 11.0 Hz, -CH=CHCH=C-); ms m/e: 900 (M$^+$), 885 (M$^+$ − CH$_3$), 869 (M$^+$ − OCH$_3$). Exact Mass (M$^+$) calcd.: 900.4507; found: 900.4502.

TTT macrocycle ***1****c*

The macrocyclization was carried out as described in the general procedure I. Thus, a solution of allylic bromide **25***c* (21.4 mg, 40 μmol) in 10 mL of DMF–THF (1:1) was added slowly to a Cs$_2$CO$_3$ (74.2 mg, 230 μmol) suspension in 14 mL of DMF–THF (1:1) at 80°C over 5 h. After the mixture was stirred for an additional 10 h, it was worked up to provide pure macrocycle **1***c* (13.1 mg, 29 μmol, 73%) and dimer **26***c* (1.0 mg, 5%).

Compound ***1****c*: ir (neat): 2960, 2860, 1738, 1450, 1220 cm^{-1}; ^{1}H nmr (CDCl$_3$) δ: 1.46 (s, 3H, -CH$_2$C(CH_3)=CH-), 1.65 (s, 3H, =CHCH=C(CH_3)-), 1.73–2.07 (m, 8H, -CH_2CH_2C(CH$_3$)=CHCH_2CH_2-), 2.66 (d, 2H, J = 7.0 Hz, -CH_2CH=CHCH=), 2.80 (s, 2H, -CH_2C(CH$_3$)=CHCH=), 3.73 (s, 12H, 4 × -OCH_3), 4.98 (t, 1H, J = 7.0 Hz, -CH$_2$CH=C(CH$_3$)-), 5.67 (dt, 1H, J = 14.9 Hz, 7.0 Hz, -CH=CHCH=C), 5.90 (d, 1H, J = 10.7 Hz, -CH=CHCH=C-), 6.11 (dd, 1H, J = 14.9 Hz, 10.8 Hz, -CH=CHCH=C); ms m/e: 450 (M$^+$).

Compound ***26****c*: ir (neat): 3020, 2950, 2860, 1735, 1440, 1200 cm^{-1}; ^{1}H nmr (CDCl$_3$) δ: 1.56 (s, 12H, 4 × =C(CH_3)-), 1.75–2.00 (m, 16H, -CH_2CH_2C(CH$_3$)=CHCH_2CH_2-), 2.72 (d, 4H, J = 7.5 Hz, -CH_2CH=CHCH=C-), 2.76 (s, 4H, =CH-CH=C(CH$_3$)CH_2-), 3.70 and 3.72 (2s, 24H, 8 × -OCH_3), 5.11 (m, 2H, -CH$_2$CH=C(CH$_3$)CH$_2$-), 5.39 (dt, 2H, J = 15.1 Hz, 7.5 Hz, -CH=CHCH=C-), 5.87 (d, 2H, J = 10.6 Hz, -CH=CHCH=C-), 6.25 (dd, 2H, J = 15.1 Hz, 10.8 Hz, -CH=CHCH=C-); ms m/e: 900 (M$^+$), 869 (M$^+$ − OCH$_3$).

Triene diether ***28***

The coupling reaction of diene and dienophile was carried out as described in the general procedure G. Thus, treatment of dimethyl malonate **4** (622.0 mg, 1.7 mmol) with NaH (89.0 mg, 60%, 2.2 mmol) in 20 mL of THF–DMF (1:1) followed by addition of allylic chloride **5***a* (507.4 mg, 2.2 mmol) afforded coupling product **28** (578.0 mg, 61%) as a colorless oil; ir (neat): 2950, 1735, 1255, 1220, 1025, 838 cm^{-1}; ^{1}H nmr (CDCl$_3$) δ: 0.04 (s, 6H, (CH_3)$_2$Si-), 0.88 (s, 9H, -(CH_3)$_3$C), 1.49–1.83 (m, 6H, -OCH$_2$(CH_2)$_3$-), 1.58 (d, 3H, J = 1.0 Hz, CH_3C=CHCH$_2$CH$_2$-), 1.67 (s, 3H, CH_3C=CHCH=CH-), 1.85–1.90 (m, 4H, -C=CH-CH_2CH_2-), 2.18 (t, 2H, J = 7.5 Hz, -CH_2CH$_2$OSi-), 2.79 (s, 2H, =CHCH=C(CH$_3$)CH_2-), 3.47–3.56 and 3.82–3.93 (2m, 2H, -OCH_2(CH$_2$)$_3$-), 3.64 (t, 2H, J = 7.5 Hz, -SiOCH_2CH$_2$-), 3.71 (s, 6H, -C(CO$_2$CH_3)$_2$), 4.11–4.21 and 4.30–4.39 (2m, 2H, -CH_2OTHP), 4.64 (t, 1H, J = 2.5 Hz, -OCHO-), 5.10 (m,

Can. J. Chem. Downloaded from www.nrcresearchpress.com by 213.200.69.106 on 09/08/12
For personal use only.

1H, -C=C*H*CH_2CH_2-), 5.55 (dt, 1H, J = 10.0 Hz, 5.0 Hz, -CH_2C*H*=CHCH=C-), 6.11 (d, 1H, -CH=CHC*H*=C-), 6.30 (ddt, 1H, J = 10.0 Hz, 11.0 Hz, 1.0 Hz, -CH=C*H*CH=C-); ms m/e: 495 ($M^+ - C_4H_9$).

Allylic alcohol ***29***

The desilylation was carried out as described in the general procedure E. Thus, treatment of silyl ether **28** (578.0 mg, 1.05 mmol) with tetrabutylammonium fluoride solution (1 M in THF, 1.93 mL, 1.93 mmol) in 10 mL of THF afforded allylic alcohol **29** (385.0 mg, 81%) as an oil; ir (neat): 3650–3200, 2950, 1735, 1440, 1270, 1220, 1117, 1025 cm^{-1}; ^1H nmr ($CDCl_3$) δ: 1.47 (t, 1H, J = 5.0 Hz, -CH_2O*H*), 1.49–1.83 (m, 6H, -$OCH_2(CH_2)_3$-), 1.60 (d, 3H, J = 1.0 Hz, -(CH_3)C=$CHCH_2CH_2$-), 1.67 (d, 3H, J = 1.0 Hz, -(CH_3)C=CHCH=), 1.86–1.95 (m, 4H, -(CH_3)C=$CHCH_2CH_2$-), 2.23 (t, 2H, J = 5.0 Hz, -CH_2CH_2OH), 2.79 (s, 2H, -CH_2C(CH_3)=CHCH=CH-), 3.47–3.56 and 3.83–3.93 (2m, 2H, -$OCH_2(CH_2)_3$-), 3.66 (dt, 2H, J = 5.0 Hz, 5.0 Hz, -CH_2CH_2OH), 3.72 (s, 6H, -C(CO_2CH_3)$_2$), 4.11–4.21 and 4.30–4.39 (2m, 2H, -CH_2OTHP), 4.64 (t, 1H, J = 2.5 Hz, -OC*H*O-), 5.18 (m, 1H, -C=C*H*CH_2CH_2-), 5.55 (dt, 1H, J = 10.0 Hz, 5.0 Hz, -C*H*=CHCH=C-), 6.11 (d, 1H, J = 11.0 Hz, -CH=CHC*H*=C-), 6.30 (ddt, 1H, J = 10.0 Hz, 11.0 Hz, 1.0 Hz, -CH=C*H*CH=C-); ms m/e: 438 (M^+). Exact Mass (M^+) calcd: 438.2617; found: 438.2614.

Methanesulfonate ester ***30***

The mesylation reaction was carried out as described in the general procedure F. Thus, the alcohol **29** (380.0 mg, 0.87 mmol) was treated with methanesulfonyl chloride (84 μL, 122.0 mg, 1.06 mmol) in the presence of triethylamine (183 μL, 142.0 mg, 1.32 mmol) to afford sulfonate ester **30** (440.5 mg, 0.85 mmol), 98%) as an oil that was used immediately for the next reaction without further purification and characterization.

Tetraester ***31***

The introduction of dimethyl malonate unit into triene **30** was carried out as described in the general procedure H. Thus, the mesylate **30** (440.5 mg, 0.85 mmol) was treated with NaH (196.0 mg, 60% in oil, 4.86 mmol) in a mixture of DMF and THF (1:1, 12 mL), followed by addition of dimethyl malonate (0.61 mL, 705.0 mg, 5.4 mmol) and a catalytic amount of KI (77.0 mg) to give alkylated product **31** (338.0 mg, 0.61 mmol, 72%) as an oil; ir (neat): 2950, 1735, 1435, 1080, 1025 cm^{-1}; ^1H nmr ($CDCl_3$) δ: 1.46–1.83 (m, 6H, -$OCH_2(CH_2)_3$-), 1.56 (d, 3H, J = 1.0 Hz, -(CH_3)C=$CHCH_2CH_2$-), 1.68 (s, 3H, -(CH_3)C=CHCH=CH-), 1.85–1.90 (m, 4H, -C=C*H*CH_2CH_2-), 1.96–2.02 (m, 4H, -CH_2CH_2CH(CO_2CH_3)$_2$), 2.79 (s, 2H, =C(CH_3)-CH_2C(CO_2CH_3)$_2$-), 3.28–3.36 (m, 1H, -C*H*(CO_2CH_3)$_2$), 3.46–3.56 and 3.82–3.92 (2m, 2H, -$OCH_2(CH_2)_3$-), 3.71 and 3.73 (2s, 12H, 4 × -OCH_3), 4.11–4.21 and 4.30–4.39 (2m, 2H, -CH_2OTHP), 4.64 (t, 1H, J = 2.5 Hz, -OC*H*O-), 5.09 (m, 1H, -C=C*H*CH_2CH_2-), 5.55 (dt, 1H, J = 10.0 Hz, 5.0 Hz, -C*H*=CHCH=C-), 6.11 (d, 1H, J = 11.0 Hz, -CH=CHC*H*=C-), 6.30 (ddt, 1H, J = 10.0 Hz, 11.0 Hz, 1.0 Hz, -CH=C*H*CH=C-); ms m/e: 552 (M^+). Exact Mass (M^+) calcd.: 552.2934; found: 552.2922.

Allylic alcohol ***32***

The deprotection of THP–ether was carried out in the same way as described in the general procedure D. Thus, treatment of THP–ether **31** (330.0 mg, 0.59 mmol) with pyridinium p-toluenesulfonate (17.0 mg, 0.07 mmol) in 6 mL of CH_3OH afforded alcohol **32** (268.0 mg, 97%) as a viscous oil; ir (neat): 3600–3200, 2950, 1730, 1435, 1270, 1210 cm^{-1}; ^1H nmr ($CDCl_3$) δ: 1.55 (t, 1H, J = 5.0 Hz, -CH_2O*H*), 1.56 (d, 3H, J = 1.0 Hz, -(CH_3)C=$CHCH_2CH_2$-), 1.66 (s, 3H, -(CH_3)C=CHCH=CH-), 1.84–1.88 (m, 4H, -C=C*H*CH_2CH_2-), 1.96–2.01 (m, 4H, -CH_2CH_2CH(CO_2CH_3)$_2$), 2.78 (s, 2H, =C(CH_3)CH_2C(CO_2CH_3)$_2$-), 3.28–3.35 (m, 1H, -C*H*(CO_2CH_3)$_2$), 3.71 and 3.73 (2s, 12H, 4 × -OCH_3), 5.29 (dt, 2H, J = 1.0 Hz, 5.0 Hz, -CH_2OH), 5.08 (m, 1H, -C=C*H*CH_2CH_2-), 5.58 (dt, 1H, J = 10.0 Hz, 5.0 Hz, -C*H*=CHCH=C-), 6.08 (d, 1H, J = 11.0 Hz, -CH=CHC*H*=C-), 6.29 (ddt, 1H, J = 10.0 Hz, 11.0 Hz, 1.0 Hz, -CH=C*H*CH=C-); ms m/e: 450 ($M^+ - H_2O$). Exact Mass ($M^+ - H_2O$) calcd.: 450.2253; found: 450.2253.

CTT macrocycle ***1***a

The preparation of allylic chloride **33** was carried out as described in the general procedure B. Thus, treatment of allylic alcohol **33** (35.0 mg, 75 μmol) with LiCl (12.6 mg, 299 μmol), s-collidine (40 μL, 299 μmol), and methanesulfonyl chloride (23 μL, 299 μmol) in 0.5 mL of DMF yielded allylic chloride **33** (35 mg) as a crude oil that was used immediately in the next cyclization step without characterization and further purification.

The cyclization of allylic chloride **33** was carried out in as described in the general procedure I. Thus, a solution of crude oil **33** (35 mg) in a mixture of DMF and THF (1:1, 5 mL) was added at 70°C over 5 h slowly to a Cs_2CO_3 (122 mg, 375 μmol) suspension in a mixture of DMF and THF (1:1, 12 mL). The stirring was continued for an additional 8 h after completion of the addition. Work-up of the reaction mixture followed by flash chromatography and recrystallization (CH_2Cl_2–hexane) furnished a crystalline compound ***1a*** (19 mg, 57% from alcohol **33**); mp 173–176°C; ^1H nmr ($CHCl_3$) δ: 1.53 (s, 3H, -(CH_3)C=CHCH=CH-), 1.59 (d, 3H, J = 1.0 Hz, -(CH_3)C=$CHCH_2CH_2$), 1.80–2.03 (m, 8H, -CH_2CH_2C(CH_3)=CHCH_2CH_2-), 2.76 (d, 2H, J = 8.0 Hz, -CH_2CH=CHCH=C-), 2.89 (s, 2H, CH=CHCH=C(CH_3)CH_2-), 3.728 and 3.730 (2s, 12H, 4 × -OCH_3), 5.05 (m, 1H, -C*H*=CHCH=C-), 5.32 (t, 1H, J = 7.5 Hz, -C=C*H*CH_2CH_2-), 5.95 (d, 1H, J = 11.0 Hz, -CH=CHC*H*=C-), 6.36 (dd, 1H, J = 10.0 Hz, 11.0 Hz, -CH=C*H*CH=C-); ms m/e: 450 (M^+). Exact Mass (M^+) calcd.: 450.2253; found: 450.2246.

Diels–Alder reaction of ***1***a

Solid macrocycle ***1a*** (5.0 mg, 11 μmol) was heated in a vacuum-sealed quartz tube (20 cm long, 8 mm diameter) at 360°C for 80 min. After the tube was cooled to room temperature, the residue in the tube was dissolved in CH_2Cl_2 and then transferred into a flask. After the solvent was evaporated, the residue was purified by flash chromatography with a 12:7:1 mixture of $CHCl_3$, hexane, and Et_2O to provide a mixture (3.1 mg, 62%) that displayed only one spot on tlc but contained several tricyclic isomers as observed by gc. Attempts to separate each isomer of the mixture by flash chromatography using different solvent systems were unsuccessful. Proton nmr of the mixture is very complicated, but it does contain all the characteristic peaks for tricycle **34** whose spectral data are provided below.

The gc analysis of the reaction mixture before flash chromatography reveals four major products, each contributing between 10 and 19% yield, along with a number of minor ones (<9%).

Diels–Alder reaction of ***1***b

Solid macrocycle ***1b*** (18.8 mg, 41.7 μmol) was placed in the bottom of a quartz tube, which was then sealed under vacuum. The tube was heated to 300°C for 2 h. The crude residue was transferred to a flask with CH_2Cl_2 and then purified by flash chromatography with a 97:3 mixture of hexane and ethyl acetate to give tricycle **41** (12.4 mg, 66%) as a crystalline solid; mp 119–122°C; ir (neat): 2960, 2850, 1738, 1450, 1240, 1100 cm^{-1}; ^1H nmr ($CDCl_3$) δ: 0.92 (d, 3H, J = 6.9 Hz, CH_3CH-), 1.25–2.60 (m, 15H, all other CH_2 and C*H*), 1.62 (s, 3H, CH_3C=), 3.63–3.75 (m, 12H, 4 × -OCH_3), 5.19 (s, 1H, -C*H*=CCH_3); ^1H nmr (C_6D_6) δ: 0.82 (d, 3H, J = 6.9 Hz, C*H*CH-), 1.05–2.60 (m, 15H, all other CH_2 and C*H*), 1.62 (s, 3H, CH_3C=CH), 3.30–3.35 (m, 12H, 4 × -OCH_3), 5.20 (s, 1H, -C*H*=CCH_3). The relative stereochemistry for compound **41** was further confirmed by X-ray crystallography.

Diels–Alder reaction of ***1***c

A solution of macrocycle ***1c*** (13.0 mg, 28.9 μmol) in 2 mL of toluene was heated in a vacuum-sealed quartz tube at 200°C for 17 h. After the tube was opened, the reaction mixture was trans-

ferred into a flask with CH_2Cl_2 and then evaporated. The residue was purified by flash chromatography using a 5:1 mixture of hexane and ethyl acetate to give TAC tricyclic compound **34** (12.5 mg, 27.8 μmol, 96%) as a crystalline solid; mp 146–148°C; ir (neat): 2945, 2870, 1738, 1435, 1230 cm^{-1}; ^1H nmr ($CDCl_3$) δ: 0.88 (s, 3H, -CH_3), 0.91 (s, 3H, -CH_3), 1.10–2.23 (m, 14H, all other CH_2 and CH), 3.68, 3.70, 3.73 and 3.74 (4s, 12H, 4 × -OCH_3), 5.19 (d, 1H, J = 9.9 Hz, -CH=C*H*C-), 5.40 (dd, 1H, J = 9.9 Hz, 1.9 Hz, CHC*H*=CH-). The structure of the compound **34** was further confirmed by X-ray crystallography.

Acknowledgements

This research was supported by the Natural Sciences and Engineering Research Council of Canada (NSERCC, Ottawa) and by the "Ministère de l'Enseignement supérieur et de la Science (Fonds FCAR, Québec)." We also acknowledge the support of IBM Canada Ltd (Cooperative Project Program) and the Tripos Company that allowed us to use the Sybyl Software, and thank Professor A. Michel for helpful discussions.

1. P. Deslongchamps. Aldrichimica Acta, **24**, 43 (1991).
2. (*a*) S. Lamothe, A. Ndibwami, and P. Deslongchamps. Tetrahedron Lett. **29**, 1639 (1988); (*b*) Tetrahedron Lett. **29**, 1641 (1988); (*c*) A. Marinier and P. Deslongchamps. Tetrahedron Lett. **29**, 6215 (1988); (*d*) Y.C. Xu, M. Cantin, and P. Deslongchamps. Can. J. Chem. **68**, 2137 (1990); (*e*) M. Cantin, Y.C. Xu, and P. Deslongchamps. Can. J. Chem. **68**, 2144 (1990); (*f*) K. Baettig, C. Dallaire, R. Pitteloud, and P. Deslongchamps. Tetrahedron Lett. **28**, 5249 (1987); (*g*) K. Baettig, A. Marinier, R. Pitteloud, and P. Deslongchamps. Tetrahedron Lett. **28**, 5253 (1987); (*h*) G. Berube and P. Deslongchamps. Tetrahedron Lett. **28**, 5255 (1987); (*i*) Can. J. Chem. **68**, 404 (1990); (*j*) A. Marinier, K. Baettig, C. Dallaire, R. Pitteloud, and P. Deslongchamps. Can. J. Chem. **6741**, 1609 (1989).
3. (*a*) D. Taub. *In* The total synthesis of natural products. Vol. 6. *Edited by* J. Apsimon. John Wiley and Sons, New York. 1984. pp. 1–49; (*b*) K. Nakanishi. *In* Natural products chemistry. Vol. 3. *Edited by* K. Nakanishi et al. Kodansha Ltd, Tokyo. 1983. Chap. 4.
4. (*a*) P. Deslongchamps, S. Lamothe, and H.-S. Lin. Can. J. Chem. **62**, 2395 (1984); (*b*) Can. J. Chem. **65**, 1298 (1987); (*c*) D. Brillon and P. Deslongchamps. Can. J. Chem. **65**, 43 (1987); (*d*) Can. J. Chem. **65**, 56 (1987).
5. T. Takahashi, K. Shimizu, T. Doi, and T. Tsuji. J. Am. Chem. Soc. **110**, 2674 (1988), and references therein.
6. Y. Tamaru, H. Ochiai, T. Nakamura, K. Tsubaki, and Z. Yoshida. Tetrahedron Lett. **26**, 5559 (1985).
7. C.L. Rand, D.E. Van Horn, M.W. Moor, and E. Negishi. J. Org. Chem. **46**, 4093 (1981).
8. O.P. Goel and R.E. Seamans. Synthesis, 538 (1973).
9. S.K. Chaudhary and O. Hernandez. Tetrahedron Lett. 99 (1979).
10. A.P. Krapcho, E.G.E. Jahngen, Jr., and D.S. Kashdan. Tetrahedron Lett. **32**, 2721 (1974).
11. M. Miyashita, A. Yoshikoshi, and P.A. Grieco. J. Org. Chem. **42**, 3772 (1977).
12. A.J. Mancuso, S.L. Huang, and D. Swern. J. Org. Chem. **43**, 2480 (1978).
13. H. Nagaoka and Y. Kishi. Tetrahedron, **37**, 3873 (1981).
14. E.W. Collington and A.I. Meyers. J. Org. Chem. **36**, 3044 (1971).
15. E.J. Corey and J.W. Suggs. Tetrahedron Lett. 2647 (1975).
16. W.C. Still and C. Gennari. Tetrahedron Lett. **24**, 4405 (1983).
17. S. Hanessian and P. Lavallee. Can. J. Chem. **53**, 2975 (1975); **55**, 562 (1977).
18. E.J. Corey, A. Venkateswarlu. J. Am. Chem. Soc. **94**, 6190 (1972).
19. B.M. Trost and W.C. Vladuchick. J. Org. Chem. **44**, 148 (1979).
20. J. Hooz and S.S.H. Gilani. Can. J. Chem. **46**, 86 (1968).
21. A.G. Michel, M. Drouin, N. Michel-Dewez, A.L. Roughton, and P. Deslongchamps. Acta Crystallogr. Sect. C: Cryst. Struct. Commun. **C47**, 1032 (1991).
22. M. Drouin, A.G. Michel, Y.C. Xu, and P. Deslongchamps. Acta Crystallogr. Sect. C: Cryst. Struct. Commun. **C46**, 1884 (1990).
23. A. Ndibwami, S. Lamothe, P. Soucy, S. Goldstein, and P. Deslongchamps. Can. J. Chem. **71**, 714 (1993).
24. F.K. Brown and K.N. Houk. Tetrahedron Lett. **25**, 4609 (1984).
25. L.V. Manes, P. Crews, M.R. Kernan, J.D. Faulkner, F.R. Fronczek, and R.D. Gandour. J. Org. Chem. **53**, 570 (1988).
26. T.K. Devon and A.I. Scott. *In* Handbook of naturally occurring compounds, Vol. II. Terpenes. Academic Press, New York. 1972.

Can. J. Chem. Downloaded from www.nrcresearchpress.com by 213.200.69.106 on 09/08/12
For personal use only.

Stereocontrolled construction of 1,7-dimethyl A.B.C.[6.6.6] tricycles. Part II. Transannular Diels–Alder reaction of 14-membered macrocycles containing *cis*-dienophiles

YAO-CHANG XU, ANDREW L. ROUGHTON, PIERRE SOUCY, SOLO GOLDSTEIN, and PIERRE DESLONGCHAMPS[1]

Laboratoire de synthèse organique, Département de chimie, Faculté des sciences, Université de Sherbrooke, Sherbrooke (Québec), Canada J1K 2R1

Received February 18, 1993

YAO-CHANG XU, ANDREW L. ROUGHTON, PIERRE SOUCY, SOLO GOLDSTEIN, and PIERRE DESLONGCHAMPS. Can. J. Chem. **71**, 1169 (1993).

The synthesis and transannular Diels–Alder reactions of 14-membered macrocyclic trienes containing a methyl-substituted diene and a methyl-substituted *cis*-dienophile moiety are described. As a result of the dienophile *cis* geometry the 1,7-dimethyl A.B.C.[6.6.6] tricycles obtained from the Diels–Alder reaction have a different stereochemistry at the four chiral centers than similar tricycles that were the subject of the preceding paper in this series. Thus *trans-syn-cis* (TSC) tricycle **30** was the sole product obtained from the *trans-cis-cis* (TCC) macrocycle **1***b*. In a similar fashion TCC macrocycle **1***d* afforded only *trans-syn-cis* (TSC) tricycle **31**. On the contrary, the transannular Diels–Alder reaction in *cis-trans-cis* (CTC) macrocycle **1***a* and *trans-trans-cis* (TTC) macrocycle **1***c* led to a mixture of the same four tricyclics (**30**, **32–34**) but in different ratio. The above experimental results are rationalized by taking into consideration the interconversion of macrocyclic trienes **1***a*, **1***b*, and **1***c*. Pathways for these interconversions are also proposed.

YAO-CHANG XU, ANDREW L. ROUGHTON, PIERRE SOUCY, SOLO GOLDSTEIN et PIERRE DESLONGCHAMPS. Can. J. Chem. **71**, 1169 (1993).

La synthèse ainsi que la réaction de Diels–Alder transannulaire, des triènes macrocycliques à 14 chaînons dont l'unité diène et l'unité *cis*-diénophile portent un substituant méthyle, seront décrites. La cycloaddition transannulaire génère des tricycles A.B.C.[6.6.6]-1,7-diméthyle. Cependant, dû à la géométrie *cis* du diénophile, la stéréochimie observée pour les quatre centres chiraux est différente de celle obtenue pour des composés similaires qui ont été examinés dans l'article précédent de cette série. Ainsi le tricycle **30**, de stéréochimie *trans-syn-cis* (TSC), a été le seul produit obtenu à partir du macrocycle **1***b*, de stéréochimie *trans-cis-cis* (TCC). De la même manière le macrocycle TCC **1***d* a fournit uniquement le tricycle TSC **31**. Contrairement à ces résultats, les macrocycles *cis-trans-cis* (CTC) **1***a* et *trans-trans-cis* (TTC) **1***c* ont fourni, dans des proportions différentes, un mélange des mêmes quatre produits (**30**, **32–34**). Ces résultats expérimentaux ont été rationalisés prenant en considération l'interconversion des triènes macrocycliques **1***a*, **1***b* et **1***c*. On a proposé aussi des mécanismes pour ces interconversions.

Can. J. Chem. Downloaded from www.nrcresearchpress.com by 213.200.69.106 on 09/08/12
For personal use only.

Introduction

In the preceding article (1), we reported the syntheses and transannular Diels–Alder reactions of 14-membered macrocyclic trienes containing *E* dienophiles. As indicated in Scheme 1, the A.B.C.[6.6.6] tricyclic compound **2**, which may be derived from macrocycle **1**, contains two methyl groups at the quaternary C1 and C7 positions and could be constructed in a stereoselective manner by changing the geometry of the diene double bonds. This new methodology, which is complementary to other methods such as aldol condensations (2), biomimetic cyclization (3), intramolecular Diels–Alder reaction (4), and intramolecular Michael addition (5), provides a powerful tool for the synthesis of polycyclic natural products such as steroids and terpenes (6).

In this article, we would like to report our continued investigation (7) of this new methodology specifically applied to the macrocyclic system **1**, which contains a *cis* dienophile.

Preparation of dienophiles and dienes

In the preceding publication, a stereoselective synthesis of an *E* dienophile was reported, and this basic building block was used in the syntheses of three macrocycles (1). In this series, a *Z* dienophile was used as a basic building block in constructing four other macrocyclic trienes. Since both *Z* and *E* dienophiles are required for our systematic studies, a method for the simultaneous synthesis of both isomers was desirable.

Scheme 2 illustrates the synthetic route to both dienophiles via a Wittig reaction as the key step. The coupling reaction of commercially available (ethyl)triphenylphosphonium bromide with tetrahydropyranyl bromide ether **3**, which was prepared from 2-bromoethanol and 3,4-dihydro-2*H*-pyran (8), gave rise in the presence of potassium bis(trimethylsilyl)amide as a base to phosphonium salt **4**, in good yield (9). Swern oxidation (10) of alcohol **5**, which was obtained by mono-protection of commercially available 1,3-propanediol (11), furnished aldehyde **6** in 86% yield, thus setting the stage for the olefination reaction.

The Wittig olefination reaction was carried out in tetrahydrofuran at 0°C by adding aldehyde **6** to a solution of the phosphonium ylide, generated from **4** and butyllithium, to provide an isomeric mixture of *Z* and *E* dienophiles **7** with both hydroxyl groups protected. The ratio of *Z* and *E* isomers is roughly 43:57 as determined by integration of the proton nmr signals.

Attempts to separate the isomeric mixture **7** by chromatography met with little success. It was finally found, however, that after selective removal of the tetrahydropyranyl protecting group with pyridinium *p*-toluenesulfonate in isopropanol at 75°C[2] the resulting alcohols of the isomeric mixture **8** could be separated by the use of medium-pres-

[1]Author to whom correspondence may be addressed.

[2]L. Ruest, S. Lamothe, and P. Deslongchamps. Unpublished results.

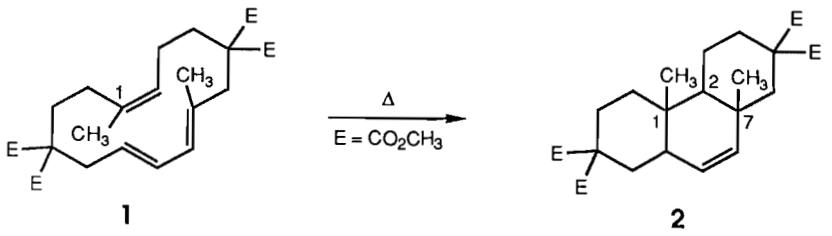

SCHEME 1

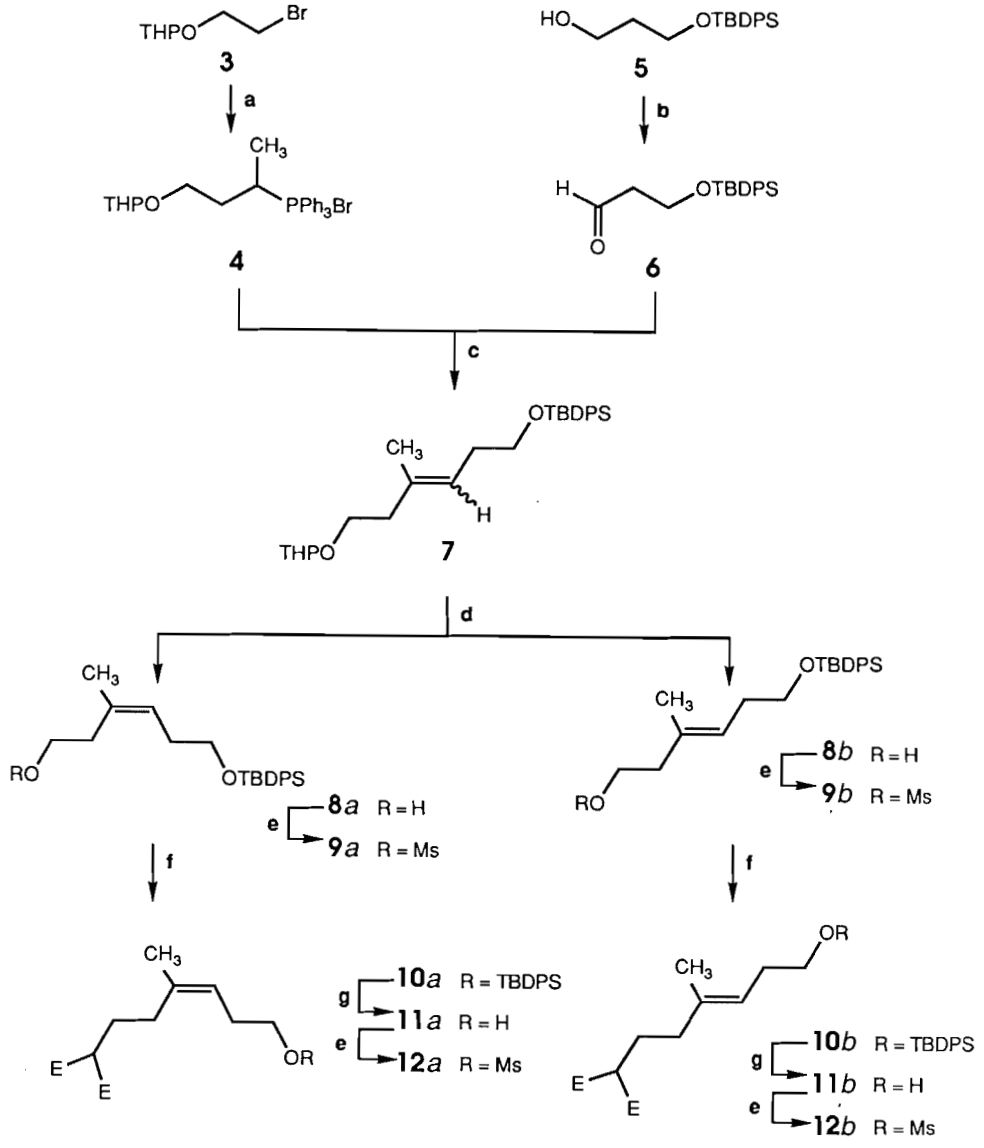

(a) $EtPPh_3Br$, $KN(TMS)_2$, THF, 0°C to r.t., 88%;
(b) $(COCl)_2$, DMSO, CH_2Cl_2, Et_3N, -78°C to r.t., 86%;
(c) nBuLi, THF, 0°C, 61%;
(d) PPTS, iPrOH, 80°C, 98%;
(e) MsCl, Et_3N, CH_2Cl_2, 0°C, 93-97%;
(f) NaH, CH_2E_2, KI, DMF, THF, 0° to 70°C, 87-88%;
(g) nBu_4NF, THF, 0°C to r.t., 74-91%.

SCHEME 2

Can. J. Chem. Downloaded from www.nrcresearchpress.com by 213.200.69.106 on 09/08/12
For personal use only.

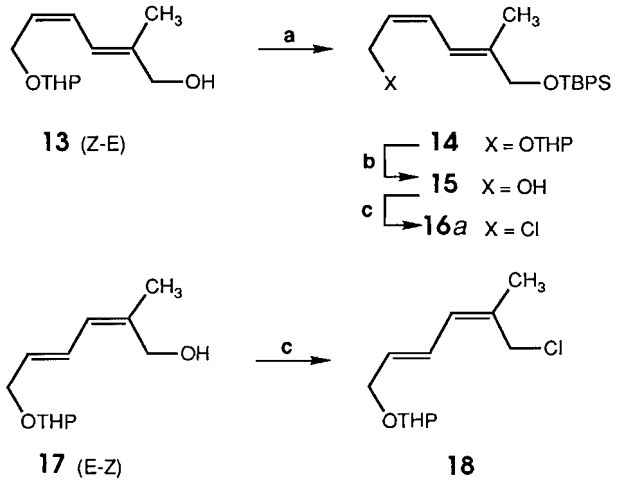

(a) *t*-BuPh$_2$SiCl, imidazole, THF, 0°C, 99%;

(b) PPTS, iPrOH, 80°C, 86%;

(c) LiCl, MsCl, *s*-collidine, DMF, 0°C to r.t., 99%.

SCHEME 3

sure chromatography. It is interesting to note that the isomeric mixture of alcohols resulting from desilylation of **7** was practically inseparable.

After separation, both alcohols **8***a* and **8***b* were subjected, in separate experiments, to the same transformations as indicated in Scheme 2, in order to produce the proper functionality necessary for the coupling reaction with dienes. Thus, **8***a* and **8***b* were converted in good yields to their respective methanesulfonate esters **9***a* and **9***b*. Potassium-iodide-catalyzed alkylation of methanesulfonate esters **9***a* and **9***b* with the sodium-hydride-generated enolate of dimethyl malonate in a mixture of DMF and THF (1:1) at 85°C afforded methyl octenoates **10***a* and **10***b*, respectively. Desilylation of **10***a* and **10***b* by tetrabutylammonium fluoride (12) in THF then gave alcohols **11***a* and **11***b*, which were similarly converted, as described above, to their methanesulfonate esters **12***a* and **12***b* as the desired dienophiles. A stereoselective synthesis of *Z* dienophile **12***a* was also developed in our laboratory; the details will be reported in near future (13).

In the studies of transannular Diels–Alder reactions for this series, four different diene moieties were required. Syntheses of dienes **16***b* (*E-Z*) and **16***c* (*E-E*) used as depicted in Scheme 4 were reported in the preceding article (1). The other two dienes **16***a* (*Z-E*) and **18** (*E-Z*) were derived from dienes **13** and **17** (1), respectively, by functional group manipulations. As presented in Scheme 3, hydroxyl group protection in **13** with *tert*-butylchlorodiphenylsilane gave diene diether **14** (11). Selective deprotection of the tetrahydropyranyl ether (THP) with pyridinium *p*-toluenesulfonate (PPTS) ether was performed with isopropanol[2] to give allylic alcohol **15**, which could be transformed into allylic chloride **16***a* by use of Meyers' method (14). Similarly, allylic alcohol **17** could be converted to allylic chloride **18** (14).

Preparation of macrocycles

Our basic strategy for the synthesis of acyclic trienes, which are the immediate precursors of macrocycles, is based on the coupling reaction of dienes and dienophiles, which has been used extensively in our laboratory (7). As presented in Scheme 4, the coupling reactions were conducted by alkylation of the sodium-hydride-generated enolate of dimethyl malonate **12***a* with allylic chlorides **16***a*, **16***b*, or **16***c* in a mixture of THF and DMF (15), which provided three acyclic trienes **19***a* (*Z-E-Z*), **19***b* (*E-Z-Z*), and **19***c* (*E-E-Z*), respectively, in good yields. Introduction of the malonate connector was accomplished by substitution of the methanesulfonate ester groups of **19***a*, **19***b*, and **19***c* with the sodium salt of dimethyl malonate in the presence of a catalytic amount of potassium iodide to produce **20***a*, **20***b*, and **20***c*, respectively. Deprotection of the silyl ether groups was carried out by treatment of **20***a*, **20***b*, and **20***c* with tetrabutylammonium fluoride in THF (12) to give **21***a*, **21***b*, and **21***c*. The allylic alcohol **21***b* was converted to allylic chloride **22***b* by Meyers' method (LiCl, CH_3SO_2Cl, and *s*-collidine in DMF (14)). The allylic chloride has been used very often for the preparation of macrocycles in our laboratory (7). However, it was recently found that the corresponding allylic bromide is superior to the allylic chloride for the macrocyclization process (1). Therefore, allylic alcohols **21***a* and **21***c* were transformed into allylic bromides **22***a* and **22***c*, respectively, using PPh_3 and CBr_4 in CH_2Cl_2 (16). Allylic halides **22***a*, **22***b*, and **22***c* decomposed slowly when they were purified by flash chromatography; however, this problem could be avoided if the newly prepared allylic halides were filtered through a short-path silica gel column and then used immediately for the next cyclization reaction.

Having synthesized the requisite carbon chain and appropriate functional groups at each end, the acyclic trienes **22***a–c* were ready for the construction of macrocycles. All macrocyclizations were performed in the same way by slowly adding a solution of allylic halides **22***a*, **22***b*, **22***c* in THF to a stirred suspension of cesium carbonate in a mixture of DMF and THF (1:1) at about 80°C under dilute conditions to avoid dimerization (7). Macrocyclic products **1***a* (*cis-trans-cis*, CTC), **1***b* (TCC), and **1***c* (TTC) were formed as white solids in very good yields (66–93%) via an intramolecular displacement of allylic halides by the base-generated dimethyl malonate anion. In all cases, no detectable amount of dimerization product was observed by ^{1}H nmr spectra. However, a side-product **23**, which was derived from an S_N2'-like mechanism, was obtained from **22***c* but in less than 5% yield.

The structures of macrocycles **1***a*, **1***b*, and **1***c* were rigorously established by spectroscopic data including ^{13}C and ^{1}H nmr, ir, and high- and low-resolution ms. The conservation of the double bond geometries in the macrocyclic products has been confirmed by comparing the ^{1}H nmr data with those of their triene precursors such as **22** or **21**. Further confirmation of the structures by X-ray crystallography was also obtained for macrocycles **1***a*[3] and **1***b* (17).

Macrocycle **1***d*, which has methyl substituents at the C2 and C7 positions and which possesses the same olefin geometries (*trans-cis-cis*) as macrocycle **1***b*, was synthesized via a slightly different procedure than that used for the preparation of other macrocycles. As presented in Scheme 5, the *Z* dienophile **24**, previously prepared in our laboratory (1), was first converted to its enolate anion with sodium hydride in tetrahydrofuran. The coupling reaction (15)

[3]A.G. Michel, Y.C. Xu, and P. Deslongchamps. Unpublished results.

Can. J. Chem. Downloaded from www.nrcresearchpress.com by 213.200.69.106 on 09/08/12
For personal use only.

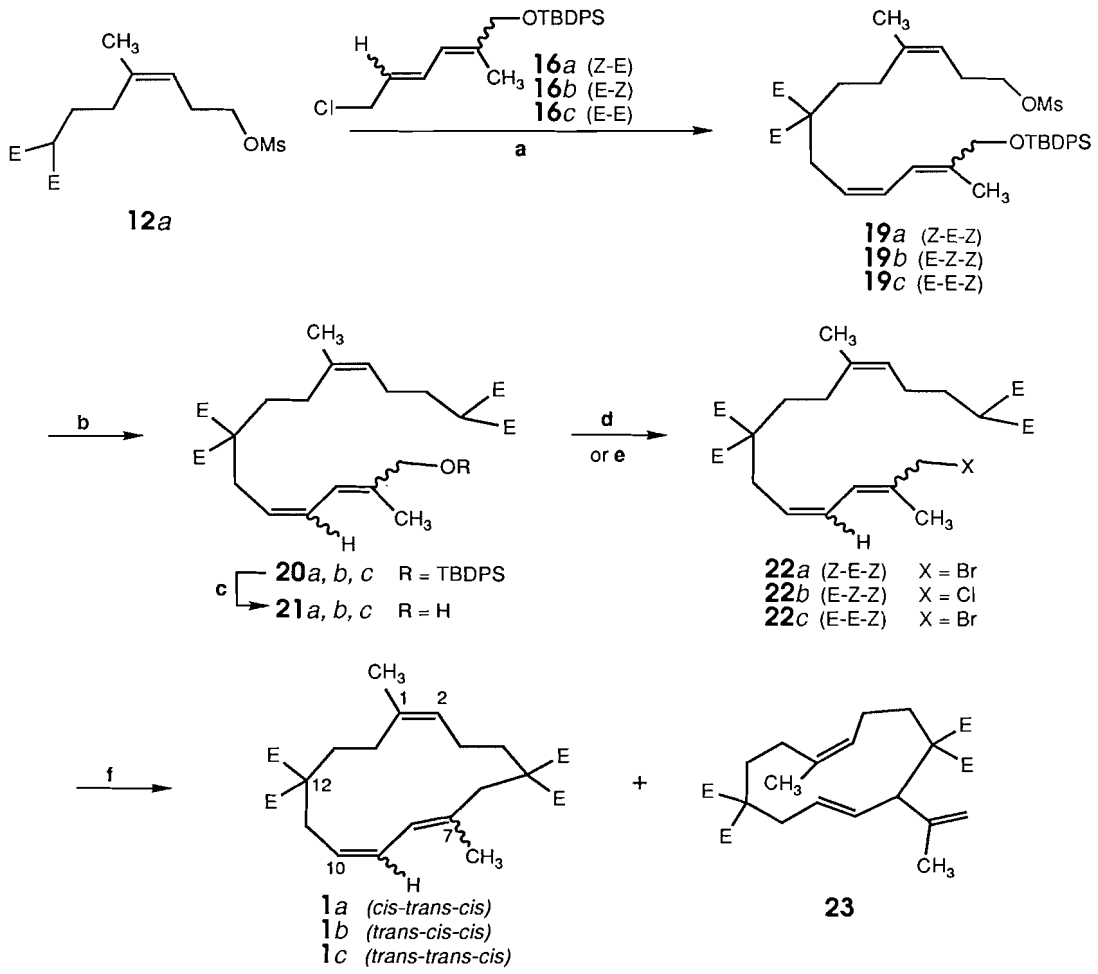

(a) NaH, THF, DMF, 0°C to r.t., 59-77%;

(b) NaH, CH_2E_2, KI, DMF, THF, 0°C to r.t., 76-91%;

(c) nBu_4NF, THF, 0°C to r.t., 60-90%;

(d) CBr_4, PPh_3, CH_2Cl_2, 0°C to r.t., 74-87%;

(e) LiCl, MsCl, *s*-collidine, DMF, 0°C to r.t.;

(f) Cs_2CO_3, DMF, THF, 70°C, 63-90%.

SCHEME 4

of this enolate with allylic chloride **18** took place at room temperature (DMF–THF) to give *E-Z-Z* triene **25**. After treatment of **25** with tetrabutylammonium fluoride in THF (12), the resulting alcohol **26** was converted to its methanesulfonate ester **27** with methanesulfonyl chloride and triethylamine. Introduction of the malonate connector to give **28***a* was accomplished according to the previously described procedures. Treatment of compound **28***a* with pyridium *p*-toluenesulfonate in methanol at 55°C (8) resulted in the formation of alcohol **28***b*, which was subsequently transformed into allylic chloride **29** by Meyers' procedure (14). Without further purification, triene allylic chloride **29** was immediately subjected to the previously described cyclization conditions. TCC macrocycle **1***d* was thus obtained as a crystalline solid in 69% overall yield from alcohol **28**. Again, the structure of macrocycle **1***d* was rigorously established by spectroscopic analysis including nmr, ir, and ms as well as X-ray crystallography (17).

Diels–Alder reaction of TCC macrocycles **1***b and* **1***d*

In the case of TCC macrocycle **1***b*, the cycloaddition reaction was carried out at 320°C in a sealed tube for 90 min, providing the crystalline *trans-syn-cis* (TSC) tricycle **30** (Scheme 6) in 87% isolated yield. The structure of **30** was rigorously established by X-ray crystallographic analysis (18).

In principle, a macrocyclic triene can yield two different diastereoisomeric products. However, and as previously discussed (7*a*), there are cases where a particular diastereoisomer cannot be formed because of conformational restrictions due to the fact that the Diels–Alder reaction must take place via a boat transition state. Such a situation occurs in the case of a TCC macrocycle, which is predicted to give exclusively a TSC tricycle since a CST tricycle cannot be

Can. J. Chem. Downloaded from www.nrcresearchpress.com by 213.200.69.106 on 09/08/12
For personal use only.

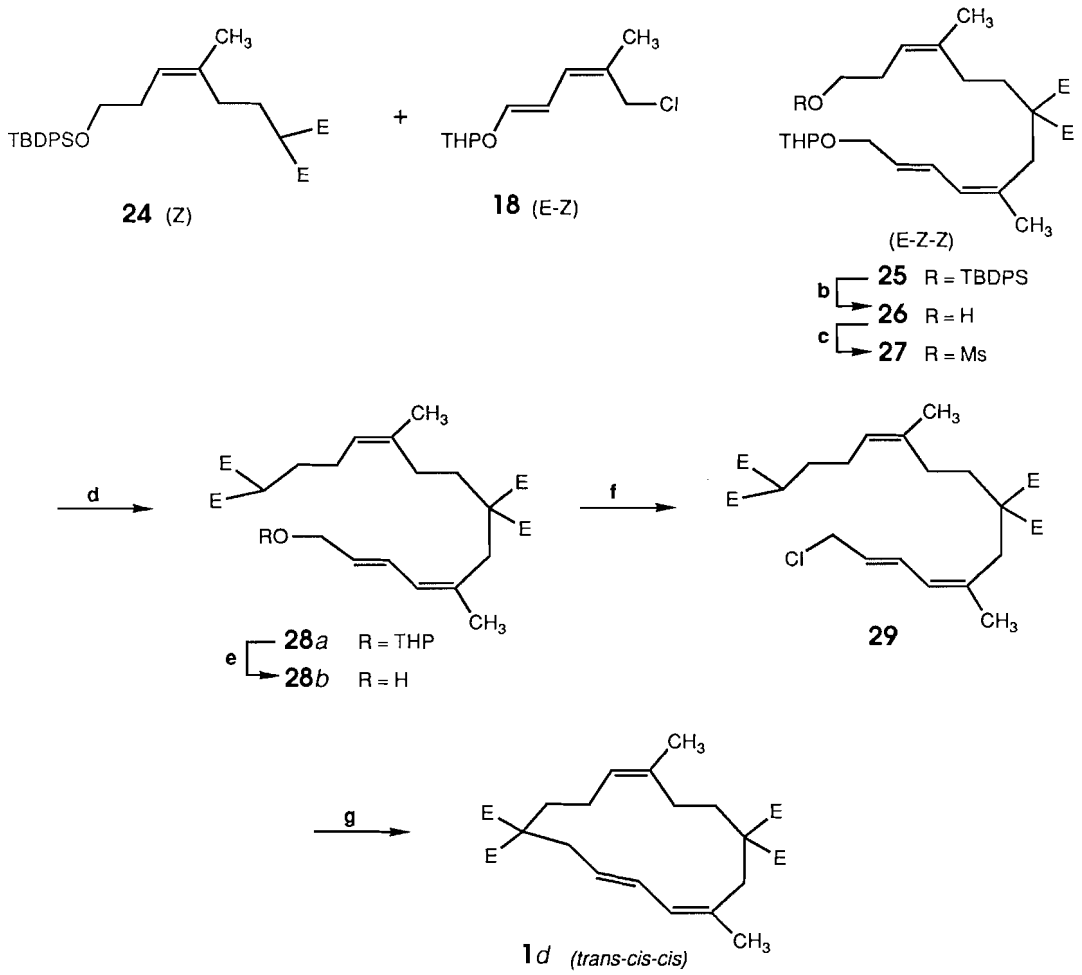

(a) NaH, THF, DMF, 0°C to r.t., 35%;

(b) nBu_4NF, THF, 0°C to r.t., 99%;

(c) MsCl, Et_3N, CH_2Cl_2, 0°C;

(d) NaH, CH_2E_2, KI, DMF, THF, 0°C to 85°C, 73% from **26**;

(e) PPTS, iPrOH, 55°C, 95%;

(f) LiCl, MsCl, *s*-collidine, DMF, 0°C to r.t.;

(g) Cs_2CO_3, DMF, THF, 70°C, 69% from **28B**.

SCHEME 5

formed. The above experimental result is thus readily explained. Indeed, macrocycle **1***b* must react via conformation **1***bi* to produce the TSC tricycle **30** in the chair–boat–chair conformation **30***i*. The high temperature (320°C) required is primarily due to a steric repulsion that occurs when the *trans-cis* diene takes the *cisoid* conformation necessary for the cycloaddition as shown in **1***bi*. There is also a steric interaction between the methyl group of the diene and one of the ester functions. This is best visualized in conformation **30***i* of the Diels–Alder product where the methyl group at C7 is in a 1,3 diaxial disposition relative to the axial ester of ring C. The above result is also in complete agreement with the previously reported (7*b*) cycloaddition of a TCC macrocyclic triene having only one methyl group on the dienophile. In this case, a TSC macrocycle is again exclusively formed but a slightly lower temperature (300°C) appears to be required because there is less steric hindrance due to the absence of the methyl group on the diene moiety.

In a similar fashion, TCC macrocycle **1***d* was transformed into TSC tricycle **31** in 90% yield (Scheme 6). The stereochemistry of **31** was confirmed by X-ray diffraction analysis (19). Thus, as expected, the macrocyclic triene reacted via the *cisoid* conformation **1***di*, which gave **31** in conformation **31***i*, having steric interactions similar to those taking place during the conversion of TCC macrocycle **1***b* into TSC tricycle **30**.

Diels–Alder reaction of CTC macrocycle **1***a and TTC macrocycle* **1***c*

Upon heating at 325°C in toluene in a sealed quartz tube for 18 h, CTC macrocycle **1***a* was converted into a mixture

Can. J. Chem. Downloaded from www.nrcresearchpress.com by 213.200.69.106 on 09/08/12
For personal use only.

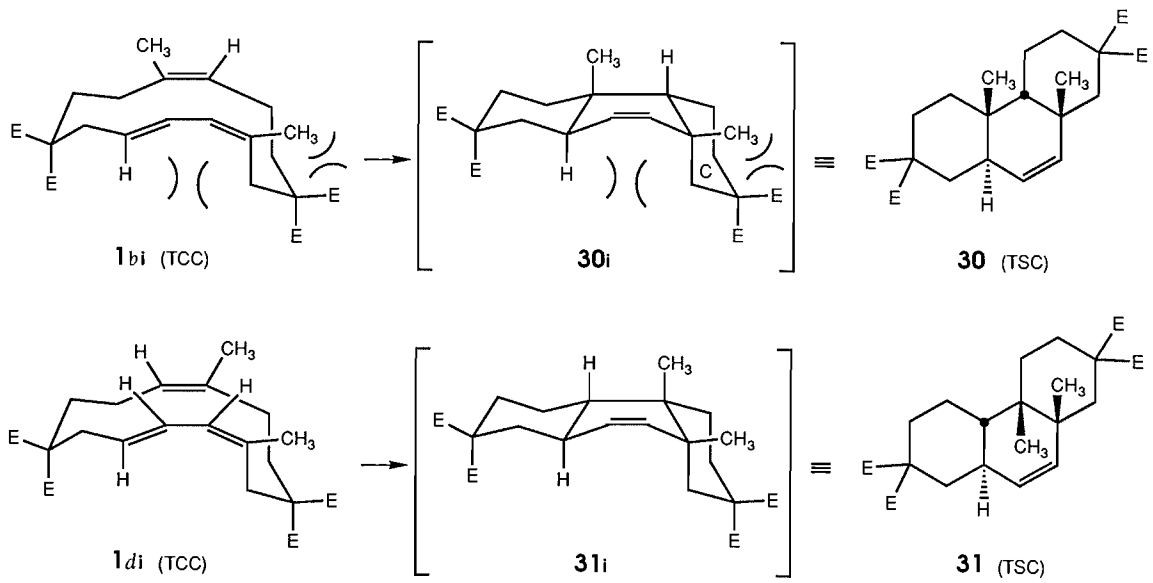

SCHEME 6

of four tricyclic isomers **30** and **32–34** in a 7:20.6:5.9:1 ratio as determined by ^{1}H nmr spectroscopy. The first isomer **30** was shown to have the TSC tricyclic geometry by comparison with an authentic sample obtained from the Diels–Alder reaction of macrocycle **1***b*. Isomers **33** and **34** could be obtained pure by chromatography and characterized by the usual spectroscopic techniques. Isomer **33** was shown to have the CSC stereochemistry by X-ray diffraction analysis.[4] Assignment of the basic skeleton of isomer **32** could be made by ^{1}H nmr spectroscopic analysis of the mixture. Isomers **32** and **34** have been tentatively assigned the CST and TST relative stereochemistry.

We have found that when TTC macrocycle **1***c* is heated at 200°C for 4 h, it is quantitatively isomerized into CTC macrocyclic triene **1***a*, indicating that the triene having a second *cis* olefin is more stable. It was also found that upon heating at 310°C, TTC macrocycle **1***c* gave the same mixture of tricyclic isomers as that observed with **1***a*, but in a different ratio, namely, 2.3:1:29.9:5.3.

It is thus very likely that **1***a* and **1***c* are interconverted prior to the Diels–Alder reactions. Also, **1***a* and (or) **1***c* must probably undergo an isomerization into macrocycle **1***b* since we previously observed that **1***b* yields exclusively the TSC isomer **30**, which is one of the four isomers observed from **1***a* and **1***c*.

It is possible to understand why such a complex mixture was obtained and to propose pathways for the interconversion of macrocyclic trienes **1***a*, **1***b*, and **1***c*. The facile conversion of macrocyclic triene **1***a* into **1***c* can be explained by two consecutive hydrogen migrations via the intermediate formation of macrocycle **35** as shown in Scheme 7. The isomerization of macrocycle **1***a* into macrocycle **1***b* is a more complex process that can take place via four consecutive 1,5 hydrogen migrations. Macrocycle **1***a* would first be converted to TCC macrocycle **36**, which can then give CCC macrocycle **37**. Finally, CTC macrocycle **38** would be obtained from **37**, and converted into TCC macrocycle **1***b*. The isomerization of a CC diene into a CT or TC diene has previously been observed in our laboratory (*7b*).

Assuming that macrocycles **35**, **36**, and **38** do not undergo a cycloaddition because they would produce tricycles containing a seven-membered ring, the formation of the mixtures of stereoisomers **30** and **32–34** having respectively the TSC, CST, CSC, and TST stereochemistry would be the result of cycloaddition of macrocycles CTC (**1***a*), TCC (**1***b*), TTC (**1***c*), and CCC (**37**), which would be thermally interconvertible prior to the Diels–Alder reaction. These interconversions are summarized in Fig. 1.

First, CTC macrocyclic trienes are predicted (*7a*) to give only one tricyclic isomer having the *cis-syn-trans* (CST) stereochemistry. In the case of CTC macrocycle **1***a*, this means that it should react via conformation **1***ai*, which would undergo a cycloaddition to produce CST tricycle **32** in conformation **32***i* as illustrated in Scheme 8. The required *cisoid* conformation of the diene moiety is highly hindered (cf. **1***ai*), and the resulting product will have ring B in a boat form that is very severely encumbered by the presence of the methyl group at C7. In addition, this methyl group also experiences a 1,3 diaxial steric interaction with the axial ester of ring C. The energy barrier for this cycloaddition must be quite high and it is therefore not surprising that other processes can compete with the formation of this CST tricycle.

We have previously shown that TCC macrocycle **1***b* gives TSC tricycle **30** exclusively and this result has been already rationalized (Scheme 6).

TTC macrocyclic trienes are predicted (*7a*) to give the TST and the CSC tricycles. Indeed, TTC macrocycle **1***c* can either take conformation **1***ci* (Scheme 9) to produce the TST tricycle **34** (via **34***i*) or conformation **1***cii* to yield the CSC tricycle **33** (via **33***i*). Both processes are somewhat hindered, but the formation of the TST isomer should be favored since it appears to be less sterically crowded.

Finally, the cycloaddition of CCC macrocycle **37** is predicted to give the CSC tricycle **33**. This cycloaddition involves rather severe steric interactions at the transition state, resulting from a diene having a *cis-cis* configuration. In-

[4]A.G. Michel, M. Drouin, and P. Soucy. Unpublished results.

Can. J. Chem. Downloaded from www.nrcresearchpress.com by 213.200.69.106 on 09/08/12
For personal use only.

Can. J. Chem. Downloaded from www.nrcresearchpress.com by 213.200.69.106 on 09/08/12
For personal use only.

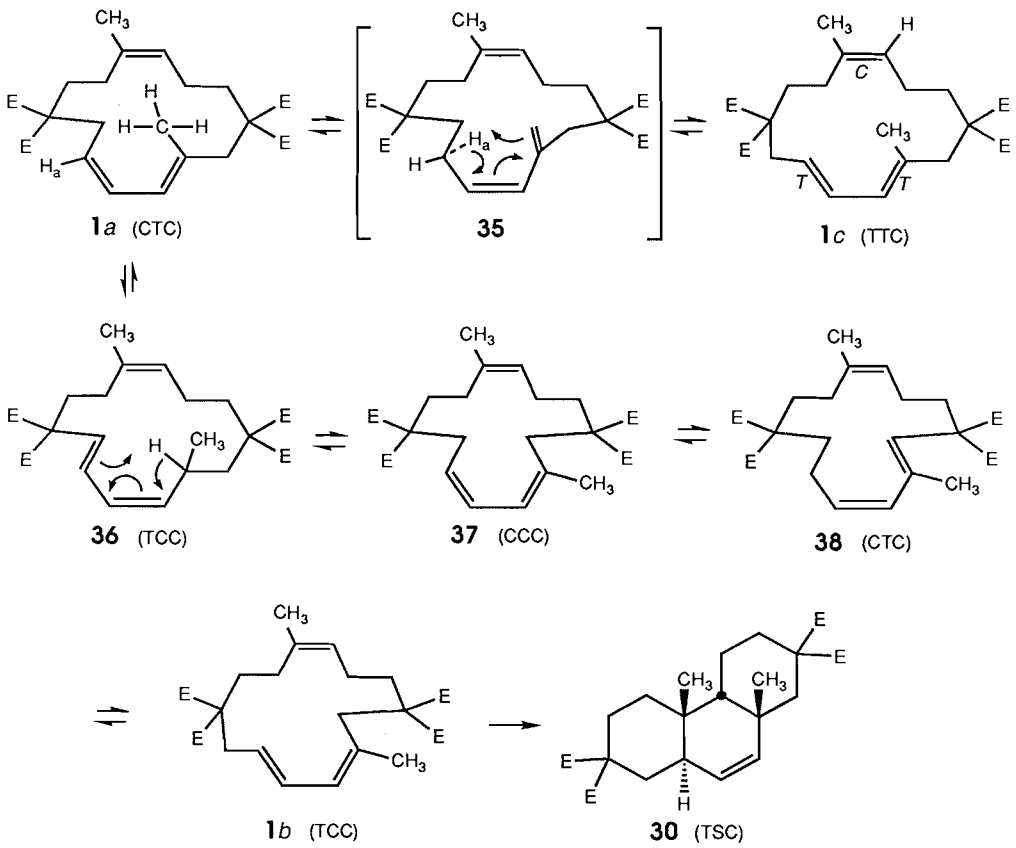

SCHEME 7

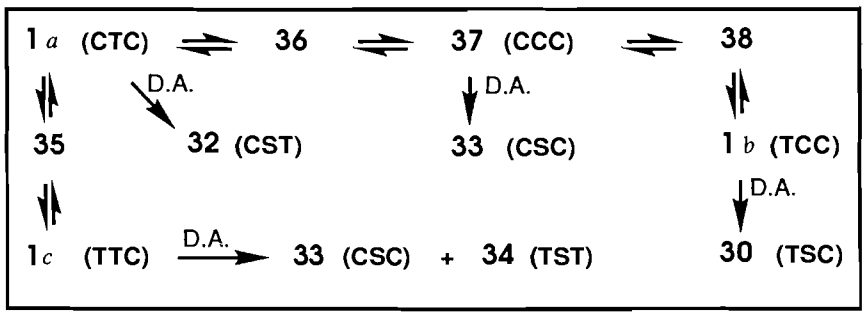

FIG. 1. Summary of possible interconversion.

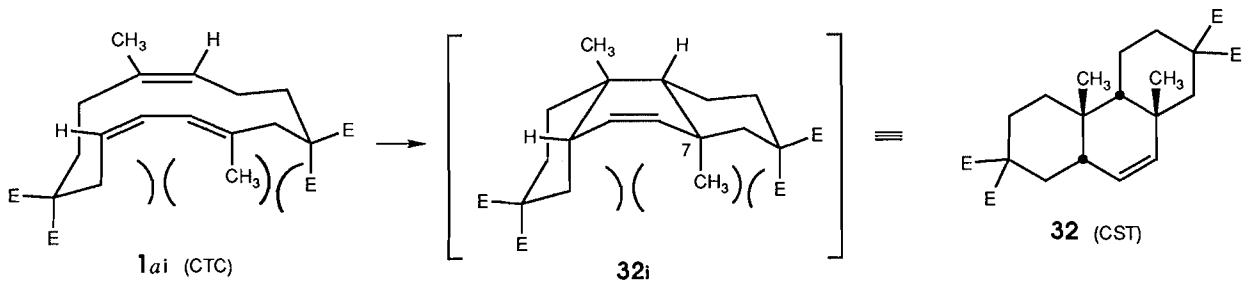

SCHEME 8

deed, CCC macrocycle **37** must react via the very crowded *cisoid* conformation **37***i* (Scheme 10) to yield tricycle **33** in the high-energy conformation **33***i*.

All the cycloadditions must take place via transition states that experience severe steric repulsions. It is therefore not surprising that the macrocycles are thermally interconverted

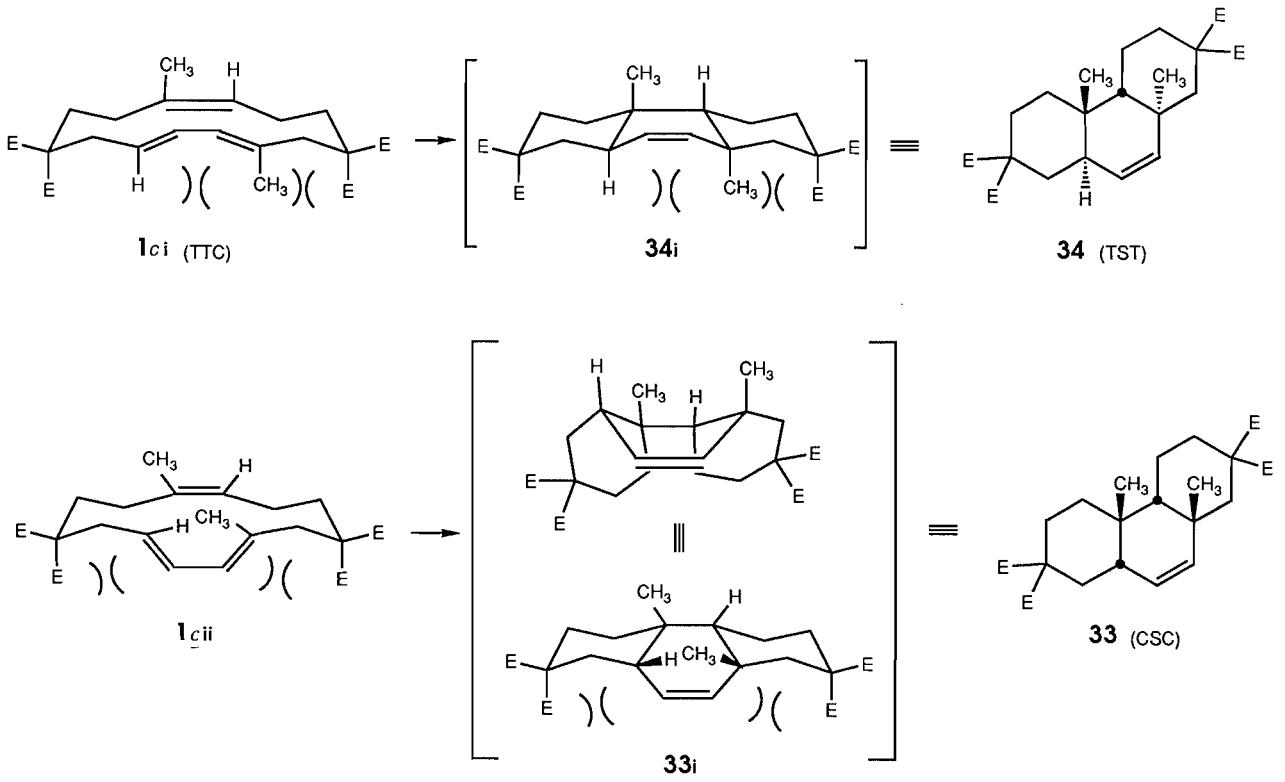

SCHEME 9

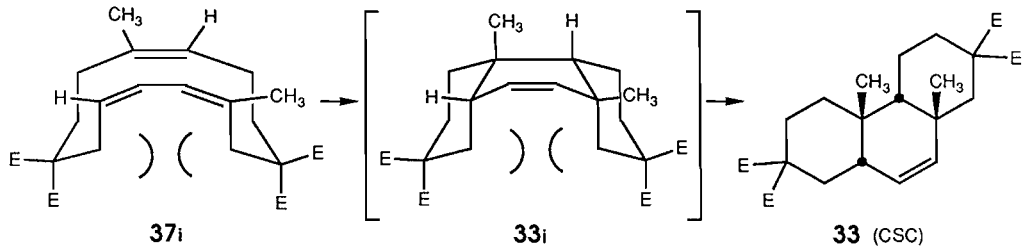

SCHEME 10

prior to the cycloaddition reaction. The exclusive formation of TSC tricycle **30** from TCC macrocycle **1***b* shows that its thermal isomerization to the other macrocycles is, however, higher is energy than the cycloaddition reaction to give TSC tricycle **30**. The different ratios of stereoisomers obtained from macrocycles **1***a* and **1***c* indicate that the Diels–Alder reaction can compete to some extent with the isomerization process of the macrocycles, although this process is known to take place at lower temperature. This may be because the Diels–Alder reaction is probably more favorable from an entropy point of view than the sigmatropic 1,5 hydrogen migration. Finally, an unexplained result is the large percentage of CSC tricycle **33** obtained from **1***c*. On the basis of steric effect arguments, it can be predicted that TST tricycle **34** and CSC tricycle **33** should have been the major and the minor isomer, respectively (Scheme 9). Of course, CSC tricycle **33** can also be obtained from CCC macrocycle **37**. However, on that basis CSC tricycle **33** should have been produced in large amount from CTC macrocycle **1***a*, as **1***a* is an intermediate in the interconversion of macrocycles **1***c* (TTC) and **37** (CCC).

In conclusion, four macrocyclic trienes (two TCC, one CTC, and one TTC) were successfully synthesized in good yield. The TCC macrocycles **1***b* and **1***d* gave, respectively, the TSC tricycles **30** and **31** via a transannular Diels–Alder reaction. On the other hand, the transannular Diels–Alder reaction of CTC macrocycle **1***a* and TTC macrocycle **1***c* led to a mixture of the same four tricycles (**30** (TSC), **32** (CST), **33** (CSC), and **34** (TST)) but in a different ratio. These results are explained by taking into consideration the interconversion of macrocyclic trienes **1***a* (CTC), **1***b* (TCC), **1***c* (TTC), and **37** (CCC) prior to the Diels–Alder reaction. A useful summary of the results obtained with the various dimethyl-substituted macrocyclic trienes reported in this paper and the preceding one (1) is shown in Fig. 2. This information is presently being used for the elaboration of new routes for the synthesis of various polycyclic natural products of the diterpene and triterpene family.

Experimental

2-(2-Bromoethyloxy)tetrahydropyran 3

To a stirred solution of 2-bromoethanol (19.2 g, 154 mmol) in 200 mL of CH_2Cl_2 were added at 0°C under argon pyridinium *p*-toluenesulfonate (PPTS) (387 mg, 1.5 mmol) and 3,4-dihydro-

Can. J. Chem. Downloaded from www.nrcresearchpress.com by 213.200.69.106 on 09/08/12
For personal use only.

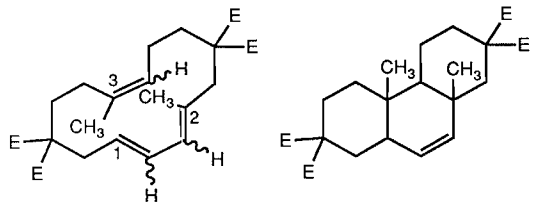

Macrocycle geometry	Tricycle expected	Experimental results
TCC	TSC	TSC
TTC	TST + CSC	TST + CST + CSC + TSC
CTC	CST	TST + CST + CSC + TSC
TTT	TAC + CAT	TAC only
CTT	CAC	TAC + 3 uncharacterized isomers
TCT	CAC	≡ CAC (rearranged)

FIG. 2. Summary of transannular Diels–Alder reactions of disubstituted macrocyclic trienes.

2*H*-pyran (21.0 mL, 230 mmol). The resulting mixture was stirred at room temperature for 2.3 h and then poured into a saturated $NaHCO_3$ solution (120 mL). The organic phase was washed with water, dried, and concentrated to a crude residue that was purified by distillation (1.4 Torr (1 Torr = 133.3 Pa), 63–64°C) to give colorless oil **3** (25.7 g, 81%); ir (neat): 2945, 2850, 1125, 1030 cm^{-1}; ^1H nmr ($CDCl_3$) δ: 1.50–1.86 (m, 6H, -OCHOCH$_2$(CH_2)$_3$-), 3.48–3.54 (m, 2H, BrCH_2-), 3.48–3.57 and 3.85–3.94 (2m, 2H, -OCHOCH_2-), 3.72–3.82 and 3.97–4.06 (2dt, 2H, J = 11.2 Hz, 6.2 Hz, -CH_2OTHP), 4.68 (t, 1H, J = 3.3 Hz, -OC*H*O).

2-Triphenylphosphonium bromide ***4***

To a stirred solution of (ethyl)triphenylphosphonium bromide (32.3 g, 87 mmol) in 200 mL of THF was added dropwise, at 0°C under argon, potassium hexamethyldisilazane (0.5 M in toluene, 174 mL, 87 mmol). The resulting suspension was stirred at 0°C for 0.5 h and then a solution of compound **3** (25.8 g, 125 mmol) in 70 mL of THF was introduced dropwise over 20 min. The orange mixture was warmed to room temperature and then stirred for 50 h. The resulting thick, pink mixture was filtered through a Buchner funnel and the solid was washed several times with THF. The filtrate collection flask was changed and the solid was washed with CH_2Cl_2 until only solid, grey, KBr remained in the funnel. The CH_2Cl_2 filtrate was concentrated to an off-white crude salt (40.8 g) that was recrystallized from CH_2Cl_2 and hexane to give pure compound **4** (38.0 g, 88%) as clear crystals; ir ($CHCl_3$): 3060–3010, 2950–2860, 1442, 1115, 1038 cm^{-1}; ^1H nmr ($CDCl_3$) δ: 1.44 (dd, 3H, J = 19.8 Hz, 7.1 Hz, -CH(CH_3)-), 1.32–1.64 (m, 6H, -OCH$_2$(CH_2)$_3$-), 1.70–1.87 and 2.20–2.30 (2m, 2H, -CHCH_2-CH$_2$OTHP), 3.45–3.54 and 3.79–3.85 (2m, 2H, -CHOCH_2-), 3.88–4.17 (m, 2H, -CH_2OTHP), 4.57–4.59 and 4.62–4.64 (2m, 1H, -OC*H*O-), 4.87–5.08 and 5.13–5.28 (2m, 1H, -C*H*PCH$_2$-), 7.62–8.01 (m, 15H, P*Ph*$_3$).

*3-*tert*-Butyldiphenylsilyloxy 1-propanol* ***5***

To a stirred solution of 1,3-propanediol (20.0 g, 263 mmol) and imidazole (3.58 g, 52.6 mmol) in 180 mL of THF was added at room temperature under argon *tert*-butylchlorodiphenylsilane (13.7 mL, 52.6 mmol). After the mixture was stirred for 25 h, 100 mL of water was introduced. The aqueous layer was extracted with hexane (5 × 100 mL) and the combined organic layers were washed with H_2O, dried over $MgSO_4$, filtered, and concentrated to a crude brown residue that was purified by flash chromatography (hexane – ethyl acetate, 9:1) to afford **5** (15.86 g, 96%) as a colorless oil; ir ($CHCl_3$): 3620–3510, 3080–3020, 2960–2860, 1430, 1115, 1068 cm^{-1}; ^1H nmr ($CDCl_3$) δ: 1.05 (9H, s, -(CH_3)$_3$CSi-), 1.52–1.98 (m, 2H, -CH_2CH$_2$OH), 2.35 (t, 1H, J = 5.4 Hz, -CH$_2$O*H*), 3.86 (q, 2H, J = 5.7 Hz, -CH_2OH), 3.88 (t, 2H, J = 5.7 Hz, -CH_2OSi-), 7.46–7.66 (m, 10H, *Ph*$_2$Si-).

Aldehyde ***6***

To a stirred solution of oxalyl chloride (4.8 mL, 55.3 mmol) in 115 mL of CH_2Cl_2 was added dropwise, at −78°C under argon over a period of 20 min, a solution of DMSO (7.9 mL, 110.6 mmol) in 25 mL of CH_2Cl_2. The stirring was continued for 20 min before adding a solution of alcohol **5** (15.8 g, 50.3 mmol) in 50 mL of CH_2Cl_2 over 25 min. After the mixture was stirred at −78°C for 45 min, triethylamine (35 mL) was introduced. The reaction mixture was warmed to room temperature for 1 h, followed by addition of 100 mL of water. The aqueous layer was extracted with CH_2Cl_2 (3 × 100 mL) and the combined organic phases were washed with water and brine, dried over $MgSO_4$, filtered, and concentrated to a yellow residue that was purified by flash chromatography (hexane – ethyl acetate, 9:1) to give aldehyde **6** (13.6 g, 86%); ir ($CHCl_3$): 3080–3010, 2960–2860, 2740, 1728, 1430, 1115 cm^{-1}; ^1H nmr ($CDCl_3$) δ: 1.05 (s, 9H, -(CH_3)$_3$CSi-), 2.61 (dt, 2H, J = 5.6 Hz, 2.8 Hz, -CH_2CHO), 4.03 (t, 2H, J = 6.1 Hz, -CH_2OSi-), 7.35–7.81 (m, 10H, *Ph*$_2$Si-), 9.83 (t, 1H, J = 2.4 Hz, -C*H*O); ms m/e: 255 ($M^+ - C_4H_9$).

3-Hexene diether ***7***

To a stirred solution of phosphonium bromide **4** (25.9 g, 51.9 mmol) in 200 mL of THF, butyllithium (1.6 M in hexane, 29.7 mL, 47.6 mmol) was added dropwise at 0°C under argon. After the mixture was stirred for 40 min, a solution of aldehyde **6** (13.5 g, 43.3 mmol) in 70 mL of THF was introduced dropwise over 35 min. The stirring was continued at 0°C for 3 h, followed

Can. J. Chem. Downloaded from www.nrcresearchpress.com by 213.200.69.106 on 09/08/12
For personal use only.

Can. J. Chem. Downloaded from www.nrcresearchpress.com by 213.200.69.106 on 09/08/12
For personal use only.

by addition of a mixture (petroleum ether – hexane, 1:1). After the mixture was filtered through a Celite plug on a fritted-disk funnel, the filtrate was concentrated to a crude yellow oil (15.2 g). The solid remaining in the funnel was dissolved in H_2O, which was then extracted with ether (5 × 100 mL). The combined organic phases were dried, filtered, and concentrated to a crude residue (5.0 g) that was combined with the original crude material. Purification by flash chromatography (hexane – ethyl acetate, 96:4) gave pure product **7** (12.0 g, 61%) as a colorless oil. The following spectral data were obtained from a mixture of *Z*- and *E*-**7**; ir (neat): 3075, 2940, 2860, 1430, 1115, 1036 cm^{-1}; ^1H nmr ($CDCl_3$) δ: 1.04 (s, 9H, -(CH_3)$_3$C), 1.59 (s, 3H, -CH=C(CH_3)-, *E*), 1.71 (d, 3H, *J* = 1.3 Hz, -CH=C(CH_3)-, *Z*), 1.30–1.89 (m, 6H, -OCH$_2$(CH_2)$_3$-), 2.20–2.35 (m, 4H, CH_2CH=C(CH_3)CH_2-), 3.62 and 3.63 (2t, 2H, *J* = 7.1 Hz, -CH_2OSi-), 3.32–3.52 and 3.71–3.88 (2m, 4H, -OCH_2-CH$_2$-, -CH_2OTHP), 4.54–4.58 (m, 1H, -OC*H*O-), 5.12–5.24 (m, 1H, -C*H*=C(CH_3)-), 7.33–7.49 and 7.62–7.70 (2m, 10H, Ph_2Si-). The ratio for *Z* and *E* isomers is approximately 43:57 as determined by ^1H nmr.

Alcohols ***8***a *and* ***8***b

General procedure A

To a stirred solution of *Z*- and *E*-**7** (8.0 g, 17.7 mmol) in 370 mL of isopropanol was added under argon pyridinium *p*-toluenesulfonate (0.89 g, 3.2 mmol) and the resulting mixture was heated to 80°C for 4 h. The reaction was stopped by addition of H_2O (200 mL) and ether (300 mL). The aqueous phase was extracted with ether (2 × 100 mL). The combined organic phases were dried, filtered, and concentrated to a crude oil (6.7 g). Initial attempts to separate the isomers by flash chromatography met with only limited success. Considerably better separation was obtained by the use of medium-pressure chromatography under a pressure of 30 psi (1 psi = 6.9 kPa) with a 85:15 mixture of hexane and ethyl acetate as eluant. Purification of 1 g crude oil gave rise to *Z* isomer **8***a* (355 mg) and *E* isomer **8***b* (522 mg) along with a mixture of **8***a* and **8***b* (80 mg). Based on this set of data, the yield for this reaction is 98%.

Spectral data for ***8***a: ir ($CHCl_3$): 3618, 3460, 3075–3055, 2960–2860, 1430, 1385, 1110, 1055 cm^{-1}; ^1H nmr ($CDCl_3$) δ: 1.04 (s, 9H, -(CH_3)$_3$C), 1.72 (d, 3H, *J* = 1.3 Hz, -CH=C(CH_3)-), 2.26 (t, 2H, *J* = 6.4 Hz, -CH=C(CH_3)CH_2-), 2.32 (qd, 2H, *J* = 6.8 Hz, 0.7 Hz, SiOCH$_2$CH_2-), 3.62 (t, 2H, *J* = 6.4 Hz, -CH_2OH), 3.64 (t, 2H, *J* = 6.7 Hz, -SiOCH_2-), 5.31 (t, 1H, *J* = 7.0 Hz, -C*H*=C(CH_3)-), 7.34–7.47 and 7.64–7.73 (2m, 10H, Ph_2Si-).

Spectral data for ***8***b: ir (neat): 3360, 3070–3045, 2925–2858, 1430, 1385, 1110, 1050 cm^{-1}; ^1H nmr ($CDCl_3$) δ: 1.04 (s, 9H, -(CH_3)$_3$C), 1.45 (s, 1H, -CH$_2$O*H*), 1.59 (m, 3H, -CH=C(CH_3)-), 2.24 (t, 2H, *J* = 6.6 Hz, -CH=C(CH_3)CH_2-), 2.29 (q, 2H, *J* = 6.9 Hz, -SiOCH$_2$CH_2-), 3.64 (t, 2H, *J* = 6.2 Hz, -CH_2OH), 3.65 (t, 2H, *J* = 6.8 Hz, -SiOCH_2-), 5.25 (td, 1H, *J* = 7.3 Hz, 1.3 Hz, -C*H*=C(CH_3)-), 7.27–7.46 and 7.63–7.70 (2m, 10H, Ph_2Si-); ms *m/e*: 311 ($M^+ - C_4H_9$).

Mesylates ***9***a *and* ***9***b

General procedure B

To a stirred solution of alcohol **8***a* (130 mg, 0.35 mmol) and triethylamine (180 g, 1.75 mmol) in 8 mL of CH_2Cl_2, methanesulfonyl chloride (50 mg, 0.42 mmol) was added dropwise at 0°C under argon. The stirring was continued at 0°C for 1 h before the mixture was poured into H_2O (40 mL). The aqueous phase was extracted with CH_2Cl_2 (4 × 10 mL) and the combined organic phases were washed with H_2O, dried over $MgSO_4$, filtered, and concentrated to a crude residue that was purified by flash chromatography (hexane – ethyl acetate, 9:1) to furnish mesylate **9***a* (145 mg, 93%) as a clear oil; ^1H nmr ($CDCl_3$) δ: 1.04 (s, 9H, -(CH_3)$_3$C), 1.73 (m, 3H, -CH=C(CH_3)-), 2.26 (m, 2H, -CH_2CH=), 2.42 (t, 2H, *J* = 7.2 Hz, =C(CH_3)CH_2-), 2.91 (s, 3H, -SO_2CH_3), 3.64 (t, 2H, *J* = 6.8 Hz, -SiOCH_2-), 4.18 (t, 2H, *J* = 7.0 Hz, -CH_2OSO_2-), 5.32 (m, 1H, -C*H*=C-), 7.34–7.44 and 7.65–7.68 (m, 10H, Ph_2Si-).

The mesylation for alcohol **8***b* was carried out exactly as described above. Thus, treatment of alcohol **8***b* (580 mg, 1.6 mmol) with triethylamine (0.33 mL, 1.9 mmol) and methanesulfonyl chloride (0.15 mL, 1.9 mmol) in 20 mL of CH_2Cl_2 yielded *Z*-mesylate **9***b* (685 mg, 97%); ir (neat); 3070–3018, 2930, 2860, 1430, 1380, 1358, 1175, 1110 cm^{-1}; ^1H nmr ($CDCl_3$) δ: 1.06 (s, 9H, -(CH_3)$_3$C), 1.63 (m, 3H, -CH=C(CH_3)-), 2.25–2.51 (m, 4H, -CH_2CH=C(CH_3)CH_2-), 2.95 (s, 3H, -SO_2CH_3), 3.67 (t, 2H, *J* = 6.7 Hz, -SiOCH_2-), 4.26 (t, 2H, *J* = 7.1 Hz, -CH_2OSO_2-), 5.28 (m, 1H, -C*H*=C(CH_3)-), 7.28–7.85 (m, 10H, Ph_2Si-); ms *m/e*: 389 ($M^+ - C_4H_9$).

Dimethyl malonates ***10***a *and* ***10***b

General procedure C

To a stirred suspension of NaH (130 mg, 5.4 mmol) in a mixture of DMF and THF (1:1, 40 mL) was added dropwise, over 20 mins at 0°C under argon, dimethyl malonate (800 mg, 6.0 mmol). The stirring was continued at 0°C for 1 h before adding a solution of mesylate **9***a* (540 mg, 1.2 mmol) in 2 mL of THF and KI (20 mg, 0.12 mmol). The resulting mixture was heated at 70°C for 36 h, then poured into 200 mL of water. The aqueous phase was extracted with hexane–ether (1:1, 3 × 200 mL), and the combined organic phases were washed with H_2O, dried over $MgSO_4$, filtered, and concentrated to a crude residue that was purified by flash chromatography (hexane – ethyl acetate, 9:1) to give **10***b* (509 mg, 88%) as a colorless oil; ^1H nmr ($CDCl_3$) δ: 1.04 (s, 9H, -(CH_3)$_3$C), 1.67 (m, 3H, -CH=C(CH_3)-), 1.92–2.04 (m, 4H, -CH=(CH_3)CH_2CH_2-), 2.18–2.28 (m, 2H, -SiOCH$_2$CH_2-), 3.32 (t, 1H, *J* = 7.0 Hz, -C*H*(CO_2CH_3)$_2$), 3.62 (t, 2H, *J* = 6.9 Hz, -SiOCH_2-), 3.73 (s, 6H, 2 × -OCH_3), 5.19 (m, 1H, -C*H*=C-), 7.34–7.43 and 7.65–7.69 (2m, 10H, Ph_2Si-).

The preparation of **10***b* was carried out in the same way as described above. Thus, treatment of dimethyl malonate (0.865 mL, 7.6 mmol) with NaH (272 mg, 60%, 6.8 mmol) in THF–DMF mixture (1:1), followed by addition of mesylate **9***b* (675 mg, 1.5 mmol) in 2 mL of THF, afforded product **10***b* (631 mg, 87%) as a colorless oil; ir (neat): 3070–3000, 2950, 2860, 1738, 1430, 1385, 1230, 1155, 1115 cm^{-1}; ^1H nmr ($CDCl_3$) δ: 1.05 (s, 9H, -(CH_3)$_3$C), 1.57 (s, 3H, -CH=C(CH_3)-), 1.99–2.03 (m, 4H, -CH=C(CH_3)CH_2CH_2-), 2.27 (q, 2H, *J* = 6.8 Hz, -SiOCH$_2$CH_2-), 3.36 (m, 1H, -C*H*(CO_2CH_3)$_2$), 3.64 (t, 2H, *J* = 6.6 Hz, -SiOCH_2-), 3.72 and 3.73 (2s, 6H, 2× -OCH_3), 5.17 (m, 1H, -C*H*=C-), 7.35–7.78 (2m, 10H, Ph_2Si-); ms *m/e*: 425 ($M^+ - C_4H_9$).

Alcohols ***11***a *and* ***11***b

General procedure D

To a stirred solution of silyl ether **10***a* (316 mg, 0.655 mmol) in 6 mL of THF, tetrabutylammonium fluoride (1.0 M in THF, 1.2 mL, 1.2 mmol) was added at 0°C under argon. The mixture was warmed to room temperature and stirred for 2.5 h. The solvent was removed by evaporation and the oily residue was purified by flash chromatography (hexane – ethyl acetate, 7:3) to give alcohol **11***a* (119 mg, 74%) as a viscous oil; ir (neat): 3420, 2955, 2870, 1738, 1438, 1230, 1155, 1050 cm^{-1}; ^1H nmr ($CDCl_3$) δ: 1.71 (d, 3H, -CH=C(CH_3)-), 1.95–2.12 (m, 4H, =C(CH_3)CH_2CH_2-), 2.22 (qd, 2H, *J* = 6.7 Hz, 1.0 Hz, HOCH$_2$CH_2-), 3.35 (t, 1H, *J* = 7.0 Hz, -C*H*(CO_2CH_3)$_2$), 2.61 (t, 2H, *J* = 6.4 Hz, HOCH_2-), 3.74 (s, 6H, 2× -OCH_3), 5.20 (td, 1H, *J* = 6.8 Hz, 1.1 Hz, -C*H*=C-); ms *m/e*: 244 ($M^+ - H_2O$).

The desilylation of **10***b* was carried out in the same way as described above. Thus, treatment of silyl ether **10***b* (603 mg, 1.3 mmol) with tetrabutylammonium fluoride (1.0 M in THF, 1.4 mL, 1.4 mmol) in THF yielded alcohol **11***b* (277 mg, 91%) as a colorless oil that has spectral data identical with the same compound reported in the preceding article.

Mesylates ***12***a *and* ***12***b

The mesylation of **12***a* was carried out in the same way as described in the general procedure B. Thus, treatment of alcohol **11***a*

Can. J. Chem. Downloaded from www.nrcresearchpress.com by 213.200.69.106 on 09/08/12
For personal use only.

(100 mg, 0.41 mmol) with triethylamine (86.1 μL, 0.45 mmol) and methanesulfonyl chloride (35 μL, 0.45 mmol) at 0°C in CH_2Cl_2 yielded mesylate **12***a* (110 mg, 83%) as a colorless oil; ir (neat): 2960, 2866, 1732, 1435, 1355, 1225, 1172 cm^{-1}; ^1H nmr ($CDCl_3$) δ: 1.72 (d, 3H, J = 1.2 Hz, -CH=C(CH_3)-), 1.93–2.11 (m, 4H, -CH=C(CH_3)CH_2CH_2-), 2.42 (q, 2H, J = 7.0 Hz, $MsOCH_2$-CH_2-), 3.01 (s, 3H, $-SO_2CH_3$), 3.33 (t, 1H, -$CH(CO_2CH_3)_2$), 3.74 (s, 6H, 2× -OCH_3), 4.17 (t, 2H, J = 6.9 Hz, -CH_2OMs), 5.17 (t, 1H, J = 7.5 Hz, -CH=C-); ms m/e: 322 (M^+), 290 (M^+ – CH_3OH).

The preparation of **12***b* from **11***b* was reported in the preceding article: the same reaction procedure as described in the general procedure B was used.

(Z,E)-Diene diether ***14***

To a solution of alcohol **13** (619.2 mg, 2.9 mmol) and imidazole (453.0 mg, 6.7 mmol) in 18 mL of THF, *tert*-butylchlorodiphenylsilane (0.89 mL, 3.4 mmol) was added at 0°C under argon. The mixture was stirred for 1 h before a saturated ammonium chloride solution (25 mL) was added. The aqueous layer was extracted with a mixture of hexane and ether (2:1, 3 × 25 mL). The combined organic layers were washed with water, dried over $MgSO_4$, filtered, and concentrated to a crude residue that was purified by flash chromatography (hexane – ethyl acetate, 98:2) to give **14** (1298.7 mg, 2.88 mmol, 99%). The clear oil was used immediately for the next reaction without characterization.

Diene alcohol ***15***

The hydrolysis of the THP ether was carried out in a similar fashion as described in the general procedure A. Thus, treatment of THP ether **14** (1298.7 mg, 2.88 mmol) with pyridinium *p*-toluenesulfonate (131.0 mg) in 35 mL of isopropanol afforded alcohol **15** (911.6 mg, 2.49 mmol, 86%) as a colorless oil; ir (neat): 3340, 3040, 2950, 2860, 1450, 1375, 1110 cm^{-1}; ^1H nmr ($CDCl_3$) δ: 1.08 (s, 9H, -(CH_3)$_3$C), 1.26 (t, 1H, J = 5.7 Hz, -CH_2OH), 1.70 (s, 3H, -CH_3), 4.13 (s, 2H, -CH_2OSi-), 4.34 (t, 2H, J = 6.2 Hz, -CH_2OH), 5.62 (dt, 1H, J = 10.3 Hz, 6.9 Hz, $HOCH_2CH$=CH-), 6.30–6.51 (m, 2H, $HOCH_2CH$=CHCH=C-), 7.35–7.48 and 7.65–7.73 (2m, 10H, Ph_2Si-).

Allylic chloride ***16***a

General procedure E

To a round-bottom flask containing flame-dried LiCl (69.6 mg, 1.64 mmol) was introduced, under argon, a solution of alcohol **15** (150.2 mg, 0.41 mmol) in 2.5 mL of DMF and *s*-collidine (0.11 mL, 99.9 mg, 0.82 mmol). The solution was then cooled to 0°C before methanesulfonyl chloride (63μL, 93.2 mg, 0.81 mmol) was added dropwise over 10 min. The resulting mixture was stirred at 0°C for 1 h and at 25°C for an additional hour. The reaction was stopped by adding 15 mL of ice water. The aqueous phase was extracted with ether (5 × 10 mL) and the combined organic phases were washed with cold, saturated, copper nitrate solution, and then with water. After drying over $MgSO_4$, the mixture was filtered through a short-path column containing silica gel and Celite. The filtrate was evaporated to a crude oil, **16***a* (155.7 mg, 0.40 mmol, 99%), which was used immediately for the next coupling reaction without further purification and characterization.

Allylic chloride ***18***

The preparation of allylic chloride **18** was accomplished in a similar fashion as described in the general procedure E. Thus, treatment of allylic alcohol **17** (2.2 g, 10.4 mmol) with LiCl (1.32 g, 31.2 mmol), *s*-collidine (2.1 mL, 15.6 mmol), and methanesulfonyl chloride (1.2 mL, 15.6 mmol) in DMF (37 mL) at 0°C yielded **18** (2.4 g) as a crude oil that was used immediately in the coupling reaction without further purification and characterization.

Mesylate triene ***19***a

General procedure F

To a stirred suspension of NaH (12.3 mg, 60%, 0.31 mmol) in 2 mL of THF was added at 0°C under argon a solution of dimethyl malonate **12***a* (90.1 mg, 0.28 mmol) in 2 mL of THF. The mixture was stirred at 0°C for 45 min, at room temperature for 30 min, and then cooled to 0°C. A solution of the crude allylic chloride **16***a* (155.7 mg, 1.40 mmol) in 4 mL of DMF was introduced dropwise by syringe. The stirring was continued at 0°C for 2 h and then at room temperature for 15 h. The mixture was poured into a saturated ammonium chloride solution (15 mL). The aqueous layer was extracted with ether–hexane (2:1, 4 × 10 mL). The combined organic phases were washed with H_2O, $NaHCO_3$ solution (5%), and brine and dried over $MgSO_4$. After removal of the solvents, the residue was purified by flash chromatography (hexane – ethyl acetate, 85:15) to give triene **19***a* (127.1 mg, 0.19 mmol, 68%) along with recovered starting material (12.6 mg, 14%); ir (neat): 3060–3020, 2950, 2855, 1732, 1430, 1360, 1175, 1110 cm^{-1}; ^1H nmr ($CDCl_3$) δ: 1.08 (s, 9H, -(CH_3)$_3$C), 1.68 (s, 3H, -CH_2C(CH_3)=$CHCH_2$-), 1.65–1.75 (m, 4H, -CH_2CH_2C-(CH_3)=CH-), 1.90 (s, 3H, -CH-CHCH=C(CH_3)-), 2.36 (q, 2H, J = 7.2 Hz, -$CH_2CH_2OSO_2$-), 2.85 (d, 2H, J = 8.1 Hz, -CH_2CH=CHCH=C-), 2.97 (s, 3H, $-SO_2CH_3$), 3.71 (s, 6H, 2× -OCH_3), 4.13 (s, 2H, -CH_2OSi-), 4.14 (t, 2H, J = 7.0 Hz, -CH_2SO_2-), 5.10 (t, 1H, J = 7.0 Hz, -CH_2C(CH_3)=$CHCH_2$-), 5.24 (dt, 1H, J = 11.0 Hz, 6.0 Hz, -CH=CHCH=C-), 6.38 (t, 1H, J = 11.2 Hz, -CH=CHCH=C-), 6.52 (d, 1H, J = 11.3 Hz, -CH=CHCH=C-), 7.35–7.45 and 7.65–7.71 (2m, 10H, Ph_2Si-); ms m/e: 670 (M^+), 613 (M^+ – C_4H_9).

Mesylate triene ***19***b

A similar procedure as that described above was employed. Thus, treatment of **12***a* (110 mg, 0.34 mmol) with NaH (15 mg, 60%, 0.63 mmol), followed by allylic chloride **16***b* (162 mg, 0.42 mmol) in a mixture of THF and DMF, afforded triene **19***b* (175 mg, 77%) as a colorless oil; ir (neat): 3070–3020, 2950, 2860, 1730, 1428, 1357, 1174, 1110 cm^{-1}; ^1H nmr ($CDCl_3$) δ: 1.04 (s, 9H, -(CH_3)$_3$C), 1.64 (d, 3H, J = 1.2 Hz, -CH_2CH_2C(CH_3)=), 1.84–1.86 (m, 7H, -CH_2CH_2- and -CH=CHCH=C(CH_3)-), 2.35 (q, 2H, J = 6.3 Hz, -CH_2CH_2OMs), 2.60 (d, 2H, J = 7.6 Hz, -CH_2CH=CHCH=C-), 2.97 (s, 3H, $-SO_2CH_3$), 3.68 (s, 6H, 2 × -OCH_3), 4.12 (t, 2H, J = 6.8 Hz, -CH_2OMs), 4.25 (s, 2H, -CH_2OSi-), 5.08 (t, 1H, J = 7.4 Hz, -CH_2CH_2CH=), 5.32 (dt, 1H, J = 14.8 Hz, 7.4 Hz, -CH=CHCH=C-), 5.80 (d, 1H, J = 11.0 Hz, -CH=CHCH=C-), 6.08 (dd, 1H, J = 14.8 Hz, 11.0 Hz, -CH=CHCH=C-), 7.35–7.44 and 7.65–7.70 (m, 10H, Ph_2Si-); ms m/e: 670 (M^+), 613 (M^+ – C_4H_9).

Mesylate triene ***19***c

The general procedure F described above was employed. Thus, treatment of **12***a* (380.1 mg, 1.18 mmol) with NaH (52.4 mg, 60%, 1.31 mmol), followed by crude allylic chloride **16***c* (589.9 mg, 1.53 mmol) in a mixture of THF and DMF, furnished triene **19***c* (461.9 mg, 0.69 mmol, 59%) along with recovered starting material (121.3 mg, 32%); ir (neat): 3070–3020, 2950, 2858, 1735, 1440, 1360, 1265, 1170, 1110 cm^{-1}; ^1H nmr ($CDCl_3$) δ: 1.06 (s, 9H, -(CH_3)$_3$C), 1.70, (s, 3H, -CH_2CH=C(CH_3)CH_2-), 1.71 (s, 3H, -CH=CHCH=C(CH_3)-), 1.90–1.94 (m, 4H, =C(CH_3)CH_2CH_2-), 2.40 (q, 2H, J = 7.0 Hz, -CH_2CH_2OMs), 2.75 (d, 2H, J = 7.5 Hz, -CH_2CH=CHCH=C), 2.98 (s, 3H, $-SO_2CH_3$), 3.74 (s, 6H, 2× -OCH_3), 4.07 (s, 2H, -CH_2OSi-), 4.16 (t, 2H, J = 6.8 Hz, -CH_2OMs), 5.12 (t, 1H, J = 6.7 Hz, -CH_2CH_2CH=), 5.43 (dt, 1H, J = 14.9 Hz, 7.4 Hz, -CH=CHCH=C-), 6.08 (d, 1H, J = 10.0 Hz, -CH=CHCH=C-), 6.36 (dd, 1H, J = 15.0 Hz, 11.0 Hz, -CH=CHCH=C-), 7.35–7.44 and 7.65–7.70 (m, 10H, Ph_2Si-); ms m/e: 670 (M^+), 639 (M^+ – OCH_3), 613 (M^+ – C_4H_9).

Dimethyl malonate triene ***20***a

The general procedure C described before was employed. Thus, treatment of dimethyl malonate (0.11 mL, 127.1 mg, 0.96 mmol) with NaH (33.6 mg, 60%, 0.84 mmol), followed by mesylate triene **19***a* (125.2 mg, 0.19 mmol) and KI (3.1 mg, 19 μmol) in a mixture of THF and DMF (1:1, 8 mL), at 80°C for 20 h yielded dimethyl malonate triene **20***a* (121.0 mg, 0.17 mmol, 90%) as a

viscous oil, which was used for the following reaction without characterization.

Dimethyl malonate triene ***20***b

The general procedure C described before was employed. Thus, treatment of dimethyl malonate (0.145 mL, 1.3 mmol) with NaH (45 mg, 60%, 1.1 mmol), followed by mesylate triene **19***b* (170 mg, 0.253 mmol) and KI (4.2 mg, 25 μmol) in a mixture of THF and DMF (8 mL), at 85°C for 16 h yielded **20***b* (136 mg, 76%) as a viscous oil; ir (neat): 3070–3000, 2950, 2855, 1735, 1435, 1200, 1110 cm^{-1}; ^1H nmr ($CDCl_3$) δ: 1.04 (s, 9H, -(CH_3)$_3$C), 1.60 (s, 3H, -$CH_2CH_2C(CH_3)$=), 1.80 (s, 4H, -CH_2CH_2-CR(CO_2CH_3)$_2$), 1.85 (s, 3H, =CHCH=C(CH_3)-), 1.92 (m, 4H, -CH_2CH_2CH-(CO_2CH_3)$_2$), 2.58 (d, 2H, J = 7.5 Hz, =CHCH_2CR(CO_2CH_3)$_2$), 3.33 (t, 1H, J = 7.1 Hz, -CH(CO_2CH_3)$_2$), 3.67, 3.71 (2s, 12H, 4 × -OCH_3), 4.25 (s, 2H, -CH_2OSi-), 5.04 (t, 1H, J = 7.0 Hz, -CH_2CH_2CH=), 5.33 (dt, 1H, J = 14.9 Hz, 7.6 Hz, -CH_2CH=CH-), 5.80 (d, 1H, J = 11.2 Hz, =CHCH=C(CH_3)-), 6.07 (dd, 1H, J = 14.7 Hz, 11.0 Hz, -CH_2CH=CH-), 7.34–7.47 and 7.64–7.70 (2m, 10H, *Ph*Si-); ms *m/e*: 706 (M^+), 675 ($M^+ - OCH_3$), 649 ($M^+ - C_4H_9$).

Dimethyl malonate triene ***20***c

The general procedure **20***c* described before was employed. Thus, treatment of dimethyl malonate (0.231 mL, 2.02 mmol) with NaH (71.8 mg, 60%, 1.80 mmol), followed by mesylate triene **19***c* (267.3 mg, 0.40 mmol) and KI (6.6 mg, 0.04 mmol) in a mixture of THF and DMF (1:1, 18 mL), at 85°C for 15 h yielded **20***c* (256.2 mg, 0.36 mmol, 91%) as a viscous oil; ir (neat): 3070–3000, 2950, 2855, 1740, 1435, 1340, 1200, 1110 cm^{-1}; ^1H nmr ($CDCl_3$) δ: 1.06 (s, 9H, -(CH_3)$_3$C), 1.68 (br, s, 7H, -CH_2CH=C(CH_3)-CH_2CH_2-), 1.87 (s, 3H, =CHCH=C(CH_3)-), 1.88–2.01 (m, 4H, -CH_2CH_2CH=), 2.73 (d, 2H, J = 7.5 Hz, -CH=CHCH_2-), 3.35 (t, 1H, J = 7.2 Hz, -CH(CO_2CH_3)$_2$), 3.72 and 3.74 (2s, 12H, 4 × -OCH_3), 4.07 (s, 2H, -CH_2OSi-), 5.07 (t, 1H, J = 6.8 Hz, -$CH_2C(CH_3)$=$CH$$CH_2$-), 5.43 (dt, 1H, J = 14.7 Hz, 7.1 Hz, -CH=CHCH=C-), 6.07 (d, 1H, J = 11.0 Hz, -CH=CHCH=C-), 6.35 (dd, 1H, J = 14.6 Hz, 10.8 Hz, -CH=CHCH=C-), 7.34–7.47 and 7.64–7.70 (2m, 10H, Ph_2Si-); ms *m/e*: 706 (M^+), 675 ($M^+ - OCH_3$), 649 ($M^+ - C_4H_9$).

Allylic alcohol ***21***a

The general procedure D described before was employed. Thus, treatment of silyl ether **20***a* (121.0 mg, 0.17 mmol) with nBu$_4$NF (1 M in THF, 0.37 mL, 0.37 mmol) in 3 mL of THF at room temperature for 5 h yielded allylic alcohol **21***a* (70.6 mg, 0.15 mmol, 88%) as a viscous oil; ir (neat): 3530, 3020, 1950, 1860, 1735, 1438, 1200, 1100 cm^{-1}; ^1H nmr ($CDCl_3$) δ: 1.65 (s, 3H, -(CH_3)C=CH-), 1.76 (s, 3H, -CH=CHCH=C(CH_3)-), 1.78–2.02 (m, 9H, -$CH_2CH_2C(CH_3)$=$CHCH_2CH_2$- and -CH_2OH), 2.84 (d, 2H, J = 7.5 Hz, -CH_2CH=CHCH=), 3.34 (t, 1H, J = 7.2 Hz, -CH(CO_2CH_3)$_2$), 3.72 and 3.73 (2s, 12H, 4 × -OCH_3), 4.10 (d, 2H, J = 5.6 Hz, -CH_2OH), 5.06 (t, 1H, J = 6.0 Hz, -$CH_2C(CH_3)$=$CH$$CH_2$-), 5.21–5.34 (m, 1H, -$CH$=CHCH=), 6.28–6.39 (m, 2H, -CH=$CHCH$=); ms *m/e*: 468 (M^+), 466 ($M^+ - H_2$), 450 ($M^+ - H_2O$). Exact Mass ($M^+ - H_2$) calcd.: 466.2203; found: 466.2195.

Allylic alcohol ***21***b

The general procedure D described before was employed. Thus, treatment of silyl ether **20***b* (112 mg, 0.159 mmol) with nBu$_4$NF (1.0 M in THF, 0.286 mL, 0.286 mmol) in 2 mL of THF at room temperature for 2.5 h yielded allylic alcohol **21***b* (45 mg, 60%) as a colorless oil; ir (neat): 3500, 2950, 2860, 1735, 1435, 1200 cm^{-1}; ^1H nmr ($CDCl_3$) δ: 1.65 (d, 3H, J = 1.0 Hz, -$CH_2C(CH_3)$=$CHCH_2$-), 1.85 (br s, 7H, -CH_2CH_2CR(CO_2CH_3)$_2$ and =CHCH=C(CH_3)-), 1.89–2.00 (m, 4H, -CH_2CH_2CH-(CO_2CH_3)$_2$), 2.70 (d, 2H, J = 7.5 Hz, =CHCH_2CR(CO_2CH_3)$_2$), 3.35 (t, 1H, J = 7.2 Hz, -CH(CO_2CH_3)$_2$), 3.73 (s, 12H, 4 × -OCH_3), 4.22 (s, 2H, -CH_2OH), 5.06 (t, 1H, J = 6.0 Hz, -CH_2CH_2CH=), 5.41 (dt, 1H, J = 14.9 Hz, 7.5 Hz, -CH_2-CH=CH-), 5.89 (d, 1H, J = 10.9 Hz, -CH=CHCH=C-), 6.40 (dd, 1H, J = 14.9 Hz, 11.1 Hz, -CH=CHCH=C-); ms *m/e*: 450 ($M^+ - H_2O$).

Allylic alcohol ***21***c

The general procedure D described before was employed. Thus, treatment of silyl ether **20***c* (406.1 mg, 0.57 mmol) with nBu$_4$NF (1.0 M in THF, 1.15 mL, 1.15 mmol) in 8 mL of THF at room temperature for 2 h yielded allylic alcohol **21***c* (241.1 mg, 0.515 mmol, 90%) as a viscous oil; ir (neat): 3530, 3020, 2960, 2855, 1435, 1440, 1220, 1170 cm^{-1}; ^1H nmr ($CDCl_3$) δ: 1.66 (s, 3H, -CH_2CH=C(CH_3)CH_2-), 1.76 (s, 3H, -CH=CHCH=C(CH_3)-), 1.83–2.02 (m, 9H, -CH_2CH_2CH=C(CH_3)CH_2CH_2- and -CH_2OH), 2.74 (d, 2H, J = 7.6 Hz, -CH_2CH=CHCH=), 3.34 (t, 1H, J = 7.1 Hz -CH(CO_2CH_3)$_2$), 3.73 (s, 12H, 4 × -OCH_3), 4.05 (d, 2H, J = 6.2 Hz, -CH_2OH), 5.09 (t, 1H, J = 6.2 Hz, -CH_2CH=C(CH_3)CH_2-), 5.49 (dt, 1H, J = 15.0 Hz, 7.5 Hz, -CH=CHCH=), 6.03 (d, 1H, J = 10.7 Hz, -CH=CHCH=C(CH_3)-), 6.35 (dd, 1H, J = 15.0 Hz, 10.8 Hz, -CH=CHCH=C-); ms *m/e*: 468 (M^+), 450 ($M^+ - H_2O$).

Allylic bromide ***22***a

General procedure G

To a stirred solution of allylic alcohol **21***a* (52.5 mg, 0.11 mmol) and CBr_4 (42.0 mg, 0.127 mmol) in 1.2 mL of CH_2Cl_2 was added dropwise at 0°C under argon over a period of 15 min a solution of PPh_3 (37.6 mg, 0.143 mmol) in 0.7 mL of CH_2Cl_2. The resulting mixture was allowed to warm to room temperature and then stirred for 2 h. The volatile was evaporated to dryness and the residue was purified by flash chromatography (hexane – ethyl acetate) using a short-path column to afford allylic bromide **22***a* (43.2 mg, 0.081 mmol, 74%) and recovered starting material **21***a* (8.8 mg, 17%). Compound **22***a* was used immediately for the next macrocyclization without characterization.

Allylic chloride ***22***b

The general procedure E described before was employed. Thus, treatment of allylic alcohol **21***b* (45 mg, 96 μL) with LiCl (12.7 mg, 288 μmol), *s*-collidine (38 μL, 288 mmol), and methanesulfonyl chloride (22 μL, 288 mmol) in DMF (0.5 mL) at 0°C for 6 h yielded allylic chloride **22***b* as a crude oil (45 mg), which was used immediately in the cyclization step without further purification and characterization.

Allylic bromide ***22***c

The general procedure G described before was employed. Thus, treatment of alcohol **21***c* (46.4 mg, 99 μmol) with CBr_4 (37.8 mg, 114 μmol) and PPh_3 (33.8 mg, 129 μmol) in 1.6 mL of CH_2Cl_2 at room temperature for 2 h yielded allylic bromide **22***c* (46.0 mg, 87 μmol, 87%) as an oil; ir (neat): 3030, 2950, 2860, 1740, 1440, 1250, 1200 cm^{-1}; ^1H nmr (C_6D_6) δ: 1.59 (s, 3H, -CH_2CH=C(CH_3)CH_2-), 1.64 (s, 3H, -CH=CHCH=C(CH_3)-), 1.94–2.21 (m, 8H, -CH_2CH_2CH=C(CH_3)CH_2CH_2-), 2.91 (d, 2H, J = 7.5 Hz), 3.34 and 3.38 (2s, 12H, 4 × -OCH_3), 3.41 (t, 1H, J = 7.0 Hz, -CH(CO_2CH_3)$_2$), 3.59 (s, 2H, -CH_2Br), 5.01 (t, 1H, J = 6.0 Hz, -CH_2CH=C(CH_3)CH_2-), 5.65 (dt, 1H, J = 15.0 Hz, 7.6 Hz, -CH=CHCH=), 5.78 (d, 1H, J = 10.9 Hz, -CH=CHCH=C(CH_3)-), 6.20 (dd, 1H, J = 15.0 Hz, 10.9 Hz, -CH=CH=); ms *m/e*: 532 (M^+), 530 (M^+), 501 ($M^+ - OCH_3$), 499 ($M^+ - OCH_3$), 451 ($M^+ - Br$).

CTC macrocycle ***1***a

General procedure H

To a stirred suspension of Cs_2CO_3 (152.0 mg, 0.467 mmol) in THF–DMF (1:1, 40 mL) at 74°C was added slowly, by automatic syringe pump over a period of 5.5 h under argon, a solution of allylic bromide **22***a* (43.2 mg, 81 μL) in THF–DMF (1:1, 15 mL). After completion of the addition, the stirring was continued for 17 h at 74°C. The solid was removed by filtration and the filtrate was evaporated to dryness, in vacuo. The crude residue thus obtained was purified by flash chromatography (hexane – ethyl ace-

Can. J. Chem. Downloaded from www.nrcresearchpress.com by 213.200.69.106 on 09/08/12
For personal use only.

Can. J. Chem. Downloaded from www.nrcresearchpress.com by 213.200.69.106 on 09/08/12
For personal use only.

tate, 5:1) to give cyclized product **1***a* (32.9 mg, 73 μmol, 90%) as a solid; mp 185–187°C; ir (neat): 3025, 2950, 2850, 1735, 1448, 1275, 1220, 1170, 1070 cm^{-1}; ^1H nmr ($CDCl_3$) δ: 1.56 (s, 3H, $-CH_2CH{=}C(CH_3)CH_2-$), 1.66 (s, 3H, $=CHCH{=}C(CH_3)-$), 1.70–1.98 (m, 8H, $-CH_2CH_2CH{=}C(CH_3)CH_2CH_2-$), 2.85 (d, 2H, J = 7.8 Hz, $-CH_2CH{=}CH-$), 2.86 (s, 2H, $-CH_2C(CH_3){=}$), 3.72–3.74 (2s, 12H, 4 × $-OCH_3$), 5.00 (q, 1H, J = 8.8 Hz, $-CH{=}CHCH{=}$), 5.11 (t, 1H, J = 6.0 Hz, $-CH_2CH{=}C(CH_3)CH_2-$), 6.27–6.45 (m, 2H, $-CH{=}CHCH{=}$), ms *m/e*: 450 (M^+), 435 ($M^+ - CH_3$), 432 ($M^+ - H_2O$), 418 ($M^+ - CH_3OH$). Exact Mass (M^+) calcd.: 450.2253; found: 450.2250. The structure of compound **1***a* was further confirmed by X-ray crystallography.

TCC macrocycle ***1***b

The general procedure H described above was employed. Thus, a solution of crude allylic chloride **22***b* (45 mg) in THF–DMF (1:1, 6 mL) was added slowly at 70°C over a period of 1.5 h to a Cs_2CO_3 (150 mg, 0.46 mmol) suspension in THF–DMF (1:1, 50 mL). The stirring was continued for an additional 2.5 h after addition. Work-up of the reaction mixture followed by flash chromatography and crystallization (CH_2Cl_2–hexane) furnished a crystalline compound **1***b* (27 mg, 63% for two steps from alcohol **21***b*); mp 178–181°C; ir ($CHCl_3$): 3035–3000, 2950, 2860, 1730, 1435, 1220 cm^{-1}; ^1H nmr (C_6D_6): δ: 1.52 (s, 3H, $-CH_2CH_2C(CH_3){=}$), 1.57 (s, 3H, $=CHCH{=}C(CH_3)-$), 1.76–2.32 (m, 8H, $-CH_2CH_2CH{=}C(CH_3)CH_2CH_2-$), 2.88–3.30 (m, 4H, $-H_2CH{=}CHCH{=}C(CH_3)CH_2-$), 3.32 and 3.34 (2s, 12H, 4 × $-OCH_3$), 4.98 (t, 1H, J = 6.6 Hz, $-CH_2CH_2CH{=}$), 5.38 (dt, 1H, J = 15.0 Hz, 7.7 Hz, $-CH_2CH{=}CH-$), 5.80 (d, 1H, J = 11.0 Hz, $-CH{=}CHCH{=}C-$), 6.32 (dd, 1H, J = 14.7 Hz, 11.1 Hz, $-CH{=}CHCH{=}C-$); ms *m/e*: 450 (M^+). Exact Mass (M^+) calcd.: 450.2253; found: 450.2250. The structure of this compound was further confirmed by X-ray crystallography.

TTC macrocycle ***1***c

The general procedure H described above was employed. Thus, a solution of allylic bromide **22***c* (42.8 mg, 80.6 μmol) in THF–DMF (1:1, 10 mL) was added slowly at 72°C over a period of 13.5 h to a Cs_2CO_3 (131.0 mg, 402.0 μmol) suspension in THF–DMF (1:1, 34 mL). The stirring was continued for an additional 36 h after completion of the addition. Work-up of the reaction mixture followed by flash chromatography (hexane – ethyl acetate; 5:1) furnished macrocycle **1***c* (28.0 mg, 62.2 μmol, 77%) and by-product **23** (1.0 mg, 2.2 mmol, 3%).

Compound ***1***c: mp 115–117°C; ir (neat): 3025, 2950, 1740, 1440, 1240 cm^{-1}; ^1H nmr ($CDCl_3$) δ: 1.64 (s, 3H, $-CH_2CH{=}C(CH_3)-CH_2-$), 1.67 (s, 3H, $-CH{=}CHCH{=}C(CH_3)-$), 1.68–2.50 (br m, 8H, $-CH_2CH_2CH{=}C(CH_3)CH_2CH_2-$), 2.60–3.22 (br m, 4H, $-CH_2CH{=}CHCH{=}C(CH_3)CH_2-$), 3.72 and 3.74 (2s, 12H, 4 × $-OCH_3$), 5.01 (t, 1H, J = 6.0 Hz, $-CH_2CH{=}C(CH_3)CH_2-$), 5.80 (dt, 1H, J = 15.1 Hz, 7.6 Hz, $-CH{=}CHCH{=}$), 6.10 (d, 1H, J = 10.9 Hz, $-CH{=}CHCH{=}$), 6.29 (dd, 1H, J = 14.6 Hz, 10.8 Hz, $-CH{=}CHCH{=}$); ms *m/e*: 450 (M^+), 445 ($M^+ - CH_3$), 442 ($M^+ - H_2O$), 418 ($M^+ - CH_3OH$). Exact Mass (M^+) calcd.: 450.2253; found: 450.2250.

Compound ***23***: mp 140–142°C; ir (neat): 3090–3000, 2960, 2860, 1740, 1450, 1200 cm^{-1}; ^1H nmr ($CDCl_3$) δ: 1.40–1.85 and 1.95–2.27 (2m, 8H, $-CH_2CH_2CH{=}C(CH_3)CH_2CH_2-$), 1.67 and 1.72 (2s, 6H, $=C(CH_3)-$ and $CH_2{=}C(CH_3)-$), 2.58–2.70 and 2.88–3.00 (2m, 2H, $-CH_2CH{=}CH-$), 3.61–3.67 (m, 1H, $-CHRC(CH_3){=}CH_2$), 3.71, 3.73, 3.74 (3s, 12H, 4 × $-OCH_3$), 4.74 and 4.86 (2s, 2H, $-C(CH_3){=}CH_2$), 5.18 (t, 1H, J = 7.2 Hz, $-CH{=}C(CH_3)-$), 5.49 (dt, 1H, J = 15.4 Hz, 7.8 Hz, $-CH_2CH{=}CH-$), 6.10 (dd, 1H, J = 15.4 Hz, 7.7 Hz, $-CH_2CH{=}CH-$); ms *m/e*: 450 (M^+). Exact Mass (M^+) calcd. 450.2253; found: 450.2258.

Triene diether ***25***

The general procedure F previously described was employed. Thus, treatment of dimethyl malonate **24** (2.89, 7.8 mmol) with NaH (344 mg, 60% in oil, 14.3 mmol), followed by crude allylic chloride **18** (2.2 g, 9.4 mmol) in a mixture of THF and DMF (1:1, 180 mL) at room temperature for 16.5 h, yielded acyclic triene **25** (1.5 g, 35%) as a colorless oil; ir (neat): 2950, 2860, 1738, 1450, 1200, 1110 cm^{-1}; ^1H nmr ($CDCl_3$) δ: 0.04 (s, 6H, $(CH_3)_2Si-$), 0.88 (s, 9H, $-(CH_3)_3C$), 1.64 (d, 3H, J = 1.3 Hz, $-CH_2CH{=}C(CH_3)CH_2-$), 1.89 (d, 3H, J = 1.6 Hz, $=CHCH{=}C(CH_3)-$), 1.45–1.99 (m, 10H, $=C(CH_3)CH_2CH_2-$ and $-OCHOCH_2(CH_2)_3-$), 2.13 (qd, 2H, J = 7.1 Hz, 1.1 Hz, $-CH_2CH_2OSi-$), 2.90 (s, 2H, $=CHCH{=}C(CH_3)CH_2-$), 3.54 (t, 2H, J = 7.0 Hz, $-CH_2OSi-$), 3.71 (s, 6H, 2 × $-OCH_3$), 3.40–3.53 and 3.80–3.92 (2m, 2H, $-OCHOCH_2-$), 4.01 (dd, 1H, J = 12.3 Hz, 6.9 Hz, $-CHHOTHP$), 4.26 (dd, 1H, J = 12.9 Hz, 5.6 Hz, $-CHHOTHP$), 4.63 (t, 1H, J = 3.0 Hz, $-OCHO-$), 5.12 (td, 1H, J = 7.2 Hz, 1.4 Hz, $-CH_2CH_2CH{=}$), 5.70 (dt, 1H, J = 14.9 Hz, 6.5 Hz, $-CH_2CH{=}CH-$), 5.98 (d, 1H, J = 11.0 Hz, $=CHCH{=}C(CH_3)-$), 6.48 (dd, 1H, J = 15.0 Hz, 11.1 Hz, $-CH_2CH{=}CH-$); ms *m/e*: 552 (M^+), 537 ($M^+ - CH_3$), 495 ($M^+ - C_4H_9$).

Triene alcohol ***26***

The general procedure D previously described was employed. Thus, treatment of silyl ether **25** (504 mg, 0.91 mmol) with nBu$_4$NF (1 M in THF, 1.6 mL, 1.6 mmol) in 8 mL of THF at room temperature for 2 h yielded triene alcohol **26** (397 mg, 0.90 mmol, 99%) as a colorless oil, which was used in the following mesylation without further characterization.

Triene mesylate ***27***

The general procedure B previously described was employed. Thus, treatment of alcohol **26** (397 mg, 0.91 mmol) with triethylamine (0.19 mL, 1.4 mmol) and methanesulfonyl chloride (77 μL, 1.0 mmol) in CH_2Cl_2) (12 mL) at 0°C for 1 h gave mesylate **27** (480 mg) as a crude oil, which was used immediately for the following alkylation without further purification and characterization.

Dimethyl malonate triene ***28***a

The general procedure C previously described was employed. Thus, treatment of dimethyl malonate (0.52 mL, 4.6 mmol) with NaH (164 mg, 60%, 4.1 mmol), followed by mesylate **27** (480 mg, obtained as a crude oil from the above reaction) and KI (15 mg, 91 μmol) in THF–DMF (1:1, 24 mL) at 85°C for 17 h, yielded **28***a* (366 mg, 73% for two steps from alcohol **26**) as a colorless oil; ir (neat): 2950, 2860, 1734, 1437, 1210 cm^{-1}; ^1H nmr ($CDCl_3$) δ: 1.64 (s, 3H, $-CH_2CH_2CH{=}C(CH_3)-$), 1.71 (s, 3H, $=CHCH{=}C(CH_3)-$), 1.45–1.80 (m, 6H, $-OCHOCH_2(CH_2)_3-$), 1.80–2.04 (m, 8H, $-CH_2CH_2CH{=}C(CH_3)CH_2CH_2-$), 2.89 (s, 2H, $=CHCH{=}C(CH_3)CH_2-$), 3.34 (t, 1H, J = 7.0 Hz, $-CH(CO_2CH_3)_2$), 3.71 and 3.73 (2s, 12H, 4 × $-OCH_3$), 3.45–3.90 (m, 2H, $-OCHOCH_2-$), 4.00 (dd, 1H, J = 12.0 Hz, 7.0 Hz, $-CHHOTHP$), 4.26 (dd, 1H, J = 13.1 Hz, 5.6 Hz, $-CHHOTHP$), 4.63 (t, 1H, J = 3.0 Hz, $-OCHO-$), 5.05 (t, 1H, J = 6.0 Hz, $-CH_2CH_2CH{=}$), 5.70 (dt, 1H, J = 15.1 Hz, 6.1 Hz, $-CH_2CH{=}CH-$), 5.97 (d, 1H, J = 11.3 Hz, $=CHCH{=}C(CH_3)-$), 6.47 (dd, 1H, J = 15.0 Hz, 11.1 Hz, $-CH_2CH{=}CH-$); ms *m/e*: 552 (M^+), 534 ($M^+ - H_2O$), 520 ($M^+ - CH_3OH$), 467 ($M^+ - THP$).

Triene allylic alcohol ***28***b

The general procedure A previously described was employed. Thus, treatment of THP ether **28***a* (366 mg, 0.663 mmol) with pyridinium *p*-toluenesulfonate (20 mg, 80 μmol) in methanol (7 mL) at 55°C for 75 min yielded allylic alcohol **28***b* (295 mg, 95%) as a viscous oil; ir (neat): 3500, 2955, 2860, 1735, 1435, 1210 cm^{-1}; ^1H nmr ($CDCl_3$) δ: 1.25 (m, 1H, $-CH_2OH$), 1.64 (s, 3H, $-CH_2CH_2CH{=}C(CH_3)-$), 1.70 (s, 3H, $=CHCH{=}C(CH_3)-$), 1.78–2.04 (m, 8H, $-CH_2CH_2CH{=}C(CH_3)CH_2CH_2-$), 2.91 (s, 2H, $=CHCH{=}C(CH_3)CH_2-$), 3.43 (t, 1H, J = 7.0 Hz, $-CH(CO_2CH_3)_2$), 3.72, 3.73 (2s, 12H, 4 × $-OCH_3$), 4.19 (t, 2H, J = 5.8 Hz, $-CH_2OH$), 5.05 (t, 1H, J = 6.0 Hz, $-CH_2CH_2CH{=}$), 5.76 (dt, 1H, J = 15.0 Hz, 5.8 Hz, $-CH_2CH{=}CH-$), 5.97 (d, 1H, J = 11.1 Hz, $=CHCH{=}C(CH_3)-$), 6.49 (dd, 1H, J = 15.0 Hz, 11.1 Hz, $-CH_2CH{=}CH-$).

Can. J. Chem. Downloaded from www.nrcresearchpress.com by 213.200.69.106 on 09/08/12
For personal use only.

Allylic chloride ***29***

The general procedure E previously described was employed. Thus, treatment of allylic alcohol **28***b* (150 mg, 0.32 mmol) with LiCl (41 mg, 0.96 mmol), *s*-collidine (63 μL, 0.48 mmol), and methanesulfonyl chloride (37 μL, 0.48 mmol) in DMF (1.2 mL) at 0°C for 3 h yielded allylic chloride **29** as a crude oil (140 mg), which was used immediately in the next cyclization without purification and characterization.

TTC macrocycle ***1***d

The general procedure H previously described was employed. Thus, a solution of allylic chloride **29** (140 mg, obtained as a crude oil from the above reaction) in THF–DMF (1:1, 18 mL) was added slowly by syringe pump at 70°C over 1 h to a Cs_2CO_3 (469 mg, 1.4 mmol) suspension in THF–DMF (1:1, 50 mL). The stirring was continued for an additional 2 h after completion of the addition. Work-up of the reaction mixture followed by flash chromatography (hexane – ethyl acetate – CH_2Cl_2; 75:9:16) and crystallization (CH_3OH) provided macrocycle **1***d* (100 mg, 69% for two steps from alcohol **28***b*) as a crystalline solid; mp 167–170°C; ir ($CHCl_3$): 3030, 2960, 2860, 1730, 1450, 1215 cm^{-1}; ^1H nmr ($CDCl_3$) δ: 1.57 (s, 3H, -$CH_2CH_2C(CH_3)$=), 1.66 (d, 3H, J = 1.0 Hz, =CHCH=C(CH_3)-), 1.15–1.70 (br m, 8H, -CH_2CH_2-CH=C(CH_3)CH_2CH_2-), 2.77 (d, 2H, J = 7.9 Hz, =CHCH_2CR-(CO_2CH_3)$_2$), 2.80–3.10 (m, 2H, =C(CH_3)CH_2CR(CO_2CH_3)$_2$), 3.73 (s, 12H, 4 × -OCH_3), 5.14 (m, 1H, -CH_2CH_2CH=), 5.31 (dt, 1H, J = 14.9 Hz, 7.9 Hz, -CH_2CH=CH-), 6.00 (d, 1H, J = 10.9 Hz, =CHCH=C(CH_3)-), 6.48 (dd, 1H, J = 14.8 Hz, 11.1 Hz, -CH_2CH=CH-); ms *m/e*: 450 (M^+). Exact Mass (M^+) calcd.: 450.2253; found: 450.2246. The structure of this macrocycle was further characterized by X-ray crystallography.

Diels–Alder reaction of ***1***a

A solution of macrocycle **1***a* (10.4 mg, 23.1 μmol) in 0.8 mL of toluene was sealed in a quartz tube (20 cm long, 8 mm diameter) under vacuum and then heated at 320°C for 18 h. After the tube was opened, the mixture was transferred into a flask and then evaporated to dryness. The residue thus obtained was eluted through a silica gel column (hexane – ethyl acetate, 7:3) to give a mixture (8.8 mg, 19.6 μmol, 85%), containing four tricyclic compounds **30**, **32**, **33**, and **34**. The characteristic spectral data for the mixture were obtained; ir (neat): 2960, 2870, 1735, 1440, 1250, 1170 cm^{-1}; ^1H nmr ($CDCl_3$) δ: 0.78–1.12 (8s, -CH_3), 1.13–2.90 (m, all other CH and CH_2), 3.60–3.80 (14s, -OCH_3), 5.13–6.00 (m, -CH=CH-). The ratio for compounds **30**, **32**, **33**, and **34** was found to be 7.0:20.6:5.9:1.0 as determined by the ^1H nmr integration of their methyl peaks and olefin proton peaks. The assignment is the following:

Compound ***30***: 0.95 (s, 3H, -CH_3), 1.12 (s, 3H, -CH_3), 5.16 (d, 1H, J = 10.5 Hz, -CHRCH=CH-), 5.31 (dd, 1H, J = 10.5 Hz, 3.0 Hz, -CHRCH=CH-).

Compound ***32***: 0.78 (s, 3H, -CH_3), 1.07 (s, 3H, -CH_3), 1.12–2.68 (br m, 14H, all other CH and CH_2), 3.74, 3.72, 3.69, 3.68 (4s, 12H, 4 × -OCH_3), 5.45 (dd, 1H, J = 10.5 Hz, 1.8 Hz, -CHRCH=CH-), 5.97 (dt, 1H, J = 10.5 Hz, 1.8 Hz, -CHRCH=CH-).

Compound ***33***: 0.87 (s, 3H, -CH_3), 1.10 (s, 3H, -CH_3), 5.22 (dd, 1H, J = 10.5 Hz, 1.8 Hz, -CHRCH=CH-), 5.35 (dd, 1H, J = 10.5 Hz, 3.0 Hz, -CHRCH=CH-). The structure of this compound was further characterized by X-ray crystallography and shown to have the CSC stereochemistry.

Compound ***34***: 0.83 (s, 3H, -CH_3), 0.85 (s, 3H, -CH_3), 5.50 (dd, 1H, J = 10.5 Hz, 2.8 Hz, -CHRCH=CH-), 5.72 (dd, 1H, J = 10.5 Hz, 1.6 Hz, -CHRCH=CH-).

Separation of the four isomers from the mixture was attempted by flash chromatography with different solvent systems. A mixture of hexane and ethyl acetate (9:1) was found to be the best system, the use of which in flash chromatography of the mixture provided two fractions. Fraction 1, which contained tricycles **32** and **34**, was then purified by plate chromatography with silica gel (toluene–acetone, 9:1) to give pure tricycle **34**. Fraction 2, which contained tricycles **30** and **33**, was purified by plate chromatography with silica gel (toluene–acetone, 98:2) to give pure tricycle **33**.

Thermolysis of TTC macrocycle ***1***c

Neat macrocycle **1***c* (4.0 mg, 8.9 μmol) was sealed in a quartz tube under vacuum and then heated in an oven at 200°C for 4 h. After the tube was opened, the product was transferred into a flask with CH_2Cl_2 and then evaporated to dryness. Purification of the residue by flash chromatography (hexane – ethyl acetate; 7:3) furnished CTC macrocycle **1***a* (4.0 mg, 100%), which had spectral properties identical with the compound obtained from the cyclization of acyclic triene **22***a*.

Diels–Alder reaction of ***1***c

A solution of **1***c* (20.1 mg, 44.7 μmol) in 1.5 mL of toluene was sealed in a quartz tube under vacuum and then heated in an oven at 310°C for 18 h. After the tube was opened, the mixture was transferred into a flask and then evaporated to dryness. The ^1H nmr of the crude residue indicated the presence of the same four tricyclic compounds **30**, **32**, **33**, and **34**. The crude residue was then purified by flash chromatography (hexane – ethyl acetate, 9:1) to give two fractions (fraction 1: 3.2 mg, 7.1 μmol, 16%; fraction 2: 16.3 mg, 36.2 mmol, 81%). Fraction 1 contained tricycles **32** and **34** in a ratio of 1:5 by ^1H nmr and 1:5.6 by gc. Fraction 2 contained tricycles **30** and **33** in a ratio of 1:14 by ^1H nmr and 1:12 by gc. The overall ratio of **30**, **32**, **33**, and **34** was found to be 2.3:1.0:29.9:5.3.

Spectral data for fraction 1: ir (neat): 1960, 1860, 1740, 1440, 1250 cm^{-1}; ms *m/e*: 450 (M^+). The ^1H nmr data for fraction 1 are identical with those of tricycles **32** and **34** obtained from the Diels–Alder reaction of **1***a*.

The ir spectral data for fraction 2: (neat): 2960, 2860, 1735, 1450, 1200 cm^{-1}; ^1H nmr data for fraction 2 are identical with those of tricycles **33** and **30** obtained from the Diels–Alder reaction of **1***c*.

Diels–Alder reaction of ***1***b

The crystalline macrocycle **1***b* (11.5 mg, 26 μmol) was sealed in a quartz tube under vacuum and then heated in an oven at 320°C for 1.5 h. After the tube was opened, the mixture was transferred into a flask with CH_2Cl_2 and then evaporated to dryness. The residue thus obtained was purified by flash chromatography (hexane – ethyl acetate, 9:1) to give tricycle **30** (10 mg, 87%) as a crystalline compound: mp 68–71°C; ir ($CHCl_3$): 3022, 2950, 2870, 1730, 1435, 1250 cm^{-1}; ^1H nmr (C_6D_6) δ: 0.88 (s, 3H, -CH_3), 1.06 (s, 3H, =CHCR(CH_3)-), 1.43–2.60 (m, 14H, all CH and CH_2), 3.27, 3.28, 3.31, 3.32 (4s, 12H, 4 × -OCH_3), 5.17 (dd, 1H, J = 10.0 Hz, 1.4 Hz, -CHRCH=CH-), 5.25 (dd, 1H, J = 10.0 Hz, 2.7 Hz, -CHRCH=CH-); ms *m/e*: 450 (M^+). Exact Mass (M^+) calcd.: 450.2253; found: 450.2246. The structure of this tricycle was further characterized by X-ray crystallography.

Diels–Alder reaction of ***1***d

The crystalline macrocycle **1***d* (25.0 mg, 56 μmol) was sealed in a quartz tube under vacuum and then heated in an oven at 360°C for 1 h. After the tube was opened, the mixture was transferred into a flask with CH_2Cl_2 and then evaporated to dryness. The residue thus obtained was purified by flash chromatography (hexane – ethyl acetate, 4:1) to give tricycle **31** (22.6 mg, 90%) as a crystalline solid; mp 138–140°C; ir ($CHCl_3$): 3020, 2955, 2870, 1730, 1435, 1245 cm^{-1}; ^1H nmr (C_6D_6) δ: 0.69 (s, 3H, -CH_3), 0.78 (s, 3H, =CHCR(CH_3)-), 1.20–2.78 (m, 14H, all CH and CH_2), 3.26, 3.27, 3.30, and 3.34 (4s, 12H, 4 × -OCH_3), 5.26 and 5.31 (2d, 2H, J = 11.0 Hz, -CH=CH-); ms *m/e*: 450 (M^+). Exact Mass (M^+) calcd.: 450.2253; found: 450.2246. The structure of this compound was further characterized by X-ray crystallography.

Acknowledgements

This research was supported by the Natural Sciences and Engineering Research Council of Canada (NSERCC, Ottawa)

and by the "Ministère de l'Enseignement supérieur et de la Science (Fonds FCAR, Québec)". We acknowledge the help of Dr Solo Goldstein in writing this manuscript.

1. Y.C. Xu, A.L. Roughton, R. Plante, and P. Deslongchamps. Can. J. Chem. **71**, 000 (1993).
2. (*a*) R.A. Micheli, Z.G. Hajos, N. Cohen, D.R. Parrish, L.A. Portland, W. Sciamanna, M.A. Scott, and P.A. Wherli. J. Org. Chem. **40**, 675 (1975); (*b*) Z.G. Hajos and D.R. Parrish. J. Org. Chem. **38**, 3244 (1973).
3. W.S. Johnson, B.E. McCarry, R.L. Harkezich, and S.G. Boots. J. Am. Chem. Soc. **102**, 352 (1980), and references therein.
4. (*a*) T. Kametani and H. Nemoto. Tetrahedron, **37**, 3 (1981); (*b*) W. Oppolzer. Angew. Chem. Int. Ed. Engl. **16**, 10 (1977); (*c*) A.G. Fallis. Can. J. Chem. **62**, 183 (1984), and references therein; (*d*) M. Ihara, I. Sudow, and K. Fukumoto. J. Chem. Soc. Perkin Trans. **1**, 117 (1986); (*e*) M.E. Jung and K.M. Halweg. Tetrahedron Lett. 2121 (1984).
5. (*a*) J.F. Lavallee and P. Deslongchamps. Tetrahedron Lett. **29**, 6033 (1988); (*b*) Tetrahedron Lett. **28**, 3457 (1987).
6. (*a*) D. Taub. *In* The total synthesis of natural products. Vol. 6. *Edited by* J. Apsimon. John Wiley and Sons, New York. 1984. pp. 1–49; (*b*) K. Nakanishi. *In* Natural products chemistry. Vol. 3. *Edited by* K. Nakanishi et al. Kodansha Ltd., Tokyo. 1983. Chap. 4.
7. (*a*) S. Lamothe, A. Ndibwami, and P. Deslongchamps. Tetrahedron Lett. **29**, 1639 (1988); (*b*) Tetrahedron Lett. **29**, 1641 (1988); (*c*) A. Marinier and P. Deslongchamps. Tetrahedron Lett. **29**, 6215 (1988); (*d*) Y.C. Xu, M. Cantin, and P. Deslongchamps. Can. J. Chem. **68**, 2137 (1990); (*e*) M. Cantin, Y.C. Xu, and P. Deslongchamps. Can. J. Chem. **68**, 2137 (1990); (*f*) K. Baettig, C. Dallaire, R. Pitteloud, and P. Deslongchamps. Tetrahedron Lett. **28**, 5249 (1987); (*g*) K. Baettig, A. Marinier, R. Pitteloud, and P. Deslongchamps. Tetrahedron Lett. **28**, 5253 (1987); (*h*) G. Bérubé and P. Deslongchamps. Tetrahedron Lett. **28**, 5255 (1987); (*i*) Can. J. Chem. **68**, 404 (1990); (*j*) A. Marinier, K. Baettig, C. Dallaire, R. Pitteloud, and P. Deslongchamps. Can. J. Chem. **67**, 1609 (1989).
8. M. Miyashita, A. Yoshikoshi, and P.A. Grieco. J. Org. Chem. **42**, 3772 (1977).
9. H.J. Bestmann and H. Schulz. Tetrahedron Lett. **4**, 5 (1960).
10. A.J. Mancuso, S.L. Huang, and D. Swern. J. Org. Chem. **43**, 2480 (1978).
11. S. Hanessian and P. Lavallee. Can. J. Chem. **53**, 2975 (1975); **55**, 562 (1977).
12. E.J. Corey and A. Venkateswarlu. J. Am. Chem. Soc. **94**, 6190 (1972).
13. S. Lamothe. Ph. D. Thesis, Université de Sherbrooke (1989).
14. E.W. Collington and A.I. Meyers. J. Org. Chem. **36**, 3044 (1971).
15. B.M. Trost and W.C. Vladuchick. J. Org. Chem. **44**, 148 (1979).
16. J. Hooz and S.S.H. Gilani. Can. J. Chem. **46**, 86 (1968).
17. A.G. Michel, N. Michel-Dewez, A.L. Roughton, J.P. Springer, and K. Hoogsteen. Acta Crystallogr. Sect. C: Cryst. Struct. Commun. **C45**, 932 (1989).
18. A.G. Michel, N. Michel-Dewez, and A.L. Roughton. Acta Crystallogr. Sect. C: Cryst. Struct. Commun. **C45**, 327 (1989).
19. A.G. Michel, N. Michel-Dewez, A.L. Roughton, J.P. Springer, and K. Hoogsteen. Acta Crystallogr. Sect. C: Cryst. Struct. Commun. **C45**, 9092 (1989).

Can. J. Chem. Downloaded from www.nrcresearchpress.com by 213.200.69.106 on 09/08/12
For personal use only.

Spruce budworm (*Choristoneura fumiferana*) antifeedants 3. Structure–activity relationship among some angularly functionalized decalin compounds[1]

A.E. SCHWERDTFEGER AND T.H. CHAN[2]
Department of Chemistry, McGill University, Montréal, Que., Canada H3A 2K6

AND

A.W. THOMAS, G.M. STRUNZ, A. SALONIUS, AND M. CHIASSON
Forestry Canada – Maritimes Region, Fredericton, N.B., Canada E3B 5P7

Received November 4, 1992

A.E. SCHWERDTFEGER, T.H. CHAN, A.W. THOMAS, G.M. STRUNZ, A. SALONIUS, and M. CHIASSON. Can. J. Chem. **71**, 1184 (1993).

Several angularly functionalized decalins, synthethized during the preparation of three keto diacetate decalins, models for clerodane diterpenoids, were tested for antifeedant activity against the spruce budworm, *Choristoneura fumiferana*. Definite biological activity was observed for some of these compounds. A structure–activity relationship was discussed on the basis of these results.

A.E. SCHWERDTFEGER, T.H. CHAN, A.W. THOMAS, G.M. STRUNZ, A. SALONIUS et M. CHIASSON. Can. J. Chem. **71**, 1184 (1993).

On a synthétisé plusieurs décalines, fonctionnalisées à la position angulaire, au cours de la préparation de trois cétones diacétates. On a vérifié l'activité biologique de ces composés contre la tordeuse des bourgeons de l'épinette, *Choristoneura fumiferana*. Quelques-uns de ces composés présentent une activité biologique non ambiguë. Sur la base de ces résultats, on discute d'une relation structure–activité.

Can. J. Chem. Downloaded from www.nrcresearchpress.com by 213.200.69.106 on 09/08/12
For personal use only.

Introduction

The spruce budworm, *Choristoneura fumiferana* (Clem.), is one of the most widely distributed and destructive defoliators of spruce–fir forests in eastern North America (2). In eastern Canada the larvae of the budworm begin to feed on the buds or the newly opened shoots of the host tree in mid-May, while they consume the greatest amount of foliage during their sixth instar in late June. A pest control strategy involving the use of antifeedants, to interfere with the feeding behaviour of insects, may offer advantages over conventional pest control methods since the antifeedant could protect current year foliage while leading indirectly to budworm mortality without being generally toxic.

Clerodin (**1**) (3) and azadirachtin (**2**) (4) are two natural products that possess marked antifeedant properties. Chang and Nakanishi (5) have isolated the iridoid specionin (**3**), from leaves of *Catalpa speciosa* and found it to be an effective antifeedant against the spruce budworm. Specionin has recently been synthesized (6, 7).

Because of the complexity of structures of known antifeedants such as clerodin (**1**) and azadirachtin (**2**), synthetic chemists have turned to the more practical approach of preparing simpler analogs of these compounds. In 1981 Kojima and Kato (8) prepared the clerodin homologs **4** and **5**, which were found to be biologically active against *Spodoptera litura* at 500 and 250 ppm, respectively. At the same time Ley and co-workers (9) prepared the *trans* and *cis* epoxydiacetate clerodin analogs **6** and **7**, which were found to be biologically active at 100 and 1000 ppm when tested against *Locusta migratoria*. Ley and co-workers (10) have also prepared azadirachtin analogs such as **8** and **9**, of which **9** (active at 1 ppm) is almost as active as azadirachtin itself in some bioassays.

A few years ago we found that the specionin analog **10** exhibits moderate activity against the spruce budworm (11). More recently we reported the synthesis and biological activity of several polyoxygenated decalins, of which compounds **11**–**14** were found to exhibit moderate antifeedant activity against the spruce budworm at a concentration of 0.2% wet weight (1).

A common structural feature of all natural insect antifeedants is the close proximity of the polyoxygenated functions. It is possible that such a dense array of oxygen functions may be required for biological activity. As part of our effort to study the structure–activity relationship of insect antifeedants, we describe here the preparation of three polyoxygenated angularly functionalized decalins **15**–**17**, possessing some structural features in common with the clerodanes, as potential antifeedants against the spruce budworm.

Chemical synthesis

Previously in our laboratory (12) it was found that the decalin **20** could be prepared by a tandem Michael–Claisen annelation sequence (see Scheme 1). The conjugate addition of siloxy diene **18** to 2-cyclohexen-1-one provided the isomeric Michael adducts **19**, which were cyclized by a Claisen condensation.

We then reported the angular hydroxymethylation of decalin **20** with diisopropylethylamine and benzyl chloromethyl ether in the presence of paraformaldehyde to provide the benzyloxymethoxymethyl derivative **22** in 75% yield (13) (see Scheme 2).

The trapping of intermediate aldol **21** could also be accomplished with acetic anhydride to form compound **23**. The hydroxymethylation procedure was then also applied to keto ester **24** as well as to decalin **27** to prepare compounds **25** and **26** as well as angularly functionalized decalin **28** (13) (see Scheme 3). It is interesting to note that in the case of the keto ester **24**, the unprotected aldol **26** was isolated directly.

[1]For previous paper on this subject, see ref. 1.
[2]Author to whom correspondence may be addressed.

Can. J. Chem. Downloaded from www.nrcresearchpress.com by 213.200.69.106 on 09/08/12
For personal use only.

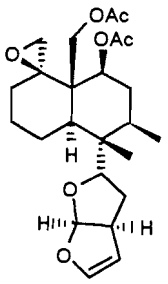

1

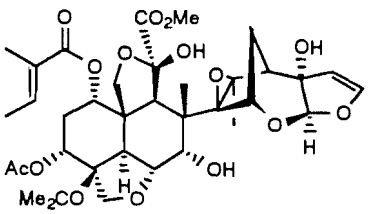

2

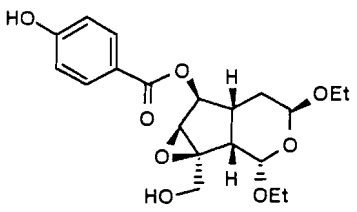

3

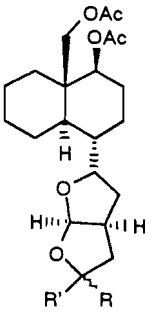

4 R = OH, R'= H
5 R, R'= O

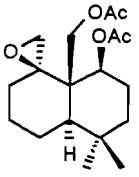

6

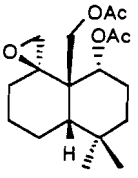

7

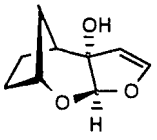

9

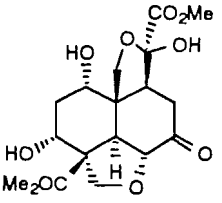

8

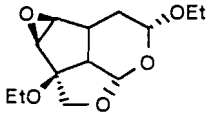

10

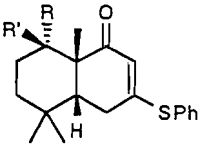

11 R = OTBDMS, R'= H
12 R, R'= O

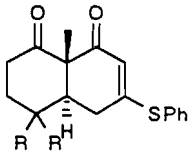

13 R = Me
14 R = H

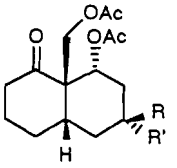

15 R = R'= H
16 R = Me, R'= H
17 R = R'= Me

In the hope of preparing a decalin compound functionalized at the angular position with an ester moiety, decalin **20** was treated with potassium *tert*-butoxide in THF and the resulting anion was quenched with 3 equivalents of methyl chloroformate. However, this provided the O-alkylated product **29** in 93% yield (see Scheme 4). This is not surprising since it is known that ethyl chloroformate frequently gives predominantly O-alkylation (14, 15). The O-alkylation as confirmed by the presence of only one (unsaturated) carbonyl signal in the ^{13}C nmr spectrum at 183.8 ppm, as well as by the presence of the carbonate signal at 163.6 ppm.

Recently Mander and Sethi (16) described the C-acylation of lithium enolates by methyl cyanoformate, which provided high yields of β-keto esters. These reaction conditions were modified and applied to Michael adduct **19**. Thus, compound **19*E*** was treated with potassium *tert*-butoxide in THF, to promote the Claisen condensation, and the resulting anion quenched with methyl cyanoformate, providing after 30 h at room temperature the diacylated product **30** in 23% yield together with 29% of compound **31** and 38% recovered decalin **20** (see Scheme 5).

Subjecting decalin **20** to the same conditions provided **31** as the sole product in 48% yield together with 25% starting material. The structure of compound **31** was confirmed by the presence of an unsaturated carbonyl carbon signal at 189.2 ppm and a carbonate signal at 165.1 ppm in the ^{13}C nmr spectrum. The presence of the CN functionality was

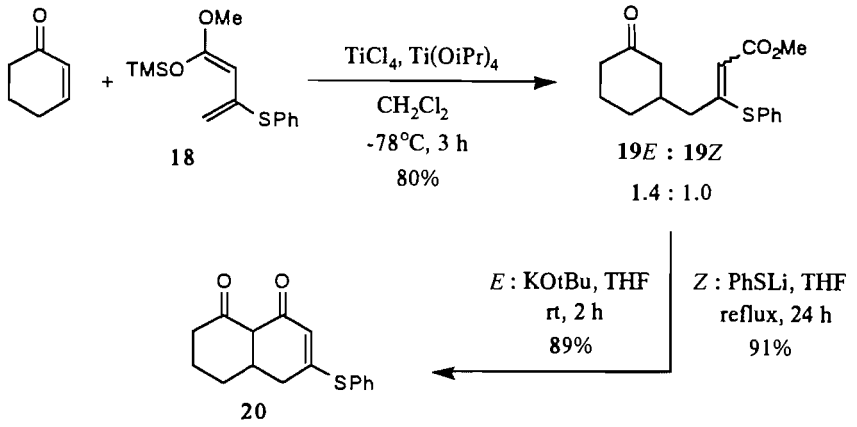

SCHEME 1

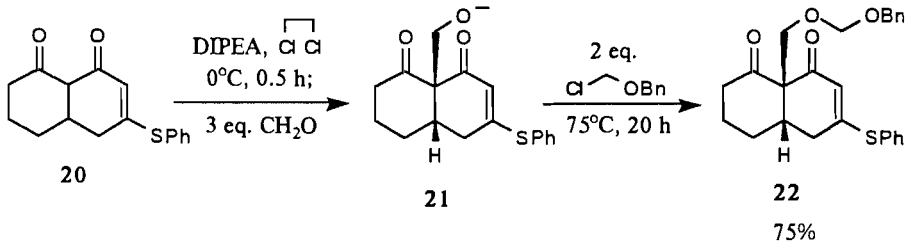

SCHEME 2

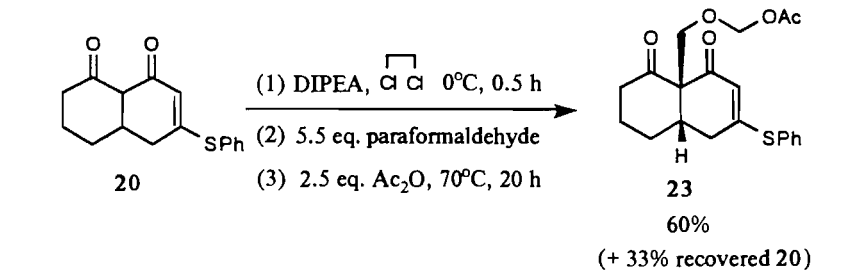

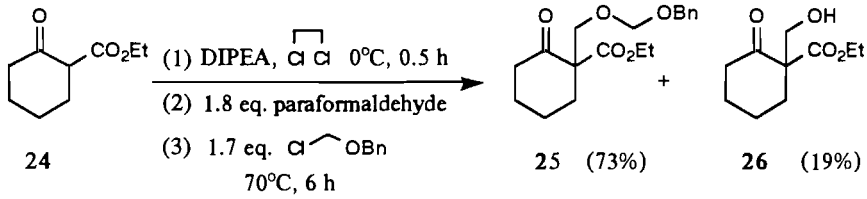

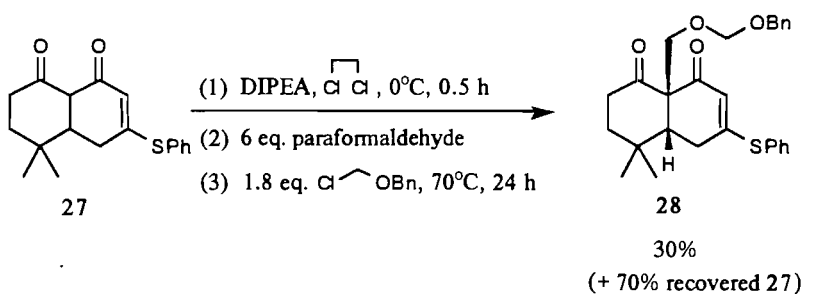

SCHEME 3

Can. J. Chem. Downloaded from www.nrcresearchpress.com by 213.200.69.106 on 09/08/12
For personal use only.

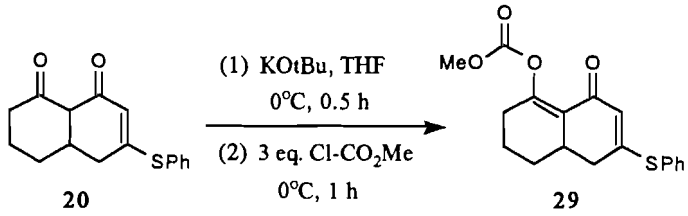

SCHEME 4

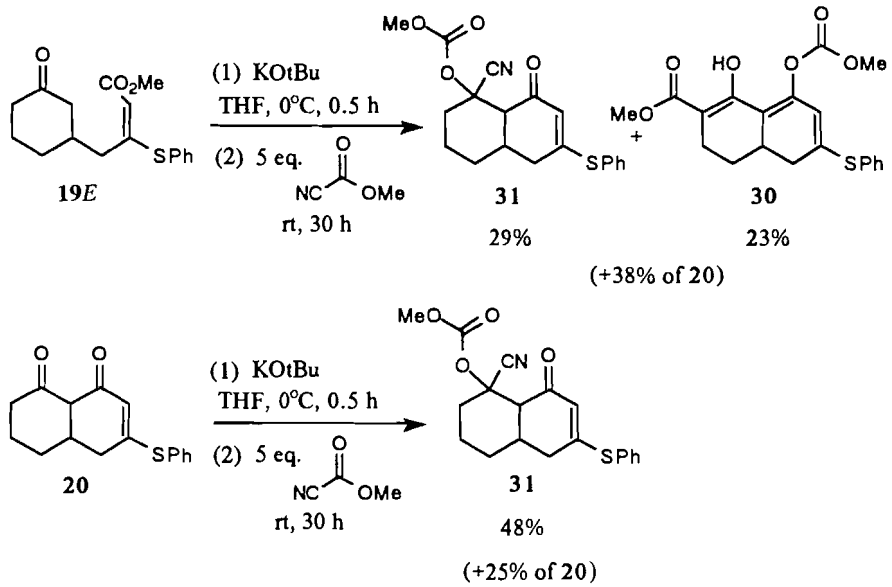

SCHEME 5

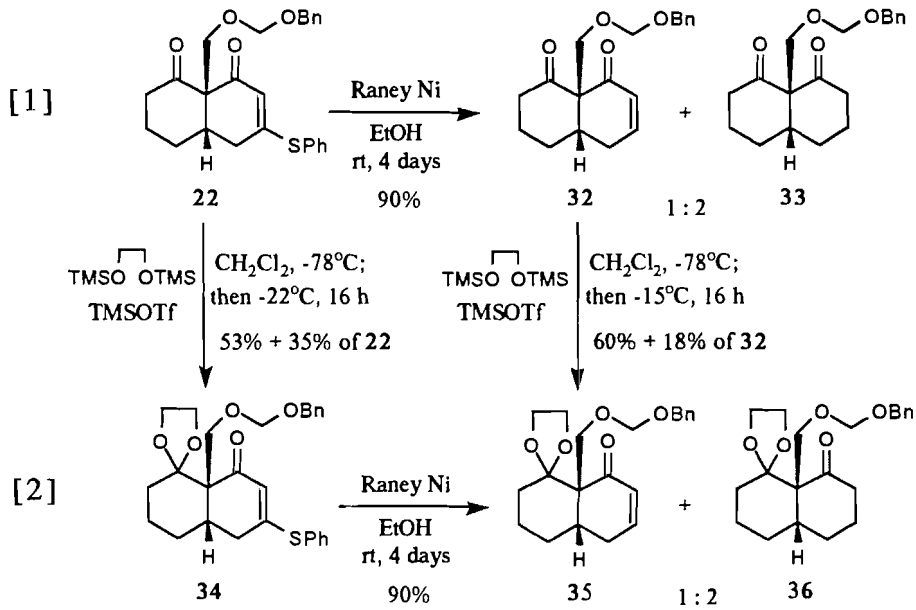

SCHEME 6

evident from the weak peak at 2361 cm^{-1} in the ir spectrum.

In our report on the angular hydroxymethylation of decalin **20** we have detailed the utility of the following chemical transformation (eq. [1] in Scheme 6) in establishing the structure of compound **22** (13). Treatment of **22** with Raney nickel provided both the desulfurized product (**32**) and the product resulting from overreduction (**33**).

Can. J. Chem. Downloaded from www.nrcresearchpress.com by 213.200.69.106 on 09/08/12
For personal use only.

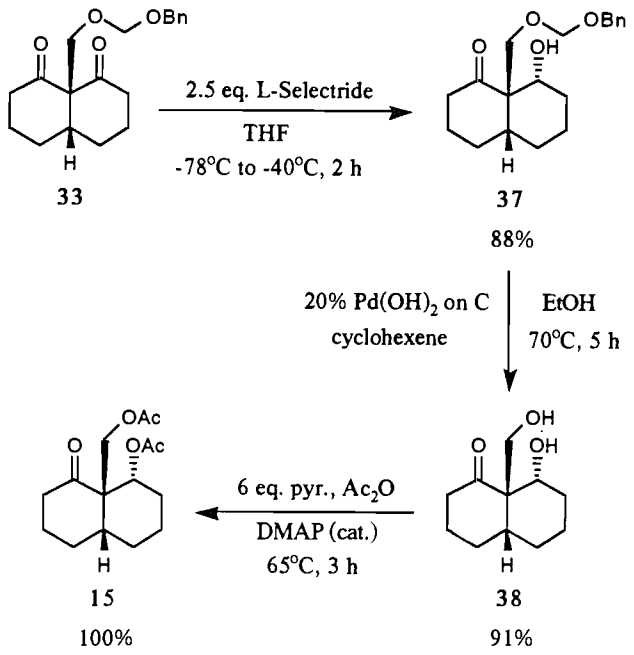

SCHEME 7

These same reaction conditions could also be applied to ketal **34**, which was obtained in 53% yield, together with 35% recovered starting material, from compound **22** via a variation of the Noyori (17) reaction conditions (13). When ketal **34** was treated with Raney nickel in absolute ethanol for 4 days, a 1:2 mixture of enone **35** and compound **36** was produced in 90% yield. Enone **35** was also obtained in 60% yield together with 18% recovered **32** by subjecting compound **32** to the modified Noyori (17) reaction conditions. The symmetrical diketone **33** and the two ketals **34** and **35** served as intermediates in the preparation of the angularly functionalized decalin compounds **15**–**17**.

Preparation of keto diacetate ***15***

The synthesis of compound **15** began with the reduction of ketone **33** with L-Selectride, which afforded keto-alcohol **37** in 88% yield (see Scheme 7). D_2O exchange indicated that the proton α to the newly formed secondary alcohol was axial (J = 11.1 Hz and J = 3.7 Hz). Since the substrate is a *cis*-fused decalin, there are two possible chair–chair conformers: one in which the secondary (equatorial) alcohol is *cis* to the protected hydroxymethylene unit, **37c** in Fig. 1, and the other where the two moieties exist in a *trans* relationship, **37t** in Fig. 1. A sterically hindered base such as L-Selectride would be expected to approach the *cis*-fused decaline from the convex face, thus leading to the formation of **37t**, where the secondary alcohol and the protected hydroxymethylene moiety are oriented *trans* to each other. The relative stereochemistry was later established as *trans* through the X-ray structure determination[3] **40**, thus confirming that indeed α alcohol **37** was formed in the L-Selectride reduction.

Subsequent catalytic hydrogenolysis (18) of keto-alcohol **37** with 20% palladium hydroxide on carbon in ethanol at 70°C using cyclohexene as a hydrogen source provided keto-diol **38** in 91% yield. Keto-diol **38** was treated with pyridine in acetic anhydride in the presence of a catalytic amount of DMAP (19) to give the corresponding diacetate (**15**) in quantitative yield (see Scheme 7).

Compound **37** could also be acetylated to provide the monoacetate (**39**) in 75% yield (see Scheme 8).

Keto-diol **38** was converted to its isopropylidene derivative by treatment with 2,2′-dimethoxypropane in dry acetone in the presence of 10-camphorsulfonic acid (20) at room temperature to provide the crystalline ketal **40** in 90% yield (see Scheme 9 and Fig. 2).

Preparation of keto diacetate ***16***

The keto diacetate **16** was prepared starting from intermediate **35**. The conjugate addition of an excess of lithium dimethylcuprate to enone **35** gave, after 4 h at −35°C, the β-alkylated ketone **41** as a single isomer in 95% yield after purification (see Scheme 10). The approach of the lithium dimethylcuprate reagent from the α face would have been sterically hindered due to the concave nature of the *cis*-fused decaline. The crude ketone **41** could be directly treated with lithium aluminum hydride in ether at 0°C for 3 h to provide the alcohol (**42**) in 89% overall yield for the two steps after purification. The alcohol is a 3:1 mixture of isomers.

When the alcohol mixture (**42**) was subjected to mildly acidic treatment (5% HCl) for 3 h at room temperature, keto-alcohols **43***a* and **43***b* were obtained in a 3:1 ratio in 80% combined yield.

The keto-alcohols (**43***a* and **43***b*) proved to be suitable candidates for nOe experiments, which served to establish the stereochemistry of the secondary alcohols (see Fig. 3). The ^{1}H nmr spectrum of the major isomer (**43***a*) in $CDCl_3$ solvent is rather complex with most of the proton signals appearing together in selected narrow regions of the spectrum. However, the ^{1}H nmr spectrum run in C_6D_6 was simplified, allowing the individual proton signals to be more easily distinguished. Thus an nOe experiment was carried out in C_6D_6, which confirmed the structure of **43***a* to be as shown in Scheme 10.

The mutual enhancement of the signals of protons H_a and H_b suggests that these protons are both axial, thus indicating that the secondary alcohol and the benzyloxymethoxymethylene moiety exist in a *trans* relationship in the major keto-alcohol isomer **43***a*. The β orientation of the methyl group, already alluded to earlier, is further confirmed by the fact that irradiation of this signal enhances the signals of both the H_a and H_b protons.

Similarly for the minor isomer (**43***b*), the ^{1}H nmr spectrum of the compound in C_6D_6 solvent proved to be less complex than the ^{1}H nmr spectrum of the same compound in $CDCl_3$. An nOe experiment was carried out to establish the stereochemistry of compound **43***b*. In this case there was no mutual enhancement of protons H_a and H_b or of proton H_a and the methyl group. Irradiation of the methyl group signal did effect a 6% enhancement of the signal of proton H_b. Irradiation of the proton H_b signal effected a 3% enhancement of the methyl group signal. It was thus concluded that the structure of keto-alcohol isomer **43***b* is as shown in Scheme 10 and that in this case the secondary alcohol and the benzyloxymethylene functionality exist in a *cis* relationship.

The keto-alcohol major isomer **43***a* was then subjected to hydrogenolysis conditions (18) to give, after 20 h at 70°C,

[3]We thank Dr. Rosi Hynes from the McGill X-ray Facility for the X-ray structure determination.

Can. J. Chem. Downloaded from www.nrcresearchpress.com by 213.200.69.106 on 09/08/12
For personal use only.

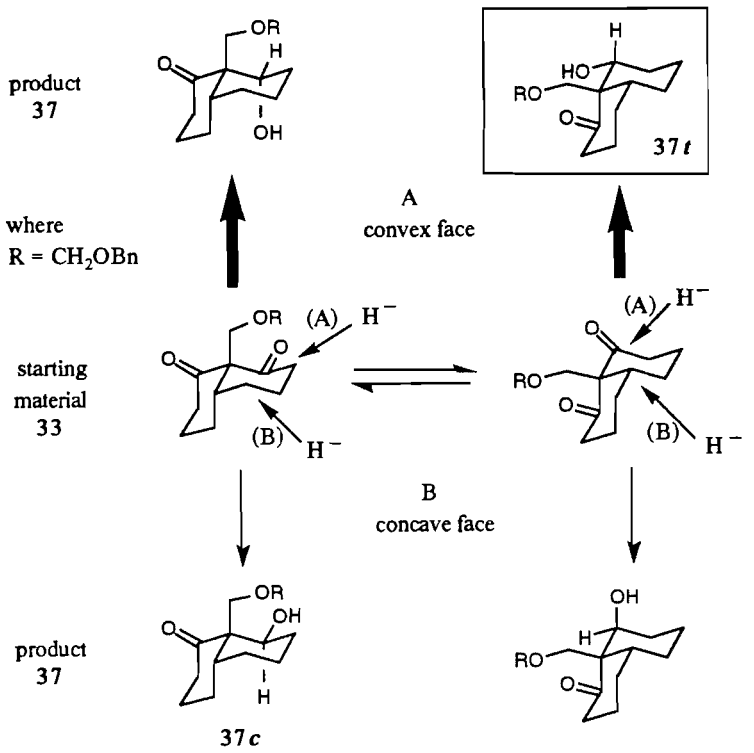

FIG. 1

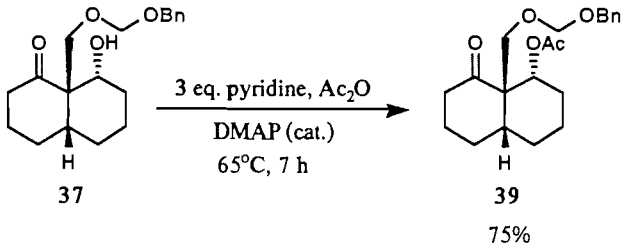

SCHEME 8

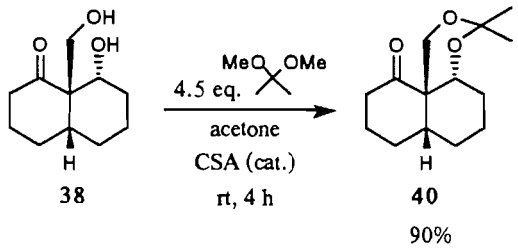

SCHEME 9

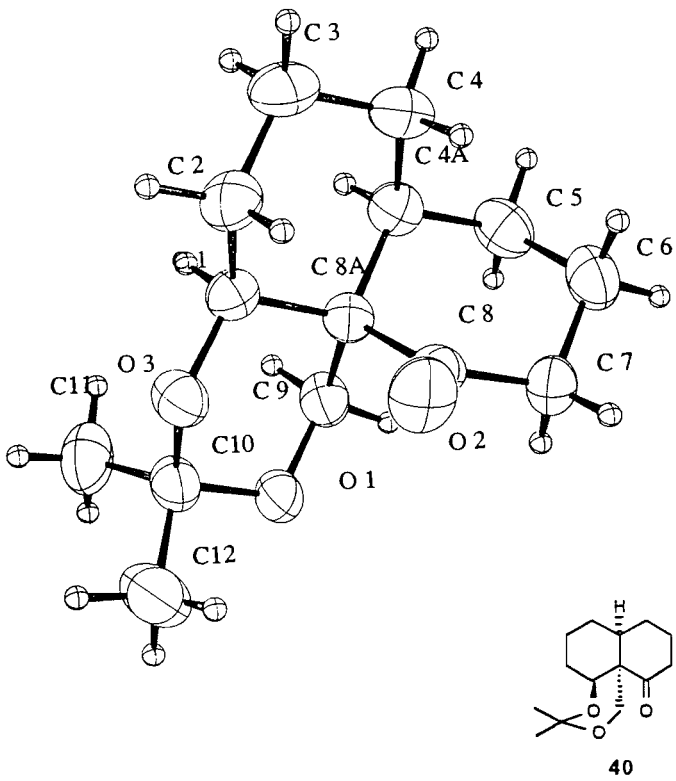

FIG. 2

65% of keto-diol **44***a* together with 35% recovered **43***a*. The keto-diol **44***a* was then treated with acetic anhydride in pyridine in the presence of a catalytic amount of dimethylaminopyridine (19) to afford the monomethyl keto diacetate **16**.

Preparation of keto diacetate 17

The ketal **34** served a precursor to the *gem*-dimethyl decalin compound **17**. When the ketal was treated with 2 equivalents of lithium dimethylcuprate the β-alkylated enone **45** was produced in 86% yield after stirring for 3 h at −30°C. When a larger excess of lithium dimethylcuprate was employed, the desired β,β-dialkylated ketone **46** was formed in 85% yield after purification (see Scheme 11). The crude product could be directly treated with lithium aluminum hydride to provide alcohol **47** in 78% overall yield for the two steps after purification (see Scheme 12).

Can. J. Chem. Downloaded from www.nrcresearchpress.com by 213.200.69.106 on 09/08/12
For personal use only.

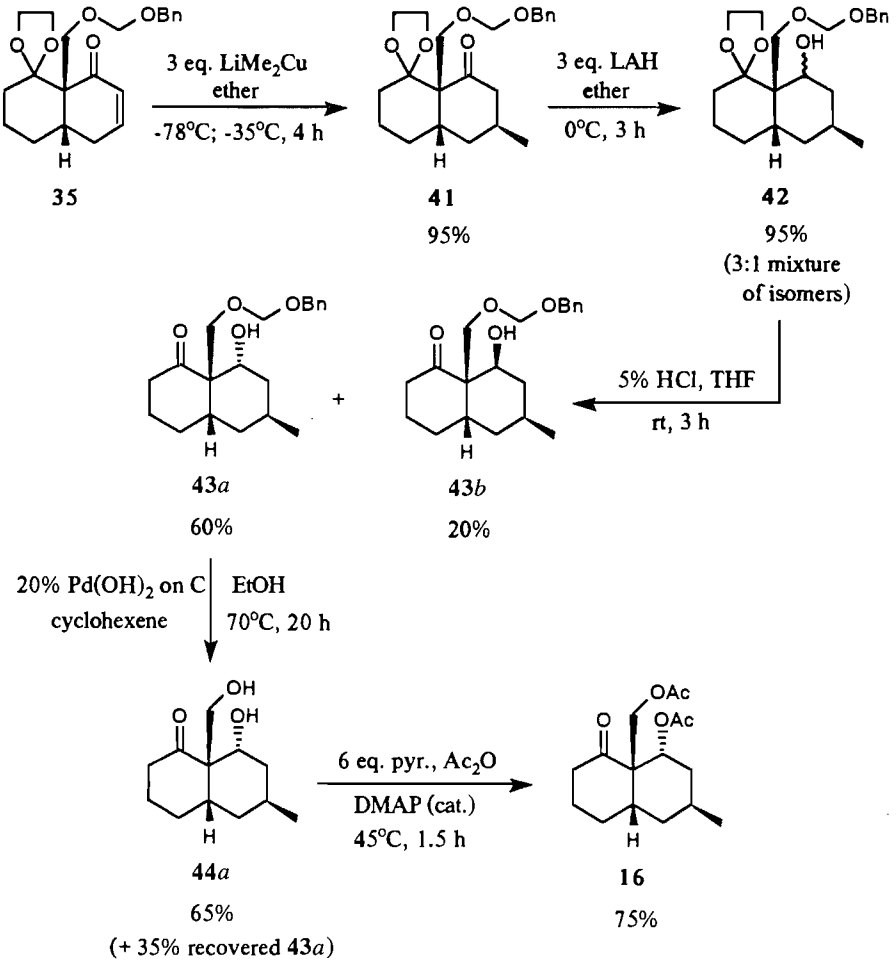

SCHEME 10

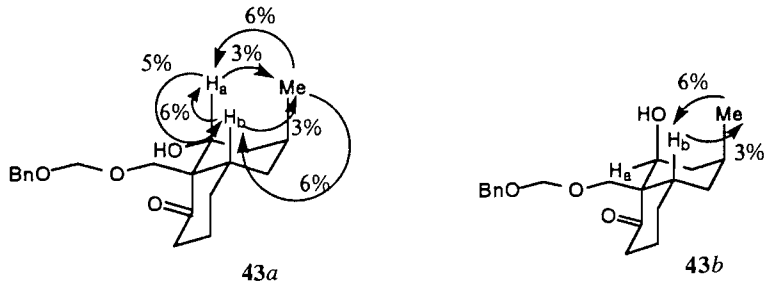

FIG. 3

The alcohol was then subjected to the catalytic hydrogenolysis conditions (18), which produced a mixture of three products together with 35% recovered starting material as shown in Scheme 12. The desired keto-diol **48** was formed in 20% yield along with 15% keto-alcohol **49** and 7% of the diol **50** with the protected carbonyl. Compound **50** could be deprotected under mildly acidic conditions (5% HCl) to provide 95% of the desired keto-diol **48**. Keto-alcohol **49** could be resubjected to the reaction conditions to provide the keto-diol **48** in quantitative yield. The stereochemistry of keto-diol **48** was confirmed by an X-ray structure determination (see Fig. 4).[4]

[4]We thank Dr. J. Britten from the McGill X-ray Facility for the X-ray structure determination.

Keto-diol **48** was then treated wth 2:1 acetic anhydride:dichloromethane in pyridine containing a catalytic amount of DMAP (19) to provide, after 1.5 h at room temperature, a mixture of the monoacetate **51** and the desired diacetate **17** (see Scheme 13). When monoacetate **51** was resubjected to the reaction conditions at 45°C for 1.5 h it was smoothly transformed into the diacetate **17** in 95% yield.

Biological assay

Four sets of biological assays were conducted on 23 of the synthetic compounds. Each set involved the simultaneous bioassay of six compounds plus a control and used 350 larvae, except the 4th set which had only five compounds plus a control and used 300 larvae. Each bioassay involved feed-

Can. J. Chem. Downloaded from www.nrcresearchpress.com by 213.200.69.106 on 09/08/12
For personal use only.

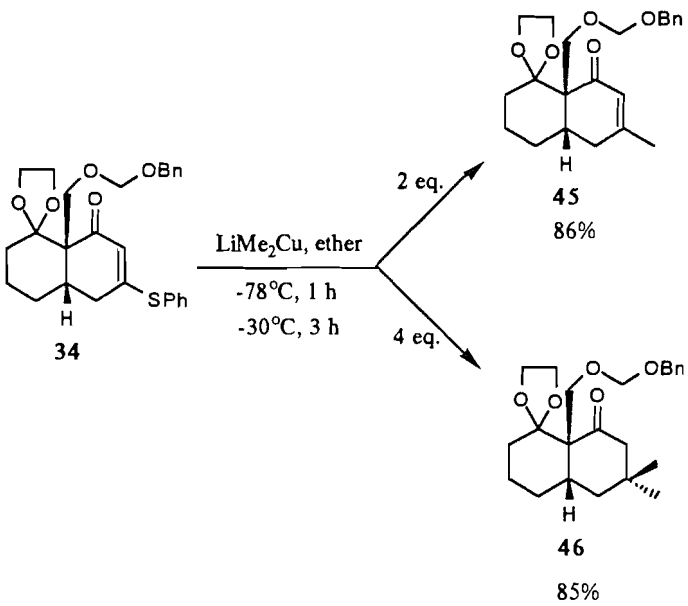

SCHEME 11

ing laboratory-colony spruce budworm larvae on artificial diet (21) containing 0.2% (wet weight) of the test compounds. In each bioassay, newly emerged larvae were reared individually at 26°C, 17 h photoperiod, 50 replicates per test compound. At the point when approximately 50% of the control larvae had reached the final (6th) instar, all the larvae were sacrificed and their developmental stage determined. Because the data were nonparametric, the rank transformation approach, RT-1 (22), was used prior to statistical analysis. For each set of data, the entire set of observations was ranked from smallest to largest, with the least developed larvae, instar 2, having rank 1, the second least developed, instar 3, having rank 2, etc. Average ranks were assigned in the case of ties (23). A one-way analysis of variance on the rank values allowed us to test for differences between compounds using the F-test; when significant differences were detected, a Tukey-type multiple comparison test, using rank sums, was performed to locate the differences (23, 24). For each set of bioassays, the compounds are listed in descending order according to their mean rank values (Tables 1–4). Compounds in the same set having the same code were not significantly different at the 5% level ($P > 0.05$) in their effect on the development rate of budworm larvae. Because the mean rank values, per se, have no biological meaning, mean instar values and the proportion of 6th instars are included in Tables 1–4. Both variables showed the same trend as the ranked values; as mean rank values decreased, both mean instar and the proportion of 6th instars decreased.

Discussion

The biological assay showed that the development of larvae reared from second instar on test diets was significantly retarded by compounds **22**, **30**, **31**, **32**, **35**, **37**, and **28**, but not by the other compounds. The level of activity of compounds, **30**, **35**, **37**, and **28** is comparable to that of the specionin analog **10**, as well as compounds **11–14** reported previously by our laboratory (1, 11). However, the activity of compounds **22** and **32** is slightly better than the activity of the latter compounds. The activity of compound **31** is superior to the activity exhibited by all the other compounds.

Several conclusions can be drawn from the structure–activity relationship observed. The nature of the oxygen function is of critical importance, with the hydroxy and ketal groups generally giving the inactive compounds, with the exception of the moderate activity demonstrated by compounds **35** and **37**. Surprisingly, the diacetates **15**, **16**, and **17** showed no significant activity. It was expected that since both the *trans*- and *cis*-fused epoxy diacetate decalins **6** and **7** synthesized by Ley and co-workers (9) showed definite activity against *Locusta migratoria*, the diacetates **15–17** would also show some activity against *Choristoneura fumiferana*. This suggests that the oxirane functionality at C-8 contributes signficantly to the activity. Interestingly, the simple decalins **28**, **22**, and **32**, featuring an angular benzyloxymethoxymethyl moiety, are active. The definite activity exhibited by compound **31** may be due to the presence of a nitrile functionality in this molecule.

For all the compounds (**46**, **45**, **47**, **16**, **41**, **48**, **17**) bearing a methyl group at the C-3 position, little or no biological activity was observed. Equally interesting is the observation that all of the active compounds (except **37**) in the present series are conjugated enones. It is possible that the ability to alkylate a biological nucleophile by the oxygen function is required for biological activity. Thus, the presence of either an oxirane (as in clerodine and specionin), dihydrofuran (as in azadirachtin and clerodin), or an enone (for Michael addition) may fulfill this role. We intend to further investigate the structure–activity relationship.

Conclusion

The biological activity exhibited by the simple decalins **22**, **28**, and **32** suggests that the angular benzyloxymethoxymethyl moiety and the enone function may be in part responsible for the observed activity. The nitrile functionality also promotes activity, as illustrated by the definite biological activity exhibited by decalin **31**.

Experimental

Melting points were determined on a Gallenkamp block and are uncorrected. The ^{1}H nmr spectra were taken on Varian XL-200 and XL-300 instruments and the data are reported in ppm relative to the $CHCl_3$ reference line with the multiplicity, coupling constants, and the number of protons given in parentheses. The ^{13}C nmr spectra were recovered on a Varian XL-300 (75.4 MHz) spectrometer. The ir spectra were obtained on an Analect AQS-18 FT-IR instrument. Solution spectra were obtained using sodium chloride solution cells of 0.2 mm thickness. Low-resolution mass spectra were recorded on a Du Pont 21-492B mass spectrometer operating at an ionization potential of 70 eV or on a Hewlett–Packard 5980A mass spectrometer using ammonia chemical ionization and are reported as m/z (relative intensity %). All high-resolution mass spectra were recorded on a ZAB 2F HS instrument using ammonia chemical ionization. Column chromatography was performed on Merck silica gel 60 (230–400 mesh). For all moisture-sensitive reactions, glassware was oven-dried at ca. 200°C and cooled in a desiccator. X-ray diffraction measurements were made on a Rigaku AFC6S diffractometer and the calculations were performed using the NRCVAX (25) and the TEXSAN (26) crystallographic software packages.

3-Phenylthio-8-(methoxycarbonyl)oxy-2,4,4a,5,6,7-hexahydronaphthalene-1-one (29)

To a solution of decalin **20** (0.203 g; 0.744 mmol) in 15 mL THF at 0°C under argon was added KO*t*Bu (0.086 g; 0.768 mmol).

Can. J. Chem. Downloaded from www.nrcresearchpress.com by 213.200.69.106 on 09/08/12
For personal use only.

Can. J. Chem. Downloaded from www.nrcresearchpress.com by 213.200.69.106 on 09/08/12
For personal use only.

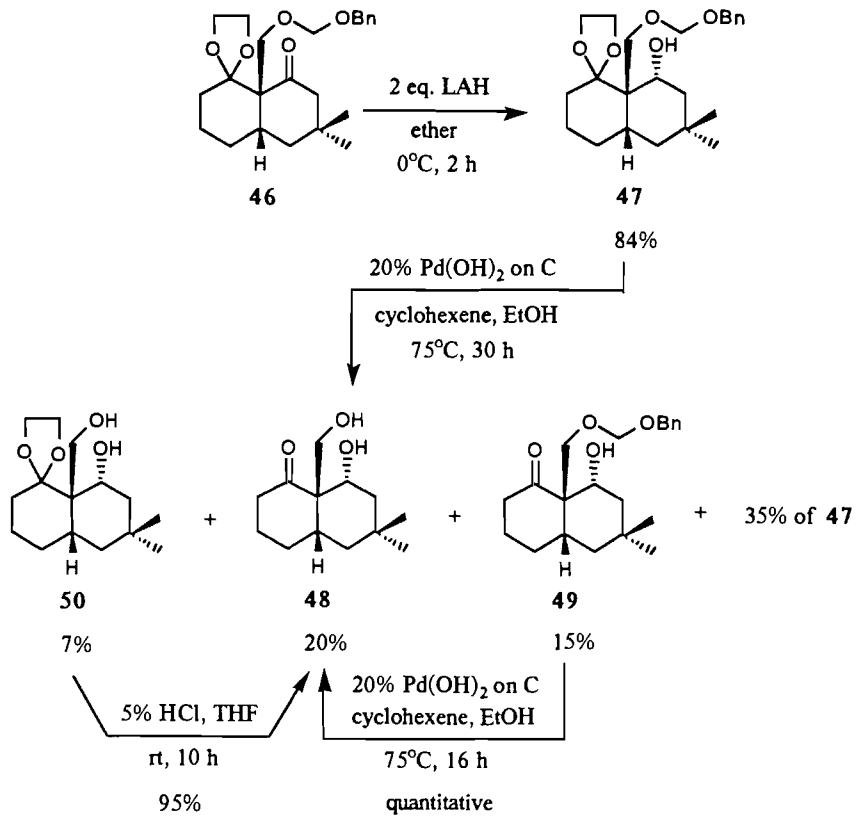

SCHEME 12

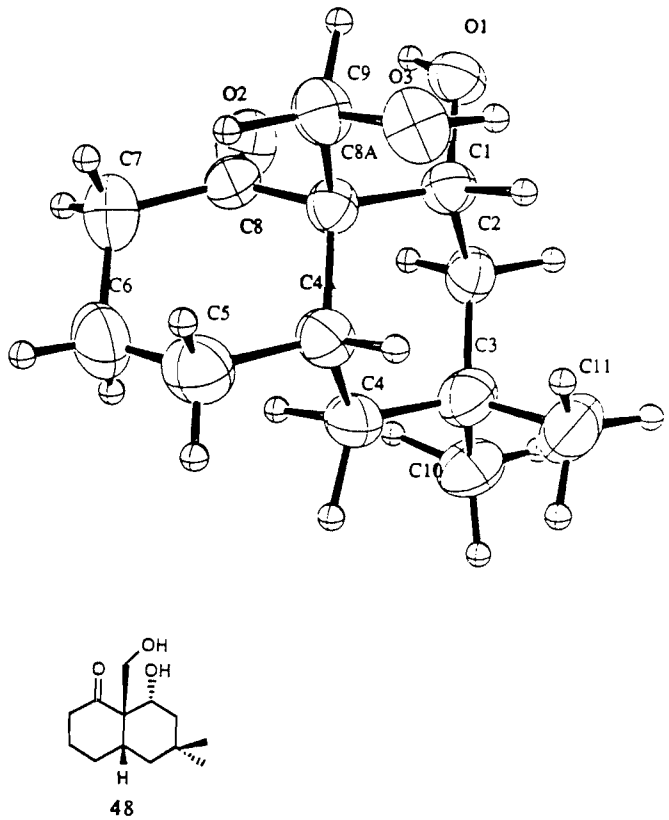

FIG. 4

After 20 min methyl chloroformate (0.17 mL; 2.22 mmol) was added. The reaction mixture was stirred for 1 h and then quenched by the addition of saturated ammonium chloride solution. The mixture was extracted with ether (3 × 25 mL) and the combined extracts were dried ($MgSO_4$), filtered, and the solvent removed to provide 0.260 g crude material. Column chromatography (1:4 EtOAc:hexane) provided the O-alkylated product **29** (0.228 g, 93%) as a beige oil that crystallized on standing (mp 77–78°C); ir ($CHCl_3$, cm^{-1}): 3012, 1762, 1664, 1608, 1586, 1443, 1268, 1196, 784; ^1H nmr ($CDCL_3$, ppm): 7.36–7.53 (m, 5H), 5.42 (s, 1H), 3.80 (s, 3H), 2.80–3.03 (m, 1H), 2.40–2.55 (m, 2H), 2.26–2.39 (m, 2H), 1.55–2.07 (m, 4H); ^{13}C nmr ($CDCl_3$, ppm): 183.8, 163.6, 153.8, 152.5, 135.3, 130.1, 129.8, 127.8, 122.2, 121.9, 55.1, 36.7, 35.7, 29.3, 29.0, 20.3; ms: 330 (19, M^+), 270(32), 77(23), 55(25), 44(100), 31(75), 28(34).

*1-(Methoxycarbonyl)oxy-3-phenylthio-7-methoxycarbonyl-8-hydroxy-4,4a,5,6-tetrahydronaphthalene (**30**) and 3-phenylthio-8-(methoxycarbonyl)oxy-8-cyano-2,4,4a,5,6,7-hexahydronaphthalene-1-one (**31**)*

Potassium *tert*-butoxide (0.050 g; 0.44 mmol) was added to a solution of *E* Michael adduct **19***E* (0.124 g; 0.41 mmol) in 5 mL THF at 0°C under argon. After stirring for 20 min, methyl cyanoformate (0.18 mL; 2.27 mmol) was added. The reaction mixture was allowed to warm to room temperature and stirred for 8 h. The red mixture was then diluted with 5 mL ether and quenched with 10 mL water. The aqueous layer was extracted with ether (3 × 15 mL) and the combined organic extracts were dried ($MgSO_4$), filtered, and the solvent removed to provide 0.127 g crude material. Column chromatography (1:4 EtOAc: hexane) provided **30** (0.036 g, 23%) and **31** (0.038 g, 29%), along with some recovered decalin **20** (0.042 g, 38%).

30: ir (neat, cm^{-1}): 2948, 1752, 1743, 1709, 1603, 1582, 1437,

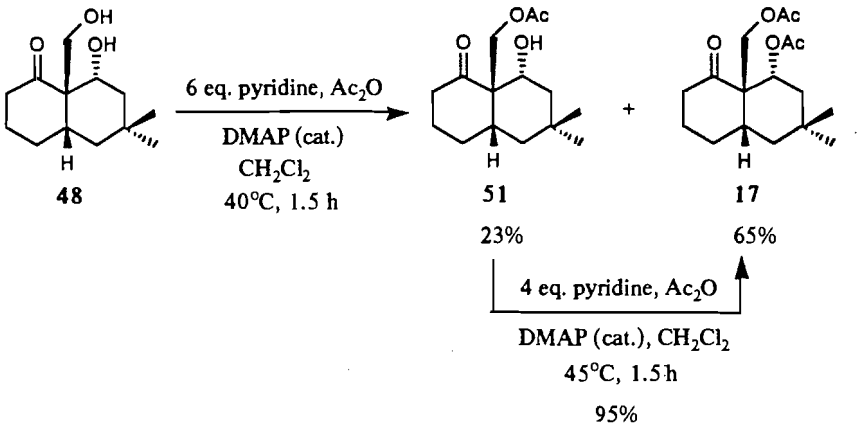

SCHEME 13

TABLE 1. Biological assays

Compound	Code	Mean instar	% of 6th instars
Control	a	5.36	42
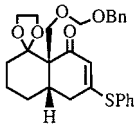 **34**	a	5.32	42
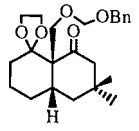 **46**	a	5.30	50
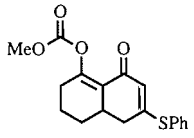 **29**	ab	5.06	24
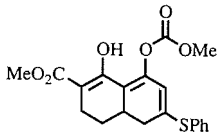 **30**	b	4.87	18
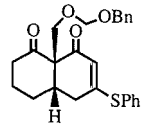 **22**	c	4.28	0
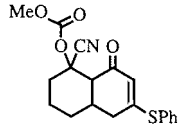 **31**	c	3.52	0

TABLE 2. Biological assays

Compound	Code	Mean instar	% of 6th instars
Control	a	5.00	36
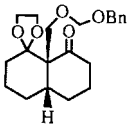 **36**	ab	4.80	30
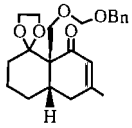 **45**	ab	4.56	32
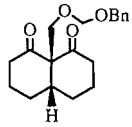 **33**	ab	4.50	14
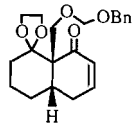 **35**	b	4.42	10
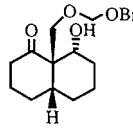 **37**	b	4.38	14
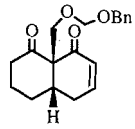 **32**	bc	4.18	10

Can. J. Chem. Downloaded from www.nrcresearchpress.com by 213.200.69.106 on 09/08/12
For personal use only.

TABLE 3. Biological assays

Compound	Code	Mean instar	% of 6th instars
Control	a	5.64	70
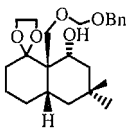 **47**	ab	5.48	56
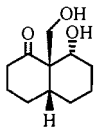 **38**	ab	5.46	52
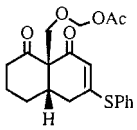 **23**	ab	5.30	50
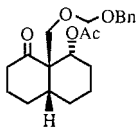 **39**	ab	5.28	48
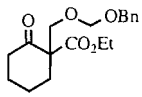 **25**	ab	5.28	46
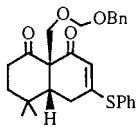 **28**	b	5.22	34

TABLE 4. Biological assays

Compound	Code	Mean instar	% of 6th instars
Control	a	5.54	60
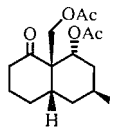 **16**[a]	a	5.24	54
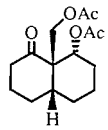 **15**	a	5.12	48
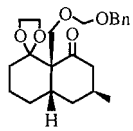 **41**	a	5.10	34
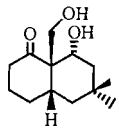 **48**[a]	a	5.08	40
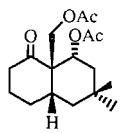 **17**	a	4.96	38

[a]Tested at 0.1% wet weight.

1234, 1192, 1175, 1147; ^{1}H nmr ($CDCl_3$, ppm): 7.43–7.55 (m, 5H), 5.24 (s, 1H), 3.83 (s, 3H), 3.58 (s, 3H), 1.08–3.05 (m, 7H); ^{13}C nmr ($CDCl_3$, ppm): 165.4, 162.4, 152.9, 135.7, 130.1, 129.9, 129.1, 117.8, 111.8, 55.2, 50.9, 40.6, 35.0, 30.8, 22.3; ms: 389(29, M + H^+), 272(86), 208(52), 172(26), 163(31), 147(55), 135(100), 134(71), 110(80), 109(43), 77(55), 59(23), 55(31), 41(25).

31: ir ($CHCl_3$, cm^{-1}): 3028, 2950, 2361, 1757, 1666, 1577, 1442, 1285, 1245, 1181; ($CDCl_3$, ppm): 7.42 (s, 5H), 5.45 (s, 1H), 3.76 (s, 3H), 1.25–3.10 (m, 9H); ^{13}C nmr ($CDCl_3$, ppm): 189.2, 165.1, 152.6, 135.5, 130.5, 130.0, 127.5, 120.6, 118.1, 70.6, 55.9, 55.2, 37.1, 34.9, 34.2, 31.5, 19.0; ms: 375 (19, M + NH_4^+), 358 (100, M + H^+), 282(60).

*3-Phenylthio-8-(methoxycarbonyl)oxy-8-cyano-2,4,4a,5,6,7-hexahydronaphthalene-1-one (**31**)*

Potassium *tert*-butoxide (0.195 g; 1.74 mmol) was added to a solution of decalin **20** (0.330 g; 1.20 mmol) in 15 mL THF at 0°C under argon. After stirring for 20 min at 0°C, methyl cyanoformate (0.80 mL; 10.1 mmol) was added and the reaction mixture was allowed to warm to room temperature and stirred for 30 h. The red mixture was then diluted with 200 mL ether and quenched with 200 mL saturated ammonium chloride solution. The aqueous layer was extracted with ether (3 × 75 mL) and the combined extracts were dried ($MgSO_4$), filtered, and the solvent removed to provide 0.460 g crude material. Column chromatography (1:4 EtOAc:hexane) provided the product **31** (0.192 g, 48%) along with some recovered decalin **20** (0.079 g, 25%). See procedure above for spectral data of **31**.

Ethylene ketal of cis-*8a-[[(benzyloxy)methoxy]methyl]-4a,5,6,8a-tetrahydronaphthalene-1,8(4*H*,7*H*)-dione (**35**) and ethylene ketal of* cis-*8a-[[(benzyloxy)methoxy]methyl]-3,4,4a,5,6,8a-hexahydronaphthalene-1,8-(2*H*,7*H*)-dione (**36**)*

To a solution of the ethylene ketal **34** (0.224 g; 0.48 mmol) in 17 mL absolute ethanol at room temperature under argon was added Raney nickel (1.421 g). The mixture was stirred for 4 days at room temperature at which time the catalyst was removed by filtration and the solvent removed to provide 0.198 g crude material. Column chromatography (1:4 EtOAc:hexane) provided **35** (0.065 g, 37%) and **36** (0.109 g, 62%).

35: ir ($CHCl_3$, cm^{-1}): 3012, 2949, 1662, 1217, 1078; ^{1}H nmr ($CDCl_3$, ppm): 7.28–7.35 (m, 5H), 6.92–7.06 (m, 1H), 6.06(d, J = 10 Hz, 1H), 4.73 and 4.70 (AB, J = 6 Hz, 2H), 4.55 (s, 2H), 4.39 (AB, J = 10 Hz, 1H), 3.65–3.89 (m, 5H), 2.78–2.98 (m, 2H), 2.05–2.30 (m, 1H), 1.39–1.99 (m, 6H); ^{13}C nmr ($CDCl_3$, ppm): 200.3, 150.3, 138.0, 130.6, 128.4, 127.9, 127.6, 110.8,

Can. J. Chem. Downloaded from www.nrcresearchpress.com by 213.200.69.106 on 09/08/12
For personal use only.

Can. J. Chem. Downloaded from www.nrcresearchpress.com by 213.200.69.106 on 09/08/12
For personal use only.

95.2, 69.5, 67.1, 65.1, 64.6, 56.6, 33.7, 32.7, 29.2, 25.5, 18.8; ms: 359(25, M + H^+), 329(19), 251(93), 189(100). Exact Mass calcd. for $C_{21}H_{26}O_5$ + H^+: 359.1857; found: 359.1858.

36: ir ($CHCl_3$, cm^{-1}): 2958, 1734, 1699, 1457, 1232, 1077; ^1H nmr ($CDCl_3$, ppm): 7.27–7.45 (m, 5H), 4.75 and 4.70(AB, J = 6 Hz, 2H), 4.57 (s, 2H). 4.34 (AB, J = 9.5 Hz, 1H), 3.65–3.90 (m, 5H), 1.39–2.59 (m, 13H); ^{13}C nmr ($CDCl_3$, ppm): 210.5, 138.0, 128.5, 128.3, 127.8, 127.6, 110.1, 95.2, 69.5, 67.1, 66.2, 64.1, 59.6, 42.1, 37.0, 32.8, 26.9, 26.8, 23.8, 19.2; ms: 361 (10, M + H^+), 331(24), 329(13), 254(17), 253(100), 223(10). Exact Mass calcd. for $C_{21}H_{28}O_5$ + H^+: 361.2017; found: 361.2015.

Ethylene ketal of cis-*8a-[[(benzyloxy)methoxy]methyl]-4a,5,6,8a-tetrahydronaphthalene-1,8(4*H*,7*H*)-dione (35)*

To a solution of trimethylsilyltriflate (0.01 mL; 0.052 mmol) in 0.10 mL CH_2Cl_2 at −78°C under argon was added 1,2-bis(trimethylsiloxy)ethane (1.70 mL; 6.93 mmol), followed by the starting material **32** (0.075 g; 0.24 mmol) in 0.40 mL CH_2Cl_2. The reaction mixture was then slowly warmed to −45°C and stirred at this temperature for 20 h. The mixture was then further warmed to −15°C and stirred for an additional 20 h. The reaction was then quenched by the addition of pyridine (0.02 mL; 0.25 mmol) at −15°C, and poured into saturated sodium bicarbonate. The aqueous layer was extracted with ether (3 × 10 mL) and the combined extracts were dried ($MgSO_4$), filtered, and the solvent removed to provide 0.090 g crude material. Column chromatography 1:4 EtOAc:hexane) provided the product **35** (0.050 g, 60%) as a clear oil. For spectral data: see the preceding experiment.

cis-*8a-[[(Benzyloxy)methoxy]methyl]-1α-hydroxy-1,3,4,4a,5,6,8a-septahydronaphthalene-8(2*H*,7*H*)-one (37)*

To a solution of the starting material **33** (0.222 g; 0.701 mmol) in 11.5 mL THF at −78°C under argon was added 1 M L-Selectride (1.75 mL; 1.75 mmol). The solution was stirred for 1 h at −78°C, followed by 2 h at −40°C. The reaction mixture was then diluted with 10 mL ether and quenched with 10 mL saturated ammonium chloride solution at −40°C. The organic layer was separated and the aqueous layer was extracted with ether (3 × 15 mL). The combined extracts were dried ($MgSO_4$), filtered, and the solvent removed to provide 0.425 g crude material. Column chromatography (1:4 EtOAc:hexane) provided the keto-alcohol **37** (0.197 g, 88%) as a clear oil; ir ($CHCL_3$, cm^{-1}): 3500, 2939, 1694, 1453, 1288, 1028, 748, 697; ^1H nmr ($CDCl_3$, ppm): 7.31–7.44 (m, 5H), 4.79 (s, 2H), 4.62 (s, 2H), 3.98 (s, 2H), 3.49–3.51 (m, 2H), 1.25–2.50 (m, 13H); D_2O exchange clarifies the multiplet at 3.49–3.51 to: 3.51 (dd, J = 11.8 Hz and J = 4.4 Hz, 1H); ^{13}C nmr ($CDCl_3$, ppm): 217.0, 137.7, 128.4, 128.0, 127.8, 95.0, 72.8, 69.7, 67.3, 58.3, 40.1, 39.2, 31.9, 28.3, 25.4, 23.8, 21.5; ms: 319 (37, M^+), 289(8) (212)(18), 211(100). Exact Mass calcd. for $C_{19}H_{26}O_4$ (M^+): 319.1910; found: 319.1909.

cis-*8a-(Hydroxymethyl)-1α-hydroxy-1,3,4,4a,5,6,8a-septahydronaphthalene-8(2*H*,7*H*)-one (38)*

To a solution of the keto-alcohol **37** (0.148 g; 0.46 mmol) in 6.5 mL absolute ethanol was added 20% palladium hydroxide on carbon (0.282 g), followed by cyclohexene (6.60 mL; 65.7 mmol). The mixture was heated to 70°C and stirred for 5 h. The catalyst was then removed by filtration and the solvent removed. Column chromatography (1:1 EtOAc:hexane) provided the keto-diol **38** (0.085 g, 91%); ir ($CHCl_3$, cm^{-1}): 3505, 3015, 2947, 1693, 1226, 1066, 792; ^1H nmr ($CDCL_3$, ppm): depending on the concentration of the sample in $CDCl_3$, the spectrum is either 4.43 (t, J = 11.5 Hz, 1H), 3.87 (t, J = 9.8 Hz, 2H), 3.80 (d, J = 10 Hz, 1H), 3.47 (dt, J = 4.4 Hz and J = 11.5 Hz, 1H), 2.54–2.79 (m, 1H), 1.16–2.38 (m, 12H) or ^1H nmr ($CDCl_3$, ppm): 4.39 (d, J = 11 Hz, 2H), 3.85 (d, J = 11.5 Hz, 3H), 3.42 (dd, J = 11 Hz and J = 2 Hz, 1H), 2.54–2.79 (m, 1H), 1.16–2.38 (m, 12H); D_2O exchange: 4.38 (d, J = 11.5 Hz, 1H), 3.77–3.97 (m, 1H), 3.36–3.52 (dd, J = 3.8 Hz and J = 11.2 Hz, 1H); ^{13}C nmr ($CDCl_3$, ppm): 217.2, 80.5, 71.5, 57.9, 40.8; 39.6, 32.3, 28.2, 25.8, 23.9, 22.1; ms: 216 (11, M + NH_4^+), 200 (22, M + $2H^+$), 199 (100, M + H^+).

cis-*8a-[[(Benzyloxy)methoxy]methyl]-1α-acetoxy-1,3,4,4a,5,6,8a-septahydronaphthalene-8(2*H*,7*H*)-one (39)*

To a solution of the monoalcohol **37** (0.060 g; 0.19 mmol) in 1.80 mL acetic anhydride at room temperature under argon was added pyridine (0.05 mL; 0.62 mmol), followed by dimethylaminopyridine (0.0210 g; 0.17 mmol). The mixture was heated to 70°C and stirred at this temperature for 48 h, by which time the yellow solution had turned brown. The mixture was allowed to cool to room temperature, was diluted with ether (2 mL), and quenched with saturated ammonium chloride solution (5 mL). The aqueous layer was extracted with ether (3 × 10 mL) and the combined ether extracts were dried ($MgSO_4$), filtered, and the solvent removed to provide the monoacetate **39** (0.049 g, 75%) as a clear oil; ir (neat, cm^{-1}): 2931, 2867, 1749, 1714, 1453, 1378, 1233, 1105, 1029, 738, 699; ^1H nmr ($CDCl_3$, ppm); 7.24–7.38 (m, 5H), 4.86 (dd, J = 3.8 Hz and 8.2 Hz, 1H), 4.71 and 4.67 (AB, J = 8 Hz, 2H), 4.55 (s, 2H), 3.94 and 3.70 (AB, J = 9.4 Hz, 2H), 2.11–2.63 (m, 3H), 2.00 (s, 3H), 1.28–1.96 (m, 8H); ^{13}C nmr ($CDCl_3$, ppm): 211.2, 170.1, 137.6, 128.4, 127.8, 127.7, 95.1, 76.6, 74.0, 69.6, 68.3, 56.2, 40.4, 37.4, 27.2, 26.1, 22.5, 21.4, 19.9; ms: 378 (34, M + NH_4^+), 361 (4, M + H^+), 348(8), 331(25), 281(6), 271(26), 254(16), 253(100), 223(26), 193(22), 179(6), 163(6), 151(7), 108(6). Exact Mass calcd. for $C_{21}H_{28}O_5$ + H^+: 361.2017; found: 361.2015.

cis-*8a-Oxymethyl-9,1α,*O*-isopropylidene-1,3,4,4a,5,6,8a-septahydronaphthalene-8-(2*H*,7*H*)-one (40)*

To a solution of the starting material **38** (0.062 g; 0.311 mmol) in 2.0 mL spectrograde acetone under argon at room temperature was added 2,2′-dimethoxypropane (0.17 mL; 1.40 mmol) and a catalytic amount of camphor sulphonic acid. The mixture was stirred at room temperature for 3 h, at which time a few drops of concentrated aqueous ammonium hydroxide were added and the solvent was evaporated. Ether and water were added and the aqueous layer was extracted with ether. The combined ether extracts were dried ($MgSO_4$), filtered, and the solvent evaporated to provide 0.068 g crude material. The crude material was purified by simply filtering it through a silica gel plug to provide the product **40** (0.068 g, 90%) as white crystals (mp 86–88°C); ir ($CHCl_3$, cm^{-1}): 2944, 1711, 1453, 1384, 1234, 1197, 1102, 1059; ^1H nmr ($CDCl_3$, ppm): 4.43 and 3.83 (AB, J = 12 Hz, 2H), 3.51 (dd, J = 4.2 Hz and 12 Hz, 1H), 2.69–2.87 (m, 1H), 2.05–2.33 (m, 2H), 1.54–2.05 (m, 10H), 1.44 (s, 3H), 1.36 (s, 3H); ^{13}C nmr ($CDCl_3$, ppm): 210.5, 99.5, 75.7, 69.4, 52.9, 41.4, 39.1, 29.7, 27.5, 27.1, 25.2, 24.1, 22.6, 18.6; ms: 256 (7, M + NH_4^+), 239 (100, M + H^+), 181(19), 151(9). Exact Mass calcd. for $C_{14}H_{22}O_3$ + H^+: 239.1647; found: 239.1648.

X-ray structure determination of ***40***

The data were collected on a Rigaku AFC6S diffractometer with a graphite monochromator with CuKα radiation (λ = 1.5405 Å). The linear absorption coefficient for CuKα is 6.4 cm^{-1}. Cell constants and an orientation matrix for data collection, obtained by least squares using the setting angles of 22 reflections with 2θ angle in the range 84.00–109.00°, corresponded to a monoclinic cell with dimensions: a = 6.7423(4) Å; b = 16.354(2) Å; c = 12.149(1) Å; β = 105.012(7)°; V = 1293.9(2) $Å^3$. For Z = 4 and F. W. = 238.32, the calculated density is 1.223 Mg/m^3. The space group was determined to be $P2_1/n$. The data were collected at a temperature of 20 ± 1°C using the ω–2θ scan technique to a maximum 2θ value of 110.0°. A correction for secondary extinction (coefficient = 1.917373) was applied; σ = 0.077671. The standard intensities dropped an average of 2.83%; merging R = 0.9% for 163 symmetry equivalent pairs. No correction was made for absorption. The structure was solved by direct methods. All non-H atoms were refined anisotropically and H atoms were found in a difference map and refined isotropically. Full-matrix least-squares refinement converged to R = 0.036, R_w = 0.035. The standard

Can. J. Chem. Downloaded from www.nrcresearchpress.com by 213.200.69.106 on 09/08/12
For personal use only.

deviation of an observation of unit weight was 4.82. The maximum shift/σ ratio was 0.032. The weighting scheme was based on counting statistics. The weight modifier K in KF_o^2 is 0.000010. The maximum and minimum peaks on the final difference Fourier map correspond to 0.14 and −0.13 e/Å^3, respectively. All calculations were made with the NRCVAX (25) crystallographic software package. Figure 2 was prepared from the output of ORTEPII (27).

cis-*8a-Acetoxymethyl-1α-acetoxy-1,3,4a,4,5,6,8a-septahydronaphthalene-8(2H,7H)-one* (**15**)

To a solution of the diol **38** (0.028 g; 0.14 mmol) in 2.0 mL acetic anhydride at room temperature under argon was added pyridine (0.070 mL; 0.87 mmol), followed by a catalytic amount of dimethylaminopyridine. The mixture was heated at 50°C and stirred for 3 h at which time the reaction was complete. The mixture was allowed to cool down and was then diluted with ether (2 mL) and quenched with saturated ammonium chloride solution (5 mL). The aqueous layer was extracted with ether (3 × 10 mL). The combined ether extracts were dried ($MgSO_4$), filtered, and the solvent was removed to provide 0.059 g crude material. Column chromatography (eluting first with 1:4 EtOAc:hexane and then with 1:1 EtOAc:hexane) provided the diacetate **15** as a pale orange oil (0.054 g, quantitative) that crystallized on standing (mp 83–85°C); ir ($CHCl_3$, cm^{-1}): 3029, 2947, 1741, 1736, 1374, 1233, 1212, 1042, 784; ^{1}H nmr ($CDCl_3$, ppm): 4.76 (dd, J = 3.7 Hz and J = 9.5 Hz, 1H), 4.36 (s, 2H), 2.41–2.59 (m, 2H), 2.04 (s, 3H), 2.02 (s, 3H), 1.37–2.39 (m, 11H); ^{13}C nmr ($CDCl_3$, ppm): 210.0, 170.6, 170.2, 73.7, 63.6, 55.5, 40.4, 38.2, 27.2, 27.1, 26.1, 22.6, 21.4, 20.8, 20.3; ms: 300 (100, M + NH_4^+), 283 (9, M + H^+), 223(33). Exact Mass calcd. for $C_{15}H_{22}O_5$ + H^+: 283.1544; found: 283.1544.

Ethylene ketal of cis-*8a-[[(benzyloxy)methoxy]methyl]-3β-methyl-4,4a,5,6,8a-pentahydronaphthalene-1,8(2H,7H)-dione* (**41**)

To a suspension of cuprous iodide (0.1224 g; 0.62 mmol) in 1.3 mL dry ether at −35°C under argon was added 1.4 M MeLi (0.89 mL; 1.25 mmol). The mixture was then cooled to −78°C and the starting enone **35** (0.075 g; 0.21 mmol) in 3.3 mL dry ether was added. After stirring at −78°C for 15 min, the reaction mixture was warmed to −35°C and stirred for 4 h. The reaction was then quenched by the addition of saturated ammonium chloride solution (4.0 mL). The aqueous phase was extracted with ether (3 × 10 mL) and the combined ether extracts were dried ($MgSO_4$), filtered, and the solvent removed. Column chromatography (1:4 EtOAc:hexane) provided the monomethyl product **41** (0.076 g, 95%) as a clear oil; ir ($CHCl_3$, cm^{-1}): 2958, 1711, 1456, 1229, 1170, 1041, 720; ^{1}H nmr ($CDCl_3$, ppm): 7.25–7.34 (m, 5H), 4.72 (s, 2H), 4.58 (s, 2H), 4.19 (AB, J = 10 Hz, 1H), 3.78–3.95 (m, 5H), 1.30–2.61 (m, 12H), 0.98 (d, J = 6.5 Hz, 3H); ^{13}C nmr ($CDCl_3$, ppm): 210.8, 138.0, 128.4, 127.8, 127.7, 110.4, 95.3, 70.3, 69.6, 64.6, 63.9, 59.7, 48.9, 34.2, 32.2, 28.9, 27.5, 25.5, 21.4, 20.4; ms: 375 (19, M + H^+), 345(13), 268(17), 267(100), 237(12). Exact Mass calcd. for $C_{22}H_{30}O_5$ + H^+: 375.2172; found: 375.2171.

Ethylene ketal of cis-*8a-[[(benzyloxy)methoxy]methyl]-1α-hydroxy-3β-methyl-1,4,4a,5,6,8a-hexahydronaphthalene-8(2H,7H)-one* (**42**)

To a solution of the crude starting material **41** (0.073 g; 0.20 mmol) in 9.0 mL ether at 0°C under argon was added lithium aluminum hydride (0.024 g; 0.62 mmol). After stirring for 3 hr at 0°C, the reaction was quenched with 5 mL saturated ammonium chloride solution. The aqueous layer was extracted with ether (3 × 10 mL ether) and the combined ether extracts were dried ($MgSO_4$), filtered, and the solvent removed. Column chromatography of the crude material (1:4 EtOAc:hexane) provided the product **42** (0.077 g, 89% from enone **35**), a pale yellow oil, as a mixture of two isomers in a ratio of 3:1. These isomers could not be separated in an EtOAc:hexane or a benzene:acetone solvent system and were thus carried on to the next step as a mixture; ir ($CHCl_3$, cm^{-1}): 3494, 2952, 1456, 1176, 1081, 1041; ^{1}H nmr ($CDCl_3$, ppm): 7.30–7.41 (m, 5H), 4.76 and 4.79 (two s in a 3:1 ratio, 2H), 4.61 and 4.64 (two s in a 3:1 ratio, 2H), 4.13–4.37 (m, 1H), 3.83–4.08 (m, 4H), 3.74–3.82 (m, 2H), 1.10–2.80 (m, 12H), 0.88 and 0.95 (two d in a 1:3 ratio, J = 6.2 Hz, 3H); D_2O exchange simplifies one of the multiplets to: 1.10–2.56 (m, 11H); ^{13}C nmr ($CDCl_3$, ppm): 138.0, 128.4, 128.0, 127.7, 114.4, 95.4, 69.5, 69.0, 65.6, 64.9, 63.7, 47.6, 38.9, 38.3, 36.1, 33.7, 30.4, 27.3, 25.2, 22.5. All signals in the ^{13}C nmr spectrum are doubled.

cis-*8a-[[(Benzyloxy)methoxy]methyl]-1α-hydroxy-3β-methyl-1,4,4a,5,6,8a-hexahydronaphthalene-8(2H,7H)-one* (**43**a) *and* cis-*8a-[[(benzyloxy)methoxy]methyl]-1β-hydroxy-3β-methyl-1,4,4a,5,6,8a-hexahydronaphthalene-8-(2H,7H)-one* (**43**b)

To a solution of the alcohol mixture **42** (0.065 g; 0.17 mmol) in 1.20 mL THF at room temperature was added 5% HCl (0.39 mL; 0.54 mmol). After stirring for 4 h at room temperature, sodium bicarbonate solution and ether were added. The aqueous layer was extracted with ether and the combined ether extracts were dried ($MgSO_4$), filtered, and the solvent removed. Column chromatography (1:3 EtOAc:hexane) of the crude material provided the keto-alcohols **43***a* (0.034 g, 60%) and **43***b* (0.011 g, 20%).

43*a*: ir ($CHCl_3$, cm^{-1}): 2949, 1691, 1457, 1111, 1036; ^{1}H nmr ($CDCl_3$, ppm): 7.25–7.42 (m, 5H), 4.78 (s, 2H), 4.60 (s, 2H), 3.93 and 3.78 (AB, J = 9.2 Hz, 2H), 3.69–3.85 (m, 1H), 1.35–2.90 (m, 12H), 1.20–1.35 (m, 1H), 0.97 (d, J = Hz, 3H); ^{1}H nmr (200 MHz, C_6D_6): 7.10–7.50 (m, 5H, hidden under C_6D_6 solvent), 4.69 and 4.64 (AB, J = 6 Hz, 2H), 4.61 and 4.55 (AB, J = 11.2 Hz, 2H), 3.93 and 3.69 (AB, J = 9 Hz, 2H), 3.75 (dt, J = 3 Hz and J = 8 Hz, 1H), 2.40–2.54 (m, 1H), 2.33 (t, J = 6 Hz, 2H), 2.10–2.25 (m, 1H), 1.82–2.06 (m, 1H), 1.48–1.82 (m, 4H), 1.24–1.46 (m, 2H), 1.01–1.17 (m, 1H), 0.84 (d, J = 6.8 Hz, 3H); ^{13}C nmr ($CDCl_3$, ppm): 216.6, 137.7, 128.4, 128.0, 127.7, 95.0, 69.7, 69.6, 67.8, 57.3, 40.6, 38.3, 34.7, 33.8, 26.2, 24.7, 21.9, 19.7.

43*b*: ^{1}H nmr ($CDCl_3$, ppm): 7.26–7.44 (m, 5H), 4.77 (s, 2H), 4.62 (s, 2H), 4.15–4.18 (dd, J = 4 Hz and J = 10 Hz, 1H), 4.11 and 3.85 (AB, J = 10 Hz, 2H), 3.09 (d, J = 5 Hz, 1H), 2.34–2.72 (m, 2H), 2.16–2.34 (m, 1H), 1.65–2.09 (m, 5H), 1.16–1.65 (m, 4H), 0.94 (d, J = 6.6 Hz, 3H); ^{1}H nmr (200 MHz, C_6D_6): 7.06–7.46 (m, 5H, hidden under C_6D_6 solvent), 4.68 (s, 2H), 4.50 (s, 2H), 4.32 and 3.88 (AB, J = 10 Hz, 2H), 3.88–3.99 (m, 1H), 2.94 (d, J = 5.2 Hz, 1H), 2.25–2.37 (m, 1H), 2.03–2.24 (m, 1H), 1.74 (dt, J = 4 Hz and J = 12 Hz, 1H), 1.32–1.61 (m, 4H), 1.01–1.21 (m, 4H), 0.78 (d, J = 6 Hz, 3H); ^{13}C nmr ($CDCl_3$, ppm): 215.2, 137.9, 128.5, 128.1, 127.8, 95.2, 70.1, 69.8, 66.5, 56.9, 39.3, 38.5, 38.3, 35.5, 27.0, 26.6, 24.4, 22.2.

cis-*8a-Hydroxymethyl-1α-hydroxy-3β-methyl-1,4,4a,5,6,8a-hexahydronaphthalene-8(2H,7H)-one* (**44**a)

To a solution of the alcohol **43***a* (0.018 g; 0.05 mmol) in 0.8 mL absolute ethanol under argon was added 20% palladium hydroxide on carbon (0.030) g) and cyclohexene (0.80 mL; 7.9 mmol). The mixture was stirred at 70°C for 20 h, whereupon the catalyst was removed by filtration through a Celite pad. Column chromatogrpahy (1:3 EtOAc:hexane) of the crude material provided the keto-diol **44***a* (0.009 g, 65%) together with some recovered keto-monoalcohol **43***a* (0.006 g, 35%).

44*a*: ir ($CHCl_3$, cm^{-1}): 3503, 2949, 1693, 1421, 1230, 1073; ^{1}H nmr ($CDCl_3$, ppm): 4.38 (t, J = 11.7 Hz, 1H), 3.70–3.90 (m, 3H), 3.34 (d, J = 11.7 Hz, 1H), 2.55–2.73 (m, 1H), 2.26–2.43 (m, 1H), 1.82–2.22 (m, 5H), 1.45–1.74 (m, 3H), 1.14–1.34 (m, 2H), 0.98 (d, J = 7.2 Hz, 3H); D_2O simplifies the region downfield of 3.5 ppm to: 4.27 and 3.84 (AB, J = 11.7 Hz, 2H), 3.82 (dd, J = 3 Hz and J = 8 Hz, 1H); ^{13}C nmr ($CDCl_3$, ppm): 218.0, 75.0, 70.5, 57.9, 40.0, 37.9, 35.3, 34.0, 26.3, 26.1, 22.4, 18.7.

cis-*8a-Acetoxymethyl-1α-acetoxy-3β-methyl-1,4,4a,5,6,8a-hexahydronaphthalene-8(2H,7H)-one* (**16**)

To a solution of the methyl keto-diol **44***a* (0.016 g; 0.075 mmol) in 1.50 mL acetic anhydride under argon was added pyridine (0.04 mL; 0.50 mmol) and a catalytic amount of DMAP. The

Can. J. Chem. Downloaded from www.nrcresearchpress.com by 213.200.69.106 on 09/08/12
For personal use only.

mixture was stirred at 45°C for 1.5 h, whereupon saturated ammonium chloride solution and ether were added. The aqueous layer was extracted with ether and the ether extracts were dried ($MgSO_4$), filtered, and the solvent removed. Column chromatography (1:3 EtOAc:hexane) of the crude material afforded the diacetate **16** (0.017 g, 75%); ir ($CHCl_3$, cm^{-1}): 2949, 1731, 1702, 1458, 1378, 1248, 1035; ^1H nmr ($CDCl_3$, ppm): 4.86 (br t, J = 3 Hz, 1H), 4.27 and 4.22 (AB, J = 10.6 Hz, 2H), 2.45–2.63 (m, 1H), 2.10 (s, 6H), 1.07–2.37 (m, 11H), 0.88 (d, J = 6.1 Hz, 3H); ^{13}C nmr ($CDCl_3$, ppm): 211.7, 170.6, 169.0, 74.2, 64.4, 53.1, 40.9, 35.9, 35.6, 35.0, 27.4, 22.5, 21.8, 21.4, 20.9; ms: 314 (100, M + NH_4^+), 237(40). Exact Mass calcd. for $C_{16}H_{24}O_5 + H^+$: 297.1073; found: 297.2702.

Ethylene ketal of cis-*8a-[[(benzyloxy)methoxy]methyl]-3-methyl-4a,5,6,8a-tetrahydronaphthalene-1,8(4*H,7H*)-dione (**45**)*

To a suspension of copper iodide (0.030 g; 0.16 mmol) in 0.50 mL dry ether at −30°C under argon was added 1.4 M MeLi (0.23 mL; 0.32 mmol). The first few drops cause the appearance of a bright yellow precipitate, due to the presence of excess copper iodide. As one approaches the "end-point," this precipitate disappears. Enough MeLi is added so that there is only a slight excess of copper iodide. The mixture was then cooled down to −78°C and the protected enone **44** (0.041 g; 0.088 mmol) in 1.5 mL dry ether was added, causing the mixture to turn orange and thicken. The mixture was stirred for 1 h at −78°C and then quenched by the addition of saturated ammonium chloride solution at −30°C and extracted with ether (3 × 10 mL). The organic extracts were dried ($MgSO_4$), filtered, and the solvent removed to provide 0.031 g crude material. Column chromatography (1:4 EtOAc:hexanes) provided the product **45** (0.027 g, 86%) as a clear oil; ir ($CHCl_3$, cm^{-1}): 3016, 1654, 1205, 1026, 774, 738, 675; ^1H nmr ($CDCl_3$, ppm): 7.29–7.40 (m, 5H), 5.91 (s, 1H), 4.73 and 4.68 (AB, J = 8 Hz, 2H), 4.55 (s, 2H), 4.38 (AB, J = 10 Hz, 1H), 3.67–3.86 (m, 5H), 2.78–2.95 (m, 2H), 1.94 (s, 3H), 1.50–2.05 (m, 7H); ^{13}C nmr ($CDCl_3$, ppm): 198.8, 162.1, 138.0, 128.4, 127.9, 127.6, 127.5, 110.8, 95.2, 69.5, 67.2, 65.1, 64.6, 55.1, 34.3, 33.5, 32.9, 25.5, 24.5, 18.7; ms: 373 (55, M + H^+), 265(100), 203(50). Exact Mass calcd. for $C_{22}H_{28}O_5 + H^+$: 373.2014; found: 373.2015.

Ethylene ketal of cis-*8a-[[(benzyloxy)methoxy]methyl]-3,3-dimethyl-2,4a,5,6,8a-pentahydronaphthalene-1,8(4*H,7H*)-dione (**46**)*

To a suspension of copper iodide (0.206 g; 1.09 mmol) in 4 mL dry ether at −30°C under argon was added 1.4 M MeLi (1.5 mL; 2.13 mmol). The mixture was cooled down to −78°C and a solution of the ketal **34** (0.130 g; 0.278 mmol) in 2.0 mL dry ether was added. The thick orange mixture was stirred for 15 min at −78°C, followed by 4 h at −30°C. The reaction was then quenched by the addition of saturated ammonium chloride solution at −30°C and extracted with ether (3 × 10 mL). The combined ether extracts were dried ($MgSO_4$), filtered, and the solvent removed to provide 0.099 g crude material. Column chromatography provided the β,β-dialkylated product **46** (0.091 g, 85%) as a clear oil, which crystallized (mp 79–80°C) upon standing; ir ($CHCl_3$, cm^{-1}): 2958, 1696, 1229, 1049, 759; ^1H nmr ($CDCl_3$, ppm): 7.22–7.43 (m, 5H), 4.72 (q, J = 6 Hz, 2H), 4.57 (s, 2H), 4.38 (AB, J = 10 Hz, 1H), 3.67–3.84 (m, 5H), 2.74–2.88 (m, 1H), 2.11–2.50 (m, 4H), 1.34–1.90 (m, 5H), 1.13–1.28 (m, 1H), 1.01 (s, 3H), 0.93 (s, 3H); ^{13}C nmr ($CDCl_3$, ppm): 211.0, 138.1, 128.4, 128.0, 127.6, 110.0, 95.2, 69.5, 67.0, 64.1, 64.0, 58.0, 55.7, 40.5, 33.1, 32.6, 32.3, 31.4, 26.8, 26.5, 18.8; ms: 388 (7, M^+), 297(32), 267(47), 112(70), 99(99), 91(100), 86(86), 55(48), 41(30), 28(39). Exact Mass calcd. for $C_{23}H_{32}O_5 + H^+$: 389.2329; found: 389.2328.

Ethylene ketal of cis-*8a-[[(benzyloxy)methoxy]methyl]-1α-hydroxy-3,3-dimethyl-1,4,4a,5,6,8a-hexahydronaphthalene-1,8(2*H,7H*)-dione (**47**)*

To a solution of the crude starting material **46** (0.114 g; 0.294 mmol) in 8.0 mL ether at 0°C under argon was added lithium aluminum hydride (0.024 g; 0.63 mmol). The mixture was stirred for 2.5 h at 0°C and then diluted with more ether (5 mL) and quenched with saturated ammonium chloride solution (7 mL). The aqueous layer was extracted with ether (3 × 10 mL) and the ether extracts were dried ($MgSO_4$), filtered, and the solvent evaporated to provide 0.099 g crude material. Column chromatograph (1:4 EtOAc:hexane) provided the alcohol **47** (0.085 g, 78% from ketal **34**) as a pale yellow oil; ir ($CHCl_3$, cm^{-1}): 3493, 3009, 2965, 1455, 1208, 1168, 1107, 1034, 1006, 924; ^1H nmr ($CDCl_3$, ppm): 7.22–7.41 (m, 5H), 4.82 (s, 2H), 4.63 (s, 2H), 3.65–4.18 (m, 8H), 2.12–2.31 (m, 1H), 1.99 (t, J = 17 Hz, 2H), 1.40–1.80 (m, 6H), 1.10–1.31 (m, 1H), 0.95 (s, 3H), 0.94 (s, 3H); ^{13}C nmr ($CDCl_3$, ppm): 138.0, 128.4, 128.0, 127.7, 114.3, 95.2, 70.6, 69.6, 67.9, 63.5, 62.2, 46.8, 44.1, 40.3, 33.2, 31.8, 31.3, 30.8, 26.4, 26.0, 18.5; ms: 391 (22, M + H^+), 373(23), 329(18), 299(57), 284(18), 283(100), 269(42), 265(31), 253(20), 251(8), 238(10), 237(64), 235(23), 222(15), 221(77), 191(11), 175(41), 99(20). Exact Mass calcd. for $C_{23}H_{34}O_5 + H^+$: 391.2483; found: 391.2485.

cis-*8a-(Hydroxymethyl)-1α-hydroxy-3,3-dimethyl-1,4,4a,5,6,8a-hexahydronaphthalene-8(2*H,7H*)-one (**48**)*

To a solution of the protected dimethyl monoalcohol **47** (0.089 g; 0.228 mmol) in 2.2 mL absolute ethanol was added 20% palladium hydroxide on carbon (0.151 g), followed by cyclohexene (4.70 mL; 46.5 mmol). After stirring the mixture overnight at 70°C, the catalyst was removed by filtration and the solvent removed, providing 0.035 g crude material. Column chromatography (1:1 EtOAc:hexane) provided the dimethyl keto-diol **48** (0.011 g, 20%) as a white solid (mp 149–151°C), the protected dimethyl diol **50** (0.005 g, 7%) as a white solid (mp 120–121°C), the deprotected dimethyl keto-alcohol **49** (0.011 g, 15%), and some recovered starting material **47** (0.031 g, 35%). Resubjecting **49** to the reaction conditions provided **48** in quantitative yield.

48: ir ($CHCl_3$, cm^{-1}): 3511, 1691, 1223, 1074, 785; ^1H nmr ($CDCl_3$, ppm): 4.38–4.52 (br d, J = 11 Hz, 1H), 3.88 (d, J = 11 Hz, 1H), 3.60–4.09 (m, 3H), 2.57–2.79 (m, 1H), 2.07–2.36 (m, 2H), 1.88–2.07 (m, 2H), 1.61 (d, J = 9.2 Hz, 2H), 1.21–1.50 (m, 3H), 0.90–1.12 (m, 1H), 0.93 (s, 3H), 0.90 (s, 3H); D_2O exchange: 4.40 (d, J = 11.5 Hz, 1H), 3.87 (d, J = 11.5 Hz, 1H), 3.66 (br t, J = 8 Hz, 1H); ^{13}C nmr ($CDCl_3$, ppm): 217.3, 77.4, 71.5, 57.5, 44.7, 41.1, 39.4, 36.5, 32.9, 31.4, 25.6, 24.7, 22.1; ms: 244 (7, M + NH_4^+), 228 (26, M + $2H^+$), 227 (100, M + H^+), 209(5). Exact Mass calcd. for $C_{13}H_{22}O_3 + H^+$: 227.1647; found: 227.1647.

49: ^1H nmr ($CDCl_3$, ppm): 7.35 (s, 5H), 4.82 (s, 2H), 4.64 (s, 2H), 4.00 (s, 2H), 3.49–3.81 (m, 2H), 1.05–2.55 (m, 11H), 0.95 (s, 3H), 0.93 (s, 3H).

50: ir ($CHCl_3$, cm^{-1}): 3510, 2959, 1418, 1199, 1118, 1016; ^1H nmr ($CDCl_3$, ppm): 4.40 and 3.57 (AX, J = 11.8 Hz, 2H), 3.80–4.18 (m, 7H), 1.88–2.06 (m, 2H), 1.35–1.83 (m, 7H), 1.18–1.30 (m, 1H), 0.93 (s, 6H), 0.75–0.88 (m, 1H).

*Preparation of dimethyl keto-diol **48** from the ketal **50***

To a solution of the ketal **50** (0.023 g; 0.082 mmol) in 0.40 mL THF at room temperature was added 5% HCl (0.18 mL; 0.25 mmol). After stirring for 10 h at room temperature, sodium bicarbonate solutions and ether were added. The aqueous layer was extracted with ether and the combined ether extracts were dried ($MgSO_4$), filtered, and the solvent removed. Column chromatography (1:2 EtOAc:hexane) of the crude material provided the keto-diol **48** (0.022 g, 95%). The spectral data for the keto-diol are given at the end of the preceding experimental procedure.

*X-ray structure determination of **48***

All measurements were made on a Rigaku AFC6S diffractometer with graphite monochromated CuKα radiation (λ = 1.54178 Å). Cell constants and an orientation matrix for data collection, obtained from a least-squares refinement using the setting angles of 16 carefully centered reflections in the range $21.22° < < 37.88°$, corresponded to a triclinic cell with dimensions a = 8.455(6) Å; b = 12.68(1) Å; c = 6.241(8) Å; V = 621(1) $Å^3$; α = 96.8 (1)°;

Can. J. Chem. Downloaded from www.nrcresearchpress.com by 213.200.69.106 on 09/08/12
For personal use only.

$\beta = 105.25(8)°$; $\gamma = 101.94(8)°$. For $Z = 2$ and F. W. = 226.31, the calculated density is 1.210 g/cm^3. Based on packing considerations, a statistical analysis of intensity distribution, and the successful solution and refinement of the structure, the space group was determined to be $P\bar{1}$ (no. 2). The data were collected at a temperature of 20 ± 1°C using the ω–2θ scan technique to a maximum 2θ value of 119.6° Omega scans of several intense reflections, made prior to data collection, had an average width at half-height of 0.59° with a take-off angle of 6.0°. Scans of $(1.78 + 0.30 \tan \theta)°$ were made at a speed of 32.0°/min (in omega). The weak reflections ($I < 10.0\sigma(I)$) were rescanned (maximum of 2 rescans) and the counts were accumulated to assure good counting statistics. Stationary background counts were recorded on each side of the reflection. The ratio of peak counting time to background counting time was 2:1. The intensities of three representative reflections that were measured after every 150 reflections remained constant throughout data collection. No decay correction was applied. The linear absorption coefficient for CuKα is 6.4 cm^{-1}. An empirical absorption correction, using the program DIFABS (28), was applied, which resulted in transmission factors ranging from 0.61 to 1.49. The data were corrected for Lorentz and polarization effects. The structure was solved by direct methods. Full-matrix least-squares refinement with anisotropic factors given to all non-H atoms converged to $R = 0.055$, $R_w = 0.037$. The standard deviation of an observation of unit weight was 4.04. The weighting scheme was based on counting statistics and included a factor ($p = 0.00$) to downweight the intense reflections. The maximum shift/error in the final cycle was 0.00. The maximum and minimum peaks on the final difference Fourier map correspond to 0.18 and −0.21 e/Å^3, respectively. Neutral atom scattering factors were taken from Cromer and Waber (29). Anomalous dispersion effects were included in F_{calc} (30); the values for $\Delta f'$ and $\Delta f''$ were those of Cromer (31). All calculations were performed using the TEXSAN (26) crystallographic software package of Molecular Structure Corporation. Figure 4 was prepared from the output of ORTEPII (27).[5]

cis-*8a-(Acetoxymethyl)-1α-acetoxy-3,3-dimethyl-1,4,4a,5,6,8a-hexahydronaphthalene-8(2*H,*7*H)*-one (17)*

To a solution of the dimethyl keto-diol **48** (0.021 g; 0.095 mmol) in 3 mL of 2:1 acetic anhydride:methylene chloride (as the starting material would not dissolve in acetic anhydride alone) under argon at room temperature was added pyridine (0.050 mL; 0.58 mmol) and a catalytic amount of DMAP. The mixture was then stirred at 50°C for 1.5 h, at which time the solvent was removed. To the residue was added ether and saturated ammonium chloride solution. The aqueous layer was extracted with ether and the combined ether extracts were dried ($MgSO_4$), filtered, and the solvent removed to give 0.032 g crude material. Column chromatography (1:10 spectrograde acetone:benzene) provided both the monoacetate **51** (0.006 g, 23%) and the diacetate **17** (0.019 g, 65%). These two compounds were inseparable in an EtOAc:hexane solvent system. Resubjecting the monoacetate to the reaction conditions for 1.5 h at 45°C, with 4 equivalents rather than 6 equivalents of pyridine, smoothly transformed it into the diacetate.

[5]Details of experimental procedures and tables of all atomic positional and thermal parameters, and atomic distances and angles, for the crystallographic structure of compounds **40** and **48** have been deposited as Supplementary Material and may be purchased from: The Depository of Unpublished Data, Document Delivery, CISTI, National Research Council Canada, Ottawa, Canada K1A 0S2.

Tables of positional parameters and atomic distances and angles have also been deposited with the Cambridge Crystallographic Data Centre and can be obtained on request from The Director, Cambridge Crystallographic Data Centre, University Chemical Laboratory, 12 Union Road, Cambridge, CB2 1EZ, U.K.

51: ir ($CHCl_3$, cm^{-1}): 3545, 2958, 1736, 1694, 1419, 1248, 1039; ^{1}H nmr ($CDCl_3$, ppm): 4.71 and 4.37 (AB, J = 11 Hz, 2H), 3.69 (dt, J = 5.1 Hz and 11.7 Hz, 1H), 3.43 (d, J = 11.7 Hz, 1H), 2.09 (s, 3H), 1.01–2.55 (m, 11H), 0.93 (s, 6H); ^{13}C nmr ($CDCl_3$, ppm): 216.2, 170.7, 69.7, 63.1, 60.0, 44.2, 41.0, 40.0, 35.1, 32.9, 31.2, 25.2, 24.7, 21.2, 20.9.

17: ir ($CHCl_3$, cm^{-1}): 2960, 1736, 1728, 1250, 1037; ^{1}H nmr ($CDCl_3$, ppm): 4.98 (dd, J = 4.7 Hz and 12.4 Hz, 1H), 4.48 and 4.37 (AB, J = 11.4 Hz, 2H), 2.05 (s, 3H), 2.00 (s, 3H), 1.00–2.58 (m, 11H), 0.98 (s, 3H), 0.91 (s, 3H); ^{13}C nmr ($CDCl_3$, ppm): 209.0, 170.9, 170.7, 71.1, 63.4, 56.6, 40.4, 40.1, 38.2, 36.4, 32.7, 31.3, 25.5, 25.1, 22.9, 21.3, 20.9; ms: 328 (100, M + NH_4^+), 311 (25, M + H^+), 251(54), 191(21). Exact Mass calcd. for $C_{17}H_{26}O_5 + H^+$: 311.1858; found: 311.1858.

Acknowledgements

Financial support from the Natural Sciences and Engineering Research Council of Canada (NSERC) and le Fonds pour la formation de chercheurs et l'aide à la recherche (FCAR) is gratefully acknowledged. We thank Dr. Rosi Hynes and Dr. Jim Britten from the McGill X-ray Facility for the determination of the X-ray structures of compounds **40** and **48**.

1. T.H. Chan, K.R. Guertin, C.V.C. Prasad, A.W. Thomas, G.M. Strunz, and A. Salonius. Can. J. Chem. **68**, 1170 (1990).
2. D.M. Schmitt, D.G. Grimble, and J.L. Searcy. Managing the spruce budworm in eastern North America. USDA Agriculture Handbook 620. 1984.
3. D.H.R. Barton, H.T. Cheung, A.D. Cross, L.M. Jackman, and M. Martin-Smith. J. Chem. Soc. 5061 (1961).
4. (*a*) I. Kubo, A. Matsumoto, T. Matsumoto, and J.A. Klocke. Tetrahedron, 489 (1986); (*b*) W. Kraus, M. Bokel, A. Klenk, and H. Pohnl. Tetrahedron Lett. **26**, 6435 (1985); (*c*) H.B. Broughton, S.V. Ley, A.M.Z. Slawin, D.J. Williams, and E.D. Morgan, J. Chem. Soc. Chem. Commun. 46 (1986).
5. C.C. Chang and K. Nakanishi. J. Chem. Soc. Chem. Commun. 605 (1983).
6. E. Van Der Eycken, A. Janssens, and M. Vandewalle. Tetrahedron Lett. **28**, 3519 (1987).
7. D.P. Curran, P.B. Jacobs, R.L. Elliot, and B.H. Kim. J. Am. Chem. Soc. **109**, 5280 (1987).
8. Y. Kojima and N. Kato. Tetrahedron, **37**, 2527 (1981).
9. (*a*) W.P. Jackson and S.V. Ley. J. Chem. Soc. Perkin Trans. 1, 1516 (1981); (*b*) S.V. Ley, D. Neuhaus, N.S. Simpkins, and A.J. Whittle. J. Chem. Soc. Perkin Trans. 1, 2157 (1982).
10. (*a*) H.C. Kolb and S.V. Ley. Tetrahedron Lett. **32**, 6187 (1991); (*b*) S.V. Ley, D. Santafianos, W.M. Blaney, and M.S.J. Simmonds. Tetrahedron Lett. **28**, 221 (1987).
11. T.H. Chan, Y.J. Zhang, F. Sauriol, A.W. Thomas, and G.M. Strunz. Can. J. Chem. **65**, 1853 (1987).
12. T.H. Chan and C.V.C. Prasad. J. Org. Chem. **52**, 110 (1987).
13. T.H. Chan and A.E. Schwerdtfeger. J. Org. Chem. **56**, 3294 (1991).
14. R. Trave, L. Garanti, and A. Marchesini. Gazz. Chim. Ital. **93**, 1327 (1963).
15. J.P. Ferris, C.E. Sullivan, and B.G. Wright. J. Org. Chem. **29**, 87 (1964).
16. L.N. Mander and S.P. Sethi. Tetrahedron. Lett. **24**, 5425 (1983).
17. T. Tsunoda, M. Suzuki, and R. Noyori. Tetrahedron Lett. **21**, 1357 (1980).
18. S. Hanessian, T.J. Liak, and B. Vanasse. Synthesis, 396 (1981).
19. G. Hofle, W. Steglich, and H. Vorbruggen. Angew. Chem. Int. Ed. Engl. **17**, 569 (1978).

20. B.P. Bashyal, G.W.J. Fleet, M.J. Gough, and P.W. Smith. Tetrahedron, **43**, 3083 (1987).
21. A. McMorran. Can. Entomol. **97**, 58 (1965).
22. W.J. Conover and R.L. Iman. Am. Stat. **35**, 124 (1981).
23. SAS User's Guide: Statistics, Version, 5, 1985 Edition. SAS Institute Inc., Cary, N.C.
24. J.H. Zar. Biostatistical analysis. 2nd ed. Prentice–Hall, New York. 1984.
25. E.J. Gabe, Y. LePage, J.P. Charland, F.L. Lee, and P.S. White. J. Appl. Crystallogr. **22**, 384 (1989).
26. TEXSAN-TEXRAY Structure Analysis Package, Molecular Structure Corporation. 1985.
27. C.K. Johnson. ORTEPII. Report ORNL-5138, Oak Ridge National Laboratory, Oak Ridge, Tenn. 1976.
28. Walker and Stuart. Acta. Crystallogr. Sect. A: Found. Crystallogr. **A39**, 158 (1983).
29. D.T. Cromer and J.T. Waber. International tables for X-ray crystallography. Vol. IV. The Kynoch Press, Birmingham. 1974. Table 2.2A.
30. J.A. Ibers and W.C. Hamilton. Acta Crystallogr. **17**, 781 (1964).
31. D.T. Cromer. International tables for X-ray crystallography. Vol. IV. The Kynoch Press, Birmingham. 1974. Table 2.3.1.

Can. J. Chem. Downloaded from www.nrcresearchpress.com by 213.200.69.106 on 09/08/12
For personal use only.

Synthèse et propriétés de nouveaux triazaphospholes : les 5-méthylthio 1,2,4,3-triazaphospholes

YOUSSEF KANDRI RODI

Laboratoire de chimie organique hétérocyclique, Avenue Ibn Batouta Faculté des Sciences, Rabat, Maroc

LUCIEN LOPEZ,[1] CHRISTIAN MALAVAUD[1] ET MARIE-THÉRÈSE BOISDON

Synthèse, structure et réactivité de molécules phosphorées, Unité de recherche associée au Centre National de la recherche scientifique n° 454, Université Paul Sabatier, 118 Route de Narbonne, 31062 Toulouse Cédex, France

ET

JEAN-PIERRE FAYET

Laboratoire de chimie des matériaux inorganiques, Unité de recherche associée au Centre National de la recherche scientifique n° 1311, Université Paul Sabatier, 118 Route de Narbonne, 31062 Toulouse Cédex, France

Reçu le 23 juillet 1992[2]

YOUSSEF KANDRI RODI, LUCIEN LOPEZ, CHRISTIAN MALAVAUD, MARIE-THÉRÈSE BOISDON et JEAN-PIERRE FAYET. Can. J. Chem. **71**, 1200 (1993).

La synthèse de nouveaux 1,2,4,3-triazaphospholes est décrite : des 5-méthylthio 1,2,4,3-triazaphospholes substitués en 1, 2 ou 4. Le dérivé substitué en 1,5 **6** est stable tandis que les composés **14** et **16** substitués en position-2,5 sont en équilibre avec leurs tétramères $[\mathbf{14}]_4$ et $[\mathbf{16}]_4$. Les 5-méthylthio 4-alkyl 1,2,4,3-triazaphospholes n'existent que sous leurs formes tétramériques $[\mathbf{12}]_4$ et $[\mathbf{13}]_4$. La complexation dépolymérisante de $[\mathbf{12}]_4$ par un acide de Lewis, conduit au triazaphosphole complexé $\mathbf{12},BF_3$. La position du reste triméthylsilyle du composé **16**, obtenu par silylation de **15**, a été confirmée par RMN de ^{15}N. L'étude de la stabilité de ces systèmes par la méthode MNDO est en accord avec les résultats expérimentaux, comme l'action des 1,4-diaza-1,3-diènes avec les triazaphospholes qui conduit aux dérivés spiranniques du phosphore tétracoordonné : **21–25**.

YOUSSEF KANDRI RODI, LUCIEN LOPEZ, CHRISTIAN MALAVAUD, MARIE-THÉRÈSE BOISDON, and JEAN-PIERRE FAYET. Can. J. Chem. **71**, 1200 (1993).

The synthesis of new 1,2,4,3-triazaphospholes is described: a number of 5-methylthio 1,2,4,3-triazaphospholes, substituted in the 1, 2, or 4 position. The 1,5-disubstituted compound **6** is stable, whereas 2,5-disubstituted compounds **14** and **16** undergo an equilibrium with their tetrameric form, the cyclotetraphosphazanes $[\mathbf{14}]_4$ and $[\mathbf{16}]_4$. 5-Methylthio 4-alkyl 1,2,4,3-triazaphospholes exist only in the tetrameric forms $[\mathbf{12}]_4$ and $[\mathbf{13}]_4$. $[\mathbf{12}]_4$ can be depolymerized by complexation with a Lewis acid, giving the complexed triazaphosphole $\mathbf{12} \cdot BF_3$. The ^{15}N NMR spectrum of compound **16**, the N-silylated derivative of **15**, allows us to confirm the position of the trimethylsilyl group. MNDO calculations are in good agreement with experimental results, such as the reaction of 1,4-diazadienes with triazaphospholes providing new tetracoordinated phosphorus spirocompounds **21–25**.

Introduction

Les 1,2,4,3-triazaphospholes peuvent exister sous trois formes isomères : **1**, **2**, **3**.

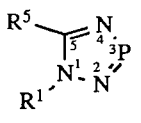

1

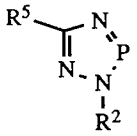

2

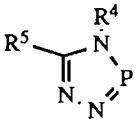

3

Seuls les dérivés disubstitués en 1,5 (**1**) et en 2,5 (**2**) par des groupements alkyles, dialkylamino- ou aryles sont stables (1, 2). La complexation par un acide de Lewis (BF_3) en position 2 stabilise l'isomère **3**; elle a permis une détermination de la structure d'un isomère **3** (R = R' = iPr) par diffraction des rayons X, ainsi que l'observation par RMN de ^{31}P d'isomères complexés par BF_3 (3), comme cela a déjà été signalé pour les 1,3,2-diazaphospholes (4). Les dérivés monosubstitués sont rares; seuls les composés **4** (2*b*) et **5** (2*c*) ont été décrits.

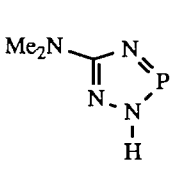

4 (2b)

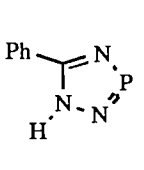

5 H-1 (2c)

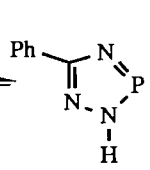

5 H-2

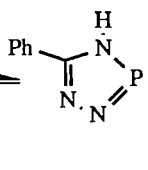

5 H-4

Nous avons récemment obtenu le 1-méthyl 5-méthylthio 1,2,4,3-triazaphosphole **6** par action de l'iodure de méthyle sur un sel de triazaphospholinium (5) :

1. Auteurs à qui adresser toute correspondance.
2. Revision reçue le 3 mai 1993.

Can. J. Chem. Downloaded from www.nrcresearchpress.com by 213.200.69.106 on 09/08/12
For personal use only.

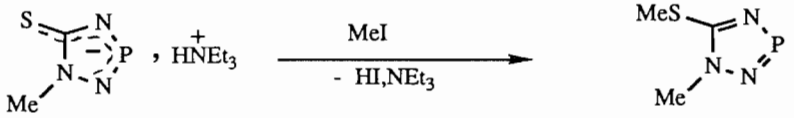

6

La présence de l'atome de soufre en position 5 introduit un facteur de délocalisation électronique dans ces molécules et nous a incité à étudier la synthèse de triazaphospholes substitués par des groupements 5-méthylthio. Nous avons effectué des calculs MNDO sur divers 1,2,4,3-triazaphospholes pour essayer d'interpréter leurs différences de stabilité. Enfin nous avons étudié l'addition des 1,4-diaza 1,3-dienes sur ces 5-méthylthio triazaphospholes : la réaction dépend de l'électrophilie de l'atome de phosphore.

Résultats et discussion

1. Synthèse des iodhydrates de 3-méthylthio semicarbazides

Les triazaphospholes **1**, **2**, **3** sont obtenus, le plus souvent, par action de la tris(diméthylamino)phosphine sur les chlorhydrates (ou iodhydrates) d'amidrazones correspondants (1, 2*b*, 2*d*, 3), dont la synthèse nécessite plusieurs étapes (3, 6).

Nous avons utilisé une réaction analogue à partir des iodhydrates de 3-méthylthio semicarbazides **7**–**11**, qui sont obtenus avec de bons rendements par addition de l'iodure de méthyle sur les thiosemicarbazides correspondantes (7).

2. Synthèse des 5-méthylthio 1,2,4,3-triazaphospholes

L'ensemble des réactions de la tris(diméthylamino)-phosphine effectuées sur les iodhydrates des 3-méthylthio semicarbazides **7**–**11** est présenté dans le schéma 1.

Les 3-méthylthio semicarbazides conduisent, suivant la position et la nature du substituant sur l'azote, à trois types de dérivés : (*i*) des composés stables du phosphore dicoordonné **6** et **15**; (*ii*) des composés du phosphore dicoordonné **14** et **16** en équilibre thermique observable avec leurs tétramères : composés du phosphore tricoordonné $[\mathbf{14}]_4$ et $[\mathbf{16}]_4$; (*iii*) des tétramères $[\mathbf{12}]_4$ et $[\mathbf{13}]_4$.

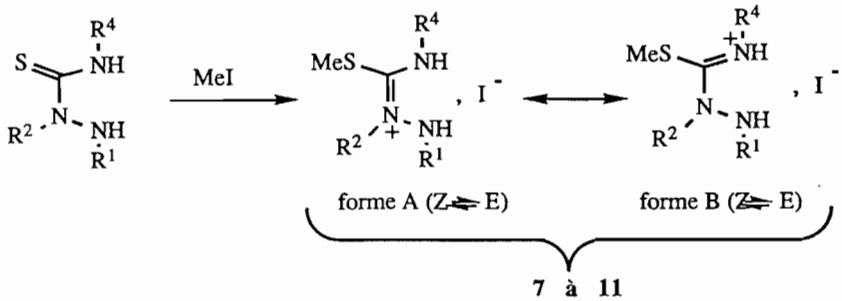

forme A (Z ⇌ E) forme B (Z ⇌ E)

7 à 11

	7	**8**	**9**	**10**	**11**
R^1	Ph	H	H	H	H
R^2	H	H	Me	H	H
R^4	H	H	H	Me	Et

Synthèse des tétramères [12]$_4$ et [13]$_4$

À partir des 3-méthylthio semicarbazides **10** et **11**, on obtient respectivement les tétramères $[\mathbf{12}]_4$ et $[\mathbf{13}]_4$, mis en évidence par RMN de ^{31}P et par spectrométrie de masse par ionisation chimique, dans le méthane. Par chauffage de $[\mathbf{12}]_4$ et de $[\mathbf{13}]_4$, dans le toluène ou la pyridine à l'ébullition, on n'observe pas en RMN de ^{31}P, d'équilibre tétramère ⇌ monomère, comme dans le cas de cyclotétraphosphazanes dérivant de 4,5-benzo 1,3,2-diazaphospholes (4). Le composé $[\mathbf{12}]_4$ est facilement dépolymérisable par action du trifluorure de bore. Le monomère complexé **12**,BF_3 a été caractérisé par analyse et par spectrographie de RMN de ^1H, ^{31}P, ^{13}C, ^{11}B, par IR et par son spectre de masse. Ces données sont en faveur d'une complexation de BF_3 en position 2 (J_{PF} = 35 Hz), comme dans le 4,5-diisopropyl 1,2,4,3-triazaphosphole (3).

*Synthèse des monomères **6** et **15***

Le composé **6** a déjà été préparé par action de l'iodure de méthyle sur un sel de triazaphospholinium (5). Il s'obtient également à partir de l'iodhydrate de 3-méthylthio semicarbazide **9** et de la tris(diméthylamino)phosphine. Le dérivé **15**, obtenu à partir de la 3-méthylthio semicarbazide **8**, est solide à la température ordinaire. Ses caractéristiques physicochimiques (RMN ^1H, ^{13}C, IR, spectre de masse) indiquent qu'il s'agit d'un dérivé du phosphore dicoordonné monomère; cependant il peut exister sous trois formes isomères selon la position du proton sur les azotes 1, 2 ou 4. Le spectre RMN de ^{31}P du mélange réactionnel de **15** dans le toluène montre deux signaux P^{II} à 250 et 246 ppm et un massif bien résolu entre 71,15 et 63,8 ppm, alors que le spectre de **15** isolé puis dissous dans la pyridine présente, à température ambiante, un seul signal large entre 254 et 250 ppm. Ce signal pourrait correspondre à un échange rapide entre les trois isomères facilité par la basicité de la pyridine. Quand on chauffe la solution jusqu'à 90°C, l'allure du signal reste inchangée; par contre, quand on refroidit

Can. J. Chem. Downloaded from www.nrcresearchpress.com by 213.200.69.106 on 09/08/12
For personal use only.

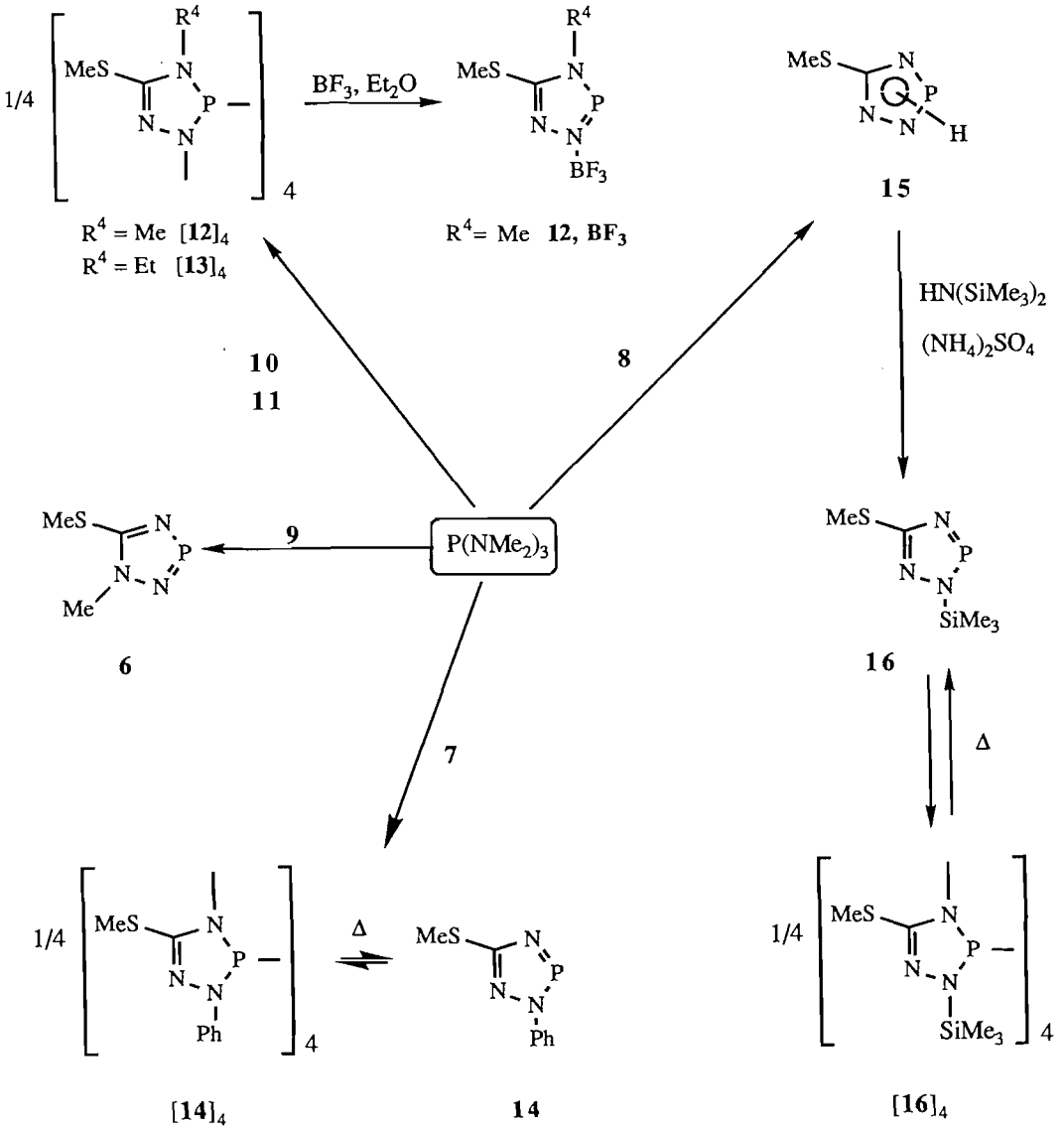

SCHÉMA 1. Synthèse des 5-méthylthio 1,2,4,3-triazaphospholes.

jusqu'a −35°C, on observe un affinement du signal vers 252 ppm et l'apparition de plusieurs signaux dans le domaine des composés du phosphore tricoordonné : un signal large vers 58 ppm, qui pourrait être l'oligomère du composé **15** H-2 et un système AA'XX' (δ = 74,1 et 63,3 ppm; $J_{PNP} + J'_{PNP}$ = 136 Hz) analogue à ceux que l'on observe dans les 1,2,4,3-triazaphospholes 4,5-disubstitués (3); nous pensons donc que ce système est dû à la présence de l'oligomère de **15** H-4. Quand on revient à la température ordinaire, les signaux des composés du phosphore tricoordonnè disparaissent, et on observe à nouveau le signal large vers 252 ppm, montrant qu'il s'agit d'un équilibre thermique.

À partir des composés du phosphore dicoordonné **15** et **6**, nous avons préparé les composés du phosphore tétracoordonné **17** et **18** par addition d'ammoniac en présence de soufre (schéme 2).

Cette addition d'ammoniac, en présence de soufre, a déjà été observés sur des 1,2,4,3-triazaphospholes disubstitués par des groupements aryles ou alkyles (8). Le composé **18** réagit lentement avec la pyridine. Au bout d'une heure, on observe la précipitation d'un nouveau produit **19**, forme salifiée de **18**.

Synthèse des tétramères [14]$_4$ et [16]$_4$ en équilibre avec leur forme monomère

Le dérivé [**14**]$_4$ obtenu par action de la méthylthiosemicarbazide **7** sur la tris(diméthylamino)phosphine et le dérivé [**16**]$_4$ est obtenu à partir de **15** (schéma 1). Leurs spectres de masse obtenus par ionisation chimique (CH_4), montrent qu'il s'agit de tétramères. À la température ordinaire, ces dérivés sont des oligomères de composés du phosphore dicoordonné; si on les chauffe en solution dans la pyridine, on observe en RMN de ^{31}P les signaux des monomères **14** et **16**. Les caractéristiques de ces équilibres sont rassemblées dans le tableau 1.

Lors de la silylation de **15** par action de l'hexaméthyldisilazane (schéma 1), le groupement $SiMe_3$ pourrait se fixer en 1, 2 ou 4. Les spectres RMN de ^{15}N (9) permettent de distinguer les 1,2,4,3-triazaphospholes disubstitués en 1,5 ou en 2,5 (les monomères disubstitués en 4,5 ne sont pas stables). Nous n'avons pas enregistré le spectre de RMN de ^{15}N de **14**, sa solubilité étant insuffisante dans le toluène à

Can. J. Chem. Downloaded from www.nrcresearchpress.com by 213.200.69.106 on 09/08/12
For personal use only.

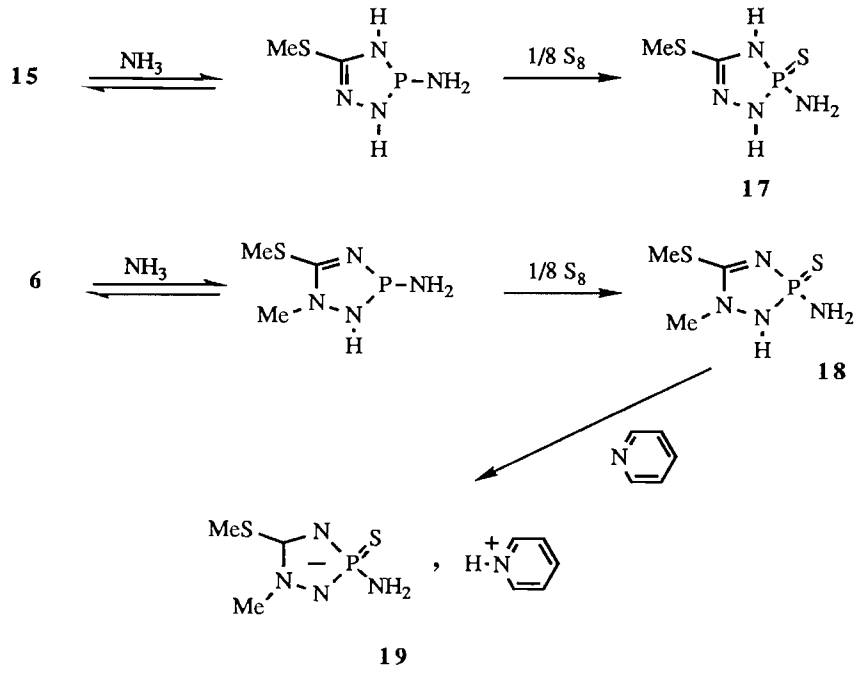

SCHÉMA 2. Synthèse des composés **17–19**.

TABLEAU 1. RMN de ^{31}P à température variable des composés $[\mathbf{14}]_4$ et $[\mathbf{16}]_4$ dans C_5D_5N

	Tétramères		Monomères	
	$[\mathbf{14}]_4$	$[\mathbf{16}]_4$	**14**	**16**
$\delta^{31}P$ (ppm)	79,6	72	247	274
T = 30°C	100%	75%	0%	25%
T = 110°C	20%	0%	80%	100%

chaud. Dans le tableau 2, nous comparons les spectres RMN de ^{15}N de **6** et **16** à ceux de **1** (R^1=Me, R=Ph) et **2** (R^2=Me, R=Ph) (9).

La valeur de $\delta^{15}N^{1}$ (−165 ppm) du composé **6** est bien caractéristique d'un triazaphosphole disubstitué en 1,5; quant à la valeur de $\delta^{15}N^{1P}$ (−50 ppm) du dérivé **16**, elle correspond bien à celle d'un isomère disubstitué en 2,5.

3. Etude de la stabilité relative des 1,2,4,3-triazaphospholes

Généralement les hétérocycles du phosphore dicoordonné présentent une bonne stabilite : phosphinines (17), 1,2,3-diazaphospholes (18), etc. Pourtant nous venons de voir que certains triazaphospholes à double liaison P=N peuvent donner lieu à des équilibres monomère–oligomère ou s'oligomériser spontanément de façon irreversible. L'expérience montre que les dérivés des trois triazaphospholes isomères **1**, **2**, **3** ont des stabilités différentes : les plus stables sont les dérivés de l'isomère **2** alors que ceux de l'isomère **3** existent seulement sous forme complexée ou sous forme de tetramère (3); quant aux derivés de l'isomère **1**, leur stabilité dépend des substituants. Plusieurs études théoriques ont été consacrées à des composés du phosphore dicoordonné : HP=NH (10, 11), $HP=CH_2$ (11), HP=O (14); triazaphospholes (12), dérivés de phosphinines (15, 16), etc.

Nous avons essayé d'expliquer la stabilité relative des triazaphospholes et certains aspects de leur réactivité en utilisant la méthode MNDO (21, 22), moins rigoureuse que les méthodes employées dans les exemples précédents mais beaucoup plus simple et qui donne souvent des résultats intéressants. Les calculs théoriques ont été effectués pour l'ensemble des conformations des triazaphospholes. Les approximations de base dans la méthode MNDO utilisée inclue un modéle semi-empirique pour les intégrales à deux centres (21). Pour juger de la fiabilité de cette méthode, on peut comparer les valeurs calculées en MNDO pour les chaleurs de formation, les géométries moléculaires, les potentiels d'ionisation et les moments dipolaires aux valeurs expérimentales (22); on constate le bon accord, ce qui justifie l'utilisation de la methode. Dans le tableau 3, sont rassemblées les énergies totales et les charges électroniques portées par les atomes de quelques 1,2,4,3-triazaphospholes : les trois isomères monosubstitués (R-1 = R-2 = R-4 = H, R-5 = SCH_3), leurs complexes et enfin une série d'isomères disubstitués (R-1 = R-4 = CH_3, R-2 = CH_3 ou $Si(CH_3)_3$, R-5 = CH_3, SCH_3).

Les énergies totales sont voisines (ΔE = 3 eV) dans les trois isomères non substitués. La monosubstitution en 5 (R^5 = SCH_3) stabilise fortement les formes monomères, puisque les valeurs des énergies électroniques totales diminuent de prés de 400 eV. Dans la série des isomères disubstitués par des groupements CH_3 (R^1, R^2, R^4, R^5 = CH_3), l'isomère 4,5-dimethyl 1,2,4,3-triazaphosphole a une énergie électronique totale très supérieure à celle des autres isomères (+150 eV). Ce résultat pourrait expliquer le fait que les triazaphospholes disubstitués en 4,5 monomères ne sont pas connus, contrairement aux derivés substitués en 1,5 et 2,5. Enfin le calcul montre la très grande stabilisation des trois isomères par un acide de Lewis, le trifluorure de bore, les énergies passant de −1200 à −2400 eV.

Charges partielle

La liaison P=N est fortement polarisée dans tous les dérivés étudiés, comme cela avait déjà été montré dans le cas

Can. J. Chem. Downloaded from www.nrcresearchpress.com by 213.200.69.106 on 09/08/12
For personal use only.

TABLEAU 2. Caractéristiques des spectres RMN de ^{15}N des 5-Ph 1-Me et 5-Ph 2-Me 1,2,4,3-triazaphospholes et des composés **6** et **16**

	δN^1	$^2J_{NP}$	δN^2	$^1J_{NP}$	δN^4	$^1J_{NP}$	Référence
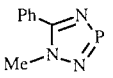	156,5(s)	0	−10,4(d)	85,6	−87(d)	85,6	9
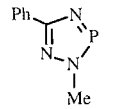	−42,7(d)	6	−117,8(d)	86,6	−99(d)	87,6	9
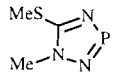	−165(s)		−9,2(d)	85,3	−98,1(d)	87,5	5[a]
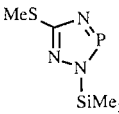	−50,4(s)	0	−97,8(d)	89,3	−95,6(d)	82,0	

[a]Ces valeurs remplacent celles données dans la référence 5.

TABLEAU 3. Calculs MNDO de 1,2,4,3-triazaphospholes **1**, **2**, **3** (charges des différents atomes, moment dipolaire et énergie totale de la molécule)

R-5	N-R	*E* totale (eV)	$\mu_{(D)}$	N-1	N-2	P-3	N-4	C-5
H	H-1	−934,015	4.13	−0,1754	−0,2596	+0,3455	−0,3709	+0,0708
CH_3	CH_3-1	−1246,95	4,60	−0,1858	−0,2577	+0,3361	−0,606	+0,0377
SCH_3	H-1	−1297,49	4,19	−0,1755	−0,2619	+0,3706	−0,334	+0,1713
H	H-1 $BF_3$4	−2447,74	10,15	−0,1535	−0,2735	+0,6043	−0,3481	+0,1887
H	H-2	−934,272	2,08	−0,1234	−0,3156	+0,4204	−0,3700	+0,0082
CH_3	CH_3-2	−1247,41	2,37	−0,1129	−0,3347	+0,4153	−0,3599	−0,0277
SCH_3	H-2	−1328,66	3,54	−0,1387	−0,3151	+0,4444	−0,3470	−0,0104
SCH_3	CH_3-2	−1485,10	3,99	−0,1392	−0,3353	+0,4418	−0,3474	−0,0098
SCH_3	$Si(CH_3)_3$-2	−1924,81	4,42	−0,1410	−0,4683	+0,4071	−0,3438	−0,0121
H	H-2 BF_3-4	−2447,95	10,21	−0,0910	−0,3309	+0,7213	−0,3271	+0,0867
H	H-4	−931,206	5,26	−0,1722	+0,1692	+0,1987	−0,2355	+0,0386
CH_3	CH_3-4	−1087,40	5,75	−0,1748	−0,1696	+0,1941	−0,2607	+0,0413
SCH_3	H-4	−1328,68	3,35	−0,1173	−0,2314	+0,3205	−0,3276	−0,076
H	H-4 BF_3-2	−2444,57	13,43	−0,0747	−0,1676	+0,5505	−0,2657	+0,0441

[a]Dans la colonne N-R, est indiquée la nature du reste R suivie du numéro de l'atome d'azote concerné, puis, le cas échéant, du site de complexation.

de HP=NH (11), avec une séquence décroissante : dérivés 2-substitués > dérivés 1-substitués > dérivés 4-substitués.

L'atome d'azote N-4 porte la charge négative la plus grande, ce que confirme l'expérience puisque la complexation avec BF_3 se fait bien sur cet azote pour les isomères disubstitués-1,5 (*2f*) et 2,5 (9). Dans l'isomère CH_3-4, la complexation avec BF_3 se fait en N-2 (3), sans doute à cause de la substitution de N-4, L'atome de phosphore, compte tenu de son électronégativité, est toujours polarisé positivement par rapport aux atomes d'azote. Cette charge varie en fonction des isomères selon la même séquence.

L'action des diazadiènes sur les 1,2,4,3-triazaphospholes illustre parfaitement ce résultat : ce sont les 1,2,4,3-triazaphospholes disubstitués en 2,5 qui sont les plus réactifs (13).

Moment dipolaire

Les moments expérimentaux sont en bon accord avec les moments calculés.[3] Remarquons que les molécules les moins polarisées sont H-2 et Me-2 (cf. tableau 3) dont les moments dipolaires respectifs sont 2,08 et 2,37 D. Les moments dipolaires théoriques sont ordonnés suivant la séquence : $\mu(R4) > \mu(R\text{-}1) > \mu(R\text{-}2)$.

On remarque que les molécules qui ont tendance à s'oligomériser possèdent un moment dipolaire élevé : les dérivés substitués en 4,5.

4. Action des 1,4-diaza 1,3-diènes sur les 5-méthylthio 1,2,4,3-triazaphospholes

La caractérisation par voie chimique des composés du phosphore dicoordonné est un problème intéressant, puisque ces composés peuvent être en équilibre avec leurs oligomères quelquefois en quantité si faible que les méthodes spectroscopiques ne permettent pas leur detection. Donc nous avons proposé une méthode de caractérisation spécifique des hétérocycles à motif -N-P=N-, basée sur l'électrophilie du phosphore, en utilisant comme réactifs les diazadiènes (13) et non une cycloaddition [2 + 4] sur la double liaison P=N. On obtient des composés spiranniques du schéme 3. Ces composés spiranniques du phosphore tétracoordonné, possédant un environnement de quatre atomes d'azote, sont

3. Avec le 5-phényl 1-méthyl 1,2,4,3 triazaphosphole (μ_{exp} 5.66 D) et avec le 2-méthyl 5-isopropyl 1,2,4,3 triazaphosphole (μ_{exp} 2.28 D).

Can. J. Chem. Downloaded from www.nrcresearchpress.com by 213.200.69.106 on 09/08/12
For personal use only.

rares. À notre connaissance, seuls, deux dérivés de composés analogues, préparés par d'autres voies, sont décrits (19, 20) :

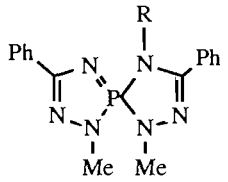

R = H, Me (19)

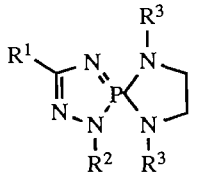

(20)

Il nous a paru intéressant d'étudier l'action des 1,4-diaza 1,3-diènes **20** sur les différents 5-méthylthio 1,2,4,3-triazaphospholes que nous avons synthétisés (schéma 3). Quand la réactivité du triazaphosphole est insuffisante, nous avons utilisé son complexe avec BF_3, car la complexation augmente la charge positive de l'atome de phosphore et probablement son électrophilie (schéma 3).

Le diaza-4,5 diène-1,3 **20***a* (R=*n*Pr) est plus réactif, car plus nucléophile, que le diazadiène **20***b* (R=Ph). On remarque aussi que les triazaphospholes disubstitués en 2,5 sont les dérivés qui réagissent le mieux. Par exemple **15** qui existe exclusivement sous forme monomère réagit totalement en un quart d'heure, à température ambiante. La réaction est plus lente (2–3 h) et nécessite une température plus élevée quand le triazaphosphole est en équilibre avec sa forme tétramère : c'est le cas des dérivés **14** et **16**. On a montré que l'étape initiale de cette réaction est une attaque nucléophile du doublet libre de l'un des atomes d'azote du diazadiène, sur l'atome de phosphore dicoordonné. Les tétramères P^{III} qui ne sont pas en équilibre avec la forme monomère P^{II}, ne réagissent pas; ce réactif peut donc constituer un test pour cet équilibre. D'autre part, les triazaphospholes disubstitués-2,5 réagissent en 1 h à la température ordinaire, tandis que les composés disubstitués-1,5 réagissent en 60 h à 80–100°C (13). Lorsque l'on chauffe **6** avec **20***a* pendant 2 jours dans le benzène à 80°C, on obtient seulement 10% du dérivé spirannique **24***a*, caractérisé par son déplacement chimique de RMN de ^{31}P. Dans les mêmes conditions, **20***b* ne réagit pas avec **6**. Notons que **20***a* n'a pas réagi sur $[\mathbf{12}]_4$ aprés 48 h à 100°C dans le toluène ou la pyridine. Nous avons déjà étudié l'action de **20***a* sur les tétramères $[\mathbf{26}]_4$ et $[\mathbf{27}]_4$, dont la forme monomère P^{II} n'est pas observable par RMN de ^{31}P.

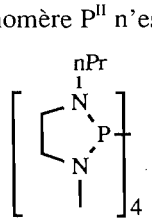

$[\mathbf{26}]_4$

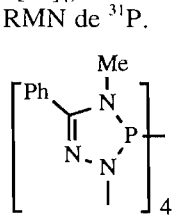

$[\mathbf{27}]_4$

$[\mathbf{26}]_4$ n'a pas réagi, même après chauffage pendant plusieurs jours à 100°C dans la pyridine (ou $NO_2C_6H_5$), tandis que $[\mathbf{27}]_4$ réagit quand on le chauffe à 100°C pendant 2 h dans la pyridine (14). Il semble donc que $[\mathbf{12}]_4$ n'est pas en équilibre avec son monomère, le groupement SMe augmentant la stabilité de $[\mathbf{12}]_4$ qui devient alors comparable à celle de $[\mathbf{26}]_4$. On peut aussi supposer que l'électrophilie de l'atome de phosphore de **12** est réduite par la présence de SMe. Cette dernière hypothèse semble plus plausible, si la réaction se fait sous contrôle des charges, puisque la complexation de **6** par BF_3, en augmentant la charge positive sur P, entraine une réaction instantanée de **20** pour donner les dérivés spiranniques **24**,BF_3. De même la réaction entre **12**,BF_3 et **20** est instantanée (schéme 3). D'aprés les spectres RMN de ^1H, le spirophosphazène obtenu est probablement complexé sur l'azote N-2 du cycle triazaphospholique. La liaison azote–bore est trés forte : en effet la décomplexation de **24**,BF_3 par addition d'une quantité stoechiométrique de DBU nécessite 2 jours à température ambiante.

Ainsi les diazadiénes **20** constituent non seulement des réactifs de détection du phosphore dicoordonné à enchainement -N-P=N- mais aussi peuvent permettre une appréciation qualitative de son électrophilie.

Conclusion

La synthèse de ces nouveaux 1,2,4,3-triazaphospholes indique clairement que l'introduction d'un groupement thiométhyle en position 5 conduit à une destabilisation par rapport aux triazaphospholes issus d'amidrazones. Les 5-méthylthio 1,2,4,3-triazaphospholes substitués en position 2 illustrent ce comportement. C'est ainsi que l'on a pu mettre en évidence, l'existence d'un équilibre thermique : phosphazane $P^{III} \rightleftharpoons$ phosphazène P^{II}. Il en est de même du 5-méthylthio 1,2,4,3-triazaphosphole **15** en solution dans la pyridine, mis en évidence à basse température.

Les résultats (ènergie totale et charges) des calculs effectués par la méthode MNDO apportent un élément de prévision de la réactivité de ces hétérocycles; les résultats expérimentaux confirment ces prévisions : site de complexation, addition des diazadiènes ou observation de l'équilibre. Cependant la stabilité relative des trois isomères est conservée.

L'introduction d'un reste fonctionnel en position-5 ou -2 des groupements -SMe ou -$SiMe_3$ ouvre des possibilités de réaction trés intéressantes.

Partie expérimentale

Les spectres IR ont été réalisés sur un spectromètre Perkin Elmer à transformée de Fourier, modèle 1760 X.

Les spectres de masse ont été effectués sur spectromètre Varian Mat 311 A, soit par impact électronique, soit par desorption de champ (NH_3, CH_4).

Les spectres de RMN de ^{31}P (32,44 MHz) et de ^1H (80 MHz) ont été obtenus sur un spectromètre Bruker AC 80, ceux de ^{13}C sur spectromètres Bruker AC 80 (20,15 MHz), AC 200 (50,32 MHz), AC 250 (62,90 MHz).

Les spectres de RMN de ^{15}N et ^{19}F ont été réalisés sur un spectromètre Bruker AM 300 WB; les déplacements chimiques sont donnés par rapport à CH_3NO_2 pour l'azote ^{15}N et CF_3COOH pour le fluor ^{19}F (en réf. externe).

Les analyses élémentaires ont été effectuées par le service central de microanalyse de CNRS et par le laboratoire d'analyse de l'École Nationale Supérieure de Chimie de Toulouse.

Iodhydrates de 3-méthylthio semicarbazide 7–11

Ils ont été préparés selon la référence 7. Certains sont nouveaux.

1-Phényl 3-méthylthio semicarbazide 7 : (68%) *F* 183°C; δH (80 MHz; C_5D_5N) : 2,81 (3H, s, CH_3), 6,8–7,2 (5H, m, Ph), 10,5 (4H, s, NH); δC (50,32 MHz; DMSO-D_6) : 13,60 (CH_3), 110–145 (m, CHPh), 170,50 (>C=N-). Anal. calc. pour $C_8H_{12}IN_3S$: C 31,17; H 3,90; N 13,64%. Tr. : C 31,06; H 3,97; N 14,09%.

3-Méthylthio semicarbazide 8 : (75%) *F* 137°C (lit. (7) *F* 136–140°C (7)); δH (80 MHz; C_5D_5N) : 2,74 (3H, s, CH_3), 8,71 (4H, s, NH); δC (50,32 MHz; DMSO-d_6) : 13,63 (CH_3), 167,60 (>C=N-).

Can. J. Chem. Downloaded from www.nrcresearchpress.com by 213.200.69.106 on 09/08/12
For personal use only.

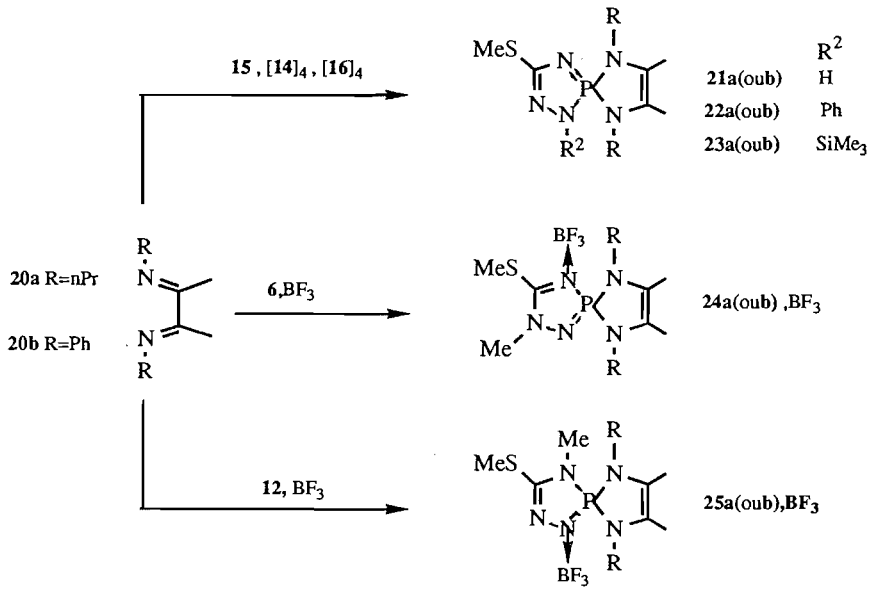

SCHÉMA 3. Réaction des 1,4-diaza 1,3-diène **20** sur les 5-méthylthio 1,2,4,3-triazaphospholes.

2-Méthyl 3-méthylthio semicarbazide ***9*** *:* (79%) *F* 166°C; δH (80 MHz; C_5D_5N) : 2,51 (3H, s, SCH_3), 3,35 (3H, s, NCH_3), 5,52 (2H, s, NH); 8.29 (2H, s, NH); δC (50,32 MHz; DMSO-d_6) : 14,1 (SCH_3), 42,26 (N-CH_3), 171,0 (>C=N-). Anal calc. pour $C_3H_{10}N_3S$: C 14,63; H 4,06; N 17,07%.Tr. : C 14,47; H 4,00; N 17,01%.

3-Méthylthio 4-méthyl semicarbazide ***10*** *:* (70%) *F* 170°C (lit. (7) *F* (163°C); δH (80 MHz; C_5D_5N) : 2,44 (3H, s, SCH_3), 2,92 (3H, s, NCH_3), 8,1 (4H, s, NH); δC (50,32 MHz; DMSO-d_6) : 12,96 (SCH_3), 30,24 (N-CH_3), 168,10 (>C=N-).

3-Méthylthio 4-éthyl semicarbazide ***11*** *:* (73%) *F* 174%C; δH (80 MHz; C_5D_5N) : 1,07 (3H, t, *J* 7,1, CH_3-C-N), 2,42 (3H, s, SCH_3), 3,29 (2H, q, *J* 7,1, C-CH_2-N), 6,0 (4H, s, NH); δC (50,3 MHz; DMSO-d_6) : 13,79 (CH_3-CN), 14,70 (S-CH_3), 38,80 (C-CH_2-N), 166,70 (<C=N-). Anal. calc. pour $C_4H_{12}IN_3S$: C 18,46; H 4,62; N 16,15%. Tr. : C 18,31; H 4,57; N 16,09%.

5-Méthylthio 1,2,4,3-triazaphosphole ***6****, 15 et cyclotétraphosphazanes* ***[12]4****,* ***[13]4***

Un mélange équimoléculaire de tris(diméthylamino)phosphine et d'iodhydrate de méthylthiosemicarbazide (2×10^{-3} mol) dans 10 mL de toluène fraîchement distillé, est chauffé au reflux. La diméthylamine formée, entraînée par un courant d'azote sec, est titrée par une solution molaire d'acide chlorhydrique. On neutralise environ 90% de la quantité théorique d'amine en 3 heures. On décante très rapidement, à chaud sous argon, pour éliminer l'iodhydrate de diméthylamine.

Pour **6**, la solution obtenue est concentrée sous vide puis distillée sous pression réduite.

Pour **15**, $[\mathbf{12}]_4$ et $[\mathbf{13}]_4$: dans le filtrat apparaît très rapidement, en refroidissant, un précipité que l'on recristallise dans le toluène. La précipité, lavé à l'hexane, est séché sous vide sur P_2O_5.

1-Méthyl 5-méthylthio 1,2,4,3-triazaphosphole ***6*** *:* (82%) Eb 45°C/0,5 Torr (1 Torr = 133,3 Pa); ν_{max}, cm^{-1} (CH_2Cl_2) : 1619 (C=N); δP (32,44 MHz; C_6D_6) : 261 (s); δH (80 MHz, $CDCl_3$) : 2,67 (3H, s, SCH_3), 3,86 (3H, d, *J* 0,9, NCH_3); δC (50,32 MHz; C_6D_6) : 16,42 (SCH_3), 32,60 (d, *J* 3,6, NCH_3), 160,40 (d, *J* 15,9, >C=N-); SM (70 eV) *m/z* : 63 [12, $(CH_3)_2$ SH^+], 74 (100, PN_2CH_3), 89 (34, M^+-58), 102 (43, M^+-PN), 119 (12, M^+-28), 147 (35, M^+). Anal. calc. pour $C_3H_6N_3PS$: C 24,49; H 4,08; N 28,60; P 21,08; S 21,67%. Tr. : C 24,45; H 4,17; N 28,87; P 20,66; S 21,68%.

5-Méthylthio 1,2,4,3-triazaphosphole ***15*** *:* (86%) *F* 101°C; ν_{max}, cm^{-1} (CH_2Cl_2) : 3325 (NH), 1625 (C=N); δP (32,44 MHz; C_6D_6) : 251,4 (s); δH (80 MHz; C_5D_5N : 2,42 (3H, s, SCH_3), 10,78 (1H, s, NH); δC (50,32 MHz; C_6D_6) : 15,5 (SCH_3), 167 (>C=N-); SM (70 eV) *m/z* : 28 (57,5, N_2), 88 (100, $M^+ - PN$), 105 (17,3, CH_3SCNP), 133 (61, M^+). Anal. calc. pour $C_2H_4N_3PS$: C 18,05; H 3; N 31,58; P 23,31; S 24,06%. Tr. : C 18,03; H 3,04; N 32; P 22,83; S 24%.

[12]4 : (68%) *F* 159°C; ν_{max}, cm^{-1} (CH_2Cl_2) : 1602 (C=N); δP (32,44 MHz; C_5D_5N) : 70–82 (m); δH (80 MHz; C_5D_5N) : 1,30 (3H, m, SCH_3), 2,45 (3H, m, NCH_3); SM (DCI, NH_3) *m/z* : 134 (21, $M/4^+ + 1 - N_2$), 162 100, $M/4^+ + 1$), 322 (58, $M/2^+$), 353 (3, $M/2^+ + 31$), 483 (2, $3M/4^+$), 644 (1, M^+). Anal. calc. pour $C_3H_6N_3PS$: C 24,49; H 4,08; N 28,60; P 21,08; S 21,67%. Tr. : C 25,31; H 4,87; N 29,01; P 20,21; S 20,60%.

([13]4 : (72%) *F* 166°C; ν_{max}, cm^{-1} (CH_2Cl_2) : 1595 (C=N); δP (32,44 MHz; C_5D_5N) : 69–87 (m); δH (80 MHz; C_5D_5N) : 1,25 (3H, m, N-CH_2-CH_3), 2,50 (3H, m, SCH_3), 3,25 (2H, m, N-CH_2-CH_3). Anal. calc. pour $C_4H_8N_3PS$: C 29,81; H 4,97; N 26,09; P 19,25; S 19,86%. Tr. : C 29,92; H 5,04; N 25,84; P 18,95; S 21,25%.

[14]4 : (81%) *F* 198°C; δP (32,44 MHz; C_5D_5N) : 76–81 équilibre observable 1/4 $[\mathbf{14}]_4 \rightleftharpoons$ **14** (cf. tableau 1); δH (80 MHz; C_5D_5N; 110°C) : 2,57 (3H, s, SCH_3), 7,0–8,0 (m, Ph); SM (DCI, NH_3) *m/z* : 104 (68,2 $M/4^+ - N_2Ph$), 181 (100,$M/4^+ - N_2$), 209 (95, $M/4^+$), 388 (15, $M/2^+ - 30$), 418 (12, $M/2^+$), 836 (1, M^+). Anal. calc. pour $C_8H_8N_3PS$: C 45,93; H 3,83; N 20,10; P 14,83; S 15,31%. Tr. : C 46,23; H 4,18; N 19,80; P 14,96; S 14,74%.

2-Triméthylsilyl 5-méthylthio 1,2,4,3-triazaphosphole ***16***

À une suspension de 3 g de **15** ($2,25 \times 10^{-2}$ mol) dans 60 mL de dichloroéthane sont ajoutés 4,03 g ($2,5 \times 10^{-2}$ mol) d'hexaméthyldisilazane; on catalyse la réaction avec 20 mg de sulfate d'ammonium. Le mélange réactionnel est chauffé au reflux du solvant. L'ammoniac formé au cours de la réaction est dosé par une solution molaire d'acide chlorhydrique. Quand de dégagement est fini, on concentre la solution, et on distille le résidu obtenu. (75%). Eb 68°C/5 $\times 10^{-3}$ Torr; δP (32,44 MHz; C_5D_5N; cf. tableau 1) : 274 (25% **16**), 70–80 (75% $[\mathbf{16}]_4$); δH (80 MHz; C_5D_5N; 110°C) : 0,49 (9H, d, *J* 0,52, $Si(CH_3)_3$), 2,48 (3H, s, SCH_3); δC (50,3 MHz; C_5D_5N; 92°C) : -0,38 (d, *J* 3,6, $Si(CH_3)_3$), 14,83, (SCH_3), 170,5 (d, *J* 21, >C=N); δN (cf. tableau 2). SM (DCI, NH_3) *m/z* : 105 (100, $C_2H_4SNP^+$), 134 (83, $C_3H_{11}N_2PSi$), 147 (32, $C_3H_{10}N_3PSi$), 206 (24, $M/4^+ + 1$), 227 (15), 373 (11), 419 (3), 579 (3), 819 (3, $M^+ - 1$). Anal. calc. pour $C_5H_{12}N_3PSSi$: C 29,27; H 5,87; N 20,49; P 15,12; S 15,61; Si 13,66%. Tr. : C 29,25; H 5,94; N 19,88; P 15,03; S 15,01; Si 13,49%.

Can. J. Chem. Downloaded from www.nrcresearchpress.com by 213.200.69.106 on 09/08/12
For personal use only.

Can. J. Chem. Downloaded from www.nrcresearchpress.com by 213.200.69.106 on 09/08/12
For personal use only.

2-Trifluoroborate 4-méthyl 5-méthylthio 1,2,4,3-triazaphosphole. ***12***$,BF_3$

On met en suspension dans 50 mL de toluène 7.35 g (0,05 mol) de $[\mathbf{12}]_4$, et on ajoute lentement, en agitant, 6.15 mL (0,05 mol) d'étherate de trifluorure de bore. Après 30 min d'agitation, on observe une dissolution complète, et après 6 h d'agitation, un précipité blanc apparaît. On filtre et on sèche sur P_2O_5 sous un vide de 10^{-3} Torr. (75%) *F* 140–142°C; δP (32,44 MHz; CD_2Cl_2) : 2,59 (s); δH (80 MHz; CDCl3) : 2,89 (3H, s, SMe), 3,79 (3H, d, 7,8, NMe); δC (50,32 MHz; CD_2Cl_2) : 16,1 (S-CH_3), 33,10 (d, *J* 14,6, N-CH_3), 166,00 (>C=N); δB (25.71 MHz, C_6D_6) : -0,1 (q, $J_{B\text{-}F} = J_{B\text{-}P} = 11$); δF (282.39 MHz, C_6D_6) : -71,30 (d, $J_{F\text{-}B} = 11$; $J_{F\text{-}P} = 35$). Anal. calc. pour $C_3H_6BF_3N_3PS$: C 16,74; H 2,79; N 19,53; P 14,42; S 14,81%. Tr. : C 16,69; H 3,25; N 18,26; P 13,96; S 15,21%.

*3-Thio 3-amino 5-méthylthio 4*H *1,2,4,3-triazaphospholine* ***17*** *et 3-thio 3-amino 5-méthylthio 1-methyl 1,2,4,3-triazaphospholine* ***18***

On ajoute 0,16 g (5×10^{-3}) de soufre à 5×10^{-3} mol de **6** ou de **15** en solution dans 20 mL de benzène. On fait barboter 15 min, un courant d'ammoniac seché par passage sur potasse, dans le mélange précédent. On constate tout d'abord une dissolution complète, puis apparition d'un précipité blanc abondant.

17 *:* (81%) *F* 173–175°C; ν_{max}, cm^{-1} (CH_2Cl_2) : 3467 (NH_2 anti-sym), 3351 (NH_2 sym), 3301 (NH), 1601 (C=N); δP (32,44 MHz; C_5H_5N) : 68; δH (80 MHz; C_5D_5N) : 2,25 (3H, s, SCH_3), 9,5 (4H, s, NH). Anal. calc. pour $C_2H_7N_4PS_2$: C 13, 19; H 3,85; N 30,77; P 17,03; S 35,16%. Tr. : C 13,74; H 4,02; N 30,47; P 16,79; S 35,52%.

18 *:* (78%) F 119°C; ν_{max}, cm^{-1} (CH_2Cl_2) : 3467 (NH_2 anti-sym), 3373 (NH_2 sym), 3307 (NH) 1605 (C=N); δP (32,44 MHz; C_5H_5N) : 82; δH (80 MHz; C_5D_5N) : 2, 12 (3H, s, SCH_3), 2,35 (3H, s, NCH_3), 10,4 (3H, s, NH); δC (62,89 MHz; $CDCl_3$) : 15,54 (S-CH_3), 37,89 (d, $^3J_{P\text{-}C}$ 8,43, NCH_3), 169,12 (d, $^2J_{PC}$ 5,16, C=N). Anal. calc. pour $C_3H_9N_4PS_2$: C 18,37; H 4,59; N 28,57; P 15,82; S 32,65%. Tr. : 18,99; H 4,57; N 27,83; P 15,47; S 32,41%.

Sel de pyridinium de l'3-amino 5-méthylthio 1,2,4,3-triazaphospholine ***19***

On dissout 0,1 g de **18** dans 3 mL de pyridine. Au bout d'une heure, se forme un précipité que l'on sépare par centrifugation. δP (32,44 MHz; D_2O) : 75,7; δH (80 MHz; D_2O) : 2,28 (3H, s, SCH_3) 2,75 (3H, s, NCH_3); δC (50,32; D_2O) : 15,20 (SCH_3), 42, 26 (NCH_3), 171,95 (C=N).

1,4-Dipropyl (ou diphényl) 2,3-diméthyl 1,4,6,8,9-penta-aza 6-méthylthio $\sigma^4\lambda_5$ *5-phospha (4,4) spiro 2,5,7-nonatriène substitués* ***21–25***

À une suspension de 2 g de **15** fraichement preparé ($1,55 \times 10^{-2}$) mol) dans 20 mL de dichloroéthane, on ajoute ($1,55 \times 10^{-2}$ mol) de ***20****a* ou ***20****b*. On observe un léger échauffement de la solution et la dissolution complète de **15**. On poursuit l'agitation 15 min.

Après évaporation du solvant, l'huile obtenue est séchée sous un vide de 10^{-2} Torr pendant 2 h. Cependant les spectres RMN de ^1H montrent que l'élimination du solvant n'est pas totale; ces produits n'étant pas distillables sous cette pression, nous n'avons pas pu obtenir des analyses satisfaisantes.

Les autres dérivés ont étè preparés selon la même méthode.

21*a* *:* (70%) 15 min, huile δP (32,44 MHz; C_6D_6) : 50,0 (q, $^3J_{PNCH_2}$ 12,90); δH (80 MHz, C_6D_6) : 0,67 (6H, t, 7,56, $CH_3CH_2CH_2$), 1,21 (4H, m, $CH_3CH_2CH_2$), 1,43 (6H, s, CH_3-C=C), 2,42, (3H, d, 0,9, SCH_3), 3,05 (4H, m, $CH_3CH_2CH_2$), 6,65 (1H, d, 24,7, NH); NH); δC (50,32 MHz, C_6D_6) : 10,11 (CH_3-C=C), 12,38 ($CH_3CH_2CH_2$), 16,18 (SCH_3), 24,8 (CH_3CH_2), 43,31 (N-$CH_2CH_2CH_3$), 112,52 (d, 14,10, C=C), 158,8 (d, 17,93, C=N). Anal. calc. pour $C_{12}H_{24}N_5PS$: C 47,29; H 7,97; N 23,26%. Tr. : C 46, 92; H 7,5; N 22,10%.

21*b* *:* (75%) 15 min, *F* = 128°C; δP (32,44 MHz; $CDCl_3$) : 43,6; δH (80 MHz, $CDCl_3$) : 1,68 (6H, t, 3,87, CH_3-C=C), 2,17 (3H, s, SCH_3), 6,7–7,5 (10H, m, N-Ph et NH); δC (50,32 MHz, $CDCl_3$) : 10,98 (d, 5,04, CH_3-C=C), 13,64 (s, SCH_3), 114,57 (d, 23,0, C=C), 120–139 (m, N-Ph), 158,49 (d, 16,7, C=N).

22*a* *:* (69%) 3 h, *F* = 124–126°C; $\delta^{33}P$ (32,44 MHz, CH_2Cl_2) : 58,27 (q, $^3J_{PNCH_2}$ 13,10); δH (80 MHz, $CDCl_3$) : 0,62 (6H, t, 7,24, $CH_3CH_2CH_2$), 1,17 (4H, m, $CH_3CH_2CH_2$), 1,33 (6H, s, CH_3-C=C), 2,54 (3H, d, 1,1, SCH_3) 2,87 (4H, m, $CH_3CH_2CH_2$), 7–7,6 (5H, m, NPh); δC (50,32 MHz, $CDCl_3$) : 11,19 (CH_3-C=C), 12,46 ($CH_3CH_2CH_2$), 17,06 (SCH_3), 25,51 (CH_3CH_2), 42,9 (N-$CH_2CH_2CH_3$), 111,89 (d, 15,10, C=C), 120–141 (m, N-Ph), 157,2 (d, 16,40, C=N). Anal calc. pour $C_{18}H_{28}N_5PS$: C 57,29; H 7,43; N 18,27; P 8,22; S 8,49%. Tr. : C 55,54; H 7,49; N 16,57; P 8,40; S 7,80%.

22*b* *:* (68%) 3 h; $\delta^{31}P$ (32,44 MHz, $CDCl_3$) : 54,27; δH (80 MHz, $CDCl_3$) : 1,68 (6H, t, 3,87, CH_3-C=C), 2,17 (3H, s, SCH_3), 6,7–7,5 (10H, m, N-Ph et NH); δC (50,32 MHz, $CDCl_3$) : 10,98 (d, 5,04, CH_3-C=C), 13,64 (s, SCH_3), 114,57 (d, 23,0, C=C), 120–139 (m, N-Ph), 158,49 (d, 16,7, C=N).

23*a* *:* (71%) 3 h, huile; δP (32,44 MHz, C_6D_6) : 58,4 (quint., $^3J_{PNHCH_2}$ 13,3); δH (80 MHz, C_6D_6) : 0,22 (9H, s, N-Si$(CH_3)_3$, 0,70 (6H, t, 6,97, $CH_3CH_2CH_2$), 1,41 (4H, m, $CH_3CH_2CH_2$), 1,49 (6H, s, CH_3C=C), 2,40 (3H, s, SCH_3), 2,90 (4H m, N-CH_2CH_2); δC (50,32 MHz, C_6D_6) : 0,65 (Si$(CH_3)_3$), 9,88 (d, 6,05, CH_3-C=C), 11,33 ($CH_3CH_2CH_2$), 12,35 (SCH_3), 24,68 ($CH_3CH_2CH_2$), 43,19 (d, 5,6, N-CH_2CH_2), 112,57 (d, 13,5, C=C), 161,27 (d, 19,2 C=N). Anal. calc. pour $C_{15}H_{32}PSSi$: C 48,26; H 8, 58; N 18,77; P 8,31; S 8,58; Si 7,50%. Tr. : C 48,64; H 8,31; N 19,07; P 9,13; S 8,30; Si 7,46%.

23*b* *:* (69%) 2 jours, huile; $\delta^{31}P$ (32,44 MHz, tol.) : 54,28; δC (62,9 MHz, $CDCl_3$) : -1,05 (s, Si$(CH_3)_3$), 11,42 (d, 5,0, CH_3C=C), 15,40 (s, SCH_3), 114,71 (d, 13,0 C=C), 160,6 (d, 20, C=N). Anal. calc. pour $C_{21}H_{28}N_5PSSi$: C 57,14; H 6,35; N 15,87%. Tr. : C 58,07; H 6,34; N 14,48%.

24*a*$,BF_3$ *:* (76%) 30 min; *F* = 96–98°C; ν_{max}, cm^{-1} (Nujol) : 1632 (C=N). δP (32,44 MHz, $CDCl_3$) : 46,5; δH (80 MHz, C_5D_5N) : 0,35 (6H, t, 7,14, $CH_3CH_2CH_2$), 1,15 (4H, m, $CH_3CH_2CH_2$), 1,36 (6H, s, CH_3-C=C), 2,20 (3H, s, S-CH_3), 2,90 (4H, m, N-CH_2CH_2), 3,23 (3H, s, N-CH_3); δC (50, 32 MHz, $CDCl_3$) : 10,08 (d, 7,05, CH_3-C=C), 11,60 (s, $CH_3CH_2CH_2$), 15,70 (s, SCH_3), 24,59 (s, $CH_3CH_2CH_2$), 35,76 (s, NCH_3), 43,50 (d, 5,18, N-CH_2CH_2), 114,25 (d, 6,19, C=C), 160,75 (s, C=N). Anal. calc. pour $C_{13}H_{26}BF_3N_5PS$: C 40,73; H 6,79; N 18,28; P 8,09; F 14,88; S8,36%. Tr.: C 38,74; H 7,00; N 16,72; P 6,95; F 14,19; S 6,70%.

24*b*$,BF_3$ *:* (73% min, *F* = 185°C; ν_{max}, cm^{-1} (Nujol) : 1655 (C=N). δP (32,44 MHz, C_6D_6) 38,8; δH (80 MHz, C_6D_6) : 1,66 (6H, s, CH_3-C=C), 2,39 (3H, s, SCH_3), 3,16 (3H, d, 0,7, NCH_3), 7,35 (10H, m, N-*P*h); δC (50,32 MHz, C_6D_6) : 10,44 (d, 5,99, CH_3C=C), 14,52 (s, SCH_3), 34,66 (d, 8,15, N-CH_3), 115,15 (d, 16,05, C=C), 120–140 (m, N-Ph), 160,46 (s, C=N). Anal. calc. pour $C_{19}H_{22}BF_3NPS$: C 50,55; H 4,88; N 15,52; P 6,87; F 12,64; S 7,10%. Tr. : C 49,62; H 5,02; N 14,87; P 6,54; F 13,32; S 6,52%.

25*a*$,BF_3$ *:* (75%) 30 min, *F* = 101°C; δP (32,44 MHz, $CDCl_3$) : 40,7; δH (80 MHz, $CDCl_3$) : 0,82 (6H, t, CH_3-CH_2CH_2), 1,54 (4H, m, $CH_3CH_2CH_2$), 1,86 (6H, s, CH_3-C=C), 2,46 (3H, s, CH_3), 2,82 (3H, d, 8,60, N-CH_3), 3,00 (4H, m, N-CH_2CH_2); δC (50,32 MHz, $CDCl_3$) : 9,7 (d, 6,9, CH_3-C=C), 10,94 (s, $CH_3CH_2CH_2$), 12,29 (s, CH_3), 27,34 (d, 6,1, NCH_3), 43,09 (d, 4,7, N-CH_2CH_2), 44,41 (s, N-CH_2CH_2), 114,57 (d, 2,16, C=C), 146,17 (d, 42,7, C=N). Anal. calc. pour $C_{13}H_{26}N_5PSBF_3$: C 40,73; H 6,79; N 18,28; P 8,09; F 14,88; S, 8,36%. Tr. : C 40,31; H 6,47; N 17,98; P 8,39; F 14,48; S 7,96%.

25*b*$,BF_3$ *:* (73%) 30 min, *F* = 198°C δP (32,44 MHz, C_5D_5N) : 33,9; δH (80 Hz, $CDCl_3$) : 1,66 (6H, s, CH_3-C=C), 2,18 (3H, s, SCH_3), 2,81 (3H, d, 9, N-CH_3), 7,22 (10H, m, N-*P*h); δC (50,32 MHz, $CDCl_3$) : 10,89 (d, 5,3, CH_3C=C), 16,19 (s, SCH_3), 36,52 (d, 8, N-CH_3), 115,76 (d, 9,8, C=C), 129–140 (m, N-Ph), 146,1 (s, C=N). Anal. calc. pour $C_{19}H_{22}BF_3NPS$: C 50,55; H

4,88; N 15,52; P 6,87; F 12,64; S 7,10%. Tr. : C 48,92; H 5,03; N 15,08; P 6,54; F 13,05; S 6,52%.

1. Y. Charbonnel et J. Barrans. C.R. Acad. Sci. **278**, 35 (1974); Tetrahedron, **32**, 2039 (1976).
2. (*a*) A. Schmidpeter, J. Luber et H. Tautz. Angew. Chem. Int. Ed. Engl. **16**, 546 (1977); (*b*) A. Schmidpeter et H. Tautz. Z. Naturforsch. **35B**, 1228 (1980); (*c*) L. Lopez, J.P. Majoral, A. Meriem, T. N'Gando M'Pondo, J. Navech et J. Barrans. J. Chem. Soc. Chem. Commun. 183 (1984); (*d*) T. N'Gando M'Pondo, C. Malavaud, L. Lopez et J. Barrans. Tetrahedron Lett. **28**, 6049 (1987); (*e*) C.K. Karaghiosoff et A. Schmidpeter. Phosphorus Sulfur, **36**, 217 (1988); (*f*) M. Haddad, J.P. Legros, L. Lopez, M.T. Boisdon et J. Barrans. Phosphorus Sulfur, **69**, 189 (1992); (*g*) A. Schmidpeter et K. Karaghiosoff. Multiple bonds and low coordination in phosphorus chemistry. *Editeurs :* M. Regitz et O.I. Scherrer. Georg Thieme Verlag, Stuttgart. 1990.
3. M. Haddad, F. Dahan, J.P. Legros, L. Lopez, M.T. Boisdon et J. Barrans. J. Chem. Soc. Perkin Trans. 2, 671 (1992).
4. (*a*) C. Malavaud, M.T. Boisdon, Y. Charbonnel et J. Barrans. Tetrahedron Lett. **20**, 447 (1979); (*b*) C. Malavaud, T. N'Gando M'Pondo, L. Lopez, J. Barrans et J.P. Legros. Can. J. Chem. **62**, 43 (1984).
5. Y. Kandri Rodi, L. Lopez, C. Malavaud, M.T. Boisdon et J. Barrans. J. Chem. Soc. Chem. Commun. 23 (1991).
6. (*a*) A. Pinner. Die Iminoäther und ihre Derivate. Oppenhein, Berlin. 1892; (*b*) A. Pinner et F. Klein. Chem. Ber. **10**, 1877 (1889).
7. M. Frend et Th. Paradies. Chem. Ber. **34**, 3110 (1901).
8. M.T. Boisdon, L. Lopez, C. Malavaud, J. Barrans, A. Chabane et R. Mathis. Can. J. Chem. **64**, 1725 (1986).
9. M. Haddad, M.T. Boisdon, L. Lopez, C. Malavaud, G. Pelletier, J. Barrans, G. Pfister-Guillouzo et J.P. Legros. J. Chem. Res (M), 1815 (1989).
10. G. Trinquier. J. Am. Chem. Soc. **104**, 6969 (1982).
11. D. Gonbeau, G. Pfister-Guillouzo et J. Barrans. Can. J. Chem. **61**, 1371 (1983).
12. D. Gonbeau, G. Pfister-Guillouzo, J. Barrans et M.H. Palmer. Chem. Phys. **95**, 243 (1985).
13. O.S. Diallo, M.T. Boisdon, L. Lopez, C. Malavaud et J. Barrans. Tetrahedron Lett. 2971 (1986).
14. W.W. Schoeller et E. Niecke. J. Chem. Soc. Chem. Commun. 569 (1982).
15. M.H. Palmer, R.H. Findlay, W. Moyes et A.J. Gaskell. J. Chem. Soc. Perkin Trans. 2, 841 (1975).
16. W. Schafer, A. Schweig, K. Dimroth et K. Kauter. J. Am. Chem. Soc. **98**, 4410 (1976).
17. (*a*) G. Märkl. Angew. Chem. Int. Ed. Engl. **5**, 846 (1966); (*b*) A. Ashe. J. Am. Chem. Soc. **93**, 3293 (1971).
18. A.F. Vasil'ev, L.V. Vilkov, N.P. Ignatova. N.N. Mel'nikov, V.V. Negrebetski, N.I. Shvetsov-Shilovskii et L.S. Khaikin. Dokl. Chem. (Engl. Transl.), **183**, 945 (1968).
19. A. Schmidpeter, M. Nagibi, P. Mayer et H. Tautz. Chem. Ber. **116**, 1468 (1983).
20. O.S. Diallo, L. Lopez, Y. Kandri Rodi et J. Barrans. Phosphorus, Sulfur Relat. Elem. Silicon **56**, 17 (1991).
21. M.J. Dewar et W. Thiel. J. Am. Chem. Soc. **99**, 4899 (1977).
22. M.J. Dewar et W. Thiel. J. Am. Chem. Soc. **99**, 4907 (1977).

Can. J. Chem. Downloaded from www.nrcresearchpress.com by 213.200.69.106 on 09/08/12
For personal use only.

Laser flash photolysis study of the photochemistry of *ortho*-benzoylbenzaldehyde

J.C. NETTO-FERREIRA
Departamento de Química, Universidade Federal Rural do Rio de Janeiro, Itaguaí, Rio de Janeiro, Brazil, 23851

AND

J.C. SCAIANO
Department of Chemistry, University of Ottawa, Ottawa, Ont., Canada K1N 6N5

Received March 10, 1993

Can. J. Chem. Downloaded from www.nrcresearchpress.com by 213.200.69.106 on 09/08/12
For personal use only.

J.C. NETTO-FERREIRA and J.C. SCAIANO. Can. J. Chem. **71**, 1209 (1993).

Ketene-enols **4** and **5** have been generated by laser flash photolysis of *ortho*-benzoylbenzaldehyde (**3**) and kinetically and spectroscopically characterized. In benzene or acetonitrile, the *E* ketene-enol, **4**, shows absorption at 340 and 400 nm and a lifetime in excess of 1 ms, whereas the *Z* ketene-enol, **5**, shows maxima at 360 and 430 nm and a lifetime of only 1.5 μs. At shorter time scales we observed a weak absorption (λ_{max} = 580 nm) tentatively assigned to biradical **6** with a lifetime of 140 ns. The *E* ketene-enol is readily quenched by oxygen, dienophiles, methanol, and water, with quenching rate constants ranging from 3.6×10^3 M^{-1} s^{-1} (for methanol as a quencher) to 2.2×10^8 M^{-1} s^{-1} (for diethyl ketomalonate). At high water concentrations (typically >10 M) a new species, **7**, was detected showing maximum absorption at 510 nm and a growth lifetime of 7 μs. In deuterated water and using the same concentration as before we observed a formation lifetime for **7** of 10 μs, which results in an isotope effect of ~1.5. It is proposed that **5** is the main precursor for **7**. Steady-state irradiation of **3** in deaerated methanol leads to the formation of dihydroanthraquinone (**9**), a strongly colored and fluorescent (λ_{max} = 475 nm, τ_f = 29 ns) species, whereas 3-phenylphthalide (**2**, R = Ph) is the main product when the irradiation is performed in benzene. Steady-state quenching of product formation by diethyl ketomalonate gives a Stern–Volmer constant of 380 M^{-1} from which we conclude that **5** is the ketene-enol responsible for product formation, in agreement with the laser flash photolysis results.

J.C. NETTO-FERREIRA et J.C. SCAIANO. Can. J. Chem. **71**, 1209 (1993).

On a préparé les cétènes-énols **4** et **5** par photolyse flash au laser de l'*ortho* benzoylbenzaldéhyde (**3**) et on les a caractérisés cinétiquement et spectroscopiquement. Dans le benzène ou dans l'acétonitrile, le *E* cétène-énol, **4**, absorbe à 340 et à 400 nm et a un temps de vie de >1 ms tandis que le *Z* cétène-énol, **5**, montre des maxima à 360 et à 430 nm avec un temps de vie de 1,5 μs. Nous avons observé, dans des intervalles de temps plus courts, une faible absorption (λ_{max} = 580 nm) que nous avons attribué au biradical **6**, avec un temps de vie de 140 ns. Le *E* cétène-énol est facilement bloqué par l'oxygène, les diénophiles, le méthanol et l'eau avec des constantes de blocage allant de $3,6 \times 10^3$ M^{-1} s^{-1} (pour le méthanol comme agent de blocage) à $2,2 \times 10^8$ M^{-1} s^{-1} (pour le cétomalonate d'éthyle). Des concentrations élevées en eau (typiquement >10 M) permettent de déceler une nouvelle espèce présentant une absorption à 510 nm et un temps de croissance de 7 μs. Dans l'eau deutériée aux mêmes concentrations, on observe un temps de formation de **7** à 10 μs résultant d'un effet isotopique de 1,5 environ. On suggère que le composé **5** est le précurseur principal du composé **7**. L'irradiation à l'état stationnaire du composé **3** dans le méthanol désaéré conduit à la formation de la dihydroanthraquinone (**9**), un composé fortement coloré et fluorescent (λ_{max} = 475 nm, τ_f = 20 ns) tandis que le phthalide de phényl-3 (**2**, R = Ph) est le produit majoritaire lorsque l'irradiation a lieu dans le benzène. Le blocage à l'état stationnaire des produits obtenus à partir du cétomalonate d'éthyle donne une constante de Stern–Volmer de 380 M^{-1} qui nous porte à conclure que le composé **5** est le cétène-énol responsable de la formation des produits en accord avec les résultats de la photolyse flash au laser.

[Traduit par la rédaction]

Introduction

Photoenolization of *ortho*-alkyl ketones is now a very well understood process. In most cases the transients involved in this intramolecular hydrogen abstraction reaction are well characterized as is the mechanism for the photoenolization process (1–20).

This is not the case for *ortho*-formyl aromatic aldehydes or ketones. Similarly to *ortho*-alkyl-substituted aromatic ketones, these compounds can form *ortho*-quinodimethane-like structures by intramolecular hydrogen abstraction (reaction [1]). However, little is known about the transients involved in this process, especially for the case of *ortho*-acylbenzaldehydes.

From the photochemical point of view, *ortho*-phthaldehyde (**1**; R = H) is the most studied *ortho*-dicarbonyl compound (21–26). In this case, intramolecular hydrogen abstraction leads to the formation of a 1,4 biradical (τ = 1.6 μs). Two triplet states, which are not responsible for product formation, are the precursors of this biradical, having lifetimes of 6 and 36 ns. Photolysis of *ortho*-phthalaldehyde leads to the formation of phthalide (**2**, R = H) and an isomeric mixture of dimeric products (21–25). Similar photochemical behavior has been observed for 2,3- and 3,4-diformylpyridines (27), 2,3-diformylquinolines (27), and 2,3- and 3,4-diformylthiophenes and selenophenes (28).

[1]

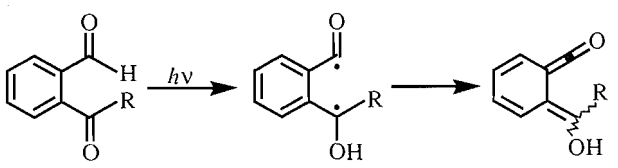

1; R = alkyl, aryl, H

Recently, the ketene-enol probably involved in the decay

of the biradical from *ortho*-phthalaldehyde has been characterized by nitrogen matrix isolation studies (29).

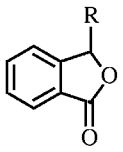

2

The involvement of this kind of ketene-enol intermediate was also confirmed by low-temperature infrared studies on *ortho*-benzoylbenzaldehyde (**3**) (30). This compound is known to form 3-phenylphthalide (**2**, R = Ph) in an almost quantitative yield upon irradiation at low temperature (reaction [2]) (31).

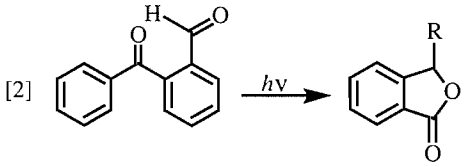

[2]

3 **2**; R = Ph

The reactions of ketenes have been the subject of a recent review (32), and their reaction with water has been the subject of theoretical studies (33, 34).

In this paper we report an extensive study of the photochemistry of **3** in which we identify and characterize the transients involved in the phototransformation of reaction [2]. Our approach involves a combination of laser flash photolysis, steady-state irradiation, and emission and absorption spectroscopy.

Experimental part

Materials

The solvents benzene (Aldrich), acetonitrile (Fisher), and methanol (Aldrich) were used as received and were all Spectrograde.

Maleic anhydride (Aldrich), diethyl ketomalonate (Aldrich), dimethyl acetylenedicarboxylate (Aldrich), water (Omni, HPLC grade), and deuterated water (MSD isotopes) were used as received.

ortho-Benzoylbenzaldehyde was synthesized from the methyl ester of *ortho*-benzoylbenzoic acid using a literature procedure (35, 36). Its physical and spectroscopic properties agree well with the values found in the literature and are in accord with the proposed structure: mp 66–67°C (lit. (36) mp 64–67°C); ^{1}H NMR ($CDCl_3$) δ (ppm): 9.98 (s, 1H), 7.75 (m, 9H); MS *m/z* (%): 210 (100, M^+), 181(94), 105(28), 77(39).

General techniques

UV–VIS spectra were recorded with a HP-8451A diode array spectrometer. Phosphorescence and fluoroescence spectra were recorded with a Perkin Elmer LS-50 spectrofluorimeter.

GC analyses were carried out on a Perkin Elmer model 8320 capillary gas chromatograph employing a 12-m J&W bonded-phase vitreous BP1 silicone column. GC–MS analyses were performed in a Hewlett–Packard model 5995 system using a similar column.

Melting points were determined in a Mel-Temp apparatus and were not corrected.

The ^{1}H NMR spectrum was recorded on a Varian 200 MHz spectrometer model Gemini-200, using $CDCl_3$ as a solvent.

Product studies and quantum yield determinations

Typical samples were 1.0 mL containing 0.02 M ketone in benzene or methanol and were deaerated by bubbling with oxygen-free nitrogen. The samples were contained in Pyrex tubes and irradiated in a merry-go-round with nine RPR-3000 Å lamps. The products were characterized by GC–MS. Dodecane was used as internal standard in the steady-state quenching experiments.

For the quantum yield determinations the photofragmentation of valerophenone in benzene was employed as actinometer, taking the quantum yield of acetophenone formation as 0.30 (37).

Laser flash photolysis

Samples were contained in cells constructed of 7 mm × 7 mm Suprasil tubing and were deaerated by bubbling oxygen-free nitrogen. The samples were irradiated with the pulses (308 nm, ~5 ns, ≤25 mJ/pulse) from a Lumonics model 510 excimer laser operated with Xe–HCl–He mixtures. The signals from an RCA-4840 photomultiplier were initially captured by a Tektronix 2440 transient digitizer and then transferred to a Macintosh IIci computer that controlled the experiment and provided suitable storage, processing, and hard-copy capabilities. This system operated under LabVIEW-2.2 software and will be described in detail elsewhere. The system is otherwise similar to that employed in earlier work (38, 39).

Results

Phosphorescence spectroscopy

The phosphorescence spectrum for ketone **3** in an EPA (diethylether:isopentane:ethanol) glass at 77 K shows vibrational structure characteristic of a n,π^* triplet ketone. From the 0,0 emission band in this spectrum we obtain a triplet energy of 69.5 kcal/mol, which is very close to the value of 69 kcal/mol for benzophenone (40, 41). Clearly the emitting chromophore is localized on the benzophenone moiety. The small difference may reflect out-of-plane twisting of the *o*-formyl phenyl system.

Laser flash photolysis studies

(a) Transient characterization

Irradiation of a 3.0 mM solution of **3** in benzene or acetonitrile with the 308-nm pulses from an excimer laser leads to the formation of a readily detectable transient that shows absorptions at 340 and 400 nm (Fig. 1*a*). The decay monitored at either of these two maxima shows short- and long-lived transients; the latter has a lifetime in excess of 1 ms. It was not quenched by the usual triplet quenchers such as dienes and was only moderately quenched by oxygen. To this species we assign the structure **4**, corresponding to the *E* ketene-enol, consistent with the intramolecular hydrogen transfer mechanism usually observed in the case of photoenolizable ketones (vide infra) (3, 16).

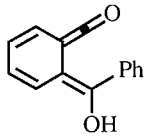

4

On shorter time scales, the spectrum recorded 0.5 μs after laser excitation is considerably different from that recorded at a delay of 5 μs (Fig. 1*b*). In the former case the decay shows contributions from a short- and a long-lived transient (Fig. 2). Subtracting the spectrum at 5 μs delay, i.e., that due to **4**, from the early spectrum corresponding to the sum of the short- and long-lived transients, we obtain maxima at 360 and 430 nm for the short-lived species (Fig. 3). To this intermediate, having a lifetime of 1.5 μs, we assign structure **5**, corresponding to the *Z* ketene-enol. This is the first example where the *Z* and *E* enols show significant spectral differences.

Can. J. Chem. Downloaded from www.nrcresearchpress.com by 213.200.69.106 on 09/08/12
For personal use only.

Can. J. Chem. Downloaded from www.nrcresearchpress.com by 213.200.69.106 on 09/08/12
For personal use only.

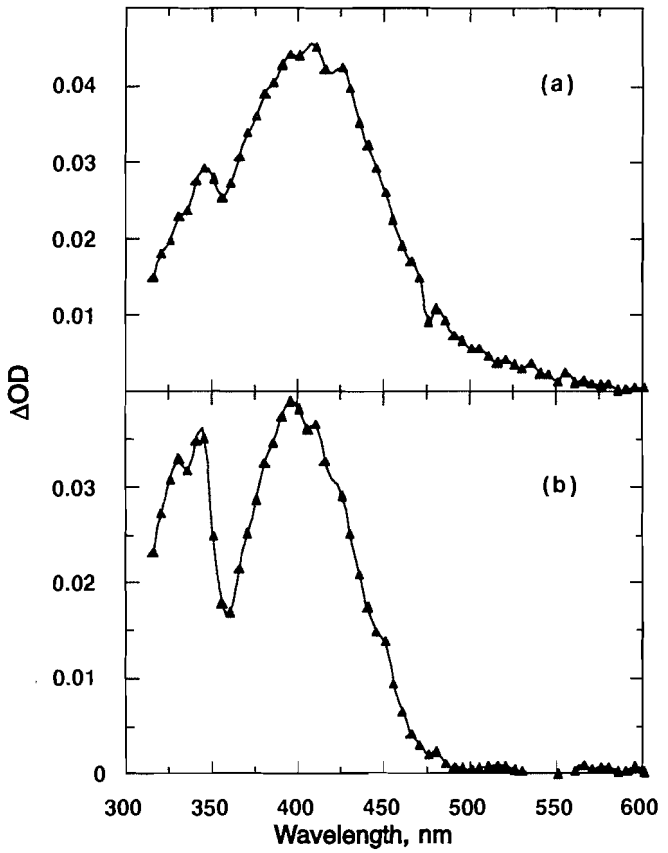

FIG 1. (*a*) Transient absorption spectrum obtained on 308-nm excitation of 3.0 mM *ortho*-benzoylbenzaldehyde (**3**) in benzene and recorded 0.5 μs after the laser pulse. (*b*) Same as above but recorded 5 μs after the laser pulse.

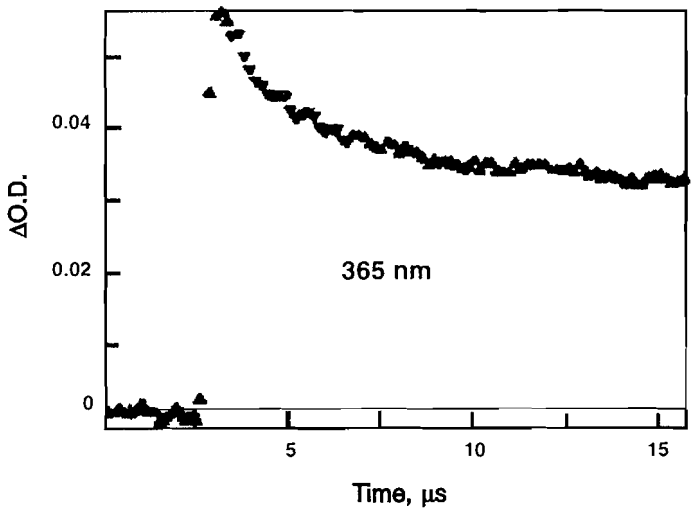

FIG. 2. Decay trace monitored at 365 nm due to the transient generated by excitation of 3.0 mM *ortho*-benzoylbenzaldehyde (**3**) in benzene.

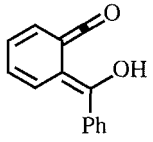

5

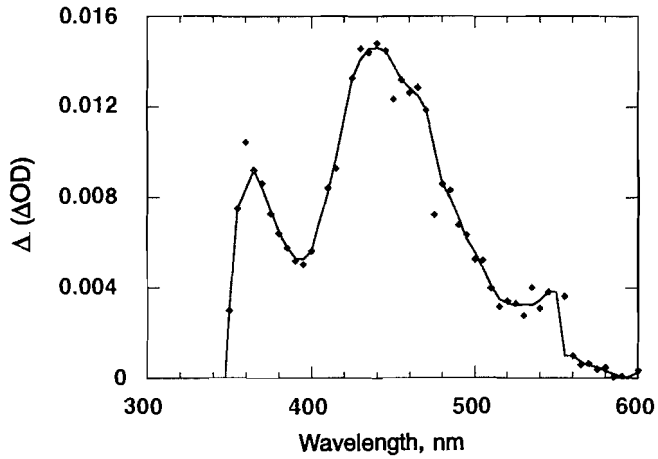

FIG. 3. Difference spectrum from the subtraction of spectrum in Fig. 1*b* from the one in Fig. 1*a* and attributed to the *Z* ketene-enol.

In benzene, at 320 nm, we observe the formation of a new species, that grows-in with first-order kinetics and a lifetime of 1.5 μs at room temperature. Since **2** (R = Ph) has a strong absorption at this wavelength we can attribute this signal to product formation. The fact that **5** is decaying with the same lifetime as **2** is growing-in indicates that the former species is the precursor of the latter (**2**, R = Ph).

The biradical **6**, precursor of the ketene-enols **4** and **5**, has a very weak absorption (only 0.005 absorbance units) at 580 nm, as previously indicated (31), with a lifetime of 140 ns. This species is quenched by oxygen (k_q = 2.8 × 10^9 M^{-1} s^{-1}) in benzene, but not by 1,3-cyclohexadiene, a typical triplet quencher, which is fully consistent with its assignment as the 1,4-biradical. We note that, just as in other systems involving photoenolization, this biradical can also be viewed as the triplet state of the ketene-enol.

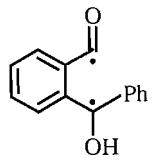

6

Attempts to detect the triplet state of **3** were (not surprisingly) unsuccessful. Addition of 1,3-cyclohexadiene in concentrations of 0.025 M had virtually no effect (≤10%) on the yield of ketene in benzene. Thus, if the precursor of the ketene is the triplet ketone one must conclude that its lifetime is less than 2 ns. Naturally, an alternative explanation would be that the reaction leading to the ketene does not take place from the triplet manifold; given the phosphorescence spectrum of **3** (vide supra) and the fact that benzophenones normally undergo intersystem crossing with unit efficiency this explanation appears unlikely.

(b) Intermolecular reactivity

The *E* ketene-enol **4** can be quenched by dienophiles, methanol, water, and oxygen. For example, oxygen quenching is rather sluggish with k_q = 2.5 × 10^6 M^{-1} s^{-1}; reaction of photoenols with oxygen has been reported before (42, 43). For diethyl ketomalonate we measured a quenching rate constant of 2.2 × 10^8 M^{-1} s^{-1}. Dimethyl

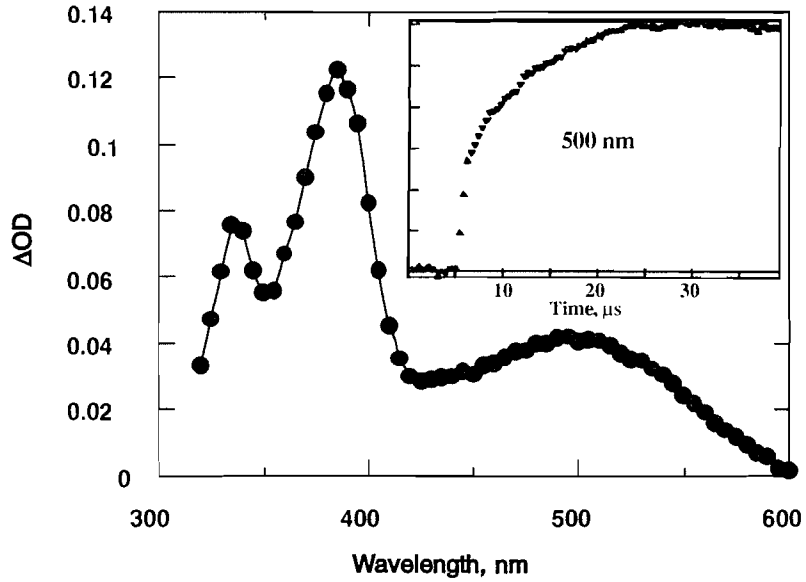

FIG. 4. Absorption spectrum obtained on 308-nm excitation of *ortho*-benzoylbenzaldehyde (**3**) in acetonitrile:water (4:1). Insert: Growth recorded at 500 nm due to **7**, generated as above.

TABLE 1. Quenching rate constants for the *E* ketene-enol **4** derived from **3**[a]

Quencher	$k_q(M^{-1}\ s^{-1})$	
	4	**8**[b]
Oxygen	2.5×10^6	
Maleic anhydride	4.1×10^6	1.4×10^4
Diethyl ketomalonate	2.2×10^8	7.8×10^5
Dimethyl acetylenedicarboxylate	$<10^3$	
Methanol	3.6×10^3	7.9×10^3
Water	1.1×10^3	

[a]In acetonitrile.
[b]From Ref. 48.

acetylenedicarboxylate in concentrations up to 0.08 M did not have any effect on the lifetime of the *E* ketene-enol.

In neat methanol (ca. 25 M) the lifetime for **4** is greatly decreased (τ = 12 μs). A plot of the rate constant for ketene decay as a function of methanol concentration in the 0–6 M range led to a linear plot and a quenching rate constant of $\sim 3 \times 10^3\ M^{-1}\ s^{-1}$. Interestingly, extrapolation to neat methanol yields almost exactly the observed lifetime of 12 μs.

Quenching by water follows a linear dependence with water concentration (0–12 M range examined) and is remarkable since, besides the considerable shortening of the lifetime for **4**, one can observe the formation of a new species. The formation of this new intermediate is most readily observed when the water concentration exceeds 10 M. The broad absorption centered at 510 nm (Fig. 4) grows-in with first-order kinetics and a lifetime of 7 μs for its formation (see insert in Fig. 4). That this quenching process involves some form of hydrogen transfer can be shown by using deuterated water as a quencher. In this case the species absorbing at 510 nm grows-in with a lifetime of 10 μs, resulting in a deuterium isotope effect of ~1.5 (44). To this species we assign structure **7**, corresponding to the ketene-hydrate, formed by a nucleophilic attack of water on the ketene. It should be noted that the formation of **7** is much faster than the decay of **4**, by at least an order of magnitude. We were initially puzzled by this observation; however, we believe that **7** results from water addition to **5**, rather than **4**. While the extensive spectral overlap in the presence of water makes it difficult to carry out accurate kinetic measurements on **5**, the traces at 430 nm reveal quite clearly that **5** is decaying in the same time scale in which **7** is formed. From the growth kinetics for **7**, one can estimate a rate of reaction of **5** with water of $\sim 1.5 \times 10^4\ M^{-1}\ s^{-1}$. Of course, the ketene-hydrate (or carboxylic acid enol) is expected to form the carboxylic acid (in a process too slow for our detection system) and ultimately to form the same lactone as reaction [2]. This mechanism is similar to that proposed for the reaction of arylketenes with alcohols (45). Other ketene hydrates have recently been reported (46, 47). Quenching of the ketene-enol by water in methanol solvent was slightly faster than in acetonitrile ($k_q > \sim 1 \times 10^4\ M^{-1}\ s^{-1}$).

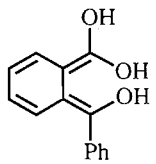

7

Table 1 shows quenching rate constants for several quenchers. These values are comparable to those reported for the quenching of the vinylketene **8** (10, 48).

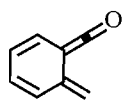

8

Product studies and quantum yield determinations

Irradiation of deaerated samples containing **3** in benzene leads to the formation of 3-phenylphthalide (**2**, R = Ph) as

Can. J. Chem. Downloaded from www.nrcresearchpress.com by 213.200.69.106 on 09/08/12
For personal use only.

Can. J. Chem. Downloaded from www.nrcresearchpress.com by 213.200.69.106 on 09/08/12
For personal use only.

the main product (see Scheme 1), together with a small amount of anthraquinone. In methanol, which as already pointed out is a good quencher for the *E* ketene-enol (**4**), we observed the development of an intense yellow color in the solution after a few minutes of irradiation. In fact, this colored species is so long-lived in the absence of oxygen that under continuous irradiation its formation could be monitored in a conventional UV–visible spectrophotometer (Fig. 5). This new species is strongly fluorescent, showing emission with λ_{max} 475 nm, and a fluorescence lifetime of 29 ns. Oxygen bubbling causes an almost complete disappearance of the yellow color and eliminates the fluorescence emission. Surprisingly, GC analysis of the irradiation product from **3** in methanol did not show the formation of any new product, although the amount of anthraquinone formed in this case is considerably higher than in benzene. Interestingly no evidence was found for the formation of **11**, a possible product from the rearrangement of **10**.

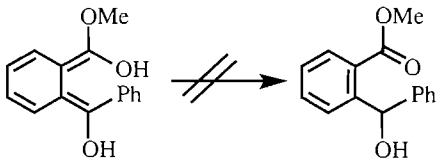

10 **11**

This observation can be explained by assuming that in methanol the formation of dihydroanthraquinone (**9**), a highly colored and fluorescent species (10, 11, 49–51), is probably favored by an increase in the electrophilicity of the carbon atom responsible for the cyclization reaction. The overall process is shown in Scheme 1.

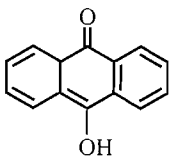

9

Quantum yield determinations were carried out using the formation of acetophenone from valerophenone as a relative actinometer (Φ = 0.30) (37). In benzene we measured a value of 0.18 ± 0.02 for the quantum yield of formation of 3-phenylphthalide (**2**, R = Ph) under nitrogen.

Steady state quenching

As proposed before, the irradiation of *ortho*-benzoylbenzaldehyde (**3**) can lead to the formation of two isomeric ketene-enols, **4** and **5**, and inspection of their structures and transient behavior leads us to assume that product formation must come from the short-lived species, the *Z* isomer **5**. To confirm this reasoning we decided to use the fact that diethyl ketomalonate is an excellent quencher for the *E* ketene-enol **4** (vide supra), and tried to quench product formation under steady-state irradiation conditions. To carry out these measurements, several samples, each containing 1 mL of a stock solution of **3** in benzene and different concentrations for the quencher, were irradiated in a merry-go-round inside a Rayonet photoreactor equipped with nine RPR-3000 Å lamps. Figure 6 shows a plot of relative quantum yield against diethyl ketomalonate from which one can obtain K_{SV} = 380 M^{-1}. Assuming the reactive species is **5**, and taking into account its lifetime, leads to a rate constant for quenching of 2.5 × 10^8 M^{-1} s^{-1}, a value remarkably similar to that measured directly for **4** (2.2 × 10^8 M^{-1} s^{-1}). In contrast, if one were to assume the reactive species to be **4**, then, given the known lifetime (>1 ms) and experimentally measured rate constant, one would have predicted a Stern–Volmer slope of ≥2 × 10^5 M^{-1}, in sharp disagreement with the experimental value of 380 M^{-1}. Thus, comparison of transient and quantum yield data identify **5** as the reactive species leading to product formation.

Discussion

The excited triplet state of *ortho*-benzoylbenzaldehyde, **3**, shows typical benzophenone-like characteristics. Compound **3** can be viewed as having two chromophores, resembling benzophenone and benzaldehyde. The triplet state from the latter is expected to be located at higher energy (~4–5 kcal/mol higher) than the benzophenone triplet.

Photolysis of **3** involves the expected photoenolization, a process that has been well characterized in many other aromatic ketones with labile hydrogens in the *ortho* position (3, 16). The case of **3** is rather special since the transient products are the ketene-enols **4** and **5**. We assume that the precursor to these enols is the triplet state of **3**; while this species has not been detected, its lifetime would be expected to be very short. The observation is in line with those for other photoenolizable benzophenones (10–12, 50, 52).

Interestingly, **4** and **5** show significant differences in their absorption spectra, as illustrated in Figs. 1*b* and 3. MM2 calculations suggest that the enol moiety can approach planarity most easily in the case of **5**; increased conjugation presumably leads to the red shift in the case of the short-lived **5**.

Two results are rather surprising: (*a*) that reaction of the ketene with water and alcohols would follow first-order kinetics and (*b*) that formation of **7** would involve either **5** (the *Z* ketene-enol) exclusively, or at least that formation from this precursor would be much faster and more efficient than from **4**.[2] There are clear examples in the literature where water addition has been demonstrated to frequently (but not always) (44) require two molecules of water (47, 53, 54) and theoretical work provides an interpretation for this observation (33, 34). If we think of these two water molecules as one for adding and the second one as "assisting" the addition, we can conceive that in the case of **5** the hydroxylic group already present can provide this assistance in an intramolecular fashion. Naturally, in the case of **4** the -OH group is not suitably oriented to assist water addition or at least not to do this with comparable efficiency. In addition, the fact that **5** is more planar than **4** may facilitate the nucleophilic attachment by water by delocalizing more easily the negative charge generated, in a manner similar to that proposed for phenylketene (55).

The isotope effect observed in the hydration reaction (H/D ~ 1.5) is in line with those observed by other groups for other ketene reactions with water, which values frequently fluctuate between 1.5 and 2.5 (44, 54–57).

Acknowledgements

Some of the early experiments in this work were carried out at the National Research Council laboratories in Ottawa,

[2]We cannot exclude some slow underlying formation of **7** from **4**.

Can. J. Chem. Downloaded from www.nrcresearchpress.com by 213.200.69.106 on 09/08/12
For personal use only.

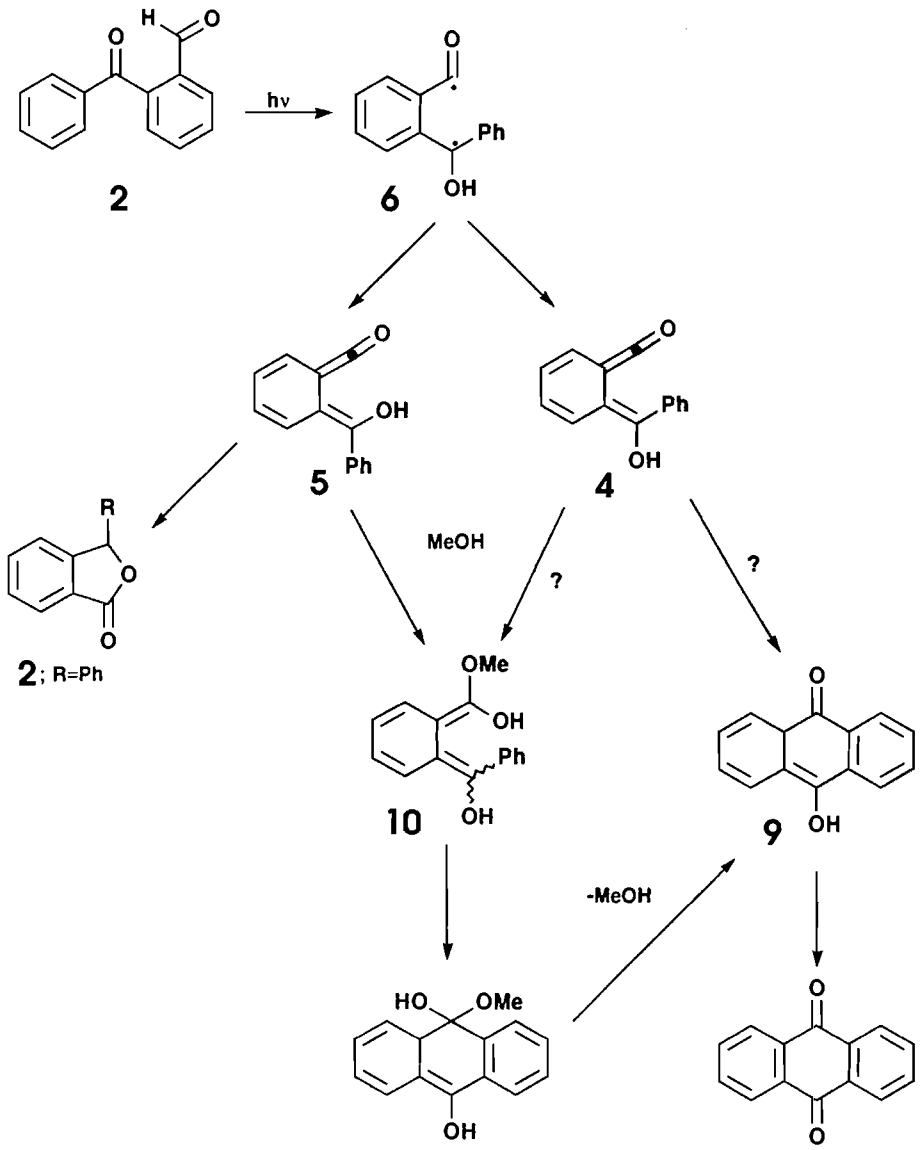

SCHEME 1

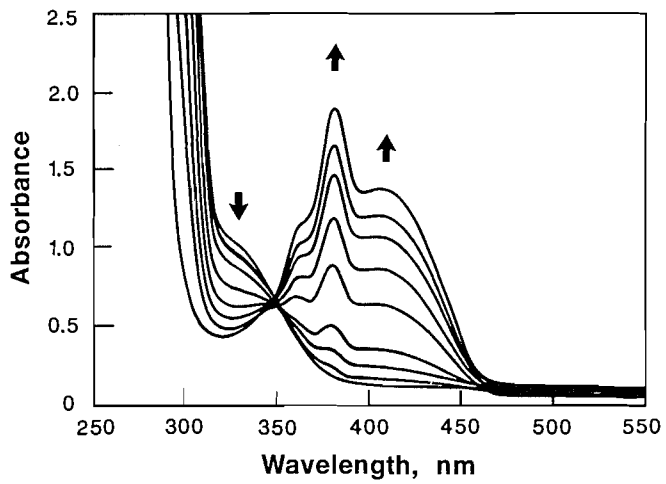

FIG. 5. Absorption spectra at different times (0, 1, 2, 4, 8, 12, 16, 20, and 28 min) obtained on steady state irradiation ($\lambda_{irradiation}$ = 300 nm) of **3** in methanol.

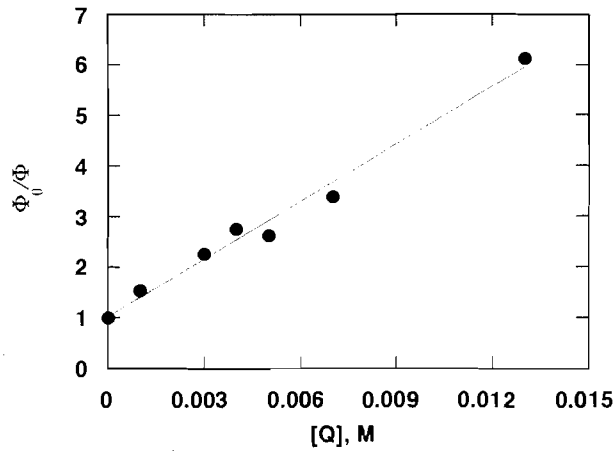

FIG. 6. Quenching plot of relative quantum yield for phthalide (**2**, R = Ph) formation from **3** vs. [diethyl ketomalonate].

Canada; the support received during that stage of the work is gratefully acknowledged. Thanks are due to Mr. D. Lindsay (NRC, Ottawa) for carrying out the GC–MS measurements. This research has been supported by an operating grant (J.C.S.) from the Natural Sciences and Engineering Research Council of Canada.

1. N.C. Yang and C. Rivas. J. Am. Chem. Soc. **83**, 2213 (1961).
2. E.F. Zwicker, L.I. Grossweiner, and N.C. Yang. J. Am. Chem. Soc. **85**, 2671 (1963).
3. P.G. Sammes. Tetrahedron, **32**, 405 (1976).
4. R. Haag, J. Wirz, and P.J. Wagner. Helv. Chim. Acta, **60**, 2595 (1977).
5. P.K. Das, M.V. Encinas, R.D. Small, Jr., and J.C. Scaiano. J. Am. Chem. Soc. **101**, 6965 (1979).
6. J.C. Scaiano. Chem. Phys. Lett. **73**, 319 (1980).
7. K.H. Grellmann, H. Weller, and E. Tauer. Chem. Phys. Lett. **95**, 195 (1983).
8. A. Beckett and G. Porter. Trans. Faraday Soc. **59**, 2051 (1963).
9. E.F. Ullman and K.R. Huffman. Tetrahedron Lett. 1863 (1965).
10. G. Porter and M.F. Tchir. Chem. Commun. 1372 (1970).
11. G. Porter and M.F. Tchir. J. Chem. Soc. A, 3772 (1971).
12. P.K. Das and J.C. Scaiano. J. Photochem. **12**, 85 (1980).
13. K. Uji-Ie, K. Kikuchi, and H. Kokubun. J. Photochem. **10**, 145 (1979).
14. P.J. Wagner and C.-P. Chen. J. Am. Chem. Soc. **98**, 239 (1976).
15. N.D. Heindel, E.W. Sarver, and M.A. Pfau. Tetrahedron Lett. 3579 (1968).
16. P.J. Wagner. Pure Appl. Chem. **49**, 259 (1977).
17. B. Guérin and L.J. Johnston. Can. J. Chem. **67**, 473 (1989).
18. J.C. Netto-Ferreira and J.C. Scaiano. J. Am. Chem. Soc. **113**, 5800 (1991).
19. M. Pfau, S. Combrisson, J.E. Rowe, Jr., and N.D. Heindel. Tetrahedron, **34**, 3459 (1978).
20. P.J. Wagner, D. Subrahmanyam, and B.S. Park. J. Am. Chem. Soc. **113**, 709 (1991).
21. A. Schönberg and A. Mustafa. J. Am. Chem. Soc. **77**, 5755 (1955).
22. J. Kagan. Tetrahedron Lett. 6097 (1966).
23. S.P. Pappas and J.E. Blackwell, Jr. Tetrahedron Lett. 3337 (1968).
24. K.F. Cohen, J.T. Pinhey, and R.J. Smith. Tetrahedron Lett. 4729 (1968).
25. D.A. Harrison, R.N. Schwartz, and J. Kagan. J. Am. Chem. Soc. **92**, 5793 (1970).
26. J.C. Scaiano, M.V. Encinas, and M.V. George. J. Chem. Soc. Perkin Trans. 2, 724 (1980).
27. G. Quequiner and A. Godard. C. R. Seances Acad. Sci. Ser. C.: **269**, 1648 (1969).
28. C. Paulmier, J. Bourguinon, J. Morel, and P. Pastour. C. R. Seances Acad. Sci. Ser. C: **270**, 494 (1970).
29. J. Gebicki and S. Kuberski. J. Chem. Soc. Chem. Commun. 1364 (1988).
30. M. Tada and T. Maeda. Chem. Ind. (London), 742 (1976).
31. M. Pfau, J. Molnar, and N.D. Heindel. Bull. Chim. Soc. Fr. **34**, 164 (1983).
32. T.T. Tidwell. Acc. Chem. Res. **23**, 273 (1990).
33. M.T. Nguyen and A.F. Hegarty. J. Am. Chem. Soc. **106**, 1552 (1984).
34. J. Andraos, A.J. Kresge, M.R. Peterson, and I.G. Csizmadia. J. Mol. Struct. (Theochem), **232**, 155 (1991).
35. W.A. Bonner. J. Am. Chem. Soc. **85**, 439 (1963).
36. M. Metlesics, T. Anton, M. Chaykovsky, V. Toome, and L.H. Sternbach. J. Org. Chem. **33**, 2874 (1968).
37. P.J. Wagner, P.A. Kelso, A.E. Kemppainen, J.M. McGrath, H.N. Schott, and R.G. Zepp. J. Am. Chem. Soc. **94**, 7506 (1972).
38. J.C. Scaiano. J. Am. Chem. Soc. **102**, 7747 (1980).
39. J.C. Scaiano, M. Tanner, and D. Weir. J. Am. Chem. Soc. **107**, 4396 (1985).
40. S.L. Murov. Handbook of photochemistry. Marcel Dekker, New York. 1973.
41. I. Carmichael and G.L. Hug. Spectroscopy and intramolecular photophysics of triplet states. *In* Handbook of organic photochemistry. *Edited by* J.C. Sciano. CRC Press, Boca Raton, Fla. 1989. p. 369.
42. M. Pfau, E.W. Sarver, and N.D. Heindel. C.R. Acad. Sci. 1167 (1969).
43. M. Juliard and M. Pfau. J. Chem. Soc. 184 (1976).
44. E. Bothe, A.M. Dessouki, and D. Schulte-Frohlinde. J. Phys. Chem. **84**, 3270 (1980).
45. J. Jähme and C. Rüchard. Tetrahedron Lett. **23**, 4011 (1982).
46. B. Urwyler and J. Wirz. Angew. Chem. Int. Ed. Engl. **29**, 790 (1990).
47. M. Barra, T.A. Fisher, G.J. Cernigliaro, R. Sinta, and J.C. Scaiano. J. Am. Chem. Soc. **114**, 2630 (1992).
48. P. Schiess, M. Eberle, M. Huys-Francotte, and J. Wirz. Tetrahedron Lett. **25**, 2201 (1984).
49. P.G. Sammes and T.W. Wallace. J. Chem. Soc. Perkin Trans. 1, 1845 (1975).
50. N.D. Heindel, J. Molnar, and M. Pfau. J. Chem. Soc. Chem. Commun. 1373 (1970).
51. W.A. Henderson, Jr. and E.F. Ullman. J. Am. Chem. Soc. **87**, 5424 (1965).
52. K. Uji-ie, K. Kikuchi, and H. Kokubun. Chem. Lett. **5**, 499 (1977).
53. P.J. Lillford and D.P.N. Satchell. J. Chem. Soc. B, 889 (1968).
54. D.P.N. Satchell and R.S. Satchell. Chem. Soc. Rev. **4**, 231 (1975).
55. A.D. Allen, A.J. Kresge, N.P. Schepp, and T.T. Tidwell. Can. J. Chem. **65**, 1719 (1987).
56. E. Bothe, H. Meier, D. Schulte-Frohlinde, and C. von Sonntag. Angew. Chem. Int. Ed. Engl. **15**, 380 (1976).
57. S.H. Kabir, H.R. Saikaly, and T.T. Tidwell. J. Am. Chem. Soc. **101**, 1059 (1979).

Can. J. Chem. Downloaded from www.nrcresearchpress.com by 213.200.69.106 on 09/08/12
For personal use only.

Synthesis and fluorescence studies of oligoethylene glycols labeled with naphthalene by a phosphate triester linkage

SAM LEE AND MITCHELL A. WINNIK[1]

Department of Chemistry and Erindale College, University of Toronto, 80 St. George St., Toronto, Ont., Canada M5S 1A1

Received October 28, 1992

SAM LEE and MITCHELL A. WINNIK. Can. J. Chem. **71**, 1216 (1993).

A series of oligoethylene glycols, incorporating two pendant naphthyl groups along the interior of the chain using a phosphate triester linkage, have been prepared. The synthetic methodology has been discussed in the context of eventually providing a route to polymers labeled in a similar fashion. The steady state fluorescence behavior of these compounds is reported briefly. Relatively little excimer emission is observed. The synthetic intermediates to the phosphates, the 2-(1-naphthyl)ethyl *N*,*N*-diisopropylphosphoramidites of triethylene glycol and tetraethylene glycol, show exciplex fluorescence. The fluorescence from these latter compounds exhibits some sensitivity to solvent quality.

SAM LEE et MITCHELL A. WINNIK. Can. J. Chem. **71**, 1216 (1993).

On a préparé une série d'oligoéthylène glycols incorporant deux groupes naphtyles pendants à l'intérieur de la chaîne au moyen d'un lien triésterphosphorique. On discute de la méthode de synthèse dans le but de trouver éventuellement une voie d'accès aux polymères marqués de la même façon. On rapporte brièvement le comportement de la fluorescence de ces composés à l'état stationnaire. On observe relativement peu d'émission d'excimère. Les intermédiaires obtenus, lors de la synthèse des phosphates, les (naphtyl-1)éthyl-2 *N*,*N*-diisopropylphosphoramidites du triéthylène glycol et du tétraéthylène glycol montrent la fluorescence de l'exciplexe. La fluorescence de ces derniers composés est d'une certaine manière sensible à la qualité du solvant.

[Traduit par la rédaction]

Introduction

We have used fluorescence techniques extensively to study the kinetics of end-to-end cyclization in polymer chains (1, 2). Our interest in cyclization experiments stems from the idea that when chromophores are attached to the ends of flexible molecules (or polymers), the quenching kinetics can be used as a tool to study issues of conformation and dynamics in these molecules (3, 4). The cyclization rate is sensitive not only to the chain length and the chemical structure (chain stiffness) of the polymer, but also to polymer–solvent interactions.

An interesting variation on this theme would be to examine the case where the two excimer-forming chromophores occupy well-defined sites in the chain interior. Such experiments would probe the backbone-to-backbone cyclization of a linear polymer chain. It is well known that the ends of a polymer chain move faster than the interior segments: the dangling chain ends introduce extra drag on the interior groups undergoing large amplitude motion. Recently, Perico et al. developed a model that describes the relaxation behavior of bond segments at specified locations within the polymer chain (5–8). This model suggests that the rate of cyclization will depend on the specific location of the cyclizing groups within the chain interior. We believe that it is important to have a means of testing these ideas.

We require linear polymers that contain two chromophores separated by a well-defined number of monomer units and that are symmetrically positioned within the chain. These polymers must exhibit a narrow molecular weight distribution and be free from any adventitious quenchers and fluorescent impurities. At present, no synthetic strategies have been developed to generate the desired materials.

Our approach to this synthetic problem is to couple an alcohol-derivatized fluorescent label to hydroxy-terminated polymers. The chosen protocol is an adaptation of the "phosphite triester" method currently used in solid-phase oligonucleotide synthesis (9–14). This report describes the adopted strategy and the synthesis of some model compounds (oligomers) to test this strategy.

Results and discussion

Synthesis

The well-established synthetic protocols that have been developed for DNA synthesis are based on features that are equally attractive to our work with polymers. The key step, involving the reaction of a derivatized phosphoramidite with an appropriate alcohol to form a phosphite bond, proceeds through a rapidly generated and highly reactive tetrazoylphosphoramidite (11, 12, 15). Exceptional reactivity is required when a polymer with an excess of 10^3 monomer units contains only a single hydroxyl group on each end with possible limited accessibility due to steric constraints presented by the coiled chain. Phosphoramidite chemistry is a particularly efficient reaction, generating internucleotide links in near-quantitative yields. Since the purification of a polymer sample, where the distinctiveness of the product is based only on the presence of two functional groups, is difficult and time consuming, highly efficient reactions are desirable. The final product, after oxidative work-up, is a phosphate triester linking together three different alcohols, which is the exact type of connectivity required for linking a pendant probe molecule to a fixed point within a linear polymer chain. Finally, the polymers studied most frequently, polyethylene glycol and polystyrene, are stable to the reactive phosphite intermediates generated in each step of this synthetic sequence.

In adapting this methodology to polymers, we began by examining the reactions with oligomeric model compounds. This allows us to carry out functionalization reac-

[1]Author to whom correspondence may be addressed.

Can. J. Chem. Downloaded from www.nrcresearchpress.com by 213.200.69.106 on 09/08/12
For personal use only.

Can. J. Chem. Downloaded from www.nrcresearchpress.com by 213.200.69.106 on 09/08/12
For personal use only.

tions in which the intermediates and products can be well characterized. Hence, polyethylene glycols have been used as models for the chemistry of larger polymers. In the study of polymers, pyrene would be the natural choice of the excimer-forming chromophore. For these shorter chains, we speculated that pyrene excimer formation might be too extensive. With the ready availability of 2-(1-naphthyl)-ethanol as a reagent, we chose to prepare molecules containing two naphthyl groups attached to the ends of the polyethylene glycol oligomers.

Scheme 1 outlines the synthesis of the desired phosphoramidites. The dichloridite of 1-naphthalene ethanol was prepared by the reaction of the alcohol with phosphorus trichloride using a modification of the standard literature procedure for such compounds (16, 17): by using a five-fold excess of phosphorus trichloride, the phosphorodichloridite, **1**, can be obtained in near quantitative yield, compared to a maximum of 80% often reported in literature preparations of similar derivatives (17). A high conversion becomes important when we eventually use the precious starting material, 4-(1-pyrenyl)butanol, which gives derivatives that are more difficult to isolate. The phosphitylating agent, **2**, was also prepared by using standard literature procedures. Both the dichloridite, **1**, and the chloridite, **2**, were isolated by simple vacuum distillation.

The phosphitylating agent, **2**, can be used in two distinct approaches to generate the desired end products. We chose to react **2** with triethylene glycol and with tetraethylene glycol to obtain the bis-phosphoramidites **3** and **4**, respectively. These two intermediates exhibit interesting fluorescence behavior on their own.

The final reaction in the sequence involves the activation and removal of each of the two diisopropylamino protecting groups on the bis-phosphoramidite with a weak acid, tetrazole. A highly reactive tetrazoylphosphoramidite intermediate is generated, which undergoes nucleophilic displacement in the presence of an alcohol to form a phosphite. The optimal conditions for this step were not investigated. Taking guidance from the work of Ogilvie, Damha, and co-workers (18, 19), who synthesized branched RNA fragments using a similar coupling approach, a reactant ratio of 1:3:12 bis-phosphoramidite:alcohol:tetrazole was used in THF at room temperature. This is an extremely rapid reaction. Monitored by TLC for the disappearance of the bis-phosphoramidite (as the hydrolysis product) and the appearance of the bis-phosphite, the reaction was found to be complete within 5–10 min in comparison to an average of 2 h used by Damha et al. to synthesize branched RNA fragments. The difference in the rate of reaction may be due, in part, to reduced steric constraints from an extremely flexible oligoethylene glycol chain, and to the ease of activation of these bis-phosphoramidites by tetrazole compared to the RNA derivatives (19). The corresponding bis-phosphate triester was obtained after oxidative work-up, by adding an excess of aqueous iodine solution to the bis-phosphite. In this manner, two sets of compounds were obtained. The first set, obtained from the bis-phosphoramidite **3**, are oligoethylene glycols where the two naphthalene probes are separated by three oxyethylene monomer units. The ends of this labelled glycol are flanked by either one or two monomer units (compounds **131** and **232**, respectively). The second set, obtained from the bis-phosphoramidite **4**, have four oxyethylene monomer units separating the two chromophores. The ends of this labelled glycol are also flanked by either one or two monomer units (compounds **141** and **242**, respectively)

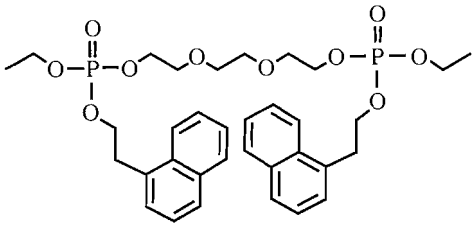

131

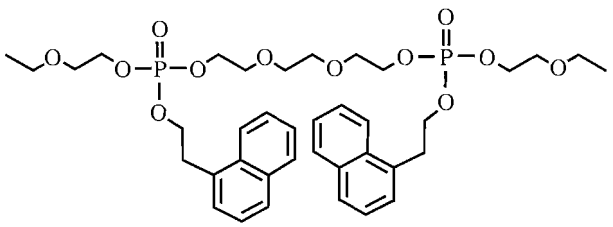

232

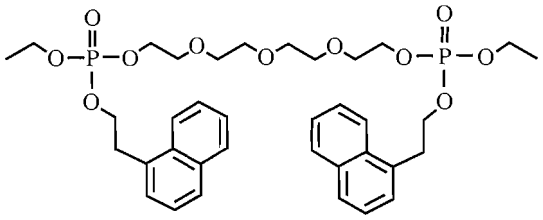

141

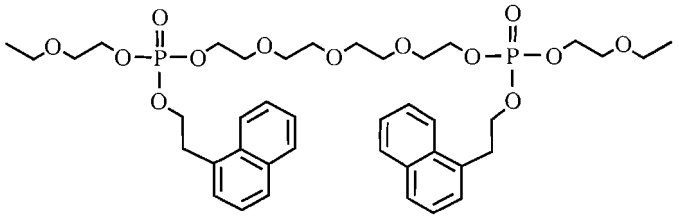

242

An alternative coupling strategy involves the synthesis of the simple phosphoramidites, **5** and **6**, from the phosphitylating agent **2**. Each of these two phosphorylating reagents can be coupled to triethylene glycol and to tetraethylene glycol to give the same bis-phosphates. Reaction of 3:1:12 phosphoramidite (**6**):tetraethylene glycol:tetrazole in THF at room temperature gave **242** in 72% yield, comparable to the yields obtained using the former coupling strategy.

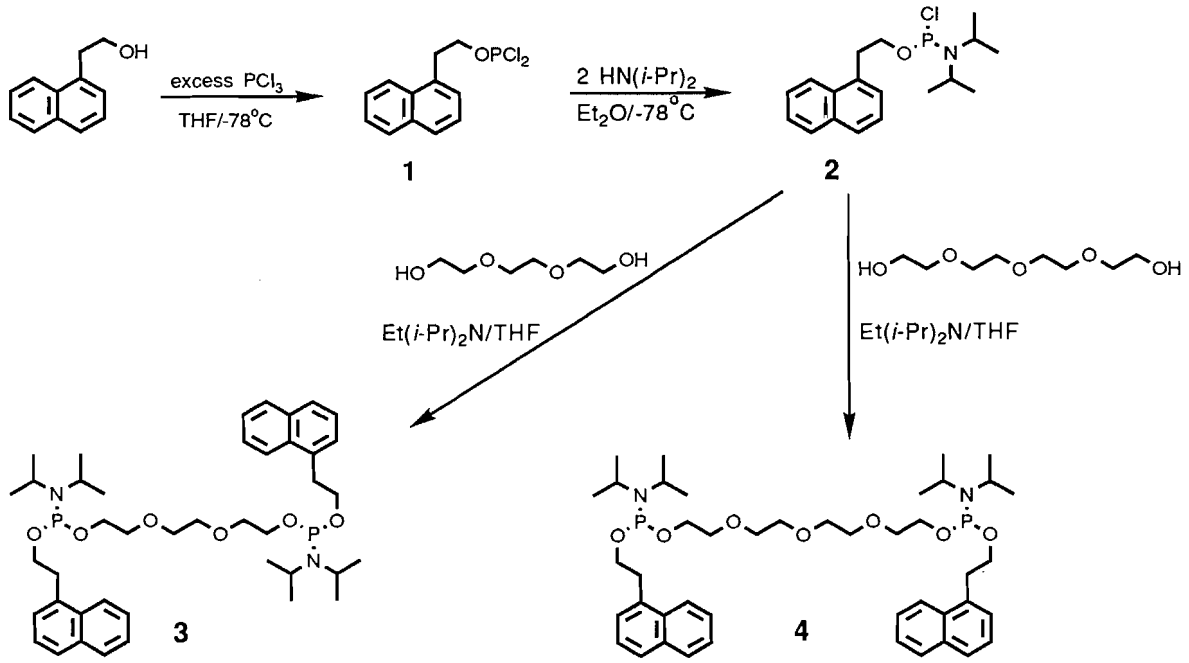

SCHEME I

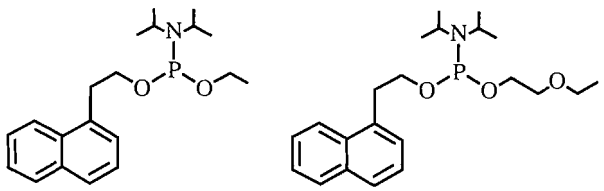

5 6

For fluorescence studies, the phosphate, **7**, was also synthesized to serve as a model compound.

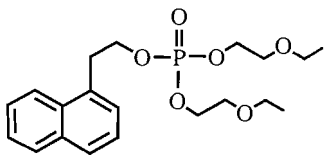

7

Fluorescence

The steady state fluorescence spectrum of the model phosphate **7**, in THF, is shown in Fig. 1. The fluorescence spectra of the phosphoramidites **3**, **4**, and **6**, also presented in Fig. 1, are normalized to the 0–0 fluorescence band of the model phosphate at 323 nm. All four compounds exhibit the structured fluorescence characteristic of the locally excited naphthalene chromophore with two major peaks at 323 and 338 nm, two smaller peaks at 328 and 333 nm, and a shoulder at 350 nm. However, the phosphoramidites all show an additional long tail, extending to longer wavelengths, which peaks at about 485 nm. The proportionate size of this tail does not change from a concentration of 3×10^{-6} to 4×10^{-5} M. This extra emission comes from the *intramolecular* exciplex formed from the interaction of the excited naphthalene moiety with the amino (or the phosphoramidite) group.[2] While the amount of intramolecular exciplex emission is not extensive, the amount of fluorescence self-quenching in these molecules is considerable. When the total fluorescence intensity from the phosphate **7** is compared with the total fluorescence intensity from the phosphoramidite **6**, at equal concentrations, the phosphoramidite only exhibits 17% of the total fluorescence emission from **7**.

The bis-phosphoramidites **3** and **4** show even more exciplex emission than **6**. The excited chromophore can form a complex, either with the "proximal" amino group in a way similar to that of the model phosphoramidite **6**, or with the "distal" amino group at the other end of the molecule via end-to-end cyclization. In the case of **4**, where the phosphoramidite groups are separated by four monomer units, the exciplex emission is indeed greater than in **6**, but only by a small amount. The shorter bis-phosphoramidite **3**, where the phosphoramidite groups are separated by three monomer units, exhibits substantially greater exciplex emission than either **4** or **6**.

These observations provide some qualitative information about the timescale of terminal cyclization in triethylene glycol and tetraethylene glycol when they are "end-labelled" with exciplex-forming phosphoramidites. Exciplex formation between excited state naphthalene and the proximal amino group is, clearly, very fast. In the longer bis-phosphoramidite **4**, the effect of the distal amino group is minimal because the excited naphthalene is, on average,

[2]The phosphate group alone does not appear to have an effect on exciplex formation or fluorescence quenching. The fluorescence spectrum and the total fluorescence intensity of **6**, **7**, and 2-(1-naphthyl)ethanol in THF do not change when either triethyl phosphate or triethyl phosphite is present at a concentration of 0–10^{-2} M.

Can. J. Chem. Downloaded from www.nrcresearchpress.com by 213.200.69.106 on 09/08/12
For personal use only.

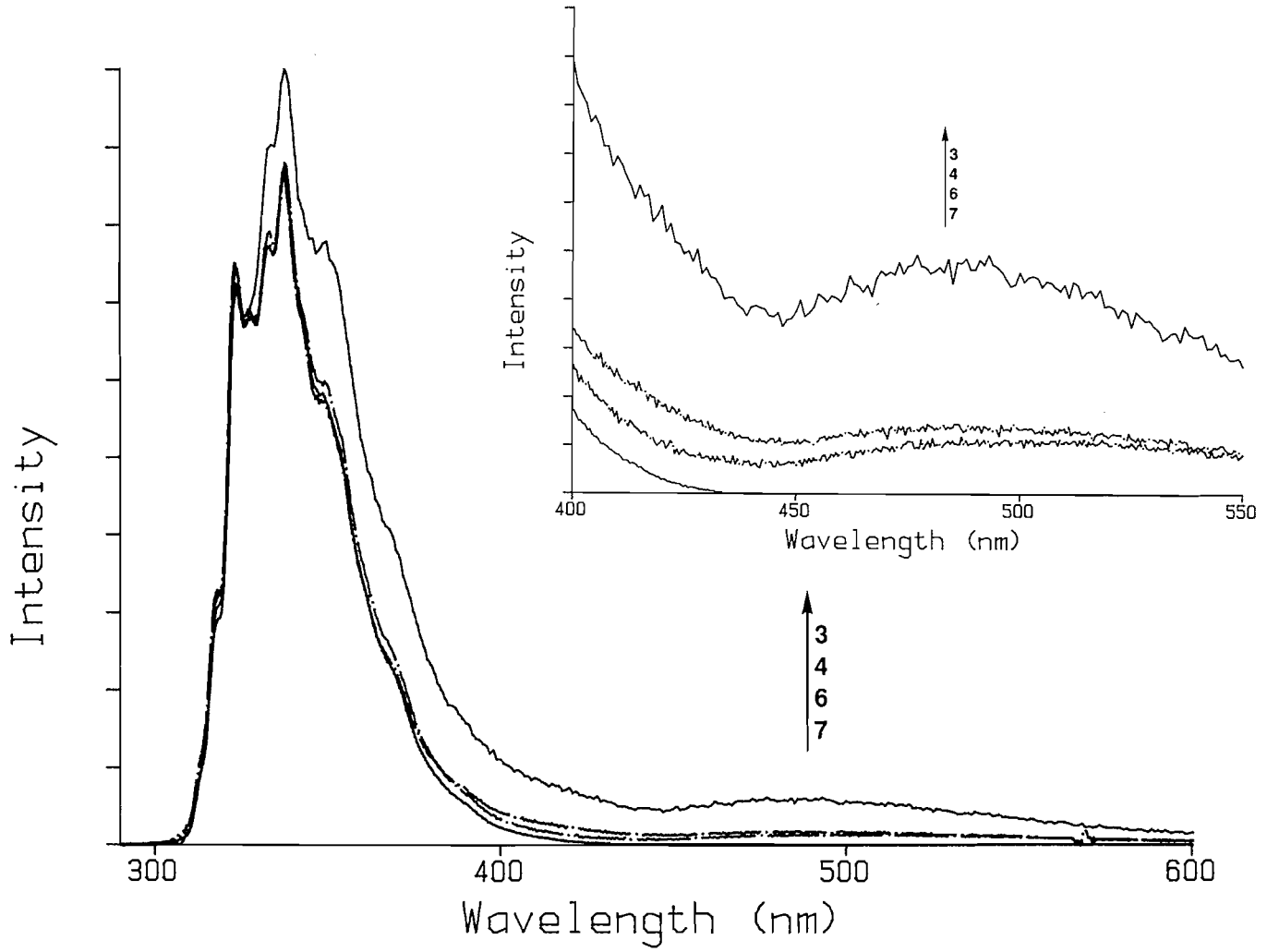

FIG. 1. Normalized fluorescence spectra of the model phosphate (**7**), model phosphoramidite (**6**), and the bis-phosphoramidites (**3** and **4**) in THF at room temperature. [Chromophore] = 10^{-6} M for all four compounds. $\lambda_{excitation}$ = 282 nm. Inset: expansion of the 400–550 nm region.

quenched by the proximal amino group before it can encounter the amino group at the other end of the chain. In the shorter bis-phosphoramidite **3**, cyclization of the chain ends is much faster, and quenching of the excited naphthalene chromophore by the distal amino group is now competitive with quenching by the proximal amino group. If the lifetime of **6** were known, a lower limit for the rate of terminal cyclization by **3** and an upper limit for the terminal cyclization by **4** could be established.

The fluorescence spectra of these same compounds in diethyl ether were also recorded (Fig. 2). The broad, structureless exciplex band of each phosphoramidite was obtained by subtracting the normalized fluorescence spectrum of the model phosphate from each of the corresponding phosphoramidites. Two broad peaks are observed: one centred at 360 nm and the other at 485 nm. The band centred at 360 nm might be due to a second, higher energy, exciplex. The increased amount of exciplex emission by the phosphoramidites in this solvent can be explained, in part, by the polarity of the solvent. It is well known that exciplex intensity increases with decreasing solvent polarity. However, while the bis-phosphoramidite **3** shows the greatest amount of exciplex fluorescence, as expected, the bis-phosphoramidite **4** exhibits less exciplex emission than that of the model phosphoramidite **6**. The nature of this reversal might be due to the solvent quality. Diethyl ether is a non-solvent for polyethylene oxide and a very poor solvent for polyethylene glycol. The degree of incompatibility depends on the number of monomer units in the polymer chain. While triethylene glycol is solvated as a random coil by diethyl ether, it is possible that tetraethylene glycol contains a sufficient number of oxyethylene monomer units to cause the coil to collapse. This might then raise the conformational barriers to exciplex formation.

Excitation spectra can provide some information about the ground state conformation of the chromophores within the coil. Figure 3 compares the excitation spectrum obtained by monitoring the emission at 323 nm (fluorescence from locally excited naphthalene) with the spectrum obtained by monitoring the emission at 485 nm (fluorescence from the exciplex). If a ground state naphthalene–amine complex existed prior to excitation, the excitation spectrum for the exciplex would be red-shifted relative to the spectrum for the single naphthalene. The identical excitation spectra ob-

Can. J. Chem. Downloaded from www.nrcresearchpress.com by 213.200.69.106 on 09/08/12
For personal use only.

Can. J. Chem. Downloaded from www.nrcresearchpress.com by 213.200.69.106 on 09/08/12
For personal use only.

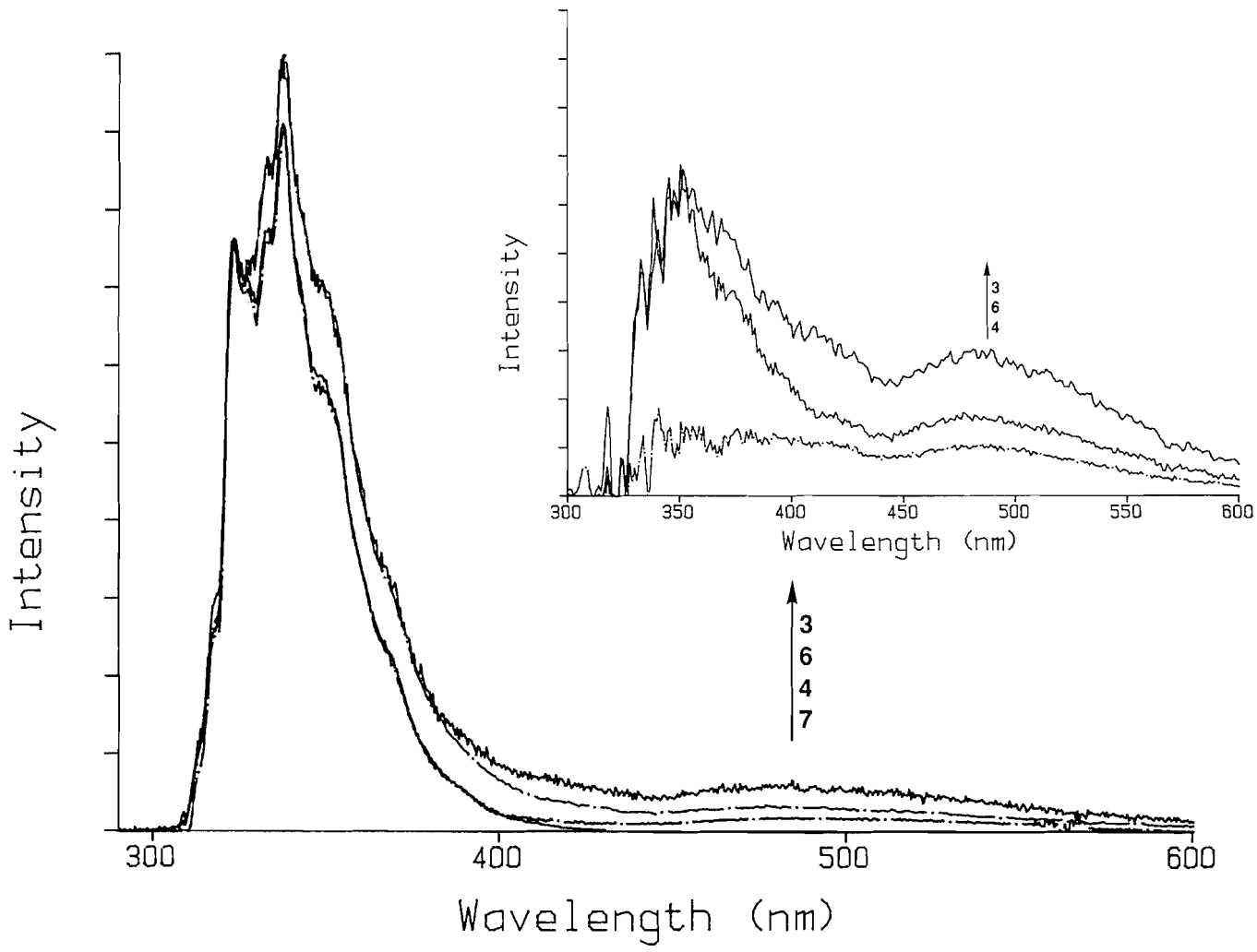

FIG. 2. Normalized fluorescence spectra of the model phosphate (**7**), model phosphoramidite (**6**), and the bis-phosphoromadites (**3** and **4**) in diethyl ether at room temperature. [Chromophore] = 10^{-6} M for all four compounds. $\lambda_{excitation}$ = 282 nm. Inset: exciplex bands obtained by subtraction of the phosphate fluorescence spectrum from the corresponding phosphoramidite fluorescence spectrum.

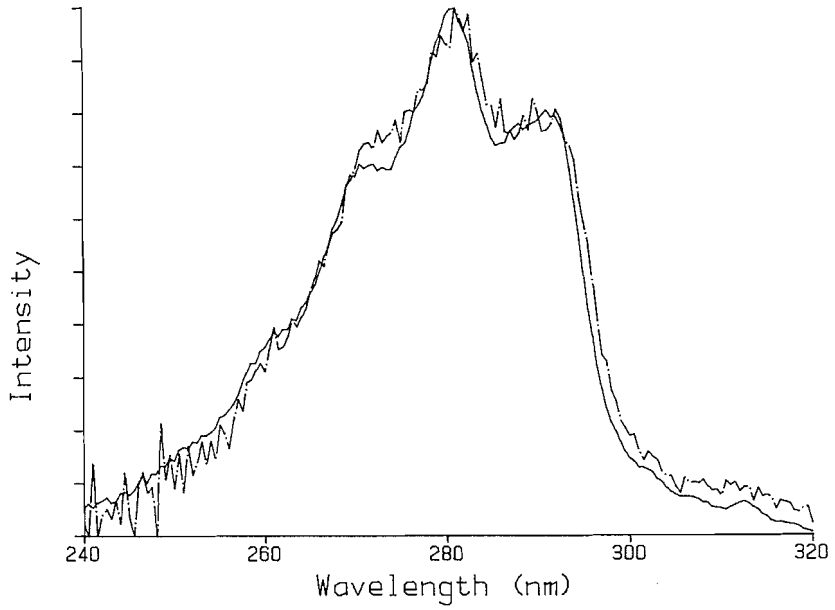

FIG. 3. Excitation spectra of the bis-phosphoramidite **4** in diethyl ether monitored at 323 nm (——) and at 485 nm (–·–·–).

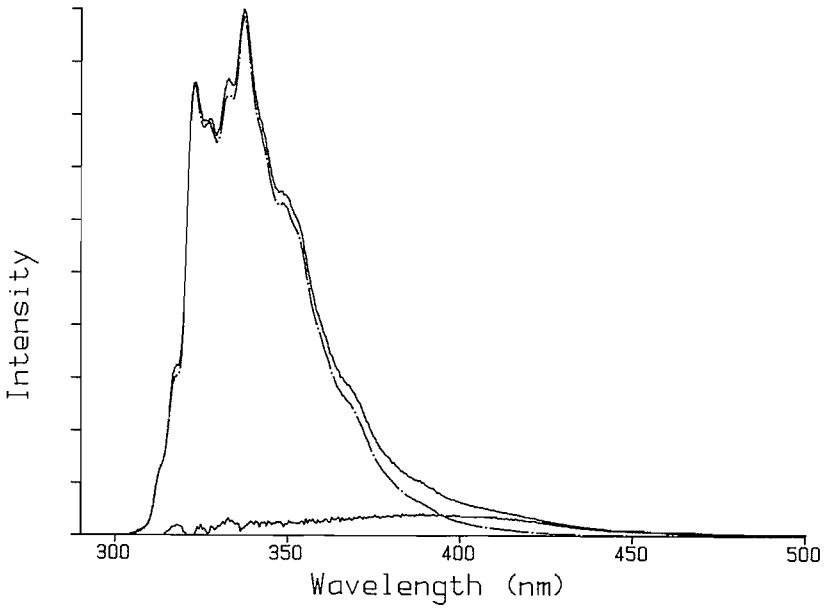

FIG. 4. Normalized fluorescence spectra of the bis-phosphate **242** (——) and the model phosphate **7** (—·—) in diethyl ether, normalized at 323 nm. [Glycol] = 10^{-6} M for both compounds. $\lambda_{excitation}$ = 282 nm. The excimer band was obtained from subtraction of the normalized spectra.

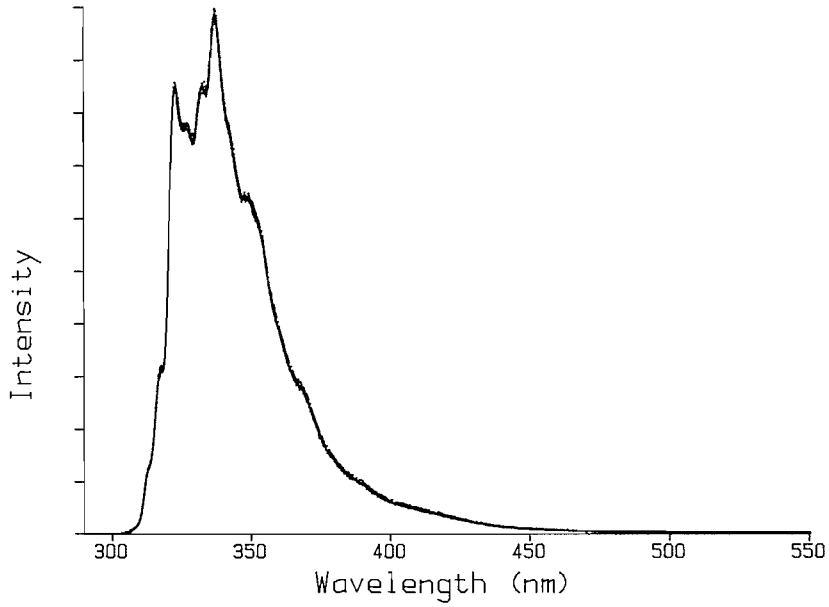

FIG. 5. Normalized fluorescence spectra of **131**, **232**, **141**, and **242** in diethyl ether, normalized to the 0–0 band at 323 nm. [Bis-phosphate] = 10^{-6} M for all four compounds. $\lambda_{excitation}$ = 282 nm.

served in this system indicate an absence of any strong preassociation between the naphthalene and amine groups prior to excitation. If the coil of the bis-phosphoramidite **4** is indeed collapsed relative to that of **3**, it is still swollen with enough solvent to permit conformational changes.

The fluorescence spectrum of the bis-phosphate **242** is compared with the model phosphate **7** in Fig. 4. The structured fluorescence characteristic of the single excited naphthalene chromophore is apparent in the fluorescence of **242**. In this case, the long tail extending to longer wavelengths is due to excimer emission. This broad, structureless band, centred at 400 nm, can be obtained by subtraction of the normalized spectra. Since the intramolecular excimer is formed via backbone-to-backbone cyclization of the oligoethylene glycol, the bis-phosphates, where the naphthalene probes are separated by three monomer units, would be expected to show more excimer emission than the bis-phosphates with the naphthalene probes separated by four monomer units. Furthermore, since longer dangling side chains present greater drag on the interior groups undergoing cyclization, the **232** and **242** bis-phosphates should cyclize at a slower rate (i.e., show less excimer emission) than the **131** and **141** bis-phosphates, respectively.

All four bis-phosphates have identical fluorescence spec-

Can. J. Chem. Downloaded from www.nrcresearchpress.com by 213.200.69.106 on 09/08/12
For personal use only.

tra in diethyl ether (Fig. 5). Similar results are also obtained in THF. The fact that they all show the same relative amount of excimer emission suggests that the rate of backbone-to-backbone cyclization is the same for all four compounds. This would mean that the rates of cyclization are affected similarly by the bulky end groups to a point where variations in the rate, resulting from a closer spacing between the naphthalene probes or from introducing longer dangling chain ends, cannot be detected. Fluorescence decay data have been obtained to support these conclusions. They will be presented in a future publication.

Experimental

General methods

All reactions were performed under an argon atmosphere. Thin-layer chromatography was performed on no. 5735 or no. 5554 Merck Kieselgel 60 F-254 analytical silical gel sheets. Preparative column chromatography was performed on 70–230 mesh silica gel (Aldrich, 60A). 4A Molecular sieves (BDH) were activated by heating at 450°C overnight.

NMR spectra were recorded on a Varian Associates XL-200 (^{31}P and ^{13}C), Gemini-300 (^{31}P), or XL-400 (^{1}H and ^{13}C) spectrometer at room temperature. ^{31}P NMR chemical shifts were referenced to 85% H_3PO_4 (external standard) where positive values indicate shifts downfield from the reference. All deuterated solvents (Aldrich) were used as received. ^{13}C and ^{31}P spectra were recorded in the proton decoupled mode. ^{13}C and ^{1}H NMR peak assignments were made with the aid of ^{13}C-APT, ^{1}H-COSY, and ^{1}H–^{13}C HETCOR spectra recorded on a Varian XL-400 spectrometer. IR spectra were recorded on a Nicolet 5DX FT-IR spectrometer. Mass spectra were recorded on a VG 70-250S mass spectrometer. UV spectra were recorded on an HP 8452A diode array spectrometer. Elemental analyses were performed by Galbraith Laboratories (Knoxville, Tenn.).

Reagents and chemicals

THF (Caledon) and diethyl ether (Caledon) were refluxed and distilled from sodium benzophenone ketyl. Dichloromethane (Caledon), triethylamine (BDH), diisopropylamine (BDH), diisopropylethylamine (Aldrich), acetonitrile (Caledon), and all glycols (Aldrich) were refluxed and distilled from calcium hydride. Absolute ethanol (Caledon) was refluxed and fractionally distilled from sodium. Phosphorus trichloride (BDH) was freshly distilled before use. Tetrazole (Dalton) was sublimed before use. A 0.1 M aqueous iodine solution, used for oxidative work-up, was made by dissolving iodine (2.6 g) in a mixture of 2,6-lutidine (80 mL) and water (2 mL).

Fluorescence spectra

Reagent grade diethyl ether (Caledon) and spectroscopic grade THF (Caledon) were refluxed and distilled from lithium aluminum hydride. Sample solutions were degassed by vigorously bubbling with argon (Union Carbide, <0.5 ppm oxygen, <3 ppm water), saturated with the solvent, for 20 min. Steady state fluorescence spectra were recorded at room temperature on a SPEX Fluorolog 2 spectrometer, at a right angle geometry, using 1-mm slits on both the excitation and emission sides. Emission spectra were corrected for scattering and the wavelength sensitivity of the photomultiplier tube.

*2-(1-Naphthyl)ethyl phosphorodichloridite (**1**)*

1-Naphthalene ethanol (Aldrich, 9.0 g, 0.05 mol in 100 mL THF) was added dropwise over 1 h to a cooled solution (−78°C) of phosphorus trichloride (25 mL, 0.29 mol) dissolved in THF (50 mL). The resulting solution was allowed to warm to room temperature and was stirred magnetically for an additional 5 h. The THF and excess phosphorus trichloride were removed under reduced pressure at room temperature to leave a clear, colourless liquid. This oil was vacuum distilled to give 13.7 g (96%) of the desired product: bp 111°C (0.05 Torr; 1 Torr = 133.3 Pa); IR (neat): 740, 775, 800, 1020, 1390, 1470, 1510, 1600 cm^{-1}; ^{31}P NMR ($CDCl_3$): 178.56; ^{1}H NMR ($CDCl_3$): 3.37 (t, 2H, $^{3}J_{HH'}$ = 7.4 Hz, $C_{10}H_7CH_2$), 4.46 (dt, 2H, $^{3}J_{PH}$ = 8.6 Hz, $^{3}J_{HH'}$ = 7.4 Hz, $POCH_2$), 7.26–7.95 (m, 7H, naphthyl-*H*); ^{13}C NMR ($CDCl_3$): 33.39 (d, $^{3}J_{PC}$ = 2.9 Hz, $C_{10}H_7CH_2$), 68.13 (d, $^{2}J_{PC}$ = 10.1 Hz, $POCH_2$), 123.18, 125.46, 125.71, 126.34, 127.25, 127.76, 128.93, 131.84, 132.47, 133.84 (naphthyl-*C*); mass spectrum, *m/e* (rel. intensity): 276 M + 4$^+$ (5), 274 M + 2$^+$ (17), 272 M$^+$ (19), 155 (100), 141 (56), 128 (13), 115 (25).

2-(1-Naphthyl)ethyl N,N-*diisopropylphosphoramidochloridite (**2**)*

Freshly distilled 2-(1-naphthyl)ethyl phosphorodichloridite (13.7 g, 0.05 mol) was distilled in diethyl ether (50 mL). The magnetically stirred solution was cooled to −78°C and diisopropylamine (14.1 mL, 0.10 mol in 100 mL diethyl ether) was added dropwise over 90 min. The resulting white slurry was stirred and allowed to slowly warm to room temperature overnight. The mixture was filtered through a coarse sintered-glass Schlenk tube under argon and the filtrate was concentrated to a cloudy, colourless oil under reduced pressure at room temperature. This material was purified by vacuum distillation to yield 13.4 g (79%) of the product as a clear, colourless oil: bp 137°C (0.05 Torr); IR (neat): 780, 880, 920, 980, 1160, 1370, 1400, 1460, 1510, 1600 cm^{-1}; ^{31}P NMR ($CDCl_3$): 182.05; ^{1}H NMR ($CDCl_3$): 0.97 (d, 6H, $^{3}J_{HH'}$ = 6.9 Hz, diastereotopic $CH(CH_3)_2$), 1.13 (d, 6H, $^{3}J_{HH'}$ = 6.8 Hz, diastereotopic $CH(CH_3)_2$), 3.23 (t, 2H, $^{3}J_{HH'}$ = 7.1 Hz, $C_{10}H_7CH_2$), 3.58 (m, 2H, $NCHMe_2$), 4.01 (m, 1H, diastereotopic $POCH_2$), 4.15 (m, 1H, diastereotopic $POCH_2$), 7.11–7.88 (m, 7H, naphthyl-*H*); ^{13}C NMR ($CDCl_3$): 23.23 (d, $^{3}J_{PC}$ = 10.6 Hz, diastereotopic $CH(CH_3)_2$), 23.96 (d, $^{3}J_{PC}$ = 5.6 Hz, diastereotopic $CH(CH_3)_2$), 34.19 (d, $^{3}J_{PC}$ = 6.9 Hz, $C_{10}H_7CH_2$), 45.91 (d, $^{2}J_{PC}$ = 12.9 Hz PNCH), 66.39 (d, $^{2}J_{PC}$ = 16.8 Hz, $POCH_2$), 123.98, 125.64, 125.72, 126.25, 127.43, 127.58, 129.04, 132.61, 134.20, 134.35 (naphthyl-*C*); mass spectrum, *m/e* (rel. intensity): 339 M + 2$^+$ (3), 337 M$^+$ (9), 302 (5), 155 (100), 141 (19), 128 (8), 115 (11).

Representative procedure for the synthesis of the phosphoramidites: 2-(1-naphthyl)ethyl-(2-ethoxyethyl N,N-*diisopropylphosphoramidite) (**6**)*

Freshly distilled 2-(1-naphthyl) *N,N*-diisopropylphosphoramidochloridite (3.0 g, 8.9 mmol) and diisopropylethylamine (15 mL, 86 mmol) were dissolved in dichloromethane (50 mL). The resulting solution was stirred magnetically at room temperature while 2-ethoxyethanol (0.9 mL, 9 mmol) was added dropwise to the solution over 5 min. The resulting mixture was stirred for an additional 2 h. At the end of the reaction, the mixture was diluted with 50 mL dichloromethane and washed twice with saturated brine. The organic layer was dried over sodium sulfate and the solution was concentrated under reduced pressure. The crude product was flash chromatographed on silica gel (90% hexane – 10% triethylamine eluent) to yield 3.0 g (86%) of the product as a clear, colourless oil: R_f 0.58 (90% hexane – 10% triethylamine); IR (neat): 780, 1020, 1125, 1185, 1360, 1395, 1460, 1510, 1600 cm^{-1}; UV (THF) λ_{max} nm (ε): 226 (3.36 × 10^4), 274 (6450), 282 (7560), 314 (370); ^{31}P NMR (C_6D_6): 147.69; ^{1}H NMR (C_6D_6): 1.07 (t, 3H, $^{3}J_{HH'}$ = 7.0 Hz, CH_2CH_3), 1.11 (d, 6H, $^{3}J_{HH'}$ = 6.8 Hz, diastereotopic $CH(CH_3)_2$), 1.15 (d, 6H, $^{3}J_{HH'}$ = 6.8 Hz, diastereotopic $CH(CH_3)_2$), 3.306 (q, 1H, $^{3}J_{HH'}$ = 7.0 Hz diastereotopic OCH_2CH_3), 3.309 (q, 1H, $^{3}J_{HH'}$ = 7.0 Hz diastereotopic OCH_2CH_3), 3.367 (br t, 1H, diastereotopic $POCH_2CH_2O$), 3.373 (br t, 1H, diastereotopic $POCH_2CH_2O$), 3.47 (t, 2H, $^{3}J_{HH'}$ = 5.5 Hz, $C_{10}H_7CH_2$), 3.58 (m, 2H, $NCH(CH_3)_2$), 3.75 (m, 1H, diastereotopic $C_{10}H_7CH_2CH_2$), 3.84 (m, 1H, diastereotopic $C_{10}H_7CH_2CH_2$), 4.02 (m, 2H, $POCH_2CH_2O$), 7.18–8.02 (m, 7H, naphthyl-*H*); ^{13}C NMR (C_6D_6): 15.46 (OCH_2CH_3), 24.67 (d, $^{3}J_{PC}$ = 7.4 Hz, $CH(CH_3)_2$), 35.37 (d, $^{3}J_{PC}$ = 6.6 Hz, $C_{10}H_7CH_2$), 43.13 (d, $^{2}J_{PC}$ = 12.4 Hz, PNCH), 63.07 (d, $^{2}J_{PC}$ = 16.4 Hz, $C_{10}H_7CH_2CH_2$), 64.16 (d, $^{2}J_{PC}$ = 16.6 Hz, $POCH_2CH_2O$), 66.48 (OCH_2CH_3), 70.96 (d, $^{3}J_{PC}$ = 7.3 Hz, $POCH_2CH_2O$), 124.15, 125.57, 125.68, 126.02, 127.28,

Can. J. Chem. Downloaded from www.nrcresearchpress.com by 213.200.69.106 on 09/08/12
For personal use only.

Can. J. Chem. Downloaded from www.nrcresearchpress.com by 213.200.69.106 on 09/08/12
For personal use only.

127.32, 128.99, 132.71, 134.36, 135.16 (naphthyl-*C*); mass spectrum, *m/e* (rel. intensity): 392 M + 1$^+$ (5), 391 M$^+$ (10), 348 (14), 190 (39), 155 (83), 141 (100), 115 (29). Anal. calcd. for $C_{22}H_{34}NO_3P$: C 67.50, H 8.75, N 3.58, P 7.91; found: C 67.96, H 8.93, N 3.82, P 7.70.

α,ω-Triethylene glycol-bis-[2-(1-naphthyl)ethyl N,N-*diisopropylphosphoramidite] (**3**)*

Addition of triethylene glycol (1.8 mL, 13 mmol) to a solution containing freshly distilled 2-(1-naphthyl) *N,N*-diisopropylphosphoramidochloridite (10.5 g, 31 mmol), diisopropylethylamine (60 mL, 340 mmol), and THF (120 mL) was followed by 90 min of stirring to yield 8.6 g (85%) of the product as a clear, colourless oil after work-up and flash chromatography (90% pentane – 10% triethylamine eluent): R_f 0.41 (90% pentane – 10% triethylamine); IR (neat): 740, 780, 980, 1020, 1130, 1185, 1360, 1395, 1460, 1510, 1595 cm^{-1}; ^{31}P NMR (C_6D_6): 147.68; ^{1}H NMR (C_6D_6): 1.11 (d, 12H, $^3J_{HH'}$ = 6.8 Hz, diastereotopic CH(CH_3)$_2$), 1.15 (d, 12H, $^3J_{HH'}$ = 6.8 Hz, diastereotopic CH(CH_3)$_2$), 3.377 (br t, 2H, diastereotopic POCH$_2$C*H*$_2$O), 3.383 (br t, 2H, diastereotopic POCH$_2$C*H*$_2$O), 3.47 (s, 4H, OC*H*$_2$C*H*$_2$O), 3.52 (t, 4H, $^3J_{HH'}$ = 5.4 Hz, $C_{10}H_7CH_2$), 3.58 (m, 4H, C*H*(CH$_3$)$_2$), 3.73 (m, 2H, diastereotopic $C_{10}H_7CH_2CH_2$), 3.82 (m, 2H, diastereotopic $C_{10}H_7$-CH_2CH_2), 4.03 (m, 4H, POC*H*$_2$CH$_2$O), 7.12–8.03 (m, 14H, naphthyl-*H*); ^{13}C NMR (C_6D_6): 24.70 (d, $^3J_{PC}$ = 7.4 Hz, diastereotopic CH(*C*H$_3$)$_2$), 24.72 (d, $^3J_{PC}$ = 7.2 Hz, diastereotopic CH(*C*H$_3$)$_2$), 35.41 (d, $^3J_{PC}$ = 6.5 Hz, $C_{10}H_7CH_2$), 43.16 (d, $^2J_{PC}$ = 12.4 Hz, PN*C*H), 63.04 (d, $^2J_{PC}$ = 16.3 Hz, $C_{10}H_7CH_2CH_2$), 64.21 (d, $^2J_{PC}$ = 16.6 Hz, PO*C*H$_2$CH$_2$O), 70.97 (O*C*H$_2$CH$_2$O), 71.68 (d, $^3J_{PC}$ = 7.3 Hz, POCH$_2$*C*H$_2$O), 124.22, 125.63, 125.75, 126.09, 127.33, 127.39, 129.03, 132.76, 134.40, 135.21 (naphthyl-*C*); mass spectrum, *m/e* (rel. intensity): 752 M$^+$ (2), 653 (1), 624 (2), 498 (10), 434 (8), 390 (5), 302 (8), 155 (100), 115 (8). Anal. calcd. for $C_{42}H_{62}N_2O_6P_2$: C 67.00, H 8.30, N 3.72, P 8.23; found: C 67.16, H 8.23, N 3.61, P 8.05.

α,ω-Tetraethylene glycol-bis-[2-(1-naphthyl)ethyl N,N-*diisopropylphosphoramidite] (**4**)*

Addition of tetraethylene glycol (2.6 mL, 15 mmol) to a solution containing freshly distilled 2-(1-naphthyl) *N,N*-diisopropylphosphoramidochloridite (11.4 g, 34 mmol), diisopropylethylamine (60 mL, 340 mmol), and THF (120 mL) was followed by 90 min of stirring to yield 10.6 g (88%) of the product as a clear, colourless oil after work-up and flash chromatography (90% pentane – 10% triethylamine eluent): R_f 0.28 (90% pentane – 10% triethylamine); IR (neat): 780, 975, 1025, 1130, 1185, 1360, 1395, 1460, 1510, 1595 cm^{-1}, ^{31}P NMR (C_6D_6): 147.64; ^{1}H NMR (C_6D_6): 1.11 (d, 12H, $^3J_{HH'}$ = 6.8 Hz, diastereotopic CH(CH_3)$_2$), 1.15 (d, 12H, $^3J_{HH'}$ = 6.7 Hz, diastereotopic CH(CH_3)$_2$), 3.370 (br t, 2H, diastereotopic POCH$_2$C*H*$_2$O), 3.376 (br t, 2H, diastereotopic POCH$_2$C*H*$_2$O), 3.45 (m, 8H, OC*H*$_2$C*H*$_2$OC*H*$_2$O), 3.52 (t, 4H, $^3J_{HH'}$ = 5.5 Hz, $C_{10}H_7CH_2$), 3.58 (m, 4H, C*H*(CH$_3$)$_2$), 3.72 (m, 2H, diastereotopic $C_{10}H_7CH_2CH_2$), 3.81 (m, 2H, diastereotopic $C_{10}H_7CH_2CH_2$), 4.02 (m, 4H, POC*H*$_2$CH$_2$O), 7.22–8.02 (m, 14H, naphthyl-*H*); ^{13}C NMR (C_6D_6): 24.70 (d, $^3J_{PC}$ = 7.4 Hz, diastereotopic CH(*C*H$_3$)$_2$), 24.72 (d, $^3J_{PC}$ = 7.3 Hz, diastereotopic CH(*C*H$_3$)$_2$), 35.39 (d, $^3J_{PC}$ = 6.5 Hz, $C_{10}H_7CH_2$), 43.15 (d, $^2J_{PC}$ = 12.5 Hz, PN*C*H), 63.03 (d, $^2J_{PC}$ = 16.4 Hz, $C_{10}H_7CH_2CH_2$), 64.20 (d, $^2J_{PC}$ = 16.6 Hz, PO*C*H$_2$CH$_2$O), 70.96 (O*C*H$_2$*C*H$_2$O-*C*H$_2$*C*H$_2$O), 71.65 (d, $^3J_{PC}$ = 7.2 Hz, POCH$_2$*C*H$_2$O), 124.20, 125.63, 125.74, 126.09, 127.32, 127.38, 129.02, 132.74, 134.38, 135.20 (naphthyl-*C*); mass spectrum, *m/e* (rel. intensity): 796 M$^+$ (2), 754 (1), 697 (1), 668 (2), 542 (9), 478 (4), 434 (6), 302 (8), 155 (100), 115 (7). Anal. calcd. for $C_{44}H_{66}N_2O_7P_2$: C 66.31, H 8.35, N 3.51, P 7.77; found: C 66.62, H 8.48, N 3.22, P 7.74.

*2-(1-Naphthyl)ethyl-di-(2-ethoxyethyl) phosphate (**7**)*

2-Ethoxyethanol (4.4 mL, 45 mmol) was added to a cooled solution (0°C) of freshly distilled 2-(1-naphthyl)ethyl phosphorodichloridite (5.3 g, 19 mmol) and triethylamine (10 mL, 72 mmol) in THF (100 mL). The resulting white slurry was stirred for 5 h at room temperature before it was oxidized by the dropwise addition of 0.1 M aqueous iodine solution until a pale yellow colour persisted. The mixture was diluted with dichloromethane (50 mL) and washed twice with 5% aqueous sodium bisulfite and twice with saturated brine. The aqueous layers were combined and back-extracted twice with dichloromethane. The combined organic layers were dried over sodium sulfate and concentrated to a clear, pale yellow liquid. The crude product was flash chromatographed on silica gel (diethyl ether – methanol, gradient 0–5% methanol, eluent) to give 6.0 g (78%) of the purified material: R_f 0.24 (50% diethyl ether – 50% dichloromethane); IR (neat): 780, 800, 1040, 1130, 1275, 1390, 1455, 1510, 1595 cm^{-1}; UV (THF) λ_{max} nm (ε): 226 (6.79 × 10^4), 272 (5580), 282 (6430), 292 (4430), 314 (335); ^{31}P NMR (C_6D_6): 0.44; ^{1}H NMR (C_6D_6): 1.00 (t, 6H, $^3J_{HH'}$ = 7.0 Hz, C*H*$_3$), 3.19 (q, 4H, $^3J_{HH'}$ = 7.0 Hz, C*H*$_2$CH$_3$), 3.29 (m, 4H, POCH$_2$C*H*$_2$O), 3.36 (t, 2H, $^3J_{HH'}$ = 7.4 and 7.5 Hz, $C_{10}H_7CH_2$), 4.07 (m, 4H, POC*H*$_2$CH$_2$O), 4.36 (dt, 2H, $^3J_{HH'}$ = 7.4 Hz, $^3J_{PH}$ = 8.6 Hz, $C_{10}H_7CH_2CH_2$); 7.17–7.98 (m, 7H, naphthyl-*H*); ^{13}C NMR (C_6D_6): 15.26 (*C*H$_3$), 34.05 (d, $^3J_{PC}$ = 6.0 Hz, $C_{10}H_7CH_2$), 66.38 (*C*H$_2$CH$_3$), 66.75 (d, $^2J_{PC}$ = 5.7 Hz, $C_{10}H_7CH_2CH_2$), 67.39 (d, $^2J_{PC}$ = 5.7 Hz, PO*C*H$_2$CH$_2$O), 69.48 (d, $^3J_{PC}$ = 6.9 Hz, POCH$_2$*C*H$_2$O), 123.96, 125.72, 125.78, 126.41, 127.47, 127.68, 129.03, 132.56, 133.60, 134.35 (naphthyl-*C*); mass spectrum, *m/e* (rel. intensity): 397 MH$^+$ (11), 269 (1), 243 (2), 154 (100), 115 (5). Anal. calcd. for $C_{20}H_{39}O_6P$: C 60.60, H 7.37, P 7.81; found: C 60.55, H 7.41, P 7.86.

*Representative procedure for the synthesis of the bis-phosphates: α,ω-triethylene glycol-bis-[2-(1-naphthyl)ethylethyl phosphate] (**131**)*

The freshly chromatographed phosphoramidite, **3** (3.0 g, 4.0 mmol), was coevaporated four times with dry diethyl ether to remove the residual triethylamine in the oil. This oil was dissolved in THF (90 mL) and 1 g of molecular sieves was added to the solution, which was then stirred magnetically for 10 min at room temperature, to dry the phosphoramidite. Ethanol was added to this mixture (1.0 mL, 17 mmol) and the coupling reaction was started by the addition of tetrazole (4.0 g, 60 mmol in 60 mL acetonitrile). The reaction was monitored by silica gel TLC (50% diethyl ether – 40% hexane – 10% triethylamine) by observing the disappearance of the bis-phosphoramidite (as the hydrolysis product) and the appearance of the bis-phosphite. In all cases, the reaction was essentially complete within 5–10 min. After 15 min, the phosphite triester intermediate was oxidized with an excess of 0.1 M aqueous iodine solution. The iodine solution was added dropwise until the orange-red colour persisted for over 5 min in the reaction mixture. The mixture was diluted with diethyl ether (150 mL) and washed twice with 5% aqueous sodium bisulfite and twice with saturated brine. The aqueous layers were combined and back-extracted three times with dichloromethane. The combined organic layers were dried over sodium sulfate and concentrated to a pale yellow oil. The crude product was flash chromatographed on silica gel (50% dichloromethane – 50% diethyl ether, followed by 50% dichloromethane – 40% diethyl ether – 10% methanol) to give 1.3 g (48%) of the purified material: R_f 0.66 (50% dichloromethane – 40% diethyl ether – 10% methanol); IR (neat): 780, 805, 1010, 1275, 1395, 1455, 1510, 1595 cm^{-1}; ^{31}P NMR ($CDCl_3$): −0.46; ^{1}H NMR ($CDCl_3$): 1.24 (br t, 6H, C*H*$_3$), 3.46 (t, 4H, $^3J_{HH'}$ = 7.3 Hz, $C_{10}H_7CH_2$), 3.52 (s, 4H, C*H*$_2$C*H*$_2$), 3.54 (m, 4H, POCH$_2$C*H*$_2$O), 4.03 (m, 8H, POC*H*$_2$CH$_2$O and C*H*$_2$CH$_3$), 4.36 (q, 4H, $C_{10}H_7CH_2CH_2$); 7.36–8.04 (m, 14H, naphthyl-*H*); ^{13}C NMR ($CDCl_3$): 15.84 (d, $^3J_{PC}$ = 6.8 Hz, *C*H$_3$), 33.53 (d, $^3J_{PC}$ = 6.6 Hz, $C_{10}H_7CH_2$), 63.68 (d, $^2J_{PC}$ = 5.9 Hz, *C*H$_2$CH$_3$), 66.25 (d, $^2J_{PC}$ = 5.9 Hz, PO*C*H$_2$CH$_2$O), 67.12 (d, $^2J_{PC}$ = 6.1 Hz, $C_{10}H_7CH_2CH_2$), 69.74 (d, $^3J_{PC}$ = 6.9 Hz, POCH$_2$*C*H$_2$O), 70.27 (*C*H$_2$*C*H$_2$), 123.19, 125.27, 125.46, 126.02, 127.06, 127.34, 128.62, 131.72, 132.75, 133.62 (naphthyl-*C*); mass spectrum (FAB, *p*-nitrobenzyl alcohol), *m/e* (rel. intensity): 675 MH$^+$ (18), 155 (100); high-resolution mass spectrum (FAB, *p*-nitrobenzyl alcohol), calcd. for $C_{34}H_{45}O_{10}P_2$: 675.2488 MH$^+$; found: 675.2513.

Can. J. Chem. Downloaded from www.nrcresearchpress.com by 213.200.69.106 on 09/08/12
For personal use only.

*α,ω-Triethylene glycol-bis-[2-(1-naphthyl)ethyl-2-ethoxyethyl phosphate] (**232**)*

The phosphoramidite, **3** (3.4 g, 4.5 mmol), was dissolved in THF (90 mL) along with 2-ethoxyethanol (1.5 mL, 15 mmol). The coupling reaction was initiated by adding tetrazole (5.0 g, 71 mmol) and the mixture was stirred for 15 min before it was oxidized to give 2.4 g (71%) of the product as a clear, colourless oil following work-up and flash chromatography: R_f 0.61 (50% dichloromethane – 40% diethyl ether – 10% methanol); IR (neat): 780, 800, 1040, 1130, 1275, 1355, 1395, 1455, 1510, 1595 cm^{-1}; ^{31}P NMR ($CDCl_3$): −0.39; ^1H NMR ($CDCl_3$): 1.14 (t, 6H, $^3J_{HH'}$ = 7.0 Hz, CH_3), 3.46 (q, 4H, $^3J_{HH'}$ = 7.0 Hz, CH_2CH_3), 3.47 (t, 4H, $^3J_{HH'}$ = 7.3 Hz, $C_{10}H_7CH_2$), 3.52 (s, 4H, CH_2CH_2), 3.54 (m, 8H, $POCH_2CH_2OEt$ and $POCH_2CH_2OCH_2CH_2$), 4.07 (m, 8H, $POCH_2CH_2OCH_2CH_2$ and $POCH_2CH_2OEt$), 4.38 (q, 4H, $C_{10}H_7CH_2CH_2$); 7.36–8.04 (m, 14H, naphthyl-*H*); ^{13}C NMR ($CDCl_3$): 14.90 (CH_3), 33.48 (d, $^3J_{PC}$ = 6.5 Hz, $C_{10}H_7CH_2$), 66.34 (CH_2CH_3), 66.37 (d, $^2J_{PC}$ = 6.5 Hz, $POCH_2CH_2OCH_2CH_2$), 66.56 (d, $^2J_{PC}$ = 6.0 Hz, $POCH_2CH_2OEt$), 67.24 (d, $^2J_{PC}$ = 6.0 Hz, $C_{10}H_7CH_2CH_2$), 68.92 (d, $^3J_{PC}$ = 7.0 Hz, $POCH_2CH_2OEt$), 69.71 (d, $^3J_{PC}$ = 6.0 Hz, $POCH_2CH_2OCH_2CH_2$), 70.27 (CH_2CH_2), 123.22, 125.27, 125.46, 126.03, 127.05, 127.33, 128.61, 131.73, 132.75, 133.62 (naphthyl-*C*); mass spectrum (FAB, *p*-nitrobenzyl alcohol), *m/e* (rel. intensity): 763 MH^+ (9), 155 (100); high-resolution mass spectrum (FAB, *p*-nitrobenzyl alcohol), calcd. for $C_{38}H_{53}O_{12}P_2$: 763.3012 MH^+; found: 763.3045.

*α,ω-Tetraethylene glycol-bis-[2-(1-naphthyl)ethylethyl phosphate] (**141**)*

The phosphoramidite, **4** (5.2 g, 6.5 mmol), was dissolved in THF (60 mL) and activated with tetrazole (6.0 g, 86 mmol). Ethanol (1.1 mL, 19 mmol) was added to the mixture, which was oxidized after 15 min, to give 3.2 g (68%) of the product as a clear, colourless oil following work-up and flash chromatography: R_f 0.66 (50% dichloromethane – 40% diethyl ether – 10% methanol); IR (neat): 780, 800, 1030, 1270, 1395, 1450, 1510, 1595 cm^{-1}, ^{31}P NMR ($CDCl_3$): −0.49; ^1H NMR ($CDCl_3$): 1.24 (br t, 6H, $^3J_{HH'}$ = 7.0 and 7.3 Hz, CH_3), 3.46 (t, 4H, $^3J_{HH'}$ = 7.2 and 7.3 Hz, $C_{10}H_7CH_2$), 3.51 (m, 8H, $CH_2CH_2OCH_2$), 3.57 (t, 4H, $^3J_{HH'}$ = 4.7 and 4.8 Hz, $POCH_2CH_2O$), 4.02 (q, 4H, $^3J_{HH'}$ = 7.0 Hz, CH_2CH_3), 4.05 (m, 4H, $POCH_2CH_2O$) 4.36 (q, 4H, $C_{10}H_7CH_2CH_2$); 7.30–8.04 (m, 14H, naphthyl-*H*); ^{13}C NMR ($CDCl_3$): 15.68 (d, $^3J_{PC}$ = 6.7 Hz, CH_3), 33.37 (d, $^3J_{PC}$ = 6.5 Hz, $C_{10}H_7CH_2$), 63.48 (d, $^2J_{PC}$ = 5.9 Hz, CH_2CH_3), 66.13 (d, $^2J_{PC}$ = 5.9 Hz, $POCH_2CH_2O$), 66.94 (d, $^2J_{PC}$ = 6.0 Hz, $C_{10}H_7CH_2CH_2$), 69.55 (d, $^3J_{PC}$ = 7.1 Hz, $POCH_2CH_2O$), 70.11 ($CH_2CH_2OCH_2CH_2$), 123.04, 125.11, 125.29, 125.86, 126.90, 127.17, 128.45, 131.56, 132.60, 133.46 (naphthyl-*C*); mass spectrum (FAB, *p*-nitrobenzyl alcohol), *m/e* (rel. intensity): 719 MH^+ (8), 155 (100); high-resolution mass spectrum (FAB, *p*-nitrobenzyl alcohol), calcd. for $C_{36}H_{49}O_{11}P_2$: 719.2750 MH^+; found: 719.2772.

*α,ω-Tetraethylene glycol-bis-[2-(1-naphthyl)ethyl-2-ethoxyethyl phosphate] (**242**)*

Addition of tetrazole (6.0 g, 86 mmol in 90 mL acetonitrile) to a solution containing the phosphoramidite **4** (5.3 g, 6.7 mmol), 2-ethoxyethanol (1.7 mL, 18 mmol), and THF (60 mL) was followed by 15 min of stirring to give 4.2 g (78%) of the product as a clear, colourless oil after oxidative work-up and flash chromatography: R_f 0.61 (50% dichloromethane – 40% diethyl ether – 10% methanol); IR (neat): 780, 800, 1030, 1270, 1350, 1395, 1455, 1510, 1595 cm^{-1}; ^{31}P NMR ($CDCl_3$): −0.40; ^1H NMR ($CDCl_3$): 1.14 (t, 6H, $^3J_{HH'}$ = 7.0 Hz, CH_3), 3.46 (q, 4H, $^3J_{HH'}$ = 7.0 Hz, CH_2CH_3), 3.48 (t, 4H, $^3J_{HH'}$ = 7.4 and 7.5 Hz, $C_{10}H_7CH_2$), 3.51 (m, 8H, $CH_2CH_2OCH_2CH_2$), 3.54 (m, 4H, $POCH_2CH_2OCH_2CH_2$), 3.59 (m, 4H, $POCH_2CH_2OEt$), 4.08 (m, 8H, $POCH_2CH_2OCH_2CH_2$ and $POCH_2CH_2OEt$), 4.38 (q, 4H, $C_{10}H_7CH_2CH_2$); 7.36–8.04 (m, 14H, naphthyl-*H*); ^{13}C NMR ($CDCl_3$): 14.86 (CH_3), 33.43 (d, $^3J_{PC}$ = 6.6 Hz, $C_{10}H_7CH_2$), 66.28 (CH_2CH_3), 66.35 (d, $^2J_{PC}$ = 5.9 Hz, $POCH_2CH_2OCH_2CH_2$), 66.50 (d, $^2J_{PC}$ = 6.0 Hz, $POCH_2CH_2OEt$), 67.17 (d, $^2J_{PC}$ = 6.1 Hz, $C_{10}H_7CH_2CH_2$), 68.88 (d, $^3J_{PC}$ = 7.0 Hz, $POCH_2CH_2OEt$), 69.64 (d, $^3J_{PC}$ = 7.1 Hz, $POCH_2CH_2OCH_2CH_2$), 70.24 ($CH_2CH_2OCH_2CH_2$), 70.25 ($CH_2CH_2OCH_2CH_2$), 123.18, 125.22, 125.41, 125.98, 127.00, 127.28, 128.56, 131.68, 132.70, 133.57 (naphthyl-*C*); mass spectrum (FAB, *p*-nitrobenzyl alcohol), *m/e* (rel. intensity): 807 MH^+ (12), 155 (100); high-resolution mass spectrum (FAB, *p*-nitrobenzyl alcohol), calcd. for $C_{40}H_{57}O_{13}P_2$: 807.3274 MH^+; found: 807.3297.

Acknowledgments

The authors thank the Natural Sciences and Engineering Research Council of Canada (NSERC) for support of this research, and Prof. M. J. Damha for many helpful suggestions.

1. M.A. Winnik, T. Redpath, and D.H. Richards. Macromolecules, **13**, 328 (1980).
2. M.A. Winnik. Acc. Chem. Res. **18**, 73 (1985).
3. M.A. Winnik. Acc. Chem. Res. **10**, 173 (1977).
4. (*a*) K. Horie and I. Mita. Macromolecules, **11**, 1175 (1978); (*b*) K. Horie, W. Schnabel, I. Mita, and H. Ushiki. Macromolecules, **14**, 1422 (1981).
5. A. Perico and M. Guenza. J. Chem. Phys. **83**, 3103 (1985).
6. A. Perico, F. Ganazzoli, and G.J. Allegra. J. Chem. Phys. **87**, 3677 (1987).
7. A. Perico. J. Chem. Phys. **88**, 3996 (1988).
8. A. Perico. Acc. Chem. Res. **22**, 336 (1989).
9. R.L. Letsinger, J.L. Finnan, G.A. Heavner, and W.B. Lunsford. J. Am. Chem. Soc. **97**, 3278 (1975).
10. R.L. Letsinger and W.B. Lunsford. J. Am. Chem. Soc. **98**, 3655 (1976).
11. S.L. Beaucage and M.H. Caruthers. Tetrahedron Lett. **22**, 1859 (1981).
12. L.J. McBride and M.H. Caruthers. Tetrahedron Lett. **24**, 245 (1983).
13. S.P. Adams, K.S. Kavka, E.J. Wykes, S.B. Holder, and G.R. Galluppi. J. Am. Chem. Soc. **105**, 661 (1983).
14. T. Atkinson and M. Smith. *In* Oligoribonucleotide synthesis — a practical approach. *Edited by* M.J. Gait. IRL Press, Oxford. 1984. pp. 35–80.
15. M.F. Moore and S.L. Beaucage. J. Org. Chem. **50**, 2019 (1985).
16. H. Tolkmith. J. Org. Chem. **23**, 1682 (1958).
17. K.K. Ogilvie, N.Y. Theriault, J.-M. Seifert, R.T. Pon, and M.J. Nemer. Can. J. Chem. **58**, 2686 (1980).
18. M.J. Damha, R.T. Pon, and K.K. Ogilvie. Tetrahedron Lett. **26**, 4839 (1985).
19. M.J. Damha and K.K. Ogilvie. J. Org. Chem. **53**, 3710 (1988).

Crystalline complexes of 18-crown-6 with methyl sulfonates

ROBERT CHÊNEVERT[1], RENÉ GAGNON, AND DANIEL CHAMBERLAND
Département de chimie, Faculté des sciences et de génie, Université Laval, Québec, PQ G1K 7P4, Canada

AND

MICHEL SIMARD
Département de chimie, Université de Montréal, C.P. 6128, Succ. A. Montréal, PQ H3C 3J7, Canada

Received August 24, 1992[2]

ROBERT CRÊNEVERT, RENÉ GAGNON, DANIEL CHAMBERLAND, and MICHEL SIMARD. Can. J. Chem. **71**, 1225 (1993).

The macrocyclic polyether 18-crown-6 forms crystalline complexes with methyl sulfonates. Most complexes have a 2:1 (sulfonate:crown) stoichiometry whereas small aliphatic sulfonates give a 1:1 ratio. In the 2:1 ratio complexes, the guest molecules are coordinated above and below the crown in such a way that the dipoles are compensated. In the 1:1 ratio complexes, there is a polymeric type association with the two ends of the sulfonate interacting with different crown molecules. A crystal structure is reported for each type of complex. The complex 18-crown-6 · $CH_3SO_3CH_3$ (**7**) crystallizes in the monoclinic system, space group $P2_1/c$ with $Z = 4$. The unit cell dimensions are as follows: $a = 8.525(4)$, $b = 16.401(7)$, $c = 15.071(6)$ Å, $\beta = 113.92(3)°$. Final $R_w = 0.064$ for 3650 reflections. The complex 18-crown 6 · $(C_6H_5SO_3Me)_2$ (**1**) crystallizes in the monoclinic system, space group $P2_1/c$ with $Z = 2$. The unit cell dimensions are as follows: $a = 8.101(3)$, $b = 17.136(5)$, $c = 12.990(5)$ Å, $\beta = 121.30(3)°$. Final $R_w = 0.048$ for 2913 reflections.

ROBERT CHÊNEVERT, RENÉ GAGNON, DANIEL CHAMBERLAND et MICHEL SIMARD. Can. J. Chem. **71**, 1225 (1993).

Le polyéther macrocyclique 18-couronne-6 forme des complexes cristallins avec des sulfonates de méthyle. La plupart des complexes ont un rapport sulfonate/couronne de 2 : 1 alors que deux sulfonates de petite taille conduisent à des rapports 1 : 1. Dans les complexes de rapport 2 : 1, les sulfonates sont situés de part et d'autre de la couronne de façon à compenser les dipôles. Dans les autres complexes, il y a une association de type polymérique où les deux extrémités du sulfonate interagissent avec des couronnes différentes. Une structure cristalline est rapportée pour chaque type de complexes. Le complexe 18-couronne-6 · $CH_3SO_3CH_3$ (**7**) cristallise dans le système monoclinique, groupe d'espace $P2_1/c$ avec $a = 8{,}525(4)$, $b = 16{,}401(7)$, $c = 15{,}071(6)$ Å, $\beta = 113{,}92(3)°$ et $Z = 4$. La valeur finale de $R_w = 0.064$ avec 3650 reflexions. Le complexe 18-couronne-6 · $(C_6H_5SO_3Me)_2$ (**1**) cristallise dans le système monoclinique, groupe d'espace $P2_1/c$ avec $a = 8{,}101(3)$, $b = 17{,}136(5)$, $c = 12{,}990(5)$ Å, $\beta = 121{,}30(3)°$ et $Z = 2$. La valeur finale de $R_w = 0{,}048$ avec 2913 réflexions.

Can. J. Chem. Downloaded from www.nrcresearchpress.com by 213.200.69.106 on 09/08/12
For personal use only.

Introduction

The ability of synthetic receptor molecules such as crown ethers to complex inorganic or organic cations has been the subject of numerous reports during the last two decades (1). The study of well-defined complexes formed between crown compounds and neutral molecules represents a much less explored area. The latter complexes are widely recognized as model systems for molecular recognition of neutral polar molecules, which play an important role in biological systems. Small neutral molecules can form adducts with crown ethers if they present one or both of the following structural features: a relatively large dipole moment and X—H bonds (X = O, N, C) able to form hydrogen bonds with oxygens of the crown ligand in a complementary spatial arrangement (2–5). Several complexes of this kind have a 1:2 stoichiometric ratio of host/guest and the guest molecules are coordinated above and below the crown in such a way that the dipoles are compensated. All complexes are far reported contain either polar O—H bonds (2, 6) (water, alcohols, gem-diols, diacids), polar N—H bonds (urea and analogues (7, 8), amides (9)), or polar C—H bonds (nitriles (10, 11), nitro compounds (10–12), dimethyl sulfone (13), dimethyl sulfate (14), dimethyl diesters (15, 16)).

Another type of neutral component complex has been obtained with weakly acidic compounds such as phenols, carboxylic acids, and weak inorganic acids (17–20). The guest usually contains only one hydrogen suitable for hydrogen bonding and one water molecule per guest serves as a linkage between the acid and the crown (2–4).

Although a number of crystallographic, thermodynamic, and molecular mechanics studies have been performed, the nature of the interactions between the partners in such complexes is only partly understood (21–29). We report here the formation of well-defined complexes between 18-crown-6 and several methyl sulfonates.

TABLE 1. Crystal data for complexes **1** and **7**

Parameter	Complex **1**	Complex **7**
Formula	$C_{26}H_{40}O_{12}S_2$	$C_{14}H_{30}O_9S$
FW	608.72	374.46
$F(000)$	648	808
Crystal system	Monoclinic	Monoclinic
Space group	$P2_1/c$	$P2_1/c$
a, Å	8.101 (3)	8.525 (4)
b, Å	17.136 (5)	16.401 (7)
c, Å	12.990 (5)	15.071 (6)
β, deg	121.30 (3)	113.92 (3)
V, Å^3	1540.8 (9)	1926.2 (15)
D_{calc}, Mg m^{-3}	1.312	1.291
Z	2	4
μ, mm^{-1}	2.02	1.82
λ, Kᾱ, Å	1.54178	1.54178
Crystal size, mm	0.11 × 0.12. × 0.25	0.16 × 0.30 × 0.34
T, K	190	190

[1]Author to whom correspondence may be addressed.
[2]Revision received May 10, 1993.

TABLE 2. Data collection and refinement

Parameter	Complex **1**	Complex **7**
Radiation	CuKα̅	CuKα̅
Scan	ω	ω
Scan width, deg	(0.80 + 0.14 tan θ)	(0.80 + 0.14 tan θ)
Octant measured	$-9 \leq h \leq 8$	$-10 \leq h \leq 9$
	$0 \leq k \leq 20$	$0 \leq k \leq 19$
	$0 \leq l \leq 15$	$0 \leq l \leq 18$
Number of measured reflections	5923	7309
Acceptance level $I/\sigma(I)$	3.0	3.0
Number of unique reflections	2913	3650
R_f	0.041	0.051
R_w	0.048	0.064
G.O.F.	2.00	2.89
w^{-1}	$\sigma^2(F_0) + 0.0001(F_0)^2$	$\sigma^2(F_0) + 0.0001(F_0)^2$
Residual fluctuations in electron density map, e Å^{-3}	−0.51, 0.27	−0.57, 0.51
Maximum shift/σ ratio	0.29	0.49

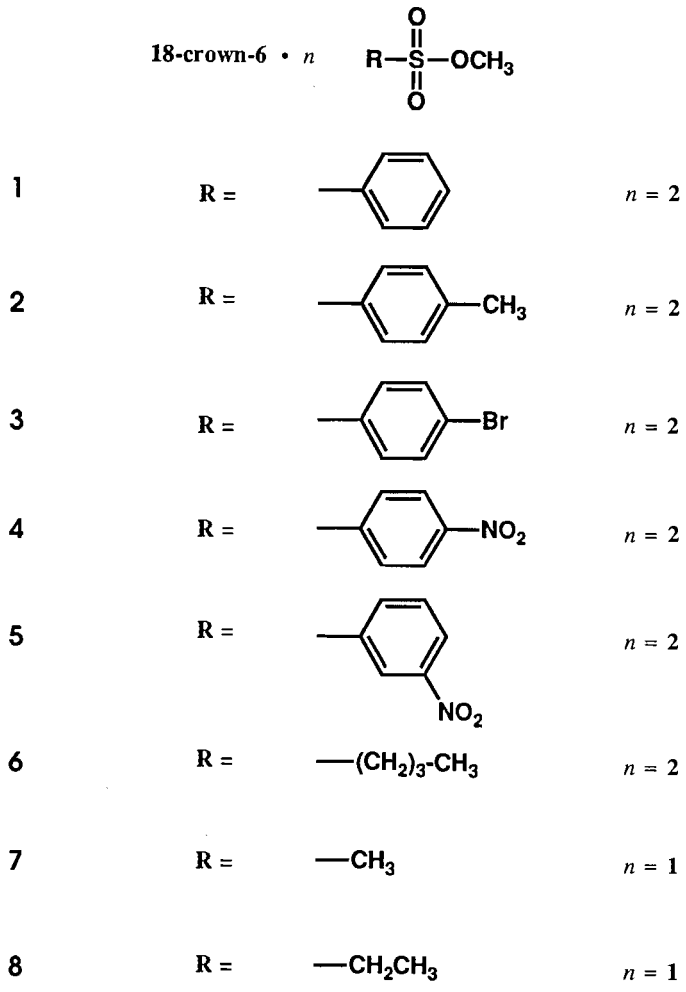

SCHEME 1

Experimental

The NMR spectra were taken on a Varian XL-200 multinuclear spectrometer. The infrared spectra, obtained from a KBr pressed disc, were run on a Beckman 4250 or an FT-IR Bomem MB 102 spectrometer. The microanalyses were performed on a Carlo Erba Strumentazione-1106 elemental analysis instrument.

TABLE 3. Final atomic coordinates with their esd's (× 10^4; S, × 10^5) and equivalent isotropic temperature factors (× 10^3) for the $C_{26}H_{40}O_{12}S_2$ compound **1**

Atom	x	y	z	U_{eq}
S	7256(8)	74210(3)	2036(5)	42
O(1)	8703(2)	4392(1)	823(1)	40
O(4)	7527(2)	4731(1)	2508(1)	44
O(7)	4201(2)	5714(1)	1699(1)	46
O(10A)[a]	6474(3)	6651(1)	−540(2)	34
O(11A)[a]	8798(3)	7295(2)	1351(2)	51
O(12A)[a]	7454(4)	7923(2)	−646(3)	58
O(10B)[a]	7519(8)	6499(3)	759(5)	48
O(11B)[a]	9048(11)	7695(4)	1296(6)	56
O(12B)[a]	7073(9)	7401(4)	−848(6)	55
C(2)	9585(4)	4077(2)	1997(3)	49
C(3)	9478(3)	4655(2)	2818(2)	49
C(5)	7307(4)	5289(2)	3232(2)	53
C(6)	5196(4)	5339(2)	2825(2)	51
C(8)	2178(4)	5756(2)	1216(3)	51
C(9)	1238(4)	6126(2)	7(3)	50
C(10)	6147(4)	5991(2)	31(3)	50
C(11)	5257(3)	7768(1)	255(2)	35
C(12)	5376(3)	7863(1)	1347(2)	41
C(13)	3780(4)	8151(1)	1352(2)	46
C(14)	2098(4)	8319(1)	283(2)	48
C(15)	1981(4)	8213(1)	−801(3)	47
C(16)	3571(3)	7940(1)	−828(2)	41

[a]Labels A and B stand for major (occ.: 0.70) and minor (occ.: 0.30) disorder model.

Preparation of the complexes (general procedure)

The methyl sulfonate (2 mmol) is dissolved in dry tetrahydrofuran (10 mL) and this solution is added to a solution of 18-crown-6 (2 mmol) in dry tetrahydrofuran (10 mL). The complex crystallizes upon addition of diethyl ether an cooling. The colorless solid complex is filtered and dried under vacuum. The complex is recrystallized in the appropriate solvent and dried under vacuum until constant melting point is obtained. Physical data pertaining to the individual complexes are given below.

*$(C_6H_5SO_3CH_3)_2 \cdot$18-crown-6, **1***

Yield: 76%; mp 69–70°C (from ether). IR(KBr): 3050, 2870, 1465, 1440, 1345, 1215, 1180, 1030, 1010, 955, 825 cm^{-1}. ^{1}H NMR ($CDCl_3$) δ: 3.62 (24H, s, crown), 3.69 (6H, s, OCH_3), 7.55

Can. J. Chem. Downloaded from www.nrcresearchpress.com by 213.200.69.106 on 09/08/12
For personal use only.

Can. J. Chem. Downloaded from www.nrcresearchpress.com by 213.200.69.106 on 09/08/12
For personal use only.

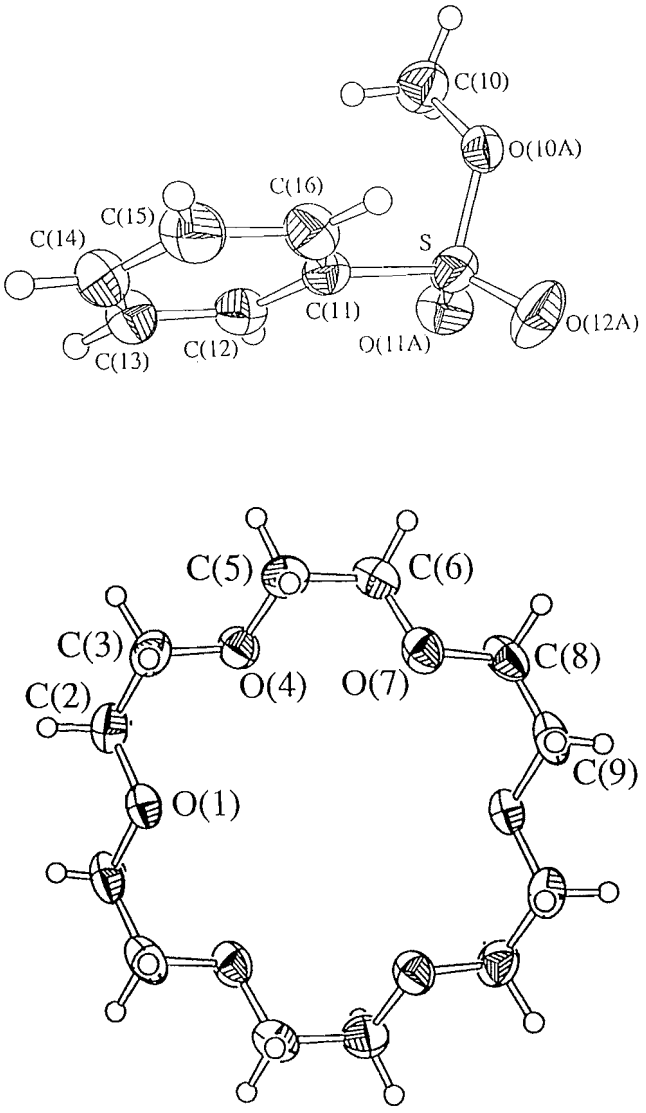

FIG. 1. ORTEP view of the two molecules in complex **1** with the numbering scheme adopted. Ellipsoids drawn at 50% probability level. Hydrogen represented by spheres of arbitrary size.

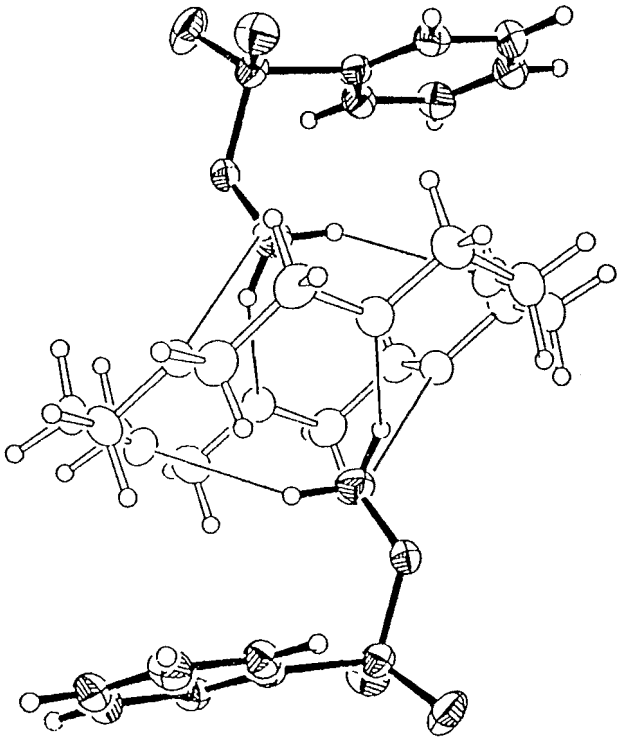

FIG. 2. ORTEP view of the association of the 2:1 complex for the $C_{13}H_{20}O_6S$ compound (**1**). Pseudo hydrogen bonds represented by thin bonds.

(6H, m), 7.85 (4H, m). ^{13}C NMR ($CDCl_3$) δ: 56.2 (OCH_3), 70.4 (crown), 127.8, 129.1, 133.7, 134.9. Anal. calcd. for $C_{26}H_{40}O_{12}S_2$: C 51.30, H 6.62; found: C 51.61, H 6.50.

(p-$CH_3C_6H_4SO_3CH_3)_2$·18-crown-6, 2

Yield: 80%; mp 63–65°C (from ether). IR(KBr): 2900, 1600, 1475, 1460, 1350, 1225, 1190, 1105, 1045, 1030, 1010, 960, 835, 810 cm^{-1}. ^1H NMR ($CDCl_3$) δ: 2.38 (6H, s), 3.62 (24H, s, crown), 3.67 (6H, s, OCH_3), 7.30 (4H, d, J = 8 Hz), 7.72 (4H, d, J = 8 Hz). ^{13}C NMR ($CDCl_3$) δ: 21.5, 55.1 (OCH_3), 70.5 (crown), 127.8, 129.6, 132.1, 144.8. Anal. calcd. for $C_{28}H_{44}O_{12}S_2$: C 52.81, H 6.96; found: C 52.47, H 7.14.

(p-$BrC_6H_4SO_3CH_3)_2$·18-crown-6, 3

Yield: 74%; mp 54–56°C (from ether). IR(KBr): 2900, 1580, 1475, 1355, 1240, 1195, 1105, 1030, 1005, 960, 835, 820 cm^{-1}. ^1H NMR ($CDCl_3$) δ: 3.65 (24H, s, crown), 3.75 (6H, s, OCH_3), 7.68 (4H, d, J = 8 Hz), 7.75 (4H, d, J = 8 Hz). ^{13}C NMR ($CDCl_3$) δ: 56.5 (OCH_3), 70.5 (crown), 128.9, 129.3, 132.4, 134.1. Anal. calcd. for $C_{26}H_{38}O_{12}S_2Br_2$: C 40.74, H 5.00; found: C 41.09, H 4.88.

(p-$NO_2C_6H_4SO_3CH_3)_2$·18-crown-6, 4

Yield: 71%; mp 87–88.5°C (from THF–hexane). IR(KBr) : 3100, 2970, 1610, 1530, 1365 1350, 1190, 1105, 1095, 970, 860, 850 cm^{-1}. ^1H NMR ($CDCl_3$) δ: 3.67 (24H, s, crown), 3.84 (6H, s, OCH_3), 8.11 (4H, d, J = 9 Hz), 8.41 (4H, d, J = 9 Hz). ^{13}C NMR ($CDCl_3$) δ: 57.0 (OCH_3), 70.3 (crown), 123.3, 124.4, 129.3, 141.0. Anal. calcd. for $C_{26}H_{38}O_{16}N_2S_2$: C 44.69, H 5.48; found: C 45.02, H 5.38.

(m-$NO_2C_6H_4SO_3CH_3)_2$·18-crown-6, 5

Yield: 84%; mp 68–70°C (from ether). IR(KBr): 3075, 2880, 1520, 1465, 1345, 1235, 1200, 1085, 1025, 955, 870, 835 cm^{-1}. ^1H NMR ($CDCl_3$) δ: 3.65 (24H, s, crown), 3.83 (6H, s, OCH_3), 7.80 (2H, t, J = 8 Hz), 8.22 (2H, ddd, J_1 = 8 Hz, J_2 = 2 Hz, J_3 = 1 Hz), 8.50 (2H, ddd, J_1 = 8 Hz, J_2 = 2 Hz, J_3 = 1 Hz), 8.72 (2H, t, J = 2 Hz). ^{13}C NMR ($CDCl_3$) δ: 57.0 (OCH_3), 70.6 (crown), 123.2, 128.3, 130,8, 133.4, 137.4, 148.3. Anal. calcd. for $C_{26}H_{38}N_2O_{16}S_2$: C 44.69, H 5.48; found: C 44.94, H 5.76.

[$CH_3(CH_2)_3SO_3CH_3]_2$·18-crown-6, 6

Yield: 75%; mp 38–39°C (from ether–hexane). IR (KBr): 2900, 1470, 1355, 1345, 1280, 1250, 1190, 1110, 1060, 965, 840 cm^{-1}. ^1H NMR ($CDCl_3$) δ: 0.92 (6H, t, J = 7 Hz), 1.45 (4H, m), 1.80 (4H, m), 3.06 (4H, m), 3.64 (24H, s, crown), 3.85 (6H, s, OCH_3). ^{13}C NMR ($CDCl_3$) δ: 13.4, 21.4, 25.3, 49.4, 55.0 (OCH_3), 70.6 (crown). Anal. calcd. for $C_{22}H_{48}O_{12}S_2$: C 46.46, H 8.51; found; C 46.91, H 8.27.

$CH_3SO_3CH_3$·18-crown-6, 7

Yield: 71%; mp 88–89.5°C (from benzene). IR (KBr): 2900, 1475, 1355, 1345, 1280, 1250, 1195, 1110, 1060, 965, 835 cm^{-1}. ^1H NMR ($CDCl_3$) δ; 3.00 (3H, s), 3.67 (24H, s, crown), 3.90 (3H, s, OCH_3). ^{13}C NMR ($CDCl_3$) δ: 36.5, 55.4, (OCH_3), 70.5 (crown). Anal. calcd. for $C_{14}H_{30}O_9S_1$: C 44.91, H 8.07; found: C 45.22, H 7.69.

CH_3-CH_2-SO_3CH_3·18-crown-6, 8

Yield: 84%; mp 56–57°C (from ether). IR(KBr): 2900, 1475, 1355, 1345, 1280, 1250, 1190, 1110, 1060, 965, 835 cm^{-1}. ^1H NMR ($CDCl)_3$ δ: 1.40 (3H, t, J = 7 Hz), 3.11 (2H, q, J = 7 Hz), 3.65 (24H, s, crown), 3.87 (3H, s, OCH_3). ^{13}C NMR ($CDCl_3$)δ 8.2,

Can. J. Chem. Downloaded from www.nrcresearchpress.com by 213.200.69.106 on 09/08/12
For personal use only.

TABLE 4. Distances and angles for the $C_{26}H_{40}O_{12}S_2$ compound **1**

Bond	Distances (esd's), Å	Bond	Distances (esd's), Å
S—O(10A)	1.562(2)	S—O(10B)	1.703(6)
S—O(11A)	1.377(3)	S—O(11B)	1.485(8)
S—O(12A)	1.474(3)	S—O(12B)	1.297(7)
S—C(11)	1.756(3)		
O(10A)—C(10)	1.450(4)	O(10B)—C(10)	1.340(7)
C(11)—C(12)	1.381(3)	C(11)—C(16)	1.391(3)
C(12)—C(13)	1.387(5)	C(13)—C(14)	1.379(4)
C(14)—C(15)	1.373(4)	C(15)—C(16)	1.388(4)
O(1)—C(2)	1.413(3)	O(1)—C(9)[a]	1.416(3)
C(2)—C(3)	1.491(4)	C(3)—O(4)	1.420(4)
O(4)—C(5)	1.416(4)	C(5)—C(6)	1.507(5)
C(6)—O(7)	1.406(3)	O(7)—C(8)	1.420(4)
C(8)—C(9)	1.485(4)		

Bonds	Angles (esd's), deg	Bonds	Angles (esd's), deg
O(10A)—S—O(11A)	112.64(15)	O(10B)—S—O(11B)	92.5(4)
O(10A)—S—O(12A)	101.32(15)	O(10B)—S—O(12B)	110.0(4)
O(11A)—S—O(12A)	120.66(18)	O(11B)—S—O(12B)	122.2(5)
O(10A)—S—C(11)	103.04(12)	O(10B)—S—C(11)	102.4(2)
O(11A)—S—C(11)	110.44(15)	O(11B)—S—C(11)	108.7(3)
O(12A)—S—C(11)	107.04(15)	O(12B)—S—C(11)	116.6(3)
S—O(10A)—C(10)	117.7(2)	S—O(10B)—C(10)	115.3(4)
S—C(11)—C(12)	120.3(2)	S—C(11)—C(16)	118.2(2)
C(12)—C(11)—C(16)	121.5(2)	C(11)—C(12)—C(13)	118.6(2)
C(12)—C(13)—C(14)	120.4(3)	C(13)—C(14)—C(15)	120.7(3)
C(14)—C(15)—C(16)	120.0(3)	C(11)—C(16)—C(15)	118.8(2)
C(2)—O(1)—C(9)[a]	112.6(2)	O(1)—C(2)—C(3)	109.5(2)
C(2)—C(3)—O(4)	109.1(2)	C(3)—O(4)—C(5)	112.3(2)
O(4)—C(5)—C(6)	108.5(2)	C(5)—C(6)—O(7)	108.9(2)
C(6)—O(7)—C(8)	112.9(2)	O(7)—C(8)—C(9)	109.2(2)
O(1)[a]—C(9)—C(8)	109.6(2)		

[a] $1 - x, 1 - y, - z$.

TABLE 5. Torsion angles for the crown molecule in complex **1**

Bonds	Torsion angles (esd's), deg	Bonds	Torsion angles (esd's), deg
O(10A)—S—C(11)—C(12)	119.3(2)	O(10A)—S—C(11)—C(16)	−60.5(2)
O(11A)—S—C(11)—C(12)	−1.2(3)	O(11A)—S—C(11)—C(16)	178.9(2)
O(12A)—S—C(11)—C(12)	−134.4(2)	O(12A)—S—C(11)—C(16)	45.8(2)
O(10B)—S—C(11)—C(12)	64.7(3)	O(10B)—S—C(11)—C(16)	−115.1(3)
O(11B)—S—C(11)—C(12)	−32.2(4)	O(11B)—S—C(11)—C(16)	148.0(4)
O(12B)—S—C(11)—C(12)	−175.2(4)	O(12B)—S—C(11)—C(16)	5.0(4)
O(1)—C(2)—C(3)—O(4)	69.3(3)		
C(2)—C(3)—O(4)—C(5)	−178.4(2)		
C(3)—O(4)—C(5)—C(6)	179.0(2)		
O(4)—C(5)—C(6)—O(7)	−71.6(3)		
C(5)—C(6)—O(7)—C(8)	177.3(2)		
C(6)—O(7)—C(8)—C(9)	−177.4(2)		
O(7)—C(8)—C(9)—O(1)[a]	70.7(3)		
C(8)—C(9)—O(1)[a]—C(2)[a]	179.7(2)		
C(9)—O(1)[a]—C(2)[a]—C(3)[a]	−179.6(2)		
O(1)[a]—C(2)[a]—C(3)[a]—O(4)[a]	−69.3(3)		
C(2)[a]—C(3)[a]—O(4)[a]—C(5)[a]	178.4(2)		
C(3)[a]—O(4)[a]—C(5)[a]—C(6)[a]	−179.0(2)		
O(4)[a]—C(5)[a]—C(6)[a]—O(7)[a]	71.6(3)		
C(5)[a]—C(6)[a]—O(7)[a]—C(8)[a]	−177.3(2)		
C(6)[a]—O(7)[a]—C(8)[a]—C(9)[a]	177.4(2)		
O(7)[a]—C(8)[a]—C(9)[a]—O(1)	−70.7(3)		
C(8)[a]—C(9)[a]—O(1)—C(2)	−179.7(2)		
C(9)[a]—O(1)—C(2)—C(3)	179.6(2)		

[a] $1 - x, 1 - y, - z$.

Can. J. Chem. Downloaded from www.nrcresearchpress.com by 213.200.69.106 on 09/08/12
For personal use only.

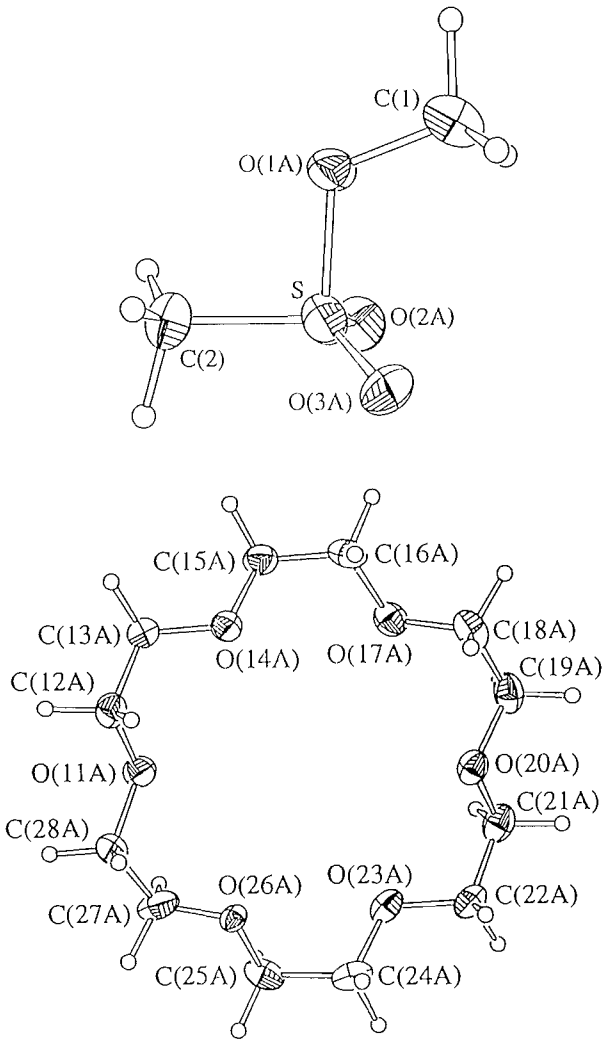

FIG. 3. ORTEP view of the two molecules in complex **7** (models A only) with the numbering scheme adopted. Ellipsoids drawn at 40% probability level. Hydrogens represented by spheres of arbitrary size.

44.3, 55.1 (OCH_3), 70.6 (crown). Anal. calcd. for $C_{15}H_{32}O_9S_1$: C 46.38, H 8.29; found: C 46.77, H 7.96.

Crystallographic characterization of complexes 1 and 7

The intensity data were collected on a Nonius diffractometer using the $\omega/2\theta$ mode and graphite monochromatized CuKα radiation. The unit cell dimensions were computed from the angular settings of 24 well-centered reflections in the range $40 \leq 2\theta \leq 50°$ (**1**) or $45 \leq 2\theta \leq 55°$ (**2**). The final parameters and other crystal data of interest are presented in Table 1 and data collection and refinement indicators are in Table 2. The structures were solved by direct methods using NRCVAX and difference Fourier synthesis using SHELX-76.[3] Disorder model introduced to account for high residual peaks in the sulfonate vicinity, with occupancies initially refined, then fixed in final refinement cycles. Full-matrix least-squares refinement based on F's all non-hydrogen atoms anisotropic, hydrogen atoms isotropic. Hydrogen atoms found from a difference Fourier map and (or) calculated, disorder H-atoms introduced at ideal positions ($D_{C-H} = 0.95$ Å) with B_{iso} refined.

[3]The programs used here are NRCVAX, program system for structure analysis (Gabe, LePage, Charland, and Lee (30)), SHELX-76, program for structure analysis (Sheldrick (31)), and ORTEP, stereodrawings (Johnson (32)).

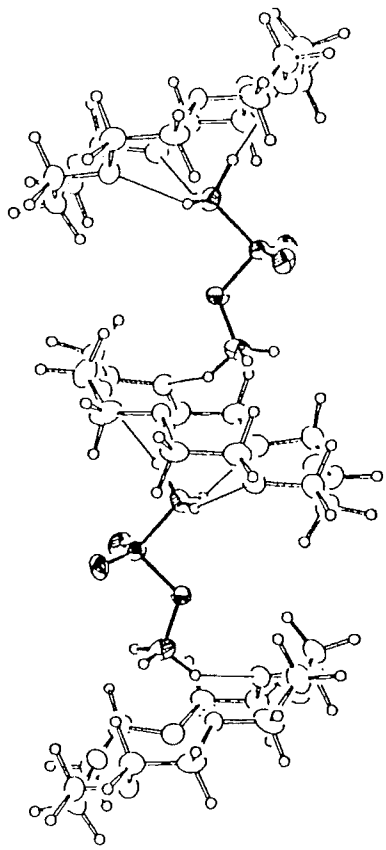

FIG. 4. ORTEP view of the association (sulfonate model A, crown model A) of the polymeric type 1:1 complex of the $C_{14}H_{30}O_9S$ compound (**7**). Pseudo hydrogen bonds represented by thin bonds.

Secondary extinction coefficients not refined. The scattering curves for the non-hydrogen atoms were taken from Cromer and Mann (33) and those for the H-atoms from Stewart, Davidson, and Simpson (34). Anomalous dispersion contributions (df' and df'') were from Cromer and Liberman (35).

Results and discussion

The methyl sulfonates were prepared under phase-transfer catalysed conditions according to a known procedure (36). Sulfonate – crown ether complexes were prepared in good yield (71–86%) by mixing the methyl sulfonate and 18-crown-6 in tetrahydrofuran. The complexes **1**–**8** (Scheme 1) are stable solids with sharp melting points. In most cases, the melting point of the complex is above those of the constituents. For instance, the melting point of complex **1** (69–70°C) is above those of the crown (40°C) or the sulfonate (liquid at room temperature). The stoichiometry of compounds **1**–**8** was determined by elemental analysis (carbon, hydrogen) and by integration of signals of the constituents in NMR. The analyses are in agreement with those observed in the X-ray determination for compounds **1** and **7**. Both the frequencies and spectral activity of the crown ether bands in the infrared spectra of the complexes are comparable to those found in various complexes in which the crown is known to have a regular D_{3d} symmetry. CH_2 rocking bands at ~960 cm^{-1} and C—C stretching at ~835 cm^{-1} are singlets in complexes **1**–**8**. Distortion of the crown causes a splitting of these vibrational bands (3, 20). These observations suggest that the shape of the crown in the complexes described here is es-

TABLE 6. Bond distances (Å) and angles (deg) related to the pseudo hydrogen bonding in complex **1**

Bond (A—H···B)	Distances (esd's) A—B	A—H	H—B	Angles (esd's) A—H—B
C(10)—H(101A)...O(1)	3.262(3)	0.93(6)	2.64(6)	125(4)
C(10)—H(102A)...O(4)[a]	3.327(4)	0.98(6)	2.53(6)	138(5)
C(10)—H(103A)...O(7)	3.310(4)	1.04(7)	2.42(7)	143(5)
C(10)—H(101B)[b]...O(1)	3.262(3)	0.95	2.51	137

Bonds	Angles (esd's), deg	Bonds	Angles (esd's), deg
O(10A)—C(10)...O(1)	124.17(19)	O(10A)—C(10)—H(101A)	113(4)
O(10A)—C(10)...O(4)[a]	95.16(17)	O(10A)—C(10)—H(102A)	103(4)
O(10A)—C(10)...O(7)	136.24(20)	O(10A)—C(10)—H(103A)	111(3)
		H(101A)—C(10)—H(102A)	108(5)
		H(101A)—C(10)—H(103A)	102(5)
		H(102A)—C(10)—H(103A)	120(5)
C(2)—O(1)...C(10)	122.93(16)	C(2)—O(1)...H(101A)	112.2(13)
C(9)[a]—O(1)...C(10)	123.59(16)	C(9)[a]—O(1)...H(101A)	135.2(13)
C(3)—O(4)...C(10)[a]	123.54(16)	C(3)—O(4)...H(102A)[a]	132.1(14)
C(5)—O(4)...C(10)[a]	122.58(16)	C(5)—O(4)...H(102A)[a]	112.6(14)
C(6)—O(7)...C(10)	122.41(17)	C(6)—O(7)...H(103A)	129.9(15)
C(8)—O(7)...C(10)	122.44(17)	C(8)—O(7)...H(103A)	116.8(15)
O(10B)—C(10)...O(1)	99.5(3)		
C(2)—O(1)...C(10)	122.93(16)	C(2)—O(1)...H(101B)	115.0
C(9)[a]—O(1)...C(10)	123.59(16)	C(9)[a]—O(1)...H(101B)	128.7

[a]1 − x, 1 − y, − z.
[b]Hydrogen calculated at ideal position.

Can. J. Chem. Downloaded from www.nrcresearchpress.com by 213.200.69.106 on 09/08/12
For personal use only.

sentially that of a regular crown of symmetry D_{3d}, although some distortion is probably present, especially in the 1:1 ratio complexes.

The ^1H and ^{13}C NMR signals of the crown protons and carbons in complexes **1–8** are on average close to the shifts of the free crown hydrogens and carbons in the same solvent ($CDCl_3$). The average chemical shift of protons is 3.65 ppm compared to 3.67 ppm for the free crown and the average position of carbons is 70.51 ppm compared to 70.76 ppm for the free crown.

To gain further insight in the structures, X-ray analyses were undertaken. We report here the structures of 18-crown-6 · 2 methyl benzenesulfonate (**1**) and 18-crown-6-methyl methanesulfonate (**7**).[4]

Crystal structure of 18-crown-6 · 2(methyl benzenesulfonate) complex (*1*)

The final atomic coordinates and the equivalent U values of the anisotropic temperature factors are given in Table 3. A stereoview showing the molecular conformations and the atomic numberings of both constituents is shown in Fig. 1.

The centrosymmetrical 18-crown-6 ligand adopts approximative D_{3d} conformation with C—O—C—C and O—C—C—O torsion angles near 180° (average value 178.6°) and 70° (average value 70.5°), which is the expected *gauche* conformation of the ethyleneoxy units (Table 5). The C—O and C—C bond distances average 1.41 and 1.49 Å while the O—C—C and C—O—C angles average 109.1° and 112.6°, respectively (Table 4). The values are consistent with those reported for the majority of 18-crown-6 complexes that exhibit the pseudo D_{3d} conformation.

The sulfonate molecule is disordered over two conformations of unequal proportion (70:30). A view of the major model association is shown in Fig. 2. The sulfonate molecules are coordinated above and below the crown in such a way that the dipoles are compensated. The methyl group of each sulfonate molecule yields three C—H---O contacts to alternate oxygen atoms of the crown.

The hydrogen bonding contacts and geometries can be found in Table 6. The C—H---O bridge angles are 125°, 138°, and 143° with methyl C---O distances of 3.262, 3.327, and 3.310 Å and CH---O distances of 2.64, 2.53, 2.42, shorter than the sum of the van der Waals radii (2.7 Å). The most important geometrical characteristic of hydrogen bonds is that the distance between the proton and the acceptor atom is shorter than the sum of their van der Waals radii (37, 38). The existence of only one H---O short contact indicates the lower stability of the minor association (supplementary data).

Crystal structure of 18-crown-6-methyl methanesulfonate complex (7)

This complex contains more disorder than the previous one; the crown has two occupancies (A and B) of almost equal population (55:45) and the sulfonate molecule is dis-

[4]A satisfactory X-ray analysis of complex **2** (18-crown-6 · methyl *p*-toluenesulfonate) has also been obtained. This structure is very similar to the structure of **1** and is not described here.

TABLE 7. Final atomic coordinates with their e.s.d's (S × 10^5; O, C, × 10^4) and equivalent isotropic temperature factors (× 10^3) for the $C_{14}H_{30}O_9S$ compound **7**

Sulfonate

Atom	*x*	*y*	*z*	U_{eq}	Occ.
S	14163(8)	14828(4)	25562(4)	42	1.00
O(1A)	1792(5)	2156(4)	3425(4)	43	0.50
O(1B)	495(11)	1728(6)	3230(6)	43	0.20
O(1C)	1186(9)	2096(8)	3306(7)	43	0.30
O(2A)	2897(23)	1137(8)	2942(13)	56	0.35
O(2B)	2956(23)	915(10)	2776(10)	56	0.30
O(2C)	2900(23)	945(9)	3019(13)	56	0.35
O(3A)	−202(22)	1042(9)	2281(15)	50	0.30
O(3B)	−267(12)	944(5)	1909(6)	50	0.30
O(3C)	−32(18)	1171(7)	2286(11)	50	0.40
C(1)	1589(4)	1854(2)	4256(2)	64	1.00
C(2)	1480(4)	2202(2)	1736(2)	48	1.00

Crown

Atom	*x*	*y*	*z*	U_{eq}
O(11A)[a]	1141(5)	1038(3)	−182(3)	45
O(14A)[a]	4482(6)	1794(3)	737(3)	40
O(17A)[a]	4830(6)	3241(3)	1878(4)	47
O(20A)[a]	1842(6)	4245(3)	1235(3)	43
O(23A)[a]	−1549(7)	3542(3)	446(4)	46
O(26A)[a]	−1795(8)	2173(3)	−745(5)	31
O(11B)[a]	1930(7)	988(3)	126(4)	49
O(14B)[a]	4822(8)	2067(3)	974(4)	42
O(17B)[a]	4518(7)	3564(4)	1938(4)	40
O(20B)[a]	1104(7)	4238(4)	1135(5)	43
O(23B)[a]	−1815(8)	3208(4)	251(5)	46
O(26B)[a]	−1513(9)	1863(4)	−726(4)	46
C(12A)[a]	2574(8)	844(3)	−374(4)	50
C(13A)[a]	4151(8)	948(4)	533(5)	47
C(15A)[a]	5842(7)	1928(4)	1655(4)	49
C(16A)[a]	6189(8)	2824(5)	1759(5)	46
C(18A)[a]	4851(8)	4094(5)	1757(4)	54
C(19A)[a]	3455(10)	4466(4)	1979(4)	53
C(21A)[a]	479(10)	4495(4)	1479(4)	54
C(22A)[a]	−1179(9)	4370(3)	624(6)	49
C(24A)[a]	−2929(7)	3357(4)	−449(4)	50
C(25A)[a]	−3216(9)	2436(5)	−578(5)	50
C(27A)[a]	−1797(8)	1352(6)	−767(4)	62
C(28A)[a]	−470(8)	952(4)	−998(4)	55
C(12B)[a]	3546(13)	853(5)	114(8)	55
C(13B)[a]	4901(10)	1195(5)	1018(6)	59
C(15B)[a]	6131(11)	2423(7)	1763(6)	53
C(16B)[a]	5876(8)	3346(5)	1668(5)	48
C(18B)[a]	4107(11)	4406(5)	1803(5)	43
C(19B)[a]	2504(10)	4949(4)	1950(5)	49
C(21B)[a]	−479(11)	4379(5)	1176(7)	52
C(22B)[a]	−1885(9)	4068(6)	272(6)	55
C(24B)[a]	−3061(10)	2831(8)	−599(6)	57
C(25B)[a]	−2827(13)	1961(6)	−596(6)	78
C(27B)[a]	−1234(13)	959(5)	−680(5)	63
C(28B)[a]	541(12)	768(5)	−759(6)	61

[a]Labels A and B stand for major (occ.:0.55) and minor (occ.: 0.45) crown disorder.

equal population (55:45) and the sulfonate molecule is disordered over one major and two minor orientations. The atomic numbering is given in the diagram in Fig. 3. The bond distances and angles, calculated from the final atomic coordinates (Table 7), are given in Table 8. The crown ligand has a pseudo D_{3d} symmetry in both conformation A and B with C—O—C—C and O—C—C—O torsion angles (Table 9) near 180° (average values 173.1° (A) and 176.1° (B)) and 70° (average values 71.1° (A) and 72.1° (B)). The C—O and C—C bond distances average 1.41 (A), 1.41 (B) and 1.51

Can. J. Chem. Downloaded from www.nrcresearchpress.com by 213.200.69.106 on 09/08/12
For personal use only.

Can. J. Chem. Downloaded from www.nrcresearchpress.com by 213.200.69.106 on 09/08/12
For personal use only.

TABLE 8. Distances and angles for the $C_{14}H_{30}O_9S$ compound **7**

Bond	Distances (esd's), Å	Bond	Distances (esd's), Å
S—O(1A)	1.642(6)	S—O(2A)	1.288(19)
S—O(1B)	1.567(10)	S—O(2B)	1.532(19)
S—O(1C)	1.583(11)	S—O(2C)	1.466(18)
S—O(3A)	1.461(20)	O(1A)—C(1)	1.421(6)
S—O(3B)	1.630(9)	O(1B)—C(1)	1.461(9)
S—O(3C)	1.243(16)	O(1C)—C(1)	1.388(10)
S—C(2)	1.725(3)		
O(11A)—C(12A)	1.401(8)	O(11B)—C(12B)	1.403(14)
C(12A)—C(13A)	1.488(10)	C(12B)—C(13B)	1.493(14)
C(13A)—O(14A)	1.424(8)	C(13B)—O(14B)	1.432(10)
O(14A)—C(15A)	1.416(8)	O(14B)—C(15B)	1.387(11)
C(15A)—C(16A)	1.495(11)	C(15B)—C(16B)	1.528(14)
C(16A)—O(17A)	1.418(10)	C(16B)—O(17B)	1.420(10)
O(17A)—C(18A)	1.412(9)	O(17B)—C(18B)	1.420(10)
C(18A)—C(19A)	1.491(11)	C(18B)—C(19B)	1.489(13)
C(19A)—O(20A)	1.424(9)	C(19B)—O(20B)	1.416(10)
O(20A)—C(21A)	1.414(10)	O(20B)—C(21B)	1.395(12)
C(21A)—C(22A)	1.491(11)	C(21B)—C(22B)	1.493(13)
C(22A)—O(23A)	1.424(8)	C(22B)—O(23B)	1.413(11)
O(23A)—C(24A)	1.411(8)	O(23B)—C(24B)	1.431(11)
C(24A)—C(25A)	1.530(11)	C(24B)—C(25B)	1.440(16)
C(25A)—O(26A)	1.402(11)	C(25B)—O(26B)	1.224(14)
O(26A)—C(27A)	1.347(11)	O(26B)—C(27B)	1.500(10)
C(27A)—C(28A)	1.466(11)	C(27B)—C(28B)	1.596(16)
C(28A)—O(11A)	1.431(8)	C(28B)—O(11B)	1.425(10)

Bonds	Angles (esd's), deg	Bonds	Angles (esd's), deg
O(1A)—S—O(2A)	95.6(8)	O(1A)—S—O(3A)	114.6(8)
O(1A)—S—O(2B)	111.3(7)	O(1A)—S—O(3B)	133.0(4)
O(1A)—S—O(2C)	100.0(7)	O(1A)—S—O(3C)	112.6(7)
O(1B)—S—O(2A)	118.5(8)	O(1B)—S—O(2C)	114.1(8)
O(1B)—S—O(2B)	128.8(7)	O(1B)—S—O(3B)	88.6(5)
O(1C)—S—O(2A)	109.9(9)	O(1C)—S—O(3A)	98.1(8)
O(1C)—S—O(2B)	125.1(8)	O(1C)—S—O(3B)	116.0(5)
O(1C)—S—O(2C)	112.0(8)	O(1C)—S—O(3C)	95.8(8)
O(2A)—S—O(3A)	123.4(11)	O(2B)—S—O(3A)	112.8(10)
O(2A)—S—O(3B)	119.7(8)	O(2B)—S—O(3B)	105.6(7)
O(2A)—S—O(3C)	129.0(10)	O(2B)—S—O(3C)	118.1(9)
O(2C)—S—O(3A)	111.8(10)	O(1A)—S—C(2)	93.4(2)
O(2C)—S—O(3B)	109.8(8)	O(1B)—S—C(2)	117.3(4)
O(2C)—S—O(3C)	117.3(10)	O(1C)—S—C(2)	97.2(4)
O(2A)—S—C(2)	108.4(8)	O(3A)—S—C(2)	115.8(8)
O(2B)—S—C(2)	107.3(6)	O(3B)—S—C(2)	102.6(3)
O(2C)—S—C(2)	118.7(7)	O(3C)—S—C(2)	111.2(7)
S—O(1A)—C(1)	114.5(4)	S—O(1B)—C(1)	116.7(6)
S—O(1C)—C(1)	120.3(7)		
C(12A)—O(11A)—C(28A)	114.4(5)	C(12B)—O(11B)—C(28B)	113.3(7)
O(11A)—C(12A)—C(13A)	108.8(5)	O(11B)—C(12B)—C(13B)	109.2(8)
C(12A)—C(13A)—O(14A)	109.6(6)	C(12B)—C(13B)—O(14B)	109.2(7)
C(13A)—O(14A)—C(15A)	112.0(5)	C(13B)—O(14B)—C(15B)	112.0(7)
O(14A)—C(15A)—C(16A)	107.7(5)	O(14B)—C(15B)—C(16B)	107.6(8)
C(15A)—C(16A)—O(17A)	110.5(6)	C(15B)—C(16B)—O(17B)	108.9(6)
C(16A)—O(17A)—C(18A)	114.1(6)	C(16B)—O(17B)—C(18B)	112.8(6)
O(17A)—C(18A)—C(19A)	108.9(6)	O(17B)—C(18B)—C(19B)	108.7(7)
C(18A)—C(19A)—O(20A)	108.8(6)	C(18B)—C(19B)—O(20B)	108.4(7)
C(19A)—O(20A)—C(21A)	110.8(5)	C(19B)—O(20B)—C(21B)	113.1(7)

TABLE 8 (*concluded*)

Bonds	Angles (esd's), deg	Bonds	Angles (esd's), deg
O(20A)—C(21A)—C(22A)	109.0(6)	O(20B)—C(21B)—C(22B)	109.6(8)
C(21A)—C(22A)—O(23A)	110.9(6)	C(21B)—C(22B)—O(23B)	109.6(7)
C(22A)—O(23A)—C(24A)	113.8(5)	C(22B)—O(23B)—C(24B)	115.4(7)
O(23A)—C(24A)—C(25A)	110.0(5)	O(23B)—C(24B)—C(25b)	111.9(8)
C(24A)—C(25A)—O(26A)	102.8(6)	C(24B)—C(25B)—O(26B)	105.3(8)
C(25A)—O(26A)—C(27A)	108.6(6)	C(25B)—O(26B)—C(27B)	105.1(7)
O(26A)—C(27A)—C(28A)	117.4(7)	O(26B)—C(27B)—C(28B)	109.2(7)
O(11A)—C(28A)—C(27A)	108.4(6)	O(11B)—C(28B)—C(27B)	109.5(7)

TABLE 9. Torsion angles for the crown part of the $C_{14}H_{30}O_9S$ compound **7**

Bonds	Torsion angles (esd's), deg	
	Major occ. (A. 0.55)	Minor occ. (B, 0.45)
O(11)—C(12)—C(13)—O(14)	−73.0(6)	−70.8(0)
C(12)—C(13)—O(14)—C(15)	172.6(5)	−175.6(8)
C(13)—O(14)—C(15)—C(16)	175.0(5)	−177.4(7)
O(14)—C(15)—C(16)—O(17)	70.7(7)	76.4(8)
C(15)—C(16)—O(17)—C(18)	−166.1(6)	−175.6(7)
C(16)—O(17)—C(18)—C(19)	−175.4(6)	170.9(6)
O(17)—C(18)—C(19)—C(20)	−69.5(7)	−73.5(8)
C(18)—C(19)—O(20)—C(21)	172.4(6)	−176.9(7)
C(19)—O(20)—C(21)—C(22)	171.4(6)	177.4(7)
O(20)—C(21)—C(22)—O(23)	69.8(7)	68.2(9)
C(21)—C(22)—O(23)—C(24)	−169.2(6)	−177.8(8)
C(22)—O(23)—C(24)—C(25)	179.5(6)	175.9(8)
O(23)—C(24)—C(25)—O(26)	−71.5(7)	−70.8(10)
C(24)—C(25)—O(26)—C(27)	173.4(6)	177.7(7)
C(25)—O(26)—C(27)—C(28)	176.1(6)	−175.6(8)
O(26)—C(27)—C(28)—O(11)	72.3(8)	73.0(8)
C(27)—C(28)—O(11)—C(12)	−166.7(5)	−179.0(7)
C(28)—O(11)—C(12)—C(13)	−179.2(5)	173.1(7)

TABLE 10. Bond distances (Å) and angles (deg) related to the pseudo hydrogen bonding in complex **7**

Bond (A—H···B)	Distances (esd's)			Angles (esd's)
	A—B	A—H	H—B	A—H—B
C(1)—H(11A)[a]...O(14A)[b]	3.394(6)	0.95	2.64	137
C(1)—H(11B)[a]...O(14A)[b]	3.394(6)	0.95	2.64	138
C(1)—H(12B)[a]...O(26A)[b]	3.296(8)	0.95	2.54	136
C(1)—H(11C)[a]...O(26A)[b]	3.296(8)	0.95	2.69	122
C(1)—H(11A)[a]...O(14B)[b]	3.412(7)	0.95	2.70	132
C(1)—H(11B)[a]...O(14B)[b]	3.412(7)	0.95	2.73	130
C(1)—H(12B)[a]...O(26B)[b]	3.388(8)	0.95	2.68	132
C(1)—H(11C)[a]...O(26B)[b]	3.388(8)	0.95	2.70	130
C(2)—H(21)...O(11A)	3.377(6)	0.95(3)	2.32(3)	175(2)
C(2)—H(22)...O(17A)	3.257(6)	0.90(3)	2.46(3)	147(2)
C(2)—H(23)...O(23A)	3.328(6)	1.05(3)	2.46(3)	152(2)
C(2)—H(21)...O(11B)	3.279(6)	0.95(3)	2.26(3)	163(2)
C(2)—H(22)...O(17B)	3.339(7)	0.90(3)	2.53(3)	148(2)
C(2)—H(23)...O(23B)	3.244(7)	1.05(3)	2.38(3)	151(2)

Can. J. Chem. Downloaded from www.nrcresearchpress.com by 213.200.69.106 on 09/08/12
For personal use only.

TABLE 10 (*concluded*)

Bonds	Angles (esd's), deg	Bonds	Angles (esd's), deg
O(1A)—C(1)...O(14A)[b]	92.1(3)	O(1A)—C(1)...O(26A)[b]	104.5(3)
O(1B)—C(1)...O(14A)[b]	140.4(4)	O(1B)—C(1)...O(26A)[b]	83.4(4)
O(1C)—C(1)...O(14A)[b]	107.6(5)	O(1C)—C(1)...O(26A)[b]	90.6(5)
O(1A)—C(1)...O(14B)[b]	98.0(3)	O(1A)—C(1)...O(26B)[b]	99.5(3)
O(1B)—C(1)...O(14B)[b]	148.1(4)	O(1B)—C(1)...O(26B)[b]	86.0(4)
O(1C)—C(1)...O(14B)[b]	114.9(5)	O(1C)—C(1)...O(26B)[b]	87.9(5)
C(13A)—O(14A)...C(1)[c]	117.8(4)	C(13A)—O(14A)...H(11A)[c]	112.8
		C(13A)—O(14A)...H(11B)[c]	112.6
C(15A)—O(14A)...C(1)[c]	129.0(4)	C(15A)—O(14A)...H(11A)[c]	130.4
		C(15A)—O(14A)...H(11B)[c]	135.5
C(25A)—O(26A)...C(1)[c]	91.6(3)	C(25A)—O(26A)...H(12B)[c]	125.3
		C(25A)—O(26A)...H(11C)[c]	137.4
C(27A)—O(26A)...C(1)[c]	118.4(5)	C(27A)—O(26A)...H(12B)[c]	122.0
		C(27A)—O(26A)...H(11C)[c]	108.9
C(13B)—O(14B)...C(1)[c]	124.2(5)	C(13B)—O(14B)...H(11A)[c]	116.2
		C(13B)—O(14B)...H(11B)[c]	116.4
C(15B)—O(14B)...C(1)[c]	123.6(5)	C(15B)—O(14B)...H(11A)[c]	129.4
		C(15B)—O(14B)...H(11B)[c]	131.4
C(25B)—O(26B)...C(1)[c]	133.5(6)	C(25B)—O(26B)...H(12B)[c]	124.6
		C(25B)—O(26B)...H(11C)[c]	136.8
C(27B)—O(26B)...C(1)[c]	120.3(5)	C(27B)—O(26B)...H(12B)[c]	125.8
		C(27B)—O(26B)...H(11C)[c]	112.6
S—C(2)...O(11A)	102.13(15)	S—C(2)—H(21)	106(2)
S—C(2)...O(17A)	126.30(17)	S—C(2)—H(22)	106(2)
S—C(2)...O(23A)	128.43(17)	S—C(2)—H(23)	108(2)
S—C(2)...O(11B)	99.33(16)	H(21)—C(2)—H(22)	116(2)
S—C(2)...O(17B)	129.84(18)	H(21)—C(2)—H(23)	104(2)
S—C(2)...O(23B)	124.89(18)	H(22)—C(2)—H(23)	117(2)
C(12A)—O(11A)...C(2)	121.7(4)	C(12A)—O(11A)...H(21)	121.0(8)
C(28A)—O(11A)...C(2)	120.7(4)	C(28A)—O(11A)...H(21)	120.8(8)
C(16A)—O(17A)...C(2)	118.6(4)	C(16A)—O(17A)...H(22)	121.1(8)
C(18A)—O(17A)...C(2)	124.5(4)	C(18A)—O(17A)...H(22)	124.2(8)
C(22A)—O(23A)...C(2)	117.7(4)	C(22A)—O(23A)...H(23)	120.0(8)
C(24A)—O(23A)...C(2)	125.5(4)	C(24A)—O(23A)...H(23)	125.2(7)
C(12B)—O(11B...C(2)	121.0(5)	C(12B)—O(11B)...H(21)	124.9(9)
C(28B)—O(11B)...C(2)	123.0(5)	C(28B)—O(11B)...H(21)	118.0(9)
C(16B)—O(17B)...C(2)	119.9(4)	C(16B)—O(17B)...H(22)	120.5(8)
C(18B)—O(17B)...C(2)	120.0(5)	C(18B)—O(17B)...H(22)	123.3(8)
C(22B)—O(23B)...C(2)	121.7(5)	C(22B)—O(23B)...H(23)	119.7(8)
C(24B)—O(23B)...C(2)	121.2(5)	C(24B)—O(23B)...H(23)	124.6(8)

[a]Calculated hydrogen atoms.
[b]$x, 1/2 - y, 1/2 + z$.
[c]$x, 1/2 - y, -1/2 + z$.

(A), 1.44 (B), respectively. The O—C—C and C—O—C angles average 109.4° (A), 108.9° (B) and 112.3° (C), 112.0° (B).

In this 1:1 ratio complex, the sulfonate molecule acts as a bifunctional guest linking the crown molecules and thus giving rise to infinite chains. Similar complexes were observed with dimethyl sulfate or dimethyl acetylenecarboxylate (14, 16) but complex **7** is unique because two different methyl groups, CH_3—O and CH_3—SO_3, are involved in the association. A view of the major model association (sulfonate A, crown model A) of the polymeric type 1:1 complex **7** is shown in Fig. 4. The hydrogen bonding contacts and geometries can be found in Table 10. On the CH_3—SO_3 end of the sulfonate molecule, all three methyl hydrogen atoms participate in interactions with altemate oxygen atoms of the crown. The C—H---O bridge angles are 175°, 147°, and

Can. J. Chem. Downloaded from www.nrcresearchpress.com by 213.200.69.106 on 09/08/12
For personal use only.

152°; the corresponding C---O distances are 3.377, 3.257, and 3.328 Å whereas CH---O distances are 2.32, 2.46, and 2.46 Å, shorter than the sum of the van der Waals radii.

On the CH_3—O end of the sulfonate molecule, where hydrogens are much less acidic than CH_3—SO_3 methyl hydrogens, interactions are very weak. In the association model in Fig. 4, there is only one weak interaction (C---O = 3.394 Å, CH---O = 2.64 Å, and C—H---O angle = 137°). The other two hydrogens are directed away from the crown ether.[5]

The hydrogen bond is one of the significant factors in the formation of natural or synthetic supramolecular structures. The recent reports on molecular recognition are concerned almost exclusively with strong hydrogen bonding of the conventional type (O—H---O, N—H---O). The present work shows that molecular arrays can be constructed with weaker C—H---X hydrogen bonds.

Acknowledgements

We acknowledge the financial support of this work by the Natural Sciences and Engineering Research Council of Canada and the "Ministère de l'Éducation du Québec."

1. R.M. Izatt, K. Pawlak, J.S. Bradshaw, and R.L. Bruening. Chem. Rev. **91**, 1721 (1991).
2. F. Vögtle, W.M. Müller, and W.H. Watson. Top. Curr. Chem. **125**, 131 (1985).
3. A. Elbasyouny, H.J. Brügge, K. von Deuten, M. Dickel, A. Knöchel, K.U. Koch, J. Kopf, D. Melzer, and G. Rudolph. J. Am. Chem. Soc. **105**, 6568 (1983).
4. W.H. Watson, J. Galloy, D.A. Grossie, F. Vögtle, and W.M. Müller. J. Org. Chem. **49**, 347 (1984).
5. F. Vögtle, W.M. Müller, and E. Weber. Chem. Ber. **113**, 1130 (1980).
6. J. van Eerden, M. Skowronska-Ptasinska, P.D.J. Grootenhuis, S. Harkema, and D.N. Reinhoudt. J. Am. Chem. Soc. **111**, 700 (1989).
7. S. Harkema, G.J. van Hummel, K. Daasvatn, and D.N. Reinhoudt. J. Chem. Soc. Chem. Commun. 368. (1991).
8. C.J. Pedersen. J. Org. Chem. **36**, 1690 (1971).
9. G.W. Buchanan, C. Morat, J.P. Charland, C.I. Ratcliffe, and J.A. Ripmeester. Can. J. Chem. **67**, 1212 (1989).
10. R.D. Rogers, L.K. Kurihara, and P.D. Richards. J. Chem. Soc. Chem. Commun. 604. (1987).
11. E. Weber, S. Franken, J. Ahrendt, and H. Puff. J. Org. Chem. **52**, 5291 (1987).
12. R.D. Rogers and P.D. Richards. J. Inclusion Phenom. **5**, 631 (1987).
13. J.A. Bandy and M.R. Truter. Acta Crystallogr. Sect. B: Struct. Crystallogr. Cryst. Chem. **B37**, 1568 (1981).
14. G. Weber, J. Mol. Struct. **98**, 333 (1983).
15. A. van Zon, F. de Jong, D.N. Reinhoudt, G.J. Torny, and Y. Onverzen. Recl. Trav. Chim. Pays-Bas, **100**, 453 (1981).
16. I. Goldberg. Acta Crystallogr. Sect. B: Struct. Crystallogr. Cryst. Chem. **B31**, 754 (1975).
17. L. Parenteau and F. Brisse. Can. J. Chem. **67**, 1293 (1989).
18. S. Deguise, F. Brisse, J. Ouellet, and R. Savoie. Can. J. Chem. **64**, 142 (1986).
19. D. Belamri and C. Baroux. Acta Crystallogr. Sect. C: Cryst. Struct. Commun. **C44**, 2173 (1988).
20. R. Savoie, A. Rodrigue, M. Pigeon-Gosselin, and R. Chênevert. Can. J. Chem. **63**, 1457 (1985).
21. C.I. Tarcliffe, J.A. Ripmeester, G.W. Buchanan, and J.K. Denike. J. Am. Chem. Soc. **114**, 3294 (1992).
22. C.J. van Staveren, V.M.L.J. Aarts, P.D.J. Grootenhuis, J. van Eerden, S. Hardema, and D.N. Reinhoudt. J. Am. Chem. Soc. **108**, 5271 (1986).
23. P.D.J. Grootenhuis, J. van Eerden. P.J. Dijkstra, S. Harkema, and D.N. Reinhoudt. J. Am. Chem. Soc. **109**, 8044 (1987).
24. J.W.H.M. Uiterwijk, S. Harkema, and D. Feil. J. Chem. Soc. Perkin Trans. 2, 721 (1987).
25. P.D.J. Grootenhuis and P.A. Kollman. J. Am. Chem. Soc. **111**, 4046 (1989).
26. T. Koritsanszky, J. Buschmann, L. Denner, P. Luger, A. Knöchel, M. Haarich, and M. Patz. J. Am. Chem. Soc. **113**, 8388, 1991.
27. R.A. Kumpf and J.R. Damerwood. J. Chem. Soc. Chem. Commun. 621 (1988).
28. J.A.A. de Boer, D.N. Reinhoudt, S. Harkema, G.J. van Hummel, and F. de Jong. J. Am. Chem. Soc. **104**, 4073 (1982).
29. A.R. van Doorn, R. Schaafstra, M. Bos, S. Harkema, J. van Eerden, W. Vergoom, and D.N. Reinhoudt. J. Org. Chem. **56**, 6083 (1991).
30. E.J. Gabe, Y. Le Page, J.-P. Charland and F.L. Lee. NRCVAX, an interactive program system for structure analysis. J. Appl. Crystallogr. **22**, 384 (1989).
31. G. Sheldrick. SHELX 76, A crystallographic computation system for crystal structure determination. Univ. of Cambridge, England. 1976.
32. C.K. Johnson. ORTEP, Report ORNL-3794, Oak Ridge National Laboratory, Tenn. 1965.
33. D.T. Cromer and J.B. Mann. Acta Crystallogr. Sect. A: Cryst. Phys. Diffr. Theor. Gen. Crystallogr. **A24**, 321 (1968).
34. R.F. Stewart, E.R. Davidson, and W.T. Simpson. J. Chem. Phys. **42**, 3175 (1965).
35. D.T. Cromer and D. Liberman. J. Chem. Phys. **53**, 1891 (1970).
36. W. Szeja. Synthesis, 822 (1979).
37. G.R. Desiraju. Acc. Chem. Res. **24**, 290 (1991).
38. R. Taylor and O. Kennard. J. Am. Chem. Soc. **104**, 5063 (1982).

[5]Tables of atomic coordinates, bond distances and angles, temperature factors, and structure factor amplitudes, as well as stereoviews of **1** and **7** may be purchased from: The Depository of Unpublished Data, Document Delivery, CISTI, National Research Council Canada, Ottawa, Canada K1A 052.

Tables of atomic coordinates, bond distances and angles, and stereoviews of **1** and **7** have also been deposited with the Cambridge Crystallographic Data Centre and can be obtained on request from The Director, Cambridge Crystallographic Data Centre, University of Chemical Laboratory, 12 Union Road, Cambridge, CB2 1EZ, U.K.

Can. J. Chem. Downloaded from www.nrcresearchpress.com by 213.200.69.106 on 09/08/12
For personal use only.

Styrylbenzodiazinones 2. Chromo- et fluoroionophores dérivés du monoaza-15-couronne-5. Synthèse et structure

LOUIS CAZAUX,[1] MOURAD FAHER, CLAUDE PICARD ET PIERRE TISNÈS

Synthèse et physicochimie organique, Unité de recherche associée au Centre national de la recherche scientifique n° 471, Université Paul Sabatier, 118 route de Narbonne, 31062 Toulouse Cédex, France

Reçu le 25 février 1993

LOUIS CAZAUX, MOURAD FAHER, CLAUDE PICARD et PIERRE TISNÈS. Can. J. Chem. **71**, 1236 (1993).

Au cours d'un travail sur les dérivés styryliques de benzodiazinones, nous avons préparé la 7-*N*,*N*-diméthylamino-3-méthyl-1,4-benzodiazine-2-one **4***a* ainsi que deux chromo- et fluoroionophores dérivés du monoaza-15-couronne-5 et de styrylbenzodiazinones. Une étude structurale de ces composés par RMN ^1H et ^{13}C, spectrophotométrie UV et modélisation moleculaire a été réalisée. Contrairement aux styrylbenzoxazinones, les styrylbenzodiazinones présentent une isomérisation *Z*/*E* dans l'acétonitrile. Cette isomérisation est photoinduite, catalysée par les ions métalliques et constitue un phénomène réversible. D'autre part, une réaction d'alkylation efficace de la fonction lactame des benzodiazinones est décrite.

LOUIS CAZAUX, MOURAD FAHER, CLAUDE PICARD, and PIERRE TISNÉS. Can. J. Chem. **71**, 1236 (1993).

In connection with our work on styryl derivatives of benzodiazinones, we have prepared the 7-*N*,*N*-dimethylamino-3-methyl-1,4-benzodiazin-2-one **4***a* and two chromo- and fluoroionophores derived from the monoaza-15-crown-5 and styrylbenzodiazinones. A structural study of these compounds by ^1H and ^{13}C NMR, UV spectrophotometry, and molecular modelling was carried out. Unlike styrylbenzoxazinones, styrylbenzodiazinone derivatives showed a *Z*/*E* isomerization in acetonitrile solution. The isomerization was photoinduced, was catalysed by metallic ions, and was a reversible process. As well, an efficient alkylation reaction of the lactam function of benzodiazinones is described.

Can. J. Chem. Downloaded from www.nrcresearchpress.com by 213.200.69.106 on 09/08/12
For personal use only.

Les chromo- et fluoroionophores ont été largement développés ces dernières années en particulier en relation avec des macrocycles de type éther-couronne (1). La sensibilité des sondes spectrophotométriques et plus encore fluorométriques peut être ainsi liée à la sélectivité de ces derniers vis-à-vis des cations métalliques et plus généralement au phénomène de reconnaissance ionique ou moléculaire. L'observation du phénomène et sa quantification à des fins, par exemple, de dosage nécessite la perturbation d'un système conjugué sous l'effet de l'association supramoléculaire. Pour cette raison les systèmes styryliques ont été l'objet de plusieurs études sur les combinaisons suivantes : dinitrostilbène (2), styrylbenzoxazinone (1), mérocyanine (3) ou coumarine 153 (4) couplés au monoaza-15-couronne-5, styrylbenzothiazole associé au benzo-15-couronne-5 (5).

Dans cette étude, nous décrirons d'abord la synthèse et l'analyse structurale des aminobenzodiazinones **4***a*,*b* et **5***a*,*b* et de deux nouveaux ionophores **1** et **2** dérivés du monoaza-15-couronne-5 et de deux styrylbenzodiazinones (schéma 1). Une discussion sur les caractéristiques structurales et spectrales des ionophores s'appuiera notamment sur l'étude des styrylbenzodiazinones (6) où le composé **6** dépourvu du motif ether-couronne peut servir de modèle au système **1**.

Nous examinerons le problème structural propre à ces systèmes styryliques, à savoir l'isomérie rotationnelle autour de la liaison N–C (7, 8) et l'existence d'une liaison H intramoléculaire entre un CH éthylénique et le groupe carbonyle qui favoriserait l'un des rotamères (8).

À ce problème nous en ajouterons un autre mis en évidence dans la seule série des styrylbenzodiazinones. C'est une modification structurale photoréversible catalysée par les ions métalliques.

Résultats

Synthèse

Les *aminobenzodiazinones* n'ont pas été décrites jusqu'à présent. Le schéme logique de leur synthèse était bien évidemment l'hétérocyclisation par un ester α cétonique de la 4-*N*,*N*-diméthylamino-1,2 phénylène-diamine **8** (schéma 2).

Cette triamine a été précédemment décrite (9), sous forme de trichlorhydrate, par réduction de la 3,4-dinitro-*N*,*N*-diméthylaniline dans l'acide chlorhydrique avec du chlorure d'étain(II). Plusieurs essais de neutralisation de ce trichlorhydrate, suivis de la condensation avec le pyruvate d'éthyle, se sont révélés infructueux. Nous avons toujours observé une détérioration rapide de la benzodiazinone **4** dans le milieu réactionnel. Dans le cas des diméthylamino-benzoxazinones, Le Bris (10) avait également noté une dégradation rapide, catalysée par des impuretés, de ce type de colorant.

Au vu de ces résultats, nous avons préféré utiliser comme synthon la 3-amino-4-nitro-*N*,*N*-diméthylaniline **9** et procéder à une hydrogénation catalytique du groupement nitro afin d'atteindre le composé **8**. La diamine **9** a été préparée en quatre étapes à partir de la 3-fluoroaniline **13** selon les méthodes de Hodgson et Nicholson (11) et de Arcos et Miller (12). Le traitement de la 3-fluoroaniline par l'anhydride acétique, suivie d'une réaction de nitration nous a fourni le 5-fluoro-2-nitro acétanilide **11**. L'action du chlorhydrate de diméthylamine sur ce dernier composé conduit au 5-*N*,*N*-diméthylamino-2-nitro acétanilide qui, par hydrolyse basique afin de régénérer la fonction amine primaire, nous a permis d'atteindre le synthon **9** avec un rendement global de 22% à partir de la fluoroaniline de départ. L'hydrogénation catalytique de **9**, puis la réction in situ en milieu éthanolique, sous atmosphère inerte, du pyruvate d'éthyle conduit quantitativement à la benzodiazinone **4**, plus exactement à un mélange des deux isomères **4***a* et **4***b*.

En effet, le spectre RMN ^1H du produit **4** à 200 MHz dans $CDCl_3$ montre la présence de deux groupes méthyle à 2,54 et 2,62 ppm ainsi que deux types de groupes diméthylamino ($\Delta\delta$ = 0,07 ppm). Une analyse en chromatographie HPLC permet de quantifier les isomères **4***a* et **4***b* dans des proportions respectives 70 : 30. Une purification par recristallisation dans l'éthanol et par chromatographie HPLC préparative nous a permis d'isoler chacun de ces deux isomères (**4***a*, Rdt = 70%; **4***b*, Rdt = 25%).

1. Auteur à qui adresser toute correspondance.

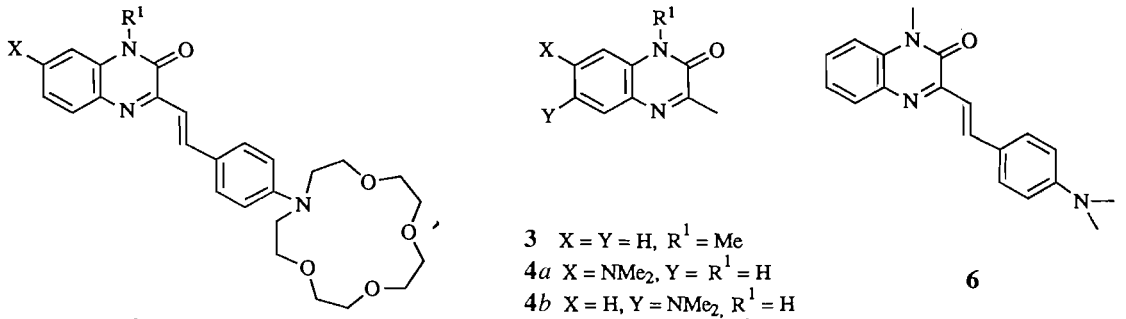

1 X = H, R^1 = Me
2 X = NMe_2, R^1 = H

3 X = Y = H, R^1 = Me
4*a* X = NMe_2, Y = R^1 = H
4*b* X = H, Y = NMe_2, R^1 = H
5*a* X = NMe_2, Y = H, R^1 = Me
5*b* X = H, Y = NMe_2, R^1 = Me

6

SCHÉMA 1

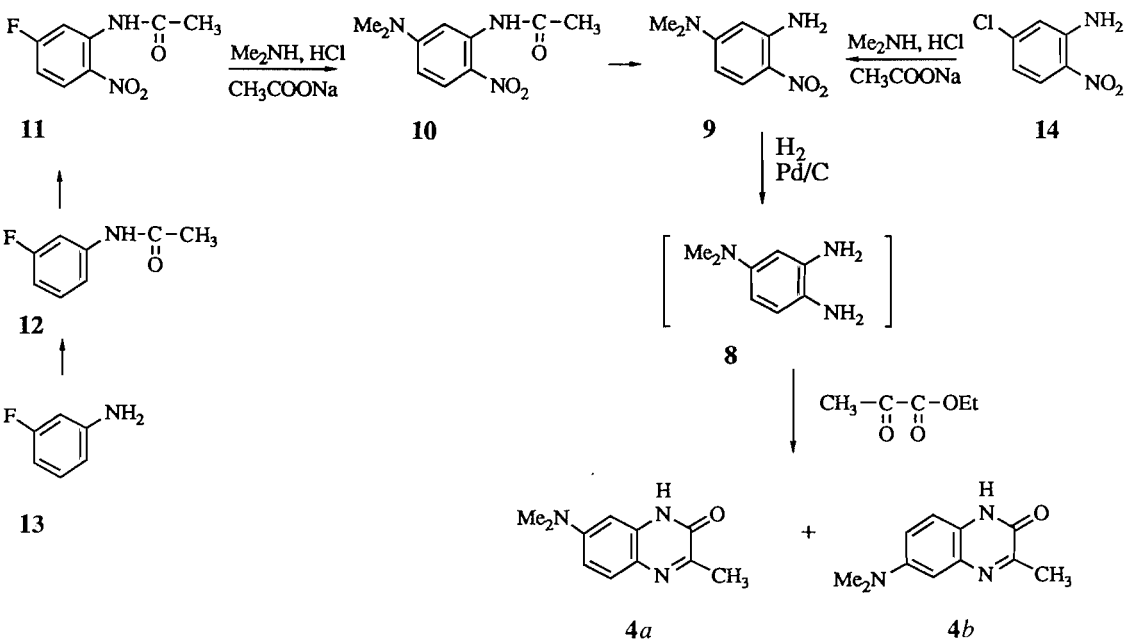

11 **10** **9** **14** **12** **8** **13** **4***a* **4***b*

SCHÉMA 2

Cette première approche nous ayant permis d'accéder aux benzodiazinones **4***a* et **4***b*, nous avons envisagé de préparer le synthon **9** par une voie plus directe. En nous inspirant des travaux de Arcos et Miller (12) sur la substitution d'un fluor par le groupement diméthylamino, nous avons appliqué cette réaction sur la 5-chloro-2-nitroaniline **14**, produit commercial. Bien que la substitution nucléophile soit rendue plus délicate dans ce cas (chlore à la place du fluor, présence sur le noyau aromatique d'un groupement donneur amino) nous avons pu optimiser les conditions de la réaction (durée de chauffage, proportion des réactifs) et obtenir ainsi **9** en une seule étape avec un rendement de 67% en produit isolé.

Nous avons également cherché à obtenir des *diméthylamino-benzodiazinones alkylées sur l'azote lactamique* afin, par exemple, de pouvoir moduler leur lipophilie. Deux approches peuvent être envisagées : la première consiste à effectuer l'hétérocyclisation à partir d'une triamine présentant les fonctions amines primaire, secondaire et tertiaire, et présente l'avantage de ne conduire qu'à un seul isomère analogue de **4***a*; la seconde, d'une utilisation plus générale, consiste à effectuer l'alkylation de l'atome d'azote lactamique de la benzodiazinone elle-même. Lorsque l'on oppose (schéma 3) la triamine **15**, obtenue par réduction de **10** avec AlH_3, au pyruvate d'éthyle, aucun produit de condensation n'a pu être détecté. En ce qui concerne la seconde approche, nous n'avons pas réussi à alkyler la benzodiazinone **4***a* par l'action du paratoluène sulfonate de méthyle et de K_2CO_3 en utilisant les mêmes conditions opératoires que pour l'obtention de **3** (6). Cependant le recours à l'iodure de méthyle et au carbonate de césium dans l'acétone, à température ambiante, nous a permis d'obtenir les composés **5***a* et **5***b* avec des rendements quantitatifs à partir de leurs précurseurs **4***a* et **4***b* (schéma 3).

Les *fluoroionophores* **1** et **2** ont été préparés suivant des méthodes décrites (6) par condensation entre le *N*-(4-formylphényl)-aza-15-couronne-5 et la benzodiazinone correspondante (**3** et **4***a* respectivement). La méthode à l'anhydride acétique fournit **1** avec un rendement de 35% et celle à la pipéridine **2** avec un redement de 10%.

Caractéristiques structurales

Les caractéristiques structurales RMN ^1H et ^{13}C, dans $CDCl_3$, des styrylbenzodiazinones **1**, **2** et des aminobenzodiazinones **4***a*,*b* et **5***a*,*b* sont reportées dans les tableaux 1 et 2. Nous y avons également reporté les caractéristiques

Can. J. Chem. Downloaded from www.nrcresearchpress.com by 213.200.69.106 on 09/08/12
For personal use only.

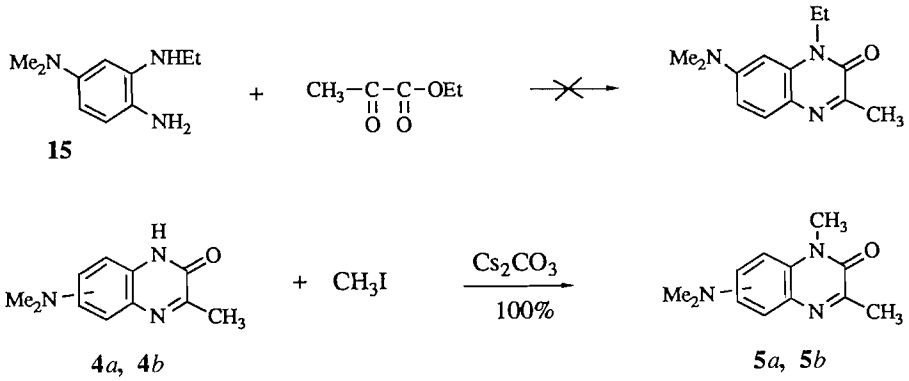

SCHÉMA 3

TABLEAU 1. Caractéristiques RMN ^{1}H des styrylbenzodiazinones **1**, **2**, **6** et des benzodiazinones **3**, **4***a*, **4***b*, **5***a*, **5***b* dans $CDCl_3$ à 250 MHz (δ en ppm et *J* en Hz)

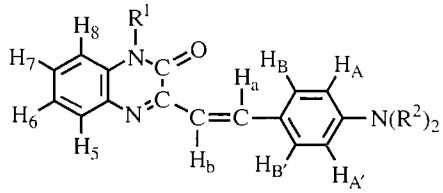

Composé	Proton														
	δ_a	δ_b	J_{ab}	$\delta_{A,A'}$	$\delta_{B,B'}$	$J_{AB,A'B'}$	δ_5	δ_6	δ_7	δ_8	$J_{5,6}$	$J_{5,7}$	$J_{6,7}$	$J_{6,8}$	$J_{7,8}$
1	8,02	7,59	16,0	6,65	7,55	8,9	7,81	7,29	7,43	7,23	7,85	1,5	7,85	1,5	8,1
2	7,96	7,42	16,0	6,65	7,53	8,5	7,64	6,74	—	6,20	9,0	—	—	2,5	—
3	–	–	–	—	—	—	7,78	7,31	7,51	7,27	7,8	1,55	7,8	1,55	8,3
4*a*	—	—	—	—	—	—	7,63	6,75	—	6,43	9,0	—	—	2,6	—
4*b*	—	—	—	—	—	—	7,07	—	7,04	7,24	—	3,0	—	—	9,0
5*a*	—	—	—	—	—	—	7,59	6,71	—	6,23	9,0	—	—	2,6	—
5*b*	—	—	—	—	—	—	7,15	—	7,09	7,19	—	2,8	—	—	9,1
6	8,07	7,56	16,3	6,69	7,58	9,0	7,85	7,30	7,47	7,35	7,8	1,5	7,6	1,5	8,2

spectrales des composés **3** et **6** étudiés dans notre publication à suivre (6).

En RMN ^{13}C les attributions ont été effectuées sur la base des spectres ^{13}C couplés ^{1}H off resonance à 6,29 MHz, des spectres *J* modulé ou des spectres corrélés ^{1}H–^{13}C.

Aminobenzodiazinones

Les analyses centésimales et les déterminations de la masse moléculaire par spectrométrie de masse des composés **4***a* et **4***b* ont permis de démontrer sans ambiguïté l'existence d'une isomérie de position dans ces deux composés.

La structure des aminobenzodiazinones **4***a*, **4***b* et **5***a*, **5***b* a été établie par RMN ^{1}H par comparaison des valeurs de déplacement chimique expérimentales et calculées. Ces dernières ont été déterminées à partir de la benzodiazinone **3** et de son homologue non méthylé sur l'atome d'azote lactamique (6) et des incréments du groupe diméthylamino en *ortho* (−0,66 ppm) et en *méta* (−0,18 ppm) déduits du benzène et du diméthylaminobenzène (13). À titre d'exemple nous avons reporté dans le tableau 3 les valeurs calculées et expérimentales, ainsi que les écarts correspondants dans le cas des composés **5***a* et **5***b*.

Une démarche analogue effectuée en RMN ^{13}C en utilisant les incréments du groupe diméthylamino sur un noyau aromatique (14) permet de confirmer cette attribution. Dans ce cas, la différenciation des deux isomères se fait sur les carbones k et n du noyau benzénique (notation du tableau 2). En effet les valeurs calculées pour ces deux carbones tertiaires sont respectivement 98,1 et 130,2 ppm pour la structure **4***a*, **5***a* et 114,9 et 113,9 ppm pour la structure **4***b*, **5***b*.

Les propriétés photophysiques de ces quatre diaminobenzodiazinones permettent également une attribution de structures. En effet **4***a* et **5***a* présentent des propriétés marquées de fluorescence, alors que **4***b* et **5***b* en sont dépourvues. Ceci peut s'expliquer du fait que, dans la structure **a** (groupe NMe_2 en position 7), le chromophore peut être décrit par les deux formes mésomères **a** et **a'** (schéma 4), la forme **a'** étant prédominante dans l'état excité, tandis que pour l'isomère **b** (groupe NMe_2 en position 6) il ne peut y avoir extension de conjugaison du doublet et l'azote du groupe diméthylamino vers le cycle diazinone, d'où l'absence de fluorescence dans ce cas.

Cette attribution de structures pour **4***a* et **4***b* est également en accord avec les proportions relatives de ces deux composés obtenues lors de la réaction d'hétérocyclisation à partir de la triamine **8** (schéma 5). Un calcul de distribution de charge par MNDO sur cette triamine **8** a permis d'établir que l'atome d'azote en *para* du groupe NMe_2 est plus nucleophile (−0,4320) que celui situé en *méta* (−0,4274). D'autre

Can. J. Chem. Downloaded from www.nrcresearchpress.com by 213.200.69.106 on 09/08/12
For personal use only.

TABLEAU 2. Caractéristiques RMN ^{13}C des styrylbenzodiazinones **1**, **2**, **6** et des benzodiazinones **3**, **4***a*, **4***b*, **5***a*, **5***b* dans $CDCl_3$ à 50,32 MHz (δ en ppm)

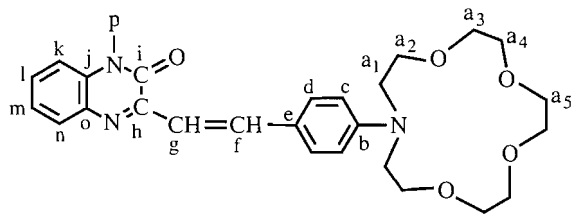

Composé	Carbone																				
	a_1	a_2	a_3	a_4	a_5	b	c	d	e	f	g	h	i	j	k	l	m	n	o	p	NMe_2
1	52,7	66,5	70,1	70,3	71,3	148,7	111,6	129,9	124,5	138,9	116,9	152,3	155,3	132,6[a]	113,6	129,3	123,8	128,8	133,6	29,2	—
2	52,7	66,6	70,2	70,3	71,4	148,3	111,6	129,4	124,7	132,5	117,4	153,5	157,0	132,5	95,2	150,9	110,7	129,4	125,2	—	40,4
3	–	–	–	–	–	–	–	–	–	–	21,5	155,0	158,2	132,5[a]	113,5	129,4	123,4	129,3	133,1[a]	28,9	–
4*a*	–	–	–	–	–	–	–	–	–	–	20,2	152,1	157,0	133,1	95,6	151,0	110,3	129,2	125,3	–	40,6
4*b*	–	–	–	–	–	–	–	–	–	–	21,0	158,2	156,3	123,0	116,2	117,1	147,7	110,4	133,9	–	41,3
5*a*	–	–	–	–	–	–	–	–	–	–	21,1	151,3	156,0	135,0	94,3	151,1	109,2	130,1	124,8	28,9	40,6
5*b*	–	–	–	–	–	–	–	–	–	–	21,8	158,9	154,7	125,5	114,3	116,8	146,5	112,3	133,6	29,1	41,6
6	40,2	–	–	–	–	151,2	112,0	129,6	124,6	138,7	117,1	153,0	155,2	132,7[a]	113,6	129,4	123,7	128,2	133,7[a]	29,2	–

[a]Ces carbones peuvent être échangés.

TABLEAU 3. Déplacements chimiques en RMN ^1H dans $CDCl_3$ pour les composés **5***a* et **5***b* comparés avec les valeurs calculées à partir de **3** et des incréments pour le groupe NMe_2 ($\Delta\delta = \delta_{calc} - \delta_{exp}$)[a]

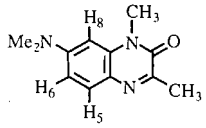

	δ_5	δ_6	δ_8
Valeurs calculées	**7,60**	**6,65**	**6,61**
5*a*	**7,59** (+0,01)	**6,71** (−0,06)	**6,23** (+0,38)
5*b*	7,19 (+0,41)	7,09 (−0,44)	7,15 (−0,54)

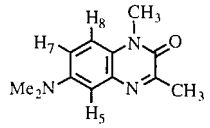

	δ_5	δ_7	δ_8
Valeurs Calculées	**7,12**	**6,85**	**7,09**
5*a*	6,23 (+0,89)	6,71 (+0,14)	7,59 (−0,50)
5*b*	**7,15** (−0,03)	**7,09** (−0,24)	**7,19** (−0,10)

[a]Les doublets à 6,23 et 7,15 ppm correspondent au proton isolé entre les deux fonctions azote.

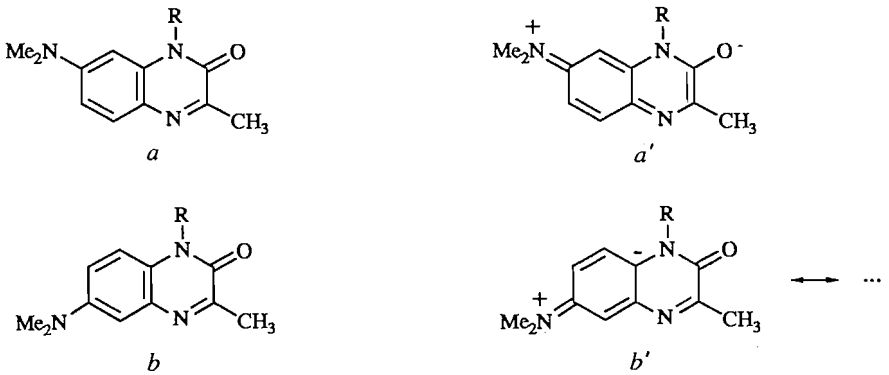

a *a'*

b *b'*

SCHÉMA 4

Can. J. Chem. Downloaded from www.nrcresearchpress.com by 213.200.69.106 on 09/08/12
For personal use only.

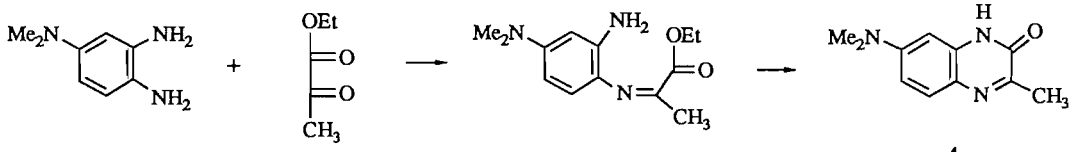

8 **4*a***

SCHÉMA 5

TABLEAU 4. Variation de la DO des composés **1**, **2** et **6** en présence de perchlorate de calcium

Composé	Ligand pur		$[Ca^{2+}]/[L]$ (ρ = 0,04)		
	Concentration (mol/l)	DO/λ_{max} (nm)	DO/λ_{max} obscurité	DO/λ_{max} lumière blanche	DO/λ_{max} obscurité
1[a]	$4,78 \times 10^{-5}$	1,096/448	→ 1,586/446	→ 1,114/448	→ 1,514/446
2[a]	$5,38 \times 10^{-5}$	1,345/465	→ 1,712/464	→ 1,346/465	→ 1,702/464
6[a]	$4,08 \times 10^{-5}$	1,026/441	→ 1,342/440	→ 1,030/441	→ 1,340/440
6[b]	$3,44 \times 10^{-5}$	0,88/444	→ 1,21/442	→ 0,83/444	→ 1,20/442

[a]Dans l'acetonitrile.
[b]Dans le dioxanne.

TABLEAU 5. Influence sur la DO_{max} du composé **6** dans l'acétonitrile de deux types d'irradiation en *absence* ou en *présence* de Ca^{2+}[a]

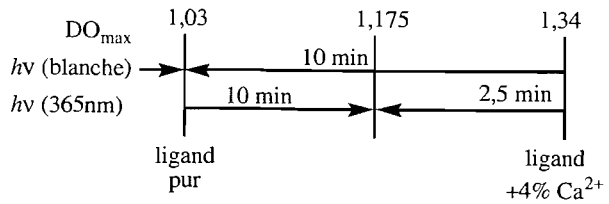

[a]Le temps nécessaire pour atteindre la position d'équilibre est indiqué au-dessus de chaque flèche.

part il a été montré par Le Bris que les 2-aminophénols réagissent dans un premier temps sur la fonction cétone du pyruvate d'éthyle pour former la liaison imine de l'hétérocycle (15). Nous retrouvons ce même mécanisme dans le cas de l'addition de 1,2-diaminobenzènes sur des β-céto-esters conduisant à des benzodiazépines (16). En tenant compte de ces deux considérations, nucléophilie plus grande de l'atome d'azote en *para* du NMe_2 de **8** et formation de la liaison imine dans une première étape, la réaction d'hétérocyclisation est donc orientée préférentiellement vers l'isomère **4*a***, obtenu expérimentalement avec un rendement de 70%.

Styrylbenzodiazinones

Les spectres RMN ^1H des composés **1** et **2** réalisés dans $CDCl_3$ montrent un systéme AB attribué aux protons H_a et H_b de la liaison styrylique avec une constante de couplage de 16 Hz qui indique une configuration *E*. La largeur à mi-hauteur du signal du proton H_a (1,5 Hz) est supérieure à celle du signal de H_b (1,0 Hz) du fait du couplage ^4J avec les protons BB′ de la partie benzénique portant l'éther-couronne. Le système AA′BB′ de cette dernière partie et les protons aromatiques du motif benzodiazinone ont d'autre part des déplacements chimiques et des constantes de couplage très proches de ceux de **6** et du leurs précurseurs **3** et **4*a*** respectivement.

Les attributions RMN ^{13}C ont été effectuées pour **1** par analogie avec la styrylbenzodiazinone homologue **6** et pour **2** par analogie avec **6** pour la partie styrylique et avec **4*a*** pour le motif aminobenzodiazinone.

Équilibre photoréversible

Lors de l'étude de complexation des ionophores **1** et **2** par les ions alcalins et alcalino-terreux dans l'acétonitrile nous avons constaté que la densité optique (DO) à la longueur d'onde d'absorption maximale de ces composés variait beaucoup dès l'ajout d'une petite quantité de sel métallique.

L'analyse sommaire de ce phénomène en préalable à l'étude de complexation[2] nous a donc paru indispensable. Nous l'avons menée à la fois sur les ionophores **1** et **2** ainsi que sur l'analogue linéaire **6**, dépourvu de motif éther-couronne pour lequel nous avons montré[2] qu'il ne possède pas de propriétés complexantes significatives contrairement aux composés **1** et **2**.

Absorption UV

On suit les variations en fonction du temps de la densité optique de ces composés dans l'acétonitrile à la longueur d'onde d'absorption maximale après addition d'une quantité catalytique de perchlorate de calcium (rapport Ca^{2+}/ligand, ρ = 0,04) avant et après irradiation à la lumière blanche ou à longueur d'onde de 365 nm (tableaux 4 et 5, figure 1).

On observe avec les trois composés un phénomène identique décomposable en quatre stades (figures 1*a*, *b*). Avec la styrylbenzodiazinone **6**, par exemple, une solution $4,08 \times 10^{-5}$ M dans l'acétonitrile présente (*i*) un maximum d'absorption à 441 nm (bande de transfert électronique) et une DO égale à 1,026; (*ii*) l'addition d'une faible quantité de perchlorate de calcium (ρ = 0,04) à la solution précédente, directement dans la cuve, provoque une forte augmentation de DO (31%) en l'espace d'environ 1 h; (*iii*) l'exposition de cette solution pendant environ 10 min à la lumière blanche ramène la DO à sa valeur en absence d'ion Ca^{2+}; puis (*iv*)

2. Résultats soumis pour publication à J. Photochem. Photobiol.

Can. J. Chem. Downloaded from www.nrcresearchpress.com by 213.200.69.106 on 09/08/12
For personal use only.

Can. J. Chem. Downloaded from www.nrcresearchpress.com by 213.200.69.106 on 09/08/12
For personal use only.

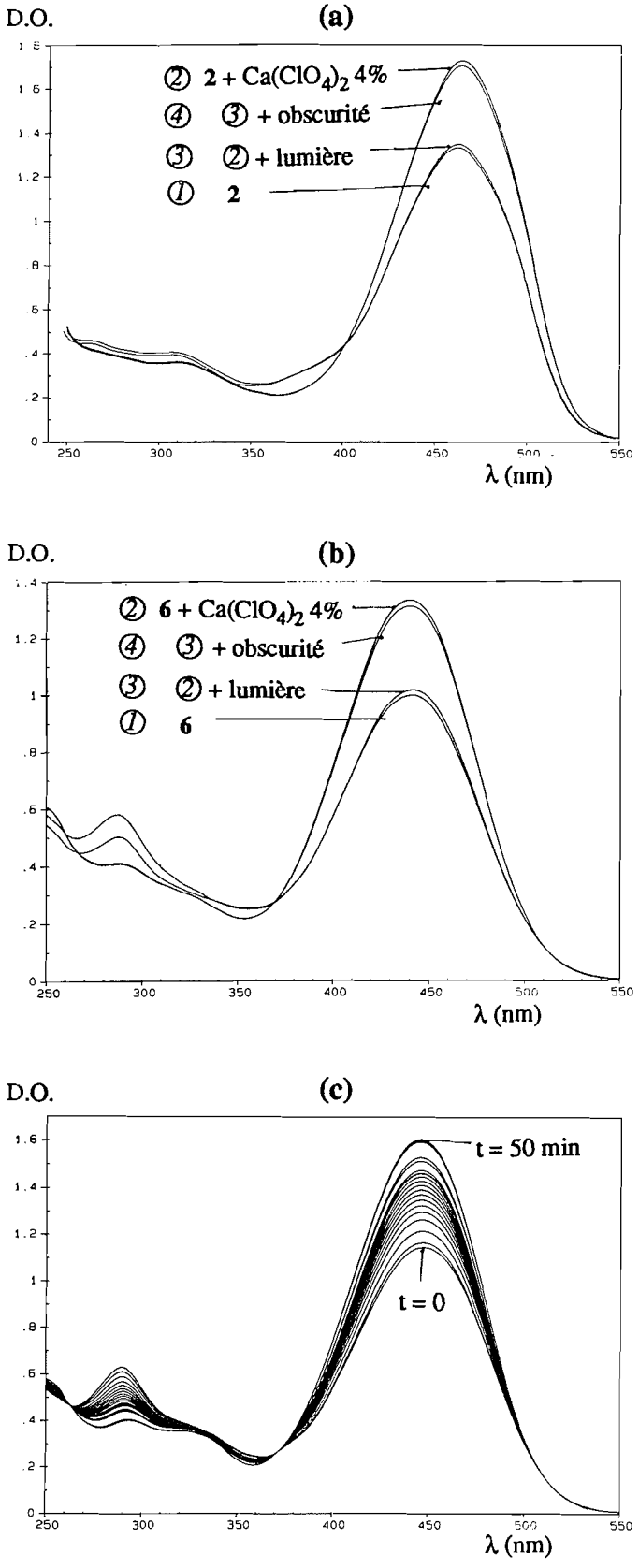

FIG. 1. Evolution du spectre d'absorption UV dans l'acétonitrile des composés **2** (*a*) et **6** (*b*) : ligand seul (1), après ajout de 4% de $Ca(ClO_4)_2$ (2), exposition à la lumière blanche (3) et retour à l'obscurité (4); (*c*) étude cinétique de la transformation du composé **1** dans l'acétonitrile après ajout de 4% de $Ca(ClO_4)_2$.

un maintien de 2 h à l'obscurité permet de retrouver la valeur maximale (1,342). Le phénomène est donc important (27–45% selon les composés) et réversible, et la longueur d'onde maximale ne varie pas de manière significative au cours du cycle.

De plus, le même phénomène a été observé lors de l'étude de complexation avec les différents ions étudiés (alcalins, alcalino-terreux et Zn^{2+}) dans l'acétonitrile ($\varepsilon = 34$). Un essai sur le composé **6** dans le dioxanne ($\varepsilon = 2$) avec le perchlorate de calcium conduit au même résultat. La nature de l'ion et du solvant semble donc avoir peu d'effet sur le phénomène étudié.

Il est aussi à noter qu'une irradiation sous lampe UV à vapeur de mercure (6 W) à 365 nm (tableau 5) du composé **6** dans l'acétonitrile augmente la DO de 18% lorsque l'équilibre est atteint (t = 10 min) alors que l'exposition à la lumière blanche ne la modifie pas; la même expérience en présence du perchlorate de calcium indique une décroissance du même ordre. Cependant, alors que l'action de la lumière blanche ramène la DO à sa valeur sans Ca^{2+}, l'action de l'autre source lumineuse tend à la ramener à une valeur intermédiaire. Le phénomène est ici encore réversible par mise à l'obscurité.

Enfin, aucune variation de DO n'est observée sur la benzodiazinone **3** par addition de 4% de perchlorate de calcium.

Une *étude cinétique* de la variation de DO dans l'acétonitrile après addition de 4% de perchlorate de calcium sur les trois composés a montré la présence de deux points isosbestiques (figure 1*c*) indiquant la non accumulation d'un intermédiaire. Après traitement des données par le programme LSG (Least Squares Guggenheim) les trois constantes de vitesse de la cinétique de pseudo premier ordre ont été déterminées à 25°C :

$$k_1\,(\mathbf{1}) = 3{,}98 \times 10^{-4} \pm 0{,}1\ s^{-1}$$
$$k_1\,(\mathbf{2}) = 2{,}48 \times 10^{-3} \pm 0{,}05\ s^{-1}$$
$$k_1\,(\mathbf{6}) = 1{,}24 \times 10^{-3} \pm 0{,}05\ s^{-1}$$

RMN ^1H

Afin de mieux préciser le phénomène nous avons essayé de le suivre par RMN ^1H sur le composé **6** en solution dans CD_3CN la plus diluée possible ($3{,}5 \times 10^{-3}$ M). Contrairement à notre observation dans $CDCl_3$ (6), le composé pur présente (figure 2) deux types de doublets pour les protons styryliques : l'un à grande constante de couplage (16 Hz) représente environ 80%, l'autre à constante de couplage moyenne (9 Hz) environ 20%. Les valeurs de ces constantes de couplage sont en accord avec une isomérie *E*/*Z*. Les déplacements chimiques observés pour les protons H_a et H_b des espèces *Z* (6,66 et 7,90 ppm) et *E* (7,51 et 8,00 ppm) présentent une différence notable sur H_a. Un comportement proche a été relevé récemment (17) pour le 4-(dicyanométhylène)-2-méthyl-6-[*p*-(diméthylamino)styryl]-4*H*-pyrane (DCM) dans DMSO-d_6; soit respectivement 6,2 et 6,9 ppm pour H_a et H_b de l'espèce *Z*, 7,04 et 7,44 ppm pour les mêmes protons de l'espèce *E*. Les constantes de couplage observées sont de 12,6 (*Z*) et 16 Hz (*E*).

D'autre part, l'addition de 3% de perchlorate de calcium à la solution précédente entraîne une disparition complète de l'espèce *Z* au profit de *E*. Toutefois, une exposition à la

Can. J. Chem. Downloaded from www.nrcresearchpress.com by 213.200.69.106 on 09/08/12
For personal use only.

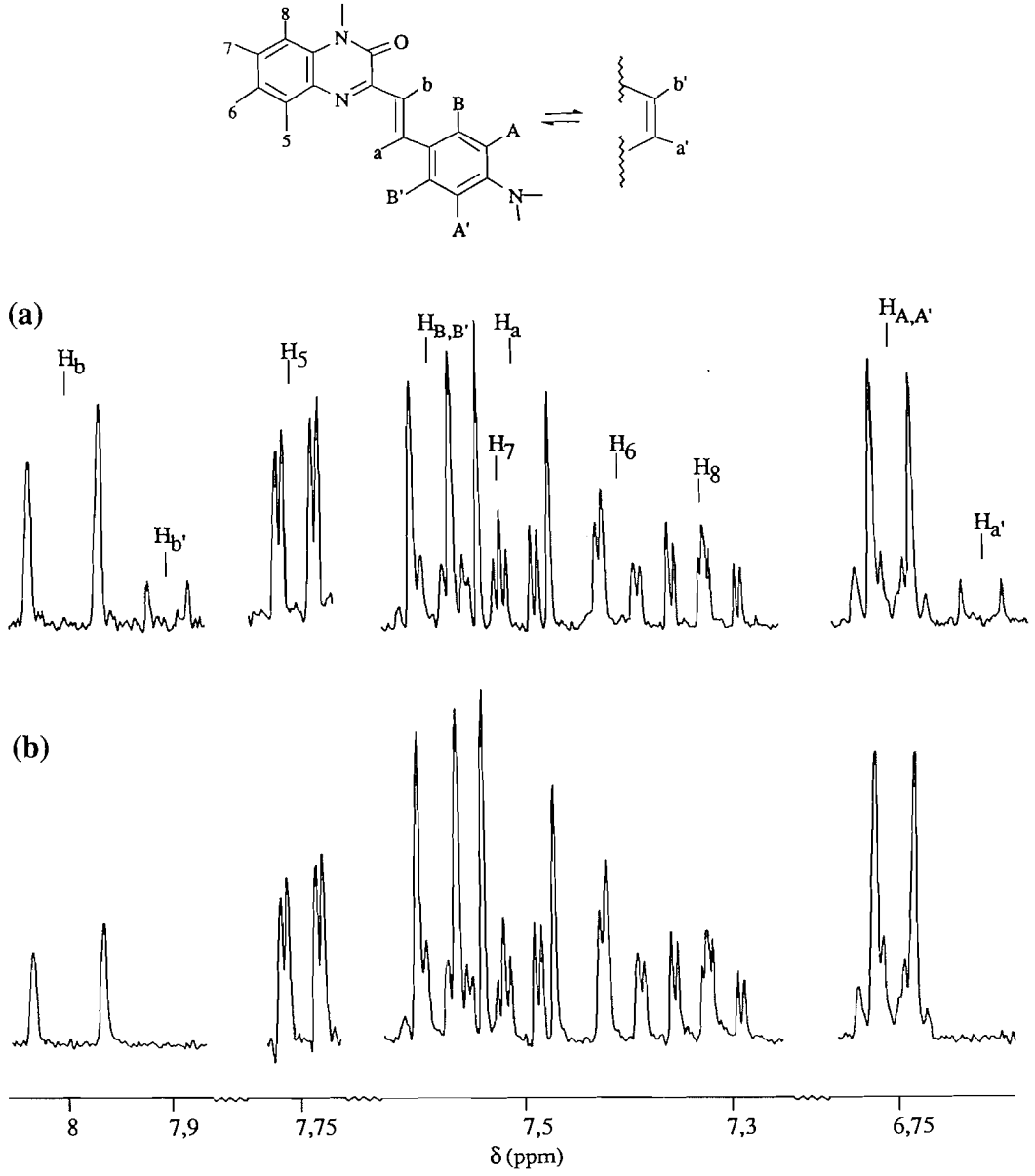

FIG. 2. Spectres RMN ^1H à 250 MHz du composé **6** ($3,5 \times 10^{-3}$ M dans CD_3CN) en absence (*a*) ou en présence (*b*) de 3% de perchlorate de calcium.

lumière du jour pendant 5 h ne fait pas réapparaître l'espèce *Z*.

Modélisation moléculaire

En complément à une étude de mécanique moléculaire (6) et dans des conditions identiques, nous avons calculé l'énergie des isomères *Z* (s-*cis* et s-*trans*) du composé **6** (schéma 6). Ainsi, avec le champ de force MM2*, nous trouvons des énergies respectives de 47,2 et 48,3 kcal/mol pour les isomères *Z*,s-*cis* et *Z*, s-*trans* respectivement. Pour les isomères *Z*, comme pour les isomères *E*, le rotamère s-*cis* est favorisé; dans ce cas, d'un peu plus de 1 kcal/mol. En raison de la gène stérique introduite par les interactions entre l'hydrogène H_B du groupe phényle et soit l'azote iminique soit le carbonyle des déviations importantes par rapport à la planéité sont observées : les angles de torsion φ_1 et φ_2 sont ainsi respectivement de 33° et −55° pour l'isomère *Z*,s-*cis*, −136° et −43° pour l'isomère *Z*, s-*trans*. À titre de comparaison les valeurs correspondantes pour les isomères *E*,s-*cis* et *E*,s-*trans* sont respectivement de 16° et −28° et de −154° et −30°.

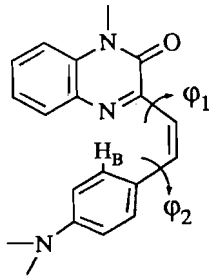

Z, s-*cis*

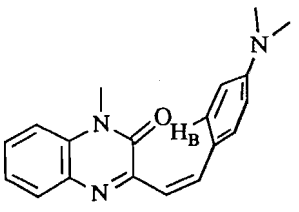

Z, s-*trans*

SCHÉMA 6

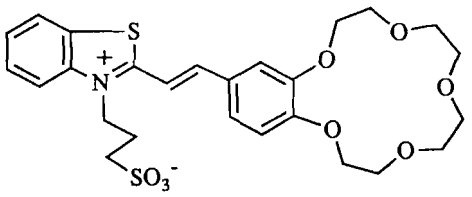

SCHÉMA 7

Discussion

Modification structurale photoréversible catalysée par les ions métalliques

Le phénomène observé implique une augmentation de DO à 440–464 nm en présence de quantités catalytiques (4%) d'ion métallique dans l'acétonitrile ou le dioxanne ($\sim 5 \times 10^{-5}$ M). Il n'est observé ni avec la benzodiazinone **3** ni avec les styrylbenzoxazinones (8). Il implique donc la participation d'un groupe lactame (plus polarisé que le groupe lactone) et d'un système styrylique. L'autoassociation ne peut en être l'explication[3] car nous avons montré (partie expérimentale) qu'elle était négligeable vraisemblablement en raison de la non planéité du système révélé par modélisation moléculaire du composé **6**. La deuxième étape du phénomène observé est une diminution de la bande à forte longueur d'onde par irradiation à la lumière blanche retrouvant rapidement une valeur proche de sa valeur primitive notée en absence de Ca^{2+}. Lorsque l'irradiation (à 365 nm) s'écarte de la longueur d'onde d'absorption maximale (440–464 nm) l'équilibre primitif n'est pas retrouvé. Un retour à la DO maximale à l'obscurité (3ème étape) referme le cycle et montre bien que nous sommes en présence d'un équilibre photo réversible catalysé par les ions métalliques.

Pour expliquer ces phénomènes on postulera un équilibre *Z*/*E* au niveau de la liaison styrylique pour lequel les arguments suivants militent. D'abord, de tels équilibres sont courants avec les systèmes styryliques, par exemple références 5*a*, 17, 19–21.

Ainsi on observe par photoisomérisation de *trans*-stilbène (21) un abaissement très important de la longueur d'onde d'absorption de la bande de transfert électronique (295 → 224 nm) et une diminution de son intensité importante (>50%). Pour les isomères *Z* et *E* du dérivé styrylique du benzothiazole (5*a*) (schéma 7) une diminution de 15 nm dans l'acétonitrile est observée pour les bandes d'absorption à forte longueur d'onde quand on passe du *E* (440 nm) au *Z* (425 nm) accompagnée d'une baisse de DO d'environ 80%. Toutefois la photoisomérisation par irradiation à 365 nm ne conduit pas à une complète transformation de l'isomère *E* en *Z*. Dans ces conditions pour nos composés, une proportion importante d'isomère *Z* peut très bien n'être décelée que par la diminution de la bande propre à l'isomère *E*, sa bande caractéristique étant masquée précisément par cette dernière.

La deuxième argument est l'observation pour **6** (CD_3CN, $3{,}5 \times 10^{-3}$ M) en l'absence de Ca^{2+} de deux doublets dont la constante de couplage (J = 9 Hz) est caractéristique d'un isomère *Z* (~20%) aux côtés des deux doublets de forte constante de couplage (J = 16 Hz) attribuables à l'isomère *E*. De plus, l'addition de 3% de $Ca(ClO_4)_2$ fait disparaître les deux doublets de 9 Hz. D'après ce résultat et la variation de DO en UV on peut déduire que l'état photostationnaire atteint dans l'acétonitrile représenterait de 20 à 30% d'isomère *Z* à la concentration 5×10^{-5} M en absence d'ion métallique. La transformation en présence d'ion Ca^{2+} est un processus lent ($k \sim 10^{-3}$ s^{-1}) et direct (sans accumulation d'intermédiaire) conduisant au seul isomère *E*; elle est photoréversible.

Un essai d'irradiation d'une solution de **6** (5×10^{-5} M) dans l'acétonitrile dans une cuve en quartz à 350 nm pendant 1 h (voir partie expérimentale) conduit à une décoloration complète de la solution. La bande à 445 nm disparaît complètement sans apparition de bande nouvelle; un retour à l'état stationnaire antérieur n'intervenant pas après ajout de 4% de perchlorate de Ca^{2+}, la cuve étant maintenue à l'obscurité jusqu'à 12 h. Il est possible qu'une réaction photochimique irréversible se soit alors produite comme, par example, la dimérisation qui a été observée récemment pour les benzodiazinones (22) ou plus vraisemblablement des polymérisations en raison de la disparition presque complète des signaux en RMN ^1H. L'isomère *Z* attendu n'est pas observé dans ces conditions.

Cet isomère *Z* serait en fait, d'après notre résultat de mécanique moléculaire, l'isomère s-*cis*.

Dans ces conditions, l'isomérisation catalysée par les ions métalliques pourrait impliquer (schéma 8) un chélate intermédiaire par transfert de charge déstabilisant la forme *Z* et donc favorisant le passage à la forme *E* la plus stable à l'obscurité. La barrière de l'isomérisation $Z \rightleftharpoons E$ serait abaissée par suite de contraintes stériques dans cet intermédiaire. La formation de cet intermédiaire serait elle-même facilitée par la torsion φ_1 autour de la liaison C—C ($\varphi_1 = 32°$ d'après notre calcul de mécanique moléculaire) dans l'isomère *Z*,s-*cis* et par l'abaissement de la barrière à la rotation autour de cette liaison induite par la chélation du carbonyle lactamique avec un cation M^{n+}.

Lorsqu'à partir de la forme *E* pure, en présence de M^{n+} et à l'obscurité, on irradie l'échantillon, on observe des équilibres photostationnaires dont la position varie selon la longueur d'onde du rayonnement et sa puissance. Le maximum de forme *Z* est obtenu par irradiation à la lumière blanche, seul rayonnement utilisé englobant la longueur d'onde maximale d'absorpiton des composés étudiés. En l'absence de M^{n+} les mêmes positions de l'équilibre photostationnaire tendent à être atteintes mais plus lentement, l'action catalytique du métal ne jouant plus.[4]

À propos du schéma 8, il nous paraît difficile de dire si une liaison H stabilisante intervient dans l'isomère *E*,s-*trans* dont nous avons vu (6) qu'il en existerait 30% dans le chloroforme d'après les durées de vie de fluorescence. Par contre, dans l'acétonitrile, en présence d'un excès de sel alcalino-terreux cette forme est très vraisemblablement exclue en raison de l'affinité des oxygènes lactamiques pour ces ions.

Le phénomène observé dans l'acétonitrile est donc compatible avec une isomérie *Z*/*E*, l'isomère *E* étant le seul isomère en présence de quantité catalytique de sel métallique (3–4%). Les phénomènes spécifiques à un ion donné, dûs à la présence du motif éther-couronne dans les composés **1** et

3. Des augmentations de DO analogues sont par exemple observées avec les acides nucléiques (18) ou l'orthophénantroline (voir partie expérimentale).

4. Comme dans le cas des *cis*- et *trans*-stilbène (23), la répulsion stérique entre cycles aromatiques est responsable des torsions (φ_1 et φ_2) observées et leur couplage avec la torsion autour de la liaison éthylénique (θ) conduit à l'isomérisation.

Can. J. Chem. Downloaded from www.nrcresearchpress.com by 213.200.69.106 on 09/08/12
For personal use only.

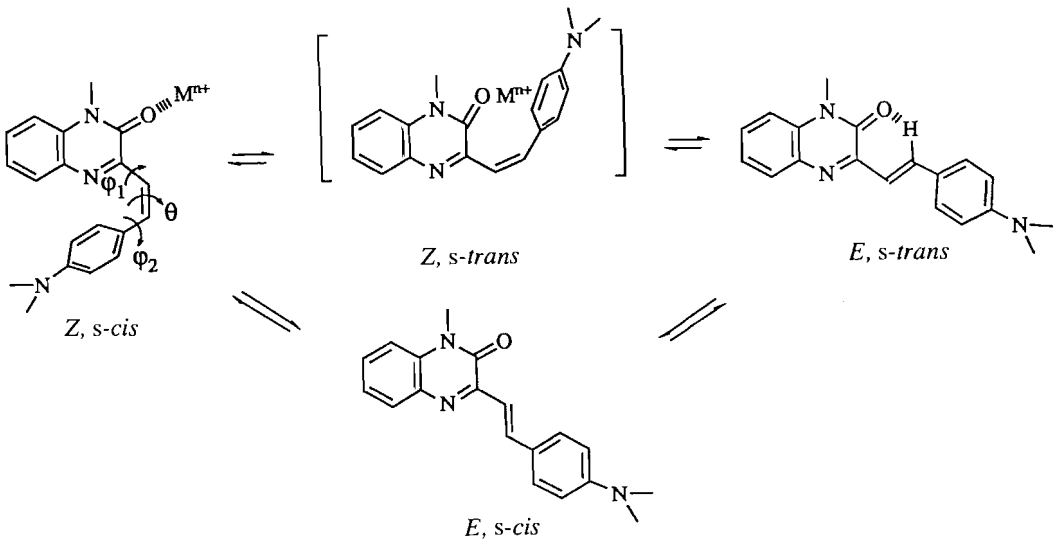

SCHÉMA 8

2, ne sont observés que pour des ajouts supplémentaires de sels métalliques.[2] On peut considérer que, quelque soit l'équilibre de complexation étudié, seul l'isomère *E* participe à cet équilibre rendant possible la détermination des constantes de complexation et l'utilisation du composé **1** au dosage sélectif de l'ion calcium.[2]

Partie expérimentale

Les points de fusion (*F*) ont été déterminés au banc Köfler. Les spectres de RMN ^1H et ^{13}C ont été enregistrés sur les appareils Bruker AC-200 et AC-250 (avec le TMS comme référence interne, les déplacements étant exprimés en ppm). Pour une description détaillée des spectres RMN ^1H, il faut se reporter au tableau 1 et pour les spectres RMN ^{13}C au tableau 2. Les spectres infrarouge ont été mesurés sur un spectrophotomètre Perkin–Elmer 833 (en pastille de KBr à moins de spécification contraire). Les spectres de masse ont été efectués sur un appareil Nermag R 10--10C (mode d'ionisation : DCI/NH_3). Les analyses centésimales ont été réalisées au service commun de microanalyse élémentaire UPS-INP à Toulouse. Les spectres d'absorption ont été effectués sur un spectrophotomètre Perkin–Elmer Lambda 17 et les spectres d'émission sur un spectrofluorimètre Perkin–Elmer LS-3B, les cuves de mesure étant thermostatées à 25 ± 1°C.

Les calculs de mécanique moléculaire ont été effectués sur une station Silicon Graphics IRIS 4D30 à l'aide du programme MACROMODEL V3.5X.

Les séparations par chromatographie liquide (CPL) sont réalisées sur colonne de silice Merck Kieselgel 60 (70–230 mesh). La pureté des produits a été vérifiée par chromatographie sur couche mince (CCM) sur plaque de gel de silice Merck 60 F 254 prête à l'emploi.

L'acétonitrile de chez BDH (Hipersolv) a été utilisé comme solvant pour les mesures d'absorption. Les perchlorates de cations alcalins et alcalinoterreux, provenant de chez Strem et Aldrich, étaient de la plus haute qualité disponible et ont été utilisés sans purification supplémentaire.

Les composés **3** et **6** ont été préparés selon la référence 6.

*3-Fluoro acétanilide : **12***

Il a été préparé par action de l'anhydride acétique sur la 3-fluoroaniline dans l'acide acétique. La recristallisation a été effectuée dans l'eau; Rdt 70%, cristaux blancs, *F* = 85°C (litt. (11) 85%C); IR : 3330 (NH), 1670 (C=O) cm^{-1}; RMN ^1H ($CDCl_3$) : 2,16 (s, 3H, CH_3), 6,53–7,60 (m, 5H, NH et arom.).

*5-Fluoro-2-nitro acétanilide : **11***

Il a été préparé à partir de **12** selon la référence 11 et purifié par CPL (éluant dichlorométhane); Rdt 56%, aiguilles jaune pâle, *F* = 87°C (litt. (11) 85°C); IR : 3340 (NH), 1710 (C=O), 1490 (NO_2 asym.), 1310 (NO_2 sym.) cm^{-1}; RMN ^1H ($CDCl_3$) : 2,30 (s, 3H, CH_3), 6,76 (m, 1H, H4, $J_{4\text{-}F}$ = 12, $J_{4\text{-}3}$ = 9 et $J_{4\text{-}6}$ = 3 Hz), 8,17 (dd, 1H, H3, $J_{3\text{-}F}$ = 6 Hz), 8,52 (dd, 1H, H6, $J_{6\text{-}F}$ = 12 Hz).

*5-(*N,N*-Diméthylamino)-2-nitro acétanilide : **10** :* 3,54 g (0,0179 mol) de **11**, 2,19 g (0,027 mol) de chlorhydrate de diméthylamine et 2,73 g (0,033 mol) d'acétate de sodium anhydre dans 14 mL d'éthanol sont chauffés à 100°C dans un tube de verre scellé pendant 8 h. Après refroidissement, le milieu réactionnel est versé dans de l'eau froide. Le précipité formé est filtré et recristallisé dans l'éthanol. Rdt 55%, fines aiguilles jaunes, *F* = 188°C (litt. (12) 187,5–188,5°C); IR : 3310 (NH), 1705 (C=O), 1490 (NO_2 asym.), 1310 (NO_2 sym.) cm^{-1}; RMN ^1H ($CDCl_3$) : 3,10 (s, 6H, $N(CH_3)_2$), 2,23 (s, 3H, CH_3), 6,30 (dd, 1H, H4, $J_{4\text{-}3}$ = 9 et $J_{4\text{-}6}$ = 3 Hz), 8,07 (d, 1H, H6), 8,08 (d, 1H, H3). Anal. calc. pour $C_{10}H_{13}N_3O_3$: C 53,81, H 5,87, N 18,82; trouvée : C 53,65, H 5,78, N 18,63.

*3-Amino-4-nitro-*N,N*-diméthylaniline : **9***

*À partir de **10** :* **10** subit une hydrolyse basique dans la soude aqueuse 1 N à 50°C pendant 8 h pour donner **9**. Rdt 100%, solide jaune clair, *F* = 138–140°C (litt. (12) 134–135°C); IR : 3475, 3360 (NH_2), 1525 (NO_2 asym.), 1365 (NO_2 sym.) cm^{-1}; RMN ^1H ($CDCl_3$) : 3,07 (s, 6H, $N(CH_3)_2$), 5,74 (d, 1H, H2, $J_{2\text{-}6}$ = 3 Hz), 6,08 (dd, 1H, H6, $J_{6\text{-}5}$ = 9 Hz), 6,17 (s élargi, 2H, NH_2), 7,99 (d, 1H, H5). Anal. calc. pour $C_8H_{11}N_3O_2$: C 53,03, H 6,12, N 23,19; trouvée : C 53,60, H 6,29, N 23,29.

*À partir de **14** :* 3,09 g (0,0179 mol) de **14**, 2,93 g (0,036 mol) de chlorhydrate de diméthylamine et 4,4 g (0,054 mol) d'acétate de sodium anhydre dans 15 mL d'éthanol sont chauffés à 130°C dans un tube de verre scellé pendant 3 jours. Après refroidissement, le milieu réactionnel est versé dans de l'eau froide. Après extraction de la phase aqueuse par du dichlorométhane, séchage de la phase organique sur $MgSO_4$ et évaporation du solvant, le milieu réactionnel est purifié par CPL (éluant acétate d'éthyle – éther de pétrole 50 : 50). On obtient ainsi 2,27 g de **9** (Rdt 70%).

*7-*N,N*-Diméthylamino-3-méthyl-1,4-benzodiazine-2-one : **4**a et 6-*N,N*-diméthylamino-3-méthyl-1,4-benzodiazine-2-one : **4**b*

Le composé **9** (1 g, 5,52 mmol) dans 70 mL d'éthanol absolu est soumis à une hydrogénation catalytique en présence de Pd/C à 10% (0,4 g) à température ambiante et sous pression atmosphérique. On additionne ensuite au milieu réactionnel, conservé sous atmosphère inerte, 0,77 g (6,63 mmol) de pyruvate d'éthyle

Can. J. Chem. Downloaded from www.nrcresearchpress.com by 213.200.69.106 on 09/08/12
For personal use only.

et on chauffe à reflux pendant 4 h. On filtre à chaud la solution sur Célite et le solvant est évaporé. Une recristallisation dans l'éthanol du résidu d'évaporation fournit 0,729 g de **4***a*. Une purification des eaux-mères par HPLC préparative (colonne RSIL C18, éluant méthanol–eau 40 : 60) fournit 0,056 g de **4***a* et 0,28 g de **4***b*.

4*a* : Rdt 70%, cristaux jaunes, F = 260°C; IR ($CHCl_3$) : 3388 (NH), 1660 (C=O), 1624 (C=N) cm^{-1}; UV et fluorescence dans chloroforme (éthanol) : λ_{max}^{abs} = 380 (381) nm, ε = 15 600 (16 000) M^{-1} cm^{-1}, λ_{max}^{em} = 448 (501,5) nm, Φ_f (référence sulfate de quinine) (0,29); RMN ^1H ($CDCl_3$) : 2,54 (s, 3H, CH_3), 3,07 (s, 6H, NMe_2); SM : *m/e* 204 $[M+H]^+$, 100%. Anal. calc. pour $C_{11}H_{13}N_3O$: C 65,01, H 6,45, N 20,67; trouvée : C 65,05, H 6,43, N 20,24.

4*b* : Rdt 25%, cristaux jaunes, F = 258°C; IR ($CHCl_3$) : 3388 (NH), 1662 (C=O), 1626 (C=N) cm^{-1}; UV dans chloroforme (éthanol) : λ_{max}^{abs} = 263 (260) nm, ε = 31 300 (34 000) M^{-1} cm^{-1}; RMN ^1H ($CDCl_3$) : 2,62 (s, 3H, CH_3), 3,0 (s, 6H, NMe_2); SM : *m/e* 204 $[M+H)^+$, 100%. Anal. calc. pour $C_{11}H_{13}N_3O$: C 65,01, H 6,45, N 20,67; trouvée : C 64,94, H 6,69, N 20,83.

*1,3-Diméthyl,7-*N,N*-diméthylamino-1,4-benzodiazine-2-one :* **5**a

À une solution de 0,200 g (9,85 × 10^{-4} mol) de **4***a* dans 25 mL d'acétone sec, on ajoute 0,160 mL (2,57 × 10^{-3} mol) d'iodure de méthyle et 0,609 g (1,87 × 10^{-3} mol) de carbonate de césium. Le milieu hétérogène est chauffé à reflux pendant 1,5 h, sous atmosphère d'azote. Une purification par CPL (éluant : dichlorométhane – acétate d'éthyle 40 : 60) fournit 0,201 g de **5***a*. Rdt 94%, cristaux jaunes, F = 170°C; IR : 1644 (C=O), 1620 (ep., C=N) cm^{-1}; UV et fluorescence dans chloroforme (éthanol) : λ_{max}^{abs} = 379 (384) nm, ε = 17 300 (16 100) M^{-1} cm^{-1}, λ_{max}^{em} = 439 nm; RMN ^1H ($CDCl_3$) : 2,51 (s, 3H, CH_3), 3,07 (s, 6H, $N(CH_3)_2$), 3,63 (s, 3H, NCH_3). Anal. calc. pour $C_{12}H_{15}N_3O$: C 66,34, H 6,96, N 19,34; trouvée : C 66,40, H 6,95, N 19,38.

*1,3-Diméthyl,7-*N,N*-diméthylamino-1,4-benzodiazine-2-one :* **5**b

Il a été préparé à partir de **4***b* selon la méthode utilisée pour **5***a*. Rdt 98%, cristaux jaunes, F = 141°C; IR : 1637 (C=O), 1620 (ép., C=N) cm^{-1}; UV dans chloroforme (éthanol) : λ_{max}^{abs} = 261 (260) nm, ε = 21 100 (27 100) M^{-1} cm^{-1}; RMN ^1H ($CDCl_3$) : 2,58 (s, 3H, CH_3), 3,01 (s, 6H, $N(CH_3)_2$), 3,66 (s, 3H, NCH_3). Anal. calc. pour $C_{12}H_{15}N_3O$: C 66,34, H 6,96, N 19,34; trouvée : C 66,02, H 6,82, N 19,24.

*1-Méthyl-3-(*p*-13-aza-1,4,7,10-tétraoxacyclopentadécane-13-ylstyryl)-1,4-benzodiazine-2-one :* **1** : 0,150 g (4,64 × 10^{-4} mol) de *p*-formyl-*N*-phénylaza-15-c-5 éther préparé selon la référence 24 et 0,080 g (4,60 × 10^{-4} mol) de benzodiazinone **3** sont chauffés en présence d'anhydride acétique (1 mL) à 135°C pendant 2 h. L'excès d'anhydride acétique est éliminé par coévaporation avec de l'eau. Le résidu sec est traité à l'acétone à froid et la suspension solide obtenue est filtrée. On obtient ainsi 0,077 g de **1**. Rdt 35%, cristaux rouge-brun, F = 199°C; IR : 1650 (C=O) cm^{-1}; UV dans acétonitrile : λ_{max}^{abs} = 448 nm, ε = 22 900 M^{-1} cm^{-1}; RMN ^1H ($CDCl_3$) : 3,6 (massif, 23H, CH_3 et éther couronne); SM : *m/e* 480 $[M+H]^+$, 100%. Anal. calc. pour $C_{27}H_{33}N_3O_5$: C 67,62, H 6,94, N 8,76; trouvée : C 67,29, H 6,80, N 8,86.

*3-(*p*-13-Aza-1,4,7,10-tétraoxacyclopentadécane-13-ylstyryl)-7-(*N,N*-diméthylamino)-1,4-benzodiazine-2-one :* **2**

On chauffe à 110–120°C pendant 24 h 0,400 g (1,24 × 10^{-3} mol) de *p*-formyl-*N*-phénylaza-15-c-5-éther et 0,252 g (1,24 × 10^{-3} mol) de **4***a* dans 10 mL de pyridine et 2 mL de pipéridine. Après avoir laisser revenir le milieu réactionnel à température ambiante, on filtre le précipité et le filtrat de couleur orange-rouge fluorescent est coévaporé plusieurs fois avec du toluène. Le résidu d'évaporation est ensuite purifié par CPL (éluant dichlorométhane–méthanol 95 : 5). Après recristallisation dans le toluène, on obtient 0,063 g de **2**. Rdt 10%, cristaux rouge-brun, **F** = 254°C; IR ($CHCl_3$) : 1653 (C=O) cm^{-1}; UV dans acétonitrile : λ_{max}^{abs} = 465 nm, ε = 25 000 M^{-1} cm^{-1}; RMN ^1H ($CDCl_3$) : 3,08 (s, 6H, NMe_2), 3,67 (m, 20H, éther couronne); SM : *m/e* 509 $[M+H]^+$, 100%. Anal. calc. pour $C_{28}H_{36}N_4O_5$: C 66,12, H 7,13, N 11,02; trouvée : C 66,20, H 7,15, N 10,96.

Autoassociation

Le phénomène d'autoassociation se traduit par une variation du coefficient d'absorption molaire en fonction de la concentration. Cette évolution en fonction de la molalité de grandeurs spectrales caractéristiques du substrat comme le coefficient d'extinction molaire ε (25) ou de grandeurs volumiques caractéristiques de la solution (masse volumique (26)), résulte de processus autoassociatifs qui conduisent à des agrégats dynamiques (dimère : A_2, ..., i-mère : A_i), en équilibre avec le monomère A_1. La constante d'équilibre pour le $(i-1)i^{ième}$ équilibre a pour expression

$$K_{i-1} = C_i/(C_{i-1} \cdot C_1)$$

C_i, C_{i-1} et C_1 étant respectivement les concentrations en entités i-mère, $(i-1)$- mère et monomère. Dans la littérature ce type d'association indéfini est traité principalement sur la base du modèle isodesmique (25). Il implique l'égalité de toutes les constantes d'équilibre régissant les processus élémentaires d'autoassociation : $K_1 = K_2 = \ldots = K_{i-1} = K$. De plus, sachant que le coefficient d'extinction molaire est la résultante des contributions additives des coeffificients d'extinction caractéristiques des molécules individuelles (27) et qu'il est fonction de leur environnement (état monomère ou molécules associées) il nous est possible de simplifier ce constat en retenant la dichotomie suivante. Seules trois contributions au coefficient d'extinction molaire seront prises en compte : celle des molécules monomère (ε_1) et, pour un agrégat de i molécules, celles des deux molécules à l'extérieur de l'agrégat (ε_{ext}) et des $i-2$ molécules à l'intérieur de l'agrégat (ε_{int}). Ainsi le coefficient d'extinction molaire observé (ε_{obs}) à une longueur d'onde donnée variera en fonction de la concentration des espèces selon :

$$\varepsilon_{obs} = (C_1 \cdot \varepsilon_1 + C_{int} \cdot \varepsilon_{int} + C_{ext} \cdot \varepsilon_{ext})/C_t$$

la concentration totale (C_t) étant donnée par :

$$C_t = C_1 + 2\sum_{i=2}^{\infty} C_i + \sum_{i=2}^{\infty} (i-2)C_i$$

Le traitement informatique (26) des variations de ε_{obs} en fonction de la concentration en soluté (C_t) permet d'atteindre de manière itérative la constante d'association K contenue dans le modèle $\varepsilon_{obs} = f(\varepsilon_1, \varepsilon_{int}, \varepsilon_{ext}, K)/C_t$.

Avec l'orthophénantroline dans l'acétonitrile, on trouve K = $8 \times 10^4 \pm 3 \times 10^3$ M^{-1}. Par contre, aucune variation de ε_{obs} n'a été notée avec la styrylbenzodiazinone **6** dans ce même solvant pour des concentrations variant de 5×10^{-7} à 10^{-4} M avec ou sans 4% Ca^{2+}.

Equilibre photoréversible

On ajoute à l'obscurité 0,04 équivalents de perchlorate de calcium à une solution de ligand (~5×10^{-5} M) dans l'acétonitrile ou le dioxanne; après stabilisation de la densité optique on irradie cette solution à la lumière blanche. Quelques minutes (~10 min) après irradiation on obtient une DO minimale voisine de la DO initiale du ligand pur. On remet enfin cette solution à l'obscurité jusqu'à stabilisation de la DO (~2 h) qui retrouve sa valeur maximale.

Cinétique d'isomérisation par un sel métallique

Après addition à l'obscurité de 0,04 équivalent de perchlorate de calcium à une solution de ligand (~5×10^{-5} M) dans l'acétonitrile, un balayage répété du spectre UV entre 250 et 550 nm est effectué jusqu'à stabilisation de la densité optique (~1,57). La cinétique elle-même a été effectuée dans les mêmes conditions au maximum d'absorption (440 nm) avec un temps de cycle de 1 min. Le traitement des données a été réalisé avec le programme LSG (Least Squares Guggenheim).

Can. J. Chem. Downloaded from www.nrcresearchpress.com by 213.200.69.106 on 09/08/12
For personal use only.

Essai de photoisomérisation

Une solution 5×10^{-5} M du composé **6** dans l'acétonitrile placée dans une curve en quartz a été irradiée à 350 nm en utilisant un récteur Rayonet pendant 1 h. La décoloration totale de la solution jaune de départ correspond à la disparition complète de la bande à 440 nm sans apparition de bande nouvelle. La même expérience réalisée sur une solution $3{,}5 \times 10^{-3}$ M dans CD_3CN donne un spectre RMN ^1H ne présentant aucun signal bien résolu.

Remerciements

Les auteurs remercient A. Lopez (UPR CNRS 8221, Toulouse) pour nous avoir permis de traiter les problèmes relatifs à l'autoassociation et pour ses utiles conseils, ainsi que le Centre National de la Recherche Scientifique et la Direction de la Recherche et des Études Doctorales pour leur soutien financier.

1. S. Fery-Forgues, M.T. Le Bris, J.P. Guetté et B. Valeur. J. Phys. Chem. **92**, 6233 (1988) et références citées.
2. H.G. Löhr et F. Vögtle. Acc. Chem. Res. **18**, 65 (1985).
3. J. Bourson et B. Valeur. J. Phys. Chem. **93**, 3871 (1989).
4. J. Bourson, M.N. Borrel et B. Valeur. Anal. Chim. Acta, **257**, 189 (1992).
5. (*a*) M.V. Alfimov, S.P. Gromov et I.K. Lednev. Chem. Phys. Lett. **185**, 455 (1991); (*b*) A.V. Barzykin, M.A. Fox, E.N. Ushakov, O.B. Stanislavsky, S.P. Gromov, O.A. Fedorova et M.V. Alfimov. J. Am. Chem. Soc. **114**, 6381 (1992).
6. L. Cazaux, M. Faher, C. Picard et P. Tisnès. Sous presse.
7. U. Mazzucato et F. Momicchioli. Chem. Rev. **91**, 1679 (1991).
8. S. Fery-Forgues, M.T. Le Bris, J.C. Mialocq, J. Pouget, W. Rettig et B. Valeur. J. Phys. Chem. **96**, 701 (1992).
9. (*a*) E. Sawicki et A. Carr. J. Org. Chem. **22**, 503 (1957); (*b*) D. Demeyere et J. Hoste. Anal. Chim. Acta, **27**, 288 (1962).
10. M.T. Le Bris. J. Heterocycl. Chem. **22**, 1275 (1985).
11. H.H. Hodgson et D.E. Nicholson. J. Chem. Soc. 766 (1941).
12. J.C. Arcos et J.A. Miller. J. Am. Chem. Soc. **77**, 3128 (1955).
13. A.J. Gordon et R.A. Ford. *Dans* The chemist's companion. John Wiley and Sons, London. 1972. p. 262.
14. H.O. Kalinowski, S. Berger et S. Braun. *Dans* Carbon-13 NMR spectroscopy. John Wiley and Sons, London. 1988. p. 315.
15. M.T. Le Bris. J. Heterocycl. Chem. **21**, 551 (1984).
16. (*a*) A. Rossi, A. Hunger, J. Kebrle et K. Hoffmann. Helv. Chim. Acta, **43**, 1298 (1960); (*b*) G. Kaupp, H. Frey et G. Behmann. Synthesis, 555 (1985).
17. M. Meyer, J.-C. Mialocq et B. Perly. J. Phys. Chem. **94**, 98 (1990).
18. W. Saenger. *Dans* Principles of nucleic acid structure. Springer Verlag, Berlin. 1984. pp. 142–143.
19. G. Grynkiewicz, M. Poenie et R.Y. Tsien. J. Biol. Chem. **260**, 3440 (1985).
20. J.M. Drake, M.L. Lesiecki et D.M. Camaioni. Chem. Phys. Lett. **113**, 530 (1985).
21. R.M. Silverstein et G.C. Bassler. *Dans* Spectrometric identification of organic compounds. 2ème ed. John Wiley and Sons, New York. 1967. p. 165.
22. T. Nishio. J. Chem. Soc. Perkin Trans. 1, 565 (1990).
23. D.H. Waldeck. Chem. Rev. **91**, 415 (1991).
24. J.P. Dix et F. Vögtle. Chem. Ber. **113**, 457 (1980).
25. M.P. Heyn et R. Bretz. Biophys. Chem. **3**, 35 (1975).
26. A. Lopez, F. Loussayre, R. Martino et A. Lattres. Nouv. J. Chim. **9**, 267 (1985).
27. J. Tannelat. *Dans* Biophysique. Vol. 2. Masson, Paris. 1973.

Can. J. Chem. Downloaded from www.nrcresearchpress.com by 213.200.69.106 on 09/08/12
For personal use only.

Solvent effect on the reactivity of monosubstituted phenols towards singlet molecular oxygen ($O_2(^1\Delta_g)$) in alkaline media

MARTA LUIZ, MARÍA I. GUTIÉRREZ, AND GRACIELA BOCCO

Departamento de Química, Facultad de Ciencias Naturales, Universidad Nacional de la Patagonia, San Juan Bosco, 9000 Comodoro Rivadavia, Argentina

AND

NORMAN A. GARCÍA[1]

Departamento de Química y Física, Universidad Nacional de Rio Cuarto, 5800 Rio Cuarto, Argentina

Received January 7, 1993

MARTA LUIZ, MARÍA I. GUTIÉRREZ, GRACIELA BOCCO, and NORMAN A. GARCÍA. Can. J. Chem. **71**, 1247 (1993).

The influence of solvent polarity on the dye-sensitized photooxidation (singlet molecular oxygen ($O_2(^1\Delta_g)$) mediated) of a series of *para*-substituted phenolates was studied. Kinetic evidence obtained shows that the overall and the pure chemical interactions, phenolate–$O_2(^1\Delta_g)$, depend on the solvent polarity in a different way. This is clearly reflected in the efficiency of $O_2(^1\Delta_g)$ photooxidation of the substrates: surprisingly, the photooxidation quantum yield increases as the overall quenching rate constant decreases. The substrate photooxidation quantum yields obtained ranged from 0.05 to 0.15, the upper limit corresponding to a moderately polar medium (a benzene–methanol mixture) and the lower to an aqueous medium. We conclude that a high solvent polarity favours only the obtainment of the encounter complex ($O_2(^1\Delta_g)$–phenolate), whereas the reactive step is affected in much the same way as those processes where charges are neutralized along the reaction pathway. The results obtained are discussed in terms of a partly polar excited state complex between $O_2(^1\Delta_g)$ and the phenolates. The rate constant for the reactive pathway in both organic and aqueous media is correlated with the Hammet-type substituent constant R^-.

MARTA LUIZ, MARÍA I. GUTIÉRREZ, GRACIELA BOCCO et NORMAN A. GARCÍA. Can. J. Chem. **71**, 1247 (1993).

On a étudié l'influence de la polarité du solvant sur la sensibilisation par photo-oxydation du colorant (via l'oxygène moléculaire à l'état singulet ($O_2(^1\Delta_g)$), d'une série de phénolates substitués en position *para*. Les preuves cinétiques obtenues démontrent que l'interaction globale et l'interaction purement chimique phénolate–$O_2(^1\Delta_g)$ dépendent de manière différente de la polarité du solvant. Cet effet se manifeste clairement dans l'efficacité de la photo-oxydation $O_2(^1\Delta_g)$ des substrats : de façon surprenante, le rendement quantique de la photo-oxydation augmente lorsque la constante globale de blocage diminue. Les rendements quantiques de la photo-oxydation des substrats se situent entre 0,05 et 0,15, la limite supérieure correspondant à un milieu modérément polaire (un mélange de benzène–méthanol), et la limite inférieure correspondant à un milieu aqueux. Nous concluons qu'une forte polarité du solvant favorise uniquement le complexe de rencontre phénolates–$O_2(^1\Delta_g)$, où l'étape réactive est affectée comme le sont les processus où les charges sont neutralisées au cours de la réaction. On discute des résultats obtenus en fonction d'un complexe à l'état excité partiellement polaire entre $O_2(^1\Delta_g)$ et les phénolates. On établit une corrélation entre la constante de vitesse pour l'étape réactive dans un milieu organique et dans un milieu aqueux avec une constante R^- de substituant du type Hammett.

[Traduit par la rédaction]

Introduction

Type II (singlet molecular oxygen ($O_2(^1\Delta_g)$) mediated) photooxidation of phenols and, especially, dye-sensitized reactions, have received much attention over the last few years in connection with the behaviour role of compounds involved in biological media (1–6) as well as the possibility of processing waste water by sunlight irradiation (7–17). More specifically, the importance of understanding environmental pathways for phenolic chlorinated and nitro derivatives (the main parent compounds employed in industrial syntheses of phenolic pesticides) led us to carry out a variety of studies (8–15, 17).

Most $O_2(^1\Delta_g)$ reactions, including those of phenols, involve parallel physical and chemical interactions of the excited oxygen species with the oxidizable substrate P (eqs. [1] and [2]):

$$[1] \quad O_2(^1\Delta_g) + P \xrightarrow{k_q} O_2(^3\Sigma_g) + P$$

$$[2] \quad O_2(^1\Delta_g) + P \xrightarrow{k_r} \text{products}$$

$$[3] \quad O_2(^1\Delta_g) \xrightarrow{k_d} O_2(^3\Sigma_g^-)$$

The sum $k_q + k_r$ is usually denoted by k_t, the overall rate constant for the whole quenching process. Equation [1] represents the physical event that gives rise to the ground-state triplet oxygen species [$O_2(^3\Sigma_g^-)$]. On the other hand, chemical interaction yields photooxidation products (eq. [2]). A third way of deactivating $O_2(^1\Delta_g)$, by collision with solvent molecules, is represented by eq. [3].

The actual significance in terms of real photodegradation of a $O_2(^1\Delta_g)$-mediated event is given by the effective quantum yield of photooxidation (18) (ϕ_r; eq. [4]):

$$[4] \quad \phi_r = \phi_\Delta k_r[P]/(k_d + k_t[P])$$

The only data required to solve eq. [4] are the kinetic rate constants and the quantum yield of $O_2(^1\Delta_g)$ generation by the dye sensitizer (ϕ_Δ).

It is surprising that even though the rate constants k_t for a vast number of compounds have been reported (for compilations see refs 19 and 20), kinetic discrimination between chemical and physical $O_2(^1\Delta_g)$ quenching has been achieved in only a few cases (19). Kinetic discrimination is of paramount significance not only for distinguishing between the

[1]Author to whom correspondence may be addressed

Can. J. Chem. Downloaded from www.nrcresearchpress.com by 213.200.69.106 on 09/08/12
For personal use only.

Can. J. Chem. Downloaded from www.nrcresearchpress.com by 213.200.69.106 on 09/08/12
For personal use only.

two types of interactions, but is also indispensable in predicting reactivity towards $O_2(^1\Delta_g)$ and the extent of physical interaction, which are of utmost importance in terms of biological protection. The above examples suggest that a basic knowledge of the factors affecting the distribution of physical and chemical contributions is crucial to understanding $O_2(^1\Delta_g)$-mediated photooxidations.

In this work we carried out a kinetic study on the interaction of a series of *para*-substituted phenols with $O_2(^1\Delta_g)$ in alkaline media with emphasis on the solvent effect on the reactive and the purely physical pathways for the overall $O_2(^1\Delta_g)$ scavenging process.

Experimental

Chemicals

Rubrene, eosin (Eos), Rose Bengal (RB) 4-chlorophenol (4-CP), 4-bromophenol (4-BrP), 4-iodophenol (4-IP), 4-phenylphenol (4-PhP), and 9,10-dimethyl anthracene (DMA) were purchased from Aldrich. The phenols and DMA were purified by double sublimation. Purified 4-fluorophenol (4-FP) was kindly provided by Dr. Gerardo Arguello. Methionine was supplied by Sigma. The solvents benzene (Bz), methanol (MeOH), and acetonitrile (MeCN) were all of the highest available purity. Water was triply distilled. All measurements were made on freshly prepared solutions. A Na_2HPO_4/NaOH buffer was employed to adjust aqueous solutions to pH 11. Solutions in organic solvent mixtures (Bz–MeOH 4:1 by volume and MeCN–MeOH 1:1 by volume) labelled as "alkaline" contained 0.01 M KOH. Only the ionized (phenolate) form of the substituted phenols was spectrophotometrically detected in all described solvents.

Methods

Ground-state absorption spectra were recorded on a Hewlett Packard 8452A diode array spectrophotometer. A Metrolab RC 325B digital instrument was employed for single wavelength measurements.

Singlet molecular oxygen was generated photochemically (eq. [5]) by the sensitizers (S) (either rubrene (2×10^{-5} M), Eos ($abs_{530} = 0.5$ nm) or RB ($abs_{560} = 0.5$ nm)) through energy transfer from the excited triplet S ($^*S^3$) to dissolved ground-state oxygen.

$$[5] \quad {}^*S^3 + O_2(^3\Sigma_g^-) \xrightarrow{k_{ET}} S + O_2(^1\Delta_g)$$

In organic solvents k_t was determined according to Carlsson *et al.* (21) on the basis of self-sensitized photooxidation of rubrene. The ratio of initial rates of rubrene photooxidation in the absence (V_0) and presence (V) at different concentrations of the phenols was plotted against the phenol concentration, and k_t was calculated from eq. [6]:

$$[6] \quad V_0/V = 1 + k_t[P]/(k_{rRub} \times [\text{rubrene}])$$

Under our experimental conditions, $k_{rRub} \times$ [rubrene], i.e., the product of the rate constant for rubrene photooxidation times the hydrocarbon concentration, was very small compared to k_d and was thus negligible (21). The k_d values employed in the calculations were 3.8×10^4 s^{-1} in Bz–MeOH (19) and 3×10^4 in MeCN–MeOH, the last being determined by time-resolved phosphorescence detection of $O_2(^1\Delta_g)$ emission. It was assumed that the rate constant k_d is pH-independent.

For water solutions (pH 11), k_t was calculated from eq. [7] (graphical method) (19) by using Eos as dye sensitizer and assuming eq. [2] to be the only source of both phenol and oxygen uptake.

$$[7] \quad (\text{rate})^{-1} = (I_a\,\phi_\Delta)^{-1}\{(k_t/k_r) + k_d/k_r\,[P]\}$$

where rate and I_a denote the velocity of P uptake and the intensity of light absorbed by the sensitizer, respectively. A k_d value of 2.5×10^5 s^{-1} was employed in the calculations (23).

The k_r values obtained for P in all water solutions at pH 11 and in alkaline organic solvents were determined by the method of Foote and Ching (24) (eq. [8]):

$$[8] \quad k_r = k_{rR}\,\text{slope}_T/\text{slope}_R$$

which compares the slopes of the first-order plots for substrate irradiation time for the oxidizable substrate and a reference of known k_r (k_{rR}). The references used were DMA (in organic media) and methionine (in water). Both compounds have proven to be *exclusive* chemical (reactive) quenchers of $O_2(^1\Delta_g)$ (19, 25, 26). The k_{rR} values employed for the hydrocarbon (1) and the amino acid (25, 26) were 1.2×10^7 M^{-1} s^{-1} and 2.0×10^7 M^{-1} s^{-1}, respectively.

The rate of P photooxidation in organic media was determined spectrophotometrically. In water, the oxygen uptake instead of the P uptake was measured. The accuracy of this methodology for substituted phenols has been discussed elsewhere (15).

Estimated error margins were in the range of ±10–12% for k_t and ±5–7% for k_r.

The ϕ_r values were calculated by means of eq. [4] at a phenolate concentration of 1 mM and a ϕ_Δ value of 0.75 for RB in water (27).

The irradiation setup, including the specific electrode (Orion 97-08) has already been described (8). The temperature was kept at 22 ± 1°C throughout.

Results and discussion

Irradiation of air-equilibrated solutions of P with visible light in the presence of either Eos or RB in water (pH 11) strongly modifies their absorption spectra, as shown for 4-ClP in Fig. 1. Similar qualitative spectral changes were observed for all P compounds studied (also in alkaline organic solvents) provided appropriate $O_2(^1\Delta_g)$ sensitizers were used.

The reaction is virtually stopped by the presence of 1 mM NaN_3 and halted altogether when N_2-bubbled solutions are used. For 4-PhP it was established that the spectral changes were greater, at the same irradiation fluence, when H_2O was substituted by D_2O as a solvent (17). According to currently accepted criteria (28), these observations indicate that the dye-sensitized photooxidation occurs largely via a $O_2(^1\Delta_g)$-mediated process. This is also consistent with a number of reported findings on the photooxidizability of the ionized form of variously substituted phenols (6–17).

The overall and reactive rate constants for $O_2(^1\Delta_g)$ scavenging were determined as described in the experimental section. Typical results are shown in Figs. 2 (main: k_t in water; inset: k_t in organic medium) and 3 (k_r in water), respectively.

We chose the *para*-substituted phenolate series for three reasons: (*a*) to maintain a unique ring-substitution pattern; (*b*) because of the large k_t values of these compounds, which exceed those of the non-ionized forms at least by one order of magnitude (3, 4, 7); and (*c*) because of the high proportion of reactive interaction with $O_2(^1\Delta_g)$ (very much higher than that for the molecular form).

The results obtained are shown in Table 1.

Bimolecular reactions of $O_2(^1\Delta_g)$ with substrates such as indoles, amines, sulphides, and phenols (4, 23, 29–31) can take place through a mechanism involving an excited encounter complex (see scheme, eq. [9]).

The data compiled in Table 1, particularly the general correlation of k_t for each P (Table 1) with the solvent polarity (H_2O > MeCN–EtOH > Bz–MeOH), provide evidence for a mechanism involving a charge transfer component

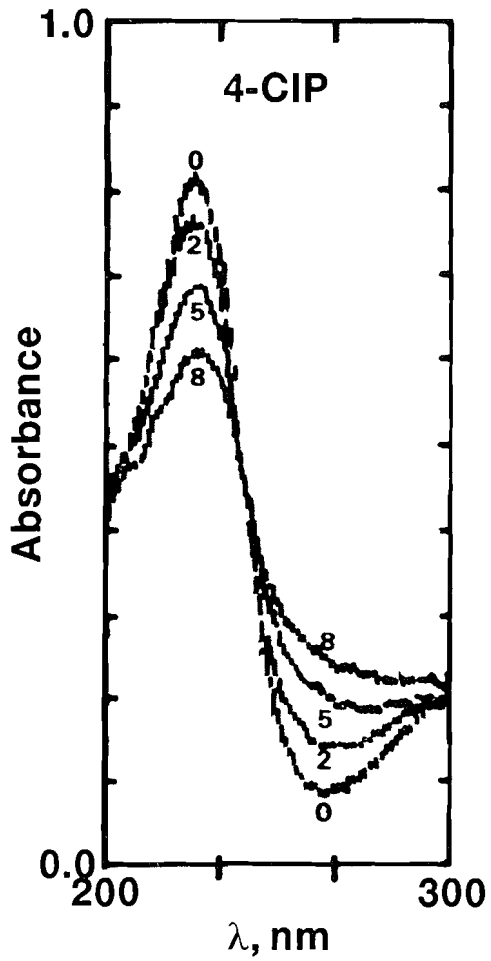

FIG. 1. Changes in the absorption spectrum of a solution (2×10^{-4} M) of 4-ClP in water, pH 11. Sensitizer: Eos, $Abs_{517} = 0.4$. Numbers correspond to irradiation time, in minutes.

within the intermediate complex. The dramatically smaller k_t value of 4-NO_2P, where the electron-releasing ability of the phenolate is diminished, also supports this hypothesis.

$$[9]\quad O_2(^1\Delta_g) + P \underset{k_{-D}}{\overset{k_D}{\rightleftarrows}} [O_2(^1\Delta_g)\text{--}P] \xrightarrow{k_P} \text{products}$$
$$\downarrow k_{ISC}$$
$$[O_2(^3\Sigma_g^-)\text{--}P] \longrightarrow O_2(^3\Sigma_g^-) + P$$

According to eq. [9], competition between the excited complex photochemistry and photophysics controls the photooxidative pathway.

Careful observation of the data in Table 1 in terms of the solvent polarity reveals some facts that were not immediately apparent in a combined analysis, namely, both the reactive and overall rate constants increase as the solvent polarity increases; also, their relative weight (k_r / k_t ratio), which is higher for the less polar media, varies from the value unity for pure chemical interactions to a very small value in the organic-solvent mixture for most of the phenolates studied. Furthermore, the effect on the rate constants of a given phenolate is not proportional to that of the solvent polarity; in fact it is much higher for k_t than for the corresponding k_r value. In addition, this holds whether physical interaction or chemical reaction controls the whole $O_2(^1\Delta_g)$ quenching, even though it is more pronounced for *exclusively* chemical quenchers. In other words, the fraction of encounter complex that yields products increases as the polar environment decreases. As a result, even when the overall quenching process seems to be considerably more efficient in aqueous medium, the effective quantum yields (ϕ_r) for photooxidation are slightly higher in the Bz–MeOH mixture (column six in Table 1).

We believe that these apparently intricate results can be interpreted in a simple manner in terms of the evolution of the excited encounter complex: as all the experimental evidence indicates, increasing solvent polarity markedly favours the overall quenching process because of the charge transfer component involving the encounter complex. The encounter complex can undergo both deactivation (thereby resulting in physical quenching, which can be regarded as a photophysical deactivation step yielding the unstable ground-state complex) and chemical reaction. The reactive pathway, favoured by less polar media, appears to be an entropy-controlled step, as hypothesized for the phenolic derivative α-tocopherol (29). As a consequence, the reactive step is affected by the solvent polarity in much the same way as those processes in which charges are neutralized along the reaction pathway.

We tried to correlate the kinetic data shown in Table 1 through a Hammett equation or one of its extended forms, which have been widely employed for studying and interpretating organic reactions and their mechanisms. Although it is not always easy to find an appropriate *Hammett-type* substituent constant for a given class of chemical reaction, we adopted the R^- constant, developed by Hansch *et al.* (32), which we attempted to correlate with the k_r values in Table 1. The R^- constant was defined for molecules such as phenolates and anilinium ions possessing lone electron pairs and substituents conjugated with the reaction site, as in the case with our *para*-substituted phenolates. In 1978, Thomas and Foote (4) reported one such treatment (Hammett plot) involving σ^+ values for a series of trisubstituted phenols (molecular species) in organic solvents. The substituents were highly electron-releasing alkyl derivatives and the $O_2(^1\Delta_g)$ interaction was, in practice, entirely due to physical quenching. In our case, we employed the rate constant for the chemical reaction since this step occurs in all cases (only chemical interaction occurs with 4-ClP, 4-BrP, and 4-IP) and can be quantified by direct individual measurements (see Methods). This is shown graphically in Fig. 4, which includes the data for 4-PhP in water (17) and those for 4-nitrophenol (4-NO_2P) (13) in organic and aqueous media. As can be seen, there is a fairly linear relationship in both aqueous and organic media.

The extrapolation of the curve obtained in Bz–MeOH *predicts* a very small reactive rate constant for 4-NO_2P, which is consistent with previously reported data (13). We detected no photooxidation of 4-NO_2P in Bz–MeOH even upon prolonged sensitized irradiation (13).

Concluding remarks

In conclusion, the evidence obtained in this work demonstrates that there is no simple straightforward interpretation for the solvent effect on the kinetics of $O_2(^1\Delta_g)$ interactions with a series of *para*-substituted phenolates. This is clearly reflected in the efficiency of $O_2(^1\Delta_g)$ photooxidation of the substrates. The results can be rationalized by postulating the intermediacy of an encounter complex from

Can. J. Chem. Downloaded from www.nrcresearchpress.com by 213.200.69.106 on 09/08/12
For personal use only.

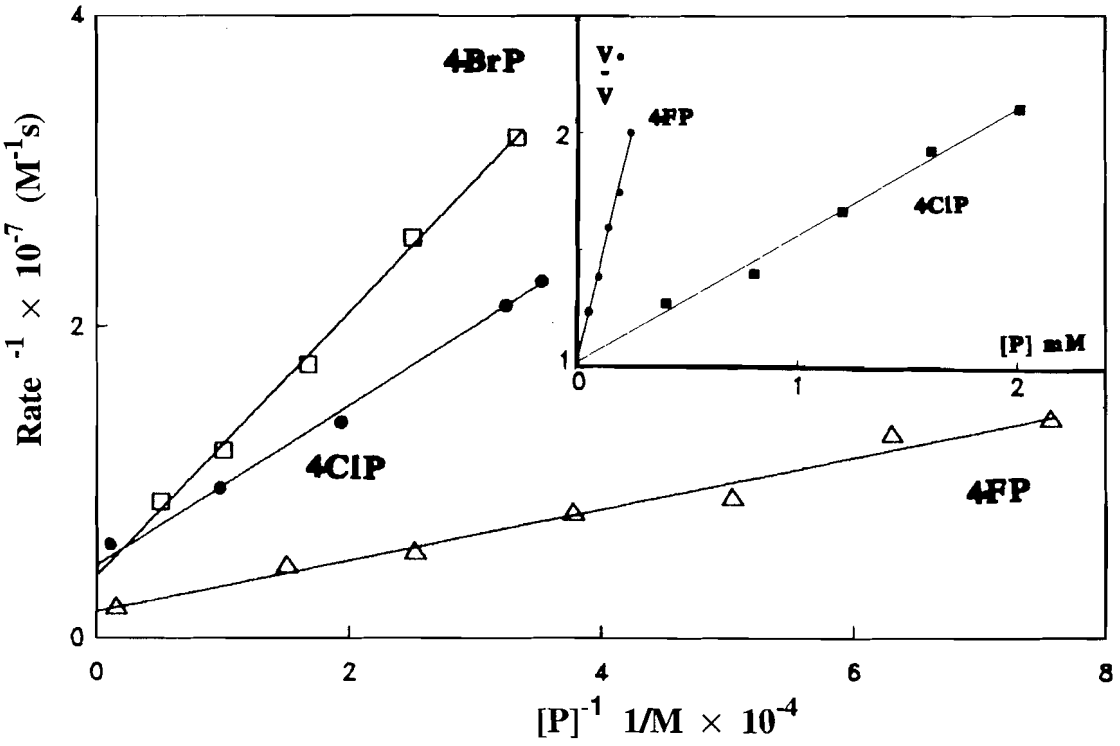

FIG. 2. Dependence of the rate of oxygen consumption on phenolate concentration in water, pH 11. Sensitizer Eos, Abs_{517} = 0.4. Inset: Stern–Volmer plot for the inhibition of rubrene photooxidation by phenolates in Bz–MeOH alkaline.

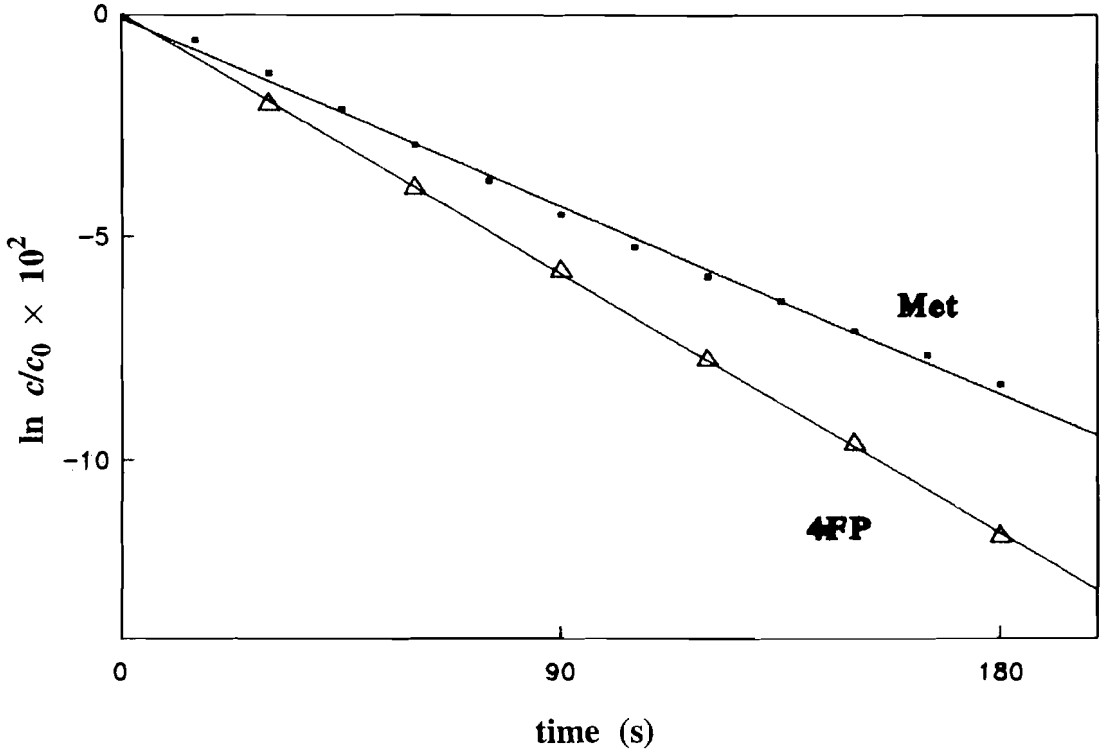

FIG. 3. First-order plots for oxygen uptake during sensitized irradiation of air-equilibrated solutions containing methionine and 4-FP. Both substrates in concentration 0.2 mM. Sensitizer Eos, Abs_{517} = 0.4. c_0 and c represent the concentration of oxygen at time = 0 and time = t respectively (see Methods).

Can. J. Chem. Downloaded from www.nrcresearchpress.com by 213.200.69.106 on 09/08/12
For personal use only.

TABLE 1. Overall (k_t, M^{-1} s^{-1}), and reactive (k_r, M^{-1} s^{-1}) rate constants for $O_2(^1\Delta g)$ quenching, k_r/k_t ratios, and photooxidation quantum yields (ϕ_r) for various *para*-substituted phenolates, in alkaline media at room temperature

Compound	Solvent	$k_t \times 10^{-8}$	$k_r \times 10^{-8}$	k_r/k_t	ϕ_r
4-FP	Bz–MeOH, alk.	2.0	0.57	0.28	0.14
	H_2O, pH 11	25	3.5	0.14	0.095
4-ClP	Bz–MeOH, alk.	0.3	0.3	1	0.17
	MeCN–MeOH, alk.	0.6			
	H_2O, pH 11	8.0	1.0	0.13	
4-BrP	Bz–MeOH, alk.	0.15	0.15	1	0.098
	MeCN–MeOH, alk.	0.6			
	H_2O, pH 11	11	1.5	0.14	
4-IP	Bz–MeOH, alk.	0.14	0.10	0.71	0.065
	H_2O, pH 11	10	0.8	0.08	0.048
4-PhP	Bz–MeOH, alk.	0.4	0.1	0.25	0.053
	H_2	0.8[a]	0.4[b]		
4-NO_2P	Bz–MeOH[c]	<0.001			
	H_2O, pH 11[c]	0.6	0.03	0.05	0.0026

[a]pD 11.8 (17).
[b]pH 11 (17).
[c]Reference 13.

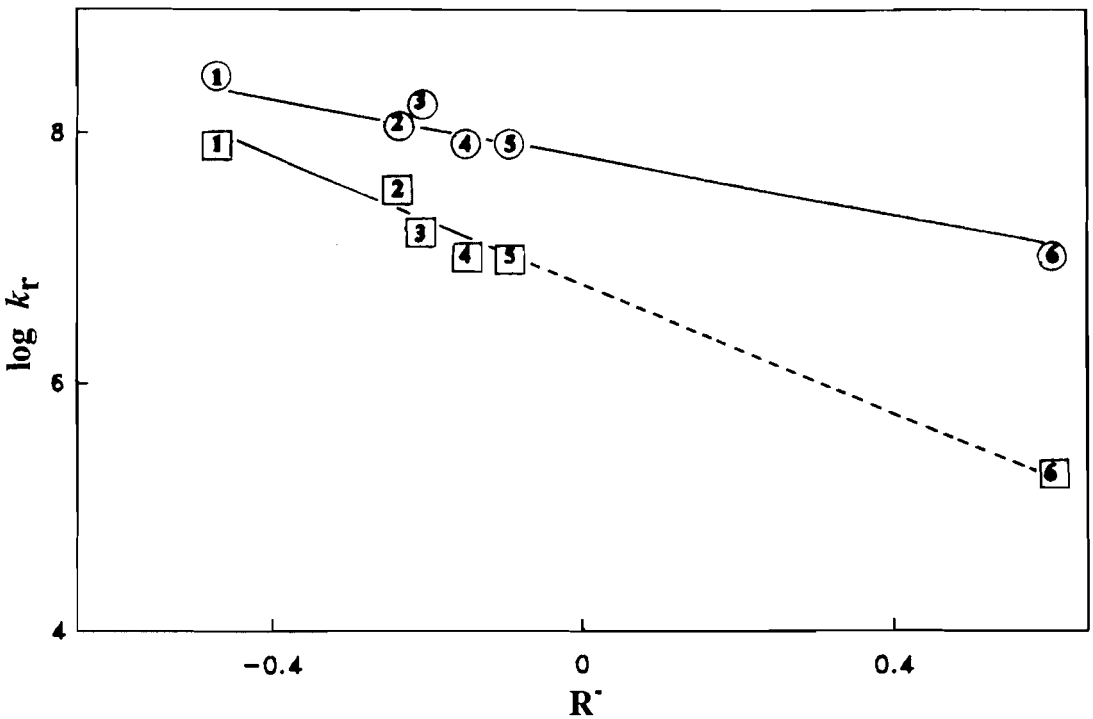

FIG. 4. Log k_r as a function of the constant R^- (see text) for several *para*-substituted phenolates. (1) 4-FP, (2) 4-ClP; (3) 4-BrP; (4) 4-IP; (5) 4-PhP; (6) 4-NO_2P. Upper line in H_2O, pH 11; lower line in Bz–MeOH 4:1 (v/v).

which both reactive and pure physical interactions can take place.

In summary, a substantial amount of information on the photooxidative kinetic behaviour of phenols under environmental conditions is discussed. This information can contribute to the understanding of the photochemical fate of these compounds, widely distributed in nature, from both the biological and the chemical point of view.

Acknowledgements

Financial support from the Consejo Nacional de Investigaciones Científicas y Técnicas de Argentina (CONICET), Consejo de Investigaciones de Córdoba, Argentina (CONICOR), Universidad Nacional de Río Cuarto and Universidad Nacional de La Patagonia, San Juan Bosco, is gratefully acknowledged. We also thank Dr. Gustavo Arguello (U. N. de Córdoba, Argentina) for the communication of his re-

Can. J. Chem. Downloaded from www.nrcresearchpress.com by 213.200.69.106 on 09/08/12
For personal use only.

sults on the lifetime of singlet molecular oxygen in MeCN–MeOH 1:1 (v/v) determined by time-resolved phosphorescence detection.

1. T. Matsuura, H. Matsushima, S. Kato, and I. Saito. Tetrahedron, **28**, 5119 (1972).
2. I. Saito, N. Yoshimura, T. Arai, K. Omura, A. Nishinaga, and T. Matsuura. Tetrahedron, **28**, 5131 (1972).
3. F. Jensen and C.S. Foote. Photochem. Photobiol. **46**, 325 (1987).
4. M.J. Thomas and C.S. Foote. Photochem. Photobiol. **27**, 683 (1978).
5. K.I. Okamoto, F. Hondo, A. Itayamand, and S. Kusabayashi. J. Chem. Eng. Jpn. **15**, 368 (1982).
6. S.G. Bertolotti, N.A. García, and G. Arguello. J. Photochem. Photobiol. B: **10**, 57 (1991).
7. F.E. Scully and J. Hoigne. Chemosphere, **16**, 681 (1987).
8. H.E. Gsponer, C.M. Previtali, and N.A. García. J. Photochem. **36**, 247 (1987).
9. H.E. Gsponer, C.M. Previtali, and N.A. García. Toxicol. Environ. Chem. **16**, 23 (1987).
10. M.C. Palumbo and N.A. García. Toxicol. Environ. Chem. **17**, 103 (1988).
11. S.G. Bertolotti, H.E. Gsponer, and N.A. García. Toxicol. Environ. Chem. **22**, 229 (1988).
12. S. Miskoski and N.A. García. Toxicol. Environ. Chem. **25**, 33 (1989).
13. M.C. Palumbo, N.A. García, M.I. Gutiérrez, and M. Luiz. Toxicol. Environ. Chem. **29**, 85 (1990).
14. M.I. Gutiérrez, M. Luiz, G. Bocco, and N.A. García. Toxicol. Environ. Chem. **35**, 115 (1992).
15. D.O. Martire, S.E. Braslavsky, and N.A. García. J. Photochem. Photobiol. A: **61**, 113 (1991).
16. R. Scurlok, M. Rougee, and R.V. Bensasson. Free Radical Res. Commun. **8**, 251 (1990).
17. D. Martire, C. Evans, S. Bertolotti, S.E. Braslavsky, and N.A. García. Chemosphere. In press.
18. N.A. García. J. Photochem. Photobiol. B: **14**, 381 (1992).
19. F. Wilkinson and J.G. Brummer. J. Phys. Chem. Ref. Data, **10**, 809 (1981).
20. R.C. Straight and J.D. Spikes. *In* Singlet oxygen. Vol. 4. *Edited by* A.A. Frimer. CRC Press, Boca Raton, Fla. 1985. pp. 91–95.
21. D.J. Carlsson, T. Suprunchuk, and D.M. Wiles. Can. J. Chem. **52**, 3728 (1974).
22. M.C. Palumbo, N.A. García and G. Arguello. J. Photochem. Photobiol. B: **7**, 33 (1990).
23. M.A.J. Rodgers and P.T. Snowden, J. Am. Chem. Soc. **104**, 5541 (1982).
24. C.S. Foote and T.-Y. Ching. J. Am. Chem. Soc. **97**, 6209 (1975).
25. B.A. Lindig and M.A.J. Rodgers. Photochem. Photobiol. **33**, 627 (1981).
26. S. Miskoski and N.A. García. Photochem. Photobiol. **57**, 447 (1993).
27. D.C. Neckers. J. Photochem. Photobiol. A: **47**, 1 (1989).
28. C.S. Foote. *In* Mechanisms of photooxygenation in porphyrin localization and treatment of tumors. Alan R. Liss, New York. 1984.
29. A.A. Gorman, I.R. Gould, I. Hamblett, and M.C. Standen. J. Am. Chem. Soc. **106**, 6956 (1984).
30. C.S. Foote, R.W. Denny, L. Weaver, Y. Chang, and J. Peters. Ann. N.Y. Acad. Sci. **171**, 139 (1970).
31. R.H. Young, R.L. Martin, D. Feriozzi, D. Brewer, and R. Kayser. Photochem. Photobiol. **17**, 283 (1973).
32. C. Hansch, A. Leo, and R.W. Taft. Chem. Rev. **91**, 165 (1991).

Can. J. Chem. Downloaded from www.nrcresearchpress.com by 213.200.69.106 on 09/08/12
For personal use only.

Solution and solid state studies of mixed ligand binuclear complexes containing one binucleating ligand

PUSHPA PATEL AND P.K. BHATTACHARYA[1]

Department of Chemistry, Faculty of Science, M.S. University of Baroda, Baroda-390 002, India

Received June 18, 1992[2]

PUSHPA PATEL and P.K. BHATTACHARYA. Can. J. Chem. **71**, 1253 (1993).

Stability constants of homobinuclear binary Cu(II) complexes of the dinucleating ligands, having equivalent coordination sites, 5,5′-methylene-bis-salicylaldehyde (H_2A^1), 5,5′-methylene-bis-(3-bromosalicylaldehyde) (H_2A^2), and 5,5′-methylene-bis-(3-nitrosalicylaldehyde) (H_2A^3), and mixed ligand Cu(II) complexes with one of the above ligands and bipyridyl (L^1) or 1,10-phenanthroline (L^2) as second ligand, have been determined potentiometrically in water:dioxane medium (50:50 and 30:70, v/v using a computer programme. The values of $\Delta \log K' = [\log K^{M}_{MAHL} - (\log K^{M}_{MAH} + \log K^{M}_{ML})]$ and $\Delta \log K'' = [\log K^{M_2}_{M_2AL_2} - (\log K^{M_2}_{M_2A} + 2 \log K^{M}_{ML})]$ have been compared within the series of complexes having different H_2A and L. Probable explanations for the stability order have been extended. The complexes $(Cu_2AL_2)(ClO_4)_2$ have been isolated and characterized by elemental analysis, electronic and ESR spectral, and magnetic studies.

PUSHPA PATEL et P.K. BHATTACHARYA. Can. J. Chem. **71**, 1253 (1993).

Opérant dans un milieu formé d'eau et dioxane (50 : 50 ou 30 : 70, v/v), faisant appel à la potentiométrie et à un programme pour ordinateur, on a déterminé les constantes de stabilité des complexes homobinucléaires binaires du Cu(II) avec les ligands bivalents comportant des sites de coordination équivalents, 5,5′-méthylène-bis-salicylaldéhyde (H_2A^1), 5,5′-méthylène-bis-(3-bromosalicylaldéhyde) (H_2A^2) et 5,5′-méthylène-bis-(3-nitrosalicylaldéhyde) (H_2A^3), et les complexes du Cu(II) avec des ligands mixtes comportant un de ceux mentionnés ci-dessus et soit le bipyridyl (L^1) ou la 1,10-phénanthroline (L^2) comme second ligand. On a comparé les valeurs du $\Delta \log K' = [\log K^{M}_{MAHL} - (\log K^{M}_{MAH} + \log K^{M}_{ML})]$ et du $\Delta \log K'' = [\log K^{M_2}_{M_2AL_2} - (\log K^{M_2}_{M_2A} + 2 \log K^{M}_{ML})]$ pour la série de complexes portant divers H_2A et L. On a étendu les explications possibles pour l'ordre des stabilités. On a isolé et caractérisé les complexes $(Cu_2AL_2)(ClO_4)$ par analyse élémentaire, par leurs spectres électronique et RPE et par des études magnétiques.

[Traduit par la rédaction]

Introduction

The study of binuclear complexes is a topic of considerable current interest, (see, for example, ref. 1) because of their use as models for a number of important biological systems containing two active metal sites (2). It has been shown that ligands having two or more coordinating sites can easily form homo- and heteropolynuclear complexes (3–11).

From a literature survey, it appears that there are mainly two types of ligands that can simultaneously coordinate with two metal ions. In the first type, the two coordinating sites are equivalent, while they are nonequivalent in the second type. The study of homo- and heterobinuclear complexes of such ligands in solution has at least two interesting aspects. Firstly, such study leads to the advancement of the knowledge, in coordination chemistry, of binucleating ligands and, secondly, to the possible application of these results to speciation of natural multicomponent systems.

Some of the polyfunctional ligands that form binuclear complexes in solution are amino acids such as histidine (4), L-(3,4-dihydroxyphenyl) alanine (L-dopa) (6), and DL-isoserine (11); dipeptides such as β-alanyl L-histidine (5) and L-histidyl glycine (10); hydroxypolycarboxylate ligands such as citrate (3, 8); and aminopolycarboxylates such as EDTA (12).

Binary (13) and ternary complexes containing salicylaldehyde have been studied earlier. In ternary complexes (dipyridyl–Cu–salicylaldehyde), it was shown that $\Delta \log K$ is less negative because of the π-acidic nature of dipyridyl and the affinity of M–dipyridyl for O^-–O coordinating salicyl aldehyde (14). The stability of the ternary complexes was shown to be dependent on substitution on the dipyridyl or salicylaldehyde (15).

In the present study we synthesized dinucleating ligands, comprising two chelating arms (salicylaldehyde), attached to the methylene group. 5,5′-Methylene-bis-salicylaldehyde (H_2A^1), 5,5′-methylene-bis-(3-bromosalicylaldehyde) (H_2A^2), and 5,5′-methylene-bis-(3-nitrosalicylaldehyde) (H_2A^3) were synthesized and their binary mono- and binuclear Cu(II) complexes, CuAH and Cu_2A, and the mixed ligand complexes CuAHL and Cu_2AL_2, where L = bipyridyl (L^1) or 1,10-phenanthroline (L^2), were studied in solution.

The complexes Cu_2AL_2 were isolated and characterized. The general structural formula of the ligand H_2A is as follows:

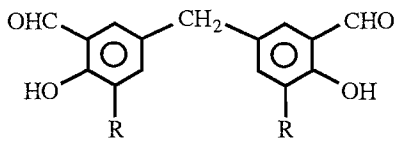

R = H, Br, NO_2

Experimental

All the reagents used were of A.R. grade. The ligand 5,5′-methylene-bis-salicylaldehyde (H_2A^1) was prepared by the method reported in the literature (16). 5,5′-Methylene-bis-(3-bromosalicylaldehyde) (H_2A^2) and 5-5′-methylene-bis-(3-nitrosalicylaldehyde) (H_2A^3) were prepared by bromination and nitration of 5,5′-methylene-bis-salicylaldehyde, as was done in the case of salicylaldehyde (17, 18). The titrations were carried out in water-dioxane (50:50, v/v and 30:70, v/v) for the system Cu–H_2A^3–L. The correction in pH parameters has been made using the method detailed earlier (15). The summary of other experimental parameters for the Cu(II) binary and mixed ligand systems is given as follows:

[1]Author to whom correspondence may be addressed.

[2]Revision received March 2, 1993.

Can. J. Chem. Downloaded from www.nrcresearchpress.com by 213.200.69.106 on 09/08/12
For personal use only.

TABLE 1. Proton–ligand formation constants of the ligands and formation constants of homobinuclear binary complexes of Cu(II) in water:dioxane medium (50:50, v/v) at 0.2 M ($NaClO_4$) and 30 ±1°C with standard deviations in parentheses

Ligand (A)	log K_1H	log β_2H	log K^{Cu}_{Cu+A+H}	log K^{Cu}_{CuAH}	log $K^{CuAH}_{Cu_2A}$	log $K^{Cu_2}_{Cu_2A}$
H_2A^1	9.30 (0.02)	17.80 (0.03)	15.45 (0.04)	6.15 (0.04)	6.95 (0.08)	13.10 (0.08)
H_2A^2	8.09 (0.01)	15.39 (0.07)	13.85 (0.05)	5.76 (0.05)	6.07 (0.11)	11.83 (0.11)
H_2A^3	7.02 (0.00)	12.98 (0.06)	11.55 (0.09)	4.53 (0.09)	5.22 (0.12)	9.75 (0.12)

TABLE 2. Stability constants of mixed ligand complexes in water:dioxane medium (50:50 or 30:70, v/v) and 0.2 M ($NaClO_4$) at 30 ± 1°C with standard deviations in parentheses

Ligand (A)	log K^{M}_{MAHL}	Δ log K' (Cu–H_2A – bipyridyl)	log $K^{M_2}_{M_2AL_2}$	Δ log K''	log K^{M}_{MAHL}	Δ log K' (Cu–H_2A – 1:10 phen)	log $K^{M_2}_{M_2AL_2}$	Δ log K''
H_2A^1	13.90 (0.08)	(+0.75)	27.95 (0.07)	(+0.85)	15.37 (0.06)	(+0.40)	31.26 (0.12)	(+0.52)
H_2A^2	14.09 (0.12)	(+1.33)	27.33 (0.20)	(+1.50)	15.27 (0.15)	(+0.69)	30.19 (0.16)	(+0.72)
H_2A^3	13.18 (0.09)	(+1.45)	25.30 (0.14)	(+1.55)	14.31 (0.16)	(+0.76)	28.21 (0.18)	(+0.82)

Solution compositions

Ligand systems:

(*a*) 0.02 M $HClO_4$:0.003 M lig H_2A:0.177 M $NaClO_4$

(*b*) 0.02 M $HClO_4$:0.002 M lig H_2A:0.178 M $NaClO_4$

Binary systems:

(*a*) 0.02 M $HClO_4$:0.003 M $Cu(ClO_4)_2$:0.0015 M lig H_2A:0.1755 M $NaClO_4$

(*b*) 0.02 M $HClO_4$:0.003 M $Cu(ClO_4)_2$:0.001 M lig H_2A:0.176 M $NaClO_4$

Mixed ligand systems:

(*a*) 0.02 M $HClO_4$:0.003 M $Cu(ClO_4)_2$:0.0015 M lig H_2A:0.003 M lig. L:0.1725 M $NaClO_4$

(*b*) 0.02 M $HClO_4$:0.003 M $Cu(ClO_4)_2$:0.001 M lig. H_2A:0.003 M lig. L:0.173 M $NaClO_4$

Ionic strength, electrolyte: 0.2 M dm^{-3}, $NaClO_4$

Experimental method: pH titration using pH meter (G.P. Electronics, Accuracy ±0.01 pH unit)

pH range: protonation: 6.00–10.8 pH, Cu(II) complexation: 3.20–5.50 pH

Temperature: 30°C

Method of calculation: SCOGS (ref. 19)[3]

Species considered: protonation: AH_2, AH, A

Cu(II) binary system: AH_2, AH, A, Cu(II), CuAH, and Cu_2A

Cu(II) mixed ligand system: AH_2, AH, A, LH, L, Cu(II), CuAH, Cu_2A, CuL, CuL_2, LCuAH, and Cu_2AL_2

The refined values of the protonation constants were used as fixed parameters for the refinement of binary complexes and the values of the protonation constants and the binary constants were used as fixed parameters for the refinements of mixed ligand species. The values of proton–ligand formation constants of ligands H_2A and formation constants of the binary and mixed ligand complexes and their Δ log K values are presented in Tables 1 and 2. The deviations in values indicate random error in the titrations, dependent on the precision of the instruments.

Isolation of some complexes

The mixed ligand binuclear complexes (Cu_2AL_2, $ClO_4)_2$ were isolated by addition of Cu:Bipyridyl or Cu:1,10-phenanthroline (1:1) complex (4 mmol) in water:ethanol (60:40, v/v) (70 mL) to a potassium salt of 5,5′-methylene-bis-salicylaldehyde (2 mmol) in 40 mL ethanol, with stirring. A dark green coloured clear solution was obtained. Stirring was continued for half an hour. $NaClO_4$ (4 mmol), in water:ethanol (50:50 v/v) (30 mL), was added to the resultant solution. A dark green solid separated out. This was filtered, washed with ethanol, dried, and crystallized from 1:1 DMF:water. These isolated complexes were characterized by metal estimation, elemental analysis, spectral studies, and magnetic moment measurement at room temperature.

The electronic spectra were recorded on a UV-Shimadzu-240 spectrophotometer and the ESR spectra of the complexes were recorded on a Bruker ESP-300 X-band spectrometer at room temperature as well as in DMF solution at 77 K.

Discussion

In the proton NMR spectra of the ligands H_2A, the δ values for -CHO, -OH, and aromatic ring protons are comparable with those for salicylaldehyde. This indicates that both aldehyde moieties are equivalent and there are no external aryl–aryl interactions between the two aromatic phenyl rings in the dinucleating ligands.

The binucleating ligands (H_2A) have two dissociable phenolic -OH groups on two phenyl rings separated from each other. It is, therefore, expected that the two -OH groups should dissociate independently of each other and both proton–ligand formation constants (K_1H and K_2H) of the dinucleating ligands H_2A^1, H_2A^2, and H_2A^3 should be similar and comparable with the protonation constant of the salicylal-

[3]SCOGS: Stability Constants of Generalized Species.

Can. J. Chem. Downloaded from www.nrcresearchpress.com by 213.200.69.106 on 09/08/12
For personal use only.

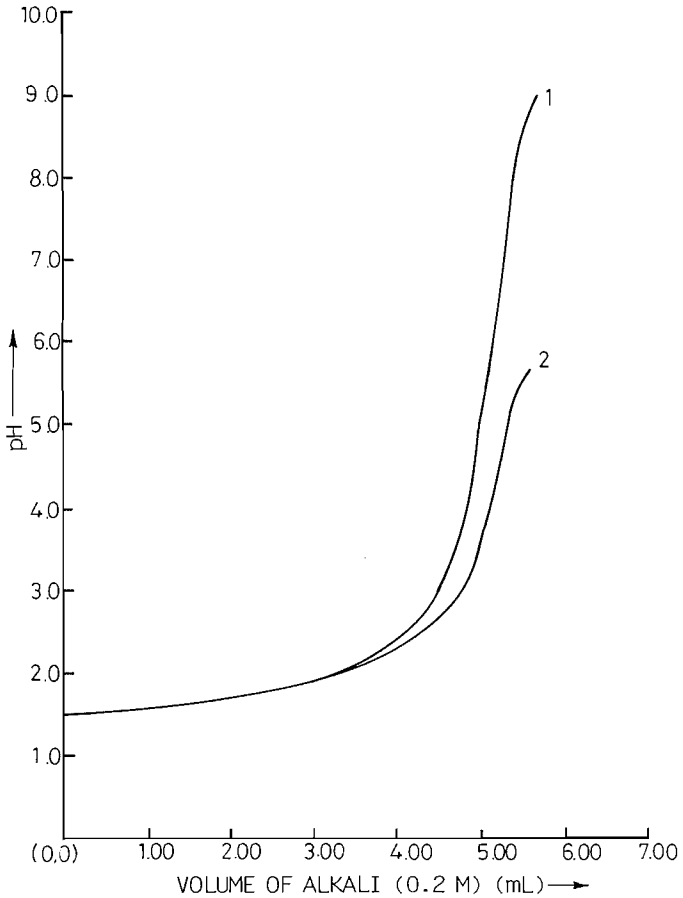

FIG. 1. 1. H_2A^3(0.001 M); 2. Cu:H_2A^3((0.003:0.001 M) (70:30 v/v, dioxane:water).

dehyde, bromosalicylaldehyde, and nitrosalicylaldehyde, respectively. However, it was observed that the values of the first proton-ligand formation constants are slightly higher than those of salicylaldehyde and derivatives, indicating that the dissociation of the two phenolic -OH groups takes place in steps, i.e., the dissociation of proton at one phenolic end may be affecting the dissociation of the other phenolic proton due to internal electronic effects.

It has been noted in the literature (3–12) that ligands with two well-separated coordinating sites behave like two individual ligands. In ligands H_2A^1, H_2A^2, and H_2A^3, also, both coordinating sites are equivalent and separated from each other; therefore it is interesting to study the tendency of the two sites to coordinate with the metal ions.

On coordination of the metal ion to the dinucleating ligand AH_2, complex MAH is first formed, and on coordination of a second metal ion to MAH, formation of the second complex M_2A takes place. The reactions can be shown as follows:

[1] $H_2A + Cu^{2+} \rightleftharpoons CuAH^+ + H^+$

[2] $CuAH^+ + Cu^{2+} \rightleftharpoons Cu_2A^{2+} + H^+$

As is evident from the ligand and Cu + A curve (Fig. 1), there is no hydroxo complex formation until pH 5.5, beyond which precipitation takes place. Consideration of mixed hydroxo species Cu_2AOH and $Cu_2A(OH)_2$ in the calculation of formation constants for CuAH and Cu_2A (in the pH range 3.2–5.5) does not give refinement of results. As is observed in the species distribution curves (Fig. 2), total Cu(II) is present in the form of free Cu(II), CuAH, and Cu_2A. The percentage of Cu(II) in Cu_2A is to be considered twice the percentage of Cu_2A.

As there are two well-separated coordination sites, the coordination of a metal ion to one coordination site should not affect the coordination of a second metal ion to the second coordination site, i.e., the values of log K^{Cu}_{CuAH} and log $K^{CuAH}_{Cu_2A}$ should be comparable. If electrostatic repulsion between CuAH and Cu^{2+} is considered, log $K^{CuAH}_{Cu_2A}$ should be lower than log K^{Cu}_{CuAH}. However, in the present investigation the value of log K^{Cu}_{CuAH} is lower than that of log $K^{CuAH}_{Cu_2A}$. The value of log $K^{Cu_2}_{Cu_2A}$ is more than twice that of log $K^{Cu}_{Cu\text{-}sal}$. This may be because of the restriction of rotation of the two phenyl rings around the central C atom of the methylene group, on coordination of Cu(II) at both the sites. An alternate explanation could be that there is a favourable electronic effect at the second $O\text{–}O^-$ site on coordination of Cu(II) to the first $O\text{–}O^-$ site and hence the coordination of the second Cu(II) to the binucleating ligand is facilitated. These move the equilibrium reaction [2] more to the right side. These are, however, probable additional explanations and further confirmation will be needed.

In the case of ligands H_2A^2 and H_2A^3, log K^{Cu}_{CuAH} and log $K^{CuAH}_{Cu_2A}$ values are less than the values in the case of H_2A^1. This is because of electron-withdrawing groups over the salicylaldehyde moieties, which result in a decrease in the π-electron-donating tendency of the ligands H_2A^2 and H_2A^3 to the Cu(II) ions, resulting in lower formation constants for the complexes.

In the case of mixed ligand complexes, the formation constants of the species CuAHL and Cu_2AL_2 could be refined. The distribution curve (Fig. 3) (plot of concentration of the species vs. pH) of the system Cu–H_2A^2–bipy shows that CuAHL formation takes place at lower pH (below pH 3). The formation of the Cu_2AL_2 complex starts around pH 3.5 and increases with pH. The concentration of species CuAH and Cu_2A is very low. The formation of CuL is almost complete at very low pH. At pH 3, there are mainly two species, CuL (~58%) and CuAHL (~38%).

Hence, the reaction can be shown as follows in three steps.

1. $Cu + L \rightleftharpoons CuL$
2. $CuL + H_2A \rightleftharpoons CuAHL + H^+$
3. $CuL + CuAHL \rightleftharpoons Cu_2AL_2 + H^+$

L = bipyridyl or 1,10-phenanthroline

The values of the formation constants of the ternary complexes. CuAHL and Cu_2AL_2 are higher than expected from statistical considerations.

$$\Delta \log K' = [\log K^{M}_{MAHL} - (\log K^{M}_{MAH} + \log K^{M}_{ML})]$$

and

$$\Delta \log K'' = [\log K^{M_2}_{M_2AL_2} - (2 \log K^{M}_{ML} + \log K^{M_2}_{M_2A})]$$

The values of $\Delta \log K'$ and $\Delta \log K''$ are observed to be positive. This can be explained on the basis of π-acidity of ligands L, as in the case of Cu–dipy–salicylaldehyde complex (14).

In ternary complexes the electron density over the metal ion gets reduced due to $M \rightarrow L$ π-interaction and hence ML

Can. J. Chem. Downloaded from www.nrcresearchpress.com by 213.200.69.106 on 09/08/12
For personal use only.

Can. J. Chem. Downloaded from www.nrcresearchpress.com by 213.200.69.106 on 09/08/12
For personal use only.

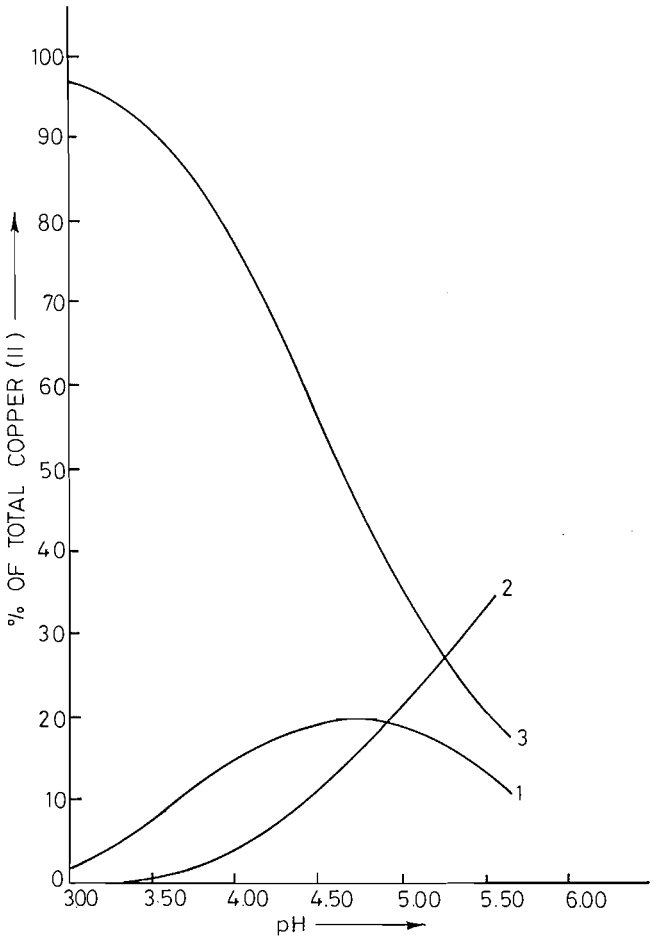

FIG. 2. Species distribution for the [$Cu^{(II)}$–H_2A^2] binary system at an M:A ratio of 2:1 (0.003:0.0015 M). 1. (CuAH); 2. (Cu_2A); 3. free Cu(II).

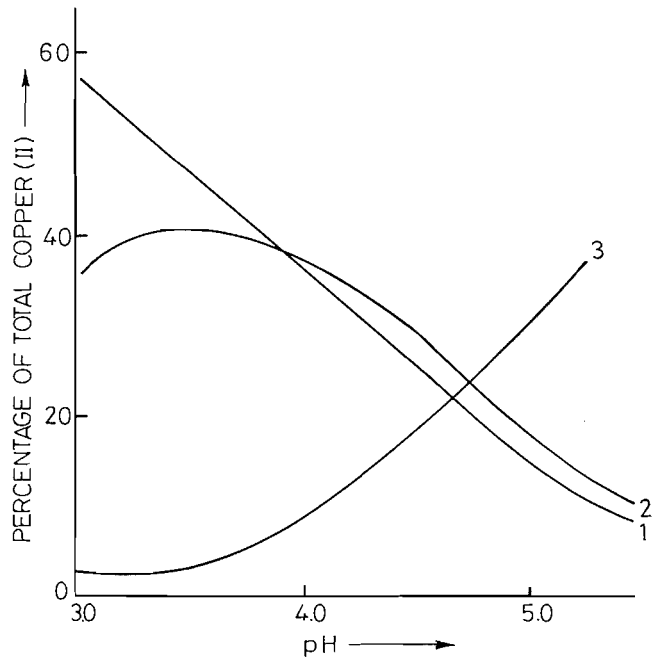

FIG. 3. Species distribution for the [Cu(II)–H_2A^2–bipy] ternary system at an M:A:L ratio of 2:1:2. 1. CuL; 2. CuAHL; 3. Cu_2Al_2.

attains a more class A character, preferring coordination with O^-–O coordinating ligands. This results in the greater stabilization of the ternary complexes and positive Δ log K values.

It is also interesting to observe the effect of the nature of substitution over the ligand A on the formation of the ternary complexes. It was observed earlier (14) that in the case of mononuclear complexes CuAL, where L = bipyridyl or 1,10 phen and A = bromo- or nitrosalicylaldehyde, the stabilization of the ternary complex is lower and hence Δ log K is less positive than in the case of complexes CuAL where A = salicylaldehyde. This is because the electron-withdrawing effect of the bromo and nitro groups causes reduction in the electron density over the coordinating atoms O^-–O and hence the stabilization of the ternary complexes is lower.

In the present study it has been observed that the Δ log K values of the complexes CuAHL and Cu_2AL_2, where A = A^2 and A^3, i.e., dibromo- and dinitro-substituted 5,5′-methylene-bis-salicylaldehyde, are more positive than those of complexes CuA^1HL and $Cu_2A^1L_2$. This can be explained by considering that the presence of substituents on the phenyl rings will further restrict the rotation of the CuL bound to the phenyl rings, around the -CH_2 group. This will orient the two rings of A suitably for coordination with CuL, which was not the case for H_2A^1 without substituents. This will result in greater stabilization of the complexes CuAHL and Cu_2AL_2, where A = H_2A^2 or H_2A^3, compared to the complexes CuA^1HL and $Cu_2A^1L_2$, respectively.

Characterization and magnetic study

The elemental analysis (Table 3) of the binuclear Cu(II) mixed ligand complex corresponds to the expected formula. The general structure of the complexes is shown in Fig. 4.

The electronic spectral studies of the complexes show the expected bands in the visible range. The presence of only one band at 610 nm, as in mononuclear Cu(II) complexes (14), indicates that both Cu(II) centres are behaving as equivalent independent centres.

To ensure that the complex does not break apart in DMF solution, the electronic spectrum of the complex was obtained in this solution. It was compared with the solid reflectance spectra. The peak positions in the two spectra are similar, showing that the mixed ligand complex remains as such in the solution.

IR spectra of the complexes exhibit the expected bands of H_2A and L, supporting the mixed ligand character of the complexes. IR spectral bands corresponding to ClO_4 were used to establish its ionic nature. There is one band obtained at ~1100 cm^{-1}, corresponding to ν_{asy} (Cl-O). The absence of ν_{sym} (Cl-O) at 900 cm^{-1} indicates T_d symmetry and the presence of ionic ClO_4^-.

The magnetic moments of the complexes were measured at room temperature. The value of magnetic susceptibility for each Cu(II) centre corresponds to one unpaired electron. This indicates the absence of magnetic interaction between the two Cu(II) centres, and was further confirmed by ESR spectral studies of the complexes in DMF in the glassy state at liquid nitrogen temperature as well as at room temperature. The spectra exhibit $g_{\|}$ = 2.26 and $g_{\perp}$ = 2.06, corre-

TABLE 3. Analytical and magnetic moment data of Cu(II) binuclear ternary complexes

	Compounds	Formula	Found (calcd.), % M	N	C	H	μ_{eff}[a] for one Cu(II)
1.	$[Cu_2A^1L^1{}_2]$ $(ClO_4)_2$ (dark green)	$[C_{35}H_{26}O_4N_4Cu_2]$ $(ClO_4)_2$	14.25 (14.09)	6.28 (6.00)	47.13 (47.03)	2.91 (2.83)	1.93
2.	$[Cu_2A^2L^1{}_2]$ $(ClO_4)_2$ (dark green)	$[C_{35}H_{24}O_4N_4Cu_2Br_2]$ $(ClO_4)_2$	12.09 (11.95)	5.33 (5.03)	40.00 (39.79)	2.28 (2.15)	1.95
3.	$[Cu_2A^1L^2{}_2]$ $(ClO_4)_2$ (dark green)	$[C_{39}H_{26}O_4N_4Cu_2]$ $(ClO_4)_2$	13.52 (13.38)	5.96 (5.60)	49.84 (49.50)	2.76 (2.68)	1.89
4.	$[Cu_2A^3L^2{}_2]$ $(ClO_4)_2$ (yellowish green)	$[C_{39}H_{24}O_6N_6Cu_2]$ $(ClO_4)_2$	12.31 (12.45)	8.11 (8.20)	45.39 (45.60)	2.32 (2.21)	1.90

[a]In BM (Bohr magneton).

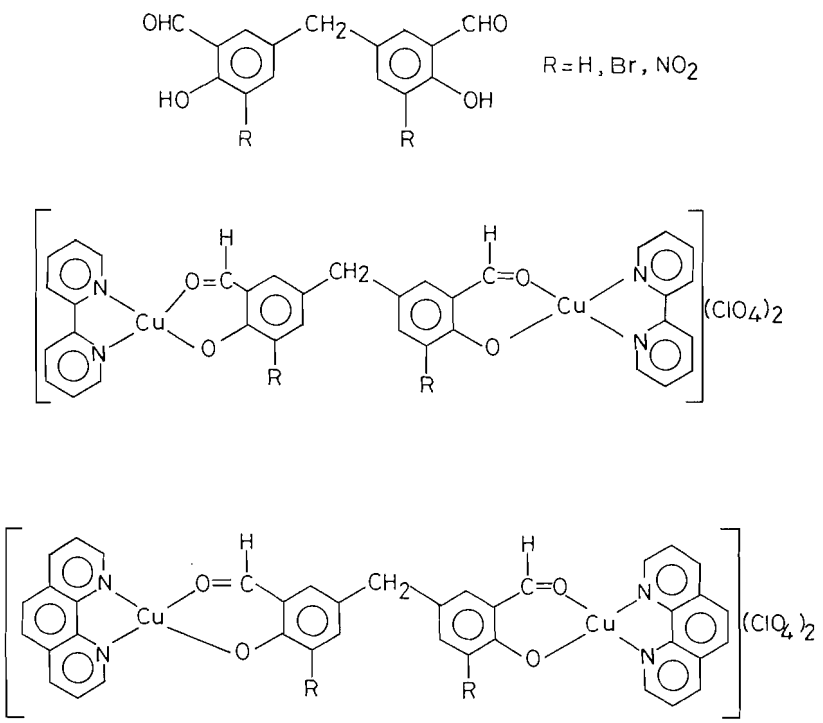

FIG. 4

sponding to the distorted octahedral symmetry. No half-filed transition at $g = 4$ is observed, indicating the absence of spin exchange interactions between the Cu(II) centres. This supports the distant orientation of the two Cu(II) centres, as indicated by the formation constant studies in solution.

Acknowledgements

We are grateful to Prof. A.C. Shah, Head, Department of Chemistry, M.S. University of Baroda, for providing the necessary laboratory facilities. Thanks are also due to Prof. P. Natarajan (Director, CSMCRI, Bhavnagar) and his group for providing ESR instrumental and library facilities.

1. K.D. Karline and J. Zubieta (*Editors*). Biological and inorganic copper chemistry. Adenine, Guilerland, New York, 1986.
2. E.I. Solomon. *In* Copper proteins. *Edited by* T.G. Spiro. Wiley Interscience, New York. (1981); J.A. Fee. Struct. Bonding (Berlin), **23**, 1 (1975).
3. P. Amico, P.G. Daniele, G. Ostacoli, G. Arena, E. Rizarelli, and S. Sammaratano. Inorg. Chim. Acta, **44**, L219 (1980).
4. P. Amico, G. Arena, P.G. Daniele, G. Ostacoli, E. Rizzarelli, and S. Sammaratano. Inorg. Chem. **20**, 772 (1981).
5. P.G. Daniele, P. Amico, and G. Ostacoli. Inorg. Chim. Acta, **66**, 65 (1982).
6. P.G. Daniele, P. Amico, G. Ostacoli, and V. Zelano. Ann. Chim. (Rome), **73**, 199 (1983).
7. P.G. Daniele, P. Amico, G. Ostacoli, and M. Marzona. Ann. Chim. (Rome), **73**, 299 (1983).
8. P. Amico, G. Daniele, G. Ostacoli, G. Arena, E. Rizzarelli, and S. Sammartano. Transition Met. Chem. (Weinheim, Ger.), **10**, 11 (1985).
9. P. Amico, G. Arena, P.G. Daniele, G. Ostacoli, E. Rizzarelli, and S. Sammartano. Environ. Inorg. Chem. 285 (1985).

Can. J. Chem. Downloaded from www.nrcresearchpress.com by 213.200.69.106 on 09/08/12
For personal use only.

10. P.G. Daniele, O. Zerbinati, R. Aruga, and K. Ostacoli. J. Chem. Soc. Dalton Trans. 1115 (1988).
11. G. Arena, V. Cucinotta, E. Rizzarelli, P.G. Daniele, G. Ostacoli, and S. Sammartano. J. Chem. Soc. Dalton Trans. 1267 (1988).
12. (*a*) M.V. Leont'eva and N.M. Dyatlova. Koord. Khim. **16**, 673 (1990); (*b*) Koord. Khim, **16**, 960 (1990).
13. (*a*) L.E. Maley and D.P. Mellor. Nature, **159**, 370 (1947); (*b*) Aust. J. Sci. Res. **2A**, 92 (1949).
14. P.J. Patel and P.K. Bhattacharya. J. Coord. Chem. **13**, 113 (1984).
15. N.D. Kulkarni and P.K. Bhattacharya. Can. J. Chem. **65**, 348 (1987).
16. C.S. Marvel and N. Torkoy. J. Am. Chem. Soc. **79**, 6000 (1957).
17. K. Auwers and O. Burger. Ber. Dtsch. Chem. Ges. **37**, 3934 (1904).
18. S. Dandegaonkar and S.G. Shet. J. Indian Chem. Soc. **42**, 323 (1965).
19. (*a*) I.G. Sayce. Talanta, **15**, 1397 (1968); (*b*) Talanta, **18**, 653 (1971); (*c*) I.G. Sayce and V.S. Sharma. Talanta, **19**, 831 (1972).

Can. J. Chem. Downloaded from www.nrcresearchpress.com by 213.200.69.106 on 09/08/12
For personal use only.

Solubility and activity coefficients of lead chloride in potassium nitrate solutions at 25°C and at boiling. Calculation of the supersaturation

JOAN TORRENT-BURGUÉS[1]

Departament d'Enginyeria Química, Universitat Politècnica de Catalunya, C/ Colom 1, 08222 Terrassa, Spain

AND

SABINO VEINTEMILLAS-VERDAGUER

Institut de Ciència de Materials de Barcelona, Consejo Superior de Investigaciones Científicas, Campus UAB, 08193 Cerdanyola, Spain

Received June 30, 1992[2]

JOAN TORRENT-BURGUÉS and SABINO VEINTEMILLAS-VERDAGUER. Can. J. Chem. **71**, 1259 (1993).

The solubility and activity coefficients of lead chloride in aqueous potassium nitrate solutions, at 25°C and at boiling, are reported. The activity product constant of lead chloride at boiling has been determined. The Pitzer equations have been applied to the system and have allowed us to determine unknown ionic interaction parameters at 25°C. The calculation of the lead chloride supersaturation is illustrated using the activities instead of the concentrations.

JOAN TORRENT-BURGUÉS et SABINO VEINTEMILLAS-VERDAGUER. Can. J. Chem. **71**, 1259 (1993).

On a déterminé la solubilité et les coefficients d'activité du chlorure de plomb en solution aqueuse de nitrate de potassium, à 25°C et à l'ébullition. On a déterminé la constante du produit d'activité du chlorure de plomb à l'ébullition. On a appliqué les équations de Pitzer au système et elles nous ont permis de déterminer des paramètres d'interactions ioniques inconnues, à 25°C. On illustre le calcul de la sursaturation du chlorure de plomb à l'aide d'activitiés au lieu de concentrations.

[Traduit par la rédaction]

Introduction

Lead chloride crystals have found new applications as acousto-optical material (1, 2). In spite of the low solubility of the salt, it is possible to grow monocrystals of centimetric size from solution by adding a salt that increases the solubility of the lead chloride and (or) by using high temperatures with the techniques of growth from boiling solutions (3, 4). Knowledge of the solubility and activity coefficients of the salt is important in order to calculate the supersaturation and to define the best conditions for nucleation and crystal growth.

In this paper a physico-chemical study of saturated lead chloride solutions in the presence of potassium nitrate, at 25°C and at boiling, is presented. A revision of the data treatment for lead chloride solutions at 25°C, ranging from dilution to saturation, is made, following which the activity coefficients at boiling are estimated using an extrapolation method from solubility measurements, and an estimated activity product constant is reported. Carmody (5) reported the activity coefficients of lead chloride from emf measurements as well as the value of E^0 (Pb^{2+}/Pb) calculated with an extrapolation process (see eq. [3] below). The same set of data were treated by Scatchard and Tefft (6) using a different extrapolation process, which led to slightly different values of E^0 and the activity coefficients. The Pitzer equations have enabled us to adjust the experimental data of emf and to obtain a reliable value for the activity coefficient at saturation and also for the standard potential of the system Pb^{2+}/Pb. The mixture parameters of the system $PbCl_2$–KNO_3 at 25°C are obtained using the Pitzer equations. The activity coefficients are used in the calculation of the supersaturation of lead chloride in $PbCl_2$–H_2O solutions.

[1]Author to whom correspondence may be addressed.

[2]Revision received May 10, 1993.

Experimental method

Solubility measurements of lead chloride were made using Carlo Erba A.R. lead chloride, Merck A.R. potassium nitrate, and concentrated nitric acid.

Solubility measurements of lead chloride at 25°C were made in a closed thermostatted cell (±0.1°C). An excess of lead chloride was added to the aqueous KNO_3 solution, of known concentration. The pH was adjusted to 4 by adding nitric acid, in order to prevent the formation of the hydroxy compound, and the solution was then stirred during 24–48 h to ensure saturation. The measurements at boiling and atmospheric pressure were made in a special reactor formed, basically, by a distillation balloon, heated uniformly by a heating blanket, and a reflux column. The top of the distillation balloon was isolated to minimize the heat loss. An excess of lead chloride was added to the aqueous KNO_3 solution, of known concentration, and the pH was adjusted to 2.8. The boiling bubbles, as well as the convection flow, ensured the stirring of the solution. The saturation procedure finished when we observed lead chloride recrystallization, which usually occurred after 24 h.

When saturation was established, the composition of the solution was determined, as well as its density. The lead chloride concentration was determined for an accurately weighed quantity of solution, using a standardized titration method of lead with EDTA. The solubilities, reported in units of molality (m), have an uncertainty of ±0.001

Densities were determined by weighing a known volume of the saturated solution. For boiling conditions, a Lunge–Rey pipette was employed. The densities reported have a precision of ±0.001 at 25°C and of ±0.01 at boiling.

Results and discussion

The experimental results of solubility and density, at 25°C and at boiling, are presented in Tables 1 and 2, respectively. The dependence of the lead chloride solubility, m_1, on the potassium nitrate concentration, m_2, can be expressed at 25°C by the relation:

Can. J. Chem. Downloaded from www.nrcresearchpress.com by 213.200.69.106 on 09/08/12
For personal use only.

Can. J. Chem. Downloaded from www.nrcresearchpress.com by 213.200.69.106 on 09/08/12
For personal use only.

TABLE 1. Solubility and mean ionic activity coefficients of lead chloride in potassium nitrate solutions at 25°C

Molality			$PbCl_2$		
KNO_3	$PbCl_2$	d/g cm^{-3}	γ_{exp}	$\gamma_{\Theta,\Psi=0}$	γ_{calc}
—	0.0396	1.007	0.412	0.412	0.412
0.0401	0.0431	1,010	0.379	0.383	0.375
0.0701	0.0462	1.012	0.353	0.366	0.353
0.1105	0.0494	1.015	0.330	0.350	0.332
0.1612	0.0523	1.020	0.312	0.335	0.311
0.2123	0.0557	1.023	0.293	0.323	0.295
0.2635	0.0581	1.027	0.281	0.313	0.280
0.3143	0.0611	1.030	0.267	0.305	0.268
0.3762	0.0640	1.034	0.255	0.297	0.256
0.4796	0.0689	1.042	0.237	0.285	0.237
0.5632	0.0726	1.048	0.225	0.278	0.225
0.7231	0.0791	1.059	0.206	0.267	0.204
1.0475	0.0930	1.080	0.175	0.252	0.175

[1a] $$m_1 = 0.0401 + 0.0855m_2 - 0.0682m_2^2 + 0.0334m_2^3$$

At boiling, the relation:

[1b] $$m_1 = 0.141 + 0.0722m_2$$

can reasonably be applied over the entire potassium nitrate concentration range, but shows significant deviations at low concentrations. For this reason, a double adjustment is preferred:

[1c] $$m_1 = 0.124 + 0.1266m_2 - 0.0217m_2^2$$

in the range 0–2.14 molal, and

[1d] $$m_1 = 0.143 + 0.0714m_2$$

in the range 2.14–7 molal. The data at 25°C are more accurate than at boiling due to the experimental conditions.

Since the lead chloride activity is constant at saturation of the salt, when the temperature is fixed, we can calculate the activity coefficients of $PbCl_2$ in the different solutions with the expression

[2] $$m\gamma_\pm = (m\gamma_\pm)_0$$

where the subscript zero refers to a known saturated solution, which can be a single saturated solution of lead chloride.

Activity coefficients at 25°C

The literature data on the activity coefficients at saturation present some scatter due, principally, to the calculation method. We revised it using the more recent treatment of Pitzer (7) for electrolyte solutions, which has been proven to work well in a number of systems. Carmody (5) obtained the emf data for the cell $Pb(Hg)/PbCl_2(aq.)/AgCl,Ag$:

[3] $$E = E^0 - RT/(2F)\ln a(PbCl_2) = E^0 - 3RT/(2F)\ln(4^{1/3}m\gamma_\pm)$$

The differences between the reported values of E^0 (5, 6), are due to the method of extrapolation to infinite dilution of the experimental values.

It is known that the lead ion and the chloride ion are associated in solution. The activity coefficients of lead chloride at 25°C show values lower than those predicted by the limiting equation of Debye–Hückel at all concentrations, and in consequence the Guggenheim equation shows a high negative value of the β parameter. But the Guggenheim equation does not fit the experimental values very well. Thus it seems convenient to use the Pitzer equation, which accounts for the ionic association through the term in $\beta^{(2)}$ (8, 9), even though it was proposed originally for 2:2 electrolytes. The Pitzer equation for lead chloride takes the following form:

TABLE 2. Solubility and mean ionic activity coefficients of lead chloride in potassium nitrate solutions at boiling

Molality				
KNO_3	$PbCl_2$	d/g cm^{-3}	t_b/°C	γ_{exp}
—	0.119	1.00	100	0.24
0.107	0.142	1.015	100	0.20
0.214	0.147	1.022	100	0.19
0.321	0.155	1.023	100	0.18
0.348	0.175	1.038	100	0.16
0.454	0.170	1.030	100	0.17
0.481	0.183	1.038	101	0.16
0.802	0.204	1.060	101	0.14
1.069	0.236	1.07	101	0.12
1.604	0.272	1.14	102	0.105
2.138	0.296	1.14	102	0.097
2.673	0.325	1.20	103	0.088
3.742	0.417	1.24	104	0.068
4.277	0.448	1.24	104	0.064
4.811	0.487	1.27	104	0.059
5.346	0.532	1.31	104	0.054
5.881	0.571	1.32	105	0.050
6.949	0.628	1.38	105	0.045

[4] $$\ln\gamma_\pm = 2f^\gamma + 4/3\,mB^\gamma + 2^{3/2}m^2C^\Phi$$

[5a] $$f^\gamma = -A_\Phi\left[\frac{I^{1/2}}{1 + 1.2I^{1/2}} + \frac{2}{1.2}\ln(1 + 1.2I^{1/2})\right]$$

[5b] $$B^\gamma = 2\beta^{(0)} + 2\beta^{(1)}/(\alpha_1^2I)\,[1 - (1 + \alpha_1I^{1/2} - 0.5\alpha_1^2I)\exp(-\alpha_1I)] + 2\beta^{(2)}/(\alpha_2^2I)\,[1 - (1 + \alpha_2I^{1/2} - 0.5\alpha_2^2I)\exp(-\alpha_2I)]$$

The activity coefficient in eq. [3] can be replaced by the Pitzer equation and the resulting expression can be reordered to perform a regression of least squares, in order to determine the parameters of the Pitzer equation and the value of E^0. Due to the ion association of the lead chloride, the term in $\beta^{(2)}$ will be retained in the fit, while the term in C^Φ, which accounts for the triple ion interactions, will be eliminated because of the low values of the ionic strengths. This simplification is also justified by the small standard deviation of the fit ($\sigma = 0.0026$) and the good correlation coefficient ($r = 0.9995$). The values of α_1 and α_2 used were 2.0 and 12.0 (8, 9), respectively. The three parameters β of the fit are reported in Table 3. This set of parameters have more physical meaning than the set of parameters $\beta^{(0)}$, $\beta^{(1)}$, and C^Φ, also reported in Table 3, which give slightly better fit, but the large values obtained have little physical sense and also work badly in further applications, i.e., in the mixture equation.

TABLE 3. Pitzer equation parameters for different electrolytes at 25°C

Electrolyte	$\beta^{(0)}$	$\beta^{(1)}$	C^{Φ}	$\beta^{(2)}$	σ
$PbCl_2$[a]	1.2031	−4.8081		−12.9063	0.0026
$PbCl_2$[b]	17.3018	−28.5171	−79.214		0.0023
$Pb(NO_3)_2$[c]	−0.03615	0.285	0.00533		
KCl[c]	0.04835	0.2122	−0.00084		
KNO_3[c]	−0.0816	0.0494	0.00660		

[a]This work, eqs. [4] and [5] with $\alpha_1 = 2$, $\alpha_2 = 12$, and $C^{\Phi} = 0$.
[b]The same, with $\alpha_1 = 2$ and $\beta^{(2)} = 0$.
[c]In ref. 18.

The obtained value of $E^0 = 343.0$ mV is the same as that reported by Scatchard and Tefft (6). Taking the potential of the silver chloride electrode to be 222.3 mV (10) and the lead – lead amalgam potential to be 5.8 mV (5, 10), the standard potential of the redox pair Pb/Pb^{2+} is E^0 (Pb/Pb^{2+}) = 126.5 mV.

With the value of E^0 and the experimental value of E at saturation, we obtain from eq. [3] $\gamma_{\pm}$(sat) = 0.413, a value that is reproduced by the Pitzer equation with the reported parameters. This value is very close to that of 0.412 recommended by Goldberg (11). With this value of $(\gamma_{\pm})_0$ and eq. [2], the activity coefficients reported in Table 1 were obtained for the $PbCl_2$(sat)–KNO_3 mixtures at 25°C.

It is possible to estimate the activity coefficients of the components in a mixture, using the corresponding Pitzer equations (9, 12) and the corresponding parameters of each single electrolyte resulting from combination of an anion and a cation in the mixture. The activity coefficient of the lead chloride (noted by MX, M = Pb and X = Cl) in a mixture with potassium nitrate (noted by NY, N = K and Y = NO_3), with the corresponding molalities m_1 and m_2, is

$$[6]\quad \ln \gamma_{MX} = 2f^{\gamma} + 4m_1[2/3\, B_{MX} + m_1 B'_{MX} + 2/3\, IC_{MX}] + m_2[2/3\, B_{MY} + 2m_1 B'_{MY} + 2/3\,(I + m_1)\, C_{MY}] + m_2[4/3\, B_{NX} + 4m_1 B'_{NX} + 4/3\,(I + m_1)\, C_{NX}] + m_2^2[2B'_{NY} + 4/3\, C_{NY}] + 2/3\, m_2(2\Theta_{XY} + \Theta_{MN}) + 4/3\, m_1 m_2(\Psi_{MXY} + \Psi_{MNX}) + 1/3\, m_2^2(\Psi_{MNY} + 2\Psi_{NXY})$$

where the term f^{γ} is expressed as indicated in eq. [5*a*], and the terms B_{MY}, B_{NX}, B'_{MY}, B'_{NX}, B'_{NY}, and C are

$$[7a]\quad B = \beta^{(0)} + 2\beta^{(1)}/(\alpha_1^2 I)\,[1 - (1 + \alpha_1 I^{1/2})\exp(-\alpha_1 I^{1/2})]$$

$$[7b]\quad B' = 2\beta^{(1)}/(\alpha_1 I)^2[-1 + (1 + \alpha_1 I^{1/2} + 0.5\alpha_1^2 I)\exp(-\alpha_1 I^{1/2})]$$

$$[7c]\quad C = C^{\Phi}/(2|Z_M Z_X|^{1/2})$$

and the terms for lead chloride B_{MX} and B'_{MX} are

$$[7d]\quad B_{MX} = \beta^{(0)} + 2\beta^{(1)}/(\alpha_1^2 I)\,[1 - (1 + \alpha_1 I^{1/2})\exp(-\alpha_1 I^{1/2})] + 2\beta^{(2)}/(\alpha_2^2 I)\,[1 - (1 + \alpha_2 I^{1/2})\exp(-\alpha_2 I^{1/2})]$$

$$[7e]\quad B'_{MX} = 2\beta^{(1)}/(\alpha_1 I)^2\,[-1 + (1 + \alpha_1 I^{1/2} + 0.5\alpha_1^2 I)\exp(-\alpha_1 I^{1/2})] + 2\beta^{(2)}/(\alpha_2 I)^2\,[-1 + (1 + \alpha_2 I^{1/2} + 0.5\alpha_2^2 I)\exp(-\alpha_2 I^{1/2})]$$

The values of all parameters appearing in eqs. [7*a*]–[7*e*] are given in table 3.

Table 1 shows the large difference between the experimental activity coefficients of $PbCl_2$ and those estimated assuming $\Theta,\Psi = 0$. Therefore it is necessary to introduce the mixture parameters. A regression of $\ln(\gamma_{exp}) - \ln(\gamma_{\Theta,\Psi=0})$ using eqs. [6] and [7] ($\sigma = 0.005$) allows us to determine the following combinations of mixture parameters;

$$2\Theta(ClNO_3) + \Theta(PbK) = -1.791$$

$$\Psi(PbClNO_3) + \Psi(PbKCl) = 12.025$$

$$\Psi(PbKNO_3) + 2\Psi(KClNO_3) = -1.840$$

Taking $\Theta(ClNO_3) = 0.016$ and $\Psi(KClNO_3) = -0.006$ (12) we obtain $\Theta(PbK) = -1.823$ and $\Psi(PbKNO_3) = -1.828$, the combination $\Psi(PbClNO_3) + \Psi(PbKCl) = 12.025$ remaining unresolved.

With the values of the mixture parameters, the activity coefficients of $PbCl_2$ in the mixture can be reproduced with great precision (see Table 1). These parameters can also be used to calculate the activity coefficients of KNO_3 in the mixture:

$$[8]\quad \mathrm{Ln}\,\gamma_{NY} = f^{\gamma} + m_2[2B_{NY} + m_2 B'_{NY} + (4m_1 + 3m_2)\, C_{NY}] + 2m_1[B_{NX} + m_2 B'_{NX} + 2(m_1 + m_2)\, C_{NX}] + m_1[B_{MY} + m_2 B'_{MY} + 2(m_1 + m_2)\, C_{MY}] + 2m_1^2[B'_{MX} + C_{MX}] + m_1(2\Theta_{XY} + \Theta_{MN}) + m_1^2(\Psi_{MXY} + \Psi_{MNX}) + m_1 m_2(\Psi_{MNY} + 2\Psi_{NXY})$$

where B, B', and C have the same meaning as indicated before in eqs. [7].

Can. J. Chem. Downloaded from www.nrcresearchpress.com by 213.200.69.106 on 09/08/12
For personal use only.

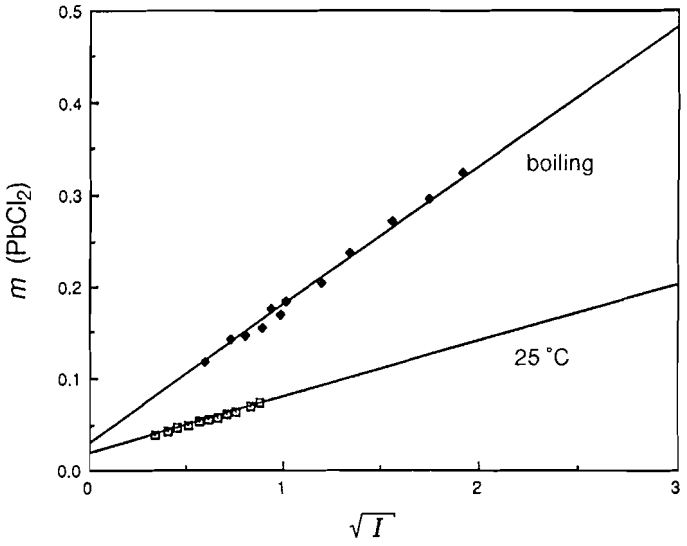

FIG. 1. Lead chloride solubility as a function of the square root of the ionic strength in $PbCl_2$–KNO_3 solutions, at 25°C and at boiling.

Activity coefficients at boiling

At boiling temperature there are no previous data for the activity coefficients of lead chloride. The approach is reduced to knowing the activity coefficient at saturation of a single lead chloride solution, and then to applying eq. [2]. We tested some extrapolation methods reported in the literature (13, 14) for salts of low solubility, but the problem is that the solubility of lead chloride is relatively high for applying these methods. Nevertheless, we observed that the plot of the lead chloride solubility ($m(PbCl_2)$) versus the square root of the ionic strength ($I^{1/2}$), for the different potassium nitrate solutions, shows a good linearity at the lower concentrations and allows us to make a less problematic extrapolation at $I = 0$. According to ref. 13 the extrapolation gives us $(K_{SP}/4)^{1/3} = (m\gamma_{\pm})_0$. This method was tested at 25°C (Fig. 1) using all the solutions of Table 1 except the two most concentrated, which start to deviate from linearity. We obtain $(\gamma_{\pm})_0 = 0.45$ for the activity coefficient at saturation of lead chloride. This activity coefficient shows an error of +0.04 with respect to that determined from emf measurements, but could be considered acceptable for the characteristics of the method.

We applied the same method to the boiling solutions, and a good linearity is also observed in Fig. 1 for the first 12 solutions of Table 2 (no consideration was taken of the small differences, less than 1°C, in the boiling temperatures of the solutions used in the fit). The extrapolation at $I = 0$ gives us the activity product constant of 8.8×10^{-5} and a value of $(\gamma_{\pm})_0 = 0.24$. Using this value and eq. [2] the values of activity coefficients reported in table 2 were obtained. Though the concentrated solutions have boiling temperatures that differ appreciably from 100°C (up to 5°C for the most concentrated), the correction due to this difference in temperature is small and lower than the experimental error. Therefore, it has been neglected.

Due to the approximate character of the method proposed before and in order to compare results, we employed another method making use of the following equation (15, 16):

$$[9] \qquad \Delta_{sol}H = \nu RT^2 \left(\frac{\delta \ln m}{\delta T}\right)_{sat} \left[1 + \left(\frac{\delta \ln \gamma}{\delta \ln m}\right)_T\right]$$

where $\Delta_{sol}H$ is the heat absorbed per mole of solute dissolved in the nearly saturated solution, or the heat evolved per mole of crystallization. From the data on solubility (16) and on activity coefficients at 25°C we calculated $(\delta \ln m/\delta T)_{sat} = 0.0184$ and $(\delta \ln \gamma/\delta \ln m)_{25°C} = -0.342$. From eq. [9], with $\nu = 3$ for lead chloride, we obtain the value of $\Delta_{sol}H = 26.85$ kJ at 25°C. With the assumption that $(\delta \ln \gamma/\delta \ln m)_T$ is practically independent of temperature (16), we can determine $\Delta_{sol}H$ at 100°C in the same way. We have calculated $(\delta \ln m/\delta T)_{sat} = 0.0112$ and then $\Delta_{sol}H = 25.6$ kJ, at 100°C. It can be assumed that $\Delta_{sol}H$ depends linearly on the temperature, $\Delta_{sol}H = K_1 + K_2T$, over a sufficiently broad temperature range (16). With the values of $\Delta_{sol}H$ at 25°C and 100°C, the resulting values of K_1 and K_2 are 31.9 kJ and -17 J K^{-1}, respectively.

To obtain the value of the activity product constant, K_{ap}, at 100°C we use the van't Hoff equation, $d \ln K/dT = \Delta H°/RT^2$, and the activity product constant at 25°C, $K_{ap} = 1.6 \times 10^{-5}$. The value of $\Delta H°$, at 25°C, obtained from literature values (17) of $\Delta_f H°$ for $Pb^{2+}(aq)$, $Cl^-(aq)$, and $PbCl_2(2)$, is 23.4 kJ mol^{-1}. This value is very different from the value of $\Delta_{sol}H$ obtained at 25°C, which is usual in electrolyte solu-

TABLE 4. Supersaturation of lead chloride, expressed as $\sigma = (\beta - 1) \times 100$, (*a*) in pure aqueous solutions, and (*b*) in 0.11 *m* potassium nitrate aqueous solutions, at 25°C

(*a*)

m	σ_m	σ_a*
0.0395	1.2	0.8
0.0400	2.4	1.6
0.0405	3.7	2.4
0.0410	5.0	3.3
0.0415	6.3	4.1
0.0420	7.6	4.9
0.0430	10.1	6.5
0.0440	12.7	8.1
0.0450	15.2	9.7

$m_{sat} = 0.03905$

(*b*)

m	σ_m	σ_a*
0.0495	1.0	0.8
0.050	2.0	1.6
0.051	4.1	3.3
0.052	6.1	4.9
0.053	8.2	6.5
0.055	12.2	9.8
0.057	16.3	13.0
0.060	22.4	17.8

$m_{sat} = 0.049$

Can. J. Chem. Downloaded from www.nrcresearchpress.com by 213.200.69.106 on 09/08/12
For personal use only.

TABLE 5. The supersaturation ratio β_m and β_a^* for different lead chloride supersaturated solutions, at boiling

$m - m_{sat}$	$\beta_m{}^a$	$\beta_a{}^{*a}$	$\beta_m{}^b$	$\beta_a{}^{*b}$	$\beta_m{}^c$	$\beta_a{}^{*c}$
0.002	1.014	1.010	1.009	1.006	1.004	1.002
0.004	1.027	1.019	1.017	1.013	1.008	1.005
0.006	1.041	1.029	1.026	1.020	1.012	1.008
0.008	1.054	1.039	1.035	1.027	1.016	1.011
0.012	1.081	1.057	1.052	1.040	1.024	1.015
0.017	1.115	1.080	1.074	1.056	1.034	1.021
0.022	1.149	1.104	1.096	1.073	1.044	1.028
0.032	1.216	1.148	1.140	1.105	1.064	1.040
0.052			1.227	1.168	1.104	1.064
0.072					1.144	1.086

[a] $m(KNO_3) = 0{,}2$, $m_{sat} = 0.148$.
[b] $m(KNO_3) = 1.0$, $m_{sat} = 0.229$.
[c] $m(KNO_3) = 5.0$, $m_{sat} = 0.500$.

tions since the heat of dilution is very large. Comparing the values of $\Delta_{sol}H$ at 25 and 100°C, it is seen that the influence of the temperature is less than that of dilution. Consequently, we take, in the van't Hoff equation, $\Delta H°$ as a constant value equal to 23.4 kJ mol^{-1}. After integration of the van't Hoff equation we obtain, at 100°C, $K_{ap} = 1.1 \times 10^{-4}$, and from it an activity coefficient $(\gamma_\pm)_0 = 0.25$, which are in accordance with the previously obtained values, taking into account the experimental and method errors.

Supersaturation

In industrial crystallization and growth of monocrystals it is important to know and control the driving force for crystallization in the system. The stoichiometric supersaturation ratio

$$[10a] \quad \beta_m = m/m_{sat}$$

or the stoichiometric relative supersaturation

$$[10b] \quad \sigma_m = \beta_m - 1$$

are usually used because they are the most simple, but they are not correct thermodynamically. According to the definition of the driving force for crystallization

$$[11] \quad \Delta\mu = \mu - \mu_{sat} = RT \ln(a/a_{sat}) = RT \ln(\beta_a)$$

where β_a is the supersaturation ratio. For electrolytes the previous expression can be transformed to

$$[12] \quad \Delta\mu = vRT \ln(m\gamma_\pm/(m\gamma_\pm)_{sat}) = vRT \ln(\beta_a{}^*)$$

where the supersaturation ratio $\beta_a{}^* = \beta_a{}^{1/\nu}$. It is simple to see that $\beta_a{}^*$ reduces to β_m when the activity coefficients are not considered or when the simplification $\gamma = \gamma_{sat}$ is assumed.

Table 4 shows the differences between the values of σ_m and $\sigma_a{}^*$ for supersaturated solutions of lead chloride at 25°C, and for supersaturated solutions of lead chloride in the presence of potassium nitrate 0.11 *m* at 25°C. The activity coefficients have been calculated with the Pitzer equations and the parameters reported in this work.

At boiling, we do not have the parameters of the Pitzer or another electrolyte equation. To calculate the activity coefficients at saturated and supersaturated solutions we used the activity coefficient dependence observed in Fig. 1 and we adjusted them to the empirical equation

$$[13] \quad 1/\gamma_\pm = 1 + 5.389\, I^{1/2} - 0.413 m_1 - 0.443 m_2 + 2.026 m_1 m_2$$

where $m_1 = m(PbCl_2)$ and $m_2 = m(KNO_3)$. Table 5 shows the dependence of β_m and $\beta_a{}^*$ versus $m - m_{sat}$ for three concentrations of KNO_3.

The activity-based supersaturation is generally lower than the concentration-based supersaturation, and this difference increases as the solution complexity increases (as is usual in many industrial processes). If we consider that nucleation and crystal growth phenomena are strongly nonlinear with supersaturation, any empirical correlation for the estimation of nucleation or crystal growth rate will work better if done as a function of the true thermodynamic supersaturation. The kinetic coefficients obtained in this way for one substance will work better in many chemical environments. A relation between concentration and activity coefficients that can be obtained from solubility measurements is needed.

Acknowledgements

This work was carried out under Project MAT88-0259 financed by the Comisión Interministerial de Ciencia y Tecnología (CICYT) (Spanish government).

1. N. Singh, J. Gottlieb, J. Conroy, R. Hopkins, and R. Mazelsky. J. Cryst. Growth **87**, 113 (1988).
2. A.V. Zamkov, I.T. Kopkov, and A.T. Amistratov. Soviet Phys. Crystallogr. (Engl. Transl.), **24**, 87 (1979).
3. S. Veintemillas, J. Torrent and R. Rodriguez. J. Cryst. Growth. **128**, 1282 (1993).
4. R. Rodriquez, S. Veintemillas, F. Rull, and K. Sangwal. Prog. Cryst. Growth Charact. **17**, 1, (1988).
5. W.R. Carmody. J. Am. Chem. Soc. **51**, 2905 (1929).
6. G. Scatchard and R.F. Tefft. J. Am. Chem. Soc. **52**, 2272 (1930).
7. K.S. Pitzer. J. Phys. Chem. **77**, 268 (1973).
8. K.S. Pitzer and G. Mayorga. J. Solution Chem. **3**, 539 (1974).
9. K.S. Pitzer. *In* Activity coefficients in electrolyte solutions. Vol. 1. *Edited by* R. Pytkowicz. CRC Press, Boca Raton, Fla. 1979. pp. 157–208.
10. A.J. Bard, R. Parsons, and J. Jordan. Standard potentials in aqueous solution. Marcel Dekker, New York. 1985.

Can. J. Chem. Downloaded from www.nrcresearchpress.com by 213.200.69.106 on 09/08/12
For personal use only.

11. R.N. Goldberg. J. Phys. Chem. Ref. Data, **8**, 1005 (1979).
12. K.S. Pitzer and J.J. Kim. J. Am. Chem. Soc. **96**, 5701 (1974).
13. S. Glasstone. Textbook of physical chemistry. Van Nostrand Company, Inc., New York. 1949.
14. R.A. Robinson and R.H. Stokes. Electrolyte solutions. Butterworths, London. 1955.
15. A.T. Williamson. Trans. Faraday Soc. **40**, 421 (1944).
16. M. Broul, J. Nyvlt, and O. Sohnel. Solubility in inorganic two-component systems. Academia, Prague. 1981.
17. R.A. Robie, B.S. Hemingway, and J.R. Fisher. Thermodynamic properties of minerals and related substances. Geological Survey Bulletin 1452. Government Printing Office, Washington, D.C. 1978.
18. K.S. Pitzer and G. Mayorga. J. Phys. Chem. **77**, 2300 (1973).

Can. J. Chem. Downloaded from www.nrcresearchpress.com by 213.200.69.106 on 09/08/12
For personal use only.

Thermodynamic behaviour of some electrolytes in ethane-1,2-diol from −10 to +80°C

FULVIO CORRADINI, LUIGI MARCHESELLI, LORENZO TASSI,[1] AND GIUSEPPE TOSI
Department of Chemistry, University of Modena, via G. Campi, 183 41100 Modena, Italy

AND

SALVATORE FANALI
Istituto di Cromatografia del Consiglio Nazionale della Ricerche, Area della Ricerca di Roma, C.P. 10, 00016 Monterotondo Scalo, Rome, Italy

Received December 22, 1992

FULVIO CORRADINI, LUIGI MARCHESELLI, LORENZO TASSI, GIUSEPPE TOSI, and SALVATORE FANALI. Can. J. Chem. **71**, 1265 (1993).

Conductivities of the electrolytes NaBr, NaPi, HPi, $NaBPh_4$, and Ph_4PBr in ethane-1,2-diol were determined in the $-10 \leq t \leq +80$°C temperature range. The experimental data were analyzed by the Fuoss–Hsia equation, which provides further informative parameters such as the dissociation constant (K) of the ion pairs formed in solution, the limiting equivalent conductivity (Λ_0), and the ion-size parameter ($\mathring{a}$). Thermodynamic behaviour of these electrolytes was derived from analysis of the K values. Single-ion conductivities were evaluated on the basis of the assumption of Ph_4PBPh_4 as reference electrolyte.

FULVIO CORRADINI, LUIGI MARCHESELLI, LORENZO TASSI, GIUSEPPE TOSI et SALVATORE FANALI. Can. J. Chem. **71**, 1265 (1993).

On a déterminé la conductivité des électrolytes NaBr, NaPi, HPi, $NaBPh_4$ et Ph_4PBr dans l'éthane-1,2-diol, à des températures allant de −10 à +80°C. On a analysé les données par l'équation de Fuoss–Hsia qui fournit d'autres paramétres plus utiles, comme la constante de dissociation (K) des paires d'ions qui se forment en solution, la conductivité équivalente limite (Λ_0) et le paramètre de la grosseur de l'ion ($\mathring{a}$). On a dérivé le comportement thermodynamique de ces électrolytes par une analyse des valeurs de K. On a évalué les conductivités des ions uniques en se basant sur l'hypothèse que le Ph_4PBPh_4 est l'électrolyte de référence.

[Traduit par la rédaction]

Introduction

Ethane-1,2-diol (ED) has attracted much attention in recent years as a nonaqueous solvent for many electrochemical investigations as well as for various practical applications (1). The great interest that this medium holds for many authors can probably be ascribed to its unusual chemical-physical properties, which make it a very singular solvent. ED is amphiprotic in nature, thoroughly miscible with a variety of other solvents (polar, such as water, and quasi-apolar, such as dioxane); because of its high density and viscosity it may be considered an excellent viscoelastic regulating medium for reaction bath and as thermoregulator fluid. Further, its high dipole moment (μ = 2.28 D) (2) and a moderately high dielectric constant (ε = 40.97 at 25°C) (3) cause it to be placed between the dissociating solvents in the general classification of Charlot and Trémillon (4).

Although a number of precise conductivity measurements of electrolytes in other solvents are reported in the literature, relatively few such studies have been made on ethane-1,2-diol. Now, following our interest in this field, an attempt has been made to investigate the nature of ion–ion and ion–solvent interactions of such electrolytes as sodium picrate (NaPi), NaBr, $NaBPh_4$, Ph_4PBr (all ionophore solutes because of their ionic structure in the crystalline state), and the ionogen picric acid (HPi) dissolved in ED, through the measurement of their conductivities at 19 temperatures ranging from −10 to +80°C.

Since few transference-number data for ED solutions of these salts are available in the literature, single-ion conductivities have been evaluated employing the two reference tetraphenyl derivative electrolytes, in an effort to provide reliable values of ionic mobilities.

Experimental section

Materials

The solvent ethane-1,2-diol (containing less than 0.10% g of water, as determined by Karl–Fischer titrations) was high purity grade reagent from Carlo Erba (Milan). It was stored over 3Å molecular sieves for many days before use and the final purity was checked by gas chromatography, confirming the absence of other significant organic components. The solvent has a density of 1.109913 g cm^{-1}, viscosity 17.14 cP, and a specific conductivity of 0.255 μS cm^{-1} at 25°C.

The NaBr was from Aldrich Chemicals, of Suprapure guaranteed quality, and was utilized without further purification after desiccation at 105°C and preservation in vacuo over P_2O_5 prior to use.

Tetraphenylphosphonium bromide (Fluka) was purified by recrystallization (×2) from a binary mixture of acetone and 2-propanol (v:v 9:1), while $NaBPh_4$ (Fluka) was recrystallized (×2) from pure acetone. Both salts were dried at 80°C and preserved in vacuo over P_2O_5 for some time before use.

Sodium picrate was prepared from picric acid and NaOH, starting from their equimolar solutions in water–ethanol (v:v 1:1) and working at high temperature. The precipitate was filtered and washed many times with the same solvent mixture and dried in vacuo over P_2O_5. The final product was checked by elemental analysis before use and the results are reported here: Anal. calcd. for $C_6H_2N_3O_7Na$: C 28.70, N 16.74, H 0.80%; found: C 28.42, N 16.81, H 0.75%.

Apparatus and procedures

Conductivity measurements were made by a Wayne Kerr 6425 Precision Component Analyzer, operating in the 2.5×10^{-9}–10 S

[1]Author to whom correspondence may be addressed.

Can. J. Chem. Downloaded from www.nrcresearchpress.com by 213.200.69.106 on 09/08/12
For personal use only.

TABLE 1. Experimental dissociation constant values (K mol^{-1} dm^{-3}) for some electrolytes in ethane-1,2-diol at different temperatures

t/°C	$NaBPh_4$ $K \times 10^2$	Ph_4PBr $K \times 10^2$	NaBr $K \times 10^2$	NaPi $K \times 10^2$	HPi $K \times 10^3$
−10	2.93 ± 0.01	2.75 ± 0.01	6.34 ± 0.01	3.51 ± 0.01	1.81 ± 0.01
−5	3.84 ± 0.01	3.24 ± 0.01	7.39 ± 0.02	4.64 ± 0.01	1.91 ± 0.01
0	4.47 ± 0.01	3.96 ± 0.01	7.99 ± 0.06	5.59 ± 0.02	2.06 ± 0.01
5	4.96 ± 0.01	4.47 ± 0.02	8.54 ± 0.04	6.33 ± 0.02	2.08 ± 0.01
10	5.61 ± 0.01	4.97 ± 0.02	9.16 ± 0.06	6.88 ± 0.04	2.18 ± 0.01
15	6.17 ± 0.01	5.26 ± 0.02	9.66 ± 0.06	7.48 ± 0.02	2.26 ± 0.01
20	6.50 ± 0.01	5.63 ± 0.01	10.5 ± 0.1	7.95 ± 0.05	2.31 ± 0.01
25	6.69 ± 0.01	5.68 ± 0.02	10.2 ± 0.1	8.09 ± 0.05	2.40 ± 0.01
30	6.74 ± 0.02	5.70 ± 0.02	9.98 ± 0.06	8.31 ± 0.07	2.43 ± 0.01
35	6.79 ± 0.01	5.71 ± 0.01	9.94 ± 0.05	8.22 ± 0.07	2.45 ± 0.01
40	6.67 ± 0.02	5.62 ± 0.01	9.66 ± 0.07	8.00 ± 0.08	2.43 ± 0.01
45	6.40 ± 0.01	5.55 ± 0.01	9.07 ± 0.07	7.95 ± 0.07	2.41 ± 0.01
50	6.18 ± 0.01	5.29 ± 0.01	8.70 ± 0.06	7.47 ± 0.07	2.36 ± 0.02
55	5.84 ± 0.01	4.94 ± 0.01	8.13 ± 0.05	6.96 ± 0.05	2.31 ± 0.01
60	5.34 ± 0.01	4.52 ± 0.01	7.59 ± 0.06	6.56 ± 0.04	2.28 ± 0.01
65	4.79 ± 0.01	3.90 ± 0.01	6.89 ± 0.06	6.32 ± 0.04	2.21 ± 0.02
70	3.99 ± 0.01	3.17 ± 0.01	6.04 ± 0.06	5.01 ± 0.03	2.13 ± 0.02
75	3.34 ± 0.01	2.52 ± 0.01	5.01 ± 0.06	3.78 ± 0.02	2.04 ± 0.02
80	2.36 ± 0.01	1.66 ± 0.01	3.80 ± 0.06	2.59 ± 0.02	1.97 ± 0.02

TABLE 2. Coefficients a_i and standard deviations σ(ln K) of eq. [2] for some electrolytes in ethane-1,2-diol

Solute	a_0	a_1	a_2	a_3	$10^2\sigma(\ln K)$
$NaBPh_4$	−1844.9	−0.68700	38575	336.57	4.7
Ph_4PBr	−3343.4	−1.1265	77838	599.43	6.0
NaBr	−1705.5	−0.61055	37539	308.79	3.7
NaPi	−2358.4	−0.84134	51784	427.03	7.5
HPi	−279.43	−0.12219	4310.9	51.839	5.4

range (end scale), with a sensitivity ±0.01 nS, and employing platinized platinum electrodes (cell constant k = 10.538 cm) with a field frequency of 1 kHz. The measuring cell was embedded in a polyurethane protective jacket, and the temperature control was provided by a Lauda K2R thermostatic bath maintained to within ±0.02°C over the investigated temperature range.

The constancy of temperature was checked by a thermoresistance Pt 100 (Tersid, Milan) immersed in the sample in the measurement cell, and by recording the resistance values by the same WK 6425 PCA bridge cited above.

Densities and viscosities were measured as previously reported (5).

Karl–Fischer titrations were performed with an automatic titration system (Crison model KF 431) equipped with a digital buret (Crison model 738).

Solutions of electrolytes at different concentrations were obtained by successive dilution of stock solutions, freshly prepared by weight; concentrations in volume were then calculated from weight concentrations and densities.

Conductivity readouts were recorded when they become invariant with time; this took about 30 min for each measurement.

Several independent solutions were prepared and as many runs as necessary were performed to ensure the reproducibility of the results. Solvent conductivity corrections were applied to all the data at the different temperatures.

Results and discussion

The measured equivalent conductivities and the corresponding molarities of solutions for the chosen salts in ED are given in Tables 1–5 of the Supplementary Material[2] available for $NaBPh_4$, Ph_4PBr, NaBr, NaPi, and HPi, respectively. The data were analyzed by means of the more general Fuoss–Hsia equation (6, 7):

$$[1] \quad \Lambda = \Lambda_0 - S(c\gamma)^{1/2} + Ec\gamma \lg c\gamma + J_1 c\gamma - J_2(c\gamma)^{3/2} - K_A c\gamma f_{\pm}^2 \Lambda$$

where the symbols have their usual meaning (8).

The above equation provides the limiting equivalent conductivity Λ_0, the ionic association constant K_A (dissociation constant $K = K_A^{-1}$), and the interionic distance parameter $\mathring{a}$. The calculations were performed on a computing program by means of an iterative procedure. The initial Λ_0 values were obtained from an Onsager plot at each selected temperature, and the first $\mathring{a}$ value was fixed at 5 Å. Generally, only a few iterations were necessary to obtain the final results.

The dissociation constant

The K values provided by the Fuoss–Hsia theory are summarized in Table 1 for all the chosen electrolytes and for any selected temperature in the range from −10 to +80°C.

[2]Supplementary Material available: Tables 1–7 (7 pages) of experimental conductivity measurements and thermodynamic data may be purchased from: The Depository of Unpublished Data, Document Delivery, CISTI, National Research Council Canada, Ottawa, Canada K1A 0S2.

Can. J. Chem. Downloaded from www.nrcresearchpress.com by 213.200.69.106 on 09/08/12
For personal use only.

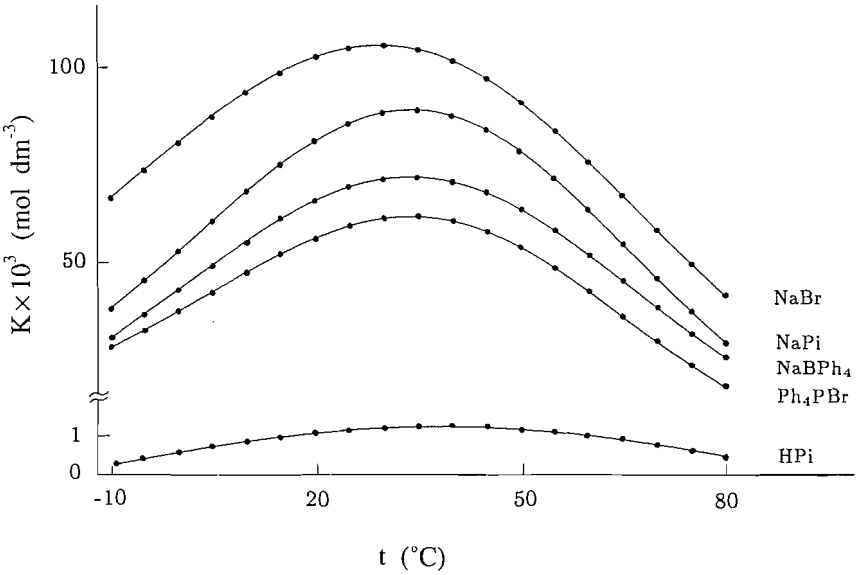

FIG. 1. Experimental dissociation constant (K mol^{-1} dm^{-3}) of some electrolytes in ethane-1,2-diol at different temperatures.

TABLE 3. K_{max} and corresponding values of t_{max} for the dissociation of some electrolytes in ethane-1,2-diol

Solute	Equation [2]		Harned's theory	
	K_{max}	t_{max}	K_{max}	t_{max}
$NaBPh_4$	7.04×10^{-2}	33.9	3.09×10^{-2}	34.3
Ph_4PBr	6.08×10^{-2}	34.0	2.77×10^{-2}	33.5
NaBr	1.03×10^{-1}	29.4	5.39×10^{-2}	33.0
NaPi	8.68×10^{-2}	34.1	3.81×10^{-2}	34.1
HPi	2.49×10^{-3}	34.4	2.47×10^{-3}	38.4

Each set of dissociation constant values for each solute was fitted by means of the integrated van't Hoff equation

$$[2] \qquad \ln K = a_0 + a_1 T + a_2/T + a_3 \ln T$$

which represents the most reliable data-fit model for analyses of this type. In fact eq. [2], whose a_i coefficients for each electrolyte in this solvent are reported in Table 2, reproduces the experimental values of Table 1 with a good approximation, as one can deduce from the standard deviation values $\sigma(\ln K)$ summarized in the last column.

Figure 1 reproduces the trend of experimental K values and the best-fitting curves expressed by eq. [2]. A brief examination of this figure provides some particularly interesting suggestions that may be pointed out as follows.

1. The dissociation of picric acid and of ion pairs of the other electrolytes shows a generally convex trend of the K vs. T curves and, as a consequence, all the curves are characterized by a relative maximum in the temperature range investigated.

2. The two precursor reference electrolytes, $NaBPh_4$ and Ph_4PBr, show slightly different dissociation constant values over all the studied temperature range, with a moderately high value for the sodium salt. Probably, the large delocalization of the electrical charge on the "bolaform" tetraphenyl ions reduces the degree of interaction with other charged species, releasing in this way the counterion in solution and

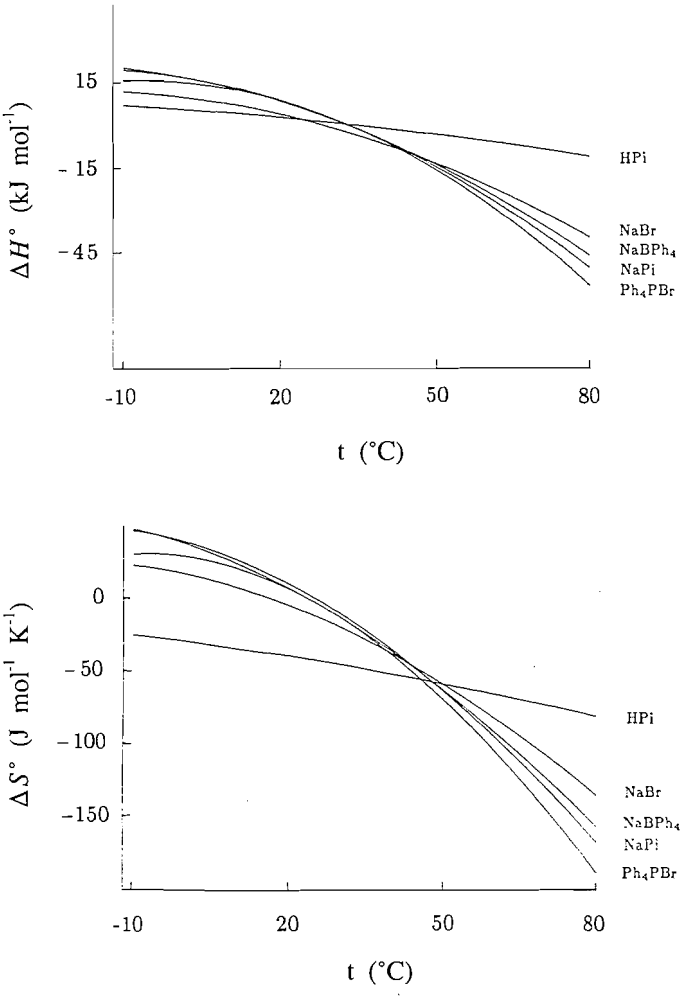

FIG. 2. Dependence on the temperature of ΔH^0 (kJ mol^{-1}) (top) and ΔS^0 (J mol^{-1} K^{-1}) (bottom) for the dissociation of some electrolytes in ethane-1,2-diol.

Can. J. Chem. Downloaded from www.nrcresearchpress.com by 213.200.69.106 on 09/08/12
For personal use only.

TABLE 4. Limiting equivalent conductivities (Λ_0/cm^2 S mol^{-1}) for some electrolytes in ethane-1,2-diol at different temperatures

t/°C	$NaBPh_4$	Ph_4PBr	NaBr	NaPi	HPi
−10	0.81 ± 0.01	1.42 ± 0.01	1.48 ± 0.01	0.97 ± 0.01	7.1 ± 0.1
−5	1.02 ± 0.01	1.62 ± 0.01	2.25 ± 0.01	1.21 ± 0.01	8.1 ± 0.1
0	1.37 ± 0.01	1.96 ± 0.01	2.85 ± 0.01	1.57 ± 0.01	9.0 ± 0.1
5	1.82 ± 0.01	2.58 ± 0.01	3.47 ± 0.01	1.98 ± 0.01	11.0 ± 0.1
10	2.36 ± 0.01	3.29 ± 0.01	3.79 ± 0.01	2.50 ± 0.01	13.0 ± 0.2
15	3.01 ± 0.01	4.11 ± 0.01	5.41 ± 0.01	3.14 ± 0.01	15.6 ± 0.2
20	3.80 ± 0.01	5.10 ± 0.01	6.94 ± 0.01	4.06 ± 0.01	18.3 ± 0.2
25	4.68 ± 0.01	6.35 ± 0.01	8.72 ± 0.01	5.14 ± 0.01	21.2 ± 0.2
30	5.67 ± 0.01	7.63 ± 0.01	10.57 ± 0.01	6.25 ± 0.01	24.8 ± 0.3
35	6.79 ± 0.01	9.00 ± 0.01	12.49 ± 0.01	7.47 ± 0.01	28.5 ± 0.3
40	8.07 ± 0.01	10.65 ± 0.01	14.62 ± 0.01	8.85 ± 0.01	32.6 ± 0.4
45	9.51 ± 0.01	12.40 ± 0.01	16.91 ± 0.01	10.31 ± 0.01	37.0 ± 0.4
50	11.04 ± 0.01	14.24 ± 0.01	19.32 ± 0.02	12.00 ± 0.01	41.6 ± 0.5
55	12.91 ± 0.01	16.64 ± 0.01	22.47 ± 0.02	13.98 ± 0.01	46.5 ± 0.5
60	14.82 ± 0.01	18.87 ± 0.01	25.47 ± 0.03	15.97 ± 0.01	51.6 ± 0.6
65	16.86 ± 0.01	21.23 ± 0.01	28.52 ± 0.05	18.06 ± 0.01	56.7 ± 0.6
70	19.15 ± 0.01	24.03 ± 0.01	32.05 ± 0.10	20.54 ± 0.01	62.0 ± 0.7
75	21.78 ± 0.01	27.26 ± 0.01	36.30 ± 0.18	23.48 ± 0.01	67.9 ± 0.9
80	24.55 ± 0.01	31.24 ± 0.01	41.14 ± 0.26	27.02 ± 0.01	74.5 ± 0.9

TABLE 5. Coefficients b_i and standard deviations $\sigma(\Lambda_0)$ of eq. [5] for some electrolytes in ethane-1,2-diol

Solute	b_0	b_1	$b_2 \times 10^3$	$b_3 \times 10^5$	$10^5\sigma(\Lambda_0)$
$NaBPh_4$	−121.25	1.65	−7.47	1.12	0.44
Ph_4PBr	−155.19	2.08	−9.27	1.38	1.9
NaBr	−32.91	0.960	−6.14	1.14	3.1
NaPi	−184.29	2.33	−9.88	1.41	1.8
HPi	833.86	−7.56	2.11	−1.64	1.9

freeing it from the electrical attractions responsible to a large extent for ion-pair formation.

3. The higher K values are observed for NaBr and NaPi, showing these electrolytes to have similar behaviour in ED solutions. A probable explanation for this experimental evidence could be the relative strength of the solvation bonds towards the different ions. In fact, the sodium ion appears strongly solvated in these solutions and, as a consequence, the solvation shell could mask the central ion towards the counterions. Similar considerations may apply for the salifiable anions, Br^- and Pi^- respectively, taking into account that on progressively increasing the ionic dimensions may observe a progressive decrease in the relative strength of the solvation network; this should lead to a parallel decrease in the dissociation constant values of the electrolyte considered.

Table 3 reports a comparison of the K_{max} and the corresponding t_{max} values for these electrolytes. These values have been obtained by fitting eq. [2] and applying Harned's theory (9), but poor agreement is observed in this case for the weak electrolyte HPi.

Starting from eq. [2], the thermodynamic data for the apparent dissociation reaction of picric acid (10) and the true dissociation of other electrolytes in ED solutions were evaluated by applying the standard equations in the form:

$$[3] \quad \Delta H^0 = R(a_1T^2 - a_2 + a_3T)$$

$$[4] \quad \Delta S^0 = R[a_0 + 2a_1T + a_3(1 + \ln T)]$$

where the a_i terms are the coefficients of Table 2. The results are summarized in Tables 6 and 7 of the Supplementary Material[2] and in graphic form in Fig. 2.

As can be noted, many uncertainties affect ΔG^0, ΔH^0, and ΔS^0 values, owing to the experimental errors in K evaluation and partly associated with the interpolating function $K = K(T)$, i.e., the van't Hoff equation [2].

In spite of these difficulties, the thermodynamic data could be a powerful tool in accounting for the solute-solvent interactions. As appears from Fig. 2, enthalpic and entropic variations seem to be comparable in magnitude on the whole for all the salts, excluding HPi, which is a medium-weak electrolyte in ED solution. However, the common trend of Fig. 2 is represented by a negative temperature coefficient $d\Delta Y/dT$, where $Y = H^0$ and S^0 respectively.

We next attempt to obtain some useful structural information by considering the entropy changes in detail. One may assume that at the highest temperatures an ordered structure exists in the neighbourhood of the charged solute species, in the form of ion pairs or free ions. This, however, is in apparent contrast to the thermokinetic steady state that is reached at each selected temperature.

A reliable explanation probably lies in the decreasing value of the dielectric constant of the solvent as the temperature increases (3), reducing in this way the electrostriction effects between moving species. Furthermore, the dramatic decrease in the viscosity with rising temperature (11) should provide a considerable decrease of the mechanical friction and viscokinetic delay for all constituent species of the system, i.e., ion pairs, free ions, and molecules. This situation should facilitate the arrangement and the correct orientation, induced by the strong and thermally unaffected electrical fields of the charged species, of the solvent molecules forming the solvation shell.

It should be noted that ED probably solvates anions by a more effective hydrogen bonding network, and cations through dipole and induced-dipole interactions. Thus, at the highest temperatures, its solvation power seems to increase with the size and polarizability of the ions in the series

Can. J. Chem. Downloaded from www.nrcresearchpress.com by 213.200.69.106 on 09/08/12
For personal use only.

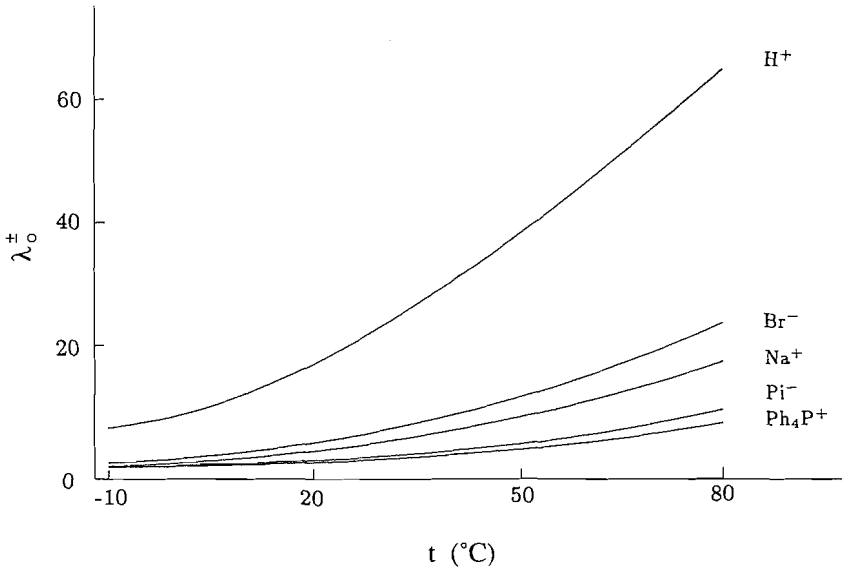

FIG. 3. Limiting ionic conductivities ($\lambda_0^{\pm}$/cm^2 S mol^{-1}) of some species in ethane-1,2-diol at different temperatures.

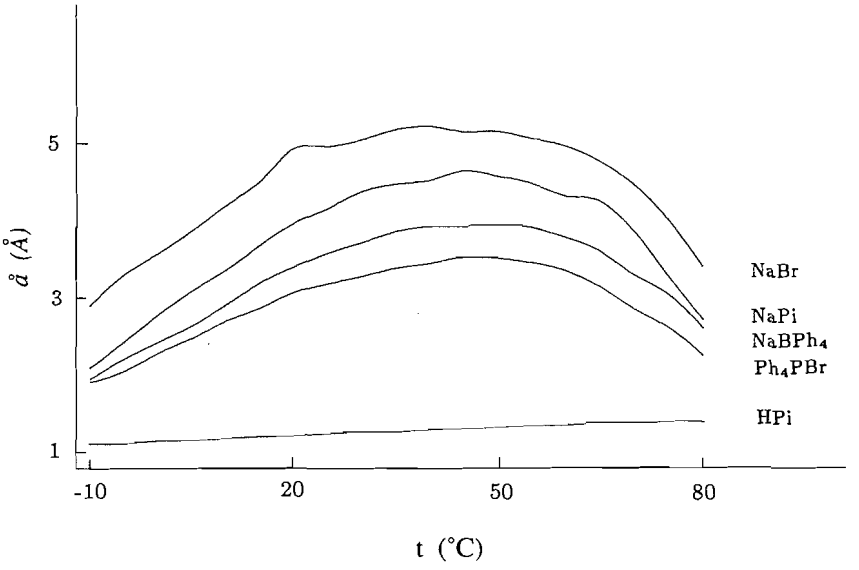

FIG. 4. Interionic distance parameter ($\mathring{a}$/Å) versus temperature for some electrolytes in ethane-1,2-diol at different temperatures.

$Br^- < BPh_4^- < Pi^-$ and $H^+ < Na^+ < Ph_4P^+$. The negative charge on the Pi^- anion is widely spread over all three nitro groups and hence is more delocalized than is the case for other isocharged species. It is to be expected, therefore, that the first anion should be solvated by ED molecules more strongly than the others.

From these arguments and from the evidence obtained about the chosen electrolytes, it may be concluded that the dissociation of salts in ED solutions is a process controlled by enthalpic rather than entropic factors.

The limiting equivalent conductivity

Table 4 shows the limiting equivalent conductivities (Λ_0) obtained by the Fuoss–Hsia equation applied to these solute–solvent systems. These values, too, being strictly related to the solute dissociation constant, are strongly dependent on temperature variation and on thermomechanical properties of the solvent.

The Λ_0 values vs. temperature were fitted by a polynomial equation of the type (12)

$$[5] \qquad \Lambda_0 = \sum_{i=0}^{3} b_i T^i \qquad T/\mathrm{K}$$

which reproduces the experimental data within an average uncertainty $\overline{\Delta\Lambda_0}$, evaluated as follows:

$$[6] \qquad \overline{\Delta\Lambda_0} = \frac{1}{N}\sum_{N} |\Lambda_0^{\mathrm{calcd}} - \Lambda_0^{\mathrm{exptl}}|$$

where N is the number of experimental points, equal to $\pm$ 0.13 cm^2 S mol^{-1}.

Table 5 summarizes the b_i (i = 0, 1, 2, 3) coefficients of eq. [5] along with the standard deviations $\sigma(\Lambda_0)$ for each electrolyte. The trend Λ_0 vs. t/°C for these species is char-

Can. J. Chem. Downloaded from www.nrcresearchpress.com by 213.200.69.106 on 09/08/12
For personal use only.

TABLE 6. Ionic mobilities ($\lambda_0^{\pm}$/cm^2 S mol^{-1}) of some species in ethane-1,2-diol at different temperatures

t/°C	Ph_4P^+	Na^+	H^+	Br^-	Pi^-
−10	0.25	0.51	6.70	0.98	0.34
−5	0.33	0.72	7.50	1.30	0.47
0	0.41	0.99	8.68	1.69	0.60
5	0.52	1.33	10.24	2.17	0.74
10	0.64	1.75	12.15	2.74	0.90
15	0.79	2.24	14.39	3.42	1.09
20	0.97	2.81	16.93	4.19	1.32
25	1.18	3.47	19.77	5.08	1.59
30	1.44	4.21	22.89	6.08	1.91
35	1.74	5.05	26.25	7.19	2.29
40	2.09	5.98	29.85	8.44	2.73
45	2.49	7.00	33.66	9.81	3.24
50	2.96	8.13	37.66	11.32	3.84
55	3.49	9.36	41.84	12.97	4.52
60	4.10	10.69	46.17	14.76	5.29
65	4.78	12.14	50.64	16.70	6.17
70	5.54	13.70	55.22	18.80	7.15
75	6.39	15.37	59.90	21.07	8.26
80	7.33	17.17	64.65	23.49	9.48

acterized by a continuous and regular increase with temperature for all the selected electrolytes.

The single-ion conductivities were evaluated by splitting the limiting equivalent conductivities (Λ_0) into ionic contributions on the basis of the fundamental assumption of a reference electrolyte (Ph_4PBPh_4 in this case), using the following relationships (13):

$$[7] \quad \lambda_0^+(Ph_4P^+) \equiv \lambda_0^-(BPh_4^-) \equiv \frac{1}{2}\Lambda_0(Ph_4PBPh_4)$$

In practice, one assumes that the two voluminous tetraphenyl derivative ions (opposite charge but similar structure) can be characterized by the same thermodynamic behaviour, and therefore by the same ionic activity coefficients and the same ionic mobility when dissolved in any solvent and at any temperature.

The limiting ionic conductivities ($\lambda_0^{\pm}$) for all the species investigated in this work were obtained by applying the relations:

$$[8] \quad \Lambda_0(Ph_4PBPh_4) = \Lambda_0(Ph_4PBr) + \Lambda_0(NaBPh_4) - \Lambda_0(NaBr)$$

$$[9] \quad \lambda_0^+(Na^+) = \Lambda_0(NaBPh_4) - \lambda_0^-(BPh_4^-)$$

$$[10] \quad \lambda_0^-(Br^-) = \Lambda_0(Ph_4PBr) - \lambda_0^+(Ph_4P^+)$$

$$[11] \quad \lambda_0^-(Pi^-) = \Lambda_0(NaPi) - \lambda_0^+(Na^+)$$

$$[12] \quad \lambda_0^+(H^+) = \Lambda_0(HPi) - \lambda_0^-(Pi^-)$$

starting from the smoothed Λ_0 values fitted by eq. [5]. The results of this analysis are reported in Table 6 and displayed, in a graphic form, in Fig. 3.

For comparison purposes, Table 7 shows the limiting ionic conductivities in some different solvents. As is particularly evident, the hydrogen ion appears to be the species with the highest mobility in all the cases collected in Table 7. For the Na^+ ion, for example, the limiting conductivity values seem to be comparable with those obtained in HMPT solutions, even if generally lower than the values obser solvents characterized by solvent properties suc ascribable to ED, but where the thermokinetic r effects are not equal to those provided in this solv one may observe that the mobility values of tetraphe picrate ions in ED are the lowest of those ions lis Table 7.

The Walden products, $\lambda_0^{\pm}\eta_0$, of the selected ions ar ported in Table 8. As one can see, the rule appears to substantially obeyed over this wide temperature range fro the large tetraphenyl derivatives to the picrate anion, in cluding the relatively small Na^+ ion, which is probably strongly solvated. The greatest exception to this rule, limited because its empirical nature is nowadays largely utilized to assess the values of ionic mobilities under different experimental conditions, is represented by the hydrogen ion.

The imperfectly defined chemical nature of this species in nonaqueous solvents, in conjunction with the observed high values of ionic mobility in almost all the alcoholic solvents, suggests a hypothetical mechanism for electrical conductivity in these media similar to the well-known mechanism proposed for water solutions. In this mechanism the hydrogen ion could act alternatively as structure maker and structure breaker in the network bonding between neighbouring solvent molecules, in order to explain the transport phenomenon described above.

The interionic distance parameter

Table 9 summarizes the ion-size fitting parameter $\mathring{a}$ provided by the Fuoss–Hsia equation for analysis of the experimental conductivity data for the selected electrolytes in this nonaqueous solvent (ED). As one can see from Fig. 4, the trend of $\mathring{a}$ vs. t/°C seems perfectly delineated with respect to the temperature variable, and it follows those trends described above for $K = K(T)$.

However, a careful examination of the ion-size fitting parameter $\mathring{a}$ and the K values of Table 1 suggests a prudent evaluation of the former quantity. In fact, Skinner and Fuoss (14) studied the conductometric behaviour of $NaBPh_4$ in water, and these authors found $\mathring{a} = 6.64 \pm 0.06$ Å for $K_A = 0$. Later, Covington and Tait (15) reexamined the same problem, and provided the value $\mathring{a} = 9.9 \pm 0.9$ Å for $K_A = 0$. These authors also showed that the calculated ion size $\mathring{a} = 6.64$ Å as determined by Skinner and Fuoss for $K_A = 0$ can be increased to $\mathring{a} = 10$ Å, using the experimental data of Skinner and Fuoss if a small association constant is imposed. From these considerations, it is clear that the ion-size parameter $\mathring{a}$ is not completely independent of the association constant in solution, because an identical set of conductivity data can be fitted with a smaller $\mathring{a}$ if it is assumed that any association phenomenon takes place in solution, and vice versa.

Moreover, for those electrolytic solutions with a consistent association investigated here, determination of the $\mathring{a}$ parameter and K values should be less ambiguous. For the $NaBPh_4$ electrolyte in ED solutions, our $\mathring{a}$ values seem to agree with those reported by other authors working in DMSO (16), which is an aprotic but almost isodielectric solvent if compared with ED.

Conclusions

Some closing notes can now be written about our electroanalytical studies in ethane-1,2-diol.

Can. J. Chem. Downloaded from www.nrcresearchpress.com by 213.200.69.106 on 09/08/12
For personal use only.

TABLE 7. Limiting equivalent conductivities ($\lambda_0^{\pm}$/cm^2 S mol^{-1}) of some ions in different solvents

	CH_3OH	DMAC	DMF	DMSO	HMPT	TMU	PC	ED	H_2O
H^+	142.2	—	—	—	—	—	12.9	19.77	349.8
Na^+	42.5	25.8	29.9	14.2	5.7	15.1	9.46	3.47	50.1
Br^-	—	43.2	53.6	23.4	18.2	30.1	18.90	5.08	78.1
Pi^-	49.2	31.5	—	16.7	—	—	12.50	1.59	30.4
BPh_4^-	—	—	—	—	6.7	—	8.10	16.02	1.18
Ref.	18	19	20	21	22	23	24	This work	25

TABLE 8. Walden products of some ionic species in ethane-1,2-diol at different temperatures

t/°C	Ph_4P^+	Na^+	H^+	Br^-	Pi^-
−10	0.28	0.57	7.52	1.10	0.39
−5	0.26	0.57	6.03	1.04	0.37
0	0.25	0.58	5.13	1.00	0.35
5	0.23	0.59	4.55	0.96	0.33
10	0.22	0.60	4.14	0.94	0.31
15	0.21	0.60	3.84	0.91	0.29
20	0.21	0.60	3.59	0.89	0.28
25	0.20	0.59	3.39	0.87	0.27
30	0.20	0.59	3.21	0.85	0.27
35	0.20	0.59	3.04	0.83	0.27
40	0.20	0.58	2.90	0.82	0.27
45	0.20	0.57	2.76	0.81	0.27
50	0.21	0.57	2.63	0.79	0.27
55	0.21	0.56	2.52	0.78	0.27
60	0.21	0.56	2.41	0.77	0.28
65	0.22	0.55	2.30	0.76	0.28
70	0.22	0.55	2.20	0.75	0.29
75	0.23	0.54	2.11	0.74	0.29
80	0.23	0.54	2.02	0.73	0.30

TABLE 9. Interionic distance centre-to-centre parameters ($\mathring{a}$/Å) of some electrolytes in ethane-1,2-diol at different temperatures

t/°C	$NaBPh_4$	Ph_4PBr	NaBr	NaPi	HPi
−10	1.96	1.92	2.91	2.11	1.12
−5	2.23	2.07	3.32	2.45	1.13
0	2.45	2.31	3.60	2.80	1.16
5	2.66	2.50	3.89	3.11	1.17
10	2.93	2.72	4.22	3.38	1.19
15	3.21	2.88	4.52	3.70	1.21
20	3.42	3.09	4.95	3.99	1.23
25	3.60	3.20	4.97	4.17	1.25
30	3.73	3.29	5.05	4.39	1.27
35	3.87	3.40	5.18	4.49	1.28
40	3.94	3.46	5.23	4.53	1.30
45	3.94	3.54	5.15	4.66	1.32
50	3.96	3.53	5.16	4.59	1.33
55	3.93	3.47	5.07	4.50	1.35
60	3.80	3.37	4.98	4.34	1.36
65	3.63	3.16	4.79	4.48	1.38
70	3.31	2.87	4.49	3.89	1.39
75	3.06	2.63	4.03	3.30	1.41
80	2.62	2.27	3.42	2.73	1.40

At first, we found that all the salts studied are moderately dissociated in this solvent medium, this fact being expected because of the medium dielectric constant of the solvent at all the temperatures investigated. The most outstanding feature of the dissociation constants reported in this work is that the salts containing larger ions show a progressive amount of association. However, excluding the ionogen solute HPi, the dissociation constant seems to decrease with increasing size of the anion, and the decrease is also observed in the case of the largest cation if compared to that of the smaller cation. These observations can be accounted for by assuming that the stabilization of the anions in ED solution increases in the order $BPh_4^- < Pi^- < Br^-$, and the stabilization of the cations is in the order $Ph_4P^+ < Na^+$. Thus, the behaviour in ED of the selected sodium salts appears perfectly consistent with measurements in other simple alcohols (17) where K decreases with the increasing anion size.

Concerning the single-ion conductivity, it should be noted that the mobility of the small Na^+ cation is less than that of the Br^- anion. This fact suggests that the Na^+ ion could be more strongly solvated by ED molecules than the Br^- species. Furthermore, the transport behaviour of Pi^- and $PH_4P^+ \equiv BPh_4^-$ ions appears small and slightly different in this solvent. A reliable explanation for this can probably be found in the low-density surface charge, masked by an extensive delocalization, and from the high viscosity of the medium, which makes difficult any ionic migration in solution.

Acknowledgments

It is a pleasure to thank Prof. C. Preti for his continuous encouragement to carry out this work and for constructive suggestions concerning this paper. L.M. wishes to thank the Hospal-Dasco s.p.a. (Modena, Italy) for the award of a research fellowship. We also gratefully acknowledge the financial support of The Consiglio Nazionale della Ricerche (C.N.R.) of Italy.

1. F. Franks and D.J.G. Ives. Q. Rev. Chem. Soc. **20**, 1 (1966).
2. W. Caminati and G. Corbelli. J. Mol. Spectrosc. **90**, 572 (1981).
3. G.C. Franchini, A. Marchetti, M. Tagliazucchi, L. Tassi, and G. Tosi. J. Chem. Soc. Faraday Trans. **87**, 2583 (1991).
4. G. Charlot and B. Trémillon. *In* Les reactions chimique dans les solvants et les sels fondus. Gautiers-Villars, Paris. 1963.
5. A. Marchetti, C. Preti, M. Tagliazucchi, L. Tassi, and G. Tosi. J. Chem. Eng. Data, **36**, 360 (1991).
6. R.M. Fuoss and K.L. Hsia. Proc. Natl. Acad. Sci. U.S.A. **58**, 1818 (1967).

Can. J. Chem. Downloaded from www.nrcresearchpress.com by 213.200.69.106 on 09/08/12
For personal use only.

7. R.M. Fuoss and K.L. Hsia. J. Am. Chem. Soc. **90**, 3055 (1968).
8. J.H. Roberts. *In* The chemistry of nonaqueous solvents. *Edited by* J.J. Lagowski. Academic Press, New York. 1978.
9. H.S. Harned and I. Kazanijian. J. Am. Chem. Soc. **58**, 1912 (1936).
10. G.C. Franchini, A. Marchetti, L. Tassi, and G. Tosi. Anal. Chem. **62**, 1004 (1990).
11. F. Corradini, L. Marcheselli, A. Marchetti, M. Tagliazucchi, L. Tassi, and G. Tosi. Bull. Chem. Soc. Jpn. **65**, 503 (1992).
12. M. Nakahara. J. Phys. Chem. **88**, 2138 (1984).
13. O. Popovych. Crit. Rev. Anal. Chem. **7**, 73 (1970).
14. J.F. Skinner and R. M. Fuoss. J. Phys. Chem. **68**, 1882 (1964).
15. A.K. Covington and M.J. Tait. Electrochim. Acta, **12**, 113 (1967).
16. N.P. Yao and D.N. Bennion. J. Electrochem. Soc. **118**, 1097 (1971).
17. R.L. Kay and D.F. Evans. J. Phys. Chem. **70**, 2325 (1966).
18. E.C. Evers and A.G. Knox. J. Am. Chem. Soc. **73**, 1739 (1951).
19. G.R. Lester, T.A. Gover, and P.G. Sears. J. Phys. Chem. **60**, 1076 (1956).
20. J.E. Prue and P.J. Sherrington. Trans. Faraday Soc. **57**, 1795 (1961).
21. M. Della Monica, D. Masciopinto, and G. Tessari. Trans. Faraday Soc. **66**, 2872 (1970).
22. J.C. Bollinger, T. Yvernault, J.Y. Gal, and F. Persin. Can. J. Chem. **54**, 3060 (1976).
23. E.M. Hanna and A.A. Tossonian. Can. J. Chem. **66**, 1605 (1988).
24. J.F. Reardon. Electrochim. Acta, **32**, 1595 (1987).
25. R.A. Robinson and R.H. Stokes. *In* Electrolyte solutions. 2nd ed. Butterworths, London. 1959.

Can. J. Chem. Downloaded from www.nrcresearchpress.com by 213.200.69.106 on 09/08/12
For personal use only.

3202

1992 Alfred Bader Award Lecture
Probing the specificity of synthetically useful enzymes[1]

J. BRYAN JONES
Department of Chemistry, University of Toronto, Toronto, ON M5S 1A1, Canada

Received April 13, 1993

J. BRYAN JONES. Can. J. Chem. **71**, 1273 (1993).

Factors involved in controlling and predicting the structural specificity and stereospecificity of synthetically useful enzymes, including pig liver esterase, subtilisin BPN' and Carlsberg, α-chymotrypsin, and an L-lactate dehydrogenase, are discussed.

J. BRYAN JONES. Can. J. Chem. **71**, 1273 (1993).

On discute des divers facteurs impliqués dans le contrôle et dans la prédiction de la spécificité structurale et de la stéréospécificité d'enzymes synthétiques utiles, y compris l'estérase du foie de cochon, la subtilisine BPN' et Carlsberg, l'α-chymotrypsine et une déshydrogénase de la L-lactate.

[Traduit par la rédaction]

Can. J. Chem. Downloaded from www.nrcresearchpress.com by 213.200.69.106 on 09/08/12
For personal use only.

Enzymes are now broadly accepted as useful catalysts for a broad range of organic synthesis, with their capacities for inducing asymmetric transformations being the most exploited (1). However, despite the widespread uses of both enzymes and microorganisms in asymmetric synthesis, relatively little is known of the factors that determine the structural specificity and stereospecificity of enzymes. In view of the increasingly broad spectrum of new and unnatural substrate structures that synthetically useful enzymes are being called on to accommodate, it is becoming more and more essential to delineate the enzyme–substrate interactions that regulate and control enzyme specificity. This will then permit the selection of the enzymes that are best suited for any given chiral synthon preparation, and will facilitate the development of active-site models capable of accurately forecasting whether an enzyme will accept a new structure as a substrate, and of reliably predicting what the stereochemical outcome of the reaction will be. Knowledge of the factors determining specificity will also facilitate the rational tailoring of enzyme specificity by the site-directed mutagenesis techniques of protein engineering.

The classes of enzymes most widely applied are the hydrolases and the oxidoreductases and this lecture will focus on probing the specificity of representative, synthetically useful, members of both of these groups.

Hydrolases

An active site model for pig liver esterase

Hydrolases are currently the enzyme group receiving the most attention. Within this group, the esterase that has seen the most extensive utilization is pig liver esterase (PLE, EC 3.1.1.1)) (2). PLE is a serine protease that catalyzes the hydrolysis of a broad range of carboxylic acid esters. It is capable of enantiomeric and enantiotopic group specificity and has been widely employed for resolving racemic esters and for producing chiral acid-ester synthons from prochiral diester substrates. Despite its proven value in asymmetric synthesis, organic chemists became somewhat uneasy in their continued use of PLE because of some uncertainty about the fidelity of its stereospecificity.

For an enzyme to receive universal approval as a routine catalyst for synthetic applications, it is important that its stereospecificity be seen to be unwavering in its absolute configuration preferences from one substrate to another. In this regard, PLE posed a dilemma in that its stereochemistry appeared to be somewhat fickle towards certain substrate groups. For example, within the homologous series of monocyclic meso diesters **1**–**3**, the stereoselectivity of PLE hydrolysis reverses itself. For the cyclobutane diester **1**, the *S*-ester is hydrolyzed to give **4**, while for the cyclohexane substrate **3**, the acid-ester **5** from *R*-ester cleavage is formed. Both **4** and **5** are enantiomerically pure. The cyclopentane substrate **2** represents the changeover point, with the acid-ester **5** being virtually racemic (3*a*). This behaviour turned out to be general, with similar stereospecificity reversals being observed in other substrate series also (3*b*).

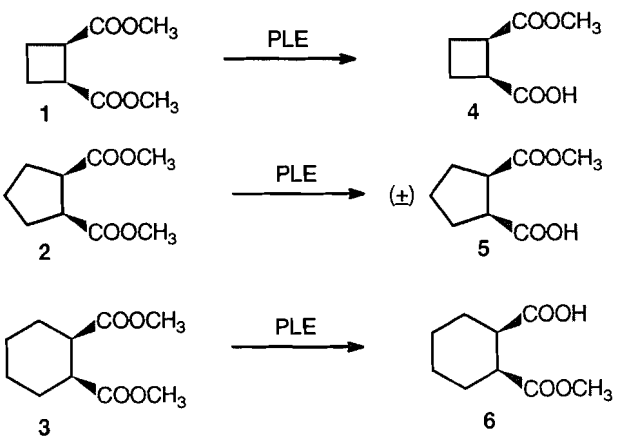

Initially we felt that the apparent variability of PLE's stereospecificity was due to the fact that the commercially available material was a melange of similar proteins, with some having *R*, and others *S*, stereospecificity preferences and that separating the mixture into its components would provide us with enzymes of both *R* and *S* types. Separation of PLE into its components by isoelectric focussing gave six distinct fractions of different isoelectric points. However, when each of these fractions was employed to hydrolyze diesters such as **1**–**3**, the stereospecificity results were un-

[1]This is an invited personal review article based on the Alfred Bader Award Lecture presented by Professor Jones at the Annual Conference of the Canadian Society for Chemistry, Edmonton, Alberta, 3 June 1992.

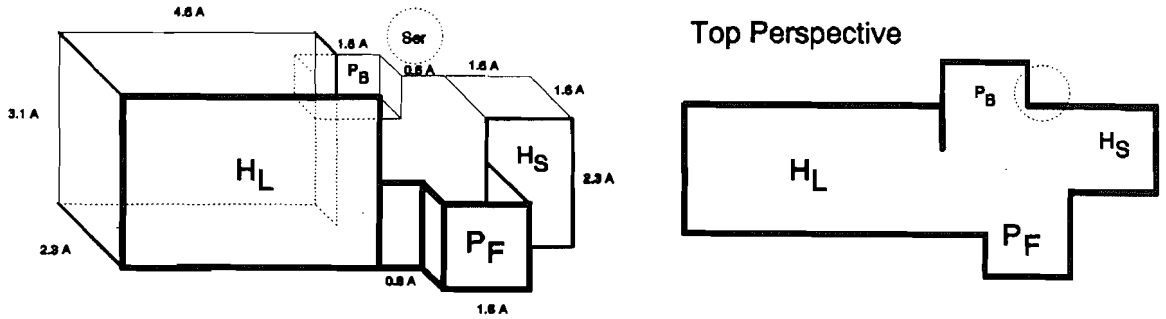

FIG. 1. Active-site model for PLE.

changed (4), thereby demonstrating that, although commercial PLE is a mixture, it behaves as if it is a single species. Thus the stereospecificity reversal patterns observed are a fundamental attribute of PLE's active site. This stimulated us to create an active-site model that would permit all PLE's specificity characteristics to be interpreted.

As with other active-site model proposals (5), the lack of an X-ray structure dictated an empirical approach. We surveyed all the known literature substrates and, using computer graphics, overlaid them to determine the active site volumes and orientations that permitted each substrate to be accommodated satisfactorily in steric terms, and in accord with the experimentally observed stereospecificities. The picture that emerged was surprisingly simple (6), and is depicted in Fig. 1.

The model comprises five binding loci. The boundaries of the binding pockets represent the physical restrictions that amino acids of the enzyme place on substrates binding in the active site and, with the exceptions noted below, substrates may not penetrate them. The catalytically essential region is that of the serine residue that initiates hydrolysis by its attack of the carbonyl group of the susceptible ester function. The binding regions controlling specificity are composed of four pockets, of which two are hydrophobic. Two others are more polar in character. The two hydrophobic zones, which interact with the aliphatic or aromatic hydrocarbon portions of a substrate, are designated $H_{L(arge)}$ and $H_{S(mall)}$. The larger of the two, H_L, has a volume of approximately 33 Å^3, while the smaller H_S pocket has a volume of roughly 5.5 Å^3. Polar groups such as hydroxyl, amino, carbonyl, nitro, etc. are excluded from these areas. However, the hydrophobic pockets can accommodate less polar heteroatom functions such as halogen, and ether or ketal oxygen atoms, if necessary. The remaining two sectors accept groups that are more polar (P) or hydrophilic. They are located at the front (P_F) and back (P_B) of the active site, respectively. Unlike the other binding regions, the rear boundary of the P_B pocket is open, and hydrogen-bonding or similar groups may extend out beyond the back of this region. The area above the model is also open, and is completely accessible to any substrate moiety that needs to locate there. Such groups may extend in this direction without restriction.

This model reveals the structural basis for the stereospecificity reversals in that, for homologous series of substrates such as **1–3**, small hydrophobic groups bind in H_S until they become too large to do so, at which point the substrate orientation must be turned around to place the larger hydrophobic group in the H_L pocket, where there is room to accommodate it. It is this "turning over" requirement that is responsible for the *S*-to-*R* (and vice versa) switches observed experimentally. The situation is exemplified in Fig. 2 for the **1–3** substrate series (6).

The pocket sizes created in the initial Fig. 1 model represented the minimum volumes. Their actual sizes have subsequently been systematically probed with substrates of varying steric requirements (7). The dimensions of H_S, P_B, and P_F have been confirmed as originally identified, but H_L's capacity for large groups turned out to be greater than first specified. Its maximum dimensions have now been established[2] as 6.1Å × 4.6Å × 3.1Å. To the best of our knowledge, when applied correctly (6), this final model now permits all known PLE specificity to be satisfactorily interpreted, and also enables the stereospecificity of PLE-catalyzed hydrolysis to be correctly forecast for new substrate structures.

Probing enzyme specificity

Because of their simplicity, active-site specifications of the Fig. 1 type are presently the models of choice of organic chemists using enzymes synthetically, even when X-ray structures are available. However, they do not provide the understanding of enzyme specificity that in the long term is essential for identifying the range of substrate structures any synthetically useful enzyme can accept, and for selecting the most appropriate enzyme for transforming a given substrate structure into a desired synthon. Accordingly, in order to gain insights into the factors that control and determine enzyme specificity, we have begun to probe the nature of enzyme–substrate interactions in a systematic manner. This involves studying only synthetically useful enzymes for which good X-ray structures are available, using graphics analyses to select substrate or inhibitor structures that address a particular specificity question most appropriately, and, after kinetic studies on the selected structures, analyzing the experimental data with the aid of graphics and molecular modelling methods. The eventual goal of this approach is to maximize the synthetic potential of each enzyme. However, no natural enzyme can be expected to handle the ever-increasing range of substrate structures imposed by the chiral synthon demands of asymmetric synthesis. An important corollary of this strategy is thus its potential for identifying unfavourable amino acid residues at an active site that preclude conversion of a synthetically desirable substrate structure. This opens up the possibility of using the site-directed mutagenesis techniques of protein engineering to correct unsuitable amino acid positions, and eventually to

[2]A. Krawczyk, H. Wynn, E.J. Toone, and L.R. Provencher. Unpublished results.

Can. J. Chem. Downloaded from www.nrcresearchpress.com by 213.200.69.106 on 09/08/12
For personal use only.

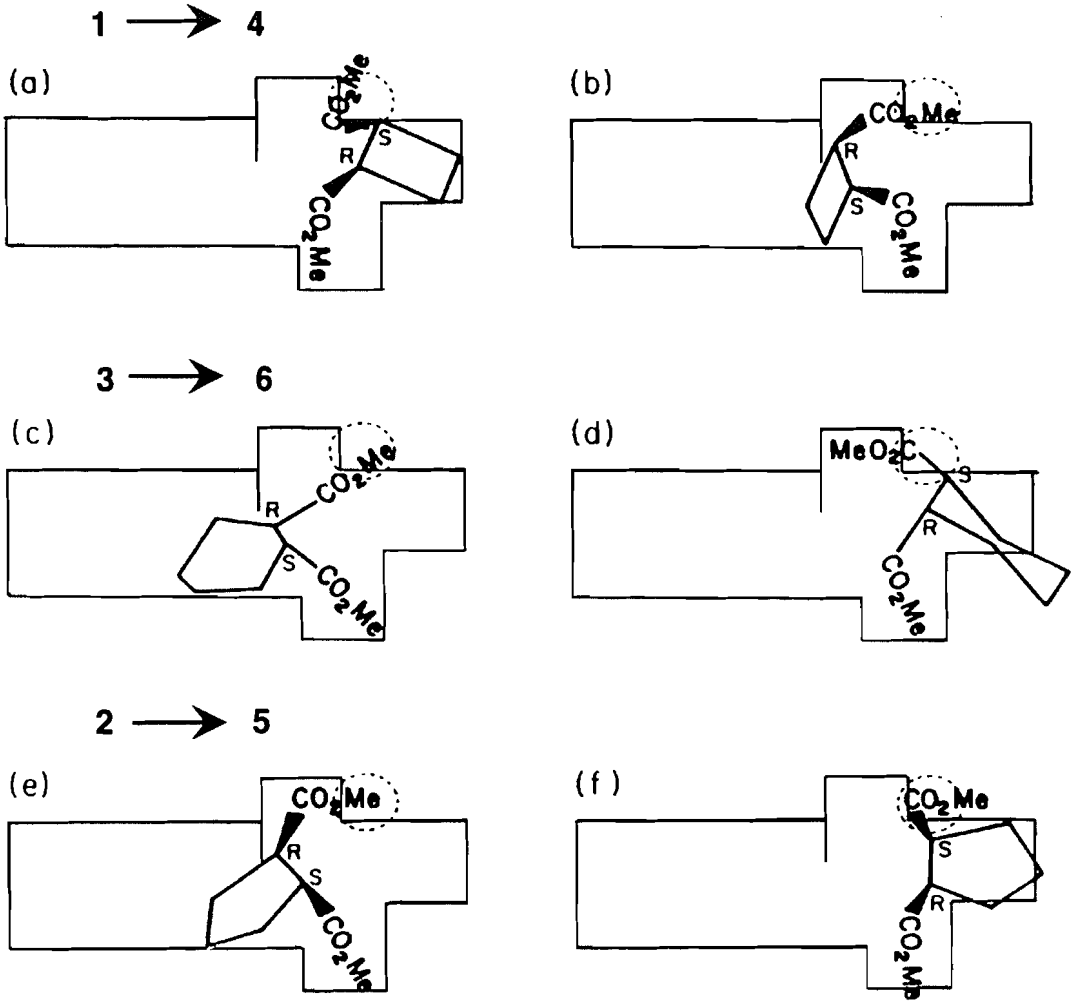

FIG. 2. The top-perspective view of the active-site model is used to illustrate the binding-mode selections for diesters **1**–**3**. Hydrolysis of an ester group can only occur when it locates within the spherical locus of the catalytically active serine function. **Dimethyl cyclobutane-1,2-dicarboxylate (1).** The *S*-centre ester hydrolysis orientation shown in (*a*) permits all substrate groups to be accommodated in the active site binding pockets, with the cyclobutane ring fitting cleanly into, and filling, the H_S pocket. The alternative binding mode required for hydrolysis of the *R*-centre ester would place a portion of the cyclobutane ring in the H_L pocket (*b*). Since binding of hydrophobic groups must occur in the H_S rather than the H_L site if sterically possible, substrate binding as in (*a*) is preferred, in accord with the observed formation of the 2*S*-acid product **4**. **Dimethyl cyclohexane-1,2-dicarboxylate (3).** The binding depicted in (*c*) shows the preferred ES-complex for hydrolysis of the *R*-center ester to the 2*R*-acid **6**, with the cyclohexane ring bound in the large hydrophobic pocket. Hydrolysis of the *S*-ester would require the orientation shown in (*d*). This is precluded since the H_S pocket is clearly too small to accept the six-membered ring. **Dimethyl cyclopentane-1,2-dicarboxylate (2).** In this instance, both *R*- and *S*-centre ester functions can be acceptably located in the serine sphere, as shown in (*e*) and (*f*), respectively. The cyclopentane group is marginally too large for optimum fit into H_S, resulting in a slight preference for hydrolysis via (*e*) that translates into a 17%ee of the corresponding 2*R*-acid **5**.

tailor an enzyme's specificity so that any given structural requirement will be accommodated.

Probing the structural specificity of hydrolases

The target enzymes selected as being representative of synthetically useful hydrolases were subtilisin BPN′ (SBPN, EC 3.4.21.14), subtilisin Carlsberg (SC, EC 3.4.21.14), and α-chymotrypsin (CT, EC 3.4.21.1). These serine proteases favour ester substrates possessing hydrophobic groups that bind well into the S_1 active site pocket, as represented schematically in Fig. 3(*a*) for the ES-complex formed by SBPN and its excellent substrate *N*-acetyl-L-phenylalanine methyl ester (NAPME). In this ES-complex, the hydrophobic benzyl group of NAPME fits nicely into the S_1 pocket, which in this case provides an appropriate environment as a result of the hydrophobic amino acid residues that form it. However, the unnatural substrates that SBPN may in the future be called on to hydrolyze could well include polar residues, towards which the natural S_1 environment would be hostile. We therefore decided to see if the S_1 pocket of the wild-type (WT) enzyme could be protein-engineered to be more accommodating of polar groups.

N-Tosyl-L-argininine methyl ester (TAME) was selected as a substrate structure whose positively charged side chain was much more polar than that of NAPME, and for which a poor interaction was anticipated between its guanidinium group and the hydrophobic S_1 environment of WT-SBPN if binding in the Fig. 3(*b*) manner took place. We therefore explored the prospect of making the S_1 trough more receptive to TAME-like side chains by changing the Gly166 residue at the bottom of S_1 to amino acids such as Asn or Ser

Can. J. Chem. Downloaded from www.nrcresearchpress.com by 213.200.69.106 on 09/08/12
For personal use only.

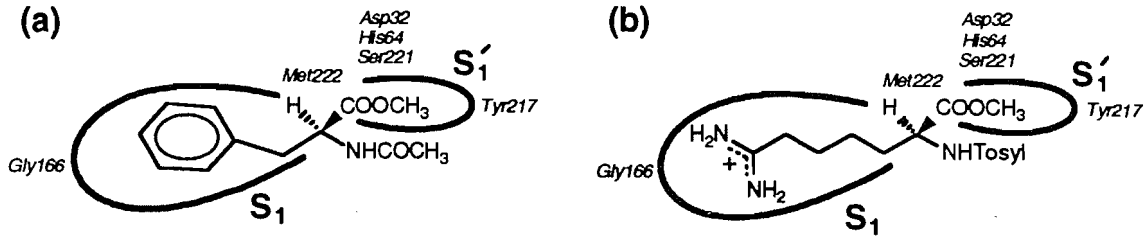

FIG. 3. Schematic representation of the active site of subtilisin BPN'. In (*a*) the nonpolar benzyl group of NAPME binds well in the hydrophobic S_1 pocket, which has a Gly166 located at its end. The S'_1 region that accommodates the leaving group is not very large, being blocked off at the end by Tyr217. S'_1 also contains the serine residue of the catalytically vital Ser221-His64-Asp32 serine protease triad. In (*b*) TAME is depicted in an orientation that site-directed mutagenesis of Gly166 to Asn or Ser should promote by creating a favourable hydrogen-bonding environment for the guanidinium function, thereby ameliorating the inhospitality of the hydrophobic milieu of S_1 towards polar groups.

whose side chains are capable of hydrogen bonding to polar groups such as guanidinium. The results obtained supported the validity of this strategy, with the effectiveness of TAME binding being increased by up to 2.4-fold, as reflected by the improvement in K_m from 34 mM for WT-SBPN to 21 and 14 mM for the Gly166Asn and Gly166Ser mutants, respectively. The G166S enzyme was the most effective catalyst of this series for TAME hydrolysis, and graphics analysis indicated it to be the optimum 166 mutant for this substrate (8).

The S'_1 site is also an important region in terms of specificity control. It is the zone in which the leaving groups of amide and ester substrates locate prior to, and during, the acylation step. In SBPN, the S'_1 site is not very large, having at its end a bulky hydroxybenzyl side chain of Tyr217 (Fig. 3) with the potential to restrict its ability to accept large leaving groups. In such situations, replacement of the relatively large Tyr217 at the end of the S'_1 region of SBPN by the smaller Leu residue (as present in subtilisin Carlsberg) should increase the space available for accommodating leaving groups. This was confirmed for the Tyr217Leu mutant, prepared by the Genencor International group (9), using the tetrapeptide substrates **7***a*,*b*. For **7***a*, its *p*-nitroanilide leaving group is still present in the rate-determining acylation step, and the catalytic constant k_{cat} is increased by a factor of 5.6 when the volume of S'_1 is increased by substituting the smaller Leu side chain for that of Tyr217 of the WT-SBPN. In contrast, for the ester substrates such as TAME or **7***b*, for which leaving groups have already departed prior to the deacylation rate-determining step, the k_{cat} values for the Tyr217Leu and WT enzymes are virtually identicial, as expected, with the differences in size between the thiobenzyl and methoxy functions being without effect on the catalytic constant (8).

Succinyl-L-Ala-L-Ala-L-Pro-L-Phe-X

7*a*, X = *p*-nitroanilide; **7***b*, X = thiobenzyl

Mutation of Met222 to Phe represents the converse situation in that the volume of S'_1 is markedly reduced by the substitution of the benzyl side chain for that of methionine. The rate of hydrolysis of the amide substrate **7***a*, with its medium-sized leaving moiety, is now reduced by this mutation, with the k_{cat} value observed for hydrolysis of **7***a* with the Met222Phe being 14-fold lower than for the WT enzyme. Once again, as expected because deacylation is rate determining for esters, the k_{cat}'s for WT and Met222Phe-catalyzed hydrolyses of TAME and **7***b* are unaffected. While reducing catalytic effectiveness is seldom a worthwhile goal, in this case the combination of the sharply reduced amide hydrolysis efficiency and unchanged esterase activity of SBPN Met222Phe is of particular synthetic interest. This mutant should be an excellent catalyst for the preparation of peptides by coupling of amino acid ester components in that the ester-to-acyl enzyme steps will proceed normally, but little subsequent hydrolysis of the newly formed peptide bond can occur. The potential thus exists for practical peptide synthesis in aqueous solution.

Probing hydrolase stereospecificity

So far, the use of enzymes in asymmetric synthesis has often been confined to the creation of chiral synthons with only one stereocentre. However, in principle, the large chiral environments provided by enzymes have the capacity to discriminate and control many stereocentres concurrently, potentially providing access to any multiple-stereocentre combination desired in syntheses of chiral targets. We have begun to explore this with the two-stereocentre substrates **9** and **10**, in which the natural L (*S*) configuration preferred by esterases is maintained at the α-amino position, but with either an *S*(**9**) or *R*(**10**) configuration at C-3. These *p*-nitro compounds were selected because of their synthetic potential as chloramphenicol precursors (10). The question was: will serine proteases such as subtilisin Carlsberg (SC) or α-chymotrypsin (CT) discriminate the second, C-3, centre?

The kinetic results, together with those on the *p*-nitrophenylalanyl parent **8** of **9** and **10**, showed that the replacement of either the *pro-R* or *pro-S* C-3-H by an OH group caused a $>10^4$-fold reduction in the hydrolysis rates, as reflected by the specificity constants, k_{cat}/K_M, for both SC- and CT-catalyzed reactions. While the rates of SC and CT hydrolyses of **9** and **10** were low, they remained preparatively viable. However, the SC, the hydrolysis rates of **9** and **10** were about the same, being 126 and 360 M^{-1} s^{-1}, respectively, showing that the enzyme did not distinguish significantly between a C-3 *S* or *R* centre and that separation of a diastereomeric mixture of **9** and **10** could not be achieved using SC hydrolysis. On the other hand, while the rate of CT hydrolysis of **9** was also low (k_{cat}/K_M 70 M^{-1} s^{-1}), **10** was not a substrate at all so that CT could very effectively be applied to separate the individual diastereomers from a mixture of **9** and **10**.

The reasons for the dramatic rate reductions for both SC

Can. J. Chem. Downloaded from www.nrcresearchpress.com by 213.200.69.106 on 09/08/12
For personal use only.

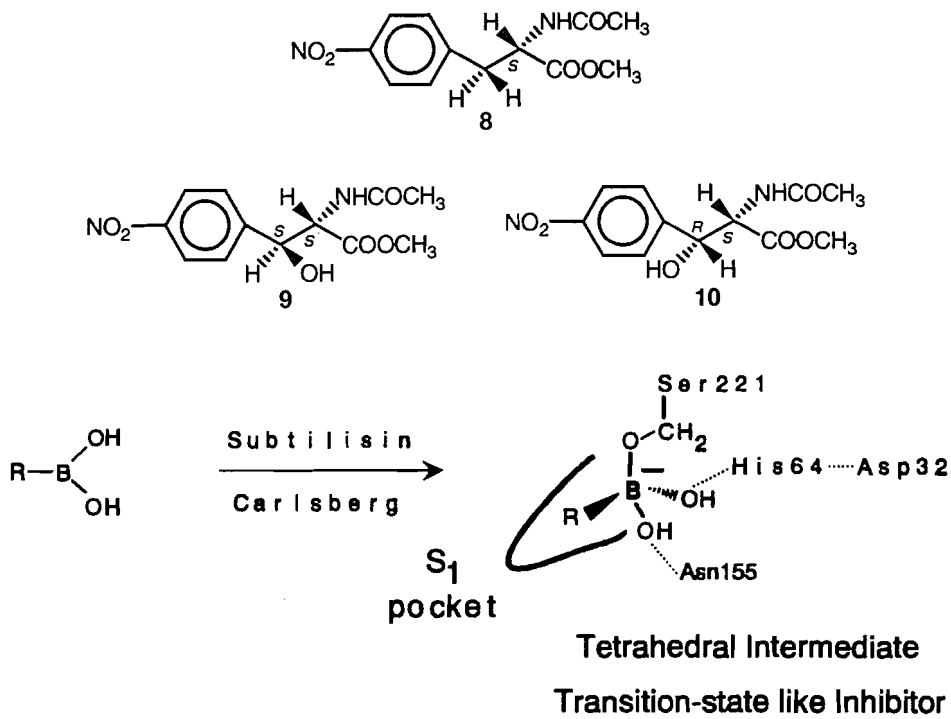

FIG. 4. Schematic representation of boronic acid inhibitor binding to subtilisin Carlsberg.

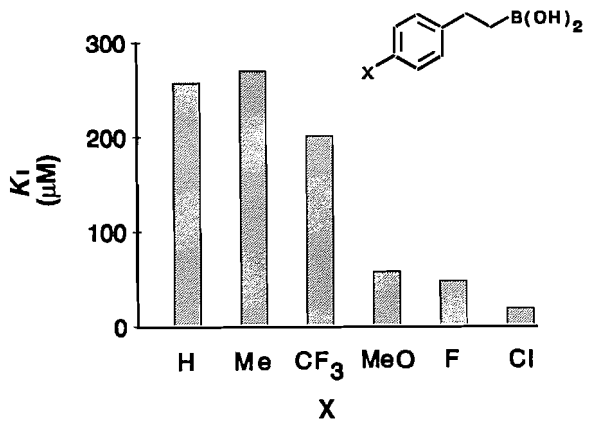

FIG. 5. *para*-Substituent effects on phenylboronic acid inhibitors of subtilisin Carlsberg.

and CT on introducing a C-3 OH substituent of either configuration, and for the differences in the abilities of the two enzymes to distinguish between the two C-3 configurations, were revealed by molecular modelling. The acyl enzyme intermediates derived from the *p*-nitrophenylalanyl parent compound **8** for each of SC and CT were minimized by molecular mechanics and molecular dynamics using the BioSym DISCOVER program. For the SC-complex, the C-3 hydrogens of **8** were located in the bottom of the S_1 pocket in environments of about equal steric constraints that are large enough to accept either an *S*- or *R*-centre hydroxyl group, but not without engendering some unfavourable steric interactions, specifically with Ala152 and Asn155 for an *S* OH and with Ser 125 for an *R* OH. Thus the consequences of replacing either the C3 *pro-S* or *pro-R* hydrogens by hydroxyl, as in **9** or **10**, respectively, both result in reduced hydrolysis rates, and to approximately the same degree. On the other hand, while the situation for the *pro-S* C-3 H of **9** in the CT-complex parallels closely that of the SC situation, the *pro-R* C-3 H of **10** is already in van der Waals contact with Cys191, Met192, Gly193, and Asp194 and this site cannot accommodate anything larger than hydrogen. Thus when the *pro-R* C-3 H is replaced by OH, as in **10**, formation of an acyl enzyme is precluded and the *S*, *R* diastereomer **10** is a non-substrate. In fact, **10** does not bind at all to CT, as demonstrated by its ineffectiveness ($K_I > 150$ mM) as a competitive inhibitor.

Exploiting electrostatic contributions to binding

When the electrostatic potential surfaces of SC and CT are calculated using the BioSym DELPHI programme, the patterns for the two enzymes are very different. We wondered if such electrostatic differences could be exploited to improve the strength or selectivity of binding to enzymes for appropriately designed substrates or inhibitors. For example, the calculations showed that, at the bottom of the S_1 pocket of SC, there was a region of positive potential that could contribute to increased binding strength of a substrate or inhibitor possessing a group of negative potential capable of interacting with this positive enzyme locus. The initial evaluations of this concept were carried out with the boronic acid inhibitors **11**. When bound to serine proteases, boronic acids of this type are transition state inhibitors that form EI-complexes of the type represented in Fig. 4, in which the aromatic group binds in S_1.

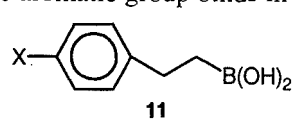

11

a, X = H *d*, X = OCH_3
b, X = CH_3 *e*, X = F
c, X = CF_3 *f*, X = Cl

In such orientations, the *para* substituents should then project into the positive region at the base of S_1. The results observed with the series of inhibitors **11***a–f* support this concept, as shown in Fig. 5, with the strength of binding increasing, as reflected by the decreasing K_I values, as the

Can. J. Chem. Downloaded from www.nrcresearchpress.com by 213.200.69.106 on 09/08/12
For personal use only.

negative potential character of the *para* substituent increases (11). For the *p*-chloro inhibitor **11***f*, with the most negative *para* group and thus the greatest electrostatic attraction with the base of S_1, binding is 13.5-fold stronger than for the parent compound **11***a*. The possibility that the observed trends simply reflected desolvation energy differences between the inhibitors on forming the respective EI-complexes was excluded by calculations and from literature tabulations of experimental solvation data.

Oxidoreductases

Oxidoreductases, such as horse liver alcohol dehydrogenase (HLADH) have proven of considerable interest in asymmetric synthesis. Illustrative examples of HLADH use include resolution, combined with diastereotopic face selectivity, of racemic ketones such as **12**, and additionally of regioselectivity, as in the oxidation of **13**, and of the enantiotopic group and face distinctions involved in the conversions of **14** and **15** (1*c*).

With the potential of a broad specificity oxidoreductase like HLADH well documented, we decided to examine an enzyme of this group with narrower specificity, with the intent of probing the factors determining structural and stereospecificity. The oxidoreductase selected was the L-lactate dehydrogenase of *Bacillus stearothermophilus* (BSLDH). BSLDH is an excellent candidate for such exploratory studies since it is a very stable, thermophilic, enzyme of known protein sequence and its properties have already been the subject of several studies (12). Also, its gene has been cloned and the protein very efficiently overexpressed, thereby enabling large quantities of BSLDH to be produced inexpensively from small fermentation volumes (13). Furthermore, the feasibility of altering the specificity of the native enzyme by site-directed mutagenesis of key active-site amino acid residues has been established (12).

On the structural specificity of BSLDH

BSLDH is an NAD/H coenzyme-dependent, fructose-1,6-diphosphate (FDP) activated, enzyme whose in vivo function is to catalyze pyruvate $\rightleftharpoons$ L-lactate oxidoreductions of the type

$$\underset{\mathbf{16}}{\text{RCOCOOH}} + \text{NADH} + \text{H}^+ \rightleftharpoons \underset{\mathbf{17}}{\text{RCH(OH)COOH}} + \text{NAD}^+$$

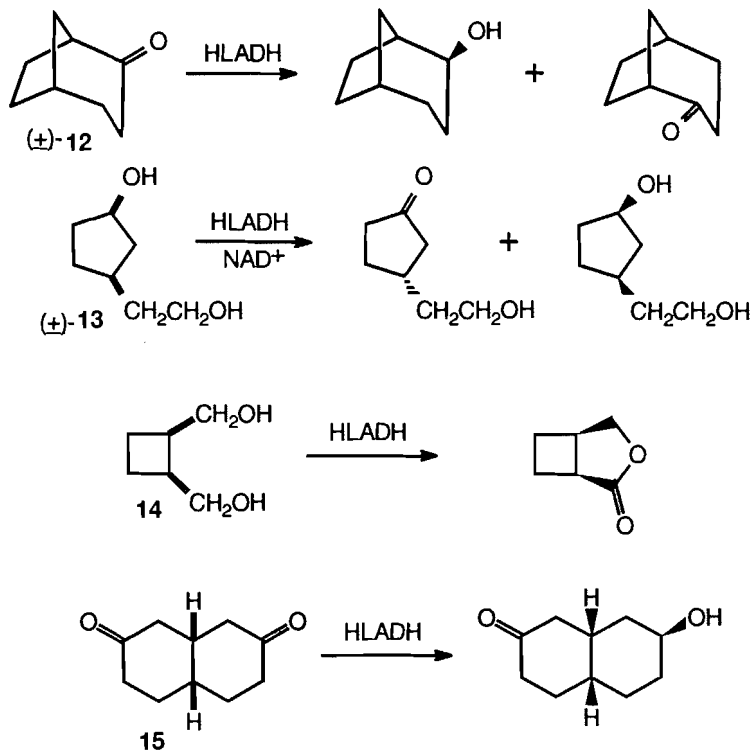

While its strongly preferred substrate is pyruvate (**16**, R = Me) with its small R group, BSLDH will accept as substrates a broad range of α-ketoacids, albeit with substantial rate penalties for large or branched R groups. Nevertheless, preparative-scale reactions to produce a range of enantiomerically pure L-α-hydroxyacids **17** are feasible, as illustrated in Fig. 6 (12).

Much is known about the structure of the active site of BSLDH (14). The key features are represented in Fig. 7. The narrow substrate specificity is due, at least in part, to the fact that the 98–110 and 235–248 loops close over the ketoacid substrate during the formation of the active ES-complex, thereby leaving only a restricted volume for the R side chains. Graphics analyses revealed that, in the productive ES-complex, large R groups would engender a bad steric interaction with the loop residue Gln102 and indicated that these adverse interactions with bulky, especially branched-chain, substrates could be diminished by reducing the size of the 102-position amino acid side chain. The validity of this analysis was tested by using site-directed mutagenesis to replace Gln102 by Asn, an amino acid of similar hydrophobicity but having one fewer CH_2 group in its side chain and thus providing more room for bigger side chains. The results obtained supported the application of such protein en-

Can. J. Chem. Downloaded from www.nrcresearchpress.com by 213.200.69.106 on 09/08/12
For personal use only.

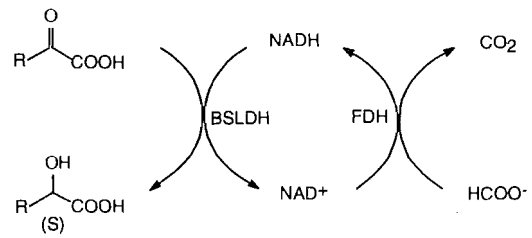

R	Rel. Rate	%Yield	% ee
CH_3	++++		
CH_3CH_2	+++	88	>99
$CH_3(CH_2)_2$	+	89	>99
H_3C, CH_3	<+	88	>99
cyclopropyl	+	89	>99
CH_2-phenyl	++	90	>99

FIG. 6. Preparative-scale BSLDH-catalyzed reductions.

gineering approaches to expand the structural specificity of enzymes, with the Gln102Asn mutant now being a better enzyme than WT-BSLDH for substrates such as **16**, R = $CH_3(CH_2)_{2-5}$, $(CH_3)_2CH$, $(CH_3)_2CHCH_2$, $CH_3CH_2CH(CH_3)$, and C_6H_5 (15).

Probing BSLDH stereospecificity

The stereospecificity of enzymes is their most important property for asymmetric synthetic applications. However, as noted already, little is known about the factors that determine and control enzyme stereospecificity. With L-LDH's being so committed to *Re*-face carbonyl attack to give (*S*)-α-hydroxyacids, BSLDH provides an excellent instrument for beginning to identify and understand important stereospecificity determinants, initially of oxidoreductases, but eventually of all enzymes. Among the methods of probing the factors controlling enzyme stereospecificity, evaluating how effectively an enzyme resists attempts to change this capability is potentially one of the most powerful. The natural L stereospecificity of BSLDH is determined by the orientation of 2-ketoacids, such as pyruvate (**16**, R = CH_3), in the ES-complex such that the hydride equivalent from NADH is delivered to the *Re* face of the carbonyl group. This is depicted schematically in Fig. 8(*a*). An important interaction helping to maintain this pyruvate orientation is that between the substate's COO^- and Arg171. As one measure of BSLDH's commitment to the L pathway, we elected to evaluate its resistance to being induced to catalyze D-lactate formation. Reduction of pyruvate to D-lactate requires delivery of the NADH-"hydride" to the *Si* face of pyruvate. One of the ways that can be envisaged of inducing this *Si*-face attack would be via an ES-complex in which the orientation of pyruvate was reversed, as illustrated in Fig. 8(*b*).

Towards this goal, Arg171 was replaced by Tyr and Trp. Despite the elimination of the key Arg171-COO^- binding

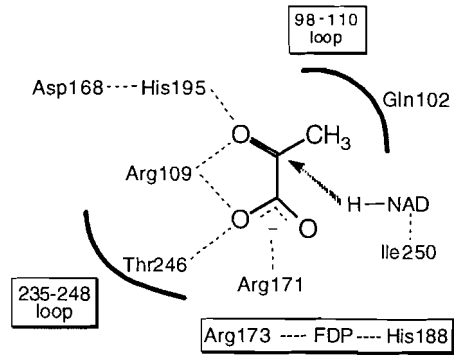

FIG. 7. Important active-site amino acid residues of BSLDH.

orientation, the Arg171Trp/Tyr mutants were still completely L-stereospecific (16). In a subsequent study, the WT-Arg171 was retained but a second COO^--binding Arg residue was introduced in place of Gln102, thereby providing a competitive possibility between the Fig. 8(*a*) and 8(*b*) pyruvate orientations and the prospect of formation of racemic products. As expected (17), the best substrates for this mutant were dicarboxylic α-ketoacids that concurrently exploit both the Arg171 and 102Arg binding sites. However, once again, this Gln102Arg mutation did not disturb the L proclivity of BSLDH in any preparatively significant way, with only L-α-hydroxyacids being produced in preparative-scale reeactions. Nevertheless, this mutant provided the first indication that it was possible to disturb the natural L-stereospecificity of BSLDH in that, in contrast to the WT situation for which oxidation of L-malate was much faster than for the D enantiomer, the rates of oxidation of L- and D-malate for the Gln102Arg mutant had become approximately equal (12). In the latest experiments, the 171 Trp/Tyr and 102Arg mutations were combined in order to eliminate any prospect of the natural Arg171-COO^- interaction and at the same time to provide the opportunity for a reversal of pyruvate orientation via 102Arg-COO^- binding. Furthermore, the formation of the natural, Arg171-directed, Fig. 8(*a*) type complex is clearly impossible for the Arg171Trp/Tyr;Gln102Arg double mutants. Despite the binding constraints designed into these double mutants, their fidelity with respect to L-stereospecificity remained dominant, with preparative-scale reductions of α-ketoacids affording only the L-hydroxyacids.

The question of how the above BSLDH mutants maintain their control of L-stereospecificity is thus an intriguing one. The X-ray structure of the 171Trp/102Arg/97Gly triple mutant that is now being refined should provide new insights into these questions. Already it is clear that Arg171Trp replacement is not wholly benign, and that the 171Trp side chain shifts out of the active site (18). Because none of the 171 or 102 mutations disturbs the natural stereospecificity of BSLDH, it is evident that there must be fail-safe, L-directing, interactions that take over when Arg 171 is not present. One such fail-safe candidate is Thr246. Other X-ray data (14) indicate that the Thr246 side chain is close enough to the substrate carboxylate function for effective hydrogen bonding (Fig. 7), although explaining how such a secondary, hydrogen-bonding, interaction could override carboxylate binding to 102Arg-containing mutants in the productive ES-complexes remains a quandary. This is particularly true for small substrates such as pyruvate for which, other than

Can. J. Chem. Downloaded from www.nrcresearchpress.com by 213.200.69.106 on 09/08/12
For personal use only.

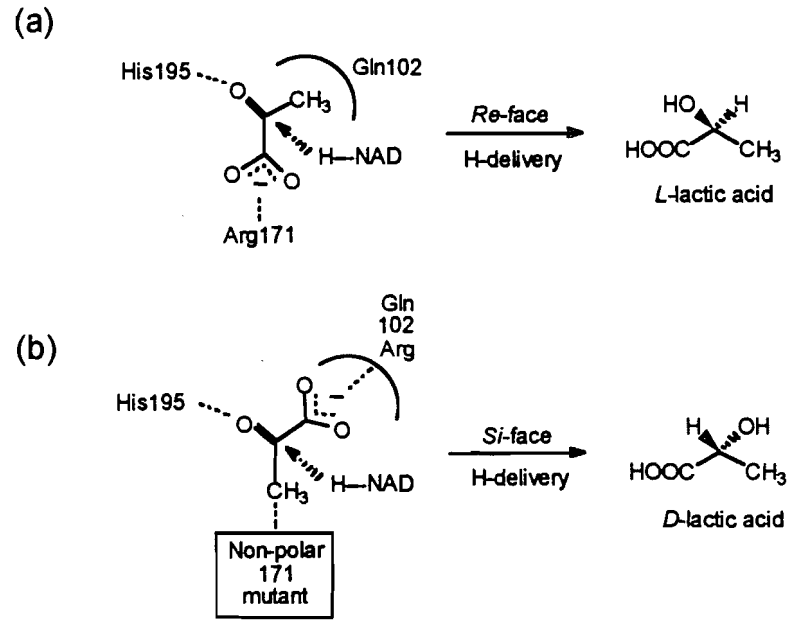

FIG. 8. Schematic representation of pyruvate bound at the active site of BSLDH in orientations leading to L- or D-lactic acid formation. Part (*a*) represents the natural binding mode that results in L-lactate formation. Part (*b*) illustrates a reversal of the natural binding orientation of pyruvate that might be induced by mutations such as Arg171Trp/Tyr, Gln102Arg, and combinations thereof, that would lead to D-lactate as the product.

the carbonyl group being reduced, the carboxylate group is the only function capable of binding strongly to the enzyme.

We have started to investigate the role of Thr246 by studying the catalytic properties of several 246 mutants, including Thr246Ala/Val/Leu/Ser. Although none of the mutants was as effective an oxidoreductase as WT-BSLDH, they did exhibit some interesting catalytic properties with respect to substrate inhibition. Substrate inhibition is a common phenomenon in enzyme-catalyzed reactions and can be a major problem in preparative-scale applications because of the very high substrate concentrations that are employed in large-scale transformations. In fact, substate inhibition can be very serious for BSLDH, particularly with pyruvate as substrate, and can result in reductions being brought to a virtual standstill. However, when no hydroxyl group is present in the 246 side chain, as for Thr246Val/Ala, substrate inhibition is virtually eliminated, as shown by the constant V_{max} values at high [S] for these two mutants (Fig. 9). Substrate inhibition of BSLDH arises from the strong complexation of pyruvate with the E.NAD$^+$ complex in the catalytic cycle. This does not occur with Thr246Val/Ala because pyruvate no longer binds effectively to E.NAD$^+$, as reflected by the dramatic increases in apparent K_I for pyruvate for this step for these two mutants (Fig. 10) (19). The effect is especially evident for the smaller 246Ala side chain where, with a K_I(app) of almost 800 mM, pyruvate is clearly not binding at all to E.NAD$^+$. Also, for WT-BSLDH, the rate-determining step (k 250 s^{-1} (13)) for pyruvate reduction is closure of the 98–110 loop. Mutation of Thr246 to Ala slows the loop closure rate such that the hydride transfer process becomes at least partially rate limiting, as refleted by the k_H/k_D kinetic isotope effect of 2.4.

Although the Arg171 and Gln102 mutations did not disturb the stereospecificity of the enzyme, there were serendipitous benefits to these changes in that thermal stability of BSLDH was further increased, dramatically so for the Arg171Tyr enzyme, for which the T_m(app) was increased by 9.4°C over that of WT-BSLDH. The greatest increase in T_m(app) was 10.7°C for Arg171Tyr, Gln102Arg. At high ionic strength, even higher thermal stabilization was manifest. Notably, in the presence of 100 mM K_2SO_4, the Arg171Tyr, Gln102Arg mutant retains 30% activity even after heating for 30 min at 100°C, conditions under which the already moderately thermostable WT-enzyme is completely inactivated in less than 2 min (18). This has considerable potential synthetic benefits since preparative-scale BSLDH-catalyzed reactions at temperatures of up to 100°C can now be contemplated, subject to NAD-coenzyme survival for sufficient time. The reason for the increased thermal stabilizations on replacing the Arg171 by hydrophobic residues such as Trp seems due to more favourable hydrophobic subunit contacts. This view is supported by preliminary X-ray structural evidence for a mutant BSLDH containing tryptophan in the 171 position. In this structure, the 171W side chain is rotated around the C_a—C_b bond, relative to the wild-type arginine side chain. The mutant indolyl group is thus located completely outside of the active site, and it projects into the space occupied by the other subunit in the BSLDH dimer in a manner that increases the hydrophobic subunit interface area (ref. 20 and footnote 3).

While the data presented in this lecture represent a beginning towards identifying the factors that determine enzyme specificity, it is evident that much needs to be done before enzymes and substrates can be tailored with confidence to permit optimum results in all asymmetric synthetic applications, and to maximize their performance and stability as catalysts. However, in view of the tremendous progress now being made in protein research, many exciting new insights

[3]R. Kodandapani and M.N.G. James. Unpublished results.

Can. J. Chem. Downloaded from www.nrcresearchpress.com by 213.200.69.106 on 09/08/12
For personal use only.

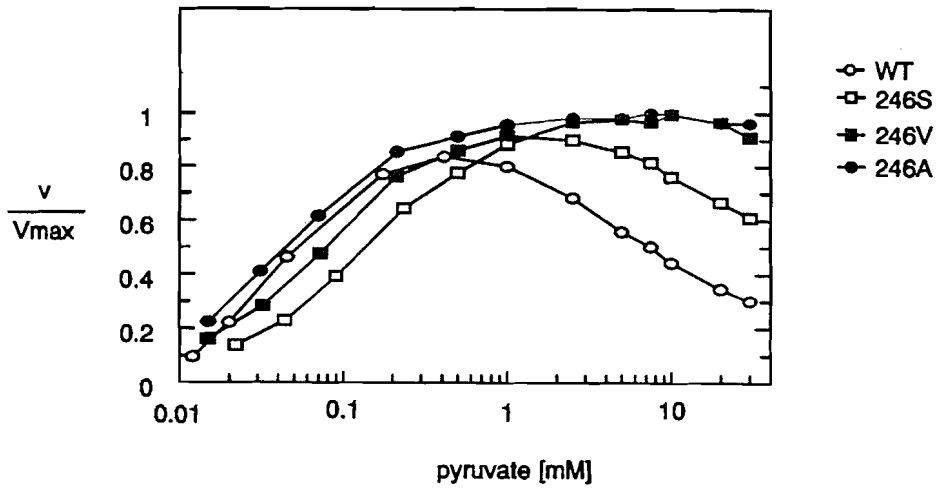

FIG. 9. Elimination of substrate inhibition by pyruvate by T246V/A mutations.

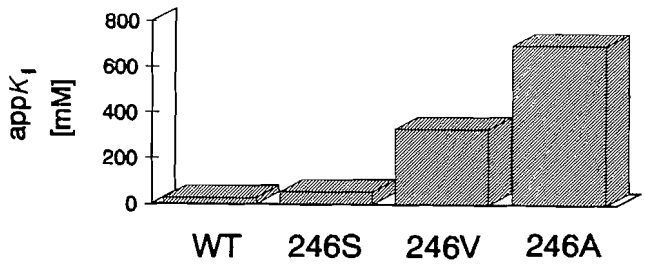

FIG. 10. Apparent K_I's for pyruvate inhibition of 246 mutant BSLDH's.

into enzyme catalysis and specificity can be anticipated in the next few years.

Acknowledgments

I am grateful to have this opportunity to acknowledge the many excellent students and postdoctoral fellows who have contributed, either directly or indirectly, to the body of knowledge of which the work described was built, and with whom it has been such a privilege to work. Most of the results presented were obtained by Pierre Bonneau, Jim Hogan, Helmut Kallwass, Tom Keller, Valeri Martichonok, Wendy Parris, Louis Provencher, Roman Sakowicz, Peter Seufer-Wasserthal, and Eric Toone. The subtilisin–mutants work was done in collaboration with Dave Estell and Tom Graycar of Genencor International and the BSLDH mutant X-ray structures by Michael James and R. Kodandapani at the University of Alberta. I am particularly indebted to my colleague and long-term collaborator, Marv Gold, without whose protein and molecular biology insights and expertise the BSLDH work would not have been possible. I also thank the Natural Sciences and Engineering Research Council of Canada and the Protein Engineering Network of the Canadian Centres of Excellence for generous financial support. Finally, I express my appreciation to Dr. Alfred Bader for setting up the Bader Award of the Canadian Society for Chemistry, for which I feel very privileged and honoured to have been selected. This is also an appropriate occasion to recognize the long-standing commitment and support by Dr. Bader of Canadian, and world, chemistry in other areas, not the least of which is the huge range of routine and state-of-the-art research chemicals that the company that he founded, Aldrich, has made available over the years and without which our research could never have been done.

1. (*a*) H.G. Davies, R.H. Green, D.R. Kelly, and S.M. Roberts. *In* Biotransformations in preparative organic chemistry. Academic Press, London. 1990; (*b*) D.H.G. Crout and M. Christen. Biotransformations in organic synthesis. *In* Modern synthetic methods. Vol. 5. *Edited by* R. Scheffold, Springer-Verlag, Berlin. 1989. pp. 1–114; (*c*) J.B. Jones. Tetrahedron, **42**, 3351 (1986).
2. (*a*) M. Ohno and M. Otsuka. Org. React. **37**, 1 (1989); (*b*) L.-M. Zhu and M.C. Tedford. Tetrahedron, **46**, 6587 (1990).
3. (*a*) G. Sabbioni and J.B. Jones, J. Org. Chem. **52**, 4565 (1987); (*b*) L.K.P. Lam, R.A.H.F. Hui, and J.B. Jones. J. Org. Chem. **51**, 2047 (1986).
4. L.K.P. Lam, C.M. Browne, B. DeJeso, L. Lym, E.J. Toone, and J.B. Jones. J. Am. Chem. Soc. **110**, 4409 (1988).
5. (*a*) P. Mohr, N. Waespe-Sarcevic, C. Tamm, K. Gawronska, and J.K. Gawronski. Helv. Chim. Acta, **66**, 2501 (1983); (*b*) M. Ohno. *In* Enzymes in organic synthesis (Ciba Found. Symp. **111**). *Edited by* R. Clark and S. Porter. Pitman, London. 1985. p. 171; (*c*) L.K.P. Lam, R.A.H.F. Hui, and J.B. Jones. J. Org. Chem. **51**, 2047 (1986); (*d*) J. Boutelje, M. Hjalmarsson, P. Szmulik, T. Norin, and K. Hult. *In* Biocatalysis in organic media. *Edited by* C. Laane, J. Tramper, and M.D. Lilly. Elsevier, Amsterdam. 1987.
6. E.J. Toone, M.J. Werth, and J.B. Jones. J. Am. Chem. Soc. **112**, 4946 (1990).
7. E.J. Toone, and J.B. Jones. Tetrahedron: Asymmetry, **2**, 207 (1991); **2**, 1041 (1991).
8. P.R. Bonneau, T.P. Graycar, D.A. Estell, and J.B. Jones. J. Am. Chem. Soc. **113**, 1026 (1990).
9. J.A. Wells, B.C. Cunningham, T.P. Graycar, and D.A. Estell. Proc. Natl. Acad. Sci. U.S.A. **84**, 5167 (1987).
10. R. Chenevert and S. Thiboutot. Synthesis, 444 (1989).
11. T. Keller, P. Seufer-Wasserthal, and J.B. Jones. Biochem. Biophys. Res. Commun. **176**, 401 (1991).
12. H.K.W. Kallwass, M.A. Luyten, W. Parris, M. Gold, C.M. Kay, and J.B. Jones. J. Am. Chem. Soc. **114**, 4551 (1992), and references therein.
13. (*a*) J.J. Holbrook, A. Liljas, S.J. Steindal, and M.G. Rossmann. *In* The enzymes. 3rd ed. *Edited by* P.D. Boyer. Academic Press, New York. 1975. pp. 191–292; (*b*) D.A. Barstow, A.R. Clarke, W.N. Chia, D.B. Wigley, A.S. Sharman, J.J. Holbrook, T. Atkinson, and N.T. Mington.

Can. J. Chem. Downloaded from www.nrcresearchpress.com by 213.200.69.106 on 09/08/12
For personal use only.

Gene, **46**, 47 (1986); (*c*) D. Stangl, F. Wiederkehr, F. Suter, and H. Zuber. Biol. Chem. Hoppe-Seyler, **368**, 1157 (1987).
14. (*a*) D.B. Wigley, S.J. Gamblin, J.P. Turkenburg, E.J. Dodson, K. Piontek, H. Muirhead, and J.J. Holbrook. J. Mol. Biol. **223**, 317 (1992); (*b*) K. Piontek, P. Chakrabarti, H.-P. Schaer, M.G. Rossmann, and H. Zuber. Proteins, **7**, 74 (1990).
15. M.A. Luyten, D. Bur, H. Wynn, W. Parris, M. Gold, J.D. Friesen, and J.B. Jones. J. Am. Chem. Soc. **111**, 6800 (1989).
16. M.A. Luyten, M. Gold, J.D. Friesen, and J.B. Jones. Biochemistry, **28**, 6605 (1989).
17. H. Wilks, K. Hart, R. Feeney, C. Dunn, H. Muirhead, W. Chia, D. Barstow, T. Atkinson, A. Clarke, and J.J. Holbrook. Science, **242**, 1541 (1988).
18. H.K.W. Kallwass, W.K. Surewicz, W. Parris, E.L.A. Macfarlane, M.A. Luyten, C.M. Kay, M. Gold, and J.B. Jones. Protein Eng. **5**, 769 (1992).
19. R. Sakowicz, H.K.W. Kallwass, W. Parris, M. Gold, and J.B. Jones. Biochem. Biophys. Res. Commun. **182**, 1305 (1992).
20. K. Huang, R. Kodandapani, H.K.W. Kallwass, J.K. Hogan, W. Parris, J.D. Friesen, M. Gold, J.B. Jones, and M.N.G. James. Proteins, **13**, 158 (1992).

Can. J. Chem. Downloaded from www.nrcresearchpress.com by 213.200.69.106 on 09/08/12
For personal use only.

Reversible electrode potentials for formation of solid and liquid chlorozirconate and chlorohafnate compounds

G.J. KIPOUROS

Technical University of Nova Scotia, Department of Mining and Metallurgical Engineering, P.O. Box 1000, Halifax, NS B3J 2X4, Canada

AND

S.N. FLENGAS[1]

University of Toronto, Department of Metallurgy and Materials Science, Toronto, ON M5S 1A4, Canada

Received October 1, 1992[2]

G.J. KIPOUROS and S.N. FLENGAS. Can. J. Chem. **71**, 1283 (1993).

The standard electrode potentials for the formation of the pure solid and molten compounds Li_2ZrCl_6, Li_2HfCl_6, Na_2ZrCl_6, Na_2HfCl_6, K_2ZrCl_6, K_2HfCl_6, Cs_2ZrCl_6, and Cs_2HfCl_6 have been calculated from measured vapour pressures corresponding to their thermal decomposition at equilibrium and from available thermochemical data. Reversible potentials for the formation of Na_2ZrCl_6 and of K_2ZrCl_6 in solution according to the reaction

$$Zr(s) + 2ACl\ (\text{in } ACl\text{–}A_2MCl_6) + 2Cl_2(g,\ 1\ atm) = A_2MCl_6\ (\text{in } ACl\text{–}A_2MCl_6)$$

where A is Na or K, have been calculated from available equilibrium vapour pressures as functions of the mole fractions of the alkali hexachlorocompounds. Standard potentials for the above reaction and "formal" potentials are also given. The latter are useful in predicting the electrochemical behaviour of dilute solutions of the hexachlorozirconates in alkali metal chlorides.

G.J. KIPOUROS et S.N. FLENGAS. Can. J. Chem. **71**, 1283 (1993).

Utilisant les pressions de vapeur correspondantes à leur décomposition thermique à l'équilibre ainsi que des données thermochimiques disponibles, on a calculé les potentiels standard d'électrode pour la formation des composés purs solide ainsi que fondu suivants : Li_2ZrCl_6, Li_2HfCl_6, Na_2ZrCl_6, Na_2HfCl_6, K_2ZrCl_6, K_2HfCl_6, Cs_2ZrCl_6 et Cs_2HfCl_6. On a calculé les potentiels réversibles pour la formation du Na_2ZrCl_6 et du K_2ZrCl_6 en solution, selon la réaction :

$$Zr(s) + 2ACl\ (\text{dans } ACl\text{–}A_2MCl_6) + 2Cl_2(g,\ 1\ atm) \rightleftarrows A_2MCl_6\ (\text{dans } ACl\text{–}A_2MCl_6)$$

dans laquelle A représente Na ou K; pour ce faire, on a utilisé les équilibres disponibles de tension de vapeur en fonction des fractions molaires des composés hexachloroalcalins. On rapporte aussi les potentiels standard et «formels» des réactions mentionnées ci-dessus. Les derniers sont utiles pour prédire le comportement électrochimique de solutions diluées d'hexachlorozirconates dans des chlorures de métaux alcalins.

[Traduit par la rédaction]

Introduction

The knowledge of the thermodynamic and electrochemical properties of $ZrCl_4$ and of $HfCl_4$ and of their solutions of alkali chloride melts is important for the development of new processes for the recovery of the corresponding refractory metals by high-temperature fused-salt electrolysis. Pure $ZrCl_4$ and $HfCl_4$ are non-ionic, covalently bonded compounds that do not conduct electricity and are very volatile. However, $ZrCl_4$ and $HfCl_4$ vapours at specific partial pressures and temperatures react with alkali chlorides and form stable stoichiometric complex compounds of the general formula A_2MCl_6, where A represents an alkali metal like Li, Na, K, or Cs and M is a refractory metal such as Hf or Zr. The compounds have been investigated extensively in this laboratory and equilibrium vapour pressures representing the reactions

$$[1] \quad A_2MCl_6(s, l, \text{solution}) = 2ACl(s, l, \text{solution}) + MCl_4(v)$$

have been measured (1–5). Some phase relationships in the binary mixtures ACl–A_2MCl_6 have also been determined.

The use of such solutions in the electrolytic cells for the recovery of Hf or Zr by fused-salt electrolysis has been considered (6–11). However, the corresponding reversible electrode potentials for the formation of the complex compounds from the elements have not been measured. Direct emf measurements would require the construction of an electrochemical cell consisting of a metal M indicator electrode and of a chlorine electrode, where both are immersed in a melt consisting of pure A_2MCl_6 or a solution of A_2MCl_6 in ACl. These measurements, however, are impossible experimentally, as previous work in this laboratory has shown (12, 13) that the tetravalent specie M^{4+} is reduced by the metal M to lower valence specie, according to chemical reactions like

$$[2] \quad \left(\frac{4}{n} - 1\right) M(s) + MCl_4(\text{solution}) = \frac{4}{n} MCl_n(\text{solution})$$

where n could have values like 1, 2, or 3.

Even under very careful experimental conditions the measured emf's are time dependent and should only be described as "mixed potentials" (14). In a high-temperature electrolytic cell the anodic and the cathodic overvoltages are expected to have low values. Therefore, in addition to the internal voltage drop due to the resistance of the electrolyte (IR drop), most of an applied potential should be used for the reversible decomposition of the complex chlorocompounds. This potential is the reverse of the reversible emf for the formation of the complexes.

In the present investigation a method is presented for calculating standard cell potentials from thermodynamic data from the equilibrium vapour pressures measured in this lab-

[1]Author to whom correspondence may be addressed.

[2]Revision received May 14, 1993.

Can. J. Chem. Downloaded from www.nrcresearchpress.com by 213.200.69.106 on 09/08/12
For personal use only.

Can. J. Chem. Downloaded from www.nrcresearchpress.com by 213.200.69.106 on 09/08/12
For personal use only.

oratory (1–5). From this information reversible decomposition potentials for the recovery of Zr metal from solutions of A_2ZrCl_6 in alkali chlorides at various compositions were also calculated from available activity data (15).

Procedure

The formation of the pure A_2MCl_6 solid compounds (1–5), at temperatures below the eutectic temperature of the corresponding A_2MCl_6–ACl binary mixtures, proceeds according to the reaction

[3] $2ACl(s) + M(s) + 2Cl_2(g, 1\ atm) = A_2MCl_6(s)$

where A_2MCl_6, ACl, and M are, respectively, pure solids. Similarly, the formation of pure molten A_2MCl_6 compounds occurs only at temperatures higher than their melting temperatures according to the reaction

[4] $2ACl(l) + M(s) + 2Cl_2(g, 1\ atm) = A_2MCl_6(l)$

where A_2MCl_6 and ACl are, respectively, pure liquids.

For the formation of A_2MCl_6 as a solute in a solution containing n_1 moles of A_2MCl_6 and n_2 moles of ACl, the corresponding reaction may be written as

[5] $M(s) + 2Cl_2(g, 1\ atm) + [(A_2MCl_6)_{n_1} \cdot (ACl)_{n_2}] = [(A_2MCl_6)_{n_1+1} \cdot (ACl)_{n_2-2}]$

where the quantities in brackets indicate solutions and n_1, n_2 are, respectively, infinitely large mole numbers. Through this requirement, solutions to the left or to the right of the equal sign represent solute species having partial molar Gibbs free energies defined by a constant mole fraction, $x_1 = n_1/(n_1 + n_2)$.

Information on the formation potentials in reactions [3], [4], and [5] may be obtained by thermodynamic cycles using available Gibbs free energies for the reactions given below as

[6] $2ACl(s) + MCl_4(v, 1\ atm) = A_2MCl_6(s)$ $\quad \Delta G_6^0$

[7] $M(s) + 2Cl_2(g, 1\ atm) = MCl_4(v, 1\ atm)$ $\quad \Delta G_7^0$

[8] $A_2MCl_6(s) = A_2MCl_6(l)$ $\quad \Delta G_8^0$

[9] $2ACl(l) = 2ACl(s)$ $\quad -2\Delta G_9^0$

From reactions [6] and [7], by addition, reaction [3] is readily obtained, for which

[10] $\Delta G_3^0 = \Delta G_6^0 + \Delta G_7^0$

where ΔG^0_3 is the Gibbs free energy of formation of pure solid A_2MCl_6, as in reaction [3].

From reactions [6], [7], [8], and [9], reaction [4] is readily derived for which

[11] $\Delta G_4^0 = \Delta G_6^0 + \Delta G_7^0 + \Delta G_8^0 - 2\Delta G_9^0$

where ΔG_4^0 is the Gibbs free energy of formation of pure molten A_2MCl_6, as in reaction [4].

For the formation of A_2MCl_6 in solution, as in reaction [5],

[12] $\Delta G_5 = \overline{G}_{A_2MCl_6} - 2\overline{G}_{ACl} - G_M^0 - G_{Cl_2}^0$

where $\overline{G}_{A_2MCl_6}$, $\overline{G}_{ACl}$ and, respectively, the partial molar Gibbs free energy contents of A_2MCl_6 and ACl in a solution having a mole fraction of x_1.

From the Gibbs free energies for reactions [5] and [4], by subtraction,

[13] $\Delta G_5 - \Delta G_4^0 = \overline{\Delta G}_{A_2MCl_6} - 2\,\overline{\Delta G}_{ACl}$

where $\overline{\Delta G}_{A_2MCl_6}$ and $\overline{\Delta G}_{ACl}$ are, respectively, the Gibbs partial molar free energies of mixing for A_2MCl_6 and ACl with respect to the standard states of the pure molten salts at the same temperatures. The latter are related to the activities by the relationships

[14] $\overline{\Delta G}_{A_2MCl_6} = RT \ln a_{A_2MCl_6}$

and

[15] $\overline{\Delta G}_{ACl} = RT \ln a_{ACl}$

From the well-known relationship between the Gibbs free energy for a chemical reaction, ΔG_R, and the corresponding electrode potential

[16] $\Delta G_R = -zFE$

the standard potentials for reactions [3] and [4] are calculated as

[17] $\Delta G_3^0 = -4FE_3^0$

[18] $\Delta G_4^0 = -4FE_4^0$

for which E_3^0 and E_4^0 are, respectively, the standard formation potentials for A_2MCl_6 with respect to the solid and the molten pure salt states as standard. F is the Faraday constant given as 23 060 cal mol^{-1} V^{-1}.

From eqs. [13], [14], [15], and [18], the expression for the formation Nernst potential of A_2MCl_6, representing eq. [5], is given as

[19] $$E_5 = E_4^0 - \frac{RT}{4F} \ln \frac{a_{A_2MCl_6}}{a_{ACl}^2}$$

where E_4^0 is defined by eq. [18] and E_5 is the emf of an electrochemical cell containing metal M and gaseous chlorine electrodes at standard chlorine pressure, when both are immersed in a molten salt solution containing A_2MCl_6 and ACl at mole fractions x_1 and $1 - x_1$, respectively. This potential is also the potential at which the metal M will first appear at the cathode during molten salt electrolysis, assuming reversible behaviour.

Results and discussion

Calculations of standard electrode potentials

Equilibrium vapour pressures representing reaction [6] were measured in this laboratory for the pure solid stoichiometric compounds Li_2ZrCl_6, Li_2HfCl_6 (2); K_2ZrCl_6, K_2HfCl_6 (3); Na_2ZrCl_6, Na_2HfCl_6 (4); and Cs_2ZrCl_6, Cs_2HfCl_6 (5). Based on the reported data the standard Gibbs free energies of formation of the pure solid chlorozirconate and chlorohafnate compounds were calculated as functions of temperature of the form

[20] $\Delta G_6^0 = A + BT$

The results are given in Table 1 where A and B are constants and T is in degrees K.

The standard Gibbs free energy of formation of the pure zirconium or hafnium tetrachloride vapours, representing reaction [7], were calculated as functions of temperature from

TABLE 1. Standard free energies of formation of the pure solid chlorohafnate and chlorozirconate compounds according to reaction [6], given as functions of temperature

Reaction	$\Delta G_3^0 = A + BT$ (cal/mol) A	B	Temperature (K)	Reference
$2LiCl(s) + ZrCl_4(v) = Li_2ZrCl_6(s)$	−7 888	9.97	623–808	2
$2LiCl(s) + HfCl_4(v) = Li_2HfCl_6(s)$	−7 570	−9.32	623–830	2
$2NaCl(s) + ZrCl_4(v) = Na_2ZrCl_6(s)$	−7 807	4.16	821–919	3
$2NaCl(s) + HfCl_4(v) = Na_2HfCl_6(s)$	−7 485	−3.09	813–933	3
$2KCl(s) + ZrCl_4(v) = K_2ZrCl_6(s)$	−4 570	−1.08	893–1072	4
$2KCl(s) + HfCl_4(v) = K_2HfCl_6(s)$	−2 678	4.66	877–1081	4
$2CsCl(s) + ZrCl_4(v) = Cs_2ZrCl_6(s)$	−2 766	−5.47	862–1083	5
$2CsCl(s) + HfCl_4(v) = Cs_2HfCl_6(s)$	−3 052	5.53	864–1100	5

TABLE 2. Standard free energies of formation of hafnium and zirconium tetrachloride vapours, according to reaction [7], given as functions of temperature

$$\Delta G_7^0 = a_1 + a_2T + a_3T \ln T + a_4T^2 + a_5T^{-1} \text{ (cal mol}^{-1}\text{)}$$

Reaction	a_1	a_2	a_3	$a_4 \times 10^3$	$a_5 \times 10^{-5}$	Temperature range (K)
$Zr(s) + 2Cl(g, 1 atm) = ZrCl_4(v)$	−203 080	35.9	−1.59	0.85	−1.1	604–1135
$Hf(s) + 2Cl(g, 1 atm) = HfCl_4(v)$	−229 750	−40.10	−2.00	0.55	−0.65	590–2500

TABLE 3. Standard free energies of fusion of alkali chlorohafnate and chlorozirconate compounds as functions of temperature

$$\Delta G_8^0 = b_1 + b_2T + b_3T \ln T + b_4T^2 \text{ (cal mol}^{-1}\text{)}$$

Compound	b_1	b_2	b_3	$b_4 \times 10^3$	Melting point (K)
Li_2ZrCl_6	−2 108	212.64	−34.40	25.10	808
Li_2HfCl_6	−6 367	400.70	−65.50	56.9	830
Na_2ZrCl_6	5 838	−20.05	2.00		919
K_2ZrCl_6	−8 556	99.41	−13.10		1072
Cs_2ZrCl_6	−8 501	102.849	−16.71	20.38	1083

TABLE 4. Standard free energies of fusion of the alkali chlorides as functions of temperature

$$\Delta G_9^0 = c_1 + c_2T + c_3T \ln T + c_4T^2 \text{ (cal mol}^{-1}\text{)}$$

Compound	c_1	c_2	c_3	$c_4 \times 10^3$	Melting point (K)
LiCl	1 183	40.505	−6.537	2.82	883
NaCl	3 558	29.628	−5.020	1.95	1074
KCl	2 730	37.098	−6.110	2.60	1045
CsCl	−2 471	85.708	−13.055	6.66	918

available data (16). The data were expressed by equations of the general form

[21] $$\Delta G_7^0 = a_1 + a_2T + a_3T \ln T + a_4T^2 + a_5T^{-1}$$

and the values for the coefficients are given in Table 2. T is in degrees K.

The standard Gibbs free energies of fusion for the alkali chlorozirconate and the alkali chlorohafnate compounds were calculated as functions of temperature from heat capacities measured in this laboratory (16–18) and the data for ΔG_8^0 were expressed as functions of temperature in eq. [22].

[22] $$\Delta G_8^0 = b_1 + b_2T + b_3T \ln T + b_4T^2$$

The coefficients for these equations are given in Table 3. Also, the standard free energies of fusion for the alkali chlorides, ΔG_9^0, were obtained from available thermochemical data (19) and their temperature dependence expressed by eq. [23].

[23] $$\Delta G_9^0 = c_1 + c_2T + c_3T \ln T + c_4T^2 + c_5T^{-1}$$

The coefficients for these equations are given in Table 4 and T is in degrees K.

From the data in Tables 1 and 2, the standard formation electrode potentials for the alkali chlorozirconate and chlorohafnate compounds representing reaction [3] were calculated using eqs. [10] and [16], with respect to pure solids as

Can. J. Chem. Downloaded from www.nrcresearchpress.com by 213.200.69.106 on 09/08/12
For personal use only.

Can. J. Chem. Downloaded from www.nrcresearchpress.com by 213.200.69.106 on 09/08/12
For personal use only.

TABLE 5. Standard cell potential for the formation of A_2MCL_6 with respect to solid standard states, according to $E_3^0 = d_1 + d_2T + 2.17 \times 10^{-5}T \ln T - 5.96 \times 10^{-9}T^2$ (V)

	Standard formation potential coefficients[a]		Melting temperature (K)	E_3^0 at 923 K
	d_1	$d_2 \times 10^4$		
Li_2ZrCl_6	2.287	−4.97	808	1.965
Na_2ZrCl_6	2.286	−4.34	919	2.022
K_2ZrCl_6	2.251	−3.77	1072	2.039
Cs_2ZrCl_6	2.232	−3.29	1083	2.064
Li_2HfCl_6	2.573	−5.36	830	2.215
Na_2HfCl_6	2.572	−4.68	953	2.277
K_2HfCl_6	2.520	−3.84	1081	2.165
Cs_2HfCl_6	2.524	−3.74	1100	2.315

[a]Only two coefficients needed for each chloro compound.

the standard states of reference. These potentials are tabulated in Table 5 as functions of temperature of the general form

$$[24] \quad E_3^0 = d_1 + d_2T + 2.17 \times 10^{-5}\,T \ln T - 5.96 \times 10^{-9}\,T^2$$

where the constants d_1 and d_2 are given for each compound and T is in degrees K.

The standard formation potentials at 923 K are plotted as a function of the radius of the alkali metal cation in Fig. 1. It is readily seen that the hafnium compounds are more stable than the corresponding zirconium compounds. The relationship is nearly linear, as observed for the thermal decomposition temperatures of the pure solid compounds (1, 2).

A similar procedure was followed for the calculation of the standard formation potentials of the alkali chlorozirconate and alkali chlorohafnate compounds with respect to pure liquids as the standard states for A_2MCl_6 and ACl, as per reaction [4]. All data needed for this calculation may be found in Tables 1–4, and were used in connection with eq. [11]. These calculations were performed only for the compounds for which the necessary data were available.

The temperature dependence for the electrode potentials for each of these compounds is given in Table 6 in the form of the general equation

$$[25] \quad E_4^0 = e_1 + e_2T + e_3T \ln T - e_4T^2 \qquad (T \text{ in K})$$

Standard potentials with respect to the liquid state of reference were calculated at the melting temperature of the pure complex compounds.

The standard free energies in Tables 1–4 are given in cal mol^{-1}. These may be converted to the SI units of joule mol^{-1} by multiplication by 4.184.

Calculation of the reversible decomposition potentials of solutions containing alkali chlorozirconate and chlorohafnate compounds

In a real high-temperature electrolytic cell for the recovery of zirconium or hafnium metals by fused-salt electrolysis, the electrolyte could be chosen to be a solution of the alkali chlorozirconate or chlorohafnate compounds in a molten bath of alkali chlorides. Metal recovery during electrolysis should proceed by the reverse of reaction [5]. The corresponding reversible decomposition potentials may be calculated from eq. [19], in which the standard formation potentials for the pure molten alkali chlorozirconate or chlorohafnate compounds are given in Table 6. The necessary values for the activities of the alkali chlorides in the binary systems NaCl-Na_2ZrCl_6 and KCl-K_2ZrCl_6 were reported previously (15, 20). The calculations were based on a modified form of the Gibbs-Duhem equation in which the unit activity states for the complex compounds are the pure molten stoichiometric compounds A_2ZrCl_6, where A is an alkali metal cation. Complex stoichiometry occurs in a solution containing 66.7 mol% alkali chloride within the overall primary system ACl-$ZrCl_4$. However, at this composition, the activities of ACl are not zero but have finite values representing the activities of ACl within a complex A_2ZrCl_6, which is also a congruently melting compound. Activities for both the ACl and A_2ZrCl_6 compounds at the corresponding melting temperatures are given in Table 7. The plot of the calculated potentials from eq. [19] is given as Fig. 2. The "true" standard electrode potential representing reaction [5] is obtained from eq. [19], in which A_2ZrCl_6 activities are set to unity and the activities of ACl have the corresponding limiting values of the activities of the alkali chlorides within each compound. These are 0.28 for NaCl in the Na_2ZrCl_6 and 0.24 for KCl in K_2ZrCl_6. The corresponding "true" standard potentials are 1.959 V for Na_2ZrCl_6 and 1.890 V for K_2ZrCl_6.

Formal potentials may also be calculated from the limiting values for the activity coefficients for the complex compounds A_2MCl_6 at $x_{A_2MCl_6} = 0$. Formal potentials define the infinitely dilute solution standard state at unit mole fraction of A_2MCl_6. The overall concentration dependence of the activity coefficients within the pseudobinary systems ACl–A_2MCl_6 has been given (15, 20) by the equation

$$[26] \quad \log_{10} \gamma_{A_2MCl_6} = \frac{0.06}{2.3RT} + \frac{x_{ACl}^2 b}{2.3RT}$$

where b are constants specific to Na_2ZrCl_6 and K_2ZrCl_6 and are given in Table 7. At $x_{ACl} = 1$, $x_{A_2MCl_6} = 0$ and the corresponding Henrian activity coefficients are readily calculated from eq. [26] as

$$\gamma'_{Na_2ZrCl_6} = 2.913$$

and

$$\gamma'_{K_2ZrCl_6} = 1.995$$

Formal potentials are obtained from the expression,

$$[27] \quad E_{5(\text{formal})} = E_4^0 - \frac{RT}{4F} \ln \gamma'_{A_2ZrCl_6}$$

For Na_2ZrCl_6 at its melting temperature of 919 K and for K_2ZrCl_6 at its melting temperature of 1072 K, the corresponding formal potentials are 1.988 and 1.940 V. The limiting potentials for unity and zero mole fractions of the alkali chlorozirconates, respectively, are also shown in Fig. 2.

For Cs_2ZrCl_6, vapour pressure data within the CsCl-Cs_2ZrCl_6 pseudobinary were available only over a limited composition range and calculations of its activities were only approximate. Accordingly, plots of E_5 versus $\log_{10} x_{Cs_2ZrCl_6}$ were not constructed. However, its formal potential at its melting temperature of 1090 K could be calculated from eqs.

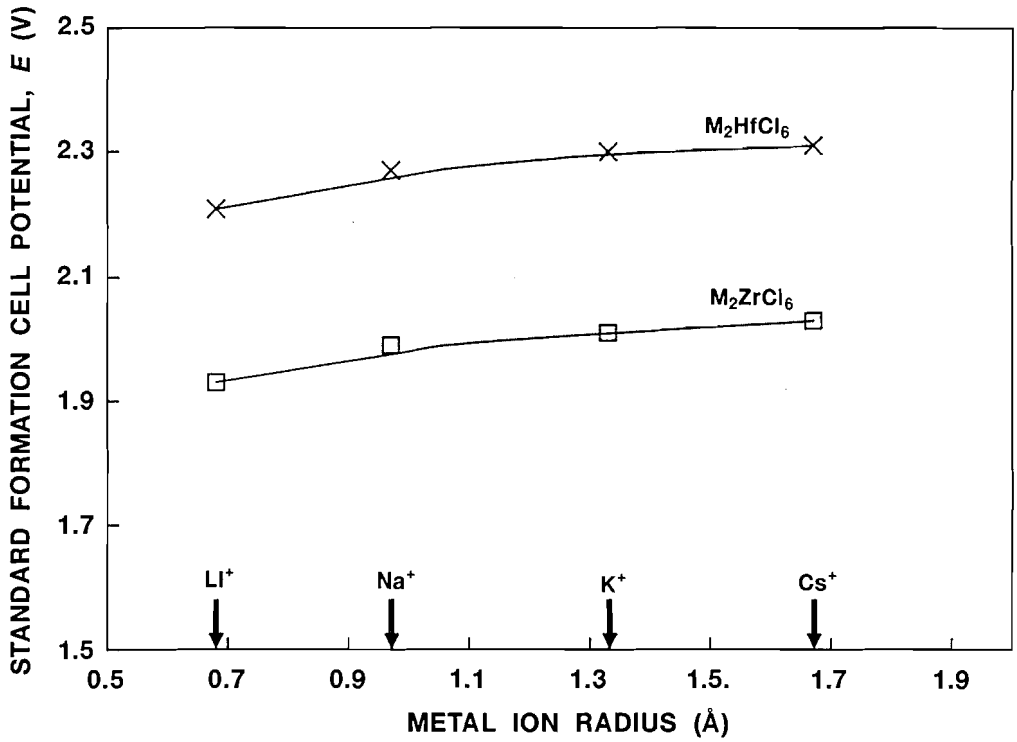

FIG. 1. Standard formation cell potentials of the solid alkali chlorozirconate and chlorohafnate compounds plotted as functions of the radii of the alkali metal cations.

TABLE 6. Standard cell potential for the formation of A_2MCl_6 with respect to liquid standard states

$$E_4^0 = e_1 + e_2T + e_3T \ln T - e_4T^2 \text{ (V)}$$

Compound	e_1	$e_2 \times 10^3$	$e_3 \times 10^4$	$e_4 \times 10^8$	E^0 at melting temperature (K)	
Li_2ZrCl_6	2.336	−1.92	2.48	4.94	2.157	808
Li_2HfCl_6	2.667	−400	5.90	−56.14	2.251	830
Na_2ZrCl_6	2.300	0.42	−1.13	3.30	2.009	919
K_2ZrCl_6	2.403	−0.65	0.26	4.71	1.960	1072
Cs_2ZrCl_6	2.270	0.41	−0.84	−8.56	1.973	1090

TABLE 7. Activities of ACl and of A_2MCl_6 in the two respective solutions NaCl-Na_2ZrCl_6 and KCl-K_2ZrCl_6 at the melting temperatures of the complex compounds

$$\log_{10} \gamma_{Na_2ZrCl_6} = \frac{0.06}{2.3RT} + \frac{x^2_{NaCl}1950}{2.3RT}$$

$$\log_{10} \gamma_{K_2ZrCl_6} = \frac{0.06}{2.3RT} + \frac{x^2_{KCl}1470}{2.3RT}$$

where $R = 1.987$ cal deg^{-1} mol^{-1} and T is in degrees K

x_{ACl} overall system ACl-MCl_4	x_{ACl} subsystem ACl-A_2MCl_6	$x_{A_2MCl_6}$ subsystem ACl-A_2MCl_6	NaCl–Na_2ZrCl_6 at 919 K		KCl–K_2ZrCl_6 at 1072 K	
			a_{NaCl}	$a_{Na_2ZrCl_6}$	a_{KCl}	$a_{K_2ZrCl_6}$
1.0	1.0	0.0	1.0	0.0	1.0	0.0
0.857	0.8	0.2	0.835	0.396	0.830	0.311
0.778	0.6	0.4	0.675	0.587	0.675	0.513
0.728	0.4	0.6	0.550	0.712	0.50	0.670
0.692	0.2	0.8	0.405	0.835	0.32	0.822
0.667	0.0	1.0	0.28	1.0	0.24	1.0

Can. J. Chem. Downloaded from www.nrcresearchpress.com by 213.200.69.106 on 09/08/12
For personal use only.

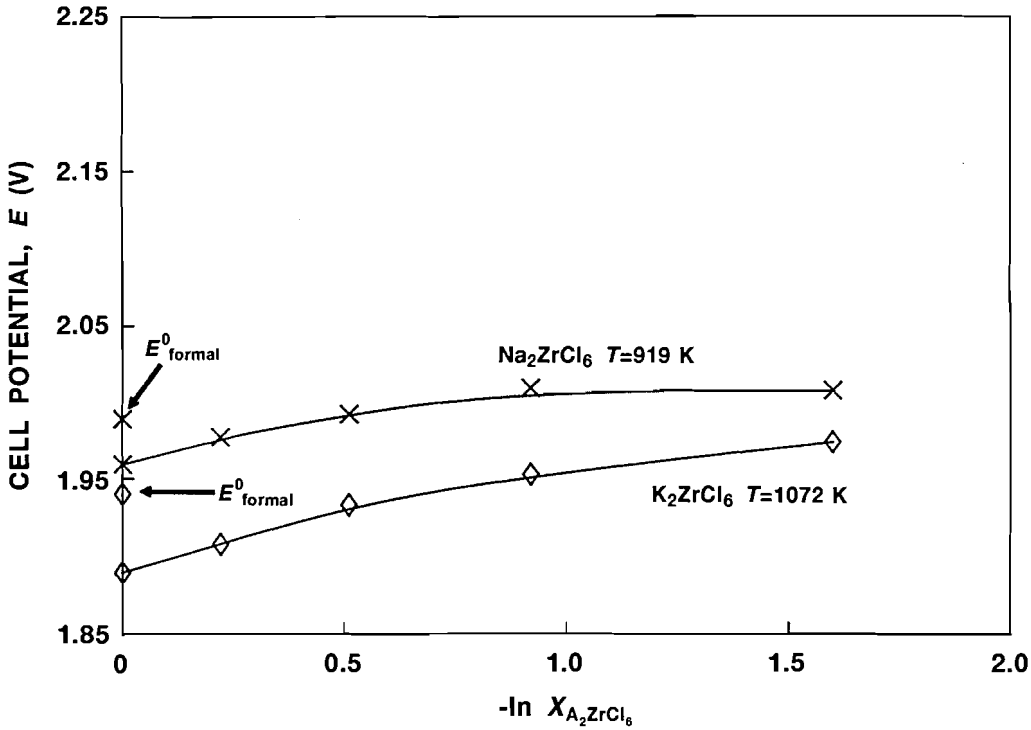

FIG. 2. Cell potentials in the solutions of Na_2ZrCl_6 in NaCl and K_2ZrCl_6 in KCl, as functions of the mole fractions of the complex compounds. Cell potentials represent the reactions for the formation of the complexes from the elements, according to eq. [5]. The "true" standard potentials with respect to the liquid standard states are shown at the extrapolation of these curves to unit mole fractions. Also, "formal" potentials are given as 1.989 V for Na_2ZrCl_6 and 1.940 V for K_2ZrCl_6.

[26] and [27], using the approximate value (15, 20) for b of 930 cal/mol. For $x_{Cs_2ZrCl_6} = 0$, the Henrian activity coefficient is 1.534. The approximate formal potential at 1090 K was calculated from the standard formation potential in Table 6, using eq. [27], as 2.167 V. Current-voltage curves obtained during the electrowinning of Zr metal by fused-salt electrolysis from solutions of Cs_2ZrCl_6 in CsCl containing about 5 mol% Cs_2ZrCl_6, at 950 K, indicated a decomposition voltage of 2.1 V. Instantaneous emf measurements obtained in a previous investigation (14) at 973 K indicated a formal potential having the value of 2.218 V. This value could be significantly different from the true equilibrium value because of the changes in the initial composition of the solution due to the metal solubility reactions mentioned earlier. Nevertheless, the calculated formal potential of 2.167 V appears to be a reasonable value that is compatible with experimental evidence. Comparable calculations for melts containing $HfCl_4$ could not be made because the required vapour pressure data on the A_2HfCl_6-ACl pseudobinary systems are not available.

Conclusions

The standard formation cell potentials for Li_2ZrCl_6, Li_2HfCl_6, Na_2ZrCl_6, Na_2HfCl_6, K_2ZrCl_6, K_2HfCl_6, Cs_2ZrCl_6, and Cs_2HfCl_6 have been calculated, with respect to solid and liquid standard states, from available thermochemical data and experimentally measured vapour pressures. Cell potentials for the ACl–A_2ZrCl_6 melts at various compositions were also calculated from the standard formation cell potentials and existing activity data.

It is shown that the correct form of the Nernst equation for a cell representing the formation of a complex compound according to reaction [5] is eq. [19]:

$$E_5 = E_4^0 - \frac{RT}{4F} \ln \frac{a_{A_2MCl_6}}{a_{ACl}^2}$$

From the limiting condition that the solutions of A_2MCl_6 in ACl are expected to obey Henry's law when $x_{A_2MCl_6} = 0$, formal potentials for Na_2ZrCl_6, K_2ZrCl_6, and Cs_2ZrCl_6, respectively, have been calculated. These potentials are useful in that they predict the decomposition potentials of dilute solutions as

$$[28] \quad E_{(decomposition)} = E_{5(formal)} - \frac{RT}{4F} \ln x_{A_2MCl_6}$$

The calculated standard formation potentials from eq. [19] indicate that thermodynamically the Na_2ZrCl_6 complex compound is slightly more stable than K_2ZrCl_6 and that solid Cs_2ZrCl_6 appears to be the most stable of these compounds. This also explains why the CsCl–Cs_2ZrCl_6 melts have shown the least ability to react with Zr metal, as compared with melts containing NaCl and KCl (12, 13).

Acknowledgements

The financial assistance by the Natural Sciences and Engineering Research Council of Canada (NSERC) and by the Technical University of Nova Scotia (TUNS) is gratefully acknowledged.

1. R.L. Lister and S.N. Flengas. Can. J. Chem. **43,** 2947 (1965).
2. J.E. Dutrizac and S.N. Flengas. Adv. Extr. Metall. Proc.

Can. J. Chem. Downloaded from www.nrcresearchpress.com by 213.200.69.106 on 09/08/12
For personal use only.

Symp. paper 24. April 17–20, 1967. The Institution of Mining and Metallurgy, London, England. (1968).
3. G.J. Kipouros and S.N. Flengas. Can. J. Chem. **50,** 990 (1981).
4. G.J. Kipouros and S.N. Flengas. Can. J. Chem. **56,** 1549 (1978).
5. G.J. Kipouros and S.N. Flengas. Can. J. Chem. **61,** 2183 (1983).
6. G.W. Mellors and S. Senderoff. J. Electrochem. Soc. **113,** 60 (1966).
7. M.A. Steinberg, M.E. Siebert, and E. Wainer. Zirconium and zirconium alloys. Am. Soc. Met. Cleveland. 1953. pp. 37–72.
8. A.N. Baraboshkin and K.P. Lebedeva. Transl. no. 6. Tr. Inst. Elektrokhim. Ural. Fil. Akad. Nauk SSSR, **3,** 83 (1966).
9. A.N. Baraboshkin and K.P. Lebedeva. Transl. no. 7. Tr. Inst. Elektrokhim. Ural. Fil. Akad. Nauk SSSR, **4,** 55 (1967).
10. M.M. Wong, J.M. Hiegel, and G.M. Martinez. Electrolytes for electrorefining hafnium. U.S. Bureau of Mines, Report of Investigation RI-6818. 1966.
11. W.R. Opie and K. Svaanstrom. Trans. Metall. Soc. AIME, **215,** 253 (1959).
12. P. Pint and S.N. Flengas. Trans. Inst. Min. Metall. **87,** C29 (1978).
13. G.J. Kipouros and S.N. Flengas. J. Electrochem. Soc. **132,** 1087 (1985).
14. G.J. Kipouros and S.N. Flengas. Proc. 7th Int. Symp. Molten Salts. *Edited by* S.N. Flengas, C.L. Hussey, Y. Ito, and J.S. Wilkes. The Electrochemical Society, Pennington, N.J. Vol. 90-17. 1990. pp. 626–651.
15. S.N. Flengas, J.E. Dutrizac, and R.L. Lister. Can. J. Chem. **46,** 495 (1968).
16. A. Glassner. The thermochemical properties of the oxides, fluorides and chlorides to 2500 K. ANL-5750, Argonne National Laboratory, Argonne, Ill. 1965.
17. J.E. Dutrizac and S.N. Flengas. Can. J. Chem. **45,** 2313 (1967).
18. A.S. Kucharski and S.N. Flengas. Can. J. Chem. **52,** 946 (1974).
19. O. Kubaschewski and C.B. Alcock. Metallurgical thermochemistry. 5th ed. Pergamon Press, New York. 1979.
20. S.N. Flengas and P. Pint. Can. Metall. Q. **8,** 151 (1969).

Can. J. Chem. Downloaded from www.nrcresearchpress.com by 213.200.69.106 on 09/08/12
For personal use only.

An examination of β-enolization in benzobicyclo[2.2.2], [3.2.1], and [3.2.2] ketones[1]

DAVID J. MUIR AND J. B. STOTHERS
Department of Chemistry, University of Western Ontario, London, ON N6A 5B7 Canada

Received March 11, 1993

DAVID J. MUIR and J. B. STOTHERS. Can. J. Chem. **71**, 1290 (1993).

Under homoenolization conditions (*t*-BuO$^-$/*t*-BuOH/185°C), the 3,3-dimethylbenzobicyclo[2.2.2]- and [3.2.1]octen-2-ones (**7**, **8**) and their [3.2.2] homolog (**9**) each undergo β-enolate rearrangement to a single ketone. These rearrangement processes, however, are in competition with Haller–Bauer cleavage, in contrast to the behavior of bicyclo-[2.2.2]octenone, which is not cleaved under these reaction conditions, although Haller–Bauer cleavage was found as a minor process for the [3.2.1] and [3.2.2] analogs. The structures of all products were determined primarily from their ^{1}H and ^{13}C magnetic resonance spectra.

DAVID J. MUIR et J.B. STOTHERS. Can. J. Chem. **71**, 1290 (1993).

Dans des conditions d'homoénolisation (*t*-BuO$^-$/*t*-BuOH/185°C), les 3,3-diméthylbenzobicyclo[2.2.2]- et [3,2,1]oct-2-énones (**7** et **8**) et leur homologue [3.2.2] (**9**) subissent toutes une transposition β-énolique conduisant à une seule cétone. Ces réactions de réarrangements sont toutefois en compétition avec le clivage de Haller–Bauer; ce comportement est en opposition à ce qui est observé avec la bicyclo[2.2.2]octénone qui n'est pas clivée dans ces conditions, même si le clivage de Haller–Bauer est un processus mineur avec ses analogues [3.2.1] et [3.2.2]. La détermination de la structure des produits a été réalisée principalement par résonance magnétique nucléaire du ^{1}H et du ^{13}C.

[Traduit par la rédaction]

Can. J. Chem. Downloaded from www.nrcresearchpress.com by 203.198.23.82 on 09/08/12
For personal use only.

Introduction

Since the discovery of the homoenolization process whereby proton abstraction occurs from a carbon remote from the carbonyl group under strongly basic conditions (1), many examples have been reported for polycyclic ketones (2), as well as for some acyclic systems (3), and a few monocyclic cases (4). In the majority of these examples, the process involves abstraction from β-carbons to form β-enolate intermediates, although there are a few examples involving γ-enolate formation (5).

Several years ago, we investigated β-enolate rearrangements of bicyclo[2.2.2]- and [3.2.1]octanones **1** and **2** under homoenolization conditions (*t*-BuO$^-$/*t*-BuOH/185°C) and, recently, the behavior of the [3.2.2] homolog **3** was examined. While **1** is slowly equilibrated with **4** (6), both **2** and **3** are irreversibly transformed slowly to **5** (7) and **6** (8), respectively. In another study, we found that the reactivity of **1** contrasts sharply with that of bicyclooctenone Δ^5-**1**, which is rapidly equilibrated with a mixture of Δ^2- and Δ^3-**4** under the same conditions (9). Ketone Δ^5-**1** had a half-life of ca. 8 h, rearranging >100 times faster than **1**, with the equilibrium more strongly biased toward the [3.2.1] skeleton and with no evidence of any other product. This activating effect of the double bond in the [2.2.2] system gave rise to the notion that introduction of a double bond in the [3.2.1] and [3.2.2] systems could enhance their rates of rearrangement and thereby provide viable synthetic routes to other carbon skeletons. For example, the isomerization of Δ^6-**2** could offer a route to substituted 3,3-dimethylbicyclo[3.3.0] octane derivatives, a number of which have been employed in the syntheses of various natural products (10). Upon examination, however, it was found that Δ^6-**2** (11) and Δ^6-**3** (8) are each converted to six products, in distinct contrast to the simple rearrangements observed for **1**, Δ^5-**1**, **2**, and **3**.

From these results, it was clear that the olefinic bond enhanced β-enolate formation over that exhibited by the saturated counterparts **1**, **2**, **3**, and **6**, but subsequent migration of the double bond in the [3.3.0] and [4.3.0] skeletons led to reduction of these α,β-unsaturated ketones. Therefore, it seemed reasonable that an investigation of the behavior of the benzo analogs **7**–**9** under typical homoenolization conditions would be interesting since migration of the double bond cannot occur, but the activating effect of a π-system is retained. In this paper, we present the results of these experiments.

Results and discussion

Ketone **7** was prepared as outlined in Scheme 1. As reported previously (12), the reaction of benzyne with 1,3-cyclohexadiene gave a mixture of four addition products in which the major Diels–Alder component **10** was accompanied by two minor components arising from ene addition and one from [2+2] addition. Since these were not easily separated, the total product was hydroborated and then oxidized with alkaline H_2O_2. Upon oxidation by Swern's method (13), this material gave a product containing >85% **11**. Methylation with MeI/$NaNH_2$/Et_2O afforded **7**, which was readily purified by column chromatography.

The preparation of **8** is outlined in Scheme 2. Treatment of benzonorbornadiene, generated from benzyne and cyclopentadiene (12, 14), with borane – methyl sulfide complex followed by reaction with alkaline H_2O_2 gave benzonorbornenol, which was oxidized by Swern's method (13) to benzonorbornenone (**12**). Ring expansion of **12** was accomplished by cyclopropanation of its silyl enol ether **13** to **14**, homoketonization of which gave **15**, a sequence we have found to be effective for many related bicyclic ketones (15). Methylation with MeI/$NaNH_2$/Et_2O furnished **8**.

Ring expansion of **11** following the sequence analogous to that employed for **12** → **15** gave 6,7-benzobicyclo-[3.2.2]nonen-2-one, which was dimethylated to furnish **9**.

Following our usual procedures (16), ketone **7** was dissolved in anhydrous *t*-BuO$^-$/*t*-BuOH (1.0 M) to furnish a solution 0.25 M in **7**. Aliquots of this solution were quickly transferred to glass tubes under nitrogen, sealed under vacuum, and heated to 185°C for varying periods of time (3, 6, 9, 12, 24, 48 h). Neutral material from each tube was iso-

[1]Part 145 in the series ^{13}Cmr studies; for Part 144 see ref. 8.

lated by pentane extraction. The aqueous washings were acidified before extraction with ether to isolate the acidic material. Upon analysis by glc and ^{13}Cmr, each neutral fraction was found to contain **7** and one new ketone. Within 6 h, their relative proportions became constant (47:53), with the new compound in small excess, but the yield of the neutral fraction dropped as that of the acidic fraction slowly increased with time to constitute 43% of the total product after 48 h.

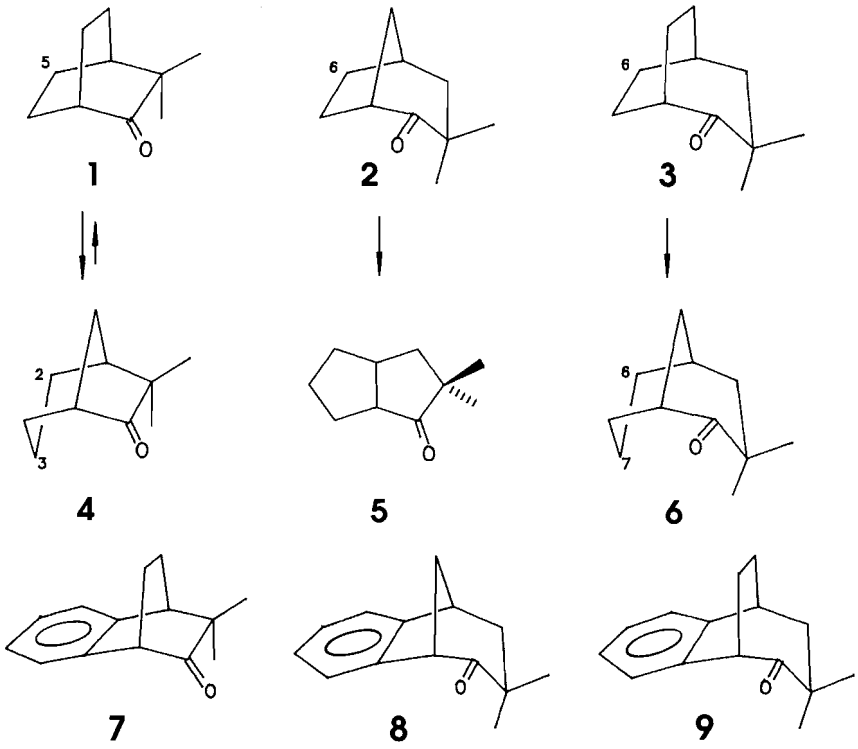

The new ketone, easily isolated from **7** by chromatography on silica, contained a cyclopentanone ring, to judge from its carbonyl absorption (δ_C 225.6, 1742 cm^{-1}), and could be assigned structure **16** by analogy with the rearrangement of **1**. Generation of β-enolate **17** by proton abstraction from C-7 in **7**, with subsequent cleavage of the original C-1,C-2 bond, gives **16** directly. The ^{1}Hmr spectrum fully supported this assignment containing two methyl singlets, two methylene groups absorbing as AB portions of larger spin systems, and two bridgehead methine absorptions as well as the aryl pattern of the benzo substituent.

Each of the acidic fractions contained one acid, which was assigned structure **18** on the basis of the observed spectral data. Haller–Bauer cleavage of **19**, formed by attack of the base at the carbonyl carbon in **7**, can lead to the formation of a benzylic anion and would readily account for the generation of **18**. While the *tert*-butyl ester of **18** must be the initial product, it has been found that these esters do not survive the reaction conditions and are isolated as the corresponding carboxylic acids (17). One can conclude that benzylic stabilization of the intermediate anion from cleavage of **19** renders this process strongly competitive with the β-enolate rearrangement of **7**.

As anticipated, the same ratio of **7** and **16** was found from experiments with **16** as the initial ketone. Their equilibration within 6 h is distinctly faster than that found earlier for their olefinic counterparts, since equilibration of Δ^5-**1** requires ca. 20 h. The [3.2.1] skeleton, however, is favored by a factor of >10 in the olefinic system (9). Another difference is the fact that Haller–Bauer cleavage is a major mode of reaction for **7** but is not observed for Δ^5-**1**.

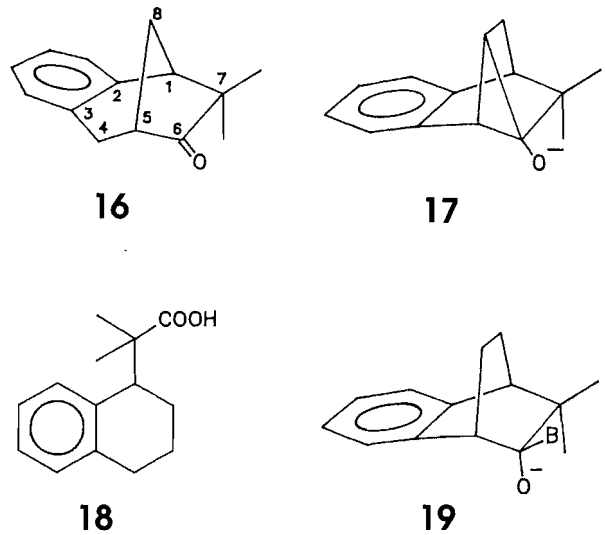

A series of runs with **8** in *t*-BuO$^-$/*t*-BuOH at 185°C was carried out as described for **7**. The yields of neutral products steadily decreased with time and each fraction contained **8** and an isomer, the proportion of which increased with time. The acidic fraction contained a single component constituting nearly half of the total product after 96 h.

Can. J. Chem. Downloaded from www.nrcresearchpress.com by 203.198.23.82 on 09/08/12
For personal use only.

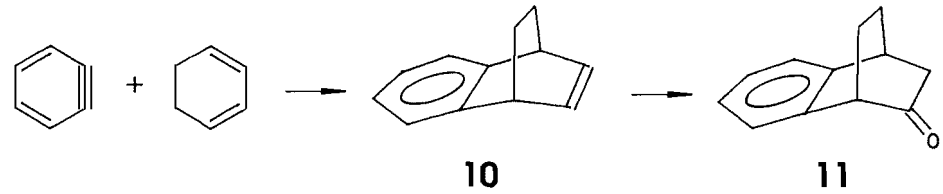

SCHEME 1

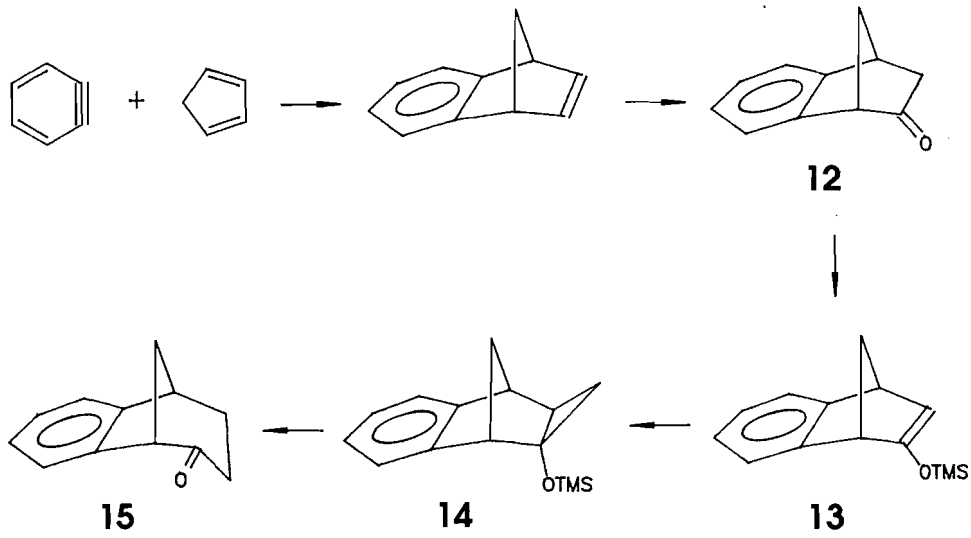

SCHEME 2

The new ketone was readily separated by preparative thin-layer chromatography and shown to be isomeric with **8** by precise mass measurement. Its carbonyl absorption (δ_C 226.0, 1738 cm^{-1}) was distinctly different from that of **8** (δ_C 214.3, 1705 cm^{-1}) and indicated the presence of a cyclopentanone ring. Thus, the ketone was assigned structure **20**, arising by rearrangement after proton abstraction from C-8 in **8** to form **21**, or an equivalent β-enolate. This assignment was confirmed by the nmr results.

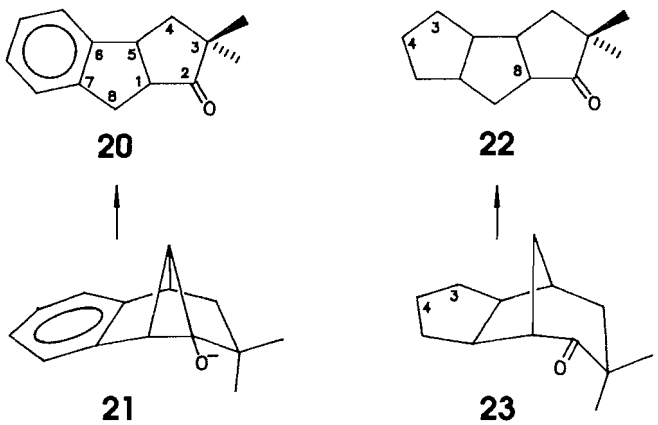

Ketone **22** is formed by β-enolate rearrangement of **23** under strongly basic conditions; Δ^3- and Δ^4-**23** also undergo this process (20). With **8**, however, a substantial acidic fraction was obtained in contrast to the findings for **23** and its unsaturated derivatives from which no acidic products were formed. A single component was present in each of the acidic fractions from **8**, according to the ^{13}Cmr spectra, and was found to be **24**. The generation of **24** must be similar to that of **18**, with Haller–Bauer cleavage enhanced by benzylic stabilization of the intermediate anion formed upon opening of the [3.2.1] species corresponding to **19**. These processes may be compared to that for Δ^6-**2** for which this cleavage is presumably facilitated by allylic stabilization of the resulting anion. The lower yields of acids from Δ^6-**2** (20% after 96 h) indicate that the allylic species is less stabilized than the benzylic intermediate generated through cleavage of **8**.

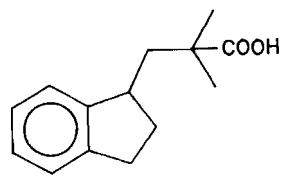

The distribution of the components in the products from the runs with **8** as a function of time is listed in Table 1. From these data, **8** exhibited a half-life of ~16 h, which may be compared with the value of ~40 h found for its olefinic analog Δ^6-**2** under the same conditions (11).

In a third series of experiments, the behavior of **9** upon treatment with *t*-BuO^-/*t*-BuOH at 185°C was found to be analogous to that of **8**. The yields of the neutral fractions decreased with time and each contained a new ketone, the proportion of which increased with time. The acidic fractions contained one component that made up ca. 45% of the product after 48 h.

Preparative tlc of the neutral fractions provided samples

Can. J. Chem. Downloaded from www.nrcresearchpress.com by 203.198.23.82 on 09/08/12
For personal use only.

TABLE 1. Composition[a] of the products from homoenolization of **8** (t-BuO$^-$/t-BuOH/185°C)

Time (h)	**8**	**20**	**24**
12	40	15	31
24	27	25	35
48	11	28	46
72	7	37	43
96	3	36	47

[a]Listed as percentage of the isolated material; the relative amounts of **8** and **20** were determined by glc and ^{13}Cmr.

TABLE 2. Composition[a] of the products from homoenolization of **9** (t-BuO$^-$/t-BuOH/185°C)

Time (h)	**9**	**25**	**27**
3	63	8	14
6	53	17	22
12	41	25	25
24	22	43	22
48	6	44	36
96	<2	49	38

[a]Listed as percentage of the isolated material; the relative amounts of **9** and **25** were determined by glc and ^{13}Cmr.

of the new ketone, which was found to be isomeric with **9** by precise mass measurement. Its carbonyl absorption (δ_C 220.5, 1698 cm^{-1}) is very similar to that for 3,3-dimethylbicyclo[3.3.1]non-6-en-2-one (δ_C 221.3, 1700 cm^{-1}) (8). The ^{1}H, ^{13}C, ^{1}H{^{1}H}, and ^{13}C{^{1}H} COSY nmr data led to the assignment of structure **25**, readily envisaged to arise from **9** by proton abstraction at C-8 to form β-enolate **26**, or an equivalent species, with subsequent cleavage of the original C-1,C-2 bond.

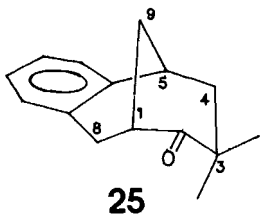

25

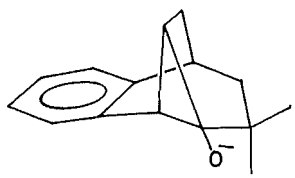

26

As found for **7** and **8**, ^{13}Cmr spectra showed that the acidic fractions from **9** contained a single component. This carboxylic acid, $C_{15}H_{20}O_2$ by precise mass measurement, exhibited signals for eight sp^3 carbons from two methyl, four methylene, one methine, and a quaternary site, together with those for the benzo group and the carboxyl carbon. This acid, assigned structure **27**, presumably arises from Haller–Bauer cleavage of the species analogous to **19**. The composition of the product isolated in these experiments with **9** is listed in Table 2. These data permit comparison of the half-life of **9** with that of its olefinic counterpart Δ^6-**3** under the same conditions, namely, ~8 vs. ~24 h, respectively.

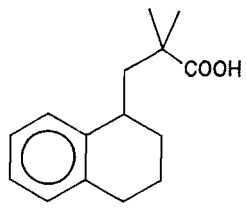

27

Both **3** and **9** undergo rearrangement to stable isomeric ketones **6** and **25**, respectively, whereas their olefinic analog Δ^6-**3** is isomerized to Δ^6-**6**, which, in turn, rapidly equilibrates with Δ^7-**6**, which undergoes a second β-enolate rearrangement. In **25**, the double bond is "locked" in position and cannot activate a suitable proton abstraction for a second β-enolate rearrangement. In both Δ^6-**3** and **9**, the π-system renders each susceptible to Haller–Bauer cleavage, a process that is not observed for **3**.

In summary, we have found that the benzo grouping increases the rate of disappearance of **7**, **8**, and **9** relative to that of Δ^5-**1**, Δ^6-**2**, and -**3**, respectively. Although this appears to supprt our notion that benzylic stabilization of the intermediate carbanions arising through putative β-enolates **17**, **21**, and **26** could accelerate rearrangement, the benzo group renders **7**–**9** susceptible to Haller–Bauer cleavage and precludes synthetic applications of β-enolate rearrangement in these systems, at least with t-BuO$^-$/t-BuOH as base.

Experimental

Boiling points and melting points are uncorrected. Gas–liquid chromatography was carried out on Varian 3300 and 3700 instruments using columns of 5% OV-101 on Chromosorb G and 5% SE-30 on Chromosorb W, respectrively. Tetrahydrofuran (THF) and ether were dried over sodium/benzophenone and freshly distilled before use.

Infrared spectra were recorded using a Bruker/IBM FTIR spectrometer. Mass spectral data were obtained with a Finigan MAT 8230 instrument at 70 eV for routine spectra and at 20 eV for exact mass measurements. Proton and carbon nmr spectra were recorded with Varian Gemini-200, XL-200, or XL-300 spectrometers. The protonation level for each carbon was found by recording the APT or DEPT spectra. Specific assignments for the sp^3 carbon signals of the ketones employed for the homoenolization experiments and their isomeric products were obtained by heteronuclear correlation with the ^{1}H signals. The HETCOR sequence of the Varian software with a 2048 × 512 data point matrix was used to reveal the one-bond interactions and the FLOCK (18) sequence served to identify the two- and three-bond interactions. The HOMCOR sequence of the Varian software was employed for ^{1}H{^{1}H} COSY-45 spectra with a 1024 × 1024 data matrix.

3,3-Dimethyl-5,6-benzobicyclo[2.2.2]octen-2-one (7)

Benzenediazonium-2-carboxylate was prepared according to Logullo, Seitz, and Friedman (14) from anthranilic acid (33.2 g), isoamyl nitrite (53.4 mL), and trifluoroacetic acid (0.2 mL) in tetrahydrofuran (150 mL) in the glassware described by Crews and Beard (12). After draining the solvent and washing with THF, the solvent was replaced with CH_2Cl_2 (150 mL). Then, freshly prepared cyclohexadiene (33 mL) was added rapidly and the reaction mixture was refluxed for 4 h. After the solvent was removed, the black oil was taken up in pentane and the solids removed by filtration and washed thoroughly with pentane. After removal of the solvent, the product was distilled to furnish a mixture of four olefins (27.3 g, 72% yield), bp 102–106°C/15 Torr (1 Torr = 133.3 Pa). The major component was benzobicyclo[2.2.2]octadiene (**10**), constituting ca. 50% of the product, together with two products from ene addition (each ca. 20%) and one from [2+2] addition (ca. 10%) (12). With two additional runs, 87.5 g of the mixture of olefins was obtained. Since these products were not

Can. J. Chem. Downloaded from www.nrcresearchpress.com by 203.198.23.82 on 09/08/12
For personal use only.

Can. J. Chem. Downloaded from www.nrcresearchpress.com by 203.198.23.82 on 09/08/12
For personal use only.

easily separated by chromatography, the mixture was used in the following step.

This mixture of olefins (87.5 g, 560 mmol) was dissolved in hexane (250 mL) and the solution cooled to 0°C before 10 M $BH_3 \cdot Me_2S$ (45 mL) was added dropwise. This reaction mixture was stirred for 3 h at room temperature and then refluxed for another hour. The solution was cooled to 0°C before the sequential, dropwise addition of ethanol (150 mL), 3 M NaOH (100 mL), and 30% H_2O_2 (100 mL). This mixture was refluxed for 1.5 h, and then cooled before its addition to brine (100 mL). The layers were separated and the aqueous phase extracted with hexane (5 × 200 mL). The combined extracts were washed with brine (150 mL) before drying over anhydrous $MgSO_4$. The solvent was removed to afford 67.8 g of waxy product consisting of a 4:2:1 mixture of three alcohols according to its ^{13}Cmr spectrum.

Dimethyl sulfoxide (0.9 mL, 12.6 mmol) and CH_2Cl_2 (10 mL) were combined and cooled to −78°C under nitrogen before oxalyl chloride (2.0 M in CH_2Cl_2, 3.2 mL) was added dropwise. The solution was stirred for 15 min and then a portion of the product from the preceding step (1.0 g, 5.75 mmol) in CH_2Cl_2 (5 mL) containing DMSO (1 mL) was added dropwise. After rapid addition of Et_3N (4 mL), the solution was allowed to warm to room temperature before it was poured into water (50 mL). The layers were separated and the aqueous phase was extracted with CH_2Cl_2 (50 mL). The combined extracts were washed with HCl (50 mL, 1 M) and brine (50 mL) before drying over anhydrous $MgSO_4$. Removal of the solvent gave a yellow oil (0.9 g) containing ca. 80% of benzobicyclo[2.2.2]octenone (**11**), judging from its ^{13}Cmr spectrum, which represented a 50% yield from the mixture of olefins; ^{13}Cmr ($CDCl_3$) δ_C: CH_2, 23.4, 24.9, 36.3; CH, 41.8, 52.4; aryl CH, 123.7, 125.4, 126.8, 127.2; aryl C, 136.4, 142.8; C=O, 211.7.

To a stirred suspension of freshly powdered $NaNH_2$ (2.87 g, 73.5 mmol) in dry ether (10 mL) was added a solution of impure **11** (2.0 g, 11.6 mmol) in dry ether (10 mL) and this mixture heated under reflux for 2 h with vigorous stirring. The mixture was then cooled and methyl iodide (4.4 mL) was added slowly before refluxing the mixture for 16 h after which time a second addition of methyl iodide (1.4 mL) in dry ether (5 mL) was made. After refluxing for 3 h, the mixture was cooled to 0°C and the excess $NaNH_2$ destroyed by the addition of cold water (50 mL). The ether layer was separated and the aqueous phase extracted with ether (2 × 75 mL). The combined extracts were washed with brine before drying over anhydrous $MgSO_4$. Removal of the solvent gave ketone **7** (2.13 g, 92% yield) as a yellow oil that glc analysis indicated to be >90% pure. Chromatography on silica furnished suitable samples for the homenolization experiments. An analytical sample was obtained by sublimation at 100°C/1 Torr; mp 37.0–37.5°C; ir ($CHCl_3$): 1725 cm^{-1}; ^{1}Hmr ($CDCl_3$) δ: 0.73 (s, 3H, *endo*-3-Me), 1.23 (s, 3H, *exo*-3-Me), 1.47 (dddd, 1H, J = 12.6, 11.8, 5.2, 2.6 Hz, *syn*-H-8), 1.71 (ddt, 1H, J = 12.8, 11.8, 3.2 Hz, *syn*-H-7), 1.99 (dddd, 1H, J = 12.8, 10.2, 5.2, 2.0 Hz, *anti*-H-7), 2.20 (dddd, 1H, J = 12.6, 10.2, 3.2, 3.0 Hz, *anti*-H-8), 2.93 (dd, 1H, J = 2.6, 3.0 Hz, H-4), 3.55 (dd, 1H, J = 2.0, 3.2 Hz, H-1), 7.13–7.24 (m, 4H, aryl H); ^{13}Cmr ($CDCl_3$) δ_C: 23.8 (*exo*-3-Me), 26.0 (*endo*-3-Me), 21.4 (C-8), 23.1 (C-7), 44.3 (C-3), 48.1 (C-4), 52.6 (C-1), 124.8, 125.3, 126.8, 127.1 (aryl CH), 135.2, 143.6 (aryl C), 216.7 (C=O). Exact Mass calcd. for $C_{14}H_{16}O$: 200.1202; found: 200.1201.

*Benzonorbornenone (**12**)*

Benzenediazonium-2-carboxylate was prepared from anthranilic acid (34.5 g), isoamyl nitrite (54 mL), and trichloroacetic acid (250 mg) in THF (200 mL) following the procedure of Logullo, Seitz, and Friedman (14) using the glassware described by Crews and Beard (12). The solvent was replaced with CH_2Cl_2 (150 mL) and freshly distilled cyclopentadiene (50 mL) was added before the mixture was heated under reflux for 5 h. After removal of the solvent, the residue was taken up in pentane and the insoluble material removed by filtration through Celite. After the pentane was removed, the residue was distilled to furnish benzonorbornadiene (22.0 g, 65% yield), bp 84–86°C/12 Torr (lit. (21) bp 82.5–83.0°/12 Torr).

This product was dissolved in dry hexane (75 mL) in a flame-dried flask under dry nitrogen and cooled to 0°C before dropwise addition of 10 M $BH_3 \cdot Me_2S$ (9.5 mL) with stirring. The ice-bath was removed and stirring was continued for 3 h before cooling again to 0°C. The temperature was maintained at <40°C during the sequential dropwise addition of absolute ethanol (100 mL), 30 M NaOH (40 mL), and 30% H_2O_2 (40 mL). This reaction mixture was refluxed for 1 h and, after cooling to room temperature, the product was recovered by pentane extraction (4 × 100 mL). These extracts were washed with water (50 mL) and brine (50 mL); these washings were back-extracted with pentane (25 mL). The combined extracts were dried over anhydrous $MgSO_4$ before the solvent was removed to furnish white, crystalline benzonorbornenol (22.3 g, 90% yield), mp 67–70°C (lit. (22) mp 74.1–75.4°C), which was used without further purification.

A solution of anhydrous dimethyl sulfoxide (0.7 mL) in dry CH_2Cl_2 (5 mL) was cooled to −78°C, under nitrogen. This solution was rapidly stirred during the dropwise addition of a solution of trifluoroacetic anhydride (1.0 mL) in CH_2Cl_2 (3 mL) and stirring was continued for 10 min. Then a solution of benzonorbornenol (800 mg) in CH_2Cl_2 (5 mL) was slowly added and the solution stirred for 10 min before the cold bath was removed. After this mixture had warmed to room temperature, triethylamine (2 mL) was added and stirring was continued for 45 min before the addition of brine (10 mL). The organic layer was separated and the aqueous layer extracted with CH_2Cl_2 (10 mL). The combined organic extracts were dried over anhydrous magnesium sulfate before removal of the solvent. Distillation of the residue through a short-path column gave **12** (760 mg, 95% yield) bp 98–102°C/2 Torr (lit. (23) bp 65–75°C/0.02 Torr).

*6,7-Benzobicyclo[3.2.1]octen-2-one (**15**)*

A solution of lithium diisopropylamide (LDA) was prepared in a flame-dried flask under nitrogen at −78°C by dropwise addition of diisopropylamine (5.8 mL, 41.5 mmol) to *n*-butyllithium (14.5 mL, 2.5 M in hexane, 36.3 mmol) in dry THF (25 mL). After stirring for 15 min, a solution of **12** (4.1 g, 25.9 mmol) in THF (5 mL) was added and stirring continued for 1 h at −78°C. A quenching solution of trimethylsilyl chloride (6.6 mL) and triethylamine (2 mL) in dry THF (5 mL) was prepared in a flamed, nitrogen-purged centrifuge tube. The precipitate was removed by centrifugation and the clear solution rapidly added at −78°C to the reaction mixture, which was then allowed to warm to room temperature before the addition of cold, saturated aqueous Na_2CO_3 solution (100 mL). The product was extracted with pentane (3 × 100 mL) and the extracts washed with brine (50 mL) before drying over anhydrous $MgSO_4$. After removal of the solvent, Kugelrohr distillation afforded **13** (5.6 g, 94% yield), bp 115°C/2 Torr; ^{1}Hmr ($CDCl_3$) δ: 0.17 (s, 9H, $SiMe_3$), 2.30 (ddt, 1H, J = 6.9, 0.5, 1.7 Hz, *anti*-H-7), 2.51 (dt, 1H, J = 6.9, 1.6 Hz, *syn*-H-7), 3.47 (m, 1H, H-1), 3.75 (dt, 1H, J = 3.3, 1.7 Hz, H-4), 5.35 (bd, 1H, J = 3.3 Hz, H-3), 6.9–7.3 (m, 4H, aryl H); ^{13}Cmr ($CDCl_3$) δ_C: $SiMe_3$, −0.1; CH_2, 67.4; CH, 48.3, 53.8, 110.5; aryl CH, 120.4, 121.6, 123.8, 124.5; C, 150.5, 153.3, 171.0. Exact Mass calcd. for $C_{14}H_{18}OSi$: 230.1127; found: 230.1133.

To a flask fitted with a reflux condenser, nitrogen purge, and magnetic stirrer was added zinc–silver couple (3.82 g, 58.4 mmol). The apparatus was flame-dried and then cooled to room temperature before the addition of CH_2I_2 (2.6 mL, 32.9 mmol) in dry ether (10 mL). The mixture was warmed with stirring until refluxing occurred without external heating. Upon cessation of reflux, a solution of **13** (4.5 g, 19.6 mmol) in ether (30 mL) was added and the mixture refluxed for 17 h before cooling to room temperature. While the mixture was stirred, pyridine–ether (1:1, 14 mL) was added slowly until precipitation ceased. Then the precipitate was removed by filtration and thoroughly washed with ether. After evaporation of the ether, the residue was taken up in pentane and

Can. J. Chem. Downloaded from www.nrcresearchpress.com by 203.198.23.82 on 09/08/12
For personal use only.

passed through Celite to remove the last traces of precipitate before drying over anhydrous $MgSO_4$. Kugelrohr distillation of the material remaining after the removal of the solvent gave the cyclopropanated ether **14** (2.9 g, 61% yield), bp 125–128°C/2 Torr; ^{13}Cmr ($CDCl_3$) δ_C: $SiMe_3$, 0.8; CH_2, 21.2, 42.0; CH, 26.1, 43.0, 49.2; quat C, 67.5; aryl CH, 120.8, 122.9, 124.7, 125.1; aryl C, 149.0, 150.6. Exact Mass calcd. for $C_{15}H_{20}OSi$: 244.1284; found: 244.1283.

To a methanolic NaOH solution (3 M, 20 mL) was added ether **14** (2.84 g). The reaction mixture was stirred at room temperature for 24 h before the addition of brine (50 mL) and extraction with pentane (3 × 50 mL). The combined extracts were washed with brine (50 mL) before drying over anhydrous $MgSO_4$. The solvent was removed to furnish ketone **15** (1.98 g, 98% yield; ir (liq. film): 1719 cm^{-1}; ^{13}Cmr ($CDCl_3$) δ_C: CH_2, 29.4, 34.3, 43.2; CH, 40.1, 57.3; aryl CH, 123.1_6, 123.2_2, 126.8, 127.9; aryl C, 142.2, 146.0; C=O, 209.4. Exact Mass calcd. for $C_{12}H_{12}O$: 172.0889; found: 172.0885.

3,3-Dimethyl-6,7-benzobicyclo[3.2.1]octen-2-one (8)

To a stirred suspension of freshly powdered $NaNH_2$ (1.14 g, 29.2 mmol) in dry ether (5 mL) was added a solution of **15** (837 mg, 4.87 mmol) in dry ether (5 mL) and the mixture heated under reflux for 2 h with vigorous stirring. The mixture was cooled and methyl iodide (1.8 mL, 29 mmol) was added slowly before the mixture was refluxed for 16 h after which time a second addition of methyl iodide (0.6 mL, 9.8 mmol) in dry ether (5 mL) was made. After refluxing for 3 h, the mixture was cooled to 0°C and the excess $NaNH_2$ destroyed by the addition of cold water (25 mL). The ether layer was separated and the aqueous phase extracted with ether (2 × 25 mL). The combined ether extracts were washed with brine before drying over anhydrous $MgSO_4$. Removal of the solvent gave essentially pure **8** (912 mg, 93% yield) from which trace impurities were readily removed by chromatography on neutral alumina; ir (liq. film): 1705 cm^{-1}; ^{1}Hmr ($CDCl_3$) δ: 0.38 (s, 3H, *endo*-3-Me), 1.14 (s, 3H, *exo*-3-Me), 1.85 (dt, 1H, J = 13.5, 2.8 hz, *endo*-H-4), 2.04 (dd, 1H, J = 13.5, 3.9 Hz, *exo*-H-4), 2.21 (d, 1H, J = 11.4 Hz, *syn*-H-8), 2.71 (ddt, 1H, J = 11.4, 2.8, 4.8 Hz, *anti*-H-8), 3.41 (m, 1H, H-5), 3.69 (d, 1H, J = 4.8 Hz, H-1), 7.1–7.4 (m, 4H, aryl H); ^{13}Cmr ($CDCL_3$) δ_C: 29.8 (*exo*-3-Me), 32.0 (*endo*-3-Me), 41.0 (C-5), 42.0 (C-8), 43.6 (C-3), 44.3 (C-4), 57.2 (C-1), 123.2, 123.5, 126.9, 127.9, (aryl CH), 142.0, 147.0 (aryl C), 214.3 (C=O). Exact Mass calcd. for $C_{14}H_{16}O$: 200.1202; found: 200.1206.

3,3-Dimethyl-6,7-benzobicyclo[3.2.2]nonen-2-one (9)

To a solution of LDA prepared at −78°C from diisopropylamine (4.0 mL) and *n*-butyllithium (10 mL, 2.5 M in hexane) in THF (10 mL) was added **11** (3.1 g) in THF (5 mL) and this mixture was stirred at −78°C for 45 min. During this time, a flame-dried, nitrogen-purged centrifuge tube was charged with trimethylsilyl chloride (4.5 mL), triethylamine (1.5 mL), and THF (2 mL). The precipitate was removed by centrifugation and the clear supernatant liquid was injected rapidly into the reaction mixture. The solution was allowed to warm to 0°C and then was poured into a saturated aqueous solution of Na_2CO_3 (100 mL) in a separatory funnel. The layers were separated and the aqueous layer extracted with ether (3 × 75 mL). The combined extracts were washed with brine before drying over $MgSO_4$. After removal of the solvent, the residual yellow oil (5.2 g) was purified by Kugelrohr distillation at 120°C/1.5 Torr to furnish the trimethylsilyl enol ether of **11** (3.6 g, 81% yield).

Following the preparative procedure described above for **14**, a solution of methylene iodide (2.0 mL) in ether (5 mL) was added to Zn–Ag couple (2.5 g) and the mixture heated until reflux proceeded without external heating. When reflux ceased, the grey solution was sonicated for 15 min before the silyl enol ether of **11** (3.0 g) was added. The reaction mixture was refluxed for 40 h and then cooled to 0°C before a 1:1 pyridine–ether solution was added until no more white precipitate formed (5 mL). The precipitate was removed by filtration and the solid was washed with ether (3 × 30 mL). After the ether washings were dried over $MgSO_4$, removal of the solvent gave a yellow oil (2.9 g). Kugelrohr distillation gave the desired cyclopropanated ether (2.4 g, 71% yield); bp 120°C/1.5 Torr; ^{13}Cmr ($CDCl_3$) δ_C: $SiMe_3$, 1.1; CH_2, 11.1, 21.7, 25.4; CH, 19.1, 35.5, 42.6; quat C, 57.7; aryl CH, 123.8, 124.0, 125.8, 126.3; aryl C, 139.7, 141.4. Exact Mass calcd. for $C_{16}H_{22}OSi$: 218.1441; found: 218.1443.

The cyclopropyl ether (2.4 g) was dissolved in 3 M methanolic NaOH solution (25 mL) and stirred for 18 h. The solution was then poured into 100 mL of 10% aqueous NaCl solution and the product extracted with pentane (3 × 75 mL). After washing with brine, the extracts were dried over $MgSO_4$. The solvent was removed to furnish 6,7-benzobicyclo[3.2.2]nonen-2-one (1.7 g, 98% yield); ir (liquid film): 1705 cm^{-1}; ^{1}Hmr ($CDCl_3$) δ: 1.84–2.05 (m, 5H), 2.10–2.27 (m, 2H), 2.44 (m, 1H), 3.29 (m, 1H, H-5), 3.61 (m, 1H, H-1), 7.13–7.29 (m, 4H); ^{13}Cmr ($CDCl_3$) δ_C: CH_2, 24.5, 26.3, 31.1, 38.3; CH, 37.1, 55.0; aryl CH, 126.7, 127.0, 127.2, 127.7; aryl C, 136.9, 141.9; C=O, 211.6. Exact Mass calcd. for $C_{13}H_{14}O$: 186.1045; found: 186.1046.

This ketone (1.7 g) was methylated as described above for **7** and **8** using $NaNH_2$ (2.15 g) and methyl iodide (3.4 mL, 1.7 mL). The usual work-up gave **9** as an oily liquid (1.7 g, 89% yield). This product was chromatographed through silica with hexane – ethyl acetate as eluent and this material sublimed at 100°C/1 Torr to yield **9** as long, white needlelike crystals: mp 97.5–98.5°C; ir ($CHCl_3$): 1692 cm^{-1}; ^{1}Hmr ($CDCl_3$) δ: 0.42 (s, 3H, *endo*-3-Me), 1.07 (s, 3H, *exo*-3-Me), 1.7–2.1 (m, 6H), 3.26 (m, 1H, H-5), 3.76 (m, 1H, H-1), 7.0–7.3 (m, 4H, aryl H); ^{13}Cmr ($CDCl_3$) δ_C: CH_3, 29.4, 30.1; CH_2, 24.3, 28.1, 45.9; CH, 37.9, 55.2; quat C, 45.3; aryl CH, 126.4, 126.8, 127.1, 127.6; aryl C, 137.0, 141.9; C=O, 211.7. Exact Mass calcd. for $C_{15}H_{18}O$: 214.1358; found: 214.1362.

Homoenolization experiments

Following the general procedure described previously (16), solutions of **7**, **8**, and **16** in *t*-BuO^-/*t*-BuOH, prepared from potassium metal and *t*-BuOH (H_2O content <50 μg/mL), were made up under N_2 in a mole ratio: ketone/*t*-BuO^-/*t*-BuOH, 1:4:40. Aliquots were then quickly transferred to predried, thick-walled glass tubes and the solutions degassed before sealing under vacuum. In the case of **9**, samples of the solid ketone (27 mg) were weighed directly in the reaction tubes and aliquots of the base solution (0.5 mL) added to each under nitrogen. These tubes were degassed and sealed under vacuum. The tubes were heated in an oil bath at 185°C for varying periods of time. After cooling, the reaction mixture was washed from the tube with brine and the product was extracted with pentane. The combined extracts were washed with 3 M NaOH solution (10 mL) and brine before drying over anhydrous $MgSO_4$. Evaporation of the solvent gave the neutral fraction, which was initially examined by glc and identified by ^{13}Cmr spectra. The aqueous alkaline washings were acidified with 6 M HCl solution to pH 1 and then extracted with ether. After drying, the solvent was removed to furnish an acidic product that was identified by ^{13}Cmr.

7,7-Dimethyl-2,3-benzobicyclo[3.2.1]octen-6-one (16)

The new ketone was separated from **7** by column chromatography on silica and was assigned structure **16** from the following data: ir (liq. film): 1742 cm^{-1}; ^{1}Hmr ($CDCl_3$) δ: 0.72 (s, 3H, *endo*-7-Me), 1.25 (s, 3H, *exo*-7-Me), 2.06 (dd, 1H, J = 1.0, 11.9 Hz, *anti*-H-8), 2.56 (dddd, 1H, J = 1.3, 4.1, 5.5, 11.9 Hz, *syn*-H-8), 2.85 (dddd, 1H, J = 2.0, 2.1, 5.5, 5.9 Hz, H-5), 2.94 (bd, 1H, J = 17.2 Hz, *endo*-H-4), 2.95 (bd, 1H, J = 4.1 Hz, H-1), 3.16 (dd, 1H, J = 5.9, 17.2 Hz, *exo*-H-4), 7.0–7.25 (m, 4H, aryl H); ^{13}Cmr ($CDCl_3$) δ_C: 21.7 (*endo*-7-Me), 24.7 (*exo*-7-Me), 30.3 (C-8), 34.6 (C-4), 45.4 (C-1), 49.6 (C-5), 52.9 (C-7), 125.7, 126.9, 128.8, 129.2 (aryl CH), 132.5, 141.5 (aryl C), 225.6 (C-6). The assignments were completed with the aid of a ^{13}C{^{1}H}COSY spectrum obtained using the HETCOR sequence of the Varian software. Exact Mass calcd. for $C_{14}H_{16}O$: 200.1202; found: 200.1197.

*2-Methyl-2-(1',2',3',4'-tetrahydro-1'-naphthyl)-propionic acid (**18**)*

The acid obtained from **7** was purified by sublimation at 120°C/1 Torr, mp 99–101°C, and identified as **18** from the following data: ir (KBr disc): 2400–3400, 1709 cm^{-1}; ^{1}Hmr ($CDCl_3$) δ: 1.11 (s, 3H, Me), 1.13 (s, 3H, Me), 1.5–1.7 (m, 2H, H-3'), 1.9–2.2 (m, 2H, H-2'), 2.67 (m, 2H, H-4'), 3.46 (m, 1H, H-1'), 7.05–7.20 (m, 4H, aryl H); ^{13}Cmr ($CDCl_3$) δ_C: CH_3, 22.6, 22.7; CH_2, 22.7, 25.5, 30.4; CH, 43.6; quat C, 47.6; aryl CH, 125.4, 125.9, 128.9, 129.4; aryl C, 136.8, 140.2; COOH, 185.3. Exact Mass calcd. for: $C_{14}H_{18}O_2$: 218.1307; found: 218.1305.

*3,3-Dimethyl-6,7-benzobicyclo[3.3.0]octen-2-one (**20**)*

The new ketone was separated from **8** by preparative tlc on Silica Gel 60 F-254 plates (0.5 mm) with petroleum ether – ether (90:10) as eluent and was assigned structure **20** from the following data: ir (liq film): 1738 cm^{-1}; ^{1}Hmr ($CDCl_3$) δ: 0.68 (s, 3H, 3-Me), 1.14 (s, 3H, 3-Me), 2.06 (dd, 1H, J = 13.4, 4.0 Hz, *endo*-H-4), 2.34 (dd, 1H, J = 8.3, 13.4 Hz, *exo*-H-4), 3.1–3.3 (m, 2H, H-8), 3.20 (m, 1H, H-1), 3.90 (ddd, 1H, J = 4.0, 8.0, 8.3 Hz, H-5), 7.14–7.30 (m, 4H, aryl H); ^{13}Cmr ($CDCl_3$) δ_C: 25.2, 25.9 (3-Me's), 35.4 (C-8), 43.4 (C-4), 43.8 (C-5), 46.3 (C-3), 50.6 (C-1), 124.0, 124.9, 127.0(2) (aryl CH), 142.1, 146.2 (aryl C), 226.0 (C=O). These assignments were confirmed from the results of ^{1}H{^{1}H}COSY-45 and one-bond ^{13}C{^{1}H}COSY spectra, using the HOMCOR and HETCOR sequences of the Varian software at 200 and 300 MHz, respectively, and a long-range ^{13}C{^{1}H}COSY spectrum, using the FLOCK sequence (18) at 300 MHz (2048 × 128 matrix, 2.2 kHz (^{13}C), 1.2 kHz (^{1}H) spectral widths, 1.0 s relaxation delay, Δ_1 = 0.09 s and Δ_2 = 0.024 s). Exact Mass calcd. for $C_{14}H_{16}O$: 200.1202; found: 200.1196.

*3-(1'-Indanyl)-2,2-dimethylpropionic acid (**24**)*

The acidic product isolated from **8** was recrystallized from aqueous EtOH to give beige, powdery crystals, mp 105–107°C, and identified as **24** on the basis of these data: ir (KBr disc): 2400–3400, 1696 cm^{-1}; ^{1}Hmr ($CDCl_3$) δ: 1.39 (s, 6H, $(Me)_2$), 1.65–1.90 (m, 2H, H-2'), 2.25–2.50 (m, 2H, H-3'), 2.75–3.05 (m, 2H, H-3), 3.18 (m, 1H, H-1'), 7.18–7.32 (m, 4H, aryl H); ^{13}Cmr ($CDCl_3$) δ_C: 26.2, 25.4 (2-Me's), 31.8 (C-2'), 34.0 (C-3), 41.9 (C-1'), 42.4 (C-2), 46.4 (C-3'), 123.4, 124.3, 126.2, 126.4 (aryl CH), 143.6, 147.5 (aryl C), 184.9 (COOH). Exact Mass calcd. for $C_{14}H_{18}O_2$: 218.1307; found: 218.1305.

*3,3-Dimethyl-6,7-benzobicyclo[3.3.1]nonen-2-one (**25**)*

The ketone obtained from **9** was purified by tlc, as described above for **20**, and recrystallized from aqueous EtOH, mp 112–115°C. It was assigned structure **25** on the basis of the following data: ir ($CHCl_3$): 1698 cm^{-1}; ^{1}Hmr ($CDCl_3$) δ: 0.49 (s, 3H, *endo*-3-Me), 1.09 (s, 3H, *exo*-3-Me), 1.95 (dt, 1H, J = 13.6, 2.7 Hz, *endo*-H-4), 2.05 (dd, 1H, J = 13.6, 4.7 Hz, *exo*-H-4), 2.07–2.25 (m, 2H, H-9), 2.85 (bd, 1H, J = 17.1 Hz, *endo*-H-8), 2.92 (m, 1H, H-1), 3.15 (m, 1H, H-5), 3.16 (dd, 1H, J = 17.1, 7.0 Hz, *exo*-H-8), 7.01 (d, 1H, $J \sim 3$ Hz), 7.12–7.17 (m, 3H); ^{13}Cmr ($CDCl_3$) δ_C: 28.9 (*exo*-3-Me), 29.7 (*endo*-3-Me), 30.2 (C-9), 33.7 (C-5), 34.6 (C-8), 43.0 (C-3), 43.6 (C-1), 48.0 (C-4), 126.4, 126.6, 128.6, 128.8 (aryl CH), 134.8, 140.7 (aryl C), 220.5 (C=O). Exact Mass calcd. for $C_{15}H_{18}O$: 214.1358; found: 214.1352.

*2,2-Dimethyl-3-(1',2',3',4'-tetrahydro-1'-naphthyl)-propionic acid (**72**)*

The single acid isolated from the runs with **9** was purified by recrystallization from EtOH to yield white needles, mp 87–88°C, and identified as **27** on the basis of the following data: ir ($CHCl_3$): 2400–3400, 1698 cm^{-1}; ^{1}Hmr ($CDCl_3$) δ: 1.33 (s, 3H, 2-Me), 1.34 (s, 3H, 2-Me), 1.70 (m, 2H, H-3'), 1.84 (m, 2H, H-2'), 1.87 (dd, 1H, J = 14.5, 2.9 Hz, H-3), 2.09 (dd, 1H, J = 14.5, 10.0, H-3), 2.73 (m, 2H, H-4'), 2.94 (m, 1H, H-1'), 7.03–7.18 (m, 4H, aryl H); ^{13}Cmr ($CDCl_3$) δ_C: CH_3, 24.6, 27.2; CH_2, 19.3, 28.1, 29.5, 47.2; CH, 34.7; quat C, 42.1; aryl CH, 125.6, 125.7, 128.9, 129.1; aryl C, 140.2, 141.7; COOH, 184.8. Exact Mass calcd. for $C_{15}H_{20}O_2$: 232.1464; found: 232.1462.

Acknowledgments

We are grateful for the continued financial support of the Natural Sciences and Engineering Research Council of Canada and we thank Professor W. F. Reynolds for kindly providing the FLOCK pulse sequence and for his helpful comments on the selection of appropriate operating parameters.

1. A. Nickon and J.L. Lambert. J. Am. Chem. Soc. **84**, 4604 (1962); **88**, 1905 (1966).
2. N.H. Werstiuk. Tetrahedron, **39**, 205 (1983).
3. R.A. Dyllick-Brenzinger, V. Patel, M.B. Rampersad, J.B. Stothers, and S.E. Thomas. Can. J. Chem. **68**, 1106 (1990).
4. W. Sifton, J.B. Stothers, and S.E. Thomas. Can. J. Chem. **70**, 1274 (1992).
5. A.K. Cheng, A.K. Ghosh, and J.B. Stothers. Can. J. Chem. **62**, 1385 (1984).
6. A.K. Cheng, J.B. Stothers, and C.T. Tan. Can. J. Chem. **55**, 447 (1977).
7. A.L. Johnson, N.O. Petersen, M.B. Rampersad, and J.B. Stothers. Can. J. Chem. **52**, 4143 (1974).
8. D.J. Muir and J.B. Stothers. Can. J. Chem. **71**, 1099 (1993).
9. A.K. Cheng and J.B. Stothers. Can. J. Chem. **56**, 1342 (1978).
10. M. Demuth and K. Schaffner. Angew. Chem. Int. Ed. Engl. **21**, 820 (1982).
11. G.A. Antoniadis, M.T.M. Clements, S. Pieris, and J.B. Stothers. Can. J. Chem. **65**, 1557 (1987).
12. P. Crews and J. Beard. J. Org. Chem. **38**, 522 (1973).
13. A.J. Mancuso and D. Swern. Synthesis, 165 (1981).
14. F.M. Logullo, A.H. Seitz, and L. Friedman. Org. Synth. **48**, 12 (1969).
15. V. Patel, A.J. Ragauskas, J.B. Stothers. Can. J. Chem. **64**, 1440 (1986).
16. A.L. Johnson, J.B. Stothers, and C.T. Tan. Can. J. Chem. **53**, 212 (1975).
17. A. Nickon, J.L. Lambert, J.E. Oliver, D.F. Covey, and J. Morgan. J. Am. Chem. Soc. **98**, 2593 (1976).
18. W.F. Reynolds, S. McLean, M. Perpick-Dumont, and R. A. Enriquez. Magn. Reson. Chem. **27**, 162 (1989).
19. J.L. Jurlina, A.J. Ragauskas, and J.B. Stothers. Magn. Reson. Chem. **23**, 689 (1985).
20. B.A. Dawson, A.K. Ghosh, J.L. Jurlina, A.J. Ragauskas, and J.B. Stothers. Can. J. Chem. **62**, 2521 (1984).
21. G. Wittig and E. Knauss. Chem. Ber. **91**, 895 (1958).
22. P.D. Bartlett and W.P. Giddings. J. Am. Chem. Soc. **82**, 1240 (1960).
23. D.J. Sandman, K. Mislow, W.P. Giddings, J. Dirlam, and G.C. Hanson. J. Am. Chem. Soc. **90**, 4877 (1968).

Can. J. Chem. Downloaded from www.nrcresearchpress.com by 203.198.23.82 on 09/08/12
For personal use only.

Switchover of reactions of solvated electrons with nitrate ions and ammonium ions in propanol–water solvents

TAE BUM KANG[1] AND GORDON R. FREEMAN[2]
Chemistry Department, University of Alberta, Edmonton, AB T6G 2G2, Canada

Received December 8, 1992

TAE BUM KANG and GORDON R. FREEMAN. Can. J. Chem. **71**, 1297 (1993).

The reaction rate constants of e_s^- with ammonium nitrate (~0.1 mol m^{-3}) in 1-propanol–water and 2-propanol–water binary solvents correspond to $[e_s^- + (NO_3^-)_s]$ reaction in the water-rich solvents, and to $[e_s^- + (NH_4^+)_s]$ reaction in alcohol-rich solvents. The overall rate constant is smaller in solvents with 40–99 mol% water, with a minimum at 70 mol% water. The Arrhenius temperature coefficient is 26 kJ mol^{-1} in each pure propanol solvent, increases to 29 kJ mol^{-1} at 40 mol% water, then decreases to 17 kJ mol^{-1} in pure water solvent. The high reaction rates in the single component solvents, alcohol or water, are limited mainly by solvent processes related to shear viscosity (diffusion) and dielectric relaxation (dipole reorientation). Rate constants reported for concentrated solutions (50–1000 mol m^{-3}) of ammonium and nitrate salts in methanol (Duplâtre and Jonah. J. Phys. Chem. **95**, 897 (1991)) have been quantitatively reinterpreted in terms of the ion atmosphere model.

TAE BUM KANG et GORDON R. FREEMAN. Can. J. Chem. **71**, 1297 (1993).

Les constantes de vitesse de la réaction des e_s^- avec le nitrate d'ammonium (environ 0,1 mol m^{-3}) dans les solvants binaires 1-propanol–eau et 2-propanol–eau ressemblent à celles de la réaction des $[e_s^- + (NH_4^+)_s]$ dans des solvants riches en alcool. La constante globale de vitesse est plus faible dans les solvants ayant de 40 à 99 mol% d'eau; on observe un minimum à 70 mol% d'eau. Le coefficient de température d'Arrhénius, qui est de 26 kJ mol^{-1} dans chacun des deux propanols, augmente à 29 kJ mol^{-1} à 40 mol% d'eau avant de diminuer jusqu'à 17 kJ mol^{-1} dans l'eau pure. Les vitesses de réaction élevées observées dans les solvants purs, alcool ou eau, sont principalement limitées par des processus de solvant reliés à la viscosité de cisaillement (diffusion) et à la relaxation diélectrique (réorientation dipolaire). On a fait appel au modèle ionique atmosphérique pour réinterpréter les constantes de vitesse rapportées antérieurement (Duplâtre et Jonah. J. Phys. Chem. **95**, 897 (1991)) pour des solutions concentrées de sels d'ammonium et de nitrate dans le méthanol.
[Traduit par la rédaction]

Introduction

The reaction of e_s^- with $(NO_3^-)_s$ in alcohol solvents is complex (1–5). An intermediate product apparently undergoes a relatively irreversible further reaction with a solvent molecule to complete the capture of the electron by the nitrate (4). Addition of Ca^{2+} or Mg^{2+} in an equimolar amount to lithium nitrate solutions in ethanol, increases the rate of electron reaction with nitrate by a factor of 30 (1). The catalytic effect is due to ion pairing, which reverses the Coulumbic interaction from the repulsion between e_s^- and $(NO_3^-)_s$ to attraction between e_s^- and $(M^{2+}NO_3^-)_s$ (1), and possibly also offers an easier irreversible step to form $M\langle^{OH}_{ONO}$ rather than the $(NO_2^- + OH^-)_s$ that might form in the absence of the M^{2+} (3, 4).

The initial, transient product of the $e_s^- + (NO_3^-)_s$ reaction is presumably $(NO_3^{2-})_s$. In alkaline water solvent at pH = 9.5 a broad optical absorbance band with a maximum at 250 nm has been attributed to it (6). This absorbance, measured at 290 nm, is formed during the 1-μs radiolysis pulse and decays with a half-life of 12.5 μs at room temperature (~295 K?). In neutral or acidic water (pH ≤ 7.0) the absorbance is weaker and the half-life is only 3 μs. The suggested reactions were (6)

[1] $NO_3^{2-} + H_2O \rightarrow NO_2 + 2OH^-$ pH = 9.0 – 9.5, $t_{1/2}$ = 12.5 μs

[2] $HNO_3^- \rightarrow NO_2 + OH^-$ pH = 4.5 – 7.0, $t_{1/2}$ = 3 μs

An optical absorption at 400 nm was attributed to NO_2. However, at pH = 9.5 and with 0.1 M *tert*-butanol to scavenge OH radicals, there was an absorbance at 400 nm immediately after the 1-μs radiolysis pulse and it increased by only 30% when the NO_3^{2-} decomposed over a 30-μs period (6). At 100 μs after the pulse the absorbance at 400 nm had returned to the end-of-pulse value, after which it decayed on a much longer timescale. The reactions

[3] $2NO_2 \rightarrow N_2O_4$

[4] $N_2O_4 + 2OH^- \rightarrow NO_2^- + NO_3^- + H_2O$

were suggested to occur on a millisecond timescale (6). The end-of-pulse absorbance at 400 nm has not been explained, nor its relatively small increase when the NO_3^{2-} decayed, nor the decay back to the end-of-pulse value at 100 μs. Thus the reaction mechanism in water is not completely known.

Electrons in a higher energy state, before the water has relaxed around them to form the solvated state, have much higher apparent rate constants with concentrated solutions (10^2–10^3 mol m^{-3}) of sodium nitrate than do solvated electrons with dilute solutions (~0.1 mol m^{-3}) of the salt (7). Electrons prior to solvation, e_{ps}^-, might react directly with $(NO_3^-)_s$ to form $(NO_3^{2-})_s$, or with ion pairs to form $(NaNO_3^-)_s$. The reverse of the reaction between the solvated species, $e_s^- + (NO_3^-)_s \rightleftharpoons (NO_3^{2-})_s$, is perhaps not observed after capture of e_{ps}^- because the local solvent structure in that case does not contain an adequate site for e_s^-.

In pure alcohol solvents the overall rate constant for $e_s^- + (NO_3^-)_s$ at 298 K is much smaller than that in pure water (Table 1). This would be consistent with a more rapid protolysis of NO_3^{2-} by water, followed by reaction [2], be-

[1]Permanent address: Chemistry Dept., Sang Myung Women's University, 7 Hong Ji Dong, Jong Ro Gu, Seoul 110-743, Korea.
[2]Author to whom correspondence may be addressed.

Can. J. Chem. Downloaded from www.nrcresearchpress.com by 203.198.23.82 on 09/08/12
For personal use only.

TABLE 1. Solvent parameters at 298 K

Solvent	ε_r[a]	pK_s[b]	D[$R_2C(OH)$—H][c]	$k[e_s^- + (NO_3^-)_s]$ (10^5 m^3 mol^{-1} s^{-1})
HOH	78.5	14.0	(498, HO—H)	94. (ref. 3)
CH_3OH	32.6	16.4	385	0.26 (ref. 3)
C_2H_5OH	24.3	18.8	377	0.68 (ref. 3)
n-C_3H_7OH	20.1	19.3	~377[d]	0.9 (ref. 4)
i-C_3H_7OH	18.4	20.7	~368[d]	6.5 (ref. 4)

[a]Reference 16.
[b]Reference 8.
[c]Reference 9.
[d]By analogy with D[R_3C—H] in alkanes, where R = H or CH_3 (9).

cause the ionic dissociation of water, and hence the concentration of H_s^+ in water, is greater than that of alcohols (the negative exponents pK_s of the autoprotolysis constants (8) are listed in Table 1). However, the rate constants for $e_s^- + (NO_3^-)_s$ in pure alcohol solvents vary inversely with the autoprotolysis constants (vary directly with the negative exponents of the constants, Table 1). This suggests that, while protolysis of NO_3^{2-} is important in water, a different reaction, such as H-atom abstraction, probably occurs in alcohols. The dissociation energies of the $R_2C(OH)$—H bonds (9) decrease in the appropriate order to correlate with the increasing reactivity of the solvent (Table 1). The reaction might be

[5] $(NO_3^{2-})_s + R_2CHOH \rightarrow (NO_2^-)_s + OH_s^- + R_2\dot{C}OH$

Hydrogen atom transfer is sometimes associated with electron transfer reactions, as in the $[(H_2O)_5FeOH]^{2+} + [(H_2O)_6Fe]^{2+}$ exchange (10, 11), and might involve correlated electron and proton transfers.

It is certain that in pure alcohol solvents the solvent participates chemically in the overall $e_s^- (NO_3^-)_s$ reaction.

The recent suggestion (5) that NH_4^+ catalyses e_s^- capture by NO_3^- in methanol through ion pairing is not valid, because pairing of NH_4^+ and NO_3^- in methanol is negligible (12). We have investigated the high reactivity by measuring reaction rate constants and activation energies for (e_s^- + ammonium nitrate) in 1-propanol–water and 2-propanol–water solvents. The rate constant for lithium nitrate is much smaller in 1-propanol than in 2-propanol, and this is a clue to the reaction mechanism (4). Solvated electron reactivity in methanol (3) is similar to that in 1-propanol (4), because solvation properties are similar in different primary alcohols. The measured behavior in 1-propanol can therefore be extrapolated to that in methanol.

Experimental

Materials

The solvents were purified as described earlier (4). Ammonium nitrate (Aldrich, 99.999%), after opening the bottle, was stored in a vacuum desiccator that contained P_2O_5.

Samples were prepared as described in ref. 13.

Methods of temperature control, irradiation, optical measurement, and determination of reaction rate constants were similar to those in refs. 14 and 15. The 100-ns pulses of 336 fJ (2.10 MeV) electrons delivered doses of ~4 J kg^{-1}. The temperature was controlled to ±0.1 K.

Briefly, a 10^{-3} mol m^{-3} solution of solvated electrons was generated by ionizing ~10^{-7} of the solvent molecules with a 100-ns pulse of high-energy electrons. The decay of the solvated electrons was followed by kinetic absorption spectroscopy. The rate of decay was continually processed by computer and the value of the decay half-life was plotted as a function of time on the oscilloscope along with the optical absorbance trace. The decay half-life was independent of time for the reactant solutions, where the concentration of, say, ammonium nitrate was at least an order of magnitude greater than that of e_s^-. This meant that the decay of e_s^- was first order. In pure solvent, where ~10^{-3} mol m^{-3} of H_s^+ and free radicals were produced along with the e_s^- by the radiation, the decay half-life increased with time, and the order was between one and two.

Results and discussion

Second-order rate constants k_2 were determined from the slopes of plots of the measured first-order decay rates of e_{solv}^- in ammonium nitrate solutions over a 5- to 10-fold concentration range within the overall range 0.02–0.6 mol m^{-3}. The solvent composition was varied from pure 1-propanol or 2-propanol to pure water. The temperatures were within the overall range 208–364 K.

Arrhenius plots of k_2 were linear for solvent compositions ≤50 mol% water, and were curved for ≥70 mol% water (Figs. 1 and 2). The change in linearity and in the average slope of the Arrhenius plots of k_2 on going from alcohol-rich to water-rich solvents reflects behavior of Arrhenius plots of shear viscosity (16, 17) and dielectric relaxation time (18–20) in pure 1- or 2-propanol and pure water. Thus the rates of the reactions seem limited mainly by solvent processes, such as the solvent rearrangement involved in solvation and desolvation of reactants and products, or the reaction of solvent with NO_3^{2-}.

The values of k_2 for ammonium nitrate were similar in the two isomeric propanols, contrary to the behavior of lithium nitrate (Fig. 3). The rate constant for ammonium nitrate was about 100 times greater than that for lithium nitrate in 1-propanol, and 10 times greater in 2-propanol (Table 2). The large rate constants for ammonium nitrate in the alcohol-rich solvents are attributed to the reaction of e_s^- with $(NH_4^+)_s$. By contrast, the rate constant for $e_s^- + (NH_4^+)_s$ in water at room temperature has been reported to be very small, (2 or 1.3) × 10^3 m^3 mol^{-1} s^{-1} (21). A recent value of k_2 for e_s^- reaction with ammonium perchlorate in pure water solvent at 298 K is 1.5 × 10^3 m^3 mol^{-1} s^{-1} (22). However, in the primary alcohol 1-butanol containing 20 mol% water, the value of k_2 for ammonium perchlorate at 298 K is 1.2 × 10^7 m^3 mol^{-1} s^{-1} (22). The rate constant for lithium perchlorate is <10^2 m^3 mol^{-1} s^{-1}, so the high rate constant is due to $(NH_4^+)_s$ (22). The rate constant for $(NH_4^+)_s$ in pure 1-propanol sol-

Can. J. Chem. Downloaded from www.nrcresearchpress.com by 203.198.23.82 on 09/08/12
For personal use only.

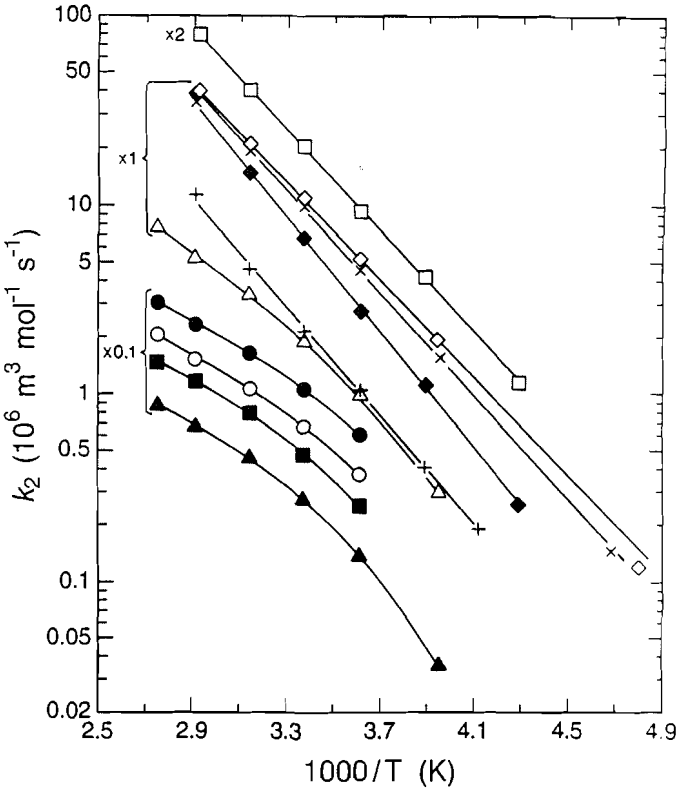

FIG. 1. Arrhenius plots of k_2 of e_s^- reaction with ammonium nitrate in 1-propanol–water solvents. Mol% water: X, 0; ◇, 10; □, 20; ◆, 35; +, 50; △, 70; ▲, 80; ■, 93; ○, 97; ●, 100. To separate the lines the values of k_2 have been multiplied by the factors indicated.

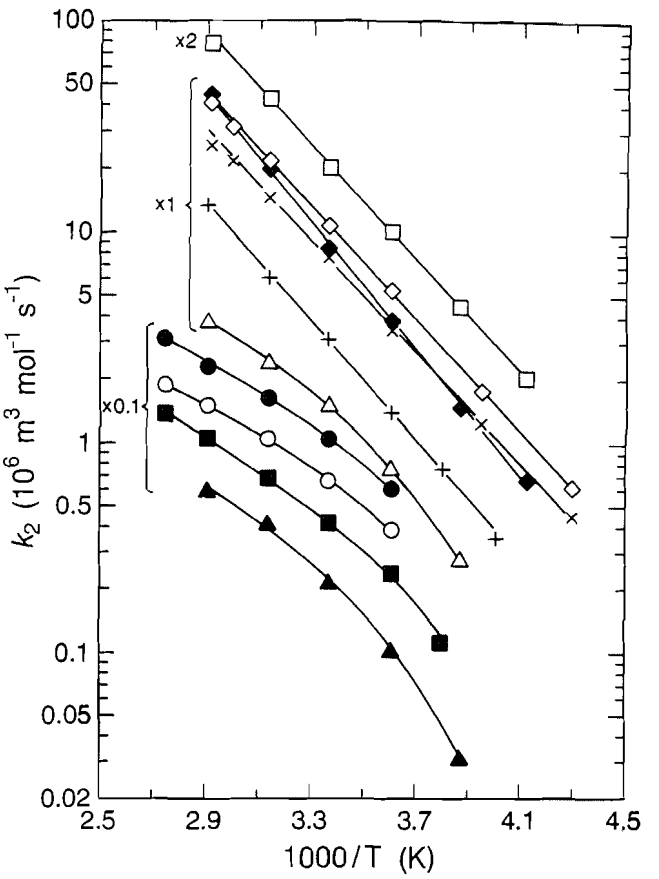

FIG. 2. As Fig. 1, but in 2-propanol–water.

vent, which is also a primary alcohol, would be about 1×10^7 m^3 mol^{-1} s^{-1}; the 20 mol% water has relatively little effect on the $(NH_4^+)_s$ reaction (Fig. 3).

In the secondary alcohol 2-propanol, k_2 for ammonium nitrate is tenfold larger than that for lithium nitrate (Table 2); the large value is attributed to reaction of $(NH_4^+)_s$. Thus the reactivity of e_s^- with $(NH_4^+)_s$ in both primary and secondary alcohols is $\sim 10^4$ times larger than in water (Table 2 and ref. 22). This great difference cannot be attributed to the different electron trap depths, because the optical absorption energy of e_s^- in water is smaller than that in primary alcohols, but larger than that in secondary alcohols (23). We attribute the difference of reactivity of e_s^- with $(NH_4^+)_s$ in water and alcohols to different solvation structures of the NH_4^+. We suggest that NH_4^+ is symmetrically solvated in water and has little tendency to accept an electron. For example, the hydrogen-bonded NH_4^+ fits easily into the liquid water structure. We suggest that NH_4^+ is unsymmetrically solvated in an alcohol. A tetrahedrally hydrogen-bonded NH_4^+ would not fit into the liquid alcohol structure. This asymmetric structure evidently facilitates electron attachment and the subsequent decomposition of $NH_4 \rightarrow H + NH_3$. A similar, but much smaller, effect occurs for the reaction ($e_s^- + H_s^+$) on going from water to an alcohol (24).

The S-curve for $k_2(e_s^-$ + ammonium nitrate) in Fig. 3 represents reaction of e_s^- with $(NO_3^-)_s$ in the water-rich solvents, and with $(NH_4^+)_s$ in the alcohol-rich solvents. The Arrhenius temperature coefficient E_2 of the overall reaction has a small maximum in the transition region (Fig. 3). By contrast, the values of E_2 for the lithium nitrate reactions reach a high maximum in the pure alcohols: 46 kJ mol^{-1} in 1-propanol, and 42 kJ mol^{-1} in 2-propanol (Table 2). These high activation energies are attributed to reaction of e_s^- with $(NO_3^-)_s$, involving an alcohol molecule.

The high values of k_2 and E_2 for ammonium nitrate in the propanols containing 35 mol% water (Fig. 3) correspond to an Arrhenius pre-exponential factor of $A_2 = 1.1 \times 10^{12}$ m^3 mol^{-1} s^{-1}. This large value must contain an entropy factor for solvent rearrangement around the transition state.

Reinterpretation of Duplâtre and Jonah data (5)

Solvated electron reaction rate constants in methanol containing various combinations of the ions NH_4^+, ClO_4^-, Li^+, and NO_3^- at high concentrations, 50–1000 mol m^{-3}, were measured with 25-ps pulses of electrons (5). The temperature was ~296 K.[3] Their interpretation of the data included the assumption that the association constant of ammonium and nitrate ions in methanol,

$$[6] \quad (NH_4^+)_s + (NO_3^-)_s \rightleftharpoons (NH_4NO_3)_s$$

was $K_6 >> 10^4$ M^{-1} (10 m^3 mol^{-1}). However, electrical conductance measurements of ammonium nitrate solutions in methanol, at concentrations from 1 to 995 mol m^{-3} and temperatures from 283 to 328 K, have shown that ion pairing is negligible (12), so reaction [6] can be neglected. The rate constant data in ref. 5 therefore require reinterpretation.

At ion concentrations between 100 and 1000 mol m^{-3} (0.1

[3] C. D. Jonah. Private communication, 24 March 1992.

Can. J. Chem. Downloaded from www.nrcresearchpress.com by 203.198.23.82 on 09/08/12
For personal use only.

Can. J. Chem. Downloaded from www.nrcresearchpress.com by 203.198.23.82 on 09/08/12
For personal use only.

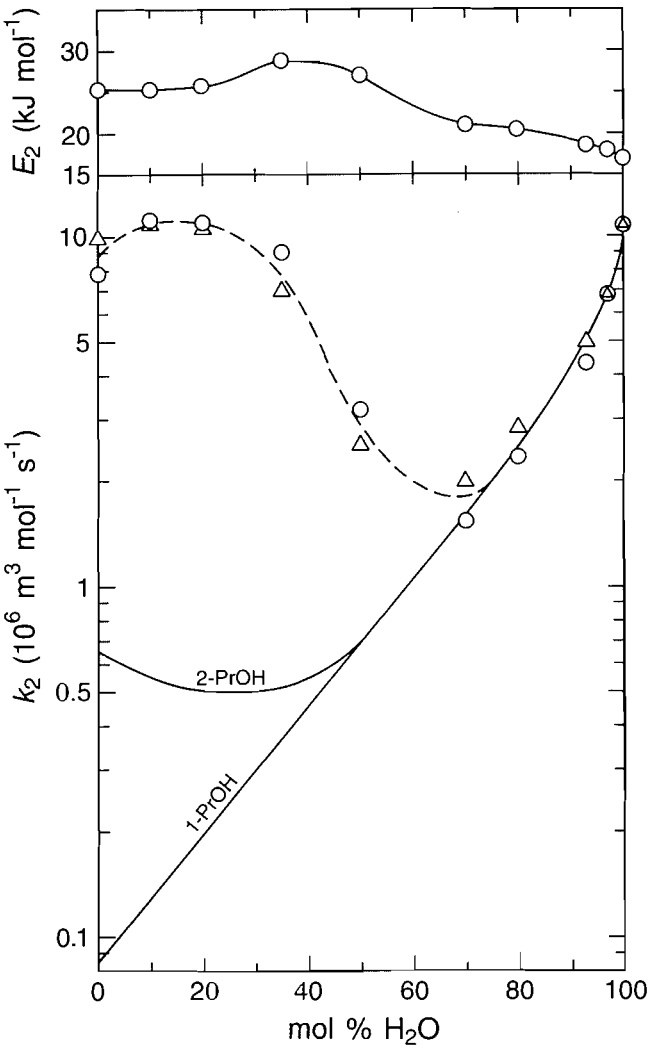

FIG. 3. Arrhenius temperature coefficients E_2 at temperatures near 298 K in both propanols, and values of k_2 (e_s^- + ammonium nitrate) at 298 K in 1-propanol–water (△) and 2-propanol–water (○). The k_2 full lines represent the e_s^- + lithium nitrate reaction (ref. 4). The values of E_2 for the ammonium nitrate reactions in the 1-propanol and 2-propanol systems at a given water content were the same within 1 kJ mol^{-1}.

and 1.0 M) the Debye–Hückel-type eq. [1] of ref. 5 becomes progressively less applicable. (The authors neglected the solvent density, so the ionic strength I in their eqs. [1] and [2] was actually the molar concentration C. This error did not affect the curve-fitting procedure.) At such high concentrations it is preferable to add another term in the manner of the Debye–Hückel–Onsager equation for conductivity (25*a*). We thereby obtain

$$[7] \quad \ln k_2(e_s^- + S) = \ln k_2^0(e_s^- + S) - \frac{aZ_S C^{1/2}}{1 + bC^{1/2}} - dZ_S C$$

where $k_2^0(e_s^- + S)$ is the rate constant at very low ion concentrations, Z_S is the number of protonic charges on the reactant S, b and d are empirical constants that are fitted to the data (25*b*), and (25*c*, *d*)

$$[8] \quad a = \frac{eF^2}{\pi}\left(\frac{1}{2\varepsilon RT}\right)^{3/2}$$

where e = protonic charge, F = Faraday, $\varepsilon = \varepsilon_0\varepsilon_r$ = electric permittivity of the solvent, R = gas constant, and all units are SI. The value of a is related to that of B in the Debye–Hückel–Onsager equation for molar conductivity, which is (12)

$$[9] \quad B = \frac{0.586eF^2}{6\pi}\left(\frac{1}{2\varepsilon RT}\right)^{3/2}$$

In the simpler form of eq. [7] with $d = 0$, the parameter b used to be thought of as a measure of the closest approach of the ions in relatively dilute solutions. However, b is best regarded as an adjustable parameter even for dilute solutions (25*b*). For the concentrated solutions considered here, the model is inadequate to give detailed interpretation to either b or d. This remains a challenge for theorists.

For reaction of e_s^- with $(NH_4^+)_s$ in methanolic ammonium perchlorate at 296 K, $\varepsilon_r = 33.0$ and $a = 0.275$ (m^3 mol^{-1})$^{1/2}$, which gives the full curve in Fig. 4 with $k_2^0 = 1.9 \times 10^6$ m^3 mol^{-1} s^{-1}, $b = 0.466$ (m^3 mol^{-1})$^{1/2}$, and $d = 1.06 \times 10^{-3}$ m^3 mol^{-1}. The value of k_2^0 was taken from the plateau value in Fig. 3 of ref. 5, rather than using k_2^0 as an adjustable parameter. The curve calculated from eq. [7] fits the data at least as well as did the curve of Duplâtre and Jonah (Fig. 4).

For reaction of e_s^- with $(NO_3^-)_s$ in methanolic solutions of lithium nitrate, some of which contained additional lithium perchlorate, the curves calculated from eq. [7] fit the experimental data better than the qualitative curves drawn in Fig. 2 of ref. 5 (see present Fig. 5). Duplâtre and Jonah had neglected the value of $k_2^0 = 2.6 \times 10^4$ m^3 mol^{-1} s^{-1}, obtained at lithium nitrate concentrations 0.02–1.4 mol m^{-3} (3). The value of a is 0.275 (m^3 mol^{-1})$^{1/2}$ as in Fig. 4, but $b = 0.182$ (m^3 mol^{-1})$^{1/2}$ and $d = 1.38 \times 10^{-4}$ m^3 mol^{-1}. The concentration C used in eq. [7] is the total salt concentration, and all of the experimental data in Fig. 5 are fitted by the same equation.

The values of b and d for the methanolic ammonium perchlorate solutions are larger than those for the lithium nitrate/perchlorate solutions. This is probably related to the fact that dissolution of lithium nitrate in methanol at 298 K is 19 kJ mol^{-1} exothermic, while for ammonium nitrate it is 11 kJ mol^{-1} endothermic (26). The ammonium nitrate solutions are therefore "less ideal" electrolytes than are the lithium nitrate solutions, which is indicated by the larger values of b and d for the former.

The value $k_2 = 1.9 \times 10^6$ m^3 mol^{-1} s^{-1} for ammonium nitrate in methanol did not vary with ionic strength (Fig. 3 of ref. 5). The overall reaction of e_s^- with $(NO_3^-)_s$ is multistep, electron capture by $(NO_3^-)_s$ being followed by reaction [5], for example. We suggest that $(NH_4^+)_s$ reacts rapidly with $(NO_3^{2-})_s$:

$$[10] \quad (NO_3^{2-})_s + (NH_4^+)_s \rightarrow NO_2 + OH_s^- + NH_3$$

Thus the net reaction is rapid whether e_s^- first encounters an $(NH_4^+)_s$ or a $(NO_3^-)_s$. Since the $(NH_4^+)_s$ and $(NO_3^-)_s$ ions "screen" each other in ammonium nitrate solutions, and the two ions have opposite ionic strength effects for the reactions with e_s^-, there is no net effect of ionic strength.

There is some uncertainty about the location of the charge in the products of reaction [10], and possibly of reactions [1], [2], and [5]. In the gas phase, the electron affinity (27) of

TABLE 2. Kinetic parameter values in single component solvents at 298 K

Process	Parameter	Solvent H_2O	Solvent 1-PrOH	Solvent 2-PrOH	Ref.
e_s^- + Li^+, NO_3^-	k_2 (10^4 m^3 mol^{-1} s^{-1})	940	9	65	4
	E_2 (kJ mol^{-1})	17	46	42	4
e_s^- + NH_4^+, NO_3^-	k_2 (10^4 m^3 mol^{-1} s^{-1})	1080	990	780	Present
	E_2 (kJ mol^{-1})	17	25	25	Present
e_s^- + NH_4^+, ClO_4^-	k_2 (10^4 m^3 mol^{-1} s^{-1})	0.15	(1200)[a]		22
e_s^- + Li^+, ClO_4^-	k_2 (10^4 m^3 mol^{-1} s^{-1})	0.01	(<0.01)[b]		22
Li^+, NO_3^- conductance	Λ_0 (10^{-3} S m^2 mol^{-1})	11.5	2.0	2.0	4
	E_Λ (kJ mol^{-1})	14	16	22	4
Shear viscosity	η (mPa s)	0.90	2.0	2.0	17
	E_η (kJ mol^{-1})	17	18	22	17
Dielectric relaxation	τ (ps)	8.3[c]	350[d]	350[e]	
	E_τ (kJ mol^{-1})	20[c]	24[d]	27[e]	

[a]1-Butanol solvent containing 20 mol% water. The rate constant in pure 1-propanol solvent would be similar to this.
[b]Pure 1-butanol solvent. The rate constant in pure 1-propanol solvent would be similar to this.
[c]Reference 18.
[d]Reference 19.
[e]Reference 20.

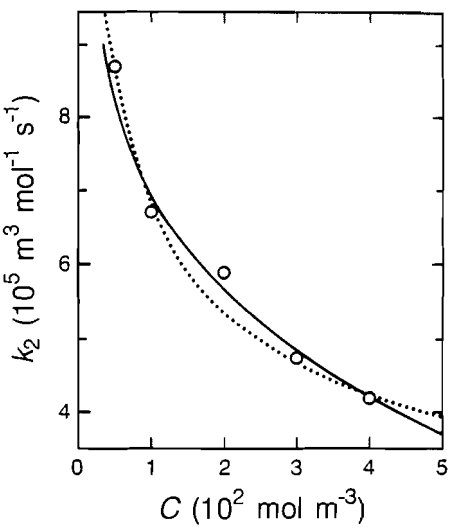

FIG. 4. Reaction of e_s^- with ammonium perchlorate in methanol at ~296 K. Data from Fig. 1 of ref. 5. ——, eq. [7] with parameter values given in the text; . . ., calculated curve from ref. 5.

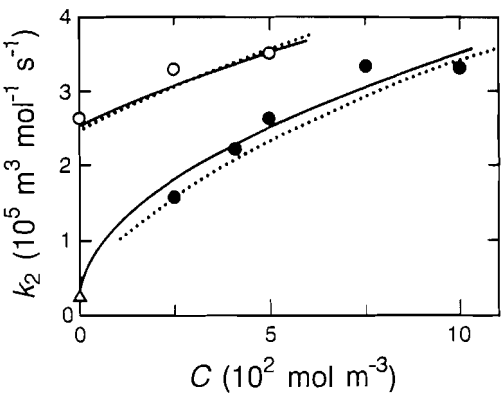

FIG. 5. Reaction of e_s^- with $(NO_3^-)_s$ in lithium nitrate solutions in methanol at ~296 K. Data from Fig. 2 of ref. 5 (●), with the infinite dilution value from ref. 3 (△). For ○, the C axis represents the concentration of lithium perchlorate added to 0.5 M lithium nitrate. ——, eq. [7] with parameter values given in the text; . . ., qualitative curves from ref. 5.

NO_2 (220 kJ/mol) is ≥42 kJ mol^{-1} greater than that of OH (117 kJ mol^{-1}) or $(CH_3)_2CHO$ (178 kJ/mol), and probably of $(CH_3)_2COH$. This would tend to favor initial formation of NO_2^- rather than OH^- or $(CH_3)_2\bar{C}OH$. However, the free energy of solvation of the smaller OH^- in water is 100 kJ mol^{-1} greater than that of the larger NO_2^- (28), which favors the ultimate formation of NO_2 + OH_s^- in reactions [1] and [2]. The free energy of solvation of OH^- in alcohols is probably also greater than that of NO_2^-, which would favor formation of OH_s^- in reaction [10]. Relative solvation energies might favor formation of $(NO_2^-)_s$ rather than $(R_2\bar{C}OH)_s$ in reaction [5].

The approximately linear increase of the *apparent* $k_2[e_s^- + (NO_3^-)_s]$ with addition of ammonium perchlorate to 0.5 M lithium nitrate solutions (Fig. 3 of ref. 5) is attributed to reaction [10] and to the direct reaction of $(NH_4^+)_s$ with e_s^-. Thus ammonium ions dominate the reaction rate in alcohols.

1. B. Hickel. J. Phys. Chem. **82**, 1005 (1978).
2. P.C. Senanayake and G.R. Freeman. (*a*) J. Phys. Chem. **92**, 5142 (1988); (*b*) J. Chem. Phys. **87**, 7007 (1987).
3. C.C. Lai and G.R. Freeman. J. Phys. Chem. **94**, 4891 (1990).
4. A.P. Sedigallage and G.R. Freeman. Can. J. Phys. **68**, 940 (1990).
5. G. Duplâtre and C.D. Jonah. J. Phys. Chem. **95**, 897 (1991).
6. M. Grätzel, A. Henglein, and S. Taniguchi. Ber. Bunsen-Ges. Phys. Chem. **74**, 292 (1970).

Can. J. Chem. Downloaded from www.nrcresearchpress.com by 203.198.23.82 on 09/08/12
For personal use only.

7. J.E. Aldrich, M.J. Bronskill, R.K. Wolff, and J.W. Hunt. J. Chem. Phys. **55**, 530 (1971).
8. (*a*) A.P. Kreshkov, N.Sh. Aldarova, and B.B. Tanganov. Russ. J. Phys. Chem. **44**, 279 (1970); (*b*) A. P. Kreshkov, N.Sh. Aldarova, N.T. Smolova, and A.I. Ryaguzov. Russ. J. Phys. Chem. **44**, 628 (1970); (*c*) R. C. Weast (*Editor*). CRC handbook of chemistry and physics. 70th ed. CRC Press, Boca Raton, Fla. 1989. p. D-166.
9. J.A. Kerr. Chem. Rev. **66**, 465 (1966).
10. S. Fukushima and W.L. Reynolds. Talanta, **11**, 283 (1964).
11. B.S. Brunschwig, C. Creutz, D.H. Macartney, T.-K. Sham, and N. Sutin. Faraday Discuss. Chem. Soc. **74**, 113 (1982).
12. R. Chen and G.R. Freeman. J. Phys. Chem. **96**, 7107 (1992).
13. Y. Maham and G.R. Freeman. J. Phys. Chem. **89**, 4347 (1985).
14. K. Okazaki and G.R. Freeman. Can. J. Chem. **56**, 2313 (1978).
15. F.-Y. Jou and G.R. Freeman. (*a*) Can. J. Chem. **54**, 693 (1976); (*b*) J. Phys. Chem. **81**, 909 (1977); (*c*) J. Phys. Chem. **83**, 2383 (1979).
16. R.W. Gallant. Physical properties of hydrocarbons. Gulf Publishing, Houston, Tex. Vol. 1. 1968; Vol. 2. 1970.
17. R.C. Reid, J.M. Prausnitz, and T.K. Sherwood. The properties of gases and liquids. 3rd ed. McGraw–Hill, New York. 1977. pp. 454, 640.
18. F. Buckley and A.A. Maryott. NBS Circ. 589, US Govt. Printing Off., Washington, D.C. 1958.
19. S.K. Garg and C.P. Smyth. J. Phys. Chem. **69**, 1294 (1965).
20. L.M. Imanov, F.G. Mirzoev, and K.E. Zul'fugarzade. Russ. J. Phys. Chem. **39**, 1518 (1965).
21. M. Anbar and P. Neta. Int. J. Appl. Radiat. Isotopes **18**, 493 (1967).
22. R. Chen and G.R. Freeman. Can. J. Chem. **71**, 1303 (1993).
23. A.-D. Leu, K.N. Jha, and G.R. Freeman. Can. J. Chem. **61**, 1115 (1983).
24. S.A. Peiris and G.R. Freeman. Can. J. Chem. **69**, 884 (1991).
25. P.W. Atkins. Physical chemistry. 4th ed. Freeman, New York. 1990. (*a*) pp. 760–761; note that B requires F^2; (*b*) p. 252; (*c*) p. 277, eq. (A8), note that ln 10 should be in the denominator for log to base 10, and that the solvent density is not included when concentration C is used instead of molality; (*d*) p. 861.
26. A.K. Covington and T. Dickson. Physical chemistry of organic solvent systems. Plenum, London. 1973. pp. 101–102.
27. S.G. Lias, J.E. Bartmess, J.F. Liebman, J.L. Holmes, R.D. Levin, and W.G. Mallard. J. Phys. Chem. Ref. Data, **17**, Suppl. 1 (1988). pp. 689, 781, 789.
28. Y. Marcus. Ion solvation. Wiley, New York. 1985. p. 108.

Can. J. Chem. Downloaded from www.nrcresearchpress.com by 203.198.23.82 on 09/08/12
For personal use only.

Solvent effects on the reactivity of solvated electrons with ammonium and nitrate ions in 1-butanol–water solvents

RUZHONG CHEN AND GORDON R. FREEMAN[1]

Chemistry Department, University of Alberta, Edmonton, AB T6G 2G2, Canada

Received December 8, 1992

RUZHONG CHEN and GORDON R. FREEMAN. Can. J. Chem. **71**, 1303 (1993).

Values of the rate constants, k_2 (10^6 m^3 mol^{-1} s^{-1}), of solvated electrons, e_s^-, with several related salts, in pure water and pure 1-butanol solvents at 298 K are, respectively, as follows: $LiNO_3$, 9.2, 0.19; NH_4NO_3, 10, 8.3; NH_4ClO_4, 1.5×10^{-3}, 12 in 20 mol% water; $LiClO_4$, 1.0×10^{-4}, $<1.0 \times 10^{-4}$. The value of $k_2(e_s^- + NO_{3,s}^-)$ in water solvent is 48 times larger than that in 1-butanol solvent, whereas $k_2(e_s^- + NH_{4,s}^+)$ in water is 10^{-4} times smaller than the value in 1-butanol. This enormous reversal of solvent effects on e_s^- reaction rates is the first observed for ionic reactants. The solvent participates chemically in the $(e_s^- + NO_{3,s}^-)$ reaction, and the overall rate constant *increases* with *increasing* viscosity and dielectric relaxation time. This unusual behavior is attributed to a greatly increased probability of reaction of an encounter pair with increasing duration of the encounter. Effective reaction radii κR_r for $(e_s^- + NO_{3,s}^-)$ and $(e_s^- + NH_{4,s}^+)$ were estimated with the aid of measured electrical conductances of the salt solutions in all the solvents. Values of κR_r are $(2–7) \times 10^{-10}$ m, except for $NH_{4,s}^+$ in 100 and 99 mol% water, which are 2.6 and 2.7×10^{-14} m, respectively. The effective radii of the ions for mutual diffusion increase with increasing butanol content of the solvent, from ~50 pm in water to ~150 pm in 1-butanol, due to the increasing average size of the molecules that solvate the ions.

RUZHONG CHEN et GORDON R. FREEMAN. Can. J. Chem. **71**, 1303 (1993).

Les valeurs des constantes de vitesse, k_2 (10^6 m^3 mol^{-1} s^{-1}), des électrons solvatés, e_s^-, avec plusieurs sels apparentés, dans l'eau pure et dans le 1-butanol, à 298 K, sont les suivantes : $LiNO_3$, 9,2, 0,19; NH_4NO_3, 10, 8,3; NH_4ClO_4, $1,5 \times 10^{-3}$, 12 (avec 20% d'eau); $LiClO_4$, $1,0 \times 10^{-4}$, $<1,0 \times 10^{-4}$. La valeur de $k_2(e_s^- + NO_{3,s}^-)$ dans l'eau est 48 fois plus forte que dans le 1-butanol comme solvant; par ailleurs, la valeur de $k_2(e_s^- + NH_{4,s}^+)$ dans l'eau est 10^{-4} fois plus faible que dans le 1-butanol comme solvant. Cet énorme différence des effets de solvant sur les vitesses de réaction des e_s^- est la première à être observée avec des réactifs ioniques. Le solvant participe chimiquement dans la réaction de $(e_s^- + NO_{3,s}^-)$ et la constante globale de vitesse augmente avec une augmentation de la viscosité et du temps de relaxation diélectrique. On attribue ce comportement inhabituel à une grande augmentation de la probabilité de réaction d'une paire de rencontre avec une augmentation de la durée de la rencontre. Faisant appel à des mesures de conductances électriques des solutions de sels dans tous les solvants, on a évalué les rayons efficaces de réaction, κR_r, des réactions $(e_s^- + NO_{3,s}^-)$ et $(e_s^- + NH_{4,s}^+)$. Les valeurs de κR_r s'étalent de 2 à 7×10^{-10} m, excepté pour le $NH_{4,s}^+$ dans les solutions contenant 99 ou 100 mol% d'eau alors que les valeurs sont respectivement de 2,7 et $2,6 \times 10^{-14}$ m. De ~50 pm en eau à ~150 pm en 1-butanol, les rayons efficaces des ions pour la diffusion mutuelle augmentent avec une augmentation de la concentration de butanol dans le solvant; ce résultat est causé par une augmentation de la grosseur moyenne des molécules qui solvatent les ions.

[Traduit par la rédaction]

Introduction

In the present work we report solvent effects on the rate of reaction of solvated electrons with solvated ions, and on the transport (conductance) of ions in solution. Rates of reaction between two species depend on the coming together (transport) of the species, and on the probability that they react when they encounter each other. Division of the reaction rate constant by the ionic conductance in the same solvent partially separates the solvent effect on transport from that on the probability of reaction of the encounter pair. We used 1-butanol–water binary solvents over the entire range of miscibility (1), and the newly discovered "switchover" reactant, ammonium nitrate (2).

Alcohols (3) and alcohol binary solvents (4, 5) have a wide range of physical and solvation properties (6, 7), so they are excellent media in which to study solvent effects on reaction kinetics.

Experimental

All chemicals and 1-butanol were from Aldrich Chemical Co. Lithium nitrate (99.999%), ammonium nitrate (99.999%), lithium perchlorate (reagent grade), and ammonium perchlorate (99.8%) were used as received; after opening a bottle, it was stored in a vacuum desiccator that contained P_2O_5. 1-Butanol (spectrometric grade, 99.5%, gold label) was dried for 1 week on Davison molecular sieves (3 Å), then treated for 1 day under UHP argon (99.999%, Liquid Carbonic Canada Ltd.) with sodium borohydride (2 g L^{-1}) at 330 K. The alcohol was then fractionally distilled under argon, through an 80 × 2.3 cm column packed with glass helices, discarding the first 20% and last 40%. The middle 40% portion was collected and stored in a flask under argon. The water content, measured by Karl–Fisher titration, was 0.05 mol%. The solvated electron half-life after a 100-ns pulse of 2.1 MeV electrons (4 J kg^{-1}) at 298 K was about 10 μs.

Water was purified in a Barnstead Nanopure II ion exchange system. The solvated electron half-life after a 100-ns pulse of 2.1 MeV electrons was about 12 μs.

Techniques

The methods of sample preparation and kinetic optical absorption spectroscopy were the same as those in the preceding work (2).

Electrical conductivity measurements were done with an impedance bridge (model 1608-A, General Radio Co.) at 1 kHz. Most of the time the conductance mode (Gp) was used. For conductances <0.6 μS, the bridge was set to one of the capacitance modes (Cp) and the conductance was calculated from the capacitance data. The conductance cells were obtained from Yellow Springs Instruments (model YSI-3403), and calibrated at 298.15 K using the secondary standard solution YSI-1361. Temperature was controlled to within ±0.01 K at 273 K, and to ±0.02 K at 344 K. Conductances were measured when the specified temperature had

[1]Author to whom correspondence may be addressed.

Can. J. Chem. Downloaded from www.nrcresearchpress.com by 213.200.69.106 on 09/08/12
For personal use only.

Can. J. Chem. Downloaded from www.nrcresearchpress.com by 213.200.69.106 on 09/08/12
For personal use only.

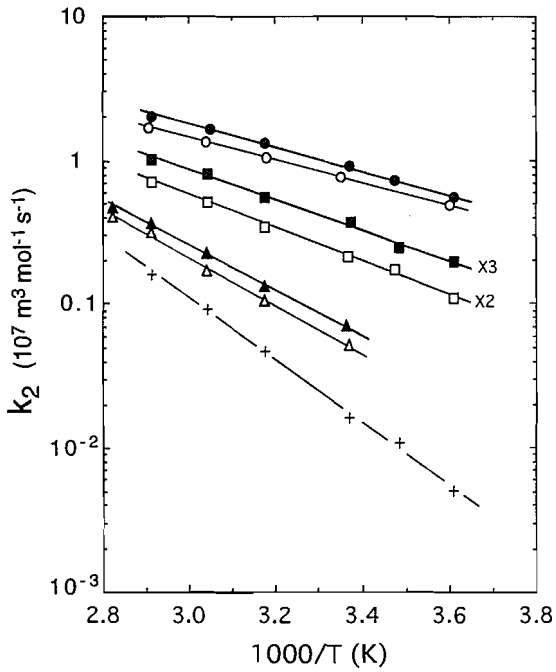

FIG. 1. Arrhenius plots of k_2 of e_s^- reaction with $LiNO_3$ in 1-butanol–water mixed solvents. Symbols representing mol% water are given in Table 1. To separate the lines, some values of k_2 have been multipled by the factors indicated.

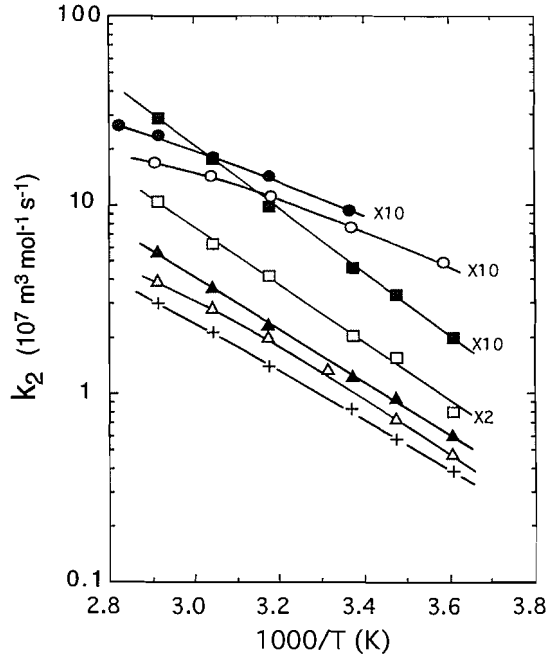

FIG. 2. Arrhenius plots of k_2 of e_s^- reaction with NH_4NO_3 in 1-butanol–water mixed solvents. Symbols representing mol% water are given in Table 1. To separate the lines, some values of k_2 have been multipled by the factors indicated.

been constant for 30 min. The molar conductance (Λ) was obtained from the plot of specific conductance against solute concentration.

Results and discussion

Physical properties

1-Butanol is not completely miscible with water (8). The rate constants were measured over the miscible range. The following mol% water were used: 0, 10.0, 20.0, 35.0, 45.0, 99.0, and 100.0. The values of viscosities for the mixed solvents were obtained from ref. 1. The values of relative permittivities for the mixed solvents were obtained from ref. 9. However, only data in the range of 0–23 mol% water were available, so we use those for isobutanol–water mixed solvents (10) as an approximation for other compositions.

Rate constants

Arrhenius plots of k_2 for $LiNO_3$, NH_4NO_3, and NH_4ClO_4 in mixed solvents are given in Figs. 1–3. The mol% of water represented by the symbols in these figures are shown in Table 1. Due to the low solubility of NH_4ClO_4 in solvents of 0 and 10 mol% water, its k_2 was not measured at these compositions.

For the reaction of e_s^- with $NH_{4,s}^+$ in NH_4ClO_4 solutions at 100 and 99 mol% water, the equilibrium $NH_{4,s}^+ \rightleftharpoons NH_3 + H_s^+$ affects the measured rate constants. The value of k_2 for $NH_{4,s}^+$ in water is $\sim 10^{-4}$ times smaller than that for H_s^+, so a small amount of dissociation of NH_4^+ causes a significant increase in the observed rate of reaction of e_s^-. The concentration of H_s^+ when $[NH_{4,s}^+] = 1$–140 mol m^{-3} is $[H_s^+] \approx \sqrt{K_a[NH_{4,s}^+]}$, where K_a is the dissociation constant. Values of K_a in water at different temperatures (11) are listed in Table 2. Values of K_a in the 99 mol% H_2O mixed solvent

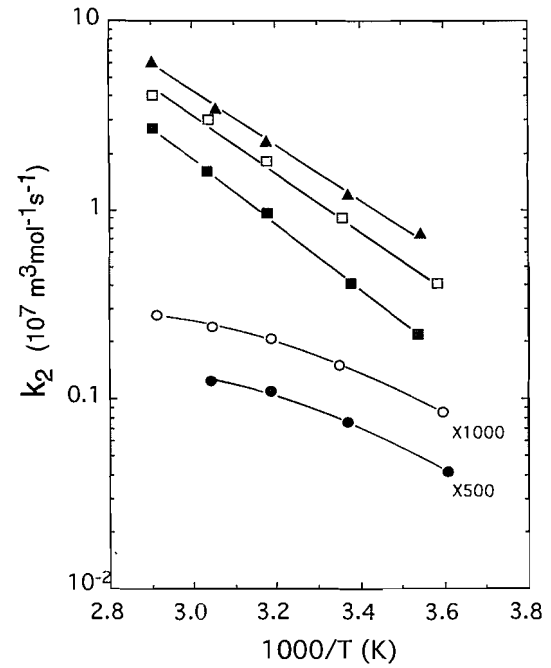

FIG. 3. Arrhenius plots of k_2 of e_s^- reaction with NH_4ClO_4 in 1-butanol–water mixed solvents. Symbols representing mol% water are given in Table 1. To separate the lines, some values of k_2 have been multipled by the factors indicated.

are not available, so we used those for water as an approximation. The values of k_2 ($e_s^- + NH_{4,s}^+$) were calculated from the slopes of plots of ($k_{obs} - k_2'[H_s^+]$) against $[NH_{4,s}^+]$, where k_2' is the rate constant for the reaction of e_s^- with H_s^+ in water (5).

In alcohol solvent we have the following equilibrium:

Can. J. Chem. Downloaded from www.nrcresearchpress.com by 213.200.69.106 on 09/08/12
For personal use only.

TABLE 1. Symbols in Figs. 1–3

Symbol	mol% H_2O	Symbol	mol% H_2O
+	0	■	45
△	10	○	99
▲	20	●	100
□	35		

TABLE 2. pK_a for $NH_{4,s}^+ \rightleftharpoons NH_3 + H_s^+$ in water[a]

T(K)	pK_w	pK_b	pK_a
277.0	14.78	4.84	9.94
298.0	14.00	4.75	9.25
313.5	13.54	4.73	8.81
328.5	13.13		8.41
343.2			8.08

[a]Values of pK_w and pK_b from ref. 11. $pK_a = pK_w - pK_b$. Values of pK_a at 328.5 and 343.2 are extrapolated from a plot of pK_a against T.

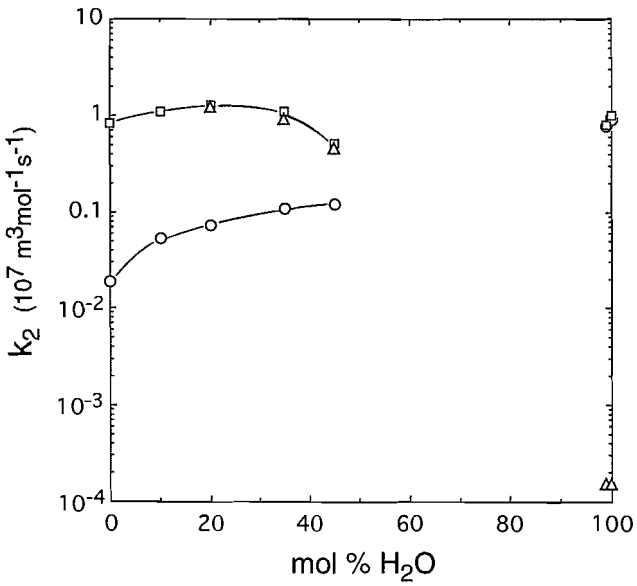

FIG. 4. Solvent composition dependence of k_2 at 298 K in 1-butanol–water mixed solvents. ○ $LiNO_3$, □ NH_4NO_3, △ NH_4ClO_4.

TABLE 3. Properties[a] of $NH_{4,s}^+$ and H_2O (liquid) compared

Molecule	Mass (g mol^{-1})	Partial molar volume (mL/mol^{-1})	H—X—H angle (°)	X—H distance (nm)
NH_4^+	18.05	18.0	109.5	0.103
H_2O	18.02	18.0	104.5	0.101

[a]From ref. 32, p. 2241.

$NH_{4,s}^+ + BuOH \rightleftharpoons NH_3 + BuOH_{2,s}^+$. Values of K_a for 1-BuOH–H_2O are not available, but those for methanol–water and ethanol–water have been reported (12*a*); K_a in pure ethanol is about 6 times larger than that in pure water (12*b*). In the alcohol-rich region k_{obs} is $>1 \times 10^5$ s^{-1} at 298 K for the concentration range of $[NH_{4,s}^+] = 0.02$–0.2 mol m^{-3}. Based on K_a in ethanol, the estimated $k_2'[H_s^+]$ is $<10^4$ s^{-1} for the range of $[NH_{4,s}^+]$ we used. Therefore, the influence of $[H_s^+]$ on k_{obs} is negligible and the values of $k_2(e_s^- + NH_{4,s}^+)$ were directly calculated from the slopes of plots of k_{obs} against $[NH_{4,s}^+]$.

The solvent composition dependences of k_2 at 298 K are shown in Fig. 4. In the water-rich region the reaction of e_s^- with $NH_{4,s}^+$ is very slow ($k_2 = 1.5 \times 10^3$ m^3 mol^{-1} s^{-1} in water, which agrees with a recently reported value (13)). However, in the alcohol-rich region, the reaction is fast ($k_2 \approx 10^7$ m^3 mol^{-1} s^{-1}). Therefore, the observed rate constants with NH_4NO_3 are mainly due to $NO_{3,s}^-$ in the water-rich region and mainly due to $NH_{4,s}^+$ in the alcohol-rich region.

The rate constants at 297 K for the reaction of e_s^- with the lithium perchlorate are 1.0×10^2 m^3 mol^{-1} s^{-1} in water, and $<1.0 \times 10^2$ m^3 mol^{-1} s^{-1} in 1-butanol (Table 3), so these ions did not contribute appreciably to the measured e_s^- reaction rates in the other solutions.

In models of the kinetics of chemical reactions in solution, the solvent is generally assumed to be a uniform continuum, and two effects determine how fast the reaction will be (14). Foremost is the intrinsic rate at which the reaction occurs, which is a molecular-level quantity that requires a quantum or semiclassical theory for its evaluation. The other effect for biomolecular reaction rates is statistical and accounts for the probability of existence of adjacent reactive entities in solution. The Smoluchowski–Debye–Stokes–Einstein model is such an example (15–18). We here use it to examine the reactions of solvated electrons with ionic solutes. Once the effects of the bulk fluid are accounted for, the unexplained features are attributed to effects of the nonhomogeneous structure of the solvent.

For a diffusion-controlled reaction between species i and j (18):

$$[1] \quad k_2 = 4\pi N_A(D_i + D_j)\kappa R_r f$$

where 4π steradians indicates that all directions of approach of i and j lead to reaction, N_A is Avogadro's constant, D_i, and D_j (m^2 s^{-1}) are the diffusion coefficients of i and j, R_r is the reaction radius of the reacting pair, and κ is the probability of reaction during one encounter. The factor f reflects the effect of Coulombic interaction between the reactants on their probability of obtaining the closeness of approach at which reaction occurs (17),

$$[2] \quad f = \frac{U(R_r)}{k_B T}\left[\exp\left(\frac{U(R_r)}{k_B T}\right) - 1\right]^{-1}$$

where, $U(R_r)$ is the potential energy of interaction between the reactants at distance R_r, k_B is Boltzmann's constant, and T is the temperature.

The potential energy when S is an ion of charge $z\xi$ is given by:

$$[3] \quad U(R_r) = -\frac{z\xi^2}{4\pi\varepsilon_0\varepsilon R_r}$$

where $-\xi$ is the charge on the electron, ε_0 is the permittivity of vacuum, and ε is the relative permittivity of the solvent between the electron and the ion.

Can. J. Chem. Downloaded from www.nrcresearchpress.com by 213.200.69.106 on 09/08/12
For personal use only.

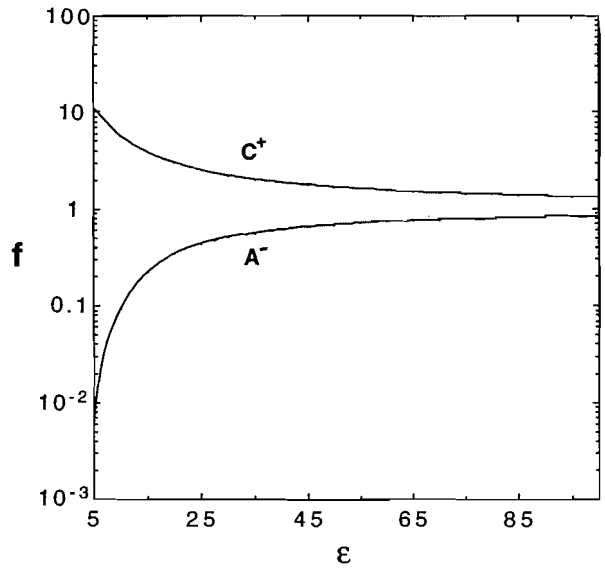

FIG. 5. Dielectric permittivity dependence of the Debye factor f at 298 K. C^+, $NH_{4,s}{}^+$, using R_r = 1.0 nm; A^-, $NO_{3,s}{}^-$, using R_r = 1.5 nm.

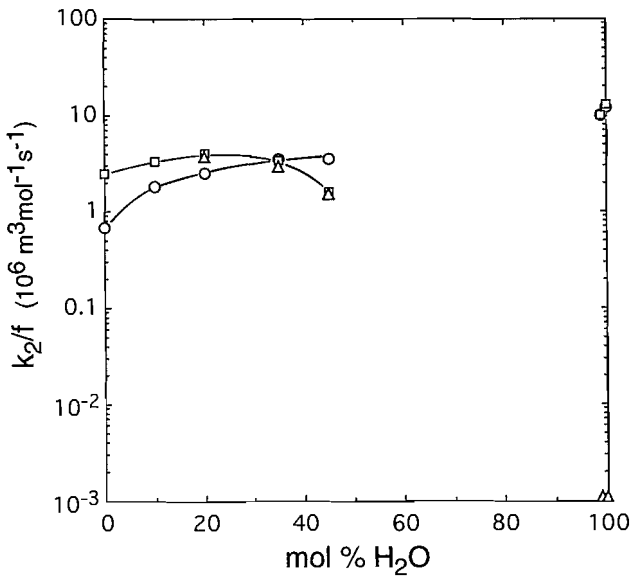

FIG. 6. Solvent composition dependence of k_2/f at 298 K in 1-butanol–water mixed solvents. Symbols are as in Fig. 4.

Values of f were calculated for a range of ε, using a value of R_r appropriate to each solute. The results for 298 K are shown in Fig. 5. When the reactants attract each other (z = +1), the value of f is >1; for repulsion (z = −1), f is <1. The solvent composition dependences of k_2/f at 298 K are shown in Fig. 6. For the reaction of (e_s^- + $NO_{3,s}{}^-$) the observed values of k_2 decrease monotonically with increasing alcohol content of the solvent (Fig. 4). Removal of the Coulombic interaction (k_2/f) reduces the apparent difference between the water-rich and alcohol-rich regions.

Values of f at other temperatures were not calculated, because values of ε are not available.

The Coulombic interaction does not explain the shape of the curve of $k_2(e_s^-$ + $NH_{4,s}{}^+)$ against solvent composition (Fig. 6). The diffusion coefficients and effective reaction radii (κR_r) also influence the reaction rates.

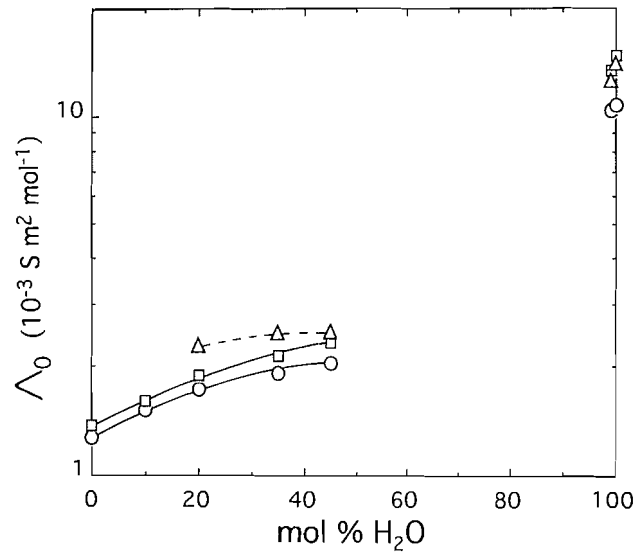

FIG. 7. Solvent composition dependence of the molar conductivities Λ_0 of salts at 298 K in 1-butanol–water mixed solvents. Symbols as in Fig. 4.

Electrical conductivities

The diffusion coefficients in eq. [1] are related to the molar electrical conductivities λ (S m^2 mol^{-1}) of the respective ions (19):

$$[4] \quad D = \lambda k_B T / z_i^2 \xi^2 N_A$$

Combining eq. [1] with eq. [4] we get:

$$[5] \quad \kappa R_r = \frac{\xi^2}{4\pi k_B} \times \frac{k_2}{fT\left[\frac{\lambda_i}{z_i^2} + \lambda_e\right]}$$

$$= 1.48 \times 10^{-16} k_2/fT\,[(\lambda_i/z_i^2) + \lambda_e]$$

where λ_i and λ_e are the molar conductivities of the reactant ion and e_s^-, respectively.

The values of the individual ionic conductivities in the mixed solvents are not known, so we have used approximations based on measured salt conductances. In pure water at 298 K the ratios of the λ's of e_s^- (20):$NH_{4,s}{}^+$ (21):$NO_{3,s}{}^-$ (21) are 2.59:1.04:1.00. The diffusion coefficients ($\propto\lambda_i/z_i^2$) are in the same ratios. Thus, diffusion of e_s^- dominates the relative motion of each reactant pair.

In water we have the following ratios: $[\lambda(e_s^-) + \lambda(NO_{3,s}{}^-)]/\Lambda_0$ (Li_s^+ + $NO_{3,s}{}^-$) = 2.3; $[\lambda(e_s^-) + \lambda(NH_{4,s}{}^+)]/\Lambda_0(NH_{4,s}{}^+$ + $ClO_{4,s}{}^-$) = 1.8; $[\lambda(e_s^-) + \lambda(NH_{4,s}{}^+)]/\Lambda_0$ ($NH_{4,s}{}^+$ + $NO_{3,s}{}^-$) = 1.7; and $[\lambda(e_s^-) + \lambda(NO_{3,s}{}^-)]/\Lambda_0$ ($NH_{4,s}{}^+$ + $NO_{3,s}{}^-$) = 1.7. Thus, eq. [5] can be approximated as

$$[6] \quad \kappa R_r \approx 1 \times 10^{-16} k_2/fT\,\Lambda_0$$

where Λ_0 is the molar conductance in the dilute solutions.

The solvent composition dependence of the molar conductivities Λ_0 of the salts at 298 K, and the approximate values of κR_r at 298 K, are shown in Figs. 7 and 8, respectively. The most interesting observation is that κR_r for the reaction (e_s^- + $NH_{4,s}{}^+$) increases by a factor of more than 10^3 when the mixed solvent changes from the water-rich region to the alcohol-rich region. The activation energy of the reactions, E_2, and the activation energy of the conductance, E_Λ, of the salts are plotted against solvent composition in Figs.

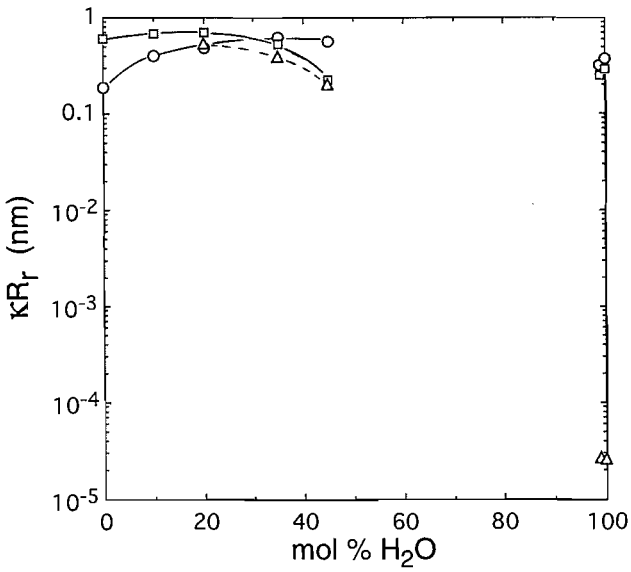

FIG. 8. Solvent composition dependence of κR_r, eq. [6], at 298 K in 1-butanol–water mixed solvents. Symbols as in Fig. 4.

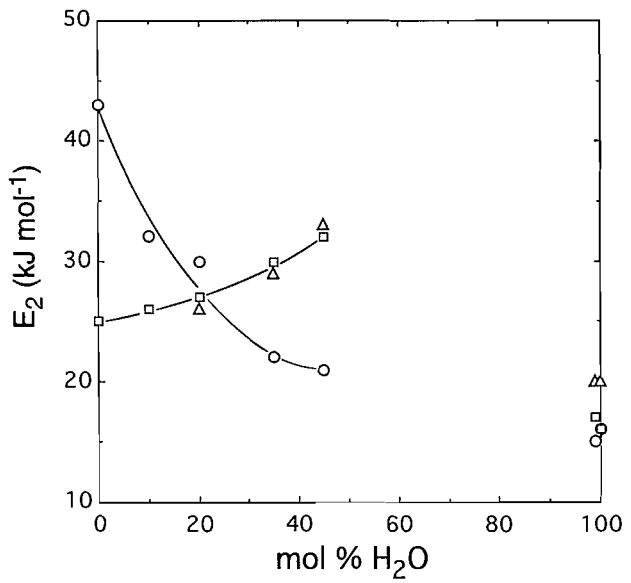

FIG. 9. Solvent composition dependence of the activation energies E_2 near 298 K in 1-butanol–water mixed solvents. Symbols as in Fig. 4.

9, and 10, respectively. For a diffusion-controlled reaction, E_2 is essentially that for the mutual diffusion of e_s^- and S, which encounter each other at random,

[7] $e_s^- + S \rightarrow (e_s^-, S)$

and react,

[8] $(e_s^-, S) \rightarrow$ product

In slow reactions most encounter pairs diffuse apart again,

[9] $(e_s^-, S) \rightarrow e_s^- + S$

in which case the measured E_2 is mainly due to the activation energy of reaction [8].

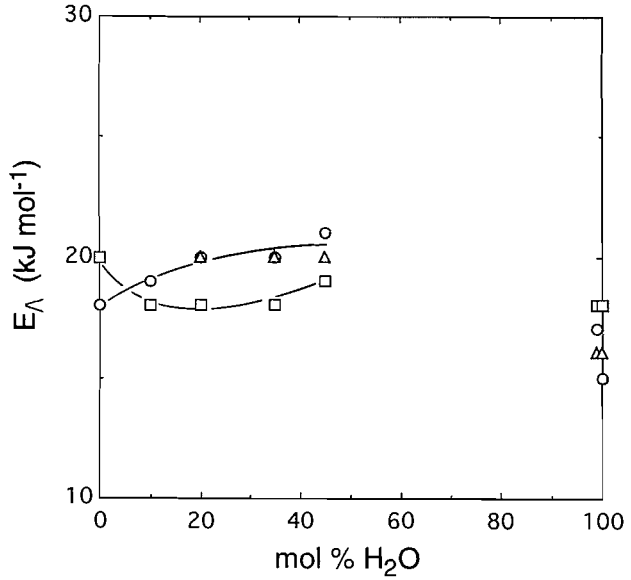

FIG. 10. Solvent composition dependence of the activation energies E_Λ of conductance near 298 K in 1-butanol–water mixed solvents. Symbols as in Fig. 4.

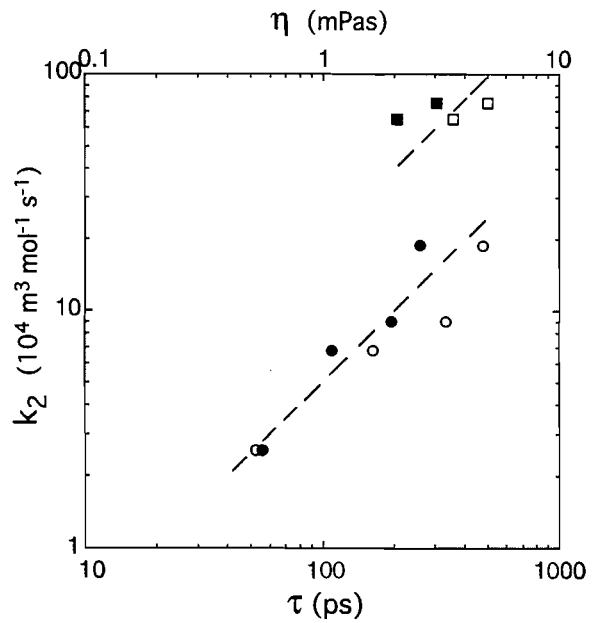

FIG. 11. k_2 (e_s^- + $NO_{3,s}^-$) in pure C_1–C_4 alcohol solvents at 298 K, as functions of viscosity η (●, ■) and dielectric relaxation time τ (○, □). ○, ● primary alcohols; ■, □ secondary alcohols. References for k_2: C_1 and C_2 (22); C_3 (18); 1–C_4 (present work); 2–C_4 (5). Solvent properties: η (23); τ (24, 25). The dashed lines have slopes = 1.0.

$e_s^- + NO_{3,s}^-$

E_Λ of the reactant salts is similar to the E_2 that might be expected for a diffusion-controlled reaction. The values of E_2 for the reaction (e_s^- + $NO_{3,s}^-$) increase with increasing alcohol content, reaching a maximum in pure 1-butanol that is about 3 times larger than that in pure water (Fig. 9). The values of E_Λ decrease with increasing alcohol content in the alcohol-rich region, and the magnitude of change is much smaller than that of E_2. This agrees with the observation that

Can. J. Chem. Downloaded from www.nrcresearchpress.com by 213.200.69.106 on 09/08/12
For personal use only.

TABLE 4. Rate parameters for the reaction of solvated electrons with solutes in 1-butanol–water mixed solvents at 298 K

ε^a	η^b (10^{-3} Pa s)	$X_{H_2O}{}^c$	f^d	k_2 (10^6 m^3 mol^{-1} s^{-1})	k_2/f (10^6 m^3 mol^{-1} s^{-1})	$E_2{}^e$ (kJ mol^{-1})	$\Lambda_0{}^f$ (10^{-3} S m^2 mol^{-1})	$E_\Lambda{}^g$ (kJ mol^{-1})
				$NO_{3,s}{}^{-h}$				
78.5	0.89	1.00	0.78	9.2	12.	16.	10.8	15
75.8	1.09	0.99	0.77	7.7	10.	15.	10.4	17
19.8	2.92	0.45	0.34	1.2	3.5	21.	2.05	21
18.4	2.81	0.35	0.31	1.1	3.5	22.	1.92	20
17.8	2.70	0.20	0.29	0.72	2.5	30.	1.74	20
17.5	2.66	0.10	0.29	0.53	1.8	32.	1.52	19
17.4	2.60	0.00	0.28	0.19	0.68	43.	1.28	18
				$NH_{4,s}{}^+$, $NO_{3,s}{}^{-i}$				
		1.00	0.78	10.	13.	16.	14.8	18
		0.99	0.77	8.0	10.	17.	13.4	18
		0.45	3.01	5.2	1.6	32.	2.35	19
		0.35	3.20	11.	3.4	30.	2.14	18
		0.20	3.29	13.	4.0	27.	1.89	18
		0.10	3.34	11.	3.3	26.	1.60	18
		0.00	3.35	8.3	2.5	25.	1.37	20
				$NH_{4,s}{}^{+j}$				
		1.00	1.40	1.5×10^{-3}	1.1×10^{-3}	20	14.0	16
		0.99	1.42	1.5×10^{-3}	1.1×10^{-3}	20	12.6	16
		0.45	3.01	4.6	1.5	33	2.50	20
		0.35	3.20	9.2	2.9	29	2.47	20
		0.20	3.29	12.	3.6	26	2.30	20
				$Li_s{}^+$, $ClO_{4,s}{}^{-k}$				
		1.00	1.0×10^{-4}		20			
		0.00	$<1.0 \times 10^{-4}$		—			

[a]Static dielectric permittivity. Those for 99%, 45%, and 35% are for isobutanol–water mixtures. Data from refs. 9 and 10.
[b]Viscosity. Data from ref. 1.
[c]Mole fraction of water.
[d]Debye factor.
[e]Temperature coefficient at 298 K from Arrhenius plots of k_2.
[f]Molar conductivity of the solutions.
[g]Temperature coefficient at 298 K from Arrhenius plots of Λ_0.
[h]$NO_{3,s}{}^-$ in $LiNO_3$ solutions, concentrations 0.02–1.8 mol m^{-3}.
[i]$NH_{4,s}{}^+$, $NO_{3,s}{}^-$ in NH_4NO_3 solutions, concentrations 0.02–0.2 mol m^{-3}. The value of f was calculated according to $z = -1$ ($NO_{3,s}{}^-$) in 100 and 99 mol% H_2O; in the other compositions, f was calculated according to $z = +1$ ($NH_{4,s}{}^+$).
[j]$NH_{4,s}{}^+$ in NH_4ClO_4 solutions, concentrations 1–140 mol m^{-3} for mol% H_2O of 100, 99; 0.02–0.2 for mol% H_2O of 45, 35, and 20.
[k]$LiClO_4$ concentrations 60–600 mol m^{-3} in water, and 90–440 mol m^{-3} in 1-butanol.

the reaction (e_s^- + $NO_{3,s}{}^-$) is a nearly diffusion-controlled reaction in water and gradually deviates from it as the alcohol content is increased.

The reaction (e_s^- + $NO_{3,s}{}^-$) in alcohol solvents is complex. The proposed reaction sequence is (2, 5, 18, 22):

$$[10] \quad e_s^- + NO_{3,s}{}^- \rightleftharpoons (e_s^-, NO_{3,s}{}^-)$$

$$[11] \quad (e_s^-, NO_{3,s}{}^-) + ROH \rightarrow NO_{2,s}{}^- + OH_s^- + \dot{R}OH$$

Alcohol molecules apparently participate chemically in the reaction. The changes in k_2 for the reaction (e_s^- + $NO_{3,s}{}^-$) in different pure alcohol solvents are shown in Fig. 11 as functions of solvent viscosity (23) and dielectric relaxation time (24, 25). As the length of the alkyl group in the primary alcohols is increased, the solvent fluidity *decreases* and k_2 *increases*. This inverse relationship between k_2 and solvent fluidity is attributed to the increasing duration of reactant encounter pairs as solvent fluidity decreases, and a greatly enhanced probability of reaction [11] with increasing encounter duration.

For secondary alcohol solvents, k_2 is 4–7 times larger than in their primary alcohol counterparts. This is attributed to the relatively reactive α-C—H group on the secondary alcohol.

e_s^- + $NH_{4,s}{}^+$

The reaction (e_s^- + $NH_{4,s}{}^+$) is nearly diffusion controlled in the alcohol-rich region and much slower in the water-rich region. The value of κR_r in pure 1-butanol is 10^3 times larger than that in pure water at 298 K (Fig. 8). In ammonium nitrate solution, E_2 represents the reaction (e_s^- + $NH_{4,s}{}^+$) in the alcohol-rich region and (e_s^- + $NO_{3,s}{}^-$) in the water-rich region. The value of E_2 for the reaction (e_s^- + $NH_{4,s}{}^+$) is larger in pure 1-butanol than in pure water (Fig. 9).

The rate constants in water for several other cations, Ag_s^+ (4*c*), H_s^+, Tl_s^+, Cu_s^{2+} (5), are all (2.5–4.2) × 10^7 m^3 mol^{-1} s^{-1}, so the respective values of κR_r are much larger than that for $NH_{4,s}{}^+$ in water.

Can. J. Chem. Downloaded from www.nrcresearchpress.com by 213.200.69.106 on 09/08/12
For personal use only.

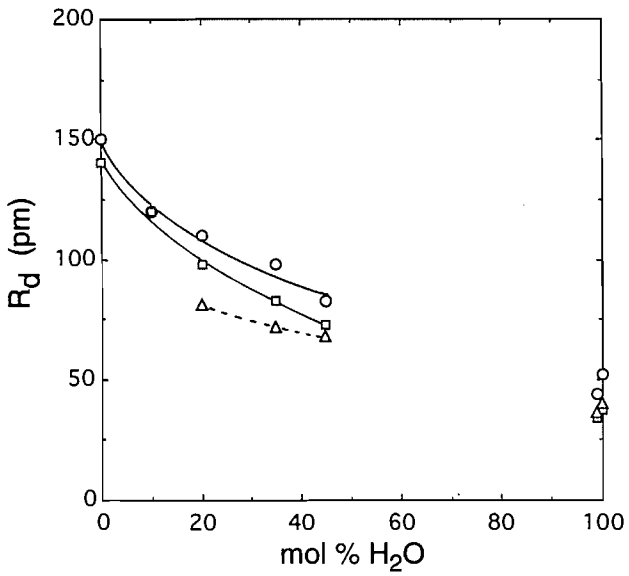

FIG. 12. Solvent composition dependence of R_d at 298 K in 1-butanol–water mixed solvents. Symbols as in Fig. 4.

The solvation of ammonium ions in aqueous solution has been extensively studied by the method of apparent volume of individual ions (26); of entropies of dilution (27); of viscosities (28); of water activity (29); of NMR (30); and of IR and Raman spectra (31, 32). All these studies show that the ammonium ion in aqueous solution has properties similar in many respects to those of a water molecule (structure, volume, molecular weight, charge distribution; see Table 3). Its influence on water properties is usually negligible compared with the change caused by the other cations.

In a study of entropies of solution, Frank and Robinson stated that (27) ". . . the difference [between NaCl and NH_4Cl] is in the direction to be expected if the NH_4^+ exerts an additional stabilizing influence on the water structure by virtue of its tetrahedral shape and its ability to form hydrogen bonds." In a study of Raman spectra of aqueous electrolyte solutions, Vollmar wrote (32) ". . . the electrostatic forces exerted on their nearest neighbors by H_2O and by NH_4^+ are probably very similar. In particular both H_2O and NH_4^+ form hydrogen bonds of about the same strength." As this unique property of solvated ammonium ions in water is responsible for many thermodynamic and spectroscopic properties of the aqueous solutions of ammonium salts, we believe that it is also responsible for the kinetic behavior of solvated ammonium ion reaction in water. Since $NH_{4,s}^+$ is symmetrically solvated in water, it has little tendency to accept an electron.

Relatively little is known about behavior of electrolyte solutions in alcohols. Each alcohol molecule contains one -OH group that can bond with others to form a chain or ring structure in the liquid, but not a three-dimensional structure like that of water. This would greatly influence the solvation structure of an ammonium ion in it. It is, therefore, reasonable to suggest that $NH_{4,s}^+$ is unsymmetrically solvated in an alcohol, and that this greatly facilitates electron attachment and subsequent decomposition, $NH_4 \rightarrow H + NH_3$. More thermodynamic and spectroscopic studies of electrolyte solutions in alcohols would be of great help for our embryonic understanding of solvation effects in different solvents.

The rate parameters for the reactions in 1-butanol–water mixed solvents are summarized in Table 4.

Effective radii for mutual diffusion

The Stokes radius, R_d, for mutual diffusion of ions in an electrolyte solution is given by (19)

$$[12] \quad R_d = \left(\frac{1}{R_{d_i}} + \frac{1}{R_{d_j}}\right)^{-1} = 8.2 \times 10^{-16} \Big/ \eta\left(\frac{\lambda_i}{z_i^2} + \frac{\lambda_j}{z_j^2}\right)$$

In our case, $i = e_s^-$, $j = NH_{4,s}^+$ or $NO_{3,s}^-$, so $|z_i| = |z_j| = 1$. As discussed before for κR_r, we use the approximation $(\lambda_{e_s^-} + \lambda_j) = 1.8\ \Lambda_0$, so

$$[13] \quad R_d \approx 5 \times 10^{-16}/\eta\Lambda_0$$

The solvent composition dependences of R_d are shown in Fig. 12. Equation [12] shows that R_d emphasizes the more mobile ion. In the alcohol-rich region, R_d increases as the alcohol content increases. This is attributed to the larger size of the molecules that solvate the ions. The decrease of R_d as a small amount of alcohol is added to water indicates that the microscopic viscosity of the liquid in the vicinity of the ions is lower than the shear viscosity of the bulk liquid; the ions remain in the disordered water.

Acknowledgements

We thank the Natural Sciences and Engineering Research Council for financial assistance, and the personnel of the Radiation Research Centre for aid with the electronics and for maintaining the equipment.

1. Y. Maham and G.R. Freeman. J. Phys. Chem. **91**, 1561 (1987).
2. T.B. Kang and G.R. Freeman. Can. J. Chem. **71**, 1297 (1993).
3. A.M. Afanassiev, K. Okazaki, and G.R. Freeman. (*a*) J. Phys. Chem. **83**, 1244 (1979); (*b*) Can. J. Chem. **57**, 839 (1979).
4. P.C. Senanayake and G.R. Freeman. (*a*) J. Chem. Phys. **87**, 7007 (1987); (*b*) J. Phys. Chem. **91**, 2123 (1987); (*c*) J. Phys. Chem. **92**, 5142 (1988).
5. S.A. Peiris and G.R. Freeman. Can. J. Chem. **69**, 884 (1991).
6. A.-D. Leu, K.N. Jha, and G.R. Freeman. Can. J. Chem. (*a*) **60**, 2342 (1982); (*b*) **61**, 1115 (1983).
7. K.M. Idriss-ali and G.R. Freeman. Can. J. Chem. **62**, 2217 (1984).
8. J.M. Sorensen and W. Arlt. Liquid–liquid equilibrium data collection. DECHEMA Chem. Data Series, Frankfurt. 1979. p. 237.
9. A. D'Aprano, D. Donato, and E. Caponetti. J. Solution Chem. **8**, 135 (1979).
10. A.C. Brown and D.G. Ives. J. Chem. Soc. 1608 (1962).
11. R.C. Weast. Handbook of chemistry and physics. 70th ed. CRC Press, Boca Raton, Fla. 1989. pp. D165–166.
12. (*a*) O. Popovych. Anal. Chem. **46**, 2009 (1974); (*b*) R. P. Bell. Acids and bases, their quantitative behavior. 2nd ed. Methuen, London. 1969. p. 27.
13. H.A. Schwarz. J. Phys. Chem. **95**, 6697 (1991).
14. J. Keizer. J. Phys. Chem. **86**, 5053 (1982).
15. M.V. Smoluchowski. Z. Phys. Chem. **92**, 129 (1917).
16. R. Fürth (*Editor*). A. Einstein's investigations on the theory of Brownian movement. Dover Publications, New York. 1956.

Can. J. Chem. Downloaded from www.nrcresearchpress.com by 213.200.69.106 on 09/08/12
For personal use only.

p. 75. *Translation by* A.D. Cowper of Z. Elektrochem. **14**, 235 (1908).
17. P. Debye. Trans. Electrochem. Soc. **82**, 265 (1942).
18. A. Peiris Sedigallage and G.R. Freeman. Can. J. Phys. **68**, 940 (1990).
19. P.W. Atkins. Physical chemistry. 2nd ed. Freeman, New York. 1982. pp. 904–905.
20. K.H. Schmidt, P. Han, and D.M. Bartels. J. Phys. Chem. **96**, 199 (1992).
21. A.L. Horvath. Handbook of aqueous electrolyte solutions. Wiley, New York. 1985. pp. 262–263.
22. C.C. Lai and G.R. Freeman. J. Phys. Chem. **94**, 302 (1990).
23. R.W. Gallant. Physical properties of hydrocarbons. Vol. 1. Gulf Publishing, Houston, Tex. 1968.
24. J. Barthel, K. Bachhuber, R. Buchner, and H. Hetzenauer. Chem. Phys. Lett. **165**, 369 (1990).
25. F. Buckley and A.A. Maryott. Tables of dielectric dispersion data for pure liquids and dilute solutions. NBS Circular 589, Washington, D.C. 1958.
26. K. Fajans and O. Johnson. J. Am. Chem. Soc. **64**, 668 (1942).
27. H.S. Frank and A.L. Robinson. J. Chem. Phys. **8**, 933 (1940).
28. M. Kaminsky. Discuss. Faraday Soc. **24**, 171 (1957).
29. Z. Libus and K. Chachulska. J. Mol. Liq. **46**, 53 (1990).
30. J.C. Hindman. J. Chem. Phys. **36**, 1000 (1962).
31. E. Ganz. Z. Phys. Chem. Abt. B: **35**, 1 (1937).
32. P.M. Vollmar. J. Chem. Phys. **39**, 2236 (1963).

Can. J. Chem. Downloaded from www.nrcresearchpress.com by 213.200.69.106 on 09/08/12
For personal use only.

Formation of 2,2-disubstituted 1,3-cyclopentanediones from ketals with 1,2-bis(trimethylsilyloxy)cyclobutene

YONG-JIN WU, DEAN W. STRICKLAND, TRACY J. JENKINS, PEI-YING LIU, AND D. JEAN BURNELL[1]

Department of Chemistry, Memorial University of Newfoundland, St. John's, NF A1B 3X7, Canada

Received February 16, 1993

This paper is dedicated to Professor Robert H. Burnell on the occasion of his 65th birthday

YONG-JIN WU, DEAN W. STRICKLAND, TRACY J. JENKINS, PEI-YING LIU, and D. JEAN BURNELL. Can. J. Chem. **71**, 1311 (1993).

The direct formation of 2,2-disubstituted 1,3-cyclopentanedione compounds by a Lewis acid catalysed reaction with 1,2-bis(trimethylsilyloxy)cyclobutene proceeds in good to excellent yields with unhindered ketals, but steric hindrance reduces the yields considerably. A carbonyl group α or β to the ketal, or a carbon–carbon double bond α to the ketal, stops the reaction completely. Orthoesters do not give geminally acylated products in synthetically useful yields.

YONG-JIN WU, DEAN W. STRICKLAND, TRACY J. JENKINS, PEI-YING LIU et D. JEAN BURNELL. Can. J. Chem. **71**, 1311 (1993).

La formation directe des cyclopentane-1,3-diones 2,2-disubstituées par la réaction catalysée par les acides de Lewis du 1,2-bis(triméthylsilyoxy)cyclobutène se produit avec des rendements allant de bon à excellent avec les acétals non empêchés; toutefois, l'empêchement stérique réduit considérablement les rendements. Un groupement carbonyle en α ou en β de l'acétal ou une double liaison carbone–carbone en α de l'acétal inhibe complètement la réaction. Les orthoesters ne conduisent pas à des rendements utiles de produits acylés d'une façon géminée.

[Traduit par la rédaction]

Can. J. Chem. Downloaded from www.nrcresearchpress.com by 213.200.69.106 on 09/08/12
For personal use only.

Introduction

Kuwajima and coworkers (1, 2) reported that methyl, ethyl, and benzyl ketals, for example, the cyclohexanone ketal **1** in Scheme 1, in the presence of boron trifluoride etherate react with 1,2-bis(trimethylsilyloxy)cyclobutene (**2**) (3) to give a cyclobutanone derivative **3**. Treatment of that intermediate with trifluoroacetic acid results in rearrangement to a geminally acylated product, such as **4**. This two-step process for the construction of 2,2-disubstituted 1,3-cyclopentanediones has been used in a number of syntheses (2, 4, 5). However, in conjunction with our synthetic approaches to sesquiterpenes with the tricyclo[6.2.1.0^{1,5}]-undecane ring system (6), to triquinane sesquiterpenes (7), and to A-ring aromatic steroids (8) we showed that the aldol step and the subsequent rearrangement can be executed in a single synthetic operation when one employs a large excess of the Lewis acid. Furthermore, the yields of the 1,3-cyclopentanediones obtained in this way are superior to the yields by the two-step method. The reaction with 1,2-bis(trimethylsilyloxy)cyclopentene proceeds in an analogous fashion (9). Results similar to ours with **2** were reported by Ayyangar's group (10), and our procedure found application in a method of direct conversion of alkynyl ketals to polycyclic ketones (11). This method of geminal acylation has been examined with a variety of simple substrates in order to ascertain its applicability to the synthesis of more complex natural products. The results are presented here.

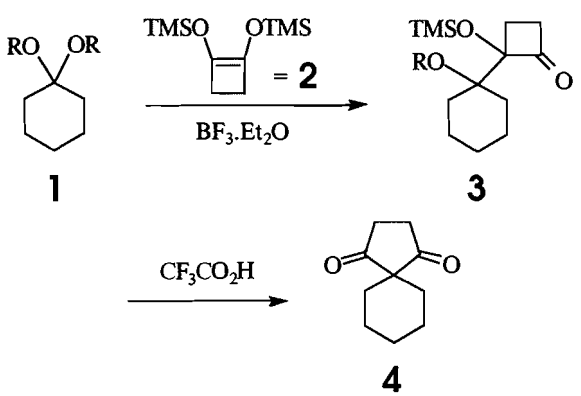

SCHEME 1

Results and discussion

By and large, reactions followed the procedure, which is herein referred to as the "standard conditions," that was developed for the synthesis of isokhusimone (6*b*). This can be summarized as addition over 5–10 min of a dichloromethane solution of 2–3 equivalents of **2** to a dichloromethane solution of the ketal and 10–15 equivalents of freshly distilled boron trifluoride etherate at −78°C.[2] The reaction mixture was stirred for approximately 12 h during which time it was allowed to attain room temperature. An aqueous reaction work-up was followed by purification by flash column chromatography.

Use of different ketals

Whereas Kuwajima and co-workers (1, 2) used mainly methyl and ethyl ketals, we successfully employed ketals derived from 1,2-ethanediol and 2,2-dimethyl-1,3-propanediol in syntheses (6–8). Under the standard conditions we obtained a 68% yield of 2,2-dimethyl-1,3-cyclopentanedione (cf. 40% from 2,2-dimethoxypropane in ref. 5) from 2,2,5,5-tetramethyl-1,3-dioxane, and from 2-ethyl-2-methyl-1,3-dioxolane we obtained a 91.5% yield of 2-ethyl-2-methyl-1,3-cyclopentanedione (6*b*). The cyclopentanone-derived

[1]Author to whom correspondence may be addressed.

[2]The concentrations of the reactants were not critical, but it was important that **2** be pure. Therefore, redistillation of **2** under vacuum (3) is recommended strongly if impurities are evident in its ^{1}H nmr spectrum. The procedure described in ref. 6*b* may be carried out entirely at room temperature, but the isolated yields tend to be a little lower.

Can. J. Chem. Downloaded from www.nrcresearchpress.com by 213.200.69.106 on 09/08/12
For personal use only.

ketal **5** gave a lower yield than the cyclohexanone counterpart **6**. The ketal derived from (±)-2,3-butanediol **7** gave a much poorer yield of **4**, and ketal **8** derived from (±)-1,2-diphenyl-1,2-ethanediol completely resisted the conditions, so that such a ketal may be considered as a protecting group during a geminal acylation under standard conditions (Table 1).

Alkyl groups in the α position

The reaction proved to be very sensitive to congestion about the ketal carbon. A series of ketals derived from ketones with α-methyl groups and 1,2-ethanediol were examined. The yields of their bisacylation products ranged from modest to nonexistent (Table 2). One reason for poor yields was a tendency for the 1,2-ethanediol generated during the reaction to participate in an acid-catalysed ring opening of the double acylation product to lead ultimately to a ketoester. Indeed, with the ketal **9*a*** derived from 3-methylbutanone only a very small amount of the desired cyclopentanedione was detected in the ^{1}H nmr spectrum of the crude product, and the keto-ester **18** was the only product that was isolated by chromatography, albeit in low yield. Evidence for a similar ring-opening process was apparent in the ^{1}H nmr

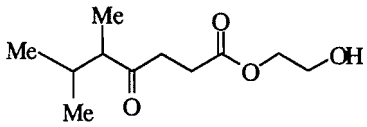

18

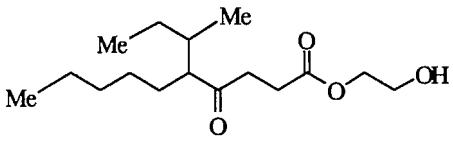

19

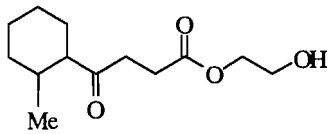

20

spectrum of the crude product of **12**, and the reactions of **11** and **13** gave significant amounts of ring-opened products **19** and **20**, respectively, as a 1:1 mixture of diastereomers. There is some precedence for ring-opening in work by Kuwajima (2, 12) in which $SnCl_4$ was the Lewis acid catalyst. This could be overcome to a degree by the use of a ketal derived from a more hindered diol, e.g., **9*b***. A ketal derived from a more hindered ketone, i.e., **10**, proved unreactive, and it was recovered unchanged after being subjected to the standard conditions. Ketals **12**, **13**, and **14** derived from cyclic α-methyl ketones fared better, but the yields were still poor compared to **5** and **6**. This sensitivity to substitution places a serious limit on the utility of the geminal acylation process, but sometimes a lack of reactivity can be used to advantage. Thus, in the synthesis of isokhusimone (Scheme 2) the doubly ketalized substrate **21** was treated with excess **2** and $BF_3 \cdot Et_2O$. The less hindered ketal underwent geminal acylation efficiently while the more hindered side-chain ketal was merely hydrolysed during work-up to give **22** in

TABLE 1. Reactions with different ketals

Substrate	Yield	Substrate	Yield
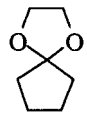 **5**	68%	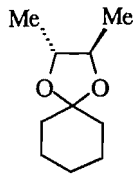 **7**	48%
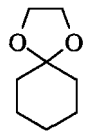 **6**	96% (6*b*)	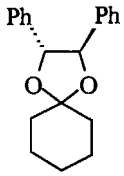 **8**	0%

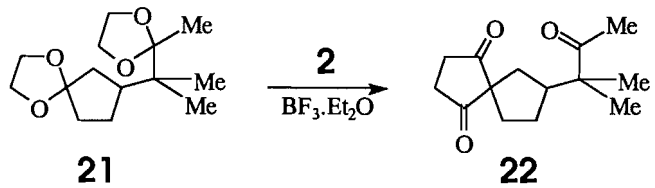

21 **22**

SCHEME 2

very good yield (6*b*). The bicyclic systems in ketals **15**, **16**, and **17** can be considered as α-substituted, but these were more reactive than the α-methyl cases. Ketal **15** appeared by gc–ms to react efficiently under standard conditions, but chromatography led to considerable destruction of the product. Ketals **16** and **17** gave good yields of the expected geminal acylation products.

Oxygen functions near the ketal

Kuwajima claimed that ketones do not react with **2** in the presence of $BF_3 \cdot Et_2O$ (2). In fact, ketones can give good yields of geminal acylation products.[3] Nevertheless, a ketone next to the target ketal will completely stop the reaction of both the ketal and the ketone. No geminal acylation product was observed when the 2,3-butanedione monoketal **23** was treated with **2** under the standard conditions. Also,

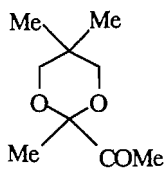

23

in no case could we obtain a geminal acylation product with any ketal bearing an ester or lactone carbonyl in its β-position (i.e., **24**, **25**, **28**, **29**, or **30** in Table 3). An ester group

[3]Details of our work with ketones will be described elsewhere.

TABLE 2. Reactions of substrates bearing an α-alkyl group

Substrate	Yield	Substrate	Yield	Substrate	Yield
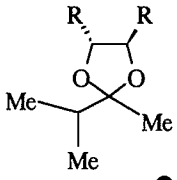		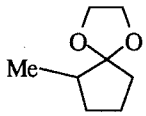	36%	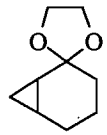	30%
R = H **9***a*	0%	**12**		**15**	
R = Me **9***b*	56%[a]				
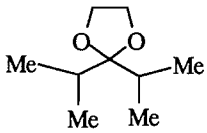	0%	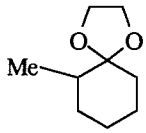	30%	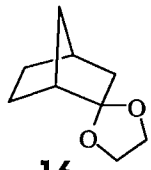	82% (*6b*)
10		**13**		**16**	
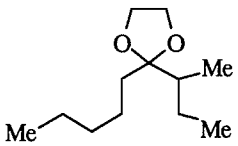	28%	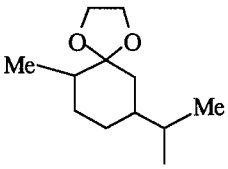	36%	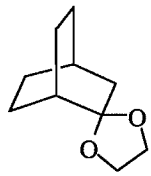	74%
11		**14**		**17**	

TABLE 3. Reactions of substrates bearing other oxygen functions

Substrate	Yield	Substrate	Yield
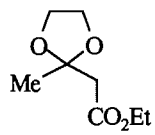	0%	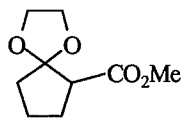	0%
24		**28**	
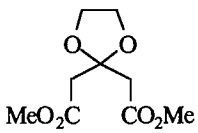	0%	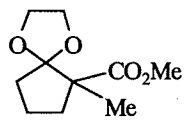	0%
25		**29**	
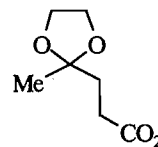	91%	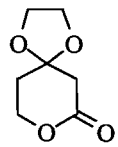	0%
26		**30**	
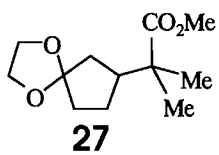	80% (*6b*)	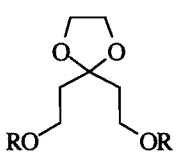	**31** R = Ac 0% **32** R = H 0% **33** R = Me 74% **34** R = Bn 86%
27			

Can. J. Chem. Downloaded from www.nrcresearchpress.com by 213.200.69.106 on 09/08/12
For personal use only.

TABLE 4. Reactions of unsaturated substrates

Substrate	Yield	Substrate	Yield
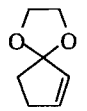 **35**	0%	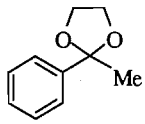 **39**	77%
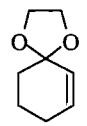 **36**	0%	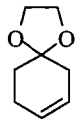 **40**	75%
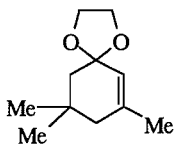 **37**	0%	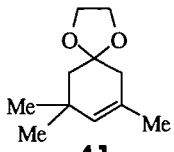 **41**	72%
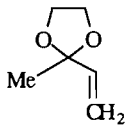 **38**	0%	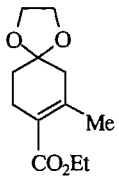 **42**	72%

at a γ-position, as in **26**, or further away, as in **27** (*6b*), was not deleterious. However, under standard conditions neither the diacetate **31** nor, not surprisingly, its corresponding diol **32** gave any diketone product, but the reaction was compatible with dimethyl (**33**) and dibenzyl (**34**) ethers.

Unsaturation near the ketal

Geminal acylation failed with conjugated cyclic enones when the unsaturation remained in its original position during ketalization, such as with **35**, **36**, and **37** (Table 4). Attempts at reactions with such substrates led invariably to recovery of the enone itself, which must have resulted largely by hydrolysis during the aqueous work-up. A ketal **38** derived from butenone gave a complex mixture with much of the product in a polymeric form. However, ketal **39**, derived from acetophenone, underwent geminal acylation smoothly, and substrates in which the double bond had migrated to the β,γ-position during acid-catalysed ketalization, i.e., **40** and **41**, also underwent the desired reaction with very good yields. A 72% yield was realized for the geminal acylation of ketal **42**, which also had a distant ester function. In this instance there was a small amount of double bond isomerization.[4]

[4]Prolonged exposure to the acidic reaction medium led to some isomerization of the double bond in the products of **40** and **41**, also.

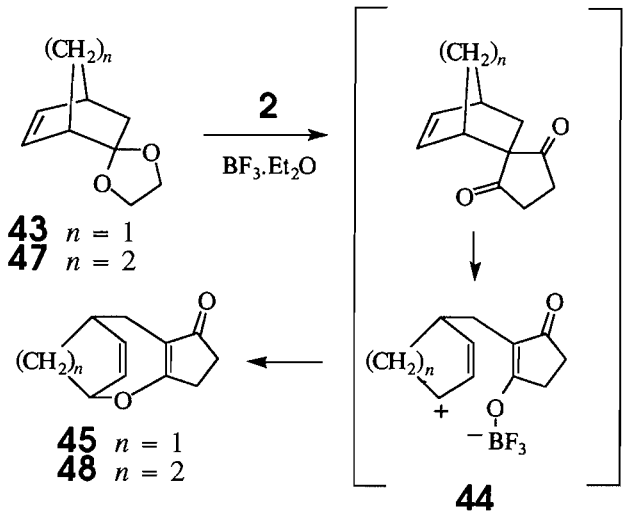

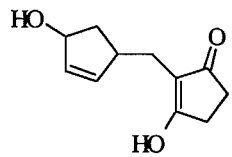

46

SCHEME 3

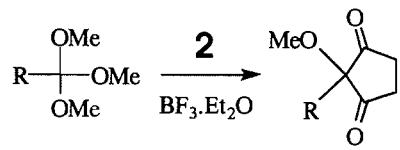

R = *n*Bu : **49** **51** 16%
R = Ph : **50** **52** 0%

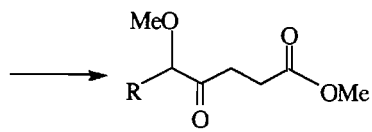

53 4%
54 15%

SCHEME 4

Some unsaturated bicyclic ketones gave only products that must have been derived by initial geminal acylation followed by rupture of the bicyclic framework (Scheme 3). Ketal **43** gave a 12% yield of **45**, the consequence of closure of an intermediate allylic cation (**44**) on to an enol oxygen. The major product (42%) was **46**, which was, considering our efforts to exclude moisture from the reaction medium, likely the result of hydrolysis of **45** during work-up rather than of capture of adventitious water by **44**. On the other hand the similar ketal **47** gave **48** in 56% yield as the only isolated product.

Reactions of orthoesters

The reaction of orthoesters with **2** seemed like an interesting entry to 1,3-cyclopentanediones with an oxygen

Can. J. Chem. Downloaded from www.nrcresearchpress.com by 213.200.69.106 on 09/08/12
For personal use only.

function at C-2. However, with the simple examples **49** and **50**, hydrolysis to the corresponding ester, presumably during work-up, was the predominant result. A small amount of geminal acylation did lead to the cyclopentanedione **51** from **49** (Scheme 4), but it was unstable under the reaction conditions, and concomitant acid-catalysed opening of the cyclopentanedione ring yielded some keto-ester **53**. In the case of **50** the intermediate **52** was not detected, and the only recognizable product was the keto-ester **54**. The appalling yields of both types of geminally acylated product preclude any synthetic application of this reaction with orthoesters.

Experimental

General

For details of the instruments, the format of the spectral data, and the abbreviations see ref. 13. All nmr spectra were recorded in $CDCl_3$ unless otherwise noted.[5] Ketalizations were by the acid-catalysed action (*p*-toluenesulfonic acid or Amberlyst-15) of a large excess of 1,2-ethanediol in benzene with azeotropic removal of water. In more sluggish cases and with some enones a method involving 1,2-bis(trimethylsilyloxy)ethane and trimethylsilyl trifluoromethanesulfonate (TMSOTf) was employed (14). Monoketal **23** was prepared by the method of Levine and Mauney (15). Ketals were purified by distillation or column chromatography. The reactions were run under an atmosphere of dry N_2 following the procedure described in ref. 6*b*, as outlined in the above section. Aqueous "work-up" followed one of these procedures: (*i*) the reaction mixture was poured into ice-cold saturated $NaHCO_3$ solution, the organic layer was washed again with saturated $NaHCO_3$ solution, then washed with saturated NaCl solution (×2), dried over anhydrous $MgSO_4$, and concentrated in vacuo; (*ii*) the reaction mixture was poured into ice-water, the organic layer was washed again with water (×2), then washed with saturated $NaHCO_3$ solution and saturated NaCl solution, dried over anhydrous $MgSO_4$, and concentrated in vacuo; (*iii*) the reaction mixture was poured into water at room temperature, the organic layer was washed again with water (×2) then saturated NaCl solution, dried over anhydrous $MgSO_4$, and concentrated in vacuo. (In some instances *i* gave emulsions in the initial $NaHCO_3$ wash.) Flash column chromatography ("chromatography") used 230–400 mesh silica gel, and elution was normally with hexane containing an increasing proportion of ethyl acetate, the approximate proportion of ethyl acetate at the initial point of elution being noted below as a percentage. Care was required in determining which chromatographic fractions contained the desired diketone products because these compounds generally are very poorly detected using standard tlc visualization methods, e.g., uv light, I_2, and acid-based sprays (ceric ammonium nitrate – H_2SO_4, phosphomolybdic acid, and anisaldehyde–H_2SO_4). In some instances we used gc–ms to identify the correct fractions.

Reaction of 5

Addition of **2** (1.1 mL, 4.1 mmol) in CH_2Cl_2 (6.0 mL) to a solution of ketal **5** (208 mg, 1.63 mmol) and $BF_3 \cdot Et_2O$ (3.0 mL, 24 mmol) in CH_2Cl_2 (60 mL), then work-up *i*, led, after chromatography (5%), to *spiro[4.4]nonane-1,4-dione* (168 mg, 68%) as colorless crystals: mp 58–59.5°C; ir ν_{max}: 1720 cm^{-1}; ^1H nmr δ: 2.48 (4H, br s), 1.61 (8H, br s); ^{13}C nmr δ: 215.8 (2C, 0), 63.0 (0), 34.7 (2C, 2), 34.6 (2C, 2), 26.6 (2C, 2); ms: 152 (100, M^+), 124 (35), 111 (48), 97 (52), 96 (44), 95 (33), 69 (28), 68 (52), 67 (61), 56 (61), 41 (37). Exact Mass calcd. for $C_9H_{12}O_2$: 152.0837; found: 152.0831.

Reaction of 7

Addition of **2** (2.0 mL, 7.5 mmol) in CH_2Cl_2 (8.0 mL) to a solution of ketal **7** (425 mg, 2.29 mmol) and $BF_3 \cdot Et_2O$ (4.6 mL, 37 mmol) in CH_2Cl_2 (20 mL), then work-up *ii*, led, after chromatography (10%), to 183 mg (48%) of *spiro[4.5]decane-1,4-dione* (**4**), which was identical with a sample previously prepared in this laboratory (6*b*).

*Reaction of 9*a

Addition of **2** (1.6 mL, 6.0 mmol) in CH_2Cl_2 (8.0 mL) to a solution of ketal **9***a* (0.26 g, 2.0 mmol) and $BF_3 \cdot Et_2O$ (3.7 mL, 30 mmol) in CH_2Cl_2 (20 mL), then work-up *ii*, led, after chromatography (5%), to *2-hydroxyethyl 5,6-dimethyl-4-oxoheptanoate* (**18**) (59 mg, 19%) as a pale yellow liquid; ir ν_{max}: 3459 (br), 1737, 1711 cm^{-1}; ^1H nmr δ: 4.23 (2H, nar m), 3.82 (2H, nar m), 2.81 (1H, very br), 2.80 (2H, br t, J = 6.7 Hz), 2.60 (2H, br t, J = 6.7 Hz), 2.36 (1H, quintet, $J \approx$ 7.0 Hz), 1.97 (1H, octet, $J \approx$ 6.8 Hz), 1.04 (3H, d, J = 7.0 Hz), 0.91 (3H, d, J = 6.7 Hz), 0.87 (3H, d, J = 6.8 Hz); ^{13}C nmr δ: 213.3, 173.1, 66.1, 60.9, 52.7, 36.4, 30.2, 27.8, 21.2, 18.7, 12.8; ms: no M^+, 199 (2), 186 (2), 174 (7), 155 (22), 145 (24), 112 (21), 101 (100), 85 (24), 71 (73), 45 (29), 43 (70). Exact Mass calcd. for $C_8H_{14}O_4$ ($M^+ - C_3H_6$ via McLafferty): 174.0892; found: 174.0890.

*Reaction of 9*b

Compound **2** (2.0 mL, 7.4 mmol) in CH_2Cl_2 (8.0 mL) was added over 1 h to a solution of ketal **9***b* (390 mg, 7.46 mmol) and $BF_3 \cdot Et_2O$ (4.5 mL, 37 mmol) in CH_2Cl_2 (20 mL) at −78°C, then the mixture was stirred for 27 h during which time it attained room temperature. Work-up *ii* gave material that was a mixture of the spirodiketone and unreacted **9***b*, so $BF_3 \cdot Et_2O$ (4.5 mL, 37 mmol) and **2** (2.0 mL, 7.4 mmol) were added again to a CH_2Cl_2 solution of the product mixture. After stirring for 19 h, work-up *ii* yielded 213 mg (56%) of product that ^1H nmr revealed was very largely *2-methyl-2-methylethyl-1,3-cyclopentanedione*. Attempts to purify this product by chromatography led largely to its destruction, but a small amount (50 mg) of homogeneous material was recovered: ir ν_{max}: 1759 (m), 1721 (s) cm^{-1}; ^1H nmr δ: 2.74 (4H, symmetrical m), 2.01 (1H, septet, J = 6.9 Hz), 1.06 (3H, s), 0.93 (6H, d, J = 6.9 Hz); ^{13}C nmr δ: 216.8 (2C), 59.5, 35.6 (2C), 33.8, 17.3 (2C), 15.3; ms: 154 (28, M^+), 139 (100), 112 (24), 111 (32), 83 (25), 56 (18), 55 (27), 43 (12), 41 (20). Exact Mass calcd. for $C_9H_{14}O_2$: 154.0993; found: 154.0989.

Reaction of 11

Addition of **2** (0.88 mL, 3.3 mmol) in CH_2Cl_2 (8.0 mL) to a solution of ketal **11** (0.22 g, 1.1 mmol) and $BF_3 \cdot Et_2O$ (2.0 mL, 16 mmol) in CH_2Cl_2 (20 mL), then work-up *ii*, led, after chromatography (15%), to *2-(1-methylpropyl)-2-pentyl-1,3-cyclopentanedione* (0.68 g, 28%) as a very pale yellow liquid: ir ν_{max}: 1719 cm^{-1}; ^1H nmr δ: 2.66 (4H, nar m), 1.80–1.61 (3H, m), 1.45 (1H, m), 1.31–0.95 (7H, m), 0.92 (3H, d, J = 6.9 Hz), 0.85 (3H, t, J = 7.2 Hz), 0.83 (3H, t, J = 7.0 Hz); ^{13}C nmr δ: 218.5, 218.1, 64.1, 41.0, 36.9, 36.8, 32.9, 32.2, 24.4 (2C), 22.2, 13.9, 13.2, 12.3; ms: no M^+, 195 (34), 169 (53), 168 (25), 154 (33), 139 (54), 126 (28), 125 (56), 112 (100), 69 (27), 55 (65), 41 (80). Exact Mass calcd. for $C_{12}H_{19}O_2$ ($M^+ - C_2H_5$): 195.1384; found: 195.1380. A later chromatographic fraction contained a mixture of the diastereomers of *2-hydroxyethyl 6-methyl-4-oxo-5-pentyloctanoate* (**19**) (46 mg, 15%) as an oil: ir ν_{max}: 3457 (br), 1736, 1709 cm^{-1}; ^1H nmr δ: 4.26 (2H, m), 3.85 (2H, m), 2.96–2.38 (6H, m), 1.76–1.05 (11H, m), 0.96–0.84 (9H, nar m).

Reaction of 12

Addition of **2** (2.0 mL, 7.4 mmol) in CH_2Cl_2 (8.0 mL) to a solution of ketal **12** (0.35 g, 2.5 mmol) and $BF_3 \cdot Et_2O$ (4.5 mL, 37 mmol) in CH_2Cl_2 (20 mL), then work-up *ii*, led, after chromatography (15%), to *6-methylspiro[4.4]nonane-1,4-dione* (146 mg, 36%) as a colorless liquid: ir ν_{max}: 1718 cm^{-1}; ^1H nmr δ: 2.81–2.57 (4H, br m), 2.25 (1H, br m), 1.85 (5H, br m), 1.54 (1H, br m),

[5]The complete set of ^1H and ^{13}C nmr spectra of the products of the reactions of ketals **5**, **7**, **9***a*, **9***b*, **11**–**15**, **17**, **26**, **33**, **34**, **39**–**43**, **47**, and of the orthoesters **49** and **50** may be purchased from: The Depository of Unpublished Data, Document Delivery, CISTI, National Research Council Canada, Ottawa, Canada K1A 0S2.

Can. J. Chem. Downloaded from www.nrcresearchpress.com by 213.200.69.106 on 09/08/12
For personal use only.

Can. J. Chem. Downloaded from www.nrcresearchpress.com by 213.200.69.106 on 09/08/12
For personal use only.

0.95 (3H, d, J = 7.2 Hz); ^{13}C nmr δ: 217.3, 216.6, 66.7, 46.9, 36.2, 35.8, 34.5, 33.5, 24.6, 15.2; ms: 166 (64, M^+), 151 (100), 125 (15), 109 (52), 95 (41), 81 (20), 67 (41), 55 (31), 41 (30). Exact Mass calcd. for $C_{10}H_{14}O_2$: 166.0993; found: 166.0997.

Reaction of ***13***

Addition of **2** (1.7 mL, 6.5 mmol) in CH_2Cl_2 (6.0 mL) to a solution of ketal **13** (339 mg, 2.17 mmol) and $BF_3 \cdot Et_2O$ (4.0 mL, 33 mmol) in CH_2Cl_2 (30 mL), then work-up *iii*, gave a mixture of two products. This material was subjected to chromatography twice (5%) to provide *6-methylspiro[4.5]decane-1,4-dione* (116 mg, 30%) as a pale yellow oil: ir ν_{max}: 1715 cm^{-1}; ^{1}H nmr δ: 2.90–2.48 (4H, m), 1.95–1.17 (9H, m), 0.75 (3H, d, J = 6.3 Hz); ^{13}C nmr δ: 217.4 (0), 216.3 (0), 60.0 (0), 35.6 (2), 35.5 (1), 35.3 (2), 32.0 (2), 28.9 (2), 25.2 (2), 20.0 (2), 18.0 (3); ms: 180 (74, M^+), 165 (65), 126 (21), 125 (39), 123 (24), 112 (100), 111 (23), 109 (22), 95 (24), 81 (38), 67 (45), 56 (32), 55 (31), 53 (25), 41 (46). Exact Mass calcd. for $C_{11}H_{16}O_2$: 180.1149; found: 180.1149. Chromatography also provided, in a more polar fraction, a 3:1 diastereomeric mixture of *(2-hydroxyethyl) 4-(2-methylcyclohexyl)-4-oxobutanoate* (**20**) (186 mg, 36%) as a pale yellow oil: ir ν_{max}: 3451 (br), 1737, 1709 cm^{-1}; ^{1}H nmr δ: 4.24 (m), 3.85 (m), 3.12 (br, O*H*), 2.98–2.59 (m), 2.34 (m from major isomer), 2.17 (m from minor isomer), 1.90–0.90 (m), 0.87 (methyl d of major isomer, J = 7.1 Hz), 0.86 (methyl d of minor isomer, J = 6.3 Hz); ms: 242 (3, M^+), 224 (4), 181 (18), 145 (13), 125 (19), 101 (50), 97 (100), 85 (25), 55 (87), 41 (21). Exact Mass calcd. for $C_{13}H_{22}O_4$: 242.1517; found: 242.1506.

Reaction of ***14***

Addition of **2** (1.6 mL, 6.3 mmol) in CH_2Cl_2 (8.0 mL) to a solution of ketal **14** (500 mg, 2.52 mmol) and $BF_3 \cdot Et_2O$ (4.6 mL, 38 mmol) in CH_2Cl_2 (20 mL), then work-up *ii*, led, after chromatography (7%), to *6-methyl-9-(methylethyl)spiro[4.5]decane-1,4-dione* as a yellow oil (204 mg, 36%): ir ν_{max}: 1717 cm^{-1}; ^{1}H nmr δ: 2.92–2.49 (4H, complex m), 1.81 (3H, m), 1.57 (3H, m), 1.39 (1H, m), 1.28–1.00 (2H, m), 0.83 (3H, d, J = 6.7 Hz), 0.82 (3H, d, J = 6.7 Hz), 0.75 (3H, d, J = 6.0 Hz); ^{13}C nmr δ: 217.8 (0), 216.7 (0), 60.5 (0), 36.5 (1), 36.0 (1), 35.7 (2), 35.4 (2C, 2), 32.2 (1), 29.3 (2), 28.5 (2), 19.6 (3), 19.2 (3), 17.7 (3); ms: 222 (3, M^+), 179 (1), 138 (10), 125 (15), 106 (48), 105 (23), 91 (100), 86 (25), 84 (40), 43 (31). Exact Mass calcd. for $C_{14}H_{22}O_2$: 222.1619, found: 222.1614.

Reaction of ***15***[6]

Addition of **2** (0.92 mL, 3.4 mmol) in CH_2Cl_2 (7.0 mL) to a solution of ketal **15** (209 mg, 1.37 mmol) and $BF_3 \cdot Et_2O$ (2.6 mL, 25 mmol) in CH_2Cl_2 (16 mL), then work-up *iii*, gave 254 mg of a crude product, of which 81% (by gc–ms) was the geminally acylated product. Serious losses were incurred during chromatography (5%), which nevertheless provided some homogeneous *spiro(bicyclo[4.1.0]heptane-2,2'-cyclopentane-1,3-dione)* as a low-melting solid (64 mg, 30%): mp 38–41°C; ir ν_{max}: 1759 (m), 1720 (s) cm^{-1}; ^{1}H nmr (CD_2Cl_2) δ: 2.88 (2H, m), 2.64 (2H, m), 1.80 (1H, m), 1.66 (1H, m), 1.25–1.52 (4H, m), 1.10 (1H, m), 0.78 (1H, m), 0.52 (2H, m); ^{13}C nmr (CD_2Cl_2) δ: 215.1 (0), 214.8 (0), 53.7 (0), 34.7 (2), 34.5 (2), 24.7 (2), 22.3 (2), 15.7 (2), 14.7 (1), 10.6 (1), 6.4 (2); ms: 178 (73, M^+), 163 (18), 150 (18), 136 (15), 135 (17), 123 (15), 122 (37), 121 (18), 111 (32), 94 (26), 93 (31), 91 (21), 79 (100), 77 (29), 55 (34). Exact Mass calcd. for $C_{11}H_{14}O_2$: 178.0993; found: 178.1003.

Reaction of ***17***

Addition of **2** (2.0 mL, 7.6 mmol) in CH_2Cl_2 (5.0 mL) to a solution of ketal **17** (428 mg, 2.54 mmol) and $BF_3 \cdot Et_2O$ (4.8 mL, 38 mmol) in CH_2Cl_2 (50 mL), then work-up *i*, gave, after chromatography (4%), the hydrolysis product *bicyclo[2.2.2]octan-2-one* (72 mg, 17%) and *spiro(bicyclo[2.2.2]octane-2,2'-cyclopentane-1,3-dione)* as colorless crystals (362 mg, 74%): mp 99–100°C; ir ν_{max}: 1738 (sh), 1718 cm^{-1}; ^{1}H nmr δ: 3.00 (2H, m), 2.56 (2H, m), 1.83 (1H, br s), 1.76 (1H, br s), 1.61–1.68 (6H, m), 1.35–1.49 (4H, m); ^{13}C nmr δ: 213.1 (2C, 0), 62.4 (0), 34.0 (2C, 2), 32.1 (1), 26.5 (2), 24.1 (2C, 2), 23.0 (1), 21.2 (2C, 2); ms (from gc–ms): 192 (25, M^+), 112 (100), 81 (23), 80 (15), 79 (40), 77 (21), 55 (20), 53 (20), 41 (27). Exact Mass calcd. for $C_{12}H_{16}O_2$: 192.1150; found: 192.1141.

Reaction of ***26***

Addition of **2** (1.0 mL, 3.8 mmol) in CH_2Cl_2 (6.0 mL) to a solution of ketal **26** (290 mg, 1.54 mmol) and $BF_3 \cdot Et_2O$ (2.8 mL, 23 mmol) in CH_2Cl_2 (40 mL), then work-up *i*, gave, after chromatography (10% acetone in petroleum ether), *2-((2-carbethoxy)ethyl)-2-methyl-1,3-cyclopentanedione* (298 mg, 91%) as a colorless oil: ir ν_{max}: 1724 cm^{-1}; ^{1}H nmr δ: 4.06 (2H, q, J = 7.1 Hz), 2.82 (4H, s), 2.26 (2H, t, J = 7.5 Hz), 1.96 (2H, t, J = 7.5 Hz), 1.23 (3H, t, J = 7.1 Hz), 1.13 (3H, s); ^{13}C nmr δ: 215.5 (2C, 0), 172.6 (0), 60.4 (2), 55.1 (0), 34.6 (2C, 2), 28.6 (2C, 2), 19.7 (3), 13.9 (3); ms: 212 (11, M^+), 184 (9), 167 (15, $M^+ - CH_3CH_2O$), 166 (17), 138 (36), 125 (100), 110 (20), 97 (24), 69 (22), 55 (36), 43 (20), 41 (34). Exact Mass calcd. for $C_{11}H_{16}O_4$: 212.1048; found: 212.1046.

Reaction of ***33***

Addition of **2** (1.26 mL, 4.74 mmol) in CH_2Cl_2 (6.0 mL) to a solution of ketal **33** (301 mg, 1.58 mmol) and $BF_3 \cdot Et_2O$ (1.94 mL, 15.8 mmol) in CH_2Cl_2 (50 mL), then work-up *i*, gave, after chromatography (5% acetone in petroleum ether), *2,2-bis(2-methoxyethyl)-1,3-cyclopentanedione* (251 mg, 74%) as a colorless oil: ir ν_{max}: 1760, 1720 cm^{-1}; ^{1}H nmr δ: 3.12 (4H, t, J = 6.0 Hz), 3.04 (6H, s), 2.54 (4H, s), 1.85 (4H, t, J = 6.0 Hz); ^{13}C nmr δ: 217.9 (2C, 2), 68.4 (2C, 2), 58.5 (2C, 3), 55.5 (0), 37.8 (2C, 2), 36.2 (2C, 2); ms: no M^+, 156 (14, $M^+ - CH_2{=}CH\text{-}OMe$ by McLafferty), 141 (42), 125 (7), 112 (8), 109 (23), 81 (10), 55 (12), 53 (10), 45 (100), 41 (12). Exact Mass calcd. for $C_8H_{12}O_3$ ($M^+ - CH_2{=}CH\text{-}OMe$): 156.0786; found 156.0783. Another small chromatographic fraction was tentatively identified as *2-methoxyethyl-2-methyl-1,3-cyclopentanedione*, a colorless oil (17 mg): ir ν_{max}: 1759 (shoulder), 1715 cm^{-1}; ^{1}H nmr δ: 3.20 (2H, t, J = 7.2 Hz), 3.08 (3H, s), 2.67 (4H, s), 2.00 (2H, t, J = 7.2 Hz), 1.03 (3H, s); ^{13}C nmr δ: 217.2 (2C, 0), 68.3 (2), 58.7 (3), 53.6 (0), 35.8 (2), 35.0 (2C, 2), 21.6 (3); ms: 170 (1, M^+), 156 (5), 140 (14), 125 (42), 109 (11), 69 (53), 59 (30), 55 (28), 45 (100), 43 (16), 41 (61).

Reaction of ***34***

Addition of **2** (0.33 mL, 1.2 mmol) in CH_2Cl_2 (5.0 mL) to a solution of ketal **34** (211 mg, 0.62 mmol) and $BF_3 \cdot Et_2O$ (1.1 mL, 9.3 mmol) in CH_2Cl_2 (30 mL), then work-up *i*, gave, after chromatography (5% acetone in petroleum ether), *2,2-bis(2-benzyloxyethyl)-1,3-cyclopentanedione* (194 mg, 86%) as an oil: ir ν_{max}: 1757, 1710 cm^{-1}; ^{1}H nmr δ: 7.39 (10H, m), 4.43 (4H, s), 3.48 (4H, t, J = 7.0 Hz), 2.50 (4H, s), 2.15 (4H, t, J = 7.0 Hz); ^{13}C nmr δ: 217.6 (2C, 0), 137.2 (2C, 0), 128.2 (4C, 1), 127.6 (2C, 1), 127.5 (4C, 1), 72.8 (2C, 2), 65.8 (2C, 2), 55.5 (0), 37.3 (2C, 2), 35.8 (2C, 2); ms: 366 (2, M^+), 169 (18), 141 (14), 126 (8), 125 (4), 108 (3), 107 (3), 91 (100), 78 (3), 77 (4), 65 (10).

Reaction of ***39***

Addition of **2** (1.1 mL, 4.3 mmol) in CH_2Cl_2 (6.0 mL) to a solution of ketal **39** (232 mg, 1.43 mmol) and $BF_3 \cdot Et_2O$ (2.6 mL, 21 mmol) in CH_2Cl_2 (30 mL), then work-up *iii*, led, after chromatography (15%), to *2-methyl-2-phenyl-1,3-cyclopentanedione* as a yellow oil (206 mg, 77%): ir ν_{max}: 1765 (m), 1724 cm^{-1}; ^{1}H nmr δ: 7.38–7.19 (5H, m), 2.82 (4H, wide symmetrical m), 1.43 (3H, s); ^{13}C nmr δ: 213.0 (0), 136.8 (0), 129.3 (1), 127.9 (1), 126.3 (1), 61.9 (0), 35.2 (2), 19.7 (3); ms: 188 (100, M^+), 145 (36), 132 (32), 105 (26), 104 (74), 103 (30), 78 (24), 77 (26), 51 (21). Exact Mass calcd. for $C_{12}H_{12}O_2$: 188.0837; found: 188.0835.

Reaction of ***40***

Addition of **2** (0.57 mL, 2.1 mmol) in CH_2Cl_2 (5.0 mL) to a solution of ketal **40** (119 mg, 0.85 mmol) and $BF_3 \cdot Et_2O$ (1.57 mL,

[6]We thank Mr. Sheldon Crane for performing this reaction.

Can. J. Chem. Downloaded from www.nrcresearchpress.com by 213.200.69.106 on 09/08/12
For personal use only.

12.8 mmol) in CH_2Cl_2 (50 mL), then work-up *i*, led, after chromatography (3% acetone in petroleum ether), to *spiro[4.5]dec-7-ene-1,4-dione* (91 mg, 75%) as colorless crystals: mp 53–54°C; ir ν_{max}: 1749, 1716, 1438 cm^{-1}; ^1H nmr δ: 5.76 (2H, m), 2.82 (4H, symmetrical m), 2.13 (4H, m), 1.73 (2H, t, J = 6.1 Hz); ^{13}C nmr δ: 214.4 (2C, 0), 125.1 (1), 122.9 (1), 55.3 (0), 34.1 (2C, 2), 27.0 (2), 25.8 (2), 20.8 (2); ms: 164 (100, M^+), 149 (11), 136 (44), 135 (36), 122 (28), 121 (24), 108 (22), 107 (43), 80 (53), 79 (93), 77 (37), 55 (25). Exact Mass calcd. for $C_{10}H_{12}O_2$: 164.0837; found: 164.0843.

Reaction of ***41***

Addition of **2** (3.0 mL, 11 mmol) in CH_2Cl_2 (10 mL) to a solution of ketal **41** (722 mg, 3.42 mmol) and $BF_3 \cdot Et_2O$ (7.0 mL, 57 mmol) in CH_2Cl_2 (60 mL), then work-up *i*, led, after chromatography (10–16% EtOAc in hexane), to 37 mg (16%) of recovered isophorone and *7,9,9-trimethylspiro[4.5]dec-7-ene-1,4-dione* (601 mg, 85%) as colorless crystals: mp 85–86°C; ir ν_{max}: 1721 cm^{-1}; ^1H nmr δ: 5.20 (1H, br s, irradiation of this signal resulted in a 1% nOe for δ 1.76 and a 1.5% nOe at δ 0.94), 3.05 (2H, m), 2.63 (2H, m), 2.03 (2H, br s), 1.76 (3H, s), 1.65 (2H, s), 0.94 (6H, s, irradiation of this signal resulted in a 17% nOe for δ 5.20 and a 7% nOe for δ 1.65); ^{13}C nmr δ: 214.2 (2C, 0), 129.6 (1), 128.6 (0), 59.0 (0), 43.3 (2), 34.7 (2C, 2), 32.8 (0), 30.1 (2C, 3), 29.1 (2), 23.6 (3); ms: 206 (100, M^+), 191 (22), 178 (11), 163 (31), 145 (28), 131 (31), 107 (21), 91 (21). Exact Mass calcd. for $C_{13}H_{18}O_2$: 206.1306; found: 206.1306.

Reaction of ***42***

Addition of **2** (0.70 mL, 2.5 mmol) in CH_2Cl_2 (5.0 mL) to a solution of ketal **42** (225 mg, 1.24 mmol) and $BF_3 \cdot Et_2O$ (2.3 mL, 18 mmol) in CH_2Cl_2 (40 mL), then work-up *i*, gave a mixture of double bond isomers in a ratio of 11:1. The major product, *8-carbethoxy-7-methylspiro[4.5]dec-7-ene-1,4-dione*, was isolated by chromatography (7%) as a colorless oil (223 mg, 72%): ir ν_{max}: 1721 (s), 1645 (m) cm^{-1}; ^1H nmr δ: 4.18 (2H, q, J = 6.9 Hz), 3.03–2.64 (4H, m), 2.38 (2H, br s), 2.24 (2H, s), 2.11 (3H, s), 1.74 (2H, t, J = 6.3 Hz), 1.29 (3H, t, J = 7.2 Hz); ^{13}C nmr δ; 213.8 (2C, 0), 167.5 (0), 143.4 (0), 122.7 (0), 59.8 (2), 56.4 (0), 34.2 (2C, 2), 33.6 (2), 28.2 (2), 22.2 (2), 21.5 (3), 14.2 (3); ms (from gc-ms): 250 (6, M^+), 205 (26), 204 (100), 177 (26), 176 (75), 175 (24), 91 (45), 77 (32), 55 (27). Exact Mass calcd. for $C_{14}H_{18}O_4$: 250.1204; found: 250.1206. The minor isomer was not obtained homogeneously, but from a fraction containing the major isomer the following data suggested its structure to be *8-carbethoxy-9-methylspiro[4.5]dec-7-ene-1,4-dione*: ^1H nmr δ: 5.11 (s) with the remaining signals masked by those of the major isomer; ^{13}C nmr δ: 213.2 (2C, 0), 172.9 (0), 137.5 (0), 117.5 (1), 60.8 (2), 56.4 (0), 44.4 (1), 34.7 (2C, 2), 25.0 (2), 22.9 (3), 14.1 (3) with one methylene signal hidden; ms (from gc–ms): 250 (25, M^+), 177 (100), 131 (41), 121 (41), 93 (28), 91 (59), 77 (53), 55 (27).

Reaction of ***43***

Addition of **2** (0.89 mL, 3.3 mmol) in CH_2Cl_2 (6.0 mL) to a solution of ketal **43** (202 mg, 1.33 mmol) and $BF_3 \cdot Et_2O$ (2.5 mL, 20 mmol) in CH_2Cl_2 (40 mL), then work-up *i*, led, after chromatography (5%), to *8-oxatricyclo[7.2.1.0^{3,7}]dodeca-3(7),10-dien-4-one* (**45**) (29 mg, 12%) as a colorless oil: ir ν_{max}: 1690 (m), 1611, 1386 cm^{-1}; ^1H nmr δ: 6.29 (1H, dd, J = 2.7, 5.5 Hz), 5.81 (1H, dd, J = 2.6, 5.5 Hz), 5.33 (1H, dd, J = 2.6, 6.1 Hz), 3.06 (1H, m), 2.60–2.21 (7H, m), 1.93 (1H, d, J = 14.0 Hz); ^{13}C nmr δ: 207.7 (0), 179.6 (0), 144.4 (1), 126.8 (1), 115.4 (0), 85.2 (1), 40.1 (2), 38.1 (1), 33.4 (2), 32.2 (2), 28.0 (2); ms (from gc–ms): 194 (14, M^+), 91 (36), 89 (12), 66 (100), 65 (27). A more polar chromatographic fraction was composed of *2-((3-hydroxycyclopent-4-enyl)methyl)cyclopentane-1,3-dione* (**46**, mainly in its enol form) as a colorless oil (108 mg, 42%): ir ν_{max}: 3404 (br), 1683 (m), 1621, 1411 cm^{-1}; ^1H nmr δ: 6.14 (1H, m), 6.00 (1H, m), 5.10 (1H, d, J = 5.5 Hz), 2.67–2.18 (9H, m); ^{13}C nmr δ: 203.6 (0), 184.5 (0), 137.4 (1), 134.8 (1), 110.0 (0), 84.2 (1), 36.9 (2), 34.2 (1), 32.6 (2), 26.5 (2), 17.5 (2); ms: no M^+, 176 (6, $M^+ - H_2O$), 66 (100), 65 (20), 55 (17), 54 (24). Exact Mass calcd. for $C_{11}H_{12}O_2$ ($M^+ - H_2O$): 176.0851; found: 176.0841.

Reaction of ***47***

Addition of **2** (0.73 mL, 2.8 mmol) in CH_2Cl_2 (6.0 mL) to a solution of ketal **47** (182 mg, 1.10 mmol) and $BF_3 \cdot Et_2O$ (2.0 mL, 16 mmol) in CH_2Cl_2 (40 mL), then work-up *i*, gave, after chromatography (6%), *8-oxatricyclo[7.2.2.0^{3,7}]triscadeca-3(7),10-dien-4-one* (**48**) (117 mg, 56%) as a colorless solid: mp 72–74°C; ir ν_{max}: 1682 (m), 1619, 1415 (m) cm^{-1}; ^1H nmr δ: 6.10 (1H, m), 5.90 (1H, m), 4.65 (1H, br s), 2.77–2.08 (9H, m), 1.62–1.55 (2H, m); ^{13}C nmr δ: 204.1 (0), 182.4 (0), 133.4 (1), 124.5 (1), 112.7 (0), 74.6 (1), 33.1 (2), 29.2 (1), 26.3 (2), 24.7 (2), 22.9 (2), 21.0 (2); ms: 190 (6, M^+), 112 (52), 111 (24), 80 (100), 79 (72), 76 (31), 55 (20), 53 (18), 51 (20). Exact Mass calcd. for $C_{12}H_{14}O_2$: 190.0993; found: 190.0988.

*Reaction of trimethyl orthovalerate (****49****)*

A solution of **2** (1.2 mL, 4.1 mmol) in CH_2Cl_2 (6.0 mL) was added over 20 min to a solution of trimethyl orthovalerate (**49**) (275 mg, 1.70 mmol) and $BF_3 \cdot Et_2O$ (3.1 mL, 25 mmol) in CH_2Cl_2 (30 mL) at room temperature. The reaction was stirred for 90 h. Work-up *iii* gave 260 mg of a volatile brown oil for which gc–ms analysis indicated that the major product was *methyl valerate*. Chromatography (10%) provided only 52 mg (16%) of *2-butyl-2-methoxy-1,3-cyclopentanedione* (**51**) as a yellow oil: ir ν_{max}: 1775 (m), 1731 cm^{-1}; ^1H nmr δ: 3.26 (3H, s), 2.93 and 2.68 (2H each, coupled multiplets), 1.74 (2H, m), 1.30 (4H, br m), 0.88 (3H, t, J = 7.0 Hz); ^{13}C nmr δ: 210.9 (2C, 0), 87.5 (0), 54.5 (3), 34.9 (2), 34.0 (2C, 2), 24.3 (2), 22.6 (2), 13.7 (3); ms (from gc–ms): 184 (38, M^+), 169 (0.2), 141 (55), 113 (10), 100 (14), 85 (54), 71 (86), 57 (100), 55 (35), 41 (65). Exact Mass calcd. for $C_{10}H_{16}O_3$: 184.1099; found: 184.1104. A less polar chromatographic fraction (5%) yielded *methyl 5-methoxy-4-oxononanoate* (**53**) (16 mg, 4%) as a yellow oil (contaminated with a little methyl valerate): ir ν_{max}: 1742, 1719 cm^{-1}; ^1H nmr δ: 3.68 (3H, s), 3.62 (1H, apparent t, J = 6.3 Hz), 3.38 (3H, s), 2.84 (2H, complex m), 2.61 (2H, apparent t, J = 6.5 Hz), 1.65 (2H, m), 1.34 (4H, br m), 0.90 (3H, distorted t, $J \approx$ 6.7 Hz); ^{13}C nmr δ: 211.5 (0), 173.2 (0), 87.1 (1), 58.2 (3), 51.8 (3), 32.3 (2), 31.8 (2), 27.2 (2C, 2), 22.5 (2), 13.9 (3); ms (from gc–ms): no M^+, 185 (4), 153 (1), 131 (15), 115 (9), 101 (70), 71 (30), 69 (83), 59 (17), 55 (24), 45 (100). Exact Mass calcd. for $C_{10}H_{17}O_4$ ($M^+ - CH_3$): 185.1177; found: 185.1168.

*Reaction of trimethyl orthobenzoate (****50****)*

A solution of **2** (1.1 mL, 3.9 mmol) in CH_2Cl_2 (6.0 mL) was added over 30 min to a solution of trimethyl orthobenzoate (**50**) (240 mg, 1.32 mmol) and $BF_3 \cdot Et_2O$ (2.4 mL, 19 mmol) in CH_2Cl_2 (30 mL) at −78°C. The reaction was stirred for 26.5 h during which time the reaction was allowed to attain room temperature. Work-up *iii* provided a brown oil (331 mg), but chromatography (5%) yielded only 47 mg (15%) of *methyl 5-methoxy-4-oxo-5-phenylpentanoate* (**54**) as a yellow oil: ir ν_{max}: 1729 cm^{-1}; ^1H nmr δ: 7.42–7.35 (5H, m), 4.72 (1H, s), 3.61 (3H, s), 3.40 (3H, s), 2.81 (2H, complex m), 2.52 (2H, m); ^{13}C nmr δ: 206.9, 173.0, 135.8, 128.7 (2C), 128.6, 126.9 (2C), 88.9, 57.3, 51.7, 32.3, 27.4; ms: 236 (0.6, M^+), 205 (1), 204 (2), 131 (14), 121 (100), 115 (15), 105 (16), 91 (18), 77 (41), 55 (12). Exact Mass calcd. for $C_{13}H_{16}O_4$: 236.1048; found: 236.1057.

Acknowledgements

We thank Ms. N. Brunet and Dr. C. R. Jablonski for nmr spectra, and Miss M. Baggs and Dr. B. Gregory for mass spectra. We are grateful to the Natural Sciences and Engineering Research Council of Canada for financial support.

1. E. Nakamura and I. Kuwajima. J. Am. Chem. Soc. **99**, 961 (1977); Org. Synth. **65**, 17 (1987).
2. J. Shimada, K. Hashimoto, B.H. Kim, E. Nakamura, and I. Kuwajima. J. Am. Chem. Soc. **106**, 1759 (1984).

3. J.J. Bloomfield. Tetrahedron Lett. 587 (1968); J.J. Bloomfield and J.M. Nelke. Org. Synth. Coll. Vol. **VI**, 167 (1988).
4. W.K. Anderson and G.E. Lee. J. Org. Chem. **45**, 501 (1980); Synth. Commun. **10**, 351 (1980); W. Oppolzer and R.D. Wylie. Helv. Chim. Acta, **63**, 1198 (1980); W.H. Bunnelle and W.R. Shangraw. Tetrahedron, **43**, 2005 (1987); J.C. Evans, R.C. Klix, and R.D. Bach. J. Org. Chem. **53**, 5519 (1988).
5. K.A. Parker, K.A. Koziski, and G. Breault. Tetrahedron Lett. **26**, 2181 (1985).
6. (*a*) Y.-J. Wu and D.J. Burnell. Tetrahedron Lett. **29**, 4369 (1988); (*b*) D.J. Burnell and Y.-J. Wu. Can. J. Chem. **68**, 804 (1990).
7. Y.-J. Wu and D.J. Burnell. J. Chem. Soc. Chem. Commun. 764 (1991).
8. D.J. Burnell and Y.-J. Wu. Can. J. Chem. **67**, 816 (1989).
9. Y.-J. Wu and D.J. Burnell. Tetrahedron Lett. **30**, 1021 (1989).
10. B. Pandey, U.R. Khire, and N.R. Ayyangar. Synth. Commun. **19**, 2741 (1989).
11. J. Sisko, A. Balog, and D.P. Curran, J. Org. Chem. **57**, 4341 (1992).
12. I. Kuwajima and I. Azegami. Tetrahedron Lett. 2369 (1979).
13. J.R. Gillard and D.J. Burnell. Can. J. Chem. **70**, 1296 (1992).
14. T. Tsunoda, M. Suzuki, and R. Noyori. Tetrahedron Lett. **21**, 1357 (1980); J.R. Hwu, L.-C. Leu, J.A. Robl, D.A. Anderson, and J.M. Wetzel. J. Org. Chem. **52**, 188 (1987).
15. S.G. Levine and C.U. Mauney. Synth. Commun. **18**, 689 (1988).

Can. J. Chem. Downloaded from www.nrcresearchpress.com by 213.200.69.106 on 09/08/12
For personal use only.

Phthalocyanine-modified silica gels and their application in the purification of unsymmetrical phthalocyanines

CLIFFORD C. LEZNOFF,[1] COLIN R. MCARTHUR, AND YONGNIAN QIN
Department of Chemistry, York University, North York (Toronto), ON M3J 1P3, Canada

Received February 8, 1993

CLIFFORD C. LEZNOFF, COLIN R. MCARTHUR, and YONGNIAN QIN. Can. J. Chem. **71**, 1319 (1993).

Five species of phthalocyanine-modified silica gels were prepared. The loadings of phthalocyanine on these silica gels were determined by acidic hydrolysis. The concept of using the aggregation phenomenon to advantage to aid chromatographic separation of unsymmetrical phthalocyanines was investigated by employing these modified silica gels as chromatographic media to purify unsymmetrical phthalocyanines. Four groups of phthalocyanine mixtures were prepared by mixed condensation. One of the desired unsymmetrical phthalocyanines was successfully purified by conventional column chromatography while others were separated by the new method described herein.

CLIFFORD C. LEZNOFF, COLIN R. MCARTHUR et YONGNIAN QIN. Can. J. Chem. **71**, 1319 (1993).

On a préparé cinq espèces de gels de silice modifiés par des phtalocyanines. On a déterminé la quantité de phtalocyanine présente sur ces gels de silice en faisant appel à une hydrolyse acide. On a étudié le concept de l'utilisation du phénomène d'agrégation pour faciliter la séparation chromatographique de phtalocyanines non symétriques en utilisant ces gels de silice modifiés comme milieux chromatographiques pour la purification de phtalocyanines non symétriques. On a préparé quatre groupes de mélanges de phtalocyanines par condensations mixtes. On a réussi à purifier une des phtalocyanines non symétriques désirées par chromatographie conventionnelle sur colonne alors que les autres ont été séparées par la méthode décrite ici.

[Traduit par la rédaction]

Unsymmetrical phthalocyanines present challenges in the development of new methods of synthesis and separation. The potential use of phthalocyanines for photodynamic therapy (PDT) of cancer has sparked considerable interest in the photobiology of these compounds (1–9). To find a suitable phthalocyanine as photosensitizer, it is necessary to tune the position of its absorption band. Such fine tuning can be achieved by the stepwise introduction of peripheral substituent groups or by the stepwise adjustment of the size of the π-conjugated macrocyclic systems (10–13). Thus, unsymmetrical phthalocyanines are important goals in synthesis. Although symmetrical tetra- and octasubstituted phthalocyanines are well known, the synthesis of simple mono- and disubstituted and other unsymmetrical phthalocyanines remains a difficult problem (10–21). For instance, all tetrasubstituted phthalocyanines so far synthesized contain one substituent in each of the benzene rings, and no phthalocyanines such as 1,2,3,4- or 1,2,3,8-tetrasubstituted phthalocyanines have been reported.

Successful methods for the synthesis of unsymmetrical phthalocyanines can be divided into three groups according to strategy: (1) the polymer support route (14, 16, 19, 20); (2) the homogeneous mixed condensation route (12–14, 21); and (3) the subphthalocyanine route (11). There are difficulties with all three routes for large-scale preparation of unsymmetrical alkoxy-substituted phthalocyanines.

Route 1 is not suitable for large-scale preparation of unsymmetrical phthalocyanines. Route 3 is not suitable for the preparation of alkoxy-substituted phthalocyanines, as this method uses BBr_3, an ether-cleaving reagent. Route 2, the ordinary method of forming unsymmetrical phthalocyanines by mixed condensation of different phthalonitriles, most often gives statistical mixtures of phthalocyanines, which are very difficult to separate by common chromatographic methods. Although purifications of desired unsymmetrical phthalocyanines from mixed condensations by common chromatographic methods have been reported, success has been achieved only with those phthalocyanines having greatly differing polarities and after numerous repetitions of chromatographic separations. There appear to be two reasons for such difficulties. First, a number of very similar phthalocyanine species exist in the mixture. With site-isomers considered, a mixture from a mixed condensation conceivably can contain more than 20 species of similar phthalocyanines! Second, strong aggregation (22–24) exists among the different phthalocyanine species. Generally speaking, one of the basic premises and presumptions of chromatography is that each gradient to be separated should behave independently without interfering with another. The premise is not valid if aggregation occurs. Thus, a well-defined band on column chromatography or a single spot on thin-layer chromatography (TLC) is by itself insufficient evidence of purity and should be accompanied by mass spectral and other spectroscopic data (15).

In this investigation, the homogeneous mixed condensation route was used, together with work aimed at developing a more powerful method of separation. For the latter, we envisioned and investigated a new strategy which *takes advantage of the aggregation* that would be expected to occur between immobilized phthalocyanines and those in the synthetic mixture.

Five species of phthalocyanine-modified silica gels (Pc-Si-Gels) were prepared. These Pc-Si-Gels can be divided into three groups. In the first group, flash grade silica gel (**1**), preactivated with concentrated hydrochloric acid (25), reacted with thionyl chloride to give chlorinated silica gel (**2**). A reaction between **2** and 2,9,16,23-tetrakis(2-hydroxymethyl-2-methylbutoxy)phthalocyanine (**3**) (14) gave a modified silica gel (**4**), which contained phthalocyanine entities bonded to silica through Si—O—C linkages (Scheme 1). It should be noted that the phthalocyanine entities could be bonded to silica through more than one Si—O—C linkage (26), so its structure shown in Scheme 1 represents a simplified model.

[1]Author to whom correspondence may be addressed.

Can. J. Chem. Downloaded from www.nrcresearchpress.com by 213.200.69.106 on 09/08/12
For personal use only.

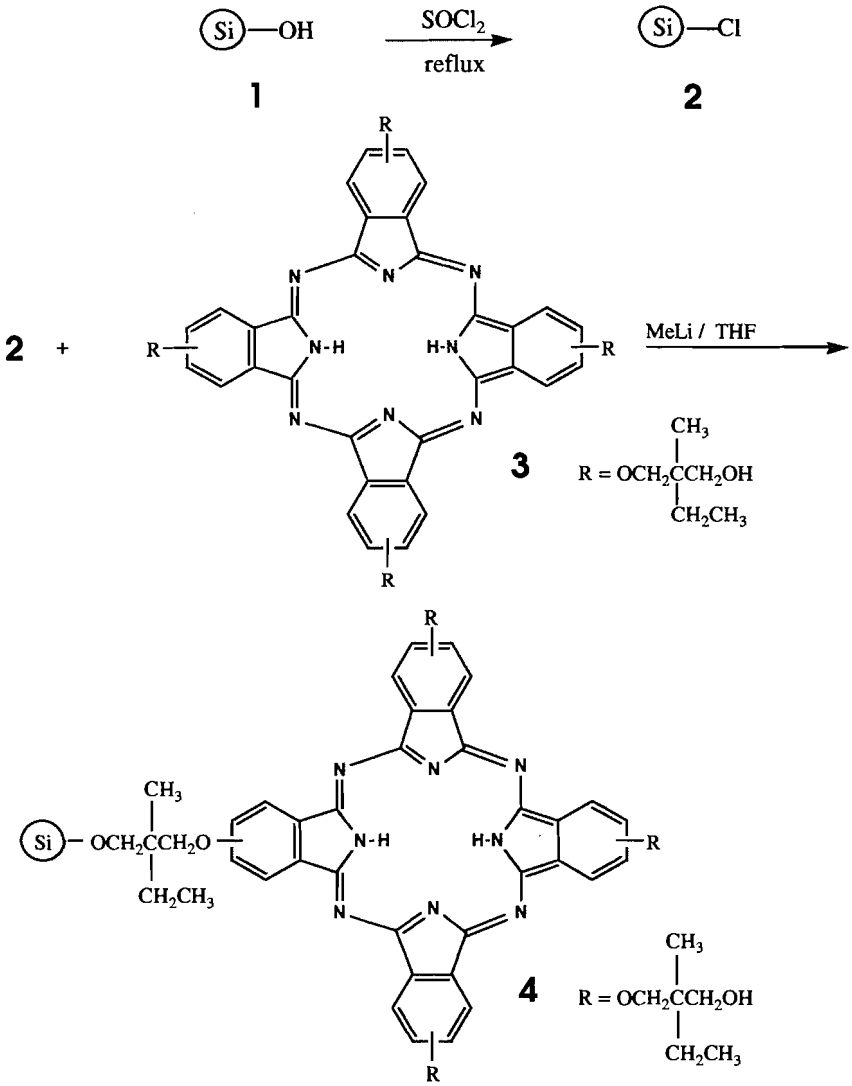

SCHEME 1

In the second group of Pc-Si-Gels, the metal atoms of metallophthalocyanines are bonded with the oxygen atoms of silica gels (Scheme 2). Thus, reactions of 2,9,16,23-tetra-*tert*-butylphthalocyanine (**5**) (27), 2,9,16,23-tetraneopentoxyphthalocyanine (**6**) (28), or unsubstituted phthalocyanine (**7**) with trimethyl aluminum and **1** gave 2,9,16,23-tetra-*tert*-butylphthalocyaninato aluminum(III) silica (**8**), 2,9,16,23-tetraneopentoxyphthalocyaninato aluminum(III) silica (**9**), or phthalocyaninato aluminum(III) silica (**10**), respectively.

In the third group, the metal atom of the phthalocyanine is bonded to the nitrogen atom of an aminopropyl derivative of silica (29) (Scheme 3). During the process of preparation, **1** reacted with (3-aminopropyl)trimethoxysilane (**11**) to give 3-aminopropylsilyl silica (**12**), which then reacted with methylaluminum(III) phthalocyanine (**13**) and gave phthalocyaninato aluminum(III) aminopropylsilyl silica (**14**).

To determine the loadings of immobilized Pc in the Pc-Si-Gels, three accurately weighed samples of each of the Pc-Si-Gels were hydrolysed with hydrochloric acid. Comparison of the UV spectra of the filtrates with reference solutions, also under acidic conditions, gave the values of the loadings, which are summarized in Table 1. In all examples the silica gels recovered from acidic hydrolyses were colourless and indeed hydrolyses were continued until the silica gels were colourless. Three species of the Pc-Si-Gels, namely **4**, **9**, and **14**, were chosen to pack columns. One of the Pc-Si-Gels, **4**, was abandoned as it was found to be unstable in the alcoholic solvent (2-methoxyethanol:toluene = 4:6) used in the column-cleaning process. Among the Pc-Si-Gels **8–10**, compound **8** was formed in lower yield while **10** was abandoned in favour of **14**, a chain-extended analog of **10**, and hence **8** and **10** were not examined further.

Four homogeneous mixed condensations were used to prepare mixtures of unsymmetrical phthalocyanines. The mixed condensation of 2,3-dihydro-1,3-diimino-1*H*-benz[*f*]isoindole (**15**) with 5-neopentoxy-1,3-diiminoisoindoline (**16**) or 5-*tert*-butyl-1,3-diiminoisoindoline (**17**) gave mixtures containing 2,9,16-trineopentoxy-31*H*,33*H*-tribenzo[*b*,*g*,*l*]-naptho[2,3-*q*]porphyrazine (**18**) or 2,9,16-tri-*tert*-butyl-31*H*,33*H*-tribenzo[*b*,*g*,*l*]naphtho[2,3-*q*]porphyrazine (**19**) (Scheme 4). The mixed condensation of **16** and **17** gave a mixture containing 2-*tert*-butyl-9,16,23-trineopentoxyphthalocyanine (**20**) (Scheme 5). The mixed condensation of 4,5-di-(1-octyn-1-yl)phthalonitrile (**21**)[2] and 4-methoxy-

[2]C. C. Leznoff and K. Nolan. Unpublished work.

Can. J. Chem. Downloaded from www.nrcresearchpress.com by 213.200.69.106 on 09/08/12
For personal use only.

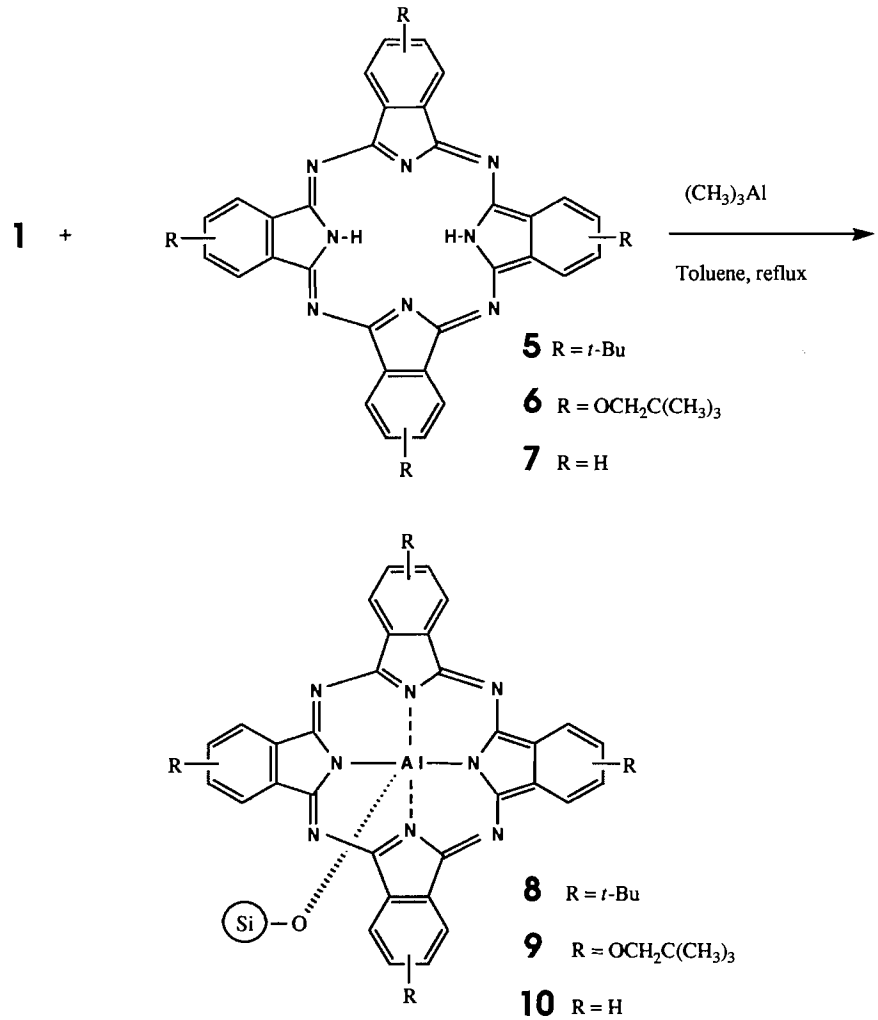

SCHEME 2

methyloxyphthalonitrile (**22**) (30) with DBU and zinc acetate gave a mixture containing 2,3-di-(1-octyn-1-yl)-9,16,26-tri-(methoxymethyloxy)phthalocyanine zinc(II) (**23**) (Scheme 6).

Among those desired phthalocyanines, **23** was successfully purified by ordinary column chromatography with the help of reverse phase HPLC as a monitor. The other three species, **18**, **19**, and **20**, could not be completely purified by ordinary column chromatography, but were successfully purified by Pc-Si-Gel column chromatography with the help of reverse phase HPLC or UV as a monitor.

The mass spectra and other data showed that complete separations were achieved. For instance, the mass spectrum of **18** showed that none of the phthalocyanines (porphyrazines) containing di-, tri-, or tetrabenzo groups or tetraneopentoxyphthalocyanines contaminated the desired unsymmetrical phthalocyanine. As a comparison, the same crude products were subjected to ordinary flash chromatography for as many as four repetitive columns. Even so, the mass spectra of the purest fractions showed that substantial contamination by undesired phthalocyanines still occurred (e.g., *m/z* 858, tetraneopentoxyphthalocyanine; 786, dibenzodineopentoxyphthalocyanine (dibenzodinaphthoporphyrazines)).

It should be noted that each of the unsymmetrical phthalocyanines (**18**–**20**, **23**) are likely a mixture of several closely related site-isomers. So far, we have not seen any successful example of the separation of such phthalocyanine isomers by chromatographic methods. This method does not readily separate similar isomers such as 2,9,16,23-, 2,10,16,24-, 2,9,17,24-, and 2,9,16,24-tetraneopentoxyphthalocyanine (**6**) and this mixture has normally been represented as the 2,9,16,23 isomer.

The experiments showed that the Pc-Si-Gels have some enhanced ability relative to standard silica gel for the purification of phthalocyanines. The separation ability of Pc-Si-Gels may depend on a number of complicated factors: amongst others, the nature of the phthalocyanines to be separated, the solvent system employed, and the chemical nature and physical condition of the phthalocyanines bonded to the polymer. Further studies of this new strategy are required before a general statement in this regard can be made. As well, additional work will be aimed at further enhancement of the capabilities of Pc-Si-Gels in practical applications.

Experimental

High-purity argon was used to maintain inert atmosphere conditions. Infrared (IR) spectra were recorded on a Pye Unicam SP-3200 infrared spectrophotometer using KBr discs for solids or

Can. J. Chem. Downloaded from www.nrcresearchpress.com by 213.200.69.106 on 09/08/12
For personal use only.

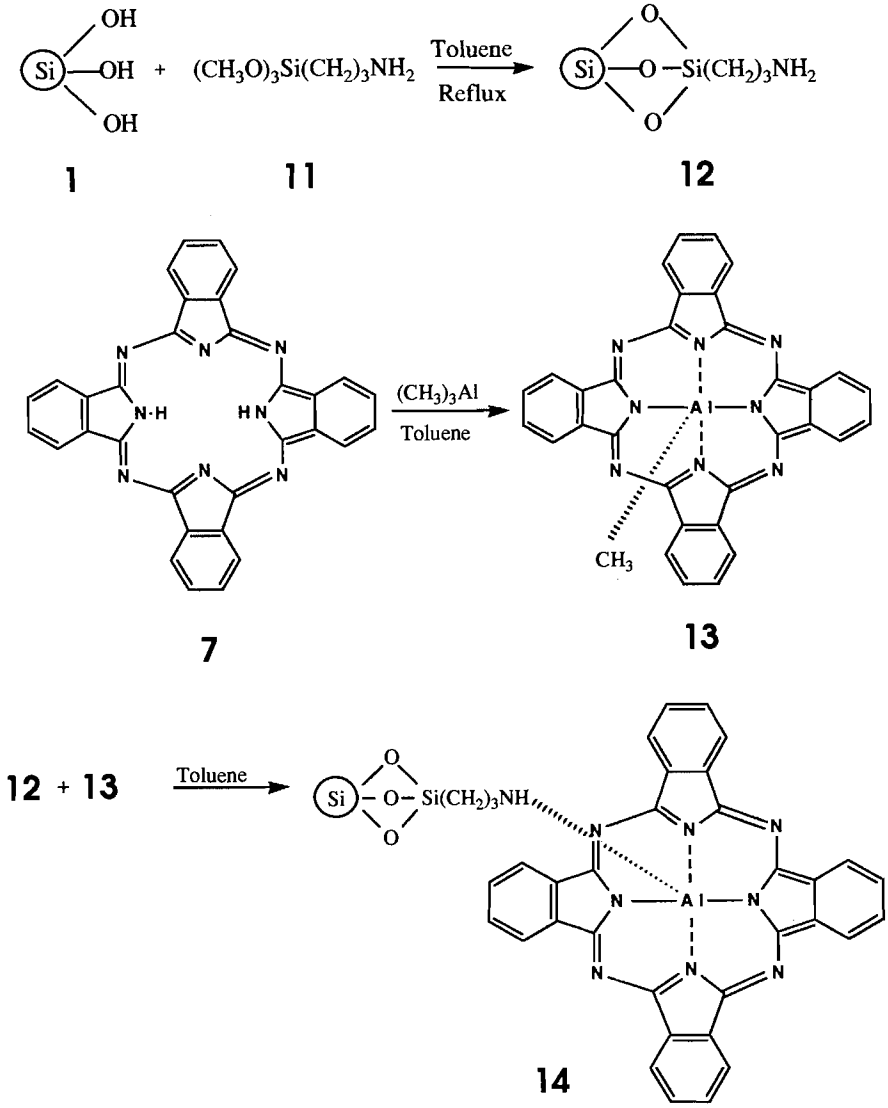

SCHEME 3

TABLE 1. Some properties of Pc-Si-Gels

Pc-Si-Gels	Pc loading (mg/g) (mmol/g)	Yield[a] (%)	Colour
4	18.7 (0.020)	66.5	Dark green
8	14.4 (0.019)	47.0	Dark blue
9	28.7 (0.033)	~100	Dark green
10	22.3 (0.044)	55.6	Dark blue
14	29.9 (0.056)	~100	Dark blue-grey

[a]Usually, the functional groups on silica gel are used as the limiting reagents, but in these cases, since the functional groups on silica gel were in excess, the yields were calculated using the phthalocyanines as the limiting reagents.

as neat films between NaCl discs for liquids. Nuclear magnetic resonance (NMR) spectra for carbons and protons were recorded on a Bruker AM300 NMR spectrometer using tetramethylsilane as the internal standard. The positions of the signals are reported in δ units. The splittings of the signals are described as singlets (s), doublets (d), triplets (t), quartets (q), or multiplets (m). The ^1H NMR spectra of 10^{-4} M solutions of the phthalocyanines were obtained by averaging 500–3000 scans over the absorption range. The ^{13}C NMR spectra of 5×10^{-4} M solutions of the phthalocyanines were obtained by averaging 7000–15 000 scans. The ultraviolet–visible spectra (UV–VIS) were recorded on a Hewlett Packard HP8451A diode array spectrophotometer. Mass spectra (MS) were recorded at 70 eV on a VG Micromass 16F mass spectrometer in the El mode for relatively small molecules (generally less than 800 amu). The Fast Atom Bombardment mode (FAB) spectra were obtained with a Kratos Profile or Kratos MS-50 analyzer mass spectrometer equipped with a FAB ion source of standard Kratos design and Ion Tech atom gun for relatively large molecules (generally greater than 800 amu).

Melting points (mp) were determined using a Kofler hot stage

Can. J. Chem. Downloaded from www.nrcresearchpress.com by 213.200.69.106 on 09/08/12
For personal use only.

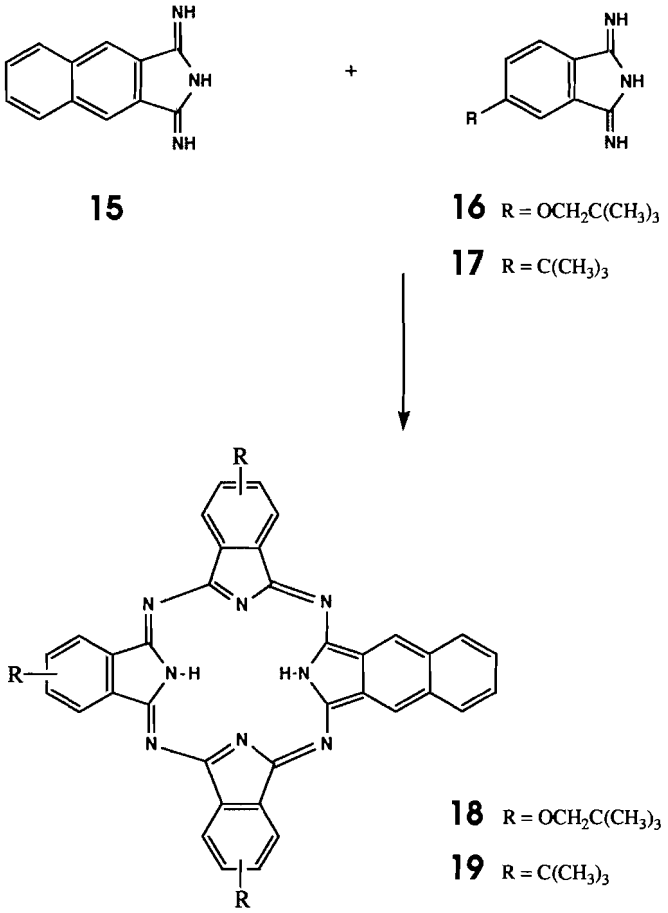

SCHEME 4

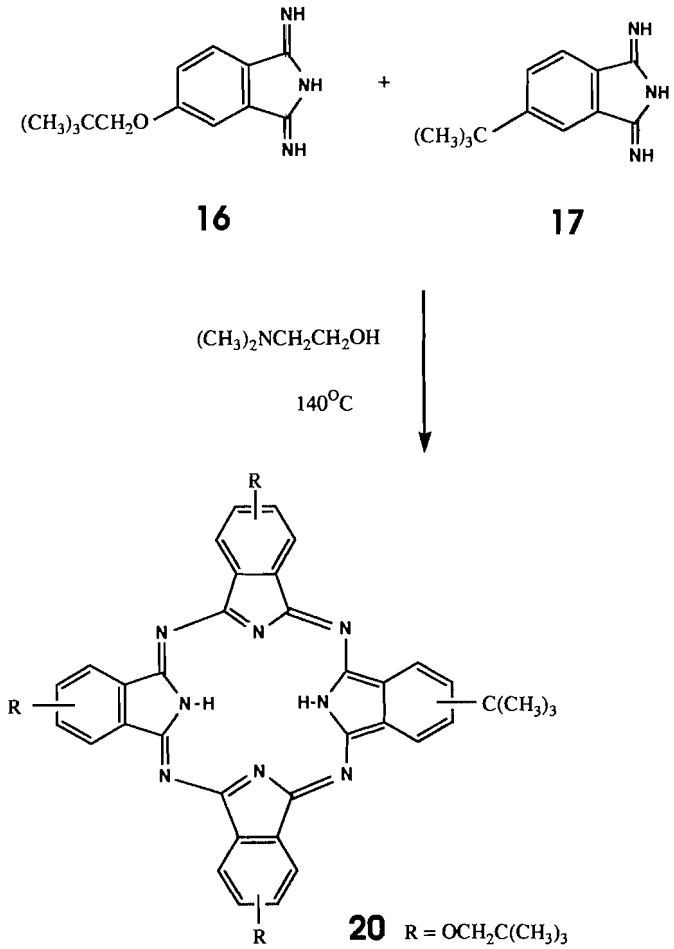

SCHEME 5

melting point apparatus and are uncorrected. Thin-layer chromatography (TLC) was performed using Kodak 13181 silica gel TLC sheets unless otherwise stated. Flash chromatography was performed using silica gel of particle size 20–45 μm (purchased from Terochem Laboratories Ltd., equivalent to Merck 9385). Neutral alumina column chromatography was performed using Brockmann I standard grade (150 mesh, 155 m^2/g). Reaction mixtures were stirred with a magnetic stirrer, except those that required sonication. Ultrasound treatment was carried out using a Branson 1200 sonicator. Microanalyses were performed by Guelph Chemical Laboratories Ltd., Guelph, Ont. All diiminoisoindolines were used directly without purification, after evaporation of the solvent in condensation experiments. All yields were not optimized by detailed investigation of the effects of temperature, reaction time, and other conditions.

Activated flash silica gel (1)

Flash grade silica gel (20–45 μm, purchased from Terochem Laboratories Ltd.) was heated under reflux with concentrated hydrochloric acid for 4 h. The ratio of concentrated hydrochloric acid to **1** was 4–5 mL/g. After cooling to room temperature, **1** was filtered, washed with distilled water until the filtrate was neutral, preliminarily dried in an oven, and thoroughly dried under vacuum (140°C, 0.05 Torr (1 Torr = 133.3 Pa), 3 h).

Chlorinated silica gel (2)

Freshly distilled thionyl chloride (30 mL) was injected into a round-bottom flask that contained 5.7 g of **1** under argon. After heating under reflux with stirring for 24 h, the mixture was filtered under argon in a Schlenk tube. After washing with dry dichloromethane (20 mL, three times) by injection, the chlorinated silica gel was obtained as a white powder.

To determine the chlorine loading, three accurately weighed samples of **2** (about 50 mg each) were taken out and immediately treated with 10 mL of distilled water with stirring. After 10 min, the suspensions were titrated with a 0.1 M aqueous solution of potassium hydroxide and compared with a blank assay. The chlorine loadings were determined to be ~1.0 ± 0.1 mmol per gram of silica gel. Different batches of silica gel yielded chlorine loadings of 0.8–1.8 mmol/g.

2,9,16,23-Tetrakis(2-hydroxymethyl-2-methylbutoxy)phthalocyanine (3) modified silica gel (4)

A solution of **3** (162 mg, 0.17 mmol) (14) in 30 mL of dry tetrahydrofuran (THF) and 0.5 mL of 1.4 M methyllithium solution in toluene was injected into a round-bottom flask that contained 5.7 g of **2**. The mixture was stirred at room temperature for 24 h. After filtering and washing with dry toluene and dry THF (three times each), a dark green powder of Pc-Si-Gel **4** was obtained.

To determine the loading of phthalocyanine on silica gel, three accurately weighed samples of **4** (about 50 mg each) were hydrolysed in 10 mL of hydrochloric acid solution (HCl:THF:H_2O = 1:8:1) by heating under reflux for 1 h, and then were filtered. Comparison of the UV–VIS spectra of the filtrate with a solution of **3** as a reference showed that the loading of phthalocyanine on **4** was 18.7 mg per gram of silica gel (0.020 mmol/g). The yield was 66% with **3** as the limiting reactant.

2,9,16,23-Tetra-tert-butylphthalocyaninatoaluminum(III) silica (8)

Trimethylaluminum (8.5 mL of 2 M solution in toluene) was injected into a round-bottom flask that contained 8.5 g of **1** and 30 mL of dry toluene under argon. The suspension was stirred at room temperature overnight, then filtered and washed once with

Can. J. Chem. Downloaded from www.nrcresearchpress.com by 213.200.69.106 on 09/08/12
For personal use only.

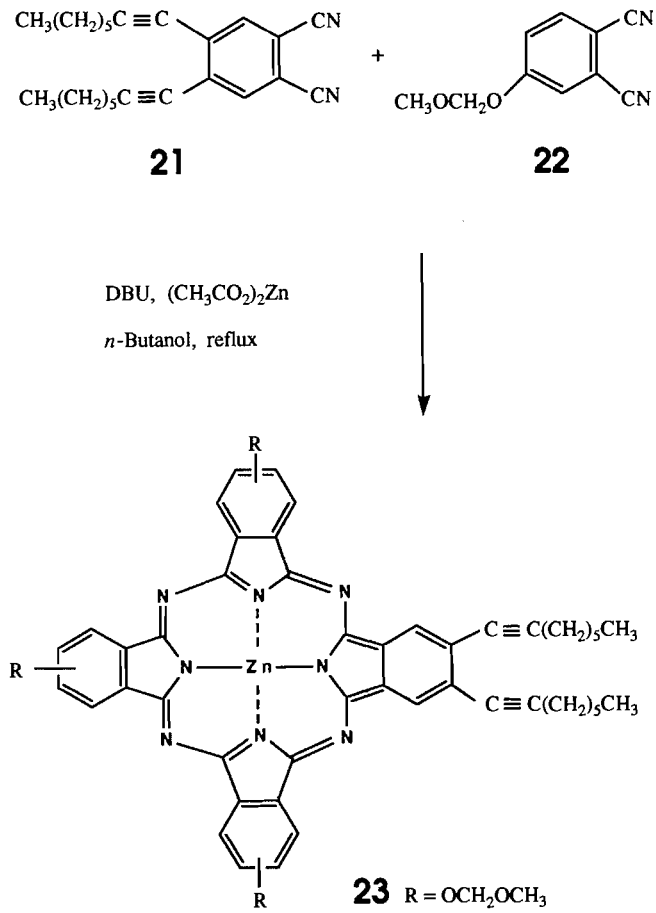

SCHEME 6

dry toluene. A solution of 2,9,16,23-tetra-*tert*-butylphthalocyanine (**5**) (27) (260 mg, 0.35 mmol) in 40 mL of dry toluene was then injected. The reaction was monitored by removal of an aliquot and examination by UV–VIS spectroscopy to ensure that all of **8** was consumed. The suspension was stirred under reflux for 48 h, at which time the reaction was complete, and then was filtered. The dark blue powder was first washed with dry toluene until the solvent was almost colourless, then washed with dry THF three times, with dry dichloromethane three times, and dried in the air.

Three accurately weighed samples (about 50 mg each) were hydrolysed by heating under reflux for 2 h with 10 mL of hydrochloric acid solution (HCl:THF:H_2O = 1:8:1). After filtration, the comparison of the UV–VIS spectrum of the filtrate with that of a similar acidic reference solution of the starting material **5** showed that the loading of **5** on **8** was 14.4 mg per gram of silica gel (0.019 mmol/g). The yield was 47% with **5** as the limiting reactant.

2,9,16,23-Tetraneopentoxyphthalocyaninatoaluminum(III) silica (9)

Trimethylaluminum (6.0 mL of 2 M solution in toluene) was injected under argon into a round-bottom flask that contained 6.0 g of **1** and 25 mL of dry toluene. The suspension was stirred at room temperature overnight, then filtered and washed once with dry toluene. A solution of 2,9,16,23-tetraneopentoxyphthalocyanine (**6**) (28) (168 mg, 0.20 mmol) in 30 mL of dry toluene was then injected. The suspension was stirred under reflux for 48 h until the reaction was complete (as monitored for **8** above) and then was filtered. The filtrate was almost colourless. The dark green powder was then washed with dry toluene three times, with dry THF three times, with dry dichloromethane three times, and dried in the air. Three accurately weighed samples (about 50 mg each) were taken and hydrolysed by heating under reflux for 2 h with 10 mL of hydrochloric acid solution (HCl:THF:H_2O = 1:8:1). After filtration, comparison of the UV–VIS spectrum of the filtrate with that of a reference solution of the starting material **6** showed that the loading of **6** on **9** was 28.7 mg per gram of silica gel (0.033 mmol/g). The yield was 100% with **6** as the limiting reactant.

Phthalocyaninatoaluminum(III) silica (10)

Unsubstituted phthalocyanine **7** (1.28 g, 2 mmol) was mixed with 50 mL of a 1.9 M solution of trimethylaluminum in toluene under argon. This mixture was treated with ultrasound for 24 h to improve solubility and then filtered through a Schlenk tube into a flask containing 24 g of **1**. After heating under reflux for 48 h under argon, the mixture was filtered in the Schlenk tube and washed with dry toluene and dry dioxane. The dark blue modified silica gel was then treated with dry dioxane, which allowed the unbound unsubstituted phthalocyanine to be removed by floatation. After the floatation procedure was repeated a few times, no visible unbound phthalocyanine remained and the Pc-Si-Gel **10** was obtained as a dark blue powder.

To determine the loading of **7** on **10**, three accurately weighed samples of **10** (about 50 mg each) were taken and hydrolysed by heating for 2 h under reflux with 10 mL of hydrochloric acid solution (HCl:THF:H_2O = 1:8:1). After filtration, comparison of the UV–VIS spectrum of the filtrate with that of an acidic reference sample, which was prepared by hydrolysis of **13** and diluted to a suitable concentration for the UV–VIS spectrum, showed that the loading of **7** on **10** was 22.3 mg per gram of silica gel (0.044 mmol/g). The yield was 55.6%, with **7** as the limiting reactant.

3-Aminopropylsilyl silica (12)

Activated dry silica gel (**1**, 55 g) was mixed with 30 mL (160 mmol) of (3-aminopropyl)trimethoxysilane (**11**) and 250 mL of dry toluene. The suspension was stirred under reflux overnight, and then filtered. The solids were washed with dry toluene and anhydrous ether to give **12**.

To determine the amino group loading, three accurately weighed samples (about 50 mg each) were treated with 5 mL of 0.05 M aqueous solution of sulphuric acid for 10 min, then filtered and titrated with a 0.1 M aqueous solution of potassium hydroxide. Comparison with a blank assay showed that the amino loading on **12** was 0.8–1.3 mmol per gram of silica gel.

Phthalocyaninato methylaluminum(III) (13)

A mixture of 1.6 g (3.1 mmol) of metal-free unsubstituted phthalocyanine **7**, 10 mL of a 1.9 M solution of trimethylaluminum (19 mmol) in toluene, and 100 mL of dry toluene was treated with ultrasound for 24 h to give a solution of phthalocyaninato methylaluminum(III) **13**. Without purification and characterization, **13** was used to prepare **14** immediately.

Phthalocyaninatoaluminum(III) aminopropylsilyl silica (14)

The newly prepared **12** (55 g) and 100 mL of dry toluene were poured with vigorous stirring into a round-bottom flask containing 110 mL of a hot solution of **13** under argon. After heating under reflux for 1 h, at which time reaction was complete (as monitored for **8** above), the suspension was filtered to give a dark blue-grey powder and an almost colourless filtrate. The powder was then washed with dry toluene three times, followed by dry dioxane three times, to give **14**.

To determine the phthalocyanine loading on **14**, three accurately weighed samples of **14** (about 50 mg each) were taken and hydrolysed by heating for 1 h under reflux with 10 mL of hydrochloric acid solution (HCl:THF:H_2O = 1:8:1). After filtration, comparison of the UV–VIS spectrum of the filtrate with that of an acidic reference sample, prepared by hydrolysis of **13** and diluted to a suitable concentration for the UV–VIS spectrum, showed that the loading of **7** was 29.0 mg per gram of **14** (0.056 mmol/g). The yield was ~100% with **7** as the limiting reactant.

Can. J. Chem. Downloaded from www.nrcresearchpress.com by 213.200.69.106 on 09/08/12
For personal use only.

Can. J. Chem. Downloaded from www.nrcresearchpress.com by 213.200.69.106 on 09/08/12
For personal use only.

*2,9,16-Trineopentoxy-31*H,*33*H-*tribenzo*[b,g,l]*naphtho-[2,3,*-q]*porphyrazine (18)*

A solution of **15** derived from 178 mg (1 mmol) of 2,3-dicyanonaphthalene (**12**) (Tokyo Kasei) and **16** derived from 642 mg (3 mmol) of 4-neopentoxyphthalonitrile (**15**) (28) in 4 mL of 2-*N*,*N*-dimethylaminoethanol was heated under reflux for 48 h. The dark green mixture was then poured into 100 mL of water, and the precipitate was filtered and washed with methanol a few times until the filtrate was colourless. After flash chromatography with toluene as solvent, 356 mg of a phthalocyanine mixture was obtained in about 43.5% yield. The phthalocyanine mixture was then subjected to common flash silica gel chromatography using carbon tetrachloride/toluene (30/0–70/100) as the eluting solvent, while monitoring with UV–VIS spectroscopy, to afford crude **18**. Further purification was effected by column chromatography with **14** or **9** as the static phase. After evaporation of the solvent and precipitation from methanol, the desired 2,9,16-trineopentoxy-31*H*,33*H*-tribenzo[*b*,*g*,*l*]naphtho[2,3-*q*]porphyrazine (**18**, 104.5 mg) was obtained, in 12.7% yield, as a purple solid; IR (KBr, cm^{-1}): 3300 (w, NH), 1620 (vs, C=C), 1240 (s, COC), 1100 (s, COC), 1020 (vs, NH), 750 (s, CH_{arom}); UV–VIS (1,2-dichlorobenzene, nm) (log ϵ): 734 (5.00), 690 (4.94), 670 (4.70), 622 (4.22), 400 (4.49), 344 (4.72), 300 (4.51); ^{1}H NMR ($CDCl_3$) δ: 7.0–9.1 (vbr, aromatic), 4.0–4.2 (m, -O*CH*$_2$C-, 6H), 1.1–1.6 (m, -*CH*$_3$, 27H), −3.6 (br N-*H*); ^{13}C NMR (toluene-d_8) δ: 116–162 (C_{arom}), 78 (*C*H$_2$-O), 27.2(*C*-CH$_3$), 19.7–21.2 (C-*C*H$_3$); MS (FAB) *m/z*: 823 (M^+ + 1 100%), 752 (19%), 681 (9%). Anal. calcd. for $C_{51}H_{50}N_8O_3$: C 74.42, H 6.12, N 13.61; found: C 73.84, H 6.32, N 13.26.

The mass spectrum of **18** showed no contamination by undesired phthalocyanines. As a comparison, the same crude product was subjected four times to ordinary flash silica gel chromatography. The mass spectrum of its purest components indicated that it still contained some 2,9,16,23-tetraneopentoxyphthalocyanine.

*2,9,16-Tri-*tert*-butyl-31*H,*33*H-*tribenzo*[b,g,l]*naphtho-[2,3-*q]*porphyazine (19)*

A solution of **15** derived from 178 mg (1 mmol) of 2,3-dicyanonaphthalene (Tokyo Kasei) and **17** derived from 552 mg (3 mmol) of 4-*tert*-butylphthalonitrile (27) (Toyko Kasei) in 4 mL of 2-*N*,*N*-dimethylaminoethanol was heated under reflux for 48 h. The dark blue mixture was then poured into 100 mL of water to form a precipitate. The precipitate was filtered and washed with methanol a few times until the filtrate was colourless. After column chromatography with ordinary flash silica gel as the static phase and toluene as the eluting solvent, 198 mg of a phthalocyanine mixture was obtained in about 27% yield. The phthalocyanine mixture was then separated again by flash silica gel chromatography to get the crude **19**. Further purification was effected by column chromatography with Pc-Si-Gel **14** or **9** as the static phase, with carbon tetrachloride/toluene (70/30–0/100) as the eluting solvent and using UV–VIS spectroscopy as a monitor. After evaporation of the solvent and precipitation from methanol, 52.8 mg of pure 2,9,16-tri-*tert*-butyl-31*H*,33*H*-tribenzo-[*b*,*g*,*l*]naphtho[2,3-*q*]porphyazine (**19**) was obtained, in 7.2% yield, as a purple solid, IR (KBr, cm^{-1}): 3300 (w, NH), 1620 (vs, C=C), 1010 (vs, NH), 750 (s, CH_{arom}); UV–VIS (1,2-dichlorobenzene, nm) (log ϵ): 730 (5.10), 686 (5.09), 666 (4.82), 618 (4.47), 346 (4.85), 302 (4.52); ^{1}H nmr (toluene-d_8) δ: 6.9–8.1, 8.6–9.5 (vbr, aromatic), 1.7–1.8 (m, -*CH*$_3$, 27 H), −2.3 (br N-*H*); ^{13}C nmr (toluene-d_8) δ: 122.5–152.8 (C_{arom}), 35.8–36.0 (*C*-CH$_3$), 32.1–32.3 (C-*C*H$_3$); MS *m/z*: 733 (M^+ +1, 100%), 718 (22%), 703 (9%), 676 (17%). Anal. calcd. for $C_{48}H_{44}N_8$: C 78.66, H 6.05, N 15.29; found: C 78.19, H 6.25, N 15.14.

The mass spectrum of **19** showed no contamination by undesired phthalocyanines. As a comparison, an attempt was made to purify the same crude **19** by a series of four ordinary flash chromatographic operations. The mass spectrum of its purest part showed that it still contained some 2,9,16,23-tetra-*tert*-butylphthalocyanine.

*2-*tert*-Butyl-9,16,23-trineopentoxyphthalocyanine (20)*

A solution of **16** derived from 107 mg (0.5 mmol) of 4-neopentoxyphthalonitrile (28) and **17** derived from 276 mg (1.5 mmol) of 4-*tert*-butylphthalonitrile (27) in 2 mL of 2-*N*,*N*-dimethylaminoethanol was heated under reflux for 48 h. The dark blue mixture was then poured into 50 mL of distilled water to form a precipitate. The precipitate was filtered and washed with methanol for a few times until the filtrate was colourless. After column chromatography with flash silica gel as the static phase and toluene as the eluting solvent, 115 mg of a phthalocyanine mixture was obtained, in about 28% yield, as a purple solid. The phthalocyanine mixture was then subjected to both ordinary flash chromatography and chromatography using Pc-Si-Gels **9** or **14** with carbon tetrachloride/toluene (70/30–0/100) as the eluting solvent. Reverse phase HPLC was used as the monitor to check the purity of the eluted fractions. After six repetitive chromatographic separations and precipitation from methanol, 10.5 mg of the desired 2-*tert*-butyl-9,16,23-trineopentoxyphthalocyanine (**20**) was obtained, in 2.5% yield, as a purple solid; IR (KBr, cm^{-1}): 3300 (w, NH), 1620 (vs, C=C), 1240 (s, COC), 1100 (s, COC), 1020 (vs, NH); 750 (s, CH_{arom}); UV–VIS (1,2-dichlorobenzene, nm) (log ϵ): 708 (5.20), 674 (5.11), 640 (4.66), 607 (4.47), 348 (4.85); ^{1}H nmr ($CDCl_3$) δ: 7.3–9.7 (vbr, aromatic), 4.1–4.6 (m, -O*CH*$_2$C-, 6H), 1.1–1.6 (m, -*CH*$_3$, 36H), −3.5 (br N-*H*); ^{13}C nmr (toluene-d_8) δ: 118–160 (C_{arom}), 78 (*C*H$_2$-O), 27.2 (*C*-CH$_3$), 19.7–21.2 (C-*C*H$_3$); MS (FAB) *m/z*: 829 (M^+ + 1, 100%), 759 (20%). Anal. calcd. for $C_{51}H_{56}N_6O_3$: C 73.89, H 6.81, N 13.52; found: C 73.98, H 6.84, N 13.12.

2,3-Di-(1-Octyn-1-yl)-9,16,23-trimethoxymethyloxyphthalocyaninato zinc(II) (23)

A mixture of **21** (425 mg, 1.24 mmol) (19), **22** (467 mg, 2.48 mmol) (19), DBU (2 mL), and 1-butanol (4 mL) was heated under reflux with stirring in an argon atmosphere. After 5–10 min, 184 mg (1.0 mmol) of dry zinc acetate was added. After heating for 4–5 h, the dark green-blue mixture was poured into 400 mL of water, and then extracted three times with toluene. The organic phase was washed with water until it was neutral, then dried with magnesium sulphate. After filtration and evaporation, the crude product underwent a preliminary silica flash column chromatography with toluene/ethyl acetate (50/50–0/100) as the eluting solvent. A mixture of phthalocyanines (320 mg) was obtained in about 40% yield, and reverse phase HPLC showed it contained about 40% of the desired phthalocyanine **23**. After three more separations by flash column chromatography with toluene/ethyl acetate (92/8–86/14) as the eluting solvent, 100 mg of the desired 2,3-dioctynyl-9,16,23-trimethoxymethyloxyphthalocyaninato zinc(II) (**23**) was obtained, as a purple solid, in 12.4% yield with **22** as the limiting reactant; IR (KBr, cm^{-1}): 1620 (vs, C=C), 1240 (s, COC), 1100 (s, COC), 750 (s, CH_{arom}); UV–VIS (1,2-dichlorobenzene, nm) (log ϵ): 698 (5.12), 682 (5.02), 624 (4.39), 357 (4.80); ^{1}H nmr (Benzene-d_6) δ: 6.94–8.81 (vbr, aromatic, 11H), 4.73–5.02 (m, -O-C*H*$_2$-O, 6H), 2.97–3.16 (m, C*H*$_3$-O, 9H), 2.57–2.70 (m, C≡C-C*H*$_2$-, 4H), 1.07–1.87 (m, -C-C*H*$_2$-C-, 16 H), 0.54–0.64 (tri, CH$_2$-C*H*$_3$, 6H); MS (FAB) *m/z*: 972 (M^+, 100%), 928 (85%), 888 (50%). Anal. calcd. for $C_{54}H_{52}N_8O_8Zn$: C 66.56, H 5.38, N 11.50, Zn 6.71; found: C 65.81, H 5.14, N 11.12, Zn 6.64.

Acknowledgements

We are grateful to the Natural Sciences and Engineering Research Council of Canada for financial support of this research.

1. I. Rosenthal and E. Ben-Hur. *In* Phthalocyanines: properties and applications. Vol. 1. *Edited by* C.C. Leznoff and A.B.P. Lever. VCH, New York. 1989. p. 393.
2. J.E. van Lier. *In* Biology and medicine. Vol. 1. *Edited by* R.H.

Douglas, J. Moan, and F. Dall'Acqua. Plenum Press, New York. 1988. p. 435.
3. B. Paquette, H. Ali, R. Langlois, and J.E. van Lier. Photochem. Photobiol. **51**, 313 (1990).
4. D. Wöhrle, N. Iskander, G. Graschew, H. Sinn, E.A. Friedrich, W. Maier-Borst, J. Stern, and P. Schlag. Photochem. Photobiol. **51**, 351 (1990).
5. C.C. Leznoff, S. Vigh, P.I. Svirskaya, S. Greenberg, D.M. Drew, E. Ben-Hur, and I. Rosenthal. Photochem. Photobiol. **49**, 279 (1989).
6. I. Rosenthal, E. Ben-Hur, S. Greenberg, A. Concepcion-Lam, D.M. Drew, and C.C. Leznoff. Photochem. Photobiol. **46**, 959 (1987).
7. J.D. Spikes. Photochem. Photobiol. **43**, 691 (1986).
8. E. Ben-Hur. *In* From photophysics to photobiology. *Edited by* A. Favre, R. Tyrrell, and J. Cadet. Elsevier, New York. 1987. p. 407.
9. J.E. van Lier and J.D. Spikes. *In* Photosensitizing compounds: their chemistry, biology and clinical use. *Edited by* T.J. Dougherty, G.H. Bock, and S. Harnett. Ciba Found. Symp. **146**, 17 (1987).
10. C.C. Leznoff. *In* Phthalocyanines: properties and applications. Vol. 1. *Edited by* C.C. Leznoff and A.B.P. Lever. VCH, New York. 1989. p. 1.
11. N. Kobayashi, R. Kondo, S. Nakajima, and T. Osa. J. Am. Chem. Soc. **112**, 9640 (1990).
12. Y. Ikeda, H. Konami, M. Hatano, and K. Mochizuki. Chem. Lett. 763 (1992).
13. H. Konami and M. Hatano. Chem. Lett. 1359 (1988).
14. C.C. Leznoff, P.I. Svirskaya, B. Khouw, R.L. Cerny, P. Seymour, and A.B.P. Lever. J. Org. Chem. **56**, 82 (1991).
15. C.C. Leznoff, S. Greenberg, B. Khouw, and A.B.P. Lever. Can. J. Chem. **65**, 1705 (1987).
16. D. Wöhrle and G. Krawczyk. Polym. Bull. **15**, 193 (1986).
17. C. Piechocki and J. Simon. J. Chem. Soc. Chem. Commun. 259 (1985).
18. H. Shirai, K. Hanabusa, M. Kitamura, and E. Masuda. Makromol. Chem. **185**, 2537 (1984).
19. C.C. Leznoff and T.W. Hall. Tetrahedron Lett. **23**, 3023 (1982).
20. T.W. Hall, S. Greenberg, C.R. McArthur, B. Khouw, and C.C. Leznoff. Nouv. J. Chim. **6**, 653 (1982).
21. M.J. Cook, M.F. Daniel, K.J. Harrison, N.B. McKeown, and A.J. Thomson. J. Chem. Soc. Chem. Commun. 1148 (1987).
22. W.A. Nevin, W. Liu, S. Greenberg, M.R. Hempstead, S.M. Marcuccio, M. Melnik, C.C. Leznoff, and A.B.P. Lever. Inorg. Chem. **26**, 891 (1987).
23. A. Giraudeau, A. Lovati, M. Gross, J.J. Andre, J. Simon, C.H. Su, and K.M.J. Kadish. J. Am. Chem. Soc. **105**, 2917 (1983).
24. M. Abkowitz and A.R.J. Monahan. J. Phys. Chem. **58**, 2281 (1973).
25. M.P. McDaniel. J. Phys. Chem. **85**, 532 (1981).
26. T. Buck, D. Wöhrle, G. Schulz-Ekloff, and A. Andreev. J. Mol. Catal. **70**, 259 (1991).
27. M. Hanack, J. Metz, and G. Pawlowski. Chem. Ber. **115**, 2836 (1982).
28. C.C. Leznoff, S.M. Marcuccio, S. Greenberg, A.B.P. Lever, and K.B. Tomer. Can. J. Chem. **63**, 623 (1985).
29. E. Angeletti, C. Canepa, G. Martinetti, and P. Venturello. J. Chem. Soc. Perkin Trans. 1, 105 (1989).
30. Y. Qin. M. Sc. Thesis, York University, Toronto. 1991. pp. 67–68.

Can. J. Chem. Downloaded from www.nrcresearchpress.com by 213.200.69.106 on 09/08/12
For personal use only.

Synthesis and preliminary in vitro biological activity of non-steroidal cytotoxic estrogens designed for the treatment of breast cancer

G. BÉRUBÉ[1] AND P. WHEELER
School of Pharmacy, Memorial University, of Newfoundland, St. John's, NF A1B 3V6, Canada

AND

C.H.J. FORD, M. GALLANT, AND Z. TSALTAS
Oncology Research Laboratory, Memorial University of Newfoundland, and The Newfoundland Cancer Foundation, St. John's, NF A1B 3V6, Canada

Received March 3, 1993

G. BÉRUBÉ, P. WHEELER, C.H.J. FORD, M. GALLANT, and Z. TSALTAS. Can J. Chem. **71**, 1327 (1993).

The development of resistance to endocrine therapy as well as chemotherapy is presently a major problem in the treatment of breast cancer. To minimize this obstacle, new, more selective and potent, chemotherapeutic agents should be designed. One way to improve selectivity is to link a cytotoxic moiety to a molecule possessing an affinity to the estrogen receptor (ER). The latter would be used to direct the cytotoxic portion of the molecule towards the target cells. Our initial approach led us to the synthesis of new triphenylethylene–platinum(II) complexes **1***a–c*. The commercially available desoxyanisoin (**10**) was efficiently transformed in seven steps into the platinum(II) complexes **1***a–c* with an overall yield exceeding 30%. The biological activity of compounds **1***a–c* was evaluated in vitro on ER+ and ER− human breast tumor cell lines: MCF-7 and MDA-MD-231.

G. BÉRUBÉ, P. WHEELER, C.H.J. FORD, M. GALLANT et Z. TSALTAS. Can. J. Chem. **71**, 1327 (1993).

Le dévelopement de la résistance aux thérapies hormonales aussi bien qu'à la chimiothérapie est présentement un problème majeur dans le traitement du cancer du sein. De manière à minimiser cet obstacle, de nouveaux agents chemothérapeutiques plus selectifs et puissants devraient être conçus. Afin d'améliorer la sélectivité, il est possible de lier une portion cytotoxique à une molécule possédant une affinité pour le récepteur de l'estrogène (ER). Cette dernière serait utilisée pour diriger la portion cytotoxique de la molécule aux cellules cibles. Notre approche initiale nous a mené à la synthèse de complexes de triphényléthylène–platine(II) **1***a–c*. La désoxyanisoïne (**10**) commerciale fut transformée, en sept étapes, en complexes de platine(II) **1***a–c* avec un rendement global excédent 30%. L'activité biologique des composés **1***a–c* fut évaluée in vitro sur des cellules cancéreuses du sein : ER+ (MCF-7) et ER− (MDA-MD-231).

Introduction

Breast cancer is the most common form of cancer among women in North America. In 1993, it is estimated that more than 5000 women will die of this disease in Canada. Much progress has been accomplished for the treatment and the detection of this malady. Unfortunately, resistance to endocrine therapy as well as cytotoxic chemotherapy is still considered one of the major obstacles to successful treatment of breast cancer (1). Thus, many researchers are developing new drugs that are designed to overcome the problem of drug resistance. An attractive solution to this impediment is drug targeting. As we know, the aim of drug targeting is to deliver drugs only to those sites needing treatment; when this objective is met, not only the efficacy of the treatment will be improved, but toxic side effects will also be minimized (2). Therefore, we believe that new, more selective and potent, chemotherapeutic agents should be designed to rapidly eradicate the disease, preferably before any sign of resistance occurs.

The concept of linking an anti-cancer agent to a ligand with affinity for a tumor cell has some encouraging experimental precedent. As early as the 1960s, researchers investigated the possibility of linking nitrogen mustard groups to the steroidal skeleton in order to induce cytotoxic effects on hormone-dependent tumor cells (3). Since that time, several compounds (steroids and others) have been linked to various alkylating agents, including nitrogen mustards (4), nitrosoureas (5), and platinum complexes (6). However, in the early attempts, the cytotoxic moiety was often inappropriately linked to the estrogenic portion at the binding sites of the molecules, i.e., carbon 3 or 17 (steroid numbering, **3**, Scheme 1). This resulted in an inefficient interaction with the ER, and consequently a low biological activity. More recently, compounds **5** and **6**, synthesized in Germany (7, 8), showed very promising biological activities. The platinum complex **5** was found to be more potent than the parent drug cisplatin (**2**) and was selective on hormone-dependent breast cancer in vivo (in vitro, no selectivity was shown (7)). On the other hand, compound **6** showed selectivity on hormone-dependent breast cancer in both situations, i.e., in vitro and in vivo (8). In both cases, the exact mechanism(s) of action remains to be elucidated.

The new derivatives **1***a–c* were synthesized on the structural basis of the steroidal antiestrogens ICI 164 384 (**3**) and ICI 182 780 (**4**) recently described in the literature (9). Cytotoxic triphenylethylene with a long alkyl chain in the middle part of the molecule will, therefore, mimic the pure antiestrogens ICI 164 384 and ICI 182 780 bearing a 7-α side chain (see Scheme 1). This structural analogy should confer upon the new platinum(II) complexes both antiestrogenic and cytotoxic activity. We wish to report the details of our initial effort towards the synthesis of such derivatives (10) as well as their in vitro biological activity on MCF-7 (ER+) and MDA-MD-231 (ER−) human breast cancer cell lines.

Results and discussion

Synthesis of platinum(II) complexes

As shown in Scheme 3, three new (1,2-diaminoethane)

[1]Author to whom correspondence may be addressed. Present address: Département de chimie, Université du Québec à Trois-Rivières, CP 500, Trois-Rivières, QC G9A 5H7, Canada.

Can. J. Chem. Downloaded from www.nrcresearchpress.com by 213.200.69.106 on 09/08/12
For personal use only.

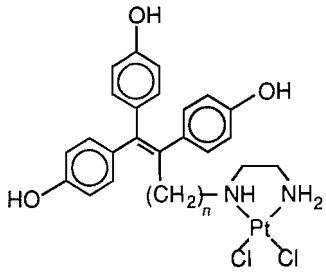

1 *a-c*

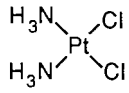

2

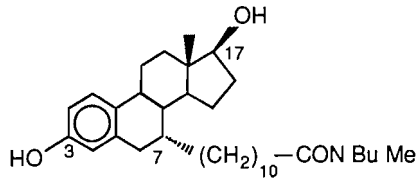

3

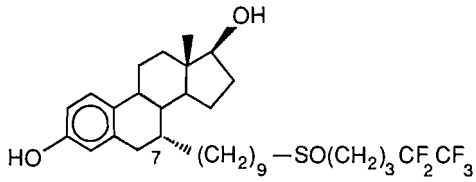

4

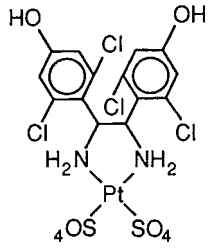

5

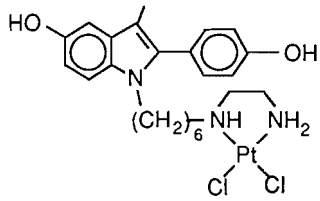

6

n = 6(*a*), 8(*b*), 10(*c*)

SCHEME 1

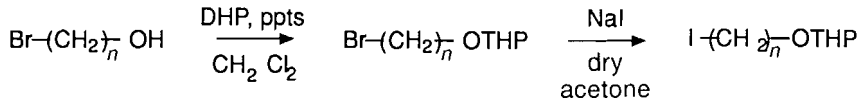

7 *a-c* **8** *a-c* **9** *a-c*

n = 6(*a*), 8(*b*), 10(*c*)

SCHEME 2

dichloroplatinum(II) complexes **1***a–c* were synthesized from commercially available desoxyanisoin (**10**). Initially the appropriate iodotetrahydropyranyl ethers were prepared. The choice of the length of the starting bromoalcohol **7** with 6, 8, and 10 carbon atoms is important since it has been observed that at least 6 carbon atoms are needed to give platinum derivatives such as compound **6** good estrogen receptor binding activity (11). The high affinity of compound **6** was possibly due to the interaction with an additional binding site removed from the receptor (11). As illustrated in Scheme 2, the alcohols **7***a–c* were protected as a tetrahydropyranyl ether (12) to give compounds **8***a–c*, which, upon treatment with sodium iodide in dry acetone, gave the iodotetrahydropyranyl ethers **9***a–c* (95% average yield for the two steps).

Alkylation of desoxyanisoin (**10**) with the iodotetrahydropyranyl ethers **9***a–c* was achieved using sodium hydride in tetrahydrofuran to give compounds **11***a–c* with an average yield of 65% (98% taking in consideration the alkyl iodide recovered, Scheme 3). Addition of an excess of *p*-methoxyphenylmagnesium bromide to ketones **11***a–c* and subsequent treatment of the crude tertiary alcohols with pyridinium-*p*-toluenesulfonate in ethanol at reflux afforded directly the triphenylethylene alcohols **12***a–c* with an average yield of 90% as the result of dehydration of the tertiary alcohol intermediates and simultaneous deprotection of the tetrahydropyranyl ethers (12). With the desired triphenylethylenes in hand the following sequence of reactions are simple functional group transformations. Initially, alcohols **12***a–c* were transformed to the bromides **13***a–c* (85% average yield) with carbon tetrabromide and triphenylphos-

Can. J. Chem. Downloaded from www.nrcresearchpress.com by 213.200.69.106 on 09/08/12
For personal use only.

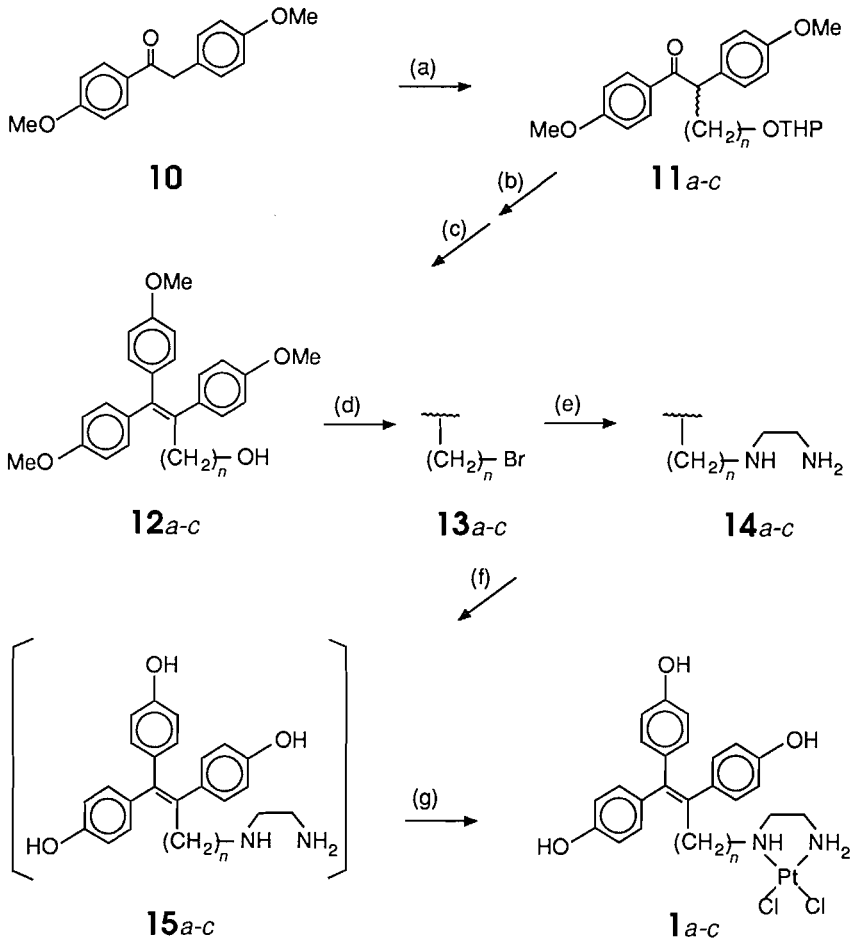

Reagents: (a) NaH, I-$(CH_2)_n$-OTHP, THF, 25°C, 17 h, 65% (98%); (b) $MeOC_6H_4MgBr$, ether, 25°C, 17 h; (c) crude tertiary alochol, ethanol, PPTS, reflux, 5 h, 90% from **11**; (d) CBr_4, Ph_3P, ether, 25°C, 24 h, 85%; (e) $H_2NCH_2CH_2NH_2$, methanol, reflux, 24 h, 95% crude; (f) BBr_3, CH_2Cl_2, -60°C to 25°C (15 h) to reflux (2 h); (g) K_2PtCl_4, DMF: H_2O, 2 days, 60% from **14**

SCHEME 3

phine in dry ether (13). The amines **14***a–c* were obtained with an average yield of 95% by refluxing bromides **13***a–c* in the presence of an excess of ethylenediamine in dry methanol (11). Finally, demethylation with boron tribromide gave the intermediate tris-phenols **15***a–c*, which, upon treatment with potassium tetrachloroplatinate(II) in a mixture of dimethylformamide and water, led to the desired platinum(II) complexes **1***a–c* (60% average yield for the two steps (11, 14, 15)).

In vitro antitumor activity

Two human breast tumor cell lines were chosen, based on their estrogen receptor content, to evaluate the antitumor activity of our new platinum(II) complexes (16). The "cytotoxic antiestrogens" (**1***a* = Pt-6, **1***b* = Pt-8, **1***c* = Pt-10) were tested along with controls (vehicle, cisplatin = Cis-Pt, tamoxifen = TAM) on both ER+, i.e., MCF-7, and ER−, i.e., MDA-MD-231, human mammary carcinomas in order to assess the potential selective anti-neoplastic effect on hormone-dependent breast cancer. The antitumor activity was evaluated with a colorimetric assay that uses the ability of viable cells to reduce a soluble tetrazolium salt, 3(4,5-dimethylthiazol)-2,5-diphenyltetrazolium bromide (MTT), into an insoluble formazan precipitate (17). A recent report (18) indicates that the MTT assay can be used to replace the [^{3}H]-uridine assay for chemosensitivity screening. The colorimetric assay has the advantages of being safer, less costly, and simpler than the radiometric assay.

As shown by the MTT assays on human breast cancer cell lines, the new compounds demonstrated similar activity on either MCF-7 (ER+) or MDA-MD-231 (ER−) cells (see Table 1). Interestingly, the longer the side chain, the better the activity. This could be explained in the following fashion: a more lipophilic compound (Pt-10) could theoretically penetrate more easily the lipophilic cell membranes, therefore killing the cells more readily and (or), assuming an identical rate of infiltration in the cells, a compound with a longer chain could possibly alkylate DNA more efficiently due to fewer steric interactions between the triphenylethylene moiety and DNA. These interesting biological results also indicate that our new products are not selective to-

Can. J. Chem. Downloaded from www.nrcresearchpress.com by 213.200.69.106 on 09/08/12
For personal use only.

TABLE 1. Inhibitory concentration on breast tumor cells[a]

	MCF-7 (ER+) IC_{50} (μM)	MDA-MD-231 (ER−) IC_{50} (μM)
Cis-Pt	31	14
TAM	14	22
Pt-6	225	188
Pt-8	100	94
Pt-10	48	47

[a]IC_{50} as obtained by the MTT assay (see Experimental).

wards ER+ human breast cancer cells. It is important to indicate that the desired selectivity might be expressed more clearly (and possibly only) in vivo as was demonstrated previously for compound **5**. The fact that these compounds exhibit activity against both ER+ and ER− tumor cells may have advantages in that selective accumulation in the ER+ tumor could quench any ER− tumor cells that are known to spring up from the initial ER+ cells or destroy any ER− cells already present in the original, and predominantly ER+, tumor. This hypothesis will be further evaluated both in vitro and in vivo in the future.

Three new platinum(II) complexes have been synthesized and tested for biological activity. The synthesis of this type of compound is straightforward and efficient. The strategy described could be used to synthesize other types of DNA alkylating agents such as nitrogen mustards and nitrosoureas. Work is in progress in our laboratory to synthesize similar derivatives with improved biological activity.

Experimental

Synthesis of Pt(II) complexes

General procedures

Anhydrous reactions were performed under an inert atmosphere, the setup assembled and cooled under dry nitrogen. Unless otherwise noted, starting material, reactant, and solvents were obtained commercially and were used as such or purified and (or) dried by standard means (19). Organic solutions were dried over magnesium sulphate ($MgSO_4$), and evaporated on a rotatory evaporator and under reduced pressure. All reactions were monitored by thin-layer chromatography (TLC). The plates were visualized by UV fluorescence, or by staining with iodine or spraying with an aqueous solution of phosphomolybdic acid followed by heating the plate at ~135°C. Commercial TLC plates were Sigma T 6145 (polyester silica gel 60 Å (0.25 mm)). Preparative TLC was performed on 1 mm silica gel 60 Å, 20 × 20 plates (Whatman, 4861 840). Flash chromatography was performed according to the method of Still et al. (20) on Merck grade 60 silica gel, 230–400 mesh. All solvents used in chromatography had been distilled. Melting points (mp) were recorded on an Electrothermal 9100 apparatus and are uncorrected. The infrared spectra (IR) were taken on a Nicolet model 205 FT-IR spectrophotometer. Mass spectral assays (MS, *m/e*) were obtained using a VG Micromass 7070 HS instrument using an ionization energy of 70 eV. Elemental analyses were conducted by Microanalysis Laboratories Limited, Markham, Ontario. Nuclear magnetic resonance (NMR) spectra were obtained in $CDCl_3$ solution, unless otherwise noted, on a General Electric GE 300-NB (300 MHz) instrument: chemical shifts were measured relative to internal standards: tetramethylsilane (TMS, δ 0.0 ppm) for ^1H and $CDCl_3$ (δ 77.0 ppm) for ^{13}C NMR. Multiplicities are described by the following abbreviations: s (singlet), d (doublet), t (triplet), q (quartet), m (multiplet), dd (double doublet), tq (triple quartet), mm (multiple multiplets), and so on. The NMR assignments were assisted by ^{13}C–^1H correlation (HETCORR) 2-D spectra.

General procedure for conversion of bromoalcohols to iodotetrahydropyranyl ethers

*1-Tetrahydropyranyloxy-6-bromohexane (**8**a).* A solution of 6-bromo-1-hexanol **7***a* (5.0 g, 27.6 mmol), dihydropyran (2.58 g (2.8 mL), 30.6 mmol), and pyridinium *p*-toluenesulfonate (PPTS, 10 mg, 3.97×10^{-5} mol) in dichloromethane (CH_2Cl_2, 50 mL) was stirred for 5 h under nitrogen. Afterwards, sodium bicarbonate ($NaHCO_3$, 500 mg) and $MgSO_4$ (5.0 g) were added to the reaction mixture and stirred 15 min before being filtered on a short pad of Celite/silica gel (1 cm/4 cm) using CH_2Cl_2 as eluent. The filtrate was evaporated to a viscous oil **8***a* (7.16 g, 98%), which was used without further purification in the next step. IR (neat): 1170–1000 (C—O), cm^{-1}. ^1H NMR (δ ppm): 4.57 (1H, t apparent, J = 3.2 Hz, -OCHO-), 3.87, 3.74, 3.50, and 3.38 (4H, 4 × m, -CH_2OCHOCH_2-), 3.41 (2H, t, J = 6.7 Hz, -CH_2Br), 1.3–2.0 (14H, m, BrCH$_2$-(CH_2)$_4$-CH$_2$O-THP). MS (*m/e*): 265 (M^+ +1), 163 (M^+ −OTHP).

*1-Tetrahydropyranyloxy-6-iodohexane (**9**a).* To a solution of crude bromide **8***a* (7.16 g, 27 mmol) in dry acetone was added sodium iodide (6.07 g, 40.5 mmol). The reaction mixture was stirred at 25°C for 5 h. Then, most of the solvent was evaporated and the residue was transferred to an extraction flask with ether (100 mL) and water (100 mL). The organic phase was washed with water (6 × 50 mL), dried, filtered, and concentrated to a viscous liquid. The crude iodide **9***a* (8.26 g, 98%) was used as such at the alkylation step. IR (neat): 1170–1000 (C—O) cm^{-1}. ^1H NMR (δ ppm): 4.57 (1H, t apparent, J = 3.2 Hz, -OCHO-), 3.87, 3.74, 3.50, and 3.38 (4H, 4 × m, -CH_2OCHOCH_2-), 3.19 (2H, t, J = 7.0 Hz, -CH_2I), 1.3–2.0 (14H, m, ICH$_2$-(CH_2)$_4$-CH$_2$O-THP). MS (*m/e*): 311 (M^+ −H), 211 (M^+ −OTHP).

*1-Tetrahydropyranyloxy-8-bromooctane (**8**b):* 98% yield. IR (neat): 1170–1000 (C—O) cm^{-1}. ^1H NMR (δ ppm): 4.58 (1H, t apparent, J = 3.5 Hz, -OCHO-), 3.87, 3.73, 3.50, and 3.38 (4H, 4 × m, -CH_2OCHOCH_2-), 3.41 (2H, t, J = 6.8 Hz, -CH_2Br), 1.2–2.0 (18H, m, BrCH$_2$-(CH_2)$_6$-CH$_2$O-THP). MS (*m/e*): 293 (M^+ +1).

*1-Tetrahydropyranyloxy-8-iodooctane (**9**b):* 98% yield. IR (neat): 1170–1000 (C—O) cm^{-1}. ^1H NMR (δ ppm): 4.58 (1H, t apparent, J = 3.5 Hz,-OCHO-), 3.87, 3.73, 3.50, and 3.38 (4H, 4 × m, -CH_2OCHOCH_2-), 3.19 (2H, t, J = 7.0 Hz, -CH_2I), 1.2–2.0 (18H, m, ICH$_2$-(CH_2)$_6$-CH$_2$O-THP). MS (*m/e*): 339 (M^+ −H), 239 (M^+ −OTHP).

*1-Tetrahydropyranyloxy-10-bromodecane (**8**c):* 99% yield. IR (neat): 1170–1000 (C—O) cm^{-1}. ^1H NMR (δ ppm): 4.58 (1H, t apparent, J = 3.5 Hz, -OCHO-), 3.87, 3.73, 3.50, and 3.38 (4H, 4 × m, -CH_2OCHOCH_2-), 3.41 (2H, t, J = 6.8 Hz, -CH_2Br), 1.2–2.0 (22H, m, BrCH$_2$-(CH_2)$_8$-CH$_2$O-THP). MS (*m/e*): 321 (M^+ +1).

*1-Tetrahydropyranyloxy-10-iododecane (**9**c):* 98% yield. IR (neat): 1170–1000 (C—O) cm^{-1}. ^1H NMR (δ ppm): 4.58 (1H, t apparent, J = 3.5 Hz, -OCHO-), 3.87, 3.73, 3.50, and 3.38 (4H, 4 × m, -CH_2OCHOCH_2-), 3.19 (2H, t, J = 7.0 Hz, -CH_2I), 1.2–2.0 (22H, m, ICH$_2$-(CH_2)$_8$-CH$_2$O-THP). MS (*m/e*): 367 (M^+ −H).

General procedure for conversion of desoxyanisoin to triphenylethylene platinum(II) complexes

*A. Synthesis of 1,2-bis(4-methoxyphenyl)-X-tetrahydropyranyloxy-alkylones **11**a–c.* To a stirred suspension of sodium hydride (732 mg, 18.3 mmol, 60% dispersion in mineral oil) in dry tetrahydrofuran (THF, 150 mL) was added rapidly desoxyanisoin (**10**) (4.47 g, 17.4 mmol). The reaction mixture was heated (50°C) with a water bath for 1 h under a nitrogen atmosphere. After cooling, the iodotetrahydropyranyl ether (18.3 mmol) was added dropwise and the resulting mixture stirred overnight (17 h). Most of the solvent was then evaporated and the residue was diluted with ether (200 mL) and treated with water (50 mL). The ethereal phase was washed thoroughly with water (6 × 50 mL), dried, and evaporated to give an oil that was purified by flash chromatography (hexane:acetone, 85:15). A viscous oil was obtained. The aver-

Can. J. Chem. Downloaded from www.nrcresearchpress.com by 213.200.69.106 on 09/08/12
For personal use only.

Can. J. Chem. Downloaded from www.nrcresearchpress.com by 213.200.69.106 on 09/08/12
For personal use only.

age yield was 65% (98% taking into account the alkyl iodide recovered).

*1,2-Bis(4-methoxyphenyl)-8-tetrahydropyranyloxy-octanone (**11**a):* IR (neat): 1674 (C=O), 1599 (C=C), 1254 (C=O) cm^{-1}. ^1H NMR (δ ppm): 7.95, 6.84 and 7.21, 6.80 (8H, 2 × two d, J = 8.88 and 8.66 Hz, 2 × *para*-substituted anisyl group), 4.55 (1H, t, J = 3.45 Hz, -OCHO-), 4.44 (1H, t, J = 7.23 Hz, -CH-), 3.82 and 3.47 (2H, two m, -CH_2OTHP), 3.70 and 3.34 (2H, two m, -CHOCH_2-), 3.77 and 3.71 (6H, two s, 2 × -OCH_3), 2.20–1.10 (16H, br singlets, 8 × -CH_2-). ^{13}C NMR (δ ppm): 198.57, 162.97, 158.23, 132.03, 130.69(2), 129.69, 128.91(2), 113.98(2), 113.44(2), 98.62, 67.37, 62.13, 55.17, 54.93, 52.08, 33.83, 30.60, 29.50, 29.30, 27.47, 25.92, 25.32, 19.53. MS (*m/e*): 440 (M^+), 356 (M^+ −DHP).

*1,2-Bis(4-methoxyphenyl)-10-tetrahydropyranyloxy-decanone (**11**b):* IR (neat): 1674 (C=O), 1599 (C=C), 1255 (C—O) cm^{-1}. ^1H NMR (δ ppm): 7.95, 6.86 and 7.21, 6.81 (8H, 2 × two d, J = 8.87 and 8.62 Hz, 2 × *para*-substituted anisyl group), 4.56 (1H, t, J = 3.45 Hz, -OCHO-), 4.44 (1H, t, J = 7.23 Hz, -CH-), 3.82 and 3.47 (2H, two m, -CH_2OTHP), 3.70 and 3.35 (2H, two m, -CHOCH_2-), 3.81 and 3.74 (6H, two s, 2 × -OCH_3), 2.20–1.10 (20H, br singlets, 10 × -CH_2-). ^{13}C NMR (δ ppm): 198.77, 163.07, 158.32, 132.20, 130.82(2), 129.84, 129.03(2), 114.09(2), 113.55(2), 98.75, 67.58, 62.26, 55.32, 55.10, 52.24, 33.98, 30.72, 29.65, 29.53, 29.33(2), 27.64, 26.14, 25.44, 19.64. MS (*m/e*): no molecular ion, 384 (M^+ −DHP).

*1,2-Bis(4-methoxyphenyl)-12-tetrahydropyranyloxy-dodecanone (**11**c):* IR (neat): 1674 (C=O), 1599 (C=C), 1254 (C—O) cm^{-1}. ^1H NMR (δ ppm): 7.95, 6.87 and 7.21, 6.81 (8H, 2 × two d, J = 8.88 and 8.67 Hz, 2 × *para*-substituted anisyl group), 4.57 (1H, t, J = 3.45 Hz, -OCHO-), 4.40 (1H, t, J = 7.23 Hz, -CH-), 3.82 and 3.47 (2H, two m, -CH_2OTHP), 3.70 and 3.34 (2H, two m, -CHOCH_2-), 3.80 and 3.73 (6H, two s, 2 × -OCH_3), 2.20–1.10 (24H, br singlets, 12 × -CH_2-). ^{13}C NMR (δ ppm): 198.74, 163.04, 158.31, 132.18, 130.78(2), 129.82, 129.00(2), 114.05(2), 113.52(2), 98.73, 67.58, 62.24, 55.28, 55.04, 52.20, 33.97, 30.69, 29.65, 29.55, 29.44(2), 29.39(2), 27.61, 26.14, 25.42, 19.63. MS (*m/e*): no molecular ion, 412 (M^+ −DHP).

*B. Synthesis of X,Y,Y-tris(4-methoxyphenyl)-X-alken-1-ols **12**a–c.* A Grignard reagent was prepared from 460 mg (18.9 mmol) of magnesium and 2.98 g (2 mL, 15.9 mmol) of 4-bromoanisole in the presence of a crystal of iodine in 100 mL of dry ether. The Grignard reagent was usually ready after stirring at room temperature overnight (17 h), but sometimes required heating at reflux to initiate the reaction. A solution of ketone **11** (3.0 mmol) in dry ether was treated with the excess of Grignard reagent for 3 h under nitrogen at 25°C and was then hydrolysed with 50 mL of 10% aqueous ammonium chloride. The ethereal phase was washed with water (5 × 50 mL), dried, and evaporated to give the crude tertiary alcohol intermediate. The oily residue was dehydrated and deprotected in 100 mL of 95% ethanol in the presence of PPTS (100 mg, 0.34 mmol) at reflux for 2.5 h. After evaporation of the solvent, the residue was taken with ether and extracted with water (5 × 50 mL), dried, and evaporated to an oil. Flash chromatography (hexanes:acetone, 85:15) gave **12** in 90% average yield as a viscous oil.

*7,8,8-Tris(4-methoxyphenyl)-7-octen-1-ol (**12**a):* IR (neat): 3640–3150 (OH), 1605 (C=C), 1242 (C—O), cm^{-1}. ^1H NMR (δ ppm): 7.13, 6.85 and 7.01, 6.69 and 6.78, 6.54 (12H, 3 × two d, J = 8.70, 8.70, and 8.78 Hz, 3 × *para*-substituted anisyl group), 3.78, 3.71, and 3.64 (9H, 3 × s, 3 × -OCH_3), 3.51 (2H, t, J = 6.65 Hz, -CH_2OH), 2.40 (2H, m, -C=CCH_2-), 1.90 (1H, br s, -OH), 1.50–1.10 (8H, m, -CH_2-(CH_2)$_4$-CH_2-). ^{13}C NMR (δ ppm): 157.93, 157.48, 157.09, 139.06, 137.40, 136.34, 135.88, 134.88, 131.76(2), 130.46(4), 113.25(2), 113.11(2), 112.58(2), 62.61, 55.02, 54.88, 54.82, 35.69, 32.43, 29.35, 28.81, 25.25. MS (*m/e*): 446 (M^+), 359 (M^+ −$C_5H_{10}OH$).

*9,10,10-Tris(4-methoxyphenyl)-9-decen-1-ol (**12**b):* IR (neat): 3690–3150 (OH), 1605 (C=C), 1242 (C—O) cm^{-1}. ^1H NMR (δ ppm): 7.13, 6.87 and 7.02, 6.72 and 6.78, 6.55 (12H, 3 × two d, J = 8.70, 8.73, and 8.81 Hz, 3 × *para*-substituted anisyl group), 3.81, 3.75, and 3.68 (9H, 3 × s, 3 × -OCH_3), 3.59 (2H, t, J = 6.65 Hz, -CH_2OH), 2.40 (2H, m, -C=CCH_2-), 1.90 (1H, br s, -OH), 1.60–1.10 (12H, m, -CH_2-(CH_2)$_6$-CH_2-). ^{13}C NMR (δ ppm): 158.02, 157.55, 157.22, 139.29, 137.42, 136.50, 136.03, 135.04, 131.87(2), 130.56(4), 113.34(2), 113.19(2), 112.67(2), 62.99, 55.16, 54.99(2), 35.82, 32.71, 29.59(2), 29.19, 28.91, 25.62. MS (*m/e*): 474 (M^+), 359 (M^+ −$C_7H_{14}OH$).

*11,12,12-Tris(4-methoxyphenyl)-11-dodecen-1-ol (**12**c):* IR (neat): 3640–3150 (OH), 1605 (C=C), 1242 (C—O), cm^{-1}. ^1H NMR (δ ppm): 7.13, 6.87 and 7.02, 6.70 and 6.78, 6.55 (12H, 3 × two d, J = 8.70, 8.73, and 8.80 Hz, 3 × *para*-substituted anisyl group), 3.81, 3.74, and 3.67 (9H, 3 × s, 3 × -OCH_3), 3.62 (2H, t, J = 6.65 Hz, -CH_2OH), 2.40 (2H, m, -C=CCH_2-), 1.80 (1H, br s, -OH), 1.60–1.10 (16H, m, -CH_2-(CH_2)$_8$-CH_2-). ^{13}C NMR (δ ppm): 157.92, 157.47, 157.12, 139.29, 137.32, 136.46, 136.02, 135.02, 131.84(2), 130.54(4), 113.28(2), 113.14(2), 112.63(2), 62.92, 55.10, 54.98, 54.92, 35.80, 32.62, 29.62, 29.45, 29.32(2), 29.19, 28.90, 25.63. MS (*m/e*): 502 (M^+), 359 (M^+ −$C_9H_{18}OH$).

*C. Synthesis of 1-bromo-X,Y,Y-tris(4-methoxyphenyl)-X-alkenes **13**a–c.* A solution of alcohol **12** (5.83 mmol), carbon tetrabromide (7.73 g, 23.3 mmol), and triphenylphosphine (6.11 g, 23.3 mmol) in dry ether (250 mL) was stirred at room temperature (25°C) for 20 h under a nitrogen atmosphere. The triphenylphosphine oxide precipitate was filtered and the resulting solution was washed thoroughly with water (5 × 50 mL), dried, and evaporated to an oil. The crude material was purified by flash chromatography (hexanes:acetone, 95:5) to give the bromide **13** in 85% average yield as a viscous oil.

*1-Bromo-7,8,8-tris(4-methoxyphenyl)-7-octene (**13**a):* IR (neat): 1605 (C=C), 1242 (C—O), cm^{-1}. ^1H NMR (δ ppm): 7.13, 6.86 and 7.02, 6.69 and 6.78, 6.54 (12H, 3 × two d, J = 8.67, 8.69, and 8.74 Hz, 3 × *para*-substituted anisyl group), 3.79, 3.72, and 3.64 (9H, 3 × s, 3 × -OCH_3), 3.30 (2H, t, J = 6.84 Hz, -CH_2Br), 2.41 (2H, m, -C=CCH_2-), 1.73 (2H, p, J = 7.20 Hz, -CH_2CH_2Br), 1.26 (6H, m, -CH_2-(CH_2)$_3$-CH_2CH_2Br). ^{13}C NMR (δ ppm): 158.02, 157.55, 157.19, 138.91, 137.55, 136.31, 135.83, 134.80, 131.77(2), 130.46(4), 113.29(2), 113.17(2), 112.61(2), 55.06, 54.91, 54.84, 35.62, 33.87, 32.53, 28.66(2), 27.72. MS (*m/e*): 508 (M^+), 510 (M^+ +2), 359 (M^+ −C_5H_{10}Br).

*1-Bromo-9,10,10-tris(4-methoxyphenyl)-9-decene (**13**b):* IR (neat): 1605 (C=C), 1242 (C—O), cm^{-1}. ^1H NMR (δ ppm): 7.13, 6.87 and 7.02, 6.71 and 6.77, 6.55 (12H, 3 × two d, J = 8.73, 8.79, and 8.79 Hz, 3 × *para*-substituted anisyl group), 3.82, 3.76, and 3.69 (9H, 3 × s, 3 × -OCH_3), 3.37 (2H, t, J = 6.87 Hz, -CH_2Br), 2.42 (2H, m, -C=CCH_2-), 1.80 (2H, p, J = 7.35 Hz, -CH_2CH_2Br), 1.40–1.10 (10H, m, -CH_2-(CH_2)$_5$-CH_2CH_2Br). ^{13}C NMR (δ ppm): 158.05, 157.57, 157.21, 139.22, 137.46, 136.46, 136.01, 134.00, 131.87(2), 130.57(4), 113.33(2), 113.19(2), 112.67(2), 55.18, 55.04, 54.98, 35.80, 34.08, 32.74, 29.53, 29.02, 28.87, 28.56, 28.05. MS (*m/e*): 536 (M^+), 538 (M^+ +2), 359 (M^+ −C_7H_{14}Br).

*1-Bromo-11,12,12-tris(4-methoxyphenyl)-11-dodecene (**13**c):* IR (neat): 1605 (C=C), 1242 (C—O) cm^{-1}. ^1H NMR (δ ppm): 7.13, 6.85 and 7.02, 6.69 and 6.78, 6.54 (12H, 3 × two d, J = 8.70, 8.77, and 8.84 Hz, 3 × *para*-substituted anisyl group), 3.78, 3.71, and 3.64 (9H, 3 × s, 3 × -OCH_3), 3.36 (2H, t, J = 6.86 Hz, -CH_2Br), 2.40 (2H, m, -C=CCH_2-), 1.81 (2H, p, J = 7.35 Hz, -CH_2CH_2Br), 1.40–1.10 (14H, m, -CH_2-(CH_2)$_7$-CH_2CH_2Br). ^{13}C NMR (δ ppm): 157.98, 157.51, 157.14, 139.20, 137.36, 136.39, 135.95, 134.94, 131.80(2), 130.50(4), 113.24(2), 113.11(2), 112.60(2), 55.04, 54.89, 54.83, 35.78, 33.95, 32.68, 29.60, 29.28(2), 29.14, 28.88, 28.62, 28.05. MS (*m/e*): 564 (M^+), 566 (M^+ +2), 359 (M^+ −C_9H_{18}Br).

*D. Synthesis of 1-[(2-aminoethyl)amino]-X,Y,Y-tris(4-methoxyphenyl)-X-alkenes **14**a–c.* Under a nitrogen atmosphere, ethylenediamine (592 mg (658 μL), 9.84 mmol) was added to a solution of triphenylethylene bromide **13** (0.984 mmol) in 50 mL of dry methanol. After boiling for 2 days under reflux (sometimes a longer

Can. J. Chem. Downloaded from www.nrcresearchpress.com by 213.200.69.106 on 09/08/12
For personal use only.

reaction period is required), the solvent was evaporated. The resulting residue was dissolved in ether (100 mL) and washed with a solution of $NaHCO_3$ (30 mL, 5% aqueous) and with water (5 × 50 mL). The ethereal phase was dried and evaporated to a viscous oil. The average yield was 75%.

*1-[(2-Aminoethyl)amino]-7,8,8-tris(4-methoxyphenyl)-7-octene (**14**a):* IR (neat): 3565–3130 (N—H), 1605 (C=C), 1242 (C—O) cm^{-1}. ^1H NMR (δ ppm): 7.13, 6.85 and 7.01, 6.67 and 6.78, 6.52 (12H, 3 × two d, J = 8.28, 8.33, and 8.21 Hz, 3 × *para*-substituted anisyl group), 3.74, 3.64, and 3.59 (9H, 3 × s, 3 × $-OCH_3$), 2.75 (2H, br s, $-CH_2NH_2$), 2.61 (2H, br s, $-CH_2CH_2NH_2$), 2.51 (2H, t, J = 7.0 Hz, $-CH_2NH$-), 2.42 (2H, t, J = 7.0 Hz, $-C{=}CCH_2$-), 2.29 (3H, br s, -NH and $-NH_2$), 1.50–1.10 (8H, m, $-CH_2-(CH_2)_4-CH_2$-). ^{13}C NMR (δ ppm): 157.68, 157.21, 156.87, 138.76, 137.11, 136.00, 135.55, 134.53, 131.47(2), 130.16(4), 112.96(2), 112.82(2), 112.28(2), 54.66, 54.50, 54.44, 51.69, 49.32, 41.02, 35.44, 29.49, 29.22, 28.56, 26.62. MS (*m/e*): 488 (M^+), 458 ($M^+ - CH_2NH_2$), 445 ($M^+ - CH_2CH_2NH$).

*1-[(2-Aminoethyl)amino]-9,10,10-tris(4-methoxyphenyl)-9-decene (**14**b):* IR (neat): 3660–3130 (N—H), 1605 (C=C), 1242 (C—O) cm^{-1}. ^1H NMR (δ ppm): 7.13, 6.86 and 7.02, 6.68 and 6.78, 6.53 (12H, 3 × two d, J = 8.32, 8.35, and 8.52 Hz, 3 × *para*-substituted anisyl group), 3.95 (3H, br s, -NH and $-NH_2$), 3.77, 3.70, and 3.63 (9H, 3 × s, 3 × $-OCH_3$), 2.93 (2H, m, $-CH_2NH_2$), 2.82 (2H, m, $-CH_2CH_2NH_2$), 2.66 (2H, m, $-CH_2NH$-), 2.40 (2H, m, $-C{=}CCH_2$-), 1.60–1.10 (12H, m, $-CH_2-(CH_2)_6-CH_2$-). ^{13}C NMR (δ ppm): 157.77, 157.30, 156.94, 138.95, 137.17, 136.15, 135.73, 134.70, 131.60(2), 130.29(4), 113.06(2), 112.95(2), 112.40(2), 54.85, 54.69, 54.64, 50.24, 48.85, 39.60, 35.58, 29.38, 28.95(2), 28.69, 28.37, 26.84. MS (*m/e*): 516 (M^+), 486 ($M^+ - CH_2NH_2$), 473 ($M^+ - CH_2CH_2NH$).

*1-[(2-Aminoethyl)amino]-11,12,12-tris(4-methoxyphenyl)-11-dodecene (**14**c):* IR (neat): 3660–3140 (N—H), 1605 (C=C), 1242 (C—O) cm^{-1}, ^1H NMR (δ ppm): 7.13, 6.86 and 7.02, 6.70 and 6.78, 6.55 (12H, 3 × two d, J = 8.66, 8.70, and 8.80 Hz, 3 × *para*-substituted anisyl group), 3.81, 3.74, and 3.67 (9H, 3 × s, 3 × $-OCH_3$), 2.80 (2H, t, J = 6.0 Hz, $-CH_2NH_2$), 2.66 (2H, t, J = 6.0 Hz, $-CH_2CH_2NH_2$), 2.59 (2H, t, J = 7.2 Hz, $-CH_2NH$-), 2.40 (2H, m, $-C{=}CCH_2$-), 2.04 (3H, br s, -NH and $-NH_2$), 1.50–1.10 (16H, m, $-CH_2-(CH_2)_8-CH_2$-). ^{13}C NMR (δ ppm): 157.97, 157.49, 157.14, 139.26, 137.31, 136.42, 136.00, 134.99, 131.81(2), 130.51(4), 113.25(2), 113.12(2), 112.61(2), 55.08, 54.91(2), 52.32, 49.81, 41.55, 35.80, 30.02, 29.66, 29.46(3), 29.23, 28.92, 27.28. MS (*m/e*): 544 (M^+), 514 ($M^+ - CH_2NH_2$), 501 ($M^+ - CH_2CH_2NH$).

*E. Synthesis of 1-[(2-aminoethyl)amino]-X,Y,Y-tris(4-hydroxyphenyl)-X-alkenes **15**a–c.* A solution of trimethyl ether **14** (0.665 mmol) in dry CH_2Cl_2 (30 mL) was treated with a solution of boron tribromide (2.33 mL (1 M), 2.33 mmol) at −60°C, under a nitrogen atmosphere. After the addition, the reaction mixture was allowed to warm to room temperature (25°C) and was stirred for 17 h. The mixture was refluxed during 2 h. The reaction was cooled with an ice bath before adding 15 mL of methanol. The resulting solution was concentrated to 2–3 mL, treated with saturated $NaHCO_3$ solution (30 mL), and extracted with ethyl acetate (5 × 30 mL). The crude yields range from 50 to 85%. Compounds **15***a–c* were used without further purification in the next step.

*F. Synthesis of 1-[*cis*-[(2-aminoethyl)amino]dichloroplatinum-(II)]-X,Y,Y-tris(4-hydroxyphenyl)-X-alkenes **1**a–c.* A solution of potassium tetrachloroplatinate(II) (219 mg, 0.527 mmol) in 7.5 mL of a mixture of dimethylformamide (DMF) and water (2:1) was added to a warm (35°C) solution of diamine **15** (0.527 mmol) in 5 mL of DMF. The resulting mixture (pH 9–10) was stirred in the dark for 2–3 days until the pH value reached 4–5. Then, 1 drop of dimethyl sulfoxide was added and the stirring was continued for 2 h. The solvent was evaporated and the residue was suspended in saturated potassium chloride solution (30 mL; **note**: a vigorous stirring was essential to pulverized the lumps of platinum(II) complex). The resulting suspension was filtered, washed with water (100–250 mL), and dried in a desiccator. The product can be further purified either by flash chromatography or by preparative TLC (CH_2Cl_2:methanol, 9:1). The crude yields range from 70 to 95%.

*1-[*cis*-[(2-Aminoethyl)amino]dichloroplatinum(II)]-7,8,8-tris(4-hydroxyphenyl)-7-octene (**1**a):* mp >148°C (dec.). IR (KBr): 3640–3050 (N—H, O—H), 1605 (C=C), 1223 (C—O) cm^{-1}. ^1H NMR (acetone-d_6, δ ppm): 8.6–8.2 (3H, br s, 3 × -OH), 7.02, 6.83 and 6.94, 6.64 and 6.69, 6.48 (12H, 3 × two d, J = 8.57, 8.59, and 8.59 Hz, 3 × *para*-substituted phenol), 5.64, 5.08, and 4.97 (3H, 3 × br s, $-NHCH_2CH_2NH_2$), 3.15 (6H, br s, $-CH_2NHCH_2CH_2NH_2$), 3.03 (2H, br s, $-CH_2CH_2NH$-), 2.80–2.55 (2H, br s, $CH_2CH_2-CH_2NH$-), 2.39 (2H, m, $-C{=}CCH_2$-), 1.80–1.10 (4H, m, $-C{=}CCH_2-(CH_2)_2$-). ^{13}C NMR (acetone-d_6, δ ppm): 156.70, 156.20, 155.88, 139.39, 138.78, 136.16, 135.93, 134.64, 132.55(2), 131.43(2), 131.26(2), 115.61(2), 115.44(2), 114.84(2), 56.11, 53.43, 47.67, 36.21, 27.58, 26.81. (N.B. 2 carbons are hidden by acetone.) Anal. calcd. for $C_{28}H_{34}Cl_2N_2O_3Pt$: C 47.26, H 4.78, N 3.94; found: C 47.52, H 4.50, N 3.81.

*1-[*cis*-[(2-Aminoethyl)amino]dichloroplatinum(II)]-9,10,10-tris(4-hydroxyphenyl)-9-decene (**1**b):* mp >150°C (dec.). IR (KBr): 3700–3000 (N—H, O—H), 1605 (C=C), 1223 (C—O) cm^{-1}. ^1H NMR (acetone-d_6, δ ppm): 8.53, 8.39, and 8.32 (3H, 3 × br s, 3 × -OH), 7.02, 6.83 and 6.94, 6.64 and 6.69, 6.48 (12H, 3 × two d, J = 8.50, 8.60, and 8.64 Hz, 3 × *para*-substituted phenol), 5.75, 5.19, and 5.05 (3H, 3 × br s, $-NHCH_2CH_2NH_2$), 3.24 (6H, br s, $-CH_2NHCH_2CH_2NH_2$), 3.08 (2H, br s, $-CH_2CH_2NH$-), 2.73 (2H, br s, $-CH_2CH_2CH_2NH$-), 2.39 (2H, m, $-C{=}CCH_2$-), 1.80–1.10 (8H, m, $-C{=}CCH_2-(CH_2)_4$-). ^{13}C NMR (acetone-d_6, δ ppm): 156.01, 155.62, 155.20, 138.87, 138.10, 135.54, 135.25, 134.03, 131.88(2), 130.71(2), 130.58(2), 114.91(2), 114.76(2), 114.19(2), 55.43, 52.90, 46.99, 35.69, 27.12, 26.54. (N.B. 4 carbons are hidden by acetone.) Anal. calcd. for $C_{30}H_{38}Cl_2N_2O_3Pt$: C 48.71, H 5.14, N 3.79; found: C 48.82, H 5.14, N 3.68.

*1-[*cis*-[(2-Aminoethyl)amino]dichloroplatinum(II)]-11,12,12-tris(4-hydroxyphenyl)-11-dodecene (**1**c):* mp >150°C (dec.). IR (KBr): 3775–3050 (N—H, O—H), 1605 (C=C), 1223 (C—O) cm^{-1}. ^1H NMR (δ ppm): 8.53, 8.39, and 8.32 (3H, 3 × s, 3 × -OH), 7.02, 6.81 and 6.93, 6.63 and 6.69, 6.48 (12H, 3 × two d, J = 8.51, 8.62, and 8.65 Hz, 3 × *para*-substituted phenol), 5.72, 5.11, and 4.98 (3H, 3 × br s, $-NHCH_2CH_2NH_2$), 3.14 (6H, br s, $-CH_2NHCH_2CH_2NH_2$), 3.05 (2H, br s, $-CH_2CH_2NH$-), 2.72 (2H, br s, $-CH_2CH_2CH_2NH$-), 2.39 (2H, m, $-C{=}CCH_2$-), 1.80–1.10 (12H, m, $-C{=}CCH_2-(CH_2)_6$-). ^{13}C NMR (acetone-d_6, δ ppm): 156.72, 156.23, 155.88, 139.59, 138.70, 136.23, 135.63, 134.70, 132.58(2), 131.39(2), 131.27(2), 115.52(2), 115.40(2), 114.89, 114.84, 56.13, 53.51, 47.82, 36.43, 27.82, 27.26. (N.B. 6 carbons are hidden by acetone.) Anal. calcd. for $C_{32}H_{42}Cl_2N_2O_3Pt$: C 50.20, H 5.49, N 3.66; found: C 50.53, H 5.62, N 3.70.

In vitro antitumor activity

Microcytostasis assay

MTT was dissolved in phosphate-buffered saline (PBS) at a concentration of 5 mg/mL and stored in a dark environment at 4°C for a maximum of 3 weeks. Cell lines were grown until they were subconfluent, then trypsinized, washed in PBS, and resuspended in fresh media. A total of 100 μL medium containing 10^4 viable cells was plated per well into 96-well microtitre plates. Cells were allowed to attach to the plates for 24 h at 37°C in a 5% CO_2 atmosphere. The new drugs were dissolved in 0.25 mL of 95% ethanol and 4.75 mL of fresh media to a concentration of 1000 μ*m*. Drug dilutions were prepared in culture medium (range 1–1000 μ*m*). Medium was removed from the cells and test dilutions were added in 100 μ*m* fresh medium. Tests were carried out with 10 control wells (cells, no drug treatment) and 3 wells for each test dilution. Cells were exposed to the drug for 24 h at 37°C in 5% CO_2. Medium was removed and the cells were washed three times with sterile PBS. Next, 100 μL fresh medium was added to each well, followed by a 24 h recovery period. Subsequently, the medium was aspirated from each well and 100 μL 1:10 dilution of

MTT stock (5 mg/mL) was added to each well, followed by a 4 h incubation period at 37°C. MTT/medium blank controls with no cells also received 100 μM MTT/well. After incubation, medium was aspirated from each well, 100 μL DMSO was added per well, and the plates were agitated on a plate shaker for 20 min at room temperature (RT). The plates were read spectrophotometrically using a dual wavelength filter (570 and 630 nm) with a BIO-Tek EL310 E1A reader interfaced with a Samsung Deskmaster 386 microcomputer. Absorbance at 630 nm was used as the reference wavelength for detecting artefacts in the plastic plates and was subtracted from the 570 nm values. Wells with medium only (no cells) were processed in exactly the same manner as the rest of the plate, and the mean absorbance for these wells was subtracted from the absorbance values in the other wells.

Acknowledgments

We are grateful to the School of Pharmacy, Memorial University of Newfoundland, and to The Newfoundland Cancer Foundation for financial support of this work. We wish to thank members of the Chemistry Department (MUN): Dr. C. R. Jablonski, Ms. N. Brunet for NMR spectra, and Dr. B. Gregory and Miss M. Baggs for MS spectra.

1. D.E. Merkel, S.A.W. Fuqua, and W.L. McGuire. *In* Drug resistance in cancer therapy. *Edited by* R.F. Ozols. Kluwer, Academic Publishers, Boston/Dordrecht/London. 1989. pp. 97–105; P. Selby, J.-P. Bizzari, and R.N. Buick. Cancer Treat. Rep. **67**, 659 (1983).
2. R.K.-Y. Zee-Cheng and C.C. Cheng. Methods Find. Exp. Clin. Pharmacol. **11**, 439 (1989); E. Tomlinson and C. Livingstone. Pharm. J. 619 (1989).
3. I. Niculescu-Duvaz, A. Cambanis, and E. Tarnauceanu. J. Med. Chem. **10**, 172 (1966).
4. M.E. Wall, G.S. Abernethy, Jr., F.I. Carroll, and D.J. Taylor. J. Med. Chem. **12**, 810 (1969); P.O. Gunnarsson, T. Davidsson, S.-B. Andersson, C. Backman, and S.-A. Johansson. Eur. J. Clin. Pharmacol. **38**, 189 (1990); P. Catsoulacos and D. Catsoulacos. Anticancer Res. **11**, 1773 (1991).
5. H.-Y.P. Lam, A. Begleiter, C.J. Goldenberg, and C.-M. Wong. J. Med. Chem. **22**, 200 (1979); L.L. Wei, B.S. Katzenellenbogen, D.W. Robertson, D.M. Simpson, and J.A. Katzenellenbogen. Breast Cancer Res. Treat. **7**, 77 (1986); J.E. McCormick and R.S. McElhinney. Eur. J. Cancer, **26**, 207 (1990); B. Betsch, M.R. Berger, B. Spiegelhalder, D. Schmahl, and G. Eisenbrand. Eur. J. Cancer, **26**, 895 (1990).
6. A. Passini and F. Zumino. Angew. Chem. Int. Ed. Engl. **26**, 615 (1987); P.C. Hydes and M.J.H. Russell. Cancer Metastasis Rev. **7**, 67 (1988); J. Kozelka and J.-C. Chottard. Biophys. Chem. **35**, 165 (1990); V. Brabec, V. Kleinwachter, J.-L. Butour, and N.P. Johnson. Biophys. Chem. **35**, 129, (1990); M. Sip, A. Schwartz, F. Vovelle, M. Ptak, and M. Leng. Biochemistry, **31**, 2508 (1992).
7. A.M. Otto, M. Faderl, and H. Schonenberger. Cancer Res. **51**, 3217 (1991).
8. N. Knebel, C.-D. Schiller, M.R. Schneider, H. Schonenberger, and E. von Angerer. Eur. J. Cancer Oncol. **25**, 293 (1989).
9. J. Bowler, T.J. Lilley, J.D. Pittam, and A.E. Wakeling. Steroids, **54**, 71 (1989); A.E. Wakeling and J. Bowler. J. Endocrinol. **112**, R7 (1987); J. Steroid Biochem. **30**, 141 (1988); J. Steroid Biochem. **31**, 645 (1988); R. Poulin, Y. Merand, D. Poirier, C. Levesque, J.-M. Dufour, and F. Labrie. Breast Cancer Res. Treat. **14**, 65 (1989); A.E. Wakeling. J. Steroid Biochem. **34**, 183 (1989); A.P.M. Wilson, P.J. Weatherill, R.I. Nicholson, P. Davies, and A.E. Wakeling. J. Steroid Biochem. **35**, 421 (1990); M.S. Galman, S.A. Sundstrom, and C.R. Lyttle. J. Steroid Biochem. **36**, 281 (1990); J.R. Pasqualini, N. Giambiagi, C. Gelly, and G. Chetrite. J. Steroid Biochem. Mol. Biol. **37**, 343 (1990); A.E. Wakeling. J. Steroid Biochem. Mol. Biol. **37**, 771 (1990); S.E. Fawell, R. White, S. Hoare, M. Sydenham, M. Page, and M.G. Parker. Proc. Natl. Acad. Sci. U.S.A. **87**, 6883 (1990); M. Sabbah, F. Gouilleux, B. Sola, G. Redeuilh, and E.-E. Baulieu. Proc. Natl. Acad. Sci. U.S.A. **88**, 390 (1991); J.R. Pasqualini and B.-L. Nguyen. Breast Cancer Res. Treat. **18**, 93 (1991); N. Giambiagi and J.R. Pasqualini. J. Mol. Endocrinol. **7**, 9 (1991); M.K. Gibson, L.A. Nemmers, W.C. Beckman, Jr., V.L. Davis, S.W. Curtis, and K.S. Korach. Endocrinology, **129**, 2000 (1991); A. Claussner, L. Nedelec, F. Nique, D. Philibert, G. Teutsch, and P. Van de Velde. J. Steroid Biochem. Mol. Biol. **41**, 609 (1992); A.E. Wakeling, M. Dukes, and J. Bowler. Cancer Res. **51**, 3867 (1991).
10. P. Wheeler and G. Bérubé. Inorg. Chim. Acta, **209**, 97 (1993).
11. N. Knebel and E. von Angerer. J. Med. Chem. **31**, 1675 (1988); E. von Angerer, H. Birnbock, and N.G. Knebel. Anti-Cancer Drug Des. **4**, 21 (1989); N. G. Knebel and E. von Angerer. J. Med. Chem. **34**, 2145 (1991).
12. M. Miyashita, A. Yoshikoshi, and P.A. Grieco. J. Org. Chem. **42**, 3772 (1977).
13. J. Hooz and S.S.H. Gillani. Can. J. Chem. **46**, 86 (1968).
14. M.P. Georgiadis and S.A. Haroutounian. Inorg. Chim. Acta, **138**, 249 (1987).
15. K. Krohn, K. Kulikowski, and G. Leclerq. J. Med. Chem. **32**, 1532 (1989); H. Kohle, K. Krohn, and G. Leclerq. J. Med. Chem. **32**, 1538 (1989).
16. K.B. Horwitz, D.T. Zava, A.K. Thilagar, E.M. Jensen, and W.L. McGuire. Cancer Res. **38**, 2434 (1978), and references cited therein.
17. J. Carmichael, W.G. DeGraff, A.F. Gazdar, J.D. Minna, and J.B. Mitchell. Cancer Res. **47**, 943 (1987); F. Denizot and R. Lang. J. Immunol. Methods, **89**, 271 (1986); D.J. Adams. Cancer Res. **49**, 6615 (1989).
18. C.H.J. Ford, V.J. Richardson, and G. Tsaltas. Cancer Chemother. Pharmacol. **24**, 295 (1989).
19. D.D. Perrin and L.F. Armarego. *In* Purification of laboratory chemicals. 3rd ed. Pergamon Press, Oxford, New York. 1988.
20. W.C. Still, M. Kahn, and A. Mitra. J. Org. Chem. **43**, 2923 (1978).

Can. J. Chem. Downloaded from www.nrcresearchpress.com by 213.200.69.106 on 09/08/12
For personal use only.

Solvent influence on the conformation of cyclosporin. An FT-IR study[1]

R.A. SHAW AND H.H. MANTSCH[2]
Institute for Biodiagnostics, National Research Council of Canada, Winnipeg, MN R3B 1Y6, Canada

AND

B.Z. CHOWDHRY
University of Greenwich, Woolwich, London, SE18 6PF, U.K.

Received May 21, 1993

R.A. SHAW, H.H. MANTSCH, and B.Z. CHOWDHRY. Can. J. Chem. **71**, 1334 (1993).

Infrared spectra of the cyclic peptide cyclosporin A and three analogues have been measured in a number of organic solvents (CCl_4, $CDCl_3$, acetonitrile, DMSO, and 50:50 acetonitrile:D_2O). Seven of the eleven amide groups of cyclosporin A are methylated, the remaining four N-H protons forming strong intramolecular hydrogen bonds in the crystal and in $CDCl_3$ solution. These hydrogen bonds give rise to amide I (C=O stretching) bands at positions characteristic of β-turns, γ-turns, and β-sheet domains in proteins and model polypeptides. Increasing the polarity of the solvent eliminates some of these features; however, the spectra in DMSO and acetonitrile–D_2O retain strong amide I absorptions characteristic of hydrogen-bonded carbonyl groups. The conformation of cyclosporin A in water cannot be observed directly due to low solubility; these findings suggest that the structure likely retains strong intramolecular hydrogen bonding. Spectra of the three analogues are consistent with this interpretation. Implications respecting the mechanism of pharmacological action of cyclosporin A are discussed.

R.A. SHAW, H.H. MANTSCH et B.Z. CHOWDHRY. Can. J. Chem. **71**, 1334 (1993).

On a mesuré les spectres infrarouges du peptide cyclique, cyclosporine A, et de trois de ses analogues dans divers solvants organiques (CCl_4, $CDCl_3$, acétonitrile, DMSO et mélange 50 : 50 d'acétonitrile : D_2O). Sept des onze groupes amides de la cyclosporine sont méthylés et les quatre autres groupes N-H forment de fortes liaisons hydrogènes dans le cristal et en solution dans le $CDCl_3$. Ces liaisons hydrogènes donnent lieu à des bandes amides I (élongation C=O) à des positions caractéristiques des domaines des tours β et γ et des feuillets β des protéines et des polypeptides modèles. Une augmentation de la polarité du solvant élimine une partie de ces caractéristiques; toutefois, les spectres dans le DMSO et dans le mélange acétonitrile–eau retiennent les fortes absorptions caractéristiques des groupes carbonyles fortement impliqués dans des liaisons hydrogènes. On ne peut pas observer directement la conformation de la cyclosporine A dans l'eau à cause de sa faible solubilité; ces observations suggèrent que la structure la plus probable conserve une forte liaison hydrogène intramoléculaire. Les spectres des trois analogues sont en accord avec cette interprétation. On discute des implications de ces résultats sur le mécanisme d'action pharmacologique de la cyclosporine A.

[Traduit par la rédaction]

Introduction

Cyclosporin A (CsA, see Scheme 1) is a cyclic undecapeptide that serves as an immunosuppressive agent, inhibiting the rejection of transplanted organs. The mechanism underlying this effect is not understood, but one of the first steps is believed to involve binding to the protein cyclophilin, a *cis–trans* isomerase whose activity in vitro is inhibited by complexation with CsA (1).

Cyclosporin A contains only hydrophobic amino acids, seven of which are N-methylated. The crystal (2, 3) and solution (chloroform) (2, 4) structures of cyclosporin A are virtually identical to one another. Structural features include the following:

(*i*) Three H-bonds forming a twisted β-sheet involving residues 11 through 1 to 7 (11-1-7), with (*a*) a type II′ β-turn (10-membered ring) formed by hydrogen bonding between the C=O of Abu-2[3] and the N-H of Val-5; (*b*) the adjacent H-bond connecting the N-H of Abu-2 to the C=O of Val-5; (*c*) a third H-bond connecting the C=O of MeVal-11 to the N-H of Ala-7.

(*ii*) A γ-turn (7-membered ring) formed by hydrogen bonding between the N-H of D-Ala-8 and the C=O of MeLeu-6 (C_6=O ← H-N_8).

(*iii*) An open loop structure for residues 7 through 8 to 11 (7-8-11).

Cyclosporin has 11 amide carbonyl groups, but only four amide protons, all of which form intramolecular H-bonds. This conformer of CsA is also stabilized by the N-CH_3 group of MeVal-11, which extends into the centre of the open loop to form close van der Waals contacts with several of the backbone atoms. No experimental structures are available for the analogues CsC, CsD, or CsH.

The similarity between the crystal and NMR structures of cyclosporin A might reasonably be taken to suggest that the active conformation is very similar. It turns out that this is not the case: the structure of CsA bound to cyclophilin has been measured using both NMR and X-ray crystallography, and has been shown to differ substantially from any known structure of the free molecule (5–11). This finding has spurred renewed interest in the solvent dependency of the conformation. The conformation in aqueous solution is of particular interest, as this structure may more closely resemble that of the molecule bound to cyclophilin.

The very low solubility of cyclosporin precludes direct studies of the conformation in water. Molecular dynamics calculations suggest that the backbone conformation is largely

[1]Issued as NRCC No. 34728.

[2]Author to whom correspondence may be addressed.

[3]**Abbreviations**: MeLeu, *N*-methylleucine; Sar, sarcosine (*N*-methylglycine); Abu, L-α-aminobutyric acid; Val, valine; Ala, alanine; MeVal, *N*-methylvaline; MeBmt, (4*R*)-4-[(*E*)-but-2-enyl]-4,*N*-dimethyl-L-threonine; CsX, cyclosporin A with Abu-2 → Thr-2 (CsC), Abu-2 → Val-2 (CsD), and L-MeVal-11 → D-MeVal-11 (CsH)

Can. J. Chem. Downloaded from www.nrcresearchpress.com by 213.200.69.106 on 09/08/12
For personal use only.

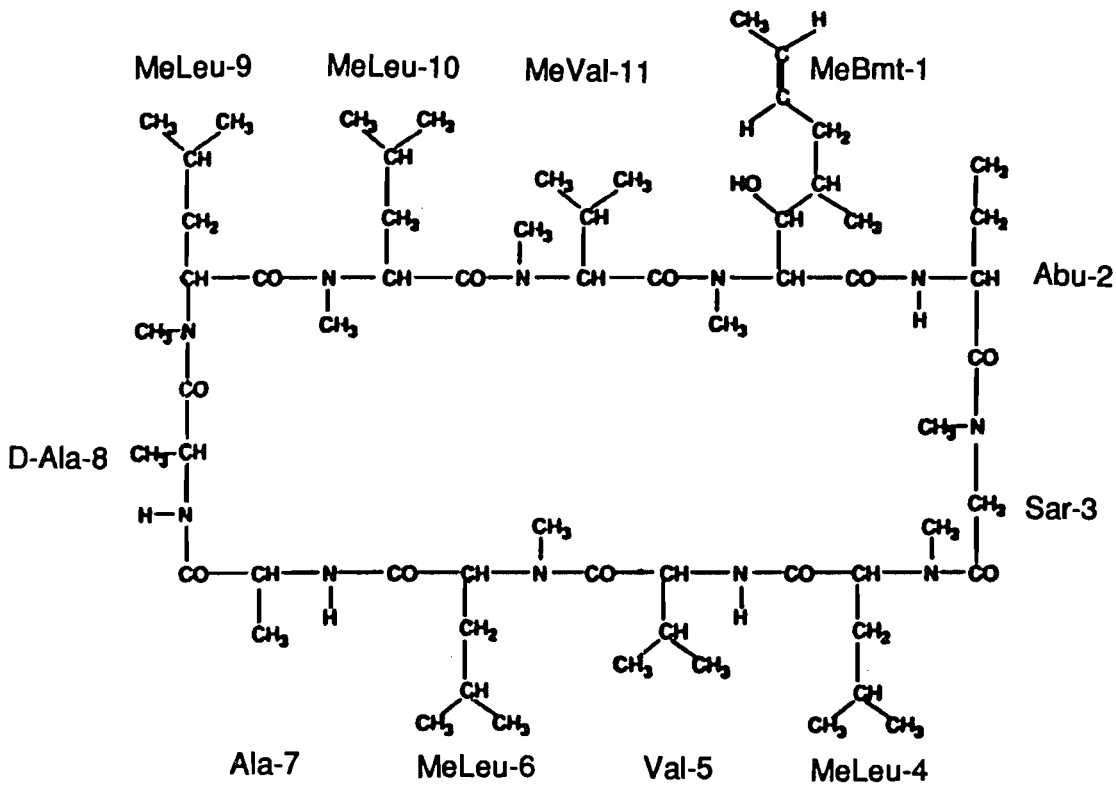

SCHEME 1. Cyclosporin A. The other cyclosporins differ from CsA in the following; cyclosporin C (CsC) has Abu-2 replaced by Thr-2, cyclosporin D (CsD) has Abu-2 replaced by Val-2, and cyclosporin H (CsH) has L-MeVal-11 replaced by D-MeVal-11.

independent of the solvent polarity (12). NMR spectra in DMSO suggest the presence of a variety of geometries, apparently showing conformational differences in the backbone as well as in the side chains (2, 13). NMR studies of CsA in various mixtures of $CDCl_3$ and CD_3OD suggest that the $CDCl_3$ conformer is also the dominant one in CD_3OD, although the relative abundance is reduced to ~30% (14). Recent CD studies of CsA, CsC, CsD, and CsH (see Scheme 1) indicate that the dominant conformational features are similar for CsA, CsC, and CsD, but significantly altered for CsH (15).

Infrared spectra are easily measured in a variety of solvents including CCl_4, $CDCl_3$, and DMSO, which are unsuitable for CD work due to spectral cutoff in the 185–260 nm region. Hydrogen bonding and distortion (rehybridization) of the amide linkages give rise to a range of amide I (C=O stretching) bands between 1600 and 1700 cm^{-1}. Analysis of this spectral region has become a powerful technique for determining the secondary structure of proteins and polypeptides, the absorption pattern for these amide I modes providing a signature that can be interpreted to reveal the relative importance of characteristic structures such as α-helix, β-sheet, and turns (for a recent review, see ref. 16).

To examine the influence of the nature of the solvent on the conformation of cyclosporin, we have measured the FT-IR spectra of cyclosporin A and three analogues (CsC, CsD, CsH) in CCl_4, $CDCl_3$, acetonitrile, DMSO, and 50:50 acetonitrile:D_2O.

Experimental

Cyclosporins A, C, D, and H were kindly supplied by Dr. T.G. Payne (Sandoz Ltd., Basel, Switzerland). Infrared spectra were obtained using 20 mg/mL cyclosporin (~17 mM) at pathlengths of 10 μm. Spectra were run in acetonitrile, DMSO, carbon tetrachloride, deuterochloroform, and 50:50 acetonitrile:D_2O using a Digilab FTS-60 spectrometer and MCT detector; 256 scans were typically coadded at a resolution of 2 cm^{-1}, and Fourier self-deconvolution was performed using software developed in our laboratory. All figures display spectra that have been deconvolved, using bandwidths of 11 cm^{-1} (CCl_4), 13 cm^{-1} ($CDCl_3$), 14 cm^{-1} (CH_3CN), 14 cm^{-1} (DMSO), and 20 cm^{-1} (CH_3CN–D_2O), and K values of 1.3 (CH_3CN–D_2O) and 1.8 (all others).

Results

Figure 1 shows the spectra of CsA in five different solvents, plotted together for comparison. Figures 2–5 show the spectra of the various cyclosporins measured in carbon tetrachloride, chloroform-d_1, acetonitrile, and acetonitrile–D_2O, respectively. Under all conditions the spectrum of CsD is virtually identical to that of CsA, as demonstrated by the spectra measured in CCl_4 (see Fig. 2). Therefore, the spectra of CsD are not plotted in the other figures.

The interpretation of the cyclosporin spectra is based on general rules derived from infrared studies of proteins and model peptides. The success of infrared spectroscopy in probing these structures is largely founded upon the fact that the amide I (C=O stretch) frequency is sensitive to hydrogen bonding. These modes generally appear between 1610 and 1690 cm^{-1}; a band at 1610 cm^{-1} denotes a very strongly H-bonded C=O group, while an absorption at 1690 cm^{-1} indicates the complete absence of H-bonding and possibly a deviation from coplanarity of the amide group. Between these extremes lies a gradient of H-bonding strengths, strongest at lowest frequencies and absent at the highest. Generally, bands above 1660 cm^{-1} arise from non-H bonded structures while

Can. J. Chem. Downloaded from www.nrcresearchpress.com by 213.200.69.106 on 09/08/12
For personal use only.

Can. J. Chem. Downloaded from www.nrcresearchpress.com by 213.200.69.106 on 09/08/12
For personal use only.

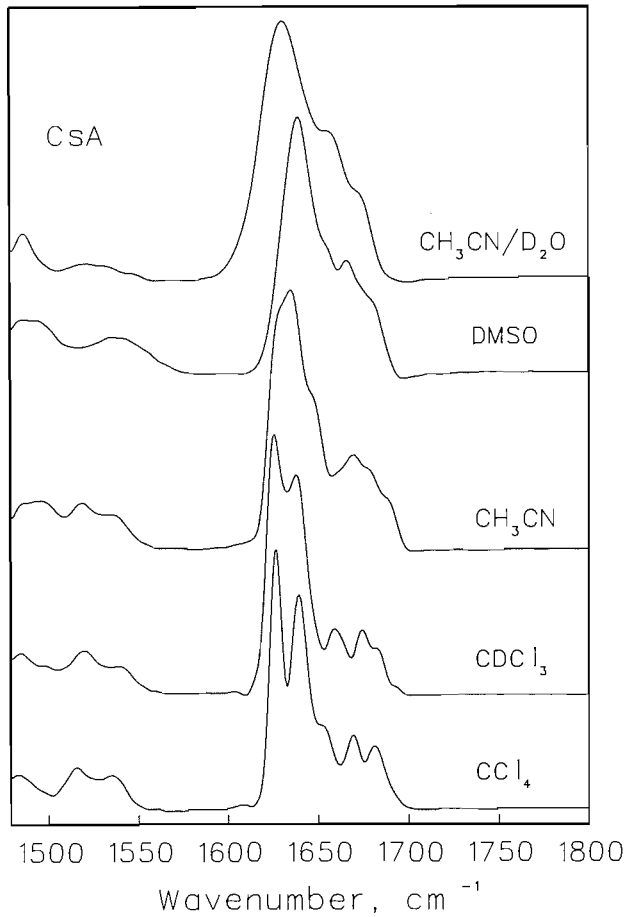

FIG. 1. FT-IR spectra of cyclosporin A in various solvents.

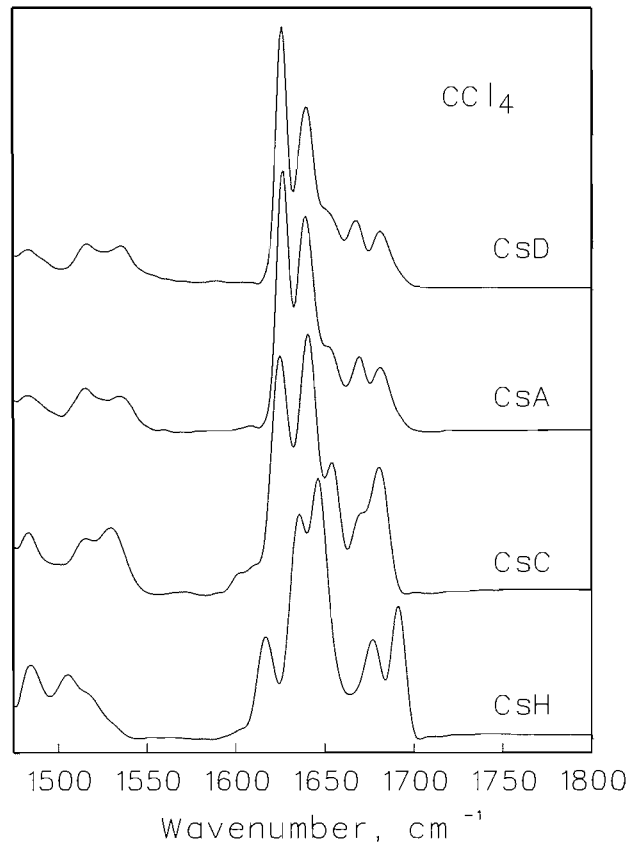

FIG. 2. FT-IR spectra of cyclosporins in CCl_4.

bands below 1645 cm^{-1} correspond to strong H-bonds such as those found in β-type structures (17). Features in the 1645–1660 cm^{-1} range may arise from weaker H-bonds, e.g., α-helices, or unordered structures. A recent study of model cyclic peptides (18) has shown that the two C=O groups defining a β-turn and adjacent H-bond give rise to infrared absorptions that cannot be resolved one from another, appearing at 1645 cm^{-1} in acetonitrile, 1642 cm^{-1} in chloroform, 1642 cm^{-1} in DMSO, and 1644 (1640) cm^{-1} in H_2O (D_2O).

The NMR structure of CsA in $CDCl_3$ includes a β-sheet domain, with one H-bond defining the type II′ β-turn (C_2=O ← H-N_5) and two other H-bonds extending the β-sheet (C_5=O ← H-N_2 and C_{11}=O ← H-N_7), as well as a γ-turn centered around Ala-7 (C_6=O ← H-N_8). These features, which define the backbone structure, should give rise to characteristic signatures below 1645 cm^{-1} in the infrared spectra.

The CsA spectrum in $CDCl_3$ shows two strong features in the 1620–1645 cm^{-1} range typical of strongly H-bonded C=O groups. By analogy with the model peptide study, we assign the band at 1638 cm^{-1} as a superposition of two amide I bands corresponding to the first two carbonyl groups (C_2=O ← H-N_5 and C_5=O ← H-N_2) involved in the β-sheet structure. The amide I band observed at 1625 cm^{-1} for CsA, CsC, and CsD also denotes even more strongly H-bonded C=O groups. We assign this band as a superposition of the absorptions arising from the third H-bond of the β-structure (C_{11}=O ← H-N_7) and the H-bond forming the γ-turn (C_6=O ← H-N_8).

With seven of the 11 amide protons replaced by methyl groups, these four intramolecular H-bonds play a major role in stabilizing the backbone structure of CsA in $CDCl_3$. The stability of this conformer in other solvents may be assessed by monitoring changes in those amide I bands that most clearly reflect the H-bonding in $CDCl_3$ solution, i.e., the bands at 1625 and 1638 cm^{-1}. Therefore the remainder of our interpretation focuses largely upon these bands.

The CsH spectrum is unique in that there is no band at 1625 cm^{-1}, this feature being replaced by a new absorption at 1616 cm^{-1}. This position indicates a very strongly H-bonded C=O, likely due to strengthening of the γ-turn or the C_{11}=O ← H-N_7 H-bond relative to the analogous bond in CsA. For CsH inversion of the MeVal-11 chiral center, compared to CsA, disrupts van der Waals interactions of the N-CH_3 group that stabilize the conformation of CsA and presumably also CsC and CsD (2). This effect is likely to lead to a weakening of the C_{11}=O ← H-N_7 H-bond, leaving the γ-turn as the more plausible source of the band at 1616 cm^{-1}. The feature at 1693 cm^{-1} may then be assigned as the C_7=O enclosed by the γ-turn, with the high frequency induced by strain (non-coplanarity) associated with formation of the 7-membered ring. The weakened C_{11}=O ← H-N_7 bond may give rise to the band at ~1649 cm^{-1} in the spectrum of CsH.

Surprisingly, the spectra measured in CCl_4 differ substantially from counterparts measured in $CDCl_3$ solution, particularly above 1650 cm^{-1}. The spectra of CsH are particularly informative, as the feature at 1616 cm^{-1} is notice-

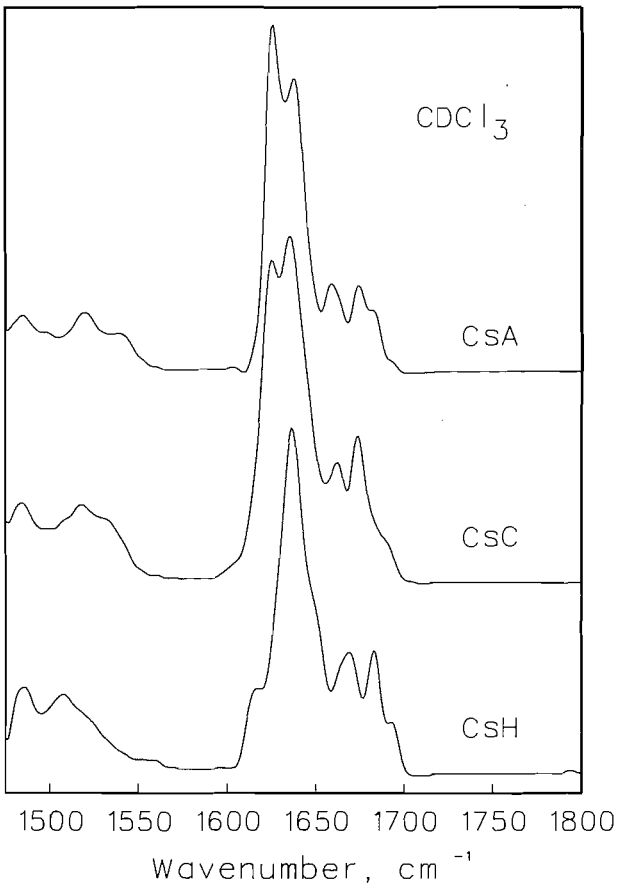

FIG. 3. FT-IR spectra of cyclosporins in $CDCl_3$.

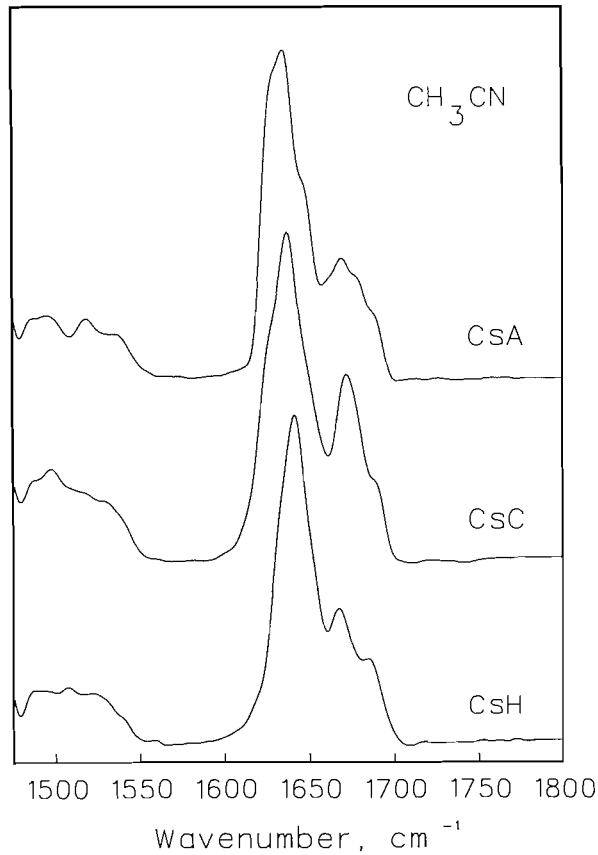

FIG. 4. FT-IR spectra of cyclosporins in acetonitrile.

ably less intense in $CDCl_3$ than in CCl_4. This suggests that in $CDCl_3$ the H-bond responsible for the 1616 cm^{-1} band is disrupted by the solvent, likely through formation of weak C=O ← D-C type hydrogen bonds with the solvent deuterium.

The same phenomenon seems likely as the cause of analogous changes in the spectra of CsA and CsC. For each molecule the structure in which all N-H's form intramolecular H-bonds, i.e., the dominant structure found in $CDCl_3$ solution, is most highly populated in the completely apolar solvent CCl_4. Figure 1 shows a gradual loss of the lowest frequency amide I band and broadening of the remaining features with increasing solvent polarity. Against this background, differences between the spectra in CCl_4 and $CDCl_3$ solutions may be ascribed to $CDCl_3$ competing with N-H in the C_{11}=O ← H-N_7 and (or) C_6=O ← H-N_8 H-bonds. This effect would account for the minor (6%) conformer inferred from the NMR spectra in $CDCl_3$ (2).

For CsA in acetonitrile, the 1635 cm^{-1} band remains as an indicator that the first two H-bonds of the β-structure (10- and 14-membered rings) remain intact. The lower frequency amide I band at ~1625 cm^{-1} is weakened relative to the analogous absorptions in CCl_4 and $CDCl_3$. This suggests a relatively low, yet still significant, population of the intramolecular H-bonds responsible for this absorption. In contrast, the CsH spectrum loses all features below 1642 cm^{-1} in the spectra of more polar solvents (see bottom trace, Figs. 2–5). Hydrogen bonds giving rise to peaks at 1616 and ~1638 cm^{-1} in CCl_4 are broken, indicating that these bonds in CsH are more exposed to the solvent than are the analogous H-bonds in CsA.

The amide II features between 1500 and 1550 cm^{-1} are distinct and well resolved for all spectra measured in CCl_4. In acetonitrile, bands in this spectral region become particularly broad and overlapped for CsC and CsH. This reflects two related influences: hydrogen bonding of the amide hydrogens to the solvent, and the presence of a distribution of structures as opposed to the single rigid conformer in CCl_4. For CsA the relatively clean amide II features confirm that although there is some solvent perturbation of the intramolecular H-bonds, this effect is much less pronounced than is the case for CsC and CsH.

DMSO has been shown to disrupt protein secondary structures through strong H-bonding to the amide N-H protons (19). Typically, the result is that the amide I region is dominated by a strong band in the 1660–1670 cm^{-1} range that is characteristic of "free" C=O oscillators. All cyclosporin spectra in DMSO solution show a moderately strong feature in this region; however, the dominant feature in each case is a band at 1639 cm^{-1} (Fig. 6). This indicates that the β-sheet structure is retained in DMSO, as previously found for model hexapeptides (18). The elimination of the lower frequency bands observed in the CCl_4 solution spectra at 1627 (CsA), 1624 (CsC), and 1616 cm^{-1} (CsH) implies compete disruption of the C_{11}=O ← H-N_7 and C_6=O ← H-N_8 hydrogen bonds in DMSO. For CsH there is no counterpart to the band observed at 1691 cm^{-1} in CCl_4 and ascribed to the C_7=O enclosed by the γ-turn in that solvent; this provides further evidence supporting both the original assignment and

Can. J. Chem. Downloaded from www.nrcresearchpress.com by 213.200.69.106 on 09/08/12
For personal use only.

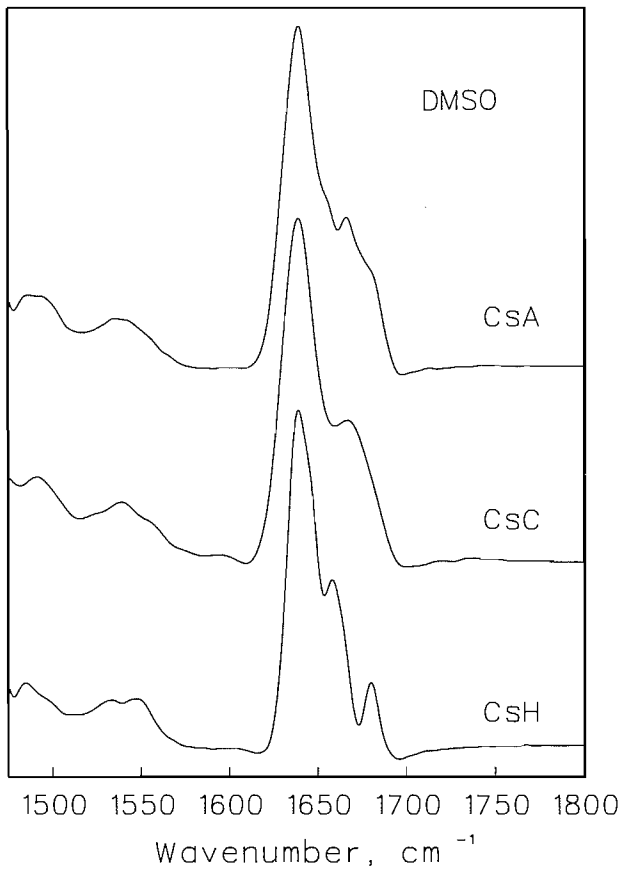

FIG. 5. FT-IR spectra of cyclosporins in DMSO.

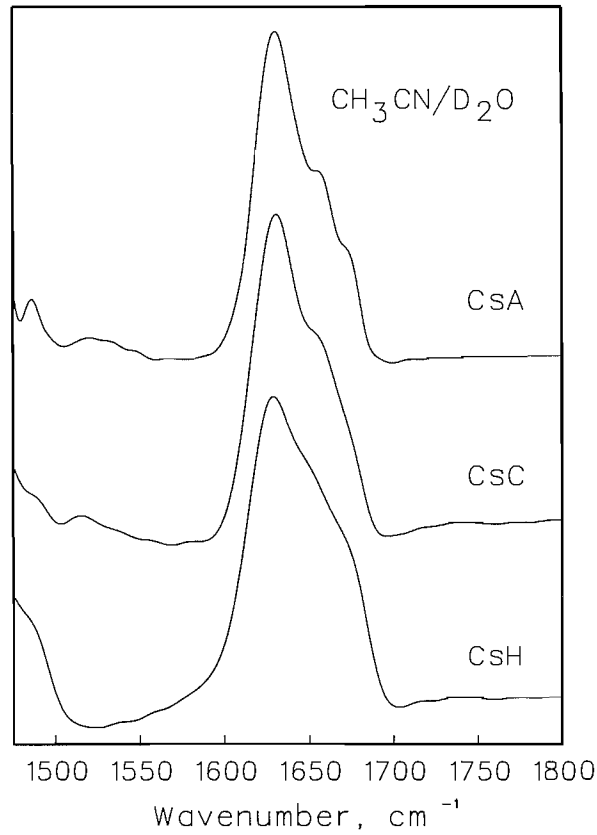

FIG. 6. FT-IR spectra of cyclosporins in 50:50 acetonitrile:D_2O.

the suggestion that DMSO disrupts the γ-turn of all three cyclosporins.

The three spectra in acetonitrile–D_2O show very similar profiles to one another, dominated by the lowest frequency amide I band at 1630 (CsA), 1631 (CsC) and 1628 cm^{-1} (CsH). These bands demonstrate that the β-sheet structure is retained, the relatively low frequencies arising from H/D exchange of the amide NH groups. The broad, featureless bands suggest a situation analogous to that for DMSO; retention of the β-sheet structure, with the remaining loop free to adopt a variety of conformations. Weak residual features in the region of the amide II bands also indicate incomplete H/D exchange.

Discussion

The above analysis gauges solvent effects in terms of conformational *changes* relative to the CsA structure in $CDCl_3$ established independently by NMR spectroscopy. This is the kind of application for which infrared spectroscopy is ideally suited, and we are confident that the major conclusions drawn from this study are soundly based.

The more subtle features of the NMR structure are also consistent with the infrared spectra. It is unreasonable to postulate that only four C=O absorptions contribute to the pair of bands at lowest frequency in the CCl_4 and $CDCl_3$ solution spectra. While we are confident that these bands are associated *predominantly* with the specific H-bonds discussed above, it should be recognized that other H-bonds are present and will contribute intensity in the 1620–1645 cm^{-1} region. For example the OH of MeBmt forms a hydrogen bond to the C=O of the same residue, likely contributing intensity to the band at ca. 1640 cm^{-1} in most of the spectra. A variety of γ-turn type interactions are also populated, e.g., C_5=O ← H-7_7, C_{11}=O ← H-N_2, and C_3= O ← H-N_5, and the relative populations of these are undoubtedly influenced by changing the solvent.

It should be noted that this study serves as a useful calibration for further infrared studies of cyclic polypeptides. Each of the two common types of turn are represented in the structure of cyclosporin: the assignments of the γ-turn at ~1625 cm^{-1} and the β-turn at ~1640 cm^{-1} serve as benchmarks for subsequent studies, as does the assignment of the 1693 cm^{-1} band to the C=O bond enclosed by the strong γ-turn in CsH. General trends observed here can also be useful as a guide in *selecting* appropriate solvents for related studies. The infrared spectral differences introduced by varying the solvent clearly correspond to structural changes induced by different solvents. The trends observed here confirm that solvation in CCl_4 maximizes intramolecular H-bonding. Particularly for cyclic polypeptides, it should prove useful to approach spectral interpretation by comparing to the "simplified" spectrum measured in CCl_4. The inherently narrow bands and the appearance of the spectrum in comparison to those measured in $CDCl_3$ and acetonitrile strongly suggest that a single conformer predominates in CCl_4 solution.

The structure of cyclophilin-bound CsA contains no intramolecular H-bonds (5–7), leaving the question of whether aqueous solvation might induce a conformer similar to the bound structure. Spectra measured in acetonitrile–D_2O all show bands characteristic of strong intramolecular D-bonds.

Can. J. Chem. Downloaded from www.nrcresearchpress.com by 213.200.69.106 on 09/08/12
For personal use only.

It thus seems unlikely that any dominant conformer in this solvent resembles the bound structure, and in turn we conclude that it appears that aqueous solvation does not disrupt intramolecular H-bonds to the extent required to produce a structure resembling that of bound cyclophilin.

Concluding remarks

Infrared spectra of CsA measured in $CDCl_3$ are in complete accord with the NMR structure of CsA determined in the same solvent. The spectral changes observed in other solvents suggest that increasing the solvent polarity does not disrupt the β-turn or the adjacent H-bond. The infrared spectra also indicate that CsA, CsC, and CsD adopt very similar backbone conformations.

As indicated previously by CD measurements (15), the conformation of CsH is markedly different from that of CsA, CsC, and CsD, both in structure and in the susceptibility to solvent disruption. Strong H-bonds that are evident in apolar solvents are broken in acetonitrile, whereas the analogous bonds in the other cyclosporins remain relatively strong.

Solvation in DMSO or acetonitrile–D_2O clearly leaves strong intramolecular H-bonds intact in all the cyclosporins studied. This finding indicates that interactions with physiological solvents alone (e.g., H_2O) are unlikely to produce cyclosporin conformers that mimic the conformation of the cyclophilin-bound molecule.

1. S.S. Schreiber. Cell, **70**, 365 (1992).
2. H.-R. Loosli, H. Kessler, H. Oschkinat, H.-P. Weber, T.J. Petcher, and A. Widmer. Helv. Chim. Acta, **68**, 682 (1985).
3. R.B. Knott, J. Schefer, and B.P. Schoenborn. Acta. Crystallogr. Sect. C: Cryst. Struct. Commun. **C46**, 1528 (1990).
4. H. Kessler, M. Kock, T. Wein, and M. Gehrke. Helv. Chim. Acta, **73**, 1818 (1990).
5. C. Weber, G. Wider, B. von Freyberg, R. Traber, W. Braun, H. Widmer, and K. Wuthrich. Biochemistry, **30**, 6563 (1991).
6. S.W. Fesik, R.T. Gampe, Jr., H.L. Eaton, G. Gemmecker, E.T. Olejniczak, P. Neri, T.F. Holzman, D.A. Egan, R. Edalji, R. Simmer, R. Helfrich, J. Hochlowski, and M. Jackson. Biochemistry, **30**, 6574 (1991).
7. K. Wuthrich, B. von Freyberg, C. Weber, G. Wider, R. Traber, H. Widmer, and W. Braun. Science, **254**, 953 (1991).
8. S.W. Fesik, P. Neri, R. Meadows, E.T. Olejniczak, and G. Gemmecker. J. Am. Chem. Soc. **114**, 3165 (1992).
9. D. Altschuh, O. Vix, B. Rees, and J.-C. Thierry. Science, **256**, 92 (1992).
10. Y. Theriault, T.M. Logan, R. Meadows, L. Yu, E.T. Olejniczak, T.F. Holzman, R.S. Simmer, and S.W. Fesik. Nature, **361**, 88 (1993).
11. G. Pflugl, J. Kallen, T. Schirmer, J.N. Jansonius, M.G.M. Zurini, and M.D. Walkinshaw. Nature, **361**, 91 (1993).
12. J. Lautz, H. Kessler, W.F. van Gunsteren, H.-P. Weber, and R.M. Wenger. Biopolymers, **29**, 1669 (1990).
13. H. Kessler, M. Gehrke, J. Lautz, M. Kock, D. Seebach, and A. Thaler. Biochem. Pharm. **40**, 169 (1990); Additions and Corrections: Biochem. Pharm. **40**, 2185 (1990).
14. S.Y. Ko and C. Dalvit. Int. J. Peptide Protein Res. **40**, 380 (1992).
15. S. Senior, S.C.J. Cole, S.A. Leharne, B.Z. Chowdhry, and A.F. Drake. Biophys. Chem. In press.
16. W. Surewicz, H.H. Mantsch, and D. Chapman. Biochemistry, **32**, 391 (1993).
17. S. Krimm and J. Bandekar. Adv. Protein Chem. **38**, 181 (1986).
18. H.H. Mantsch, A. Perczel, M. Hollosi, and G.D. Fasman. Biopolymers, **33**, 201 (1993).
19. M. Jackson and H.H. Mantsch. Biochim. Biophys. Acta, **1078**, 231 (1991).

Can. J. Chem. Downloaded from www.nrcresearchpress.com by 213.200.69.106 on 09/08/12
For personal use only.

Photochemistry of lignin model compounds on solid supports[1]

L. HURRELL, L.J. JOHNSTON,[2] N. MATHIVANAN, and D. VONG
Steacie Institute for Molecular Sciences, National Research Council of Canada, Ottawa, ON K1A 0R6, Canada

Received April 15, 1993

L. HURRELL, L.J. JOHNSTON, N. MATHIVANAN, and D. VONG. Can. J. Chem. **71**, 1340 (1993).

The photochemistry of several substituted α-(aryloxy)acetoveratrones that are models for chromophores in lignin has been studied using a combination of laser flash photolysis and product studies in solution and on silica, Na-X zeolite, and cellulose. The lifetimes of the triplet ketones vary substantially with the electron-donating ability of the substituents in the α-aryloxy ring, with values ranging from 30 ns for the 4-methoxy derivative to 5.5 μs for the 4-cyano ketone in acetonitrile. The triplet ketones are considerably longer lived on a silica surface than in solution and do not decay with first-order kinetics; however, they are all shorter lived than triplet acetoveratrone under the same conditions, indicating that β-phenyl quenching and (or) β-cleavage dominate their decay. The same triplets show quite different kinetic behavior in Na-X or cellulose and there is no indication in these systems for the importance of either β-phenyl quenching or β-cleavage in determining the rates of triplet decay. Product studies for α-guaiacoxyacetoveratrone indicate that β-cleavage from the singlet excited state is responsible for product formation; in contrast to solution results, the phenacyl–phenoxyl radical pairs react exclusively by geminate recombination to give rearranged ketones resulting from *ortho* and *para* ring coupling of the two radicals. Product formation is very inefficient for this ketone in cellulose, indicating either a low singlet reactivity or efficient geminate recombination of the initial radical pair to regenerate starting material.

L. HURRELL, L.J. JOHNSTON, N. MATHIVANAN et D. VONG. Can. J. Chem. **71**, 1340 (1993).

Utilisant une combinaison de photolyse éclair au laser et une étude des produits en solution, sur de la silice, sur une zéolite Na-X et sur de la cellulose, on a étudié la photochimie de plusieurs α-(aryloxy)acétovératrones qui sont des modèles pour les chromophores de la lignine. Les temps de vie des cétones triplet varient beaucoup avec les capacités des substituants du cycle aryloxy à donner des électrons; les valeurs varient de 30 ns pour le dérivé 4-méthoxy à 5,5 μs pour la 4-cyanocétone dans l'acétonitrile. Les cétones triplet ont des temps de vie beaucoup plus élevés sur une surface de silice qu'en solution et leur dégénérescence n'est pas du premier ordre; toutefois, leurs temps de vie sont tous plus courts que celui du triplet de l'acétovératrone dans les mêmes conditions et ces résultats indiquent que la relaxation β-phényle et (ou) un clivage β dominent leur dégénérescence. Les mêmes triplets présentent un comportement cinétique très différent avec Na-X ou la cellulose et il ne semble pas que, dans ces systèmes, la relaxation β-phényle ou un clivage β joue un rôle important dans la détermination de la vitesse de dégénérescence de l'état triplet. Des études de produit pour l'α-guaïacoxyacétovératrone indiquent que le clivage β à partir de l'état singulet excité est responsable pour la formation des produits; par opposition aux résultats obtenus en solution, les paires de radicaux phénacyle–phénoxyle réagissent exclusivement par recombinaison géminée conduisant à des cétones transposées résultant de couplages en *ortho* et en *para* des deux radicaux. Pour cette cétone dans la cellulose, la formation de produits est très inefficace; ce résultat suggère que la réactivité du singulet est faible ou que la recombinaison géminée de la paire initiale de radicaux pour régénérer le produit de départ est efficace.

[Traduit par la rédaction]

Introduction

There is currently a large amount of interest in studying the basic reaction mechanisms that are responsible for the light-induced yellowing of low-grade paper products made from high-yield mechanical pulps. It has been established that the rapid photoreversion results from photooxidation of lignin in the wood pulp and it is believed that reactions of phenoxyl radicals, probably to give quinones, are key steps in the process (1–3). One of the major routes for the formation of phenoxyl radicals is hydrogen abstraction by excited ketone chromophores from phenolic groups within the lignin framework. However, it is known that pulps with fully alkylated phenol groups still undergo some photoyellowing, indicating that other reactions are also important (4). One of these is β-cleavage of α-aryloxyacetophenone ketone units to yield phenoxyl and phenacyl radicals. Cleavage reactions of ketyl radicals produced by hydrogen abstraction reactions of triplet ketones provide a second potential source of phenoxyl radicals (5, 6). Recently, the photochemistry of α-guaiacoxyacetoveratrone (**1**) and related compounds in solution and in heterogeneous environments has been studied as a model for the β-cleavage processes in lignin (7–12).

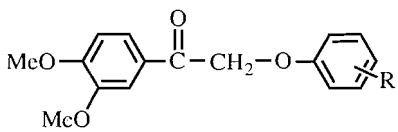

1, R = 2-MeO
2, R = H
3, R = 3-MeO
4, R = 4-MeO
5, R = 2,6-$(MeO)_2$
6, R = 4-CN

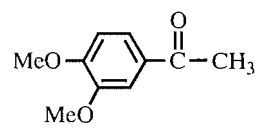

7

The photochemistry of a variety of substituted α-aryloxyacetophenones has been studied in solution. The earlier work suggested that the triplet excited ketone decayed by a competition between β-phenyl quenching and β-cleavage (13, 14). In simple aryloxyacetophenones the triplet lifetimes were short (<1 ns) and the products resulted from (*a*) scavenging of the phenacyl and phenoxyl radicals by hydrogen donors, (*b*) *ortho* and *para* coupling of the phenacyl and phenoxyl

[1]Issued as NRCC 35276.
[2]Author to whom correspondence may be addressed.

Can. J. Chem. Downloaded from www.nrcresearchpress.com by 213.200.69.106 on 09/08/12
For personal use only.

radicals to give α-arylacetophenones isomeric with starting materials, and (*c*) dimerization of phenacyl radicals (14). Similar chemistry has been observed for the lignin model ketone **1**, except that in this case substantial amounts of oligomeric materials were formed (reaction [1]) (7). Recently, detailed CIDNP studies have demonstrated that a variety of phenacyl- and aryloxy-substituted α-phenoxyacetophenones undergo β-cleavage primarily from the excited singlet state, in contrast to the usual triplet reactivity of most aromatic ketones (15, 16). Irradiation of ketone **1** in solution in the presence of triplet quenchers has also provided evidence that β-cleavage occurs predominantly, if not exclusively, from the singlet ketone in aprotic solvents; in alcohols both singlet and triplet reactions lead to products (11). The solvent effects on both the triplet lifetime and quantum yield for disappearance of starting ketone have been rationalized on the basis of a slower rate of β-phenyl quenching for the triplet in hydrogen-bonding solvents, thus allowing β-cleavage to compete as a triplet deactivation mechanism.

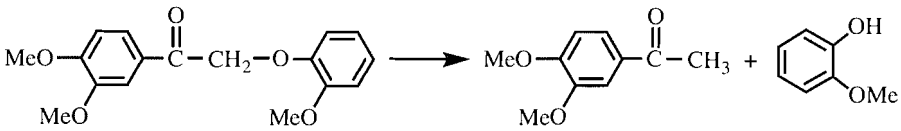

1

[1]

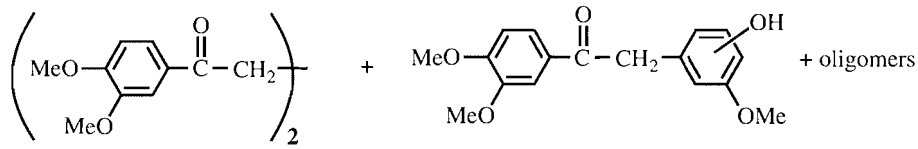

8a, 2-OH
8b, 4-OH

Despite the many studies of model compounds in solution, there have been relatively few detailed examinations of product studies or time-resolved experiments for these materials in heterogeneous environments that mimic the behavior of pulp itself. A recent diffuse reflectance laser flash photolysis study of bleached thermomechanical pulp samples has detected a long-lived transient assigned to an aryl ketone triplet distributed over a variety of sites in the lignin macromolecule (17). It is obvious that a detailed understanding of the effects of an organized environment on the behavior of both the excited states and the radicals generated from them is essential for understanding the chemistry involved in the photoreversion process. Accordingly, we have examined the behavior of several model ketones (**1**–**7**) on three solid supports (silica gel, Na-X zeolite, and cellulose) using a combination of diffuse reflectance laser flash photolysis and product studies. The diffuse reflectance flash photolysis techniques developed by Wilkinson and coworkers over the last decade have considerable potential for studying transients such as triplets, radicals, and radical ions in opaque solids (18–26). The present studies provide insight into the manner in which the initial photochemistry and the behavior of photogenerated radical pairs are modified for lignin model ketones in a constrained environment. They also provide useful background information to aid in the interpretation of transient results on lignin and pulp samples.

Results

Laser flash photolysis in solution

For comparison with the diffuse reflectance work, absorption spectra and lifetimes for triplets **1**–**6** were also measured in acetonitrile and ethanol, using either 266 or 308 nm excitation. The low ketone concentrations (~5 × 10^{-5} M) used in these experiments necessitated the use of flow samples in order to replenish the solution for every laser shot and prevent the rapid buildup of products that generated longer lived transients. The triplet lifetime for **1** was approximately 250 ns in acetonitrile, which is comparable to the previously reported value of 230 ns in that solvent (11). The triplet lifetime was substantially longer in ethanol (~1 μs), again in agreement with the literature results (11).

Either 308 or 266 nm excitation of ketones **2**–**6** in acetonitrile generated triplet–triplet absorptions with λ_{max} at 390–400 nm, as shown for **5** in Fig. 1. The measured triplet lifetimes in acetonitrile and ethanol are listed in Table 1. The 3-methoxy derivative (**3**) has a substantially longer lifetime in acetonitrile (0.75 μs) than does triplet **1**. The unsubstituted and 4-cyano ketones (**2**, **6**) have even longer lifetimes of 1.8 and 5.5 μs, respectively; in the latter case traces of residual oxygen that are difficult to remove from flow samples may account for the observed decay kinetics. In contrast, both the 4-methoxy and 2,6-dimethoxy derivatives (**4**, **5**) have quite short triplet lifetimes: 30 and 16 ns, respectively. The decay of triplet **5** is shown as an insert in Fig. 1. The triplet lifetimes for **1**, **2**, and **3** are all significantly longer in ethanol than in acetonitrile; in contrast, the short-lived triplets (**4** and **5**), as well as the long-lived 4-cyano derivative, show much less effect of changing to a hydrogen-bonding solvent.

Diffuse reflectance laser flash photolysis

Laser excitation of ketone **1** on either silica or Na-X zeolite (2% by weight, ~6 × 10^{-5} mol g^{-1} loading) gave a strongly absorbing transient with λ_{max} at 390 nm. Similar results were observed upon excitation of **1** on microcrystalline cellulose, although in this case the observed transient was broader and the signals were weaker. In each case the ob-

Can. J. Chem. Downloaded from www.nrcresearchpress.com by 213.200.69.106 on 09/08/12
For personal use only.

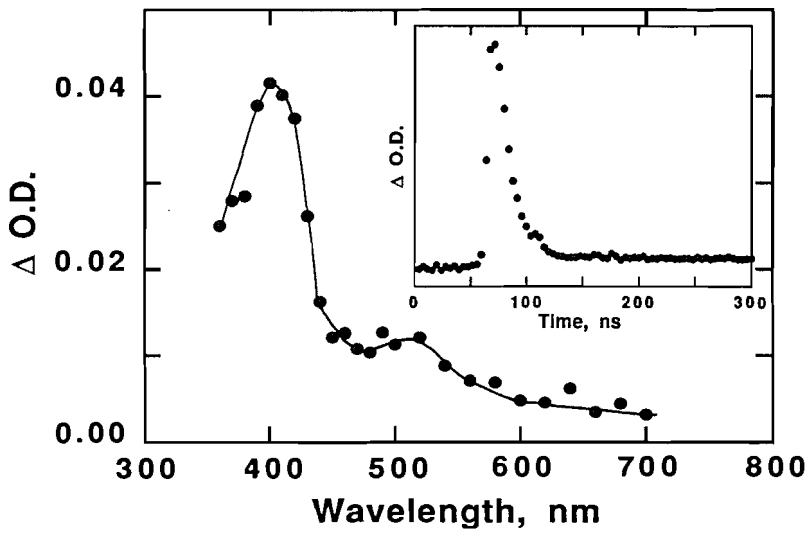

FIG. 1. Transient absorption spectrum measured 10 ns after 308 nm laser excitation of ketone **5** in nitrogen-purged acetonitrile. Insert: Decay trace at 400 nm for the same sample.

TABLE 1. Lifetimes and half-lives for decay of triplet α-(aryloxy)acetoveratrones in solution and on silica

Ketone	τ, μs (CH_3CN)	τ, μs (EtOH)	Half-life, μs (silica)
1	0.25	1	6
2	1.8	7	70
3	0.75	2.1	30
4	0.03	0.02	4
5	0.016	0.035	4.5
6	5.5	~7	>100

served transient can be assigned to the triplet–triplet absorption spectrum of the ketone, based on the known solution spectrum for this species (11) and on the observed quenching by triplet quenchers such as oxygen and dienes on silica. Representative spectra for each support are shown in Fig. 2. The broadness of the spectrum on cellulose may be related to aggregation effects, as observed previously for methoxyacetophenones in various heterogeneous environments (19, 27). Transient absorption spectra for acetoveratrone (**7**) on the three solid supports were also recorded and showed virtually identical results to those for ketone **1**.

The decay kinetics for ketones **1** and **7** were examined under matched conditions for each of the supports. The triplet decay for a deaerated sample of **1** on silica is shown in Fig. 3. The decay cannot be fitted with single exponential kinetics; however, a half-life of 6 μs (Table 1) can be estimated from the data. In contrast to these results, triplet acetoveratrone on silica was much longer lived (Fig. 3), with ~80% of the initial signal remaining 100 μs after laser excitation and with a half-life in excess of 400 μs. The marked difference in decay kinetics for triplets **1** and **7** suggests that an additional decay pathway (either β-cleavage or β-phenyl quenching) contributes to the decay of triplet **1** on silica.

As noted above, triplet **1** on silica was efficiently quenched by oxygen and dienes (e.g., 2,4-hexadiene or *trans,trans*-2,4-hexadienol). In the presence of relatively minor amounts of either oxygen or diene the kinetics for decay of triplet **1** gave reasonably good fits to a single exponential. For example, a sample of **1** plus 6×10^{-5} mol g^{-1} hexadienol decayed with a rate constant of 2.8×10^6 s^{-1}. Addition of higher concentrations of dienol further shortened the triplet lifetime, although luminescence problems made it difficult to obtain reliable rate constants under these conditions. The more rapid triplet decay in the presence of dienol indicates a dynamic quenching mechanism, involving some mobility of either the triplet ketone or dienol. A rough estimate based on a single dienol concentration gives a value of $\sim 2 \times 10^{15}$ dm^2 mol^{-1} s^{-1} for the rate constant for diene quenching. This value has been obtained by using a surface area of 480 m^2 g^{-1} for the silica and assuming a flat two-dimensional surface. The estimated rate constant is in reasonable agreement with measured numbers for energy transfer quenching of triplet benzophenone on silica (25). The initial signal intensity was also decreased in the presence of higher concentrations of dienol, consistent with a component due to a static quenching mechanism under these conditions.

The triplet decay kinetics for **1** and **7** in Na-X were also nonexponential and occurred over a wide range of timescales. Individual decay traces for each ketone on two different timescales that differ by a factor of 10 are shown in Fig. 4. These do not give adequate fits to either second-order kinetics or to a combination of two monoexponential decays, and probably reflect a distribution of decay kinetics arising from multiple sites. Comparison of the data in Fig. 4 for the two ketones shows that triplet **1** decays more rapidly than triplet **7** in the zeolite cavity. However, it is also obvious that triplet **1** is very substantially longer lived in the zeolite than in either solution or on a silica surface. Again

Can. J. Chem. Downloaded from www.nrcresearchpress.com by 213.200.69.106 on 09/08/12
For personal use only.

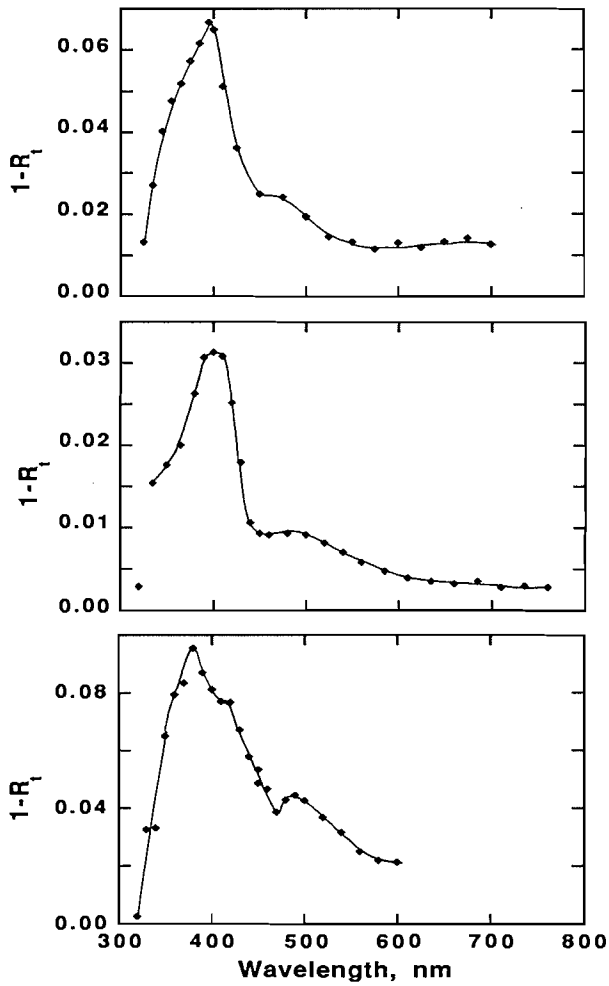

FIG. 2. Triplet diffuse reflectance spectra measured after 308 nm laser excitation of ketone **1** on silica (top), Na-X zeolite (middle), and cellulose (bottom).

this behavior is typical of that observed for other triplets in zeolites (19, 23, 25).

The decay kinetics for triplets **1** and **7** in cellulose are also complex. However, in this case there is some evidence for two distinct types of kinetics. For example, there is a component (~30–50% of initial signal) that decays within 1–2 μs, while most of the residual long-lived signal remains after 100 μs (Fig. 5). Spectra recorded at different time delays after laser excitation are very similar, indicating that the fast and slow components are both due to triplets. There is little difference between the results for **1** and **7**, except for the observation of a slightly larger amount of the fast component for the latter. The similar decay kinetics for both **1** and **7** may indicate similar decay processes for both. It is also noteworthy that the signal intensities for cellulose samples are weaker than for either silica or zeolite even after correction for differences in the amount of light absorbed. This may be the result of a fraction of rapidly decaying triplets that are not observable on our shortest timescale for the cellulose samples.

Neither the intensity of the triplet-triplet absorption nor the decay kinetics for triplet **1** on cellulose was affected by the presence of oxygen. These results are in good agreement with earlier studies for triplet benzophenone on cellulose (28, 29)

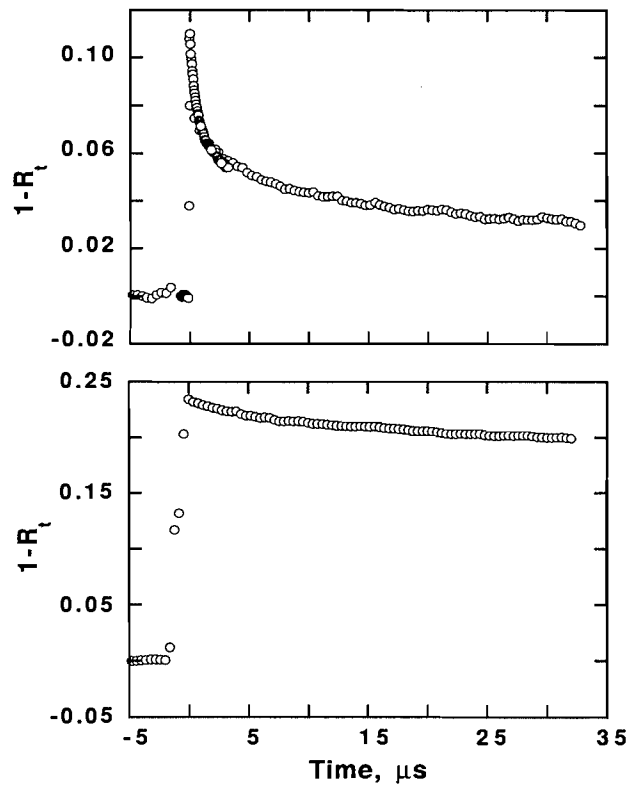

FIG. 3. Decay of triplets **1** (top) and **7** (bottom) at 400 nm on silica. The decay trace for **1** is a combination of two kinetic traces recorded on two different timescales, in order to better capture the early part of the decay.

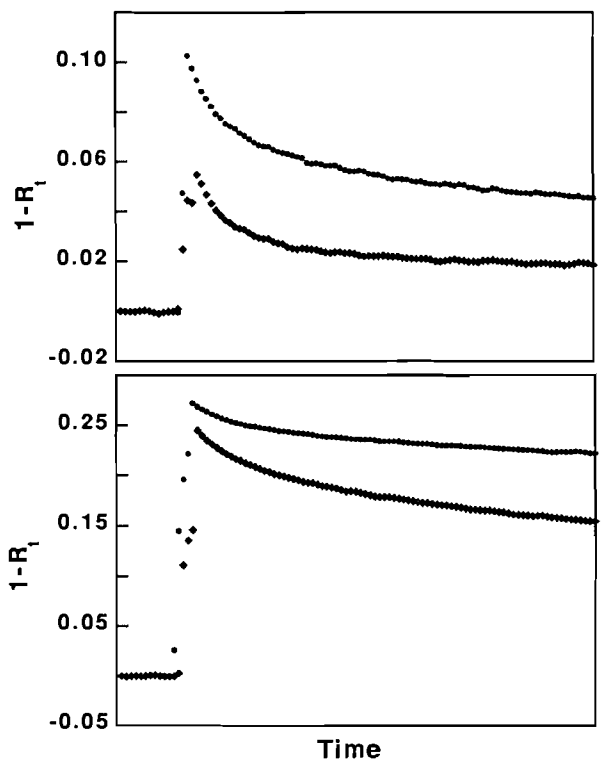

FIG. 4. Decay of triplets **1** (top) and **7** (bottom) at 400 nm on Na-X zeolite. The total time windows correspond to 8 (●) and 80 (◆) μs.

Can. J. Chem. Downloaded from www.nrcresearchpress.com by 213.200.69.106 on 09/08/12
For personal use only.

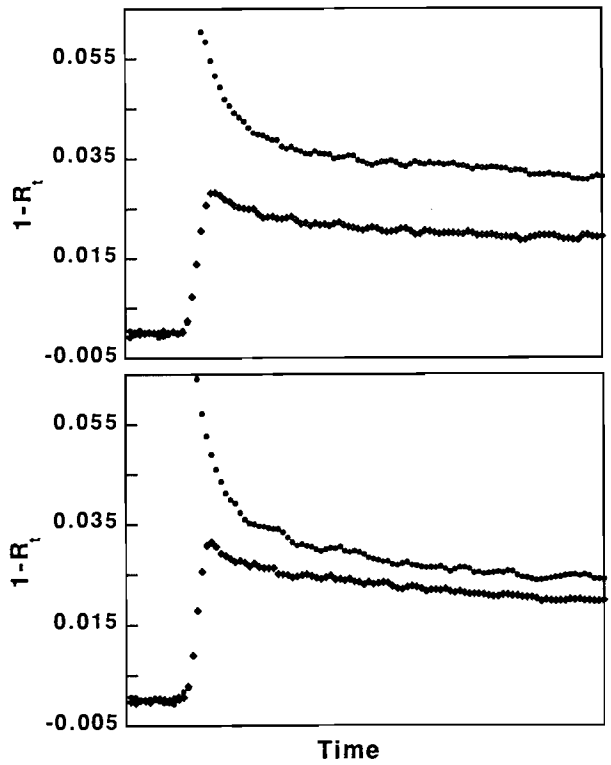

FIG. 5. Decay of triplets **1** (top) and **7** (bottom) at 400 nm on cellulose. The total time windows correspond to 8 (●) and 80 (◆) μs.

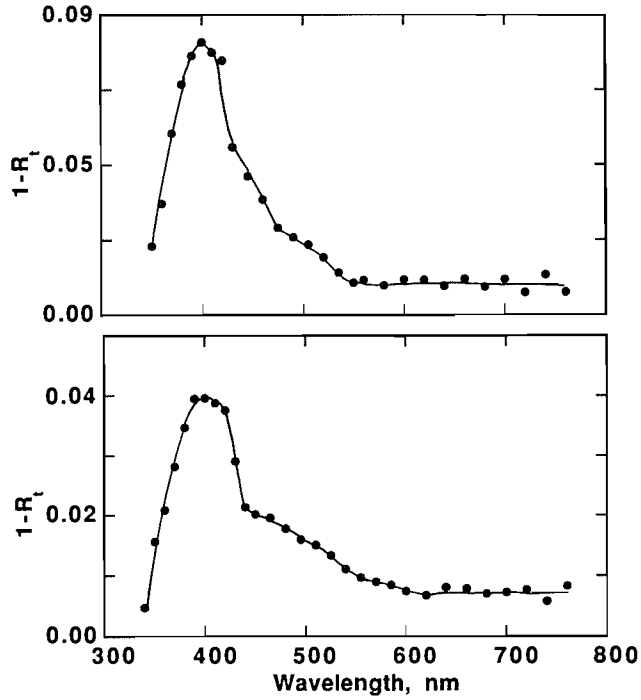

FIG. 6. Triplet diffuse reflectance spectra measured after 308 nm laser excitation of ketone **3** on silica (top) and cellulose (bottom).

and indicate that oxygen penetration throughout the cellulose framework is very slow.

There is no evidence in any of our results for ketone **1** on solids for the intermediacy of the phenoxyl radicals that are known to be formed by β-cleavage. Since these species have relatively low extinction coefficients (30) and are only formed with moderate quantum yields (7, 11), this is perhaps not too surprising. However, we had hoped that radicals would be more readily detectable for some of the other ketones (e.g., **3** and **4**) since these would generate phenoxyl radicals with higher extinction coefficients. For example, the relative extinction coefficients for the 2-methoxy, 3-methoxy, unsubstituted, and 4-methoxyphenoxyl radicals of 0.25, 0.8, 1.0, and 2.3 indicate that compound **1** would give the weakest phenoxyl signals, assuming equal quantum yields for radical formation (30). Accordingly, we investigated ketones **2**–**6** on both silica and cellulose.

The transient absorption spectra for ketones **2**–**6** at 2% loading on silica all have λ_{max} at 390–400 nm in good agreement with the results for **1** and **7**. None of these ketones gave decays that could be fitted with single exponential kinetics. However, the half-lives given in Table 1 indicate that changes in substitution do result in substantial differences in the rates of triplet decay. Furthermore, the overall trends on silica are qualitatively similar to those observed in acetonitrile solution. Thus, the 4-methoxy and 2,6-dimethoxy ketones decay the most rapidly both in solution and on silica, while the 4-cyano ketone is the longest lived. On cellulose each of these ketones gives results that are similar to those obtained for **1** and **7** on this support, both in terms of spectrum and decay kinetics. However, we were unable to provide any definitive spectroscopic evidence for phenoxyl radical formation following excitation of any of these ketones on solid supports. Representative spectra for **3** on silica and cellulose are shown in Fig. 6.

Product studies

Irradiation of **1** on silica for short periods of time followed by extraction of the sample as outlined in the experimental section gives a mixture of two products that are isomeric with starting material, based on GC-MS analysis. The relative amounts of the two compounds vary considerably from one sample to the next, although there is usually twice as much of the longer retention time material. The mass balance is typically ≥85% at low conversions (≤20%) but prolonged irradiation leads to the formation of a variety of additional products that appear to result from further photochemistry of the two primary products. The mass balance also decreases for longer irradiation times, probably as a result of oligomerization reactions. The two primary photoproducts are assigned to the α-arylacetoveratrones (**8***a*,*b*) formed as a result of *ortho* and *para* coupling of the phenacyl and phenoxyl radicals. These two products have been reported previously following irradiation of **1** in solution. The two isomers were identified on the basis of comparison of retention times and spectroscopic data with those of an authentic sample and with literature data, as outlined in the experimental section. The silica irradiations always led to a larger amount of the *ortho* isomer, although the relative yields varied from one sample to the next. Minor amounts (5–10%) of the hydrogen abstraction products (acetoveratrone and guaiacol) were recovered in some early experiments in which the solvent was not rigorously removed by vacuum drying before irradiation. These are assumed to arise from residual solvent rather than by hydrogen abstraction from the parent ketone, since they disappeared for well-dried samples.

There was no evidence for the production of the phenacyl

Can. J. Chem. Downloaded from www.nrcresearchpress.com by 213.200.69.106 on 09/08/12
For personal use only.

radical dimer, suggesting that **8** is formed via in-cage radical coupling. Such a reaction could in principle occur from either the singlet or triplet state of the ketone since the slow mobility of the radicals on the surface would allow intersystem crossing for a triplet radical pair to compete with diffusional cage escape of the radicals. To examine whether triple **1** was involved in product formation on silica, the photochemistry of **1** on silica was examined in the presence of 2×10^{-4} mol g^{-1} *trans,trans*-2,4-hexadienol; this concentration of dienol is sufficient to react with >90% of the triplet ketones. Two samples of **1** (6.6×10^{-5} mol g^{-1}) on silica that were identical except for the presence of dienol were irradiated using 350 nm Rayonet lamps to eliminate absorption of incident light by the dienol. Product extraction and analysis indicated that the yields of **8** and of recovered **1** were identical within experimental error for the samples with and without dienol. Further, no additional products were observed in the diene sample and the amount of recovered ketone was the same for the two samples. It should be pointed out that complications due to trapping of phenoxyl or phenacyl radicals by diene should lead to increased yields of either hydrogen abstraction or diene addition products and these were not detected; further, a lower mass balance would have been expected in the diene experiment if increased yields of nonextractable materials were formed.

Irradiation of **1** in either Na-X or cellulose for prolonged periods of time resulted in pronounced yellowing of the samples. However, extraction of the samples showed only recovered starting material (80–90% recovery) with undetectable amounts of the usual solution products. The loss of starting material is presumably due to the formation of oligomeric products. Inspection of ground state UV spectra for the samples before and after irradiation indicated that the low product yields were *not* primarily due to screening of the light by photoproducts. These results are in agreement with previous experiments in which inefficient product formation (relative to solution) was observed when **1** was irradiated on lignin-free paper fibers (7).

Discussion

The combination of product studies and triplet lifetimes for ketone **1** in solution indicates that the triplet decay is dominated by β-phenyl quenching in aprotic solvents such as acetonitrile and by a combination of β-phenyl quenching and β-cleavage in protic solvents such as alcohols (11). The slower triplet decays in ethanol have been rationalized on the basis of a slower rate of β-phenyl quenching due to hydrogen bonding. Our solution results for the substituted ketones indicate that there are substantial substituent effects on the triplet lifetimes for ketones **1–6** in acetonitrile. Both *meta* and *para* methoxy substituents decrease the triplet lifetime relative to the parent (**2**) while a 4-cyano substituent lengthens it. The β-phenyl quenching mechanism in β-arylpropiophenones and α-phenoxyacetophenones is well established to occur via charge transfer quenching involving the carbonyl n,π^* state for ketones with either n,π^* or π,π^* lowest excited triplet states (13, 31–34). Thus, our results are consistent with a faster rate of β-phenyl quenching for those ketones containing β-aryl groups with stronger electron-donating properties (i.e, methoxy). Such effects have been observed previously upon comparison of triplet lifetimes for 4-methoxy-β-phenylpropiophenones with and without methyl substituents in the β-aryl ring (34).

The substituent effects on the solution lifetimes for ketones **1–6** are consistent with β-phenyl quenching as the controlling factor, particularly as this has been demonstrated to be the case for **1**. The fact that the triplet lifetimes for most of the ketones are substantially longer in ethanol than in acetonitrile also points towards similar mechanisms for triplet decay in each case. However, it is also possible that the substituents are altering the rate of β-cleavage. Of particular interest in this regard is recent work in which the rate constants for β-cleavage for α-(aryloxy)acetophenones were shown to be substantially higher when the α-aryloxy ring was substituted with electron-releasing groups such as 4-methoxy (14). These results suggest that electron-donating substituents may be expected to increase the rates for both β-cleavage and β-phenyl quenching. However, given the recent conclusions regarding the importance of singlet processes for these ketones (15, 16), detailed product studies with and without triplet quenchers and under conditions where all radicals are scavenged would be required to determine whether or not β-cleavage is a significant triplet decay pathway in any particular case. Despite this, the long lifetime for the 4-cyano ketone (**6**) suggests that both of the possible deactivation pathways are slow for electron-withdrawing substituents.

Product studies indicate that the chemistry of **1** on silica occurs via β-cleavage, as in solution. In the absence of hydrogen donors, the radical pairs recombine to give the rearranged ketone (**8**) and presumably also to regenerate starting material. The absence of the phenacyl radical dimer that is formed in solution indicates that geminate recombination dominates and suggests that singlet chemistry may be largely responsible for product formation. This hypothesis is confirmed by product studies in the presence of triplet quenchers, in which no change in the relative product yields was observed in the presence of sufficient diene to completely quench all triplet excited states. The high cage effect for recombination of phenacyl-phenoxyl radicals demonstrates that these radicals are not very mobile on the silica surface. These results are in contrast to those obtained for other radical pairs on silica surfaces. For example, on silica, benzyl radicals generated from a triplet precursor recombine with product ratios that are very close to the statistical ratio obtained in solution, leading to cage effects of ~0 (35). Similar radicals generated as a singlet pair show a cage effect of 40% (36). The predominance of ketone **8***a*, which corresponds to *ortho* coupling of the two radicals, is also indicative of restricted mobility of the radicals. For example, ring coupling of phenylacetyl–benzyl radical pairs has been shown to yield both *ortho* and *para* products with the *ortho* isomer being favored when the mobility of the radical pairs is more severely restricted (37).

The triplet states of ketones **1–6** are all substantially longer lived on a silica surface than in solution. The nonexponential nature of the decay kinetics suggests that there may be a distribution of triplet decays on the surface. It is also of interest to note that triplets **1–6** all decay more rapidly than triplet acetoveratrone. This sugests that additional decay pathways, presumably β-phenyl quenching and (or) β-cleavage, are responsible for the enhanced triplet decay. The results for **1** in the presence of diene quencher indicate that product formation on silica arises primarily, if not ex-

Can. J. Chem. Downloaded from www.nrcresearchpress.com by 213.200.69.106 on 09/08/12
For personal use only.

Can. J. Chem. Downloaded from www.nrcresearchpress.com by 213.200.69.106 on 09/08/12
For personal use only.

clusively, from singlet excited state chemistry, demonstrating that, at least for this ketone, β-phenyl quenching is the dominant triplet decay pathway. It is also interesting to note that the relative decay rates for the series of ketones that we have examined show exactly the same trends on silica as in solution. Although surface adsorption obviously imposes substantial restrictions to the mobility of the triplet ketone and leads to pronounced decreases in the kinetics for triplet decay, the triplet lifetimes still reflect the substituent effects that are observed in solution. Similar results have been observed previously for triplet valerophenone and butyrophenone as compared to acetophenone included in Silicalite (19).

The results for ketone **1** included in Na-X are markedly different from those in solution or on a silica surface. Firstly, product formation is very inefficient in this case and only starting material is isolated even after lengthy irradiations. Secondly, the triplet ketone decays much more slowly than on the silica surface. Interestingly, there is still some difference between the decay kinetics for acetoveratrone and **1**, although it is certainly less pronounced than on the silica surface. This could be taken as evidence that either β-phenyl quenching or β-cleavage contributes to the triplet decay for **1**. However, it is likely that complexation with cations (i.e., Na^+) present in the zeolite cavities is responsible for the long and nonexponential triplet decays for both ketones in Na-X (38). Thus, the different sizes and polarities of **1** and **7** may also lead to substantial differences in either the strength of interaction between the ketone and the Na cations or in the type and (or) number of accessible complexation sites; such effects will certainly contribute to the observed differences in the triplet decays of **1** and **7**.

Product studies for ketone **1** in cellulose are similar to those in Na-X, in that product formation is a relatively inefficient process. In terms of the behavior of the triplet ketones on this support, the results are intermediate between those of silica and Na-X. The triplet decays show both a fast and a slow component and the results for acetoveratrone are similar to those for **1** and the other α-(aryloxy)acetoveratrones. Therefore, there is no reason to postulate that the fast component in the decay of triplet **1** results from ketones for which either β-phenyl quenching or β-cleavage is an important decay pathway. One possible explanation for the two different types of kinetics is that some ketones are close together and decay by self-quenching, which is known to be an efficient triplet deactivation mechanism in solution and on silica (25). The lower signal intensities for cellulose compared to those for either silica or Na-X zeolite, even after accounting for differences in absorption at the excitation laser wavelength, may indicate that a fraction of the triplets generated on this support decay on a timescale that is too short for our detection window. The 1–2 μs component that is observed may represent triplets that undergo self-quenching in the time window that we can monitor, while the longer lived fraction is due to isolated ketones, probably in a distribution of different sites. An alternate explanation is that the ketones responsible for the fast component are in an environment where they can decay by interaction with the cellulose framework; one possibility could be hydrogen abstraction from the cellulose to generate a ketyl radical, although such processes are usually less efficient for π,π^* ketones. In this regard it should be noted that similar ketyl radicals have recently been shown to have lifetimes shorter than 0.5 μs in solution and, thus, would not be easily observable in our experiments (6). This explanation seems less likely, given that we have been unable to extract any of the expected products of ketyl radical fragmentation from irradiated samples on cellulose.

It is clear that product formation from ketone **1** on cellulose is an inefficient process. Further, there is no evidence that β-cleavage of the triplet occurs to a significant extent. It is likely that some singlet β-cleavage still occurs since this has been demonstrated to be an important pathway in solution (11, 15, 16) and on a silica surface. However, the low product yields suggest either that this is a minor process or that geminate recombination of the initial radical pair to regenerate starting material predominates over *ortho* or *para* ring addition to give rearranged ketones **8**. If the latter is true, it indicates that the cellulose framework imposes very substantial restrictions on both the translational and rotational mobility of the phenacyl–phenoxyl radical pairs.

The present results demonstrate that the behavior of the excited states of α-(aryloxy)acetoveratrones and of the radical pairs generated from them is quite sensitive to environmental factors. It is clear that one cannot simply extrapolate directly from solution results in order to understand the behavior in any particular heterogeneous system. However, studies of model compounds in structured environments such as cellulose that mimic many of the features of wood pulps can provide valuable insight into the primary steps involved in the photoreversion of lignin-rich paper products.

Experimental

Instrumentation

Melting points were measured on a Mel-Temp II melting point apparatus and are uncorrected. ^1H and ^{13}C NMR spectra were recorded on a Bruker AM400 spectrometer with deuterochloroform as solvent and residual chloroform (7.24 ppm) as the reference. Gas chromatograph – mass spectra (GC/MS) were recorded on a Hewlett-Packard model 5790A instrument equipped with a 12 m × 0.2 mm cross-linked methyl silicone (HP-1) column. Gas chromatographs were obtained with a Hewlett-Packard 5890 system equipped with the same column. UV-visible spectra were recorded on a Varian Cary 3 spectrometer equipped with a diffuse reflectance accessory for measuring solid samples.

Materials

Davisil 634 silica gel (480 $m^2\ g^{-1}$, 60 Å pore diameter, 100–200 mesh), acetoveratrone, phenols, and *trans,trans*-hexa-2,4-dienol were obtained from Aldrich. Microcrystalline cellulose DS-0 and 13X zeolite (NaX) were obtained from Fluka and BDH, respectively. Ketones **1–6** were synthesized by reaction of α-bromoacetoveratrone with the corresponding phenol in acetone in the presence of potassium carbonate according to the literature procedure reported for α-guaiacoxyacetoveratrone (39). The ketones were recrystallized from ethanol before use. The physical and spectroscopic data for ketone **1** are in agreement with the reported values in the literature (39). Melting points and spectral data for ketones **2–6** are given below.

α-(Phenoxy)acetoveratrone (2): mp 95–96°C; ^1H NMR: 3.90 (s, 6H, 3- and 4-OCH_3), 5.18 (s, 2H,CH_2), 6.86 (d, J = 8.4 Hz, 1H, 5-H), 6.89–6.95 (m, 3H, 2′-, 4′-, and 6′-H), 7.21–7.27 (m, 2H, 3′- and 5′-H), 7.52 (d, J = 2 Hz, 1H, 2-H), 7.79 (dd, J = 8.4 and 2 Hz, 1H, 6-H); ^{13}C NMR: 55.87, 55.97, 70.5, 110.0, 110.2, 114.7, 121.4, 122.7, 127.6, 129.4, 149.1, 153.8, 157.9, 193.0; MS, *m/e*: 272 (M^+), 165 (M^+ − 107). Anal. calcd. for $C_{16}H_{16}O_4$: C 70.55%, H 5.93%; found: C 70.80%, H 5.97%.

α-(3-Anisoxy)acetoveratrone (3): mp 90°C; ^1H NMR: 3.71 (s, 3H), 3.88 (s, 3H), 3.90 (s, 3H), 5.16 (s, 2H), 6.46–6.49 (m, 3H), 6.85 (d, J = 8.4 Hz, 1H), 7.10–7.15 (m, 1H), 7.50 (d, J = 2 Hz,

Can. J. Chem. Downloaded from www.nrcresearchpress.com by 213.200.69.106 on 09/08/12
For personal use only.

1H), 7.58 (dd, J = 8.4 and 2 Hz, 1H); ^{13}C NMR: 55.12, 55.86, 55.95, 70.47, 101.4, 106.5, 107.0, 110.0, 110.2, 122.6, 127.6, 129.8, 149.1, 153.8, 159.2, 160.7, 192.8; MS, *m/e*: 302 (M^+), 165 ($M^+ - 137$). Anal. calcd. for $C_{17}H_{18}O_5$: C 67.52%, H 6.01%; found: C 68.63%, H 6.14%.

α-(4-Anisoxy)acetoveratrone (4): mp 104°C; ^{1}H NMR: 3.72 (s, 3H), 3.92 (s, 3H), 3.93 (s, 3H), 5.15 (s, 2H), 6.79 (d, J = 8 Hz, 2H), 6.84–6.88 (m, 3H), 7.53 (d, J = 2 Hz, 1H), 7.62 (dd, J = 8.4 and 2 Hz, 1H); ^{13}C NMR: 55.63, 55.99, 56.07, 71.62, 110.1, 110.3, 114.7, 115.9, 122.8, 127.8, 149.2, 152.3, 153.8, 154.4, 193.5; MS, *m/e*: 302 (M^+), 165 ($M^+ - 137$). Anal. calcd. for $C_{17}H_{18}O_5$: C 67.52%, H 6.01; found: C 68.45%, H 6.03%.

α-(2,6-Dimethoxyphenoxy)acetoveratrone (5): mp 103–104°C (lit. (40) mp 100–103°C); ^{1}H NMR: 3.77 (s, 6H), 3.90 (s, 6H), 5.12 (s, 2H), 6.54 (d, J = 8.4 Hz), 6.86 (d, J = 8.4 Hz, 1H), 6.97 (t, J = 8.4 Hz, 1H), 7.60 (d, J = 2 Hz, 1H), 7.68 (dd, J = 8.4 and 2 Hz, 1H); ^{13}C NMR: 55.98, 75.16, 105.2, 109.9, 110.6, 122.9, 123.9, 128.3, 136.5, 148.9, 153.3, 193.6; MS, *m/e*: 332 (M^+), 165 ($M^+ - 167$).

α-(4-Cyanophenoxy)acetoveratrone (6): mp 131–132°C; ^{1}H NMR: 3.94 (s, 3H), 3.97 (s, 3H), 5.33 (s, 2H, CH_2), 6.90–6.99 (m, 3H), 7.53–7.61 (m, 4H); ^{13}C NMR: 55.79, 55.94, 69.91, 104.4, 109.9, 110.1, 115.3, 118.8, 122.4, 126.9, 133.8, 149.2, 154.0, 161.2, 191.4; MS, *m/e*: 297 (M^+), 165 ($M^+ - 137$). Anal. calcd. for $C_{17}H_{15}NO_4$: C 68.69%, H 5.05%, N 4.71%; found: C 68.26%, H 5.06%, N 4.86%.

Sample preparation

Silica and zeolite were activated by heating at 100°C and 200°C, respectively, for about 12 h and the activated solids were stored in a desiccator before use. Cellulose was used as received. The solid support and known amounts of the ketone (plus coadsorbate, if required) were stirred in 1:3 dichloromethane–hexane (3 mL g^{-1}) for 3 h. The solvent was then removed on a vacuum pump and the sample was dried at 60°C under vacuum for 2 h.

Laser flash photolysis

The experimental setup for diffuse reflectance and transmission laser flash photolysis has been described elsewehere (25). Either a Lumonics HY-750 Nd:YAG laser (fourth harmonic; 266 nm; 10-ns pulses; <30 mJ/pulse) or a Lumonics EX-530 excimer laser (XeCl gas mixture; 308 nm; 8-ns pulses; <45 mJ/pulse) was used for sample excitation. Solutions of ketones ($\sim 6 \times 10^{-5}$ M) in acetonitrile were deaerated by purging with nitrogen. All the solution experiments were done using a 7 mm × 7 mm quartz flow cell attached to a sample reservoir to minimize problems related to sample depletion and buildup of products. For the diffuse reflectance experiments, the solid samples were contained in 3 mm × 7 mm quartz cells and were purged with nitrogen for 30 min. The solid sample was either moved or shaken during the experiments to provide a fresh sample surface for each laser shot. The diffuse reflectance data are reported as $1 - R_t$, where $R_t = J_t/J_0$; J_t is the reflected light from the sample at time t after laser excitation and J_0 is the initial reflected light from the sample.

Product studies

A sample containing ketone **1** on silica (5% loading by weight) was prepared as described earlier. The sample was placed in a Pyrex tube, degassed by purging with nitrogen, and irradiated with 300 nm lamps in a Rayonet reactor. The irradiation cells were mounted on a vertically rotating bar in order to provide uniform exposure of the sample. After 16 h photolysis, the products were extracted by continuous extraction of the sample with 1:2 chloroform-methanol at 60°C. GC and GC–MS analysis of the extract revealed the presence of two materials that were isomeric with the starting ketone. The retention time and mass spectrum for the minor component of the mixture are in agreement with those for an authentic sample of α-(4-hydroxy-3-methoxyphenoxy)acetoveratrone. Additional evidence for this assignment is provided by conversion of the free phenolic groups in the product mixture to their silicon-protected analogs by treatment with *tert*-butyldimethylchlorosilane and pyridine in dichloromethane. This led to the disappearance of the two primary products and the appearance of two new silicon-protected isomers. These were isolated as a mixture by column chromatography on silica gel using 5% ethyl acetate – dichloromethane as the eluent. The ^{1}H NMR, GC, and GC–MS data for one component corresponded to the data for an authentic sample of α-[(4-*tert*-butyldimethylsilylhydroxy)-3-methoxyphenoxy]acetoveratrone. The ^{1}H NMR and GC–MS data for the second component are consistent with the silicon-protected form of α-(2-hydroxy-3-methoxyphenoxy)acetoveratrone.

For product studies in the presence of the triplet quencher, silica samples containing 2% each of α-guaiacoxyacetoveratrone and *trans,trans*-hexa-2,4-dienol were prepared. The samples with and without dienol were irradiated with 350 nm Rayonet lamps and extracted as outlined above. Product yields were determined by GC using hexadecane as an internal standard. No significant difference in either the amount of recovered ketone or the product yields were observed for the samples containing diene as compared to those with ketone alone.

Acknowledgments

This work was supported by a National Centres of Excellence grant to the Mechanical and Chemimechanical Wood Pulps Network. We thank Dr. Ross Barclay and Dr. James Hilborn (Mount Allison University) for their generous gift of α-(4-hydroxy-3-methoxyphenoxy)acetoveratrone and its *tert*-butyldimethylsilyl derivative.

1. G. Leary. Nature, **217**, 672 (1968).
2. J.A. Schmidt, C. Heitner, G.P. Kelly, and F. Wilkinson. J. Pulp Paper Sci. **16**, J111 (1990).
3. S.E. Lebo, W.F.W. Lonsky T.J. McDonough, P.J. Medvecz, and D.R. Dimmel. J. Pulp Paper Sci. **16**, J139 (1990).
4. J. Gierer and S.Y. Lin. Sven. Papperstidn. **75**, 233 (1972).
5. J.K.S. Wan, M.Y. Tse, and M.C. Depew. Res. Chem. Intermed. **17**, 59 (1992).
6. J.C. Scaiano, J.C. Netto-Ferreira, and V. Wintgens. J. Photochem. Photobiol. A: **59**, 265 (1991).
7. C. Vanucci, P.F. de Violet, H. Bouas-Laurent, and A. Castellan. J. Photochem. Photobiol. A: **41**, 251 (1988).
8. M.G. Neumann and A.E.H. Machado. J. Photochem. Photobiol. B: **3**, 473 (1989).
9. A. Castellan, N. Colombo, C. Vanucci, P.F. de Violet, and H. Bouas-Laurent. J. Photochem. Photobiol. A: **51**, 451 (1990).
10. A. Castellan, N. Colombo, A. Nourmamode, J.H. Zhu, D. Lachenal, R.S. Davidson, and L. Dunn. J. Wood Chem. Technol. **10**, 461 (1990).
11. J.A. Schmidt, A.B. Berinstain, F. de Rege, C. Heitner, L.J. Johnston, and J.C. Scaiano. Can. J. Chem. **69**, 104 (1991).
12. J.C. Scaiano, A.B. Berinstain, M.K. Whittlesey, P.R.L. Malenfant, and C. Bensimon. Chem. Mater. **5**, 700 (1993).
13. J.C. Scaiano and J.C. Netto-Ferreira. J. Photochem. **32**, 253 (1986).
14. J.C. Netto-Ferreira, I.G.J. Avellar, and J.C. Scaiano. J. Org. Chem. **55**, 89 (1990).
15. W.U. Palm and H. Dreeskamp. J. Photochem. Photobiol. A: **52**, 439 (1990).
16. W.U. Palm, H. Dreeskamp, H. Bouas-Laurent, and A. Castellan. Ber. Bunsen-Ges. Phys. Chem. **96**, 50 (1992).
17. J.A. Schmidt, C. Heitner, G.P. Kelly, P.A. Leicester, and F. Wilkinson. J. Photochem. Photobiol. **57**, 111 (1991).
18. R.W. Kessler, G. Krabichler, S. Uhl, D. Oelkrug, W.P. Hagan, J. Hyslop, and F. Wilkinson. Opt. Acta, **30**, 1099 (1983).
19. F. Wilkinson, C.J. Willsher, H.L. Casal, L.J. Johnston, and J.C. Scaiano. Can. J. Chem. **64**, 539 (1986).
20. F. Wilkinson and C.J. Willsher. Tetrahedron, **43**, 1197 (1987).

21. D. Oelkrug, G. Krabichler, W. Honnen, F. Wilkinson, and C.J. Willsher. J. Phys. Chem. **92**, 3589 (1988).
22. F. Wilkinson and G. Kelly. *In* Handbook of photochemistry. Vol. 1. *Edited by* J.C. Scaiano. CRC Press, Inc., Boca Raton, Fla. Chap. 12. 1991.
23. D. Oelkrug, S. Uhl, F. Wilkinson, and C.J. Willsher. J. Phys. Chem. **93**, 4551 (1989).
24. G. Kelly, C.J. Willsher, F. Wilkinson, J.C. Netto-Ferreira, A. Olea, D. Weir, L.J. Johnston, and J.C. Scaiano. Can. J. Chem. **68**, 812 (1990).
25. S. Kazanis, A. Azarani, and L.J. Johnston. J. Phys. Chem. **95**, 4430 (1991).
26. D. Oelkrug, S. Reich, F. Wilkinson, and P. Leicester. J. Phys. Chem. **95**, 269 (1991).
27. J.C. Selwyn and J.C. Scaiano. Polymer, **21**, 1365 (1980).
28. F. Wilkinson, P.A. Leicester, L.F.V. Ferreira, and V.M.M.R. Freire. Photochem. Photobiol. **54**, 599 (1991).
29. J. Murtagh and J.K. Thomas. Chem. Phys. Lett. **148**, 445 (1988).
30. P.K. Das, M.V. Encinas, S. Steenken, and J.C. Scaiano. J. Am. Chem. Soc. **103**, 4162 (1981).
31. J.C. Scaiano, H.L. Casal, and J.C. Netto-Ferreira. ACS Symp. Ser. **278**, 211 (1985).
32. J.C. Netto-Ferreira, W.J. Leigh, and J.C. Scaiano. J. Am. Chem. Soc. **107**, 2617 (1985).
33. W.J. Leigh. J. Am. Chem. Soc. **107**, 6114 (1985).
34. R. Boch, C. Bohne, J.C. Netto-Ferreira, and J.C. Scaiano. Can. J. Chem. **69**, 2053 (1991).
35. N.J. Turro. Tetrahedron, **43**, 1589 (1987).
36. B. Frederick, L.J. Johnston, P. de Mayo, and S.K. Wong. Can. J. Chem. **62**, 403 (1984).
37. N.J. Turro and M. Garcia-Garibay. *In* Photochemistry in organized and constrained media. *Edited by* V. Ramamurthy. VCH Publishers, New York. 1991. Chap. 1.
38. V. Ramamurthy, D.R. Corbin, and L.J. Johnston. J. Am. Chem. Soc. **114**, 3870 (1992).
39. E. Adler, B.O. Lindgren, and U. Saeden. Sven. Papperstidn. **55**, 245 (1952).
40. G. Gellerstedt and J. Gierer. Acta Chem. Scand. **24**, 1645 (1970).

Can. J. Chem. Downloaded from www.nrcresearchpress.com by 213.200.69.106 on 09/08/12
For personal use only.

5-Nitroimidazoles. II[1]: Unexpected reactivity of ronidazole and dimetridazole with thiols

MICHEL GIRARD,[2] FRANÇOIS CLAIRMONT, ASPI MANECKJEE, NICOLE MOUSSEAU, BRIAN A. DAWSON, AND LARRY W. WHITEHOUSE

Bureau of Drug Research, Health and Welfare Canada, Tunney's Pasture, Ottawa, ON K1A 0L2, Canada

Received March 17, 1993

MICHEL GIRARD, FRANÇOIS CLAIRMONT, ASPI MANECKJEE, NICOLE MOUSSEAU, BRIAN A. DAWSON, and LARRY W. WHITEHOUSE. Can. J. Chem. **71**, 1349 (1993).

Ronidazole and dimetridazole, two important veterinary drugs, were found to react readily in the presence of cysteine, under neutral aqueous conditions, leading to the formation of 5-*S*-cysteinyl-1-methylimidazole-2-methanol carbamate and 5-*S*-cysteinyl-1,2-dimethylimidazole respectively through nitro displacement. The reaction products were identified by spectroscopic techniques. The rate of reaction was accelerated by increasing the pH of the medium and was accompanied by a slight change in the product distribution. The reaction was also observed, albeit at a slower rate than that of cysteine, with glutathione, another ubiquitous thiol substrate found in biological systems. While this type of nucleophilic reaction has previously been observed for suitably substituted nitrobenzene derivatives, to the best of our knowledge its occurrence with nitro-heteroaromatics has never been reported. The ready reaction of the parent nitro drugs under such mild aqueous conditions suggests that this may be an alternative path for the formation of nonextractable bound residues in tissues.

MICHEL GIRARD, FRANÇOIS CLAIRMONT, ASPI MANECKJEE, NICOLE MOUSSEAU, BRIAN A. DAWSON et LARRY W. WHITEHOUSE. Can. J. Chem. **71**, 1349 (1993).

On démontre que le ronidazole et le dimétridazole, deux médicaments vétérinaires importants, réagissent facilement avec la cystéine, dans des conditions aqueuses neutres, pour former le carbamate du 5-*S*-cystéinyl-1-méthylimidazole-2-méthanol et le 5-*S*-cystéinyl-1,2-diméthylimidazole respectivement par déplacement du groupe nitro. Les produits de la réaction ont été identifiés à l'aide de techniques spectroscopiques. L'augmentation du pH du milieu réactionnel a eu pour effet d'accélérer la réaction ce qui, par ailleurs, conduit à une légère modification de la distribution des produits. La même type de réaction a été observé avec le glutathion, un autre thiol retrouvé fréquemment dans les systèmes biologiques. Cette réaction de substitution nucléophilique avait déjà été rapportée pour certains nitrobenzènes convenablement substitués, mais n'avait jamais encore été décrite avec les nitro-hétéroaromatiques. En considérant la facilité avec laquelle cette réaction s'effectue à partir des 5-nitroimidazoles, il apparait plausible de considérer ce processus comme voie alternative pour la formation de résidus entre ces médicaments et les macromolécules tissulaires.

Can. J. Chem. Downloaded from www.nrcresearchpress.com by 203.198.23.82 on 09/08/12
For personal use only.

Introduction

Ronidazole (RNZ, 1-methyl-5-nitroimidazole-2-methanol carbamate) (**1**) and dimetridazole (DMZ, 1,2-dimethyl-5-nitroimidazole) (**2**) are veterinary drugs widely used for the treatment of microbial infections in food-producing animals. Metabolism studies (1, 2) have shown that small amounts of these drugs are retained in tissues as nonextractable protein-bound adducts of unknown toxicity. While the nature of these adducts remains unknown, a general structure has been proposed, based on the widely accepted mechanism of activation for these nitroimidazoles (2) involving formation of reduced 4-thiosubstituted imidazoles. To gain further insight into the structure of these biomolecular adducts, the reactivity of ronidazole and dimetridazole towards thiol-containing substrates has been studied. Thus, the preparation of 5-amino derivatives of DMZ and RNZ, bearing thio substituents at C-4 of the imidazole ring, and obtained through Michael type nucleophilic reactions performed under strongly reducing conditions, was reported (3). In the present study, the reactivity of DMZ and RNZ towards thiol substrates under neutral and basic aqueous conditions was examined and it was found that both compounds react readily with loss of the characteristic strong UV maximum associated with the conjugated nitro group. Herein, the structural identification of the reaction products, parameters of the reaction, and the possible metabolic relevance of these findings are reported.

Experimental

Instrumentation

HPLC experiments were performed using a Waters 600E multisolvent delivery system, a Waters 990+ photodiode array detector, and a Waters 700 satellite WISP autosampler. Proton and carbon-13 NMR spectra were recorded at 300 K on a Bruker AM400 spectrometer equipped with an Aspect 3000 computer and process controller, using DISNMR version 891101.0. Standard microprograms from the Bruker Software Library were employed. $^{1}H-^{13}C$ direct and long range correlation spectra were obtained in inverse detection mode. The nOe difference experiments were carried out using a 2.0 s delay after irradiation for 2.0 s. After subtraction of the off-resonance control free-induction-decay (FID) from those acquired for each decoupling frequency, the resulting FID was processed with a line-broadening of 2.0 Hz. FAB mass spectra were obtained on a VG ZAB 2F at a resolution of 2000, a mass range of 100–950 in 5 s, an accelerating votage of 7000 V, an M-Scan FAB source, and using Xe at 10 kV. "Magic bullet," thioglycerol, and glycerol were used as matrices.

Materials and methods

Dimetridazole, cysteine, and glutathione were purchased from Sigma Co. (St. Louis, Mo.). Ronidazole was obtained from MSD-AGVET (Merck Frosst, Kirkland, Qué.). Chemicals used were analytical reagent grade or better; solvents were HPLC grade. HPLC separations were on Brownlee Spheri-5 phenyl columns (250 × 4.6 mm i.d., 5 μm for analytical, and 250 × 7.5 mm i.d. for semi-preparative; Brownlee Laboratories, Santa Clara, Calif.) with a mobile phase consisting of pH 3.6 (adjusted with acetic acid)

[1]For Part I, see ref. 3.

[2]Author to whom correspondence may be addressed.

TABLE 1. Reaction of 5-nitroimidazoles with thiols[a]

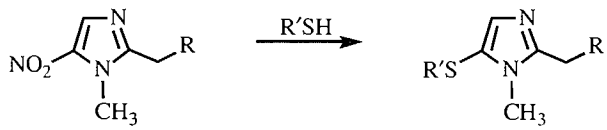

1 R = $OCONH_2$ (RNZ)
2 R = H (DMZ)

3 R = $OCONH_2$ R'S = Cys
4 R = H R'S = Cys
5 R = H R'S = GSH
6 R = H R'S = -Cys-Gly

Entry	Imidazole	Thiol[b]	Conditions	Major product[c]	Unreacted imidazole[d]
1	RNZ	Cys	pH 7/93 h	**3** (25%)	67%
2	RNZ	Cys	pH 9/120 h	**3** (36%)	12%
3	DMZ	Cys	pH 7/42 h	**4** (70%)	8%
4	DMZ	Cys	pH 9/18 h	**4** (62%)	n.d.
5	RNZ	GSH	pH 9/120 h	n.i.	20%
6	DMZ	GSH	pH 9/120 h	**5** (35%); **6** (17%)	16%
7	DMZ	Met	pH 7/120 h	No reaction	100%

[a]Reactions were carried using of a substrate-to-thiol ratio of 1:3.
[b]Cys: cysteine; GSH: glutathione; Met: methionine.
[c](Percent yield measured by HPLC at 230 nm); n.i.: not identified — see text.
[d]Measured by HPLC at 230 nm; n.d : not detectable.

Can. J. Chem. Downloaded from www.nrcresearchpress.com by 203.198.23.82 on 09/08/12
For personal use only.

0.05 M ammonium acetate:acetonitrile (95:5) at a flow rate of 1 mL/min. For preparative experiments, fractions containing the desired product were pooled and freeze-dried.

*Preparation of 5-thiosubstituted imidazoles **3**, **4**, **5**, and **6***

The 5-thiosubstituted imidazoles were obtained from the appropriate combination of starting imidazole and thiol substrate as reported in Table 1. The reaction proceeded at the indicated pH and with the same substrate-to-thiol molar ratio (1:3) as in the following example.

The following procedure was used in a typical experiment: dimetridazole (71 mg, 0.5 mmol) was added to a 0.01 M NaH_2PO_4 buffer solution (5 mL) containing cysteine (187 mg, 1.5 mmol) under inert atmosphere, and the pH adjusted to 9 with 1 M NaOH. The mixture was placed in a water-bath incubator/shaker at 37°C and the progress of the reaction was monitored by HPLC. At completion, the reaction mixture was neutralized with phosphoric acid. The majority of the buffer salts and unreacted starting material were removed by a pre-purification step on a short C-18 or phenyl-bonded silica column (Sep-Pak or Bond-Elut). Typically, an aliquot (1 mL) was adsorbed on a 3 mL column and the eluate was discarded. Aqueous washings (3 × 1 mL) were combined, concentrated under reduced pressure, and the resulting solution purified by semi-preparative HPLC using the conditions described in the previous section. The fractions containing the desired product were pooled and the solvent was removed by lyophilization. The purified product was identified as 5-*S*-cysteinyl-1,2-dimethylimidazole (**4**) by spectroscopic methods. Structural data for the imidazoles **3**–**6** were as follows:

*5-S-Cysteinyl-1-methylimidazole-2-methanol carbamate **3**:* C-13 and proton NMR chemical shifts, see Table 2; UV λ_{max} (from HPLC): 229 nm; FAB-MS: *m/z* 275 [M^++1]; high-resolution FAB-MS: *m/z* 275.0863 for $C_9H_{15}N_4O_4S$ (M+H), calcd. 275.0814.

*5-S-Cysteinyl-1,2-dimethylimidazolec **4**:* C-13 and proton NMR chemical shifts, see Table 2; UV λ_{max} (from HPLC): 231 nm; FAB-MS: *m/z* 216 [M^++1].

*5-S-Glutathionyl-1,2-dimethylimidazole **5**:* C-13 and proton NMR chemical shifts, see Table 2; UV λ_{max} (from HPLC): 241 nm; FAB-MS: 402 [M^++1].

*5-S-Cysteinylglycinyl-1,2-dimethylimidazole **6**:* C-13 and proton NMR chemical shifts, see Table 2; UV λ_{max} (from HPLC): 225 nm; FAB-MS: 273 [M^++1].

Results

Reactivity towards cysteine

Reverse-phase HPLC (RP-HPLC) monitoring of the reaction between ronidazole and excess cysteine, incubated under neutral aqueous conditions, showed the formation of an unknown product, reaching 25% of the integrated area after 93 h of incubation (Table 1, entry 1). Due to the poor solubility of RNZ in neutral aqueous media a large amount of unreacted RNZ (67%) was detected. Using photodiode array detection it was possible to examine the UV spectrum of the unknown. The 310 nm maximum characteristic of 5-nitroimidazoles was not observed, a finding not unlike that observed under strong reducing reaction conditions (3), and suggesting the loss of the nitro group. The UV spectrum featured a single maximum at 229 nm, again consistent with the absence of the conjugated nitro group. Upon isolation, the unknown was identified using standard spectroscopic techniques. The proton and carbon-13 NMR spectra displayed signals (Table 2) indicating the presence of one unit of cysteine and one unit of the imidazole ring moiety. The proton chemical shift assignments were straightforward and unambiguous. The carbon-13 chemical shifts were assigned using carbon–proton correlation experiments with inverse detection. Standard experiments were used to obtain both direct and multiple-bond correlation. Results were consistent with the presence of a sulfur substituent at C-5 of the imidazole ring and chemical shifts correlated well with values calculated from additivity rules. Further evidence for the position of the cysteine substituent was obtained from nOe experiments which showed enhancements for the olefinic resonance upon irradiation of the cysteine resonances. The high-resolution FAB mass spectrum showed a fragment at *m/z* 275.0863, corresponding to molecular formula

TABLE 2. Proton and carbon-13 chemical shifts of 5-thiosubstituted imidazoles[a]

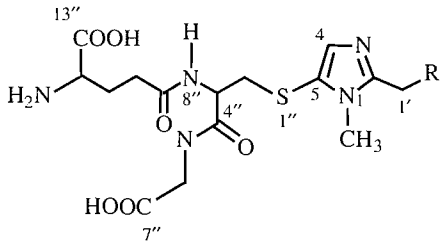

	Compounds							
	3		**4**		**5**		**6**	
C/H	δ_C	δ_H	δ_C	δ_H	δ_C	δ_H	δ_C	δ_H
C-2	147.6	—	148.1	—	150.7	—	150.7	—
C-4 H	130.3	7.40 s	126.4	7.15 s	130.2	7.33 s	129.5	7.31 s
C-5	130.2	—	128.8	—	124.9	—	126.5	—
C-1′ H3	—	—	12.5	2.34 s	13.2	2.48 s	13.8	2.43 s
C-1′ H2	60.2	5.18 s	—	—	—	—	—	—
C-3′	161.1	—	—	—	—	—	—	—
C-2″ H2	39.0	3.20 dd	38.6	2.96 dd	39.3	3.06 m	38.5	3.26 m
		3.40 dd		3.35 dd		3.23 m		
C-3″ H	56.6	3.85 dd	55.9	3.61 dd	55.5	4.42 m	55.3	4.10 m
C-4″	175.3	—	172.5	—	178.8	—	178.5	—
C-6″ H2					45.9	3.68 m	45.8	3.64 AB q
C-7″					173.9	—	171.0	—
C-9″					176.6	—		
C-10″ H2					36.2	2.51 m		
C-11″ H2					28.7	2.13 m		
C-12″ H	56.7	3.74 m						
C-13″					177.51			
N-CH_3	35.4	3.78 s	33.3	3.57 s	34.1	3.66 s	35.6	3.63 s

[a]s = singlet, dd = doublet of doublets, m = multiplet, ABq = AB quartet.

$C_9H_{15}N_4O_4S$ (calcd. 275.0814) for $[M^+ + 1]$, consistent with the proposed structure. Thus, on the basis of the previous considerations, the structure of the unknown was assigned as 5-*S*-cysteinyl-1-methylimidazole-2-methanol carbamate (**3**). Unlike that observed under strong reducing conditions (3), the carbamate group remained unsubstituted under these conditions. The reaction was conducted under inert atmosphere or in the presence of air without any apparent change in product distribution.

The reactivity of dimetridazole (DMZ) towards cysteine was examined under similar reaction conditions, readily leading to the formation of 5-*S*-cysteinyl-1,2-dimethylimidazole (**4**) as the major reaction product (Table 1, entry 3). The structural identification was based mainly on the similarity of the chemical shifts and coupling pattern observed in the proton and carbon-13 NMR spectra (Table 2) with those of **3**. The rate of reaction, monitored by following the disappearance of dimetridazole by HPLC, appeared faster than that of RNZ, with only 8% of the original imidazole detectable after 42 h.

Both RNZ and DMZ showed increased reactivity when the reactions were conducted at pH 9. Only 12% of the initial RNZ remained unreacted after 120 h of incubation while no DMZ was detectable after 18 h (Table 1, entries 2 and 4, respectively). However, this increased reaction rate at higher pH did not translate into comparable increases in the amounts of 5-thiosubstituted imidazoles formed. The yield of RNZ-derived imidazole **3** was only marginaly higher, while the relative amount of the DMZ-related compound **4** appeared slightly lower. In both cases the use of basic reaction conditions may have facilitated the formation of side reaction products, often observable as early eluting peaks in the HPLC traces. Probable side reactions would include carbamate hydrolysis, imidazole ring opening, and nitro reduction products.

Reactivity towards glutathione

Ronidazole and excess glutathione (GSH) reacted at pH 9 (Table 1, entry 5) and led to the formation of a complex mixture of unidentified compounds, likely products of carbamate and partial glutathione hydrolysis, ronidazole ring opening, and possibly nitro group reduction. Reaction under neutral conditions resulted in almost complete recovery of starting RNZ. On the other hand, when dimetridazole was reacted with excess GSH at pH 9 (Table 1, entry 6), the expected imidazole **5** was formed as the major reaction product (35%) along with a minor constituent (17%), easily separated by HPLC, which was identified as the 5-thiosubstituted imidazole dipeptide **6**. Structures were deduced mainly from carbon-13 and proton NMR data presented in Table 2. The latter compound lacked the glutamine residue present in glutathione. The reaction monitored by HPLC proceeded at a slower rate than that observed with cysteine, a likely consequence of the steric hindrance due to the larger glutathione molecule.

Indirect evidence that the reaction proceeded through attack by the thiol group was obtained when methionine, a

Can. J. Chem. Downloaded from www.nrcresearchpress.com by 203.198.23.82 on 09/08/12
For personal use only.

natural amino acid bearing a methyl substituted thiol group, failed to react with dimetridazole (Table 1, entry 7).

Discussion

The reactivity of the two nitroimidazoles examined in this study involved substitution of the nitro group by thiol-containing compounds in fair to good yield. The rate enhancement observed by raising the pH of the reaction is consistent with the nucleophilic reaction proceeding through the thiolate ion. Such thiol-mediated nitro group displacements have been shown to occur readily in appropriately substituted aromatic compounds, and were the subject of a review (4). The classical addition/elimination mechanism has usually been suggested to account for the formation of most products (5). The ease with which the reaction proceeded was explained in terms of the polarizability of the thiolate ion, which would minimize repulsion in the transition state. Reaction conditions generally reported for the preparation of these aromatic thioethers usually involve in situ generation of the thiol anion in polar aprotic solvent. However, to the best of our knowledge, the reaction observed in this study is the first example of this type of reaction occurring with nitro-substituted heteroaromatic compounds and proceeding under aqueous (protic) conditions.

The formation of appreciable amounts of cystine (dicysteine) in the RNZ and DMZ reactions conducted under inert atmosphere suggests that the reaction more likely proceeds via a radical anion mechanism, involving the formation of the nitro anion radical intermediate **8**. In such a case, cystine would be formed upon dimerization of the thiyl radical generated upon one-electron reduction of the thiolate to form the radical anion **8** (eq. [1]). In a recently published article (6), the RNZ-derived nitro radical anion **8** (R = $OCONH_2$) was detected in intact rat hepatocytes, lending support to its intermediacy in the biological activation mechanism of 5-nitroimidazole drugs.

Consideration of the ease with which 5-thiosubstituted imidazoles are formed from their parent nitro compounds, notably under such mild aqueous conditions, leads us to hypothesize that this process may have some biological significance. Until now the only mechanism to account for the formation of thiosubstituted imidazole adducts was one involving a reductive process that was shown to occur in mammalian cells under very specific conditions (1, 2), the end product being 4-thiosubstituted imidazoles. The results presented in this study describe an alternative chemical mechanism for the substitution of 5-nitroimidazoles. This mechanism was demonstrated to lead to the formation of 5-thiosubstituted imidazoles and offers an alternative pathway by which drug-bound residues are formed with tissue macromolecules.

[1] $RS^- + RNZ\,(DMZ) \longrightarrow RS^{\bullet} +$ 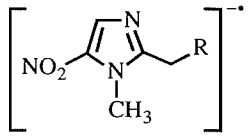

8

Acknowledgements

We are grateful to Dr. T. Cyr who diligently provided FAB mass spectra. This study was financially supported by grant No. FD-U-00428–3 from the Food and Drug Administration of the United States of America.

1. A. Maneckjee, A. Menzies, B.C. Foster, P. Andrews, and L.W. Whitehouse. Metabolism and adduct formation of the antimicrobial veterinary drugs, dimetridazole and ronidazole, following *in vitro* incubation with mouse liver microsomes. Canadian Federation of Biological Societies, 1990 Annual Meeting, Halifax, N.S.
2. P.G. Wislocki, E.S. Bagan, W.J.A. Vandenheuvel, R.W. Walker, R.F. Alvaro, B.H. Arison, A.Y.H. Lu, and F.J. Wolf. Chem.–Biol. Interact. **49**, 13 (1984).
3. M. Girard, G. Carignan, N. Mousseau, and B.A. Dawson. J. Pharm. Biomed. Anal. **9**, 151 (1991).
4. J.R. Beck. Tetrahedron, **34**, 2057 (1978).
5. (*a*) P. Cogolli, L. Tesstaferri, M. Tingoli, and M. Tiecco. J. Org. Chem. **44**, 2636 (1979); (*b*) J.R. Beck and J.A. Yahner. J. Org. Chem. **43**, 2048 (1978).
6. D.N. Ramakrishna Rao, S. Jordan, and R.P. Mason. Biochem. Pharmacol. **37**, 2907 (1988).

Can. J. Chem. Downloaded from www.nrcresearchpress.com by 203.198.23.82 on 09/08/12
For personal use only.

Fourier transform infrared spectroscopy studies of cyanide ion solutions of dimethylformamide and aqueous dimethylformamide

DAVID J. JOBE[1] AND KENNETH CHARLES WESTAWAY[2]

Department of Chemistry and Biochemistry, Laurentian University, Sudbury, ON P3E 2C6, Canada

Received February 25, 1993

DAVID J. JOBE and KENNETH CHARLES WESTAWAY. Can. J. Chem. **71**, 1353 (1993).

Fourier transform infrared spectroscopy has been used to investigate the behaviour of HCN and alkali metal and tetraethylammonium cyanides in DMF and aqueous DMF. The cyanide ion exists as free ions and ion pairs in pure DMF but as water-solvated and DMF-solvated ions in aqueous DMF. The aqueous DMF solutions can be treated as a pseudo two-phase system with a distribution coefficient of 0.018 between the aqueous and DMF-rich pseudo phases. A kinetic analysis of the cyanide ion – benzyl chloride reaction in DMF and aqueous DMF has shown that the rate constant for the S_N2 reaction is markedly decreased with the addition of as little as 2.5% water. This decrease is primarily due to changes in transition state solvation. The S_N2 reactions between cyanide ion and benzylmethyl-4-substituted phenylsulphonium perchlorates in 20% aqueous DMF have also been investigated.

DAVID J. JOBE et KENNETH CHARLES WESTAWAY. Can. J. Chem. **71**, 1353 (1993).

On a utilisé la spectroscopie infrarouge par transformation de Fourier pour étudier le comportement du HCN et des cyanures de tétraéthylammonium et des métaux alcalins dans le DMF et le DMF aqueux. Dans le DMF pur, les ions cyanures existent sous la forme d'ions libres et de paires d'ions alors que, dans le DMF aqueux, ils existent sous la forme d'ions solvatés par l'eau ou par le DMF. On peut traiter les solutions aqueuses de DMF comme un système à pseudo deux phases avec un coefficient de partage de 0,018 entre les phases pseudo aqueuses et pseudo DMF. Une analyse cinétique de la réaction de l'ion cyanure avec le chlorure de benzyle dans le DMF et dans le DMF aqueux démontre que la constante de vitesse de la réaction S_N2 est de beaucoup diminuée par l'addition d'aussi peu que 2,5% d'eau. Cette diminution est principalement due à des changements dans la solvatation de l'état de transition. On a aussi étudié les réactions S_N2 de l'ion cyanure avec les perchlorates de benzylméthyl(substitués en position 4)phénylsulfonium dans de DMF contenant 20% d'eau.

[Traduit par la rédaction]

Introduction

Loupy and Seyden-Penne investigated the effect of counterion association on the nucleophilicity of the cyanide ion in dipolar aprotic solvents (1–3). Their studies demonstrated that the rates of substitution and elimination reactions are dependent on both the cation of the cyanide salt (MCN) and the solvent. To assist in their interpretation of the kinetic results, solutions of cyanide salts were characterized in dipolar aprotic solvents using infrared (IR) spectroscopy (4, 5). This work showed that the cyanide ion IR absorptions are strongly dependent on the cation but show only a slight dependence on the solvent. From these studies, Loupy et al. concluded that the alkali and alkaline earth metal cyanide salts exist as ion pairs having stoichiometries of $M^+/solvent/CN^-$, M^+/CN^-, and $M^+/CN^-/M^+$ in dimethylformamide (DMF) and dimethyl sulphoxide (DMSO). The "free" or non-complexed cyanide anion was observed only when the cation was the larger tetraphenylarsonium ion. The effect of mixed solvents on the form and nucleophilicity of the cyanide ion has not been studied.

In this study, DMF and aqueous DMF solutions containing either potassium cyanide, sodium cyanide, tetraethylammonium cyanide (Et_4NCN), or hydrogen cyanide were characterized using Fourier Transform Infrared Spectroscopy (FT-IR). Then, FT-IR spectroscopy was used to determine the rate constants for the S_N2 displacement reactions between cyanide ion and several substrates in these solvents. This study was undertaken to determine if the addition of water decreased ion pairing and hence removed the dependence of the reaction rate on the cation.

Experimental

Reagents

The alkali metal salts, potassium cyanide and sodium cyanide (Fisher, analytical grade), and tetraethylammonium cyanide (Sigma, 94%) were used as purchased. All the cyanide solutions were prepared on a percent volume (v/v) basis with spectroscopic grade DMF (Caledon) and deionized, double-distilled water. The benzyl chloride (Aldrich >99%) was washed with an aqueous sodium bisulfite solution (6), dried over $CaCl_2$, and purified by distillation, bp 126°C at 26 Torr (1 Torr = 133.3 Pa).

The salts, benzylmethyl-4-chlorophenylsulphonium perchlorate (CS) and benzylmethyl-4-methoxyphenylsulphonium perchlorate (MeOS), were synthesized by passing an aqueous solution of the tosylate salt through an Amberlite IRA-400, 60–100 mesh anion (Cl^-) exchange column that had been converted to the ClO_4^- form. After the solvent had been removed on a rotary evaporator, the resulting salt was recrystallized from ethanol. The tosylate salts were synthesized according to the procedure described by Schowen (7).

HCN was synthesized by adding a 50% H_2SO_4–water mixture to a three-necked flask containing 5 g of potassium cyanide (8). The resulting $HCN_{(g)}$ was passed through a $CaCl_2$ drying tube and collected in a 50-mL round-bottomed flask cooled in an ice bath. The HCN was stored as a solution in dry DMF to keep it from evaporating.

FT-IR spectra

All spectra were recorded at room temperature (ca. 23°C) on a Bomem Michelson 100 FT-IR spectrometer using a CaF_2 solution cell. The path length for the cell was determined by a diffraction method to be 0.0104 cm. Due to the low IR absorption for DMF in the 2000–2300 cm^{-1} region, only 25–40 scans were required to obtain good quality spectra. However, between 100 and 500 scans

[1]Present address: Research Chemistry Branch, AECL Research, Whiteshell Laboratories, Pinawa, MB R0E 1L0, Canada.

[2]Author to whom correspondence may be addressed.

Can. J. Chem. Downloaded from www.nrcresearchpress.com by 213.200.69.106 on 09/08/12
For personal use only.

TABLE 1. The second-order rate constants for the reaction:

$$\text{Substrate} + CN^- \xrightarrow{k_2} \text{products}$$

Substrate	MCN	[Substrate] (mol L^{-1})	[MCN] (mol L^{-1})	% H_2O	T (°C)	$k_2/10^{-3}$ (L mol^{-1} s^{-1})
Benzyl chloride	Et_4NCN	0.1792	0.1065	2.5	30.00	4.4
Benzyl chloride	Et_4NCN	0.1795	0.1072	5.0	30.00	3.2
Benzyl chloride	Et_4NCN	0.1476	0.09739	15	30.00	0.52
Benzyl chloride	Et_4NCN	0.1792	0.01046	20	30.00	0.57
Benzyl chloride	KCN	0.1736	0.09517	5.0	30.00	5.3
ClS	Et_4NCN	0.1355	0.08182	20	23.0	9.0
MeOS	Et_4NCN	0.1753	0.1179	20	23.0	0.84

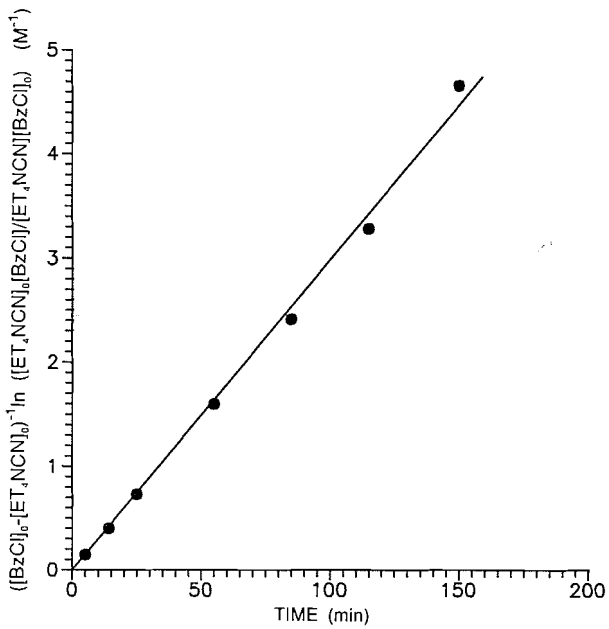

FIG. 1. A typical rate plot of $([BzCl]_0 - [Et_4NCN]_0)\ln([Et_4NCN][BzCl]_0/[Et_4NCN]_0[BzCl])$ versus time for the reaction of benzyl chloride with tetraethylammonium cyanide in 15% aqueous DMF at 30.00°C.

were needed to obtain acceptable spectra for samples containing more than 20% water. In some cases, these spectra had to be background corrected due to slight differences in the solvent composition between the reference and sample solutions.

Kinetic studies

The rate constants for the S_N2 reactions between benzyl chloride (BzC) and cyanide ion were determined at 30.00 ± 0.01°C, Table 1. One-millilitre aliquots were removed from the thermostated solution and the FT-IR spectra were taken using an average of 25 scans. Since the samples could not be quenched before analysis, the average time between the removal of the sample and the termination of the acquisition was used to calculate the rate constant. This period was typically 2 min. Using the average time rather than the time the aliquot was removed does not alter the slope (rate constant) of the second-order plot.

For those kinetic studies where a sulphonium salt was the substrate, a 5.0-mL sample containing tetraethylammonium cyanide and the appropriate sulphonium salt was prepared, Table 1. A portion of this solution was transferred to the CaF_2 cell and the rate constant was measured at 23.0 ± 0.5°C. For the benzylmethyl-4-chlorophenylsulphonium perchlorate reaction with cyanide ion, only 10 scans were used to obtain a spectrum so more data points could be collected for this fast reaction.

The percent reaction was calculated from the decrease in the water-solvated cyanide ion peak in the FT-IR spectrum. Then, the rate constants (k_2), Table 1, were determined from the slopes of the least-squares fit of the second-order plots (9). A typical rate plot for the reaction of benzyl chloride with cyanide ion in aqueous DMF is shown in Fig. 1. The plots had correlation coefficients between 0.992 and 0.997. All reactions were followed to 80% of completion, except for the reaction in 20% aqueous DMF, which was monitored to 54% of completion. The rate constants obtained by this method are precise to within ±5%.

Results and discussion

FT-IR characterization

FT-IR spectra for MCN in DMF

Figure 2 shows the FT-IR spectra obtained for various concentrations of tetraethylammonium cyanide in both dry and aqueous DMF. The spectra of tetraethylammonium cyanide in dry DMF, Fig. 2(*a*), have two concentration-dependent absorptions, at 2054 and 2062 cm^{-1}. The FT-IR spectrum for this salt has identical maxima and similar intensity ratios to the spectrum obtained by Loupy and Corset for tetraphenylarsonium cyanide (4, 5). The similarity is not unexpected given that the tetraethylammonium cation is also large and would be expected to promote the formation of the "free" cyanide ion. The FT-IR absorption for the "free" cyanide ion has been assigned to the peak at 2054 cm^{-1} while the peak at 2062 cm^{-1} has been assigned to either a M^+/CN^- or a $M^+/DMF/CN^-$ ion pair. The assignment of the cation-associated form to the absorption at 2062 cm^{-1} was confirmed by adding tetraethylammonium chloride to a DMF solution containing tetraethylammonium cyanide. The increase in the absorption at 2062 cm^{-1} and the slight decrease in the absorption at 2054 cm^{-1} indicates that more of the cyanide ion pair is formed in the presence of the excess tetraethylammonium ion.

The assignment of the FT-IR absorption peak at 2054 cm^{-1} to the "free" cyanide ion is supported by the change in the sodium cyanide spectrum when the macrocyclic crown ether, 15-crown-5 ether, is added. The FT-IR spectrum for sodium cyanide in DMF in the absence of 15-crown-5 ether has strong FT-IR absorption maxima at 2062 and 2080 cm^{-1}. The addition of 15-crown-5, which is known to complex sodium ions (10), results in a decrease in the absorption at both 2062 and 2080 cm^{-1} and an increase in the absorption at 2054 cm^{-1}. Presumably the decrease in the absorptions at 2062 and 2080 cm^{-1} occurs because the Na^+/CN^- and $Na^+/DMF/CN^-$ ion pairs are converted into the "free" cyanide ion.

Due to the low solubility, obtaining an FT-IR absorption

Can. J. Chem. Downloaded from www.nrcresearchpress.com by 213.200.69.106 on 09/08/12
For personal use only.

Can. J. Chem. Downloaded from www.nrcresearchpress.com by 213.200.69.106 on 09/08/12
For personal use only.

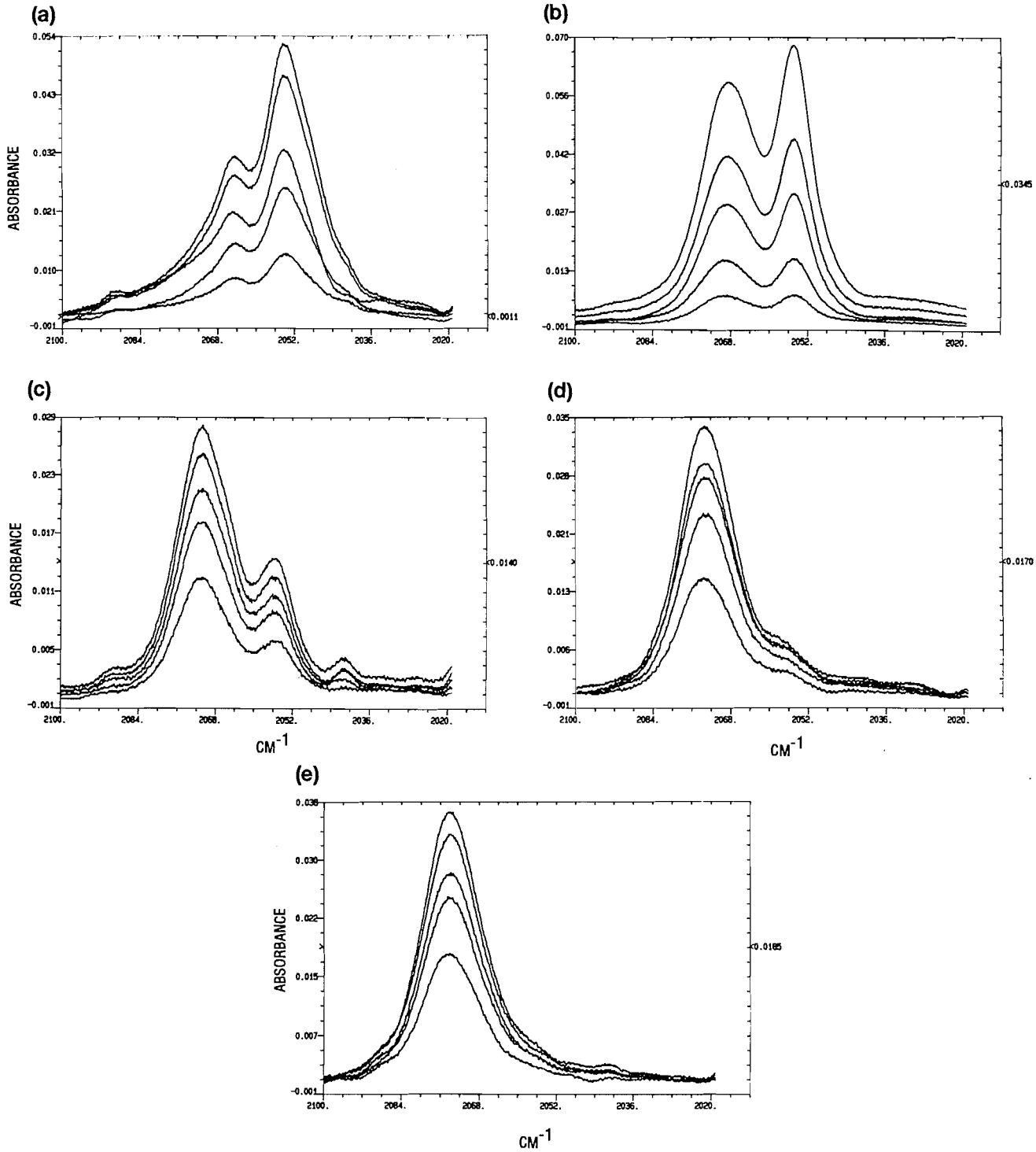

FIG. 2. Spectra obtained for tetraethylammonium cyanide in (*a*) dry DMF and (*b*) 2%, (*c*) 5%, (*d*) 15%, and (*e*) 20% aqueous DMF.

spectrum of potassium cyanide in DMF was difficult. The spectrum obtained for a saturated potassium cyanide – DMF solution after 500 scans has FT-IR absorption maxima at 2054 and 2070 cm^{-1}. The same absorption maxima were observed by Loupy and Corset for potassium cyanide in DMSO (4). The absorption at 2054 cm^{-1} would indicate that potassium cyanide is either strongly dissociated in DMF or, as Loupy and Corset reported for potassium cyanide in DMSO, the potassium cyanide ion pair absorbs at a lower wave number than the sodium cyanide ion pair. If Loupy and Corset are correct, the wave number for the K^+/CN^- ion pair just happens to coincide with the wave number for the absorption of the "free" anion.

In contrast to the spectra obtained for tetraethylammonium cyanide, potassium cyanide, and sodium cyanide, the spectrum of HCN in dry DMF is much simpler. The FT-IR absorption spectrum for a 0.16 M HCN solution in DMF has a single absorption with a maximum at 2079 cm^{-1} and $\epsilon_{2079} = 160$. Thus, the only cyanide species in dry DMF is the unionized HCN.

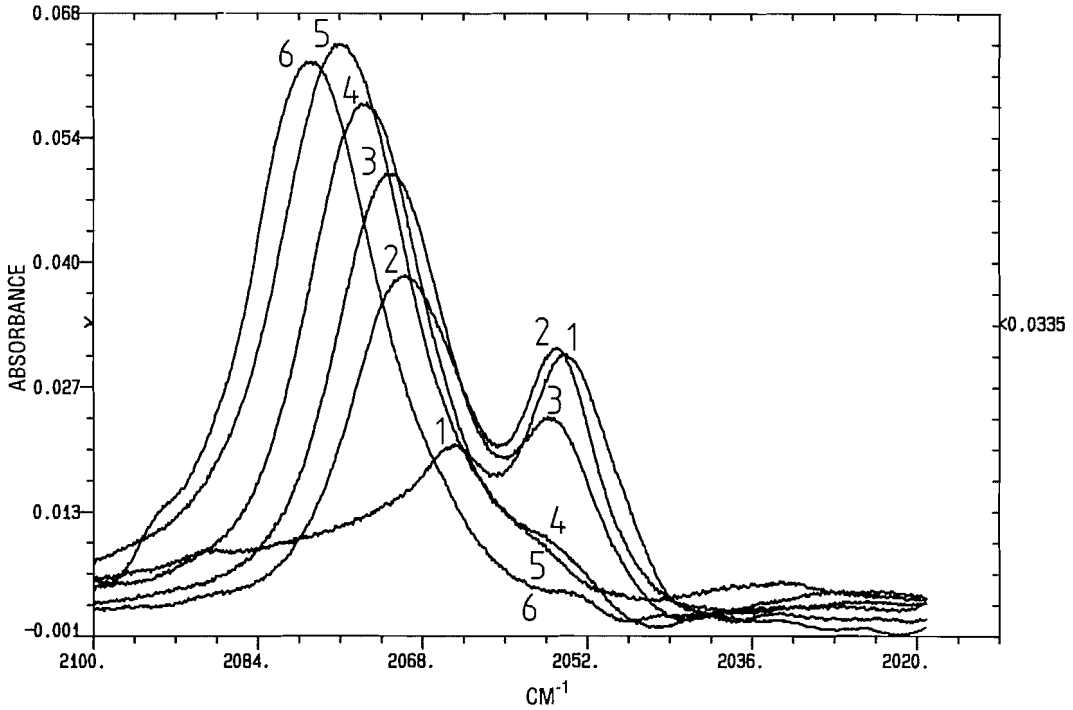

FIG. 3. Spectra obtained for a 0.20 M tetraethylammonium cyanide solution in (1) 0%, (2) 2.5%, (3) 5.0%, (4) 15%, (5) 38%, and (6) 80% aqueous DMF.

Addition of water to MCN–DMF solutions

Adding water to a solution containing 0.20 M tetraethylammonium cyanide in DMF alters the cyanide ion absorptions significantly, Fig. 3. The addition of 2.5% water results in a very small increase in the 2054 cm^{-1} peak, the apparent disappearance of the absorption at 2062 cm^{-1}, and a new absorption at approximately 2071 cm^{-1}. This new absorption at 2071 cm^{-1} could be due to either a shift in the wave number for the ion pair or to the formation of a new species. It is important to note that this new absorption has a much greater intensity than the absorption at 2062 cm^{-1} in dry DMF. Thus, if this absorption were due to a shift in the wave number of the ion pair, the increase in the intensity of the peak at 2071 cm^{-1} would have to be accompanied by a decrease in the absorption at 2054 cm^{-1}. However, the absorption at 2054 cm^{-1} has increased slightly and it is reasonable to assume that the new absorption is due to the formation of a new species, either a water-solvated cyanide ion or a DMF solvent-separated ion pair. Since the DMF solvent-separated ion pair would be expected to absorb at a wave number between the tight ion pair (2062 cm^{-1}) and the "free" cyanide ion (2054 cm^{-1}), one must conclude that the absorption at 2071 cm^{-1} is due to a water-solvated cyanide ion.

The presence of the water-solvated cyanide ion, $(CN^-)_W$, means an equilibrium exists between it and the "free" or DMF solvated cyanide ion, $(CN^-)_{DMF}$.

[1] $$(CN^-)_W \rightleftarrows (CN^-)_{DMF}$$

Given that cyanide ion in pure water absorbs at 2079 cm^{-1} (11), the solvation shell around the water-solvated cyanide ion in the 2.5% solution must contain some DMF because the wave number for this species is between the wave numbers for the cyanide ion in pure water and pure DMF.

The addition of more water to form a 5% solution results in a marked decrease in the absorption at 2054 cm^{-1} and an increase in both the intensity and wave number of the water-solvated cyanide ion. This trend continues up to 38% water. Presumably, increasing the water content converts more of the DMF-solvated cyanide ion into the water-solvated form. In fact, at $\geq$20% water, the absorbance due to the DMF-solvated cyanide ion is very small (negligible) with respect to the total cyanide ion absorbance. In 80% water, the wave number of the water-solvated species is 2079 cm^{-1} and the intensity of the absorption is identical to that obtained for a solution containing the same concentration of tetraethylammonium cyanide in pure water.

The spectra obtained for potassium cyanide in 5%, 15%, and 20% aqueous DMF were identical to those obtained using the same concentrations of tetraethylammonium cyanide (cf. Fig. 2). Since the spectra for the two salts are identical even though the cation is different, one must conclude that the absorption at the higher wave number is due to a water-solvated ion and not an ion pair. This supports the existence of the equilibrium between the DMF- and water-solvated cyanide ions.

The intensities of the peaks for tetraethylammonium cyanide in aqueous DMF are also concentration dependent. Due to the strong overlap of the two cyanide ion absorptions in these spectra, a computer program was developed to resolve the spectra into multiple Gaussian peaks (12, 13). The resulting absorptions and their wave number maxima are given in Table 2. The constant ratio of the 2054 to 2072 cm^{-1} intensities in 5% aqueous DMF with increasing salt concentration indicates that the distribution of the DMF- and water-solvated cyanide ions is independent of the $[Et_4NCN]/[H_2O]$ ratio. This is also observed in the 15% and 20% aqueous DMF solutions. This behaviour would be expected only if

Can. J. Chem. Downloaded from www.nrcresearchpress.com by 213.200.69.106 on 09/08/12
For personal use only.

TABLE 2. The molar extinction coefficients and distribution coefficients obtained from the deconvolution of the FT-IR spectra of tetraethylammonium cyanide in 2.0%, 5.0%, 15%, and 20% aqueous DMF

% H_2O	ν_{DMF} (cm^{-1})	A_{DMF}	ν_W (cm^{-1})	A_W	[Et_4NCN] (mol L^{-1})	[CN^-]$_W$ (mol L^{-1})	[CN^-]$_{DMF}$ (mol L^{-1})	ϵ_{DMF} (M^{-1} cm^{-1})	A_1/A_2	ϕ_W	K_D
2.0	2054	0.053	2068	0.049	0.340	0.150	0.190	28	1.08	0.020	0.024
2.0	2055	0.036	2069	0.034	0.210	0.110	0.100	35	1.03	0.020	0.019
2.0	2055	0.026	2069	0.025	0.140	0.079	0.061	40	1.00	0.020	0.016
2.0	2055	0.012	2069	0.013	0.071	0.041	0.030	40	0.95	0.020	0.015
5.0	2056	0.010	2070	0.024	0.110	0.073	0.037	28	0.42	0.050	0.024
5.0	2055	0.009	2070	0.022	0.088	0.067	0.021	41	0.42	0.050	0.017
5.0	2055	0.008	2070	0.019	0.077	0.060	0.017	46	0.41	0.050	0.015
5.0	2055	0.007	2070	0.016	0.066	0.050	0.016	41	0.41	0.050	0.016
15	2057	0.004	2073	0.031	0.100	0.096	0.004	[a]	0.15	0.15	—
15	2058	0.004	2073	0.027	0.087	0.084	0.003	[a]	0.14	0.15	—
15	2058	0.003	2073	0.024	0.076	0.074	0.002	[a]	0.11	0.15	—
15	2058	0.002	2073	0.020	0.065	0.063	0.002	[a]	0.12	0.15	—
15	2058	0.002	2073	0.014	0.043	0.042	0.001	[a]	0.14	0.15	—
20	2060	0.003	2074	0.033	0.100	0.100	—	—	0.080	0.20	—
20	2062	0.002	2074	0.028	0.087	0.087	—	—	0.070	0.20	—
20	2063	0.002	2074	0.025	0.077	0.077	—	—	0.072	0.20	—
20	2060	0.002	2074	0.021	0.064	0.064	—	—	0.071	0.20	—

[a]The concentrations of cyanide ion in DMF were too small to give an accurate ϵ value.

Can. J. Chem. Downloaded from www.nrcresearchpress.com by 213.200.69.106 on 09/08/12
For personal use only.

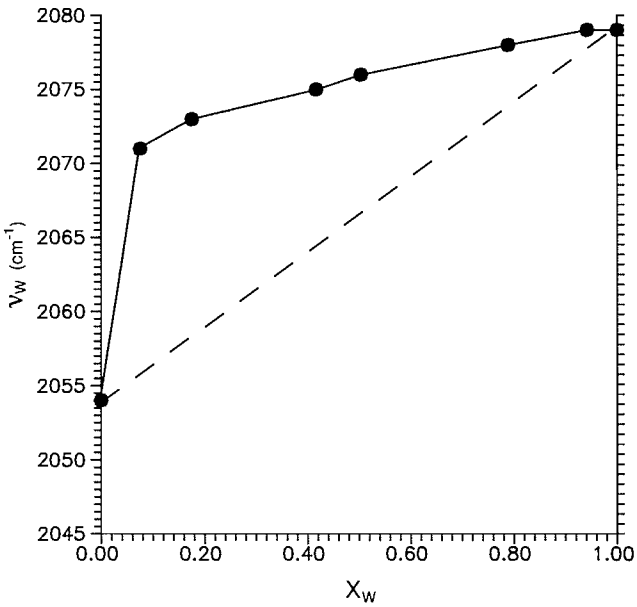

FIG. 4. The absorption wave number for the water solvated cyanide ion (ν_W) versus the mole fraction of water (x_W) in aqueous DMF solutions.

more water than the amount necessary to solvate the ions were present. Assuming this to be the case, the mixed solvent system can be treated as a pseudo two-phase system with the cyanide ion distributed between a water- and a DMF-rich phase.

The ratio of the absorbances at 2054 to those at 2069 cm^{-1} for the 2% aqueous DMF solutions, on the other hand, decreases slightly in a regular fashion from 1.08 to 0.95 as the concentration decreases from 0.34 M to 0.071 M, Table 2. When the [Et_4NCN]/[H_2O] ratio is large, the distribution of the cyanide ions between the two pseudo phases is shifted in favour of the DMF-rich phase because the solvent shell around the water-solvated cyanide ion contains fewer water molecules. As the [Et_4NCN]/[H_2O] ratio decreases, there are more water molecules available to solvate the cyanide ions and the equilibrium shifts towards the water-solvated ion.

For the 20% aqueous DMF solutions, the absorption due to the DMF-solvated cyanide ion accounts for 7% of the total absorbance, Table 2. If one assumes the concentration of this species is negligible, a Beer's Law plot of the absorption at 2074 cm^{-1} versus [Et_4NCN] yields $\epsilon_{2074} = 31 \pm 1$ M^{-1} cm^{-1} for the water-solvated cyanide ion. To compare this value to the molar extinction coefficient for cyanide ion in water, FT-IR spectra were obtained for 0.065–0.31 M aqueous solutions of both potassium cyanide and tetraethylammonium cyanide. A single absorption at 2079 cm^{-1} was observed for all these solutions, indicating that only water-solvated cyanide ions exist in water. A plot of the absorption at 2079 cm^{-1} versus [CN^-] yielded $\epsilon_{2079} = 31 \pm 1$ M^{-1} cm^{-1}, comparable to the value 29 M^{-1} cm^{-1} reported by Jones and Penneman (11) for a 10 M aqueous potassium cyanide solution. It is worth noting that the molar extinction coefficients for cyanide ion in water and in 20% aqueous DMF are identical.

Although the molar extinction coefficients of the cyanide ion in water and in 20% aqueous DMF are identical, the wave numbers for their maxima are different. The lower wave number in the 20% aqueous DMF indicates that the environment around the water-solvated cyanide ion is different than that in pure water. This suggests that the solvent shell around the cyanide ion in mixed solvents contains some DMF. The wave number for the water-solvated cyanide ion absorption (ν_W) increases with the mole fraction of water in the mixed solvent, Fig. 4. At 80% water, the wave number for this absorption is, within experimental error, equal to that for cyanide ion in water and has shifted 10 cm^{-1} relative to that for the cyanide ion in 2% aqueous DMF. This shift of ν_W to higher wave numbers as the mole fraction of water increases is expected because the solvation shell of the water-solvated cyanide ion becomes less like DMF (ν = 2054 cm^{-1}) and more like water (ν = 2079 cm^{-1}). The nonlinear change in ν_W with increasing mole fraction of water in the mixed

Can. J. Chem. Downloaded from www.nrcresearchpress.com by 213.200.69.106 on 09/08/12
For personal use only.

solvent also supports the solvent sorting (two-phase) model. If DMF and water formed an ideal single phase, the variation in ν_W for the water-solvated cyanide ion should follow the dashed line in Fig. 4.

The absorption maximum for the DMF-solvated cyanide ion, Table 2, also increases as the water content increases. As with the water-solvated cyanide ion, this wave number shift indicates that the solvation shell for the DMF-solvated cyanide ion changes slightly with water content. Given the direction of the wave number shift, there is likely more water in the DMF solvent shell as the water content increases.

The treatment of the 2% and 5% aqueous DMF solutions is more difficult because they contain significant amounts of the water-solvated and DMF-solvated ions. The molar extinction coefficient for the water-solvated cyanide ion is the same in water and in 20% aqueous DMF ($\epsilon = 31\ M^{-1}\ cm^{-1}$) even though ν_W differs by 5 cm^{-1}. Since the molar extinction coefficient for the water-solvated cyanide ion is not sensitive to significant changes in the composition of the solvent, one can assume that the molar extinction coefficient for the water-solvated form is 31 $M^{-1}\ cm^{-1}$ in all the aqueous DMF solutions. Using this value, the concentration of cyanide ion in the aqueous phase can be calculated and, by subtraction, the concentration of cyanide ion in the DMF phase can be obtained. The resulting concentrations from the 2% and 5% aqueous DMF solutions give $\epsilon = 37 \pm 7\ M^{-1}\ cm^{-1}$ for the DMF-solvated cyanide ion in aqueous DMF, Table 2. This is 3 times larger than the apparent extinction coefficient reported by Loupy and Corset (4). However, these authors were unable to determine the concentrations of the contributing species.

If one assumes the pseudo two-phase model, a distribution coefficient for the cyanide ion between the two pseudo phases, K_D, is given by:

$$[2] \quad K_D = c_{DMF}/c_W$$

where c_{DMF} and c_W are the cyanide ion concentrations in the DMF and water pseudo phases, respectively. These concentrations are:

$$[3] \quad c_i = n_i/V_i$$

where n_i and V_i are the number of moles of cyanide ion and the volume, respectively, of pseudo phase i. Assuming the volume of the pseudo phase i is equal to the volume of solvent i used to prepare the solution, the volume fraction of pseudo phase i, ϕ_i, is given by:

$$[4] \quad \phi_i = V_i/V_T$$

where V_T is the total volume of the solution.

The ratio of the number of moles of cyanide ion in the DMF phase to the water phase (n_{DMF}/n_W) is given by:

$$[5] \quad n_{DMF}/n_W = A_{2054}\epsilon_{2074}/A_{2074}\epsilon_{2054} = [CN^-]_{DMF}/[CN]_W$$

where $[CN^-]_{DMF}$ and $[CN^-]_W$ are the bulk concentrations of the DMF- and water-solvated cyanide ion, respectively.

Since $\phi_W + \phi_{DMF} = 1$, substituting eqs. [3]–[5] into eq. [2] yields:

$$[6] \quad K_D = \{\phi_W/(1 - \phi_W)\}\, A_{2054}\epsilon_{2074}/A_{2074}\epsilon_{2054}$$
$$= \{\phi_W/(1 - \phi_W)\}[CN^-]_{DMF}/[CN^-]_W$$

The values of K_D calculated using this model are given in Table 2. An examination of the K_D values shows that it is constant within experimental error at $0.018_2 \pm 0.004$. Given that the K_D value does not change significantly over a wide range of solvent composition, the assumption of a pseudo two-phase model is valid.

It is also worth noting that the values for K_D in the 2% aqueous DMF increase slightly as the ratio of salt to water increases. This trend, which is within the error associated with K_D, probably reflects the fact that the solvation shell around both the cyanide ion species varies with water content. However, this does not affect the validity of the pseudo two-phase model.

It is worth noting that the cyanide ion in water and HCN in DMF both have a single absorption at 2079 cm^{-1}. However, the molar extinction coefficient for HCN is 160, or 5 times that for the cyanide ion in water. Also, adding water to dry DMF solutions containing HCN does not alter the wave number of the C≡N bond absorption although there is a slight (<10%) reduction in the intensity of the peak when the water content is increased to 20%. When enough KOH is present to neutralize the HCN in the 20% aqueous DMF solution, the intensity of the peak decreases fivefold to the absorption expected for a potassium cyanide solution of the same concentration. These results indicate that even in a 20% aqueous DMF solution all, or virtually all, of the HCN stays in the molecular form.

Kinetic studies

Reaction of benzyl chloride with tetraethylammonium cyanide

Figure 5 shows the time-dependent FT-IR spectra obtained for the S_N2 reaction between benzyl chloride and tetraethylammonium cyanide in 2.5%, 5%, 15%, and 20% aqueous DMF. In these spectra, the decrease in the intensity of the cyanide ion absorptions (2054–2074 cm^{-1}) is accompanied by an increase in the intensity of a peak at 2250 cm^{-1}, where the product, benzyl nitrile, absorbs. An interesting feature of the spectra for the reaction in 2.5% and 5% aqueous DMF is that the peak ratio for the two solvated cyanide ions (2054–2074 cm^{-1}) does not change throughout the reaction. This indicates that the interconversion between the two forms of the cyanide ion is much faster than the reaction between cyanide ion and benzyl chloride. Therefore, the rate-determining step in the mechanism is the S_N2 reaction between cyanide ion and benzyl chloride.

This reaction in dry DMF was too fast to measure. Even at 0°C, the reaction was at least 95% complete in 4 min. White and Baizer (14) also found that the reaction between tetraalkylammonium cyanides and alkyl halides in dry DMF was extremely fast. Presumably this is because there is a high concentration of the DMF-solvated cyanide ion in the reaction mixture. White and Baizer also found that the reaction was considerably slower when sodium cyanide rather than tetraalkylammonium cyanide was used. This probably occurs because the cyanide ion exists as the less reactive ion pair when sodium cyanide is the nucleophile.

Adding water to the solvent decreases the rate constant (k_2) markedly, Table 1. Even in 2.5% aqueous DMF, the reaction is slow; it is only 91% complete after 1.5 h at 30.00°C. The rate continues to decrease as the amount of water in the solvent increases. Haberfield et al. (15, 16) showed that changing a dipolar aprotic to a protic solvent reduces the free energy of the reactants only slightly but markedly increases

Can. J. Chem. Downloaded from www.nrcresearchpress.com by 213.200.69.106 on 09/08/12
For personal use only.

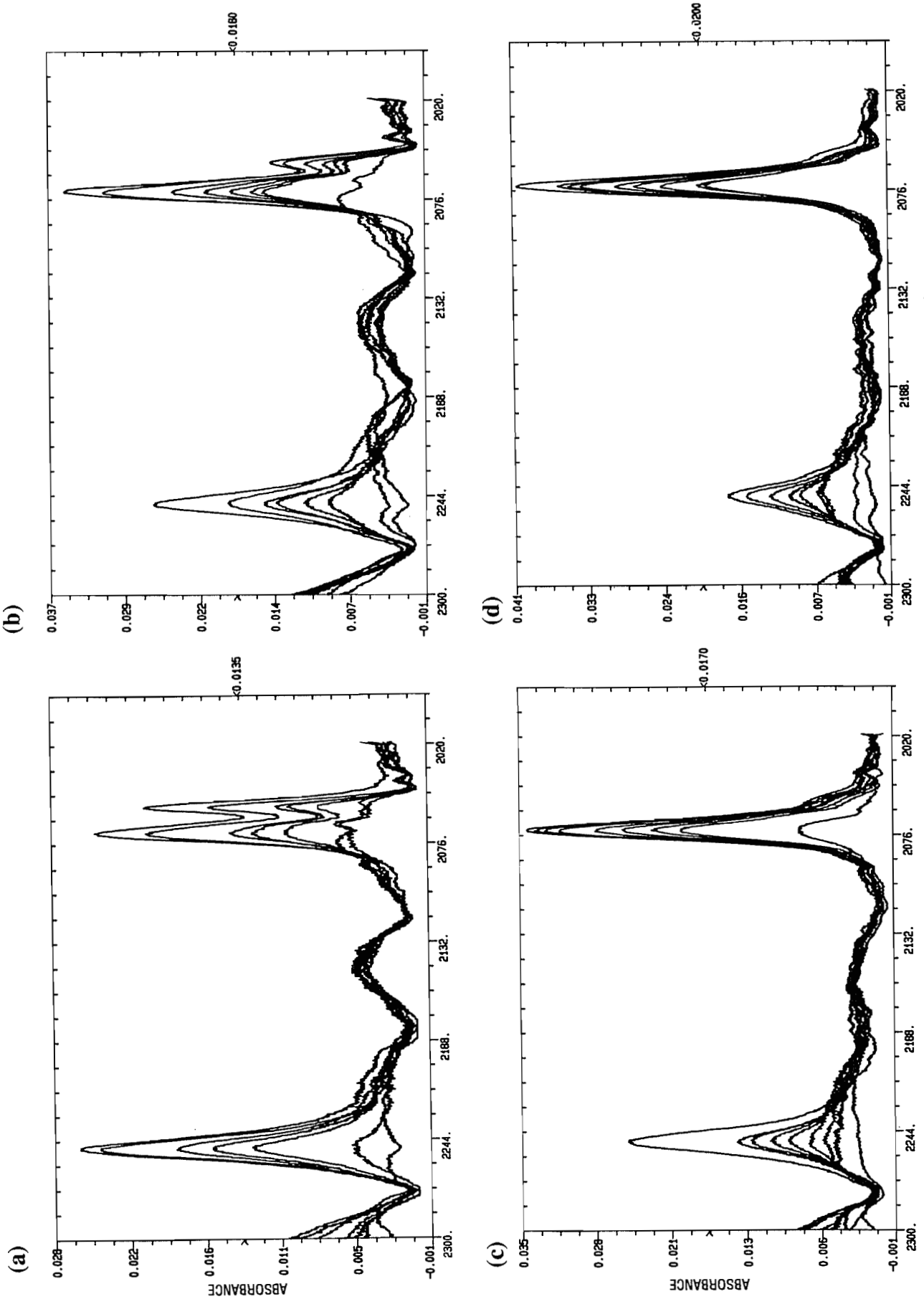

FIG. 5. Time-resolved spectra for the S_N2 reaction of benzyl chloride with tetraethylammonium cyanide in (*a*) 2.5%, (*b*) 5%, (*c*) 15%, and (*d*) 20% aqueous DMF at 30.00°C.

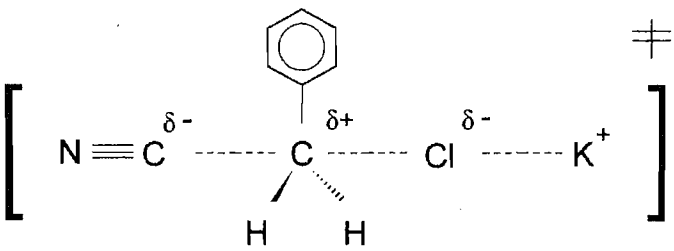

FIG. 6. Electrophilic catalysis in the removal of the leaving group by potassium ion in the S_N2 reaction between cyanide ion and benzyl chloride.

the free energy of the ionic S_N2 transition state. Since both of these effects increase the free energy of activation, the rate of reaction decreases as the percent water increases. Adding water also reduces the rate by shifting the equilibrium between the DMF- and water-solvated cyanide ions towards the less reactive water-solvated cyanide ion.

Another noteworthy observation is the 20% increase in k_2 when the cyanide salt is changed from tetraethylammonium cyanide to potassium cyanide in 5% aqueous DMF, Table 1. A possible explanation for this is that the potassium ion provides electrophilic catalysis in the removal of the leaving group, Fig. 6. Electrophilic catalysis has been proposed for elimination reactions in organic solvents (17, 18).

Finally, when HCN and benzyl chloride were added to dry DMF or 20% aqueous DMF at 30.00°C, the HCN absorption did not decrease and there was no evidence of any product absorption at 2250 cm^{-1} even after 48 h. Thus, no reaction occurs in either DMF or 20% aqueous DMF when the cyanide ion is added as HCN. Therefore, HCN does not ionize and react with benzyl chloride in either solvent.

Reaction of benzylmethyl-4-substituted phenylsulphonium salts with tetraethylammonium cyanide in 20% aqueous DMF

The S_N2 reactions of cyanide ion with benzylmethyl-4-chlorophenylsulphonium perchlorate and benzylmethyl-4-methoxyphenylsulphonium perchlorate in 20% aqueous DMF yielded spectra similar to those obtained when benzyl chloride was the substrate. The absorption at 2074 cm^{-1} for the water-solvated cyanide ion decreased and the benzyl cyanide absorption at 2250 cm^{-1} increased. The least-squares fits of the second-order plots for these reactions had correlation coefficients of 0.996 and 0.992 for the benzylmethyl-4-chlorophenylsulphonium perchlorate and benzylmethyl-4-methoxyphenylsulphonium perchlorate, respectively. The rate constants for these reactions are also given in Table 1. The ratio of the rate constants for the two substrates (k_{Cl}/k_{MeO}) is ca. 11. A similar ratio was obtained when these two substituents were present in the leaving group in the S_N2 reactions between benzyldimethyl-4-substituted phenylammonium ions with thiophenoxide ion in DMF (19). The large k_{Cl}/k_{MeO} value shows that these reactions are very susceptible to changes in the leaving group and will be useful for elucidating how substituents alter the structure of the S_N2 transition state.

Kinetic analysis of the benzyl chloride – cyanide ion reactions

The FT-IR spectra clearly demonstrate that there are two forms of cyanide ion in these systems, a DMF- and a water-solvated species. Given that (*i*) the rate constant was too large to measure in dry DMF and (*ii*) the rate decreases as the water content in the solvent increases, the DMF-solvated ion must be the more reactive species. This conclusion is supported by the work of Parker (20), who demonstrated that anions are much less strongly solvated and, therefore, are much more reactive in dipolar aprotic solvents than in protic solvents.

TABLE 3. Rate constants, k_2', for the reaction of the DMF-solvated cyanide ion with benzyl chloride in various aqueous DMF solutions at 30.00°C

% H_2O	$k_2'/10^{-3}$ (L mol^{-1} s^{-1})
2.5	10.6
5.0	12.5
15	5.5_6
20	8.4_0

The ratio of the absorptions, and hence the ratio of the concentrations of the two cyanide ion species, remains constant throughout the reaction. This means there is a rapid pre-equilibrium between the two forms of the cyanide ion followed by a rate-determining reaction between the DMF-solvated cyanide ion and benzyl chloride, eq. [7]:

$$[7] \quad (CN^-)_W \overset{K_D}{\rightleftharpoons} (CN^-)_{DMF} + BzCl \xrightarrow{k_2'} BzCN + Cl^-$$

where the subscripts W and DMF refer to the water and DMF pseudo phases, respectively, k_2' is the second-order rate constant for the reaction between the DMF-solvated cyanide ion and benzyl chloride, and K_D is the distribution coefficient for the cyanide ion between the two pseudo phases, eq. [6].

The kinetic expression for the rate-determining step is

$$[8] \quad \text{rate} = k_2' [CN^-]_{DMF}[BzCl]$$

Since $[CN^-] = [CN^-]_{DMF} + [CN^-]_W$, eq. [6] can be rearranged to give:

$$[9] \quad [CN^-]_{DMF} = K_D/\{\phi_W/(1 - \phi_W) + K_D\} \cdot [CN^-]$$

Substituting eq. [9] into eq. [8] yields:

$$[10] \quad \text{rate} = k_2 [CN^-][BzCl]$$

where the experimentally determined rate constant, k_2, is

$$[11] \quad k_2 = k_2' K_D/\{\phi_W/(1 - \phi_W) + K_D\}$$

The k_2' values were determined in the various aqueous DMF solvents using the average K_D, and the second-order rate constants, k_2, Table 1. These k_2' values, along with the percent water in the mixed solvent, are given in Table 3.

Given the error in K_D (22%) and k_2 (5%), the error in the k_2' values is in the order of 30%. Although the k_2' values could be the same in all the aqueous DMF solutions (the average is 9.3 ± 3.0), it seems more likely that they decrease slightly as the water content in the mixed solvent increases. This is more likely because k_2' in 15% aqueous DMF is lower than k_2' in 5% aqueous DMF, even when the sizable error in k_2' is considered.

Using the above model, the k_2' values should be independent of solvent composition and equal to the rate constant for

Can. J. Chem. Downloaded from www.nrcresearchpress.com by 213.200.69.106 on 09/08/12
For personal use only.

the reaction in dry DMF. However, these rate constants are at least two orders of magnitude lower than the rate constant for this reaction in dry DMF. Since K_D accounts for the shift in the equilibrium between the DMF- and the water-solvated cyanide ion, the much smaller values for k_2' in aqueous DMF must be due to changes in the solvation of the reactants and (or) the transition state.

As noted above, the absorption wave number for the DMF-solvated cyanide ion, and hence the number of water molecules in the solvation shell, increases with increasing water content. The increased number of water molecules will lower the free energy of the cyanide ion, increase the activation energy, and decrease k_2'. However, it is unlikely that this effect is large because the shift in the wave number for the peak is small and Haberfield et al. (15, 16) showed that the free energy of the transition state is much more sensitive to changes in solvent than the free energy of the reactants. Therefore, it must be concluded that the decrease in k_2' is primarily due to an increase in the free energy of the transition state. It is important to note that this conclusion would be reached even if the reaction were assumed to occur in a single homogeneous phase.

Finally, it is interesting to note that k_2' decreases markedly when the solvent is changed from dry DMF to 2.5% aqueous DMF and decreases only slightly as the water content is increased further to 20%. This means that the change that occurs in transition state solvation when a protic solvent is added to a dipolar aprotic solvent is virtually complete when as little as 2.5% water is present.

Conclusion

This FT-IR study has shown that cyanide salts exist as both water-solvated and DMF-solvated ions, and not as ion pairs, in aqueous DMF solutions. The concentrations of these two species are dependent upon the composition of the solvent, and the equilibrium between the two forms of the cyanide ion can be described using a pseudo two-phase model.

The rate constants for the S_N2 reaction between tetraethylammonium cyanide and benzyl chloride have been analyzed using the pseudo two-phase model. The reaction proceeds in two steps: a fast pre-equilibrium between the two forms of the cyanide ion followed by a rate-determining reaction between the DMF-solvated cyanide ion and benzyl chloride. The rate constant for the rate-determining step decreases markedly with as little as 2.5% water and then only slightly as the water content is further increased to 20%. These changes are primarily due to solvation effects in the transition state.

Changing the cyanide salt to KCN from tetraethylammonium cyanide increased the rate of reaction slightly. This may be due to electrophilic catalysis in the removal of the leaving group. Both spectroscopic and kinetic studies have shown that HCN does not ionize in DMF or aqueous DMF solutions and no reaction was found even in 20% aqueous DMF. This clearly demonstrates that cyanide ion is the reactive species in the S_N2 reaction with benzyl chloride.

Finally, the cyanide ion displacement reaction of sulphonium salts with different leaving groups is sensitive to changes in the substituent on the leaving group. Thus, these reactions make a good system for studying substituent effects on the structure of the S_N2 transition state.

Acknowledgements

The authors gratefully acknowledge the financial support provided by the Natural Sciences and Engineering Research Council of Canada.

1. A. Loupy. Bull. Chim. Soc. Fr. 2662 (1975).
2. A. Loupy and J. Seyden-Penne. Bull. Chim. Soc. Fr. 2306 (1971).
3. A. Loupy and J. Seyden-Penne. C.R. Seances Acad. Sci. Ser. C: **273**, 1665 (1971).
4. A. Loupy and J. Corset. J. Solution Chem. **5**, 817 (1976).
5. A. Loupy and J. Corset. C.R. Seances Acad. Sci. Ser. C: **279**, 713 (1978).
6. R.L. Shriner, R.C. Fuson, and D.Y. Curtin. The systematic identification of organic compounds. 4th ed. J. Wiley and Sons, New York. 1959. p. 149.
7. B. Schowen. Ph.D. Thesis, Massachussets Institute of Technology, 1960.
8. G.D. Parkes. Mellor's modern inorganic chemistry. Longman, Green and Co. Ltd., 1967. pp. 410–411.
9. K.J. Laidler. Chemical kinetics, 2nd ed. McGraw–Hill Book Co., New York. 1965. p. 9.
10. J.J. Christensen, D.J. Eatough, and R.M. Izatt. Chem. Rev. **74**, 351 (1974).
11. L.H. Jones and R.A. Penneman. J. Chem. Phys. **22**, 965 (1954).
12. M. Bachellan, P. Gans, and J. Bernard Gill. J. Chem. Soc. Faraday Trans. **88**, 3327 (1992).
13. P. Gans. Comput. Chem. **1**, 291 (1977).
14. D.A. White and M.M. Baizer. J. Chem. Soc. Perkin Trans. I, 2230 (1973).
15. P. Haberfield, L. Clayman, and J.S. Cooper. J. Am. Chem. Soc. **91**, 787 (1969).
16. P. Haberfield, A. Nudelman, A. Bloom, R. Romm, H. Ginzberg, and P. Steinhertz. Chem. Commun. 194 (1968).
17. P.J. Smith, K.S. Rangappa, and K.C. Westaway. Can. J. Chem. **63**, 100 (1985).
18. P.J. Smith and K.C. Westaway. Can. J. Chem. **65**, 2149 (1987).
19. K.C. Westaway and S.F. Ali. Can. J. Chem. **57**, 1354 (1979).
20. A.J. Parker. Chem. Rev. **69**, 1 (1969).

Can. J. Chem. Downloaded from www.nrcresearchpress.com by 213.200.69.106 on 09/08/12
For personal use only.

Novel quinazolinones and enniatins from *Fusarium lateritium* Nees

YOULA S. TSANTRIZOS[1] AND XIAO-JIN XU
Department of Chemistry and Biochemistry, Concordia University, Montréal, QC H3G 1M8, Canada

AND

FRANÇOISE SAURIOL AND ROSEMARY C. HYNES
Department of Chemistry, McGill University, Montréal, QC H3A 2K6, Canada

Received January 18, 1993

YOULA S. TSANTRIZOS, XIAO-JIN XU, FRANÇOISE SAURIOL, and ROSEMARY C. HYNES. Can. J. Chem. **71**, 1362 (1993).

Fusarium lateritium Nees is a natural antagonist of the plant pathogen *Eutypa armeniacae*. In an effort to show that this biological phenomenon is chemically mediated, the bioactive metabolites of *F. lateritium* were investigated. The cytotoxic alkaloids 2-(1-hydroxyethyl)-4(3*H*)quinazolinone (**1**) and 2-acetyl-4(3*H*)quinazolinone (**2**), and the three cyclohexadepsipeptides, enniatins B (**3**), B_1 (**4**), and A_1 (**5**), were isolated and characterized. Metabolites **3**, **4**, and **5** were found to exhibit strong antifungal activity against *E. armeniacae*. The structures of the novel metabolites **1** and **2** were elucidated by spectroscopic analysis and that of **2** was confirmed by X-ray crystallography. The absolute stereochemistry of **1** was investigated by ^1H and ^{19}F NMR analysis of its Mosher ester derivative.

YOULA S. TSANTRIZOS, XIAO-JIN XU, FRANÇOISE SAURIOL et ROSEMARY C. HYNES. Can. J. Chem. **71**, 1362 (1993).

Le *Fusarium lateritium* Nees est un antagoniste naturel de la plante pathogène *Eutypa armeniaceae*. Dans le but de démontrer que ce phénomène biologique est d'origine chimique, on a étudié les métabolites bioactifs du *F. lateritium*. On a isolé et caractérisé les alcaloïdes cytotoxiques 2-(1-hydroxyéthyl)-(3*H*)quinazolin-4-one (**1**) et 2-acétyl-(3*H*)quinazolin-4-one (**2**) ainsi que les trois cyclohexadepsipeptides enniatines B (**3**), B_1 (**4**) et A_1 (**5**). On a trouvé que les métabolites **3**, **4** et **5** montrent une forte activité antifongique envers la *E. armenacieae*. On a élucidé les structures de ces nouveaux métabolites **1** et **2** par analyse spectroscopique et on a confirmé celle du composé **2** par cristallographie de rayons X. On a étudié la stéréochimie absolue du composé **1** par analyse RMN du ^1H et du ^{19}F de son dérivé ester de Mosher.

[Traduit par la rédaction]

Introduction

In 1983, Carter (1*a*) described the use of *Fusarium lateritium* Nees macroconidia as a biofungicide for the protection of commercial apricot orchards from *Eutypa armeniacae* infections (1). *Eutypa armeniacae* is an aggressive plant pathogen associated with sapwood necrosis (commonly known as "dieback disease") in fruit trees, grapevines, and ornamental plants around the world (2). Thus, an investigation into the metabolites of *F. lateritium* that exhibit antifungal activity against *E. armeniacae* was undertaken.

A biologically active mixture of metabolites was obtained from *F. lateritium* cultures grown on solid Czapex-Dox plus yeast medium. The subsequent bioassay-guided separation of the active components led to the isolation of the novel alkaloids 2-(1-hydroxyethyl)-4(3*H*)quinazolinone (**1**) and 2-acetyl-4(3*H*)-quinazolinone (**2**), and the three enniatins B (**3**), B_1 (**4**), and A_1 (**5**). The structural identity of these compounds was explored extensively by 2D-NMR studies using COSY, HMQC, and HMBC experiments. It is noteworthy that the general structure of the enniatin cyclodepsipeptides has been known since the late 1940s (3). However, the complete NMR data, for all nine of the known enniatins (Fig. 1), were reported only very recently; during preparation of this manuscript, the ^1H and ^{13}C NMR of enniatins A_1 and B_1 were reported by Blackwell, Miller and co-workers for the first time (4).

Results and discussion

The agricultural importance of *F. lateritium* as both a biofungicide (2, 5) and a bioherbicide (6) has been known for some time, although investigations into the metabolites of this organism have been limited to the isolation of the antibiotic lateropyrone (7), the mycotoxin diacetoxyscirpenol (8), and the insecticidal cyclodepsipeptide beauvericin (5, 9). The production of enniatins from *F. lateritium* has also been described; however, they were isolated as a mixture and only partly identified (5, 9).

In this work, a bioassay-guided purification scheme was developed for the isolation of *F. lateritium* metabolites exhibiting antifungal activity against the plant pathogen *E. armeniacae*. A crude metabolite mixture of *F. lateritium* was extracted from infected solid Czapex-Dox medium with CH_2Cl_2 and partitioned by reversed phase flash column chromatography (10). Metabolite **1** eluted from the column in 45–55% aqueous MeOH and it was isolated as an amorphous white solid after further purification by normal phase flash column chromatography.

The ^1H NMR of **1** (Table 1) revealed the presence of a methyl group at δ 1.53 (d, 3H), coupled to an adjacent -CH-O- moiety at δ 4.73 (q, 1H). The remaining signals were assigned to four neighboring aromatic protons (δ 7.49, 7.66, 7.79, and 8.18) whose relative positions were determined by selective decoupling experiments. The ^{13}C NMR indicated the presence of 10 nonequivalent carbon atoms, a methyl at δ 22.4, a -CH-O- at δ 68.6, three quaternary olefinic carbons at δ 122.2, 149.6, and 161.6 (two of which had to be attached to a heteroatom), four protonated olefinic carbons at δ 127.2, 127.5, 127.8, and 135.9, and an amide carbonyl at δ 164.3. Although the signal at δ 127.5 was unusually broad and of very low intensity for a protonated carbon, HMQC NMR clearly showed its ^1J coupling to the proton at δ 7.66. This effect may be due to further long-range coupling with ^{15}N.

High-resolution CI-MS of **1** gave a molecular ion at 191.08201 for the ($M^+ + 1$) ion (calculated: 191.08205), indicating an elemental composition of $C_{10}H_{10}N_2O_2$. Its IR

[1]Author to whom correspondence may be addressed.

Can. J. Chem. Downloaded from www.nrcresearchpress.com by 203.198.23.82 on 09/08/12
For personal use only.

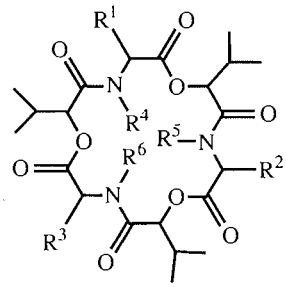

Enniatin	R^1	R^2	R^3	R^4	R^5	R^6
A	*s*-Bu	*s*-Bu	*s*-Bu	Me	Me	Me
(**5**) A_1	i-Pr	*s*-Bu	*s*-Bu	Me	Me	Me
(**3**) B	i-Pr	i-Pr	i-Pr	Me	Me	Me
(**4**) B_1	i-Pr	i-Pr	*s*-Bu	Me	Me	Me
B_2	i-Pr	i-Pr	i-Pr	H	Me	Me
B_3	i-Pr	i-Pr	i-Pr	H	H	Me
B_4 (D)	i-Pr	i-Pr	i-Bu	Me	Me	Me
E	i-Pr	*s*-Bu(i-Bu)	i-Bu(*s*-Bu)	Me	Me	Me
F	i-Bu	*s*-Bu	*s*-Bu	Me	Me	Me

FIG. 1. Structures of enniatins.

TABLE 1. ^1H and ^{13}C NMR data of the quinazoline metabolites **1** and **2**

	Metabolite **1** (500 MHz, CD_3OD)			Metabolite **2** (290 MHz, $CDCl_3$)	
C	^1H (δ)	^{13}C (δ)[a]	HMBC (δ)[b]	^1H (δ)	^{13}C (δ)[a]
2		161.6			147.7
NH				~9.9	
4		164.3			160.5
5		122.2			123.5
6		149.6			145.3
7	7.66	127.5	122.2, 127.8	7.80[c]	129.4
8	7.79	135.9	127.2, 149.6	7.80[c]	134.8
9	7.49	127.8	122.2, 127.2	7.60	126.9
10	8.18	127.2	135.9, 149.6	8.33	129.2
1′	4.73	68.6	22.4, 161.6		194.1
2′	1.53	22.4	68.6, 161.6	2.75	24.5

[a]Assignments based on the HMQC spectral data.
[b]^{13}C shifts that are correlated to ^1H shifts in the HMBC spectra.
[c]Overlapping signals in the ^1H NMR (δ 7.78–7.88).

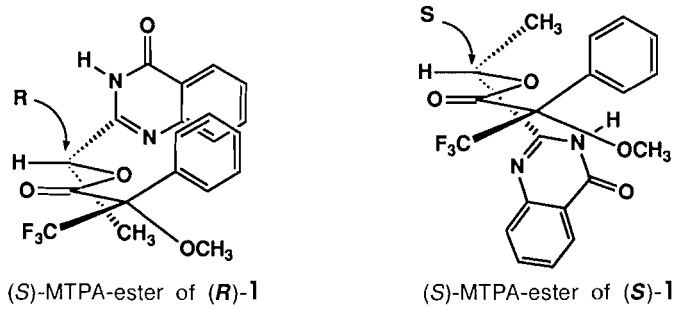

FIG. 2. Absolute stereochemistry of metabolite (**1**).

spectrum supported the existence of N—H, O—H, C=N, and amide C=O bonds. Based on this data, as well as the long-range H–C connectivity suggested by the HMBC NMR, the structure of 2-(1-hydroxyethyl)-4(3*H*)quinazolinone was assigned to metabolite **1**.

The absolute stereochemistry of **1** was investigated using Mosher's method (11). In this technique, the absolute stereochemistry of a carbinol center is based on the assumption that the most stable conformation of its Mosher's ester (MTPA-esters) is that which places the carbonyl proton, the ester carbonyl, and the trifluoromethyl group of the MTPA moiety on the same plane (12). Consequently, in the case of the MTPA-esters of **1** (Fig. 2), the methyl substituent of the **S** enantiomer will be located under the shielding effects of the phenyl group and appear upfield from the equivalent signal in the **R** enantiomer. Using the same argument, the methoxy substituent of the MTPA moiety will be exposed to the shielding effects of the quinazolinone ring system and it should be shifted upfield in the (*S*)-MTPA-ester of the **S** enantiomer but not in that of the **R**.

Can. J. Chem. Downloaded from www.nrcresearchpress.com by 203.198.23.82 on 09/08/12
For personal use only.

TABLE 2. ^1H and ^{19}F NMR data of the (*S*)-MTPA-esters **1**[a] (270 MHz, $CDCl_3$)

	(*S*)-MTPA-ester (**R**)-**1**		(*S*)-MTPA-ester (**S**)-**1**	
	^1H (δ)	^{19}F (δ)	^1H (δ)	^{19}F (δ)
$-CH_3$	1.71 (d, J = 6.6 Hz)		1.63 (d, J = 6.6 Hz)	
$-OCH_3$	3.55		3.49	
-CON*H*-	8.9		9.2	
$-CF_3$		−71.7		−71.4

[a]Only the signals shown above were unambiguously assigned (due to multiple overlapping, the remaining signals in the ^1H NMR spectrum of the MTPA-esters of **1** were not assigned).

Fluorine NMR analysis has also been used for making stereochemical assignments of MTPA-esters. The fundamental argument is again based on the preferred coplanar conformation of the trifluoromethyl group and the ester carbonyl. However, the relative extent of this preference has been shown to depend on the magnitude of steric interactions between the phenyl group of the MTPA moiety and the adjacent carbinol substituent (13). Therefore, it is expected that the destabilizing quinazolinone–phenyl interactions in the (*S*)-MTPA-ester (**R**)-**1** will force the trifluoromethyl group away from the carbonyl deshielding plane and result in an upfield shift of the $-CF_3$ signal (relative to that of the (*S*)-MTPA-ester (**S**)-**1**) in the ^{19}F NMR.

The (*S*)-MTPA-ester of metabolite **1** was prepared from the (*R*)-MTPA chloride following standard literature procedures (12). Both the ^1H and ^{19}F NMR spectra were consistent with the presence of a diastereomeric mixture, composed of the (*S*)-MTPA-ester (**R**)-**1** and the (*S*)-MTPA-ester (**S**)-**1** in a ratio of ~1.5:1 (Table 2). Thus, the small, negative optical rotation observed for metabolite **1** was attributed to the major **R** enantiomer. It has been speculated that the loss of optical purity is perhaps due to an equilibrium between compound **1** and its **1′** tautomer.

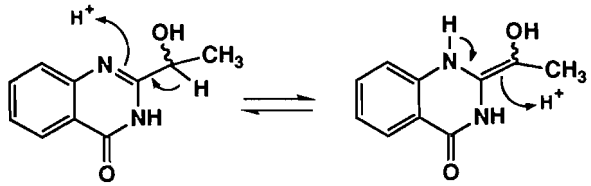

1 **1′**

The closely related metabolite **2** was eluted from the reversed phase column in 60–70% aqueous MeOH and it was further purified by crystallization from CH_2Cl_2. Unlike the enniatin metabolites (**3**, **4**, and **5**), metabolites **1** and **2** were not produced in liquid cultures of *F. lateritium* in any appreciable amounts (liquid Czapex-Dox plus 5% yeast and malt extract were tried). The ^1H NMR of **2** (Table 1) revealed the presence of an acetyl methyl at δ 2.75, four aromatic protons (δ 7.6–8.3), and a very broad signal at δ ~9.9 (1H). The ^{13}C NMR was consistent with the presence of an acetate unit (C=O, δ 194.1; Me, 24.5) and an amide (δ 160.5), in addition to seven other aromatic or olefinic carbons: four protonated and three quaternary, of which two had chemical shifts consistent with the presence of =C-N moieties (δ 147.7 and 145.3). The CI-MS data of metabolite **2** gave a molecular ion at 189 (M^+ + 1) suggesting an elemental composition of $C_{10}H_8N_2O_2$, and its IR data supported the existence of N—H, N=C, and C=O bonds (a strong, very broad carbonyl absorption at 1692 cm^{-1} was observed which was attributed to both an amide and a conjugated ketone). Based on this data, the structure of 2-acetyl-4(3*H*)quinazolinone was assigned to **2**, which was later confirmed by X-ray crystallography (ORTEP diagram shown in Fig. 3).[2]

Metabolites **1** and **2** are new members of the quinazoline family of natural products (Fig. 4). Such compounds exhibit a variety of biological properties and have been isolated from both plant and microbial sources. Among the best known examples are the plant metabolites rutaecarpine (**6**, hypertensive agent (14)), arborine (**7**, antipyretic and anthelmintic agent (15)), febrifugine **8** and isofebrifugine **9** (antimalarial (16)), and the microbial metabolites tryptanthrin (**10**, antibiotic (17)), fumiquinazolines A (**11**), B (**12**), and C (**13**) (cytotoxic agents (18)).

The enniatin metabolites **3**, **4**, and **5** were first eluted from the reversed phase flash column as a mixture (with 80–100% aqueous MeOH) and subsequently purified by semipreparative HPLC. FAB MS showed the characteristic molecular ions of enniatins B (**3**), B_1 (**4**), and A_1 (**5**), along with several metal complex ions (Na^+, K^+, and Cs^+) indicative of the ionophoric properties of these compounds (19). All of the IR and NMR data of metabolites **3**, **4**, and **5** were consistent with their identification as the enniatins B (20), B_1 and A_1 (5), respectively.

The enniatin metabolites are known to exhibit insecticidal (21, 22), antibiotic (23), and phytotoxic activities (24), and to also inhibit cholesterol biosynthesis (25). In this work, the antagonistic effect of *F. lateritium* against the important plant pathogen *E. armeniacae* was investigated. Potent antifungal activity against *E. armeniacae* was observed with metabolites **3**, **4**, and **5**. Therefore, it appears that the production of enniatins B (**3**), B_1 (**4**), and A_1 (**5**) by *F. lateritium* may play a key role in the biological effects of this organism as a biofungicide (1).

As part of a broader biological screening work of microbial metabolites, some of the compounds presented in this paper were evaluated for their ability to inhibit HIV replication in C8166 cells (as evidenced by a reduction of HIV-

[2]X-ray data for metabolite **2** (16 pages) have been deposited as supplementary material and may be purchased from: The Depository of Unpublished Data, Document Delivery, CISTI, National Research Council Canada, Ottawa, Canada K1A 0S2.

Tables of atomic parameters and of bond lengths and angles (5 pages) have also been deposited with the Cambridge Crystallographic Data Centre, and can be obtained on request from The Director, Cambridge Crystallographic Data Centre, University Chemical Laboratory, 12 Union Road, Cambridge, CB2 1EZ, U.K.

Can. J. Chem. Downloaded from www.nrcresearchpress.com by 203.198.23.82 on 09/08/12
For personal use only.

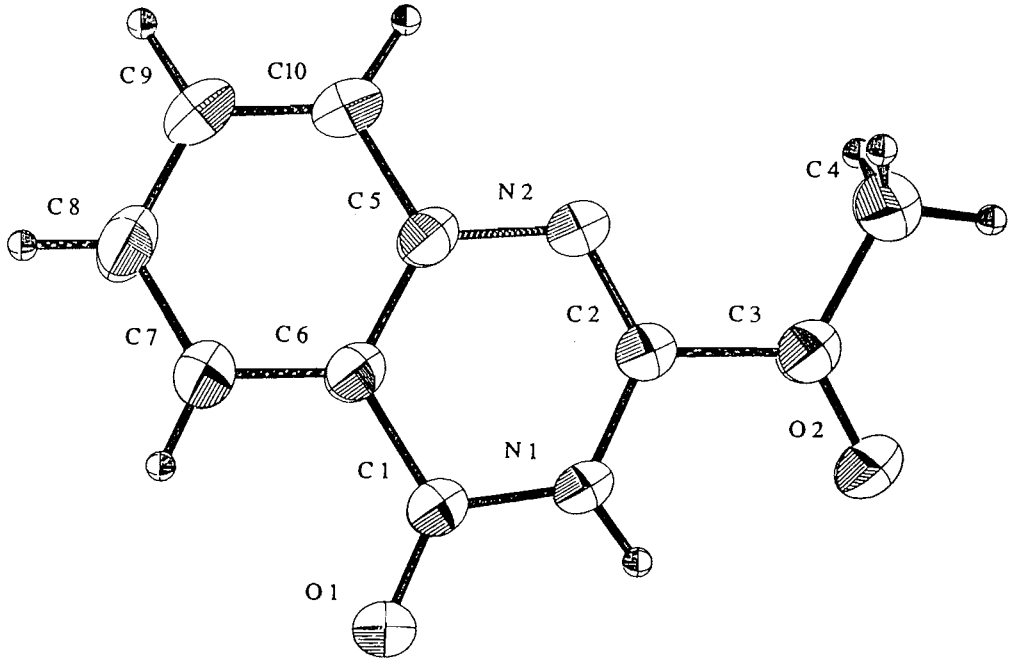

FIG. 3. ORTEP diagram of metabolite **2**.

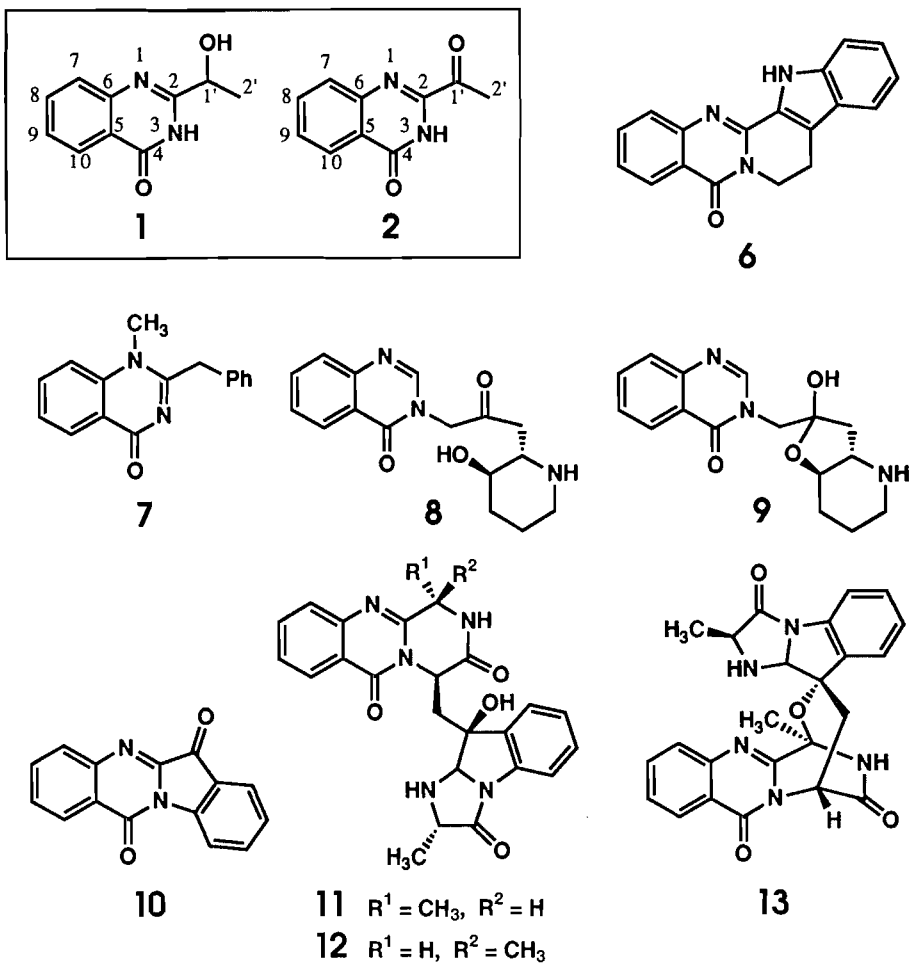

FIG. 4. Quinazoline natural products.

Can. J. Chem. Downloaded from www.nrcresearchpress.com by 203.198.23.82 on 09/08/12
For personal use only.

induced cytopathogenic effects (26)). Metabolite **2** was found to cause 23% inhibition of syncytia formation at concentrations of 3 μg/mL. Higher concentrations were not tested since it was found to be cytotoxic to the host cells at concentrations >6 μg/mL. Strong cytotoxicity at concentrations >0.8 μg/mL was also observed with enniatin B_1 (**4**), which was found to cause a 41% inhibition of the HIV protease enzyme at concentrations of 100 μg/mL. (Details on the biological properties of all five metabolites will be published elsewhere.)

Experimental

General

Nuclear magnetic resonance spectra were obtained at 20–22°C using Jeol 270 MHz-CPF, Varian XL-200 MHz, Varian Gemini 200, and Varian Unity 500 MHz instruments. ^1H and ^{13}C NMR chemical shifts are quoted in ppm and are referenced to the internal deuterated solvent downfield from tetramethylsilane (TMS). ^{19}F NMR was recorded in $CDCl_3$; $CFCl_3$ was used as an external reference.

Mass spectra were performed at the Biomedical Mass Spectrometry Unit, McGill University, and the Mass Spectrometry Centre, Department of Chemistry, University of Ottawa. FAB mass (Cs^+ particles, diethanolamine matrix) spectra were obtained using a Concept 2H Kratos instrument, EI mass spectra were obtained using a VG 7070 instrument, and high-resolution $(NH_3)Cl$ mass spectra were obtained using a ZAB 2F HS instrument (resolution: 10^4).

Melting points were measured using a Gallenkamp capillary apparatus and they are uncorrected. Ultraviolet spectra were recorded on a Hewlett Packard 8452A diode array spectrophotometer. Infrared spectra were recorded on a Bomem Michelson 102 FTIR spectrophotometer calibrated to the 1602 cm^{-1} line of polystyrene.

Chromatography

Reversed phase flash column chromatography was carried out on silica gel (Merck Kieselgel 60, 230–400 mesh, no. 9385) reacted with *n*-octadecyltrichlorosilane. C18 reversed phase silica gel was prepared following previously reported procedures (10*a*).

HPLC

Doubly distilled H_2O and HPLC grade MeOH and MeCN were filtered through a 0.45 μm filter membrane (Millipore Corp., Bedford, Mass.) before they were used in HPLC. Analysis and purification were carried out on a semipreparative, reversed phase, C18 column; Waters Nova-Pak (25 mm × 100 mm, 6 μm, 60A) using a Waters instrument (pump model W600EP, UV/VIS detector model M486P, Rheodyne injector). All retention times were automatically recorded from the time of injection.

General extraction of active metabolites from F. lateritium

Stock cultures of *F. lateritium* were maintained on Czapex-Dox (Difco) plus 5% yeast agar in slant tubes at 4°C. A small amount of mycelium was used to inoculate 40 Czapex-Dox plus 5% yeast agar plates, which were then incubated in the dark, at room temperature, for a period of 5 weeks. A crude metabolite mixture was isolated from the infected agar plates by soaking the agar in CH_2Cl_2 (2 × 500 mL) over a period of 24 h. Evaporation of the CH_2Cl_2 led to the isolation of a metabolite mixture (~240 mg) exhibiting strong antifungal activity against *E. armeniacae*.

The crude metabolite mixture was first purified by flash column chromatography on a C18 reversed phase column (20 mm × 20 cm) (11*a*), using a linear solvent gradient from 0.1% aqueous AcOH to 100% MeOH, at a flow rate of ~4 cm/min. Metabolites **1** and **2** eluted from the column in 45–55% and 60–70% aqueous MeOH, respectively, while metabolites **3**, **4**, and **5** eluted in 80–100% aqueous MeOH. Metabolite **1** was further purified by normal phase flash column chromatography using EtOAc, whereas metabolite **2** was purified by crystallization from CH_2Cl_2. Approximately 5–8 mg of each metabolite **1** and **2** were isolated. Pure metabolites **3**, **4**, and **5** were isolated after semipreparative HPLC on a C18 reversed phase column, eluted with 55% MeOH, 15% H_2O, and 30% MeCN. At a flow rate of 5 mL/min, the retention times for metabolites **3**, **4**, and **5** were 22–23, 26–27, and 33–34 min, respectively. The yields of pure enniatins isolated from 40 infected plates were approximately 12 mg of B (**3**), 15 mg of B_1 (**4**), and 3 mg of A_1 (**5**).

2-(1-Hydroxyethyl)-4(3H)quinazolinone (1): TLC: EtOAc, R_f = 0.34; mp 155–156°C, $[\alpha]_D$ −26.6 (the calculated $[\alpha]_D$ for the *R* enantiomer was based on ~20% ee of *R* in the sample of metabolite **1** isolated, *c* 0.258, MeOH, 20°C). UV (MeOH, nm): max 226, min 264, 304: IR (MeCN): 3550, 3542 (NH, OH), 1690 (-CO-NH-), and 1605 (C=N) cm^{-1}. ^1H NMR (500 MHz, CD_3OD) δ: 1.53 (d, J = 6.6 Hz, 3H, -C*H*$_3$), 4.73 (q, J = 6.6 Hz, 1H, C*H*-OH), 7.49 (ddd, J_{9-10} = 8.1 Hz, J_{8-9} = 7.8 Hz, J_{7-9} = 2.4 Hz, 1H, H9), 7.66 (d, J_{7-8} = 8.1 Hz , 1H, H7), 7.79 (ddd, J_{7-8} = 8.1 Hz, J_{8-9} = 7.8, J_{8-10} = 2.3 Hz, 1H, H8), and 8.18 (dd, J_{9-10} = 8.1 Hz, J_{8-10} = 2.3 Hz, 1H, H10) ppm. ^{13}C NMR: Table 1. MS (HR, $(NH_3)Cl$): *m/z* calcd. for (M^+ + 1) ion: 191.08205; found: 191.08201.

Preparation of the (S)-MTPA-ester 1

(*R*)-MTPA chloride (10 μL, 52 μmol) was added to a solution of **1** (3.3 mg, 17.4 μmol) in pyridine (~100 μL). After the reaction mixture was allowed to stir at room temperature for 15 h, it was diluted with 10 mL CH_2Cl_2 and the pyridine was removed by extraction with 5% aqueous $CuSO_4$ solution (3 × 10 mL). The residue obtained from the CH_2Cl_2 layer after evaporation was purified by preparative TLC (CH_2Cl_2–EtOAc (1:1), R_f = 0.75). ^1H NMR (270 MHz, $CDCl_3$) δ: 1.63 and 1.71 (d, J = 6.6 Hz, ratio ~1:1.5, Me), 3.49 and 3.55 (s, ratio ~1:1.5, -OMe), 5.9 (m, carbinol C*H*), 7.3–8.2 (overlapping aromatic signals), 8.9 and 9.2 (s, ratio ~1.5:1, -CON*H*-) ppm. ^{19}F NMR (270 MHz, $CDCl_3$) δ: −71.7 and −71.4 (ratio 1.5:1) ppm.

2-Acetyl-4(3H)quinazolinone (2): TLC: CH_2Cl_2/EtOAc (3:1), R_f = 0.59; mp 188.0–188.5°C. UV (H_2O, nm): max 232, min 302. IR ($CDCl_3$): 3351 (NH), 1692 (-CO-NH- and -CO-Me), and 1606 (C=N) cm^{-1}. ^1H NMR (270 MHz, $CDCl_3$) δ: 2.75 (s, 3H, -CO-C*H*$_3$), 7.60 (ddd, J_{9-10} = 8.0 Hz, J_{8-9} = 6.1 Hz, J_{7-9} = 2.3 Hz, 1H, H9), 7.78–7.88 (m, 2H, H7 and H8), 8.33 (dd, J_{9-10} = 8.0 Hz, J_{8-9} = 2.3 Hz, 1H, H10), and ~9.9 (bs, 1H, CO-N*H*) ppm. ^{13}C NMR: Table 1. MS (EI, VG 7070E mass spectrometer), *m/z* (% relative intensity, assignment): 189 (100, M^+ + 1), 175 [25, (M^+ + 1) − CH_2], 133 [20, (M^+ + 1) − (CH-CO-CH_3)].

Enniatin B (3): TLC: CH_2Cl_2/EtOAc (1:3), R_f = ~0.73, mp 167–169°C. $[\alpha]_D$ −114.6 (*c* 0.32, $CHCl_3$, 20°C). IR ($CHCl_3$): 1664 (C=O, amide) and 1732 (C=O, ester) cm^{-1}. ^1H NMR (500 MHz, $CDCl_3$): N-Me-Val δ: 0.88 (d, $J_{\beta-\gamma}$ = 6.8 Hz, 3H, γ-Me), 1.05 (d, $J_{\beta-\gamma}$ = 6.3 Hz, 3H, γ-Me), 2.30 (m, 1H,*[3] H_β), 3.12 (s, 3H, N-Me), 4.51 (d, $J_{\alpha-\beta}$ = 9.3 Hz, 1H, H_α) ppm. Hiv δ: 0.95 (d, $J_{\beta-\gamma}$ = 6.8 Hz, 3H, γ-Me), 0.97 (d, $J_{\beta-\gamma}$ = 5.9 Hz, 3H, γ-Me), 2.27 (m, 1H,* H_β), 5.13 (d, $J_{\alpha-\beta}$ = 8.8 Hz, 1H, H_α) ppm. ^{13}C NMR[4] (500 MHz, $CDCl_3$): N-Me-Val δ: 19.1 and 20.2 (2 γ-Me), 27.7 (C_β), 33.06 (N-Me), 63.0 (C_α), and 169.1 (C=O, amide) ppm. Hiv δ: 18.3 and 18.5 (2 γ-Me), 29.7 (C_β), 75.5 (C_α), and 170.1 (C=O, ester) ppm. FAB MS (Cs^+ particles, diethanolamine matrix), *m/z* (assignment): 640 (M + H)$^+$, 662 (M + Na)$^+$, 678 (M + K)$^+$, 745 (M + DEA + H)$^+$, 772 (M + Cs)$^+$.

Enniatin B_1 (4): TLC: CH_2Cl_2/EtOAc (1:3), R_f ~0.73, mp 122–123°C; $[\alpha]_D$ −106.7 (*c* 0.34, $CHCl_3$, 20°C).[5] IR ($CHCl_3$): 1664

[3]An asterisk (*) indicates overlapping signals; integration and (or) *J* values not clear.

[4]Assignments based on the HMQC and HMBC NMR data.

[5]Enniatin B_1 was isolated by Blackwell, Miller and co-workers (4) as a pale yellow oil having $[\alpha]_D$ +173.8; however, the sign of the optical rotation is a typographical error (private communication).

Can. J. Chem. Downloaded from www.nrcresearchpress.com by 203.198.23.82 on 09/08/12
For personal use only.

(C=O, amide) and 1732 (C=O, ester) cm^{-1}. ^1H NMR (500 MHz, $CDCl_3$): N-Me-Val δ: 0.88 (d, $J_{\beta-\gamma}$ = 6.8 Hz, 3H, γ-Me), 1.05 (d, $J_{\beta-\gamma}$ = 6.4 Hz, 3H, γ-Me), 2.30 (m, 2H,* H_β), 3.13 (s, 6H, 2(N-Me)), 4.45 (d, $J_{\alpha-\beta}$ = 9.3 Hz, 1H, H_α), 4.50 (d, $J_{\alpha-\beta}$ = 9.8 Hz, 1H, H_α) ppm. Hiv δ: 0.93–0.98 (6d, $J_{\beta-\gamma}$ = 6–8 Hz,* 18H, 6 γ-Me), 2.25 (m, 3H,* 3H_β), 5.09 (d, $J_{\alpha-\beta}$ = 9.3 Hz, 1H, H_α), 5.12 (d, $J_{\alpha-\beta}$ = 8.8 Hz, 1H, H_α), 5.15 (d, $J_{\alpha-\beta}$ = 8.8 Hz, 1H, H_α) ppm. N-Me-ILe δ: 0.86 (t, $J_{\gamma-\delta}$ = 7.6 Hz, 3H, δ-Me), 0.99 (d, $J_{\beta-\gamma}$ = 6.8 Hz, 3H, γ-Me), 1.42 and 1.08 (2m, γ-CH_2), 2.16 (m, 1H, H_β), 3.10 (s, 3H, N-Me), 4.72 (d, $J_{\alpha-\beta}$ = 9.3 Hz, H_α). ^{13}C NMR[5] (500 MHz, $CDCl_3$): N-Me-Val δ: 19.17 and 20.28 (4 γ-Me), 27.77 and 27.85 (2 C_β), 33.16 and 33.31 (2 N-Me), 63.12 and 63.30 (2 C_α), and 169.04 (2 C=O, amide) ppm. Hiv δ: 18.2, 18.3, and 18.5 (6 γ-Me), 29.7 (3 C_β), 75.20, 75.61, and 75.62 (3 C_α), and 170.04, 170.08, and 170.2 (3 C=O, ester) ppm. N-Me-ILe δ: 10.67 (δ-Me), 15.96 (γ-Me), 25.08 (γ-CH_2), 32.54 (N-Me), 33.66 (C_β), 61.24 (C_α), 169.0 (C=O, amide) ppm. FAB MS (Cs^+ particles, diethanolamine matrix), *m/z* (assignment): 654 $(M + H)^+$, 676 $(M + Na)^+$, 692 $(M + K)^+$, 759 $(M + DEA + H)^+$, 786 $(M + Cs)^+$.

Enniatin A_1 (5): TLC: CH_2Cl_2/EtOAc (1:3), $\mathbf{R}_f$ = ~0.73. $[\alpha]_D$ −110.9 (c 0.08, $CHCl_3$, 20°C). IR ($CHCl_3$): 1664 (C=O, amide) and 1732 (C=O, ester) cm^{-1}. ^1H NMR (500 MHz, $CDCl_3$): N-Me-Val δ: 0.90 (d, $J_{\beta-\gamma}$ = 7.3 Hz, 3H, γ-Me), 1.07 (d, $J_{\beta-\gamma}$ = 6.3 Hz, 3H, γ-Me), 2.30 (m, 1H, H_β), 3.14 (s, 3H, N-Me), 4.45 (d, $J_{\alpha-\beta}$ = 9.3 Hz, 1H, H_α) ppm. Hiv α: 0.94–1.0 (6d, $J_{\beta-\gamma}$ = 6–8 Hz,* 18H, 6 γ-Me), 2.25 (m, 3H,* 3H_β), 5.09 (d, $J_{\alpha-\beta}$ = 8.3 Hz, 1H, H_α), 5.12 (d, $J_{\alpha-\beta}$ = 8.3 Hz, 1H, H_α), 5.15 (d, $J_{\alpha-\beta}$ = 8.9 Hz, 1H, H_α) ppm. N-Me-ILe δ: 0.87 (t, $J_{\gamma-\delta}$ = 7.3 Hz, 6H, 2 δ-Me), 1.00 (d, $J_{\beta-\gamma}$ = 6.3 Hz, 6H, γ-Me), 1.10 and 1.42 (2m, 4H, 2 γ-CH_2), 2.06 (m, 2H, 2H_β), 3.11 (s, 6H, 2 N-Me), 4.69 (d, $J_{\alpha-\beta}$ = 12.0 Hz, 1H, H_α), 4.71 (d, $J_{\alpha-\beta}$ = 11.2 Hz, 1H, H_α) ppm. ^{13}C NMR[3] (500 MHz, $CDCl_3$): N-Me-Val δ: 19.3 and 20.4 (2 γ-Me), 27.9 (C_β), 33.4 (N-Me), 63.4 (C_α), and 169.1 (2 C=O, amide) ppm. *Hiv* δ: 18.3, 18.4, and 18.5 (6 γ-Me), 29.7 (3 C_β), 75.3 and 75.8 (3 C_α), and 170.1 and 170.2 (3 C=O, ester) ppm. N-Me-ILe δ: 10.7 (2 δ-Me), 16.0 (2 γ-Me), 25.2 (2 γ-CH_2), 32.6 (2 N-Me), 33.7 and 33.8 (2 C_β), 61.4 and 61.5 (2 C_α), 169.1 (2 C=O, amides) ppm. FAB MS (Cs^+ particles, diethanolamine matrix), *m/z* (assignment): 668 $(M + H)^+$, 690 $(M + Na)^+$, 706 $(M + K)^+$, 773 $(M + DEA + H)^+$, 800 $(M + Cs)^+$; (Cs^+ particles, glycerol matrix), *m/z* (assignment); 668 $(M + H)^+$.

Bioassays against E. armeniacae

Biological testing of enniatins B (**3**), B_1 (**4**), and A_1 (**5**) for their ability to inhibit the grown of *E. armeniacae* were carried out on Czapex-Dox plus 5% yeast agar plates. Samples of each compound ranging in amounts from 8 to 170 μg were absorbed onto sterile paper disks and each was placed at the edge of a sterile plate. The plates were inoculated at the center with a constant size plug of *E. armeniacae* mycelium, cut from the edge of an actively grown colony of this fungus. The inhibition zone from the center of the paper disk to the edge of the *E. armeniacae* growth was measured from 1 to 3 days after the growth on the control plates had reached its maximum (i.e., plates were completely covered with mycelium).

Initially, all samples showed an inhibition zone of 8–14 mm, however, after an incubation period of ~15 days there was little or no inhibition observed with enniatins B and B_1, whereas the plates tested with enniatin A_1 showed a consistent and persisting inhibition zone of 5–10 mm. The difference observed between the 8 μg and the 170 μg samples was very small, most likely due to the poor solubility and absorption of the compounds into the agar medium; thus a dose versus inhibition response could not be evaluated.

Acknowledgements

The authors are indebted to Drs. M. V. Carter (Hawthorndene, South Australia) and D. Ramsdell (Department of Botany and Plant Pathology, Michigan State University) for providing us with the isolate of *F. lateritium* used in this work. We are also indebted to Bio-Méga Inc. for carrying out all of the antiviral and cytotoxicity bioassays. We are most grateful to the Natural Sciences and Engineering Research Council (NSERC) of Canada and to Concordia University for financial support.

1. (*a*) M.V. Carter. Aust. J. Exp. Agric. Anim. Husb. **23**, 429 (1983); (*b*) M.V. Carter and T.V. Price. Aust. J. Agric. Res. **26**, 537 (1975).
2. E.H. Gendloff, D.C. Ramsdell, and C.L. Burton. Plant Dis. **67**, 754 (1983).
3. E. Gaumann, S. Roth, L. Ettlinger, P.A. Plattner, and U. Nager. Experientia, **3**, 202 (1947).
4. L.A. Blais, J.W. ApSimon, B.A. Blackwell, R. Greenhalgh, and J.D. Miller. Can. J. Chem. **70**, 1281 (1992).
5. E.H. Gendloff, D.C. Ramsdell, and C.L. Burton. Plant Dis. **67**, 754 (1983).
6. (*a*) H.L. Walker. Weed Sci. **29**, 629 (1981); (*b*) Eur. Pat. 207653 A 17 Jan. 1987; (*c*) U.S. Pat. 85-747511 21 Jun. 1985.
7. (*a*) C.P. Gorst-Allman, P.H. van Rooyen, S. Wnuk, P. Golinski, and J. Chelkowski. S.-Afr. Tydskr. Chem. **39**, 116 (1986); (*b*) G.W. Bushnell, Y.-L. Li, and G.A. Poulton. Can. J. Chem. **62**, 2101 (1984).
8. M. Cole and G.N. Rolinson. Appl. Microbiol. **24**, 660 (1972).
9. G.C. Bishop and A.H. Isley. Aust. J. Biol. Sci. **31**, 93 (1978).
10. (*a*) Y.S. Tsantrizos, K.K. Ogilvie, and A.K. Watson. Can. J. Chem. **70**, 2276 (1992); (*b*) J.W. Blunt, V.L. Calder, G. D. Fenwick, R.J. Lake, J.D. McCombs, M.H.G. Munro, and N.B. Perry. J. Nat. Prod. **50**, 290 (1987).
11. (*a*) J.A. Dale and H.S. Mosher. J. Am. Chem. Soc. **95**, 512 (1973); (*b*) G.R. Sullivan, J.A. Dale, and H.S. Mosher. J. Org. Chem. **38**, 2143 (1973).
12. I. Ohtani, T. Kusumi, Y. Kashman, and H. Kakisawa. J. Am. Chem. Soc. **113**, 4092 (1991).
13. M.J. Rieser, Y. Hui, J.K. Rupprecht, J.F. Kozlowski, K.V. Wood, J.L. McLaughlin, P.R. Hanson, Z. Zhuang, and T.R. Hoye. J. Am. Chem. Soc. **114**, 10203 (1992).
14. (*a*) I.J. Pachter, R.F. Raffauf, G.E. Ullyot, and O. Ribeiro. J. Am. Chem. Soc. **82**, 5187 (1960); (*b*) T. Kametani, C.V. Loc, T. Higa, M. Koizumi, M. Ihara, and K. Fukumoto. J. Am. Chem. Soc. **99**, 2306 (1977); (*c*) J. Kökösi, I. Hermecz, G. Szász, and Z. Mészáros. Tetrahedron Lett. **22**, 4861 (1981).
15. D.G. O'Donovan and H. Horan. J. Chem. Soc. (C), 2466 (1970).
16. D.F. Barringer, Jr., G. Berkelhammer, and R.S. Wayne. J. Org. Chem. **38**, 1937 (1973).
17. E. Fiedler, H.-P. Fiedler, A. Gerhard, W. Keller-Schierlein, W.A. König, and H. Zähner. Arch. Microbiol. **107**, 349 (1976).
18. A. Numata, C. Takahashi, T. Matsushita, T. Miyamoto. K. Kawai, Y. Usami, E. Matsumura, M. Inoue, H. Ohishi, and T. Shingu. Tetrahedron Lett. **33**, 1621 (1992).
19. B.C. Pressman. Annu. Rev. Biochem. **45**, 501 (1976).
20. J.F. Hinton and G.L. Turner. J. Magn. Reson. **58**, 262 (1984).
21. D.B. Strongman, G.M. Strunz, P. Giguere, C.-M. Yu, and L. Calhoun. J. Chem. Ecol. **14**, 753 (1988).
22. J.F. Grove and M. Pople. Mycopathologia, **70**, 103 (1980).
23. H. Tomoda, H. Nishida, X.-H. Huang, R. Masuma, Y.K. Kim, and S. Omura. J. Antibiot. **45**, 1207 (1992).
24. (*a*) E. Gaumann, St. Naef-Roth, and H. Kern. Phytopathol. Z. **40**, 45 (1960); (*b*) H. Burmeister and R.D. Plattner. Phytopathology, **77**, 1483 (1987).
25. H. Tomoda, X.-H. Huang, J. Cao, H. Nishida, R. Nagao, S. Okuda, H. Tanaka, and S. Omura. J. Antibiot. **45**, 1626 (1992).
26. P.C. Anderson, S. Rakhit, and C. Yoakim. European Patent Application, Publication No. 443 560, published August 28, 1991.

Can. J. Chem. Downloaded from www.nrcresearchpress.com by 203.198.23.82 on 09/08/12
For personal use only.

Structures, binding energies, and thermodynamic functions of NH_4^+, $NH_3^{\cdot+}$, and their H_2O complexes

DAVID A. ARMSTRONG, ARVI RAUK,[1] AND DAKE YU
Department of Chemistry, The University of Calgary, Calgary, AB T2N 1N4, Canada

Received March 30, 1993

DAVID A. ARMSTRONG, ARVI RAUK, and DAKE YU. Can. J. Chem. **71**, 1368 (1993).

Ab initio calculations are performed for $(H_2O)_n \cdots H_4N^+$ and $(H_2O)_n \cdots H_3N^{\cdot+}$ complexes for $n = 0$–5. For $n = 0$ and 1, the geometries of the complexes are optimized at the HF/6-31+G* and MP2/6-31+G* levels, and the energies are evaluated at the G2 level. For $n = 2$–5, the geometry optimizations and frequency calculations are carried out at the HF/6-31+G* level, and the MP2/6-31+G* energies are calculated at the HF optimized geometries. Basis set superposition errors are corrected by the Boys–Bernardi scheme at the HF/6-31+G* level. The gas phase thermodynamic properties C_P^0, S^0, and $H^0 - H_0^0$, are evaluated as functions of temperature using standard statistical methods. Based on the calculated binding energies and the thermodynamic functions, the incremental changes in enthalpies and free energies, ΔH_n and ΔG_n, for the gas phase equilibria $(H_2O)_{n-1}M^+ + H_2O \rightarrow (H_2O)_nM^+$ for $M^+ = NH_4^+$ and $NH_3^{\cdot+}$, are evaluated in comparison with the experimental data for $(H_2O)_n \cdots H_4N^+$, the present results suggest conformations for the hydrated complexes observed in the experiments. The total free energy change for filling the first hydration shell is significantly more negative for $NH_3^{\cdot+}$ than for NH_4^+.

DAVID A. ARMSTRONG, ARVI RAUK et DAKE YU. Can. J. Chem. **71**, 1368 (1993).

On a effectué des calculs *ab initio* sur les complexes $(H_2O)_n \cdots H_4N^+$ et $(H_2O)_n \cdots H_3N^{\cdot+}$ dans lesquels $n = 0$–5. Pour $n = 0$ et 1, on a optimisé les géométries aux niveaux HF/6-31+G* et MP2/6-31+G* et les énergies au niveau G2. Pour $n = 2$–5, on a effectué les calculs des optimisations de géométrie et de fréquence au niveau HF/6-31+G* et on a calculé les énergies au niveau MP2/6-31+G* sur des géométries optimisées au niveau HF. On a corrigé les erreurs dues aux superpositions d'ensembles en faisant appel à la méthode de Boys–Bernardi au niveau HF/6-31+G*. Faisant appel à des méthodes statistiques standard, on a évalué les propriétés thermodynamiques C_P^0, S^0 et $H^0 - H_0^0$ en phase gazeuse en fonction de la température. En se basant sur les énergies de liaison calculées et sur les fonctions thermodynamiques, on a évalué les augmentations incrémentielles des enthalpies et des entropies libres, ΔH_n et ΔG_n, pour les équilibres gazeux $(H_2O)_{n-1}M^+ + H_2O \rightarrow (H_2O)_nM^+$ dans lesquels $M^+ = NH_4^+$ et $NH_3^{\cdot+}$. Par comparaison avec les résultats expérimentaux pour $(H_2O)_n \cdots H_4N^+$, ces calculs suggèrent les conformations des complexes hydratés observées dans les expériences. Le changement total d'énergie libre pour remplir la première couche d'hydration est beaucoup plus négative pour le $NH_3^{\cdot+}$ que pour le NH_4^+.

[Traduit par la rédaction]

1. Introduction

Experimental and theoretical investigations of gas phase ion–solvent clusters for solvents such as water have been of interest for many years (1–6). Mass spectrometric investigations provide accurate thermodynamic data on the binding of solvent molecules, but do not as a rule lead to explicit structural information (1, 2). Vibrational data on aquo ion complexes is also rare (7). *Ab initio* calculations, which yield structures and vibrational frequencies as well as binding energies that can be correlated with those obtained experimentally, therefore play an important complementary role (3). In particular, they make comparisons of the relative stabilities of different structures possible (3, 4). They can also be carried out on systems where experiment is technically difficult.

This publication describes a study of the gas phase aquo complexes of the ammonium and amminium ions, NH_4^+ and $NH_3^{\cdot+}$. The specific interest in amminium ions arises from a prior (8) interpretation of experimental data that showed that the solution free energy of the trialkyl amminium system, $(CH_3)_3N^{\cdot+}$, is probably some 30 kJ mol^{-1} larger in magnitude than that of the corresponding ammonium species, $(CH_3)_3NH^+$. For these larger species high-level *ab initio* calculations of "solvation" are of course not practical. The $NH_3^{\cdot+}$ species was chosen so that the effect of the difference in forming aquo complexes between it and ammonium could be examined by *ab initio* methods at reasonably high levels. The NH_4^+ ion serves as a standard since the free energies for $(H_2O)_{n-1}H_4N^+ + H_2O \rightarrow (H_2O)_nH_4N^+$ have been studied experimentally in the gas phase by a number of research groups (9, 10). Therefore there are accurate experimental results with which comparisons of the theoretical predictions can be made.

The binding energies and structures for the complexes formed by successive addition of water molecules to ammonium and amminium ions in reaction [1]

[1] $(H_2O)_{n-1}M^+ + H_2O \rightarrow (H_2O)_nM^+$

were determined by carrying out *ab initio* calculations at the HF and MP2 levels with 6-31+G* basis sets on all complexes with n up to 5. The complexes $H_2O \cdots HNH_3^+$ and $H_2O \cdots HNH_2^{\cdot+}$ were also studied at the G2 level (11) to provide an indication of the level of accuracy to be expected from the HF and MP2 calculations.

Computational details are provided in Sect. 2, and the results are reported in Sect. 3. In Sect. 4, the results are discussed in comparison with the experimental and theoretical studies in the literature. Conclusions have been summarized in Sect. 5.

2. Computational details

Ab initio *calculations*

All *ab initio* calculations presented here were performed with the Gaussian 90 molecular orbital packages (12). In the

[1]Author to whom correspondence may be addressed.

Can. J. Chem. Downloaded from www.nrcresearchpress.com by 213.200.69.106 on 09/08/12
For personal use only.

Can. J. Chem. Downloaded from www.nrcresearchpress.com by 213.200.69.106 on 09/08/12
For personal use only.

cases of calculations on the free radical species, $\langle S^2 \rangle$ was invariably close to 0.76, indicating negligible spin contamination of the UHF wave function. For $(H_2O)_n \cdots H_4N^+$ and $(H_2O)_n \cdots H_3N^{\cdot+}$, with $n = 0$ and 1, it is possible to evaluate their energies at the G2 level (11) of theory. The G2 procedure includes the following: a geometry optimization with the standard Hartree–Fock (HF) method and the 6-31G* split-valence basis set; a vibrational frequency calculation at the HF optimized geometry; the second-order Moller–Plesset (MP2) geometry optimization with 6-31G* basis set; and a series of single-point post-HF calculations carried out on the MP2 optimized geometry, to obtain an accurate evaluation of the correlation energies. The geometries of these complexes are also optimized at the HF and MP2 levels with the 6-31+G* basis set, to include diffuse functions that are important in studying hydrogen-bonding systems. The procedure proposed by Boys and Bernardi (13) was used to estimate and correct for the basis set superposition error (BSSE) at the HF/6-31+G* level on the HF/6-31+G* optimized geometries. It should be noted that the Boys–Bernardi scheme represents an overestimate of the BSSE (14).

For the complexes associated with more than one water molecule, the geometry optimizations were performed at the HF/6-31+G* level. The H-bonded complexes are characterized by very flat potential energy surfaces. Convergence of the geometries was to the limit imposed internally in Gaussian 90 without symmetry constraints.[2] All structures are energetically close to minima, as confirmed by frequency calculations that yield all real frequencies. All the vibrational frequencies calculated at the HF/6-31G* and HF/6-31+G* levels were scaled by a factor of 0.89 (15) in considering the zero-point energy (ZPE) and in the calculations of thermodynamic properties. Correlation corrections to the total energies were estimated by single-point calculations with the same basis set at the level of MP2 theory.

Thermodynamic functions

Ideal gas thermodynamic functions C_P^0, S^0, and $H^0 - H_0^0$ in the temperature range 100–298.15 K and 1 bar (1 bar = 100 kPa) pressure were calculated by standard statistical thermodynamic methods based on the rigid rotor – harmonic oscillator model. The lowest vibrational modes, which correspond to torsional motions of bound H_2O molecules, were treated as internal rotations. As the barriers for the internal rotations around the hydrogen bonds are very small, the calculations were carried out using the free rotor model. Without symmetry constraints, the geometry optimization usually resulted in low (or no) symmetry structures. For the hydrogen-bonded systems, more than one conformer is often accessible without significant change in the total energy. Therefore, in calculating the entropies of the complexes, the symmetry numbers used were taken as the number of rotation operations in the molecular point group of the highest possible symmetry of the complex.[2] Calculations of accurate $\Delta_f H^0$ and $\Delta_f G^0$ values for NH_4^+, $NH_3^{\cdot+}$, and $H_2O \cdots HNH_2^{\cdot+}$ have been presented in ref. 16.

[2]Optimizations without symmetry constraints invariably yield C_1 symmetry structures. Many of the structures converged to geometries with apparently higher symmetry. The actual presence of higher symmetry has no energetic consequences and was not pursued. For the purpose of evaluation of the rotational partition functions, however, structures of the highest symmetry close to the converged geometries were assumed.

The binding energies of the complexes at 0 K are defined as E(complex) $- \Sigma E$(fragment), where E is the *ab initio* total energy (including the ZPE contribution). The *incremental* energy changes, ΔE_n, for reaction [1] at 0 K, were also calculated from the E values with $n = 1$–5. Based on that information and the calculated thermodynamic functions for the fragments and complexes, the corresponding incremental changes in enthalpy (ΔH_n), entropy (ΔS_n), and free energy (ΔG_n) for reaction [1] at 298 K were then found.

3. Results

The HF/6-31+G* optimized structures of the isolated NH_4^+ and $NH_3^{\cdot+}$, and some of their water complexes, are plotted in Figs. 1 and 2, respectively. The main geometric features of the complexes can be determined by the listed characteristic parameters and the symmetry types. The energies evaluated at different levels are reported in Table 1, and the incremental binding energies, $\Delta E_n (= E[(H_2O)_n M^+] - E[(H_2O)_{n-1} M^+] - E(H_2O))$, with and without BSSE correction, are listed in Table 2. For the purpose of BSSE correction, $E[(H_2O)_{n-1}M^+]$ was evaluated in the presence of the basis functions of the nth H_2O, and similarly, the energy of the nth H_2O, $E(H_2O)$, was calculated in the presence of the basis functions of $(H_2O)_{n-1}M^+$ (13).

For clarity, we introduce a condensed notation (i,j,k) to denote the number and distribution of bound H_2O molecules on M^+, where i, j, and k stand for the number of H_2O bonded to H atoms of M^+, to H atoms of H_2O, and to the N atom of M^+, respectively. The total number of H_2O molecules bonded to M^+ is $n = i + j + k$.

Throughout the paper, three dots (···) have been used to separate complexed partners and proximity denotes the nature of the interaction. Thus $(H_2O)_2 \cdots H_2NH_2^+$ denotes a complex formed by bonding two water molecules on the H atoms of NH_4^+. The "isomeric" complex with the second water bonded to the first one would be denoted as $H_2O \cdots H_2O \cdots HNH_3^+$. Subsequently complexes of these two kinds are identified as (2,0,0) and (1,1,0) in our condensed notation. Similar notations are used for $M^+ = NH_3^{\cdot+}$ species.

The thermodynamic functions for H_2O, $(H_2O)_n \cdots H_4N^+$, and $(H_2O)_n \cdots H_3N^{\cdot+}$ are reported in Table 3. The enthalpy and free energy changes for reaction [1] calculated from the S^0 and $H^0 - H_0^0$ values, and the BSSE corrected ΔE_n of Table 2, are given in Table 4. The ΔH_n vs. the number of bonded H_2O molecules are also plotted in Fig. 3, compared with the available experimental data.

4. Discussion

Equilibrium structures and energetic considerations

The structures of the isolated H_2O, NH_4^+, and $NH_3^{\cdot+}$ have been discussed elsewhere (16) and it may be noted here that the optimized geometries at the HF/6-31+G* level are in reasonable agreement with experimental geometries.

Basis set superposition errors were expected to be small for the hydrogen-bonded species because of the large separations involved. Comparison of columns I and I_{BSSE} in Table 2 reveals that the magnitude of BSSE falls in the range of 3.1–3.8 kJ mol^{-1} except in the cases of (3,0,1) and (3,0,2) of $H_3N^{\cdot+}$ complexes, where the correction for the axially coordinated H_2O is less than 1 kJ mol^{-1}.

$(H_2O)_n \cdots H_4N^+$ complexes.

Pullman et al. (4) investigated three possible configurations of the complex formed with one H_2O and NH_4^+, namely

Can. J. Chem. Downloaded from www.nrcresearchpress.com by 213.200.69.106 on 09/08/12
For personal use only.

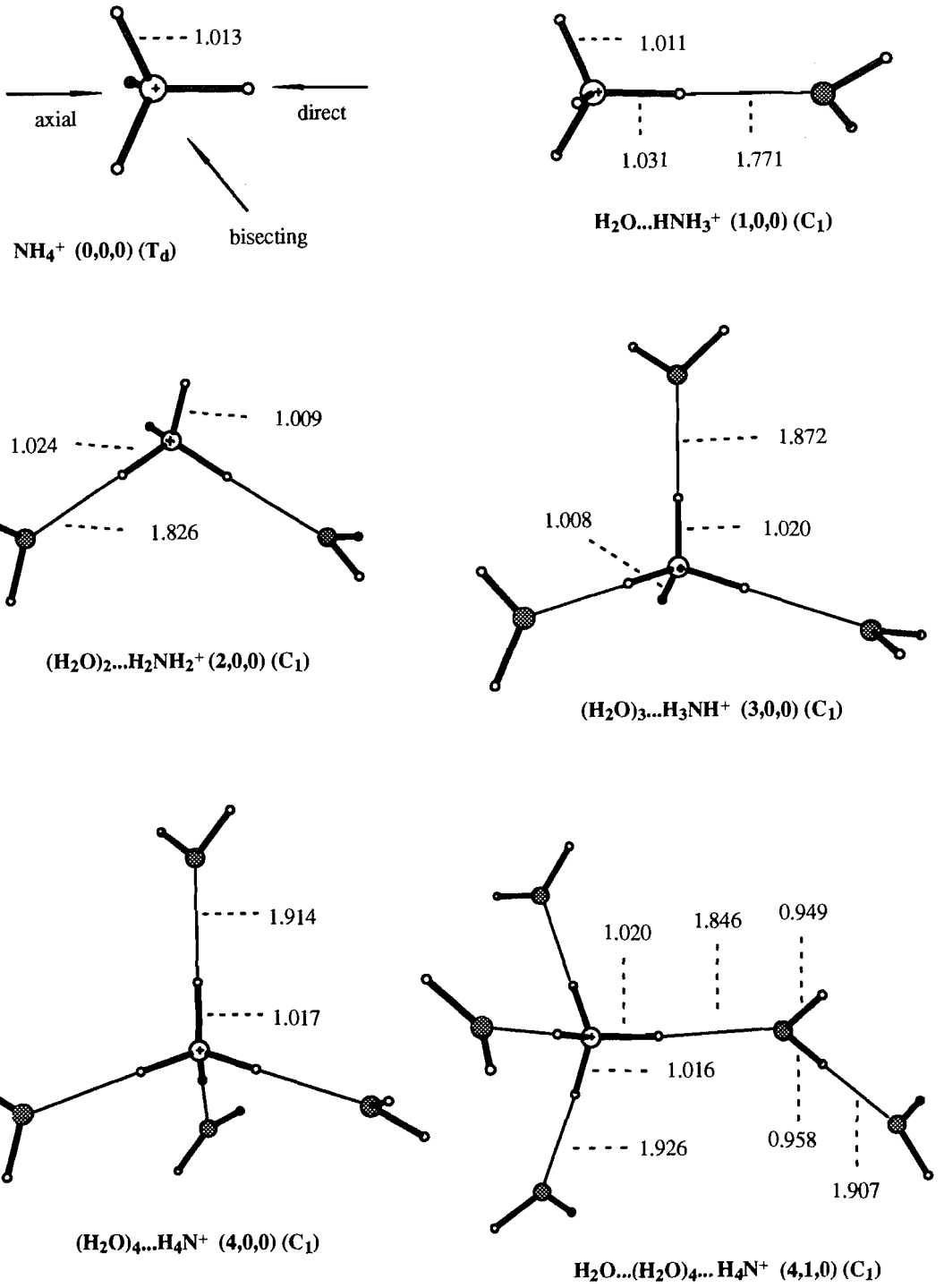

FIG. 1. HF/6-31+G* optimized structures for NH_4^+ and its water complexes. Filled circles represent oxygen atoms, large open circles are nitrogen, and small open circles are hydrogen. Bond lengths in Å, angles in degrees.

the direct (1,0,0), and bisecting and axial approaches of H_2O to NH_4^+ (see Fig. 1 for the definitions). The last two would both be denoted as (0,0,1) in our condensed notation. The direct approach was found to form the most stable complex at the HF level with an extended polarized basis set, and the bisecting and axial species were found to be 13 and 17 kJ mol^{-1} higher in energy, respectively. In the present study, only one stable complex was found, i.e., the (1,0,0) structure formed from direct approach. With C_s and C_2 symmetry constraints on the bisecting and axial complexes, respectively, the estimated relative stabilities (referring to the (1,0,0) structure) are 12 and 15 kJ mol^{-1} from the HF/6-31+G* energies evaluated at the HF/6-31+G* optimized geometries (HF/6-31+G*//HF/6-31+G*), which are similar to those found by Pullman et al. (4). However, frequency calculations suggest these complexes are not stable. In the present publication, we will only discuss the NH_4^+ complexes that arise from direct approaches.

The first H_2O molecule forms a linear complex (1,0,0) with the H atom of NH_4^+. The O ··· H distance is 1.77 Å, well

Can. J. Chem. Downloaded from www.nrcresearchpress.com by 213.200.69.106 on 09/08/12
For personal use only.

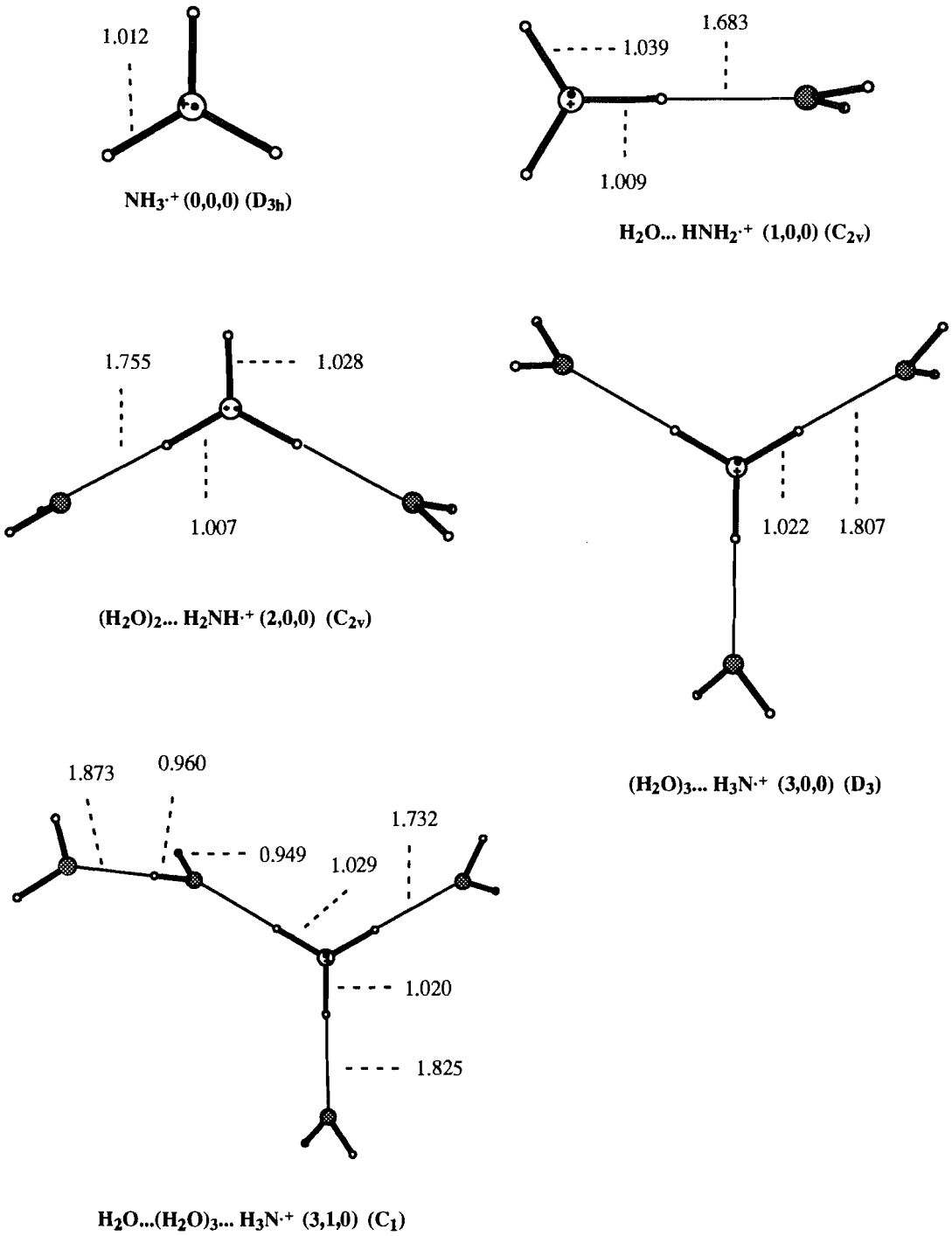

FIG. 2. HF/6-31+G* optimized structures for $NH_3^{\cdot+}$ and its water complexes. Filled circles represent oxygen atoms, large open circles are nitrogen, and small open circles are hydrogen. Bond lengths in Å, angles in degrees.

within the van der Waals separation 2.6 Å. The hydrogen-bonded N—H distance is 0.018 Å longer than that of isolated NH_4^+, while the other N—H bonds are almost identical to those of isolated NH_4^+. The changes in H_2O bond structure are minor. The orientation of the H_2O is not tipped as it is for the donor H_2O of the water dimer (16), indicating that the structure is dominated by charge–dipole interaction. For this species, the structure was also optimized at the MP2/6-31+G* level. The general features of the MP2/6-31+G* geometry are very similar to those of HF/6-31+G*, but the H bond is stronger; and the O—H distance is 1.713 Å, 0.058 Å shorter than that predicted at the HF level.

The binding energy of $H_2O \cdots HNH_3^+$ was evaluated at several levels of theory up to G2. The G2 level binding energy is -77.2 kJ/mol^{-1}, and served as reference for the performance of lower levels of theory, which must be employed for the larger species. The BSSE uncorrected HF/6-31+G*/HF/6-31+G* energies including the ZPE corrections give a value within 1 kJ/mol^{-1} of the G2 value, being -76.4 kJ mol^{-1}. The MP2/6-31+G*//HF/6-31+G*

Can. J. Chem. Downloaded from www.nrcresearchpress.com by 213.200.69.106 on 09/08/12
For personal use only.

TABLE 1. Energies at different levels of *ab initio* calculations
I: HF/6-31+G*//HF/6-31+G*; II: MP2/6-31+G*//HF/6-31+G*; III: MP2/6-31+G*//MP2/6-31+G*

	$(i,j,k)^a$	Symmetry[b]	I (hartree)	ZPE (kJ mol^{-1})	II (hartree)	III (hartree)	G2 (hartree)
H_2O		C_{2v}	−76.017743	60.2	−76.208740	−76.212295	−76.33205[c]
NH_4^+	(0,0,0)	T_d	−56.531277	139.9	−56.700411	−56.704510	−56.78140[c]
	(1,0,0)	C_1	−132.581024	208.6	−132.944415	−132.946354	−133.142869
	(2,0,0)	C_1	−208.626347	276.8	−209.183481		
	(3,0,0)	C_1	−284.668082	344.3	−285.418739		
	(4,0,0)	C_1	−360.706657	410.6	−361.650675		
	(1,1,0)	C_1	−208.620250	278.2	−209.178560		
	(2,1,0)	C_1	−284.663890	346.1	−285.415612		
	(3,1,0)	C_1	−360.703934	413.1	−361.648875		
	(4,1,0)	C_1	−436.741305	479.3	−437.879486		
$NH_3^{\cdot+}$	(0,0,0)	D_{3h}	−55.873340	91.7	−56.004030	−56.007574	−56.08410[c]
	(1,0,0)	C_{2v}	−131.927847	161.6	−132.253254	−132.260764	−132.450892
	(2,0,0)	C_{2v}	−207.976603	230.3	−208.495927		
	(3,0,0)	D_3	−284.021081	298.2	−284.733986		
	(1,1,0)	C_1	−207.968293	230.5	−208.488919		
	(2,1,0)	C_1	−284.014948	299.4	−284.728969		
	(3,1,0)	C_1	−360.057676	367.0	−360.964983		
	(3,0,1)	C_1	−360.053822	364.1	−360.959909		
	(3,0,2)[d]	C_1	−436.083999	428.2	−437.183050		

[a] i, j, and k are the number of H_2O molecules bonded to H atoms of M^+, to H atoms of H_2O, and to the N atom of M^+, respectively.
[b] See footnote 2.
[c] From ref. 11.
[d] The optimized structure has one imaginary frequency.

TABLE 2. Incremental binding energies ΔE_n (= $E((H_2O)_nM^+) - E((H_2O)_{n-1}M^+) - E(H_2O)$) in kJ mol^{-1}

	Complex $(i,j,k)^a$	n^b	I^c	$I_{BSSE}{}^d$	II[c]	III[c]	G2
NH_4^+	(1,0,0)	1	−76.4	−72.6	−85.0	−70.0	−77.2
	(2,0.0)	2	−65.2	−61.7	−72.4		
	(3,0,0)	3	−56.5	−53.0	−63.2		
	(4,0,0)	4	−49.2	−45.8	−55.4		
	(1,1,0)	2	−48.0	−44.8	−58.3		
	(2,1,0)	3	−43.9	−40.5	−53.3		
	(3,1,0)	4	−39.9	−36.8	−48.5		
	(4,1,0)	5	−36.8	−33.4	−45.1		
$NH_3^{\cdot+}$	(1,0,0)	1	−87.9	−84.5	−97.7	−98.7	−91.2
	(2,0,0)	2	−73.8	−70.5	−81.5		
	(3,0,0)	3	−63.3	−60.0	−70.0		
	(1,1,0)	2	−51.8	−48.7	−62.9		
	(2,1,0)	3	−46.1	−42.9	−55.8		
	(3,1,0)	4	−41.9	−38.3	−50.8		
	(3,0,1)	4	−34.3	−33.5	−40.1		
	(3,0,2)[e]	5	−29.2	−28.7	−34.3		

[a] i, j, and k are the number of H_2O molecules bonded to H atoms of M^+, to H atoms of H_2O, and to the N atom of M^+, respectively.
[b] $n = i + j + k$.
[c] Defined as those of Table 1 + 0.89 ZPE from the HF/6-31+G* calculations.
[d] Same as I, corrected for BSSE using the Boys–Bernardi compromise scheme, see text.
[e] The optimized structure has an imaginary frequency.

+ ZPE binding energy is 8 kJ mol^{-1} larger than that of G2. The MP2/6-31+G* binding energy with MP2/6-31+G* optimized geometry was found to be 15.0 kJ mol^{-1} smaller than that obtained on HF/6-31+G* optimized geometry, indicating the extent of correlation effects on geometry. Pullman et al. (4) studied $H_2O \cdots HNH_3^+$ in some detail and

TABLE 3. Ideal gas thermodynamic properties

Complex $(i,j,k)^a$	T (K)	NH_4^+ C_P^0 (J K^{-1} mol^{-1})	NH_4^+ S^0 $(\sigma)^b$ (J K^{-1} mol^{-1})	NH_4^+ $H^0 - H_0^0$ (kJ mol^{-1})	$NH_3^{\cdot+}$ C_P^0 (J K^{-1} mol^{-1})	$NH_3^{\cdot+}$ S^0 $(\sigma)^b$ (J K^{-1} mol^{-1})	$NH_3^{\cdot+}$ $H^0 - H_0^0$ (kJ mol^{-1})
(0,0,0)	100	33.3	149.0(12)	3.3	33.3	155.5(6)	3.3
	200	33.4	172.1	6.7	34.2	178.8	6.7
	298	34.7	185.6	10.0	36.7	192.8	10.2
(1,0,0)	100	49.8	220.6(1)	4.1	47.8	215.7(2)	4.0
	200	66.6	261.1	10.0	64.7	254.6	9.7
	298	74.2	289.3	16.9	73.7	282.2	16.5
(2,0,0)	100	72.7	264.1(2)	5.3	68.7	267.1(2)	5.2
	200	102.7	325.3	14.3	98.7	325.3	13.8
	298	115.0	368.9	25.1	113.0	367.6	24.2
(3,0,0)	100	99.7	308.3(3)	7.0	95.5	306.8(6)	6.9
	200	140.6	392.3	19.3	135.1	386.9	18.7
	298	156.9	451.8	34.0	153.7	444.6	32.9
(4,0,0)	100	130.5	350.9(4)	8.9			
	200	180.3	459.5	24.8			
	298	199.8	535.6	43.6			
(1,1,0)	100	69.0	278.5(1)	5.1	67.1	282.9(1)	5.0
	200	95.5	335.8	13.5	93.2	338.5	13.2
	298	108.1	376.5	23.5	107.1	378.5	23.1
(2,1,0)	100	93.8	319.2(1)	6.4	89.7	321.7(1)	6.3
	200	132.7	398.3	18.1	128.4	397.5	17.5
	298	149.7	454.8	32.0	147.3	452.6	31.1
(3,1,0)	100	122.1	363.2(1)	8.1	118.1	368.3(1)	8.1
	200	171.6	465.7	23.2	165.9	467.0	22.6
	298	192.2	538.5	41.2	188.8	538.0	40.1
(4,1,0)	100	153.9	408.5(1)	10.1			
	200	211.9	536.3	28.9			
	298	235.5	625.8	51.0			
(3,0,1)	100				127.2	355.6(1)	8.4
	200				177.5	462.0	24.1
	298				198.7	537.2	42.6
(3,0,2)	100				155.6	381.0(2)	9.9
	200				213.5	510.2	28.8
	298				236.2	600.2	51.0

[a] i, j, and k are the number of H_2O molecules bonded to H atoms of M^+, to H atoms of H_2O, and to the N atom of M^+, respectively.
[b] Symmetry number used in calculating S^0.

found a binding energy of 77 kJ mol^{-1} at the HF level with extended polarized basis set. The values reported by Welti et al. (5) including configuration interaction are −84.7 and −83.1 kJ mol^{-1} at the CISD and CISDQ levels, respectively. The BSSE at HF/6-31+G* for this interaction energy was found to be 3.8 kK mol^{-1}, yielding an value of interaction energy −72.6 kJ mol^{-1}.

The results for this complex suggest that the true binding energies may lie in between those evaluated at HF/6-31+G*//HF/6-31+G* + ZPE and MP2/6-31+G*//HF/6-31+G* + ZPE levels. If the G2 values for $H_2O \cdots HNH_3^+$ (and $H_2O \cdots HNH_2^{\cdot+}$) are used as references, the results listed in Table 2 also indicate that for the HF/6-31+G*//HF/6-31+G* + ZPE binding energies there is a fortuitous cancellation of correlation errors. Therefore, we will discuss the bond strength based on the values obtained at this level from now on.

In $(H_2O)_2 \cdots H_2NH_2^+$, (2,0,0) structure, the two water molecules form almost symmetric hydrogen bonds with the H atoms of NH_4^+; both are within 2° from linear. The O ··· H separations are both 1.826 Å, increased by 0.055 Å from that of $H_2O \cdots HNH_3^+$. The local structures of NH_4^+ and H_2O are altered little. The binding energy of the second H_2O molecule is calculated to be 61.7 kJ mol^{-1}. Thus the incremental binding energy of the second water is reduced by 10.9 kJ mol^{-1} from that of the first.

An exhaustive search of all possible local minima of the $(H_2O)_2 \cdots H_2NH_2^+$ potential surface was not conducted. However, a second configuration was examined, in which the second water molecule is H bonded to the first one, i.e., a (1,1,0) structure, $H_2O \cdots H_2O \cdots HNH_3^+$. This complex was found to be 16.9 kJ mol^{-1} less stable than the (2,0,0) isomer, $(H_2O)_2 \cdots H_2NH_2^+$. The hydrogen bond length of O ··· HN is reduced by 0.178 Å, compared with that of $H_2O \cdots HNH_3^+$. The O ··· HO hydrogen bond length is 1.821 Å and 3° from linear. It is of interest to note that this hydrogen bond length is 0.193 Å shorter than the corresponding one in water dimer $H_2O \cdots HOH$ (16), and the binding energy ($E(1,1,0) - E(1,0,0) - E(H_2O)$) of 44.8 kJ mol^{-1} is substantially larger than that of $H_2O \cdots HOH$, 10.0 kJ mol^{-1} at the same level. This indicates a strong "secondary" effect of the central charge of NH_4^+.

The additions of the third H_2O molecule to NH_4^+ were also

Can. J. Chem. Downloaded from www.nrcresearchpress.com by 213.200.69.106 on 09/08/12
For personal use only.

TABLE 4. ΔH_n, $T\Delta S_n$, and ΔG_n (kJ mol^{-1}) of $[(H_2O)_{n-1}M^+]_g + (H_2O)_g \rightarrow [(H_2O)_nM^+]_g$ calculated at HF/6-31+G*//HF/6-31+G* + ZPE level at 298.15 K and 1 bar

	Complex $(i,j,k)^a$	n^b	$-\Delta H_n$			$-T\Delta S_n$			$-\Delta G_n$		
			Calcd.[c]	Expt.[d]	Expt.[e]	Calcd.[c]	Expt.[d]	Expt.[e]	Calcd.	Expt.[d]	Expt.[e]
NH_4^+	(1,0,0)	1	75.6	72.4	83.3	25.2	24.6	28.8	50.8	47.7	54.4
	(2,0,0)	2	63.4	61.5	61.9	32.4	27.3	30.1	31.0	34.3	31.4
	(3,0,0)	3	54.0	56.1	51.0	31.4	31.3	26.5	22.6	24.7	24.7
	(4,0,0)	4	46.1	51.0	45.2	31.1	34.1	28.7	15.0	17.2	16.3
	$\Sigma_{i=1}^4$								119.4	123.9	126.8
	(1,1,0)	2	48.1			30.3			17.8		
	(2,1,0)	3	43.6			30.5			13.1		
	(3,1,0)	4	39.5			30.3			9.2		
	(4,1,0)	5	35.9	40.6	44.4	30.9	27.9	33.7	5.0	12.6	10.9
$NH_3^{\bullet+}$	(1,0,0)	1	88.1			29.5			58.6		
	(2,0,0)	2	72.7			30.6			42.1		
	(3,0,0)	3	61.2			33.2			28.0		
	$\Sigma_{i=1}^3$								128.7		
	(1,1,0)	2	52.0			27.4			24.6		
	(2,1,0)	3	45.9			30.8			15.1		
	(3,1,0)	4	41.0			28.3			12.7		
	(3,0,1)	4	33.7			28.5			5.2		
	(3,0,2)	5	30.2			37.3			−7.1		

[a] i, j, and k are the number of H_2O molecules bonded to H atoms of M^+, to H atoms of H_2O, and to the N atom of M^+, respectively.
[b] $n = i + j + k$.
[c] The corresponding values for H_2O (16) at 298.15 K are $S^0 = 188.2$ kJ^{-1} K^{-1} mol^{-1}; $H^0 - H_0^0 = 9.9$ kJ mol^{-1}.
[d] Reference 9.
[e] Reference 10.

investigated for two configurations, namely, $(H_2O)_3 \cdots H_3NH^+$ and $H_2O \cdots (H_2O)_2 \cdots H_2NH_2^+$, structures (3,0,0) and (2,1,0) of Fig. 1. The three nearly equivalent O ··· H hydrogen bond lengths are 1.872 Å in $(H_2O)_3 \cdots H_3NH^+$, and the hydrogen bonds are within 2° deviation from linear. The incremental binding energy of the third H_2O is found to be 53.0 kJ mol^{-1}, 8.7 kJ mol^{-1} less than the second. $H_2O \cdots (H_2O)_2 \cdots H_2NH_2^+$ is 11.9 kJ mol^{-1} higher in energy than $(H_2O)_3 \cdots H_3NH^+$. The water dimer bonded O ··· HN bond length is shorter by 0.1 Å than water monomer O ··· HN, reflecting the effect of the "secondary" water molecule. The O ··· HO hydrogen bond of structure (2,1,0) is longer by 0.048 Å than that in $H_2O \cdots H_2O \cdots HNH_3^+$ (1,1,0) but still substantially shorter than that of $H_2O \cdots HOH$. The corresponding binding energy, 40.5 kJ mol^{-1}, reduced by 4.3 kJ mol^{-1} from that of (1,1,0) is 4 times that of $H_2O \cdots HOH$.

The binding of a fourth H_2O to the remaining H atom of NH_4^+ forms $(H_2O)_4 \cdots H_4N^+$, (4,0,0), and fills the first hydration shell of NH_4^+. The four O ··· H hydrogen bond lengths are 1.914 Å, and the bonds are within 2° of being linear. The incremental binding energy of the last water in the first hydration shell is 45.8 kJ mol^{-1}, about 63% that of the first one. The average binding energy for the first shell H_2O molecules is 53.8 kJ mol^{-1}. A complex $H_2O \cdots (H_2O)_3 \cdots H_3NH^+$ (3,1,0) is also found to be a local minimum but less preferred by 9.0 kJ mol^{-1} than $(H_2O)_4 \cdots H_4N^+$. The O ··· HO distance is 1.891 Å and the angle is only 1° from linear. The length of the O ··· HN from the "water dimer" is also found to be about 0.1 Å shorter than the two O ··· HN bonds from water monomers. Again, the binding energy for the "water dimer" in (3,1,0) was found to be reduced by 3.7 kJ mol^{-1} from that of the (2,1,0) structure. It is clear from the above investigation that, given a choice, attachment of water to H—N^+ is preferred to attachment to H—O.

Three possibilities of adding a fifth water molecule to the (4,0,0) structure $(H_2O)_4 \cdots H_4N^+$ have been examined: binding to N in an axial or bisected fashion (Fig. 1) or attachment to one of the H atoms of one of the hydrogen-bonded water molecules. The geometry optimizations indicated that the preferred binding sites of the fifth H_2O are the H atoms of the water molecules, to form complex (4,1,0), $H_2O \cdots (H_2O)_4 \cdots NH_4^+$. No stable axial or bisected structures, which would be denoted as (4,0,1), were found. Attempts at optimization of a (4,0,1) structure from reasonable starting points yield a (4,1,0) structure. Similar to $(n - 1,1,0)$ structures, $H_2O \cdots (H_2O)_n \cdots H_nNH_{4-n}^+$, the O ··· HN bond with the second water attached is reduced by about 0.1 Å, compared with the other three O ··· HN distances. The O ··· HO forms a fairly strong hydrogen bond, with an O ··· H distance 0.7 Å shorter than the corresponding van der Waals separation and only 1° deviation from linear. The incremental binding energy ΔE_5 is 33.4 kJ mol^{-1} at the HF level.

$(H_2O)_n \cdots H_3N^{\bullet+}$ complexes.

The optimized $H_2O \cdots HNH_2^{\bullet+}$ structure, (1,0,0) in our condensed notation, has C_{2v} symmetry, the radical center $N^{\bullet+}$ being planar and the OH_2 molecule lying in a plane perpendicular to it (Fig. 2). The hydrogen bond is stronger by 11.9 kJ mol^{-1} than that in $H_2O \cdots HNH_3^+$, as reflected by the O ··· H separation, which is 0.088 Å shorter (1.683 vs. 1.771 Å). The hydrogen-bonded N—H bond is lengthened by 0.027 Å but there are no significant changes in local H_2O structure from the isolated one. The binding energy was found to be 87.9 kJ mol^{-1} at the HF level, and 91.2 kJ mol^{-1} at the G2 level. The BSSE corrected value is 84.5 kJ mol^{-1}. Again,

Can. J. Chem. Downloaded from www.nrcresearchpress.com by 213.200.69.106 on 09/08/12
For personal use only.

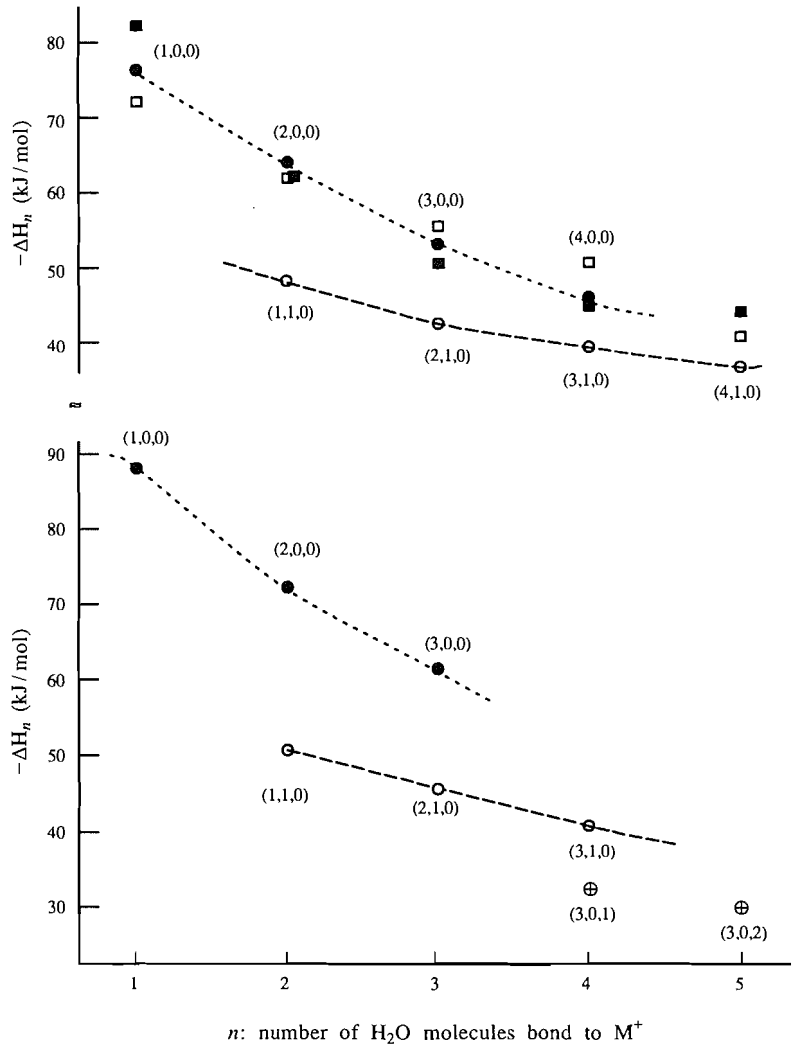

FIG. 3. Experimental and calculated $\Delta_r H_{n-1}$ for NH_4^+ and $NH_3^{\bullet+}$. Experimental values for NH_4^+ are taken from refs. 9 (□) and 10 (■). Circles display calculated data: ● indicates n H_2O molecules bonded to H atoms of NH_4^+ or $NH_3^{\bullet+}$; ○ indicates $n-1$ H_2O molecules bonded to NH_4^+ or $NH_3^{\bullet+}$, and one H_2O bonded to an H atom of H_2O; ⊕ indicates one or two H_2O bonded to the N atom while the rest are bonded to H atoms of $NH_3^{\bullet+}$.

the G2 value is between the HF and MP2 (97.7 kJ mol^{-1}) binding energies, and HF is slightly closer to the G2 value.

The possibility of forming a $H_2O \cdots NH_3^+$ complex through three-electron or one-electron bonding involving the singly occupied molecular orbital of N, i.e., a (0,0,1) complex, was examined previously (16). It was found that $H_2O \cdots NH_3^{\bullet+}$ (0,0,1) does not correspond to a stationary point on the potential energy surface, in the gas phase.

The preferred addition sites for the second and third H_2O molecules to $NH_3^{\bullet+}$ are also the H atoms of $NH_3^{\bullet+}$. The optimized $(H_2O)_2 \cdots H_2NH^{\bullet+}$ has C_{2v} symmetry, with the water H atoms perpendicular to the radical plane. The two symmetric hydrogen bond lengths equal 1.752 Å, longer by 0.069 Å than that in $H_2O \cdots HNH_2^{\bullet+}$. The incremental binding energy, ΔE_2, of the second water molecule is 70.5 kJ mol^{-1}, smaller by 14.0 kJ mol^{-1} than ΔE_1. For NH_4^+, the difference between ΔE_1 and ΔE_2 is smaller, being 10.9 kJ mol^{-1}, suggesting the incremental binding energy decreases faster for $NH_3^{\bullet+}$ complexes.

On binding the second water molecule to the H atom of H_2O, a slightly less stable isomer of $H_2O \cdots H_2O \cdots HNH_2^{\bullet+}$ (1,1,0), which is 21.8 kJ mol^{-1} higher in energy than $(H_2O)_2 \cdots H_2NH^{\bullet+}$, is obtained. The hydrogen bond lengths of O ··· HO are 1.821 Å with corresponding binding energy of 48.7 kJ mol^{-1}. The O ··· HN distance is reduced by 0.09 Å from that of the complex with single water, $H_2O \cdots HNH_2^{\bullet+}$. The "secondary" effect of the central charge is even stronger than the cases for NH_4^+ complexes, reflected by the binding energy for the $H_2O \cdots HOH$ in their (1,1,0) structures (48.7 vs. 44.8 kJ mol^{-1}). Note that these binding energies are much larger than that for the water dimer, 10.0 kJ mol^{-1} at the same level of theory.

In the (3,0,0) structure, $(H_2O)_3 \cdots H_3N^{\bullet+}$, the planes defined by the water molecules form angles of 67.3° with the $NH_3^{\bullet+}$ plane and give this complex D_3 symmetry. The D_{3h} structure has an almost identical total energy but with a small imaginary frequency (58i cm^{-1}). In fact, the internal rotations in the hydrogen-bonded complexes are essentially unhindered, more than one rotational conformer being accessible without a significant change in total energy (16). The hydrogen bond lengths in $(H_2O)_3 \cdots H_3N^{\bullet+}$ are 1.807 Å, 0.124 Å longer than that of $H_2O \cdots HNH_2^{\bullet+}$. The incremen-

Can. J. Chem. Downloaded from www.nrcresearchpress.com by 213.200.69.106 on 09/08/12
For personal use only.

Can. J. Chem. Downloaded from www.nrcresearchpress.com by 213.200.69.106 on 09/08/12
For personal use only.

tal binding energy of the third H_2O is 60.0 kJ mol^{-1}. The (2,1,0) isomer, $H_2O \cdots (H_2O)_2 \cdots H_2NH^{\cdot+}$, is found to be less stable by 17.9 kJ mol^{-1} at the HF level, 3.9 kJ mol^{-1} less than the difference between the (2,0,0) and (1,0,0) structures.

For the addition of the fourth water molecule to the (3,0,0) structure, two possible sites need to be considered, binding to one of the H atoms of the first-shell water molecules, to form a (3,1,0) structure $H_2O \cdots (H_2O)_3 \cdots H_3N^{\cdot+}$ and an axial binding to form (3,0,1) structure $(H_2O)_3 \cdots H_3N^{\cdot+} \cdots OH_2$. Both structures are found. The more stable (3,1,0) complex has a linear O ··· HO hydrogen bond with a bond length 1.873 Å. The corresponding O ··· HN distance is shorter by 0.075 Å and the other two O ··· HN separations are lengthened by 0.018 Å from those in $(H_2O)_3 \cdots H_3N^{\cdot+}$. The binding energy is found to be 38.3 kJ mol^{-1} at the HF level, only half of that for the first H_2O bonded on the first hydration shell. The secondary interaction can be seen clearly by comparing the successive reductions in binding energies. Thus $\Delta E_1 - \Delta E_2 = 14.0$ and $\Delta E_2 - \Delta E_3 = 10.5$, while $\Delta E_3 - \Delta E_4 = 21.7$ kJ mol^{-1}.

The (3,0,1) complex $(H_2O)_3 \cdots H_3N^{\cdot+} \cdots OH_2$ is also predicted to be stable, though in a very shallow potential well. The binding energies were found to be 33.5 kJ mol^{-1} at the HF level. Compared with the (3,1,0) complex, $H_2O \cdots (H_2O)_3 \cdots H_3N^{\cdot+}$, the binding energy is 4.8 kJ mol^{-1} less, indicating that the H atoms of the H_2O molecules are still the preferred positions of attachment.

In $(H_2O)_3 \cdots H_3N^{\cdot+} \cdots OH_2$, (3,0,1), the radical center is little altered from planarity. This leads us to explore the possibility of adding another water molecule to the N atom of (3,0,1) structure. A structure $(H_2O)_3 \cdots H_3N^{\cdot+} \cdots (OH_2)_2$, i.e., (3,0,2), optimized with constraints has an imaginary frequency of 37i cm^{-1}, indicating the tendency of the fifth H_2O to transfer to a H atom of another H_2O, possibly to form a (3,1,1) structure. The estimated binding energies, with the (3,0,2) structure that undoubtedly would be present in solution, are 28.7 at HF levels. We did not pursue structures of the (3,1,1) type further.

Vibrational frequencies and zero-point energy (ZPE)

The calculated vibrational frequencies indicate that the complexes correspond to minima in the potential energy surfaces, with the exception of $(H_2O)_3 \cdots H_3N^{\cdot+} \cdots (OH_2)_2$. For many of the complexes, the first few vibrational frequencies are very small, confirming that the corresponding potential wells are very flat, permitting different conformers to be reached without significantly increasing the total energies of the complexes.

For a complex with n hydrogen bonds, there are $6 \times n$ vibrational modes more than the sum of those in the fragments. Even if the torsional modes are treated as free internal rotations, the remaining $5 \times n$ modes may contribute to the ZPE change in a significant way. It is found that even for weakly interacted systems, the ZPE correction to the binding energy ranges from 4 to 10 kJ mol^{-1} per hydrogen bond, and thus plays an important role in evaluating accurately the binding energies.

Gas phase thermodynamic functions

In the case of NH_4^+, values of ΔH_n, ΔS_n, and ΔG_n for reaction [1] have been measured for $n = 1$–5 in the gas phase (9, 10). These are compared with the present calculated values in Table 4 and the ΔH_n values are also plotted as a function of n in Fig. 3. The plots of Fig. 3 and the data for the $(n,0,0)$ and $(n-1,1,0)$ clusters listed in Table 4 suggest that the experimentally measured incremental free energy values are for structures of the $(n,0,0)$ type for $n \leq 4$. The level of agreement between the calculated and experimental data is excellent. Indeed it is a clear confirmation that the species studied experimentally are all of the $(n,0,0)$ type.

From Fig. 3 it is evident that the curves for $(n,0,0)$ and $(n-1,1,0)$ complexes will merge at approximately $n = 5$. The present data, which are still in reasonable agreement with experiment at that point, showed that the structure with the fifth water bonded to it is a structure of (4,1,0) type.

A search of the literature on ion clusters did not reveal any studies of $NH_3^{\cdot+}$ complexes with water. However, from Table 4 and Fig. 3 one can see that the trends for the $(n,0,0)$ and $(n-1,1,0)$ complexes with increasing n resemble those for NH_4^+ in that $(n-1,1,0)$ species are bound less strongly. There are, however, three points of particular interest. First, the binding of the initial three waters in $NH_3^{\cdot+}$ is much stronger than in the case of the first four waters bound to NH_4^+. This is such that $\Delta_r G_g(3) = \Sigma_{n=1}^{3} \Delta G_n$ for this species is slightly more negative than $\Delta_r G_g(4) = \Sigma_{n=1}^{4} \Delta G_n$ for NH_4^+ (−128.7 vs. −119.4 kJ mol^{-1}). Secondly, for $(n-1,1,0)$ type complexes, the ΔG_n are also more negative for $NH_3^{\cdot+}$ species than for NH_4^+. For $n = 2$–4, the differences in free energy change between $NH_3^{\cdot+}$ and NH_4^+ species are 6.8, 2.0, and 3.5 kJ mol^{-1}, respectively. Third, at least one, and possibly two H_2O molecules can occupy sites axial to the N^+ center of $NH_3^{\cdot+}$ (above and below the plane of the H atoms) with a further stabilization. As indicated in Table 4, the addition of the fourth water molecule (from (3,0,0) structure to (3,0,1) structure) gives a free energy change of −7.1 kJ mol^{-1}. In the gas phase the structure (3,0,2) is unstable and corresponds to a similar amount of destabilization. However, in liquid water both sites will undoubtedly be occupied. These considerations imply that the solution free energy of $NH_3^{\cdot+}$ could be more negative than that of NH_4^+.

5. Conclusions

The present study confirmed that the experimentally observed incremental changes in free energies for $(H_2O)_n \cdots H_4N^+$ $(n \leq 4)$ are due to the formation of $(n,0,0)$-type complexes, i.e., water molecules binding to the H atoms of H_4N^+. The calculated incremental changes for enthalpy and free energy are in good agreement with the experimental data. The results for $NH_3^{\cdot+}$ aquo complexes provide new information on the hydration of $NH_3^{\cdot+}$. The change in free energies also suggests that water molecules form stronger aquo complexes with $NH_3^{\cdot+}$ than they do with NH_4^+.

6. Acknowledgement

The financial support of the Natural Sciences and Engineering Research Council of Canada is gratefully acknowledged.

1. P. Kebarle. Annu. Rev. Phys. Chem. **28**, 445 (1977).
2. A.W. Castleman, Jr. and R.G. Keesee. Chem. Rev. **86**, 589 (1986).
3. J.W. Caldwell and P.A. Kollman. J. Phys. Chem. **96**, 8249 (1992), and references cited therein.
4. A. Pullman, P. Claverie, and M-C. Cluzan. Chem. Phys. Lett. **117**, 419 (1985).
5. M. Welti, T-K. Ha, and E. Pretsch. J. Chem. Phys. **83**, 2959 (1985).

6. J.E. Del Bene. J. Comput. Chem. **10**, 603 (1988).
7. H.A. Schwarz. J. Chem. Phys. **72**, 284 (1980).
8. D.A. Armstrong, A. Rauk, and D. Yu. J. Am. Chem. Soc. **115**, 666 (1993).
9. J.D. Payzant, A.J. Cunningham, and P. Kebarle. Can. J. Chem. **51**, 3242 (1973).
10. M. Meot-Ner. J. Am. Chem. Soc. **106**, 1265 (1984).
11. L.A. Curtiss, K. Raghavachari, G.W. Trucks, and J.A. Pople. J. Chem. Phys. **94**, 7221 (1991).
12. M.J. Frisch, M. Head-Gordon, G.W. Trucks, J.B. Foresman, H.B. Schlegel, K. Raghavachari, M.A. Robb, J.S. Binkley, C. Gonzalez, D.J. Defrees, D.J. Fox, R.A. Whiteside, R. Seeger, C.F. Melius, J. Baker, R.L. Martin, L.R. Kahn, J.J.P. Stewart, S. Topiol, and J.A. Pople. Gaussian, Inc., Pittsburgh, Pa. 1990.
13. S.F. Boys and B. Bernardi. Mol. Phys. **19**, 55 (1970).
14. D. Yu, R.A. Poirier, and P.R. Surjan. Chem. Phys. Lett. **183**, 25 (1991).
15. J.A. Pople, H.B. Schlegel, R. Krishnan, D.J. Defrees, J.S. Binkley, M.J. Frisch, R.A. Whiteside, R.F. Hout, and W.J. Hether. Int. J. Quantum Chem. Symp. **15**, 269 (1981).
16. D. Yu, A. Rauk, and D.A. Armstrong. Can. J. Chem. In press.

Can. J. Chem. Downloaded from www.nrcresearchpress.com by 213.200.69.106 on 09/08/12
For personal use only.

Étude thermodynamique des trois isomères de l'acide hydroxybenzoïque

RAPHAËL SABBAH[1] ET THI HUY DUC LE

Centre de thermodynamique et de microcalorimétrie du Centre national de la recherche scientifique, 26, rue du 141e R.I.A., 13003 Marseille, France

Reçu le 21 avril 1993

RAPHAËL SABBAH et THI HUY DUC LE. Can. J. Chem. **71**, 1378 (1993).

L'étude thermodynamique des trois isomères de l'acide hydroxybenzoïque a été réalisée par calorimétrie de combustion, de sublimation, par mesures de capacités calorifiques par la méthode de chute et par analyse thermique différentielle. Elle nous a permis de déterminer les fonctions thermodynamiques suivantes (exprimées en kJ mol^{-1}) :

	ortho	*méta*	*para*
$-\Delta_c H^0_m$(s, 298,15 K)	3020,0 ± 1,3	3017,9 ± 1,1	3005,4 ± 2,1
$-\Delta_f H^0_m$(s, 298,15 K)	592,1 ± 1,3	594,1 ± 1,1	606,6 ± 2,1
$\Delta_{sub} H^0_m$(298,15 K)	96,27 ± 0,49	124,99 ± 0,74	114,05 ± 0,69
$-\Delta_f H^0_m$(g, 298,15 K)	495,8 ± 1,4	469,1 ± 1,3	492,6 ± 2,2
$\Delta_{fus} H_m(T_{fus}$ K)	18,2	26,2	
T_{pt}/K	433	475	

À partir de ces résultats expérimentaux, il nous a été possible de déterminer l'énergie de conjugaison des trois isomères, de constater que l'isomère *ortho* serait le plus stable et d'en discuter la raison. Par ailleurs, les valeurs de l'enthalpie d'atomisation expérimentale sont compatibles avec celle que nous avons calculée par voie incrémentale.

RAPHAËL SABBAH and THI HUY DUC LE. Can. J. Chem. **71**, 1378 (1993).

A thermodynamic study of the three hydroxybenzoic acids was carried out by combustion and sublimation calorimetry, heat capacity measurements, and differential thermal analysis. The experimental results (in kJ mol^{-1}) are summarized as :

	ortho	*meta*	*para*
$-\Delta_c H^0_m$(s, 298,15 K)	3020.0 ± 1.3	3017.9 ± 1.1	3005.4 ± 2.1
$-\Delta_f H^0_m$(s, 298,15 K)	592.1 ± 1.3	594.1 ± 1.1	606.6 ± 2.1
$\Delta_{sub} H^0_m$(298,15 K)	96.27 ± 0.49	124.99 ± 0.74	114.05 ± 0.69
$-\Delta_f H^0_m$(g, 298,15 K)	495.8 ± 1.4	469.1 ± 1.3	492.6 ± 2.2
$\Delta_{fus} H_m(T_{fus}$ K)	18.2	26.2	
T_{tp}/K	433	475	

From these experimental results, it was possible to determine for the three isomers (*i*) the resonance energies. From their comparison, the *ortho* isomer seems to be the most stable. This result is discussed using a structural consideration; (*ii*) the enthalpies of atomization. These values are in good agreement with that calculated using a contribution method.

I. Introduction

Dans le cadre de nos études sur l'énergétique des liaisons intra- et intermoléculaires dans les substances organiques, nous avons décidé de nous intéresser à l'étude des trois isomères de l'acide hydroxybenzoïque. C'est une suite logique aux travaux précédemment réalisés au laboratoire sur les acides aminés (1) si l'on souhaite mettre en évidence et comprendre l'effet des substituants sur les propriétés des molécules étudiées.

Si l'on consulte les travaux thermodynamiques consignés dans la littérature au sujet des trois acides traités dans ce mémoire, on se rend compte qu'il sont peu nombreux (cf. III.3. Résultats).

Compte tenu de leurs propriétés et de leurs applications directes et indirectes dans différents secteurs économiques (2), nous avons entrepris leur étude par nos moyens expérimentaux d'investigation (cf. II.2. Appareillage, techniques et mode opératoire) afin d'élucider certaines questions liées à leur structure et à leur utilisation courante.

1. Auteur à qui adresser toute correspondance.

II. Partie expérimentale

II.1. Produits

L'acide hydroxy-2 benzoïque (communément appelé acide salicylique) est un produit Baker, pureté initiale 99,6%. Il a été repurifié par sublimation sous une pression résiduelle de 10^{-2} Torr (1 Torr = 133,322 Pa) à 150°C. L'acide hydroxy-3 benzoïque est un produit Aldrich, pureté initiale 98%. Il a été recristallisé dans le méthanol absolu puis sublimé sous une pression résiduelle de 10^{-2} Torr à 200°C. L'acide hydroxy-4 benzoïque est un produit Aldrich, pureté initiale 99%. Il a été recristallisé dans l'éthanol absolu puis sublimé sous une pression résiduelle de 10^{-2} Torr à 200°C.

Il ne nous a pas été possible de déterminer par ATD le degré de pureté de l'acide hydroxy-4 benzoïque car cette substance se décompose à la fusion. Par contre, dans les deux autres cas, nos expériences d'ATD nous ont permis de déterminer le degré de pureté des échantillons repurifiés (tableau 1).

II.2. Appareillage, techniques et mode opératoire

Pour mener à bien cette étude, nous avons utilisé la calorimétrie de combustion de faibles quantités de substance, la calorimétrie de sublimation, l'analyse thermique différentielle et la mesure des capacités calorifiques.

II.2.1. Calorimétrie de combustion

Pour réaliser les expériences par calorimétrie de combustion, nous avons utilisé l'appareillage décrit dans la référence 3. La micro-

Can. J. Chem. Downloaded from www.nrcresearchpress.com by 213.200.69.106 on 09/08/12
For personal use only.

TABLEAU 1. Degré de pureté, température du point triple et enthalpie molaire de fusion des isomères *ortho* et *méta* de l'acide hydroxybenzoïque

Substance	Pureté (mol%)	Température du point triple[a] (K)	$\Delta_{fus}H_m$ (kJ mol^{-1})
Acide hydroxy-2 benzoïque	99,96	433	18,2
Acide hydroxy-3 benzoïque	99,93	475	26,2

[a]Définie par rapport à l'EIT-90 (24).

TABLEAU 2. Grandeurs physiques des molécules étudiées à 298,15 K

Substance	M[a] (g mol^{-1})	ρ (g cm^{-3})	$(\delta U/\delta P)_T$ (J g^{-1} atm^{-1})[b]
Acide hydroxy-2 benzoïque	138,1228	1,443 (réf. 25)	(0,013)
Acide hydroxy-3 benzoïque	138,1228	1,167	(0,013)
Acide hydroxy-4 benzoïque	138,1228	1,173	(0,013)

[a]Les masses molaires ont été calculées à partir du tableau des masses atomiques de 1991 (26).
[b]1 atm = 101,325 kPa.
Les valeurs placées entre parenthèses ont été estimées.

bombe qui lui est associée a été décrite dans un précédent mémoire (4). La sensibilité de la pile du calorimètre CRMT est de 62,4 μV mW^{-1} à 298,15 K; celle de l'amplificateur est de 30 mV. L'oxygène N45, utilisé dans nos expériences, provient de l'Air Liquide; son degré de pureté est égal à 99,995%.

II.2.2. Calorimétrie de sublimation

Pour mesurer directement la quantité de chaleur mise en jeu par la sublimation des substances étudiées, nous avons utilisé un calorimètre Tian–Calvet, dont la sensibilité de la pile est de 64,3 μV mW^{-1} entre 333 et 363 K, associé à une cellule d'effusion de Knudsen. L'appareillage et le mode opératoire ont été décrits dans la référence 5. Seule a été ajoutée par la suite la robotisation de l'ouverture et de la fermeture des cellules d'effusion. Le signal issu du calorimètre est amplifié par un nanovoltmètre Keithley modèle 147 (sensibilité utilisée 100 μV) puis digitalisé à l'aide d'un voltmètre numérique Keithley modèle 175. L'acquisition et le traitement des données ont été réalisés à l'aide d'un programme écrit par nos soins et traité par un ordinateur Zénith modèle 158.

La très faible pression de vapeur saturante des substances étudiées ne nous a pas permis de les sublimer à 298,15 K. En conséquence, l'isomère *ortho* a été étudiée à 333 K et les deux autres isomères à 368 K avec un trou d'effusion de 0,5 mm (*ortho*), 1 mm (*méta*) et 2 mm (*para*).

II.2.3. Analyse thermique différentielle

En utilisant l'appareillage et le mode opératoire décrits dans la référence 6, cette technique nous a permis de suivre le comportement thermique des trois acides hydroxybenzoïques et de mesurer la température du point triple ainsi que l'enthalpie de fusion des isomères *ortho* et *méta* (tableau 1).

III. Résultats

Nous avons consigné dans le tableau 2 les grandeurs physiques à 298,15 K des substances étudiées intervenant dans les calculs menant aux résultats expérimentaux.

III.1. Calorimétrie de combustion

L'èquivalent énergétique du calorimètre (U_{calor}) a été obtenu à partir d'une série de 10 combustions d'acide benzoïque, échantillon 39i du NBS, pour lequel $\Delta_c u^0$(s, 298,15 K) = −(26 414 ± 3) J g^{-1}. Dans ces expériences, nous avons utilisé environ 5 mg d'acide et 0,2 mg de coton (dont l'énergie de combustion, préalablement déterminée au laboratoire, a pour valeur $\Delta_c u^0$(s, 298,15 K) = −(16 399 ± 23) J g^{-1} (7)). Nous trouvons pour U_{calor}(298,15 K) la valeur (16,05 ± 0,01) J V^{-1} s^{-1}.

Les résultats expérimentaux obtenus par calorimétrie de combustion sont consignés dans les tableaux 3, 4 et 5. Ces résultats correspondent à la réaction :

$$C_7H_6O_3\ (s) + 7\ O_2\ (g) \rightarrow 7\ CO_2\ (g) + 3\ H_2O\ (l)$$

En ce qui concerne l'acide hydroxy-2 benzoïque, notre valeur de l'enthalpie de combustion, $\Delta_c H^0$(s, 298,15 K) = −(3020,0 ± 1,3) kJ mol^{-1}, est compatible avec celles de la littérature comprises entre −3017,5 et −3026,1 kJ mol^{-1} (7, 8). Quant aux deux autres isomères, nous trouvons dans la littérature, pour cette grandeur thermodynamique, les valeurs de Colomina et al. (9) : −(3021,6 ± 0,4) kJ mol^{-1} pour l'acide hydroxy-3 benzoïque et −(3017,6 ± 0,5) kJ mol^{-1} pour l'acide hydroxy-4 benzoïque. Comme on peut le constater, ces valeurs diffèrent légèrement des nôtres.

III.2. Calorimétrie de sublimation

L'étalonnage de notre système calorimétrique a été réalisé par effet Joule avant et après les expériences.

À cause de la très faible pression de vapeur saturante des substances étudiées, nous avons admis l'identité $\Delta_{sub}H_m(T) \equiv \Delta_{sub}H^0_m(T)$. Par ailleurs, pour calculer $\Delta_{sub}H^0_m$(298,15 K) à partir de $\Delta_{sub}H^0_m(T)$, nous avons utilisé la relation suivante :

$$\Delta_{sub}H^0_m(298{,}15\ \text{K}) = \Delta_{sub}H^0_m(T) + \int_T^{298{,}15\ \text{K}} [C^0_{p,m}(g) - C^0_{p,m}(s)]dT$$

après nous être assurés par ATD que la substance ne présente aucun changement de phase entre 298,15 K et T. En ce qui concerne l'intègrale

$$\int_T^{298{,}15\ \text{K}} C^0_{p,m}(s)dT$$

elle a été obtenue par la méthode de chute en utilisant un

Can. J. Chem. Downloaded from www.nrcresearchpress.com by 213.200.69.106 on 09/08/12
For personal use only.

TABLEAU 3. Combustion de l'acide hydroxy-2 benzoïque à 298,15 K[a]

m(subst.) (mg)	m(coton) (mg)	S (V s)	$-\Delta U$ (J)	$-w_1$ (J)	w_2 (J)	$-\Delta_c U^0_m$(s, 298,15 K) (kJ mol^{-1})
7,290	0,135	10,063 341	161,56	2,216	0,207	3015,30
6,780	0,214	9,445 509	151,64	3,516	0,194	3013,72
6,910	0,208	9,648 733	154,90	3,408	0,198	3024,46
7,818	0,168	10,824 723	173,78	2,749	0,223	3017,64
6,216	0,216	5,815 548	139,79	3,543	0,178	3023,85
6,946	0,221	6,466 983	155,45	3,625	0,199	3015,41
5,115	0,281	4,847 220	116,52	4,609	0,148	3018,17
5,688	0,207	5,320 490	127,89	3,395	0,163	3019,50
4,631	0,221	4,374 180	105,15	3,625	0,133	3024,24
5,153	0,221	4,851 183	116,61	3,625	0,148	3024,84
7,617	0,237	7,104 528	170,78	3,887	0,218	3022,58

$-\Delta_c U^0_m$ (s, 298,15 K) = (3020,0 ± 1,3) kJ mol^{-1}
$-\Delta_c H^0_m$ (s, 298,15 K) = (3020,0 ± 1,3) kJ mol^{-1}
$-\Delta_f H^0_m$ (s, 298,15 K) = (592,1 ± 1,3) kJ mol^{-1}

[a]S = aire des thermogrammes; ΔU = variation de l'énergie interne de la bombe et de son contenu; w_1 = énergie de combustion du coton; w_2 = corrections pour passer à l'état standard.

TABLEAU 4. Combustion de l'acide hydroxy-3 benzoïque à 298,15 K[a]

m(subst.) (mg)	m(coton) (mg)	S (V s)	$-\Delta U$ (J)	$-w_1$ (J)	w_2 (J)	$-\Delta_c U^0_m$(s, 298,15 K) (kJ mol^{-1})
6,9765	0,3960	9,916 431	159,20	6,494	0,203	3019,36
6,4825	0,2705	9,107 130	146,21	4,437	0,186	3016,83
6,7656	0,3722	9,596 889	154,07	6,104	0,197	3016,85
7,1574	0,3279	10,083 054	161,88	5,378	0,207	3016,16
7,4458	0,3230	10,498 005	168,54	5,298	0,215	3024,22
7,1078	0,3625	10,055 076	161,43	5,945	0,206	3017,43
6,3020	0,3710	8,979 579	144,16	6,085	0,183	3022,26
6,0476	0,2922	8,541 321	137,13	4,792	0,174	3018,42
7,0492	0,2735	9,868 866	158,44	4,486	0,202	3012,60
7,0245	0,2239	9,792 192	157,21	3,672	0,201	3015,02

$-\Delta_c U^0_m$ (s, 298,15 K) = (3017,9 ± 1,1) kJ mol^{-1}
$-\Delta_c H^0_m$ (s, 298,15 K) = (3017,9 ± 1,1) kJ mol^{-1}
$-\Delta_f H^0_m$ (s, 298,15 K) = (594,1 ± 1,1) kJ mol^{-1}

[a]S = aire des thermogrammes; ΔU = variation de l'énergie interne de la bombe et de son contenu; w_1 = énergie de combustion du coton; w_2 = corrections pour passer à l'état standard.

TABLEAU 5. Combustion de l'acide hydroxy-4 benzoïque à 298,15 K[a]

m(subst.) (mg)	m(coton) (mg)	S (V s)	$-\Delta U$ (J)	$-w_1$ (J)	w_2 (J)	$-\Delta_c U^0_m$(s, 298,15 K) (kJ mol^{-1})
7,0411	0,3386	9,883 125	158,67	5,553	0,204	2999,63
7,4225	0,4269	10,486 038	168,35	7,002	0,216	2998,43
6,7122	0,3826	9,511 347	152,70	6,275	0,195	3009,11
8,4166	0,4612	11,909 742	191,21	7,564	0,246	3009,67
7,0602	0,3458	9,956 613	159,85	5,672	0,205	3012,27
7,3012	0,2979	10,222 230	164,11	4,886	0,210	3008,26
6,0383	0,3577	8,547 381	137,23	5,867	0,175	3000,73

$-\Delta_c U^0_m$(s, 298,15 K) = (3005,4 ± 2,1) kJ mol^{-1}
$-\Delta_c H^0_m$(s, 298,15 K) = (3005,4 ± 2,1) kJ mol^{-1}
$-\Delta_f H^0_m$(s, 298,15 K) = (606,6 ± 2,1) kJ mol^{-1}

[a]S = aire des thermogrammes; ΔU = variation de l'énergie interne de la bombe et de son contenu; w_1 = énergie de combustion du coton; w_2 = corrections pour passer à l'état standard.

Can. J. Chem. Downloaded from www.nrcresearchpress.com by 213.200.69.106 on 09/08/12
For personal use only.

TABLEAU 6. Sublimation des trois isomères de l'acide hydroxybenzoïque

Substance	T (K)	m (mg)	$\Delta_{sub}H^0_m(T)$ (kJ mol^{-1})	$\Delta_{sub}H^0_m(T)$ (kJ mol^{-1})	$\Delta^T_{298,15K}H^0_m(s)$ (kJ mol^{-1})	$\Delta^T_{298,15K}H^0_m(g)$ (kJ mol^{-1})	$\Delta_{sub}H^0_m(298,15K)$ (kJ mol^{-1})	$P(T)$ (Torr)
Acide hydroxy-2 benzoïque	333	10,1742	93,44					
		10,5091	94,65					
		10,4892	95,20					
		10,5726	94,44	95,12 ± 0,49	5,76 ± 0,01	4,61 ± 0,03	96,27 ± 0,49	$7,3 \times 10^{-3}$
		10,4566	96,58					
		10,3207	96,39					
Acide hydroxy-3 benzoïque	363	9,9509	120,22					
		10,5286	124,19					
		10,6674	122,69					
		10,4512	124,67	123,49 ± 0,73	10,36 ± 0,10	8,86 ± 0,03	124,99 ± 0,74	$1,1 \times 10^{-3}$
		10,6782	124,23					
		10,4280	124,95					
Acide hydroxy-4 benzoïque	363	10,8634	114,78					
		10,3227	113,89					
		10,1846	111,73					
		10,1865	112,45	112,39 ± 0,68	10,52 ± 0,12	8,86 ± 0,03	114,05 ± 0,69	$3,4 \times 10^{-4}$
		10,1232	110,93					
		10,8291	110,56					

calorimètre Tian–Calvet et un four maintenus respectivement à 298,15 K et T. Quant à l'intégrale

$$\int_T^{298,15\ K} C^0_{p,m}(g)dT$$

elle a été déterminée à l'aide d'une méthode incrémentale utilisant les données des capacités calorifiques à l'état gazeux de la littérature pour les molécules de benzène, de phénol et d'acide benzoïque (10).

Nous avons consigné dans le tableau 6 les différents résultats expérimentaux obtenus.

Quant aux valeurs de la littérature, celles-ci sont peu nombreuses. En effet, seuls les acides hydroxy-2 et hydroxy-4 benzoïques ont fait l'objet de mesures indirectes. Pour l'acide hydroxy-2 benzoïque, nous avons trouvé trois valeurs de l'enthalpie de sublimation qui sont cohérentes avec la nôtre :

Colomina et al. (9) : $\Delta_{sub}H_m(315,4\ K) = (95,7 \pm 0,1)$ kJ mol^{-1}

Davies et Jones (11) : $\Delta_{sub}H_m(368 < T/K < 408) = (94,8 \pm 0,4)$ kJ mol^{-1}

de Kruif et Van Ginkel (12) : $\Delta_{sub}H_m(312 < T/K < 332) = (94,9 \pm 0,4)$ kJ mol^{-1}

Pour l'acide hydroxy-4 benzoïque, il existe une seule valeur : 116,1 kJ mol^{-1}, obtenue par Davies et Jones (11) dans l'intervalle $398 < T/K < 432$.

III.3. Enthalpie de formation des trois acides hydroxybenzoïques à l'état gazeux

Il est possible, à partir des résultats consignés dans les tableaux 3–6 de déterminer l'enthalpie de formation des substances étudiées à l'état gazeux et à 298,15 K. Celle-ci est respectivement égale à $(-495,8 \pm 1,4)$, $(-469,1 \pm 1,3)$ et $(-492,6 \pm 2,2)$ kJ mol^{-1} dans le cas des isomères *ortho*, *méta* et *para*.

III.4. Pression de vapeur saturante des trois acides hydroxybenzoïques

Comme indiqué dans la référence 13, il nous est possible, à partir de nos essais, d'évaluer la pression de vapeur saturante des substances étudiées (tableau 6) en utilisant la relation suivante :

$$P(T) \approx \Delta P(T) = dm/dt(2\pi RT/M)^{1/2}1/aF$$

dans laquelle $\Delta P(T)$ est la pression de part et d'autre du trou d'effusion; $P(T)$, la pression mesurée par effusion à la température T; dm/dt, la masse effusée par unité de temps; R, la constante des gaz parfaits; M, la masse molaire de la substance; F, le facteur de Clausing (14) et a, l'aire de l'orifice d'effusion.

III.5. Analyse thermique différentielle

Les résultats expérimentaux obtenus sont rassemblés dans le tableau 1. Le manque de valeurs thermodynamiques consignées dans la littérature pour les deux isomères *ortho* et *para* ne nous a pas permis de les comparer à nos résultats expérimentaux.

L'analyse thermique différentielle des trois isomères de l'acide hydroxybenzoïque nous a posé quelques problèmes. En effet, l'acide hydroxy-4 benzoïque se décompose à la fusion avec bris d'ampoule, dû vraisemblablement à un dégagement gazeux d'anhydride carbonique (décarboxylation) qui augmente la pression à l'intérieur de l'ampoule de verre mince (2). Quant aux deux autres isomères, en fin d'expérience, nous avons constaté un changement de coloration laissant supposer une décomposition de ces substances à la fusion. Ce changement de coloration est léger dans le cas de l'isomère *ortho*, beaucoup plus prononcé dans celui de l'isomère *méta*. Ne possédant pas les moyens expérimentaux permettant l'analyse en fonction du temps des produits soumis au traitement thermique et compte tenu du manque de travaux consignés dans la littérature à ce sujet, il ne nous a pas été possible de tirer des conclusions plus concrètes sur le comportement thermique de ces substances.

Enfin précisons que l'incertitude qui accompagne les résultats expérimentaux représente l'écart moyen, σ_m, et tient compte des erreurs sur les termes et facteurs de l'expression utilisée pour calculer ces résultats.

Can. J. Chem. Downloaded from www.nrcresearchpress.com by 213.200.69.106 on 09/08/12
For personal use only.

Can. J. Chem. Downloaded from www.nrcresearchpress.com by 213.200.69.106 on 09/08/12
For personal use only.

IV. Discussion

IV.1. Existence d'une liaison hydrogène intramoléculaire dans l'isomère ortho

L'enthalpie de sublimation d'une substance organique est liée aux interactions intermoléculaires qui comprennent les énergies relatives aux forces de van der Waals et, le cas échéant, aux liaisons hydrogène.

Dans ce travail, l'acide hydroxy-2 benzoïque a une enthalpie de sublimation inférieure de 17,78 kJ mol^{-1} à celle de l'acide hydroxy-4 benzoïque. Cette différence doit être attribuée au fait que la molécule d'acide hydroxy-2 benzoïque présente moins de liaisons hydrogène intermoléculaires que les deux autres isomères. En effet, cet acide est le seul à pouvoir former une liaison hydrogène intramoléculaire entre l'atome d'oxygène du groupement carboxyle et celui d'hydrogène de la fonction hydroxyle (15). Dans un précédent travail (1) l'un de nous (R.S) a mis en évidence, à partir d'une étude sur les acides aminobenzoïques, que l'enthalpie de sublimation de l'isomère *ortho* était inférieure de 11,2 kJ mol^{-1} à celle de l'isomère *para*. En conséquence, la chélation s'affaiblit en passant des acides hydroxybenzoïques aux aminobenzoïques. Une confirmation à cette constatation peut être trouvée dans l'ouvrage de Julg (16) à propos de l'énergie mise en jeu par les liaisons hydrogène dans les deux cas précédents : O—H···O (25 kJ mol^{-1}), N—H···O (11 kJ mol^{-1}).

D'autres observations faites sur les propriétés physicochimiques des acides hydroxybenzoïques tendent à prouver l'existence de cette liaison intramoléculaire dans le cas de l'acide hydroxy-2 benzoïque.

1. À partir de nos expériences de sublimation, il s'avère que la pression de vapeur saturante de l'acide hydroxy-2 benzoïque est, quelle que soit la température, toujours plus forte que celle de l'acide hydroxy-4 benzoïque.

2. L'acide hydroxy-4 benzoïque présente, à l'état liquide, des associations intermoléculaires, par liaisons hydrogène, plus nombreuses que l'acide hydroxy-2 benzoïque. En conséquence, il est moins soluble que l'isomère *ortho* dans un liquide non associé comme le benzène.

3. La température du point triple (ou de fusion), qui renseigne sur la force des liaisons intermoléculaires, est plus élevée dans le cas de l'acide hydroxy-4 benzoïque. Il en est de même pour l'enthalpie de fusion (tableau 1).

4. La constante d'acidité de l'acide hydroxy-2 benzoïque est plus de 10 fois plus forte que celle de l'isomère *méta* et près de 40 fois plus forte que celle de l'isomère *para* (2). On ne peut expliquer cette différence qu'en admettant la présence d'une chélation dans l'isomère *ortho* donnant ainsi à l'oxygène du groupement carboxyle la possibilité de drainer vers lui les électrons de façon à favoriser, d'une part, la formation d'une liaison hydrogène intramoléculaire avec l'hydrogène du groupement hydroxyle et, d'autre part, la dissociation de la fonction carboxylique.

IV.2. Calcul de l'enthalpie de sublimation de l'acide hydroxy-4 benzoïque par voie incrémentale

Comme nous l'avons déjà fait, nous avons essayé de retrouver par le calcul, à partir des contributions énergétiques apporteés par le noyau benzénique et les deux fonctions acide et hydroxyle, l'enthalpie de sublimation de l'acide hydroxy-4 benzoïque. Dans le réseau cristallin, celui-ci se trouve à l'état moléculaire et ne présente pas de liaison hydrogène intramoléculaire. Afin de tenir compte des interactions que peuvent avoir le noyau benzénique et les fonctions acide et hydroxyle au sein du cristal d'acide hydroxy-4 benzoïque, nous avons cherché à calculer ces contributions à partir des grandeurs énergétiques de molécules ayant une nature chimique voisine de celle qui nous intéresse. Dans le cas présent, le problème se simplifie du fait que nous possédons l'enthalpie de sublimation de l'acide benzoïque à 298,15 K; celle-ci est égale à 89,74 kJ mol^{-1} (17). Il suffit donc d'ajouter à cette valeur la contribution du chaînon OH. Nous avons déterminé la contribution de ce chaînon à partir des deux composés : benzène et phénol, en cherchant dans la littérature les principales données qui nous permettaient d'obtenir leur enthalpie de sublimation à 298,15 K. Pour le benzène, il nous a fallu calculer cette grandeur à partir de $\Delta_{vap}H^0_m$(298,15 K) et $\Delta_{fus}H_m$(298,15 K). La première de ces deux grandeurs est empruntée à la littérature (18). Quant à la seconde, nous l'avons calculée à partir de $\Delta_{fus}H_m$(278,68 K) = 9,84 kJ mol^{-1} (10) et en utilisant la règle de Sidgwick (19) :

$$\Delta_{fus}H_m(T) = \Delta_{fus}H_m(298{,}15\ \text{K}) + k(T - 298{,}15)$$

avec k = 0,055 kJ mol^{-1} K^{-1}. Nous trouvons : $\Delta_{sub}H^0_m$(298,15 K) = 44,83 kJ mol^{-1}. En ce qui concerne le phénol, son enthalpie de sublimation à 298,15 K est égale à 68,7 kJ mol^{-1} (8). En conséquence, la part du chaînon OH est égale à ± 23,87 kJ mol^{-1}. Il s'ensuit que l'enthalpie de sublimation de l'acide hydroxy-4 benzoïque, calculée à partir des différentes contributions, égale à 113,61 kJ mol^{-1}, est en parfait accord avec la valeur expérimentale.

IV.3. Energie de conjugaison

L'énergie de conjugaison est, par définition, égale à la différence entre l'énergie de la molécule réelle conjuguée et celle qu'elle aurait si les systèmes insaturés qu'elle comporte étaient indépendants. Nous l'avons déterminée en utilisant les enthalpies de combustion à l'état gazeux de la molécule dans ses états réel et fictif. La première de ces grandeurs est déterminée expérimentalement tandis que la seconde nécessite le recours aux systématiques. Pour notre part, nous avons utilisé celle de Klages consignée dans la référence 20. Les résultats obtenus sont pour l'*ortho* : E_{conj} = 268 kJ mol^{-1}, pour le *méta* : E_{conj} = 238 kJ mol^{-1} et pour le *para* : E_{conj} = 262 kJ mol^{-1}.

Comme nous pouvons le constater, l'isomère *ortho* possède l'énergie de conjugaison la plus élevée. Ceci est vraisemblablement dû à la présence dans la molécule de cet isomère d'une liaison hydrogène intramoléculaire entre l'oxygène du groupement carboxyle et l'hydrogène de la fonction hydroxyle formant ainsi un second cycle. Signalons que le même classement et la même observation ont été faits lors de l'étude des acides aminobenzoïques (1).

IV.4. Enthalpie d'atomisation

L'enthalpie d'atomisation est liée à la transformation suivante : molécule (considérée comme gaz idéal, état fondamental, T) → atomes (chacun d'eux considéré comme gaz idéal, état fondamental, T).

À partir de l'enthalpie de formation d'une molécule à l'état gazeux et de celle des différents constituants C, H, O, que l'on emprunte aux tables (21) et dont les valeurs sont respectivement égales à (716,67 ± 0,44), (217,997 ± 0,006) et (249,17 ± 0,10) kJ mol^{-1}, il est possible de calculer son enthalpie d'atomisation expérimentale. Nous trouvons pour nos trois isomères les valeurs suivantes : *ortho* : $\Delta_{a,exp}H^0_m$(298,15 K) = (7568 ± 2) kJ mol^{-1}; *méta* :

$\Delta_{a,exp}H^0_m(298,15\ K) = (7541 \pm 2\ kJ)\ mol^{-1}$ et *para* : $\Delta_{a,exp}H^0_m(298,15\ K) = (7565 \pm 3)\ kJ\ mol^{-1}$. Ces résultats sont cohérents si on les compare à la valeur de l'enthalpie d'atomisation calculée ($\Delta_{a,calc}H^0_m(298,15\ K) = 7542\ kJ\ mol^{-1}$) à partir de celle de l'acide benzoïque (7117 kJ mol^{-1})(8, 21) en remplaçant la contribution enthalpique de la liaison C_b—H = 415,88 kJ mol^{-1} (22) par celle de la liaison C_b—OH = 841 kJ mol^{-1} (23).

1. M. Nabavian, R. Sabbah, R. Chastel et M. Laffitte. J. Chim. Phys. **74**, 115 (1977).
2. V. Grignard, G. Dupont et R. Locquin. Traité de chimie organique. Tome XI. Masson, Paris. 1945.
3. R. Sabbah et I. Antipine. Bull. Soc. Chim. Fr. 392 (1987).
4. R. Sabbah et L. El Watik. Thermochim. Acta, **176**, 163 (1991).
5. R. Sabbah, I. Antipine, M. Coten et L. Davy. Thermochim. Acta, **115**, 153 (1987).
6. (*a*) R. Sabbah et I. Antipine. J. Therm. Anal. **32**, 1929 (1987); (*b*) R. Sabbah et L. El Watik. J. Therm. Anal. **36**, 2299 (1990).
7. R. Sabbah et M. Coten. Thermochim. Acta, **49**, 307 (1981).
8. J.B. Pedley, R.D. Naylor et S.P. Kirby. Thermochemical data of organic compounds. 2nd ed. Chapman et Hall, London. 1986.
9. M. Colomina, P. Jiménez, M.V. Roux et C. Turrion. Bull. Journ. Calorim. Anal. Therm. **11**, 3-19-1 (1980).
10. D.R. Stull, E.F. Westrum, Jr. et G.C. Sinke. The chemical thermodynamics of organic compounds. J. Wiley, New York. 1969.
11. M. Davies et J.I. Jones. Trans. Faraday Soc. **50**, 1042 (1954).
12. C.G. de Kruif et C.H.D. Van Ginkel. J. Chem. Thermodyn. 9, 725 (1977).
13. R. Sabbah, R. Chastel et M. Laffitte. Thermochim. Acta, **5**, 117 (1972); Can. J. Chem. **52**, 2201 (1974).
14. R.D. Freeman et A.W. Searcy. J. Chem. Phys. **22**, 762 (1954).
15. W. Cochran. Acta Crystallogr. **6**, 260 (1953).
16. A. Julg. Chimie théorique. Dunod, Paris. 1964.
17. R. Chastel, F. Steckel et H. Tachoire. Proc. 1st Int. Conf. Calorimetry and Thermodynamics, Warsaw, 1969. Polish Scientific Publishers, Warsaw. 1969. p. 155.
18. V. Majer, V. Svoboda et H.V. Kehiaian. Enthalpies of vaporization of organic compounds: a critical review and data compilation. IUPAC Chemical Series N° 32, Blackwell, Oxford. 1985.
19. T.L. Cottrell. The strengths of chemical bonds. Butterworths, London. 1958. p. 145.
20. G.W. Wheland. Resonance in organic chemistry. Wiley, New York. 1955.
21. Report of the Codata task group on key values for thermodynamics 1977. J. Chem. Thermodyn. **10**, 903 (1978).
22. R. Sabbah et M. Laffitte. Thermochim. Acta, **25**, 376 (1978).
23. R. Sabbah et E.N.L.E. Buluku. Can. J. Chem. **69**, 481 (1991).
24. H. Preston-Thomas. Metrologia, **27**, 3 (1990).
25. D.R. Lide. Handbook of chemistry and physics. 71st ed. CRC, Boca Raton, Fla. 1990–1991.
26. Atomic weights of the elements 1991. Pure Appl. Chem. **64**, 1519 (1992).

Can. J. Chem. Downloaded from www.nrcresearchpress.com by 213.200.69.106 on 09/08/12
For personal use only.

^{1}H and ^{13}C nuclear magnetic resonance studies of the conformational equilibrium of 2-(diphenylphosphino)benzaldehyde in polar and nonpolar solutions. Signs of the proximate coupling constants, $^{4}J(CHO, ^{31}P)$ and $^{3}J(^{13}CHO, ^{31}P)$

TED SCHAEFER, RUDY SEBASTIAN, ROBERT W. SCHURKO, AND FRANK E. HRUSKA
Department of Chemistry, University of Manitoba, Winnipeg, MN R3T 2N2, Canada

Received March 10, 1993

Can. J. Chem. Downloaded from www.nrcresearchpress.com by 213.200.69.106 on 09/08/12
For personal use only.

TED SCHAEFER, RUDY SEBASTIAN, ROBERT W. SCHURKO, and FRANK E. HRUSKA. Can. J. Chem. **71**, 1384 (1993).

The analyses of the ^{1}H nuclear magnetic resonance spectra of 2-(diphenylphosphino)benzaldehyde in CS_2/C_6D_{12} and acetone-d_6 solutions yield stereospecific coupling constants from which the populations of the O-*cis* and O-*trans* conformers are derived. The free energy differences favouring the O-*trans* conformer at 300 K are 2.7 and 0.9 kJ/mol, in the polar and nonpolar solutions, respectively; in the crystal only the O-*cis* conformer exists. The coupling constant, $^{4}J(CHO, P)$, is estimated as $-7.1(2)$ Hz in the O-*trans* confomer and $^{3}J(CHO, P)$ as $+29.4(1.3)$ Hz. Their magnitudes depend on the proximity of the C—H bond to the lone pair on phosphorus. $^{n}J(C, P)$ are reported for triphenylphosphine and for the benzaldehyde derivative as dilute solutions in the two solvents, demonstrating a significant solvent dependence for some of these coupling constants. Some simple relationships are proposed between $^{n}J(C, P)$ and the torsion angle about the C—P bond, estimates of the latter coming from AM1 and STO 3G MO computations. $^{n}J(C, P)$ are also sensitive to intrinsic ring substituent perturbations, as are the $^{n}J(H, P)$; for example, $^{5}J(H, P)$ is negative in the disubstituted ring of 2-(diphenylphosphino)benzaldehyde but positive in the phenyl groups. The $^{n}J(H, P)$ are also discussed with respect to their dependence on the torsion angles about the C—P bonds. It appears that the conformational properties of the aromatic rings in triphenylphosphine and its formyl derivative are very similar. Further, the phosphorus atom is polarized such that the carbonyl bond is attracted towards the positive region near phosphorus, and the C—H bond of the formyl group more towards the lone-pair region; the actual torsion angles represent a compromise between these attractive forces and the repulsive forces between bonds on neighbouring aromatic moieties. CNDO/2 MO and INDO MO FPT computations of $^{n}J(C, P)$ and $^{n}J(H, P)$ are of mixed utility, although the former bear out the idea that the proximate O=C—H···lone-pair interaction dominates $^{3}J(CHO,P)$ and $^{4}J(CHO,P)$.

TED SCHAEFER, RUDY SEBASTIAN, ROBERT W. SCHURKO et FRANK E. HRUSKA. Can. J. Chem. **71**, 1384 (1993).

L'analyse des spectres de résonance magnétique nucléaire du ^{1}H du 2-(diphénylphosphino)benzaldéhyde en solution soit dans le CS_2/C_6D_{12} ou dans l'acétone-d_6 permet d'obtenir les constantes de couplage stéréospécifiques à partir desquelles on peut déterminer les populations des conformères O-*cis* et O-*trans*. Les différences d'énergie libre favorisant le conformère O-*trans*, à 300 K, sont de 2,7 et 0,9 kJ/mol respectivement pour les solutions polaires et non polaires; dans la forme cristalline, seul le conformère O-*cis* existe. On a évalué que la constante de couplage $^{4}J(CHO, P)$ est de $-7,1(2)$ Hz dans le conformère O-*trans* alors que la constante $^{3}J(CHO, P)$ est de $+29,4(1,3)$ Hz. Leurs amplitudes varient avec la distance entre la liaison C—H et la paire libre du phosphore. On rapporte les constantes $^{n}J(C, P)$ pour la triphénylphosphine et pour le dérivé benzaldéhyde en solutions diluées dans les deux solvants et on démontre ainsi une forte dépendence sur le solvant pour quelques-unes de ces constantes. On propose quelques relations simples entre des $^{n}J(C, P)$ et l'angle de torsion autour de la liaison C—P évalué par des calculs OM AM1 et STO 3G. Comme c'est le cas pour les constantes $^{n}J(H, P)$, les constantes $^{n}J(C, P)$ sont aussi sensibles aux perturbations intrinsèques causées par les substituants du cycle; par exemple, la constante $^{5}J(H, P)$ est négative dans le cycle disubstitué 2-diphénylphosphino)-benzaldéhyde, mais elle est positive dans les groupes phényles. On discute aussi des constantes $^{n}J(H, P)$ en fonction de leur dépendance sur les angles de torsion autour des liaisons C—P. Il semble que les propriétés conformationnelles des cycles aromatiques de la triphénylphosphine et de son dérivé formylé soient très semblables. De plus, l'atome de phosphore est polarisé d'une telle manière que la liaison carbonyle est attirée vers la région positive près du phosphore alors que la liaison C—H du groupe formyle s'approche de la région de la paire libre; les angles de torsion réels représentent un compromis entre les forces d'attraction et de répulsion entre les liaisons des portions aromatiques voisines. Les calculs d'OM CNDO/2 et INDO FPT des constantes $^{n}J(C, P)$ et $^{n}J(H, P)$ ne sont pas toujours utiles même si les premiers relient correctement le fait que la proximité de l'interaction O=C—H···paire libre domine les constantes $^{3}J(CHO, P)$ et $^{4}J(CHO, P)$.

[Traduit par la rédaction]

Introduction

In the crystal, 2-(diphenylphosphino)benzaldehyde (DPPB) exists as the O-*cis* conformer (1). The P···O distance, 2.83 Å, is considered (1) as too long for a strong interaction. Of course, the direction of the lone pair of electrons on phosphorus need not lie in the plane of the formyl group, nor does it. As expected on steric grounds, however, the formyl group is in the *exo* position, that is, it lies above the plane containing the three ipso carbon atoms of the aromatic rings. This arrangement is conveniently described with reference to **1**. In the absence of the formyl group,**1** would represent one of the two C_{3v} conformers of triphenylphosphine. The other conformer of C_{3v} symmetry, defined by vanishing torsion angles, θ, would be that in which the C_3 axis lies in the planes of the phenyl groups. The C_3 axis in triphenylphosphine forms a normal to the plane containing the three ipso carbon atoms and also lies along the direction of the lone pair. Both of the C_{3v} conformers of triphenylphosphine are unstable because of close approaches of the *ortho* C—H bonds in neighbouring phenyl groups. On average, the stable conformer will have C_3 symmetry (2) with $0 < \theta < 90°$, although at a given instant none of the three torsional angles need be equal.

[1]Author to whom correspondence may be addressed.

In DPPB, however, none of the torsion angles will be equal on average. For steric reasons the formyl group mainly occupies a region near the lone-pair but the direction of the lone-pair does not lie in the plane of the formyl group; such an arrangement implies lone-pair, lone-pair repulsions (O-*cis* conformer). To a first approximation, the formyl group lies in the plane of its benzene ring because the barrier to internal rotation in benzaldehyde is much larger than thermal energies available at ambient temperatures (3). Consequently, the disubstituted ring twists about the P—C bond so as to relieve the lone-pair repulsion. The two phenyl groups also twist about their P—C bonds to relieve *ortho* C—H interactions; the twist direction has the same sense for all the aromatic moieties, clockwise, say, as viewed along the vectors from each *para* carbon atom to the phosphorus atom (see **1**). As θ increases from zero for the disubstituted ring the P···O distance in the O-*cis* conformer remains constant, apart from small changes caused by slight alterations in bond lengths and angles. At some value of θ, less than 90°, it is then surmised that a compromise is reached between lone-pair, lone-pair repulsions and those between the C=O bond and the π cloud of the nearest phenyl group.

In the light of this discussion, it is perhaps unexpected that DPPB exists as the O-*cis* conformer in the solid. Because the carbonyl group is highly polar (4), the carbon and hydrogen atoms are both positively charged (most of the positive charge resides at carbon, however). Intuition therefore suggests the O-*trans* as more stable than the O-*cis* conformer of DPPB; the formyl group lies in the region of the lone pair on phosphorus. Such intuition is supported by the conformational properties of some 2-(alkylthio)benzaldehydes in solution (5), in which the orientation of the 3*p* lone pair on sulfur controls the orientation of the formyl substituent, repelling the C=O bond.

Alternatively, it might be argued that the net charge on phosphorus is positive and, while the lone-pair region is one of negative charge,[2] the twist of the disubstituted benzene ring about the P—C bond is such that, perhaps together with some extra polarization of the phosphorus atom caused by the C=O bond dipole, a net small stabilization of the O-*cis* conformer occurs. It is also possible, however, that packing forces in the crystal determine the observed conformation.

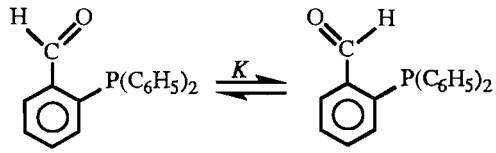

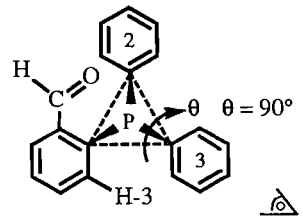

1

Accordingly, the first aim of this work is to establish the conformational behaviour of the formyl group of DPPB in a nonpolar as well as in a polar solution. The long-range spin–spin coupling constant over five formal bonds, ^5J(H, CHO), between the formyl and ring protons, is a sensitive indicator (10, 11) of the equilibrium constant, *K*. The values of *K* can then be compared with some semiempirical, AM1, and ab initio, STO-3G, molecular orbital calculations of the stabilities of the free O-*cis* and O-*trans* conformers.

If, as it does, *K* turns out to be of order unity in solution and dependent on the solvent, then the possibility exists that the through-space, or, better, proximate, coupling constants, $^4J(CHO, P)$ and $^3J(CHO, P)$, can be characterized as to sign and magnitude in the two conformers. A recent discussion (12) of proximate $^{5,6}J$(H, F) and $^{4,5}J$(C, F), for which the ^{13}C nuclei and protons exist in the same C—H bond, points out the importance of sign determinations and also that, while the theoretical treatments are promising, they do not agree very well with experiment. Nevertheless, it is clear (12) that the orientation of the C—H bond with respect to the in-plane lone-pair on fluorine, the one in the plane defined by coplanar C—F and C—H vectors, will likely determine the sign of $^{5,6}J$(H, F). In DPPB, the lone-pair sits on phosphorus and, in the O-*trans* conformer, a proximate coupling pathway can be represented by P···H—C=O. It is unlikely that the lone-pair direction and the formyl group are coplanar, so that, by analogy to ^nJ(H,F) and ^{n-1}J(C, F), either sign of $^4J(CHO, P)$ is a possibility. Furthermore, the proximate contribution to $^3J(CHO, P)$ is of interest.

Therefore, the second aim of the present work is the measurement of the signs and magnitude of $^4J(CHO, P)$ and of $^3J(CHO, P)$. Their values are then extrapolated to those appropriate to the individual conformers; the results are of interest in theoretical approaches to coupling mechanisms and in conformational analysis.

From the experiments of Jakobsen and co-workers (13, 14), the signs of ^nJ(C, P), n = 1–3, in triphenylphosphine are known. Their studies of tri(*o*-tolyl)phosphine indicate (14) a remarkable stereospecificity of ^2J(C, P) in that the coupling constant is +26.44(3) Hz when the aromatic C—C bond in question is oriented towards the region of the lone pair on phosphorus[3] and is less than 1 Hz in magnitude for

[2]The lone-pair on phosphorus in DPPB is not a pure lone-pair like, for example, the oxygen $p\pi$ orbital in water, but a quasi lone-pair in the sense that it is a molecular orbital consisting perhaps predominantly of orbitals located on phosphorus (6–9). The available STO-3G* molecular orbital computations on triphenylphosphine (9) imply that the lone-pair is an sp^2 hybrid in the sense that in the HOMO the ratio of the sum of the squares of the coefficients of the *s* orbitals on phosphorus to that of the *p* orbitals is 1 to 2. Our own STO-3G computations on DPPB imply that, of the phosphorus orbitals, it is predominantly the 3*s* and $3p_z$ orbitals that contribute to the HOMO and that the lone-pair on phosphorus can be thought of as an $sp^{1.9}$ hybrid in the O-*cis* conformer and $sp^{1.8}$ in the O-*trans*. The degree of localization of the HOMO at phosphorus, however, defined as the sum of the squares of the coefficients of the phosphorus orbitals divided by the sum of the squares of the coefficients of *all* contributing orbitals, is only 45% for the O-*cis* conformer of DPPB (compare 47% for triphenylphosphine (9) using the STO 3G* basis). The lone-pair on phosphorus is thus a quasi lone-pair. A naive approach, in which the bond angles at phosphorus are used to define hybridization states, would yield the lone-pair hybrid in triphenylphosphine as $sp^{1.2}$.

[3]For a recent review on the qualitative influence of electron lone pairs on spin–spin coupling constants, see ref. 15. If the lone-pair were completely localized it would have minimal influence on the conformational dependence of ^nJ(X, P); see also footnote 2.

Can. J. Chem. Downloaded from www.nrcresearchpress.com by 213.200.69.106 on 09/08/12
For personal use only.

TABLE 1. The ^{1}H nmr spectral parameters for the disubstituted benzene ring of 2-(diphenylphosphino) benzaldehyde in CS_2/C_6D_{12} and acetone-d_6 solutions at 300 K

Parameter	Solvent		Parameter	Solvent	
	CS_2/C_6D_{12}[a]	Acetone-d_6[b]		CS_2/C_6D_{12}[a]	Acetone-d_6[b]
υ(CHO)	3128.176(2)[c]	3138.767(2)	^5J(H-3, CHO)	0.219(2)	0.336(2)
υ_3	2071.263(2)	2098.301(2)	^5J(H-5, CHO)	0.631(2)	0.485(3)
υ_4	2196.107(2)	2264.444(2)	^6J(H-4, CHO)	−0.029(2)	−0.034(3)
υ_5	2211.464(2)	2276.773(2)	^4J(CHO, P)	−5.853(3)	−5.136(4)
υ_6	2350.798(2)	2403.888(2)	^3J(H-3, P)	4.456(3)	4.495(3)
$^3J_{34}$	7.715(2)[d]	7.735(3)	^4J(H-4, P)	0.447(3)	0.480(3)
$^3J_{45}$	7.350(2)	7.405(2)	^4J(H-6, P)	3.777(3)	3.713(3)
$^3J_{56}$	7.664(2)	7.673(3)	^5J(H-5, P)	−0.376(3)	−0.421(4)
$^4J_{35}$	1.221(2)	1.187(3)	Calcd. transitions	166	176
$^4J_{46}$	1.472(2)	1.439(3)	Assigned trans.	128	115
$^5J_{36}$	0.530(2)	0.536(2)	Peaks observed	131	110
^4J(H-6, CHO)	−0.184(2)	−0.204(2)	Largest diff.	0.022	0.014
^6J(H-3, H_o)	±0.05(2)	±0.05(2)	rms deviation	0.007	0.008

[a]For a saturated, ca. 2.5 mol%, solution in CS_2, containing also 10 mol% C_6D_{12} and 0.5 mol% tetramethylsilane (TMS).
[b]For a saturated, <3 mol%, solution in acetone-d_6, containing also 0.5 mol% TMS.
[c]In Hz at 300.135$_2$ MHz to high frequency of internal TMS.
[d]Numbers in parentheses are the standard deviations in the last significant figure.

the opposite orientation (below the plane of the ipso carbon atoms; see **1**). ^3J(C, P) displays a somewhat less remarkable but similar dependence on the orientation of the lone-pair direction. It is of interest whether ^nJ(H, P) in triphenylphosphine and its derivatives behave like the corresponding ^{n-1}J(C, P). The analysis of the somewhat complex ^{1}H nmr spectra of 2-substituted triphenylphosphines has not been reported.

The third aim of the present work is thus the extraction of ^nJ(H, P) for DPPB and their comparison with ^{n-1}J(C, P), not only in the same molecule but also with ^{n-1}J(C, P) for triphenylphosphine (TPP) in a similar state. Hence dilute solutions of DPPB and of TPP in CS_2/C_6D_{12}/TMS and acetone-d_6/TMS solvent mixtures are here the subject of nmr investigations.

Experimental

Saturated solutions, less than 3 mol% in 2-(diphenylphosphino)-benzaldehyde (Aldrich), were prepared in CS_2/C_6D_{12}/TMS and acetone-d_6/TMS solvent mixtures, the comparisons of which are given in Table 1. Similar data are given for triphenylphosphine solutions in Table 4. These solutions were filtered into 5-mm o.d. nmr sample tubes. The tubes were degassed by five cycles of the freeze–pump–thaw procedure and were then flame-sealed to yield fairly symmetrical tops (smooth spinning).

The ^{1}H nmr spectra were obtained by our standard techniques (16, 17) on a Bruker AM300 spectrometer, taking care to shim finally on the free induction decay arising from internal tetramethylsilane. Acquisition times were 51.2 s in ordinary accumulations of free induction decays and were 47.0 s during the double resonance experiments. Spectral windows were sufficiently small to ensure digital resolutions as high as 0.01 Hz/real point; digitization was further improved by zero-filling to four or six times the original number of data points.

Because $|^4J(CHO, P)| > 5$ Hz, relative sign determinations were most easily performed by partial decoupling procedures (18), ^{1}H{*CH*O}, in which transitions of the formyl proton corresponding to different spin states of ^{31}P were irradiated in separate experiments. A similar set of experiments, in which proton transitions of the ^{13}CHO group corresponding to distinct ^{31}P spin states were irradiated while recording the coupled ^{13}C nmr spectrum of this group, gave the relative signs of $^4J(CHO, P)$ and $^3J(CHO, P)$.

The proton-decoupled ^{13}C nmr spectra of the four samples of TPP and DPPB were acquired in a manner designed to define small ^nJ(C, P) values with a precision of at least 0.02 Hz. One coupling constant, ^3J(C-3, P) in the disubstituted ring of DPPB in acetone-d_6 solution, was not very cleanly resolved and may be 0.03 Hz larger in magnitude than that reported in Table 4.

Molecular orbital computations on various conformations of DPPB utilized the program GAUSSIAN 86 (19) and employed the AM1 (20) and STO-3G (21) parameterizations.

Results and discussion

Spectral analyses

The ^{1}H nmr spectra of DPPB were analyzed as due to two separate 6-spin systems, one for the C_5H_4(CHO)P fragment and the other for the two equivalent C_6H_5P fragments. The formyl proton does not couple with the protons in the two phenyl groups, to within experimental error. H-3 in the C_6H_4(CHO)P moiety displays a through-space coupling interaction of ±0.05 ± 0.02 Hz with the *ortho* protons of the two phenyl groups, added as a simulation during the formal analysis with the program NUMARIT (22), completely reworked by R. Sebastian. The ensuing spectral parameters are presented in Tables 1 and 2.

The ^{1}H{C^1*HO*} partial decoupling experiments give $^4J(CHO, P)/^4J(H\text{-}6, P) < 0$, $^4J(CHO), P)/^5J(H\text{-}5, P) > 0$, $^4J(CHO, P)/^4J(H\text{-}4, P) < 0$, and $^4J(CHO, P)/^3J(H\text{-}3, P) < 0$. The ^{13}CHO{*CH*O} experiments showed that $^4J(CHO, P)/^3J(CHO, P) < 0$. Because all ^nJ(H, P) in triphenylphosphine are positive (23–25), it appears that $^4J(CHO, P)$ is negative and $^3J(CHO, P)$ positive. Then ^5J(H, P) in the disubstituted aromatic ring is negative.

Tables 3 and 4 contain the ^{13}C nmr chemical shifts and values of ^nJ(C, P) for DPPB and TPP in the polar and nonpolar solutions.

*The O-*trans, *O-*cis *equilibrium*

It has been demonstrated (10, 11) that the ratio of the values of ^5J(H, CHO) in *ortho*-substituted benzaldehydes is

Can. J. Chem. Downloaded from www.nrcresearchpress.com by 213.200.69.106 on 09/08/12
For personal use only.

TABLE 2. The ^{1}H nmr spectral parameters for the equivalent phenyl groups of 2-(diphenylphosphino) benzaldehyde at 300 K[a]

Parameter	Solvent		Parameter	Solvent	
	CS_2/C_6D_{12}	Acetone-d_6		CS_2/C_6D_{12}	Acetone-d_6
ν_o	2153.316(1)	2184.785(1)	^3J(H, P)	7.717(2)	7.836(2)
ν_m	2169.575(1)	2213.870(1)	^4J(H, P)	1.531(2)	1.504(3)
ν_p	2174.891(1)	2217.359(2)	^5J(H, P)	0.744(3)	0.831(4)
$^3J_{om}$	7.642(3)	7.654(3)	Calcd. transitions	160	151
$^3J_{mp}$	7.452(2)	7.479(2)	Assigned trans.	125	121
$^4J_{op}$	1.283(2)	1.273(3)	Peaks observed	106	118
$^4J_{oo}$	1.718(2)	1.731(3)	Largest diff.	0.015	0.016
$^4J_{mm}$	1.396(2)	1.395(3)	rms deviation	0.007	0.007
$^5J_{op}$	0.624(1)	0.636(1)			

[a]See the footnotes to Table 1 for concentrations of solute and spectral parameter specifications.

TABLE 3. The ^{13}C nmr chemical shifts and ^nJ(C, P) for the disubstituted benzene ring of 2-(diphenylphosphino) benzaldehyde in CS_2/C_6D_{12} and acetone-d_6 solutions at 300 K

Parameter	Solvent	
	CS_2/C_6D_{12}[a]	Acetone-d_6[a]
δ_1[b]/^2J[c]	140.765/27.37	141.381/27.42
$\delta_2/^1J$	138.656/−14.93	141.381/−14.70
$\delta_3/^2J$	133.624/0.19[e]	134.411/0.11[e]
$\delta_4/^3J$	132.840/0.64[e]	134.395/0.74[e]
$\delta_5/^4J$	128.506/0.26	129.830/0.35
$\delta_6/^3J$	129.423/3.90	131.795/3.87
δ(CHO)/^3J	188.605/+21.80	191.737/+17.34[d]

[a]For the samples described in Table 1.
[b]In ppm relative to internal TMS at a transmitter frequency of 75.4834 MHz.
[c]With an accuracy of 0.02 Hz or better, with the exception of ^3J for the acetone solution, which may be too small by 0.03 Hz.
[d]Sign determined by ^{13}C {^{1}H} experiments as described in the text.
[e]The assignment is interchangeable in both solutions. The one given agrees best with the values of $^{2,3}J$(C, P) for tri(*o*-toyl)phosphine (15).

TABLE 4. The ^{13}C nmr chemical shifts and ^nJ(C, P) for triphenylphosphine and the two phenyl groups in 2-(diphenylphosphino) benzaldehyde in CS_2/C_6D_{12} and acetone-d_6 solutions at 300 K

	Solvent			
	CS_2/C_6D_{12}		Acetone-d_6	
	TPP[a]	2-DPPB[b]	TPP[c]	2-DPPB[b]
δ_{ipso}	137.326	136.196	138.052	137.344
δ_o	133.586	133.925	134.240	134.623
δ_m	128.175	128.474	129.284	129.497
δ_p	128.265	128.742	129.502	129.839
^1J	−12.92[d]	(−)11.43	−11.73	(−)10.49
^2J	+19.68	(+)20.47	+19.73	(+)20.36
^3J	+6.76	(+)7.16	+6.88	(+)7.24
^4J	0.34	0.43	0.34	0.51

[a]For a 3.0 mol% solution in CS_2 containing also 10.0 mol% of C_6D_{12} and 0.5 mol% of TMS.
[b]For the sample described in Table 1.
[c]For a 5.0 mol% solution in acetone-d_6, containing also 0.5 mol% of TMS.
[d]See ref. 14 for the signs of $^{1,2,3}J$(C, P).

a reliable measure of the equilibrium between the O-*trans* and O-*cis* conformers. This statement implies that ^5J essentially vanishes for an antizigzag arrangement of the intervening bonds and that the intrinsic substituent perturbation of ^5J is small. These assumptions have been examined in detail, particularly for relatively electronegative substituents such as fluorine (10) and chlorine (11). It is noted here that the electronegativities of phosphorus and hydrogen are very similar. Application of the ratio to DPPB yields $K = P_t/P_c = {}^5J$(H-5, CHO)/^5J(H-3, CHO) = 0.631(2)/0.219(2) = 2.9 for the CS_2/C_6D_{12} solution and, similarly, $K = 1.4$ for the acetone-d_6 solution, at 300 K. Hence the free energy differences favoring the O-*trans* conformer are 2.7 and 0.9 kJ/mol; the latter value pertains to the polar solution.

The predominance of the O-*trans* conformer in both solutions contrasts sharply with its absence in the crystal. Furthermore, both AM1 and STO-3G MO computations, to be described below, predict a dipole moment lower by 0.3 D for the O-*cis* than for the O-*trans* conformer. Therefore, to first order in reaction field theory (26) the O-*trans* conformer should become more stable in the more polar solvent, contrary to our results.

The proximate coupling constants, ^{4}J(CHO, P) and ^{3}J(CHO, P)

^4J(C*H*O, P) is −5.853(3) Hz in the CS_2/C_6D_{12} solution and is −5.136(4) Hz in the acetone-d_6 solution. A two-site analysis, using these numbers and the values of ^5J(H, CHO) as indicators of the O-*cis*/O-*trans* equilibrium constants, yields ^4J(O=C—H···P) as −7.1(2) Hz and ^4J(H—C=O···P) as −2.3(3) Hz. ^4J(O=C—H···P), the coupling constant in the O-*trans* conformer, is the proximate coupling constant mediated by the lone-pair on phosphorus. However, ^4J(H—C=O···P) is not zero in the O-*cis* conformer, although the C—H bond of the formyl group points away from the lone-pair. These matters are discussed further below.

^3J(C*H*O, P) is 21.80(2) Hz in CS_2/C_6D_{12} and 17.34(2) Hz in acetone-d_6. A two-site equilibrium entails ^3J(O=C—H···P) as 29.4 ∓ 1.3 Hz and ^3J(H—C=O···P) as 0.0 ± 3.2 Hz. If $^3J \geq 0$, then the maximum value of ^3J(O=C—H···P) is 29.4 Hz. In any event, ^3J(C*H*O, P) has a large component transmitted via a proximate C—H···lone-pair interaction. Some information about the P—C torsion angles is now sought from AM1 and STO-3G MO computations.

Can. J. Chem. Downloaded from www.nrcresearchpress.com by 213.200.69.106 on 09/08/12
For personal use only.

Can. J. Chem. Downloaded from www.nrcresearchpress.com by 213.200.69.106 on 09/08/12
For personal use only.

TABLE 5. Torsion angles and relative AM1 and STO-3G MO energies of the most stable conformers of 2-(diphenylphosphino) benzaldehyde[a]

	Solvent			
	CS_2/C_6D_{12}		Acetone-d_6	
Torsion angle/deg	AM1	STO-3G	AM1	STO-3G
CHO ring[b,c]	31.3	42.3	32.4	50.4
C_2 ring[b,c]	25.6	44.8	11.5	40.1
C_3 ring[b,c]	29.8	42.5	46.1	38.4
CHO group[d]	0.0	5.7	0.0	8.2
Relative energy (kJ/mol)[e]	0.00	0.47	22.9	0.00[f]

[a]See structures **1–3** in the text.
[b]The torsion angle is the angle by which the plane of the phenyl group deviates from the normal (lone-pair direction) to the pyramid base defined by the three carbon atoms bonded to phosphorus. The sense of twist is such that, were these angles equal and the formyl group absent, the molecule would have C_3 symmetry (propeller).
[c]For triphenylphosphine, these torsion angles are equal to 29.2° and 43.2°, respectively, as given by the AM1 and STO-3G MO optimizations; a vanishing torsion angle implies C_{3v} symmetry.
[d]The angle by which the formyl group twists out of the plane of its phenyl group; see structures **2** and **3**.
[e]The text described the geometry-optimization procedures.
[f]The total energy is −1130.130 066 au.

Torsion angles from AM1 and STO-3G MO calculations

During the computations of the torsion angles about the three P—C bonds in the O-*cis* and O-*trans* conformers of DPPB, the only constraint on the geometries was that the nuclei of each benzene ring remain in their plane; otherwise all bond angles and bond lengths were allowed to vary during the optimization procedures, including the angle by which the formyl group turned out of the plane of its bonded benzene ring. Table 5 contains the computed torsion angles and the relative energies of the conformers. The torsion angle is the angle by which the plane of the aromatic group (see **1**) deviates from the normal (lone-pair direction) to the pyramid base defined by the three carbon atoms bonded to phosphorus. The sense of twist about the P—C bond is the same for the three planes; if the formyl group were absent and all torsion angles the same, then the molecule would have C_3 symmetry (propeller).

The torsion angles differ considerably for the AM1 and STO-3G MO minimizations. Comparison of the computed bond lengths and angles with those for the crystal (1) shows reasonable agreement for the minimal basis set and some marked disagreements for the semiempirical parameterization. For example, for the O-*cis* conformer the experimental P—C lengths are 1.839, 1.833, and 1.838 Å; the corresponding STO-3G (AM1) values are 1.845(1.765), 1.838(1.751), and 1.842(1.753) Å. Again, the P···O distance in the crystal is 2.83 Å whereas it is computed as 2.83 Å with the STO-3G basis set and as 2.89 Å by AM1 (O-*cis* conformer). Another comparison involves the C—C—C bond angles at the ipso positions: they are 117.4°, 118.2°, and 118.8° in the crystal, range from 117.1° to 117.9° for the STO-3G structure, but from 119.4° to 119.9° for that from AM1. Furthermore, AM1 has the O-*cis* conformer as 22.9 kJ/mol less stable than the O-*trans* conformer, a result somewhat unlikely in view of its sole presence in the crystal and its similar stability to that of the O-*trans* conformer in solution; the O-*cis* is computed as 0.47 kJ/mol less energetic than the O-*trans* conformer with the minimal basis set, a more likely estimate (albeit at absolute zero). Accordingly, the STO-3G results are taken as more reliable for DPPB and the corresponding torsion angles are used in the discussion below. Their magnitudes (Table 5) for the O-*trans* conformer are also rather similar to the mean torsion angle of 43.7° found in the crystal for tri(*o*-tolyl)phosphine (27); it should be noted, however, that neither this compound nor triphenylphosphine (28) has C_3 symmetry in the crystal, very likely due to packing constraints.

The torsion angles presumably represent an energetic compromise among intramolecular repulsions between *ortho* C—H bonds and (or) the formyl substituent on neighbouring aromatic groups, having maxima either at 0° or 90°. Conjugative interactions of the lone-pair on phosphorus with the aromatic π system, favoring torsion angles of 90°, are probably small, as for triphenylphosphine (29). Consequently, the conjugative contribution to the intrinsic barrier to rotation about the P—C bonds is very likely small. Hence it is also likely that the minima in the internal potential surface, represented by the structures in Table 5, are fairly shallow over a significant range near the torsion angles given in Table 5; the repulsive parts of the potential are probably steeply dependent on the distances between atoms on neighbouring rings. Although our computing resources did not allow an extensive exploration of this problem for such a large molecule, one AM1 procedure, with geometry optimization and allowance for relaxation of the other two torsion angles, predicted that the molecular energy did not change by more than 1.5 kJ/mol as the disubstituted ring was rotated by ±15° from its optimum value of 31° in the O-*trans* conformer. This result implies substantial excursion of the torsion angles in Table 5, at least at ambient temperatures (floppy molecule). With these qualifications in mind, the following remarks about the O-*cis* and O-*trans* conformers are of interest.

The torsion angles for the O-*trans* conformer, 42.3°–44.8°, suggest that the formyl group can be accommodated easily in the *exo* conformation, as does our STO-3G optimization for triphenylphosphine for which the three torsion angles are calculated as 42.5°. Alternatively, the *ortho* C—H repulsions determine the torsion angles, and the small twist of 5.7° of the formyl group out of its aromatic plane, as in **2**, is caused by repulsion from the neighboring phenyl group or attraction towards the lone-pair direction.

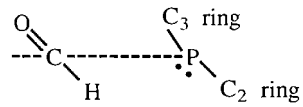

2 **3**

In the O-*cis* conformer, the largest change in the torsional angles is that for the ring carrying the formyl group, which increases by 8° from its value in the O-*trans* conformer, while the aldehydic function twists out of its aromatic plane by 8°, as in **3**, that is, away from the lone-pair region on phosphorus.

Structural implications for ^4J(CHO, P) and ^3J(CHO, P)

The values of ^4J(C*H*O), P) deduced above for the O-*cis* and O-*trans* conformers refer to structures in which the for-

myl group and the lone-pair vector are not coplanar. An INDO MO FPT (30) computation of $^4J(CHO, P)$, perturbing the 1*s* orbital at the formyl proton site, was done for AM1 optimized geometries, those in which rotation occurred about the C-2, P bond (see **4**). Between $\theta = 0$, lone-pair in the formyl plane, and $\theta = 68°$, the computed $^4J(CHO, P)$ closely

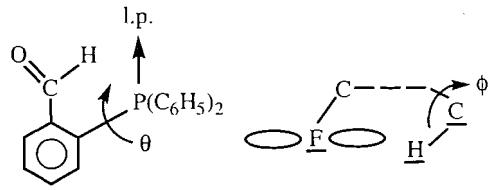

4 **5**

follows $-13.8 \cos^2 \theta$ in units of Hz. For a θ of 42.3° (Table 5), $^4J(CHO, P)$ is then −7.5 Hz, not far from the −7.1 Hz deduced from experiment for the O-*trans* conformer. Of course, the agreement is somewhat accidental, in that the computed value depends on the parameterization of the calculational scheme, as well as on the computed bond lengths and angles for a given θ, which will also oscillate about the equilibrium value. The computation does emphasize the importance of the proximity of the C—H bond of the formyl group and the lone-pair direction.

The computed $^4J(CHO, P)$ becomes positive at a θ of 75° in **4**. This result is reminiscent of a recent set of relative sign determinations (12), from which it appears that the negative proximate $J(H, F)$, for $\phi = 0$, can become positive for sufficiently large ϕ values (see **5**). An assessment of the critical ϕ awaits improvements in the theory of coupling constants and (or) reliable computations or measurements of ϕ for the molecules in question.

The estimate of −7.1 Hz for $^4J(CHO, P)$ in the O-*trans* conformer of DPPB can be compared with the −7.9 Hz obtained for $^4J(CH(CH_3)_2, P)$ in 2-isopropylphenyl diphenylphosphine (31); the sign is deduced from the measurement of $^4J(CH(CH_3)_2, P)/^3J(CH(CH_3)_2, P)$ as negative, it being likely that ^3J is positive. The torsion angle for the isopropylphenyl moiety is not known, nor is the conformational distribution of the isopropyl group. From models, the predominance of the arrangement $(CH_3)_2C$—H···P appears probable. By how much the C—H bond of the isopropyl group twists out of the plane of its bonded aromatic ring is also not known. The barrier to rotation about the Csp^2—Csp^3 bond in isopropylbenzene is much smaller than the internal rotational barrier in benzaldehyde (32). For the O-*cis* conformer of DPPB, $^4J(CHO, P)$, at −2.3(3) Hz, corresponds to a *cis–trans* arrangement of the intervening bonds, consistent with a σ electron coupling mechanism. The analogous situation for $^4J(CHO, F)$ in 2-fluorobenzaldehyde has been reviewed (33).

The large value of 29.4 ± 1.3 Hz for $^3J(O{=}C{-}H{\cdots}P)$, as compared to 0.0 ± 3.2 Hz for $^3J(H{-}C{=}O{\cdots}P)$, implicates the C—H lone-pair interaction in the coupling mechanism for the former coupling constant. A model CNDO MO FPT calculation was done for four conformations of 2-formylphenylphosphine, whose geometries had been optimized by STO 3G MO computations. The lone-pair direction on phosphorus lies in the aromatic plane. The computed coupling constants are displayed in the diagrams. Qualitatively, these numbers, in sign and relative magnitude, bear out the importance of the C—H lone-pair proximity for the coupling mechanism. $^3J(CHO, P)$ and $^4J(CHO, P)$ are indeed small in magnitude unless the C—H bond lies near the lone pair.

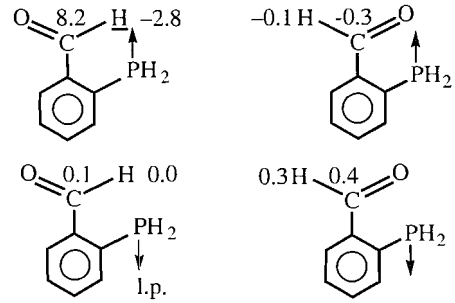

$^nJ(C, P)$ in DPPB and TPP

In Table 4 it is demonstrated that $^nJ(C, P)$ in TPP are solvent dependent, particularly $^1J(C, P)$, which changes from −12.92(2) Hz in CS_2/C_6D_{12} to −11.73(2) Hz in acetone-d_6 solution. In a 36% w/w solution of TPP in CS_2/acetone-d_6 (52:12 w/w), $^1J(C, P)$ is −12.51(3) Hz (14), consistent with such a result. $^2J(C, P)$ and $^3J(C, P)$ are less sensitive to solvent, the former increasing by only 0.05(4) Hz in the polar solvent. $^2J(C, P)$ is very sensitive to orientation of the lone pair on phosphorus with respect to the aromatic plane (14, 34), so that the solvent effect on $^1J(C, P)$ must be intrinsic, that is, the two solvents perturb the internal rotational potential in TPP in a similar manner.

$^1J(C, P)$ in the phenyl rings of DPPB is smaller in magnitude than in TPP, but (Table 3) the solvent perturbations of $^1J(C, P)$ are roughly the same in size as those caused by the presence of the formyl substituent on the neighbouring aromatic group. $^1J(C, P)$ in the disubstituted ring (Table 4) is less susceptible to solvent effects and is −14.93(2) Hz in the nonpolar solvent, as compared to −12.92(2) Hz in TPP. The sum of the three $^1J(C, P)$ values for DPPB is close to that in TPP. For example, in acetone-d_6 solution the two sums differ by 0.5 ± 0.1 Hz, so that, while the individual values of $^1J(C, P)$ differ by as much as 4.2 Hz, the perturbation by the formyl substituent is distributed in a compensatory manner among the three P—C bonds. There is no simple relationship (13) between $^1J(C, P)$ and the *s*/*p* ratio of the bonding orbitals employed by phosphorus. A proper theory of $^1J(C, P)$, not yet available, will also need to account for its solvent susceptibility.[4]

Again, for the two phenyl rings in DPPB, the solvent perturbations of $^{2,3,4}J(C, P)$ are not in general negligible compared to those caused by the formyl substituent on the neighbouring benzene moiety (Table 3). In a given solvent, $\Sigma^nJ(C, P)$ is the same for the two phenyl groups of DPPB and TPP, to within 0.1–0.2 Hz in about 40 Hz. This result may be indicative of a substituent perturbation of $^nJ(C, P)$ as distinct from a change in the average torsion angle for the two

[4]The dipole moment of TPP is dominated by the lone-pair contribution (44), meaning that the orbital is an *s*/*p* hybrid. If the more polar solvent increases the lone-pair "polarity," thereby increasing its *p* character, then the orbitals used to bond to carbon will have reduced *p* character. Via an exchange interaction (spin polarization) this *p* character makes a negative contribution (45) to $^1J(C,P)$. Therefore $^1J(C,P)$ should increase algebraically in acetone, as confirmed in Table 4.

Can. J. Chem. Downloaded from www.nrcresearchpress.com by 213.200.69.106 on 09/08/12
For personal use only.

Can. J. Chem. Downloaded from www.nrcresearchpress.com by 213.200.69.106 on 09/08/12
For personal use only.

phenyl groups of DPPB; the MO computations described above suggest as much.

That, however, ^2J(C, P) is very sensitive to torsion about the P—C bond (15, 35) is confirmed by the data in Table 4 for the disubstituted ring in DPPB (see also **1** for the numbering of the ring positions and **6** for an extreme torsion angle, $\theta = 0$). ^2J(C-1, P) is 27.4 Hz while ^2J(C-3, P) is

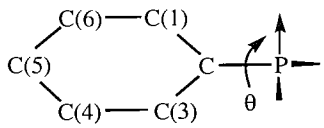

6 $\theta = 0$

± 0.2 Hz.[5] A negative sign for this small coupling constant is suggested by the -3.9 ± 2.0 Hz measured for the analogous coupling constant in 1,6-diphosphatriptycene (34), in which the lone pair on phosphorus is situated in the aromatic plane. The ^2J(C, P) in the triptycene derivative, corresponding to ^2J(C-1, P), is 44.4 ± 0.15 Hz. If this number is taken as defined by a torsion angle, θ, of 0° then the value of $-3.9 + 2.0$ Hz corresponds to a θ of 180°. Hence, write $^2J(C, P) = A + B\cos^2(\theta/2)$. Then, A is $-3.9 + 2.0$ Hz and B is 48.3 ± 1.8 Hz. Our STO-3G computations on the internal barrier to rotation in TPP yield a potential given by the sum of evenfold terms in θ. For such a potential the expectation value of $\cos^2(\theta/2)$ must be 0.5. Hence ^2J(C, P) in TPP is predicted to be 20.3 ± 3.0 Hz; it is measured as 19.7 Hz (Table 4). As to ^2J(C-1, P) in DPPB, the STO-3G MO value for θ is 42.3°, which, if the molecule were rigid, would entail a predicted value of 38.1 ± 3.6 Hz. For ^2J(C-3, P), the θ would be 137.7°, so that its value would follow as 2.4 ± 2.2 Hz, compatible with its measurement. Of course, the molecule is not rigid and the disubstituted ring will oscillate by an unknown value about the optimum θ. Nevertheless, it is clear that ^2J(C-1, P) is reduced substantially in magnitude by the formyl substituent.

An analogy has previously been drawn between ^3J(H, P) in TPP and ^3J(H, F) in fluorobenzene (35). If such an analogy holds for ^2J(C, P) and ^2J(C, F), it may be noted that ^2J(C, F) in fluorobenzene is +21.0 Hz (35), whereas ^2J(C-1, F) and ^2J(C-3, F) in 2-fluorobenzaldehyde are 8.2 and 20.5 Hz, respectively (36). The sharp reduction in ^2J(C-1, F) is analogous to that suggested above for ^2J(C-1, P) in DPPB. Of course, in DPPB the conformational behaviour is more complex than in a fluorobenzene derivative; it may well be that the substituent perturbation of ^2J(C-1, P) is θ dependent. Its dependence on the O-*cis*–O-*trans* equilibrium appears small, ^2J(C-1, P) being invariant to solvent (Table 3). Our computations of ^2J(C, P) by the INDO MO FPT technique were not very useful[6] in assessing the θ and substituent dependencies of ^nJ(C, P) or ^nJ(H, P).

Turning to ^3J(C, P), the coupling corresponding to $\theta = 0°$ (see **6**) is $+13.8 \pm 0.5$ Hz in the diphosphatriptycene and is $+1.4 \mp 0.15$ Hz for $\theta = 180°$ (35). An equation for ^3J(C, P) similar in form to that postulated for ^2J(C, P) above, together with the arguments presented there, implies ^3J(C, P) as $(1.4 \mp 0.15) + (13.8 \pm 0.5)0.5$ or $+ 8.3 \pm 0.4$ Hz; its actual value is +6.8 Hz (Table 4), a number more compatible with a ^3J(C, P) vanishing at $\theta = 180°$. Be that as it may, the ^3J(C-6, P) of 3.9 Hz in DPPB once more implies a substantial reduction due to the formyl substituent at C-1. The analogy with ^3J(C, F) in fluorobenzene is again appropriate in that ^3J(C, F) changes from +7.8 Hz in fluorobenzene (36) to 1.9 Hz for ^3J(C-6, F) and to 9.1 Hz for ^3J(C-4, F) in 2-fluorobenzaldehyde (36). Hence, although ^3J(C, P) is stereospecific, it also seems very sensitive to substituent perturbations.

Finally, ^4J(C, P) is -1.4 ± 0.5 Hz in the triptycene derivative, so that its small magnitudes in TPP and DPPB, ≤ 0.5 Hz, may correspond to negative values or, perhaps, to either sign among these magnitudes. Certainly, ^5J(H, P) in DPPB is also small and varies in sign for DPBP, as discussed below.

$^nJ(H, P)$ in TPP and DPPB

For TPP, in benzene solution two analyses of the ^{1}H nmr spectra yield ^3J(H, P) as 7.58(3) and 7.52(1) Hz (24, 25). As mentioned above, the barrier to internal rotation about the P—C bonds is calculated to be evenfold. If it is assumed that ^3J(H, P) follows a relationship $A + B\cos^2(\theta/2)$, one has $7.56(4)\text{ Hz} = A + 0.5B$. For the disubstituted ring of DPPB, ^3J(H-3, P) is 4.46 Hz in CS_2/C_6D_{12} solution and 4.50 Hz in acetone-d_6 (Table 1). According to the STO-3G MO computations in Table 5, θ is 42.3° for the O-*trans* and 50.4° for the O-*cis* conformer. Were these expectation values and not simply minima, a weighting of these angles according to the values of K deduced in a previous section would be appropriate. As it is, an approximation to ^3J(H-3, P) is given by $A + B(1 - \cos^2(\theta/2))$ with θ as 46°, so that $4.48 = A + B(0.15)$. The two relationships yield A as 3.2(3) and B as 8.8(3) Hz; the quoted errors are meant to indicate the concomitant ambiguities that may well include intrinsic solvent effects on ^3J(H, P), see Table 2, as well as intrinsic substituent perturbations. That the latter are not very large, or at least roughly equal for CH_3 and CHO groups, is indicated by a recent report of ^3J(H-3, P) as 4.4 Hz in tri(*o*-tolyl)phosphine in solution (37). In the crystal, θ values for this compound are close to those given for DPPB in Table 5.

Turning to ^4J(H, P), its θ dependence is relatively strong. Thus, ^4J(H, P) is 1.49(3) or 1.43(1) Hz for TPP (25, 26), similar to the 1.51 Hz for the phenyl groups in DPPB. The disubstituted ring of the latter, however, has ^4J(H-4, P) as 0.447(3) and 0.480(3) Hz in the polar and nonpolar solutions, respectively, as contrasted to 3.777(3) and 3.713(3) Hz for ^4J(H-6, P). Now, for ^4J(H-6, P) the formyl substituent is at-

[5]The assignment of C-3 is based on that in tri(*o*-tolyl)phosphine (14) in which ^2J(C-3, P) is smaller in magnitude than ^3J(C-4, P) in the present notation. The torsion angles for this molecule have an average value of 43.7° in the crystal (27), very similar to those calculated for DPPB (Table 5). Furthermore, the ^2J(C, P) values are 26.4 and 0.4 Hz, implying only small or similar perturbations by the methyl and formyl substituents. The available evidence indicates the existence only of the *exo* conformer of tri(*o*-tolyl)phosphine in solution (2, 37), that in which the three methyl groups lie near the lone pair on phosphorus, that is, above the plane defined by the three carbon atoms bonded to phosphorus (see **1**).

[6]For example, for model calculations on geometry-optimized STO 3G MO structures of phenylphosphine, the INDO MO FPT values of ^3J(C, P) and ^3J(H, P) are negative for all likely torsion angles (lone-pair directions with respect to the aromatic plane), although for ^2J(C, P) the numbers are qualitatively compatible with the θ dependence used here.

Can. J. Chem. Downloaded from www.nrcresearchpress.com by 213.200.69.106 on 09/08/12
For personal use only.

tached to the coupling fragment and, by analogy to ^3J(C-6, P), a substantial substituent perturbation, either an increase or decrease, of ^4J(H-6, P) may be anticipated. Hence, the use of ^4J(H, P) in TPP and ^4J(H-4, P) in DPPB in a treatment analogous to that of ^3J(H, P) yields ^4J(H, P) = 0.0(2) + 2.9(2) $\cos^2(\theta/2)$, where, of course, the θ applicable to ^4J(H-4, P) is (180 − 46). The error indications are meant to allow for thermal averaging of θ in DPPB. Application of this relationship to ^4J(H-6, P) yields 2.5(4) Hz compared to the measured value of 3.7 Hz. If the latter had been used in the treatment above, instead of ^4J(H-4, P) one would have had $^4J = -1.8 + 6.5 \cos^2(\theta/2)$ and ^4J(H-4, P) would be calculated as −0.8 Hz. However, ^4J(H-4, P) is positive, ^4J(H-4, P)/^4J(C*H*O, P) being determined as negative in the double resonance experiments. Consequently, within the assumptions concerning the θ dependence, it follows that a substantial intrinsic substituent dependence exists for ^4J(H-6, P). As far as the analogy with J(H, F) holds, ^4J(H, F) being 5.8 Hz in fluorobenzene (39) and ^4J(H-6, F) being 7.0 Hz in 2-fluorobenzaldehyde (10), the conclusion above appears valid.

^5J(H, P) is positive in TPP (25), as it is for the phenyl groups in DPPB, 0.7–0.8 Hz. By way of contrast, ^5J(H, P) in the disubstituted ring is −0.4 Hz. Because of the similar θ values for the two kinds of rings in DPPB (Table 5), the negative sign is likely a consequence of a perturbation from the formyl substituent. Again, ^5J(H, F) is 0.3 Hz in fluorobenzene (38), but −0.2 Hz in 2-fluorobenzaldehyde (10). ^5J(H, F) has almost equal contributions from σ and π electron mechanisms, which, however, differ in sign; the σ electron mechanism is thought to be the most sensitive to ring substitution (39). A determination of ^6J(P, CH_3) in tri(*p*-tolyl)phosphine is in order because its magnitude will give the π electron contribution to ^5J(H, P) (39); ^6J(P, CH_3) is anticipated as negative in sign.

The present discussion shows that a reliable theoretical treatment of ^nJ(C, P) and ^nJ(H, P) would enhance the utility of these coupling constants in conformational analysis. In particular, their intrinsic perturbations by ring substituents, which themselves may be dependent on θ, that is, on the lone-pair orientation, need a theoretical elucidation.

*Coupling between H-3 and H-*ortho *of the phenyl groups*

The coupling constant, ^6J(H-3, H-*ortho*), formally one over six bonds and of magnitude 0.05 ± 0.02 Hz, is attributable to the proximity of the C—H-3 bond of the disubstituted aromatic ring and the *ortho* C—H bonds of the two phenyl groups. A similar coupling interaction occurs in a derivative of 2,2′-dihydroxybenzophenone, in which two intramolecular C=O···HO hydrogen bonds constrain the phenyl groups to a conformation leading to close contacts of the hydrogen atoms of two C—H bonds on neighbouring aromatic rings (40). Models of DPPB imply that the conformation, in which the lone-pair lies near the plane of the disubstituted benzene and is oriented towards the formyl group, could have minimum distances as small as 1.3 Å between the protons in the relevant C—H bonds. Such a distance would no doubt lead to a large through-space coupling constant. Of course, the coupling constant must be averaged over all excursions of the phenyl groups about the C—P bonds and the closest contact distance would no doubt occur only in a conformation of high relative energy. Nevertheless, the existence of this ^6J is consistent with the predominance of the lone-pair orientation under discussion.

The chemical shift of H-3

In CS_2 solution, $\delta(C_6H_6)$ is 7.218 (16). Using the chemical shifts of the phenyl protons in DPPB and in benzaldehyde (4.0 mol% in the same solvent mixture (41)) as reference points, H-3 is more screened by 0.5 ppm than expected on the basis of additivity. Qualitatively, this is a consequence of its proximity to the phenyl groups, H-3 being, on average, in the screening volume of these diamagnetically anisotropic rings for the conformation in which the lone pair points towards the formyl group. H-4 and H-5, being more distant from the phenyl groups, experience excess shieldings of only 0.22 and 0.10 ppm, respectively.

Other spectral parameters

The solvent perturbation of the coupling constants within the phenyl groups (Table 2) displays the pattern common to a variety of C_6H_5X molecules, for instance, for X = CHO, C≡CH, C≡N, C≡C, CHO, as measured in this laboratory. The pattern displays increases in ^3J, $^4J_{oo}$, and ^5J in the more polar solvent and a decrease in $^4J_{op}$; $^4J_{mm}$ is insensitive to solvent. It is most unlikely that this pattern is an artefact of the analyses. Hence the solvent dependence of ^nJ(H, P) for the phenyl groups is interesting in that ^4J(H, P) also decreases in the more polar solvent. However, the generally larger solvent dependence of ^nJ(H, P) may also indicate slightly different excursional motion about the two C—P bonds in the two solvents.

^nJ(H, H) for ring protons in the disubstituted ring are also solvent dependent. Here an added complication comes from the different proportions of O-*cis* and O-*trans* conformers in the two solvents because the unsymmetric formyl substituent may, after all, perturb a given J in a manner dependent on its orientation with respect to the bonds in question. That the solvent does not strongly perturb the long-range coupling constants of the formyl proton is suggested by the 0.430(1) and 0.432(2) Hz found for ^5J(H, CHO) in benzaldehyde in the two solvents (41). In 2-chlorobenzaldehyde, it appears that a small solvent dependence of ^5J(H, CHO) exists, but that the *cis* and *trans* values are affected in a compensatory manner (11). In other words, the ratio of ^5J(H-3, CHO) to ^5J(H-5, CHO) is still a good measure of the equilibrium constant.

The C—H···P and C=O···P interactions

The small free energy differences between the O-*cis* and O-*trans* conformers in the two solutions prompt the following remarks. It is accepted (29, 42) that conjugation between the π orbitals of the phenyl group and the lone pair on phosphorus is very weak in phenylphosphines. The conjugational barrier to torsion about the P—C bonds is therefore small. Hence the average conformation of triphenylphosphine is a consequence mainly of the minimization of the repulsions between *ortho* C—H bonds of different phenyl groups, these having maxima at $\theta = 0°$ and $\theta = 90°$ (see **1**). The average torsion angles at equilibrium, substantial excursions of which will occur at ambient temperatures, appear to be about 40 ± 5°. Addition of one *ortho* substituent to each phenyl group, as in tri(*o*-tolyl)phosphine, does not alter the torsion angles dramatically because these substituents can lie near the lone pair, therby avoiding repulsions from the neighbouring moieties.

Can. J. Chem. Downloaded from www.nrcresearchpress.com by 213.200.69.106 on 09/08/12
For personal use only.

In DPPB in solution the nmr parameters and the STO-3G MO computations are consistent only with a proximity of the lone pair to the formyl substituent. However, the molecular orbital computations imply that the lone-pair electrons on phosphorus and oxygen are not directly opposed to each other in the O-*cis* conformer (see **3**). Furthermore, the Mulliken population analysis has the charge on phosphorus as +0.52 (electron units) while that on oxygen is −0.21. For a torsion angle of 50° (Table 5) the oxygen atom may well avoid the electron density due to the lone pair and experience a net attraction to the phosphorus region. In contrast, the charge on hydrogen in the formyl group is +0.05, so that in the O-*trans* conformer a smaller torsion angle is anticipated, calculated as 42°, because of a net attractive interaction with the lone-pair region on phosphorus (see **2**).

This rationalization is consistent with the computed out-of-plane torsions of the formyl group — 8° in the O-*cis* and 5° in O-*trans* conformer — in the sense pictured in **2** and **3**. In the O-*trans* conformer both the C—H bond of the formyl group and the lone-pair vector lie above the aromatic plane carrying the formyl group. However, in the O-*cis* conformer the C═O and the lone-pair lie on opposite sides of this plane. Parenthetically, the negative values of ^6J(H, CHO) are consistent with an average out-of-plane conformation of the formyl group in DPPB. ^6J(H, CHO) should be negative for significant values of the out-of-plane angles (43) and is possibly largest in the acetone-d_6 solution. Furthermore, the larger reaction field in the polar solvent, acetone-d_6, can increase the magnitude of the local C═O dipole relative to its value in the CS_2/C_6D_{12} solution, thereby stabilizing the O-*cis* conformer, as measured. What the reaction field is in the crystal in which only the O-*cis* conformer appears is a moot point.

A comparison of the conformational behaviour of the formyl groups in DPPB and 2-(alkylthio)benzaldehydes is instructive. In 2-methylthiobenzaldehyde the thiomethyl group is situated in the benzene plane and the directional, mainly 3*p*, lone-pair on sulfur lies perpendicular to that plane (5); the O-*cis* and O-*trans* conformers have very similar stability. As the size of the alkyl group increases, the population of the O-*cis* conformer decreases until, for a *tert*-butyl group on sulfur, only the O-*trans* conformer is detected (5). In 2-(*tert*-butylthio)benzaldehyde, the *tert*-butyl moiety lies in a plane roughly perpendicular to the benzene plane. In consequence, the directional lone-pair on sulfur is twisted into the benzene plan and repels the C═O bond. By analogy, if the torsion angle of the disubstituted aromatic ring in DPPB were zero, then only the O-*trans* conformer would be detected. An equivalent statement would be that, for trivalent phosphorus, there are regions that attract electrophilic groups and others that attract nucleophilic substituents. One may therefore infer that the lone-pair on phosphorus has considerable *p* character, as deduced from the molecular orbital calculations described at the outset.

Acknowledgment

We thank the Natural Sciences and Engineering Research Council of Canada for financial assistance.

1. E.F. Landvatter and T.B. Rauchfuss. Organometallics, **1**, 506 (1982).
2. E.J. Halpern and K. Mislow. J. Am. Chem. Soc. **89**, 5224 (1967).
3. K. Unemoto and K. Ouchi. Proc. Indian Acad. Sci. Chem. Sci. **94**, 1 (1985), and references therein.
4. K.B. Wiberg, C.M. Hadad, P.R. Rablen, and J. Cioslowski. J. Am. Chem. Soc. **114**, 8644 (1992).
5. T. Schaefer, G.H. Penner, K.J. Davie, and R. Sebastian. Can. J. Chem. **63**, 777 (1985).
6. M.B. Hall. J. Am. Chem. Soc. **100**, 6333 (1978); E. Shustorovich and P.A. Dobosh. J. Am. Chem. Soc. **101**, 4090 (1979).
7. D.M. Chipman, W.E. Palke, and B. Kirtman. J. Am. Chem. Soc. **102**, 3377 (1980).
8. E. Magnusson. J. Am. Chem. Soc. **106**, 1177, 1185 (1984).
9. E. Magnusson. Aust. J. Chem. **38**, 23 (1985).
10. T. Schaefer and C.S. Takeuchi. Can. J. Chem. **68**, 339 (1990).
11. R. Laatikainen, K. Tuppurainen, Y. Hiltunen, and S. Lötjönen. Magn. Reson. Chem. **28**, 939 (1990).
12. I.D. Rae, J.A. Weigold, R.H. Contreras, and G. Yamamoto. Magn. Reson. Chem. **30**, 1047 (1992)
13. T. Bundgaard and H.J. Jakobsen. Acta Chem. Scand. **26**, 2548 (1972).
14. S. Sørensen, R.S. Hansen, and H.J. Jakobsen. J. Am. Chem. Soc. **94**, 5900 (1972).
15. V.M.S. Gill and W. v. Philipsborn. Magn. Reson. Chem. **27**, 409 (1989).
16. T. Schaefer, R. Sebastian, and G.H. Penner. Can. J. Chem. **63**, 2597 (1985).
17. T. Schaefer, R. Sebastian, and R.W. Schurko. Can. J. Chem. **70**, 2365 (1992).
18. J.P. Maher and D.F. Evans. Proc. Chem. Soc. London, 208 (1961).
19. M.F. Frisch, J.S. Binkley, H.B. Schlegel, K. Raghavachari, C.F. Melius, F.L. Martin, J.J.P. Steward, F.W. Bobrowicz, D.F. Rohlfing, L.R. Kahn, D.J. DeFrees, R. Seeger, R.A. Whiteside, K.J. Fox, E.M. Fluder, and J.A. Pople. Carnegie-Mellon Quantum Publishing Unit, Pittsburgh, Pa. 1984.
20. M.J.S. Dewar, E.J. Zoebisch, E.F. Healy, and J.J.P. Stewart. J. Am. Chem. Soc. **107**, 3902 (1985).
21. W.J. Hehre, R. Ditchfield, R.F. Stewart, and J.A. Pople. J. Chem. Phys. **52**, 2769 (1970).
22. J.S. Martin, A.R. Quirt, and K.E. Worvill. The NMR Program Library, Daresbury Laboratory, Daresbury, U.K.
23. W. McFarlane. Org. Magn. Reson, **1**, 3 (1969).
24. S. Sørensen and H.J. Jakobsen. Acta Chem. Scand. Ser. A, **28**, 249 (1974)
25. L. Radics, E. Baitz-Gács, and A. Neszmélyi. Org. Magn. Reson. **6**, 60 (1974).
26. F.J. Abraham and E. Bretschneider. *In* Internal rotation in molecules. *Edited by* W.J. Orville-Thomas. J. Wiley and Sons, New York. 1974. Chap. 13.
27. T.S. Cameron and B. Dahlèn. J. Chem. Soc. Perkin Trans. 2, 1737 (1975).
28. J.J. Daly. J. Chem. Soc. London, 3799 (164).
29. M.A. Winer, M. Lattman, and S.O. Grim. J. Org. Chem. **40**, 1292 (1975).
30. J.A. Pople, J.W. McIver, Jr., and N.S. Ostlund. J. Chem. Phys. **49**, 2960 (1968); **49**, 2965 (1968).
31. H.J. Jakobsen, T. Liptaj, T. Bundgaard, and S. Sørensen. J. Magn. Reson. **26**, 71 (1977).
32. T. Schaefer, R. Sebastian, and G.H. Penner. Can. J. Chem. **66**, 1495 (1988).
33. R.H. Contreras, M.A. Natiello, and G.E. Scuseria. Magn. Reson. Rev. **9**, 239 (1985).
34. S. Sorensen and H.J. Jakobsen. Org. Magn. Reson. **9**, 101 (1977)
35. W.S. Brey, L.W. Jaques, and H.J. Jakobsen. Org. Magn. Reson. **12**, 243 (1979).

36. F.J. Weigert and J.D. Roberts. J. Am. Chem. Soc. **93**, 2361 (1971).
37. J.A.S. Howell, M.G. Palin, P.C. Yates, P. McArdle, D. Cunningham, Z. Goldschmidt, H.E. Gottlieb, and D. Hezroni-Langerman. J. Chem. Soc. Perkin Trans. **2**, 1769 (1992).
38. J.E. Loemker and J.H. Goldstein. Spectrosc. Lett. **1**, 153 (1968).
39. R. Wasylishen and T. Schaefer. Can. J. Chem. **49**, 94 (1971).
40. T. Schaefer and K. Chum. Can. J. Chem. **54**, 2231 (1976).
41. T. Schaefer and C.S. Takeuchi. Can. J. Chem. **67**, 827 (1989).
42. R. Benassi, M.L. Schenetti, F. Taddei, P. Vivarelli, and P. Dembech. J. Chem. Soc. Perkin Trans. 2, 1338 (1974).
43. T. Schaefer, J. Peeling, G.H. Penner, A. Lemire, and R. Laatikainen. Can. J. Chem. **64**, 1859 (1986).
44. M.P. Warchol, E.N. DiCarlo, C.A. Maryanoff, and K. Mislow. Tetrahedron Lett. 917 (1975)
45. C.J. Jameson and H.S. Gutowsky. J. Chem. Phys. **51**, 2790 (1969).

Can. J. Chem. Downloaded from www.nrcresearchpress.com by 213.200.69.106 on 09/08/12
For personal use only.

Kinetics and mechanism of the oxidation of alcohols by ferrate ion

DONALD G. LEE[1] AND HUIFA GAI
Department of Chemistry, University of Regina, Regina, SK S4S 0A2, Canada

Received February 24, 1993

DONALD G. LEE and HUIFA GAI. Can. J. Chem. **71**, 1394 (1993).

A kinetic study of the reduction of ferrate ion under basic conditions has been completed. The observation that a typical aliphatic ether, tetrahydrofuran, is oxidized at a rate comparable to that of aliphatic alcohols, such as cyclopentanol, indicates that the reaction between ferrate and alcohols is likely initiated by attack of the oxidant at an α-C—H bond, a conclusion that is consistent with the occurrence of primary deuterium kinetic isotope effects (2.8–4.3 at 25°C) when α-hydrogens are replaced by deuterium. Because only acyclic products are obtained from the oxidation of cyclobutanol by ferrate, it may be concluded that free radical intermediates are involved in the reaction. The insensitivity of the reaction rates to substituent effects during the oxidation of substituted mandelic acids indicates that substantial charges are not built up in the transition state. All of these observations are most readily accommodated by a mechanism in which the reaction is initiated by a 2+2 addition of an Fe=O bond to the α-C—H of an alcohol to give an organometallic intermediate that subsequently decomposes by homolytic cleavage of the resulting C—Fe bond. Comparisons are made with the reactions between alcohols and other high-valent transition metal oxides.

DONALD G. LEE et HUIFA GAI. Can. J. Chem. **71**, 1394 (1993).

On a réalisé une étude cinétique de la réduction de l'ion ferrate dans des conditions basiques. Le fait qu'un éther typique, le tétrahydrofurane, est oxydé à une vitesse comparable à celle des alcools, comme le cyclopentanol, indique que la réaction entre le ferrate et les alcools est probablement initiée par une attaque de l'oxydant sur la liaison α-C—H; cette hypothèse est en accord avec le fait que l'on observe un effet isotopique primaire du deutérium (2,8–4,3, à 25°C) lorsqu'on remplace les hydrogènes-α par du deutérium. En se basant sur le fait que l'on n'obtient que des produits aliphatiques lors de l'oxydation du cyclobutanol par le ferrate suggère que des intermédiaires radicalaires sont impliqués dans la réaction. Le fait que les vitesses de réaction d'oxydation d'acides mandéliques substitués ne soient pas sensibles à la nature des substituants indique qu'il n'y aurait pas d'accumulation de charge dans l'état de transition. Le meilleur mécanisme permettant d'expliquer tous ces résultats implique une réaction initiée par une addition 2+2 d'une liaison Fe=O sur la liaison α-C—H d'un alcool qui conduit à un intermédiaire organométallique que se décompose par la suite par un clivage homolytique de la liaison C—Fe qui en résulte. On a fait des comparaisons avec les réactions des alcools avec d'autres oxydes de métaux de transition de valence élevée.

[Traduit par la rédaction]

Introduction

The use of iron-based oxidants is attractive from an environmental standpoint because iron, unlike many other transition metals, is considered to be nontoxic. Therefore, despite its current rather high cost, it is possible that ferrate (FeO_4^{2-}) may become preferable to other common oxidants such as chromate, permanganate, or ruthenate, which contain toxic heavy metals. It is known, for example, that ferrate can be used to oxidize alcohols to the corresponding carbonyl compounds in yields comparable to those obtained with other oxidants (1), that it is particularly useful for the conversion of primary alcohols into aldehydes (2–4), and that it reacts selectively with the primary hydroxyls of carbohydrates (5). Sodium ferrate, dissolved in nonpolar solvents with the assistance of phase transfer agents (6), may also be used for the oxidation of alcohols that have limited solubility in aqueous solutions.[2]

In many ways ferrate's properties resemble those of manganate (MnO_4^{2-}) (7) and ruthenate (RuO_4^{2-}) (8, 9). In common with those reagents, ferrate is known to have only limited stability in aqueous solutions, especially below pH 7 (10).

Several possible mechanisms, including electron transfer (4), hydrogen atom transfer (11), hydride ion transfer (1), and the formation of intermediate ferrate esters (12) have been suggested for the oxidation of alcohols by ferrate. However, molecular orbital calculations indicate that other high-valent transition metal oxides react with alkanes and alcohols by 2+2 additions between a metal–oxo double bond and a carbon–hydrogen or an oxygen—hydrogen bond as illustrated in eqs. [1] and [2] (13). Addition to an O—H bond results in the formation of an ester while C—H addition yields an organometallic intermediate, which may subsequently undergo a rearrangement as in eq. [3] or cleavage of the M—C bond to produce either free radicals or carbocations as in eq. [4] (14).

Although this general mechanism readily accommodates all known experimental observations, including those for Gif and related reactions (15), and for oxidations by high-valent iron complexes (16), there is not unanimous agreement concerning some of the details. For example, it has been suggested that the reaction of other high-valent transition metal oxides with alkanes is initiated by a 2+2 reaction in which carbon becomes attached to oxygen with concomitant formation of a metal hydride as in eq. [5] (17). However, since the hydrogen of the metal hydride would likely migrate to oxygen (as depicted in eq. [6]) it is impossible to decide between a sequence involving reaction [2] followed by reaction [3] or one in which reaction [6] follows reaction [5], because they both lead to the same product.

In this paper we wish to describe the kinetics and mechanism of the reaction between alcohols and ferrate ion in alkaline solutions and to make comparisons with the mechanisms for the oxidation of alcohols by other high-valent transition metal oxidants. Because ferrate stability is of crucial importance, we began with a reinvestigation of its stability in aqueous base and then proceeded with a kinetic

[1]Author to whom correspondence may be addressed.
[2]A. Sabesan. Unpublished results.

Can. J. Chem. Downloaded from www.nrcresearchpress.com by 213.200.69.106 on 09/08/12
For personal use only.

study of its reactions with alcohols under conditions where it is most stable.

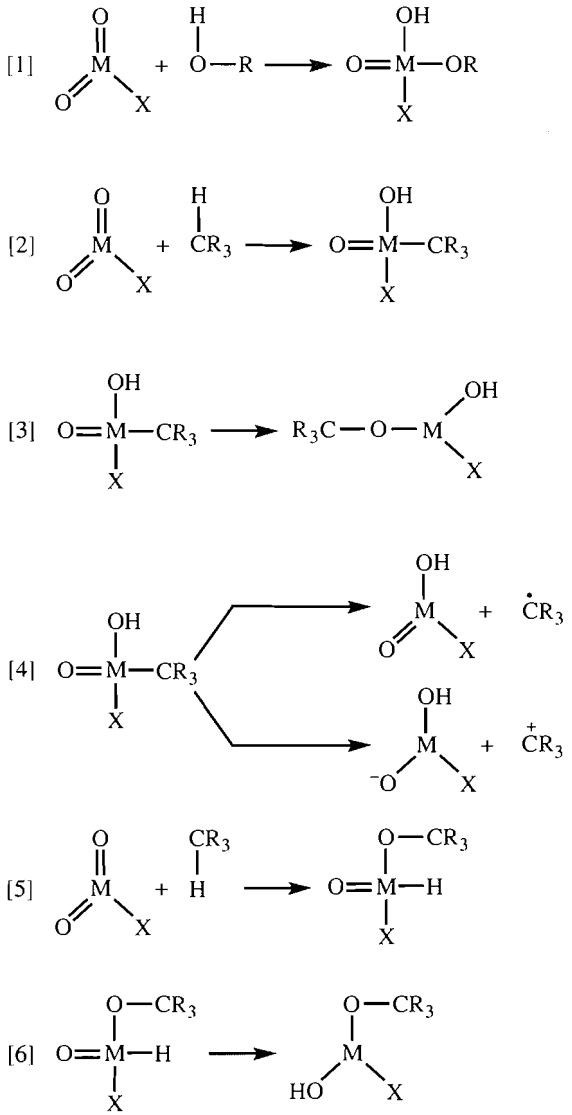

Experimental

Preparation and purity of potassium ferrate

Potassium ferrate was prepared by oxidation of ferric nitrate nonahydrate by hypochlorite using the procedure reported by Bartzatt (18). The purity of the product, determined by titration with ferrous chloride using sodium diphenylamine as an indicator (19), was 98.6 ± 0.5%.

Reduction of ferrate by water

The rates of reduction of ferrate by water were determined by monitoring the decrease in absorbance at 508 nm. For each experiment a small portion of solid potassium ferrate was added to an aqueous solution buffered at a particular pH, the volume was adjusted to give an absorbance of 0.3–0.8, and 2.0 mL were transferred to a 10-mm quartz cell in the thermostated cell compartment of an 8450A Hewlett-Packard spectrophotometer. Absorbances were then plotted against time and the initial rates $(-dA/dt)$ obtained from the slope of a tangent to the resulting curve at time zero.

Oxidation of alcohols

Oxidation rates were determined by transferring a specific amount of an alcohol (using a microlitre syringe for liquid compounds) to 2.0 mL of a freshly prepared ferrate solution and monitoring the absorbance at 508 nm. The observed rate of oxidation was then corrected (if necessary) for the rate of reduction of ferrate by water under identical conditions. (These corrections usually reduced the observed rates by 10% or less.)

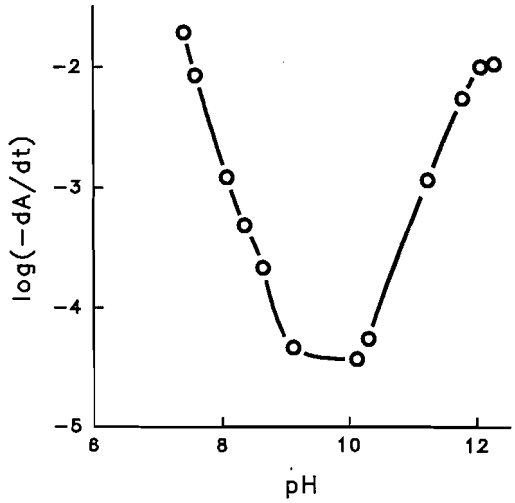

FIG. 1. The effect of pH changes on the initial rate of reduction of ferrate ion by water. Temperature = 25.0 ± 0.1°C.

Product analysis

The only product obtained from the oxidation of 2-propanol was acetone. When 2-propanol (3.9 g, 65 mmol) was reacted with potassium ferrate (10.8 g, 54.5 mmol) in 70 mL of buffered solution at pH = 9.0–9.6 and the product extracted into methylene chloride (3 × 50 mL), dried, and distilled, only acetone (2.2 g, 38 mmol, 58%) and unreacted 2-propanol (1.25 g, 21 mmol) were isolated.

The products obtained from the oxidation of mandelate ion were benzaldehyde and benzoate ion. Addition of potassium ferrate (1.5 g, 7.6 mmol) to a solution of mandelic acid (1.0 g, 6.6 mmol) in 100 mL of aqueous buffer (pH = 9.0–9.6) over a period of 1 h with good stirring followed by extraction (3 × 50 mL CH_2Cl_2), drying, and flash evaporation yielded a liquid product that exhibited an infrared spectrum identical to that of benzaldehyde. The yield was 0.23 g (2.2 mmol, 33%). When the pH of the buffered solution was reduced to 1.5 by addition of concentrated HCl and again extracted with methylene chloride, dried, and flash evaporated, a solid product (0.42 g) was obtained. ^1H NMR analysis of this product was consistent with it being a 7:3 mixture of benzoic acid and unreacted mandelic acid. The yield of benzoic acid was therefore approximately 0.29 g (2.4 mmol, 36%).

Only acyclic products and a trace of cyclobutanone were obtained when cyclobutanol was oxidized. Potassium ferrate (1.5 g, 7.6 mmol) was added slowly (over about 1 h) to cyclobutanol (0.50 g, 6.9 mmol) in 100 mL of buffered solution (pH = 9.0–9.6) with stirring. On completion of the reaction, concentrated HCl was added to reduce the pH to 1.5 and the solution was extracted with methylene chloride (3 × 100 mL). Careful distillation of the solvent gave a liquid residue that was found to contain only acyclic products and a trace of cyclobutanone (<1%).

Results

Rates of reduction of ferrate by water

A plot of initial reaction rates $(-dA/dt)_0$ against pH indicated that the lowest rate of reduction of ferrate by water occurs at pH = 9.4–9.7 (Fig. 1). From plots of log $(-dA/dt)_0$ vs. log $(A - A_f)$ it was found that the rate with respect to ferrate is second order below pH 9 (Fig. 2) and first order above pH 10 (Fig. 3). The reaction can therefore be exper-

Can. J. Chem. Downloaded from www.nrcresearchpress.com by 213.200.69.106 on 09/08/12
For personal use only.

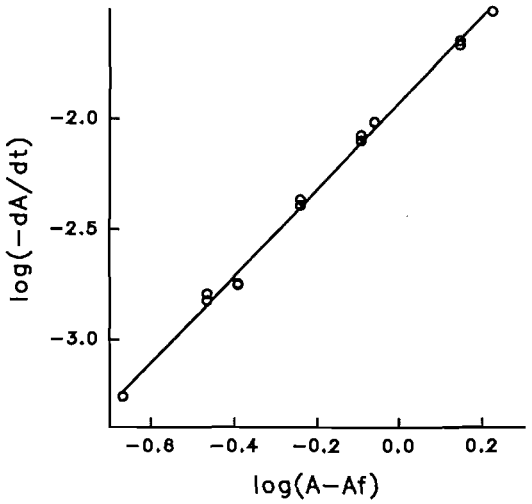

FIG. 2. The relationship between the initial rate of reduction and concentration of ferrate (as determined by the absorbance at 508 nm). pH = 8.07. Slope = 1.95 ± 0.08. r = 0.999.

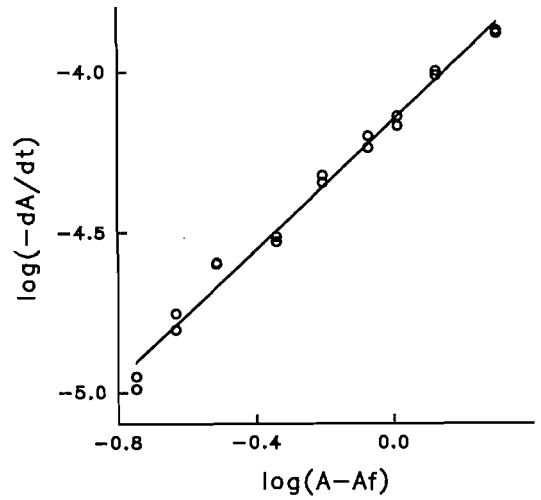

FIG. 3. The relationship between the initial rate of reduction and concentration of ferrate (as determined by the absorbance at 508 nm). pH = 10.3. Slope = 1.05 ± 0.06. r = 0.994.

essed as in eq. [7], a result that is in agreement with previously reported observations (20).

[7] $$\text{Rate} = k_1 [FeO_4^{2-}] [OH^-] + k_2 [FeO_4^{2-}]^2/[OH^-]^{1.6}$$

When the rates of reduction were studied as a function of temperature, plots of $\ln(k/T)$ vs. $1/T$ were linear for both k_1 and k_2 (Figs. 4 and 5). The activation parameters, $\Delta H^{\neq}$ and $\Delta S^{\neq}$, for these reactions were then calculated from the slopes and intercepts, respectively. The results are summarized in Table 1.

Oxidation rates

Most oxidation rates were measured at pH 9–10 where the rate of reduction of ferrate by water is minimal. Under these conditions, plots of $(A - A_f)$ vs. time are linear (Fig. 6), indicating that the reaction is first order in ferrate. Plots of log k vs. log[alcohol]$_0$ are linear with unit slope (Fig. 7), indicating that the rate of the reaction is also first order with respect to alcohol. Therefore, the total rate law for the reduction of ferrate at a particular pH (eq. [8]) has been verified.

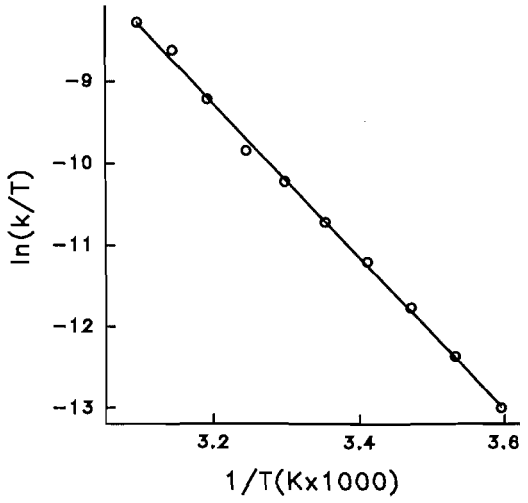

FIG. 4. Activation energy plot for the reduction of ferrate by water at pH 11.5. r = 0.999.

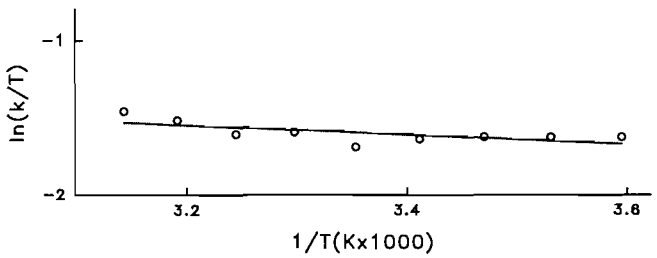

FIG. 5. Activation energy plot for the reduction of ferrate by water at pH 7.70. r = 0.68.

TABLE 1. Activation parameters for the reduction of ferrate by water

	pH	$\Delta H^{\neq}$ (kcal mol^{-1})	$\Delta S^{\neq}$ (cal mol^{-1} K^{-1})
k_1	11.52	18.6 ± 0.8	−6 ± 1
k_2	7.70	0.6 ± 0.1	−48 ± 3

[8] $$-d[FeO_4^{2-}]/dt = k_1 [FeO_4^{2-}] + k_2 [FeO_4^{2-}]^2 + k_3 [FeO_4^{2-}] [\text{Alcohol}]$$

Kinetic isotope effects

Substitution of deuterium for the α-hydrogen in both 2-propanol and mandelic acid caused a decrease in the rate of reaction as indicated by the data in Table 2. The magnitude of the decrease is indicative of a primary isotope effect.

Effect of substituents

The rate of oxidation of mandelic acid was not sensitive to the introduction of substituents into the ring as indicated by the data in Table 3. A Hammett plot for these data has a slope of zero with only a small amount of random scatter.

Variations in the structure of aliphatic alcohols caused greater effects on the rate of reaction, with alcohols containing electron-withdrawing groups exhibiting rates that are larger, in general, than for 2-propanol or alcohols bearing electron-donating substituents (Table 4).

Can. J. Chem. Downloaded from www.nrcresearchpress.com by 213.200.69.106 on 09/08/12
For personal use only.

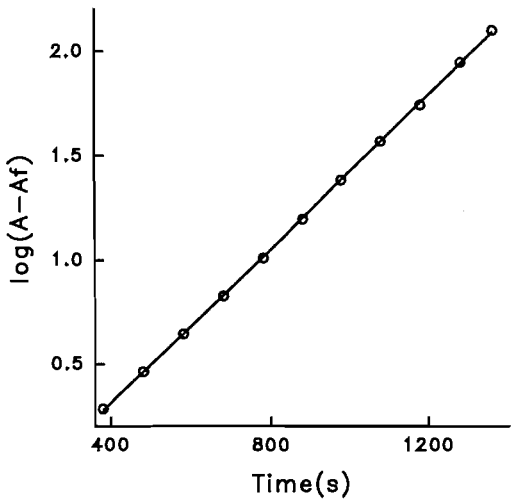

FIG. 6. Pseudo-first-order rate plot for the oxidation of 1,1,1,3,3,3-hexafluoro-2-propanol (0.0100 M). Temperature = 25.0 ± 0.1°C. Slope = 0.00185 s^{-1}. r = 0.999.

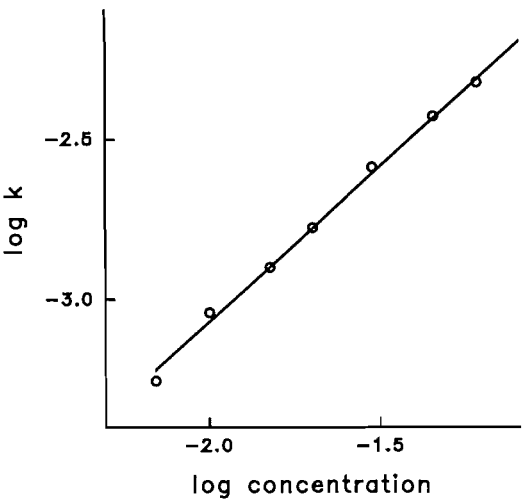

FIG. 7. Dependence of pseudo-first-order rate constants on the concentration of 1,1,1,3,3,3-hexafluoro-2-propanol. pH = 9.70. Temperature = 25.0 ± 0.1°C. Slope = 0.97 ± 0.05. r = 0.999.

TABLE 2. Isotope effects[a]

Reductant	pH	$k_2 \times 10^2$ (L mol^{-1} s^{-1})	k_H/k_D
2-Propanol	9.30	1.38 ± 0.03	
2-Propanol-2-*d*	9.30	0.480 ± 0.029	2.8 ± 0.3
Mandelic acid	8.70	35.7 ± 2.2	
Mandelic acid-α-*d*	8.70	8.33 ± 0.21	4.3 ± 0.4

[a]Temperature = 25.0 ± 0.1°C.

Activation parameters

Activation parameters for the oxidation of 2-propanol and mandelic acid were determined from measurement of the respective rate constants at different temperatures. Because pH is also temperature dependent it was necessary to correct the observed rate constants (k_{obs}) at a particular temperature for pH changes. Although plots of ln k_{cor}/T vs. $1/T$ are linear with high correlation coefficients (Figs. 8 and 9), the uncertainties in the calculated values of $\Delta H^{\neq}$ and $\Delta S^{\neq}$ are consequently somewhat larger than suggested from a consideration of plot statistics. This added uncertainty is reflected in the values for the activation parameters reported in Table 5.

TABLE 3. Rate constants for the oxidation of substituted mandelic acids by ferrate ion

Substituent	k_3 (M^{-1} s^{-1} × 10^2)[a]
4-Methoxy	44.5 ± 0.7
4-Methyl	39.8 ± 2.7
3-Methyl	43.1 ± 0.7
Unsubstituted	36.1 ± 2.2
3-Methoxy	40.6 ± 1.6
4-Fluoro	37.9 ± 2.9
4-Chloro	36.3 ± 0.7
4-Bromo	38.6 ± 1.4
3-Fluoro	32.1 ± 0.4
3-Chloro	43.6 ± 0.7

[a]pH = 8.70; temperature = 25.0 ± 0.1°C; [Reductant] = 0.0300 M.

TABLE 4. Rate constants for the oxidation of aliphatic alcohols and ethers by ferrate ion

Reductant	k_3 (M^{-1} s^{-1} × 10^2)[a]
1,1,1,3,3,3-Hexafluoro-2-propanol	11.4 ± 0.3
1,3-Dichloro-2-propanol	3.60 ± 0.1
1,1,1-Trifluoro-2-propanol	2.60 ± 0.03
1,3-Difluoro-2-propanol	2.26 ± 0.04
1-Methoxy-2-propanol	1.47 ± 0.06
3-Pentanol	1.45 ± 0.03
2-Butanol	1.40 ± 0.06
Cyclopentanol	1.34 ± 0.02
2-Propanol	1.18 ± 0.05
2-Pentanol	1.04 ± 0.04
Tetrahydrofuran	0.753 ± 0.03

[a]pH = 9.70; temperature = 25.0 ± 0.1°C; [Reductant] = 0.0300 M.

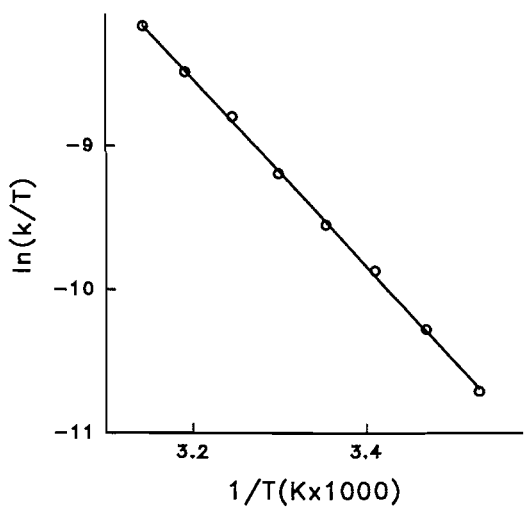

FIG. 8. Activation energy plot of the oxidation of 1,3-difluoro-2-propanol (0.0300 M) by ferrate ion. pH = 9.70. r = 0.999.

Can. J. Chem. Downloaded from www.nrcresearchpress.com by 213.200.69.106 on 09/08/12
For personal use only.

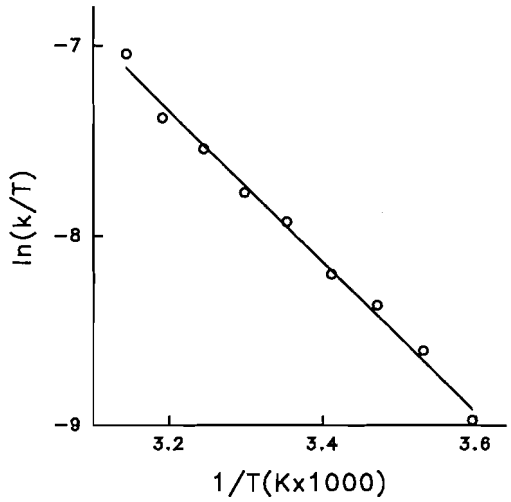

FIG. 9 Activation energy plot for the oxidation of mandelate ion by ferrate. pH = 9.70. r = 0.996.

Oxidation of tetrahydrofuran

Previous results from several laboratories have shown that it is possible to distinguish between reactions that are initiated by O—H addition and those that are initiated by addition to the α-C—H bond from a comparison between the rates of oxidation of alcohols and ethers of similar structure (14). The rates of oxidation of several aliphatic alcohols and tetrahydrofuran were consequently compared. The results are presented in Table 4.

Discussion

Reduction of ferrate by water

The data summarized in Fig. 1 indicate that ferrate exhibits its greatest stability at pH 9–10, below which decomposition occurs by a reaction that is second order with respect to ferrate ion concentration and approximately first order in hydronium ion concentration. These kinetics suggest a reaction scheme in which hydrogen ferrate ion reacts with another ferrate ion to give a dimer that undergoes reduction by loss of dioxygen as summarized in eqs. [9]–[11]. The enhanced reactivity of $HFeO_4^-$ as compared to FeO_4^{2-} is consistent with the known chemistry of chromate (CrO_4^{2-}) and manganate (MnO_4^{2-}) ions (20, 21).

[9] $FeO_4^{2-} + H_2O \rightleftharpoons HFeO_4^- + OH^-$

[10] $HFeO_4^- + FeO_4^{2-} \rightleftharpoons Fe_2O_7^{2-} + OH^-$

[11] $Fe_2O_7^{2-} + 2H_2O \longrightarrow O_2 + H_2FeO_4^- + H_2FeO_3^-$

The increased reactivity of ferrate in solutions with pH above 10 is unusual when compared to the established chemistry of CrO_4^{2-}, RuO_4^{2-}, and MnO_4^{2-}. It is more reminiscent of permanganate, which undergoes reduction to manganate in sodium hydroxide solutions with concentrations of 1 M or greater (7). Although it is not possible on the basis of these kinetic data to define with confidence a reaction mechanism, a possible sequence of reactions that is consistent with the observed kinetics and results in the reduction of ferrate ion has been summarized in Scheme 1.

The observation (Table 1) that the entropy of activation is much less favorable for the reaction below pH 10 is consistent with the suggestion that a dimer is involved.

The oxidation of aliphatic alcohols

As previously discussed, alcohols can react with high-valent transition metal oxides such as ferrate by a 2+2 addition of a carbon–hydrogen bond to a metal–oxo double bond (eq. [2]) or by a 2+2 addition of the oxygen–hydrogen bond to a metal–oxo bond (eq. [1]). Distinction between these two possibilities can usually be made by comparing the rates of oxidation of aliphatic alcohols and ethers. Oxidants that react preferentially with O—H bonds will exhibit higher rates of reaction with alcohols than with ethers (which lack O—H bonds). For example, Westheimer and co-workers (22), noting that chromic acid reacts approximately 1500 times faster with isopropyl alcohol than diisopropyl ether, concluded that the initial reaction between chromic acid and alcohols involved ester formation (as in eq. [1]). Conversely, oxidants that react by way of 2+2 additions to α-C—H bonds oxidize alcohols and ethers with approximately equal ease. For example, it has been observed that ruthenium tetroxide reacts with 2-propanol and tetrahydrofuran at comparable rates (at 25°C, $k_{2\text{-propanol}} = 1.58 \times 10^{-2}\ M^{-1}\ s^{-1}$ while $k_{THF} = 5.38 \times 10^{-2}\ M^{-1}\ s^{-1}$ in 0.9 M $HClO_4$) (23).

From the data in Table 4, it is apparent that ferrate also reacts with aliphatic alcohols and THF at similar rates and, consequently, suggests that the mechanism involves an initial 2+2 addition between an α-C—H bond and a Fe=O double bond to give an organometallic intermediate, **1**, as in eq. [12]. A primary kinetic isotope effect for the oxidation of 2-propanol-2-*d* (Table 2) is also consistent with this conclusion.

[12] 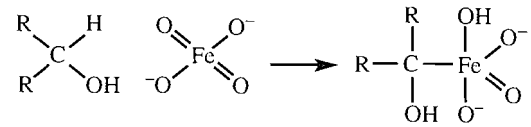

1

The observation that the unusually large rate constant observed for the oxidation of 1,1,1,3,3,3-hexafluoro-2-propanol (Table 4) is due almost entirely to a more favorable entropy of activation (Table 5) suggests that it is not unreasonable to propose a tightly structured intermediate for these reactions.

Decomposition of **1** could occur by either homolysis or heterolysis of the C—Fe bond (14). Heterolysis would yield an α-hydroxy carbocation while homolysis would give an α-hydroxy free radical. Distinction between these two possibilities can be made by observing the products obtained from the oxidation of cyclobutanol because it has been shown by Rocek and co-workers (24) that the α-hydroxycyclobutyl free radicals undergo a very rapid ring-opening reaction with consequent formation of acyclic products. When free radicals are not involved, the only product obtained is cyclobutanone (25).

Since the oxidation of cyclobutanol by ferrate resulted in the formation of only acyclic products, it seems likely that cleavage of the C—Fe bond occurs homolytically as in eq. [13].

For alcohols not containing a strained ring, homolytic cleavage of the C—Fe bond of the intermediate (**1**) would

Can. J. Chem. Downloaded from www.nrcresearchpress.com by 213.200.69.106 on 09/08/12
For personal use only.

TABLE 5. Activation parameters for the oxidation of alcohols by ferrate ion

Alcohol	pH	$\Delta H^{\neq}$ (kcal mol^{-1})	$\Delta S^{\neq}$ (cal mol^{-1} K^{-1})	$\Delta G^{\neq}$ (kcal mol^{-1})
1,1,1,3,3,3-Hexafluoro-2-propanol	9.72	13.2 ± 0.6	−19 ± 2	18.9 ± 1.2
1,3-Difluoro-2-propanol	9.72	12.9 ± 0.2	−23 ± 2	19.8 ± 0.8
2-Propanol	9.72	12.9 ± 0.4	−24 ± 2	20.1 ± 1.0
Mandelic acid	8.76	5.03 ± 0.30	−44 ± 3	18.1 ± 1.2
Mandelic acid	9.70	7.90 ± 0.52	−37 ± 3	18.9 ± 1.4
4-Methoxymandelic acid	8.76	6.24 ± 0.52	−39 ± 2	17.9 ± 1.1
4-Chloromandelic acid	8.76	4.95 ± 0.80	−44 ± 3	18.1 ± 1.7

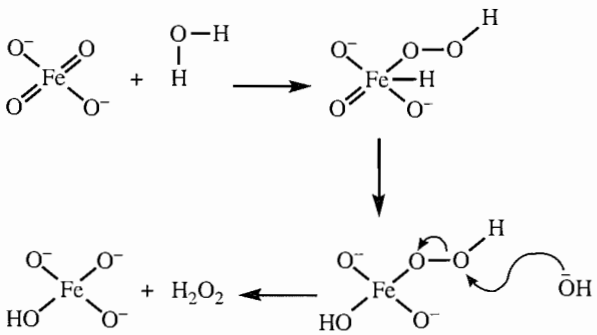

SCHEME 1

likely be followed by hydrogen transfer to yield a ketone as in eqs. [14] and [15].

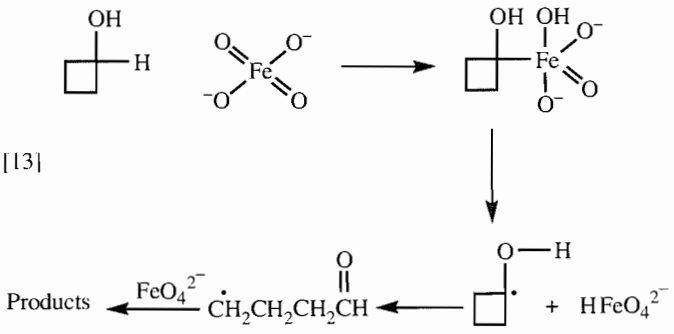

[13]

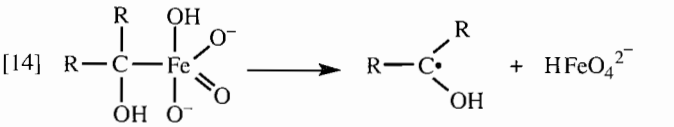

[14]

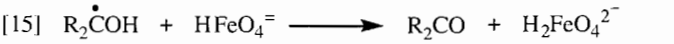

[15]

The oxidation of mandelic acid

A primary deuterium kinetic isotope effect is also observed for the oxidation of mandelic acid (Table 2), suggesting that the reaction mechanism may be similar to that proposed for 2-propanol. The enthalpy of activation (Table 5), much less than for 2-propanol, reflects a decrease in the strength of C—H bonds adjacent to an aromatic ring. The less favorable entropy of activation for mandelic acid as compared to 2-propanol is likely associated with additional solvation that would be required for a transition state bearing three (rather than two as in the case of 2-propanol) negative charges.

The insensitivity of the rate of reaction to substituents on the ring (Table 3) is also consistent with a 2+2 rate-limiting step in which additional charge is not built up adjacent to the ring in the transition state.

Conclusion

The results obtained from a kinetic study of the oxidation of 2-propanol and mandelic acid by ferrate ion at pH 9–10 are readily accounted for by assuming that the reaction is initiated by a 2+2 addition of the α-C—H bond to an iron–oxo double bond, followed by subsequent homolytic cleavage of the resulting carbon—iron bond.

Acknowledgments

The authors are pleased to acknowledge the financial assistance of the National Research Council of Canada. We are grateful to the Carus Chemical Co. for the gift of a sample of potassium ferrate.

1. R.J. Audette, J.W. Quail, and P.J. Smith. Tetrahedron Lett. 279 (1971).
2. Y. Tsuda and S. Nakajima. Chem. Lett. 1397 (1978).
3. D.H. Williams and J.T. Riley. Inorg. Chim. Acta, **8**, 177 (1974).
4. R.J. Audette, J.W. Quail, and P.J. Smith. J. Chem. Soc. Chem. Commun. 38 (1972).
5. J.N. BeMiller and S.D. Darling. U.S. Patent 3 632 802 (1972); J.N. BeMiller, V.G. Kumari, and S.D. Darling. Tetrahedron Lett. 4143 (1972).
6. C.M. Starks. Phase transfer catalysis. ACS Symp. Ser. 326. 1987; C.M. Starks and C. Liotta. Phase transfer catalysis. Academic Press, New York. 1978; W.P. Weber and G.W. Gokel. Phase transfer catalysis in organic synthesis. Springer-Verlag, New York. 1977; D.G. Lee. *In* Oxidation in organic chemistry. Part D. *Edited by* W.S. Trahanovsky. Academic Press, New York. 1982.
7. D. Arndt. Manganese compounds as oxidizing agents in organic chemistry. Open Court, La Salle, Ill. 1981. Chap. 4.
8. D.G. Lee and L.N. Congson. Can. J. Chem. **68**, 1774 (1990).
9. A. Rauk and T. Ziegler. Theor. Chim. Acta (Berlin), **34**, 49 (1974).
10. B.H.J. Bielski. Free Radical Res. Commun. **12**, 469 (1991); R.L. Bartzatt. Transition Met. Chem. **11**, 116 (1986); T. Ernst, M. Wawrzenczyk, M. Cyfert, and M. Wronska. Bull. Acad. Polon. Sci. **27**, 773 (1979); H. Goff and R.K. Murmann. J. Am. Chem. Soc. **93**, 6058 (1971); B. Jezowska-Trzebiatowska and M. Wronska. Bull. Acad. Polon. Sci. **5**, 659 (1957).
11. J.E. Cyr and B.H.J. Bielski. Free Radical Biol. Med. **11**, 157 (1991).
12. R. Bartzatt, A. Tabatabai, and J. Carr. Synth. React. Inorg. Met. Org. Chem. **15**, 1171 (1985).
13. A.K. Rappe and W.A. Goddard III. J. Am. Chem. Soc. **104**, 3287 (1982).
14. D.G. Lee and T. Chen. J. Org. Chem. **56**, 5341 (1991).
15. D.H.R. Barton, S.D. Beviere, W. Chavasiri, E. Csuhai, D. Doller, and W-G. Liu. J. Am. Chem. Soc. **114**, 2147 (1992);

Can. J. Chem. Downloaded from www.nrcresearchpress.com by 213.200.69.106 on 09/08/12
For personal use only.

D.H.R. Barton and D. Doller. Acc. Chem. Res. **25**, 504 (1992).
16. C-M. Che, C. Ho, and T-C. Lau. J. Chem. Soc. Dalton Trans. 1259 (1991); A.L. Balch, C.R. Cornman, L. Latos-Grazynski, and W. Renner. J. Am. Chem. Soc. **114**, 2230 (1992); N. Kitajima, M. Ito, H. Fukui, and Y. Moro-oka. J. Chem. Soc. Chem. Commun. 102 (1991).
17. A. Tenaglia, E. Terranova, and B. Waegell. J. Org. Chem. **57**, 5523 (1992).
18. R.L. Bartzatt. Ph.D. Thesis, University of Nebraska–Lincoln, 1982. p. 21.
19. J.M. Schreyer, G.W. Thompson, and L.T. Ockerman. Anal. Chem. **22**, 1426 (1950).
20. K.B. Wiberg. *In* Oxidation in organic chemistry. Part A. *Edited by* K.B. Wiberg. Academic Press, New York. 1965. Chap. 2.
21. T. Chen. Ph.D. Thesis, University of Regina. 1991.
22. R. Brownell, A. Leo, Y.W. Chang, and F.H. Westheimer. J. Am. Chem. Soc. **82**, 406 (1960).
23. D.G. Lee and M. van den Engh. Can. J. Chem. **50**, 2000 (1972); **50**, 3129 (1972).
24. K. Meyer and J. Rocek. J. Am. Chem. Soc. **94**, 1209 (1972); J. Rocek and D.E. Aylward. J. Am. Chem. Soc. **97**, 5452 (1975); J. Rocek and A.E. Radkowsky. J. Am. Chem. Soc. **90**, 2986 (1968); **95**, 7123 (1973).
25. D.G. Lee, U.A. Spitzer, J. Cleland, and M.E. Olson. Can. J. Chem. **54**, 2124 (1976).

Can. J. Chem. Downloaded from www.nrcresearchpress.com by 213.200.69.106 on 09/08/12
For personal use only.

Novel access to (3*R*)- and (3*S*)-3-hydroxy-L-aspartic acids, (4*S*)-4-hydroxy-L-glutamic acid, and related amino acids

STEPHEN HANESSIAN[1] AND BENOIT VANASSE
Department of Chemistry, Université de Montréal, Montréal, QC H3C 3J7, Canada

Received April 12, 1993

STEPHEN HANESSIAN and BENOIT VANASSE. Can. J. Chem. **71**, 1401 (1993).

Derivatives of L-aspartic and L-glutamic acids can be converted into α-hydroxy acids via oxygenation of the corresponding enolates.

STEPHEN HANESSIAN et BENOIT VANASSE. Can. J. Chem. **71**, 1401 (1993).

Des dérivés de l'acide L-aspartique et L-glutamique sont convertis en α-hydroxy acides via des réactions d'oxygénation des énolates correspondants.

Can. J. Chem. Downloaded from www.nrcresearchpress.com by 213.200.69.106 on 09/08/12
For personal use only.

There is at present much interest in the asymmetric synthesis of non-proteinogenic as well as unusual amino acids of natural occurrence (for recent excellent monographs, see ref. 1; for selected recent reviews, see ref. 2). In this regard, the β- and γ-hydroxy α-amino acid motif, which can be found in a number of natural products (e.g., cyclosporin (3*a*) and lysobactin (3*b*); see also ref. 4), presents a challenging area for studies in stereocontrolled synthesis. Most of the synthetic routes to β- and γ-hydroxy α-amino acids and their derivatives have been developed only recently and they rely basically on chemical (1, 2), or enzymatic methods (4, 5). In connection with other ongoing projects in our laboratory, we became interested in the synthesis of (3*R*)- and (3*S*)-3-hydroxy-L-aspartic acids. Although the four optical isomers have been obtained by resolution (6) and by individual synthesis (7), recent reports have described alternative methods relying on asymmetric processes using amino acids (8, 9), on utilizing (*R*, *R*)-(+)-tartaric acid as a chiral template (10–16), and on other methodology.

We wish to disclose a novel access to (3*R*)- and (3*S*)-3-hydroxy-L-aspartic acids and (4*S*)-4-hydroxy-L-glutamic acid, as well as to α,γ-dihydroxy amino acids (17), by the stereocontrolled hydroxylation of the dianions derived from appropriate amino acids or their functional equivalents. Although there are ample precedents for the hydroxylation of ester (18),[2] lactone (19), and lactam (20) enolates, there are few practical examples in the amino acid series (21), one, to the best of our knowledge, in the case of acidic amino acids (22), and none with amino lactones. Our choice of L-aspartic and L-glutamic acids as substrates was instigated by the fact that the corresponding β- and γ-hydroxy acids, respectively, are found in nature. In planning our strategy for the stereocontrolled hydroxylation of dianions we wished to control the process by capitalizing on internal asymmetric induction resulting from the inherent chirality and functional disposition of a resident *N*-substituted amino group. We reasoned that by the judicious choice of oxidation reagent, we could alter the stereochemical course of the hydroxylation by taking advantage of the steric bulk in the substrate on the one hand, and chelation of proximal *N*-substituted groups on the other, as illustrated by paths A and B for the enolate resulting from L-aspartic acid in Scheme 1.

To test our plan, we chose the readily available (23) lactone **1** as a model in which the geometry of the dianion is fixed. Thus, lactone **1** was treated with a variety of bases, and the resulting enolate was treated with the Davis oxaziridine reagent (24) on the one hand, and the Mimoun-Vedejs, oxodiperoxymolybdenum pyridine hexamethylphosphoric triamide (MoOPH) reagent (25) on the other (Scheme 2).

As can be appreciated from the results in Table 1, regardless of the nature of the base, hydroxylation with MoOPH led to the preponderance of the *syn* product, albeit in modest yields. The isomeric lactones **2** and **3** were easily separated by chromatography, and variable quantities (up to 20%) of unreacted starting materials were recovered, which is not uncommon with dianions of this type (26). We rationalize the preponderance of this *syn* product by an initial coordination with the carbamate anion (N or O) followed by intramolecular delivery of oxygen as shown in Fig. 1. In view of the initial coordination with MoOPH, the nature of the cation seems to play little or no role in the selectivity.

With the oxaziridine, however, the major product is the *anti* isomer **2**, which most likely results from an approach of the oxidant from a position opposite to the bulky NHCbz group. Moreover, there appears to be an important difference in the ratio of the product **2** and **3**, particularly in the presence of NaHMDS, which gives the highest proportion of the *anti* isomer **2**. The origin of this dependence of selectivity on the nature of the cation is not clear, but could, in part, be due to the states of aggregation of mono and dianions as well as to the reactivity of the intermediate hemiaminal-type species formed with the reagent (18*b*).

Having confirmed the validity of the plan for a reagent and resident functional group-based strategy of hydroxylation with the cyclic model, we investigated the same reactions with *N*-benzyloxycarbonyl-L-asparate **4**. Table 2 summarizes the results in this series, where once again, the combination of the oxaziridine reagent with NaHMDS was found to give the highest selectivity (7:1) in favor of the *erythro* (2*S*,3*R*) isomer **6**.

Acid hydrolysis of **5** and **6**, respectively, gave (3*S*)-3-hydroxy-L-aspartic acid (14) and (3*R*)-4-hydroxy-L-aspartic acid (7), respectively.

With MoOPh, the *threo* isomer (*syn* attack) was favored (Table 2, entries 5–7), but the effect was much less pronounced than in the cyclic model. It is possible that chelation is also taking place in this series although, contrary to the lactone case (Table 1), there seems to be a dependence

[1]Author to whom correspondence may be addressed.

[2]For some examples using molecular oxygen and lead tetracetate, etc., see ref. 18*a*; for the use of 2-sulfonyloxaziridines, see ref. 18*b*; for the use of MoOPH, see ref. 18*c*.

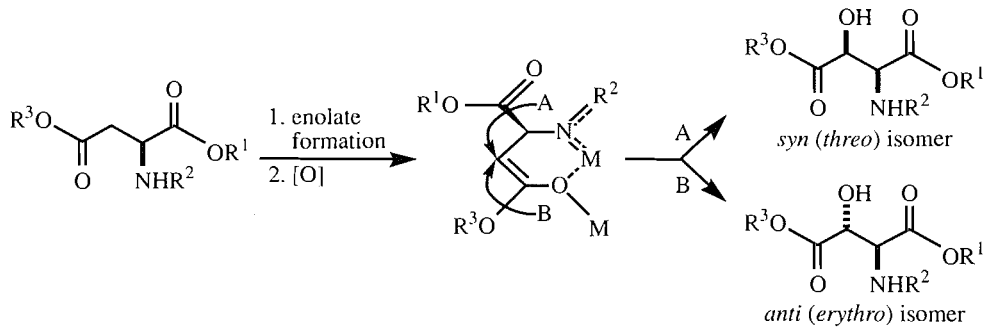

SCHEME 1

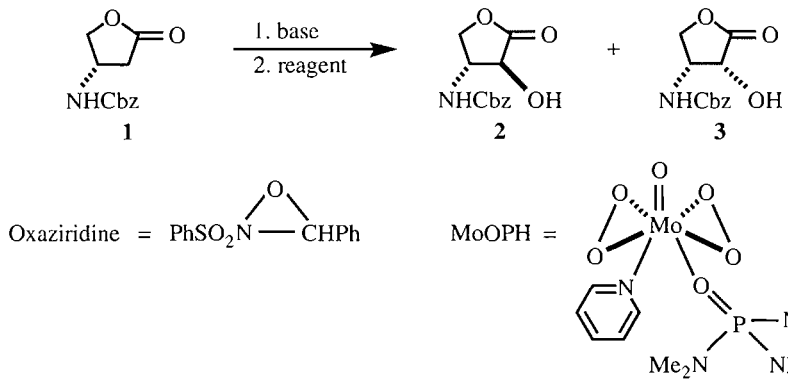

SCHEME 2

TABLE 1. Hydroxylation of lactone **1**

	Base	Reagent	Conditions[a] lactone/base/reagent	Yield[b,c] (%)	Ratio[d,e] 2:3
1	LiHMDS	MoOPH	1:4:1.5	30	1:9
2	KHMDS	MoOPH	1:4:1.5	40	1:9
3	NaHMDS	MoOPH	1:4:1.5	36	1:9
4	LiHMDS	Oxaziridine	1:3:1.5	50	4.5:1
5	KHMDS	Oxaziridine	1:3:1.5	70	6.5:1
6	NaHMDS	Oxaziridine	1:3:1.5	56	14:1

[a]THF, −78°C, 6 h (entries 1–3), 1 h (entries 4–6).
[b]Isolated major product.
[c]Varying amounts of starting material were also recovered (10–20%).
[d]Determined by HPLC and by isolation.
[e]Average of three different runs.

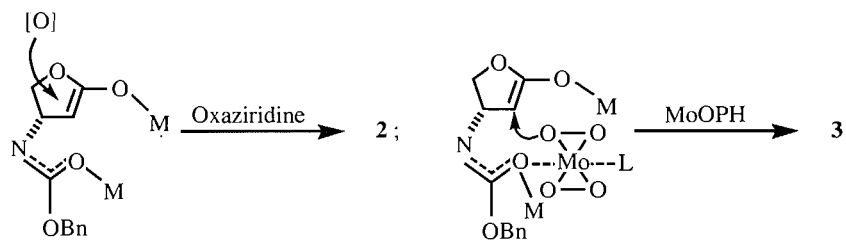

FIG. 1

on the nature of the cation. In an effort to clarify the nature of the dianionic species and the influence of the ester group on the selectivity of hydroxylation, we investigated the *N*-tosyl series with different combinations of methyl and *tert*-butyl ester groups (Scheme 4, Table 3).

Thus, localizing the charge on nitrogen (*N*-Ts series) (Scheme 1, R^2 = Ts), in combination with the presence of the bulky α-ester groups, clearly favors the formation of the *erythro* isomer, where a ratio of 45:1 can be obtained (Table 3, entry 5). Interestingly, the bulk of the ester group also has

Can. J. Chem. Downloaded from www.nrcresearchpress.com by 213.200.69.106 on 09/08/12
For personal use only.

TABLE 2. Hydroxylation of **4**

	Base	Reagents[a]	Yield (%)[b]	Ratio 6:5[c,d]
1	LDA	Oxaziridine	60	1.5:1
2	LiHMDS	Oxaziridine	60	2.5:1
3	KHMDS	Oxaziridine	70	1.1:1
4	NaHMDS	Oxaziridine	70	7:1
5	LiHMDS	MoOPH	36 (50)	1:2
6	KHMDS	MoOPH	50 (60)	1:1
7	NaHMDS	MoOPH	30 (40)	1:1

[a]THF, −78°C, 15 min (entries 1–4), 4 h (entries 5–7); ester/base/reagent, 1:3:1.5 (entries 1–4), ester/base/reagent, 1:4:2 (entries 5–7).
[b]Yield based on recovered starting material.
[c]Determined by HPLC and by isolation.
[d]Average of three different runs.

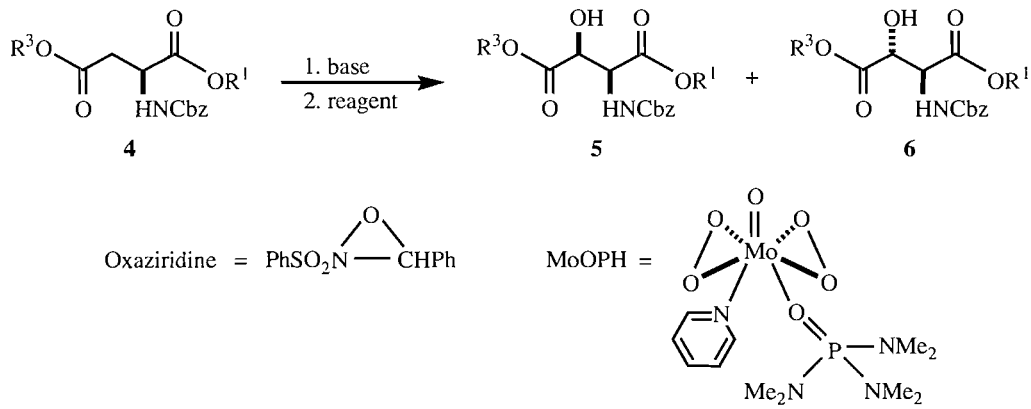

SCHEME 3

a synergistic effect in the case of MoOPH, where the selectivity can be increased to 1:4 in favor of the *threo* isomer (Table 3, entry 6), compared to the dimethyl ester series. Evidently in the *N*-Cbz series, selectivity is decreased, possibly due to the larger size of the chelated dianionic species, or due to its different state of aggregation. It should be pointed out that Tamm and co-workers (27) also postulated internal chelation in the hydroxylations with MoOPH.

In view of the limited number of methods for the preparation of enantiomerically pure γ-hydroxy-L-glutamic acid (4, 28–30), it was of interest to extend the hydroxylation reaction to *N*-benzyloxycarbonyl dimethyl L-glutamate **7** (Scheme 5, Table 4). Treatment of the dianion of **7** with MoOPH under a variety of conditions resulted in complete recovery of unchanged starting material, as was recently observed in a related case (21). However, when the oxaziridine was used as oxidant, hydroxylation took place to give the (4*S*)-hydroxy analog as the major (9:1) isomer, when LiHMDS was used as the base. In this series, KHMDS and NaHMDS proved to be much less selective than with **4**. Acid hydrolysis gave (4*S*)-4-hydroxy-L-glutamic acid (28).

The selectivity in this case is intriguing in view of the relative nonproximity of the carbamate to the enolate function. It is possible that the lithium enolate in this case is more conducive to the formation of a π-complex (31) with the aromatic ring of the carbamate, thus imposing an element of conformational constraint, and favoring an approach of the electrophilic reagent that leads to the observed product.

The methodology developed in this work provides an expeditious access to optically pure β- and γ-hydroxylated amino acids in the aspartic and glutamic acid series, respectively. The ability to control the stereochemistry of hydroxylation of dianions of the type reported here, based on the nature of the reagent used, and on the choice of functional group present, should stimulate further development in asymmetric synthesis[3] of related amino acids.

Experimental section

General data

Tetrahydrofuran was distilled over benzophenone and sodium prior to use. Analytical thin-layer chromatography (TLC) was carried out on Merck Kieselgel silica gel 60 F_{254} glass plates. Flash chromatography was performed according to the procedure of Still et al. (33) with Merck silica gel, 230–400 mesh. Infrared (IR) spectra were recorded in chloroform on a Perkin–Elmer 781 spectrometer. The wavenumbers reported are referenced to the polystyrene 1601 cm^{-1} absorption. Nuclear magnetic resonance spectra were obtained on a Bruker WH-400 (^1H 400 MHz) spectrometer with chloroform-*d* as solvent and tetramethylsilane as an internal standard, unless otherwise indicated. ^1H NMR multiplicities are recorded by use of the following abbreviations: s, singlet; d, doublet; dd, double doublet; t, triplet; q, quartet; m, multiplet; b, broad; *J*, coupling constant (hertz). High-resolution FAB mass spectra were obtained by means of Kratos MS5OTCTA and AEI-MS 902 spectrometers at the Université de Montréal. Melting points were mea-

[3]The reactivity of dianions resulting from various N-substituted dialkyl aspartates and glutamates depends on the nature of the electrophile, see for example, ref. 32.

Can. J. Chem. Downloaded from www.nrcresearchpress.com by 213.200.69.106 on 09/08/12
For personal use only.

Can. J. Chem. Downloaded from www.nrcresearchpress.com by 213.200.69.106 on 09/08/12
For personal use only.

TABLE 3. The effect of different ester and *N*-protective group combinations on the hydroxylation of L-aspartic acid

	Base	Reagent/conditions[a]	R^1	R^2	R^3	Yield[b] (%)	Ratio[d,e] 6:5
1	LiHMDS	Oxaziridine	Me	Cbz	*t*-Bu	40	10:1
2	LiHMDS	Oxaziridine	*t*-Bu	Cbz	Me	60	10:1
3	LiHMDS	Oxaziridine	*t*-Bu	Cbz	*t*-Bu	70	10:1[f]
4	LiHMDS	Oxaziridine	Me	Ts	Me	60	7:1
5	LiHMDS	Oxaziridine	*t*-Bu	Ts	*t*-Bu	57	45:1
6	LiHMDS	MoOPH	*t*-Bu	Cbz	*t*-Bu	40[c]	1:4

[a]THF, −78°C, 5–10 min, ester/base/reagent, 1:3:1.5 (entries 1–5).
[b]Yield of mixture.
[c]Starting material was recovered (20%).
[d]Determined by HPLC and by isolation.
[e]Average of three different runs.
[f]Ratio with KHMDS, 4:1, NaHMDS, 6:1.

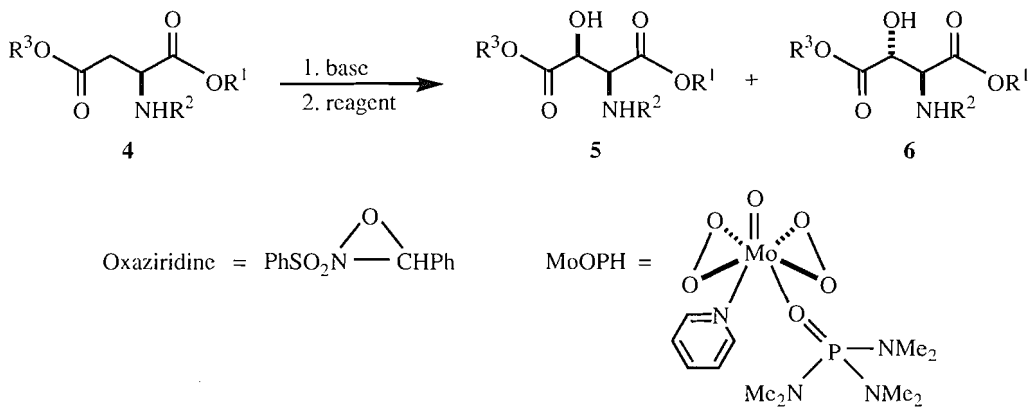

SCHEME 4

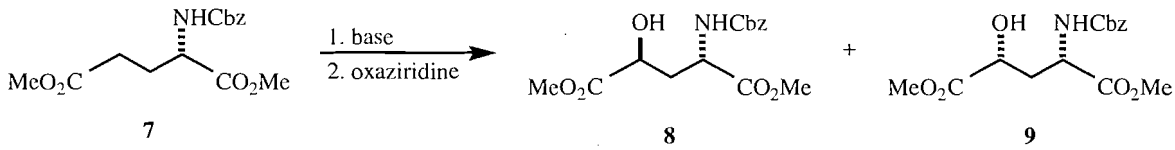

SCHEME 5

TABLE 4. Hydroxylation of dimethyl *N*-benzyloxycarbonyl-L-glutamate

	Base/conditions[a]	Yield (%)[b,c]	Ratio[d] 8:9
1	LiHMDS	70	9:1
2	KHMDS	70	1:1
3	NaHMDS	56	2.6:1

[a]THF, −78°C, 5–10 min, ester/base/reagent, 1:3:1.5.
[b]Yield of isolated products.
[c]Starting ester was recovered (ca. 10%).
[d]Determined by HPLC.

sured on a Büchi apparatus and are uncorrected. Optical rotations were measured on a Perkin–Elmer 241 polarimeter at 25° C.

Hydroxylation of ***1*** *with 3-phenyl-*N*-phenylsulfonyloxaziridine*

To a solution of lactone **1** (235 mg, 1 mmol) and 3-phenyl-*N*-phenylsulfonyloxaziridine (392 mg, 1.5 mmol) in THF (5 mL) was added a solution of sodium bis(trimethylsilyl)amide (1 M, 2 mL, 2 mmol) in THF (4 mL) at −78°C. After 15 min, the solution was quenched by addition of camphorsulfonic acid (1.0 g, 4 mmol) in THF (1.0 M), diluted with ethyl acetate, then washed with aqueous solutons of 10% HCl, 5% sodium bicarbonate, and brine. The organic layers were combined, dried ($MgSO_4$), and evaporated to dryness. The crude products were then purified by flash chromatography (ethyl acetate – hexanes, 4:6) to give (2*S*,3*S*)-3-benzyloxycarbonylamino-2-hydroxy-γ-butyrolactone, **2** (140 mg, 56%), and (2*R*,3*S*)-3-benzyloxycarbonylamino-2-hydroxy-γ-butyrolactone, **3** (10 mg, 4%).

For **2**: mp 105–106°C; $[\alpha]_D$ −30 (*c* 1, $CHCl_3$); IR ν_{max} (film): 3600–3200 (OH + NHCbz), 1785 (γ-lactone), 1720–1690 (carbamate) cm^{-1}; ^1H NMR (400 MHz, *O*-acetyl derivative) δ: 2.21 (3H, s, OAc), 3.9 (1H, dd, $J_{4,3}$ = 8.8 Hz, and J_{gem} = 8.8 Hz, H-4a), 4.2–4.16 (1H, m, H-3), 4.34 (1H, d, $J_{2,3}$ = 9.3 Hz, H-2), 4.39 (1H, dd, $J_{4,3}$ = 8.2 Hz, and J_{gem} = 8.8 Hz, H-4b), 5.0 (2H, s, CH_2Ph), 5.5–5.7 (1H, s, *NH*), 7.3–7.40 (5H, s, Ph); MO (O-Acetyl-derivative), *m/z*: 274 (MH^+); $C_{14}H_{15}NO_6$ (273.279).

For **3**: $[\alpha]_D$ +10.75 (*c* 1, $CHCl_3$); IR ν_{max} (film): 3600–3200 (OH + NHCbz), 1785 (γ-lactone), 1740 (ester and carbamate) cm^{-1}; ^1H NMR (400 MHz, O-acetyl derivative) δ: 2.21 (3H, s, OAc), 3.9 (1H, dd, $J_{4,3}$ = 8.8 Hz, and J_{gem} = 8.8 Hz, H-4a), 4.2–

Can. J. Chem. Downloaded from www.nrcresearchpress.com by 213.200.69.106 on 09/08/12
For personal use only.

4.16 (1H, m, H-3), 4.34 (1H, d, $J_{2,3}$ = 6.8 Hz, H-2), 4.39 (1H, dd, $J_{4,3}$ = 8.2 Hz, and J_{gem} = 8.8 Hz, H-4b), 5.0 (2H, s, CH_2Ph), 5.5–5.7 (1H, s, *NH*), 7.3–7.40 (5H, s, Ph); MO (O-acetyl derivative), *m/z*: 294 (MH^+); $C_{14}H_{15}NO_6$ (293.279).

Hydroxylation of ***1*** *with MoOPH*

To a solution of lactone **1** (117 mg, 0.5 mmol) in THF at −78°C was added a solution of potassium bis(trimethylsily)amide (0.5 M, 4 mL, 2 mmol) in THF (4 mL) followed by MoOPH (434 mg, 1 mmol). After 15 min, the reaction mixture was quenched by addition of aqueous 10% HCl. The solution was diluted with ethyl acetate, then washed with successively aqueous solutions of 10% HCl, 5% sodium bicarbonate, and brine. The organic layers were combined, dried ($MgSO_4$), and evaporated to dryness. The crude products were then purified by flash chromatography (ethyl acetate – hexanes 4:6) to give **2** (5 mg, 4%) and **3** (45 mg, 65%).

Hydroxylation of ***4*** *with 3-phenyl-*N*-phenylsulfonyloxaziridine*

To a solution of dimethyl *N*-benzyloxycarbonyl-L-asparate **4** (295 mg, 1 mmol) and 3-phenyl-*N*-phenylsulfonyloxaziridine (392 mg, 1.5 mmol) in THF (5 mL) at −78°C was added, dropwise, a solution of sodium bis(trimethylsilyl)amide (1 M, 2.0 mL, 2 mmol) in THF (5 mL). After 15 min, the reaction mixture was quenched by addition of camphorsulfonic acid and processed as described for the synthesis of **2**. The products were then purified by flash chromatography (ethyl acetate – hexanes 4:6) to give (2*S*,3*R*)-dimethyl 3-hydroxy-*N*-benzyloxycarbonyl-L-aspartate **6**, isolated as an oil (190 mg, 61%) and (2*S*,3*S*)-dimethyl 3-hydroxy-*N*-benzyloxycarbonyl-L-aspartate **5**, isolated as an oil (27 mg, 9%).

For **6**: $[\alpha]_D$ +14.58 (*c* 1, $CHCl_3$); IR ν_{max} (film): 3400–3300 (NHCbz), 1750–1730 (esters and carbamate) cm^{-1}; ^1H NMR (300 MHz) δ: 3.34 (1H, d, *J* = 5.3 Hz, OH), 3.78 (3H, s, C(4)OOMe), 3.80 (3H, s, C(1)OOMe), 4.72 (1H, d, $J_{2,3}$ = 3.9 Hz, H-2), 4.75 (1H, d, $J_{3,NH}$ = 9.3 Hz, H-3), 5.10 (2H, s, CH_2Ph), 5.61 (1H, d, $J_{NH,2}$ = 9.3 Hz, NH), 7.34 (5H, s, Ph); MS, *m/z*: 312 (MH^+, 100%); $C_{14}H_{17}NO_7$ (311.294).

For **5**: $[\alpha]_D$ +24.2 (*c* 1, $CHCl_3$); IR ν_{max} (film): 3400–3300 (NHCbz), 1750–1730 (esters and carbamate) cm^{-1}; ^1H NMR (300 MHz) δ: 3.46 (1H, d, *J* = 5.0 Hz, OH), 3.73 (3H, s, C(4)OOMe), 3.83 (3H, s, C(1)OOMe), 4.53 (1H, d, $J_{2,3}$ = 2.0 Hz, H-2), 4.64 (1H , dd, $J_{3,2}$ = 2.2 Hz and $J_{3,NH}$ = 8.4 Hz, H-3), 5.14 (2H, s, CH_2Ph), 5.79 (1H, d, $J_{NH,2}$ = 8.4 Hz, NH), 7.34 (5H, s, Ph); MS, *m/z*: 312 (MH^+, 100%); $C_{14}H_{17}NO_7$ (311.294).

Hydroxylation of ***4*** *with MoOPH*

To a solution of dimethyl *N*-benzyloxycarbonyl-L-aspartate **4** (158 mg, 0.53 mmol) in THF at −78°C was added a solution of potassium bis(trimethylsilyl)amide (0.5 M, 4 mL, 2 mmol) in THF (4 mL) followed by addition of MoOPH (434 mg, 1 mmol). After 15 min, the reaction mixture was quenched by addition of an aqueous solution of 1 N HCl and processed as described above. The crude products were then purified by flash chromatography (ethyl acetate – hexanes 4:6) to give **6** (27 mg, 16%) and **5** (55 mg, 34%), isolated as oils.

*Hydroxylation of di-*tert*-butyl-*N*-p-tolylsulfonyl-*L*-aspartate with 3-phenyl-*N*-phenylsulfonyl oxaziridine*

To a solution of di-*tert*-butyl-*N*-*p*-tolylsulfonyl-L-aspartate (104 mg, 0.27 mmol) at −78°C was added, dropwise, a solution of lithium hexamethyldisilazane (0.78 mmol) in THF (5 mL). After 2 h, 3-phenyl-*N*-phenylsulfonyl oxaziridine (102 mg, 0.39 mmol) in THF (2 mL) was added. The reaction was quenched, after 15 min, by addition of camphorsulfonic acid (0.26 g, 1.1 mmol) in THF (1.0 M). The solution was diluted with ethyl acetate and processed as described above. The crude products were purified by flash chromatography (ethyl acetate – hexanes 1:1) to give (2*S*-3*R*)-di-*tert*-butyl-3-hydroxy-*N*-tosyl-L-aspartate and (2*S*,3*S*)-di-*tert*-butyl-3-hydroxy-*N*-tosyl-L-aspartate as a 45:1 (*anti*:*syn*) mixture of diastereomers (62 mg, 57%); IR ν_{max} (film): 3400–2900 (OH + NHCbz), 1750–1730 (esters) cm^{-1}; ^1H NMR (300 MHz) δ: 1.23 (9H, s, *tert*-butyl), 1.57 (9H, s, *tert*-butyl), 2.40 (3H, s, CH_3), 3.02 (1H, m, OH-3), 4.275 (1H, dd, $J_{2,OH}$ = 10.8 Hz and $J_{2,3}$ = 2.26 Hz, H-2), 4.39–4.42 (1H, M, H-3), 5.3 (1H, d, $J_{NH,2}$ = 10.8 Hz, NH), 7.29 (2H, d, *J* = 8 Hz, Ph), 7.75 (2H, d, *J* = 6.5 Hz, Ph).

*Hydroxylation of di-*tert*-butyl-*N*-benzyloxycarbonyl-*L*-aspartate with MoOPH*

To a solution of di-*tert*-butyl-*N*-benzyloxycarbonyl-L-aspartate (100 mg, 0.264 mmol) in THF (10 mL) at −78°C was added a solution of lithium bis(trimethylsilyl)amide (2.1 mmol) in THF (4 mL). After 2 h, MoOPH (229 mg, 0.527 mmol) was added as a solid in one portion at −78°C. After 4 h, the solution was quenched by addition of an aqueous solution of 1 N HCl, then processed as described above. The crude products were purified by flash chromatography (ethyl acetate – hexanes 2:8) to give 42 mg, 40%) of (2*S*,3*R*)-di-*tert*-butyl-3-hydroxy-*N*-benzyloxycarbonyl-L-aspartate and (2*S*,3*S*)-di-*tert*-butyl-3-hydroxy-*N*-benzyloxycarbonyl-L-aspartate isolated as a 1:4 (*anti*:*syn*) mixture of diastereomers; IR ν_{max} (film): 3600–3300 (OH + NHCbz), 1730 (esters) cm^{-1}; ^1H NMR (300 MHz, for the OAc derivative) δ: 1.469 (9H, s, *tert*-butyl), 1.496 (9H, s, *tert*-butyl), 2.109 (3H, s, OAc), 4.852 (1H, dd, $J_{2,NH}$ = 8,1 Hz and $J_{2,3}$ = 3.2 Hz, H-2), 5.125 (2H, s, CH_2Ph), 5.355 (1H, d, $J_{2,3}$ = 3.2 Hz, H-3), 5.585 (1H, d, $J_{NH,2}$ = 8.1 Hz, NH), 7.36 (5H, s, Ph); MS, *m/z*: 278 (50%) 222 (55%), 89 (95%); HRMS, calcd. for $C_{20}H_{29}NO_7$: 395.1944; found: 395.4520.

Hydroxylation of dimethyl N*-benzyloxycarbonyl-*L*-glutamate (7) with 3-phenyl-*N*-phenylsulfonyl oxaziridine*

To a solution of dimethyl *N*-benzyloxycarbonyl-L-glutamate (120 mg, 0.408 mmol) and 3-phenyl-*N*-phenylsulfonyl oxaziridine (160 mg, 0.612 mmol) in THF (5 mL) at −78°C (acetone – Dry Ice) was added, dropwise, a solution of lithium bis(trimethylsilyl)amide (1 M, 1.22 mL, 1.22 mmol) in THF (5 mL). After 15 min, the solution was quenched by addition of camphorsulfonic acid (0.408 g, 1.8 mmol) in THF (1.0 M). The solution was diluted with ethyl acetate, washed with an aqueous solution of 10% HCl, then processed as described above. The crude products were purified by flash chromatography (ethyl acetate – hexanes 1:1) to give (92 mg, 70%) of (2*S*,4*S*)-dimethyl 4-hydroxy-*N*-benzyloxycarbonyl-L-glutamate as a 9:1 mixture of inseparable diastereomers; $[\alpha]_D$ +9.0 (*c* 1, $CHCl_3$); IR ν_{max} (film): 3600–3200 (NHCbz + OH), 1760–1690 (esters and carbamate) cm^{-1}; ^1H NMR (300 MHz) δ: 2.2 (2H, m, H-3a and H-3b), 3.5 (1H, d, *J* = 4.4 Hz, OH), 3.73 (3H, s, COOMe), 3.75 (3H, s, COOMe), 4.25 (1H, m, H-2), 4.64 (1H, m, H-4), 5.11 (2H, s, CH_2Ph), 5.8 (1H, d, $J_{NH,4}$ = 7.8 Hz, NH), 7.34 (5H, s, Ph); MS, *m/z*: 326 (30%, MH^+), 282 (100%, $-CO_2$); HRMS, calcd. for $C_{15}H_{19}NO_7$: 325.1161; found: 325.1120.

*(3*R*)-3-Hydroxy-*L*-aspartic acid*

A solution of **6** (100 mg, 0.321 mmol), in 6 N HCl, was heated at reflux for 1.5 h. The solution was cooled, diluted with EtOAc, processed in the usual way, and the aqueous layer was evaporated to a volume of 2 mL. Acetone was then added and the resulting crystals were isolated by filtration to give the title compound as a white crystalline solid (33 mg, 69%); mp >200°C, $[\alpha]_D$ +45.6 (*c* 0.5, HCl 1 N) (lit. (16) mp >220°C, $[\alpha]_D$ +49 (*c* 2.85, HCl 1 N)).

*(3*S*)-3-Hydroxy-*L*-aspartic acid*

A solution of **5** (100 mg, 0.321 mmol), in 6 N HCl, was heated at reflux for 1.5 h. The solution was processed as described above to give the title compound as a white crystalline solid (33 mg, 69%); mp >200°C, $[\alpha]_D$ +1 (*c* 2, HCl 1 N) (lit. (7) mp >200°C, $[\alpha]_D$ +1.3 (*c* 2, HCl 1 N)).

*(4*S*)-4-Hydroxy-*L*-glutamic acid*

A solution of **8** (100 mg, 0.308 mmol), in 6 N HCl, was heated at reflux for 1.5 h. The solution was cooled, then processed as described above to give the title compound as a white crystalline solid (35 mg, 69%); mp >200°C, $[\alpha]_D$ +55 (*c* 1, HCl 5 N) (lit. (28) mp >200°C, $[\alpha]_D$ +61 (*c* 1, HCl 5 N)).

Can. J. Chem. Downloaded from www.nrcresearchpress.com by 213.200.69.106 on 09/08/12
For personal use only.

Acknowledgments

We thank the Natural Sciences and Engineering Research Council of Canada (NSERCC) and the Fonds pour la formation de chercheurs et l'aide à la recherche (Québec) (FCAR) for financial assistance, and the Mass Spectrometry Laboratory of l'Université de Montréal for analyses.

1. R.M. Williams. *In* Synthesis of optically active α-amino acids. Pergamon Press, Oxford, U.K. 1989; G.M. Coppola and H.F. Schuster. Asymmetric synthesis; construction of chiral molecules using amino acids. John Wiley & Sons, New York. 1987, and references cited therein.
2. P. Cintas. Tetrahedron, **47**, 6079 (1991); M.J. O'Donnell. Tetrahedron, **44**, 5253 (1988); K.A. Kochetkov and J.M. Belikov. Russ. Chem. Rev. **56**, 1045 (1987); I. Wagner and H. Musso. Angew. Chem. Int. Ed. Engl. **22** (1983); C.G. Barrett. *In* Chemistry and biochemistry of amino acids. Chapman and Hall, London. 1985. p. 246.
3. (*a*) R.M. Wenger. Angew. Chem. Int. Ed. Engl. **24**, 77 (1985); (*b*) A.A. Tymiak, T.J. McCormick, and S.E. Unger. J. Org. Chem. **54**, 1149 (1989).
4. N. Passerat and J. Bolte. Tetrahedron, **28**, 1277 (1987).
5. H.J. Sallach and T.H. Peterson. J. Biol. Chem. **223**, 629 (1956); H.J. Sallach and M.L. Kornguth. Biochim. Biophys. Acta, **34**, 582 (1959).
6. J. Oh-hashi and K. Harada. Bull. Chem. Soc. Jpn. **40**, 2977 (1967).
7. T. Kaneko and H. Katsura. Bull Chem. Soc. Jpn. **36**, 899 (1963).
8. C. Palomo, F. Cabré, and J.M. Ontoria. Tetrahedron Lett. **33**, 4819 (1992).
9. R. Wagner and J.W. Tilley. J. Org. Chem. **55**, 6289 (1990).
10. J. Legters, L. Thijs, and B. Zwanenburg. Tetrahedron Lett. **47**, 5287 (1991).
11. B.B. Lohray and J.R. Ahuja. J. Chem. Soc. Chem. Commun. 95 (1991).
12. R. Wagner, J.W. Tilley, and K. Lovey. Synthesis, 785 (1990).
13. T.G. Hausson and J.O. Kihlberg. J. Org. Chem. **51**, 4490 (1986).
14. Y. Gao and K.B. Sharpless. J. Am. Chem. Soc. **110**, 7538 (1988).
15. S. Saito, N. Bunya, M. Inaba, T. Moriwake, and S. Torii. Tetrahedron Lett. **26**, 5309 (1985).
16. P.G. Mattingley, M.J. Miller, R.D.G. Cooper, and B.W. Daugherty. J. Org. Chem. **48**, 3556 (1983).
17. E.E. Hamel and E.P. Painter. J. Am. Chem. Soc. **75**, 1362 (1953).
18. (*a*) G.W. Moersch and M.L. Zwiesler. Synthesis, 647 (1971); H.H. Wasserman and B.H. Lipshutz. Tetrahedron Lett. 1731 (1975); G.M. Rubottom, J.M. Gruber, R. Marrero, H.D. Juve, Jr., and C.W. Kim. J. Org. Chem. **48**, 4940 (1983); W. Oppolzer and P. Dudfield. Helv. Chim. Acta, **68**, 216 (1985); M.P. Gore and J.C. Vederas. J. Org. Chem. **51**, 3700 (1986); (*b*) F.A. Davis, L.C. Vishwakarma, J.M. Billmers, and J. Finn. J. Org. Chem. **49**, 3243 (1984); D.A. Evans, M.M. Morrissey, and R.L. Dow. J. Am. Chem. Soc. **107**, 4346 (1985); (*c*) E. Vedejs, D.A. Engler, and J.E. Telschow. J. Org. Chem. **43**, 188 (1978); R. Gamboni and Ch. Tamm. Tetrahedron Lett. **27**, 3999 (1986).
19. M.J. Taschner and A.S. Aminbhavi. Tetrahedron Lett. **30**, 1029 (1989); S. Takano, M. Morimoto, and K. Ogasawara. J. Chem. Soc. Chem. Commun. **82** (1984); G. Stork and S.D. Rychnovsky. J. Am. Chem. Soc. **109**, 1564 (1987); S. Hanessian, S. Sahoo, and M. Botta. Tetrahedron Lett. **28**, 1147 (1987); S. Hanessian. Aldrichimica Acta, **3**, 1 (1989).
20. T. Ohta, A. Hosoi, and S. Nozoe. Tetrahedron Lett. **29**, 329 (1988); W.W. Ogilvie and T. Durst. Can. J. Chem. **66**, 304 (1988).
21. J.B. Burkhart, G.W. Holbert, and B.W. Metcalf. Tetrahedron Lett. **46**, 5267 (1984).
22. F.J. Sardina, M. Paz, E. Fernandez-Megía, R. de Boer, and P. Alvarez. Tetrahedron Lett. **33**, 4637 (1992).
23. (*a*) G.J. McGarvey, R.H. Hiner, Y. Matsubara, and T. Oh. Tetrahedron Lett. **24**, 2733 (1983); (*b*) Y. Takahashi, H. Yamashita, S. Kobayashi, and M. Ohno. Chem. Pharm. Bull **34**, 2732 (1986).
24. L.C. Vishwakarma, O.D. Stringer, and F.A. Davis. Org. Synth. **66**, 203 (1986).
25. H. Mimoun, I. Seree de Roche, and L. Sajus. Bull. Soc. Chim. Fr. 1481 (1969); E. Vedejs and S. Larsen. Org. Synth. **64**, 127 (1984).
26. S. Hanessian, B. Vanasse, H. Yang, and M. Alpegiani. Can. J. Chem. **71**, 1407 (1993); H. Nitta, M. Hatanaka, and T. Ishimaru. J. Chem. Soc. Chem. Commun. 51 (1987).
27. R. Gamboni, P. Mohr, N. Sarcevic, and C. Tamm. Tetrahedron Lett. **26**, 203 (1985).
28. L. Benoiton, M. Winitz, S.M. Birnbaum, and J.P. Greenstein. J. Am. Chem. Soc. **79**, 6192 (1957).
29. T. Kusumi, H. Kakisawa, S. Suzuki, K. Harada, and C. Kashima. Bull. Chem. Soc. Jpn. **51**, 1261 (1978).
30. E.P. Kristensen, L.M. Larsen, O. Olsen, and H. Sorensen. Acta Chim. Scand. B, **34**, 497 (1980).
31. G.H. Posner and C.M. Lentz. J. Am. Chem. Soc. **101**, 934 (1979).
32. J.E. Baldwin, M.G. Moloney, and M. North. Tetrahedron, **45**, 6309, 6319 (1989); A.M.P. Koskinen and H. Rapoport. J. Org. Chem. **54**, 1859 (1989); D. Seebach and D. Wasmuth. Angew. Chem. Int. Ed. Engl. **20**, 971 (1981).
33. W.C. Still, M. Kahn, and A. Mitra. J. Org. Chem. **43**, 2923 (1978).

Highly stereocontrolled syntheses of 2,3-disubstituted 1,4-butyrolactones using ionic and free radical reactions

STEPHEN HANESSIAN,[1] BENOIT VANASSE, HUA YANG, AND MARCO ALPEGIANI
Department of Chemistry, Université de Montréal, Montréal, QC H3C 3J7, Canada

Received April 12, 1993

STEPHEN HANESSIAN, BENOIT VANASSE, HUA YANG, and MARCO ALPEGIANI. Can. J. Chem. **71**, 1407 (1993).

N-Substituted 3-amino-1,4-butyrolactones undergo highly stereocontrolled substitution reactions via anionic and free radical processes.

STEPHEN HANESSIAN, BENOIT VANASSE, HUA YANG et MARCO ALPEGIANI. Can. J. Chem. **71**, 1407 (1993).

Les dérivés des 3-amino-1,4-butyrolactones *N*-substitués réagissent de façon hautement stéréocontrollée dans de réactions de type anioniques et radicalaires.

Can. J. Chem. Downloaded from www.nrcresearchpress.com by 213.200.69.106 on 09/08/12
For personal use only.

The past decade has seen a resurgence in asymmetric processes in virtually all facets of preparative organic chemistry where chirality is an issue (1). Efforts in the area of amino acid chemistry (2) have focused on the synthesis of natural and unnatural analogs in connection with natural product synthesis (for some recent examples, see ref. 3), and a continuing interest in the design of enzyme inhibitors and peptidomimetics (ref. 4 for recent reviews). Thus, the search for enantiomerically pure "small" molecules as mimics and surrogates of proteinogenic amino acids has become an important area of research activity.

In the preceding paper (5), we described methods for the stereocontrolled hydroxylation of enolates derived from *N*-substituted dialkyl aspartates and glutamates, as well as from 3-*N*-substituted butyrolactones. It was shown that by utilizing steric control, influenced by resident functionality, hydroxylation of enolates took place from a side opposite to a bulky substituent. On the other hand, using a reagent capable of coordinating with the *N*-substituent, hydroxylation could be directed to produce significant amounts of the other diastereomer.

We now report on the utilization of (*S*)-3-benzyloxycarbonylamino butyrolactones, **1** and **2**, readily available from *L*-aspartic acid (6), as chiral templates for site-selective and stereocontrolled functionalizations at C-2 via the corresponding enolates and radicals. In this context, the 2-azido and 2-bromo products would constitute versatile 4-carbon chirons with preparatively useful applications (see, for example, ref. 7), as shown in Scheme 1.

Previous studies (6) with the same lactone showed that treatment of the dianion with methyl iodide led to the expected *anti* product (X = Me) as the preponderant isomer (88:12 *anti*:*syn*). More recently, this work was extended by Ohno and co-workers (8) to the corresponding ethyl (55%) and 2-propyl (15%) products, with high selectivity. Such 2-alkyl butyrolactones were subsequently transformed into monocyclic β-lactams (9).

We first addressed the problem of electrophilic bromination of the dianion **3** generated in the presence of LiHMDS. Using *N*-bromosuccinimide and bromine as the brominating reagents produced a single crystalline product **4**, in yields of 45% and 51%, respectively, with recovery of starting material. The stereochemical outcome of the reaction was proved by detailed NMR studies. Changing the base to LDA or KHMDS, among others, did not affect the reaction or the stereochemistry. Surprisingly, when bromodimethylsulfonium bromide (10) was used as the brominating reagent, a crystalline 2,2-dibromo lactone **5** was formed in 55% yield. Once again, starting material could be recovered from the reaction mixture.

Attempts to displace the bromine atom in **4** with azide ion, under different conditions (solvent, temperature), led to decomposition, presumably due to participation of the *N*-benzyloxycarbonyl group followed by subsequent reactions of the resulting 2-benzyloxy-1,3-oxazolinium ion.

We next investigated electrophilic amination of the dianion of **1**, as well as of the corresponding *N*-*tert*-butoxycarbonyl analog **2**. Since we sought to have two functional groups that could be chemically manipulated independently of one another, we looked into the prospects of electrophilic azidation reactions. Enolate anions of simple 2-azetidinones have been transformed into the 3-azido derivatives by treatment with arylsulfonyl azides in 30–76% yield (11). Evans and Britton (12) showed that treatment of the potassium enolate of anions bearing a chiral oxazolidone auxiliary with triisopropylbenzenesulfonyl azide produces the corresponding 2-azido derivatives in good yields and high selectivity. While our work was in progress, Nitta et al. (9) reported the azidation of the dianion **3** (R = *t*-Bu) with tosyl azide in the presence of trimethylsilyl chloride, to give the corresponding azido derivative **7** in 58% yield (Scheme 2).

Treatment of the dilithium dianion of **1** with tosyl azide produced a single crystalline azido derivative **6** in 55% yield with recovery of starting material. The same reaction with the *N*-Boc derivative also produced the expected 2-azido derivative **7** in agreement with the published results (9). Several attempts to improve the yield, including changes in the nature of the base (e.g., KHMDS) and the use of tripsyl azide, were not successful. The lower reactivity of such dianions toward weak electrophiles is not uncommon (9, 11).

The lactones **6** and **7** offer the flexibility of differentiating the two vicinal amino groups with different protective groups. Thus, the azido group can be transformed to *N*-Cbz or *N*-Boc groups simply by reduction in the presence of the appropriate carbamoylating agent, as shown in Scheme 2.

With the availability of the 2-bromo derivative **4**, we became interested in their utilization in a free-radical *C*-allylation reaction (ref. 13, and, for a recent application to carbohydrate lactones, ref. 14), with a particular emphasis on the stereochemical outcome as compared to the analogous anionic reaction (6, 7). As a parallel study, we also

[1]Author to whom correspondence may be addressed.

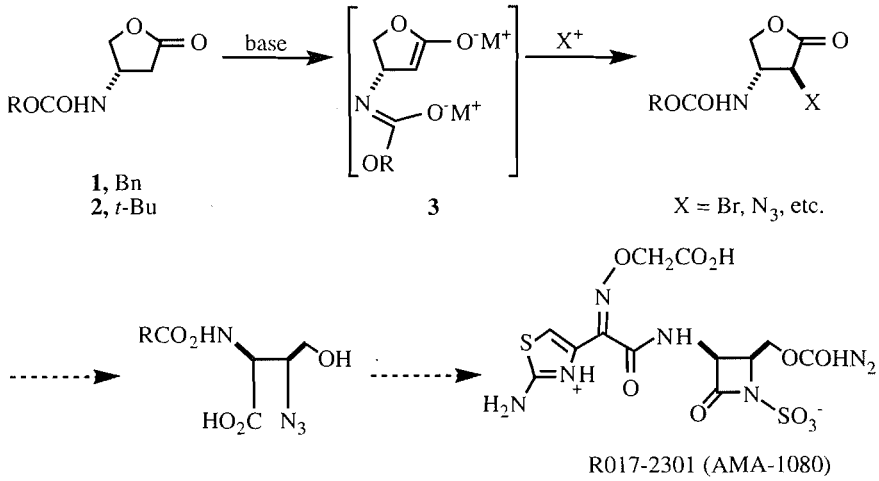

SCHEME 1

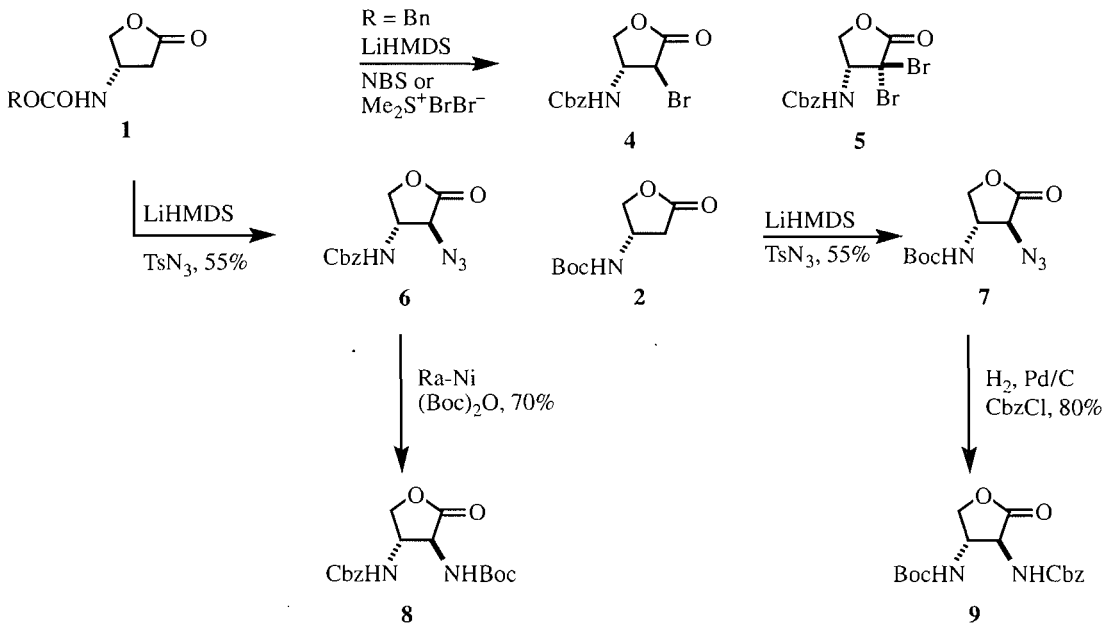

SCHEME 2

prepared the 2-phenylseleno lactone **10** for a series of reactions shown in Scheme 3.

Thus, treatment of either the 2-bromo or the 2-phenylseleno lactones **4** or **10** with allyltributylstannane, in refluxing benzene and in the presence of a radical initiator, led to the formation of the *C*-allyl derivative **11** in yields of 82% and 55%, respectively. It is of interest that the allylation of the dianion of **1** gave an 88:12 (*anti*:*syn*) mixture of *C*-allyl derivatives (6, 8). In spite of the more modest yield obtained with the phenylseleno derivative, the method is more practical since the bromination is sometimes accompanied by the dibromo compound **5**. When subjected to the same radical-induced *C*-allylation, **5** afforded the *gem* di-*C*-allyl product **13** accompanied by the monoallyl derivative. The two-step sequence proceeding through the phenylseleno derivative **12** gave an excellent and reproducible yield of **13**. Thus the lactone motifs **1** and **2** can be readily functionalized with a high degree of stereocontrol to provide chirons useful in a number of synthetic endeavors related to natural and unatural products.

Experimental

General data

Tetrahydrofuran was distilled over benzophenone and sodium prior to use. Analytical thin-layer chromatography (TLC) was carried out on Merck Kieselgel silica gel 60 F_{254} glass plates. Flash chromatography was performed according to the procedure of Still et al. (15) with Merck silica gel, 230–400 mesh. Infrared (IR) spectra were recorded in chloroform on a Perkin–Elmer 781 spectrometer. The wavenumbers reported are referenced to the polystyrene 1601 cm^{-1} absorption. Nuclear magnetic resonance spectra were obtained on a Bruker WH-400 (^1H 400 MHz) spectrometer with chloroform-*d* as solvent and tetramethylsilane as an internal standard, unless otherwise indicated. ^1H NMR multiplicities are recorded by use of the following abbreviations: s, singlet; d, doublet; dd, doublet doublet; t, triplet; q, quartet; m, multiplet; b, broad; *J*, coupling constant (hertz). High-resolution FAB mass spectra were

Can. J. Chem. Downloaded from www.nrcresearchpress.com by 213.200.69.106 on 09/08/12
For personal use only.

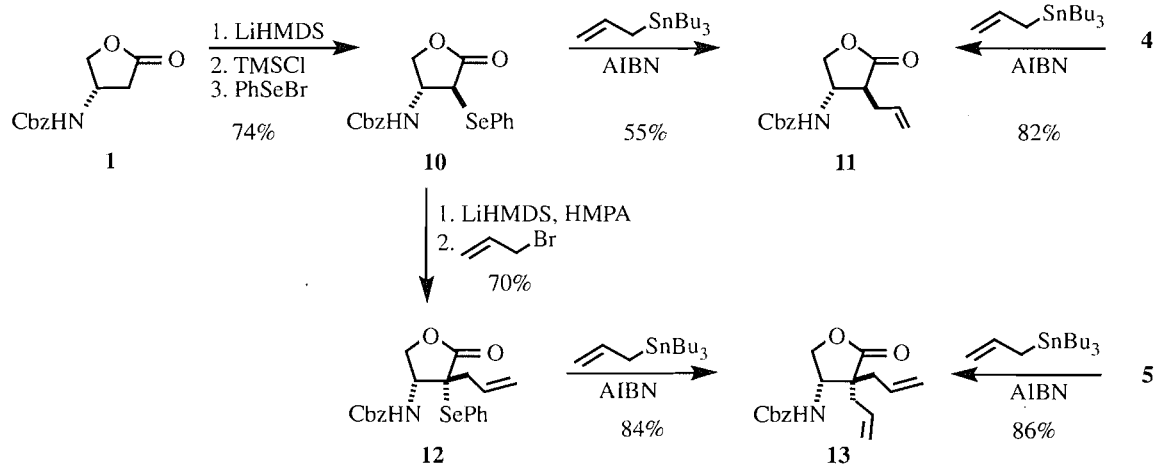

SCHEME 3

obtained by means of Kratos MS5OTCTA and AEI-MS 902 spectrometers at the Université de Montréal. Melting points were measured on a Büchi apparatus and are uncorrected. Optical rotations were measured on a Perkin–Elmer 241 polarimeter at 25°C.

(2S,3S)-3-Benzyloxycarbonylamino-2-bromo-1,4-butyrolactone (4)

Method A

A solution of butyllithium in hexanes (1.52 M, 1.3 mL, 2 mmol) was added dropwise to a solution of hexamethyldisilazane (0.422 mL, 2 mmol) in THF (4 mL) at 0°C. After 15 min, the solution was cooled down to −78°C, a solution of the lactone **1** (235 mg, 1 mmol) in THF (5 mL) was added, and the mixture was stirred at that temperature for 30 min. The reaction flask was covered with aluminum foil and a solution of *N*-bromosuccinimide (267 mg, 1.5 mmol), in THF (3 mL) was then added to the resulting dianion mixture at −78°C. After 3 min, trimethylsilyl chloride (0.33 mL, 2.6 mmol) was added to quench the reaction. The mixture was diluted with ether and washed successively with 10% aqueous HCl, 5% aqueous $NaHCO_3$, and brine and dried over $MgSO_4$. Concentration and flash column chromatography (EtOAc–hexanes 3:7) furnished the title compound **4** (160 mg, 51%) as a white solid, and the starting material (35 mg, 15%). Recrystallization from a mixture of ethyl acetate and hexanes gave colorless crystals, mp 97–99°C; $[\alpha]_D$ −32 (*c* 1, THF); IR ν_{max} (film): 3400 (NHCbz), 1800 (γ-lactone), 1740 (carbamate) cm^{-1}; ^1H NMR (400 MHz) δ: 4.28–4.31 (1H, d, $J_{2,3}$ = 9 Hz, H-2), 4.42–4.48 (2H, m, H-3 and H-4a), 4.70–4.74 (1H, m, H-4b), 5.13 (2H, CH_2Ph), 5.28 (1H, NH), 7.3–7.45 (5H, Ph); MS, *m/z*: 315 (MH^+). Anal. calcd. for $C_{12}H_{12}NO_4Br$: C 45.87, H 3.82, N 4.46; found: C 45,81, H 3.79, N 4.42.

Method B

The dianion was generated as described in Method A. Then a solution of bromine (0.077 mL, 1.5 mmol) in THF (3 mL) was added dropwise, in the dark at −78°C. After 3 min, the reaction was quenched with trimethylsilyl chloride (0.33 mL, 2.6 mmol) and worked up as described above to afford the title compound **4** (141 mg, 45%), as a white solid, and the starting material (35 mg, 15%).

(3S)-3-Benzyloxycarbonylamino-2,2-dibromo-1,4-butyrolactone (5)

A solution of the lactone **1** (235 mg, 1 mmol) in THF (5 mL) was added dropwise to a solution of lithium hexamethyldisilazide (2 mmol) in THF (4 mL) at −78°C. The mixture was stirred at −78°C for 30 min, then the flask was covered with aluminum foil, and a solution of bromodimethylsulfonium bromide (333 mg, 1.5 mmol) in THF (3 mL) was added dropwise. After stirring for 15 min at −78°C, the reaction was quenched with trimethylsilyl chloride (0.33 mL, 2.6 mmol). After allowing to warm up to room temperature, the resulting mixture was diluted with ether and washed successively with 10% aqueous HCl, 5% aqueous $NaHCO_3$, and brine and dried over $MgSO_4$. Evaporation of the solvent and flash column chromatography (ethyl acetate – hexanes 3:7) yielded starting material (35 mg, 15%), and the title compound **5** (200 mg, 51%) as a white solid. Recrystallization from a mixture of ethyl acetate and hexanes gave colorless crystals, mp 87–88°C; $[\alpha]_D$ +18.0° (*c* 1, THF); IR ν_{max} (film): 3400–3100 (NHCbz), 1800 (γ-lactone), 1740 (carbamate) cm^{-1}; ^1H NMR (400 MHz) δ: 4.42–4.48 (2H, m, H-3 and H-4a), 4.70–4.74 (1H, m, H-4b), 5.13 (2H, s, CH_2Ph), 5.28 (2H, NH), 7.3–7.45 (5H, Ph); MS, *m/z*: 394 (MH^+). Anal. calcd. for $C_{12}H_{11}NO_4Br_2$: C 36.66, H 2.80, N 3.56; found: C 36.34, H 2.76, N 3.49.

(2S,3S)-2-Azido-3-benzyloxycarbonylamino-1,4-butyrolactone (6)

A solution of the lactone **1** (1.0 g, 4.25 mmol) in THF (20 mL) was added dropwise to a solution of lithium hexamethyldisilazide (9.5 mmol) in THF (20 mL) at −78°C. The mixture was stirred at −78°C for 30 min, and a solution of *p*-toluenesulfonyl azide (1.0 g, 5.08 mmol) in THF (10 mL) was added rapidly, at −78°C. After stirring for 5 min, the reaction was quenched with trimethylsilyl chloride (1.6 mL, 12.75 mmol). The resulting mixture was diluted with ether and washed successively with 10% aqueous HCl, 5% aqueous $NaHCO_3$, and brine and dried over $MgSO_4$. Concentration and flash column chromatography (ethyl acetate – hexanes 3:7) gave the title compound **6** (0.65 g, 55%) as an oil that solidified upon standing. A small quantity of starting material (0.1 g, 10%) was also isolated. The product was recrystallized from a solvent mixture of ethyl acetate – hexanes, mp 86–87°C; $[\alpha]_D$ −99 (*c* 1, THF); IR ν_{max} (film): 2130 (azide), 1785 (γ-lactone), 1700 (carbamate) cm^{-1}; ^1H NMR (400 MHz) δ: 4.1–4.2 (1H, d, $J_{2,3}$ = 8 Hz), 4.42–4.48 (2H, m, H-3 and H-4a), 4.70–4.74 (1H, m, H-4b), 5.13 (2H, s, CH_2Ph), 5.28 (1H, NH), 7.3–7.45 (5H, Ph); MS, *m/z*: 277 (MH^+), 91 (100%, C_7H_7). Anal. calcd. for $C_{12}H_{12}N_4O_4$: C 52.17, H 4.35, N 20.29; found: C 51.92, H 4.31, N 20.04.

*(2S,3S)-3-Benzyloxycarbonylamino-2-*tert*-butoxycarbonylamino-1,4-butyrolactone (8)*

Raney nickel (0.5 g) and di-*tert*-butyl dicarbonate (1.09 g, 5.0 mmol) were added successively to a solution of the lactone **6** (1.03 g, 3.73 mmol) in THF (20 mL). Filtration of the suspension through Celite and concentration of the filtrate furnished a crude sample, which was purified through flash column chromatography (ethyl acetate – hexanes 45%) to give the title compound **8** (0.887 g, 70%) as a white solid, mp 150–152°C; $[\alpha]_D$ +25.3

Can. J. Chem. Downloaded from www.nrcresearchpress.com by 213.200.69.106 on 09/08/12
For personal use only.

Can. J. Chem. Downloaded from www.nrcresearchpress.com by 213.200.69.106 on 09/08/12
For personal use only.

(*c* 1, $CHCl_3$); IR ν_{max} (film): 3300 (NHBoc, NHCbz), 1780 (γ-lactone), 1720 (carbamate) cm^{-1}; ^1H NMR (60 MHz) δ: 1.47 (9H, s, *tert*-butoxy), 3.8–4.35 (3H, m, H-2, H-3, and H-4a), 4.70–4.74 (1H, m, 4-Hb), 5.03 (2H, s, CH_2Ph), 5.28 (1H, m, NH), 6.3 (1H, m, NH), 7.3–7.45 (5H, Ph); MS, *m/z*: 351 (80%, MH^+).

*(3S)-3-*tert*-Butoxycarbonylamino-1,4-butyrolactone (2)*

10% Palladium-on-charcoal (0.4 g) and di-*tert*-butyl dicarbonate (4.09 g, 18.7 mmol) were added successively to a solution of the lactone **1** (4.0 g, 17.0 mmol) in THF (10 mL). The resulting mixture was vigorously stirred overnight under an atmosphere of hydrogen. Filtration of the suspension through Celite and concentration of the filtrate yielded a crude sample, which was purified through flash column chromatography (ether) to give the title compound **2** (3.2 g, 85%) as a white solid, mp 113–114°C; $[\alpha]_D$ −54.3 (*c* 1.15, $CHCl_3$) (lit. (8) mp 106–108°C; $[\alpha]_D^{25}$ −61 (*c* 1.0, EtOH); IR ν_{max} (film): 1780 (γ-lactone), 1700 (carbamate) cm^{-1}; ^1H NMR (400 MHz) δ: 1.45 (9H, s, *tert*-butyl), 2.45 (1H, dd, $J_{2,3}$ = 3.9 Hz and J_{gem} = 17.9 Hz, H-2a), 2.85 (1H, dd, $J_{2,3}$ = 7.7 Hz and J_{gem} = 17.9 Hz, H-2b), 4.2 (1H, m, H-4b), 4.5–4.8 (2H, m, H-3 and H-4a), 5.09 (2H, s, CH_2Ph), 5.5 (1H, NH), 7.3–7.40 (5H, Ph); MS, *m/z*: 202 (MH^+), 146 (*tert*-butyl).

*(2S,3S)-2-Azido-3-*tert*-butoxycarbonylamino-1,4-butyrolactone (7)*

A solution of the lactone **2** (0.854 g, 4.25 mmol) in THF (20 mL) was added dropwise to a solution of lithium hexamethyldisilazide (9.5 mmol) in THF (20 mL) at −78°C. The mixture was stirred at −78°C for 30 min. A solution of *p*-toluenesulfonyl azide (1.0 g, 5.08 mmol) in THF (10 mL) was then added rapidly to the resulting dianion suspension at −78°C. After stirring for 5 min, the reaction was quenched with trimethylsilyl chloride (1.6 mL, 12.75 mmol). After warming up to room temperature, the resulting mixture was diluted with ether and washed successively with 10% aqueous HCl, 5% aqueous $NaHCO_3$, and brine and dried over $MgSO_4$. Concentration and flash column chromatography (ethyl acetate – hexanes 3:7) furnished the title compound **7** (0.57 g, 55%) as an oil that solidified upon standing. Starting material (0.1 g, 11.7%) was also recovered. Compound **7** was recrystallized from a mixture of ethyl acetate and hexanes, mp 107–109°C; $[\alpha]_D$ −70 (*c* 1.0, EtOH) (lit. (9) mp 110–111°C; $[\alpha]_D$ −69 (*c* 1.0, EtOH)); IR ν_{max} (film): 2130 (azido), 1800 (γ-lactone), 1735 (carbamate) cm^{-1}; ^1H NMR (400 MHz) δ: 1.45 (9H, s, *tert*-butyl), 4.1–4.2 (1H, d, $J_{2,3}$ = 8 Hz, H-2), 4.42–4.48 (2H, m, H-3 and H-4a), 4.70–4.74 (1H, m, H-4b), 5.28 (1H, m, NH). Anal. calcd. for $C_9H_{14}N_4O_4$: C 44.63, H 5.79, N 23.14; found: C 44.59, H 5.71, N 23.11.

*(2S,3S)-2-Benzyloxycarbonylamino-3-*tert*-butoxycarbonylamino-1,4-butyrolactone (9)*

10% Palladium-on-charcoal (50 mg) was added to a solution of the lactone **7** (0.25 g, 1.03 mmol) in THF (5 mL). The resulting mixture was stirred under an atmosphere of hydrogen for 40 min, and the suspension was filtrated through Celite. Triethylamine (0.153 mL, 1.1 mmol) and benzyl chloroformate (0.142 mL, 1 mmol) were then added successively to the filtrate, which was precooled down to 0°C. After allowing the mixture to stir overnight, water was added, and the solution extracted several times with ether. The combined organic phases were dried ($MgSO_4$) and concentrated to give a crude sample as an oil, which was purified through flash column chromatography (ethyl acetate – hexanes, 1:1) to give the title compound **9** (0.28 g, 80%) as a white crystalline solid, mp 118–120°C; $[\alpha]_D$ −33.2 (*c* 1, $CHCl_3$); IR ν_{max} (film): 3300 (NHBoc + NHCbz), 1780 (γ-lactone), 1720 (carbamate) cm^{-1}; ^1H NMR (60 MHz); δ: 1.47 (9H, s, *tert*-butoxy), 3.8–4.35 (3H, m, H-2, H-3 and H-4a), 4.70–4.74 (1H, m, H-4b), 5.03 (2H, s, CH_2Ph), 5.28 (1H, m, NH), 6.3 (1H, m, NH), 7.3–7.45 (5H, Ph); MS, *m/z*: 351 (10%, MH^+).

(2S,3S)-3-Benzyloxycarbonylamino-2-phenylselenyl-1,4-butyrolactone (10)

A solution of the lactone **1** (1.0 g, 4.25 mmol) in 10 mL THF was added dropwise to a solution of LiHMDS (9.00 mmol) in 25 mL THF at −78°C under an argon atmosphere with stirring. After 1 h at that temperature, trimethylsilyl chloride (1.8 mL, 14.18 mmol) was added, and the resulting mixture was stirred at 0°C for 2 h. It was then recooled down to −78°C, followed by addition of *N*-(phenylseleno)phthalimide (1.28 g, 4.24 mmol) in THF (15 mL) at −78°C through a canal. After 30 min stirring at −78°C, the mixture was poured into a mixed solution of 200 mL 5% aqueous HCl, 100 mL ether, and 100 mL pentane. The organic phase was separated and washed successively with water, 10% aqueous $NaHCO_3$, and brine and dried over sodium sulfate. Concentration and flash column chromatography (ethyl acetate – hexanes 3:7) afforded the title compound as an off-white solid (1.22 g, 74%). IR ν_{max} (film): 1780 (lactone), 1710 (carbamate) cm^{-1}; ^1H NMR (300 MHz, $CDCl_3$) δ: 3.83 (1H, d, *J* = 4 Hz, H-2), 4.10 (1H, dd, J_{gem} = 10 Hz and $J_{4,3}$ = 3 Hz, H-4), 4.25 (1H, dd, J_{gem} = 10 Hz and $J_{4,3}$ = 4 Hz, H-4), 4.35 (1H, m, H-3), 5.10 (2H, s, CH_2Ph), 5.60 (1H, bd, NH), 7.50–7.25 (8H, m, Ph and SePh), 7.70 (2H, m, SePh); MS (EI), *m/z*: 391 (M), 300 (M − Bn), 284 (M − BnO); HRMS calcd. for $C_{18}H_{17}NO_4Se$: 391.0322; found: 391.0348.

(2S,3S)-2-C-Allyl-3-benzyloxycarbonylamino-1,4-butyrolactone (11)

A solution of **10** (320 mg, 0.82 mmol), allyl tributyltin (0.31 mL, 0.99 mmol), and AIBN (15 mg, 0.0914 mmol) in benzene (3.7 mL) was degassed and brought to reflux under an argon atmosphere for 16 h. The volume of the mixture was reduced and the residue was purified through flash column chromatography (ethyl acetate – hexanes 0:1–3:7) to yield the title compound as a colorless thick oil (125 mg, 55%); $[\alpha]_D$ −34 (*c* 1.0, $CHCl_3$); IR ν_{max} (film): 1780 (lactone), 1720 (carbamate) cm^{-1}; ^1H NMR (300 MHz, $CDCl_3$) δ: 2.70–2.35 (3H, m, H-2, CH_2 CH=CH_2), 4.01 (1H, dd, J_{gem} = 8 Hz and $J_{4,3}$ = 7 Hz, H-4), 4.28 (1H, m, H-3), 4.52 (1 H, dd, J_{gem} = 8 Hz and $J_{4,3}$ = 7 Hz, H-4), 4.98 (1H, bs, NH), 5.11 (2H, s, CH_2Ph), 5.15 (1H, bd, *J* = 11.5 Hz, CH=CH_2-*cis*), 5.20 (1H, bd, *J* = 18 Hz, CH=CH_2-*anti*), 5.90–5.70 (1H, m, *CH*=CH_2), 7.43–7.31 (5H, m, Ph); MS (EI), *m/z*: 275 (M), 184 (M − Bn), 167 (M − HOBn), 140 (M − O=C − OBn); HRMS calcd. for $C_{15}H_{17}NO_4$: 275.1157; found: 275.1174.

(3S)-2-C-Allyl-3-benzyloxycarbonylamino-2-phenylselenyl-1,4-butyrolactone (12)

A solution of compound **10** (208 mg, 0.53 mmol) in 3 mL THF was added dropwise to a solution of LiHMDS (1.20 mmol) in 3 mL THF at −78°C under an argon atmosphere. After being stirred at −78°C for 30 min, HMPA (2 mL) was then added, followed by addition of allyl bromide (0.23 mL, 2.66 mmol). The resulting mixture was allowed to stir at −78°C for 2 h, and then treated with 10% aqueous HCl. The mixture was extracted with ether several times and the combined organic phases were washed successively with water, $NaHCO_3$, and brine and dried over $MgSO_4$. The solvent was removed to give a crude sample, which was purified by flash column chromatography (ethyl acetate – hexanes 3:7) to furnish the title compound as a colorless viscous oil (160 mg, 70%). IR ν_{max} (film): 1770 (lactone), 1725 (carbamate) cm^{-1}; ^1H NMR (300 MHz, $CDCl_3$) δ: 2.70–2.50 (2H, m, CH_2CH=CH_2), 4.15–4.05 (1H, m, H-4), 4.70–4.50 (2H, m, H-3, H-4), 5.11 (2H, s, CH_2Ph), 5.23–5.15 (2H, m, CH=CH_2), 5.28 (1H, b, NH), 6.00–5.85 (1H, m, *CH*=CH_2), 7.50–7.30 (8H, m, Ph and SePh), 7.65 (2H, m, SePh); MS, *m/z*: 431 (M); HRMS, calcd. for $C_{21}H_{21}NO_4Se$: 431.0635; found: 431.0700.

(3S)-2,2-Di-C-Allyl-3-benzyloxycarbonylamino-1,4-butyrolactone (13)

A solution of **12** (0.35) g, 0.814 mmol), allyl tributyltin (0.38 mL, 1.226 mmol), and a catalytic amount of AIBN in 3 mL benzene was degassed and brought to reflux under an atmosphere of argon for 1.45 h. The solvent was removed and the residue was subjected to flash column chromatography (ethyl acetate – hexanes 0:1–3:7) to give the title compound as a colorless thick oil (0.217 g, 84%); $[\alpha]_D$ +23 (*c* 2.1, $CHCl_3$). IR ν_{max} (film): 1770 (lactone), 1720 (carbamate) cm^{-1}; ^1H NMR (300 MHz, $CDCl_3$) δ:

2.55–2.27 (4H, m, $CH_2CH{=}CH_2$), 3.80 (1H, t, J = 9 Hz, H-4), 4.47 (1H, t, J = 9 Hz, H-4), 4.71 (1H, q, J = 9 Hz, H-3), 5.03 (1H, bd, J = 9 Hz, NH), 5.11 (1H, d, J_{gem} = 12 Hz, *CH*Ph), 5.17 (1H, d, J_{gem} = 12 Hz, *CH*Ph), 5.35–5.18 (4H, m, $CH{=}CH_2$), 5.90–5.70 (2H, m, $CH{=}CH_2$), 7.38 (5H, m, Ph); MS (EI), m/z: 315 (M), 224 (M − Bn); HRMS, calcd. for $C_{18}H_{21}NO_4$: 315.1471; found: 315.1475.

Acknowledgments

We thank the Natural Sciences and Engineering Research Council of Canada (NSERCC) and the Fonds pour la formation de chercheurs et l'aide à la recherche (Québec) (FCAR) for financial assistance. We thank the Mass Spectrometry Laboratory, Université de Montréal, for services.

1. J.D. Morrison (*Editor*). Asymmetric synthesis. Vols. 1–5. Academic Press, Orlando, Fla. 1983–1986; S. Hanessian. Total synthesis of natural products: the chiron approach. *Edited by* J. Baldwin. Pergamon Press, New York. 1983.
2. (*a*) R.M. Williams. Synthesis of optically active α-amino acids. Pergamon Press, Oxford, U.K. 1989; (*b*) G.M. Coppola and H.F. Schuster. Asymmetric synthesis: construction of chiral molecules using amino acids. John Wiley & Sons, New York. 1987, and references cited therein.
3. E.J. Corey and G.A. Reichard. J. Am. Chem. Soc. **114**, 106 (1992); R.M. Williamson, T. Glinka, E. Kwast, H. Coffman, and J.K. Stille. J. Am. Chem. Soc. **112**, 808 (1990); J.D. White and M. Kawasaki. J. Am. Chem. Soc. **112**, 4991 (1990); A.B. Smith III, T.A. Rano, N. Chida and G.A. Sulikowski. J. Org. Chem. **55**, 1136 (1990).
4. R. Hirschmann. Angew. Chem. Int. Ed. Engl. **30**, 1278 (1991); W. Bauer. Trends Drug Res. **13**, 85 (1990); B.A. Morgan and J.A. Gainor. Annu. Rep. Med. Chem. **24**, 243 (1989); J.-L. Faucher. Adv. Drug. Res. **15**, 29 (1986).
5. S. Hanessian and B. Vanasse. Can. J. Chem. **71**, 1401 (1993).
6. G.J. McGarvey R.N. Hiner, Y. Matsubara, and T. Oh. Tetrahedron Lett. **24**, 2733 (1983); G.J.M. McGarvey, J.M. Williams, R.N. Hiner, Y. Matsubara, and T. Oh. J. Am. Chem. Soc. **108**, 4943 (1986).
7. C.C. Wei, J. De Bernado, J.-P Tengi, J. Borgese, and M. Weigele. J. Org. Chem. **50**, 3462 (1985); M. Kondo, S. Kishimoto, M. Ochiai, K. Okonagi, and A. Imada. Proc. Int. Congr. Chemother. 13th, Vienna, Austria. August 28 – September 2, 1983; Abstract SE 4.2/15-1.
8. Y. Takahashi, H. Yamashita, S. Kobayashi, and M. Ohno. Chem. Pharm. Bull. **34**, 2732 (1986).
9. H. Nitta, M. Hatanaka, and T. Ishimaru. J. Chem. Soc. Chem. Commun. 51 (1987).
10. G.A. Olah, Y.D. Vankar, M. Arranaghi, and G.K.S. Prakash. Synthesis, 720 (1979).
11. (*a*) K. Kuhlein and H. Jensen. Ann. Chem. 369 (1974); (*b*) H.H. Wasserman, D.J. Hlasta, A.W. Tremper, and J.S. Wu. J. Org. Chem. **46**, 2999 (1981); (*c*) P.F. Belivacqua, D.D. Keith, and J.L. Roberts. J. Org. Chem. **49**, 1430 (1984); A. Nishida, M. Shibasaki, and S. Ikegami, Tetrahedron Lett. **25**, 765 (1984); M. Shibuya, Y. Jonbo, and S. Kubota. Chem. Pharm. Bull. **32**, 1303 (1984).
12. D.A. Evans and T.C. Britton. J. Am. Chem. Soc. **109**, 6881 (1987).
13. G.E. Keck and J.B. Yates. J. Am. Chem. Soc. **104**, 5829 (1982).
14. S. Hanessian, R. Léger, and M. Alpegiani. Carbohydr. Res. **228**, 145 (1992).
15. W.C. Still, M. Kahn, and A. Mitra. J. Org. Chem. **43**, 2923 (1978).

Can. J. Chem. Downloaded from www.nrcresearchpress.com by 213.200.69.106 on 09/08/12
For personal use only.

Metal pyrazolate polymers. Part 4. Synthesis, characterization, and magnetic properties of $[Co(pz^*)_2]_x$ complexes (where pz* = pyrazolate, 3-methylpyrazolate, and 4-substituted 3,5-dimethylpyrazolate)

MARTIN K. EHLERT, ALAN STORR,[1] AND ROBERT C. THOMPSON[1]

Department of Chemistry, University of British Columbia, 2036 Main Mall, Vancouver, BC V6T 1Z1, Canada

Received February 8, 1993

MARTIN K. EHLERT, ALAN STORR, and ROBERT C. THOMPSON. Can. J. Chem. **71**, 1412 (1993).

The title compounds were prepared and characterized by X-ray powder diffraction, scanning electron microscopy, vibrational and electronic spectroscopy, and magnetic susceptibility measurements. Indirect evidence supports polymeric one-dimensional chain structures involving double pyrazolate bridges linking pseudo-tetrahedrally coordinated metal centres in all six compounds. The spectroscopic studies indicate a greater degree of distortion of the CoN_4 chromophore from regular stereochemistry in the 4-substituted 3,5-dimethylpyrazolate complexes. The magnetic studies reveal anisotropy in the susceptibilities and the presence of significant antiferromagnetic exchange. Magnetic modelling employing both Ising and Heisenberg models suggests the exchange behaviour is probably of the Heisenberg type with zero-field splitting effects producing Ising-like exchange at low temperatures. The derived J values (~ -2 to -6 cm^{-1}) have been used to qualitatively rank the magnitude of exchange as follows: 4-Hpz ≈ 3-Mepz ≫ 4-Medmpz ≈ 4-Cldmpz ≈ 4-Brdmpz ≈ 4-Hdmpz.

MARTIN K. EHLERT, ALAN STORR et ROBERT C. THOMPSON. Can. J. Chem. **71**, 1412 (1993).

On a préparé les composés mentionnés dans le titre et on les a caractérisé par diffraction des rayons X par des poudres, microscopie électronique à balayage, spectroscopies vibrationnelle et électronique et par mesures de susceptibilité magnétique. Des données indirectes sont en accord avec des structures de chaines polymériques unidimensionnelles impliquant dans les six composés des ponts pyrazolates doubles reliant des centres métalliques à coordination pseudo-tétraédrique. Les études spectroscopiques indiquent que, par rapport à sa stéréochimie habituelle dans les complexes de 3,5-diméthylpyrazolates substitués, le chromophore CoN_4 est plus déformé. Les études magnétiques révèlent l'existence d'une anisotropie dans les susceptibilités et la présence d'échanges antiferromagnétiques importants. Le modelage magnétique réalisé à l'aide de modèles de Ising et de Heisenberg suggère que le comportement d'échange est probablement du type Heisenberg avec des effets de couplage de champ zéro produisant un échange de type Ising à basses températures. On a utilisé les valeurs de J (de ~ -2 à -6 cm^{-1}) qui en découlent pour établir que l'amplitude de l'échange diminue dans l'ordre suivant : 4-Hpz ≈ 3Mepz ≫ 4-Medmpz ≈ 4-Cldmpz ≈ 4-Brdmpz ≈ 4-Hdmpz.

[Traduit par la rédaction]

Introduction

Previous papers in this series described the results of investigations of copper(II)-based pyrazolate polymers, compounds in which the metal ions are linked by double pyrazolate bridges to form extended chain structures (1–3). These materials exhibit intrachain antiferromagnetic coupling between the d^9 metal centres, the magnitude of which has been discussed in terms of differences in structural detail between different compounds. Further information about the structures adopted by binary metal pyrazolates and, in particular, about the nature of pyrazolate ligand-mediated magnetic exchange requires the study of systems with other d-electron configurations. In this paper we report on the synthesis, characterization, and magnetic properties of a series of Co(II) complexes incorporating the pyrazolate anion and several of its C-substituted derivatives. These compounds possess the general formula $[Co(pz^*)_2]_x$ (where pz* = pyrazolate (4-Hpz), 3-methylpyrazolate (3-Mepz), 3,5-dimethylpyrazolate (4-Hdmpz), 3,4,5-trimethylpyrazolate (4-Medmpz), 4-chloro-3,5-dimethylpyrazolate (4-Cldmpz), and 4-bromo-3,5-dimethylpyrazolate (4-Brdmpz)).

Cobalt pyrazolates have formed the basis of a few studies in the past. In the early part of this century, Fischer (4) and Heim (5) noted that insoluble solids could be precipitated from cobalt-containing aqueous solutions of pyrazole in the presence of base. Interest in 3,5-dimethylpyrazole as a reagent for the gravimetric determination of cobalt was more thoroughly pursued in the late 1950's by Pflaum and Dieter (6) who determined that the blue-violet precipitate formed from Co(II) salts and 3,5-dimethylpyrazole in basic aqueous solution had the formulation $[Co(4\text{-}Hdmpz)_2]_x$. In 1970, Bagley, Nicholls, and Warburton published a study of pyrazole, and of pyrazolate complexes of Co(II) (7). Pyrazole, 3-methylpyrazole, and 3,5-dimethylpyrazole were employed in the preparation of compounds. Infrared and electronic spectroscopic studies were conducted on the compounds and room temperature magnetic moments were measured from which the authors suggested that the compounds possess polymeric structures in which the (substituted)pyrazolate ions act as bridging ligands and the Co(II) ions are tetrahedrally coordinated. In 1973, Singh, Satpathy, and Sahoo reported the synthesis of $[Co(4\text{-}Hdmpz)_2]_x$ by condensation of $[Co(acac)_2]_4$ with hydrazine (8). Their characterization of the compound included the only variable temperature magnetic susceptibility measurements (90–300 K) of a cobalt pyrazolate system prior to the present study. In the late 1970's, Vos and Groeneveld prepared a number of 4-substituted pyrazolates of cobalt (9–11); however, it is not clear whether pure samples of these compounds were actually obtained in the work because analytical results deviated significantly from the expected values.

In spite of numerous attempts in the course of the present work, none of the binary cobalt(II) pyrazolates could be isolated in crystalline form suitable for single crystal X-ray diffraction studies. Hence it was necessary to employ a va-

[1]Authors to whom correspondence may be addressed.

Can. J. Chem. Downloaded from www.nrcresearchpress.com by 213.200.69.106 on 09/08/12
For personal use only.

TABLE 1. Preparation conditions and analytical results

$[Co(3\text{-}Mepz)_2]_x$:

Co powder (0.8 g, 14 mmol), 3-MepzH (6 g, 75 mmol)
100°C, 18 h
CH_2Cl_2 extraction, product yield ~3 g
Anal. calcd. for $C_8H_{10}CoN_4$: C 43.5, H 4.6, N 25.3
found: C 44.1, H 4.7, N 25.3

$[Co(4\text{-}Hdmpz)_2]_x$:

Co powder (2.32 g, 39.4 mmol), 4-HdmpzH (6.00 g, 62.4 mmol)
115°C, 6 days
THF extraction, product yield 0.851 g
Anal. calcd. for $C_{10}H_{14}CoN_4$: C 48.2, H 5.7, N 22.5
found: C 48.0, H 5.6, N 22.3

$[Co(4\text{-}Medmpz)_2]_x$:

Co powder (2.00 g, 33.9 mmol), 4-MedmpzH (5.51 g, 50.0 mmol)
128°C, 24 h
THF extraction, product yield 4.00 g
Anal. calcd. for $C_{12}H_{18}CoN_4$: C 52.0, H 6.5, N 20.2
found: C 52.2, H 6.5, N 20.4

$[Co(4\text{-}Cldmpz)_2]_x$:

Co massive (4.623 g, 78.44 mmol), 4-CldmpzH (2.7 g, 21 mmol)
130°C, 48 h
THF extraction, product yield 0.180 g (57% yield)
Anal. calcd. for $C_{10}H_{12}Cl_2CoN_4$: C 37.8, H 3.8, N 17.6
found: C 37.5, H 3.8, N 17.4

$[Co(4\text{-}Brdmpz)_2]_x$:

Co massive (4.566 g, 77.48 mmol), 4-BrdmpzH (6.79 g, 38.8 mmol)
130°C, 40 h
THF extraction, product yield 0.312 g (81% yield)
Anal. calcd. for $C_{10}H_{12}Br_2CoN_4$: C 29.5, H 3.0, N 13.8
found: C 29.8, H 3.0, N 14.0

Can. J. Chem. Downloaded from www.nrcresearchpress.com by 213.200.69.106 on 09/08/12
For personal use only.

riety of indirect methods to obtain structural information on these materials.

Experimental

Syntheses

Pyrazole (4-HpzH), 3-methylpyrazole (3-MepzH), and 3,5-dimethylpyrazole (4-HdmpzH) were purchased from Aldrich and used without further purification. 4-Chloro-3,5-dimethylpyrazole (4-CldmpzH), 4-bromo-3,5-dimethylpyrazole (4-BrdmpzH), and 3,4,5-trimethylpyrazole (4-MedmpzH) were prepared as described previously (3).

$[Co(4\text{-}Hpz)_2]_x$

All solvents employed in this synthesis were degassed and all manipulations were performed under dinitrogen atmosphere. $CoCl_2 \cdot xH_2O$ (3.31 g, <14 mmol) and pyrazole (6.08 g, 89.3 mmol) were dissolved in 80 mL of water. NaOH (1.60 g, 40.0 mmol) was dissolved in 40 mL of water. The NaOH solution was added dropwise to the vigorously stirred $CoCl_2$–pyrazole solution at room temperature. The reaction mixture was suction filtered and the product was washed sequentially with water, ethanol, and, finally, petroleum ether. This afforded a purple filtercake, which was dried under vacuum for 1.5 h at room temperature. This yielded ~2 g of $[Co(4\text{-}Hpz)_2]_x$ as a fine purple powder. Anal. calcd. for $C_6H_6CoN_4$: C 37.3, H 3.1, N 29.0; found: C 37.5, H 3.2, N 29.3.

$[Co(3\text{-}Mepz)_2]_x$ and $[Co(4\text{-}Xdmpz)_2]_x$ (X = H, Me, Cl, and Br)

The remaining five binary Co(II) (substituted)pyrazolates were all synthesized in essentially the same manner. Cobalt metal (either powdered or massive) was combined with the appropriate molten substituted pyrazole and the mixture was heated with stirring in a dioxygen atmosphere. This resulted in formation of the product as a fine purple powder admixed with excess cobalt and substituted pyrazole. The pyrazole was removed by washing with polar solvent. If the excess cobalt metal was in powdered form it was removed by dredging a slurry of the reaction mixture in a solvent with a magnet until all of the cobalt metal was removed, and if the cobalt was present in massive form it was removed manually. In all cases the Co(II) pyrazolates were obtained as purple powders. Specific reaction conditions and analytical results are presented in Table 1.

Physical characterization

Infrared spectra (4000–250 cm^{-1}) were recorded using a Perkin–Elmer model 598 spectrometer and calibrated against polystyrene film. Samples were mulled in Nujol and sandwiched between KBr plates or KRS-5 plates (Harshaw Chemical Co.). Infrared frequencies have been deposited.[2] Electronic spectra (200–2500 nm) were recorded using a Cary 5 spectrometer. Samples were mulled in Nujol and sandwiched between quartz plates.

Powder X-ray diffractograms were recorded using either an automated Rigaku Rotaflex RU-200BH rotating anode powder X-ray diffractometer (Ni filtered or graphite monochromated, Cu $K\alpha$ radiation) or a Philips powder X-ray diffractometer equipped with a

[2]Supplementary material mentioned in the text may be purchased from: The Depository of Unpublished Data, Document Delivery, CISTI, National Research Council Canada, Ottawa, Canada K1A OS2.

Can. J. Chem. Downloaded from www.nrcresearchpress.com by 213.200.69.106 on 09/08/12
For personal use only.

Philips PW 1830 generator (Mn filtered, Fe $K\alpha$ radiation). Samples were prepared by applying a thin film of compound slurried in octane to a glass slide and allowing the slurry to dry. In such cases the sample packing force is perpendicular to the glass sample support (cf. Results and discussion). For a preferred orientation study conducted on $[Co(4\text{-}Medmpz)_2]_x$, a sample packed with the force directed parallel to the sample support was prepared using a glass slide with a U-shaped brass ridge glued to the surface. A second glass plate was held firmly on top of this ridge, creating a thin cavity running parallel to the glass support surface. This cavity was then filled with sample powder by packing from the open end. The top plate was then removed to reveal the suitably prepared sample.

Differential scanning calorimetry (DSC) measurements were obtained with a Mettler DSC 20 standard cell and TC10 TA processor.

Scanning electron micrographs (SEM) of samples were recorded with a Hitachi S-570 scanning electron microscope. Samples were prepared by applying a thin suspension of a given compound in petroleum ether to an aluminum stub, allowing the suspension to dry, and then sputter-coating the stub and sample with a thin layer of a gold–palladium alloy.

Magnetic measurements were performed using either a Princeton Applied Research vibrating sample magnetometer (VSM) described previously (12), or a Quantum Design MPMS SQUID magnetometer. Studies conducted with the SQUID magnetometer employed pressed pellet samples held inside a gelatin capsule suspended in a quartz tube. Variable temperature magnetic susceptibility data using this instrument were recorded in the temperature range 2–300 K in an applied field of 10 kOe. Magnetic data for the compounds were corrected for the diamagnetism of the sample and the sample holder. The following corrections were applied (all values $\times 10^{-6}$ cm^3 mol^{-1}): Co(II), −12; 4-Hpz, −38; 3-Mepz, −50; 4-Hdmpz, −62; 4-Medmpz, −74; 4-Cldmpz, −79; and 4-Brdmpz, −90. Corrections for the temperature-independent paramagnetism of the Co(II) ion were also applied using the formula, $\chi_{TIP} = 8N\mu_B{}^2/10Dq$, with the Dq (ligand field parameter) values (see below) estimated from the electronic spectra of the complexes. Field dependence studies were performed with the same instrument in the field range 0–55 kOe.

Elemental analyses were performed by Mr. P. Borda of this department.

Results and discussion

Synthesis and thermal properties

Reaction of cobalt metal with molten C-substituted pyrazoles in the presence of dioxygen has permitted the synthesis of five Co(II) substituted pyrazolates. Because $[Co(4\text{-}Hpz)_2]_x$ slowly oxidizes in air when exposed to moisture, the molten ligand precursor – metal reaction described above could not be used to synthesize this compound. Instead, a metathetical reaction employing $CoCl_2$, 4-HpzH, and NaOH under anaerobic conditions was used (9). The Co(II) (substituted)pyrazolates are insoluble, infusible, involatile solids; all six compounds considered here were obtained as fine purple powders and, with the exception of $[Co(4\text{-}Hpz)_2]_x$, they are air-stable. The Co(II) (substituted)pyrazolates are thermally robust. In the case of $[Co(3\text{-}Mepz)_2]_x$, DSC studies demonstrated that the complex undergoes an endothermic event at 405°C with concomitant decomposition. Qualitative observation of the other Co(II) compounds using a melting point apparatus revealed that the compounds can be heated to temperatures >360°C without decomposing.

Scanning electron microscopy and X-ray powder diffraction

The particle morphologies of these compounds were examined by SEM, and images of the $[Co(4\text{-}Hpz)_2]_x$, $[Co(3\text{-}Mepz)_2]_x$, $[Co(4\text{-}Hdmpz)_2]_x$, and $[Co(4\text{-}Medmpz)_2]_x$ complexes are presented in Figs. 1(*a*)–(*d*). The 4-Hpz, 4-Hdmpz, and 4-Medmpz derivatives possess elongated, crystallite morphologies, whereas the 3-Mepz derivative consists of particles that are quasi-spherical agglomerations of microcrystallites. In the case of $[Co(4\text{-}Hdmpz)_2]_x$ the particles are extremely small, with dimensions in the submicron regime. These morphologies become important in the discussion of the magnetic properties of these complexes.

Although attempts were made, no X-ray diffraction quality single crystals of the cobalt(II) pyrazolates were prepared; however, some powder diffraction studies were undertaken. Initial studies were made using a diffractometer equipped with a copper anode in the X-ray generator. The X-ray absorption edge of cobalt is coincident with the Cu $K\alpha$ X-radiation generated by the instrument and, because of this, the cobalt in these compounds undergoes X-ray fluorescence (13) and high-intensity, noisy backgrounds result in the recorded diffractograms. Because of the poor quality of the diffractograms and the possibility that the high background contribution might be masking an amorphous component of the materials, diffractograms were also recorded using an apparatus equipped with an iron anode X-ray generator. Diffractograms for the alkylated Co(II) pyrazolates were recorded using this instrument (there were insufficient amounts of the halogenated Co(II) pyrazolates to conduct such studies) and showed these materials to be highly crystalline. The *d*-spacings and relative intensities of the diffraction lines for these compounds have been deposited.[2] Furthermore, comparison of the diffractogram of $[Co(4\text{-}Hdmpz)_2]_x$ with that of $[Zn(4\text{-}Hdmpz)_2]_x$ (14) reveals the two complexes to be isomorphous.

Compounds with elongated crystallite morphologies (as seen in the SEM images described above) tend to have their crystallites oriented such that the longitudinal axes of the particles are arrayed perpendicular to the direction of the original packing force (in this case, gravity). Advantage was taken of the geometry of the iron anode X-ray diffractometer to see if this preferred orientation of microcrystallites occurs in the bulk compounds. Two samples of $[Co(4\text{-}Medmpz)_2]_x$ were prepared such that the packing force used in preparation was in one case perpendicular to the sample support (a glass slide) and in the other case parallel to the support. The first indication of preferred orientation comes from the relative intensity of the most intense line at the *d*-spacing 9.982 Å. In the perpendicular packed sample the most intense line is relatively more intense compared to the lesser lines than it is in the parallel packed sample. There are other observations that further demonstrate the presence of preferred orientation in this material. Comparison between the two diffractograms of the pairs of diffraction lines at *d*-spacings 7.451 and 7.061 Å, 4.610 and 4.460 Å, and 3.378 and 3.338 Å shows that their relative intensities are reversed, hence preferred orientation of the crystallites is present in this compound. Studies of magnetic properties conducted on the Co(II) (substituted)pyrazolates, which are discussed below, revealed orientation effects. The results of these X-ray diffraction experiments are important because, at least in the case of $[Co(4\text{-}Medmpz)_2]_x$, they provide independent experimental verification of the presence of preferred particle orientation.

Electronic spectra

The electronic spectra of the cobalt(II) (substituted)-pyrazolates are shown in Figs. 2(*a*) and (*b*). It is apparent

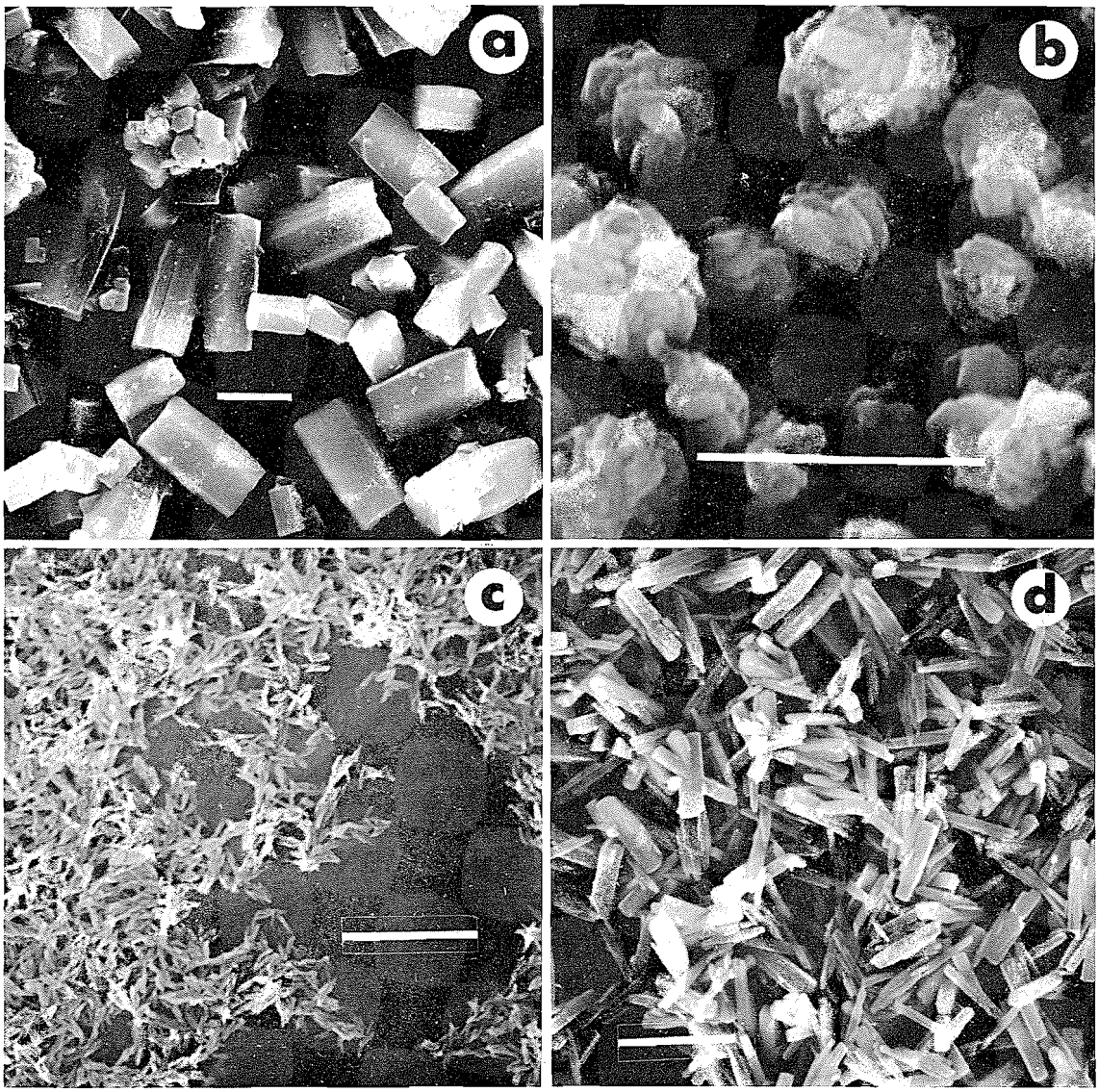

FIG. 1. SEM images of (*a*) $[Co(4\text{-}Hpz)_2]_x$, (*b*) $[Co(3\text{-}Mepz)_2]_x$, (*c*) $[Co(4\text{-}Hdmpz)_2]_x$, and (*d*) $[Co(4\text{-}Medmpz)_2]_x$. The white bar in each image represents a length of 5 μm.

from these figures that the compounds can be divided into two groups, the 3,5-dimethyl derivatives forming one group, and $[Co(4\text{-}Hpz)_2]_x$ and $[Co(3\text{-}Mepz)_2]_x$ forming the other group. With regard to possible chromophore geometries, the structured band at ~550 nm (ν_3) in these compounds is too low in energy for an octahedral complex with aromatic, nitrogen donor ligands (15); the complexes are more likely to possess four-coordinate Co(II) ions. The spectra do not have the general appearance of the spectra of square-planar Co(II) species (16) and the intense colour of the cobalt(II) (substituted)pyrazolates suggests a non-centrosymmetric chromophore. In addition, the spectra for both groups are similar in general appearance to the spectra of some oligometallic Co(II) 3,5-dimethylpyrazolate complexes, which have been shown by single crystal X-ray diffraction to contain pseudo-tetrahedral cobalt centres (17). Therefore, it is concluded that the $[Co(pz^*)_2]_x$ complexes studied here possess (pseudo-)tetrahedral CoN_4 chromophores. Band positions and relative intensities for the compounds have been tabulated in Table 2.

Using visually estimated band centres for ν_2 and ν_3 and the tetrahedral formalism, Dq and B values were estimated (18) to be 485 ± 20 and 770 ± 40 cm^{-1}, respectively, for the 3,5-dimethyl derivatives and 545 ± 20 and 690 ± 40 cm^{-1}, respectively, for the other two complexes. These Dq and B values are similar to those found for a number of $[Co(py^*)_4]^{2+}$ cations (py* = pyridine, 4-methylpyridine, and 3-methylpyridine) (19–21). The smaller values of Dq and larger values of B observed for the 3,5-dimethyl derivatives are consistent with weaker metal–ligand interactions in this group of compounds. Based on absorption band widths and fine-structure resolution, we propose that the 3,5-dimethyl derivatives possess CoN_4 chromophores that are more distorted from regular tetrahedral geometry than are the CoN_4 chromophores of $[Co(4\text{-}Hpz)_2]_x$ and $[Co(3\text{-}Mepz)_2]_x$. It is this basic difference in chromophore geometry which likely contributes most to the differences in the electronic spectra (and hence calculated "tetrahedral" ligand field parameters) between these two groups of compounds.

Can. J. Chem. Downloaded from www.nrcresearchpress.com by 213.200.69.106 on 09/08/12
For personal use only.

Can. J. Chem. Downloaded from www.nrcresearchpress.com by 213.200.69.106 on 09/08/12
For personal use only.

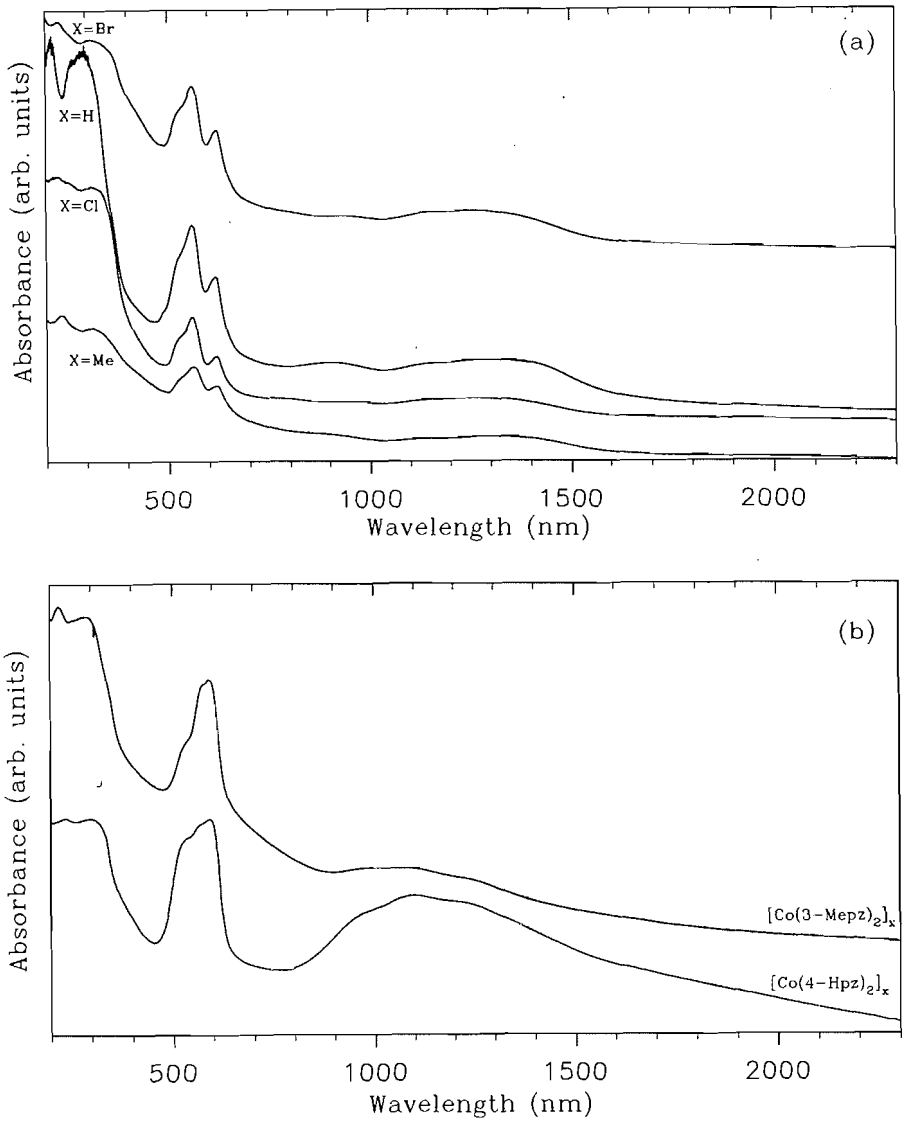

FIG. 2. Electronic spectra of the Co(II) (substituted)pyrazolates: (*a*) the 4-Xdmpz derivatives and (*b*) $[Co(4\text{-}Hpz)_2]_x$ and $[Co(3\text{-}Mepz)_2]_x$.

Infrared spectra

Infrared spectra for the compounds considered here were recorded mainly as "fingerprints" and as preliminary checks of product purity. In the case of $[Co(4\text{-}Hpz)_2]_x$, comparison of its infrared spectrum with those of $[Cu(4\text{-}Hpz)_2]_x$ (1), $[Ni(4\text{-}Hpz)_2]_x$ (22), and Na[4-Hpz] (22) provides some additional support for the proposed stereochemistry of the CoN_4 chromophore. The $[M(4\text{-}Hpz)_2]_x$ (M = Co, Ni, Cu) complexes each show two strong bands in the 250–600 cm^{-1} region. It is suggested that the bands observed for the $[M(4\text{-}Hpz)_2]_x$ compounds in this region are due principally to M–N vibrations since Na[4-Hpz] shows no absorptions in this region. For $[Co(4\text{-}Hpz)_2]_x$ and $[Cu(4\text{-}Hpz)_2]_x$, these bands occur at similar positions (334 and 322 cm^{-1} in the Co(II) species and 362 and 342 cm^{-1} in the Cu(II) species) with the same relative intensities (the higher energy band in each pair being of lower intensity). On the other hand, the M–N bands in $[Ni(4\text{-}Hpz)_2]_x$ occur at substantially higher energies (459 and 414 cm^{-1}) and their relative intensities are reversed compared to the above. This difference suggests that the coordination environment in the nickel complex is quite different from the environments of the other two. The electronic spectrum and magnetic properties of the nickel(II) complex are consistent with a square-planar coordination geometry (22), this suggesting that $[Co(4\text{-}Hpz)_2]_x$ possesses a chromophore similar to that of $[Cu(4\text{-}Hpz)_2]_x$ (1): a pseudo- or more regular tetrahedral stereochemistry (supported also by the electronic spectrum as described above).

Structural considerations

Since diffraction-quality single crystals of the Co(II) (substituted)pyrazolates could not be prepared, a discussion of their magnetic properties is preceded by a consideration of their probable structures. Their thermal and solubility properties are consistent with polymeric structures. The empirical formulae of the compounds could be satisfied if their structures consisted of chains of Co(II) ions doubly bridged by (substituted)pyrazolate ligands as confirmed in the $[Cu(4\text{-}Xpz)_2]_x$ compounds (1, 2) and proposed for the $[Cu(4\text{-}Xdmpz)_2]_x$ species (3). The electronic spectra of the Co(II) complexes indicate that they possess (pseudo-)tetrahedral CoN_4 chromophores and, furthermore, that the 4-X-3,5-dimethylpyrazolate compounds have geometries quite

TABLE 2. Electronic spectral data[a]

Compound	Assignment[b] $^4T_1(F)\leftarrow{}^4A_2(F)$ (ν_2)	$^4T_1(P)\leftarrow{}^4A_2(F)$ (ν_3)	SF	IL/CT
$[Co(4\text{-}Hpz)_2]_x$	8.10 m,sh 9.13 m 10.4 m,sh	16.9 s 17.7 s,sh 18.9 s,sh		33.3 s 42.6 s
$[Co(3\text{-}Mepz)_2]_x$	8.10 m,sh 9.25 m 10.1 m,sh	16.9 s 17.5 s,sh 18.9 s,sh		34.5 vs 45.1 vs
$[Co(4\text{-}Hdmpz)_2]_x$	7.30 m,sh 7.75 m 8.81 m 11.1 m	16.2 s 17.9 s 19.2 s	20.5 w,sh	35.1 vs 46.7 vs
$[Co(4\text{-}Medmpz)_2]_x$	7.12 m,sh 7.72 m 8.73 m,sh 11.1 m,sh	16.2 s 17.8 s 19.1 s,sh		32.2 vs 41.8 vs
$[Co(4\text{-}Cldmpz)_2]_x$	7.27 m,sh 7.92 m 8.85 m,sh 10.3 w,sh 10.6 m	16.2 s 17.9 s 19.1 s,sh	20.6 w,sh	32.0 vs 38.8 vs,sh 43.9 vs
$[Co(4\text{-}Brdmpz)_2]_x$	7.25 m,sh 7.97 m 8.81 m,sh 10.7 m	16.1 s 17.8 s 19.1 s,sh		32.3 vs 42.9 vs

[a]Band positions in units of kilo Kaser (kK) (10^3 cm^{-1}). Abbreviations: w, weak; m, medium; s, strong; vs, very strong; sh, shoulder.

[b]Assignments are based on the tetrahedral formalism. Abbreviations: SF, spin-forbidden; IL/CT, internal ligand or charge transfer.

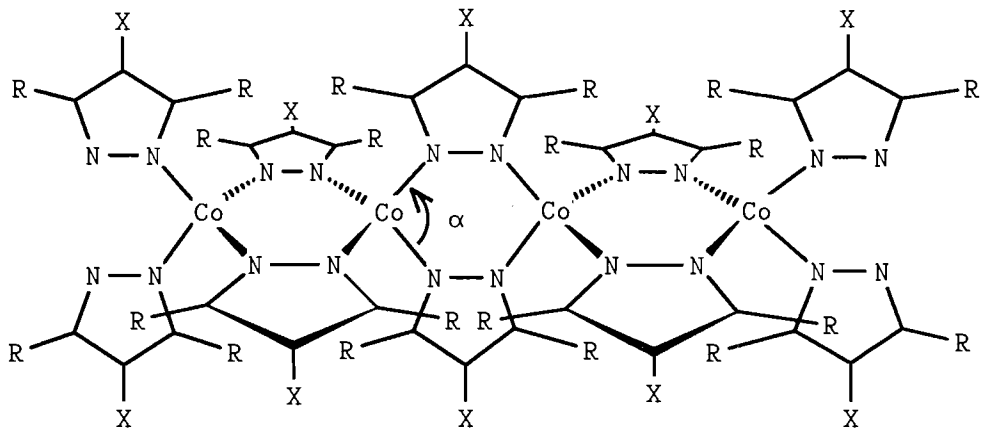

FIG. 3. Proposed structure for the Co(II) (substituted)pyrazolate polymers (where R is H or Me and X is H, Me, Cl, or Br).

distorted from the ideal tetrahedral stereochemistry. Such chromophores preclude the formation of oligometallic species analogous to the one proposed by Blake et al. for Ni(II) pyrazolates (23). There are other indirect pieces of evidence that suggest that the Co(II) compounds considered here consist of chains of (pseudo-)tetrahedrally coordinated metal ions. The structures of the dimetallic and trimetallic Co(II) 3,5-dimethylpyrazolates (described above), which contain pseudo-tetrahedrally coordinated cobalt ions, may easily be envisaged as being small segments of an extended linear chain (17). Finally, $[Zn(4\text{-}Hdmpz)_2]_x$ most certainly consists of chains of tetrahedrally coordinated Zn(II) ions as this ion contains a spherically symmetric, filled, 3*d* electronic shell and the polymer is derived from the dimeric species in which the Zn(II) ions are tetrahedrally coordinated (13). The cobalt analogues of these zinc compounds are isomorphous with the latter (14, 17) and this lends further credence to the proposed structures for the binary cobalt pyrazolates. Thus, a picture emerges of the general structure of these compounds and it is illustrated in Fig. 3.

Can. J. Chem. Downloaded from www.nrcresearchpress.com by 213.200.69.106 on 09/08/12
For personal use only.

Can. J. Chem. Downloaded from www.nrcresearchpress.com by 213.200.69.106 on 09/08/12
For personal use only.

Earlier it was noted that the electronic spectra indicate the 4-X-3,5-dimethylpyrazolates of cobalt(II) possess more distorted tetrahedral geometries than $[Co(4\text{-}Hpz)_2]_x$ or $[Co(3\text{-}Mepz)_2]_x$. The structure proposed in Fig. 3 may account for this experimental observation. When the R groups on each pyrazolate ring in the figure are both hydrogen atoms ($4\text{-}Hpz^-$) or if only one R group per ring is a methyl group ($3\text{-}Mepz^-$), molecular models indicate that there is negligible steric interaction between one pyrazolate ring and its adjacent, translational, equivalent. In these two cases there is no obvious intra-chain, inter-ligand effect to cause distortion of the chromophores away from the ideal T_d symmetry in which the angle, α (Fig. 3), would be 109.47° and the dihedral angle between fused $Co(N—N)_2Co$ rings would be 90°. However, if the CoN_4 chromophores are strictly tetrahedral and both R groups on each pyrazolate ring are methyl substituents, then there would be a substantial repulsive steric interaction between adjacent, translationally equivalent, pyrazolate ligands. The structure could minimize this repulsion by lengthening the Co—N bonds and (or) undergoing an S_4 elongation of the chromophore along the chain axis. The latter process would entail a compression of α to a value less than the tetrahedral angle and, as bond angle deformations are generally lower energy processes than bond length changes, the α-angle compression is likely to account for most of the deformation described above. The proposed large chromophore distortion in the 4-X-3,5-dimethylpyrazolates relative to the pyrazolate and 3-methylpyrazolate species is also supported by the magnetic properties of these compounds, which are considered below.

Magnetic properties

Magnetic susceptibility studies on random oriented powders (see below) show $[Co(4\text{-}Hpz)_2]_x$, $[Co(3\text{-}Mepz)_2]_x$, $[Co(4\text{-}Hdmpz)_2]_x$, and $[Co(4\text{-}Medmpz)_2]_x$ to exhibit susceptibility maxima at 38, 25, 11, 15 K, respectively. The halogenated dimethyl cobalt(II) derivatives show incipient maxima at ~10 K. These findings indicate the presence of antiferromagnetic coupling in all of the compounds. The susceptibility data for $[Co(4\text{-}Hdmpz)_2]_x$ are in excellent agreement with those reported by Singh et al. (8). At the lowest temperatures studied, the magnetic susceptibilities of all six compounds rise with decreasing temperature. This phenomenon is commonly observed in antiferromagnetically coupled systems and has been ascribed to small amounts of structural paramagnetic impurity (3). In addition, magnetization studies over a range of fields (0–55 kOe) revealed that two of the compounds, $[Co(3\text{-}Mepz)_2]_x$ and $[Co(4\text{-}Medmpz)_2]_x$, contained traces of ferromagnetic impurity (estimated <0.1% metallic cobalt). As the susceptibility measurements were made in an applied field above the saturation field for metallic cobalt, the presence of this impurity made a temperature-independent contribution to the susceptibility data for these compounds and the data have been corrected for this (22).

During initial magnetic studies of these compounds, discrepancies were observed between the data collected using the VSM and SQUID magnetometers. Both instruments subject the samples to homogeneous applied fields, but the orientations of the fields with respect to the way in which the samples are packed into their holders are orthogonal; in the VSM instrument the applied field is perpendicular to the sample packing force direction and in the SQUID magnetometer the field is parallel to that direction. Co(II) complexes often exhibit considerably anisotropic magnetic properties. The elongated crystallite morphologies observed in the SEM images of $[Co(4\text{-}Hpz)_2]_x$, $[Co(4\text{-}Hdmpz)_2]_x$, and $[Co(4\text{-}Medmpz)_2]_x$ and the preferred orientation observed in the powder X-ray diffraction study of $[Co(4\text{-}Medmpz)_2]_x$ led to the hypothesis that the crystallites in the samples used for magnetic studies were subject to a certain degree of preferred orientation that was partially resolving the anisotropic magnetic properties of these complexes. To test this hypothesis, pellets of the samples were pressed under high pressure in the hope that this would maximize the preferred orientation of the sample particles. Based on the morphologies of the crystallites, the model depicted in Fig. 4 is proposed for the preferred orientation exhibited by these compounds. If one assumes that the polymer chain axes of these complexes run parallel to the long axes of the crystallites, one then recognizes that application of an external field normal to the pellet face depicted in Fig. 4 (referred to as the perpendicular direction) will permit an enhanced sampling of the magnetic properties of these compounds in the plane normal to the chain axis. Application of the external field in the direction parallel to the pellet face (referred to as the random orientation) should actually result in random sampling of crystallite orientations because there is little difference in the crystallite edge lengths perpendicular to the long axis and, of course, there is a random distribution of long-axis orientations within the plane perpendicular to the packing-force direction.

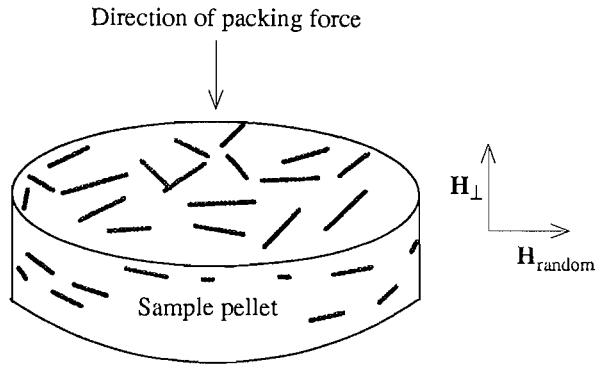

FIG. 4. Diagram showing the preferred orientation of crystallites in samples used for magnetic studies of the Co(II) (substituted)pyrazolates.

Susceptibility versus temperature studies were conducted on all of the compounds in the two orientations depicted in Fig. 4 and the results are shown in Fig. 5. The SQUID magnetometer was used for both orientations for five of the compounds; in the case of $[Co(4\text{-}Hpz)_2]_x$, the random orientation values were obtained from the VSM instrument and the perpendicular orientation values were obtained with the SQUID instrument. Magnetic susceptibility and effective magnetic moment versus temperature data for the compounds are tabulated and have been deposited.[2] The 4-X-3,5-dimethylpyrazolates show essentially no difference between the random and perpendicular orientation susceptibilities from room temperature down to approximately 30 K; however, below this temperature the susceptibilities of the two orientations begin to diverge, with the perpendicular orientation values larger than the random orientation values in all four cases. In the case of $[Co(3\text{-}Mepz)_2]_x$ (Fig.

Can. J. Chem. Downloaded from www.nrcresearchpress.com by 213.200.69.106 on 09/08/12
For personal use only.

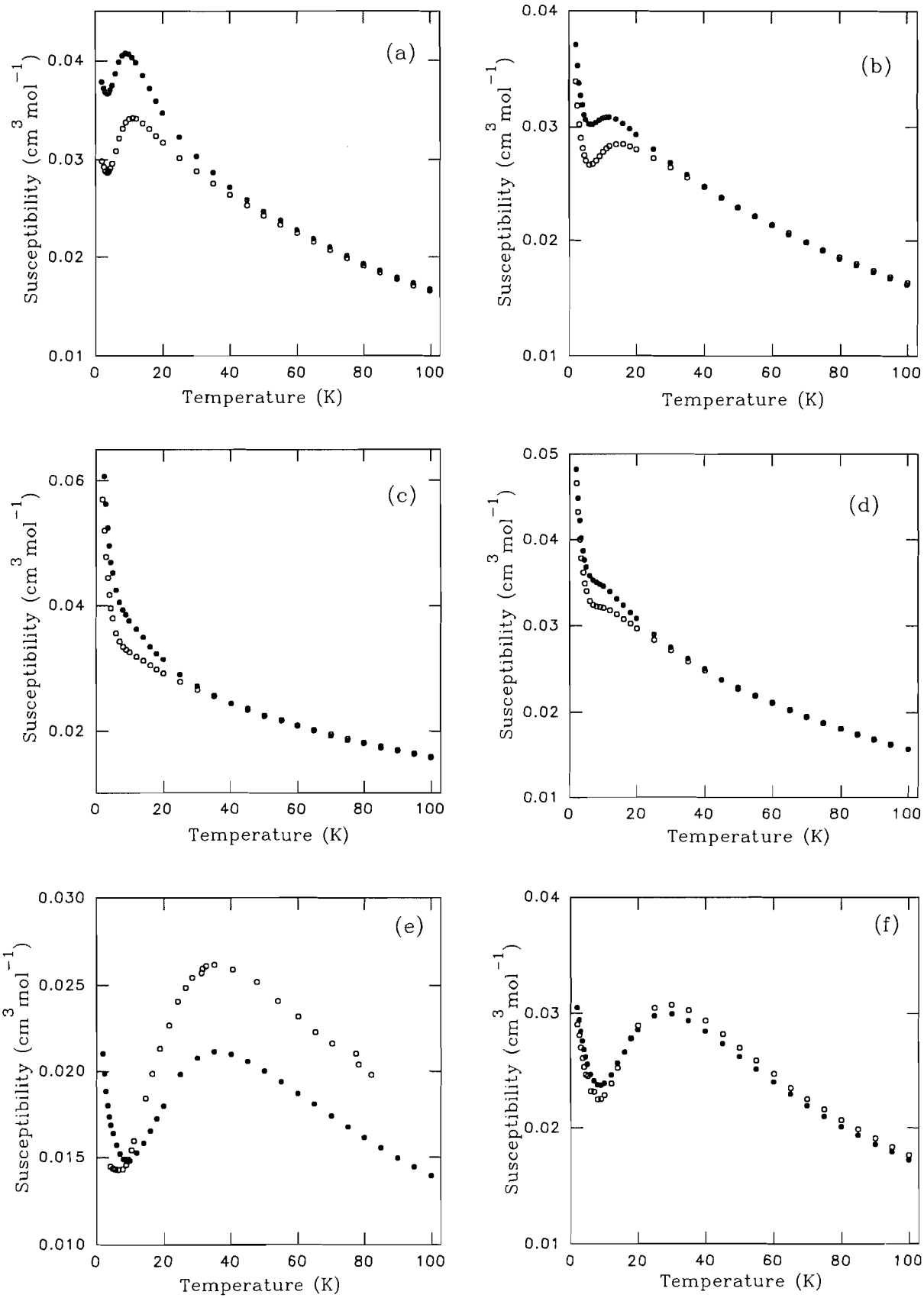

FIG. 5. Oriented pellet susceptibility versus temperature plots for the Co(II) (substituted)pyrazolate polymers: (*a*) $[Co(4\text{-}Hdmpz)_2]_x$, (*b*) $[Co(4\text{-}Medmpz)_2]_x$, (*c*) $[Co(4\text{-}Cldmpz)_2]_x$, (*d*) $[Co(4\text{-}Brdmpz)_2]_x$, (*e*) $[Co(4\text{-}Hpz)_2]_x$, and (*f*) $[Co(3\text{-}Mepz)_2]_x$. The open circles represent the random orientation and the solid circles represent the perpendicular orientation.

Can. J. Chem. Downloaded from www.nrcresearchpress.com by 213.200.69.106 on 09/08/12
For personal use only.

5(*f*)), there is little difference between the measured susceptibilities in the two orientations at the lower temperatures, and the divergence that is observed is the opposite of what was observed in Figs. 5(*a*) through (*d*). The poorer resolution of susceptibilities in the two orientations with this complex may be due either to a smaller anisotropy in its magnetic properties and (or) to the fact that the particles of this material appear to be roughly spherical aggregates of smaller microcrystallites (see Fig. 1(*b*)). As a result, they are not likely to exhibit much preferred orientation. These oriented pellet studies have clearly demonstrated anisotropy in the magnetic properties of four of the cobalt(II) (substituted)pyrazolates considered in this section; however, the studies do not yield quantitative information about the magnitudes of anisotropies.

Finally, we note that the procedures employed in the orientation studies utilizing the SQUID magnetometer required exposing the samples to the atmosphere for up to 1 h. This generally presented no problems since all of the compounds are air-stable except one. $[Co(4\text{-}Hpz)_2]_x$ undergoes slow oxidation in moist air and for this reason we used the VSM instrument for the random orientation study of this sample (Fig. 5(*e*)). The perpendicular orientation study, however, required the use of the SQUID instrument and, while there was no visible evidence of sample decomposition, some partial oxidation to diamagnetic cobalt(III) may have occurred. Having stated this, it is very unlikely that the apparent anisotropy exhibited by this compound is totally due to decomposition because such a degree of decomposition would be visually detected.

Magnetic modelling

Attempts to model the random-orientation susceptibility data for all of the complexes were made using published models that employ the Hamiltonian:

$$[1] \quad \hat{H}_{spin} = -2J \sum_{i \neq j}^{n} (S_i^z S_j^z) + \alpha(S_i^x S_j^x + S_i^y S_j^y)$$

where, when $\alpha = 1$ the Heisenberg model is obtained and when $\alpha = 0$ the Ising model results. The Heisenberg model for antiferromagnetically coupled linear chains of $S = 3/2$ metal centres developed by Hiller et al. (24) based on the numerical calculations of Weng (25) is

$$[2] \quad \chi_{chain} = \frac{Ng^2\mu_B{}^2}{kT}\left[\frac{1.2500 + 17.041x^2}{1 + 6.7360x + 238.47x^3}\right]$$

where $x = |J|/kT$. In our work the Weng equation was combined with a Curie law term,

$$[3] \quad \chi_{para} = \frac{Ng^2\mu_B{}^2 S(S+1)}{3kT}$$

in the following way;

$$[4] \quad \chi_M = [1 - P]\chi_{chain} + P\chi_{para}$$

to account for the presence of paramagnetic impurities in the compounds. Fits to the susceptibility data were achieved using a nonlinear least-squares procedure with the following as the function minimized:

$$[5] \quad F = \left[\frac{1}{n}\sum_{i=1}^{n}\frac{(\chi_i^{obs} - \chi_i^{calc})^2}{(\chi_i^{obs})^2}\right]^{1/2}$$

The F value provides a measure of the goodness of fit between theory and experiment.

The derived best-fit parameters over various temperature ranges are listed in Table 3 and the curves calculated from these fits are shown in Figs. 6(*a*) through (*f*). For $[Co(4\text{-}Hpz)_2]_x$ and $[Co(3\text{-}Mepz)_2]_x$, fits to the data over the full temperature ranges studied reproduce reasonably well the temperatures at which the maxima in the susceptibilities are observed; however, the fits do not adequately model the sharpness of the maxima. For the $[Co(4\text{-}Xdmpz)_2]_x$ complexes, the low-temperature data are modelled poorly as the temperatures at which the calculated susceptibility maxima appear are too high. Modelling of the high-temperature data yields very good fits for all six compounds with only two parameters, J and g, but extrapolation of these fits to low temperatures, as shown in the figures, reveals shortcomings. Modelling of the low-temperature data only reveals that the quality of the fits to the data for $[Co(4\text{-}Hpz)_2]_x$ and $[Co(3\text{-}Mepz)_2]_x$ is poor and, while the fits for the $[Co(4\text{-}Xdmpz)_2]_x$ compounds are excellent, the calculated g values are unrealistically low, suggesting the fits are probably fortuitous. The $S = 3/2$, Heisenberg model accounts for the magnetic behaviour over limited temperature ranges (particularly at higher temperatures), but it does not describe the behaviour of the complexes over the full temperature ranges examined.

Generally, for antiferromagnetic systems, stronger exchange should lead to maxima at higher temperatures and to lower overall susceptibilities. In spite of the fact that the compounds in the present group exhibit susceptibilities of similar overall magnitude, the dimethyl derivatives show maxima at significantly lower temperatures than $[Co(4\text{-}Hpz)_2]_x$ or $[Co(3\text{-}Mepz)_2]_x$. This inconsistency may be due to zero-field splitting (ZFS), which manifests itself in powder susceptibility measurements as a reduction of the observed susceptibility (particularly at lower temperatures). Referring to the proposed structure of the compounds under consideration (Fig. 3), if compression of the α angle is the only significant distortion in these complexes, then an axially symmetric CoN_4 chromophore results and single-ion susceptibilities are influenced by the ZFS parameter, D. A priori, it is difficult to predict the sign of D, but angular overlap model calculations performed on idealized Co(II) chromophores (15) predict that for values of α lower then the tetrahedral angle, D should be negative, in which case $m_s = \pm 3/2$ would be the ground state. Such a ZFS effect would have important consequences for exchange coupling in these systems because at temperatures where $kT < 2D$ the $m_s = \pm 1/2$ state becomes depopulated and the spin vector is essentially restricted to alignment along the principal axis of the CoN_4 chromophore (it is proposed, but not required, that the principal chromophore axis is parallel to the polymer chain axis). In this case, the coupling can occur only through that single component of the spin vector and the single-ion anisotropy will have caused the coupling to appear Ising-like. Conversely, if D is positive, then the $m_s = \pm 1/2$ state becomes the ground state and in an exchange-coupled system, the coupling will appear to be XY-like at temperatures where $kT < 2D$. Thus, attempts to quantify exchange interactions were made employing available anisotropic models.

Smith and Friedberg (26) have developed expressions for modelling susceptibility data that account for axial ZFS and Heisenberg exchange coupling simultaneously provided

TABLE 3. Derived magnetic parameters using the Heisenberg, $S = 3/2$, antiferromagnetically coupled chain model with estimated standard deviation in the last digit in parentheses

Compound	Temperature range (K)	$-J$ (cm^{-1})	g	$\%P$	F
$[Co(4\text{-}Hpz)_2]_x$	4.2–41	5(3)	2.1(7)	0[a]	0.16
	35–82	5.00(8)	2.35(1)	0[a]	0.0077
	4.2–82	7(1)	2.5(2)	0	0.15
$[Co(3\text{-}Mepz)_2]_x$	2–35	5(2)	2.4(4)	0.4(2)	0.057
	50–300	3.68(2)	2.242(1)	0[a]	0.027
	2–300	4.43(8)	2.29(1)	0.46(7)	0.042
$[Co(4\text{-}Hdmpz)_2]_x$	2–20	1.89(6)	1.64(2)	0.30(8)	0.016
	50–300	4.6(1)	2.24(1)	0[a]	0.024
	2–300	3.31(9)	2.15(2)	0.5(1)	0.062
$[Co(4\text{-}Medmpz)_2]_x$	2–20	2.63(9)	1.76(3)	1.73(8)	0.0091
	50–300	5.74(8)	2.341(7)	0[a]	0.015
	2–300	4.4(1)	2.24(2)	1.2(1)	0.051
$[Co(4\text{-}Cldmpz)_2]_x$	2–20	2.2(1)	1.62(4)	6.3(3)	0.014
	50–300	5.08(3)	2.238(2)	0[a]	0.0048
	2–300	4.3(1)	2.17(1)	3.9(1)	0.043
$[Co(4\text{-}Brdmpz)_2]_x$	2–20	2.16(5)	1.63(2)	4.06(9)	0.0075
	50–300	4.42(9)	2.168(7)	0[a]	0.016
	2–300	3.75(8)	2.11(1)	2.7(1)	0.041

[a]Fixed at zero.

$|J| >> |D|$. It is possible to estimate whether this condition is met in the present compounds by considering the modelling results and the oriented pellet studies together. The Heisenberg modelling studies suggest that the $|J|$ values for the complexes lie in the range ~2–6 cm^{-1}. Assuming that the anisotropy exhibited in the oriented pellet studies is due to ZFS effects, a crude estimate of its magnitude may be made. The temperatures at which the susceptibilities of the two orientations begin to diverge (which is a lower limit to the magnitude of the anisotropy) indicate that $|D|$ is of the order of 10 cm^{-1}. Clearly, the condition required to apply the expressions of Smith and Friedberg (26) is not met in these compounds. If $|D|$ is much greater than the lower limit suggested by the oriented pellet studies, then at low temperatures only the lowest Kramers' doublet of the electronic states manifold is populated and the Co(II) ions will behave as $S' = 1/2$ ions. Anisotropically coupled, $S = 1/2$, linear chain models have been studied theoretically. Closed-form expressions have been derived for the magnetic susceptibility (27, 28) and they are presented below:

$$[6a] \quad \chi_{\parallel} = \frac{Ng_{\parallel}^2\mu_B^2}{4kT}\exp(-|J|/kT)$$

$$[6b] \quad \chi_{\perp} = \frac{Ng_{\perp}^2\mu_B^2}{4|J|}\left[\tanh\left(\frac{J}{2kT}\right) + \left(\frac{J}{2kT}\right)\mathrm{sech}^2\left(\frac{J}{2kT}\right)\right]$$

$$[6c] \quad \chi_p = \tfrac{1}{3}\chi_{\parallel} + \tfrac{2}{3}\chi_{\perp}$$

Implicit in the assumption that $S' = 1/2$ models apply to the behaviour of these compounds is the condition that $g_{\parallel}$ and $g_{\perp}$ are anisotropic *effective* components of the true g-tensor for the $S = 3/2$ Co(II) ion. In an axially distorted system, the relationships between the effective, g', components and the true g values are as follows (15): $g'_{\parallel} = 3g_{\parallel}$ and $g'_{\perp} = 0$. Thus, if Ising-like exchange is present in these compounds, use of eq. [6*a*] alone in eq. [6*c*] should provide an adequate fit to the observed data. It is important to note that, according to the model, $\chi_{\parallel} \rightarrow 0$ as $T \rightarrow 0$, while the measured susceptibilities show an increase in magnitude as $T \rightarrow 0$, behaviour ascribed to the presence of paramagnetic impurity. Because of the anisotropy in these compounds, inclusion of a Curie law term may be inadequate to account for the lowest temperature susceptibility data. Consequently, the low-temperature data were fit using eq. [6*c*] with $\chi_{\perp}$ fixed at zero and this was combined with a Curie–Weiss law paramagnetic impurity term,

$$[7] \quad \chi_{para} = \frac{Ng^2\mu_B^2S(S+1)}{3k(T-\Theta)}$$

where $g = \frac{1}{3}g'$. The best-fit results are presented in Table 4 where the F values show this model to provide excellent fits to the low-temperature data, better, in fact, than does the Heisenberg model with a Curie law paramagnetic impurity term. Of course, the former is a four-parameter model while the latter is only a three-parameter model. Fits to the low-temperature data using the Heisenberg model coupled with the Curie–Weiss paramagnetic impurity term only yield marginal decreases in the F values at the expense of indeterminate $\%P$. It should be noted that the $\%P$ values and Weiss constants obtained with the Ising parallel susceptibility model are rather large in magnitude.

A major problem in analyzing the magnetic data arises from the presence of paramagnetic impurities and the fact that their contributions to the overall susceptibilities are maximized in the low-temperature region. Accordingly, an attempt was made to fit the data in the region of susceptibility maxima without correcting for paramagnetic impurities, using both the Ising and Heisenberg models. The halogenated derivatives do not exhibit discrete susceptibility maxima and

Can. J. Chem. Downloaded from www.nrcresearchpress.com by 213.200.69.106 on 09/08/12
For personal use only.

Can. J. Chem. Downloaded from www.nrcresearchpress.com by 213.200.69.106 on 09/08/12
For personal use only.

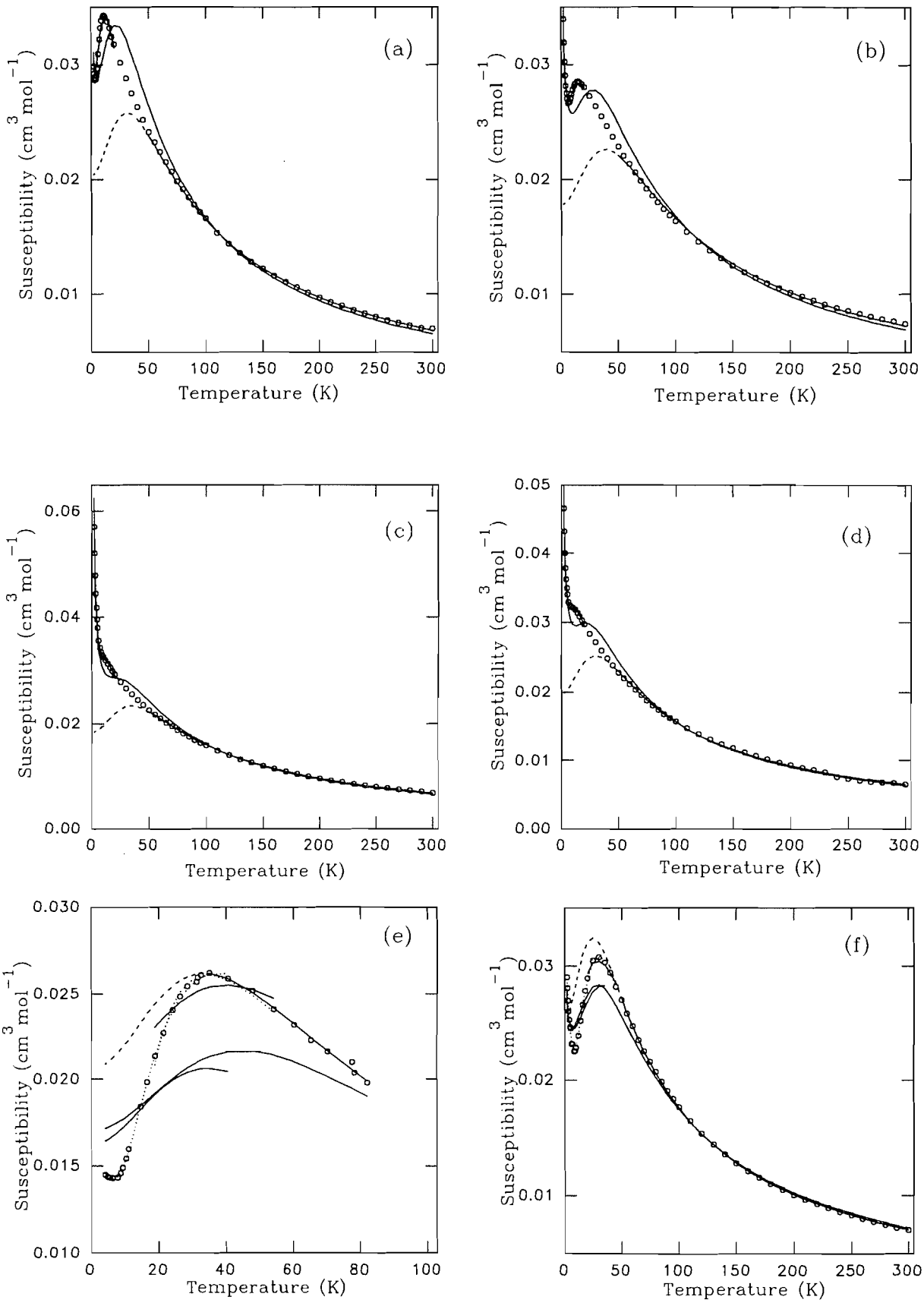

FIG. 6. Magnetic susceptibility (random orientation) versus temperature plots for the Co(II) (substituted)pyrazolate polymers: (*a*) $[Co(4\text{-}Hdmpz)_2]_x$, (*b*) $[Co(4\text{-}Medmpz)_2]_x$, (*c*) $[Co(4\text{-}Cldmpz)_2]_x$, (*d*) $[Co(4\text{-}Brdmpz)_2]_x$, (*e*) $[Co(4\text{-}Hpz)_2]_x$, and (*f*) $[Co(3\text{-}Mepz)_2]_x$. The lines are the calculated curves for the best-fit parameters listed in Tables 3 through 5. The solid lines correspond to the Heisenberg model with the broken lines as extrapolations of these fits. The dotted lines seen in (*e*) and (*f*) correspond to the Ising model.

TABLE 4. Derived magnetic parameters for low-temperature data fits of the $S = 1/2$, Ising $\chi_\parallel$ model coupled with a Curie–Weiss law paramagnetic impurity component (estimated standard deviation in the last digit in parentheses)

Compound	Temperature range (K)	$-J$ (cm^{-1})	$g'_\parallel$	%P	$-\Theta$ (K)	F
$[Co(4\text{-}Hpz)_2]_x$	4.2–41	32.6(2)	9.34(5)	18(2)	51(5)	0.0044
$[Co(3\text{-}Mepz)_2]_x$	2–35	28.6(4)	9.58(8)	15.3(4)	13(1)	0.0061
$[Co(4\text{-}Hdmpz)_2]_x$	2–20	12.5(1)	6.06(2)	24(2)	13(1)	0.0041
$[Co(4\text{-}Medmpz)_2]_x$	2–20	16.6(2)	6.42(3)	13.8(3)	6.8(2)	0.0031
$[Co(4\text{-}Cldmpz)_2]_x$	2–20	16.2(1)	6.27(2)	14.2(1)	3.1(1)	0.0020
$[Co(4\text{-}Brdmpz)_2]_x$	2–20	15.0(2)	6.22(3)	14.1(3)	4.1(2)	0.0039

TABLE 5. Derived magnetic parameters fits of the $S = 1/2$, Ising $\chi_\parallel$ and $S = 3/2$, Heisenberg models to data in the region of the susceptibility maxima (estimated standard deviation in last digit in parentheses)

Compound	Temperature range (K)	Model	$-J$ (cm^{-1})	g or $g'_\parallel$	F
$[Co(4\text{-}Hpz)_2]_x$	19–54	Ising	24.0(2)	8.86(5)	0.0097
		Heisenberg	5.9(5)	2.5(1)	0.033
$[Co(3\text{-}Mepz)_2]_x$	20–45	Ising	19.8(1)	8.74(3)	0.0033
		Heisenberg	4.3(1)	2.36(3)	0.0097
$[Co(4\text{-}Hdmpz)_2]_x$	10–20	Ising	8.6(2)	6.09(6)	0.011
		Heisenberg	1.81(3)	1.62(1)	0.0068
$[Co(4\text{-}Medmpz)_2]_x$	12–20	Ising	10.4(3)	6.12(9)	0.0089
		Heisenberg	2.15(4)	1.62(2)	0.0072

were not included in this analysis. The results are presented in Table 5 and the calculated curves corresponding to the best-fit parameters are shown in Figs. 6(*a*) through (*f*) (these curves span only the susceptibility maxima and the Ising curves are seen as distinct from the Heisenberg ones only for 6(*e*) and (*f*)). Only in the case of $[Co(4\text{-}Hpz)_2]_x$ does the Ising model provide a substantially better fit than the Heisenberg model. In fact, the Heisenberg model provides a marginally better fit to the data for the 4-Hdmpz and 4-Medmpz derivatives; however, the resulting g values are unrealistically low.

EPR studies on monometallic analogues provide some support for application of the Ising susceptibility model to these compounds. Compounds with the general formula $Co[R_2B(pz^*)]_2$ (R = H or phenyl and pz* = 4-Hpz, 4-Hdmpz, or 4-Medmpz) were found to exhibit $g_\parallel >> g_\perp$ (29), which is the condition required for application of the Ising exchange model. In light of this, we attempted to fit the data for $[Co(4\text{-}Hpz)_2]_x$ and $[Co(3\text{-}Mepz)_2]_x$ over wide temperature ranges employing the Ising model, but allowing a contribution due to $\chi_\perp$. In the case of $[Co(4\text{-}Hpz)_2]_x$, the full random-orientation powder susceptibility data set was modelled allowing J, $g'_\parallel$, and $g'_\perp$ to vary with the resulting best-fit values of $-39.5(2)$ cm^{-1}, 7.56(2), and 3.59(1), respectively ($F = 0.0080$). With $[Co(3\text{-}Mepz)_2]_x$, data over the range 2–300 K were modelled in a similar fashion. The derived values of J, $g'_\parallel$, $g'_\perp$, and %P were $-38.3(5)$ cm^{-1}, 6.19(7), 4.24(5), and 0.82(3)%, respectively ($F = 0.010$). When such modelling efforts were made with the data for the $[Co(4\text{-}Xdmpz)_2]_x$ species, $g_\parallel$ invariably tended to zero and for the halogenated species, J became indeterminate.

In the Hamiltonian, eq. [1], if the z-component is set at zero and $\alpha = 1$, then another important form of anisotropic exchange coupling, X–Y exchange, is obtained. Katsura (30) derived an open-form expression for $\chi_\perp$ in X–Y coupled $S = 1/2$ linear chains and Duxbury et al. (31) developed numerical approximations to Katsura's expression; however, they did not provide explicit expressions for those approximations. Another important shortcoming in the application of the X–Y model here is that no expression for $\chi_\parallel$ in linear chain systems is available and, within the framework of an axially distorted, $S = 3/2$ chromophore, $g'_\parallel = g$ and $g'_\perp = 2g$ (15). Thus, neglect of $\chi_\parallel$ would incur considerable error in the fitting procedure.

Summary and conclusions

Synthetic routes to six binary pyrazolate and substituted pyrazolate complexes of Co(II) are described. The materials are microcrystalline and, although none could be obtained in a form suitable for single crystal X-ray diffraction studies, indirect evidence supports polymeric doubly pyrazolate-bridged chain structures with pseudo-tetrahedral cobalt centres. Magnetic susceptibility studies reveal anisotropy in the susceptibilities and the presence of significant antiferromagnetic exchange. No single model currently available for quantification of exchange interactions adequately describes the observed magnetic properties over wide temperature ranges. In spite of this difficulty, the modelling exercises facilitate the qualitative interpretation of the magnetic properties. The high-temperature susceptibility data for all of the compounds can be adequately fit with the antiferromagnetically coupled $S = 3/2$ linear chain model. This procedure yields true g values in the range expected for (pseudo)tetrahedrally coordinated Co(II) ions. At temperatures below those of the susceptibility maxima, the ob-

Can. J. Chem. Downloaded from www.nrcresearchpress.com by 213.200.69.106 on 09/08/12
For personal use only.

served susceptibilities decrease more rapidly than can be accounted for by the Heisenberg model. This fact, along with the results of the oriented pellet studies, reveals the presence of anisotropy effects. Application of the $S' = 1/2$, Ising parallel susceptibility model to the low-temperature data yields excellent fits and reasonable $g_{\parallel}'$ values. The derived J values from the Ising and Heisenberg models can be used to qualitatively rank the magnitude of exchange coupling in these complexes as follows:

$$\text{4-Hpz} \approx \text{3-Mepz} >> \text{4-Medmpz} \approx \text{4-Cldmpz} \approx \text{4-Brdmpz} \approx \text{4-Hdmpz}$$

This division of the compounds into two exchange strength groups also correlates with their ligand field properties and proposed chromophore distortions. A weaker ligand field is consistent with the type of distortion proposed in the dimethyl species relative to the other two complexes. The pyrazolate ligands are most certainly the medium of magnetic exchange in these complexes and one might reasonably expect that a weaker interaction between the ligands and Co(II) centres would manifest itself in smaller magnitudes of exchange. As a final comment on the nature of the exchange interaction, the true exchange behaviour is probably of the Heisenberg type and, although the modelling results indicate that low-temperature, 1-D, Ising-like exchange may be manifest in these compounds, the anomalously sharp susceptibility maxima most likely result from single-ion ZFS effects. Further interpretation of the order of the magnitudes of exchange coupling or of its nature is not warranted without detailed knowledge of the structures of these compounds.

Acknowledgements

We thank the Natural Sciences and Engineering Research Council of Canada for financial support. We also thank Drs. J. Carolan and W. Hardy of the Department of Physics at the University of British Columbia for use of the SQUID magnetometer.

1. M.K. Ehlert, S.J. Rettig, A. Storr, R.C. Thompson, and J. Trotter. Can. J. Chem. **67**, 1970 (1989).
2. M.K. Ehlert, S.J. Rettig, A. Storr, R.C. Thompson, and J. Trotter. Can. J. Chem. **69**, 432 (1991).
3. M.K. Ehlert, A. Storr, and R.C. Thompson. Can. J. Chem. **70**, 1121 (1992).
4. E.J. Fischer. Wiss. Veröff. Siemens-Konzern. **4**, 178 (1925).
5. O. Heim. Ind. Eng. Chem. Anal. Ed. **2**, 38 (1930).
6. R.T. Pflaum and L.H. Dieter. Proc. Iowa Acad. Sci. **64**, 235 (1957).
7. M.J. Bagley, D. Nicholls, and B.A. Warburton. J. Chem. Soc. (A), 2694 (1970).
8. C.B. Singh, S. Satpathy, and B. Sahoo. J. Inorg. Nucl. Chem. **35**, 3947 (1973).
9. J.G. Vos and W.L. Groeneveld. Inorg. Chim. Acta, **24**, 123 (1977).
10. J.G. Vos and W.L. Groeneveld. Inorg. Chim. Acta, **26**, 71 (1978).
11. J.G. Vos and W.L. Groeneveld. Transition Met. Chem. (London), **4**, 137 (1979).
12. J.S. Haynes, K.W. Oliver, S.J. Rettig, R.C. Thompson, and J. Trotter. Can. J. Chem. **62**, 891 (1984).
13. A.R. West. Solid state chemistry and its applications. John Wiley & Sons, New York. 1984. p. 177.
14. M.K. Ehlert, S.J. Rettig, A. Storr, R.C. Thompson, and J. Trotter. Can. J. Chem. **68**, 1494 (1990).
15. L. Banci, A. Bencini, C. Benelli, D. Gatteschi, and C. Zanchini. *In* Structure and bonding. Vol. 52. *Edited by* M.J. Clarke et al. Springer-Verlag, Berlin. 1982. p. 37.
16. C. Daul, C.W. Schlapfer, and A. von Zelewsky. *In* Structure and bonding. Vol. 36. *Edited by* J.D. Dunitz et al. Springer-Verlag, Berlin. 1979. p. 129.
17. M.K. Ehlert, S.J. Rettig, A. Storr, R.C. Thompson, and J. Trotter. Can. J. Chem. **71**, 1425 (1993).
18. Y. Dou. J. Chem. Educ. **67**, 134 (1990).
19. R.M. Morrison and R.C. Thompson. Inorg. Nucl. Chem. Lett. **12**, 937 (1976).
20. R.M. Morrison and R.C. Thompson. Can. J. Chem. **56**, 985 (1978).
21. R.M. Morrison and R.C. Thompson. Can. J. Chem. **61**, 1651 (1983).
22. M.K. Ehlert. Ph.D. Thesis. University of British Columbia. 1992.
23. A.B. Blake, D.F. Ewing, J.E. Hamlin, and J.M. Lockyer. J. Chem. Soc. Dalton Trans. 1897 (1977).
24. W. Hiller, J. Strahle, A. Datz, M. Hanack, W.E. Hatfield, L.W. ter Haar, and P. Gutlich. J. Am. Chem. Soc. **106**, 329 (1984).
25. C.H. Weng. Ph.D. Dissertation, Carnegie-Mellon University. 1968.
26. T. Smith and S.A. Friedberg. Phys. Rev. **176**, 660 (1968).
27. J.C. Bonner and M.E. Fisher. Phys. Rev. A, **135**, 640 (1964).
28. M.E. Fisher. J. Math. Phys. **4**, 124 (1963).
29. L.J. Guggenberger, C.T. Prewitt, P. Meakin, S. Trofimenko, and J.P. Jesson. Inorg. Chem. **12**, 508 (1973).
30. S. Katsura. Phys. Rev. **127**, 1508 (1962); **129**, 2835 (1963).
31. P.M. Duxbury, J. Oitmaa, M.N. Barber, A. van der Bilt, K.O. Joung, and R.L. Carlin. Phys. Rev. B, **24**, 5149 (1981).

Can. J. Chem. Downloaded from www.nrcresearchpress.com by 213.200.69.106 on 09/08/12
For personal use only.

Oligometallic cobalt 3,5-dimethylpyrazolate complexes: synthesis, structural and magnetic studies

MARTIN K. EHLERT, STEVEN J. RETTIG, ALAN STORR,[1] ROBERT C. THOMPSON,[1] AND JAMES TROTTER
Department of Chemistry, University of British Columbia, 2036 Main Mall, Vancouver, BC V6T 1Z1, Canada

Received February 12, 1993

MARTIN K. EHLERT, STEVEN J. RETTIG, ALAN STORR, ROBERT C. THOMPSON, and JAMES TROTTER. Can. J. Chem. **71**, 1425 (1993).

Three oligometallic 3,5-dimethylpyrazolate (dmpz) bridged Co(II) compounds have been synthesized and characterized spectroscopically: dimeric $[Co(dmpz)_2(Hdmpz)]_2$, the related oligometallic compound, $Co(dmpz)_2 \cdot 0.344(Hdmpz)$, and the trimetallic $[Co(dmpz)_2Cl(Hdmpz)]_2Co$. The first and last of these compounds have been studied magnetically and by single crystal X-ray diffraction. Crystals of $[Co(dmpz)_2(Hdmpz)]_2$ are orthorhombic, $a = 17.022(1)$, $b = 29.224(2)$, $c = 13.576(3)$ Å, $Z = 8$, space group *Fddd*; and those of $[Co(dmpz)_2Cl(Hdmpz)]_2Co$ are triclinic, $a = 11.742(3)$, $b = 18.604(4)$, $c = 8.950(2)$ Å, $\alpha = 99.76(2)°$, $\beta = 102.32(2)°$, $\gamma = 93.36(2)°$, $Z = 2$, space group $P\bar{1}$. The structures were solved by the Patterson method and were refined by full-matrix least-squares procedures to $R = 0.035$ and 0.042 ($R_w = 0.034$, 0.047) for 938 and 3853 reflections with $I \geq 3\sigma(F^2)$, respectively. Magnetic susceptibility studies on the dimeric and trimetallic complex show them to exhibit antiferromagnetic behaviour. Analysis of the magnetic data (2–300 K) for the trimetallic complexes reveals antiferromagnetic coupling between the terminal and central Co(II) ions with J (Heisenberg) ≈ -3 cm^{-1}. Either intramolecular next-nearest neighbour or intermolecular antiferromagnetic exchange is also present in this compound. The dimeric complex shows significant antiferromagnetic exchange between cobalt centres. Susceptibility data over the range 12–300 K are adequately modelled with the Ising $S = 1/2$ dimer model ($J \approx -23$ cm^{-1}).

MARTIN K. EHLERT, STEVEN J. RETTIG, ALAN STORR, ROBERT C. THOMPSON, et JAMES TROTTER. Can. J. Chem. **71**, 1425 (1993).

On a synthétisé trois composés oligométalliques du Co(II) portant du 3,5-diméthylpyrazolate (dmpz) ponté et on les a caractérisés par des méthodes spectroscopiques : le $[Co(dmpz)_2(Hdmpz)]_2$, le composé oligométallique apparenté, $Co(dmpz)_2 \cdot 0{,}344(Hdmpz)$, et le composé trimétallique, $[Co(dmpz)_2Cl(Hdmpz)]_2Co$. On a étudié les premier et dernier composés magnétiquement et par diffraction des rayons X par des cristaux uniques. Les cristaux du $[Co(dmpz)_2(Hdmpz)]_2$ sont orthorhombiques, groupe d'espace *Fddd*, avec $a = 17{,}022(1)$, $b = 29{,}224(2)$ et $c = 13{,}576(3)$ Å, $Z = 8$ alors que ceux du $[Co(dmpz)_2Cl(Hdmpz)]_2Co$ sont tricliniques, groupe d'espace $P\bar{1}$, avec $a = 11{,}742(3)$, $b = 18{,}604(4)$ et $c = 8{,}950(2)$ Å, $\alpha = 99{,}76(2)°$, $\beta = 102{,}32(2)°$ et $\gamma = 93{,}36(2)°$ et $Z = 2$. On a résolu les structures par la méthode de Patterson et on les a affinées par la méthode des moindres carrés (matrice entière) jusqu'à des valeurs de $R = 0{,}035$ et 0,042 ($R_w = 0{,}034$ et 0,047) pour respectivement 938 et 3853 réflexions avec $I \geq 3\sigma(F^2)$. Les études de susceptibilité magnétique sur le complexe dimère et trimétallique montrent qu'ils présentent un comportement antiferromagnétique. Une analyse des données magnétiques (2–300 K) du complexe trimétallique révèle l'existence d'un couplage antiferromagnétique entre les ions Co(II) terminal et central, avec J (Heisenberg) ≈ -3 cm^{-1}. Dans ce composé, il existe aussi un échange antiferromagnétique intramoléculaire ou intermoléculaire avec le deuxième voisin. Le complexe dimère présente un échange antiferromagnétique important entre les centres de cobalt. Le modèle dimère de Ising, $S = 1/2$ ($J = -23$ cm^{-1}), permet d'expliquer adéquatement les données de susceptibilité entre 12 et 300 K.

[Traduit par la rédaction]

Introduction

We recently reported on a number of metal pyrazolate complexes containing copper or zinc (1–6). Particular emphasis was placed on studies of the magnetic properties of copper(II) oligometallic and polymeric systems (1, 4–6), studies in which it was demonstrated that pyrazolate and substituted pyrazolate ligands are efficient mediators of antiferromagnetic exchange between copper centres.

As part of our investigations of binary metal pyrazolates, generally, we have synthesized a number of polymeric cobalt(II) pyrazolates (7). In the course of this work, two 3,5-dimethylpyrazolate-bridged complexes, the dimeric $[Co(dmpz)_2(Hdmpz)]_2$ and the trimetallic $[Co(dmpz)_2Cl(Hdmpz)]_2Co$, were isolated in crystalline form suitable for single crystal X-ray diffraction studies. The structures and magnetic properties of these complexes, together with some studies on a dimeric–oligometallic material with the empirical formula $Co(dmpz)_2 \cdot 0.344(Hdmpz)$, form the basis of this communication. These materials provide important insights into the structure – magnetic property relationships in pyrazolate-bridged cobalt(II) systems. In addition, they provide structural models for interpreting systems such as the polymeric cobalt(II) pyrazolates where, due to the microcrystalline nature of the samples, no single crystal X-ray data are available (7).

Experimental

Syntheses

3,5-Dimethylpyrazole (Hdmpz) was purchased from Aldrich and used without further purification.

$[Co(dmpz)_2(Hdmpz)]_2$

A mixture of $CoCO_3 \cdot xH_2O$ (0.465 g) and 3,5-dimethylpyrazole (2.88 g), in sufficient acetone to dissolve the 3,5-dimethylpyrazole (~1–2 mL), was reacted, with stirring, at 75°C for 24 h. The solid mixture obtained on cooling was extracted with acetone to yield an insoluble dark purple powder and a solution of 3,5-dimethylpyrazole. Collection of the purple powder yielded 1.22 g $[Co(dmpz)_2(Hdmpz)]_2$. Anal. calcd. for $C_{30}H_{44}Co_2N_{12}$: C 52.2, H 6.4, N 24.3; found: C 51.8, H 6.5, N 24.6.

The sample of this material on which the single crystal X-ray diffraction studies were performed formed one half of a larger,

[1]Authors to whom correspondence may be addressed.

Can. J. Chem. Downloaded from www.nrcresearchpress.com by 203.198.23.82 on 09/08/12
For personal use only.

Can. J. Chem. Downloaded from www.nrcresearchpress.com by 203.198.23.82 on 09/08/12
For personal use only.

elongated octahedral crystal from the sample of $Co(dmpz)_2 \cdot 0.344(Hdmpz)$. An X-ray powder diffraction study on the bulk sample confirmed it to be the same as the single crystal sample.

$Co(dmpz)_2 \cdot 0.344(Hdmpz)$

This material was produced in a manner similar to that of $[Co(dmpz)_2(Hdmpz)]_2$ with the following differences. Approximately 0.1 g of $CoCO_3 \cdot xH_2O$ and 4 g of 3,5-dimethylpyrazole were used. The reaction mixture was heated at 100°C for 40 h, without stirring. This yielded 0.18 g of large purple crystals with the nominal formulation $Co(dmpz)_2 \cdot 0.344(Hdmpz)$. Anal. calcd. for $C_{11.7}H_{16.8}CoN_{4.7}$: C 49.9, H 6.0, N 23.3; found: C 49.9, H 6.2, N 23.2.

$[Co(dmpz)_2Cl(Hdmpz)]_2Co$

$[Co(acac)_2]_4$ (0.551 g, 2.14 mmol) and excess 3,5-dimethylpyrazole (mp = 108–110°C) were combined and heated, with stirring, at 160°C for 2 h under a dinitrogen atmosphere. The mixture was then cooled to room temperature and the resultant solid extracted with 40 mL of CH_2Cl_2. Filtration, followed by removal of solvent from the filtrate, yielded a pink solid. The pink solid was heated at 130°C (above the mixture melting point), without stirring, for 18 h. During this heating period the reaction mixture was exposed to a slow flow of dinitrogen gas carrying CH_2Cl_2 vapour (Cl source). After this time, a dark purple solid remained at the bottom of the reaction vessel and excess 3,5-dimethylpyrazole and acetylacetone had collected on cooler parts of the apparatus. The purple solid was washed with 80 mL of acetone in small portions to leave the product as insoluble, well-formed purple crystals together with a small amount of light blue material. The latter was removed by washing with methanol and the remaining product was then dried in air yielding 0.142 g (23%) of $[Co(dmpz)_2Cl(Hdmpz)]_2Co$ as dark purple crystals. Anal. calcd. for $C_{30}H_{44}Cl_2Co_3N_{12}$: C 43.9, H 5.4, N 20.5; found: C 44.2, H 5.5, N 20.3

Physical characterization

Infrared spectra (4000–400 cm^{-1}) were recorded as Nujol mulls between KBr plates using a Perkin–Elmer model 598 spectrometer and were calibrated against polystyrene film. Electronic spectra (200–2500 nm) were recorded using a Cary 5 spectrometer on Nujol mull samples between quartz plates. Electronic band positions and assignments are listed in Table 1.

Differential scanning calorimetry measurements were obtained with a Mettler DSC 20 standard cell and TC10 TA processor.

Magnetic measurements were performed using a Quantum Design MPMS SQUID magnetometer. Powdered samples (approximately 30 mg) were packed into a PVC sample holder specially designed to possess a constant cross-sectional area. Magnetic susceptibility data were recorded in the temperature range 2–300 K in an applied field of 10 kOe. Susceptibility data were corrected for diamagnetism: Co, −12; Cl, −26; dmpz(H), −62 (all values × 10^{-6} cm^3 mol^{-1}). A correction of 4.0×10^{-4} cm^3 mol^{-1}, derived from ligand field *D*q values, was also applied for the temperature-independent paramagnetism of the Co(II) ion. The estimated uncertainty in the susceptibility data is ±1%.

Elemental analyses were performed by Mr. P. Borda of this department.

X-ray crystallographic analyses of $[Co(dmpz)_2(Hdmpz)]_2$ and $[Co(dmpz)_2Cl(Hdmpz)]_2Co$

Crystallographic data for both complexes appear in Table 2. The final unit-cell parameters were obtained by least squares on the setting angles for 25 reflections with 2θ = 55.6–92.0° for $[Co(dmpz)_2(Hdmpz)]_2$, and 11.6–34.7° for $[Co(dmpz)_2Cl(Hdmpz)]_2Co$. The intensities of three standard reflections, measured every 200 reflections throughout the data collections, showed only small random variations. The data were processed,[2] corrected for Lorentz and polarization effects, and for absorption (empirical, based on azimuthal scans for three reflections).

TABLE 1. Electronic spectral data for $[Co(dmpz)_2(Hdmpz)]_2$, $Co(dmpz)_2 \cdot 0.344(Hdmpz)$, and $[Co(dmpz)_2Cl(Hdmpz)]_2Co$[a]

Compound	Band position[b] (kK)	Assignment[c]
$[Co(dmpz)_2(Hdmpz)]_2$	7.92 m 8.70 m 9.84 m	$^4T_1(F) \leftarrow {}^4A_2(F)$ (ν_2)
	16.8 s 17.3 s,sh 18.4 s 18.9 s,sh	$^4T_1(P) \leftarrow {}^4A_2(F)$ (ν_3)
	34.5 vs,sh 45.0 vs 48.3 vs	IL/CT
$Co(dmpz)_2 \cdot 0.344(Hdmpz)$	7.94 m,sh 8.79 m 9.85 m	$^4T_1(F) \leftarrow {}^4A_2(F)$ (ν_2)
	16.9 s 17.3 s 18.8 s,sh	$^4T_1(P) \leftarrow {}^4A_2(F)$ (ν_3)
	24.7 w,sh	SF
	35.1 vs 46.3 vs	IL/CT
$[Co(dmpz)_2Cl(Hdmpz)]_2Co$	5.90 w,sh 7.05 m,sh 8.10 m 10.0 m 12.3 w,sh	$^4T_1(F) \leftarrow {}^4A_2(F)$ (ν_2)
	16.0 s,sh	
	16.8 s 18.5 s,sh	$^4T_1(P) \leftarrow {}^4A_2(F)$ (ν_3)
	22.0 w	SF
	34.7 vs 39.7 vs 46.1 vs	IL/CT

[a]Recorded in the solid state using Nujol mulls.

[b]kK = 10^3 cm^{-1}. Abbreviations: w, weak; m, medium; s, strong; vs, very strong; sh, shoulder.

[c]Assignments are based on the tetrahedral formalism. Abbreviations: SF, spin-forbidden; IL/CT, internal ligand or charge transfer.

$[Co(dmpz)_2(Hdmpz)]_2$ is isomorphous and isostructural with the corresponding zinc complex (3), the structure analysis being initiated with the coordinates of the non-hydrogen atoms of the zinc analog. The $[Co(dmpz)_2(Hdmpz)]_2$ molecule lies on a crystallographic twofold axis. The analysis of the structure of $[Co(dmpz)_2Cl(Hdmpz)]_2Co$ was initiated in the centrosymmetric space group $P\bar{1}$ on the basis of the Patterson functions, this choice being confirmed by the subsequent successful solution and refinement of the structure. The structure of $[Co(dmpz)_2Cl(Hdmpz)]_2Co$ was solved by conventional heavy atom methods, the coordinates of the metal atoms being determined from the Patterson function and those of the remaining non-hydrogen atoms from subsequent difference Fourier syntheses. The non-hydrogen atoms were fixed in idealized positions (methyl group orientations based on observed difference map positions, C—H = 0.98 Å, $B_H = 1.2\ B_{\text{bonded atom}}$). Corrections for secondary extinction were applied for [Co-

[2]TEXAN/TEXRAY structure analysis package (Molecular Structure Corp. 1985) that includes versions of the following: ORFLS, full-matrix least squares, and ORFFE, function and errors, by W.R. Busing, K.O. Martin, and H.A. Levy; ORTEP II, illustrations, by C.K. Johnson.

TABLE 2. Crystallographic data[a]

Compound	$[Co(dmpz)_2(Hdmpz)]_2$	$[Co(dmpz)_2Cl(Hdmpz)]_2Co$
Formula	$C_{30}H_{44}Co_2N_{12}$	$C_{30}H_{44}Cl_2Co_3N_{12}$
fw	690.62	820.46
Crystal system	Orthorhombic	Triclinic
Space group	*Fddd*	$P\bar{1}$
a, Å	17.022(1)	11.742(3)
b, Å	29.224(2)	18.604(4)
c, Å	13.576(2)	8.950(2)
α°	90	99.76(2)
β°	90	102.32(2)
γ°	90	93.36(2)
V, Å^3	6754(1)	1873(2)
Z	8	2
ρ_{calc}, g cm^{-3}	1.358	1.454
F(000)	2896	846
Radiation (λ, Å)	Cu (1.54178)	Mo (0.71069)
μ, cm^{-1}	83.9	14.9
Crystal size, mm	0.12 × 0.18 × 0.22	0.10 × 0.25 × 0.25
Transmission factors	0.62–1.00	0.88–1.00
Scan type	ω–2θ	ω–2θ
Scan range, deg in ω	0.89 + 0.20 tan θ	1.21 + 0.35 tan θ
Scan speed, deg min^{-1}	16	16
Data collected	$+h, +k, +l$	$+h, \pm k, \pm l$
$2\theta_{max}$, deg	155	55
Crystal decay	Negligible	Negligible
Total reflections	1873	9033
Total unique reflections	1873	8607
R_{merge}	—	0.043
Reflections with $I \geq 3\sigma(I)$	938	3853
No. of variables	102	424
R	0.035	0.042
R_w	0.034	0.047
gof	2.08	1.50
Max Δ/σ (final cycle)	0.01	0.004
Residual density e Å^{-3}	−0.26 to 0.26	−0.34 to 0.66

[a]Temperature 294 K, Rigaku AFC6S diffractometer, graphite monochromator, takeoff angle 6.0°, aperture 6.0 × 6.0 mm at a distance of 285 mm from the crystal, stationary background counts at each end of the scan (scan/background time ratio 2:1, up to 8 rescans), $\sigma^2(F^2) = [S^2(C + 4B) + (pF^2)^2]/Lp^2$ (S = scan rate, C = scan count, B = normalized background count, $p = 0.005$ for $[Co(dmpz)_2(Hdmpz)]_2$ and 0.04 for $[Co(dmpz)_2Cl(Hdmpz)]_2Co$,), function minimized $\Sigma w(|F_o| - |F_c|)^2$ where $w = 4F_o^2/\sigma^2(F_o^2)$, $R = \Sigma||F_o| - |F_c||/\Sigma|F_o|$, $R_w = (\Sigma w(|F_o| - |F_c|)^2/\Sigma w|F_w|^2)^{1/2}$, and gof = $[\Sigma w(|F_o| - |F_c|)^2/(m - n)]^{1/2}$. Values given for R, R_w, and gof are based on those reflections with $I \geq 3\sigma(F^2)$.

$(dmpz)_2(Hdmpz)]_2$, the final value of the extinction coefficient being 4.72×10^{-7}. Neutral atom scattering factors for all atoms and anomalous dispersion corrections for the non-hydrogen atoms were taken from the *International tables for X-ray crystallography* (8).

Final atomic coordinates and equivalent isotropic thermal parameters, bond lengths, and bond angles appear in Tables 3–5, respectively. Hydrogen atom parameters, anisotropic thermal parameters, torsion angles, intermolecular contacts, least-squares planes, and measured and calculated structure factor amplitudes for the two structures are included as supplementary material.[3]

[3]Supplementary material mentioned in the text may be purchased from: The Depository of Unpublished Data, Document Delivery, CISTI, National Research Council Canada, Ottawa, Canada K1A 0R6.

Tables of hydrogen atom coordinates and bond lengths and angles involving hydrogen atoms have also been deposited with the Cambridge Crystallographic Data Centre and can be obtained on request from The Director, Cambridge Crystallographic Data Centre, University Chemical Laboratory, 12 Union Road, Cambridge CB2 1EZ, U.K.

Results and discussion

Synthesis and structural studies

During attempts to prepare X-ray diffraction quality single crystals of poly(cobalt(II) 3,5-dimethylpyrazolate), three oligometallic Co(II) species were obtained in macroscopic crystalline form: a dimeric complex with the formula, $[Co(dmpz)_2(Hdmpz)]_2$, a dimeric–oligometallic material with the empirical formula, $Co(dmpz)_2 \cdot 0.344(Hdmpz)$, and a trimetallic complex with the formula $[Co(dmpz)_2Cl(Hdmpz)]_2Co$. The dimeric and dimeric–oligometallic Co(II) compounds were prepared by heating $CoCO_3 \cdot xH_2O$ in very concentrated acetone solutions of 3,5-dimethylpyrazole. More specifically, the pure dimer was prepared by heating a stirred reaction mixture at 75°C and the dimeric–oligometallic mixture was prepared by heating a quiescent reaction mixture at 100°C. The behaviours of these compounds closely parallel those of the analogous Zn(II) compounds, $[Zn(dmpz)_2(Hdmpz)]_2$ and $Zn(dmpz)_2 \cdot 0.323(Hdmpz)$ (3). For example, at lower reaction temperatures (≤90°C), samples

Can. J. Chem. Downloaded from www.nrcresearchpress.com by 203.198.23.82 on 09/08/12
For personal use only.

TABLE 3. Fractional atomic coordinates and B_{eq} (Å^2) with estimated standard deviations in the last digit in parentheses

Atom	x	y	z	B_{eq}
$[Co(dmpz)_2(Hdmpz)]_2$				
Co(1)	0.51405(4)	1/8	1/8	2.97(3)
N(1)	0.4375(1)	0.1774(1)	0.1248(4)	3.4(1)
N(2)	0.3578(1)	0.1693(1)	0.1240(4)	3.8(1)
N(3)	0.5844(1)	0.1229(1)	0.2427(2)	3.0(1)
C(1)	0.4466(2)	0.2231(1)	0.1215(8)	3.5(2)
C(2)	0.3737(3)	0.2441(1)	0.1183(3)	4.2(2)
C(3)	0.3198(2)	0.2093(1)	0.1196(8)	3.8(2)
C(4)	0.5270(2)	0.2438(1)	0.1230(6)	5.1(2)
C(5)	0.2315(2)	0.2100(1)	0.1183(6)	5.3(2)
C(6)	0.5607(2)	0.1218(2)	0.3368(3)	3.2(2)
C(7)	5/8	5/8	0.3991(3)	3.5(2)
C(8)	0.4754(2)	0.1173(2)	0.3629(4)	4.9(2)
$[Co(dmpz)_2Cl(Hdmpz)]_2Co$				
Co(1)	0.32659(6)	0.24762(4)	0.67164(8)	3.04(3)
Co(2)	0.06121(6)	0.20371(4)	0.36453(8)	3.41(3)
Co(3)	0.61861(6)	0.28921(4)	0.91779(8)	3.55(3)
Cl(1)	0.0440(1)	0.2523(1)	0.1485(2)	4.75(6)
Cl(2)	0.7530(1)	0.2125(1)	0.8631(2)	6.07(8)
N(1)	0.2945(4)	0.1597(2)	0.5027(5)	3.3(2)
N(2)	0.1907(3)	0.1400(2)	0.3931(5)	3.2(2)
N(3)	0.1758(3)	0.2910(2)	0.6774(5)	3.4(2)
N(4)	0.0742(3)	0.2732(2)	0.5623(5)	3.5(2)
N(5)	0.3819(3)	0.2167(2)	0.8764(5)	3.2(2)
N(6)	0.4858(3)	0.2437(2)	0.9840(5)	3.3(2)
N(7)	0.4459(3)	0.3227(2)	0.6484(5)	3.4(2)
N(8)	0.5544(4)	0.3424(2)	0.7485(5)	3.3(2)
N(9)	−0.0918(4)	0.1391(3)	0.3176(5)	4.4(2)
N(10)	−0.1694(4)	0.1271(3)	0.1781(5)	4.3(2)
N(11)	0.7188(4)	0.3646(3)	1.0957(5)	4.0(2)
N(12)	0.8377(4)	0.3658(3)	1.1358(5)	4.3(2)
C(1)	0.3643(5)	0.1061(3)	0.4819(6)	4.0(2)
C(2)	0.3065(5)	0.0506(3)	0.3609(6)	4.3(2)
C(3)	0.1996(5)	0.0744(3)	0.3085(6)	3.4(2)
C(4)	0.1513(5)	0.3375(3)	0.7963(6)	3.9(2)
C(5)	0.0354(5)	0.3505(4)	0.7597(7)	5.0(3)
C(6)	−0.0097(5)	0.3095(3)	0.6136(6)	4.1(2)
C(7)	0.3166(5)	0.1777(3)	0.9474(6)	3.8(2)
C(8)	0.3759(5)	0.1797(3)	1.0984(6)	4.2(2)
C(9)	0.4798(5)	0.2210(3)	1.1166(6)	3.9(2)
C(10)	0.4368(5)	0.3633(3)	0.5369(6)	3.8(2)
C(11)	0.5382(5)	0.4097(3)	0.5634(6)	4.0(2)
C(12)	0.6086(5)	0.3954(3)	0.6960(6)	3.4(2)
C(13)	−0.1359(6)	0.0966(4)	0.4004(8)	6.0(3)
C(14)	−0.2396(6)	0.0585(4)	0.312(1)	6.6(3)
C(15)	−0.2590(5)	0.0786(4)	0.1710(8)	5.1(3)
C(16)	0.6934(5)	0.4263(4)	1.1718(7)	4.4(2)
C(17)	0.7954(6)	0.4682(4)	1.2599(7)	5.5(3)
C(18)	0.8850(6)	0.4277(4)	1.2354(8)	5.7(3)
C(19)	0.4850(6)	0.1114(4)	0.5823(8)	6.2(3)
C(20)	0.1014(6)	0.0381(3)	0.1741(6)	4.9(3)
C(21)	0.2427(5)	0.3671(4)	0.9412(7)	5.6(3)
C(22)	−0.1328(5)	0.3020(4)	0.5143(8)	6.2(3)
C(23)	0.1986(5)	0.1420(3)	0.8624(7)	5.2(3)
C(24)	0.5802(6)	0.2409(4)	1.2585(7)	5.3(3)
C(25)	0.3276(6)	0.3538(4)	0.4080(7)	5.9(3)
C(26)	0.7289(5)	0.4310(3)	0.7776(7)	5.1(3)
C(27)	−0.0749(8)	0.0974(5)	0.565(1)	10.1(5)
C(28)	−0.3571(6)	0.0573(4)	0.031(1)	8.1(4)
C(29)	0.5688(6)	0.4445(4)	1.1538(7)	5.7(3)
C(30)	1.0151(6)	0.4422(4)	1.299(1)	9.0(4)

Can. J. Chem. Downloaded from www.nrcresearchpress.com by 203.198.23.82 on 09/08/12
For personal use only.

TABLE 4. Bond lengths (Å) with estimated standard deviations in the last digit in parentheses[a]

Atom	Atom	Distance	Atom	Atom	Distance
$[Co(dmpz)_2(Hdmpz)]_2$					
Co(1)	N(1)	2.010(3)	C(1)	C(2)	1.385(5)
Co(1)	N(3)	1.998(2)	C(1)	C(4)	1.498(5)
N(1)	N(2)	1.377(3)	C(2)	C(3)	1.371(5)
N(1)	C(3)	1.344(4)	C(3)	C(5)	1.504(4)
N(2)	C(1)	1.337(4)	C(6)	C(7)	1.388(4)
N(3)	N(3)′	1.387(4)	C(6)	C(8)	1.500(4)
N(3)	C(6)	1.340(4)			
$[Co(dmpz)_2Cl(Hdmpz)]_2Co$					
Co(1)	N(1)	1.988(4)	N(10)	C(15)	1.329(7)
Co(1)	N(3)	1.996(4)	N(11)	N(12)	1.363(6)
Co(1)	N(5)	2.001(4)	N(11)	C(16)	1.316(7)
Co(1)	N(7)	1.988(4)	N(12)	C(18)	1.340(7)
Co(2)	Cl(1)	2.246(2)	C(1)	C(2)	1.387(7)
Co(2)	N(2)	1.983(4)	C(1)	C(19)	1.495(8)
Co(2)	N(4)	1.978(4)	C(2)	C(3)	1.370(7)
Co(2)	N(9)	2.025(5)	C(3)	C(20)	1.508(7)
Co(3)	Cl(2)	2.263(2)	C(4)	C(5)	1.377(8)
Co(3)	N(6)	1.977(4)	C(4)	C(21)	1.493(7)
Co(3)	N(8)	1.988(4)	C(5)	C(6)	1.375(7)
Co(3)	N(11)	2.034(5)	C(6)	C(22)	1.512(8)
N(1)	N(2)	1.377(5)	C(7)	C(8)	1.375(7)
N(1)	C(1)	1.341(7)	C(7)	C(23)	1.487(8)
N(2)	C(3)	1.346(6)	C(8)	C(9)	1.366(7)
N(3)	N(4)	1.381(5)	C(9)	C(24)	1.513(8)
N(3)	C(4)	1.345(6)	C(10)	C(11)	1.381(7)
N(4)	C(6)	1.343(6)	C(10)	C(25)	1.510(8)
N(5)	N(6)	1.389(5)	C(11)	C(12)	1.370(7)
N(5)	C(7)	1.348(6)	C(12)	C(26)	1.501(7)
N(6)	C(9)	1.340(6)	C(13)	C(14)	1.380(9)
N(7)	N(8)	1.380(5)	C(13)	C(27)	1.49(1)
N(7)	C(10)	1.340(6)	C(14)	C(15)	1.36(1)
N(8)	C(12)	1.345(6)	C(15)	C(28)	1.490(0)
N(9)	N(10)	1.355(6)	C(16)	C(17)	1.393(8)
N(9)	C(13)	1.326(7)	C(16)	C(29)	1.502(8)
C(17)	C(18)	1.362(9)	C(18)	C(30)	1.502(9)

[a]The primed atom has coordinates related to those in Table 3 by the symmetry operations: 5/4-x, 1/4-y, z.

Can. J. Chem. Downloaded from www.nrcresearchpress.com by 203.198.23.82 on 09/08/12
For personal use only.

of pure $[M(dmpz)_2(Hdmpz)]_2$ (M = Co, Zn) may be prepared, but at higher temperatures (≥100°C), materials with the empirical formula $M(dmpz)_2 \cdot x(Hdmpz)$ (M = Co, Zn; $x < 1$) are formed instead. It was previously suggested in the case of $Zn(dmpz)_2 \cdot 0.323(Hdmpz)$ that the material consists of a mixture of dimeric and longer chain oligometallic species (3). We propose that $Co(dmpz)_2 \cdot 0.344(Hdmpz)$ possesses an analogous composition, and evidence in support of this will be presented after discussion of the structure of $[Co(dmpz)_2(Hdmpz)]_2$.

$[Co(dmpz)_2(Hdmpz)]_2$ is isomorphous and isostructural with $[Zn(dmpz)_2(Hdmpz)]_2$ (3). The molecular structure (Fig. 1) consists of two cobalt ions bridged by two dmpz anions with each cobalt being end-capped by a pyrazolate ion and a neutral Hdmpz molecule. The coordination geometry about the cobalt centres is pseudo-tetrahedral (crystallographic D_2 point symmetry) with Co—N bond lengths between the bridging and terminal dmpz moieties of 1.998(2) and 2.010(3) Å, respectively. N—Co—N bond angles range from 99.2(1)° to 114.4(2)° (average = 107.8°) and the dihedral angle between the normals of the central $Co(N–N)_2Co$ and terminal $Co(N–N)_2H$ planes is 87.8°. The cobalt centres in the molecule are separated by a nonbonding distance of 3.777 Å. Figure 2 depicts the unit cell packing of $[Co(dmpz)_2(Hdmpz)]_2$. The figure shows how individual molecules lie in sheets parallel to the *ab*-plane of the crystal lattice such that all of their terminal ligands are coplanar. Within each sheet, Co–Co vectors of individual molecules align in a coparallel manner and, moreover, chains of Co–Co vectors running along the *a*-axis are not only coparallel, but collinear. Adjacent sheets are oriented such that the dimer molecules in the neighbouring sheets are staggered by translation of one dimer length along the *a*-axis. This structural arrangement has important consequences for the formation of $Co(dmpz)_2 \cdot 0.344(Hdmpz)$, as will be discussed below.

The infrared data for $[Co(dmpz)_2(Hdmpz)]_2$ reflect the presence of strong hydrogen bonding in the molecule with the appearance of two broad ν_{NH} bands at ~2380 and ~1870 cm^{-1} and a γ_{NH} band appearing at 865 cm^{-1} (cf. $[Zn(dmpz)_2(Hdmpz)]_2$ (3)).

Returning to discussion of the structural composition of

Can. J. Chem. Downloaded from www.nrcresearchpress.com by 203.198.23.82 on 09/08/12
For personal use only.

TABLE 5. Bond angles (°) with estimated standard deviations in the last digit in parentheses[a]

Atom	Atom	Atom	Angle	Atom	Atom	Atom	Angle
$[Co(dmpz)_2(Hdmpz)]_2$							
N(1)	Co(1)	N(1)″	99.2(1)	N(2)	C(1)	C(2)	109.9(3)
N(1)	Co(1)	N(3)	114.4(2)	N(2)	C(1)	C(4)	120.4(3)
N(1)	Co(1)	N(3)″	111.3(2)	C(2)	C(1)	C(4)	129.7(3)
N(3)	Co(1)	N(3)″	106.3(1)	C(1)	C(2)	C(3)	105.6(3)
Co(1)	N(1)	N(2)	120.5(2)	N(1)	C(3)	C(2)	109.0(3)
Co(1)	N(1)	C(3)	133.0(2)	N(1)	C(3)	C(5)	119.7(4)
N(2)	N(1)	C(3)	106.4(3)	C(2)	C(3)	C(5)	131.3(4)
N(1)	N(2)	C(1)	109.2(3)	N(3)	C(6)	C(7)	110.0(3)
Co(1)	N(3)	N(3)′	126.47(8)	N(3)	C(6)	C(8)	121.3(3)
Co(1)	N(3)	C(6)	125.6(2)	C(7)	C(6)	C(8)	128.7(3)
N(3)′	N(3)	C(6)	107.6(2)	C(6)	C(7)	C(6)′	104.8(4)
$[Co(dmpz)_2Cl(Hdmpz)]_2Co$							
N(1)	Co(1)	N(3)	108.1(2)	N(4)	N(3)	C(4)	107.8(4)
N(1)	Co(1)	N(5)	109.2(2)	Co(2)	N(4)	N(3)	124.1(3)
N(1)	Co(1)	N(7)	113.9(2)	Co(2)	N(4)	C(6)	128.6(3)
N(3)	Co(1)	N(5)	107.1(2)	N(3)	N(4)	C(6)	107.2(4)
N(3)	Co(1)	N(7)	110.1(2)	Co(1)	N(5)	N(6)	125.5(3)
N(5)	Co(1)	N(7)	108.4(2)	Co(1)	N(5)	C(7)	126.0(3)
Cl(1)	Co(2)	N(2)	113.2(1)	N(6)	N(5)	C(7)	107.3(4)
Cl(1)	Co(2)	N(4)	116.5(1)	Co(3)	N(6)	N(5)	120.6(3)
Cl(1)	Co(2)	N(9)	101.6(1)	Co(3)	N(6)	C(9)	131.2(4)
N(2)	Co(2)	N(4)	108.4(2)	N(5)	N(6)	C(9)	107.2(4)
N(2)	Co(2)	N(9)	107.9(2)	Co(1)	N(7)	N(8)	124.7(3)
N(4)	Co(2)	N(9)	108.6(2)	Co(1)	N(7)	C(10)	127.3(4)
Cl(2)	Co(3)	N(6)	114.9(1)	N(8)	N(7)	C(10)	107.9(4)
Cl(2)	Co(3)	N(8)	114.5(1)	Co(3)	N(8)	N(7)	123.5(3)
Cl(2)	Co(3)	N(11)	100.9(1)	Co(3)	N(8)	C(12)	128.8(3)
N(6)	Co(3)	N(8)	108.3(2)	N(7)	N(8)	C(12)	107.2(4)
N(6)	Co(3)	N(11)	110.7(2)	Co(2)	N(9)	N(10)	123.5(4)
N(8)	Co(3)	N(11)	107.1(2)	Co(2)	N(9)	C(13)	131.6(4)
Co(1)	N(1)	N(2)	125.2(3)	N(10)	N(9)	C(13)	104.8(5)
Co(1)	N(1)	C(1)	126.9(4)	N(9)	N(10)	C(15)	112.6(5)
N(2)	N(1)	C(1)	107.7(4)	Co(3)	N(11)	N(12)	122.1(4)
Co(2)	N(2)	N(1)	123.8(3)	Co(3)	N(11)	C(16)	130.8(4)
Co(2)	N(2)	C(3)	128.7(3)	N(12)	N(11)	C(16)	105.9(5)
N(1)	N(2)	C(3)	107.3(4)	N(11)	N(12)	C(18)	110.7(5)
Co(1)	N(3)	N(4)	125.0(3)	N(1)	C(1)	C(2)	109.8(5)
Co(1)	N(3)	C(4)	127.0(3)	N(1)	C(1)	C(19)	120.9(5)
C(2)	C(1)	C(19)	129.3(6)	N(7)	C(10)	C(25)	120.5(5)
C(1)	C(2)	C(3)	104.8(5)	C(11)	C(10)	C(25)	130.1(5)
N(2)	C(3)	C(2)	110.4(5)	C(10)	C(11)	C(12)	105.6(5)
N(2)	C(3)	C(20)	120.9(5)	N(8)	C(12)	C(11)	109.9(5)
C(2)	C(3)	C(20)	128.7(5)	N(8)	C(12)	C(26)	122.2(5)
N(3)	C(4)	C(5)	109.5(5)	C(11)	C(12)	C(26)	127.9(5)
N(3)	C(4)	C(21)	121.5(5)	N(9)	C(13)	C(14)	109.8(6)
C(5)	C(4)	C(21)	129.0(6)	N(9)	C(13)	C(27)	120.0(6)
C(4)	C(5)	C(6)	105.5(5)	C(14)	C(13)	C(27)	130.2(7)
N(4)	C(6)	C(5)	110.0(5)	C(13)	C(14)	C(15)	107.3(6)
N(4)	C(6)	C(22)	120.8(5)	N(10)	C(15)	C(14)	105.6(6)
C(5)	C(6)	C(22)	129.3(5)	N(10)	C(15)	C(28)	122.7(7)
N(5)	C(7)	C(8)	109.5(5)	C(14)	C(15)	C(28)	131.7(7)
N(5)	C(7)	C(23)	120.4(5)	N(11)	C(16)	C(17)	110.4(6)
C(8)	C(7)	C(23)	130.1(5)	N(11)	C(16)	C(29)	120.8(6)
C(7)	C(8)	C(9)	105.8(5)	C(17)	C(16)	C(29)	128.7(6)
N(6)	C(9)	C(8)	110.2(5)	C(16)	C(17)	C(18)	105.7(6)
N(6)	C(9)	C(24)	120.7(5)	N(12)	C(18)	C(17)	107.3(5)
C(8)	C(9)	C(24)	129.0(5)	N(12)	C(18)	C(30)	121.1(7)
C(7)	C(10)	C(11)	109.3(5)	C(17)	C(18)	C(30)	131.6(7)

[a]Primed and double-primed atoms have coordinates related to those in Table 3 by the symmetry operations: 5/4-x, 1/4-y, z; and x, 1/4-y, 1/4-z, respectively.

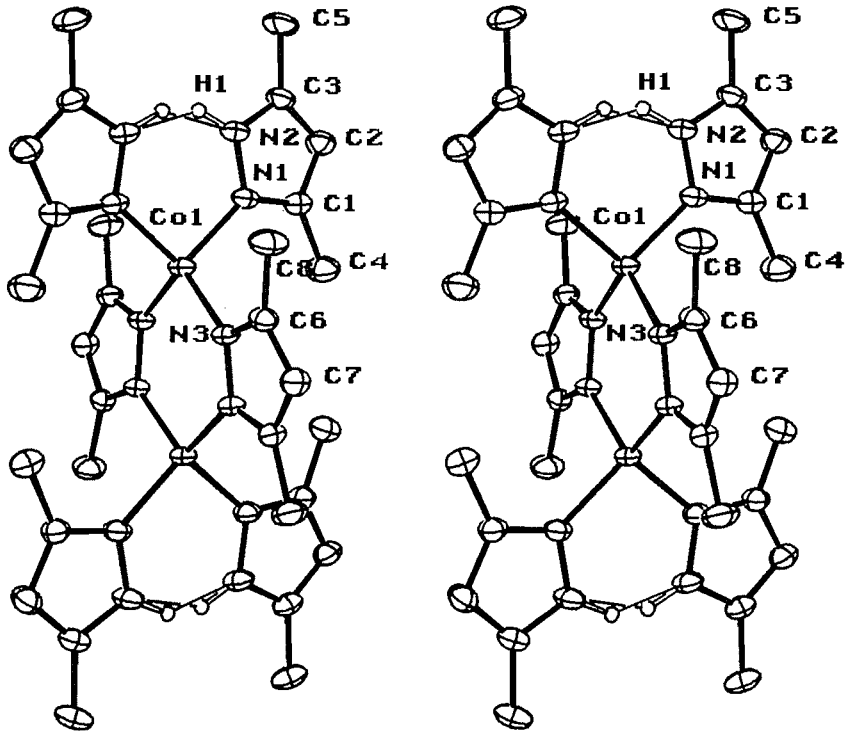

FIG. 1. Stereoscopic view of the $[Co(dmpz)_2(Hdmpz)]_2$ molecule; 50% probability thermal ellipsoids are shown for the non-hydrogen atoms.

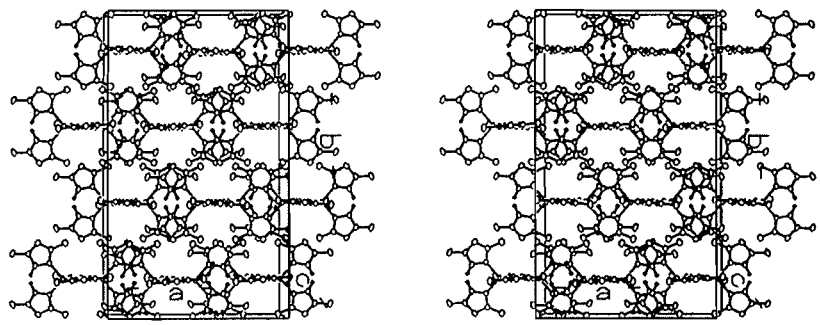

FIG. 2. Stereoscopic view of the unit cell packing in the crystal structure of $[Co(dmpz)_2(Hdmpz)]_2$.

$Co(dmpz)_2 \cdot 0.344(Hdmpz)$, if a structure consisting of a doubly pyrazolate-bridged chain of Co(II) ions with end-capping neutral ligands is assumed for this compound, then the nominal formulation corresponds to a mean chain length of 5.8 Co(II) ions. One possible composition is a biphasic distribution; the bulk compound consists of a mixture of the dimeric phase and the infinite polymer phase such that their ratio yields the observed empirical formula. Electronic spectroscopy indicates that such a dispersion is very unlikely. The electronic spectra of $Co(dmpz)_2 \cdot 0.344(Hdmpz)$ and $[Co(dmpz)_2(Hdmpz)]_2$ (Table 1) are very similar and are consistent with that of a fairly regular tetrahedral CoN_4 chromophore (9) like the type structurally characterized in the dimer. Pure polymeric $[Co(dmpz)_2]_x$ exhibits a distinctly different electronic spectrum (7), one consistent with a more distorted tetrahedral geometry about cobalt (9). There is no evidence of this polymer in the spectrum of $Co(dmpz)_2 \cdot 0.344(Hdmpz)$, thus disproving the biphasic distribution model, which requires the sample to be ~66% (by mole Co(II) ions) polymer phase. Moreover, microscopic examination of the sample revealed it to consist entirely of macroscopic crystals, all of the same colour and morphology. Most of the crystals were opaque, but a few of the smaller crystals were quite transparent. One might expect the presence of two crystal morphologies in a biphasic distribution.

Observation of a small sample of crystals of $Co(dmpz)_2 \cdot 0.344(Hdmpz)$ heated in a melting point apparatus indicated that, between 180 and 200°C, colourless crystals of Hdmpz sublimed from the sample. There appeared to be no physical deterioration of the sample crystals at that point. Heating of the sample to the apparatus limit of 360°C revealed no further change. Microscopic examination of the sample before the heating process revealed it to consist of large, almost opaque, dark purple crystals whose morphology is best described as elongated octahedral. The crystal facets were shiny and the crystal edges sharp. After heating, microscopic examination showed that the crystal facets had now become dull and chalky; however, the crystal edges were still sharp and the crystals had maintained their me-

Can. J. Chem. Downloaded from www.nrcresearchpress.com by 203.198.23.82 on 09/08/12
For personal use only.

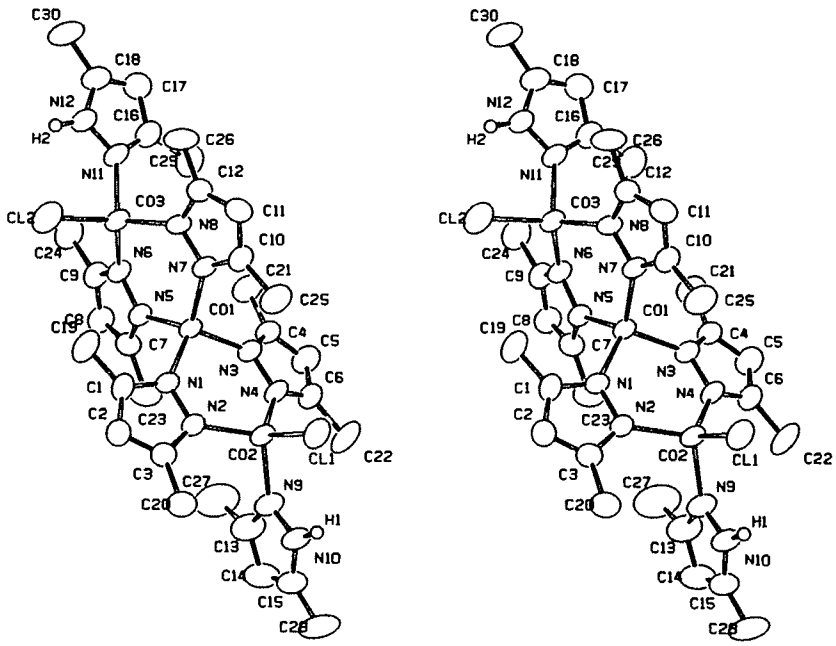

FIG. 3. Stereoscopic ORTEP diagram of the $[Co(dmpz)_2Cl(Hdmpz)]_2Co$ molecule; 33% probability thermal ellipsoids are shown for the non-hydrogen atoms.

chanical integrity. Evidently the thermolysis of this material, resulting in volatilization of Hdmpz consistent with polymerization, left the original crystals largely intact. This suggests that either the crystal lattice of this material can tolerate considerable molecular reorganization, or that relatively little reorganization occurs during volatilization of Hdmpz.

The results of the single crystal diffraction study of $[Co(dmpz)_2(Hdmpz)]_2$ are important in this discussion because the crystal selected for X-ray study formed one half of a larger, elongated octahedral crystal from the sample of $Co(dmpz)_2 \cdot 0.344(Hdmpz)$! This particular half crystal was chosen because it was much more transparent than the remainder of the whole crystal or the other crystals in the sample. A well-formed, but opaque, crystal that had been selected previously for study was found to diffract X-rays too poorly to be useful. In other words, the crystal structure of the dimeric species appears to be compatible with the bulk sample of $Co(dmpz)_2 \cdot 0.344(Hdmpz)$, but not necessarily representative of the molecular contents of most of the crystals in the bulk sample.

The information presented about $Co(dmpz)_2 \cdot 0.344(Hdmpz)$ above suggests that most of the sample consists of oligometallic species with the general formula, $[Co(dmpz)_2]_n(Hdmpz)_2$. Figure 2 illustrates that the crystal lattice of $[Co(dmpz)_2(Hdmpz)]_2$ contains columns, parallel to the *c*-axis, of overlapped terminal pyrazolyl rings with the ring planes normal to the *c*-axis. Thus, the structure of the dimeric phase appears particularly amenable to polymerization of the dimer molecules. This may occur through a process of molecular dislocation in which a dimer molecule from one *ab*-sheet in the lattice moves into the gap between dimer molecules in an adjacent sheet (Fig. 2) with the concomitant release of four molecules of Hdmpz. If such a process occurs in this material, then one might expect chain lengths to increase by steps of four. In other words, oligometallic chains would be present in the bulk material containing 2, 6, 10, etc. metal ions. That both the zinc (3) and cobalt oligometallic species possess mean chain lengths close to six (6.2 and 5.8, respectively) is consistent with (but by no means proof for) such a process.

As mentioned above, the trimetallic complex $[Co(dmpz)_2Cl(Hdmpz)]_2Co$ was prepared during attempts to grow diffraction-quality single crystals of $[Co(dmpz)_2]_x$. Once it was recognized that the trimetallic complex could be prepared, the reaction conditions were modified to intentionally prepare this compound in bulk quantities. This is described in the experimental section. The compound is air-insensitive and sparingly soluble in CH_2Cl_2 and acetone. The DSC thermogram of the complex shows an endothermic event at 293°C (probably melting) followed immediately by exothermic decomposition.

$[Co(dmpz)_2Cl(Hdmpz)]_2Co$ crystallizes in the space group $P\bar{1}$ as a trimetallic molecule with the Co(II) ions in an approximately linear arrangement (Fig. 3). The terminal Co(II) ions are linked to the central cobalt by double 3,5-dimethylpyrazolate bridges. The central cobalt is coordinated by four pyrazolate nitrogen atoms in a pseudo-tetrahedral fashion with Co—N bond lengths ranging from 1.988(4) to 2.001(4) Å (average = 1.993 Å), N—Co—N bond angles ranging from 107.1(2)° to 113.9(2)°, and a dihedral angle between the fused N—Co—N planes running along the approximate molecular Co–Co–Co axis of 90.2° (the angle formed by these three cobalt centres is 169.2°). The terminal Co(II) ions are each coordinated by two bridging pyrazolate nitrogen atoms, one terminal 3,5-dimethylpyrazole nitrogen atom, and one terminal chloride ion in a distorted tetrahedral manner. The average terminal Co—N bond length is somewhat longer than the average bridging Co—N bond length (2.030(5) versus 1.981(5) Å, respectively) and the average Co—Cl bond length is 2.25(1) Å. Both $Co(N–N)_2Co$ rings in the complex exhibit a half-boat conformation in which the terminal cobalt is displaced from the mean plane defined by the central cobalt and the four nitrogen atoms. The average dis-

Can. J. Chem. Downloaded from www.nrcresearchpress.com by 203.198.23.82 on 09/08/12
For personal use only.

Can. J. Chem. Downloaded from www.nrcresearchpress.com by 203.198.23.82 on 09/08/12
For personal use only.

tance between cobalt centres within the $Co(N–N)_2Co$ rings is nonbonding at 3.627 Å. There are two molecules per unit cell related by an inversion centre. The "pyrrolic" hydrogen atom of the terminal Hdmpz ligand is hydrogen bonded to the chloride ligand of an adjacent molecule and vice versa (average N...Cl = 3.376 Å), creating chains of the trimetallic complex running along the *a*-direction of the crystal lattice. The infrared spectrum of $[Co(dmpz)_2Cl(Hdmpz)]_2Co$ exhibits a strong, relatively sharp, ν_{NH} band at 3265 cm^{-1}, consistent with the hydrogen bonding, which is significantly weaker than that in the dimeric compound, as indicated in its crystal structure.

The electronic spectrum of $[Co(dmpz)_2Cl(Hdmpz)]_2Co$ (Table 1) reveals considerable structure in the formally ν_2 and ν_3 transitions with bandwidths of the order of 6000 and 2500 cm^{-1} in the former and latter transitions, respectively. The large bandwidths and band structure are principally due to the presence of two different chromophores revealed by the X-ray diffraction study on the complex. The compound possesses a central CoN_4 chromophore of close to regular tetrahedral symmetry and two terminal CoN_3Cl chromophores of lower symmetry; the crystallographic symmetry of the CoN_3Cl chromophores is C_1 and they have very approximate C_{3v} point symmetry (see Fig. 3).

Magnetic properties

Magnetic susceptibility measurements (2–300 K) were made on powdered samples of $[Co(dmpz)_2Cl(Hdmpz)]_2Co$ and $[Co(dmpz)_2(Hdmpz)]_2$. Susceptibility and effective magnetic moment data have been deposited.[3] Data for $[Co(dmpz)_2Cl(Hdmpz)]_2Co$ are presented as a magnetic moment versus temperature plot in Fig. 4. The magnetic moment of the compound decreases from a value of 7.44 μ_B at 300 K to 2.96 μ_B at 2 K. This decrease in moment as the sample is cooled may reflect one or both of zero-field splitting (ZFS) and antiferromagnetic exchange effects. A plot of χ_M versus temperature for $[Co(dmpz)_2(Hdmpz)]_2$ is given in Fig. 5. The presence of a maximum in χ_M at ~27 K indicates antiferromagnetic coupling between the Co(II) centres. At the lowest temperatures studied the magnetic susceptibility begins to increase again and this is most likely due to the presence of structural paramagnetic impurity in the sample. In an effort to quantify the magnitudes of the exchange interaction in these complexes, we have attempted to fit their magnetic data to two types of theoretical exchange models: isotropic Heisenberg models and anisotropic Ising models. The specific models employed for the dimeric and trimetallic complexes are discussed separately below.

In the case of $[Co(dmpz)_2Cl(Hdmpz)]_2Co$, a spin vector coupling scheme first proposed by Kambe for trimetallic systems (10), and later generalized by Sinn (11), was used to derive an expression for the magnetic susceptibility of a Heisenberg, exchange-coupled, $S = 3/2$ linear trimetallic system. The expression is rather long and has been deposited.[3] The equation assumes no difference between central and terminal Co(II) *g* values and allows one to vary the exchange coupling constants, J (nearest neighbour) and J_{13} (next-nearest neighbour), independently. In addition to applying this equation, fits to various temperature ranges of data were made using a trimetallic $S' = 1/2$ Ising model (12), an $S' = 1/2$ Heisenberg model (13), and the trimetallic Heisenberg $S = 3/2$ equation combined with the molecular field equation (14):

$$\chi'_{calc} = \frac{\chi_{calc}}{1 - (2zJ'/Ng^2\mu_B{}^2)\chi_{calc}}$$

where z is the number of interacting neighbouring molecules and J' is the magnitude of exchange coupling with those molecules. The equation above compensates for secondary intermolecular interactions. Fits of the experimental data to the models were achieved using a nonlinear least-squares procedure with the following as the function minimized:

$$F = \left[\frac{1}{n}\sum_{i=1}^{n}\frac{(\chi_i^{obs} - \chi_i^{calc})^2}{(\chi_i^{obs})^2}\right]^{1/2}$$

The F value provides a measure of the goodness of fit between theory and experiment. Experimental susceptibility versus temperature data are compared with theory in Fig. 4 and values of the exchange coupling constant, J, the other fitting parameters, and the fitting function, F, for various fits are listed in Table 6.

Table 6 shows clearly that the models based on the $S' = 1/2$ formalism yield very poor fits, even over a narrow temperature range. Though not shown here, allowing J_{13} to vary in these models causes only a marginal improvement in the quality of the fits, but at the expense of an indeterminate J_{13}. It is only the $S = 3/2$ based models that have yielded good fits to the susceptibility data. A good quality fit was achieved for the data from 12–300 K by neglecting J_{13} (Fig. 4). At the lowest temperatures, however, the observed magnetic moment can be seen (Fig. 4) to drop well below the moment predicted by the model. Recalling that the molecular structure demonstrates considerable distortion of the terminal Co(II) ions away from ideal tetrahedral symmetry and that the electronic spectrum for the complex supports this observation, it is possible that the low observed magnetic moments at low temperatures are due to zero-field splitting effects. Attempts to model the lower temperature data (<10 K) with the ZFS expression for $S = 3/2$ ions (14), however, yielded a poor fit ($F = 0.10$) and an indeterminate D.

The best fit over the full data range was achieved by allowing both J and J_{13} to vary (Fig. 4). If the best fit results are to be believed, then $[Co(dmpz)_2Cl(Hdmpz)]_2Co$ exhibits a next-nearest neighbour exchange interaction that is ~60% of the nearest neighbour interaction. Some precedence for this is found in the work of Mackey and Martin on the magnetic properties of the linear trimetallic nickel(II) complex, $[(Ni(1,2,4\text{-triazole})_3,(OH_2)_3)_2Ni][NO_3]_6 \cdot 2H_2O$ (15). It was concluded in this work that the complex experiences a next-nearest neighbour exchange coupling of a magnitude ~50% of that of the nearest neighbour exchange. Reedijk and co-workers reported studies of trimetallic and bimetallic, first row transition metal complexes in which the bridging ligands were alkylated 1,2,4-triazolyl moieties (12, 16–22) and several of these reports describe work performed on Co(II) species. In their analyses of the magnetic properties of these compounds, however, J_{13} was assumed to be zero and they cited several experimental findings to justify neglect of J_{13} in their modelling procedures (12, 17, 19, 21). Moreover, in a recent communication, Antolini et al. described the structural and magnetic characterization of a mixed valence Co(II)–Co(III) complex in which a central Co(III) ion is connected to two terminal Co(II) ions by tri-

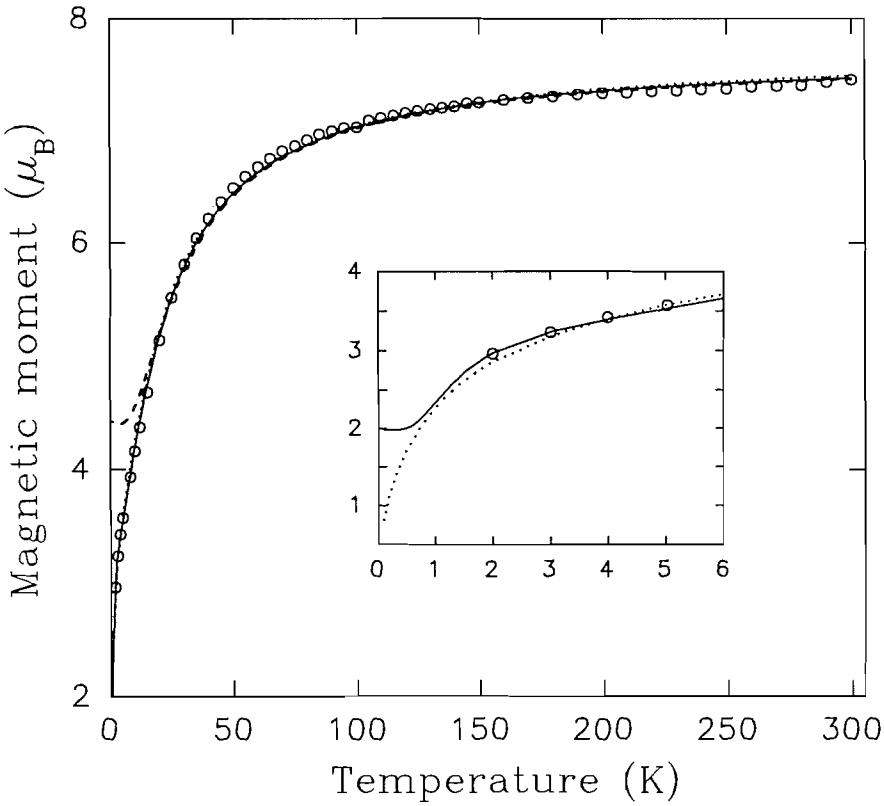

FIG. 4. Plot of effective magnetic moment versus temperature for $[Co(dmpz)_2Cl(Hdmpz)]_2Co$. The solid line represents the best fit of the trimetallic Heisenberg model with J and J_{13} variable. The dashed line represents the same model with J_{13} fixed at zero. The dotted line represents the preceding model coupled with a molecular field term.

Can. J. Chem. Downloaded from www.nrcresearchpress.com by 203.198.23.82 on 09/08/12
For personal use only.

ple triazolyl bridges (23). The terminal Co(II) ions of the mixed valence complex were found to be magnetically uncoupled.

Consideration of the crystal structure of $[Co(dmpz)_2Cl(Hdmpz)]_2Co$ suggests an alternative interpretation of the exchange interactions in the complex. In the crystal lattice each $[Co(dmpz)_2Cl(Hdmpz)]_2Co$ molecule is linked to two adjacent neighbours through hydrogen bonds. There is considerable precedence for the mediation of magnetic exchange via hydrogen-bonded bridges (24), and, to explore this possibility, the magnetic susceptibility of the complex was modelled using the trimetallic Heisenberg $S = 3/2$ equation with J_{13} fixed at zero and coupled with the molecular field expression to account for intermolecular interaction. This model yields a good fit to the data over the whole temperature range and an even better fit if only the data above 12 K are considered (dotted curve Fig. 4). However, application of the molecular field correction is justifiable only if $J/zJ' > 5$–10 (14) and the results in Table 6 correspond to smaller ratios. Further experimentation might provide additional insight regarding the low-temperature properties of this trimetallic compound. The inset of Fig. 4 shows μ_{eff} predicted by the two models extrapolated to very low temperature. If susceptibility measurements could be made to these low temperatures, then the two modes of coupling could possibly be distinguished. Furthermore, magnetization studies could also shed light on the problem. A caveat here, though, is that if paramagnetic impurity is present in the sample it may be masking the true low-temperature behaviour of the complex as paramagnetic impurity contributions to the magnetic properties of antiferromagnetically coupled systems are greatest at the lowest temperatures.

We turn now to a discussion of the magnetic properties of the dimeric molecule, $[Co(dmpz)_2(Hdmpz)]_2$. The dimeric Heisenberg model for $S = 3/2$ gives

$$\chi_{dimer} = \frac{Ng^2\mu_B{}^2}{kT} \cdot \frac{e^{2x} + 5e^{6x} + 14e^{12x}}{1 + 3e^{2x} + 5e^{6x} + 7e^{12x}}$$

where $x = J/kT$ (14). The dimeric Ising model for $S = 1/2$ gives

$$\chi_{dimer} = \frac{1}{3}\left[\frac{Ng^2\mu_B{}^2}{2kT} \cdot \frac{e^x}{1 + e^x}\right]$$

where $x = J/kT$ (25). Attempts were made to fit the data over various temperature ranges and when the lowest temperature data were included in fits, the expressions shown above were combined with the Curie law term,

$$\chi_{para} = \frac{Ng^2\mu_B{}^2S(S + 1)}{3kT}$$

or the Curie–Weiss law term.

$$\chi_{para} = \frac{Ng^2\mu_B{}^2S(S + 1)}{3k(T - \theta)}$$

in the following way;

$$\chi_M = [1 - P]\chi_{dimer} + P\chi_{para}$$

Can. J. Chem. Downloaded from www.nrcresearchpress.com by 203.198.23.82 on 09/08/12
For personal use only.

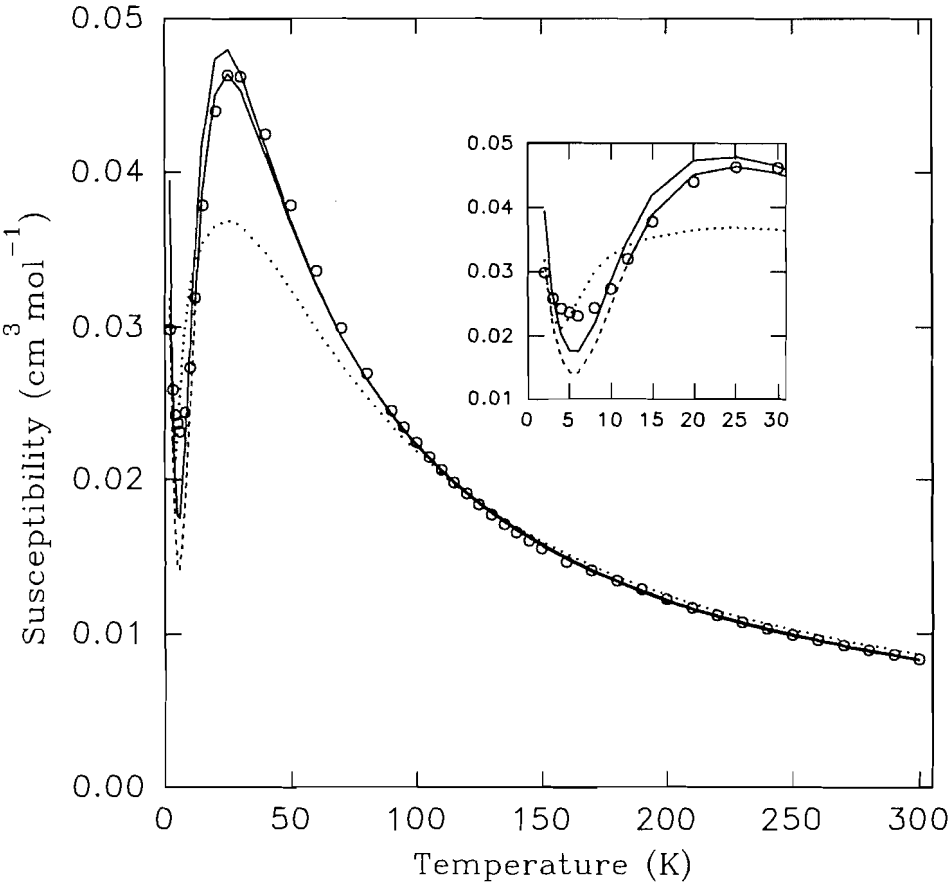

FIG. 5. Plot of magnetic susceptibility versus temperature for $[Co(dmpz)_2(Hdmpz)]_2$. The solid lines represent the best fits of the dimeric Ising model (with a Curie–Weiss law term) from 2–300 K (upper line) and 12–300 K (lower line, the dashed line is an extrapolation of the fit). The dotted line represents the best fit of the Heisenberg model (with a Curie–Weiss law term).

TABLE 6. Derived magnetic parameters for $[Co(dmpz)_2Cl(Hdmpz)]_2Co$ with uncertainties in the last digit in parentheses

Model[a]	Temperature range (K)	$-J$ (cm^{-1})	$-J_{13}$ (cm^{-1})	$-zJ'$ (cm^{-1})	g	F
HT1/2	2–300	9(1)	0[b]	—	4.63(8)	0.19
	2–40	4.9(9)	0[b]	—	3.9(1)	0.14
IT1/2	2–50	7(2)	—	—	11.9(5)	0.17
HT3/2	2–40	1.2(4)	0[b]	—	1.72(8)	0.15
	2–300	2.3(4)	0[b]	—	2.08(4)	0.20
	12–300	3.6(1)	0[b]	—	2.287(9)	0.027
	2–300	2.84(3)	1.76((2)	—	2.292(3)	0.011
HT3/2MF	2–300	2.48(5)	0[b]	0.75(1)	2.304(5)	0.015
	12–300	2.3(3)	0[b]	0.8(2)	2.305(5)	0.013

[a]Abbreviations: HT1/2, Heisenberg trimetallic $S' = 1/2$; IT1/2, Ising trimetallic $S' = 1/2$; HT3/2, Heisenberg trimetallic $S = 3/2$; HT3/2MF, Heisenberg trimetallic $S = 3/2$ plus molecular field exchange.
[b]Fixed at zero.

where $100P$ represents the percent paramagnetic impurity ($\%P$). In addition, fits were made combining the Heisenberg and Ising equations listed above with the molecular field equation. The data were fit in the same manner for the dimer as described for $[Co(dmpz)_2Cl(Hdmpz)]_2Co$ and the results of these modelling efforts are listed in Table 7 and depicted in Fig. 5.

It is clear that the data in the 12–300 K region can be reasonably well fit with either the Heisenberg $S = 3/2$ or Ising $S' = 1/2$ models, with a generally better fit employing the Ising model. Fits employing the full data set (2–300 K) are significantly poorer for both models. Modifications to each model involving the inclusion of a molecular field term or a Curie–Weiss law paramagnetic impurity term gave a significant improvement to the fit in only one case. The fit involving the Ising model and a Curie–Weiss term is excellent

TABLE 7. Derived magnetic parameters for $[Co(dmpz)_2(Hdmpz)]_2$ with uncertainties in the last digit in parentheses

Model[a]	Temperature range (K)	$-J$ (cm^{-1})	g	$\%P$	$-zJ'$ (cm^{-1})	θ (K)	F
HD3/2	2–300	6.4(2)	2.46(2)	2.2(1)	—	—	0.089
	12–300	5.2(1)	2.41(1)	0[b]	—	—	0.049
HD3/2MF	2–300	7.1(2)	2.26(3)	2.9(1)	8(1)	—	0.062
HD3/2θ	2–300	6.4(4)	2.46(3)	2.1(6)	—	0.1(6)	0.089
ID1/2	2–300	22.0(5)	9.16(7)	3.0(1)	—	—	0.082
	12–300	22.9(4)	9.22(2)	2.4(7)	—	—	0.014
ID1/2MF	2–300	21.4(5)	9.3(1)	2.8(2)	9(6)	—	0.080
ID1/2θ	2–300	25.2(2)	9.26(2)	10.2(8)	—	−7.2(8)	0.020

[a]Abbreviations: HD3/2, Heisenberg dimeric $S = 3/2$; HD3/2MF, Heisenberg dimertic $S = 3/2$ plus molecular field exchange; ID1/2, Ising dimeric $S' = 1/2$; ID1/2MF, Ising dimeric $S' = 1/2$ plus molecular field exchange; ID1/2θ, Ising dimeric $S' = 1/2$ with Curie–Weiss law paramagnetic impurity.

[b]When allowed to vary, $\%P$ took on a physically unrealistic negative value. Consequently, $\%P$ was fixed at zero.

over the whole temperature range (Table 7); however, this fit comes at the expense of a significantly larger paramagnetic impurity content.

Our inability to satisfactorily fit the data below 12 K may rise from our inability to explicitly model ZFS effects or the paramagnetic impurity (the effect of which is greatest at low temperatures). It should be noted that the dimer possesses a $S = 0$ magnetic ground state, which precludes one from treating ZFS effects and exchange separately in different temperature regimes.

In summary, our studies on the trimetallic complex $[Co(dmpz)_2Cl(dmpzH)]_2Co$ have revealed the presence of antiferromagnetic exchange coupling between the terminal and central Co(II) ions with J(Heisenberg) ≈ -3 cm^{-1} and, furthermore, that this exchange coupling alone is insufficient to account for the magnetic behaviour at low temperatures. Either intramolecular next-nearest neighbour or intermolecular antiferromagnetic exchange may also be present. The magnetic properties of the dimeric molecule, $[Co(dmpz)_2(Hdmpz)]_2$, reveal significant antiferromagnetic exchange between the metal centres. Magnetic susceptibility data over the temperature range 12–300 K are adequately modelled with either the Heisenberg $S = 3/2$ ($J \approx -5$ cm^{-1}) or the Ising $S' = 1/2$ ($J \approx -23$ cm^{-1}) dimer model, with a better fit obtained using the Ising model.

Acknowledgements

We thank the Natural Sciences and Engineering Research Council of Canada for financial support. We also thank Drs. J. Carolan and W. Hardy of the Department of Physics at the University of British Columbia for use of the SQUID magnetometer.

1. M.K. Ehlert, S.J. Rettig, A. Storr, R.C. Thompson, and J. Trotter. Can. J. Chem. **67**, 1970 (1989).
2. M.K. Ehlert, S.J. Rettig, A. Storr, R.C. Thompson, and J. Trotter. Can. J. Chem. **68**, 1444 (1990).
3. M.K. Ehlert, S.J. Rettig, A. Storr, R.C. Thompson, and J. Trotter. Can. J. Chem. **68**, 1494 (1990).
4. M.K. Ehlert, S.J. Rettig, A. Storr, R.C. Thompson, and J. Trotter. Can. J. Chem. **69**, 432 (1991).
5. M.K. Ehlert, A. Storr, and R.C. Thompson. Can. J. Chem. **70**, 1121 (1992).
6. M.K. Ehlert, S.J. Rettig, A. Storr, R.C. Thompson, and J. Trotter. Can. J. Chem. **70**, 2161 (1992).
7. M.K., Ehlert, A. Storr, and R.C. Thompson. Can. J. Chem. **71**, 1412 (1993).
8. International tables for X-ray crystallography. Vol. IV. Kynoch Press, Birmingham. 1974. pp. 99–102 and 149.
9. L. Banci, A. Bencini, C. Benelli, D. Gatteschi, and C. Zanchini. Struct. Bonding (Berlin), **52**, 37 (1982).
10. K. Kambe. J. Phys. Soc. Jpn. **5** 48 (1950).
11. E. Sinn. Coord. Chem. Rev. **5**, 313 (1970).
12. L.R. Groeneveld, R.A. le Febre, R.A. de Graaff, J.G. Haasnoot, G. Vos, and J. Reedijk. Inorg. Chim. Acta, **102**, 69 (1985).
13. D.B. Brown, J.R. Wasson, J.W. Hall, and W.E. Hatfield. Inorg. Chem. **16**, 2526 (1977).
14. C.J. O'Connor. Prog. Inorg. Chem. **29**, 203 (1982).
15. D.J. Mackey and R.L. Martin. J. Chem. Soc. Dalton Trans. 702 (1978).
16. G. Vos. Ph.D. Thesis, State University Leiden, 1983.
17. G. Vos, R.A. le Febre, R.A.G. de Graaff, J.G. Haasnoot, and J. Reedijk. J. Am. Chem. Soc. **105**, 1682 (1983).
18. G.A. van Albada, R.A.G. de Graaff, J.G. Haasnoot, and J. Reedijk. Inorg. Chem. **23**, 1404 (1983).
19. G. Vos, R.A.G. de Graaff, J.G. Haasnoot, A.M. van der Kraan, P. de Vaal, and J. Reedijk. Inorg. Chem. **23**, 2905 (1984).
20. G. Vos, J.G. Haasnoot, G.C. Verschoor, and J. Reedijk. Inorg. Chim. Acta, **102**, 187 (1985).
21. G. Vos, J.G. Haasnoot, G.C. Verschoor, J. Reedijk, and P.E.L. Schaminee. Inorg. Chim. Acta, **105**, 31 (1985).
22. W. Vreugdenhil, J.G. Hasnoot, M.F.J. Schoondergang, and J. Reedijk. Inorg. Chim. Acta, **130**, 235 (1987).
23. L. Antolini, A.C. Fabretti, D. Gatteschi, A. Giusti, and R. Sessoli. Inorg. Chem. **30**, 4858 (1991).
24. E. Colacio, J.P. Costes, R. Kivekas, J.P. Laurent, J. Ruiz, and M. Sundberg. Inorg. Chem. **30**, 1474 (1991), and references therein.
25. R.L. Carlin and A.J. van Duyneveldt. Magnetic properties of transition metal compounds. Springer-Verlag, Berlin. 1977. p. 204.

Can. J. Chem. Downloaded from www.nrcresearchpress.com by 203.198.23.82 on 09/08/12
For personal use only.

The synthesis and characterization of $W(SeMes)_4 \cdot THF$ (Mes = mesityl): a possible homoleptic mononuclear tungsten selenolate. Its reaction with CN^tBu to yield $(^tBuNC)(MesSe)_2W(\mu\text{-}Se)_2W(SeMes)_2(Cn^tBu)$[1]

HEINZ-BERNHARD KRAATZ,[2] P. MICHAEL BOORMAN,[3] AND MASOOD PARVEZ

Department of Chemistry, University of Calgary, 2500 University Dr. N.W., Calgary, AB T2N 1N4, Canada

Received April 15, 1993

HEINZ-BERNHARD KRAATZ, P. MICHAEL BOORMAN, and MASOOD PARVEZ. Can. J. Chem. **71**, 1437 (1993).

The reaction of NaSeMes (Mes = mesityl, 2,4,6-$(CH_3)_3C_6H_2$) with $WCl_4(PPh_2Me)_2$ in THF leads to the formation of $W(SeMes)_4 \cdot THF$ (**1**), a possible mononuclear tetrakis(selenolato) complex of tungsten. The identity of the red crystalline material has been confirmed by elemental analysis and NMR spectroscopic methods (^1H, ^{13}C, and ^{77}Se NMR). The reaction of $W(SeMes)_4 \cdot THF$ with *tert*-butyl isocyanide results in the formation of $(^tBuNC)(MesSe)_2W(\mu\text{-}Se)_2W(SeMes)_2(CN^tBu)$ (**2**). Compound **2** crystallized in the monoclinic space group $C2/c$ (no. 15) with a = 23.933(2) Å, b = 16.776(2) Å, c = 15.595(2) Å, β = 122.98(2)°, and four formula units per unit cell. Refinement by full-matrix least squares gave final residuals of R = 0.038 and R_w = 0.028. The two metal centres in **2** are in a trigonal bipyramidal (tbp) coordination environment. The two tbps are connected via a common edge (axial–equatorial). The W—W bond length of 2.732(1) Å and the diamagnetism of **2** indicate the presence of a metal–metal bonding interaction.

HEINZ-BERNHARD KRAATZ, P. MICHAEL BOORMAN et MASOOD PARVEZ. Can. J. Chem. **71**, 1437 (1993).

La réaction du NaSeMes (Mes = mésityle, 2,4,6-$(CH_3)_3C_6H_2$) avec le $WCl_4(PPh_2Me)_2$ dans le THF conduit à la formation de $W(SeMes)_4 \cdot THF$ (**1**), un complexe tétrakis(sélénolato) mononucléaire du tungstène. On a confirmé l'identité du produit cristallin rouge par analyse élémentaire et par RMN du ^1H, du ^{13}C et du ^{77}Se. La réaction du $W(SeMes)_4 \cdot THF$ avec l'isocyanure de *tert*-butyle conduit à la formation du $(t BuNC)(MesSe)_2W(\mu\text{-}Se)_2W(SeMes)_2(CNtBu)$ (**2**). Le composé **2** cristallise dans le groupe d'espace $C2/c$ (n° 15) avec a = 23,933(2), b = 16,776(2) et c = 15,595(2) Å, β = 122,98(2)° et quatre unités de formule par unité élémentaire. L'affinement de la structure par la méthode des moindres carrés (matrice complète) conduit à des valeurs finales de R = 0,038 et R_w = 0,028. Deux des centres métalliques du composé **2** se trouvent dans un environnement de coordination trigonale bipyramidale (tbp). Les deux centres tbp sont reliés par une arête commune (axiale-équatoriale). La longueur de la liaison W—W (2,732(1) Å) et le diamagnétisme du composé **2** indiquent la présence d'une interaction liante métal–métal.

[Traduit par la rédaction]

Introduction

The coordination chemistry of the selenolato ligand (RSe^-, R = alkyl or aryl) is still an underdeveloped field (1). Over recent years, fueled partly by the quest for precursors for new materials possessing useful properties, efforts have been concentrated on selenolato complexes of group 12 metals (2). The use of bulky aryl substituents has proven extremely helpful in obtaining characterizable complexes with sometimes unexpected structural features. Although numerous examples of mononuclear and multinuclear thiolato complexes of early transition metals are known (3, 4), selenolato complexes of early transition metals are very rare (1). Despite an earlier report by Andrä about the synthesis of homoleptic group 5 and 6 metal selenolates from $Al(SeR)_3$ (R = phenyl and naphthyl) and metal halides, the true nature of these complexes has not been established (5). A review of the recent literature shows that structural data for complexes possessing terminal selenolates in particular are rare and to the best of our knowledge there are no mononuclear homoleptic selenolato complexes of any early transition metal known.[4] In fact, $CpCr(CO)_3(SePh)$ (7), $(OC)_4Cr(CNEt)(SePh)$ (8), and $(\eta^7\text{-}C_7H_7)W(CO)_2(SePh)$ (9) are the only structurally characterized mononuclear selenolato complexes of any early transition metal. Very recently, Chisholm and co-workers reported the first two examples of homoleptic binuclear selenolato complexes of molybdenum and tungsten (10) of the type $M_2(SeMes)_6$ (Mes = 2,4,6-trimethylphenyl).[5] Mononuclear tetrakis(thiolato) complexes of molybdenum (11, 12) and tungsten (13), and more recently hexakis(thiolato) complexes of niobium and tantalum (14), are easily accessible. They can be valuable starting materials for the preparation of larger clusters and have been used in HDS modelling reactions (15). Analogous selenolato complexes are of interest in their own right, but also in terms of their reactivity as compared to that of thiolato complexes. ^{77}Se NMR spectroscopy may be an additional probe for the characterization of the complexes in solution.

As part of our ongoing investigation of the reactivity of aryl selenolates with group 6 metal centres, we now report the synthesis of $W(SeMes)_4 \cdot THF$ (**1**) and provide evidence for its identity. Additional evidence stems from its reactivity towards *tert*-butyl isocyanide and the formation of the centrosymmetric binuclear complex $(^tBuNC)(MesSe)_2W(\mu\text{-}Se)_2W(SeMes)_2(CN^tBu)$ (**2**) of which the crystal structure is reported.

Experimental section

All operations were carried out under an argon atmosphere, using standard double manifold techniques. Analytical grade THF was dried with sodium and distilled from Na/benzophenone. NaSeMes (16) and $WCl_4(PPh_2Me)_2$ (17) were prepared according to litera-

[1]Taken in parts from H.-B. Kraatz, Ph.D. Thesis, University of Calgary, 1993.

[2]Present address: Department of Chemistry and Biochemistry, University of Maryland, College Park, MD 20742, U.S.A.

[3]Author to whom correspondence may be addressed.

[4]The X-ray structure of the homoleptic anion $[Fe(SePh)_4]^-$ has been reported (6).

[5]$M_2(SeMes)_6$ (M = Mo, W; Mes = 2,4,6-trimethylphenyl).

Can. J. Chem. Downloaded from www.nrcresearchpress.com by 213.200.69.106 on 09/08/12
For personal use only.

Can. J. Chem. Downloaded from www.nrcresearchpress.com by 213.200.69.106 on 09/08/12
For personal use only.

ture procedures. 2,4,6-$(CH_3)_3C_6H_2SeH$ was prepared in 52% yield by a modified version of the literature procedure (18). ^1H NMR (δ in ppm; $CDCl_3$): 6.98 (s, 2H $HSeC_6H_2(CH_3)_3$, 2.44 (s, 6H, 2,6-Me), 2.34 (s, 3H, 4-Me), 1.31 (s, 1H, *H*SeMes, J_{HSe} = 54 Hz). ^{13}C NMR (δ in ppm, $CDCl_3$): 138.2 (*p*-C), 135.47 (*o*-C), 128.58 (*m*-C), 124.67 (i-C), 24.24 (*o*-CH_3), 20.62 (*p*-CH_3). ^{77}Se NMR (δ in ppm; $CDCl_3$): 14.1 (d, J_{HSe} = 54 Hz). Elemental analyses (C,H N) were performed by the University of Calgary, Department of Chemistry, Analytical Service Laboratory. IR spectra (2000–200 cm^{-1}) were recorded as Nujol mulls between CsI plates using a Mattson 4030 Galaxy Series FT-IR spectrometer. Routine ^1H NMR spectra were recorded on a Bruker ACE-200 spectrometer (referenced to external $SiMe_4$). ^{31}P NMR spectra were recorded on a Varian XL-200 spectrometer (referenced to external H_3PO_4). ^{77}Se NMR spectra were recorded on a Bruker AM-400 spectrometer (referenced to external PhSeSePh, δ = 460 ppm). The pulse width was 9 μs (40°) with an acquisition time of 0.082 s and a dead time of 1–2 s.

Synthesis of W(SeMes)$_4$·THF (1)

A 100 mL round-bottom flask with sidearm was charged with $WCl_4(PPh_2Me)_2$ (0.42 g; 0.58 mmol), NaSeMes (0.50 g; 2.31 mmol), and a stirring bar. The vessel was cooled to −196°C and degassed THF (20 mL) was added to the cold reactants. The mixture was degassed three times using freeze–thaw cycles and then allowed to warm up to room temperature. The solution was stirred for 3 h. The deep red solution was then filtered through a pad (1 cm) of Celite 545. The volume of the solution was reduced to 10 mL. After addition of *n*-hexane (5 mL) and storage of the solution at −20°C overnight, 0.35 g of red crystals were deposited (58% based on $WCl_4(PPh_2Me)_2$). ^1H NMR (δ in ppm, CD_3CN): 7.11 (s, 2H, Se-2,4,6-$(CH_3)_3C_6H_2$), 3.65 (m, 2,5-H of THF), 2.18 (s, 6H, *o*-CH_3 of Se-2,4,6-$(CH_3)_3C_6H_2$), 2.17 (s, 3H, *p*-CH_3 of Se-2,4,6-$(CH_3)_3C_6H_2$), 1.81 (m, 3,4-H of THF). $^{13}C\{^1H\}$ NMR (δ in ppm, CD_3CN): 143.4 (i-C of SeMes), 135.0 (*m*-C of SeMes), 132.1 (*o*-C of SeMes), 129.3 (*p*-C of SeMes), 68.3 (2,5-C of THF), 26.3 (3,4-C of THF), 25.7 (2,6-CH_3 of SeMes), 24.6 (4-CH_3 of SeMes). $^{77}Se\{^1H\}$ NMR (δ in ppm relative to Me_2Se; THF, D_2O insert): 1128 ($\nu_{1/2}$ = 116 Hz). Anal. calcd. for $C_{40}H_{52}OSe_4W$ (MW = 1048.55): C 45.82, H 5.00; found: C 46.0, H 5.1.

Preparation of (^{t}BuNC)(MesSe)$_2$W(μ-Se)$_2$W(μ-SeMes)$_2$(CN^{t}Bu) (2)

MesSeH (0.54 g, 2.75 mmol) was dissolved in degassed DME (15 mL) and the solution was cooled to −78°C. A solution of *n*-butyllithium in *n*-hexane (1.25 mL of a 2.5 M solution) was added slowly to the selenol, giving a colourless solution of LiSeMes. This solution was added to a stirring slurry of $WCl_4(PPh_2Me)_2$ (0.5 g, 0.69 mmol) in DME (15 mL) via a canula. The reaction mixture was allowed to warm up to room temperature. Over a period of 3 h, the reaction solution turned deep red. *tert*-Butyl isocyanide (0.31 mL, 2.75 mmol) was added via a syringe upon which the solution turned green immediately. After stirring for an additional hour, the solvent was removed in vacuo and the remaining residue was extracted with *n*-hexane (2 × 25 mL). The green *n*-hexane extracts were collected, reduced in volume to 15 mL, and stored at −20°C overnight. After this time, orange X-ray quality crystals deposited on the bottom of the flask. Yield: 0.28 g = 55% (based on $WCl_4(PPh_2Me)_2$. IR (Nujol mull): 2041 vs (ν(NC)), 1312s, 1206s, 968m, 947w, 873w, 843w, 507s, 486s, 426s. ^1H NMR (δ in ppm; $CDCl_3$): 6.83 (s, 4H, Se-2,4,6-$(CH_3)_3C_6H_2$), 2.35 (s, 12H, *o*-CH_3 of Se-2,4,6-$(CH_3)_3C_6H_2$), 2.27 (s, 6H, *p*-CH_3 of Se-2,4,6-$(CH_3)_3C_6H_2$), 1.45 (s, 9H, $(CH_3)_3CNC$). $^{13}C\{^1H\}$ NMR (δ in ppm; $CDCl_3$): 141.1 (Me_3CNC), 133.9 (i-C of SeMes), 131.9 (*m*-C of SeMes), 128.4 (*o*-C of SeMes), 127.4 (*p*-C of SeMes), 31.5 Me_3CNC), 24.8 (2,6-CH_3 of SeMes), 20.6 (4-CH_3 of SeMes). ^{77}Se NMR (δ in ppm; $CDCl_3$): 508 ($\nu_{1/2}$ = 10 Hz), 369 ($\nu_{1/2}$ = 15 Hz). ^{14}N NMR (δ in ppm; $CDCl_3$): −170 ($\nu_{1/2}$ = 162 Hz). Anal. calcd. for $C_{46}H_{62}N_2Se_6W_2$ (MW = 1484.48): C 37.22, H 4.21, N 1.89; found: C 37.5, H 4.2, N, 2.1.

TABLE 1. Crystallographic data for (^{t}BuNC)(MesSe)$_2$W(μ-Se)$_2$W(SeMes)$_2$(CN^{t}Bu) (2)

Parameter	2
Empirical formula	$C_{46}H_{62}N_2Se_6W_2$
fw	1484.47
Crystal system	Monoclinic
Space group	C2/c (no. 15)
a, Å	23.933(2)
b, Å	16.776(2)
c, Å	15.595(2)
α, deg	—
β, deg	122.98(2)
γ, deg	—
V, Å^3	5252(1)
Z	4
ρ (calcd), g cm^{-3}	1.877
μ, cm^{-1}	85.71
Radiation; λ, Å	MoK_α; 0.71069
F_{000}	2816

X-ray crystallography of (^{t}BuNC)(MesSe)$_2$W(μ-Se)$_2$W(SeMes)$_2$(CN^{t}Bu) (2)

Data collection and refinement

A dark red triangular crystal of **2** of dimensions 0.13 × 0.30 × 0.28 mm was mounted onto a glass fiber and coated with epoxy resin. Accurate cell dimensions and the crystal orientation matrices were determined on a Rigaku AFC6S diffractometer by a least-squares refinement of 25 reflections ($20.0 < \theta < 36.3°$); 2346 reflections with $I > 3\sigma(I)$ were observed. The intensity data were collected at a temperature of −103°C ± 1°C, using the ω–2θ scan method and monochromatized MoK_α radiation (λ = 0.71069 Å) in the range $2° < \theta < 25°$. To monitor crystal decay, the intensities of three standard reflections were measured after every 200 reflections. An empirical absorption correction was applied (transmission factor: 0.4230–0.9987). The data were corrected for Lorentz and polarization effects and absorption ($\mu(MoK_\alpha)$ = 85.71 cm^{-1}). The structure was solved by direct methods using the TeXsan program package (19). The refinement was by full-matrix least-squares calculations, initially with isotropic and finally with anisotropic temperature factors for the non-hydrogen atoms. H-atoms were included in the model at geometrically idealized positions (C—H 0.95 Å) with a fixed common isotropic temperature factor. The refinement converged with R = 0.038 and R_w = 0.028. Scattering factors were those of Cromer and Mann (20) and Stewart et al. (21). Allowance was made for anomalous dispersion (22). A difference map at the end of the refinement showed no chemically significant features (Δρ of −1.82–1.73 e Å^{-3}, which were close to the W and Se atoms). All crystallographic plots were obtained using ORTEP II (23).

A summary of crystal data is given in Table 1 and atomic positional parameters are given in Table 2. Anisotropic thermal parameters (Table S1), hydrogen positional parameters (Table S2), a full listing of bond distances and bond angles (Table S3), and a listing of calculated and observed structure factors (Table S4) have been deposited as supplementary material.[6]

[6]Supplementary material mentioned in the text can be purchased from: The Depository of Unpublished Data, Document Delivery, CISTI, National Research Council Canada, Ottawa, ON K1A 0S2, Canada.

Tables of hydrogen positional parameters and of bond lengths and angles have also been deposited with the Cambridge Crystallographic Data Centre, and can be obtained on request from The Director, Cambridge Crystallographic Data Centre, University Chemical Laboratory, 12 Union Road, Cambridge, CB2 1EZ, U.K.

Can. J. Chem. Downloaded from www.nrcresearchpress.com by 213.200.69.106 on 09/08/12
For personal use only.

TABLE 2. Positional parameters and B(eq) values for (^{t}BuNC)-(MesSe)$_2$W(μ-Se)$_2$W(SeMes)$_2$(CN^{t}Bu) (**2**)

Atom	x	y	z	B(eq)[a]
W(1)	0.23681(3)	0.24999(5)	0.57489(4)	1.69(2)
Se(1)	0.23872(8)	0.13001(8)	0.49489(15)	2.17(6)
Se(2)	0.33877(7)	0.28559(9)	0.73798(11)	2.52(6)
Se(3)	0.12924(7)	0.31588(9)	0.50720(12)	2.55(6)
N(1)	0.2021(5)	0.1207(7)	0.6956(8)	2.4(5)
C(1)	0.2145(6)	0.1672(9)	0.6540(10)	2.5(7)
C(2)	0.1912(7)	0.0490(8)	0.7404(12)	3.1(7)
C(3)	0.1786(8)	0.0795(11)	0.8191(15)	7.0(9)
C(4)	0.1316(7)	0.0058(8)	0.6546(13)	6.9(8)
C(5)	0.2543(7)	0.0016(9)	0.7894(11)	4.1(7)
C(6)	0.3578(6)	0.2090(8)	0.8446(9)	2.3(6)
C(7)	0.3335(6)	0.2196(9)	0.9074(11)	3.3(7)
C(8)	0.3558(7)	0.1666(9)	0.9893(10)	3.1(7)
C(9)	0.3987(7)	0.1041(9)	1.0098(11)	2.9(7)
C(10)	0.4216(6)	0.0940(9)	0.9478(11)	2.7(6)
C(11)	0.4025(6)	0.1442(8)	0.8652(11)	2.4(6)
C(12)	0.2851(7)	0.2860(10)	0.8878(12)	4.9(8)
C(13)	0.4188(8)	0.0475(10)	1.0946(12)	5.1(9)
C(14)	0.4293(6)	0.1304(9)	0.7989(11)	4.0(8)
C(15)	0.0744(5)	0.2547(12)	0.5416(9)	2.9(6)
C(16)	0.0672(6)	0.2820(9)	0.6193(9)	2.6(6)
C(17)	0.0245(6)	0.2414(13)	0.6368(10)	3.8(7)
C(18)	−0.0093(6)	0.1719(11)	0.5815(12)	3.9(8)
C(19)	−0.0017(7)	0.1482(10)	0.5054(12)	3.3(7)
C(20)	0.0399(6)	0.1865(9)	0.4831(11)	2.6(7)
C(21)	0.1003(7)	0.3595(10)	0.6785(12)	4.4(8)
C(22)	−0.0553(8)	0.1274(11)	0.6046(13)	5.2(10)
C(23)	0.0446(7)	0.1555(10)	0.3946(12)	4.2(8)

[a] $B_{eq} = 8/3\ \pi^2(U_{11}(aa^*)^2 + U_{22}(bb^*)^2 + U_{33}(bb^*)^2 + 2U_{12}aa^*bb^*\cos\gamma + 2U_{13}aa^*cc^*\cos\beta + 2U_{23}bb^*cc^*\cos\alpha)$.

Results

*Reaction of WCl$_4$(PPh$_2$Me)$_2$ with MesSe$^-$: preparation of W(SeMes)$_4$·THF (**1**)*

The reaction between WCl$_4$(PPh$_2$Me)$_2$ and sodium mesityl selenolate in THF or DME results in the formation of a deep red solution. Lithium mesityl selenolate, prepared in situ by the addition of butyllithium to a cooled solution of mesityl selenol in THF or DME, gives the same red solution. From this solution, dark red crystals can be obtained by adding an approximately equal amount of *n*-hexane and storing overnight at −20°C. These crystals are very soluble in organic solvents, such as methylene chloride, acetone, or acetonitrile. ^{1}H and ^{13}C NMR spectroscopy confirms the presence of only one selenolate environment. The integration of the THF and aromatic selenolate resonances gives a ratio of four selenolates per molecule of THF. The ^{13}C–{^{1}H} NMR spectrum of the crystals in CD$_3$CN confirms the presence of only one selenolate environment. The ^{77}Se–{^{1}H} NMR spectrum of the red crystals in THF shows a single broad resonance at 1128 ppm (Me$_2$Se = 0 ppm). No coupling between the ^{77}Se nuclei and the ^{183}W nucleus (I = 1/2; 14.4% abundance) is observed. In view of the broadness of the signal this is not too surprising, since the gyromagnetic ratio of tungsten is small (1.1131×10^7 rad T^{-1} s^{-1}); the W–Se coupling constants are generally small since coupling constants are directly proportional to γ for both coupling nuclei (24). Ibers and co-workers reported $^1J_{W-Se}$ between 34 Hz for the diselenene complex [W(Se$_2$C$_2$(COOCH$_3$)$_2$)$_3$]$^{2-}$ (25) and 113 Hz for the coupling of the bridging selenides to one of the tungsten centers in (Ph$_4$P)$_2$[W$_3$Se$_8$O] (26). This shift is much more deshielded than that of d^{10} metal systems of group 12 elements (27, 28). However, similar shifts have been observed for other tungsten(IV) systems, such as for the confacial bioctahedral complex [Cl$_3$W(μ-Se)(μ-SePh)$_2$WCl$_3$]$^{2-}$ (923 ppm) (29), for the mononuclear tungsten-diselenene complex [W(Se$_2$C$_2$(COOCH$_3$)$_2$)$_3$]$^{2-}$ (839 ppm), and for [W$_2$Se$_2$(Se$_2$C$_2$(COOCH$_3$)$_2$)$_4$]$^{2-}$ (1360 ppm) (26). The fact that W(SeMes)$_4$·THF is diamagnetic (based on the observation of sharp and unshifted resonances in the ^{1}H and ^{13}C spectra), is not unexpected. [W(O-2,6-(CH(CH$_3$)$_2$)$_2$C$_6$H$_3$)$_4$] and [W(S-C(CH$_3$)$_3$)$_4$], the only known examples of WX$_4$-type complexes, where X is an anionic ligand, are diamagnetic d^2 species (13). Similarly, the Mo(IV) complexes [Mo(S-C(CH$_3$)$_3$)$_4$)] (11) and [Mo(S-2,4,6-(CH(CH$_3$)$_2$)$_3$C$_6$H$_2$)$_4$] (12) are diamagnetic. It is possible to consider that all four complexes are being derived from a tetrahedron. Distortion from an ideal tetrahedral environment leads to the pairing of the electrons, which renders the complexes diamagnetic. The distortion from ideal T_d symmetry is the largest for [W(O-2,6-(CH(CH$_3$)$_2$C$_6$H$_3$)$_4$], which has the metal center in a nearly square-planar coordination environment.

The spectroscopic evidence and the elemental analysis are compatible with the formulation of the red diamagnetic crystalline material as W(SeMes)$_4$·THF (**1**). **1** crystallizes from solution as very thin plates and all attempts to grow crystals suitable for a single-crystal X-ray diffraction study have failed.

To confirm that **1** is present in the initial reaction solution and to get more information about the formation of **1**, we monitored the reaction between WCl$_4$(PPh$_2$Me)$_2$ and LiSeMes in DME by ^{31}P and ^{77}Se NMR spectroscopy. The ^{31}P NMR spectrum of the reaction solution shows that in the course of the reaction PPh$_2$Me is liberated as expected (^{31}P–{^{1}H} δ of PPh$_2$Me −25.9 ppm). The ^{77}Se NMR spectrum of the reaction solution shows that the resonance due to free mesityl selenolate is absent (^{77}Se{^{1}H} δ of LiSeMes in THF 721 ppm), indicating the consumption of all free selenolate. The red reaction solution contains essentially only one selenium-containing species, which gives rise to a signal in the ^{77}Se NMR spectrum at 1128 ppm; this is identical to the chemical shift of **1**.

*Reaction of W(SeMes)$_4$ with CN^{t}Bu: synthesis of the complex (^{t}BuNC)(MesSe)$_2$W(μ-Se)$_2$W(μ-SeMes)$_2$(CN^{t}Bu) (**2**)*

Since it was not possible to obtain suitable crystals of **1**, we thought that the characterization of a predictable reaction product might provide further evidence for the identity of **1** as the tungsten tetrakis(selenolate).

The two known M(SR)$_4$ systems (Mo(S^{t}Bu)$_4$ and Mo(TIPT)$_4$) react with simple ligands. For example *tert*-butyl isocyanide reduces Mo(S^{t}Bu)$_4$ to give the Mo(II) complex Mo(S^{t}Bu)$_2$(CN^{t}Bu)$_4$ (30). ^{t}BuSS^{t}Bu is a by-product of this reaction. In contrast to that, the aromatic tetrathiolato complex, Mo(TIPT)$_4$ (TIPT = 2,4,6-triisopropylphenylthiolate), resists reduction in the presence of ^{t}BuNC and forms the simple adduct, Mo(TIPT)$_4$(CN^{t}Bu) (12). It was anticipated that the reactivity of **1** would be similar to that of Mo(TIPT)$_4$, leading to a related product.

Addition of LiSeMes to a stirring slurry of WCl$_4$(PPh$_2$Me)$_2$ in DME produced a deep red reaction solution. This solution shows a single resonance in the ^{77}Se {^{1}H} NMR spec-

Can. J. Chem. Downloaded from www.nrcresearchpress.com by 213.200.69.106 on 09/08/12
For personal use only.

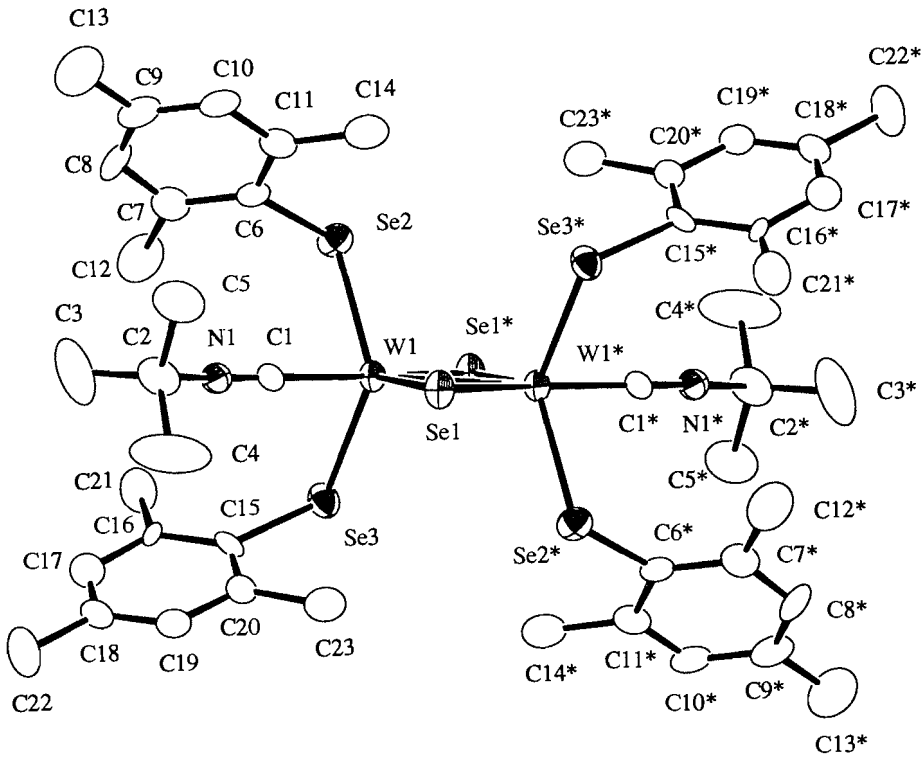

FIG. 1. An ORTEP plot (50% probability) of the centrosymmetric complex (^{t}BuNC)(MesSe)$_2$W(μ-Se)$_2$W(MesSe)$_2$(CN^{t}Bu) (**2**).

TABLE 3. Selected bond (*a*) distances (Å) and (*b*) angles (deg) for (^{t}BuNC)-(MesSe)$_2$W(μ-Se)$_2$W(SeMes)$_2$(CN^{t}Bu) (**2**)

(*a*)

Bond	Distance	Bond	Distance
W(1)—W(1*)	2.732(1)	W(1)—Se(1)	2.382(2)
W(1)—Se(1*)	2.505(2)	W(1)—Se(2)	2.454(2)
W(1)—Se(3)	2.451(2)	W(1)—C(1)	2.11(1)
Se(2)—C(6)	1.95(1)	Se(3)—C(15)	1.96(1)
N(1)—C(1)	1.15(2)	N(1)—C(2)	1.48(2)
C(2)—C(3)	1.48(2)	C(2)—C(4)	1.51(2)
C(2)—C(5)	1.50(2)		

(*b*)

Bonds	Angle	Bonds	Angle
Se(1)—W(1)—Se(1*)	112.08(4)	Se(1)—W(1)—Se(2)	117.18(6)
Se(1)—W(1)—Se(3)	118.09(6)	Se(1)—W(1)—C(1)	80.4(4)
Se(1)—W(1)—Se(2)	85.35(6)	Se(1)—W(1)—Se(3)	83.66(5)
Se(1*)—W(1)—C(1)	167.5(4)	Se(2)—W(1)—Se(3)	123.74(6)
Se(2)—W(1)—C(1)	88.8(3)	Se(3)—W(1)—C(1)	90.5(3)
W(1)—Se(1)—W(1*)	67.92(4)	W(1)—Se(2)—C(6)	111.2(3)
W(1)—Se(3)—C(15)	110.5(4)	C(1)—N(1)—C(2)	168(1)
W(1)—C(1)—N(1)	179(1)	N(1)—C(2)—C(3)	106(1)
N(1)—C(2)—C(4)	107(1)	N(1)—C(2)—C(5)	106(1)
C(3)—C(2)—C(4)	112(1)		

trum at 1128 ppm, indicating the presence of **1**. Upon the addition of *tert*-butyl isocyanide to the stirring solution, it immediately changed colour from dark red to green. Extraction with *n*-hexane yielded a green solution, which deposited large orange crystals upon cooling to −20°C. These crystals have been identified as (^{t}BuNC)(MesSe)$_2$W(μ-Se)$_2$W(μ-SeMes)$_2$(CN^{t}Bu) (**2**) by X-ray crystallography. **2** crystallizes without any solvent of crystallization in the lattice. The complex is moderately air stable. An ORTEP representation of **2** is shown in Fig. 1. Bond distances and angles are listed in Table 3. **2** is isostructural with (MePh$_2$P)(PhSe)$_2$W(μ-Se)$_2$W(SePh)$_2$(PPh$_2$Me), which has been obtained from the reaction of WCl$_2$(PPh$_2$Me)$_4$ with Me$_3$SiSePh in THF (31) (vide infra). **2** can be described as

Can. J. Chem. Downloaded from www.nrcresearchpress.com by 213.200.69.106 on 09/08/12
For personal use only.

a centrosymmetric dimer with distorted trigonal bipyramidal geometry around each tungsten center, and an overall structure of an edgesharing bitrigonal bipyramid. The two trigonal bipyramids are connected via a common axial edge and not via an equatorial edge. At this point it should be mentioned that the reaction of Otsuka's $Mo(S^tBu)_4$ with PPh_2Me was shown to lead to the formation of (Me_2PhP)-$(^tBuS)_2Mo(\mu\text{-}S)_2Mo(S^tBu)_2(PPhMe_2)$ (30).

Each tungsten center in **2**, formally W(IV), is bonded to two equatorial mesityl selenolates, an axial isocyanide, and two Se atoms that bridge the two W atoms. Both mesityl substituents of the selenolates are pointing up towards the axial isocyanide. This geometry maximizes the π-type interaction between the lone pair on the selenolates with the empty $d_{x^2-y^2}$ orbital of the metal center. However, this geometry causes steric congestion and is probably the cause for the ^{t}Bu group of the isocyanide ligand bending away from the mesityl rings (C(1)—N(1)—C2) = 168(1)°). The W(1)—C(1)(isocyanide) distance (2.11(1) Å) is similar to those reported for the seven coordinated W(II) isocyanide complexes, $[W(CN^tBu)_7]^{2+}$ (range 2.069(6)–2.142(8) Å; mean 2.108 Å) (32) and $[(^tBuNC)_3W(CO)_2I_2]$ (2.092(13), 2.145(13), 2.099(13) Å) (33). The W—Se (selenolate) and Se—C distances are comparable to those observed for $W_2(SeMes)_6$, $W_2(O^iPr)_2(SeMes)_4$ (10), and η^7-$C_7H_7W(CO)_2$-SePh (9). The W—Se—C angles are significantly larger than those observed for the aforementioned tungsten–selenolate complexes.

The selenide bridge is asymmetric, with the W(1)—Se(1) and W(1)—Se(1*) distances differing in length by 0.123 Å. The W_2Se_2 cores of the polyselenide complexes $W_2Se_9^{2-}$ and $W_2Se_{10}^{2-}$ show a similar distortion of the bridging region (26). The W(1)—W(1*) separation of 2.732(1) Å and the diamagnetism of the complex indicate the presence of an attractive metal–metal interaction. However, the W(IV)—W(IV) separation is longer than expected for a formal W=W double bond (34).

For spectroscopic purposes, the crystals were dissolved in $CDCl_3$ to give a green solution. The ^{1}H NMR spectrum shows a single sharp resonance for the aromatic protons of the mesityl selenolate with a chemical shift of 6.83 pm and two signals for the methyl substituents at 2.35 and 2.27 ppm. In addition, there is a singlet for the isocyanide ^{t}Bu group at 1.45 ppm. The methyl protons of the ^{t}Bu groups are somewhat more shielded than in the thiolato complex $Mo(S^tBu)_2(CN^tBu)_4$ (δ 1.98) (30).

The ^{13}C–$\{^1H\}$ NMR signal for the ^{t}Bu group appears at 31.5 ppm, which is deshielded compared to free ^{t}BuNC. However, this is comparable to values obtained for $Mo(S^tBu)_2(CN^tBu)_4$ (δ 31.4, 30.8) and the related acetylene complexes $Mo(S^tBu)_2(CN^tBu)_2(HCCH)$ (δ 30.3), $Mo(S^tBu)_2(CN^tBu)_2(HCCPh)$ (δ 29.7, 30.3), and $Mo(S^tBu)_2(CN^tBu)_2(PhCCPh)$ (δ 29.8) (35, 36). The ^{14}N NMR spectrum of **2** reveals a broad resonance at −170 ppm ($\nu_{1/2}$ = 162 Hz), deshielded compared to free ^{t}BuNC (−185 ppm). The IR spectrum of **2** shows a strong ν(NC) band at 2141 cm^{-1}. The ^{77}Se NMR spectrum shows two resonances, but the position of the signals is surprising compared to that of known tungsten–selenide–selenolate species (25, 26, 29). A very sharp resonance appears at 508 pm ($\nu_{1/2}$ = 10 Hz); a second resonance appears at 369 ppm ($\nu_{1/2}$ = 15 Hz). The ratio of the two signals is approximately 1:2, so that we tentatively assign the resonance at 508 ppm to μ-Se and the resonance at 369 ppm to -SeMes. Unfortunately, the quality of the spectrum does not permit a definite assignment of coupling constants ($J_{^{183}W-^{77}Se}$).

The formation of **2** might be rationalized by assuming that $W(SeMes)_4$ will react similarly to $Mo(TIPT)_4$ with CN^tBu. A plausible first step may involve adduct formation to give the five-coordinate 12-electron species $W(SeMes)_4(CN^tBu)$. The documented lability of the Se—C bond, even for Se—C(aryl) bonds, (29, 31, 37) can then lead to Se—C bond cleavage and formation of a selenido species, which can dimerize to give **2**. Since only a handful of homoleptic thiolato complexes of group 6 metals are known, direct quantitative comparisons between M—S—C and analogous M—Se—C are not yet possible. However, based on results by Schrock and co-workers (12, 13) and Otsuka and co-workers (30) and our own studies, we come to the conclusion that in terms of the tendency towards chalcogen–carbon bond cleavage the Se–aryl bond closely resembles the S–alkyl bond. A more detailed theoretical comparative analysis will be necessary to evaluate this problem in more detail. We will continue our efforts in the search for homoleptic selenolato complexes of the early transition metals.

Acknowledgements

The financial support of the Natural Sciences and Engineering Research Council of Canada is gratefully acknowledged. H.-B.K. is the recipient of The Department of Chemistry Scholarship.

1. H.J. Gysling. *In* The chemistry of organic selenium and tellurium compounds. Vol. 1. *Edited by* S. Patai and Z. Rappoport. Wiley, Chichester. 1986. pp. 679–855.
2. (*a*) M.L. Steigerwald and C.R. Sprinkle. J. Am. Chem. Soc. **109**, 7200 (1987); (*b*) S.M. Stuczynski, J.G. Brennan, and M.L. Steigerwald. Inorg. Chem. **28**, 4431 (1989); (*c*) M. Bochman, K. Webb, M. Harman, and M.B. Hursthouse. Angew. Chem. Int. Ed. Engl. **29**, 638 (1990); (*d*) M. Bochman, A.P. Coleman, K.J. Webb, M.B. Hursthouse, and M. Mazid. Angew. Chem. Int. Ed. Engl. **30**, 973 (1991); (*e*) M. Bochman, K.J. Webb, M.B. Hursthouse, and M. Mazid. J. Chem. Soc. Chem. Commun. 1735 (1991).
3. I.G. Dance. Polyhedron, **5**, 1037 (1986).
4. P.J. Blower and J.R. Dilworth. Coord. Chem. Rev. **76**, 121 (1987).
5. K. Andrä. Z. Anorg. Allg. Chem. **373**, 209 (1970).
6. J.M. McConnachie and J.A. Ibers. Inorg. Chem. **30**, 1770 (1991).
7. L.Y. Goh, Y.Y. Lim, M.S. Tay, T.C.W. Mak, and Z.-Y. Zhou. J. Chem. Soc. Dalton Trans. 1239 (1992).
8. H. Fischer, E.O. Fischer, D. Himmelreich, R. Cai, U. Schubert, and K. Ackermann. Chem. Ber. **114**, 3220 (1981).
9. A. Rettenmeier, K. Weidenhammer, and M.L. Ziegler. Z. Anorg. Allg. Chem. **473**, 91 (1981).
10. M.H. Chisholm, I.P. Parkin, J.C. Huffman, and W.B. Streib. J. Chem. Soc. Chem. Commun. 920 (1990).
11. S. Otsuka, M. Kamata, K. Hirotsu, and T. Higuchi. J. Am. Chem. Soc. **103**, 3011 (1981).
12. E. Roland, E.C. Walborski, J.C. Dewan, and R.R. Schrock. J. Am. Chem. Soc. **107**, 5795 (1985).
13. M.L. Listemann, J.C. Dewan, and R.R. Schrock. J. Am. Chem. Soc. **107**, 7207 (1985).
14. S.-M. Koo, R. Bergero, A. Salifoglou, and D. Coucouvanis. Inorg. Chem. **29**, 4846 (1990).
15. P.M. Boorman, J.F. Fait, and G.K.W. Freeman. Polyhedron, **8**, 1762 (1989).
16. J.M. Ball, P.M. Boorman, J.F. Fait, A.S. Hinman, and P.J. Lundmark. Can. J. Chem. **67**, 751 (1988).

17. P.T. Bishop and J.R. Dilworth. Inorg. Synth. **28**, 37 (1990).
18. H. Rheinboldt. Herstellung and Umwandlung organischer Selen- und Tellur-Verbindungen. *In* Methoden der Organischen Chemie. Bd. 9. Houben-Weyl-Müller, Georg Thieme Verlag, Stuttgart. 1955. pp. 958–960.
19. TeXsan (1992). Single crystal structure analysis software. Version 1.2. Molecular Structures Corporation, Woodland, Tex.
20. D.T. Cromer and J.B. Mann. Acta Crystallogr. Sect. A: Cryst. Phys. Diffr. Theor. Gen. Crystallogr. **A24**, 321 (1968).
21. R.F. Stewart, E.R. Davidson, and W.T. Simpson. J. Chem. Phys. **42**, 3175 (1965).
22. D.T. Cromer and D. Liberman. J. Chem. Phys. **53**, 1891 (1970).
23. C.K. Johnson. ORTEPII. Report ORNL-5138, Oak Ridge National Laboratory, Oak Ridge, Tenn. 1976.
24. B.E. Mann. Annu. Rep. NMR Spectrosc. **23**, 141 (1991).
25. M.A. Ansari, C.H. Mahler, and J.A. Ibers. Inorg. Chem. **28**, 2669 (1989).
26. R.W.M. Wardle, S. Bhaduri, C.-N. Chau, and J.A. Ibers. Inorg. Chem. **27**, 1747 (1988).
27. P.A.W. Dean and J.J. Vittal. Inorg. Chem. **26**, 278 (1987).
28. P.A.W. Dean, J.J. Vittal, and N.C. Payne. Inorg. Chem. **26**, 1683 (1987).
29. J.M. Ball, P.M. Boorman, J.F. Fait, H.-B. Kraatz, J.F. Richardson, D. Collison, and F.E. Mabbs. Inorg. Chem. **29**, 3290 (1990).
30. M. Kamata, T. Yoshida, S. Otsuka, K. Hirotsu, and T. Higuchi. J. Am. Chem. Soc. **103**, 3572 (1981).
31. P.M. Boorman, H.-B. Kraatz, and M. Parvez. J. Chem. Soc. Dalton Trans. 3281 (1992).
32. D.J. Szalda, J.C. Dewan, and S.J. Lippard. Inorg. Chem. **20**, 3851 (1981).
33. E.B. Dreyer, C.T. Lam, and S.J. Lippard. Inorg. Chem. **18**, 1904 (1979).
34. F.A. Cotton and R.A. Walton. Multiple bonds between metal atoms. R.E. Krieger Publishing Company, Inc., Malabar, Fla. 1988.
35. M. Kamata, T. Yoshida, S. Otsuka, K. Hirotsu, T. Higuchi, M. Kido, K. Tatsumi, and R. Hoffmann. Organometallics, **1**, 227 (1982).
36. M. Kamata, K. Hirotsu, T. Higuchi, M. Kido, K. Tatsumi, T. Yoshida, and S. Otsuka. Inorg. Chem. **22**, 2417 (1983).
37. L. Batt. *In* The chemistry of organic selenium and tellurium compounds. Vol. 1. *Edited by* S. Patai and Z. Rappoport. John Wiley, London and New York. 1986. Chap. 4. pp. 157–160.

Can. J. Chem. Downloaded from www.nrcresearchpress.com by 213.200.69.106 on 09/08/12
For personal use only.

Molecular structure and tautomerism of 3,5-bis(4-methylpyrazol-1-yl)-4-methylpyrazole

MONIQUE PERRIN[1] AND ALAIN THOZET

Laboratoire de minéralogie–cristallographie, Unité de recherche associée n° 805 du Centre national de la recherche scientifique, Université Claude Bernard Lyon 1, 43, boulevard du 11 Novembre 1918, 69622 Villeurbanne Cédex, France

PILAR CABILDO AND ROSA MA CLARAMUNT

Departamento de Química Orgánica y Biología, Facultad de Ciencias, Universidad Nacional de Educación a Distancia, Ciudad Universitaria, 28040 Madrid, Spain

EDUARD VALENTI

Laboratorios Dr. Esteve, S.A., Av. Mare de Déu de Montserrat, 221, 08026 Barcelona, Spain

AND

JOSÉ ELGUERO[1]

Instituto de Química Médica, Consejo Superior de Investigaciones Cientificas, Juan de la Cierva, 3, 28006 Madrid, Spain

Received January 18, 1993

MONIQUE PERRIN, ALAIN THOZET, PILAR CABILDO, ROSA MA CLARAMUNT, EDUARD VALENTI, and JOSÉ ELGUERO. Can. J. Chem. **71**, 1443 (1993).

The title compound $C_{12}N_6H_{14}$, **1**, crystallizes in the space group $P2_1/n$ (a = 8.222(2) Å, b = 27.336(8) Å, c = 5.574(2) Å, α = 90.00°, β = 100.97(4)°, γ = 90.00°), Z = 4, d = 1.308 g cm^{-3}. The conformation about the N—C bonds linking the pyrazole rings can be defined as *EZ*, with "pyridine-like" nitrogen atoms in an *anti* disposition (ϕ_1 = −155.3(3)°) and "pyridine-like" and "pyrrole-like" nitrogen atoms in a *syn* disposition (ϕ_2 = −6.2(5)°), with regard to the central pyrazole. Intermolecular hydrogen bonds between the central and the terminal pyrazole ring of configuration *Z* form centrosymmetric dimers. They pack in sheets nearly parallel to the (−2 3 1) plane. Its tautomerization barrier has been determined in methanol-d_4; the value, 11.9 kcal mol^{-1}, is similar to those of 3,5-dimethyl-4-chloropyrazole (12.8 kcal mol^{-1}) and 3,5-dimethyl-4-nitropyrazole (12.1 kcal mol^{-1}). These values together with the shape of the conformational potential surface (calculated using the AM1 Hamiltonian) suggest that, in compound **1**, prototropy and rotation about the N—C bonds linking the three pyrazole rings take place simultaneously.

MONIQUE PERRIN, ALAIN THOZET, PILAR CABILDO, ROSA MA CLARAMUNT, EDUARD VALENTI et JOSE ELGUERO. Can. J. Chem. **71**, 1443 (1993).

3,5-Bis(4-methylpyrazol-1-yl)-4-methylpyrazole **1**, $C_{12}N_6H_{14}$, cristallise dans le groupe spatial $P2_1/n$ (a = 8.222(2) Å, b = 27.336(8) Å, c = 5.574(2) Å, α = 90.00°, β = 100.97(4)°, γ = 90.00°), Z = 4, d = 1.309 g cm^{-3}. La conformation autour des deux liaisons N—C qu'unissent les trois noyaux de pyrazole peut être définie comme *EZ*, avec les atomes d'azote du type pyridinique dans une disposition *anti* (ϕ_1 = −155.3(3)°) et les atomes d'azote pyridinique et pyrrolique dans une disposition *syn* (ϕ_2 = −6.2(5)°) par rapport au pyrazole central. Des liaisons hydrogène intermoléculaires entre un pyrazole central et un pyrazole lateral de configuration *Z* forment des dimères centrosymétriques. L'enchaînement intermoléculaire donne lieu à des feuilles presque parallèles au plan (−2 3 1). La barrière à la tautomérie a été mesurée dans méthanol-d_4; la valeur obtenue, 11.9 kcal mol^{-1} est analogue à celles du 3,5-diméthyl-4-chloropyrazole (12.8 kcal mol^{-1}) et du 3,5-diméthyl-4-nitropyrazole (12.1 kcal mol^{-1}). Ces valeurs ainsi que la forme de la surface de potential (calculée avec la méthode AM1) suggèrent que dans le composé **1**, prototropie et rotation autour des laisons N—C unissant les trois noyaux de pyrazole, ont lieu simultanement.

Our interest in polydentate ligands led us to prepare and study the rhodium(I) complexes of 3,5-bis(4-methylpyrazol-1-yl)-4-methylpyrazole **1** (1), but the structure of the ligand itself was not determined. We describe here its molecular structure and a detailed NMR and semi-empirical study of the annular tautomerism involving the nitrogen atoms of the central ring. This molecule presents an interesting case in which tautomerism of the central ring is linked to conformational isomerism of the lateral pyrazoles.

Chemistry

3,5-Bis(4-methylpyrazol-1-yl)-4-methylpyrazole **1** was first prepared by bromination of 4-methylpyrazole (2) although its correct structure was established afterwards (3). Compound **1**, together with 3,5-bis(4-chloropyrazol-1-yl)-4-chloropyrazole (obtained by chlorination of pyrazole) (4), are the only representatives of this class of polydentate ligands. In fact, halogenation of pyrazoles unsubstituted on the nitrogen is a rather complex reaction (5–7). If position 4 of an *N*H-pyrazole is unsubstituted, then the reaction proceeds normally and the 4-bromo derivative is obtained. When position 4 is substituted, then an *N*-bromopyrazole is formed. These last compounds have been isolated in some cases but, normally, they rearrange to 5-bromopyrazoles, either by an intramolecular shift or, more probably, by an intermolecular mechanism (4). *N*-Bromopyrazoles are generally considered brominating agents (pz^- Br^+) but, owing to the pseudohalogen character of the pyrazol-1-yl substituent, they can react as "pyrazolating" agents (pz^+ Br^-). This explains the formation of *N*–*C* dimers (2, 4). If R = H, they can be further "pyrazolated" and trimers **1** result (2–4). If $R \neq$ H, *N*-bromination leads to a cyclic trimer (2, 8, 9). Finally, if

[1]Authors to whom correspondence may be addressed.

Can. J. Chem. Downloaded from www.nrcresearchpress.com by 213.200.69.106 on 09/08/12
For personal use only.

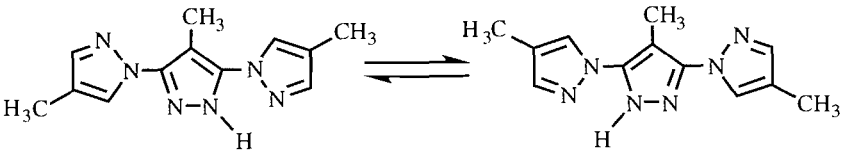

1*a* 1*b*

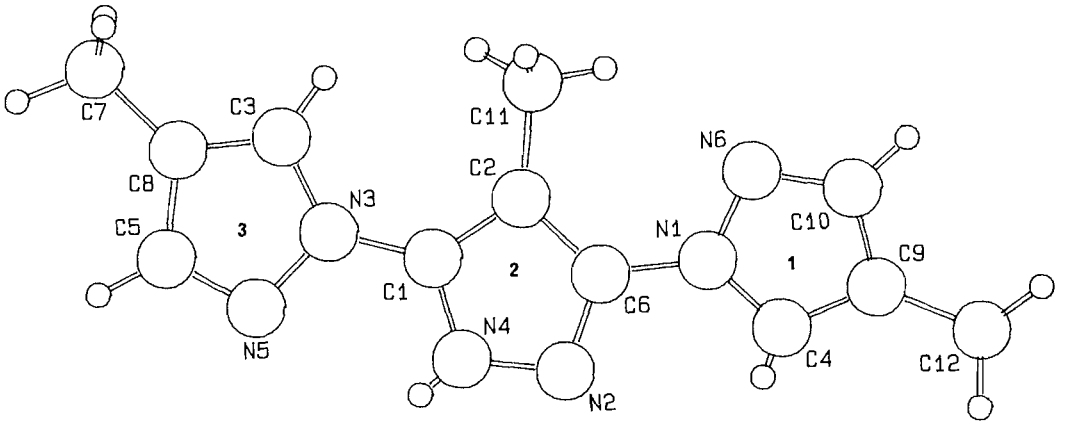

FIG. 1. An isolated molecule of compound **1** with the numbering system adopted in the crystallographic work.

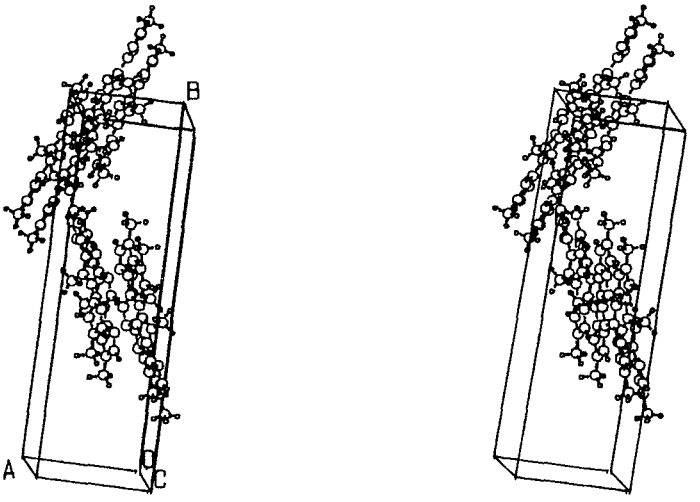

FIG. 2. Stereodrawing of the two dimers.

the substituents *R* and *R'* are too bulky, such as in campho[*c*]pyrazole, then, instead of trimers, only a *C*-brominated pyrazole is obtained.[2]

Stepwise preparation of *N–C* dimers (useful building blocks for supramolecular structures) is conveniently carried out using 3(5)-hydrazinopyrazoles (10). Although possible in principle, the stepwise preparation of trimers **1** is not known and some preliminary attempts indicated that it would involve some difficulties. Thus, we have optimized Hüttel's synthesis (2) (see experimental part) to improve the yield of compound **1** (R = CH_3).

[2]W. Meutermans and J. Elguero. Unpublished results.

Crystal and molecular structure of compound 1

Figure 1 shows the numbering scheme for compound **1** and Fig. 2 is a stereoview of the two dimers. Bond lengths and angles are listed in Tables 1 and 2. The three pyrazole rings can be considered as planar (to within ±0.01 Å). The angle between rings 1 and 2 is 23.6(1)° and that between rings 2 and 3 is 6.3(1)°. The related torsional angles are N6—N1—C6—N2 = −155.3(3)° and N4—C1—N3—N5 = −6.2(5)°. The three pyrazole rings deviate from C_{2v} symmetry (11), their geometry being quite similar to that of other pyrazoles (12).

The five most characteristic hydrogen bond interactions are summarized in Table 3 and the hydrogen bond network

Can. J. Chem. Downloaded from www.nrcresearchpress.com by 213.200.69.106 on 09/08/12
For personal use only.

TABLE 1. Bond distances in angstroms

Atom 1	Atom 2	Distance[a]	Atom 1	Atom 2	Distance	Atom 1	Atom 2	Distance
N1	N6	1.366(4)	N3	C3	1.367(4)	C3	C8	1.350(5)
N1	C4	1.342(5)	N4	C1	1.351(4)	C4	C9	1.346(5)
N1	C6	1.395(4)	N5	C5	1.325(5)	C5	C8	1.415(5)
N2	N4	1.348(4)	N6	C10	1.322(6)	C7	C8	1.501(5)
N2	C6	1.333(4)	C1	C2	1.376(4)	C9	C10	1.404(6)
N3	N5	1.358(4)	C2	C6	1.406(5)	C9	C12	1.485(6)
N3	C1	1.386(4)	C2	C11	1.502(5)	N4	H2	0.72(4)
C7	H72	1.080(6)	C11	H113	0.89(4)	C3	H3	0.90(3)
C7	H73	1.080(6)	C12	H121	1.080(6)	C4	H4	0.75(4)
C10	H10	0.93(4)	C12	H122	1.080(9)	C5	H5	1.00(3)
C11	H111	1.05(4)	C12	H123	1.080(7)	C7	H71	1.080(5)
C11	H112	1.03(4)						

[a]Numbers in parentheses are estimated standard deviations in the least significant digits.

TABLE 2. Bond angles in degrees

Atom 1	Atom 2	Atom 3	Angle[a]	Atom 1	Atom 2	Atom 3	Angle	Atom 1	Atom 2	Atom 3	Angle
N6	N1	C4	110.5(3)	N3	C1	N4	119.7(3)	N1	C6	C2	129.0(3)
N6	N1	C6	121.3(3)	N3	C1	C2	132.3(3)	N2	C6	C2	113.8(3)
C4	N1	C6	128.2(3)	N4	C1	C2	108.0(3)	C3	C8	C5	103.5(3)
N4	N2	C6	103.0(3)	C1	C2	C6	102.5(3)	C3	C8	C7	129.2(3)
N5	N3	C1	119.8(2)	C1	C2	C11	129.3(3)	C5	C8	C7	127.3(3)
N5	N3	C3	110.4(3)	C6	C2	C11	128.2(3)	C4	C9	C10	102.5(4)
C1	N3	C3	129.9(3)	N3	C3	C8	109.0(3)	C4	C9	C12	130.4(4)
N2	N4	C1	112.6(3)	N1	C4	C9	110.0(3)	C10	C9	C12	127.1(4)
N3	N5	C5	104.7(3)	N5	C5	C8	112.4(3)	N6	C10	C9	113.5(4)
N1	N6	C10	103.5(3)	N1	C6	N2	117.2(3)	N2	N4	H2	131.(3)
C8	C7	H73	107.4(3)	H111	C11	H113	110.(3)	C1	N4	H2	115.(3)
H71	C7	H72	109.5(5)	H112	C11	H113	113.(3)	N3	C3	H3	118.(2)
H71	C7	H73	109.5(5)	C9	C12	H121	112.7(5)	C8	C3	H3	133.(2)
H72	C7	H73	109.5(4)	C9	C12	H122	110.6(5)	N1	C4	H4	117.(3)
N6	C10	H10	126.(3)	C9	C12	H123	105.0(5)	C9	C4	H4	133.(3)
C9	C10	H10	121.(3)	H121	C12	H122	109.5(6)	N5	C5	H5	123.(2)
C2	C11	H111	111.(2)	H121	C12	H123	109.5(6)	C8	C5	H5	125.(2)
C2	C11	H112	106.(2)	H122	C12	H123	109.5(6)	C8	C7	H71	114.5(4)
C2	C11	H113	109.(2)	C8	C7	H72	106.4(4)	H111	C11	H112	108.(3)

[a]Numbers in parentheses are estimated standard deviations in the least significant digits.

TABLE 3. Intra- and intermolecular hydrogen bonds, H-bond distances (in Å), and angles (in deg)

Intra			
N4—H2···N5	N4—H2 = 0.72(4)	H2···N5 = 2.41	N4—H2···N5 = 110(3)
C11—H112···N6	C11—H112 = 1.04(4)	H112···N6 = 2.51(4)	C11—H112···N6 = 115(3)
Inter			
N4—H2···N5	N4—H2 = 0.72(4)	H2···N5 = 2.33(4)	N4—H2···N5 = 140(4)
C5—H5···N2	C5—H5 = 0.99(4)	H5···N2 = 2.77(4)	C5—H5···N2 = 124(3)

is represented in Fig. 3. Two strong intermolecular N—H···N interactions hold together the two molecules of the dimer. The two C—H···N intermolecular bonds, although weaker, also contribute to the stabilization of the dimer. In pyrazoles formed by only one ring, cyclic dimers, trimers, and tetramers are formed by N—H···N hydrogen bonds of the same pyrazole (13). In the case of compound **1**, this situation would correspond to intermolecular N4—H2···N5 hydrogen bonds. The reason this "standard" situation is not followed in compound **1** may be related to the possibility of an extra stabilization due to C5—H5···N2 hydrogen bonds. From the intramolecular hydrogen bonds, the one between the methyl group and the adjacent nitrogen atom belongs to the class of weak C—H···N interactions that are related to the stabilization of one of the conformations of the methyl groups (14). The N4—H2···N5 is weaker than the intramolecular hydrogen bond of the same proton; in particular, the angle is not very favorable for the interaction (15). The situation corresponds to a 3-centered hydrogen bond (a theoretical study of water

Can. J. Chem. Downloaded from www.nrcresearchpress.com by 213.200.69.106 on 09/08/12
For personal use only.

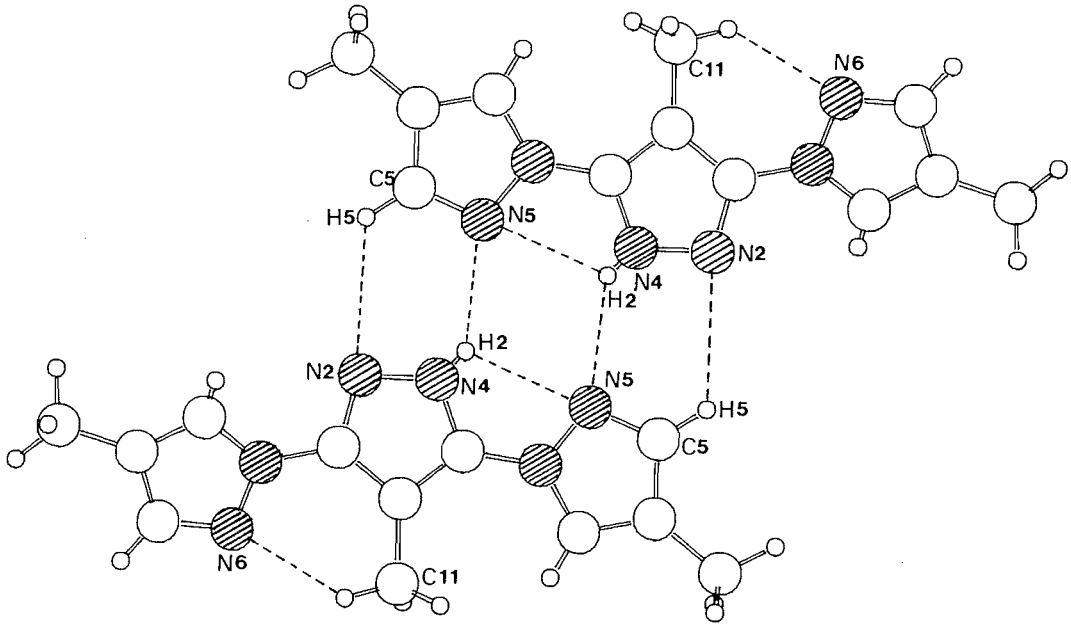

FIG. 3. The hydrogen bond network in the dimers.

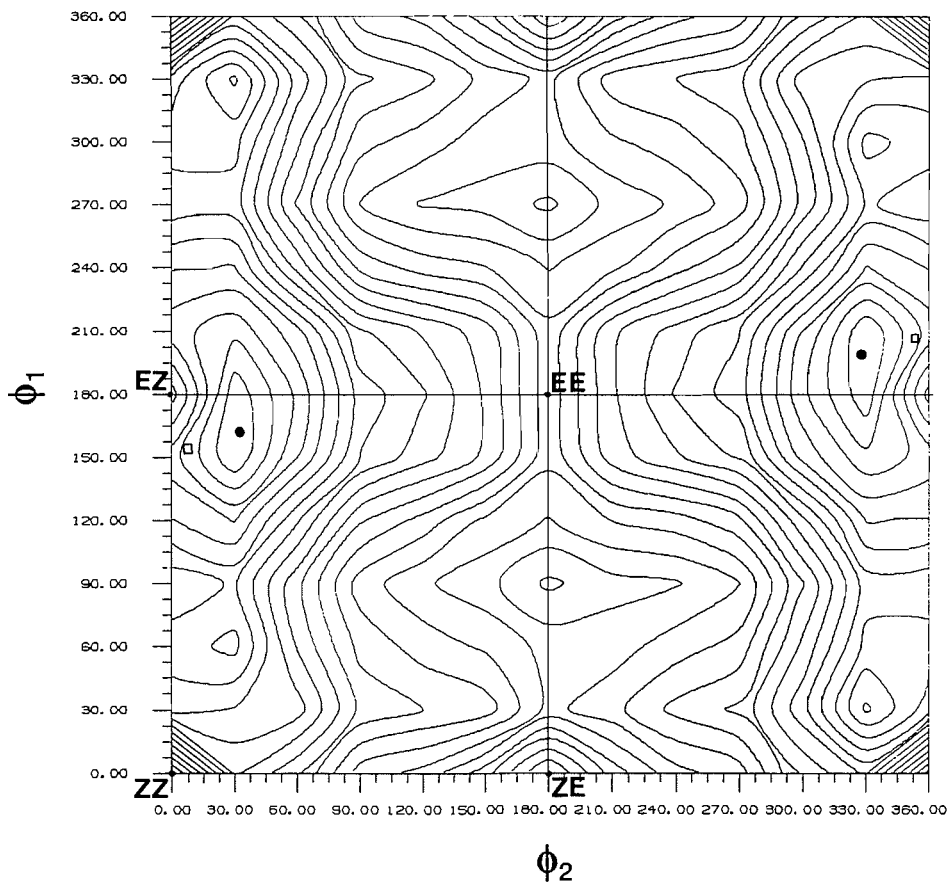

FIG. 4. Map of the potential surface. Separation between lines corresponds to 0.3 kcal mol^{-1}. Large black points: absolute minimum; small black points: conformations of Scheme 1; white squares: X-ray structure.

trimers (16) shows that this situation is not a stationary point of the energy hypersurface) but we prefer to describe it as the combination of a "normal" hydrogen bond (the intermolecular) characterized by the presence of charge density along the hydrogen bond with an "electrostatic" interaction (the intramolecular).

Can. J. Chem. Downloaded from www.nrcresearchpress.com by 213.200.69.106 on 09/08/12
For personal use only.

TABLE 4. Activation barriers to proton transfer in pyrazoles (^{1}H NMR in CD_3OD solution)

Compound	Temperature (K)	Chemical shifts (ppm)[a]	$\Delta G^{\neq}$ (kcal mol^{-1})
9	298	Me3 = Me5 = 2.35	
	248 (T_c)		12.8
	230	Me3 = 2.32, Me5 = 2.38, $\Delta\nu$ = 12.1 Hz	
10	298	Me3 = Me5 = 2.70	
	236 (T_c)		12.1
	230	Me3 = 2.67, Me5 = 2.74, $\Delta\nu$ = 14.0 Hz	
1[b]	298	Me4 = 2.36, Me4′ = Me4″ = 2.35 H3′ = H3″ = 7.77, H5′ = H5″ = 8.01	
	228(T_c)	H3′H3″; 238 H5′/H5″ (T_c)	11.9
	198	Me4 = 2.38, Me4′ = 2.38, M4″ = 2.38 H3′ = 7.87, H3″ = 7.91, $\Delta\nu$ = 7.3 Hz H5′ = 8.09, H5″ = 8.15, $\Delta\nu$ = 11.8 Hz	

[a]The chemical shifts are referred to the signal of residual protons of CD_3OD at 3.50 ppm.
[b]Me4 = C11, Me4′ = C7, Me4″ = C12.

^{1}H NMR study of the prototropy of compound 1 and related pyrazoles

Very few activation energies for pyrazole tautomerism have been reported. Grant and co-workers (17) determined the values for pyrazole itself and for 3,5-dimethylpyrazole in hexamethylphosphorotriamide (HMPA): 14 and 15 kcal mol^{-1}, respectively. We report in Table 4 the results obtained in the case of compound **1** and for 3,5-dimethyl-4-chloropyrazole **2** and 3,5-dimethyl-4-nitropyrazole **3**. The preparation of compounds **2** and **3** is described in the literature (5).

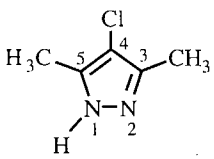

2

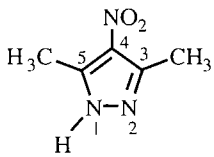

3

In methanol-d_4, the three barriers are similar and a little lower than in HMPA, which is normal taking into account the strong solvating properties of the latter. The results of Table 4 correspond to N-D pyrazoles and a small primary isotope effect is included in the value of $\Delta G^{\neq}$ (the values reported by Nesmeyanov *et al.* (18) for isotope effects on the tautomerism of pyrazoles are probably much exaggerated).[3]

Semiempirical calculations of the potential surface of compound 1

Tautomerism between the *a* and *b* forms of compound **1** involves the rotation of the two pyrazole rings about the C3(5)—N bonds. To explore if this rotation is simultaneous or consecutive to the prototropy, we decided to analyze the complete potential conformational hypersurface. The semiempirical SCF-MO AM1 method (19*a–c*) was selected because of its ability to reproduce the experimental strength of hydrogen bonds (19*b*). The surface was explored by rotating ϕ_1 and ϕ_2 every 30° (Fig. 4), while forcing the planarity of each pyrazole ring. The absolute minimum lies at ϕ_1 = 162.85° and ϕ_2 = 32.92° near the molecular structure found in the crystal (ϕ_1 = −155.3(3)°, ϕ_2 = −6.2(5)°). Both correspond to a conformation that can be denoted *EZ*, with "pyridine-like" nitrogen atoms in the *anti* disposition and "pyridine-like" and "pyrrole-like" nitrogen atoms of the central pyrazole in a *syn* disposition.

This molecule can adopt four planar conformations (Scheme 1), which are useful for the following discussion. $\delta\Delta H_f$ is the difference, in kcal mol^{-1}, of the heats of formation of the absolute minimum (ΔH_f = 209.474 kcal mol^{-1}) and each one of the four conformations. Those four planar conformations are not local minima of the AM1 hypersurface as the structures are not fully minimized. It should be noted that planarity has been forced within the five atoms of each pyrazole ring, and thus the differences in energy with the absolute minimum would not only be due to changes in ϕ_1 and ϕ_2 but to the inability of the pyrazole rings to distort as well. However, this contribution is negligible except for ϕ_1 = ϕ_2 = 0°, a conformation for which the contribution can be evaluated as 1.70 kcal mol^{-1}. In this case, distortion relieves steric hindrance between the methyl group of the central pyrazole ring and the adjacent 5′ hydrogens.

The tautomerization/isomerization process (from ϕ_1 = 162.85 and ϕ_2 = 32.92° to ϕ_1 = 197.18 and ϕ_2 = 327.08°) through the transition state *ZE* requires an activation energy of 2.14 kcal mol^{-1}. (This value corresponds to a full optimisation of the absolute minimum and the transition state.) The different values of $\delta\Delta H_f$ of Scheme 1 roughly represent two kinds of repulsive interactions: N lone pair/N lone pair (ϕ_1 = 0°) and N—H/C—H (ϕ_2 = 180°). These interactions amount to 3.0 and 2.1 kcal mol^{-1}, respectively, values that must be considered at the uppermost limit due to the lack of complete optimization. In rhodium(I) dinuclear complexes (1), the N lone pair/N lone pair interaction becomes attractive and the structure of the pyrazolate ligands corresponds to the *ZZ* conformation.

Tautomerization without rotation of the lateral pyrazole rings leads to a conformation ϕ_1 = 32.92, ϕ_2 = 162.85°. To this *ZE*-like structure corresponds an $\delta\Delta H_f$ of 4.9 kcal mol^{-1}. Since the activation energy (see NMR discussion) is similar to those of other pyrazoles where there is no need to account for rotational isomerism, the conclusion is that in compound **1** the rotation of the lateral pyrazole rings should

[3]H. H. Limbach. Personal communication.

Can. J. Chem. Downloaded from www.nrcresearchpress.com by 213.200.69.106 on 09/08/12
For personal use only.

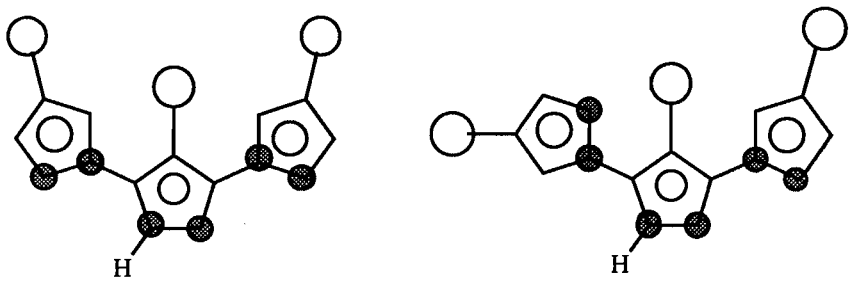

ZZ, ϕ_1=0°, ϕ_2=0°, $\delta\Delta H_f$ = 5.45

ZE, ϕ_1=0°, ϕ_2=180°, $\delta\Delta H_f$=6.87

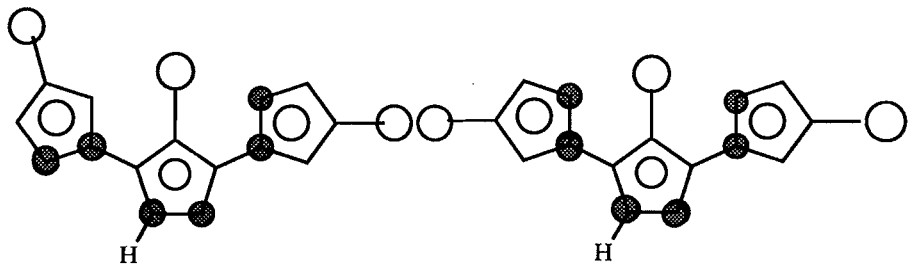

EZ, ϕ_1=180°, ϕ_2=0°, $\delta\Delta H_f$=2.14

EE, ϕ_1=180°, ϕ_2=180°, $\delta\Delta H_f$=4.61

SCHEME 1

TABLE 5. Crystal analysis parameters at room temperature

Crystal data	
Formula	$C_{12}H_{14}N_6$
Crystal habit	Colourless needles
Crystal size, mm	0.08 × 0.2 × 0.7
Symmetry	Monoclinic, $P2_1/n$
Unit cell determination	Least-squares fit from 25 reflections ($\theta < 50°$)
Unit cell dimensions, Å, deg	a = 8.222(2), α = 90.00° b = 27.336(8), β = 100.97(4)° c = 5.574(2), γ = 90.00°
Packing: V/Å^3, Z	1230.0(7), 4
D_c, g cm^{-3}, M, F(000)	1.308, 242.283, 512
μ, cm^{-1}	6.554
Experimental data	
Technique	Enraf–Nonius CAD4 diffractometer Graphite-oriented monochromator: CuKα $\omega/2\theta$ scans, θ range, 1–73°
Number of reflections	
Independent	2210
Observed	1890 (2.5 σ(I) criterion)
Standard reflections	3 reflections every 60 min. No variation
Solution and refinement	
Solution	MULTAN (25)
Number of variables	193
Weighting scheme	Unit
Max. thermal value	U11(N(6)) = 0.131(4) Å^2
Final ΔF peaks	0.34 e Å^{-3}
Final R	0.063

be synchronous with prototropy. Although the energy required to rotate the 3- and 5-pyrazolyl substituents and the conformations of minimum energy are not known for the transition state of the prototropy (where there is no longer an NH and an N atom with a lone pair (20)), the conclusion of synchronicity is probably true.

Can. J. Chem. Downloaded from www.nrcresearchpress.com by 213.200.69.106 on 09/08/12
For personal use only.

Can. J. Chem. Downloaded from www.nrcresearchpress.com by 213.200.69.106 on 09/08/12
For personal use only.

Experimental section

Preparation of 3,5-bis(4-methylpyrazol-1-yl)-4-methylpyrazole (1)

4-Methylpyrazole was prepared in 70% yield from hydrazine and methylmalonaldehyde tetraethylacetal (21; see ref. 5, p. 407). Following Hüttel's procedure (2) but with a 4-methylpyrazole (2.46 g)/bromine (1.6 g) 3:2 stoichiometry and 3 h reflux, 1.16 g of compound **1** was obtained, yield 48% (Lit. (2) yield 24%); mp 165–166°C (lit. (2) mp 167–168°C). Anal. calcd for $C_{12}N_6H_{14}$: C 59.48, H 5.82, N 34.69; found: C 59.27, H 5.93, N 34.73.

X-ray crystallography

Table 5 shows the crystal analysis parameters. Crystals were obtained by slow evaporation of a dichloromethane–hexane solution. The intensities collected on the diffractometer were corrected for Lorentz and polarisation factors. An empirical absorption correction was applied using the measurement of Ψ scans. The SDP (22) system was used for initial computation. The crystalline structure was solved by direct methods using MULTAN (23) and SHELX-76 (24). The nonhydrogen atoms were refined, allowing for isotropic and then anisotropic vibrations. The hydrogens of the methyl groups were included at calculated positions and were refined first as a rigid group, then freely. The other hydrogens were found on a difference map. In each case, isotropic thermal parameters were kept fixed. Geometrical computations were done with PARST (25), and plots were made with PLUTO (27).[4]

NMR measurements

The variable temperature proton NMR spectra were recorded on a Bruker AC 200 spectrometer operating at 200.13 MHz in a 5-mm dual probe with CD_3OD as solvent. The temperature of the probe was calibrated by the methanol standard method and there was a delay of 15 min before registering the NMR spectra at each temperature. The rotational barriers were measured by line shape analysis of the signals of protons H3 and H5 in the case of compound **1** and Me3 and Me5 signals in the case of compounds **2** and **3** (27). The middles of the signals of compound **1** at low temperature (H3′ and H3″, 7.885 ppm; H5′ and H5″, 8.12 ppm) are slightly different from the averaged values at room temperature (7.77 and 8.01 ppm).

Computational details

Calculations were performed on a VAX-8350 belonging to "Laboratorios Dr. Esteve", with the standard version of AM1 (19*a*), as implemented in the MOPAC package of programs (19*c*). The RHF method was used throughout. The geometries of the conformational hypersurface points were determined by minimizing the energy with respect to all geometrical variables except for the three that define ϕ_1 and ϕ_2, and for those that maintain the planarity of the pyrazole rings (10 extra dihedral angles were set to 0° or 180°), using the BFGS algorithm until the gradient norm of the energy was less than 1.0. The absolute minimum was determined by minimizing the energy with regard to all geometrical variables from the lower energy points in the conformational hypersurface.

Acknowledgment

The "Laboratorios Dr. Esteve, S. A." provided the computational facilities.

[4]Atomic coordinates for this structure can be purchased from: The Depository of Unpublished Data, Document Delivery, CISTI, National Research Council Canada, Ottawa, ON K1A 0S2, Canada.

Tables of positional parameters have also been deposited with the Cambridge Crystallographic Data Centre, and can be obtained on request from The Director, Cambridge Crystallographic Data Centre, University Chemical Laboratory, 12 Union Road, Cambridge, CB2 1EZ, U.K.

1. R.M. Claramunt, C. Lopez, D. Sanz, J. Elguero, D. Carmona, M. Esteban, L.A. Oro, and M. Begtrup. J. Organomet. Chem. **412**, 259 (1991).
2. R. Hüttel, H. Wagner, and P. Jochum. Ann. Chem. **593**, 179 (1955).
3. P. Bouchet, J. Elguero, R. Jacquier, and F. Forissier. C.R. Seances Acad. Sci. Ser. C; **269C**, 570 (1969).
4. H. Reimlinger, A. Noels, J. Jadot, and A.V. Overstraeten. Chem. Ber. **103**, 1942 (1970).
5. R. Fusco. *In* Pyrazoles, pyrazolines, pyrazolidines, indazoles and condensed rings. *Edited by* R. H. Wiley. Interscience, New York. 1967. p. 84.
6. K. Schofield, M.R. Grimmett, and B.R.T. Keene. The azoles. Cambridge University Press, Cambridge. 1976. p. 45.
7. J. Elguero. *In* Comprehensive heterocyclic chemistry. *Edited by* A.R. Katritzky and C.W. Rees. Pergamon Press, Oxford. 1984. p. 167.
8. B. Björkqvist, E. Helgstrand, and N.E. Stjernström. Acta Chem. Scand. **21**, 2296 (1967).
9. J. de Mendoza, P. Prados, and J. Elguero. Heterocycles, **23**, 2629 (1985).
10. G. Tarrago, I. Zidane, C. Marzin, and A. Tep. Tetrahedron, **44**, 91 (1988).
11. A. Baldy, J. Elguero, R. Faure, M. Pierrot, and E.J. Vincent. J. Am. Chem. Soc. **107**, 5290 (1985).
12. P. Cabildo, R.M. Claramunt, D. Sanz, M.C. Foces-Foces, F.H. Cano, J. Catalan, and J. Elguero. Tetrahedron, **41**, 471 (1985).
13. F. Aguilar-Parrilla, G. Scherer, H.H. Limbach, M.C. Foces-Foces, F.H. Cano, J.A.S. Smith, C. Toiron, and J. Elguero. J. Am. Chem. Soc. **114**, 9657 (1992).
14. G.R. Desiraju. Crystal engineering. Elsevier, Amsterdam. 1989.
15. A. Llamas-Saiz, C. Foces-Foces, O. Mo, M. Yañez, and J. Elguero. Acta Crystallogr. Sect. B: Struct. Sci. **B48**, 700 (1992).
16. O. Mo, M. Yañez, and J. Elguero. J. Chem. Phys. **97**, 6628 (1992).
17. M.T. Chenon, C. Coupry, D.M. Grant, and R.J. Pugmire. J. Org. Chem. **42**, 659 (1977).
18. A.N. Nesmeyanov, E.B. Zavelovich, V.N. Babin, N.S. Kochetkova, and E.I. Fedin. Tetrahedron, **31**, 1461 (1975); **31**, 1463 (1975); A.N. Nesmeyanov, V.N. Babin, E.V. Zavelovich, and N.S. Kochetkova. Chem. Phys. Lett. **37**, 184 (1976).
19. (*a*) M.J.S. Dewar, E.G. Zoebish, E.F. Healy, and J.J.P. Stewart. J. Am. Chem. Soc. **107**, 3902 (1985); (*b*) J.J.P. Stewart. J. Comput. Aided Mol. Des. **4**, 1 (1990); (*c*) MOPAC version 6.0, QCPE 455.
20. J. Catalan, J.L.G. de Paz, M. Sanchez-Cabezudo, and J. Elguero. Bull. Chem. Soc. Fr. 429 (1986).
21. P. Zeller, F. Bader, H. Lindlar, M. Montavon, P. Müller, R. Rüegg, G. Ryser, G. Saucy, S.F. Schaeren, U. Schwieter, K. Stricker, R. Tamm, P. Zürcher, and O. Isler. Helv. Chim. Acta, **42**, 841 (1959).
22. Enraf–Nonius, SDP Structure Determination Package 1983. Enraf–Nonius, Delft, The Netherlands.
23. P. Main, S. Fiske, S.E. Hull, L. Lessinger, G. Germain, J.P. Declercq, and M.M. Woolfson. MULTAN 80 system; 1980, a system of computer programs for the automatic solution of crystal structures from X-ray diffraction data, Universities of York, England, and Louvain-la-Neuve, Belgium.
24. G.M. Sheldrick. SHELX-76, 1976, a program for crystal structure determination, University of Cambridge, England.
25. M. Nardelli. Comput. Chem. **7**, 95 (1983).
26. W.D.S. Motherwell. PLUTO, 1976, a program for plotting molecular and crystal structures, University of Cambridge, England.
27. (*a*) M. Oki. Applications of dynamic NMR spectroscopy, VCH Publishers, Deerfield Beach, Fla. 1985; (*b*) J. Sandström. Dynamic NMR spectroscopy. Academic Press, London. 1982.

Electron ionization mass spectrometry of aryl- and fluoroalkyl-substituted nickel(II) β-diketonates and monothio-β-diketonates

MARK L.J. REIMER[1] AND JOHN B. WESTMORE[2]
Department of Chemistry, University of Manitoba, Winnipeg, MB R3T 2N2, Canada

AND

MANORANJAN DAS[3]
School of Chemistry, University of New South Wales, P. O. Box 1, Kensington, N.S.W. 2033, Australia

Received January 20, 1993

MARK L.J. REIMER, JOHN B. WESTMORE, and MANORANJAN DAS. Can. J. Chem. **71**, 1450 (1993).

Electron ionization positive-ion mass spectra are reported for 18 substituted nickel(II) β-diketonates and monothio-β-diketonates, $Ni^{II}(RCXCHCOR')_2$, where X = O or S; R = phenyl, 2-thienyl, 5-methyl-2-thienyl, or 2-naphthyl; and R′ = difluoromethyl, trifluoromethyl, pentafluoroethyl, or *n*-heptafluoropropyl. Each mass spectrum contains a prominent molecular ion, $[NiL_2]^+$, which, for β-diketonates, fragments mainly by elimination of the odd-electron R″˙ species; the resulting ion decomposes by losses of one or more even-electron neutral species to yield ions containing nickel(II). In contrast, the major fragmentation of the molecular ion of monothio-β-diketonates is loss of $Ni^{I}L$ to yield an abundant L^+ ion. Furthermore, while most ions contain nickel(II), some prominent ions contain nickel(I); among these are $[Ni^{I}SC(R)=CH]^+$ and $[Ni^{I}(HCCR)]^+$. Interesting ions are formed by hydrogen transfer processes. The $[NiHL]^+$ ion is favored in the spectra of β-diketonates having a phenyl substituent, consistent with hydrogen transfer to the metal from the aryl group. On the other hand, the $[Ni(L-H)]^+$ ion, favored for the monothio-β-diketonates, could be formed by hydrogen transfer from the central position of the chelate ring or from an aryl substituent. Alternative mechanisms of formation are discussed. Some minor ions are formed by fluorine transfer to nickel. The trends in their abundances are influenced by the hardness of nickel as an acid in its different oxidation states, under the influence of the ligand donor atoms, and by the hardness of the carbon atoms of the perfluoroalkyl substituents.

MARK L.J. REIMER, JOHN B. WESTMORE et MANORANJAN DAS. Can. J. Chem. **71**, 1450 (1993).

On a déterminé les spectres de masse des ions positifs par ionisation électronique de 18 β-dicétonates et monothio-β-dicétonates de nickel(II), $Ni^{II}(RCXCHCOR')_2$, dans lesquels X = O ou S; R = phényle, 2-thiényle, 5-méthyl-2-thiényle ou 2-naphtyle; et R′ = difluorométhyle, trifluorométhyle, pentafluoroéthyle ou *n*-heptafluoropropyle. Chaque spectre de masse comporte un ion moléculaire important, $[NiL_2]^+$, qui, pour les β-dicétonates, se fragmente principalement par élimination de l'espèce R″˙ à électron célibataire; l'ion qui en résulte se décompose par perte d'une ou de plusieurs espèces neutres comportant un nombre pair d'électrons, pour fournir des ions contenant du nickel(II). Par opposition, la fragmentation principale de l'ion moléculaire des monothio-β-dicétonates comporte une perte de $Ni^{I}L$ qui conduit à un ion L^+ abondant. De plus, alors que la plupart des ions contiennent du nickel(II), quelques ions importants contiennent du nickel(I); parmi ceux-ci, on remarque le $[Ni^{I}SC(R)=CH]^+$ et le $[Ni^{I}(HCCR)]^+$. Il se forme des ions intéressants par des processus de transfert d'hydrogène. L'ion $[NiHL]^+$ est favorisé dans les spectres des β-dicétonates possédant un substituant phényle; ce résultat est en accord avec un transfert d'hydrogène du groupe aryle vers le métal. D'autre part, l'ion $[Ni(L-H)]^+$, favorisé pour les monothio-β-dicétonates, pourrait se former par un transfert d'hydrogène de la position centrale du cycle chélate ou d'un substituant aryle. On discute des mécanismes alternatifs à ces formations. Il se forme des ions mineurs par transfert de fluor vers le nickel. Les tendances dans les abondances sont influencées par la dureté du nickel, agissant comme acide dans ses différents états d'oxydation, sous l'influence d'atomes ligands donneurs et par la dureté des atomes de carbone des substituants perfluoroalkyles.

[Traduit par la rédaction]

Introduction

We pointed out in the previous publication (1) that many metal β-diketonates are thermally stable and have sufficient volatility for study by gas chromatography (2). Because of these properties, they have recently been used as precursors for chemical vapor deposition (3–5), a promising technique for the preparation of thin films of high T_c superconducting oxides (6). The alkaline earth complexes used for this purpose have been characterized by mass spectrometry (7). Analytical methods can also be devised for metals by combining mass spectrometry with gas chromatography.

The mass spectra of these complexes are of interest in their own right because the wide variety of compounds available permits assessment of the influence exerted by bonding and structure factors, i.e., (*i*) the central metal atom, (*ii*) the ligand donor atoms, and (*iii*) different organic substituents attached to the ligand. Conversely, because of this, the mass spectra can often be used to draw conclusions about the condensed phase chemistry of the metals. Much of the early mass spectral work, starting from the first extended study (8), has been reviewed (9–12).

The electron ionization (EI) positive-ion mass spectra of organic compounds often show an abundant molecular ion ($M^{+\cdot}$), which initially eliminates an odd-electron ($OE^{\cdot}$) neutral species; generally, the resulting ion then loses one or more even-electron (EE^0) neutral species. In the case of transition metal compounds the odd- ($OE^{+\cdot}$) or even-electron (EE^+) character of the metal-containing ions can be altered by a formal change of the oxidation state of the metal (8, 13, 14). For example, we may depict the molecular ion, $[NiL_2]^+$, of a nickel complex either as $[Ni^{II}L_2]^{+\cdot}$ or as

[1]Present address: Biomedical Mass Spectrometry Unit, McGill University, 1130 Pine Ave. W., Montreal, QC H3A 1A3, Canada.
[2]Author to whom correspondence may be addressed.
[3]Present address: 9 Golmuri Market, Jamshedpur-3, Bihar, India

Can. J. Chem. Downloaded from www.nrcresearchpress.com by 203.198.23.82 on 09/08/12
For personal use only.

Can. J. Chem. Downloaded from www.nrcresearchpress.com by 203.198.23.82 on 09/08/12
For personal use only.

$[Ni^{III}L_2]^+$ by formal movement of an electron between nickel and ligand (L).

While the major features of the mass spectra of complexes of many metals conform to a number of broad generalizations including, for example, the relative stabilities of metal oxidation states, there are often more subtle features associated with a particular metal or ligand. These features include the formation of new bonds between the metal and an atom, or substituent, originally part of the ligand. Thus, formation of metal–hydrogen, metal–halogen, or metal–carbon bonds has been noted in the reviews cited above. In the case of nickel, there is a marked tendency for formation of nickel–hydrogen bonds. In this paper we present the EI mass spectra of a series of fluorinated β-diketonate complexes of nickel(II), having the general form $Ni^{II}(RCXCHCOR')_2$, as listed in Table 1. Particularly noteworthy in these spectra are the $[NiHL]^+$ and $[Ni(L-H)]^+$ ions, which result by hydrogen transfer either from the aryl substituent or from the central position of the chelate ring; for these ions mechanisms of formation are suggested. In contrast, ions arising by fluorine transfer to nickel are of limited number and of low abundance. While the prominent ions in the spectra can be assigned structures containing Ni(II), there are also ions for which the less favored, but well-known, Ni(III) or Ni(I) states seem more reasonable. Trends in observed ion abundances are interpreted in light of the ability of nickel to undergo a change in valency, the principle of Hard and Soft Acids and Bases (HSAB), and the inductive effects of the ligand donor atoms and of the R and R′ groups. We have discussed these concepts previously (1). For two compounds ion decomposition pathways were supported by linked electric–magnetic field scans. The work described here is a continuation of our survey of transition metal β-diketonate and monothio-β-diketonate complexes.

TABLE 1. The nickel chelates examined and their molecular masses

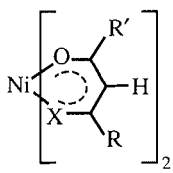

Complex	X	R	R′	M_r
1*a*	O	$-C_6H_5$	$-CHF_2$	452
2*a*	O	$-C_4H_3S$	$-CHF_2$	464
3*a*	O	$-C_6H_5$	$-CF_3$	488
3*b*	S	$-C_6H_5$	$-CF_3$	520
4*a*	O	$-C_4H_3S$	$-CF_3$	500
4*b*	S	$-C_4H_3S$	$-CF_3$	532
5*a*	O	$-C_5H_5S$	$-CF_3$	528
5*b*	S	$-C_5H_5S$	$-CF_3$	560
6*a*	O	$-C_6H_5$	$-C_2F_5$	588
6*b*	S	$-C_6H_5$	$-C_2F_5$	620
7*a*	O	$-C_4H_3S$	$-C_2F_5$	600
7*b*	S	$-C_4H_3S$	$-C_2F_5$	632
8*b*	S	$-C_{10}H_7$	$-C_2F_5$	720
9*a*	O	$-C_6H_5$	$-C_3F_7$	688
9*b*	S	$-C_6H_5$	$-C_3F_7$	720
10*a*	O	$-C_4H_3S$	$-C_3F_7$	700
10*b*	S	$-C_4H_3S$	$-C_3F_7$	732
11*b*	S	$-C_{10}H_7$	$-C_3F_7$	820

Experimental

Mass spectrometry

For these studies a VG 7070E-HF double-focusing (EB geometry) mass spectrometer (VG Analytical Ltd., Manchester, England) equipped with a data system based on a DEC PDP-11/73 microcomputer (Digital Equipment Corp., Maynard, Mass.) was used. Samples were admitted to the ion source on a direct insertion probe. In many cases ambient heating from the ion source was sufficient to obtain steady evaporation and reproducible mass spectra; in other cases the probe temperature was raised but it never exceeded 100°C. Low-resolution EI mass spectra were recorded under the following conditions: ion accelerating voltage, 6 kV; ionizing energy, 70 eV; trap current, 200 μA; source temperature, 200°C, scan rate, 1.0 s/decade; resolution, 1400 (10% valley definition). Ion decomposition mass spectra of selected ions in the spectra of **2***a*, **3***a*, and **3***b* were recorded by linked scanning, at a scan rate of 5.0 s/decade, as follows: (*a*) product ion scans at a constant magnetic field/electric field ratio (i.e., B/E constant with accelerating voltage (V) fixed), and (*b*) constant neutral loss scans such that $B[1-(E/E_0)]^{1/2}/E$ was constant, with V fixed. Precursor ions were collisionally activated in the first field-free region of the instrument by adjusting the helium pressure in the collision cell to achieve approximately 50% attenuation of the parent ion signal.

Ligand synthesis

The fluorinated β-diketones used in the syntheses of complexes **3***a* and **4***a* were purchased from Aldrich Chemical Co. (Milwaukee, Wis.). The remaining β-diketones were synthesized by a Claisen condensation of the appropriate methyl ketone ($RCOCH_3$) with the fluorinated ethyl ester ($R'COOC_2H_5$), as previously described (15, 16). The fluorinated monothio-β-diketones were synthesized from their corresponding β-diketones (16–20).

Synthesis of nickel chelates

(a) β-Diketonates

Upon addition of nickel(II) acetate tetrahydrate (0.22 mmol) in water (5 mL) to a solution of the ligand (0.44 mmol) in absolute ethanol (3 mL) a cloudy, pale green suspension formed. The suspension was heated on a steam bath for 15 min and then cooled in an ice bath for 1 h. The precipitate was filtered off under mild suction, washed with cold water, and dried in an oven (100°C) for 3 h to give the desired product (15, 21).

(b) Monothio-β-diketonates

Nickel(II) acetate tetrahydrate (0.5 mmol) in hot ethanol (10 mL) was added to a solution of the ligand (1.0 mmol) in ethanol (5 mL). The resulting brown precipitate was filtered off and recrystallized from a 1:1 acetone/light petroleum (bp 40–60°C) solution. The products were dark brown solids (20, 22–24).

Results and discussion

Although these complexes may exist as polymeric species in the solid state, the mass spectra indicate that they vaporize as monomers; thus, no trace of polymeric ions could be detected in the mass spectra of **2***a* and **3***a* when scanning to an upper mass limit greater than twice the molecular mass. Neither was $[NiL_2H]^+$ observed. Thus, there is no evidence for species that could have been formed by ionization of polymeric neutrals, or by ion-neutral reactions.

Nickel(II) β-diketonates

Table 2 lists assignments and relative abundances for significant ions in the mass spectra of the nine Ni(II) β-diketonates; representative mass spectra are shown in Fig. 1. The mass spectrum of **4***a* agrees well with one reported previously (25). Also obtained for **2***a* (but not shown) were product ion mass spectra of collisionally activated $[NiL_2]^+$, $[Ni^{II}L(L-R')]^+$, and $[Ni^{II}L]^+$ ions.

Scheme 1 depicts decomposition pathways proposed for

TABLE 2. EI mass spectra, m/z (%RA), of β-diketonates of nickel(II)[a]

Ion R,R′:	**1***a* C_6H_5, CHF_2	**2***a* C_4H_3S, CHF_2	**3***a* C_6H_5, CF_3	**4***a* C_4H_3S, CF_3	**5***a* C_5H_5S, CF_3	**6***a* C_6H_5, C_2F_5	**7***a* C_4H_3S, C_2F_5	**9***a* C_6H_5, C_3F_7	**10***a* C_4H_3S, C_3F_7
$[NiL_2]^+$	452 (28)	464 (58)	488 (24)	500 (14)	528 (20)	588 (39)	600 (12)	688 (14)	700 (3.3)
$[NiL(L-F)]^+$						569 (1.7)	581 (0.4)	669 (1.1)	
$[NiL(L-COF)]^+$						541 (1.0)	553 (0.3)	641 (0.6)	
$[NiFL(L-CF_3)]^+$						538 (1.1)	550 (0.7)		
$[NiL(L-R')]^+$	401 (34)	413 (57)	419 (19)	431 (9.1)	459 (13)	469 (38)	481 (13)	519 (19)	531 (3.4)
$[NiL(HCCR)]^+$			375 (0.5)	387 (0.2)	415 (0.8)	425 (1.0)	437 (0.4)	475 (0.9)	
$[NiRL]^+$			350 (0.3)	362 (0.2)	390 (1.3)				
$[NiHL]^{+b}$	256 (0.5)	262 (1.3)	274 (3.3)	280 (0.7)	294 (1.7)	324 (3.4)	330 (1.0)	374 (1.3)	380 (0.3)
$[NiL]^{+b}$	255 (3.2)	261 (7.9)	273 (4.0)	279 (3.9)	293 (4.8)	323 (5.5)	329 (4.9)	373 (2.8)	379 (1.4)
$[Ni(L-H)]^+$		260 (0.5)	272 (0.4)		292 (0.7)	322 (0.3)	328 (0.3)		
$[Ni(L-CO)]^+$	227 (3.3)	233 (6.1)							
$[NiF(L-R')]^+$	223 (2.0)	229 (2.4)	223 (3.1)		243 (2.6)				
$[Ni(L-CHF-HF)]^+$	203 (1.4)	209 (4.4)							
$[Ni(L-CF_2-HF)]^+$			203 (1.0)	209 (1.3)	223 (1.1)				
$[NiR]^+$	135 (3.6)	141 (7.6)	135 (4.0)	141 (3.5)	155 (4.6)	135 (5.0)	141 (5.1)	135 (3.4)	141 (1.4)
$[Ni]^+$	58 (3.5)	58 (4.6)	58 (2.6)		58 (5.7)		58 (3.9)	58 (1.3)	58 (7.2)
Ni-free ions:									
$[HL]^{+b}$		204 (16)	216 (20)	222 (50)	236 (37)	266 (7.8)	272 (34)	316 (5.0)	322 (31)
$[L]^+$			215 (2.8)	221 (0.9)	235 (0.9)	265 (1.3)	271 (0.4)	315 (0.9)	321 (0.3)
$[L-S]^+$				189 (4.2)	203 (9.6)				
$[L-F]^+$	178 (3.1)	184 (2.5)							
$[L-2F]^+$	159 (2.9)	165 (3.7)							
$[HL-R']^+$	147 (5.1)	153 (34)	147 (26)	153 (55)	167 (36)	147 (24)	153 (66)	147 (32)	153 (100)
$[L-CO-2F]^+$	131 (5.7)	137 (4.3)							
$[RCO]^+$	105 (100)	111 (100)	105 (100)	111 (100)	125 (100)	105 (100)	111 (100)	105 (100)	111 (94)
$[RCCH]^+$	102 (12)	108 (5.4)				102 (2.1)	108 (2.7)	102 (2.8)	108 (3.6)
$[R]^+$	77 (39)	83 (6.7)	77 (42)	83 (9.8)	97 (14)	77 (35)	83 (8.9)	77 (35)	83 (5.6)
$[R']^+$	51 (7.2)		69 (43)[c]	69 (80)[c]	59 (60)[c]	119 (2.2)	119 (3.5)		169 (1.9)
m/z 69	69 (5.8)[c]	69 (34)[c]				69 (34)[c]	69 (86)[c]	69 (40)[c]	69 (45)[c]
$[HL-R']^{2+}$		76.5 (2.2)	73.5 (3.5)	76.5 (5.7)	83.5 (2.3)	73.5 (1.8)	76.5 (5.7)	73.5 (2.5)	76.5 (3.4)
Base peak as $\%\Sigma_{50}$	38	28	33	30	32	33	29	38	33

[a]Relative abundances are calculated for the m/z values cited, which are the biggest signals for the group of peaks corresponding to the listed ion type. Thus, a correction factor should be applied to calculate the true relative abundance ratios among nickel-containing and nickel-free ions.

[b]Since these abundances are calculated as indicated in footnote [a] their values will be lower when a contribution from isotopes of an ion type of lower mass are significant. For $[HL]^+$ the correction is negligible.

[c]Probably CF_3^+, except for **1***a* and **2***a*, for which the assignment can be $C_3HO_2^+$.

1*a* and **2***a* (R′ = CHF_2; Fig. 1(*a*) shows the mass spectrum of **2***a*). The two most abundant nickel-containing ions are $[NiL_2]^+$ and $[Ni^{II}L(L-R')]^+$, the latter formed from $[Ni^{II}L_2]^{+\bullet}$ by elimination of the OE$^\bullet$ radical $CHF_2^\bullet$ (R″) (confirmed for **2***a* by the product ion spectrum of $[NiL_2]^+$). A product ion scan also confirmed subsequent consecutive EE^0 neutral losses of (L−R′) and (L−R) from $[Ni^{II}L(L-R')]^+$ to give $[Ni^{II}L]^+$ and $[Ni^{II}R]^+$, respectively. We can also propose a parallel pathway of EE^0 eliminations of (L−F), HF, and C_3O_2 to give $[Ni^{II}F(L-R')]^+$, $[Ni^{II}(L-CHF-HF)]^+$, and $[Ni^{II}R]^+$, respectively. The $[Ni^{II}L]^+$ ion, which is probably also directly formed from $[Ni^{II}L_2]^{+\bullet}$ by loss of L$^\bullet$, decomposes by loss of CO, to give $[Ni^{II}(L-CO)]^+$ (confirmed for **2***a* by the product ion scan) or by loss of :CHF, to give $[Ni^{II}F(L-R')]^+$. Although not supported here, the latter decomposition has been confirmed for an analogous cobalt complex by a product ion scan (1). The formation of the bare Ni^+ ion, which has also been reported in the mass spectrum of nickel(II) acetylacetonate (26, 27), confirms that reduction of nickel(II) has occurred. A probable formation route is by loss of (L−R′) and F$^\bullet$ from $[Ni^{II}F(L-R')]^+$, since we have confirmed the analogous decomposition for a similar cobalt complex (1). We infer that the nickel-free $[L-2F]^+$ and $[L-CO-2F]^+$ ions are formed by losses of the neutral species $Ni^{II}F_2$ from the $[Ni^{II}L]^+$ and $[Ni^{II}(L-CO)]^+$ ions, respectively. Precedents for such reactions are known (28) but our attempts to confirm these decompositions by product ion scanning were unsuccessful.

We note, for later discussion, the presence of $[NiHL]^+$ and $[Ni(L-H)]^+$ ions, formed from $[NiL_2]^+$ by hydrogen transfer reactions.

Scheme 2 shows fragmentation pathways proposed for **3***a*, **4***a*, and **5***a* (R′ = CF_3; Fig. 1(*b*) shows the mass spectrum of **4***a*). Once again, the major nickel-containing ions are $[NiL_2]^+$ and $[Ni^{II}L(L-R')]^+$. Many of the mechanisms discussed for Scheme 1 in the preceding paragraph still apply. A new decomposition pathway involves sequential elimination of the EE^0 neutrals CO_2, HCCR, and :CF_2 from $[Ni^{II}L(L-R')]^+$ to give $[Ni^{II}L(HCCR)]^+$, $[Ni^{II}L]^+$, and $[Ni^{II}F(L-R')]^+$, respectively (although elimination of :CF_2

Can. J. Chem. Downloaded from www.nrcresearchpress.com by 203.198.23.82 on 09/08/12
For personal use only.

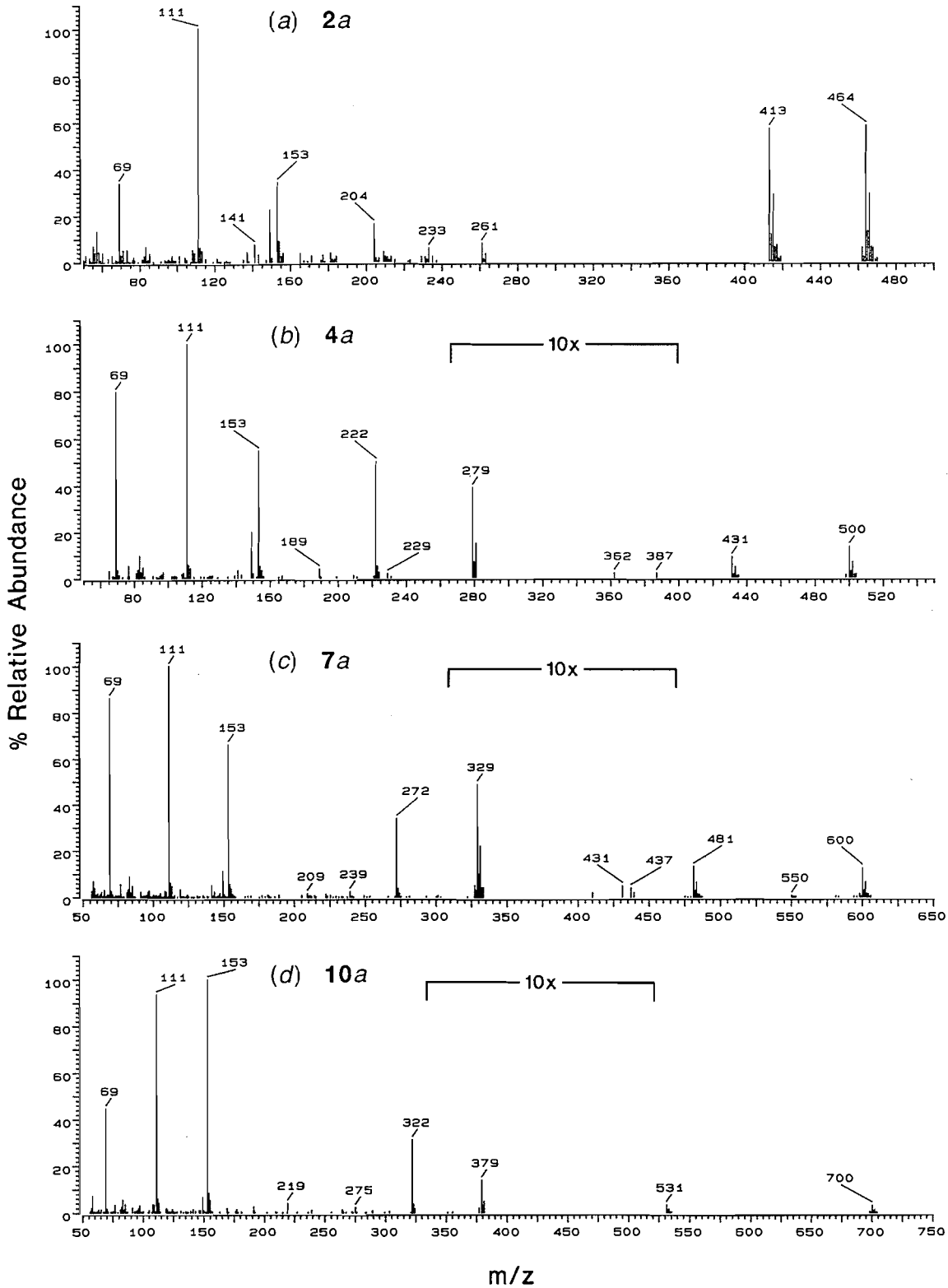

FIG. 1. EI mass spectra of (*a*) bis-[1,1-difluoro-4-(2-thienyl)-2,4-butanedionato]nickel(II), **2***a*; (*b*) bis-[1,1,1-trifluoro-4-(2-thienyl)-2,4-butanedionato]nickel(II), **4***a*; (*c*) bis-[1,1,1,2,2-pentafluoro-5-(2-thienyl)-3,5-pentanedionato]nickel(II), **7***a*; (*d*) bis-[1,1,1,2,2,3,3-heptafluoro-6-(2-thienyl)-4,6-hexanedionato]nickel(II), **10***a*.

Can. J. Chem. Downloaded from www.nrcresearchpress.com by 203.198.23.82 on 09/08/12
For personal use only.

Can. J. Chem. Downloaded from www.nrcresearchpress.com by 203.198.23.82 on 09/08/12
For personal use only.

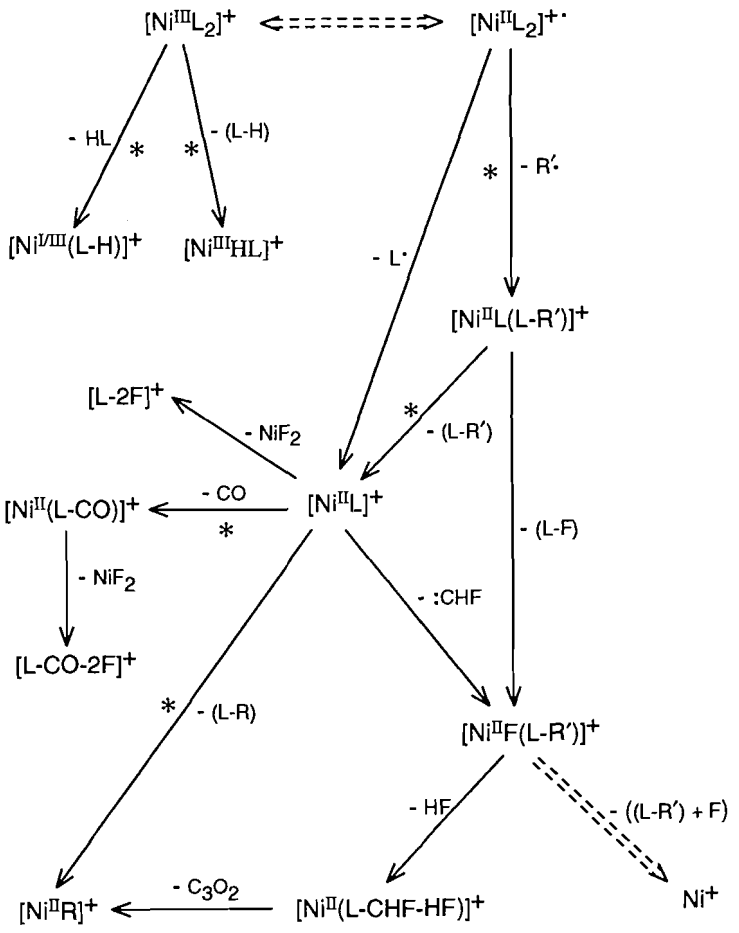

*decomposition confirmed for **2***a* by product ion scan
⇒ step involving metal valence change

SCHEME 1. Fragmentation pathways proposed for compounds **1***a* and **2***a* (R′ = CHF_2).

mimics loss of :CHF, noted above). For **3***a*, elimination of HF from $[Ni^{II}F(L-R')]^+$ has been confirmed by a product ion scan. It is interesting that the proposed, partially supported, stepwise eliminations of $:CF_2$ and HF from $[Ni^{II}L]^+$ have been confirmed from the analogous $[Co^{II}L]^+$ ion, even though elimination of CHF_3 is more favorable energetically. The formation of $[Ni^{III}RL]^+$ from $[NiL_2]^+$ by the loss of (L−R) implies formation of a nickel–carbon bond, and has a parallel in the mass spectrum of a similar cobalt complex (R = C_4H_3S, R′ = CF_3) (1). In contrast to **1***a* and **2***a*, the presence of $[Ni^{II}F(L-R')]^+$ is the only evidence supporting transfer of fluorine to nickel; nickel-free ions formed by elimination of NiF_2 are not observed.

Scheme 3 shows fragmentation routes suggested for **6***a*, **7***a* (R′ = C_2F_5), **9***a*, and **10***a* (R′ = *n*-C_3F_7). (The mass spectra of **7***a* and **10***a* are shown in Figs. 1(*c*) and 1(*d*).) As before, the major nickel-containing ions are $[NiL_2]^+$ and $[Ni^{II}L(L-R')]^+$. A new feature is the loss of the OE· neutral F· from $[NiL_2]^+$ to yield the low-abundance $[Ni^{II}L(L-F)]^+$ ion that, in turn, can lose the EE^0 neutral CO to give $[Ni^{II}L(L-COF)]^+$. For **6***a* and **7***a*, a minor ion formed by elimination of $:CF_2$ from $[NiL_2]^+$ indicates fluorine-to-nickel transfer.

Ni(II) Monothio-β-diketonates

Table 3 lists ion assignments and relative abundances for significant ions in the mass spectra of the nine Ni(II) monothio-β-diketonates; as examples of representative mass spectra those of **4***b*, **7***b*, and **10***b* are shown in Fig. 2. The mass spectra of **3***b* and **4***b* agree well with those previously reported (24). Also obtained for **3***b* (but not shown), and used in the elucidation of fragmentation pathways, were product ion mass spectra of collisionally activated $[NiL_2]^+$, $[Ni^{II}L(L-R'CO)]^+$, $[Ni^{II}L]^+$, and $[Ni^{I}SC(R)=CH]^+$ ions.

Scheme 4 shows decomposition pathways proposed for **3***b*, **4***b*, and **5***b* (R′ = CF_3; Fig. 2(*a*) shows the mass spectrum of **4***b*). In each spectrum, $[NiL_2]^+$ is the most abundant nickel-containing ion, but L^+ gives rise to the base peak for **3***b* and **4***b*; in the case of **3***b* the product ion mass spectrum indicates that L^+ is formed from $[NiL_2]^+$ by elimination of $Ni^{I}L$. We have proposed (1) that L^+ adopts a cyclic structure that is highly stabilized by the presence of sulfur. From $[NiL_2]^+$, losses of the OE· neutrals F·, R″·, and L· yield the $[Ni^{II}L(L-F)]^+$, $[Ni^{II}L(L-R')]^+$, and $[Ni^{II}L]^+$ ions, respectively. The pathway $[Ni^{II}L(L-R')]^+ \rightarrow [Ni^{II}L(L-R'CO)]^+ \rightarrow [Ni^{II}L]^+$ involves stepwise elimination of the EE^0 neutrals CO and $R(C_2S)H$. An alternative route to $[Ni^{II}L]^+$ involves elimination of COS from $[Ni^{II}L(L-R')]^+$ to give $[Ni^{II}L(HCCR)]^+$, which then loses HCCR. Loss of the OE· species R′C·(=O) from $[Ni^{II}L]^+$ through reduction of nickel produces the $[EE]^+$ ion $[Ni^{I}SC(R)=CH]^+$. The subsequent loss of $R(C_2S)H$ should be the preferred pathway to Ni^+. Elimination of atomic sulfur is inferred in formation of

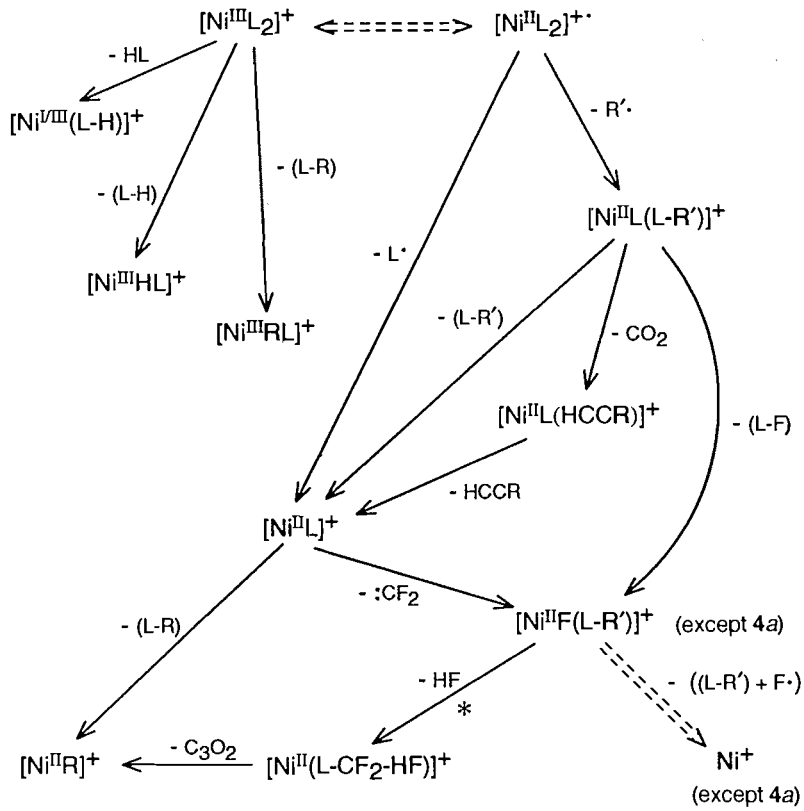

*decomposition confirmed for **3***a* by product ion scan
⇒ step involving metal valence change

SCHEME 2. Fragmentation pathways proposed for compounds **3***a*, **4***a*, and **5***a* (R′ = CF_3). Pathways are common to all complexes, except where noted.

$[Ni^{II}(L-S)]^+$ from $[Ni^{II}L]^+$ and of $[Ni^{I}(HCCR)]^+$ from $[Ni^{I}SC(R)=CH]^+$; this inference is supported by the formation of $[Ni^{III}L(L-S)]^+$ from $[Ni^{III}L_2]^+$ in the mass spectrum of **11***b*, where no alternative fragmentation is possible. Elimination of neutral $Ni^{II}S$ from $[Ni^{II}L(L-R'CO)]^+$ gives the metal-free ion $[2L-2S-R'CO]^+$, a documented reaction for Co(III) monothio-β-diketonates (1). A small peak at *m/z* 321 in the mass spectrum of **3***b* is assigned as $[NiSL]^+$; its formation by retention of a sulfur atom and elimination of the OE· neutral RC·(=CHC(=O)R′) from $[NiL_2]^+$ is supported by a product ion scan.

Scheme 5 shows decomposition pathways suggested for complexes substituted with pentafluoroethyl (**6***b*, **7***b*, and **8***b*) and *n*-heptafluoropropyl (**9***b*, **10***b*, and **11***b*) groups. (Mass spectra of **7***b* and **10***b* are shown in Figs. 2(*b*) and 2(*c*).) In all spectra, L^+ gives rise to the base peak and $[NiL_2]^+$ is, once again, the most abundant nickel-containing ion. Many of the fragmentation pathways parallel those observed for the trifluoromethyl derivatives, as discussed above. A new feature of these spectra is the increased abundance of ions formed by fluorine transfer to nickel. Thus, the analogues of the $[Ni^{III}FL(L-CF_3)]^+$ and $[Ni^{III}FL(L-C_2F_5)]^+$ ions observed here are not detected for complexes **3***b*, **4***b*, and **5***b*. The inferred elimination of $Ni^{II}F_2$ from $[Ni^{II}L]^+$ to give $[L-2F]^+$ also provides support for fluorine-to-metal transfer.

The $[Ni^{II}L(L-F-HF)]^+$ ion, observed only in the mass spectra of **9***b* and **10***b*, could arise by loss of HF from $[Ni^{II}L(L-F)]^+$, with formation of a five-membered ring and stabilization of the positive charge by sulfur, as shown in mechanism A. The difficulty of forming strained four- and three-membered rings, respectively, may explain the ab-

A

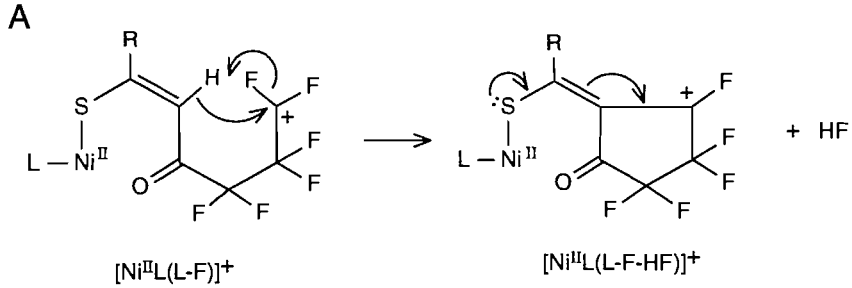

$[Ni^{II}L(L-F)]^+$ $[Ni^{II}L(L-F-HF)]^+$

Can. J. Chem. Downloaded from www.nrcresearchpress.com by 203.198.23.82 on 09/08/12
For personal use only.

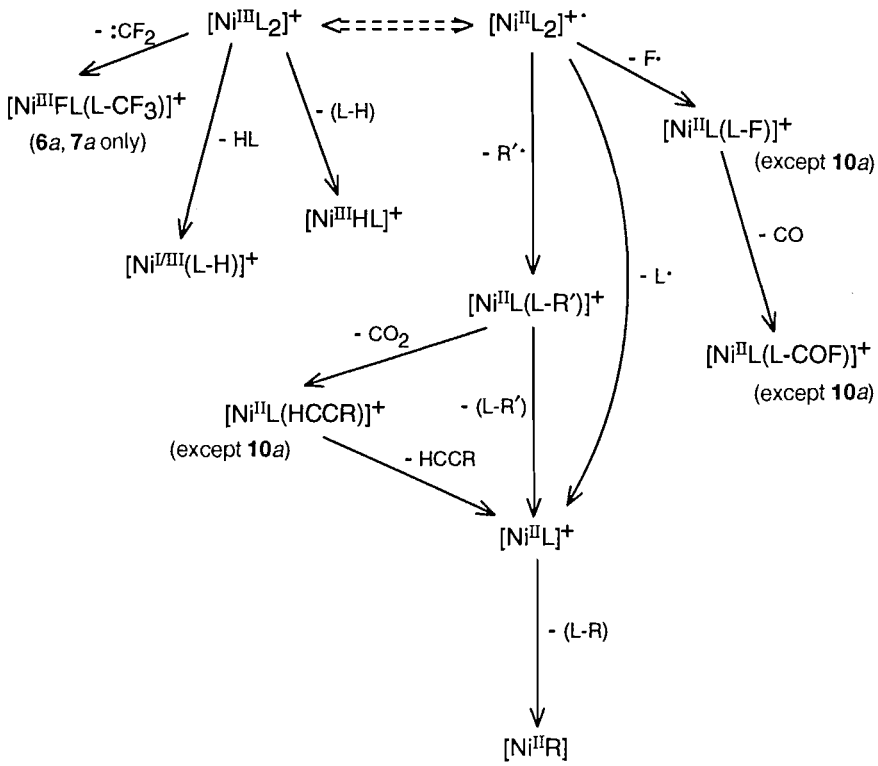

⇒ step involving metal valence change

SCHEME 3. Fragmentation pathways proposed for **6***a* and **7***a* (R′ = C_2F_5), and **9***a* and **10***a* (R′ = *n*-C_3F_7). Pathways are common to all complexes, except where noted.

sence of analogous ions from the mass spectra of the perfluoroethyl and perfluoromethyl substituted complexes. The absence of the corresponding ion from the mass spectra of the corresponding β-diketonates may be attributed to less effective stabilization of the positive charge by oxygen.

Ions formed by hydrogen transfer

An interesting feature of the mass spectra of many metal-containing compounds is the presence of ions formed by reactions involving hydrogen transfer, for which reactions the mechanistic and electronic requirements are not well

B

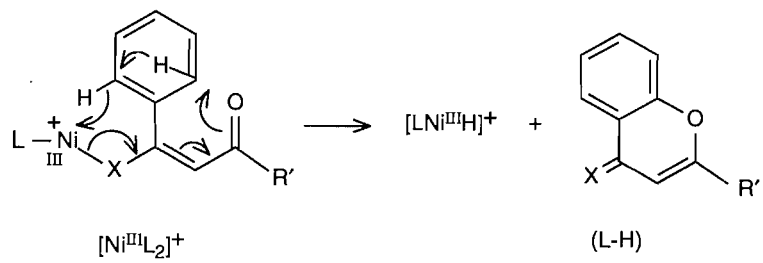

C

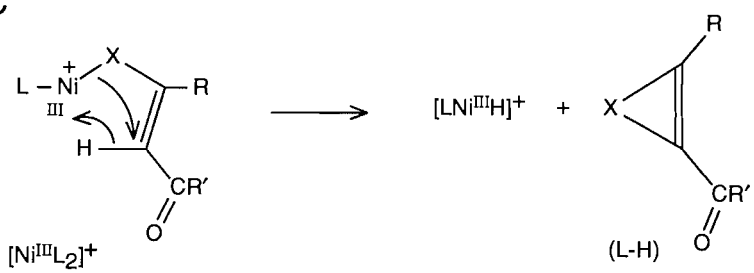

Can. J. Chem. Downloaded from www.nrcresearchpress.com by 203.198.23.82 on 09/08/12
For personal use only.

TABLE 3. EI mass spectra, m/z (% RA), of monothio-β-diketonates of nickel(II)[a]

	3*b*	**4***b*	**5***b*	**6***b*	**7***b*	**8***b*	**9***b*	**10***b*	**11***b*
Ion R,R′:	C_6H_5, CF_3	C_4H_3S, CF_3	C_5H_5S, CF_3	C_6H_5, C_2F_5	C_4H_3S, C_2F_5	$C_{10}H_7$, C_2F_5	C_6H_5, C_3F_7	C_4H_3S, C_3F_7	$C_{10}H_7$, C_3F_7
$[NiL_2]^+$	520 (55)	532 (57)	560 (100)	620 (45)	632 (65)	720 (48)	720 (62)	732 (81)	820 (80)
$[NiL(L-F)]^+$	501 (1.3)	513 (1.4)	541 (3.0)		613 (1.1)	701 (0.8)	701 (1.6)	713 (2.3)	801 (2.4)
$[NiL(L-S)]^+$									788 (2.4)
$[NiL(L-F-HF)]^+$							681 (0.9)	693 (1.5)	
$[NiFL(L-CF_3)]^+$				570 (2.6)	582 (7.3)	670 (1.0)		682 (0.7)	770 (14)
$[NiFL(L-C_2F_5)]^+$									720 (2.4)
$[NiL(L-R')]^+$	451 (1.0)	463 (2.7)	491 (4.8)	501 (1.1)	513 (3.8)	601 (1.3)	551 (1.9)	563 (6.2)	651 (2.4)
$[NiL(L-R'CO)]^+$	423 (0.5)	435 (1.0)	463 (1.0)	473 (0.9)	485 (1.4)	573 (0.5)	523 (1.9)	535 (2.3)	623 (0.7)
$[NiL(HCCR)]^+$	391 (0.3)	403 (1.0)	431 (0.8)	441 (0.8)	453 (1.7)	541 (0.9)		503 (2.4)	591 (2.4)
$[NiSL]^+$	321 (0.5)				377 (0.4)		421 (1.2)	427 (0.5)	
$[NiHL]^{+b}$	290 (1.9)	296 (2.0)	310 (3.6)	340 (1.5)	346 (1.9)	390 (2.0)	390 (1.6)	396 (2.3)	440 (5.0)
$[NiL]^{+b}$	289 (4.4)	295 (7.8)	309 (6.9)	339 (5.7)	345 (11)	389 (2.3)	389 (5.6)	395 (13)	439 (3.8)
$[Ni(L-H)]^+$	288 (1.3)	294 (1.3)	308 (2.8)	338 (0.9)	344 (1.1)	388 (1.7)	388 (0.8)	394 (1.1)	
$[Ni(L-F)]^+$	270 (0.2)								
$[Ni(L-S)]^+$	257 (1.5)	263 (2.2)	277 (3.8)	307 (1.2)	313 (2.3)	357 (1.2)	357 (1.8)	363 (2.4)	407 (1.9)
$[NiSC(R)=CH]^+$	192 (6.2)	198 (4.8)	212 (2.6)	192 (16)	198 (11)	242 (13)	192 (17)	198 (14)	242 (24)
$[NiSCR]^+$	179 (1.6)	185 (1.9)	199 (1.7)						
$[Ni(HCCR)]^+$	160 (4.0)	166 (6.5)	180 (2.2)	160 (6.0)	166 (11)	210 (5.5)	160 (7.4)	166 (12)	210 (11)
$[Ni]^+$	58 (6.7)	58 (6.1)	58 (8.3)	58 (11)	58 (6.9)	58 (3.8)	58 (9.3)	58 (5.9)	58 (14)
Ni-free ions:									
$[2L-2S-R'CO]^+$	301 (0.4)	313 (1.3)		351 (0.6)	363 (1.8)	451 (0.3)	401 (0.7)	413 (2.8)	501 (1.0)
$[HL]^{+b,c}$	232 (15,12)	238 (16,10)	252 (25,8)	282 (20,13)	288 (19,12)	332 (21,18)	332 (14,13)	338 (14,13)	382 (13,18)
$[L]^+$	231 (100)	237 (100)	251 (69)	281 (100)	287 (100)	331 (100)	331 (100)	337 (100)	381 (100)
$[L-F]^+$				262 (2.5)	268 (1.7)	312 (0.9)			
$[L-S]^+$		205 (81)	219 (81)	249 (0.6)	255 (86)	299 (1.4)		305 (87)	349 (2.7)
$[L-2F]^+$				243 (6.8)	249 (6.5)	293 (3.2)	293 (5.9)	299 (8.7)	343 (3.2)
$[L-CF_2]^+$				231 (4.9)	237 (5.7)	281 (1.1)			
$[L-S-CF_2]^+$	149 (4.5)	155 (12)	169 (17)		205 (5.3)				
$[HL-R']^+$		169 (4.8)	183 (9.2)	163 (12)	169 (9.7)	213 (4.1)			
$[R(C_2S)H]^+$	134 (18)	140 (25)	154 (25)	134 (23)	140 (31)	184 (30)	134 (21)	140 (34)	184 (32)
$[RC_3O]^+$	129 (5.2)	135 (7.0)	149 (8.5)	129 (8.2)	135 (8.3)	179 (4.7)	129 (6.9)	135 (9.7)	
$[RCS]^+$	121 (7.6)	127 (14)	141 (20)	121 (14)	127 (17)	171 (8.0)	121 (9.8)	127 (16)	171 (14)
$[RCO]^+$				105 (3.8)	111 (4.1)	155 (1.3)	105 (1.6)	111 (4.6)	155 (5.5)
$[RCCH]^+$	102 (4.9)	108 (14)	122 (22)	102 (17)	108 (20)	152 (20)	102 (6.1)	108 (20)	152 (26)
$[R]^+$	77 (3.6)		97 (8.3)	77 (9.0)		127 (2.9)	77 (3.3)		127 (8.4)
$[R']^+$	69 (3.6)	69 (18)	69 (13)	119 (16)	119 (4.9)	119 (0.6)		169 (6.7)	
$[CF_3]^+$				69 (58)	69 (9.4)	69 (2.0)	69 (5.2)	69 (11)	69 (38)
Base peak as $\%\Sigma_{50}$	40	26	23	26	23	35	35	22	24

[a] and [b]See footnotes to Table 2.
[c]The isotopic contributions of L^+ to the observed peak height (first number shown in the parentheses) is the second number shown in the parentheses.

understood. The availability of both phenyl- and thienyl-substituted complexes in the present study permits further investigation of these mechanisms. As noted earlier, the mass spectra exhibit the ions $[NiHL]^+$ and $[Ni(L-H)]^+$, which the product ion mass spectra of **2***a* and **3***b* indicate are formed from $[NiL_2]^+$ by losses of the EE^0 neutrals (L−H) and LH, respectively. Table 4 shows relative ion currents, %TIC(Ni), carried by these ions. (In a given mass spectrum we have computed the %TIC(Ni) value as the current carried by an ion expressed as a percentage of the total ion current (TIC) carried by all nickel-containing ions.)

The %TIC(Ni) values of these ions formed by hydrogen transfer are sensitive to the nature of the chelate ring donor atoms and also to the substituents on the ring. Thus, for phenyl-substituted β-diketonate complexes with corresponding perfluoroalkyl substituents, formation of $[NiHL]^+$ is strongly favored over formation of $[Ni(L-H)]^+$. For 2-thienyl and 5-methyl-2-thienyl substituents the prominences of the $[NiHL]^+$ ions relative to the $[Ni(L-H)]^+$ ions are less marked. For corresponding monothio-β-diketonate complexes, formation of $[NiHL]^+$ is less likely than formation of $[Ni(L-H)]^+$, even for the phenyl-substituted complexes.

The formation of these ions can be discussed in terms of the origins of the transferred hydrogens. While these origins have not been determined here, the mass spectra of related complexes, and their deuterium-labelled analogues, have been studied. Thus, in the mass spectrum of bis(1,3-diphenyl-1,3-propanedionato-2-*d*)nickel(II) (R = R′ = phenyl), the $[NiHL]^+$ ion is more abundant than $[Ni(L-H)]^+$, while $[Ni^{II}L]^+$ is even less significant (29). In the formation of $[NiHL]^+$, hydrogen rearrangement from the *ortho* position of a phenyl ring is the major process (~76%) (30); this was rationalized (29) by mechanism B (X = O). A minor process involves a contribution by hydrogen transfer from the central position of the chelate ring, for which we propose

Can. J. Chem. Downloaded from www.nrcresearchpress.com by 203.198.23.82 on 09/08/12
For personal use only.

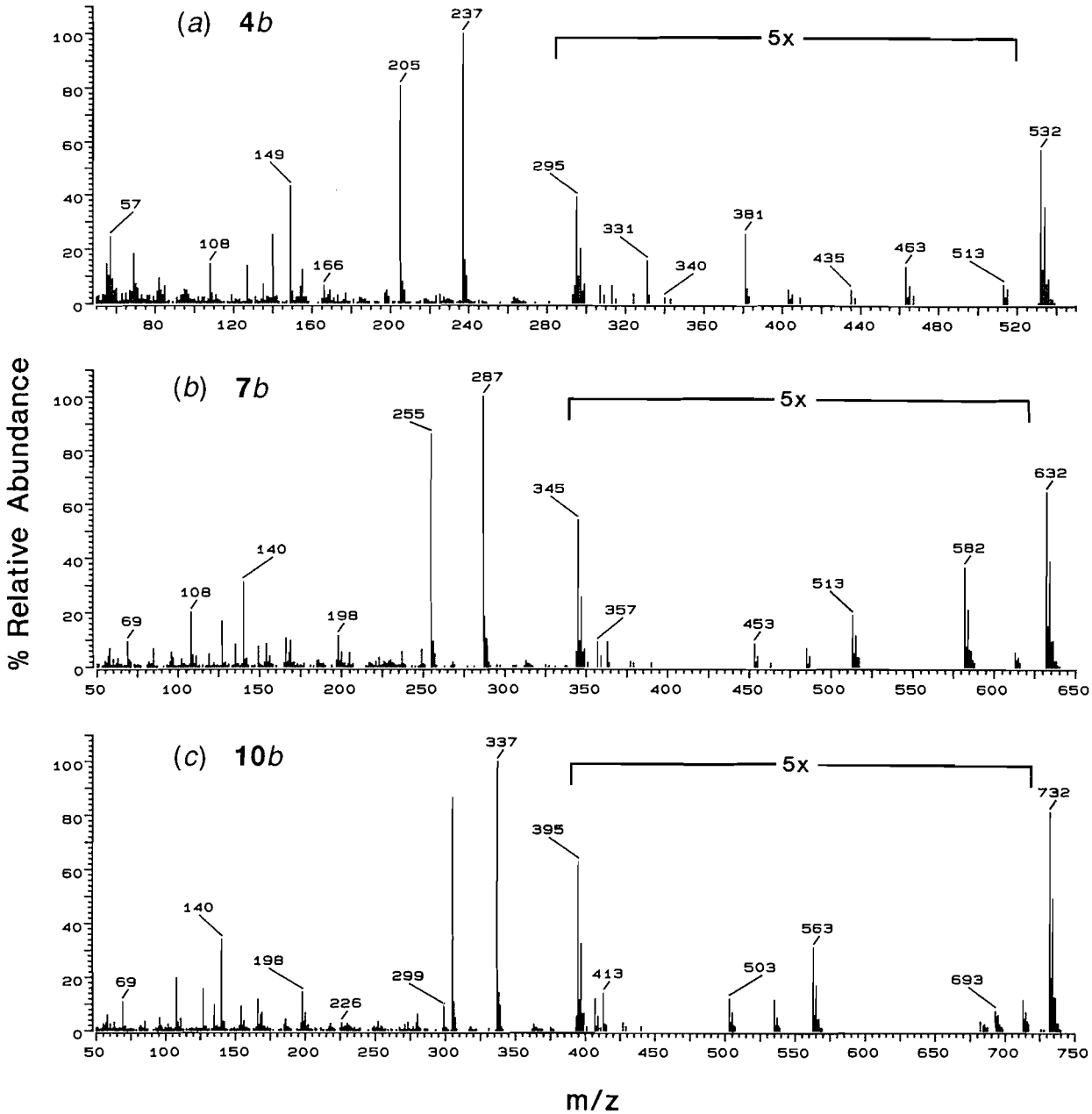

FIG. 2. EI mass spectra of (*a*) bis-[1,1,1-trifluoro-4-mercapto-4-(2-thienyl)-but-3-en-2-onato]-nickel(II), **4***b*; (*b*) bis-[1,1,1,2,2-pentafluoro-5-mercapto-5-(2-thienyl)-pent-4-en-3-onato]nickel(II), **7***b*; (*c*) bis-[1,1,1,2,2,3,3-heptafluoro-6-mercapto-6-(2-thienyl)-hex-5-en-4-onato]nickel(II), **10***b*.

mechanism C, although it was suggested (30) that the results are also consistent with extensive scrambling of the *o*-phenyl and chelate ring hydrogens prior to fragmentation. Similar results were reported for formation of $[CoHL]^+$ from cobalt(II) (29) and of $[RhHL]^+$ from rhodium(III) analogues (31). For either mechanism the structure of the $[NiHL]^+$ ion formed is the same, with nickel in the +3 oxidation state if we regard the hydrogen ligand as the two-electron donor hydride ion.

If, as is probable, hydrogen migration from the phenyl group to nickel is also the more important process for the current complexes then the favored formation of $[Ni^{III}HL]^+$ can be rationalized because mechanism B is not applicable to thienyl-substituted complexes (i.e., the thienyl group lacks a second "*ortho*" hydrogen). It is conceivable that, instead of the concerted mechanism shown, a two-step process operates, i.e., after hydrogen transfer to nickel, rotation about the phenyl–carbon bond permits oxygen to bind to the aryl carbon vacated by the transferred hydrogen. In principle, this mechanism is available to thienyl-substituted complexes. The low abundance of the product ion in this case may mean that this mechanism is not important, or that differing electronic effects may play a role.

The origin of the transferred hydrogen in the formation of $[Ni(L-H)]^+$ is less well known. For a number of copper(II) complexes the hydrogen transferred to the neutral species originates from the central position of the chelate ring (29, 30, 32); these results are consistent with mechanism D

Can. J. Chem. Downloaded from www.nrcresearchpress.com by 203.198.23.82 on 09/08/12
For personal use only.

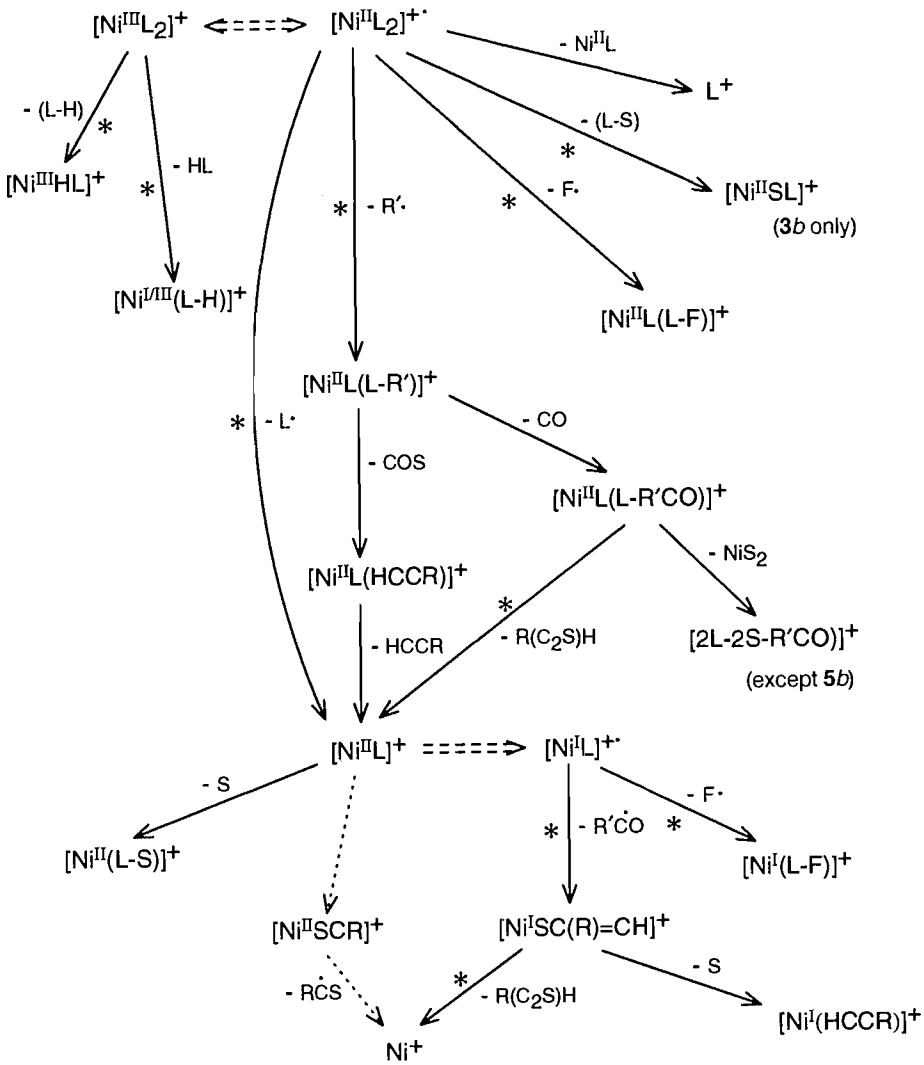

*decomposition confirmed for **3***b* by product ion scan
⇒ step involving metal valence change
---> probable, but unconfirmed, decomposition

SCHEME 4. Fragmentation pathways proposed for **3***b*, **4***b*, and **5***b* (R′ = CF_3). Pathways are common to all complexes, except where noted.

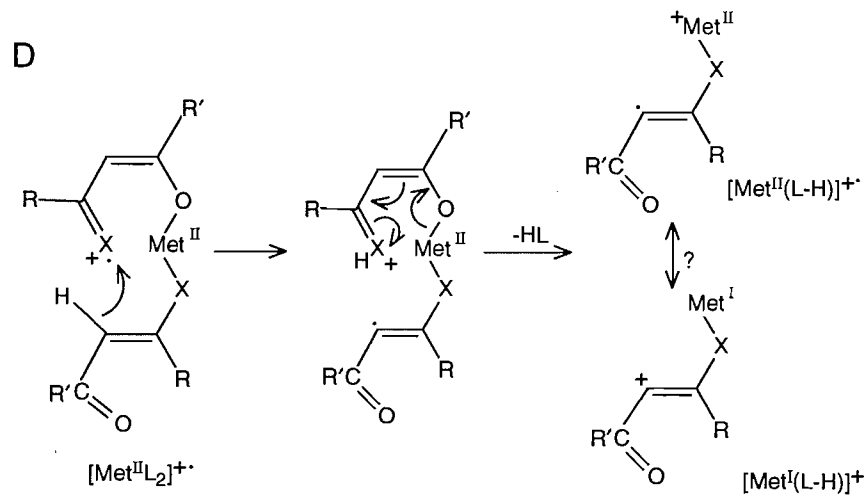

Can. J. Chem. Downloaded from www.nrcresearchpress.com by 203.198.23.82 on 09/08/12
For personal use only.

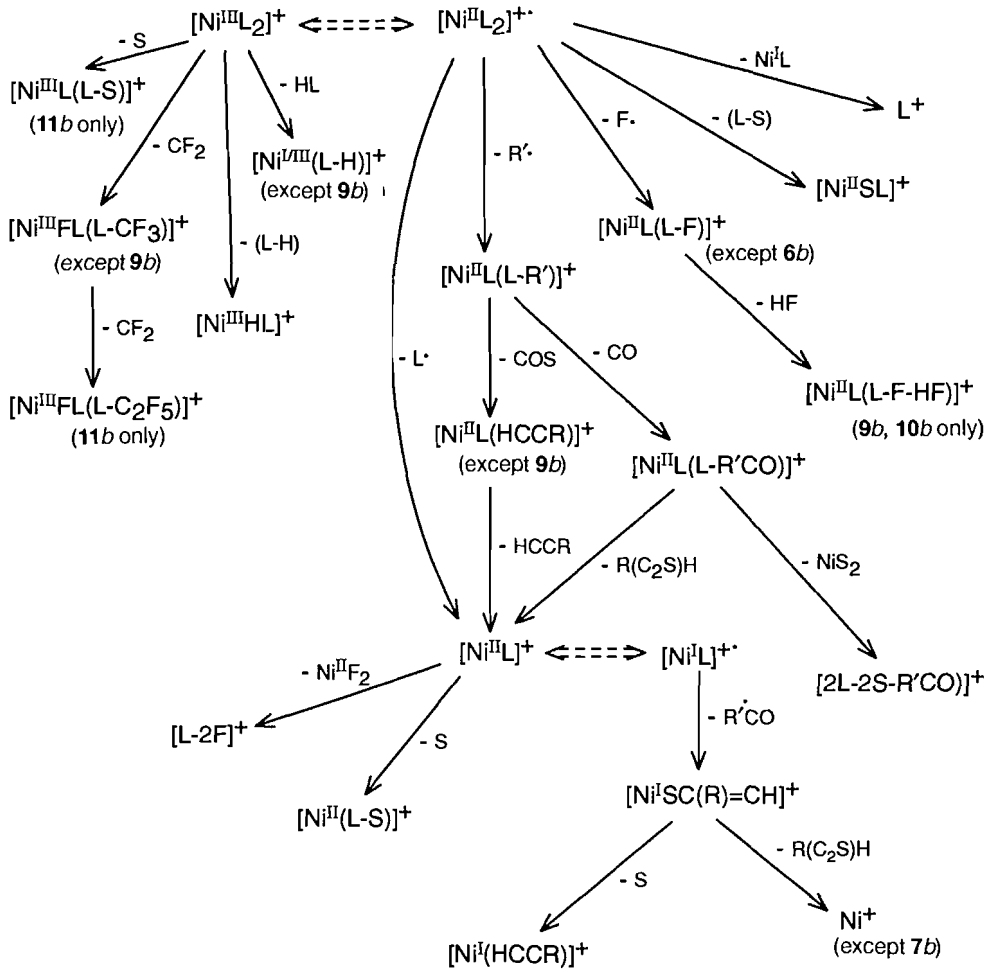

SCHEME 5. Fragmentation pathways proposed for **6***b*, **7***b*, and **8***b* (R′ = C_2F_5) and **9***b*, **10***b*, and **11***b* (R′ = n-C_3F_7). Pathways are common to all complexes, except where noted.

(Met = Cu, X = O), proposed earlier (29). Unfortunately, the data in Table 4 do not reveal any clear trend to support or oppose this mechanism for nickel.

For monothio-β-diketonate complexes the formation of $[Ni^{III}HL]^+$ is suppressed relative to the β-diketonates. We may speculate that the charge site in mechanism B is less well developed when X is the less electronegative S atom. On the other hand, formation of $[Ni(L-H)]^+$ seems to be enhanced for monothio-β-diketonates. This enhancement is even more striking in the formation of $[Rh(L-H)]^+$ from a rhodium(III) analogue, for which we have observed that ~93% of the hydrogen transferred to the neutral fragment originates from

TABLE 4. Relative abundance, %TIC(Ni), for $[NiHL]^+$ and $[Ni(L-H)]^+$ ions

		R substituent and donor atoms							
		C_6H_5 phenyl		$C_{10}H_7$ 2-naphthyl		C_4H_3S 2-thienyl		$CH_3C_4H_2S$ 5-methyl-2-thienyl	
Ion	R′ substituent	O,O	O,S	O,O	O,S	O,O	O,S	O,O	O,S
$[NiHL]^{+a}$	CHF_2	**1***a*, 0.61				**2***a*, 0.23			
	CF_3	**3***a*, 3.4	**3***b*, 0.95			**4***a*, 1.05	**4***b*, 0.57	**5***a*, 1.61	**5***b*, 1.08
	C_2F_5	**6***a*, 2.7	**6***b*, 0.34		**8***b*, 1.06	**7***a*, 0.89	**7***b*, 0.11		
	n-C_3F_7	**9***a*, 2.2	**9***b*, 0.42		**11***b*, 2.6	**10***a*, 1.40	**10***b*, 0.11		
$[Ni(L-H)]^+$	CHF_2	**1***a*, —				**2***a*, 0.32			
	CF_3	**3***a*, 0.64	**3***b*, 1.5			**4***a*, —	**4***b*, 1.36	**5***a*, 1.24	**5***b*, 2.08
	C_2F_5	**6***a*, 0.32	**6***b*, 0.88		**8***b*, 2.05	**7***a*, 0.94	**7***b*, 0.89		
	n-C_3F_7	**9***a*, —	**9***b*, 0.73		**11***b*, —	**10***a*, —	**10***b*, 0.73		

[a]Abundances are now corrected for isotopic contributions from ions of lower mass.

Can. J. Chem. Downloaded from www.nrcresearchpress.com by 203.198.23.82 on 09/08/12
For personal use only.

the phenyl group (31). Thus, in this case, mechanism E (Met = Rh, X = S) may be preferable.

The structures of the $[Met(L-H)]^+$ ion, the electronic environment of the metal, and its formal oxidation state, differ for mechanisms D and E. The preference of copper complexes for mechanism D may be related to the ease of formation of the copper(I) oxidation state, whereas the preference of the rhodium complexes for mechanism E may be influenced by the reluctance of rhodium(III) to be reduced to lower oxidation states. In the case of nickel, both nickel(I) and nickel(III) states can be formed with relatively little difficulty so that both mechanisms D and E are feasible. Thus, nickel chelates appear to be particularly suitable for further studies of the role of the metal, ligand donor atoms, and substituents on hydrogen transfer reactions.

E

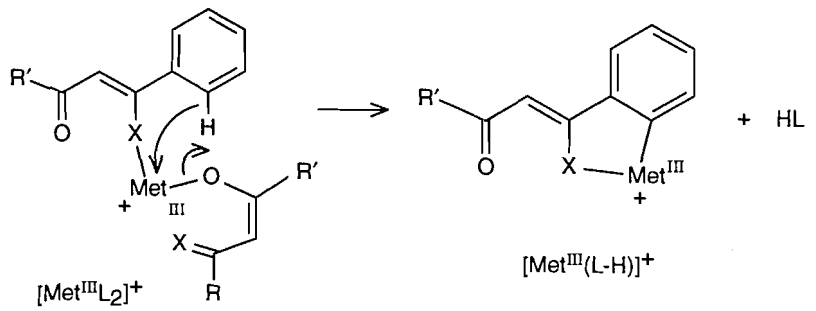

Fluorine transfer reactions

The mass spectra of the β-diketonates show evidence, albeit minor, of fluorine transfer to nickel. Thus, compounds **1***a* and **2***a* show the $[Ni^{III}F(L-R')]^+$ ion (R′ = CHF_2), a probable decomposition product ($[Ni(L-CHF-HF)]^+$), and the $[L-F]^+$, $[L-2F]^+$, and $[L-CO-2F]^+$ ions formed by the inferred elimination of NiF_2. Compared to **1***a* and **2***a*, compounds **3***a* and **5***a* show comparable abundances of $[NiF(L-R')]^+$ (R′ = CF_3), somewhat lower abundances of the analogous daughters $[Ni(L-CF_2-HF)]^+$, and no evidence for elimination of NiF_2. Compounds **6***a*, **7***a*, **9***a*, and **10***a* show none of these species but **6***a* and **7***a* show low-abundance $[NiFL(L-CF_3)]^+$ ions, discussed below, formed by a different reaction. These observations can be rationalized by the hard acid–soft base (HSAB) concept, in terms of which Ni^{II} has borderline hard acid properties. We see that fluorine migrations to nickel decrease in both number and significance with increasing fluorine content of R′. Thus, nickel(II) is able to abstract a hard fluorine atom from the carbon of a CHF_2 substituent but is less effective at abstracting fluorine from the harder carbons of CF_3, C_2F_5, or n-C_3F_7 groups. We have discussed the relative hardnesses of the carbon atoms in the perfluoroalkyl substituents in more detail in the previous publication (1).

For compounds **6***a* and **7***a* the fluorine transfer ion, noted above, can be formulated as $[Ni^{III}FL(L-CF_3)]^+$ (Scheme 5). Noting that an increase of valence hardens a metal, nickel(III) is evidently hard enough to abstract a fluorine atom from the perfluoroethyl group. We have argued previously that fluorine should be abstracted more readily from an α-carbon (1).

The mass spectra of the monothio-β-diketonates having CF_3 substituents show no evidence of ions formed by fluorine transfer to nickel; this is consistent with the softening of nickel by sulfur. The observation of $[Ni^{III}FL(L-CF_3)]^+$ for compounds **6***b*, **7***b*, and **8***b*, which have C_2F_5 substituents, and of $[Ni^{III}FL(L-C_2F_5)]^+$ for **11***b*, which has the n-C_3F_7 substituent, and of $[L-F]^+$ and $[L-2F]^+$ indicate that nickel(III) is still hard enough to abstract fluorine from these substituents, presumably from their α-carbons.

Conclusions

A prominent molecular ion in each mass spectrum reflects the capacity of the ligand to accommodate the positive charge and (or) the ability of nickel(II) to undergo oxidation to nickel(III). Subsequent fragmentation of the β-diketonates proceeds mainly by elimination of the $OE^{\bullet}$ radical $R''^{\bullet}$ followed by one or more EE^0 neutral losses. Conversely, the major fragmentation of the $M^{+\bullet}$ ion of the monothio-β-diketonates is loss of $Ni^{I}L$ to yield an abundant L^+ ion. While the major ions of both series of complexes contain nickel(II), the monothio-β-diketonates show a greater tendency to form some important nickel(I)-containing ions (e.g., $[Ni^{I}SC(R)=CH]^+$ and $[Ni^{I}(HCCR)]^+$). This is consistent with the HSAB concept; nickel(I) is a soft acid and the ligands are soft bases.

The formation of the $[Ni^{III}HL]^+$ ion by hydrogen transfer to nickel agrees with mechanism B. On the other hand, formation of the $[Ni^{I/III}(L-H)]^+$ ion may occur by transfer of hydrogen from the central position of the chelate ring (mechanism D) or from an aryl group (mechanism E). Such reactions are sensitive to the nature of the metal, and to donor atoms and substituents of the ligand. Nickel chelates appear to be particularly suitable for further studies of these effects.

Acknowledgements

We thank Mr. Wayne Buchannon for assistance in the operation and maintenance of the mass spectrometer and the Natural Sciences and Engineering Research Council (NSERC) of Canada for financial support. We also thank NSERC and the University of Manitoba for grants to purchase the mass spectrometer.

1. M.L.J. Reimer, J.B. Westmore, and M. Das. Can. J. Chem. **70**, 952 (1992).
2. R.W. Moshier and R.E. Sievers. Gas chromatography of metal chelates. Pergamon Press, Oxford. 1965.
3. J. Zhao, K.H. Dahmen, H.O. Marcy, L.M. Tonge, T.J. Marks, B.W. Wessels, and C.R. Kannewurf. Appl. Phys. Lett. **53**, 1750 (1988).

Can. J. Chem. Downloaded from www.nrcresearchpress.com by 203.198.23.82 on 09/08/12
For personal use only.

4. D.S. Richeson, L.M. Tonge, J. Zhao, J. Zhang, H.O. Marcy, T.J. Marks, B.W. Wessels, and C.R. Kannewurf. Appl. Phys. Lett. **54**, 2154 (1989).
5. A.J. Panson, R.G. Charles, D.N. Schmidt, J.R. Szedon, G.J. Machiko, and A.I. Braginski. Appl. Phys. Lett. **53**, 1756 (1988).
6. A.R. Barron. *In* The Strem Chemiker. Vol XIII. No. 1. Strem Chemicals, Inc., Newburyport, Mass. 1990. p. 1.
7. S B. Turnipseed, R.M. Barkley, and R.E. Sievers. Inorg. Chem. **30**, 1164 (1991).
8. C.G. Macdonald and J.S. Shannon. Aust. J. Chem. **19**, 1 (1966).
9. R.C. Mehrotra, R. Bohra, and D.P. Gaur. Metal β-diketonates and allied derivatives. Academic Press, London. 1978.
10. K.C. Joshi and V.N. Pathak. Coord. Chem. Rev. **22**, 37 (1977).
11. J.B. Westmore. *In* Mass spectrometry of metal compounds. *Edited by* J. Charalambous. Butterworths, London. 1975. Chap. 9.
12. I.K. Gregor and M. Guilhaus. Mass Spectrom. Rev. **3**, 39 (1984).
13. J.S. Shannon and J.M. Swan. Chem. Commun. 33 (1965).
14. M.J. Lacey and J.S. Shannon. Org. Mass Spectrom. **6**, 931 (1972).
15. M. Das. Trans. Met. Chem. **5**, 17 (1980).
16. M. Das and S.E. Livingstone. Org. Mass Spectrom. **9**, 781 (1974).
17. R.K.Y. Ho and S.E. Livingstone. Aust. J. Chem. **21**, 1781 (1968).
18. M. Das. Inorg. Chim. Acta, **36**, 79 (1979).
19. S.E. Livingstone and D.S. Moore. Aust. J. Chem. **29**, 283 (1976).
20. M. Das. Inorg. Chim. Acta, **48**, 33 (1981).
21. W.C. Fernelius and B.E. Bryant. Inorg. Synth. **5**, 105 (1957).
22. M. Das and S.E. Livingstone. J. Chem. Soc. Dalton Trans. 662 (1977).
23. M. Das. J. Inorg. Nucl. Chem. **43**, 1803 (1981).
24. M. Das and S.E. Livingstone. Aust. J. Chem. **27**, 53 (1974).
25. J.K. Terlouw and W. Heerma. Z. Anal. Chem. **257**, 177 (1971).
26. C.G. Macdonald and J.S. Shannon. Aust. J. Chem. **19**, 1545 (1966).
27. M.N. Bhattacharjee, M.K. Chaudhuri, M. Devi, R.N. Dutta Purkayastha, and Z. Hiese. Int. J. Mass Spectrom. Ion Processes, **71**, 109 (1986).
28. A.L. Clobes, M.L. Morris, and R.D. Koob. J. Am. Chem. Soc. **91**, 3087 (1969).
29. M.J. Lacey, C.G. Macdonald, and J.S. Shannon. Org. Mass Spectrom. **1**, 115 (1968).
30. M.J. Lacey, C.G. Macdonald, and J.S. Shannon. Aust. J. Chem. **25**, 2559 (1972).
31. J.B. Westmore and G.A. Stern. Proc. 37th ASMS Conf. on Mass Spectrometry and Allied Topics, Miami Beach, Fla. May 21–26, 1989.
32. C. Reichert, G.M. Bancroft, and J.B. Westmore. Can. J. Chem. **48**, 3213 (1970).

Can. J. Chem. Downloaded from www.nrcresearchpress.com by 203.198.23.82 on 09/08/12
For personal use only.

Synthesis of functionalized hexahydro-, octahydro-, and decahydro-1*H*-phenalenes via Diels–Alder reactions of 1-methylene-4a-methoxycarbonyl-1,2,3,4,4a,5,6,7-octahydronaphthalene and related dienes

EDWARD PIERS,[1] RICHARD W. FRIESEN, PAUL KAO, STEVEN J. RETTIG, AND JAMES TROTTER

Department of Chemistry, University of British Columbia, 2036 Main Mall, University Campus, Vancouver, BC V6T 1Z1, Canada

Received April 2, 1993

EDWARD PIERS, RICHARD W. FRIESEN, PAUL KAO, STEVEN J. RETTIG, and JAMES TROTTER. Can. J. Chem. **71**, 1463 (1993).

The results of a study of Diels–Alder reactions of the bicyclic dienes **6**–**8** with a variety of dienophiles are reported. Although **6** and **7** undergo cycloaddition reactions smoothly and efficiently, thermal Diels–Alder reactions of **8** are generally sluggish or, under the conditions investigated, do not proceed at all. Additions of tetracyanoethylene (TCNE) to **6**–**8** are highly face-selective, with preferential attack of the dienophile on the side of the dienes opposite to the angular methoxycarbonyl group. Reaction of **7** with maleic anhydride (MAN) is completely face-selective and proceeds preferentially via an *endo* transition state. Diels–Alder reactions of **6** and **7** with methyl acrylate (MAC) and nitroethylene (NE) are entirely regioselective, but the face-selectivities, which vary from ~2:1 to ~3:1, are rather low. The use of this chemistry as a method for the synthesis of functionalized, stereochemically defined, perhydro-1*H*-phenalenes is demonstrated.

EDWARD PIERS, RICHARD W. FRIESEN, PAUL KAO, STEVEN J. RETTIG et JAMES TROTTER. Can. J. Chem. **71**, 1463 (1993).

On rapporte les résultats d'une étude sur des réactions de Diels–Alder des dienes bicycliques **6**–**8** avec divers diénophiles. Même si les composés **6** et **7** subissent des réactions de cycloadditions faciles et efficaces, les réactions de Diels–Alder thermiques du composé **8** sont généralement difficiles ou, dans les conditions utilisées, elles ne se produisent pas du tout. Les additions du tétracyanoéthylène (TCNE) sur les composés **6**–**8** se font d'une façon très face-sélectives avec une attaque préférentielle du diénophile sur le côté du diène qui est opposé au groupe méthoxycarbonyle angulaire. La réaction du composé **7** avec l'anhydride malélique (ANM) est complètement face-sélective et se produit préférentiellement par le biais d'un état de transition *endo*. Les réactions de Diels–Alder des composés **6** et **7** avec l'acrylate de méthyle (ACM) et le nitroéthylène (NE) sont complètement régiosélectives, mais les sélectivités relatives à la face, qui varient d'environ 2 : 1 à environ 3 : 1, sont relativement basses. On démontre l'utilité de cette chimie comme méthode de synthèse de perhydro-1*H*-phénalènes fonctionnalisés de stéréochimie définie.

[Traduit par la rédaction]

Can. J. Chem. Downloaded from www.nrcresearchpress.com by 213.200.69.106 on 09/08/12
For personal use only.

Introduction

The structurally novel marine natural product (−)-8,15-diisocyano-11(20)-amphilectene, obtained from the sponge *Hymeniacidon amphilecta*, has been shown by X-ray diffraction analysis to possess the constitution and relative stereochemistry depicted in structural formula **1** (1). This substance is a member of the small family of biologically active amphilectane-type diterpenoids that share the carbon skeleton **2** (1–3).

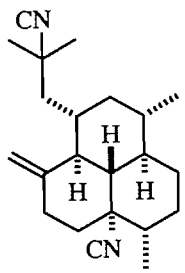

1

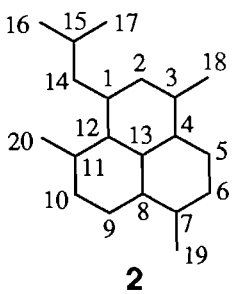

2

Recently, we described, inter alia, the synthesis of the structurally unique dienes **6**–**8** via effective routes that employed, as the key steps, the palladium(0)-catalyzed ring closure of the enol triflate-vinylstannanes **3**–**5**, respectively (4, 5) (eq. [1]). One of the reasons for developing the methods that led to the preparation of **6**–**8** and related dienes (4, 5) was related to the possibility of using these substances as substrates for Diels–Alder reactions. It was hoped that an investigation into the Diels–Alder chemistry of **6**–**8** would set the stage for subsequent use of similar methodology for effecting the total synthesis of 8,15-diisocyano-11(20)-amphilectene (**1**) and related amphilectane diterpenoids. We report herein the details of a study (6) of the reaction of the dienes **6**–**8** with symmetrically and unsymmetrically substituted dienophiles.

Results and discussion

General considerations

Prior to a description of the work carried out during the course of this study, it may be helpful to point out that four questions were to be addressed during the exploration of Diels–Alder reactions of the dienes **6**–**8**. These may be formulated as follows. (*a*) What is the face-selectivity of dienophile addition to the diene system present in **6**–**8**? A preference for attack on the β face[2] of the dienes would be expected, but the extent of this preference could, of course, vary with the structure of the dienophile. (*b*) For each of those dienophiles in which there is the potential for *endo*- or *exo*-selectivity in the cycloaddition transition states, which mode of attack is favored upon addition of the dienophile to each

[1]Author to whom correspondence may be addressed.

[2]Throughout this discussion, the α face of the diene refers to the side of the molecule on which the methoxycarbonyl group is situated, while the β face refers to the side of the diene opposite to the CO_2Me moiety.

of the α and β faces of the dienes? (*c*) In the case of unsymmetrically substituted dienophiles, what will be the preferred regiochemistry of addition of these reagents to the dienes? (*d*) Of the geometrically isomeric dienes **7** and **8**, one would expect the *cisoid-trans* diene **7** to undergo Diels–Alder reactions at rates much faster than those associated with the *cisoid-cis* diene **8**. Will the latter substance undergo cycloaddition reactions with dienophiles, particularly with those that are rather unreactive? The investigations outlined below provide useful information about each of these points.

[1]

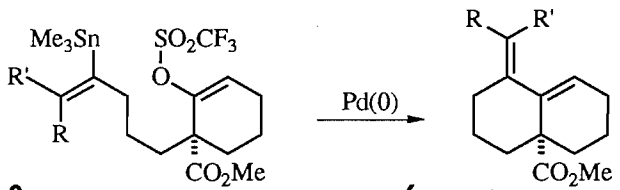

3 R = R' = H
4 R = $CH_2OSi(t\text{-}Bu)Me_2$, R' = H
5 R = H, R' = $CH_2OSi(t\text{-}Bu)Me_2$

6 R = R' = H
7 R = $CH_2OSi(t\text{-}Bu)Me_2$, R' = H
8 R = H, R' = $CH_2OSi(t\text{-}Bu)Me_2$

Diels–Alder reactions of the dienes ***6–8*** *with symmetrical dienophiles*

Reaction of the "parent" diene **6** with two equivalents of dimethyl acetylenedicarboxylate (DMAD) in benzene (reflux, 6 h) (eq. [2]) gave, in 78% yield, a crystalline material that exhibited mp 136–137°C. Analyses (gas–liquid chromatography (glc) – low-resolution mass spectrometry (lrms) and ^1H nmr spectroscopy) of this material showed that it consisted of a mixture of isomers of molecular mass 348, in a ratio of approximately 3:1. These two substances were inseparable by flash chromatography on silica gel (7). Recrystallization of the mixture from Et_2O–$CHCl_3$ produced colorless cubic crystals with mp 137.5–138.5°C. The ^1H nmr analysis of this material showed that the ratio of isomers was substantially unchanged. X-ray crystallographic analysis of the mixture (vide infra) revealed that the major isomer was the triester **9** and, consequently, the minor Diels–Alder product was assigned structure **10**. Thus, the face-selectivity of the reaction of **6** with the linear, sterically undemanding dienophile DMAD is modest. Nevertheless, there is a small preference for attack of DMAD on the β face of **6**.

[2]

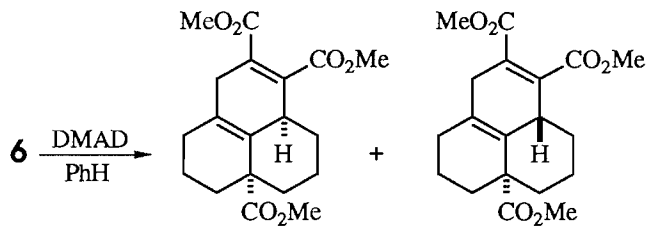

9 **10**

The issue of face-selectivity in the Diels–Alder reactions of the dienes **6–8** was investigated further by use of the symmetrical dienophiles tetracyanoethylene (TCNE) and maleic anhydride (MAN). In terms of its ability to approach the diene systems present in **6–8**, TCNE would be expected to be sterically more demanding than the (linear) dienophile DMAD. On the other hand, use of MAN would provide information not only about face-selectivity, but would also shed light on the issue of *endo*- versus *exo*-selectivity in the cycloaddition reactions. The structural formulas of the products formed from the reactions involved are shown in Chart 1 and the results derived from this part of the study are summarized in Table 1.

Treatment of the diene **6** with TCNE (Table 1, entry 1) provided a white solid that consisted of two products in a ratio of 96:4 (glc analysis). Fractional crystallization of this material gave a pure sample of the major isomer as colorless cubic crystals that exhibited mp 146–147°C. This substance was expected to be the tricyclic ester **11**, resulting from preferential attack of the dienophile on the β face of the diene **6**. In the ^1H nmr spectrum of this material, the tertiary allylic proton H_A gives rise to a broad doublet (J = 12.5 Hz) at δ 3.31. Although the size of the observed coupling constant is consistent with a *trans* diaxial coupling between H_A and H_B in **11**, molecular models indicate that a similar strong coupling between H_A and H_B in **12** would be expected. Thus, ^1H nmr spectroscopy did not easily lead to an ambiguous structural assignment. Therefore, a single crystal X-ray analysis of the major isomer was undertaken (vide infra). This exercise confirmed that the major Diels–Alder adduct has the constitution and relative stereochemistry depicted in **11**. The minor product, although not isolated, was shown by glc–lrms to be isomeric with **11** and, therefore, was assumed to be **12**.

Reaction of the *cisoid-trans* diene **7** with TCNE at room temperature (Table 1, entry 2) afforded a mixture of two products in a combined yield of 74%. Integration of the signals due to the *t*-Bu groups in the ^1H nmr spectrum of this material indicated that the two substances were present in a ratio of approximately 7:1. The fact that the two compounds could not be separated by chromatography on silica gel precluded the acquisition of a pure sample of the minor product. However, based on the previous results derived from

Can. J. Chem. Downloaded from www.nrcresearchpress.com by 213.200.69.106 on 09/08/12
For personal use only.

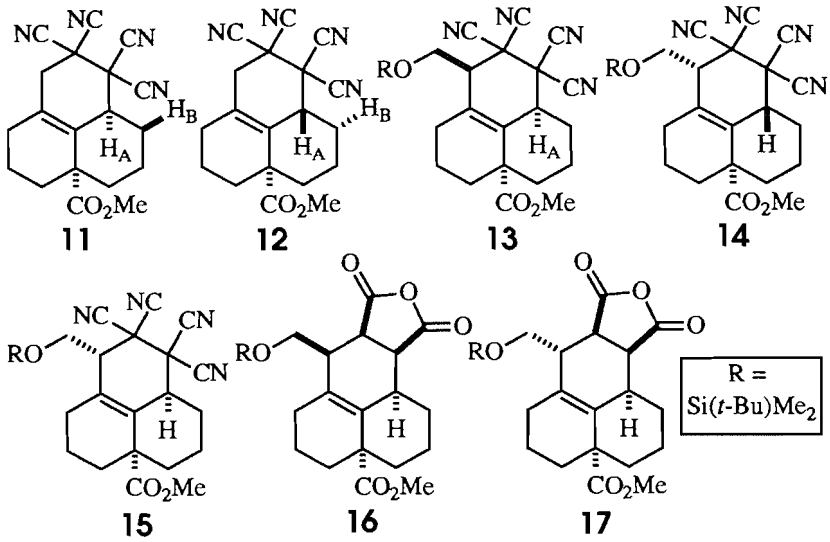

CHART 1

TABLE 1. Diels–Alder reactions of the dienes **6–8** with symmetrical dienophiles

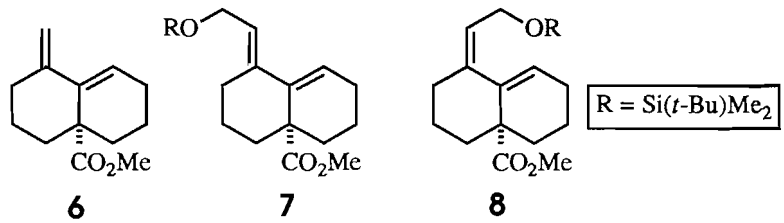

Entry	Diene	Dienophile[a]	Reaction conditions	Product(s) (ratio; combined yield, %[b])
1	**6**	TCNE	THF,[c] r.t.,[d] 30 min	**11**, **12**[e] (96:4;[f] 83)
2	**7**	TCNE	THF, r.t., 30 min	**13**, **14**[e] (7:1;[g] 74)
3	**7**	TCNE	THF, −78°C, 2 h	**13** (84)
4	**8**	TCNE	Et_2O, reflux, 15 h	**15** (72)
5	**7**	MAN	PhH, reflux, 18 h	**16** (63)
6	**8**	MAN	PhH, reflux, 3 days	**17** (18)

[a]TCNE = tetracyanoethylene; MAN = maleic anhydride.
[b]Yield of (combined) isolated, purified product(s). See Chart 1 for structural formulas.
[c]THF = tetrahydrofuran.
[d]r.t. = room temperature.
[e]This substance was not obtained in pure form.
[f]Ratio determined by analysis of the crude product mixture by glc.
[g]Ratio determined by analysis of the crude product mixture by ^1H nmr spectroscopy.

the reaction of TCNE with the diene **6**, it is reasonable to conclude that the major and minor products possess structures **13** and **14**, respectively.

When the reaction of diene **7** with TCNE was carried out at −78°C (Table 1, entry 3), a single isomer **13** was produced in 84% yield. This substance (mp 119–120°C) was shown to be identical with the major product of the room temperature Diels–Alder reaction. In the ^1H nmr spectrum of **13**, H_A gives rise to a broad doublet (J = 12.5 Hz) at δ 3.10.

The cycloaddition reaction between the *cisoid-cis* diene **8** and TCNE proved to be very slow at or below ambient temperatures. However, when a solution of the two reactants in diethyl ether was refluxed for 15 h, a single crystalline product was obtained in 72% yield (Table 1, entry 4). In the ^1H nmr spectrum of this substance, the two tertiary allylic protons give rise to an unresolved multiplet centered at δ 3.26, while the CH_2O protons produce well-separated signals at δ 3.93 (doublet of doublets, J = 7.5, 10.5 Hz) and 4.25 (doublet of doublets, J = 4.0, 10.5 Hz). The expectation that the product was the result of face-selective attack of TCNE on the β face of the diene **8** was confirmed by a single crystal X-ray analysis (vide infra), which showed conclusively that the cycloadduct has the constitution and relative stereochemistry shown in **15**.

A single Diels–Alder adduct was obtained from the reaction of the *cisoid-trans* diene **7** with MAN (Table 1, entry 5). It is known (8) that MAN has a strong predilection for an *endo* transition state. For example, the reaction of cyclopentadiene with MAN provides the *endo* adduct with a stereoselectivity of greater than 98%. Thus, it appears very likely that the reaction of MAN with **7** would proceed via an

Can. J. Chem. Downloaded from www.nrcresearchpress.com by 213.200.69.106 on 09/08/12
For personal use only.

Can. J. Chem. Downloaded from www.nrcresearchpress.com by 213.200.69.106 on 09/08/12
For personal use only.

endo transition state. In this event, approach of MAN to the α face of the diene would be precluded, since, in this arrangement, there would be a strong steric interaction between the angular CO_2Me function of **7** and the anhydride portion of the dienophile. On the basis of these predictions and the results of the TCNE experiments (Table 1, entries 1–4), it was concluded that the sole product of the reaction of the diene **7** with MAN possesses the structure shown in **16**.

The reaction of MAN with the *cisoid-cis* diene **8** was very sluggish. The starting material **8** was completely consumed only after a solution of the two reactants in benzene had been refluxed for approximately 3 days. A single Diels–Alder product was isolated in low yield (18%) (Table 1, entry 6). On the basis of the arguments presented above (reaction of MAN with **7**) and taking into account the result of the reaction of diene **8** with TCNE (Table 1, entry 4), it was concluded that this adduct possesses structure **17**.

The major material obtained from this reaction was an amorphous white solid that precipitated from the reaction mixture. This substance was found to be quite insoluble in common solvents (chloroform, acetone, methanol, benzene) and resisted crystallization. The ir spectrum included absorptions due to anhydride and ester functions and the ^1H nmr spectrum (CD_3SOCD_3) did not contain signals for the $OSi(t\text{-}Bu)Me_2$ moiety. The peak of highest mass in the mass spectrum of this material corresponds to a molecular formula of $C_{22}H_{22}O_8$. Although this substance was not investigated further, it is clear that it is not a simple, primary, Diels–Alder adduct.

Diels–Alder reactions of the dienes **6–8** *with unsymmetrical dienophiles*

Theoretically, it is possible that each of the Diels–Alder reactions of the dienes **6–8** with an unsymmetrical dienophile could produce eight isomeric products. Fortunately, in practice, this worst case scenario was not realized. In fact, each of the cycloaddition reactions studied produced, at most, three products. Even so, conclusive determination of the structures of the products obtained was not straightforward. In particular, ^1H nmr spectroscopy did not lead to unambiguous conclusions regarding the constitution and relative stereochemistry of the cycloadducts. Consequently, the structures of four products were determined directly or indirectly by X-ray crystallographic analyses. Once these structures were secured, ^1H nmr spectroscopy was of considerable use in assigning structures to related substances.

The reactions of each of the dienes **6–8** with the unsymmetrical dienophiles methyl acrylate (MAC) and nitroethylene (NE) (9) were investigated. The results obtained are summarized in Table 2 and the structural formulas of the various products produced are shown in Chart 2.

Reaction of the diene **6** with MAC gave an excellent yield of a colorless oil that, on the basis of analyses by glc and ^1H nmr spectroscopy, consisted of a mixture of three Diels–Alder adducts in a ratio of about 2.7:1:1.7. These substances were shown, as outlined below, to be compounds **18**, **19**, and **20**, respectively.

The three products were difficult to separate by chromatography. However, subjection of the mixture to drip column chromatography on silica gel gave pure samples of **18** and **20**, as well as fractions that contained only mixtures of compounds **18** and **19**.

The first product to be eluted was **20**, a colorless oil. In the ^1H nmr spectrum of this material the two CO_2Me functions produced singlets at δ 3.67 and 3.68, while H_A appeared as a doublet of triplets (J = 3, 12 Hz) at δ 2.31. Reduction of **20** with lithium aluminum hydride in refluxing diethyl ether provided the diol **30** in 83% yield (eq. [3]). A single crystal X-ray crystallographic analysis (vide infra) on the latter substance (mp 162.5–164°C) confirmed its structure and, thereby, the structure of the diester **20**.

[3] 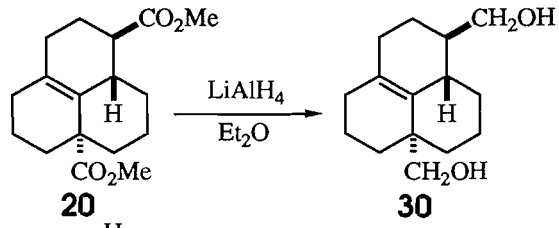

20 **30**

[4] 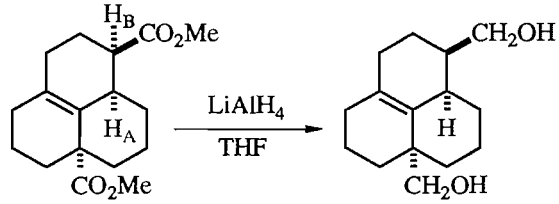

18 **31**

The second component to be eluted was the major Diels–Alder product **18**. Although the ^1H nmr spectrum of **18** did not provide conclusive evidence for the structure of this cycloadduct, two signals (δ 2.35, broad doublet, J = 13 Hz; 2.73, doublet of doublet of doublets, J = 2.8, 6, 13 Hz) were distinctive. These one-proton resonances can be assigned with confidence to protons H_A and H_B, respectively, in structural formula **18**. Reduction ($LiAlH_4$, THF) of **18** gave the corresponding diol in 97% yield (eq. [4]). An X-ray crystallographic analysis (vide infra) showed that the latter substance (mp 182.5–184°C) possesses structure **31**. Consequently, the major Diels–Alder product derived from reaction of the diene **6** with MAC is **18**.

The product **18** arises from attack of MAC on the β face of the diene **6** via an *endo* transition state, while **20** is produced via a pathway involving α-face attack and an *exo* transition state. It seemed reasonable to assume that the minor Diels–Alder adduct should be that arising from an approach of MAC to the β face of **6** and an *exo* transition state and should, therefore, possess structure **19**. That this conclusion was correct was shown as follows. A solution of a mixture of **18** and **19** (ratio 3:1, respectively) in methanol containing sodium methoxide was refluxed for 2 weeks. The isolated material (86% yield) consisted of a mixture of **18** and **19** in a ratio of 1:6, respectively. Thus, these two substances are epimeric at the stereogenic center associated with the secondary CO_2Me function.

Reaction of the *cisoid-trans* diene **7** with MAC (Table 2, entry 2) produced a crude product that, on the basis of its ^1H nmr spectrum, consisted of at least three components. Unfortunately, extensive overlap of the potentially diagnostic resonances precluded a determination of the product ratios. Medium-pressure column chromatography of the product mixture on silica gel gave, in order of elution, pure adduct **23** (31%), a trace of an unidentified diester, and a 3:1 mixture of the major and minor products **21** and **22** (56%). The

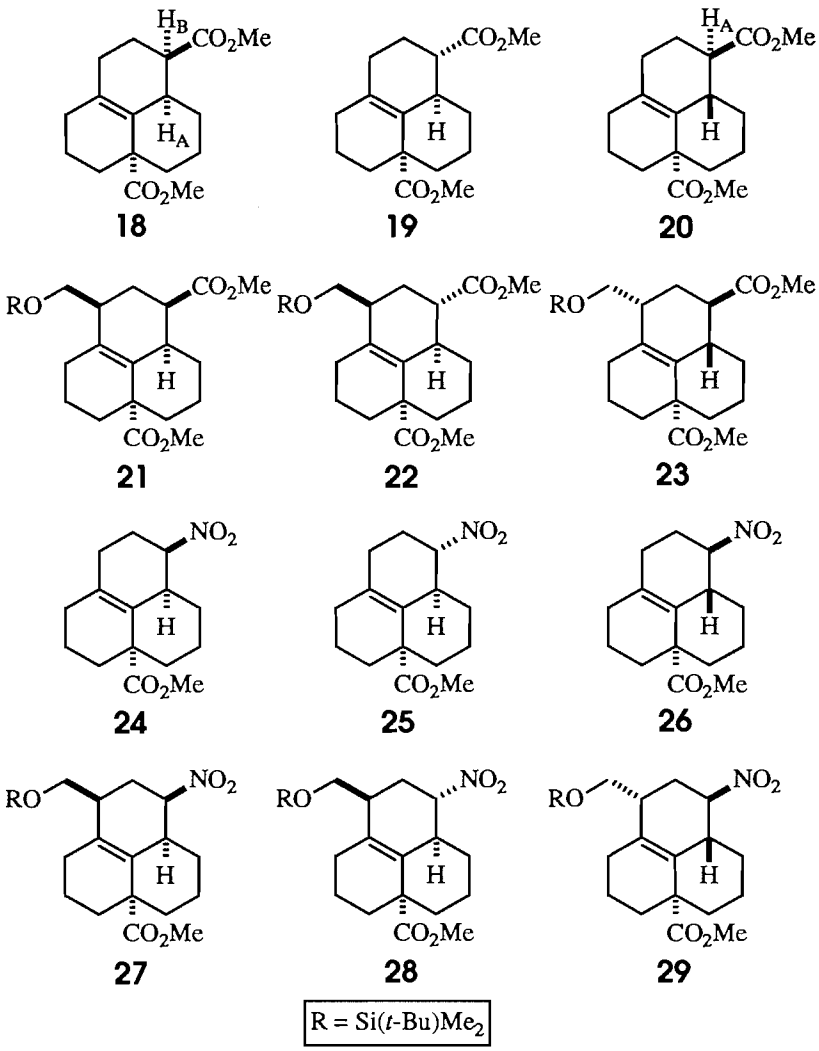

CHART 2

ratio of the latter substances was determined by ^{1}H nmr spectroscopy (integration of the *t*-Bu groups).

A pure sample of the major product **21** was obtained by subjecting the 3:1 mixture of **21** and **22** to drip column chromatography on silica gel. Treatment of pure **21** with sodium methoxide in refluxing methanol produced a 1:9 mixture of **21** and **22** and, thus, as expected, the major and minor Diels–Alder adducts were found to be epimeric at the chiral center bearing the secondary CO_2Me function. A pure sample of **22** was procured by chromatography of the 1:9 mixture of **21** and **22**.

At this stage, by analogy with the results obtained from the reaction of the diene **6** with MAC (Table 2, entry 1), it seemed reasonable to conclude that the three products (48:16:36) derived from reaction of **7** with MAC possess structures **21**, **22**, and **23**, respectively. Comparison of certain signals in the ^{1}H nmr spectra of these substances with the corresponding resonances in the spectra of the products derived from reaction of **7** with nitroethylene provided strong evidence for this conclusion (vide infra).

A successful Diels–Alder reaction between MAC and the *cisoid-cis* diene **8** was not achieved (Table 2, entry 3). After a benzene solution of **8** and MAC was refluxed for 4 days, 92% of the diene was recovered. Heating of a benzene solution of the two substances at 180°C (sealed tube) for 42 h led only to decomposition of the diene. Interestingly, treatment of **8** with DMAD under a variety of conditions did not produce any Diels–Alder adducts either.

It appears that, in the case of substrate **8**, successful thermal Diels–Alder reactions with relatively unreactive dienophiles such as MAC and DMAD are precluded. In fact, the Diels–Alder adducts produced by the reactions of **8** with the more reactive dienophiles TCNE and MAN (Table 1, entries 4 and 6) may well have been formed via a two-step mechanism (10), as illustrated in eq. [5] for the TCNE reaction. In this case, since the reaction is stereospecific (compare entries 3 and 4, Table 1), ring closure would have to be faster than rotation about the (formal) single bond between carbons **a** and **b** in the intermediate **32**.

Treatment of the parent diene **6** with nitroethylene (NE) in diethyl ether (Table 2, entry 4) gave, in 83% yield, a mixture of the cycloaddition adducts **24**, **25**, and **26** (~3:1:2, respectively, by glc analysis). The *CH*NO_2 proton signals in the ^{1}H nmr spectrum of this mixture were observed at δ 4.44 (compound **26**), ~4.71 (m, compound **25**), and ~4.74 (m, compound **24**). The relative intensity of the signals at δ 4.44 and 4.70–4.76 was found to be about 1:2, respectively. Subjection of the mixture to column chromatography on sil-

Can. J. Chem. Downloaded from www.nrcresearchpress.com by 213.200.69.106 on 09/08/12
For personal use only.

Can. J. Chem. Downloaded from www.nrcresearchpress.com by 213.200.69.106 on 09/08/12
For personal use only.

TABLE 2. Diels–Alder reactions of the dienes **6–8** with unsymmetrical dienophiles

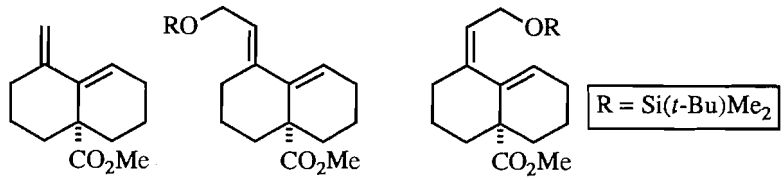

6 **7** **8**

Entry	Diene	Dienophile[a]	Reaction conditions	Product(s) (ratio; combined yield, %[b])
1	**6**	MAC	PhH, reflux, 3 days	**18, 19, 20** (2.7:1:1.7;[c,d] 85)
2	**7**	MAC	PhH, reflux, 3 days	**21, 22, 23** (48:16:36;[e] 87)
3	**8**	MAC	See text	No Diels–Alder products
4	**6**	NE	Et_2O, r.t.,[f] 3 h	**24, 25, 26** (3:1:2;[d] 83)
5	**7**	NE	Et_2O, r.t., 3 h	**27, 28, 29** (3:tr[g]:1;[c] 81)
6	**8**	NE	Et_2O, reflux, 7 h	**27, 28, 29** (2.5:tr:1;[c] 78)

[a]MAC = methyl acrylate; NE = nitroethylene.
[b]Yield of (combined) isolated, purified product(s). See Chart 2 for structural formulas.
[c]Composition was determined by analysis of the crude product mixture by ^1H nmr spectroscopy.
[d]Composition was determined by analysis of the crude product mixture by glc.
[e]See text.
[f]r.t. = room temperature.
[g]tr = trace.

[5] 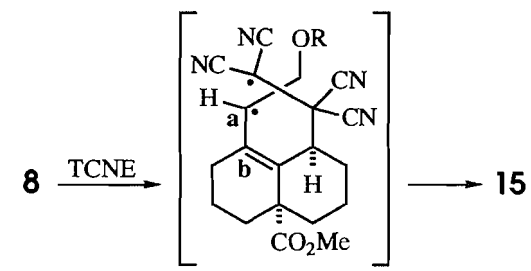

32

ica gel provided a pure sample of product **26**, the first substance to be eluted. Although the adducts **24** and **25** were not obtained in pure form, these substances were found to be epimeric at the stereogenic center containing the nitro function. Thus, treatment of a small sample of a mixture of **24**, **25**, and **26** (3:1:2) with potassium *tert*-butoxide in *tert*-butyl alcohol provided a mixture of the same three substances (composition 0.7:3.1:2, respectively, by glc analysis) in 87% yield.

On the basis of these results, along with those obtained from the reaction of **6** with MAC (vide supra), the three products (~3:1:2) derived from the cycloaddition of **6** with NE were assigned structures **24**, **25**, and **26**, respectively. Further evidence for these assignments was obtained by ^1H nmr spectra comparisons. Specifically, the chemical shift and coupling constants associated with the C*H*NO_2 protons in each of the substances **24–26** are similar to those of the structurally analogous nitro esters **27–29**, respectively. The structures of the latter trio of compounds have been assigned unambiguously (vide infra). The C*H*NO_2 protons in **24** and **27** give rise to multiplets at δ 4.74 and 4.75 while, in **25** and **28**, the corresponding signals appear at 4.71 (multiplet) and 4.68 (doublet of doublet of doublets, J = 4, 9, 12 Hz). In compounds **26** and **29**, the resonances for the C*H*NO_2 protons are found at δ 4.44 (doublet of triplets, J = 3.8, 10.5 Hz) and 4.58 (doublet of doublet of doublets, J = 3, 10.5, 12 Hz).

Further evidence for the completely regioselective nature of the Diels–Alder reaction of **6** with NE was obtained as follows. Treatment of a 3:1:2 mixture of **24–26** with sodium methoxide in methanol, followed by addition of an aqueous solution of titanium trichloride and ammonium acetate (11), provided a single ketone in 90% yield (eq. [6]). Apparently, under the reaction conditions, the primary product **34** derived from the nitro ester **26** epimerizes to the more stable diastereomer **33**.[3] The carbonyl group of **33** produces an absorption at 1710 cm^{-1} in the infrared spectrum. The relative stereochemistry of this substance was confirmed by a ^1H nmr nuclear Overhauser enhancement (nOe) difference experiment, in which irradiation at δ 3.69 (CO_2Me) increased the intensity of the resonance (2.82, br d, J = 13 Hz) due to the angular allylic proton.

Treatment of **33** with potassium *tert*-butoxide in THF caused isomerization of the substrate into the more stable α,β-unsaturated ketone **35** (eq. [7]). The infrared (1668 cm^{-1}) and ^{13}C nmr (δ 133.8, 155.3, 199.6) spectra of the latter substance confirmed the presence of the enone moiety.

[3]Molecular models indicate that, in compound **34**, the six-membered ring B must adopt a twist-boat conformation. On the other hand, in substance **33**, the three rings can comfortably adopt half-chair (A, C) or chair (B) conformations. Molecular mechanics calculations predict that **33** should be approximately 2.6 kcal/mol more stable than **34**. We are grateful to Professor L. Weiler for carrying out these calculations.

Can. J. Chem. Downloaded from www.nrcresearchpress.com by 213.200.69.106 on 09/08/12
For personal use only.

[6]

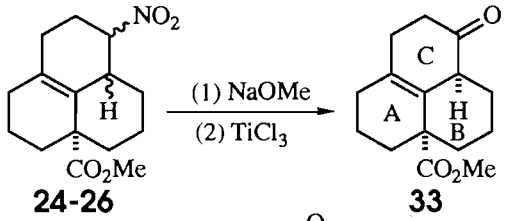

24-26 33

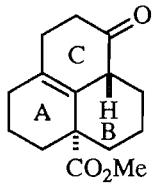

34

[7]

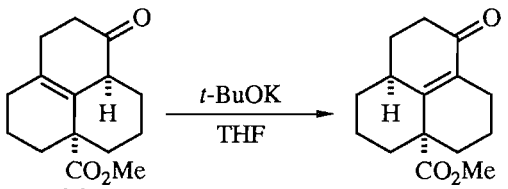

33 35

Reaction of the *cisoid-trans* diene **7** with NE was carried out in diethyl ether at room temperature (Table 2, entry 5). Analysis of the crude product by ^{1}H nmr spectroscopy showed the presence of essentially two products **27** and **29**, ratio ~3:1), along with a trace of a third substance (**28**). Column chromatography of the mixture gave compounds **29** (the first substance to be eluted) and **27** in isolated yields of 24 and 57%, respectively. Recrystallization of **27** from chloroform produced crystals (mp 89–90°C) suitable for X-ray crystallographic analysis (vide infra), which showed conclusively that **27** correctly represents the structure of the major Diels–Alder adduct.

The adduct that was produced in trace amounts was shown to possess the structure **28**. Thus, treatment of **27** with potassium *tert*-butyl alcohol at 100°C caused epimerization at the stereogenic center associated with the nitro function and produced, in 92% yield, compound **28** (eq. [8]). Diagnostic signals in the ^{1}H nmr spectrum of **28** were found to be identical (chemical shift, multiplicity) with the corresponding resonances of the trace component present in the crude Diels–Alder product mixture.

[8]

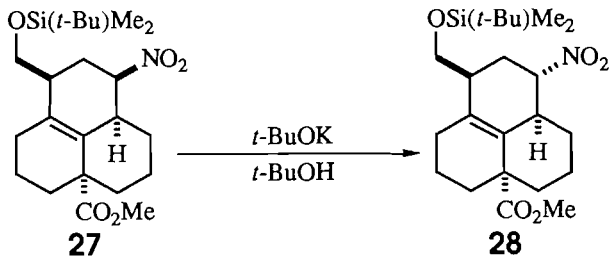

27 28

[9]

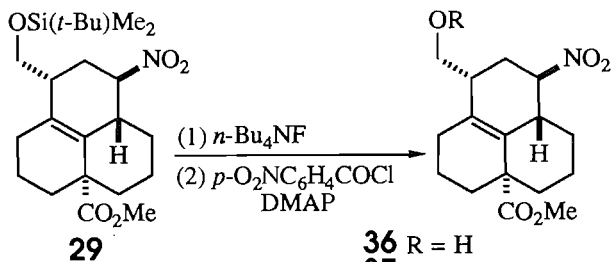

29

36 R = H
37 R = *p*-$O_2NC_6H_4CO$

TABLE 3. Signals for the $CH_2OSi(t\text{-Bu})Me_2$ protons in the ^{1}H nmr spectra of **21–23** and **27–29**

Compound	Chemical shift(s)	Multiplicity (coupling constant(s), Hz)
21	3.63–3.70[a]	—
27	3.66	dd (3, 10)
	3.73	dd (5, 10)
22	3.47	dd (8.5, 10)
	3.66–3.72[b]	—
28	3.59	dd (6.3, 10)
	3.68	dd (3.4, 10)
23	3.44	t (10)
	3.74	dd (3.8, 10)
29	3.50	dd (8, 10)
	3.75	dd (4, 10)

[a]The signals for both protons are partially hidden under the CO_2Me resonances.
[b]This signal is partially hidden under the CO_2Me resonances.

Treatment of the Diels–Alder adduct **29** (an oil) with tetra-*n*-butylammonium fluoride in THF, followed by reaction of the resultant alcohol **36** with *p*-nitrobenzoyl chloride in the presence of 4-(*N*,*N*-dimethylamino)pyridine (DMAP), gave the crystalline *p*-nitrobenzoate **37** (eq. [9]). An X-ray crystallographic analysis (vide infra) of this substance confirmed its structure and, thereby, the structure of the Diels–Alder adduct **29**.

In the ^{1}H nmr spectra of the series of compounds **21–23** and **27–29**, the signals due to the $CH_2OSi(t\text{-Bu})Me_2$ protons were particularly diagnostic and were helpful in making structural assignments. In each case, these two protons are magnetically nonequivalent and, thus, typically give rise to a pair of doublets, with the geminal coupling constant being 10 Hz. The appropriate data is summarized in Table 3. As can be seen from this data, each pair of structurally related compounds (**21**, **27**; **22**, **28**; **23**, **29**) exhibit signals for the $CH_2OSi(t\text{-Bu})Me_2$ protons that, in terms of chemical shifts and, where determinable, coupling constants, are similar. Since the structures of **27–29** are firmly established (vide supra) these data provide additional evidence for the structural assignments with respect to compounds **21–23**.

Reaction of the *cisoid-cis* diene **8** with NE did not proceed at room temperature. However, when a solution of the reactants in diethyl ether was refluxed for 7 h (Table 2, entry 6) no diene remained. Analysis of the crude product by ^{1}H nmr spectroscopy indicated the presence of three components (~2.5: trace:1). These substances, which could be separated by column chromatography and were obtained in isolated yields of 54%, 3%, and 21%, were shown to possess ^{1}H nmr spectra identical with those of the nitro esters (**27**, **28**, **29**, respectively) obtained from the Diels–Alder reaction of NE with the *cisoid-trans* diene **7**.

Since the composition of the product mixture derived from **8** and NE is essentially identical with that obtained from **7** and NE, it appears that, under the conditions of the former reaction, the *cisoid-cis* diene **8** isomerizes to the geometric isomer **7** prior to the Diels–Alder reaction. When solutions of **8** in diethyl ether or THF were refluxed in the absence of NE, the diene could be recovered unchanged in high yields, even after extended reflux times. Thus, it appears that the isomerization of **8** into **7** is promoted by NE itself (electron-transfer mechanism?) or by traces of impurity arising from

Can. J. Chem. Downloaded from www.nrcresearchpress.com by 213.200.69.106 on 09/08/12
For personal use only.

the preparation of NE. In any case, it was clear that the Diels–Alder reaction of **8** itself with NE is, not unexpectedly, sluggish.

Discussion of results from Diels–Alder studies

With respect to face-selectivity, the Diels–Alder reactions that were investigated varied considerably. The reactions of the dienes **6–8** with the dienophiles TCNE and MAN (Table 1) are highly face-selective and produce predominantly or exclusively the products resulting from attack of the reagents on the β face of the substrates. These results can be rationalized on the basis of steric effects. Thus, the transition states derived from α-face attack of TCNE would be destabilized by severe steric repulsion between the angular CO_2Me function and one of the cyano groups (see **38**). Similarly, attack of MAN on the α faces of **7** and **8** via *endo* transition states (MAN has a strong preference for *endo* orientations) would lead to a substantial steric repulsion (see **39**). Clearly, transition states derived from β-face attack of TCNE or MAN (*endo* orientation) would be expected to be considerably more stable than those (e.g., **38**, **39**) involving α-face attack.

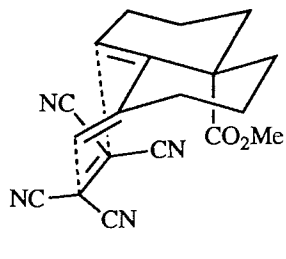

38 (**6** + TCNE)

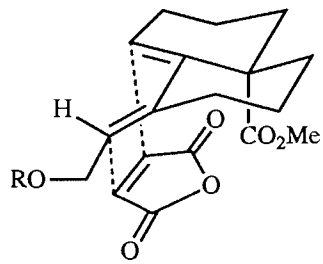

39 (**7** + MAN)

On the other hand, face-selectivities associated with the linear dienophile DMAD and the unsymmetrical dienophiles MAC and NE are quite low. Thus, reaction of **6** with DMAD proceeds via β- and α-face attack in a ratio of about 3:1, respectively (eq. [2]), while, in the reactions of **6** and **7** with MAC and NE, the ratios of β- to α-face attack vary from about 1.8:1 to 3:1 (Table 2). Not surprisingly, the products of α-face attack of MAC and NE on the dienes **6** and **7** are formed only via *exo* transition states. On the other hand, β-face attacks proceed predominantly via *endo* transition states (Table 2, entries 1, 2, 4, 5).

The Diels–Alder reactions of the dienes **6** and **7** with the unsymmetrical dienophiles MAC and NE are highly regioselective (Table 2). The regioselective nature of the reactions involving the diene **7** are particularly interesting. Although different models may be used to rationalize these observations, the biradical arguments developed by Dewar et al. (12) will be employed here.[4]

On the reasonable assumption that the presence of the angular CO_2Me function has little or no effect on the regiochemistry of the cycloaddition reactions, the dienes **6** and **7** may be represented in general terms by **41** and **42**, respectively (Scheme 1). Reaction of **41** with MAC or NE can, theoretically, provide two intermediate biradicals, **44** and **47**. Consideration of the relative stability of these two species allows one to predict which regioisomer should predominate in the product mixture (12). The allyl radical is stabilized by more alkyl substituents in **44** than in **47** and, therefore, the latter species should be less stable than the former. Hence, the regioisomers predicted to be preferred from the reactions of **41** (equivalent to **6**) with MAC and NE are those with general structure **50**. In fact, these are the only regioisomers formed (Table 2, entries 1 and 4). None of the regioisomeric substances (general structure **53**) were produced.

The interaction of **42** with MAC and NE can, theoretically, lead to the intermediate biradicals **45** and **48**. In **45**, the allyl radical is stabilized by three alkyl substituents. On other hand, the allyl radical system in **48** is also trisubstituted. However, although the alkyl-type substituents would be expected to have a stabilizing effect on this radical, it may be proposed that the inductively electron-withdrawing CH_2OR' function destabilizes the species. On this basis, one would predict that **45** is more stable than **48** and that, therefore, the preferred Diels–Alder products from the reaction of **42** (equivalent to **7**) with MAC and NE should possess the general structure **51**. In practice, the cycloadditions produced only **51** and none of the isomeric substances of general structure **54** could be observed in the crude product mixtures.

To demonstrate further that the $CH_2OSi(t\text{-}Bu)Me_2$ function does play an important role in directing the regiochemistry of the cycloaddition reactions of the diene **7**, the Diels–Alder reaction of the diene **40** (5) with the unsymmetrical dienophile MAC was investigated. The two biradicals **46** and **49** that could be (theoretically) formed from the diene system of general structure **43** (equivalent to **40**, see Scheme 1) would possess very similar substitution patterns and, consequently, would be expected to be of similar stability. In turn, one would expect the formation of mixtures of **52** and **55** in ratios approaching 1:1.

In the event (see Scheme 2), treatment of the diene **40** (5) with MAC in refluxing benzene provided (84%) an oil that, on the basis of analysis by glc–lrms, was shown to be a mixture of at least five isomeric diesters **56**. Reaction of this mixture with an excess of lithium diisopropylamide in THF, followed by treatment of the resultant mixture of enolate anions with benzeneselenenyl chloride, gave a mixture of selenides. This mixture was treated immediately with aqueous hydrogen peroxide and acetic acid in THF and the resultant mixture of dienes was allowed to react with 2,3-dichloro-5,6-dicyano-1,4-benzoquinone in benzene. Chromatography of the crude product gave, in 82% yield from **56**, a mixture of the isomeric diesters **57** and **58** in a ratio of about 1.4:1, respectively (analysis by ^1H nmr spectroscopy). The structural assignments were made on the basis of the relative chemical shifts of the signals due to the CH_2CH_3 protons in the ^1H nmr spectra of **57** and **58**. In **57**, this resonance (quartet, J = 7.5 Hz) appears at δ 2.60. The corresponding signal (quartet, J = 7.5 Hz) in **58**, which would be expected to be at lower field due to the proximity of the ethyl and methoxycarbonyl groups, appears at δ 2.86.

The results summarized above show that the regioselectivity of the Diels–Alder reaction of the diene **40** with MAC is, not unexpectedly, low. In contrast, the cycloadditions of the diene **7** with unsymmetrical dienophiles (MAC, NE) are

[4]The following discussion is not meant to imply a two-step mechanism for the cycloaddition reactions. These processes, in terms of the proposals of Dewar et al. (12), are considered to occur via *concerted, non-synchronous* pathways in which the transition state energies differ little from those of the corresponding biradicals.

Can. J. Chem. Downloaded from www.nrcresearchpress.com by 213.200.69.106 on 09/08/12
For personal use only.

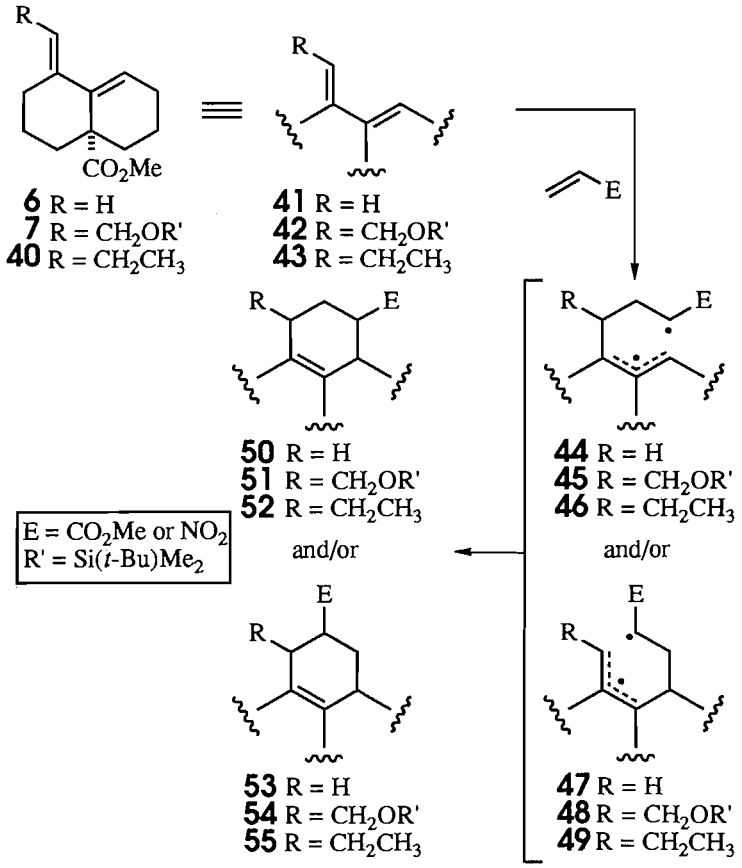

SCHEME 1

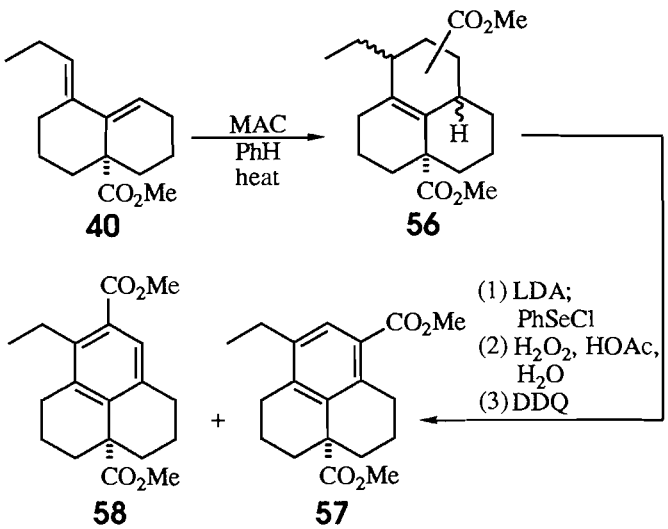

SCHEME 2

highly regioselective. Thus, the $CH_2OSi(t\text{-Bu})Me_2$ group in **7** has a notable directing effect on the regiochemistry of the cycloaddition reactions.

The "parent" diene **6**, as well as the *cisoid-trans* dienes **7** and **40**, are reasonably reactive substrates for Diels–Alder cycloadditions. In contrast, the *cisoid-cis* diene **8** is very reluctant to undergo Diels–Alder reactions. Indeed, only the reactions of **8** with very reactive dienophiles (TCNE, MAN) gave "normal" Diels–Alder adducts (Table 1, entries 4, 6) and, even then, the yield in one case (entry 6) was very low.

As mentioned previously, it is likely that these products are formed via a two-step process rather than a concerted cycloaddition pathway. With less reactive dienophiles, either no cycloaddition was observed (Table 2, entry 3; dimethyl acetylenedicarboxylate) or alternative processes took place (Table 2, entry 6).

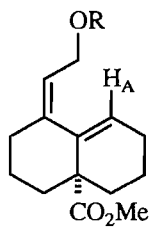

8 R = $Si(t\text{-Bu})Me_2$
59 R = $p\text{-}O_2NC_6H_4CO$

An X-ray crystallographic study (5) has shown that in the *p*-nitrobenzoate **59** (derived from the diene **8**), the diene system is twisted away from planarity to the extent of about 54°. If the crystal structure data accurately reflect the ground state conformation of substance **59** (and, thereby, of **8**) in solution, the sluggish nature of the Diels–Alder reactions of **8** would not be unexpected. Probably more important, however, is the fact that, if the diene unit in **8** is to attain planarity, a strong steric interaction between the CH_2OR group and H_A (see **8**, **59**) would be introduced. Clearly, this repulsion would destabilize cycloaddition transition states.

Additional synthetic applications

The studies summarized above show that Diels–Alder cycloadditions involving dienes **6** and **7** constitute an effec-

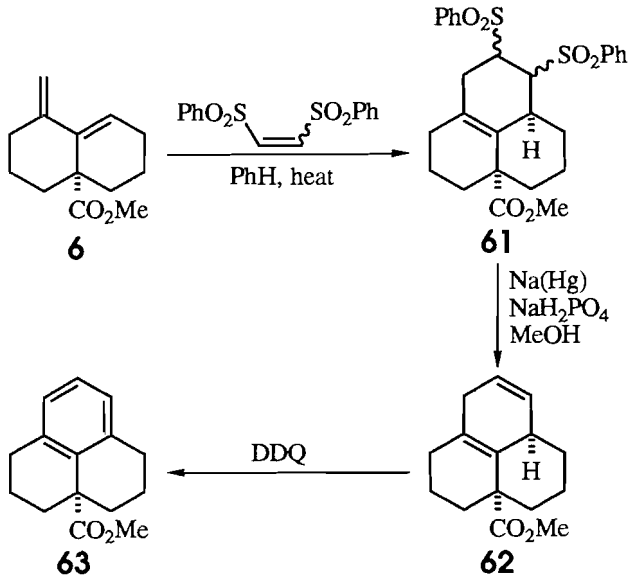

SCHEME 3

tive method for the preparation of functionalized perhydrophenalenes. With respect to a possible synthetic approach to amplilectane-type diterpenoids such as the natural product **1**, the fact that **21**, the major cycloaddition product from **7** and MAC, can be equilibrated to give primarily **22** is particularly noteworthy. Furthermore, the conversion of a mixture of cycloadducts (**24–26**, derived from **6** and NE, Table 2, entry 4) into the stereochemically homogeneous keto esters **33** and **35** illustrates the synthetic utility of the developed chemistry. We record here two additional examples that demonstrate the preparative value of Diels–Alder adducts derived from the dienes **7** and **6**.

The nitro ester **27**, the major product obtained from **7** and NE (Table 2, entry 5), upon sequential treatment with sodium methoxide and titanium trichloride under conditions identical with those employed earlier (conversion of **24–26** into **33**) provided, in excellent yield, the β,γ-unsaturated ketone **60** (eq. [10]). The ir spectrum of this stereochemically homogeneous substance exhibited carbonyl absorptions at 1740 and 1729 cm^{-1}.

[10]

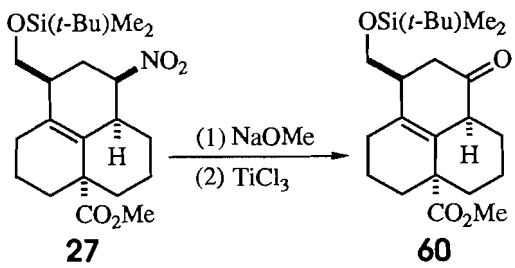

Reaction of the diene **6** with 1,2-bis(phenylsulfonyl)-ethylene in refluxing benzene gave the Diels–Alder adduct **61** (see Scheme 3). Although the latter material appeared to be a single isomer, its relative stereochemistry was not determined. Nevertheless, on the basis of previous results, it seems highly likely that the cycloaddition had proceeded via attack of the dienophile on the β face of **6** and that, therefore, the angular allylic proton and the CO_2Me function are in a *syn* relationship, as shown in **61**.

Treatment of **61** with sodium amalgam in methanol in the presence of sodium dihydrogen phosphate gave the diene ester **62** (mp 51–52°C) in 85% yield. Dehydrogenation of the latter material with 2,3-dichloro-5,6-dicyano-1,4-benzoquinone in benzene produced (87%) the tricyclic aromatic ester **63**. The symmetrical nature of the structure of the latter substance was clearly shown by the ^1H and ^{13}C nmr spectra.

*X-ray crystal structures of compounds **9**, **11**, **15**, **30**, **31**, **27**, and **37***

The main purpose of the structure analyses was to establish the relative stereochemistries at the chiral centres of the compounds studied. All seven of these compounds crystallize in centrosymmetric space groups, therefore each crystal is racemic and is composed of equal numbers of the stereoisomers shown in Figs. 1–3 and their mirror images. The absolute configurations for the chiral centres of the molecules depicted in Figs. 1–3 are given in Table 4. It should be noted that the crystallographic numbering scheme employed for **9** (**10**) differs from that employed for the remaining six structures. The conformations of the individual six-membered rings constituting the central ring systems are summarized in Table 5.

The crystal structures of **30** and **31** are dominated by hydrogen bonding. In **30** each disordered OH group is hydrogen bonded either to the same group on another molecule related by a centre of symmetry or to the other OH group on a molecule related by a translation along the *ab* diagonal (O(1)—H(O1a)···O(1)(2 − *x*, 2 − *y*, 1 − *z*), O(1)—H(O1b)···O(2)(1 + *x*, 1 + *y*, *z*), O(2)—H(O2a)···O(2)(−*x*, 1 − *y*, 1 − *z*), and O(2)—H(O2b)···O(1)(*x* − 1, *y* − 1, *z*); H···O = 1.95(5), 1.95(6), 2.02(4), 2.00(7) Å; O···O = 2.814(3), 2.754(2), 2.792(3), 2.754(2) Å, O—H···O = 170(6), 165(5), 170(5), 178(6)°; respectively). The equivalence of the two possible O—H···O hydrogen bonds that can be formed for each OH group is the reason for the statistical disordering of the OH protons in **30**. Molecules of **31** are each linked to four others by O—H···O hydrogen bonding (O(1)—H(O1)···O(2)(*x* − 1, *y*, *z* − 1) and O(2)—H(O2)···O(1)(1 + *x*, 1/2 − *y*, 1/2 + *z*), H···O = 2.04(8) and 1.82(5) Å, O···O = 2.690(5) and 2.695(6) Å, O—H···O = 165(11) and 168(5)°, respectively). Normal van der Waals interactions dominate the crystal structures of the five remaining compounds.

Experimental

General information

Distillation temperatures, which refer to short-path (Kugelrohr) distillations, and melting points are uncorrected. Proton (^1H) and carbon (^{13}C) nuclear magnetic resonance spectra were recorded on $CDCl_3$ solutions. For the ^{13}C nmr data, signals with negative intensities in attached proton test (APT) experiments are designated as −ve following the chemical shift value. Conventional column chromatography and flash chromatography (7) were carried out with 230–400 mesh silica gel (E. Merck). Gas–liquid chromatography (glc) was carried out on instruments equipped with 25 m × 0.21 mm fused silica columns coated with cross-linked SE-54. Thin-layer chromatography (tlc) was performed with commercial, aluminum-backed silica gel plates. Reagents and solvents were purified and dried using standard methods.

Note. Unless otherwise noted, all reactions were carried out under an atmosphere of argon in flame or oven-dried glassware.

*Reaction of the diene **6** with dimethyl acetylenedicarboxylate (DMAD)*

A stirred solution of the diene **6** (50 mg, 0.24 mmol) and DMAD (70 mg, 0.49 mmol) in dry benzene (10 mL) was refluxed and the

Can. J. Chem. Downloaded from www.nrcresearchpress.com by 213.200.69.106 on 09/08/12
For personal use only.

Can. J. Chem. Downloaded from www.nrcresearchpress.com by 213.200.69.106 on 09/08/12
For personal use only.

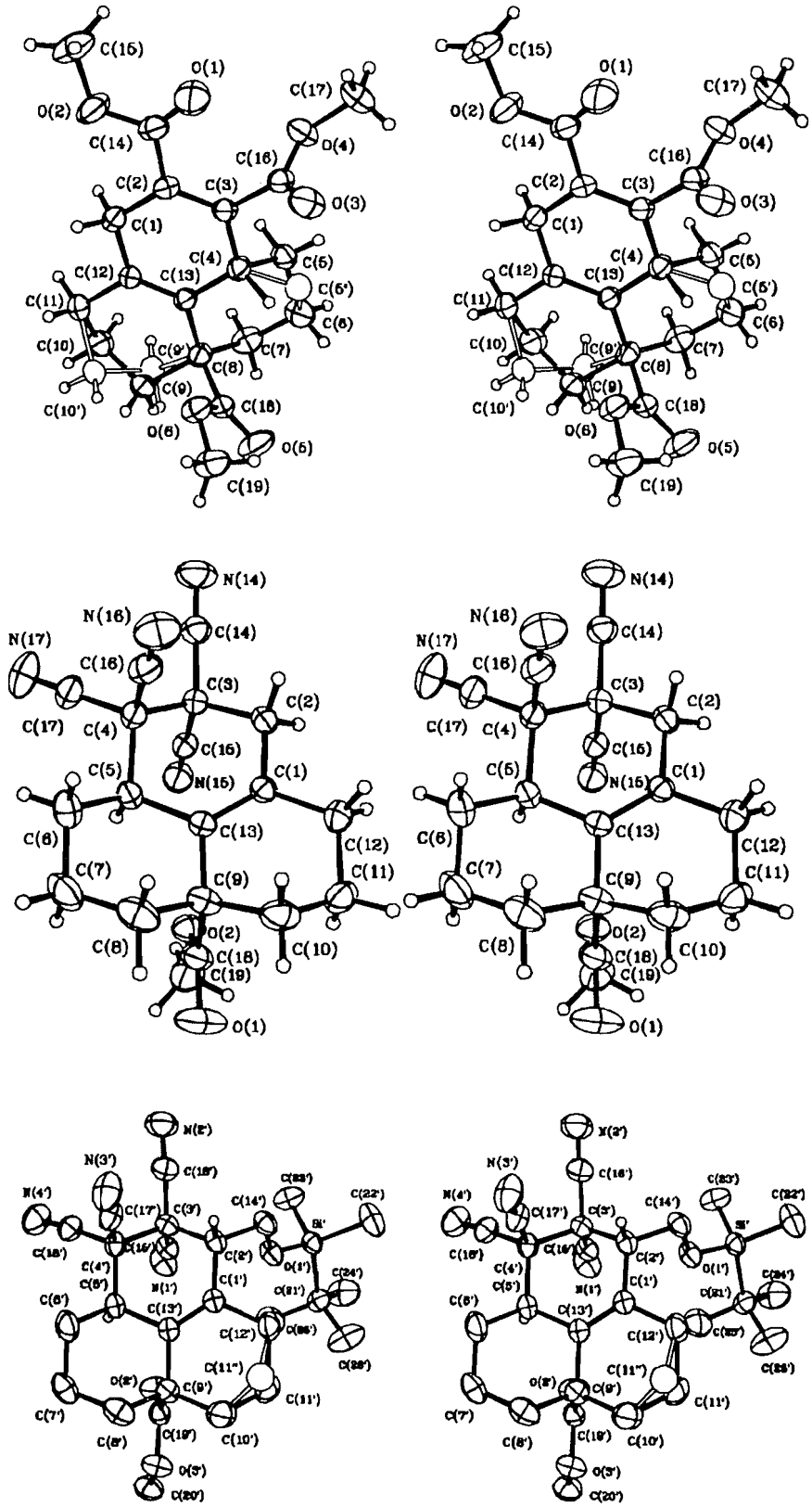

FIG. 1. Stereoviews of **9** (top), **11** (middle), and one of the two independent molecules of **15** (bottom) showing the crystallographic atom numbering schemes; 33% probability thermal ellipsoids are shown for the non-hydrogen atoms.

disappearance of the diene was monitored by glc. After 6 h, the solvent was removed under reduced pressure. Flash chromatography (15 g silica gel, 3:1 petroleum ether – Et_2O) of the residual material provided 66 mg (78%) of a slightly off-white solid (mp 136–137°C). Analysis (glc–lrms) of this material showed that it consisted of a mixture of two isomers with molecular mass of 348, while the ^1H nmr spectrum revealed that the two substances were present in a ratio of 3:1. Recrystallization (Et_2O–$CHCl_3$) of the solid

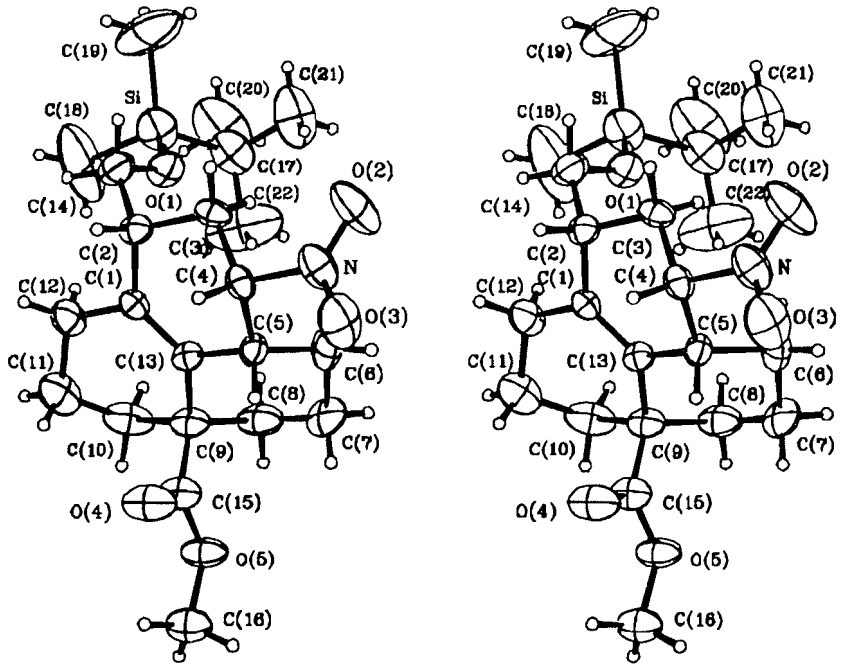

FIG. 2. Stereoview of **27** showing the crystallographic atom numbering scheme; 25% probability thermal ellipsoids are shown for the non-hydrogen atoms.

Can. J. Chem. Downloaded from www.nrcresearchpress.com by 213.200.69.106 on 09/08/12
For personal use only.

provided colorless, cubic crystals (mp 137.5–138.5°C), the ^{1}H nmr spectrum of which showed that the two isomers were still present in a ratio of 3:1. X-ray crystallographic analysis of this crystalline mixture disclosed that the major isomer was the triester **9**. The minor component of the mixture was assigned structure **10**. The mixture exhibited ir ($CHCl_3$): 1719, 1199 cm^{-1}; ^{1}H nmr (400 MHz) δ: 1.12–2.34 (m, 12H), 2.67–2.90 (m, 1H), 2.98–3.15 (m, 2H), 3.67, 3.70 (s, s, 3H, ratio 1:3), 3.75, 3.76 (s, s, 3H, ratio 1:3), 3.78, 3.80 (s, s, 3H, ratio 3:1). Exact Mass calcd. for $C_{19}H_{24}O_6$: 348.1573; found: 348.1580.

*Reaction of the diene **6** with TCNE (Table 1, entry 1)*

To a cold (0°C), stirred solution of the diene **6** (225 mg, 1.09 mmol) in dry THF (10 mL) was added, dropwise, a solution of TCNE (147 mg, 1.15 mmol) in dry THF (10 mL). The mixture was warmed to room temperature and stirred for 30 min. Removal of the solvent, followed by flash chromatography (35 g silica gel, 5:1 petroleum ether – ethyl acetate) of the residual material gave 302 mg (83%) of a white solid. Analysis of this material by glc and by glc–lrms showed that it consisted of a mixture of two isomers (**11** and, presumably, **12**) in a ratio of 96:4. Recrystallization of the mixture from diethyl ether – chloroform provided the pure, major isomer **11** as colorless, cubic crystals that exhibited mp 146–147°C. An X-ray crystallographic study on this material confirmed the structural assignment. Compound **11** exhibited ir ($CHCl_3$): 2255, 1728, 1603 cm^{-1}; ^{1}H nmr (400 MHz) δ: 1.33 (dt, 1H, J = 3, 13 Hz), 1.38–1.75 (m, 5H), 1.90 (m, 1H), 2.00 (br d, 1H, J = 18 Hz), 2.14–2.38 (m, 4H), 2.89 (d, 1H, J = 18 Hz), 3.19 (br d, 1H, J = 18 Hz), 3.31 (br d, 1H, J = 12.5 Hz), 3.73 (s, 3H). In decoupling experiments, irradiation at δ 2.89 simplified the m at 2.14–2.38, changed the br d at 3.19 to a br s, and sharpened the br d at 3.31; irradiation at δ 3.19 simplified the multiplets at 1.38–1.75 and 2.14–2.38 and converted the resonance at 2.89 to a br s; ^{13}C nmr (75.3 MHz) δ: 18.4, 21.2, 29.7, 30.7, 35.5, 36.4, 36.6, 37.5, 41.3 (−ve), 45.3, 48.1, 52.4 (−ve), 109.4, 110.1, 111.1, 111.2, 126.0, 127.7, 174.7. Anal. calcd. for $C_{19}H_{18}O_2N_4$: C 68.25, H 5.43, N 16.76; found: C 68.29, H 5.44, N 16.78. Exact Mass calcd.: 334.1431; found: 334.1435.

*Reaction of the diene **7** with TCNE (Table 1, entries 2 and 3)*

To a stirred solution of the diene **7** (50 mg, 0.143 mmol) in dry THF (10 mL) at room temperature was added solid TCNE (21.5 mg, 0.168 mmol). The yellow solution was stirred for 1 h. Concentration of the reaction mixture, followed by flash chromatography of the residual oil on silica gel (18 g, 4:1 petroleum ether – diethyl ether) gave 50.5 mg (74%) of a 7:1 mixture of the esters **13** and **14**, respectively, as a colorless foam. These isomers were found to be inseparable by chromatography on silica gel. The mixture exhibited ^{1}H nmr (400 MHz) δ: 0.15, 0.16, 0.17, 0.18 (all s, 6H, ratio ~1:1:7:7), 0.94, 0.97 (s, s, 9H, ratio ~1:7), 1.20–2.33 (series of m), 2.44 (br d, major isomer), 2.91 (br s, minor isomer), 3.10 (br d, major isomer), 3.25 (m, major isomer), 3.74, 3.75 (s, s, 3H, ratio ~1:7), 3.98 (br t, major isomer), 4.23 (dd, major isomer), 4.34 (dd, minor isomer).

To a cold (−78°C), stirred solution of the diene **7** (100 mg, 0.285 mmol) in dry THF (4 mL) was added, dropwise, a solution of TCNE (73 mg, 0.57 mmol) in dry THF (5 mL). After the solution had been stirred for 2 h at −78°C, it was concentrated and the residual material was subjected to flash chromatography (27 g silica gel, 4:1 petroleum ether – diethyl ether). A single isomer **13** (114 mg, 84%) was obtained as a colorless foam. Crystallization of this material from hexane–acetone gave colorless, needle-like crystals of **13**. This substance exhibited ir (KBr): 2253, 1729, 840, 782 cm^{-1}; ^{1}H nmr (400 MHz) δ: 0.17, 0.18 (s, s, 3H each), 0.97 (s, 9H), 1.27 (dt, 1H, J = 3.5, 13.5 Hz), 1.37–1.50 (m, 3H), 1.72 (m, 1H), 1.87–2.32 (series of m, 6H), 2.44 (br d, 1H, J = 13 Hz), 3.10 (br d, 1H, J = 12.5 Hz), 3.25 (m, 1H), 3.75 (s, 3H), 3.98 (m, 1H), 4.23 (dd, 1H, J = 4.5, 10.5 Hz). In decoupling experiments, irradiation at δ 3.25 simplified the signals at 3.98 and 4.23 to a br d (J = 10.5 Hz) and a d (J = 10.5 Hz), respectively, while irradiation at δ 4.23 changed the resonances at 3.25 and 3.98 to broad doublets (J = 4.5 Hz and 7.0 Hz, respectively); ^{13}C nmr (75.3 MHz) δ: 18.4, 18.5, 23.6, 25.8 (−ve), 28.7, 30.5, 35.7, 38.0, 39.8 (−ve), 43.0, 43.8, 47.6 (−ve), 50.0, 52.7 (−ve), 62.1, 110.3, 110.5, 114.4, 112.3, 126.3, 129.6, 174.9. Exact Mass calcd. for $C_{25}H_{31}O_3N_4Si$ (M^+ − Me): 463.2166; found: 463.2168.

*Reaction of the diene **8** with TCNE (Table 1, entry 4)*

A stirred solution of the diene **8** (60 mg, 0.171 mmol) and TCNE (180 mg, 1.41 mmol) in diethyl ether (10 mL) was refluxed gently for 15 h. Concentration of the mixture, followed by flash chromatography of the residual material on silica gel (18 g, 4:1 petroleum ether – diethyl ether), afforded 59.1 mg (72%) of the tricyclic

Can. J. Chem. Downloaded from www.nrcresearchpress.com by 213.200.69.106 on 09/08/12
For personal use only.

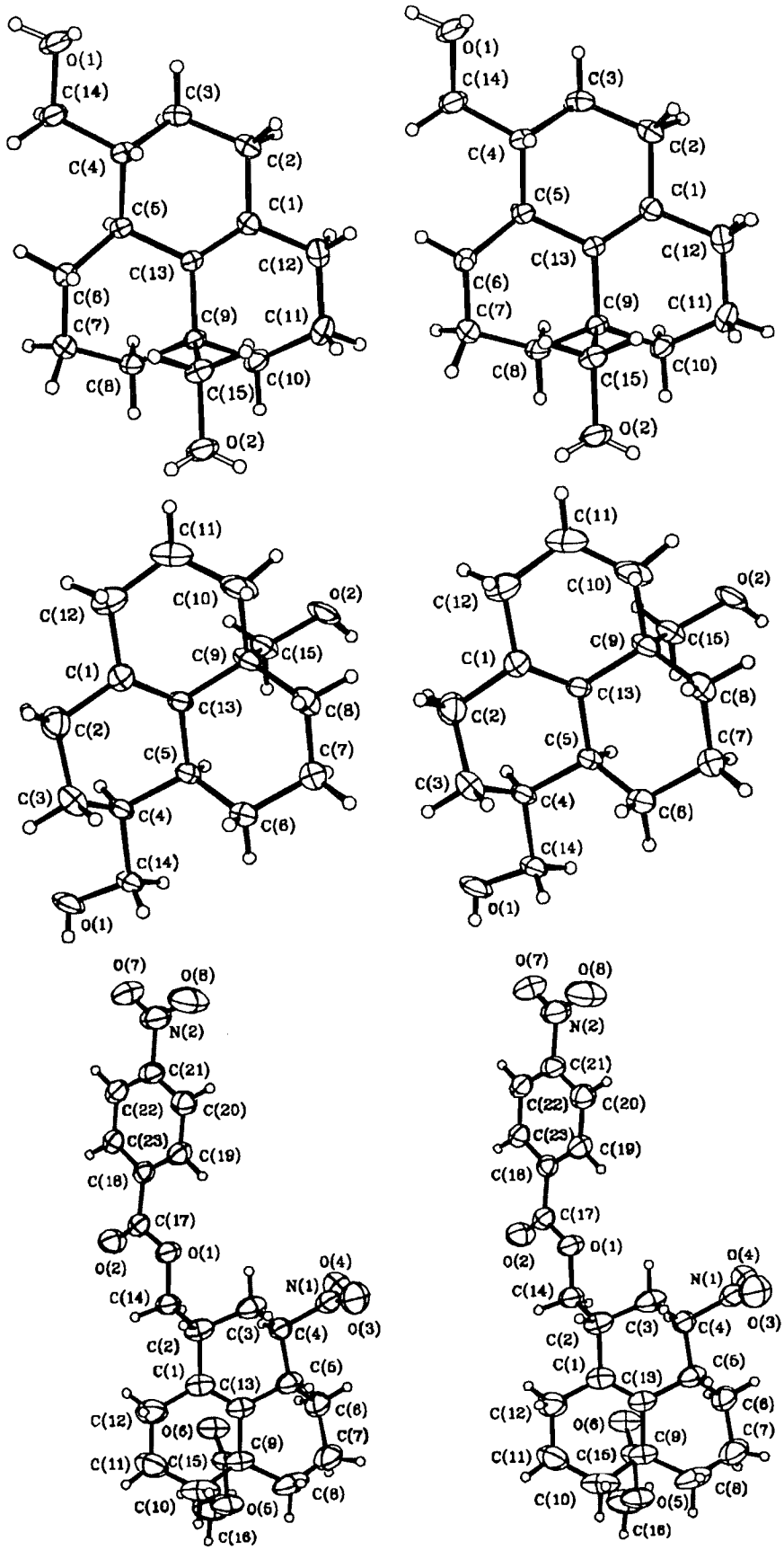

FIG. 3. Stereoviews of **30** (top), **31** (middle), and **37** (bottom) showing the crystallographic atom numbering schemes; 33% probability thermal ellipsoids are shown for the non-hydrogen atoms.

Can. J. Chem. Downloaded from www.nrcresearchpress.com by 213.200.69.106 on 09/08/12
For personal use only.

TABLE 4. Stereochemistries of the chiral centres of the structurally characterized compounds[a]

Compound	Assignments
9	4*R*,8*S*
10[b]	4*S*,8*S*
11	5*R*,9*S*
15	2*R*,5*R*,9*S*
27	2*R*,4*S*,5*R*,9*S*
30	4*R*,5*S*,9*R*
31	4*S*,5*S*,9*S*
37	2*R*,4*R*,5*R*,9*R*

[a]Atom numbering as shown in Figs. 1–3.
[b]Minor component of the disordered structure **9**.

TABLE 5. Ring conformations for the structurally characterized compounds[a]

Compound	Conformations		
	A ring	B ring	C ring
9[b]	Planar	Chair	Half-chair
10[c]	Planar	Boat	Half-chair
11	Half-chair	Chair	Half-chair
15[b,d]	Half-chair	Chair	Half-chair
27	Half-chair	Chair	Half-chair
30	Half-chair	Twist	Half-chair
31	Half-chair	Chair	Half-chair
37	Half-chair	Twist	Half-chair

[a]All of the rings show some degree of distortion from ideal geometry. The conformations designated as "half-chair" are intermediate between ideal half-chair (four adjacent atoms coplanar) and sofa (five atoms coplanar) forms.
[b]Conformational disordering of the C ring.
[c]Minor component in the disordered structure of **9**.
[d]Applies to both of the crystallographically independent molecules.

ester **15** as a colorless glass. Analysis of this material by ^{1}H nmr spectroscopy showed the presence of only one isomer. Crystallization from hexane–acetonitrile gave compound **15** as colorless, needle-like crystals that exhibited mp 127–128°C. An X-ray crystallographic analysis of this substance confirmed the structural assignment. Compound **15** displayed ir ($CHCl_3$): 2254, 1718 cm^{-1}; ^{1}H nmr (400 MHz) δ: 0.17, 0.18 (s, s, 3H each), 0.96 (s, 9H), 1.41–1.77 (m, 6H), 1.82–1.94 (m, 2H), 1.98–2.17 (m, 2H), 2.21–2.36 (m, 2H), 3.26 (m, 2H), 3.70 (s, 3H), 3.93 (dd, 1H, J = 7.5, 10.5 Hz), 4.25 (dd, 1H, J = 4.0, 10.5 Hz). Decoupling experiment: irradiation at δ 4.24 sharpened the m at 3.26 and changed the dd at 3.93 into a d (J = 7.5 Hz); ^{13}C nmr (75.3 MHz) δ: 18.4, 19.3, 21.7, 25.8 (−ve), 28.0, 30.5, 35.3, 36.0, 41.7 (−ve) 42.0, 46.6, 46.9 (−ve), 48.7, 52.6 (−ve), 61.9, 109.4, 110.1, 111.5, 112.1, 129.1, 129.6, 175.1. Anal. calcd. for $C_{26}H_{34}O_3N_4Si$: C 65.24, H 7.16; found: C 65.40, H, 7.12. Exact Mass calcd.: 478.2400; found: 478.2406.

Reaction of the diene 7 with MAN (Table 1, entry 5)

A stirred solution of the diene **7** (100 mg, 0.285 mmol) and MAN (56 mg, 0.57 mmol) in dry benzene (20 mL) was refluxed gently for 18 h. The solvent was removed under reduced pressure. Flash chromatography (27 g silica gel, 3:2 petroleum ether – diethyl ether) of the residual solid gave 80 mg (63%) of the anhydride **16** as a white solid. Recrystallization from hexane afforded colorless, cubic crystals that exhibited mp 103.5–105°C; ir (KBr): 1860, 1781, 1730, 838 cm^{-1}; ^{1}H nmr (400 MHz) δ: 0.04, 0.07 (s, s, 3H each), 0.89 (s, 9H), 1.21 (dt, 1H, J = 4, 13 Hz), 1.29–1.68 (m, 5H), 1.74 (m, 1H), 1.92–2.02 (m, 2H), 2.11 (m, 1H), 2.26 (br d, 1H, J = 12.5 Hz), 2.40 (m, 1H), 2.51–2.64 (m, 2H), 3.35 (m, 2H), 3.65 (dd, J = 5.5, 10.5 Hz), 3.66 (s, 3H), 3.74 (dd, 1H, J = 4, 10.5 Hz). In decoupling experiments irradiation at δ 3.35 simplified the m at 2.51–2.64 to two signals, a br d at 2.59 (J = 12 Hz) and a dd at 2.53 (J = 4, 5.5 Hz), while irradiation at δ 3.74 changed the resonance at 2.53 to a br t (J = 5.5 Hz) and simplified the dd at 3.65 to a d (J = 5.5 Hz). Exact Mass calcd. for $C_{24}H_{36}O_6Si$: 448.2281; found: 448.2276.

Reaction of the diene 8 with MAN (Table 1, entry 6)

A stirred solution of the diene **8** (100 mg, 0.285 mmol) and MAN (56 mg, 0.57 mmol) in dry benzene (5 mL) was refluxed gently for 3 days. During this time, a white solid precipitated from the colorless solution. The cooled mixture was filtered and the filtrate was concentrated. Flash chromatography of the residual oil on silica gel (15 g, 5:1 petroleum ether – diethyl ether) produced 22.4 mg (18%) of the anhydride **17** as a colorless oil. This material exhibited ir (neat): 1864, 1784, 1729, 837, 779 cm^{-1}; ^{1}H nmr (400 MHz) δ: 0.06, 0.07 (s, s, 3H each), 0.89 (s, 9H), 1.15 (m, 1H), 1.35–2.20 (series of m, 11H), 2.56 (m, 1H), 2.68 (m, 1H), 3.43 (t, 1H, J = 9 Hz), 3.50 (dd, 1H, J = 1, 9 Hz), 3.51 (dd, 1H, J = 7, 10 Hz), 3.67 (s, 3H), 3.72 (dd, 1H, J = 4, 10 Hz). Decoupling experiments: irradiation at δ 2.56 simplified the t at 3.43 to a d (J = 9 Hz); irradiation at δ 2.68 changed the signals at 3.50, 3.51, and 3.72 to doublets (J = 9, 10, 10 Hz, respectively); irradiation at δ 3.43 changed the resonance at 2.56 to a br d (J = 12 Hz); irradiation at δ 3.72 sharpened the signals at 2.68 and 3.51 to a br d (J = 7 Hz) and a d (J = 7 Hz), respectively. Exact Mass calcd. for $C_{24}H_{36}O_6Si$: 448.2281; found: 448.2276.

The white solid (75 mg) that had precipitated during the course of the reaction was washed with diethyl ether and dried. This material exhibited ir (KBr): 1849, 1779, 1718 cm^{-1}; ^{1}H nmr (400 MHz, CD_3SOCD_3): no signals due to the OSi(*t*-Bu)Me_2 group. Exact Mass calcd. for $C_{22}H_{22}O_8$: 414.1315; found: 414.1315.

Reaction of the diene 6 with MAC (Table 2, entry 1)

A stirred solution of the diene **6** (500 mg, 2.43 mmol) and MAC (0.44 mL, 4.8 mmol) in dry benzene (50 mL) was refluxed gently and the disappearance of the diene was monitored by glc. Additional amounts of MAC were added after reaction times of 22 and 46 h (4.8 and 2.4 mmol, respectively). After a total reaction time of 72 h, the reaction mixture was concentrated. Flash chromatography (70 g silica gel, 10:1 petroleum ether – diethyl ether) of the residual oil afforded 603 mg (85%) of a colorless oil. Analysis of this material by ^{1}H nmr spectroscopy and glc–lrms showed that it consisted of a mixture of three isomers (each of molecular mass 292) in a ratio of about 2.7:1:1.7. These substances were eventually identified as compounds **18**, **19**, and **20**, respectively.

Subjection of the mixture to drip column chromatography on silica gel (80 g, 15:1 petroleum ether – diethyl ether) provided pure samples of the major product **18** (the second component to be eluted) and of substance **20** (the first compound to be eluted). Although a pure sample of the minor, most polar, product was not obtained, this substance was subsequently identified as the diester **19**.

The major Diels–Alder adduct **18** (distillation temperature 195–200°C/0.5 Torr (1 Torr = 133.3 Pa)) exhibited ir (neat): 1732 cm^{-1}; ^{1}H nmr (400 MHz) δ: 1.15 (dt, 1H, J = 4, 8 Hz), 1.24 (dt, 1H, J = 4, 12.5 Hz), 1.28–1.73, 1.77–2.12 (series of m, 13H), 2.35 (br d, 1H, J = 13 Hz), 2.73 (ddd, 1H, J = 2.8, 6, 13 Hz), 3.67, 3.71 (s, s, 3H each). Exact Mass calcd. for $C_{17}H_{24}O_4$: 292.1674; found: 292.1674.

The diester **20** (distillation temperature 160–162°C/0.5 Torr) displayed ir (neat): 1720 cm^{-1}; ^{1}H nmr (400 MHz) δ: 1.21 (m, 1H), 1.33–1.70, 1.75–2.05 (series of m, 14H), 2.17 (m, 1H), 2.31 (dt, 1H, J = 3, 12 Hz), 2.38 (m, 1H), 3.67, 3.68 (s, s, 3H each). Exact Mass calcd. for $C_{17}H_{24}O_4$: 292.1674; found: 292.1676.

Can. J. Chem. Downloaded from www.nrcresearchpress.com by 213.200.69.106 on 09/08/12
For personal use only.

To a stirred solution of a mixture of the diesters **18** and **19** (ratio 3:1, respectively, obtained from fractions of the column chromatography described above, 24.9 mg) in dry methanol (20 mL) was added sodium methoxide (10 mg) and the resulting solution was refluxed gently for 2 weeks. The mixture was concentrated and diethyl ether (25 mL) was added to the residual slurry. The mixture was filtered and the filtrate was dried ($MgSO_4$) and concentrated. Distillation (160–170°C/0.6 Torr) of the residual oil provided 22 mg (88%) of a colorless oil that consisted of a mixture of **18** and **19** in a ratio of 1:6 (glc analysis). The ^{1}H nmr spectrum (400 MHz) of the material exhibited the following unique signals for compound **19**: δ 0.99 (dq, 1H, J = 4, 12 Hz), 2.19–2.27 (m, 2H), 2.49 (br t, 1H, J = 11 Hz), 3.69 (s, 6H).

*Reduction of the diester **18**. Preparation of the diol **31***

Solid $LiAlH_4$ (17 mg, 0.45 mmol) was added to a stirred solution of the diester **18** (85 mg, 0.29 mmol) in dry THF (10 mL) and the resulting slurry was refluxed for 1 h and then was cooled to room temperature. Hydrochloric acid (1 M, 5 drops) was added cautiously and then the mixture was treated with cold water (5 mL). The phases were separated and the aqueous phase was extracted with diethyl ether (3 × 25 mL). The combined extracts were dried ($MgSO_4$) and concentrated to provide 66.8 mg (97%) of the diol **31** as a white solid. Recrystallization from ethanol–hexane gave colorless cubes that exhibited mp 182.5–184.5°C. The structure of **31** was confirmed by an X-ray crystallographic analysis. This material displayed ir (Nujol): 3271, 3189 cm^{-1}. It was not sufficiently soluble in common deuterated solvents ($CDCl_3$, CD_3SOCD_3, C_6D_6, CD_3COCD_3) to allow for acquisition of a satisfactory ^{1}H nmr spectrum. Anal. calcd. for $C_{15}H_{24}O_2$: C 76.23, H 10.24; found: C 76.17, H 10.24. Exact Mass calcd.: 236.1777; found: 236.1777.

*Reduction of the diester **20**. Preparation of the diol **30***

To a stirred suspension of $LiAlH_4$ (43 mg, 1.13 mmol) in dry diethyl ether (20 mL) at 0°C was added, dropwise, a solution of the diester **20** (218 mg, 0.747 mmol) in dry diethyl ether (10 mL). After the mixture had been stirred at 0°C for 30 min, it was refluxed for 6.5 h. Hydrochloric acid (1 M, 5 mL) and water (10 mL) were added cautiously. The organic phase was separated and the aqueous phase was extracted with diethyl ether (3 × 10 mL). The combined organic extracts were dried ($MgSO_4$) and concentrated to give 146 mg (83%) of the diol **30** as a crystalline solid. Recrystallization from methanol produced colorless cubic crystals that displayed mp 162.5–164°C. An X-ray crystallographic analysis confirmed that this substance possessed structure **30**. This material showed ir (Nujol): 3310, 3195 cm^{-1}. It was sparingly soluble in common deuterated solvents and its ^{1}H nmr spectrum in CD_3OD was uninformative. Anal. calcd. for $C_{15}H_{24}O_2$: C 73.23, H 10.24; found: C 73.17, H 10.21. Exact Mass calcd.: 236.1777; found: 236.1776.

*Reaction of the diene **7** with MAC (Table 2, entry 2)*

A stirred solution of the diene **7** (170 mg, 0.485 mmol) and MAC (0.18 mL, 1.95 mmol) in dry benzene (10 mL) was refluxed gently. Additional amounts (1 mmol) of MAC were added to the reaction mixture after reaction times of 24, 48, and 56 h. After a total reaction time of 72 h, the solution was concentrated. Analysis (^{1}H nmr spectroscopy) of the crude product indicated the presence of at least three components. Medium-pressure column chromatography of the crude oil on silica gel (40 g, 8:1 petroleum ether – diethyl ether) provided, in addition to a trace amount of an unidentified compound, two major fractions. The first material to be eluted (65.7 mg, 31%) was a single compound that was identified as the Diels–Alder adduct **23**, while the second fraction (118.3 mg, 56%) was shown by ^{1}H nmr spectroscopy to consist of a 3:1 mixture of the diesters **21** and **22**. Thus, the cycloaddition reaction involving the diene **7** and MAC gave, in 87% yield, a mixture of **21**, **22**, and **23** (48:16:36, respectively).

Subjection of the 3:1 mixture of **21** and **22** to drip column chromatography (27 g silica gel, 8:1 petroleum ether – diethyl ether) provided a pure sample of the major adduct **21**.

A pure sample of the minor isomer **22** was obtained as follows. A stirred solution of the diester **21** (20 mg) and sodium methoxide (~2 mg) in dry methanol (5 mL) was refluxed gently for 6 days and then was concentrated. Analysis of the crude material by ^{1}H nmr spectroscopy indicated the presence of **21** and **22** in a ratio of ~1:9, respectively. Drip column chromatography of this material on silica gel (10 g, 5:1 petroleum ether – diethyl ether) gave a pure sample of **22**.

The major adduct **21**, a colorless oil, displayed ir (neat): 1733, 837, 776 cm^{-1}; ^{1}H nmr (400 MHz) δ: 0.04, 0.05 (s, s, 3H each), 0.89 (s, 9H), 1.09 (dt, 1H, J = 4, 13 Hz), 1.20–2.08 (series of m, 12H), 2.20 (m, 1H), 2.30 (m, 1H), 2.39 (br d, 1H, J = 13.5 Hz), 2.76 (ddd, 1H, J = 2.7, 6, 13.5 Hz), 3.63–3.70 (m, 2H), 3.67, 3.71 (s, s, 3H each). Exact Mass calcd. for $C_{24}H_{40}O_5Si$: 436.2645; found: 436.2643.

The minor product **22**, a colorless oil, exhibited ir (neat): 1735, 837, 777 cm^{-1}; ^{1}H nmr (400 MHz) δ: 0.06 (s, 6H), 0.91 (s, 9H), 1.16 (dt, 1H, J = 3.5, 13.5 Hz), 1.30 (m, 1H), 1.39–1.64, 1.70–2.06, 2.16–2.32, 2.36–2.48 (series of m, 5H, 5H, 3H, 2H), 3.47 (dd, 1H, J = 8.5, 10 Hz), 3.66–3.72 (m, 1H, buried under OMe signals), 3.68, 3.69 (s, s, 3H each). Exact Mass calcd. for $C_{24}H_{40}O_5Si$: 436.2645; found: 436.2645.

Compound **23**, a colorless oil, showed ir (neat): 1733, 838, 777 cm^{-1}; ^{1}H nmr (400 MHz) δ: 0.06, 0.07 (s, s, 3H each), 0.91 (s, 9H), 1.15–1.72 (series of m, 8H), 1.78 (dt, 1H, J = 6, 12.5 Hz), 1.87–2.02, 2.06–2.27, 2.34–2.46 (series of m, 3H, 3H, 2H), 3.44 (t, 1H, J = 10 Hz), 3.65, 3.67 (s, s, 3H each), 3.74 (dd, 1H, J = 3.8, 10 Hz). Exact Mass calcd. for $C_{24}H_{40}O_5Si$: 436.2644; found: 436.2645.

*Reaction of the diene **6** with NE (Table 2, entry 4)*

To a solution of the diene **6** (150 mg, 0.728 mmol) in dry diethyl ether (7 mL) was added neat NE (9) (0.5 mL) and the resultant mixture was stirred at room temperature for 3 h. Concentration of the mixture, followed by flash chromatography (27 g silica gel, 15:1 petroleum ether – ethyl acetate) of the residual oil afforded 168 mg (83%) of a very pale-green solid. Analysis of this material by glc and by glc–lrms indicated that it consisted of a mixture of three isomers (3:1:2), each with molecular mass 279. These substances were assigned structures **24**, **25** and **26**, respectively. The ^{1}H nmr spectrum (400 MHz) of this mixture exhibited δ: 1.14–2.43 (series of m, 16H), 2.75 (m, 1H, angular allylic protons of all three isomers), 3.69, 3.72 (s, s, 3H, ratio 1:2), 4.44 (dt, ~0.33 H, J = 3.8, 10.5 Hz, CHNO$_2$ of **26**), ~4.71, 4.74 (overlapping multiplets, minor and major, respectively, ~0.67 H total, CHNO$_2$ of **25** and **24**, respectively).

A 30 mg sample of this mixture was added to dry *tert*-butyl alcohol (4 mL) containing 4 mg of potassium *tert*-butoxide and the resultant stirred mixture was heated at 80°C for 16 h. Dilute (1%) aqueous acetic acid (5 mL) and water (5 mL) were added sequentially to the cooled reaction mixture. The phases were separated and the aqueous phase was extracted with diethyl ether (2 × 10 mL). The combined organic extracts were washed with saturated aqueous sodium bicarbonate (2 × 10 mL), dried ($MgSO_4$), and concentrated. Flash chromatography of the residual oil on silica gel (10 g, 10:1 petroleum ether – ethyl acetate) gave 26 mg (87%) of a mixture of the nitro esters **24**, **25**, and **26** (0.7:3.1:2, respectively, by glc analysis).

Drip column chromatography of the 3:1:2 mixture of **24**, **25**, and **26** (135 mg) on silica gel (18 g, 20:1 petroleum ether – diethyl ether) gave a pure sample of **26**, the first component to be eluted. This material exhibited ir ($CHCl_3$): 1718 cm^{-1}; ^{1}H nmr (400 MHz) δ: 1.20–1.75, 1.90–2.35 (series of m, 8H, 8H), 2.75 (m, 1H), 3.69 (s, 3H), 4.44 (dt, 1H, J = 3.8, 10.5 Hz). In a decoupling experiment, irradiation at δ 4.44 simplified the m at 2.75 to a br d (J = 13 Hz).

*Preparation of the keto ester **33***

To a stirred solution of the mixture of the nitro esters **24**, **25**, and **26** (3:1:2, 162 mg, 0.581 mmol) in spectral grade methanol (8 mL)

Can. J. Chem. Downloaded from www.nrcresearchpress.com by 213.200.69.106 on 09/08/12
For personal use only.

at room temperature was added solid sodium methoxide (31 mg, 0.57 mmol) and the resultant yellow solution was stirred for 20 min. A freshly prepared solution of titanium trichloride (358 mg, 2.32 mmol) and ammonium acetate (1.12 g, 14.5 mmol) in water (8 mL) was added. The mixture immediately turned green in color and, as the reaction progressed, became blue and finally yellow. A finely divided solid precipitated. The mixture was stirred for 3 h and then was filtered. The collected solid was washed with diethyl ether (50 mL). The phases of the combined filtrate were separated and the aqueous phase was washed with diethyl ether (3 × 25 mL). The combined organic extracts were washed with saturated aqueous sodium bicarbonate (20 mL), dried ($MgSO_4$), and concentrated. Distillation (132–133°C/0.1 Torr) of the residual oil provided 129 mg (90%) of the ketone **33**, a colorless oil that displayed ir (neat): 1710, 1450, 1226, 1160 cm^{-1}; ^1H nmr (400 MHz) δ: 1.15–130 (m, 2H), 1.36 (tt, 1H, J = 3.2, 13 Hz), 1.45–1.69 (m, 4H), 1.74 (d of quintets, 1H, J = 13, 3.4 Hz), 2.00–2.10 (m, 3H), 2.27–2.57 (m, 5H), 2.82 (br d, 1H, J = 13 Hz), 3.69 (s, 3H). In a nuclear Overhauser enhancement (nOe) difference experiment, irradiation at δ 3.69 (CO_2Me) caused enhancement of the broad d at 2.82 (angular allylic proton); ^{13}C nmr (75.3 MHz) δ: 19.3, 23.0, 30.6, 30.7, 31.0, 36.0, 37.4, 37.9, 48.4, 48.5, 52.1, 130.1, 130.6, 176.6, 213.0. Exact Mass calcd. for $C_{15}H_{20}O_3$: 248.1413; found: 248.1410.

Preparation of the enone ester ***35***

To a stirred solution of the ketone **33** (10 mg) in dry THF (5 mL) at room temperature was added approximately 1–2 mg of potassium *tert*-butoxide and the resulting mixture was stirred for 24 h. Water (5 mL) was added, the phases were separated, and the aqueous layer was extracted with diethyl ether (3 × 20 mL). The combined organic extracts were washed with brine, dried ($MgSO_4$), and concentrated. Drip column chromatography of the residual oil on silica gel (10 g, 1:5 petroleum ether – diethyl ether) produced 5.5 mg (55%) of the enone **35** as a white solid. Recrystallization from diethyl ether provided material that displayed mp 159–160°C; ir ($CHCl_3$): 1723, 1668, 1603 cm^{-1}; ^1H nmr (400 MHz) δ: 1.35–2.42 (series of m, 15H), 2.50 (ddd, 1H, J = 1.8, 5.5, 18.2 Hz), 2.89 (ddd, 1H, J = 6, 13, 18.2 Hz), 3.72 (s, 3H). In a decoupling experiment, irradiation at δ 2.89 simplified the signal at 2.50 to a dd (J = 1.8, 5.5 Hz); ^{13}C nmr (75.3 MHz) δ: 15.3, 18.3, 22.7, 29.0, 31.0, 33.0, 34.8, 36.4, 47.5, 52.4, 68.3, 133.8, 155.3, 175.8, 199.6. Exact Mass calcd. for $C_{15}H_{20}O_3$: 248.1413; found: 248.1356.

Reaction of the diene ***7*** *with NE (Table 2, entry 5)*

To a stirred solution of the diene **7** (190 mg, 0.542 mmol) in dry diethyl ether (5 mL) was added neat NE (9) (0.6 mL). After the mixture had been stirred at room temperature for 3 h, the solvent was removed under reduced pressure. The residual oil was passed through a plug of silica gel (elution with diethyl ether). Concentration of the eluate provided an oil that consisted of a mixture of three nitro esters **27**, **28**, and **29** (~3:trace:1 by ^1H nmr spectroscopy). Medium-pressure column chromatography (40 g silica gel, 10:1 petroleum ether–diethyl ether) afforded 56 mg (24%) of **29** (the first compound to be eluted, distillation temperature 180–195°C/0.03 Torr) as a colorless oil and 130.4 mg (57%) of **27** (the second product to be eluted, mp 89–90°C (from chloroform)) as a colorless crystalline material. An X-ray crystallographic analysis confirmed the structure of the latter substance.

Product **27** displayed ir ($CHCl_3$): 1728, 1547, 1384, 838, 777 cm^{-1}; ^1H nmr (400 MHz) δ: 0.06, 0.07 (s, s, 3H each), 0.90 (s, 9H), 1.11 (dt, 1H, J = 3.9, 13 Hz), 1.23–1.66 (m, 6H), 1.73 (m, 1H), 1.91–2.08 (m, 3H), 2.09–2.17 (m, 2H), 2.33 (m, 1H), 2.44 (br d, 1H, J = 13.4 Hz), 2.69 (m, 1H), 3.66 (dd, 1H, J = 3, 10 Hz), 3.72 (s, 3H), 3.73 (dd, 1H, J = 5, 10 Hz), 4.75 (m, 1H). In decoupling experiments irradiation at δ 2.69 simplified the multiplets at 1.23–1.66 and 4.75; irradiation at 3.66 sharpened the m at 2.33 to a br t; irradiation at 4.75 sharpened the m at 2.09–2.17 and changed the m at 2.69 to a br d (J = 11 Hz). Anal. calcd. for $C_{22}H_{37}O_5NSi$: C 62.38, H 8.80; found: C 62.49, H 8.92. Exact Mass calcd. for $C_{21}H_{34}O_5NSi$ (M^+ − Me): 408.2207; found: 408.2212.

Compound **29** exhibited ir (neat): 1729, 1549, 1378, 838, 778 cm^{-1}; ^1H nmr (400 MHz) δ: 0.07, 0.08 (s, s, 3H each), 0.91 (s, 9H), 1.25–1.75, 1.88–2.08, 2.16–2.33 (series of m, 8H, 3H, 3H), 2.46 (ddd, 1H, J = 0.9, 3, 12 Hz), 2.78 (br t, 1H, J = 12 Hz), 3.50 (dd, 1H, J = 8, 10 Hz), 3.67 (s, 3H), 3.75 (dd, 1H, J = 4, 10 Hz), 4.58 (ddd, 1H, J = 3, 10.5, 12 Hz). Decoupling experiments: irradiation at δ 2.46 sharpened the m at 2.16–2.33 and changed the m at 4.58 to a dd (J = 10.5, 12 Hz); irradiation at δ 2.78 simplified the multiplets at 1.25–1.75 and 1.88–2.08 and sharpened the ddd at 4.58 to a br d (J = 10.5 Hz); irradiation at δ 3.50 sharpened the m at 2.16–2.33 and changed the dd at 3.75 to a d (J = 4 Hz); irradiation at δ 4.58 sharpened the m at 2.16–2.33, simplified the signal at 2.46 to a dd (J = 0.9, 12 Hz), and changed the br t at 2.78 to a br d (J = 12 Hz). Exact Mass calcd. for $C_{21}H_{34}O_5NSi$ (M^+ − Me): 408.2207; found: 408.2203.

To a stirred solution of the nitro ester **27** (38 mg, 0.09 mmol) in dry *tert*-butyl alcohol (4 mL) was added potassium *tert*-butoxide (~1.5 mg) and the resultant solution was heated at ~100°C for 18 h. The mixture was cooled and then was treated with 5 mL of dilute aqueous acetic acid, 5 mL of diethyl ether, and 5 mL of water. The organic phase was separated and the aqueous layer was washed with diethyl ether (3 × 10 mL). The combined organic extracts were washed with brine, dried ($MgSO_4$), and concentrated. Flash chromatography (10 g silica gel, 10:1 petroleum ether–diethyl ether) of the residual oil provided 35 mg (92%) of the nitro ester **28** as a colorless crystalline solid that displayed mp 62–63°C. This substance, which showed diagnostic ^1H nmr signals with chemical shifts identical with those of the Diels–Alder adduct formed in trace amounts, exhibited ir ($CHCl_3$): 1721, 1548, 1379, 839 cm^{-1}; ^1H nmr (400 MHz) δ: 0.07, 0.08 (s, s, 3H each), 0.91 (s, 9H), 1.07 (dq, 1H, J = 3.5, 12.5 Hz), 1.17 (dt, 1H, J = 3.2, 13.1 Hz), 1.23–1.35 (m, 1H), 1.39–1.70 (m, 4H), 1.83–1.94 (m, 2H), 2.09 (m, 1H), 2.14–2.35 (m, 4H), 2.84 (m, 1H), 3.59 (dd, 1H, J = 6.3, 10 Hz), 3.68 (dd, 1H, J = 3.4, 10 Hz), 3.71 (s, 3H), 4.68 (ddd, 1H, J = 4, 9, 12 Hz). In decoupling experiments, irradiation at δ 2.84 sharpened the m at 2.14–2.35 and simplified the signals at 1.07 and 4.68 to a dt (J = 3.5, 12.5 Hz) and a dd (J = 4, 12 Hz), respectively; irradiation at δ 3.59 sharpened the m at 2.14–2.35; irradiation at δ 4.68 simplified the m at 2.14–2.35 and changed the m at 2.84 to a br d (J = 12 Hz). Exact Mass calcd. for $C_{21}H_{34}O_5NSi$ (M^+ − Me): 408.2206; found: 408.2204.

Preparation of the p*-nitrobenzoate* ***37***

To a stirred solution of the silyl ether **29** (106 mg, 0.251 mmol) in dry THF (10 mL) at room temperature was added, dropwise, a solution of tetra-*n*-butylammonium fluoride (0.5 mL, 1 M, THF). The solution was stirred for 16 h and then was concentrated. Flash chromatography of the residual oil on silica gel (27 g, 2:1 petroleum ether–diethyl ether) provided 55.6 mg (72%) of the alcohol **36** as a colorless oil. This material displayed ir (neat): 3478, 1713, 1546, 1379 cm^{-1}; ^1H nmr (400 MHz) δ: 1.19–1.79, 1.92–2.35 (series of m, 7H, 7H), 2.40 (ddt, 1H, J = 1, 6.5, 12.5 Hz), 2.80 (m, 1H), 3.60 (dd, 1H, J = 1.5, 11 Hz), 3.72 (s, 3H), 3.90 (ddd, 1H, J = 4, 10, 12.5 Hz).

To a stirred solution of the alcohol **36** (46.9 mg, 0.152 mmol) in dry THF (10 mL) at room temperature was added 4-(*N*,*N*-dimethylamino)pyridine (22.3 mg) and *p*-nitrobenzoyl chloride (42.4 mg, 0.228 mmol). The mixture was refluxed for 1 h and then was concentrated. Flash chromatography (18 g silica gel, 1:1 petroleum ether–diethyl ether) of the residual material provided 63 mg (91%) of the *p*-nitrobenzoate **37** as a white solid. Recrystallization of this material from benzene gave colorless crystals, mp 142.5–143.5°C. An X-ray crystallographic study showed that this substance possesses the constitution and relative stereochemistry shown in **37**. Compound **37** exhibited ir ($CHCl_3$): 1724, 1550, 1530, 1350 cm^{-1}; ^1H nmr (400 MHz) δ: 1.23–1.82, 1.96–2.10, 2.30–2.49 (series of m, 8H, 3H, 3H), 2.65 (m, 1H), 2.82 (br t, 1H,

Can. J. Chem. Downloaded from www.nrcresearchpress.com by 213.200.69.106 on 09/08/12
For personal use only.

J = 10 Hz), 3.65 (s, 3H), 4.40 (dd, 1H, J = 7.3, 11.2 Hz), 4.53 (dd, 1H, J = 3, 11.2 Hz), 4.63 (dt, 1H, J = 4, 11 Hz), 8.25–8.35 (m, 4H). Anal. calcd. for $C_{23}H_{26}N_2O_8$: C 60.26, H 5.72, N 6.11; found: C 60.05, H 5.70, N 6.00. Exact Mass calcd.: 458.1689; found: 458.1684.

*Reaction of the diene **8** with NE (Table 2, entry 6)*

A stirred solution of the diene **8** (500 mg, 1.426 mmol) and NE (9) (~1 mL) in dry diethyl ether (20 mL) was refluxed for 7 h and then was concentrated. The residual oil was passed through a plug of silica gel (elution with diethyl ether). Removal of the solvent from the eluant produced a mixture of three nitro esters (**27**, **28**, **29**; ~2.5:trace:1, by ^{1}H nmr spectroscopy). Medium-pressure column chromatography of this material on silica gel (90 g, 10:1 petroleum ether – diethyl ether) provided, in order of elution, 127 mg (21%) of **29**, 19 mg (3%) of **28**, and 328 mg (54%) of **27**. These materials exhibited ir and ^{1}H nmr spectra identical with those of the same substances obtained previously (vide supra).

*Reaction of the diene **40** with MAC*

A stirred solution of the diene **40** (760 mg, 3.24 mmol) and MAC (2.9 mL) in dry benzene (60 mL) was refluxed for 3 days and then was concentrated. Flash chromatography (100 g silica gel, 10:1 petroleum ether – diethyl ether) without any attempt to separate isomers provided 873 mg (84%) of a mixture of diesters **56** as a colorless oil. Analysis of this material by glc–lrms indicated the presence of at least five isomers, each with molecular mass 320.

To a cold (0°C) stirred solution of lithium diisopropylamide (2.5 equiv.) in dry THF (6 mL) was added, dropwise, a solution of the mixture of diesters **56** (50 mg, 0.156 mmol) in dry THF (2 mL). The solution was stirred at 0°C for 30 min and at room temperature for 30 min. Solid benzeneselenenyl chloride (75 mg, 2.5 equiv.) was added and the solution was stirred for 30 min. Water (1 mL), acetic acid (0.04 mL, 4 equiv.), and hydrogen peroxide (0.18 mL, 10 equiv.) were added sequentially and the mixture was stirred for 1 h. Saturated aqueous sodium bicarbonate (10 mL) was added and the organic phase separated. The aqueous phase was extracted with diethyl ether. The combined organic solutions were washed with brine, dried ($MgSO_4$), and concentrated. The residual oil was dissolved in dry benzene (10 mL) and 2,3-dichloro-5,6-dicyano-1,4-benzoquinone (40 mg) was added to the solution. The stirred mixture was refluxed for 4 h and then was concentrated. Drip column chromatography (18 g silica gel, 7:1 petroleum ether – diethyl ether) of the remaining material and distillation (130–140°C/0.1 Torr) of the oil thus obtained provided 40.3 mg (82%) of a mixture of the diesters **57** and **58** (ratio 1.4:1), a colorless oil that displayed ir (neat): 1724, 1598, 1565 cm^{-1}; ^{1}H nmr (400 MHz) δ: 1.18, 1.22 (t, t, 3H, ratio 1:1.4, J = 7.5 Hz), 1.43–1.90, 2.30–2.40 (series of m, 6H, 2H), 2.60, 2.86 (q, q, 2H, ratio 1.4:1, J = 7.5 Hz), 2.69–2.82 (m), 3.00 (ddd, J = 18, 7, 4 Hz), 3.20 (dt, J = 18, 9 Hz), 3.63, 3.86, 3.87 (s, s, s, 2.4:1.4:1), 7.38, 7.59 (s, s, 1H, ratio 1:1.4). Exact Mass calcd. for $C_{19}H_{24}O_4$: 316.1674; found: 316.1683.

*Preparation of the keto ester **60***

Using a procedure identical with that used for the preparation of the keto ester **33**, the nitro ester **27** (81 mg, 0.191 mmol) was converted into the keto ester **60**. Flash chromatography (27 g silica gel, 3:1 petroleum ether – diethyl ether) of the crude product, followed by distillation (205–215°C/0.05 Torr) of the acquired liquid, provided 62 mg (83%) of the keto ester **60**, a colorless oil that displayed ir (neat): 1740, 1729, 838, 779 cm^{-1}; ^{1}H nmr (400 MHz) δ: 0.02, 0.04 (s, s, 3H), 0.89 (s, 9H), 1.10 (dq, 1H, J = 3.8, 12.5 Hz), 1.23 (dq, 1H, J = 3, 12.8 Hz), 1.33 (tq, 1H, J = 3.5, 13.5 Hz), 1.42–1.77 (m, 4H), 1.99–2.08 (m, 2H), 2.19–2.31 (m, 3H), 2.50–2.67 (m, 3H), 2.77 (br d, 1H, J = 12 Hz), 3.44 (dd, 1H, J = 6, 10 Hz), 3.53 (dd, 1H, J = 3.4, 10 Hz), 3.70 (s, 3H). Exact Mass calcd. for $C_{22}H_{36}O_4Si$: 392.2384; found: 392.2378.

*Preparation of the tricyclic esters **62** and **63***

A stirred solution of the diene **6** (50 mg, 0.243 mmol) and 1,2-bis(phenylsulfonyl)ethylene (90 mg, 0.292 mmol) in dry benzene (10 mL) was refluxed for 24 h and then was concentrated. Flash chromatography (18 g silica gel, 7:2:5 dichloromethane – diethyl ether – petroleum ether) of the residual oil provided 102 mg (82%) of the ester **61** as a white amorphous solid. This material (Exact Mass calcd. for $C_{27}H_{30}O_6S_2$: 514.1485; found: 514.1485), which appeared to be a single isomer, was not characterized further.

A mixture of the ester **61** (179 mg, 0.348 mmol), 2% sodium amalgam (2.7 g, 6.8 equiv. of sodium), and sodium dihydrogen phosphate monohydrate (615 mg) in dry methanol (5 mL) was stirred at room temperature for 24 h. The mixture was poured into water (10 mL) and the mixture was extracted with diethyl ether (3 × 10 mL). The combined extracts were washed with brine, dried ($MgSO_4$), and concentrated. Flash chromatography (30 g silica gel, 2:1 petroleum ether – diethyl ether) of the remaining oil, followed by distillation (120–124°C/0.6 Torr) of the acquired oil, yielded 69 mg (85%) of the diene ester **62**, a white waxy solid (mp 51–52°C) that displayed ir ($CHCl_3$): 1715 cm^{-1}; ^{1}H nmr (400 MHz) δ: 1.35–1.80, 1.95–2.14 (series of m, 8H, 4H), 2.52–2.63 (m, 2H), 2.70 (m, 1H), 3.67 (s, 3H), 5.60 (br d, 1H, J = 9 Hz), 5.76 (m, 1H). Exact Mass calcd. for $C_{15}H_{20}O_2$: 232.1463; found: 232.1463.

To a stirred solution of the diene **62** (20 mg, 0.086 mmol) in dry benzene was added 2,3-dichloro-5,6-dicyano-1,4-benzoquinone (20 mg, 1.02 equiv.). The mixture was refluxed for 30 min, was cooled to room temperature, and was filtered. Concentration of the filtrate and flash chromatography (10 g silica gel, 100:1 diethyl ether – petroleum ether) of the crude solid gave 17 mg (87%) of the ester **63** as an off-white solid. Recrystallization (petroleum ether) provided a white solid (mp 60–61°C) that exhibited ir ($CHCl_3$): 3009, 1719 cm^{-1}; ^{1}H nmr (400 MHz) δ: 1.55 (dt, 2H, J = 5, 13 Hz), 1.68–1.90 (m, 4H), 2.35 (dt, 2H, J = 13, 4 Hz), 2.78–2.85 (m, 4H), 3.65 (s, 3H), 6.95 (br d, 2H, J = 7.5 Hz), 7.11 (t, 1H, J = 7.5 Hz); ^{13}C nmr (75.3 MHz) δ: 19.5, 28.5, 34.7, 47.5, 52.1, 126.1, 126.5, 135.5, 136.5, 177.2. Exact Mass calcd. for $C_{15}H_{18}O_2$: 230.1307; found: 230.1311.

*X-ray crystallographic analyses of **9**, **11**, **15**, **27**, **30**, **31**, and **37***

Crystallographic data for the seven compounds analyzed appear in Table 6. The final unit-cell parameters were obtained by least squares on sin θ/λ values for 25 reflections with 2θ = 93.0–98.7, 60.8–84.6, 59.6–83.6, 50.4–79.2, 71.8–88.0, 40.8–81.3, and 70.0–87.8° for **9**, **11**, **15**, **27**, **30**, **31**, and **37**, respectively. The intensities of three standard reflections, measured every hour of X-ray exposure time throughout the data collections, showed only small random fluctuations in each case except for compound **27**, which exhibited a linear decay of 2.7%. The data were processed[5] and corrected for Lorentz and polarization effects, linear decay for **27**, and absorption for **11**, **15**, and **30** (numerical integration, based on 104–126 sampling points).

The structure analyses of **9**, **30**, and **37** were initiated in the centrosymmetric space group $P\bar{1}$ on the basis of the E-statistics, these choices being verified by the successful completion of the structure analyses. The structures were all solved by direct methods, the coordinates of the non-hydrogen atoms being determined from E-maps and subsequent difference Fourier syntheses. The asymmetric unit of **15** contains two crystallographically independent molecules.

The structures of **9**, **15**, and **30** were found to be disordered. In **9** there are two disordered regions: a 1:1 conformational disorder of the C(8–13) ring (modeled by a split atom refinement of C(9) and C(10)) and a disordering of C(5) that results in a configurational inversion at the asymmetric carbon atom C(4) (modeled by

[5]Computer programs used include locally written programs for data processing and locally modified versions of the following: MULTAN80, multisolution program by P. Main, S.J. Fiske, S.E. Hull, L. Lessinger, G. Germain, J.P. Declercq, and M.M. Woolfson; ORFLS, full-matrix least-squares, and ORFFE, function and errors, by W.R. Busing, K.O. Martin, and H.A. Levy; FORDAP, Patterson and Fourier syntheses, by A. Zalkin; ORTEP II, illustrations, by C.K. Johnson.

Can. J. Chem. Downloaded from www.nrcresearchpress.com by 213.200.69.106 on 09/08/12
For personal use only.

TABLE 6. Crystallographic data[a]

Compound	**9, 10** (84:16)	**11**	**15**	**27**	**30**	**31**	**37**
Formula	$C_{19}H_{24}O_6$	$C_{19}H_{18}N_4O_2$	$C_{26}H_{34}N_4O_3Si$	$C_{22}H_{37}NO_5Si$	$C_{15}H_{24}O_2$	$C_{15}H_{24}O_2$	$C_{23}H_{26}N_2O_8$
fw	348.40	334.38	478.67	423.62	236.35	236.35	458.47
Crystal system	Triclinic	Orthorhombic	Monoclinic	Monoclinic	Triclinic	Monoclinic	Triclinic
Space group	$P\bar{1}$	*Pbca*	$P2_1/c$	$P2_1/n$	$P\bar{1}$	$P2_1/c$	$P\bar{1}$
a, Å	9.2190(4)	12.6415(5)	13.3676(6)	13.9274(10)	8.6943(3)	8.5889(7)	11.0580(5)
b, Å	11.4758(6)	17.5941(8)	18.036(2)	12.8578(8)	8.7576(3)	18.437(2)	15.5119(7)
c, Å	8.5341(3)	15.6240(7)	23.3524(6)	14.8272(11)	9.9939(8)	8.9424(7)	6.9053(5)
α, deg	101.160(4)	90	90	90	110.736(4)	90	78.415(4)
β, deg	89.087(4)	90	105.144(3)	109.394(6)	97.337(5)	109.893(7)	95.034(7)
γ, deg	95.720(5)	90	90	90	109.162(3)	90	103.295(5)
V, Å^3	881.37(7)	3475.0(3)	5434.6(6)	2504.5(3)	646.09(6)	1331.5(2)	1128.2(1)
Z	2	8	8	4	2	4	2
ρ_{calc}, g cm^{-3}	1.313	1.278	1.170	1.123	1.215	1.179	1.350
F(000)	372	1408	2048	920	260	520	484
μ(Cu-K$_\alpha$), cm^{-1}	7.65	6.59	10.09	10.47	5.77	5.60	8.21
Crystal size, mm	0.35 × 0.40 × 0.45	0.14 × 0.20 × 0.41	0.25 × 0.40 × 0.40	0.36 × 0.40 × 0.44	0.25 × 0.25 × 0.40	0.07 × 0.27 × 0.42	0.25 × 0.28 × 0.40
Transmission factors	—	0.71–0.89	0.65–0.80	—	0.77–0.89	—	—
Scan type	ω–2θ	ω–2θ	ω–2θ	ω–2θ	ω–2θ	ω–2θ	ω–2θ
Scan range, ω°	1.00 + 0.14 tan θ	0.60 + 0.14 tan θ	0.65 + 0.14 tan θ	0.80 + 0.14 tan θ	0.75 + 0.14 tan θ	1.00 + 0.14 tan θ	0.80 + 0.14 tan θ
Scan rate, deg min^{-1}	1.8–10.0	1.3–10.0	1.6–10.0	1.4–10.0	1.0–10.0	1.7–10.0	1.3–10.0
Data collected	$\pm h, \pm k, +l$	$-h, -k, +l$	$+h, +k, \pm l$	$+h, +k, \pm l$	$\pm h, -k, \pm l$	$\pm h, +k, +l$	$\pm h, +k, \pm l$
$2\theta_{max}$, deg	150	150	130	150	150	150	150
Crystal decay, %	Negligible	Negligible	Negligible	2.7	Negligible	Negligible	Negligible
Unique reflections	3643	3566	9195	5152	2654	2732	4627
Number with $I \geq 3\sigma(I)$	2877	2321	5375	2066	2240	1137	2443
Variables	328	299	622	263	259	163	299
R	0.055	0.042	0.043	0.092	0.037	0.065	0.051
R_w	0.070	0.053	0.050	0.103	0.050	0.069	0.059
gof	1.64	2.23	0.89	3.73	1.12	2.31	1.14
Max Δ/σ (final cycle)	0.34	0.21	0.38	0.11	0.18	0.15	0.03
Residual density e Å^{-3}	−0.25 to 0.34	−0.23 to 0.17	−0.22 to 0.19	−0.39 to 0.50	−0.14 to 0.25	−0.27 to 0.30	−0.18 to 0.26

[a]Temperature 294 K, Enraf–Nonius CAD4-F diffractometer, Cu-K$_\alpha$ radiation ($\lambda(K_{\alpha 1}) = 1.54056$, $\lambda(K_{\alpha 2}) = 1.54439$ Å) radiation, graphite monochromator, takeoff angle 2.7°, aperture (2.0 + tan θ) × 4.0 mm at a distance of 173 mm from the crystal, scan range extended by 25% on both sides for background measurement, $\sigma^2(I) = C + 2B + [0.04(C - B)]^2$ (S = scan rate, C = scan count, B = normalized background count), function minimized $\Sigma w(|F_o| - |F_c|)^2$ where $w = 4F_o^2/\sigma^2(F_o^2)$, $R = \Sigma||F_o| - |F_c||/\Sigma|F_o|$, $R_w = (\Sigma w(|F_o| - |F_c|)^2/\Sigma w|F_o|^2)^{1/2}$, and gof = $[\Sigma(|F_o| - |F_c|)^2/(m - n)]^{1/2}$. Values given for R, R_w, and gof are based on those reflections with $I \geq 3\sigma(I)$.

TABLE 7. Final positional (fractional × 10^4) and isotropic thermal parameters ($U \times 10^3$)[a]

Atom	x	y	z	U_{eq}/U_{iso}	Occupancy
			9		
O(1)	8116(2)	3196(2)	5462(3)	101	
O(2)	6640(2)	2256(2)	6959(2)	79	
O(3)	7857(2)	3466(1)	1866(2)	74	
O(4)	7296(1)	4975(1)	3763(2)	62	
O(5)	1943(2)	1636(2)	−1545(2)	90	
O(6)	3270(2)	665(1)	−192(2)	61	
C(1)	4272(2)	1958(2)	5035(2)	54	
C(2)	5633(2)	2669(2)	4655(2)	45	
C(3)	5726(2)	3201(2)	3391(2)	43	
C(4)	4500(2)	3104(2)	2218(2)	48	
C(5)	4064(3)	4325(2)	2062(3)	57	0.84
C(5′)	4568(14)	3749(12)	985(15)	55(3)	0.16
C(6)	2926(3)	4198(2)	750(4)	72	
C(7)	1608(2)	3424(2)	1132(3)	64	
C(8)	1960(2)	2179(2)	1330(2)	48	
C(9)	646(9)	1231(6)	1682(10)	58	0.50
C(10)	371(5)	1341(5)	3419(6)	72	0.50
C(9′)	516(9)	1728(6)	1995(10)	59	0.50
C(10′)	769(5)	604(4)	2664(5)	56	0.50
C(11)	1740(3)	1028(2)	4182(3)	64	
C(12)	3073(2)	1805(2)	3835(2)	44	
C(13)	3183(2)	2313(2)	2552(2)	42	
C(14)	6935(2)	2747(2)	5695(2)	55	
C(15)	7847(5)	2286(4)	8037(4)	95	
C(16)	7099(2)	3870(2)	2942(2)	47	
C(17)	8628(3)	5669(3)	3454(4)	77	
C(18)	2382(2)	1494(2)	−293(2)	51	
C(19)	3649(4)	−96(3)	−1659(3)	76	
			11		
O(1)	2866(2)	−621(1)	7546(1)	93	
O(2)	1467(1)	−203(1)	6825(1)	57	
N(14)	97(2)	2640(1)	3862(2)	85	
N(15)	−613(2)	678(1)	5455(1)	63	
N(16)	2746(2)	2991(1)	5280(2)	84	
N(17)	−367(2)	2885(2)	6374(2)	99	
C(1)	2444(2)	832(1)	5220(1)	40	
C(2)	1773(2)	1234(1)	4570(1)	45	
C(3)	820(2)	1655(1)	4967(1)	43	
C(4)	1218(2)	2094(1)	5781(1)	47	
C(5)	1632(2)	1527(1)	6461(1)	46	
C(6)	2095(3)	1965(2)	7223(2)	70	
C(7)	2586(3)	1428(2)	7870(2)	77	
C(8)	3467(2)	990(2)	7445(2)	70	
C(9)	3081(2)	502(1)	6689(1)	51	
C(10)	4038(2)	169(2)	6222(2)	65	
C(11)	3706(2)	−263(1)	5439(2)	63	
C(12)	3175(2)	266(1)	4804(2)	54	
C(13)	2394(1)	960(1)	6064(1)	40	
C(14)	385(2)	2202(1)	4342(2)	55	
C(15)	−4(2)	1108(1)	5236(1)	47	
C(16)	2079(2)	2609(1)	5504(2)	57	
C(17)	334(2)	2551(1)	6130(2)	62	
C(18)	2467(2)	−168(1)	7071(1)	55	
C(19)	876(3)	−854(2)	7122(3)	75	
			15		
Si	10027.9(8)	1679.4(6)	3942.5(4)	55	
O(1)	9554(2)	1594(1)	3221(1)	59	
O(2)	11037(2)	517(2)	1723(1)	87	

TABLE 7 (*continued*)

Atom	x	y	z	U_{eq}/U_{iso}	Occupancy
O(3)	10646(2)	−564(2)	1264(1)	74	
N(1)	11156(3)	2293(2)	2517(2)	85	
N(2)	8618(3)	3742(2)	2298(2)	101	
N(3)	7081(3)	2704(2)	855(2)	97	
N(4)	10171(3)	3361(2)	1027(2)	109	
C(1)	8653(2)	1058(2)	1998(1)	46	
C(2)	8467(2)	1815(2)	2234(1)	44	
C(3)	9163(2)	2410(2)	2055(1)	47	
C(4)	9009(3)	2372(2)	1363(1)	51	
C(5)	9331(3)	1605(2)	1178(1)	56	
C(6)	8953(4)	1526(3)	503(2)	98	
C(7)	9262(5)	775(4)	305(2)	113	
C(8)	8830(3)	163(3)	616(2)	96	
C(9)	9231(3)	208(2)	1294(2)	59	
C(10)	8717(4)	−407(2)	1567(3)	100	
C(11)	8843(4)	−317(3)	2198(3)	79	0.835
C(12)	8364(3)	408(2)	2331(2)	64	
C(13)	9020(2)	972(2)	1521(1)	48	
C(14)	8556(3)	1847(2)	2899(1)	54	
C(15)	10285(3)	2316(2)	2338(2)	57	
C(16)	8872(3)	3165(2)	2208(2)	64	
C(17)	7914(3)	2548(2)	1074(2)	64	
C(18)	9658(3)	2944(3)	1175(2)	71	
C(19)	10398(3)	88(2)	1456(2)	58	
C(20)	11735(3)	−737(3)	1393(2)	87	
C(21)	11064(3)	961(2)	4155(2)	66	
C(22)	8966(3)	1524(3)	4310(2)	97	
C(23)	10555(4)	2630(2)	4104(2)	103	
C(24)	11686(4)	1070(4)	4795(2)	141	
C(25)	11794(4)	1008(3)	3760(3)	119	
C(26)	10602(5)	185(3)	4097(3)	150	
Si′	3834.2(8)	1767.3(6)	1081.4(4)	54	
O(1′)	3979(2)	1725(1)	1806(1)	62	
O(2′)	6713(2)	583(1)	3278(1)	74	
O(3′)	6688(2)	−515(1)	3708(1)	70	
N(1′)	6199(3)	2430(2)	2559(1)	81	
N(2′)	3831(3)	3861(2)	2773(2)	98	
N(3′)	3460(3)	2698(2)	4145(2)	90	
N(4′)	6465(3)	3412(2)	4110(2)	91	
C(1′)	4089(2)	1164(2)	3000(1)	46	
C(2′)	3720(2)	1934(2)	2773(1)	48	
C(3′)	4585(3)	2522(2)	2992(1)	49	
C(4′)	5015(3)	2445(2)	3681(1)	50	
C(5′)	5501(2)	1669(2)	3843(1)	49	
C(6′)	5713(3)	1541(2)	4514(2)	74	
C(7′)	6192(3)	790(3)	4697(2)	78	
C(8′)	5469(3)	198(2)	4363(2)	69	
C(9′)	5270(3)	275(2)	3684(2)	50	
C(10′)	4504(3)	−327(2)	3391(2)	82	
C(11′)	4073(4)	−217(3)	2774(3)	70	0.77
C(12′)	3463(3)	530(2)	2657(2)	68	
C(13′)	4877(2)	1051(2)	3476(1)	44	
C(14′)	3257(3)	1985(2)	2105(2)	59	
C(15′)	5476(3)	2441(2)	2726(2)	56	
C(16′)	4164(3)	3275(2)	2854(2)	66	
C(17′)	4134(3)	2581(2)	3948(2)	61	
C(18′)	5815(3)	3010(2)	3922(2)	62	
C(19′)	6299(3)	152(2)	3527(2)	53	
C(20′)	7674(3)	−696(2)	3597(2)	78	
C(21′)	4693(3)	1023(2)	924(2)	62	
C(22′)	2456(3)	1621(3)	697(2)	100	
C(23′)	4231(4)	2688(2)	890(2)	89	
C(24′)	4828(4)	1105(3)	293(2)	112	

Can. J. Chem. Downloaded from www.nrcresearchpress.com by 213.200.69.106 on 09/08/12
For personal use only.

Can. J. Chem. Downloaded from www.nrcresearchpress.com by 213.200.69.106 on 09/08/12
For personal use only.

TABLE 7 (*continued*)

Atom	*x*	*y*	*z*	U_{eq}/U_{iso}	Occupancy
C(25′)	5764(4)	1075(3)	1360(2)	109	
C(26′)	4268(5)	255(3)	991(3)	117	
C(11*)	8008(22)	−272(15)	1891(13)	77(8)	0.165
C(11″)	3485(14)	−124(10)	3096(8)	68(5)	0.23
		27			
Si	3835(2)	3429(3)	3363(2)	125	
O(1)	3055(3)	3833(4)	3887(3)	88	
O(2)	2804(5)	4833(6)	7176(4)	144	
O(3)	1276(5)	4787(5)	7249(4)	124	
O(4)	−1324(4)	2980(4)	4403(5)	115	
O(5)	−1239(3)	1278(4)	4489(4)	94	
N	1903(6)	4753(5)	6824(4)	95	
C(1)	976(4)	3766(5)	3906(4)	59	
C(2)	1659(4)	4699(4)	4178(5)	63	
C(3)	2199(4)	4762(4)	5254(5)	63	
C(4)	1448(4)	4565(5)	5745(4)	60	
C(5)	1034(4)	3459(5)	5597(4)	60	
C(6)	1713(6)	2611(7)	6212(5)	95	
C(7)	1155(7)	1541(7)	5942(8)	112	
C(8)	842(6)	1324(6)	4900(8)	106	
C(9)	179(5)	2154(4)	4290(5)	72	
C(10)	−20(6)	1882(7)	3205(8)	108	
C(11)	−312(7)	2802(9)	2578(6)	114	
C(12)	553(5)	3540(7)	2844(5)	90	
C(13)	732(4)	3172(4)	4546(4)	56	
C(14)	2434(6)	4726(6)	3669(5)	89	
C(15)	−842(5)	2211(6)	4405(5)	77	
C(16)	−2254(6)	1245(6)	4482(6)	102	
C(17)	4397(8)	2238(9)	3982(8)	134	
C(18)	3098(10)	3106(17)	2083(7)	289	
C(19)	4816(10)	4443(12)	3419(13)	248	
C(20)	5017(9)	1682(13)	3435(10)	239	
C(21)	5112(11)	2504(13)	4967(10)	203	
C(22)	3580(14)	1521(10)	4085(16)	270	
		30			
O(1)	9320(2)	10283(2)	3798(2)	57	
O(2)	572(2)	3767(2)	4147(2)	49	
C(1)	5015(2)	3866(2)	2066(2)	33	
C(2)	6821(2)	4586(2)	2003(2)	39	
C(3)	7429(2)	6424(2)	2016(2)	41	
C(4)	6743(2)	7625(2)	3049(2)	32	
C(5)	4799(2)	6767(2)	2450(2)	31	
C(6)	3916(2)	7857(2)	3332(2)	42	
C(7)	1973(2)	6981(2)	2693(2)	48	
C(8)	1276(2)	4962(2)	1775(2)	37	
C(9)	2273(2)	4079(2)	2381(2)	30	
C(10)	1477(2)	2063(2)	1424(2)	39	
C(11)	2526(2)	1135(2)	1859(2)	50	
C(12)	4332(2)	1925(2)	1772(2)	51	
C(13)	4100(2)	4857(2)	2319(1)	28	
C(14)	7523(2)	9521(2)	3187(2)	44	
C(15)	2252(2)	4460(2)	4008(2)	37	
		31			
O(1)	−2952(5)	2157(3)	1766(5)	67	
O(2)	5823(5)	2012(2)	8585(4)	63	
C(1)	382(6)	1061(3)	7125(6)	43	
C(2)	−1442(6)	1022(3)	6152(7)	55	
C(3)	−1754(6)	1075(3)	4383(6)	53	
C(4)	−810(5)	1701(3)	4064(5)	38	
C(5)	1060(5)	1597(3)	4857(5)	37	

TABLE 7 (*concluded*)

Atom	*x*	*y*	*z*	U_{eq}/U_{iso}	Occupancy
C(6)	1881(6)	1148(3)	3906(6)	54	
C(7)	3760(6)	1099(3)	4730(7)	57	
C(8)	4192(6)	819(3)	6433(6)	52	
C(9)	3372(6)	1241(3)	7449(6)	43	
C(10)	3714(7)	817(4)	9011(7)	69	
C(11)	2562(9)	962(4)	9834(8)	92	
C(12)	785(7)	796(4)	8812(7)	68	
C(13)	1503(5)	1288(3)	6541(5)	34	
C(14)	−1295(6)	1882(3)	2298(6)	51	
C(15)	4080(6)	2002(3)	7806(6)	50	
		37			
O(1)	7285(2)	3909(1)	6871(3)	71	
O(2)	8874(2)	3266(2)	8065(4)	87	
O(3)	3168(3)	4622(2)	8767(7)	149	
O(4)	4028(3)	4096(2)	11487(7)	131	
O(5)	2126(2)	−284(1)	9674(4)	91	
O(6)	3849(2)	704(2)	10267(4)	89	
O(7)	12550(3)	7555(2)	7279(6)	132	
O(8)	10938(4)	8111(2)	6437(6)	142	
N(1)	3727(3)	4108(2)	9759(7)	93	
N(2)	11445(4)	7483(3)	6902(5)	96	
C(1)	4304(3)	2258(2)	6222(5)	71	
C(2)	5222(3)	3164(2)	6057(5)	72	
C(3)	4716(3)	3853(2)	6858(6)	79	
C(4)	4072(3)	3405(2)	8774(5)	67	
C(5)	2917(3)	2708(2)	8383(6)	73	
C(6)	2210(3)	2227(2)	10225(6)	91	
C(7)	1018(4)	1576(3)	9754(8)	113	
C(8)	1100(3)	1205(3)	7892(7)	102	
C(9)	2424(3)	1123(2)	7546(5)	70	
C(10)	2458(5)	706(3)	5722(6)	106	
C(11)	3773(5)	683(3)	5361(6)	109	
C(12)	4616(4)	1625(3)	5034(6)	95	
C(13)	3294(3)	2054(2)	7305(5)	67	
C(14)	6444(3)	3027(2)	7080(5)	69	
C(15)	2908(3)	516(2)	9321(5)	67	
C(16)	2543(4)	−952(2)	11200(7)	116	
C(17)	8468(3)	3927(2)	7468(5)	63	
C(18)	9219(3)	4865(2)	7278(4)	56	
C(19)	8678(3)	5610(2)	6742(5)	69	
C(20)	9403(3)	6463(2)	6623(5)	75	
C(21)	10656(3)	6562(2)	7038(5)	68	
C(22)	11220(3)	5843(3)	7566(5)	69	
C(23)	10475(3)	4985(2)	7683(5)	63	

[a] U_{eq} = 1/3 trace diagonalized *U*.

a split atom refinement of C(5)). As a result of the latter disordering, the crystals actually contain both of the diastereomers **9** and **10** in a ratio of 84:16. In each of the two independent molecules of **15**, conformational disordering of one of the cyclohexene rings was modeled by split atom refinement of C(11). In **30** the hydrogen atoms of both of the hydroxyl groups were 1:1 disordered and were modeled by split-atom refinement. Site occupancy factors for the disordered structures were initially estimated from relative Fourier map peak heights and were subsequently adjusted[6] to result in approximately equal equivalent isotropic thermal parameters for the two component atoms at each disordered site. The disordering in both **9** and **15** probably extends beyond the mod-

[6] Attempts to refine even some of the population parameters led to nearly singular matrices due to high correlations with the thermal parameters.

eled regions, but attempts at more sophisticated and extensive treatment of the disorder were not attempted. As a result, some of the geometrical parameters involving the disordered regions show significant deviations from expected values, in particular when the minor components are involved. Compound **27** displays substantial thermal motion at room temperature, particularly for the peripheral substituents, and may be disordered. The poor quality of the data for **27** precludes any attempts at refining a disordered model.

The low-occupancy disordered carbon atoms C(5′) in **9**, C(11*) and C(11″) in **15** were refined with isotropic thermal parameters. All other non-hydrogen atoms were refined with anisotropic thermal parameters. The ordered hydrogen atoms for **9**, all hydrogen atoms for **11** and **30**, and the O-H hydrogen atoms for **31** were refined with isotropic thermal parameters. The remaining hydrogen atoms were fixed in idealized positions ($C(sp^2)$—H = 0.97, $C(sp^3)$—H = 0.98 Å, $U_H \propto U_{\text{bonded atom}}$) with the exception of the 16% occupancy disordered component of **9**.

Isotropic Type I extinction corrections were applied for **11**, **15**, **27**, **30**, **31**, and **37**, the final values of the extinction parameter g being $3.0(5) \times 10^4$, $3.9(2) \times 10^4$, $0.72(5) \times 10^4$, $0.25(3) \times 10^4$, $0.57(9) \times 10^4$, and $0.28(4) \times 10^4$, respectively. Neutral atom scattering factors and anomalous dispersion corrections for the non-hydrogen atoms were taken from the *International tables for X-ray crystallography* (13). Final atomic coordinates and equivalent isotropic thermal parameters are given in Table 7. Bond lengths, bond angles, general and intra-annular torsion angles, hydrogen atom parameters, anisotropic thermal parameters, and measured and calculated structure factor amplitudes for the seven structures are provided as supplementary material.[7]

[7]Supplementary material mentioned in the text may be purchased from: The Depository of Unpublished Data, Document Delivery, CISTI, National Research Council Canada, Ottawa, Canada K1A 0S2.

Tables of bond lengths and angles and hydrogen atom parameters have also been deposited with the Cambridge Crystallographic Data Centre, and can be obtained on request from The Director, Cambridge Crystallographic Data Centre, University Chemical Laboratory, 12 Union Road, Cambridge, CB2 1EZ, U.K.

Acknowledgement

We are very grateful to the Natural Sciences and Engineering Research Council of Canada for financial support and for a 1967 Centennial Science and Engineering Scholarship (to R.W.F.).

1. S.J. Wratten, D.J. Faulkner, K. Hirotsu, and J. Clardy. Tetrahedron Lett. 4345 (1978).
2. R. Kazlauskas, P.T. Murphy, R.J. Wells, and J.F. Blount. Tetrahedron Lett. **21**, 315 (1980).
3. T.F. Molinski, D.J. Faulkner, G.D. Van Duyne, and J. Clardy. J. Org. Chem. **52**, 3334 (1987).
4. E. Piers, R.W. Friesen, and B.A. Keay. Tetrahedron, **47**, 4555 (1991).
5. E. Piers, R.W. Friesen, and S.J. Rettig. Can. J. Chem. **70**, 1385 (1992).
6. E. Piers and R.W. Friesen. Can. J. Chem. **65**, 1681 (1987).
7. W.C. Still, M. Kahn, and A. Mitra. J. Org. Chem. **43**, 2923 (1978).
8. H. Stockmann. J. Org. Chem. **26**, 2025 (1961).
9. S. Ranganathan, D. Ranganathan, and A.K. Mehrotra. J. Am. Chem. Soc. **96**, 5261 (1974).
10. J. Sauer and R. Sustmann. Angew. Chem. Int. Ed. Engl. **19**, 779 (1980).
11. J.E. McMurry and J. Melton. J. Org. Chem. **38**, 4367 (1973); J.E. McMurry. Acc. Chem. Res. **7**, 281 (1974).
12. M.J.S Dewar, S. Olivella, and J.J.P. Stewart. J. Am. Chem. Soc. **108**, 5771 (1986).
13. International tables for X-ray crystallography. Vol. IV. Kynoch Press, Birmingham, U.K. (present distributor Kluwer Academic Publishers, Dordrecht, The Netherlands). 1974. pp. 99–102 and 149.

Can. J. Chem. Downloaded from www.nrcresearchpress.com by 213.200.69.106 on 09/08/12
For personal use only.

Total synthesis of amphilectane-type diterpenoids: (±)-8,15-diisocyano-11(20)-amphilectene

EDWARD PIERS,[1] MONTSE LLINAS-BRUNET, AND RENATA M. OBALLA
Department of Chemistry, University of British Columbia, 2036 Main Mall, University Campus, Vancouver, BC V6T 1Z1, Canada

Received April 6, 1993

EDWARD PIERS, MONTSE LLINAS-BRUNET, and RENATA M. OBALLA. Can. J. Chem. **71**, 1484 (1993).

A total synthesis of the structurally novel, antimicrobial diterpenoid (±)-8,15-diisocyano-11(20)-amphilectene (**2**) is described. Alkylation of 2-methoxycarbonyl-3-methylcyclohexanone (**13**) with (*E*)-1-(*tert*-butyldimethylsiloxy)-6-iodo-3-(trimethylstannyl)-2-hexene (**14**) provided, stereoselectively, the functionalized keto ester **15**, which was converted efficiently into the diene **17**. Diels–Alder reaction of **17** with acrolein, followed by base-catalyzed equilibration of the resultant product mixture, gave the aldehydes **19** (58%) and **20** (29%). Allylic oxidation of the alkene **24** (derived from **19**) afforded the enone **25**. Reduction (Na, NH_3, *t*-BuOH) of **25** gave **28**, which was converted, via a sequence of eight synthetic steps, into the diacid **45**. Efficient transformation of the carboxyl functions of **45** into isonitrile groups completed the synthesis of (±)-**2**.

EDWARD PIERS, MONTSE LLINAS-BRUNET et RENATA M. OBALLA. Can. J. Chem. **71**, 1484 (1993).

On décrit une synthèse totale du diterpéne antimicrobien, (±)-8,15-diisocyanoamphilect-11(20)-ène (**2**) qui est structuralement nouveau. L'alkylation de la 2-méthoxycarbonyl-3-méthylcyclohexanone (**13**) avec le (*E*)-1-(*tert*-butyldiméthylsiloxy)-6-iodo-3-(triméthylstannyl)hex-2-ène (**14**) permet d'accéder stéréosélectivement au cétoester fonctionnalisé **15**, que l'on transforme efficacement en un diène **17**. La réaction de Diels–Alder du composé **17** avec l'acroléine, suivie de l'équilibration catalysée par une base du mélange de produits résultant, donne les aldéhydes **19** (58%) et **20** (29%). L'oxydation allylique de l'alcène **24** (dérivé du composé **19**) fournit l'énone **25**. La réduction (par Na, NH_3, *t*-BuOH) du composé **25** conduit au composé **28** qui, par une synthèse à huit étapes, donne le diacide **45**. La transformation efficace des fonctions carboxyles du composé **45** en groupes isonitriles complète la synthèse du composé (±)-**2**.

[Traduit par la rédaction]

Can. J. Chem. Downloaded from www.nrcresearchpress.com by 213.200.69.106 on 09/08/12
For personal use only.

Introduction

The small family of amphilectane-type diterpenoids share the structurally interesting tricyclic carbon skeleton **1** (1–3). One member of this group of marine natural products, (−)-8,15-diisocyano-11(20)-amphilectene, was isolated from *Hymeniacidon amphilecta*, a sponge of the Order Halichondrida collected at Glover Reef, Belize (1). This substance, which was shown by X-ray diffraction analysis to possess the constitution and relative configuration shown in formula **2** (1), exhibits antibiotic activity against *Staphyloccocus aureus, Bacillus subtilis*, and *Candida albicans*.

Recently, we have reported, inter alia, the efficient preparation of the dienes **3**–**5** (4, 5) and have studied in some detail the Diels–Alder reactions of these substrates with a variety of dienophiles (6). For the present work, the cycloaddition reaction of the diene **4** with methyl acrylate (eq. [1]) is particularly pertinent. This process produced, in high yield (87%), a mixture of products **6**, **7**, and **10** (~3:1:2, respectively). With regards to the possibility of using this chemistry to effect a total synthesis of **2**, the completely regioselective nature of the transformation was gratifying. Thus, substances structurally related to **6** and **7** (e.g., **8** and **9**) should serve as suitable intermediates for the synthesis of **2**. In this regard, it has been shown (6) that, upon treatment with sodium methoxide in methanol, compound **6** epimerizes to give primarily the "desired" isomer **7**. By analogy, equilibration of **8** and **9** should produce predominately **9**. Similarly, although the relative configuration at C* in **9** is "incorrect" for the synthesis of **2**, it should be possible to make the necessary stereochemical adjustment at some (later) stage of the synthesis.

Unfortunately, the face-selectivity of the Diels–Alder reaction of **4** with methyl acrylate is mediocre (**6** + **7**:**10** ≈ 2:1). Furthermore, it would appear to be rather difficult to make efficient use of an intermediate structurally related to **10** (e.g., **11**) for the synthesis of **2**. Nevertheless, the overall efficiency of the reactions involved (synthesis of dienes such as **4** (5), Diels–Alder reactions of **4** (6)) encouraged us to attempt a total synthesis of (±)-**2** via a route that makes use of this chemistry. We report herein the details of this study (7).

Results and discussion

(a) Preparation of the tricyclic enone 25 (Scheme 1)

The synthesis of (±)-**2** began with methyl 2-methyl-6-oxocyclohexanecarboxylate (**13**) (see Scheme 1). This substance had been prepared previously in our laboratory (8) by reaction of methyl 6-oxo-1-cyclohexenecarboxylate (**12**) (9) with lithium methyl(phenylthio)cuprate (10). However, we found subsequently that this conversion is generally more efficient and less capricious if lithium methyl(cyano)cuprate (11) is used in place of the (phenylthio)cuprate. Thus, treatment of **12** with Me(CN)CuLi in tetrahydrofuran (THF)–Et_2O at −78°C gave **13** in 86% yield.

Alkylation of **13** with (*E*)-1-(*tert*-butyldimethylsiloxy)-6-iodo-3-(trimethylstannyl)-2-hexene (**14**) (5) was attempted under a variety of conditions. Use of potassium or sodium hydride as base and THF or 1,2-dimethoxyethane as solvent produced good yields (70–75%) of alkylated material. However, the product invariably consisted of a mixture of the desired C-alkylation product **15** and the corresponding O-alkylation substance (~3–4:1, respectively). Eventually, it was found that alkylation of the potassium enolate of **13** with **14** in refluxing toluene gave the required keto ester **15**, accompanied by only traces of the O-alkylation product. The isolated yield of **15** was 66% (~70% based on recovered **14**).

[1]Author to whom correspondence may be addressed.

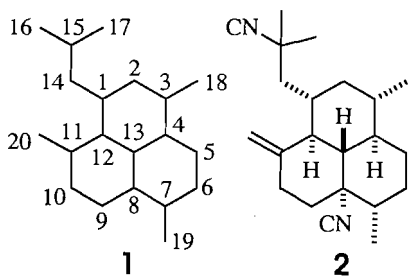

1 **2**

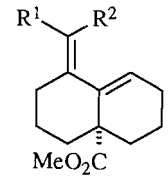

3 $R^1 = R^2 = H$
4 $R^1 = CH_2OSi(t\text{-}Bu)Me_2$, $R^2 = H$
5 $R^1 = H$, $R^2 = CH_2OSi(t\text{-}Bu)Me_2$

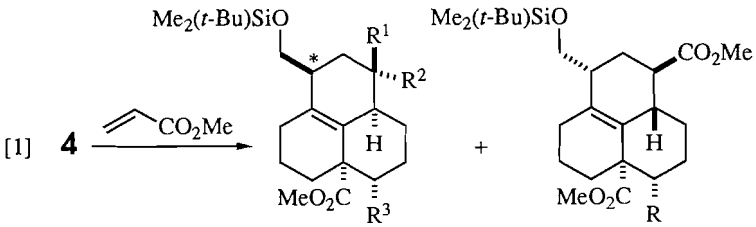

6 $R^1 = CO_2Me$, $R^2 = R^3 = H$
7 $R^1 = R^3 = H$, $R^2 = CO_2Me$
8 $R^1 = CO_2Me$, $R^2 = H$, $R^3 = Me$
9 $R^1 = H$, $R^2 = CO_2Me$, $R^3 = Me$

10 R = H
11 R = Me

For steric reasons, alkylation at C-1 of the enolate anion of **13** would be expected to occur from the face of the enolate opposite to the adjacent secondary methyl group. Thus, the relative configuration of the alkylation product **15** could be assigned with confidence.

Sequential treatment of the intermediate **15** with lithium diisopropylamide (LDA) and *N*-phenyltrifluoromethanesulfonimide (12) in THF gave a solution of the enol trifluoromethanesulfonate (triflate) **16**. Although the latter substance could be isolated and subsequently cyclized in a separate step, the overall conversion of **15** into the required diene **17** could be achieved more conveniently and more efficiently by use of a one-pot protocol (5). Thus, direct treatment of the reaction mixture containing **16** with ~0.06–0.07 equivalents of tetrakis(triphenylphosphine)palladium(0), followed by a period of reflux and an appropriate work-up procedure, provided the diene **17** in 86% overall yield from **15**.

The tricyclic carbon skeleton necessary for the synthesis of the amphilectene **2** was to be derived from the diene **17** via a Diels–Alder reaction. In this connection, the earlier work (6) on the cycloaddition reaction of the diene **4** with methyl acrylate served as an informative prelude to the present study. However, since the reaction of **4** with methyl acrylate is quite sluggish (6), we chose, in the current work, to use the more reactive dienophile acrolein.

Treatment of the diene **17** with an excess of acrolein in refluxing benzene gave a high yield of four Diels–Alder adducts. The composition (~62:8:28:2) of this mixture was determined by ^1H nmr spectroscopy, involving integration of the aldehydic proton signals at δ 9.79, 9.62, 9.65, and 9.87, respectively. On the basis of the earlier work (6) (vide supra), the four cycloaddition products were assigned structures **18–21**, respectively. Compounds **18** and **19** are the result of attack of the dienophile on the face of the diene opposite to the angular CO_2Me function (*endo* and *exo* transition states, respectively), while substances **20** and **21** are derived from approach of acrolein to the bottom face of **17** (*syn* to the CO_2Me group) via *exo* and *endo* transition states, respectively. Thus, as expected (6), the face-selectivity (~7:3 in favor of top-side attack of the dienophile) of the cycloaddition reaction is modest and, although an *endo* transition state is favored in the approach of acrolein to the top face of **17**, bottom-side attack takes place predominately via an *exo* orientation of the dienophile.

Flash chromatography of the mixture on silica gel (13) gave a mixture of **19–21** (~4:14:1) (33%) and pure **18** (53%). In compound **18**, the CHO group has a pseudoaxial orientation on the cyclohexene ring and is in a 1,3-diaxial-type relationship with the $CH_2OSi(t\text{-}Bu)Me_2$ function. Consequently, one would expect that equilibration of **18** and **19** would favor the latter epimer. Indeed, treatment of **18** with sodium methoxide in methanol produced **19** in 92% yield. In the ^1H nmr spectrum of **19**, the coupling constants associated with the proton α to the CHO function show clearly that this hydrogen is pseudoaxially oriented (see experimental).

Molecular models indicate that equilibration of the epimers **20** (pseudoequatorial CHO) and **21** (pseudoaxial CHO) should favor the former isomer. Evidence for this expectation was acquired from the observation that treatment of a mixture of **19–21** (4:14:1, see above) with sodium methoxide in methanol provided cleanly an oil that consisted only of substances **19** and **20**.

Of the four aldehydes **18–21**, intermediate **19** was required for the synthesis of (±)-**2**. To optimize the acquisition of **19** from the diene **17**, the crude product derived from the reaction of **17** with acrolein was immediately subjected to equilibration with sodium methoxide in methanol. As expected (vide supra), this protocol produced cleanly and efficiently a mixture that consisted only of the aldehydes **19** and **20**. Fortunately, separation of these substances by flash chromatography (13) was readily accomplished and, by this means, **19** and **20** were obtained in isolated yields of 58 and 29%, respectively.

Reductive conversion of the formyl function in **19** into a methyl group was accomplished efficiently by known meth-

Can. J. Chem. Downloaded from www.nrcresearchpress.com by 213.200.69.106 on 09/08/12
For personal use only.

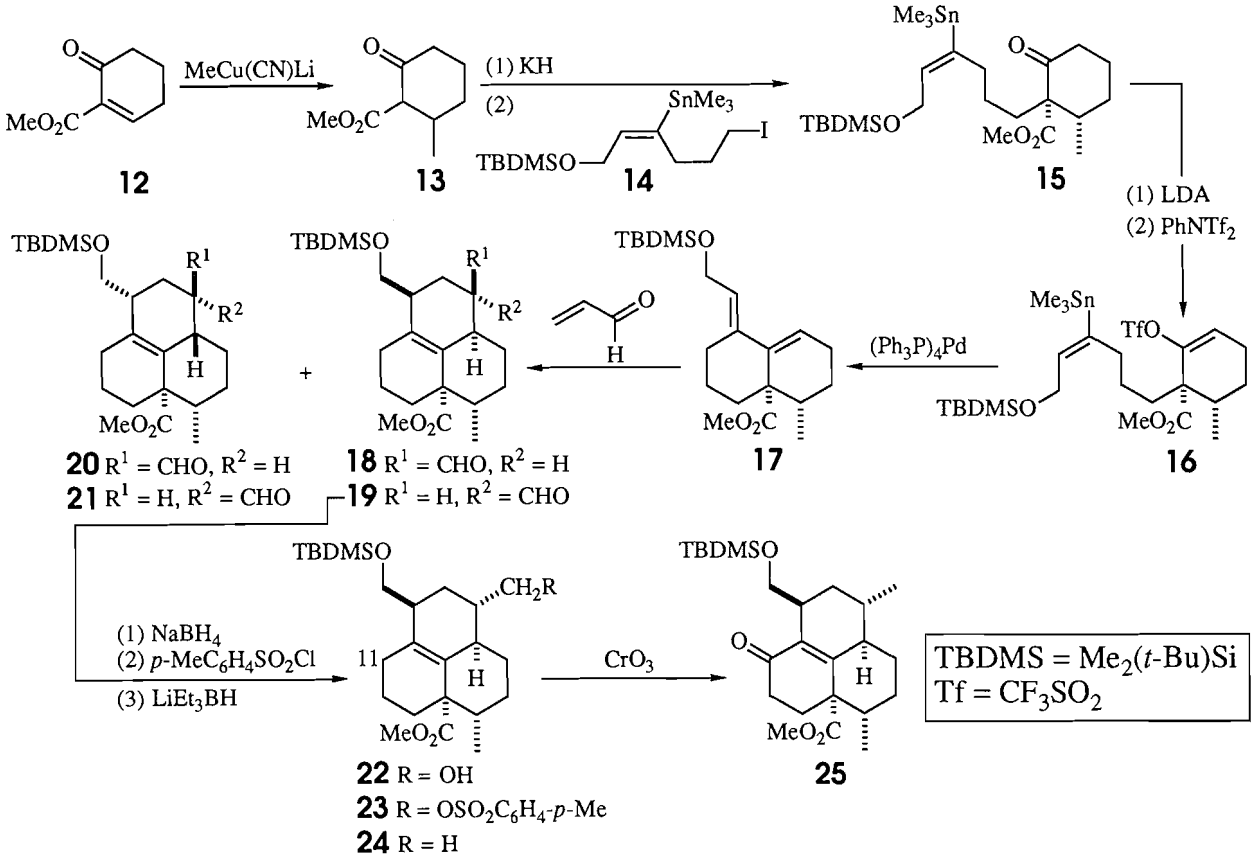

SCHEME 1

ods. Reduction of **19** with sodium borohydride in methanol, followed by treatment of the resultant alcohol **22** with *p*-toluenesulfonyl chloride in dichloromethane containing 4-*N*,*N*-dimethylaminopyridine (DMAP), provided the *p*-toluenesulfonate **23** (87% from **19**). Reaction of **23** with lithium triethylborohydride in THF (14) afforded the tricyclic olefinic ester **24** (90%).

At this stage of our envisaged synthesis of (±)-**2**, a carbonyl function had to be introduced at C-11 (amphilectane numbering) of the intermediate **24**. Not only would this function subsequently serve as a precursor for the required exocyclic methylene group, but, in theory, it would also provide a "handle" for effecting the necessary, stereochemically controlled, reduction of the olefinic double bond in **24**. In the event, treatment of **24** with chromium trioxide-3,5-dimethylpryazole complex (15) in dichloromethane afforded the α,β-unsaturated ketone **25** in 77% yield.

(b) Conversion of the enone 25 into the ketone 28

A successful, chemoselective reduction of the enone **25** with an alkali metal in ammonia (16) could, in theory, produce either or both of the intermediate enolate anions **27** and **29** (see Scheme 2). Protonation of these species during work-up would give the ketones **28** (the desired product) and (or) **30**, respectively. The question as to which pathway should be preferred may be addressed on the basis of proposals originally set forth by Robinson (17) (see also ref. 18).

Transfer of the two electrons to the enone system of **25** would afford (16) an anionic intermediate that can adopt two "reasonable" conformations, **26***a* and **26***b*. It has been proposed (17) that the allylic anion portion of intermediates such as these should be planar. Furthermore, protonation of **26***a* would be expected (17) to take place face-selectively to provide, via transition state **A**, the enolate **27**, in which the three rings are produced directly in chair (or half-chair) conformations. Similarly, selective protonation (17) of the allylic anion of **26***b* from the bottom face of the molecule would give **29**, which, again, has the three six-membered rings in stable conformations.

It has been convincingly argued (17) that the transition states for protonation of intermediates such as **26** have, in terms of molecular shape, a significant amount of reactant-like character. Consequently, the relative stability of the transition states **A** and **B** should be related to the relative stability of **26***a* and **26***b*. Of the latter two conformers, it appears that **26***b* is, due to the presence of more angle and torsional strain and, perhaps more importantly, due to a notable steric repulsion between the $ROCH_2$ and MO moieties, considerably less stable than **26***a*. On this basis, one would predict that transition state **A** would be preferred to transition state **B** and that, therefore, the predominant product derived from dissolving metal reduction of **25** should be substance **28**.

Top-face protonation of **26***a* via **A** is sterically hindered by the pseudoaxial CH_2OR function. However, protonation of **26***b*, via **B**, is impeded by the pseudoaxial methyl group and by the fact that the proton must be delivered in an orientation *gauche* to the angular CO_2Me group. Thus, in terms of ease of approach of a proton source, transition state **A** is, again, preferred.

In practice, finding a suitable procedure for successful alkali metal – ammonia reduction of **25** was not straightforward. Treatment of **25** with an excess (~15 equiv.) of lith-

Can. J. Chem. Downloaded from www.nrcresearchpress.com by 213.200.69.106 on 09/08/12
For personal use only.

Can. J. Chem. Downloaded from www.nrcresearchpress.com by 213.200.69.106 on 09/08/12
For personal use only.

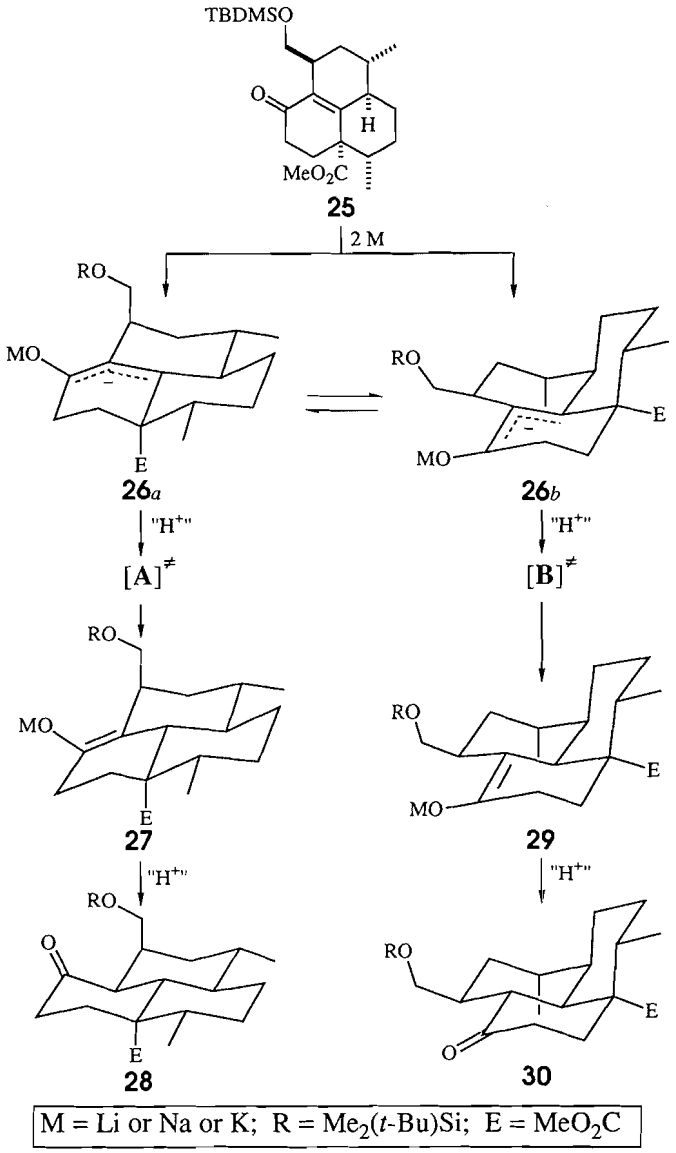

SCHEME 2

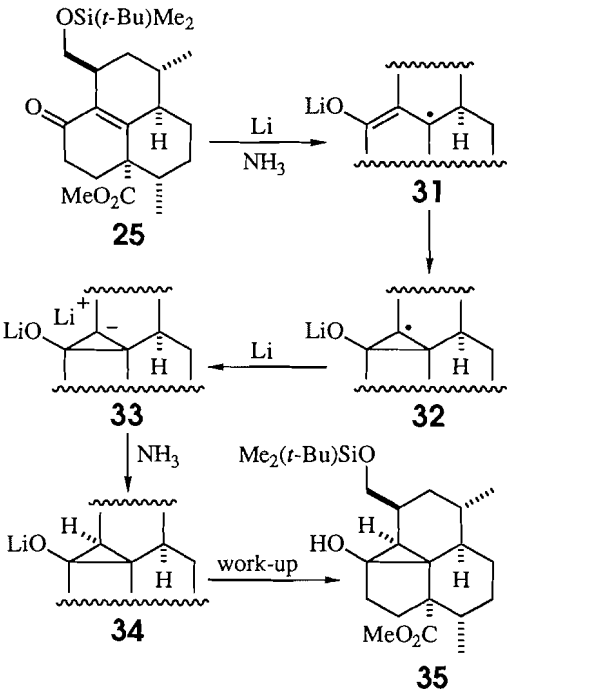

SCHEME 3

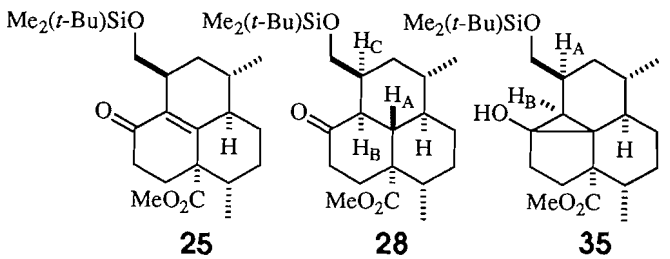

ium in ammonia – diethyl ether gave cleanly one product. The ir spectrum of this (quite unstable) material showed absorptions due to ester (1719 cm^{-1}) and hydroxyl (3240 cm^{-1}) groups. In the ^1H nmr spectrum, a singlet due to the OH function (D_2O exchange) appeared at δ 5.01. Although signals due to the $CH_2OSi(t\text{-Bu})Me_2$ protons were present, no resonance for a CHOH hydrogen was observed. On the other hand, a high-field one-proton signal (δ 1.02, d, J = 8 Hz) was present and, on this basis, it was tentatively concluded that the product possesses the cyclopropanol structure shown in **35**. Further evidence for this conclusion was derived from a ^1H nmr decoupling experiment. Thus, irradiation at δ 2.44 (m, unequivocally assigned to proton H_A in **35**) caused the doublet at δ 1.02 (H_B) to collapse to a singlet. The configuration of the stereogenic center bearing H_B is (provisionally) assigned on the basis of the size of J_{AB} (8 Hz). Molecular models indicate that a *trans* relationship between H_A and H_B would have resulted in a much weaker coupling between these hydrogens.

Mechanistically, it may be proposed that conversion of the enone **25** into **35** proceeds via a pathway summarized in Scheme 3. Transfer of an electron to **25** would produce the radical anion **31**. Cyclization of **31** to give the isomeric radical anion **32**, followed by a second electron transfer, would provide the anionic intermediate **33**. Protonation of **33** with ammonia to give the alkoxide **34** and a subsequent work-up would afford the tetracyclic product **35**.

Reaction of the enone with excess lithium in NH_3–Et_2O in the presence of *tert*-butyl alcohol (2 equiv.) gave better results. However, the desired product **28** was accompanied by varying amounts of the cyclopropanol **35** and, at times, by the starting material **25**. The capricious nature of this reaction was discouraging. On the other hand, when **25** was treated with excess lithium in the presence of *t*-BuOH and *N*,*N*,*N*′,*N*′-tetramethylethylenediamine (TMEDA), the starting material was consumed and the cyclopropanol **35** was not produced. However, the desired ketone **28** was accompanied by products resulting from reduction of the ester function.

Replacement of lithium with other alkali metals was investigated. The results obtained from reaction (NH_3, Et_2O, 2 equiv. of *t*-BuOH) of **25** with 10–15 equivalents of potassium metal also proved to be variable. Gratifyingly, these conditions did not produce any of the cyclopropanol **35**. However, although some experiments gave good yields of **28**, others produced mixtures of the desired product and the

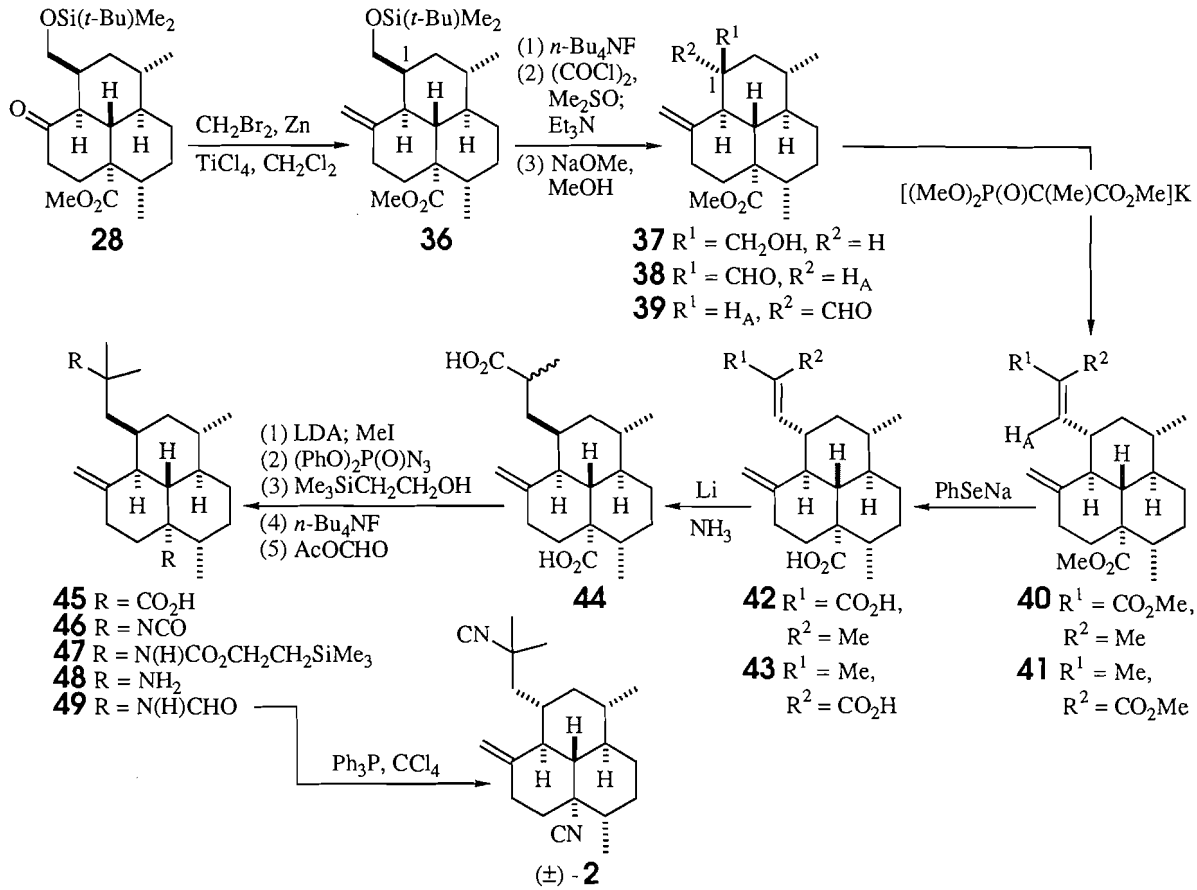

SCHEME 4

starting material **25**. Since the latter substances are inseparable by chromatography on silica gel, this method for effecting an efficient conversion of **25** into **28** also proved to be unsatisfactory.

The best, most consistent results were obtained from use of sodium metal. Treatment of **25** with sodium (15 equiv.) and *t*-BuOH (2 equiv.) in NH_3–Et_2O consistently gave excellent yields of the required tricyclic ketone **28**.

The ^1H nmr spectrum of the reduction product provided strong evidence for the conclusion that this substance possesses the (expected) relative configuration shown in **28**. Explicitly, the signal due to the proton H_A (δ 1.56) is a doublet of doublets (J = 13, 11 Hz), while the hydrogen H_B gives rise to a dd (J = 13, 4 Hz) at δ 2.32. The observed coupling constants (J_{AB} = 13 Hz, J_{BC} = 4 Hz) are consistent with the stereostructure **28**, but are incompatible with the alternative possibility **30** (see Scheme 2 for conformational representations).

(c) Conversion of the ketone 28 into the (±)-8,15-diisocyano-11(20)-amphilectene (2) (Scheme 4)

Attempted conversion of the carbonyl group of **28** into an exocyclic methylene group by treatment of this material with methylenetriphenylphosphorane under a variety of conditions gave back only starting material. Presumably, competition between the reagent acting as a base (enolate anion formation) and a nucleophile favors the former process. Similarly, starting material was obtained from treatment of **28** with $Ph_3P{=}CHLi$ (19). On the other hand, reaction of **28** with a reagent derived from dibromomethane, zinc dust, and titanium tetrachloride (20) afforded the required alkene **36** in very good yield (Scheme 4).

For a successful synthesis of (±)-**2** from **36**, the configuration at C-1 (amphilectane numbering) of the latter substance had to be inverted. Since the $CH_2OSi(t\text{-}Bu)Me_2$ group on this stereogenic center is axially oriented, the required epimerization was envisaged to be effected via an appropriate, thermodynamically driven, equilibration process. In the event, cleavage of the silyl ether function of **36** with tetra-*n*-butylammonium fluoride in THF, followed by oxidation (21) of the resultant alcohol **37**, provided the aldehyde **38** (83% from **36**). As expected, treatment of **38** with sodium methoxide in MeOH provided cleanly and efficiently (95%) the epimeric substance **39**.

Decoupling experiments in ^1H nmr spectroscopy verified that the formyl groups in compounds **38** and **39** are axially and equatorially oriented, respectively. In the spectrum of **38**, irradiation at δ 9.92 (CHO signal) changed the resonance (multiplet, δ 2.88) due to H_A (see Scheme 4) to a quartet (overlapped ddd), with a coupling constant of 3 Hz. On the other hand, irradiation at δ 9.45 in the spectrum of **39** modified the signal (δ 2.50) due to H_A to a ddd (J = 10, 10, 4 Hz). Thus, it is evident that the H_A protons in **38** and **39** are equatorial and axial, respectively.

Reaction of the aldehyde **39** with the potassium salt of trimethyl 2-phosphonopropionate in the presence of 18-crown-6 (22) provided, in excellent yield, a mixture of the geometrically isomeric α,β-unsaturated esters **40** and **41** in a ratio of ~4:1, respectively. The configurations of the en-

Can. J. Chem. Downloaded from www.nrcresearchpress.com by 213.200.69.106 on 09/08/12
For personal use only.

Can. J. Chem. Downloaded from www.nrcresearchpress.com by 213.200.69.106 on 09/08/12
For personal use only.

oate double bonds in these substances, which were readily separated by flash chromatography (13) on silica gel, were determined by ^{1}H nmr spectroscopy. The olefinic enoate proton H_A in **40**, being *cis* to the CO_2Me function, should resonate at lower field than the corresponding hydrogen in **41** (H_A *trans* to the CO_2Me group). In the ^{1}H nmr spectra of the minor and major products, H_A gives rise to signals at δ 5.73 (broad doublet, J = 10 Hz) and 6.56 (broad doublet, J = 9 Hz), respectively. Thus, it was clear that the major enoate product possesses the *E* configuration.

Attempts to effect efficient, chemoselective reduction of the enoate carbon–carbon double bond of **40** proved to be fruitless. Consequently, the required reduction was carried out on the corresponding diacid **42**. Treatment of **40** with PhSeNa in refluxing THF–hexamethylphosphoramide (HMPA) (23) for 78 h[2] gave **42** in 88% yield. Reaction of the latter substance with lithium in ammonia–THF (24) gave, in excellent yield, the diacid **44**, which consisted of a mixture of epimers in a ratio of approximately 4:1. The major isomer could be obtained in pure form by flash chromatography (13) of the mixture on silica gel.[3]

An alkylation reaction was employed to introduce the last carbon atom necessary to complete the synthesis. Treatment of **44** (mixture of epimers) with an excess of LDA in THF, followed by reaction of the resultant trianion with methyl iodide, gave the required diacid **45**.

Completion of the total synthesis of (±)-**2** required the degradation of the carboxyl groups of **45** to isonitrile functions. These synthetic operations were carried out conveniently and efficiently as follows.

Treatment of **45** with diphenyl phosphorazidate and triethylamine (25) in toluene at 80°C, followed by reaction of the resultant diisocyanate **46** (ir: 2170 cm^{-1}) with 2-(trimethylsilyl)ethanol (26) in the presence of triethylamine in the same solvent (100°C), produced the dicarbamate **47** (colorless oil, ir: 1731 cm^{-1}). Acquisition of the diamine **48** was accomplished by reaction of **47** with tetra-*n*-butylammonium fluoride in warm THF (26). Treatment of **48** with acetic formic anhydride in diethyl ether (27) gave the diformamide **49**, which, as expected, consisted of a mixture of rotamers associated with the amide functions.

The final step for the synthesis of the amphilectene **2** required the overall dehydration of the two formamide functions present in **49**. Although a number of methods for the transformation of formamides into isonitriles are known, we found that the protocol developed by Appel et al. (28) is, at least in the present case, particularly effective. Thus, treatment of **49** with triphenylphosphine – carbon tetrachloride in the presence of triethylamine (28) afforded crystalline (±)-8,15-diisocyano-11(20)-amphilectene (**2**) (41% from the diacid **45**). Racemic **2** (mp 84–86°C) exhibited ^{1}H and ^{13}C nmr spectra identical with those derived from natural (−)-**2**.[4]

[2]With shorter reaction times, it is possible to effect the chemoselective cleavage of the α,β-unsaturated ester function.

[3]Treatment of the α,β-unsaturated ester **41** with PhSeNa in refluxing THF–HMPA (23) provided the diacid **43**, which, like **42**, could be cleanly reduced (Li, NH_3–THF (24)) to **44**. Alternatively, a mixture of **40** and **41** could be converted efficiently, via the corresponding mixture of diacids **42** and **43**, into the diacid **44**.

[4]We are very grateful to Dr. D.J. Faulkner for a sample of natural (−)-**2**.

Conclusion

The structure of the antimicrobial diterpenoid (−)-8,15-diisocyano-11(20)-amphilectene (**2**) contains seven contiguous stereogenic centers. In the work reported above, which culminated in the first recorded total synthesis of (±)-**2**, the relative configurations at carbons 4, 7, 8, 12, and 13 (amphilectane numbering) were established under conditions of kinetic control. The reactions involved consisted of an alkylation of the keto ester **13** with the iodide **14** (centers 7 and 8), a key Diels–Alder reaction of the diene **17** with acrolein (center 4), and a reduction (Na, NH_3, *t*-BuOH) of the enone **25** (centers 12 and 13). On the other hand, the correct relative stereochemical orientations at carbons 3 and 1, the two remaining stereogenic centers, were secured by thermodynamically controlled epimerizations of the aldehydes **18** and **38**, respectively. Starting from the keto ester **13**, the synthesis of (±)-**2** involved approximately 20 synthetic operations and was accomplished in an overall yield of about 1.5%.

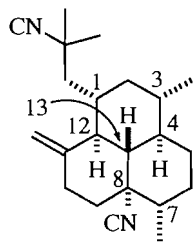

2

Experimental

General information

Distillation temperatures, which refer to short-path (Kugelrohr) distillations, and melting points are uncorrected. Proton nuclear magnetic resonance (^{1}H nmr) spectra were recorded on $CDCl_3$ solutions, unless otherwise noted. Signal positions (δ values) were measured relative to the resonances of Me_4Si (internal standard) or $CHCl_3$ (δ 7.25). Carbon nuclear magnetic resonance (^{13}C nmr) spectra were taken on $CDCl_3$ solutions (unless otherwise noted) and signal positions are given relative to the signal for $CDCl_3$ (δ 77.0). Flash chromatography (13) was carried out with 230–400 mesh silica gel (E. Merck). Thin-layer chromatography (tlc) was carried out with commercial aluminum-backed silica gel plates. Gas–liquid chromatography (glc) was performed on instruments equipped with 25 m × 0.21 mm fused silica columns coated with cross-linked SE-54. Reagents and solvents were purified and dried using standard methods. Aqueous NH_4Cl–NH_4OH (pH 8) refers to a solution prepared by addition of ~50 mL of aqueous NH_4OH (30%) to ~950 mL of saturated aqueous NH_4Cl.

Note: Unless otherwise noted, all reactions were carried out under an atmosphere of dry argon in flame- or oven-dried glassware.

Note: All compounds for which high-resolution mass measurements are given exhibited one spot on tlc analyses and produced clean ^{1}H nmr spectra.

Methyl 2-methyl-6-oxocyclohexanecarboxylate (13)

To a cold (−78°C) stirred solution of lithium methyl(cyano)cuprate (11) (28.3 mmol) in dry THF–Et_2O (10:1, 220 mL) was added a solution of methyl 6-oxo-1-cyclohexenecarboxylate (**12**) (9) (3.36 g, 21.8 mmol) in 10 mL of dry THF. The clear yellow solution was stirred at −78°C for 2 h. Aqueous NH_4Cl–NH_4OH (pH 8) (250 mL) and Et_2O (125 mL) were added and the mixture was allowed to warm to room temperature. The mixture was opened to the atmosphere and was stirred vigorously until the aqueous layer was deep blue. The phases were separated and the aqueous layer was extracted three times with Et_2O. The combined organic extracts were washed sequentially with saturated aqueous NH_4Cl and

Can. J. Chem. Downloaded from www.nrcresearchpress.com by 213.200.69.106 on 09/08/12
For personal use only.

brine, dried ($MgSO_4$), and concentrated. Distillation (80–90°C/0.1 Torr (1 Torr = 133.3 Pa)) of the residual oil gave 3.19 g (86%) of compound **13**, the spectral data of which agreed with those obtained previously (8).

*Methyl (±)-[1α, 1(*E*), 2α]-1[6-[[(1,1-dimethylethyl)-dimethylsilyl]oxy]-4-(trimethylstannyl)-4-hexenyl]-2-methyl-6-oxocyclohexanecarboxylate (**15**)*

To a stirred suspension of KH (9.8 mmol) in dry toluene (80 mL) at room temperature was added, dropwise, a solution of the keto ester **13** (1.66 g, 9.8 mmol) in dry toluene (10 mL). After the mixture had been stirred for 30 min, a solution of (*E*)-1-(*tert*-butyldimethylsiloxy)-6-iodo-3-(trimethylstannyl)-2-hexene (**14**) (5) (4.44 g, 8.8 mmol) in dry toluene (10 mL) was added and the reaction mixture was refluxed for 48 h. The mixture was cooled to 0°C and aqueous NH_4Cl–NH_4OH (pH 8) (~50 mL) was added. The phases were separated and the aqueous phase was washed with brine, dried ($MgSO_4$), and concentrated. Flash chromatography of the residual material on silica gel (600 g, 98:2 and 94:6 petroleum ether – Et_2O) gave 250 mg of the iodide **14** and 3.18 g (66%; 70% based on recovered **14**) of the keto ester **15**. The latter material, a colorless oil, exhibited ir (neat): 1743, 1715, 1088, 836 cm^{-1}; ^1H nmr (400 MHz) δ: 0.06 (s, 6H), 0.11 (s, 9H, $^2J_{Sn-H}$ = 54 Hz), 0.90 (s, 9H), 1.11 (d, 3H, J = 7 Hz), 1.11–1.20 (m, 2H), 1.22–1.32 (m, 1H), 1.57–1.87 (m, 4H), 1.90–2.02 (m, 2H), 2.24 (m, 2H), 2.39 (br d, 1H, J = 15 Hz), 2.63 (ddd, 1H, J = 15, 13.5, 6.5 Hz), 3.65 (s, 3H), 4.27 (d, 2H, J = 5.5 Hz, $^4J_{Sn-H}$ = 17 Hz), 5.65 (t, 1H, J = 5.5 Hz, $^3J_{Sn-H}$ = 79 Hz). Exact Mass calcd. for $C_{23}H_{43}O_4{}^{120}Sn$ (M^+ − Me): 531.1952; found: 531.1957.

*Methyl (±)-1(1*E*, 4aα, 5α)-1-[2-[[(1,1-dimethylethyl)-dimethylsilyl]oxy]ethylidene]-1,3,4,5,6,7-hexahydro-5-methyl-4a(2*H*)-naphthalenecarboxylate (**17**)*

To a cold (−48°C), stirred solution of LDA (5.14 mmol) in dry THF (50 mL) was added a solution of the keto ester **15** (2.55 g, 4.67 mmol) in dry THF (10 mL). After the solution had been stirred at −48°C for 1 h, *N*-phenyltrifluoromethanesulfonimide (2.84 g, 7.93 mmol) was added as a solid. The yellow solution was warmed to room temperature and was stirred at this temperature for 30 min. Analysis of the reaction mixture by tlc showed that all of the starting material **15** had been converted into the enol trifluoromethanesulfonate **16**. Solid $(Ph_3P)_4Pd$ (0.37 g, 0.32 mmol) was added and the resulting solution was refluxed overnight. The solution was cooled to room temperature and the solvent was removed under reduced pressure. The remaining crude material was filtered through a short column of silica gel (100 g, elution with 1:1 petroleum ether – Et_2O). Concentration of the eluate gave a yellowish oil, which was subjected to flash chromatography (500 g silica gel, 96:4 petroleum ether – Et_2O). Concentration of the appropriate fractions, followed by removal of last traces of solvent (vacuum pump), gave 1.46 g (86%) of the diene **17**, a colorless oil that displayed ir (neat): 1728, 1655, 837, 776 cm^{-1}; ^1H nmr (400 MHz) δ: 0.02 (s, 6H), 0.87 (s, 9H), 1.13 (ddd, 1H, J = 13, 13, 4 Hz), 1.42–1.63 (m, 4H), 1.71–1.82 (m, 2H), 2.15 (m, 2H), 2.52 (br d, 1H, J = 15 Hz), 2.64 (br d, 1H, J = 13 Hz), 3.64 (s, 3H), 4.18, 4.22 (ddd, ddd, 1H, 1H, J = 13, 7, 1 Hz in each case), 5.42 (ddd, 1H, J = 7, 1.5, 1.5 Hz), 5.73 (br t, 1H, J = 7 Hz). In decoupling experiments, irradiation at δ 1.13 caused collapse of the signal at 2.64 to a br s, while irradiation at δ 2.64 converted the signal at 1.13 into a dd (J = 13, 4 Hz). Exact Mass calcd. for $C_{21}H_{36}O_3Si$: 364.2434; found: 364.2428.

*Diels–Alder reaction of the diene **17** with acrolein. Isolation of methyl (±)-(3α, 3aα, 7β, 9β, 9aα)-7-[[[(1,1-dimethylethyl)dimethylsilyl]oxy]methyl]-9-formyl-2,3,5,6,7,8,9,9a-octahydro-3-methyl-1*H*-phenalene-3a(4*H*)-carboxylate (**18**)*

A stirred solution of the diene **17** (73 mg, 0.20 mmol) and acrolein (0.5 mL, 7.48 mmol) in dry benzene was refluxed for 20 h. After the mixture had been cooled to room temperature, the volatile material was removed under reduced pressure and the crude residual oil was subjected to flash chromatography (50 g silica gel, 9:1 petroleum ether – Et_2O). The initial fractions produced 28 mg (33%) of a mixture of three aldehydes. Analysis of this mixture by ^1H nmr spectroscopy (integration of the *CH*O signals, δ 9.62, 9.65, 9.87) showed that the three substances were present in a ratio of ~4:14:1. These Diels–Alder adducts were assigned structures **19**, **20**, and **21**, respectively. The later fractions from the flash chromatography provided 45 mg (53%) of the aldehyde **18**, a colorless oil that showed ir (neat): 2852, 1724, 837, 775 cm^{-1}; ^1H nmr (400 MHz) δ: 0.05 (s, 6H), 0.89 (s, 9H), 1.09 (d, 3H, J = 7 Hz), 1.19 (ddd, 1H, J = 13, 13, 3 Hz), 1.25–1.40 (m, 2H), 1.49–1.71 (m, 6H), 1.86–2.07 (m, 3H), 2.2 (m, 1H), 2.33 (br d, 1H, J = 13 Hz), 2.60 (ddd, 1H, J = 13, 5, 2 Hz), 2.82 (br d, 1H, J = 13 Hz), 3.67 (s, 3H), 3.66 (m, 2H), 9.79 (s, 1H). Exact Mass calcd. for $C_{24}H_{40}O_4Si$: 420.2695; found: 420.2695.

*Epimerization of the aldehyde **18**. Preparation of methyl (±)-(3α, 3aα, 7β, 9α, 9aα)-7-[[[(1,1-dimethylethyl)-dimethylsilyl]oxy]-methyl]-9-formyl-2,3,5,6,7,8,9,9a-octahydro-3-methyl-1*H*-phenalene-3a(4*H*)-carboxylate (**19**)*

A solution of the aldehyde **18** (42 mg, 0.115 mmol) in 3 mL of 0.1 M sodium methoxide in dry methanol was stirred at room temperature for 1 h. Water (10 mL) was added and the mixture was extracted with pentane. The combined extracts were washed with water, dried ($MgSO_4$), and concentrated. Flash chromatography (15 g silica gel, 9:1 petroleum ether – Et_2O) of the residual material gave 40 mg (92%) of the aldehyde **19**, a colorless oil that displayed ir (neat): 2858, 1724, 838, 776 cm^{-1}; ^1H nmr (400 MHz) δ: 0.06 (s, 6H), 0.90 (s, 9H), 1.02 (d, 3H, J = 7 Hz), 1.09 (m, 1H), 1.23 (ddd, 1H, J = 13, 13, 3 Hz), 1.34–1.37 (m, 6H), 1.80–1.90 (m, 2H), 1.98 (ddd, 1H, J = 13, 4, 4 Hz), 2.19 (m, 2H), 2.27 (dddd, 1H, J = 11, 8, 3.5, 2.5 Hz), 2.46 (br d, 1H, J = 13 Hz), 2.83 (br s, 1H), 3.50 (dd, 1H, J = 10, 8 Hz), 3.67 (s, 3H), 3.68 (dd, 1H, J = 10, 4 Hz), 9.62 (d, 1H, J = 2.5 Hz). In a decoupling experiment, irradiation at δ 9.62 changed the signal at 2.27 to a ddd (J = 11, 8, 3.5 Hz). Anal. calcd. for $C_{24}H_{40}O_4Si$: C 68.53, H 9.58; found: C 68.78, H 9.59. Exact Mass calcd.: 420.2695; found: 420.2693.

*Diels–Alder reaction of the diene **17** with acrolein. Equilibration of the crude product mixture. Isolation of the aldehydes **19** and methyl (±)-(3α, 3aα, 7α, 9β, 9aβ)-7-[[[(1,1-dimethylethyl)dimethylsilyl]oxy]methyl]-9-formyl-2,3,5,6,7,8,9,9a-octahydro-3-methyl-1*H*-phenalene-3a(4*H*)-carboxylate (**20**)*

A stirred solution of the diene **17** (233 mg, 0.64 mmol) and acrolein (1.2 mL, 18 mmol) in dry benzene (20 mL) was refluxed for 20 h. The mixture was cooled and concentrated under reduced pressure. The crude material was passed through a small column of silica gel (10 g, 1:1 petroleum ether – Et_2O). Concentration of the eluate gave a mixture of aldehydes. This material was dissolved in a 0.1 M solution of sodium methoxide in dry methanol (10 mL) and the solution was stirred at room temperature for 1 h. Water (20 mL) was added and the mixture was extracted three times with pentane. The combined organic extracts were washed with water, dried ($MgSO_4$), and concentrated. Flash chromatography (90 g silica gel, 9:1 petroleum ether – Et_2O) of the residual material gave 158 mg (58%) of the aldehyde **19** (spectra identical with those obtained previously, vide supra) and 77 mg (29%) of the aldehyde **20**. The latter substance, a colorless oil, displayed ir (neat): 2707, 1724 (br), 838, 777 cm^{-1}; ^1H nmr (400 MHz) δ: 0.06 (s, 6H), 0.91 (s, 9H), 1.03 (d, 3H, J = 7 Hz), 1.15–1.25 (m, 2H), 1.36–1.97 (m, 8H), 2.08–2.22 (m, 3H), 2.31–2.36 (m, 2H), 2.55 (m, 1H), 3.43 (dd, 1H, J = 10, 10 Hz), 3.64 (s, 3H), 3.72 (dd, 1H, J = 10, 4 Hz), 9.65 (d, 1H, J = 3.5 Hz). Exact Mass calcd. for $C_{24}H_{40}O_4Si$: 420.2695; found: 420.2700.

*Methyl (±)-(3α, 3aα, 7β, 9α, 9aα)-7-[[[(1,1-dimethylethyl)-dimethylsilyl]oxy]methyl]-2,3,5,6,7,8,9,9a-octahydro-9-(hydroxymethyl)-3-methyl-1*H*-phenalene-3a(4*H*)-carboxylate (**22**)*

To a cold (0°C), stirred solution of the aldehyde **19** (722 mg, 1.72 mmol) in methanol (60 mL) was added solid sodium boro-

Can. J. Chem. Downloaded from www.nrcresearchpress.com by 213.200.69.106 on 09/08/12
For personal use only.

hydride (79 mg, 2.08 mmol) and the mixture was stirred for 1 h. Saturated aqueous NH_4Cl (40 mL) was added and the mixture was extracted with dichloromethane. The combined extracts were washed with brine, dried ($MgSO_4$), and concentrated to give 687 mg (95%) of the alcohol **22**, a colorless oil that showed ir (neat): 3406 (br), 1723, 837, 776 cm^{-1}; ^1H nmr (400 MHz) δ: 0.04 (s, 6H), 0.90 (s, 9H), 1.04 (d, 3H, J = 7 Hz), 1.27 (m, 2H), 1.34–1.67 (m, 10H), 1.90 (m, 2H), 2.15 (m, 2H), 2.36 (br d, 1H, J = 13 Hz), 3.50 (dd, 1H, J = 10, 7 Hz), 3.55 (dd, 1H, J = 10, 7 Hz), 3.64 (s, 3H), 3.65 (m, 2H). Anal. calcd. for $C_{24}H_{42}O_4Si$: C 68.20, H 10.01; found: C 68.13, H 10.10. Exact Mass calcd.: 422.2852; found: 422.2846.

*Methyl (±)-(3α, 3aα, 7β, 9α, 9aα)-7-[[[(1,1-dimethylethyl)-dimethylsilyl]oxy]methyl]-2,3,5,6,7,8,9,9a-octahydro-3-methyl-9-[[[(4-methylphenyl)sulfonyl]oxy]methyl]-1H-phenalene-3a(4H)-carboxylate (**23**)*

A solution of the alcohol **22** (678 mg, 1.61 mmol), *p*-toluenesulfonyl chloride (614 mg, 3.22 mmol), and 4-*N*,*N*-dimethylaminopyridine (492 mg, 4.03 mmol) in dry dichloromethane (20 mL) was stirred at room temperature overnight. Water (30 mL) and diethyl ether (40 mL) were added and the phases were separated. The aqueous layer was washed with diethyl ether. The combined organic phases were washed with brine, dried ($MgSO_4$), and concentrated. Flash chromatography (80 g silica gel, 4:1 petroleum ether – Et_2O) of the crude material gave 851 mg (92%) of the *p*-toluenesulfonate **23**, a colorless oil that displayed ir (neat): 1723, 1178, 837, 776 cm^{-1}; ^1H nmr (400 MHz) δ: 0.02 (s, 6H), 0.87 (s, 9H), 1.01 (d, 3H, J = 6 Hz), 1.09–1.50 (m, 5H), 1.60 (m, 2H), 1.68–1.85 (m, 4H), 2.00–2.15 (m, 4H), 2.35 (br d, 1H, J = 12 Hz), 2.44 (s, 3H), 3.43 (dd, 1H, J = 10, 7.5 Hz), 3.58 (dd, 1H, J = 10, 4 Hz), 3.62 (s, 3H), 3.91 (dd, 1H, J = 9.5, 7.5 Hz), 4.03 (dd, 1H, J = 9.5, 5 Hz), 7.34, 7.78 (d, d, 2H each, J = 8 Hz in each case). Exact Mass calcd. for $C_{24}H_{40}O_3Si$ (M^+ – $MeC_6H_4SO_3H$): 404.2747; found: 404.2757.

*Methyl (±)-(3α, 3aα, 7β, 9α, 9aα)-7-[[[(1,1-dimethylethyl)-dimethylsilyl]oxy]methyl]-3,9-dimethyl-1H-phenalene-3a(4H)-carboxylate (**24**)*

To a cold (0°C) solution of the *p*-toluenesulfonate **23** (1.242 g, 2.16 mmol) in dry THF (25 mL) was added a solution of lithium triethylborohydride in THF (5.4 mmol). The solution was warmed to room temperature, was stirred for 3 h, and was recooled to 0°C. Aqueous sodium hydroxide (3 N, 8 mL) and aqueous hydrogen peroxide (30%, 8 mL) were added slowly and the mixture was stirred at 0°C for 40 min. Water (25 mL) was added and the mixture was extracted thoroughly with pentane. The combined organic extracts were washed with brine, dried ($MgSO_4$), and concentrated. Flash chromatography (500 g silica gel, 95:5 petroleum ether – Et_2O) of the residual material gave 785 mg (90%) of the ester **24**, a colorless oil that showed ir (neat): 1725, 837, 775 cm^{-1}; ^1H nmr (400 MHz) δ: 0.06 (s, 6H), 0.91 (s, 9H), 0.93 (d, 3H, J = 6 Hz), 1.01 (d, 3H, J = 6 Hz), 1.25 (m, 2H), 1.26–1.70 (m, 7H), 1.76 (ddd, 1H, J = 13, 4, 4 Hz), 1.85 (br d, 1H, J = 16 Hz), 1.95 (m, 2H), 2.05 (m, 1H), 2.19 (m, 1H), 2.41 (br d, 1H, J = 13 Hz), 3.45 (dd, 1H, J = 10, 9.5 Hz), 3.64 (s, 3H), 3.66 (dd, 1H, J = 10, 5 Hz). Anal. calcd. for $C_{24}H_{42}O_3Si$: C 70.88, H 10.41; found: C 71.00, H 10.50. Exact Mass calcd.: 406.2903; found: 406.2895.

*Methyl (±)-(3aα, 4α, 6aα, 7α, 9β)-9-[[[(1,1-dimethylethyl)-dimethylsilyl]oxy]methyl]-2,3,5,6,6a,7,8,9-octahydro-4,7-dimethyl-1-oxo-1H-phenalene-3a(4H)-carboxylate (**25**)*

To a cold (−20°C), stirred suspension of chromium trioxide (2.25 g, 22.5 mmol) in dry dichloromethane (25 mL) was added, in one portion, 3,5-dimethylpyrazole (2.18 g, 22.5 mmol). The mixture was stirred at −20°C for approximately 30 min. A solution of the alkene **24** (365 mg, 0.899 mmol) in dry dichloromethane (10 mL) was added; the mixture was warmed to 0°C and then was stirred for 1.5 h. Dry diethyl ether (30 mL) was added and the mixture was filtered through a column of Florisil (elution with dry diethyl ether). The eluate was concentrated and the residual material was subjected to flash chromatography (80 g silica gel, 9:1 petroleum ether – Et_2O). Concentration of the appropriate fractions gave 291 mg (77%) of the enone **25**, a crystalline solid, mp 53–54°C, that exhibited ir (KBr): 1725, 1672, 1596, 836, 776 cm^{-1}; ^1H nmr (400 MHz) δ: 0.03 (s, 3H), 0.06 (s, 3H), 0.89 (s, 9H), 1.02 (d, 3H, J = 6 Hz), 1.04 (d, 3H, J = 6 Hz), 1.08 (m, 1H), 1.14 (ddd, 1H, J = 13, 13, 5 Hz), 1.58 (m, 4H), 1.68 (ddd, 1H, J = 14, 14, 5 Hz), 1.97 (ddd, 1H, J = 13, 4, 2 Hz), 2.24 (m, 2H), 2.44 (ddd, 1H, J = 18, 5, 3 Hz), 2.50 (ddd, 1H, J = 18, 14, 5 Hz), 2.69 (ddd, 1H, J = 13, 5, 3 Hz), 2.98 (m, 1H), 3.32 (dd, 1H, J = 9.5, 9.5 Hz), 3.62 (dd, 1H, J = 9.5, 4 Hz), 3.70 (s, 3H). Anal. calcd. for $C_{24}H_{40}O_4Si$: C 68.53, H 9.58; found: C 68.66, H 9.69. Exact Mass calcd.: 420.2696; found: 420.2702.

*Methyl (±)-(3aα, 4α, 6aα, 7α, 9α, 9aα, 9bβ)-9-[[[(1,1-dimethylethyl)dimethylsilyl]oxy]-methyl]decahydro-4,7-dimethyl-1-oxo-1H-phenalene-3a(4H)-carboxylate (**28**)*

A solution of the enone **25** (35 mg, 0.083 mmol) and *tert*-butyl alcohol (17 μL, 0.18 mmol) in dry diethyl ether (0.8 mL) was added via cannulation to a stirred solution of sodium (29 mg, 1.26 mmol) in ammonia (3 mL, freshly distilled from sodium). The mixture was refluxed for 40 min. Isoprene was added dropwise until the blue color of the solution disappeared. Saturated aqueous NH_4Cl (10 mL) and diethyl ether (5 mL) were added. While the mixture was stirred for 4 h, it was warmed occasionally with a water bath (~40–45°C) until the ammonia was distilled. During this time, diethyl ether was added occasionally to the mixture. The phases were separated and the aqueous phase was extracted with diethyl ether (2 × 10 mL). The combined organic extracts were washed with water, dried ($MgSO_4$), and concentrated. Flash chromatography of the crude material on silica gel (20 g, 9:1 petroleum ether – Et_2O) afforded 30 mg (86%) of the ketone **26**, a white solid (mp 79–81°C, from pentane) that exhibited ir (KBr): 1724, 1707, 836, 776 cm^{-1}; ^1H nmr (400 MHz) δ: 0.03 (s, 3H), 0.05 (s, 3H), 0.89 (s, 9H), 0.90 (d, 3H, J = 6 Hz), 0.95 (d, 3H, J = 6 Hz), 0.79–1.00 (m, 1H), 1.12 (ddd, 1H, J = 13.5, 13.5, 3.5 Hz), 1.28 (m, 1H), 1.32–1.47 (m, 3H), 1.52 (m, 1H), 1.56 (dd, 1H, J = 13, 11 Hz), 1.74 (dddd, 1H, J = 11, 11, 11, 3 Hz), 1.88 (ddd, 1H, J = 13.5, 3, 3 Hz), 2.08 (dddd, 1H, J = 13, 3, 3, 3 Hz), 2.32 (dd, 1H, J = 13, 4 Hz), 2.35–2.50 (m, 2H), 2.53 (m, 1H), 2.62 (ddd, 1H, J = 13.5, 8, 3.5 Hz), 3.60 (dd, 1H, J = 10, 10 Hz), 3.65 (dd, 1H, J = 10, 5.5 Hz), 3.68 (s, 3H). In decoupling experiments, irradiation at δ 1.12 simplified the m at 2.53 and collapsed the signal at 1.88 to a br s; irradiation at δ 1.88 sharpened the m at 2.53 and changed the resonance at 1.12 to a dd (J = 13.5, 3.5 Hz); irradiation at δ 2.32 simplified the m at 2.53 and changed the dd at 1.56 to a d (J = 11 Hz). Exact Mass calcd. for $C_{23}H_{39}O_4Si$ (M^+ – Me): 407.2618; found: 407.2610.

*Methyl (±)-(3aα, 4α, 6aα, 7α, 9β, 9aα, 9bβ)-9-[[[(1,1-dimethylethyl)dimethylsilyl]oxy]-methyl]decahydro-4,7-dimethyl-1-methylene-1H-phenalene-3a(4H)-carboxylate (**36**)*

To a stirred solution of the ketone **28** (51 mg, 0.05 mmol) in dry dichloromethane (3 mL) was added, in small portions over a period of about 30 min, a THF slurry of a reagent prepared from CH_2Br_2, Zn dust, and $TiCl_4$ as described by Lombardo (20). After about 1 mL of the reagent solution had been added, analysis of an aliquot of the reaction mixture by glc showed that the reaction was complete. The mixture was diluted with Et_2O (15 mL) and saturated aqueous sodium bicarbonate (10 mL) was added. The mixture was stirred vigorously until a clear organic phase was obtained. The phases were separated and the aqueous layer was washed with Et_2O. The combined organic solutions were washed (brine), dried ($MgSO_4$), and concentrated. Flash chromatography (10 g silica gel, 95:5 petroleum ether – Et_2O) of the residue gave 40 mg (79%) of the alkene **36**, a white solid (mp 46–48°C) that displayed ir (KBr): 1726, 1636, 1095, 840, 788 cm^{-1}; ^1H nmr (400 MHz) δ: 0.02 (s, 6H), 0.88 (d, 3H, J = 6 Hz), 0.89 (s, 9H), 0.90 (d, 3H, J = 6 Hz),

Can. J. Chem. Downloaded from www.nrcresearchpress.com by 213.200.69.106 on 09/08/12
For personal use only.

1.06 (dd, 1H, J = 12.5, 11 Hz), 1.09–1.60 (diffuse m, 8H), 1.79 (dddd, 1H, J = 11, 11, 11, 3.5 Hz), 1.98 (ddd, 1H, J = 13, 3, 3 Hz), 2.02 (dddd, 1H, J = 13, 3.5, 3.5, 3.5 Hz), 2.11–2.29 (m, 3H), 2.42 (br d, 1H, J = 12 Hz), 2.52 (ddd, 1H, J = 13, 6, 6 Hz), 3.60 (dd, 1H, J = 10, 10 Hz), 3.63 (s, 3H), 3.76 (dd, 1H, J = 10, 3.5 Hz), 4.75 (br s, 1H), 4.81 (dd, 1H, J = 1.5, 1.5 Hz). Exact Mass calcd. for $C_{25}H_{44}O_3Si$: 420.3060; found: 420.3058.

*Methyl (±)-(3aα, 4α, 6aα, 7α, 9β, 9aα, 9bβ)-decahydro-9-(hydroxymethyl)-4,7-dimethyl-1-methylene-1*H*-phenalene-3a(4*H*)-carboxylate (**37**)*

A solution of compound **36** (40 mg, 0.095 mmol) in 3 mL of dry THF was added to 0.3 mL of a 1 M solution of n-Bu_4NF in THF and the resultant mixture was stirred at room temperature for 4 h. Water (5 mL) and Et_2O (5 mL) were added, the phases were separated, and the aqueous layer was washed with Et_2O. The combined organic solutions were washed (brine), dried ($MgSO_4$), and concentrated. Flash chromatography (10 g silica gel, 3:2 petroleum ether – Et_2O) of the residue gave 28 mg (96%) of the alcohol **37**, a white solid (mp 60–62°C) that showed ir (KBr): 3348, 1724, 1636 cm^{-1}; ^1H nmr (400 MHz) δ: 0.89 (d, 3H, J = 6 Hz), 0.92 (d, 3H, J = 6 Hz), 1.06 (dd, 1H, J = 12.5, 11 Hz), 1.12 (ddd, 1H, J = 13, 9, 7 Hz), 1.22–1.40 (m, 5H), 1.48 (dddd, 1H, J = 13, 3.5, 3.5, 3.5 Hz), 1.81 (dddd, 1H, J = 10, 10, 10, 4 Hz), 1.93 (dd, 1H, J = 10, 3 Hz), 2.03 (dddd, 1H, J = 13, 3.5, 3.5, 3.5 Hz), 2.21 (m, 3H), 2.48 (br d, 1H, J = 13 Hz), 2.53 (ddd, 1H, J = 13.5, 6, 6 Hz), 3.64 (s, 3H), 3.65 (dd, 1H, J = 10, 10 Hz), 3.87 (dd, 1H, J = 10, 4 Hz), 4.77, 4.84 (s, s, 1H each). Exact Mass calcd. for $C_{19}H_{30}O_3$: 306.2195; found: 306.2195.

*Methyl (±)-(3aα, 4α, 6aα, 7α, 9β, 9aα, 9bβ)-9-formyldecahydro-4,7-dimethyl-1-methylene-1*H*-phenalene-3a(4*H*)-carboxylate (**38**)*

To a cold (−78°C), stirred solution of dimethyl sulfoxide (9.3 μL, 0.131 mmol) in dry CH_2Cl_2 (2 mL) was added oxalyl chloride (10 μL, 0.117 mmol) and the solution was stirred at −78°C for 15 min. A solution of alcohol **37** (20 mg, 0.065 mmol) in dry CH_2Cl_2 (0.8 mL) was added, stirring was continued for 20 min, Et_3N (45 μL, 0.325 mmol) was added, stirring was continued (−78°C) for 5 min, and then the mixture was allowed to warm to room temperature. Water (5 mL) and Et_2O (10 mL) were added, the phases were separated, and the aqueous layer was washed with Et_2O. The combined organic extracts were washed (brine), dried ($MgSO_4$), and concentrated. Flash chromatography (6 g silica gel, 94:6 petroleum ether – Et_2O) of the remaining material gave 17.3 mg (87%) of the aldehyde **38**, a white solid (mp 68–70°C) that exhibited ir (KBr): 2857, 1720, 1638 cm^{-1}; ^1H nmr (400 MHz), δ: 0.89 (d, 3H, J = 6 Hz), 0.91 (m, 1H), 0.96 (d, 3H, J = 6 Hz), 1.03 (m, 1H), 1.15 (ddd, 1H, J = 13, 13, 4 Hz), 1.18–1.32 (m, 2H), 1.38–1.58 (m, 4H), 2.03 (m, 3H), 2.15 (br dd, 1H, J = 15, 13 Hz), 2.38 (ddd, 1H, J = 15, 4, 4 Hz), 2.53 (ddd, 1H, J = 13, 4, 4 Hz), 2.60 (dd, 1H, J = 12, 3 Hz), 2.88 (m, 1H), 3.69 (s, 3H), 4.42, 4.85 (br s, br s, 1H each), 9.92 (d, 1H, J = 2 Hz). In decoupling experiments, irradiation at δ 2.15 changed the ddd at 1.15 to a dd (J = 13, 4 Hz), sharpened the ddd at 2.38 to a broad, unresolved signal, altered the ddd at 2.53 to a dd (J = 13, 4 Hz), and changed the broad singlets at 4.42 and 4.85 to sharp doublets (J = 2 Hz in each case); irradiation at δ 2.38 changed the signals at 1.15, 2.15, and 2.53 to a dd (J = 13, 13 Hz), a broad d (J = 13 Hz), and a dd (J = 13, 4 Hz), respectively; irradiation at δ 2.88 simplified the multiplets at 1.38–1.58 and 2.03, sharpened the dd at 2.60 to a d (J = 12 Hz), and converted the d at 9.92 to a s; irradiation at δ 9.92 caused the m at 2.88 to collapse to a ddd (J = 3, 3, 3 Hz). Exact Mass calcd. for $C_{19}H_{28}O_3$: 304.2038; found: 304.2035.

*Methyl (±)-(3aα, 4α, 6aα, 7α, 9α, 9aα, 9bβ)-9-formyldecahydro-4,7-dimethyl-1-methylene-1*H*-phenalene-3a(4*H*)-carboxylate (**39**)*

A solution of the aldehyde **38** (17 mg, 0.056 mmol) in 1.5 mL of dry 0.1 M sodium methoxide in methanol was stirred at room temperature for 1 h. Water (5 mL) was added and the mixture was extracted thoroughly with pentane. The combined organic extracts were washed (brine), dried ($MgSO_4$) and concentrated. Flash chromatography (5 g silica gel, 93:7 petroleum ether – Et_2O) of the residual material gave 16 mg (95%) of the aldehyde **39**, a white solid (mp 65–67°C) that showed ir (KBr): 2853, 1723, 1645 cm^{-1}; ^1H nmr (400 MHz) δ: 0.85 (dddd, 1H, J = 13, 13, 13, 4 Hz), 0.94 (d, 3H, J = 6 Hz), 0.95 (m, 1H), 0.96 (d, 3H, J = 6 Hz), 1.05 (m, 1H), 1.09 (ddd, 1H, J = 13, 13, 4 Hz), 1.14 (ddd, 1H, J = 12, 12, 12 Hz), 1.26 (ddd, 1H, J = 13, 13, 4 Hz), 1.37 (m, 1H), 1.52 (dddd, 1H, J = 13, 4, 4, 4 Hz), 1.67 (ddd, 1H, J = 13, 4, 4 Hz), 2.04 (m, 2H), 2.12 (ddd, 1H, J = 14, 14, 3.5 Hz), 2.29 (ddd, 1H, J = 14, 3.5, 3.5 Hz), 2.45 (dd, 1H, J = 10, 10 Hz), 2.50 (dddd, 1H, J = 10, 10, 4, 4 Hz), 2.64 (ddd, 1H, J = 13, 3.5, 3.5 Hz), 3.73 (s, 3H), 4.45, 4.75 (s, s, 1H each), 9.45 (d, 1H, J = 4 Hz). In a decoupling experiment, irradiation at δ 9.45 changed the dddd at 2.50 to a ddd (J = 10, 10, 4 Hz). Exact Mass calcd. for $C_{19}H_{28}O_3$: 304.2038; found: 304.2035.

*Methyl (±)-(3aα, 4α, 6aα, 7α, 9α(*E*), 9aα, 9bβ)-decahydro-9-(3-methoxy-2-methyl-3-oxo-1-propenyl)-4,7-dimethyl-1-methylene-1*H*-phenalene-3a(4*H*)-carboxylate (**40**) and the geometric isomer **41***

A 35% dispersion of KH in mineral oil (~23 mg) was washed three times with dry THF (3 mL) and the remaining KH (~8 mg, 0.2 mmol) was covered with 4 mL of dry THF. To this stirred suspension (0°C) was added trimethyl 2-phosphonopropionate (35 μL, 0.2 mmol) and 18-crown-6 (~1 mmol, recrystallized from MeCN) and the mixture was stirred at room temperature for 20 min. A solution of the aldehyde **39** (40 mg, 0.132 mmol) in dry THF (1.5 mL) was added and the mixture was stirred at room temperature for 3.5 h. Water (10 mL) and Et_2O (15 mL) were added and the phases were separated. The aqueous layer was extracted twice with Et_2O. The combined extracts were washed (brine), dried ($MgSO_4$), and concentrated. Flash chromatography (15 g silica gel, 94:6 pentane–Et_2O) of the residual material gave 9.5 mg (19%) of the Z ester **41** (the first product to be eluted) and 38 mg (77%) of the E ester **40**.

The ester **41**, a white solid with mp 100–103°C, exhibited ir (KBr): 1718, 1648, 1212, 1151, 1110 cm^{-1}; ^1H nmr (400 MHz) δ: 0.83 (dddd, 1H, J = 13, 13, 13, 4 Hz), 0.89 (d, 3H, J = 6 Hz), 0.90 (d, 3H, J = 6 Hz), 0.93 (dd, 1H, J = 11, 11 Hz), 1.03 (m, 2H), 1.23 (dddd, 1H, J = 13, 13, 13, 4 Hz), 1.35 (m, 1H), 1.48 (dddd, 1H, J = 14, 14, 14, 4 Hz), 1.59 (m, 2H), 1.85 (d, 3H, J = 1 Hz), 1.90–2.10 (m, 4H), 2.23 (ddd, 1H, J = 14, 3.5, 3.5 Hz), 2.62 (ddd, 1H, J = 13, 3.5, 3.5 Hz), 3.32 (dddd, 1H, J = 10, 10, 10, 4 Hz), 3.70 (s, 3H), 3.75 (s, 3H), 4.56 (s, 1H), 4.68 (d, 1H, J = 1 Hz), 5.73 (br d, 1H, J = 10 Hz). Exact Mass calcd. for $C_{23}H_{34}O_4$: 374.2456; found: 374.2454.

The ester **40**, a white solid with mp 106–108°C, displayed ir (KBr): 1718, 1642, 1277, 1224, 1157 cm^{-1}; ^1H nmr (400 MHz) δ: 0.85 (dddd, 1H, J = 13, 13, 13, 4 Hz), 0.91 (d, 6H, J = 6 Hz), 0.95 (dd, 1H, J = 11, 11 Hz), 1.06 (m, 3H), 1.26 (ddd, 1H, J = 13, 13, 3 Hz), 1.36 (m, 1H), 1.48 (m, 2H), 1.89 (s, 3H), 2.06 (m, 4H), 2.23 (ddd, 1H, J = 14, 4, 4 Hz), 2.53 (dddd, 1H, J = 11, 11, 9, 4 Hz), 2.63 (ddd, 1H, J = 13, 3.5, 3.5 Hz), 3.70 (s, 3H), 3.71 (s, 3H), 4.35 (s, 1H), 4.67 (s, 1H), 6.56 (d, 1H, J = 9 Hz). Exact Mass calcd. for $C_{23}H_{34}O_4$: 374.2456; found: 374.2462.

*(±)-[(3aα, 4α, 6aα, 7α, 9α(*E*), 9aα, 9bβ]-9-(2-Carboxy-1-propenyl)-decahydro-4,7-dimethyl-1-methylene-1*H*-phenalene-3a(4*H*)-carboxylic acid (**42**)*

To a stirred suspension of oil-free NaH (75 mg, 3.1 mmol) in dry THF (1 mL) were added benzeneselenol (0.33 mL, 3.1 mmol) and dry HMPA (1.11 mL, 6.4 mmol). The deep red solution was treated with a solution of the diester **40** (48 mg, 0.128 mmol) in dry THF (1 mL) and the mixture was refluxed for 78 h. The solution was allowed to cool to room temperature and was concentrated under reduced pressure. The residual material was treated with water (4 mL), and the basic mixture was washed with pentane

Can. J. Chem. Downloaded from www.nrcresearchpress.com by 213.200.69.106 on 09/08/12
For personal use only.

(5 mL). The aqueous phase was acidified with 10% hydrochloric acid and the mixture was extracted with Et_2O (3 × 5 mL). The combined extracts were washed (brine), dried ($MgSO_4$), and concentrated. Flash chromatography of the residue (15 g silica gel, Et_2O) produced 39 mg (88%) of the diacid **42**, a white solid (mp 273–275°C) that exhibited ir (KBr): 1687, 1665, 1648 cm^{-1}; ^1H nmr (400 MHz) δ: 0.90 (m, 1H), 0.91 (d, 3H, J = 6 Hz), 0.99 (d, 3H, J = 6 Hz), 1.00–1.15 (m, 3H), 1.32 (m, 1H), 1.39 (m, 2H), 1.52 (m, 2H), 1.87 (s, 3H), 2.05 (m, 3H), 2.22 (m, 2H), 2.60 (m, 2H), 4.40 (s, 1H), 4.68 (s, 1H), 6.54 (br d, 1H, J = 9 Hz). Exact Mass calcd. for $C_{21}H_{30}O_4$: 346.2144; found: 346.2152.

*Preparation of the dicarboxylic acid **44***

To a stirred solution of lithium metal (4.5 mg) in dry ammonia (3 mL, freshly distilled from sodium metal) was added, via cannulation, a solution of the diacid **42** (20 mg, 0.058 mmol) in dry THF (1 mL) and the mixture was refluxed for 30 min. Solid ammonium chloride was added in small portions until the blue color was discharged. Diethyl ethyl (4 mL) was added, the mixture was warmed gently to distill the ammonia, and the residual mixture was acidified with 6 N hydrochloric acid. The mixture was extracted with Et_2O (3 × 5 mL). The combined extracts were washed (brine), dried ($MgSO_4$), and concentrated. Flash chromatography (10 g silica gel, 55:45 pentane–Et_2O) gave 10 mg (50%) of **44** as a single isomer (white solid, mp 248–250°C) and 8 mg (40%) of **44** as a mixture of two epimers (ratio ~1.5:1, by ^1H nmr spectroscopy). The single isomer exhibited ir (KBr): 1702, 1644 cm^{-1}; ^1H nmr (400 MHz, acetone-d_6) δ: 0.75 (m, 1H), 0.80–0.92 (m, 5H), 0.94 (d, 3H, J = 6 Hz), 1.04 (ddd, 1H, J = 13, 13, 5 Hz), 1.10 (d, 3H, J = 6 Hz), 1.30–1.40 (m, 2H), 1.46 (m, 1H), 1.59 (m, 1H), 1.71 (m, 1H), 1.77 (m, 1H), 1.97 (m, 3H), 2.12–2.30 (m, 4H), 2.64 (m, 2H), 4.74 (s, 1H), 4.79 (s, 1H). Exact Mass calcd. for $C_{21}H_{32}O_4$: 348.2295; found: 348.2300.

*(±)-(1α, 3α, 3aα, 6α, 6aα, 9aα, 9bβ)-6a-Carboxydecahydro-α,α,3,6-tetramethyl-9-methylene-1H-phenalene-1-propanoic acid (**45**)*

To a cold (0°C), stirred solution of LDA (1.0 mmol) in dry THF (1.5 mL) was added a solution of the diacid **44** (35 mg, 0.1 mmol, mixture of epimers) in dry THF (2 mL). The mixture was allowed to warm to room temperature and was stirred for 2.5 h. Methyl iodide (~0.5 mL, passed through a small, dry basic alumina column) was added and the mixture was stirred at room temperature for 1 h. The solution was acidified with 10% hydrochloric acid and the mixture was extracted with Et_2O (3 × 5 mL). The combined extracts were washed (brine), dried ($MgSO_4$), and concentrated. Flash chromatography (5 g silica gel, 1:1 pentane–Et_2O) gave 20 mg (55%) of the diacid **45**, a white solid (mp 245–247°C) that showed ir (KBr): 1705 cm^{-1}; ^1H nmr (400 MHz, acetone-d_6) δ: 0.79–0.92 (m, 5H), 0.93 (d, 3H, J = 6 Hz), 1.01–1.12 (m, 2H), 1.15 (s, 3H), 1.18 (s, 3H), 1.30–1.50 (m, 5H), 1.60 (m, 1H), 1.78–2.00 (m, 5H), 2.12–2.32 (m, 2H), 2.65 (ddd, 1H, J = 12, 4, 4, 4 Hz), 4.69 (s, 1H), 4.79 (s, 1H). Exact Mass calcd. for $C_{22}H_{34}O_4$: 362.2457; found: 362.2463.

*(±)-(1α, 3α, 3aα, 6α, 6aα, 9aα, 9bβ)-Dodecahydro-6a-isocyano-1-(2-isocyano-2-methylpropyl)-3,6-dimethyl-9-methylene-1H-phenalene [(±)-8,15-diisocyano-11(20)-amphilectene (**2**)]*

To a stirred solution of the diacid **45** (19 mg, 0.052 mmol) in dry toluene (0.4 mL) were added dry Et_3N (38 μL, 0.273 mmol) and diphenyl phosphorazidate (38 μL, 0.186 mmol) and the mixture was heated to 80°C. Evolution of nitrogen began immediately. After a period of 2 h, the ir spectrum of the material obtained from a small sample of the mixture showed an absorption at 2170 cm^{-1} (-N=C=O, compound **46**). No carbonyl absorption was present. Dry 2-(trimethylsilyl)ethanol (0.15 mL, 1.06 mmol) and dry Et_3N (76 μL, 0.546 mmol) were added and the mixture was heated at 100°C for 60 h. During this time, after periods of 20 h and 40 h, additional amounts of $Me_3SiCH_2CH_2OH$ (0.15 mL) and Et_3N (76 μL) were added. The reaction mixture was cooled, diluted with Et_2O, and passed through a small column of silica gel (2 g, elution with Et_2O). The eluate was concentrated and the residue was subjected to flash chromatography (15 g silica gel, 9:1 pentane–Et_2O) to provide 16 mg (52%) of the dicarbamate **47**, a colorless oil that exhibited ir (neat): 3448, 3371, 1731, 1645, 1505 cm^{-1}; ^1H nmr (400 MHz) δ: 0.04 (s, 9H), 0.06 (s, 6H), 0.64–0.86 (m, 3H), 0.87 (d, 3H, J = 6 Hz), 0.93 (d, 3H, J = 6 Hz), 0.90–1.10 (m, 7H), 1.22–1.32 (m, 2H), 1.31 (s, 3H), 1.34 (s, 3H), 1.42 (m, 1H), 1.68–2.10 (m, 7H), 2.21 (br ddd, 1H, J = 13, 3.5, 3.5 Hz), 3.52 (br d, 1H, J = 13 Hz), 4.10 (m, 4H), 4.43 (s, 1H), 4.50 (s, 1H), 4.55 (s, 1H), 4.80 (s, 1H).

To a stirred solution of the dicarbamate (16 mg, 0.027 mmol) in dry THF (0.6 mL) was added a solution of tetra-*n*-butylammonium fluoride in THF (0.21 mL) and the mixture was heated at 50°C for 2 h. The mixture was cooled and concentrated. The residue was treated with pentane (3 mL) and aqueous NH_4Cl–NH_4OH (2 mL, 1.6 mL of saturated aqueous NH_4Cl diluted with 0.4 mL of concentrated aqueous NH_4OH) and the mixture was stirred rapidly for 15 min. The phases were separated and the aqueous layer was washed with pentane (2 × 2 mL). The combined organic extracts were concentrated to provide the crude diamine **48** (~9 mg) as a pale yellow oil. This material was dissolved in dry Et_2O (0.5 mL) containing 30 μL (0.23 mmol) of acetic formic anhydride and the solution was stirred at room temperature for 2 h. Water (2 mL) and Et_2O (3 mL) were added and the phases were separated. The aqueous layer was extracted with Et_2O (2 × 2 mL) and the combined extracts were washed (brine), dried ($MgSO_4$), and concentrated to give the diformamide **49** (~10 mg) as a white solid. The ^1H nmr spectrum of this material showed that it was a mixture of *cis* and *trans* isomers with respect to the formamide functions. A solution of this material in dry CH_2Cl_2 (0.5 mL) was treated with Ph_3P (22.5 mg, 0.086 mmol), dry CCl_4 (8 μL, 0.08 mmol) and dry Et_3N (30 μL, 0.18 mmol) and the mixture was heated at 55°C for 6.5 h. The mixture was concentrated and the solid residue was extracted (triturated) with 1:1 pentane–Et_2O. The combined organic extracts were concentrated and the residue was subjected to flash chromatography (2 g silica gel, 93:7 pentane–Et_2O) to afford 7 mg (41% from the diacid **45**) of (±)-8,15-diisocyano-11(20)-amphilectene (**2**), a crystalline solid (mp 84–86°C) that displayed ir (KBr): 2127, 1647 cm^{-1}; ^1H nmr (400 MHz) δ: 0.78–0.94 (m, 2H), 0.92 (d, 3H, J = 6 Hz), 1.00 (d, 3H, J = 6 Hz), 1.02–1.15 (m, 2H), 1.20–1.50 (m, 4H), 1.45 (t, 3H, J = 2 Hz), 1.47 (t, 3H, J = 2 Hz), 1.54 (m, 2H), 1.85 (dd, 1H, J = 11, 11 Hz), 1.93–2.04 (m, 2H), 2.09 (dd, 1H, J = 15, 2 Hz), 2.23–2.36 (m, 4H), 4.68 (s, 1H), 4.87 (s, 1H); ^{13}C nmr (75.3 MHz, C_6D_6) δ: 15.9, 19.9, 30.0, 30.2, 30.5, 31.5, 33.5, 33.9, 35.6, 39.7, 40.9, 41.2, 42.9, 45.7, 46.3, 55.5, 56.5 (t, J = 4 Hz), 66.9 (t, J = 4 Hz), 106.6, 150.0, 158.1 (t, J = 4 Hz), 159.9 (t, J = 4 Hz). Exact Mass calcd. for $C_{22}H_{32}N_2$: 324.2565; found: 324.2556.

Acknowledgements

We thank the Natural Sciences and Engineering Research Council of Canada for financial support and for an Undergraduate Student Research Award (to R.M.O.). We are grateful to Dr. Miguel Romero for carrying out model studies related to the conversion of the diacid **45** into (±)-**2**.

1. S.J. Wratten, D.J. Faulkner, K. Hirotsu, and J. Clardy. Tetrahedron Lett. 4345 (1978).
2. R. Kazlauskas, P.T. Murphy, R.J. Wells, and J.F. Blount. Tetrahedron Lett. **21**, 315 (1980).
3. T.F. Molinski, D.J. Faulkner, G.D. Van Duyne, and J. Clardy. J. Org. Chem. **52**, 3334 (1987).
4. E. Piers, R.W. Friesen, and B.A. Keay. Tetrahedron, **47**, 4555 (1991).
5. E. Piers, R.W. Friesen, and S.J. Rettig. Can. J. Chem. **70**, 1385 (1992).
6. E. Piers and R.W. Friesen. Can. J. Chem. **65**, 1681 (1987);

E. Piers, R.W. Friesen, P. Kao, S.J. Rettig, and J. Trotter. Can J. Chem. **71**, 1463 (1993).
7. E. Piers and M. Llinas-Brunet. J. Org. Chem. **54**, 1483 (1989).
8. E. Piers and H.L.A. Tse. Tetrahedron Lett. **25**, 3155 (1984).
9. H.J. Reich, J.M. Renga, and I.L. Reich. J. Am. Chem. Soc. **97**, 5434 (1975).
10. G.H. Posner, C.E. Whitten, and J.J. Sterling. J. Am. Chem. Soc. **95**, 7788 (1973).
11. J.-P. Gorlier, L. Hamon, J. Levisalles, and J. Wagnon. J. Chem. Soc. Chem. Commun. **88** (1973); L. Hamon and J. Levisalles. J. Organomet. Chem. **251**, 133 (1983).
12. J.E. McMurry and W.J. Scott. Tetrahedron Lett. **24**, 979 (1983).
13. W.C. Still, M. Kahn, and A. Mitra. J. Org. Chem. **43**, 2923 (1978).
14. S. Krishnamurthy and H.C. Brown. J. Org. Chem. **41**, 3064 (1976).
15. W.G. Salmond, M.A. Barta, and J.L. Havens. J. Org. Chem. **43**, 2057 (1978).
16. D. Caine. Org. React. **23**, 1 (1976).
17. M.J.T. Robinson. Tetrahedron, **21**, 2475 (1965).
18. E. Piers, W.M. Phillips-Johnson, and C. Berger. Can. J. Chem. **53**, 1291 (1975).
19. E.J. Corey, J. Kang, and K. Kyler. Tetrahedron Lett. **26**, 555 (1985).
20. L. Lombardo. Tetrahedron Lett. **23**, 4293 (1982).
21. K. Omura and D. Swern. Tetrahedron, **34**, 1651 (1978).
22. W.C. Still and C. Gennari. Tetrahedron Lett. **24**, 4405 (1983).
23. D. Liotta, U. Sunay, H. Santiesteban, and W. Markiewicz. J. Org. Chem. **46**, 2605 (1981).
24. J.E. Shaw and K.K. Knutson. J. Org. Chem. **36**, 1151 (1971).
25. T. Shioiri, K. Ninomiya, and S. Yamada. J. Am. Chem. Soc. **94**, 6203 (1972).
26. T.L. Capson and C.D. Poulter. Tetrahedron Lett. **25**, 3515 (1984).
27. C.W. Huffman. J. Org. Chem. **23**, 727 (1958).
28. R. Appel, R. Kleinstuck, and K.-D. Ziehn. Angew. Chem. Int. Ed. Engl. **10**, 132 (1971).

Can. J. Chem. Downloaded from www.nrcresearchpress.com by 213.200.69.106 on 09/08/12
For personal use only.

Crystal chemistry of tetraradial species. Part 3. Salts of aliphatic Schiff bases crystallizable from aqueous media: crystal structures of five iminium tetraphenylborates and a 6-31G* *ab initio* study of simple iminium ions[1]

OSVALD KNOP, T. STANLEY CAMERON, PRADIP K. BAKSHI,[2] WITOLD KWIATKOWSKI, S.C. CHOI, AND D. ADHIKESAVALU[3]

Department of Chemistry, Dalhousie University, Halifax, NS B3H 4J3, Canada

Received March 24, 1993

Can. J. Chem. Downloaded from www.nrcresearchpress.com by 213.200.69.106 on 09/08/12
For personal use only.

OSVALD KNOP, T. STANLEY CAMERON, PRADIP K. BAKSHI, WITOLD KWIATKOWSKI, S.C. CHOI, and D. ADHIKESAVALU. Can. J. Chem. **71**, 1495 (1993).

Recrystallization of a primary or secondary alkylammonium tetraphenylborate (TB) from approximately 1:1 mixtures of Me_2CO (or MeEtCO) and water yields, against expectation, the TB of the corresponding iminium cation and thus provides an easy route to a variety of aliphatic Schiff bases. The crystal structures of five such salts have been determined: **A**, $[Me_2C{=}NHMe]BPh_4$ (*Cmcm*, a = 10.747(2) Å, b = 15.641(4) Å, c = 13.453(4) Å, Z = 4); **B**, $[Me_2C{=}NMe_2]BPh_4$ (*Cmca*, a = 13.196(4) Å, b = 14.469(3) Å, c = 25.122(4) Å. Z = 8); **C**, $[Me_2C{=}NHEt]BPh_4$ ($P2_1/n$, a = 12.146(3) Å, b = 14.099(2) Å, c = 14.177(3) Å, β = 96.23(2)°, Z = 4); **D**, $[MeEtC{=}NHMe]BPh_4$ ($Cmc2_1$, a = 10.967(5) Å, b = 15.642(5) Å, c = 13.430(4) Å, Z = 4); **E**, $[Me_2C{=}NH(\beta\text{-}CH_2CH_2Ph)]BPh_4 \cdot H_2O$ ($C2/c$, a = 30.747 Å, b = 9.845(4) Å, c = 19.741(5) Å, β = 97.12(2)°, Z = 8). The building principles of these and related TBs are discussed in detail, as also is the tendency of the small iminium ions to orientational disorder. The range of the C=N bond length in these and other iminium salts is quite narrow, with 1.283(12) Å as the mean (uncorrected) value. Where a hydrogen atom(s) is attached to the iminium nitrogen, it will form a hydrogen bond (simple or bifurcated) with the aromatic π system of the nearest phenyl ring(s). The narrowness of the C=N bond-length range with respect to substitution on the cation has prompted a detailed 6-31G* *ab initio* study of the effect, on the geometry of the $[H_2C{=}NH_2]^+$ ion, of a partial or complete replacement of the H atoms by one of the following substituents: F, Cl, CN, Li, and Na. The 46 structures optimized in planar geometry were supplemented by a number of optimizations of similarly substituted ethylenes as well as by a few optimizations in perpendicular geometry. Analysis of the numerical results involves the bond lengths and angles, Mulliken ε_M and (in part) Löwdin ε_L net charges on the atoms, and electron densities $\rho_c = \rho(r_c)$ at the bond critical points. Only a limited use has been made of comparisons involving the total electronic energies E (substitutional isomerism). Since the above substituents span the entire electronegativity scale, and CN provides for the possibility of conjugation, the effects they produce are expected to bracket the effects that would be produced by any other substituents. The calculations confirm the essential narrowness of the C=N bond-length range in iminium ions. They also show that, at least in the 6-31G* scheme, the nitrogen in $[H_2C{=}NH_2]^+$ carries a significant *negative* net charge (both in terms of ε_M and ε_L), which is contrary to the conventional representation of the ion as $H_2C{=}N^+H_2$. The *trends* observed in the parameters are smooth and highly self-consistent except for the tri- and tetrasubstituted ions containing Li or Na, where interligand repulsions may invalidate the assumption of planarity. Many of the parameters can be represented to a high degree of correlation as linear functions $\alpha_0 + \alpha_C n_C(X) + \alpha_N n_N(X)$ of the numbers n of substituent atoms X on the C and N atoms. This representation makes it possible to estimate the contribution to the parameter value from the substitution at the distant atom of the C=N bond, i.e., the extent of localization of the effect produced by the substituent. The success of the linearization of the parameter variation raises the important question of whether the apparent additivity is genuine and intrinsic or merely a property of the 6-31G* optimization scheme. In other words, will additivity be retained, functionally, for sets of parameters obtained from higher level *ab initio* calculations, and will it be eventually verified by experiment?

OSVALD KNOP, T. STANLEY CAMERON, PRADIP K. BAKSHI, WITOLD KWIATKOWSKI, S.C. CHOI et D. ADHIKESAVALU. Can. J. Chem. **71**, 1495 (1993).

La recristallisation d'un tétraphénylborate d'alkylammonium primaire ou secondaire (TB) dans des mélanges approximativement 1 : 1 d'acétone (ou de butanone) et d'eau conduit, contre toute attente, au TB du cation iminium correspondant; ceci fournit une voie de synthèse facile pour une variété de bases de Schiff aliphatiques. On a déterminé les structures cristallines de cinq de ces sels : **A**, $[Me_2C{=}NHMe]BPh_4$ (*Cmcm*, a = 10,747(2), b = 15,641(4) et c = 13,453(4) Å, Z = 4); **B**, $[Me_2C{=}NMe_2]BPh_4$ (*Cmca*, a = 13,196(4), b = 14,469(3) et c = 25,122(4) Å, Z = 8); **C**, $[Me_2C{=}NHEt]BPh_4$ ($P2_1/n$, a = 12,146(3), b = 14,099(2) et c = 14,177(3) Å, β = 96,23(2)°, Z = 4); **D**, $[MeEtC{=}NHMe]BPh_4$ ($Cmc2_1$, a = 10,967(5), b = 15,642(4) et c = 13,430(4) Å, Z = 4); **E**, $[(Me_2C{=}NH(\beta\text{-}CH_2CH_2Ph)BPh_4 \cdot H_2O$ ($C2/c$, a = 30,747, b = 9,845(4) et c = 19,741(5) Å, β = 97,12(2)° et Z = 8). On discute en détail des principes d'empilement de ces TB et de leurs composés apparentés ainsi que de la tendance des petits ions iminium à se trouver dans un désordre orientationnel. La plage des longueurs des liaisons C=N de ces sels d'iminium et d'autres composés apparentés est très mince, avec une valeur moyenne (non corrigée) de 1,283(12) Å. Lorsqu'un (ou des) hydrogène(s) est (ou sont) attaché(s) à l'azote de l'iminium, il(s) forme(nt) une liaison hydrogène simple (ou bifurquée) avec le système π aromatique du (ou des) noyau(x) phényle(s) le(s) plus proche(s). L'étroitesse de la plage des longueurs des liaisons C=N en fonction de la substitution sur le cation nous conduit à réalisé une étude détaillée *ab in-*

---

[1]For Part 2 see ref. 1.

[2]Holder of a graduate scholarship, Canadian Commonwealth Scholarship and Fellowship Plan, and of a Killam Graduate Scholarship.

[3]Present address: Muthurangam Government Arts College, Vellore, India 632 002.

itio 6-31G* complète de l'effet, sur la géométrie de l'ion $[H_2C{=}NH_2]^+$, du remplacement complet ou partiel des atomes de H par un des groupes suivants : F, Cl, CN, Li et Na. On a optimisé 46 structures en géométrie planaire ainsi qu'un certain nombre d'éthylènes substitués de la même manière en plus de quelques optimisations dans la géométrie perpendiculaire. L'analyse des résultats numériques implique les longueurs de liaison et les angles, les charges nettes de Mulliken, ϵ_M, et (en partie) de Löwdin, ϵ_L, sur les atomes et les densités électroniques, $\rho_c = \rho(r_c)$, aux points critiques de la liaison. On n'a fait qu'une utilisation restreinte de comparaisons impliquant les énergies électroniques totales, *E* (isomérie de substitution). Puisque les substituants utilisés couvrent l'ensemble de l'échelle de l'électronégativité et que le CN offre la possibilité de conjugaison, on s'attend à ce que les effets produits recouvrent l'ensemble des effets qui pourraient être provoqués par d'autres substituants. Pour l'essentiel, les calculs confirment que la plage des longueurs des liaisons C=N est étroite dans les ions iminium. Ils montrent aussi, au moins au niveau 6-31G*, que l'azote du $[H_2C{=}NH_2]^+$ porte une charge nette *négative* importante (tant en termes de ϵ_M que de ϵ_L), ce qui est contraire à la représentation conventionnelle de l'ion, $H_2C{=}N^+H_2$. Les *tendances* observées dans les paramètres sont graduelles et très autocohérentes, excepté pour les ions tri- et tétracoordinés contenant du Li ou du Na; dans ces cas, les répulsions intercoordinats peuvent invalider l'hypothèse de planéité. On peut obtenir une bonne corrélation de plusieurs paramètres par les fonctions linéaires $\alpha_0 + \alpha_C n_C(X) + \alpha_N n_N(X)$ des nombres *n* de substituants X sur les atomes C et N. Grâce à cette corrélation, on peut évaluer la contribution à la valeur du paramètre à partir de la substitution sur l'atome éloigné de la liaison C=N, c'est-à-dire l'étendue de la localisation de l'effet produit par le substituant. Le succès de la linéarisation de la variation du paramètre soulève une question importante : est-ce que l'additivité apparente est réelle et intrinsèque ou s'agit-il simplement d'une propriété du schéme d'optimisation 6-31G*? En d'autres termes, est-ce que l'additivité sera fonctionnellement maintenue pour des ensembles de paramètres obtenus par des calculs *ab initio* à des niveaux plus élevés et permettra-t-elle éventuellement de vérifier des expériences?

[Traduit par la rédaction]

Aliphatic $[RR'C{=}NR''R''']^+$ Schiff cations are notorious for the ease with which they hydrolyze to the corresponding aldehyde or ketone and the alkylammonium cation (2). Because of this their synthesis and use require rigorously anhydrous conditions (for example, refs. 2–11). It came therefore as a surprise to find that solutions of $MeNH_3^+$ and $Me_2NH_2^+$ tetraphenylborates in mixtures of acetone and water, when concentrated by evaporation at room temperature, yield crystals of the $Me_2C{=}NHMe^+$ and $Me_2C{=}NMe_2^+$ iminium tetraphenylborates, and that these crystals can be handled without special precautions in atmospheric air. The simple expedient of recrystallization from an acetone–water solution thus provides an easy synthetic route to the two iminium salts.

Encouraged by this discovery, we have successfully used this method to prepare several other tetraphenylborates of this type and determined the crystal structures of $[Me_2C{=}NHMe]BPh_4$ (**A**), $[Me_2C{=}NMe_2]BPh_4$ (**B**), $[Me_2C{=}NHEt]BPh_4$ (**C**), $[MeEtC{=}NHMe]BPh_4$ (**D**), and $[Me_2C{=}NH(\beta\text{-phenethyl})]BPh_4 \cdot H_2O$ (**E**). (Table 1). Formation of the iminium cation was ascertained by the appearance of the diagnostic ν(C=N) ir absorption band at ca. 1680 cm^{-1} (Table 2).[4] From the crystal structures of **A**–**E** and those of other tetraphenylborates (15–22) we have been able to elucidate some of the principles of ion packing in tetraphenylborates of small cations, and also to provide evidence for the existence of hydrogen bonding between cation or H_2O hydrogens and the aromatic π system of the phenyl ring(s). In addition, *ab initio* (6-31G*) calculations on a variety of substituted $[LL'C{=}NL''L''']^+$ cations have made it possible to examine the effects of substitution on the geometry and the net charges in such cations, as well as the existence of a correlation between the C=N bond length and the electron density $\rho(r_c)$ at the bond critical point (cf. ref. 23).

Crystal structures

The positional parameters of non-hydrogen atoms in **A**–**E** are listed in Table 3 and the bond lengths and angles in the cations of **A**–**E** in Table 4. Tables of other parameters and derived quantities have been deposited.[5] The contents of the deposited tables are as follows:

A. Positional parameters and isotropic temperature factors of hydrogen atoms.

B. Anisotropic thermal parameters of non-hydrogen atoms.

C. Bond lengths and bond angles in the anions of **A**–**E**.

D. CBC valence angles α and α' in **A**–**E**.

E. Deviations from best planes through phenyl rings and through cations in **A**–**E**.

F. Dihedral angles between best planes through the phenyl rings.

G. Molecular parameters for the CN groups of the cyano-substituted iminium ions of Tables 7 and 8.

H. Power regressions $\rho_c = sd^{-v}$ of the electron density at the bond critical point on the corresponding bond lengths in iminium ions.

J–N. Observed and calculated structure factors for **A**–**E**.

P. Coefficients of the linear regressions $d = a_0 + a_C n_C + a_N n_N$ for the bond lengths and interligand distances (Å) in X-substituted planar iminium ions.

Q. Coefficients of the linear regressions $\epsilon = b_0 + b_C n_C + b_N n_N$ for the Mulliken ϵ_M and Löwdin ϵ_L net charges in X-substituted planar iminium ions.

R. Coefficients of the linear regressions $\rho_c = c_0 + c_C n_C + c_N n_N$ for the electron densities at the bond critical points in X-substituted planar iminium ions.

S. Comparison of Mulliken ϵ_M and Löwdin ϵ_L net charges (e) in planar F and CN substituted iminium ions.

T. Coefficients of the exponential regressions $\epsilon_M(X) = p + q \exp[-s\epsilon_M(C \text{ or } N)]$ for the mono- and disubstituted iminium ions and ethylenes.

[4]Only values directly relevant to **A**–**E** are listed. For a comprehensive list of ν(C=N) frequencies in other iminium salts see Table I of ref. 14.

[5]This material may be purchased from: The Depository of Unpublished Data, Document Delivery, CISTI, National Research Council Canada, Ottawa, Canada K1A 0S2.

Tables A, C, and G have also been deposited with the Cambridge Crystallographic Data Centre, and can be obtained on request from The Director, Cambridge Crystallographic Data Centre, University Chemical Laboratory, 12 Union Road, Cambridge, CB2 1EZ, U.K.

Can. J. Chem. Downloaded from www.nrcresearchpress.com by 213.200.69.106 on 09/08/12
For personal use only.

TABLE 1. Crystal data of $[Me_2C{=}NHMe]BPh_4$ (**A**), $[Me_2C{=}NMe_2]BPh_4$ (**B**), $[Me_2C{=}NHEt]BPh_4$ (**C**), $[MeEtC{=}NHMe]BPh_4$ (**D**), and $[Me_2C{=}NH(\beta\text{-phenethyl})]BPh_4 \cdot H_2O$ (**E**)[a]

Parameter	**A**	**B**	**C**	**D**(LT)	**E**
Formula	$BC_{28}H_{30}N$	$BC_{29}H_{32}N$	$BC_{29}N_{32}N$	$BC_{29}H_{32}N$	$BC_{35}H_{36}NO$
fw	391.4	405.4	405.4	405.4	497.5
Crystal size, mm^3	0.27 × 0.35 × 0.25	0.4 × 0.2 × 0.4	0.4 × 0.5 × 0.2	0.27 × 0.2 × 0.4	0.8 × 0.05 × 0.4
θ-range, deg[b]	12.0–15.0/25	10.2–16.4/21	10.2–14.5/23	12.0–15.0/25	3.9–10.8/21
Space group	*Cmcm* (no. 63)	*Cmca* (no. 64)	$P2_1/n$ (no. 14)	$Cmc2_1$ (no. 36)	$C2/c$ (no. 15)
a, Å	10.747(2)	13.196(4)	12.146(3)	10.967(5)	30.747(10)
b, Å	15.641(4)	14.469(3)	14.099(2)	15.642(5)	9.845(4)
c, Å	13.453(4)	25.122(4)	14.177(3)	13.430(4)	19.741(5)
β, deg	90	90	96.23(2)	90	97.12(2)
V, $Å^3$	2261(2)	4797(4)	2413(2)	2304(3)	5930(6)
Z	4	8	4	4	8
ρ_c, g/cm^3	1.150(1)	1.123(2)	1.116(1)	1.169(2)	1.115(1)
F(000), e	840	1744	872	872	2128
Reflections:					
θ-range, deg	3–25	2–23	2–23	2–23	2–30
Max/min[c]	1.21/0.75	1.69/0.71	1.04/0.92	1.24/0.73	1.39/0.59
Total measured	1474	1892	3725	1871	6117
Unique measured	1105	1887	3539	1770	5957
Unique used[d]	624	832	1605	708	1378
R_{merg}, %	2.7	1.9	2.2	8.3	11.7
d/p[e]	5.9[f]	4.4[f]	5.7[g]	4.1[g]	4.0[g]
R, %; R_w, %	5.5; 5.8	4.8; 5.3	4.2; 3.8	4.8; 5.4	5.0; 5.1
G.O.F.	2.41	2.09	1.67	1.26	2.50
Residual ed.,[h] $e/Å^3$	−0.16/0.23	−0.20/0.17	−0.18/0.14	−0.20/0.30	−0.18/0.19

[a]Mo *K*α, λ = 0.71069 Å (**B**, **C**, **E**), 0.70926 Å (**A**, **D**-LT); graphite monochromator; *T* = 18(1)°C (**A**–**C**, **E**), −70(1)°C (**D**-LT).
[b]$\theta_{min} < \theta < \theta_{max}/n$. The lattice parameters and orientation matrices were obtained by least squares from the setting angles θ of *n* suitable reflections.
[c]Max/min empirical absorption corrections, cf. ref. 12.
[d]$I > 3\sigma(I)$.
[e]Data-to-parameters ratio.
[f]H(C) atoms placed geometrically (C—H, 1.08 Å) and refined isotropically.
[g]H(C) atoms placed geometrically (C—H, 1.08 Å, $U_{iso}(H) = 1.2B_{eq}(C)$) and not refined.
[h]Minimum and maximum residual electron density in final difference map.

TABLE 2. Frequencies (cm^{-1}) of the ir C=N and NH stretching absorptions in iminium ions[a]

Compound	ν(C=N)	ν(NH)	Reference
$[H_2C{=}NMe_2]I$[b]	1682	—	7
	1681.7		13
$[Me_2C{=}NHMe]BPh_4$ (**A**)	1688.2(1)	3246.5	This work
		3165.5[c]	
$[Me_2C{=}NMe_2]ClO_4$	1687	—	4
$[Me_2C{=}NMe_2]BPh_4$ (**B**)	1674.0(1)	—	This work
$[Me_2C{=}NHEt]BPh_4$ (**C**)	1681.1	3238.0	This work
		3161.0	
$[MeEtC{=}NHMe]BPh_4$ (**D**)	1685.0	3228.0	This work
		3159.0	
$[Me_2C{=}NH(\beta\text{-phenethyl})]BPh_4 \cdot H_2O$ (**E**)[d]	1689.5		This work

[a]This work: FT-ir spectra of fluorolube mulls on CaF_2 plates.
[b]ν(CH) = 3115, 3011.2 cm^{-1}.
[c]Higher-frequency component of an unresolved doublet.
[d]ν(OH) = 3590.5, 3529.5 cm^{-1}.

Preliminary observations

Because of its bulk the tetraphenylborate (TB) ion is often used as a counter-anion of convenience when it is desired to prepare well-crystallized salts of large composite cations or simply to stabilize such cations. This is reflected in the generous number of crystal structure determinations of tetraphenylborates in the literature. By the same token, however, in the majority of these structures the large cation, often of awkward shape, dominates the packing geometry and this tends to obscure, in all but a small number of the known

Can. J. Chem. Downloaded from www.nrcresearchpress.com by 213.200.69.106 on 09/08/12
For personal use only.

Can. J. Chem. Downloaded from www.nrcresearchpress.com by 213.200.69.106 on 09/08/12
For personal use only.

TABLE 3. Positional parameters ($\times 10^4$ except for special positions) of nonhydrogen atoms in **A**–**E**

Atom	*x*	*y*	*z*
	$[Me_2C{=}NHMe]BPh_4$ (**A**)		
B	1/2	1666(4)	3/4
C(11)	1/2	2313(2)	6542(3)
C(12)	3899(3)	2641(1)	6127(2)
C(13)	3893(3)	3237(1)	5367(2)
C(14)	1/2	3535(2)	4973(3)
C(21)	3802(4)	1024(2)	3/4
C(22)	3294(3)	0694(1)	6626(2)
C(23)	2336(3)	0090(1)	6622(2)
C(24)	1871(5)	−0215(3)	3/4
N	1/2	1079(5)	2145(5)
C(N)	1/2	1311(4)	1097(4)
C	1/2	1639(5)	2819(5)
C(C1) ≡ C(1)′	1/2	2566(4)	1/4
C(2) ≡ C(N)′	1/2	1311(4)	3903(4)
	$[Me_2C{=}NMe_2]BPh_4$ (**B**)		
B	1/2	1647(3)	3788(2)
C(11)	4009(2)	0962(1)	3777(1)
C(12)	3557(3)	0635(2)	3309(1)
C(13)	2733(3)	0031(2)	3305(1)
C(14)	2333(3)	−0290(2)	3773(1)
C(15)	2771(3)	−0013(2)	4243(1)
C(16)	3595(3)	0595(2)	4242(2)
C(21)	1/2	2344(3)	4292(2)
C(22)	4110(3)	2713(2)	4510(1)
C(23)	4106(4)	3386(2)	4909(1)
C(24)	1/2	3711(4)	5110(3)
C(31)	1/2	2362(3)	3264(2)
C(32)	4110(3)	2721(2)	3048(1)
C(33)	4107(3)	3376(2)	2642(1)
C(34)	1/2	3708(3)	2435(2)
N	5335(4)	2066(4)	1417(2)
C(N1) ≡ C(C2)′	6430(2)	2307(3)	1325(1)
C(N2) ≡ C(N2)′	1/2	1255(4)	1752(2)
C	4652(4)	2591(3)	1207(2)
C(C1) ≡ C(C1)′	1/2	3410(3)	0881(2)
C(2) ≡ C(N1)′	3570(2)	2307(3)	1325(1)
	$[Me_2C{=}NHEt]BPh_4$ (**C**)		
B	9836(3)	1732(3)	2504(3)
C(11)	8671(3)	1196(3)	2685(2)
C(12)	8568(3)	0240(3)	2907(3)
C(13)	7575(4)	−0164(3)	3119(3)
C(14)	6642(4)	0375(4)	3122(3)
C(15)	6694(3)	1321(4)	2901(3)
C(16)	7686(3)	1717(3)	2687(3)
C(21)	10797(3)	0973(2)	2284(2)
C(22)	11902(3)	0975(3)	2682(2)
C(23)	12683(3)	0338(3)	2401(3)
C(24)	12398(4)	−0321(3)	1717(3)
C(25)	11316(4)	−0348(3)	1291(3)
C(26)	10548(3)	0289(3)	1572(3)
C(31)	9685(3)	2412(2)	1562(2)
C(32)	8872(3)	2266(3)	0800(3)
C(33)	8804(3)	2802(3)	−0028(3)
C(34)	9554(4)	3516(3)	−0119(3)
C(35)	10363(3)	3684(3)	0604(3)
C(36)	10429(3)	3142(3)	1429(3)
C(41)	10155(3)	2359(2)	3475(2)
C(42)	10657(3)	1962(3)	4316(3)
C(43)	10898(3)	2480(3)	5152(3)
C(44)	10611(4)	3418(3)	5176(3)
C(45)	10083(4)	3828(3)	4375(3)
C(46)	9868(3)	3305(3)	3551(3)
N	7840(3)	2335(3)	5070(2)
C(N1)	7441(4)	3298(3)	5198(3)
C(N2)	6830(5)	3676(4)	4330(4)
C	8349(3)	1806(3)	5706(3)
C(C1)	8657(4)	2149(3)	6692(3)
C(C2)	8624(4)	0831(3)	5472(3)
	$[MeEtC{=}NHMe]BPh_4$ (**D**-LT)		
B	0	3346(4)	0904(0)
C(11)	0	2713(6)	−0101(7)
C(12)	1094(6)	2366(4)	−0488(5)
C(13)	1091(8)	1764(5)	−1242(6)
C(14)	0	1418(8)	−1629(10)
C(21)	0	2688(6)	1815(8)
C(22)	1051(7)	2381(4)	2245(5)
C(23)	1072(7)	1767(4)	2989(5)
C(24)	0	1473(6)	3371(7)
C(31)	1173(3)	3998(2)	0859(7)
C(32)	1673(8)	4316(4)	−0017(5)
C(33)	2620(10)	4933(5)	0034(8)
C(34)	3082(4)	5227(2)	0915(9)
C(35)	2619(7)	4920(4)	1786(6)
C(36)	1682(7)	4322(4)	1746(5)
N	0295(0)	3923(4)	5496(6)
C(N)	−0034(4)	3746(7)	4457(7)
C	0197(10)	3373(5)	6188(6)
C(C1)	0295(0)	3636(8)	7290(10)
C(C21)	0515(6)	2484(5)	5881(15)
C(C22)	−0624(8)	1944(6)	5855(14)
	$[Me_2C{=}NH(CH_2CH_2Ph)]BPh_4 \cdot H_2O$ (**E**)		
B	1465(3)	0469(9)	0669(4)
C(11)	1041(2)	−0201(8)	0962(4)
C(12)	0883(2)	−1494(9)	0754(4)
C(13)	0553(3)	−2150(10)	1050(5)
C(14)	0365(2)	−1550(10)	1575(5)
C(15)	0514(3)	−0290(10)	1805(4)
C(16)	0848(2)	0353(9)	1501(4)
C(21)	1889(2)	−0318(9)	1075(4)
C(22)	2057(2)	0050(10)	1742(4)
C(23)	2385(3)	−0690(10)	2130(4)
C(24)	2563(3)	−1830(10)	1852(6)
C(25)	2403(3)	−2230(10)	1206(5)
C(26)	2076(2)	−1486(9)	0821(4)
C(31)	1487(2)	2112(8)	0771(4)
C(32)	1881(2)	2840(10)	0907(4)
C(33)	1899(3)	4250(10)	0934(4)
C(34)	1518(3)	5023(9)	0821(4)
C(35)	1122(3)	4360(10)	0674(4)
C(36)	1112(2)	2950(10)	0642(4)
C(41)	1424(2)	0289(8)	−0168(4)
C(42)	1019(2)	0290(10)	−0583(4)
C(43)	0978(3)	0270(10)	−1306(4)
C(44)	1344(3)	0240(10)	−1613(4)
C(45)	1751(3)	0250(10)	−1230(5)
C(46)	1792(2)	0294(9)	−0529(4)
N	1469(2)	5106(7)	7982(3)
C(N1)	1243(2)	6137(9)	7523(4)
C(N2)	0751(3)	5770(10)	7375(4)
C(N3)	0529(2)	5800(10)	8003(4)
C(N4)	0498(3)	4650(10)	8388(5)

TABLE 3 (*concluded*)

Atom	*x*	*y*	*z*
C(N5)	0328(3)	4720(10)	8996(6)
C(N6)	0197(3)	5960(20)	9252(6)
C(N7)	0220(3)	7110(10)	8856(6)
C(N8)	0391(3)	7020(10)	8255(5)
C	1577(2)	5190(10)	8634(4)
C(C1)	1798(3)	4000(10)	8982(5)
C(C2)	1494(2)	6400(10)	9050(4)
O	6506(2)	2240(6)	2218(3)

structures, the basic principles that govern the ion packing and the conformational behaviour of the anion in TB structures with small or medium-size cations.[6]

To understand the crystal chemistry of the title compounds it is instructive to compare the alkali TBs, as exemplified by the K^+ (16) and NH_4^+ (18) salts, with the tetramethylammonium salt Me_4NBPh_4 = 4MTB (16). The tetragonal (*I*4*m*, *Z* = 2) TBs form an isostructural series (25), in which the cation size ranges from Na to Cs; 4MTB is orthorhombic (*Cmcm*, *Z* = 4). In both cases the structure consists of columns in which cations alternate with anions. In the alkali salts the axes of these columns coincide with the 4 axes, in 4MTB they are parallel to the *b* axis. In the former, the quasi-spherical cation is inside a "tetrahedral" cavity formed by two pairs of phenyl rings, one pair from the anion above and the other from the anion below the cation, all three ions in the same column (Fig. 1*a*). In 4MTB, however, the cation is too large for this type of packing to remain favourable: the phenyl-ring coordination of the cation is still "tetrahedral," but now only one pair of rings comes from an anion neighbour in the same column, the other two rings come one each from anions in neighbouring columns (Fig. 1*b*). To achieve such partial hetero-column coordination the vertical positions of the N and B atoms in neighbouring columns must be adjusted, which results in a lowering of the space-group symmetry.

In $KBPh_4$ the ions are arranged in a tetragonally distorted NaCl-type packing, with the N and B atoms on tetragonal Bravais *I* sublattices (Fig. 2*a*)[7] In 4MTB the orthorhombic distortion of the N and B sublattices is appreciable but the NaCl-type packing is still recognizable (Fig. 2*b*). Moderate increase in the effective cation size may thus be expected to bring about a change in the space-group symmetry consistent with the transition from homo-column to partial hetero-column cation coordination, i.e., from *I*42*m* to *Cmcm* or subgroup as a likely candidate.

*Compounds **A**, **B**, and **D***

Projections on (100) of these three structures and of 4MTB are shown in Fig. 3. **A** and **D** have unit cells of roughly similar shapes, while that of **B** is doubled along *c*. The space-group relations of these orthorhombic structures can be represented as $Cmc2_1$ (**D**) ⊂ [*Cmcm* (**A**), *Cmca* (**B**)] ⊂ *Fmmm* ⊂ *Fm*3*m*. The ion packing in all three is of the same type as in 4MTB (*Cmcm*). The structure of the latter is closely similar to both **A** and **D**: columns of alternating ions are parallel to *b*. The structure of **B** consists of $a \times b \times (c/2)$ segments, each of almost *Cmcm* symmetry, translated along *c* and related by the *a* translations of *Cmca* in the $z = \pm\frac{1}{4}$ planes. As in 4MTB, **A**, and **D**, the cation in **B** is coordinated by four phenyl rings, one pair from an anion in the same column and the other two, one each, from neighbouring columns. However, because of the presence of the *a* glide mirrors the "tetrahedral" coordination cage is not completely enclosed but open on one side (Fig. 1c).

The structures of **A**, **D**, and 4MTB may be regarded as distorted NaCl-type packings based on dichromatic C_A Bravais lattices; the chromatic reversal changes the orientation of the anion.

Insertion of the carbon atom into the $Me_2NMe_2^+$ cation in 4MTB to form $[Me_2C{=}NMe_2]^+$ in **B** expands the volume per formula unit by approximately 18 Å^3; the tabulated increment for the insertion of an ethylenic carbon, $CH_2 \rightarrow C{=}CH_2$, is 13.1 Å^3 (26).

*Compound **C***

The ion packing in **C** may be regarded as of a very distorted zincblende type. The cations form an approximate fc arrangement; the anions are arranged in columns of quasi-2_1 symmetry parallel to *c* (Fig. 4). The $[Me_2C{=}NHEt]^+$ cation, in a general position and with a skeleton not far from planar (Table E), is enclosed by rings 1 and 4 from one and rings 2 and 3 from another anion neighbour (Fig. 5). The cavity formed by the four rings is less symmetric than in 4MTB, **A**, **D**, or **B** (cf. Figs. 1 and 8). The N—H vector is directed at ring 1 (see below and Fig. 9). Since **C** and **B** have the same molecular weight, their volumes per formula unit would be expected to be closely similar: indeed, V_1(**C**) = 603(1) Å^3, V_1(**B**) = 600(1) Å^3.

*Compound **E***

The anions, the cations, and the water molecules in this structure are arranged in layers ∥(100), each layer containing all three component species (Fig. 6). Within a layer the anions form columns generated by the *c* glide reflection. The phenyl rings are segregated in double layers ∥(100) at $z = 0, \frac{1}{2}$; the water molecules are dispersed between the anion columns. The N—H group of the cation is hydrogen-bonded to the water molecule, which in turn forms hydrogen bonds to an anion (see below and Fig. 9). The hydrogen-bonding system is thus of the same type as that found in $(n\text{-}Bu_3NH)BPh_4 \cdot H_2O$ and presumably also in $(n\text{-}Pr_3NH)BPh_4 \cdot H_2O$ (17), whereas in the anhydrous Me_3NH^+ and Et_3NH^+ TBs the N—H group interacts directly with a phenyl ring (19, 21; Knop et al., to be published).

Cation disorder

As shown above, the packing in the structures of 4MTB, **A**, **B**, and **D** is dominated by the anion geometry. The volume of the "tetrahedral" inter-anion space that is available to the cation within the anion–cation columns is regulated by the B...B distances, which in turn depend on the shape and dimensions of the cation. In 4MTB the regular shape of the tetrahedral cation permits the cation to wedge itself between the nearest pair of phenyl rings, in a symmetric orientation and with little freedom of movement inside the phenyl-ring coordination cage (Fig. 2*b*). As a result the structure is completely ordered. In **B**, however, the cation is rectangular, and the cation shapes in **A** and **D** are even less

[6]Crystal structures of the corresponding "*anti*" compounds $[Ph_4X]^+[an]^-$ and of $[Ph_4Y]^0$ (X from Group V, Y from Group IV) have been classified by Müller (24).

[7]For the present purpose the tetragonal *I* lattice (*Z* = 2) may be represented as a tetragonal *F* lattice (*Z* = 4). In Fig. 2*a* the tetragonal bc cell has been transformed into the corresponding fc cell, the correct space-group designation now being *F*4*m*2.

Can. J. Chem. Downloaded from www.nrcresearchpress.com by 213.200.69.106 on 09/08/12
For personal use only.

Can. J. Chem. Downloaded from www.nrcresearchpress.com by 213.200.69.106 on 09/08/12
For personal use only.

TABLE 4. Bond lengths (Å) and bond angles (deg) in the cations of compounds **A**–**E**[a]

Atoms	Distance	Atoms	Angle
		Compound **A**	
C—N	1.261(7)	C(C1)—C—N	117.5(4)
C—C(C1)	1.512(6)	C(C2)—C—N	116.6(4)
C—C(C2)	1.546(6)	C(C1)—C—C(C2)	125.9(4)
N—C(N)	1.457(6)	C—N—C(N)	121.5(4)
N—H(N)	1.02	H(N)—N—C	118.6
		H(N)—N—C(N)	119.9
		Compound **B**	
C—N	1.291(8)	C(C1)—C—N	118.0(5)
C—C(C1)	1.513(7)	C(C2)—C—N	114.7(5)
C—C(C2)	1.515(7)	C(C1)—C—C(C2)	127.2(5)
N—C(N1)	1.505(7)	C—N—C(N1)	118.2(5)
N—C(N2)	1.509(7)	C—N—C(N2)	118.7(5)
		C(N1)—N—C(N2)	123.1(4)
		Compound **C**	
C—N	1.277(4)	C(C1)—C—N	121.7(4)
C—C(C1)	1.489(5)	C(C2)—C—N	119.7(4)
C—C(C2)	1.461(5)	C(C1)—C—C(C2)	118.6(4)
N—C(N1)	1.460(5)	C(N1)—N—C	126.7(4)
C(N1)—C(N2)	1.467(6)	N—C(N1)—C(N2)	112.2(4)
N—H(N)	1.02	H(N)—N—C	117.6
		H(N)—N—C(N1)	115.7
		Compound **D**-LT	
C—N	1.271(11)	C(C1)—C—N	121.0(8)
C—C(C1)	1.539(12)	C(C21)—C—N	114.1(8)
C—C(C21)	1.49(2)	C(C1)—C—C(C21)	119.9(8)
C(C21)—C(C22)	1.51(2)	C(C22)—C(C21)—C	109.6(10)
N—C(N)	1.47(2)	C(N)—N—C	123.2(10)
N—H(N)	1.02	H(N)—N—C	116.2(6)
		H(N)—N—C(N)	111.6(9)
		Compound **E**	
C—N	1.291(9)	C(C1)—C—N	117.2(9)
C—C(C1)	1.48(1)	C(C2)—C—N	124.3(9)
C—C(C2)	1.48(1)	C(C1)—C—C(C2)	118.5(8)
N—H(N)	1.02	C—N—C(N1)	127.7(8)
N—C(N1)	1.475(9)	N—C(N1)—C(N2)	109.3(7)
C(N1)—C(N2)	1.55(1)	H(N)—N—C	118.8
C(N2)—C(N3)	1.49(1)	H(N)—N—C(N1)	112.9
C(N3)—C(N4)	1.38(1)	C(N1)—C(N2)—C(N3)	112.3(6)
C(N4)—C(N5)	1.37(1)	C(N2)—C(N3)—C(N4)	120.8(9)
C(N5)—C(N6)	1.40(1)	C(N2)—C(N3)—C(N8)	120.8(9)
C(N6)—C(N7)	1.38(1)	C(N3)—C(N4)—C(N5)	120(1)
C(N7)—C(N8)	1.36(1)	C(N4)—C(N5)—C(N6)	121(1)
C(N8)—C(N3)	1.38(1)	C(N5)—C(N6)—C(N7)	118(1)
O—H(O1)	1.00	C(N6)—C(N7)—C(N8)	119(1)
O—H(O2)	1.01	C(N7)—C(N8)—C(N3)	123(1)
		C(8)—C(N3)—C(N4)	118.0(8)
		H(O1)—O—H(O2)	104.8

[a]Bond lengths and angles are not corrected for thermal motion.

regular. Introduction of a cation less "tetrahedral" than Me_4N^+ into the symmetric wedge-shaped space inside the pair of phenyl rings results in orientational disorder. The existence of the disorder complicated the structure determinations of **A**, **B**, and **D**, especially as initially it was not realized that recrystallization of $MeNH_3BPh_4$ and $Me_2NH_2BPh_4$ from aqueous acetone would yield the iminium TBs **A** and **B** instead of the expected original compounds.

The electron-density map in the cation plane of **A** (*m* in (100), Fig. 7*a*) shows clearly the twofold positional disorder across $m \| (001)$ at $z = \pm\frac{1}{4}$ (cf. Fig. 3), which interchanges z and $z' = \frac{1}{2} - z$. The almost exact coincidence of C(N) and C(C2)′, and of C(C1) and C(C1)′, precludes resolution of the corresponding composite peaks. The presence of disorder is also manifested in some of the U_{ii} values, notably in the U_{11} of C(C1) and C(N),

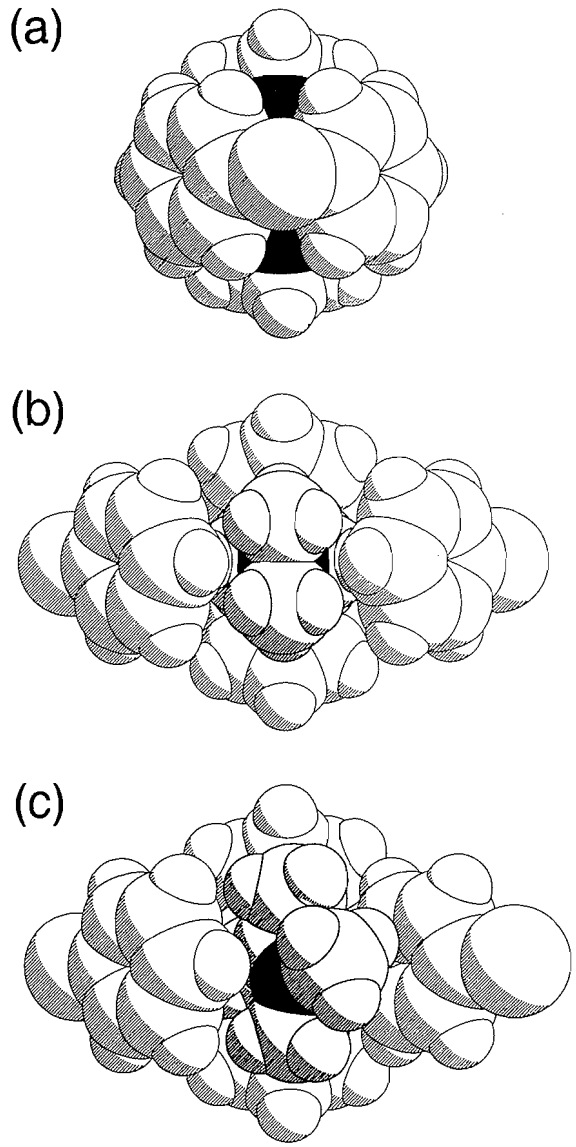

FIG 1. The quasi-tetrahedral enclosure of the cation by (*a*) two pairs of phenyl rings belonging to neighbouring anions in the same vertical cation–anion column (in $KBPh_4$); (*b*) a pair of phenyl rings of an anion neighbour in the cation–anion column and two phenyl rings each belonging to an anion in different neighbouring columns (in 4MTB); and (*c*) ditto in **B** (see text). The cation is inside the heavy outline, with the K and N atoms shown in black. Since the effective coordination number of the K^+ ion is ill-defined, the choice of $r(K^+)$ is arbitrary; however, the exact choice of the ionic radius matters little, as the cation coordination is the same in all the alkali TBs, from Na to Cs.

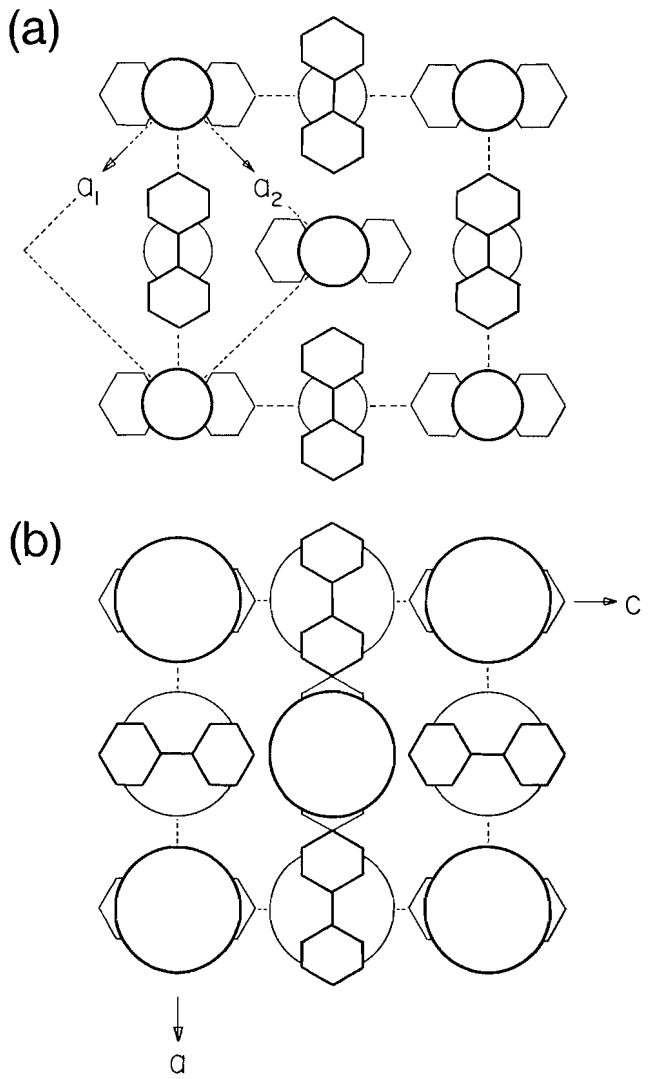

FIG. 2. Schematic representation of the ion packing and anion orientation is (*a*) $KBPh_4$ and (*b*) Me_4NBPh_4 (see text). All the phenyl rings shown are tilted upward from the page.

and to a smaller extent in the U_{11}(N) and U_{22}[C(N)] (Fig. 7*a*).

In **B** the plane of the cation is perpendicular to (100); the disorder is across a mirror plane ∥(100) (Figs. 7*b* and 8*e*). Here again the very close coincidence of the C(N1) and C(C2)′, C(C1) and C(C1)′, and C(N2) and C(N2)′ peaks renders resolution impossible.

The cation disorder that is present in **D** is of a simpler kind. The cation, in a general position, is disordered across *m*(100), i.e., $x' = -x$ (Figs. 3 and 8*b*).

While the peak heights in the electron-density maps through the cations are not a reliable guide to distinguishing between the C and N atoms in the C=N bond, in **A** the absence of a methyl carbon on the nitrogen permits unique identification. In **B**, refinement with the C and N positions of Table 3 reversed produced peak contours of unsatisfactory shapes and thus confirmed the present assignment.

Attempts to refine the three structures as fully ordered in subgroups of lower symmetry produced less satisfactory results (see Experimental).

It is interesting to note that an orientational disorder even greater than in **B** has been reported for the cation in the tetragonal (*I*4/*mmm*, $Z = 2$) $[Me_2C{=}NMe_2]ClO_4$ (27), in which crystal the ion packing is of the NaCl-type. In this even less constraining environment of nearest ClO_4^- neighbours in twofold disorder the cations are situated in mirror planes ∥(001), and their orientations are distributed over four symmetry-equivalent C—N directions. Not surprisingly, therefore, the "C=N" bond length resulting from the structure determination of the perchlorate, 1.30(4) Å, approximates the mean of the azo N=N and ethylenic C=C bond lengths.

Can. J. Chem. Downloaded from www.nrcresearchpress.com by 213.200.69.106 on 09/08/12
For personal use only.

Can. J. Chem. Downloaded from www.nrcresearchpress.com by 213.200.69.106 on 09/08/12
For personal use only.

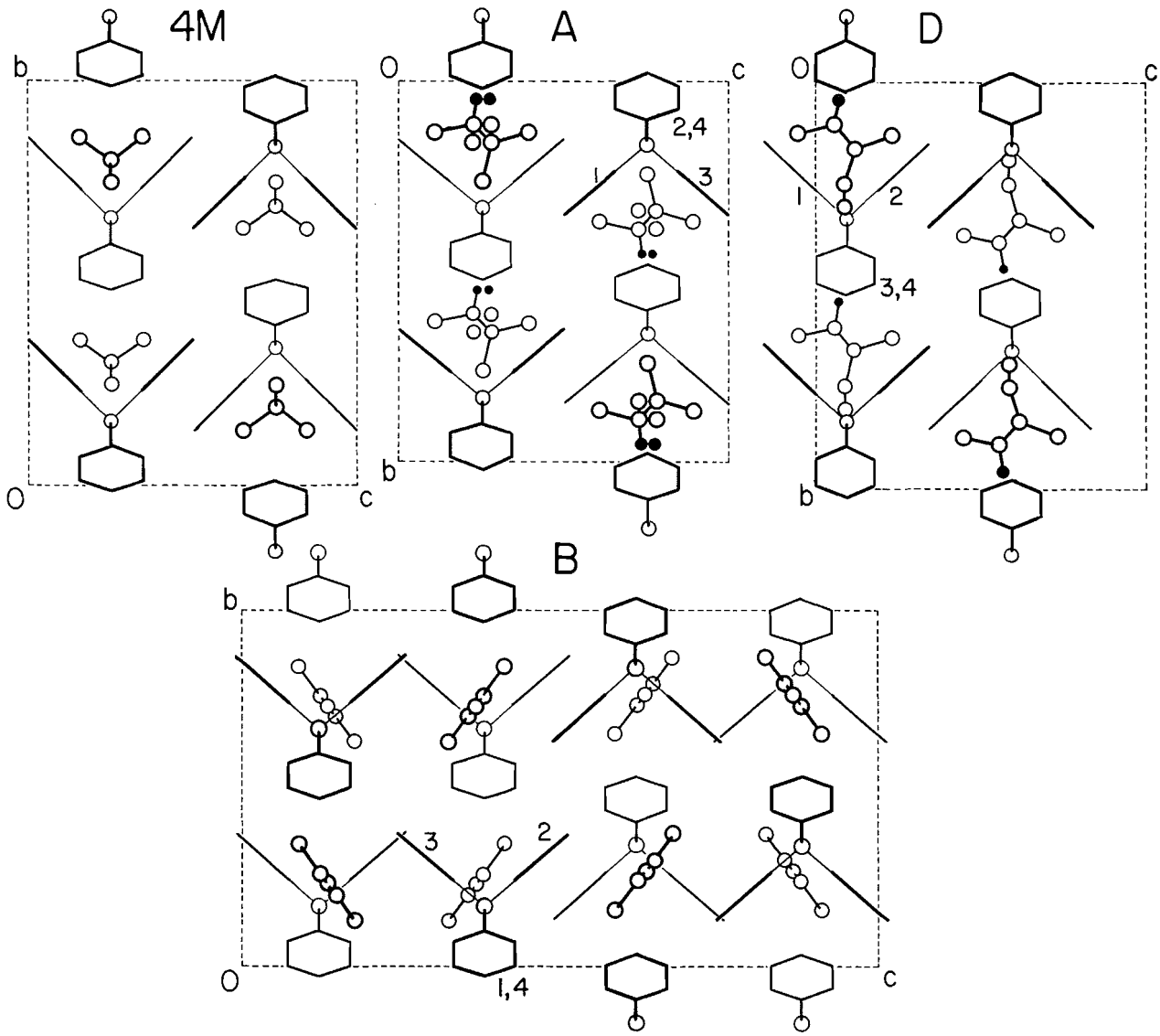

FIG. 3. Projection on (100) of the unit-cell contents of 4MTB (16), **A**, **B**, and **C**. The packing in the segment of **B** between $z = 1/4$ and $z = 3/4$ corresponds to that in the unit cells in the upper row.

Tetraphenylborate anion

The maximum possible symmetry of the anion, D_{2d}, is realized only in its unsolvated alkali and ammonium salts (16, 18, 25). Of the five proper subgroups of D_{2d}, C_{2v} is observed as the anion symmetry in **A** and 4MTB, while the crystallographic anion symmetry in **B** and **D** is C_s; the skeletal symmetry of the anion is very close to D_{2d}. The anion is asymmetric in **C** and **E**, but even in the latter its conformation is not far from D_{2d}.

The overall mean of the CBC valence angles α in **A**–**E** and 4MTB (Table D) is 104.0(10)° and that of α', 112.8(13)°. Here α represents the angle that in the D_{2d} conformation of the anion would be bisected by the S_4 axis; for conformations of subgroup symmetries other than S_4 there are two such angles, α_1 and α_2 (Tables D and 5). The valence angle α appears to be influenced by the size, shape, and position of the cation that it encloses and possibly also by hydrogen bonding betweeen the cation and the rings (Table 5 and next section).

The phenyl rings in all five structures exhibit satisfactory planarity (Table E), the mean deviation of the C atoms from the respective best planes through the 20 rings being 0.006 Å. The boron atoms are not coplanar with their phenyl rings: the mean deviation for the 20 rings is 0.12(4) Å. The non-coplanarity is seen particularly clearly in the anions of **A**, **B**, **D**, and 4MTB, in which the B atom is situated in a mirror (or pseudo mirror) plane bisecting the valence angle α. Comparison of the dihedral angle ϕ between the two rings that define α (i.e., the angle between the best planes through these rings) with the corresponding α (Tables 5, D, and F) shows that $\phi < \alpha$ instead of $\phi = \alpha$, which would be the case if the B atom were coplanar with each ring plane. The angle $\delta = \frac{1}{2}(\alpha - \phi)$ between the B–C vector and a ring plane can be appreciable (cf. Table 5); the tilt, with respect to the B–C vector, of the ring planes is toward the bisector of the CBC angle α.

The mean endocyclic CCC angles in the phenyl rings of **A**–**E** and 4MTB (Tables 4 and C) are 114.7(6)° at the C(α) carbon, 122.9(10)° at C(β), 120.4(9)° at C(γ), and 118.8(8)° at C(δ), showing clearly the effect of the bonding to the B

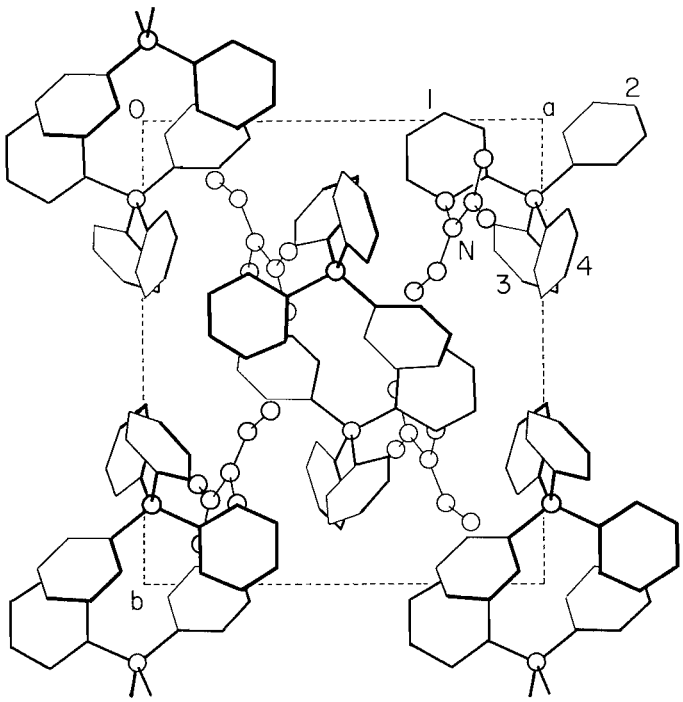

FIG. 4. Projection of the unit-cell contents of **C** on (001).

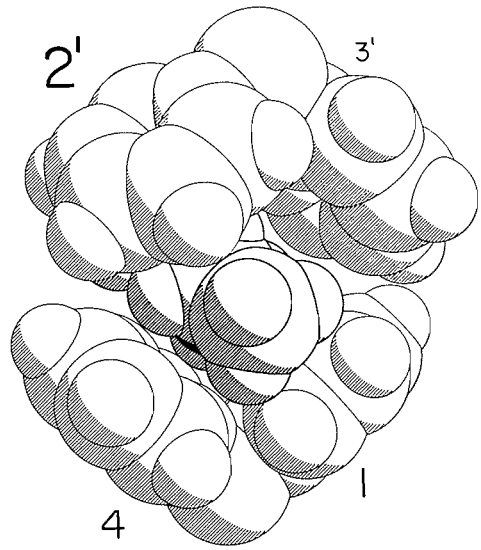

FIG. 5. The asymmetric enclosure of the cation in **C** by two pairs of phenyl rings, each pair from a different anion. Compare with Figs. 1 and 4.

atom at C(α) and the attendant compensation at the other carbon atoms.

Hydrogen bonding

The N–H vectors in **A**, **C**, and **D**, and the O–H vectors in **E**, are seen to point into a phenyl ring (**C**, **E**) or between a pair of phenyl rings enclosing the cation (**A**, **D**) (Figs. 8 and 9). These geometries suggest the formation of N^+—H...π^- and N^+—H...O—H...π^- bonds between the cation or the water molecule and the aromatic π system. More specifically, a single N–H vector points into a ring (**C**) or forms a bifurcated hydrogen bond (**A**, **D**). The two O–H vectors of the water molecule in **E** form a hydrogen bond each, analogous to the situation involving the two N–H vectors in the azoniacycloheptane TB, $[(CH_2)_6NH_2]BPh_4$, of ref. 20 (Fig. 8*c*). The geometric relation between the H-bonded cation and the phenyl ring is not affected by the presence of orientational disorder of the cation in **A** and **D**, since the alternative cation orientations are symmetric with respect to the H-bonding geometry. In **E** the situation is more complicated in that the N^+–H vector forms a hydrogen bond to the ring via the intermediary of the H_2O molecule. This type of situation has previously (17) been found in $(n\text{-}Bu_3NH)BPh_4 \cdot H_2O$, in which structure the local geometry is essentially the same as in **E** (Fig. 3 of ref. 17).

The distance of the N or O atom from the centre c_π of the associated phenyl ring varies from approximately 3.1 to approximately 3.8 Å. In **C**, N...c_π is 3.76 Å, whereas in $[(CH_2)_6NH_2]BPh_4$ (20) the corresponding two distances are much shorter, 3.08 and 3.10 Å. In **A**, N...c_π is 3.32 Å, and in **D** at low temperature the corresponding two distances are 3.10 and 3.55 Å, respectively (the N atom is in an asymmetrically bifurcated position). In the hydrated species, the two O_w...c_π distances are, respectively, 3.26 and 3.44 Å in **E**, and 3.12 and 3.19 Å in the n-Bu_3NH salt (17). These observed O_w...c_π values are in the same range as the estimates obtained from *ab initio* or other calculations (28–30) for the C_6H_6...H_2O complex, 3.1–3.4 Å. The N or O atom in general is not exactly above the centre of the associated phenyl ring, nor does the N–H or O–H vector point to the centre of the ring. Rather it appears to be directed at some point in the π-electron density region above the ring.

In contrast, in 4MTB and **B**, where no H(N) are available, the cation is farther away from its coordinating rings (in 4MTB, N...c_π = 4.40 Å, C(Me)...c_π = 3.93 Å; Fig. 8*d*) and the H(C) vectors tend to avoid the rings. The tendency of an H(N)-containing cation to orient itself preferentially to form a N^+—H...π^- grouping is shown even more clearly in anhydrous R_3NH TBs, especially when these are compared with $R_3S^+BPh_4^-$ (19, 21).[8] In **B**, in the absence of hydrogen bonding, the NMe_2 end of the cation is turned away from the nearest ring pair (Fig. 8*e*).

Although the formation of a N^+—H...π^- bond would be expected to reduce the valence angle α or the angle φ between the planes of the phenyl rings involved or both, the available data (Table 5) do not provide clear-cut evidence of such a reduction. In $KBPh_4$ and NH_4 BPh_4 the simplicity and small size of the cation result in a high-symmetry packing in which the inter-ion distances and angles are too equalized for these structures to be used as reference. However, the dihedral angle ϕ_1 in pairs of rings enclosing the cation in **A**, **D**, and **C** (possibly also in $[(CH_2)_6NH_2]BPh_4$) are consistently smaller than in 4MTB and **B**, where there is no hydrogen bonding; a similar claim could be made for the valence angle α_1 (Table 5). Details of additional TB structures containing the anion in situations of suitable symmetry are desirable before more definite conclusions can be drawn.

While structurally documented only here and there, formation of a hydrogen bond to an aromatic π system is not a novelty and may in fact be more common than the available

[8]A detailed discussion of these matters, with additional new crystal-structure determinations of TBs, is in preparation and is planned to appear as a sequel in this series.

Can. J. Chem. Downloaded from www.nrcresearchpress.com by 213.200.69.106 on 09/08/12
For personal use only.

Can. J. Chem. Downloaded from www.nrcresearchpress.com by 213.200.69.106 on 09/08/12
For personal use only.

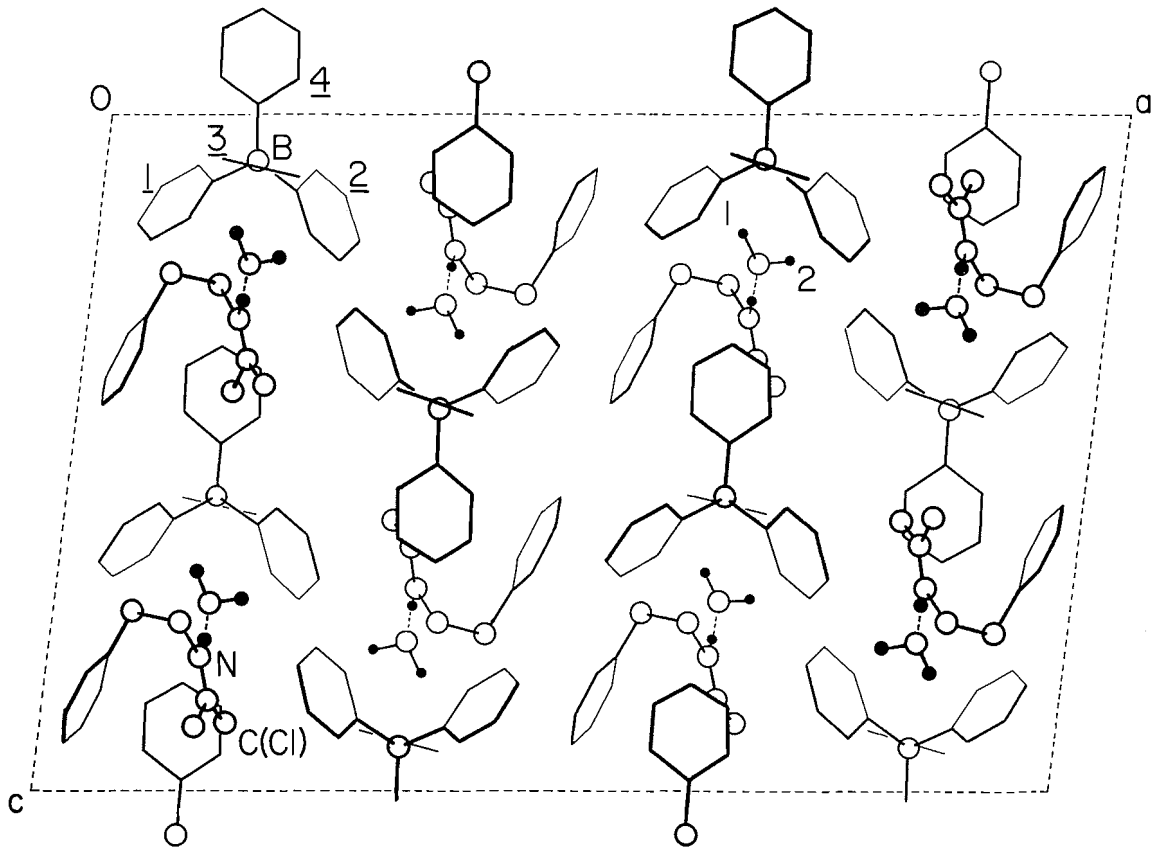

FIG. 6. Projection of the unit-cell contents of **E** on (010). The underlined numbers refer to the phenyl rings. The hydrogen atoms H(01) and H(02) of the water molecule are labelled 1 and 2.

documentation[9] might suggest. The view that X—H...π and X^+—H...π^- (X = N, O) groupings indeed constitute H-bonded systems receives support from the observed lowering of the ν(XH) ir stretching frequencies relative to a non-H-bonded reference frequency (17, 18). However, caution is indicated when invoking spectroscopic evidence: the ir spectrum *and* the crystal structure must be available, and the reference frequency must be judiciously chosen and clearly and unambiguously defined. When X—H...π involves a water molecule, i.e., X = O_w, the ultimate reference frequency is that in water vapour. The two absorption bands in the spectrum of $(n\text{-}Bu_3NH)BPh_4 \cdot H_2O$, observed at 3564 and 3508 cm^{-1} and interpreted as ν_w(OH) (Fig. 5 of ref. 17), would thus suggest significant O_w—H...π interaction. However, in ammonium and alkylammonium TBs, the problem of how to establish a reference frequency that would serve for detecting frequency lowering induced by the formation of N^+—H...π^- bonds is much more difficult. Here frequency comparisons intended to demonstrate the presence of hydrogen bonding must be interpreted with great caution.[10] In the particular case of NH_4BPh_4 the conclusion from a detailed X-ray and ir study (18) is that a ν(NH) frequency lowering indeed exists and is attributable to a weak N^+—H...π^- interaction. By implication, it is reasonable to assume that a similar interaction exists also in the structures discussed in this paper.

Iminium ions: *ab initio* study

The experimental geometry of the unsubstituted $[H_2C{=}NH_2]^+$ ion and thus the C—N distance do not appear to be known. However, the mean of the limited number of the available C—N distances in substituted iminium ions (uncorrected for thermal motion; Table 6) is 1.283(12) Å, i.e., corresponding to a double bond. This value may thus be accepted, provisionally, as a representative (uncorrected) length of the polar C=N bond in iminium ions.

The range of *d*(C=N) in Table 6 is quite narrow. Although a number of C=N bonds with lengths between 1.30 and 1.38 Å are listed in Table XX of ref. 14, these bonds are untypical in that they appear to be subject to steric or electronic interactions that would be absent is simple $[RR'C{=}NR''R''']^+$ ions with H, alkyl, or halogen assubstituents. To substantiate or otherwise the narrowness of the *d*(C=N) range as well as to obtain a clearer idea of the effect of substitution, we undertook 6-31G* optimization of the equilibrium geometries of substituted iminium ions (Tables 7, 8, and G). Aiming at maximum economy of the computational effort we chose F and Cl as the monatomic substituents with the most substantial electron-withdrawing powers, and Li and Na as substituents acting in the opposite direction, in the expectation that the changes induced by these substitutions would bracket the *d*(C=N) variation. Substitution by cyano groups was included to probe the effect of

[9] N^+—H...π^- (15, 18–21); N^+—H...O_w—H...π^- (17); O—H...π (22, 31, 32). See also Addendum.

[10] For a full discussion see refs. 18 and 33 and subsequent papers on the subject in this journal by Knop et al.

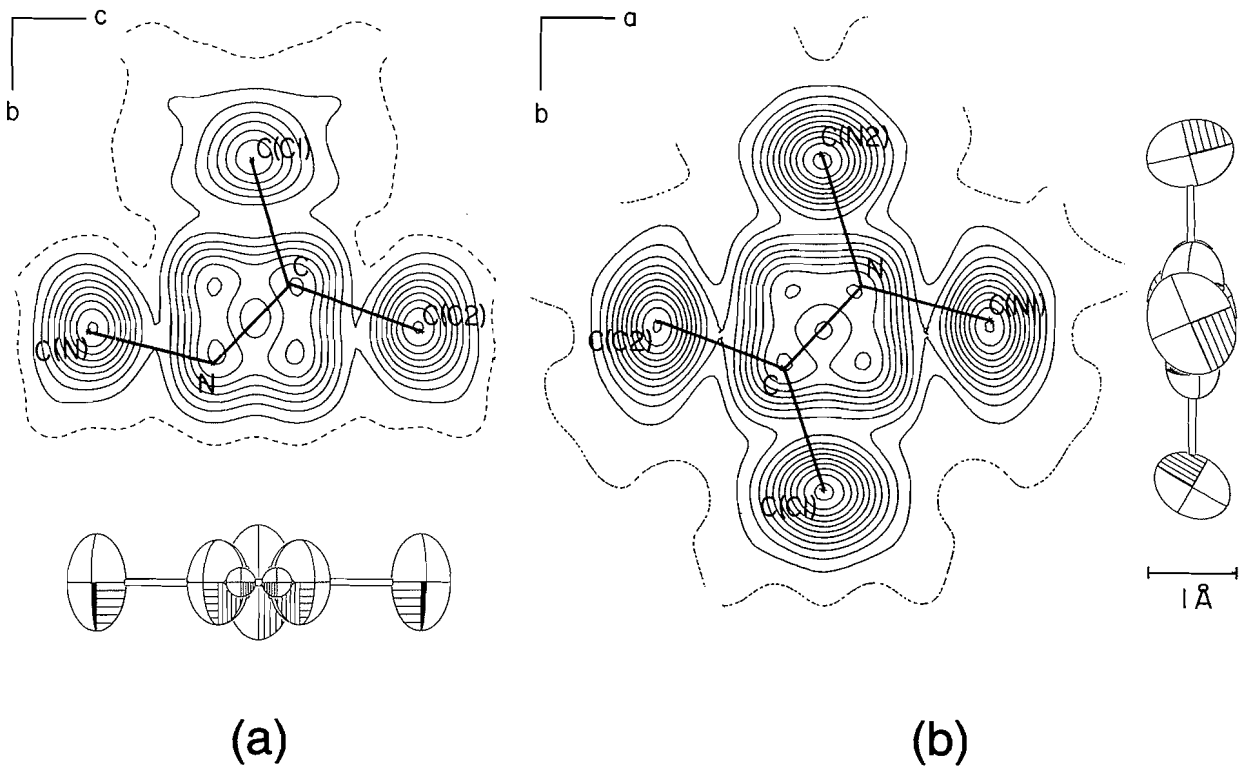

FIG. 7. Electron-density maps in the plane of the cation. Contour intervals, 0.4 e/Å^3. (*a*) $Me_2C{=}NHMe^+$ in **A**. Cation plane is $m\|(100)$, cation disorder is across the vertical $m\|(001)$. A projection of the cation on the (010) plane (perpendicular to the page) is also shown. (*b*) $Me_2C{=}NMe_2^+$ in **B**; the cation plane is about 45° inclined to (001). The cation disorder is across the vertical $m\|(100)$. A projection of the cation on the (100) plane (perpendicular to the page) is also shown.

TABLE 5. Comparison of the CBC valence angle α with the dihedral angle φ between the ring planes enclosing the cation in BPh_4^- salts[a]

Salt	Valence angle		Dihedral angle		(B–C)/ring angle	
	α_1	α_2	ϕ_1	ϕ_2	δ_1	δ_2
Cation not hydrogen-bonded to ring						
K (16)	102.7	102.7	89.2	89.2	6.8	6.8
Me_4N (16)	105.8	102.1	101.7	92.6	2.1	4.8
B	105.6	103.4	101.7	87.0	2.0	8.2
Cation hydrogen-bonded to ring(s)						
NH_4 (18)	103.2	103.2	89.4	89.4	6.9	6.9
$(CH_2)_6NH_2$ (20)	103.0	103.3	92.8	90.1	5.1	6.6
A (bifurcated)	103.6	103.8	94.3	84.4	4.7	9.7
D (bifurcated)	103.1	103.7	94.9	86.9	4.1	8.4
C	104.1	104.3	94.8	86.8	4.7	8.8
E[b]	105.0	103.1	91.5	92.7	6.8	5.2

[a]Angles in deg. Subscript 1 refers to the rings involved in the hydrogen bonding or closest to the cation. The (B—C)/ring plane angles $\delta_1 = (\alpha_1 - \phi_1)/2$ and $\delta_2 = (\alpha_2 - \phi_2)/2$ measure the tendency of the two rings to close up on the bisector of α (see text).

[b]Water molecule bonded to phenyl rings (Figs. 6 and 9).

π conjugation. This choice of substituents was furthermore intended to make unnecessary an investigation of the effect of individual composite substituents (e.g., CH_3, NH_2), which would have added significantly to the already extensive projected computer requirements.[11] The optimizations were carried out in planar geometry, C_{2v} or C_s (but see below).

The choice of the 6-31G* basis set (see Experimental) represents a compromise between wishing to obtain reasonably realistic molecular geometry and keeping the computational effort within practical bounds. While we are well aware of the limitations imposed by this choice as concerns the values of the individual optimized parameters, we would expect that the *trends* that may emerge will constitute a sufficiently valid and realistic approximation to the actual, as yet unknown trends.

We have also included in the optimizations a limited number of similarly substituted ethylene derivatives as well as $[H_2C{=}BH_2]^-$ (Table 9). Comparison of the experimental with the optimized geometry of ethylene itself shows that the C—C and C—H distances are underestimated by 0.022 and 0.009 Å, respectively, and the HCH angle by 1.4° (Table 9). These are not serious discrepancies; one would expect the calculated distances and angles in the optimized iminium geometries to be consistently underestimated by similar amounts.

The optimized molecular parameters can, in general, be

[11]In particular, the above choice was hoped to encompass the effects of substitution in species such as $[Me_2C{=}NMe_2]^+$, for which Kollman (34) suggested that the C—N distance might be expected to be larger than in $[H_2C{=}NH_2]^+$ because of Me hyperconjugation with the carbonium ion centre and C...C repulsions.

Can. J. Chem. Downloaded from www.nrcresearchpress.com by 213.200.69.106 on 09/08/12
For personal use only.

Can. J. Chem. Downloaded from www.nrcresearchpress.com by 213.200.69.106 on 09/08/12
For personal use only.

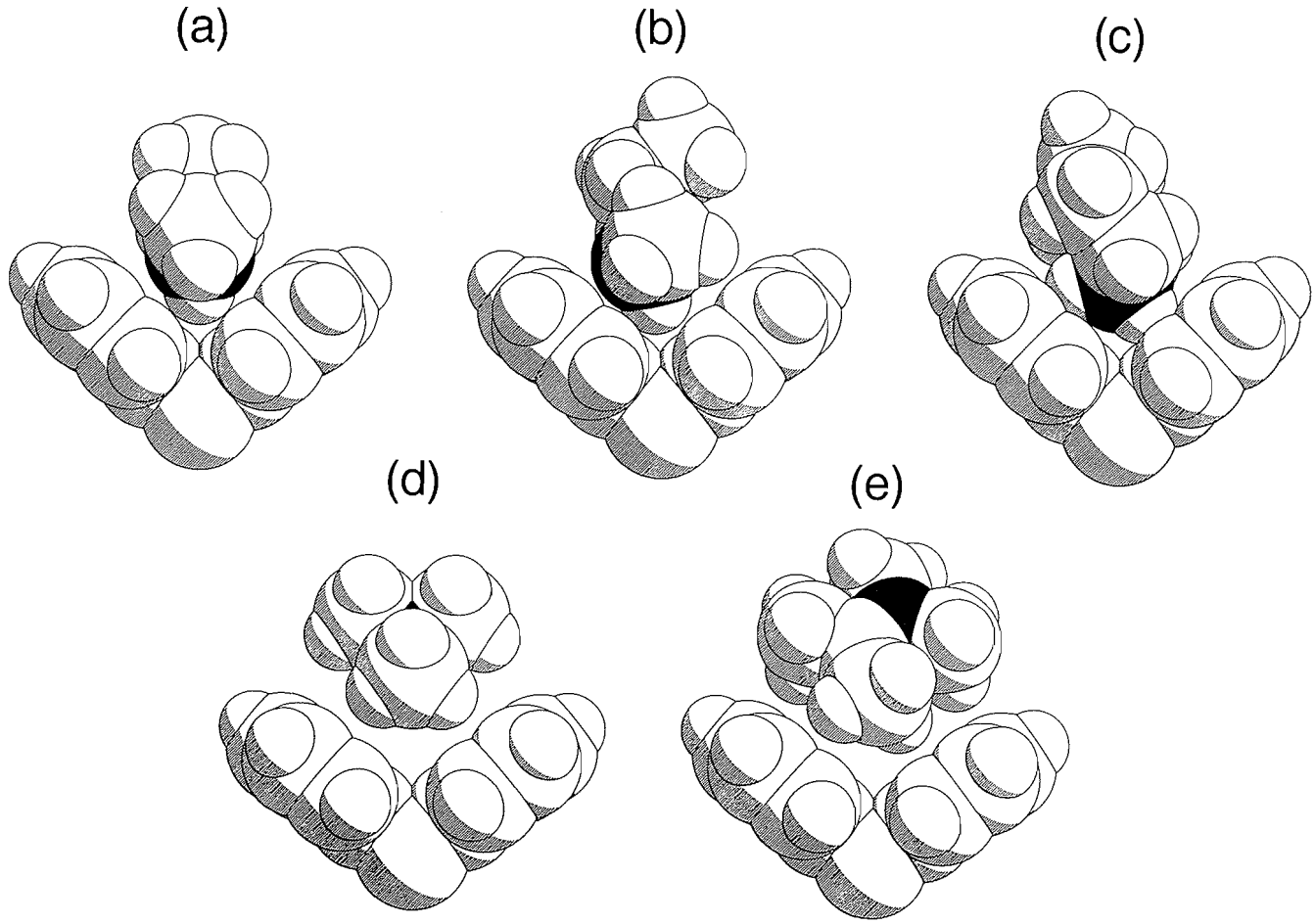

FIG. 8. Coordination of the cation in **A** (*a*), **D** (*b*), $[(CH_2)_6NH_2]BPh_4$ (20) (*c*), 4MTB (16) (*d*), and **B** (*e*), by the nearest pair of phenyl rings of the anion. The N atoms are shown in black. For the disordered cations in *a*, *b*, and *c* only one orientation is shown. The N atom is *a*–*c* is H-bonded to the ring(s), by bifurcated bonds in *a* and *b*, and by normal bonds in *c*. The cation is either symmetric with respect to (*a*, *d*), or disordered across (*b*, *e*), a vertical plane bisecting the boron atom; in *a*, *c*, and *d* the plane of the paper is parallel to a crystallographic mirror plane.

represented as linear functions $\alpha_0 + \alpha_C n_C + \alpha_N n_N$ of n_C and n_N, the numbers of substituents on the C and N atoms, respectively (Tables P–R). These approximations are on the whole remarkably successful, giving r^2 mostly well over 0.9 and not often below this value. They show that the changes resulting from the substitution are essentially additive, and their uniform functional form makes it possible to separate the contributions from the C and N atoms to the changes in the optimized parameters and thus to assess the relative importance of these contributions. The linear parametric representation in n_C and n_N also permits looking for possible relationships between the coefficients of the regressions.

The validity of the observations and conclusions that follow is of course contingent on the presumed self-consistency of the 6-31G* scheme for elements of the first and second rows of the periodic system, as well as on the assumption that each of the optimized geometries corresponds to the *global* E(6-31G*) minimum for that ion or molecule in the prescribed symmetry. Attention will be drawn to situations where there are reasons for thinking that these assumptions may not hold.

No effort was made to analyze the results for orbital populations and similar features. This and further calculations will have to await another occasion.

Notation

The optimized parameters discussed below are the bond lengths and interligand distances d, the bond angles, the Mulliken ε_M and Löwdin ε_L net charges on the atoms, the electron densities $\rho_c = \rho(\boldsymbol{r}_c)$ at the bond critical points, and the dipole moments μ. The following numbering scheme has been adopted to specify the substitutions:

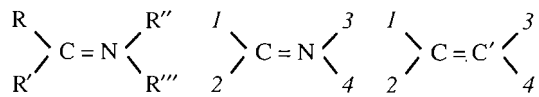

Thus FHFH and *13* in the fluoro iminium set both designate $[F^1H^2C{=}NF^3H^4]^+$, and HCyCyH and *23* both stand for $[H^1(NC)^2C{=}N(CN)^3H^4]^+$ in the cyano set; and similarly for the ethylene derivatives. Where confusion might arise, the iminium and the ethylene derivatives are distinguished as, for example, $LiHHH^+$ and LiHHH.

For reasons that will be apparent later it will be convenient to refer to X = H, F, Cl, and CN as group **A** and to X = Li and Na as group **B** substituents.

Relative stability of substitution isomers

Substitution in $HHHH^+$ yields two types of planar isomers, the *cis/trans* $XHXH^+/XHHX^+$ (*13*/*14*), and the pairs

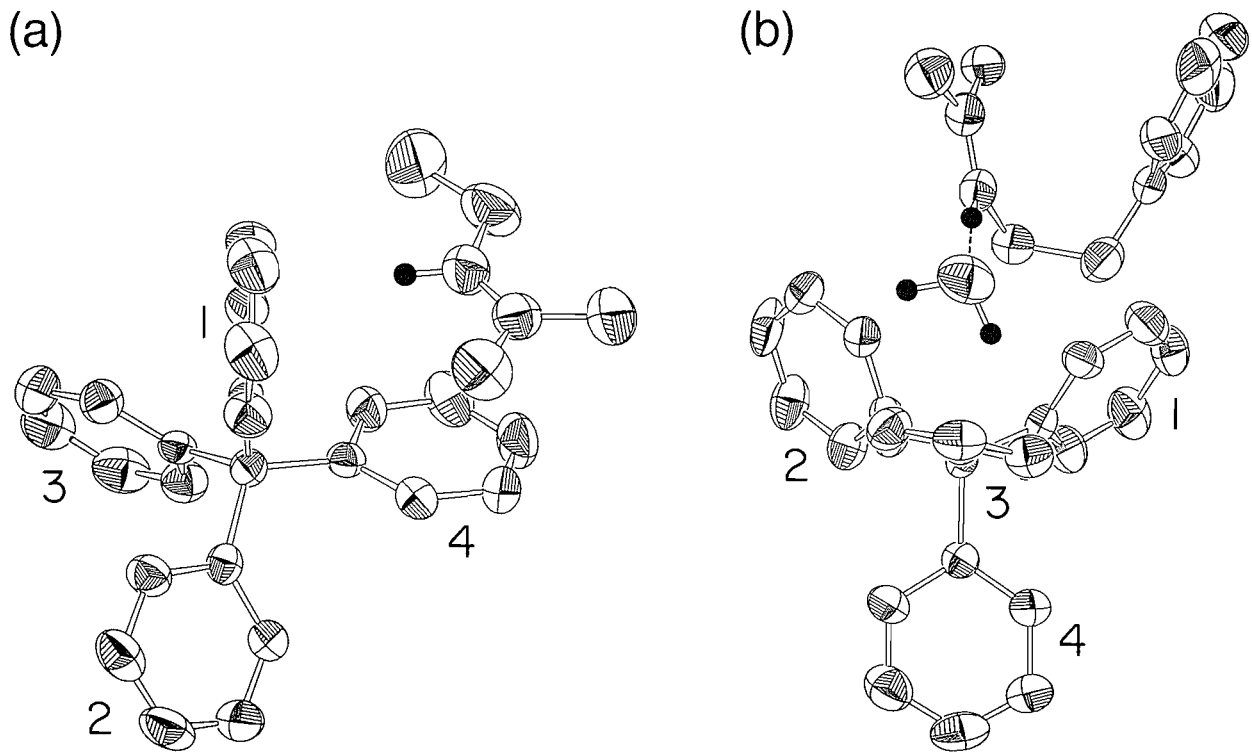

FIG. 9. (*a*) The N^+—H...π^- hydrogen bond in **C**. The projection plane contains the N—H bond. The filled circle represents the H(N) atom. (*b*) The N^+—H...O—H...π^- hydrogen bonds in **E**. The projection is on the plane of the water molecule.

TABLE 6. Cation symmetry and C=N bond length (Å) in iminium salts

Compound	P.G.[a]	Bond length	Reference
$[H_2C{=}NMe_2]Cl$	C_{2v}	1.264(9)	11
$[ClMeC{=}NH_2]Cl$	C_s	1.265(7)[b]	5
$[Me_2C{=}NHMe]BPh_4$ (**A**)	C_s	[1.261(7)][c]	This work
$[Me_2C{=}NHEt]BPh_4$ (**C**)	C_1	1.277(4)	This work
$[Me_2C{=}NMe_2]ClO_4$	[C_{2v}]	[1.302(43)][c]	27
$[Me_2C{=}NMe_2]BPh_4$ (**B**)	$C_1 \sim C_s$	[1.291(8)][c]	This work
$[Me_2C{=}NH(CH_2CH_2Ph)]BPh_4 \cdot H_2O$ (**E**)	C_1	1.291(9)	This work
$[MeEtC{=}NHMe]BPh_4$ (**D**-LT)	$C_1 \sim C_s$	1.271(11)[c]	This work
$[PhC{=}C{-}C{=}NMe_2]ClO_4$	C_s	1.284(9)	10
[*p*-MeO—$C_5H_4C{=}C{-}C{=}NMe_2]ClO_4$	C_1	1.290(6)	10
$[Me_2C{-}CH{=}C(t\text{-}Bu){-}C{=}NMe_2]BF_4$	C_1	1.287(6)	[d]
$[Me_2C{-}CMe{=}CMe{-}C{=}NMe_2]ClO_4$	C_1	1.296(7)	[d]

[a]Point-group symmetry.
[b]Neutron diffraction. *Ab initio* value for $[ClHC{=}NH_2]^+$ is 1.270 Å (cf. Table 7).
[c]Cation positionally disordered. Bond length values in brackets are from resolved disorder.
[d]F.J. Chentli-Benchikha, J.-P. Declercq, G. Germain, and M. Van Meersche. Cited in ref. 14.

that arise from substitution either on the C or on the N atom, viz. $XXHH^+/HHXX^+$ (*12/34*) and the complementary pairs $XHHH^+/HHXH^+$ (*1/3*) and $XXXH^+/XHXX^+$ (*123/134*). For the **B**-substituted *cis/trans* pairs the difference $\Delta E = E(13) - E(14)$ is of the order of 5 kcal/mol, favouring the *trans* form. For X = **A** the $|\Delta E| < 0.5$ kcal/mol (−0.03 kcal/mol for X = Cl) are too small to claim, even in terms of the 6-31G* scheme, the existence of a trend. However, X = H requires $\Delta E = 0$ by definition, and if the ΔE values are regressed parabolically on $\chi(X)$, $\chi(\Delta E = 0)$ would fall at 3.3 (Fig. 10). The error estimate derived from 1σ of the regression is $|0.7|$, so that the existence of a trend favouring the *trans* form over the entire $\chi(X)$ range cannot be ruled out, given the flatness of the regression line in the vicinity of $\Delta E = 0$.

For the *C*- and the *N*-substituted isomers the respective ΔE differences show strong and clear trends (Fig. 10). The ΔE in each of the three series can be regressed linearly on $\chi(X)$, resulting in $r^2 > 0.99$. With the effective $\chi(CN)$ taken as 2.43, $\sigma(12/34) = 0.00543$ au ~ 2% of range, $\sigma(1/3) = 0.00156$ au ~ 1% of range. For *123/134* the ΔE values for **B** fall slightly below the straight line through the points for

Can. J. Chem. Downloaded from www.nrcresearchpress.com by 213.200.69.106 on 09/08/12
For personal use only.

TABLE 7. 6-31G* parameters of $[12C{=}N34]^+$ iminium cations optimized in C_{2v} or C_s symmetry: total electronic energies E (au), bond lengths (Å) and bond angles (deg)[a]

1234	*E*	C=N	*1*-C	*2*-C	N-*3*	N-*4*	*1*CN	*2*CN	*1C2*	CN*3*	CN*4*	*3*N*4*
HHHH	−94.38318	1.263	1.075	1.075	1.006	1.006	119.8	119.8	120.4	121.9	121.9	116.2
FHHH	−193.23024	1.265	1.260	1.074	1.008	1.005	119.8	123.2	117.0	121.2	121.0	117.8
HHFH	−193.12602	1.254	1.075	1.075	1.313	1.007	119.3	118.0	122.7	120.1	128.1	111.8
FFHH	−292.07893	1.269	1.247	1.247	1.006	1.006	122.0	122.0	116.0	120.6	120.6	118.8
FHFH	−291.96278	1.266	1.252	1.075	1.312	1.007	120.2	120.7	119.1	119.4	126.7	113.9
FHHF	−291.96306	1.265	1.257	1.076	1.009	1.314	118.4	122.1	119.5	127.7	118.0	114.3
HHFF	−291.86935	1.249	1.075	1.075	1.290	1.290	117.8	117.8	124.4	124.5	124.5	111.0
FFFH	−390.80540	1.273	1.239	1.245	1.314	1.008	122.1	119.9	118.0	117.9	126.6	115.5
FHFF	−390.69918	1.264	1.252	1.076	1.289	1.291	118.8	120.2	121.0	124.2	122.5	113.3
FFFF	−489.53577	1.272	1.240	1.240	1.291	1.291	120.3	120.3	119.4	122.7	122.7	114.7
ClHHH	−553.27498	1.270	1.662	1.075	1.006	1.005	123.0	119.4	117.6	122.2	120.8	117.0
HHClH	−553.21931	1.263	1.075	1.076	1.687	1.008	120.2	118.5	121.3	124.5	121.3	114.2
ClClHH	−1012.16065	1.278	1.673	1.673	1.005	1.005	120.4	120.4	119.2	121.2	121.2	117.6
ClHClH	−1012.10960	1.274	1.656	1.076	1.683	1.007	125.0	117.2	117.9	126.4	119.2	114.4
ClHHCl	−1012.10955	1.272	1.663	1.076	1.008	1.687	122.1	119.4	118.5	121.5	123.4	115.3
HHClCl	−1012.05357	1.265	1.075	1.075	1.697	1.697	119.2	119.2	121.6	121.9	121.9	116.2
ClClClH	−1470.99359	1.283	1.666	1.678	1.684	1.007	122.5	118.4	119.1	126.2	119.3	114.4
ClHClCl	−1470.94233	1.278	1.657	1.075	1.691	1.700	124.8	117.5	117.8	124.1	119.8	116.1
ClClClCl	−1929.82225	1.293	1.672	1.672	1.697	1.697	121.3	121.3	117.5	122.9	122.9	114.3
CyHHH	−186.07973	1.267	1.431	1.076	1.008	1.006	121.6	119.7	118.7	122.3	121.1	116.6
HHCyH	−186.05157	1.276	1.075	1.075	1.371	1.010	119.9	118.9	121.4	123.6	120.3	116.1
CyCyHH	−277.76950	1.272	1.434	1.434	1.008	1.008	120.7	120.7	118.7	121.4	121.4	117.1
CyHCyH	−277.74560	1.283	1.421	1.077	1.369	1.011	122.8	118.1	119.2	124.8	119.0	116.2
CyHHCy	−277.74631	1.282	1.423	1.078	1.012	1.369	120.8	119.5	119.7	120.5	122.9	116.6
HHCyCy	−277.71020	1.290	1.076	1.076	1.380	1.380	118.9	118.9	122.2	121.4	121.4	117.3
CyCyCyH	−369.43425	1.290	1.425	1.428	1.366	1.012	121.7	119.3	119.1	124.2	119.2	116.6
CyHCyCy	−369.40333	1.299	1.414	1.078	1.378	1.378	122.1	118.0	119.9	122.5	120.2	117.4
CyCyCyCy	−461.09045	1.311	1.420	1.420	1.376	1.376	120.5	120.5	119.0	121.4	121.4	117.1
LiHHH	−101.29640	1.288	2.122	1.085	1.000	1.003	131.3	109.6	119.1	121.8	123.6	114.6
HHLiH	−101.33625	1.261	1.077	1.078	1.967	1.006	120.2	122.7	117.1	130.3	111.9	117.8
LiLiHH	−108.15416	1.305	2.090	2.090	1.003	1.003	118.5	118.5	123.1	124.2	124.2	111.5
LiHLiH	−108.20377	1.291	2.072	1.097	1.893	1.009	138.8	112.0	109.2	131.0	112.8	116.2
LiHHLi	−108.21148	1.290	2.081	1.097	1.004	1.901	132.1	110.1	117.9	112.2	124.8	123.0
HHLiLi	−108.23533	1.257	1.092	1.092	1.904	1.904	124.1	124.1	111.8	113.3	113.3	133.3
LiLiLiH	−115.05628	1.289	1.929	2.020	1.830	1.083	167.9	81.4	110.8	82.3	123.8	154.0
LiHLiLi	−115.08613	1.264	2.059	1.194	1.822	1.858	135.7	114.5	109.8	146.4	84.1	129.5
LiLiLiLi	−121.91766	1.157	2.293	2.293	2.124	2.124	107.0	107.0	145.9	131.5	131.5	97.0
NaHHH	−255.69805	1.291	2.474	1.086	0.999	1.003	133.0	108.7	118.3	121.6	123.9	114.5
HHNaH	−255.73937	1.259	1.078	1.079	2.327	1.006	120.1	123.2	116.7	131.2	111.3	117.5
NaNaHH	−416.94118	1.308	2.437	2.437	1.004	1.004	117.4	117.4	125.2	124.4	124.4	111.2
NaHNaH	−416.99179	1.290	2.401	1.102	2.227	1.010	143.0	111.7	105.3	131.7	112.4	115.9
NaHHNa	−417.00105	1.289	2.413	1.102	1.005	2.237	133.1	109.4	117.5	111.4	123.3	125.4
HHNaNa	−417.02160	1.251	1.099	1.099	2.249	2.249	124.7	124.7	110.6	109.5	109.5	141.0
NaNaNaH	−578.21721	1.280	2.300	2.537	2.193	1.011	163.8	97.9	98.3	88.9	119.2	151.8
NaHNaNa	−578.24653	1.254	2.364	1.152	2.222	2.196	168.6	116.8	74.6	80.8	132.8	146.6
NaNaNaNa	−739.54121	1.161	3.091	3.091	1.341	2.341	127.6	127.6	104.8	104.2	104.2	151.5

[a]For ligand numbering see text. Parameters for the cyano groups Cy are listed in Table G (see footnote 5).

X = **A**. This is probably a consequence of nonplanarity (see below). If these two points are disregarded the lines for the *1/3* and *123/134* pairs practically coincide.

The sign of ΔE for the *1/3*, *12/34*, and *123/134* sets reverses between X = CN and X = Li, i.e., the *C*-substituted isomers are more stable than the corresponding *N*-substituted isomers when X = **A** but less stable when X = **B**. This appears to relate to the electronegativity difference $\chi(X) - \chi(H)$, which changes sign between X = Cl (and CN) and X = Li. The effect of the *gem* substitution on the relative stability appears to be additive: $a_1(12/34) = 2a_1(1/3)$, where a_1 is the slope of the ΔE regression.

The regression lines for *1/3* and *12/34* (and *123/134* ?) intersect at $\Delta E = 0$, $\chi = 1.8$. This point would be expected to correspond to $HHHH^+$, i.e., to X = H and $\chi(\Delta E = 0) = \chi(H) \sim 2.2$. The observed $\chi(\Delta E = 0)$ is thus 0.4 lower than $\chi(H)$. This difference seems to arise from the symmetry of the substitution in the pairs with respect to the C=N bond:

Can. J. Chem. Downloaded from www.nrcresearchpress.com by 213.200.69.106 on 09/08/12
For personal use only.

TABLE 8. 6-31G* parameters of [*12*C=N*34*]$^+$ iminium ions optimized in C_{2v} or C_s symmetry: Mulliken net charges ε_M (e), electron densities $\rho_c = \rho(r_c)$ at the bond critical points (au), and dipole moments μ (D)[a]

1234	ε_M(C)	ε_M(N)	ε_M(*1*)	ε_M(*2*)	ε_M(*3*)	ε_M(*4*)	ρ_c(CN)	ρ_c(*1*C)	ρ_c(*2*C)	ρ_c(N*3*)	ρ_c(N*4*)	μ
HHHH	0.038	−0.657	0.323	0.323	0.486	0.486	0.3842	0.3014	0.3014	0.3354	0.3354	0.08
FHHH	0.618	−0.738	−0.200	0.330	0.496	0.494	0.4005	0.3222	0.3087	0.3278	0.3315	3.73
HHFH	−0.017	−0.009	0.360	0.342	−0.184	0.508	0.3838	0.2977	0.2983	0.3749	0.3364	4.19
FFHH	1.133	−0.794	−0.173	−0.173	0.504	0.504	0.4111	0.3435	0.3435	0.3272	0.3272	4.09
FHFH	0.589	−0.108	−0.176	0.348	−0.167	0.514	0.3937	0.3311	0.3061	0.3751	0.3329	5.02
FHHF	0.587	−0.099	−0.191	0.363	0.516	−0.175	0.3946	0.3261	0.3056	0.3298	0.3735	0.51
HHFF	−0.062	0.642	0.374	0.374	−0.164	−0.164	0.3711	0.2965	0.2965	0.4083	0.4083	4.72
FFFH	1.133	−0.176	−0.150	−0.167	−0.161	0.522	0.4036	0.3521	0.3463	0.3739	0.3281	2.75
FHFF	0.555	0.553	−0.171	0.379	−0.154	−0.162	0.3789	0.3332	0.3040	0.4074	0.4057	1.62
FFFF	1.118	0.478	−0.147	−0.147	−0.152	−0.152	0.3888	0.3529	0.3529	0.4045	0.4045	0.81
ClHHH	0.097	−0.682	0.253	0.352	0.491	0.489	0.3884	0.2513	0.3034	0.3320	0.3328	4.78
HHClH	0.042	−0.590	0.334	0.331	0.381	0.503	0.3796	0.3003	0.2990	0.2237	0.3347	4.87
ClClHH	0.129	−0.699	0.291	0.291	0.494	0.494	0.3904	0.2477	0.2477	0.3315	0.3315	4.34
ClHClH	0.101	−0.626	0.273	0.354	0.394	0.504	0.3796	0.2536	0.3015	0.2231	0.3333	4.20
ClHHCl	0.106	−0.619	0.262	0.360	0.506	0.384	0.3825	0.2501	0.3025	0.3317	0.2216	0.20
HHClCl	0.050	−0.545	0.338	0.338	0.409	0.409	0.3738	0.2995	0.2995	0.2186	0.2186	4.43
ClClClH	0.140	−0.649	0.313	0.289	0.389	0.509	0.3810	0.2503	0.2446	0.2216	0.3320	1.95
ClHClCl	0.112	−0.583	0.282	0.362	0.420	0.407	0.3726	0.2523	0.3023	0.2190	0.2163	2.14
ClClClCl	0.152	−0.618	0.311	0.311	0.422	0.422	0.3693	0.2469	0.2469	0.2159	0.2159	0.26
CyHHH	0.303	−0.689	0.275	0.376	0.502	0.495	0.3875	0.3024	0.3011	0.3316	0.3331	6.86
HHCyH	0.064	−0.620	0.351	0.344	0.596	0.513	0.3723	0.3015	0.3018	0.3126	0.3302	7.47
CyCyHH	0.570	−0.730	0.328	0.328	0.508	0.508	0.3895	0.3015	0.3015	0.3296	0.3296	6.66
CyHCyH	0.355	−0.690	0.274	0.391	0.625	0.518	0.3728	0.3073	0.3008	0.3107	0.3288	7.94
CyHHCy	0.349	−0.662	0.274	0.401	0.524	0.602	0.3741	0.3065	0.3003	0.3269	0.3113	0.93
HHCyCy	0.087	−0.603	0.367	0.367	0.622	0.622	0.3618	0.3015	0.3015	0.3039	0.3039	7.46
CyCyCyH	0.633	−0.733	0.336	0.325	0.628	0.528	0.3735	0.3056	0.3044	0.3100	0.3257	3.90
CyHCyCy	0.393	−0.675	0.277	0.412	0.647	0.624	0.3605	0.3111	0.3001	0.3029	0.3033	4.59
CyCyCyCy	0.689	−0.751	0.334	0.334	0.649	0.649	0.3583	0.3082	0.3082	0.3024	0.3024	1.43
LiHHH	−0.067	−0.724	0.710	0.214	0.432	0.435	0.3558	0.0296	0.2924	0.3465	0.3421	5.74
HHLiH	0.000	−0.750	0.232	0.252	0.854	0.412	0.3942	0.2979	0.2970	0.0325	0.3422	5.70
LiLiHH	−0.177	−0.743	0.576	0.576	0.383	0.383	0.3310	0.0348	0.0348	0.3475	0.3475	6.00
LiHLiH	−0.085	−0.832	0.626	0.147	0.778	0.367	0.3654	0.0346	0.2804	0.0405	0.3426	6.84
LiHHLi	−0.079	−0.812	0.622	0.124	0.366	0.779	0.3669	0.0342	0.2795	0.3474	0.0397	0.46
HHLiLi	−0.016	−0.808	0.156	0.156	0.756	0.756	0.3984	0.2835	0.2835	0.0408	0.0408	5.70
LiLiLiH	−0.115	−0.793	0.570	0.462	0.541	0.334	0.3564	0.0367	0.0336	0.0391	0.3204	4.31
LiHLiLi	−0.039	−0.816	0.606	0.036	0.728	0.484	0.3894	0.0357	0.2099	0.0456	0.0429	2.99
LiLiLiLi	0.041	−0.508	0.396	0.396	0.337	0.337	0.4793	0.0124	0.0124	0.0171	0.0171	4.16
NaHHH	−0.092	−0.740	0.786	0.195	0.424	0.427	0.3522	0.0236	0.2911	0.3473	0.3424	3.75
HHNaH	−0.029	−0.724	0.218	0.237	0.904	0.395	0.3965	0.2953	0.2953	0.0253	0.3436	4.12
NaNaHH	−0.197	−0.763	0.607	0.607	0.373	0.373	0.3277	0.0280	0.0280	0.3466	0.3466	4.13
NaHNaH	−0.138	−0.825	0.673	0.110	0.838	0.342	0.3667	0.0284	0.2745	0.0329	0.3420	5.82
NaHHNa	−0.132	−0.810	0.670	0.086	0.345	0.841	0.3681	0.0282	0.2739	0.3477	0.0320	0.48
HHNaNa	−0.077	−0.762	0.115	0.115	0.805	0.805	0.4029	0.2761	0.2761	0.0322	0.0322	4.36
NaNaNaH	−0.143	−0.813	0.609	0.381	0.638	0.328	0.3717	0.0285	0.0226	0.0306	0.3388	3.21
NaHNaNa	−0.134	−0.806	0.616	0.012	0.530	0.782	0.3972	0.0261	0.2339	0.0315	0.0349	0.27
NaNaNaNa	0.033	−0.651	0.242	0.242	0.566	0.566	0.4781	0.0065	0.0065	0.0208	0.0208	1.18

[a]For ligand numbering see text. Parametrs for the cyano groups Cy are listed in Table G (see footnote 5).

in reality, $\chi(\Delta E = 0) \sim 1.8$ corresponds not to the tabulated χ(H) but to the difference $[\chi(N) - \chi(H)] - [\chi(C) - \chi(H)] = \chi(N) - \chi(C) \sim 0.5$.

Bond lengths

In answer to the question that had prompted this investigation, viz. what is the total variability of d(C=N) in iminium ions, the d(C=N) values of Table 7 range from 1.249 to 1.311 Å if the values for LiLiLiLi$^+$ and NaNaNaNa$^+$ are disregarded (see below). The total range is thus only 0.06 Å, i.e., smaller than the 6-31G* estimate for the similarly substituted ethylenes, 0.09 Å (Table 9), and this in spite of the fact that the χ(X) of the substituents span practically the entire electronegativity scale and that the C≡N bond of the cyano group provides for the possibility of π conjugation. In view of this it is reasonable to believe that the d(C=N) for substituents such as CH_3, NH_2, or OH,[11] when similarly optimized, would be amply accommodated within the 0.06 Å range. The experimental d(C=N) values of Table 6 fall easily within the calculated limits. Allowing for the underestimation of bond lengths in the 6-31G* optimizations, it would seem that explanations for uncorrected experimental d(C=N) values larger than, say, 1.33 Å should

Can. J. Chem. Downloaded from www.nrcresearchpress.com by 213.200.69.106 on 09/08/12
For personal use only.

TABLE 9. 6-31G* parameters of *12*C=C'*34* and $[H_2C{=}BH_2]^-$ optimized in planar (D_{2h} or C_s) or perpendicular (D_{2d}, ⊥) geometries: total electronic energies E (au), bond lengths (Å) and angles (deg), Mulliken ε_M and Löwdin ε_L net charges (e), electron densities $\rho_c = \rho(r_c)$ at the bond critical points (au), and dipole moments μ (D)[a]

1234	*E*	C=C'	*1*-C	*2*-C	*3*-C'	*4*-C'	*1*CC'	*2*CC'	*1C2*	CC'*3*	CC'*4*	3C'*4*
HHHH[b]	−78.03172	1.317	1.076	1.076	1.076	1.076	121.8	121.8	116.4	121.8	121.8	116.4
FHHH	−176.88195	1.308	1.329	1.072	1.074	1.073	122.4	125.7	111.9	121.5	119.8	118.7
FFHH	−275.74000	1.304	1.303	1.303	1.070	1.070	125.2	125.2	109.6	119.9	119.9	120.2
FFFF	−473.41567	1.300	1.302	1.302	1.302	1.302	123.5	123.5	113.1	123.5	123.5	113.1
ClHHH	−536.93369	1.311	1.737	1.071	1.074	1.074	123.3	123.9	112.8	122.5	119.6	117.9
ClClHH	−995.82603	1.311	1.728	1.728	1.073	1.073	122.8	122.8	114.5	120.6	120.6	118.7
ClClClCl	−1913.60370	1.322	1.717	1.717	1.717	1.717	128.8	128.8	114.4	128.8	128.8	114.4
CyHHH[c]	−169.76801	1.320	1.443	1.074	1.074	1.074	122.2	122.0	155.8	122.0	120.7	117.4
CyCyHH[d]	−261.49054	1.325	1.445	1.445	1.073	1.073	121.5	121.5	117.0	120.9	120.9	118.2
LiHHH	−84.86139	1.337	1.975	1.089	1.084	1.084	119.3	112.4	128.3	122.5	124.3	113.2
LiLiHH[e]	−91.67590	1.349	1.922	1.922	1.129	1.129	77.7	77.7	204.5	128.5	128.5	102.9
LiLiLiLi	−105.42041	1.233	2.055	2.055	2.055	2.055	138.1	138.1	83.9	138.1	138.1	83.9
LiLiLiLi ⊥	−105.42750	1.235	2.049	2.049	2.049	2.049	136.0	136.0	87.9	136.0	136.0	87.9
NaHHH	−239.29556	1.335	2.300	1.090	1.084	1.086	120.5	112.3	127.3	122.7	124.2	113.1
NaNaHH	−400.44359	1.333	2.372	2.372	1.090	1.090	116.9	116.9	126.3	124.5	124.5	110.9
NaNaNaNa	−723.02117	1.245	2.339	2.339	2.339	2.339	120.0	120.0	120.0	120.0	120.0	120.0
NaNaNaNa ⊥	−723.01047	1.241	2.365	2.365	2.365	2.365	133.5	133.5	93.1	133.5	133.5	93.1
$[H_2C{=}BH_2]^-$	−64.81069	1.444	1.089	1.089	1.227	1.227	124.1	124.1	111.0	122.9	122.9	114.2

1234	ε(C)	ε(C')	ε(*1*)	ε(*2*)	ε(*3*)	ε(*4*)	ρ_c(C=C')	ρ_c(*1*-C)	ρ_c(*2*-C)	ρ_c(*3*-C')	ρ_c(*4*-C')	μ
HHHH	−0.353	−0.353	0.176	0.176	0.176	0.176	0.3628	0.2863	0.2863	0.2863	0.2863	0
	−0.325	−0.325	0.162	0.162	0.162	0.162						
FHHH	0.257	−0.473	−0.366	0.187	0.203	0.192	0.3719	0.2564	0.3001	0.2850	0.2858	1.53
	0.062	−0.388	−0.198	0.165	0.180	0.179						
FFHH	0.785	−0.559	−0.327	−0.327	0.215	0.215	0.3162	0.2835	0.2835	0.2858	0.2858	1.25
	0.336	−0.438	−0.141	−0.141	0.192	0.192						
FFFF	0.636	0.636	−0.318	−0.318	−0.318	−0.318	0.3842	0.2859	0.2859	0.2859	0.2859	0
ClHHH	−0.252	−0.352	−0.033	0.234	0.210	0.200	0.3670	0.2056	0.2955	0.2880	0.2866	1.85
	−0.215	−0.327	−0.005	0.186	0.181	0.179						
ClClHH	−0.188	−0.344	0.041	0.041	0.225	0.225	0.3650	0.2145	0.2145	0.2827	0.2827	1.82
	−0.152	−0.327	0.048	0.048	0.192	0.192						
ClClClCl	−0.194	−0.194	0.097	0.097	0.097	0.097	0.3629	0.2199	0.2199	0.2199	0.2199	0
CyHHH[c]	−0.172	−0.377	0.280	0.245	0.223	0.210	0.3622	0.2839	0.2903	0.2905	0.2903	4.26
	−0.173	−0.250	0.004	0.194	0.186	0.182						
CyCyHH[d]	0.045	−0.314	0.303	0.303	0.252	0.252	0.3607	0.2861	0.2861	0.2931	0.2931	4.81
	−0.026	−0.198	0.009	0.009	0.202	0.202						
LiHHH	−0.393	−0.362	0.431	0.098	0.103	0.124	0.3482	0.0427	0.2726	0.2780	0.2784	5.95
	−0.260	−0.348	0.205	0.140	0.132	0.132						
LiLiHH[e]	−0.238	−0.459	0.263	0.263	0.086	0.086						2.16
	−0.069	−0.221	−0.030	−0.030	0.175	0.175						
LiLiLiLi	−0.353	−0.353	0.176	0.176	0.176	0.176	0.4247	0.0284	0.0284	0.0284	0.0284	0
LiLiLiLi ⊥	−0.335	−0.335	0.168	0.168	0.168	0.168						
NaHHH	−0.407	−0.395	0.497	0.094	0.097	0.114	0.3495	0.0349	0.2719	0.2775	0.2762	7.27
	−0.269	−0.383	0.274	0.128	0.124	0.127						
NaNaHH	−0.301	−0.436	0.253	0.253	0.115	0.115						4.15
	−0.046	−0.382	0.083	0.083	0.132	0.132						
NaNaNaNa	−0.428	−0.428	0.214	0.214	0.214	0.214	0.4218	0.0243	0.0243	0.0243	0.0243	0
NaNaNaNa ⊥	−0.433	−0.433	0.216	0.216	0.216	0.216						
	−0.074	−0.074	0.037	0.037	0.037	0.037						
$[H_2C{=}BH_2]^-$	−0.568	−0.009	0.021	0.021	−0.232	−0.232	0.2069	0.2626	0.2626	0.1502	0.1502	1.39

[a]For $[H_2C{=}BH_2]^-$ read B instead of C'. First line, ε_M; second line, ε_L.
[b]Experimental values for C_2H_4: C—C, 1.339 Å; C—H, 1.085 Å; HCH, 117.8°.
[c]In the CN group, C≡N, 1.136 Å; CCN, 179.3°; ε_M(N) = −0.448; ε_L(N) = −0136; ρ_c(C≡N) = 0.4891 au.
[d]In the CN group, C≡N, 1.135 Å; CCN, 179.4°; ε_M(N) = −0.421; ε_L(N) = −0.098; ρ_c(C≡N) = 0.4892 au.
[e]This result may not represent the global E(6-31G*) minimum.

Can. J. Chem. Downloaded from www.nrcresearchpress.com by 213.200.69.106 on 09/08/12
For personal use only.

Can. J. Chem. Downloaded from www.nrcresearchpress.com by 213.200.69.106 on 09/08/12
For personal use only.

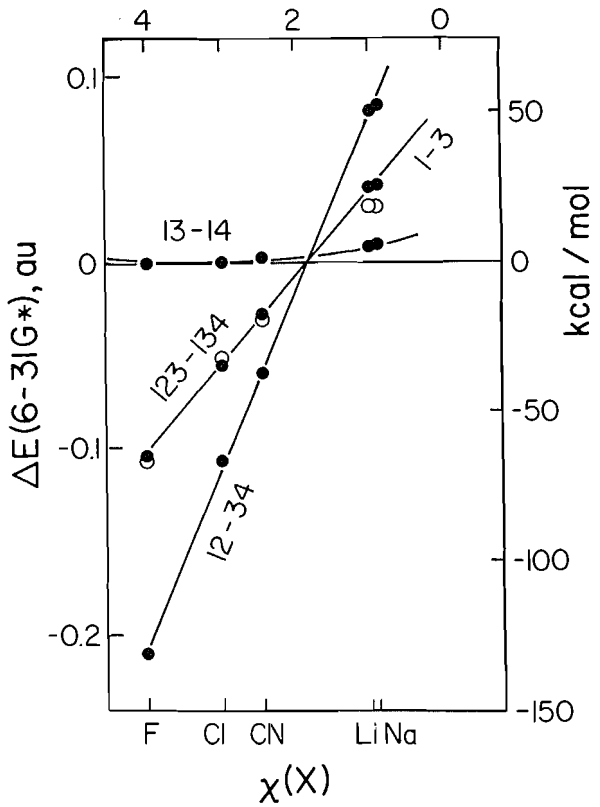

FIG. 10. Variation of the difference in the 6-31G* total electronic energy of substitutional iminium isomers $\Delta E = E(12) - E(34) = E(XXHH^+) - E(HHXX^+)$, etc. with Pauling's electronegativity $\chi(X)$.

be looked for elsewhere than in substitution on C or N per se.[12]

Although the vagaries of the 6-31G* treatment might be expected, given the narrowness of the d(C=N) range, to perturb the trend in d(C=N), the $d(C{=}N)_X$ for a particular X can be represented as a function of n_C and n_N in a reasonably clear-cut manner (Table P). The effect of the substitution at C is dominant in the lengthening (relative to $HHHH^+$) of C=N when X = **B**; that of the substitution at N is dominant in the lengthening of C=N when X = CN; and for F and Cl the substitution at C lengthens C=N modestly, although for X = F this change is opposed by the contribution from N. The mean a_0 from the regressions, $\bar{a}_0$ = 1.262(3) Å, is indistinguishable from d(C=N) = 1.263 Å in the unsubstituted ion.

The change in d(C=N) on substitution is displayed even more dramatically when $\Delta d(C{=}N) = d(C{=}N)_X - d(C{=}N)_H$ is examined in conjunction with $\Delta\rho_c(C{=}N) = \rho_c(C{=}N)_X - \rho_c(C{=}N)_H$ (Fig. 11); ρ_c may be regarded as an estimator of bond covalency (23). As the plot shows, Δd(C=N) and $\Delta\rho_c$(C=N) do not necessarily go hand in hand: a C=N bond lengthening on substitution may correspond to an increase *or* a decrease in the C=N covalency, and similarly for bond contraction. Thus the C=N bond lengthens on *any* substitution by Cl or CN, but $\Delta\rho_c$(C=N) is positive for substitution at C and negative for substitution at N. F-substitution produces a C=N expansion and an increase in ρ_c(C=N) in $FHHH^+$ and $FFHH^+$, but it has the opposite effect in $HHFH^+$ and $HHFF^+$. The reverse is observed for Li and Na, for which the magnitude of the change is appreciable.

Interestingly, the effect of the corresponding substitutions in ethylene is not always in the same direction as that in $HHHH^+$. Substitution by F and Cl results in a C=N bond expansion in $XHHH^+$ and $XXHH^+$ but in a C=C *contraction* of comparable magnitude in XHHH and XXHH (Fig. 11). The lowering of ρ_c(C=C) in FFHH on introduction of the second fluorine atom is striking.

The variation of the X—C and X—N bond lengths with X and with the degree of substitution is successfully represented by the regressions in Table P, more closely so for d(X—N) than for d(X—C). The exception is X = Cl, for which the fit is not as close as for the other X. The **B**—C and **B**—N bonds contract with increasing substitution, as do the F—C (and F—N) bonds, though to a lesser extent. For Cl and CN the dominant a term (a_C for X—C and a_N for X—N) is positive.

The a_0 values in Table may be regarded as the "limiting" d(X—C) and d(X—N), i.e., the bond lengths resulting from extrapolation to zero substitution. These limiting bond lengths are found to correlate to a high degree ($r^2 = 0.985$; $a_0^N - a_0^C = 0.084 - 0.077a_0^C$, σ = 0.07 Å ~ 5% of range; Fig. 12*a*).

The C—C_{CN} and N—C_{CN} bonds are contracted owing to the proximity of the C=N and C≡N bonds: d(C—C_{CN}) = 1.425(6) Å, d(N—C_{CN}) = 1.373(5) Å. Their lengths show a weak dependence on the variation in the associated d(C=N) and d(C≡N):

$$d(C{-}C_{CN}) = 8.337 + 0.022d(C{=}N) - 6.111d(C{\equiv}N),$$
$$r^2 = 0.89,\ \sigma = 0.003\ \text{Å} \sim 13\%\ \text{of range}$$

$$d(N{-}C_{CN}) = 8.949 + 0.264d(C{=}N) - 7.000d(C{\equiv}N),$$
$$r^2 = 0.84,\ \sigma = 0.003\ \text{Å} \sim 20\%\ \text{of range.}$$

The total variation in d(C=N) and d(C≡N) in the iminium ions is 0.044 and 0.003 Å, respectively, for the substitution at C, and 0.035 and 0.002 Å, respectively, for the substitution at N; the corresponding ranges for d(C—C_{CN}) and d(N—C_{CN}) are 0.020 and 0.014 Å, respectively. The length of the N—C_{CN} bond is more than 10 times as sensitive to changes in d(C=N) as that of the C—C_{CN} bond.

The H—C and H—N bond lengths do not vary substantially with X, even though they tend to increase slightly, for a given X, with the degree of substitution. That mean d(H—C) tends to increase with the decreasing χ(X):

X =	F	Cl	CN	Li	Na
$\bar{d}$(H—C) =	1.075(1)	1.075(1)	1.075(1)	1.088(9)	1.091(10) Å
$\bar{d}$(H—N) =	1.007(1)	1.007(1)	1.010(2)	1.004(3)	1.005(3) Å

The overall means for the C—F, N—F, C—Cl, and N—Cl bonds in Table 7 are 1.249(7), 1.302(12), 1.666(7), and 1.691(6) Å, respectively.

Bond angles

The variation in the bond angles is less regular than in the bond lengths and the trends are on the whole qualitative rather than quantitative. In the $XHHH^+$ and $HHXH^+$ sets, for ex-

[12]This would not apply to extreme cases of substitution, such as that with mixed X = F, Li ligands (see below), unlikely to be encountered in practical circumstances.

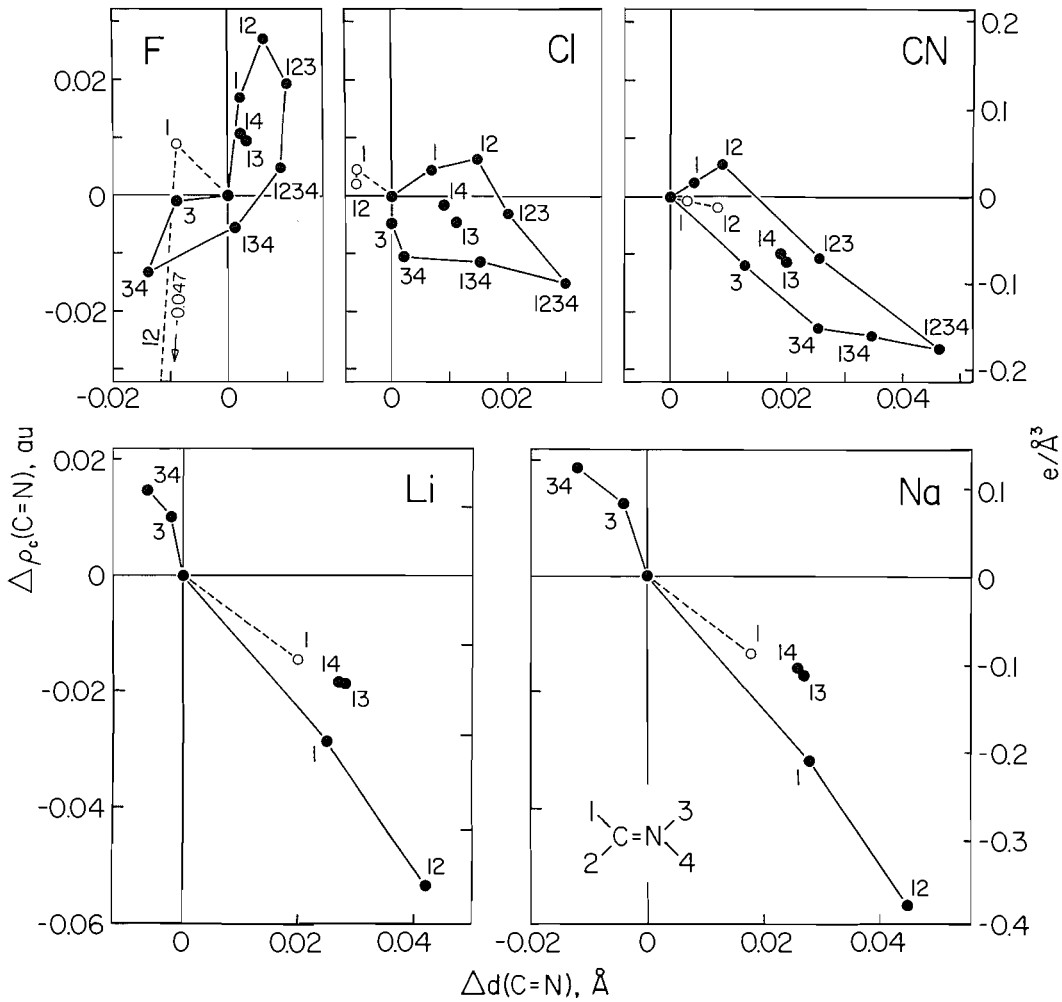

FIG. 11. Variation of the change $\Delta\rho_c$(C=N) in the electron density at the critical point in the C=N bond with the change Δd(C=N) in the C=N bond length in substituted iminium ions, both changes with respect to $[H_2C{=}NH_2]^+ = HHHH^+$. The corresponding changes in $XHC{=}C'H_2$ and $X_2C{=}C'H_2$ relative to $H_2C{=}CH_2$ are shown by the open circles (for these, read C=C′ instead of C=N).

ample, the *1*CN and CN*3* angles increase with $d(1\text{–C})$ and $d(\text{N–}3)$, respectively. For the F-substituted series these expressions have been obtained for the *gem* angles:

$$(1C2)_F = 120.20 - 2.35n_C + 1.90n_N,$$
$$r^2 = 0.95, \sigma = 0.7^\circ \sim 8\% \text{ of range}$$

$$(3N4)_F = 115.36 + 1.67n_C - 2.30n_N,$$
$$r^2 = 0.89, \sigma = 0.9^\circ \sim 12\% \text{ of range}$$

$$(3N4)_F = 1383.9 - 20.237(1C2)_F + 0.080347[(1C2)_F]^2,$$
$$r^2 = 0.97, \sigma = 0.5^\circ \sim 6\% \text{ of range}$$

For the other X, the variations are more erratic. Nevertheless, even partial regressions may be informative in that they indicate the relative importance and sign of the individual contributions to the angle variation with the degree of substitution. Thus including only the *1*, *3*, *12*, and *34* species one finds

$$(1C2)_{Cl} = 118.5 + 0.10n_C + 1.80n_N,$$
$$r^2 = 0.77, \sigma = 1.5^\circ \sim 30\% \text{ of range}$$

$$(3N4)_{Cl} = 114.3 + 1.86n_C + 0.74n_N,$$
$$r^2 = 0.73, \sigma = 1.3^\circ \sim 38\% \text{ of range}$$

$$(1C2)_{Li} = 118.8 + 1.81n_C - 3.11n_N,$$
$$r^2 = 0.92, \sigma = 2.3^\circ \sim 20\% \text{ of range}$$

$$(3N4)_{Li} = 110.0 + 1.52n_C + 10.88\, n_N,$$
$$r^2 = 0.92, \sigma = 4.9^\circ \sim 23\% \text{ of range}$$

$$(1C2)_{Na} = 117.1 + 3.48n_C - 2.68n_N,$$
$$r^2 = 0.88, \sigma = 3.6^\circ \sim 25\% \text{ of range}$$

$$(3N4)_{Na} = 105.9 + 3.84n_C + 16.36n_N,$$
$$r^2 = 0.90, \sigma = 7.6^\circ \sim 26\% \text{ of range}$$

$$(3N4)_{Li} = -12.58 + 2.4849(1C2)_{Li} - 0.011891[(1C2)_{Li}]^2,$$
$$r^2 = 0.97, \sigma = 2.1^\circ \sim 10\% \text{ of range}$$

While *statistically* these regressions may be found wanting, the coefficients of n_C and n_N show that the *gem* angle at C is substantially influenced by the substitution at N and vice versa. They also show that the contraction of the $(1C2)_X$ angle arises (with the exception of X = F) from the substitution at N, whereas (again excepting F) the $(3N4)_X$ angle increases with *any* substitution at N *and* C. Furthermore, the sum

Can. J. Chem. Downloaded from www.nrcresearchpress.com by 213.200.69.106 on 09/08/12
For personal use only.

Can. J. Chem. Downloaded from www.nrcresearchpress.com by 213.200.69.106 on 09/08/12
For personal use only.

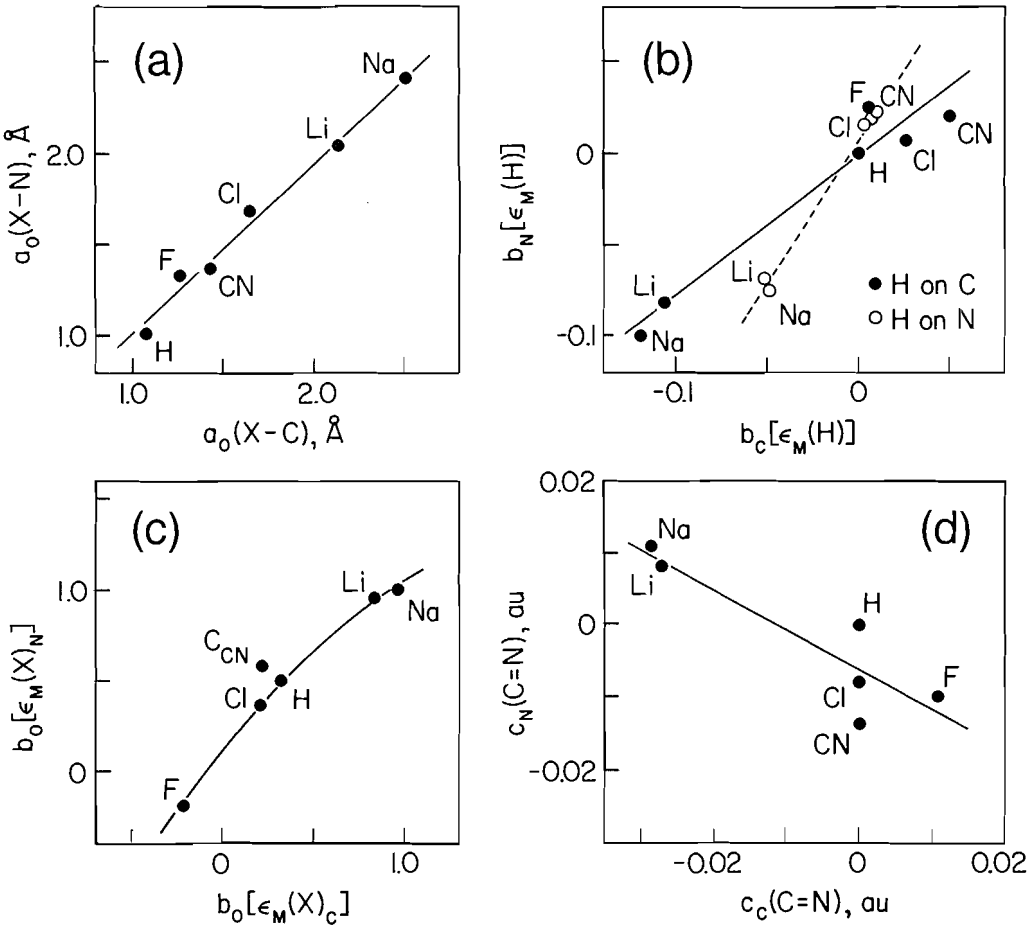

FIG. 12. Relations between regression coefficients of Tables P–R. (*a*) $a_0[d(X—N)]$ vs. $a_0[d(X—C)]$. (*b*) Full circles, $b_N[\varepsilon_M(H)_C]$ vs. $b_C[\varepsilon_M(H)_C]$; open circles, $b_N[\varepsilon_M(H)_N]$ vs. $b_C[\varepsilon_M(H)_N]$. On substitution, $\varepsilon_M(H)$ on the remaining H atoms increases with the degree of substitution when X = **A** but decreases when X = **B**, regardless of whether the H atoms are on C or on N. (*c*) Dependence of $\varepsilon_M(X)$ on the substitution site when $\varepsilon_M(X)$ is extrapolated to zero substitution, i.e., $n_C = n_N = 0$, $\varepsilon_M(X)_0 = b_0[\varepsilon_M(X)]$. (*d*) c_N vs. c_C for $\rho_c(C{=}N)_X$.

$(1C2)_X + (3N4)_X$ (X ≠ F) of the *gem* angles also increases with *any* substitution. This means that the substituents other than F reduce, at least in the mono- and *gem*-disubstituted species, the sum of the non-*gem* angles $720° - (1C2)_X - (3N4)_X$, with consequences for interligand repulsion.

The very large bond angles obtained for the highly **B**-substituted species may be open to question, as they possibly arise from the planarity constraint (see below).

Net charges

Both Mulliken ε_M and Löwdin ε_L net charges are discussed in the following, but only the former constitute a comprehensive set.[13] As we are about to demonstrate, the ε_L charges (Table S) differ considerably from the corresponding ε_M (subject of course to $\Sigma\varepsilon_M = \Sigma\varepsilon_L = +1$ or 0), but the trends they exhibit are much the same, at least to the extent we have investigated. Our detailed analysis is therefore confined to ε_M.

Linear regressions of ε_M and ε_L on n_C and n_N yield, with only a few exceptions, high correlations. Of the 50 such regressions in Table Q only seven have r^2 between 0.78 and 0.9; of the remaining 43, 38 have $r^2 > 0.95$. The ε_M set for the substituted iminium ions is thus not only highly self-consistent but also additive with respect to the degree of substitution. The condition (not used in the independent individual regressions) $b_0[\varepsilon_M(C)]_X + b_0[\varepsilon_M(N)]_X + 2b_0[\varepsilon_M(H)_C]_X + 2b_0[\varepsilon_M(H)_N]_X = 1$ is satisfied to ~0.7% for X = F on to ~3.3% for X = Na.

Of the individual results, that of fundamental interest concerns the unsubstituted ion and the conventional way of representing the charge on it, viz. $H_2C{=}N^+H_2$. If this formula implies that the N atom carries a positive net charge, then on the present evidence this representation is incorrect. Neither $\varepsilon_M(N) = -0.657$ nor $\varepsilon_L = -0.250$ is positive; in fact, both are strongly negative. When these charges on N are contrasted with those on C, $\varepsilon_M(C) = 0.038$ and $\varepsilon_L(C) = 0.042$, the difference is seen to be substantial. The sum $\varepsilon_M(C) + 2\varepsilon_M(H)_C = 0.684$ and $\varepsilon_M(N) + 2\varepsilon_M(H)_N = 0.315$ (0.526 and 0.473, respectively, for ε_L) indicate that the

[13]The reason for the incomplete coverage of ε_L is historico-practical: in the final stages of this investigation GAUSSIAN 86, which was used throughout and which calculates ε_M but not ε_L, was supplemented by GAMESS, which calculates both ε_M and ε_L (see Experimental). The last-named program was used in a limited way for special purposes other than obtaining ε_L, but as the desirability to compare ε_M and ε_L became apparent, some of the optimizations were repeated using GAMESS solely to generate ε_L.

Can. J. Chem. Downloaded from www.nrcresearchpress.com by 213.200.69.106 on 09/08/12
For personal use only.

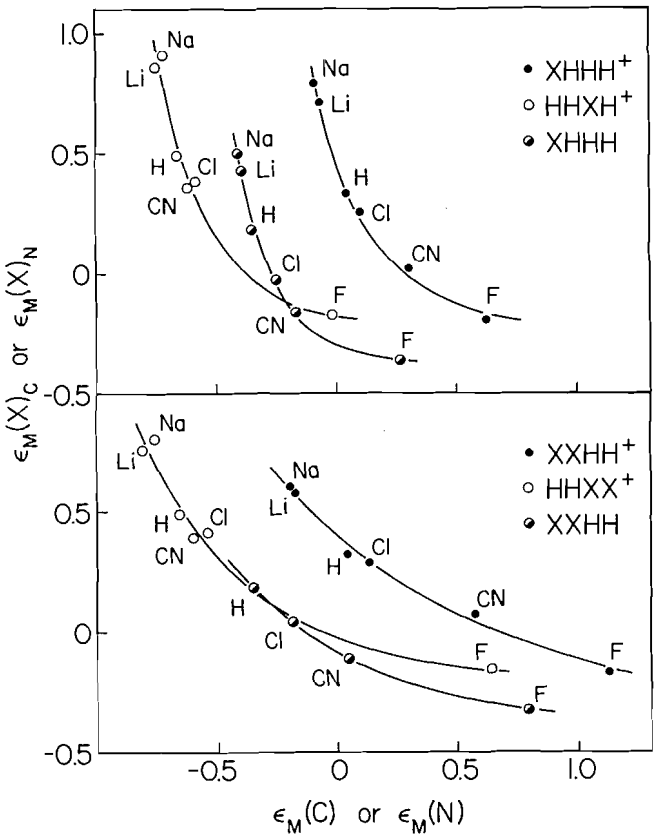

FIG. 13. Variation of the Mulliken net charges ε_M on X with $\varepsilon_M(C)$ and $\varepsilon_M(N)$ in X-monosubstituted iminium ions and ethylenes. For X = CN, $\varepsilon_M(X) = \varepsilon_M(CN) = \varepsilon_M(C) + \varepsilon_M(N)$. The fitted curves represent exponential regressions of $\varepsilon_M(X)$ on $\varepsilon_M(C)$ and $\varepsilon_M(N)$, respectively (see text and Table T).

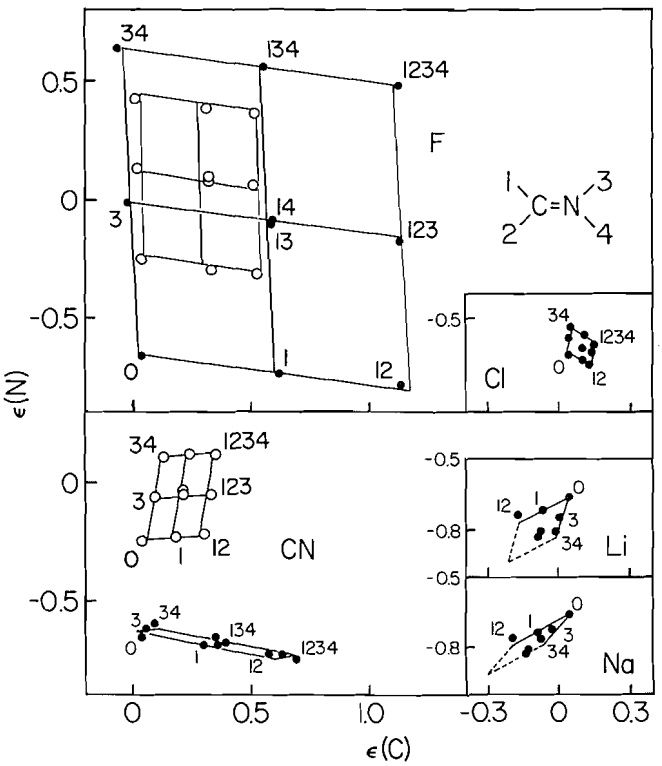

FIG. 14. Correlation of the Mulliken net charges $\varepsilon_M(C)$ and $\varepsilon_M(N)$ (and the Löwdin net charges $\varepsilon_L(C)$ and $\varepsilon_L(N)$ for X = F and CN) in X-substituted iminium ions. For notation see text. Full circles, ε_M; open circles, ε_L.

charge on the nitrogen half of the ion remains less positive even on inclusion of the charges on the H atoms.

As is evident from Table Q, $\varepsilon_M(N)$ will become positive only on *N*-substitution by F, whereas $\varepsilon_M(C)$ can become negative for X = F and Li, and *will* be negative when X = Na.

As for the net charges on the H atoms, $\varepsilon_M(H)$ is always positive for X = **A**, but $\varepsilon_M(H)_C$ is negative in $NaNaNaH^+$ and almost zero in $NaHNaNa^+$. The $\varepsilon_L(H)$ are available only for X = F and CN; they are positive for both ligands. The sensitivity of $\varepsilon_M(H)$ to substitution is displayed in a plot of the coefficients of the regressions of $\varepsilon_M(H)_C$ and $\varepsilon_M(H)_N$ on n_C and n_N (Fig. 12*b*). The two fits ($\varepsilon_M(H)_C$, $r^2 = 0.944$; $\varepsilon_M(H)_N$, $r^2 = 0.990$) show a neat separation between X = **A** and X = **B** (**B** being the electron-donating substituents).

The relationship between $\varepsilon_M(X)$ and $\varepsilon_M(C)$ or $\varepsilon_M(N)$ in the mono- and the *gem*-disubstituted ions is shown in Fig. 13.[14] There is a clear division between the *C*- and the *N*-substituted ions, the curve for the XHHH ethylenes occupying a more or less intermediate position. The position of the curve for XXHH is less well defined. Remarkably, the $\varepsilon_M(X)$ vs. $\varepsilon_M(C)$ or $\varepsilon_M(N)$ curves can be fitted to exponential expressions $\varepsilon_M(X) = p + q \exp[-s\varepsilon_M(C \text{ or } N)]$ to $r^2 > 0.96$, as can the curves for the ethylenes (Table T).

The $XHXH^+$, $XHHX^+$, and the tri- and tetrasubstituted sets yield similar functional dependence, as far as it is possible to determine from the somewhat uncertain ε_M values for the higher-substituted iminium ions and ethylenes (see later). In fact, the curves corresponding to $\varepsilon_M(C)$ and $\varepsilon_M(X)_C$ in $XHXH^+$ and $XHHX^+$, and those corresponding to $\varepsilon_M(N)$ and $\varepsilon_M(X)_N$, differ very little from the curves for $XHHH^+$ and $HHXH^+$, respectively, thus pointing to the largely localized character of the $\varepsilon_M(C)$ vs. $\varepsilon_M(X)_C$ and $\varepsilon_M(N)$ vs. $\varepsilon_M(X)_N$ relationship.

A synoptic impression of the ε(N) vs. ε(C) relationship is obtained from Fig. 14. The expected difference in the electron-transfer properties of the **A** and **B** substituents is immediately apparent. The plot for X = F conveys at a glance the essentially additive nature of the relationship and of the difference between the effect of substitution at C and that at N. Comparison of this plot with the plot for Cl shows that the range of ε_M for X = Cl is about six times smaller than that for F. This, in a somewhat different way, is also true of the effects produced by CN substitution.

For X = **B** approximate additivity obtains only for the mono- and disubstituted ions. When the ε values from the optimizations for the higher-substituted ions are entered in Fig. 14, the parallellogram geometry disappears and the points, especially those for $XXXX^+$, fall in unexpected places. Since the expectation stems from a preconceived notion that assumes persistence of the additivity and is thus a self-fulfilling prophecy, one cannot exclude the possibility that the answers provided by the calculation *are* correct and that the additivity breaks down. It is more likely, however, that either the optimizations of Tables 7–9 for the tri- and tetrasubstituted Li and Na species do not correspond to

[14]For X = CN, $\varepsilon(CN) = \varepsilon(C_{CN}) + \varepsilon(N_{CN})$.

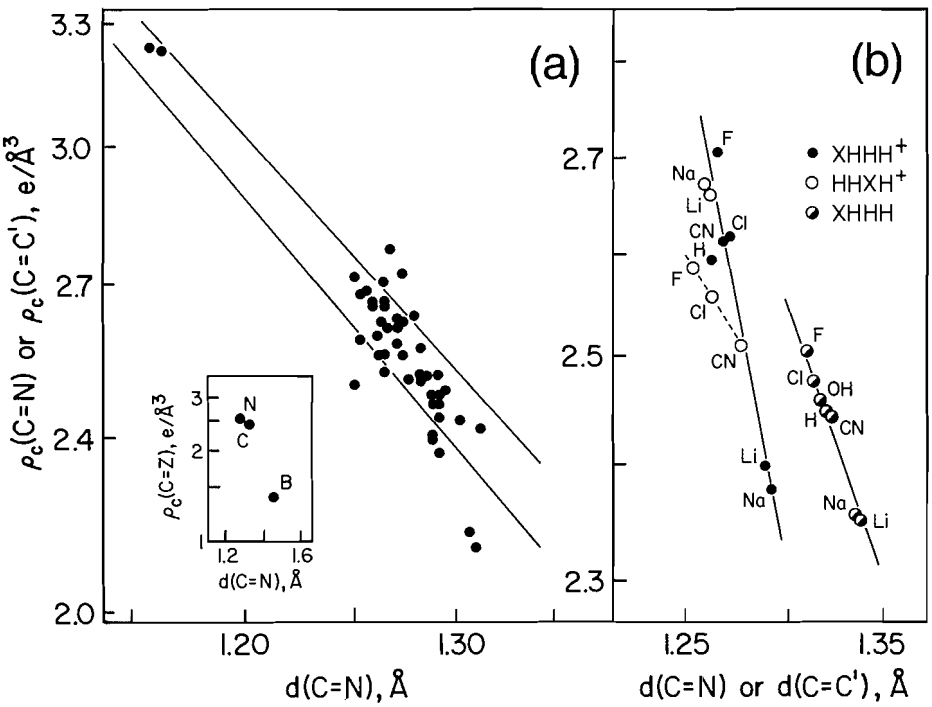

FIG. 15. (*a*) Logarithmic plot of ρ_c(C=N) vs. d(C=N) for the iminium ions of Table 7. The band corresponds to the $\pm 1\sigma$ limits of a section of the $\rho_c = sd^{-v}$ correlation for C—N bonds of all orders (cf. text and ref. 23). (*b*) Logarithmic plot of ρ_c(C=N) vs. d(C=N) for monosubstituted iminium ions, and of ρ_c(C=C) vs. d(C=C) for monosubstituted ethylenes. Inset: plot of log ρ_c(C=Z) vs. log d(C=Z) for $[H_2C{=}NH_2]^+$, $H_2C{=}CH_2$, and $[H_2C{=}BH_2]^-$.

the *global* E(6-31G*) minima for planar geometry, or that interligand repulsions in these species begin to interfere with the planarity, in which case optimization in nonplanar geometries is indicated. This matter is discussed in more detail below.

Figure 14 also displays the differences that arise when ε_L rather than ε_M values are used in the analaysis of trends in the net charges. Numerically, the ε_L values generally are smaller than the corresponding ε_M. In the X = F set it makes little difference to the trends whether ε_M or ε_L are employed. In the CN set, however, the range of the ε_M(N) values is markedly compressed, whereas the ε_L values generate a parallellogram of the expected shape.

The coefficients b_0 of the regressions of ε_M(X) on n_C and n_N (Table Q) represent the net charges on X extrapolated to zero substitution, i.e., $n_C = n_N = 0$. The $\varepsilon_M(X)_0 = b_0[\varepsilon_M(X)]$ for substitution at N correlate smoothly with those for substitution at C (Fig. 12*c*), with the exception of X = CN. A parabolic fit yields $b_0[\varepsilon_M(X)_N] = -0.153 + 1.394b_0[\varepsilon_M(X)_C] - 0.534\{b_0[\varepsilon_M(X)_C]\}^2$, $r^2 = 0.97$, $\sigma = 0.10 \sim 8\%$ of range. The anomaly for X = CN is not unexpected, given the composite nature of the ligand and the presence of the C≡N bond.

Electron density at the bond critical point

Results of the regressions of ρ_c on n_C and n_N are presented in Table R. The coefficients for $\rho_c(C{=}N)_C$ show modest degree ($r^2 = 0.80$) of correlation (Fig. 12*d*).

The ρ_c(C—X) and ρ_c(N—X) would be expected to be approximated by simple power functions of the corresponding d(C—X) and d(N—X) bond lengths, $\rho_c = sd^{-v}$ (cf. ref. 23). With the exceptions of ρ_c(N—Cl), which correlates poorly with d(N—Cl), this is indeed the case (Table H). For X = F this relationship is satisfied to $r^2 > 0.98$. For the other bonds the regressions are not quite as good but still satisfactory. It must be remembered, however, that the ranges of these ρ_c,d are narrow and the results of the regressions may therefore be somewhat misleading. A proper test of conformity to the power dependence would be the success of immersion of these pairs in the global 6-31G* ρ_c(C—X) vs. d(C—X) and ρ_c(N—X) vs. d(N—X) regressions, which span the entire range of bond orders. Such a test will have to await the completion of our comprehensive investigation of the global regressions now in progress.[15]

These remarks apply equally or even more to the relationship between ρ_c(C=N) and d(C=N). In the rectified plot of Fig. 15*a* the distribution of the ρ_c,d points for the iminium ions of Table 7 would largely lack orientation were it not for the two points for LiLiLiLi$^+$ and NaNaNaNa$^+$, about which there may be certain reservation (see below). However, when these and all the other points are mapped on the previously established[15] 6-31G* $\rho_c = sd^{-v}$ power regression comprising C—N bonds of *all* orders, the majority of the points by far fall inside the $\pm 1\sigma$ limits of this overall regression. There is thus no doubt that the points for the iminium ions conform, within reasonable statistics, to the ρ_c,d behaviour established for C—N bonds in general.[16]

The gross features of the overall ρ_c,d regressions for C—N bonds may, however, tend to obscure the behaviour of the ρ_c,d pairs *in the small*. In Fig. 15*b* the ρ_c(C=N),d(C=N)

[15]O. Knop, S.C. Choi, and R.J. Boyd, to be published. See also ref. 23.

[16]When the ρ_c,d values for the C≡N and those for the C—C_{CN} bonds of the cyano-substituted ions (Tables 7,8, and G) are entered in Fig. 15*a*, the points fall within the $\pm 1\sigma$ band. The positions of the ρ_c,d points for C=N in LiLiLiLi$^+$ and NaNaNaNa$^+$ are then seen to be very close to the C≡N group of points.

Can. J. Chem. Downloaded from www.nrcresearchpress.com by 213.200.69.106 on 09/08/12
For personal use only.

Can. J. Chem. Downloaded from www.nrcresearchpress.com by 213.200.69.106 on 09/08/12
For personal use only.

values for the monosubstituted $XHHH^+$ and $HHXH^+$, as well as the $\rho_c(C{=}C'),d(C{=}C')$ values for XHHH, not only satisfy separate linear regressions to high r^2, but they even mimic the break between X = **A** and X = **B** for $HHXH^+$ (see below). The linearity of the rectified plot for XHHH is particularly impressive.

The inset of Fig. 15*a* gives an idea of the variation of $\rho_c(C{=}Z)$ with $d(C{-}Z)$ in the unsubstituted species, viz. in $[H_2C{=}NH_2]^+$, $H_2C{=}CH_2$, and $[H_2C{=}BH_2]^-$ (cf. Table 9).

The cyano group as ligand

The parameters of the CN groups in Tables 7, 8, and G vary only slightly with substitution: $d(C{\equiv}N)_C$ of CN on the C atom, 1.136(2) Å; $d(C{\equiv}N)_N$, 1.131(1) Å; $\langle CC{\equiv}N\rangle$, 179.0(8)°; $\langle NC{\equiv}N\rangle$, 179.6(2)°; $\bar{\varepsilon}_M(C_{CN})_C$, 0.309(28); $\bar{\varepsilon}_M(N_{CN})_C$, −0.244(11); $\bar{\varepsilon}_M(C_{CN})_N$, 0.626(17); $\bar{\varepsilon}_M(N_{CN})_N$, −0.230(9); $\bar{\rho}_c(C{\equiv}N)_C$, 0.4864(8) au; $\bar{\rho}_c(C{\equiv}N)_N$, 0.4823(5) au. Nevertheless, the ε_M and ε_L show a weak dependence on n_C and n_N, both for C_{CN} and N_{CN} individually and for the CN group as a unit, $\varepsilon(CN) = \varepsilon(C_{CN}) + \varepsilon(N_{CN})$ (Table Q). Perhaps not surprisingly, the $\varepsilon_M(N_{CN})_C$ and $\varepsilon_M(N_{CN})_N$ values are about the same, while the $\varepsilon_M(C_{CN})_N$ value is on the average about twice that for $\varepsilon_M(C_{CN})_C$.

The individual contributions to the joint effect, which conjugation with the C≡N bond and the net charge on the distant atom of the C=N bond have on the cyano-substituted atom of the C=N bond, are detailed as follows:

$$\varepsilon_M(C)_{CN} = -0.502 - 0.386\varepsilon_M(N) + 4.493\varepsilon_M(C_{CN}) + 2.637\varepsilon_M(N_{CN}),$$
$$r^2 = 0.986,\ \sigma = 0.024 - 6\%\ \text{of range}$$

$$\varepsilon_M(N)_{CN} = -0.122 - 0.246\varepsilon_M(C) - 0.235\varepsilon_M(C_{CN}) + 1.378\varepsilon_M(N_{CN}),$$
$$r^2 = 0.984,\ \sigma = 0.009 \sim 6\%\ \text{of range}$$

$$\varepsilon_L(C)_{CN} = 0.773 + 0.190\varepsilon_L(N) + 11.05\varepsilon_L(C_{CN}) - 0.949\varepsilon_L(N_{CN}),$$
$$r^2 = 0.942,\ \sigma = 0.021 \sim 12\%\ \text{of range}$$

$$\varepsilon_L(N)_{CN} = -0.553 - 0.171\varepsilon_L(C) + 12.82\varepsilon_L(C_{CN}) + 2.204\varepsilon_L(N_{CN}),$$
$$r^2 = 0.984,\ \sigma = 0.015 \sim 8\%\ \text{of range}$$

The difference in sign and magnitude of the individual ε_M and ε_L components of these expressions for ε(C) and ε(N) elucidates the difference in the appearance of the two ε(N) vs. ε(C) plots in Fig. 14, in particular the compression of the $\varepsilon_M(N)$ range compared to the $\varepsilon_L(N)$ range.

The electron density at the critical point of the C≡N bond decreases with the increasing number of CN groups in the ion (Table R). Here, too, the parameter is more sensitive to the substitution on the N atom of C=N: $(c_N/c_C)_C = 1.6$, $(c_N/c_C)_N = 4.5$.

The effect of the adjacent C=N and C≡N bonds on ρ_c in the $C{-}C_{CN}$ and $N{-}C_{CN}$ bonds can be expressed as

$$\rho_c(C{-}C_{CN}) = -0.5459 - 0.397\rho_c(C{=}N) + 2.056\rho_c(C{\equiv}N),$$
$$r^2 = 0.907,\ \sigma = 0.0011\ \text{au} \sim 12\%$$

$$\rho_c(N{-}C_{CN}) = -1.9021 + 0.259\rho_c(C{=}N) + 4.383\rho_c(C{\equiv}N),$$
$$r^2 = 0.992,\ \sigma = 0.0005\ \text{au} \sim 5\%$$

On the one hand, these ρ_c values are much more sensitive to changes in $\rho_c(C{\equiv}N)$; on the other hand, the latter changes are much smaller than the changes in $\rho_c(C{=}N)$ on substitution.

Mixed F,Li ligands

The effect of substitution can be maximized by replacing all four H atoms in $HHHH^+$ by a combination of ligands from the opposite ends of the electronegativity scale, viz. F and Li. The three substitutions in Table 10, $LiLiFF^+$, $FFLiLi^+$, and $LiFFLi^+$, were chosen to accentuate the effect. Indeed, the effect on $d(C{=}N)$ and $\rho_c(C{=}N)$ is seen to be dramatic (Fig. 16). In both *gem* isomers the C=N bond contracts by about 0.05 Å with respect to $d(C{=}N)$ in $FFFF^+$, 1.272 Å, i.e., over three times the maximum contraction observed on pure F substitution in $HHHH^+$. However, $\rho_c(C{=}N)$ in $LiLiFF^+$ has decreased by about 0.03 au ~ 0.2 e/Å^3 and that of $FFLiLi^+$ has *increased* by about 0.06 au ~ 0.4 e/Å^3 with respect to the $FFFF^+$ reference. Thus while the $d(C{=}N)$ contraction is about the same, the substitution with Li at C in $FFFF^+$ decreases, and that at N increases, the covalent character of the C=N bond. As indicated in Fig. 16, the transfer of electronic charge (in terms of ε_M) on Li substitution is almost entirely between Li and C in $LiLiFF^+$, and almost entirely between Li and N in $FFLiLi^+$, whereas on H substitution in $FFFF^+$ the situation for $FFHH^+$ is similar to $FFLiLi^+$ but in $HHFF^+$ a non-negligible electronic charge is transferred also to the N atoms.[17]

The electronic charges transferred to the C and N atoms, respectively, when $FFFF^+ \rightarrow LiFFLi^+$ and $FFFF^+ \rightarrow HFFH^+$ are almost equal and, in these two *trans* substitutions, of comparable magnitude. Yet the changes in the C=N bond length are in the opposite directions, even though numerically they are quite similar. This seems to indicate that in $LiFFLi^+$ the interligand repulsion dominates the electronic effects and results in a net expansion of the C=N bond.

Interligand separations

When the $X^1{-}H^3$ separation in $XHHH^+$ is regressed linearly on the $X^1{-}H^2$ separation, a very good correlation results ($n = 6$, $r^2 = 0.997$, $\sigma = 0.033$ Å ~ 3% of range), and similarly for $d(X^3{-}H^1)$ in $HHXH^+$ regressed on $d(X^3{-}H^4)$ ($n = 6$, $r^2 = 0.994$, $\sigma = 0.036$ Å ~ 3% of range) (Fig. 17). The $X^1{-}H^3$ and $X^3{-}H^1$ distances are about 0.2 Å or less smaller than the sums of the corresponding van der Waals radii for H, F, and Cl (Pauling's values).

However, a plot of $d(X^1{-}H^3)$ against $d(X^1{-}H^2)$ for $XHC{=}C'H_2$ (Fig. 17) shows a break in the correlation line between X = Cl and X = Li, while the portion for X = **A** correlated to $r^2 = 0.993$, $\sigma = 0.019$ Å ~ 4% of range. The existence of this feature in the ethylene series calls for a closer examination of the $d(X^1{-}H^3)$ against the *gem*-d(H–H) plots for the monosubstituted iminium ions. Indeed, fitting only the **A** points for $XHHH^+$ to $d(X^1{-}H^2)$ yields $r^2 = 0.9982$, $\sigma = 0.010$ Å ~ 2.3% of range compared to the above $r^2 = 0.9968$, $\sigma = 0.033$ Å ~ 3% range for **A** + **B**. While by itself this difference does not constitute compelling evidence

[17]Interpretation of H–F calculations involving adjacent Li atoms is not without problems (cf. ref. 35) and caution is indicated.

TABLE 10. 6-31G* parameters of [*12*C=N*34*]$^+$ iminium ions in planar (C_s or C_{2v}) or perpendicular (C_{2v}, ⊥) geometries: total eletronic energies *E* (au), bond lengths (Å) and angles (deg), Mulliken ε_M and Löwdin ε_L net charges (e), electron densities $\rho_c = \rho(r_c)$ at the bond critical points (au), and dipole moments μ (D)[a]

1234	*E*	C=N	*1*-C	*2*-C	*3*-N	*4*-N	*1*CN	*2*CN	*1C2*	CN*3*	CN*4*	*3*N*4*
LiLiLiLi	−121.91766	1.157	2.293	2.293	2.124	2.124	107.0	107.0	145.9	131.5	131.5	97.0
LiLiLiLi ⊥	−121.88595	1.236	2.203	2.203	1.837	1.837	125.6	125.6	108.8	123.2	123.2	113.6
NaNaHH	−416.94118	1.308	2.437	2.437	1.004	1.004	117.4	117.4	125.2	124.4	124.4	111.2
NaNaHH ⊥	−416.90954	1.294	2.261	2.261	1.009	1.009	124.9	124.9	110.1	124.0	124.0	112.0
NaNaNaNa	−739.54121	1.161	3.091	3.091	2.341	2.341	127.6	127.6	104.8	104.2	104.2	151.5
NaNaNaNa ⊥	−739.52142	1.163	3.578	3.578	2.303	2.303	117.6	117.6	124.9	98.7	98.7	162.5
LiLiFF	−305.72476	1.222	2.098	2.098	1.362	1.362	104.6	104.6	150.7	129.5	129.5	101.1
LiFFLi	−305.87408	1.281	2.108	1.314	1.428	1.952	94.6	108.6	156.8	105.2	136.1	118.6
FFLiLi	−305.98106	1.216	1.315	1.315	1.924	1.924	126.7	126.7	106.7	109.3	109.3	141.5

1234	ε(C)	ε(N)	ε(*1*)	ε(*2*)	ε(*3*)	ε(*4*)	ρ_c(C=N)	ρ_c(*1*-C)	ρ_c(*2*-C)	ρ_c(*3*-N)	ρ_c(*4*-N)	μ
LiLiLiLi	0.041	−0.508	0.396	0.396	0.337	0.337	0.4793	0.0124	0.0124	0.0171	0.0171	4.16
LiLiLiLi ⊥	0.041	−0.820	0.214	0.214	0.676	0.676						4.07
	0.222	−0.132	0.052	0.052	0.403	0.403						
NaNaHH	−0.197	−0.763	0.607	0.607	0.373	0.373	0.3277	0.0280	0.0280	0.3466	0.3466	4.13
	−0.033	−0.387	0.429	0.429	0.281	0.281						
NaNaHH ⊥	−0.355	−0.740	0.665	0.665	0.382	0.382	0.3335	0.0245	0.0245	0.3425	0.3425	4.47
	−0.148	−0.339	0.456	0.456	0.288	0.288						
NaNaNaNa	0.033	−0.651	0.242	0.242	0.566	0.566	0.4781	0.0065	0.0065	0.0208	0.0208	1.18
NaNaNaNa ⊥	0.054	−0.658	0.078	0.078	0.724	0.724						5.32
	0.027	−0.142	0.126	0.126	0.431	0.431						
LiLiFF	−0.244	0.485	0.659	0.659	−0.280	−0.280	0.3587	0.0299	0.0299	0.3289	0.3289	9.90
LiFFLi	0.405	−0.208	0.663	−0.334	−0.361	0.835	0.3899	0.0257	0.2669	0.2513	0.0312	4.31
FFLiLi	1.090	−0.947	−0.331	−0.331	0.760	0.760	0.4464	0.2799	0.2799	0.0366	0.0366	9.95

[a]First line, ε_M; second line, ε_L.

for segregation of the points into **A** and **B**, the $HHXH^+$ set behaves in a similar way, and plots of the *gem*-(H—H) and H^1–H^3 distances against *gem*-*d*(X—H) consistently show discontinuities that correspond to the gaps in the X^1–H^3 and X^3–H^1 plots. The H—H separations in **A** and in **B**, especially the *gem* ones, remain essentially constant on substitution.

Similar discontinuities are observed in the disubstituted $XHXH^+$ and $XHHX^+$ iminium ions (Fig. 18). In the *trans* isomer the gap between **A** and **B** is clearly visible in the $d(X^4$–$H^2)$ and $d(X^4$–$H^3)$ vs. $d(X^1$–$H^2)$ plots but not in the $d(X^1$–$H^3)$ vs. $d(X^1$–$H^2)$ plot, which indicates that the substitution at N affects the geometry in a significantly different way than the substitution at C. Nonetheless, all four X–H separations in XHHX increase from X = H to X = Na.

In the *cis* isomer there are discontinuities between X = Cl and X = Li for all three separations, X^1–X^3, X^2–H^4, and H^2–H^4, when these are plotted against X^1–H^2. While the gap for the *gem*-(X—H) distances is small, those for $d(X^1$–$X^3)$ and $d(H^2$–$H^4)$ are unmistakable: the increasing X^1–H^3 repulsion can no longer be easily compensated for and necessitates a gradual decrease in the H^2–H^4 distance. This is clearly reflected in the bond angles (Table 7).

In the *gem*-disubstituted isomers (Fig. 19) the discontinuity in $d(X^1$–$H^3)$ is insignificant in the plot against $d(X^1$–$X^2)$ of $XXHH^+$ but dramatic in the plot against $d(X^3$–$X^4)$ of $HHXX^+$, and readily visible in the plots for *gem*-(H–H). This again indicates that in the *C*-substituted isomers the effect of substitution at C is continuous for **A** + **B**, while the *N*-substitution differentiates between **A** on the one hand and **B** on the other.

The effect of tri- and tetrasubstitution on the interligand separations is more difficult to assess. The **A** derivatives give clear trends, but some of the interligand separations for **B** behave in an unexpected, seemingly erratic, manner (see above for ε). For $XXXH^+$ of **A**, the X^1–X^2, X^2–H^4, and X^3–H^4 distances all increase with $d(X^1$–$X^2)$, and the same is true of the X^1–X^3, X^4–X^2, and X^1–H^2 distances in $XHXX^+$ of **A** with respect to $d(X^3$–$X^4)$ (Fig. 19). However, the positions of the X = Li points for both $XXXH^+$ and $XHXX^+$ seem to be anomalous. In particular, the X^2–H^4 and X^4–H^2 distances are extremely short, the latter especially so.

The $d(X^1$–$X^3)$ vs. $d(X^1$–$X^2)$ and $d(X^3$–$X^4)$ correlation lines in the fully substituted $XXXX^+$ (Fig. 19) are well defined and practically coincident. The X^1–X^3 vs. X^3–X^4 line accommodates the point for X = Li, but the X^1–X^3 vs. X^1–X^2 line contains only the **A** points. The point of intersection of the joint correlation line with the 45° line corresponds to the crossover of the *gem*-(X–X) and the X^1–X^3 distances; it appears to separate the "conforming" from the "nonconforming" points.

When the size and number of the X atoms in the substituted iminium ions increase, the bond lengths and angles will adjust quasi-homometrically to minimize interligand repulsions. However, *d*(C=N) can only vary within the range *d*(C—N)–*d*(C≡N) ~ 0.35 Å. This bond length is thus a limiting factor in the adjustment. Since in the optimization the ion geometry has been constrained to planar, eventually

Can. J. Chem. Downloaded from www.nrcresearchpress.com by 213.200.69.106 on 09/08/12
For personal use only.

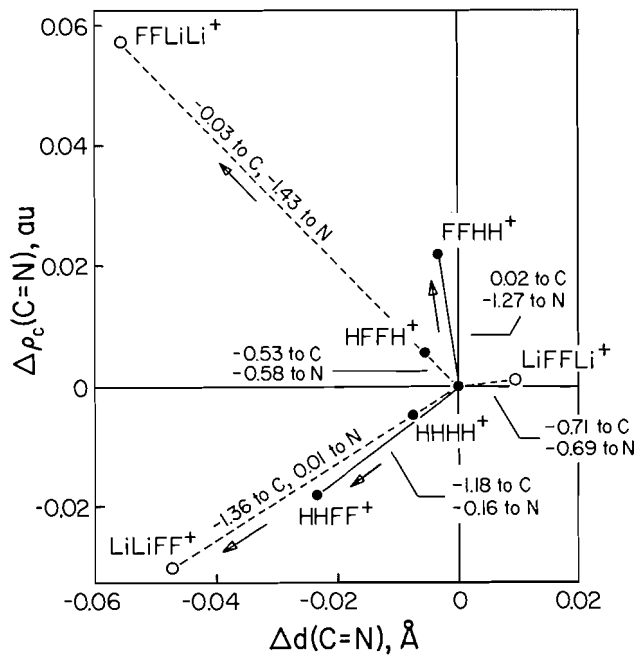

FIG. 16. Variation of the change $\Delta\rho_c$(C=N) in the electron density at the critical point in the C=N bond with the change Δd(C=N) in the C=N bond length in F- and Li,F-substituted iminium ions, both changes relative to $FFFF^+$. The amounts of ε_M charge transferred to the C and N atoms on replacing F in $FFFF^+$ by Li or H, respectively, are shown. This plot can be compared with that of Fig. 11.

the adjustment in d(C=N) will no longer be able to compensate for the increased L^1–L^3 and L^2–L^4 interactions, which compete with the *gem*-(L–L) interactions. Deviations from planarity may then be expected, reducing the C_{2v} symmetry of $XXHH^+$, $HHXX^+$ and $XXXX^+$ to C_2 (with the dihedral angles XCX/HNH, HCH/XNX, and XCX/XNX equal to 90° for the limiting, perpendicular geometry) and the C_s symmetry elsewhere to C_1.

To assess the effect of the interligand repulsions on interligand distances we have plotted the *gem* separations $d(L^3$–$L^4)$ against $d(L^1$–$L^2)$ (Fig. 20) and the non-*gem* separations $d(L^2$–$L^4)$ against $d(L^1$–$L^3)$ (Fig. 21). From Fig. 20 it is clear that, for X = **A**, $d(L^1$–$L^2)$ and $d(L^3$–$L^4)$ correlate and that the variation is in the first approximation additive, analogous to the net charges (Table P).

For **B** the additivity also holds but only up to disubstitution, and the linear combinations represent $d(L^1$–$L^2)$ and $d(L^3$–$L^4)$ less well than for **A**. Nonetheless, these representations are adequate to display the smallness of the effect that the substitution at the distant atom of the C–N bond has on the *gem*-(L–L) distances: the a_N/a_C and a_C/a_N ratios are well within ±0.1 (Fig. 20, inset). The substitution at the distant atom may have a lengthening (for X = F) or a contracting (for X = **B**) effect; for X = Cl and even more for X = CN this effect is negligible.

The points for the tri- and tetrasubstituted ions of the **B** group deviate considerably from the positions expected from additivity. This is consistent with the behaviour of these ions in Figs. 17–19.

An analogous behaviour is evident in Fig. 21. For X = CN and Cl (less so for X = F) the points for *1* and *3*; for *12*, *34*, and *14*; and for *123* and *134* bunch closely together. This indicates that in these cases it matters little to the non-*gem* interligand distances whether the substitution is at C or at N or both. For Li and Na, however, the *1* and *3*, and the *12*, *34*, and *14*, points are widely separated, as are also the *123* and *134* points for Na. The latter two points for Li fall in an unexpected region, casting suspicion on the optimization results or on the additivity hypothesis or both.

For **A** the regularity of the trends for any substitution indicates that here quasi-homometric adjustment is at work: the L^1–L^3 and L^2–L^4 repulsions are "non-crowding." For **B**, the discrepancies observed for *123* and *134* indicate significant incipient L^1–L^3 and L^2–L^4 repulsions, which tend to squeeze together the *gem* ligands and greatly distort the bond angles. The effects of these repulsions are amplified even more in the fully substituted *1234* ions.

Optimization in nonplanar geometry

The irregularities and anomalies in the parameter trends for **B** convinced us of the desirability of abandoning the planarity constraint, at least for the higher-substituted ions. Exploratory 6-31G* calculations for $XXXX^+$ in C_2 symmetry presented difficulties and led to the conclusion that the energy variation near the minimum is very flat, and that in any event it would take an inordinately large amount of computer time and effort if justice were to be done to the nonplanarity problem, important and interesting as it may be. Facing up to the practicalities of the situation, we decided not to proceed with an expansion of the present project. Nevertheless, we have attempted optimization for three ions in "perpendicular" C_{2v} geometry, i.e., with the dihedral angles LCL/L′NL′ equal to 90°. The results are compared in Table 10 with the results for the corresponding planar geometries.

In all three cases, viz. $NaNaHH^+$, $LiLiLiLi^+$, and $NaNaNaNa^+$, the energy of the planar form is lower than that of the perpendicular form, by 19.85, 19.89, and 12.42 kcal/mol, respectively, and the same is true of $Na_2C{=}CNa_2$, where the difference is 6.7 kcal/mol (Table 9). However, for $Li_2C{=}CLi_2$ the perpendicular form appears to be more stable, albeit by a relatively small amount, 4.4 kcal/mol. These results would seem to indicate that the lowest-energy conformation is the C_2-distorted planar conformation (D_2 for the two ethylenes).

There is some evidence that the conformational problem for the higher-**B**-substituted iminium ions and ethylenes may be further complicated by uncertainties involving globality of the optimizations. This would suggest even more strongly that its resolution is less straightforward and may require considerably more computational effort than originally envisaged.

Summary and conclusions

From chemistry

Recrystallization of a primary or secondary alkylammonium tetraphenylborate from approximately 1:1 mixtures of acetone (or another ketone) and water produces, against expectation, the corresponding iminium tetraphenylborate. Thus $MeNH_3BPh_4$ recrystallized from acetone and water will yield $Me_2C{=}NHMe^+BP_4^-$. Since aliphatic iminium cations generally are quite unstable in the presence of water and require anhydrous conditions for their synthesis and handling, this simple method permits the preparation, as tetraphenylborates, of a variety of iminium ions without special pre-

Can. J. Chem. Downloaded from www.nrcresearchpress.com by 213.200.69.106 on 09/08/12
For personal use only.

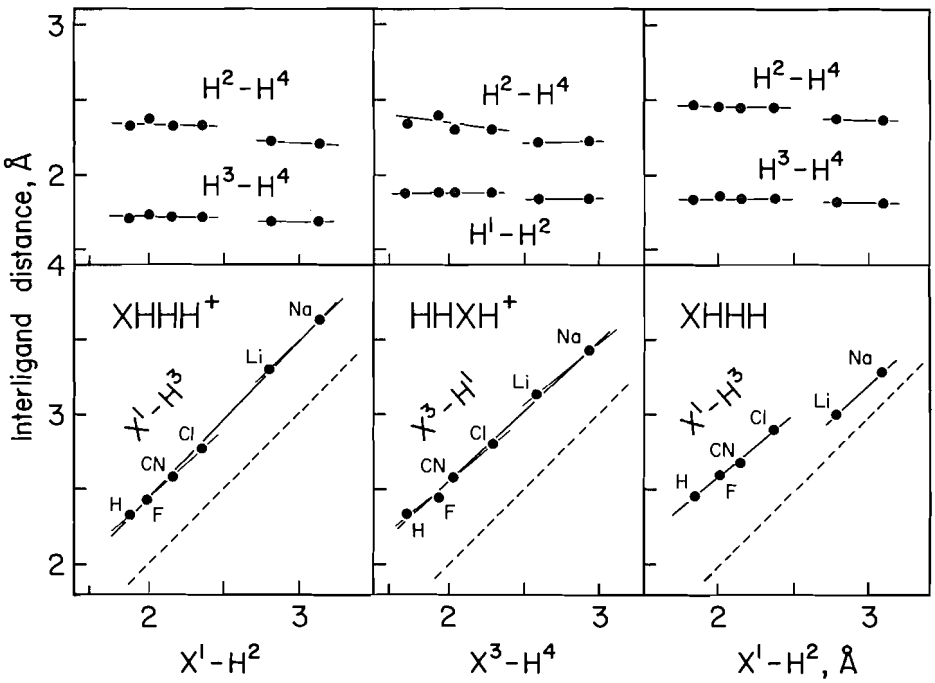

FIG. 17. Variation of the X–H and H–H interligand distances d with the *gem*-d(X—H) distances in X-monosubstituted iminium ions and ethylenes. Broken lines, d = *gem*-d(X—H).

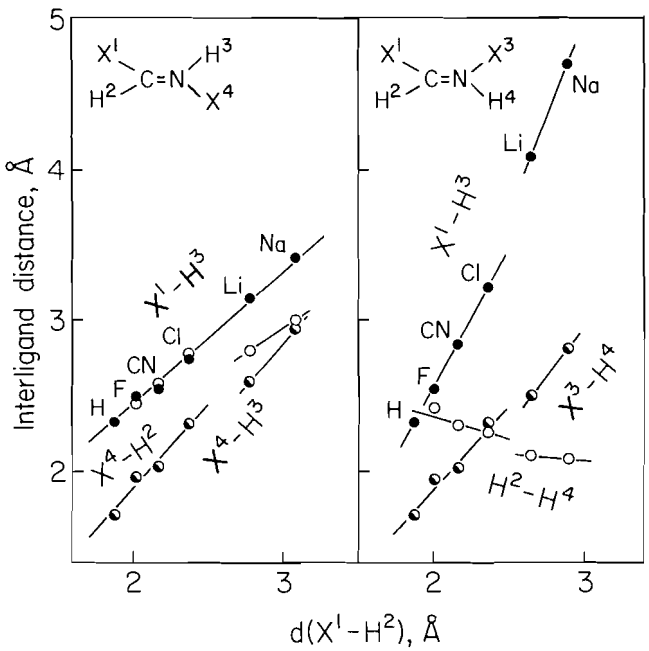

FIG. 18. Variation of the interligand distances d(X–H) with $d(X^1-H^2)$ in the *cis*/*trans* X-disubstituted iminium ions $XHXH^+$ and $XHHX^+$. Broken line, d(X–H) = $d(X^1-H^2)$.

cautions. Five such iminium tetraphenylborates, **A**–**E** (Table 1), have been prepared and their crystal structures determined.

From crystallography

The ion packing in the structures of the anhydrous **A**, **B**, **D**, and $Me_4N^+BPh_4^-$ is dominated by columns of the anions. The cations are accommodated in spaces generated by the phenyl rings of neighbouring anions. Depending on the size and shape of the cation, these phenyl rings may come from anion neighbours in the same column, or a pair of rings may come from one column and the other two rings form anions in neighbouring columns (Figs. 1–3). The structure of **C** is somewhat more complicated, with the cation less tightly enclosed between two pairs of rings, one pair each from two adjacent cations (Figs. 4 and 5). A different type of columnar arrangement of the anions is found in the hydrated **E** (Fig. 6). The small cations are prone to orientational disorder inside their cavities, which complicates determination of the true length of the C=N bond in the iminium cation.

A hydrogen atom(s) attached to the cation nitrogen will enter into a N^+—H...π^- hydrogen bond to the nearest phenyl ring(s); depending on the circumstances, this bond may be simple or bifurcated. In the hydrated **E** salt the hydrogen bonding between the cation and an anion is through the intermediary of the water molecule, N^+—H...O_w—H...π^- (Fig. 9). In these and similar iminium tetraphenylborates a hydrogen bond to the aromatic π system will form whenever the opportunity arises. This tendency will be documented more fully in a later paper.

From ab initio *studies*

6-31G* Optimization involving elements of the first and second rows of the periodic system are known to yield equilibrium molecular geometries that generally agree reasonably well with experiment. The corresponding total electronic energies can be considerably lowered by higher-level treatment, but this is of relatively little consequence for this study, since minimal use is made of energy comparisons, and then only in closely similar chemical situations (simple substitutional isomerism). We are therefore confident that the *trends* observed in the calculated parameters are substantially valid, especially as the considerable body of numerical results we have assembled shows a large measure of self-consistency

Can. J. Chem. Downloaded from www.nrcresearchpress.com by 213.200.69.106 on 09/08/12
For personal use only.

Can. J. Chem. Downloaded from www.nrcresearchpress.com by 213.200.69.106 on 09/08/12
For personal use only.

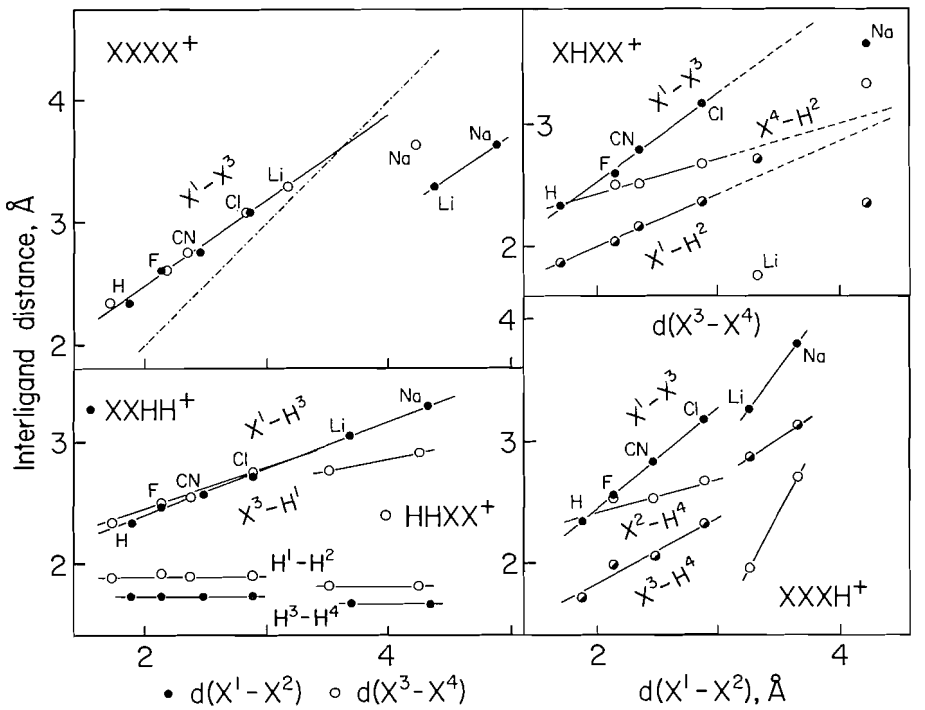

FIG. 19. Variation of the interligand distances in X-substituted iminium ions with $d(X^1–X^2)$ or $d(X^3–X^4)$. Dot-dash line, $d(X^1–X^3) = d(X^1–X^2)$, $d(X^1–X^3) = d(X^3–X^4)$.

and does not militate against standard chemical ideas. While, in the absence of an exhaustive investigation of the appropriate energy surface, questions may be raised about the *globality* of an individual, isolated, energy minimization, the present optimization of matching *series* of substituted iminium ions permits detection of anomalies and remedial action in suspect cases. The parameter variation in most of the (valence-isoelectronic) substitution series is smooth, thus lending credence to internal consistency if not necessarily to absolute validity.

The main findings can be summarized as follows:

1. The range of the C=N bond length in the substituted iminium ions is quite narrow (ca. 0.06 Å if the fully Li- and Na-substituted ions are excluded; Table 7) and in agreement with the range available from experiment (uncorrected mean, 1.283(12) Å; Table 6).

2. As would be expected, the effect of substitution on the molecular parameters of $[H_2C{=}NH_2]^+$ depends on the substitution site (C or N), the number of H atoms replaced, and on the type of substituent (**A** = H, F, Cl, CN; **B** = Li, Na). The differences are reflected clearly in the relative stabilities of the substitution isomers (Fig. 10).

3. Substitution by Cl or CN lengthens the C=N bond; that by F lengthens it except in $[H_2C{=}NHF]^+$ and $[H_2C{=}NF_2]^+$, where there is a contraction (Fig. 11). Li and Na as substituents expand the C=N bond when the substitution is at C but contract it when the substitution is at N (mono- and *gem*-disubstitution; Fig. 11). In the two cases of extreme substitution, $[Li_2C{=}NF_2]^+$ and $[F_2C{=}NLi_2]^+$, the C=N bond is shortened by over 0.04 Å relative to $[H_2C{=}NH_2]^+$ (Fig. 16).

4. The variation of several of the parameters with X substitution can be represented, to a good approximation and to a high degree of correlation, by linear functions $\alpha_0(X) + \alpha_C n_C(X) + \alpha_N n_N(X)$ of the number of X atoms on the C (n_C) and the N (n_N) atoms (Tables 10–12, Figs. 14 and 20). This mode of representation is important and informative, in that it makes it possible to estimate the contribution to the parameter values from the substitution at the distant atom of the C=N bond, i.e., the range and sign of action of that substituent. This approximate additivity is satisfied by X = **A** for any degree of substitution and by X = **B** up to and including disubstitution.

5. Both the Mulliken ε_M and the Löwdin ε_L net charges on the N atom of $[H_2C{=}NH_2]^+$ are strongly negative. This is contrary to the conventional formulation of the ion as $H_2C{=}N^+H_2$. Moreover, $[\varepsilon(C) + 2\varepsilon(H)_C] > [\varepsilon(N) + 2\varepsilon(H)_N]$, i.e., the NH_2 half of the ion also is less positively charged than the CH_2 half, both in terms of ε_M and ε_L. With the exception of $[Na_2C{=}NHNa]^+$ and $[NaHC{=}NNa_2]^+$, the net charge $\varepsilon_M(H)$ on the H atom is always positive regardless of the degree and type of substitution.

6. Complete sets of the Löwdin ε_L charges have been obtained only for X = F and CN. They are compared with the corresponding Mulliken ε_M net charges in Table S.

7. The variation of the net charge $\varepsilon_M(X)$ on the substituent atom with the net charge $\varepsilon_M(C)$ or $\varepsilon_M(N)$ on the parent atom can be approximated to $r^2 > 0.96$ by exponential functions $\varepsilon_M(X) = p + q \exp[-s\varepsilon_M(C \text{ or } N)]$ (mono- and *gem*-disubstituted ions; also the ethylene analogs; Table T, Fig. 13).

8. The correlation of the electron density $\rho_c(C{=}N)$ at the critical point in the C=N bond with the $d(C{=}N)$ bond length can be satisfactorily immersed in the "universal" $\rho_c(C{—}N) = k[d(C{—}N)]^{-v}$ correlation (Fig. 15; cf. ref. 23).

9. Detailed examination of the interligand distances (Figs. 17–21) suggests that planarity is maintained in all the iminium ions of Table 7 except for the tri- and tetrasubstituted ions with X = Li or Na as substituents. It seems likely that interligand repulsions force the latter to adopt nonplanar conformations with torsion angles LCL/LNL < 90°, of C_1

Can. J. Chem. Downloaded from www.nrcresearchpress.com by 213.200.69.106 on 09/08/12
For personal use only.

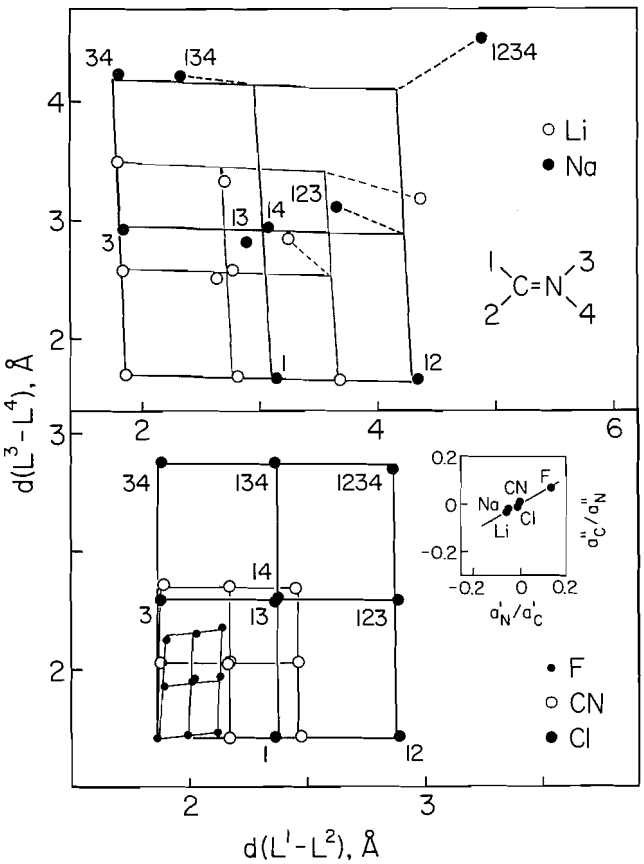

FIG. 20. Variation of the interligand distance $d(L^3–L^4)$ in substituted iminium ions with $d(L^1–L^2)$. The straight lines represent the regressions $d(L^3–L^4) = a''_0 + a''_C n_C + a''_N n_N$ and $d(L^1–L^2) = a'_0 + a'_C n_C + a'_N n_N$ of Table P. For X = Li and Na the values for *123*, *134*, and *1234* are not included in the regressions. The broken lines join the expected (from additivity) and the actual positions of the points. Note the different $d(L^3–L^4)$ scales. Inset: response of the *gem*-(L–L) distances to substitution as measured by coefficients of the regressions.

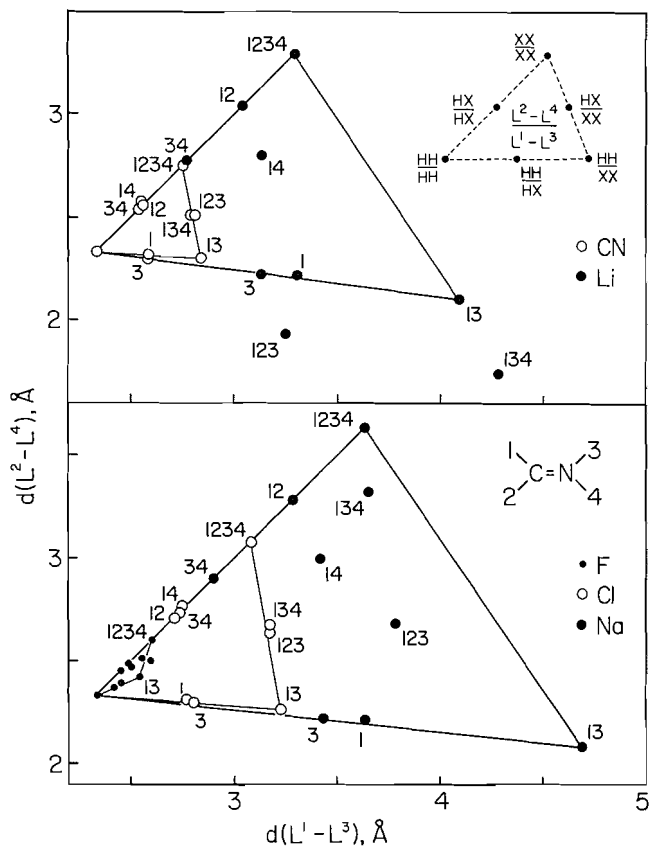

FIG. 21. Variation of the interligand distances $d(L^2–L^4)$ in X-substituted iminium ions with $d(L^1–L^3)$. HH/HX, etc. in the inset indicate the type of interligand separation: $d(H^2–H^4)$ vs. $d(H^2–X^3)$, etc.

symmetry for the tri- and of C_2 symmetry for the tetrasubstituted ions. This matter remains to be investigated.

Experimental

Preparation

An aqueous solution of $NaBPh_4$ was combined with an aqueous or ethanolic solution of an alkylammonium halide in stoichiometric amounts. The resulting precipitate of the alkylammonium tetraphenylborate was washed several times with water by decantation and then redissolved in acetone. Water was added dropwise until precipitation began to occur, upon which acetone was added only just to redissolve the solid formed. Typically, this occurred to an acetone–water volume ratio of approximately 1:1 (for compound **B** the measured ratio was 55:45 by volume), i.e., in a strongly aqueous medium. The resulting solution was allowed to recrystallize by slow evaporation at room temperature, yielding the appropriate iminium tetraphenylborate.

Structure determination

An ENRAF–Nonius CAD-4 four-circle diffractometer (**A**, **D**) and a Rigaku AFC5R diffractometer (**B**, **C**, **E**) were used in the data acquisition (cf. Table 1). The intensities ($\omega/2\theta$ scans) were reduced and corrected for Lorentz and polarization effects by routine procedures (36); empirical absorption corrections ($\mu_{Mo} \sim 0.6$ cm^{-1}) were applied (12). Scattering factors for neutral atoms and anomalous dispersion corrections were taken from ref. 37. Positions of the nonhydrogen atoms were found from an *E*-map and the remaining nonhydrogen atoms were located from successive Fourier syntheses. The H(C) atoms were placed geometrically (C—H, 1.08 Å) and refined isotropically or not refined (U_{iso}(H) = $1.2B_{eq}$(C) of the attached C atom). The function minimized by full-matrix least aquares was $\Sigma w(\Delta|F|)^2$. The anisotropic temperature factor is defined as $\exp[-2\pi^2(U_{11}h^2a^{*2} + U_{22}k^2b^{*2} + U_{33}l^2c^{*2} + 2U_{23}klb^*c^* + 2U_{13}hla^*c^* + 2U_{12}hka^*b^*)]$. Weighting schemes and other particulars of refinement are quoted below. Tables J–N of the structure factors for **A**–**E** have been deposited.[5]

It should be pointed out that, in general, alkylammonium tetraphenylborate crystals are weak scatterers. Significant reflections were seldom observed above a $(\sin\theta)/\lambda$ limit of 0.48 Å^{-1} ($\theta = 20°$ for Mo radiation). Since in this laboratory X-ray data collection routinely extends to a limit of 0.55 Å^{-1} ($\theta = 23°$), the ratios of observed reflections to total measured unique reflections never exceeded 50%. Attempts to collect the data at lower temperatures produced little if any improvement in these ratios (see, for example, **D**).

The computer preograms of refs. 36 and 38–43 were used in the crystallographic investigation.

Compound A

The systematic absences (*hkl*, $h + k$ odd; 0*kl*, *k* odd; *h*0*l*, *h*,*l* odd; *hk*0, $h + k$ odd; *h*00, *h* odd; 0*k*0, *k* odd; 00*l*, *l* odd) pointed to *Cmcm* or $Cmc2_1$ as possible space groups. The structure was successfully refined in the former, with the cations in twofold orientational disorder. The H(N) atom was located from a difference map and the N–H distance was fixed in the refinement to 1.02 Å. Weighting scheme, $w = 1.595/[\sigma^2(F) + 0.00072F^2]$.

Can. J. Chem. Downloaded from www.nrcresearchpress.com by 213.200.69.106 on 09/08/12
For personal use only.

Because of the cation disorder in *Cmcm* the structure was also refined in $Cmc2_1$, with the cations ordered. In this refinement there were many serious correlations between the atomic parameters. Refinement with constrained interatomic distances and with a large number (1000) added to each element of the leading diagonal finally converged at $R = 0.079$, with unreasonable temperature factors on the N atom. The correlations were so serious that all attempts to lower R further failed. Because of the cation disorder in *Cmcm* the space gorup *Cmca* was also considered but rejected, since its adoption would have required many reflections with large measured intensities to be absent.

Compound B

Systematic absences: hkl, $h + k$ odd; $0kl$, k odd, $h0l$, h,l odd; $hk0$, h,k odd; $h00$, h odd; $0k0$, k odd; $00l$, l odd. These and the E-statistic pointed to *Cmca* as the maximum space group. Refinement in this group was successfully carried out, with the cations in twofold positional disorder. Weighting scheme, $w = 1.000/[\sigma^2(F) + 0.000221F^2]$. The alternative refinement, in *Cc2b*, with the cations ordered, was more successful than was the alternative refinement of **A** in $Cmc2_1$. In this instance, the final converged R was 0.044, compared with 0.048 for *Cmca*. However, a Hamilton test showed that this reduction in R was not significant even at the 10% level.

Compound C

The systematic absences ($h0l$, $h + l$ odd; $h00$, h odd; $0k0$, k odd; $00l$, l odd) led to $P2_1/n$ as the correct space group. Weighting scheme, $w = 4F_o^2/\sigma^2(F_o^2)$, $\sigma^2(F_o^2) = [S^2(C + R^2B) + (pF_o^2)^2]/(\mathrm{LP})^2$ (S = scan rate, C = total integrated peak count, R = scan time to background counting time ratio, B = total background count, LP = Lorentz-polarizaiton factor, p = reduction factor).

Compound D

Intensities were collected at room temperature and later recollected at −70°C. The refinement results reported here are for the low-temperature collection. The systematic absences were the same as for **A**, i.e., pointing to *Cmcm* or $Cmc2_1$ as possible space groups. However, in *Cmcm*, neither direct methods nor difference maps revealed the positions of *all* the nonhydrogen atoms in the cation, and the noncentrosymmetric group was therefore adopted. Weighting scheme, $w = 1.388/[\sigma^2(F) + 0.00197F^2]$.

Compound E

Systematic absences: hkl, $h + k$ odd; $h0l$, h,l odd; $0kl$, k odd; $hk0$, $h + k$ odd; $h00$, h odd; $0k0$, k odd; $00l$, l odd. Space group, $C2/c$. The H(N) and H(O) hydrogens were located from a difference map; the N—H and O—H distances and the HOH angle were constrained in the refinements to 1.02 Å, 1.00 Å, and 105°, respectively. Unit weights were used in the refinement.

Ab initio *calculations*

The programs used in this part of the investigation were GAUSSIAN 86 (44), AIMPAC (45) and, in the later stages, GAMESS (46).

Acknowledgments

We thank Miss K.N. Robertson and Dr. S.P. Roe for assistance with some of the early experimental work, Dr. M. Falk for obtaining the FT-ir spectra, and Professor R.J. Boyd for occasional advice on *ab initio* calculations. This investigation was supported by grants from the Natural Sciences and Engineering Research Council of Canada to the two first-named authors.

ADDENDUM: We thank one of the reviewers for drawing our attention to references 47–53. While the results reported there refer mostly to X—H...π interactions with X other than N, they do strengthen the case for the existence of hydrogen bonding to aromatic π systems as a positive rather than passive type of bonding interaction. A recent search of the Cambridge Structural Database using a novel search procedure (54) has uncovered further examples of N—H...π bonds, often unnoticed by the original authors. In Part 4 of this series (see footnote 8) we shall report on numerous additional examples of N—H...π bonding in tetraphenylborate structures and provide a detailed discussion of the geometric scope of such bonding.

1. B.R. Vincent, O. Knop, A. Linden, T.S. Cameron, and K.N. Robertson. Can. J. Chem. **66**, 3060, (1988).
2. H. Böhme and H.G. Wiebe (*Editors*). Iminium salts in organic chemistry. Part 1. (Advances in organic chemistry. Vol. 9.) Wiley–Interscience, New York. 1976.
3. H. Böhme, W. Lehners, and G. Keitzer. Chem. Ber. **91**, 340 (1958).
4. N.J. Leonard and J.V. Paukstelis. J. Org. Chem. **28**, 3021 (1963).
5. J.M. Williams, S.W. Peterson, and G.M. Brown. Inorg. Chem. **7**, 2577 (1968).
6. H. Volz and H.H. Kiltz. Tetrahedron Lett. 1917 (1970).
7. J. Schreiber, H. Maag, N. Hashimoto, and A. Eschenmoser. Angew. Chem. Int. Ed. Engl. **10**, 330 (1971).
8. G. Kinast and L.-F. Tietze. Angew. Chem. Int. Ed. Engl. **15**, 239 (1976).
9. J.L. Roberts, P.S. Borromeo, and C.D. Poulter. Tetrahedron Lett. 1299 (1977).
10. R.F. Childs, B.D. Dickie, R. Faggiani, C.A. Fyfe, C.J.L. Lock, and R.E. Wasylishen. J. Crystallogr. Spectrosc. Res. **15**, 73 (1985).
11. A.B. Burg. Inorg. Chem. **28**, 1295 (1989).
12. N. Walker and D. Stuart. Acta Crystallogr. Sect. A: Found. Crystallogr. **A39**, 158 (1983).
13. C.J. Pouchert. The Aldrich library of FT-IR spectra. Vol. 1. Aldrich Chemical, Milwaukee, Wis. 1985. no. 814D.
14. R. Merényi. *In* Iminium salts in organic chemistry. Part 1. (Adv. Org. Chem. Vol. 9). Wiley–Interscience, New York. 1976. Chap. 2.
15. T. Davies and L.A.K. Staveley. Trans. Faraday Soc. **53**, 19 (1957).
16. K. Hoffmann and E. Weiss. J. Organomet. Chem. **67**, 221 (1974).
17. A. Aubry, J. Protas, E. Moreno-Gonzalez, and M. Marraud. Acta Crystallogr. Sect. B: Struct. Crystallogr. Cryst. Chem. **B33**, 2572 (1977)
18. W.J. Westerhaus, O. Knop, and M. Falk. Can. J. Chem. **58**, 1355 (1980).
19. A. Linden, T.S. Cameron, and O. Knop. Abstract ING-50-F2. Book of abstracts. 70th Canadian Chemical Conference, Quebec, P.Q. June 7–11, 1987.
20. B.R. Vincent. Doctoral thesis, Dalhousie University. 1987.
21. A. Linden, K.N. Robertson, O. Knop, and T.S. Cameron. Abstract 505. Book of abstracts. 3rd Chemical Conference of North America, Toronto, Ont. June 5–10, 1988.
22. J.L. Atwood, F. Hamada, K.D. Robinson, G.W. Orr, and R.L. Vincent. Nature (London), **349**, 683 (1991).
23. O. Knop, S.C. Choi, and R.J. Boyd. J. Am. Chem. Soc. **110**, 7299 (1988).
24. U. Müller. Acta Crystallogr. Sect. B: Struct. Crystallogr. Cryst. Chem. **B36**, 1075 (1980).
25. S. Arnott and S.C. Abrahams. Acta Crystallogr. **11**, 449 (1958).
26. A.I. Kitaigorodsky. Molecular crystals and molecules. Academic Press, New York and London. 1973. Table 1.
27. L.N. Trefonas, R.L. Flurry, Jr., R. Majeste, E.A. Meyers, and R.F. Copeland. J. Am. Chem. Soc. **88**, 2145 (1966).
28. G. Karlström, P. Linse, A. Wallqvist, and B. Jönsson. J. Am. Chem. Soc. **105**, 3777 (1983).
29. B.V. Cheney, M.W. Schulz, J. Cheney, and W.G. Richards. J. Am. Chem. Soc. **110**, 4195 (1988).

30. W.L. Jorgensen and D.L. Severance. J. Am. Chem. Soc. **112**, 4768 (1990).
31. A.T. McPhail, G.A. Sim, A.J. Frey, and H. Ott. J. Chem. Soc. B, 377 (1966).
32. A.D.U. Hardy and D.D. MacNicol. J. Chem. Soc. Perkin 2, 1140 (1976).
33. O. Knop, I.A. Oxton, and M. Falk. Can. J. Chem. **57**, 404 (1979); (errata) **57**, 2003 (1979).
34. P.A. Kollman. *In* Iminium salts in organic chemistry. Part 1. (Adv. Org. Chem. Vol. 9.) Wiley–Interscience, New York. 1976. Chap. 1.
35. J. Cioslowski J. Phys. Chem. **94**, 5496 (1990).
36. T.S. Cameron and R.E. Cordes. Acta Crystallogr. Sect. B: Struct. Crystallogr. Cryst. Chem. **B35**, 749 (1979).
37. International tables for X-ray crystallography. Vol. IV. The Kynoch Press, Birmingham, U.K. 1974.
38. G.M. Sheldrick. SHELX-76. Program for crystal structure determination. University of Cambridge. Cambridge, U.K. 1976.
39. C.K. Johnson. ORTEP II. Report ORNL-5138. Oak Ridge National Laboratory. Oak Ridge, Tenn. 1976.
40. S. Motherwell and W. Clegg. PLUTO. Program for plotting molecular and crystal structures. University of Cambridge. Cambridge, U.K. 1978.
41. C.G. Gilmore. MITHRIL. An integrated direct methods computer program. University of Glasgow. Glasgow, Scotland. J. Appl. Crystallogr. **17**, 42 (1984).
42. G.M. Sheldrick. SHELX-86. *In* Crystallographic computing (*Edited by* G.M. Sheldrick, C. Kruger, and R. Goddard). Oxford University Press, Oxford, U.K. 1985.
43. TEXSAN–TEXRAY Single crystal structure analysis package. Version 5.0. Moelcular Structure Corporation, The Woodlands, Tex. 1989.
44. M.J. Frisch, J.S.Binkley, H.B. Schlegel, K. Raghavachari, C.F. Melius, R.L. Martin, J.J.P. Stewart, F.W. Bobrowicz, C.M. Rohlfing, L.R. Kahn, D.J. Defrees, R. Seeger, R.A. Whiteside, D.J. Fox, E.M. Fleuder, and J.A. Pople. GAUSSIAN 86. Carnegie–Mellon Quantum Chemistry Publishing Unit, Pittsburgh, Pa. 1984.
45. R.F.W. Bader. AIMPAC series of programs. Department of Chemistry, McMaster University, Hamilton, Ont. 1983.
46. M.W. Schmidt, K.K. Baldridge, J.A. Boatz, J.H. Jensen, S. Koseki, M.S. Gordon, K.A. Nguyen, T.L. Windus, and S.T. Elbert. QCPE Bull. **10**, 52 (1990).
47. F. Toda, K. Tanaka, S. Nagamatsu, and T.C.W. Mak. Isr. J. Chem. **24**, 346 (1985).
48. Yu. T. Struchkov, A.S. Batsanov, Š. Toma, and M. Sališová. J. Organomet. Chem. **329**, 375 (1987).
49. Yu. E. Ovchinnikov, V.E. Shklover, Yu. T. Struchkov, V.V. Dement'ev, T.M. Frunze, and B.A. Antipova. J. Organomet. Chem. **335**, 157 (1987).
50. H.S. Rzepa, M.L. Webb, A.M.Z. Slawin, and D.J. Williams. J. Chem. Soc. Chem. Commun. 765 (1991).
51. L.R. Hanton, C.A. Hunter, and D.A. Purvis. J. Chem. Soc. Chem. Commun. 1134 (1992).
52. J.L. Atwood, S.G. Bott, C. Jones, and C.L. Raston. J. Chem. Soc. Chem. Commun. 1349 (1992).
53. S.S. Al-Juaid, A.K.A. Al-Nasr, C. Eaborn, and P.B. Hitchcock. J. Chem. Soc. Chem. Commun. 1482 (1991).
54. R.S. Rowland. Abstract C006. Book of abstracts. Annual Meeting of the American Crystallographic Association, Albuquerque, N.M. May 23–28, 1993.

Can. J. Chem. Downloaded from www.nrcresearchpress.com by 213.200.69.106 on 09/08/12
For personal use only.

Oxidation of H_2S to S by air with Fe(III)–NTA as a catalyst: catalyst degradation

DIAN CHEN, RAMUNAS J. MOTEKAITIS, AND ARTHUR E. MARTELL[1]
Department of Chemistry, Texas A&M University, TX 77843-3255, U.S.A.

AND

DEREK MCMANUS
ARI Technologies, Geneva, IL 60134, U.S.A.

Received January 15, 1993

DIAN CHEN, RAMUNAS J. MOTEKAITIS, ARTHUR E. MARTELL, and DEREK MCMANUS. Can. J. Chem. **71**, 1524 (1993).

The oxidation of H_2S to S by air is represented by the overall reaction:

$$2H_2S + O_2 \rightarrow 1/4S_8 + 2H_2O$$

The process is used with a catalyst for the removal of H_2S from natural gas. A typical catalyst would be an iron(III) chelate system such as iron(III)–nitrilotriacetate (NTA is a tribasic acid, H_3L, and NTA^{3-} represents the trinegative anion). The catalyst reactions are

$$2FeNTA + H_2S \rightarrow 2FeNTA^- + 1/8S_8 + 2H^+$$

$$2FeNTA^- + 1/2O_2 + H_2O \rightarrow 2FeNTA + 2OH^-$$

The main difficulty with the process is the degradation of the metal chelate catalyst. Thus the Fe(II,III)–NTA system degrades through the formation of a number of weaker chelating agents and eventually to carbon dioxide, water, and ammonia. The degradation products identified are iminodiacetic acid (IDA), glycine, and oxalate. All of these degradation products were measured quantitatively by HPLC, and a degradation scheme is presented for the catalytic process. The fact that thiosulfate greatly decreases the degradation rate, and the fact that the degradation products were observed only in the stoichiometric reactions in which the ferrous NTA was oxidized by air, led to the interpretation that the hydroxyl radical or the superoxide radical ion is the reactive species that attacks the NTA and the intermediate degradation products and is responsible for the degradation of the organic ligands present.

DIAN CHEN, RAMUNAS J. MOTEKAITIS, ARTHUR E. MARTELL et DEREK MCMANUS. Can. J. Chem. **71**, 1524 (1993).

On peut représenter l'oxydation du H_2S en S sous l'influence de l'air par la réaction globale suivante :

$$2H_2S + O_2 \rightarrow 1/4S_8 + 2H_2O$$

On utilise cette réaction catalysée pour enlever du H_2S du gaz naturel. Un catalyseur typique est un système de chélate du fer(II), comme le fer(II)–nitrilotriacétate (NTA est un acide tribasique, H_3L et NTA^{3-} représentent l'anion trinégatif). Les réactions du catalyseur sont

$$2FeNTA + H_2S \rightarrow 2FeNTA^- + 1/8S_8 + 2H^+$$

$$2FeNTA^- + 1/2O_2 + H_2O \rightarrow 2FeNTA + 2OH^-$$

La principale difficulté associée à ce processus est la dégradation du chélate métallique agissant comme catalyseur. Ainsi, le système Fe(II,III)–NTA se dégrade par formation d'un certain nombre d'agents chélatants plus faibles et éventuellement en bioxyde de carbone, en eau et en ammoniac. Les produits de dégradation qui ont pu être identifiés sont l'acide iminodiacétique (AID), la glycine et l'oxalate. Faisant appel à la CLHP, on a mesuré quantitativement tous ces produits de dégradation et on présente un schéma de dégradation pour le processus catalytique. Le fait que le thiosulfate diminue beaucoup la vitesse de dégradation et que l'on a observé les produits de dégradation uniquement lorsqu'on a effectué des réactions stoechiométriques dans lesquelles de NTA aqueux était oxydé par l'air conduit à suggérer que le radical hydroxyle (ou l'ion radicalaire superoxyde) est l'espèce réactive qui attaque le NTA et les produits intermédiaires de dégradation et qu'il est responsable de la dégradation des ligands organiques présents.

[Traduit par la rédaction]

Introduction

In 1960 a patent issued to Hartley et al. (1) reported that the Fe(III)–chelate rapidly oxidizes H_2S to sulfur and this reaction is used to remove H_2S from natural gas. The main factor that prevented industrial application was the magnitude of ligand loss. Since then, considerable work (2–5) has been done to solve this difficulty. McManus (2) described a liquid chromatographic technique that enabled quantitative measurement of aminopolycarboxylate ligands and their degradation products. Haruta and Soeta (4) described the conversion of H_2S to $Na_2S_2O_3$ with the addition of tartrate for increasing the $Na_2S_2O_3$ recovery. The use of iron(III) aminopolycarboxylates for the oxidation of H_2S was described by Diaz (6, 7) and by McManus and Kin (8). Other effective polyvalent metal chelate catalysts were identified by Bedell (9). The catalysts employed were stabilized by a number of additives, such as sulfhydryl compounds used by Diaz (6, 7) and a larger number of inorganic and organic compounds used by Bedell (9). The use of thiosulfate by McManus and Kin (8) was found to greatly lengthen the lifetime of the polyvalent metal aminopolycarboxylate catalysts, and they also described the addition of sorbitol and other polyhydroxy organic compounds to be beneficial because of their ability to form soluble complexes of iron(III) at high pH.

Although the previous work examined the chemistry of catalysts and identified major degradation products, a plausible mechanism of degradation was not established. The metal complexes of the ligands that have been identified as catalysts, and their degradation products, are stable organic

[1]Author to whom correspondence may be addressed.

Can. J. Chem. Downloaded from www.nrcresearchpress.com by 213.200.69.106 on 09/08/12
For personal use only.

Can. J. Chem. Downloaded from www.nrcresearchpress.com by 213.200.69.106 on 09/08/12
For personal use only.

compounds that would not ordinarily be expected to undergo degradation under the conditions that prevail in the process. Further information is therefore needed to explain why degradation occurs, to describe the reactions in detail, and to point the way to further improvements in the process.

This paper reports kinetic studies of the degradation of the Fe(II,III)–NTA (nitrilotriacetate) redox system under operating conditions whereby H_2S is continuously oxidized by air, as well as stoichiometric degradation reactions of the Fe(II,III)–NTA complexes with one of the reacting species (O_2, H_2S) missing. The rate of degradation of NTA and of two other ligands that act as redox catalysts for the oxidation of H_2S, EDTA (ethylenediaminetetraacetic acid) and HEDTA (hydroxyethylethylenediaminetriacetic acid), are also compared. This information, plus the fact that lowering pH increases the rates of degradation of NTA and of intermediate degradation products and that thiosulfate greatly decreases the rates of degradation, led to the conclusion that a free radical reaction is responsible for the degradation reactions. Two possible candidates, the superoxide radical ion $^{\bullet}O_2^-$, and hydroxyl radical HO$^{\bullet}$, are suggested as possible initiators of the free radical reactions. The evidence pointing to one or the other of these intermediates is discussed.

Experimental

Materials

The following materials were ordered in the highest purity available and were used without further purification: nitrilotriacetic acid trisodium salt (99+% Aldrich); $Fe(NO)_3 \cdot 9H_2O$ (Certified A.C.S.) and $Na_2S_2O_3 \cdot 5H_2O$ (Reagent A.C.S., Fisher Scientific Company); $FeCl_2 \cdot 4H_2O$ and $Ni(NO_3)_2 \cdot 6H_2O$ (Baker Analyzed Reagents); $CuCl_2 \cdot 2H_2O$ (Baker Analyzed Reagent); MeOH (Mallinckrodt Chrom AR HPLC); hexadecyltrimethyl ammonium bromide (99%, Sigma); H_2O double distilled water; H_2S (99.5%, Gas Analytical Service). Catalase (Biomedicals, Inc., Ex: Bovine liver, E.C.1.11.1.6; sterile aqueous solution; activity, 40 000 units per milligram solid; unit definition, one unit decomposes one micromole of H_2O_2 per minute; 25.0°C; pH 7.0; approx. 30 000 units per millilitre).

HPLC equipment

An IBM L. C. pump No. 771008 equipped with a chromatography accessory, UV–visible spectro monitor 3100 (LDC Analytical), and a chart recorder 6885 (Kipp and Zone) were used.

Redox reaction conditions

Iron–NTA solution: One litre of solution contained 7.24 g of $Fe(NO)_3 \cdot 9H_2O$ and 9.96 g of $N(CH_2COONa)_3 \cdot H_2O$. The redox reaction was carried out in a glass apparatus, Fig. 1, and the pH and redox potential in both the absorber and oxidizer were monitored. The H_2S flow rate was 2.0 mL min^{-1} and the air flow rate was 1.0 L min^{-1}. The temperature was maintained at 25 ± 1°C throughout.

NMR spectra

The proton NMR spectra were recorded with a Varian XL-200 NMR spectrometer, and chemical shifts are reported in ppm.

Degradation of Fe(III)–NTA with uncontrolled pH

One litre of the NTA solution described above was placed in the oxidizer compartment (Fig. 1). The pump was then started and some of the solution was pumped into the absorber compartment, with a flow rate of 100 mL min^{-1}. The pH and redox meters were then turned on. At this stage the air pump was turned on and the air flow was adjusted to 1.0 L min^{-1}. The valve of the H_2S cylinder was turned on and the H_2S flow was adjusted to 2.0 mL min^{-1}. The time of the start of the reaction was recorded, and the pH and redox meter readings were recorded from time to time. Every half hour the flow rates of H_2S and air were checked and adjusted if necessary. Any FeS and S that deposited in the tubing was cleaned out occasionally.

The operation of the other experiments were carried out in the same manner except that the sulfur was filtered off every 7 or 8 h and the pH was continuously adjusted to 8.5 by the addition of NaOH solution.

HPLC analysis procedure

The analyses of NTA, IDA, and oxalate were measured by following the method of McManus (2).

Preparation of iron-free samples

To 12.0 mL of solution taken from the continuous reactor, 140 mg of NaOH in 5 mL water was added dropwise with stirring. The stirring was continued for 10 min and the reaction mixture was allowed to stand at room temperature for 20 min. The $Fe(OH)_3$ that precipitated was filtered off carefully and was washed several times with water. The filtrate combined with the washings was transferred to a 50-mL volumetric flask. The solution was adjusted with acid to pH 4.2 and then diluted with water to 50 mL.

Analysis of NTA, IDA, and oxalate as their copper(II) complexes

A 7-mL sample of solution was taken from the volumetric flask and placed in a 10-mL volumetric flask. To this was added 2.5 mL of 0.050 M $CuCl_2$ solution and the mixture was diluted to 10 mL with water. The mobile phase contained: 0.0010 M Cu(II), 60:40 H_2O:MeOH, 2% CH_3COOH, 0.2% $CH_3(CH_2)_{15}(CH_3)_3NBr$, adjusted to pH 4.2 with NaOH solution. This phase is presumed to contain the alkyl ammonium salts of the negative copper complexes of NTA, IDA, and oxalate.

Operating conditions

Analytical column: IB-SIL 5 C8, reverse phase, 4.5 × 150 mm; column temperature: ambient; flow rate, 1.5 cm^3 min^{-1}; detection, UV absorption at 280 nm; sample, 20 μL; recorder 10 mV full scale; chart speed, 0.5 cm min^{-1}.

Analysis of glycine and glyoxylate as their Ni(II) complexes

For the analysis of glycine and glyoxylate as the complexes formed with Ni(II), the procedure is identical to that described above for the copper complexes of NTA, IDA, and oxalate, the only difference being the use of 2.5 mL of 0.050 M $Ni(NO_3)_2$ solution instead of $CuCl_2$ solution, and the mobile phase contained 0.0010 M Ni(II) rather than Cu(II) and was presumed to contain the alkylammonium salts of the negative nickel complexes of glycine and glyoxylate. For the measurement of glycine, the UV absorption was measured at 270 nm; for glyoxylate, the UV absorption was measured at 250 nm. The other operating conditions were the same as above. The retention time for IDA is about 3.0 min, 7.0 min for the oxalate, and 21 min for the NTA. The separations of these quantitative calibrations for the HPLC analysis of NTA, IDA, and oxalate and for glycine and glyoxylate were obtained from varying amounts of known samples of these compounds, and the peak heights at the indicated amplification settings vs. concentration of the species were plotted. The linear nature of these plots indicated accurate HPLC determinations of these molecular species over a considerable range of concentration.

Identification of the hydroxylation products by paper chromatography

The paper chromatographic measurements of the hydroxylation products of benzoic acid were made by the procedure of Grinstead (10). Benzoic acid and its hydroxylation products were separated from the Fe(III), the remaining NTA, and its degradation products by acidification of the reaction mixture and extracting five times with ether. The extracts were combined and reduced to a small volume by evaporation of the solvent. The ether residue was chromatographed on Whatman No. 1 filter paper, with 4:1 (by volume) isopropyl alcohol, 7 M NH_4OH as the eluant. Under ultraviolet light six spots appeared on the paper. The R_f value and the color of the spots were compared with those of standard compounds, and the six spots were assigned as follows:

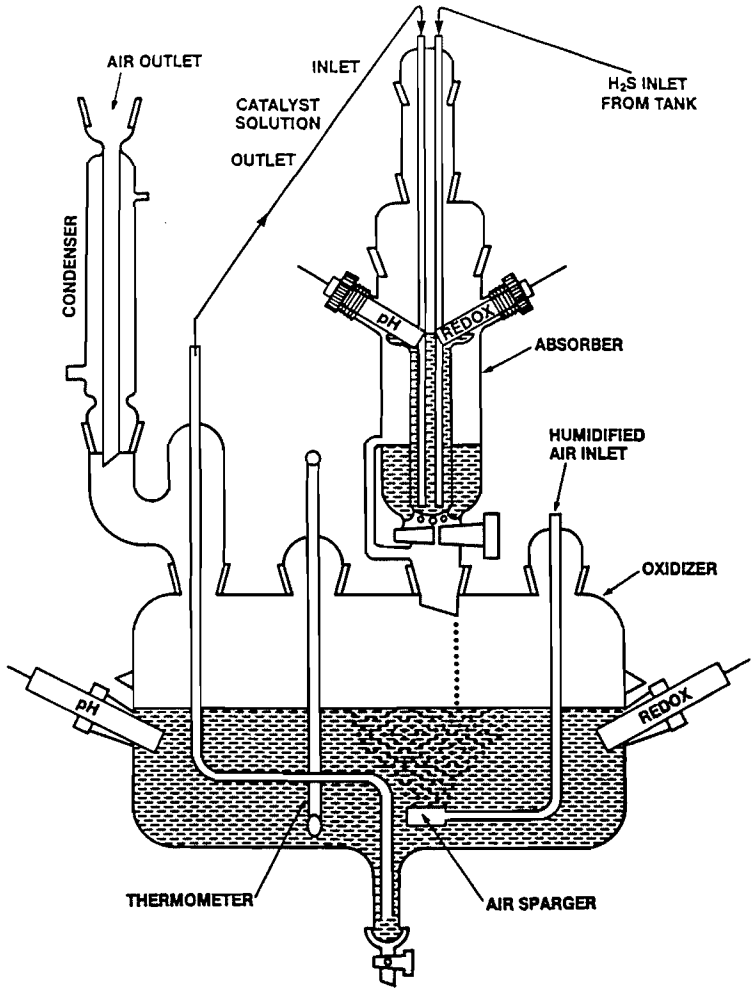

FIG. 1. Continuous apparatus.

Compound	R_f value
1. *o*-Hydroxybenzoic acid	0.78
2. Benzoic acid	0.64
3. 2,5-Dihydroxybenzoic acid	0.54
4. 2,3-Dihydroxybenzoic acid	0.41
5. *m*-Hydroxybenzoic acid	0.25
6. *p*-Hydroxybenzoic acid	0.090

Identification of the hydroxylation products by NMR

The ether residue obtained as described above was loaded on a silica gel (60 Å) column and eluted first with benzene and then with a benzene and ether mixed solvent beginning with 1% ether, which was slowly increased to 20%. At the end MeOH was used as the eluant. Each 30 mL of eluate was collected; after the solvent was removed its NMR spectrum was determined. The benzoic acid was eluted first. The second eluate was salicylic acid, which was then followed by *m*-hydroxybenzoic acid and *p*-hydroxybenzoic acid.

The NMR measurements of the silica gel separation products confirm the formation of salicylic acid, *m*-hydroxybenzoic acid, and *p*-hydroxybenzoic acid: salicylic acid: ^{1}H NMR (D_2O):6.51 (t, 1H, phenyl), 6.56 (d, 1H, phenyl), 7.00 (t, 1H, phenyl), 7.16 (d, 1H, phenyl); *m*-hydroxybenzoic acid: ^{1}H NMR (D_2O): 6.56 (d, 1H, phenyl), 6.86 (m, 2H, phenyl), 6.96 (t, 1H, phenyl); *p*-hydroxybenzoic acid: ^{1}H NMR (D_2O): 6.39 (d, 2H, phenyl), 7.45 (d, 2H, phenyl).

The dihydroxybenzoic acids were not found in the NMR measurements, and the yield of each was concluded to be less than 5%, which is the limit of sensitivity of the NMR technique.

Identification of the hydroxylation products by mass spectral measurements

The mass spectra were obtained with a VG analytical 70S high-resolution double-focusing mass spectrometer with an attached VG analytical 11/250J data system. The operator was Dr. David Jacobs of the Departmental Research Services Facility. Mass spectral data of the hydroxylation products gave the molecular weight 138 for the three monohydroxybenzoic acids, which had been partially separated on a silica gel column.

Results

The degradation of the Fe(III)–NTA catalyst in a continuous reaction system with no control of pH is shown in Table 1 and illustrated in Fig. 2. The NTA decreases rapidly with time, and over 95% of it is lost in 100 h. During this time the pH, which starts at 8.6, drifts gradually downward, reaching 3.6 at the end of the run. IDA was the first and main reaction product (Fig. 2). Its concentration increased steadily throughout the run, although its rate of formation seemed to decrease slightly toward the end. The second and subsequent degradation product containing nitrogen was glycine, as indicated in Fig. 2. The amount of glycine produced was considerably less than IDA, showing that the rate of degradation of the latter is slower than that of NTA. The sum of the concentrations of NTA, IDA, and glycine in Fig. 2 shows

Can. J. Chem. Downloaded from www.nrcresearchpress.com by 213.200.69.106 on 09/08/12
For personal use only.

TABLE 1. Degradation of Fe(III)–NTA with uncontrolled pH (8.6 → 3.6) at 25.0°C

Time (h)	NTA (M)	IDA (M)	Oxalate (M)	Gylcine (M)
0	3.62×10^{-2}			
4.0	3.45×10^{-2}	1.41×10^{-3}		
15.0	2.72×10^{-2}	5.2×10^{-3}	2.70×10^{-3}	
27.5	2.10×10^{-2}	1.00×10^{-2}	6.0×10^{-3}	
52.0	1.17×10^{-2}	1.69×10^{-2}	1.95×10^{-2}	5.7×10^{-3}
69.0	4.1×10^{-3}	2.22×10^{-2}	2.46×10^{-2}	5.9×10^{-3}
93.0	2.10×10^{-3}	2.80×10^{-2}	2.58×10^{-2}	6.0×10^{-3}

a material balance of about 100%, indicating that very little of the ligand degraded all the way to ammonia, even after 100 h. The formation of oxalate, presumably from the acetate side chains of NTA, IDA, and glycine, starts off more slowly than expected at first, but rises above the rate of IDA formation. This behavior is not considered unusual since oxalate is expected to form both in the formation and degradation of IDA. It shows a somewhat slower rate of formation near the end of the run and it is suggested that this may be due to the further oxidation of oxalate to carbon dioxide (13). It is noteworthy that no glyoxylate was found among the degradation products.

The degradation of the Fe(II,III)–NTA chelate in an experiment in which the pH was kept constant at 8.5 and in which the sulfur was removed by filtration every 6–7 h (Table 2 and Fig. 3) gave a lower rate of degradation of NTA. In fact glycine, which was produced in a small amount at pH 7, was not formed at pH 8.5. Thus, it appears degradation is promoted under acidic conditions.

To further determine the effect of pH, the redox reactions were run at pH 7.0 and 5.5. The pH was regulated by the addition of NaOH solution initially and at short time intervals (every 30 min or less). The NTA degradation at these pH values is compared in Fig. 4 with the degradation observed at pH 8.5 (also shown in Fig. 3). The results confirm that the rate of degradation of NTA increases as the pH is decreased.

Kinetic analysis of the degradation of NTA at 25.0°C at pH 8.5, 7.0, and 5.5 (Fig. 4) suggests that the degradation of NTA is a first-order reaction. The observed degradation rate constants of NTA obtained from the data in Fig. 4 are

TABLE 2. Degradation of Fe(III)–NTA at pH 8.5 at 25.0°C

Time (h)	NTA (M)	IDA (M)	Oxalate (M)
0	3.62×10^{-2}		
12.0	2.74×10^{-2}	5.7×10^{-3}	
20.0	2.38×10^{-2}	8.0×10^{-3}	1.90×10^{-3}
30.0	1.90×10^{-2}	9.1×10^{-3}	2.26×10^{-3}
40.0	1.79×10^{-3}	1.00×10^{-2}	2.68×10^{-3}
64.0	1.19×10^{-2}	1.13×10^{-2}	2.75×10^{-3}
77.0	9.5×10^{-3}	1.16×10^{-2}	2.82×10^{-3}

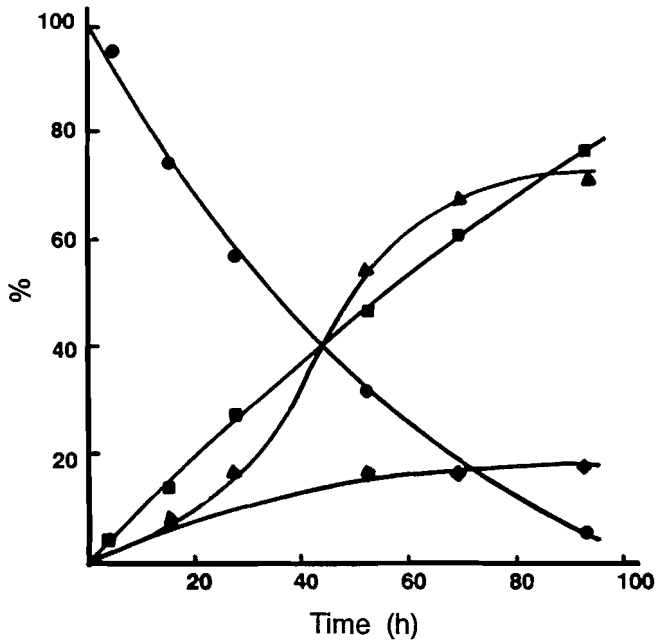

FIG. 2. Degradation of Fe(III)–NTA with uncontrolled pH (8.6 → 3.6): ●, NTA; ■, IDA; ▲, oxalate; ◆, glycine; % is mole per cent of species based on initial concentration of NTA, 0.036 M = 100%.

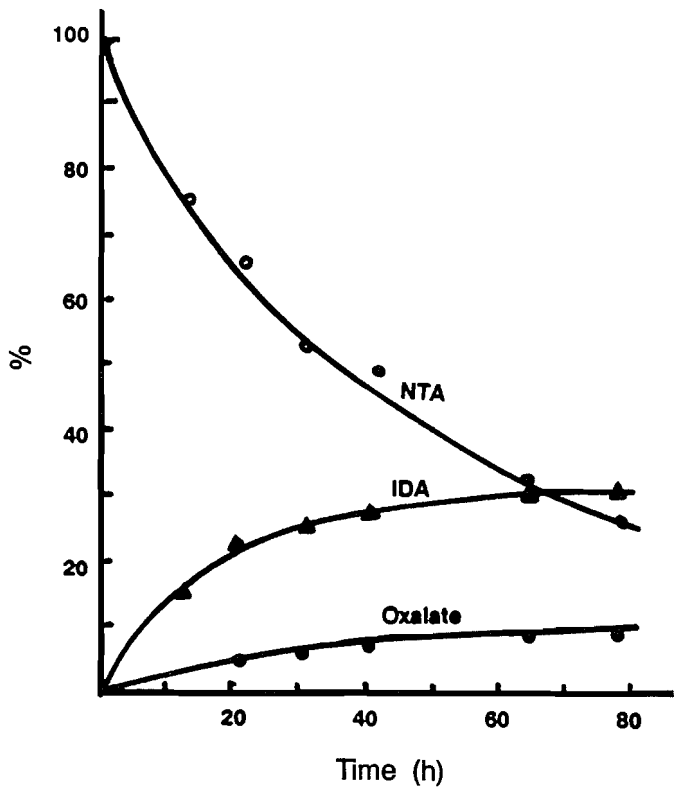

FIG. 3. Degradation of Fe(III)–NTA at pH 8.5;% is mole per cent of species based on initial concentration of NTA, 0.036 M = 100%.

Can. J. Chem. Downloaded from www.nrcresearchpress.com by 213.200.69.106 on 09/08/12
For personal use only.

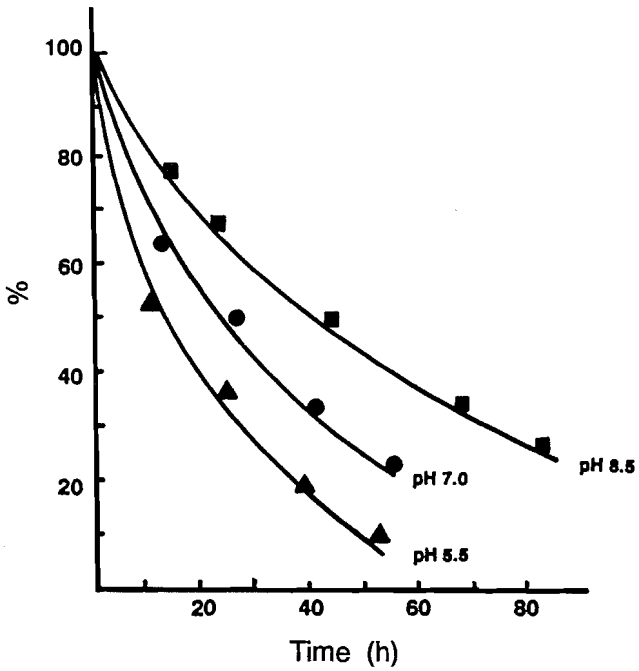

FIG. 4. Degradation of Fe(III)–NTA at pH 8.5, 7.0, and 5.5; 25.0°C; H_2S flow rate (2.0 mL/min); % is mole per cent of species based on initial concentration of NTA, 0.036 M = 100%.

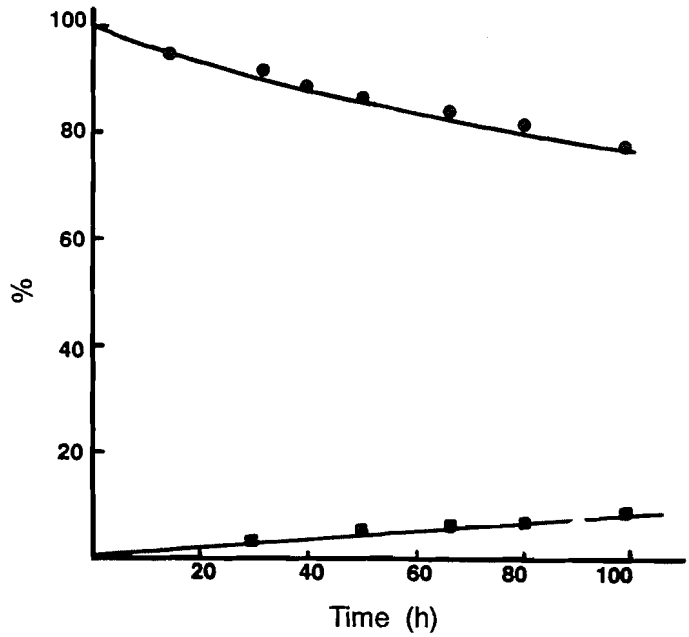

FIG. 5. Degradation of Fe(III)–NTA at pH 8.5 with 5% $Na_2S_2O_3 \cdot 5H_2O$: ●, NTA; ■, IDA; % is mole per cent of species based on initial concentration of NTA, 0.036 M = 100%.

pH 8.5, 4.4×10^{-6} s^{-1}; pH 7.0, 7.0×10^{-6} s^{-1}; pH 5.5, 1.1×10^{-5} s^{-1}. This increase in rate constant with a decrease in pH agrees with the qualitative observation, stated above, that degradation is more rapid at low pH.

A similar run at pH 8.5 with 32 g of $Na_2S_2O_3$ in the solution as a stabilizer is shown in Table 3 and illustrated in Fig. 5. It is seen that the sodium thiosulfate greatly reduces the rate of degradation of the NTA. A small amount of IDA was found as the only degradation product in concentrations large enough to measure.

To determine which part of the process involved degradation of NTA, a number of stoichiometric reactions were carried out. A ferric–NTA solution of the same concentration as used in the redox runs at pH 8.5 was treated with air for 2 days. HPLC analysis carried out as described above indicated the presence of only NTA after 1 and 2 days, and that no degradation reaction had occurred. Also, a ferric–NTA solution was treated with H_2S at the same rate as the experimental redox runs for 2 days, and analysis of the reaction products in the same manner showed the absence of degradation products. However, when a similar ferrous–NTA solution was treated with air for 2 days and the results were subjected to HPLC analysis, the results showed evidence of degradation with the formation of 1.7% of IDA and slightly less than 1.0% of oxalate. These experiments indicate that the degradation of NTA is a side reaction that occurs during the oxidation by air of the ferrous–NTA to the ferric–NTA chelate system.

TABLE 3. Degradation of Fe(III)–NTA at pH 8.5 with 32 g $Na_2S_2O_3$ at 25.0°C

Time (h)	NTA (M)	IDA (M)
0	3.62×10^{-2}	
14.0	3.44×10^{-2}	
26.0	3.33×10^{-2}	8.2×10^{-4}
39.0	3.20×10^{-2}	1.17×10^{-3}
50.0	3.17×10^{-2}	1.69×10^{-3}
66.0	3.06×10^{-2}	2.12×10^{-3}
80.0	2.97×10^{-2}	2.32×10^{-3}
99.0	2.93×10^{-2}	2.80×10^{-3}

To obtain information on the question of whether H_2O_2 is an intermediate in the reaction, the Fe(III)–NTA solution was mixed with catalase (catalase solution added to a dilution of 1:100) and the redox reaction was carried out at pH 7.0 for 50 h. The results show that the NTA degradation slowed down on the addition of catalase. This result confirms the formation of H_2O_2 as an intermediate product, because the enzyme rapidly catalyzes the decomposition of H_2O_2 and should slow down reactions requiring H_2O_2 as an intermediate.

To investigate the possible formation of the hydroxyl radical, an equimolar amount (0.0362 M) of benzoic acid was mixed with Fe(III)–NTA, and the redox reaction was carried out at pH 8.5 for 100 h, as described above. The results indicate that the benzoic acid was hydroxylated to a mixture of *o*-, *m*-, and *p*-hydroxybenzoic acid. The products were characterized by NMR, paper chromatography, and mass spectra. This is strong evidence for the formation of the hydroxyl radical, because the benzene ring is not hydroxylated by molecular oxygen. There still remains the possibility that the less reactive $\cdot O_2^-$ radical is involved. This question is addressed below.

These results are similar to those obtained by Grinstead (10). He reported that when a solution of Fe(III)–NTA is mixed with ascorbic acid and benzoic acid under oxygen, the latter is hydroxylated to a mixture of *o*-, *m*-, and *p*-hydroxybenzoic acid. He also confirmed the formation of H_2O_2 as an intermediate by the use of catalase.

Because the iron chelates of EDTA and of HEDTA have been used as redox catalysts for the oxidation of H_2S to S_8

Can. J. Chem. Downloaded from www.nrcresearchpress.com by 213.200.69.106 on 09/08/12
For personal use only.

Can. J. Chem. Downloaded from www.nrcresearchpress.com by 213.200.69.106 on 09/08/12
For personal use only.

by air, it was considered of interest to compare the rates of degradation of the iron chelates of these ligands with that described above for NTA. Figure 6 shows the measured rates of degradation of all three iron chelate systems starting with the same concentration of Fe(III) in each case, with the molar ratio of ligand to metal being 2:1 for NTA, EDTA, and HEDTA. No stabilizer or additional ligand was added. It is obvious from Fig. 6 that NTA degrades more slowly than do the other two ligands and the most rapid rate of degradation was observed in the case of HEDTA. The superiority of NTA over the other ligands with respect to degradation was first pointed out by McManus and Kin (8).

Discussion

Graphic formulas indicating the reaction of H_2S with the catalyst, the Fe(III)–NTA chelate, to produce sulfur and the Fe(II)–NTA chelate, and regeneration of the ferric–NTA catalyst by oxidation with air, are illustrated in Scheme 1. The iron(III)–NTA system is shown to consist of two complexes in equilibrium, a 1:1 monohydroxo iron – NTA complex and a 1:2 iron(III)–NTA complex, in accordance with the description given by Motekaitis and Martell.[2] The six-coordinate representation of the 1:2 complex represents one of the possibilities for this complex. It may very well be seven-coordinate, in view of the seven-coordinate crystal structure of the 1:2 complex described by Clegg et al. (11). However, it is possible that the structures and coordinate bonding of the Fe(III)–NTA complexes in the solid state and in solution may be different.

The degradation reactions illustrated by Figs. 2, 3, and 5 show that IDA is the first compound produced, and that it is followed by the formation of glycine. The oxalate that is formed apparently comes from the side chains (acetate groups) that are cleaved from the NTA, IDA, and glycine. On the basis of the evidence now available, the following degradation scheme is tentatively suggested. Because the ligands undergoing degradation are usually very stable, and the degradation occurs during the re-oxidation of the ferrous–NTA system with air (molecular oxygen), it is suggested that only free radicals have enough energy to degrade these chelating ligands. The review by Walling (12) (see also the paper by McManus (2)) indicates that the hydroxyl radical may be formed under the reaction conditions that prevail, leading to the following sequence of reactions.

[1] $2FeNTA^- + O_2 + 2H_2O \rightarrow 2FeNTA + H_2O_2 + 2HO^-$

[2] $FeNTA^- + H_2O_2 \rightarrow FeNTA + OH^- + HO^{\cdot}$

[3] $R^1R^2NCH_2COO^- \xrightarrow{{}^{\cdot}OH} R^1R^2NH + {}^-OOC{-}COO^- + 2H_2O + H^+$

$R^1\,R^2 = CH_2COO^-$ NTA

$R^1 = H;\ R^2 = CH_2COO^-$ IDA

$R^1 = R^2 = H$ Glycine

[4] $^-OOC{-}COO^- + 2HO^{\cdot} \rightarrow 2CO_2 + 2OH^-$

Equations [1] and [2] are in accord with the fact that low pH increases the rate of degradation, in that low pH favors the formation of the free radical. The formation of carbon dioxide from oxalate has been described (13).

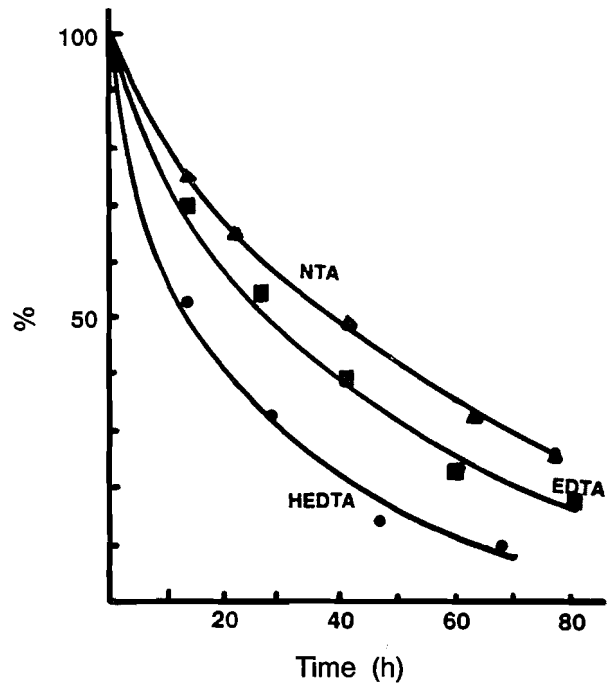

FIG. 6. Degradation of Fe(III)–NTA, Fe(III)–EDTA, and Fe(III)–HEDTA at p[H] 8.5 and 25.0°C; H_2S flow rate = 2.0 mL/min. % is mole per cent of species based on initial concentration of NTA, EDTA, and HEDTA, 0.036 M = 100%.

The stabilizing effect of thiosulfate (Fig. 4), reported previously by McManus and Kin (8), as well as other stabilizers described by Diaz (6, 7) and Bedell (9), can be understood since they have one property in common. They are all free radical scavengers, and decrease the degradation represented by eqs. [1]–[4] by decreasing the concentration of free radical in the reaction mixture.

While the above reaction sequence describes the degradation of the NTA on the basis of the intermediates actually detected in the reaction mixture, it does not give a rationale for the initial attack on the NTA, and the degradation products, iminodiacetic acid and glycine. The following reactions involve species and intermediates that have been inferred but not demonstrated to be present.

[5] $R^1R^2NCH_2COO^- + HO^{\cdot} \rightarrow R^1R^2N\dot{C}HCOO^- + H_2O$

[6] $R^1R^2N\dot{C}HCOO^- + FeNTA \rightarrow R^1R^2\overset{+}{N}CHCOO^- + FeNTA^-$

[7] $R^1R^2\overset{+}{N}CHCOO^- + H_2O \rightarrow R^1R^2\underset{|}{\overset{OH}{N}}CHCOO^- + H^+$

[8] $R^1R^2\underset{|}{\overset{OH}{N}}CHCOO^- \rightarrow R^1R^2NH + OHCCOO^-$

Reaction [5] is inferred by the presumed presence of ·OH generated by the Fenton reaction (Fe(II) + H_2O_2), and the facile hydroxylation of benzoic acid in the reaction mixture. Reactions [6] and [7], favored by the considerable concentration of Fe(III) chelate in the reaction mixture, may

[2]To be published.

Can. J. Chem. Downloaded from www.nrcresearchpress.com by 213.200.69.106 on 09/08/12
For personal use only.

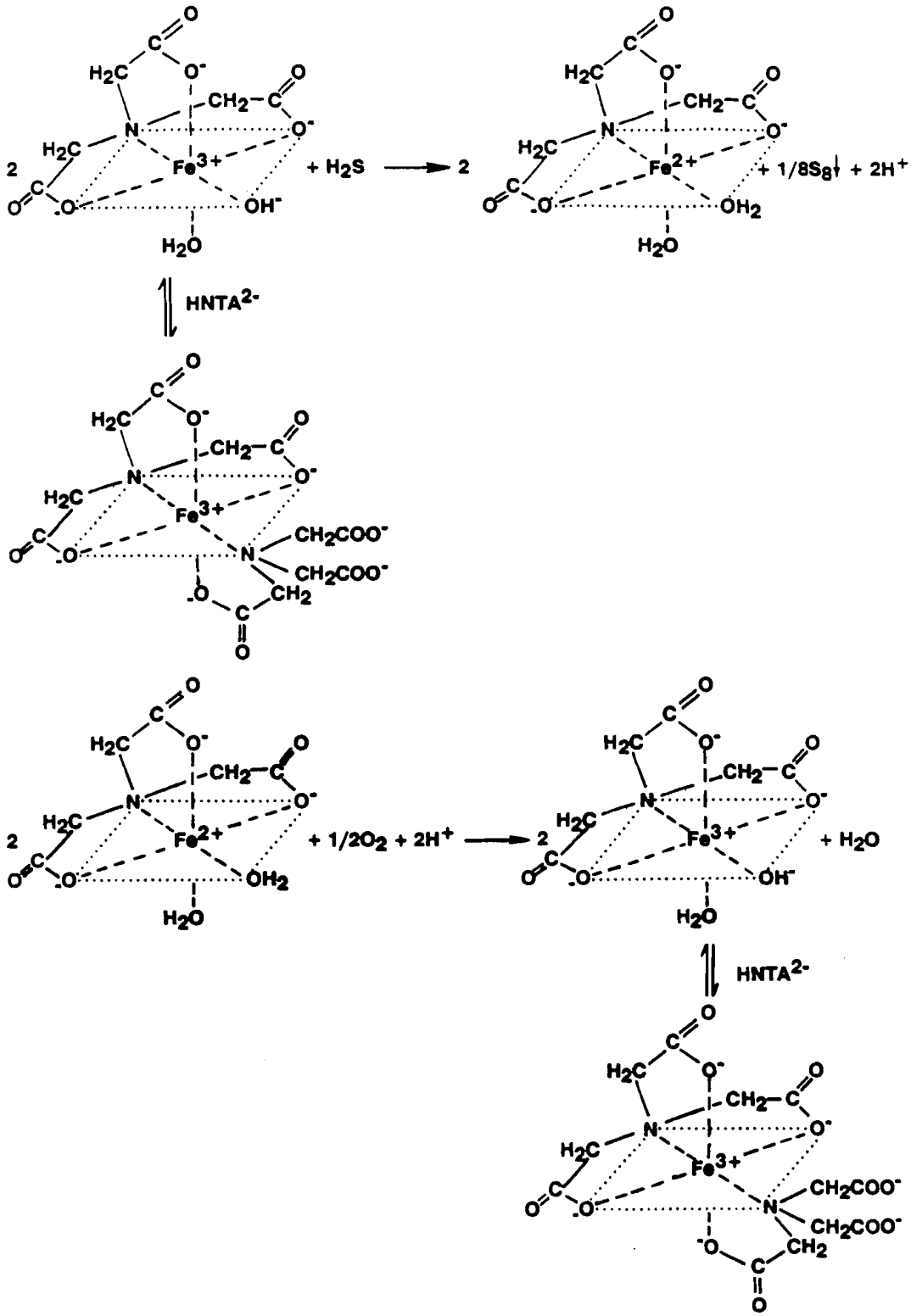

SCHEME 1. Reactions for the oxidation of H_2S to S with the Fe(II,III)–NTA system as catalyst.

be considered as occurring in sequence or as concerted. The failure to detect glyoxylate in the reaction mixture may be due simply to its rapid oxidation to oxalate. Alternatively, its absence may be due to the superoxide radical as the oxidizing agent, rather than the hydroxyl radical, leading to the following sequence of reactions:

[9] $H_2O_2 + HO^{\bullet} \rightarrow O_2^{\bullet-} + H_2O + H^+$

[10] $R^1R^2NCH_2COO^- + O_2^{\bullet-} + H^+$

$\rightarrow R^1R^2N\dot{C}HCOO^- + H_2O_2$

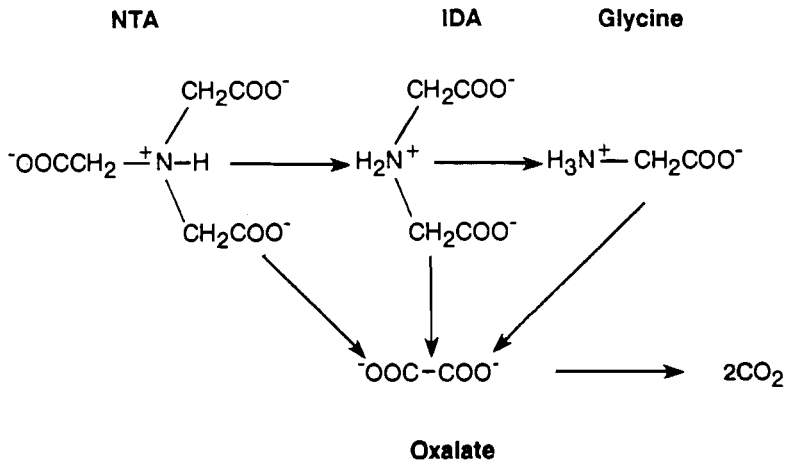

SCHEME 2. Proposed degradation scheme for NTA.

$$[11]\quad R^1R^2N\dot{C}HCOO^- + {}^{\bullet}O_2 \rightarrow R^1R^2NCHCOO^-$$
($^{\bullet}O_2$ attached to N)

$$[12]\quad R^1R^2NCHCOO^- + FeNTA^- \rightarrow R^1R^2NH + {}^-OOC{-}COO^- + FeNTA$$
($^{\bullet}O_2$ attached to C)

While the above reactions are somewhat speculative, all the reactants are present, and both $^{\bullet}OH$ and $O_2^{\bullet-}$ have been inferred as possible intermediates. The oxidation of the aminopolycarboxylate ligands is considered a free radical reaction because the ligands are not oxidized by oxygen, even in the presence of Fe(III), under the reaction conditions employed.

Acknowledgement

This work was supported by a research contract with ARI Technologies, Inc. of Palatine, Illinois.

1. W. Hartley, R.S. Craig, and R.H. Sapiro. UK, Ltd. Ger. 1,091,696, Oct. 27, 1960 (Cl. 26d).
2. D. McManus. 41st Pittsburgh Conference and Exposition on Analytical Chemistry and Applied Spectroscopy, New York City. 1990.
3. W. Nanbu, T. Nanbu, and N. Nanbu. Japan Kokai 76,133,191 (Cl. BO1J31/O4), 18 Nov. 1976, Appl. 75/57,813, 15 May 1975, 4 pp.
4. M. Haruta and M. Soeta. Kageno, Kenji Jpn. Kokai Tokyo Koho 79 57,467 (Cl. BO1D53/34) 09 May 1979, Appl, 77/124,343, 12 Oct 1977; 4 pp.
5. D.A. Van Kleeck. U.S. US 4,876,075 (Cl.423-226; CO1B17/16), 24 Oct 1989, Appl. 258,425, 17 Oct 1988; 8 pp.
6. Z. Diaz. U.S. Patent No. 4,388,239, June 14, 1983.
7. Z. Diaz. U.S. Patent No. 4,518,576, May 21, 1985.
8. D. McManus and F.R. Kin. U.S. Patent 4,622, 212, Nov. 11, 1986.
9. S.A. Bedell. U.S. Patent No. 4,891,205, Jan. 20, 1990.
10. R.R. Grinstead. J. Am. Chem. Soc. **82**, 3472 (1960).
11. W. Clegg, A.K. Powell, and M.J. Ware. Acta Crystallogr. Sect. C: Cryst. Struct. Commun. **C40**, 1822 (1984).
12. C. Walling. Acc. Chem. Res. **8**, 125 (1985).
13. Y. Zuo and J. Holgne. Environ. Sci. Technol. **26**, 1014 (1992).

Can. J. Chem. Downloaded from www.nrcresearchpress.com by 213.200.69.106 on 09/08/12
For personal use only.

The syntheses and vibrational spectra of tetrakis(carbonyl) palladium(II) and platinum(II) undecafluorodiantimonate(V), $[Pd(CO)_4][Sb_2F_{11}]_2$, and $[Pt(CO)_4][Sb_2F_{11}]_2$

G. HWANG, C. WANG, AND F. AUBKE[1]

Department of Chemistry, The University of British Columbia, Vancouver, BC V6T 1Z1, Canada

AND

H. WILLNER AND M. BODENBINDER

Institut für Anorganische Chemie der Universität, W-3000 Hannover, Callinstrasse 9, Germany

Received April 2, 1993

G. HWANG, C. WANG, F. AUBKE, H. WILLNER, and M. BODENBINDER. Can. J. Chem. **71**, 1532 (1993).

The reductive carbonylation of either platinum(IV) fluorosulfate, $Pt(SO_3F)_4$, or palladium(III) fluorosulfate, $Pd(SO_3F)_3$, either in solution of fluorosulfuric acid, HSO_3F, or in the solid state with CO at pressures of 0.5 to 2 atmospheres and at 25°C, affords in high yield complexes of the type $M(CO)_2(SO_3F)_2$, M = Pd or Pt. The square-planar complexes are readily converted by solvolysis in liquid antimony(V) fluoride in the presence of CO at a pressure of about 1 atmosphere to white, thermally stable, salts of the composition $[M(CO)_4][Sb_2F_{11}]_2$, M = Pd or Pt, which contain the novel, square-planar cations $[Pd(CO)_4]^{2+}$ and $[Pt(CO)_4]^{2+}$. The two cations exhibit the highest CO stretching frequencies reported so far, about 120 cm^{-1} higher than in free CO, which suggests the absence or near absence of π-back donation for the M—CO bond.

G. HWANG, C. WANG, F. AUBKE, H. WILLNER et M. BODENBINDER. Can. J. Chem. **71**, 1532 (1993).

La carbonylation réductrice des fluorosulfates de platine(IV), $Pt(SO_3F)_4$, ou de palladium(III), $Pd(SO_3F)_3$, soit en solution dans l'acide fluorosulfurique, HSO_3F, ou à l'état solide avec du CO à des pressions allant de 0,5 à 2 atmosphères et à 25°C fournissent, avec des rendements élevés, des complexes du type $M(CO)_2(SO_3F)_2$ dans lesquels M = Pd ou Pt. Par hydrolyse dans le fluorure d'antimoine liquide en présence de CO à une pression d'environ 1 atmosphère, on peut facilement transformer les complexes plans carrés en des sels blancs, thermiquement stables, de composition $[M(CO)_4][Sb_2F_{11}]_2$, M = Pd ou Pt, qui contiennent les nouveaux cations plans carrés $[Pd(CO)_4]^{2+}$ et $[Pt(CO)_4]^{2+}$. Les fréquences de vibration d'élongation du CO de ces deux cations sont les plus élevées à avoir été rapportées jusqu'à maintenant, soit environ 120 cm^{-1} plus haut que le CO libre; ce résultat suggère l'absence complète ou pratiquement complète de rétrodonation π pour la liaison M—CO.

[Traduit par la rédaction]

This communication describes the syntheses and vibrational spectra of two thermally stable compounds with the square-planar cations $[Pt(CO)_4]^{2+}$ and $[Pd(CO)_4]^{2+}$, stabilized in each case by $[Sb_2F_{11}]^-$. Neither cation has been reported previously. They display the highest CO stretching frequencies ($\nu_{av.} \sim 2260$ cm^{-1}) and stretching force constants ($f_r \times 10^2 \sim 20.6$ N m^{-1}) for metal CO derivatives, which suggests little or no π-backdonation for the M—CO bonds in the two cations.

Carbon monoxide, CO, is viewed as the prototype of a π-acceptor ligand (1), and synergic bonding, that is, σ-donation from the filled 5σ-molecular orbital of CO to a suitable, empty metal orbital of σ symmetry and π-backdonation from a filled metal *d*-orbital to the π_g MO's of CO, is an essential feature of transition metal carbonyl chemistry (1). Vibrational spectroscopy (2, 3), where νCO in metal carbonyls is lowered well below the value of gaseous CO at 2143 cm^{-1} (4), ^{13}C NMR (5), X-PES (6), and numerous molecular structure determinations have provided support for this bonding concept.

There are, among the longest known metal carbonyl derivatives, some examples where νCO is observed at slightly higher wavenumbers than for CO itself (7, 8). These include three platinum(II) carbonyl chlorides, first reported by Schützenberger in 1870 (9), and gold(I) carbonyl chloride, Au(CO)Cl (10), known since 1925. In spite of these early beginnings, the number of noble metal carbonyl derivatives has remained limited (11, 12) until very recently, and only two reports of carbonyl cations, $[Cu(CO)][CO_2CF_3]$ (13*a*) and $[Cu(CO)][AsF_6]$ (13*b*), involving coinage metal derivatives have appeared.

Two recent developments have suggested promising new synthetic pathways to these unusual compounds. The use of very weakly coordinating anions like $B(OTeF_5)_4^-$ has allowed the synthesis first of $Ag(CO)B(OTeF_5)_4$ (14) and later of $Ag(CO)_2B(OTeF_5)_4$ (15) and their characterization by low temperature X-ray crystallography. The latter contains a weakly coordinated, nearly linear $[Ag(CO)_2]^+$ group.

The far more thermally stable linear $[Au(CO)_2]^+$ cation has been obtained by reductive carbonylation of gold tris-(fluorosulfate), $[Au(SO_3F)_3]_2$ (16), initially in solution of fluorosulfuric acid as a solvated cation (17) and subsequently in a solid salt of the formula $[Au(CO)_2][Sb_2F_{11}]$ (18). This material is synthesized from $Au(CO)SO_3F$ (17) and liquid SbF_5 by solvolysis in a CO atmosphere. The linear cation $[Au(CO)_2]^+$ is fully characterized by ^{13}C NMR and vibrational spectroscopy including a normal coordinate analysis, valence force field calculations (18), and a spectral comparison to the isoelectronic species $[Au(CN)_2]^-$ and $Hg(CN)_2$. The average CO stretching frequency is found at

[1]Author to whom correspondence may be addressed.

Can. J. Chem. Downloaded from www.nrcresearchpress.com by 203.198.23.82 on 09/08/12
For personal use only.

Can. J. Chem. Downloaded from www.nrcresearchpress.com by 203.198.23.82 on 09/08/12
For personal use only.

2235.5 cm^{-1}, the highest reported at the time of publication (18).

We have now applied this synthetic strategy to the syntheses of $[Pt(CO)_4][Sb_2F_{11}]_2$ and $[Pd(CO)_4][Sb_2F_{11}]_2$. Reductive carbonylation of $Pt(SO_3F)_4$ in HSO_3F (19) proceeds at 25°C to yield a diamagnetic yellow solid of the composition $Pt(CO)_2(SO_3F)_3$, which is identified by ^{13}C and ^{19}F NMR and by vibrational spectra as $[Pt(CO)_4][Pt(SO_3F)_6]$ (20). The cation $[Pt(CO)_4]^{2+}$ appears to be, just like the isoelectronic anion $[Pt(CN)_4]^{2-}$ (21), square planar. The weighted average value of νCO is unprecedentedly high (2251 cm^{-1}). Band overlap with bands due to the anion $[Pt(SO_3F)_6]^{2-}$ (19) makes a complete vibrational assignment very difficult, and all attempts to obtain single crystals from HSO_3F solution have so far failed.

Under more stringent conditions (80°C and ~0.6 atm pressure of CO; 1 atm = 101.3 kPa) more extensive reduction of $Pt(SO_3F)_4$ is observed:

$$[1]\quad Pt(SO_3F)_4 + 3CO \xrightarrow[80°C]{HSO_3F} Pt(CO)_2(SO_3F)_2 + CO_2 + S_2O_5F_2$$

The reaction allows isolation of *cis*-$Pt(CO)_2(SO_3F)_2$ (22) and its characterization ($\nu CO_{avg.}$ = 2202 cm^{-1} (IR) and 2198.5 cm^{-1} (Raman)). The fluorosulfate groups appear to be coordinated to Pt in a monodentate fashion, as is the case for $Au(CO)SO_3F$ (17, 22).

The synthesis of the corresponding palladium(II) compound, $Pd(CO)_2(SO_3F)_2$, from Pd(II)Pd(IV)$(SO_3F)_6$ (23), may be performed either in a solid – gas phase reaction according to:

$$[2]\quad Pd(II)Pd(IV)(SO_3F)_{6(s)} + 5CO_{(g)} \xrightarrow[\approx 0.5\ atm\ CO]{25°C} 2Pd(CO)_2(SO_3F)_{2(s)} + S_2O_5F_{2(g)} + CO_2$$

or in HSO_3F as solvent. In both instances a yellow solid of the composition $Pd(CO)_2(SO_3F)_2$ forms. According to the vibrational spectra, the solid – gas phase reaction leads almost exclusively to the *cis* isomer while in HSO_3F an isomeric mixture forms (22). This mixture, or pure *cis*-$Pd(CO)_2(SO_3F)_2$, are both suitable for the subsequent solvolysis in liquid antimony(V) fluoride according to:

$$[3]\quad Pd(CO)_2(SO_3F)_2 + 8SbF_5 + 2CO \xrightarrow[\approx 0.5\ atm\ CO]{60–80°C} [Pd(CO)_4][Sb_2F_{11}]_2 + 2Sb_2F_9SO_3F$$

As noted previously (18), the reaction mixture is initially very viscous and gentle heating to 60–80°C is suggested, to allow magnetic stirring. The yellow colour of the starting material fades to colourless, but solid material suspended in liquid SbF_5 persists throughout the reaction. Removal of all volatiles in vacuo leaves a white, hygroscopic powder of the composition $[Pd(CO)_4][Sb_2F_{11}]_2$. Careful trap-to-trap distillation of the volatile materials from the solvolysis in the presence of CO provides no evidence for either CO_2 or $S_2O_5F_2$, which rules out any reduction to Pd(I). Since a number of palladium(I) carbonyl derivatives are known (12), further reduction is a distinct possibility. The reaction product $Sb_2F_9SO_3F$ is identified by its vibrational spectrum (24).

Formation of $[Pt(CO)_4][Sb_2F_{11}]_2$ proceeds in a very similar manner. Solid *cis*-$Pt(CO)_2(SO_3F)_2$ dissolves in liquid SbF_5 at room temperature to a clear colourless liquid. When ~0.6 atm of gaseous CO is admitted to the reactor a white solid starts forming on the surface of the solution. Since there is no colour change, the progress of the solvolysis is conveniently monitored by the uptake of CO from the gas phase, which together with the weight balance of the reaction allows an insight into the composition of the product. This is important here because, as in case of $[Au(CO)_2][Sb_2F_{11}]$ (18), no reliable metal analysis has been obtained due to interference between antimony and the noble metals. Tetrakis(carbonyl) platinum(II) undecafluorodiantimonate(V), $[Pt(CO)_4][Sb_2F_{11}]_2$, is a white, moisture-sensitive solid.

Appearance and the vibrational spectra are extremely similar for both salts, in particular in the range below 800 cm^{-1}. The slightly lower thermal stability of $[Pd(CO)_4][Sb_2F_{11}]_2$ is expected from previously reported CO derivatives of Pt(II) and Pd(II) (12, 25). Unlike $[Au(CO)_2][Sb_2F_{11}]$ (18), both $[M(CO)_4][Sb_2F_{11}]_2$ (M = Pd or Pt) are nearly insoluble in liquid SO_2 and attempts to obtain single crystals have failed for lack of an appropriate solvent. As the facile displacement of CO during the conversion of $[Au(CO)_2][Sb_2F_{11}]$ to $[Au(NCCH_3)_2][SbF_6]$ indicates (18), donor solvents may be unsuitable in recrystallization attempts. Our efforts are therefore currently directed at a complete vibrational analysis of both $[M(CO)_4]^{2+}$ cations (M = Pd or Pt), a normal coordinate analysis, and valence force field calculations, in order to allow a comparison with the corresponding data for the isoelectronic anions $[Pd(CN)_4]^{2-}$ and $[Pt(CN)_4]^{2-}$ (21).

A number of aspects discussed so far, and the molecular geometries of the cations, are very unusual in transition metal carbonyl chemistry (1). Some remote precedents will be briefly summarized.

The use of a strong protonic acid in the attempted syntheses of noble metal carbonyls is reported by Manchot et al. (26) in an attempt to obtain a silver(I) carbonyl species in a solution of concentrated H_2SO_4. Subsequently the generation of Cu(I) and Ag(I) carbonyl cations in various strong protonic acids (27, 28) and the use of these solutions as carbonylation catalysts (29–31) are reported.

The conversion of fluorosulfate into fluoroantimonate(V) derivatives has been reported previously by us, and a number of unusual and highly electrophilic cations like I_2^+ or Br_2^+ (32), $(CH_3)_2Sn^{2+}$ (33), and, most recently, $[Au(CO)_2]^+$ (18) have been stabilized by SbF_6^-, $Sb_2F_{11}^-$, or $Sb_3F_{16}^-$.

An intriguing difference from transition metal carbonyls (1) is the relative ease of formation. Reaction temperatures are usually between 25 and 80°C and CO uptake from the gas phase by solutions or suspensions is accomplished with pressures of ~0.5 atm.

The unusual nature of the compounds discussed here extends to the starting material *cis*-$Pd(CO)_2(SO_3F)_2$. There are only two precedents of the type *cis*-$Pd(CO)_2R_2$ (R = C_6F_5 or C_6Cl_5) (34). Both are only moderately stable at −30°C in a CO atmosphere, while *cis*-$Pd(CO)_2(SO_3F)_2$ is thermally stable up to 117°C (22). Previously known binary metal carbonyl cations are octahedral and are of the $[M(CO)_6]^+$ type (M = Mn, Tc, or Re) (35) with a +1 complex charge. There do not appear to be any square-planar binary carbonyl species reported (1). Carbonyls of Pd and Pt of the type $M(CO)_n$ (n = 1–4) are obtainable by matrix isolation (36, 37) only.

Can. J. Chem. Downloaded from www.nrcresearchpress.com by 203.198.23.82 on 09/08/12
For personal use only.

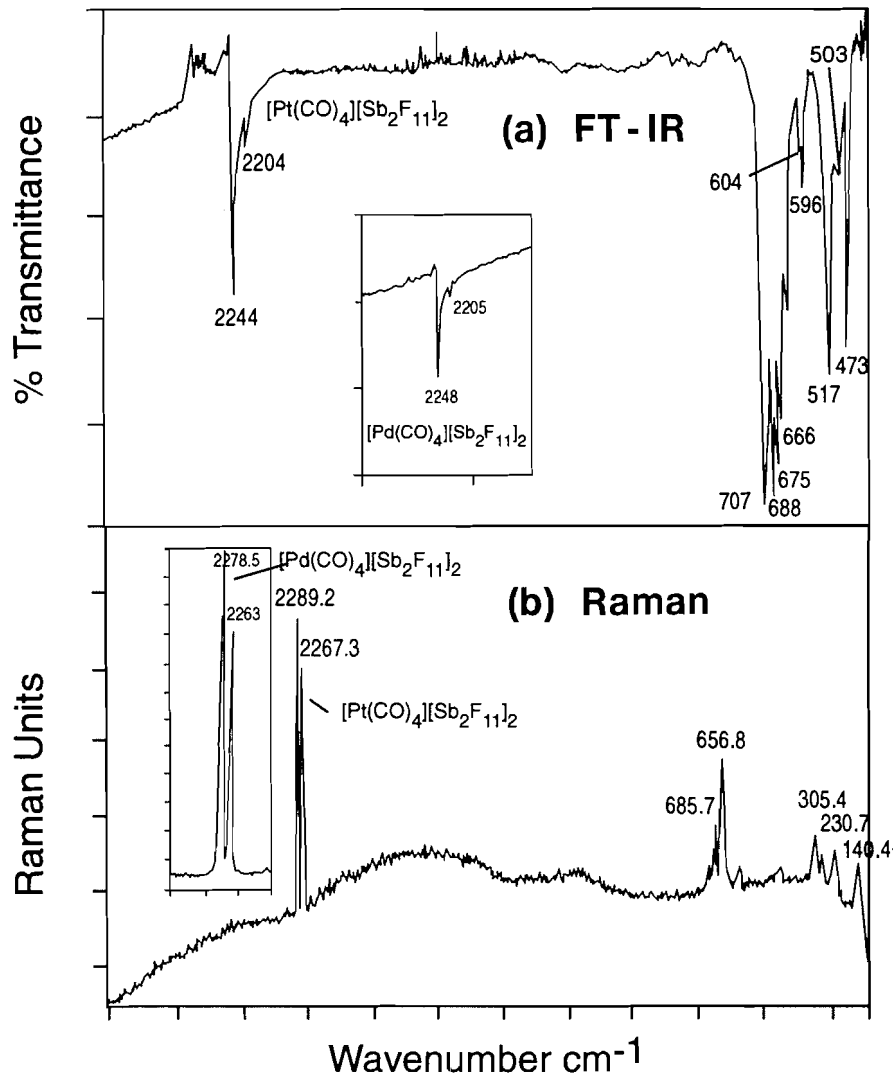

FIG. 1. Vibrational spectra of $[Pt(CO)_4][Sb_2F_{11}]_2$ and $[Pd(CO)_4][Sb_2F_{11}]_2$ (partial).

According to their vibrational spectra, the $M(CO)_4$ species appear to be tetrahedral (36, 37).

The relatively high thermal stability of $[Pd(CO)_4][Sb_2F_{11}]_2$ (to ~155°C), $[Pt(CO)_4][Sb_2F_{11}]_2$ (to ~200°C), and also of $[Au(CO)_2][Sb_2F_{11}]$ (to ~156°C) (18) is remarkable for another reason. Both $Ag(CO)B(OTeF_5)_4$ (14) and $Ag(CO)_2B(OTeF_5)_4$ (15) decompose with CO release below 25°C with formation of $AgB(OTeF_5)_4$ (14) and $AgB(OTeF_5)_4$. All three noble metal carbonyl fluoroantimonates undergo a more complex decomposition, which leads eventually to the formation of the corresponding metals rather than to a clean cleavage of CO.

It is not surprising that only $[Sb_2F_{11}]^-$ and, in the case of $[Pt(CO)_4]^{2+}$, the $[Pt(SO_3F)_6]^{2-}$ ion are capable of stabilizing the three binary carbonyl cations of the noble metals. Both anions rank, according to a scale based on ^{119}Sn Mössbauer spectroscopy (38), as the weakest nucleophiles. It is also not surprising that *cis*-$M(CO)_2(SO_3F)_2$ (M = Pd or Pt) are isolated from HSO_3F (22), even though the $[M(CO)_4]^{2+}_{(solv.)}$ cations are initially formed as indicated by the ^{13}C NMR spectra, in analogy to the $[Au(CO)_2]^+$–$Au(CO)SO_3F$ system (17, 18).

By far the most unusual aspect of the binary carbonyl cations of Pt(II) and Pd(II) are their vibrational spectra. The FT-IR and Raman spectra of $[Pt(CO)_4][Sb_2F_{11}]_2$ and the CO stretching range of $[Pd(CO)_4][Sb_2F_{11}]_2$ are shown in Fig. 1. Both compounds give identical vibrational spectra except for some small shifts in the CO stretching region and below 400 cm^{-1}. The band spacings make it obvious that the unusually high CO stretching modes cannot be the result of vibrational coupling as, for example, in BH_3CO (39).

The case for square-planar geometries for both cations rests on four observations: (*i*) the compounds are diamagnetic; (*ii*) the mutual exclusion rule is observed in the νCO range; (*iii*) vibrations due to $Sb_2F_{11}^-$ suggest the absence of significant covalent anion–cation interaction, and (*iv*) the bands in the CO stretching range display similar band positions and intensity patterns to those observed for CN vibrations of the isoelectronic anions $[Pd(CN)_4]^{2-}$ and $[Pt(CN)_4]^{2-}$ (21).

The CO stretching frequencies for $[Pd(CO)_4]^{2+}$ ($\nu_{avg.}$ = 2259 cm^{-1}) and $[Pt(CO)_4]^{2+}$ ($\nu_{avg.}$ = 2261 cm^{-1}) are unprecedentedly high, even when compared to those of $[Au(CO)_2]^+$ ($\nu_{avg.}$ = 2235.5 cm^{-1}) (18). The individual band positions are listed in Table 1 and are compared to those of related species. Also listed are stretching force constants obtained according to Jones (40), where vibrational spectra of the isotopomers are available (18, 21), or according to

TABLE 1. CO and CN stretching vibrations and force constants for selected Noble metal carbonyl and cyanide complexes

Molecule or ion	Point-group	νCX sym (cm^{-1})	ν'CX sym[a] (cm^{-1})	νCX as. (cm^{-1})	νCX av. (cm^{-1})	$f_r \times 10^2$ (Nm^{-1})	Ref.
$[Pt(CO)_4]^{2+}$[b]	D_{4h}	2289	2267	2244	2261	20.64[e]	[g]
$[Pt(CO)_4]^{2+}$[c]	D_{4h}	2281	2257	2233	2251	20.47[e]	20,[g]
$[Pd(CO)_4]^{2+}$	D_{4h}	2278	2263	2248	2259	20.63[e]	[g]
$[Pt(CN)_4]^{2-}$	D_{4h}	2168	2149	2133	2146	17.38[f]	21
$[Pd(CN)_4]^{2-}$	D_{4h}	2160	2146	2136	2144.5	17.35[f]	21
$[Au(CO)_2]^+$	$D_{\infty h}$	2254		2217	2235.5	20.18[e]	18
						20.1[f]	[g]
$[Au(CN)_2]^-$	$D_{\infty h}$	2162		2142	2152	17.60[f]	40
cis-$Pt(CO)_2(SO_3F)_2$[d]	$\sim C_{2v}$	2219		2185	2202	19.56[e]	22,[g]
cis-$Pd(CO)_2(SO_3F)_2$[d]	$\sim C_{2v}$	2227		2208	2217.5	19.87[e]	22,[g]
$Au(CO)SO_3F$[d]	$\sim C_s$	2196			2196	19.5[f]	18
CO	$C_{\infty v}$	2143			2143	18.6	4, 18
CO^+	$C_{\infty v}$	2184			2184	19.3[f]	18
HCO^+	$C_{\infty v}$	2184			2184	21.3[f]	18

[a] ν refers to the B_{1g} mode.
[b] $Sb_2F_{11}^-$ as anion.
[c] $[Pt(SO_3F)_6]^{2-}$ as anion.
[d] IR bands.
[e] Cotton–Kraihanzel values, refs. 41 and 42.
[f] According to Jones, ref. 40.
[g] This work.

Cotton and Kraihanzel (41, 42), where this is not yet the case. There is generally a very good correspondence between both sets of force constants as small differences in stretching frequencies and stretching force constants found for $[Pt(CO)_4][Sb_2F_{11}]_2$ and $[Pt(CO)_4][Pt(SO_3F)_6]$ (20) are seemingly due to differences in anion basicity (38).

It appears from the data for the noble metal carbonyl derivatives collected in Table 1 that the synergic bonding model (1) cannot be invoked. CO stretching frequencies, which for terminally bonded carbonyl groups usually absorb between 2125 and 1850 cm^{-1}, below the value of 2143 cm^{-1} for CO (4), are now generally observed between 2200 and 2290 cm^{-1}. CO stretching force constants usually between 15 and 18×10^2 N m^{-1} are now in excess of 20 in the case of the binary carbonyl cations.

Judging by the force constant $f_r = 21.3 \times 10^2$ N m^{-1} calculated for HCO^+ (18), where π-backdonation is impossible, this process can only make an insignificant contribution to the bonding in noble metal carbonyl cations. As discussed for $[Au(CO)_2]^+$ (18), the ability of gold, platinum, and apparently also palladium to form strong covalent bonds to non-metals, possibly aided by relativistic effects (43) and polar contributions, is seen as an important factor in describing the bonding in this small but interesting group of cationic coordination complexes of CO with the noble metals.

Acknowledgements

Financial support of this work by the Natural Sciences and Engineering Research Council of Canada (NSERC), the Deutsche Forschungs Gemeinschaft (DFG), and the North Atlantic Treaty Organization (NATO) is gratefully acknowledged.

1. (*a*) F.A. Cotton and G. Wilkinson. Advanced inorganic chemistry. 5th ed. John Wiley and Sons, New York. 1988. pp. 58 and 1021; (*b*) F.P. Pruchnik. Organometallic chemistry of the transition elements. Plenum Press, New York. 1990. p. 23.
2. P.S. Braterman. Metal carbonyl spectra. Academic Press, New York. 1975.
3. S.F.A. Kettle. Top. Cur. Chem. **71**, 111 (1977).
4. K. Nakamoto. Infrared spectra of inorganic compounds and coordination compounds. 1st ed. J. Wiley and Sons, New York. 1963. p. 72.
5. B.E. Mann. Adv. Organomet. Chem. **12**, **133** (1974).
6. S.C. Avazino, A.A. Bakke, H.-W. Chen, C.G. Donahue, W.L. Jolly, T.H. Lee, and R.J. Ricco. Inorg. Chem. **19**, 1931 (1980).
7. J. Browning, P.L. Goggin, R.J. Goodfellow, M.J. Norton, A.J.M. Rattray, B.F. Taylor, and J. Mink. J. Chem. Soc. Dalton Trans. 2061 (1977).
8. F. Calderazzo and D. Belli Dell'Amico. Pure Appl. Chem. **58**, 561 (1986), and references therein.
9. (*a*) P. Schützenberger. C. R. Hebd. Seances Acad. Sci. **70**, 1134 (1870); **70**, 1287 (1870); (*b*) Bull. Chim. Fr. **14**, 97 (1870).
10. (*a*) W. Manchot and H. Gall. Ber. Dtsch. Chem. Ges. B, **58**, 2175 (1925); (*b*) M.S. Kharash and H.S. Isbell. J. Am. Chem. Soc. **52**, 2919 (1930).
11. M.I. Bruce, J. Organomet. Chem. **44**, 209 (1972).
12. (*a*) S.C. Tripathi, S.C. Srivastava, R.P. Mani, and A.K. Shrimal. Inorg. Chim. Acta, **17**, 257 (1976); (*b*) M.N. Vargaftik, T.A. Stromnova, and I.I. Moiseev. Russ. J. Inorg. Chem. (Engl. Transl.), **25**, 127 (1980).
13. (*a*) A.F. Scott, L.L. Wilkening, and B. Rubin. Inorg. Chem. **8**, 2533 (1969); (*b*) C.D. Desjardins, D.B. Edwards, and J. Passmore. Can. J. Chem. **57**, 2714 (1979).
14. P.K. Hurlburt, O.P. Anderson, and S.H. Strauss. J. Am. Chem. Soc. **113**, 6277 (1991).
15. P.K. Hurlburt, J.J. Rack, S.F. Dec, O.P. Anderson, and S.H. Strauss. Inorg. Chem. **32**, 373 (1993).
16. H. Willner, S. Rettig, J. Trotter, and F. Aubke. Can. J. Chem. **69**, 391 (1991).
17. H. Willner and F. Aubke. Inorg. Chem. **29**, 2195 (1990).
18. H. Willner, J. Schaebs, G. Hwang, F. Mistry, R. Jones, J. Trotter, and F. Aubke. J. Am. Chem. Soc. **114**, 8972 (1992).

Can. J. Chem. Downloaded from www.nrcresearchpress.com by 203.198.23.82 on 09/08/12
For personal use only.

19. K.C. Lee and F. Aubke. Inorg. Chem. **23**, 2124 (1984).
20. G. Hwang, M. Bodenbinder, H. Willner, and F. Aubke. Inorg. Chem. In press.
21. G.J. Kubas and L.H. Jones. Inorg. Chem. **13**, 2816 (1974).
22. G. Hwang, C. Wang, M. Bodenbinder, H. Willner, and F. Aubke. J. Fluorine Chem. In press.
23. K.C. Lee and F. Aubke. Can. J. Chem. **57**, 2058 (1979).
24. W.W. Wilson and F. Aubke. J. Fluorine Chem. **13**, 431 (1979).
25. D.M. Roundhill. *In* Comprehensive coordination chemistry. Vol. 5. Pergamon Press, Oxford. 1987. p. 377.
26. W. Manchot, J. König, and H. Gall. Chem. Ber. **57**, 1157 (1924).
27. Y. Souma, J. Iyoda, and H. Sano. Inorg. Chem. **15**, 968 (1976).
28. A. Neppel, J.P. Hickey, and I.S. Butler. J. Raman Spectrosc. **8**, 57 (1979).
29. Y. Souma and H. Sano, J. Org. Chem. **38**, 2016 (1973).
30. Y. Souma and H. Sano. Bull. Chem. Soc. Jpn. **46**, 3273 (1973).
31. Y. Souma and H. Sano. J. Org. Chem. **38**, 3633 (1973).
32. W.W. Wilson, R.C. Thompson, and F. Aubke. Inorg. Chem. **19**, 1484 (1980).
33. S.P. Mallela, S. Yap, J.R. Sams, and F. Aubke. Rev. Chim. Miner. **23**, 572 (1986).
34. R. Usón, J. Forniés, M. Tomás, and B. Menjoń. Organometallics, **4**, 1912 (1985).
35. E.W. Abel and S.P. Tyfield. Adv. Organomet. Chem. **12**, 133 (1974).
36. J.H. Darling and J.S. Ogden. J. Chem. Soc. Dalton Trans. 1079 (1973).
37. M. Moskovits and G.A. Ozin. *In* Cryochemistry. John Wiley and Sons, New York. 1976. p. 263 and references therein.
38. S.P. Mallela, S. Yap, J.R. Sams, and F. Aubke. Inorg. Chem. **25**, 4327 (1986).
39. S. Sundaram and F.F. Cleveland. J. Chem. Phys. **32**, 166 (1960).
40. L.H. Jones. Inorganic vibrational spectroscopy. Vol. 1. Marcel Dekker, New York. 1971. p. 122.
41. F.A. Cotton and C. S. Kraihanzel. J. Am. Chem. Soc. **84**, 4432 (1962).
42. C.S. Kraihanzel and F.A. Cotton. Inorg. Chem. **2**, 553 (1963).
43. P. Pyykko. Chem. Rev. **88**, 563 (1988).

Appendix

Experimental

The sources of the chemicals used in this study (22), the preparation and (or) purification of $S_2O_6F_2$, HSO_3F, and SbF_5 (18), the equipment used for reductive carbonylation reactions in HSO_3F (17, 22) or in a solid state – gas reaction (22), and our instrumentation to obtain vibrational spectra (18, 22) have all been reported and described very recently. The synthesis of the starting material *cis*-$Pt(CO)_2(SO_3F)_2$ from $Pt(SO_3F)_4$ (19) and of *cis*-$Pd(CO)_2(SO_3F)_2$ from $Pd(SO_3F)_3$ (23), is described elsewhere as well (22). The published synthesis of $[Au(CO)_2][Sb_2F_{11}]$ by solvolysis of $Au(CO)SO_3F$ in liquid SbF_5 (18) was adopted for the syntheses of $[Pd(CO)_4][Sb_2F_{11}]_2$ and $[Pt(CO)_4][Sb_2F_{11}]_2$.

Synthetic reactions

(a) $[Pd(CO_4)][Sb_2F_{11}]_2$

A sample of 184 mg (0.511 mmol) of $Pd(CO)_2(SO_3F)_2$, obtained by reductive carbonylation of $Pd(SO_3F)_3$ in HSO_3F and analyzed (calcd:C 6.66, S 17.78; found: C 6.67, S 17.97), was placed in a round-bottom flask and an excess of SbF_5 was added by distillation. After warming to room temperature, gaseous CO was admitted to the reactor and the pressure was adjusted to 0.6 atm of CO. The reactor was sealed off. The mixture was stirred and heated for 48 h at 60°C. In this time the colour of the mixture had changed from yellow to white. After removal of all volatiles, with the reactor first at 25 and later at 60°C, 581 mg (0.517 mmol) of a white solid was obtained. The weight and microanalysis confirmed the composition as $[Pd(CO)_4][Sb_2F_{11}]_2$ (Anal. calcd.: C 4.27; found: 4.41). The extremely hygroscopic solid is thermally stable to 140°C and melts on further heating at 155°C.

(b) $[Pt(CO)_4][Sb_2F_{11}]_2$

A sample of freshly prepared $Pt(CO)_2(SO_3F)_2$ (472 mg, 1.051 mmol) (Anal. calcd.: C 5.34, S 14.27; found: C 5.41, S 14.17) was placed in a round-bottom flask. After addition of an excess of SbF_5 (~10–15 g) by distillation, a clear viscous liquid formed. Previously dried CO was admitted to the reactor and a white solid film was seen forming on the surface of the liquid phase. The CO pressure was adjusted to 0.6 atm, and the stirred mixture was kept overnight at 80°C. During this time a white solid had formed. The total CO uptake determined by measuring the pressure in a vacuum line of known volume was 2.25 mmol. Removal of all volatiles yielded 1.296 g (1.069 mmol) of a hygroscopic white solid of the composition $[Pt(CO)_4][Sb_2F_{11}]_2$ (Anal. calcd.: C 3.96, F 34.48; found: C 4.05; 3.72; F 35.6). The solid was stable in a sealed capillary to about 200°C.

Can. J. Chem. Downloaded from www.nrcresearchpress.com by 203.198.23.82 on 09/08/12
For personal use only.

An analysis of vibronic coupling in the triplet absorption spectrum of pyrazine

GAD FISCHER

Department of Chemistry, The Faculties, Australian National University, Canberra 2601, Australia

Received January 18, 1993

This paper is dedicated to Professor Gerald W. King on the occasion of his 65th birthday

GAD FISCHER. Can. J. Chem. **71**, 1537 (1993).

New measurements of the singlet–triplet ($\tilde{a}^3B_{3u} \leftarrow \tilde{X}^1A_g$) absorption spectra of pyrazine and pyrazine-d_4 at longer pathlengths and higher vapour pressures have been recorded. Particular attention was paid to the hot band region to the red of the electronic origin. The activities of the out-of-plane vibrations, ν_4 and ν_{10a}, were identified in sequence bands, and their triplet state vibrational frequencies were determined, 295 (276, -d_4) and 254 (194, -d_4) cm^{-1}, respectively. Model calculations were undertaken to match the observed singlet and triplet absorption and emission spectra for vibronic coupling induced by (*i*) $\nu_{10a}(b_{1g})$, and (*ii*) ν_4 and $\nu_5(b_{2g})$. The calculations allowed the ordering and the relative energies of the higher lying triplet states to be determined. The $^3B_{2u}$ and $^3B_{1u}$ electronic states are above the ground electronic state by about 3.9 and 4.4 eV, respectively. The ordering is in analogy with the corresponding singlet states but opposite to that predicted by most theoretical calculations.

GAD FISCHER. Can. J. Chem. **71**, 1537 (1993).

On a mesuré les spectres d'absorption singulet–triplet ($\tilde{a}^3B_{3u} \leftarrow \tilde{X}^1A_g$) de la pyrazine et de la pyrazine-d_4 à des longueurs d'onde plus grandes et à des tensions de vapeur plus élevées que celles utilisées jusqu'à maintenant. On a particulièrement fait attention à la région des bandes chaudes situées vers le rouge par rapport à l'origine électronique. On a identifié les activités des vibrations en dehors du plan, ν_4 et ν_{10a}, dans la séquence des bandes et on a déterminé les fréquences de leurs états vibrationnels triplets, respectivement 295 (276 pour le -d_4) et 254 (194 pour le -d_4). On a réalisé des calculs modèles pour comparer aux spectres d'absorption et d'émission triplet et singulet du couplage vibronique induit par (*i*) ν_{10a} (b_{1g}) et (*ii*) ν_4 et ν_5 (b_{2g}). Les calculs ont permis d'ordonner et de déterminer les énergies relatives des états triplets se trouvant à des niveaux élevés. Les niveaux des états électroniques $^3B_{2u}$ et $^3B_{1u}$ sont respectivement 3,9 et 4,4 eV au-dessus de l'état électronique fondamental. L'ordre est semblable à celui observé avec les états singulets correspondants; il est toutefois l'inverse de celui prédit par la plupart des calculs théoriques.

[Traduit par la rédaction]

1. Introduction

For a number of molecules, the increase in our knowledge of their electronic states and vibrational frequencies makes it now possible to undertake more general modelling of their electronic spectra, and to achieve a better understanding of their intramolecular dynamics. Benzene and some of the azabenzenes fall in this category. The model calculations can be based on the vibronic and spin-orbit interactions involving the relevant singlet and triplet states. The ensuing theoretical results allow for a greater understanding of the sources of transition intensity, better identification of those vibrations vibronically active — even if they are not effective in inducing intensity, more secure assignments of vibrational frequencies, and more satisfactory descriptions of the radiationless decay paths.

Pyrazine, 1,4-diazabenzene, has been the subject of very considerable investigation. The lowest singlet system of pyrazine, $\tilde{A}\ ^1B_{3u} \leftrightarrow \tilde{X}\ ^1A_g$, has been very extensively studied, experimentally in absorption and emission, and also theoretically (1–17). It has served as a prototype for modelling vibronic coupling, and has been used as a test case illustrating the nature of the vibronic interactions (15, 16). In the theory of radiationless transitions pyrazine has served as the best known and most studied example of intermediate level structure (18–23). At energies corresponding to the low-lying vibrational levels of the first excited singlet state the triplet vibrational manifold is believed to be sparse. The singlet–triplet interactions are said to be in the strong coupling regime and are responsible for the non-exponential fluorescence decay.

Much less attention has been paid to the lowest triplet system (7, 8, 24–31). This is in part due to the greater experimental difficulties encountered in measuring the singlet–triplet absorption spectrum. However, this factor does not lessen the importance of gaining a full characterization of the lowest triplet state, since in addition to obtaining a more complete picture of pyrazine electronic spectroscopy, the triplet state is believed to play a key role in the scheme of radiationless transitions involving the first excited singlet state (18, 19). The singlet–triplet spectrum also allows for testing the applicability of the models of vibronic coupling developed for the singlet state. This is of particular relevance for pyrazine since the triplet has the same electron configuration as the lowest excited singlet state. Both are $n\pi^*$-type states of B_{3u} orbital symmetry. Because intensity must be induced by spin-orbit interaction, the vibronic coupling as a mechanism-inducing intensity in the singlet–triplet spectrum of pyrazine is not as explicit as it is for the singlet state transitions. Nevertheless, this must not be viewed as an argument against the occurrence of vibronic coupling. Indeed, theoretical calculations of the triplet state energies can be interpreted to indicate heightened vibronic coupling activity involving the b_{2g} modes because of a greatly decreased electronic state energy gap. Experimental evidence to this effect is obtained indirectly from phosphorescence spectra of pyrazine in mixed crystals at low temperatures (7, 8, 29). Progressions in the $b_{2g}(\nu_4)$ and $b_{1g}(\nu_{10a})$ modes are observed, an indication of vibronic activity and of large vibrational frequency changes. Furthermore, it should be noted that some experimental results, as for example those involving microwave-induced delayed phosphorescence, have been interpreted in terms of a triplet state distorted by pseudo Jahn–Teller vibronic coupling involving the lower frequency b_{2g} vibrational mode (25, 27).

Can. J. Chem. Downloaded from www.nrcresearchpress.com by 203.198.23.82 on 09/08/12
For personal use only.

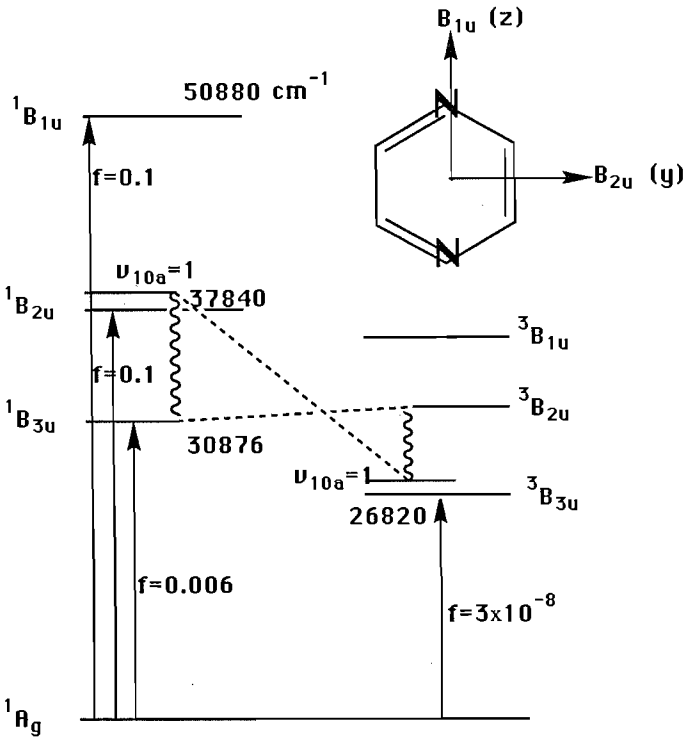

FIG. 1. Schematic representation of some of the low-lying pyrazine electronic states and delineation of the four-state model involving vibronic couplings via mode 10a, and spin-orbit interactions. The energies of the three singlet and the lowest triplet states were spectroscopically determined. The two higher triplet states are assigned according to this work. Oscillator strengths and state energies are taken from ref. 1.

In the singlet absorption spectrum, intensity is vibronically induced by both b_{1g} and b_{2g} vibrations. This is evident through the appearance in the vapour spectra of all three types of rotational contours (1). Most prominent are the allowed bands, which are type C (out-of-plane polarized), and type B (in-plane polarized).[1] The latter originate from Herzberg–Teller vibronic coupling involving the b_{1g} mode ν_{10a} with the $^1B_{2u}(\pi\pi^*)$ state some 7000 cm^{-1} to higher energy, see Fig. 1. The vibrational frequency is very considerably reduced in the excited state. It is one of the features that has focussed interest on the spectroscopy of pyrazine and that has stimulated much of the work on vibronic coupling models. Most of the frequency decrease of this vibration is attributed to vibronic coupling. Being the sole vibration of its symmetry type, no Duschinsky effect is induced by the coupling (32, 33). Vibronically induced bands, through coupling via b_{2g} modes with the $^1B_{1u}$ state removed some 20 000 cm^{-1}, are also weakly evident and are responsible for the type A rotational contours.

In modelling the vibronic coupling through the b_{1g} mode, ν_{10a}, for pyrazine and pyrazine-d_4 in the vapour and in a number of different host crystals, Chappell and Ross (14) obtained good agreement with experiment by making appropriate adjustment of the electronic energy intervals. In contrast, the other parameters in the vibronic coupling calculations, namely, the vibrational frequencies and the magnitudes of the vibronic coupling, were held constant throughout. Because of the close similarity of the lowest excited singlet and triplet states, the triplet state may be expected to provide a further testing ground for models of vibronic coupling developed for the singlet state. In particular, by employing the same input data as used in the singlet state calculations, consisting of the vibrational frequencies and coupling strengths, the triplet electronic states energy gap may be determined and compared to theoretical prediction.

The vibronically active modes are either not seen or are only weakly evident in the triplet spectra (24–31). However, information on the vibronic coupling can be obtained indirectly. One source is the vibrational frequency changes associated with the electronic excitation. Even in the absence of vibronically induced transition intensity, triplet state vibrational frequencies of vibronically active modes may be determined from sequence structure (hot bands) observed in the singlet–triplet absorption spectrum of the vapour, and from the identification of overtones.

Qualitatively, the singlet and triplet absorption spectra have much in common. The totally symmetric vibrations appear with similar relative intensities. The sequence bands deriving from the low-frequency out-of-plane vibrations also appear with similar intensities and frequencies. The isotope effect is the same, about 154 cm^{-1}. Only with respect to the appearance of the vibronically active modes are there any distinguishing features.

In this paper we report on new measurements of the absorption spectra. Particular emphasis has been placed on the hot band structure to the red of the electronic origins. It is there that sequence bands associated with vibronically active modes can be expected, and may be most readily identified. They are not subject to overlap by the more intense cold bands. It is the low-frequency out-of-plane modes that are expected to be the most vibronically active in the lowest excited singlet and triplet states (1). Their Boltzmann factors will not be too small, relative to the cold bands, to preclude observation.

In conjunction with the new experimental work a number of vibronic coupling calculations involving the lowest excited triplet state have been undertaken. The calculations include the following: (*a*) Extension of the model previously employed for the b_{1g} singlet state coupling (16) to a four-state problem involving the lowest singlet and triplet B_{3u} and B_{2u} states, where states of the same spin multiplicity are vibronically coupled by the sole b_{1g} mode, and states of different spin multiplicity are spin-orbit coupled. A four-state model was earlier proposed to explain the intensity distributions in progressions of the b_{1g} mode observed in phosphorescence and phosphorescence-excitation spectra (12). However, for the sole b_{1g} mode no consideration needed to be given to normal coordination rotation (the Duschinsky effect), and perturbation theory was satisfactorily used to account for the spin-orbit interaction. (*b*) Application and extension of the model to the four-state problem involving the $^3B_{3u}$, $^3B_{1u}$, $^1B_{3u}$, and $^1B_{1u}$ states through coupling by the two b_{2g} modes ν_4 and ν_5.

The new experimental results together with the vibronic coupling calculations undertaken have allowed a revision to be made of the vibrational frequencies in the singlet and triplet states, have suggested which modes are vibronically active in the triplet state, and have provided estimates of the locations of some of the higher lying triplet electronic states.

[1]Pyrazine is assumed a planar molecule belonging to the D_{2h} symmetry point group. The axis convention is depicted in Fig. 1.

Can. J. Chem. Downloaded from www.nrcresearchpress.com by 203.198.23.82 on 09/08/12
For personal use only.

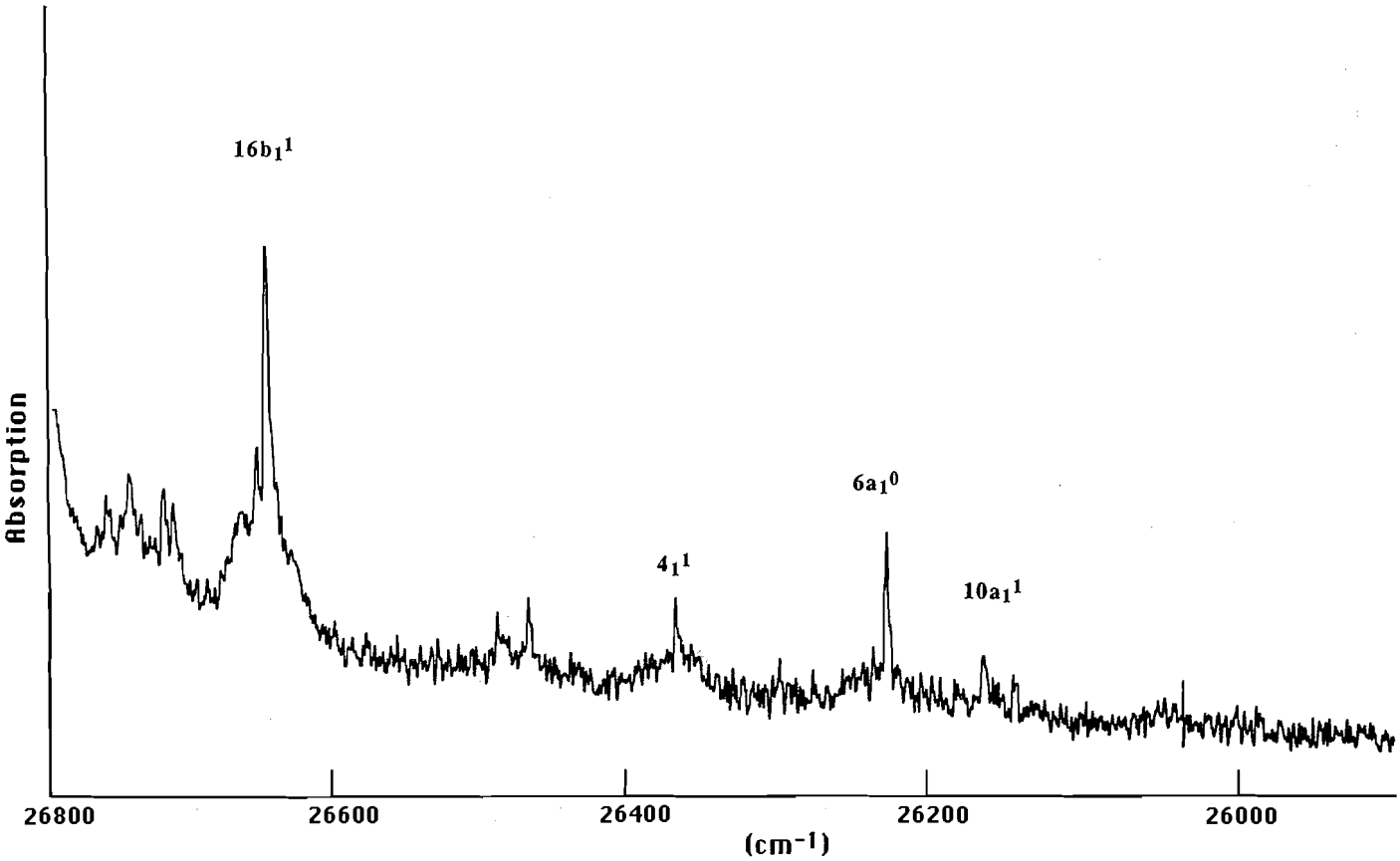

FIG. 2. Microdensitometer tracing of the singlet–triplet absorption spectrum of pyrazine vapour in the hot band region.

2. Experimental

A new series of singlet–triplet absorption spectra were recorded on a 3.4-m spectrograph, at higher vapour pressures and longer pathlengths, 264 m. A 6-m multiple-traversal cell with facilities for heating was used. Calibration was by the iron lines of an iron hollow-cathode lamp. Vapour pressures of about 7 Torr (1 Torr = 133.3 Pa) were used in all room-temperature measurements, and for the 40°C runs ambient pyrazine vapour pressures were used. The pyrazine and pyrazine-d_4 were commercially available (Aldrich) and were vacuum distilled prior to use. A mass spectrum of the deuterated sample showed the following: 93.7% -d_4, 5.5% -d_3, and 0.8% -d_2. Only one spurious band, namely the origin for pyrazine-hd_3, was identified in the pyrazine-d_4 spectra.

3. Results

The absorption spectra to the red of the electronic origins for pyrazine and pyrazine-d_4 are presented in Figs. 2 and 3, respectively, and lists of the bands and their proposed assignments are given in Table 1. Included in the table are the observed relative intensities taken from microdensitometer tracings of the photographically recorded spectra. They are compared with the relative spectral intensities calculated for the proposed assignments from approximate Franck–Condon factors[2] and from Boltzmann factors. It is seen that good agreement is achieved between the two in support of the proposed assignments. Further support for the assignments is obtained from the vibronic coupling calculations described in Sect. 5. The spectra are almost identical to the singlet absorption spectra in the same region, apart from the bands assigned 4_1^1 and $10a_1^1$.

4. Vibrational frequencies

For electronic transitions of the type encountered for the low-lying electronic states of the azines, that is, those involving the promotion of an electron from a nonbonding (n), or bonding (π) orbital to an antibonding orbital (π^*), most vibrational frequencies are reduced, although many only marginally. In addition, Herzberg–Teller vibronic coupling can induce substantial changes in the frequencies of the vibronically active modes. This is clearly the case for the b_{1g} mode ν_{10a} identified in the singlet absorption and fluorescence spectra. Much of the frequency decrease from 919 to 383 cm^{-1} can be attributed to vibronic coupling. In terms of a simple model of zero-order states chosen to correspond to the states hypothetically obtained in the absence of the vibronic interaction, an estimate of the reduction in vibrational frequency, δ, can be obtained from perturbation theory,

$$[1] \quad \delta = 2V^2/\Delta E$$

where V is the vibronic coupling matrix element and ΔE is the energy separation of the zero-order, non-interacting states. This result applies for the vibration ν_{10a} because it is the only vibration of symmetry b_{1g} and hence no Duschinsky rotation need be taken into consideration. Equation [1] gives the dependence of the vibrational frequency shift on the energy separation of the vibronically coupled states.

There are six other out-of-plane vibrations, two of each symmetry type, b_{2g}, b_{3u}, and a_u. Also for these it is possible

[2]The appropriate Franck–Condon factors have been taken from unpublished tables (J. Christie).

Can. J. Chem. Downloaded from www.nrcresearchpress.com by 203.198.23.82 on 09/08/12
For personal use only.

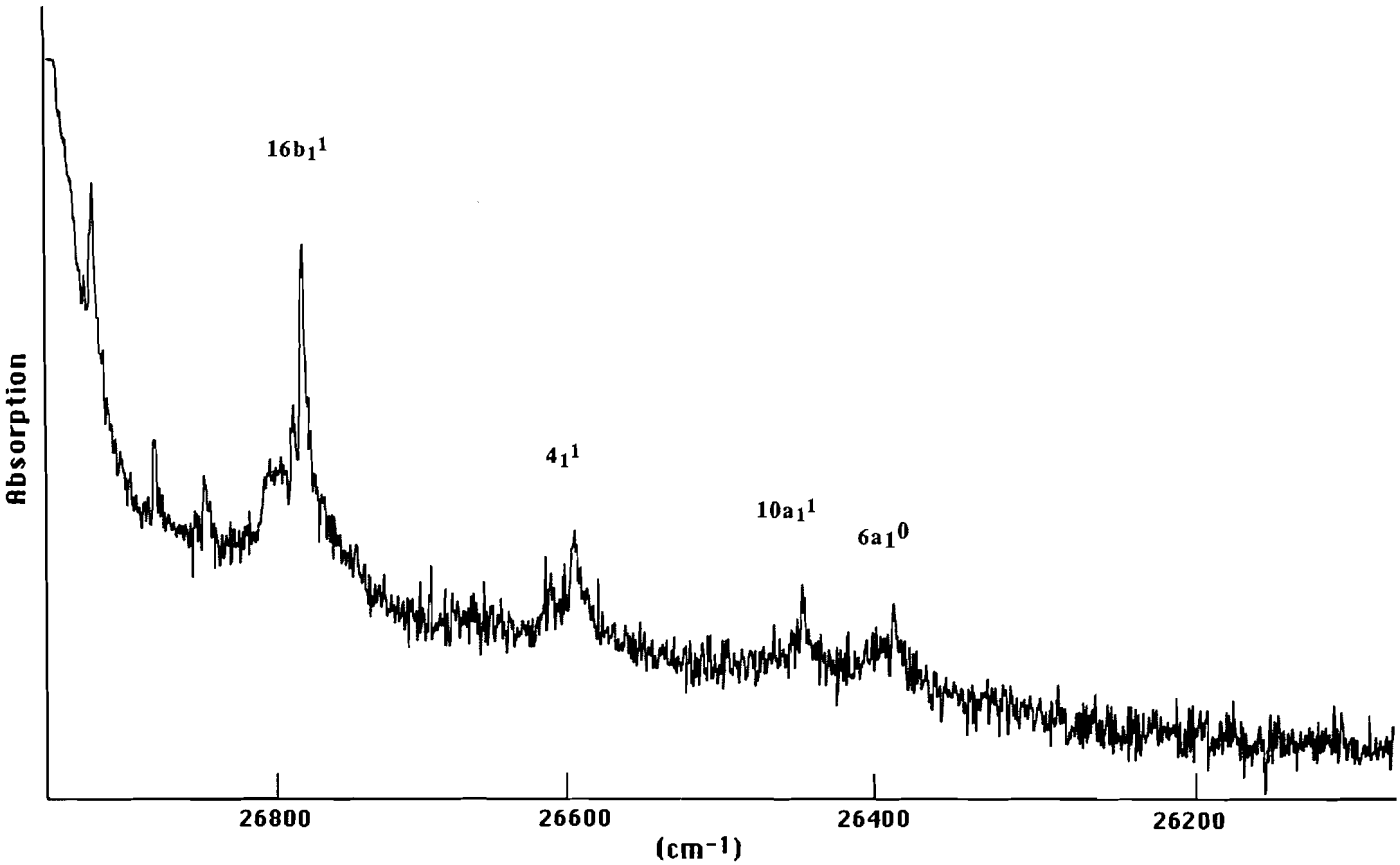

FIG. 3. Microdensitometer tracing of the singlet–triplet absorption spectrum of pyrazine-d_4 vapour in the hot band region.

to provide approximate estimates of the changes in vibrational frequencies in terms of the vibronic coupling. Because of the occurrence of a vibronically induced Duschinsky rotation, eq. [1] does not apply here. However, using a simple two-state model it can be shown (33) that for the case of two vibronically active modes of the same symmetry, the excited state frequencies relative to the ground state frequencies are approximately given by

$$[2] \quad \nu_a' = \nu_a'' - 2V_a^2/\Delta E + 4V_a^2V_b^2/\Delta E^2\Delta E_{ab}$$
$$\nu_b' = \nu_b'' - 2V_b^2/\Delta E - 4V_a^2V_b^2/\Delta E^2\Delta E_{ab}$$

where ν_a' is the larger of ν_a' and ν_b', and $\Delta E_{ab} = (\nu_a'' - \nu_b'')$.

It is clear from eqs. [1] and [2] that the frequency changes of all those vibrations vibronically active, but not necessarily inducing transition intensity, depend on the separations of the coupled states. Even under the assumption that the vibronic coupling strengths are the same for the lowest excited singlet and triplet states of pyrazine — it should be recalled that both are of the same electron configuration — the vibrational frequencies of the vibronically active modes may nevertheless differ because of differing electronic state energy gaps.

A number of calculations of the electronic state energies of pyrazine have been reported. Among the most recent are the electronic state locations as computed by Walker and Palmer (34) and listed in Table 2. It can be seen that for the relatively low-lying electronic states of pyrazine, the singlet–triplet splittings for states of the same electron configurations are small, less than 1 eV, and for many only ~0.1 eV. The $^{1,3}B_{1u}$ splitting is an exception. Thus, for example, the lowest excited singlet and triplet states, $^{1,3}B_{3u}(n\pi^*)$, are calculated to be separated by ~0.6 eV. The experimentally observed value is ~0.5 eV. However, for the $^{1,3}B_{1u}(\pi\pi^*)$ states this splitting is very much larger, estimated to be in the range 3–4 eV, although our vibronic coupling calculations show it to be much less.

It follows that a consideration of the electronic state energy gaps can provide information on the singlet and triplet state vibrational frequencies relative to the ground electronic state. Or the converse, a consideration of the vibrational frequencies in the excited states can provide estimates of the relative singlet and triplet state separations. Thus, for example, a cursory inspection of Table 2 reveals that for the case that the two b_{3u} modes are effective in coupling the $B_{3u}(n\pi^*)$ and $A_g(\pi\pi^*)$ states, the vibrations may be expected to have similar frequency reductions in both the excited singlet and triplet states. The calculated separations of the singlet states and of the triplet states are approximately the same. The frequencies of ν_{16b} in the excited states are in complete accord with this conclusion, Table 3. They are approximately the same in singlet and triplet excited states. Furthermore, because the frequencies are the same, it is possible to conclude that significant vibronic coupling of the $^1B_{3u}$ with the ground electronic state can be excluded. The excited state frequencies of ν_{11}, the other b_{3u} mode, have not been sufficiently well assigned to permit comment.

The opposite conclusions are reached for the two b_{2g} modes. They vibronically couple the lowest excited $B_{3u}(n\pi^*)$ states with the higher lying $B_{1u}(\pi\pi^*)$ states, Fig. 1. How-

Can. J. Chem. Downloaded from www.nrcresearchpress.com by 203.198.23.82 on 09/08/12
For personal use only.

TABLE 1. Analyses of the regions to the red of the origin bands in the singlet–triplet absorption spectra of pyrazine and pyrazine-d_4. The intensities are relative to those of $6a_1^0$, which have been arbitrarily set to 1.0. The conventional meaning is attached to the specification $X_j^k Y_m^n$, for a vibronic transition between j and m quanta of vibrations X and Y, respectively, in the lower state, and quanta k and n, respectively, in the upper state

Pyrazine				Pyrazine-d_4		
ν − 26 820 (cm^{-1})	Intensity		Assign	ν − 26 974 (cm^{-1})	Intensity	
	Calcd.	Obsd.			Calcd.	Obsd.
−782	0.13	0.09	$6a_1^0 16b_1^1$			
−686	0.006	0.18	$16a_2^0$			
−665	0.30	0.30	$10a_1^1$	−526	1.0	1.1
−599	1.0	1.0	$6a_1^0$	−585	1.0	1.0
−531	0.19	0.18	$6a_1^0 16a_1^1$			
−461	0.65	0.55	4_1^1	−369	1.36	1.4
−361	0.45	0.45	$16b_2^2$	−379	0.64	
−341	1.0	0.35	$6b_1^1$?	−357		
−182	3.9	2.2	$16b_1^1$	−185	5.2	4.0
−119	0.04	0.48	$6a_1^0 16b_0^2$			
−113	0.22	0.48	$16a_1^1 16b_1^1$	−119	1.32	0.81
−89		0.58		−85		0.65
−74		0.41		−41(0_0^0-d_3h)	1.4	1.4

TABLE 2. Calculated and measured electronic state energies relative to the ground state (eV). The data are from Walker and Palmer (34) unless otherwise indicated. The values in parentheses are from this work as determined from vibronic coupling calculations

State	Calculated	Measured	State	Calculated	Measured
^1A_g(GS)	0	0	$^3B_{1u}(\pi\pi^*)$	4.00 (4.4)	4.0
			$^1B_{1u}(\pi\pi^*)$	7.19	6.31[a]
$^3B_{3u}(n\pi^*)$	3.28	3.33[a]			
$^1B_{3u}(n\pi^*)$	3.87	3.83[a]	$^3A_g(\pi\pi^*)$	7.60[b]	
			$^1A_g(\pi\pi^*)$	8.70[b]	
$^3B_{2u}(\pi\pi^*)$	4.66 (3.9)	~4.4			
$^1B_{2u}(\pi\pi^*)$	4.77	4.7[a]	$^3B_{3g}(\pi\pi^*)$	7.78[b]	
			$^1B_{3g}(\pi\pi^*)$	8.81[b]	
$^3A_u(n\pi^*)$	4.12	4.2			
$^1A_u(n\pi^*)$	4.93	5.0			

[a]Reference 1.
[b]Reference 35.

ever, the measured energy separation between the two singlet states (2.5 eV) is much larger than the calculated energy separation between the two triplet states (0.7 eV). Hence, in accordance with eq. [2], the vibrational frequencies for the b_{2g} modes can be expected to be substantially different in the singlet and triplet states. A similar situation applies for the b_{1g} mode, ν_{10a}. It is the vibration effective in coupling the $B_{3u}(n\pi^*)$ and $B_{2u}(\pi\pi^*)$ states. The state separations, according to the computed values of Walker and Palmer listed in Table 2, vary significantly between the singlet (0.9 eV) and triplet manifolds (1.4 eV).

It will be seen in the following section that the locations of the B_{2u} and B_{1u} triplet states obtained in this work differ markedly from the calculated positions of Table 2. In fact, our vibronic coupling calculations give good agreement if the $^3B_{1u}$ and $^3B_{2u}$ assignments in the electron energy-loss spectra of Walker and Palmer are reversed. Nevertheless, even with the revised assignments, the relevant singlet and triplet state separations still differ, supporting the observation of different vibrational frequencies for modes 4, 5, and 10a in the singlet and triplet excited states.

The vibrational frequencies for the totally symmetric and the out-of-plane modes, for the ground and first excited singlet and triplet states, are listed in Table 3. These particular symmetry representations have been included because they contain the majority of the vibrations active in the spectra, and accordingly are the ones that have experienced frequency changes and possibly normal coordinate displacements in the case of the a_g modes. The 12 non-totally symmetric, in-plane modes have been omitted from the table. They were not identified in the absorption and emission spectra, although one, mode 6b, was tentatively identified as a sequence band.

For the a_g modes the ratio of frequencies for the two isotopes $(\nu_i)_h/(\nu_i)_d$, measured (1.98) and calculated from the product rule (2.0), are in excellent agreement for the ground electronic state. For the singlet and triplet excited states, it was assumed that the frequencies of the C—H (C—D) stretching mode have not changed significantly from their ground state values. This assumption is in accord with the very localized nature of these vibrations, and has subsequently allowed the product rule to be employed for the de-

Can. J. Chem. Downloaded from www.nrcresearchpress.com by 203.198.23.82 on 09/08/12
For personal use only.

TABLE 3. Vibrational frequencies for the a_g and out-of-plane modes of pyrazine and pyrazine-d_4

		^1A_g		$^1B_{3u}$		$^3B_{3u}$	
		-h_4	-d_4	-h_4	-d_4	-h_4	-d_4
a_g	1	1015	884	966	831	986	834
	2	3055	2274				
	6a	596	586	583	564	620	578
	8a	1582	1537	1373	(1248)	1234	1265
	9a	1230	1005	1101	978	1149	965
a_u	16a	341	286	399	351	406[S]	356[S]
	17a	960	(810)				
b_{1g}	10a	919	721	383	292	254[S]	194[S]
b_{2g}	4	756	651	517	463?	295[S]	276[S]
	5	983	860				
b_{3u}	11	785	597				
	16b	416	399	235	211	236[S]	212[S]

[a]Frequencies determined from application of the "product rule" are given in parentheses. Frequencies estimated from sequence and (or) overtone bands are marked with an "S." All other frequencies are taken from references 1, 3, and 26.

termination of the frequency of ν_{8a} for pyrazine-d_4 in the first excited singlet state. Bands at 1234 and 1265 cm^{-1} have been assigned to the vibration 8a in the triplet state spectra of pyrazine-h_4 and -d_4, respectively, although a possible Fermi resonance between 8a (1234 cm^{-1}) and $6a^2$(1221 cm^{-1}) may have perturbed the former. No band in the singlet absorption spectrum of pyrazine-d_4 has been assigned to ν_{8a}.

Formally, the b_{1g} and b_{2g} out-of-plane modes can vibronically couple the $B_{3u}(n\pi^*)$ state with the $B_{2u}(\pi\pi^*)$ and $B_{1u}(\pi\pi^*)$ states, respectively. Transitions to these $\pi\pi^*$ states in the singlet manifold are electric-dipole allowed from the ground state. Intensity is induced by this means and several of the out-of-plane vibrations were identified in the singlet absorption and fluorescence spectra. Although vibronic coupling undoubtedly occurs in the triplet manifold, it is the spin-orbit coupling mechanism that induces intensity in the singlet–triplet absorption and emission spectra. Consequently, it is not surprising that no positive identification of single quanta of these out-of-plane modes was made in the singlet–triplet absorption spectra (24, 26). Highly tentative assignments have been made in the singlet–triplet excitation spectra of pyrazine in mixed crystals at low temperatures (29). The frequencies of the vibrations 16a and 16b are based on the observed sequence and overtone bands. In the table the frequencies entered for the b_{1g} and b_{2g} modes in the triplet state were determined solely from the sequence bands.

The major revision from earlier assignments concerns the b_{2g} modes 4 and 5. A detailed four-state vibronic coupling calculation involving these modes is described later. Suffice it here to point out a general observation. If two modes of the same symmetry are active in vibronic coupling, then, because of the induced Duschinsky rotation, there is a tendency for the vibration of lower frequency to induce greater intensity in the excited state relative to its activity in the ground state. This is a consequence of the generally greater energy separation for ground state coupling than for excited state coupling. Spectra depicting this have been recorded for a number of molecules (36). Hence it follows that the frequency of 517 cm^{-1} (-d_4, 463) observed in the absorption spectrum, $^1B_{3u} \leftarrow {}^1A_g$, must be assigned to $\nu_{4'}$ and not $\nu_{5'}$ as was previously done. In the ground state the corresponding frequency is 756 cm^{-1} (-d_4, 651), and $\nu_{5''}$ is 983 cm^{-1} (-d_4, 860), in accordance with the assignments proposed by Innes, Ross, and Moomaw (1).

A similar "Duschinsky type" argument, invoking eqs. [2], is proposed to suggest that the frequency of ν_{17a} in the singlet state cannot have decreased substantially from its ground state value. For the two a_u modes, 16a and 17a, the opposite situation applies. Ground state coupling is more significant than excited state coupling. It is one of the exceptional cases where the roles of the two radiatively coupled states are reversed, leading to greater excited state than ground state frequencies for 16a and possibly also 17a.

5. Vibronic coupling calculations

In a comparison of the singlet–singlet and singlet–triplet spectra, and in the context of vibronic coupling, it is the vibrations of b_{1g} and b_{2g} symmetries that are of most interest. Progressions of these vibrations are evident in the absorption and emission spectra. Numerous models have been proposed to represent the coupling induced by the single b_{1g} mode. Some have included totally symmetric vibrations to act as tuning modes. No such, or similar, calculations have been carried out for the b_{2g} modes, although their activity has been unambiguously noted in the fluorescence and phosphorescence spectra. In the singlet–triplet absorption and emission spectra the two b_{2g} vibrations, where identified, appear with little relative intensity. But theoretically, because of the much smaller electronic energy separation in the triplet manifold, the two vibrations are expected to be involved in very significant vibronic coupling, despite the fact that they fail to induce measurable amounts of intensity in the singlet–triplet spectra. In the following a detailed description is given of the vibronic coupling calculations undertaken for (*a*) the b_{1g} mode (10a), and (*b*) the b_{2g} modes (4 and 5).

Can. J. Chem. Downloaded from www.nrcresearchpress.com by 203.198.23.82 on 09/08/12
For personal use only.

TABLE 4. Input parameters (cm^{-1}) for the $b_{1g}(\nu_{10a})$ vibronic coupling calculations, respectively: the vibrational frequency; the B_{3u}··B_{2u} vibronic coupling strength; the $n\pi^*\cdots\pi\pi^*$ spin-orbit interaction; and the separations between the electronic states

	ν_{10a}	V_{10a}	V_{so}	$\Delta E_{t't}$	ΔE_{st}	$\Delta E_{s't}$
Pyrazine-h_4	736	1020	10	4580	3958	10 593
Pyrazine-d_4	580	909	10	4740	3975	10 543

(a) b_{1g} *Mode*

Very considerable effort has been devoted to the modelling of the activity of the b_{1g} mode, 10a, in the singlet absorption and emission spectra. In this work, the model is extended to a four-level system of singlet and triplet B_{3u}, and singlet and triplet B_{2u} states coupled by vibronic and spin-orbit interactions. The vibronic interactions are restricted to linear terms ($\Delta v = \pm 1$), and only spin-orbit interactions between $n\pi^*$ and $\pi\pi^*$ states are included. Spin-orbit interactions between like states are excluded on symmetry grounds. A schematic representation of the interacting states is depicted in Fig. 1. The two interaction pathways involve comparable matrix elements and energy denominators and thus may be expected to be of the same overall magnitude. Hence, interference between the two intensity-inducing pathways can be expected to occur. Just as in the calculations of Siebrand and Zgierski (12) for the b_{1g} mode, so here the interference may be expected to cause different intensity patterns in the vibrational progressions of the vibronically active modes in the singlet–triplet absorption and emission spectra. However, this point was not investigated in the current work.

In this study the zero-order description is to be interpreted as corresponding to the energies and wavefunctions of the vibronic levels in the absence of the vibronic and spin-orbit interactions. The calculations are undertaken for both pyrazine-d_0 and -d_4. The input parameters listed in Table 4 are for each isotope, respectively: the vibrational frequency of ν_{10a}, the vibronic coupling strength, the spin-orbit interactions, and the electronic state energy separations. The different spin sublevels are assumed to be orthogonal. In the calculations one set of input parameters was used for each isotopic species. In particular, this meant that the same zero-order vibrational frequency and vibronic coupling strength were used for both the singlet and triplet states. Furthermore, the vibrational frequencies and coupling strengths for the two isotopic species have been constrained to conform with the Teller–Redlich product rule (37) and with Herzberg-Teller theory (36). Of the electronic state separations only one, namely $E_{t't}$ (where s',t' and s,t refer to the upper and lower singlet and triplet states, respectively, here $^{1,3}B_{2u}$ and $^{1,3}B_{3u}$), was not previously directly, experimentally determined. It is used as a parameter to achieve agreement with the observed singlet–triplet absorption spectra. Apart from the spin-orbit coupling strength and the separation of the triplet states, the input parameters were taken almost without change from previous calculations of Chappell and Ross (14) carried out for the singlet state vibronic coupling.

The calculated results are presented in Table 5. The observed frequencies of ν_{10a} in the triplet state listed in the table were determined from the assigned sequence bands in the absorption spectra. In view of the fact that for each isotope agreement is sought between the calculated results, which depend essentially on five input parameters, and the observed results, consisting of the energies of the first three vibrational quanta in the excited singlet state, one or more vibrational quanta in the triplet state, and two state energy separations (ΔE_{st} and $\Delta E_{s't}$), the calculations may be seen as unique. Furthermore, whereas two different sets of observed results are included for the two isotopes, the input parameters for the two isotopes are not independent. The vibrational frequencies are related by the product rule

$$\frac{\nu_{10a}(d)}{\nu_{10a}(h)} = \sqrt{\left(\frac{m_h I_z(d)}{m_d I_z(h)}\right)}$$

where the I_z are the moments of inertia about the z axis, and the m the masses of the isotopic molecules; and the vibronic coupling strengths are related by Herzberg–Teller theory (36)

$$\frac{V_h}{V_d} = \sqrt{\left(\frac{\nu_{10a}(h)}{\nu_{10a}(d)}\right)}$$

Very good overall agreement is achieved for both isotopes when the $^3B_{2u}$ states are located some 4600 cm^{-1} above the lowest triplet states. This is considerably less than the 10 000 cm^{-1} or more obtained in the majority of theoretical determinations of the electronic state energies, but it does agree with the location of a triplet state seen in the electron energy-loss spectrum (34).

The magnitude of the spin-orbit interaction was chosen by comparison of the calculated emission intensity of the transition in which one quantum of ν_{10a} is excited in the ground state with the observed intensity of this transition in the phosphorescence in mixed crystals of pyrazine in benzene (8). The experimentally measured oscillator strengths (1) for the various singlet–singlet and singlet–triplet absorptions are marked in Fig. 1. From the observed band heights in the phosphorescence spectrum (8) the oscillator strength for the transition $10a_1^0$ was estimated to be about 5×10^{-10}. The oscillator strength of the origin band in absorption has been measured to be 1.4×10^{-8} (26). For a spin-orbit coupling strength of 4 cm^{-1} a calculated oscillator strength equiva-

TABLE 5. A comparison of the calculated and observed frequencies (cm^{-1}) of the members of the ν_{10a} vibrational progressions in the singlet and triplet absorption spectra

	$^1B_{3u}$			$^3B_{3u}$	
	Calcd.	Obsd.[a]		Calcd.	Obsd.
Pyrazine-h_4					
ν_{10a}	384	383		254	254
$2\nu_{10a}$	831	823		660	
$3\nu_{10a}$	1308	1306		1091	
$\Delta E_{s's}$	6963	6963	ΔE_{st}	4056	4056
Pyrazine-d_4					
ν_{10a}	292	296		191	194
$2\nu_{10a}$	630	626		492	488
$3\nu_{10a}$	993	987		818	
$\Delta E_{s's}$	6831	6830	ΔE_{st}	4051	4055

[a]Reference 1.

Can. J. Chem. Downloaded from www.nrcresearchpress.com by 203.198.23.82 on 09/08/12
For personal use only.

TABLE 6. Input parameters (cm^{-1}) for the $b_{2g}(\nu_4$ and $\nu_5)$ vibronic coupling calculations respectively: the vibrational frequencies; the $B_{3u}\cdot\cdot B_{1u}$ vibronic coupling strengths; the $n\pi^*\cdots\pi\pi^*$ spin-orrbit interaction; and the separations between the electronic states

	ν_4	ν_5	V_4	V_5	V_{so}	$\Delta E_{t't}$	ΔE_{st}	$\Delta E_{s't}$
Pyrazine-h_4	660	845	1050	6000	10	8700	4000	24 000
Pyrazine-d_4	580	730	950	575	10	8700	4000	24 000

lent to that observed is obtained. Because of the relatively large errors associated with the estimates of the oscillator strengths, no allowance was made for the fact that the observed results referred to both vapour and mixed crystal. Furthermore, the comparison drawn between the calculated and observed results is deemed valid since it was shown through dynamic studies of microwave-induced delayed phosphorescence that the phosphorescence is very largely polarized $B_{1u}(z)$ (Fig. 1), and that the radiative rate is very much larger than the radiationless rate (30). It was also shown that the radiative rates for phosphorescence polarized along the other two axes are some one to two orders of magnitude smaller, but nevertheless much larger than the radiationless rates. Hence in the comparison with the phosphorescence, the radiationless transitions may be ignored in the model calculations. As a general point, it should be added that the calculated energies of the vibrational levels are not very sensitive to the magnitude of the spin-orbit interaction for values in the range of 4 cm^{-1}, and hence the magnitude of the spin-orbit interaction is not a critical factor insofar as the assignment of ν_{10a} and the location of the higher triplet state are concerned.

In vibronic coupling calculations of this type convergence of results with the number of zero-order states included in the calculation is always a problem. Here, the seriousness of the problem was checked by comparing the results of calculations for the cases where the maximum number of quanta was limited to 30 and 40. For the levels of concern to this study, and these include the low-lying vibrational levels of all four electronic states, convergence in energies was to better than 0.1 cm^{-1}.

(b) b_{2g} *Modes*

The activity of b_{2g} modes in the phosphorescence spectra has been experimentally observed. In the low-temperature phosphorescence spectra of pyrazine (and pyrazine-d_4) in the various hosts benzene, *p*-dioxane, and pyrazine (pyrazine-d_4), progressions in a ground state vibration with frequency of about 756 cm^{-1} (-d_4, 651) were noted (8, 29). According to the recent review of azine spectroscopy (1) the correct assignment is to the lower of the two frequencies of the b_{2g} modes, that is ν_4''. A relatively weaker band, particularly noticeable in the spectrum of pyrazine-d_4 in dioxane at 1.3 K, was assigned to ν_5''. Its frequency is 839 cm^{-1} (-h_4, 980). In the singlet–triplet absorption and phosphorescence-excitation spectra, no similar progressions involving ν_4' or ν_5' have been identified.

In the singlet absorption spectrum of pyrazine vapour, $^1B_{3u} \leftarrow {}^1A_g$, a progression in a 517 cm^{-1} frequency is evident. It is assigned as ν_4'. Analysis of the fluorescence obtained following SVL (single vibronic level) excitation of the bands at $0^0 + 517$ and at $0^0 + (2 \times 517)$ cm^{-1} indicate that in the ground state ν_4'' is 756 cm^{-1} (3). Of particular interest is the appearance of a band at $0_0 + 972$ cm^{-1} in the fluorescence following excitation of the former band. It is in approximate agreement with the ground state vibrational frequency of ν_5'', and suggests that, in accordance with theory, there is a rotation of the normal coordinate space of the b_{2g} modes upon electronic excitation. That is

$$[3] \quad Q_4' = cQ_4'' + dQ_5''$$

where the Q' and Q'' are the normal coordinates in the excited and ground states, respectively, and c and d are constants, such that $c^2 + d^2 = 1$.

The occurrence of odd members in the vibrational progressions of the b_{2g} modes in the phosphorescence spectra requires vibronic as well as spin-orbit coupling. In parallel with the model previously proposed for the b_{1g}-induced vibronic coupling, two equivalent routes are available: vibronic coupling between the two triplet states, $T_1(B_{3u})$ and $T_3(B_{1u})$, and with spin-orbit coupling between T_3 and $S_1(B_{3u})$; or spin-orbit coupling between T_1 and $S_3(B_{1u})$ and with vibronic coupling between the singlet states S_3 and S_1. A four-level model that incorporates these states and interactions is set up, but now includes two vibrational modes and not one as in the previous b_{1g} case. The vibronic coupling is induced by the two b_{2g} modes ν_4 and ν_5. A further important difference from the previous calculations concerns the very much larger energy separation of the two singlet states. It is about 20 000 cm^{-1} as compared to 7000 cm^{-1}. Finally, it should be noted that in distinction to the b_{1g} mode activity where normal coordinate rotation is absent since there is only one vibration of that symmetry representation, the normal coordinate rotation is of consequence for the b_{2g} modes. The Duschinsky effect contributes to asymmetry in the absorption and emission spectra, see above eq. [3], and must be included in the calculations. In our four-state and two-vibrational-mode model, it is automatically included.

The input parameters for the calculations are listed in Table 6, and the calculated and experimentally measured frequencies are presented in Table 7. In parallel with the approach used for the b_{1g} calculations, the same set of vibrational frequencies and coupling strengths was used for both singlet and triplet states. The requirements of conformity with the product rule and with Herzberg–Teller theory have imposed further restrictions on the choice of parameters for the two isotopes. Essentially, only five of the input parameters were allowed to be varied. They comprised the two vibrational frequencies, the two vibronic coupling strengths, and the triplet states (T_3–T_1) energy gap.

The magnitude of the spin-orbit interaction governs the intensities of the origin and the totally symmetric vibrational bands in the triplet absorption spectra, since it has been shown that these bands acquired their intensity by direct spin-orbit coupling with singlet state(s) of B_{1u} symmetry (30). It is assumed in these calculations that only S_3 is involved, solely on the basis that other B_{1u} states are energetically further removed. In consequence, very narrow limits can be

Can. J. Chem. Downloaded from www.nrcresearchpress.com by 203.198.23.82 on 09/08/12
For personal use only.

TABLE 7. A comparison of the calculated and observed frequencies (cm^{-1}) for quanta of the b_{2g} vibrations in the singlet and triplet absorption spectra

	$^1B_{3u}$			$^3B_{3u}$	
	Calcd.	Obsd.		Calcd.	Obsd.
Pyrazine-h_4					
ν_4	521	517[a]		296	295
$2\nu_4$	1047	1033[a]			659
$3\nu_4$	1576				
ν_5	823			813	
$\Delta E_{s's}$	20 148	~20 000[b]	ΔE_{st}	4132	4056
Pyrazine-d_4					
ν_4	465	456[a]		271	276
$2\nu_4$	932			539	
$3\nu_4$	1402				
ν_5	710			701	
$\Delta E_{s's}$	20 125	~20 000[b]	ΔE_{st}	4111	4055

[a]Reference 3.
[b]Reference 1.

TABLE 8. Intensity ratios for the two b_{2g} vibrations in absorption and emission

	Absorption					Emission			
	$^1B_{3u}$		$^3B_{3u}$			$^1B_{3u}$		$^3B_{3u}$	
	Calcd.	Obsd.	Calcd.	Obsd.		Calcd.	Obsd.[a]	Calcd.	Obsd.
Pyrazine									
$I(4_0^1)/I(5_0^1)$	11.6	—	19.4	—	$I(4_1^0)/I(5_1^0)$	3.2	~4	3.7	—
Pyrazine-d_4									
$I(4_0^1)/I(5_0^1)$	11.0	—	20.8	—	$I(4_1^0)/I(5_1^0)$	2.8	~3	3.3	—

[a]Reference 3.

placed on the range of values for V_{so}. It was found that V_{so} must lie in the range 5–15 cm^{-1} and, in analogy with the previous set of calculations carried out for ν_{10a}, that the calculated vibrational frequencies are insensitive to variations of V_{so} in this range. The best agreement with the measured intensity of the singlet–triplet absorption spectrum was obtained for a spin-orbit coupling of about 10 cm^{-1}.

The two energy gaps E_{st} (S_1–T_1) and $E_{s't}$ (S_3–T_1) are also known. The locations of the triplet and the two singlet states have been experimentally measured. The final choice of input parameters, Table 6, was obtained through comparison of the calculated and observed spectra. In particular, good agreement was sought with the frequencies of ν_4 in the singlet and triplet absorption spectra. Also, qualitative agreement was required with the relative intensities induced by the two b_{2g} modes, Table 8. The calculations show that in absorption the intensity ratios $I(4_0^1)/I(5_0^1)$ are so large that the bands 5_0^1 are accordingly weak and are not expected to be readily seen. On the other hand, in emission the ratios are much smaller. Some weak bands do appear in fluorescence (3) at frequencies corresponding to ν_5''. Their intensities relative to 4_1^0 are in agreement with the calculated ratios. The calculated results of Table 8 clearly illustrate the lack of mirror symmetry between the absorption and emission spectra.

In the calculation the maximum number of combined quanta for the two vibrations in each of the four electronic states was limited to 16. This resulted in two matrices of size 272 × 272. This ensured that for the low-lying vibrational states in each of the electronic states, convergence in their energies to better than 0.1 cm^{-1} was achieved.

In recent model calculations on the vibronic activity of the b_{1g} mode, some of the totally symmetric vibrations were included. Through this approach it was possible to reproduce some of the anomalies in the frequencies and intensities of those transitions involving the totally symmetric vibrations. Totally symmetric modes were not included in the calculation here. As the model already contains a large number of parameters it was argued that no justification existed to introduce further parameters by the inclusion of some of the totally symmetric modes, particularly since the number of relevant experimental observations is so limited.

Other alternative assignments of the hot bands, Fig. 2, were considered. In one, the case where the assignments of the $b_{1g}(\nu_{10a})$ and $b_{2g}(\nu_4)$ modes are interchanged was considered. To satisfy this alternative, the measured triplet state frequencies of ν_4 are required to be 91 and 120 cm^{-1} for pyrazine-h_4 and -d_4, respectively. As a general rule the vibrational frequency of the protonated species is expected to be larger than that of the deuterated species, suggesting that this alternative assignment for ν_4 cannot be correct. To check this conclusion further, calculations were undertaken in an attempt to match the totality of these triplet and the excited singlet state frequencies. No calculations were able to give

Can. J. Chem. Downloaded from www.nrcresearchpress.com by 203.198.23.82 on 09/08/12
For personal use only.

complete agreement, thus excluding this alternative assignment for the b_{1g} and b_{2g} modes in the triplet state.

6. Densities of states

The high-resolution studies on the $^1B_{3u}$–^1A_g fluorescence excitation spectrum of pyrazine allowed an estimate to be made of the density of triplet states in the region of the origin band (18). The estimate was considerably higher than the density of states calculated on the basis of the vibrational frequencies. However, because ground state frequencies were used for those vibrations whose excited state frequencies were unknown, it was argued that the calculated value must be viewed as an underestimate since, in general, excited state frequencies are less than their ground state counterparts. The assignments in this work of ν_4 and ν_{10a} in the triplet state to vibrations with very reduced frequencies relative to both the ground and excited singlet states has posed the question whether the incorporation of these frequencies in the calculation of the densities of states may lead to much better agreement with the density of states estimated from the counting of lines in the high-resolution spectra.

Using the Haarhoff approach (38), it was found that whereas the density of states at an excess energy above the triplet state of 4056 cm^{-1} is 26 cm using the ground state vibrational frequencies, it is almost an order of magnitude larger, 193 cm, when those of the triplet state frequencies that have been determined, and are listed in Table 3, are used to replace the corresponding ground state frequencies. In particular, this bears on ν_4 and ν_{10a}. The density of states value is larger than that determined in previous calculations and may go part of the way to providing an explanation for the discrepancy between the two different approaches to the estimation of the density of states. Furthermore, it should be noted that no allowance was made for anharmonicity in arriving at these estimates, that the anharmonicity may be very significant for the low-frequency vibrations, and that therefore the calculated density of states should be even larger. For the low-frequency vibrations large numbers of quanta may be involved. Thus, for example, for the vibrations ν_{10a} and ν_4 some 16 and 14 harmonic quanta, respectively, are required to match the triplet–singlet energy gap.

7. Isotope effect

It is of some interest to examine the individual contributions that the vibrations make to the overall measured isotope effect of about 154 cm^{-1} in both the singlet and triplet absorption spectra.

The isotope effect, Δ, is defined as the difference in transition frequencies for transitions between the vibrationless levels of the same two electronic states for two isotopic species,

$$[4] \quad \Delta = [\nu_0 + \tfrac{1}{2}\Sigma(\nu'_d - \nu''_d)] - [\nu_0 + \tfrac{1}{2}\Sigma(\nu'_h - \nu''_h)]$$

where the summations are over all the vibrations (ν' upper state and ν'' lower state), the subscripts h and d refer respectively to pyrazine-h_4 and -d_4, and ν_0 is the frequency separation between the minima of the two potential surfaces.

For the case of the one b_{1g} mode, one obtains by substitution

$$[5] \quad \Delta(b_{1g}) = \tfrac{1}{2}[\nu''_h(1 - R'') - \nu'_h(1 - R')]$$

where R' and R'' are the ratios of the vibrational frequencies, ν_d/ν_h, in the excited and ground states respectively. Now for the b_{1g} mode, the calculated values R' (0.7812) and R'' (0.7610) are almost the same. Assuming that they are the same and equal to R, the isotope effect is then given by

$$[6] \quad \Delta(b_{1g}) = \frac{\delta(h)}{2}(1 - R)$$

where $\delta(h)$ is defined as the decrease in frequency of the -h_4 isotope, $\delta(h) = \nu''_h - \nu'_h$. Substituting eq. [1] for the frequency decrease determined by perturbation theory, one obtains a relation between the isotope effect and the vibronic coupling strength,

$$[7] \quad \Delta(b_{1g}) = \frac{V^2}{\Delta E}(1 - R)$$

This shows that, provided the major part of the vibrational frequency reduction derives from vibronic coupling, eq. [7] holds and the isotope effect is inversely proportional to the energy separation of the coupled electronic states. For mode 10a this is the case. The isotope effect increases from 54 cm^{-1} for the singlet state absorption to 69 cm^{-1} for the triplet state absorption. There is a similar increase for mode 4 (26 to 43 cm^{-1}), although because there are two b_{2g} modes, eq. [7] does not apply for it.

It should be noted that modes 4 and 10a contribute 112 cm^{-1} to the isotope effect in triplet state absorption as compared to 80 cm^{-1} for singlet state absorption, out of a total isotope effect of about 154 cm^{-1}. This difference of 32 cm^{-1} must be accounted for by other vibrations. In this respect at least, the lowest excited singlet and triplet states do differ. However, since only a few of the triplet state vibrational frequencies are known, it is not possible at this time to identify the vibrations, nor is it possible to use the isotope effects to determine other instances of large vibronically induced frequency reductions. One vibration that may possibly qualify in this context is ν_{6b}.

8. Conclusions

The majority of theoretical calculations carried out over the past decade or two on electronic state energies of the singlet and triplet states of pyrazine have indicated significant variations in the energy separations of some singlet and triplet states of the same electronic configurations. Insofar as the relative vibronic coupling activity in the singlet and triplet electronic state manifolds is concerned, this is predicted to have some important ramifications. In particular, the b_{2g} modes are expected to be more vibronically active in the triplet ($^3B_{3u}$–^1A_g) than singlet ($^1B_{3u}$–^1A_g) state transitions because of reduced electronic state energy gaps. Analyses of the triplet absorption spectra in the hot band regions to the red of the electronic origins, for pyrazine and pyrazine-d_4 vapour, combined with vibronic coupling calculations support the prediction. The vibrational frequencies of ν_4 for pyrazine-h_4 and -d_4 in the triplet state have been determined, as well as the approximate location of the $^3B_{1u}$ state. The frequencies are less than in the excited singlet state, an indication of increased vibronic coupling resulting from the smaller energy gap.

On the other hand, the location of the $^3B_{2u}$ state following from the assignment of ν_{10a} in the triplet absorption spectra and from vibronic coupling calculations, is not in agreement with the theoretical calculations. The state lies below the $^3B_{1u}$ state, in complete analogy with the singlet state or-

Can. J. Chem. Downloaded from www.nrcresearchpress.com by 203.198.23.82 on 09/08/12
For personal use only.

dering. Furthermore, the triplet state energy gap ($^3B_{2u}$–$^3B_{3u}$), is smaller than the corresponding singlet state gap, a fact that is also in contradiction to the theoretical calculations. Of the three triplet states under discussion in this work only the $^3B_{3u}$ state lies below the $^1B_{3u}$ state in pyrazine vapour; both the $^3B_{2u}$ and $^3B_{1u}$ states are at higher energies.

Insofar as the calculated density of states at an energy corresponding to the vibrationless level of the $^1B_{3u}$ is concerned, the discrepancy with the observed value remains, but it is reduced because of the significantly smaller frequencies for ν_4 and ν_{10a}. Contributions from another triplet state to the vibrational density of states are excluded, at least insofar as the $^3B_{2u}$ and $^3B_{1u}$ states are concerned.

Acknowledgement

The help of A. Nwankwoala in the measurement of some of the spectra is gratefully acknowledged.

1. K.K. Innes, I.G. Ross, and W.R. Moomaw. J. Mol. Spectrosc. **132**, 492 (1988).
2. D.B. McDonald and S.A. Rice. J. Chem. Phys. **74**, 4893 (1981).
3. Y. Udagawa, M. Ito, and I. Suzuka. Chem. Phys. **46**, 237 (1980); Y. Udagawa, M. Ito, I. Suzuka, W. Siebrand, and M. Z. Zgierski. Chem. Phys. Lett. **68**, 258 (1979).
4. D.L. Narva and D.S. McClure. Chem. Phys. **11**, 151 (1975).
5. E.F. Zalewski, D.S. McClure, and D.L. Narva. J. Chem. Phys. **61**, 2964 (1974).
6. S.N. Thakur and K.K. Innes. J. Mol. Spectrosc. **52**, 130 (1974).
7. H. Hong and G. W. Robinson. J. Mol. Spectrosc. **52**, 1 (1974).
8. C. Marzzacco and E.F. Zalewski. J. Mol. Spectrosc. **43**, 239 (1972).
9. R. Schneider and W. Domcke. Chem. Phys. Lett. **150**, 235 (1988).
10. N. Heider and S.F. Fischer. Chem. Phys. **88**, 209 (1984).
11. J. Brickmann. Ber. Bunsen-Ges. Phys. Chem. **83**, 70 (1979).
12. W. Siebrand and M.Z. Zgierski. Chem. Phys. Lett. **67**, 13 (1979).
13. W.H. Henneker, A.P. Penner, W. Siebrand, and M.Z. Zgierski. J. Chem. Phys. **69**, 1884 (1978).
14. P.J. Chappell and I.G. Ross. Chem. Phys. Lett. **43**, 440 (1976).
15. G. Orlandi and W. Siebrand. J. Chem. Phys. **58**, 4513 (1973).
16. G. Fischer, S. Jakobson, and B. Scharf. Chem. Phys. **16**, 237 (1976).
17. K. Kamogawa and M. Ito. J. Mol. Spectrosc. **60**, 277 (1976); I. Suzuka, N. Mikami, and M. Ito. J. Mol. Spectrosc. **52**, 221 (1974).
18. W. Siebrand, W. L. Meerts, and D. W. Pratt. J. Chem. Phys. **90**, 1313 (1989).
19. J. Kommandeur. Adv. Chem. Phys. **70**, 133 (1987).
20. A. Amirav. Chem. Phys. **108**, 403 (1986).
21. G. Fischer and R. Naaman. Chem. Phys. **19**, 377 (1977).
22. F. Lahmani, A. Tramer, and C. Tric. J. Chem. Phys. **60**, 4431 (1974).
23. A. Frad, F. Lahmani, A. Tramer, and C. Tric. J. Chem. Phys. **60**, 4419 (1974).
24. J.L. Tomer, K.W. Holtzclaw, D.W. Pratt, and L.H. Spangler. J. Chem. Phys. **8**, 1528 (1988).
25. E. Villa, M. Terazima, and E.C. Lim. Chem. Phys. Lett. **129**, 336 (1986).
26. G. Fischer. Chem. Phys. Lett. **79**, 573 (1981).
27. K. Matsuzaki and T. Azumi. J. Chem. Phys. **69**, 3907 (1978).
28. S.L. Madej, G.D. Gillispie, and E.C. Lim. Chem. Phys. **32**, 1 (1978).
29. N. Nishi, M. Kinoshita, T. Nakashima, R. Shimada, and Y. Kanda. Mol. Phys. **33**, 31 (1977).
30. D.M. Burland and J. Schmidt. Mol. Phys. **22**, 19 (1971).
31. K.K. Innes and L.E. Giddings, Jr. Discuss. Faraday Soc. **35**, 192 (1963).
32. G.J. Small. J. Chem. Phys. **54**, 3300 (1971).
33. B. Sharf and B. Honig. Chem. Phys. Lett. **7**, 132 (1970).
34. I.C. Walker and M.H. Palmer. Chem. Phys. **153**, 169 (1991).
35. W.R. Wadt, W.A. Goddard III, and T.H. Dunning, Jr. J. Chem. Phys. **65**, 438 (1976).
36. G. Fischer. Vibronic coupling. Academic Press, London. 1984.
37. G. Herzberg. Molecular spectra and molecular structure. Vol. 2. Van Nostrand, New York. 1945.
38. P.C. Haarhoff. Mol. Phys. **7**, 101 (1963).

Can. J. Chem. Downloaded from www.nrcresearchpress.com by 203.198.23.82 on 09/08/12
For personal use only.

Thiophosgene monomer–dimer equilibria in perfluoroalkane solutions: spectroscopic and photophysical implications of self-association in the ground state

ANDRZEJ MACIEJEWSKI,[1] MARIAN SZYMANSKI,[2] AND RONALD P. STEER
Department of Chemistry, University of Saskatchewan, Saskatoon, SK S7N OWO, Canada

Received March 2, 1993

This paper is dedicated to Professor Gerald W. King on the occasion of his 65th birthday

ANDRZEJ MACIEJEWSKI, MARIAN SZYMANSKI, and RONALD P. STEER. Can J. Chem. **71**, 1548 (1993).

The S_2–S_0 absorption, emission, and emission excitation spectra of thiophosgene in a perfluoroalkane solvent have been measured as a function of the analytical concentration, C, of the solute. Strong evidence of the formation of van der Waals dimers at 10^{-4} M $< C < 10^{-1}$ M and of higher oligomers at $C > 10^{-1}$ M has been found. Variations in the absorption spectra at $C < 10^{-1}$ M have been analyzed successfully in terms of a single $2Cl_2CS \rightleftarrows (Cl_2CS)_2$ equilibrium, for which the value of K is $(5.0 \pm 0.4) \times 10^2$ M^{-1} at 295 K. The mole fractions of monomer and dimer have been calculated at each C, and have been used to construct the absorption spectrum of the dimer. Both the monomer and dimer have similar $S_0 \rightarrow S_1$ and $S_0 \rightarrow S_2$ absorption spectra, but the dimer has an oscillator strength that is about twice that of the monomer. The effects of self-aggregation on the S_2–S_0 emission and excitation spectra have been analyzed. Absorption by the dimer in the ultraviolet also leads to emission, but with a different quantum efficency compared with direct excitation of the monomer. The implications of these observations on the interpretation of the spectroscopy, photophysics, and photochemistry of thiophosgene in solution are assessed.

ANDRZEJ MACIEJEWSKI, MARIAN SZYMANSKI et RONALD P. STEER. Can. J. Chem. **71**, 1548 (1993).

On a mesuré les spectres d'absorption, les spectres d'émission et les spectres d'émission d'excitation S_2–S_0 du thiophosgène dans un solvant de type perfluoroalcane en fonction de la concentration analytique, C, du soluté. On démontre la formation des dimères de van der Waals à 10^{-4} M $< C < 10^{-1}$ M et la formation d'oligomères supérieurs à $C < 10^{-1}$ M. On a analysé, avec succès, les variations des spectres d'absorption à $C < 10^{-1}$ M en fonction d'un équilibre simple $2Cl_2CS \rightleftarrows (Cl_2CS)_2$, dont la valeur de K est de $(5{,}0 \pm 0{,}4) \times 10^2$ M^{-1} à 295 K. Pour chacune des concentrations, C, on a calculé les fractions molaires du monomère et du dimère et on les a utilisées pour établir le spectre d'absorption du dimère. Le monomère et le dimère ont les mêmes spectres d'absorption $S_0 \rightarrow S_1$ et $S_0 \rightarrow S_2$, mais l'amplitude d'oscillation du dimère est environ le double de celle du monomère. On a analysé l'influence de l'auto-agrégation sur les spectres d'émission et d'excitation S_2–S_0. L'absorption du dimère dans l'UV donne également un spectre d'émission mais avec un quantum d'efficacité différent si on le compare avec l'excitation directe du monomère. On a déterminé l'influence de ces observations sur l'interprétation de la spectroscopie, de la photophysique et de la photochimie du thiophosgène en solution.

[Traduit par la rédaction]

Introduction

The formation of dimers, trimers, and oligomers in solutions containing solutes that exhibit relatively strong specific interactions, such as hydrogen bonding or charge transfer, is well documented (1–8). van der Waals dimers and larger clusters of more weakly bound molecules can also be formed and can easily be isolated and studied in cold, supersonic expansions (9–13). Many such homomolecular (A_x) and heteromolecular (A_yB_z) systems have now been examined using both traditional and jet methods (1–17).

Despite the widespread occurrence of self-association, its influence on the photochemistry and photophysics of weakly interacting solutes in solution has been clearly delineated in a surprisingly small number of systems (3–7, 18–21). For example, the interpretation of the effects of self-association on the photochemistry and photophysics of hydrogen-bonding solutes is greatly complicated by the existence of multiple equilibria in which a rather large number of *n*-mers can participate (1, 3–6).

We have been studying the spectroscopy, photophysics, and photochemistry of compounds containing the thiocarbonyl (C=S) group for almost 20 years (22–25). Although mindful of the need to search for the effects of self-association, we have to date found no evidence of it in these systems. Recently we began to study the details of the photophysics of thiophosgene, Cl_2CS, in perfluoroalkane solvents. Unlike the thiocarbonyl-containing molecules we examined previously, we have found clear evidence for the existence of a monomer–dimer equilibrium in solutions of thiophosgene in perfluoroalkane solvents (26, 27).

Thiophosgene is an excellent potential model compound for multi-state photochemical and photophysical studies because it emits from all of its S_2 ($^1(\pi,\pi^*)$), S_1 ($^1(n,\pi^*)$), and T_1 ($^3(n,\pi^*)$) states and because it undergoes photodissociation from both S_1 and S_2 (22, 25, 26, 28–36). On the other hand, its spectroscopy and photophysics have been difficult to interpret because of the unexpected complexity of its S_2–S_0 spectra (33–36), the existence of a dark, weakly absorbing, excited state in the near uv (27), the low quantum yields of emission from S_1 and T_1 in solution (26), and the effects of self-association (26). Many of these problems have now been identified and solved. Moreover, we recently came to realize that the existence of ground state van der Waals dimers of Cl_2CS in solution might provide an avenue for examining the photophysics of a highly electronically excited, but weakly bound, simple dimeric system. We have been interested in exploring the photophysics of the excited electronic states of the Cl_2CS van der Waals dimer since our discovery of $2S_1 \rightarrow S_2 + S_0$ electronic energy pooling following pulsed

[1]Permanent address: Faculty of Chemistry, A. Mickiewicz University, Poznan, Poland.

[2]Permanent Address: Institute of Physics, A. Mickiewicz University, Poznan, Poland.

Can. J. Chem. Downloaded from www.nrcresearchpress.com by 203.198.23.82 on 09/08/12
For personal use only.

visible laser excitation of the vapor (37, 38). The mechanism of this process is essencially unexplored, but it must proceed via an electronically excited encounter complex. Thus the ability to from a $(Cl_2CS)_2$ van der Waals dimer in solution and excite it in a strong uv absorption band appears to be one potential means of obtaining further information about the partitioning of electronic energy among the monomeric dissociation products of the excited dimer. Our original intent was to try to accomplish this by synthesizing $(Cl_2CS)_2$ in a supersonic expansion. However, our failure to find bands associated with van der Waals dimer in the $S_2 - S_0$ fluorescence excitation spectrum of supersonically expanded thiophosgene forced us to abandon this experiment temporarily. Our recent observation of ground state dimer in perfluoroalkane soutions of Cl_2CS has now rekindled this interest.

To this end we have now characterized the monomer–dimer equilibrium of Cl_2CS in solution and have assessed its importance in interpreting the uv–visible spectra, photophysics, and photochemistry of this model compound. The general chemistry of this equilibrium is reported here, and forms the basis for the assessment of the effects of self-association on the photochemistry and photophysics of Cl_2CS and a future report of the photophysics of the S_2 dimer.

Experimental

The methods of purification of the thiophosgene solute and perfluoro-1,3-dimethylcyclohexane solvent and of preparation and degassing of the solutions have been previously described (26, 27). Solute concentrations were determined by two methods for calibration purposes. (*i*) A known pressure of pure Cl_2CS vapor ($P >$ 10 Torr (1 Torr = 133.3 Pa), measured with a Baratron pressure transducer) from a precalibrated volume was transferred quantitatively under vacuum into an accurately measured volume of solvent, thoroughly mixed and degassed. (*ii*) Weights of, first, the empty cell, then, in sequence, the cell containing pure degassed solvent and added solute, were measured accurately and the concentration calculated using the density of the pure solvent. The two methods agreed to within ±7%. Standard samples prepared in this way were used to construct calibration curves of absorbance vs. molar concentration for several wavelengths of interest. Initial concentrations of Cl_2CS in the perfluoroalkane solvent were then obtained routinely by measuring the absence of a freshly prepared degassed sample at a selected wavelength using pure solvent as a reference. A number of cells of various path lengths (10.0–0.0045 cm) connected to a common manifold enabled the same sample to be measured at various absorbances.

The equipment and the methods used to measure the absorption, emission, and emission excitation spectra have also been described in detail previously (26, 27, 36). Briefly, emission and excitation spectra were measured with a Spex Fluorolog 222 instrument using either the standard 450-W high-pressure Xe arc source or the expanded beam from a tunable dye laser. Both emission and excitation spectra were corrected for the spectral characteristics of the measuring system. The spectral correction curve for the former was extended to 900 nm using an Optronics Laboratories HTS-110 high-intensity standard of spectral irradiance. Excitation spectral corrections were accomplished by measuring the relative intensity of the source as a function of wavelength using a Rhodamine B quantum counter operating in its linear response range. The corner geometry method was used to avoid artefacts in the emission and excitation spectra due to high absorbances of the solutions (39). (Solutions whose absorbances in a 1-cm cell were as high as 10 could be examined without significant error.)

Photochemical decomposition products are formed in relatively large yield at excitation wavelengths < 280 nm in this system and were observed to absorb in a range that was coincident with the long-wavelength tail of the S_2–S_0 and the dark excited state absorptions. For this reason measurements of Cl_2CS concentration and molar extinction coefficient were always taken on freshly prepared samples. Thereafter absorption measurements at λ near λ_{max} were used only to monitor the extent of Cl_2CS photodecomposition during or after prolonged exposure to exciting light in the emission measurements.

Results and discussion

The electronic absorption spectrum of thiophosgene consists of two weak, broadly overlapping, transitions in the visible, assigned to singlet and triplet $n \rightarrow \pi^*$ promotions (26, 40), a strong, broad transition to a $^1(\pi,\pi^*)$ state in the near uv (34, 36, 41), a weak absorption that overlaps the long-wavelength tail of the $\pi \rightarrow \pi^*$ system tentatively assigned to a transition to a dark, doubly excited, $^1(n^0,\pi^{*2})$ state (27), and at least two additional unassigned strong features further to the blue in the quartz ultraviolet (41, 42). We have shown previously that excitation of Cl_2CS solutions in the visible produces weak red – near infrared emission from both the S_1 $^1(n,\pi^*)$ and T_1 $^3(n,\pi^*)$ states (26) and that excitation in the strong uv absorption band at $\lambda < 300$ nm results in the production of strong S_2 $^1(\pi,\pi^*) \rightarrow S_0$ fluorescence in the near uv – blue (35, 36). Analysis of the low-energy emission is complicated by the fact that the fluorescence and phosphorescence overlap strongly and are very weak, whereas analysis of the photophyics of the fluorescent $^1(\pi,\pi^*)$ state is complicated by the presence of a non-emissive state of only slightly lower energy (27) and the fact that its main nonradiative decay process in perfluoroalkane solution involves efficient crossing of a low (ca. 1450 cm^{-1}) barrier (36, 43).

Analysis of the spectroscopy, photochemistry, and photophysics of the entire system is further complicated by the self-association of the solute in solution (1–7, 17–21). Self-association can be detected in the absorption spectra only by a careful examination of changes in the apparent molar extinction coefficients, ε, as a function of wavelength over a wide range of concentrations.

We previously noted (26), qualitatively, that the shape of the visible absorption band only changes noticeably on its long-wavelength side on increasing the thiophosgene concentrations from ca. 10^{-4} M to ca. 1 M, that λ_{max} remains almost invariant, but that $\varepsilon(\lambda_{max})$ increases significantly at higher concentrations and, particularly, in the pure liquid compared with more dilute solutions. Changes in the uv absorption spectra with changing concentration are more dramatic, as shown in Fig. 1 where ε is plotted vs. log C for several different wavelengths. We define the "as measured" values of $\varepsilon = A/(Cl)$ in terms of the measured absorbance A, in a cell of length l, of a solution in which the analytical molar concentration of thiophosgene solute is C. Note that ε decreases with increasing C in the region of the dark excited state (DES) near 300 nm, increases with increasing C further to the blue near the maximum of the $\pi \rightarrow \pi^*$ transition (ca. 255 nm), but is relatively constant at 467 nm (λ_{max} of $S_1 \leftarrow S_0$) over the whole range of concentration up to ca. 0.1 M. No further changes in ε can be detected at $C \leq 5 \times 10^{-5}$ M, but very large differences may be noted between solutions of ca. 0.1 M concentration and the pure solute. Modest changes in the S_2–S_0 emission and emission excitation spectra are also observed when C varies from low ($<10^{-4}$ M) to high ($\sim 10^{-1}$ M) concentration (vide infra).

Can. J. Chem. Downloaded from www.nrcresearchpress.com by 203.198.23.82 on 09/08/12
For personal use only.

Can. J. Chem. Downloaded from www.nrcresearchpress.com by 203.198.23.82 on 09/08/12
For personal use only.

We attribute these observations to self-association of the thiophosgene solute in the perfluoroalkane solutions;

$$[1] \quad 2M \rightleftarrows D$$

$$[2] \quad D + M \rightleftarrows T \overset{M}{\rightleftarrows} Ol_1 \overset{M}{\rightleftarrows} Ol_2 \text{ etc.}$$

where M, D, T, and Ol represent monomer, dimer, trimer, and oligomer, respectively. We interpret the fact that the spectral and photophysical properties of the thiophosgene solutions are invariant with C at $C \lesssim 5 \times 10^{-5}$ M as indicating that the solute exists exclusively in monomeric form at these low concentrations. The large changes (not shown in Fig. 1) at $C > 10^{-1}$ M are attributed to the formation of trimers and higher oligomers. The fact that the spectroscopic and photophysical properties of the solutions of concentration 5×10^{-1} M $< C < 10^{-1}$ M can be analyzed in terms of a model that involves only two solute species, monomer and dimer (vide infra), is strong evidence that only one self-association equilibrium, eq. [1], is important in this intermediate concentration range.

If monomer–dimer equilibrium is the only important self-association process in solution and if both M and D absorb at the same wavelengths, then Dearden (44) and Ito (45) have shown that the mole fractions of monomer, α, can be found by measuring ε at various C using

$$[3] \quad \alpha_1 = \frac{(1 - Q)}{1 - (QC_1/C_2)^{1/2}}$$

$$[4] \quad Q = \frac{\varepsilon_1 - \varepsilon_M}{\varepsilon_2 - \varepsilon_M}$$

where the subscripts 1 and 2 indicate two different concentrations. Here ε_M is the molar extinction coefficient of the monomer alone, a quantity which must be determined independently. Values of ε_M can readily be found in our case by taking the limiting values of ε at low C. The equilibrium constant for the monomer–dimer equilibrium (eq. [1]) in dilute ideal solutions is given by

$$[5] \quad K = \frac{1 - \alpha}{2\alpha^2 C}$$

whereas the measured ε is related to ε_M and ε_D (the molar extinction coefficient of the dimer) by

$$[6] \quad \varepsilon = \varepsilon_M\alpha + \frac{1}{2}\varepsilon_D(1 - \alpha)$$

The most accurate values of α and K will be obtained at those wavelengths where the differences between ε_M and ε_D are greatest. For Cl_2CS in perfluoroalkane solvents this occurs in the 300–340 nm region where the DES absorption occurs most strongly, as shown in Fig. 2 and 3. Analysis of ε vs. λ data in the $330 \geq \lambda \geq 300$ nm region, for 11 concentrations of Cl_2CS such as those shown in Fig. 2, according to the above method yields the results for α and K as a function of C shown in Table 1. Note that α is independent of λ within experimental error and varies smoothly from 1.00 at $C \leq 3 \times 10^{-5}$ M to 0.085 at $C = 1.09 \times 10^{-1}$ M. The value of K is independent of C, with the possible exception of a slight apparent increase at concentrations greater than ca. 0.1 M. The average value of K at $C \leq 0.1$ M and a temperature of 295 ± 1 K is $(5.0 \pm 0.4) \times 10^2$ in units of M^{-1}. Similar though less precise results are obtained by using the ε vs. C data in other wavelength regions. The fact that α varies smoothly with changing C but that the value of K is independent of C indicates that the single monomer–dimer equilibrium, ideal solution, model adopted adequately describes the system, at least at $C \leq 0.1$ M.

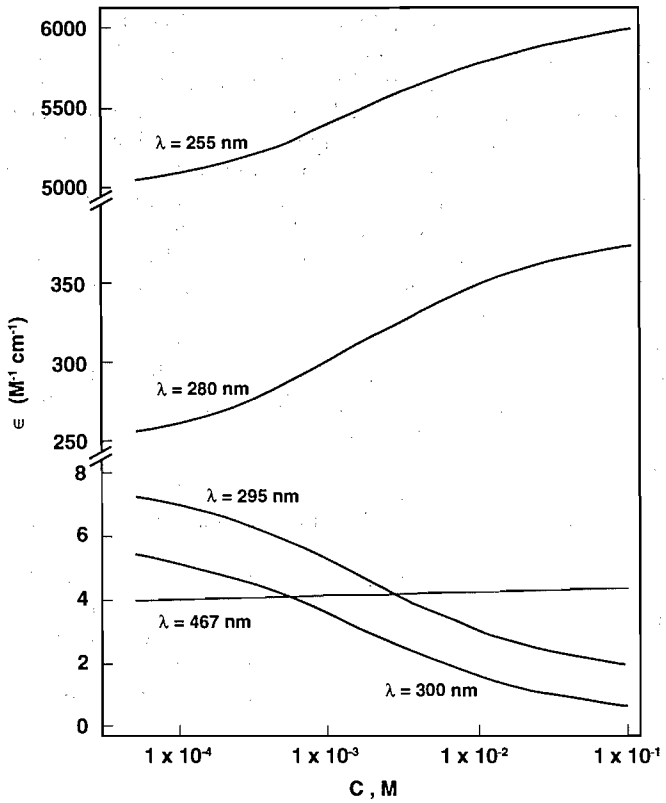

FIG. 1. Apparent values of the molar extinction coefficient for selected wavelengths within the $S_2 \leftarrow S_0$, DES $\leftarrow S_0$, and $S_1 \leftarrow S_0$ absorption bands as a function of the analytical concentrations of Cl_2CS in PF-1,3-DMCH.

With values of K and α as a function of C in hand, it is then possible to calculate the values of ε_D as a function of λ, using eq. [6], and to construct an absorption spectrum of the dimer. A representative set of data showing the consistency of the values of ε_D at a given λ over a wide range of C and α is given in Table 2. A complete set of values of ε_M and ε_D at 5- or 10-nm intervals over the range $350 \geq \lambda \geq 200$ nm is given in Table 3. For completeness, the values of $\varepsilon(\lambda)$ for the monomer have been further deconvolved into values of ε for the DES and the $^1(\pi,\pi^*)$ states using the method described in ref. 27. The results are displayed graphically in Fig. 3. Table 4 presents a representative set of $\varepsilon(\lambda)$ data obtained in the visible for various C, together with the results of a similar calculation of $\varepsilon_M(\lambda)$ and $\varepsilon_D(\lambda)$ using the accurate values of α obtained in the uv. Note from Tables 3 and 4 and Fig. 3 that the shapes of the monomer and dimer spectra are very similar, and that at all wavelengths, except those on the red wings of an absorption, the ratio $\varepsilon_D/\varepsilon_M$ is slightly greater than 2. Such a value of this ratio is consistent with the notion that the van der Waals dimer consists of two nearly independently acting chromophores each of which contributes about equally to the oscillator strength of the dimeric species. This observation is consistent with those obtained

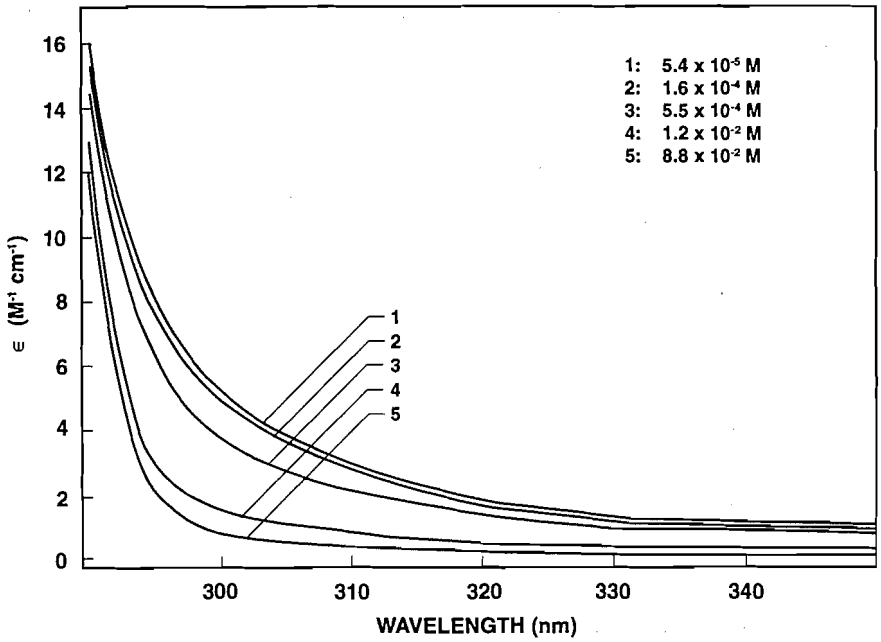

FIG. 2. Concentration effects in the long-wavelength tail of the uv absorption spectrum of Cl_2CS in PF-1,3-DMCH.

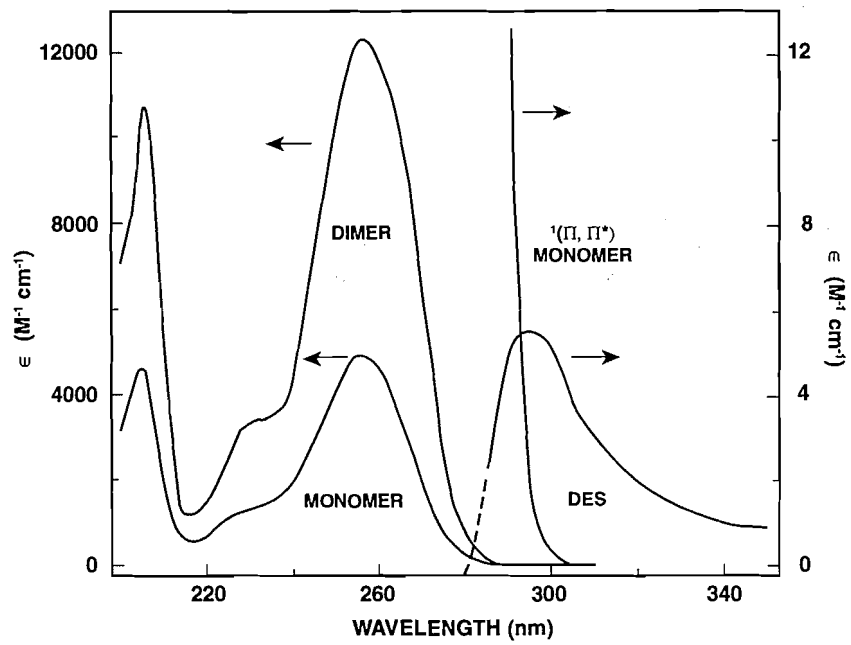

FIG. 3. Quantitative absorption spectra of Cl_2CS monomer and dimer in PF-1,3-DMCH.

in analogous systems in which a single weakly bound complex is formed from two identical monomeric molecules (1, 4–6, 14, 15, 46, 47).

With quantitative data available for the composition of the solutions as a function of C and for ε_M, ε_D, and ε_{DES} as a function of λ, it is then possible to more fully interpret the emission and emission excitation spectra of Cl_2CS in perfluoroalkane solutions in the $250 < \lambda < 500$ nm region. The DES of the monomer is dark ($\phi_f < 10^{-8}$) and contributes nothing to the emission although it absorbs weakly in the $290 < \lambda < 340$ nm range (27). No evidence of a comparable DES is found in the dimer. Changes in the uv–blue emission (Fig. 4) and near-uv emission excitation (Fig. 5) spectra with changing C can thus be attributed to changes both in the composition of the solution in the ground state and in the nature and fluorescence yields of the emitting species.

Note that the emission spectra (normalized in Fig. 4) remain almost invariant in the range $C < 0.1$ M, i.e., for solutions in which the solute composition changes from nearly pure monomer to largely dimer. We take this as evidence that either (*i*) the monomer and dimer have similar emission spectra, or (*ii*) the excited dimer dissociates to excited monomer, which is then the dominant fluorescent species over the entire $C < 0.1$ M concentration range. At $C \gtrsim 0.1$ M, a marked shift in the emission spectrum to shorter

Can. J. Chem. Downloaded from www.nrcresearchpress.com by 203.198.23.82 on 09/08/12
For personal use only.

TABLE 1. Mole percent of monomer, α_M', and equilibrium constant, K, as a function of the analytical concentration of thiophosgene, C, determined at several wavelengths in perfluoro-1,3-dimethylcyclohexane solution at room temperature

C (10^{-4} M)	α_M'[a] 330	325	320	315	310	305	300	Avg. α_M'	K[b] (M^{-1})
0.3	100	100	100	100	100	100	100	100	—
1.4	—	—	89	88	85	95	92	90	4.4×10^2
2.7	—	86	82	80	78	81	84	82	5.0×10^2
3.4	80	81	79	76	76	78	—	78	5.3×10^2
10.3	58	—	62	57	59	—	64	60	5.4×10^2
18.2	47	56	52	48	51	—	—	51	5.2×10^2
55.0	35	43	39	34	—	41	36	38	3.9×10^2
140	24	28	26	25	22	30	22	25	4.3×10^2
360	13	15	15	17	18	—	11	15	5.3×10^2
1090	10	7	8	11	8	—	8	8.5	5.8×10^2

[a]Wavelengths in nm at which α_M' was measured are given at the head of each column.
[b]Equilibrium constant for reaction [1] at 295 K. Avg. $K = (5.0 \pm 0.4) \times 10^2$ M^{-1}.

TABLE 2. Examples of calculated molar absorption coefficients of the dimer, ε_D, as a function of wavelength and mole percent of monomer, α_M', for solutions of Cl_2CS in perfluoro-1,3-dimethylcyclohexane at room temperature

λ (nm)	ε_D (M^{-1} cm^{-1}) α_M' = 80	50	25	20	15	9	Average ε_D (M^{-1} cm^{-1})
290	20	23	26	24	27	24	25 ± 4
285	158	156	153	148	147	174	156 ± 8
280	760	798	740	736	765	880	780 ± 30

TABLE 3. Molar extinction coefficients of the monomer, M, and dimer, D, of Cl_2CS in PF-1,3-DMCH in the uv range. The contributions of both the $S_2(\pi,\pi^*) \leftarrow S_0$ and DES $\leftarrow S_0$ bands to ε_M have been resolved

λ (nm)	ε_M[a]	$\varepsilon_M(\pi,\pi^*)$[a]	ε_M(DES)[a]	ε_D[a]	$\varepsilon_D/\varepsilon_M$
350	0.95	0	0.95	0	
340	1.2	0	1.2	0	
330	1.3	~0	1.3	~0	
320	1.9	$\sim 10^{-2}$	1.9	~0.01	
310	3.1	0.015	3.1	~0.1	0.03
300	5.6	0.4	5.2	0.5	0.09
295	7.5	2.0	5.5	2.9	0.39
290	16.5	11.3	5.2	25	1.51
285	62.8	60.7	2.1	156	2.48
280	250	250	~0	780	3.12
270	2020	2020	0	6200	3.07
260	4640	4640	0	11650	2.51
250	4020	4020	0	9940	2.47
240	1945	1945	0	4500	2.31
230	1295	1295	0	3350	2.59
220	700	700	0	1465	2.09
210	2005	2005	0	4950	2.47
200	3155	3155	0	7120	2.26

[a]Units: M^{-1} cm^{-1}.

wavelengths is taken as convincing evidence that the main emitting species at these higher concentrations are different from those at $C < 0.1$ M. Excited trimers and higher oligomers are again implicated. A complete analysis of the intensity and wavelength dependence of the emission on concentration is complicated by the need to account not only for the changing composition of the solution and the nature of the emitting species, but also for the different rates of self-quenching of the emitters. Such an analysis will be presented in a subsequent paper (48).

We have previously shown (35, 36) that the S_2–S_0 excitation spectrum of the monomer in perfluoroalkane solu-

Can. J. Chem. Downloaded from www.nrcresearchpress.com by 203.198.23.82 on 09/08/12
For personal use only.

TABLE 4. Examples of "as measured" molar absorption coefficients for Cl_2CS in perfluoro-1,3-dimethylcyclohexane at room temperature at several concentrations in the visible absorption range and their deconvolution into components due to monomer, ε_M, and dimer, ε_D

λ (nm)	$\varepsilon(M^{-1}\ cm^{-1})^a$ $\alpha'_M = 9$	$\alpha'_M = 30$	$\alpha'_M = 60$	$\varepsilon_M{}^b$ ($M^{-1}\ cm^{-1}$)	$\varepsilon_D{}^b$ ($M^{-1}\ cm^{-1}$)	$\varepsilon_D/\varepsilon_M{}^b$
458	4.38	4.26	4.05	3.95	8.80	2.23
467	4.60	4.43	4.12	4.00	8.98	2.25
488	4.00	3.83	3.54	3.50	7.55	2.16
513	2.28	2.20	2.06	2.01	4.52	2.25
535	0.89	0.87	0.84	0.83	1.81	2.18
545	0.59	0.57	0.55	0.55	1.18	2.15
560	0.22	0.23	0.21	0.21	0.45	2.14

[a]"As measured." See text.
[b]Determined from the complete data set for a larger number of concentrations.

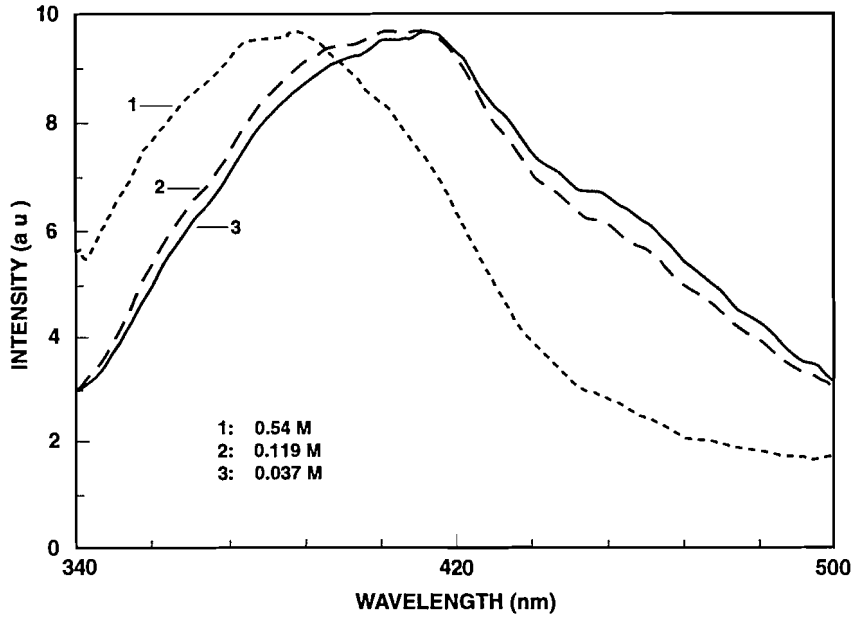

FIG. 4. Emission spectra of Cl_2CS in PF-1,3-DMCH for three samples of different analytical concentration normalized to the same peak emission intensity; $\lambda_{ex} = 295$ nm.

tion differs from the corresponding absorption spectrum because of the onset of a fast radiationless relaxation process (likely photodissociation) at modest E_{vib} in S_2 that causes abrupt fluorescence weakening at excitation wavelengths < 272 nm. Differences in the excited state behavior of the monomer and dimer must therefore be deduced by comparing the absorption and excitation spectra at each C in the 10^{-4}–10^{-1} M concentration range. In the present work, it is important to note that artefacts associated with the excitation of solutions of large absorbance are not responsible for the observed changes in the excitation spectra with changing thiophosgene concentration. Such artefacts have been avoided through the use of the corner geometry technique (vida supra). Thus the excitation spectra (normalized in Fig. 5) offer additional strong evidence not only that two (or more) different species are absorbing at thiophosgene concentrations in the $3 \times 10^{-4}\ M < C < 9 \times 10^{-2}\ M$ range, but also that the two absorbing species produce uv–visible fluorescence with different quantum efficiencies at different excitation wavelengths. We interpret the fact that the excitation spectrum retains a similar shape but shifts to slightly longer wavelengths at higher C as showing that the dimer is weakly bound, and that, like the monomer, excitation of the dimer in the red edge of its uv absorption band produces a higher quantum yield of emission than does excitation further to the blue. This interpretation is consistent with the notion that the dimer relaxes nonradiatively at higher excitation energies, but that the onset of this relaxation process occurs at a lower energy than that of the monomer. The nonradiative relaxation process in the excited dimer could involve dissociation of the dimer to two intact monomers, at least one of which is electronically excited. The spectra are also consistent with the requirement that the origin of the dimer S_2–S_0 absorption system should be located at a lower energy than that of the monomer. The dimer must be stabilized by at least a few kilojoules per mole, and the magnitude of the wavelength shift on the red edge of the excitation spectrum appears to be consistent with this stabilization requirement.

The dimer could in fact be stabilized by a number of weak

Can. J. Chem. Downloaded from www.nrcresearchpress.com by 203.198.23.82 on 09/08/12
For personal use only.

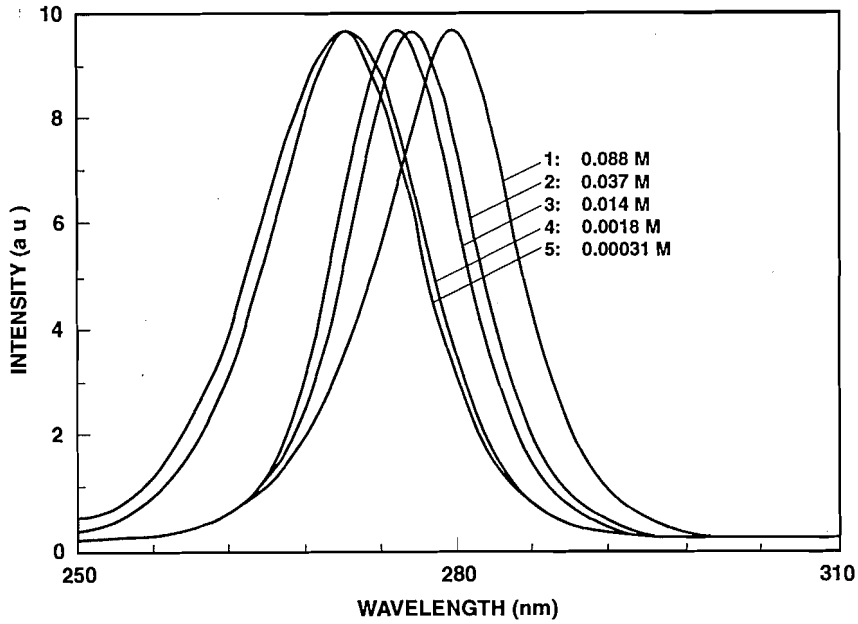

FIG. 5. Excitation spectra of Cl_2CS in PF-1,3-DMCH measured at λ_{em} = 410 nm for five samples of different analytical concentration (normalized to the same peak intensity).

electrostatic interactions. The small ground state electric dipole moment of Cl_2CS (μ = 0.28 D) (25) suggests that dipole-dipole interactions may only contribute in a minor way to the stabilization energy, and in this system stronger charge transfer and hydrogen-bonding interactions are not possible. Thus dispersive interactions are likely to provide the most important contributions to the binding energy in this species. The large polarizability of ground state Cl_2CS (10.2 $Å^3$) (25) is consistent with this view. A similar conclusion was reached recently in the case of van der Waals complexes of aromatic thiones with rare gas atoms (49), and supports in a general way the approach that Morokuma (5, 50) has taken in analyzing and describing intermolecular interactions. Theoretical calculations of the energies of van der Waals dimers of various possible geometries would be most useful for interpreting these experimental data.

Conclusions

Self-aggregation of the solute is an important phenomenon in perfluoroalkane solutions of thiophosgene at room temperature and must be accounted for in analyzing and interpreting the spectroscopy, photophysics, and photochemistry of this model system. At concentrations below ca. 5×10^{-5} M the solute is for practical purposes all in monomeric form, and at higher concentrations up to ca. 0.1 M only one self-aggregation process, formation of van der Waals dimer, need be considered. At still higher concentrations evidence of further self-aggregation can be found in both the absorption and uv–blue emission spectra.

Using a method developed by Ito (45) and by Dearden (44), the mole fractions of monomer at various concentrations have been determined and have been used to calculate the value of the equilibrium constant, $K = (5.0 \pm 0.4) \times 10^2\ M^{-1}$, for the monomer–dimer equilibrium at room temperature. Using these data the molar extinction coefficients of the dimer can be calculated as a function of wavelength and the absorption spectrum of the dimer constructed. Both monomer and dimer have similar spectra, but the dimer exhibits an oscillator strength which is ca. twice that of the monomer, a fact consistent with the notion that it contains two, almost independent, weakly interacting monomeric chromophores.

The effects of self-aggregation are also reflected in the emission and emission excitation spectra, which, among other things, show that absorption by dimer in the uv also leads to emission. Thus thiophosgene in perfluoroalkane solution presents an important opportunity to study the partitioning of electronic energy among several possible products following uv excitation of a weakly bound van der Waals dimer.

Finally we note that thiophosgene in perfluoroalkane solution appears to be a relatively uncomplicated system with respect to its self-aggregation in the ground state. The monomer can be studied in the absence of higher *n*-mers at low concentration, and relatively "clean" mixtures of monomer plus dimer are formed over a wide span of concentrations in the intermediate concentration ranges. Thus the thiophosgene system appears to be a simpler system to study than most hydrogen-bonding solutes, which generally self-aggregate in a more complex fashion.

Acknowledgements

We are grateful for support from the Natural Sciences and Engineering Research Council of Canada and the Centers of Excellence for Molecular and Interfacial Dynamics. A.M. also acknowledges partial financial support from Polish KBN Project no. 2-2617-91-02.

1. D.J.W. Grant and T. Higuchi. *In* Techniques of chemistry series. Vol. XXI. Wiley–Interscience, New York. 1990. Chaps. 4–6, and papers cited therein.
2. A.S.N. Murthy and C.N.R. Rao. Appl. Spectrosc. Rev. **2**, 69 (1968).
3. N. Mataga and T. Kubota. Molecular interactions and electronic spectra. M. Dekker, Inc., New York. 1970. Chaps. 6 and 7.
4. R. Foster (*Editor*). Molecular association. Vols. 1 and 2. Academic Press, London. 1975 and 1979.

Can. J. Chem. Downloaded from www.nrcresearchpress.com by 203.198.23.82 on 09/08/12
For personal use only.

5. H. Ratajczak and H.J. Orville-Thomas (*Editors*). Molecular interactions. Vol. 1. Wiley, New York. 1980.
6. H. Ratajczak and H.J. Orville-Thomas (*Editors*). Molecular interactions. Vol. 2. Wiley, New York. 1981.
7. V.G. Bakhisiev. Spectroscopy of intermolecular interactions. Nauka, Leningrad. 1972. (In Russian.)
8. C.N.R. Rao, S. Singh, and S. Senthilnathan. Chem. Soc. Rev. **5**, 297 (1978).
9. (*a*) J. Jortner, R.D. Levine, and S.A. Rice. Adv. Chem. Phys. **70**, 1 (1988); (*b*) F.G. Celii and K.C. Janda. Chem. Rev. **86**, 507 (1986).
10. R. Naaman. Adv. Chem. Phys. **70**, 181 (1988).
11. V. Vaida. Acc. Chem. Res. **19**, 114 (1986).
12. D.J. Nesbitt. Chem. Rev. **88**, 843 (1988).
13. J. Jortner, R.D. Levine, and S.A. Rice. Adv. Chem. Phys. **47**, (1981).
14. A. Taleb-Bendiab, K.W. Hillig II, and R.L. Kuczkowski. J. Chem. Phys. **94**, 6956 (1991).
15. E.J. Goodwin and A.C. Legon. J. Chem. Phys. **85**, 6828 (1986).
16. D. Birnbaum, D. Fichou, and B.E. Kohler. J. Chem. Phys. **96**, 165 (1992).
17. K. Nakashima and M. Koyanagi. Bull. Chem. Soc. Jpn. **55**, 3923 (1982).
18. N.J. Turro. Modern molecular photochemistry. Benjamin Cummings, Menlo Park, 1978.
19. J.B. Birks. Photophysics of aromatic molecules. Wiley Interscience, New York. 1970.
20. B. Stevens. Adv. Photochem. **8**, 162 (1971).
21. R.S. Davidson. Adv. Phys. Org. Chem. **19**, 1 (1983).
22. S.Z. Levine, A.R. Knight, and R.P. Steer. Chem. Phys. Lett. **29**, 73 (1979).
23. R.P. Steer. Rev. Chem. Intermed. **4**, 1 (1981).
24. V. Ramamurthy and R.P. Steer. Acc. Chem. Res. **21**, 380 (1988).
25. A. Maciejewski and R.P. Steer. Chem. Rev. **93**, 67 (1993).
26. M. Szymanski, A. Maciejewski, and R.P. Steer. J. Phys. Chem. **96**, 7857 (1992).
27. A. Maciejewski, M. Szymanski, and R.P. Steer. Chem. Phys. **165**, 101 (1992).
28. H. Okabe. J. Chem. Phys. **66**, 2058 (1977).
29. G.S. Ondrey and R. Bersohn. J. Chem. Phys. **79**, 175 (1983).
30. J.R. McDonald and L.E. Brus. Chem. Phys. Lett. **16**, 587 (1972).
31. D.A. Condirston, A.R. Knight, and R.P. Steer. Chem. Phys. Lett. **86**, 254 (1982).
32. M. Kawasaki, K. Kasatani, and H. Sato. Chem. Phys. **94**, 179 (1985).
33. D.J. Clouthier, A.R. Knight, R.P. Steer, and P.A. Hackett. Chem. Phys. **48**, 1 (1980).
34. T. Oka, A.R. Knight, and R.P. Steer. J. Chem. Phys. **66**, 699 (1977).
35. K.J. Falk, S.E. Sveinson, and R.P. Steer. Chem. Phys. Lett. **163**, 490 (1989).
36. M. Szymanski, S.E. Sveinson, and R.P. Steer. J. Phys. Chem. **95**, 5159 (1991).
37. D.J. Clouthier, P.A. Hackett, A.R. Knight, and R.P. Steer. J. Photochem. **17**, 319 (1981).
38. D.J. Clouthier, A.R. Knight, R.P. Steer, and P.A. Hackett. J. Chem. Phys. **72**, 1560 (1980).
39. A. Novak. Collect. Czech. Chem. Commun. **43**, 2869 (1978).
40. D.C. Moule and C.R. Subramaniam. J. Mol. Spectrsc. **48**, 336 (1973).
41. D.J. Clouthier and D.C. Moule. Top. Curr. Chem. **150**, 167 (1989).
42. R.H. Judge and D.C. Moule. J. Mol. Spectrosc. **80**, 363 (1980).
43. M. Ludwiczak, D.R. Latimer, and R.P. Steer. J. Mol. Spectrosc. **147**, 414 (1991).
44. J.C.Dearden. Can. J. Chem. **41**, 2683 (1963).
45. M. Ito. J. Mol. Spectrosc. **4**, 125 (1960).
46. B.D. Anderson, J.H. Rytting, and T. Higuchi. J. Am. Chem. Soc. **101**, 5194 (1979).
47. J.H. Lady and K.B. Whetsel. J. Phys. Chem. **68**, 1001 (1964).
48. M. Szymanski, A. Maciejewski, and R.P. Steer. Chem. Phys. In press.
49. M. Ludwiczak, H.K. Sinha, and R.P. Steer. Chem. Phys. Lett. **194**, 196 (1992).
50. K. Morokuma. Acc. Chem. Res. **10**, 294 (1977).

Can. J. Chem. Downloaded from www.nrcresearchpress.com by 203.198.23.82 on 09/08/12
For personal use only.

The a'' vibrations of singlet propynal[1]

J.K.G. WATSON
Herzberg Institute of Astrophysics, National Research Council of Canada, Ottawa, ON K1A 0R6, Canada

Received March 10, 1993

This paper is dedicated to Professor Gerald W. King on the occasion of his 65th birthday

J.K.G. WATSON. Can. J. Chem. **71**, 1556 (1993).

The a'' vibrational frequencies of all possible H and D isotopomers of propynal (HCCCHO) are shown to allow two solutions for the a'' harmonic potential constants. Equations relating the solutions are given. In the $\tilde{X}^1A'$ ground electronic state one solution can be rejected as chemically unrealistic, but in the $\tilde{A}^1A''$ excited electronic state the choice is more difficult. It is shown that a choice can be made on the basis of the observed cross-sequence intensities in the $\tilde{A}$–$\tilde{X}$ band system.

J.K.G. WATSON. Can. J. Chem. **71**, 1556 (1993).

On démontre que les fréquences de vibration a'' de tous les isotopomères H et D possibles du propynal (HCCCHO) permettent deux solutions pour les constantes du potentiel harmonique a''. On donne les équations donnant une corrélation des solutions. Dans l'état électronique fondamental $\tilde{X}^1A'$, on peut rejeter une solution sur la base qu'elle est chimiquement irréaliste, toutefois, dans l'état électronique excité $\tilde{A}^1A''$, le choix est plus difficile. On démontre qu'un choix peut quand méme être fait en se basant sur les intensités des séquences croisées du systèma de bandes $\tilde{A}$–$\tilde{X}$.

[Traduit par la rédaction]

1. Introduction

The $\tilde{A}^1A''$–$\tilde{X}^1A'$ electronic transition of propynal (1–5, footnote 2) is relatively weak, and therefore the vibronically-induced 1–0 and 0–1 bands in the out-of-plane a'' vibrations can be readily observed as in-plane-polarized type *ab* bands among the main type *c* bands of the system (3, 4, footnote 2). These observations, together with the vibrational spectrum (6, 7), make it possible to get a complete set of a'' fundamentals for both the $\tilde{X}$ and the $\tilde{A}$ electronic states of the four possible H and D isotopomers. Similar data are available for the $\tilde{a}^3A''$ electronic state (8, 9). Using these data, the harmonic potentials for the $\tilde{X}$, $\tilde{a}$, and $\tilde{A}$ states have been discussed by Lin and Moule (10) and by Williams (11). Neither of these papers mention the fact that there are two rather similar solutions for the out-of-plane harmonic potentials of the upper states that give identical calculated values for the a'' vibrational frequencies of all the H and D isotopomers. Thus other data are required to resolve this ambiguity, and the present paper is devoted to a discussion of this problem for the singlet state. There is a similar ambiguity for the ground state, but in that case the alternative solution can be ruled out as being chemically unreasonable.

The 1–1 sequence bands in the a'' modes are observed in the spectrum and, because of the change in a'' potential between the two states, cross-sequence bands of the type ν_k'–ν_l'' are also observed, where ν_k' and ν_l'' are different a'' modes in the $\tilde{A}$ and $\tilde{X}$ states. The intensities of these sequences and cross-sequences are determined by simple Condon vibrational overlap considerations, and it is shown here that the cross-sequence intensities in particular can be used to distinguish between the two possible a'' potentials for the $\tilde{A}$ state after the alternative solution for the $\tilde{X}$ state has been eliminated.

2. Theory of double solutions for potential constants

Least-squares fits of the out-of-plane vibrational frequencies of each electronic state were found to converge to one or other of two different solutions for the potential constants, depending upon the choice of the initial estimates. The two solutions yield identical values for the calculated frequencies of the various isotopomers. Such ambiguities result from multiple solutions of the algebraic relationships between the potential constants and the data, as discussed previously for XY_3 molecules (12). In general, such an ambiguity can only be resolved if it can be shown that these relations can be manipulated to give a sufficient set of equations that are **linear** in the potential constants. Such algebraic relations are useful for demonstrating the existence or otherwise of ambiguities, although they do not provide values of the potential constants that are optimised in a least-squares sense. The algebraic approach is best regarded as a way of understanding the results of a least-squares fit.

In the present case, the problem is to determine the 6 out-of-plane potential constants from a total of 12 frequencies, ν_{10}, ν_{11}, and ν_{12} of 4 isotopomers. The frequency data for one isotopomer gives us three relationships between the six potential constants F_{ij}, $i \le j$:

$$[1] \quad S_1 \equiv \lambda_{10} + \lambda_{11} + \lambda_{12} = \text{tr } \mathbf{FG}$$

$$[2] \quad S_2 \equiv \lambda_{11}\lambda_{12} + \lambda_{12}\lambda_{10} + \lambda_{10}\lambda_{11} = \frac{1}{2}\{(\text{tr } \mathbf{FG})^2 - \text{tr } (\mathbf{FGFG})\}$$

$$[3] \quad S_3 \equiv \lambda_{10}\lambda_{11}\lambda_{12} = (\det \mathbf{F})(\det \mathbf{G})$$

where $\lambda_k = (2\pi\nu_k)^2 = (2\pi c\omega_k)^2$ are the usual frequency parameters and $\mathbf{F}$ and $\mathbf{G}$ are the Wilson potential and kinetic matrices (13). Obviously, these three equations leave the six potential constants indeterminate. A second isotopomer gives a further three relationships with different $\boldsymbol{\lambda}$ and $\mathbf{G}$ matrices. However, the product [3] gives no new information, only a test of consistency. Thus the $\mathbf{F}$ matrix is still indeterminate. A third isotopomer will probably provide sufficient information to remove the indeterminacy, but there will probably still be ambiguities because there are multiple so-

[1]NRCC No. 34675.
[2]S.A. Edwards and J.E. Parkin. To be published.

Can. J. Chem. Downloaded from www.nrcresearchpress.com by 203.198.23.82 on 09/08/12
For personal use only.

TABLE 1. **B** matrix elements for the a'' modes of propynal[a,b,c,d]

Atom i	$B_{10,ic}$	$B_{11,ic}$	$B_{12,ic}$
H_1	0	ρ_{12}	0
C_2	0	$-(\rho_{12}+\rho_{23})$	ρ_{23}
C_3	$\rho_{34}\sigma \sin\theta_{546}$	ρ_{23}	$-\rho_{34}\sigma \sin(\theta_{234}-\theta_{345})-\rho_{23}$
C_4	$-\Sigma_{i\neq 4}B_{10,ic}$	0	$-\Sigma_{i\neq 4}B_{12,ic}$
O_5	$\rho_{45}\sigma \sin\theta_{346}$	0	$\rho_{45}\sigma \sin\theta_{234}$
H_6	ρ_{46}	0	0

[a]The atom numbering convention is shown in Fig. 1, and the coordinates are defined in the text before eq. [4].
[b]$\rho_{ij} = 1/r_{ij}$, $\sigma = 1/\sin\theta_{345}$.
[c]The chain 123 is assumed to be linear.
[d]The sign of $(\theta_{234}-\pi)$ is defined as positive for the chain 321 bending towards atom 5.

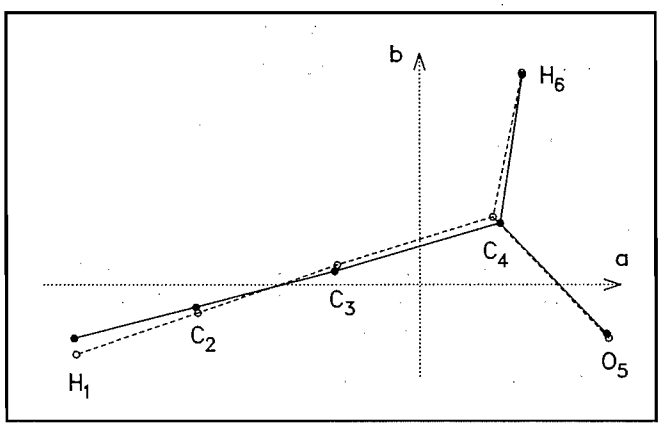

FIG. 1. Numbering convention for atoms of propynal. The structures of the $\tilde{X}$ state (full lines) and the $\tilde{A}$ state (broken lines) are each shown relative to their own principal axes of inertia.

lutions of the algebraic equations for **F**. These multiple solutions give identical frequencies for the various isotopomers, but the forms of the normal coordinates are different and so the solutions can distinguished by using data, such as vibration–rotation interaction parameters, that are sensitive to these forms.

The question of whether a unique solution can be obtained from frequency data reduces to the question of whether the equations [1]–[3], together with the corresponding equations for the other isotopomers, can be reduced to a set of independent linear equations equal to or greater in number than the number of potential constants. Such a set of linear equations has a unique solution.

In the present case, let us label the four isotopomers HCCCHO, DCCCHO, HCCCDO, and DCCCDO as HH, DH, HD, and DD, respectively. The atom numbering convention is shown in Fig. 1. The out-of-plane coordinates are taken as S_{10}, the angle of the C_4H_6 bond relative to the $C_3C_4O_5$ plane, S_{11}, the angle of the C_2H_1 bond relative to the $C_2C_3C_4$ plane, and S_{12}, the angle of the C_3C_2 bond relative to the $C_3C_4O_5$ plane. The corresponding **B** matrix elements are given in Table 1. From these, the **G** matrix elements are calculated according to

$$[4] \qquad G_{rs} = \sum_i m_i^{-1} B_{r,ic} B_{s,ic}$$

The hydrogen isotope changes in the **G** matrix are quite simple:

$$G_{rs}^{HD} = G_{rs}^{HH} + \delta_{r,10}\delta_{s,10}\Delta G_{10,10}$$

$$[5] \qquad G_{rs}^{DH} = G_{rs}^{HH} + \delta_{r,11}\delta_{s,11}\Delta G_{11,11}$$

$$G_{rs}^{DD} = G_{rs}^{HH} + \delta_{r,10}\delta_{s,10}\Delta G_{10,10} + \delta_{r,11}\delta_{s,11}\Delta G_{11,11}$$

where

$$[6] \qquad \Delta G_{10,10} = (m_D^{-1} - m_H^{-1})\rho_{46}^2$$
$$\Delta G_{11,11} = (m_D^{-1} - m_H^{-1})\rho_{12}^2$$

We now use these expressions in eqs. [1]–[3] for the four isotopomers. The linear sums [1] give one redundancy relation

$$[7] \qquad S_1^{DD} = S_1^{HD} + S_1^{DH} - S_1^{HH}$$

which is the linear sum rule (13), two unambiguous potential constants

$$[8] \qquad F_{10,10} = (S_1^{HD} - S_1^{HH})/\Delta G_{10,10}$$
$$F_{11,11} = (S_1^{DH} - S_1^{HH})/\Delta G_{11,11}$$

and the linear combination of **F** matrix elements tr (**FG**). Similarly, the quadratic sums give tr (**FGFG**), $(FGF)_{10,10}$ from the HD–HH difference, $(FGF)_{11,11}$ from the DH–HH difference, and then F_{12}^2 from the double D substitution. Finally, the products give one piece of information, det **F**. These eight data are to be solved for the **F** matrix. Extensive algebra shows that there is a fourth independent linear relation from which $F_{10,11}$ is determined unambiguously in terms of the original data by

$$[9] \qquad F_{10,11} = (G_{10,11}G_{12,12} - G_{10,12}G_{11,12}) \times \frac{[S_2^{HD}S_1^{DH} + S_2^{DH}S_1^{HD} - S_2^{HH}S_1^{DD} - S_2^{DD}S_1^{HH} - S_3^{HH} + S_3^{HD} + S_3^{DH} - S_3^{DD}]}{[S_2^{HH}(\det \mathbf{G}^{DD}) - S_2^{HD}(\det \mathbf{G}^{DH}) - S_2^{DH}(\det \mathbf{G}^{HD}) + S_2^{DD}(\det \mathbf{G}^{HH})]}$$

Can. J. Chem. Downloaded from www.nrcresearchpress.com by 203.198.23.82 on 09/08/12
For personal use only.

With this information the remaining equations can be manipulated to show that $(FG)^2_{10,12}$, $(FG)_{10,12}(FG)_{11,12}$, and $(FG)^2_{11,12}$ are determined unambiguously, where

$$[10]\quad \begin{aligned}(FG)_{10,12} &= F_{10,10}G_{10,12} + F_{10,11}G_{11,12} + F_{10,12}G_{12,12}\\ (FG)_{11,12} &= F_{11,10}G_{10,12} + F_{11,11}G_{11,12} + F_{11,12}G_{12,12}\end{aligned}$$

These together provide two possible solutions for $(FG)_{10,12}$ and $(FG)_{11,12}$. For either solution, we can combine together six linear equations to determine the six elements of **F** unambiguously. Thus there are at most two possible solutions $\mathbf{F}^{(1)}$ and $\mathbf{F}^{(2)}$, related to each other by the linear equations

$$[11]\quad \begin{aligned}F^{(2)}_{10,10} &= F^{(1)}_{10,10}\\ F^{(2)}_{11,11} &= F^{(1)}_{11,11}\\ F^{(2)}_{10,11} &= F^{(1)}_{10,11}\\ \text{tr}\,(\mathbf{F}^{(2)}\mathbf{G}) &= \text{tr}\,(\mathbf{F}^{(1)}\mathbf{G})\\ (F^{(2)}G)_{10,12} &= -(F^{(1)}G)_{10,12}\\ (F^{(2)}G)_{11,12} &= -(F^{(1)}G)_{11,12}\end{aligned}$$

If one solution **F** has been obtained by fitting the data, it is easy to obtain the other by solution of these equations, which are equivalent to

$$[12]\quad \mathbf{F}^{(2)} = \mathbf{Y}^{\mathrm{T}}\mathbf{F}^{(1)}\mathbf{Y}$$

where

$$[13]\quad \mathbf{Y} = \begin{bmatrix}1 & 0 & -2G_{10,12}/G_{12,12}\\ 0 & 1 & -2G_{11,12}/G_{12,12}\\ 0 & 0 & -1\end{bmatrix},\quad \mathbf{Y}^2 = \mathbf{E}$$

or

$$[14]\quad Y_{rs} = \delta_{rs} - 2(G_{r12}/G_{1212})\delta_{12s}$$

Substitution of these two **F** matrices into eqs. [1]–[3] for the four isotopomers shows that if one satisfies all these equations then so does the other. The basic reason for this is that

$$[15]\quad \mathbf{YGY}^{\mathrm{T}} = \mathbf{G}$$

for all four isotopomers. Thus it is not possible to distinguish these solutions on the basis of this isotopomeric frequency data. However, they may be distinguishable on the basis of data that depends on the form of the normal coordinates, and this is where the intensities of the sequence and cross-sequence bands are useful. The relationship between the two possible **L** matrices in the transformation $\mathbf{S} = \mathbf{LQ}$ is

$$[16]\quad \mathbf{L}^{(2)} = \mathbf{YL}^{(1)}$$

3. Sequence intensities

The vibration–rotation coordinate transformation between different electronic states is rather complicated because of the necessity of using different rotational Eckart conditions appropriate to the different geometries of the two states (14, 15). Using the lower-state coordinates as independent variables, we find that the upper-state normal coordinates Q'_k are given in terms of the lower-state normal coordinates Q''_l by

$$[17]\quad Q'_k = \sum_{i\alpha} m_i^{1/2} l'_{i\alpha k}\left[\sum_{\beta}\Lambda_{\alpha\beta}(r^e_{i\beta})'' - (r^e_{i\alpha})'\right] + \sum_{i\alpha\beta l} l'_{i\alpha k}\Lambda_{\alpha\beta}l''_{i\beta l}Q''_l$$

where the **l** matrices for the upper and lower states are the transformation matrices from mass-weighted Cartesian displacements to normal coordinates, given in terms of standard matrices (13) by

$$[18]\quad \mathbf{l} = \mathbf{m}^{-1/2}\mathbf{B}^{\mathrm{T}}(\mathbf{L}^{-1})^{\mathrm{T}}$$

and the matrix $\mathbf{\Lambda}$ is the Eckart rotation matrix (also called the "axis-switching matrix" (14) because it corresponds to a sudden switch from one Eckart system to the other) such that

$$[19]\quad [(\mathbf{r}^e)']^{\mathrm{T}}\,[\mathbf{m}(\mathbf{r}^e)'' + \mathbf{m}^{1/2}\mathbf{l}''\mathbf{Q}'']\Lambda^{\mathrm{T}}$$

is a symmetric matrix. $\mathbf{\Lambda}$ is a function of $\mathbf{Q}''$, and expanding it to first-degree terms we have the zero-order Eckart rotation matrix $\mathbf{\Lambda}^e$ such that

$$[20]\quad \mathbf{P} = [(\mathbf{r}^e)']^{\mathrm{T}}\,\mathbf{m}(\mathbf{r}^e)''(\mathbf{\Lambda}^e)^{\mathrm{T}}$$

is a symmetric matrix, and, from eq. [17], the expression for the dimensionless excited state normal coordinate $q'_k = (\gamma'_k)^{1/2}Q'_k$, where $\gamma_k = hcw_k/\hbar^2$, is

$$[21]\quad q'_k = (\gamma'_k)^{1/2}\sum_{i\alpha} m_i^{1/2}l'_{i\alpha k}\cdot\left[\sum_{\beta}\Lambda^e_{\alpha\beta}\,(r^e_{i\beta})'' - (r^e_{i\alpha})'\right] + \sum_l D_{kl}q''_l + O(q''^2)$$

where

$$[22]\quad \mathbf{D} = (\gamma')^{1/2}\{(\mathbf{l}')^{\mathrm{T}}\mathbf{\Lambda}^e\mathbf{l}'' + [(\mathbf{l}')^{\mathrm{T}} \times \mathbf{\Lambda}^e\mathbf{m}^{1/2}(\mathbf{r}^e)'']\,\mathbf{J}^{-1}\,[\mathbf{m}^{1/2}[(\mathbf{r}^e)']^{\mathrm{T}} \times \mathbf{\Lambda}^e\mathbf{l}'']\}\,(\gamma'')^{-1/2}$$

Here **J** is the matrix

$$[23]\quad \mathbf{J} = \mathbf{E}\,(\text{tr}\,\mathbf{P}) - \mathbf{P}$$

E being the unit matrix. The first term in eq. [21] represents the Franck–Condon shift of origin, and the second term is the Duschinsky rotation and rescaling of the normal coordinates. The main effect of $\mathbf{\Lambda}^e$ is to redistribute the intensity of the rotational lines within the bands (14), rather than on the total intensities of the bands. When the Eckart rotation is small, $\mathbf{\Lambda}^e$ can be replaced by the unit matrix and the second term in eq. [22] can be ignored.

In the harmonic approximation, the vibrational wavefunctions for the zero-point level and for the ν_k fundamental levels are

$$[24]\quad \begin{aligned}\psi(0) &= \pi^{-N/4}\exp\left(-\frac{1}{2}\sum_m q_m^2\right)\\ \psi(\nu_k) &= 2^{1/2}\pi^{-N/4}\,q_k\exp\left(-\frac{1}{2}\sum_m q_m^2\right)\end{aligned}$$

where N is the number of vibrational degrees of freedom. These functions are normalised in **q**-space. For non-totally-

Can. J. Chem. Downloaded from www.nrcresearchpress.com by 203.198.23.82 on 09/08/12
For personal use only.

TABLE 2. Observed and calculated a'' fundamental wavenumbers in the $\tilde{A}$ and $\tilde{X}$ electronic states of propynal (in cm^{-1})[a]

	Wavenumber							
	HCCCHO		DCCCHO		HCCCDO		DCCCDO	
	Obsd	Calcd	Obsd	Calcd	Obsd	Calcd	Obsd	Calcd
ν'_{10}	462.1	460.1	459.0	459.6	411.3	411.5	400.9	402.3
ν'_{11}	389.7	388.7	291.0	290.7	375.0	375.2	286.0	287.4
ν'_{12}	345.9	344.2	346.9	346.7	321.8	321.6	319.9	322.1
ν''_{10}	981.2	981.2	980.9	980.8	841.0	841.0	839.8	839.8
ν''_{11}	692.7	693.2	548.6	548.0	691.5	691.4	546.7	546.7
ν''_{12}	260.6	261.2	248.5	247.7	249.9	250.5	237.7	237.2

[a]The two solutions for the potential in each state give identical calculated wavenumbers.

symmetric vibrations such as the out-of-plane modes there is no Franck–Condon change of origin. Thus the Condon overlap integrals for the 0–0 band and the ν'_k–ν''_l sequence are obtained in the form

$$C(0\text{–}0) = \pi^{-N/2} \int (\det \mathbf{D})^{1/2} \cdot \exp\left\{-\frac{1}{2}(\mathbf{q}'')^{\mathrm{T}}(\mathbf{E} + \mathbf{D}^{\mathrm{T}}\mathbf{D})\mathbf{q}''\right\} \mathrm{d}^N q''$$

$$[25] \quad C(\nu'_k\text{–}\nu''_l) = 2\pi^{-N/2} \int (\det \mathbf{D})^{1/2} \sum_m D_{km} q''_m q''_l \cdot \exp\left\{-\frac{1}{2}(\mathbf{q}'')^{\mathrm{T}}(\mathbf{E} + \mathbf{D}^{\mathrm{T}}\mathbf{D})\mathbf{q}''\right\} \mathrm{d}^N q''$$

The factors $(\det \mathbf{D})^{1/2}$ are due to renormalisation of ψ' to $\mathbf{q}''$ space. The integrals can be evaluated (16) by transforming the exponent to a sum of squares and reducing the integral to a product of N standard one-dimensional integrals. Here we are interested in the ratio of the two integrals in eq. [25], which is found to be

$$[26] \quad \frac{C(\nu'_k\text{–}\nu''_l)}{C(0\text{–}0)} = \sum_m D_{km}(A^{-1})_{ml} = (X^{-1})_{kl}$$

Here $\mathbf{A}$ and $\mathbf{X}$ are the matrices

$$[27] \quad \mathbf{A} = \frac{1}{2}(\mathbf{E} + \mathbf{D}^{\mathrm{T}}\mathbf{D}) \qquad \mathbf{X} = \frac{1}{2}(\mathbf{D}^{\mathrm{T}} + \mathbf{D}^{-1})$$

The first form of eq. [26] involving the symmetric matrix $\mathbf{A}$ is more convenient for numerical calculations, whereas the second form involving the non-symmetric matrix $\mathbf{X}$ shows better the symmetry between the electronic states.

4. Results

The observed a'' fundamental frequencies of the four H and D isotopes of propynal in the $\tilde{X}$ and $\tilde{A}$ electronic states are given in Table 2. These are uncorrected for anharmonicity. In the calculations of the harmonic potential the $\tilde{X}$- and $\tilde{A}$-state structures shown in Fig. 1 were employed. The $\tilde{X}$-state structure is (17)

$$H_1C_2 = 1.055,\ C_2C_3 = 1.209,\ C_3C_4 = 1.445,$$
$$C_4O_5 = 1.215,\ C_4H_6 = 1.106\ \text{Å}$$
$$\angle H_1C_2C_3 = 180°,\ \angle C_2C_3C_4 = 178.4°,$$
$$\angle C_3C_4O_5 = 123.8°,\ \angle C_3C_4H_6 = 113.9°$$

where the $C_3C_2H_1$ chain is bent away from the O atom. The $\tilde{A}$-state structure is only approximate, based on the rotational constants and Franck–Condon considerations (3, 4):

$$H_1C_2 = 1.073,\ C_2C_3 = 1.238,\ C_3C_4 = 1.363,$$
$$C_4O_5 = 1.325,\ C_4H_6 = 1.091\ \text{Å}$$
$$\angle H_1C_2C_3 = 180°,\ \angle C_2C_3C_4 = 181.6°,$$
$$\angle C_3C_4O_5 = 122.8°,\ \angle C_3C_4H_6 = 118.1°$$

In this structure the $C_3C_2H_1$ chain is bent towards the O atom.

Least-squares fits of the potential constants to the frequencies in Table 2 converged fairly rapidly, and gave two well-defined solutions for each electronic state, depending on the choice of initial potential constants in the refinement. These solutions are related according to eq. [12], and give identical calculated frequencies, given in Table 2. The standard deviations are 0.6 cm^{-1} for the $\tilde{X}$ state and 1.7 cm^{-1} for the $\tilde{A}$ state. The sets of potential constants are given in Table 3.

For each electronic state, one solution is presumably the "correct" solution, and the other has no physical reality: it is merely an artefact of the shortage of information. Thus the alternative solutions in these kinds of situations are often physically or chemically ridiculous. That seems to be the case for solution 2 in the $\tilde{X}$ state, where the large value of $F_{12,12}$ and the large interaction constants $F_{10,12}$ and $F_{11,12}$ do not agree with "intuition" (i.e. experience with similar molecules). The excited state is rather different. In the first place, the solutions are much more similar to each other; and, in the second place, experience with stable ground-state molecules is a less reliable guide. Thus it is desirable to use additional data to choose between the two $\tilde{A}$-state solutions. The difference between the $\tilde{X}$ and $\tilde{A}$ states with respect to this ambiguity may be related to the different distributions of

Can. J. Chem. Downloaded from www.nrcresearchpress.com by 203.198.23.82 on 09/08/12
For personal use only.

TABLE 3. Alternative solutions for the a'' potential constants in the $\tilde{A}$ and $\tilde{X}$ electronic states of propynal (in aJ/Å^2)[a,b]

State				Solution 1	Solution 2
		S_{10}	S_{11}	S_{12}	S_{12}
$\tilde{A}$	S_{10}	0.0958(8)	0.0082(12)	0.0548(16)	0.1195(14)
	S_{11}		0.0895(6)	0.0806(20)	0.0633(12)
	S_{12}			0.3449(42)	0.4295(42)
$\tilde{X}$	S_{10}	0.3829(15)	0.0081(38)	−0.0205(45)	0.6408(38)
	S_{11}		0.2485(12)	0.0554(19)	0.3568(69)
	S_{12}			0.2033(15)	1.736(12)

[a]The solutions differ only in the final row and column of the **F** matrix.
[b]The standard deviations are given in parentheses in units of the last quoted decimal place.

TABLE 4. Observed sequence relative intensities[a] of HCCCHO and calculated values for the four possible pairs of harmonic potentials

	Obsd[b]	Solns 1–1	Solns 2–1	Solns 1–2	Solns 2–2
$\nu'_{10}-\nu''_{10}$	2.2	0.85	0.29	0.35	0.85
$\nu'_{10}-\nu''_{11}$		0.03	0.15	0.15	0.02
$\nu'_{10}-\nu''_{12}$		0.00	0.47	0.41	0.01
$\nu'_{11}-\nu''_{10}$		0.02	0.05	0.05	0.02
$\nu'_{11}-\nu''_{11}$	0.8_1	0.65	0.78	0.78	0.63
$\nu'_{11}-\nu''_{12}$	0.2_8	0.27	0.09	0.10	0.28
$\nu'_{12}-\nu''_{10}$		0.00	0.46	0.42	0.00
$\nu'_{12}-\nu''_{11}$	0.2_7	0.24	0.00	0.00	0,26
$\nu'_{12}-\nu''_{12}$	0.6_9	0.71	0.39	0.45	0.69

[a]Relative to the 0–0 band, corrected for the lower-state Boltzmann factor.
[b]Blanks indicate unobserved bands.

TABLE 5. Observed and calculated sequence relative intensities[a] for D-containing isotopes of propynal

	Relative intensity				
	DCCCHO		HCCCDO		DCCCDO
	Obsd[b]	Calcd	Obsd[b]	Calcd	Calcd[c]
$\nu'_{10}-\nu''_{10}$	1.9	0.86	1.3	0.48	0.78
$\nu'_{10}-\nu''_{11}$		0.01	0.0_2	0.26	0.00
$\nu'_{10}-\nu''_{12}$		0.00		0.17	0.10
$\nu'_{11}-\nu''_{10}$		0.00	0.3	0.32	0.03
$\nu'_{11}-\nu''_{11}$	0.8	0.78	0.9	0.56	0.62
$\nu'_{11}-\nu''_{12}$	0.1	0.13		0.01	0.27
$\nu'_{12}-\nu''_{10}$		0.00	0.0_6	0.06	0.05
$\nu'_{12}-\nu''_{11}$		0.12	0.0_3	0.09	0.29
$\nu'_{12}-\nu''_{12}$	0.7	0.84	0.6	0.80	0.61

[a]Relative to the 0–0 band, corrected for the lower-state Boltzmann factor.
[b]Blanks indicate unobserved bands.
[c]Observed intensities not available.

frequencies in the two cases. The $\tilde{X}$ state has a wide spread (721 cm^{-1}) between the highest and lowest a'' frequency, and as a result the spurious solution can be quite different from the correct solution. On the other hand, the $\tilde{A}$ state has an unusually narrow spread (116 cm^{-1}) of frequencies, and the spurious solution has to be fairly close to the correct solution.

Table 4 contains the calculated sequence intensities of the HCCCHO isotopomer for the four possible pairs of solutions. The Eckart rotation about the c axis was found to be

Can. J. Chem. Downloaded from www.nrcresearchpress.com by 203.198.23.82 on 09/08/12
For personal use only.

very small (0.47°), and essentially the same results were obtained by ignoring it. It is seen from Table 4 that the intensities come in pairs that are essentially indistinguishable experimentally. This follows from the facts that the Eckart rotation is small and that the matrix **Y** in eq. [16] is essentially the same in both electronic states. Thus if both upper- and lower-state solutions are changed to their alternatives, the **Y** matrices largely cancel out and the intensities are practically unchanged. However, the two pairs are quite different. One pair (1–1 and 2–2) gives strong ν'_{11}–ν''_{12} and ν'_{12}–ν''_{11} cross sequences, while the other pair (2–1 and 1–2) gives strong ν'_{10}–ν''_{12} and ν'_{12}–ν''_{10} cross sequences, together with a rather weak ν'_{10}–ν''_{10} sequence. The observed intensities clearly support the former.

Thus the cross-sequence intensities, in conjunction with the "intuitive" choice for the ground state, give 1–1 as the correct solutions for the $\tilde{X}$ and $\tilde{A}$ states. Calculated sequence and cross-sequence intensities for the D isotopes with these solutions are presented in Table 5. The agreement with observation is satisfactory for DCCCHO, but somewhat less good for HCCCDO. The latter isotopomer has an unusually small spread of frequencies (90 cm^{-1}), and the forms of its normal coordinates are particularly sensitive to the values of the potential constants. Thus accurate sequence and cross-sequence intensities of this isotope might be useful data for refining the potential constants.

5. Discussion

This work has shown that the ambiguity in the a'' harmonic potentials of the $\tilde{X}$ and $\tilde{A}$ states of propynal can be resolved by using the cross-sequence intensities together with the fact that one of the solutions for the ground state seems chemically unreasonable. The preferred solutions here are similar to those obtained by Williams (11), although he makes no reference to the alternative solutions. However, there seems to be some error in the results presented by Williams. For example, the calculated cross-sequence intensities in his Table IV are much weaker than those observed and calculated here. His intensities are correctly calculated from the $\mathbf{L}^{-1}$ matrices in his Table III. However, the latter do not seem correct, at least for the $\tilde{X}$ state. For example, the value of $F_{10,11}$ (his numbering) for the $\tilde{X}$ state calculated from

$$[28] \quad \mathbf{F} = (\mathbf{L}^{-1})^{\mathrm{T}} \boldsymbol{\lambda} \mathbf{L}^{-1}$$

does not agree with the value in his Table I, while $(G^{-1})_{10,11}$ (his numbering) calculated from

$$[29] \quad \mathbf{G}^{-1} = (\mathbf{L}^{-1})^{\mathrm{T}} \mathbf{L}^{-1}$$

seems to be about 10% too large.

In principle, the observed inertial defect Δ_0 of the $\tilde{A}$ state (5) might allow a distinction between the two possible harmonic potentials. The inertial defect depends on the out-of-plane potential through Coriolis coupling with in-plane vibrations (19–21). Thus a harmonic potential for the in-plane vibrations is required. To study this possibility, Δ_0 was calculated with both a'' harmonic potentials in conjunction with the a' potential of Williams (11). It was found that both gave Δ_0(calcd) = 0.20 $Å^2$ for HCCCHO, in quite good agreement with Δ_0(obsd) = 0.175 $Å^2$. Thus this test does not discriminate between the two solutions.

In formaldehyde it is well known (18) that the first excited singlet state is non-planar. The large drop in the $F_{10,10}$ potential constant in propynal to 25% of its ground-state value is a reflection of the same tendency. However, as a result of the conjugation in propynal the effect is delocalised into the ethynyl group, and $F_{11,11}$ drops to 36% of its ground-state value. The net result is that propynal in its $\tilde{A}$ state seems to be essentially planar, although possibly with a rather flat-bottomed out-of-plane potential. Evidence for the latter comes from the anharmonicity of the out-of-plane vibrations (3, 4), and also from the intensity of the relatively strong sequence band ν'_{10}–ν''_{10}.

Acknowledgment

I am grateful to Dr. J.C.D. Brand for information on the frequencies of DCCCDO.

1. J.A. Howe and J.H. Goldstein. J. Am. Chem. Soc. **80**, 4846 (1958).
2. J.C.D. Brand, J.H. Callomon, and J.K.G. Watson. Can. J. Phys. **39**, 1508 (1961).
3. J.K.G. Watson, Ph. D. thesis, University of Glasgow. 1962.
4. J.C.D. Brand, J.H. Callomon, and J.K.G. Watson. Discuss. Faraday Soc. **35**, 175 (1963).
5. J.C.D. Brand, W.H. Chan, D.S. Liu, J.H. Callomon, and J.K.G. Watson. J. Mol. Spectrosc. **50**, 304 (1974).
6. J.C.D. Brand and J.K.G. Watson. Trans. Faraday Soc. **56**, 1582 (1960).
7. G.W. King and D.C. Moule. Spectrochim. Acta, **17**, 286 (1961).
8. G.W. King and D.C. Moule. J. Mol. Spectrosc. **20**, 331 (1966).
9. C.T. Lin and D.C. Moule. J. Mol. Spectrosc. **37**, 280 (1971).
10. C.T. Lin and D.C. Moule. J. Mol. Spectrosc. **38**, 136 (1971).
11. D.R. Williams. J. Chem. Phys. **55**, 4578 (1971).
12. A.R. Hoy, J.M.R. Stone, and J.K.G. Watson. J. Mol. Spectrosc. **42**, 393 (1972).
13. E.B. Wilson, Jr., J.C. Decius, and P.C. Cross. Molecular vibrations. Dover Publications, New York. 1980.
14. J.T. Hougen and J.K.G. Watson. Can. J. Phys. **43**, 298 (1965).
15. I. Özkan. J. Mol. Spectrosc. **139**, 147 (1990).
16. T.E. Sharp and H.M. Rosenstock. J. Chem. Phys. **41**, 3453 (1964).
17. C.C. Costain and J.R. Morton. J. Chem. Phys. **31**, 389 (1959).
18. J.C.D. Brand. J. Chem. Soc. 858 (1956).
19. T. Oka and Y. Morino. J. Mol. Spectrosc. **6**, 472 (1961).
20. M.-F. Jagod and T. Oka. J. Mol. Spectrosc. **139**, 313 (1990).
21. J.K.G. Watson. J. Chem. Phys. **98**, 5302 (1993).

Can. J. Chem. Downloaded from www.nrcresearchpress.com by 203.198.23.82 on 09/08/12
For personal use only.

Predicting thermodynamic stability of diatomic dications: a case study of BeF^{2+}

MARCIN KOLBUSZEWSKI AND JAMES S. WRIGHT[1]

Ottawa–Carleton Chemistry Institute, Department of Chemistry, Carleton University, 1125 Colonel By Drive, Ottawa, ON K1S 5B6, Canada

Received February 10, 1993

This paper is dedicated to Professor Gerald W. King on the occasion of his 65th birthday

MARCIN KOLBUSZEWSKI and JAMES S. WRIGHT. Can. J. Chem. **71**, 1562 (1993).

General criteria are discussed for the prediction of thermodynamically stable diatomic dications (i.e., cations of +2 charge). For a diatomic AB^{2+}, the most useful quantity for this purpose is Δ, the difference in energy between the attractive channel with asymptote $A + B^{2+}$ and the repulsive channel with asymptote A^+ and B^+. Excluding noble gas compounds and using this measure, diatomic dications that may be thermodynamically stable include BeF^{2+}, MgO^{2+}, MgF^{2+}, $MgCl^{2+}$, and SiF^{2+}, as well as several other less likely combinations. The dication BeF^{2+} was selected for further analysis. *Ab initio* calculations show that the $X^2\Pi$ state of this ion is thermodynamically stable by 1.08 eV and undergoes an avoided crossing that causes the effective dissociation energy to be 2.07 eV. The excited state $A^2\Sigma^+$ is also very low-lying and predicted to be long-lived. The $X^2\Pi$–$A^2\Sigma^+$ band system is electric dipole allowed but very weak in intensity. Possible mechanisms of formation of BeF^{2+} are discussed.

MARCIN KOLBUSZEWSKI et JAMES S. WRIGHT. Can. J. Chem. **71**, 1562 (1993).

On discute de critères généraux permettant de prédire la stabilité thermodynamique de dications diatomiques (comme les cations de charge +2). Pour une entité diatomique AB^{2+}, la quantité la plus utile est le Δ, la différence d'énergie entre la canal attractif avec asymptote $A + B^{2+}$ et le canal répulsif avec asymptote $A^+ + B^+$. Excluant les composés des gaz rares et utilisant cette mesure, les dications diatomiques qui peuvent être thermodynamiquement stables incluent le BeF^{2+}, le MgO^{2+}, le MgF^{2+}, le $MgCl^{2+}$ et le SiF^{2+} ainsi que plusieurs autres combinaisons moins probables. On a choisi le dication BeF^{2+} pour d'autres études. Des calculs *ab initio* montrent que l'état $X^2\Pi$ de cet ion est thermodynamiquement stable par 1,08 eV avec une énergie de dissociation effective de 2,07 eV. L'état excité $A^2\Sigma^+$ est aussi très bas et sa vie devrait être longue. Le système de bande $X^2\Pi$–$A^2\Sigma^+$ est un dipôle électrique permis d'intensité très faible. On discute des mécanismes de formation possibles du BeF^{2+}.

[Traduit par la rédaction]

Introduction

The gas-phase study of molecular +2 ions (dications) is progressing rapidly, thanks to advances in charge-stripping mass spectrometry, electron impact spectroscopy, and double charge-transfer spectroscopy. Reviews of these techniques and the results obtained using them are given in refs. 1 and 2. A growing number of theoretical studies have also added to the understanding of potential curves and chemical bonding in dications. In homonuclear diatomics of the second period, so far only C_2^{2+} (3), N_2^{2+} (4), and O_2^{2+} (5) have been observed experimentally, but potential curves for ground and excited states are available for Be_2^{2+} (6), B_2^{2+} (7), and F_2^{2+} (8) from theoretical calculations. A variety of heteronuclear diatomics have also been studied. For example, NO^{2+} has been well characterized experimentally (9) and CNe^{2+} has been predicted theoretically to have a metastable ground state that could be observable (10).

To the best of our knowledge, however, no diatomic dication has yet been experimentally observed which is *thermodynamically stable,* where the minimum in the potential curve lies below the lowest dissociation products. At first sight this is not surprising in view of the strong repulsion between the monocations A^+ and B^+ in the diatomic AB^{2+}. However, in an important paper Frenking et al. (11) showed that the helium compounds $HeBe^{2+}$, HeB^{2+}, and HeC^{2+} are all thermodynamically stable by 20.1, 16.6, and 17.7 kcal/mol, respectively. The dications $NeBe^{2+}$ and $ArBe^{2+}$ were predicted to be even more stable (12), and the authors have suggested that these noble gas compounds could be observed experimentally. The bonding interaction was shown to be primarily electrostatic, arising from the polarization of the noble gas by the Be^{2+} ion.

In this paper we discuss the criteria for stability given by various authors, and consider whether diatomic dications that do not contain noble gases could also be thermodynamically stable. If such compounds do exist, they could be easier to synthesize than the noble gas compounds. Promising candidates for stability include BeF^{2+}, MgO^{2+}, MgF^{2+}, $MgCl^{2+}$, and SiF^{2+}. For the most part these dications have not been examined previously. From among these we have selected BeF^{2+} for a more thorough investigation. We use extensive *ab initio* calculations to analyze the potential curves of this molecular ion, and discuss its stability in ground and electronic excited states.

Thermodynamic stability of dications

The principles underlying the formation of diatomic dications are by now rather well understood. In a paper in 1955 that was remarkable for its foresight, Bates and Carson (13) showed that the dominant interactions in the dication of type AB^{2+} can be analyzed in terms of a repulsive channel **R** leading to A^+ and B^+, and an attractive channel **A** leading to $A + B^{2+}$. This pioneering work laid the foundation for many of the developments to follow.

For example, in a series of papers Radom and Gill and coworkers (14, 15) analyzed the dissociation of the dication AB^{2+} in terms of an avoided crossing (AC) model, where an interaction occurs between an attractive channel that correlates to $A + B^{2+}$, and a repulsive channel that correlates to $A^+ + B^+$. The location of the crossing between diabatic potential curves allows prediction of the location of the maximum in the metastable lower state. The extension of the

[1]Author to whom correspondence may be addressed.

Can. J. Chem. Downloaded from www.nrcresearchpress.com by 203.198.23.82 on 09/08/12
For personal use only.

Can. J. Chem. Downloaded from www.nrcresearchpress.com by 203.198.23.82 on 09/08/12
For personal use only.

TABLE 1. Δ values (eV) for dications of the second period[a]

	Li	Be	B	C	N	O	F	Ne
Li	70.3	12.8	19.8	19.0	24.2	29.7	29.6	35.6
Be		8.9	9.9	7.0	3.7	4.6	0.8	−3.4
B			16.9	13.9	10.6	11.5	7.7	3.6
C				13.1	9.9	10.8	7.0	2.8
N					15.1	16.0	12.2	8.0
O						21.5	17.7	13.6
F							17.6	13.4
Ne								19.4

[a]Δ = $IP_2(B) - IP_1(A)$. Ionization potential data are from ref. 18.

TABLE 2. Δ values (eV) for dications of the third period

	Na	Mg	Al	Si	P	S	Cl	Ar
Na	42.2	9.9	13.7	11.2	14.6	18.2	18.7	22.5
Mg		7.4	9.1	6.9	4.6	4.7	2.1	−0.7
Al			12.8	10.4	8.3	8.5	5.9	3.1
Si				8.2	5.9	6.0	3.4	0.6
P					9.2	9.4	6.8	4.0
S						13.0	10.4	7.6
Cl							10.8	8.1
Ar								11.9

TABLE 3. Δ values (eV) for dications of the second–third period

	Na	Mg	Al	Si	P	S	Cl	Ar
Li	41.9	9.7	13.4	11.0	14.3	17.9	18.4	22.2
Be	13.1	5.7	9.5	7.0	7.7	7.9	5.2	2.5
B	20.0	6.7	10.5	8.1	11.4	14.8	12.2	9.4
C	19.2	3.8	7.6	5.1	8.5	12.1	11.4	8.6
N	24.5	0.5	4.3	1.8	5.2	8.8	9.3	13.1
O	30.0	1.4	5.2	2.7	6.1	9.7	10.2	14.0
F	29.8	−1.1	1.4	−2.4	2.3	5.9	6.4	10.2
Ne	25.7	−6.5	−2.7	−5.2	−1.9	1.8	2.3	6.1

model (15) includes diabatic interactions and polarization (ACDCP model). This model neglects the chemical bonding along the potential curves, which may be particularly important for the A^+–B^+ interaction. The virtue of these models is that they require only the ionization potentials of the atoms and the polarizability of the atom A to make useful predictions about potential curves.

Further development along these lines by Bruna and Wright (7) extended these ideas to include higher lying electronic states with different dissociation limits, and a molecular orbital treatment of the bonding interactions. A related approach was used by Frenking et al. (11), who used an MO approach to discuss the chemical bonding in dications in terms of donor–acceptor interactions.

An alternative model, introduced by Hurley and Maslen (16), considers that the important interaction in AB^{2+} can be estimated by considering the potential curve of the isoelectronic neutral molecule, superimposed on the Coulomb repulsion potential of the monocations A^+ and B^+. This idea was also proposed in the original work of Bates and Carson (13). The model was successfully applied to O_2^{2+} and N_2^{2+} and properties were predicted for several other molecules, including F_2^{2+}. Recently an *ab initio* study of F_2^{2+} in the ground state confirmed the usefulness of this model (8). Although it would be expected to be most useful for homonuclear diatomics, it was also shown to give good predictions of potential curves in the case of CO^{2+} (17).

Because the second ionization potential of any atom is always significantly greater than the first, the dissociation channel for the homonuclear dication A_2^{2+} correlating with the monocations $A^+ + A^+$ must always lie below the asymmetric channel $A^{2+} + A$. Since the difference is in general much too large to be compensated for by any bonding interactions among the species, the consequence is that homonuclear dications will not be thermodynamically stable but can at best be metastable. We can therefore begin any search for absolute stability of diatomic dications by eliminating the homonuclear case. By extension of this argument, the heteronuclear case where the atoms lie close together in ionization potential is also unlikely to be thermodynamically stable.

Since we wish to predict stability for the case of the heteronuclear dication AB^{2+}, the single most useful criterion is Δ, the difference in energy between attractive and repulsive channels (13–15). This quantity, which is currently defined as Δ = $IP_2(B) - IP_1(A)$, was introduced by Bates and Carson (13) except with opposite sign. When Δ is positive but small, say less than 5 eV, then the combination of bonding interactions in the repulsive channel and charge-induced polarization in the attractive channel may be sufficient to cause the ground-state potential curve to lie below the lowest dissociation limit. When Δ is negative, implying that dissociation to monocations lies above the asymmetric dissociation to $A + B^{2+}$, then a thermodynamically stable ground state is essentially guaranteed. These two cases correspond to Figs. 5*b* and 5*a* in the discussion given by Frenking et al. (11). Since the calculation of Δ depends only on atomic IP data, we can tabulate values for all possible combinations of interest, in particular those that contain atoms from the second and third periods. In fact, these atomic data were also available to Bates and Carson, who therefore in 1955 could have given the same predictions that we present in this paper. What could not be done at that time, however, was to give an accurate molecular calculation that can verify the prediction for diatomics composed of atoms from the second or third periods.

Tables 1–3 show the value of Δ for combinations of atoms from the second period exclusively (Table 1), from the third period exclusively (Table 2), or mixed diatomics containing one atom from each period (Table 3). All IP data were taken from the compilation by Moore (18). For the second period, Table 1 shows that there is a generally decreasing trend in Δ, as expected, as the compound becomes more ionic. The homonuclear case has a minimum value of Δ = 8.9 eV for the Be_2^{2+} molecule, which is known to be metastable in its ground electronic state (6). Ionic compounds of Be are particularly interesting. Thus only $BeNe^{2+}$ has a negative Δ, consistent with the results of Frenking et al. that $BeHe^{2+}$ and $BeNe^{2+}$ are thermodynamically stable (11, 12). The next most likely possibility is BeF^{2+} with Δ = +0.8 eV. The dication CNe^{2+}, with Δ = +2.8 eV, is also a possibility. However, accurate calculations reported by Koch and Frenking (10) showed that CNe^{2+} lies above its lowest dissociation limit by 1.94 eV. All other possible combinations from Table 1 have Δ greater than 3 eV, and it is unlikely that any of them

TABLE 4. Dissociation channels for electronic states of BeF^{2+}

	Conf.	State		Conf.	State		Expt.[a]	CI[b]	El. states
Be^+	$2s^1$	^2S_g	F^+	$2p^4$	^3P_g	**I**	0.00	0.00	$1^2\Sigma^-$, $X^2\Pi$, $1^4\Sigma^-$, $1^4\Pi$
Be^{2+}	$1s^2$	^1S_g	F	$2p^5$	^2P_u	**a**	0.79	0.94	$A^2\Sigma^+$, $2^2\Pi$
Be^+	$2s^1$	^2S_g	F^+	$2p^4$	^1D_g	**II**	2.59	2.62	$2^2\Sigma^+$, $3^2\Pi$, $1^2\Delta$
Be^+	$2p^1$	^2P_u	F^+	$2p^4$	^3P_g	**III**	3.96	3.99	$3^2\Sigma^+$, $2,3^2\Sigma^-$, $4,5^2\Pi$ $2^2\Delta$, $1^4\Sigma^+$, $2,3^4\Sigma^-$, $2,3^4\Pi$
Be^+	$2s^1$	^2S_g	F^+	$2p^4$	^1S_g	**IV**	5.57	5.60	$4^2\Sigma^+$

[a]Values (eV) taken from ref. 18.
[b]In eV, relative to the MRCI(+Q) energy of Be^+ and F^+ of $-113.27496\ E_H$.

have sufficient bonding interactions to be thermodynamically stable.

Third-period dications (Table 2) show the expected stability of compounds of Ar, which were reported by Frenking et al. (12). Thus $MgAr^{2+}$ has the only negative entry for Δ, but $SiAr^{2+}$ is also very low-lying at 0.6 eV. For non-noble gas compounds, the most promising combination is $MgCl^{2+}$, at only 2.1 eV. Other combinations would appear to lie too high to be serious possibilities.

Table 3, which contains the mixed dications, shows a considerable number of negative entries. Four compounds of type XNe^{2+} have negative entries, where X = Mg, Al, Si, and P, and two others (S and Cl) have values near 2 eV. Among the non-noble gas compounds, MgF^{2+} and SiF^{2+} are both negative and thus predicted to be stable. The magnesium dications MgN^{2+} and MgO^{2+} are very low-lying at 0.5 and 1.4 eV, respectively, and may be stable. Other systems lying below 2 eV include AlF^{2+} and SiN^{2+}.

There are distinct advantages when trying to detect a dication to start from a stable neutral precursor, and an outstanding candidate from Table 1 is BeF^{2+}, which has the low Δ value of 0.8 eV. In addition, high-accuracy calculations can be performed for all diatomics composed of second-period atoms. We now focus on the electronic states of this particular dication.

Method of calculation

We used a flexible 6*s*4*p*2*d*1*f* basis set on Be and 6*s*5*p*2*d*1*f* on F, derived from the 10*s*6*p* primitive set of Gaussian-type orbitals given by Huzinaga (19). A 10*s*/5*s* contraction (20) and 5*p*/3*p* (21) contraction on Be was used to obtain a valence triple-zeta basis. In addition, the beryllium basis set was augmented with 2*d*1*f* polarization functions (α_d = 0.3, 0.05; α_f = 0.26) (22) and semidiffuse *sp* ($\alpha_{s,p}$ = 0.025) functions. On fluorine we used the 10*s*6*p*/5*s*4*p* valence triple-zeta basis of Dunning (20), with the addition of semidiffuse *s*,*p* functions ($\alpha_{s,p}$ = 0.074) (21) and 2*d*1*f* polarization functions (α_d = 3.107, 0.855, α_f = 1.917) (23).

The multireference single- and double-excitation (MRD-CI) method of Buenker and co-workers (24) was used to obtain total energies. The molecular orbitals of the ground state $X^2\Pi$ were used for the CI expansion. At the CI step, excitations from the two lowest σ MO's were excluded and the high-lying counterpart MO's were discarded, leaving 7 electrons to populate 79 MO's.

Thirty-six reference configurations were used for the two lowest $^2\Pi$ states and 24 reference configurations for the $^2\Sigma^+$ states. A configuration selection threshold of 5.0 microhartree (μE_h) led to CI spaces on the order of 10 000, selected from the generated space of 867 123 ($^2\Pi$) and 610 113 ($^2\Sigma^+$). Energies arising from the matrix diagonalization were extrapolated to zero selection threshold and subsequently corrected using the generalized Davidson (25) correction for higher-order excitations. These energies, denoted MRCI(+Q), were used to obtain potential curves and spectroscopic constants.

Calculations were carried out at 40 internuclear geometries spanning the range from 2.0 to 50.0 bohr. Additional calculations were carried out at 1000.0 bohr to establish the dissociation limits for the channels of interest. The calculated energy corresponding to the repulsive channels was lowered by 0.001 E_h, in order to account for the Coulomb repulsion still present at 1000 bohr.

Calculated MRCI(+Q) energy values were fitted to a polynomial function over the range R = 2.5–5.0 bohr with an rms deviation smaller than 0.1 millihartree. Vibrotational levels were calculated using the Numerov–Cooley method. The resulting $E_{v,J}$ levels were fitted to a standard spectroscopic expansion in the constants ω_e, $\omega_e x_e$, B_e, and α_e.

Radiative properties were calculated following the procedure described in ref. 26. All calculations were carried out in the subgroup C_{2v}. Transition moments were calculated using the length form of the dipole moment operator. The total transition moment squared $\Sigma R^2_{e'e''}$ is equivalent to $KR^2_{e'e''}$, where K takes into account all possible space and spin components of both states (for the $A^2\Sigma^+$–$X^2\Pi$ system, K = 4). The band strength is defined as

$$S_{v'v''} = K|\int \phi_{v'}(R)R_{e'e''}(R)\phi_{v''}(R)\mathrm{d}R|^2$$

where φ is the vibrational wavefunction and $R_{e'e''}$ is a polynomial fit to the calculated $R_{e'e''}$ values. The absorption oscillator strength is defined as

$$f_{v'v''} = \frac{2}{3}K'\Delta E_{v'v''}S_{v'v''}$$

where in this case $K' = \frac{1}{4}$ (i.e., for absorption from $X^2\Pi$), and $\Delta E_{v'v''}$ is in atomic units. For emission from the upper state $A^2\Sigma^+$, the Einstein coefficients (in s^{-1}) are given by

$$A_{v'v''} = 2.1419 \times 10^{10}K''\Delta E^3_{v'v''}S_{v'v''}$$

where $K'' = \frac{1}{2}$. Total fluorescence lifetimes involve the summation of $A_{v'v''}$ values over all v'', so that $\tau^{-1}_{v'} = \Sigma_{v''}A_{v'v''}$.

Results and discussion

Dissociation channels and electronic states

Information about the lowest dissociation channels of BeF^{2+} is summarized in Table 4. As discussed earlier, the

Can. J. Chem. Downloaded from www.nrcresearchpress.com by 203.198.23.82 on 09/08/12
For personal use only.

Can. J. Chem. Downloaded from www.nrcresearchpress.com by 203.198.23.82 on 09/08/12
For personal use only.

TABLE 5. Dominant electron configurations (near equilibrium) and term energies[a] for low-lying states of BeF^{2+}

State	Configuration	Channel	T_v (eV)
$X^2\Pi$	$\sigma^2\sigma^2\pi^3$	**I**	0.00
$A^2\Sigma^+$	$\sigma^2\sigma\pi^4$	**a**	1.60
$1^4\Sigma^-$	$\sigma^2\sigma^2\sigma\pi^2$	**I**	11.00
$1^2\Sigma^-$	$\sigma^2\sigma^2\sigma\pi^2$	**I**	11.35
$1^4\Pi$	$\sigma^2\sigma\sigma\pi^3$	**I**	11.97
$2^2\Pi$	$\sigma^2\sigma\sigma\pi^3$	**a**	12.71
$1^2\Delta$	$\sigma^2\sigma^2\sigma\pi^2$	**II**	13.77
$2^4\Pi$	$\sigma^2\sigma^2\pi^2\pi^*$	**III**	13.82
$3^2\Pi$	$\sigma^2\sigma^2\pi^2\pi^*$	**II**	14.17
$1^4\Sigma^+$	$\sigma^2\sigma\pi^3\pi^*$	**III**	14.52
$2^2\Sigma^+$	$\sigma^2\sigma^0\sigma\pi^4$	**II**	14.67

[a]Vertical excitation energy from the minimum of $X^2\Pi$ at 3.09 bohr.

lowest channel corresponds to the repulsive channel **I** correlating with Be^+ and F^+ in their ground states. The next channel **a** is the attractive channel at +0.79 eV, correlating with Be^{2+} + F in their ground states. The higher channels **II**, **III**, and **IV** correspond to $Be^+ + F^+$ in excited states. For this table the CI energy was calculated separately for the ions of Be and F. Therefore the energy of Be^+ and Be^{2+} is just the SCF energy, in the frozen core approximation. The energy of the first attractive channel **a** is overestimated at the MRCI(+Q) level by 0.15 eV, but the remaining channels agree with the experimental values to within 0.03 eV.

As shown in Table 4, channel **I** correlates with four states and channel **a** with two. The only common state for these two channels is $^2\Pi$, and it is the mixing between $^2\Pi$ states that is of greatest interest. The state $A^2\Sigma^+$ correlates with channel **a**, and therefore will be expected to be at least metastable.

The dominant configuration of the 10 lowest lying states is shown in Table 5. In this notation core orbitals (1σ and 2σ) are omitted, and the molecular orbitals 3σ,4σ,5σ and 1π,2π are designated $\sigma\sigma\sigma$ and $\pi\pi^*$, respectively. Thus the state $3^2\Pi$, which has configuration $3\sigma^24\sigma^21\pi^22\pi$, is designated $\sigma^2\sigma^2\pi^2\pi^*$, etc.

The electronic configurations of most interest are $\sigma^2\sigma^2\pi^3$, $\sigma^2\sigma\sigma\pi^3$ and $\sigma^2\sigma\pi^4$. The two former configurations belong to symmetry $^2\Pi$, whereas the latter is $^2\Sigma^+$. In $\sigma^2\sigma^2\pi^3$ the occupancy corresponds to filled $2s$,$2p_\sigma$ orbitals on F ($2p_\sigma$ lies on the bond axis), with three electrons in the $2p_\pi$ orbitals on F (perpendicular to the bond axis). This configuration is therefore ionic, and corresponds to Be^{2+} + F. The $\sigma^2\sigma\sigma\pi^3$ configuration has one σ-electron in $2p_\sigma$ on F and the other in $2s$ on Be; this configuration therefore has the covalent form $Be^+ + F^+$. For the configuration $\sigma^2\sigma\pi^4$, the second σ-MO corresponds essentially to $2p$ on F, so the best representation for this configuration is also the ionic form Be^{2+} + F. We will refer to these ionic and covalent configurations frequently in the discussion which follows.

Table 5 also shows the vertical excitation energies T_v, measured from the potential minimum in the ground electronic state. Only the state $A^2\Sigma^+$ is low-lying, with all other states lying higher than 10 eV above the ground state. This makes the discussion of the low-lying states very straightforward.

Potential energy curves

Potential energy curves for the various electronic states are shown in Fig. 1. Most of the potential curves are repulsive,

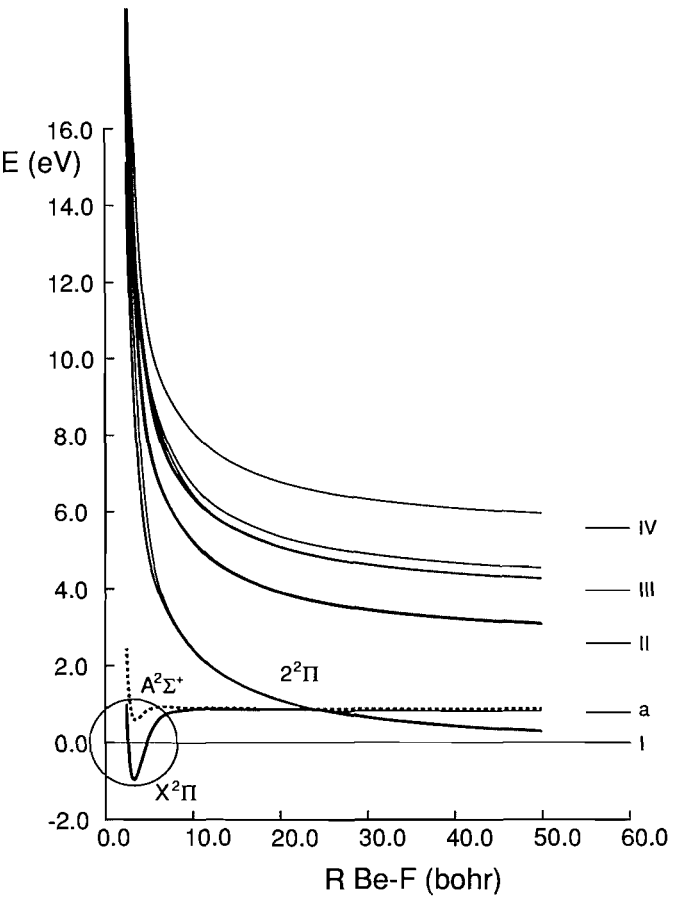

FIG. 1. Potential curves for the low-lying electronic states of BeF^{2+}. The dissociation energy of the five lowest channels is shown at the right.

including all those correlating with channels **II**, **III**, and **IV** (14 states, see Table 4). This is to be expected, since these states correlate with $Be^+ + F^+$. The repulsive states are dense and close-lying and cannot be clearly distinguished in the figure.

The ground state is $X^2\Pi$. This state shows an avoided crossing at long range with the excited state $2^2\Pi$. Most significant is the fact that the well depth in this state is such that the potential minimum, which occurs at R_e = 3.09 bohr, lies 1.08 eV below the lowest asymptote **I**. The BeF^{2+} dication is therefore thermodynamically stable. The avoided crossing, which occurs near R = 24 bohr, lies 0.99 eV above the lowest limit. The effective dissociation energy D_{eff} is 2.07 eV, measured from the potential minimum. The very broad shape of this dissociation barrier indicates that, except for vibrational levels near the very top of the barrier, the tunneling lifetime of the molecule in the ground electronic state is essentially infinite.

The $A^2\Sigma^+$ state is also bound relative to its own dissociation limit, which is channel **a**. This state is bound by 0.45 eV, and has its minimum at R_e = 3.23 bohr. Although this state is not formally thermodynamically stable, because of the presence of a lower lying dissociation limit, the coupling interaction between $A^2\Sigma^+$ and $X^2\Pi$ is probably weak except at large R. This means that lower vibrational levels in the excited state $A^2\Sigma^+$ could well be long-lived, so that spectral transitions between these two states could be observable.

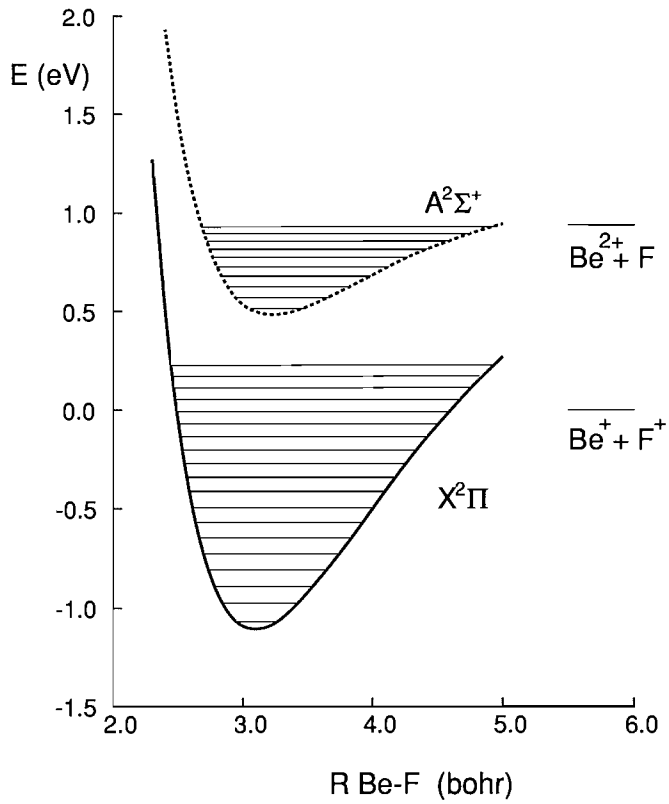

FIG. 2. Expanded view of the potential curves for the ground state $X^2\Pi$ and the lowest excited state $A^2\Sigma^+$, showing some of the bound vibrational levels for each state. The lowest dissociation limit is channel **I** and the next lowest is channel **a** (see Fig. 1).

The shapes of the two potential curves can be understood in terms of the dominant configurations in each region. Considering $^2\Pi$ states first, the attractive channel has the ionic configuration $\sigma^2\sigma^2\pi^3$ near the asymptotic limit. This configuration remains the dominant configuration in the region of the potential minimum for $X^2\Pi$. The solid curve that approaches channel **I** has the covalent configuration $\sigma^2\sigma\sigma\pi^3$. This configuration also describes the excited state $2^2\Pi$ at short R. Thus we have two diabatic potentials, one of which is attractive (ionic) and one of which is repulsive (covalent). These states interact weakly near 24 bohr so that an avoided crossing results, with the resulting potential minimum and effective barrier in the adiabatic potential curve for the ground state $X^2\Pi$. The excited state $A^2\Sigma^+$, with ionic configuration $\sigma^2\sigma\pi^4$, correlates directly to attractive channel **a** and thus has the simple Morse-like form, with a shallow potential minimum.

This interpretation of the charge distribution in each state was obtained by analysis of the configurations contributing to the CI wave function. The interpretation was checked by performing a Mulliken population analysis. At the potential minimum of the ground state, we obtained partial charges of +1.75 on Be and +0.25 on F, confirming that the interaction is essentially ionic, of the form Be^{2+} + F.

The shapes of the two lowest states are shown over a smaller range in Fig. 2. Here it can be seen that $X^2\Pi$ has 15 vibrational levels that lie below the asymptotic limit (channel **I**). The potential well in the excited state $A^2\Sigma^+$ also supports about 10 bound vibrational levels.

TABLE 6. Spectroscopic constants of bound states of BeF^{2+} and LiO

Species	BeF^{2+}		LiO[a]	
parameter	$X^2\Pi$	$A^2\Sigma^+$	$X^2\Pi$	$A^2\Sigma^+$
T_e (eV)	0.00	1.59	0.00	0.29
R_e (bohr)	3.09	3.23	3.20	3.02
D_e (eV)	1.08	0.45	3.59	—
D_{eff} (eV)	2.07	—	—	—
ω_e (cm^{-1})	717	497	852	867
$\omega_e x_e$ (cm^{-1})	9.7	14.0	12.5	6.7
B_e (cm^{-1})	1.04	0.94	1.20	1.35
α (cm^{-1})	0.019	0.029	0.015	0.020

[a]Values taken from Huber and Herzberg (27).

Spectroscopic constants for the two-lying states are shown in Table 6, along with the constants for the isoelectronic neutral molecule LiO (27). Since the LiO molecule is polarized in the form Li^+O^-, the electron configurations are analogous to those in BeF^{2+} and the ground state is $^2\Pi$ in each case. According to Partridge et al. (28), the reason that $^2\Pi$ lies lower in LiO and BeO^+ is that the electrons along the σ (bond axis) direction on O are closer to the cation and thus experience a greater attractive force. In the case of BeF^{2+}, a similar argument could be used to account for the greater stability of the state ($^2\Pi$), with two $2p_\sigma$ electrons on the bond axis, rather than the state ($^2\Sigma^+$) with only one such electron. However, the splitting between the $^2\Pi$ and $^2\Sigma^+$ states in the series of alkali oxides LiO, NaO, KO,..., which change order from a $^2\Pi$ ground state (LiO, NaO, KO) to $^2\Sigma^+$ in the higher oxides, has been analyzed in more detail by Goddard and coworkers (29). They show that the ordering of the states is actually the result of a balance between Pauli repulsion forces (favoring $^2\Sigma^+$) and quadrupole interactions (favoring $^2\Pi$). By analogy, the series of dications BeF^{2+}, MgF^{2+}, ... may also show an inversion in the order of $^2\Pi$ and $^2\Sigma^+$ states as the atomic number of the cation increases.

The bond distance in the ground state of BeF^{2+} is even shorter than in LiO (3.09 vs. 3.20 bohr). This is another indication that the BeF^{2+} dication has the strongly attractive ionic configuration (near its minimum) and is not mixed with the covalent repulsive configuration. The dissociation energy is much less than in LiO, however, partly due to the avoided crossing described earlier.

The strength of the bond in BeF^{2+} is comparable with other molecules in which charge-induced polarization is responsible for the bonding. For example, for $BeHe^{2+}$, D_e = 0.87 eV (11) and for $BeNe^{2+}$, D_e = 1.25 eV (12). In both noble gas compounds the minima correspond to a Be^{2+} + X structure, with little or no covalent bonding.

The $X^2\Pi$–$A^2\Sigma^+$ band system

The $X^2\Pi$–$A^2\Sigma^+$ band system has an electric-dipole-allowed transition near 1.6 eV, so transition between these states will occur in the near IR and could be of help in identifying the BeF^{2+} ion. Since the minima occur at 3.09 and 3.29 bohr for the X and A states, respectively, the relatively small shift of 0.14 bohr suggests that Franck–Condon factors (FCF's) should be favorable and that transitions between vibrational levels in upper and lower states should be nearly diagonal. However, as shown in Fig. 2, the levels are

Can. J. Chem. Downloaded from www.nrcresearchpress.com by 203.198.23.82 on 09/08/12
For personal use only.

TABLE 7. Radiative data[a] for the $X^2\Pi$–$A^2\Sigma^+$ system of BeF^{2+}

v''	$v' = 0$	$v' = 1$	$v' = 2$	$v' = 3$	$v' = 4$	
0	12705	13176	13621	14042	14822	ν (cm^{-1})
	0.706E 0	0.242E 0	0.456E−1	0.560E−2	0.361E−3	$q^b_{v'v''}$
	0.618E 2	0.172E 3	0.129E 3	0.544E 2	0.158E 2	$A^c_{v'v''}$
	0.287E−6	0.743E−6	0.522E−6	0.207E−6	0.568E−7	$f^d_{v'v''}$
1	12007	12478	12923	13344	13744	
	0.231E 0	0.254E 0	0.341E 0	0.136E 0	0.322E−1	
	0.401E 2	0.197E 2	0.124E 3	0.195E 3	0.148E 3	
	0.208E−6	0.951E−7	0.557E−6	0.825E−6	0.589E−6	
2	11327	11797	12243	12664	13064	
	0.533E−1	0.313E 0	0.258E−1	0.267E 0	0.221E 0	
	0.178E 2	0.645E 2	0.177E 2	0.604E 2	0.158E 3	
	0.104E−6	0.348E−6	0.886E−7	0.282E−6	0.695E−6	
3	10664	11135	11580	12001	12401	
	0.830E−2	0.144E 0	0.237E 0	0.178E−1	0.107E 0	
	0.371E 1	0.473E 2	0.558E 2	0.299E 2	0.311E 2	
	0.245E−7	0.286E−6	0.312E−6	0.155E−6	0.151E−6	
4	10017	10488	10930	11355	11754	
	0.109E−2	0.375E−1	0.224E 0	0.903E−1	0.101E 0	
	0.297E 0	0.164E 2	0.758E 2	0.243E 2	0.468E 2	
	0.222E−8	0.111E−6	0.475E−6	0.141E−6	0.254E−6	
5	9386	9856	10301	10722	11123	
	0.113E−3	0.735E−2	0.941E−1	0.228E 0	0.287E−2	
	0.597E−1	0.273E 1	0.425E 2	0.795E 2	0.739E 0	
	0.508E−9	0.211E−7	0.300E−6	0.518E−6	0.440E−8	
	8.1	3.1	2.2	1.8	1.6	τ^e (ms)

[a]v'' indicates vibrational levels of $X^2\Pi$, v' indicates vibrational levels of $A^2\Sigma^+$. The notation 0.207E−6 indicaes 0.207×10^{-6}.
[b]Franck–Condon factors.
[c]Einstein coefficients (s^{-1}).
[d]Oscillator strength.
[e]Fluorescence lifetime of v' level (ms). The series of Einstein coefficients was summed over 20 v'' levels and is converged.

closely spaced, with harmonic frequencies in lower and upper states of only 717 and 497 cm^{-1}, respectively. Thus we can anticipate that intensity of absorption from each lower vibrational level may be spread over several upper levels, and vice versa.

Table 7 shows some radiative data for emission from a given upper level v' to the lower levels $v'' = 0$–5. The table is arranged so that the top line in each block of v'' levels gives the transition energies, the next line gives the FCF's, the third line gives the Einstein coefficients, and the fourth line gives the oscillator strengths. The fluorescence lifetime of each v' level is given at the bottom of the table.

The FCF's are indeed nearly diagonal, and in fact the largest FCF (= 0.706) occurs for the 0–0 transition. Transitions from levels $v' = 1,2$ occur with $\Delta v = \pm 1$ and the range increases for higher levels. The Einstein coefficients and oscillator strengths are all very low, so that lifetimes for the v' levels are of the order of 10 ms ($v' = 0$) or 1 ms (the other v' levels). This will cause low intensity and make the A–X emission band very difficult to observe.

A very similar situation holds for the isoelectronic LiO molecule, data for which are given in Table 6. In this case the upper state $A^2\Sigma^+$ has the shorter bond length, but the shift between the minima is similar at 0.18 bohr. Detailed radiative data for the A–X band were given by Yoshimine et al. (30). FCF's are very similar to those of BeF^{2+}, e.g., their largest reported value of 0.577 also occurred for the 0–0 transition. Oscillator strengths for transitions from $X^2\Pi$ in LiO are about a factor of four higher than in BeF^{2+}, and this band system has not yet been experimentally observed in LiO (27). Thus, although the transition is electric dipole allowed in each case, the intensity is so low as to make experimental observation very difficult.

Since the polarization in each system corresponds to $Be^{2+}F$ and Li^+O^-, the reason for the low intensity is the same. In each case the (absorption) transition occurs in the perturbed $2p^5$ manifold on F or O^-, i.e., from $2p_\sigma$ to $2p_\pi$. Since this corresponds to a type of p–p transition, it is forbidden in the isolated atom. Polarization of the atom by the cation breaks the symmetry, making it partially allowed but still weak. Unfortunately, therefore, this band system will probably be of no help in identifying the BeF^{2+} dication, and we now consider its simple formation and detection in a mass spectrometer.

Formation of the ion

There are several possible ways to generate diatomic dications. It was proposed by Bates and Carson (13) that noble gas compounds of type $NeMg^{2+}$ should be formed readily in three-body collisions of Mg^{2+} + 2Ne. To the best of our

Can. J. Chem. Downloaded from www.nrcresearchpress.com by 203.198.23.82 on 09/08/12
For personal use only.

Can. J. Chem. Downloaded from www.nrcresearchpress.com by 203.198.23.82 on 09/08/12
For personal use only.

knowledge, however, this mechanism has never led to observation of any noble gas dications.

In the case of BeF^{2+}, the precursor BeF was prepared by Hildenbrand and Murad (31) by effusing vapors of Be(s) and CaF_2(s). The species BeF^+ was detected in a mass spectrometer. They also observed formation of BeF^+ above 15 eV from the reaction

$$BeF_2 + e^- \rightarrow BeF^+ + F + 2e^-.$$

Once the BeF^+ ion has been generated it has the high D_e of 6.25 eV (28). The ion is thus quite stable and could be further ionized to the dication according to $BeF^+ \rightarrow BeF^{2+} + e^-$. We estimate the IP for this reaction to be 21.4 eV.

Another mass-spectrometric experiment, described by Galindo-Uribarri et al. (32), generates XY^- ions by sputtering from solids X and Y, followed by collision with argon gas at MeV energies (accelerator mass spectroscopy) to produce XY^{2+} ions. This approach led to detection of many ions in the mass range 20–26, due to a window in this range free of interference from atomic ions with these masses. Unfortunately BeF^{2+} has mass 27 and may therefore suffer from interference with Al ions.

A more promising route to products is to generate an excited beam of Be^{2+} ions and react these with the stable reagent, gaseous F_2. The abstraction reaction is then

$$Be^{2+} + F_2 \rightarrow BeF^{2+} + F$$

For formation of BeF^{2+} ($X^2\Pi$), we estimate this reaction to be exothermic by 0.47 eV. Beams of doubly charged Be ions have been prepared in two-laser produced plasmas (33), so the experiment should be feasible. The more exothermic products $BeF^+ + F^+$ would also be formed in the same reaction, so the product ratio for formation of both channels would depend on the detailed dynamics of the reaction and on whether the products are formed under collision-free conditions. The same reaction is endothermic to produce $A^2\Sigma^+$, but since the ion beam can easily be created with energies of several electronvolts and the A-state is expected to be long-lived, mass-spectrometric detection would probably see both $X^2\Pi$ and $A^2\Sigma^+$ states on a millisecond time scale.

Conclusions

By considering energy differences for dissocation of a dication AB^{2+} into the repulsive channel $A^+ + B^+$ and the attractive channel $A + B^{2+}$, we predict that several diatomics not including noble gases may be thermodynamically stable, including BeF^{2+}, MgN^{2+}, MgO^{2+}, MgF^{2+}, $MgCl^{2+}$, SiN^{2+}, SiO^{2+}, and SiF^{2+}. *Ab initio* calculations prove that this is the case for the ground state $X^2\Pi$ of BeF^{2+}, which has the positive value of $\Delta = 0.79$ eV. The ground state is indeed thermodynamically stable and has a dissociation energy of 1.08 eV (uncorrected for zero-point energy) relative to the lowest dissociation limit $Be^+ + F^+$. Due to an avoided crossing with the upper state $2^2\Pi$, a barrier is created so that the effective dissociation energy from $X^2\Pi$ is 2.07 eV. The low-lying excited state $A^2\Sigma^+$ is metastable relative to the lowest possible dissociation limits, but is probably very long-lived since it dissociates uphill to an attractive channel and is only weakly connected by radiative transitions to the ground state. The A–X band has been shown to be of low intensity even though it is electric dipole allowed. Several mechanisms are proposed to form the dication BeF^{2+}. The most promising of these would be the exothermic ion–molecule reaction of Be^{2+} and gaseous diatomic fluorine.

Acknowledgements

We thank the Natural Sciences and Engineering Research Council of Canada (NSERC) for financial support for this work, Dr. Pablo Bruna for useful discussions, and Dr. Leo Radom for use of the program ACDCP. We also thank the referee for useful suggestions.

1. T. Ast. Adv. Mass Spectrom. A, **8**, 555 (1980).
2. M.T. Bowers (*Editor*). Gas phase ion chemistry. Vols. 1–3. Academic, New York. 1979–1984.
3. E. Dörnenburg, H. Hinterberger, and J. Franzen. Z. Naturforsch A: Astrophys. Phys. Phys. Chem. **16A**, 532 (1961).
4. (*a*) P.C. Cosby, R. Möller, and H. Helm. Phys. Rev. A, **28**, 766 (1983); (*b*) R.W. Wetmore and R.K. Boyd. J. Phys. Chem. **90**, 5540 (1986).
5. F.C. Fehsenfeld, J. Appell, P.G. Fournier, and J. Durup. J. Phys. B: At. Mol. Phys. **6**, L268 (1973).
6. (*a*) C.W. Bauschlicher, Jr. and M. Rosi. Chem. Phys. Lett. **159**, 485 (1989); (*b*) C.A. Nicolaides, M. Chrysos, and P. Valtazanos. J. Phys. B: At. Mol. Opt. Phys. **23**, 791 (1990); (*c*) P.J. Bruna, G.A. DiLabio, and J.S. Wright. J. Phys. Chem. **96**, 6269 (1992).
7. P.J. Bruna and J.S. Wright. J. Chem. Phys. **93**, 2617 (1990).
8. J. Senekowitsch and S. ONeil. J. Chem. Phys. **95**, 1847 (1991).
9. (*a*) M.J. Besnard, L. Hellner, Y. Malinovich, and G. Dujardin. J. Chem. Phys. **85**, 1316 (1986); (*b*) D. Cossart, B. Bonneau, and J.M. Robbe. J. Mol. Spectrosc. **125**, 413 (1987).
10. W. Koch and G. Frenking. J. Chem. Phys. **86**, 5617 (1987).
11. G. Frenking, W. Koch, D. Cremer, J. Gauss, and J.F. Liebman. J. Phys. Chem. **93**, 3397 (1989).
12. G. Frenking, W. Koch, J. Gauss, and D. Cremer. J. Am. Chem. Soc. **110**, 8007 (1988).
13. D.R. Bates and T.R. Carson. Proc. Phys. Soc. London, Sect. A: **68**, 1199 (1955).
14. P.M.W. Gill and L. Radom. Chem. Phys. Lett. **136**, 94 (1987).
15. L. Radom, M.W. Gill, and M.W. Wong. Int. J. Quantum Chem. Quantum Chem. Symp. **22**, 567 (1988).
16. A.C. Hurley and V.M. Maslen. J. Chem. Phys. **34**, 1919 (1961).
17. N. Levasseur, P. Millie, P. Archirel, and B. Levy. Chem. Phys. **153**, 387 (1991).
18. C.E. Moore. Atomic energy levels. National Bureau of Standards NSRDS–NBS 35, Washington, D.C. 1971.
19. S. Huzinaga. J. Chem. Phys. **42**, 1293 (1965).
20. T.H. Dunning, Jr. J. Chem. Phys. **55**, 716 (1971).
21. T.H. Dunning, Jr. and P.J. Hay. *In* Modern theoretical chemistry. Plenum, New York. 1977. p. 1.
22. P.J. Bruna and J.S. Wright. Mol. Phys. In press.
23. T.H. Dunning, Jr. J. Chem. Phys. **90**, 1007 (1989).
24. R.J. Buenker. Proceedings of Workshop on Quantum Chemistry and Molecular Physics into the 80's. *Edited by* P. Burton. University of Wollongong, Australia. 1980. p. 1.5.1.
25. S.R. Langhoff and E.R. Davidson. Int. J. Quantum Chem. **8**, 61 (1974).
26. P.J. Bruna and J.S. Wright. J. Phys. Chem. **96**, 1630 (1992).
27. K.P. Huber and G. Herzberg. Molecular spectra and molecular structure. Van Nostrand Reinhold Co., New York. 1979.
28. H. Partridge, S.R. Langhoff, and C.W. Bauschlicher, Jr. J. Chem. Phys. **84**, 4489 (1986).

29. J.N. Allison, R.J. Cave, and W.A. Goddard III. J. Phys. Chem. **88**, 1262 (1984).
30. M. Yoshimine, A.D. McLean, and B. Liu. J. Chem. Phys. **58**, 4412 (1973).
31. D.L. Hildenbrand and E. Murad. J. Chem. Phys. **44**, 1524 (1966).
32. A. Galindo-Uribarri, H. W. Lee, and K. H. Chang. J. Chem. Phys. **83**, 3685 (1985).
33. E. Jannitti, P. Nicolosi, and G. Tondello. Proc. SPIEI – Int. Soc. Opt. Eng. **664**, 172 (1986).

Can. J. Chem. Downloaded from www.nrcresearchpress.com by 203.198.23.82 on 09/08/12
For personal use only.

Proton transfer equilibrium reactions in some substituted 3*H*-indole probe molecules: role played by the TICT state

RANJIT S. SARPAL, MICHEL BELLETÊTE, and GILLES DUROCHER[1]

Département de chimie, Université de Montréal, C.P. 6128, Succ. A, Montréal, QC H3C 3J7, Canada

Received April 23, 1993

This paper is dedicated to Professor Gerald W. King on the occasion of his 65th birthday

RANJIT S. SARPAL, MICHEL BELLETÊTE, and GILLES DUROCHER. Can. J. Chem. **71**, 1570 (1993).

Five substituted derivatives of the main chromophore, 2-phenyl-3,3-dimethyl-3*H*-indole (**1**), have been studied over a wide range of acidity by UV absorption and steady state fluorescence spectroscopy. These are as follows: 2-[(*p*-amino)phenyl]-3,3-dimethyl-3*H*-indole (**2**), 2-[(*p*-dimethylamino)phenyl]-3,3-dimethyl-3*H*-indole (**3**), 2-[(*p*-amino)-phenyl]-3,3-dimethyl-5-carboethoxy-3*H*-indole (**4**), 2-[(*p*-methylamino)phenyl]-3,3-dimethyl-5-carboethoxy-3*H*-indole (**5**), and 2-[(*p*-dimethylamino)phenyl]-3,3-dimethyl-5-carboethoxy-3*H*-indole (**6**). The dependence of absorption and fluorescence spectral characteristics upon acidity has allowed us to characterize four species, namely, the anion (A), the neutral molecule (N), the cation (C), and the dication (DC), for molecules **2** and **3**. Molecules **4**, **5**, and **6** give rise to an additional anion due to the hydrolysis of the ester group. The relative order of protonations to available sites is discussed. The ring-protonated species have shown the Ph_c and indole rings to be coplanar in both the ground and first excited singlet states. A low-energy non-emissive twisted intramolecular charge transfer (TICT) state taking its origin in the dimethylamino moiety is suggested from INDO-S calculations to explain the strong fluorescence quenching of these ring-protonated species. Acidity constants for the various prototropic equilibria have been determined experimentally both in the ground and in the excited singlet states. Förster cycle calculations have been used to supplement the various equilibrium constants. Possible applications in organized assemblies are discussed.

RANJIT S. SARPAL, MICHEL BELLETÊTE et GILLES DUROCHER. Can. J. Chem. **71**, 1570 (1993).

Faisant appel à l'absorption UV et à la spectroscopie de fluorescence en état stationnaire, on a étudié cinq produits de substitution du 2-phényl-3,3-diméthyl-3*H*-indole (**1**) à diverses acidités. Il s'agit des 2-[(*p*-amino)phényl]-3,3-diméthyl-3*H*-indole (**2**), 2-[(*p*-diméthylamino)phényl]-3,3-diméthyl-3*H*-indole (**3**), 2-[(*p*-amino)phényl]-3,3-diméthyl5-carboéthoxy3*H*-indole (**4**), 2-[(*p*-méthylamino)phényl]-3,3-diméthyl-5-carboéthoxy-3*H*-indole (**5**) et 2-[(*p*-diméthylamino)-phényl]-3,3-diméthyl-5-carboéthoxy-3*H*-indole (**6**). La relation entre les caractéristiques spectrales d'absorption et de fluorescence et l'acidité nous ont permis de caractériser quatre espèces, soit l'anion (A), la molécule neutre (N), le cation (C) et le dication (DC) des molécules **2** et **3**. Les molécules **4**, **5** et **6** donnent aussi lieu à la formation d'un anion additionnel qui provient d'une hydrolyse de l'ester. On discute de l'ordre relatif des protonations des divers sites. On a démontré que les espèces protonées des cycles benzénique et indolique sont coplanaires tant dans l'état fondamental que dans le premier état excité. Sur la base de calculs INDO-S, on suggère qu'un état de transfert de charge intramoléculaire déformé, de basse énergie, non radiatif et dont l'origine se trouverait dans la portion diméthylamino peut expliquer la forte désactivation de fluorescence de ces espèces protonées sur le cycle. On a déterminé expérimentalement les constantes d'acidité des divers équilibres prototropiques tant dans l'état fondamental que dans les états excités. On a utilisé des calculs de cycles de Förster comme suppléments aux diverses constantes d'équilibre. On discute de diverses applications possibles pour des systèmes organisés.

[Traduit par la rédaction]

Introduction

Proton and electron transfer reactions are among the most elementary processes in chemistry and biochemistry (1). Since the original work of Förster (2) and Weller (3) on 1-naphthylamine-4-sulfonate, considerable research work on proton transfer has been done over the years (4–15). Due to these efforts, the acid-base behavior of various substituent groups attached to aromatic moieties in both the S_0 and S_1 electronic states is now well understood. If $\pi \rightarrow \pi^*$ is the lowest energy transition, amino and hydroxy substituents become stronger acids in the S_1 state, which shifts band wavenumber maxima to higher and lower values upon protonation and deprotonation, respectively. To the contrary, esters and tertiary ring nitrogen atoms become strongly basic in the S_1 state, which shifts wavenumber maxima to lower values upon protonation. Thus, the acid-base chemistry becomes a direct function of the electronic structures of aromatic compounds in ground as well as in excited states. Various combinations of these substituent groups with homo- and heterocyclic chromophores have been reported in the literature (16–31). Results show that for the same set of basic centers, the preferential attack of protons has varied from molecule to molecule. To name a few: in amino-substituted quinolines, acridine, and benzimidazole the first preferred protonaton site is the tertiary ring nitrogen (16–20), whereas in oxazoles and thiazoles the preferential proton attack occurs on the terminal amino group (21, 22). Also, ground state protonaton sites are reported to be different from excited state sites for the same molecule, which is attributed to the change in acidity and basicity of the reaction centers (23, 24). All these observations cast serious doubt on the reliable prediction of any kind of equilibrium reactions, and lend strong support to the benefits of their experimental determination.

Important applications, such as use of proton transfer equilibrium in sensing interfacial proton concentration of microheterogeneous media (32–34) and use of phototautomers as effective light protectors and materials in continuous lasers, have surfaced (35–37). Another aspect of acidity and basicity dependence that becomes especially important is evident when absorption and fluorescence probing of organized assemblies is done by external/internal probes that

[1]Author to whom correspondence may be addressed.

Can. J. Chem. Downloaded from www.nrcresearchpress.com by 203.198.23.82 on 09/08/12
For personal use only.

have one (or more than one) basic center(s). The nature of the species used in probing environments must be defined a priori; otherwise, observations can be misleading. The various species generated as a function of pH should then be used to make estimates about the nature of the environment in organized assemblies.

In the past few years, our laboratory has been particularly interested in examining 3*H*-indole derivatives in various environments (38–41). INDO-S, AMPAC, and X-ray crystallography have been successfully used to quantify various spectroscopic and structural parameters. Because of their spectral dependence on different environments, their fluorescence probing properties in microheterogeneous media have recently been identified (42, 43). As a further extension of these studies, we want to report in this paper the acidity dependence of the following molecules in water.

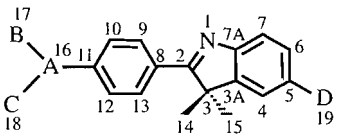

	A	B	C	D
1	H	-	-	H
2	N	H	H	H
3	N	CH_3	CH_3	H
4	N	H	H	CO_2Et
5	N	H	CH_3	CO_2Et
6	N	CH_3	CH_3	CO_2Et

Molecule **1** has already been studied in our recent communications (41, 43, 44), and is included here for comparison purposes only. The aim of this paper is manifold. We first want to investigate the order of the various protonating sites and to identify the different prototropic species. We also want to follow the order of basicity of the substituent groups in the S_0 and S_1 states and to see whether there is any kind of tautomerism. The proton-induced fluorescence quenching phenomenon will also be looked at to obtain the acidity constants of the various equilibria studied in both S_0 and S_1 states. Possible application to organized assemblies will also be discussed briefly.

2. Experimental section

Synthesis and purification of molecule **3** was done according to the method of Skrabal et al. (45), whereas the other molecules were synthesized by a modified method of Skrabal et al. (46) and will be published elsewhere.[2] Analytical grade reagents sodium hydroxide, sulfuric acid, and phosphoric acid were used as received. Deionized triply distilled water was used in all studies.

The absorption spectra were recorded on a Philips PU-8800 UV-VIS spectrophotometer. Corrected fluorescence spectra were measured on a Spex Fluorolog-2 spectrofluorimeter with a F2T11 special configuration. Fluorescence quantum yields of all the mentioned species were measured using molecule **3** in ethanol (Φ_F = 0.33) (39) as a fluorescence standard. Fluorescence lifetimes were obtained from a multiplexed time-correlated single-photon counting fluorimeter (Edinburgh Instruments, model 299T) (40). A modified Hammett's acidity scale (47) for H_2SO_4-H_2O mixtures and Yagil's basicity scale (48) for NaOH-H_2O mixtures were used below pH 1 and above pH 13, respectively. Solutions in the pH range 3–11 were prepared by adding appropriate amount of NaOH and H_3PO_4. Stock solutions of all the compounds were prepared in methanol and 0.1 mL of this was added to 10 mL of all the aqueous solutions. The concentration of the compounds used was never more than 1×10^{-5} M. Isosbestic wavelengths were used for excitation in all the acid-base equilibria. The method of Ireland and Wyatt (9) was used in the determination of the ground and excited state pK_a values.

3. Results and discussion

3.1. Acid-base concentration behavior of molecules 2 and 3

The effects of acid-base concentration on the ground and excited state spectral characteristics of molecules **2** and **3** were studied in the H_-/pH/H_0 range of 16 to −9 and are described in this section. Four major species, namely, the monoanion (A), the neutral species (N), the monocation (C), and the dication (DC), were observed. Relevant absorption and fluorescence spectral data are listed in Table 1, which also includes results on molecule **1**. Table 2 features all the proton transfer equilibrium constants determined experimentally. Figure 1 displays absorption and corrected fluorescence spectra of the various prototropic species detected over the wide range of acidity used. Scheme 1 reproduces the various prototropic reactions in equilibrium for molecule **2**.

3.1.1. Neutral-monoanion acid-base equilibrium

The absorption maximum of molecule **2** centered at $\bar{\upsilon}_A$ = 29 600 cm^{-1} remained the same from pH 7.5 to H_- = 14. With a further increase of the base concentration, this band started shifting to lower energy and the formation of the new species was incomplete even at H_- = 16, the highest base concentration used in this study. The fluorescence band maximum at $\bar{\upsilon}_F$ = 22 300 cm^{-1} did not change from pH 7.5 to H_- = 13, but the fluorescence was quenched with a further increase of the base concentration to H_- = 16. At H_- = 16, the spectrum showed a new fluorescence band peaking at lower frequency.

Based on the solvatochromic shifts observed in various nonpolar, polar, and polar protic solvents (footnote 2, (*b*)) and from the behavior of molecule **1** in different protic media (43), the absorption and fluorescence maxima at pH 7.5 should be assigned to the neutral species of molecule **2** and the low-energy absorption maximum at high base concentration should be ascribed to a monoanion formed by N-H deprotonation. Such deprotonations were also reported earlier (17, 20–22). Deprotonation of a ring carbon atom in this basicity range ($14 < H_- < 16$) is ruled out on the basis that it usually occurs at much higher base concentrations and the resulting anions are usually fluorescent with low quantum yields (49, 50). The new low-energy band at H_- = 16 might be assigned to the dianion formed by deprotonation of the amino group and one of the carbon atoms. The ground state pK_a value for the amino group deprotonation equilibrium could not be calculated due to the incompleteness of the reaction but should be higher than 16. The excited state pK_a value (pK_a^*) was found by monitoring the decay of fluorescence intensity of the neutral species. The fluorimetric titration gives a pK_a^* value of 13.9 that is close to some reported literature values for amine deprotonation (14, 20–22, 49, 50).

[2](*a*) M. Belletête, A. Popowycz, D. Héroux, D. Gravel, F. Brisse, and G. Durocher. Manuscript in preparation; (*b*) M. Belletête, A. Popowycz, D. Gravel, R.S. Sarpal and G. Durocher. Manuscript in preparation.

Can. J. Chem. Downloaded from www.nrcresearchpress.com by 203.198.23.82 on 09/08/12
For personal use only.

TABLE 1. Spectral characteristics of some prototropic species of amino phenyl 3*H*-indole derivatives in water at 298 K

Molecule	Species	$\tilde{\upsilon}_A{}^b$ (cm^{-1})	ϵ^c ($M^{-1}\,cm^{-1}$)	$\tilde{\upsilon}_A{}^d$ (cm^{-1})	$\tilde{\upsilon}_F{}^b$ (cm^{-1})	$\tilde{\upsilon}_F{}^d$ (cm^{-1})	Φ_F
1	Neutral (pH = 9)	33 300	14 600	33 400	23 900	23 500	0.0011
	Monocation (pH = 1.5)	30 300	15 600	29 800	21 100	20 700	0.0011
	Dication[a] (H_0 = −9)	29 000	15 500	28 900	21 000	20 600	0.010
2	Neutral (pH = 9)	29 600	23 300	29 600	22 300	21 800	0.17
	Monocation (pH = 2)	24 400 23 300	39 700 27 700	24 600	22 300 21 300 19 800	21 300	0.0031
	Dication (H_0 = −8)	29 300	13 100	29 600	21 100	20 500	0.0056
3	Neutral (pH = 9)	27 300	24 700	27 500	21 800	21 300	0.21
	Monocation (pH = 2)	23 000 22 200	50 900 50 900	22 900	21 100 19 900	20 400	0.0012
	Dication (H_0 = −8)	29 200	11 700	29 400	21 000	20 500	0.0071

[a]Ring protonation.
[b]Wavenumbers at the peak intensity maximum.
[c]Absorptivity coefficients at the peak intensity maximum.
[d]Wavenumbers at the center of mass of the bands.

TABLE 2. Acidity constants of the various prototropic equilibria in the ground and excited singlet states at 298 K

	Equilibrium					
	Amino group deprotonation		Ring nitrogen protonation		Amino group protonation	
Molecule	pK_a	pK_a^*	pK_a	pK_a^*	pK_a	pK_a^*
1	—	—	3.25	3.2	−3.40[b]	—[a]
2	—	13.90	5.40	—[a]	0.05	−4.00
3	—	14.50[c]	5.70	−[a]	−0.20	−4.30
4	—	13.50	4.20	−[a]	−0.50	−5.00
5	—	13.55	4.80	−[a]	−1.00	−4.60
6	—	15.30[c]	4.90	−[a]	−1.00	−4.80

[a]Too much overlap between the fluorescence profiles of the conjugate acid–base species.
[b]Ring protonation.
[c]Ring deprotonation.

The fact that $pK_a^* < pK_a$ means that the amino group becomes a stronger acid in the excited state.

For molecule **3**, on increasing the base concentration, the intensity of the absorption band of the neutral species remained invariant until H_- = 15 but was slightly red-shifted at H_- = 16. On the other hand, the fluorescence band of this species started decreasing in intensity only at H_- = 13.5 without the appearance of any other new band. It was noticed that the bandwidth at H_- = 16 is much larger than that observed for the neutral species at pH 7.5. These spectral changes can be attributed to the deprotonation of one ring carbon atom as there is no other available proton on nitrogen in this molecule, and also because the pK_a^* for methyl group deprotonation is higher than that for ring carbon deprotonation (49). The broadening of the band at H_- = 16 might be due to a mixing of the monoanion formed by deprotonation of the carbon atom with the neutral species. The ground state pK_a could not be calculated due to the incompleteness of the reaction. The excited state pK_a was calculated by using the fluorimetric titration curve of the neutral band (see Table 2).

3.1.2. Monocation – neutral species acid–base equilibrium

The absorption bands of the neutral species of molecules **2** and **3** were altered drastically by lowering the pH. The gradual appearance of a largely red-shifted, structured, highly intense band was observed at the expense of the neutral band by lowering the pH and the whole reaction was completed at pH 2.5. A clear-cut isosbestic point was observed, as exemplified in Fig. 2 for molecule **2** undergoing this equilibrium. Similarly, under these pH conditions the fluorescence intensity of the neutral species was significantly reduced, transforming into well-defined structured bands without much change in their positions, contrary to the observations made in the absorption spectra (see Fig. 1).

Because these molecules have two basic centers, the monocation can be generated by protonating either of the available sites. In these molecules, the first preferred pro-

Can. J. Chem. Downloaded from www.nrcresearchpress.com by 203.198.23.82 on 09/08/12
For personal use only.

Can. J. Chem. Downloaded from www.nrcresearchpress.com by 203.198.23.82 on 09/08/12
For personal use only.

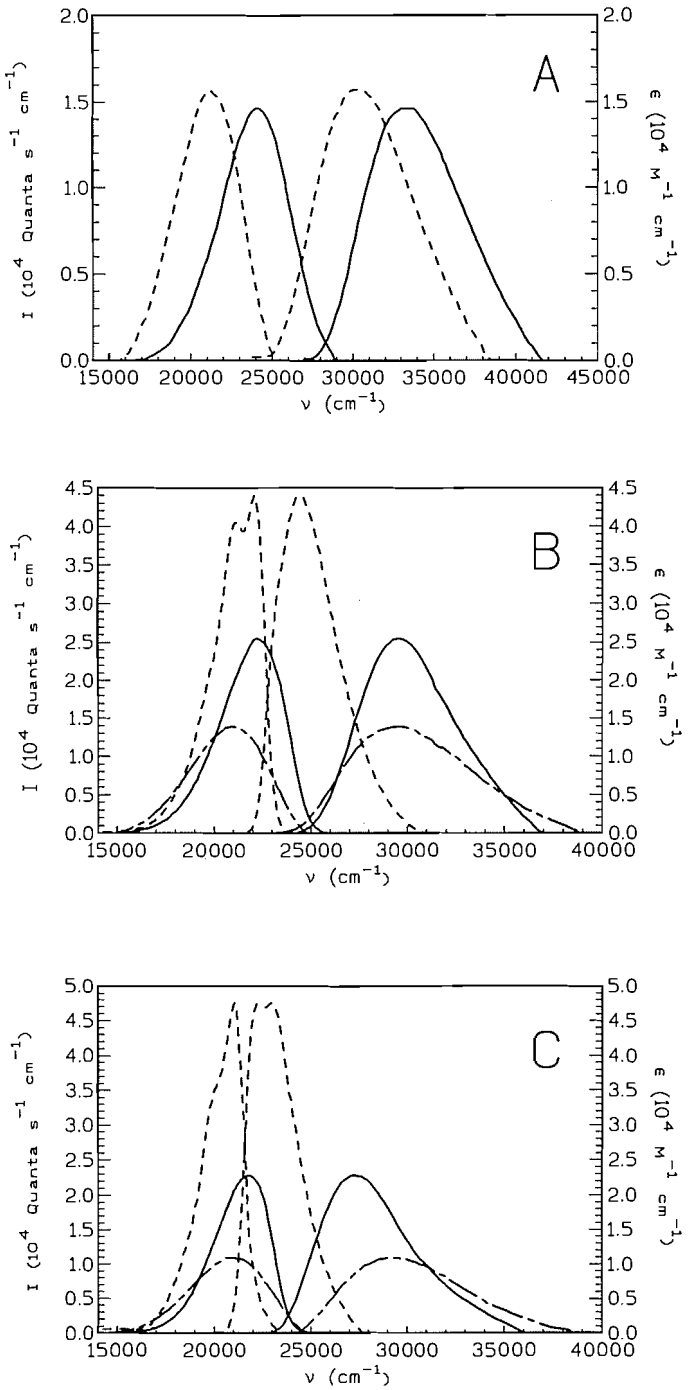

FIG. 1. Absorption and corrected fluorescence spectra of the various prototropic species of molecules **1** (*A*), **2** (*B*), and **3** (*C*); (——) neutral, (- - - - -) monocation, (–·–·–) dication.

tonation site should be the tertiary indole ring nitrogen atoms, based on the following arguments:

1. Had the protonation occurred at the terminal amino-nitrogen, the spectral characteristics of this species would have resembled those of the neutral species of molecule **1** because, once the lone pair on the amino group is coordinated by a proton, it no longer affects the total energy of the system (8, 9, 14, 21, 22).

2. Protonation of tertiary ring nitrogens leads to lowering the S_0–S_1 energy gap of the system when the lowest energy transition is $\pi\pi^*$ in character (8, 9, 16–22, 39).

3. The pK_a value of ring nitrogens is usually higher (~5) than that for terminal nitrogens (~4) (9).

3.1.2.1. Absorption spectra. Because of the large red shift (~5000 and ~4600 cm^{-1} for molecules **2** and **3**, respectively) observed in the absorption spectrum when going from the neutral to the cation species and also because of the calculated differences in the ground state structures, discussed below, the nearly planar structure C is suggested as the ground state monocation species (see Scheme 1).

As far as the absorption red shift is concerned, INDO-S calculations on molecule **3** have already shown that protonation of the ring nitrogen center increases the conjugation throughout the molecular frame in the ground electronic state, giving rise to a much more hindered phenyl ring torsional movement (higher potential barrier for rotation) (39). These calculations predicted a first singlet-singlet energy transition for the monocation at 24 770 cm^{-1} compared to 31 270 cm^{-1} for the neutral species, accounting for a red shift of approximately 6500 cm^{-1} in the gas phase. This shift is expected to be reduced in water as the neutral species is stabilized by hydrogen bonding and the monocation, since it is already protonated, is not. Table 1 shows that the first electronic absorption band for molecule **3** in water is red-shifted by 4600 cm^{-1} when protonation occurs, which seems reasonable enough when compared to theoretical calculations.

To study the effect of protonation of the ring nitrogen atom on the geometry of the molecule, the structural properties of these molecules in their neutral and cationic forms were obtained by the AMPAC molecular orbital package (Table 3). It was clearly established earlier (39) that both crystallographic measurements and AM1 geometry optimization agree very well, so that the AMPAC method has proven a valuable tool in the prediction of the ground state structures and energies for this class of molecules. The nine atoms constituting the 3*H*-indole moiety are coplanar and so is the phenyl group of atoms. It is shown in Table 3 that the two atomic planes of molecules **2** and **3** are tilted in the neutral form whereas this torsional angle is much reduced in the monocation. Accordingly, one should expect the bonds C(8)—C(2) and C(2)—N(1) to be affected by this structural change. Indeed, Table 3 shows that the length of the C(8)—C(2) bond decreases whereas the C(2)—N(1) bond length increases upon protonation. However, the C(8)—C(2) bond length is still higher than the C—C distance (1.379 Å) in a phenyl ring (51). By comparison, in molecule 3 the C(8)—C(9) and C(9)—C(10) bond distances in the Ph_c ring of the cation are 1.413 and 1.385 Å, respectively. Other parts of the molecule are practically not affected by the protonation, except for the donor group environment where the bond length N(16)—C(11) decreases in the cation. AMPAC also shows that the dimethylamino group of molecule **3** is pyramidal in the neutral form whereas this donor group is nearly coplanar with the Ph_c ring in the monocationic form (Table 3, angles θ_1 and θ_2). All these calculations strongly suggest that these molecules become more planar in their monocationic form and consequently the conjugation over the whole molecule should increase upon protonation.

3.1.2.2. Fluorescence spectra. When comparing the fluorescence of the neutral species and the monocation at room temperature in water, small red shifts of 500 and 900 cm^{-1} were observed for molecules **2** and **3**, respectively, while

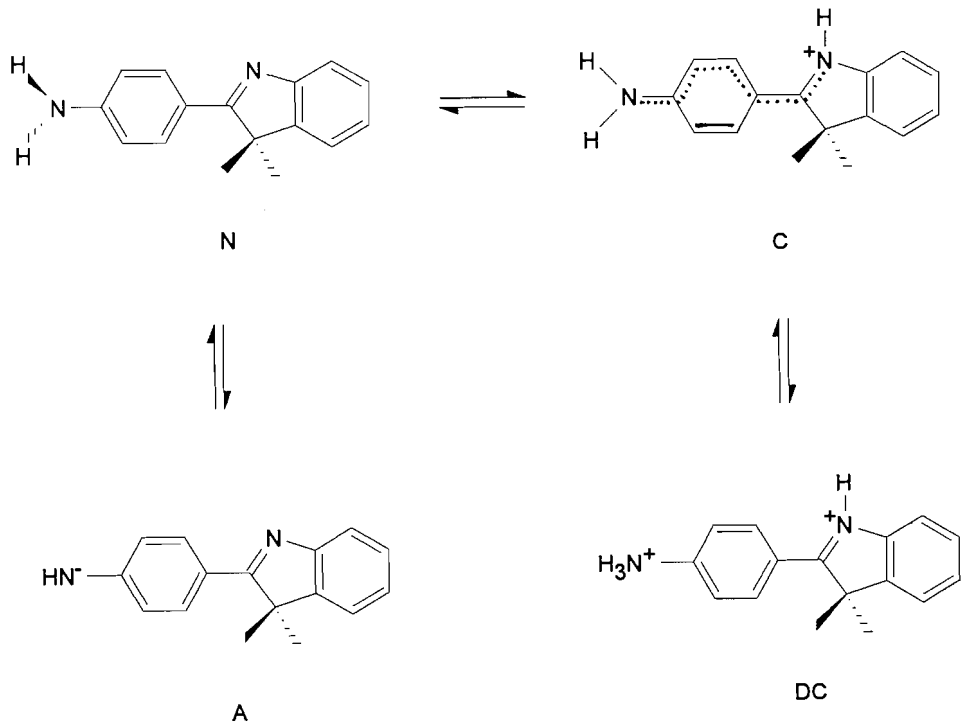

SCHEME 1

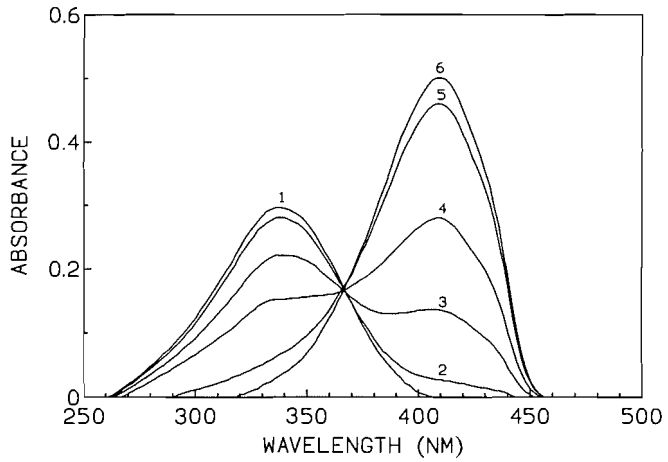

FIG. 2. Absorption spectra of molecule **2** at various pH (1 = 8.5, 2 = 6.4, 3 = 5.9, 4 = 5.7, 5 = 5.4, and 6 = 2.1).

large bathochromic shifts were observed in the absorption spectra (5000 and 4600 cm^{-1} for **2** and **3**, respectively). This might be due to (1) changes in protonation sites via photoautomerism in the excited state or (2), since it has been shown above that the ground state of the cation is much more planar than that of the neutral species, the small red shifts in the fluorescence spectra of the cations might be due to the smaller relaxation of their excited Franck–Condon (FC) states. This is equivalent to saying that the ground state cationic species give rise to fewer conformers than the neutral species. We then examined the excitation and fluorescence spectra of both species for molecule **2** in ice at 77 K, where the ground state nuclear configurations of the solutes are trapped even in the singlet excited states since the FC excited state relaxation is avoided. The fluorescence spectra of the cationic species at pH 2 at room temperature and at 77 K for molecule **2** are shown in Fig. 3. The near-equivalence of both spectra confirms that the protonation sites are similar in both the ground and excited singlet states, thus contraindicating any phototautomerism.

The vibrational structure is well resolved at 77 K. The absorption band of the neutral species (center of mass) is red-shifted by 1500 cm^{-1} at 77 K whereas the center of mass of the fluorescence band is practically not affected, causing a reduced Stokes shift that is entirely attributed to the stabilization of the ground state neutral species. This confirms quite well what is already known about molecule **3**, that no important modification of the nuclear configuration occurs during the relaxation of the Franck–Condon excited singlet state in fluid solutions (38, 39). The same pattern is observed for the cation species, where its absorption band is red-shifted by 510 cm^{-1} at 77 K and its fluorescence band is at nearly the same position. This shows that even for this species, practically no relaxation of the FC state occurs before emission takes place, even at room temperature. We then conclude that the ground state dynamics between the various possible conformers in the neutral species is responsible for the large Stokes shifts observed between the absorption and fluorescence spectra compared to those observed in the monocationic species.

On the other hand, based on what has been said above, one should expect the more planar cation (structure C) to be much more fluorescent in water than its neutral counterpart. To the contrary, Table 1 shows a completely different behavior for molecules **2** and **3** and for all the esters listed in Table 4. The quantum yield of the neutral species is reduced by nearly two orders of magnitude in the monocation. A high fluorescence quantum yield in these neutral molecules has always been interpreted as being correlated with a lack of rotational

Can. J. Chem. Downloaded from www.nrcresearchpress.com by 203.198.23.82 on 09/08/12
For personal use only.

TABLE 3. Structural properties of the 3*H*-indoles and their monocations as obtained by the AMPAC calculation method

Molecule	Species	Torsional angles			Bond lengths[d]		
		θ^a (deg)	$\theta_1{}^b$ (deg)	$\theta_2{}^c$ (deg)	N(16)—C(11) (Å)	C(8)—C(2) (Å)	C(2)—N(1) (Å)
1	Neutral	−0.1				1.464	1.322
	Monocation	0.1				1.465	1.346
2	Neutral	−0.9			1.393	1.460	1.323
	Monocation	0.1			1.353	1.423	1.356
3	Neutral	3.3	−5.9	−157.4	1.400	1.461	1.323
	Monocation	−0.7	−179.7	0.1	1.363	1.421	1.357
4	Neutral	−2.9			1.390	1.456	1.325
	Monocation	−1.9			1.352	1.422	1.358
5	Neutral	−0.1		167.2	1.393	1.460	1.325
	Monocation	−1.2		179.8	1.356	1.418	1.360
6	Neutral	−2.7	0.4	161.6	1.393	1.459	1.325
	Monocation	−5.3	−3.7	176.9	1.362	1.418	1.360

[a]Dihedral angle (tilt angle) of the Ph_c ring involving the following atoms: N(1)—C(2)—C(8)—C(9) calculated by AMPAC.
[b]Dihedral angle of the dimethylamino group involving the following atoms: C(10)—C(11)—N(16)—C(17) calculated by AMPAC.
[c]Dihedral angle of the dimethylamino group involving the following atoms: C(10)—C(11)—N(16)—C(18) calculated by AMPAC.
[d]These bond lengths were calculated by AMPAC and confirmed by X-ray for the neutral form of **3** (39).

freedom in the dimethylanilino ring. This rotational freedom can be hindered by increasing the viscosity of the media (41) or by hydrogen bonding and (or) polarity effects (38–40, 43). Since the fluorescence lifetimes and fluorescence quantum yields (2.6 ns and 0.5, respectively) of the neutral and monocation species of **2** are the same and very high in ice at 77 K when rotation is hindered, it shows that the quenching in water is of dynamic nature and that the excited FC state of the various monocations in water studied in this paper relaxes to a geometry in which some part of the dimethylanilino moiety is twisted from its planar ground state geometry. Because the fluorescence quantum yield of molecule **1** is not at all effected by protonation (see Table 1) compared to the other *para*-substituted derivatives (in the benezene ring), we tentatively assign the fluorescence quenching of the neutral species by protonation to the formation of a non-emissive twisted intramolecular charge transfer state (TICT) originating in the dimethylamino group (52*a–d*).

We have recently undertaken detailed semiempirical INDO-S molecular orbital calculations on the effect of rotating both the dimethylamino and the dimethylanilino groups in the neutral and monocation species. Preliminary results on molecule **3** and its monocation are now available. As far as molecule **3** is concerned, rotation of the $(CH_3)_2$ N- group by 90° does not give rise to any TICT state, but rotation of the dimethylanilino moiety by 90° stabilizes a highly polar TICT state. Though electron transfer to this state seems energetically allowed in all polar solvents, no decrease of the fluorescence quantum yield (Φ_F) of the emissive locally excited state in these media is observed at room temperature (40). This shows that the barrier to TICT state formation is probably too high for relaxation from the excited Franck–Condon state to occur.

The picture is totally different for the monocation of molecule **3**. Rotation of both the $(CH_3)_2$ N- and the dimethylanilino groups by 90° stabilizes the TICT state by about the same amount of energy, which is higher by 30% than that

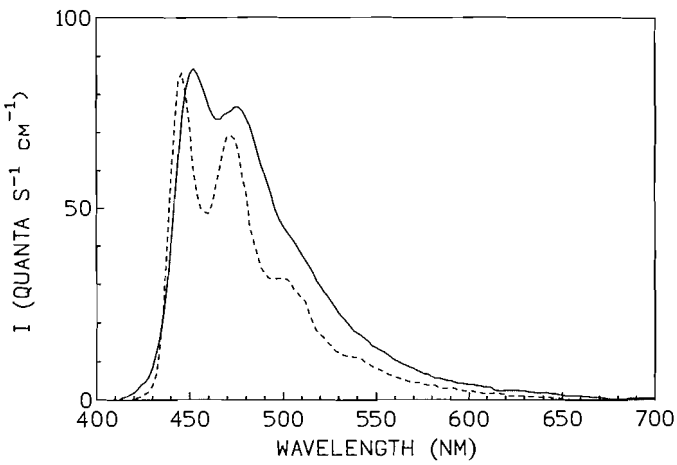

FIG. 3. Room temperature (—) and low temperature (77 K) (---) fluorescence spectra of the monocation of molecule **2**.

obtained for the case of the neutral molecule. But since the locally excited state is much less destabilized following dimethylamino torsion than for dimethylanilino twisting, a very weak rotational energy barrier of about 100 cm^{-1} is obtained for the dimethylamino torsion compared to about 1300 cm^{-1} for the dimethylanilino group. These energy barriers were obtained from the excited states correlation diagram (INDO-S) for planar and twisted forms. The stabilization energies, taking into consideration the solute-solvent interactions, have also been accounted for (52*e*). Hence, dimethylamino twisting in the monocations studied here is most likely responsible for the important fluorescence quenching of these species in water. The details of these calculations will be given in a subsequent paper where the photophysics will be emphasized.[3] These energetic and ki-

[3]R.S. Sarpal, M. Belletête, and G. Durocher. Manuscript in preparation.

Can. J. Chem. Downloaded from www.nrcresearchpress.com by 203.198.23.82 on 09/08/12
For personal use only.

TABLE 4. Spectral characteristics of some prototropic species in the ester series at 298 K

Molecule	Species	$\bar{\upsilon}_A{}^a$ (cm^{-1})	ϵ^b (M^{-1} cm^{-1})	$\bar{\upsilon}_A{}^c$ (cm^{-1})	$\bar{\upsilon}_F{}^a$ (cm^{-1})	$\bar{\upsilon}_F{}^c$ (cm^{-1})	Φ_F
4	Monoanion (pH = 12)	28 200	32 400	28 200	21 600	21 200	0.17
	Neutral (pH = 9)	27 900	32 700	27 900	20 900	20 700	0.022
	Monocation (pH = 2)	23 800 22 900	60 000 55 200	23 800	21 800 20 900	21 100	0.0018
	Dication (H_0 = −8)	29 700	19 100	29 700	21 400	20 800	0.045
5	Monoanion (pH = 13)	26 600	31 700	26 700	21 300	20 900	0.13
	Neutral (pH = 9)	26 500	30 200	26 500	20 500	20 300	0.013
	Monocation (pH = 2)	23 100 22 100	59 900 66 700	22 800	21 200 20 200	20 500	0.0010
	Dication (H_0 = −8)	29 900	18 700	29 900	21 400	20 800	0.049
6	Monoanion (pH = 13)	26 200	33 800	26 400	20 900	20 600	0.16
	Neutral (pH = 9)	25 400	32 500	25 600	20 900	19 900	0.012
	Monocation (pH = 2)	22 500 21 600	70 500 85 100	22 200	20 500 19 600	19 900	0.00094
	Dication (H_0 = −8)	29 900	20 700	29 900	21 400	20 800	0.05

[a]Wavenumbers at the peak intensity maximum.
[b]Absorptivity coefficients at the peak intensity maximum.
[c]Wavenumbers at the center of mass of the bands.

netic factors were also used recently to explain the probability of TICT formation in dimethyl-, methyl-, and aminobenzonitrile compounds (52*f*).

If the conclusion above is valid one would expect that, since the ionization potential is higher for an NH_2 group than for $NHCH_3$ or $N(CH_3)_2$ groups, the Φ_F value would be higher for **2** than for **3**, and also for **4**, **5**, and **6** in this decreasing order, for the monocation species in water. This is exactly what Tables 1 and 4 show. It was also shown recently that the 4-(*N*,*N*-dialkylamino)pyrimidines (4-DAAP), which give the usual *b** and *a** (TICT) fluorescences in polar aprotic solvents, show strong fluorescence quenching in protic solvents and no fluorescence at all for their cations (53).

The ground state pK_a value determined for the neutral species – monocation equilibrium is 5.4 for molecule **2**, higher than that for its unsubstituted derivatives reported earlier (3.25) (43). This means that the amino substituent pushes the electron density toward the ring nitrogen atom, making it more basic. The ground state pK_a value of molecule **3** for the same equilibrium is slightly higher than that of molecule **2** because the dimethylamino group is a better donor. Thus, the relative order of increasing basicity for this equilibrium is **3** > **2** > **1**. The very large overlap between the respective profiles of the neutral and monocation species in the fluorescence spectra precludes the calculation of the excited state pK_a values for this equilibrium. Since both the absorption and fluorescence intensity changes remain constant at pH ≃ 2.5 for the monocation, it can be safely concluded that both absorption and fluorescence data would yield similar pK_a values. This is probably because the rate constants for interconversion between the neutral and monocation species are low compared to the observed lifetimes of both species. Therefore, the prototropic equilibrium is not established in the excited state, so that the fluorescence intensities measured at this pH reflect the relative ground state concentration of the neutral and monocation species. Similar behavior was observed for molecule **1** (43) and has also been reported by others (19, 20).

3.1.3. Dication–monocation acid–base equilibrium. With further lowering of the pH, the intense structured absorption band of the monocation decreased in intensity for both molecules, concurrent with the appearance of a high-energy, lower intensity broad band at $\bar{\upsilon}_A$ = 29 600 cm^{-1} and $\bar{\upsilon}_A$ = 29 400 cm^{-1} for **2** and **3**, respectively. A sharp isosbestic point was also observed for this equilibrium, making chemistry simple in the sense that only two prototropic species are involved in the equilibrium reaction. It was completed at H_0 = −2 and the band remained unaffected both in position and intensity until H_0 = −9, the highest acid strength used. In a similar acidity range, the fluorescence

Can. J. Chem. Downloaded from www.nrcresearchpress.com by 203.198.23.82 on 09/08/12
For personal use only.

Can. J. Chem. Downloaded from www.nrcresearchpress.com by 203.198.23.82 on 09/08/12
For personal use only.

spectral characteristics behaved differently. The structured weak fluorescence band of the monocation was slowly transformed into a broad, highly intense, low-energy band. The reaction was completed only at $H_0 = -8$, contrary to what happens in the ground state where the reaction was completed at lower acidity.

This new high-energy absorption band can be assigned to the dication formed by protonation of both the basic centers, without involving ring carbon atom protonation. It has already been shown that molecule **1** undergoes ring protonation under these acidity conditions (43). The above assignment is based on the following:

1. The spectral characteristics of the dication are similar to those of the molecule **1** monocation (Table 1), in terms of both position and intensity. This is because, once the amino group is protonated, its effect on the spectroscopic properties of the basic chromophore is made negligible. Also, if the second protonation had occurred on the ring carbon atom, it would have caused further lowering of the energy of the system as had already been observed in molecule **1** (43).

2. The ground state pK_a value of the ring protonation is too low (−3.4), as noticed in molecule **1**, compared to what is observed for this equilibrium (see below).

It is generally observed that the fluorescence intensity of neutral aromatic amines is quenched before the formation of the monocation (20, 24) by amino group protonation. Shizuka and Tsutumi (54, 55) showed that this is due to the protonation of one of the aromatic sites if the charge transfer state is the lowest excited state. This phenomenon has been termed proton-induced fluorescence quenching, which competes with the proton transfer equilibrium. Though all the factors for molecules **2** and **3** favor this process, excessive overlap between the spectra of the respective monocation and dication species and the low quantum yield of the monocation did not allow us to draw definite conclusions regarding this aspect of our study.

The ground state pK_a value found for this equilibrium is lowered to 0.05 and −0.20 for **2** and **3**, respectively (Table 2), compared to pK_a values of around 4 normally observed for aromatic amine equilibria (9). This is ascribed to the positive charge already on the ring nitrogen, which makes the terminal nitrogen electron deficient by delocalizing the electron density toward the aromatic ring. The decrease in fluorescence intensity of the monocation with change in acidity could not be monitored due to the reasons already mentioned above. Therefore, the fluorimetric titration curve was constructed from the increase in fluorescence intensity of the dication at a wavelength where overlapping of the two species is negligible. Values of −4.0 and −4.30 were obtained for the pK_a^* of **2** and **3**, respectively. A decrease in pK_a^* compared to the pK_a value is good evidence that the lone pair of the terminal nitrogen atom is involved in conjugation with the rest of the molecule more effectively in the excited state. Due to the more efficient charge migration to the nitrogen ring for molecule **3**, the pK_a and pK_a^* values for the terminal atom protonation are lowered compared to those of molecule **2**. A difference in the ground and excited state equilibrium constants means that the rate constants for the interconversion between the two species are higher in the excited state compared to the fluorescence decay rate of both the species. This allows complete equilibrium to be established (7, 8).

*3.2. Acid-base concentration behavior of molecules **4–6***

Molecules **4**, **5**, and **6** in an acidity range similar to that mentioned in Sec. 3.1 will be described in this section. Five main prototropic species, namely, the dianion (DA), monoanion (MA), neutral species (N), monocation (C), and dication (DC), were identified in the acidity range used. The various spectroscopic quantities measured are reproduced in Table 4 and the acidity constants for all the prototropic equilibria found experimentally are listed in Table 2. Figure 4 displays the absorption and fluorescence spectra of the various prototropic species. Scheme 2 represents the various prototropic species in equilibrium.

*3.2.1. Molecule **4***

This molecule exists in the neutral form from pH 7 to 9. This assignment is based on the similarity of the spectral characteristics when compared with those in different solvents (40). When the pH was increased from 9, another absorption band, shifted to higher energy and almost as intense as that of the neutral molecule, started to appear, at the expense of the neutral band, with a clear isosbestic point. Its formation was complete at pH ≈ 12. Similar effects were observed in the fluorescence spectra except that the fluorescence intensity of this species at pH 12 was significantly higher. The new species formed at pH 12 is assigned to formation of the monoanion (MA) caused by hydrolysis of the ester group, based on the following arguments:

1. When the same pH titration was reversed by decreasing the pH from 12 to 9, the reaction was irreversible. The absorption and fluorescence spectra are not modified, either in position or intensity, between pH 9 and 12.

2. The fluorescence quantum yield of the monoanion is higher than that of the neutral species. A low fluorescence quantum yield for the neutral species in these molecules in protic-polar solvents is assumed to be linked with the formation of nonfluorescent TICT states (52 and footnote 3). It is well known that TICT state formation is highly dependent upon the strength of the donor and acceptor moieties (52). Following the hydrolysis, the acceptor property of the ester is significantly reduced due to the delocalization of the negative charge on both oxygen atoms (Scheme 2). This is also evident in the blue shifts observed in the absorption and fluorescence spectra compared with those of the neutral species.

3. This interpretation is further supported by the near similarity in fluorescence quantum yields of the monoanions of **4**, **5**, and **6** to those of the neutral molecules **2** and **3** that do not contain any ester group.

A similar kind of hydrolysis was reported earlier, though at a higher basicity (56). This can be linked with the electron-withdrawing nature of the ring nitrogen coupled with the carbonyl oxygen. Further increase in base concentration to $H_- = 16$ yielded the dianion (DA), due to amino group deprotonation as discussed for molecule **2**.

When the pH was lowered from 7, the same order of protonations as obtained for molecules **2** and **3** was observed. Similar spectral shifts (see Table 4) were obtained on increasing the acidity and therefore the same interpretation of the results follows naturally. The effect of the electron-withdrawing nature of the ester group can be seen in the pK_a values of the ring nitrogen and terminal amino group protonation equilibria (Table 2). The pK_a and pK_a^* values are lower than those of molecule **2**. We did not observe any

Can. J. Chem. Downloaded from www.nrcresearchpress.com by 203.198.23.82 on 09/08/12
For personal use only.

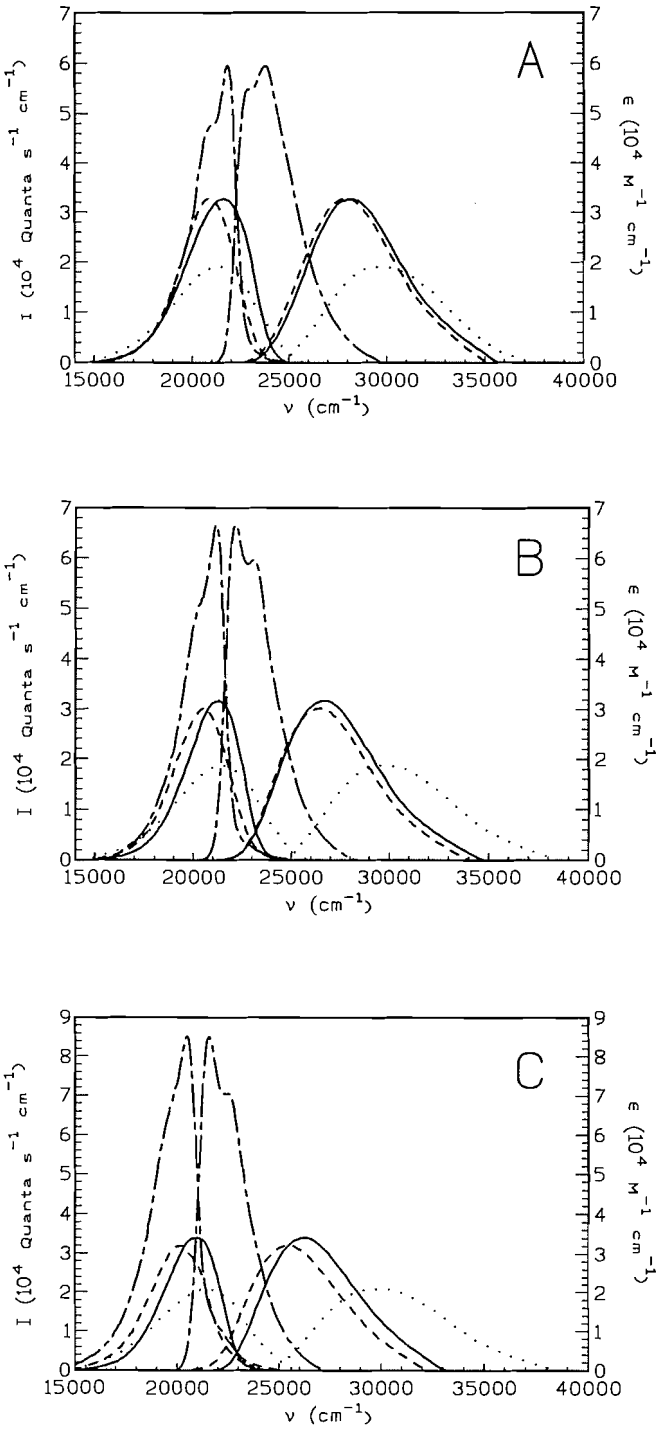

FIG. 4. Absorption and corrected fluorescence spectra of the various prototropic species of molecules **4** (A), **5** (B), and **6** (C); (——) monoanion, (- - - - -) neutral, (—·—·—) monocation, (·····) dication.

carbonyl group protonation in the acidity range studied, probably due to the presence of two positive charges already present on the molecule. Carbonyl group protonations around $H_0 \approx -6$ were reported earlier (28).

3.2.2. Molecule 5

This molecule behaves similarly to molecule **4** as far as the order of protonations and shifts in spectroscopic parameters are concerned. The magnitude of the various parameters mentioned in Tables 2 and 4 has shown the direct dependence on the donor capability of the methyl-substituted amino group.

3.2.3. Molecule 6

This molecule is a homolog of molecule **3** but with an additional ester group. As expected, it showed acidity dependence similar to that of molecules **4** and **5** from $H_- = 13$ to $H_0 = -9$. Further addition of base decreased the fluorescence intensity of the monoanion band, leading to the formation of dianion by the ring deprotonation. At $H_- = 16$, no additional broadening or appearance of any new fluorescent band was noticed, as for the other molecules. The pK_a^* value for the ring deprotonation equilibrium was found by plotting the decrease in the fluorescence intensity of the neutral species in the fluorimetric titration curve.

3.3. Förster cycle calculations

It was observed that the prototropic equilibrium is not established in the excited state when the ring nitrogen is involved in the protonation equilibrium. Thus, the Förster cycle calculation (2) can be a good means of estimating the values of pK_a^*. Also, since for the amino group protonation a complete equilibrium in the S_1 state is established, the validity of the Förster cycle calculations can be tested on these systems. Förster cycle calculations were done, using absorption (pK_a^* (Abs)) and fluorescence (pK_a^* (Flu)) center-of-mass wavelengths. All the calculated constants are listed in Table 5. This method could not be used for the neutral species – anion equilibrium due to incompleteness in the reaction.

For both the above-mentioned equilibria, the agreement between the pK_a^*(Abs) and pK_a^*(Flu) is very bad for all the molecules except molecule **1**, although the protonating sites are considered the same in the S_0 and S_1 states. From Table 5, a reduced basicity is shown by the fluorescence data compared to the absorption data. This observation is in contrast to the general behavior of the amino group (9, 16–22). One has to remember, however, that the Förster cycle strictly applies only when equal solvent relaxations exist in the ground and excited states of the species participating in the equilibrium (2). The results discussed above and the photophysical results to be published later (footnote 3) emphasize the fact that solvent relaxations differ for the species in equilibria in their ground and excited electronic states. If one had to choose between the two pK_a^* values calculated from the Förster cycle, obviously the pK_a^*(Abs) values better correlate with what is known from the literature about these basic centers. For amino group protonation the pK_a^*(Abs) emphasizes the trend in acidity observed in the pK_a (Table 2) with the donor–acceptor properties of the substituents. The pK_a^*(Abs) values shown in Table 5 are lower than the experimentally determined ones in Table 2. Such low values were also reported earlier (16).

Concluding remarks

Analysis of the absorption and fluorescence spectra of the various prototropic species of these *para*-substituted 3*H*-indole molecules, coupled with the study of the fluorescence emission and fluorescence excitation spectra of the ring protonated species at 77 K and the semiempirical AMPAC molecular orbital calculations, has shown that in these ring protonated species, the Ph_c and the indole rings are coplanar in the ground and first electronic singlet excited states

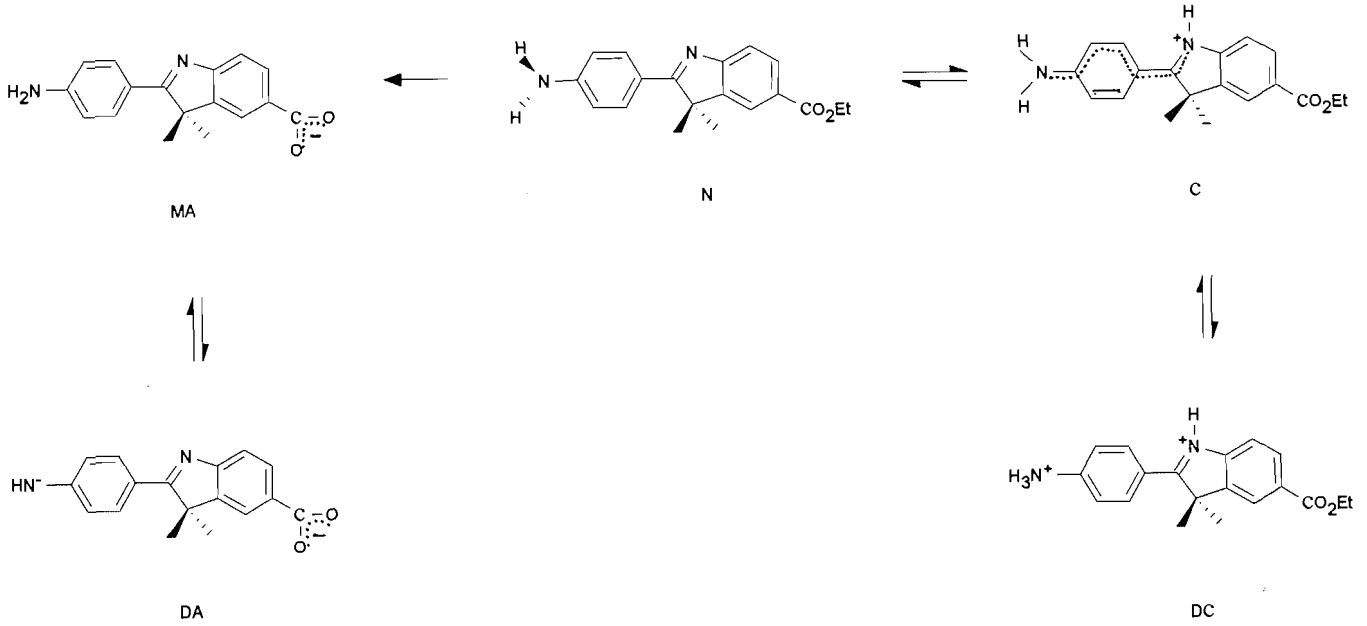

SCHEME 2

TABLE 5. Equilibrium constants for various prototropic equilibria calculated by the Förster cycle method using the center of mass of absorption (pK_a^* (Abs)) and fluorescence (pK_a^*(Flu)) wavenumbers at 298 K

	Equilibrium			
	Ring nitrogen protonation		Amino group protonation	
Molecule	pK_a^*(Abs)	pK_a^*(Flu)	pK_a^*(Abs)	pK_a^*(Flu)
1	9.55	9.13	—	—
2	15.9	6.45	−10.45	1.73
3	15.36	7.59	−13.85	−0.41
4	11.97	3.36	−12.89	0.13
5	12.57	4.38	−15.91	−1.63
6	12.04	4.9	−17.17	−2.89

in rigid as well as in fluid solutions. In the neutral species, the dimethylamino groups are rather pyramidal in the ground state, taking part in hydrogen bonding interactions with water. This effect would explain the slight fluorescence quenching of the neutral species. On the other hand, INDO-S semiempirical calculations have shown that a non-emissive low-energy TICT state might be responsible for the drastic fluorescence quenching of the monocation species.

Acid–base chemistry studies have resulted in the determination of four prototropic species in molecules **2** and **3**, whereas the ester-substituted **4**, **5**, and **6** molecules have given rise to an additional anion due to hydrolysis of the ester group. In all these molecules the first protonation site is the ring nitrogen in preference to the terminal nitrogen. Although the ring nitrogen becomes more basic upon excitation, the proton transfer equilibrium is not established in the excited state. On the other hand, the terminal amino group undergoes a complete proton transfer equilibrium in the S_1 state. The various proton transfer equilibria have shown a direct dependence upon the donor and acceptor properties of the substituent groups. Förster cycle calculations support the nature of the various substituent groups, i.e., the amino group acquires more acidity in the excited state while the ring nitrogen becomes more basic.

Because these molecules show strong dependence on pH and in turn generate charged species of various types, these species could yield good information about the nature of charged membranes (positively or negatively charged), especially, since the spectra of the charged species are well separated from the neutral entity in these molecules. The ring nitrogen prototropic equilibrium could be put to profit to sense interfacial proton concentration at anionic surfaces.

Acknowledgments

The financial assistance of the Natural Sciences and Engineering Research Council of Canada and the "Fonds pour la formation de chercheurs et l'aide à la recherche" (Québec) is gratefully acknowledged.

1. E.M. Kosower. Annu. Rev. Phys. Chem. **37**, 127 (1986).
2. Th. Förster. Z. Elektrochem. **54**, 42 (1950).
3. A. Weller. Ber. Bunsen-Ges. Phys. Chem. **56**, 662 (1952); **66**, 1166 (1956).
4. A. Weller. Prog. React. Kinet. **1**, 189 (1961).
5. E.L. Wehry and L.B. Rogers. *In* Fluorescence and phosphorescence analysis. *Edited by* D.M. Hercules. Wiley Interscience, New York. 1966. p. 125.
6. E. Vander Donckt. Prog. React. Kinet **5**, 273 (1970).
7. S.G. Schulman. *In* Modern fluorescence spectroscopy. Vol. 2. *Edited by* E.L. Wehry. Plenum, New York. 1976.
8. S.G. Schulman. *In* Fluorescence and phosphorescence spectroscopy. Pergamon, Oxford. 1977.
9. J.F. Ireland and P.A.H. Wyatt. Adv. Phys. Org. Chem. **12**, 131 (1976).
10. W.J.M. Underberg and S.G. Schulman. Anal. Chim. Acta, **105**, 311 (1979).
11. G.J. Woolfe, M. Melzig, S. Schneider, and F. Dorr. Chem. Phys. **77**, 213 (1983).
12. A.J.G. Strandjord, D.M. Couteny, and P.F. Barbara. J. Phys. Chem. **87**, 1125 (1983).

Can. J. Chem. Downloaded from www.nrcresearchpress.com by 203.198.23.82 on 09/08/12
For personal use only.

13. S.R. Flow and P.F. Barbara. J. Phys. Chem. **89**, 4489 (1985).
14. R. Manoharan and S.K. Dogra. J. Phys. Chem. **92**, 5282 (1988).
15. Y.V. Il'ichev, K.M. Solntsev, A.B. Demyashkevich, M.G. Kuzmin, H. Lemmetyinen, and E. Vuorimaa. Chem. Phys. Lett. **193**, 128 (1992).
16. S.G. Schulman and L.B. Sanders. Anal. Chim. Acta, **56**, 83 (1971).
17. S.G. Schulman and A.C. Capomacchia. Anal. Chim. Acta, **58**, 91 (1972).
18. P.J. Zavala, M.D. Radcliffe, and S.G. Schulman. Talanta, **32**, 258 (1985).
19. B.S. Vogt and S.G. Schulman. Chem. Phys. Lett. **99**, 157 (1983).
20. A.K. Mishra and S.K. Dogra. J. Photochem. **31**, 333 (1985).
21. J.K. Dey and S.K. Dogra. Bull. Chem. Soc. Jpn. **64**, 3142 (1991).
22. J.K. Dey and S.K. Dogra. Chem. Phys. **143**, 97 (1990).
23. P.L. Kovi, C.L. Miller, and S.G. Schulman. Anal. Chim. Acta, **61**, 7 (1972).
24. M. Swaminathan and S.K. Dogra. J. Am. Chem. Soc. **105**, 6223 (1983).
25. G.J. Woolfe and P.J. Thistlethwaite. J. Phys. Chem. **103**, 3849 (1981).
26. D. Brault and C. Vever-Bizet. J. Chem. Soc. Faraday Trans. **88**, 1519 (1992).
27. H.K. Sinha and S.K. Dogra. Bull. Chem. Soc. Jpn. **62**, 2668 (1989).
28. S. Srivastava and S.K. Dogra. J. Photochem. Photobiol. A: **46**, 329 (1989).
29. J.J. Aaron, A. Tine, M.E. Wojciechowska, and C. Párkányi. J. Lumin. **33**, 33 (1985).
30. F.R. Prieto, M. Mosfuera, and M. Novo. J. Phys. Chem. **94**, 8536 (1990).
31. M. Novo, M. Mosquera, and F.R. Prieto. Can. J. Chem. **70**, 823 (1992).
32. L.S. Romsted and D. Zanette. J. Phys. Chem. **92**, 4690 (1988).
33. C.J. Drummond and F. Greiser. Photochem. Photobiol. **45**, 19 (1987).
34. J.E. Hansen, E. Pines, and G.R. Fleming. J. Phys. Chem. **96**, 6904 (1992).
35. K.P. Ghiggino, A.O. Scully, and I.H. Lener. J. Phys. Chem. **90**, 5089 (1986).
36. G. Woessner, G. Groeller, J. Reiker, H. Hoier, J.J. Strezowski, E. Dattrozzo, M. Neureiter, and H.E.A. Khamer. J. Phys. Chem. **89**, 3629 (1985).
37. T. Nishiya, S. Yamanch, N. Hirota, M. Baba, and I. Hamazaki. J. Phys. Chem. **90**, 5130 (1986).
38. M. Belletête and G. Durocher. J. Phys. Chem. **93**, 1793 (1989).
39. M. Lachapelle, M. Belletête, M. Poulin, N. Godbout, F. LeGrand, A. Héroux, F. Brisse, and G. Durocher. J. Phys. Chem. **95**, 9764 (1991).
40. M. Belletête and G. Durocher. J. Phys. Chem. **96**, 9183 (1992).
41. M. Belletête, R.S. Sarpal, and G. Durocher. Chem. Phys. Lett. **201**, 145 (1993).
42. M. Belletête, M. Lachapelle, and G. Durocher. J. Phys. Chem. **94**, 5337 (1990); **94**, 7642 (1990).
43. R.S. Sarpal, M. Belletête, and G. Durocher. J. Phys. Chem. **97**, 5007 (1993).
44. M. Belletête, A. Popowycz, D. Héroux, D. Gravel, F. Brisse, and G. Durocher. J. Mol. Struct. In press.
45. P. Skrabal, J. Steiger, and H. Zollinger. Helv. Chem. Acta, **58**, 800 (1975).
46. A. Popowycz. M.Sc. Thesis, Université de Montréal. 1992.
47. M.J. Jorgenson and D.A. Hartter. J. Am. Chem. Soc. **85**, 878 (1963).
48. G. Yagil. J. Phys. Chem. **71**, 1034 (1967).
49. M. Chowdhury and N. Chattopaday. J. Photochem. Photobiol. A: **41**, 337 (1988).
50. A.K. Mishra, M. Swaminathan, and S.K. Dogra. J. Photochem. **28**, 87 (1985).
51. F. Brisse and J. Sygusch. Acta Crystallogr. Sect. B: Struct. Crystallogr. Cryst. Chem. **B30**, 480 (1974).
52. (*a*) Z.R. Grabowski, K. Rotkiewicz, A. Siemiarczuk, D.J. Cowley, and W. Baumann. Nouv. J. Chim. **3**, 443 (1979); (*b*) Z.R. Grabowski and J. Dobkowski. Pure Appl. Chem. **55**, 245 (1983); (*c*) Z.R. Grabowski. Acta Phys. Polon. A, **A71**, 743 (1987); (*d*) W. Rettig. Angew. Chem. Int. Ed. Engl. **25**, 971 (1986); (*e*) J. Lipinski, H. Chojnacki, Z.R. Grabowski, and K. Rotkiewicz. Chem. Phys. Lett. **70**, 449 (1980); (*f*) K. Rotkiewicz and W. Rettig. J. Lumin. **54**, 221 (1992).
53. J. Herbich, J. Karpink, Z.R. Grabowski, N. Tamai, and K. Yoshihara. J. Lumin. **54**, 165 (1992).
54. H. Shizuka and K. Tsutumi. J. Photochem. **9**, 334 (1978).
55. H. Shizuka. Acc. Chem. Res. **18**, 141 (1985).
56. R. Manoharan and S.K. Dogra. Spectrochim. Acta, **43**, 91 (1987).

Can. J. Chem. Downloaded from www.nrcresearchpress.com by 203.198.23.82 on 09/08/12
For personal use only.

The negative ion BN^- and its role in determining the ground state of BN via photodetachment. An MRDCI *ab initio* study

ROBERT C. MAWHINNEY, PABLO J. BRUNA, AND FRIEDRICH GREIN[1]

Department of Chemistry, University of New Brunswick, Fredericton, NB E3B 6E2, Canada

Received March 15, 1993

This paper is dedicated to Professor Gerald W. King on the occasion of his 65th birthday

ROBERT C. MAWHINNEY, PABLO J. BRUNA, and FRIEDRICH GREIN. Can. J. Chem. **71**, 1581 (1993).

Extensive multireference CI calculations using a contracted 6*s*5*p*3*d*1*f* Gaussian basis set on the B and N atoms indicate that the $X^2\Sigma^+$, $A^2\Pi$, and $B^2\Sigma^+$ states of BN^- are bound with respect to the electron attachment BN + e^-. The $1^4\Sigma^+$, $1^4\Delta$, $1^4\Sigma^-$, and $1^4\Pi$ states of BN^- are resonant states, all autodetaching into neutral BN. The electron affinity $X^3\Pi \rightarrow X^2\Sigma^+$ is predicted to be 2.84 eV (with a best estimate of 3.10 eV). Other features studied for BN^- include the infrared spectrum of the $X^2\Sigma^+$ ground state as well as the electronic radiative properties involving the excited states $A^2\Pi$ and $B^2\Sigma^+$. The present study supports a $X^3\Pi$ ground state for BN, with $a^1\Sigma^+$ lying about 0.03 eV higher. As an alternative to optical spectroscopy on BN, experimental studies of the photodetachment spectrum of BN^- are proposed in order to find the ordering and energetic separation of the lowest $^3\Pi$ and $^1\Sigma^+$ states of BN.

ROBERT C. MAWHINNEY, PABLO J. BRUNA et FRIEDRICH GREIN. Can. J. Chem. **71**, 1581 (1993).

Des calculs extensifs d'IC à références multiples réalisés à l'aide d'un ensemble de base gaussien 6*s*5*p*3*d*1*f* sur les atomes de B et de N indiquent que les états $X^2\Sigma^+$, $A^2\Pi$ et $B^2\Sigma^+$ du BN^- sont liés lors de la fixation d'électron BN + e^-. Les états $1^4\Sigma^+$, $1^4\Delta$, $1^4\Sigma^-$ et $1^4\Pi$ du BN^- sont des états de résonance qui s'autodétachent tous pour donner du BN neutre. On fait la prédiction que l'affinité électronique de $X^3\Pi \rightarrow X^2\Sigma^+$ est de 2,84 eV (la meilleure évaluation est de 3,10 eV). Les autres caractéristiques du BN^- étudiées comprennent le spectre infrarouge de l'état fondamental $X^2\Sigma^+$ ainsi que les propriétés électroniques radiatives impliquant les états excités $A^2\Pi$ et $B^2\Sigma^+$. Les résultats de notre étude sont en accord avec un état fondamental $X^3\Pi$ pour le BN ayant un état $a^1\Sigma^+$ à environ, 0,03 eV plus haut. Comme alternative à la spectroscopie optique du BN, on propose des études expérimentales du spectre de photoablation du BN^- qui devraient permettre de déterminer l'ordre et la séparation énergétique des états $^3\Pi$ et $^1\Sigma^+$ du BN.

[Traduit par la rédaction]

1. Introduction

The characterization of the ground state of the first-row isoelectronic diatomics C_2, BN, and CN^+ represents a challenging task for experimental as well as theoretical spectroscopists. The main reason for this difficulty lies in two electronic states, $^1\Sigma_{(g)}^+$ and $^3\Pi_{(u)}$, being separated energetically by less than 0.1 eV (1, 2). Despite the fact that electronic transitions into these lowest triplet and singlet states have been recorded in some instances, a *direct* spectroscopic determination of the $^3\Pi_{(u)}$–$^1\Sigma_{(g)}^+$ separation is prevented by the multiplicity selection rules. The spectroscopist is thus compelled to look at small vibrational or rotational perturbations in the available spectra (3).

The C_2 molecule, which has been studied experimentally more extensively than BN or CN^+ (1), represents a good example. For simplicity, the C_2 states are labelled according to the revised, final assignment given by Ballik and Ramsay (4). Until around 1960 the C_2 ground state was thought to be $^3\Pi_u(3\sigma_g 1\pi_u^3)$ since the intense $^3\Pi_g$–$^3\Pi_u$ (Swan) band system was observed in the laboratory as well as in spectra from outer space (4, 5). However, a seminal study by Ballik and Ramsay (4) on the band system $b^3\Sigma_g^-$–$a^3\Pi_u$ detected perturbations in the upper state caused by the lowest lying $^1\Sigma_g^+$ state. Additional analysis of the Phillips band system $A^1\Pi_u$–$X^1\Sigma_g^+$ confirmed that C_2 has a $X^1\Sigma_g^+(1\pi_u^4)$ ground state, with $a^3\Pi_u$ lying at a T_e of about 0.09 eV (6).

Unfortunately, for neither BN nor CN^+ has the question about the nature of the ground state been settled experimentally. The main reason is the lack of experimental studies on band systems equivalent to those of C_2. For instance, according to the 1977 compilation by Huber and Herzberg (1), the only experimental data available for CN^+ are restricted to the singlet manifold. On the other hand, for BN, information exists on two triplet transitions, namely $2^3\Pi$–$1^3\Pi$ (7, 8) and $n^3\Sigma^-$–$1^3\Sigma^-$ (9) as well as two singlet band systems $c^1\Sigma^+$–$a^1\Sigma^+$ and $c^1\Sigma^+$–$b^1\Pi$ (10). Since the transitions $1^3\Sigma^-$–$1^3\Pi$ and $1^1\Pi$–$1^1\Sigma^+$ of BN (corresponding to the Ballik-Ramsay and Phillips bands in C_2) have not been studied experimentally, nothing can currently be said about the existence of perturbations similar to those in the C_2 molecule.

It is well established that *ab initio* methods may provide reliable data to complement experimental results (2, 11). In principle, modern theoretical computational techniques are able to describe electronic states of different multiplicity or character (bound or unbound, valence or Rydberg, etc.) with a fairly uniform degree of accuracy. However, to achieve an accuracy of better than 0.1 eV (about 2 kcal mol^{-1} or 800 cm^{-1}) requires the use of rather large AO basis sets and extensive multireference wave functions (12).

All *ab initio* studies on BN published to date favor $X^3\Pi(5\sigma 1\pi^3)$ to be the ground state, with $a^1\Sigma^+(1\pi^4)$ lying up to 0.1 eV higher. In a prior investigation from this laboratory by Karna and Grein (ref. 13, hereafter KG1), many excited states were studied by carrying out MRD-CI calculations using an AO basis set of triple-zeta plus polarization quality. KG1 reported $T_e(a^1\Sigma^+)$ to be 0.10 eV. Later, Martin et al. (14) performed quadratic CI (QCISD(T)) calculations especially tailored to reinvestigate the $^1\Sigma^+$–$^3\Pi$ separation in BN. Unfortunately, this study was not conclusive since ΔE values ranging from −0.03 to +0.03 eV were obtained depending on the technical conditions of the calculations. They recommended a best estimate of $T_e(a^1\Sigma^+) = 0.012$ eV, with $X^3\Pi$ being the ground state.

[1]Author to whom correspondence may be addressed.

Can. J. Chem. Downloaded from www.nrcresearchpress.com by 203.198.23.82 on 09/08/12
For personal use only.

Can. J. Chem. Downloaded from www.nrcresearchpress.com by 203.198.23.82 on 09/08/12
For personal use only.

A very detailed *ab initio* study on the same topic has recently been published (15) which uses a multireference CI treatment and a fairly extended $5s4p3d2f1g$ contracted basis set. This work came to the conclusion that $X^3\Pi$ is more stable than $a^1\Sigma^+$ by 0.047 ± 0.012 eV. Taking into account the high degree of sophistication used in these studies, one can conclude that theory (nonrelativistic model and only correlating valence electrons) strongly supports $X^3\Pi$ to be the ground state.

We decided to address the question of the $^1\Sigma^+$–$^3\Pi$ separation in BN from another point of view, aimed to assist future *experimental* determinations of that quantity. In short, we propose, as an alternative to the optical spectroscopy on BN, the study of the photoelectron detachment spectrum of BN^-. This anion has a $X^2\Sigma^+$ ($4\sigma^2 5\sigma 1\pi^4$) ground state (16) and is expected to be as stable as the experimentally observed isoelectronic C_2^- species (1). Moreover, simple arguments indicate that photodetachment from the ground state of BN^- is able to generate neutral BN either in the $^3\Pi$ ($1\pi\rightarrow\infty$) or $^1\Sigma^+(5\sigma\rightarrow\infty)$ state (17). To assist future experiments in that direction, reliable potential curves and spectroscopic data on the low-lying state of BN^- will be reported here.

2. Technical details

Each atomic orbital basis set consisted of the 49 contracted Gaussian functions, $6s5p3d1f$. The primitive set $10s6p$ from Huzinaga (18) has been contracted to $5s4p$ according to Dunning (19). Additional semidiffuse $(1s,1p)$ and polarization functions $(3d,1f)$ were added to each atom, with exponents taken from the literature (19–21). In the same order as above, the exponents of the extra functions are 0.018, 0.019, 0.822, 0.187, 0.05, and 0.5 for B and 0.045, 0.048, 1.986, 0.412, 0.07, and 1.0 for N.

The potential curves were studied for internuclear distances from 1.95 to 3.40 bohr. For BN^-, all CI calculations were carried out by using the SCF MO's obtained for the ground state $X^2\Sigma^+(4\sigma^2 5\sigma 1\pi^4)$, whereas all potential curves of BN have been studied with the SCF MO's from the $^3\Sigma^-(4\sigma^2 5\sigma^2 1\pi^2)$ state of BN.

The MRD-CI method (22) has been used. This method includes selection of configurations and extrapolation techniques. The core orbitals $1\sigma(1s_N)$ and $2\sigma(1s_B)$ are kept doubly occupied throughout (frozen core approximation), while the nine highest lying virtual orbitals have been discarded (5 in a_1, 2 each in b_1 and b_2). Thus, the active MO space consists of 87 orbitals to describe the valence correlation among eight (BN) or nine (BN^-) valence electrons (VE). Single-point calculations at the respective equilibrium geometries have been carried out by using parent natural orbitals (NO). The number of reference configurations varied from 40 to 55 depending on the states. The total CI space generated had an average dimension of 1.5×10^6, with the secular equations directly diagonalized varying from 16 000 to 25 000. Configuration thresholds of 2.5 μhartree (MO's) and 1.0 μhartree (NO's) have been used.

All total and relative energies to be reported are estimated full-CI energies. The latter are obtained by applying a generalized Langhoff–Davidson correction to the extrapolated MRD-CI energies (2, 23). As shown by Knowles et al. (24) for a series of molecular species, the estimated full-CI energies reproduce the exact full-CI energies (for a given AO basis set) within ±5 kcal mol^{-1}.

TABLE 1. Relative energies, in eV, for selected atomic states of B, B^-, N, and N^-

	State	ΔE^a This work	ΔE^a Experimental
B	$^2P_u(s^2p)$	0.00[b]	0.00
	$^4P_g(sp^2)$	3.59	3.57[c]
B^-	$^3P_g(s^2p^2)$	−0.27	−0.277[d,e]
	$^1D_g(s^2p^2)$	0.23	[e]
	$^1S_g(s^2p^2)$	0.59	[e]
N	$^4S_u(s^2p^3)$	0.00[f]	0.00
	$^2D_u(s^2p^3)$	2.46	2.38[c]
	$^2P_u(s^2p^3)$	3.64	3.58[c]
N^-	$^3P_g(s^2p^4)$	0.27	0.07[d]

[a]Values tabulated for X^- correspond to −EA.
[b]Total energy = −24.59999 hartree.
[c]Reference 25.
[d]Reference 27.
[e]Compare with semiempirically corrected values of −0.30 eV for ^3P_g, 0.22 eV for ^1D_g, and 1.01 eV for ^1S_g from ref. 45.
[f]Total energy = −54.51739 hartree.

3. Atomic energies

The quality of the AO basis set has been assessed by computing several electronic states of both the neutral and negatively charged atoms. Table 1 summarizes the results.

The calculated transition energies of B and N reproduce experimental values (25) quite well, with errors of less than 0.1 eV. Thus, the transition energies of BN and BN^- should be of similar accuracy.

Electron attachment upon $B(^2P_u, s^2p)$ generates three electronic states of B^-, all arising from the global configuration s^2p^2 (26). However, only $B^-(^3P_g)$ has a positive electron affinity (EA), with a predicted value of 0.27 eV, in almost perfect agreement with the experimental value of 0.277 eV (27). The excited B^- states ^1D_g and ^1S_g are resonant states (i.e., they lie above the ground state of B), with estimated EA values of −0.23 and −0.59 eV, respectively. These results indicate that a semiempirical estimate of −1.01 eV for EA ($B,^3P_g \rightarrow B^-,^1S_g$) is about 0.40 eV too high (see footnote *e*, Table 1).

The negative ion $N^-(^3P_g,s^2p^4)$ is known to be unbound upon electron attachment on N. An experimental EA of −0.07 eV (27) has to be compared with our theoretical estimate of −0.27 eV. The predicted EA of BN might be too low by roughly 0.25 eV, similar to the error obtained for the N atom. This assumption is based on the fact that in going from BN ($X^3\Pi$,$a^1\Sigma^+$) to BN^- ($X^2\Sigma^+$), electron attachment leads to the occupation of the MO's 5σ or 1π, which are mainly localized on the N atom (see Sect. 4.1).

4. Electronic states of BN^-

A summary of several dissociation channels of BN^- and BN is given in Table 2. Spectroscopic data predicted for the low-lying doublet and quartet states of BN^- are collected in Table 3.

The second and third dissociation limits of BN^- are placed above the ground state products $B(^2P_u)$ + $N(^4S_u)$. This situation contrasts with that observed for AlP^- (17), in which the first three asymptotes lie below the ground state of Al + P. The channel $B^-(^3P_g)$ + $N(^4S_u)$ gives rise to doublet, quartet, and sextet Σ^+ and Π states of BN^-. Earlier studies on

TABLE 2. Correlation between atomic and molecular electronic states for the lower dissociation channels of BN and BN^-

	Products	Molecular states	ΔE (eV)[a] This work	ΔE (eV)[a] Experimental
BN^-	$B^-(^3P_g) + N(^4S_u)$	$^{6,4,2}(\Sigma^+,\Pi)$	0.00	0.000
	$B(^2P_u) + N^-(^3P_g)$	$^{4,2}(\Sigma^+,\Sigma^-(2),\Pi(2),\Delta)$	0.54	0.347
	$B^-(^1D_g) + N(^4S_u)$	$^4(\Sigma^-,\Pi,\Delta)$	0.50	—
BN	$B(^2P_u) + N(^4S_u)$	$^{5,3}(\Sigma^-,\Pi)$	0.27	0.277
	$B(^2P_u) + N(^2D_u)$	$^{3,1}(\Sigma^+,\Sigma^-(2),\Pi(3),\Delta(2),\Phi)$	2.73	2.657

[a]Based on the data from Table 1.

TABLE 3. Calculated spectroscopic data for BN^- obtained from MRD-CI-MO wavefunctions. Energies in eV, distances in bohr, all other data in cm^{-1} [a]

State[b,c]	T_e[d]	R_e	ω_e	$\omega_e x_e$	B_e	α_e
$X^2\Sigma^+$	0.0[e]	2.440	1709	14.5	1.611	0.004
	0.0	2.453	1781	21.3	1.625	0.006
$A^2\Pi$	0.78	2.568	1496	8.6	1.464	0.007
	1.08	2.549	1595	16.6	1.503	0.010
$B^2\Sigma^+$	2.62	2.477	1414	3.0	1.627	0.025
	2.85	2.428	1880	34.6	1.656	0.002
$1^4\Sigma^+$	3.40	2.642	1171	6.5	1.460	—
$1^4\Delta$	3.64	2.597	1476	13.3	1.375	—
$1^4\Pi$	3.63	2.542	1603	11.8	1.516	—
$1^4\Sigma^-$	3.89	2.565	1451	17.9	1.356	—

[a]Second entry (doublet states) from ref. 16.
[b]The quartet states are metastable (see text).
[c]The $X^3\Pi$ state of BN lies at T_e = 2.77 eV (MO's), and 2.84 eV (NO's). See Table 10.
[d]With NO's, T_e = 0.81 eV ($A^2\Pi$) and T_e = 2.53 eV ($B^2\Sigma^+$).
[e]Total energy (in hartree): −79.36549 (MO's) and −79.37178 (NO's).

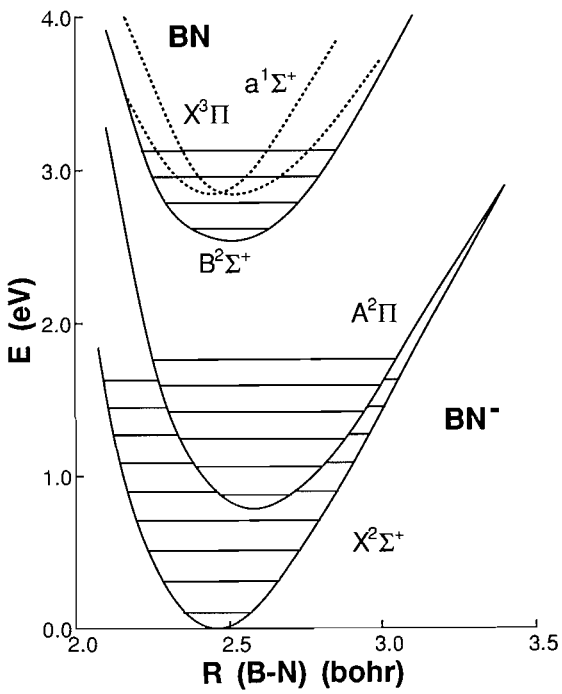

FIG. 1. Potential curves of the states $X^2\Sigma^+$, $A^2\Pi$, and $B^2\Sigma^+$ of BN^-, and $X^3\Pi$ and $a^1\Sigma^+$ of BN.

CSi^- (28) and AlP^- (17) indicated that the $^6\Sigma^+$ and $^6\Pi$ states lie well above the ground state of the neutral species. Therefore, sextet states of BN^- were not considered in this study.

4.1 Doublet states

As reported by Karna and Grein (ref. 16, hereafter KG2) the lowest doublet states of BN^- are $X^2\Sigma^+(4\sigma^2 5\sigma 1\pi^4)$, $A^2\Pi(1\pi\rightarrow 5\sigma)$, and $B^2\Sigma^+(4\sigma\rightarrow 5\sigma)$. The potential curves are shown in Fig. 1.

The transition energies of BN^- obtained in the present study are about 0.3 eV smaller than those of KG2. At the same time, we obtain an EA(BN) about 0.3 eV higher than the earlier estimates of 2.54 eV. Therefore, a relative stabilization of 0.6 eV in the excited states of $A^2\Pi$ and $B^2\Sigma^+$ of BN^- with respect to $BN(X^3\Pi)$ has a dramatic influence on the character of the $B^2\Sigma^+$ state, which is now predicted to be bound.

Our R_e values for $X^2\Sigma^+$ and $A^2\Pi$ agree within 0.02 bohr with KG2's results, but the present ω_e data are roughly 100 cm^{-1} lower. The discrepancies are somewhat larger for $B^2\Sigma^+$, namely +0.05 bohr for R_e and −470 cm^{-1} for ω_e.

The electron charge density contours as obtained from SCF calculations on the $X^2\Sigma^+$ state of BN^- (at R = 2.40 bohr) are displayed in Fig. 2. The corresponding MO's of $X^3\Pi$ (BN) look similar. Most of the valence MO's are strongly localized: 3σ is an *sp* hybrid on the B atom, whereas both 5σ and

Can. J. Chem. Downloaded from www.nrcresearchpress.com by 203.198.23.82 on 09/08/12
For personal use only.

Can. J. Chem. Downloaded from www.nrcresearchpress.com by 203.198.23.82 on 09/08/12
For personal use only.

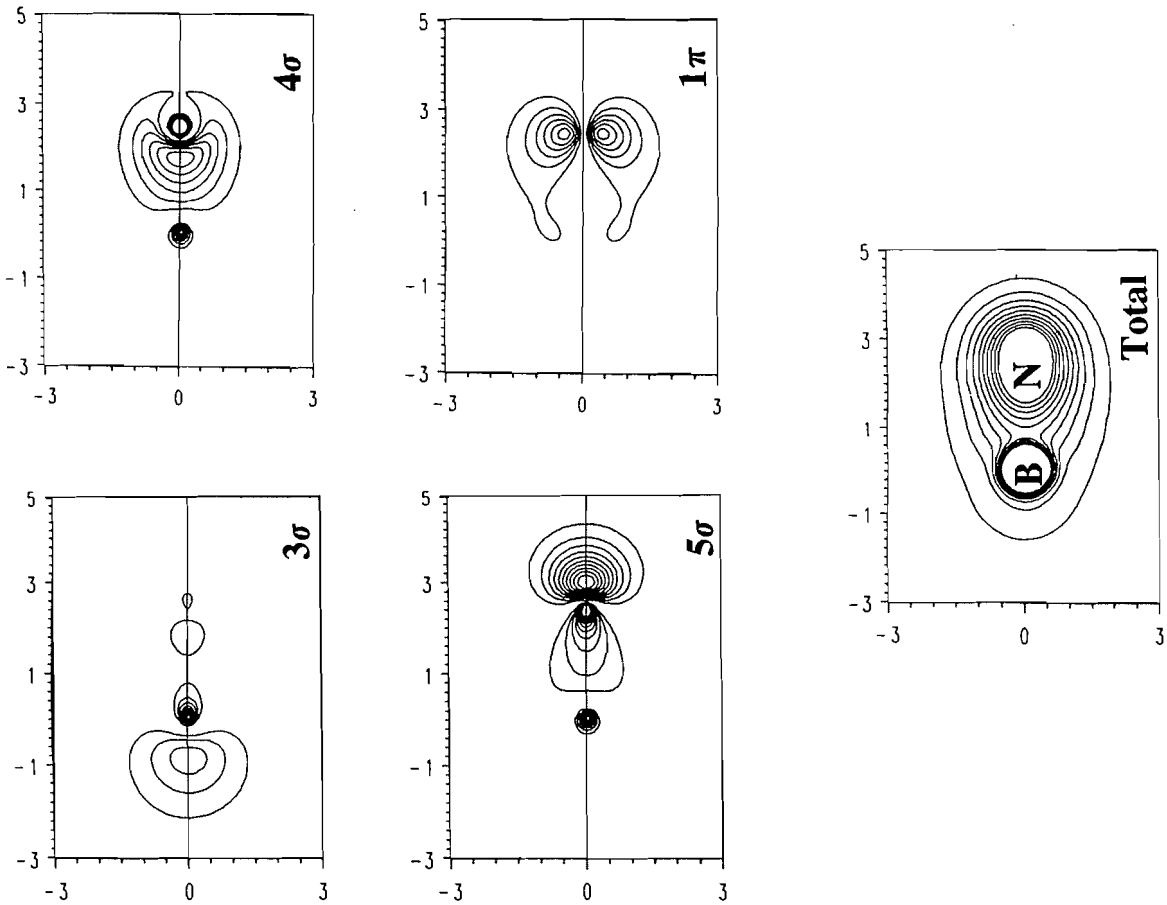

FIG. 2. Electron charge density contours for the valence MO's of ground state BN^- at R = 2.40 bohr. The contour line ranges from 0.05 (outermost) to 0.5 (innermost), in steps of 0.05.

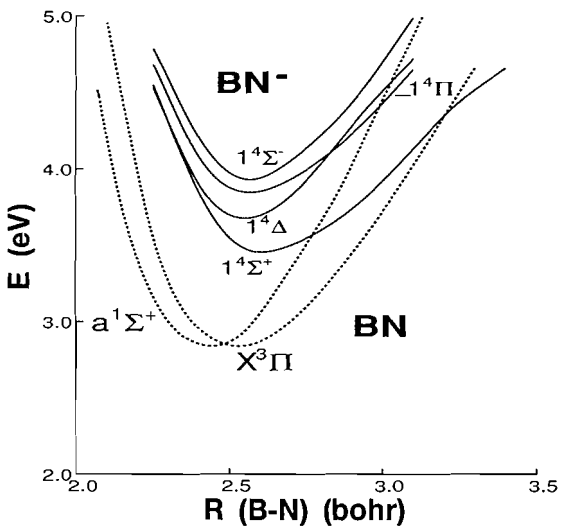

FIG. 3. Potential curves of the metastable states $1^4\Sigma^+$, $1^4\Delta$, $1^4\Pi$, and $1^4\Sigma^-$ of BN^-. Energies relative to the minimum of $X^2\Sigma^+(BN^-)$.

1π are essentially N species. Only 4σ shows some B—N bonding character.

The total density distribution reveals an excess of electronic charge around the N atom, as pointed out by contour lines that are well spread out spatially. By contrast, those around B are not only more compact but also retain a good deal of spherical symmetry (similar to a local B^+ (s^2) structure). Thus, the overall charge distribution for the ground state of BN^- corresponds to $B^{\delta+}N^{(1+\delta)-}$. Since the $X^3\Pi$ state of BN has a $B^{\delta+}N^{\delta-}$ polarity (Sect. 5), it can be concluded that in the ground state of BN^- the extra electron is attached mainly to the N center.

4.2 Quartet states

Near equilibrium, the lowest lying quartet states arise from the electronic configurations ... $5\sigma 1\pi^3 2\pi(1^4\Sigma^+ < 1^4\Delta < 1^4\Sigma^-)$ and ... $5\sigma 1\pi^3 6\sigma(1^4\Pi)$. Formally, these states can be generated by electron attachment into the 2π (π^*) or 6σ (σ^*) MO's of the $^3\Pi$(... $5\sigma 1\pi^3$) state of BN. The potential curves are displayed in Fig. 3.

These quartet states are less stable than the ground state of BN. The $1^4\Sigma^+$ and $1^4\Sigma^-$ states lie 0.56 and 1.05 eV above $X^3\Pi$, respectively; the $1^4\Pi$ state has an intermediate T_e value (Table 3). The autoionizing character of these quartets has been investigated by carrying out additional MRD-CI calculations at R = 2.55 bohr that allow the outermost s and p AO's on the B atom to become more diffuse. The original semidiffuse exponents of α_s = 0.018 and α_p = 0.02 have been reduced in two steps, each by a factor of 2. The MRD-CI results with α_s = 0.0045 and α_p = 0.005 indicate a lowering of the total energies for all four quartet states, which are finally clustered within an energy range of 0.20 eV. An additional calculation for $X^3\Pi$ of BN with this

TABLE 4. Dipole moments, in debye, for the $X^2\Sigma^+$ and $A^2\Pi$ states of BN^-, and the $X^3\Pi$ and $a^1\Sigma^+$ state of BN. Distances in bohr

	BN^- [a]		BN[b]	
R	$X^2\Sigma^+$	$A^2\Pi$	$X^3\Pi$	$a^1\Sigma^+$
1.95	−4.1658	0.3955	−1.9647	−1.1805
2.10	−4.3439	0.0040	−1.9864	−1.3646
2.25	−4.5237	−0.4109	−1.9885	−1.5987
2.40	−4.6959	−0.8485	−1.9444	−1.7695
2.55	−4.8211	−1.2896	−1.8665	−1.9751
2.70	−4.9689	−1.7315	−1.8358	−2.0956
2.95	−5.0748	−2.6256	−1.7217[c]	−2.1643[c]
3.10	−5.0902	−3.6386	−1.6308[d]	−2.1564[d]

[a]With B atom at the origin of the coordinate system.
[b]A negative value of μ corresponds to a B^+N^- polarity.
[c]R = 2.85 bohr.
[d]R = 3.00 bohr.

modified basis set indicates that they lie only from 0.1 to 0.3 eV above $X^3\Pi$ of BN.

Earlier studies on C_2^- (29) reported a similar autoionizing character for the corresponding lowest quartet states. By contrast, a prior investigation from this laboratory on AlP^- (17) found that $1^4\Sigma^+$, $1^4\Delta$, $1^4\Sigma^-$, and $1^4\Pi$ are bound.

5. Dipole moments and infrared spectrum

The dipole moment μ has been computed for the $X^2\Sigma^+$ and $A^2\Pi$ states of BN^- and the $X^3\Pi$ and $a^1\Sigma^+$ states of BN. The variation of μ with nuclear separation R is given in Table 4 and shown graphically in Fig. 4. The data for BN^- have been obtained with the B atom placed at the origin of the coordinate system.

The $X^3\Pi$ and $a^1\Sigma^+$ states of BN are highly ionic, with dipole moments slightly below 2.0 D near equilibrium. Both states have a B^+N^- polarity, as pointed out earlier by KG1 (13). The $X^2\Sigma^+$ and $A^2\Pi$ states of BN^- exhibit a significant dependence of the dipole moment on geometry, much higher than that predicted for the ground state of BN. These features are reflected in the dipole moment derivatives $\partial\mu/\partial R$ calculated at the corresponding equilibrium distances. The computed values in D/bohr are −0.8765 for $X^2\Sigma^+$ and −2.6760 for $A^2\Pi$ of BN^-, and 0.4194 for $X^3\Pi$ and −1.3235 for $a^1\Sigma^+$ of BN.

Within the double-harmonic approximation (30, 31), the infrared intensity associated with the fundamental absorption is given by the expression:

$$I = 65.53257 \times \left|\frac{\partial\mu}{\partial R}\right|^2_{R_e}$$

with I in km/mol and $\partial\mu/\partial R$ in D/bohr. The data from above thus correspond to infrared intensities (in km/mol) of 50.3 for $X^2\Sigma^+$ and 469.3 for $A^2\Pi$ of BN^- and of 11.5 for $X^3\Pi$ and 114.8 for $a^1\Sigma^+$ of BN. This simple approximation indicates that in BN^- the infrared absorption of $A^2\Pi$ is about 10 times higher than for the ground state. As already suggested by the $\mu(R)$ data given in Fig. 4, the infrared intensities for the $^3\Pi$ and $^1\Sigma^+$ states of BN are much smaller. An earlier SCF study reported IR intensities (in km/mol) of 27 for $X^3\Pi$ and 75 for $a^1\Sigma^+$ of BN (32).

Table 5 summarizes the predicted radiative data for a few vibrational levels v' of the ground state of BN^-. The diagonal matrix elements $R_{v'v'}$ represent the expectation values of the dipole moment $\mu_{v'}$, with the B atom placed at the origin of the coordinate system. The variation of μ with geometry is independent of the system of coordinates, as is also the case for the non-diagonal matrix elements $R_{v',v'-1} = \int \psi_{v'}\mu(z)\psi_{v'-1}d\tau$. The small variation of the dipole moment with geometry is indicated by an increase in polarity of only 0.076 D when going from $v' = 0$ to $v' = 5$. The lifetimes $\tau_{v'}$ (in ms) predicted for the first three excited vibrational levels are 148 for $v' = 1$, 67 for $v' = 2$, and 43 for $v' = 3$.

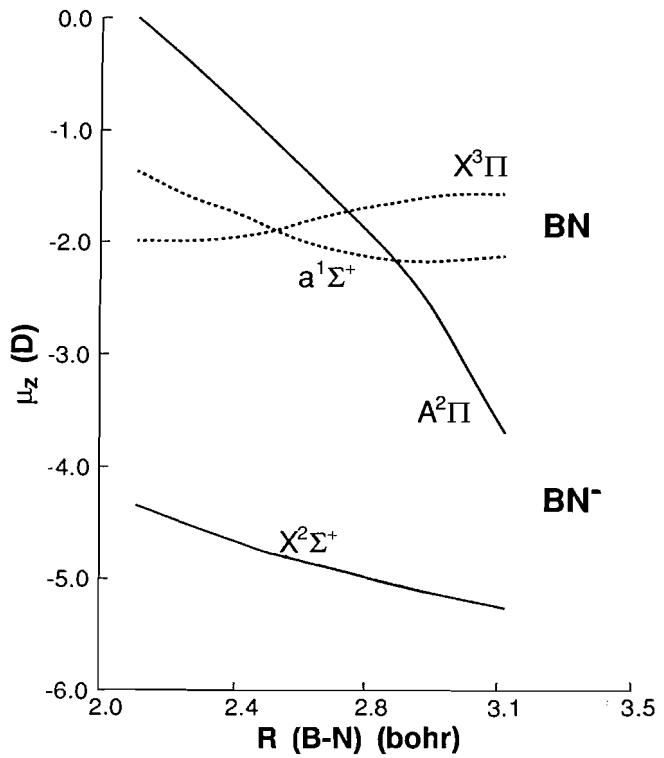

FIG. 4. Variation of the dipole moment μ with bond length R(BN) for the two lowest states of BN and BN^-.

As seen in Fig. 1, depopulation of levels with $v' \geq 4$ may occur via vibrational deexcitation within $X^2\Sigma^+$ as well as via radiative emission into the $A^2\Pi$ state (which in turn undergoes deexcitation, both vibrational and electronic). The overall rate for the cascading mechanism $X^2\Sigma^+$ ($v' \geq 4$) → $A^2\Pi(v)$ → $X^2\Sigma^+$ ($v' < 4$) is controlled by the first step since, as shown in Sect. 7, the radiative lifetime $A^2\Pi \rightarrow X^2\Sigma^+$ lies in the μs scale, and the vibrational deexcitation in $A^2\Pi$ occurs in the ms region.

Taking $v' = 8$ of $X^2\Sigma^+$ as an example, the directly calculated sum $\Sigma_f A_{if}$ of the Einstein coefficients (with $i = 8$ and $f = 0, 1, \ldots 4$) is about 2.2×10^{-2} s^{-1}. This rate constant for spontaneous emission from $v' = 8$ of $X^2\Sigma^+$ via $A^2\Pi$ intercombination corresponds to $\tau = 45$ s, much longer indeed than vibrational lifetimes of milliseconds predicted for $X^2\Sigma^+$.

A similar analysis for the $A^2\Pi$ state indicates vibrational relaxation lifetimes of about 18 ms for $v = 1$ and 9 ms for $v = 2$. This process is much longer than $\tau_0(A^2\Pi \rightarrow X^2\Sigma^+) = 14.4$ μs (Sect. 7.1), so that the vibrationally excited $A^2\Pi$ state essentially decays via emission into the electronic ground state.

Can. J. Chem. Downloaded from www.nrcresearchpress.com by 203.198.23.82 on 09/08/12
For personal use only.

TABLE 5. Dipole matrix elements $R_{v',v''}$ (in debye), Einstein coefficients for spontaneous emission $A_{v',v''}$ (in s^{-1}), and radiative lifetimes $\tau_{v'}$ (in ms) of vibrational levels of the $X^2\Sigma^+$ state of BN^- [a]

v'	$R_{v'v'} = \langle\mu_{v'}\rangle$	$R_{v',v'-1}$ [b]	$R_{v',v'-2}$ [b]	$R_{v',v'-3}$ [b]	$A_{v',v'-1}$ [c]	$A_{v',v'-2}$ [c,d]	Lifetimes $\tau_{v'}$
0	−4.740	—	—	—	—	—	—
1	−4.754	−0.692(−1)	—	—	6.778	—	148
2	−4.772	−1.041(−1)	0.71(−2)	—	14.429	0.558	67
3	−4.789	−1.296(−1)	1.15(−2)	−4.57(−3)	20.990	1.355 [0.751]	43
4	−4.804	−1.480(−1)	1.79(−2)	−4.82(−3)	25.668	3.106 [0.783]	34
5	−4.816	−1.610(−1)	2.61(−2)	−3.89(−3)	28.414	6.195 [0.479]	28

[a]Diagonal matrix elements $R_{v',v'}$ calculated with B atom at the origin of the coordinate system.
[b]$x.yz(m)$ stands for $x.yz$ times 10^m.
[c]$A_{v'v''} = 3.13602 \times 10^{-7} (\Delta E_{v'v''})^3 \langle R_{v'v''}\rangle^2$, with $\Delta E_{v'v''}$ in cm^{-1} and $R_{v'v''}$ in debye.
[d]Second entry (in brackets) corresponds to $A_{v',v'-3}$.

TABLE 6. Computed transition moments $R_{e'e''}$ (in au) for dipole-allowed transitions between the bound states of BN^- [a]

R (bohr)	$A^2\Pi$–$X^2\Sigma^+$	$B^2\Sigma^+$–$X^2\Sigma^+$	$B^2\Sigma^+$–$A^2\Pi$
1.95	0.4244	0.5573	−0.1138
2.10	0.4354	0.6380	−0.0909
2.25	0.4368	0.7030	−0.0676
2.40	0.4336	0.7512	−0.0428
2.55	0.4212	0.7830	−0.0123
2.70	0.4003	0.7748	0.0081
2.95	0.3532	0.7362	0.0304
3.10	0.3307	0.5963	0.0435
3.25	0.3040	0.4295	0.0065
3.40	0.2776	0.2795	0.0464

[a]Data tabulated do not include degeneracy factor K (see text).

6. Dissociation energies

The dissociation energy D_e for $X^2\Sigma^+$ of BN^- is found to be 6.79 eV, compared with 4.22 eV predicted for the $X^3\Pi$ state of BN. These values have been obtained by combining the total energies at equilibrium (NO results) with those of $1^6\Pi$ ($5\sigma 1\pi^2 2\pi 6\sigma$) for BN^- and $1^5\Pi(5\sigma 1\pi^2 2\pi)$ for BN at $R = 20.0$ bohr. According to a thermochemical cycle connecting ground state species, $D_e(BN^-) = D_e(BN) + [EA(BN) - EA(B)]$. An increase in the B—N bond strength of about 2.6 eV upon electron attachment implies that the EA of BN is higher than that of the B atom by the same amount.

A summary of experimentally inferred data for $D_e(BN)$ as collected by Reddy et al. (33) gives an average $D_e = 4.0 \pm 0.5$ eV for five out of nine values, with an additional estimate of about 3.36 eV, and three others from 5.4 to 6.4 eV. On the other hand, earlier *ab initio* studies reported $D_e(BN, X^3\Pi)$ values of 4.21 eV (13), 4.42 eV (32), 4.62 ± 0.1 eV (14), and 4.56 ± 0.1 eV (15). The last three results are not directly calculated D_e values but estimates obtained by adding correction terms from ±0.25 eV (15) to ±0.58 eV (32). Assuming a best estimate of 4.55 ± 0.1 eV for $D_e(X^3\Pi)$, our directly calculated value shows an error of −0.33 ± 0.1 eV. This would suggest a recommended $D_e(X^2\Sigma^+)$ of 7.12 ± 0.1 eV for BN^-.

Since the $a^1\Sigma^+$ state of BN correlates adiabatically with the second dissociation channel (Table 2), its dissociation energy should be larger by about 2.38 eV. Thus, $D_e(a^1\Sigma^+)$ is expected to lie near 6.9 eV. In refs. 14, 15, and 32, however, it has been assumed that $X^3\Pi$ and $a^1\Sigma^+$ of BN have the same dissociation products.

7. Radiative properties for electronic transitions of BN^-

Optical spectroscopy can be used to study three band systems of BN^-, namely $A^2\Pi$–$X^2\Sigma^+$, $B^2\Sigma^+$–$X^2\Sigma^+$, and $B^2\Sigma^+$–$A^2\Pi$. The purpose of this section is to discuss the radiative data associated with these bands, such as Franck–Condon factors ($q_{v'v''}$), Einstein emission coefficients ($A_{v'v''}$), oscillator strengths ($f_{v'v''}$), and radiative lifetimes ($\tau_{v'}$).

The different parameters have been calculated as outlined below. The transition moment $\bar{R}_{e'e''} = \langle\psi_{e'}{}^a/\bar{P}/\psi_{e''}{}^b\rangle$ has been calculated with $\bar{P} = e\,\bar{r}$ (length form; $\psi_{e'}{}^a$ and $\psi_{e''}{}^b$ are appropriate b_1 or b_2 (C_{2v}) components in the case of the spatially degenerate $A^2\Pi$ state. As standard notation, double and single primes label the lower and upper electronic states (same notation for the corresponding vibrational levels). The values of $R_{e'e''}$ are given in Table 6 and shown graphically in Fig. 5.

The term $\Sigma R^2_{e'e''}$ corresponds to $KR^2_{e'e''}$, with K taking into account the overall multiplicity and spatial degeneracies. In the present case, $K = 2$ for $^2\Sigma^+$–$^2\Sigma^+$ and $K = 4$ for $^2\Pi$–$^2\Sigma^+$ transitions. The band strength $S_{v'v''}$ is computed via the expression $S_{v'v''} = K|\int \phi_{v'}(R)R_{e'e''}(R)\phi_{v''}(R)dR|^2$, by using a polynomial expansion to represent the (discrete) $R_{e'e''}$ data and the appropriate vibrational wavefunctions $\phi_v(R)$ of each electronic state as weight functions (34). The absorption oscillator strength $f_{v'v''}$ is defined as $f_{v'v''} = 2/3\ K'\Delta E_{v'v''}S_{v'v''}$, with $\Delta E_{v'v''}$ in atomic units and $K' = [(2\text{-}\delta_{0\Lambda''})(2S'' + 1)]^{-1}$. Thus, $K' = {}^1/_2$ and ${}^1/_4$ for absorption from $X^2\Sigma^+$ and $A^2\Pi$, respectively.

The Einstein coefficient for spontaneous emission $A_{v'v''}$ (s^{-1}) is given by $A_{v'v''} = 2.1419 \times 10^{10}\ K''(\Delta E_{v'v''})^3 S_{v'v''}$, with $\Delta E_{v'v''}$ in atomic units and $K'' = [2\text{-}\delta_{0\Lambda'})(2S' + 1)]^{-1}$. Emission from $B^2\Sigma^+$ and $A^2\Pi$ implies $K'' = {}^1/_2$ and ${}^1/_4$, respectively. The natural fluorescence lifetime $\tau_{v'}$(s) corresponds to $\tau_{v'} = [\Sigma_{v''}A_{v'v''}]^{-1}$.

Earlier experience from the literature suggests that radiative lifetimes obtained by combining experimental $\Delta E_{v'v''}$ (when available) with theoretically derived $S_{v'v''}$ data deviate from experiments by about 10% (34, 35). Since the present estimates are based exclusively on theoretical results, the reported lifetimes might be accurate within 20%.

Can. J. Chem. Downloaded from www.nrcresearchpress.com by 203.198.23.82 on 09/08/12
For personal use only.

Can. J. Chem. Downloaded from www.nrcresearchpress.com by 203.198.23.82 on 09/08/12
For personal use only.

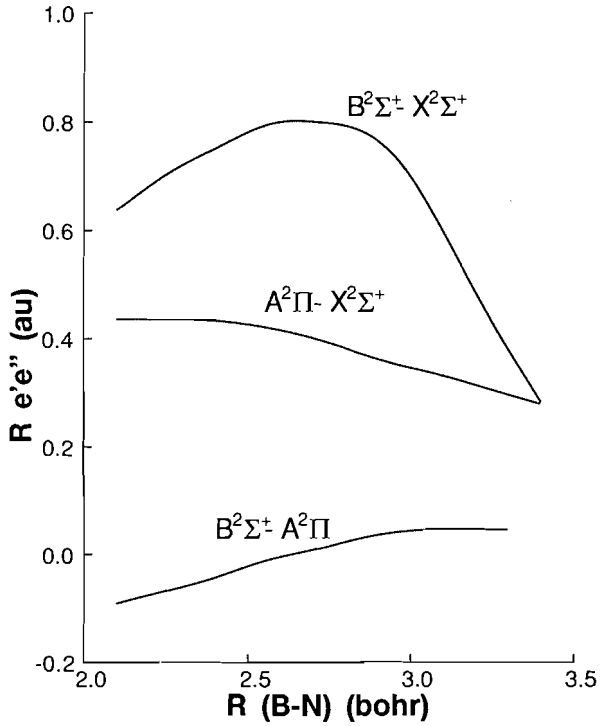

FIG. 5. Variation of the transition moment $R_{e'e''}$ (degeneracy factor K not included) with bond length R(BN) for the B–X, A–X, and B–A band systems of BN^-.

7.1 The $A^2\Pi$–$X^2\Sigma^+$ *transition*

The transition moment $R_{e'e''}$ for $A^2\Pi$–$X^2\Sigma^+$ varies smoothly with geometry (Fig. 5 and Table 6), so that changes of $\tau_{v'}(A^2\Pi)$ with v' are essentially dictated by $(\Delta E_{v'v''})^3$ and $q_{v'v''}$. Table 7 collects the corresponding radiative data.

For the upper state R_e is 0.128 bohr larger and ω_e about 210 cm^{-1} smaller than for the ground state. These changes are reflected in the existence of relatively broad Franck–Condon envelopes (see $q_{v'v''}$ data in Table 7). When compared with the equivalent $A^2\Pi_u$–$X^2\Sigma_g^+$ band of C_2^- (experimentally not yet observed), a similar Franck–Condon distribution is expected on the basis of predicted changes of $\Delta R_e = 0.12$ bohr and $\Delta\omega_e = -135$ cm^{-1} upon excitation (29, 36, 37).

The radiative lifetime $\tau_{v'}(A^2\Pi)$ decreases smoothly with vibrational excitation, namely from 14.4 μs for $v' = 0$ to 8.7 μs for $v' = 5$. Therefore, the electronic decay $A^2\Pi(v') \rightarrow X^2\Sigma^+$ is about 10^3 times faster than vibrational relaxation within the $A^2\Pi$ state (Sect. 5).

Theoretical predictions (37) on $A^2\Pi_u \rightarrow X^2\Sigma_g^+$ of C_2^- gave $\tau_{v'}$ values of 49.9 μs for $v' = 0$ and 25.0 μs for $v' = 5$, a range of lifetimes roughly 3 times longer than for BN^-. An analysis of the corresponding spectroscopic data indicates that the main difference between BN^- and C_2^- lies in the transition energy T_e of the $A^2\Pi_{(u)}$ state.

The oscillator strength $f_{v'v''}$ is estimated to be 0.40×10^{-2} for f_{00} and 0.266×10^{-2} for f_{01}. In line with the discussion above, these values are somewhat larger than those assigned to C_2^-, namely 0.34×10^{-2} and 0.129×10^{-2}, respectively (37).

7.2 The $B^2\Sigma^+$–$X^2\Sigma^+$ *transition*

The predicted radiative properties for the $B^2\Sigma^+$–$X^2\Sigma^+$ transition are summarized in Table 8. Near equilibrium this band system is associated mainly with the excitation $4\sigma \leftrightarrow 5\sigma$ (parallel band), which generally exhibits a higher intensity than that generated by the excitation $5\sigma \leftrightarrow 1\pi$ (perpendicular band). Examples have been discussed in ref. 26.

Two main factors are responsible for the higher intensity of the transition $B^2\Sigma^+$–$X^2\Sigma^+$ versus $A^2\Pi$–$X^2\Sigma^+$. First, the excitation $4\sigma \leftrightarrow 5\sigma$ is primarily of s–p type, whereas $5\sigma \leftrightarrow 1\pi$ is mainly an intrashell p–p transition. Since the former is the only one being allowed in atomic transitions, its intrinsic character is transferred to the equivalent molecular excitations. Accordingly, in terms of the $R_{e'e''}$ parameter, the values for the parallel band are higher than those of the perpendicular band. Second, the B state ($4\sigma \rightarrow 5\sigma$) lies at higher energies than the A state ($5\sigma \rightarrow 1\pi$). In summary, parallel bands are characterized by higher absorption numbers $f_{v'v''}$ (lower state) and shorter radiative lifetimes (upper state) than those of perpendicular type. The relative orders of magnitude are roughly 10 for $f_{v'v''}$ and 10^{-3} for $\tau_{v'}$.

The data shown in Tables 6–9 and in Fig. 5 confirm the expectations from above. For instance, near equilibrium the transition moment $R_{e'e''}$ ($B^2\Sigma^+$–$X^2\Sigma^+$) is roughly twice that of $R_{e'e''}$($A^2\Pi$–$X^2\Sigma^+$), whereas $T_0(B^2\Sigma^+)$ of 2.51 eV has to be compared with $T_0(A^2\Pi)$ of 0.80 eV. Moreover, the radiative lifetimes of the B and A states lie in the ns and μs time region, respectively.

As shown in Fig. 1 (MO results), the minimum of the $X^3\Pi$(BN) state lies between the v' levels 1 and 2 of $B^2\Sigma^+(BN^-)$. On the other hand, using the relative energies from the NO calculations and spectroscopic parameters from Table 3 and those discussed in Sect. 8, the zero vibrational level of $X^3\Pi$(BN) appears to lie about 0.026 eV (210 cm^{-1}) below $v' = 2$ of $B^2\Sigma^+(BN^-)$. In principle, the latter is the lowest lying vibrational level that may autodetach into $X^3\Pi + e^-$. However, since our theoretical predictions are expected to underestimate uniformly the separation BN–BN^- by not less than 0.25 eV, a more realistic picture would indicate that up to $v' = 3$ the $B^2\Sigma^+$ state is mainly depopulated via radiative emission (see below).

Since the upper and lower states of the $B^2\Sigma^+$–$X^2\Sigma^+$ band system have similar equilibrium geometries, the Franck–Condon distribution is mainly concentrated in the diagonal elements (Table 8). Accordingly, the diagonal absorption numbers $f_{v'v''}$ are about 100 times larger than the nondiagonal terms. A f_{00} ($B \leftarrow X$) value of 0.354×10^{-1} for BN^- compares with 0.436×10^{-1} reported for the equivalent transition of C_2^- (37).

7.3 The $B^2\Sigma^+$–$A^2\Pi$ *transition*

The radiative data for the $B^2\Sigma^+$–$A^2\Pi$ transition are given in Table 9. For this band system, the absolute value of the transition moment remains below 0.1 au (Fig. 5 and Table 6). However, the energy term $E_{v'v''}^3$ contributing to the Einstein coefficients is large enough to give $A_{v'v''}$ values in the order of 10^3–10^4 s^{-1}, which in turn lead to radiative lifetimes from 127 ($v' = 3$) to 175 ($v' = 0$) microseconds.

Strictly speaking, the total lifetime $\tau_{v'}$ of $B^2\Sigma^+(v')$ has to be computed via the expression $\tau_{v'} = [\Sigma_{v''}A_{v'v''}(B^2\Sigma^+(v')$–$X^2\Sigma^+(v'')) + \Sigma_{v''}A_{v'v''}(B^2\Sigma^+(v')$–$A^2\Pi(v''))]^{-1}$. Comparing the respective $A_{v'v''}$ data from Tables 8 and 9, it is seen that those for $B \rightarrow X$ emission are 10^3 times higher than those for $B \rightarrow A$ decay. Therefore, the first three or four levels of $B^2\Sigma^+$ are mainly depopulated via emission into the $X^2\Sigma^+$ ground state.

The low absorption intensity for the $B^2\Sigma^+ \leftarrow A^2\Pi$ tran-

TABLE 7. Radiative data for the $A^2\Pi(v')$-$X^2\Sigma^+(v'')$ transition of BN^-. First entry: Franck–Condon factors $q_{v'v''}$. Second entry: Einstein coefficients for spontaneous emission $A_{v'v''}$ $(s^{-1})^{a,b}$

	v'					
v''	0	1	2	3	4	5
0	0.568	0.293	0.100	0.288(−1)	0.759(−2)	0.190(−2)
	5.54(4)	5.56(4)	3.23(4)	1.43(4)	5.45(3)	1.87(3)
1	0.348	0.109	0.265	0.169	0.723(−1)	0.254(−1)
	1.31(4)	9.29(3)	4.56(4)	5.02(4)	3.34(4)	1.70(4)
2	0.767(−2)	0.401	0.895(−3)	0.152	0.180	0.110
	7.37(2)	1.32(4)	3.31(1)	2.37(4)	4.91(4)	4.69(4)
3	0.716(−2)	0.172	0.327	0.297(−1)	0.579(−1)	0.148
	6.52(0)	1.41(3)	9.47(3)	2.43(3)	8.00(3)	3.70(4)
4	0.244(−3)	0.237(−1)	0.255	0.219	0.881(−1)	0.909(−2)
	−1.59(−5)	1.69(1)	1.80(3)	5.55(3)	6.21(3)	1.02(3)
5	0.130(−5)	0.104(−2)	0.491(−1)	0.314	0.122	0.131
	−1.55(−6)	−4.78(−4)	2.82(1)	1.93(3)	2.68(3)	8.22(3)
Radiative lifetime:						
$\tau_{v'}$	14.4 μs	12.6 μs	11.2 μs	10.2 μs	9.4 μs	8.7 μs

[a]See footnote (*b*) in Table 5.

[b]Selected $f_{v'v''}$ numbers (absorption oscillator strengths) are $0.400 \times 10^{-2}(f_{00})$, $0.266 \times 10^{-2}(f_{10})$, $0.172 \times 10^{-2}(f_{01})$, and $0.714 \times 10^{-3}(f_{11})$.

TABLE 8. Radiative data for the $B^2\Sigma^+(v')$-$X^2\Sigma^+(v'')$ transition of BN^-. First entry: Franck–Condon factors $q_{v'v''}$. Second entry: Einstein coefficients for spontaneous emission $A_{v'v''}$ $(s^{-1})^{a,b}$

	v'			
v''	0	1	2	3
0	0.985	0.135(−1)	0.885(−3)	0.336(−3)
	9.69(6)	1.12(5)	2.48(4)	6.15(3)
1	0.122(−1)	0.959	0.260(−1)	0.185(−2)
	1.32(5)	8.94(6)	2.28(5)	4.95(4)
2	0.246(−2)	0.217(−1)	0.936	0.354(−1)
	1.06(4)	2.15(5)	8.30(6)	3.07(5)
3	0.197(−4)	0.587(−2)	0.281(−1)	0.919
	1.08(2)	2.36(4)	2.67(5)	7.82(6)
4	0.183(−5)	0.110(−3)	0.909(−2)	0.315(−1)
	8.44(0)	3.33(2)	3.51(4)	2.93(5)
5	0.581(−6)	0.622(−5)	0.359(−3)	0.113(−1)
	7.33(−2)	2.87(1)	8.89(2)	4.10(4)
Radiative lifetimes:				
$\tau_{v'}$	101.7 ns	107.6 ns	112.9 ns	117.4 ns

[a]See footnote (*b*) in Table 5.

[b]Selected $f_{v'v''}$ numbers (absorption oscillator strengths) are $0.354 \times 10^{-1}(f_{00})$, $0.359 \times 10^{-3}(f_{10})$, $0.574 \times 10^{-3}(f_{01})$, and $0.335 \times 10^{-1}(f_{11})$.

sition is demonstrated by an f_{00} number of about 0.9×10^{-5} (Table 9). The corresponding transition $B^2\Sigma_u^+$–$A^2\Pi_u$ of C_2^- does not contribute to the spectrum since it is dipole forbidden.

8. The $X^3\Pi$, $a^1\Sigma^+$, $1^1\Pi$, and $1^3\Sigma^-$ states of BN

Table 10 collects the spectroscopic parameters of the lowest lying state of BN that can be generated by photodetachment of BN^- (Sect. 9). Earlier theoretical and experimental results are also given.

The question of the $X^3\Pi$–$a^1\Sigma^+$ separation has recently been investigated theoretically by Martin et al. (15). Their work employed state-of-the-art computational methods (multireference CI and averaged couple-pair functional, ACPF) as well as flexible AO basis sets (van Duijneveldt's 13*s*8*p* primitive set, augmented with even-tempered 6*d*4*f*2*g* polarization functions in an atomic natural orbital (ANO) contraction scheme). The most sophisticated results were obtained with a 5*s*4*p*3*d*2*f*1*g* contracted basis. In some cases, relativistic corrections were also included.

Martin et al. (15) concluded that the ground state of BN indeed corresponds to $X^3\Pi$, the $a^1\Sigma^+$ state lying 0.05 ± 0.01 eV higher. This result confirms earlier predictions by Karna and Grein (13) about the nature of the ground state of BN and the very low excitation energy of $a^1\Sigma^+$ (T_e = 0.1 eV, MRD-CI calculations with a TZP basis set). In the

Can. J. Chem. Downloaded from www.nrcresearchpress.com by 203.198.23.82 on 09/08/12
For personal use only.

TABLE 9. Radiative data for the $B^2\Sigma^+(v')$-$A^2\Pi(v'')$ transition of BN^-. First entry: Franck–Condon factors $q_{v'v''}$. Second entry: Einstein coefficients for spontaneous emission $A_{v'v''}$ $(s^{-1})^{a,b}$

	v'			
v''	0	1	2	3
0	0.683	0.288	0.276(−1)	0.414(−3)
	2.24(4)	6.21(2)	4.35(2)	2.71(0)
1	0.222	0.260	0.434	0.811(−1)
	2.56(3)	1.21(3)	6.49(2)	1.15(3)
2	0.659(−1)	0.247	0.588(−1)	0.466
	7.60(2)	3.20(3)	4.87(2)	5.42(2)
3	0.200(−1)	0.121	0.187	0.496(−3)
	1.39(2)	1.58(3)	2.85(3)	9.21(1)
4	0.613(−2)	0.511(−1)	0.142	0.108
	1.91(1)	4.36(2)	2.10(3)	2.13(3)
5	0.190(−2)	0.201(−1)	0.798(−1)	0.132
	2.35(0)	8.40(1)	8.28(2)	2.22(3)
Radiative lifetimes:				
$\tau_{v'}$	174.7 μs	139.9 μs	131.2 μs	127.1 μs

[a]See footnote (*b*) in Table 5.

[b]Selected $f_{v'v''}$ numbers (absorption oscillator strengths) are $0.881 \times 10^{-5}(f_{00})$, $0.201 \times 10^{-5}(f_{10})$, $0.126 \times 10^{-4}(f_{01})$, and $0.482 \times 10^{-5}(f_{11})$.

TABLE 10. Calculated spectroscopic data for BN obtained from MRD-CI-MO wavefunctions. Energies (estimated full-CI) in eV, distances in bohr, all other data in cm^{-1}

State	Reference	T_e[a]	R_e	ω_e	$\omega_e x_e$	B_e	α_e
	This work	0.00[b]	2.520	1488	15.4	1.537	0.018
$X^3\Pi$	15	0.00	2.513	1491	12.9	—	0.017
$(5\sigma 1\pi^3)$	13	0.00	2.508	1518	11.5	1.552	0.022
	14	0.00	2.504	1530	16.8	1.558	0.019
Experimental	7	0.00	2.421	1515	12.3	1.666	0.025
	8[c]	0.00	2.511	1496	—	1.548	—
	This work	0.02[d]	2.425	1660	10.0	1.671	0.019
$a^1\Sigma^+$	15	0.05	2.419	1686	11.3	—	0.016
$(4\sigma^2 1\pi^4)$	13	0.10	2.425	1796	22.7	1.666	0.014
	14	0.01	2.418	1738	12.8	1.671	0.019
Experimental	10[c]	—	2.425	1712	—	—	—
$1^1\Pi$	This work	0.45	2.535	1522	24.4	1.520	0.010
$(5\sigma 1\pi^3)$	13	0.50	2.517	1573	16.0	1.540	0.016
Experimental	10[c]	—	2.515	1658	—	1.544	—
$1^3\Sigma^-$	This work	1.11	2.798	1100	14.1	1.165	0.010
$(5\sigma^2 1\pi^2)$	13	1.09	2.810	1146	11.0	1.236	0.010
Experimental	9	—	—	1049	8.9_5	1.455	—

[a]With parent NO's (estimated full CI) the T_e values are: 0.01 for $a^1\Sigma^+$, 0.47 for $1^1\Pi$, and 1.18 for $1^3\Sigma^-$.

[b]Total energy (in hartree): −79.26384 (MO's) and −79.26731 (NO's).

[c]The data tabulated correspond to R_0, $\Delta G(1/2)$, and B_0.

[d]The T_e values from extrapolated MRD-CI energies (without full-CI correction) are 0.05 eV (MO's) and 0.03 eV (NO's). The best estimate of T_e ($a^1\Sigma^+$) from the results given here is 0.03 ± 0.02 eV.

present work, using a better basis set and larger CI expansion, the energetic separation between $X^3\Pi$ and $a^1\Sigma^+$ ranges from 0.05 to 0.01 eV, depending on the option used (MO vs. NO, extrapolated energy with or without correction for full CI). Therefore, our best estimate is 0.03 ± 0.02 eV, in agreement with the result by Martin et al.

The present estimates of R_e and ω_e are in fairly good agreement with those from ref. 15. For $X^3\Pi$, our values of R_e = 2.520 bohr and ω_e = 1488 cm^{-1} have to be compared with average values R_e = 2.532 ± 0.008 bohr and ω_e = 1474 ± 15 cm^{-1} derived from Table IV in ref. 15 (their best estimates given in Table 10 are slightly different). A similar analysis for $a^1\Sigma^+$ points out a comparable degree of accuracy. The present estimates R_e = 2.425 bohr and ω_e = 1660 cm^{-1} reproduce averaged data of 2.429 ± 0.002 bohr and 1679 ± 10 cm^{-1}, respectively (ACPF and MRCI results from Table III, ref. 15).

The $1^1\Pi(5\sigma 1\pi^3)$ state constitutes the second excited state

Can. J. Chem. Downloaded from www.nrcresearchpress.com by 203.198.23.82 on 09/08/12
For personal use only.

TABLE 11. Selected photodetachment transitions from the $X^2\Sigma^+(v'')$ and $A^2\Pi(v'')$ states of BN^-

BN state	ΔE^a (eV)	ΔR_e^a (bohr)	$\Delta\omega_e^a$ (cm^{-1})	Relative Franck–Condon factors[b] v' = 0	1	2	3	4
			From $X^2\Sigma^+$ $(4\sigma^2 5\sigma 1\pi^4)$					
$X^3\Pi$ $(1\pi \rightarrow \infty)$	2.84	0.082	−221	v'' = 0: 1.000, 0.266, 0.046 v'' = 1: 0.285, 0.510, 0.385, 0.114				
$a^1\Sigma^+$ $(5\sigma \rightarrow \infty)$	2.87	−0.015	−49	v'' = 0: 1.000, 0.017 v'' = 1: 0.166, 0.964, 0.037				
$1^1\Pi$ $(1\pi \rightarrow \infty)$	3.31	0.095	−187	v'' = 0: 1.000, 0.302, 0.059				
			From $A^2\Pi(4\sigma^2 5\sigma^2 1\pi^3)$					
$X^3\Pi$ $(5\sigma \rightarrow \infty)$	2.03	−0.046	74	v'' = 0: 1.000, 0.047 v'' = 1: 0.042, 0.916, 0.085				
$1^1\Pi$ $(5\sigma \rightarrow \infty)$	2.50	−0.033	26	v'' = 0: 1.000, 0.035				
$1^3\Sigma^-$ $(1\pi \rightarrow \infty)$	3.21	0.230	−314	v'' = 0: 0.618, 1.000, 0.879, 0.561, 0.295				

[a]Relative changes $\Delta X = X(BN) - X(BN^-)$, with ΔE representing the electron affinity.
[b]The maximum absolute $q_{v'v''}$ values are 0.758 ($X^3\Pi$), 0.983 ($a^1\Sigma^+$), 0.729 ($1^1\Pi$), 0.958 ($X^3\Pi$), 0.967 ($1^1\Pi$), and 0.282 ($1^3\Sigma^-$).

Can. J. Chem. Downloaded from www.nrcresearchpress.com by 203.198.23.82 on 09/08/12
For personal use only.

of BN, with a present estimate for T_e of 0.45 eV, close to an excitation energy of 0.50 eV reported earlier by KG1 (13). Experimentally little is known for this singlet state, which has been assumed to be the lower state in a rather weak $c^1\Sigma^+$–$b^1\Pi$ emission band (10). The transition $b^1\Pi(1^1\Pi)$–$a^1\Sigma^+$ lies in the infrared region ($T_{00} \approx 3200$ cm^{-1}).

The $1^3\Sigma^-(5\sigma^1 1\pi^2)$ state lies near $T_e = 1.10$ eV. This triplet state is connected to $a^1\Sigma^+(1\pi^4)$ by the double-excitation $1\pi^2 \rightarrow 5\sigma^2$, accompanied by a significant decrease in bond strength, as pointed out by changes in R_e of +0.373 bohr and ω_e of −570 cm^{-1}.

A $^3\Sigma^-$–$^3\Sigma^-$ transition recently detected by Verma (9) has been assumed to involve this $1^3\Sigma^-$ state of BN. An experimentally determined rotational constant $B = 1.455$ cm^{-1} corresponds to an $R_e(1^3\Sigma^-)$ of 2.59 bohr, about 0.2 bohr shorter than the theoretical estimates (Table 10). Moreover, this experimental $R_e(1^3\Sigma^-)$ is longer than that of $X^3\Pi$ by only 0.07 bohr, whereas the corresponding derease in ω_e is relatively large (~450 cm^{-1}, Table 10). On the other hand, theory supports a vibrational frequency $\omega_e(1^3\Sigma^-)$ near the experimental region (1100 vs. 1049 cm^{-1}).

Neither the $1^1\Pi$–$a^1\Sigma^+$ nor $1^3\Sigma^-$–$X^3\Pi$ band systems of BN (equivalent to the Phillips and Ballik–Ramsay bands of C_2) have been observed experimentally. However, their radiative properties have been studied theoretically (39).

9. Electron affinities and photodetachment transitions

The relative energies of selected states of BN^- and BN, together with the corresponding Franck–Condon factors for photodetachment, are summarized in Table 11.

9.1 Electron affinities

At the MRD-CI-MO level of computation, $X^2\Sigma^+(BN^-)$ lies 2.77 eV below $X^3\Pi(BN)$. The electron affinity EA($^3\Pi$) increases to 2.84 eV at the more sophisticated MRD-CI-NO level of treatment. Assuming that this study underestimates the energy separation BN^-–BN by about 0.25 eV, EA($^3\Pi$) might lie close to 3.10 eV. The latter value compares with an experimental estimate of 3.40 eV for EA(C_2) (36, 38). Indeed electron attachment stabilizes both molecules in a degree comparable to that of the strongly electronegative F and Cl atoms, with EA's near 3.5 eV (27).

On a relative scale, however, electron attachment strengthens the BN bond more than it affects that of C_2. As shown in Sect. 6, dissociation energies and electron affinities are connected by the expression $D_e(XY^-) - D_e(XY) = EA(XY) - EA(X)$. Using EA data from this work and literature values for C_2 (36, 38) and C (27), the right-hand side amounts to 2.82 eV for BN and 2.13 eV for C_2. Looking for the changes in D_e, and taking into account that $D_e(BN, X^3\Pi)$ is about 4.55 eV and $D_e(C_2, X^1\Sigma_g^+)$ about 6.30 eV (1), it is easily seen that the relative increase $\Delta D_e/D_e$ upon electron attachment is more significant for BN (62%) than for C_2 (34%).

In the process $X^3\Pi(5\sigma 1\pi^3) + e^- \rightarrow X^2\Sigma^+(5\sigma 1\pi^4)$ the attached electron occupies the 1π MO. Another concurrent attachment reaction (into 5σ) may generate BN^- in the $A^2\Pi(5\sigma^2 1\pi^3)$ excited state, with an EA of 2.03 eV. In principle, the reaction $X^3\Pi$ (BN) + $e^- \rightarrow A^2\Pi$ (BN^-) could be an experimentally accessible mechanism to generate excited BN^- and to study the emission spectrum $A^2\Pi \rightarrow X^2\Sigma^+$.

Electron attachment to the $a^1\Sigma^+(4\sigma^2 1\pi^4)$ state of BN gives rise to only one bound electronic state of BN^-, namely $X^2\Sigma^+(4\sigma^2 5\sigma 1\pi^4)$. Since near equilibrium $B^2\Sigma^+$ has the configuration $4\sigma 5\sigma^2 1\pi^4$, this state of BN^- cannot be generated from $X^3\Pi$ or $a^1\Sigma^+$ of BN via a single-electron process. Electron attachment has to be accompanied simultaneously by the excitation $4\sigma \rightarrow 5\sigma$. Since these two-electron processes occur with very low probability, their contribution to the formation of BN^- states is negligible.

9.2 Photodetachment transitions

Extraction of one electron from each of the highest lying MO's of the ground state $X^2\Sigma^+(4\sigma^2 5\sigma 1\pi^4)$ formally gives rise to the following states of BN: (*i*) $X^3\Pi$, $1^1\Pi$ $(1\pi \rightarrow \infty)$; (*ii*) $a^1\Sigma^+$ $(5\sigma \rightarrow \infty)$; and (*iii*) $1^3\Sigma^+$, $(2,3)^1\Sigma^+$ $(4\sigma \rightarrow \infty)$. Similarly, single-electron photodetachment from $A^2\Pi$

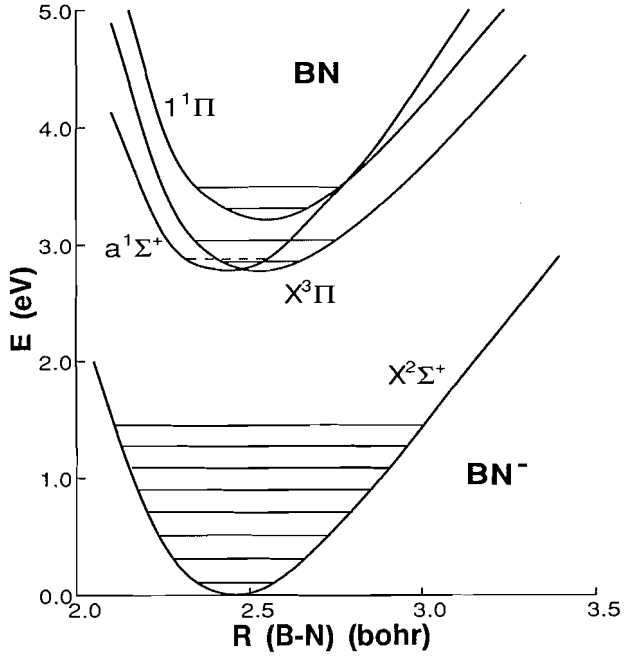

FIG. 6. Potential curves of the lowest states of BN generated via photodetachment from $X^2\Sigma^+$ of BN^-.

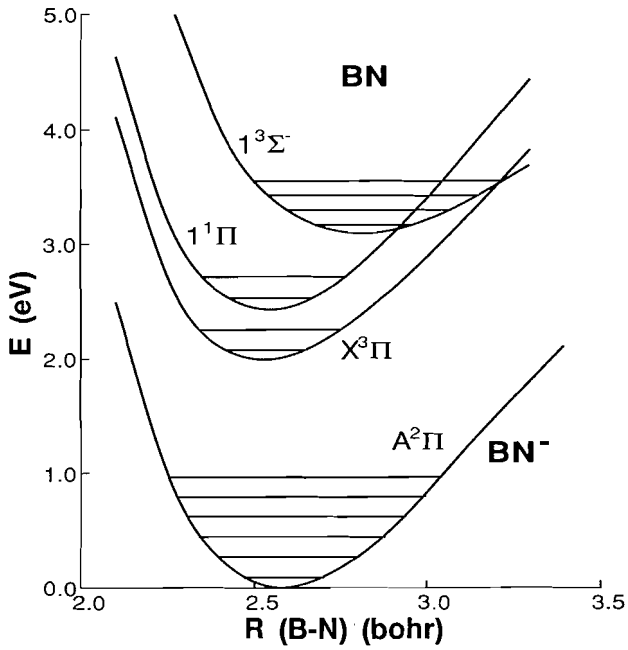

FIG. 7. Potential curves of the lowest states of BN generated via photodetachment from $A^2\Pi$ of BN^-.

$(4\sigma^2 5\sigma^2 1\pi^3)$ of BN^- leads to (*i*) $X^3\Pi$, $1^1\Pi$ $(5\sigma \rightarrow \infty)$; (*ii*) $1^3\Sigma^-$, $1^1\Delta$, $(2,3)^1\Sigma^+$ $(1\pi \rightarrow \infty)$; and (*iii*) $2^3\Pi$, $2^1\Pi$ $(4\sigma \rightarrow \infty)$.

In this paper we focus on the processes leading to the $X^3\Pi$, $1^1\Pi$, $a^1\Sigma^+$, and $1^3\Sigma^-$ states of BN. Figures 6 and 7 show the potential curves of BN and BN^- involved in the photodetachment spectrum. The corresponding relative Franck–Condon factors are given in Table 11. Other photodetachment transitions are analyzed elsewhere.[2] A diagram showing relative energies is given in Fig. 8.

[2]R.C. Mawhinney, P.J. Bruna, and F. Grein. To be published.

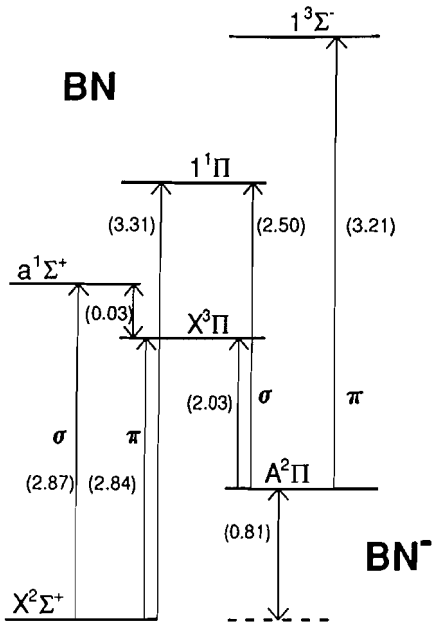

FIG. 8. Schematic diagram showing the relative energies of selected states of BN and BN^-. The labels σ and π characterize the MO's of BN^- from which photodetachment takes place.

The process $X^3\Pi(v') \leftarrow X^2\Sigma^+(v'' = 0)$ generates a short vibrational progession consisting of the strong line 0,0, and a secondary peak 1,0 with about $^1/_4$ relative intensity. Both lines are separated by $\omega_e(X^3\Pi) \simeq 1490\ cm^{-1}$ (Table 10). If hot bands from $v'' = 1$ of $X^2\Sigma^+$ contribute to the photodetachment spectrum, upper levels v' up to 3 can be populated. The corresponding transitions $1^1\Pi(v') \leftarrow X^2\Sigma^+(v'')$ are shifted to higher energies by about 0.47 eV (about 3800 cm^{-1}). As expected, the Franck–Condon distribution of this band is essentially the same as for $X^3\Pi \leftarrow X^2\Sigma^+$. The photodetachment $1^1\Sigma^+ \leftarrow X^2\Sigma^+$ $(5\sigma \rightarrow \infty)$ is accompanied by small changes in R_e and ω_e (Table 11). Therefore, the line 0,0 is the only one expected to contribute to this portion of the spectrum.

Simple rules about the relative intensities of photoelectron ionization bands discussed by Eland (40) can be applied to the equivalent photodetachment processes. One rule states that the partial cross-section for ionization (i.e., relative ionization probability) is proportional to the number of equivalent electrons available for ionization. Therefore, in the case of linear molecules, $\pi \rightarrow \infty$ bands are expected to show twice the intensity of that arising from $\sigma \rightarrow \infty$ ionization (photodetachment). A second rule states that the ionization cross section is proportional to the statistical weight of the final (ionic) state produced. For $\pi \rightarrow \infty$ detachment from $X^2\Sigma^+$ of BN^- into both $X^3\Pi$ and $1^1\Pi$ of BN, it follows that the triplet and singlet bands should appear with relative intensities in a 3:1 ratio.

Combining both rules (that is, by photodetachment $1\pi \rightarrow \infty$ as well as $5\sigma \rightarrow \infty$ from $X^2\Sigma^+$), the experimental spectrum is expected to consist of three band systems $X^3\Pi < a^1\Sigma^+ < 1^1\Pi$ with a total intensity ratio of 3:2:1. On the basis of spectroscopic information from Tables 10 and 11, these bands cover an energy region of about 5350 cm^{-1} above the transition $X^3\Pi(v' = 0) \leftarrow X^2\Sigma^+(v'' = 0)$.

To estimate the relative strength of each vibrational transition, the total band intensities have to be multiplied by the

Can. J. Chem. Downloaded from www.nrcresearchpress.com by 203.198.23.82 on 09/08/12
For personal use only.

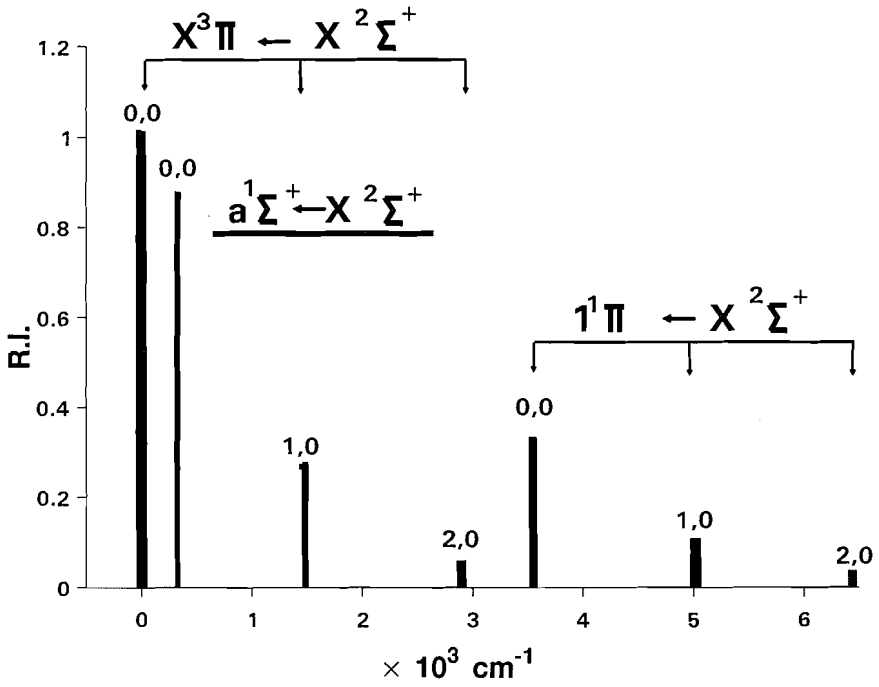

FIG. 9. Relative intensity (R.I.) and vibrational structure (v', v'') predicted for the photodetachment from $X^2\Sigma^+(v'' = 0)$ of BN^- into the $X^3\Pi$, $a^1\Sigma^+$, and $1^1\Pi$ states of BN. The $a^1\Sigma^+$ state is assumed to lie about 300 cm^{-1} above $X^3\Pi$ ($v' = 0$).

appropriate Franck–Condon factors. A total relative intensity of three for $X^3\Pi(v')$ decomposes into 2.273 for $v' = 0$, 0.605 for $v' = 1$, and 0.122 for $v' = 2$ when the vibrational structure is taken into account. Similarly, a relative intensity of one for $1^1\Pi$ decomposes into 0.729 for $v' = 0$, 0.220 for $v' = 1$, and 0.043 for $v' = 2$. The $a^1\Sigma^+$ band consists mainly of a strong $v' = 0$ peak with a relative intensity of 1.967.

For simplicity, the ratios from above are normalized with respect to the strongest line of the spectrum, namely $X^3\Pi(v' = 0)$. Figure 9 has been drawn on the basis of these intensity ratios. From this analysis the following points can be made:

1. Two close-lying peaks contribute to the maximum intensity region. The strongest line corresponds to $v' = 0$ of $X^3\Pi$ (100% relative intensity), followed by $v' = 0$ of $a^1\Sigma^+$ (~87%). According to the best theoretical estimates, both lines are separated by approximately 400 ± 100 cm^{-1}, with the strongest photodetachment peak being energetically the lowest.

2. The $v' = 1$ ($X^3\Pi$) line, shifted by about 1490 cm^{-1} relative to $v' = 0$, should appear with a 27% relative intensity. Since the energy separation between these two vibrational levels of $X^3\Pi$ is known from optical spectroscopy (1, 7, 8, 10), the location of the $v' = 1$ line in the photodetachment spectrum indirectly helps to pick up the corresponding $v' = 0$ counterpart from the low-energy region discussed above.

3. A weak line (about 5% intensity) near 2900 cm^{-1} corresponds to $v' = 2$ of $X^3\Pi$.

4. The $1^1\Pi \leftarrow X^2\Sigma^+$ band system essentially consists of the lines $v' = 0$ (32% intensity) and $v' = 1$ (about 10%), the former shifted by approximately 3800 ± 200 cm^{-1} with respect to $v' = 0$ ($X^3\Pi$). It should be pointed out that radiative emission from $1^1\Pi$ into $a^1\Sigma^+$ is dipole allowed; according to ref. 39, the radiative lifetime $\tau_{v'}(1^1\Pi)$ is 162 μs for $v' = 0$. The photodetachment process $1^1\Pi \leftarrow X^2\Sigma^+$ might constitute an appropriate experimental route to generate the $1^1\Pi$ state of BN and to study its emission spectrum.

Photodetachment from the $A^2\Pi(5\sigma^2 1\pi^3)$ state of BN^- can be recorded experimentally. A drawback to study ionization of $A^2\Pi$, however, might lie in the radiative process $A^2\Pi \rightarrow X^2\Sigma^+$ occurring in the 10-μs time scale.

As already observed for the transition $a^1\Sigma^+ \leftarrow X^2\Sigma^+$, ejection of a 5σ electron does not affect significantly the BN bonding because of the quasi-lone-pair character of the MO (Sect. 4.1 and Fig. 2). In line with this feature, no vibrational structure is expected for the bands $X^3\Pi \leftarrow A^2\Pi$ and $1^1\Pi \leftarrow A^2\Pi$ (Table 11).

Determination of the energy separation between the $v' = 0$ levels of both $X^3\Pi$ and $1^1\Pi$ via photodetachment from $A^2\Pi$ is extremely important as an independent experimental route to deconvolute the low-energy region of the composite $X^3\Pi$, $a^1\Sigma^+ \leftarrow X^2\Sigma^+$ spectrum. Moreover, the relative separation $A^2\Pi$–$X^2\Sigma^+$ of BN^- can be indirectly derived by photodetachment from $X^2\Sigma^+$ and from $A^2\Pi$ into their common $X^3\Pi$ and $1^1\Pi$ states of BN.

The transition $1^3\Sigma^- \leftarrow A^2\Pi$ ($\pi \rightarrow \infty$) is accompanied by a relatively large change in bond length and frequency (Table 11 and Fig. 7). Accordingly, the Franck–Condon envelope consists of no less than five terms separated by $\omega_e(1^3\Sigma^-) \simeq$ 1050 ± 100 cm^{-1} (Table 10). The upper state $1^3\Sigma^-$ may decay into $X^3\Pi$ via radiative emission, a process having lifetimes from 11.2 μs ($v' = 0$) to 3.9 μs ($v' = 5$) (39).

10. Summary and conclusions

The BN^- species, like isoelectronic C_2^-, has three stable electronic states, $X^2\Sigma^+(4\sigma^2 5\sigma 1\pi^4)$, $A^2\Pi$ ($1\pi \rightarrow 5\sigma$), and $B^2\Sigma^+(4\sigma \rightarrow 5\sigma)$. The low-lying states $1^4\Sigma^+$, $1^4\Delta$, $1^4\Sigma^-$, and $1^4\Pi$ autodetach into BN ($X^3\Pi$) + e^-. A detailed comparison of BN^- with C_2^-, AlP^-, $GaAs^-$, Si_2^-, and Ge_2^- is given in ref. 17. There it is shown that the heavier isoelectronic

Can. J. Chem. Downloaded from www.nrcresearchpress.com by 203.198.23.82 on 09/08/12
For personal use only.

anions exhibit a larger number of bound states. All doublet and quartet states listed above are more stable than the respective ground state of the neutral species. Such a markedly strong difference between first- and higher row compounds is mainly governed by the stabilization of the $\pi^*(\pi_g)$ MO upon substitution (2, 17, 41, 42).

An electron affinity of 3.10 eV (best estimate) for BN compares with an experimental value of 3.40 eV for C_2 (29, 36–38). A recent *ab initio* study (43) on the process $BNB \rightarrow BNB^-$ finds EA values of about 2.96 eV (directly calculated) and 3.33 eV (best estimate), quite similar to our result for $BN \rightarrow BN^-$. On the other hand, a relatively high EA(BN) is reflected in a fairly large increase in the BN bond strength as pointed out by ground state dissociation energies of 4.55 eV for BN and of 7.12 eV for BN^- (best estimates, ±0.1 eV).

Optical spectroscopy can be used to investigate BN^- as it has been done for C_2^- (1, 5, 44). The present radiative data on BN^- should be of assistance in future experiments. In general, the electronic spectrum of BN^- shows features similar to those observed experimentally for the isoelectronic first-row diatomics C_2^-, CN, and CO^+ (1). For instance, the parallel band system $B^2\Sigma^+_{(u)}$–$X^2\Sigma^+_{(g)}$ is invariably of higher intensity than the perpendicular transition $A^2\Pi_{(u)}$–$X^2\Sigma^+_{(g)}$. In line with this difference in intensities, the radiative lifetimes of the B and A states lie in the ns and μs time scale, respectively. The emission process $B \rightarrow A$ (dipole allowed only for heteronuclear species) is of secondary importance when compared with $B \rightarrow X$ decay.

The low-energy region of the photodetachment spectrum originating from $X^2\Sigma^+$ of BN^- should be instrumental in determining experimentally the nature of the ground state of BN. According to this work and literature data (13–15), the $X^3\Pi$ state is predicted to be the ground state, with $a^1\Sigma^+$ lying about 0.03 eV higher. Unfortunately, this small energy difference is comparable to the accuracy of the *ab initio* results. Therefore, the final word on the relative positioning of $X^3\Pi$ and $a^1\Sigma^+$ will have to come from experiment or future, much improved, *ab initio* studies. Since both low-lying states of BN can be generated via ionization from $X^2\Sigma^+$ of BN^-, photodetachment spectroscopy represents an alternative technique to optical spectroscopy. On the basis of a Franck–Condon analysis and simple rules governing relative intensities in photoelectron spectrocopy, we have devised a model spectrum which should be of help to experimentalists.

Can. J. Chem. Downloaded from www.nrcresearchpress.com by 203.198.23.82 on 09/08/12
For personal use only.

Acknowledgments

The authors thank the Natural Sciences and Engineering Research Council of Canada (NSERC) for financial support and the Computing Services at UNB for the allocation of computer time. They also thank Dr. M. Kolbuszewski (Ottawa) for a copy of his graphics package.

1. K.P. Huber and G. Herzberg. *In* Molecular spectra and molecular structure. Vol. 4. Constants of diatomic molecules. Van Nostrand, Princeton, N.J. 1979.
2. P.J. Bruna and S.D. Peyerimhoff. Bull. Soc. Chim. Belg. **92**, 525 (1983); Adv. Chem. Phys. **67**, 1 (1987).
3. H. Lefebvre-Brion and R. W. Field. *In* Perturbations in the spectra of diatomic molecules. Academic Press, Orlando, Fla. 1986.
4. E.A. Ballik and D.A. Ramsay. J. Chem. Phys. **31**, 1128 (1959); Astrophys. J. **137**, 61 (1963).
5. W. Weltner, Jr. and R. J. Van Zee. Chem. Rev. **89**, 1713 (1989).
6. E.A. Ballik and D.A. Ramsay. Astrophys. J. **137**, 84 (1963).
7. A.E. Douglas and G. Herzberg. Can. J. Res. A, **18**, 179 (1940).
8. H. Bredohl, I. Dubois, Y. Houbrechts, and P. Nzohabonayo. J. Mol. Spectrosc. **112**, 430 (1985).
9. R.D. Verma. J. Phys. B: At. Mol. Opt. Phys. **22**, 3689 (1989).
10. H. Bredohl, I. Dubois, Y. Houbrechts, and P. Nzohabonayo. J. Phys. B: At. Mol. Phys. **17**, 95 (1984).
11. K.P. Lawley (*Editor*). Advances in chemical physics. Vols. 67 and 69. *Ab initio* methods in quantum chemistry. Wiley, New York. 1987.
12. Ch. W. Bauschlicher, S.R. Langhoff, and P.R. Taylor. Adv. Chem. Phys. **77**, 103 (1990).
13. S.P. Karna and F. Grein. Chem. Phys. **98**, 207 (1985); Chem. Phys. Lett. **144**, 149 (1988).
14. J.M.L. Martin, J.P. François, and R. Gijbels. Z. Phys. D: At. Mol. Clusters, **21**, 47 (1991).
15. J.M.L. Martin, T.J. Lee, G.E. Scuseria, and P.R. Taylor. J. Chem. Phys. **97**, 6549 (1992).
16. S.P. Karna and F. Grein. Mol. Phys. **56**, 641 (1985).
17. P.J. Bruna and F. Grein. J. Phys. B: At Mol. Opt. Phys. **22**, 1913 (1989).
18. S. Huzinaga. J. Chem. Phys. **42**, 1293 (1965).
19. T.H. Dunning, Jr. J. Chem. Phys. **55**, 716 (1971); T.H. Dunning, Jr. and P.J. Hay. *In* Methods of electronic structure theory. Modern theoretical chemistry. Vol. 3. *Edited by* H.F. Schaefer. Plenum, New York. 1976. p. 10.
20. S. Huzinaga. Gaussian basis sets for molecular calculations. Physical Sciences Data 16. Elsevier, New York. 1984. p. 23.
21. M.J. Frisch, J.A. Pople, and J.S. Binkley. J. Chem. Phys. **80**, 3265 (1984).
22. R.J. Buenker and S.D. Peyerimhoff. Theor. Chim. Acta, **35**, 33 (1974); **39**, 217 (1975); R.J. Buenker, S.D. Peyerimhoff, and W. Butscher. Mol. Phys. **35**, 771 (1978); R.J. Buenker. *In* Proceedings of the Workshop on Molecular Physics and Quantum Chemistry into the 80's. *Edited by* P. Burton. University of Wollongong. 1980. p. 1.5.1; *In* Studies in physical and theoretical chemistry. Vol. 21. *Edited by* R. Carbó. Elsevier, Amsterdam. 1982. p. 17; Int. J. Quantum Chem. **29**, 435 (1986); R.J. Buenker and R.A. Phillips. J. Mol. Struct. (Theochem.), **123**, 291 (1985).
23. P.J. Bruna, S.D. Peyerimhoff, and R.J. Buenker. Chem. Phys. Lett. **72**, 278 (1980); R.J. Buenker, S.D. Peyerimhoff, and P.J. Bruna. *In* Computational organic chemistry. *Edited by* I.G. Csizmadia and R. Daudel. Reidel, Dordrecht. 1981. p. 55; L. Meissner. Chem. Phys. Lett. **146**, 204 (1988).
24. D.B. Knowles, J.R. Álvarez-Collado, G. Hirsch, and R.J. Buenker. J. Chem. Phys. **92**, 585 (1990).
25. C. Moore. *In* Atomic Energy Levels. U.S. Group Printing Office, Washington. 1971.
26. P.J. Bruna and J.S. Wright. J. Phys. B: At. Mol. Opt. Phys. **23**, 2197 (1990).
27. H. Hotop and W.C. Lineberger. J. Phys. Chem. Ref. Data, **14**, 731 (1985).
28. J. Anglada, P.J. Bruna, S.D. Peyerimhoff, and R.J. Buenker. J. Phys. B: At. Mol. Phys. **16**, 2469 (1983).
29. M. Zeitz, S.D. Peyerimhoff, and R.J. Buenker. Chem. Phys. Lett. **64**, 243 (1979).
30. W.B. Person and G. Zerbi. *In* Studies in physical and theoretical chemistry. Vol. 20. Vibrational intensities in infrared and Raman spectroscopy. Elsevier, Amsterdam. 1982.
31. W.D. Allen and H.F. Schaefer. Chem. Phys. **108**, 243 (1986).
32. J.M.L. Martin, J.P. François, and R. Gijbels. J. Chem. Phys. **90**, 6469 (1989).
33. R.R. Reddy, A.S.R. Reddy, and T.V.R. Rao. Physica C: **132**, 373 (1985).
34. C.F. Chabalowski, S.D. Peyerimhoff, and R.J. Buenker.

Chem. Phys. **81**, 57 (1983); S.D. Peyerimhoff. Faraday Symp. Chem. Soc. **19**, 63 (1984); R.J. Buenker. J. Mol. Struct. (Theochem), **149**, 1 (1987); P.J. Bruna and J.S. Wright. Chem. Phys. **157**, 111 (1991); J. Phys. Chem. **96**, 1630 (1992).
35. H-J. Werner and P. Rosmus. *In* Comparison of *Ab initio* quantum chemistry with experiment for small molecules. *Edited by* R.J. Bartlett. Reidel, Dordrecht. 1985. p. 267.
36. R.D. Mead, U. Hefter, P.A. Schulz, and W.C. Lineberger. J. Chem. Phys. **82**, 1723 (1985).
37. P. Rosmus and H.-J. Werner. J. Chem. Phys. **80**, 5085 (1984).
38. P.L. Jones, R.D. Mead, B.E. Kohler, S.D. Rosner, and W.C. Lineberger. J. Chem. Phys. **73**, 4419 (1980); U. Hefter, R.D. Mead, P.A. Schulz, and W.C. Lineberger. Phys. Rev. A, **28**, 1429 (1983).
39. K. Bhanuprakash and R.J. Buenker. Chem. Phys. Lett. **152**, 215 (1988).
40. J.H.D. Eland. *In* Photoelectron spectroscopy. Wiley, New York. 1974.
41. P.J. Bruna and F. Grein. J. Phys. B: At. Mol. Phys. **20**, 5967 (1987).
42. P.J. Bruna. *In* Studies in physical and theoretical chemistry. Vol. 77. Computational chemistry, structure, interactions, and reactivity. Part A. *Edited by* S. Fraga. Elsevier, Amsterdam. 1992. p. 379.
43. J.M.L. Martin, J.P. François, and R. Gijbels. Chem. Phys. Lett. **193**, 243 (1992).
44. D.R. Bates. Adv. At. Mol. Opt. Phys. **27**, 1 (1991).
45. E. Clementi, A.D. McLean, D.L. Raimondi, and M. Yoshimine. Phys. Rev. A, **133**, 1274 (1964).

Can. J. Chem. Downloaded from www.nrcresearchpress.com by 203.198.23.82 on 09/08/12
For personal use only.

Rotational analyses of bands of the $\tilde{A}^1B_1$–$\tilde{X}^1A_1$ system of *cis*-glyoxal[1]

R.Y. DONG,[2] R. NANES,[3] AND D.A. RAMSAY

Herzberg Institute of Astrophysics, National Research Council of Canada, Ottawa, ON K1A 0R6, Canada

Received March 10, 1993

This paper is dedicated to Professor Gerald W. King on the occasion of his 65th birthday

R.Y. DONG, R. NANES, and D.A. RAMSAY. Can. J. Chem. **71**, 1595 (1993).

Rotational analyses have been carried out for the 5^1_0, 5^0_1, and 5^1_1 bands of the $\tilde{A}^1B_1$–$\tilde{X}^1A_1$ system of *cis*-glyoxal, where ν_5 is the totally symmetric C—C=O bending frequency. The vibrational frequencies $\nu_5' = 302.81$ cm^{-1} and $\nu_5'' = 284.51$ cm^{-1} are smaller than the corresponding frequencies for *trans*-glyoxal by nearly a factor of two. A vibronically induced band with a different type of rotational structure has been analysed and shown to be an *a*-type band. The coupling vibration is the out-of-plane C—H wagging vibration $\nu_6(a_2)$ and is similar in form and frequency to the vibronically active $\nu_8(b_g)$ vibration for *trans*-glyoxal.

R.Y. DONG, R. NANES et D.A. RAMSAY. Can. J. Chem. **71**, 1595 (1993).

On a effectué des analyses rotationnelles des bandes 5^1_0, 5^0_1 et 5^1_1 du système $\tilde{A}^1B_1$–$\tilde{X}^1A_1$ du *cis*-glyoxal, ou ν_5 est la fréquence de déformation totalement symétrique du C—C=O. Les fréquences de vibration $\nu_5' = 302{,}81$ cm^{-1} et $\nu_5'' = 284{,}51$ cm^{-1} sont environ deux fois plus faibles que les fréquences correspondantes du *trans*-glyoxal. On a analysé une bande induite vibroniquement avec un type différent de structure rotationnelle et on démontre qu'il s'agit d'une bande de type *a*. La vibration de couplage correspond à la vibration d'oscillation hors du plan C—H $\nu_6(a_2)$ et elle est semblable du point de vue de la forme et de la fréquence à la vibration vibroniquement active $\nu_8(b_g)$ du *trans*-glyoxal.

[Traduit par la rédaction]

Introduction

The 0–0 band of *trans*-glyoxal ($C_2H_2O_2$) at 4550 Å was first rotationally analysed by Gerald King in 1957 (1) using spectra taken on a 20-ft Ebert spectrograph (2), which he had constructed at University College, London. The analysis correctly identified the sub-bands in the symmetric top portion of the band but no attempt was made to analyse the asymmetric top structure in the central portion of the band. The latter was analysed later by Paldus and Ramsay (3). The 4550 Å band is the 0–0 band of the $\tilde{A}^1A_u$–$\tilde{X}^1A_g$ (π^*–n) system of *trans*-glyoxal. Many other bands in this system for $C_2H_2O_2$, C_2HDO_2, $C_2D_2O_2$, and $^{13}C_2H_2O_2$ have been rotationally analysed (3–6), giving accurate rotational and vibrational constants for levels in the ground and excited states and also permitting a determination of the geometric structures in both states.

In 1971, the *cis* isomer was found by Currie and Ramsay (7). A band at 4875 Å had a similar structure to the 4550 Å band except that it had about twice as many sub-bands. Rotational analysis gave constants consistent with a *cis* structure for the molecule. The 4875 Å band is assigned as the 0–0 band of the $\tilde{A}^1B_1$–$\tilde{X}^1A_1$ (π^*–n) system of *cis*-glyoxal. The band had been seen but not identified in some laser-excited fluorescence studies (8). The 4880 Å line of an argon ion laser is an excellent line for exciting *cis*-glyoxal and subsequent laser studies have yielded ground state vibrational constants for *cis*-$C_2H_2O_2$, C_2HDO_2, and $C_2D_2O_2$ (9).

cis-Glyoxal has a large dipole moment (~4.8 D) and seven lines in the microwave spectrum were observed by Durig et al. (10). Two of these were shown to be misassigned by Mamleev et al. (11) who observed many more transitions, including some from vibrationally excited levels in the ground state. The rotational constants obtained for the ground state are in good agreement with those derived from the optical spectrum.

In the present work, rotational analyses are presented for four bands in the absorption spectrum, including one vibronically induced band. Accurate molecular constants are obtained for two vibrational levels in the excited state and one in the ground state.

Experimental

Glyoxal was prepared by passing ethylene over a mixture of SeO_2 and P_2O_5 heated to 200°C.

Absorption spectra were photographed in the region 4600–5200 Å using the 12th order of a 7.3-m Ebert spectrograph with a resolving power of ~600 000 and Kodak III-O plates. The absorption cell was 2 m long and was heated to 85°C to increase the amount of the *cis* isomer. Three bands of *cis*-glyoxal were found near 4805, 4816, and 4945 Å using an absorption path length of 40 m and pressures of glyoxal ranging from 5 Torr for the first two bands to 25 Torr for the long-wavelength band (1 Torr = 133.3 Pa). Another band of *cis*-glyoxal with a different type of rotational structure was also identified near 4710 Å using the same path length and 4 Torr of glyoxal at a temperature of 181°C.

An iron hollow cathode lamp was used to provide reference spectra and the plates were measured using a comparator with a photoelectric scanning device. Standard wavelengths were taken from the tables of Crosswhite (12) and the vacuum corrections of Edlén (13) were applied. There was much overlapping of the lines in the absorption spectra but for single lines the precision of measurement is ~0.003 cm^{-1}.

Rotational analysis

(a) The 4805, 4816, and 4945 Å bands

These bands have *c*-type rotational structures similar to that of the 0^0_0 band. The 4945 Å band is relatively free from overlapping absorption and a rotational analysis was carried out in the manner described earlier (7). It was found that the upper state constants were the same as for the 0^0_0 band, hence only the lower state constants were varied in the final fit of

[1]NRCC No. 34681.

[2]Former NRCC Postdoctorate Fellow; present address: Department of Physics and Astronomy, Brandon University, Brandon, MB, R7A 6A9, Canada.

[3]Former NRCC Postdoctorate Fellow; present address: Department of Physics, California State University, Fullerton, CA 92634, U.S.A.

Can. J. Chem. Downloaded from www.nrcresearchpress.com by 203.198.23.82 on 09/08/12
For personal use only.

Can. J. Chem. Downloaded from www.nrcresearchpress.com by 203.198.23.82 on 09/08/12
For personal use only.

TABLE 1. Band origins and differences of rotational constants for bands of *cis*-glyoxal (in cm^{-1})

Constant	Band 5^1_0	5^0_1	6^1_0
$A'-A''$	+0.02108(19)[a]	+0.009614(97)	+0.015987(50)
$B'-B''$	−0.008851(29)	−0.008004(11)	−0.008677(10)
$C'-C''$	−0.005549(21)	−0.005081(8)	−0.005531(9)
$10^5(D'_K-D''_K)$	+0.003(57)	−0.021(25)	+0.0247(59)
$10^5(D'_{JK}-D''_{JK})$	+0.066(30)	+0.0230(97)	+0.0253(31)
$10^6(D'_J-D''_J)$	−0.024(8)	−0.0221(18)	−0.0463(23)
ν_0	20810.385(11)	20223.056(6)	21221.299(6)
n[b]	328	952	846
σ[c]	0.019	0.018	0.019

[a]The quoted errors are three times the standard deviations.
[b]Number of lines fitted.
[c]Standard deviation of the fit.

TABLE 2. Vibrational frequencies for *cis*- and *trans*-glyoxal (in cm^{-1})

		trans-Glyoxal			*cis*-Glyoxal		
	Vibration	Species	$\tilde{X}^1A_g$	$\tilde{A}^1A_u$	Species	$\tilde{X}^1A_1$	$\tilde{A}^1B_1$
ν_1	C—H stretching	a_g	2843.27[a]	2809[f]	a_1		
ν_2	C=O stretching		1744.12[a]	1391.38[c]		1746[i]	
ν_3	C—H rocking		1352.6[a]	1195.17[g]			
ν_4	C—C stretching		1065.80[b]	952.38[g]		826[j]	
ν_5	C—C=O bending		550.53[c]	508.95[c]		284.51[k]	302.81[k]
ν_6	C—H wagging	a_u	801.36[d]	720.0[g]	a_2	1049[j]	713.73[k]
ν_7	Torsional		126.70[e]	233.25[c]		88[k]	344[j]
ν_8	C—H wagging	b_g	1048.07[b]	735.10[h]	b_1		
ν_9	C—H stretching	b_u	2835.07[d]		b_2		
ν_{10}	C=O stretching		1732.10[e]	1280.75[g]			
ν_{11}	C—H rocking		1312.4[d]	1172[g]			
ν_{12}	C—C=O bending		338.5[d]	379.29[g]		[m]	[m]

[a]Reference 15.
[b]Reference 16.
[c]Reference 4.
[d]Reference 17.
[e]Reference 18.
[f]Reference 19.
[g]Reference 20.
[h]F.W. Birss, S.D. Colson, and D.A. Ramsay, unpublished, quoted in ref. 4.
[i]Reference 8.
[j]Reference 14.
[k]This paper.
[l]Reference 9.
[m]$\nu'_{12}-\nu''_{12} = 94\ cm^{-1}$ (9).

the band. The differences between the rotational constants in the upper and lower states are given in Table 1 together with the band origin. Altogether 952 lines were fitted with a standard deviation of 0.018 cm^{-1}. Since the band originates in a totally symmetric level of the ground state at 284.51 cm^{-1} and since the inertial defect is small (Δ = +0.036 amu Å^2), the most reasonable assignment is 5^0_1, where ν_5 is the totally symmetric CCO bending frequency. This assignment is consistent with single vibronic level fluorescence studies (14).

Rotational analysis of the 4805 Å band shows that it originates in the ground state and the rotational constants for the upper state are quite reasonable if the band is assigned as 5^1_0. The band is overlapped at the high-frequency end by the 8^0_1 band of *trans*-glyoxal and at the low-frequency end by the 4816 Å band described below. Consequently only 328 lines were assigned and the standard deviation of the fit was 0.019 cm^{-1}.

Confirmation of the assignments of the 5^1_0 and 5^0_1 bands was obtained by calculating the frequencies for the 5^1_1 band. This band lies ~18 cm^{-1} on the high-frequency side of the 0^0_0 band and is heavily overlapped by it. However, many of the unassigned lines in the original measurements of the 0^0_0 band were assigned without difficulty to the stronger lines in the calculated spectrum of the 5^1_1 band. The number of lines assigned was insufficient, however, to justify any further refinement of the molecular constants.

The 4816 Å band is also heavily overlapped and so far has

resisted attempts at rotational analysis. It appears that the band does not originate in the ground state and the most reasonable assignment is 7^1_1, where ν_7 is the torsional frequency. If this assignment is correct, then $\nu'_7 - \nu''_7$ is $\sim$256 cm^{-1} and is considerably larger than the corresponding difference for *trans*-glyoxal, viz. 106.55 cm^{-1} (4). The principal rotational constants A, B, and C for the $\nu''_7 = 1$ level are known from microwave studies (11) and, using these constants, a fit can be made to the strong 0–1 and 1–0 Q branches giving a band origin in the region of 20 763.5 cm^{-1}. However, it is likely that the values of D_K in both the lower and upper states are strongly affected by Coriolis interactions with ν_{12}, as was found for *trans*-glyoxal (4). Further progress must therefore await a more complete determination of the constants for the lower state by microwave spectroscopy.

(b) The 4711 Å band

The band near 4711 Å has a different type of rotational structure characteristic of an *a*-type transition. Indeed the band was readily analysed on the basis that it originates in the ground vibrational level of the molecule and consists of ^qR, ^qQ, and ^qP branches. Altogether 846 rotational assignments were made and were fitted by least squares with a standard deviation of 0.019 cm^{-1}. Many of the lines have multiple assignments, which limits the accuracy of the fit, but the validity of the assignments is supported by the calculation of the relative intensities as well as the frequencies of the lines. The vibrational assignment of this band is discussed below.

Discussion

The vibrational frequencies for *cis*- and *trans*-glyoxal are summarized in Table 2. The C—C=O symmetric bending frequencies ν'_5 and ν''_5 for *cis*-glyoxal are well determined in the present work and differ by nearly a factor of two from the corresponding frequencies for *trans*-glyoxal. The ν''_2 frequency for *cis*-glyoxal was determined from laser-excitation studies (8, 9) and lies close to the corresponding frequency for *trans*-glyoxal. A ν''_4 frequency has also been assigned from laser-excited fluorescence studies (14) but is considerably different from the corresponding frequency for the *trans* species. The torsional frequency in the ground state ν''_7 has been estimated from relative intensity measurements in the microwave spectrum (114 ± 8 cm^{-1} (10), 108 ± 10 cm^{-1} (11)). The frequency difference $\nu'_7 - \nu''_7 =$ 256 cm^{-1} is derived from the present work. The frequency $2\,\nu'_7 =$ 688 cm^{-1} has been obtained from laser-excitation studies (14). If the torsional frequency in the excited state is assumed to be harmonic then $\nu'_7 =$ 344 cm^{-1} and $\nu''_7 =$ 88 cm^{-1}. Clearly, further studies are desirable.

The only other frequencies that are well established for *cis*-glyoxal are those that are deduced from vibronically induced bands. The rotational analysis of the 4711 Å band above shows that it is an *a*-type band. The transition is therefore vibronically $^{cv}B_2$–$^{cv}A_1$ and since the electronic transition is B_1–A_1, the coupling vibration must have a_2 symmetry species. The coupling vibration is therefore the C—H wagging vibration $\nu_6(a_2)$ (H^+—C^-—C^+—H^-) and is similar in form to the $\nu_8(b_g)$ vibration in *trans*-glyoxal (in earlier references (8, 9) the *cis* vibration was unfortunately labelled as ν_8, see ref. 14). The frequency ν'_6 deduced from the present work and the frequency ν''_6 deduced from laser-excitation studies (9) are indeed similar to the corresponding ν_8 frequencies for *trans*-glyoxal.

The mechanism for the vibronic coupling is presumably similar for the two isomers. In *trans*-glyoxal the $\nu_8(b_g)$ vibration couples the $\tilde{A}\,^1A_u$ state to electronic states with B_u symmetry of which the closest is a state arising from a π^*–π excitation. In *cis*-glyoxal the $\nu_6(a_2)$ vibration couples the $\tilde{A}\,^1B_1$ state to electronic states with B_2 symmetry of which the closest is again expected to be a π^*–π state with the electron configuration

$$\overbrace{\ldots (b_1)^2(a_2)}^{\pi}\ \overbrace{(a_1)^2(b_2)^2}^{n}\ \overbrace{(b_1)}^{\pi^*}\quad {}^{1,3}B_2$$

An important difference between the two isomers is that whereas the vibronically induced bands for the *trans* isomer are *a*- + *b*-type hybrids, the corresponding bands for *cis*-glyoxal are pure *a*-type bands.

Acknowledgments

The assistance of M. Barnett is cordially acknowledged.

1. G.W. King. J. Chem. Soc. 5054 (1957).
2. G.W. King. J. Sci. Instrum. **35**, 11 (1958).
3. J. Paldus and D.A. Ramsay. Can. J. Phys. **45**, 1389 (1967).
4. F.W. Birss, J.M. Brown, A.R.H. Cole, A. Lofthus, S.L.N.G. Krishnamachari, G.A. Osborne, J. Paldus, D.A. Ramsay, and L. Watmann. Can. J. Phys. **48**, 1230 (1970).
5. D.M. Agar, E.J. Bair, F.W. Birss, P. Borrell, P.C. Chen, G.N. Currie, A.J. McHugh, B.J. Orr, D.A. Ramsay, and J-Y. Roncin. Can. J. Phys. **49**, 323 (1971).
6. F.W. Birss, D.B. Braund, A.R.H. Cole, R. Engleman, Jr., A.A. Green, S.M. Japar, R. Nanes, B.J. Orr, D.A. Ramsay, and J. Szyszka. Can. J. Phys. **55**, 390 (1977).
7. G.N. Currie and D.A. Ramsay. Can. J. Phys. **49**, 317 (1971).
8. W. Holzer and D.A. Ramsay. Can. J. Phys. **48**, 1759 (1970).
9. R.Y. Dong and D.A. Ramsay. Can. J. Phys. **51**, 1491 (1973).
10. J.R. Durig, C.C. Tong, and Y.S. Li. J. Chem. Phys. **57**, 4425 (1972).
11. A.Kh. Mamleev, R.G. Latypova, L.N. Gunderova, V.I. Tyulin, and N.M. Pozdeev. Zh. Strukt. Khim. **21**, 46 (1980).
12. H.M. Crosswhite. J. Res. Natl. Bur. Stand. Sect. A: **79**, 17 (1975).
13. B. Edlén. J. Opt. Soc. Am. **43**, 339 (1953).
14. K.W. Butz, J.R. Johnson, D.J. Krajnovich, and C.S. Parmenter. J. Chem. Phys. **86**, 5923 (1987).
15. E.P. Peyroula, A. Delon, and R. Jost. J. Mol. Spectrosc. **132**, 123 (1988).
16. D. Frye, L. Lapierre, and H-L. Dai. J. Chem. Phys. **89**, 2609 (1988).
17. A.R.H. Cole and G.A. Osborne. Spectrochim. Acta, Part A: **27A**, 2461 (1971).
18. J. Vander Auwera, M. Godefroid, M. Herman, T.R. Huet, and J.W.C. Johns. Can. J. Phys. **65**, 1636 (1987).
19. J.C.D. Brand. Trans. Faraday Soc. **50**, 431 (1954).
20. E.B. Peyroula and R. Jost. J. Mol. Spectrosc. **121**, 177 (1987).

Can. J. Chem. Downloaded from www.nrcresearchpress.com by 203.198.23.82 on 09/08/12
For personal use only.

Electronic spectroscopy of yttrium monosulfide: molecular beam studies and density functional calculations[1]

ANDREW M. JAMES, RENÉ FOURNIER, BENOIT SIMARD, AND MARGOT D. CAMPBELL[2]

Steacie Institute for Molecular Sciences, National Research Council of Canada, 100 Sussex Drive, Ottawa, ON K1A OR6, Canada

Received April 13, 1993

This paper is dedicated to Professor Gerald W. King on the occasion of his 65th birthday

ANDREW M. JAMES, RENÉ FOURNIER, BENOIT SIMARD, and MARGOT D. CAMPBELL. Can J. Chem. **71,** 1598 (1993)

The yttrium monosulfide molecule (YS) has been investigated using the techniques of molecular beam fluorescence spectroscopy and density functional theory. Fluorescence spectra in the region of the electronic orgin of the $B^2\Sigma^+ \leftarrow X^2\Sigma^+$ system (ν_{00} = 14 826.07 cm^{-1}) were recorded using a ring dye laser, the experimental resolution being 120 MHz. The $B^2\Sigma^+ \leftarrow X^2\Sigma^+$ (0,0) band, and a cold band of a hitherto unreported $^4\Pi_{\pm 1/2} \leftarrow X^2\Sigma^+$ system ($\nu_{v'0}$ = 14 926.02 cm^{-1}) have been rotationally analysed. (The $\pm 1/2$ notation implies that the state has either $^4\Pi_{1/2}$ or $^4\Pi_{-1/2}$ symmetry.) Improved molecular rotational constants were obtained for the $v = 0$ levels of the $X^2\Sigma^+$ and $B^2\Sigma^+$ states (r_0(X) = 2.27191(17) Å, r_0(B) = 2.32202(19) Å, γ_0(B) = −0.15150(14) cm^{-1} (2σ error bounds)). The magnetic hyperfine and spin rotation parameters determined for the $X^2\Sigma^+$ state were found to be in good agreement with previous work. An accurate bond length has been derived for the upper vibrational level of the 14 926.0 cm^{-1} band ($r_{v'}$ = 2.49510(16) Å). The $v = 1$ level of the $B^2\Sigma^+$ state is found to be strongly perturbed by another vibrational level of the $^4\Pi_{\pm 1/2}$ state. The spin-forbidden $^4\Pi_{\pm 1/2} \leftarrow X^2\Sigma^+$ transition gains intensity via spin-orbit mixing between the $^4\Pi$ state and the $B^2\Sigma^+$ state. Radiative lifetimes of the observed bands were measured by digitizing the fluorescence decay traces obtained upon excitation with a pulsed dye laser. The results of the density functional treatment provide broad confirmation of the experimental measurements. A molecular orbital description of the bonding in the YS molecule is presented.

ANDREW M. JAMES, RENÉ FOURNIER, BENOIT SIMARD et MARGOT D. CAMPBELL. Can J. Chem. **71**, 1598 (1993).

On a étudié la molécule de monosulfure d'yttrium (YS) à l'aide de techniques de spectroscopie de fluorescence de rayons laser et par la théorie de la densité fonctionnelle. Pour enregistrer les spectres de fluorescence dans la région de l'origine électronique du système $B^2\Sigma^+ \leftarrow X^2\Sigma^+$ (ν_{00} = 14 826,07 cm^{-1}) on a utilisé un laser à colorant cyclique pour lequel la résolution expérimentale est de 120 MHz. On a analysé la rotation de la bande $B^2\Sigma^+ \leftarrow X^2\Sigma^+$ (0,0) et une bande froide d'un système $^4\Pi_{1/2} \leftarrow X^2\Sigma^+$ non rapporté jusqu'à mainenant ($\nu_{v'0}$ = 14 926,02 cm^{-1}). On a obtenu des constantes de rotation améliorées pour les niveaux $v = 0$ des états $X^2\Sigma^+$ et $B^2\Sigma^+$ (r_0(X) = 2,27191(17) Å, r_0(B) = 2,32202(19) Å et γ_0(B) = −0,15150(14) cm^{-1} (limites d'erreur de 2σ)). On a trouvé que les paramètres magnétiques hyperfins et de rotation de spin déterminés pour l'état $X^2\Sigma^+$ sont en bon accord avec ceux obtenus au cours d'un travail antérieur. On a déterminé une longueur de liaison précise pour le niveau vibrationnel supérieur de la bande à 14 926,0 cm^{-1} ($r_{v'}$ = 2,49510(16) Å). On a trouvé que le niveau $v = 1$ de l'état $B^2\Sigma^+$ est fortement perturbé par un autre niveau vibrationnel de l'état $^4\Pi_{\pm 1/2}$. La transition $^4\Pi_{\pm 1/2} \leftarrow X^2\Sigma^+$ non permise par les spin augmente d'intensité par le biais d'un mélange spin-orbite entre l'état $^4\Pi$ et l'état $B^2\Sigma^+$. On a mesuré les temps de vie de radiation des bandes observées en procédant à la digitalisation des courbes de dégénérescence de la fluorescence obtenues lors de l'excitation à l'aire d'un laser à colorant pulsé. Les résultats du traitement fonctionnel de la densité fournissent une large confirmation des mesures expérimentales. On présente une description de l'orbitale moléculaire de la liaison dans la molécule de YS.

[Traduit par la rédaction]

Introduction

Difficulties arise in the spectroscopic study of molecules containing a transition metal atom due to the high density of low-lying electronic states associated with partially occupied *d* orbitals (1, 2). In addition, the large nuclear spins of the transition elements can give rise to complex magnetic hyperfine structure patterns in the already congested spectra of these molecules. However, unravelling the spectroscopy of such systems can pay rich dividends when one considers how central to chemistry is an understanding of bonding involving transition metals. Our work focusses on the electronic spectroscopy of gas phase, transition-metal-containing diatomic molecules. Preparing the molecule of interest in a gaseous environment permits the extraction of detailed information on the properties of a single transition metal – ligand bond, free from interference by other ligands or a host matrix. The versatile technique of chemical reaction in a laser-generated plasma, coupled with supersonic expansion of the products, leads to the formation of intense, internally cold beams of refractory transition metal molecules, which may then be probed by laser spectroscopic techniques (3–6). We have used this approach to make detailed investigations of molecules containing a group three transition metal atom (Sc, Y, or La) bound to a simple ligand. The group three transition elements have the simplest open-*d* shell electronic structure [$(n - 1)d^1 ns^2$], and should therefore give rise to less daunting spectra than their counterparts towards the middle of the transition periods. Experimental determination of the spectroscopic properties of these transition metal molecules furnishes the theoretician with data to check the accuracy of high level *ab initio* calculations. Yttrium monosulfide is a particularly apt candidate in this respect, since the metal–ligand bond is expected to contain both covalent and ionic contributions to a significant extent.

The experimental database relating to the spectroscopy of yttrium monosulfide is rather limited. McIntyre et al. (7) have reported esr and infrared spectra of the YS molecule isolated in an argon marix at 4 K. Stringat, Fenot, and Féménias (8) have obtained electronic spectra of gas phase YS in the

[1]Issued as NRCC No. 35251.

[2]NRCC/WISE summer student 1992.

Can. J. Chem. Downloaded from www.nrcresearchpress.com by 203.198.23.82 on 09/08/12
For personal use only.

Can. J. Chem. Downloaded from www.nrcresearchpress.com by 203.198.23.82 on 09/08/12
For personal use only.

red and near-infrared spectral regions, using a hollow cathode discharge source. Several bands belonging to the $A^2\Pi \leftarrow X^2\Sigma^+$ and $B^2\Sigma \leftarrow X^2\Sigma^+$ systems were reported, a number of them perturbed. A rotational analysis of the $B^2\Sigma \leftarrow X^2\Sigma^+$ (0,0) band was effected, despite the limited resolution and high source temperature. In 1990, Azuma and Childs (9) performed an elegant laser – radio frequency double resonance study on the ground state of YS, pumping the $B^2\Sigma \leftarrow X^2\Sigma^+$ (0,0) band. The ultra-high resolution of this technique (10–15 kHz) permitted very precise determinations of the hyperfine structure and spin-rotation constants for the $X^2\Sigma^+$ state, although no attempt was made to fit the optical frequencies in order to improve the upper state rotational constants. Recently, we employed molecular beam Stark spectroscopy to determine the permanent electric dipole moments of the $X^2\Sigma^+$ and $B^2\Sigma^+$ states of YS (6). Values of 6.098(64) D ($X^2\Sigma^+$ state, $v = 0$, 2σ error bound) and 4.572(92) D ($B^2\Sigma^+$ state, $v = 0$) were obtained. The marked reduction in the dipole moment (μ) upon $B^2\Sigma \leftarrow X^2\Sigma^+$ excitation was unexpected, and warranted further investigation. The density functional calculations reported here demonstrate that the large difference between the dipole moments of the $X^2\Sigma^+$ and $B^2\Sigma^+$ states of YS can be attributed to the differing extents of valence orbital hybridization in each state. We also present experimental and theoretical evidence for a $^4\Pi$ state in the vicinity of the $B^2\Sigma^+$ state.

Experimental

A brief outline of the experimental procedure is given, as a detailed description can be found elsewhere (10). The metal atom plasma was formed by pulsed laser vaporisation of an yttrium target rod (Goodfellows, 99.9%). An excimer laser (Lumonics model 430) operating on the 308 nm line, or a Nd:YAG laser (Lumonics HY400) generating third hamonic radiation (355 nm), were employed as vaporization sources. There were no noticeable differences in the efficiency of production of YS when 355 nm radiation was substituted for 308 nm. Vaporisation took place in a Smalley-type cluster source fixture, in the presence of a flowstream of CS_2-seeded helium gas (0.5% concentration) from a molecular beam valve (Newport BV-100). The post-reaction gas mixture, containing YS molecules, was expanded into a vacuum chamber, where laser-induced fluorescence was excited 4.3 cm downstream from the molecular beam orifice. Fluorescence was imaged through a monochromator (Spex, 0.75 m, 1200 lines/mm) on to a photomultiplier (cryo-cooled Hamamatsu R943). Low-resolution survey spectra and fluorescence decay profiles were recorded using a pulsed dye laser (Lumonics Hyperdye, 0.08 cm^{-1} linewidth), operating on the dyes Kiton Red, DCM, and LD690. The decay traces were sampled by feeding the photomultiplier signal to a digitizer (Tektronix 7912AD). The high-resolution fluorescence spectra were obtained using a cw ring dye laser (Coherent CR699-29), operating on DCM dye. The resolution of the experimental arrangement was found to be 120 MHz. The high-resolution spectra were calibrated by the wavelength meter system incoporated in the ring laser, its operation being checked by a Burleigh WA-20 wavemeter. The absolute accuracy of the ring dye laser calibration system is 200 MHz.

Density functional calculations : computational details

We performed Kohn–Sham density functional calculations on the lowest doublet and quartet states of YS, and YO for comparison, using the Linear Combination of Gaussian-Type Orbitals-Density Functional program deMon (11). We used the local exchange-correlation potential of Vosko et al. (12) throughout the self-consistent field procedure and included gradient corrections to exchange (13) and correlation (14) in the final energy evaluation. The vibrational frequencies were calculated in the harmonic approximation from energy second derivatives obtained as finite differences of analytical first derivatives. The orbital basis sets we employed have the following contraction patterns, which show the number of primitive Gaussian functions in each contracted function, first for s symmetry, second for p, and then for d : oxygen : (6311/311/1); sulfur: (73111/611/1); yttrium: (633321/532111/531). The yttrium has two diffuse p functions to give extra flexibility in describing the polarization of the $5s$ orbital. The auxiliary basis sets for fitting the charge density and exchange-correlation potential were fully uncontracted and consisted of eight s, four p, and four d functions on oxygen, nine s, four p, and four d functions on sulfur, and ten s, five p, and five d functions on yttrium.

The formalism on which our method is based holds rigorously only for the lowest states of a given symmetry and spin multiplicity. The calculated doublet–quartet energy separations have physical meaning and are truly "first principles." It should be noted that methods based on the local spin density approximation seem to underestimate the energy of high-multiplicity states relative to low-multiplicity states, but the trend is apparently not systematic (15, 16). Results for states that are not the lowest of their symmetry and spin multiplicity should be viewed with some caution. They involve additional, and poorly understood, approximations. For a discussion of exact and approximate treatment of excited states in density functional theory, the reader should consult the articles listed in ref. 17.

Description of the spectra

We completed a low-resolution survey of the YS spectrum over the region 600–800 nm, observing numerous vibronic bands of the $A^2\Pi \leftarrow X^2\Sigma^+$ and $B^2\Sigma \leftarrow X^2\Sigma^+$ transitions, as well as several new bands extraneous to these systems. In this work, we concentrate on the portion of the spectrum between 630 and 700 nm, in the vicinity of the electronic origin of the $B^2\Sigma^+ \leftarrow X^2\Sigma^+$ system, where two interesting new bands were discovered and investigated. Other new features and their interaction with the $A^2\Pi \leftarrow X^2\Sigma^+$ and $B^2\Sigma^+ \leftarrow X^2\Sigma^+$ systems will be the subject of future publications.

Figure 1(a) shows a part of the low-resolution LIF spectrum in the region of the $B^2\Sigma^+ \leftarrow X^2\Sigma^+$ (0,0) band. Approximately 100 cm^{-1} to higher energy of this band, a new and considerably less intense band was detected, with rotationless origin at 14 926.02 cm^{-1}. Dispersing the emission from this band confirmed that it originated from the $v = 0$ level in the ground state of YS. Figure 1(b) shows a portion of the pulsed dye laser LIF spectrum in the vicinity of the $B^2\Sigma \leftarrow X^2\Sigma^+$ (1,0) band. In this region, two double-headed cold bands of comparable intensity were found, located at 15 264.2 cm^{-1} and 15 300.1 cm^{-1} (approximate location of rotationless origins). At the outset, it was not clear which of these bands should be designated $B^2\Sigma^+ \leftarrow X^2\Sigma^+$ (1,0), since it appeared that the (1,0) band was being strongly perturbed by an almost degenerate band from another system. (As we demonstrate below, the upper vibrational levels of the 14 926.0 cm^{-1} and 15 300.1 cm^{-1} bands are neighbouring vibrational levels of a $^4\Pi_{\pm 1/2}$ state.) Lifetime measurements on the 15 264.2 cm^{-1} and 15 300.1 cm^{-1} bands (vide infra)

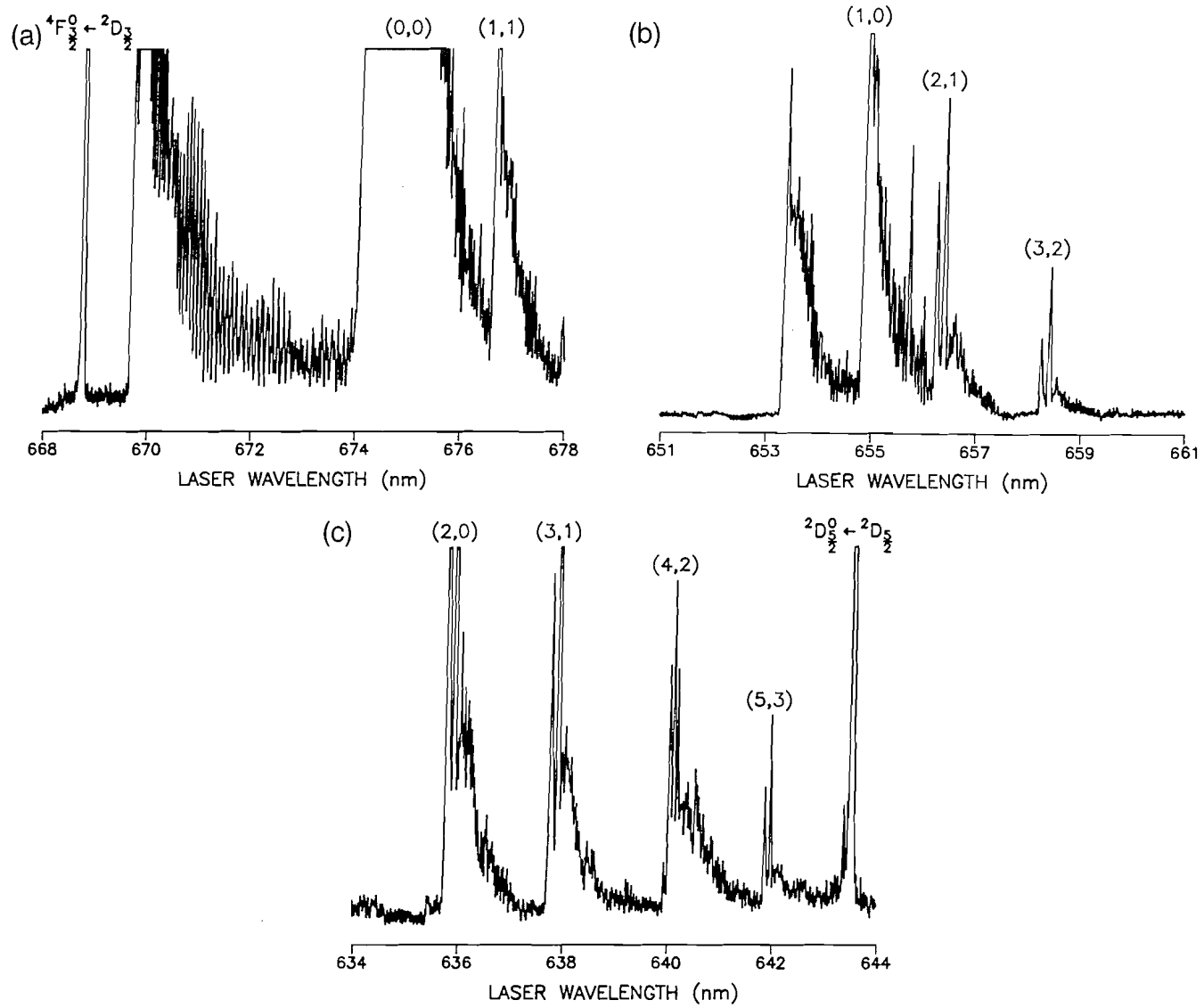

FIG. 1. Low-resolution LIF spectra recorded with the pulsed dye laser. The vertical scale is the LIF intensity. The (v', v'') labels refer to the $B^2\Sigma^+ \leftarrow X^2\Sigma^+$ system. (*a*) Spectrum in the region of the electronic origin of the $B^2\Sigma^+ \leftarrow X^2\Sigma^+$ system. The feature at 670.0 nm is the (v',0) band of the $^4\Pi_{\pm 1/2} \leftarrow X^2\Sigma^+$ system discussed in the text. (*b*) Spectrum in the region of the (1,0) band of the $B^2\Sigma^+ \leftarrow X^2\Sigma^+$ system. The feature at 653.2 nm is the (v' + 1, 0) band of the $^4\Pi_{\pm 1/2} \leftarrow X^2\Sigma^+$ system. (*c*) Spectrum in the region of the (2,0) band of the $B^2\Sigma^+ \leftarrow X^2\Sigma^+$ system.

revealed that the 15 264.2 cm^{-1} band derived more character from the $B^2\Sigma^+ \leftarrow X^2\Sigma^+$ system than did the 15 300.1 cm^{-1} band. Thus for our purposes it will henceforth be referred to as the (1,0) band, recognizing the caveat that its upper vibrational level is strongly mixed with that of the 15 300.1 cm^{-1} band. In Fig. 1(*c*), the $B^2\Sigma^+ \leftarrow X^2\Sigma^+$(2,0) band is shown, accompanied by neighbouring sequence bands, the identity of all features having been confirmed by recording dispersed emission spectra. Unlike the (1,0) band, the (2,0) band is clearly unperturbed and resembles the (0,0) band. Figures 2(*a*) and 2(*b*) show portions of the cw – ring laser LIF spectra recorded for the $B^2\Sigma^+ \leftarrow X^2\Sigma^+$(0,0) band and the 14 926.0 cm^{-1} band, respectively. Unequivocal line assignment in these bands was greatly facilitated by identification of the hyperfine structure patterns associated with each rovibronic line. The hyperfine structure observed in these spectra is due entirely to the $X^2\Sigma^+$ state. Our experimental resolution did not enable us to resolve the splittings due to the small Fermi contact interaction in the $B^2\Sigma^+$ state (b = −78 MHz (9)). Figure 3 shows how the hyperfine structure patterns arise in the $B^2\Sigma^+ \leftarrow X^2\Sigma^+$ transition. In the $X^2\Sigma^+$ state, at low rotational excitation, a $b_{\beta S}$ coupling scheme obtains in which the yttrium nuclear spin (^{89}Y, $\boldsymbol{I}$ = 1/2), is coupled to the spin of the unpaired electron ($\boldsymbol{S}$) to give a resultant $\boldsymbol{G}$, which takes values of 0 or 1. In this case, the three G = 1 hyperfine levels are almost degenerate, and the hyperfine structure is manifested in the spectra as a doublet with a 3:1 intensity ratio between the two components. The more intense component corresponds to transitions out of the G = 1 levels, the weaker one to transitions from the G = 0 level. The best example of $b_{\beta S}$ coupling is furnished by the line $R_1(0)$ in the $B^2\Sigma^+ \leftarrow X^2\Sigma^+$ (0,0) band (Fig. 2(*a*)). The splitting between the G = 0 and G = 1 components is equal to the Fermi contact interaction for the $X^2\Sigma^+$ state. With increasing rotational excitation, $b_{\beta J}$ coupling sets in, the spin-rotation interaction gradually decoupling $\boldsymbol{S}$ from $\boldsymbol{I}$, and cou-

Can. J. Chem. Downloaded from www.nrcresearchpress.com by 203.198.23.82 on 09/08/12
For personal use only.

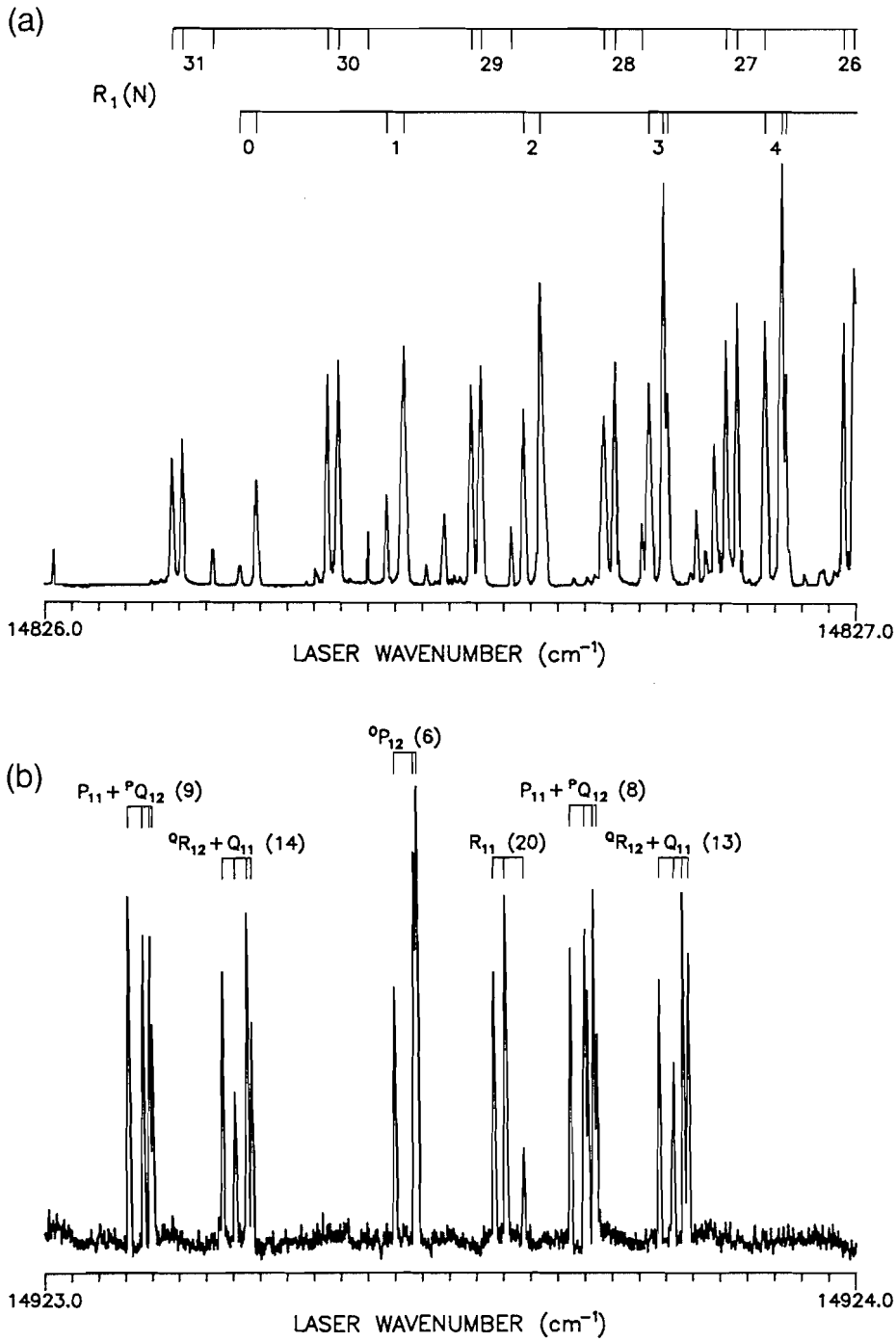

FIG. 2. Portions of the cw – ring laser LIF spectra recorded for (*a*) the (0,0) band of the $B^2\Sigma^+ \leftarrow X^2\Sigma^+$ system, and (*b*) the (v',0) band of the $^4\Pi_{\pm 1/2} \leftarrow X^2\Sigma^+$ system. Vertical scale is the LIF intensity.

pling it to N, the vector representing nuclear rotation. The three $G = 1$ levels split apart, giving, in the limiting case of fully developed $b_{\beta J}$ coupling, two pairs of hyperfine levels. The primary splitting between the levels is due to the spin-rotation interaction, the secondary splitting to the Fermi contact term. The $R_1(N)$ lines returning from the bandhead in the $B^2\Sigma^+ \leftarrow X^2\Sigma^+$ (0,0) band (Fig. 2(*a*)) provide good examples of fairly well-developed $b_{\beta J}$ coupling. Figure 3 shows the situation where the coupling is intermediate between $b_{\beta S}$ and $b_{\beta J}$ in the $X^2\Sigma^+$ state, the coupling in the $B^2\Sigma^+$ state being $b_{\beta J}$ even in the absence of rotation on account of the large spin-rotation parameter. With the selection rule $\Delta F = \pm 1$ in operation, only three hyperfine components are seen for lines of the P_2 and R_1 branches of the $B^2\Sigma^+ \leftarrow X^2\Sigma^+$ (0,0) band, while the P_1 and R_2 branches exhibit four hyperfine components. The *e*/*f* symmetry of the upper state levels in this band could thus be established unequivocally from the number of hyperfine components associated with a line. Similar arguments may be applied to rationalize the hyperfine structure in the 14 926.0 cm^{-1} band, which we demonstrate below to be a $^4\Pi_{\pm 1/2} \leftarrow X^2\Sigma^+$ transition. Figure 4 shows a typical fluorescence decay trace obtained in

Can. J. Chem. Downloaded from www.nrcresearchpress.com by 203.198.23.82 on 09/08/12
For personal use only.

Can. J. Chem. Downloaded from www.nrcresearchpress.com by 203.198.23.82 on 09/08/12
For personal use only.

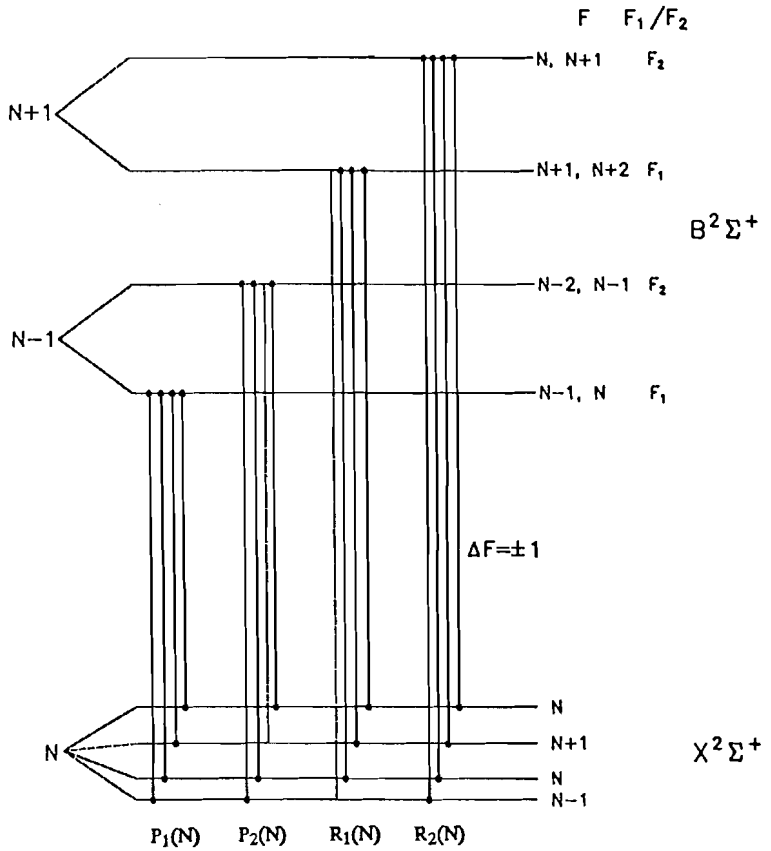

FIG. 3. Energy level diagram for the $B^2\Sigma^+ \leftarrow X^2\Sigma^+$ transition, showing allowed hyperfine transitions.

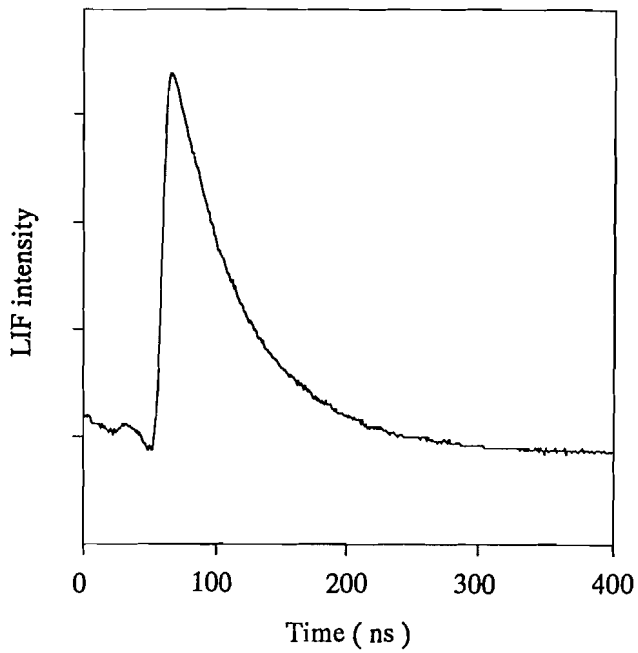

FIG. 4. Fluorescence decay trace obtained by exciting the R_1 bandhead of the $B^2\Sigma^+ \leftarrow X^2\Sigma^+$ (0,0) band.

this case by exciting the R_1 bandhead of the $B^2\Sigma^+ \leftarrow X^2\Sigma^+$ (2,0) band. Decay profiles were recorded for all the bands whose LIF spectra are presented here, excepting the 14 926.0 cm^{-1} band which was found to be too weak to permit recording of an adequate trace.

TABLE 1. Fluorescence lifetimes of some vibronic levels of the $B^2\Sigma^+$ and $^4\Pi_{\pm 1/2}$ states of YS

State	v	$T_v(cm^{-1})$	τ(ns)
$B^2\Sigma^+$	0	14 826.0	125.6(113)[a]
	1	15 264.2	188.4(108)
	2	15 717.1	114.4(22)
$^4\Pi_{\pm 1/2}$	$v' + 1$	15 300.1	232.7(234)

[a]Numbers quoted in parentheses are the uncertainties (2σ) in the units of the last quoted decimal place.

Data analysis

Fluorescence decay traces

Lifetimes were extracted from raw digitized data by first performing a background subtraction and then subjecting a portion of the trace well clear of the excitation pulse to a simple linear least-squares analysis. Deconvolution of the excitation pulse was not carried out, since the observed lifetimes were substantially longer than the laser pulse duration (9 ns). All the observed decays appeared to follow a single exponential function, and were fitted as such. Results of the analysis are presented in Table 1. Measurements are unlikely to be affected by "field of view" problems, since the molecules remain within the fluorescence collection zone for about 1 μs. Each reported lifetime is the weighted average of several independent determinations. The uncertainties quoted in parentheses represent the spread in lifetimes over repeated measurements. The rather large error bounds found for some of the bands were due to electrical noise recorded

Can. J. Chem. Downloaded from www.nrcresearchpress.com by 203.198.23.82 on 09/08/12
For personal use only.

on the decay traces that affected the analysis. As measurements were made under collision-free, molecular beam conditions, and as the fluorescence quantum yield should be unity at these energies, the data in Table 1 may be regarded as intrinsic radiative lifetimes.

The relatively short lifetimes exhibited by the $v = 0$ and $v = 2$ bands of the $B^2\Sigma^+$ state are typical of a strongly allowed radiative transition. In a system where an electronically excited state decays to a single, isolated lower state, and in which the vibrational frequency of the upper state is less than that of the lower state, the radiative lifetime of the upper state should increase with increasing vibrational quantum number (18). Such behaviour is expected in YS, where $\omega_e(B^2\Sigma^+)$ (=449.7 cm^{-1}) < $\omega_e(X^2\Sigma^+)$ (= 492.7 cm^{-1}) (8). The contradictory experimental observation that the $B^2\Sigma^+$ state $v = 0$ level is longer lived than the $v = 2$ level, is an indication that one of the vibrational levels is being perturbed by another state. Unlike the (0,0) band, which lies only 100 cm^{-1} from the 14 926.0 cm^{-1} band, the (2,0) band is quite isolated from any other experimentally observed cold bands. Thus a plausible explanation for the observed trend in lifetimes is that the $v = 0$ level is mixed with the presumably long-lived upper state level of the 14 926.0 cm^{-1} band, leading to an increase in the lifetime of the $v = 0$ level relative to the $v = 2$ level. Unfortunately, since we were unable to measure the lifetime of the upper state level in the 14 926.0 cm^{-1} band, we cannot comment further on this point.

Inspection of the data in Table 1 suggests that there is a strong interaction between the upper state levels in the 15 264.2 and 15 300.1 cm^{-1} bands, leading to an increase in the lifetime of the former, and a decrease in the lifetime of the latter. We present evidence below to demonstrate that the upper vibrational level of the 15 300.1 cm^{-1} band belongs to a $^4\Pi_{\pm 1/2}$ state. Since the upper level in the 15 264.2 cm^{-1} band has the shorter lifetime, we assign it as the $B^2\Sigma^+$ $v = 1$ level, and the other level as belonging to the $^4\Pi_{\pm 1/2}$ manifold, even though the magnitudes of the lifetimes indicate that the extent of mixing is quite considerable. The interaction between the $B^2\Sigma^+$ state $v = 1$ level and the neighbouring vibrational level of the $^4\Pi_{\pm 1/2}$ state may be understood by way of a simple two-state intensity borrowing mechanism (19). In the absence of an interaction between the $B^2\Sigma^+$ state and the $^4\Pi_{\pm 1/2}$ state, the oscillator strength for the $^4\Pi_{\pm 1/2} \leftarrow X^2\Sigma^+$ transition would be zero, and only a single bnd would be observed. If the measured radiative lifetimes of the upper state levels in the 15 264.2 and 15 300.1 cm^{-1} bands are denoted by τ_- and τ_+ respectively (the − and + referring to the directions of the energy shifts experienced by the levels when the perturbation is switched on), and the lifetimes of the parent, unperturbed $B^2\Sigma^+$ and $^4\Pi_{\pm 1/2}$ state levels by τ_1 and τ_2, respectively, then by conservation of transition intensity we may write for the radiative decay of the upper state levels:

$$[1] \quad \frac{1}{\tau_-} + \frac{1}{\tau_+} = \frac{1}{\tau_1} + \frac{1}{\tau_2}$$

The radiative lifetime for the vibrational level of the $^4\Pi_{\pm 1/2}$ state in the 15 300.1 cm^{-1} band, in the absence of the perturbation ineraction (τ_2), may be calculated using the data in Table 1. The unperturbed radiative lifetime for the $B^2\Sigma^+$ state $v = 1$, τ_1, is approximated by the lifetime of the $v = 2$ level, making a small correction for the differing v^3 factors for transitions from $v = 1$ and $v = 2$ to the ground state. The lifetime of the unperturbed $B^2\Sigma^+$ $v = 1$ level is thus estimated to be 112.4(22) ns. Substituting this value and τ_- = 188(11) ns, τ_+ = 233(24) ns in eq. [1] yields $\tau_2^{-1} = (7.1 \pm 7.6) \times 10^{-4}$ ns, implying that τ_2 could lie in the range 680 ns → infinity. The relative error on the result is very large due to the ill-conditioning of eq. [1] arising from the large errors associated with the determination of τ_- and τ_+. All we can say with certainty is that the lifetime of the perturbing state is very long, and possibly infinite. This result is quite consistent with the spin-forbidden nature of the $^4\Pi_{\pm 1/2} \rightarrow X^2\Sigma^+$ transition. We can not, however, rule out the possibility that the $^4\Pi_{\pm 1/2}$ state decays slowly to a nearby quartet state.

The $B^2\Sigma^+ \leftarrow X^2\Sigma^+$ *(0,0) band*

Line positions for the $B^2\Sigma^+ \leftarrow X^2\Sigma^+$ (0,0) band are reported in Table 2(*a*). Molecular constants were extracted from the rotational line data for the $B^2\Sigma^+ \leftarrow X^2\Sigma^+$ (0,0) band using a nonlinear least-squares procedure. There follows a description of how the pertinent eigenvalue expressions for the $B^2\Sigma^+$ and $X^2\Sigma^+$ state levels were obtained and incorporated into the fitting procedure. The effective Hamiltonian for a $^2\Sigma$ state may be written as:

$$[2] \quad H_{\text{eff}} = B\mathbf{N}^2 - D\mathbf{N}^4 + \gamma\mathbf{N}.\mathbf{S} + b_F\mathbf{I}.\mathbf{S} + [3I_zS_z - \mathbf{I}.\mathbf{S}]c/3$$

where B is the rotational constant, D the centrifugal distortion constant, γ the spin-rotation constant, b_F the Fermi contact parameter, and c the dipolar interaction parameter, the quantum numbers having their usual definition. Since with our experimental resolution there was no detectable hyperfine splitting in the $B^2\Sigma^+$ state, the last two terms in eq. [2] were dropped for the evaluation of the upper state eigenvalues. The matrix elements for the first three terms are diagonal, and give rise to the well-known pair of expressions for the energies of *e* and *f* rotational levels in a $^2\Sigma$ state (20):

$$[3] \quad F_1(N) = BN(N+1) - DN^2(N+1)^2 + \frac{1}{2}\gamma N \qquad (e \text{ levels})$$

$$[4] \quad F_2(N) = BN(N+1) - DN^2(N+1)^2 - \frac{1}{2}\gamma N(N+1) \qquad (f \text{ levels})$$

Equations [3] and [4] were used directly to represent the $B^2\Sigma^+$ state energy levels. Since the spin rotation constant in the upper state is large, it was represented by a centrifugal expansion thus:

$$[5] \quad \gamma = \gamma_0 + \gamma_1 N(N+1) + \gamma_2 N^2(N+1)^2$$

In the $X^2\Sigma^+$ state, the spin-rotation parameter is smaller than the Fermi contact term, and therefore the hyperfine energy levels were determined by diagonalization of the appropriate 4 × 4 energy matrix, which is presented in Table 3. The matrix elements are those derived by Radford using a case $b_{\beta J}$ basis set (21). Our treatment was simplified by discarding all terms involving the spin-dipolar parameter, c, as our experimental resolution did not warrant their inclusion. The observed line positions of Table 2(*a*) were fitted using a

TABLE 2(*a*). Observed line wavenumbers and residuals (obs. − calc., in parentheses) for the $B^2\Sigma^+ \leftarrow X^2\Sigma^+$ (0,0) band of $^{89}Y^{32}S$

	$P_1(N)$			
N	$F = N + 1$, $G = 1$	$F = N$, $G = 1$	$F = N - 1$, $G = 1$	$F = N$, $G = 0$
1	14 825.8024(30)	14 825.8024(15)	14 825.8024(8)	14 825.7819(30)
2	14 825.4396(63)	14 825.4396(40)	14 825.4396(27)	14 825.4158(24)
3	14 825.0539(−15)	14 825.0581(−5)	14 825.0581(−23)	14 825.0342(−19)
4	—	—	—	—
5	14 824.2619(−21)	14 824.2680(−10)	14 824.2680(−39)	14 824.2433(−24)
6	14 823.8534(29)	14 823.8604(39)	14 823.8640(41)	14 823.8401(74)
7	14 823.4233(−19)	14 823.4308(−14)	14 823.4308(−52)	14 823.4058(−20)
8	—	—	—	—
9	14 822.5394(4)	14 822.5493(12)	14 822.5541(14)	14 822.5293(70)
10	14 822.0746(−35)	14 822.0851(−32)	14 822.0902(−30)	14 822.0587(−31)
11	14 821.6050(−3)	14 821.6178(11)	14 821.6231(13)	14 821.5884(−8)
12	14 821.1157(−49)	14 821.1290(−41)	14 821.1345(−40)	14 821.1004(−44)
13	14 820.6287(48)	14 820.6401(25)	14 820.6513(80)	14 820.6165(81)
14	14 820.1120(−33)	14 820.1273(−29)	14 820.1336(−25)	14 820.0969(−31)
15	14 819.5992(45)	14 819.6172(63)	14 819.6238(68)	14 819.5835(39)
16	14 819.0574(−47)	14 819.0752(−43)	14 819.0823(−35)	14 819.0428(−44)
17	14 818.5162(−13)	14 818.5356(−5)	14 818.5429(3)	14 818.5018(−10)
18	14 817.9717(109)	—	—	—
19	14 817.3869(−51)	14 817.4088(−44)	14 817.4161(−39)	14 817.3726(−50)
20	14 816.8126(16)	14 816.8357(22)	14 816.8439(34)	14 816.7983(15)
21	14 816.2173(−6)	14 816.2415(−2)	14 816.2495(7)	14 816.2032(−6)
22	14 815.6170(44)	14 815.6451(74)	14 815.6541(92)	14 815.6022(35)
23	—	14 815.0163(−52)	14 815.0244(−44)	14 814.9907(95)
24	14 814.3602(−50)	14 814.3881(−48)	14 814.3959(−45)	14 814.3463(−52)
25	14 813.7212(−18)	14 813.7505(−16)	14 813.7589(−8)	14 813.7081(−13)
26	14 813.0653(−32)	14 813.0954(−35)	14 813.1037(−28)	14 813.0520(−29)
27	14 812.3983(−32)	14 812.4302(−30)	14 812.4387(−23)	14 812.3853(−28)
28	14 811.7220(0)	14 811.7552(1)	14 811.7637(7)	14 811.7092(5)
29	14 811.0242(−59)	14 811.0590(−56)	14 811.0672(−53)	14 811.0120(−48)
30	14 810.3265(9)	14 810.3569(−45)	14 810.3665(−29)	14 810.3133(9)
31	14 809.6143(58)	14 809.6554(97)	14 809.6654(116)	14 809.6008(54)
32	14 808.8817(30)	14 808.9227(54)	14 808.9321(67)	14 808.8689(32)
33	14 808.1311(−52)	14 808.1707(−55)	14 808.1800(−44)	14 808.1182(−51)
34	14 807.3778(−33)	14 807.4192(−32)	14 807.4284(−22)	14 807.3646(−36)
35	14 806.6131(0)	14 806.6604(47)	14 806.6702(61)	14 806.6003(1)
36	14 805.8314(−8)	14 805.8773(10)	14 805.8866(19)	14 805.8191(−3)

	$P_2(N)$			
N	$F = N + 1$, $G = 1$	$F = N$, $G = 1$	$F = N - 1$, $G = 1$	$F = N$, $G = 0$
2		14 825.6666(37)	14 825.6666(24)	14 825.6485(78)
3		—	—	—
4		14 825.1991(−7)	14 825.1991(−31)	14 825.1747(−23)
5		14 824.9592(87)	14 824.9592(58)	14 824.9321(49)
6		14 824.6931(39)	14 824.6931(5)	14 824.6576(−78)
7		14 824.4203(42)	14 824.4203(4)	14 824.3936(19)
8		14 824.1305(−5)	14 824.1305(−47)	14 824.1029(−30)
9		14 823.8368(29)	14 823.8401(17)	14 823.8099(18)
10		14 823.5238(−10)	14 823.5268(−28)	14 823.4955(−27)
11		14 823.1988(−48)	14 823.1988(−100)	14 823.1697(−65)
12		14 822.8764(61)	14 822.8804(57)	14 822.8452(32)
13		14 822.5243(−5)	14 822.5293(−12)	14 822.4942(−13)
14		14 822.1642(−29)	14 822.1684(−46)	14 822.1325(−44)
15		14 821.7989(18)	14 821.8034(2)	14 821.7661(3)
16		14 821.4108(−39)	14 821.4155(−55)	14 821.3775(−49)
17		14 821.0143(−56)	14 821.0194(−70)	14 820.9998(133)
18		14 820.6165(39)	14 820.6225(33)	14 820.5789(8)
19		14 820.1902(−25)	14 820.1961(−34)	14 820.1540(−31)

Can. J. Chem. Downloaded from www.nrcresearchpress.com by 203.198.23.82 on 09/08/12
For personal use only.

TABLE 2(*a*) (*continued*)

	$P_2(N)$			
N	$F = N + 1$, $G = 1$	$F = N$, $G = 1$	$F = N - 1$, $G = 1$	$F = N$, $G = 0$
20		14 819.7622(21)	14 819.7674(3)	14 819.7246(12)
21		14 819.3122(−26)	14 819.3185(−34)	14 819.2833(64)
22		14 818.8610(44)	14 818.8666(27)	14 818.8201(25)
23		14 818.3844(−11)	14 818.3902(−27)	14 818.3426(−27)
24		14 817.9087(74)	14 817.9147(59)	14 817.8640(41)
25		14 817.4016(−24)	14 817.4088(−28)	14 817.3578(−35)
26		14 816.9019(85)	14 816.9085(75)	14 816.8548(54)
27		14 816.3701(8)	14 816.3761(−10)	14 816.3318(76)
28		14 815.8338(20)	14 815.8404(8)	14 815.7863(10)
29		14 815.2795(−11)	14 815.2857(−28)	14 815.2306(−23)
30		14 814.7169(13)	14 814.7232(−4)	—
31		14 814.1347(−19)	14 814.1420(−27)	14 814.0849(−14)
32		14 813.5460(24)	14 813.5529(12)	14 813.4933(13)
33		14 812.9395(32)	14 812.9460(15)	—
34		14 812.3155(9)	14 812.3232(4)	14 812.2584(−20)
35		14 811.6757(−26)	14 811.6832(−34)	14 811.6242(14)
36		14 811.0242(−30)	—	—

	$R_1(N)$			
N	$F = N + 1$, $G = 1$	$F = N$, $G = 1$	$F = N - 1$, $G = 1$	$F = N$, $G = 0$
0	—	14 826.2633(−55)		14 826.2420(−49)
1	14 826.4448(−9)	14 826.4448(−23)		14 826.4240(−11)
2	14 826.6138(24)	14 826.6138(1)		14 826.5930(15)
3	14 826.7661(8)	14 826.7706(22)		14 826.7474(14)
4	14 826.9102(29)	14 826.9160(46)		14 826.8903(18)
5	14 827.0351(−24)	14 827.0413(−12)		14 827.0169(−23)
6	14 827.1521(−37)	14 827.1594(−24)		14 827.1348(−31)
7	14 827.2583(−39)	14 827.2666(−26)		14 827.2409(−39)
8	14 827.3567(0)	14 827.3663(16)		14 827.3393(−4)
9	14 827.4390(−3)	14 827.4518(34)		14 827.4226(0)
10	14 827.5091(−8)	14 827.5207(5)		14 827.4915(−21)
11	14 827.5684(−2)	14 827.5813(13)		14 827.5526(1)
12	14 827.6170(17)	14 827.6302(24)		14 827.5903(−92)
13	14 827.6450(−50)	14 827.6572(−65)		14 827.6375(31)
14	14 827.6709(−17)	14 827.6877(2)		14 827.6572(−1)
15	14 827.6820(−11)	14 827.7000(7)		14 827.6709(29)
16	14 827.6820(4)	14 827.7000(11)		14 827.6619(−48)
17	14 827.6619(−59)	14 827.6877(12)		14 827.6539(8)
18	14 827.6450(31)	14 827.6619(1)		14 827.6302(28)
19	14 827.6045(7)	14 827.6302(52)		14 827.5903(9)
20	14 827.5526(−8)	14 827.5830(71)		14 827.5388(−4)
21	14 827.4915(8)	14 827.5141(−4)		14 827.4762(−4)
22	14 827.4155(−2)	14 827.4494(86)		14 827.4020(3)
23	14 827.3260(−22)	14 827.3567(21)		14 827.3120(−24)
24	14 827.2243(−40)	14 827.2583(22)		14 827.2110(−36)
25	14 827.1128(−32)	14 827.1422(−28)		14 827.0998(−25)
26	14 827.0020(110)	—		14 826.9862(87)
27	14 826.8554(18)	14 826.8904(51)		14 826.8424(23)
28	14 826.7051(17)	14 826.7387(22)		14 826.6922(21)
29	14 826.5405(−1)	14 826.5766(15)		14 826.5276(3)
30	14 826.3644(−7)	14 826.4008(−1)		14 826.3513(6)
31	14 826.1716(−51)	14 826.2091(−48)		14 826.1592(−44)
32	14 825.9854(98)	14 826.0095(−46)		14 825.9718(93)
33	14 825.7625(10)	14 825.8024(10)		14 825.7502(17)
34	14 825.5343(−2)	14 825.5775(17)		14 825.5219(3)
35	14 825.2889(−56)	14 825.3340(−31)		14 825.2764(−52)

Can. J. Chem. Downloaded from www.nrcresearchpress.com by 203.198.23.82 on 09/08/12
For personal use only.

TABLE 2(*a*) (*concluded*)

	$R_2(N)$			
N	$F = N + 1$, $G = 1$	$F = N$, $G = 1$	$F = N - 1$, $G = 1$	$F = N$, $G = 0$
1	14 826.8276(32)	14 826.8276(17)	14 826.8276(11)	14 826.8049(11)
2	—	—	—	—
3	—	—	—	—
4	14 827.7480(79)	14 827.7480(39)	14 827.7480(15)	14 827.7231(18)
5	14 828.0204(−10)	14 828.0265(1)	14 828.0265(−28)	14 828.0001(−30)
6	14 828.2916(9)	14 828.2993(26)	14 828.2993(−7)	14 828.2715(−14)
7	14 828.5509(29)	14 828.5593(43)	14 828.5593(6)	14 828.5316(11)
8	14 828.7952(21)	14 828.8044(32)	14 828.8044(−10)	14 828.7767(6)
9	14 829.0216(−46)	14 829.0337(−16)	14 829.0337(−62)	14 829.0025(−70)
10	14 829.2448(−23)	14 829.2555(−18)	14 829.2584(−38)	14 829.2267(−40)
11	14 829.4556(−2)	14 829.4671(0)	14 829.4703(−20)	14 829.4378(−19)
12	14 829.6601(80)	14 829.6701(54)	14 829.6701(0)	14 829.6414(51)
13	14 829.8379(18)	14 829.8519(20)	14 829.8559(4)	14 829.8207(1)
14	14 830.0031(−47)	14 830.0189(−38)	14 830.0233(−53)	—
15	14 830.1653(−16)	14 830.1814(−16)	14 830.1865(−26)	14 830.1485(−33)
16	14 830.3149(15)	14 830.3328(20)	14 830.3328(−43)	14 830.2981(−4)
17	14 830.4466(−7)	14 830.4657(−3)	14 830.4708(−17)	14 830.4303(−23)
18	14 830.5729(44)	14 830.5930(46)	14 830.5988(37)	14 830.5559(19)
19	14 830.6755(−14)	14 830.6975(−6)	14 830.7027(−22)	—
20	14 830.7726(3)	14 830.7949(1)	14 830.8004(−14)	14 830.7572(−9)
21	14 830.8565(17)	14 830.8801(16)	14 830.8860(4)	14 830.8407(0)
22	14 830.9286(45)	14 830.9545(54)	14 830.9608(44)	14 830.9119(18)
23	14 830.9727(−74)	14 831.0035(−30)	14 831.0087(−52)	14 830.9608(−55)
24	14 831.0207(−21)	14 831.0487(−19)	14 831.0545(−35)	14 831.0087(−4)
25	14 831.0545(24)	14 831.0798(−13)	14 831.0905(18)	14 831.0349(−35)
26	14 831.0666(−11)	14 831.0978(−3)	14 831.1027(−31)	14 831.0545(3)
27	14 831.0666(−30)	14 831.1027(14)	14 831.1073(−18)	14 831.0545(−16)
28	14 831.0545(−31)	14 831.0859(−48)	14 831.0978(−7)	14 831.0487(45)
29	14 831.0349(34)	14 831.0666(6)	14 831.0732(−7)	14 831.0175(−8)
30	—	14 831.0270(−1)	14 831.0349(−3)	14 830.9855(73)

Residual mean square error = 109.6 MHz.

Can. J. Chem. Downloaded from www.nrcresearchpress.com by 203.198.23.82 on 09/08/12
For personal use only.

modified Levenberg–Marquardt algorithm. The energy matrix for the ground state hyperfine levels was diagonalized and the resulting eigenvalues added to $B''N(N + 1) - D''N^2(N + 1)^2$ to generate the lower state term values. These were combined with term values calculated for the upper state using eqs. [3] and [4]. The values of the various spectroscopic parameters were varied until the best fit of calculated to experimental line positions was obtained. The results of the fitting procedure are presented in Table 4(*a*). Rotational perturbations in the upper state were found to set in beyond $N = 36$, so lines terminating on these levels were not included in the fit. The random error of measurement (109 MHz) is well below the experimental accuracy of 200 MHz. The Fermi contact and spin-rotation parameters obtained for the ground state are in good agreement with those determined by Azuma and Childs (9). The sign and magnitude of the spin-rotation constant in the $B^2\Sigma^+$ state ($\gamma_0 = -0.15150(14)$ cm^{-1}) are a manifestation of an interaction of the "unique perturber" type between this state and the $A^2\Pi$ state, where Stringat et al. (8) determined the Λ-doubling parameter p to be $+0.155$ cm^{-1}.

The 14 926.0 cm^{-1} band

The band located at 14 926.0 cm^{-1} (see Fig. 2(*b*)) qualitiatively resembles the $B^2\Sigma^+ \leftarrow X^2\Sigma^+$ (0,0) band, in that it is red-degraded and possesses four discernible rotational branches with the same hyperfine structure patterns as the (0,0) band. Similarly, there was no evidence for hyperfine structure in the upper state at the experimental resolution of 120 MHz. Line assignments were confirmed in two ways. Firstly, the combination differences $\Delta_2F''(J)$ were formed for the *e* and *f* manifolds. The B'' values thus determined were found to be in good agreement with the value reported in Table 4(*a*). Secondly, the hyperfine splitting patterns of the lines in the 14 926.0 cm^{-1} band were compared with those of the corresponding lines with the same N'' values in the $B^2\Sigma^+ \leftarrow X^2\Sigma^+$ (0,0) band. The patterns were found to match, well within the limits of experimental error, confirming the assignments of the quantum number N'' and the *e*/*f* symmetry labelling for lines of the 14 926,0 cm^{-1} band. A rotational energy level diagram for the upper state level of the 14 926.0 cm^{-1} band, shown in Fig. 5, was constructed as follows. Firstly, the rotational and hyperfine parameters determined for the $X^2\Sigma^+$ state $v = 0$ level (Table 4(*a*)) were used to calculate the term values of the rotational–hyperfine levels in the lower state. The upper state rotational term values were obtained by adding the appropriate ground state term values to the experimental line positions reported in Table 2(*b*). This procedure yielded either three of four determinations of the position of each upper state rotational level, which were found to coincide, well within the experimental uncertainty. These values were averaged and are plotted for the lowest rotational levels of the upper state in

TABLE 2(*b*). Observed line wavenumbers and residuals (obs. − calc., in parentheses) for the $^4\Pi_{\pm 1/2} \leftarrow X^2\Sigma^+$ ($v = 0$) 14 926.0 cm^{-1} band of $^{89}Y^{32}S$

	$P_{11} + {}^{P}Q_{12}$ (*N*)			
N	*F* = *N* + 1, *G* = 1	*F* = *N*, *G* = 1	*F* = *N* − 1, *G* = 1	*F* = *N*, *G* = 0
1	14 926.2036(−4)	14 926.2036(−19)	14 926.2036(−26)	14 926.1815(−20)
2	14 925.9857(1)	14 925.9879(1)	—	14 925.9635(−22)
3	14 925.7176(−20)	14 925.7214(−14)	—	14 925.6970(−33)
4	14 925.4017(−45)	14 925.4070(−32)	—	14 925.3815(−59)
5	14 925.0406(−45)	14 925.0460(−41)	14 925.0416(−114)	14 925.0213(−56)
6	14 924.6327(−39)	14 924.6329(−97)	14 924.6417(−42)	14 924.6139(−49)
7	14 924.1775(−30)	14 924.1841(−34)		14 924.1593(−38)
8	14 923.6729(−39)	14 923.6844(−5)	14 923.6881(−9)	14 923.6562(−36)
9	14 923.1244(−12)	14 923.1335(−12)	14 923.1369(−23)	14 923.1065(−24)
10	14 922.5267(−1)	14 922.5363(−7)	14 922.5407(−11)	14 922.5086(−18)
11	14 921.8795(−9)	14 921.8904(−14)	14 921.8957(−12)	14 921.8620(−23)
12	14 921.1876(12)	14 921.1998(9)	14 921.2050(6)	14 921.1712(6)
13	14 920.4461(12)	14 920.4596(10)	14 920.4648(5)	14 920.4300(7)
14	—	—	—	—
15	14 918.8193(2)	14 918.8355(3)	14 918.8410(−3)	14 918.8040(0)
16	14 917.9352(4)	14 917.9524(2)	14 917.9576(−9)	14 917.9192(−7)
17	14 917.0014(−16)	14 917.0222(5)	14 917.0292(10)	14 916.9858(−25)
18	14 916.0249(12)	14 916.0445(9)	14 916.0505(2)	14 916.0106(14)
19	14 914.9984(16)	14 915.0182(2)	14 915.0251(3)	14 914.9829(5)
20	14 913.9246(22)	14 913.9465(16)	14 913.9537(18)	14 913.9091(9)
21	14 912.8016(10)	14 912.8236(−7)	14 912.8307(−7)	14 912.7858(−7)
22	14 911.6343(31)	14 911.6587(24)	14 911.6663(28)	14 911.6186(14)
23	14 910.4158(14)	14 910.4418(10)	14 910.4489(8)	14 910.4011(6)
24	14 909.1512(11)	14 909.1791(13)	14 909.1871(18)	14 909.1376(12)
25	14 907.8390(6)	14 907.8673(−2)	14 907.8740(−10)	14 907.8254(6)
26	14 906.4816(23)	14 906.5105(8)	14 906.5182(8)	14 906.4661(3)
27	14 905.0743(14)	14 905.1057(11)	14 905.1134(10)	14 905.0606(11)
28	14 903.6193(2)	14 903.6508(−14)	14 903.6593(−7)	14 903.6046(−12)
29	14 902.1181(1)	14 902.1519(−6)	14 902.1597(−7)	14 902.1045(−3)
30	14 900.5704(7)	14 900.6054(−1)	14 900.6141(6)	14 900.5552(−13)

	${}^{O}P_{12}$ (*N*)			
N	*F* = *N* + 1, *G* = 1	*F* = *N*, *G* = 1	*F* = *N* − 1, *G* = 1	*F* = *N*, *G* = 0
2		14 925.6654(1)	14 925.6654(−12)	14 925.6407(−24)
3		14 925.1856(4)	14 925.1856(−15)	14 925.1605(−23)
4		14 924.6561(−17)	14 924.6581(−21)	14 924.6414(64)
5		14 924.0829(−1)	14 924.0858(−1)	14 924.0588(−9)
6		14 923.4624(15)	14 923.4658(15)	14 923.4381(10)
7		14 922.7947(32)	14 922.7983(30)	14 922.7692(21)
8		14 922.0759(11)	14 922.0793(3)	14 922.0492(−5)
9		14 921.3141(32)	14 921.3123(−31)	14 921.2876(25)
10		14 920.5044(46)	14 920.5087(41)	14 920.4765(33)
11		14 919.6426(11)	14 919.6475(8)	14 919.6146(5)
12		14 918.7396(35)	14 918.7447(32)	14 918.7094(16)
13		14 917.7871(25)	14 917.7922(29)	14 917.7577(33)
14		14 916.7866(25)	14 916.7927(27)	14 916.7560(21)
15		14 915.7415(39)	14 915.7479(42)	14 915.7095(32)
16		14 914.6470(29)	14 914.6532(28)	14 914.6145(27)
17		14 913.5056(19)	14 913.5124(22)	14 913.4722(19)
18		14 912.3195(31)	14 912.3262(31)	14 912.2839(19)
19		14 911.0855(32)	14 911.0919(27)	14 911.0487(19)
20		14 909.8023(8)	14 909.8088(3)	14 909.7657(9)
21		14 908.4739(−1)	14 908.4807(−4)	14 908.4360(−1)
22		14 907.0985(−14)	14 907.1056(−15)	14 907.0588(−20)
23		14 905.6786(−5)	14 905.6860(−5)	14 905.6360(−29)
24		14 904.2093(−26)	14 904.2178(−15)	14 904.1668(−36)
25		14 902.6946(−35)	14 902.7027(−30)	14 902.6508(−47)

Can. J. Chem. Downloaded from www.nrcresearchpress.com by 203.198.23.82 on 09/08/12
For personal use only.

TABLE 2(*b*) (*continued*)

	$R_{11}(N)$			
N	$F = N + 1$, $G = 1$	$F = N$, $G = 1$	$F = N - 1$, $G = 1$	$F = N$, $G = 0$
0	—	14 926.8181(−29)		14 926.7958(−33)
1	14 927.1085(−14)	14 927.1085(−29)		14 927.0864(−30)
2	14 927.3493(−26)	14 927.3493(−49)		14 927.3276(−44)
3	14 927.5439(−25)	14 927.5439(−57)		14 927.5237(−34)
4	14 927.6907(−27)	14 927.6907(−67)		14 927.6708(−38)
5	14 927.7908(−19)	14 927.7908(−69)		14 927.7716(−29)
6	14 927.8421(−24)	14 927.8421(−84)		14 927.8236(−31)
7	14 927.8469(−18)	14 927.8537(−20)		14 927.8284(−29)
8	14 927.8045(−8)	14 927.8127(−7)		14 927.7861(−22)
9	14 927.7138(−6)	14 927.7232(−3)		14 927.6957(−20)
10	14 927.5752(−5)	14 927.5850(−10)		14 927.5573(−21)
11	14 927.3891(−4)	14 927.4009(0)		14 927.3720(−15)
12	14 927.1558(1)	14 927.1677(−6)		14 927.1393(−6)
13	14 926.8740(−3)	14 926.8884(4)		14 926.8550(−38)
14	14 926.5462(9)	14 926.5599(−3)		14 926.5299(−1)
15	14 926.1709(22)	14 926.1871(23)		14 926.1552(16)
16	14 925.7465(20)	14 925.7638(20)		14 925.7312(16)
17	14 925.2747(20)	14 925.2930(17)		14 925.2589(9)
18	14 924.7558(25)	14 924.7754(22)		14 924.7412(24)
19	14 924.1879(15)	14 924.2091(15)		14 924.1731(11)
20	14 923.5753(33)	14 923.5974(29)		14 923.5598(20)
21	14 922.9153(53)	14 922.9386(48)		14 922.9002(43)
22	14 922.2038(32)	14 922.2280(24)		14 922.1890(24)
23	14 921.4474(38)	14 921.4731(31)		14 921.4331(33)
24	—	—		—
25	14 919.7908(35)	14 919.8195(31)		14 919.7771(34)
26	14 918.8910(29)	14 918.9210(25)		14 918.8763(17)
27	14 917.9423(8)	14 917.9747(15)		14 917.9279(−1)
28	14 916.9462(−13)	—		14 916.9329(−12)
29	14 915.9059(−3)	—		14 915.8932(3)
30	14 914.8178(2)	—		14 914.8036(−8)
31	14 913.6825(8)	14 913.7199(10)		14 913.6697(11)
32	14 912.4992(6)	14 912.5370(−2)		14 912.4853(−3)
33	14 911.2665(−19)	14 911.3047(−36)		14 911.2539(−15)
34	14 909.9862(−48)	14 910.0300(−23)		14 909.9729(−52)
35	14 908.6619(−46)	—		14 908.6492(−45)
36	14 907.2916(−34)	—		—

	$^{Q}R_{12} + Q_{11}(N)$			
N	$F = N + 1$, $G = 1$	$F = N$, $G = 1$	$F = N - 1$, $G = 1$	$F = N$, $G = 0$
1	14 926.5818(94)	14 926.5818(80)	14 926.5818(73)	14 926.5578(60)
2	14 926.6013(18)	14 926.6013(−5)	14 926.6013(−18)	14 926.5826(30)
3	14 926.5723(−70)	14 926.5779(−46)	14 926.5779(−64)	14 926.5462(138)
4	14 926.5119(2)	14 926.5168(10)	14 926.5168(−14)	14 926.4928(−1)
5	14 926.3973(5)	14 926.4030(12)	14 926.4046(−1)	14 926.3784(−1)
6	14 926.2364(19)	14 926.2418(13)	14 926.2436(−2)	14 926.2174(7)
7	14 926.0263(14)	14 926.0338(19)	14 926.0372(15)	14 926.0078(3)
8	14 925.7712(31)	14 925.7797(35)	14 925.7841(38)	14 925.7526(15)
9	14 925.4657(16)	14 925.4749(17)	14 925.4796(18)	14 925.4483(9)
10	14 925.1159(30)	14 925.1262(30)	14 925.1311(31)	14 925.0990(24)
11	14 924.7183(37)	14 924.7299(39)	14 924.7355(44)	14 924.7009(24)
12	14 924.2716(25)	14 924.2846(29)	14 924.2893(22)	14 924.2552(18)
13	14 923.7825(59)	14 923.7960(56)	14 923.8017(57)	14 923.7660(49)
14	14 923.2398(27)	14 923.2549(28)	14 923.2605(25)	14 923.2241(23)
15	14 922.6554(47)	14 922.6775(107)	14 922.6779(50)	14 922.6400(44)
16	14 922.0197(24)	14 922.0368(21)	14 922.0429(19)	14 922.0029(5)
17	14 921.3392(22)	14 921.3586(29)	14 921.3651(29)	14 921.3262(39)
18	14 920.6142(43)	—	—	14 920.5989(35)

Can. J. Chem. Downloaded from www.nrcresearchpress.com by 203.198.23.82 on 09/08/12
For personal use only.

TABLE 2(*b*) (*concluded*)

	$^{Q}R_{12} + Q_{11}$ (*N*)			
N	*F* = *N* + 1, *G* = 1	*F* = *N*, *G* = 1	*F* = *N* − 1, *G* = 1	*F* = *N*, *G* = 0
19	14 919.8388(27)	14 919.8597(24)	14 919.8665(24)	14 919.8245(28)
20	14 919.0177(21)	14 919.0404(24)	14 919.0477(27)	14 919.0025(12)
21	14 918.1478(−6)	14 918.1709(−12)	14 918.1772(−21)	14 918.1341(−2)
22	14 917.2339(−7)	14 917.2586(−11)	14 917.2657(−12)	14 917.2201(−5)
23	14 916.2715(−28)	14 916.2974(−33)	14 916.3046(−34)	14 916.2573(−31)
24	—	14 915.2939(−13)	14 915.3018(−9)	14 915.2537(−1)
25	14 914.2102(−41)	14 914.2388(−46)	14 914.2462(−48)	14 914.1957(−50)
26	14 913.1091(−57)	14 913.1401(−51)	14 913.1475(−54)	14 913.0960(−53)
27	14 911.9643(−47)	14 911.9948(−60)	14 911.0023(−62)	14 911.9497(−59)
28	14 910.7711(−60)	14 910.8040(−62)	14 910.8113(−67)	14 910.7581(−56)
29	14 909.5333(−57)	14 909.5658(−76)	14 909.5740(−74)	14 909.5184(−73)
30	—	14 908.2818(−88)	14 908.2904(−82)	14 908.2346(−70)
31	14 906.9184(−63)	14 906.9568(−51)	14 906.9641(−59)	14 906.9059(−57)
32	14 905.5446(−41)	14 905.5811(−61)	14 905.5901(−53)	14 905.5310(−47)
33	14 904.1265(−4)	14 904.1668(0)	14 904.1732(−18)	14 904.1128(−11)
34	14 902.6612(19)	—	14 902.7109(20)	14 902.6481(17)
35	14 901.1551(90)	14 901.1958(71)	14 901.2048(77)	—
36	14 899.6038(165)	14 899.6472(159)	14 899.6553(156)	14 899.5910(165)

Residual mean square error = 106.2 MHz.

TABLE 3. Energy matrix for the rotational, spin-rotation, and magnetic hyperfine structure parts of the Hamiltonian of a $^2\Sigma^+$ state, using case $b\beta J$ basis functions

(*e*) $J = N + 1/2$		(*f*) $J = N - 1/2$	
$F = N + 1$	$F = N$	$F = N$	$F = N - 1$
$\left[b + \frac{c}{(2N+3)}\right]\frac{A}{2(2N+1)} + \frac{\gamma N}{2} + BN(N+1)$	0	0	0
0	$\left[b + \frac{c}{(2N+3)}\right]\frac{B}{2(2N+1)} + \frac{\gamma N}{2} + BN(N+1)$	$\left[b + \frac{c}{2}\right]\frac{C}{2(2N+1)}$	$\left[b + \frac{c}{2}\right]\frac{D}{2(2N+1)}$
0	$\left[b + \frac{c}{2}\right]\frac{C}{2(2N+1)}$	$\left[-b + \frac{c}{(2N-1)}\right]\frac{E}{2(2N+1)} - \frac{\gamma(N+1)}{2} + BN(N+1)$	0
0	$\left[b + \frac{c}{2}\right]\frac{D}{2(2N+1)}$	0	$\left[-b + \frac{c}{(2N-1)}\right]\frac{F}{2(2N+1)} - \frac{\gamma(N+1)}{2} + BN(N+1)$

$A = (N + 1)(N + 2) - I(I + 1) - (N + 1/2)(N + 3/2)$
$B = N(N + 1) - I(I + 1) - (N + 1/2)(N + 3/2)$
$C = \{(2N - I + 1/2)(I + 1/2)(2N + I + 3/2)(I + 1/2)\}^{1/2}$
$D = \{(2N - I + 1/2)(I - 1/2)(2N + I + 1/2)(I + 3/2)\}^{1/2}$
$E = N(N + 1) - I(I + 1) - (N - 1/2)(N + 1/2)$
$F = N(N + 1) - I(I + 1) - (N - 1/2)(N + 1/2)$

B is the rotational constant and γ the spin-rotation constant; $b = b_F - c/3$, where b_F is the Fermi contact parameter and *c* the dipolar interaction parameter. The quantum numbers have their usual definition.

Fig. 5. The derived energy level pattern is quite characteristic of a state with non-zero orbital angular momentum in Hund's case (*a*). The splitting between *e* and *f* levels with the same *J* value, which is found to increase almost linearly with $J + 1/2$, is due to Λ-doubling. The existence of a level with $J = 1/2$ indicates that the Ω value for the state is either $+1/2$ or $-1/2$. There now arises the question of how the new $\Omega = \pm 1/2$ state should be assigned. The $A^2\Pi$ state has been

Can. J. Chem. Downloaded from www.nrcresearchpress.com by 203.198.23.82 on 09/08/12
For personal use only.

TABLE 4(*a*). Spectroscopic constants for the $B^2\Sigma^+ \leftarrow X^2\Sigma^+$ (0,0) band of $^{89}Y^{32}S$

	$X^2\Sigma^+$ $v = 0$	$B^2\Sigma^+$ $v = 0$
B_0	0.138883(20)[a]	0.132953(21)
r_0(Å)	2.27191(17)	2.32202(19)
D_0	$5.7(13) \times 10^{-8}$	$1.96(13) \times 10^{-7}$
$\gamma_{0,0}$[b]	$1.437(39) \times 10^{-3}$	−0.15150(14)
$\gamma_{1,0}$[b]	—	$3.16(44) \times 10^{-6}$
$\gamma_{2,0}$[b]	—	$1.53(31) \times 10^{-9}$
b_0	−0.02120(98)	—
	ν_{00} = 14 826.07260(65)	

[a]Numbers in parentheses are the uncertainties (2σ) in the units of the last quoted decimal place.
[b]Centrifugal expansion of spin-rotation constant (see text).

TABLE 4(*b*). Spectroscopic constants for the $^4\Pi_{\pm 1/2} \leftarrow X^2\Sigma^+$ (v',0) band of $^{89}Y^{32}S$

	$^4\Pi_{\pm 1/2}$ v'
B	0.1151477(30)[a]
r(Å)	2.49510(16)[b]
D	$-1.90(24) \times 10^{-8}$
a	$-7.618(38) \times 10^{-3}$
b	$-3.421(45) \times 10^{-6}$
$T_{v'0}$	14 926.02420(65)

[a]Numbers in parentheses are the uncertainties (2σ) in the units of the last quoted decimal place.
[b]10σ error bound (see text).

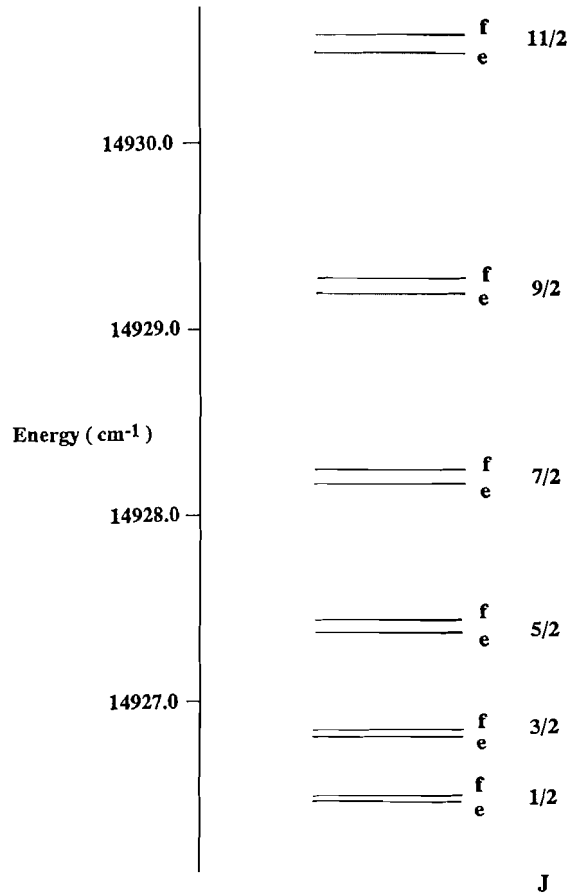

FIG. 5. Rotational energy levels in the v' level of the $^4\Pi_{\pm 1/2}$ state, derived from the experimental data reported in Table 2(*b*).

well characterized experimentally (8), so it can be ruled out immediately. Another possibility is that the new state is of doublet spin symmetry and is derived from the configuration $\sigma_2^2\pi_1^3\sigma_3^2$. (The parentage of these molecular orbitals can be found in the "Results of Calculations" section below.) Calculations on the isovalent molecule YO suggest that this "charge transfer" type state should have a bond length considerably longer than that in the ground state (22), as is found experimentally by taking combination differences for the upper state in the 14 926.0 cm^{-1} band. However, such a dramatic bond-length change upon excitation would be expected to produce an extended vibronic progression in the upper state vibrational quantum number in the allowed $^2\Pi \leftarrow X^2\Sigma^+$ transition. This expectation is at odds with the experimental observation of only one, or possibly two (including the new band at 15 300.1 cm^{-1}), bands belonging to the new system in the energy region of interest. Furthermore, transitions to both the $\Omega = 1/2$ and $\Omega = 3/2$ spin-orbit components of this doublet state would be allowed, and there is no evidence for any other bands that could be due to transitions from the ground state to the $\Omega = 3/2$ component. Similar arguments may be applied to rule out assignment to other $^2\Pi$ states based on charge transfer type excitations. There remains another possibility: that the new state belongs to the quartet spin manifold. Calculations (vide infra) place the lowest lying quartet states in approximately the same energy region as the $B^2\Sigma^+$ state. On the basis of the above arguments we assign the symmetry of the new state to be $^4\Pi_{\pm 1/2}$, arising from the configuration $\sigma_2^2\pi_1^3\sigma_3^2$. The rotational branches in the 14 926.0 cm^{-1} band are identified as $P_{11} + {}^PQ_{12}$, ${}^OP_{12}$, $Q_{11} + {}^QR_{12}$, and R_{11}. The spin-forbidden $^4\Pi_{\pm 1/2} \leftarrow X^2\Sigma^+$ transition acquires intensity through spin-orbit contamination of the $\Omega = \pm 1/2$ spin-orbit components by the $B^2\Sigma^+$ state. The other spin-orbit components of the $^4\Pi$ state, $\Omega = 3/2$ and $\Omega = 5/2$, cannot be observed in excitation from the $X^2\Sigma^+$ state on account of the strict $\Delta\Omega = 0$ selection rule for the spin-orbit operator (19), which leads to non-zero matrix elements between the $^4\Pi$ ($\Omega = \pm 1/2$) and $B^2\Sigma^+$ ($\Omega = \pm 1/2$) states only. The spin-orbit interaction mechanism explains why the 14 926.0 cm^{-1} band can be observed, despite unfavourable Franck–Condon overlap with the ground state. This point is developed further in the Discussion section.

One possible assignment for the 14 926.0 cm^{-1} band is that it arises from a $^4\Pi_{-1/2} \leftarrow X^2\Sigma^+$ excitation. In such a case, the new band at 15 300.1 cm^{-1} band could be due to the corresponding $^4\Pi_{+1/2} \leftarrow X^2\Sigma^+$ vibronic transition, implying a spin-orbit splitting in the $^4\Pi$ state of approximately +374 cm^{-1}. However, a calculation of the spin-orbit splitting for the $^4\Pi$ state using atomic spin-orbit parameters suggests that it should be of the order of +266.5 cm^{-1}, a considerable discrepancy. Furthermore, in a $^4\Pi$ state, the rotational constant for the $\Omega = 1/2$ component should be greater than that of the $\Omega = -1/2$ component. A deperturbation analysis of the 15 264.2 and 15 300.1 cm^{-1} bands is currently under way. From a preliminary centres of gravity analysis, using the data in Table 4 and the Pekeris relation to estimate the

Can. J. Chem. Downloaded from www.nrcresearchpress.com by 203.198.23.82 on 09/08/12
For personal use only.

Can. J. Chem. Downloaded from www.nrcresearchpress.com by 203.198.23.82 on 09/08/12
For personal use only.

rotational constant in the $v = 1$ level of the B state (0.13242 cm^{-1}), we calculate the rotational constant of the perturbing level to be 0.1149 cm^{-1}. This is appreciably smaller than the rotational constant determined for the upper level of the 14 926.0 cm^{-1} band, contradicting the suggested assignment. A more plausible explanation is that the upper level in the 15 300 cm^{-1} band belongs to the sam spin-orbit component of the $^4\Pi$ state as the upper level in the 14 926.0 cm^{-1} band (see Discussion).

Since we lack rotational line data on any of the other spin-orbit components of the $^4\Pi$ state, a definitive assignment of the 14 926.0 cm^{-1} band to a $^4\Pi_{+1/2} \leftarrow X^2\Sigma^+$ or $^4\Pi_{-1/2} \leftarrow X^2\Sigma^+$ transition cannot easily be made. Cheung et al. (23) have given a detailed treatment of the derivation of the matrix elements of the rotational Hamiltonian of a $^4\Pi$ state in case (*a*) coupling. In a $^4\Pi_{+1/2}$ state, the Λ doubling increases in an approximately linear fashion with $J + 1/2$ on account of the $p + 2q$ term appearing in the diagonal matrix element. However, in a $^4\Pi_{-1/2}$ state, although there is no diagonal term in $J + 1/2$ (apart from a distortion constant), the off-diagonal $o + p + q$ term connecting the $\Omega = +1/2$ and $\Omega = -1/2$ components has a similar effect upon matrix diagonalization. Thus in fitting the 14 926.0 cm^{-1} band, we decided at the outset to employ a simple expression for the rotational energies of the *e* and *f* levels of the $^4\Pi_{\pm 1/2}$ state:

$$[6] \quad E(^4\Pi_{\pm 1/2}) = T + B(z + 3) - D(z^2 + 13z + 5) \pm (J + 1/2)[a + bz]$$

where $z = (J + 1/2)^2$, the upper and lower signs referring to the *e* and *f* levels respectively. B, D, a, and b are, respectively, effective rotational, centrifugal distortion, Λ-doubling, and Λ-doubling distortion parameters. Equation [6] is simply a reduced form of the diagonal matrix elements for a $^4\Pi_{+1/2}$ state, as given by Cheung et al. The observed line positions in Table 2(*b*) were submitted to least-squares analysis in the manner described for the $B^2\Sigma^+ \leftarrow X^2\Sigma^+$ (0,0) band. In the present case, the rotational and hyperfine parameters for the $X^2\Sigma^+$ state $v = 0$ level were not varied, since these were already determined with high precision in the $B^2\Sigma^+ \leftarrow X^2\Sigma^+$ (0,0) analysis. The results of fitting the $^4\Pi_{\pm 1/2} \leftarrow X^2\Sigma^+$ band (423 hyperfine lines) are presented in Table 4(*b*). Since the rotational constant is contaminated by a number of effects, we quote a 10σ error bound on the bond length, rather than the more typical 2σ error. The negative centrifugal disortion constant and the anomalously large Λ-doubling distortion terms reflect the effects of *S*-uncoupling within the $^4\Pi$ state. The RMS error (283 MHz) is somewhat higher than the experimental resolution (120 MHz), reflecting the need for data on the other spin-orbit components. Rigorous analyses involving diagonalization of the complete Hamiltonian matrix were also attempted, using an estimated value of the spin-orbit parameter of +266.5 cm^{-1}. Due to the lack of data on any other spin-orbit parameters of the $^4\Pi$ state, several of the parameters obtained from these fits were poorly determined and highly correlated. However, whether the upper state was assumed to be of $^4\Pi_{+1/2}$ or $^4\Pi_{-1/2}$ symmetry, the rotational constant was always well determined and in reasonable agreement with the value obtained from the fit using Eq. [6]. The bond length in the $^4\Pi_{\pm 1/2}$ state is some 9.8% longer than that in the $X^2\Sigma^+$ state. This is quite consistent with the results of the density functional treatment (vide infra) where the bond length in the lowest lying quartet state is calculated to be 10% longer than in the ground state (see Table 5(*a*)). The negative sign for the Λ-doubling terms linear in $J + 1/2$ indicate that the $^4\Sigma^-$ state, which is assumed to be responsible for the Λ-doubling, lies above the $^4\Pi_{\pm 1/2}$ state.

Results of calculations

The calculated spectroscopic properties of YO and YS are shown in Table 5(*a*) along with those from the theoretical study of Langhoff and Bauschlicher (22) and experimental values. Gradient corrections are known to considerably improve the accuracy of bond energies relative to purely local functionals and bring the discrepancies down to typically a few kcal/mol (24). The generally very good agreement obtained here between experiment and theory is probably somewhat fortuitous. In YO, the lowest quartet state is calculated to lie 26 166 cm^{-1} above the ground state, in excellent agreement with the value calculated by Langhoff and Bauschlicher. In YS, the lowest quartet state is calculated to be much more stable, lying only 17 439 cm^{-1} above the ground state, on account of the lower electronegativity of sulfur relative to oxygen. The other calculated properties (ω_e, μ, $d\mu/dr$) are not highly accurate, but sufficiently so to give the correct trends. Overall, the agreement of the present calculations with those of Langhoff and Bauschlicher and with experiment is quite good. It should be noted that the density functional method does not allow us to further break down the *s*, *p*, and *d* composition of a molecular orbital into constituent contributions from individual *ns*, *np*, and *nd* orbitals. Thus in the ensuing discussion, we make the assumption that one particular *ns*, *np*, or *nd* orbital dominates the *s*, *p*, or *d* contribution to a particular molecular orbital.

The bonding can be characterized from the Mulliken populations of Table 5(*b*). As expected, bonding in YO and YS is rather similar. The valence configuration can be denoted as $\sigma_1^2\sigma_2^2\pi_1^4\sigma_3^1$. for the $X^2\Sigma^+$ state and as $\sigma_1^2\sigma_2^2\pi_1^3\sigma_3^1\delta_1^1$ for the $^4\Pi$ state. The σ_1 orbital is a low-lying *s* orbital of sulfur (oxygen) with some participation from yttrium *s*, $p\sigma$, and $d\sigma$ orbitals. The π_1 and σ_2 orbitals are bonding combinations of sulfur (oxygen) valence *p* orbitals and yttrium 4*d* orbitals, with substantially heavier weight on sulfur (oxygen). The participation of the yttrium 5*s* orbital in the σ_2 molecular orbital is calculated to be less than 8% in each case (see Table 5(*b*)). In both YO and YS, the σ_3 orbital closely resembles the yttrium 5*s* orbital, with only about 5% 5*p* character. The σ_3 orbital is semi-occupied in the lowest doublet and quartet states of YS and YO, so that the states correlate to a $4d^2\,5s^1$ yttrium atom. Note, however, that the binding energies given in Table 5(*a*) are calculated relative to the calculated (and true) ground state of the yttrium atom, which has a $4d^1\,5s^2$ configuration.

In the dissociation limit of YS (YO), there are four electrons in the 3*p* shell of sulfur (oxygen) and two in the 4*d* shell of yttrium. The "ideal covalent" populations on the sulfur for the π_1 and σ_2 orbitals are therefore $4/6 = 0.67$. The actual populations in YS are larger (0.73 and 0.69), and they are larger still on oxygen in YO (0.78 and 0.79), as expected on the basis of atomic electronegativities. The bond order in the YS ground state (2.54) is quite large and the Mulliken charges (±0.20) fairly small. The bond in YS is thus largely covalent, with a small but nevertheless significant ionic contribution. As expected, the bond in YO is more ionic.

TABLE 5(*a*). Calculated spectroscopic constants of the lowest doublet and quartet states of YO and YS

	YO					
	$X^2\Sigma^+$			$^4\Pi$, $^4\Phi$		
	DF[a]	LB[b]	Expt.	DF[a]	LB[b]	Expt.
$r_e(a_0)$	3.439	3.423	3.384[c]	3.943	4.018	—
$\omega_e(cm^{-1})$	900	855	861.0[c]	626	526	—
$D_e(eV)$	7.51	6.58	7.29[c]	—	—	—
$T_e(cm^{-1})$	—	—	—	26166	26975	—
$\mu(D)$	4.29	3.98	4.45[d]	3.25	3.42	—
$d\mu/dr(D/a_0)$	3.79	3.50	—	2.28	2.47	—
	YS					
	$X^2\Sigma^+$			$^4\Pi$, $^4\Phi$		
	DF[a]	LB[b]	Expt.	DF[a]	LB[b]	Expt.
$r_e(a_0)$	4.309	4.347	4.293[a,e]	4.742	—	4.715[a,e]
$\omega_e(cm^{-1})$	461	508	492.7[f]	355	—	—
$D_e(eV)$	5.54	5.03	5.45[c]	—	—	—
$T_e(cm^{-1})$	—	—	—	17439	—	—
$\mu(D)$	5.62	6.40	6.098[g]	3.45	—	—
$d\mu/dr$ (D/a_0)	2.57	2.32	—	1.95	—	—

[a]This work.
[b]Calculations of Langhoff and Bauschlicher (22).
[c]Reference (26).
[d]Reference (27).
[e]r_0 value.
[f]Reference (8).
[g]Reference (6).

TABLE 5(*b*). Description of bonding in the YO and YS molecules

	YO		YS	
Parameter	$X^2\Sigma^+$	$^4\Pi$, $^4\Phi$	$X^2\Sigma^+$	$^4\Pi$, $^4\Phi$
Configuration	$\sigma_1^2\sigma_2^2\pi_1^4\sigma_3^1$	$\sigma_1^2\sigma_2^2\pi_1^3\sigma_3^1\delta_1^1$	$\sigma_1^2\sigma_2^2\pi_1^4\sigma_3^1$	$\sigma_1^2\sigma_2^2\pi_1^3\sigma_3^1\delta_1^1$
Bond order	2.43	1.21	2.54	1.35
Charge on Y	+0.37	+0.27	+0.20	+0.27
	Mulliken populations			
π_1				
p on O,S	0.78	0.91	0.73	0.91
d on Y	0.20	0.08	0.23	0.08
σ_2				
p_z on O,S	0.66	0.80	0.65	0.76
s on O,S	0.13	0.04	0.04	0.02
d_{z2} on Y	0.19	0.12	0.22	0.15
s on Y	0.01	0.03	0.07	0.05

Formally, the lowest quartet state in these molecules is accessed from the ground state by "exciting" one electron from a bonding π_1 orbital, which is centred mostly on sulfur (oxygen), to a nonbonding, purely atomic, yttrium *d* orbital. The density functional calculation does not distinguish between the $^4\Phi$ and $^4\Pi$ states that are formed by promotion into the δ_1 molecular orbital. A $^4\Pi$ state could also arise by excitation from the π_1 orbital into a higher lying σ orbital, but this transition would probably lie at significantly higher energy. If a "rigid-orbital" description was strictly valid, upon excitation of the $^4\Pi$ state, the bond order would decrease by roughly 0.5, and the negative charge on the yttrium would increase by $1 - 0.25 = 0.75$. Actually, the calculated bond order decreases by 1.2 and the charge remains essentially unchanged. This is because the change in configuration is accompanied by a substantial relaxation of the orbitals: the

Can. J. Chem. Downloaded from www.nrcresearchpress.com by 203.198.23.82 on 09/08/12
For personal use only.

Can. J. Chem. Downloaded from www.nrcresearchpress.com by 203.198.23.82 on 09/08/12
For personal use only.

population on the sulfur (oxygen) atom goes from 0.73 to 0.91 (0.78 to 0.91) for the π_1 orbital and from 0.69 to 0.78 (0.79 to 0.84) for the σ_2 orbital. The tendency towards achieving approximate charge neutrality makes the π_1 and σ_2 orbitals more atomic-like and therefore weakens the bond. The reduction in bond order is manifested in the observed and calculated magnitudes of the bond length for the $^4\Pi$ state, which indicate a bond substantially weaker than in the $X^2\Sigma^+$ state (see Table 5(*a*)).

The first doublet excited state corresponds to excitation from the σ_3 orbital, which is mostly yttrium 5*s* with about 5% 5*p* character, to the σ_4 orbital. The calculated composition of the σ_4 orbital may be summarized in terms of Mulliken populations as (YS): 0.46 *pz*, 0.29 dz^2, 0.05 dx^2, 0.05 dy^2 on yttrium, 0.0 *s*, 0.13 *pz* on sulfur; (YO): 0.67 *pz*, 0.22 dz^2, 0.05 dx^2, 0.05 dy^2 on yttrium, −0.08 *s*, 0.08 *pz* on oxygen. Clearly, the σ_4 orbital is strongly hybridized and points away from the ligand. This polarization counteracts the principal component of the dipole moment. The net effect is that the dipole moments in the doublet excited states are much smaller than in the corresponding ground states, values of 3.19 D (YS) and 0.70 D (YO) being calculated. The precise values are not trustworthy, but they illustrate the general trend of excitation from the largely unhybridized σ_3 orbital to the strongly hybridized σ_4 orbital.

Discussion

The small fraction of 5*p* character (5%) calculated for the σ_3 orbital of YS is somewhat at odds with the interpretation of the hyperfine structure presented by Azuma and Childs (9). They used a simple treatment that assumed that the reduction in the Fermi contact term from the atomic value was due entirely to ligand-induced 5*s*–5*p* hybridization effects. In this way, the orbital composition of σ_3 was determined to be 53% 5*s*, 47% 5*p*. A possible explanation for the discrepancy between their analysis and our calculation is that *s* orbitals of higher principal quantum number are mixed into the σ_3 orbital by the ligand field of sulfur, reducing the electron density at the nucleus. Such a process would reduce the magnitude of the contact interaction in the molecule relative to the atom, and is known to operate in CaOH[3] and MnF (25). It is difficult to reconcile the analysis of Azuma and Childs with the experimentally observed trends in the dipole moments. Appreciable hybridization of both the σ_3 and σ_4 orbitals would not be expected to produce the experimentally observed reduction in μ upon $B^2\Sigma^+ \leftarrow X^2\Sigma^+$ excitation.

The small dipole moment calculated for the $^4\Pi$ state can be rationalized crudely in terms of the $^4\Pi \leftarrow X^2\Sigma^+$ excitation involving the back-transfer of an electron from a sulfur- (oxygen-) centred orbital (π_1) to one localized on yttrium (δ_1). In language familiar to spectroscopists, this excitation constitutes a "charge transfer" transition. In diatomic molecules where the ionic contribution to bonding dominates the covalent contribution, the reduction in bond strength accompanying such a transition would be attributed primarily to a diminution in the electrostatic contribution to the bonding. In systems such as YS and YO, where calculation indicates that covalent bonding predominates, a molecular orbital description of the excitation is more appropriate.

It seems likely that, in common with the upper level in the 14 926.0 cm^{-1} band, the upper level in the 15 300.1 cm^{-1} band also belongs to the $^4\Pi_{\pm 1/2}$ state. Analysis of the lifetimes data supports this assertion: the very long or possibly infinite lifetime determined for the upper level of the 15 300.1 cm^{-1} band is consistent with a state that is not optically coupled to the ground state. For simplicity, we denote the upper levels of the two new bands as v' and $v' + 1$, respectively. Using the vibrational constants reported by Stringat et al. (8), the $v = 1$ level of the $B^2\Sigma^+ \leftarrow X^2\Sigma^+$ system is calculated to lie 15 273.0 cm^{-1} above the ground state $v = 0$ level, in the absence of perturbations. The downward shift experienced by the $B^2\Sigma^+$ $v = 1$ level is therefore 15 273.0 − 15 264.2 = 8.8 cm^{-1}. Assuming that the $v' + 1$ level is shifted up by the same amount, its unperturbed position is calculated to be 15 300.1 − 8.8 = 15 291.3 cm^{-1}. Assuming that the v' level experiences only a small shift on account of interaction with the $B^2\Sigma^+$ $v = 0$ level, the difference in energy between the unperturbed vibrational levels of the $^4\Pi_{\pm 1/2}$ state is 15 291.3 − 14 928.0 = 365.3 cm^{-1}. The ratio of this vibrational interval to the ground state vibrational frequency is 365.3/492.7 = 0.741, in reasonable agreement with the ratio $\omega_e(^4\Pi_{1/2})/\omega_e(X^2\Sigma^+) = 0.770$ computed from the density functional data in Table 5(*a*).

The foregoing discussion begs the question as to why we observe only two vibronic bands of the $^4\Pi_{\pm 1/2} \leftarrow X^2\Sigma^+$ system in the spectral region of interest. The explanation is related to the intensity distribution in the $B^2\Sigma^+ \leftarrow X^2\Sigma^+$ system. There are basically two criteria to be met for a spin-forbidden $^4\Pi_{\pm 1/2} \leftarrow X^2\Sigma^+$ vibronic transition to exhibit observable intensity. Firstly, the spin-orbit matrix element coupling the relevant levels of the $^4\Pi_{\pm 1/2}$ and $B^2\Sigma^+$ states must be significantly non-zero. Secondly, the two interacting vibrational levels must lie fairly close in energy. A calculation of the Franck–Condon factors ($S^2_{v'v''}$) for the $B^2\Sigma^+ \leftarrow X^2\Sigma^+$ system reveals that they drop off rapidly with increasing v': $S^2_{00} = 0.659$; $S^2_{10} = 0.280$; $S^2_{20} = 0.054$; $S^2_{30} = 0.006$. Clearly, only the (0,0) and (1,0) bands are intense, as is borne out by experiment. Thus the only vibrational levels of the $^4\Pi_{\pm 1/2}$ state which can be observed experimentally are those that are energetically the closest to the $v = 0$ and $v = 1$ levels of the $B^2\Sigma^+$ state. Explicit calculation using Slater determinants to represent the wavefunctions of the $^4\Pi_{\pm 1/2}$ and $B^2\Sigma^+$ states reveals that, in a first-order approximation, the matrix element of the spin-orbit operator connecting these two states is zero. Clearly, a second-order mechanism must be invoked to explain the non-zero $^4\Pi \leftrightarrow B^2\Sigma^+$ interaction. Given that transitions to both the $\Omega = 1/2$ and $\Omega = -1/2$ spin-orbit components gain intensity through the spin-orbit interaction, our failure to observe transitions to the other spin-orbit component must remain an open question.

Conclusions

The yttrium monosulfide molecule has been investigated using molecular beam fluorescence spectroscopy and density functional theory. Improved molecular constants for the $v = 0$ levels of the $X^2\Sigma^+$ and $B^2\Sigma^+$ states have been obtained. Two vibrational levels of a state with $^4\Pi_{\pm 1/2}$ symmetry have been observed in excitation from the ground state, the spin-forbidden $^4\Pi_{\pm 1/2} \leftarrow X^2\Sigma^+$ transition gaining intensity through spin-orbit mixing between the $B^2\Sigma^+$ state and the $^4\Pi_{\pm 1/2}$ state. The bond length for one of these $^4\Pi_{\pm 1/2}$ vibrational levels was determined to be 2.49510(16) Å. The other $^4\Pi_{\pm 1/2}$ vibrational level is responsible for strongly

[3]Z.J. Jakubek and R.W. Field. Private communication.

perturbing the $v = 1$ level of the $B^2\Sigma^+$ state. Density functional calculations on low-lying states of YS (and YO) in the doublet and quartet spin manifolds have been carried out, confirming the experimental observations.

1. S.R. Langhoff and C.W. Bauschlicher, Jr. Annu. Rev. Phys. Chem. **39**, 181 (1989).
2. M.D. Morse. Chem. Rev. **86**, 1049 (1986).
3. B. Simard, S.A. Mitchell, L.M. Hendel, and P.A. Hackett. Faraday Discuss. Chem. Soc. **86**, 163 (1988).
4. B. Simard, A.M. James, and P.A. Hackett. J. Chem. Phys. **96**, 2565 (1992).
5. B. Simard and A.M. James. J. Chem. Phys. **97**, 4669 (1992).
6. A.M. James and B. Simard. J. Chem. Phys. **98**, 4422, (1993).
7. N.S. McIntyre, K.C. Lin, and W. Weltner, Jr. J. Chem. Phys. **56**, 5576 (1972).
8. R. Stringat, B. Fenot, and J.L. Féménias. Can. J. Phys. **57**, 300 (1979).
9. Y. Azuma and W.J. Childs. J. Chem. Phys. **93**, 8415 (1990).
10. B. Simard, S.A. Mitchell, M.R. Humphries, and P.A. Hackett. J. Mol. Spectrosc. **129**, 186 (1988).
11. A. St.-Amant and D.R. Salahub. Chem. Phys. Lett. **169**, 387 (1990); A. St.-Amant. Thèse de doctorat, Université de Montréal, 1992; D.R. Salahub, R. Fournier, P. Mylnarski, I. Papai, A. St.-Amant, and J. Ushio. Proceedings of the Ohio Supercomputer Center workshop on the theory and applications of density functional theory to chemistry, May 1990. *Edited by* J. Labanowsky and J. Andzelm. Springer, New York. 1991.
12. S.H. Vosko, L. Wilk, and M. Nusair. Can. J. Phys. **58**, 1200 (1980).
13. A.D. Becke. Phys. Rev. A, **38**, 3098 (1988).
14. J.P. Perdew. Phys. Rev. B, **33**, 8822 (1986).
15. A. Selmani and D.R. Salahub. J. Chem. Phys. **89**, 1529 (1988).
16. J. Andzelm and E. Wimmer. J. Chem. Phys. **96**, 1280 (1992).
17. O. Gunnarson and B.I. Lundqvist. Phys. Rev. B, **13**, 4274 (1976); L.N. Oliveira. Adv. Quantum. Chem. **21**, 135 (1990); L. Fritsche. Physica B (Amsterdam), **172**, 7 (1991).
18. G.R. Fleming, O.L.J. Gijzemann, and S.H. Lin. Chem. Phys. Lett. **21**, 527 (1973).
19. H. Lefebvre-Brion and R.W. Field. Peturbations in the spectra of diatomic molecules. Academic, Orlando. 1986.
20. G. Herzberg. Molecular spectra and molecular structure. Vol. 1. Spectra of diatomic molecules. van Nostrand, Princeton. 1950.
21. H.E. Radford. Phys. Rev. A, **136**, 1571 (1964).
22. S.R. Langhoff and C.W. Bauschlicher, Jr. J. Chem. Phys. **89**, 2160 (1988).
23. A.S.-C. Cheung, A.W. Taylor, and A.J. Merer. J. Mol. Spectrosc. **92**, 391, (1982).
24. A.D. Becke. J. Chem. Phys. **97**, 9173 (1992).
25. O. Launila, B. Simard, and A.M. James. J. Mol. Spectrosc. **159**, 161 (1993).
26. K.P. Huber and G. Herzberg. Molecular spectra and molecular structure 4. Constants of diatomic molecules. van Nostrand Reinhold, New York. 1979.
27. T.C. Steimle and J.E. Shirley. J. Chem. Phys. **92**, 3292 (1990).

Can. J. Chem. Downloaded from www.nrcresearchpress.com by 203.198.23.82 on 09/08/12
For personal use only.

Ion-pair state spectroscopy of HgCl[1]

H.A. BASCAL, K.J. JORDAN,[2] AND R.H. LIPSON[3]

Department of Chemistry, University of Western Ontario, London, ON N6A 5B7, Canada

Received March 16, 1993

This paper is dedicated to Professor Gerald W. King on the occasion of his 65th birthday

H.A. BASCAL, K.J. JORDAN, and R.H. LIPSON. Can. J. Chem. **71**, 1615 (1993).

Fluorescence excitation spectra of HgCl produced and cooled in a corona-excited supersonic jet discharge are presented. The dominant feature between ≈ 368 and 267 nm is an extensive vibrationally and isotopically resolved band system which is assigned to the $B^2\Sigma^+(v') \leftarrow X^2\Sigma^+(v'' = 0, 1,$ and 2) valence-to-ion-pair state transition of the radical. Transition wavenumbers for vibrational bands with $75 \geq v' \geq 21$ and $2 \geq v'' \geq 0$ were measured, and B-state Dunham parameters were derived which are valid between $75 \geq v' \geq 0$. The equilibrium bondlength for the B-state was determined to be 2.960(2) Å by Franck–Condon calculations. B–X Franck–Condon factors are tabulated which are expected to help in the interpretation of $HgCl_2$ photodissociation and HgCl laser spectra.

H.J. BASCAL, K.J. JORDAN et R.H. LIPSON. Can. J. Chem. **71**, 1615 (1993).

On rapporte le spectre d'excitation de fluorescence du HgCl produit et refroidi dans une décharge de jet supersonique à couronne excitée. La caractéristique dominante entre environ 368 et 267 nm est un système de bande extensif résolu tant d'un point de vue vibrationnel qu'isotopique et que l'on attribue à la transition $B^2\Sigma^+(v') \leftarrow X^2\Sigma(v'' = 0, 1$ et 2) de l'état valence à paire d'ions du radical. On a mesuré les nombres d'onde des transitions des bandes vibrationnelles avec $75 \geq v' \geq 21$ et $2 \geq v'' \geq 0$ et on a déduit des paramètres de l'état B de Dunham qui sont valides entre $75 \geq v' \geq 0$). En se basant sur des calculs de Franck–Condon, on a déterminé que la longueur à l'équilibre pour l'état B est égale à 2,960(2) Å. On présente un tableau comportant les facteurs B–X de Franck–Condon qui devraient être utiles dans l'interprétation des spectres laser du HgCl et de photodissociation du $HgCl_2$.

[Traduit par la rédaction]

Can. J. Chem. Downloaded from www.nrcresearchpress.com by 203.198.23.82 on 09/08/12
For personal use only.

1. Introduction

The ion-pair states of the group IIB metal monohalide radicals have achieved prominence as the upper level for molecular electronic transition lasing on the $B^2\Sigma^+ \rightarrow X^2\Sigma^+$ transition. The mercuric monohalides, including HgCl, have received the most attention, because their coherent outputs lie in the important blue-green spectral region (1). However, despite considerable work which began with Wieland in 1929 (2–6), an understanding of their ion-pair ↔ valence state transitions remained primarily qualitative. The reasons for this are due to the unique properties of ion-pair states, compared with their valence or Rydberg counterparts.

In the case of HgCl, the excited $B^2\Sigma^+$ ion-pair state dissociates to a pair of oppositely charged ground-state ions: $Hg^+(^2S_{1/2}) + Cl^-(^1S_0)$. The binding at large internuclear separations is predominantly Coulombic, resulting in a very deep potential energy curve (≈ 39 900 cm^{-1} (6)). In contrast, $X^2\Sigma^+$ has a much smaller binding energy (≈ 8350 cm^{-1} (6)) which is due almost entirely to covalent-ionic mixing with the B-state. However, $B^2\Sigma^+$ has a longer equilibrium bond length ($r_e(B) \approx 3.02$ Å (6)) than the ground state ($r_e(X) \approx 2.42$ Å (6)) and a much smaller vibrational frequency ($\omega_e' \approx 192$ cm^{-1} versus $\omega_e'' \approx 293$ cm^{-1} (7)).

Because of these contradictory properties, transitions from low vibrational levels in $B^2\Sigma^+$ ($v' = 0$–9) probe the outer wing of the ground state potential, exciting high closely spaced vibrational levels ($v'' = 11$–31). While this Franck–Condon condition favors bound–bound HgCl electronic transition lasing, the $B \rightarrow X$ fluorescence spectrum has a near continuum appearance due to the presence of 14 naturally occurring isotopomers, and because of spectral congestion due to transitions from the many ro-vibrational levels populated in the discharges used to generate the radical from the metal dihalide precursor.

In early studies, Wieland reported B–X transitions for excited state levels as high as $v' = 68$, corresponding to a term value which is ≈ 27% of the B-state binding energy (4). He was able to determine excited state quantum numbers by measuring the vibrational isotope shifts from spectra obtained using 92% enriched $Hg^{37}Cl$, relative to a natural abundance (and therefore, predominantly $Hg^{35}Cl$) sample. However, the residuals in his analysis were typically of the order of ≈1 cm^{-1} and in some instances, as high as 8 cm^{-1}. Recently, Tellinghuisen and co-workers (6) used a similar approach to overcome many of the difficulties associated with ion-pair ↔ valence transitions. They found that exciting single isotopomer samples ($^{200}Hg^{35}Cl$ and $^{200}Hg^{37}Cl$) in a mild Tesla discharge produced relatively uncongested spectra, also amenable to analysis. In this way they could refine Wieland's work to a precision of ≈ 0.4 cm^{-1}, and were able to determine the B-state equilibrium bond length by Franck–Condon calculations to an accuracy of ±0.01 Å. The highest observed B-state vibrational level in these later studies was $v' = 25$, whose term value is only ≈ 11% of the excited state dissociation energy.

Absorption spectra for the metal monohalide radicals are scarce. There are the inherent difficulties in producing enough of the radical to detect an appreciable direct absorption. The $B \leftarrow X$ transition is particularly challenging to study for many of the same reasons outlined above for emission work. In this case, however, Franck–Condon considerations dictate that transitions from low v'' will probe the inner wing of the B-state potential energy curve, exciting high vibrational v' levels. A knowledge of the B–X absorption spectrum is useful, because as shown for HgBr (8, 9), direct optical

[1]Publication 490 from the Photochemistry Unit, University of Western Ontario.

[2]Present address: London Regional Cancer Centre, 790 Commissioners Road E., London, ON N6A 4L6, Canada.

[3]NSERC University Research Fellow, and to whom correspondence should be addressed.

pumping of the radical is a viable means of producing a population inversion for lasing. Our group has demonstrated that vibrationally and isotopically resolved fluorescence excitation spectra of natural abundance samples of HgBr (10) and HgI (11) could be obtained by generating and cooling the radicals in a corona-excited supersonic jet discharge. In this work, we have applied similar methods to the study of the $B^2\Sigma^+ \leftarrow X^2\Sigma^+$ transition of HgCl. Analysis of the resultant spectra has yielded precise Dunham coefficients which are valid for $0 \leq v' \leq 75$, and a subsequent Franck–Condon calculation has allowed the B-state equilibrium bond length to be refined.

2. Experimental

The experimental setup used to record fluorescence excitation spectra of jet-cooled HgCl radicals is similar to that previously reported (10, 11). Briefly, $HgCl_2$ precursor (BDH, melting point = 276°C) was placed in a heated quartz bulb nozzle (pinhole diameter ≈ 0.5 mm) mounted inside a vacuum chamber, which was evacuated to ≤ 50 mTorr by a Roots blower/mechanical pump combination (Edwards EH1200/E2M80). A stainless steel electrode was placed concentrically down the long axis of the bulb, with a piece of sealing teflon press fitted around its sharpened end at the pinhole. The other end of the electrode was attached to a solenoid valve (General Valve 9-181-901) located outside the chamber, for pulsed gas operation. Gas delivery was synchronized to the arrival of the laser pulse at a repetition rate of 10 Hz by means of a home-built sequencer.

$HgCl_2$ vapor was entrained in ≈ 2 atm of He to form a supersonic jet. HgCl radicals were generated in a corona-excited supersonic expansion, produced by applying positive dc voltage (≈ 1.9 kV/1 MΩ load resistor) to the electrode. The grounded chamber served as the cathode.

Fluorescence was excited in the jet discharge ≈ 0.5–1.0 cm below the pinhole using a Nd:YAG (Spectra Physics GCR-4) pumped-dye laser (Lumonics HD500). Ultraviolet (UV) radiation was generated by second harmonic generation in a KDP crystal housed in an autotracking assembly (Inrad AT-II). Typical UV energies were 1–3 mJ/pulse. Fluorescence excitation spectra were obtained by scanning the laser at a rate of 0.04 cm^{-1}/s, and detecting undispersed emission with a photomultiplier (Hamamatsu R372). Ultraviolet transmitting filters (Corning) were placed in front of the phototube to reject visible emission from the jet discharge. The fluorescence excitation signal was processed in a gated boxcar averager, digitized, and stored in a computer.

Frequency calibration was achieved by simultaneously exciting the optogalvanic spectrum of Ne in an Fe/Ne hollow cathode lamp with a small portion of the fundamental laser beam. These signals were processed in a separate gated boxcar averager, digitized and stored on disk. At longer wavelengths ($\lambda \geq 680$ nm), where Ne lines are sparse, portions of both the fundamental beam and the generated UV output were used simultaneously to excite the optogalvanic spectrum. Since the data was digitized the calibration procedure involved fitting the Ne line wavenumbers (in cm^{-1}) as a quadratic function of data point number. The actual data point number assigned to a given optogalvanic peak was determined by visually moving a cursor over the spectrum displayed on the computer monitor, and then selecting and storing that point on disk using software developed in the lab. The Ne wavenumber versus data point number function was then used to calculate unknown transition line wavenumbers by interpolation, using the same method of visual peak determination. The relative precision for the measurement of an unknown line was estimated to be ≈ ±0.1 cm^{-1}.

3. Observed spectra, assignments, and analysis

The relevant potential energy curves, transitions, and frequencies for HgCl are presented schematically in Fig. 1.

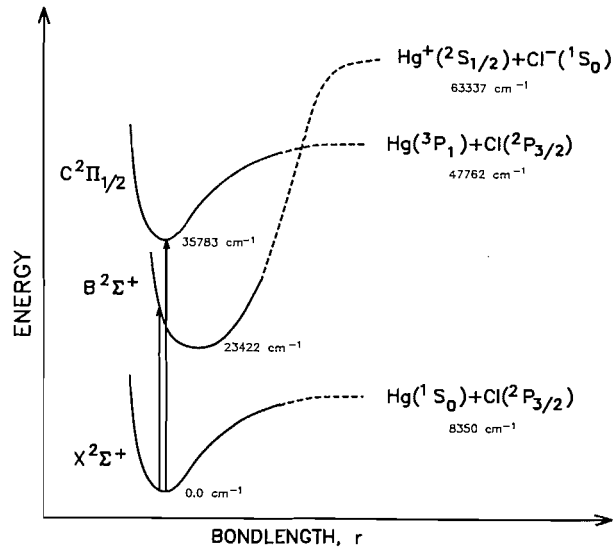

FIG. 1. A schematic of the relevant potential energy curves for HgCl showing their dissociation products. Frequencies for the potential curve minima and dissociation limits (in cm^{-1}) are referenced to the bottom of the HgCl ground state. Arrows indicate the important transitions discussed in this work.

Excitation spectra were recorded between 367 and 267 nm. The dominant features could be assigned to either members of the $B^2\Sigma^+$–$X^2\Sigma^+$ band system, or to He and Hg atomic transitions originating from metastable levels populated in the jet discharge. At the short wavelength end of the spectrum, perturbations were evident between the B-state and higher-lying Rydberg states. Consequently, the vibrational analysis described below was restricted to transitions having $\lambda > 285.5$ nm.

The presence of the atomic lines (Table 1) in the HgCl spectrum was expected, given a similar observation in our previous studies (10, 11). In this work the frequency measurements for the He lines are, for the most part, in better agreement with the literature values (12) than those for Hg, in the same frequency region. This indicates that the calibration method is sound, but that the Hg transition frequencies are more likely to shift as a result of the UV laser fluences used in this work. However, as this hypothesis was not tested experimentally the reasons for the shifts can not be stated with any certainty. Since the atomic lines provide internal calibration, the absolute accuracy for the measurement of an unknown HgCl feature is estimated to be < ±0.4 cm^{-1}.

The overall appearance of the HgCl fluorescence excitation spectrum resembles that observed for HgBr and HgI. The strongest features were readily assigned to the $B^2\Sigma^+(v') \leftarrow X^2\Sigma^+(v'' = 0)$ progression (Fig. 2*a*). Each member of the progression is a doublet composed of one strong and one weak band. The local vibrational interval which corresponds to the spacing between like components of two adjacent doublets, $(v' + 1, v'')$ and (v', v''), decreases smoothly from ≈ 169 cm^{-1} at 366 nm to ≈ 125 cm^{-1} at 285 nm. The doublet spacing for a common v' level arises from a vibrational isotope shift due to the two naturally occurring isotopes of Cl: ^{35}Cl and ^{37}Cl. That interval increases from ≈ 86 cm^{-1} near 366 nm to ≈ 217 cm^{-1} at 285 nm. The inten-

Can. J. Chem. Downloaded from www.nrcresearchpress.com by 203.198.23.82 on 09/08/12
For personal use only.

Can. J. Chem. Downloaded from www.nrcresearchpress.com by 203.198.23.82 on 09/08/12
For personal use only.

TABLE 1. Atomic line wave numbers, $\nu(cm^{-1})$, and spectral assignments

Atom	ν/cm^{-1}	Assignment
He	27665.01(−0.04)[a]	$5p\ ^1P_1^0 - 2s\ ^1S_0$
He	28997.39(−0.08)	$6p\ ^1P_1^0 - 2s\ ^1S_0$
He	29801.55(−0.16)	$7p\ ^1P_1^0 - 2s\ ^1S_0$
He	30323.71(−0.15)	$8p\ ^1P_1^0 - 2s\ ^1S_0$
He	30682.37(0.12)	$9p\ ^1P_1^0 - 2s\ ^1S_0$
He	30938.71(0.26)	$10p\ ^1P_1^0 - 2s\ ^1S_0$
He	31128.31(−0.17)	$11p\ ^1P_1^0 - 2s\ ^1S_0$
He	31361.16(0.06)	$4p\ ^3P_{2,1,0}^0 - 2s\ ^3S_1$
He	31546.24(−0.18)	$15p\ ^1P_1^0 - 2s\ ^1S_0$
He	33944.72(−0.03)	$5p\ ^3P_{2,1,0}^0 - 2s\ ^3S_1$
He	35336.78(−0.12)	$6p\ ^3P_{2,1,0}^0 - 2s\ ^3S_1$
He	36171.45(0.05)	$7p\ ^3P_{2,1,0}^0 - 2s\ ^3S_1$
He	36710.65(−0.11)	$8p\ ^3P_{2,1,0}^0 - 2s\ ^3S_1$
He	37079.20(−0.16)	$9p\ ^3P_{2,1,0}^0 - 2s\ ^3S_1$
He	37342.36(0.04)	$10p\ ^3P_{2,1,0}^0 - 2s\ ^3S_1$
Hg	27290.32(0.12)	$6d\ ^1D_2 - 6p\ ^3P_2^0$
Hg	27293.26(0.08)	$6d\ ^3D_1 - 6p\ ^3P_2^0$
Hg	27353.35(0.06)	$6d\ ^3D_2 - 6p\ ^3P_2^0$
Hg	27388.33(−0.03)	$6d\ ^3D_3 - 6p\ ^3P_2^0$
Hg	29918.26(−0.06)	$8s\ ^3S_1 - 6p\ ^3P_2^0$
Hg	33021.06(−0.06)	$7d\ ^1D_2 - 6p\ ^3P_2^0$
Hg	33041.59(−0.07)	$7d\ ^3D_1 - 6p\ ^3P_2^0$
Hg	33065.46(0.52)	$7d\ ^3D_2 - 6p\ ^3P_2^0$
Hg	33086.15(−0.41)	$7d\ ^3D_3 - 6p\ ^3P_2^0$
Hg	35617.27(−0.54)	$8d\ ^1D_2 - 6p\ ^3P_2^0$
Hg	35635.29(−0.44)	$8d\ ^3D_1 - 6p\ ^3P_2^0$
Hg	35646.99(−0.33)	$8d\ ^3D_2 - 6p\ ^3P_2^0$
Hg	35659.29(−0.37)	$8d\ ^3D_3 - 6p\ ^3P_2^0$
Hg	36225.00(−0.08)	$10s\ ^3S_1 - 6p\ ^3P_2^0$
Hg	37014.77(0)	$9d\ ^1D_2 - 6p\ ^3P_2^0$
Hg	37027.98(−0.07)	$9d\ ^3D_1 - 6p\ ^3P_2^0$
Hg	37034.57(−0.25)	$9d\ ^3D_2 - 6p\ ^3P_2^0$
Hg	37042.01(−0.14)	$9d\ ^3D_3 - 6p\ ^3P_2^0$
Hg	37373.36(−0.01)	$11s\ ^3S_1 - 6p\ ^3P_2^0$

[a]Observed — literature (ref. 12) residual/cm^{-1}.

sities of the doublet components reflect the normalized natural abundance ratios of $^{35}Cl:^{37}Cl = 1:0.33$ (13).

Both doublet components have a similar, distinctive substructure of red-shaded bands (Fig. 2*b*). The pattern arises from vibrational isotope shifts due to the seven naturally occurring isotopes of atomic Hg. The intensity of each isotopomer peak within a doublet component reflects the normalized natural abundance of the particular Hg atom involved ($^{196}Hg:^{198}Hg:^{199}Hg:^{200}Hg:^{201}Hg:^{202}Hg:^{204}Hg$ = 0.005:0.336:0.565:0.776:0.444:1.00:0.230 (13)). This made individual molecular isotopomer identification straightforward. Assignments were made for 12 of the 14 possible HgCl species. The two exceptions were $^{196}Hg^xCl$, x = 35 and 37. As expected, the isotopic transition frequencies within a doublet component are ordered $\nu(^{198}Hg^xCl) > \nu(^{199}Hg^xCl) > \nu(^{200}Hg^xCl) > \nu(^{201}Hg^xCl) > \nu(^{202}Hg^xCl) > \nu(^{204}Hg^xCl)$.

Due to Franck–Condon considerations $\Delta v = v' - v''$ will be $\geqslant 0$ for $B \leftarrow X$ transitions excited in the UV. The higher frequency component of a (v',v'') doublet can therefore be assigned to the $Hg^{35}Cl$ isotopomer. However, care must be

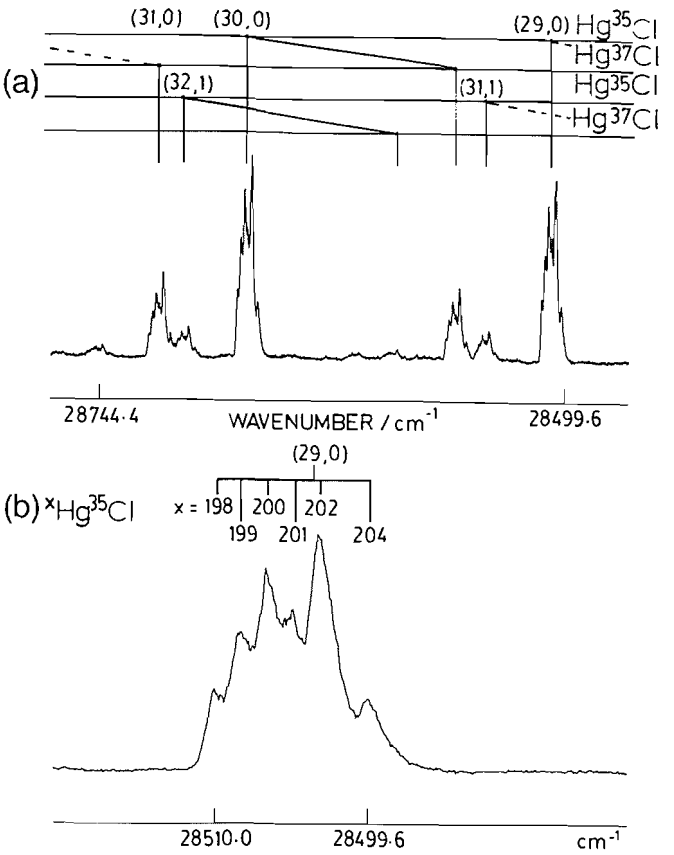

FIG. 2. (*a*) A small portion of the $B^2\Sigma^+ \leftarrow X^2\Sigma^+$ fluorescence excitation spectrum at the long wavelength region of the spectrum near 349.4 nm, showing vibrational and Hg^xCl (x = 35, 37) isotopomer assignments. (*b*) A close-up of the (29, 0) band for the $Hg^{35}Cl$ isotopomer showing the isotopic fine structure due to the numerous isotopes of Hg.

exercised in the analysis of high vibrational levels of an ion-pair state, and with HgCl in particular. Vibrational isotope shifts can equal and exceed the local vibrational spacings. As shown in Fig. 2*a*, the $Hg^{35}Cl$–$Hg^{37}Cl$ isotope splittings are already close to the local $\Delta G'_{v'+1/2}$ at the longer excitation wavelengths used in this work. To a first approximation, the vibrational level, v^0, where the isotope shift equals the vibrational spacing can be calculated from:

$$[1] \quad v^0 = \rho_i/(1 - \rho_i)$$

where ρ_i is defined here as $\rho_i = \sqrt{\mu(^{200}Hg^{35}Cl)/\mu_i}$, and μ_i is the reduced mass of a particular HgCl isotopomer.

The crossover vibrational level for Hg^xCl is calculated from eq. [1] to be $v^0 \approx 42$. As illustrated in Fig. 3, this means that the weaker $Hg^{37}Cl$ doublet component will appear at a higher frequency than the nearest $Hg^{35}Cl$ band for $v' \leqslant 42$, and at a lower frequency for $v' \geqslant 42$. However, the vibrational quantum number of the $Hg^{37}Cl$ band is actually one higher than its $Hg^{35}Cl$ partner.

Crossovers in HgCl are also expected for integer multiples of v^0 near $v' \approx 84$, 126, 168, and so on, with an additional unit increase in the relative numbering of the Hg^xCl bands per v^0 interval. As noted for the valence-to-ion-pair state transitions of the halogens (14, 15), additional information such as the electronic origin of the excited state po-

Can. J. Chem. Downloaded from www.nrcresearchpress.com by 203.198.23.82 on 09/08/12
For personal use only.

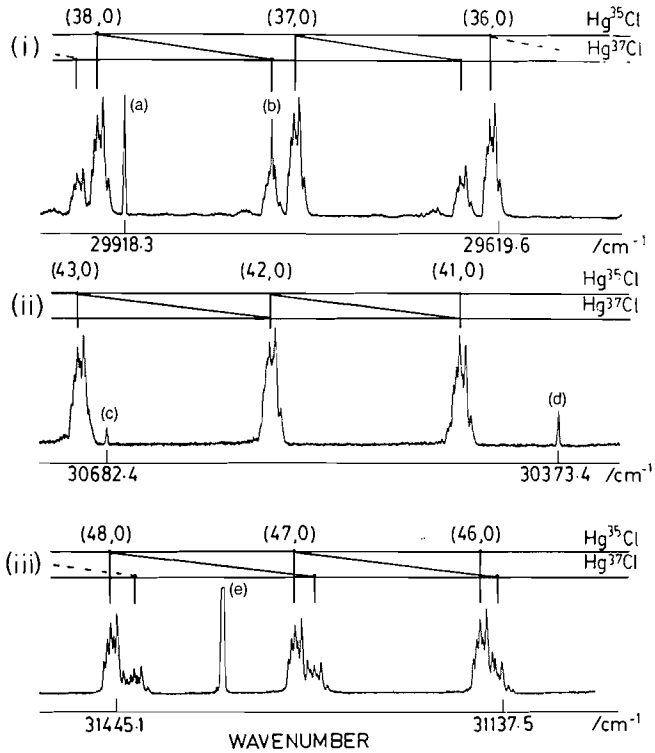

FIG. 3. An overview of the HgCl $B^2\Sigma^+ \leftarrow X^2\Sigma^+$ fluorescence excitation spectrum in the region of the first "crossover" point at (42, 0). Bands having the same vibrational assignment but belonging to a radical with a different Cl isotope are connected by a diagonal line. The features labelled (a)–(e) are atomic transition of He and Hg originating from metastable levels. Assignments and transition wavenumbers are listed in Table 1. (*i*) *B*–*X* vibrational bands just to longer wavelengths of (42, 0). In this region, the $Hg^{35}Cl$–$Hg^{37}Cl$ vibrational isotope shift is less than the local vibrational spacing. (*ii*) *B*–*X* vibrational bands near (42, 0). In this region, the $Hg^{35}Cl$–$Hg^{37}Cl$ vibrational isotope shift is approximately equal to the local vibrational spacing. (*iii*) *B*–*X* vibrational bands just to shorter wavelengths of (42, 0). In this region, the $Hg^{35}Cl$–$Hg^{37}Cl$ vibrational isotope shift is greater than the local vibrational spacing.

TABLE 2. Dunham coefficients (cm^{-1}) for the $B^2\Sigma^+$–$X^2\Sigma^+$ transition of $^{200}Hg^{35}Cl$

Dunham parameter	$B^2\Sigma^+$	$X^2\Sigma^+$
$T_e' + Y_{0,0}$	23421.8084(1218)[a]	—
$Y_{1,0}$	192.25105(1349)	293.353[b]
$Y_{2,0}$	−0.5351495(5147)	−1.7692[b]
$10^3\ Y_{3,0}$	1.011594(6686)	−0.7741[b]
$10^4\ Y_{4,0}$	—	−3.966[b]
$10^8\ Y_{5,0}$	−2.25(36)	—
r_e[c]	2.960(2)[e]	2.3948(26)[d]

[a]Quoted errors are 1σ standard errors.
[b]Constrained to values in ref. 7.
[c]Angstrom units.
[d]Value from ref. 6.
[e]Recommended value for equilibrium bondlength as discussed in text.

tential energy curve is then required to decide which crossover region is being probed because the standard deviations of "local" least squares fits for all choices of nv^0, $n = 1, 2, \ldots$, will be of similar quality. Crossovers within a doublet component for adjacent HgCl isotopomers however, are only expected to be important for $v' > 2600$.

The spectral analysis was carried out with the ground state vibrational constants constrained to the values determined by Tellinghuisen (7). The excited-state numbering was determined by fitting small portions of the spectrum to a local mass-reduced term value formula, and varying the v' numbering until the standard deviation of the fit was unambiguously minimized. When this best set of quantum numbers was used with previously published molecular vibrational constants (7), they generated transition wavenumbers which agreed with our values over a common v' range ($v' = 21$–25). For the final fit, bandhead frequencies measured at the peak of the rising edge of each rotational envelope were fitted to a mass-reduced Dunham expansion of the form (in cm^{-1}):

$$[2] \quad \nu_i = T_e' + \sum_n Y'_{n,0}[\rho_i(v' + 1/2)]^n - \sum_m Y''_{m,0}[\rho_i(v'' + 1/2)]^m$$

where T_e' is the electronic origin of the *B*-state, $Y'_{n,0}$ and $Y''_{m,0}$ are *B*-state and *X*-state Dunham parameters, respectively. No effort was made to correct the transition wavenumbers by the bandhead-to-origin shifts, which were estimated to be $< 0.16\ cm^{-1}$ from published constants (6). In this analysis $^{200}Hg^{35}Cl$ was chosen as the reference isotopomer so that the resultant excited *B*-state constants could be used with the published ground state parameters without additional scaling (7). Hotbands with $v'' = 1$, 2, and 3 were also assigned but the quality of the (v',3) bands was sufficiently poor that they were excluded from the final fit. In the end, 1026 isotopic bandhead frequencies with quantum numbers $76 \geq v' \geq 21$ and $2 \geq v'' \geq 0$ were analyzed. To establish a set of molecular constants which are also valid at the bottom of the *B*-state potential energy curve, calculated $^{200}Hg^{35}Cl$ (v',0) transition wavenumbers, $0 \leq v' \leq 21$ (7), were also included in the data set. The standard deviation of the least-squares fit was $\sigma \approx 0.26\ cm^{-1}$. Transition wavenumbers and their vibrational and isotopic assignments are provided as supplementary material.[4] The particular set of Dunham parameters chosen for data reduction, and listed in Table 2, is the ones that gave the best fit. The number of significant figures for each constant was obtained by a systematic round-off procedure (16, 17). They reproduce the calculated transition wavenumbers to better than $0.01\ cm^{-1}$.

Although the standard deviation of the fit is satisfactory, systematic trends in the observed–calculated residuals are evident. However, they fall within the $\pm 3\sigma$ error limits, and were therefore deemed acceptable. More work is necessary to determine whether these trends are due to the calibration procedure, model-dependence of the fitting function, or both.

4. The B-state potential energy curve

Since the HgCl radicals generated in the jet discharge were vibrationally warm, we were able to locate and use the

[4]A complete set of data may be purchased from the Depository of Unpublished Data, Document Delivery, CISTI, National Research Council Canada, Ottawa, Canada K1A 0S2. It may also be obtained by writing to one of the authors (R.H.L.) at the Department of Chemistry, University of Western Ontario, London, ON N6A 5B7, Canada.

TABLE 3. Franck–Condon factors, 10^3FCF, for the $B^2\Sigma^+(v')$–$X^2\Sigma^+(v'')$ transition of $^{200}Hg^{35}Cl$, $0 \leq v' \leq 30$, $0 \leq v'' \leq 31$

v''/v'	0	1	2	3	4	5	6	7	8	9	10	11	12	13	14	15	16	17	18	19	20	21	22	23	24	25	26	27	28	29	30
0	—[a]	—	—	—	—	—	—	—	—	—	—	—	—	—	—	4	0.1	0.2	0.3	0.4	0.7	1	2	2	3	4	6	8	10	12	15
1	—	—	—	—	—	—	—	—	—	—	—	—	0.1	0.2	0.4	25	1	2	3	5	7	10	13	16	20	25	29	32	35	38	39
2	—	—	—	—	—	—	—	—	—	0.1	0.3	0.6	1	2	3	39	8	12	16	21	26	31	35	38	40	39	37	32	27	20	14
3	—	—	—	—	—	—	—	0.2	0.4	1	2	4	6	10	15	12	27	33	38	41	41	39	34	27	19	12	5	1	—	1	5
4	—	—	—	—	—	0.2	0.5	1	2	5	9	14	21	28	35	5	44	42	37	29	20	10	4	0.2	0.8	5	11	16	21	22	21
5	—	—	—	—	0.3	1	2	5	10	17	25	34	42	46	45	23	29	17	7	1	0.4	4	11	18	23	23	19	13	7	2	—
6	—	—	0.1	0.5	2	4	9	17	27	38	46	49	46	35	21	1	1	0.7	6	15	22	25	21	14	7	1	0.2	3	9	14	17
7	—	0.1	0.6	2	6	14	25	38	49	53	47	34	17	4	—	15	14	23	26	21	12	4	—	2	8	15	18	17	12	6	1
8	—	0.5	3	8	18	33	48	57	53	38	18	3	0.5	9	21	8	25	15	5	—	3	11	18	19	15	8	2	—	3	9	14
9	0.3[b]	2	9	22	41	57	61	48	24	5	0.4	10	24	30	23	7	1	2	10	18	20	15	6	0.5	1	7	13	16	14	8	2
10	1	7	23	47	65	63	41	13	—	8	24	32	23	8	—	12	16	22	18	8	0.8	1	8	15	17	12	4	0.2	2	7	12
11	4	20	49	72	67	35	6	2	20	34	28	10	—	7	19	3	15	4	0.2	7	15	18	12	4	—	3	10	14	13	7	2
12	11	45	78	74	34	2	8	31	36	16	0.7	6	21	25	14	12	2	12	19	16	6	—	3	11	15	12	5	0.3	1	7	12
13	29	79	88	40	1	14	40	32	6	2	19	27	16	2	3	2	20	12	2	1	9	16	14	6	0.2	2	9	13	11	5	0.6
14	61	108	59	2	18	46	27	1	10	29	23	4	2	16	22	12	0.6	4	14	17	9	1	1	9	14	12	4	—	2	8	12
15	108	102	11	16	52	25	—	20	33	12	0.2	14	24	13	0.5	3	17	17	6	—	6	14	14	6	0.1	3	10	13	9	2	—
16	160	54	6	58	29	0.6	29	31	4	6	25	19	2	5	18	9	4	0.7	10	16	10	1	1	9	14	9	2	0.3	5	11	11
17	193	5	57	44	0.4	36	30	0.3	17	29	8	2	18	20	5	5	13	17	7	—	5	14	12	4	—	5	11	11	4	0.1	2
18	186	20	80	0.8	41	32	0.2	27	25	0.8	12	25	9	0.5	13	5	6	0.2	9	16	9	0.5	3	11	12	5	0.1	3	9	11	6
19	138	108	26	36	43	0.5	36	20	0.8	24	20	0.4	11	21	8	9	11	16	6	—	7	14	9	1	2	9	11	6	0.5	2	7
20	75	183	8	73	—	43	18	6	32	10	3	23	14	—	11	1	6	0.6	11	14	5	—	6	12	8	1	1	8	11	6	0.7
21	28	164	116	12	49	23	11	37	3	14	25	3	7	21	8	11	12	15	3	1	11	12	4	0.3	7	11	7	0.7	2	7	10
22	6	82	205	43	46	12	43	0.3	26	19	0.6	21	15	—	12	0.9	3	3	14	11	1	3	11	10	2	0.9	7	10	5	0.2	2
23	0.4	19	142	202	8	56	—	38	11	9	26	3	8	20	5	7	15	10	0.1	6	13	6	—	5	11	7	0.5	2	8	9	3
24	—	1	36	194	185	0.2	45	7	23	22	0.6	22	12	1	16	8	—	9	14	4	1	10	10	2	1	8	10	4	—	4	8
25	—	0.1	0.9	50	235	177	0.3	28	18	11	26	0.9	14	17	0.4	—	15	2	3	13	8	—	5	11	6	—	4	9	7	0.9	1
26	—	—	0.8	0.1	53	264	188	—	13	27	5	23	4	8	18	8	4	14	6	0.5	9	10	2	2	9	8	1	1	7	8	3
27	—	—	0.2	3	1	39	275	221	0.2	3	36	3	18	8	4	6	5	2	12	8	—	6	10	4	0.3	6	9	3	—	4	8
28	—	—	—	0.1	6	10	14	250	268	14	0.1	50	5	12	11	—	13	7	0.6	10	9	0.4	4	10	5	—	4	8	4	—	2
29	—	—	—	0.2	—	7	32	0.2	171	300	44	7	73	14	4	5	4	10	8	0.4	8	9	0.7	3	8	5	0.1	3	7	5	0.4
30	—	—	—	—	0.5	1	3	54	35	57	266	82	24	108	38	8	24	8	5	9	0.8	6	9	0.6	2	8	5	0.2	2	6	5
31	—	—	—	—	—	0.4	1	1	43	117	0.2	143	87	33	137	2	6	42	24	0.7	14	3	4	9	0.2	2	7	4	0.2	2	6

[a]FCF $< 10^{-4}$.
[b]For $J' = J'' = 0$.

Franck–Condon intensity minima in the hot-band vibrational progressions to establish the B-state equilibrium bond length. $B \leftarrow X$ transitions probe the inner turning points of the excited state potential energy curve where the high v' wave functions have their largest amplitudes. The intensity minima, therefore, reflect the nodal structure of the ground-state vibrational wave functions superimposed on the electronic transition Franck–Condon factors, FCFs.

A definite minimum in the $v'' = 2$ progression for $Hg^{35}Cl$ was found at $(v',v'') = (34,2)$. Another minimum at (43,1) for $Hg^{35}Cl$ was also picked out from the spectra. However, this latter assignment was made with less confidence because $v' = 43$ comes in the first crossover region where overlapping $Hg^{37}Cl$ bands are expected to have non-zero intensities.

The equilibrium bond length of the B-state potential was determined by the following procedure: RKR–Morse potential curves for both $X^2\Sigma^+$ and $B^2\Sigma^+$ were constructed (18).[5] Here, the vibrational constants in Table 2 were used in an RKR calculation to determine the width of the two potential energy curves as a function of v (19).[5] The inner wings of the potentials were then calculated using Morse functions which incorporated r_e values from the literature. Morse parameters were determined using the vibrational frequency and the dissociation energy for each electronic state. The outer turning points followed immediately.

Vibrational wave functions were evaluated numerically in the two potentials over the range $75 \geq v' \geq 0$ and $2 \geq v'' \geq 0$, and FCFs derived (20). Franck–Condon minima were predicted to lie near (57,1) and (46,2) using our initial choices for the equilibrium bond lengths: $r_e(X) = 2.3948(16)$ Å (ref. 21) and $r_e(B) = 3.02$ Å (ref. 6). The poor agreement between the predicted and experimentally observed locations of the minima suggested that the B-state r_e was too long, since the ground state bond length was established from rotational data. Consequently, a series of RKR–Morse/FCF calculations were carried out with $r_e(X)$ constrained to the initial value above, but $r_e(B)$ varied until the predicted intensity minima agree with the experimental observations. Each decrease in $r_e(B)$ of ≈ 0.004 Å dropped the minima by $\approx$ one quantum in v'. The locations of both intensity gaps were well reproduced with a B-state bond length of 2.960 Å. Since the calculation was sensitive to the relative positions of the two potentials, the error in the excited state bond length was estimated to be ±0.002 Å. FCFs for $30 \geq v' \geq 0$ and $31 \geq v'' \geq 0$ are listed in Table 3 while those for $75 \geq v' \geq 0$ and $2 \geq v'' \geq 0$ are presented graphically in Fig. 4.

[5]Computer program. A copy of the program can be obtained from R.J. LeRoy by sending a request by electronic mail to leroy@theochem.uwaterloo.ca.

Can. J. Chem. Downloaded from www.nrcresearchpress.com by 203.198.23.82 on 09/08/12
For personal use only.

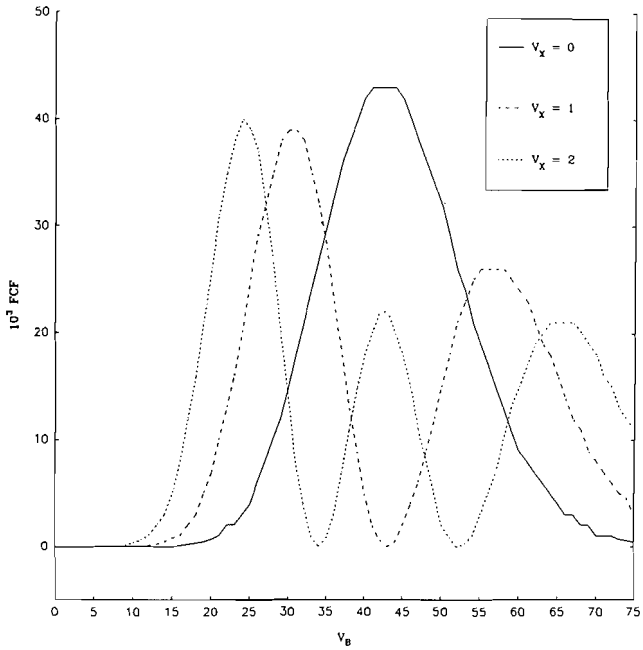

FIG. 4. B–X Franck-Condon factors, 10^3FCF, as a function of v' for the first three v'' levels in the ground state.

5. Perturbations

While the majority of the $B \leftarrow X$ bands measured in this work were accounted for, a number of strong vibrationally and isotopically resolved features at shorter wavelengths were not well reproduced by the parameters in Table 2. We assign these bands to members of the B–X band system, and attribute their poor fit to perturbations. Similar effects have been noted in our previous work on HgBr (10) and HgI (11), where $B \leftarrow X$ bands appeared to acquire strong intensity well outside the predicted Franck–Condon maximum due to excited-state interactions, possibly with the $C^2\Pi_{1/2}$ Rydberg state. However, because high order Dunham series such as those represented by the constants in Table 2 can have poor extrapolation properties (22), constants from low-order polynomial fits in $(v + 1/2)$ for HgCl bands having $75 \geq v' \geq 65$ were also used to predict (v',v'') transition frequencies beyond $v' = 75$. The shorter wavelength transitions could not be well predicted with these expressions either.

Unlike HgBr or HgI, vibrational bands of the C–X transition of HgCl are not strongly present in fluorescence excitation. Of all the mercuric halide radicals, the reported analyses for the C–X band system of HgCl are the most contradictory, although its weak intensity is well documented (3, 23–26). The latest work by Horne et al. (26) places the C–X (0,0) transition near 35 828 cm^{-1}. Indeed, although bands due to $C \leftarrow X$ are not at all obvious, some of the strongest perturbed B–X features appear in this region (Fig. 5). The B-state quantum numbers for bands predicted to lie near C–X (0,0) center around $v' \approx 84$, which corresponds to the second crossover point in the B-state potential. This numbering is corroborated spectrally by the fact that each of the irregularly spaced bands in this vicinity exhibits a more complicated isotopic substructure than expected for an isolated Hg^xCl band (x = 35 or 37), but one which is consistent with two isotopic bands, $Hg^{35}Cl$ (v',v'') and $Hg^{37}Cl$ $(v'+2,v'')$, passing through each other. A quantitative interpretation of the perturbations in HgCl will require further work.

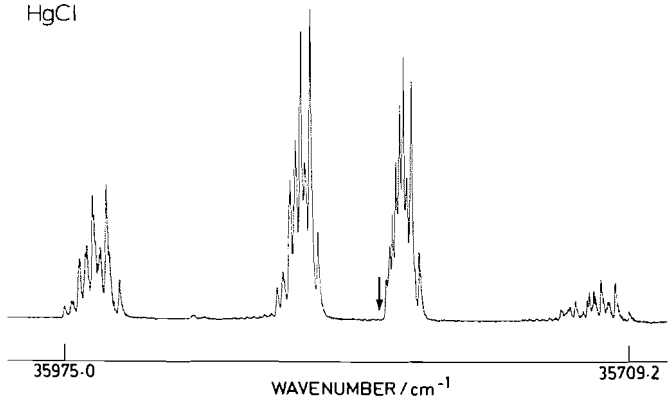

FIG. 5. Fluorescence excitation spectrum near 279.1 nm. The strongest features are assigned to perturbed members of the B–X band system which appear to derive their intensity through excited state interactions with the $C^2\Pi_{1/2}$ Rydberg state. The arrow indicates the location of the C–X (0,0) transition according to ref. 26.

6. Discussion and conclusions

The results of this work complete the $B \leftarrow X$ analyses of the HgX series (X = Cl, Br, I). Our HgCl B–X vibrational numbering and transition wavenumbers agree with Wieland's (4), but the precision of our measurements exceeds that of the older work by at least an order of magnitude. Our constants in Table 2 are also expected to be more useful since Wieland required two expressions to represent the large range of excited state vibrational levels: one for $v' \leq 30$ and the second for $v' \geq 30$. However, both our Dunham series and the older formulas will almost surely fail outside the range of fitted data, due the apparent perturbations between $B^2\Sigma^+$ and $C^2\Pi_{1/2}$ and because of the poor extrapolation properties of Dunham series in general.

The HgCl B-state bond length of $r_e(B) = 2.960(2)$ Å established in this work lies between the most recent experimental values of 3.02 Å (6) and 2.94 Å (27) (also from Franck–Condon calculations), and is larger than the theoretical estimate of 2.93 Å suggested by Wadt (28). It should be kept in mind, however, that in the absence of rotational data, Franck–Condon calculations can only give a precise value of $\Delta r_e = r_e(B) - r_e(X)$. In the older calculations the ground state equilibrium bond length was constrained to be 2.42 Å. A fairer comparison, therefore, requires an examination of Δr_e since our work used the shorter $r_e(X) = 2.3948(16)$ Å obtained from a rotational analysis of the HgCl $D^2\Pi_{3/2}$–$X^2\Sigma^+$ transition (21). Even then, our Δr_e value of $\approx$ 0.56 Å remains bracketed by that obtained by Wadt (28), and Cheung and Cool (27) ($\Delta r_e = 0.52$ Å), and Tellinghusien and co-workers (6) ($\Delta r_e = 0.60$ Å).

The behaviour of our FCFs for the $B \rightarrow X$ emission spectrum calculated using the ion-pair-state equilibrium bond length from this work agrees well with those tabulated by Cheung and Cool (27), in that both studies predict the strongest member of the $(0,v'')$ progression to be (0,17), and an intensity minimum for (1,17). However, we disagree with the detailed work of ref. 6 which places the intensity minimum at (1,19).

Since both the $(v',1)$ and $(v',2)$ intensity minima in our

Can. J. Chem. Downloaded from www.nrcresearchpress.com by 203.198.23.82 on 09/08/12
For personal use only.

fluorescence excitation spectrum could be reproduced simultaneously using an RKR–Morse potential for the $B^2\Sigma^+$ ion-pair state, it would appear then that a Morse function provides an adequate slope for the inner wall of the excited state potential. A similar conclusion was reached for HgI as well (11). We are currently reeaxamining our HgBr spectra for intensity minima which will also allow its B-state bond length to be refined in this way.[6] Nevertheless, until the disagreement between our predicted HgCl $(1,v'')$ intensity minimum and that from ref. 6 can be reconciled, general confidence in the RKR–Morse approximation must remain an open question.

Lasing on the HgCl $B \rightarrow X$ transition near 502 nm has been demonstrated using a variety of techniques. These include the photolytic dissociation of $HgCl_2$ with vacuum ultraviolet radiation (29), and electron beam pumping of Hg vapor/Cl_2 or CCl_4/high pressure rare gas mixtures (30–33). Direct optical pumping of the HgCl $B \leftarrow X$ transition has not been attempted although a similar approach was successful for HgBr (8, 9). The largest FCF for the HgCl $v' \leftarrow 0$ progression is for the (42,0) transition near 327 nm. However, the $B \leftarrow X$ aborption band is sufficiently broad ($\Delta\lambda >$ 80 nm) that either Nd:YAG or XeF pumping near 350 nm should provide a viable means of achieving laser action in this molecular system.

Acknowledgements

Funding for this research has been provided by the Networks of Centres of Excellence in Molecular and Interfacial Dynamics (CEMAID), one of the fifteen Networks of Centres of Excellence supported by the Government of Canada. Funding from the Ontario Laser and Lightwave Research Centre (OLLRC) and the Natural Sciences and Engineering Research Council of Canada (NSERC) is also gratefully acknowledged. We thank Mr. Marco Melchior for his help in measuring the spectra on which this work is based.

1. J.G. Eden, R. Burnham, L.F. Champagne, T. Donohue, and N. Djeu. IEEE Spectrum. April 1979. p. 50.
2. K. Wieland. Helv. Phys. Acta, **2**, 47 (1929).
3. K. Wieland. Z. Phys. **77**, 157 (1932).
4. K. Wieland. Helv. Phys. Acta, **14**, 420 (1941).
5. K. Wieland. Contribution à l'Étude de la Structure Moléculaire, 229 (1947).
6. J. Tellinghuisen, P.C. Tellinghuisen, S.A. Davies, P. Berwanger, and K.S. Viswanathan. Appl. Phys. Lett. **41**, 789 (1982).
7. J. Tellinghuisen. Excimer Lasers-1983, AIP Conference Proceedings No. 100. *Edited by* C.K. Rhodes, H. Egger and H. Pummer. American Institute of Physics, New York. 1983. p. 99.
8. D.P. Greene, K.P. Killeen, and J.G. Eden. Appl. Phys. Lett. **48**, 1175 (1986).
9. D.P. Greene, K.P. Killeen, and J.G. Eden. J. Opt. Soc. Am. B**3**, 1282 (1986).
10. R.H. Lipson, K.J. Jordan, and H.A. Bascal. J. Chem. Phys. **98**, 959 (1993).
11. K.J. Jordan, H.A. Bascal, R.H. Lipson, and M. Melchior. J. Mol. Spectrosc. **159**, 144 (1993).
12. C.E. Moore. Atomic energy levels. Vol. I–III. Natl. Bur. Stand. Circular No. 467. US GPO, Washington, D.C. 1971.
13. P. DeBievre, M. Gallent, N.E. Holden, and I.L. Barnes. J. Phys. Chem. Ref. Data, **13**, 809 (1984).
14. R.H. Lipson and A.R. Hoy. J. Chem. Phys. **90**, 6821 (1989).
15. R.H. Lipson and A.R. Hoy. Mol. Phys. **68**, 1311 (1989).
16. J.W. Tromp and R.J. LeRoy. J. Mol. Spectrosc. **109**, 352 (1985).
17. J. Tellinghuisen. J. Mol. Spectrosc. **137**, 248 (1989).
18. J. Tellinghuisen and S.D. Henderson. Chem. Phys. Lett. **91**, 447 (1982).
19. R.J. LeRoy. Program manual for RKR1: A computer program implementing the first-order RKR method for determining diatom potential energy curves from spectroscopic constants. University of Waterloo, Chemical Physics Research Report CP-425 (1992).
20. R.J. LeRoy. Program manual for LEVEL: A computer program for solving the radial Schrodinger equation for bound and quasibound levels and calculating (if desired) expectation values and Franck–Condon intensity factors, University of Waterloo, Chemical Physics Research Report CP-300 (1991).
21. A.K. Rai, S.B. Rai, and D.K. Rai. J. Phys. B: At. Mol. Phys. **15**, 3239 (1982).
22. K.J. Jordan, R.H. Lipson, N.A. McDonald, and R.J. LeRoy. J. Phys. Chem. **96**, 4778 (1992).
23. S.D. Cornell. Phys. Rev. **54**, 341 (1938).
24. M.G. Sastry. Proc. Natl. Inst. Sci. India, **7**, 351 (1941).
25. V.G. Krishnamurthy. Z. Phys. **150**, 287 (1958).
26. D.G. Horne, R. Gosavi, and O.P. Strausz. J. Chem. Phys. **48**, 4758 (1968).
27. N.-H. Cheung and T.A. Cool. J. Quantum Spectrosc. Radiat. Transfer, **21**, 397 (1979).
28. W.R. Wadt. Appl. Phys. Lett. **34**, 658 (1979).
29. J.G. Eden. Appl. Phys. Lett. **33**, 495 (1978).
30. J.H. Parks. Appl. Phys. Lett. **31**, 192 (1977).
31. J.G. Eden. Appl. Phys. Lett. **31**, 448 (1977).
32. W.T. Whitney. Appl. Phys. Lett. **32**, 239 (1978).
33. K.Y. Tang, R.O. Hunter, Jr., J. Oldenettel, C. Howton, D. Huestis, D. Eckstrom, B. Perry, and M. McCusker. Appl. Phys. Lett. **32**, 226 (1978).

[6]H.A. Bascal, R.H. Lipson, and P. Wang. To be published.

Can. J. Chem. Downloaded from www.nrcresearchpress.com by 203.198.23.82 on 09/08/12
For personal use only.

The $E^1\Sigma^+$–$X^1\Sigma^+$ system of GeS in emission

WALTER J. BALFOUR[1] AND BELVAI J. SHETTY[2]

Department of Chemistry, University of Victoria, Victoria, BC V8W 3P6, Canada

Received March 11, 1993

This paper is dedicated to Professor Gerald W. King on the occasion of his 65th birthday

WALTER J. BALFOUR and BELVAI J. SHETTY. Can. J. Chem. **71**, 1622 (1993).

A new group of bands has been observed in emission in the 500–600 nm region under conditions that generate known systems of GeS. It has been deduced from the appearance and position of the bands, and from their intensity distribution, that these bands constitute the long-wavelength component of the $E^1\Sigma^+$–$X^1\Sigma^+$ system of GeS, which gives rise to strong absorption and emission in the ultraviolet. E–X Franck–Condon factors have been estimated.

WALTER J. BALFOUR et BELVAI J. SHETTY. Can. J. Chem. **71**, 1622 (1993).

Opérant dans des conditions qui génèrent des systèmes connus de GeS, on a observé un nouveau groupe de bandes dans la région d'émission allant de 500 à 600 nm. On déduit de la présence et de la position des bandes, ainsi que de la distribution de leur intensité, que ces bandes constituent la composante à grande longueur d'onde du système $E^1\Sigma$–$X^1\Sigma^+$ du GeS qui donne lieu à une forte absorption et émission dans l'UV. On a évalué les facteurs E–X de Franck–Condon.
[Traduit par la rédaction]

Can. J. Chem. Downloaded from www.nrcresearchpress.com by 203.198.23.82 on 09/08/12
For personal use only.

Introduction

In recent years, considerable spectroscopic data have been gathered on the $E^1\Sigma^+$–$X^1\Sigma^+$ system of the isovalent diatomics SiO (1, 2), SiS (3, 4), and SiSe and SiTe (5, 6). One of the common features of these studies is the observation that bands belonging to the E–X system fall in two distinct spectral regions, one in the ultraviolet and the other in the visible. The bands in the visible region appear only in emission. These observations are a direct result of the substantial change in geometry that occurs upon excitation from the $X^1\Sigma^+$ state to the $E^1\Sigma^+$ state: the ultraviolet bands constitute one arm of the Condon parabola, the visible bands the other.

The corresponding germanium compounds can also be expected to exhibit similar spectroscopic properties. However, to date the bands belonging to the E–X system of germanium compounds have been reported only in the ultraviolet region. Of these, the GeS molecule has been the subject of interest of many researchers. Two ultraviolet band systems of GeS, $A^1\Pi$–$X^1\Sigma^+$ and $E^1\Sigma^+$–$X^1\Sigma^+$, are known and have been vibrationally analysed (7, 8). The rotational analysis of these band systems is made difficult because of the overlapping of bands due to significant natural abundances of the isotopomers $^{70}Ge^{32}S$, $^{72}Ge^{32}S$, $^{73}Ge^{32}S$, $^{74}Ge^{32}S$, and $^{76}Ge^{32}S$. More recently Magat et al. (9) have achieved the rotational analysis of a few bands belonging to the A–X system by making use of the accurate ground state rotational constants available from microwave spectral studies (10, 11).

In Drummond and Barrow's absorption study of the E–X system (8) a v'-0 progression was observed extending to $v' = 36$. However, the vibrational constants they reported were derived from a data set restricted to $v' \leq 17$. Linton (12) observed two new transitions, $b^3\Pi_1$–$X^1\Sigma^+$ (350–400 nm) and $a^3\Sigma^+$–$X^1\Sigma^+$ (420–650 nm), in experiments that were completely free from the previously known $A^1\Pi$–$X^1\Sigma^+$ and $E^1\Sigma^+$–$X^1\Sigma^+$ band systems: a chemiluminescent flame produced by the reaction of Ge with OCS.

We have examined the GeS spectrum in emission between 200 and 650 nm and, in addition to the known A–X (270–380 nm) bands, and the E–X ultraviolet bands, we have noted a new group of bands between 500 and 600 nm. Our conjecture that these new bands form the long-wavelength component of the E–X system has been confirmed by a combined vibrational analysis of the ultraviolet and visible bands and associated Franck–Condon calculations.

Experimental details

The spectrum of the germanium monosulfide molecule was excited in a microwave discharge (2450 MHz, 100 W) using a 5 cm long sealed quartz tube (10 mm diameter) containing milligram quantities of pure elemental germanium (in slight stoichiometric excess) and sulfur, along with neon gas at a pressure of 2–4 Torr (1 Torr = 133.3 Pa). To maintain a steady vapour pressure of GeS in the discharge column the sealed tube was heated with an electrical wire furnace wound around a quartz tube supporting the sealed tube. Further experimental details and advantages of the method can be found in a previous publication (5). The E–X bands of GeS in the ultraviolet (220–285 nm) region were photographed in the first order of a 3.4-m Ebert grating spectrograph with a 1180 groves mm^{-1} grating blazed at 750 nm. The bands in the visible (500–600 nm) region were photographed in the first order of a 1.5-m Baird-Atomic grating spectrograph. The band-heads were measured against the iron lines excited in a Fe–Ne hollow cathode lamp.

Results and discussion

In the present studies of GeS in emission we have observed extensive band structure throughout the visible and ultraviolet, including the $A^1\Pi$–$X^1\Sigma^+$ and $E^1\Sigma^+$–$X^1\Sigma^+$ systems, but not the bands found by Linton (12) in chemiluminescence. Our spectra, in the ultraviolet down to 220 nm, include bands reported by Drummond and Barrow (8) up to $v = 21$ of the E-state. Their observations extend somewhat further towards the convergence limit near 214 nm. Some 30 bands in the 500–600 nm region have been observed that have not previously been reported. Their occurrence together with known GeS bands, and the complete absence of any identifiable impurity spectra, suggested that the new bands also belong to GeS. They are red-degraded and have a similar appearance to the E–X bands in the ultraviolet. We have considered the probability that these new visible bands constitute part of the E–X system and find that they can indeed be integrated in a satisfactory way.

The detailed vibrational analysis of the ultraviolet and the

[1]Author to whom correspondence may be addressed.

[2]On leave (1991–1993) from: Spectroscopy Division, Bhabha Atomic Research Centre, Bombay - 400 085, India.

TABLE 1. Observed band-heads in the $E^1\Sigma^+$–$X^1\Sigma^+$ system of GeS in both the ultraviolet and the visible spectral regions

Band (v'-v'')	λ_{air} (nm)	ν_{vac} (cm^{-1})	Band (v'-v'')	λ_{air} (nm)	ν_{vac} (cm^{-1})
(*a*) Bands in the ultraviolet					
2-7	282.062	35 442.7	7-3	255.427	39 138.3
1-6	280.122	35 688.2	6-2	253.651	39 412.5
0-5	278.207	35 933.9	5-1	251.876	39 690.2
			4-0	250.155	39 963.1
1-5	275.839	36 242.4			
0-4	273.974	36 489.0	10-5	257.221	38 865.4
			9-4	255.352	39 149.9
3-6	275.461	36 292.1	8-3	253.587	39 422.3
2-5	273.571	36 542.8	7-2	251.800	39 702.2
1-4	271.681	36 796.9	6-1	250.029	39 983.3
0-3	269.779	37 056.4	5-0	248.295	40 262.5
3-5	271.341	36 843.1	7-1	248.245	40 270.7
2-4	269.476	37 089.0	6-0	246.498	40 556.1
1-3	267.578	37 361.1			
0-2	265.763	37 616.3	8-1	246.498	40 556.1
			7-0	244.755	40 844.9
3-4	267.276	37 403.4			
2-3	265.461	37 659.2	9-1	244.793	40 838.5
1-2	263.599	37 925.1	8-0	243.095	41 123.7
0-1	261.821	38 182.7			
			10-1	243.146	41 115.2
5-5	267.024	37 438.7	9-0	241.422	41 408.7
4.4	265.163	37 701.4			
3-3	263.334	37 963.2	11-1	241.485	41 397.8
2-2	261.518	38 226.9	10-0	239.791	41 690.3
1-1	259.688	38 496.2			
			12-1	239.900	41 671.3
5-4	263.095	37 997.8	11-0	238.200	41 968.7
4-3	261.316	38 256.4			
3-2	259.479	38 527.3	13-1	238.332	41 945.5
2-1	257.688	38 795.0	12-0	236.645	42 244.6
1-0	255.907	39 064.9			
			14-1	236.810	42 215.1
10-8	268.587	37 220.9	13-0	235.134	42 515.9
9-7	266.671	37 488.3			
8-6	264.843	37 747.0	15-1	235.325	42 481.5
7-5	262.969	38 016.0	14-0	233.618	42 791.8
6-4	261.114	38 286.0			
5-3	259.259	38 559.9	16-1	233.865	42 746.7
4-2	257.486	38 825.4	15-0	232.158	43 060.9
3-1	255.693	39 097.7			
2-0	253.949	39 366.2	16-0	230.728	43 327.8
8-5	260.975	38 306.4	17-0	229.381	43 582.1
7-4	259.171	38 573.1			
6-3	257.322	38 850.2	19-1	229.673	43 526.7
5-2	255.541	39 120.9	18-0	227.984	43 849.3
4-1	253.797	39 389.7			
3-0	252.053	39 662.3	20-1	228.319	43 784.9
10-6	260.925	38 313.8	21-1	227.018	44 035.8
9-5	259.082	38 586.2	20-0	225.417	44 348.5
8-4	257.221	38 865.4			
(*b*) Bands in the visible					
33-60	512.011	19 525.4	34-63	535.094	18 683.1
34-61	515.871	19 379.3	35-64	539.028	18 546.8
35-62	519.774	19 233.8			
36-63	523.366	19 101.8	33-63	541.240	18 471.0
37-64	527.226	18 961.9	34-64	545.323	18 332.7
38-65	531.130	18 822.6	35-65	549.377	18 197.4
39-66	535.019	18 685.7			
40-67	539.028	18 546.8	33-64	551.486	18 127.8
			34-65	555.689	17 990.7
33-61	521.630	19 165.4			
34-62	525.370	19 028.9	33-65	562.121	17 784.8
35-63	529.156	18 892.8	34-66	566.162	17 657.9
36-64	533.089	18 753.4			
37-65	536.727	18 626.3	33-66	573.147	17 442.7
38-66	540.572	18 493.8	34-67	577.458	17 312.5
39-67	544.388	18 364.2	35-68	581.918	17 179.8
40-68	548.635	18 222.0			

visible bands has revealed that while the former arise from transitional between vibrational levels $0 \leq v \leq 21$ in the $E^1\Sigma^+$ state and $0 \leq v \leq 8$ in the $X^1\Sigma^+$ state, the latter involve transitions from $33 \leq v \leq 40$ in the $E^1\Sigma^+$ state to $60 \leq v \leq 68$ in the $X^1\Sigma^+$ state of GeS. A least-squares fit, combining all of our observed band-heads in the ultraviolet and visible region, yielded the following constants: T'_e = 38 887.63(1.37), ω'_e = 308.79(19), $\omega'_e X'_e$ = 1.377(8), ω''_e = 574.51(26) and $\omega''_e X''_e$ = 1.800(4) (cm^{-1}). Values in parentheses are standard deviations. These constants from the global fit of E–X bands may be compared with those obtained from measurements of the first few vibrational intervals in the ground state from rotational analysis of A–X bands (9) and infrared emission spectra (13), where the $v = 1$ to $v = 0$ interval was found to be 571.0 cm^{-1}. The constants above give 570.9 cm^{-1}, in excellent agreement. The standard deviation of the fit (4.8 cm^{-1}) is well within the experimental uncertainties in band-head positions. Unlike the bands in the A–X system, the bands in the E–X system do not show sharp, well-defined heads. A major source of the uncertainty in the measured band-heads comes from overlapping, unresolved, isotopic structure. For the same reason no isotopic information useful to the assigning of specific vibrational quantum numbers is evident. Band-heads and their vibrational assignments are listed in Table 1.

We have used Franck–Condon calculations (14) to verify the above interpretation of the visible GeS bands. The vibrational constants necessary to compute the Rydberg–Klein–Rees (RKR) potential energy curves were taken from the present study. Equilibrium rotational data (B_e and α_e) for the ground electronic state are available from microwave studies (10, 11), but similar data for the E-state have not been measured. Initially we estimated B'_e and α'_e parameters by assuming percentage changes upon excitation to be the same for GeS as measured for the isovalent SiS (15). The estimated r'_e was 0.2356 nm. We subsequently adjusted the r'_e value to 0.22811 nm, while preserving the shape of the potential curve, to match the calculated relative intensity distribution of the v'-0 progression to experiment. The RKR curves used are given in Table 2. The Franck–Condon factors obtained from these curves are shown in Table 3. The predictions of these calculations agree well with the observations in both the ultraviolet and visible regions.

Can. J. Chem. Downloaded from www.nrcresearchpress.com by 203.198.23.82 on 09/08/12
For personal use only.

TABLE 2. RKR potential energy curves for the $X^1\Sigma^+$ and $E^1\Sigma^+$ states of GeS

$X^1\Sigma^+$ State					$E^1\Sigma^+$ State				
v	$G(v)$ (cm^{-1})	B_v (cm^{-1})	r_{min} (nm)	r_{max} (nm)	v	$G(v)$ (cm^{-1})	B_v (cm^{-1})	r_{min} (nm)	r_{max} (nm)
0	286.81	0.186 19	0.196 27	0.206 55	0	154.05	0.144 78	0.221 41	0.235 42
1	857.72	0.185 44	0.192 90	0.210 73	1	460.09	0.144 03	0.216 85	0.241 21
2	1 425.03	0.184 69	0.190 68	0.213 76	2	763.37	0.143 28	0.213 86	0.245 43
3	1 988.74	0.183 94	0.188 93	0.216 32	3	1 063.90	0.142 52	0.211 52	0.249 02
4	2 548.85	0.183 19	0.187 47	0.218 60	4	1 361.67	0.141 77	0.209 56	0.252 24
5	3 105.36	0.182 45	0.186 19	0.220 70	5	1 656.69	0.141 01	0.207 84	0.255 22
6	3 658.27	0.181 70	0.185 05	0.222 67	6	1 948.96	0.140 26	0.206 32	0.258 02
7	4 207.58	0.180 95	0.184 01	0.224 53	7	2 238.47	0.139 51	0.204 93	0.260 69
8	4 753.29	0.180 20	0.183 06	0.226 32	8	2 525.23	0.138 75	0.203 66	0.263 26
9	5 295.40	0.179 45	0.182 18	0.228 04	9	2 809.23	0.138 00	0.202 49	0.265 74
10	5 833.91	0.178 70	0.181 36	0.229 70	10	3 090.48	0.137 24	0.201 39	0.268 16
11	6 368.82	0.177 95	0.180 59	0.231 32	11	3 368.98	0.136 49	0.200 36	0.270 52
12	6 900.13	0.177 20	0.179 86	0.232 91	12	3 644.72	0.135 74	0.199 38	0.272 83
13	7 427.84	0.176 45	0.179 18	0.234 45	13	3 917.71	0.134 98	0.198 46	0.275 10
14	7 951.95	0.175 70	0.178 52	0.235 97	14	4 187.94	0.134 23	0.197 58	0.277 35
15	8 472.46	0.174 95	0.177 90	0.237 47	15	4 455.42	0.133 48	0.196 74	0.279 56
16	8 989.37	0.174 21	0.177 30	0.238 94	16	4 720.15	0.132 72	0.195 94	0.281 75
17	9 502.58	0.173 46	0.176 73	0.240 39	17	4 982.12	0.131 97	0.195 17	0.283 92
18	10 012.39	0.172 71	0.176 18	0.241 82	18	5 241.34	0.131 21	0.194 42	0.286 07
19	10 518.50	0.171 96	0.175 65	0.243 24	19	5 497.80	0.130 46	0.193 71	0.288 21
20	11 021.01	0.171 21	0.175 14	0.244 65	20	5 751.51	0.129 71	0.193 01	0.290 34
21	11 519.92	0.170 46	0.174 65	0.246 04	21	6 002.47	0.128 95	0.192 34	0.292 46
22	12 015.23	0.169 71	0.174 17	0.247 42	22	6 250.67	0.128 20	0.191 69	0.294 57
23	12 506.94	0.168 96	0.173 71	0.248 80	23	6 496.12	0.127 44	0.191 06	0.296 68
24	12 995.05	0.168 21	0.173 27	0.250 16	24	6 738.81	0.126 69	0.190 45	0.298.79
25	13 479.56	0.167 46	0.172 83	0.251 52	25	6 978.75	0.125 94	0.189 85	0.300 89
26	13 960.47	0.166 71	0.172 41	0.252 87	26	7 215.94	0.125 18	0.189 27	0.302 99
27	14 437.78	0.165 97	0.172 00	0.254 22	27	7 450.37	0.124 43	0.188 70	0.305 10
28	14 911.49	0.165 22	0.171 60	0.255 56	28	7 682.05	0.123 67	0.188 14	0.307 20
29	15 381.60	0.164 47	0.171 21	0.256 90	29	7 910.97	0.122 92	0.187 60	0.301 31
30	15 848.11	0.163 72	0.170 83	0.258 23	30	8 137.14	0.122 17	0.187 06	0.311 43
31	16 311.02	0.162 97	0.170 46	0.259 56	31	8 360.56	0.121 41	0.186 54	0.313 55
32	16 770.33	0.162 22	0.170 10	0.260 89	32	8 581.22	0.120 66	0.186 02	0.315 68
33	17 226.04	0.161 47	0.169 75	0.262 22	33	8 799.13	0.119 91	0.185 52	0.317 82
34	17 678.15	0.160 72	0.169 40	0.263 54	34	9 014.28	0.119 15	0.185 02	0.319 96
35	18 126.66	0.159 97	0.169 06	0.264 87	35	9 226.68	0.118 40	0.184 53	0.322 12
36	18 571.57	0.159 22	0.168 73	0.266 19	36	9 436.33	0.117 64	0.184 05	0.324 29
37	19 012.88	0.158 47	0.168 41	0.267 52	37	9 643.22	0.116 89	0.183 58	0.326 47
38	19 450.59	0.157 73	0.168 09	0.268 84	38	9 847.36	0.116 13	0.183 11	0.328 66
39	19 884.70	0.156 98	0.167 77	0.270 17	39	10 048.74	0.115 38	0.182 64	0.330 87
40	20 315.21	0.156 23	0.167 47	0.271 50	40	10 247.37	0.114 63	0.182 19	0.333 10
41	20 742.12	0.155 48	0.167 16	0.272 83					
42	21 165.43	0.154 73	0.166 87	0.274 16					
43	21 585.14	0.153 98	0.166 57	0.275 50					
44	22 001.25	0.153 23	0.166 29	0.276 83					
45	22 413.76	0.152 48	0.166 00	0.278 18					
46	22 822.67	0.151 73	0.165 73	0.279 52					
47	23 227.98	0.150 98	0.165 45	0.280 87					
48	23 629.69	0.150 23	0.165 18	0.282 22					
49	24 027.80	0.149 49	0.164 91	0.283 58					
50	24 422.31	0.148 74	0.164 65	0.284 95					
51	24 813.22	0.147 99	0.164 39	0.286 31					
52	25 200.53	0.147 24	0.164 13	0.287 69					
53	25 584.24	0.146 49	0.163 88	0.289 07					
54	25 964.35	0.145 74	0.163 63	0.290 45					
55	26 340.86	0.144 99	0.163 38	0.291 84					
56	26 713.77	0.144 24	0.163 14	0.293 24					
57	27 083.08	0.143 49	0.162 89	0.294 65					
58	27 448.79	0.142 74	0.162 65	0.296 06					
59	27 810.90	0.141 99	0.162 41	0.297 48					
60	28 169.41	0.141 25	0.162 18	0.298 91					
61	28 524.32	0.140 50	0.161 94	0.300 35					

Can. J. Chem. Downloaded from www.nrcresearchpress.com by 203.198.23.82 on 09/08/12
For personal use only.

TABLE 2 (*concluded*)

$X^1\Sigma^+$ State					$E^1\Sigma^+$ State				
v	$G(v)$ (cm^{-1})	B_v (cm^{-1})	r_{min} (nm)	r_{max} (nm)	v	$G(v)$ (cm^{-1})	B_v (cm^{-1})	r_{min} (nm)	r_{max} (nm)
62	28 875.63	0.139 75	0.161 71	0.301 79					
63	29 223.34	0.139 00	0.161 48	0.303 25					
64	29 567.45	0.138 24	0.161 25	0.304 71					
65	29 907.96	0.137 50	0.161 02	0.306 19					
66	30 244.87	0.136 75	0.160 80	0.307 67					
67	30 578.18	0.136 00	0.160 57	0.309 16					
68	30 907.89	0.135 25	0.160 35	0.310 67					
69	31 224.00	0.134 50	0.160 13	0.312 18					
70	31 556.51	0.133 75	0.159 91	0.313 71					

TABLE 3. Franck–Condon factors in the $E^1\Sigma^+$–$X^1\Sigma^+$ system of GeS

(*a*) Ultraviolet bands

	v''								
v'	0	1	2	3	4	5	6	7	8
0	—	0.0005	0.002	0.008	0.021	0.042	—	—	—
1	0.0004	0.004	0.014	0.037	0.068	0.095	0.100	—	—
2	0.002	0.013	0.040	0.076	0.093	0.074	—	0.001	—
3	0.006	0.032	0.072	0.090	0.059	0.012	0.003	—	—
4	0.015	0.058	0.089	0.061	0.010	—	—	—	—
5	0.030	0.082	0.077	0.018	0.005	0.043	—	—	—
6	0.050	0.092	0.042	0.0001	0.036	—	—	—	—
7	0.072	0.082	0.009	0.019	0.050	0.012	—	—	—
8	0.093	0.057		0.045	0.028	0.002	0.036	—	—
9	0.108	0.027			0.003	0.025	—	0.0001	—
10	0.114	0.006				0.039	0.006	—	0.030
11	0.112	0.0004							
12	0.101	0.012							
13	0.086	0.034							
14	0.069	0.056							
15	0.051	0.073							
16	0.036	0.079							
17	0.024	—							
18	0.015	—							
19	—	0.052							
20	0.005	0.038							
21	—	0.026							

(*b*) Visible bands

	v''								
v'	60	61	62	63	64	65	66	67	68
33	0.0001	0.021	—	0.004	0.008	0.037	0.034	—	—
34	—	0.004	0.009	0.031	0.015	0.0006	0.026	0.041	—
35			0.014	0.0007	0.024	0.026	—	—	0.040
36				0.024	0.002	—	—	—	—
37					0.025	0.011	—	—	—
38						0.018	0.021	—	—
39							0.007	0.026	—
40								0.0002	0.021

Acknowledgement

This research was supported by funds from the University of Victoria and the Natural Sciences and Engineering Research Council of Canada.

1. N. Elander and A. Lagerqvist. Phys. Scr. **3**, 267 (1971).
2. R.F. Barrow and T.J. Stone. J. Phys. B: At. Mol. Phys. **8**, L13 (1975).
3. E.E. Vago and R.F. Barrow. Proc. Phys. Soc. **58**, 538 (1946).

Can. J. Chem. Downloaded from www.nrcresearchpress.com by 203.198.23.82 on 09/08/12
For personal use only.

4. G. Lakshminarayana, B.J. Shetty, and S. Gopal. J. Mol. Spectrosc. **112**, 1 (1985).
5. G. Lakshminarayana and B.J. Shetty. J. Mol. Spectrosc. **130**, 155 (1988).
6. K. Sunanda, S. Gopal, B.J. Shetty, and G. Lakshminarayana. J. Quant. Spectrosc. Radiat. Transfer, **42**, 631 (1989).
7. C.V. Shapiro, R.C. Gibbs, and A.W. Laubengayer. Phys. Rev. **40**, 354 (1932).
8. G. Drummond and R.F. Barrow. Proc. Phys. Soc. London, Sect. A, **65**, 277 (1952).
9. P. Magat, A.C. Le Floch, and J. Lebreton. J. Phys. B: At. Mol. Phys. **13**, 4143 (1980).
10. J. Hoeft, F.J. Lovas, E. Tiemann, R. Tiescher, and T. Törring. Z. Naturforsch. A: Astrophys. Phys. Phys. Chem. **24A**, 1217 (1969).
11. W.U. Steida, E. Tiemann, T. Törring, and J. Hoeft. Z. Naturforsch., A: Phys. Phys. Chem. Kosmophys. **31A**, 374 (1976).
12. C. Linton. J. Mol. Spectrosc. **79**, 90 (1980).
13. H. Uehara, K. Horiai, K. Sueoka, and K. Nakagawa. Chem. Phys. Lett. **160**, 149 (1989).
14. (*a*) R.N. Zare. University of California Radiation Lab. Rep. UCRL-10925, University of California, Los Angeles, Calif.; (*b*) J. Chem. Phys. **40**, 1934 (1964).
15. K.P. Huber and G. Herzberg. Molecular spectra and molecular structure. IV. Constants of diatomic molecules. Van Nostrand Reinhold Co., New York. 1979.

Can. J. Chem. Downloaded from www.nrcresearchpress.com by 203.198.23.82 on 09/08/12
For personal use only.

The infrared and Raman spectra of methoxycarbonyl and thiomethoxycarbonyl isocyanates

WALTER J. BALFOUR[1] AND SCOTT G. FOUGERE
Department of Chemistry, University of Victoria, Victoria, BC V8W 3P6, Canada

AND

DIETER KLAPSTEIN AND WERNER M. NAU[2]
Department of Chemistry, St. Francis Xavier University, Antigonish, NS B2G 1C0, Canada

Received March 11, 1993

This paper is dedicated to Professor Gerald W. King on the occasion of his 65th birthday

WALTER J. BALFOUR, SCOTT G. FOUGERE, DIETER KLAPSTEIN, and WERNER M. NAU. Can. J. Chem. **71**, 1627 (1993).

The gas phase infrared and liquid phase Raman spectra of the title compounds have been recorded and vibrational analyses performed. The spectra show evidence for the presence in both the liquid and vapour phases of two rotational isomers: *cisoid-Z* and *transoid-Z* with reference to orientation of isocyanato and methyl groups relative to the carbonyl group.

WALTER J. BALFOUR, SCOTT G. FOUGERE, DIETER KLAPSTEIN et WERNER M. NAU. Can. J. Chem. **71**, 1627 (1993).

On a enregistré le spectre Raman du composé mentionné dans le titre en phase liquide ainsi que son spectre infrarouge en phase gazeuse et on a effectué des analyses vibrationnelles. Les spectres mettent en évidence, dans la phase liquide et dans la phase gazeuse, l'existence de deux isomères rotationnels : *cisoïde-Z* et *transoïde-Z* en fonction de l'orientation des groupes isocyanato et méthyle par rapport au groupe carbonyle.

[Traduit par la rédaction]

Can. J. Chem. Downloaded from www.nrcresearchpress.com by 203.198.23.82 on 09/08/12
For personal use only.

Introduction

Several papers in recent years have dealt with the infrared and Raman spectra of simple organic isocyanates (1–3). Klapstein and Nau (4) reported infrared, uv, and ^{13}C nmr data for seven carbonyl isocyanates and eight acyl isocyanates and were able to draw a number of general conclusions regarding group frequencies and conformational properties. Their results were subsequently combined with complementary Raman observations to obtain detailed vibrational analyses for acetyl and three chloroacetyl isocyanates (5). The present paper examines the vibrational spectra of the related methoxycarbonyl isocyanate (MCI) and its thio derivative (TMCI). These spectra offer clear evidence for the presence in both liquid and gas phases of more than one rotational conformer. If we neglect rotation of the methyl group and assume a planar molecular framework for the heavy atoms as resonance would favour, there are four isomeric forms to consider, with *cisoid/transoid* and *E/Z* referring to the orientations of the isocyanato and methyl groups, respectively, relative to the carbonyl group:

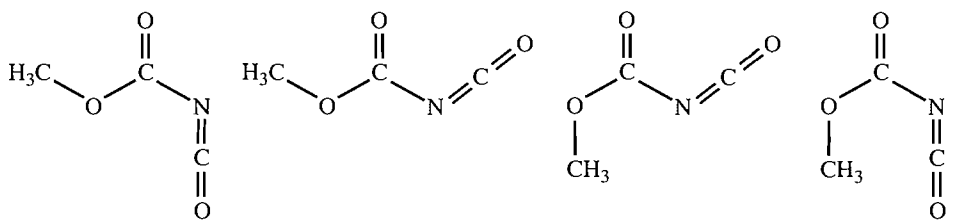

transoid-Z *cisoid-Z* *cisoid-E* *transoid-E*

A detailed analysis of the conformers of MCI, TMCI, and other carbonyl isocyanates has shown that the important contributing structures for MCI and TMCI at room temperature are the *cisoid-Z* and *transoid-Z* conformers (6). In this work we present analyses of the vapour infrared and liquid Raman spectra of MCI and TMCI.

Experimental procedure

Samples of MCI and TMCI were synthesized from commercially available (Aldrich, Milwaukee) chlorocarbonyl isocyanate following the general method of Hagemann (7). The chlorocarbonyl isocyanate was first distilled to remove traces of toluene, indicated to be present as an impurity by ^{13}C nmr, and then converted into the desired methoxy or thiomethoxy compound by reaction with the nucleophiles CH_3OH or CH_3SH, respectively. In the case of MCI, diethyl ether was used as solvent and the primary *N*-carbonyl-substituted carbamoyl chloride was isolated as a white crystalline solid which was then thermally decomposed with elimination of hydrogen chloride to yield product. For the thiomethoxy compound the product was obtained directly following reflux and removal of the 1,2-dichloroethane solvent by distillation. MCI and TMCI are colorless liquids with normal boiling points of 97 and 125°C, respectively.

Infrared spectra of the vapour phase were recorded on a Bruker IFS-25 Fourier transform spectrometer over the range 4000–

[1]Author to whom correspondence may be addressed.

[2]Present address: Department of Chemistry, University of Würzburg, 97074 Würzburg, Germany.

400 cm^{-1}, at a resolution of 2 cm^{-1}. The Raman spectra were measured perpendicular to the incident laser beam on a Jobin–Yvon RAMANOR HG2S monochromator. A Spectra Physics 2020 argon ion laser operating with 500 mW (focussed) power at 514.5 nm was used for excitation. The samples were liquids sealed in glass nmr tubes. Spectra were scanned between 3500 and 100 cm^{-1} and calibrated with reference to chloroform and known argon ion plasma lines. Raman displacements of sharp, unblended features are the average of three independent measurements and have an estimated uncertainty of ±3 cm^{-1}.

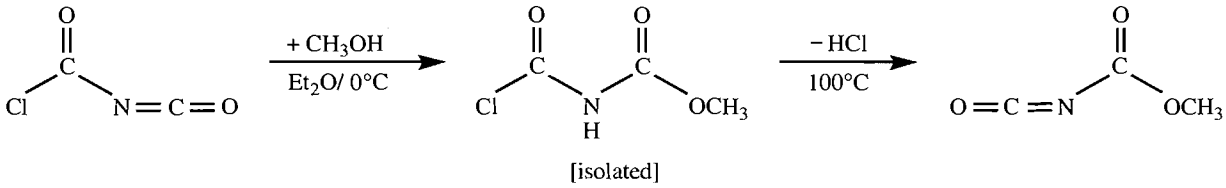

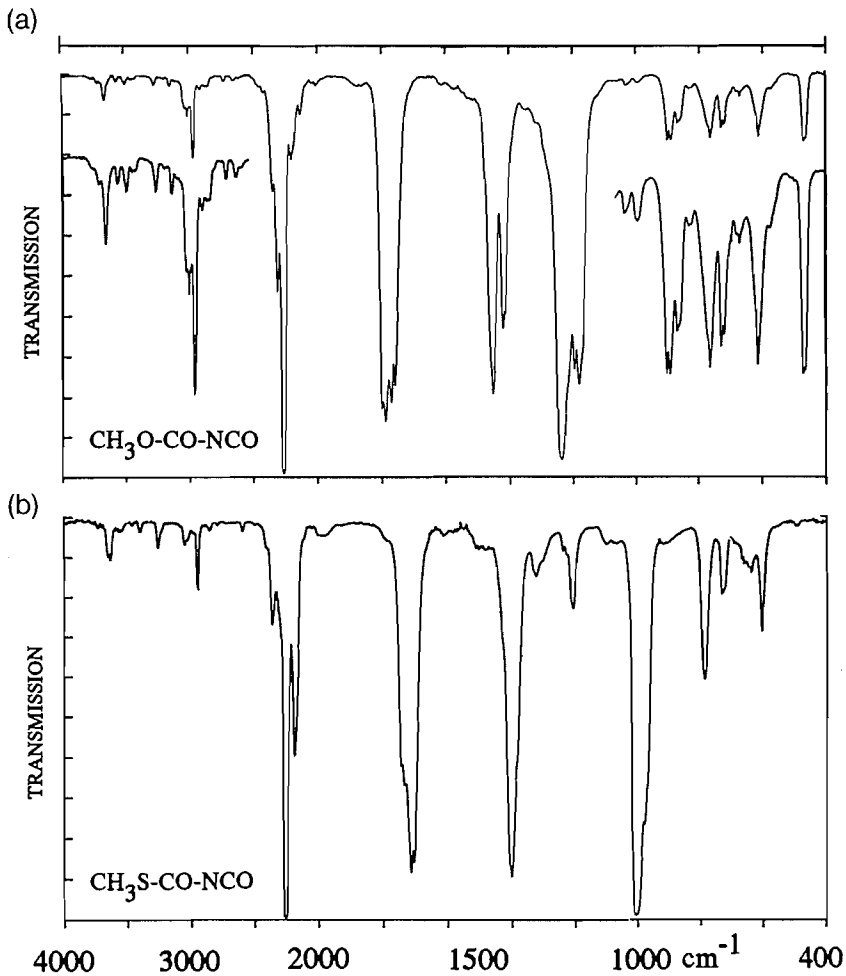

FIG. 1. The vapour phase infrared spectra of MCI and TMCI; (*a*) $CH_3OCONCO$, P = 5 Torr; insert, P = 13 Torr; (*b*) $CH_3SCONCO$, P = 7 Torr.

Results and discussion

MCI and TMCI, in any of the possible planar conformations, can be treated under C_s symmetry, the 24 normal modes spanning the irreducible representations $16a' + 8a''$. All vibrations are both infrared and Raman active. The respective spectra are presented in Figs. 1 and 2. The carbonyl stretching (infrared) region for both compounds is shown in greater detail in Fig. 3 where in each case two absorptions are evident.

A number of observations combine to favour assigning the higher frequency component to the *transoid-Z* conformer and the lower one to the *cisoid-Z* conformer (6). First, the *transoid-E* conformation is clearly improbable for steric reasons. Secondly, the higher frequency component (1795 cm^{-1}) in MCI shows an AB hybrid contour, expected only for the *transoid-Z* isomer. (The *cisoid-Z* and *cisoid-E* isomers should show B-type carbonyl stretching bands.) Thirdly, semi-empirical (AM1) calculations predict a higher frequency for the *transoid-Z* isomer. It is not possible to distinguish between the *cisoid-Z* and *cisoid-E* choices for the lower frequency component (1764 cm^{-1}) solely from observations in the car-

Can. J. Chem. Downloaded from www.nrcresearchpress.com by 203.198.23.82 on 09/08/12
For personal use only.

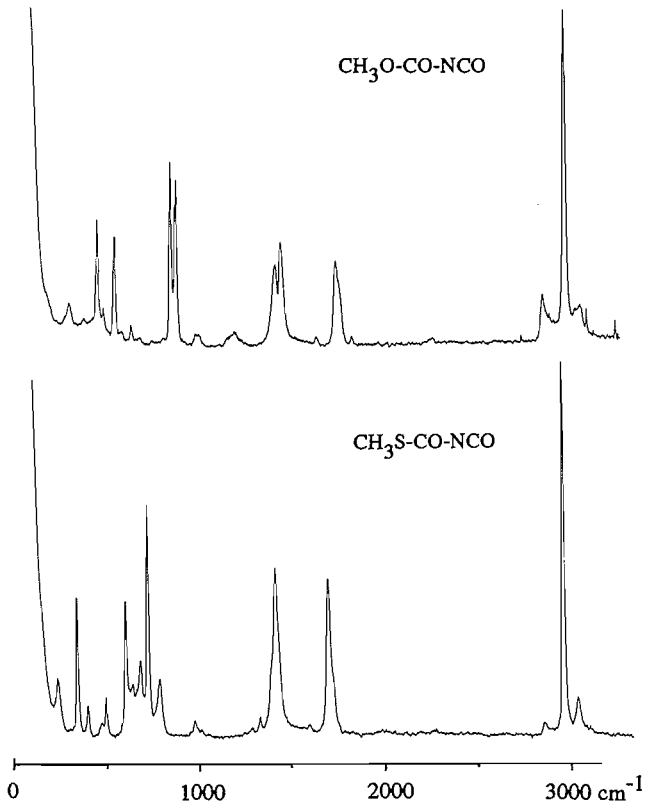

FIG. 2. Raman spectra of MCI and TMCI liquids.

bonyl stretching region. However, reference to the C—N stretching region provides a clear distinction. The C—N stretching modes for the two isomers are reasonably well resolved from each other at 892 and 862 cm^{-1} in the infrared spectrum of MCI. Experimentally the 862 cm^{-1} band gains intensity while the 892 cm^{-1} loses intensity upon heating (6). The (scaled) AM1 calculated frequencies are 888 cm^{-1} (*cisoid-Z*), 867 cm^{-1} (*transoid-Z*), and 852 cm^{-1} (*cisoid-E*). One can thus confidently assign the 862 cm^{-1} band to the *transoid-Z* isomer, with the second isomer being the *cisoid-Z* form. The temperature dependence of the 862 cm^{-1} band parallels that of the 1795 cm^{-1} carbonyl band, while the behaviour of the 892 cm^{-1} band follows that of the 1764 cm^{-1} carbonyl band. This allows unambiguous assignment of the two conformers of MCI as *transoid-Z* and *cisoid-Z*, with the latter being the more stable (6). Similar arguments hold for TMCI, allowing some conformeric vibrational assignments (see Table 2).

Vibrations of the methyl group

The stretching vibrations for a methyl group, whether attached to an oxygen atom or to a sulphur, are found in the 3050–2900 cm^{-1} region. Their assignments follow directly from the expectation that the symmetric mode will give the most intense Raman line in the region and that the frequencies of the two asymmetric counterparts will have frequencies similar to one another and lie slightly higher than the symmetric mode. The deformation modes can be assigned by comparison to methyl (8) and thiocarbamate (9) esters. The symmetric deformation lies typically near 1450 cm^{-1} for the CH_3—O group and 1320 cm^{-1} for the CH_3—S group (10). In the spectra of MCI and TMCI it is probable that the symmetric and asymmetric deformations are nearly degenerate as only one frequency attributable to CH_3 deformation can be identified. Infrared bands at 1194 and 1180 cm^{-1} have been assigned to the *a'* and *a''* CH_3—O rocking modes. The corresponding frequencies for CH_3—S, since these modes are mass-sensitive, are anticipated to be lower, e.g., 968 cm^{-1} is observed in CH_3S—CO—NH_2 (9), and a vibration with 973ir/965R cm^{-1} is assigned to the CH_3—S rocking motion.

TABLE 1. Observed frequencies (cm^{-1}) and assignments in methoxycarbonyl isocyanate

Infrared vapour	Raman liquid	Assignment
3666 vw		2262 + 1420 = 3682
3504 vvw		2262 + 1235 = 3497
3154 vvw		2262 + 892 = 3154
3036 vvw	3042 mw	$\nu_{as}(CH_3)$; *a'*
3014 vvw	3019 mw	$\nu_{as}(CH_3)$; *a''*
2969 w	2969 vvs	$\nu_s(CH_3)$
2918 vvw		2 × 1454 = 2908
2877 vvw		2262 + 612 = 2874
2856 vvw	2852 mw	2 × 1420 = 2840
2730 vvw		2262 + 466 = 2728
2652 vvw		1764 + 892 = 2656
2346 w		1453 + 892 = 2345
2312 mw		1453 + 862 = 2315
2262 vvs	2250 vw	ν_{as}(NCO)
2201 w		1453 + 763 = 2216
2130 vw		1235 + 892 = 2127
	1834 w	1236 + 604 = 1840
1795 s	1764 ms, sh	ν(C=O) *transoid*
1764 s	1750 ms	ν(C=O) *cisoid*
1453 mw	1456 ms	$\delta_{as}(CH_3)$; $\delta_s(CH_3)$
1420 ms	1424 m	ν_s(NCO) *cisoid*
1413 ms		ν_s(NCO) *transoid*
1235 vs	1236 vw	ν(C—O)
1194 s	1196 w	$\rho(CH_3)$; *a'*
1180 s	1171 w	$\rho(CH_3)$; *a''*
	1006 w	$\nu(CH_3$—O)
	993 w	Cℓ—CO—NCO impurity
892 w	896 s	ν(C—N) *cisoid*
862 w	867 s	ν(C—N) *transoid*
	821 vw	
763 w	764 vw	δ(OCO); *a''*
724 w		
	696 vw	
	658 w	δ(NCO); *a'*
612 w	604 vw	δ(NCO); *a''*
572 vw	567 ms	δ(OCO); *a'*
	507 w	321 + 190 = 511
466 w	474 ms	δ(OCN)
	397 vw	2 × 190 = 380
	321 mw	δ(COC)
	~190 vw, sh	$\tau(CH_3)$

NCO stretching vibrations

A strong infrared absorption in the 2280–2250 cm^{-1} region is characteristic of the isocyanate functional group. As with other organic isocyanates that we have studied, this asymmetric NCO stretch appears only weakly in the Raman spectra. On the other hand, the corresponding symmetric motion leads to rather weak ir absorption but intense Raman activity. These generalizations allow unambiguous assignments to be made for ν_{as} (NCO) and ν_s(NCO).

Can. J. Chem. Downloaded from www.nrcresearchpress.com by 203.198.23.82 on 09/08/12
For personal use only.

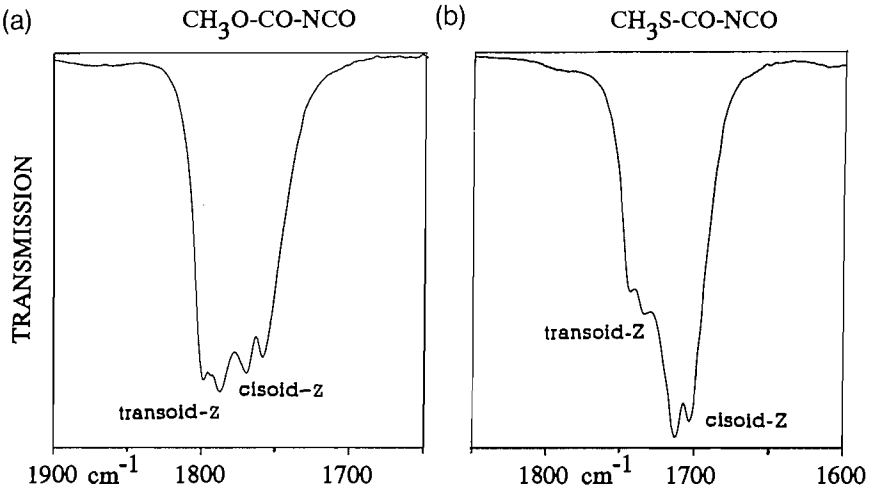

FIG. 3. The carbonyl stretching region in the infrared spectra of MCI and TMCI.

TABLE 2. Observed frequencies (cm^{-1}) and assignments in thiomethoxycarbonyl isocyanate

Infrared vapour	Raman liquid	Assignment
3653 vw		2257 + 1404 = 3661
3635 vw		2257 + 1384 = 3641
3462 vvw		2257 + 1208 = 3465
3394 vvw		2 × 1709 = 3418
3255 vvw		2257 + 1004 = 3261
3046 vvw		$\nu_{as}(CH_3)$; *a'*
3023 vvw	3021 m	$\nu_{as}(CH_3)$; *a''*
2945 w	2940 vvs	$\nu_s(CH_3)$
2850 vvw	2835 mw	
2360 mw		
2257 vvs	2241 vvw	ν_{as}(NCO)
2187 w		1404 + 787 = 2191
2177 vw, sh		1384 + 787 = 2171
1836 vvw		
1740 ms	1711 ms, sh	ν(C=O) *transoid*
1709 s	1689 s	ν(C=O) *cisoid*
	1585 w	2 × 786 = 1572
1404 s	1407 s	ν_s(NCO) *cisoid*
1384 m, sh	1385 ms, sh	ν_s(NCO) *transoid*
1323 w	1319 mw	$\delta_s(CH_3)$
1270 vvw	1265 w	2 × 637 = 1274
	1231 vvw	637 + 604 = 1241
1208 w		
1004 vs	1001 vvw	ν(C—N) *cisoid*
973 s, sh	965 vw	$\rho(CH_3)$; ν(C—N) *transoid*
787 m	786 m	
727 mw	725 vs	ν(C—S)
689 vw	684 m	$\nu(CH_3$—S)
639 vvw	637 mw	δ(NCO); *a'*
606 mw	604 ms	δ(NCO); *a''*
490 vvw	498 w	δ(OCS)
	470 vw	2 × 240 = 480
	403 w	2 × 202 = 404
	346 ms	δ(S—C—N)
	240 mw	δ(CSC)
	~202 w, sh	$\tau(CH_3)$

CH_3—O and CH_3—S stretching vibrations

The infrared spectrum of MCI shows nothing of great significance in the region between 1180 and 900 cm^{-1} where methoxy C—O stretching frequencies are to be expected. A weak Raman line at 1006 cm^{-1} is tentatively attributed to this mode. The corresponding C—S stretch in TMCI can be assigned with more confidence to a moderately intense Raman feature at 684 cm^{-1}. Again the corresponding infrared absorption is very weak. The mode is reported at 696 cm^{-1} in CH_3S—CO—NH_2 (9) and 692 cm^{-1} in CH_3—S—CH_3 (10). The adjacent bonds, from O or S to the carbonyl group, are somewhat stronger through resonance than are those to the methyl group, and this is reflected in somewhat higher values for the associated stretching frequencies: 1235 cm^{-1} for MCI and 727 cm^{-1} for TMCI.

Skeletal bending vibrations

The COC/CSC deformation mode lies at 321 and 240 cm^{-1} in MCI and TMCI, respectively. They represent the lowest frequency motions identified in the spectra, with the possible exception of poorly resolved shoulders on the rising Rayleigh scattered background, which may be due to the methyl torsion. The CNC bends are also expected to be low-lying but probably have frequencies below 150 cm^{-1}. The δ(COC/CSC) values may be compared with 320 and 253 cm^{-1} found for the analogous carbamates (9, 11). Bending vibrations within the C—NCO group can be assigned with reference to other organic isocyanates (6).

Observations and their assignments are listed for MCI and TMCI in Tables 1 and 2, respectively.

Acknowledgments

This research was supported through operating grants to W.J.B. and D.K. from the Natural Sciences and Engineering Research Council of Canada (NSERC). W.J.B. is also grateful to NSERC for an equipment grant to purchase the argon ion laser used in the Raman experiments while D.K. acknowledges support from the St. Francis Xavier University Council for Research. W.M.N. thanks the Studienstiftung des Deutschen Volkes for a graduate scholarship.

Can. J. Chem. Downloaded from www.nrcresearchpress.com by 203.198.23.82 on 09/08/12
For personal use only.

1. S.E. Ulic, C.O. Della Védova, and P.J. Aymonino. J. Raman Spectrosc. **21**, 283 (1990).
2. J.F. Sullivan, S.K. Nandy, M.J. Lee, and J.R. Durig. J. Mol. Struct. **266**, 271 (1992).
3. J.F. Sullivan, S.K. Nandy, M.J. Lee, and J.R. Durig. J. Raman Spectrosc. **23**, 51 (1992).
4. D. Klapstein and W.M. Nau. Spectrochim. Acta. In press.
5. W.J. Balfour, S.G. Fougère, D. Klapstein, and W.M. Nau. J. Mol. Struct. In press.
6. D. Klapstein and W.M. Nau. J. Mol. Struct. In press.
7. H. Hagemann. Angew. Chem. Int. Ed. Engl. **16**, 743 (1977).
8. J.K. Wilmshurst. J. Mol. Spectrosc. **1**, 201 (1957).
9. Lin Z., R. Mattes, H. Schnöckel, M. Thünemann, E. Hunting, U. Höhnke, and Ch. Mendel. J. Mol. Struct. **117**, 117 (1984).
10. M. Tranquille, P. Labarbe, M. Fouassier, and M.T. Forel. J. Mol. Struct. **8**, 273 (1971).
11. J.C. Carter and J.E. Devia. Spectrochim. Acta, **29A**, 623 (1973).

Can. J. Chem. Downloaded from www.nrcresearchpress.com by 203.198.23.82 on 09/08/12
For personal use only.

Inner shell spectroscopy of $(\eta^5\text{-}C_5H_5)_2TiCl_2$, $(\eta^5\text{-}C_5H_5)TiCl_3$, and $TiCl_4$

A.T. WEN[1] AND A.P. HITCHCOCK

Department of Chemistry, McMaster University, Hamilton, ON L8S 4M1, Canada

Received March 12, 1993

This paper is dedicated to Professor Gerald W. King on the occasion of his 65th birthday

A.T. WEN and A.P. HITCHCOCK. Can. J. Chem. **71**, 1632 (1993).

Oscillator strengths for C 1*s* excitation of gas phase Cp_2TiCl_2 and $CpTiCl_3$ (Cp = η^5-C_5H_5), and Cl 2*p* and Ti 2*p* excitation of gas phase Cp_2TiCl_2, $CpTiCl_3$, and $TiCl_4$ have been derived from electron energy loss spectra recorded under electric dipole scattering conditions. The C 1*s* spectra are interpreted with the aid of semiempirical extended Hückel calculations and comparisons with the C 1*s* spectra of other cyclopentadienyl complexes. The Ti 2*p* spectra are interpreted using the extended Hückel results and comparisons with atomic multiplet – crystal field calculations for Ti^{4+} taken from the literature.

A.T. WEN et A.P. HITCHCOCK. Can. J. Chem. **71**, 1632 (1993).

Utilisant les spectres relatifs à la perte d'énergie électronique enregistrés dans des conditions de diffusion des dipôles électriques, on a déterminé les forces de l'oscillateur pour l'excitation C 1*s* du Cp_2TiCl_2 et du $CpTiCl_3$ en phase gazeuse (Cp = η^5-C_5H_5) et les excitations Cl 2*p* et Ti 2*p* du Cp_2TiCl_2, du $CpTiCl_3$ et du $TiCl_4$ en phase gazeuse. On interprète les spectres C 1*s* à l'aide des calculs semi-empiriques étendus de Hückel et des comparaisons des spectres C 1*s* d'autres complexes du cyclopentadiényle. On interprète les spectres Ti 2*p* en utilisant des résultats de Hückel étendus et des comparaisons avec des calculs multiplet atomique – champ cristallin pour le Ti^{4+} tirés de la littérature.

[Traduit par la rédaction]

Introduction

Organometallic compounds pose interesting challenges with regard to understanding electronic structure and bonding. In addition, they provide useful models for the interaction of organic compounds with metal surfaces. Inner shell excitation spectroscopy by photoabsorption (1) or inelastic electron scattering (2) provides a site-selective probe of molecular unoccupied electronic structure. The core excitation spectra of organometallic complexes have been used in a number of recent studies to investigate the nature of metal–ligand bonding and ligand–ligand interaction via the metal centre (3–10). In this work we compare the core excitation spectra of Cp_2TiCl_2, $CpTiCl_3$, and $TiCl_4$. Improved knowledge of the spectroscopy and electronic structure of these compounds is desirable since they are involved in stereospecific polymerization of olefins (Ziegler–Natta catalysis). In addition, Cp_2TiCl_2 is being investigated as an antitumour agent (11) and a fertilizer (12).

In an early investigation of a number of 3*d*-transition metal complexes the metal 2*p* spectra were observed to have a strong dependence on ligand type, with apparently less dependence on *d*-count or symmetry (7). This empirical observation was rationalized by attributing the lower energy features to $2p \rightarrow (3d\pi\text{–}p\pi)^*$ transitions and the higher energy structure to $2p \rightarrow (3d\sigma\text{–}p\sigma)^*$ transitions since the species with strong low-energy transitions are typically species like metallocenes, which have primarily π-bonding, while those with strong higher energy transitions are metal-carbonyl species, which have strong σ-bonding as well as a π contribution. Recently Decleva et al. carried out SCF-CI ab initio calculations to explore the environmental sensitivity of metal 2*p* spectra (13). They observed a very large and characteristic sensitivity of the 2*p* spectra to the type of ligand, which they argued supports the empirical interpretation. At the same time, ab initio atomic multiplet – crystal field calculations (14–17) have met with considerable success at explaining the high-resolution metal 2*p* spectra of the elements (18), their oxides and halides (19), as well as a number of organometallic complexes (20). The physical model of this approach is qualitatively different from the empirical "π^*/σ^*" model (7); in particular, it predicts a much stronger spectral dependence on molecular geometry and 3*d*-count and a much weaker dependence on the nature of the ligand–metal bonding, which in effect only enters the crystal field calculation through the average crystal field parameter for a metal ion in a crystal field (Δ_0 or $10Dq$ in an octahedral field). Simplistically one can contrast the physical basis of the models as covalent versus ionic.

The compounds investigated in this work ($TiCl_4$, $CpTiCl_3$, and Cp_2TiCl_2) were chosen to explore the relative applicability of these two models. The Ti—Cl bond is strongly ionic and thus one might expect the crystal field approach to be more applicable to these species than to the metallocene and carbonyl complexes that were studied previously (7). As the number of Cp ligands increases, $d\pi^*\text{–}p\pi^*$ interactions should become stronger so the "π^*/σ^*" model would predict a systematic increase in the intensity of the lowest energy transition through this series of compounds that would have maximum intensity in the Ti 2*p* spectrum of $TiCp_2Cl_2$. Our goal was to use the measured spectral shape to further distinguish between these two models and, ideally, to learn which has greater predictive power.

Experimental

The inner-shell electron energy loss spectrometer and operating techniques have been described previously (2). The spectra were obtained by inelastic electron scattering with a high-velocity incident electron beam (E_0 = 2.5 keV plus the energy loss), small scattering angle (<2°), and 0.6 eV fwhm resolution. To achieve adequate vapour pressure of these low-volatility complexes in the collision region of the spectrometer, the sample cell, inlet line, and collision chamber were heated as needed. The samples were obtained commercially (Strem Chemical Co.) and used without further purification.

[1]Present address: Département de Physique, Université Laval, Ste. Foy, QC G1K 7P4, Canada.

Can. J. Chem. Downloaded from www.nrcresearchpress.com by 203.198.23.82 on 09/08/12
For personal use only.

TABLE 1. Molecular geometries of $TiCl_4$, $CpTiCl_3$, and Cp_2TiCl_2 used for EHMO calculations

Property	$TiCl_4$[a]	$CpTiCl_3$[b]	Cp_2TiCl_2[c]
Symmetry	T_d	C_{3v} (eff. O_h)	C_{2v}
R(Ti—Cl) (Å)[d]	2.170	2.20–2.25	2.36
R(Ti—Cp) (Å)[e]	—	2.01	2.06
R(Ti—C) (Å)	—	2.31	2.37
$\phi_{Cl-Ti-Cl}$ (°)	107.6	104.1, 102.2	94.5
$\phi_{Cl-Tp-Cp}$ (°)[e]	—	114.3, 117.2	106.4

[a]Gas phase electron diffraction (23).
[b]Solid state X-ray diffraction (24).
[c]Solid state X-ray diffraction (25).
[d]Differences of up to 0.05 Å are found between Ti—Cl bond lengths in gas phase and solid state $TiCl_4$ (23). Thus part of the increase in R(Ti—Cl) in the species containing Cp rings may be associated with extramolecular relaxation in the solid state.
[e]Distance (angle) to the centre of the Cp ring, which was taken to have a symmetric geometry with R(C—C) = 1.38 Å and R(C—H) = 1.10 Å.

The C 1*s*, Cl 2*p*, and Ti 2*p* spectra were converted to absolute oscillator strengths using a procedure described and tested previously (21). A precision of 5% is estimated from reproducibility of analyzing independent data sets, while absolute accuracy is about 20%, according to comparisons with other known optical oscillator strength data.

Extended Hückel calculations (EHMO) were carried out using standard methods. The default Hückel parameters were used, except that Cl 3*d* orbitals were included in the basis set since previously this was found to be important in obtaining correct (relative) energies for the lower energy unoccupied orbitals (22). The geometries were taken from gas phase electron diffraction or solid state X-ray diffraction data reported in the literature (23–25) and are summarized in Table 1. To facilitate interpretation of the core spectra, EHMO calculations relevant to the core excited states were carried out within the equivalent ionic core virtual orbital (EICVOM) model (26). EICVOM uses the "$Z + 1$" approximation to account for the core hole potential and includes an additional unit positive valence charge to give the correct number of valence electrons in the system and to account for relaxation of the valence electrons in the core excited states. Separate calculations were carried out with the C 1*s* core hole on each symmetry inequivalent site. The virtual orbital energies of the ground state of the cation were assumed to approximate the relative energies (term values) of core → valence excited states while the intensities of each transition were assumed to be proportional to the sum of the squares of the coefficients of electric dipole coupled atomic orbitals on the core excited atom for each virtual MO (27). As found in previous work (5–10, 22, 28, 29), EHMO with this approach reproduces the shapes of the discrete and, with lower quality, the near-continuum portions of core excitation spectra, giving confidence in using the virtual MO character as a guide to spectral assignment. Predicted spectra were generated from the calculations by summing Gaussian lines of position given by the eigenvalue, area given by Σc^2(N 2*p*) at the C 1*s* excited atom, and widths selected according to a graded scheme designed to approximate the observed increase in linewidth with increasing transition energy. In this work the predicted spectra were constructed using widths of 8 eV fwhm for orbitals of eigenvalue (ϵ) above 8 eV; 6 eV for $6 < \epsilon < 8$; 4 eV for $0 < \epsilon < 6$; 2 eV for $-4 < \epsilon < 0$; 1.2 eV for $-8.0 < \epsilon < -4.0$; and 0.7 eV for $\epsilon < -12$ eV. Based on comparisons with experiment, the value of 8 eV for the width of the highest energy transitions is probably underestimated.

Molecular orbital descriptions of Cp_2TiCl_2, $CpTiCl_3$, and $TiCl_4$

EHMO calculations were carried out for the ground states of all three molecules, as well as Cp^-, $TiCl_3^+$, and $TiCl_2^{2+}$, in order to provide a quantitative basis for the molecular orbital interaction diagrams presented in Fig. 1. $TiCl_4$ is a tetrahedral complex that has a ground state configuration of:

$$(1a_1)^2(1t_2)^6(1e)^4(2t_2)^6(2a_1)^2(3t_2)^6(1t_1)^6\ (2e)^0(4t_2)^0 \qquad {}^1A_1$$

The lower energy 2*e* and $4t_2$ unoccupied orbitals are almost entirely composed of Ti 3*d* orbitals. According to crystal field theory the energy difference between the 2*e* and $4t_2$ orbitals is Δ_t, the crystal field splitting of the orbitals associated with a Ti^{4+} d^0 configuration in a tetrahedral field. For the ground state of $TiCl_4$ EHMO predicts that Δ_t is 0.73 eV (see Fig. 1*a*). This separation is predicted to increase to 1.02 eV in the Ti 2*p* excited state. The EHMO ground state prediction of Δ_t for $TiCl_4$ is rather smaller than the experimental value determined by UV absorption spectroscopy (~0.95 eV (30)) or that from other semiempirical calculations (~1.0 eV) (31).

The MO diagram of $CpTiCl_3$ is presented in Fig. 1*b* together with a correlation to the orbital energies of Cp^- and $TiCl_3^+$. The symmetry of this complex is only C_s. However, the pattern of the MOs suggests that the apparent symmetry is rather close to O_h. This can be rationalized readily within a fragment MO model (32). Consider a hypothetical octahedral species ML_6 (sketch **a**) where L is a simple σ donor ligand (such as Cl^-) and has one valence orbital with two electrons pointing towards the metal centre.

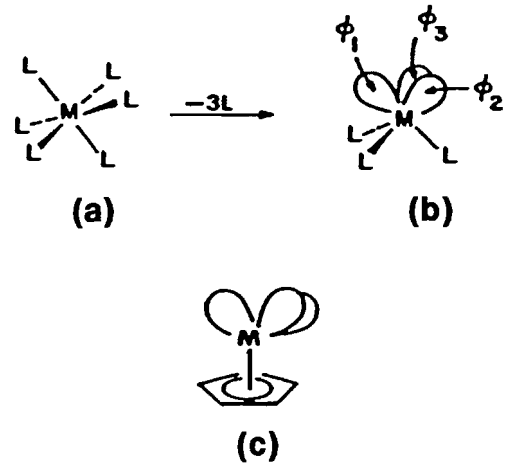

The σ-bonding skeleton can be constructed from six equivalent sp^3d^2 hybrid metal orbitals and the σ-ligand orbitals. The valence orbitals of a pyramidal ML_3 fragment (C_{3v}) can be obtained from an octahedron by removal of three facial L ligands, leaving three low-lying acceptor orbitals directed towards the vacated ligand sites (sketch **b**). If the original species has a $3d^0$ metal centre (e.g., Ti^{4+}), then there will be three unfilled valence orbitals that closely correlate to the t_{2g} set of the octahedron (31). On the other hand, if the three L ligands are removed from $CpML_3$ (such as $CpTiCl_3$), leading to the CpM fragment (sketch **c**), the resulting three hybrid orbitals will point towards the empty ligand sites. This is exactly the same pattern seen in the above generation of the ML_3 fragment from ML_6. In other words, the CpM group is expected to be very similar to ML_3. This means that the Cp^- ligand with six electrons is topologically equivalent to three facial ligands of the σ donor (Cl^- in our case) and thus $CpTiCl_3$ has a pseudo-octahedral symmetry.

Compared to $TiCl_4$, the $\pi(e_1'')$ HOMO's of the Cp^- ligand

Can. J. Chem. Downloaded from www.nrcresearchpress.com by 203.198.23.82 on 09/08/12
For personal use only.

Can. J. Chem. Downloaded from www.nrcresearchpress.com by 203.198.23.82 on 09/08/12
For personal use only.

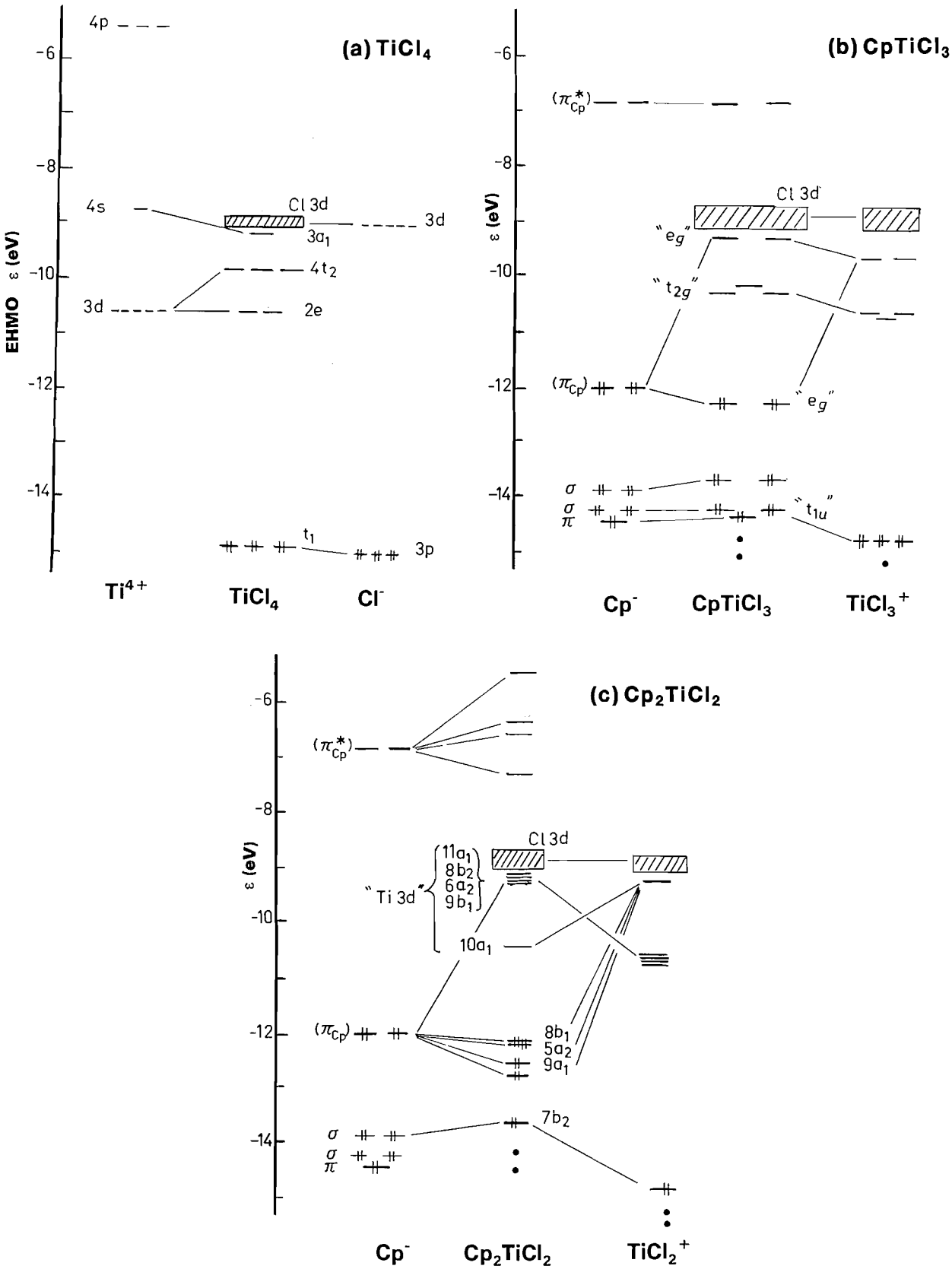

FIG. 1. Molecular orbital schemes for (*a*) $TiCl_4$, (*b*) $CpTiCl_3$, and (*c*) Cp_2TiCl_2. The orbital energies and symmetry character are based on extended Hückel calculations of the ground state. Hatched blocks represent a number of closely spaced orbitals. Only the dominant fragment origins of the MOs are shown. For $TiCl_4$ and Cp_2TiCl_2 the fragment analysis is incomplete. The "Cl_4^{4-}" (for $TiCl_4$) and Cp_2^{2-} (for Cp_2TiCl_2) units have symmetry-adapted combinations of the Cl^- and Cp^- orbitals shown, with little interaction with the Ti^{4+} AOs.

Can. J. Chem. Downloaded from www.nrcresearchpress.com by 203.198.23.82 on 09/08/12
For personal use only.

provide a better energy match with the vacant $1e$ set of $TiCl_3^+$. This can be considered to be the orbital basis for the fact that the Cp^- ligand bonds more strongly to the $TiCl_3^+$ cation than does a fourth Cl^- anion. Based on the analogy with an octahedral bonding pattern, we have labelled the three lowest energy unoccupied MOs as a "t_{2g}" MO, which, in reality, is split slightly in both the ground and excited states by about 0.15 eV. Since this splitting is much smaller than our experimental resolution we do not expect to be able to detect it. These three orbitals have primarily Ti $3d$ character (d_{z^2}, $d_{x^2-y^2}$, d_{xy}). At about 1.1 eV higher energy there are two closely spaced empty orbitals with large Ti $3d$ character, arising mainly from $TiCl_3^+$-based Ti $3d$ $1e(d_{xz}, d_{yz})$ orbitals. In accord with the octahedral analogy these two orbitals are labelled "e_g." The "e_g" orbitals also have contributions from the occupied π(Cp) e_1'' orbitals. At still higher energy one finds the π^*_{Cp} (e_2'') orbitals. Symmetry analyses of the EHMO wave functions indicates that the "e_g" MOs are of π^* character, while the "t_{2g}" are of σ^* character. For this reason, the $2e$ ("e_g") MOs of $TiCl_4$ ($CpTiCl_3$) are often referred to as $\pi^*(e$, Ti—Cl) while the t_2 ("t_{2g}") MOs are referred to as $\sigma^*(t$, Ti—Cl) (33–35). EHMO predicts that "Δ_0" for $CpTiCl_3$ is 1.10 eV in the ground state, increasing to 1.14 eV after C $1s$ excitation and to 1.28 eV after Ti $2p$ excitation. These values are significantly larger than the EHMO-predicted crystal field splitting in $TiCl_4$, consistent with the general rule that O_h are larger than T_d crystal field splittings ($\Delta_t = 5/9\ \Delta_0$ if metal–ligand bond lengths are the same). Based on applying on-site dipole selection rules to the MO scheme for $CpTiCl_3$, we expect intense peaks associated with the "t_{2g}" and "e_g" levels in the Ti $2p$ spectrum as well as strong C $1s \rightarrow \pi^*_{Cp}$ transitions and observable C $1s \rightarrow$ "$2e_g$" transitions in the C $1s$ spectrum of $CpTiCl_3$. The effect of core hole relaxation on the energy and character of the unoccupied orbitals and thus on the transition intensity should be taken into account by the EICVOM approach (10, 26). The intensities of both Ti $2p$ and C $1s$ core excitation to the "t_{2g}" and "e_g" levels should be informative with regard to Ti—Cp bonding.

The orbital scheme for Cp_2TiCl_2 is presented in Fig. $1c$. As for the other two species, the low-lying unoccupied orbitals are mainly of Ti $3d$ character. Because of the low symmetry of this complex (at best C_{2v} if the Cp rings are appropriately aligned) the five Ti $3d$ orbitals are nondegenerate and span a range of 1.38 eV in the ground state according to the EHMO results (1.38 eV with C $1s$ and 2.14 eV with Ti $2p$ excitation). The $10a_1$ LUMO has large Ti $3d_{z^2}$ and Ti $d_{x^2-y^2}$ character. The next four orbitals ($9b_1$, $6a_2$, $8b_2$ and $11a_1$) are mainly Ti $3d$ in character, but do have some admixture of Cl $3d$ and π^*_{Cp} character. The relative orbital energies and composition predicted by EHMO ground state calculations are in agreement with Fenske–Hall ($36a$) and SCF-SW-Xα ($36b$) calculations for Cp_2TiCl_2. Compared to $CpTiCl_3$, Cp_2TiCl_2 is expected to have a wider range of Ti $2p \rightarrow 3d$ transitions, with perhaps a broader and (or) structured higher energy peak, and a significant C $1s \rightarrow$ "Ti $3d$" contribution.

These considerations of the frontier orbitals of these three compounds indicate that substitution of one or two Cp^- for Cl^- ligands in $TiCl_4$ does not affect the dominant Ti $3d$ character of the low-lying unoccupied electronic structure very much, although there is a reversal of symmetry between $TiCl_4$ and $CpTiCl_3$ and a larger splitting in Cp_2TiCl_2. This suggests that all three molecules should have closely related geometries and core excitation spectra. Critical geometric parameters for all three molecules are summarized in Table 1. The Ti—Cp bond strength in $CpTiCl_3$ is 74 kcal mol^{-1} (37), similar to that of the Ti—Cl bond in $TiCl_4$. Even in Cp_2TiCl_2, where two of the Cl ligands in $TiCl_4$ have been replaced, there is relatively little change in molecular stability, although there is a significant increase in the Ti—Cl bond length.

The occupied MOs of all three molecules have been investigated by photoelectron spectroscopy (34, 38, 39). There are three major bands in the photoelectron spectrum of $CpTiCl_3$ that are associated with MOs derived largely from the Cl $3p$ orbitals but with some Ti-orbital participation. These are shifted by ~1 eV to lower energy relative to the corresponding bands of $TiCl_4$. Such a red shift has been attributed to the π-donor nature of the Cp ring pointing towards the central Ti atom, which reduces the bonding strength of the Cl lone pairs. The reduced Ti—Cl bonding is reflected in the increased Ti—Cl bond length with Cp substitution. PES has provided direct evidence that the Cp ring influences the Ti—Cl bonding through shifts in the occupied MO levels. To our knowledge, there has not been an experimental study of the *unoccupied* MOs of $CpTiCl_3$ or Cp_2TiCl_2 by electron transmission or core excitation spectroscopy.

C $1s$ spectra of $CpTiCl_3$ and Cp_2TiCl_2

The C $1s$ spectra of $CpTiCl_3$ and Cp_2TiCl_2 are presented in Fig. 2 on an oscillator-strength-per-carbon-atom intensity scale. The hatched line indicates the C $1s$ ionization potential (IP) estimated from that of $3d$ metallocenes (40). Energies, term values, and proposed assignments are summarized in Table 2.

The C $1s$ spectra are characterized by four very intense features: two sharp bands below the IP and two broader features at higher energy, above the C $1s$ IP. The first feature in the spectra of both species is attributed to C $1s$ excitations to final orbitals of mainly Ti $3d$ character, although within the EICVOM model it is the C $2p$ component of these MOs which gives rise to the transition intensity. In $CpTiCl_3$ there are two resolved components of the first band. These are attributed to the "t_{2g}" (284.4 eV) and "e_g" (285.5 eV) levels. The much higher intensity of the C $1s \rightarrow$ "e_g" transition is consistent with its larger C $2p$ admixture (see Fig. 1 and the earlier discussion of the MO structure). The "Ti $3d$" band in the C $1s$ spectrum of Cp_2TiCl_2 does not show any resolved structure although it is significantly broader than the experimental resolution and exhibits low- and high-energy shoulders on closer inspection. A Gaussian curve fit, which required three components for a satisfactory fit, was used to derive the sub-band energies reported in Table 2. The main C $1s$ spectral feature, occurring at 287.0 eV in both species, is the C $1s \rightarrow \pi^*_{Cp}$ transition. As in metallocenes (5) only a single (C $1s^{-1}$, π^*_{Cp}) feature is observed. Splittings associated with symmetry reduction or interaction of π^* orbitals on the two adjacent Cp rings in Cp_2TiCl_2 might be expected. These are either smaller than our experimental resolution or, alternatively, core hole localization distorts the electronic structure such that only the excitation to the lowest energy π^*_{Cp} orbital has appreciable intensity. The latter situation was recently determined to be operative in metal carbonyl complexes (10). The two broad bands in the C $1s$

Can. J. Chem. Downloaded from www.nrcresearchpress.com by 203.198.23.82 on 09/08/12
For personal use only.

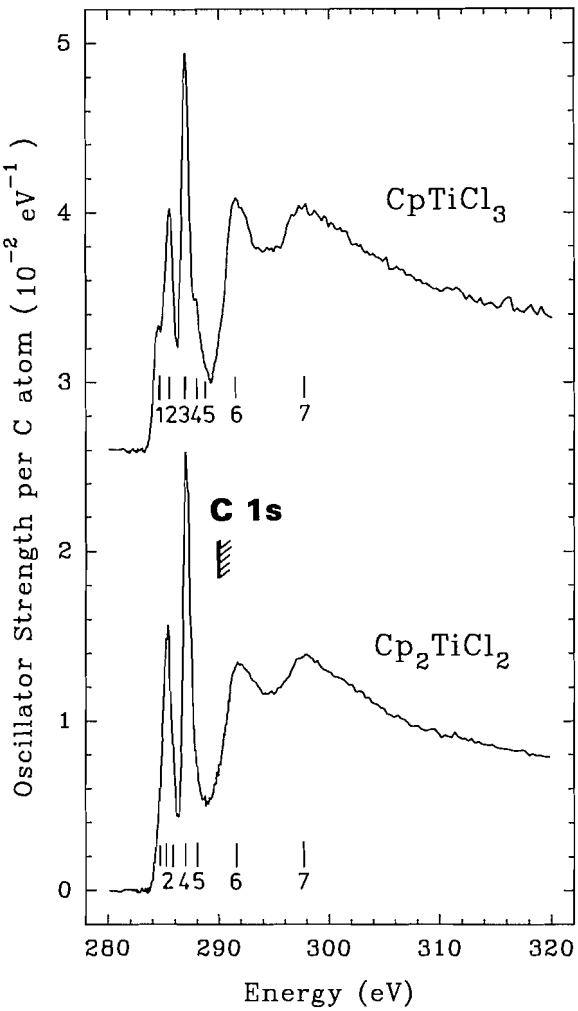

FIG. 2. Carbon 1*s* oscillator strength spectra of $CpTiCl_3$ and Cp_2TiCl_2 derived from electron energy loss spectra recorded using 2.5 keV final electron energy, 0.6 eV fwhm resolution, and 2° scattering angle. The hatched lines indicate the estimated C 1*s* IP. The spectra have been scaled on a basis of oscillator strength per carbon. The $CpTiCl_3$ spectrum has been offset vertically by 0.026 $(eV)^{-1}$ for clarity.

continuum are attributed to resonances associated with quasi-stationary states corresponding to (C $1s^{-1}$, σ^*) configurations.

The EHMO predictions of the C 1*s* spectra of $CpTiCl_3$ and Cp_2TiCl_2 are presented in Fig. 3. The EHMO spectra are plotted on the orbital energy scale. A line diagram of the spectral contributions from each of the chemically distinct carbon sites (three in $CpTiCl_3$; five in Cp_2TiCl_2) (C_s, crystal geometry (25)) is also presented. The Gaussian broadened weighted sum, scaled relative to the MO transitions in a way to approximate the experimental intensities, has been combined with the oscillator strength for ionization of atomic carbon to construct the "EHMO-predicted spectrum." The experimental C 1*s* spectrum for each species has also been plotted, with the energy scale set so as to align the sharpest feature with the maximum in the EHMO-predicted spectrum. The difference in the EHMO orbital energy scale and the experimental transition energies is 295.0 eV for $CpTiCl_3$ and 294.7 eV for Cp_2TiCl_2. Ideally the orbital energies in the EICVOM approach should be equal to the negative of the experimental term values (T = IP − E). The EHMO-EICVOM calculations for the C 1*s* spectra of these two species give orbital energies that are about 5 eV greater than the experimental term values (T = IP − E). A similar discrepancy has been found in all previous comparisons of EHMO-EICVOM predicted and experimental C 1*s* spectra (5–10, 22, 28, 29).

The splitting of the first band in the C 1*s* spectrum of $CpTiCl_3$ corresponds to the "t_{2g}"–"e_g" Δ_0 (10Dq) crystal field splitting in the quasi-octahedral field of $CpTiCl_3$. The experimental splitting (1.07 eV) is in good agreement with that predicted by EHMO (1.14 eV in the C 1*s* excited state, based on the maximum separation in the $C_{2,5}$ components). The greater intensity of the C $1s \rightarrow$ "e_g" transition (relative to the C $1s \rightarrow$ "t_{2g}" transition) is attributable to the larger C 2*p* character which arises from the interaction of $TiCl_3$ 1*e* orbitals with the Cp ring e_1'' MOs. In principle the C $1s \rightarrow$ "t_{2g}" transition should exhibit a further splitting. However, according to the EHMO results, this will be only about 0.15 eV, considerably smaller than our experimental resolution (0.6 eV).

While the C 1*s* spectrum of Cp_2TiCl_2 also contains low-lying C 1*s* excitations to MOs of large "Ti 3*d*" character, the details of the first band differ significantly from that for $CpTiCl_3$. In particular, the band is rather broad with signs of both a low-energy and a high-energy shoulder. The positions of the three features listed in Table 1 were derived from a fit of three Gaussian lines to band 1. The absence of any resolved splitting reflects the lower symmetry of this complex and thus the larger number of MOs to which the Ti 3*d* orbitals contribute. According to the EHMO calculations C 1*s* excitations to the $10a_1$ LUMO only occur from two of the five carbons of each Cp ring. Thus EHMO predicts a low-intensity first peak in the C 1*s* spectrum, which is a reasonable match, with regard to relative position and intensity, to the low-energy shoulder of the first band.

The prominent spectral feature around 287 eV in both complexes is assigned to C $1s \rightarrow \pi^*_{Cp}$ transitions. Its large oscillator strength is ascribed to the good dipole-spatial overlap between the carbon 1*s* orbital and the large C 2*p* character of the π^*_{Cp} orbitals. In the ground state of $CpTiCl_3$ the π^* e_2'' MOs are energetically well separated from other orbitals (see Fig. 1) and have little interaction with $TiCl_3$ orbitals. A dominant π^*_{Cp} character is supported by the EHMO calculation, which predicts very little variation of the transition energy for C 1*s* excitations at different sites. In Cp_2TiCl_2 the complex contains four unoccupied orbitals of mainly π^*_{Cp} character. In the ground state there is a rather large energy splitting of these orbitals (1.7 eV). If this splitting and a distributed C 2*p* character was retained in the π^*_{Cp} MOs of the C 1*s* excited states one would expect a number of resolved intense π^*_{Cp} features or at least a significant broadening of the π^*_{Cp} feature in Cp_2TiCl_2 relative to that in $CpTiCl_3$. This is not the case. The EICVOM-EHMO calculations indicate that there are a number of C $1s \rightarrow \pi^*_{Cp}$ transitions distributed over almost 3 eV. However, due to the strong polarizing effect of the core hole on the π^*_{Cp} orbitals, the only intense transition is that to the lowest energy π^*_{Cp} MO at each site (see the line diagrams in Fig. 3). Relative to $CpTiCl_3$, EHMO predicts some broadening and a higher energy shoulder for the π^*_{Cp} feature of Cp_2TiCl_2. Experimentally the π^*_{Cp} feature in Cp_2TiCl_2 is narrower than that in $CpTiCl_3$.

TABLE 2. Energies (E, eV), term values (T, eV), and proposed assignments for features in the C 1s spectra of $CpTiCl_3$ and Cp_2TiCl_2

$CpTiCl_3$			Cp_2TiCl_2			Assignment (final orbital)	
No.	E	T	No.	E	T	$CpTiCl_3$	Cp_2TiCl_2
1	284.43[a]	5.6	1 sh	284.9[a]	5.1	"t_{2g}"	$10a_1$
2	285.50[a]	4.5	2	285.3[a]	4.7	"e_g"	$9b_1$, $6a_2$, $8b_2$
			3 sh	285.7[a]	4.3		$6a_2$
3	286.93[b]	3.1	4	286.99[b]	3.0	π^*_{Cp}	π^*_{Cp}
4	287.9	2.1	5 sh	287.9	2.1	Ryd/σ^*C—H	Ryd/σ^*_{C-H}
5	288.6	0.7				Rydberg	
	290.0[c]			290.0[c]		IP	IP
6	291.5	−1.2	6	291.7	−1.7	σ_1^* (C=C)	σ_1^* (C=C)
7	298	−8	7	297.9(2)	−7.9	σ_2^* (C=C)	σ_2^* (C=C)

[a]Peak positions were determined by a curve fit of the first band to Gaussian peaks.
[b]Calibration relative to CO_2 (C 1s → π^*, 290.74 eV): ΔE = −3.81(4) and −3.75(3) eV for $CpTiCl_3$ and Cp_2TiCl_2.
[c]Estimated from the C 1s IPs of metallocenes and other compounds containing Cp^- (40).

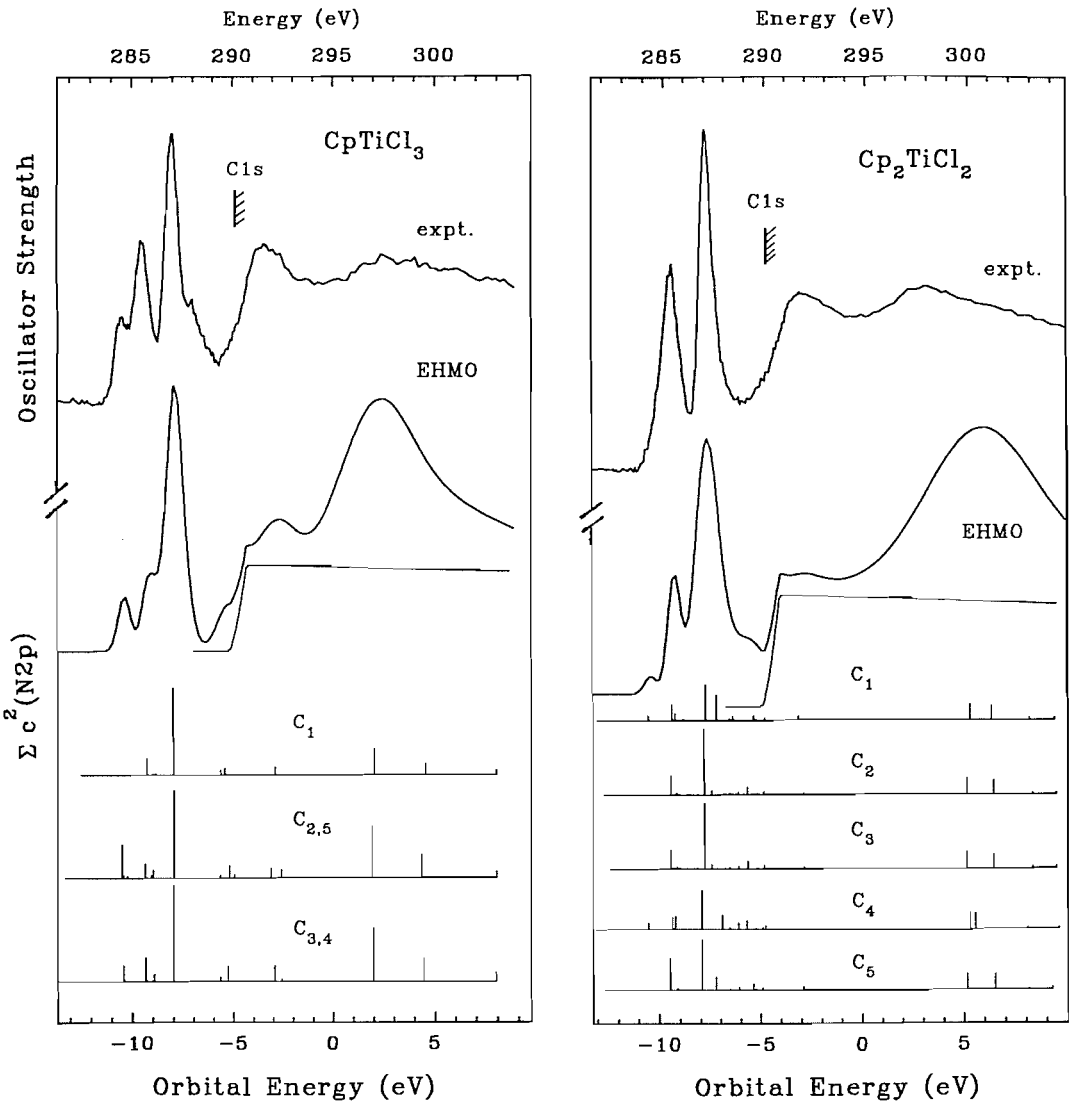

FIG. 3. Comparison of EHMO predicted and experimental C 1s spectra of $CpTiCl_3$ and Cp_2TiCl_2. The bar spectra indicate the chemically distinct components of the calculated EHMO spectrum. The C 1s continuum oscillator strength of atomic carbon (plotted under the EHMO predicted spectrum) has been added.

Can. J. Chem. Downloaded from www.nrcresearchpress.com by 203.198.23.82 on 09/08/12
For personal use only.

Can. J. Chem. Downloaded from www.nrcresearchpress.com by 203.198.23.82 on 09/08/12
For personal use only.

There is a broad peak and high-energy shoulder around 288–289 eV in the C 1*s* spectrum of $CpTiCl_3$. EHMO does not predict any spectral features in this area. This is consistent with these features arising from excitations to orbitals with a large Rydberg character, such as the 3*p*/C–H states seen in the C 1*s* spectra of many hydrocarbon species around this energy (41). A corresponding signal is not observed in Cp_2TiCl_2 but the spectrum does not return to the baseline between the π^*_{Cp} feature and the continuum onset at 290 eV, indicating that there are unresolved states at these energies.

The first band in the continuum at ~291 eV is attributed to C $1s \rightarrow \sigma_1^*$ (C=C) excitation while the broader, higher energy, asymmetric band centered around 298 eV is ascribed to C $1s \rightarrow \sigma_2^*$ (C=C) excitation. The σ_1^* and σ_2^* terminology is adopted from earlier interpretations of the C 1*s* spectra of a large number of six-member aromatic species (benzene, pyridine (42), substituted benzenes (43)) as well as other organometallic compounds containing η^5-C_5H_5 ligands (5, 10), which all show a characteristic pattern of two resonances around 291 and 298 eV in the C 1*s* continuum. The σ_1^* (C=C) band in both of these Ti species is about 1 eV below its counterpart in ferrocene (5) but the σ_2^* (C=C) band occurs at the same energy. The net effect is that there is a larger energy splitting between the two σ* resonance features in $CpTiCl_3$ or Cp_2TiCl_2 than in $FeCp_2$. This indicates there is a stronger interaction between the adjacent C—C bonds of $CpTiCl_3$ relative to that in ferrocene, consistent with the results from IR studies (44). The possible cause of this might be the difference between the partially charged $Cp^{\delta-}$ ligand in the ionically bonded $CpTiCl_3$ molecule and the relatively neutral Cp ring in the more covalently bonded $Fe(Cp)_2$ complex. The extra electron (or charge) density (δ-) transferred from Ti to Cp would partially "populate" one of the e_1'' (π) bonding orbitals of Cp, which is only half filled in free Cp. This would increase the C—C bond strength and lead to a stronger C—C bond interaction. Thus the details of the C 1*s* spectra of these complexes support the view that the Ti–Cp interaction in these complexes is strongly ionic.

Overall, the C 1*s* spectra of $CpTiCl_3$ and Cp_2TiCl_2 resemble those of other metallocenes (5, 10), especially the π^*_{Cp} feature and the positions and relative intensities of the continuum features. The resemblance reflects the fact that the virtual electronic structure of all cyclopentadienyl complexes is rather similar and that the chlorine atoms have very little influence on carbon 1*s* excitation due to poor orbital overlap. However, there are systematic trends in the intensities and energies of the two major bands below the C 1*s* ionization threshold. The most notable variation of intensity is in the first band of C $1s \rightarrow$ metal 3*d* character. It has the largest oscillator strength (peak area) in the $CpTiCl_3$ and Cp_2TiCl_2 complexes and the smallest in nickelocene (5). This intensity variation is directly related to the increasing number of 3*d* electrons as the 3*d* period is traversed, which reduces the empty 3*d* character and thus the number/density of low-lying unoccupied MOs of mixed Cp – metal 3*d* character. The smaller width of the first peak in ferrocene, cobaltocene, and nickelocene (5) relative to that of $CpTiCl_3$ is attributed to the absence of C $1s \rightarrow 2t_{2g}^*$ (3*d*) transitions in the late-period metallocenes because the $2t_{2g}^*$ orbitals are filled in these species. The particularly low intensity of the first peak in the C 1*s* spectra of cobaltocene and nickelocene is ascribed to the partial occupancy of the $4e_{1g}^*$ orbital (5).

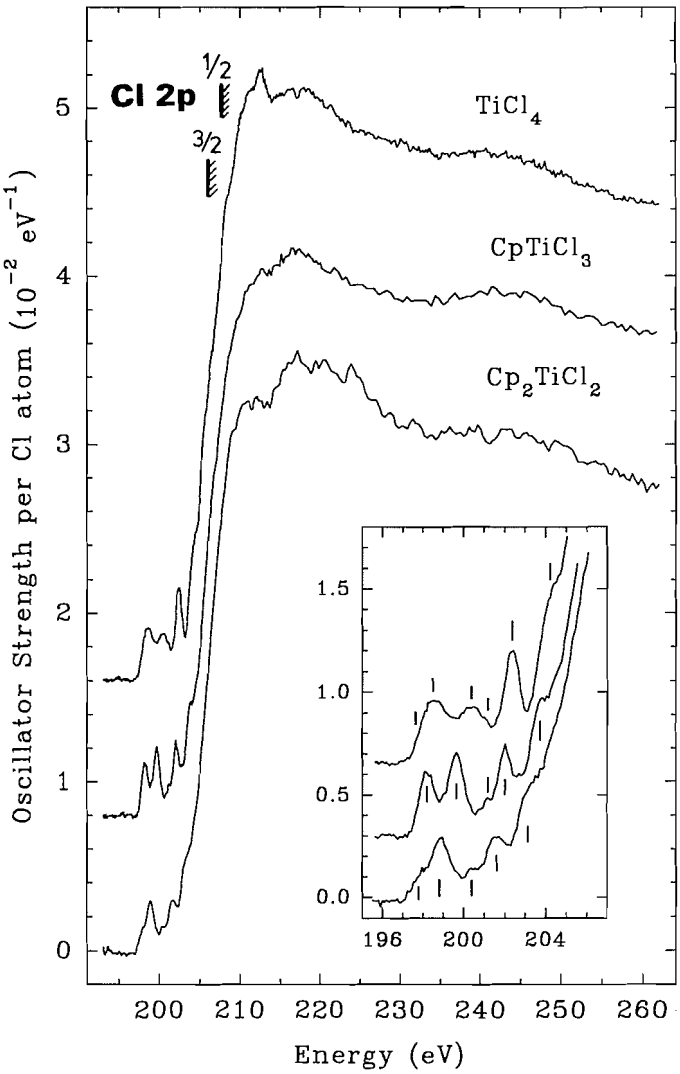

FIG. 4. Chlorine 2*p* oscillator strength spectra of $TiCl_4$, $CpTiCl_3$, and Cp_2TiCl_2 (presented on a per-Cl basis). See Fig. 2 for experimental details. The hatched lines indicate the estimated Cl 2*p* IPs. The $CpTiCl_3$ and $TiCl_4$ spectra have been offset vertically by 0.008 and 0.016 $(eV)^{-1}$ for clarity. The inset is an expansion of the pre-edge structure, plotted in the same order as the main plot.

Cl 2*p* spectra

The Cl 2*p* spectra of Cp_2TiCl_2, $CpTiCl_3$, and $TiCl_4$ are presented in Fig. 4 (on an oscillator-strength-per-Cl intensity scale), while an expansion of the weak pre-edge structure is presented as an insert. The hatched lines indicate the location of the Cl $2p_{3/2}$ and Cl $2p_{1/2}$ IPs. These have been measured for $TiCl_4$ (45) and are assumed to be the same in the other two compounds since Cl 2*p* IPs are not strong functions of the Cl environment (40). The energies, term values, and proposed assignments of the Cl 2*p* spectral features are listed in Table 3. The Cl 2*p* spectra of these three species are very similar, although there are minor variations in the pre-edge features, probably associated with the changing molecular symmetry. The similarity of these spectra is consistent with similar Ti—Cl bonding in all three compounds. Cl 3*s*/3*p* valence orbitals are completely filled in a Cl^- ligand so that core excitations to unoccupied valence

TABLE 3. Energies (E, eV), term values (T, eV), and proposed assignments for features in the Cl $2p$ spectra of $TiCl_4$, $CpTiCl_3$, and Cp_2TiCl_2

$TiCl_4$			$CpTiCl_3$			Cp_3TiCl_4			Assignment (final orbital)					
									$TiCl_4$		$CpTiCl_3$		Cp_2TiCl_2	
E	$T_{3/2}$	$T_{1/2}$	E	$T_{3/2}$	$T_{1/2}$	E	$T_{3/2}$	$T_{1/2}$	$2p_{3/2}$	$2p_{1/2}$	$2p_{3/2}$	$2p_{1/2}$	$2p_{3/2}$	$2p_{1/2}$
197.8	8.8					197.7	(8.9)		$2e$				$10a_1$	
198.5	8.1		198.2	8.4		198.8[a]	7.8		$4t_2$	$2e$	"t_{2g}"			$10a_1$
200.4	6.2	7.3	199.9	7.0	(8.1)	200.4	6.2	7.3		$4t_2$	"e_1"	"t_{2g}"	$9b_1$, $6a_2$	
201.2	5.4		201.2	5.4	6.5				$4s$		$4s$			
202.4[a]	4.2	5.3	202.0[a]	4.3	5.4	201.6	5.0	6.1	$3a_1$	$4s$	"$2a_{1g}$"	$4s$	Cl3d	$4s$
204.2		3.5	203.8		3.9	203.1		4.6		$3a_1^*$		"$2a_{1g}$"		Cl3d
206.6[b]			206.6[c]			206.6[c]			IP		IP		IP	
207.7[b]			207.7[c]			207.7[c]				IP		IP		IP
212.5	−5.3[d]		212.8	−5.6[d]		210.7	−3.5[d]		← double excitation →					
217	−10[d]		217	−10[d]		217	−10[d]		← delayed Cl $2p \rightarrow \epsilon d$ onset →					
240	−33[d]		240	−33[d]		240	−33[d]		← EXAFS →					

[a]Calibration: $TiCl_4$: −88.4(1) eV relative to CO_2 (C $1s \rightarrow \pi^*$: 290.74 eV); $CpTiCl_3$: −84.9(1) relative to C $1s \rightarrow \pi^*_{Cp}$; Cp_2TiCl_2: −89.0(1) eV relative to C $1s \rightarrow \pi^*_{Cp}$.
[b]IPs from XPS (40).
[c]IPs assumed to be the same as $TiCl_4$.
[d]Term value with respect to the mean Cl $2p_{3/2,1/2}$ IP (207.2 eV).

MOs are likely to be weak. Also, Cl $2p$ excitation samples the Cl $3s$ and Cl $3d$ character of the unoccupied MOs. This is likely to be small for low-lying unoccupied orbitals since the Cl $3s$ AOs contribute mostly to occupied MOs and the Cl $3d$ AOs are mostly involved in states above threshold rather than in the discrete structure. Both of these points explain the relatively weak character of the pre-edge structure in these Cl $2p$ spectra.

The first peak at 198.5 eV in $TiCl_4$ has a term value of more than 8 eV. This is a clear indication that the Cl $2p$ excited state has large valence character since the lowest energy Rydberg states have term values smaller than 6 eV. We assign this feature to Cl $2p \rightarrow (4t_2)$ transitions. Below this peak, there appears to be a weak shoulder around 197.8 eV, which is considered to be associated with Cl $2p \rightarrow 2e$ transitions. The 0.7 eV difference in energy between these two features is a measure of Δ_t for Cl $2p$-excited $TiCl_4$. This splitting is smaller than that found in the ground state (0.95 eV) (31). The lower value may be a consequence of differences in core hole relaxation in the two (Cl $2p^{-1}$, Ti $3d$) states. Based on the Cl $2p$ spin-orbit splitting in $TiCl_4$ (1.1 eV (45, 46)), the Cl $2p_{1/2} \rightarrow 4t_2/2e$(Ti $3d$) transitions are expected to occur under the high-energy side of the first band. The weak shoulder at 200.4 eV is attributed to Cl $2p_{3/2} \rightarrow 4s$ Rydberg transitions. The sharpest peak in the Cl $2p$ spectrum of $TiCl_4$ (202.4 eV) is assigned to Cl $2p_{3/2} \rightarrow 3a_1$ transitions, an MO derived mainly from Cl $3d$ orbitals. This feature also may contain contributions from Cl $2p_{1/2} \rightarrow$ Cl $4s$ transitions, the spin-orbit partner of the 200.4 eV feature. The large intensity is believed to be associated with the strong Cl $2p_{3/2} \rightarrow 3a_1$ resonance, as the $3d$ is usually much stronger than the $4s$ channel due to better spatial overlap. The corresponding Cl $2p_{1/2} \rightarrow 3a_1$ transition is likely the shoulder at 204.2 eV, which probably also contains other underlying Rydberg transitions and the leading edge of the Cl $2p$ continuum.

The pre-edge regions of the Cl $2p$ spectra of $CpTiCl_3$ and Cp_2TiCl_2 also exhibit particularly low-lying structures (those below 200 eV) that are attributed to Cl $2p$ excitations to the Cl $3d$ component of the low-lying "Ti $3d$" orbitals. The change from a well-structured doublet in $CpTiCl_3$ to a broader band in Cp_2TiCl_2 is similar to that observed for the first band in the C $1s$ spectra of these species and likely reflects the differences in molecular symmetry and thus Ti $3d$ splittings in these two compounds. The relatively sharp band around 202 eV seen in all three molecules is attributed primarily to Cl $2p \rightarrow 3d$ transitions.

Relative to $1s$ ionization, $2p$ ionization continua have a much more gentle rise at threshold. This is the result of a delayed onset for the dominant $2p \rightarrow \epsilon d$ ionization channel, which is associated with a centrifugal barrier. This atomic phenomenon is the cause of the broad maximum around 215 eV in the Cl $2p$ spectra. Weak structure superimposed on the top of this maximum may correspond to double excitations: monopole valence shell excitations that are a consequence of the large change in charge at the core excited Cl atom. The broad structure around 240 eV is attributed to an extended fine structure oscillation associated with backscattering by Cl or Ti. Similar broad features have been observed in the gas phase Cl $2p$ spectra of CH_xCl_{4-x} (x = 0–3) species, which has been analyzed as EXAFS (47).

Ti 2p spectra

The Ti $2p$ spectra of these three compounds are presented in Fig. 5. The hatched lines indicate the Ti $2p_{3/2}$ and $2p_{1/2}$ IPs. Those for $TiCl_4$ are taken from gas phase XPS (45). Those for Cp_2TiCl_2 are derived from its solid state IPs (48) by applying a correction of +7.1 eV, derived from XPS measurements of the Ti $2p$ IPs of gaseous and solid $TiCl_4$ (46). The Ti $2p$ IPs of $CpTiCl_3$ were determined by linear interpolation of the IPs of $TiCl_4$ and Cp_2TiCl_2. The energies, term values, and proposed assignments are listed in Table 4.

Each spectrum exhibits two main bands, with each band exhibiting a similar but not identical fine structure. The major splitting is associated with the Ti $2p_{3/2}$ (L_3) and $2p_{1/2}$ (L_2) spin-

Can. J. Chem. Downloaded from www.nrcresearchpress.com by 203.198.23.82 on 09/08/12
For personal use only.

Can. J. Chem. Downloaded from www.nrcresearchpress.com by 203.198.23.82 on 09/08/12
For personal use only.

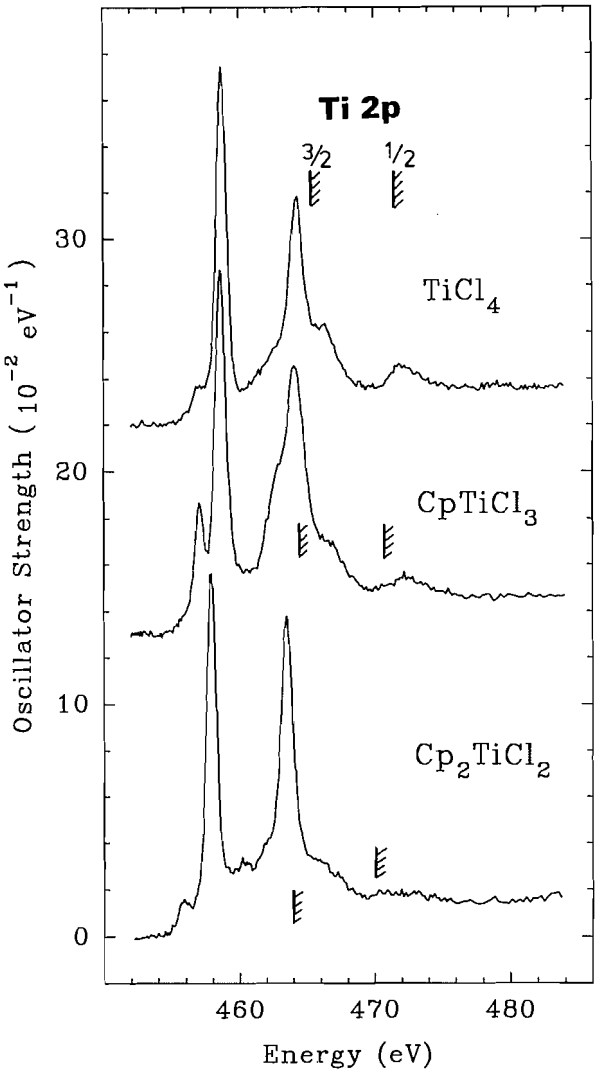

FIG. 5. Titanium 2*p* oscillator strength spectra of $TiCl_4$, $CpTiCl_3$, and Cp_2TiCl_2. The hatched lines indicated measured (45, 46, 48) or estimated Ti 2*p* IPs. See Fig. 2 for experimental details.

orbit splitting. The separation of the most intense L_3 and L_2 features is 5.6, 5.4, and 5.6 eV for $TiCl_4$, $CpTiCl_3$, and Cp_2TiCl_2, respectively. This is essentially the same L_3–L_2 splitting as observed in the Ti 2*p* X-ray absorption spectra of TiO_2 (5.5 eV (16, 49)) and $FeTiO_3$ (5.4 eV (16)). However, the excitation spin-orbit splitting is about 0.5 eV **smaller** than the spin-orbit splitting found in the XPS spectrum of $TiCl_4$ (6.1 eV (45, 46)). This difference may be associated with exchange interactions that modify the energies of the Ti 2*p* excited states (16).

Currently, there are two major theoretical models dealing with the electronic structures of transition metal complexes: the crystal field theory treating a perturbed metal atom or ion; and molecular orbital theory, which, when combined with a consideration of the crystal field splittings of the metal orbitals is denoted ligand field theory. Figure 6 presents the EHMO predictions for Ti 2*p* → 3*d* excitation in all three complexes. (Fig. 6*a*) and selected crystal field calculations for Ti^{4+} (15), in comparison with the experimental Ti 2*p* spectra. Each L_3 and L_2 band has two main components, with additional weaker structure. Within the atomic multiplet – crystal field picture (15) this splitting (e.g., that between the weak 457 eV and the much stronger 459 eV peak in $TiCl_4$) is associated with the crystal field splitting (Δ_t in $TiCl_4$) modified by a strong exchange interaction. The splittings in the Ti 2*p* experimental spectra are similar to those seen in other Ti compounds (e.g., TiO_2 (2.5 eV) (16, 49) and $FeTiO_3$ (2.2 eV) (16)) but they are larger than those found in the corresponding C 1*s* spectrum (0.8–0.9 eV) or those predicted by EHMO (0.7–1.4 eV for the ground state, and 1.0–2.1 eV for Ti 2*p* excitation). This is a clear indication of the strong coupling between crystal field and atomic multiplet (exchange) interactions in metal 2*p* excitation. Within the MO picture the separation is explained by the splitting of the "Ti 3*d*" MOs dictated by the symmetry of each compound. The splitting of the 3*d* orbitals in these three compounds is shown by the line diagrams in Fig. 6*a*, which indicate the energies and Ti 3*d* densities in the unoccupied orbitals of equivalent core species (e.g., VCl_4^+ for $TiCl_4$). The pattern in each case illustrates very clearly the preceding discussion of the lowest energy bands in the C 1*s* and Cl 2*p* spectra of these compounds: *e* lies below t_2 in $TiCl_4$; "t_{2g}" lies below "e_g" in $CpTiCl_3$ with smaller splittings of each orbital; and there are five relatively widely spaced orbitals of large 3*d* character in Cp_2TiCl_2. The assignments proposed in Table 4 are based on comparison with the EHMO calculations.

It is clear that the EHMO treatment is much less successful at describing the discrete portion of the Ti 2*p* spectra than it was at describing the C 1*s* spectra. In particular, the relative intensities of the lower and higher energy Ti 2*p* components are poorly reproduced. However, it is noteworthy that EHMO predicts that the lowest energy band of $CpTiCl_3$ should be more intense than in $TiCl_4$ or Cp_2TiCl_2. This is seen experimentally, although not to the extent that EHMO predicts. Since EHMO cannot explicitly treat the exchange interactions of atomic multiplet theory (15) it is not surprising there is only limited agreement with experiment.

One goal of investigating the core spectra of these complexes was to test the simple "π^*/σ^*" model for metal 2*p* spectra proposed earlier, based on an investigation of the metal 2*p* spectra of a series of largely covalent complexes (7). One of the predictions of that model was a continuous increase in the intensity of the lower energy "$d\pi^*$–$p\pi^*$" band relative to the higher energy "$d\sigma^*$–$p\sigma^*$" band as the number of Cp rings is increased. Clearly the experimental spectra do not show this effect. These comparisons indicate that both the simple "π^*/σ^*" model and conventional semiempirical MO treatments do not correctly account for some important interactions, such as the largely ionic ligand–metal interactions in these complexes.

Because of the dominant ionic character of these complexes the atomic multiplet – crystal field model (14–20) should be well suited to describing the Ti 2*p* spectra. If one assumes a completely ionic bonding description, their Ti 2*p* spectra should be compared to the crystal field analysis for (p^6, d^0) → (p^5, d^1) transitions in the appropriate symmetry (T_d for $TiCl_4$, O_h for $CpTiCl_3$, and C_{2v} for Cp_2TiCl_2). However, only results for cubic environments have been reported in the literature (15–17). There are significant differences between the appearance of the Ti 2*p* spectra in the two papers that report spectra for Ti^{4+} (15, 17), although similar calculational methods were used. The Ti L_2 features are much more intense than the corresponding L_3 features in the results reported by van der Laan and Kirkman

TABLE 4. Energies (E, eV), term values (T, eV), and proposed assignments for features in the Ti $2p$ spectra of $TiCl_4$, $CpTiCl_3$, and Cp_2TiCl_2

$TiCl_4$		$CpTiCl_3$		Cp_2TiCl_2		Assignment (final orbital)		
E	T	E	T	E	T	$TiCl_4$	$CpTiCl_3$	Cp_2TiCl_2
L_3								
456.9	8.5	457.0	7.7	455.8	8.2	$2e$	"t_{2g}"	$10a_1$
458.7[a]	6.7	458.6[a]	6.1	457.9[a]	6.1	$4t_2$	"e_g"	$9b_1$, $6a_2$, $8b_2$, $11a_1$
460.2	5.2	460.8	3.9	460.3	3.7			
465.4[b]		464.7[c]		464.0[c]		L_3 IP	L_3 IP	L_3 IP
466.5(5)	−0.8	467	−2	466	−2	← double excitation →		
L_2								
462.5	9.0	462.7	8.1	462.0	8.1	$2e$	"t_{2g}"	$10a_1$
464.3	7.2	464.0	6.8	463.5	6.6	$4t_2$	"e_g"	$9b_1$, $6a_2$, $8b_2$, $11a_1$
471.0[b]		471.0[c]		471.5[c]		L_2 IP	L_2 IP	L_2 IP
472.1	−0.6	472.4	−1.4	471.5(5)	−0.9	← double excitation →		

[a]Calibration: $TiCl_4$ +57.6(1) eV; $CpTiCl_3$: +57.5(1) eV; Cp_2TiCl_2: +56.8(2) relative to N $1s \rightarrow \pi^*$ in N_2 (401.1 eV).
[b]IPs from XPS (45).
[c]The Ti $2p$ IPs of Cp_2TiCl_2 were derived by adding the difference of the gas minus the solid IPs of $TiCl_4$ (7.1 eV (46)) to the IPs of solid Cp_2TiCl_2 (48). The IPs of $CpTiCl_3$ were obtained by interpolation, assuming a linear chemical shift with number of Cl atoms.

(17) compared to the results of de Groot et al. (15). The differences appear to be related to a less complete treatment of the line broadening effects in ref. 17. Since the Ti $2p$ spectra predicted for octahedral and tetrahedral fields are virtually identical for the same magnitude of crystal field parameter (17) and since the L_3:L_2 intensity ratios and relative line widths in the calculations of de Groot et al. (15) are more similar to our experimental results, we have chosen to compare our $TiCl_4$ and $CpTiCl_3$ spectra with the (Ti^{4+} in O_h) results of de Groot et al. (15). Also, since there are no results available for (Ti^{4+} in C_{2v}), we have used the (Ti^{4+} in O_h) results as a very crude first-order comparison to the Ti $2p$ spectrum of Cp_2TiCl_2.

De Groot et al. (15) report a series of spectra calculated for different crystal field strengths. We have selected the spectra that most closely match the experimental results, namely Δ_0 = 1.0, 1.2, and 1.0 eV for $TiCl_4$, $CpTiCl_3$, and Cp_2TiCl_2, respectively. These literature spectra are compared with experiment (Fig. 6*b*) after shifting the calculated energy scales by 6.5, 6.8, and 7.2 eV and scaling the intensity for best match. The chosen energy shifts are smaller but in the same sense as the Ti $2p$ chemical shifts (45, 46, 48). The decrease in the Ti $2p$ orbital energy is probably the main factor governing the shift of the main L_3 spectral feature from 456.9 eV in $TiCl_4$ down to 455.8 eV in Cp_2TiCl_2. Since IPs and excitation energies differ systematically due to differences in core hole screening, it is reasonable to postulate experimental–theory shifts in this series of compounds that differ from their Ti $2p$ chemical shifts.

As Fig. 6*b* shows, there is good agreement between the crystal field – atomic multiplet prediction and experiment for $TiCl_4$ although the intensity of the L_2 signal relative to the L_3 signal is overestimated. We note that this discrepancy would be at least a factor of two worse if we had chosen to compare with the (Ti^{4+} in T_d) results of van der Laan and Kirkman (17) even though the energy pattern is very similar. Similarly the de Groot et al. (15) prediction for the Ti $2p$ spectrum of a Ti^{4+} ion with Δ_0 = 1.2 eV is in good agreement with the Ti $2p$ spectrum of $CpTiCl_3$. In particular, increasing the crystal field parameter increases the intensity of the first band ("t_{2g}") relative to the second ("e_g"), the major change between the spectra of $TiCl_4$ and $CpTiCl_3$. The spectrum of Cp_2TiCl_2 should not be expected to be well reproduced by any of the calculations for Ti^{4+} in O_h since the symmetry of the crystal field plays a major role in determining the spectral shape. Thus it is not surprising that the best match to the O_h predictions is significantly worse for Cp_2TiCl_2 than for the other two compounds. However, we interpret the reduction in intensity of the first band relative to the second as an indication of a lower effective crystal field in Cp_2TiCl_2 than in $CpTiCl_3$, consistent with the much larger Ti—Cl bond length (Table 1). This interpretation is supported by the need to select a calculated spectrum with a lower Δ_0 value to find the best possible match to Cp_2TiCl_2.

Another possibility is that the Ti $2p$ spectra of the Cp complexes should be compared with calculations for Ti^{3+} or even Ti^{2+}, if one emphasizes a more covalent description of the Ti—Cp bond. The atomic multiplet – crystal field calculations (16, 17) indicate that a much more complex spectrum covering a wider spectral region would be expected on account of the greater number of states associated with (p^5, d^2) or (p^5, d^3) configurations than with the (p^5, d^1) configuration. Based on the relatively simple appearance of the measured spectra we do not believe a description based on Ti^{3+} or Ti^{2+} is appropriate. Thus the Ti $2p$ spectra support an ionic bonding model for all three complexes. Interestingly, based on PES and MO calculations Bruce et al. (50) have suggested that permethylation of the Cp rings in Cp_2TiCl_2 gives rise to an effective one-electron reduction. Observation of a Ti $2p$ spectrum of $Cp^*_2TiCl_2$ ($Cp^* = \eta^5$-$C^5(CH_3)_5$), which was significantly more complex than that of Cp_2TiCl_2, would be evidence in favour of this suggestion.

The relatively small difference in the crystal field values deduced from matching the experimental and calculated spectra supports the idea that Cl and Cp ligands generate a comparable ligand field. The peak separations in the experimental Ti $2p$ spectra are 1.8, 1.9, and 2.1 eV in $TiCl_4$, $CpTiCl_3$, and Cp_2TiCl_2, respectively. This is about 50% larger than the crystal field parameter estimated from the best match

Can. J. Chem. Downloaded from www.nrcresearchpress.com by 203.198.23.82 on 09/08/12
For personal use only.

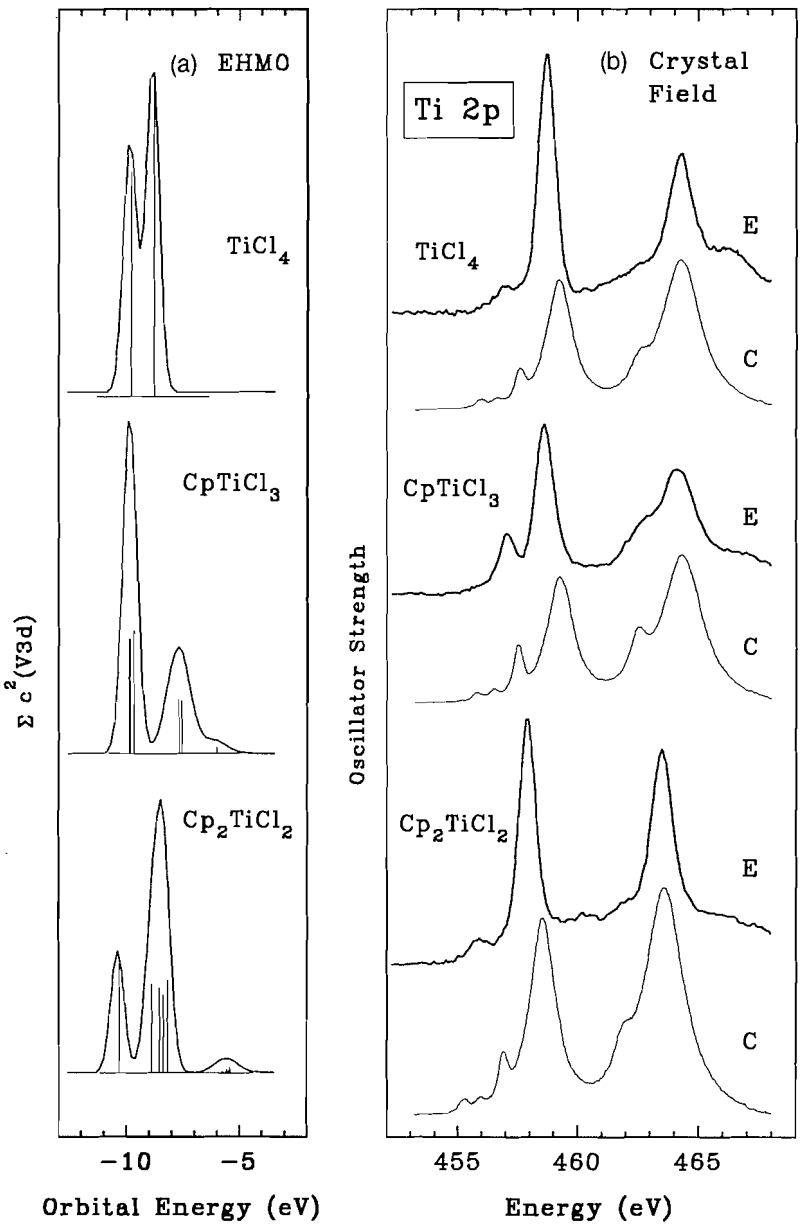

FIG. 6. (*a*) EHMO calculation of the Ti $2p \rightarrow 3d$ transitions in $TiCl_4$, $CpTiCl_3$, and Cp_2TiCl_2. (*b*) Expanded presentation of the Ti $2p$ structure compared to crystal field calculations (15) (E = experimental, C = calculated).

to the crystal field calculations. The difference arises from the complex interplay of crystal field and exchange terms (15). Due to their spatial localization, the exchange interactions are much stronger in the Ti $2p$ than the C $1s$ or Cl $2p$ states. This is consistent with the larger crystal-field-related splitting in the Ti $2p$ than in the C $1s$ or Cl $2p$ spectra. Core hole relaxation, i.e., interaction between the core hole and the valence electrons, particularly the excited electron in the upper orbital of the transition, could also have a very large effect on the Ti $2p$ spectrum since Ti $3d$ orbitals are very much localized on the Ti atom.

While the major features of the Ti $2p$ spectra are reproduced by the atomic multiplet – crystal field calculations (at least for the two cases where appropriate symmetry results are available), there are some experimental features that are not predicted, in particular, the broad maxima at 467 and 472 eV (see Fig. 5). Based on their similar appearance, these features are believed to have a common origin in all three species. They are considered to be monopole shake-up excitations in which a valence $\rightarrow$ valence transition accompanies the main $2p_{3/2} \rightarrow 3d$ and $2p_{1/2} \rightarrow 3d$ transitions. Strong shake-up satellites occur at 9.5 eV above the main line in the Ti $2p$ photoelectron spectrum of $TiCl_4$ (45, 46). In the Ti $2p$ excitation spectrum the shake-up separation ranges from 7.8 to 8.4 eV, depending on the compound (see Table 4). Ligand-to-metal charge transfer transitions, which stabilize the localized Ti core hole, have been proposed to explain the XPS shake-up satellites (45, 46, 51) and are generally considered to be an important aspect of the electronic structure of ionic $3d$ transition metal compounds (52). Ligand-to-metal charge transfers may also be involved in the double excitation features at 467 and 472 eV in these Ti $2p$ excitation spectra. However, Van de Laan (53) has studied similar structures in the Ti $2p$ X-ray absorption spectra of TiO_2 and

Can. J. Chem. Downloaded from www.nrcresearchpress.com by 203.198.23.82 on 09/08/12
For personal use only.

Can. J. Chem. Downloaded from www.nrcresearchpress.com by 203.198.23.82 on 09/08/12
For personal use only.

$SrTiO_3$ and argues that the features are better considered as polaron transitions: ligand–ligand excitations that distort the ligand charge distribution in a way that screens the core excited atom by polarization.

If one assumes that ligand–metal charge transfer is involved, $1e(Cl) \rightarrow 2e^*(Ti)$ and $3t_2(Cl) \rightarrow 4t_2^*(Ti)$ transitions are possible candidates for explaining the double excitations in $TiCl_4$. The EHMO calculation for the Ti excited state predicts that the gap between the occupied and unoccupied e MOs is ca. 4.6 eV, slightly lower than that of the two t_2 MOs (4.8 eV). Thus the 467 eV shake-up feature in $TiCl_4$, 7.8 eV above the main Ti $2p_{3/2} \rightarrow 3d$ feature, is attributed to $t_2 \rightarrow t_2^*$ transitions. A similar assignment was given by Wallbank et al. (45) for the shake-up features in the XPS spectra of $TiCl_4$. The interpretation of these bands in $CpTiCl_3$ follows similar reasoning. Two possible monopole charge transfer transitions are the "e_g" (Cl) → "e_g" (Ti 3d) and "t_{2g}" (Cl) → "t_{2g}" (Ti 3d) shake-up excitations. According to the EHMO calculation for the Ti 2p excited state, there is an occupied "e_g" MO at −15.1 eV that is constructed almost solely of Cl 3p orbitals. The separation of the occupied and unoccupied "e_g" MOs is 5.5 eV, a reasonably close match to the 7.5 eV separation between the 467 eV shake-up band and the main $2p_{3/2} \rightarrow$ Ti 3d line. The occupied "t_{2g}" MO ($\epsilon = -15.3$ eV) derives mainly from the Cl 3p orbitals but also has a sizable Ti 3d component. The energy separation of the occupied and unoccupied "t_{2g}" MOs is only 4.7 eV. Based on the better energy match, we prefer to assign the 467 eV feature to "e_g" (Cl) → "e_g" (Ti) monopole shake-up transitions accompanying the main Ti $2p_{3/2} \rightarrow 3d$ excitation. This interpretation is supported by Larsson's studies (54) on the octahedral species TiO_6^{8-} and TiF_6^{2-}. We note that the intensity of the 467 eV feature decreases systematically with the decreasing number of Cl ligands in this series of molecules. This is consistent with our assignment of this feature to a Cl → Ti charge transfer monopole excitation. However, it would also be consistent with van der Laan's polaron proposal (53) if ligand–ligand excitations at Cl are involved.

The relative intensity of corresponding L_3 ($2p_{3/2}$) and L_2 ($2p_{1/2}$) features in $CpTiCl_3$ and Cp_2TiCl_2 is about 1:1, much smaller than the 2:1 value associated with the degeneracy of $^2P_{3/2}$ and $^2P_{1/2}$ ion states. Even so, the L_3/L_2 intensity ratio in these Ti species is larger than that in Ti and TiO_2 (49). Exchange interactions and differences in core hole relaxation effects are believed to be the origin of the nonstatistical intensity ratios (18, 49). The L_2 transitions are broader than the corresponding L_3 transitions. This increased breadth reflects a shorter lifetime and increased natural linewidth, associated with additional L_2L_3M super-Coster–Kronig decay channels that are available to L_2 excited states (55). De Groot et al. (15) discussed this effect and have included it in their predictions of Ti 2p spectra in cubic environments. For L_2L_3M super-Coster–Kronig decay to occur, the difference between the $L_2(2p_{1/2})$ and L_3 ($2p_{3/2}$) core hole energy must be larger than the binding energy of the d electron (56). Thus the probability of super-Coster–Kronig decay depends on the M-shell (valence) energetics and therefore on the crystal field splitting. The increased L_2 linewidth is most evident in the Ti 2p spectrum of $CpTiCl_3$ and less so in the other two species. This observation is consistent with our interpretation that the crystal field is largest in $CpTiCl_3$.

Summary

The C 1s, Cl 2p, and Ti 2p inner shell spectra of Cp_2TiCl_2, $CpTiCl_3$, and $TiCl_4$ have been interpreted with the aid of EHMO calculations and comparison with literature atomic multiplet – crystal field calculations for $2p^63d^0 \rightarrow 2p^53d^1$ excitations in Ti^{4+}. The results support a strongly ionic character for the metal–ligand bonds in these compounds. Analysis of the Ti 2p spectra indicates that the crystal fields of $TiCl_4$ and Cp_2TiCl_2 are rather similar whereas that of $CpTiCl_3$ is larger. The spectral splittings associated with the crystal field are found to differ in the C 1s, Cl 2p, and Ti 2p spectra, because of the influence of exchange interactions and possible differences in core hole relaxation effects. The ability to detect crystal-field-related splittings in the ligand core excitation spectra has also been documented recently in a study of the N 1s spectra of TiN and N implanted into Ti (57). Relatively strong multi-electron excitations are identified in the Ti 2p spectra of all three compounds studied. The Ti 2p spectra do not support the simple "π^*/σ^*" model proposed earlier (7). Overall, the core excitation spectra of these three compounds display many similarities. This is consistent with the similar strength of the Ti—Cp and Ti—Cl bonds and the assumption commonly made in discussions of these compounds that Ti—Cp and Ti—Cl are roughly exchangeable, at least until steric hindrance becomes a factor (58).

Acknowledgements

This research was supported financially by the Natural Sciences and Engineering Research Council of Canada.

1. J. Stöhr. NEXAFS spectroscopy. Springer, Berlin. 1992.
2. (*a*) A.P. Hitchcock. Phys. Scr. T, **31**, 159 (1990); (*b*) Proc. Escola Latino-Americana de Fisica. World Sci. Publ. Co., Singapore. 1992. p. 104; (*c*) J. Electron Spectrosc. **25**, 245 (1982); (*d*) A.P. Hitchcock and D.C. Mancini. J. Electron Spectrosc. In press.
3. E. Rühl, and A.P. Hitchcock. J. Am. Chem. Soc. **111**, 2614 (1989).
4. G. Cooper, K.H. Sze, and C.E. Brion. J. Am. Chem. Soc. **111**, 5051 (1989).
5. E. Rühl and A.P. Hitchcock. J. Am. Chem. Soc. **111**, 5069 (1989).
6. A.P. Hitchcock, A.T. Wen, and E. Rühl. J. Electron Spectrosc. **51**, 653 (1990).
7. A.P. Hitchcock, A.T. Wen, and E. Rühl. Chem. Phys. **147**, 51 (1990).
8. E. Rühl, A.T. Wen, and A.P. Hitchcock, J. Electron Spectrosc. **57**, 137 (1991).
9. G. Cooper, K.H. Sze, and C.E. Brion. J. Am. Chem. Soc. **112**, 4121 (1990).
10. A.T. Wen, A.P. Hitchcock, and E. Rühl. Organometallics, **11**, 2559 (1992).
11. H. Kopf and P. Kopf-Meier. Angew. Chem. Int. Ed. Engl. **18**, 477 (1979); K.M. Petra and H. Kopf. J. Organomet. Chem. **342**, 167 (1988); P. Kopf-Meier and H. Kopf. Drugs Future, **11**, 297 (1986).
12. N. Ram, M. Verloo, and A. Cottenic. Acta Agron. Hung. **37**, 43 (1988).
13. P. Decleva, G. Fronzoni, and A. Lisini. Chem. Phys. **168**, 51 (1992).
14. F.M.F. de Groot, M. Grioni, J.C. Fuggle, J. Ghijsen, G.A. Sawatzky, and H. Petersen. Phys. Rev. B, **40**, 5715 (1989).
15. M.F. de Groot, J.C. Fuggle, B.T. Thole, and G.A. Sawatzky. Phys. Rev. B, **41**, 928 (1990).
16. M.F. de Groot, J.C. Fuggle, B.T. Thole, and G.A. Sawatzky. Phys. Rev. B, **42**, 5459 (1990).

17. G. Van der Laan and I.W. Kirkman. J. Phys. Condens. Matter, **4**, 4189 (1992).
18. J. Fink, Th. Müller-Heinzerling, B. Scheerer, W. Speier, F.U. Hillebrecht, J.C. Fuggle, J. Zaanen, and G.A. Sawatzky. Phys. Rev. B, **32**, 4899 (1985); J. Zaanen, G.A. Sawatzky, J. Fink, W. Speier, and J.C. Fuggle. Phys. Rev. B, **32**, 4905 (1985).
19. C.T. Chen and F. Sette. Phys. Scr. T, **31**, 119 (1990).
20. S.P. Cramer, F.M.F. de Groot, Y. Ma, C.T. Chen, F. Sette, C.A. Kipke, D.M. Eichhorn, M.K. Chan, W.H. Armstrong, E. Libby, G. Christou, S. Brooker, V. McKee, O.C. Mullins, and J.C. Fuggle. J. Am. Chem. Soc. **113**, 7937 (1991).
21. R. McLaren, S.A.C. Clark, I. Ishii, and A.P. Hitchcock. Phys. Rev. A, **36**, 1683 (1987).
22. A.P. Hitchcock, S.G. Urquhart, and E.G. Rightor. J. Phys. Chem. **96**, 8736 (1992).
23. (*a*) Y. Morin and H. Uehara. J. Chem. Phys. **45**, 4543 (1966); (*b*) J.L. Calderon, F. A. Colter, B.G. DeBoer, and J.J. Takats. J. Chem. Soc. **93**, 3592 (1981).
24. L.M. Engelhardt, R.I. Papasergio, C.L. Raston, and A.H. White. Organometallics, **3**, 18 (1984).
25. A. Clearwater, D.K. Warner, C.H. Saldarriaga-Molina, R. Ropal, and I. Bernal. Can. J. Chem. **53**, 1622 (1975).
26. W.H.E. Schwarz. Chem. Phys. **11**, 217 (1975).
27. I. Ishii, and A.P. Hitchcock. J. Chem. Phys. **87**, 830 (1987).
28. J.T. Francis and A.P. Hitchcock. J. Phys. Chem. **96**, 6598 (1992).
29. A.P. Hitchcock, M.J. McGlinchey, A.L. Johnson, W.K. Walter, M. Perez Jigato, D.A. King, D.L. Norman, E. Rühl, C. Heinzel, and H. Baumgärtel. Trans. Faraday Soc. In press.
30. (*a*) C.A.L. Becker, C.J. Ballhausen, and I. Trabjerg. Theor. Chim. Acta, **13**, 355 (1969); (*b*) C.A.L. Becker, and J.P. Dahl. Theor. Chim. Acta, **14**, 26 (1969).
31. R.F. Fenske and D.D. Radtke. Inorg. Chem. **7**, 479 (1968), and refs. therein.
32. T.A. Albright, J.K. Burdett, and M.H. Whangbo. Orbital interactions in chemistry. Wiley, New York. 1985, pp. 280, 381.
33. C. Dijkgraaf and J.P.G. Rousseau. Spectrochem. Acta, **25A**, 1831 (1969).
34. J.C. Green, M.L.H. Green, P.J. Joachim, A.F. Orchard, and D.W. Turner. Philos. Trans. Rev. Soc. London, A: **268**, 111, (1970).
35. M.B. Robin. Higher excited states of polyatomic molecules. Vol. 2. Academic Press, New York. 1975. p. 277.
36. (*a*) J.L. Petersen, D.L. Lichtenberger, R.F. Fenske, and L.F. Dahl. J. Am. Chem. Soc. **97**, 6433 (1985); (*b*) M.R.M. Bruce, A. Kenter, and D.R. Tyler. J. Am. Chem. Soc. **106**, 639 (1984).
37. V.I. Tel'noi, I.B. Rabinovich, V.D. Tikhonov, V.N. Latyaeva, L.I. Vyshinskaya, and G.A. Razuvaev. Dokl. Chem. Engl. Trans. **174**, 467 (1967).
38. M. Basso-Bert, P. Cassoux, F. Crasnier, D. Gervais, J.-F. Labarre, and P. de Loth. J. Organomet. Chem. **136**, 201 (1977); A. Terpstra, J.N. Louwen, A. Oskam, and J.H. Teuben. J. Organomet. Chem. **260**, 207 (1984).
39. C. Cauletti, J.P. Clark, J.C. Green, I.L. Fragala, E. Cilberto, and A.W. Coleman. J. Electron Spectrosc. **18**, 61 (1980).
40. W.L. Jolly, K.D. Bomben, and C.J. Eyermann. At. Data Nucl. Data Tables, **31**, 433 (1984).
41. J. Stöhr, D.A. Outka, K. Baberschke, D. Arvanitis, and J.A. Horsley. Phys. Rev. B, **36**, 2976 (1987).
42. J.A. Horsley, J. Stöhr, A.P. Hitchcock, D.C. Newbury, A.L. Johnson, and F. Sette. J. Chem. Phys. **83**, 6099 (1985).
43. A.P. Hitchcock, P. Fischer, A. Gedanken, and M.B. Robin. J. Phys. Chem. **91**, 531 (1987).
44. A.F. Reid, D.E. Scaife, and P.C. Wailes. Spectrochim. Acta, **20**, 1257, (1964).
45. B. Wallbank, J.S.H.Q. Perera, D.C. Frost, and C.A. McDowell. J. Chem. Phys. **69**, 5405 (1978).
46. C. Mousty-Desbuqoit, J. Riga, and J.J. Verbist. J. Chem. Phys. **79**, 26 (1983).
47. A.P. Hitchcock and C.E. Brion. J. Electron Spectrosc. **14**, 417 (1978).
48. P.G. Gassman, D.W. Macomber, and J.W. Hershberger. Organometallics, **2**, 1470 (1983).
49. R.D. Leapman, L.A. Grunes, and P.L. Fejes. Phys. Rev. B, **26**, 614 (1982); L.A. Grunes, R.D. Leapman, C.N. Wilker, R. Hoffmann, and A.B. Kunz. Phys. Rev. B, **25**, 7157 (1982).
50. M.R.M. Bruce, A. Sclafani, and D.R. Tyler. Inorg. Chem. **25**, 2546 (1986).
51. (*a*) J.A. Tossell. J. Electron Spectrosc. **8**, 1 (1976); (*b*) J. Electron Spectrosc. **10**, 169 (1977); (*c*) A. Gupta and J.A. Tossell. J. Electron Spectrosc. **26**, 223 (1982).
52. A. Fujimori, A.E. Bocquet, T. Saitoh, and T. Mizokawa. J. Electron Spectrosc. **62**, 141 (1993).
53. G. Van der Laan. Phys. Rev. B, **41**, 12366 (1990).
54. (*a*) S. Larsson. J. Electron Spectrosc. **8**, 171 (1976); (*b*) M. Braga and S. Larsson. Int. J. Quantum Chem. Symp. **11**, 61 (1977).
55. D.M. Pease. Phys. Rev. B, **44**, 6708 (1991).
56. O. Keski-Rahkonen and M.O. Krause. At. Data Nucl. Data Tables, **14**, 139 (1974).
57. L. Soriano, M. Abbate, J.C. Fuggle, C. Jiménez, J.M. Sanz, L. Galan, C. Mythen, and H.A. Padmore. Surf. Sci. **281**, 120 (1983); L. Soriano, M. Abbate, H. Pen, M.I. Czyzyk, and J.C. Fuggle. J. Electron Spectrosc. **62**, 197 (1993).
58. L.M. Hansen and D.S. Marynick. Organometallics, **8**, 2173 (1989).

Can. J. Chem. Downloaded from www.nrcresearchpress.com by 203.198.23.82 on 09/08/12
For personal use only.

High-resolution spectroscopy with a CCD array detector: application to the 2880 Å emission band system in I_2

JOEL TELLINGHUISEN
Department of Chemistry, Vanderbilt University, Nashville, TN 37235 U.S.A.

Received May 19, 1993

This paper is dedicated to Professor Gerald W. King on the occasion of his 65th birthday

JOEL TELLINGHUISEN. Can. J. Chem. **71**, 1645 (1993).

The 2880 Å system in the Tesla discharge spectrum of I_2 in Ar is reexamined using a CCD array detector to record spectra for both $^{127}I_2$ and $^{129}I_2$. This charge-transfer transition terminates on a weakly bound valence state, giving a highly congested spectrum with fine violet-degraded band structure barely perceivable on a pseudocontinuous background. The superior signal-to-noise capabilities of the array detector permit a great improvement in the precision and number of measured bandheads, as compared with previous results obtained from photographically recorded spectra. The new data span a larger range of vibrational levels in the lower state and lead to a change in the previous v'' numbering by -3 units. Both states can now be located precisely on the absolute energy axis through least-squares fits in which the lower state energy is represented as a near-dissociation expansion. The primary spectroscopic constants (cm^{-1}) are $T_e' = 47\,084$, $\omega_e' = 103.93$, $\omega_e x_e' = 0.14$, $T_e'' = 12\,260$, $\omega_e'' = 18.6$, $\omega_e x_e'' = 0.21$. The lower state has a dissociation energy of 287.5 cm^{-1} and supports 35 bound levels, subject, however, to possible further revision due to a remaining uncertainty of 1 unit in the v'' numbering. The previous tentative electronic assignment of this system remains in effect: The upper state is likely the 0_g^- state that correlates with $I^-(^1S) + I^+(^3P_1)$, while the lower state is the 0_u^- component of the lowest valence $^3\Pi_u$ multiplet.

JOEL TELLINGHUISEN. Can. J. Chem. **71**, 1645 (1993).

Utilisant un détecteur CCD qui permet d'enregistrer simultanément les spectres du $^{127}I_2$ et du $^{129}I_2$, on a réexaminé le système à 2880 Å du spectre de décharge Tesla de I_2 dans l'argon. Cette transition de transfert de charge se termine sur un état de valence faiblement lié résultant en un spectre d'une grande congestion dans lequel la structure fine de la bande violet dégradé est à peine perceptible dans un bruit de fond pseudocontinu. Les capacités supérieures signal à bruit du détecteur utilisé permettent d'obtenir une grande amélioration de la précision et du nombre de bandes mesurées par rapport aux résultats obtenus antérieurement à l'aide de spectres obtenus photographiquement. Les nouvelles données recouvrent un domaine plus étendus de niveaux vibrationnels de l'état le plus bas et elles amènent un changement de -3 unités dans la numérotation antérieure de v''. Faisant appel à la méthode des moindres carrés dans laquelle l'énergie de l'état le plus bas est représenté comme une expansion près de la dissociation, on peut maintenant localiser avec précision les deux états sur l'axe d'énergie absolue. Les constantes spectroscopiques primaires (cm^{-1}) sont les suivantes : $T_e' = 47\,084$, $\omega_e' = 103{,}93$, $\omega_e x_e' = 0{,}14$, $T_e'' = 12\,260$, $\omega_e'' = 18{,}6$, $\omega_e x_e'' = 0{,}21$. L'énergie de dissociation de l'état le plus bas est égale à 287,5 cm^{-1} et elle supporte 35 niveaux de liaison; cette évaluation est toutefois sujette à des révisions ultérieures à cause d'une incertitude résiduelle d'une unité dans la numérotation de v''. Les attributions électroniques antérieures de ce système ne sont pas changées : l'état le plus élevé est vraisemblablement l'état 0_g^- qui est relié avec $I^-(^1S) + I^+(^3P_1)$ alors que l'état le plus bas est la composante 0_u^- du multiplet $^3\Pi_u$ de la valence la plus basse.

[Traduit par la rédaction]

Introduction

Prior to 1970 the spectroscopy of the diatomic halogens was remarkably sketchy. Iodine was perhaps the most studied of this group; yet by the time of Mulliken's landmark review in 1971 (1), only two electronic states of this molecule, $X^1\Sigma_g^+$ and $B\ 0_u^+(^3\Pi)$, could be claimed to have been determined definitively. Fragmentary vibrational analyses existed for several additional states observed in both absorption and emission studies. However, as later work would demonstrate, most of the band systems recorded and described by various authors during the previous half century had been incorrectly interpreted. This was particularly true of the rich UV–visible emission spectrum, for which only two electronic transitions, $F\ 0_u^+ \rightarrow X$ and $E\ 0_g^+ \rightarrow B$, had been correctly interpreted as ion-pair → valence charge-transfer systems, and those based on vibrational assignments spanning only limited regions of v in the excited states. The situation was scarcely better in any of the other homo- or heteronuclear halogens.

In the 1970s the halogens gained prominence, both as targets of new experiments made feasible by the advent of narrow-band fixed-frequency and tunable lasers, and as lasants themselves in high-pressure discharges (2, 3). Among the players in the former arena was Gerry King, who with his research colleagues published ground-breaking papers on the high-resolution multiphoton excitation of ion-pair electronic states in I_2 (4–6). About the same time I published a new interpretation of the strong emission band systems responsible for the lasing in I_2 and Br_2 (7), according to which the emission in both molecules originated from the lowest 2_g ion-pair state and terminated on the first excited valence state, 2_u ($^3\Pi$), neither of which had been identified previously for either molecule. For I_2 this interpretation placed the upper 2_g state right in the region of the five ion-pair states analyzed by King's group; yet symmetry considerations and spectroscopic constants seemed to imply that it was distinct from the King five. This was the beginning of a string of halogen spectroscopy puzzles that prompted a number of fruitful exchanges of preprints, letters, and phone conversations between Gerry King and myself.

One of the more enduring of these puzzles was the question of precisely where the various ion-pair states lay in I_2. Mulliken had shown the lowest group of six Hund's case c states beginning around 33 000 cm^{-1} above the ground state. Within four years of King's initial multiphoton study, three other groups had interpreted multiphoton ionization experi-

Can. J. Chem. Downloaded from www.nrcresearchpress.com by 203.198.23.82 on 09/08/12
For personal use only.

Can. J. Chem. Downloaded from www.nrcresearchpress.com by 203.198.23.82 on 09/08/12
For personal use only.

ments in terms of ion-pair states lying in precisely this region. Yet the properties of the high-pressure emission spectra suggested that the lasing transition, now know as $D' \rightarrow A'$, resulted from a pooling of deposited energy in the D' state, which could be most easily understood if D' were the lowest member of its cluster of states, and if this cluster were the lowest of all, correlating ionically with $I^- + I^+(^3P_2)$. My group discussed this problem in 1980 and again in 1983 (8, 9). Interestingly, the work that appears to "put the last nail in this coffin" has come again from King's lab (10): He and McLean showed recently that those studies which found states below 40 000 cm^{-1} suffered from photon miscounting, and were actually not 2-photon but 3-photon (1 + 2) excitations, $F\ 0_u^+ \leftarrow B \leftarrow X$ and $F'\ 0_u^+ \leftarrow B \leftarrow X$, to ion-pair states correlating with $I^+(^3P_0)$ and $I^+(^1D)$, respectively.

In the last 15 years the state of knowledge of halogen spectroscopy has been vastly improved, mainly through the efforts of half a dozen groups employing laser techniques resembling those utilized in King's pioneering studies (11). The obvious advantage of such techniques is the simplicity of interpreting the resulting sparse spectral patterns; by contrast the problem of spectral congestion is particularly severe for conventional emission spectra of the halogens because of their large reduced masses. Yet some of the electronic states responsible for features in the high-pressure halogen discharge spectra have remained inaccessible to such multiple laser methods, meaning emission spectroscopy is still the only game to play with them. For the most part the D'–A' systems qualify as cases in point. Another example is the narrow band system with peak intensity near 2880 Å in the Tesla discharge spectrum of I_2 in Ar, which was the main subject of the aforementioned 1983 paper from my group (9).

In fact, the 2880 Å system in I_2 is a particularly extreme example of spectral congestion. In peak emission intensity, this system is second only to the $D' \rightarrow A'$ system (8), so not surprisingly it had been reported in prior work dating back at least to 1940. Yet our 1980 study was the first to note the presence of fine violet-degraded band structure, a dead giveaway that this system involved a weakly bound lower state. To extract the bandhead measurements reported in our 1983 paper (9), we had to push the limits of photographic technology: Since the heads could not be readily perceived on an optical comparator or on densitometer traces, we resorted to high-contrast positive enlargements, which permitted better visual interpretation than was possible at the low signal-to-noise level of the one-dimensional comparator and densitometer spectra. It is largely for this reason that I have selected this case to test the capabilities of the technology that seems destined to supplant the photographic emulsion in image recording — the charge-coupled device (CCD) array detector.

Using a commercially available CCD array detector having square pixels 25 μm on a side, I have rerecorded the 2880 Å system of I_2 for both $^{127}I_2$ and $^{129}I_2$. This pixel width is more than two times greater than the best physical resolution achievable with our spectrometer using photographic recording. Still, the results of the present study are very optimistic for the future of such detectors in application to congested spectra. As compared with the photographically recorded 1983 spectra, I have doubled the number of assigned bands while halving the standard deviation in the least-squares analysis of these bands. This improvement has removed the relative numbering ambiguity that prompted us to allow for an alternative assignment in the 1983 analysis, and it has reduced the uncertainty in the absolute numbering of the lower state from four units to one. The best guess for the electronic assignment of this system remains as given in 1983: $0_g^-(^3P_1) \rightarrow 0_u^-(^3\Pi)$, where the origin belongs to the second ion-pair cluster and the terminus is a member of the lowest $^3\Pi_u$ multiplet, having molecular orbital designation 2431 (1).

Experimental

Spectra were recorded using Tesla discharge emission sources, spectroscopic equipment, and procedures like those employed in the previous study (9) with only minor modifications, except for the substitution of a CCD array detector for the photographic plates. The sources contained excess $^{127}I_2$ or $^{129}I_2$ and 200–800 Torr Ar (1 Torr = 133.3 Pa) and were operated in open air. (The Dry Ice cooling that was used to bring out some weak heads in the 1983 work was not necessary here.) Atomic calibration spectra were obtained from microwave discharge Fe/I_2 lamps; wavelengths were taken from Crosswhite (12). The spectrometer was a Jobin–Yvon HR1500 1.5-m instrument equipped with a 3600-groove/mm holographic grating (1.55 Å/mm reciprocal dispersion near 2880 Å). Exposures were typically 20 s for the Fe calibration spectra (5 μm slit width), and 50–500 s for the I_2 spectra (20–500 μm slit widths).

The detector was a Photometrics CCD9000 array having 1024 × 256 square pixels 25 μm on a side and furnished with a UV sensitizing coating that extended its useful response range down into the VUV region. This detector was interfaced to an Intel 386SX microcomputer through a Photometrics AT200 camera controller. The accompanying software permits recording in image or trace mode for each of as many as 16 defined tracks. In trace mode, various binning options are available for the pixels contributing to a given wavelength channel; in all of the present experiments, I used pixel-by-pixel digitization of all vertical elements in each channel, followed by accumulation in the computer. Most spectra were recorded in dual tracks 42 pixels high; because of the slight curvature in the spectrometer entrance slit, the vertical displacement of these two tracks yielded about one-half channel offset of one with respect to the other. Although this offset was fortuitous, it may in fact be the ideal choice for extracting maximal information from such recordings.

After correction for a DC bias the digitized signal for each pixel and for a binned row of pixels is essentially linear in the light exposure (intensity × time) over a large range of accumulated charge. Although it is usually desirable to correct for "dark current" (thermal charge accumulation), at the ~160 K operating temperature of the CCD array the dark charge was negligible in the present experiments. It is also necessary to calibrate the detector elements for variations in effective sensitivity. For example, exposures to continuous light sources in image mode revealed a number of blemishes in the defined regions for both tracks. These may have been due to dirt on the window or on the array surface, or to imperfections in the array itself. Regardless, it is easy to compensate for such effects by ratioing the unknown spectrum to a spectrum recorded using a source of continuum light in the region of interest. I chose a slightly different tack: I used the discharge source itself as the reference "continuum," by simply opening the entrance slit to a width large enough to ensure that all fine structure would be washed out. Since the spectral features of interest represent small percentage changes on the fine wavelength scale of a spectrum that shows considerable intensity variation on the coarse scale, ratioing a high-resolution spectrum to a low-resolution spectrum in this fashion effectively amplifies the fine structure while canceling the rather severe variation in overall intensity associated with the coarse structure.

As might be expected, the Tesla discharge is a fierce source of

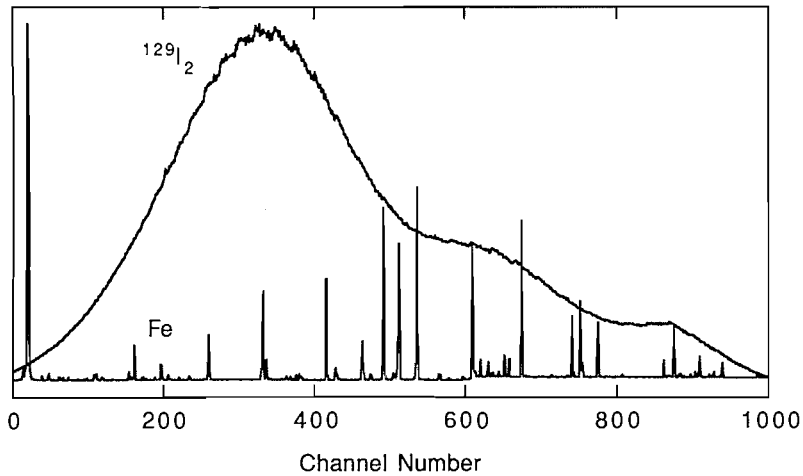

FIG. 1. Typical Tesla discharge spectrum of $^{129}I_2$ together with microwave discharge Fe calibration spectrum, recorded near 2870 Å. The intensity scales are arbitrary but relative to an approximate zero at the baseline of the Fe spectrum. Wavelength decreases with increasing channel number. Fine structure is evident in the I_2 spectrum, which was recorded using a slit width of 20 μm and an exposure of 500 s. The Fe spectrum was exposed 20 s using a 5-μm slit.

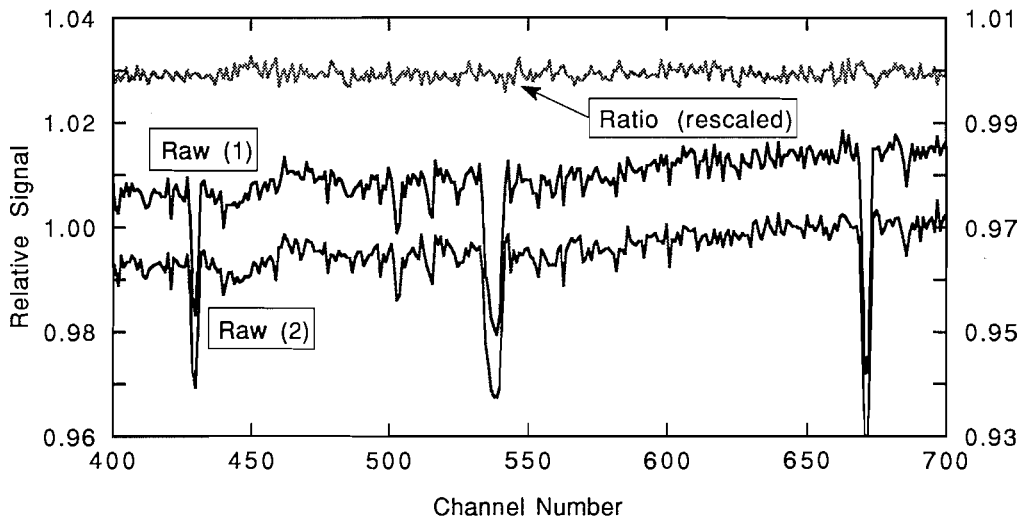

FIG. 2. Spectra recorded near 2870 Å on a single track in separate exposures of 30 and 60 s to a D_2 continuum source, using a 500 μm slit width. The raw spectra have been corrected for bias, and they and their ratio (scale to right) have been rescaled for display.

electronic noise. One might anticipate that this would play havoc with the array detector and its associated electronics. Fortunately this turns out to be only partly true: as long as the discharge was off during the readout stage (and to a much lesser extent, during array initialization), such problems were entirely negligible.

Detector performance tests

Overview

Figure 1 shows a typical I_2 discharge spectrum and its companion Fe calibration. One advantage of electronic over photographic recording is immediately evident on first use of such an array: the user can expose and reexpose in trial-and-error fashion until the result is satisfactory. By contrast, the photographic emulsion cannot be erased or examined between exposures, and so the achievement of an adequate overlay of calibration and unknown spectra necessarily entails a modicum of "flying blind," since it is crucial that the spectrometer not be perturbed in any way between these recordings. With the array detector the only interaction with the instrument is electronic (plus possibly a manual slit width adjustment) during a series of exposures. The largest drift I encountered in "before" and "after" wavelength calibration checks could be accounted for by atmospheric pressure changes over the several hours duration of that set of experiments.

Figure 2 illustrates the signal-to-noise capabilities of the array detector. The structure in the two lower "raw" spectra is mainly attributable to aberrations in the detector. However, the noise level in their ratio is less than 0.13%. Specifically, over the more extended range of channels 101–900, this ratio shows an average of 1.0000, a standard deviation of 0.00124, and maximal excursions of −0.00367 and +0.00403. Since this simple one-shot test yielded exposures below 20% of the maximum working capacity of the charge wells, it is likely that this noise figure could be significantly reduced with more effort. It is also clear that this ratioing procedure will prove essential in cases where signal-to-noise and precision are primary concerns.

Can. J. Chem. Downloaded from www.nrcresearchpress.com by 203.198.23.82 on 09/08/12
For personal use only.

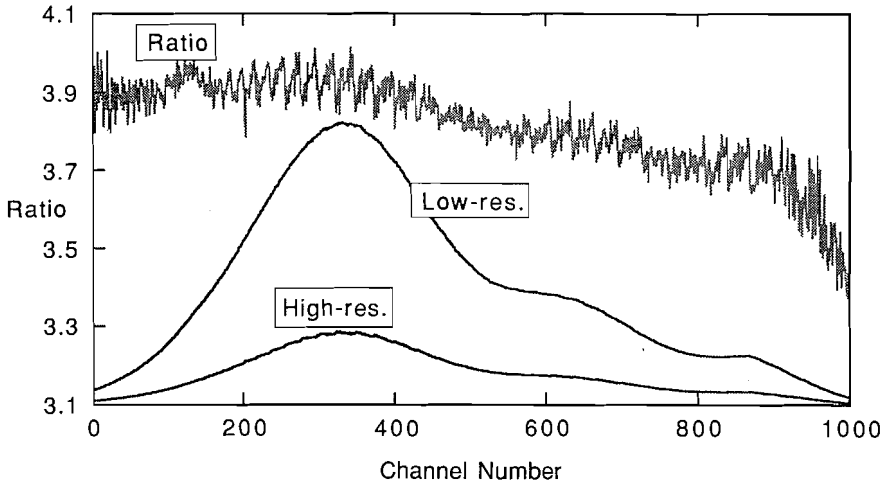

FIG. 3. Low-resolution (500 μm slit, 60 s exposure) and high-resolution (20 μm slit, 500 s exposure) spectra of $^{129}I_2$ in 2870 Å spectral region, and their ratio. (The high-resolution spectrum is the same as in Fig. 1.)

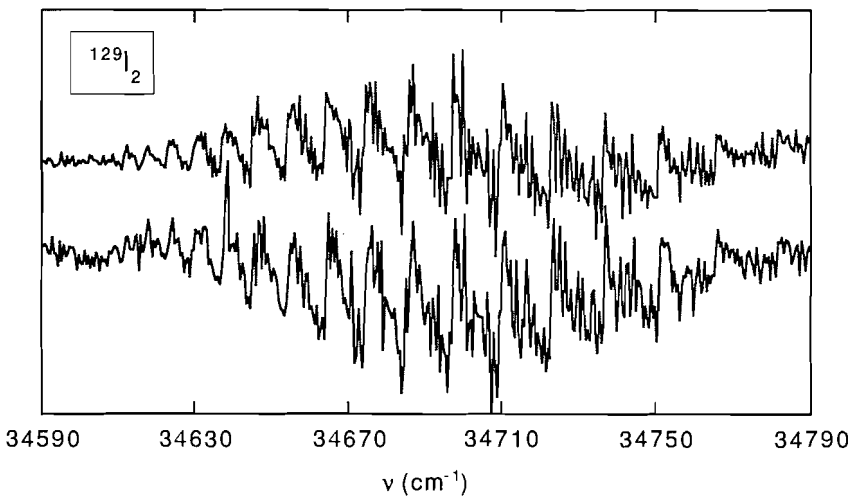

FIG. 4. Calibrated spectra for $^{129}I_2$ in the region of the 2880 Å main peak. For each of the two tracks, spectra were obtained from low- and high-resolution spectra like those in Fig. 3 by the procedure described in the text.

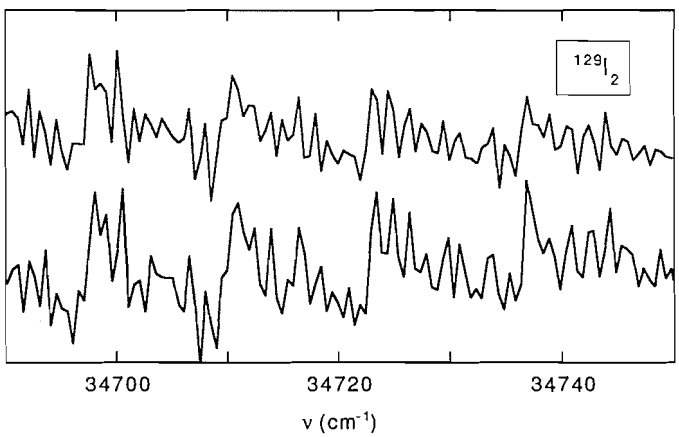

FIG. 5. A segment of Fig. 4 at expanded wavenumber scale, showing level of consistency of spectra recorded on the two tracks.

The practical significance of the S/N performance is made clearer in Fig. 3, which displays low- and high-resolution spectra of $^{129}I_2$ and their ratio. Vibrational bandhead structure is now evident across the entire spectrum, where it was barely perceptible away from the main peak in Fig. 1. In practice, working spectra were obtained by scaling the low- and high-resolution spectra to a common average intensity, then subtracting the former from the latter. Typical results of this procedure, applied to both tracks and calibrated, are displayed as a function of the wavenumber in Fig. 4. That the very fine structure is real and not artifactual is clear from the blowup in Fig. 5. The latter demonstration is made all the more compelling by the fact that the two tracks are offset by half a channel with respect to each other.

Even a cursory comparison of Fig. 4 with the photographic spectrum in Fig. 1 of ref. 9 convinces one of the impressive improvement achieved with the array detector.

Can. J. Chem. Downloaded from www.nrcresearchpress.com by 203.198.23.82 on 09/08/12
For personal use only.

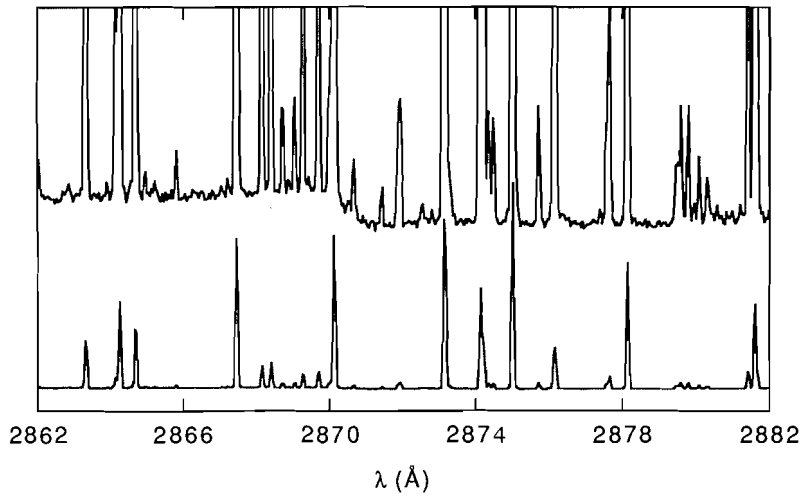

FIG. 6. A 20 Å segment of an Fe calibration spectrum recorded near 2870 Å, displayed at low and high sensitivity (× 20, upper). This region comprises ~500 array channels. The shoulder near 2870 Å in the upper trace is attributed to a light leak.

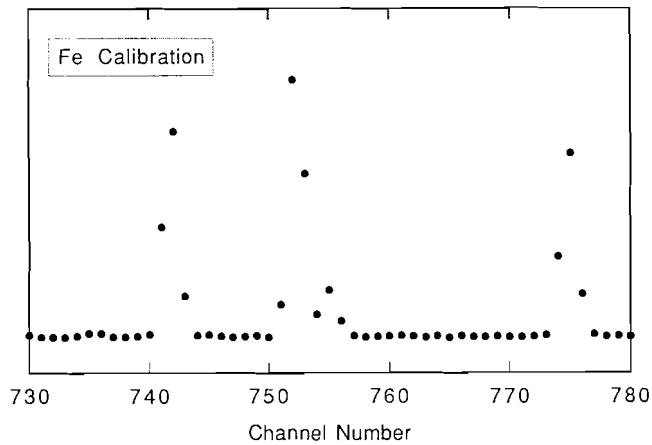

FIG. 7. A 50-channel region of a typical atomic Fe spectrum.

A less obvious advantage of spectra like those displayed in Figs. 4 and 5 is that they are free from contamination by the calibration spectra, since the two are recorded separately. In photographic mode it is necessary to measure regions of the recorded images where both calibration and unknown spectra occur together, in order to obtain a reliable plate function. Where intense atomic calibration lines occur in such spectra, they obscure the overlapping unknown features. Although it is of course possible to obtain additional densitometer records of unknowns free from this overlap, it requires extra effort and is often considered not worth the bother.

Atomic calibration spectra

The large dynamic range of the array detector is a tremendous asset when dealing with spectra that span an extreme range of intensities. Such is often the case with atomic calibration spectra, like the Fe spectrum obtained from a microwave discharge. Figure 6 shows a region of a typical Fe calibration spectrum recorded near 2870 Å, displayed at two different intensity magnifications. It is easy to locate and measure ~40 lines in this 20 Å spectrum segment. By contrast, dynamic range limitations of photographic emulsions would typically force a forfeiture of either some of the most intense lines to overexposure or some of the weakest to underexposure.

There is, however, a problem of a different sort with these array spectra. As was noted previously, the 25-μm pixel width is still large compared with the ultimate resolution achievable with photographic images. In fact it is so wide that a typical sharp atomic line recorded on the 1.5-m JY spectrometer appears in only three channels, as is shown in Fig. 7. The question arises, how best to locate the peak centers. The simplest procedure is an exact parabolic fit, and in fact this approach proved as good (in terms of the calibration fit statistics) as attempts involving more complicated procedures, like fitting Lorentzians to more than three points in the vicinity of each peak.

The statistics of a typical calibration fit are illustrated in Fig. 8. The error band on the plate function is only ~0.003 Å in width (2 σ), which is comparable to the best results achievable from photographic calibration spectra recorded on this instrument. However, this result is partly a consequence of the much larger number of Fe lines that could be measured and included in the present fits: 35–50 cf. 8–15 in a typical photographic spectrum. The estimated standard deviation in an individual measurement, typically 0.005–0.010 Å, is about a factor of two larger than achievable for spectra recorded photographically on this instrument. It is this figure that represents the limiting measurement precision for single, sharp, unknown features, and so the present array does concede a factor of two in ultimate precision to the photographic emulsion. Still, it is worth noting that this standard deviation corresponds to only ~5 μm on the image, or about one fifth of a pixel. In view of the three-point parabolic fitting procedure used to estimate peak positions, this is quite respectable.

Spectrum analysis

Data and interpretation

Calibrated spectra like those illustrated in Figs. 4 and 5 were measured directly on a Macintosh IIsi microcomputer, using the cursor tool of a graphics program (KaleidaGraph). All but one or two of the 45 bands reported in Table I of ref. 9 were also measured in the present study, most of them 6–10 times from different spectra. An additional 62

Can. J. Chem. Downloaded from www.nrcresearchpress.com by 203.198.23.82 on 09/08/12
For personal use only.

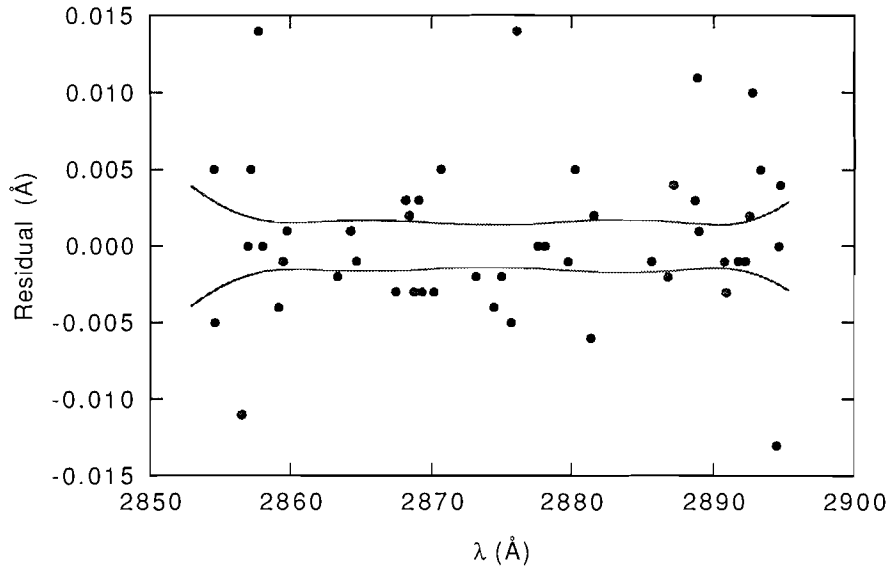

FIG. 8. Least-squares residuals from a fit of 48 Fe lines recorded near 2870 Å to a cubic polynomial (points), and 1-σ error band (curves) on the resulting fit function. The standard deviation of this fit was 0.006 Å.

bands were also assigned in the present work. Only features that appeared to be violet-degraded band edges were included in the measurements, and then only if they occurred clearly in both of the companion tracks obtained from a single exposure. The final assignment list included some weak features that were observed in only a single exposure. These were accordingly downweighted by a factor of 5 in the final fitting. This figure was crudely based on the estimated precision and number of measurements but was supported by the statistics of the fits. All (averaged) assignments for both isotopomers are presented in Table 1, together with their least-squares residuals, obtained as described below. Note that the assignment corresponds to Assignment 1 from ref. 9, which was the preferred interpretation. However the v'' numbering has been reduced by three units, for reasons discussed below.

The interpretation of this spectrum remains as given in ref. 9 and illustrated in Fig. 9. The upper state is an ion-pair state, most likely a member of the second cluster of six such states arising from $I^- + I^+(^3P_1)$ and $I^- + I^+(^3P_0)$. By analogy with the other similar ion-pair states, its internuclear distance should be about 3.6 Å. The transition terminates on the repulsive branch of a weakly bound, van der Waals type, lower state, accounting for the fine violet-degraded band structure. This state must correlated with two ground-state I atoms if the upper state belongs to the second ion-pair cluster. In the off chance that the upper state correlates with $I^- + I^+(^1D)$, the lower state would dissociate to $I(^2P_{3/2}) + I(^2P_{1/2})$. From here on, however, I will assume the lower correlation for both states.

In its intensity properties, this I_2 transition closely resembles the characteristic excimer bands observed in most of the diatomic rare-gas halide molecules and in some other rare gas van der Waals species, for example CsXe (3, 13). The piling up of intensity in the main peak at the long-wavelength end of the spectrum is attributable to nearly parallel upper and lower potentials, resulting in a nearly flat difference potential. The intensity pattern is determined almost entirely by the shapes of these potentials in the Franck–Condon region and by upper-state population distributions; it does not depend on whether the accessed region of the lower state falls below, at, or above the dissociation limit. In the present case, emission from the lowest v' levels happens to be mainly discrete, whereas, by contrast, it appears to be diffuse in most of the rare-gas halide $B \rightarrow X$ systems.

Least-squares analysis

To extract spectroscopic parameters from the assignments in Table 1, I again followed the procedures of ref. 9. Since only low v levels of the deeply bound upper state are observed, it is appropriate to represent its energy levels in terms of the usual polynomial in $(v + \frac{1}{2})$. However, the observations on the lower state extend almost to the dissociation limit, so I have examined both polynomial fits and near-dissociation expansions (NDEs) (14, 15) for it. In both cases the measured wavenumbers can be expressed as

$$[1] \quad \nu(v',v'') = \Delta T + G'_v - G''_v$$

If the polynomial representation is taken for G''_v, $\Delta T = T'_e - T''_e$. On the other hand the NDE represents the energy relative to the dissociation limit, so that its use for the lower state yields $\Delta T = T'_e - T_{\mathcal{D}}$, where $T_{\mathcal{D}}$ represents the asymptotic energy relative to the minimum of the ground-state potential. Thus the difference between these two ΔT values provides an estimate of the dissociation energy $\mathcal{D}''_e$ of the lower state.

For the NDE representation of the lower state, I have used the same form as in ref. 9,

$$[2] \quad G''_v = -X_5 (v_{\mathcal{D}} - v'')^{10/3} F(v'')$$

where $v_{\mathcal{D}}$ represents the (noninteger) vibrational quantum number at dissociation, and $F(v'')$ is an ad hoc function needed to correct for the deviation from the limiting long-range behavior. As before I have used for $F(v'')$ a simple polynomial in $z \equiv (v_{\mathcal{D}} - v'')$:

$$[3] \quad F = 1 + c_1 z + c_2 z^2 + \ldots$$

The constant X_5 is related to the limiting $-C_5/R^5$ dependence of the lower potential, assuming this state is the 0_u^-

Can. J. Chem. Downloaded from www.nrcresearchpress.com by 203.198.23.82 on 09/08/12
For personal use only.

Can. J. Chem. Downloaded from www.nrcresearchpress.com by 203.198.23.82 on 09/08/12
For personal use only.

TABLE 1. Violet-degraded bandheads (cm^{-1}) in the 2880 Å system of I_2, with residuals from least-squares fit[a,b]

$v'-v''$	$^{129}I_2$	$\Delta\nu$	$^{127}I_2$	$\Delta\nu$
0–22	34607.2	−0.3	34606.4*	0.1
0–21	34611.5	0.1	34610.5*	0.6
0–20	34616.9	0.1	(34615.5)	
0–19	34623.0	0.0	34622.8	−0.3
0–18	34629.5	0.3	34629.4	−0.2
0–17	34637.5	−0.2	34636.5	0.1
0–16	34645.0	0.5	34644.8	0.0
0–15	34654.3	0.1	34653.6	0.1
0–14	34664.0	0.1	34663.5	−0.2
0–13	34674.3	0.1	34674.1	−0.4
0–12	34685.9	−0.4	34684.7	0.1
0–11	34697.3	−0.1	34696.7	−0.1
0–10	34709.4	0.3	34709.2	−0.2
0– 9	34722.6	0.1	34721.9	0.2
0– 8	34736.3	0.1	34736.0	−0.1
0– 7	34750.6	0.1	34750.0	0.3
0– 6	34765.5	0.1	34765.2	0.1
0– 5	34781.4	−0.3	34780.8	0.0
0– 4	34797.1	0.0	34796.6*	0.3
1–12	34788.8	−0.5	34787.8*	0.6
1–11	34799.8	0.3		
1–10	34813.0	−0.5	34812.5*	0.2
1– 9	34825.6	0.0	34825.8*	0.0
1– 8	34839.2	0.1	34839.2	0.3
1– 7	34853.4	0.2	34854.3	−0.4
1– 6	34868.4	0.1	34869.1	−0.2
1– 5	34883.9	0.0	34884.5	0.0
1– 4	34899.8	0.1	34900.5	0.1
1– 3	34917.0	−0.5	34916.8	0.4
2–15	34859.3	0.5	34860.8	−0.1
2– 9	34928.9*	−0.8	34929.3	−0.1
2– 8	34941.4	0.4		
2– 7	34956.4	−0.3	34956.9	0.4
2– 6	34971.4	−0.4	34972.5	−0.2
2– 5	34986.9	−0.4	34987.6	0.2
2– 4	35002.8	−0.3	35004.2	−0.3
2– 3	35019.0*	0.1	35020.8	−0.2
3–15			34963.9	−0.1
3–13			34984.2*	−0.4
3–12	34993.3	−0.1	34994.3*	0.6
3–11			35006.3*	0.4
3– 8	35043.7*	0.4		
3– 7	35058.0*	0.4		
3– 6	35072.9*	0.4	(35074.1)	
3– 5	35088.9	−0.1	35091.0	−0.1
3– 4	35104.8*	0.0		
3– 3	35121.1	0.2	35123.2	0.5
3– 2	(35139.9)		35141.1	−0.2
3– 1	35156.0	0.0		
4–12	35095.2	0.0		
4–11			35109.5*	0.0
4– 5	35190.6	0.2	35192.5*	1.2
4– 4	35206.3	0.5		
4– 3	35223.5*	−0.1	35226.4*	0.1
4– 2	35241.1*	−0.7	35243.3*	0.4
5–11			35213.1*	−1.1
5–10	35221.8*	−0.7		
5– 9	35234.3*	−0.1		
5– 8			35251.8*	−0.5
5– 5	35292.7	−0.1		
5– 4	35308.8*	−0.2		
5– 3	35325.4	−0.3		
5– 2	35341.3*	0.9		
6– 9	35335.6	0.1		

[a]In the least-squares fits, measurements marked with an asterisk were downweighted by a factor of 5, and those in parentheses were omitted. Residuals are calculated minus observed, from polynomial/NDE fit (see text).

[b]Vibrational numbering of lower state is reduced by three units from that of Table I in ref. 9.

component of the 2431 $^3\Pi$ multiplet; I have adopted the value calculated in ref. 9 using Mulliken's (1) estimate of C_5.

In the framework of the rotating oscillator model, a single potential curve holds rigorously for all isotopic forms of a molecule in a given electronic state. In that case the vibrational energy is a unique function of the argument $\rho(v + \frac{1}{2})$, where ρ^2 is the ratio of isotopomer reduced masses. Choosing $^{127}I_2$ as the reference species makes $\rho \equiv 1.0000$ for it and 0.99221 for $^{129}I_2$. To accommodate data for multiple isotopomers in a single fit involving NDEs, one can define an effective v for all species through

$$[4] \quad \rho\left(v + \frac{1}{2}\right) = \left(v_{\text{eff}} + \frac{1}{2}\right)$$

and then use this v_{eff} in place of v where it appears in the NDE.

In the present spectra, it is not apparent that any of the observed transitions access the level $v'' = 0$ in the lower state. Thus the vibrational numbering in this state remains uncertain and can only be determined from the isotope effect. Unfortunately, weakly bound states are notoriously insensitive to isotopic substitution; thus simple calculations fail to determine this important property. Accordingly I have found it useful to incorporate an additional adjustable parameter in the fits, by defining the working v'' as $v'' + n$, where n represents a correction to the nominal v''. The latter quantity is clearly subject to an arbitrary constant shift, and the parameter n compensates for this to achieve minimum variance. Of course without data for multiple isotopomers, n is rigorously indeterminate, and the (nonlinear) fit must fail. At the outset I used the v'' numbering from ref. 9.

An additional numbering problem arose in our 1983 work. Because the anharmonicity in the lower state was small, and because the v'' progressions were short for all $v' > 0$, we were reluctant to rule out on statistical grounds an alternative *relative* numbering scheme, in which all bands for $v' = 1$ have their v'' numbers reduced by one unit, all for $v' = 2$ have theirs dropped by two, etc. The 1983 data yielded a variance 26% higher for this alternative assignment than for the preferred one, and so we presented the alternative as a possible, though unlikely, interpretation of the data. The improved quality and quantity of the present data make this alternative assignment virtually inadmissible. For example, a limited subset of 36 of the bands in Table 1 (corresponding roughly to those bands measured in 1983) gave an increase of 60% in this variance comparison. However, the full data set gave a factor of 5 increase, which suffices to eliminate this interpretation from contention.

The double polynomial and the polynomial/NDE fits both

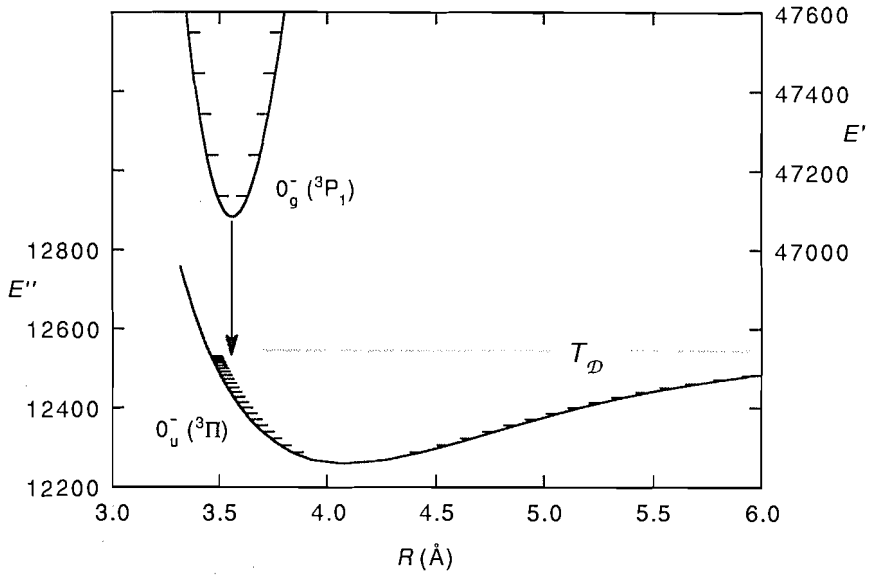

FIG. 9. Potential diagram illustrating emission process responsible for 2880 Å band system of I_2. Energies (cm^{-1}) are relative to the minimum of the ground state. (Note separate scales for lower and upper curves, to left and right, respectively.) The energy of the first dissociation limit is marked with the shaded horizontal line, and tick marks indicate observed vibrational levels.

TABLE 2. Spectroscopic parameters (cm^{-1}) for 2880 Å emission system of $^{127}I_2$, from least-squares fits of bands in Table 1 to polynomials and near-dissociation expansion[a]

	Polynomial[b]	NDE[c]
ΔT[d]	34 823.92(40)	34 536.46(35)
ω_e'	103.93(7)	103.93(7)
$\omega_e x_e'$	0.14(1)	0.14(1)
c_1''[e]	18.566(173)	$-1.974(13) \times 10^{-2}$
c_2''	−0.207(27)	—
c_3''	−0.0052(16)	$2.13(9) \times 10^{-6}$
c_4''	$6(3) \times 10^{-5}$	—
$v_{\mathcal{D}}$	—	34.67(6)
X_5^f	—	5.064×10^{-3}
σ^g	0.26	0.26
T_e'[h]	47 083.7(7)	
T_e''	12 259.8(5)	
$\mathcal{D}_e'$	32 220	
$\mathcal{D}_e''$	287.5(5)	

[a]Data span $v' = 0$–6, $v'' = 1$–22. Parameter standard errors (1 σ) in parenthesis, in terms of final digits. Parameters have been rounded by a systematic procedure that preserves their accuracy (16).

[b]Polynomials in $v + \frac{1}{2}$ for both upper and lower states.

[c]Polynomial in $v + \frac{1}{2}$ for upper state, NDE for lower state.

[d]ΔT_e for polynomial fit, $\Delta T_e - \mathcal{D}_e''$ for NDE fit.

[e]Conventional vibrational parameters for lower state in polynomial column, parameters as defined in eq. [3] in NDE column. In the latter, initial fits showed c_2'' to be uncertain by more than its magnitude, so it was set to zero.

[f]Held fixed at value given in Table III of ref. 9.

[g]Standard deviation for measurements of unit weight.

[h]T_e and $\mathcal{D}_e$ values assume dissociation of lower state to two ground-state atoms (12 547.2 cm^{-1} above the X-state minimum) and dissociation of upper state to $I^-(^1S) + I^+(^3P_1)$.

clearly indicate a reduction by three units in the v'' numbering of our 1983 paper, and it is this numbering that is used in Table 1. More specifically, the double polynomial fit of these data (as numbered in Table 1) yields, for the v'' adjustment parameter, $n = 0.16 \pm 0.56$, with very similar results from the polynomial/NDE fit. Thus I consider the new numbering quite probable, but with the possiblity that it is still in error by one unit. The two fits give virtually identical results for the upper-state G_v parameters and nearly identical estimated variances, but the double polynomial fit requires one more parameter (7 vs. 6) to accomplish this. Both sets of results are summarized along with some related derived properties in Table 2.

Compared with the 1983 results, the present reanalysis has affected mainly the parameters for the lower state that are most sensitive to the renumbering, namely T_e'', $\mathcal{D}_e''$ and ω_e''. The properties of the upper state have also changed by statistically significant amounts, e.g., $\omega_e' = 103.93(7)$ cm^{-1}, cf. 105.7(4) cm^{-1} previously. A comparison of the 1983 data with their counterparts in Table 1 reveals essentially random differences. Thus the changes in the upper-state parameters probably stem from subtle sources of model error in the fitting, relating to differences in the range of v spanned in both states and the numbers of parameters used to describe the lower state. Note, however, that the estimate of T_e' does *not* depend on the numbering, since it is based on the extrapolation to dissociation in the lower state. Thus the change in ΔT in the polynomial/NDE fit, from 34 522(6) cm^{-1} in the earlier work to the present 34 536.5(4) cm^{-1}, reflects mainly the inclusion of six higher v'' levels in the present work, which brings the observations to within 18 cm^{-1} of dissociation as compared with the previous 56 cm^{-1}.

The superior extrapolating behavior of near-dissociation

Can. J. Chem. Downloaded from www.nrcresearchpress.com by 203.198.23.82 on 09/08/12
For personal use only.

Can. J. Chem. Downloaded from www.nrcresearchpress.com by 203.198.23.82 on 09/08/12
For personal use only.

expansions for levels near dissociation argues in favor of the NDE results in Table 2 over the polynomial representation for the lower state. For this reason the residuals included in Table 1 are those from the polynomial/NDE fit. The NDE parameters are also used below to calculate the lower-state Rydberg–Klein–Rees (RKR) potential, needed for Franck–Condon calculations.

Potential curves and Franck–Condon factors

Because of the manner in which the emission terminates on the repulsive branch of the weakly bound lower potential, the intensity properties of this transition can be reliably treated using a bound-free model (13). This was done in our 1983 work and its results should remain valid now, since the earlier intensity modeling calculations utilized only low-resolution spectra, in which no vibrational structure could be perceived. Thus, for the repulsive branch of the lower potential I have simply adopted those results from ref. 9 that characterize its location and slope in the Franck–Condon region, namely $U''(R_e') = T_e' - 34\ 650(20)$, and $(dU''/dR)_{R_e'} = -850(80)\ cm^{-1}/Å$.

Of course, to calculate discrete FCFs one requires full potentials for both states. For the lower state I have accomplished this using a Morse–RKR potential (17) — a Morse repulsive branch having the above-mentioned properties, with an attractive branch constructed by adding the RKR widths to this repulsive branch. The required Morse branch was obtained using the experimental $\omega_e x_e$ value in Table 2 to define the Morse β parameter, and then solving for $\mathcal{D}_e$ and $\Delta R = R_e' - R_e''$ using the information on the location and slope given just above, together with the T_e'' value given in Table 2. The resulting parameters are included in Table 3, together with other properties of the resulting full potential.

The upper potential was represented by a Rittner-type potential, using a previously devised modification to the repulsion term (18),

$$[5]\quad U' = \mathcal{D}_e' - C_1/R - C_3/R^3 - C_4/R^4 - C_6/R^6 + b\exp(-\beta R^p)$$

The constants C_1 (rigorously known), C_3, and C_4 were obtained as before (18), and C_6 and p were adjusted in trial-and-error fashion to give a potential with the correct $\mathcal{D}_e$ and ω_e, and roughly correct R_e and $\omega_e x_e$.[1] The results of this determination are given in Table 3. Note that although the upper and lower potentials are well determined with respect to each other, there is nothing in either the 1983 results or the present work to precisely locate these potentials along the R axis. The adopted value of $R_e' \approx 3.56$ Å, which serves to anchor the pair, is purely an educated guess.

Franck–Condon factors calculated using these potentials are presented in Table 4. The assignments in Table 1 generally track these FCFs fairly well; in fact the latter were used in the final stages of the analysis to aid in the assignment of the weaker bands. The reader might notice that the FCFs sum to considerably less than unity for most of the v' levels included in this table. This is because the fraction of emission that terminates in the vibrational continuum of the lower state

[1]An incorrect sign was given for C_3 in ref. 18, when a previously derived value for the D' state was inadvertently used for $D\ 0_u^-(^3P_2)$. For the $0_g^-(^3P_1)$ state, however, the ion-quadrupole interaction *is* calculated to be identical to that for D' in both sign and magnitude.

TABLE 3. Parameters (cm^{-1} and Å units) for potentials involved in 2880 Å emission system of I_2[a]

	Upper state[b]	Lower state[c]
R_e	3.559	4.07
$\mathcal{D}_e$	32 220	538
β	0.101 29	0.882 67
b	$1.762\ 92 \times 10^5$	
p	2.8	
C_1	$1.161\ 41 \times 10^5$	
C_3	4.4×10^4	
C_4	5.8×10^5	
C_6	2.0×10^5	
ω_e[d]	103.93	18.57
$\omega_e x_e$[d]	0.184	0.21
B_e[d]	0.020 975	0.015 97
α_e[d]	2.79×10^{-5}	3.6×10^{-4}

[a]Modified Rittner potential for upper state, Morse–RKR curve for lower.

[b]As defined in eq. [5]. All parameters for upper state fixed externally except R_e, β, and b, which were obtained from condition equations for the energy, slope, and curvature of the potential at R_e'. p and C_6 were adjusted to make $R_e \approx 3.56$ Å, which is a guess based on properties of other I_2 ion-pair states (9).

[c]Parameters define the Morse repulsive branch. R_e value obtained from R_e' value and $\Delta R_e = -0.51$ Å (see text). Attractive branch obtained by adding potential widths calculated from RKR equations using NDE parameters in Table 2.

[d]Spectroscopic constants valid for derived potentials.

TABLE 4. Franck–Condon factors ($\times 10^4$) for emission from low v' levels in the 2880 Å band system of I_2[a]

	v'					
v''	0	1	2	3	4	5
0	0	1	4	10	19	34
1	2	10	25	51	89	139
2	10	36	81	145	219	293
3	32	93	181	276	354	394
4	77	187	306	388	406	355
5	153	302	409	416	333	201
6	262	411	445	341	182	50
7	397	476	394	202	48	0
8	541	476	280	71	0	52
9	673	409	149	5	38	134
10	774	297	49	13	111	176
11	831	176	3	70	163	155
12	841	75	9	132	167	96
13	809	15	45	170	132	38
14	744	0	88	174	80	5
15	659	23	119	150	34	2
16	565	68	130	112	8	17
17	472	121	123	73	0	38
18	385	169	105	41	6	54
19	309	205	81	20	17	61
20	244	226	58	7	29	61
21	191	231	39	2	37	55
22	148	225	24	0	42	46
23	114	208	14	0	42	36
24	87	185	8	2	39	28
25	65	158	4	2	34	21

[a]Computed for $J' = J'' = 0$ of $^{127}I_2$, using potentials as described in Table 3 and text.

increases with increasing v', such that for v' levels much higher than those studied here, the emission is almost entirely bound-free.

Conclusion

I have reexamined the 2880 Å emission system of I_2, using sources and methods identical to those used in a similar study 10 years ago, except for the subsitution of a CCD array detector in place of the previously used photographic plates. The high S/N capabilities of this detector have permitted me to more than double the number of identifiable violet-degraded bandheads that belong to this electronic transition, with a concomitant increase in precision by a factor of two. The new data lead to a clear rejection of an alternative assignment presented in 1983 and to a reduction by three units in the numbering of the vibrational levels of the lower state. The improved and extended data have permitted a more precise characterization of both states, particularly with respect to their absolute energies, which are now grounded on a much shorter extrapolation of the lower state to its dissociation limit.

Although the S/N performance of the CCD array detector used here is clearly superior to that of the photographic technology used in the previous study, the 25-μm pixel width limits the ultimate resolution of this array to a factor of two below that of photographic methods in equivalent applications in my laboratory. However, there are CCD array detectors now available with pixel widths a factor of four smaller. Thus in spectroscopic applications, there is every reason to expect this technology to be able to match the photographic emulsion in resolving power.

The electronic assignment of the 2880 Å system remains tentative, but no new results have surfaced in the past decade to force a change from the 1983 designation, $0_g^-(^3P_1) \rightarrow 0_u^-(^3\Pi)$. In particular, the states involved in this transition have spectroscopic properties that distinguish them from other known states of I_2 (11). Considering other diatomic halogens, only recently has this transition been convincingly identified in any other case, that in Cl_2 by Ishiwata et al. (19), who have used the label B' for the lower state. Interestingly, in Cl_2 this state has properties very similar to those of the other components of the 2431 $^3\Pi_u$ multiplet. This would appear to reflect the expected stronger tendency toward Hund's case a in Cl_2 vs. case c in I_2. However, the properties of this state in these two molecules are so strikingly different as to make the intermediate case of Br_2 of great interest.

Acknowledgments

I would like to thank Marcus Mendenhall for many valuable discussions on CCD array detectors, and for running some early proof-of-principle experiments that demonstrated the feasibility of the present experiments. I also thank my wife Patricia for help calibrating the spectra. The purchase of the CCD array detector was supported in part by National Science Foundation Grant CHE-8910823.

1. R.S. Mulliken. J. Chem. Phys. **55**, 288 (1971).
2. K.P. Huber and G. Herzberg. Constants of diatomic molecules. Van Nostrand Reinhold, New York. 1979.
3. J. Tellinghuisen. Pure Appl. Phys. **43**, 251 (1982).
4. M.D. Danyluk and G.W. King. Chem. Phys. Lett. **44**, 440 (1976).
5. M.D. Danyluk and G.W. King. Chem. Phys. **22**, 59 (1977).
6. G.W. King, I.M. Littlewood, and J.R. Robins. Chem. Phys. **56**, 145 (1981).
7. J. Tellinghuisen. Chem. Phys. Lett. **49**, 485 (1977).
8. A.L. Guy, K.S. Viswanathan, A. Sur, and J. Tellinghuisen. Chem. Phys. Lett. **73**, 582 (1980).
9. K.S. Viswanathan and J. Tellinghuisen. J. Mol. Spectrosc. **101**, 285 (1983).
10. G.W. King and T.D. McLean. J. Mol. Spectrosc. **135**, 207 (1989).
11. J.C.D. Brand and A.R. Hoy. Appl. Spectrosc. Rev. **23**, 285 (1987).
12. H.M. Crosswhite. J. Res. Natl. Bur. Stand. Sect. A: **79**, 17 (1975).
13. J. Tellinghuisen. Adv. Chem. Phys. **60**, 299 (1985).
14. R.J. LeRoy and W-H. Lam. Chem. Phys. Lett. **71**, 544 (1980).
15. J. Tellinghuisen. J. Chem. Phys. **78**, 2374 (1983).
16. J. Tellinghuisen. J. Mol. Spectrosc. **137**, 248 (1989).
17. J. Tellinghuisen. Can. J. Chem. **67**, 820 (1989).
18. J. Tellinghuisen. Can. J. Phys. **62**, 1933 (1984).
19. T. Ishiwata, Y. Kasai, and K. Obi. J. Chem. Phys. **95**, 60 (1991).

Can. J. Chem. Downloaded from www.nrcresearchpress.com by 203.198.23.82 on 09/08/12
For personal use only.

Assignment and vibrational analysis of the 600 nm absorption band in the phenoxyl radical and some of its derivatives[1]

LINDA J. JOHNSTON, N. MATHIVANAN, FABRIZIA NEGRI, AND WILLEM SIEBRAND
Steacie Institute for Molecular Sciences, National Research Council of Canada, Ottawa, ON K1A 0R6, Canada

AND

FRANCESCO ZERBETTO
Dipartimento di Chimica "G. Ciamician", Università di Bologna, 40126 Bologna, Italy

Received April 5, 1993

This paper is dedicated to Professor Gerald W. King on the occasion of his 65th birthday

LINDA J. JOHNSTON, N. MATHIVANAN, FABRIZIA NEGRI, WILLEM SIEBRAND, and FRANCESCO ZERBETTO. Can. J. Chem. **71**, 1655 (1993).

An experimental and theoretical study is reported of the 600 nm band system of phenoxyl and several methoxy substituted phenoxyls. These radicals, generated in freon, show a diffuse band in this region with a vibrational structure that is incompletely resolved but consistent with the 500 cm^{-1} "progression" observed earlier for phenoxyl in the vapour and in a rigid matrix. The low intensity of this band is considerably enhanced by *ortho*-methoxy substitution. To establish its assignment and analyze its structure, semi-empirical and *ab initio* quantum chemical calculations have been performed. It is found that, on the basis of the ordering of the states and the magnitude of their transition moments, all calculations favour a $\pi\pi^*$ ($^2B_2 \rightarrow {}^2A_2$) rather than the earlier proposed $n\pi^*$ assignment for this band. Of the methods used, only the (*ab initio*) CASSCF method is found to be able to simulate the observed vibrational structure adequately. This simulation is based on optimized structures and vibrational force fields calculated for the $1B_2$ and $1A_2$ states of phenoxyl. It identifies the dominant mode of about 500 cm^{-1} as ν_{6a}, the characteristic deformation mode of phenyl rings, but shows that higher members of the "progression" receive large intensity contributions from higher frequency modes. The chosen assignment and the assignments of higher-energy transitions reported in the literature are compared with those for the better known benzyl radical. It is shown that some of the phenoxyl assignments reported in the literature contain errors.

LINDA J. JOHNSTON, N. MATHIVANAN, FABRIZIA NEGRI, WILLEM SIEBRAND et FRANCESCO ZERBETTO. Can. J. Chem. **71**, 1655 (1993).

Une étude expérimentale et théorique est présentée concernant le système de bandes près de 600 nm du phénoxyle et de plusieurs phénoxyles comportant un ou deux groupes méthoxy. Ces radicaux, produit dans le fréon, montrent une bande diffuse dans cette région; la structure vibrationelle n'est pas complètement résolue mais est en accord avec la "progression" de bandes de 500 cm^{-1} observée plus tôt pour le phénoxyle dans la vapeur et dans une matrice rigide. L'intensité de cette bande faible est haussée considérablement par des substituants *ortho*-méthoxy. Pour établir l'attribution de cette bande et pour analyser sa structure, on a fait des calculs avec des méthodes de chimie quantique, non seulement semi-empirique mais aussi *ab initio*. On a trouvé que, selon l'ordre des états et la magnitude des moments de transition, tous ces calculs favorisent l'attribution de la bande à une transition $\pi\pi^*$ ($^2B_2 \rightarrow {}^2A_2$) au lieu de l'attribution $n\pi^*$ proposée précédemment. De toutes les méthodes utilisées, seule la méthode (*ab initio*) CASSCF peut simuler d'une façon acceptable la structure vibrationnelle observée. Cette simulation est basée sur les structures optimisées et les champs de force vibrationnels calculés pour les états $1B_2$ et $1A_2$ du phénoxyle. Elle mène à l'identification du mode normal de 500 cm^{-1}, qui domine le spectre, avec le mode ν_{6a}, c'est-à-dire le mode caractéristique pour la déformation des noyaux benzéniques; cependant, des modes normaux d'une fréquence plus élevée contribuent largement à l'intensité des membres de la progression sauf les plus bas. L'attribution choisie et les attributions rapportées dans la littérature des transitions plus hautes sont comparées avec celles du radical benzyle qui est mieux connu. On démontre des erreurs dans quelques unes des attributions des spectres du phénoxyle.

1. Introduction

Phenoxyl radicals are important intermediates in free radical reactions. Their observation and spectroscopic identification was first reported by Porter and co-workers (1, 2), who, however, did not discuss the assignment of the observed absorption spectra. Subsequent investigations by several groups (3–5) have led to assignments for the two moderately weak band systems observable in the near uv. In unsubstituted phenoxyl, these bands are situated near 400 and 315 nm and show vibrational structure consistent with $\pi\pi^*$ assignments for both. Less is known about an additional, very weak and diffuse band observed in the visible part of the spectrum, near 600 nm. Although very weak in phenoxyl itself, this band approaches the strength of the near-uv bands in some *ortho*-substituted derivatives (see, for example, ref. 6). In solution, its vibrational structure is poorly resolved, but in an early vapour-phase experiment, Ward (7) was able to observe four distinct maxima with spacings of about 500 cm^{-1}. The same maxima were observed subsequently by Pullin and Andrews (8) in a much noisier matrix-isolation spectrum of phenoxyl.

Ward (7) assigned his visible spectrum to an $n\pi^*$ transition, based on the argument that a corresponding band system is not observed in the benzyl radical. However, this argument is questionable since it is now known (9) that in benzyl there are two very weak transitions in the 450 nm region followed by a stronger transition near 320 nm. It is quite conceivable that the presence of an oxygen atom rearranges these bands so as to produce the pattern observed in phenoxyl. Neither Ward (7) nor Pullin and Andrews (8) at-

[1]NRCC No. 35269.

Can. J. Chem. Downloaded from www.nrcresearchpress.com by 203.198.23.82 on 09/08/12
For personal use only.

Can. J. Chem. Downloaded from www.nrcresearchpress.com by 203.198.23.82 on 09/08/12
For personal use only.

tempted to assign the vibrational structure; the absence of a discernable carbonyl-stretch progression would appear to argue against an $n\pi^*$ assignment.

In a more recent paper, Ebbesen and Previtali (10) have assigned what appears to be the same 600 nm band to the spectrum of a solvated electron. Their spectrum was generated by laser irradiation (266 nm) of phenol in several alcohols which resulted in the formation of a phenoxyl radical identified by its uv absorption bands. This interpretation of the visible band is based on earlier reports of solvated electrons generated by irradiation of phenolate ions and phenols in water (11–13). Although Ebbesen and Previtali (10) do not show the entire spectrum but only the absorption region from 450–750 nm, the fact that their bands show neither the solvent shifts nor the kinetics typical of solvated electrons suggests that the spectrum they observed in this region is an absorption band of phenoxyl rather than of a solvated electron.

In the present paper, we report a series of measurements and calculations aimed at securing the assignment of this band. Specifically, we measure the structure and intensity of the band for the parent radical and a number of derivatives. These measurements are compared with the results of quantum-chemical calculations. To simulate the structure of the band theoretically, we need the corresponding Franck–Condon factors. To this end we calculate the structure and the vibrational force field in the two states involved in the transition by quantum-chemical methods. For practical reasons, we use *ab initio* methods for phenoxyl itself, but semi-empirical methods for two derivatives, namely 2-methoxy- and 2,6-dimethoxyphenoxyl, both of which show much stronger absorption in the 600 nm region than the parent radical.

Although we are mostly concerned with the 600 nm band, it will prove necessary to reconsider the assignment of the higher-energy bands as well. Unfortunately, some confusion has crept into the symmetry assignments proposed in the literature. In a theoretical paper, Chang et al. (3) assumed that phenoxyl belongs to the point group C_{2v}, which seems highly probable, and assigned the ground state to the representation A_1. Tripathi and Schuler (5) followed their assignment but, assuming that the reported A_1 assignment is a misprint, reassigned the ground state to A_2. Neither assignment can be correct, however, since phenoxyl has an unpaired π-electron in an orbital that is antisymmetric with respect to the two-fold axis, so that the ground state must be either B_1 or B_2, depending on the choice of axes. Following the generally adopted notation, we choose z to be along C—O, and x to be perpendicular to the plane; with this choice, the ground state is $^2B_2$, $\pi\pi^*$ states are either $^2A_2$ or $^2B_2$ and $n\pi^*$ states are either $^2A_1$ or $^2B_1$. The assignment adopted by Tripathi and Schuler (5), following Chang et al. (3), should therefore read $^2B_2 \rightarrow {}^2B_2$ for the bands near 400 nm and $^2B_2 \rightarrow {}^2A_2$ for those near 315 nm. The observation of nontotally symmetric modes in the Raman spectrum under resonance with the 400 nm origin band (4, 5) supports the assignment of these two excited states to different symmetries, so that nontotally symmetric modes can gain Raman intensity by coupling them.

The proposed assignment implies a lowest-energy $\pi\pi^*$ state of $^2A_2$ symmetry, in agreement with the only calculation of excitation energies available to date. This calculation (3), based on the CNDO/S Hamiltonian and a model geometry, also predicts that there is a lower-energy $n\pi^*$ state of $^2B_1$ symmetry with a vanishing transition moment. There are a number of other quantum-chemical calculations on phenoxyl reported in the literature which, however, deal mostly with the ground state (14–20). They show strong disagreement with respect to the ground-state structure, in particular the CO bond length. One may therefore expect that these methods would also yield widely different values for the $^2B_2$–$^2B_1$ $n\pi^*$ transition energy. To establish the relative ordering of the lowest energy $n\pi^*$ and $\pi\pi^*$ states, it will thus be necessary to establish reliable structural parameters for the ground state. For this, we adopt a multi-configuration self-consistent-field *ab initio* method. Results for three *ab initio* methods are reported in the literature (15, 19, 20). Restricted and unrestricted Hartree–Fock (ROHF and UHF) calculations yield very different structures (19, 20). The higher level complete-active-space self-consistent-field method (CASSCF) presumably yields the most reliable structure (20). It is close to the structure obtained with the UHF approach but the latter yields a wavefunction that is unacceptable due to strong spin contamination.

In our calculations, we use the CASSCF method, after some preliminary semi-empirical calculations, to compute the structure and force field of the ground state, the ordering of the electronic states and, finally, the structure and force field of the excited state that we propose to be responsible for the 600 nm spectrum, namely the $1A_2$ $\pi\pi^*$ state.

2. Experimental

Materials

All phenols were commercially available and were purified by recrystallization or distillation. Di-*tert*-butyl peroxide was purified by passing it through an alumina column immediately before use. Solvents were spectroscopic grade and were used without further purification.

Laser flash photolysis experiments

The laser flash photolysis system has been described in detail elsewhere (21). For these experiments a Lumonics EX-530 excimer laser (Xe–Cl gas mixture; 308 nm; 8 ns pulses; ≤45 mJ/pulse) was used for sample excitation. Samples were contained in 7 × 7 mm^2 quartz flow cells connected with Teflon tubing to a flow reservoir. Flow samples were necessary to minimize problems due to product buildup. All solutions were deaerated by purging with nitrogen prior to and during the experiment. Extinction coefficients were measured using Aberchrome-540 in toluene as the actinometer (22). The yields of phenoxyl radical and the colored form of the actinometer were measured as a function of laser intensity for samples of di-*tert*-butyl peroxide plus phenol and actinometer, respectively, with matched optical densities at 308 nm. The ratio of the slopes of the two signal intensity vs. laser intensity plots was then used along with the known quantum yield and extinction coefficient for the actinometer (23) to calculate the product of the extinction coefficient times quantum yield for phenoxyl radical production. Since the experiments were carried out with sufficient phenol to ensure complete trapping of all *tert*-butoxyl radicals by phenol, the quantum yield for phenoxyl radical production can be equated to the known quantum yield for *tert*-butoxyl radical formation from di-*tert*-butyl peroxide (0.82).[2]

3. Results

Phenoxyl radicals were generated by hydrogen abstraction from the corresponding phenols by *tert*-butoxyl radi-

[2]D.D.M. Wayner, private communication.

Can. J. Chem. Downloaded from www.nrcresearchpress.com by 203.198.23.82 on 09/08/12
For personal use only.

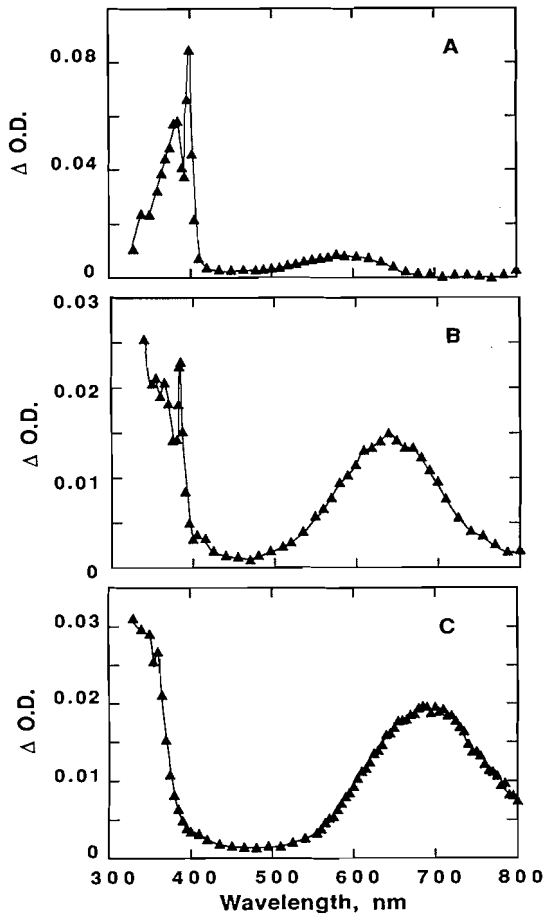

FIG. 1. Transient absorption spectra of phenoxyl (*A*), 2-methoxyphenoxyl (*B*), and 2,6-dimethoxyphenoxyl (*C*) radicals generated by 308 nm laser excitation of di-*tert*-butyl peroxide plus the appropriate phenol in Freon-113.

cals generated by 308 nm laser photolysis of di-*tert*-butyl peroxide (reaction [1]). Rate constants for hydrogen abstraction from a variety of substituted phenols in benzene

[1] 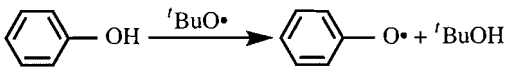

have been measured and are generally in the 10^8–10^9 M^{-1} s^{-1} range (24). All our experiments were carried out with sufficient phenol (typically 0.1 M) to ensure that all of the *tert*-butoxyl radicals decayed by hydrogen abstraction in order to maximize the phenoxyl radical signal intensities. Representative spectra for phenoxyl, 2-, 3-, and 4-methoxyphenoxyl and 2,6-dimethoxyphenoxyl in Freon-113 are shown in Figs. 1 and 2. All of these show a narrow structured absorption band in the 370–410 nm region. There is an additional broader absorption at longer wavelengths (500–700 nm) for most of these radicals. The position of this band and its intensity relative to the 400 nm band vary considerably with the substitution pattern of the phenoxyl radical.

The structured near-ultraviolet bands of phenoxyl have been studied by several groups (3–5) but not much attention has been paid to the broad band. In phenoxyl itself, this band is very weak and remains essentially structureless under our experimental conditions. In the *p*-methoxy compound, it has disappeared altogether, but in the *ortho*-substituted

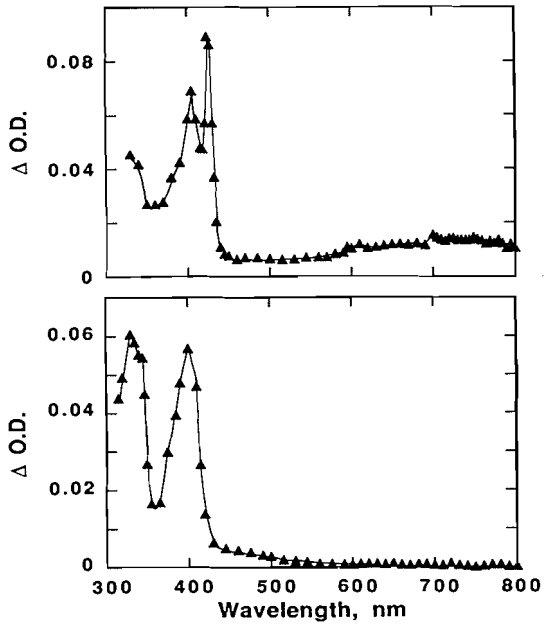

FIG. 2. Transient absorption spectra of 3-methoxyphenoxyl (top) and 4-methoxyphenoxyl (bottom) radicals generated by 308 nm laser excitation of di-*tert*-butyl peroxide plus the appropriate phenol in Freon-113.

phenoxyls, it is much stronger than in phenoxyl itself and shows some structure. It is also redshifted with maxima located near 640 nm in 2-methoxyphenoxyl and near 680 nm in 2,6-dimethoxyphenoxyl compared to the maximum near 575 nm in the parent radical. In 3-methoxyphenoxyl, the observed band is very weak but seems to be considerably broader than in the other compounds, with a maximum near 700 nm.

Among the observed broad-band spectra, that of 2-methoxyphenoxyl shows the clearest evidence of resolved vibrational structure compatible with the presence of a low-frequency progression such as that observed by Ward (7) in the vapour. However, the resolution is too poor to allow a frequency estimate.

Apart from its intrinsic interest, the visible band is valuable for monitoring phenoxyls during chemical reactions since relatively few simple organic molecules absorb in this region. Although in phenoxyl itself the band is uncomfortably weak, it appears that judiciously chosen *ortho*-substituents may render it attractive for this application.

4. Computational methods

To assign the 600 nm band, we started our analysis with a series of simple semi-empirical calculations, based on π-electron, CNDO, MNDO, and INDO Hamiltonians. Our π-electron calculations employed a modified version (25, 26) of the QCFF/PI program (27) and were based on the half-electron self-consistent-field (28) (HE-SCF) method, followed by configuration interaction (29) (CI) among all 33 determinants that are singly excited relative to the ground state configuration.

Our MNDO calculations (30) were based both on the UHF (31) and the HE-SCF + CI methods (28, 29). These methods were used to calculate the structure and force field of the ground state. At the optimized ground state structure of both QCFF/PI and MNDO-UHF, CNDO/S (32) calculations were

TABLE 1. Ground state equilibrium molecular structures of phenoxyl radical

Parameter	Value									
	QCFF/PI[a]	MNDO[b] UHF	MNDO[c] CI	INDO/1[d]	INDO[e] UHF	INDO[f] (ESR fit)	MINDO/3[g] UHF	RHF[h] 321G	UHF[h] 321G	CASSCF(7,7)[i] 321G
Bond length (Å)										
O C_1	1.2775	1.240	1.2291	1.359	1.358	1.240	1.216	1.377	1.308	1.2923
C_1C_2	1.4452	1.486	1.4943	1.397	1.399	1.500	1.489	1.385	1.422	1.4298
C_2C_3	1.3927	1.399	1.3793	1.393	1.384	1.320	1.388	1.380	1.387	1.3805
C_3C_4	1.4108	1.424	1.4273	1.395	1.389	1.440	1.425	1.386	1.404	1.4061
Bond angle (deg)										
$C_2C_1C_6$	117.94	116.4	113.95	123.04	120.0	118.00	115.2	120.	119.	117.98
$C_1C_2C_3$	120.42	120.7	122.21	117.60	119.9	119.19	121.5	120.	121.	120.71
$C_2C_3C_4$	120.47	121.1	121.01	121.02	120.3	121.68	120.8	120.	120.	120.27
$C_3C_4C_5$	120.28	120.0	119.59	117.73	120.1	120.00	120.2	120.	120.	120.07

[a]This work. The CO σ bond parameters were set to b_0 = 1.37 Å, D = 110 kcal mol^{-1}, and α = 2.0 Å^{-1}. These quantities are defined in ref. 27.
[b]Reference 18 and this work.
[c]This work, CI 4 × 3, 34 determinants included.
[d]This work.
[e]Reference 14.
[f]Reference 17.
[g]Reference 16.
[h]Reference 19.
[i]Reference 20 and this work.

carried out in order to determine the energies and transitions moments of the excited states. Similar calculations were carried out with the INDO/S method (33), followed by CI based on Rumer diagrams (34), at the structure optimized by INDO/1. These MNDO-CNDO/S and INDO/1-INDO/S methods were also used to calculate the excitation energies and transition moments of a number of substituted radicals, two of which will be considered here, namely 2-methoxy- and 2,6-dimethoxyphenoxyl, both showing strongly enhanced absorption in the 600 nm region.

The calculated ground-state equilibrium structures of phenoxyl are listed in Table 1, columns 1–4; additional structural parameters, based on calculations reported in the literature, are listed in columns 5–9. Since there is strong disagreement between the calculated structures, we carried out a higher-level *ab initio* calculation, for which we chose the CASSCF method with the split valence 3-21G basis set and an active space including the seven π electrons and orbitals of phenoxyl, for a total of 784 configurations. These calculations, labelled CASSCF(7,7)/3-21G, were performed with the GAUSSIAN 92 program package (35).

Since our CASSCF results differ in some respects from earlier results (20) obtained with the same method and basis set, we briefly outline our procedure. We started our ground-state CASSCF optimization with the ROHF molecular orbitals and the structure obtained in ref. 20 with these same orbitals. For this structure we obtained an energy of −303.3380 au and a gradient significantly different from zero. The structure (shown in Table 1) and energy obtained after optimization are identical with those obtained for the lowest energy ground state structure in ref. 20. Using the same active space of seven π orbitals, we optimized the $1A_2$ state structure starting the CASSCF calculation with the optimized ground-state molecular orbitals. The resulting structure is superior to that obtained previously in that the energy is lower by about 0.89 eV, probably because in the earlier calculations (20) two of the seven π orbitals in the active space were replaced by (ineffective) σ orbitals.

Despite the lack of agreement between the calculated ground-state structures, all methods lead to the same ordering of the lower excited states and to qualitatively similar intensities for the lower transitions, as shown in Table 2. Table 3 indicates that the presence of *ortho*-methoxy groups does not change this ordering and confirms the one-to-one correspondence between the bands in phenoxyl and those in the two substituted phenoxyls.

In the following we adopt the CASSCF(7,7)/3-21G structure, not only because it is obtained by the most elaborate method used, but also because it gives the best agreement with the available experimental data. Specifically, the presence of a quinoid distortion is indicated by the fit of the INDO results to ESR data, reported in ref. 17. In Table 4 we list the calculated vibrational frequencies (scaled by 0.95) for phenoxyl-d_0, -2,4,6-d_3, and -d_5 and compare them with the few observed frequencies. For comparison we also list the "best" semi-empirical frequencies of phenoxyl-d_0, obtained by the QCFF/PI method.

The scaling factor of 0.95 is close to unity, in keeping with the observation that CASSCF frequencies tend to be less overestimated than frequencies obtained at the HF level. The same scaling factor has been found to be appropriate for the benzyl radical.[3]

On the basis of these calculations, we assign the 1505 cm^{-1} band to mode ν_{8a} instead of the CO-stretching mode, as proposed earlier (5). For the latter, we obtain a frequency of 1269 cm^{-1}, in qualitative agreement with the calculated CO bond length. Deuteration causes mixing between the CC and CO stretching modes, leading to anomalous isotope effects. Preliminary calculations of the resonance Raman spectrum support the assignment of the most prominent band to ν_{8a}. This assignment also agrees with the observed activity of ν_{8a} in the *p*-hydroxyphenoxyl radical (4). In general, the agreement between the calculated and observed frequencies of the

[3]F. Negri. Unpublished results.

Can. J. Chem. Downloaded from www.nrcresearchpress.com by 203.198.23.82 on 09/08/12
For personal use only.

TABLE 2. Excitation energies (E, eV) and oscillator strengths (f) of the lowest electronic excited states of phenoxyl radical, as computed by semiempirical and *ab initio* methods

State		QCFF/PI[a]		CNDO/S[b]		Composition[c]	INDO/S		CIS/321G[d]		exp	
		E	f	E	f		E	f	E	f	E	ϵ
$1B_2$	D_0	0.00		0.00		$0.97(gr)$	0.00		0.00		0.00	
$1B_1$	D_1	—		1.87	—	$0.94(H-1\rightarrow S)+0.22(H-1\rightarrow L+1)+0.22(H-1\rightarrow L+1)$	0.62	—	1.26	—	—	
$1A_2$	D_2	2.25	0.008	2.31	0.002	$-0.89(H\rightarrow S)+0.40(S\rightarrow L)$	2.13	0.003	5.95 (2.94)[e]	0.017	1.85–1.98	400[f]
$2B_2$	D_3	2.54	0.075	3.36	0.002	$-0.63(H-2\rightarrow S)+0.73(S\rightarrow L+2)$	2.72	0.050	6.35	0.078	3.1	1800[f]–3000[g]
$2A_2$	D_4	4.66	0.070	4.05	0.090	$-0.41(H\rightarrow S)-0.88(S\rightarrow L)$	4.23	0.055	7.18	0.059	4.2	5500[f]
$3B_2$	D_5	4.30	0.001	4.72	0.001	$0.39(H-4\rightarrow S)+0.54(H\rightarrow L)+0.55(S\rightarrow L+2)-0.38(H\rightarrow L)$	4.31	0.039	6.32	—	4.86	sh[h]
$4B_2$	D_6	4.91	0.181	5.28	0.154	$0.58(H-2\rightarrow S)+0.24(H-4\rightarrow S)+0.56(S\rightarrow L+2)+0.21(S\rightarrow L+2)+0.30(H\rightarrow L)$	4.70	0.143	7.64	0.184	5.40	8700[h]

[a]CI 4 × 3, 34 determinants included.
[b]CI 6 × 4, 70 determinants included.
[c]The seven π orbitals correspond to the $H-4$, $H-2$, H, S, L, $L+1$, and $L+2$, respectively.
[d]The electronic states are spin-contaminated since UHF orbitals have been used.
[e]CASSCF(7,7)/321G vertical excitation energy. The corresponding 0–0 excitation energy is calculated to be 2.63 eV.
[f]Reference 2.
[g]Reference 5.
[h]Reference 38.

TABLE 3. Excitation energies (E, eV) and oscillator strengths (f) of the lowest excited states of phenoxyl radical and methoxy substituted derivatives as computed by semiempirical methods

State		CNDO/S[a]						INDO/S					
		Px		*2mPx*		*2,6dmPx*		*Px*		*2mPx*		*2,6dmPx*	
		E	f	E	f	E	f	E	f	E	f	E	f
$1B_2$	D_0	0.00		0.00		0.00		0.00		0.00		0.00	
$1B_1$	D_1	1.61	—	2.15	—	2.40	—	0.62	—	0.36	—	0.28	—
$1A_2$	D_2	2.35	0.001	2.27	0.004	2.14	0.001	2.13	0.003	1.97	0.014	1.67	0.012
$2B_2$	D_3	3.54	0.005	3.34	0.022	3.22	0.031	2.72	0.050	3.05	0.026	3.10	0.013
$2A_2$	D_5	3.90	0.100	3.58	0.113	3.58	0.144	4.23	0.055	3.81	0.043	3.94	0.052

[a]CI 6 × 4, 70 determinants included.

three isotopomers of phenoxyl is satisfactory, although the frequency of ν_{8a} is overestimated in phenoxyl-d_0 and -d_3.

In Table 5 we list the structure of the $^1A_2$ excited state of phenoxyl calculated at the CASSCF(7,7)/3-21G level. To explain the observed absorption spectra, the change in structure between the $^1B_2$ and $^1A_2$ states is the principal parameter. Since the same method is used for both states the relative rather than the absolute accuracy of these methods is crucial for our purpose. To demonstrate the proposed assignment of the 600 nm band, it will be necessary to show that the calculated displacements of the normal modes can account for the structure of this band.

5. Analysis

The ground-state structures in Table 1, obtained with the various methods used by us and by others show large divergencies. No direct experimental information is available; in the parent molecule, phenol, the benzene ring is close to a regular hexagon (36). However, the CASSCF calculations lead to a quinoid structure for phenoxyl. Support for a quinoid distortion is provided by INDO calculations of spin densities (17) which require such a structure in order to reproduce experimental results. Although the UHF/3-21G results also yield a quinoid structure (19), the resulting wavefunction is strongly spin-contaminated (S^2 is about 1.4 instead of the proper value of 0.75), so that these results are not reliable. The semi-empirical Hamiltonians tend to either overestimate or underestimate the quinoid distortion of the benzene ring, except for the QCFF/PI method which yields a structure close to that predicted by CASSCF. Table 2 shows that the order of the excited states obtained at this structure with the CNDO/S or the QCFF/PI method is the same as that obtained with an *ab initio* CI calculation at the CASSCF structure including only single excitations (37) (CIS) or even with the INDO/S method at the INDO/1 structure. The fact that all these methods yield the same ordering of the states, although the calculated energies show wide variations, indicates that this ordering is likely to be correct. It follows that the lowest excited state is an $n\pi^*$ state of B_1 symmetry, followed by a $\pi\pi^*$ state of A_2 symmetry, either of which may be responsible for the visible band.

The transition moments in Table 2 clearly favour a $\pi\pi^*$ assignment. Despite considerable scatter, they all show the pattern of a weak transition followed by two stronger tran-

Can. J. Chem. Downloaded from www.nrcresearchpress.com by 203.198.23.82 on 09/08/12
For personal use only.

TABLE 4. Vibrational frequencies of the ground state $D_0(1B_2)$ and of the lowest $\pi\pi^*$ excited state $D_2(1A_2)$ and dimensionless displacement parameters B_i for the $D_0 \rightarrow D_2$ electronic transition of phenoxyl radical

	$D_0(1B_2)$				$D_2(1A_2)$		
State	QCFF/PI	Description	CASSCF[a]	Exp[b]	CASSCF[a]	B_i	Exp
A_1	1565	CC stretch 8*a*	1567[c]/1553[d]/1492[e]	1505[c]/1487[d]/1489[e]	1529	0.746	
	1521	CC stretch 19*a*	1503/1403/1303		1412	0.577	
	1392	CO stretch	1269/1211/1180		1465	0.690	
	1155	CCH bend 9*a*	1141/1083/863	1157/1057/865	1126	0.489	
	1036	CCC bend 12	981/953/984		1019	0.214	
	1024	CCH bend 18*a*	1006/879/865	990/868/846	977	0.495	
	848	CC stretch 1	811/770/748	840/755/732	752	0.622	
	556	CCC bend 6*a*	544/532/531	528/517/514	527	1.371	519[f] 502[g]
B_1	1530	CC stretch 8*b*	1569/1500/1479		1533		
	1459	CC stretch 19*b*	1490/1447/1337		1451		
	1359	CCH bend 3	1370/1245/1102		1313		
	1245	CC stretch 14	1262/1179/1179		1210		
	1154	CCH bend 15	1153/979/888		912		
	1080	CCH bend 18*b*–9*b*	1091/867/856		1067		
	657	CCC bend 6*b*	637/626/614		599		
	468	CCO bend	439/423/419		414		
B_2	1055	CH wag	1036/976/889		1036		
	935	CH wag	945/847/797		945		
	748	CH wag	810/721/671		810		
	622	CCCC def	694/539/538		694		
	451	CCCC def	511/487/444		511		
	227	CO wag	228/215/215		228		
A_2	1043	CH wag	1020/971/825		1020		
	842	CH wag	847/710/658		847		
	408	CCCC def	419/390/367		419		

[a]Frequencies scaled by 0.95.
[b]Reference 5.
[c]-d_0 isotopomer.
[d]-2,4,6-d_3 isotopomer.
[e]-d_5 isotopomer.
[f]Reference 7.
[g]Reference 8.

TABLE 5. Computed molecular structures of the lowest $\pi\pi^*$ excited state, $1A_2$, of phenoxyl radical

	CASSCF(7,7)/321G	
	Reference 20	This work
Bond length (Å)		
O C_1	1.236	1.2383
C_1C_2	1.466	1.4649
C_2C_3	1.441	1.4404
C_3C_4	1.377	1.3975
Bond angle (deg)		
$C_2C_1C_6$	112.50	113.84
$C_1C_2C_3$	122.40	122.15
$C_2C_3C_4$	121.98	121.42
$C_3C_4C_5$	118.75	119.02

sitions of comparable strength, which in turn are followed by a strong $B_2 \rightarrow B_2$ transition at shorter wavelength (38). This pattern is close to what is observed experimentally and implies that the weakest transition corresponds to $1B_2 \rightarrow 1A_2$ $\pi\pi^*$. If an $n\pi^*$ assignment were adopted, which transition is consistently predicted to have a near-zero transition moment, one would have to explain why the stronger $\pi\pi^*$ transition at higher energies is not observed, not even in substituted phenoxyls.

The $\pi\pi^*$ assignment also agrees qualitatively with the observed spectral structure which shows no evidence of the carbonyl stretching progression expected for $n\pi^*$ transitions. On the other hand, the observed spectrum is very different from that for the $\pi\pi^*$ transitions to the $2B_2$ and $2A_2$ states and hence would seem to require a detailed explanation. This we attempt to supply by simulating the absorption spectrum on the basis of the calculated changes in structure and force field between the two states. The corresponding dimensionless displacements B_i of the equilibrium positions of the normal modes between the states, as derived from the CASSCF calculations, are listed in Table 5. These displacements yield the Franck–Condon factors which govern the vibrational intensity distribution in the spectrum.

Figure 3 depicts a simulation covering the first 2000 cm^{-1} of the $1B_2 \rightarrow 1A_2$ transition for a vibronic band width of 80 cm^{-1} chosen to allow comparison with the spectrum observed by Ward (7). The two spectra show the same four prominent bands with a spacing of about 500 cm^{-1} (~550 cm^{-1} in the calculated spectrum). To facilitate assignment of these bands, we also depict a calculated line spectrum in Fig. 3. Comparison with Table 5 shows that the 500 cm^{-1} fundamental corresponds to ν_{6a} in benzene derivatives, a ring-deformation mode active in many transitions involving a quinoid structure in the lower or upper state. This

Can. J. Chem. Downloaded from www.nrcresearchpress.com by 203.198.23.82 on 09/08/12
For personal use only.

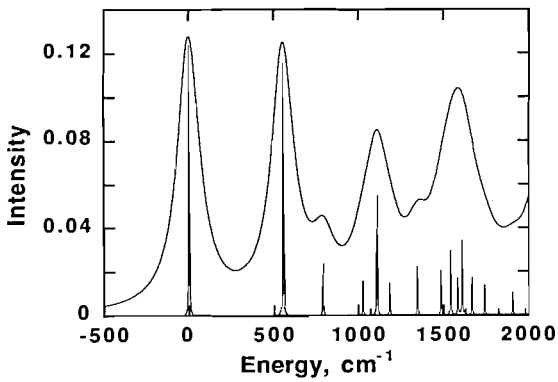

FIG. 3. Vibrational structure of the $1B_2 \rightarrow 1A_2$ absorption spectrum of the phenoxyl radical calculated for a linewidth of 80 cm^{-1}.

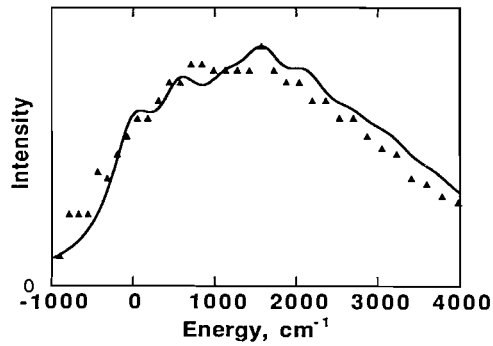

FIG. 4. Comparison of the observed (▲) and calculated spectra for the visible absorption band of the phenoxyl radical.

mode forms a prominent progression in phenoxyl, but its overtone bands also contain significant contributions of fundamentals in the ranges 1000–1200 cm^{-1} and 1500–1600 cm^{-1}, respectively. The calculated spectrum shows additional weak bands or shoulders near 800 cm^{-1} and 1300 (= 800 + 500) cm^{-1} which are not resolved in the observed spectrum (7) but whose presence is suggested by the observed intensity in these regions.

In Fig. 4 we show the entire calculated spectrum, which extends well beyond 2000 cm^{-1}, for a vibronic linewidth of 350 cm^{-1}, to allow comparison with the observed solution spectrum, measured point by point. To fit the calculated curve to the measured points, we have simply equated their two maxima. While this does not necessarily yield the best fit, it is enough to illustrate the similarity of the calculated and observed structures. The calculated spectrum does not contain hot-band contributions, which would improve the fit.

This confirms that the visible phenoxyl band can be assigned confidently to the $1B_2 \rightarrow 1A_2$ $\pi\pi^*$ transition. Theory predicts that the missing $n\pi^*$ transition is to be found at lower energies, a prediction supported by the observed diffuseness of the 600 nm band in the vapour, which suggests rapid internal conversion across a narrow energy gap. The intensity of the $n\pi^*$ transition is probably considerably smaller than that of the $1B_2 \rightarrow 1A_2$ transition, since all calculations predict a transition moment close to zero.

The calculations performed on the methoxy-substituted phenoxyls are in agreement with this conclusion within the accuracy one may expect from the two semi-empirical methods used. They both account reasonably well for the observed blue shifts upon ortho-methoxy substitution and the INDO/S method also accounts satisfactorily for the observed increase in intensity (the CNDO/S method predicts an increase only for the mono-substituted radical). These calculations refer to the lowest-energy rotamer only; the presence of other rotamers at room temperature would presumably modify these results to some extent.

6. Discussion

According to our analysis, the lowest excited state of phenoxyl is an $n\pi^*$ state which remains undetected. It is followed by the weak $1B_2 \rightarrow 1A_2$ $\pi\pi^*$ transition near 600 nm discussed in this paper, and by two medium weak $\pi\pi^*$ transitions of symmetry $1B_2 \rightarrow 2B_2$ and $1B_2 \rightarrow 2A_2$, at 400 and 315 nm, respectively. The first strong transition occurs at 230 nm (38) and is assigned to $B_2 \rightarrow B_2$. In the closely related and much studied benzyl radical (39), the lower main band structures are observed near 450, 300, and 260 nm, with an additional weak feature near 270 nm.

The quantum-chemical calculations indicate a one-to-one correspondence between the phenoxyl and benzyl transitions, with the weak 270 nm band in benzyl corresponding to a 255 nm shoulder observed in phenoxyl and assigned to $B_2 \rightarrow B_2$; the 300 and 260 nm bands in benzyl correspond to the 315 and 230 nm bands in phenoxyl and the 450 nm band in benzyl represents two nearly degenerate transitions which correspond to the 400 and 600 nm bands in phenoxyl. Thus the main difference between the two spectra is due to the large separation of the lowest two $\pi\pi^*$ transitions in phenoxyl compared to benzyl.

It is not difficult to account for this difference in terms of orbital energies. The HOMO and LUMO π orbitals are of A_2 symmetry and thus receive no contributions from the O atom or the CH_2 group. As a result, they have roughly the same energy in both radicals. The $1A_2$ state is governed, however, by contributions of the H → S and S → L configurations as shown in Table 2. While in benzyl these two configurations contribute roughly equal amounts, in phenoxyl the presence of the O atom leads to stronger contributions of the H → S component which lowers the energy of the $1A_2$ state. Similar considerations indicate that the $2B_2$ states in both radicals should have roughly the same energy, relative to the ground state, in agreement with the observed spectra. Hence comparison with benzyl lends further support to our assignment of the 600 nm transition in phenoxyl.

The larger difference in energy between the $1A_2$ and $2B_2$ states in phenoxyl relative to benzyl probably implies that vibronic coupling between these states is less important for phenoxyl than it was found to be for benzyl. In the latter radical, inclusion of this vibronic coupling was necessary in order to reproduce the observed spectrum (40). In phenoxyl, however, we obtained an adequate simulation without including vibronic coupling.

The quinoid structure calculated for the ground state of phenoxyl is similar but slightly more pronounced than that previously calculated for benzyl by the same methods, QCFF/PI (9) and CASSCF (40). The bond length changes accompanying the $1B_2 \rightarrow 1A_2$ transition are also found to be quite similar for the two radicals, but the $C_2C_1C_6$ angle undergoes a much larger change in phenoxyl (4° against 1.5° for benzyl); this implies of course that the other angles change accordingly. In particular the large change in $C_2C_1C_6$ angle

Can. J. Chem. Downloaded from www.nrcresearchpress.com by 203.198.23.82 on 09/08/12
For personal use only.

in phenoxyl is confirmed by the observed activity of ν_{6a}, which is stronger than in benzyl. Of the two radicals, phenoxyl is thus slightly less aromatic and more olefinic.

Acknowledgement

This work was supported by a National Centres of Excellence grant to the Mechanical and Chemimechanical Wood–Pulps Network.

1. G. Porter and F.G. Wright. Trans. Faraday Soc. **51**, 1469 (1955).
2. E.J. Land, G. Porter, and E. Strachan. Trans. Faraday Soc. **57**, 1885 (1961).
3. H.M. Chang, H.H. Jaffé, and C.A. Masmanidis. J. Phys. Chem. **78**, 1118 (1975).
4. S.M. Beck and L.E. Brus. J. Chem. Phys. **76**, 4701 (1982).
5. G.N.R. Tripathi and R.H. Schuler. Chem. Phys. Lett. **98**, 594 (1983); J. Chem. Phys. **81**, 113 (1984).
6. E.R. Altwicker. Chem. Rev. **67**, 475 (1967) and references therein.
7. B. Ward. Spectrochim. Acta, **A24**, 813 (1968).
8. D. Pullin and L. Andrews. J. Mol. Struct. **95**, 181 (1982).
9. F. Negri, G. Orlandi, F. Zerbetto, and M.Z. Zgierski. J. Chem. Phys. **93**, 600 (1990).
10. T.W. Ebbesen and C.M. Previtali. J. Photochem. **31**, 193 (1985).
11. J. Jortner, M. Ottolenghi, and G. Stein. J. Am. Chem. Soc. **85**, 2712 (1963).
12. L.I. Grossweiner, G.W. Swenson, and E.F. Zwicker. Science, **141**, 805 (1963).
13. G. Dobson and L.I. Grossweiner. Trans. Faraday Soc. **61**, 708 (1965).
14. R.V. Lloyd and D.E. Wood. J. Am. Chem. Soc. **96**, 659 (1974).
15. A. Hinchliffe. Chem. Phys. Lett. **27**, 454 (1974).
16. P. Bischof. J. Am. Chem. Soc. **98**, 6844 (1976).
17. Y. Shinagawa and Y. Shinagawa. J. Am. Chem. Soc. **100**, 67 (1978).
18. P. Bischof and G. Friedrich. J. Comput. Chem. **3**, 486 (1982).
19. V.B. Luzhkov and A.S. Zyubin. J. Mol. Struct. (Theochem.), **170**, 33 (1988).
20. H. Yu and J.D. Goddard. J. Mol. Struct. (Theochem.), **233**, 129 (1991).
21. S. Kazanis, A. Azarani, and L.J. Johnston. J. Phys. Chem. **95**, 4430 (1991).
22. V. Wintgens, L.J. Johnston, and J.C. Scaiano. J. Am. Chem. Soc. **110**, 511 (1988).
23. H.G. Heller and J.R. Langan. J. Chem. Soc. Perkin Trans. 2, 341 (1981).
24. P.K. Das, M.V. Encinas, S. Steenken, and J.C. Scaiano. J. Am. Chem. Soc. **103**, 4162 (1981).
25. F. Zerbetto, M.Z. Zgierski, F. Negri, and G. Orlandi. J. Chem. Phys. **89**, 3681 (1988).
26. F. Negri, G. Orlandi, A.M. Brouwer, F.W. Langkilde, and R. Wilbrandt. J. Chem. Phys. **90**, 5944 (1989).
27. A. Warshel and M. Karplus. J. Am. Chem. Soc. **94**, 5612 (1972); A. Warshel and M. Levitt. Quantum Chemistry Program Exchange No. 247, Indiana University.
28. M.J.S. Dewar, J.A. Hashmall, and C.G. Venier. J. Am. Chem. Soc. **90**, 1953 (1968).
29. D.R. Armstrong, R. Fortune, P.G. Perkins, and J.J.P. Stewart. J. Chem. Soc. Faraday Trans. 2, **68**, 1839 (1972).
30. M.J.S. Dewar and W. Thiel. J. Am. Chem. Soc. **99**, 4899 (1977); M.J.S. Dewar and W. Thiel. J. Am. Chem. Soc. **99**, 4907 (1977); M.J.S. Dewar, M.L. McKee, and H.S. Rzepa. J. Am. Chem. Soc. **100**, 3607 (1978); M.J.S. Dewar and J.J.P. Stewart. QCPE No. 506, Indiana University.
31. J.A. Pople and R.K. Nesbett. J. Chem. Phys. **22**, 571 (1954).
32. J. Del Bene and H.H. Jaffé. J. Chem. Phys. **48**, 1807 (1968).
33. J.A. Pople, D.P. Santry, and G.A. Segal. J. Chem. Phys. **43**, 5129 (1965); J.E. Ridley and M.C. Zerner. Theor. Chim. Acta, **32**, 11 (1973); J.E. Ridley and M.C. Zerner, Theor. Chim. Acta, **42**, 223 (1976); M.C. Zerner, G.H. Loew, R.F. Kirchner, and U.T. Mueller-Westerhoff. J. Am. Chem. Soc. **102**, 589 (1980); W.D. Edwards and M.C. Zerner. Theor. Chim. Acta, **72**, 347 (1987).
34. R. Pauncz. Spin eigenfunctions. Plenum, New York. 1978.
35. M.J. Frisch, G.W. Trucks, M. Head-Gordon, P.M.W. Gill, M.W. Wong, J.B. Foresman, B.G. Johnson, H.B. Schlegel, M.A. Robb, E.S. Replogle, R. Gomperts, J.L. Andres, K. Raghavachari, J.S. Binkley, C. Gonzalez, R.L. Martin, D.J. Fox, D.J. Defrees, J. Baker, J.J.P. Stewart, and J.A. Pople. Gaussian 92, Revision B. Gaussian, Inc., Pittsburgh, Pa. 1992.
36. N.W. Larsen. J. Mol. Struct. **51**, 175 (1979).
37. J.B. Foresman, M. Head-Gordon, J.A. Pople, and M.J. Frisch. J. Phys. Chem. **96**, 135 (1992).
38. Y. Kajii, K. Obi, N. Nakashima, and K. Yoshihara. J. Chem. Phys. **87**, 5059 (1987).
39. L. Grajcar and S. Leach. J. Chem. Phys. **61**, 1523 (1964); C. Cossart-Magos and S. Leach. J. Chem. Phys. **56**, 1534 (1971); P.M. Johnson and A.C. Albrecht. J. Chem. Phys. **48**, 851 (1968); G. Porter and E. Strachan. Spectrochim. Acta, **12**, 299 (1958); D.M. Friedrich and A.C. Albrecht. Chem. Phys. **6**, 366 (1974); C. Cossart-Magos and S. Leach. J. Chem. Phys. **64**, 4006 (1976); H. Hiratsuka, T. Okamura, I. Tanaka, and Y. Tanizaki. J. Phys. Chem. **84**, 285 (1980).
40. J.E. Rice, N.C. Handy, and P.J. Knowles. J. Chem. Soc. Faraday Trans. 2, **83**, 1643 (1987).

Can. J. Chem. Downloaded from www.nrcresearchpress.com by 203.198.23.82 on 09/08/12
For personal use only.

Electronic energies, dipole moment matrix elements, and static polarizabilities and hyperpolarizabilities for some diphenyl molecules

SHAHUL H. NILAR[1] AND AJIT J. THAKKAR
Department of Chemistry, University of New Brunswick, Fredericton, NB E3B 6E2, Canada

AND

ANNE E. KONDO[2] AND WILLIAM J. MEATH
Department of Chemistry, University of Western Ontario, London, ON N6A 5B7, Canada

Received March 16, 1993

This paper is dedicated to Professor Gerald W. King on the occasion of his 65th birthday

SHAHUL H. NILAR, AJIT J. THAKKAR, ANNE E. KONDO, and WILLIAM J. MEATH. Can. J. Chem. **71**, 1663 (1993).

The "giant dipole" molecules, $NR_1R_2—C_6H_4—(C{\equiv}C)_n—C_6H_4—NO_2$, n = 0, 1, 2, are studied theoretically for three sets of substituents: $R_1 = R_2 = H$, $R_1 = H$, $R_2 = CH_3$, and $R_1 = R_2 = CH_3$. For each of these nine molecules, the energies, and permanent and transition dipole moments for the 20 lowest electronic states are calculated using the intermediate neglect of differential overlap (INDO) approximation at the configuration interaction with single excitations (CIS) level. Static polarizabilities and hyperpolarizabilities for the ground states are reported for these "push–pull" molecules. The changes in the physical properties of interest due to increase in conjugation length and the inductive effect of substituents on the donor group attached to the rings are discussed. The energies and permanent and transition dipole moments for the ten lowest electronic states are tabulated for use in future studies of the spectral and dynamical effects of permanent dipole moments on laser-induced one- and multi-photon electronic transitions in realistic models for many-level giant dipole molecules.

SHAHUL H. NILAR, AJIT J. THAKKAR, ANNE E. KONDO et WILLIAM J. MEATH. Can. J. Chem. **71**, 1663 (1993).

On a étudié d'une façon théorique les molécules à "dipôle géant", $NR_1R_2—C_6H_4—(C{\equiv}C)_n—C_6H_4—NO_2$ dans lesquelles n = 0, 1 et 2 et portent trois ensembles de substituants, $R_1 = R_2 = H$, $R_1 = H$, $R_2 = CH_3$ et $R_1 = R_2 = CH_3$. Pour chacune de ces neuf molécules et utilisant l'approximation de négligence intermédiaire du recouvrement différentiel (INDO) de l'interaction de configuration avec des excitations simples (ICS), on a calculé les énergies et les moments dipolaires permanents et de transition des vingt états électroniques les plus bas. On rapporte aussi les polarisabilités et hyperpolarisabilités statiques des états fondamentaux de ces molécules qui "poussent et tirent". On discute des changements dans les propriétés physiques des propriétés intéressantes qui sont causés par une augmentation dans la longueur de la conjugaison et par l'effet inductif des substituants sur le groupe donneur attaché aux noyaux. On présente un tableau des énergies et des moments dipolaires permanents et de transition des dix états électroniques les plus bas qui pourront être utilisés dans des études futures des effets spectraux et dynamiques des moments dipolaires permanents sur les transitions électroniques mono-ou multi-photoniques induites au laser dans des modèles réels pour des molécules à plusieurs niveaux de dipôle géant.

[Tradiut par la rédaction]

1. Introduction

Materials that exhibit large nonlinear optical responses are required for a variety of applications in laser technology and optical processing of information (see, for example, ref. 1). Hence the design of molecules with such properties is of great current interest. Organic molecules with easily delocalized conjugated π electrons almost invariably have large dipole polarizabilities and hyperpolarizabilities (see, for example, refs. 2, 3). Electron donor and acceptor groups attached to opposite ends of the conjugated system are thought to facilitate charge transfer across the conjugated pathway and thus enhance the nonlinear response properties. Amino and nitro groups are prototypical donors and acceptors, respectively. Thus the prototype of a so-called "push–pull" molecule containing a conjugated pathway capped by donor and acceptor groups is *para*-nitroaniline, $NH_2—C_6H_4—NO_2$. Such molecules often have excited electronic states of a charge transfer character, and so there can be large differences between the dipole moments of the ground and charge transfer states. If this is the case, interesting spectral and dynamical effects are associated with laser-induced electronic transitions in these so-called "giant dipole molecules" (4–7).

The explicit spectral and dynamical effects of permanent dipole moments on continuous wave and pulsed laser-induced one- and multi-photon electronic transitions have been studied using few-level model systems (4–11). To extend such electronic studies to more realistic many-level molecular systems, we calculated the transition energies, and permanent and transition dipole moments for three series of giant dipole diphenyl molecules. Moreover, in view of their potential use as non-linear optical materials, we calculated the static polarizabilities and hyperpolarizabilities of these molecules. The first series consists of the *p*-amino-*p'*-nitrodiphenylacetylenes, $NH_2—C_6H_4—(C{\equiv}C)_n—C_6H_4—NO_2$ with n = 0, 1, 2, single crystals of which have been synthesized recently by Graham and co-workers (12). A more efficient donor group can be produced by replacing the hydrogen atoms in the amino substituent by methyl groups which have an inductive effect. Thus, we decided to study three sets of molecules $NR_1R_2—C_6H_4—(C{\equiv}C)_n—C_6H_4—NO_2$, n = 0, 1, 2. The first series has $R_1 = R_2 = H$ as in the work of Graham et al. (12), the second has $R_1 = CH_3$ and $R_2 = H$, and the third has $R_1 = R_2 = CH_3$. The charge transfer is ex-

[1]Present address: Biotechnology Research Institute, 6100 Ave. Royalmount, Montreal, PQ H4B 2R2, Canada.

[2]Present address: Department of Applied Mathematics, University of Waterloo, Waterloo, ON N2L 3G1, Canada.

Can. J. Chem. Downloaded from www.nrcresearchpress.com by 203.198.23.82 on 09/08/12
For personal use only.

pected to increase as one progresses from the original series to the dimethylated series.

The layout of this paper is as follows. Section 2 contains a brief description of the quantum mechanical methods we use, and section 3 deals with our calculated energies, dipole moment matrix elements, polarizabilities, and hyperpolarizabilities. Hartree atomic units are used throughout except where explicitly stated otherwise.

2. Methodology

A. Molecular geometries

The geometries for the $NH_2—C_6H_4—(C\equiv C)_n—C_6H_4—NO_2$ series of molecules were taken from the X-ray diffraction study of Graham et al. (12) with small adjustments to impose C_{2v} symmetry. These adjustments include taking the two phenyl rings to be coplanar, and averaging the two different NO bond lengths to a common value. In no case was a bond length changed by more than 0.01 A. The geometries of the other molecules $NCH_3R_2—C_6H_4—(C\equiv C)_n—C_6H_4—NO_2$, with $R_2 = H$ and $R_2 = CH_3$, were constructed as follows. All geometrical parameters in the $—N—C_6H_4—(C\equiv C)_n—C_6H_4—NO_2$ moiety and the N—H bond length were chosen to be the same as in the corresponding unmethylated molecule, and the geometry of the NCH_3 moiety was taken from X-ray structural studies of *N,N*-dimethyl aniline (13). The excited state geometries were assumed to be the same as those in the ground states, and thus all transitions are treated as vertical. Our coordinate system has its origin at the center of the bridge, the *z*-axis along the bridge axis pointing toward the nitro group, and the phenyl rings in the *xz*-plane.

B. Model Hamiltonian

The quantum mechanical calculation of transition moments and energies corresponding to a manifold of excited states requires a method that goes beyond the Hartree–Fock approximation. One suitable method is CI — configuration interaction (14, 15). However, *ab initio* CI calculations with a one-particle basis set large enough to produce useful results are not feasible for molecules as large as the ones we are considering. Therefore, we use a CI procedure based upon a semiempirical Hamiltonian in the zero differential overlap family of approximations (16, 17). The molecules considered are just small enough to allow use of an all-valence-electron scheme; higher members of these series ($n > 2$) could be studied only in a π-electron approximation with our resources.

A spectroscopically parameterized method is clearly the most suitable for our purposes. We chose INDO/S, the spectroscopic version of the intermediate neglect of differential overlap method (18), over CNDO/S, its complete neglect of differential overlap precursor (19). INDO/S retains one-centre exchange integrals that CNDO/S does not. These integrals are important for a reasonable description of singlet–triplet separations, and have a significant effect on oscillator strengths (18). The parameters in INDO/S were adjusted (18) so that the electronic spectra of benzene and the azabenzenes calculated using a single-excitation CI procedure agreed as closely as possible with experiment (18). INDO/S has been successful in predicting the frequencies and oscillator strengths of dipole-allowed transitions in conjugated systems (18, 20, 21).

A "γ-formula" for the distance dependence of the effective Coulomb repulsion between electrons located on different atoms has to be chosen. We considered three functional forms: the Mataga–Nishimoto (MN) formula (22), the Ohno–Klopman (OK) recipe (23, 24), and the Pariser–Parr (PP) approximation (25). The steepness of the variation of the repulsion with interatomic distance decreases in these formulas in the order: MN, OK, and PP. Table 1 compares ground state dipole moments for $NH_2—C_6H_4—(C\equiv C)_n—C_6H_4—NO_2$, $n = 0, 1, 2$, obtained from self-consistent-field (SCF) INDO/S calculations with these three different parameterizations. The dipole moments are large, of the order of 10 D. They increase as the number of acetylenic bonds is increased, regardless of which calculation scheme one considers. For each of the molecules, the INDO/S dipole moments increase in the order: MN, OK, and PP parameterization. For calibration purposes, we performed *ab-initio* SCF computations on these molecules with the minimal STO-3G and split-valence 3-21G basis sets (15, 26). For these molecules, the MN parameterization produces INDO/S dipole moments within 2% of the *ab initio* 3-21G values that are usually accurate to a few tenths of a Debye (3–5% in our molecules). The OK and PP parameterizations, respectively, lead to dipole moments 9–11% and 17–20% larger than the 3-21G values. On the basis of these ground state dipole moments alone, the MN scheme seems the most appropriate. However, Archibong and Thakkar (27) have found the OK parameterization leads to static polarizabilities and hyperpolarizabilities of the linear $C_{2n}H_2$ polyynes in far better agreement with accurate *ab initio* results than the MN parameterization. Since static polarizabilities and hyperpolarizabilities are among the properties of interest in this work, and since they depend on the entire spectrum of states that are also of interest in studies of laser–molecule interactions, we decided the OK formula was more appropriate for the purposes of this paper.

TABLE 1. Ground state dipole moments (in Debyes) of the "giant dipole" molecules, $NH_2—C_6H_4—(C\equiv C)_n—C_6H_4—NO_2$, $n = 0, 1, 2$[a]

	Ground state dipole moments				
n	NM	OK	PP	STO-3G	3-21G
0	8.75	9.51	10.23	6.59	8.56
1	9.10	10.00	10.73	6.94	9.14
2	9.30	10.33	11.08	7.05	9.41

[a]The table contains values obtained by the INDO/S method using the NM, OK, and PP parametrizations of the Coulomb integrals, and by *ab initio* SCF calculations using the STO-3G and 3-21G basis sets. See text for further details.

C. Selection of configurations

Since our computational resources do not permit full CI calculations to be performed on the molecules of interest, it becomes necessary to decide on the configurations to be included in the calculations. In their CNDO/S perturbation theory studies on two-photon spectroscopy, Dick and Hohlneicher (8) discussed the possibility of predicting transition energies for both dipole-allowed and dipole-forbidden transitions at a similar level of accuracy. They concluded that inclusion of double excitations in the CI procedure can be important (8, 28). Hence, we began with CI calculations including selected single and double excitations. After many

Can. J. Chem. Downloaded from www.nrcresearchpress.com by 203.198.23.82 on 09/08/12
For personal use only.

Can. J. Chem. Downloaded from www.nrcresearchpress.com by 203.198.23.82 on 09/08/12
For personal use only.

trial calculations we concluded that, given the limitations of the computer program (18) we used and our computer resources, we could not include an adequate number of double excitations to obtain results stable against small changes in the selected set of double excitations. Moreover, the INDO/S scheme was parameterized for CI calculations using single excitations only, and hence inclusion of higher excitations may require reparameterization. We then decided to restrict ourselves to single excitations only; so our calculations can be labelled INDO/S-CIS.

After numerous tests, we settled on CI calculations including all possible configurations generated by single excitations from the 20 highest occupied molecular orbitals into the 35 lowest virtual orbitals. This resulted in approximately 200 configurations for each symmetry block of the CI matrix. The transition energies, permanent dipoles and oscillator strengths obtained by this process were stable, with respect to modest changes in the number of virtual orbitals to which excitations are included, within a few hundred cm^{-1} and 1% respectively. These uncertainties are substantially smaller than the inherent errors in the INDO/S single excitation CI scheme which we estimate to be between 1000 and 3000 cm^{-1} for transition energies and 50% for permanent and transition moments. These error estimates are based on our expectation that the INDO/S CIS method is likely to do less well on systems that contain triple bonds, such as those considered in this work, than systems closer in nature to the benzenoid molecules for which it was parameterized (18).

D. Response properties

The energy E of a molecule in a weak, homogeneous, and static electric field can be expanded in a Taylor series, thus (29, 30)

$$[1]\quad E(\bar{F}) = E(\bar{O}) - \boldsymbol{\mu}_i F_i - \frac{1}{2}\boldsymbol{\alpha}_{ij}F_iF_j - \frac{1}{6}\boldsymbol{\beta}_{ijk}F_iF_jF_k - \ldots$$

in which μ_i, α_{ij}, and β_{ijk}, respectively, are components of the dipole moment vector, and the origin-independent dipole polarizability and hyperpolarizability tensors of the molecule. The subscripts denote Cartesian components (x, y, or z) and a repeated subscript implies summation over the latter. In C_{2v} molecules with the symmetry axis along the z axis, such as those with $R_1 = R_2$ in this work, the α and β tensors have three independent components each (29). In C_s molecules, such as those with R_1 different from R_2 in this work, the α and β tensors have four and six independent components, respectively. Differentiation of eq. [1] with respect to the field strength leads to an expression for the field dependent dipole moment $\bar{\boldsymbol{\mu}}(\bar{F})$:

$$[2]\quad \boldsymbol{\mu}_i(\bar{F}) = \boldsymbol{\mu}_i(\bar{O}) + \boldsymbol{\alpha}_{ij}F_j + \frac{1}{2}\boldsymbol{\beta}_{ijk}F_jF_k + \ldots$$

We used the finite perturbation method (31, 32) in which a finite field is introduced in the Hamiltonian, and the polarizabilities are obtained by numerical differentiation of the field-dependent energy or dipole moment of the molecule. We chose to differentiate the induced dipole moment following previous semiempirical work (33). The field-dependent dipole moments were computed at the INDO/S-SCF level in OK parameterization with a homogeneous field added to the Hamiltonian. The finite-field method applied at the SCF level is equivalent (34–36) to both the coupled Hartree–Fock (CHF) method and the static limit of the random phase approximation (RPA), and hence our polarizabilities are semiempirical (INDO/S) CHF polarizabilities.

TABLE 2. INDO/S (OK) ground state dipole moments (in Debyes) for three series $NR_1R_2—C_6H_4—(C{\equiv}C)_n—C_6H_4—NO_2$, n = 0, 1, 2, of "giant dipole" molecules

	Ground state dipole moments		
n	$R_1 = R_2 = H$	$R_1 = H$, $R_2 = CH_3$	$R_1 = R_2 = CH_3$
0	9.51	9.66	9.87
1	10.00	10.15	10.35
2	10.33	10.47	10.67

The finite field SCF procedure described above is theoretically more accurate than calculating polarizabilities from a sum over the INDO/S-CIS states. This is so because when only single excitations are included in a CI calculation, the sum-over-states is equivalent to the Tamm–Dancoff method (37, 38) which is an approximation to the RPA method. In quantum chemical parlance, the sum-over-CIS-states is an *un*coupled Hartree–Fock method which is an approximation to the finite-field coupled Hartree–Fock (CHF) method we use. *Ab initio* uncoupled Hartree–Fock calculations may be moderately useful for dipole polarizabilities but are completely inadequate for hyperpolarizabilities (39).

It is conceivable that these theoretical considerations fail for parametrized semiempirical methods, and that a sum over INDO/S–CIS states may produce polarizabilities closer to experiment than the INDO/S CHF method. However, we do not explore this possibility here. To resolve this issue, comparative studies are under way in our laboratory on small molecules for which both accurate *ab initio* calculations and gas-phase experiments are available.

Use of the finite-field method requires some care. Some of the precautions we took are described below. Convergence studies were carried out to verify that sufficiently small field strengths were used in the numerical differentiation to avoid contamination from even higher-order polarizabilities. Since the various components of the polarizability α and hyperpolarizability β are quite different in magnitude, different field strengths were used for different components. The stability of the finite differences was substantially improved by always using fields in pairs with the same magnitude but in opposite directions (40).

3. Results and discussion

A. Ground state dipole moments

Table 2 lists INDO/S (OK parameterization) SCF values of the ground state permanent dipole moments for each of the three series of giant dipole molecules $NR_1R_2—C_6H_4—(C{\equiv}C)_n—C_6H_4—NO_2$. Since single excitations do not mix with the ground state, the same dipole moments are predicted by the INDO/S-CIS calculation. In each series, the large dipole moments increase with the length of the conjugation path but the rate of growth seems to diminish. For a fixed number of acetylenic bonds n, the dipole moments increase as the donor amino group is increasingly methyl-

TABLE 3. Dipole moment matrix elements μ_{ij} in Debyes and transition energies ω_{ij} in cm^{-1} for the 10 lowest A_1 states of $NH_2—C_6H_4—(C\equiv C)_n—C_6H_4—NO_2$, $n = 0, 1, 2$[a]

		$n = 0$		$n = 1$		$n = 2$	
i	j	μ_{ij}	ω_{ij}	μ_{ij}	ω_{ij}	μ_{ij}	ω_{ij}
1	1	9.51	0	10.00	0	10.33	0
1	2	6.91	31136	8.24	31190	8.70	31009
1	3	0.46	38564	0.08	37036	0.48	36076
1	4	3.36	44812	−0.15	43765	−3.86	38940
1	5	−3.35	47258	3.32	45331	−3.78	45598
1	6	6.54	51320	−1.34	49084	1.83	47147
1	7	−0.13	53534	−8.26	51461	−5.40	49080
1	8	1.32	57798	−2.10	54321	−8.59	50185
1	9	0.82	61104	1.39	55657	−0.43	53826
1	10	−0.53	61607	0.76	58732	−1.41	56192
2	2	15.89	0	16.34	0	15.78	0
2	3	3.60	7428	−3.00	5846	3.00	5066
2	4	6.34	13676	−1.91	12576	−0.53	7931
2	5	−5.13	16122	8.91	14141	−9.42	14589
2	6	−6.16	20184	7.69	17894	6.10	16138
2	7	3.40	22398	2.09	20271	0.64	18070
2	8	−0.86	26662	1.22	23131	5.12	19176
2	9	−1.72	29968	−1.66	24467	−1.16	22817
2	10	−1.96	30471	−2.54	27542	1.46	25183
3	3	13.29	0	12.89	0	13.87	0
3	4	5.23	6247	−1.55	6730	−1.34	2864
3	5	1.37	8693	−4.62	8295	−5.08	9522
3	6	−2.11	12755	0.03	12048	−0.78	11071
3	7	0.93	14970	−2.07	14425	2.63	13004
3	8	−1.60	19234	−1.30	17285	1.36	14109
3	9	5.22	22540	−0.81	18621	0.27	17751
3	10	1.54	23042	−5.63	21696	−2.59	20117
4	4	18.10	0	15.88	0	11.91	0
4	5	0.35	2446	−0.29	1566	1.35	6658
4	6	−4.20	6508	−7.76	5318	3.08	8207
4	7	2.91	8723	−0.29	7695	−0.45	10140
4	8	−5.65	12987	0.85	10555	0.63	11245
4	9	6.05	16293	−0.89	11892	0.56	14887
4	10	0.59	16795	1.86	14966	−0.81	17253
5	5	19.28	0	22.71	0	27.24	0
5	6	5.52	4062	7.42	3753	−8.27	1549
5	7	−2.83	6277	4.22	6130	−2.18	3482
5	8	−1.26	10540	4.16	8990	−10.41	4587
5	9	−1.18	13846	−4.47	10326	3.44	8229
5	10	1.31	14349	8.58	13401	−4.25	10595
6	6	16.01	0	24.02	0	26.95	0
6	7	−3.11	2215	2.63	2377	−0.91	1933
6	8	3.09	6479	1.87	5237	9.00	3038
6	9	−9.64	9785	−2.59	6573	−0.85	6680
6	10	−0.26	10287	7.35	9648	0.40	9046
7	7	12.47	0	12.77	0	12.99	0
7	8	−3.19	4264	1.57	2860	0.81	1106
7	9	4.95	7570	−1.03	4196	0.03	4747
7	10	−1.59	8073	7.12	7271	−1.37	7113
8	8	16.00	0	12.71	0	18.99	0
8	9	−3.76	3306	−2.86	1336	−2.39	3641
8	10	−0.48	3809	5.11	4411	3.62	6008
9	9	21.03	0	14.90	0	12.85	0
9	10	−3.28	503	−2.39	3075	−3.22	2366
10	10	14.98	0	24.03	0	16.03	0

[a]The ground state energies, in hartrees, were −53.792249, −60.303125, and −65.960056 for $n = 0, 1, 2$, respectively.

Can. J. Chem. Downloaded from www.nrcresearchpress.com by 203.198.23.82 on 09/08/12
For personal use only.

TABLE 4. Dipole moment matrix elements μ_{ij} in Debyes and transition energies ω_{ij} in cm^{-1} between the 10 lowest A_1 states of $N(CH_3)_2$—C_6H_4—$(C{\equiv}C)_n$—C_6H_4—NO_2, n = 0, 1, 2[a]

		n = 0		n = 1		n = 2	
i	j	μ_{ij}	ω_{ij}	μ_{ij}	ω_{ij}	μ_{ij}	ω_{ij}
1	1	9.87	0	10.35	0	10.67	0
1	2	7.38	30289	8.64	30540	−9.13	30534
1	3	0.43	37790	0.09	36317	−0.28	35441
1	4	−3.14	44324	−0.03	43301	−3.90	38525
1	5	−1.52	46324	2.43	44664	−2.80	44706
1	6	5.21	49788	1.51	47959	−0.29	46583
1	7	−4.95	51204	−6.79	50221	−3.37	48931
1	8	0.42	57411	−5.34	53051	−9.49	49636
1	9	1.63	58708	1.37	55351	2.66	50848
1	10	−1.15	61005	2.25	56903	1.87	55075
2	2	17.34	0	17.52	0	16.66	0
2	3	3.84	7501	3.05	5777	2.74	4907
2	4	−7.90	14036	−4.16	12761	0.98	7991
2	5	−5.84	16036	10.30	14124	11.74	14173
2	6	−1.95	19500	−5.82	17418	−3.30	16049
2	7	5.30	20915	1.45	19681	0.22	18398
2	8	−0.24	27123	0.89	22511	−2.24	19103
2	9	−2.68	28419	−1.63	24810	2.49	20315
2	10	−1.06	30716	−2.99	26362	3.77	24542
3	3	15.22	0	14.63	0	15.23	0
3	4	−5.79	6535	−0.04	6984	1.20	3084
3	5	1.32	8535	5.60	8347	5.54	9265
3	6	−3.32	11999	1.18	11641	2.04	11142
3	7	1.66	13415	3.30	13904	−2.56	13491
3	8	−2.21	19622	1.63	16734	−3.00	14196
3	9	5.67	20918	2.07	19033	−1.95	15407
3	10	0.72	23215	5.25	20586	−6.18	19635
4	4	20.28	0	18.92	0	12.99	0
4	5	1.25	2000	−4.29	1363	0.51	6181
4	6	3.04	5464	8.86	4657	3.72	8058
4	7	−6.26	6880	−3.43	6920	−1.20	10406
4	8	8.10	13087	0.69	9750	0.68	11111
4	9	−4.67	14383	−0.27	12049	1.15	12323
4	10	1.70	16680	−0.21	13601	−1.17	16550
5	5	22.37	0	27.59	0	39.07	0
5	6	2.69	3464	−6.31	3294	−8.76	1876
5	7	−4.75	4880	5.56	5556	−0.08	4225
5	8	−0.85	11087	5.45	8387	−12.43	4930
5	9	−1.41	12383	−5.75	10686	4.63	6142
5	10	2.16	14680	10.76	12239	−3.88	10369
6	6	14.44	0	21.19	0	23.15	0
6	7	−2.23	1416	−2.85	2262	−2.44	2349
6	8	2.77	7623	−1.03	5093	4.11	3054
6	9	−5.38	8919	1.97	7392	−0.67	4266
6	10	0.29	11217	−4.36	8945	0.92	8493
7	7	16.83	0	15.74	0	14.07	0
7	8	−6.98	6207	1.64	2830	0.64	705
7	9	6.14	7504	−0.73	5130	0.26	1917
7	10	−4.16	9801	7.05	6682	5.59	6144
8	8	20.82	0	14.62	0	18.83	0
8	9	−3.75	1296	−2.35	2299	−1.11	1212
8	10	2.49	3594	7.48	3852	4.48	5438
9	9	18.22	0	18.37	0	14.94	0
9	10	−2.81	2297	−3.07	1553	0.47	4227
10	10	18.49	0	25.35	0	21.06	0

[a]The ground state energies, in hartrees, were −57.046463, −63.639557, and −69.340398 for n = 0, 1, 2, respectively.

Can. J. Chem. Downloaded from www.nrcresearchpress.com by 203.198.23.82 on 09/08/12
For personal use only.

Can. J. Chem. Downloaded from www.nrcresearchpress.com by 203.198.23.82 on 09/08/12
For personal use only.

ated. This increase can be attributed to the inductive effect of the methyl groups.

Steigman et al. (41) reported dipole moments, measured in chloroform solvent, of 14.0 and 16.0 D respectively for the $n = 1$ and $n = 2$ members of the series $NH_2—C_6H_4—(C{\equiv}C)_n—C_6H_4—NO_2$, and 15.5 D for $N(CH_3)_2—C_6H_4—(C{\equiv}C)—C_6H_4—NO_2$. These are about 50% larger than both the INDO/S values in Table 2 and the *ab initio* 3-21G values in Table 1. These large discrepancies are probably due to solvent effects since errors of the order of 5 D are highly unlikely for *ab initio* 3-21G SCF values (15). To check this possibility, we performed INDO/S (OK) self-consistent-reaction-field (SCRF) calculations for these molecules in chloroform solvent using the same Onsager radius of 6.4 Å used by Steigman et al. (41) in their data analysis. This increased our dipole moments to 12.8 and 14.6 D, respectively, for the $n = 1$ and $n = 2$ unmethylated molecules, and to 13.7 D for the $n = 1$ dimethylated molecule. The calculated solvent shifts are in the right direction but a bit too small; we think they are as good as can reasonably be expected given the uncertainty in the Onsager radius.

B. Excited state dipole moments

The permanent dipole moments μ_{ii} ($i = 1, \ldots, 10$) of the ten lowest states of A_1 symmetry are listed in Tables 3 and 4, respectively, for the $NH_2—C_6H_4—(C{\equiv}C)_n—C_6H_4—NO_2$ and $N(CH_3)_2—C_6H_4—(C{\equiv}C)_n—C_6H_4—NO_2$ series. Data for higher states and for states of A_2, B_1, and B_2 symmetry is available upon request. The dipole moments of the ten lowest states of the singly methylated series $NHCH_3—C_6H_4—(C{\equiv}C)_n—C_6H_4—NO_2$, $n = 0$, 1, 2, respectively are listed in Tables 5–7. All the states have large permanent dipole moments; quite a few are larger than 20 D and one is 39 D! Moreover, the dipole moment differences $\delta_{ij}\mu = \mu_{ii} - \mu_{jj}$ are often larger than 10 D; this is significant because it is $\delta_{ij}\mu$, and not the individual μ_{ij}, that is responsible for many of the interesting effects of permanent dipoles in laser–molecule interactions (5, 9). Some of the excited state dipole moments (μ_{ii}, $i > 1$) increase with the length of the conjugated pathway, some decrease, and some are nonmonotonic functions of n. Thus there is no simple dependence of the dipole moment differences $\delta_{ij}\mu$ on the length of the acetylenic bridge.

C. Transition energies and moments

Tables 3–7 also list transition energies ω_{ij} and transition moments μ_{ij} for pairs of states with $i, j \leq 10$. Data for states of other symmetry and for $i, j > 10$ are available upon request. These data have recently been used to study the effects of permanent dipole moments on the dynamics associated with the time evolution of molecular states populated by both one- and two-colour, single- and multi-photon, pump-probe laser–molecule interactions (42).

First consider the two C_{2v} series $NR_1R_2—C_6H_4—(C{\equiv}C)_n—C_6H_4—NO_2$. In each of these series, the lowest dipole-allowed-transition shows a small blue shift with the addition of the first acetylenic bond, followed by a red shift for the molecule with two triple bonds. The initial blue shift is due to the stabilization of the highest occupied molecular orbital (HOMO) by the triple bond. The subsequent red shift is due to the narrowing of the gap between the π and π^* molecular orbitals because of the increase in π conjugation.

The lowest dipole-allowed transition energy in the dimethylated series is red shifted relative to the unmethylated series because the inductive effect of the methyl groups stabilizes the HOMO. The transition moment for this lowest $\pi \rightarrow \pi^*$ transition increases in magnitude with conjugation in each series. The calculated transition energies for

TABLE 5. Dipole moment matrix elements μ_{ij} in Debyes and transition energies ω_{ij} in cm^{-1} between the 10 lowest states of $NHCH_3—C_6H_4—C_6H_4—NO_2$.[a]

i	j	μ_{xij}	μ_{yij}	μ_{zij}	ω_{ij}
1	1	−0.02	0.00	9.66	
1	2	0.00	0.00	0.00	29240
1	3	0.00	−0.08	0.00	30224
1	4	−0.02	0.00	−7.21	31215
1	5	−1.36	0.00	0.02	34796
1	6	0.20	0.00	0.00	36341
1	7	0.04	0.00	−0.34	38964
1	8	0.02	0.00	2.91	45470
1	9	−0.31	0.00	0.01	46700
1	10	−0.02	0.00	−2.21	47525
2	2	−0.29	0.00	7.64	
2	3	4.46	0.00	0.01	984
2	4	0.00	0.00	0.00	1975
2	5	0.00	−0.00	0.00	5556
2	6	0.00	0.01	0.00	7101
2	7	0.00	0.00	0.00	9724
2	8	0.00	−0.00	0.00	16230
2	9	0.00	−0.03	0.00	17460
2	10	0.00	−0.00	0.00	18284
3	3	0.21	0.00	8.00	
3	4	0.00	−0.03	0.00	991
3	5	0.00	−0.00	0.00	4572
3	6	0.00	0.00	0.00	6117
3	7	0.00	−0.05	0.00	8740
3	8	0.00	0.04	0.00	15246
3	9	0.00	−0.00	0.00	16476
3	10	0.00	0.06	0.00	17301
4	4	0.02	0.00	17.03	
4	5	−0.67	0.00	0.01	3581
4	6	0.51	0.00	−0.00	5126
4	7	−0.02	0.00	4.13	7749
4	8	−0.02	0.00	−7.22	14255
4	9	−0.22	0.00	−0.04	15485
4	10	0.02	0.00	6.23	16309
5	5	0.00	0.00	10.83	
5	6	0.00	0.00	−0.13	1545
5	7	−0.37	0.00	0.01	4168
5	8	−0.60	0.00	−0.01	10674
5	9	0.01	0.00	0.30	11904
5	10	−0.83	0.00	−0.01	12728
6	6	−0.01	0.00	12.50	
6	7	−0.67	0.00	0.00	2623
6	8	0.66	0.00	0.01	9129
6	9	−0.01	0.00	1.33	10359
6	10	1.19	0.00	0.01	11184
7	7	0.02	0.00	14.60	
7	8	−0.00	0.00	−5.98	6506
7	9	−1.19	0.00	0.08	7736
7	10	−0.01	0.00	−1.21	8561
8	8	−0.01	0.00	19.95	
8	9	−0.38	0.00	−0.02	1230
8	10	−0.01	0.00	−0.35	2055
9	9	−0.01	0.00	17.35	
9	10	0.24	0.00	−0.08	825
10	10	0.02	0.00	21.69	

[a]The ground state energy was −55.687356 hartrees.

TABLE 6. Dipole moment matrix elements μ_{ij} in Debyes and transition energies ω_{ij} in cm^{-1} between the 10 lowest states of $NHCH_3—C_6H_4—C\equiv C—C_6H_4—NO_2$[a]

i	j	μ_{xij}	μ_{yij}	μ_{zij}	ω_{ij}
1	1	−0.03	0.00	10.15	
1	2	0.00	0.00	0.00	28662
1	3	0.00	0.08	0.00	31210
1	4	0.02	0.00	8.51	31473
1	5	1.60	0.00	−0.01	34896
1	6	−0.28	0.00	0.00	36519
1	7	0.04	0.00	0.11	37669
1	8	0.00	−0.01	0.00	38009
1	9	−0.04	0.00	0.36	44637
1	10	0.03	0.00	2.21	45975
2	2	−0.04	0.00	7.93	
2	3	−4.38	0.00	0.00	2548
2	4	0.00	0.00	0.00	2811
2	5	0.00	−0.00	0.00	6235
2	6	0.00	−0.02	0.00	7857
2	7	0.00	0.00	0.00	9007
2	8	0.00	0.00	0.17	9347
2	9	0.00	−0.00	0.00	15975
2	10	0.00	0.00	0.00	17313
3	3	−0.01	0.00	8.43	
3	4	0.00	−0.02	0.00	262
3	5	0.00	−0.00	0.00	3686
3	6	0.00	0.00	0.00	5309
3	7	0.00	0.03	0.00	6459
3	8	−0.08	0.00	−0.00	6799
3	9	0.00	0.04	0.00	13427
3	10	0.00	−0.03	0.00	14764
4	4	0.01	0.00	17.48	
4	5	−0.57	0.00	0.04	3424
4	6	0.47	0.00	−0.03	5047
4	7	0.02	0.00	−3.46	6196
4	8	0.00	0.00	0.00	6536
4	9	0.00	0.00	3.90	13164
4	10	0.02	0.00	10.40	14502
5	5	0.00	0.00	10.89	
5	6	0.00	0.00	−0.01	1623
5	7	0.12	0.00	−0.03	2772
5	8	0.00	0.01	0.00	3113
5	9	−1.02	0.00	0.01	9741
5	10	0.27	0.00	0.06	11078
6	6	−0.02	0.00	12.38	
6	7	0.20	0.00	0.01	1150
6	8	0.00	0.01	0.00	1490
6	9	1.08	0.00	−0.00	8118
6	10	−0.71	0.00	−0.03	9456
7	7	0.02	0.00	14.24	
7	8	0.00	−0.00	0.00	340
7	9	−0.04	0.00	0.67	6968
7	10	0.01	0.00	−5.81	8306
8	8	−0.02	0.00	12.80	
8	9	0.00	0.01	0.00	6628
8	10	0.00	−0.00	0.00	7966
9	9	−0.01	0.00	18.52	
9	10	0.02	0.00	3.18	1338
10	10	0.00	0.00	27.19	

[a]The ground state energy was −62.239278 hartrees.

TABLE 7. Dipole moment matrix elements μ_{ij} in Debyes and transition energies ω_{ij} in cm^{-1} between the 10 lowest states of $NHCH_3—C_6H_4—C\equiv C—C\equiv C—C_6H_4—NO_2$.[a]

i	j	μ_{xij}	μ_{yij}	μ_{zij}	ω_{ij}
1	1	0.29	0.00	10.47	
1	2	0.00	−0.01	0.00	28146
1	3	0.00	−0.08	0.00	31013
1	4	−0.04	0.00	9.29	31726
1	5	0.00	−0.00	0.00	34102
1	6	1.66	0.00	0.08	34966
1	7	0.31	0.00	0.02	37009
1	8	0.11	0.00	0.15	37076
1	9	0.00	0.00	0.00	40329
1	10	0.02	0.00	−2.81	41533
2	2	0.94	0.00	8.23	
2	3	4.33	0.00	0.03	2868
2	4	0.00	0.00	0.00	3580
2	5	−0.01	0.00	−0.26	5956
2	6	0.00	0.00	0.00	6820
2	7	0.00	0.02	0.00	8863
2	8	0.00	0.00	0.00	8930
2	9	0.00	0.00	−0.05	12183
2	10	0.00	0.00	0.00	13388
3	3	−0.40	0.00	8.69	
3	4	0.00	0.02	0.00	712
3	5	0.11	0.00	0.04	3089
3	6	0.00	0.00	0.00	3953
3	7	0.00	0.01	0.00	5995
3	8	0.00	−0.03	0.00	6062
3	9	0.01	0.00	0.01	9315
3	10	0.00	−0.03	0.00	10520
4	4	0.29	0.00	17.41	
4	5	0.00	0.00	0.00	2376
4	6	−0.57	0.00	0.11	3240
4	7	−0.42	0.00	0.54	5283
4	8	−0.05	0.00	−2.95	5350
4	9	0.00	0.00	0.00	8603
4	10	0.00	0.00	0.47	9808
5	5	0.28	0.00	13.91	
5	6	0.00	0.00	0.00	864
5	7	0.00	−0.02	0.00	2906
5	8	0.00	−0.00	0.00	2974
5	9	−0.01	0.00	0.59	6227
5	10	0.00	−0.01	0.00	7431
6	6	0.35	0.00	10.98	
6	7	0.04	0.00	0.02	2043
6	8	−0.29	0.00	−0.08	2110
6	9	0.00	−0.16	0.00	5363
6	10	−0.49	0.00	0.01	6567
7	7	0.36	0.00	12.66	
7	8	−0.08	0.00	−0.43	67
7	9	0.00	−0.13	0.00	3320
7	10	−0.69	0.00	−0.21	4525
8	8	0.27	0.00	14.90	
8	9	0.00	−0.04	0.00	3253
8	10	−0.14	0.00	1.14	4458
9	9	0.33	0.00	14.15	
9	10	0.00	0.02	0.00	1205
10	10	0.30	0.00	14.00	

[a]The ground state energy was −67.911162 hartrees.

the other strong dipole-allowed transitions behave in a similar manner. An unequivocal comparison of the $NHCH_3—C_6H_4—(C\equiv C)_n—C_6H_4—NO_2$ results with those for the other two series is not possible because its lower symmetry effectively reduces the number of single excitations included in the CI calculation.

Steigman et al. (41) observed, in chloroform solvent, two strong transitions at 26 400 cm^{-1} and 36 500 cm^{-1} for the

Can. J. Chem. Downloaded from www.nrcresearchpress.com by 203.198.23.82 on 09/08/12
For personal use only.

TABLE 8. Static dipole polarizabilities and hyperpolarizabilities (in atomic units) of $NH_2—C_6H_4—(C\equiv C)_n—C_6H_4—NO_2$, n = 0, 1, 2

n	α_{xx}	α_{yy}	α_{zz}	β_{xxz}	β_{yyz}	β_{zzz}	β_z
0	111	22	209	395	7	5231	5633
1	119	25	285	448	8	6792	7248
2	122	27	378	465	10	7844	8319

TABLE 9. Static dipole polarizabilities and hyperpolarizabilities (in atomic units) of $N(CH_3)_2—C_6H_4—(C\equiv C)_n—C_6H_4—NO_2$, n = 0, 1, 2

n	α_{xx}	α_{yy}	α_{zz}	β_{xxz}	β_{yyz}	β_{zzz}	β_z
0	116	30	237	420	8	6969	7397
1	124	33	313	469	10	8607	9086
2	127	35	407	482	12	9681	10175

TABLE 10. Static dipole polarizabilities (in au) of $NHCH_3—C_6H_4—(C\equiv C)_n—C_6H_4—NO_2$, n = 0, 1, 2

n	α_{xx}	α_{yy}	α_{zz}	α_{xz}
0	113	27	223	0.4
1	121	29	299	0.5
2	124	31	393	0.5

n = 1 unmethylated molecule, and at 24 000 and 34 000 cm^{-1} for the n = 1 dimethylated molecule. These could correspond to the strong 1 → 2 and 1 → 5 transitions in Tables 3 and 4. To make a meaningful comparison, we estimate solvent shifts with an expression[3] obtained by a first order perturbative treatment of the reaction field (43), together with the same Onsager radius of 6.4 Å used earlier in section 3A. In this way, we find that in chloroform solvent, the transitions in Table 3 are red shifted to ω_{12} = 29 621 cm^{-1} and ω_{15} = 41 768 cm^{-1} for the n = 1 unmethylated molecule. Similarly, the transitions in Table 4 are shifted to ω_{12} = 28 680 cm^{-1} and ω_{15} = 39 299 cm^{-1} for the n = 1 dimethylated molecule. These solvent-corrected transition frequencies are in better but not perfect agreement with the measured values (41). Much closer agreement with experiment can be obtained by using an Onsager radius of 4.685 Å, but this radius produces absurd solvent shifts for the ground state dipole moments when used in a SCRF calculation of the type discussed in section 3A.

D. Polarizabilities and hyperpolarizabilities

Tables 8 and 9 list the unique non-vanishing components of the static dipole polarizability (α) and hyperpolarizability (β) tensors for the two $N(R_1)_2—C_6H_4—(C\equiv C)_n—C_6H_4—NO_2$ series with R_1 = H and R_1 = CH_3, respectively. Tables 10 and 11 list the components of the α and β tensors, respectively, for the lower symmetry $NHCH_3—C_6H_4—(C\equiv C)_n—C_6H_4—NO_2$ series. The accuracy of the calculated components should decrease in the order $\alpha_{zz} > \alpha_{xx} > \alpha_{yy}$ and $\beta_{zzz} > \beta_{zzx} > \beta_{xxz} > \beta_{yyz}$ because the INDO/S method uses a minimal basis which can be adequate for intramolecular polarization along the chain (z axis) and, to a lesser extent, in the molecular xz plane, but is quite inadequate for the description of out-of-plane polarization (27, 31, 44). However, this is not a severe limitation since the least accurate components are also the smallest ones. The longitudinal components α_{zz}, β_{zzz} are of greatest interest. Measurements of electric field induced second harmonic generation (EFISH) lead (45, 46) to the projection of the vector invariant of β upon the ground state dipole moment: $\vec{\beta} \cdot \vec{\mu}/\mu$ in which the vector invariant $\vec{\beta}$ has components given by $\beta_i = \beta_{xxi} + \beta_{yyi} + \beta_{zzi}$ for $i = x, y, z$.

First consider the two C_{2v} series $N(R_1)_2—C_6H_4—(C\equiv C)_n—C_6H_4—NO_2$. The dipole moment is along the z axis, and hence $\vec{\beta} \cdot \vec{\mu}/\mu = \beta_z$. Moreover, β_z is dominated by β_{zzz} because the longitudinal component is so large. Both the longitudinal dipole polarizability α_{zz} and hyperpolarizability β_{zzz} increase roughly linearly with the number of acetylenic links, and are larger in the dimethylated series than in the unmethylated series. Not surprisingly, the other components do not depend appreciably on either the length of the conjugated pathway or the degree of methylation of the amino group.

Tables 10 and 11 list components of the α and β tensors, respectively, for $NHCH_3—C_6H_4—(C\equiv C)_n—C_6H_4—NO_2$, n = 0, 1, 2. Table 11 also lists β_z and $\vec{\beta} \cdot \vec{\mu}/\mu$. In this case, β_{xxz} makes a substantial contribution to β_z. Although β_x is large, $\vec{\beta} \cdot \vec{\mu}/\mu \approx \beta_z$ because the x component of the dipole moment is small. Both α_{zz} and $\vec{\beta} \cdot \vec{\mu}/\mu$ increase roughly linearly with the length of the acetylenic bridge. The longitudinal polarizability α_{zz} increases as the number of methyl groups on the amino group increase, but $\vec{\beta} \cdot \vec{\mu}/\mu$ seems to be about the same whether the amino group carries one or two methyl groups. This trend is exactly that obtained in the EFISH measurements of Stiegman *et al.* (41). The measured $\vec{\beta} \cdot \vec{\mu}/\mu$ values, after conversion from their "X convention" to our "T convention" in the nomenclature of ref. 47, are 11 100, 21 300, and 21 300 au. for the n = 1 molecules with 0, 1, and 2 methyl substituents on the amino group; these are in satisfactory agreement with our values of 7248, 9051 and 9086 au, respectively, given that our values are static gas phase ones, whereas theirs are at an optical frequency and in chloroform solvent. A discussion of solvent effects on hyperpolarizabilities may be found in ref. 48.

[3]Equation [18] in ref. 43 contains a typographical error: the first factor in the second term on the right hand side should be $-1/a^3$.

Can. J. Chem. Downloaded from www.nrcresearchpress.com by 203.198.23.82 on 09/08/12
For personal use only.

TABLE 11. Static dipole hyperpolarizabilities (in au) of $NHCH_3—C_6H_4—(C\equiv C)_n—C_6H_4—NO_2$, $n = 0, 1, 2$

n	β_{xxz}	β_{yyz}	β_{zzz}	β_z	β_{xxx}	β_{yyx}	β_{zzx}	$\vec{\beta}\cdot\vec{\mu}/\mu$
0	1426	8	5972	7406	1.5	−0.5	7122	7391
1	1474	10	7589	9073	0.1	−0.5	7374	9051
2	1546	12	8706	10264	−0.7	−0.4	7731	10046

Acknowledgment

This work was supported by the Network of Centres of Excellence in Molecular and Interfacial Dynamics (CEMAID), one of fifteen networks of centres of excellence funded by the government of Canada.

1. B. Clymer and S.A. Coolins, Jr. Opt. Eng. **24**, 74 (1985); W. Blau. Phys. Technol. **18**, 250 (1987).
2. D.S. Chemla and J. Zyss (*Editors*). Nonlinear optical properties of organic molecules and crystals. Academic, New York. 1987; J.L. Bredas and R.R. Chance (*Editors*). Conjugated polymeric materials: opportunities in electronics, optoelectronics and molecular electronics. Kluwer, Dordrecht. 1990.
3. J.M. Andre and J. Delhalle. Chem. Rev. **91**, 843 (1991).
4. T. Hattori and T. Kobayashi. Phys. Rev. A: Gen. Phys. **35**, 2733 (1987); M. Terauchi and T. Kobayashi. Chem. Phys. Lett. **137**, 319 (1987).
5. M.A. Kmetic and W.J. Meath. Phys. Rev. A: Gen. Phys. **41**, 1556 (1990).
6. A.E. Kondo and W.J. Meath. Mol. Phys. **74**, 113 (1991).
7. M.A. Kmetic and W.J. Meath. Phys. Lett. A, **108**, 340 (1985).
8. B. Dick and G. Hohlneicher. J. Chem. Phys. **76**, 5755 (1982); Theor. Chim. Acta, **53**, 221 (1979).
9. W.J. Meath and E.A. Power. J. Phys. B: At. Mol. **17**, 763 (1984).
10. B.E. Scharf and Y.B. Band. Chem. Phys. Lett. **144**, 165 (1988).
11. A.E. Kondo, V.M. Blokker, and W.J. Meath. J. Chem. Phys. **96**, 2544 (1992) and references therein.
12. E.M. Graham, V.M. Miskowski, J.W. Perry, D.R. Coulten, A.E. Stiegman, W.P. Schaefer, and R.E. Marsh. J. Am. Chem. Soc. **111**, 8771 (1989).
13. M. Van Meerssche and G. Leroy. Bull. Soc. Chim. Belg. **69**, 204 (1960).
14. I. Shavitt, *In* Methods of electronic structure theory. *Edited by* H.F. Schaefer III. Plenum, New York. 1977. p. 243.
15. W.J. Hehre, L. Radom, P.V.R. Schleyer, and J.A. Pople. Ab initio molecular orbital theory. Wiley, New York. 1986.
16. J.A. Pople and D.L. Beveridge. Approximate molecular orbital theory. McGraw-Hill, New York. 1970.
17. G.A. Segal (*Editor*). Semiempirical methods of electronic structure calculations. Plenum, New York. 1977. Part A, Chap. 2; Part B, Chaps. 2, 3.
18. J. Ridley and M.C. Zerner. Theor. Chim. Acta, **32**, 111 (1973); **42**, 223 (1976).
19. J. Del Bene and H.H. Jaffe. J. Chem. Phys. **48**, 1807 (1968); **48**, 4050 (1968).
20. A.D. Bacon and M.C. Zerner. Theor. Chim. Acta, **53**, 21 (1979).
21. M.C. Zerner, G.H. Loew, R.F. Kirchner, and U.T. Mueller-Westerhoff. J. Am. Chem. Soc. **102**, 589 (1980).
22. N. Mataga and K. Nishimoto. Z. Phys. Chem. **12**, 335 (1957); **13**, 140 (1957).
23. K. Ohno. Theor. Chim. Acta, **2**, 219 (1964).
24. G. Klopman. J. Am. Chem. Soc. **86**, 4550 (1964).
25. R. Pariser and R.G. Parr. J. Chem. Phys. **21**, 466 (1953); **21**, 767 (1953).
26. M.J. Frisch, J.S. Binkley, H.B. Schlegel, K. Raghavachari, R.L. Martin, J.J.P. Stewart, F.W. Bobrowicz, D.J. Defrees, R. Seeger, R.A. Whiteside, D.J. Fox, E.M. Fleuder, and J.A. Pople. GAUSSIAN 86. Carnegie Mellon University, Pittsburgh, Pa. 1984.
27. E.F. Archibong and A.J. Thakkar. J. Chem. Phys. **98**, 8324 (1993).
28. J. Koutecky. J. Chem. Phys. **47**, 1501 (1967).
29. A.D. Buckingham. Adv. Chem. Phys. **12**, 107 (1967).
30. A.D. McLean and M. Yoshimine. J. Chem. Phys. **47**, 1927 (1967).
31. C.E. Dykstra. Ab initio calculation of the structures and properties of molecules. Elsevier, Amsterdam. 1988. Chap. 7.
32. H.D. Cohen and C.C.J. Roothaan. J. Chem. Phys. **43S**, 34 (1965).
33. J. Zyss. J. Chem. Phys. **70**, 3333 (1979); **70**, 3341 (1979); **71**, 909 (1979).
34. M. Cohen and A. Dalgarno. Rev. Mod. Phys. **35**, 506 (1963).
35. T.C. Caves and M. Karplus. J. Chem. Phys. **50**, 3649 (1969).
36. D.J. Rowe. Rev. Mod. Phys. **40**, 153 (1968).
37. A. Herzenberg, D. Sherrington, and M. Suveges. Proc. Phys. Soc. (London), **84**, 465 (1964).
38. T.H. Dunning and V. McKoy. J. Chem. Phys. **47**, 1735 (1967).
39. P. Chopra, L. Carlacci, H.F. King, and P.N. Prasad. J. Phys. Chem. **93**, 7120 (1989).
40. R.J. Bartlett and G.D. Purvis III. Phys. Rev. A: Gen. Phys. **20**, 1313 (1979).
41. A.E. Stiegman, E. Graham, K.J. Perry, L.R. Khundkar, L.T. Cheng, and J.W. Perry. J. Am. Chem. Soc. **113**, 7658 (1991).
42. A.E. Kondo. Ph.D. thesis. University of Western Ontario, London, Ont. 1992; A.E. Kondo, W.J. Meath, S.H. Nilar, and A.J. Thakkar. To be published.
43. A.T. Amos and B.L. Burrows. Adv. Quantum Chem. **7**, 289 (1973).
44. G.J.B. Hurst, M. Dupuis, and E. Clementi. J. Chem. Phys. **89**, 385 (1988).
45. B.F. Levine and C.G. Bethea. J. Chem. Phys. **63**, 2666 (1975).
46. J. Jerphagnon. Phys. Rev. B: Solid State, **2**, 1091 (1970).
47. A. Willetts, J.E. Rice, D.M. Burland, and D.P. Shelton. J. Chem. Phys. **97**, 7590 (1992).
48. M. Stahelin, D.M. Burland, and J.E. Rice. Chem. Phys. Lett. **191**, 245 (1992).

Can. J. Chem. Downloaded from www.nrcresearchpress.com by 203.198.23.82 on 09/08/12
For personal use only.

The 353 nm $^1n\pi^*$ transition of 4*H*-pyran-4-one and a deuterated derivative

ROBERT D. GORDON[1] AND WILLIAM K.C. PARK
Department of Chemistry, Queen's University, Kingston, ON K7L 3N6, Canada

Received March 12, 1993

This paper is dedicated to Professor Gerald W. King on the occasion of his 65th birthday

ROBERT D. GORDON and WILLIAM K.C. PARK. Can. J. Chem. **71**, 1672 (1993).

The 353 nm vapour absorption of 4*H*-pyran-4-one, and its 3,5-d_2 derivative, has been measured and assigned to a forbidden, $^1A_2$ ($n\pi^*$) – $^1A_1$ electronic transition, with electronic origin near 28 360 cm^{-1}, made allowed by vibrations involving out-of-plane ring and C—H motions. Although the molecule remains planar upon excitation, other effects of conjugation on the nature of the excited state are less marked than in 2-cyclopenten-1-one.

ROBERT D. GORDON et WILLIAM K.C. PARK. Can. J. Chem. **71**, 1672 (1993).

On a mesuré l'absorption (à 353 nm) de la 4*H*-pyran-4-one et de son dérivé 3,5-d_2 et on l'a attribuée à une transition électronique non permise, $^1A_2$ ($n\pi^*$) – $^1A_1$, ayant une origine électronique près de 28 360 cm^{-1} et qui est rendue permise par des vibrations impliquant des mouvements du cycle et des C—H hors-plan. Même si la molécule demeure planaire lors de son excitation, d'autres effets de conjugaison sur la nature de l'état excité sont moins marqués que dans la cyclopent-2-èn-1-one.

[Traduit par la rédaction]

Can. J. Chem. Downloaded from www.nrcresearchpress.com by 203.198.23.82 on 09/08/12
For personal use only.

Introduction

Studies of $n\pi^*$ electronic transitions in cyclic ketones, including ρ-benzoquinone (ρBQ) (1), cyclopentanone (CP) (2), cyclobutanone (CB) (3), tetramethyl-1,3-cyclobutanedione (TMCBD) (4), and 2- and 3-cyclopenten-1-one (2- and 3-CP) (5), have been a recurring theme in the work of Professor G.W. King and his former students. The present study of the 353 nm $^1n\pi^*$ absorption spectra of 4*H*-pyran-4-one (PN-h_4, Fig. 1), and its partially-deuterated derivative 3,5-d_2-4*H*-pyran-4-one (PN-d_2), continues that theme. Despite limitations imposed by the comparatively broad and diffuse nature of the observed vibronic bands, significant information has been obtained, and interesting comparisons can be made with the corresponding $^1n\pi^*$ systems in other cyclic ketones. The spectrum of PN is also of interest in the light of recent work (6) on its thione derivative.

Microwave studies (7) show that PN has a planar C_{2v} structure. Simple molecular orbital arguments predict that the lowest energy singlet electronic transition, $\tilde{A}\ ^1A_2$ ($n\pi^*$) $\leftarrow \tilde{X}\ ^1A_1$, is forbidden, and that higher energy transitions, to $^1A_1$ and $^1B_2$ $\pi\pi^*$ states, are allowed. The $^1n\pi^*$ transition is expected to gain intensity from the stronger $\pi\pi^*$ transitions by vibronic interaction involving a_2 or b_1 modes.

The near-ultraviolet absorption of PN in solution (8) is consistent with these predictions. The lowest energy absorption (λ_{max} = 300 nm, ϵ_{max} = 20 L mol^{-1} cm^{-1} in cyclohexane) is weak and shifts to higher energy in ethanol, as expected for an $n\pi^*$ transition, while the second band (λ_{max} = 240 nm, ϵ_{max} = 10^4 L mol^{-1} cm^{-1} in cyclohexane) is stronger and undergoes a small shift to lower energy in ethanol, as expected for $\pi\pi^*$ transitions.

The infrared and Raman spectra of PN have been studied (9, 10), and the assignments confirmed by *ab initio* calculations (9). Ground state fundamentals relevant to this study are listed in Table 1.

Experimental methods

PN-d_2 was prepared by refluxing PN-h_4 (Aldrich) in a DCl/D_2O solution for 28 h at 98°C. The resulting solution was neutralized with NaOD and extracted with CH_2Cl_2. The product, isolated by vacuum distillation, was shown from its NMR spectrum (11) to be the 3,5-d_2 isotopomer.

Vapour absorption spectra were photographed on a 1.5 m spectrograph, using a multiple-reflection cell with a 14 m pathlength, with PN at its saturated vapour pressure at 80–110°C.

Results

Densitometer traces of the 353 nm absorption of PN-h_4 and -d_2 are shown in Fig. 1. Observed bands and their assignments are listed in Table 2. Since the bands are broad (40–50 cm^{-1} FWHM) and featureless, their wavenumbers can be measured only to ±5 cm^{-1}, and their rotational contours cannot be used to determine their polarizations.

The strongest bands form a progression in 1240 cm^{-1}, beginning at 29 220 cm^{-1} in PN-h_4 but shifted 115 cm^{-1} to lower wavenumber in PN-d_2. We assign the 1240 cm^{-1} interval to the C=O stretching mode ν_3', significantly reduced in wavenumber from its 1702 cm^{-1} ground state value, as expected in an $n\pi^*$ transition. The 29 220 cm^{-1} band must be a vibronic origin, involving an a_2 or b_1 deuterium-sensitive mode. We assign it to the a_2 CH bending mode ν_{11}', but, as noted in Table 1, it could be of b_1 symmetry.

The isotope shift of the 11_0^1 vibronic origin suggests that the electronic origin should lie between 27 900 and 28 500 cm^{-1}, and the weak bands below 28 370 cm^{-1} seem obvious candidates for hot vibronic origins, involving one or more of the low-wavenumber out-of-plane modes ν_{18}'', ν_{17}'', or ν_{13}''. If the weak 28 210 cm^{-1} band in each isotopomer is assigned 18_1^0, the (unobserved) electronic origin would be near (28 210 + 149 ≅) 28 360 cm^{-1} in each isotopomer. This assignment is supported by the appearance of a very weak PN-h_4 band at 27 970 cm^{-1}, whose −390 cm^{-1} separation from the proposed origin corresponds to a known ground state a_2 fundamental, ν_{13}''. The stronger 28 505 and 28 780 cm^{-1} PN-h_4 bands can then be assigned as the cold vibronic origins 18_0^1 and 17_0^1, if it is assumed that ν_{18} and ν_{17} undergo small decreases in wavenumber upon excitation.

The weak 28 075 cm^{-1} PN-h_4 band, at $\Delta\tilde{\nu}$ = −285 cm^{-1}, cannot be a hot vibronic origin, since there is no 285 cm^{-1} ground state fundamental. However, if the 28 620 cm^{-1} band at $\Delta\tilde{\nu}$ = 260 cm^{-1} in each isotopic species is assigned 13_0^1,

[1]To whom correspondence should be addressed.

TABLE 1. Vibrational fundamentals in PN (cm^{-1})

Symmetry[a]	Number[a]	Description[a]	PN-h_4 Ground IR/Raman	PN-h_4 Ground this work	PN-h_4 Excited this work	PN-d_2 Ground this work	PN-d_2 Excited this work
a_1	3	$\nu_{C=O}$	1702[b]		1240		1235
	4	$\nu_{C=O}$, $\nu_{C=C}$	1652[b]		~1400		
a_2	11	γ_{CH}	960[c]		860[e]		745[e]
	13	γ_{ring}	395[c]	390	260	~390[f]	260
b_1	17	γ_{ring}, $\gamma_{C=O}$	423.92[d]		420		380
	18	γ_{ring}	148.76[d]	150	145	150	140

[a]Descriptions from ref. 9. Our choice of axes (Fig. 1) differs from theirs, so that species b_1 and b_2 are reversed and the numbering changed.
[b]Gas-phase IR, ref. 9.
[c]Raman of melt, ref. 9.
[d]Gas-phase IR, ref. 10.
[e]Could alternatively be the γ_{CH} mode ν_{12} (790 cm^{-1}, a_2) or ν_{14} (960 cm^{-1}, b_1).
[f]Approximate value from 13_1^1 sequence.

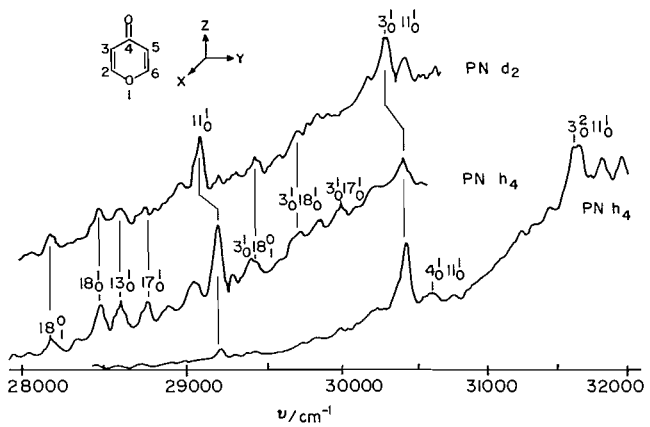

FIG. 1. Densitometer traces of the 353 nm vapour absorption spectra of PN-d_2 (top) and PN-h_4 (bottom two traces). The structure and molecular axes of PN are shown in the inset.

sequence bands with an interval of (260 − 395 =) −135 cm^{-1} would be expected in ν_{13}. The 28 075 and 28 370 cm^{-1} PN-h_4 bands can then be assigned as $18_1^0 13_1^1$ and $18_0^1 13_1^1$, respectively, and their intensities, relative to their parents, are consistent with these assignments. The −135 cm^{-1} sequence interval is also attached to the strong 11_0^1 and $3_0^1 11_0^1$ parent bands.

No sequence bands are resolved in low-wavenumber modes other than ν_{13}. As shown in Table 1, ν_{17} and ν_{18} change very little upon excitation, and sequences in these modes would be very closely spaced. Unresolved sequences in these modes may be responsible, in part, for the very broad observed bands.

In addition to the strong $3_0^{\nu'} 11_0^1$ progression, a number of weaker bands can be assigned to progressions in ν_3', attached to the vibronic origins 18_1^0, 18_0^1, 13_0^1, and 17_0^1. A weaker progression with a 1400 cm^{-1} interval, attached to 11_0^1, is assigned to the C=C stretching mode ν_4'.

A very weak band was observed at 27 292 cm^{-1} which, unlike all the other PN bands, has a sharp head. At $\Delta\tilde{\nu}$ = −1068 cm^{-1}, it is too intense to be a hot X_1^0 band. Since it does not fit into the pattern established for the $^1n\pi^*$ system, we tentatively assign it as the origin of the $^3A_2$ $n\pi^*$ transition.

The absorption of thin polycrystalline films of PN, grown from the melt between fused silica discs, was measured at 77 K. Broad bands, beginning near 31 900 cm^{-1} and separated by approximately 1200 cm^{-1}, were observed. If these bands can be identified with the strong $3_0^{\nu'} 11_0^1$ progression in the vapour, the 31 900 cm^{-1} band in the crystal can be assigned 11_0^1. The stronger bands in cyclohexane solution (8) form a similar 1200 cm^{-1} progression, beginning near 31 030 cm^{-1}. If these assignments are correct, the $^1n\pi^*$ absorption of PN shifts to higher energies, relative to the gas phase, by ca. 1800 cm^{-1} in cyclohexane solution, and by ca. 2700 cm^{-1} in the crystal.

Discussion

The weak 353 nm absorption of PN vapour is consistent with its recording a forbidden $\tilde{A}\ ^1A_2$ ($n\pi^*$) ← $\tilde{X}\ ^1A_1$ electronic transition, made allowed by vibronic interaction with a_2 and b_1 modes. The unobserved electronic origin is near 28 360 cm^{-1} in both isotopic species studied. As in the forbidden $^1n\pi^*$ transitions of ρBQ, CP, and 3CP, low-wavenumber, out-of-plane ring (or C=O) bending and twisting modes are vibronically active. In PN, however, the most active vibration is the higher-wavenumber, deuterium-sensitive CH wagging mode ν_{11}. This is also the case in the structurally similar molecule ρBQ, where a CH wagging mode of a_u (a_2 in C_{2v}) symmetry is strongly active. It is by analogy to ρBQ that we have assigned the $\Delta\tilde{\nu}$ = 860 cm^{-1} vibronic origin in PN to the a_2 mode ν_{11}'. It could, however, be of b_1 symmetry.

A very weak, comparatively sharp band at 27 292 cm^{-1} may well mark the origin of the $^3A_2$ ($n\pi^*$) system. If so, the 1068 cm^{-1} S_1–T_1 splitting is rather smaller than those in ρBQ (1) (1349 cm^{-1}) and TMCBD (4) (1410 cm^{-1}).

The effects of $n\pi^*$ excitation often extend beyond the C=O chromophore, and excited-state delocalization of this sort should be enhanced in molecules with conjugated C=O bonds. To assess the extent to which the effects of excitation are delocalized in PN, its $^1n\pi^*$ excited state is compared in Table 3 to the corresponding state in several other cyclic carbonyls.

In the spectra of most unconjugated carbonyl molecules, a progression in the C=O wagging mode indicates that the carbonyl group has become pyramidal in the $n\pi^*$ excited state. When the C=O bond is conjugated, however, as in acrolein (12), ρBQ, or 2-CP, the molecule retains its planar

Can. J. Chem. Downloaded from www.nrcresearchpress.com by 203.198.23.82 on 09/08/12
For personal use only.

TABLE 2. Observed bands (cm^{-1}) and assignments in the 353 nm absorption of PN

PN-h_4			PN-d_2			
$\tilde{\nu}$	Intensity	$\Delta\tilde{\nu}$	$\tilde{\nu}$	Intensity	$\Delta\tilde{\nu}$	Assignment[a]
27 292	VVW	(−1068)				Triplet origin?
27 970	VW	−390				13_1^0 (a_2)
28 075	VW	−285				$18_1^0 13_1^1$
28 210	W	−150	28 210	W	−150	18_1^0 (b_1)
28 360	(not obs.)		28 360	(not obs.)		0_0^0
28 370	VW	10				$18_0^1 13_1^1$
28 505	M	145	28 500	M	140	18_0^1 (b_1)
28 620	M	260	28 620	M	260	13_0^1 (a_2)
28 780	M	420	28 740	M	380	17_0^1 (b_1)
28 895	W	535				
29 090	M	730	28 965	M	605	$11_0^1 13_1^1$
29 220	S	860	29 105	S	745	11_0^1 (a_2?)[b]
			29 220	W		(PN-h_4 impurity)
29 310	VW	950	29 290	VW	930	$3_0^1 18_1^0 13_1^1$
29 440	W	1080	29 445	VW	1085	$3_0^1 18_1^0$
29 735	W	1375	29 745	VW	1385	$3_0^1 18_0^1$
29 850	W	1490	29 870	VW	1510	$3_0^1 13_0^1$
30 010	W	1650				$3_0^1 17_0^1$
30 320	W	1960	30 200	W	1840	$3_0^1 11_0^1 13_1^1$
30 460	S	2100	30 340	S	1980	$3_0^1 11_0^1$
			30 450	M		(PN-h_4 impurity)
30 630	W	2270				$4_0^1 11_0^1$
30 815	W	2455				
31 280	W	2920				
31 360	W	3000				
31 480	W	3120				
31 560	S	3300				$3_0^2 11_0^1$
31 840	M	3480				$3_0^1 4_0^1 11_0^1$
32 020	M	3660				$4_0^2 11_0^1$

[a]Symmetry of vibronic origins given in parentheses.
[b]Could be 12_0^1 (a_2) or 14_0^1 (b_1). See Table 1.

TABLE 3. Excited-state carbonyl group geometry, electronic origin, and excited state Franck–Condon active fundamentals (cm^{-1}) in the $^1n\pi^*$ spectra of some cyclic ketones

Molecule	Reference	Carbonyl geometry	Electronic origin	$\nu'_{C=O}$	$\nu'_{C=C}$
ρ-benzoquinone (ρBQ)	1	Planar	20 031	1068?[a]	
2-Cyclopenten-1-one (2CP)	5	Planar	27 211	1355	1416
4*H*-Pyran-4-one (PN)	This work	Planar	28 360	1240	1400
3-Cyclopenten-1-one (3CP)	5	Pyramidal	30 248	1239	Not observed
Cyclopentanone (CP)	2	Pyramidal	30 264	1225	Not observed

[a]Observed progression in 1068 cm^{-1} unlikely to be of pure $\nu_{C=O}$ character.

ground state geometry. PN fits into this pattern, as there is no evidence in the spectrum for a change of shape upon excitation.

Lengthening and weakening of the C=O bond upon $n\pi^*$ excitation is indicated by a progression in the C=O stretching mode, and a substantial reduction in its excited-state wavenumber, $\nu'_{C=O}$, from the ground state value of ca. 1750 cm^{-1}. The decrease in $\nu'_{C=O}$ should be less in conjugated molecules where the effects of excitation are delocalized over two or more bonds. Further evidence for this delocalization is a second progression in the stretching mode of the conjugated C=C bond. Thus, in the $^1n\pi^*$ spectra of acrolein (12) and 2CP, there are progressions of almost equal intensity in $\nu_{C=O}$ and $\nu_{C=C}$. In PN, however, the $\nu_{C=C}$ progression is much weaker than the $\nu_{C=O}$. Furthermore, as shown in Table 3, the value of $\nu'_{C=O}$ in PN is closer to that in the unconjugated molecules 3CP and CP than to that in the conjugated 2CP.

A conjugated C=O bond should also shift the $^1n\pi^*$ transition to lower energy. The PN electronic origin, though lower in energy than that of 3CP and CP, is significantly higher than that of 2CP.

Can. J. Chem. Downloaded from www.nrcresearchpress.com by 203.198.23.82 on 09/08/12
For personal use only.

Thus, although conjugation in the excited state of PN prevents its carbonyl group from becoming pyramidal, other effects of $n\pi^*$ excitation are less affected by conjugation in PN than in 2CP.

Finally, in many cyclic carbonyls, $n\pi^*$ excitation has been found to have a large effect on the low-wavenumber, out-of-plane vibrations of the ring (5). Ring bending fundamentals in ρBQ (1) and 3CP (5) increase by more than 30%, while the ring bending mode in 2CP (5), harmonic in the ground state, becomes markedly anharmonic upon excitation. In PN, on the other hand, ring bending (ν_{17} and ν_{18}) is hardly affected by excitation, while the ring twisting fundamental, ν_{13}, decreases by 34%.

Acknowledgments

We thank Mr. M. Mahon and Ms. A.R. Green for preliminary experimental work, and the Natural Sciences and Engineering Research Council of Canada for financial support. Three decades later, R.D.G. remains indebted to Dr. G.W. King for his infectious enthusiasm and wise counsel.

1. J.M. Hollas. Spectrochim. Acta, **20**, 1563 (1964).
2. H.E. Howard-Lock and G.W. King. J. Mol. Spectrosc. **36**, 53 (1970).
3. D.C. Moule. J. Chem. Phys. **64**, 3161 (1976).
4. R.D. Gordon, M. Caris, and D.G. Newman. J. Mol. Spectrosc. **60**, 130 (1976).
5. R.D. Gordon and D.R. Orr. J. Mol. Spectrosc. **129**, 24 (1988).
6. A. Maciejewski, M. Szymanski, and R.P. Steer. Chem. Phys. Lett. **143**, 559 (1988); H.K. Sinha, O.K. Abou-Zied, and R.P. Steer. Chem. Phys. Lett. **201**, 433 (1993).
7. J.N. Macdonald, S.A. Mackay, J.K. Tyler, A.P. Cox, and I.C. Ewart. J. Chem. Soc. Faraday Trans. 2, **77**, 79 (1981).
8. N. Ishibe, H. Sugimoto, and J.B. Gallivan. J. Chem. Soc. Faraday Trans. 2, **71**, 1812 (1975).
9. P. Csaszar, A. Csaszar, A. Somogyi, Z. Dinya, S. Holly, M. Gal, and J.E. Boggs. Spectrochim. Acta, **42A**, 473 (1986).
10. T.L. Smithson, N. Ibrahim, and H. Wieser. Can J. Chem. **61**, 1924 (1983).
11. P. Beak and G.A. Carls. J. Org. Chem. **29**, 2678 (1964); D.W. Mayo, P.J. Sapienza, R.C. Lord, and W.D. Phillips, J. Org. Chem. **29**, 2682 (1964).
12. J.C.D. Brand and D.G. Williamson. Discuss. Faraday Soc. **35**, 184 (1963).

Can. J. Chem. Downloaded from www.nrcresearchpress.com by 203.198.23.82 on 09/08/12
For personal use only.

Tetrakis[(trimethylsilyl)ethynyl] Group 14 metal derivatives: an examination of the electronic interaction between two Group 14 metals connected by an acetylene wire[1]

CAROL DALLAIRE,[1] MICHAEL A. BROOK,[2] ALEX D. BAIN, CHRISTOPHER S. FRAMPTON, AND JAMES F. BRITTEN

Department of Chemistry, McMaster University, 1280 Main St. W., Hamilton, ON L8S 4M1, Canada

Received March 10, 1993

This paper is dedicated to Professor Gerald W. King on the occasion of his 65th birthday

CAROL DALLAIRE, MICHAEL A. BROOK, ALEX D. BAIN, CHRISTOPHER S. FRAMPTON, and JAMES F. BRITTEN. Can. J. Chem. **71**, 1676 (1993).

The tetrakis(trimethylsilyl)ethynyl derivatives of Si, Ge, Sn, and Pb were prepared and examined spectroscopically. NMR and Mössbauer spectroscopy and X-ray crystal structure data clearly demonstrate an electronic interaction in the ground state between the distal $SiMe_3$ groups and the central metal atom, leading to a strong shielding of the central metal atom; the respective nmr signals of the central metal are among the most shielded examples reported for a tetrahedral Group 14 metal centre with four carbon ligands. The nature of these electronic interactions is discussed.

CAROL DALLAIRE, MICHAEL A. BROOK, ALEX D. BAIN, CHRISTOPHER S. FRAMPTON et JAMES F. BRITTEN. Can. J. Chem. **71**, 1676 (1993).

On a préparé les dérivés tétrakis(triméthylsilyl)éthynyles du Si, du Ge, du Sn et du Pb et on a examiné leurs spectres. Les spectres RMN et de Mössbauer et les données relatives aux structures cristallines démontrent clairement l'existence d'une interaction électronique dans l'état fondamental entre les groupes $SiMe_3$ distales et l'atome métallique central; ces interactions donnent lieu à un blindage important de l'atome métallique central et les signaux RMN respectifs de chaque métal central sont parmi les exemples les plus blindés rapportés pour un métal central tétraédrique du groupe 14 portant quatre coordinats carbonés. On discute de la nature de ces interactions électroniques.

[Traduit par la rédaction]

Can. J. Chem. Downloaded from www.nrcresearchpress.com by 203.198.23.82 on 09/08/12
For personal use only.

Introduction

Organosilicon chemistry has found extensive application in organic synthesis. This utility results primarily from the ability of silyl groups, usually trimethylsilyl groups, to behave as "super" (1) or "bulky" (2) protons. In essence, a $SiMe_3$ group is more electropositive than a proton and is thus more susceptible to nucleophilic attack on electronic grounds, but is less susceptible to nucleophilic attack for steric reasons. Thus, under conditions with which proton transfer readily takes place, the corresponding silyl groups are stable.

In the case of trimethylsilylalkynes, the materials are higher boiling and much more stable than the corresponding hydrocarbons, particularly in the case of diynes or polyynes (3). Thus, they have been used synthetically as surrogates for acetylenes and related alkynes, notably by Vollhardt (4) (Scheme 1). Polymeric versions of these compounds have also attracted attention recently as materials of potential interest for nonlinear optical applications (5); related materials have been examined as components of membranes (6). In both cases, the properties of interest in the polymers depend upon the presence of silicon in the molecules.

Silylalkynes will, however, react selectively with strong electrophiles. Indeed, under these conditions, the silylacetylenes are more reactive than the parent hydrocarbons. For example, a variety of Lewis acid activated electrophiles add cleanly to silylalkynes, leading to regioselective C—C bond formation (Scheme 2 (7), Scheme 3 (3)).

When compared with a simple alkyne, the origins of the reactivity of a silylalkyne towards electrophiles include the inductive effects of the silyl group, thermodynamic effects (the ultimate cleavage of silicon from the molecule is generally accompanied by the formation of a strong Si—X (X—Br, Cl, F, ≈96–193 kcal/mol) or Si—O bond (≈126–192 kcal/mol) at the expense of a Si—C bond (≈76 kcal/mol) (8), and the stabilization of the intermediate β-silyl vinyl cation via the β-effect.

As part of a program to try to establish the relative importance of these effects, we have been interested in studying the different mechanisms for and extent of electronic transmission from one Group 14 metal to another along an acetylene "wire" in the ground state.

During previous studies of the vinyl β-effect (9) we prepared a series of Group 14 dimetallated alkynes **1**, **2**, **3** and **4** (Fig. 1*a*) that appeared to be potential candidates for this study. The central metal is sensitive to a variety of spectroscopic techniques and can thus reflect the degree of electronic transmission from the distal $SiMe_3$ groups; any such transmission would be amplified by the presence of four distal $SiMe_3$ groups. In this paper, we report our examination of these compounds by different spectroscopic techniques to determine the extent of interaction between the two metals. The magnitude and mechanism of electronic transmission will be discussed.

Results

Preparation of compounds 1–4

The materials for this study can be conveniently prepared starting from lithium trimethylsilylacetylide, which is formed from the reaction of *n*-BuLi with trimethylsilylacetylene. With the exception of lead, the ensuing anion can be quenched by the readily available Group 14 chloro derivatives MCl_4 in THF to give, cleanly in most cases, the corresponding tetrakis(trimethylsilylethylnyl) metals

[1]Taken from the Ph.D. thesis of C.D., McMaster University, 1991.

[2]Author to whom correspondence may be addressed. Natural Sciences and Engineering Research Council University Research Fellow, 1985–1995.

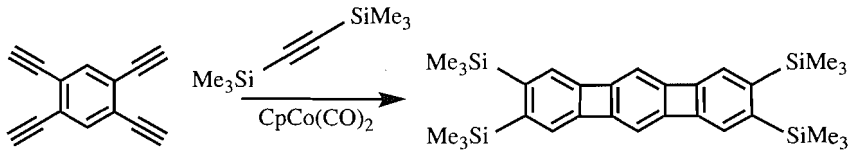

SCHEME 1

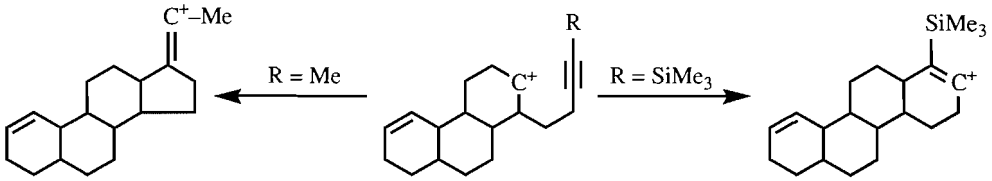

SCHEME 2

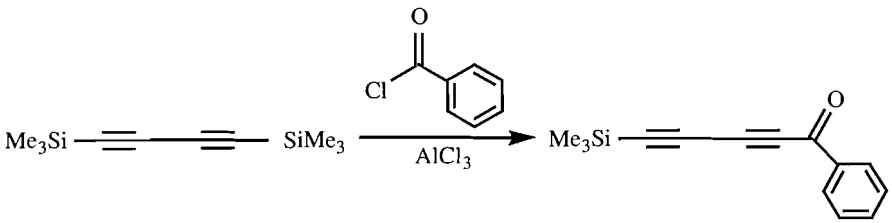

SCHEME 3

$M(C{\equiv}CSiMe_3)_4$ (M = Si **1**, Ge **2**, Sn **3**). The lead compound **4** was prepared by quenching $Pb(OAc)_4$ with $Me_3SiC{\equiv}CMgBr$ (prepared from $Me_3SiC{\equiv}CH$ and MeMgBr).

Spectroscopic characterization

These Group 14 nuclei are susceptible to examination by several spectroscopic methods; we have focused on NMR, Mössbauer spectroscopy and X-ray crystallography.

Nuclear magnetic resonance

The central metal

The nuclear magnetic resonance spectra of ^{1}H, ^{13}C, ^{29}Si and the remaining Group 14 elements (^{73}Ge for **2**, ^{119}Sn for **3**, ^{207}Pb for **4**) were measured for compounds **1**–**4**. As the chemical shifts of many Group 14 acetylides have been determined, it is relatively straightforward to evaluate by comparison the additional effect of a second Group 14 element on the alkyne.

Tetraalkynylmetals typically have large negative upfield shifts.[3] The presence of the four distal Me_3Si groups serves to substantially increase the upfield shifts of the central atom (Table 1). The chemical shifts reported here are among the furthest upfield to be reported for tetrahedral Group 14 metals substituted with four carbon ligands.

The distal Me_3Si groups

The central metal also has an effect on the terminal $SiMe_3$ groups. The ^{29}Si NMR chemical shifts show this to be small but observable; the effect of amplification has been lost (Table 2). The differences in the chemical shift correspond to increased shielding by the central atom as Si is substituted with less electronegative and more polarizable metals. The final entry in the table shows, additionally, how the degree of shielding is moderated by the type of carbon ligand on the central metal; less electronegative alkyl sp^3 hybridized carbon ligands, rather than alkyne *sp* orbital ligands, increase the degree of electronic shielding of the distal $SiMe_3$ by the central metal.

Mössbauer for tin

An additional diagnostic tool for tin compounds is Mössbauer spectroscopy. Regrettably, there are few reported values for alkynyltin compounds. Nevertheless, some general trends may be observed. An increase of *s* electron density is manifested in increased chemical isomer shifts. As *sp* orbitals are more electronegative than sp^2 or sp^3 orbitals, a decrease in chemical isomer shift is expected as sp^3 carbon ligands are sequentially replaced with sp^2 and *sp* hybridized ligands. Similarly, when electronegative groups on the alkyne terminus are replaced by electron-donating groups, an increase in isomer shift value is expected as *s* electron density is increased. However, any π-type interactions will have the effect of shielding the *s* electrons at the tin nucleus, decreasing the observed isomer shift (12). The data shown in Table 3, particular entry 12, demonstrate the latter effect (13, 14).

X-ray

We were unable to obtain suitable crystals for X-ray crystal structure analysis of the lead compound **4**. However, single crystals of compounds **2** and **3** could be readily analyzed; a structure for **1** has previously been reported (15). An ORTEP plot of the structure of **3** is shown in Fig. 1*b*; bond lengths and angles for **2** and **3** are collected in Tables 4, 5 and Tables 6, 7, respectively. A comparison of the C≡C bond lengths, the Me—Si—Me bond angles in the $SiMe_3$ groups,

[3]For a review of the NMR of the respective elements, see ref. 10*a*; see also, for Si, 10*b*, and for Sn, 10*c*.

Can. J. Chem. Downloaded from www.nrcresearchpress.com by 203.198.23.82 on 09/08/12
For personal use only.

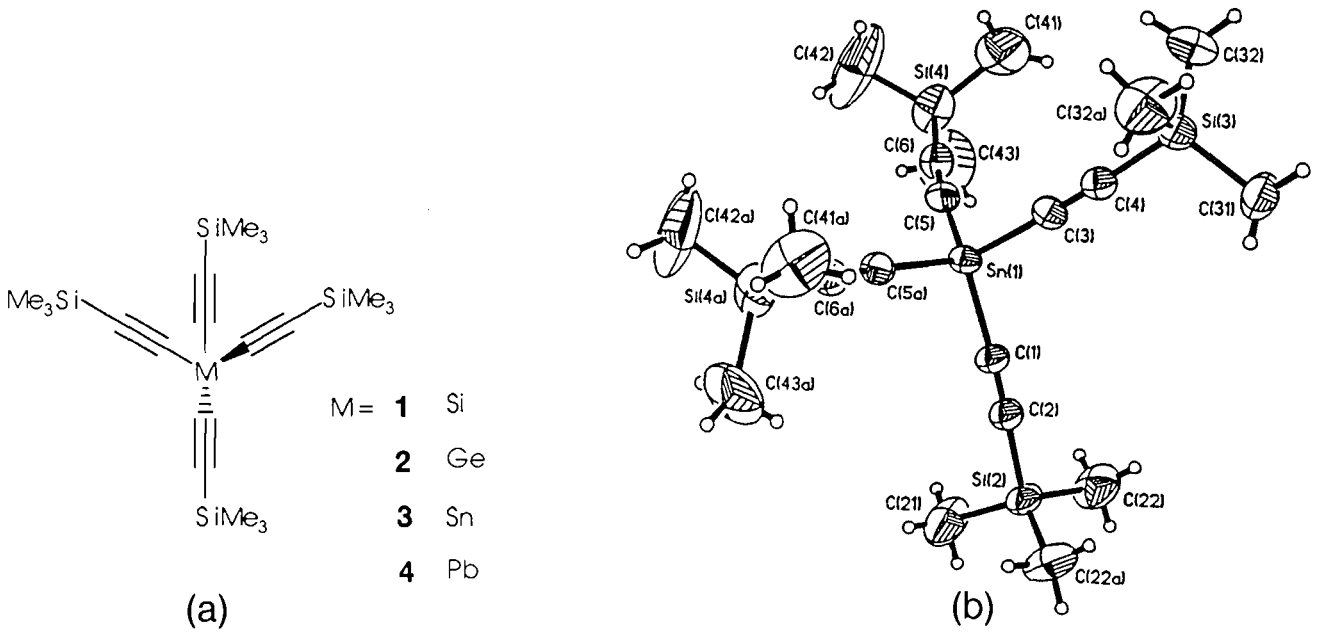

FIG 1. (*a*) The structure of compounds **1–4**; (*b*) ORTEP plot from the X-ray crystal structure of $(Me_3SiC{\equiv}C)_4Sn$ **3**.

TABLE 1. Central metal chemical shifts of the tetrakisacetylides **1–4** and related compounds

Entry	Compound	^{29}Si	^{73}Ge	^{119}Sn	^{207}Pb	Ref.
1	$(Me_3SiC{\equiv}C)_4$**Si**	−101.6				
2	$(Me_3SiC{\equiv}C)_4$**Ge**		−188.5			
3	$(HC{\equiv}C)_4$**Sn**			−356.4		11
4	$(Me_3SiC{\equiv}C)_4$**Sn**			−384.5		
5	$(MeC{\equiv}C)_4$**Pb**				−687.6	11
6	$(Me_3SiC{\equiv}C)_4$**Pb**				−760.7	
7	$(Me_3SiC{\equiv}C)_4$**Pb**				−551[a]	

[a]Solid state, non-spinning measurement. The chemical shifts of lead compounds are known to be strongly affected by solvent (10).

TABLE 2. ^{29}Si chemical shifts ($CDCl_3$) of the tetrakisacetylides and related compounds

Entry	Compound	Chemical Shift	Ref.
1	$Me_3SiC{\equiv}CH$	−17.5	11
2	$(Me_3SiC{\equiv}C)_4Si$	−17.5[a]	
3	$(Me_3SiC{\equiv}C)_4Ge$	−17.7	
4	$(Me_3SiC{\equiv}C)_4Sn$	−18.1	
5	$(Me_3SiC{\equiv}C)_4Pb$	−18.0	
6	$Me_3SiC{\equiv}CSiMe_3$	−19.3	11

[a]This study and ref. 11.

and the C≡C—**Si**—**Me** angles in the compounds we prepared and those to be found in the literature shows only small deviations. However, a comparison of R_3**M**—**C**≡C—X bond lengths is more intriguing (Table 8); clearly these bond lengths are very dependent upon the nature of the group on the other end of the acetylene wire (X) and the ligands (R) borne by the metal.

Beginning with a consideration of R_3M (R = trialkyl) compounds, a change from X = C to Si/Ge/Sn leads on average to a longer bond (1.84 Å (Table 8 entries 6 and 7) versus 1.83 Å (entries 2–4)). When that distal metal group bears electron-withdrawing ligands such as N*t*Bu or $(C{\equiv}CSiMe_3)_3$, the bond is further lengthened to 1.85 Å (entries 8–11). In contrast, if R = alkynyl, much shorter bond lengths can be seen (entry 12 versus 9–11, entry 16 versus 14 and 15).

Discussion

In all three spectroscopic techniques, we have seen evidence for electronic transmission between the two Group 14 elements linked by an acetylene. In the NMR experiments, this is manifested by significant shielding of the central metal in **1–4** by the four distal $SiMe_3$ groups and to a lesser extent of the $SiMe_3$ groups by the central metal, a significantly smaller Mössbauer isomer shift (I.S.) for the Sn derivatives when the distal $SiMe_3$ groups are present, and shorter bond lengths between the central metal and the adjacent C of the alkyne.

The electronic interaction between the two Group 14 metals could arise strictly from inductive donation through the σ-framework or from a combination of inductive effects and interactions of the π-system including resonance and π-polarization. The $SiMe_3$ group, as judged by Hammett parameters, possesses a very small capacity for σ-electronic donation (26); the parameters are −0.03 and −0.05 for σ_{meta}

Can. J. Chem. Downloaded from www.nrcresearchpress.com by 203.198.23.82 on 09/08/12
For personal use only.

TABLE 3. Mössbauer isomer shifts and quadrupole splittings for compound **3** and structurally related compounds

Entry	Compound	Chemical isomer shift[a]	Quadrupole splitting	Ref.
1	Me_3**Sn**CH=CH_2	1.30(5)	1.06(1)	13
2	Me_3**Sn**C≡C—Ph	1.23(5)	1.17(5)	13
3	Me_3**Sn**C≡C—$SiMe_3$	1.21(2)[b]	1.06(1)	
4	Me_3**Sn**C≡C—$CH(CH_3)_2$	1.15(5)	1.06(5)	13
5	Ph_3**Sn**C=CH_2	1.28(5)		13
6	Ph_3**Sn**C≡C—$SiMe_3$	1.20(4)[b]	0.84(1)	
7	**Sn**$(CH_2CH_3)_4$	1.33(8)		13
8	$(CH_3CH_2)_3$**Sn**C≡C—H	1.44(5)	1.42(5)	13
9	$(CH_3CH_2)_3$**Sn**C≡C—CH_3	1.37(5)	1.22(5)	13
10	$(CH_3CH_2)_3$**Sn**C≡C—CH_2CH_3	1.35(5)	1.05(5)	13
11	**Sn**$(CH=CH_2)_4$	1.22(5)		13
12	**Sn**$(C≡C—SiMe_3)_4$	0.82(2)[b]		

[a]Except as otherwise noted, measured against SnO_2 as the source.
[b]This study, measured against $CaSnO_3$ as the source.

TABLE 4. Bond lengths for tetrakis (trimethylsilylalkynyl)germanium **2** (Å)

Ge(1)—C(1)	1.889 (7)	Ge(1)—C(3)	1.894 (6)
Ge(1)—C(5)	1.893 (4)	Ge(1)—C(5A)	1.893 (4)
Si(2)—C(2)	1.851 (7)	Si(2)—C(21)	1.844 (9)
Si(2)—C(22)	1.855 (5)	Si(2)—C(22A)	1.855 (5)
Si(3)—C(4)	1.844 (6)	Si(3)—C(31)	1.862 (7)
Si(3)—C(32)	1.853 (5)	Si(3)—C(32A)	1.853 (5)
Si(4)—C(6)	1.847 (4)	Si(4)—C(41)	1.821 (6)
Si(4)—C(42)	1.852 (8)	Si(4)—C(43)	1.856 (7)
C(1)—C(2)	1.212 (9)	C(3)—C(4)	1.205 (8)
C(5)—C(6)	1.204 (5)		

and σ_{para}, respectively. Thus, the observations described above are better explained by a π-interaction that links the two Group 14 metals through the alkyne.

π-Type electronic interactions (conjugation) between Group 14 metals and adjacent C—C π-systems have previously been invoked for silicon, germanium, and tin compounds (27–30). The inclusion of a fourth atom in the conjugation, a distal Group 14 atom **M**—C≡C—Si, is a natural extension of this. The most compelling example of π-interactions between Group 14 substituted alkynes is in the UV spectra of silyl-terminated polyynes. These are considerably red shifted compared with the H or C terminated polyynes (20, 31).

π-Interactions may arise from either $(n–d)\pi$ or $(p–d)\pi$ (32) (or $(n–\sigma^*)\pi$ or $(p–\sigma^*)\pi$ interactions.[4] These would be anticipated to occur through σ*-orbitals in the case of silicon; *d* orbitals are apparently not very important in the interaction with first-row elements (32, 33). There is expected to be an increased propensity for *d* orbital involvement with the lower Group 14 elements. However, as has been noted by Dewar and co-workers (28), Whitesides et al. (29), and others, although *d* orbitals are energetically more available, they are increasingly mismatched in size with the C≡C π-system as one progresses down the periodic table, attenuating the resonance effect.

[4]See, however, counter arguments favouring the interaction of σ*-orbitals (33).

NMR

The chemical shift reflects the shielding a nucleus experiences. However, with the exception of protons, for which the correlation is reasonably straightforward, the nature of the electronic factors within the molecule that lead to an observed shift remains somewhat contentious. Nevertheless, it may be concluded that the observed magnitude of the change in chemical shift for the central metal is too large to originate, over three bonds, from σ-inductive effects alone. Chemical shifts are more dramatically affected by the presence of heteroatom lone pairs or π-systems on adjacent atoms. The large shift with four distal $SiMe_3$ groups (e.g., entries 3, 4, Table 1) reinforces the suggestion of a π-interaction between the two metals through the alkyne π-system.

Mössbauer

The Mössbauer results are also consistent with the proposed conjugation. Simple inductive effects by the distal $SiMe_3$ group would increase the *s* electron density and would be expected to lead to an *increase* in the Mössbauer I.S. in contrast to our observations. Again, this implies that electronic transmission between the Group 14 metals exists through the π-system of the alkyne.

X-ray

X-ray structures of polyynes and **1–3** show alternating single and triple bonds of essentially normal length (20) although some shortening of the single and lengthening of the triple bonds would be expected if π-conjugation was operative. The only significant shortening of single bonds arose with compounds **1–3** near the central atom. We attribute this to a π-polarization of the bond when the "spectator ligands" are *sp* ((R-*C*≡*C*)$_3$ **M**—**C**≡C-R′) rather than sp^3 hybridized ((R)$_3$ **M**—**C**≡C-R′).[5] Such an explanation cannot, however, account for the similarly short bond lengths in Me_3Si—$(C≡C)_4$-$SiMe_3$ (Table 8, entry 5) At the time, it was suggested that 1.20 Å was typical of C—Si bond lengths when the C ligand was *sp* hybridized. However, all crystal structures published since (Table 8) show significantly longer bond lengths (1.84 Å).

[5]We thank a referee for helpful suggestions in clarifying this.

Can. J. Chem. Downloaded from www.nrcresearchpress.com by 203.198.23.82 on 09/08/12
For personal use only.

TABLE 5. Bond angles for tetrakis(trimethylsilylalkynyl)germanium **2** (deg)

C(1)—Ge(1)—C(3)	111.0(2)	C(1)—Ge(1)—C(5)	108.9(1)
C(3)—Ge(1)—C(5)	107.8(1)	C(1)—Ge(1)—C(5A)	108.9(1)
C(3)—Ge(1)—C(5A)	107.8(1)	C(5)—Ge(1)—C(5A)	112.5(2)
C(2)—Si(2)—C(21)	106.6(3)	C(2)—Si(2)—C(22)	107.9(2)
C(21)—Si(2)—C(22)	112.0(2)	C(2)—Si(2)—C(22A)	107.9(2)
C(21)—Si(2)—C(22A)	112.0(2)	C(22)—Si(2)—C(22A)	110.2(3)
C(4)—Si(3)—C(31)	107.8(3)	C(4)—Si(3)—C(32)	107.2(2)
C(31)—Si(3)—C(32)	111.8(2)	C(4)—Si(3)—C(32A)	107.2(2)
C(31)—Si(3)—C(32A)	111.8(2)	C(32)—Si(3)—C(32A)	110.6(3)
C(6)—Si(4)—C(41)	108.3(2)	C(6)—Si(4)—C(42)	107.9(2)
C(41)—Si(4)—C(42)	109.8(4)	C(6)—Si(4)—C(43)	107.4(2)
C(41)—Si(4)—C(43)	110.7(3)	C(42)—Si(4)—C(43)	112.6(3)
Ge(1)—C(1)—C(2)	178.7(5)	Si(2)—C(2)—C(1)	179.0(5)
Ge(1)—C(3)—C(4)	176.2(5)	Si(3)—C(4)—C(3)	178.8(6)
Ge(1)—C(5)—C(6)	174.5(3)	Si(4)—C(6)—C(5)	176.7(3)

TABLE 6. Bond lengths for tetrakis(trimethylsilylalkynyl)tin **3** (Å)

Sn(1)—C(1)	2.076 (6)	Sn(1)—C(3)	2.060 (6)
Sn(1)—C(5)	2.060 (5)	Sn(1)—C(5A)	2.060 (5)
Si(2)—C(2)	1.849 (6)	Si(2)—C(21)	1.831 (8)
Si(2)—C(22)	1.848 (8)	Si(2)—C(22A)	1.848 (8)
Si(3)—C(4)	1.855 (7)	Si(3)—C(31)	1.866 (8)
Si(3)—C(32)	1.844 (7)	Si(3)—C(32A)	1.844 (7)
Si(4)—C(6)	1.842 (6)	Si(4)—C(41)	1.818 (10)
Si(4)—C(42)	1.779 (13)	Si(4)—C(43)	1.834 (10)
C(1)—C(2)	1.190 (9)	C(3)—C(4)	1.194 (9)
C(5)—C(6)	1.202 (7)		

Conclusion

Two Group 14 metals, connected by an acetylene wire, interact electronically through π-interactions. The effect is seen in the strong shielding of the central metal in compounds **1–4** and the low isomer shift in the Mössbauer spectrum of **3**. Any effect of π-conjugation is insufficiently strong to affect the C≡C bond length, as shown from the X-ray crystal structures of **1–3**; π-polarization is a better explanation of these results.

Experimental

Apparatus, materials, and methods

Due to the hydrolytic instability of the halogen derivatives of the Group 14 metals, all reactions were carried out in dry apparatus under a nitrogen atmosphere using septa and syringes for the transfer of reagents. Methylchlorosilanes were obtained from Dow Corning. Other silicon, germanium, tin, and lead compounds were obtained from Aldrich. All compounds were distilled prior to use. Tetrahydrofuran (THF) and diethyl ether were freshly distilled under a nitrogen atmoshere over benzophenone/potassium. Dichloromethane (CH_2Cl_2) was freshly distilled under a nitrogen atmosphere over calcium hydride (CaH_2) or phosphorus pentoxide (P_2O_5). Chloroform-*d* was obtained from Merck Sharp and Dohme Isotopes, Montreal, and used without further purification. (Trimethylsilyl)acetylene ($Me_3SiC{\equiv}CH$) was obtained from Aldrich or prepared according to ref. 34, by reaction of $LiC{\equiv}CH$ with Me_3SiCl.

The continuous wave ^1H NMR spectra were recorded on a Varian EM 390 (90 MHz) spectrometer and the Fourier spectra on a Bruker AM 500 (500 MHz) or Bruker AC 200 (200 MHz) spectrometer. ^{13}C, ^{29}Si, ^{73}Ge ^{119}Sn, and ^{207}Pb NMR measurements were performed on a Bruker WM 250 (at 250 MHz for protons). The ^{207}Pb solid state NMR spectrum was measured on a Bruker MS-100 spectrometer. Unless otherwise specified, the samples were dissolved in chloroform-*d* using tetramethylsilane (TMS) as internal standard ($SnMe_4$ for tin, $PbMe_4$ for lead, and $GeMe_4$ for germanium, respectively). Coupling constants (*J*) are recorded in hertz (Hz). The abbreviations s = singlet, d = doublet, t = triplet, dd = doublet of doublets, dt = doublet of triplets, dq = doublet of quartets, and m=multiplet are used in reporting the spectra.

EI mass spectra and chemical ionization (NH_3) mass spectra were recorded at 70 eV with a source temperature of ca. 200°C either on a VG Micromass 7070 F mass spectrometer equipped with a data system comprising a PDP 8A with VG 2000 software or a VG analytical ZAB E mass spectrometer equipped with a VG 11-250 data system. High-resolution mass spectral (HRMS) data were obtained with the VG-ZAB-E instrument by the electron impact (EI) method.

Infrared spectra were run on a Perkin–Elmer 283 spectrometer in $CHCl_3$ solution, $CHCl_3$ film, neat film, or as a KBr pellet.

For ^{119}Sn Mössbauer spectroscopy, thin powdered samples, prepared by grinding the crystalline material to prevent preferred orientation of the crystallites, were pressed into Kel-F sample holders. Mössbauer spectra were recorded at 80 K using an Elscint constant acceleration spectrometer with an MCDPC-IBM AT acquisition system manufactured by CMTE. The samples were cooled in a Technology Systems cryostat. The source was ^{119}Sn (5 mCi, Amersham), in a calcium stannate matrix. The velocity scale was calibrated with a standard iron foil absorber and a $^{57}Co/Rh$ source mounted on the reverse end of the transducer. Calibration spectra were thus recorded without interruption of the drive sequence. The calibration spectra were computer fitted to give a linear velocity scale and folding point. Folded ^{119}Sn spectra were computer fitted using a modified version of the program GMFP (35). All isomer shifts are referenced to a thin absorber of $CaSnO_3$ at room temperature.

Single colourless cubic crystals of $Sn(C{\equiv}CSiMe_3)_4$ and $Ge(C{\equiv}CSiMe_3)_4$ were grown from hexane. X-ray diffraction was performed on a Nicolet R3 using MoKα radiation at 183 K. The relevant information is available in Tables 9*a–f* (compound **2**) and Tables 10*a–f* (compound **3**).[6]

General preparative procedure of $(Me_3SiC{\equiv}C)_4M$

For the silicon species, the tetrakis species **1** and $Cl_3SiC{\equiv}CSiMe_3$ were prepared simultaneously.

[6]Tables 9 and 10 can be purchased from: The Depository of Unpublished Data, Document Delivery, CISTI, National Research Council Canada, Ottawa, ON K1A OS2, Canada.

These tables have also been deposited with the Cambridge Crystallographic Data Centre, and can be obtained on request from The Director, Cambridge Crystallographic Data Centre, University Chemical Laboratory, 12 Union Road, Cambridge, CB2 1EZ, U.K.

Can. J. Chem. Downloaded from www.nrcresearchpress.com by 203.198.23.82 on 09/08/12
For personal use only.

TABLE 7. Bond angles for tetrakis(trimethylsilylalkynyl)tin **3** (deg)

C(1)—Sn(1)—C(3)	110.8(2)	C(1)—Sn(1)—C(5)	108.9(1)
C(3)—Sn(1)—C(5)	107.9(1)	C(1)—Sn(1)—C(5A)	108.9(1)
C(3)—Sn(1)—C(5A)	107.9(1)	C(5)—Sn(1)—C(5A)	112.4(3)
C(2)—Si(2)—C(21)	105.8(3)	C(2)—Si(2)—C(22)	107.3(2)
C(21)—Si(2)—C(22)	113.9(3)	C(2)—Si(2)—C(22A)	107.3(2)
C(21)—Si(2)—C(22A)	113.9(3)	C(22)—Si(2)—C(22A)	108.1(5)
C(4)—Si(3)—C(31)	106.9(3)	C(4)—Si(3)—C(32)	106.8(3)
C(31)—Si(3)—C(32)	112.2(3)	C(4)—Si(3)—C(32A)	106.8(3)
C(31)—Si(3)—C(32A)	112.2(3)	C(32)—Si(3)—C(32A)	111.5(4)
C(6)—Si(4)—C(41)	107.4(4)	C(6)—Si(4)—C(42)	108.6(4)
C(41)—Si(4)—C(42)	113.1(6)	C(6)—Si(4)—C(43)	107.3(4)
C(41)—Si(4)—C(43)	106.8(4)	C(42)—Si(4)—C(43)	113.3(6)
Sn(1)—C(1)—C(2)	178.3(5)	Si(2)—C(2)—C(1)	178.4(6)
Sn(1)—C(3)—C(4)	178.4(5)	Si(3)—C(4)—C(3)	177.4(6)
Sn(1)—C(5)—C(6)	173.8(4)	Si(4)—C(6)—C(5)	177.2(4)

TABLE 8. Selected bond lengths for compounds **1–4** and related structures[a]

Entry	Compound	R_3C-C≡C—M	R_3M-C≡C—M	$(R\text{-}C{\equiv}C)_3M$—C≡C-M	Ref.
1	$Fe_2(CO)_7[Me_3Si\text{-}C{\equiv}C\text{-}C{\equiv}C\text{—}SiMe_3]_2$	1.88(2)			16
2	Steroid-CH(OH)-C≡C—$SiMe_3$	1.839			17
3	Me_3Si—C≡C-complex pyrrole	1.834			18
4	$C_6(\text{-}C{\equiv}C\text{—}SiMe_3)_6$	1.836			19
5	Me_3Si—C≡C-C≡C-C≡C-C≡C—$SiMe_3$		1.821[b]		20
6	$[\text{-}Me_2Si\text{—}C{\equiv}C\text{—}SiMe_2(CH_2)_n\text{-}]_2$				
	n = 1–4		1.843		21
7	$[\text{-}(CH_3)_2Si\text{—}C{\equiv}C\text{-}Si(CH_3)_2\text{-}]_2$		1.841		22
8	tBu$_2$(tBuNH)Si—C≡C—Si(tBuNH)tBu$_2$		1.851		23
9	$(Me_3Si\text{—}C{\equiv}C\text{-})_4$Sn **3**		1.853		
10	$(Me_3Si\text{—}C{\equiv}C\text{-})_4$Si **1**		1.854		
11	$(Me_3Si\text{—}C{\equiv}C\text{-})_4$Ge **2**		1.865		
12	$(Me_3Si\text{-}C{\equiv}C\text{—})_4$**Si 1**			1.824	
13	$(Me_3Si\text{-}C{\equiv}C\text{—})_4$**Ge 2**			1.895	
14	$o\text{-}C_6H_4(\text{-}C{\equiv}C\text{—}SnMe_3)_2$	2.09(1)			24
15	$Me_3Sn\text{-}C{\equiv}C\text{-}C{\equiv}C\text{-}SnMe_3$		2.136[b]		25
16	$(Me_3Si\text{-}C{\equiv}C\text{—})_4$**Sn 3**			2.067	

[a]The values presented are mean values from within a given structure.
[b]Because of the extended conjugation, we include this in the dimetallated group.

To a solution of $Me_3SiC{\equiv}CH$ (7.9 mL, 70.8 mmol) in THF (40 mL) at 0°C was added *n*-BuLi (1.4 in hexanes, 51 mL, 72 mmol). This solution was added slowly over 30 min at 0°C to the metal tetrachloride (e.g., $SiCl_4$; 65 mL, 8 equiv., 567 mmol) in dichloromethane (CH_2Cl_2; 200 mL) and stirred over 18 h. Then the solvent was removed by simple distillation and the residue was distilled at 55°C/15 Torr (1 Torr = 133.3 Pa) to give 3.5 g of $Cl_3Si\text{-}C{\equiv}C\text{-}SiMe_3$ (15.1 mmol, 21% yield). Afterwards, the residue was washed with water, extracted with ether, and recrystallized several times in hexane to give 3 g of **1** (7.1 mmol, 41% yield) (36).

The syntheses of the other metallated (trimethylsilyl) acetylide compounds were performed with some modifications to the procedures reported in the literature. The syntheses were done as described above by the reaction of lithium salt of (trimethylsilyl)acetylide ($Me_3Si\text{-}C{\equiv}C\text{-}$, 4.0 equiv.) with the appropriate silyl, germyl, or stannyl chloride compounds in tetrahydrofuran or ether (37). In these cases, chlorometal derivatives were not obtained as coproducts.

Spectral data

*Tetrakis[(trimethylsilyl)ethynyl]silane ($(Me_3SiC{\equiv}C)_4Si$) **1**:* mp 154–159°C (from hexane) (lit. (15) mp 160°C (from petroleum ether): IR (CH_2Cl_2) ν(cm^{-1}): 2965 h, 2900 m, 2010 m, 1950 w, 1875 w, 1400 m, 1250 st, 900-720 st, 700 st, 480 st, 290 st; ^{1}H NMR ($CDCl_3$, 200 MHz): δ(ppm) = 0.21 (s); ^{13}C NMR ($CDCl_3$, 62.9 MHz) δ(ppm): 117.2, 104.2, −0.3; ^{29}Si NMR ($CDCl_3$, 49.69 MHz) δ(ppm): −17.5, −101.6; MS (EI, *m/z*): 416 (M^+, 21), 401 (34), 343 (12), 328 (11), 313 (100), 231 (29), 179 (32), 155 (56); HRMS, mass calcd. 416.1669; observed: 416.1663.

*Tetrakis[(trimethylsilyl)ethynyl]germane ($(Me_3SiC{\equiv}C)_4Ge$) **2** (ref. 36):* Yield: 94% (lit. (36) yield 58%); mp 175–176°C (from petroleum ether) (lit. (36) mp 176°C); IR (KBr) ν(cm^{-1}) 2970 st, 2900 m, 2105 w, 2000 w, 1955 w, 1870 w, 1450 w, 1410 m, 1315 w, 1255 st, 850 st, 760 st, 820 st, 405 m, 305 m, 300 st; ^{1}H NMR ($CDCl_3$, 200 MHz) δ(ppm): 0.21 (s); ^{13}C NMR ($CDCl_3$, 62.9 MHz) δ(ppm): 114.0, 102.1, −0.3; ^{29}Si NMR ($CDCl_3$, 49.69 MHz) δ(ppm): −17.7; ^{73}Ge NMR ($CDCl_3$, 8.73 MHz) δ(ppm): −188.5 (line width of 125 Hz); MS (EI, *m/z* reported for ^{74}Ge isotope): 447 (41), 389 (18), 359 (25), 253 (10), 229 (12), 201 (53), 155 (18), 119 (100), 97 (32), 73 (95); HRMS; (M^+ reported for ^{74}Ge isotope), mass calcd. for M^+ + 1:461.1028; observed for M^+ + 1:461.1032.

*Tetrakis[(trimethylsilyl)ethylnyl]stannane ($(Me_3Si\text{-}C{\equiv}C\text{-})_4Sn$) **3** (ref. 36):* Yield: 73% (lit. (36) yield 35%); mp 170–172°C (from petroleum ether or hexane) (lit. (36) mp (dec.) 140°C (from petroleum ether)); IR (KBr) ν(cm^{-1}) 2960 st, 2900 m, 2090 w, 2010 w, 1950 w, 1865 w, 1405 m, 1310 m, 1250 st, 840 st, 755 st, 695 st, 605 m; ^{1}H NMR ($CDCl_3$, 200 MHz) δ(ppm): 0.21 (s); ^{13}C NMR ($CDCl_3$, 62.9 MHz) δ(ppm): 119.5, 103.2, −0.3; ^{29}Si NMR

Can. J. Chem. Downloaded from www.nrcresearchpress.com by 203.198.23.82 on 09/08/12
For personal use only.

Can. J. Chem. Downloaded from www.nrcresearchpress.com by 203.198.23.82 on 09/08/12
For personal use only.

($CDCl_3$, 49.69 MHz) δ(ppm): −18.1; ^{119}Sn NMR ($CDCl_3$, 93.28 MHz) δ(ppm): −384.5; MS (EI, *m/z* reported for ^{119}Sn isotope): 508 (M^+, 15), 493 (17), 405 (16), 314 (72), 247 (83), 217 (35), 179 (80), 165 (86), 119 (30), 97 (100), 73 (79); HRMS (M^+ reported for ^{119}Sn isotope), mass calcd. 508.0916; observed: 508.0915.

Trimethylstannyl(trimethylsilyl)acetylene (Me_3Si-C≡C-$SnMe_3$) (ref. 38): Yield: 71% (lit. (38) yield 68%) bp ~25°C at 1 Torr; IR (neat) ν(cm^{-1}): 2965 st, 2920 st, 2905 st, 2370 w, 2075 w, 1450 m, 1405 m, 1305 w, 1245 st, 1190 w, 830 st, 750 st, 690 st; ^{1}H NMR ($CDCl_3$, 200 MHz) δ(ppm): 0.28 (s, 9H), 0.16 (s, 9H); ^{13}C NMR ($CDCl_3$, 62.9 MHz) δ(ppm): 117.6, 113.2, 0.5, −7.4; ^{29}Si NMR ($CDCl_3$, 49.69 MHz) δ(ppm): −20.9; ^{119}Sn NMR ($CDCl_3$, 93.28 MHz) δ(ppm): −73.6; MS (EI, *m/z* reported for ^{119}Sn isotope): 247 ($M^+ - CH_3$, 100), 217 (12), 185 (6); HRMS (M^+ reported for ^{119}Sn isotope), mass calcd. for $M^+ - CH_3$: 246.9965; observed for $M^+ - CH_3$: 246.9984.

Triphenylstannyl(trimethylsilyl)acetylene (Me_3SiC≡$CSnPh_3$) (ref. 39): Yield: 92% (lit. (39) yield 61%); mp 73–74°C (lit. (39) mp 74–76°C); ^{1}H NMR ($CDCl_3$, 200 MHz) δ(ppm): 7.75–7.65 (m, 6H), 7.5–7.4 (m, 9H), 0.3 (s, 9H); ^{13}C NMR ($CDCl_3$, 62.9 MHz) δ(ppm): 139.9, 136.7, 129.5, 129.2, 121.4, 108.7, 0.17; ^{29}Si NMR ($CDCl_3$, 49.69 MHz) δ(ppm): −19.5; ^{119}Sn NMR ($CDCl_3$, 93.28 MHz) δ(ppm): −175.4; MS (EI, *m/z* reported for ^{119}Sn isotope): 448 (M^+, 3), 433 (5), 371 (39), 341 (4), 294 (3), 274 (35), 221 (27), 197 (37), 159 (50), 135 (32), 120 (100), 97 (18); HRMS (M^+ reported for ^{119}Sn isotope), mass calcd.: 448.0669; observed: 448.0677.

*Tetrakis[(trimethylsilyl)ethynyl]plumbane ($(Me_3Si$-C≡C$)_4Pb$) **4***

A solution of methylmagnesium bromide (3 M in ether, 5.9 mL, 17.7 mmol) was added slowly to a solution of (trimethylsilyl)acetylene (Me_3Si-C≡C-MgBr, 2.5 mL, 17.7 mmol) in tetrahydrofuran (20 mL) at 0°C. The solution was stirred 1 h at 0°C and about 1.5 h at room temperature until no more bubbles were observed. After cooling at 0°C, lead tetraacetate (0.8 g, 1.8 mmol) was added through glass tubing under a nitrogen atmosphere over 30 min. The mixture was stirred 1 h at 0°C and 4.5 h at room temperature (brown solution). After work-up with 1% aqueous HCl and water, the product was extracted with diethyl ether and the solution dried over magnesium sulfate. The crude compound was recrystallized in hexane. Yield: 37% (lit. (36) yield 47%); mp 155°C (dec.) (lit. (36) mp 108°C (from petroleum ether)); ^{1}H NMR ($CDCl_3$, 200 MHz) δ(ppm): 0.21 (s); ^{13}C NMR ($CDCl_3$, 62.9 MHz), δ(ppm): 117.4, 111.7, −0.3; ^{29}Si NMR ($CDCl_3$, 49.69 MHz) δ(ppm): −18.0; ^{207}Pb NMR ($CDCl_3$, 52.33 MHz) δ(ppm): −760.7 (line width of 40 Hz); ^{207}Pb NMR (solid state without spinning, 20.93 MHz) δ(ppm): −551 (line width of 100 Hz); MS (EI, *m/z* reported for ^{208}Pb isotope): 581 ($M^+ - CH_3$, 11), 551 (4), 493 (41), 402 (20), 335 (13), 305 (100), 290 (95), 261 (23).

Acknowledgments

We gratefully acknowledge the financial support of the Natural Sciences and Engineering Research Council of Canada. We also thank Dow Corning Canada for providing some of the methylchlorosilanes used in this study.

1. I. Fleming. Organosilicon compounds. *In* Comprehensive organic chemistry. *Edited by* D.H.R. Barton and W.D. Ollis. Pergamon, New York. 1979. Vol. 3, Chap. 13, p. 544.
2. J.R. Hwu and N. Wang. Chem. Rev. **89**, 1599 (1989); J.R. Hwu and J.M. Wetzel. J. Org. Chem. **50**, 3946 (1985).
3. D.R.M. Walton and F. Waugh. J. Organomet. Chem. **37**, 45 (1972), and references cited therein.
4. K.P.C. Vollhardt. Angew. Chem. Int. Ed. Engl. **23**, 539 (1984), and references cited therein.
5. R. Bortolin, S.S.D. Brown, and B. Parbhoo. Macromolecules, **23**, 2465 (1990); T.J. Barton and S. Ijadi-Maghsoodi. Macromolecules, **24**, 1257 (1991); Macromolecules, **23**, 4485 (1990); T.J. Barton, Y. Pang, and S. Ijadi-Maghsoodi. J. Polym. Sci. Part A: Polym. Chem. **28**, 935 (1990).
6. T. Masuda and T. Higashimura. *In* Silicon-based polymer Science. *Edited by* J.M. Ziegler and F.W.G. Fearon. Adv. Chem. Ser. 224, Washington, D.C. 1990. Chap. 35, pp. 641–661; T. Masuda, T. Hamano, K. Tsuchihara, and T. Higashimura. Macromolecules, **23**, 1374 (1990); T. Masuda, M. Takatsuka, B.Z. Tang, and T. Higashimura. J. Membr. Sci. **49**, 69 (1990).
7. W.S. Johnson, T.M. Yarell, R.F. Myers, D.R. Morton, and S.G. Boots. J. Org. Chem. **45**, 1254 (1980).
8. E. Colvin. Silicon in organic synthesis. Butterworths, London 1981. p. 4.
9. M.A. Brook and C. Dallaire. Organometallics, **9**, 2873 (1990); C. Dallaire and M.A. Brook. Organometallics, **12**, 2332 (1993).
10. (*a*) R.K. Harris and B.E. Mann *Editors* NMR and the periodic table. Academic, London. 1978; (*b*) R.B. Taylor, B. Parbhoo, and D.M. Fillmore. *In* The analytical chemistry of silicones. *Edited by* A.L. Smith. Wiley, New York. 1991; (*c*) P.J. Smith and A.P. Tupciauskas. Annu. Rep. NMR Spectrosc. **8**, 291 (1978); V.S. Petroxyan. Prog. NMR Spectrosc. **11**, 115 (1977).
11. S. Kerschl, A. Sebald, and B. Wrackmeyer. Magn. Reson. Chem. **23**, 514 (1985).
12. K. Schlosser, E. Hoyer, and D. Arnold. Spectrochim. Acta, Part A: **30A**, 1431 (1974); W.R. Cullen, J.R. Sams, and J.A. Thompson. Inorg. Chem. **10**, 843 (1971); D.E. Williams and C.W. Kocher. J. Chem. Phys. **52**, 1480 (1970).
13. J.J.Zuckerman. Adv. Organomet. Chem. **9**, 22 (1971).
14. P.J. Smith. Organomet. Chem. Rev. A, **5**, 373 (1970); T.C. Gibb. Principles of Mössbauer spectroscopy. Chapman and Hall, London. 1976; P.A. Flinn. *In* Mössbauer isomer shifts. *Edited by* G.K. Shenoy and F.E. Wagner. North Holland, Amsterdam. 1978.
15. H. Schmidbaur, J. Ebenhoch, and G. Müller. Z. Naturforsch. B: Chem. Sci. **43**, 49 (1988).
16. R.C. Pettersen and G.G. Cash. Inorg. Chim. Acta, **34**, 261 (1979).
17. F.H. Allen, W.B.T. Cruse, and O. Kennard. Acta Crystallogr. Sect. B: Struct. Crystallogr. Cryst. Chem. **B36**, 2337 (1980).
18. T. Kusumoto, T. Hiyama, and K. Ogata. Tetrahedron Lett. **35**, 4197 (1986).
19. R. Diercks. J.C. Armstrong, R. Boese, and K.P.C. Vollhardt. Angew. Chem. Int. Ed. Engl. **25**, 268 (1986).
20. B.F. Coles, P.B. Hitchcock, and D.R.M. Walton. J. Chem. Soc. Dalton Trans. 445 (1975).
21. G.Å. Eliassen, E. Kloster-Jensen, and C. Rømming. Acta Chem. Scand. Ser. B: **40**, 574 (1986).
22. H. Sakurai, Y. Nakadaira, A. Hosomi, Y. Eriyama, and C. Kabuto. J. Am. Chem. Soc. **105**, 3359 (1983).
23. W. Clegg, W. Klingebiel, J. Neemann, G.M. Sheldrick, and N. Vater. Acta Crystallogr. Sect. B: Struct. Crystallogr. Cryst. Chem. **B37**, 987 (1981).
24. G. Adiwidjaja and G. Grouhi-Witte. J. Organomet. Chem. **188**, 91 (1980).
25. C. Brouty, P. Spinal, and P. Whuler. Acta Crystallogr. Sect. B: Struct. Crystallogr. Cryst. Chem. **B36**, 2624 (1980).
26. A.R. Bassindale and P.G. Taylor. *In* The chemistry of organic silicon compounds. *Edited by* S. Patai and Z. Rappoport. Wiley, Chichester. 1989. Chap. 13, pp. 893–963.
27. Yu.V. Kolodyazhnyi, N.I. Sizova, I.G. Lorents, L.I. Kuznetsova, A.P. Sadimenko, L.I. Ol'khovskaya, and N.V. Komarov. Zh. Obshch. Khim. **52**, 1855 (1982); Yu. V. Kolodyazhnyi, I.G. Lorents, S.B. Bulgarevich, A.P. Sadimenko, L.I. Ol'khovskaya, N.V. Komarov, and O.A. Osipov. Zh. Obshch. Khim. **54**, 2594 (1984).
28. P.K. Bischof, M.J.S. Dewar, D.W. Goodman, and T.B. Jones. J. Organomet. Chem. **82**, 89 (1974).

29. G.M. Whitesides, J.G. Segestad, S.P. Thomas, D.W. Andrews, B.A. Morrison, E.J. Panek, and J. san Filippio, Jr. J. Organomet. Chem. **22**, 365 (1970); G. Eng and C.R. Dillard. Inorg. Chim. Acta, **31**, 227 (1978); Inorg. Chim. Acta, **28**, 99 (1978); N.W. Alcock, M. Pierce-Butler, G.R. Willey, and K. Wade. J. Chem. Soc. Chem. Commun. 183 (1975); D.R. Eaton and W.R. McClellan. Inorg. Chem. **6**, 2134 (1967).
30. C. Cauletti, C. Furlani, G. Granozzi, A. Sebald, and B. Wrackmeyer. Organometallics, **4**, 290 (1985).
31. R. Eastmond, T.R. Johnson, and D.R.M. Walton. Tetrahedron, **28**, 4601 (1972).
32. W. Adcock and G.L. Aldous. Tetrahedron Lett. **28**, 3387 (1970); H. Janes and E. Oldfield. J. Am. Chem. Soc. **108**, 5743 (1986); E. Kupce, E. Liepin, E. Zicmane, and E. Lukevics. J. Chem. Soc. Chem. Commun. 819 (1989).
33. B.T. Luke, J.A. Pople, M.-B. Krogh-Jespersen, Y. Apeloig, J. Chandrasekhar, and P. von R. Schleyer. J. Am. Chem. Soc. **108**, 260 (1986); E.R. Reed, C. Schade, P. von R. Schleyer, P.V. Kamath, and J. Chandrasekhar. J. Chem. Soc. Chem. Commun. 67 (1988); B. Rempfer, H. Oberhammer, and N. Auner. J. Am. Chem. Soc. **108**, 3893 (1986).
34. L. Brandsma and H.D. Verkruijsse. Synthesis of acetylenes, allenes and cumulenes. *In* Study in organic chemistry. Vol. 8. Elsevier, New York. 1981. p. 55.
35. K. Ruebenbauer and T. Birchall. Hyperfine Interact. **7**, 125 (1979).
36. (*a*) N.V. Komarov and O.G. Yarosh. J. Gen. Chem. USSR (Engl. Transl.), **37**, 260 (1967); (*b*) M.F. Shostakovskii, N.V. Komarov, and O.G. Yarosh. Bull. Acad. Sci. URSS Div. Chem. Sci. 2458 (1967).
37. N.J. Fitzmaurice, R. Jackson, and P. Perlmutter. J. Organomet. Chem. **285**, 375 (1985).
38. W. Findeiss, W.E. Davidsohn, and M.C. Henry. J. Organomet. Chem. **9**, 435 (1967).
39. C.S. Kraihanzel and M.L. Losee. J. Organomet. Chem. **10**, 427 (1967).

Can. J. Chem. Downloaded from www.nrcresearchpress.com by 203.198.23.82 on 09/08/12
For personal use only.

x–y Coriolis interaction in the ν_5 and ν_8 bands of propyne-d_3

GEETHA RAJAPPAN AND V.A. JOB[1]

Spectroscopy Division, Bhabha Atomic Research Centre, Bombay, 400 085, India

Received March 22, 1993

This paper is dedicated to Professor Gerald W. King on the occasion of his 65th birthday

GEETHA RAJAPPAN and V.A. JOB. Can. J. Chem. **71**, 1684 (1993).

High resolution Fourier transform spectra of the ν_5 and ν_8 bands of $CD_3C{\equiv}CH$ have been recorded and analyzed taking into account the strong x–y Coriolis interaction between these fundamentals. Fermi resonance of the ν_8 state with the $\nu_9 + \nu_{10}$ state, l-type doubling interaction between the $\pm l$ components of ν_8 and a weak k-type doubling interaction between the ν_5 and ν_8 states have also been included in the perturbation treatment. The parameters of the ν_5 and ν_8 states as well as some of the parameters of the unobserved $\nu_9 + \nu_{10}$ state have been determined. An estimate of the relative value of the transition moments has been obtained from the line intensities, which are strongly affected by the x–y Coriolis interaction.

GEETHA RAJAPPAN et V.A. JOB. Can. J. Chem. **71**, 1684 (1993).

On a enregistré les spectres à haute résolution par transformation de Fourier des bandes ν_5 et ν_8 du $CD_3C{\equiv}CH$ et on les a analysées en tenant compte de l'importante interaction x–y de Coriolis entre ces fondamentales. Dans le traitement de perturbation, on a aussi inclus la résonance de Fermi de l'état ν_8 avec l'état $\nu_9 + \nu_{10}$, l'interaction de duplication de type l entre les composantes $\pm l$ de ν_8 et la faible interaction de duplication de type k entre les états ν_5 et ν_8. On a déterminé les paramètres des états ν_5 et ν_8 ainsi que d'autres paramètres qui n'ont pas été observés pour l'état $\nu_9 + \nu_{10}$. On a pu évalué la valeur relative des moments de transition à partir des intensités des raies qui sont fortement affectées par l'interaction x–y de Coriolis.

[Traduit par la rédaction]

I. Introduction

The rotational structure of the ν_5 and ν_8 bands of propyne, $CH_3C{\equiv}CH$, has been studied by laser Stark spectroscopy (1–4) and Fourier transform spectroscopy (5). Even though the possibility of vibration–rotation interactions between these two fundamentals has been recognized (5), no attempt was made to include these interactions in the analyses. In propyne, these two fundamentals are separated by more than 100 cm^{-1} and, indeed, the interactions are weak. However, in the deuterated species, $CD_3C{\equiv}CH$, they are separated by only ~4.2 cm^{-1} and a strong interaction results. The dominant interaction between a nondegenerate a_1 mode and a degenerate e mode of a molecule belonging to the C_{3v} point group is x–y Coriolis interaction. It was pointed out by Di Lauro and Mills (6) that, in addition to shifting the line positions, the interaction can have a striking effect on the observed intensities of the spectral lines.

The ν_5 and ν_8 bands of $CD_3C{\equiv}CH$ have been studied under medium resolution by Speirs and Duncan (7). The resolution that was available to them permitted only a band contour analysis of the Q subband structure. Nevertheless, they were able to determine some of the molecular parameters, including the x–y Coriolis coupling constant and the relative values of the two transition moments. We have obtained the high-resolution Fourier transform spectrum of $CD_3C{\equiv}CH$ in the ν_5/ν_8 band region, and the analysis is presented in this paper.

II. Experimental details

A commercial sample of $CD_3C{\equiv}CH$ (Merck, Sharpe & Dohme, Canada) of 99% isotopic purity was used to record the spectrum in the region 800–900 cm^{-1} on a BOMEM DA3.002 Fourier transform spectrometer (globar source, KBr beam splitter, and HgCdTe detector) at an apodized resolution of 0.004 cm^{-1}. A sample pressure of 66 Pa was used in a folded cell of fixed path length 10 m. A total of 121 scans were coadded. Wavenumber calibration was done with respect to the NH_3 lines in this region (8), recorded in a separate run. A spectrum at a lower resolution of 0.1 cm^{-1} was also recorded at 195 K.

III. Results and discussion

Rotation about the x–y axes couples the ν_5 (a_1) and ν_8 (e) modes of $CD_3C{\equiv}CH$ through a second-order Coriolis interaction. A comprehensive treatment of this interaction may be found in ref. 6. All interactions as well as the allowed spectroscopic transitions in a C_{3v} molecule follow the selection rule

$$\Delta|k - l| = 0 \bmod 3$$

where l and k are signed quantities representing the components of the vibrational and total angular momenta along the C_3 axis. In addition, we have the selection rules based on the classification of the rovibrational levels under the full symmetry group (9), $A_1 \leftrightarrow A_1$, $A_2 \leftrightarrow A_2$, and $E \leftrightarrow E$ for all interactions, and $A_1 \leftrightarrow A_2$ and $E \leftrightarrow E$ for all electric dipole transitions.

In x–y Coriolis interaction, the relevant selection rules are $\Delta l = \pm 1$ and $\Delta k = \pm 1$. The energy levels of ν_5 and ν_8 are shown schematically in Fig. 1, with the interacting levels connected by dotted lines. We found that a complete interpretation of the spectrum required that three other interactions — a Fermi resonance with the E component of $\nu_9 + \nu_{10}$, "$\pm 2, \pm 2$" l-type resonance within the ν_8 manifold, and weak k-type doubling interaction between the ν_5 and ν_8 states — be taken into account. The Fermi interaction with the $\nu_9 + \nu_{10}$ state is also shown in Fig. 1 (broken lines). The l-type resonance connects the $-l$ and $+l$ components differing in k by two units. The $\pm l$ components connected through this interaction are the same two levels that interact with a particular K level of the ν_5 state through x–y Coriolis interaction. In addition, the $+l$ components of $K = |k| = 1$, i.e., $k = -1$, $l = -1$, and $k = +1$, $l = +1$, are coupled through

[1]Author to whom correspondence may be addressed.

Can. J. Chem. Downloaded from www.nrcresearchpress.com by 203.198.23.82 on 09/08/12
For personal use only.

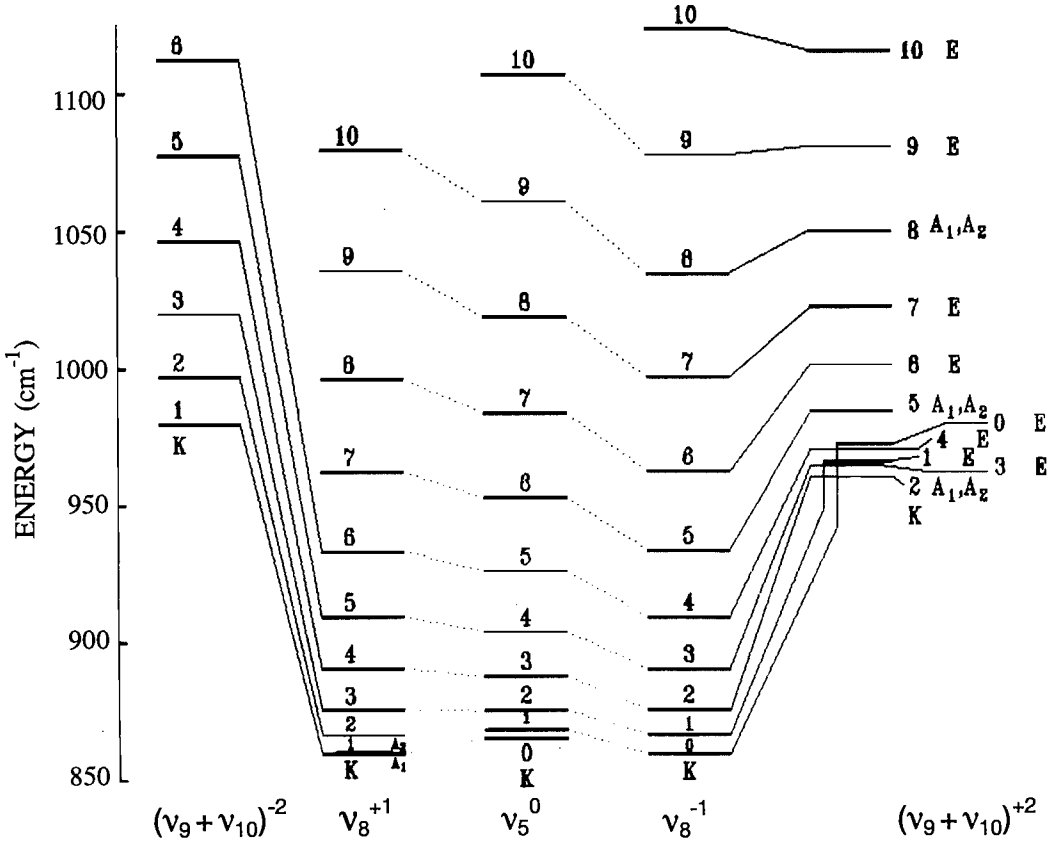

FIG. 1. Energy level diagram of ν_5 and ν_8 states and other interacting levels for $J = 10$. The levels connected through dotted lines are involved in x–y Coriolis interaction, and those connected by broken lines are in Fermi resonance.

this interaction, which results in the splitting of the A_1 A_2 pairs: the l-type doubling. The $K = 0$ levels of the nondegenerate state belong to either A_1 or A_2 species depending on whether J is even or odd. It is thus able to interact with only one component of the A_1 A_2 pairs of $K = 1$ of a degenerate state through x–y Coriolis coupling, leading to the so called "giant l-type doubling." The k-type doulbing interaction, which is not shown in Fig. 1, connects levels with $\Delta k = \pm 2$ and $\Delta l = \mp 1$. This interaction can cause A_1 A_2 splittings in the $-l$ component of $K = 2$.

An overview of the ν_5 and ν_8 bands of $CD_3C{\equiv}CH$, taken at a resolution of 0.1 cm^{-1} at 195 K is shown in Fig. 2. The low temperature suppresses the hot band transitions as well as high J transitions, making the Q branches more prominent. The different shapes of these subbands can easily be understood with the aid of Fig. 1. If two sets of levels are involved in a J-dependent perturbation, the upper(lower) set is pushed further up(down), the magnitude of the shift increasing with J. The net effect is an apparent increase in the B value of the upper set and an apparent decrease for the lower set. If the unperturbed B value of the upper state involved in a spectroscopic transition is slightly smaller than that of the lower state, the Q branches will be slightly "red"-degraded. A change in the apparent B value due to an interaction can increase this degradation or reverse it, depending on the relative position and closeness of the perturbing levels. The B value of the ν_8 state of $CD_3C{\equiv}CH$ is slightly smaller than that of the ground state, and thus the Q branches are expected to be red-degraded. The $^RQ_0$ branch, the upper state of which is unperturbed by the x–y Coriolis interaction, appears with the expected red degradation, in spite of the fact that the l-type resonance modifies it to some extent. We see from Fig. 1 that the $+l$ components of $K = 1$ and $K = 2$ are below the corresponding interacting levels of ν_5 while for $K > 3$ they lie above. The $^RQ_1$ branch thus appears strongly red-degraded, and the degradation is reversed from $^RQ_2$ onwards. With increasing K, the energy difference between the interacting levels also increases and the "violet" degradation decreases until at $K'' = 9$ the Q-branch appears as a line-like feature. The degradation changes direction for $K'' > 9$. All the K levels of the $-l$ component of ν_8 lie below the perturbing levels of ν_5, with the energy difference, ΔE, increasing with K. Thus the ^PQ branches are strongly red-degraded at low K, but become narrower with increasing K.

One notices from Fig. 2 that $^PQ_{10}$ appears shifted towards lower frequencies. All the J components show more or less the same shift, which seems to indicate a Fermi resonance. If the two levels involved in a Fermi resonance are both nondegenerate, all the K levels also are usually uniformly shifted since the ΔE's are nearly the same. When the interacting levels are degenerate, because of the different values of the z-axis Coriolis coupling constant, the different K stacks can get in and out of resonance.[2] In the case of the ν_8 state of $CD_3C{\equiv}CH$, the only suitable candidate as a Fermi res-

[2]The same situation prevails even in the case of two nondegenerate states where at least one of them is a combination of two degenerate states, for the second-order z-axis Coriolis interaction between the A_1 A_2 pairs can produce the same effect (10).

Can. J. Chem. Downloaded from www.nrcresearchpress.com by 203.198.23.82 on 09/08/12
For personal use only.

Can. J. Chem. Downloaded from www.nrcresearchpress.com by 203.198.23.82 on 09/08/12
For personal use only.

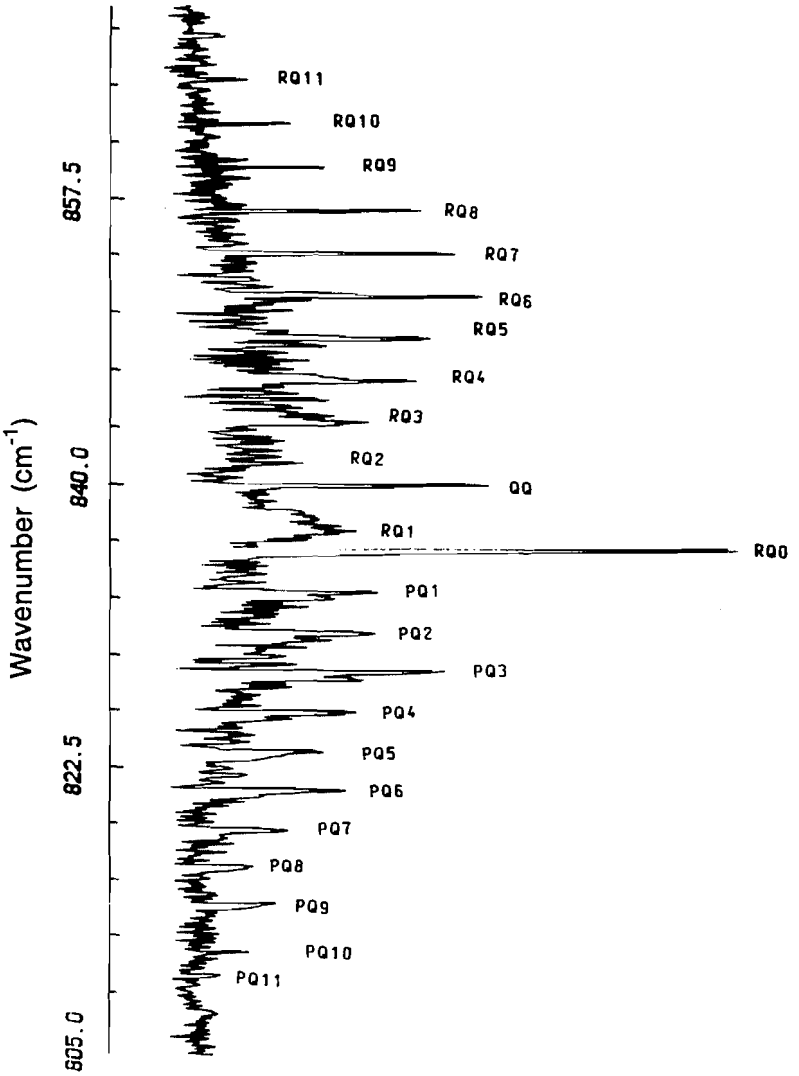

FIG. 2. The spectrum of the ν_5 and ν_8 bands of $CD_3C{\equiv}CH$ recorded at a resolution of 0.1 cm^{-1} at 195 K.

onance partner is the $\nu_9 + \nu_{10}$ (E) state, with a harmonic value of 942 cm^{-1} for G_v (7). With a $(A\zeta^z)_{\text{eff}}$ value of 4.855 cm^{-1} (i.e., $A(\zeta_9 + \zeta_{10})$) (7), the $k = \pm 9$, $l = \pm 2$ component of this state is shifted down by ~87 cm^{-1}, while the $k \cdot l = -9$ component of ν_8, for which $(A\zeta^z)_{\text{eff}}$ is ~1.159 cm^{-1} (7), is shifted up by ~21 cm^{-1} by the z-axis Coriolis coupling, bringing them into close resonance. The other K levels in the $-l$ manifold of ν_8 are also slightly affected by Fermi resonance, but the effect is negligible for the $+l$ components because of the large ΔE.

Energy level calculations

The energy levels are calculated by the diagonalization of a combined energy matrix of ν_5, ν_8, and $(\nu_9 + \nu_{10})$, with appropriate off-diagonal interaction matrix elements. The energy matrix can be factored into three smaller submatrices corresponding to the A_1, A_2, and E rovibrational species. The diagonal matrix elements are the unperturbed energy levels given by the standard polynomial expression,

$$[1]\quad E_{v,r} = G_v + B_v J(J+1) + (A_v - B_v)K^2 - D_v^J J^2(J+1)^2 - D_v^{JK} J(J+1)K^2 - D_v^K K^4 - [(2A\zeta^z)_v k \cdot l - \eta_v^J J(J+1)k \cdot l - \eta_v^K k^3 \cdot l]$$

where $K = |k|$ and the splitting of the $\pm l$ components through z-axis Coriolis coupling, given by the terms in square brackets, is relevant only for degenerate states. The choice of the relative vibrational phases is such that all off-diagonal matrix elements are real. The off-diagonal matrix elements we have used are given below and conform with those given by Di Lonardo, Fusina, and Johns (11) and Olson, Maki, and Sams (12). The numerical factors preceding these matrix elements and the relative signs are given differently by various authors, and this aspect should be taken into consideration while comparing the various results.

x–y *Coriolis interaction*

$$[2]\quad \langle \nu_5^0; k|\mathrm{H}|\nu_8^{\pm 1}; k \pm 1\rangle = \pm\sqrt{2}\, B\Omega_{58}\zeta_{58}[J(J+1) - k(k \pm 1)]^{1/2} = \pm\sqrt{2}\,\xi[J(J+1) - k(k \pm 1)]^{1/2}$$

where

$$[3]\quad \xi = B\Omega_{58}\zeta_{58} = \xi_0 + \xi_j J(J+1) + \xi_k[k^2 + (k \pm 1)^2]$$

and

$$[4]\quad \Omega_{58} = 1/2[(\nu_5/\nu_8)^{1/2} + (\nu_8/\nu_5)^{1/2}]$$

TABLE 1. Molecular parameters of the ground, ν_5, ν_8, and $\nu_9 + \nu_{10}$ states of CD_3CCH[a]

Parameter	Ground state[bc]	ν_5	ν_8	$\nu_9 + \nu_{10}$
G_v	0.0	840.281 62 (18)	836.144 62 (6)	946.1842 (16)
B_v	0.245 361 28	0.244 856 66(90)	0.245 045 78(29)	0.246 332 85(247)
$(A_v - B_v)$	2.409	2.408 983 (17)	2.421 294 2 (22)	2.409[b]
$D_v^J \times 10^7$	0.723 70	0.752 48 (183)	0.705 37 (66)	0.723 70[b]
$D_v^{JK} \times 10^5$	0.341 774	0.341 25 (85)	0.356 044 (165)	0.341 774[b]
$D_v^K \times 10^4$	0.225	0.291 35 (409)	0.232 360 (157)	0.225[b]
$(A\zeta^z)_v$			1.159 179 0 (63)	4.855[b,d]
$\eta_v^J \times 10^4$			−0.014 392(1690)	
$\eta_v^K \times 10^4$			−0.751 343(1480)	
$q_8 \times 10^4$			0.747 037(1910)	
ξ_0		0.056 897 8(82)		
$\xi_j \times 10^6$		0.151 9 (15)		
$\xi_k \times 10^4$		0.375 03 (869)		
$\kappa \times 10^4$		0.584 40 (252)		
W			1.219 87(46)	

[a]All values are in cm^{-1}. The standard deviations given in parentheses are in the units of the last digit quoted.
[b]Constrained value.
[c]From ref. 10.
[d]$(A\zeta^z)_{eff}$ value included $|l|$.

k-*Type doubling*

$$[5] \quad \langle v_5^0; k|H|v_8^{\mp 1}; k \pm 2\rangle = \sqrt{2}\,\kappa f(k, k \pm 2)$$

where

$$[6] \quad f(k, k \pm 2) = [\{J(J+1) - k(k \pm 1) \cdot \{J(J+1) - (k \pm 1)(k \pm 2)\}]^{1/2}$$

Equations [2] and [5] should be multiplied by $\sqrt{2}$ where $K = 0$ for the nondegenerate state.

"±2, ±2" l-Type resonance

$$[7] \quad \langle v_8^{\mp 1}; k|H|v_8^{\pm 1}; k \pm 2\rangle = 2\,q_8\,f(k, k \pm 2)$$

Fermi resonance

$$[8] \quad \langle v_8^{\mp 1}; K|H|(v_9 + v_{10})^{\pm 2}; K\rangle = W$$

In equations [2]–[8] the upper and lower signs are correlated throughout.

Intensity calculations

In the calculation of intensities of transitions involving unperturbed states, the relative signs of the direction cosine matrix elements are of little consequence as the intensities are proportional to the square of these matrix elements. In the present case, the upper state is a mixture of ν_5, the $\pm l$ components of ν_8, and to a smaller extent $(\nu_9 + \nu_{10})$. It is necessary to sum the products of appropriate vibrational transition moments, eigenvectors, and direction cosine matrix elements before squaring, and the relative signs of the direction cosine matrix elements become important. The intensity expression and the direction cosine matrix elements we used are consistent with those given by Di Lauro and Mills (6). The nuclear spin statistical weight factors that we used for the A_1, A_2, and E rovibrational levels were 11, 11, and 16, respectively. These also include the k-degeneracy factor and it is not necessary to use the factor 2 when $K > 0$. It is, however, necessary to include a factor of 2 for transitions involving $K = 0$ of a nondegenerate state and $K = 1$ of a degenerate state.

Analysis of the spectra

The initial assignments were made in the ^RR, ^RQ, ^PP, and ^PQ branches of the ν_8 band corresponding to high K values, where the perturbation is not severe, and counterchecked with $Q(J) - P(J+1)$ and $R(J) - Q(J+1)$ combination differences calculated from the known ground state parameters (10). A least-squares fit of these frequencies gave an initial set of paramters that was used to calculate the frequencies and intensities of the low K transitions and make further assignments. The only clearly recognizable feature of the ν_5 band was the Q head. Therefore, in the initial stages of the analysis, the ν_5 state had to be included in the calculations only as a "shadow" state. Recently we carried out the analysis of the ν_9 (13) and $2\nu_9$ (10) bands of $CD_3C{\equiv}CH$, where it was necessary to include one of more shadow states, i.e., states to which transitions are not directly observed, but which manifest their presence only through the perturbations. Even though we were able to derive some of the parameters of these shadow states from the magnitude of the perturbations, there was always a lingering doubt about their accuracy, as many other parameters were constrained. Therefore, it was gratifying to see that the perturbation treatment predicted the ν_0 and B' of the ν_5 band with fairly good accuracy even when ν_5 was used only as a shadow state. In the final stages it was possible to identify many transitions of the ν_5 band and assign over 2000 transitions.[3] The A_1 A_2 splitting in the $K \cdot \Delta K = -3$ transitions, caused by k-type doubling, was resolvable only for $J > 40$. Only a few such transitions could be identified because of the diminished intensity at high J values. In the final fit 1592 transitions, 243 of which are parallel type, have been included. In the parallel band, $K = 0$, 1 are intense in the P branch, while it is the $K = 2$, 3 that are intense in the R branch. The standard deviation of the fit was 0.00068 cm^{-1}. The parameters derived from our analysis are given in Table 1.

[3]A complete list of frequencies and assignments is available from the authors or may be purchased from: The Depository of Unpublished Data, Document Delivery, CISTI, National Research Council Canada, Ottawa, Canada K1A 0S2.

Can. J. Chem. Downloaded from www.nrcresearchpress.com by 203.198.23.82 on 09/08/12
For personal use only.

Can. J. Chem. Downloaded from www.nrcresearchpress.com by 203.198.23.82 on 09/08/12
For personal use only.

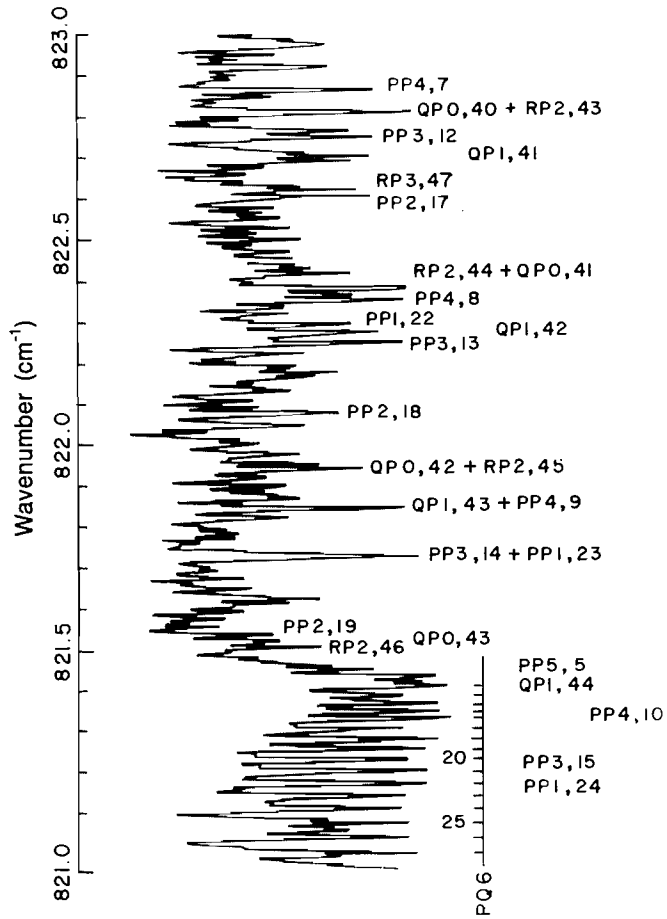

FIG. 3. A portion of the high-resolution spectrum of the ν_5 and ν_8 bands.

Figure 3 shows a section of the high-resolution spectra and the ν_5 and ν_8 transitions. The ν_5 transitions do not have the typical parallel band appearance in which the K components of a given J are clustered together. Not only do the K components appear in a haphazard manner, but their relative intensities also are unusual, and it would have been impossible to assign these transitions without the calculation of the perturbed frequencies and intensities. The most striking intensity changes are in the ${}^{Q}P_0$, ${}^{Q}P_1$, ${}^{Q}R_2$, ${}^{Q}R_3$, ${}^{P}R_1$, ${}^{P}R_2$, ${}^{P}R_3$, ${}^{R}P_2$, ${}^{R}P_3$, ${}^{R}P_4$, ${}^{R}R_0$, and ${}^{R}R_1$ branches, which are enhanced, and ${}^{Q}P_2$, ${}^{Q}P_3$, ${}^{Q}R_0$, ${}^{Q}R_1$, ${}^{P}P_1$, ${}^{P}P_2$, ${}^{R}P_0$, ${}^{R}P_1$, ${}^{R}R_2$, and ${}^{R}R_3$ branches, which are depleted in intensity. Even though we have not made any quantitative intensity measurements, from the relative intensities of the spectral lines we estimate the ratio of the transition moments, $(\mu_x \pm i\mu_y):\mu_z$, as 1.0:0.6, which corresponds to $M_5/M_8 = 0.85$. The value of 1.0 for this parameter, used by Speirs and Duncan (7) in their band contour analysis, appears to be on the high side, but their values of ζ_8 and ζ_{58} compare well with our values (0.4338 and 0.2325, respectively) derived from the parameters given in Table 1. The intensity perturbation is positive in the sense defined by Di Lauro and Mills (6), i.e., the relative sign of the transition moments is the same as the sign of the x–y Coriolis coupling parameter. It is interesting to note that, in a recent analysis of the corresponding bands of CD_3CN, Koivusaari and Anttila (14) have invoked similar perturbations, and the values of the interaction parameters are also comparable.

IV. Acknowledgments

We thank Dr. V.B. Kartha for his interest in this work and Dr. Romola D'Cunha for a critical reading of the manuscript. The assistance given by S.S. Bhattacharya in the preparation of the manuscript is gratefully acknowledged.

1. P.M. Burrell, E. Bjarnov, and R.H. Schwendeman. J. Mol. Spectrosc. **82**, 193 (1980).
2. F. Meyer, J. Dupre, C. Meyer, C. Lambeau, M. De Vleeschouwer, J.G. Lahaye, and A. Fayt. Int. J. Infrared Millimeter Waves, **3**, 83 (1982).
3. F. Meyer, J. Dupre, C. Meyer, J.G. Lahaye, and A. Fayt. Can. J. Phys. **63**, 1184 (1985).
4. T. Al Adlouni, F. Meyer, C. Meyer, J.G. Lahaye, and A. Fayt. Int. J. Infrared Millimeter Waves, **7**, 405 (1986).
5. T. Al Adlouni, F. Meyer, C. Meyer, D.E. Jennings, and J.J. Hillman. Int. J. Infrared Millimeter Waves, **8**, 1083 (1987).
6. C. Di Lauro and I.M. Mills. J. Mol. Spectrosc. **21**, 386 (1966).
7. G.K. Speirs and J.L. Duncan. J. Mol. Spectrosc. **51**, 277 (1974).
8. S. Urban, D. Papousek, J. Kauppinen, K. Yamada, and G. Winnewisser. J. Mol. Spectrosc. **101**, 1 (1983).
9. J.T. Hougen. J. Chem. Phys. **37**, 1433 (1962).
10. K. Singh, G. Rajappan, V.A. Job, V.B. Kartha, A. Weber, and W.B. Olson. J. Mol. Spectrosc. **157**, 467 (1993).
11. G. Di Lonardo, L. Fusina, and J.W.C. Johns. J. Mol. Spectrosc. **104**, 282 (1984).
12. W.B. Olson, A.G. Maki, and R.L. Sams. J. Mol. Spectrosc. **55**, 252 (1975).
13. N.S. Sule, R.J. Kshirsagar, and V.A. Job. J. Mol. Spectrosc. **160**, 502 (1993).
14. M. Koivusaari and R. Anttila. J. Mol. Spectrosc. **155**, 201 (1992).

High-resolution laser spectroscopy of excited bending vibrations ($v_2 \leq 2$) of the $\tilde{B}^2\Sigma^+$ and $\tilde{X}^2\Sigma^+$ electronic states of SrOH: analysis of ℓ-type doubling and ℓ-type resonance

P.I. PRESUNKA AND J.A. COXON[1]

Department of Chemistry, Dalhousie University, Halifax, NS B3H 4J3, Canada

Received March 15, 1993

This paper is dedicated to Professor Gerald W. King on the occasion of his 65th birthday

P.I. PRESUNKA and J.A. COXON. Can. J. Chem. **71**, 1689 (1993).

The $(02^00)\Sigma^+ \leftarrow (000)\Sigma^+$, $(02^20)\Delta \leftarrow (010)\Pi$, $(02^00)\Sigma^+ \leftarrow (010)\Pi$, and $(010)\Pi \leftarrow (000)\Sigma^+$ bands in the $\tilde{B}^2\Sigma^+ \leftarrow \tilde{X}^2\Sigma^+$ electronic system of SrOH have been recorded at Doppler limited resolution using CW dye laser excitation with selective detection. Fluorescence from selected rotational levels of the $\tilde{B}^2\Sigma^+(02^00)\Sigma^+$ and $\tilde{B}^2\Sigma^+(02^20)\Delta$ vibronic states has been dispersed, providing access to the $(02^00)\Sigma^+$ and $(02^20)\Delta$ levels of the ground electronic state. Over 1200 line positions from all transitions were included in a global least-squares fit. The effects of a weak ℓ-type resonance between the $\ell = 0$ and $\ell = 2$ components of the $v_2 = 2$ vibrational level were observed in both electronic states and the off-diagonal matrix elements were evaluated in a case (b) basis. A previous analysis of the $\tilde{B}^2\Sigma^+(010)\Pi$ level that attributes the anomalous ℓ-type doubling to an electronic perturbation arising from the $\tilde{A}^2\Pi(010)$ polyad is inconsistent with our experimental results.

P.I. PRESUNKA et J.A. COXON. Can. J. Chem. **71**, 1689 (1993).

Travaillant à une résolution Doppler limitée et utilisant un colorant CW à excitation au laser avec détection sélective, on a enregistré les bandes $(02^00)\Sigma^+ \leftarrow (000)\Sigma^+$, $(02^20)\Delta \leftarrow (010)\Pi$, $(02^00)\Sigma^+ \leftarrow (010)\Pi$ et $(010)\Pi \leftarrow (000)\Sigma^+$ dans le système électronique $\tilde{B}^2\Sigma^+ \leftarrow \tilde{X}^2\Sigma^+$ du SrOH. La dispersion de la fluorescence obtenue à partir de certains niveaux rotationnels des états vibroniques $\tilde{B}^2\Sigma^+(02^00)\Sigma^+$ et $\tilde{B}^2\Sigma^+(02^00)\Delta$ permet d'accéder aux niveaux $(02^00)\Sigma^+$ et $(02^20)\Delta$ de l'état électronique fondamental. On a inclus plus de 1200 positions de lignes provenant de toutes les transitions dans une procédure globale des moindres carrés. On a observé les effets d'une faible résonance de type ℓ entre les composantes $\ell = 0$ et $\ell = 2$ du niveau vibrationnel $v_2 = 2$ dans les deux états électroniques et on a évalué les éléments situés en dehors de la diagonale de la matrice en se basant sur le cas (b). Nos résultats expérimentaux ne concordent pas avec une analyse antérieure du niveau $\tilde{B}^2\Sigma^+(010)\Pi$ qui attribue le dédoublement anormal de type ℓ à une pertubation électronique provenant de la polyade $\tilde{A}^2\Pi(010)$.

[Traduit par la rédaction]

Introduction

Although high-resolution laser spectroscopy has been invaluable in elucidating the congested structure of electronic transitions involving the low-lying $\tilde{A}^2\Pi$ and $\tilde{B}^2\Sigma^+$ states of SrOH, previous investigations (1, 2) of the $\tilde{B}^2\Sigma^+$–$\tilde{X}^2\Sigma^+$ and $\tilde{A}^2\Pi$–$\tilde{X}^2\Sigma^+$ systems have provided detailed information only on vibrational levels with $v_i \leq 1$. In contrast, a substantial amount of data on excited vibrational levels exist for the related alkaline earth monohydroxide CaOH (3–6). However, access to excited vibrational levels of the group IIA hydroxides is experimentally difficult: not only do the Franck–Condon factors strongly favour $\Delta v_i = 0$ sequences, but the spectra contain strongly overlapped sequence structure due to small differences in the vibrational frequencies of the ground and excited electronic states. In the present work, vibrational selective detection leads to a substantial enhancement of laser induced fluorescence (LIF) arising from transitions involving excited bending vibrational levels in the $\tilde{B}$–$\tilde{X}$ system of SrOH. Since overlapping band systems are essentially completely suppressed, the complexity of the resulting spectra is greatly reduced, rendering assignment and analysis fairly straightforward.

Some of the bands observed in this work, specifically the $\tilde{B}^2\Sigma^+(02^20)\Delta \leftarrow \tilde{X}^2\Sigma^+(010)\Pi$, $\tilde{B}^2\Sigma^+(010)\Pi \leftarrow \tilde{X}^2\Sigma^+(000)\Sigma^+$, and $\tilde{B}^2\Sigma^+(02^00)\Sigma^+ \leftarrow \tilde{X}^2\Sigma^+(010)\Pi$ systems, are forbidden components of an allowed electronic transition. The notation used here to label the different vibrational levels follows that of Jarman and Bernath (7). Since the $\tilde{B}^2\Sigma^+$ and $\tilde{A}^2\Pi$ electronic states of SrOH are separated by only 1703.173 cm^{-1} (1, 2), the $\tilde{B}$ state can acquire $^2\Pi$ character through vibronic mixing. Jungen and Merer (8) have attributed this to a special case of the Herzberg–Teller interaction, whereby the mixing occurs via Renner–Teller coupling. Based on this mechanism, vibronically induced transitions are expected for most unsymmetrical linear triatomics. Other notable examples where nominally forbidden $\Delta v_2 = \pm 1$ bands in the bending mode of linear triatomics have been observed include NCS (9), HCN^+ (10), NCO (11, 12), and CaOH (7; see also footnote 2).

We report in this paper the first observation and rotational analysis of the $\ell = 0$ and $\ell = 2$ components of the (020) vibrational level in the $\tilde{B}^2\Sigma^+$ and $\tilde{X}^2\Sigma^+$ electronic states of SrOH. Although the $^2\Sigma^+$ and $^2\Delta$ vibronic states are well separated, by 32.703 and 30.259 cm^{-1} for the $\tilde{B}^2\Sigma^+$ and $\tilde{X}^2\Sigma^+$ electronic states, respectively, the effects of an ℓ-type resonance have been observed, and the off-diagonal matrix element connecting these states has been evaluated in a case (b) basis. An earlier investigation (1) of the $\tilde{B}^2\Sigma^+(010)\Pi \leftarrow \tilde{X}^2\Sigma^+(010)\Pi$ transition determined the relative magnitude of the ℓ-type doublings; however, absolute e/f parity assignments were not possible. We have observed the $(010)\Pi$ levels of both states in perpendicular-type transitions, thereby enabling unambiguous parity assignment and accurately establishsing the vibrational term values. All data have been

[1]Author to whom correspondence may be addressed.

[2]J.A. Coxon, M. Li, and P.I. Presunka. J. Mol. Spectrosc. In press.

Can. J. Chem. Downloaded from www.nrcresearchpress.com by 203.198.23.82 on 09/08/12
For personal use only.

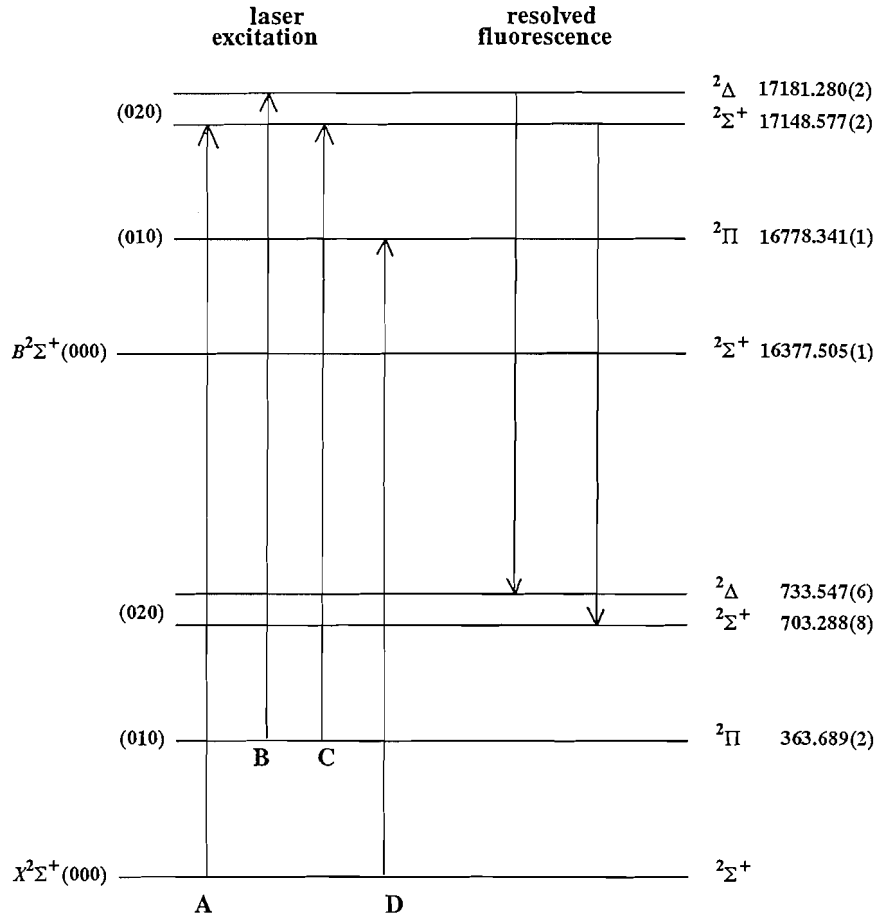

FIG. 1. Energy level diagram summarizing the six transitions analyzed in the present work. Frequency differences used in selective detection were 703, 368, 339, and 363 cm^{-1} for the A, B, C, and D transitions, respectively. The term value for $\tilde{B}^2\Sigma^+(000)\Sigma^+$ is taken from ref. (1).

combined in a simultaneous fit to obtain single-valued estimates of the molecular parameters for the $(010)\Pi$, $(02^00)\Sigma^+$, and $(02^20)\Delta$ vibronic levels of the $\tilde{B}^2\Sigma^+$ and $\tilde{X}^2\Sigma^+$ electronic states.

Experimental

Gas phase SrOH radicals were produced in a modified Broida oven by the reaction of Sr metal vapour with H_2O_2. Under our experimental conditions, the reaction was accompanied by an intense visible chemiluminescence. The flame was probed with the output of a Coherent 699-29 ring dye laser operating in single mode with rhodamine 6G dye. Excitation frequency measurements were provided directly by the internal wavemeter of the 699-29, the integrity of which was verified by recording I_2 fluorescence spectra during all scans. Comparison to the more precise measurements of the standard I_2 atlas (13, 14) resulted in small corrections ($\leq$0.005 cm^{-1}) to the wavemeter measurements where necessary.

Two distinct experimental schemes were used for this work: vibrational selective laser excitation and resolved fluorescence. In both cases the image of the laser-induced fluorescence was focused on the entrance slit of a 1.26-m Spex monochromator fitted with a 2400 groove mm^{-1} grating (Bausch and Lomb) blazed at 500 nm. The signal was detected with a selected GaAs photomultiplier tube (RCA C31034A-02) cooled to -20°C in an RF shielded housing. For the excitation scans, the laser beam was chopped at 269 Hz and phase-sensitive detection was employed. The vibrational selective detection scheme is described in more detail elsewhere (4). Briefly, the monochromator and laser were scanned simultaneously such that a constant frequency difference (corresponding to a ground state vibrational spacing) between the two was maintained. For example, during the $\tilde{B}^2\Sigma^+(02^00)^2\Sigma^+ \leftarrow \tilde{X}^2\Sigma^+(000)^2\Sigma^+$ excitation scans, the monochromator frequency was tuned ~703 cm^{-1} to the red of the laser frequency such that fluorescence to $\tilde{X}^2\Sigma^+(02^00)\Sigma^+$ is seletively detected. We have found this technique particularly effective in suppressing LIF due to coincident excitations. Laser excitation was used to record spectra for the following transitions; $\tilde{B}^2\Sigma^+(02^00)\Sigma^+ \leftarrow \tilde{X}^2\Sigma^+(000)\Sigma^+$, $\tilde{B}^2\Sigma^+(02^20)\Delta \leftarrow \tilde{X}^2\Sigma^+(010)\Pi$, $\tilde{B}^2\Sigma^+(02^00)^2\Sigma^+ \leftarrow \tilde{X}^2\Sigma^+(010)\Pi$, and $\tilde{B}^2\Sigma^+(010)\Pi \leftarrow \tilde{X}^2\Sigma^+(000)\Sigma^+$. These transitions and the frequency differences used are summarized in Fig. 1.

The experimental arrangement for resolved fluorescence is identical to that used in our previous investigations of excited vibrational levels of CaOH (3). The phase-sensitive detection equipment used in the excitation experiments was replaced by more sensitive photon counting electronics (PAR 1120 amplifier/discriminator and PAR 1105 photon counter). Depending on the strength of the LIF signal, the slit width was varied from 40 to 50 μm. The monochromator and detection system were interfaced to a MINC PDP-11 (Digital Equipment Corporation) allowing direct computer control of experiments as well as electronic data acquisition. Each resolved fluorescence scan of selected excitation features varied in range from 10 to 30 Å and was calibrated by 10 to 12 atomic uranium lines recorded simultaneously with the SrOH spectra. Using the U line positions of ref. 15, the drum wavelength was calibrated by least-squares fits to a five-parameter function (16). The accuracy of the resolved fluorescence measurements was periodically verified by determining the frequency of the output of the 699-29 using our monochromator set-up and comparing it to the value given by the wavemeter. No systematic error

Can. J. Chem. Downloaded from www.nrcresearchpress.com by 203.198.23.82 on 09/08/12
For personal use only.

Can. J. Chem. Downloaded from www.nrcresearchpress.com by 203.198.23.82 on 09/08/12
For personal use only.

was evident and the accuracy was determined on average to be better than 0.03 cm^{-1}.

In the present work, the technique of resolved fluorescence was applied to the parallel $\tilde{B}^2\Sigma^+(02^00)\Sigma^+ \rightarrow \tilde{X}^2\Sigma^+(02^00)\Sigma^+$ and $\tilde{B}^2\Sigma^+(02^20)\Delta \rightarrow \tilde{X}^2\Sigma^+(02^20)\Delta$ transitions to provide access to $v_2 = 2$ components of the $\tilde{X}$ state (see Fig. 1). In the former case, selected rovibronic levels of the $\tilde{B}^2\Sigma^+(02^00)\Sigma^+$ level are populated via optical pumping of both the $\tilde{B}^2\Sigma^+(02^00)\Sigma^+ \leftarrow \tilde{X}^2\Sigma^+(000)\Sigma^+$ and $\tilde{B}^2\Sigma^+(02^00)\Sigma^+ \leftarrow \tilde{X}^2\Sigma^+(010)\Pi$ transitions. Similarly, the $\tilde{X}^2\Sigma^+(02^20)\Delta$ level is observed following excitation of the $\tilde{B}^2\Sigma^+(02^20)\Delta \leftarrow \tilde{X}^2\Sigma^+(010)\Pi$ system.

Rotational analysis and discussion

Rotational assignments of the laser excitation spectra were generally straightforward. Since excitation was from either the $(000)\Sigma^+$ or $(010)\Pi$ level of the ground state, for which molecular constants have been previously determined (1), the rotational quantum number of the P and R branches could be assigned by use of combination differences. Owing to a small effective spin-rotation splitting of the ground state, however, the rotational numbering could be changed by one unit depending on whether the line belonged to the F_1 or F_2 spin manifold. This ambiguity was resolved in the least-squares fits since only one of the two possibilities yielded an effective spin-rotation constant for the $\tilde{B}$ state levels of the same sign as that established by Nakagawa et al. (1). This method was not reliable for the intense Q branches, which are associated with the perpendicular transitions observed in excitation. The presence of a combination defect on account of the ℓ-type doubling, as well as the compact rotational structure of the Q branches, made such assignments questionable. Rotational assignments for the Q branches were therefore made on the basis of P–R separations in the resolved fluorescence scans. Moreover the rotational structure was often extremely congested and, despite the use of selective detection, overlapping band systems could not always be completely suppressed. In particular, the overlapping was somewhat problematic for the $\tilde{B}^2\Sigma^+(02^20)\Delta \leftarrow \tilde{X}^2\Sigma^+(010)\Pi$ and $\tilde{B}^2\Sigma^+(02^00)\Sigma^+ \leftarrow \tilde{X}^2\Sigma^+(010)\Pi$ transitions. The vibronic energies of these transitions are 16 817.591 and 16 784.888 cm^{-1}, respectively. Furthermore, since the frequency differences used in the detection schemes are similar (368 and 363 cm^{-1}, respectively), the P branches of the $\tilde{B}^2\Sigma^+(02^20)\Delta \leftarrow \tilde{X}^2\Sigma^+(010)\Pi$ transition are overlapped by the stronger $\tilde{B}^2\Sigma^+(010)\Pi$–$\tilde{X}^2\Sigma^+(000)\Sigma^+$ R lines. To eliminate the possibility of erroneous assignments of rotational quantum number, resolved fluorescence spectra of adjacent rotational lines in each of the P and R (and Q) branches of all transitions were recorded. Tables 1–4 give the line positions for the four transitions investigated by laser excitation. Line positions are measured to an estimated accuracy of approximately 0.004 cm^{-1}.

The rotational assignments of the resolved fluorescence scans followed directly from the excitation spectra. For these transitions $\Delta K = 0$; consequently only two single (P and R) lines were observed in fluorescence provided only one rotational level of the upper state was populated. Tables 5 and 6 contain the line positions for the resolved fluorescence measurements.

Expressions for the rotational term energies of linear triatomic molecules in $^2\Sigma^+$ electronic states are given by (11, 12, 17);

(a) $v_2 = 0$ or 2, $\ell = 0$; $^2\Sigma^+$ vibronic state:

$$[1]\quad F_1(N,e) = B_vN(N+1) - D_vN^2(N+1)^2 + H_vN^3(N+1)^3 + 1/2\,\gamma_vN + 1/2\gamma_v^DN^2(N+1)$$

$$[2]\quad F_2(N,f) = B_vN(N+1) - D_vN^2(N+1)^2 + H_vN^3(N+1)^3 - 1/2\,\gamma_v(N+1) - 1/2\,\gamma_v^DN(N+1)^2$$

(b) $v_2 = 1$, $\ell = 1$; $^2\Pi$ vibronic state:

$$[3]\quad F_1(N,^e_f) = B_v[N(N+1)-1] - D_v[N(N+1)-1]^2 + H_v[N(N+1)-1]^3 + 1/2\,\gamma_vN + 1/2\gamma_v^DN^2(N+1) \pm 1/2\,q_vN(N+1) \pm 1/2\,q_v^D[N(N+1)]^2$$

$$[4]\quad F_2(N,^e_f) = B_v[N(N+1)-1] - D_v[N(N+1)-1]^2 + H_v[N(N+1)-1]^3 - 1/2\,\gamma_v(N+1) - 1/2\,\gamma_v^DN(N+1)^2 \mp 1/2\,q_vN(N+1) \mp 1/2\,q_v^D[N(N+1)]^2$$

(c) $v_2 = 2$, $\ell = 2$; $^2\Delta$ vibronic state:

$$[5]\quad F_1(N,^e_f) = B_v[N(N+1)-4] - D_v[N(N+1)-4]^2 + H_v[N(N+1)-4]^3 + 1/2\,\gamma_vN + 1/2\,\gamma_v^DN^2(N+1) + \Phi(N,^e_f)$$

$$[6]\quad F_2(N,^e_f) = B_v[N(N+1)-4] - D_v[N(N+1)-4]^2 + H_v[N(N+1)-4]^3 - 1/2\,\gamma_v(N+1) - 1/2\,\gamma_v^DN(N+1)^2 + \Phi(N,^e_f)$$

The designation of e/f parity throughout this work follows the definition given by Kopp and Hougen (18). The sign of the ℓ-type doubling parameter q_v is consistent with that used by Mulliken and Christy (19) for the Λ-doubling parameter q. The constants γ^D and q_v^D take account of centrifugal distortion on the effective spin-rotation and ℓ-type doubling parameters, respectively. The γ_v^D term was included only for the $\tilde{B}$ state vibrational levels, which exhibit an anomalously large γ_v due to the effects of an electronic perturbation caused by the nearby $\tilde{A}^2\Pi$ state. The $\Phi(N,^e_f)$ terms in eqs. [5] and [6] lead to ℓ-type splitting between the e and f parity levels of the $^2\Delta$ vibronic levels, given approximately as $q_{eff}N(N+1)[N(N+1)-2]$. Recent microwave measurements on the $\tilde{X}^2\Sigma^+$ ground sate of SrOH by Anderson et al. (20) have provided very accurate determinations of the molecular constants for the (000) level. Accordingly the parameters B_v'', D_v'', and γ_v'' were held fixed to the microwave values.

Initially, data from each of the vibronic transitions observed in this work were treated separately by least-squares fitting. As pointed out by Albritton et al. (21), molecular constants determined in this way are highly correlated and may differ significantly from their true values. In the present study several of the observed vibrational levels are common to more than one transition. Consequently, the final least-squares fit of the entire data simultaneously served to lessen the correlation of errors for the $\tilde{B}$ and $\tilde{X}$ state molecular constants. Resolved fluorescence data were given a lower weight than the more accurate excitation measurements, in accord with their respective uncertainties. In this fit the en-

TABLE 1. Line positions[a] (cm^{-1}) for the $B^2\Sigma^+$–$X^2\Sigma^+$ $(02^00)\Sigma^+$-$(000)\Sigma^+$ band of SrOH. The table shows $\bar{\nu}_{obs}$, the measured wavenumbers (cm^{-1}), and the residuals, $\bar{\nu}_{obs} - \bar{\nu}_{calc}$

N	P_1		R_1		P_2		R_2	
1			17 149.338	−0.100[c]			17 149.608	−0.192[c]
2	17 147.391	−0.118[c]	17 149.782	−0.091[c]	17 147.562	−0.168[c]	17 150.160	−0.220[c]
3	17 146.839	−0.105[c]	17 150.227	−0.083[c]	17 147.123	−0.187[c]		
4	17 146.292	−0.090[c]	17 150.684	−0.066[c]	17 146.669	−0.224[c]	17 151.244	−0.304[c]
5	17 145.751	−0.071[c]	17 151.131	−0.062[c]	17 146.219	−0.260[c]	17 151.778	−0.358[c]
6	17 145.195	−0.070[c]	17 151.584	−0.055[c]	17 145.751	−0.317[c]	17 152.289	−0.439[c]
7	17 144.651	−0.061[c]	17 152.040	−0.047[c]	17 145.298	−0.362[c]	17 152.784	−0.538[c]
8	17 144.107	−0.054[c]	17 152.496	−0.043[c]	17 144.813	−0.442[c]	17 153.258	−0.661[c]
9	17 143.563	−0.050[c]	17 152.954	−0.039[c]	17 144.312	−0.540[c]	17 155.487	0.969[c]
10	17 143.026	−0.042[c]	17 153.418	−0.032[c]	17 143.782	−0.671[c]	17 155.904	0.783[c]
11	17 142.508	−0.018[c]	17 153.884	−0.026[c]	17 145.022	0.966[c]	17 156.363	0.637[c]
12	17 141.956	−0.031[c]	17 154.351	−0.022[c]	17 144.441	0.778[c]	17 156.859	0.525[c]
13	17 141.424	−0.027[c]	17 154.819	−0.020[c]	17 143.908	0.636[c]	17 157.365	0.420[c]
14	17 140.892	−0.026[c]	17 155.288	−0.019[c]	17 143.409	0.525[c]	17 157.960	0.401[c]
15	17 140.367	−0.021[c]	17 155.764	−0.014[c]	17 142.918	0.418[c]	17 158.517	0.342[c]
16	17 139.841	−0.020[c]	17 156.238	−0.014[c]	17 142.507	0.389[c]	17 159.097	0.302[c]
17	17 139.327	−0.010[c]	17 156.719	−0.010[c]	17 142.083	0.344[c]	17 159.679	0.263[c]
18	17 138.801	−0.014[c]	17 157.199	−0.009[c]	17 141.633	0.301[c]	17 160.278	0.237[c]
19	17 138.281	−0.016[c]	17 157.685	−0.005[c]	17 141.256	0.267[c]	17 160.883	0.215[c]
20	17 137.770	−0.011[c]	17 158.169	−0.006[c]	17 140.858	0.239[c]	17 161.495	0.197[c]
21	17 137.257	−0.012[c]	17 158.659	−0.004[c]	17 140.467	0.216[c]	17 162.110	0.179[c]
22	17 136.751	−0.008[c]	17 159.152	−0.001	17 140.084	0.197[c]	17 162.733	0.167[c]
23	17 136.247	−0.005[c]	17 159.662	0.016[b]	17 139.705	0.180[c]	17 163.357	0.153[c]
24	17 135.742	−0.006	17 160.141	0.000	17 139.327	0.161[c]	17 163.983	0.139[c]
25	17 135.238	−0.009	17 160.640	0.001	17 138.961	0.151[c]	17 164.618	0.131[c]
26	17 134.743	−0.006	17 161.142	0.002	17 138.595	0.138[c]	17 165.245	0.113[c]
27	17 134.250	−0.004	17 161.646	0.003[b]	17 138.233	0.127[c]	17 165.888	0.108[c]
28	17 133.763	0.001	17 162.151	0.002	17 137.876	0.117[c]	17 166.531	0.100[c]
29	17 133.268	−0.005	17 162.661	0.003	17 137.525	0.111[c]	17 167.176	0.092[c]
30	17 132.789	0.003	17 163.172	0.003	17 137.172	0.100[c]	17 167.824	0.085[c]
31	17 132.297	−0.005	17 163.685	0.003	17 136.825	0.092[c]	17 168.475	0.078[c]
32	17 131.823	0.001	17 164.202	0.004	17 136.483	0.086[c]	17 169.129	0.071[c]
33	17 131.345	0.001	17 164.722	0.005	17 136.143	0.079[c]	17 169.787	0.066[c]
34	17 130.870	0.002	17 165.247	0.009	17 135.803	0.070[c]	17 170.447	0.061[c]
35	17 130.398	0.002	17 165.766	0.005	17 135.468	0.063[c]	17 171.107	0.054[c]
36	17 129.948	0.021[b]	17 166.290	0.003	17 135.135	0.055[c]	17 171.773	0.050[c]
37	17 129.462	0.002	17 166.818	0.003	17 134.808	0.051[c]	17 172.430	0.034[c]
38	17 128.997	0.001	17 167.346	0.000	17 134.486	0.049[c]	17 173.112	0.042[c]
39	17 128.534	−0.001	17 167.880	0.001	17 134.164	0.044[c]	17 173.783	0.036[c]
40	17 128.069	−0.008	17 168.417	0.003	17 133.846	0.040[c]	17 174.452	0.026[c]
41	17 127.620	−0.001	17 168.953	0.002	17 133.530	0.036[c]	17 175.134	0.027[c]
42	17 127.168	0.000	17 169.493	0.002	17 133.215	0.030[c]	17 175.817	0.026[c]
43	17 126.723	0.005	17 170.032	−0.001	17 132.908	0.029[c]	17 176.496	0.020[c]
44	17 126.271	0.000	17 170.582	0.004	17 132.599	0.024[c]	17 177.182	0.018[c]
45	17 125.822	−0.004	17 171.116	−0.008	17 132.297	0.023[c]	17 177.859	0.005[c]
46	17 125.385	0.001	17 171.676	0.003	17 131.993	0.017[c]	17 178.559	0.013[c]
47	17 124.946	0.001	17 172.224	0.000	17 131.697	0.017[c]	17 179.248	0.008[c]
48	17 124.509	0.000	17 172.772	−0.005	17 131.399	0.012[c]	17 179.950	0.014[c]
49	17 124.076	0.001	17 173.332	0.000	17 131.103	0.007[c]	17 180.641	0.006
50	17 123.641	−0.003	17 173.890	0.000	17 130.821	0.013[c]	17 181.333	−0.002[b]
51	17 123.214	−0.001	17 174.452	0.003[b]	17 130.527	0.005	17 182.042	0.005
52	17 122.788	−0.001	17 175.006	−0.005[b]	17 130.243	0.004	17 182.740	−0.001
53	17 122.361	−0.005	17 175.572	−0.002	17 129.948	−0.010[b]	17 183.451	0.004
54	17 121.943	−0.002	17 176.138	−0.001	17 129.681	0.001	17 184.156	0.001
55	17 121.523	−0.004	17 176.700	−0.007	17 129.407	0.002	17 184.858	−0.007[b]
56	17 121.108	−0.003	17 177.274	−0.002	17 129.129	−0.002	17 185.578	0.002
57	17 120.696	−0.002	17 177.859	0.011[b]	17 128.859	−0.002	17 186.292	0.002
58	17 120.287	−0.001	17 178.416	−0.005	17 128.588	−0.004	17 187.003	−0.002
59	17 119.878	−0.002	17 178.994	−0.002	17 128.323	−0.003	17 187.721	−0.001
60	17 119.470	−0.004	17 179.574	0.001	17 128.069	0.006[b]	17 188.450	0.010[b]
61	17 119.068	−0.003	17 180.148	−0.004	17 127.798	−0.003	17 189.157	−0.004
62	17 118.667	−0.004	17 180.734	0.001	17 127.539	−0.004	17 189.881	−0.002
63	17 118.273	0.000	17 181.333	0.018[b]	17 127.279	−0.007	17 190.609	0.002

Can. J. Chem. Downloaded from www.nrcresearchpress.com by 203.198.23.82 on 09/08/12
For personal use only.

TABLE 1 (*concluded*)

N	P_1		R_1		P_2		R_2	
64	17 117.874	−0.003	17 181.903	0.004	17 127.028	−0.004	17 191.330	−0.002
65	17 117.486	0.002	17 182.479	−0.006	17 126.780	0.000	17 192.064	0.005
66	17 117.094	0.001	17 183.078	0.005	17 126.527	−0.004	17 192.795	0.008
67	17 116.704	−0.001	17 183.674	0.012	17 126.271	−0.012[b]	17 193.519	0.002
68	17 116.319	0.000	17 184.252	−0.001	17 126.035	−0.003	17 194.250	0.001
69	17 115.934	−0.001	17 184.858	0.012	17 125.796	0.001	17 194.983	0.001
70	17 115.553	−0.001	17 185.440	0.000	17 125.548	−0.007	17 195.715	−0.001
71	17 115.173	−0.002	17 186.033	−0.003	17 125.324	0.008	17 196.454	0.002
72	17 114.796	−0.003	17 186.634	0.001	17 125.083	0.003		
73	17 114.426	0.001	17 187.232	0.000	17 124.852	0.006		
74	17 114.055	0.002	17 187.834	0.001	17 124.615	0.001		
75	17 113.684	0.001			17 124.382	−0.003		
76	17 113.321	0.005			17 124.148	−0.009		
77	17 112.955	0.004						
78	17 112.592	0.004						
79	17 112.229	0.001						
80	17 111.871	0.002						
81	17 111.515	0.002						
82	17 111.160	0.001						
83	17 110.810	0.002						
84	17 110.461	0.003						
85	17 110.110	−0.001						
86	17 109.767	0.001						
87	17 109.422	−0.001						
88	17 109.081	−0.001						
89	17 108.744	0.001						
90	17 108.403	−0.004						
91	17 108.067	−0.006						

[a]Unless indicated otherwise, line positions have an assigned uncertainty of 0.004 cm^{-1}.
[b]Blended line with assigned uncertainty of 0.02 cm^{-1}.
[c]Perturbed line, excluded from the fit.

Can. J. Chem. Downloaded from www.nrcresearchpress.com by 203.198.23.82 on 09/08/12
For personal use only.

ergy level expressions of eqs. [5] and [6] were not employed directly; rather, the ℓ-type doubling was modelled by inclusion of the off-diagonal $(02^00)\Sigma^+ \sim (02^20)\Delta$ matrix element in the matrix describing the Σ and Δ vibronic states for $v_2 = 2$. The combined data set contained over 1700 individual lines; however, owing to local perturbations in the $\tilde{B}$ state vibrational levels, only some 1200 lines were included in the final fit. These perturbations are clearly evident in Figs. 2–5, where reduced rotational term values of the $(02^00)\Sigma^+$, $(010)\Pi$, and $(02^20)\Delta$ vibronic levels of the $\tilde{B}$ state are plotted as functions of the rotational quantum number. The fitted parameters are listed in Table 7; we now consider each of the bands individually.

$\tilde{B}^2\Sigma^+(02^00)\Sigma^+ \leftarrow \tilde{X}^2\Sigma^+(000)\Sigma^+$

As with $^2\Sigma^+$–$^2\Sigma^+$ transitions of diatomic molecules, strong P_1, P_2, R_1, and R_2 branches are observed for this transition. A strong perturbation occurs in the F_2 spin component as a result of a level crossing between $N = 9$ and 10 (see Fig. 2). In the region of the crossing, energy levels are shifted up to 1 cm^{-1}, and the effects of the perturbation in terms of high residuals are observed over an unusually long range in N ($N \leq 49$). Low N values of the F_1 spin component ($N \leq 22$) are also perturbed, but to a much lesser extent.

$\tilde{B}^2\Sigma^+(02^20)\Delta \leftarrow \tilde{X}^2\Sigma^+(010)\Pi$

Since the $^2\Delta$ and $^2\Pi$ vibronic states follow Hund's case (b) coupling, strong Q_1 and Q_2 branches appear in addition to the P_1, P_2, R_1, and R_2 branches. Satellite branches, for which $\Delta N \neq \Delta J$, are not observed with any appreciable intensity. Each of the six main branches are doubled owing to ℓ-type doubling in both states. However, splitting of the e/f parity levels is much larger in the ground state $^2\Pi$ level so that doubled branches are observed even for low N values ($N \geq 9$). The F_1 levels are well behaved, but the e and f parity components of the $\tilde{B}^2\Sigma^+$ $(02^20)\Delta$ F_2-spin manifold both show indications of interactions with several different states (see Figs. 4 and 5). As a consequence, many line positions associated with the F_2 levels are omitted from the fit. The magnitude of the ℓ-type doubling constant q was well determined for both states, but the absolute sign and hence the actual parity assignments could not be established unequivocally from this transition alone; two equally satisfactory fits could be achieved by switching the parity assignments and adjusting the rotational quantum number accordingly. The effective ℓ-type doubling constant for the $^2\Delta$ state was determined to be $|q_{\text{eff}}| = 4.37(7) \times 10^{-9}$ cm^{-1} and is of opposite sign to that of the $^2\Pi$ state, $|q| = 3.9503(46) \times 10^{-4}$ cm^{-1}.

$\tilde{B}^2\Sigma^+(02^00)\Sigma^+ \leftarrow \tilde{X}^2\Sigma^+(010)\Pi$

Although data for both levels of this band were available from other transitions observed in this work, an analysis of the $\tilde{B}^2\Sigma^+(02^00)\Sigma^+ \leftarrow \tilde{X}^2\Sigma^+(010)\Pi$ band was undertaken to confirm on a purely experimental basis the e/f parity assignments of the $\tilde{X}^2\Sigma^+(010)\Pi$ level, thereby eliminating any ambiguity in the assignments of the $\tilde{B}^2\Sigma^+(02^20)\Delta$–$\tilde{X}^2\Sigma^+(010)\Pi$ band. The Q_1 and Q_2 branches accompanying a $^2\Sigma^+$–$^2\Pi$(b) transition are governed by the selection rule $e \leftrightarrow f$. The P and R branches follow different selection rules,

TABLE 2. Line positions[a] (cm^{-1}) for the $B^2\Sigma^+$–$X^2\Sigma^+$ (02^20)Δ–(010)Π band of SrOH. The table shows $\bar{\nu}_{obs}$, the measured wavenumbers (cm^{-1}), and the residuals, $\bar{\nu}_{obs} - \bar{\nu}_{calc}$

N	P_{1f}		P_{1e}		R_{1f}		R_{1e}	
3	16 815.220	0.009[b]	16 815.220	0.001[b]	16 818.592	0.016[b]	16 818.592	0.008[b]
4	16 814.655	0.003[b]	16 814.655	−0.008[b]	16 819.023	0.005[b]	16 819.023	−0.006[b]
5	16 814.101	0.005[b]	16 814.101	−0.008[b]	16 819.477	0.013[b]	16 819.477	0.000[b]
6	16 813.550	0.007[b]	16 813.550	−0.010[b]	16 819.937	0.025[b]	16 819.937	0.008[b]
7	16 813.007	0.014[b]	16 813.007	−0.009[b]	16 820.389	0.025[b]	16 820.389	0.003[b]
8	16 812.455	0.008	16 812.474	−0.002	16 820.823	0.004	16 820.849	0.002
9	16 811.905	0.001	16 811.936	−0.004	16 821.289	0.012	16 821.305	−0.007
10	16 811.364	0.000	16 811.407	−0.001	16 821.743	0.005	16 821.784	0.003
11	16 810.832	0.004	16 810.880	0.000	16 822.201	−0.001	16 822.257	0.002
12	16 810.300	0.006	16 810.360	0.004	16 822.673	0.003	16 822.733	0.002
13	16 809.782	0.018[b]	16 809.845	0.009	16 823.142	0.002	16 823.218	0.006
14	16 809.240	0.002	16 809.323	0.002	16 823.612	−0.002	16 823.697	0.000
15	16 808.706	−0.008	16 808.811	0.002	16 824.091	0.000	16 824.181	−0.005
16	16 808.199	0.005	16 808.306	0.005	16 824.577	0.006[b]	16 824.671	−0.007
17	16 807.679	0.002	16 807.800	0.002	16 825.055	0.001	16 825.175	0.000
18	16 807.168	0.005	16 807.310	0.011	16 825.539	−0.001	16 825.673	−0.002
19	16 806.659	0.006	16 806.797	−0.006[b]	16 826.024	−0.005	16 826.179	0.000
20	16 806.142	−0.004[b]	16 806.315	0.003	16 826.532	0.011[b]	16 826.689	0.002
21	16 805.643	0.001	16 805.835	0.010[b]	16 827.018	0.002	16 827.202	0.003
22	16 805.142	0.001	16 805.337	−0.005	16 827.516	0.002	16 827.715	0.000
23	16 804.646	0.002	16 804.864	0.001	16 828.017	0.001	16 828.235	0.000
24	16 804.159	0.009	16 804.392	0.004	16 828.518	−0.002	16 828.758	0.000
25	16 803.663	0.004	16 803.928	0.011[b]	16 829.023	−0.004	16 829.285	−0.001
26	16 803.176	0.005	16 803.453	0.003	16 829.537	−0.001	16 829.814	−0.003
27	16 802.686	−0.001	16 802.998	0.011	16 830.052	0.001	16 830.351	0.000
28	16 802.203	−0.003	16 802.524	−0.005	16 830.565	−0.002	16 830.889	−0.001
29	16 801.708	−0.021[b]	16 802.073	−0.001	16 831.081	−0.005	16 831.429	−0.004
30	16 801.256	0.002	16 801.623	−0.001	16 831.604	−0.005	16 831.977	−0.002
31	16 800.786	0.003	16 801.188	0.011[b]	16 832.131	−0.003	16 832.528	−0.001
32	16 800.304	−0.011[b]	16 800.735	0.000	16 832.660	−0.002	16 833.078	−0.005
33	16 799.856	0.005	16 800.304	0.007[b]	16 833.192	−0.001	16 833.638	−0.002
34	16 799.376	−0.013[b]	16 799.856	−0.007	16 833.726	−0.001	16 834.200	−0.002
35	16 798.931	0.000	16 799.435	0.002	16 834.265	0.002	16 834.761	−0.006
36	16 798.473	−0.004	16 799.007	−0.001	16 834.802	−0.001	16 835.337	0.002
37	16 798.021	−0.004	16 798.585	−0.001	16 835.337	−0.009	16 835.899	−0.009[b]
38	16 797.578	0.001	16 798.169	0.001	16 835.899	0.008[b]	16 836.480	−0.004
39	16 797.123	−0.009[b]	16 797.736	−0.019[b]	16 836.442	0.003[b]	16 837.063	−0.001
40	16 796.686	−0.005	16 797.343	−0.003	16 836.988	−0.003	16 837.646	−0.002
41	16 796.252	0.000	16 796.939	−0.002	16 837.544	−0.001	16 838.236	0.001
42	16 795.812	−0.005	16 796.549	0.009[b]	16 838.103	0.002[b]	16 838.826	0.000
43	16 795.376	−0.009[b]	16 796.144	0.001	16 838.660	−0.001	16 839.422	0.001
44	16 794.967	0.010[b]	16 795.746	−0.004	16 839.217	−0.006	16 840.023	0.003
45	16 794.518	−0.014[b]	16 795.376	0.014[b]	16 839.790	0.001	16 840.624	0.002
46	16 794.107	−0.003	16 794.967	−0.010[b]	16 840.357	0.000	16 841.228	0.000
47	16 793.692	0.001	16 794.595	−0.002	16 840.926	−0.002	16 841.837	0.000
48	16 793.277	0.001	16 794.225	0.004	16 841.501	0.000	16 842.452	0.001
49	16 792.859	−0.004	16 793.847	−0.002	16 842.082	0.005	16 843.068	0.001
50	16 792.453	−0.002	16 793.484	0.002	16 842.658	0.001	16 843.689	0.001
51	16 792.030	−0.019[b]	16 793.118	0.000	16 843.240	0.002	16 844.313	0.001
52	16 791.656	0.009[b]	16 792.756	−0.003	16 843.815	−0.008[b]	16 844.958	0.018[b]
53	16 791.246	−0.002	16 792.401	−0.003	16 844.412	0.002	16 845.587	0.015[b]
54	16 790.850	−0.002	16 792.030	−0.023[b]	16 844.999	−0.001	16 846.200	−0.007[b]
55	16 790.459	−0.001	16 791.711	0.004	16 845.587	−0.006[b]	16 846.844	−0.002
56	16 790.066	−0.005[b]	16 791.370	0.006	16 846.200	0.011[b]	16 847.490	0.001
57	16 789.672	−0.013[b]	16 791.012	−0.015[b]	16 846.784	−0.003	16 848.135	−0.001
58	16 789.299	−0.003	16 790.691	−0.002	16 847.389	0.001	16 848.781	−0.005[b]
59	16 788.919	−0.004	16 790.356	−0.008[b]	16 847.992	0.001	16 849.443	0.003
60	16 788.538	−0.009	16 790.066	0.027[b]	16 848.586	−0.012[b]	16 850.100	0.003
62					16 849.816	−0.002	16 851.419	−0.005
63					16 850.431	−0.002		

Can. J. Chem. Downloaded from www.nrcresearchpress.com by 203.198.23.82 on 09/08/12
For personal use only.

TABLE 2 (*continued*)

N	Q_{1ef}		Q_{1fe}		Q_{2ef}		Q_{2fe}	
9					16 817.732	0.002		
10					16 817.842	0.001		
11					16 817.959	0.003	16 817.909	0.005
12					16 818.075	0.000	16 818.017	0.003
13					16 818.201	0.003	16 818.136	0.009[b]
14					16 818.330	0.005	16 818.242	−0.001
15					16 818.459	0.003	16 818.364	0.002
16					16 818.592	0.001[b]	16 818.482	−0.002
17					16 818.732	0.002	16 818.592	−0.017[b]
18					16 818.868	−0.005	16 818.732	−0.006
19					16 819.017	−0.002[b]	16 818.868	−0.002
20					16 819.168	−0.002	16 819.017	0.013[b]
21					16 819.318	−0.006	16 819.141	−0.001
22					16 819.475	−0.007	16 819.279	−0.005
23					16 819.639	−0.006	16 819.417	−0.011[c]
24					16 819.802	−0.009	16 819.595	0.020[c]
25					16 819.966	−0.015[c]	16 819.734	0.008[c]
26					16 820.129	−0.026[c]	16 819.881	0.002
27							16 820.035	−0.001
28			16 816.456	−0.002			16 820.195	−0.001
29			16 816.498	−0.004			16 820.358	−0.001
30			16 816.549	0.000			16 820.520	−0.005[c]
31			16 816.603	0.002			16 820.685	−0.009[c]
32			16 816.659	0.003			16 820.854	−0.012[c]
33			16 816.721	0.006	16 821.492	0.012[c]	16 821.022	−0.020[c]
34	16 816.311	−0.003	16 816.786	0.007	16 821.695	0.011[c]	16 821.200	−0.020[c]
35	16 816.354	−0.001	16 816.853	0.007	16 821.901	0.008	16 821.362	−0.040[c]
36	16 816.397	−0.001	16 816.910	−0.007	16 822.111	0.006	16 821.583	−0.003[c]
37	16 816.456	0.012	16 816.996	0.005	16 822.338	0.017[b]	16 821.790	0.016[c]
38	16 816.498	0.004	16 817.076	0.006	16 822.540	−0.001	16 821.967	0.002[c]
39	16 816.549	0.002	16 817.154	0.002	16 822.766	0.002		
40	16 816.603	0.001	16 817.242	0.003	16 822.992	0.000		
41	16 816.659	−0.002	16 817.330	0.001	16 823.219	−0.004[b]		
42	16 816.721	−0.003	16 817.425	0.002				
43	16 816.786	−0.003	16 817.521	0.000				
44	16 816.854	−0.003	16 817.621	−0.001				
45	16 816.910	−0.019[b]	16 817.725	−0.003				
46	16 816.996	−0.008	16 817.827	−0.010[b]				
47	16 817.076	−0.006	16 817.947	−0.003[b]				
48	16 817.154	−0.009	16 818.065	−0.002				
49	16 817.242	−0.005	16 818.186	−0.002				
50	16 817.330	−0.004	16 818.313	0.001				
51	16 817.425	0.000	16 818.443	0.003				
52	16 817.521	0.002	16 818.572	0.000[b]				
53	16 817.621	0.005	16 818.711	0.003				
54	16 817.725	0.009	16 818.853	0.005				
55	16 817.827	0.008[b]	16 818.994	0.003				
56	16 817.947	0.021[b]	16 819.158	0.020[b]				
57	16 818.030	−0.006	16 819.291	0.002				
58	16 818.158	0.009	16 819.454	0.010				
59	16 818.272	0.007	16 819.604	0.002				
60	16 818.394	0.009	16 819.762	−0.003				
61	16 818.509	0.001	16 819.925	−0.006				
62	16 818.639	0.005	16 820.100	−0.001				
63	16 818.765	0.002	16 820.269	−0.005				
64	16 818.897	0.001	16 820.455	0.003				
65	16 819.032	0.000	16 820.631	−0.002				
66	16 819.158	−0.014[b]	16 820.821	0.003				
67	16 819.311	−0.004	16 821.012	0.005				
68	16 819.455	−0.006[b]						
69	16 819.605	−0.006						
70	16 819.762	−0.002						
71	16 819.926	0.005[b]						
72	16 820.084	0.002						
73	16 820.242	−0.004						

Can. J. Chem. Downloaded from www.nrcresearchpress.com by 203.198.23.82 on 09/08/12
For personal use only.

TABLE 2 (*concluded*)

N	P_{2f}		P_{2e}		R_{2f}		R_{2e}	
4	16 815.175	0.014[b]	16 815.175	0.025[b]	16 819.809	0.001[b]	16 819.809	0.012[b]
5	16 814.753	0.001[b]	16 814.753	0.015[b]	16 820.389	−0.011[b]	16 820.389	0.002[b]
6	16 814.345	−0.001[b]	16 814.345	0.015[b]	16 821.000	0.004[b]	16 821.000	0.021[b]
7	16 813.940	−0.005[b]	16 813.940	0.017[b]	16 821.587	−0.009[b]	16 821.587	0.014[b]
8	16 813.550	0.003[b]	16 813.550	0.031[b]	16 822.178	−0.021[b]	16 822.178	0.007[b]
9	16 813.156	0.002	16 813.119	0.001	16 822.805	−0.002	16 822.769	−0.002
10					16 823.415	−0.003	16 823.379	0.004
11	16 812.382	0.003	16 812.329	0.002	16 824.034	0.000	16 823.980	−0.002
12	16 811.997	−0.001	16 811.936	0.000	16 824.656	0.003	16 824.577	−0.015[b]
13	16 811.621	0.000	16 811.548	−0.001	16 825.269	−0.008	16 825.202	−0.003
14	16 811.251	0.004	16 811.163	−0.001	16 825.902	−0.002	16 825.818	−0.003
15	16 810.880	0.002	16 810.782	−0.001	16 826.532	−0.003	16 826.440	0.000
16	16 810.513	0.000	16 810.404	−0.001	16 827.166	−0.004	16 827.059	−0.003
17	16 810.153	0.001	16 810.016	−0.015[b]	16 827.804	−0.004	16 827.680	−0.007
18	16 809.782	−0.013[b]	16 809.658	−0.001	16 828.448	−0.003	16 828.314	−0.001[b]
19	16 809.432	−0.010	16 809.281	−0.010	16 829.090	−0.007	16 828.943	−0.004
20	16 809.089	−0.004	16 808.929	0.003	16 829.747	−0.001	16 829.577	−0.004
21	16 808.741	−0.007	16 808.559	−0.006	16 830.397	−0.005	16 830.219	0.001[c]
22	16 808.402	−0.005	16 808.199	−0.007	16 831.049	−0.011[c]	16 830.843	−0.016[c]
23	16 808.063	−0.007	16 807.834	−0.017[c]			16 831.486	−0.016[c]
24	16 807.721	−0.016[c]	16 807.488	−0.011[c]	16 832.389	0.002[c]	16 832.131	−0.017[c]
25			16 807.132	−0.018[c]	16 833.056	0.000	16 832.767	−0.031[c]
26	16 807.086	0.003[c]	16 806.797	−0.008[c]	16 833.726	−0.003		
27	16 806.762	0.000	16 806.447	−0.015[c]	16 834.401	−0.004		
28	16 806.447	0.001			16 835.078	−0.008		
29	16 806.142	0.009			16 835.758	−0.012[c]		
30	16 805.835	0.011			16 836.442	−0.016[c]	16 836.121	0.033[c]
31	16 805.509	−0.011[c]			16 837.136	−0.013[c]	16 836.772	0.018[c]
32	16 805.210	−0.009[c]	16 804.834	0.035[c]	16 837.829	−0.016[c]	16 837.434	0.010[c]
33	16 804.910	−0.012[c]	16 804.497	0.021[c]	16 838.521	−0.023[c]	16 838.103	0.007[b]
34	16 804.618	−0.012[c]	16 804.157	0.001[c]	16 839.217	−0.029[c]	16 838.778	0.007
35	16 804.326	−0.016[c]	16 803.850	0.010[b]			16 839.451	0.001
36	16 804.014	−0.043[c]	16 803.527	0.001	16 840.681	0.018[c]	16 840.131	0.001
37			16 803.226	0.010	16 841.377	0.001[c]	16 840.815	0.001
38	16 803.527	0.026[c]	16 802.925	0.016	16 842.082	−0.012[c]	16 841.501	0.000[b]
39	16 803.226	−0.002[c]	16 802.612	0.007	16 842.802	−0.013[c]	16 842.188	−0.002
40			16 802.307	0.002	16 843.520	−0.019[c]	16 842.880	−0.002
41	16 802.686	−0.010[c]	16 802.012	0.005	16 844.239	−0.028[c]	16 843.573	−0.004[c]
42					16 844.958	−0.041[c]	16 844.262	−0.012[c]
43	16 802.154	−0.026[c]	16 801.416	−0.006[c]	16 845.674	−0.061[c]	16 844.958	−0.017[c]
44	16 801.891	−0.037[c]			16 846.402	−0.072[c]	16 845.674	−0.003[c]
45			16 800.843	−0.007[c]	16 847.122	−0.094[c]	16 846.370	−0.013[c]
46			16 800.557	−0.011[c]	16 847.863	−0.100[c]	16 847.070	−0.022[c]
47					16 848.586	−0.126[c]	16 847.777	−0.026[c]
48	16 800.856	−0.105[c]					16 848.484	−0.032[c]
49	16 800.605	−0.124[c]						
50							16 849.899	−0.053[c]
51							16 850.604	−0.069[c]

[a]Unless indicated otherwise, line positions have an assigned uncertainty of 0.004 cm^{-1}.
[b]Blended line with assigned uncertainty of 0.02 cm^{-1}.
[c]Perturbed line, excluded from the fit.

$e \leftrightarrow e, f \leftrightarrow f$. Accordingly the P_1 and R_1 branches involve excitation from only $\tilde{X}^2\Sigma^+(010)\Pi$ F_1,e levels, whilst the P_2 and R_2 branches arise from the corresponding F_2,f levels. In contrast, the Q_1 and Q_2 branches fix the energy positions of the F_1,f and F_2,e parity levels, respectively. Thus unperturbed data from the three main branches of either the F_1 or F_2 spin manifofld are sufficient to specify the magnitude and sign of q_v for the $\tilde{X}(010)\Pi$ level. In the present case, data are available from both spin components, and the sign of the ℓ-type doubling constant is established unequivocally. Our determination of $q_v = -3.9503(46) \times 10^{-4}$ cm^{-1} agrees remarkably well with the estimate by Nakagawa et al. (1) of the magnitude of q, $4.05(13) \times 10^{-4}$ cm^{-1}. The negative sign of q_v is consistent with the expression [13] of Nielsen and, moreover, a negative value for q_v of similar magnitude has also been observed for the $\tilde{X}^2\Sigma^+(010)\Pi$ vibrational level of CaOH (13). The $\tilde{X}^2\Sigma^+(010)\Pi$ vibrational level of SrOH is more accurately located at 363.689(2) cm^{-1}, as compared with the previous estimate of 360 ± 3 cm^{-1} (1). This establishes the splitting in the $\tilde{B}$ state between the $v_2 = 2$, $\ell = 0$ and $\ell = 2$ components as 32.703 cm^{-1}, yielding $g_{22} = 8.1758(7)$ cm^{-1}.

Can. J. Chem. Downloaded from www.nrcresearchpress.com by 203.198.23.82 on 09/08/12
For personal use only.

TABLE 3. Line positions[a] (cm^{-1}) for the $B^2\Sigma^+$–$X^2\Sigma^+$ $(02^00)\Sigma^+$–$(010)\Pi$ band of SrOH. The table shows $\bar{\nu}_{obs}$, the measured wavenumbers (cm^{-1}), and the residuals, $\bar{\nu}_{obs} - \bar{\nu}_{calc}$

N	P_1		Q_1		R_1		P_2		Q_2		R_2	
2	16 783.974	−0.100[c]			16 786.348	−0.089[c]						
3	16 783.411	−0.106[c]			16 786.811	−0.072[c]						
4	16 782.868	−0.092[c]			16 787.262	−0.067[c]						
5	16 782.327	−0.080[c]			16 787.713	−0.065[c]						
6	16 781.787	−0.072[c]			16 788.173	−0.059[c]						
7	16 781.255	−0.062[c]										
8	16 780.721	−0.058[c]			16 789.111	−0.046[c]						
9	16 780.181	−0.065[c]			16 789.583	−0.043[c]						
10	16 779.672	−0.046[c]			16 790.063	−0.037[c]						
11	16 779.153	−0.041[c]			16 790.547	−0.031[c]						
12	16 778.651	−0.023[c]			16 791.037	−0.023[c]						
13	16 778.132	−0.027[c]			16 791.522	−0.025[c]					16 794.069	0.416[c]
14	16 777.609	−0.040[c]			16 792.012	−0.026[c]					16 794.681	0.391[c]
15	16 777.119	−0.024[c]			16 792.516	−0.018[c]			16 787.090	0.343[c]	16 795.271	0.340[c]
16	16 776.620	−0.022[c]			16 793.017	−0.017[c]					16 795.878	0.302[c]
17	16 776.129	−0.017[c]			16 793.529	−0.009[c]			16 787.283	0.268[c]	16 796.492	0.267[c]
18	16 775.641	−0.013[c]			16 794.036	−0.011[c]	16 778.480	0.279[c]			16 797.120	0.241[c]
19	16 775.150	−0.017[c]			16 794.552	−0.008[c]	16 778.132	0.273[c]	16 787.535	0.237[c]	16 797.738	0.200[c]
20	16 774.670	−0.014[c]			16 795.069	−0.009[c]	16 777.756	0.235[c]	16 787.660	0.215[c]	16 798.397	0.197[c]
21	16 774.191	−0.015[c]			16 795.592	−0.008[c]	16 777.401	0.213[c]	16 787.795	0.200[c]	16 799.043	0.176[c]
22	16 773.722	−0.010[c]			16 796.124	−0.002	16 777.056	0.197[c]	16 787.938	0.189[c]	16 799.704	0.166[c]
23	16 773.254	−0.009[c]			16 796.657	0.001	16 776.711	0.176[c]	16 788.065	0.158[c]	16 800.368	0.154[c]
24	16 772.790	−0.008			16 797.187	−0.004	16 776.377	0.161[c]	16 788.216	0.148[c]	16 801.044	0.151[c]
25	16 772.331	−0.007			16 797.738	0.008[b]	16 776.057	0.157[c]	16 788.369	0.136[c]	16 801.707	0.130[c]
26	16 771.875	−0.008			16 798.273	−0.001	16 775.728	0.138[c]	16 788.527	0.126[c]	16 802.383	0.118[c]
27	16 771.426	−0.006			16 798.824	0.003	16 775.411	0.127[c]	16 788.685	0.122[c]	16 803.068	0.110[c]
28	16 770.997	0.011[b]	16 784.604	−0.006	16 799.375	0.002	16 775.100	0.118[c]	16 788.856	0.108[c]	16 803.759	0.105[c]
29	16 770.545	0.001[b]	16 784.643	−0.001	16 799.930	0.001	16 774.795	0.110[c]	16 789.025	0.098[c]	16 804.451	0.096[c]
30	16 770.107	0.000[b]	16 784.681	−0.001[b]	16 800.492	0.003	16 774.491	0.098[c]	16 789.204	0.094[c]	16 805.132	0.072[c]
31	16 769.676	0.002[b]	16 784.721	−0.002	16 801.044	−0.010[b]	16 774.191	0.087[c]	16 789.378	0.082[c]	16 805.847	0.078[c]
32	16 769.255	0.009[b]	16 784.769	0.000	16 801.626	0.003[b]	16 773.903	0.082[c]	16 789.562	0.076[c]	16 806.556	0.074[c]
33	16 768.824	0.002	16 784.817	0.000	16 802.200	0.005	16 773.620	0.078[c]	16 789.749	0.070[c]	16 807.263	0.064[c]
34	16 768.404	0.001	16 784.870	0.001	16 802.776	0.004	16 773.337	0.070[c]	16 789.943	0.068[c]	16 807.981	0.061[c]
35	16 767.991	0.003[b]	16 784.928	0.003	16 803.359	0.006	16 773.254	0.258[c]	16 790.132	0.057[c]	16 808.703	0.058[c]
36	16 767.577	−0.001	16 784.975	−0.009[b]	16 803.939	0.001	16 772.790	0.060[c]	16 790.345	0.067[c]	16 809.425	0.051[c]
37	16 767.174	0.002	16 785.048	0.001	16 804.531	0.003	16 772.519	0.050[c]	16 790.534	0.049[c]	16 810.151	0.044[c]
38	16 766.770	−0.001	16 785.114	0.001	16 805.132	0.011	16 772.260	0.048[c]	16 790.737	0.041[c]	16 810.887	0.042[c]
39	16 766.375	0.000	16 785.186	0.003	16 805.727	0.009	16 772.001	0.042[c]	16 790.951	0.042[c]	16 811.622	0.036[c]
40	16 765.984	0.002	16 785.260	0.004	16 806.320	0.001	16 771.750	0.039[c]	16 791.160	0.034[c]	16 812.360	0.029[c]
41	16 765.585	−0.009[b]	16 785.332	−0.001	16 806.924	−0.001	16 771.499	0.032[c]	16 791.379	0.032[c]	16 813.110	0.030[c]
42	16 765.215	0.004	16 785.414	0.001	16 807.531	−0.003	16 771.257	0.030[c]	16 791.601	0.031[c]	16 813.853	0.020[c]
43	16 764.833	0.001	16 785.497	0.000	16 808.147	0.000	16 770.997	0.005[c]	16 791.822	0.024[c]	16 814.613	0.024[c]
44	16 764.457	−0.001	16 785.585	0.002	16 808.766	0.001	16 770.786	0.025[c]	16 792.046	0.018[c]	16 815.371	0.021[c]
45	16 764.087	−0.001	16 785.676	0.002	16 809.385	−0.001	16 770.545	0.010[c]	16 792.288	0.026[c]	16 816.130	0.015[c]
46	16 763.704	−0.018[b]	16 785.770	0.002	16 810.012	0.001	16 770.330	0.017[c]	16 792.516	0.017[c]	16 816.897	0.014[c]
47	16 763.358	−0.003	16 785.869	0.004	16 810.639	−0.001	16 770.107	0.012[c]	16 792.751	0.012[c]	16 817.665	0.010[c]
48	16 763.001	−0.003			16 811.273	0.001	16 769.895	0.014[c]	16 792.983	0.000[c]	16 818.455	0.014[c]
49	16 762.653	0.001	16 786.069	0.000	16 811.908	−0.001	16 769.676	0.004[c]	16 793.224	−0.006[c]		
50	16 762.309	0.005[b]	16 786.180	0.004	16 812.548	−0.002	16 769.482	0.015[c]	16 793.487	0.007	16 819.997	0.003
51	16 761.959	−0.001	16 786.287	0.000	16 813.189	−0.005	16 769.255	−0.011[b]			16 820.780	−0.001
52	16 761.621	0.001	16 786.400	0.000	16 813.853	0.011[b]	16 769.078	0.009	16 793.994	0.005	16 821.570	−0.001
53	16 761.285	0.000	16 786.518	0.001[b]	16 814.496	0.002	16 768.882	0.005[b]	16 794.254	0.005	16 822.366	0.000
54	16 760.954	−0.001	16 786.637	−0.001	16 815.147	−0.002	16 768.692	0.003	16 794.520	0.008[b]	16 823.160	−0.004
55	16 760.628	0.000	16 786.761	0.000	16 815.809	0.000	16 768.507	0.002[b]	16 794.777	−0.001	16 823.967	0.002
56	16 760.305	−0.001	16 786.885	−0.003	16 816.470	−0.002	16 768.327	0.001	16 795.030	−0.017	16 824.765	−0.005
57	16 759.995	0.006[b]	16 787.018	0.000	16 817.138	0.000	16 768.151	0.001	16 795.322	0.003	16 825.578	−0.001
58	16 759.677	0.002	16 787.169	0.018[b]	16 817.814	0.005[b]			16 795.593	−0.002	16 826.389	−0.002
59	16 759.364	−0.002	16 787.290	0.002	16 818.484	0.001	16 767.812	0.000	16 795.873	0.000	16 827.205	−0.002
60	16 759.062	0.001	16 787.438	0.010[b]	16 819.151	−0.009	16 767.646	−0.003	16 796.144	−0.010	16 828.023	−0.003
61	16 758.759	−0.002	16 787.572	0.002	16 819.842	0.000			16 796.436	−0.003	16 828.845	−0.004
62	16 758.463	−0.001	16 787.720	0.004	16 820.521	−0.005	16 767.335	0.000	16 796.723	−0.003	16 829.671	−0.004
63	16 758.173	0.001	16 787.868	0.002	16 821.215	0.000			16 797.004	−0.013[b]		
64	16 757.886	0.001	16 788.020	0.002	16 821.904	−0.003			16 797.312	0.001		

Can. J. Chem. Downloaded from www.nrcresearchpress.com by 203.198.23.82 on 09/08/12
For personal use only.

TABLE 3 (*concluded*)

N	P_1		Q_1		R_1		P_2		Q_2		R_2	
65	16 757.604	0.003	16 788.177	0.004	16 822.598	−0.004	16 766.893	−0.003	16 797.605	−0.002		
66	16 757.323	0.001	16 788.335	0.003	16 823.295	−0.006			16 797.908	0.001		
67	16 757.046	0.000			16 823.995	−0.009	16 766.628	0.004	16 798.212	0.003		
68	16 756.774	−0.001			16 824.705	−0.005	16 766.501	0.008	16 798.521	0.007		
69	16 756.507	−0.002			16 825.420	0.001						
70	16 756.247	0.001			16 826.124	−0.008	16 766.247	0.002				
71	16 755.991	0.003			16 826.848	0.000	16 766.135	0.008				
72	16 755.737	0.004			16 827.567	−0.001						
73	16 755.487	0.004			16 828.289	−0.002						
74	16 755.238	0.001			16 829.015	−0.002						
75	16 754.999	0.004			16 829.748	0.001						

[a]Unless indicated otherwise, line positions have an assigned uncertainty of 0.004 cm^{-1}.
[b]Blended line with assigned uncertainity of 0.02 cm^{-1}.
[c]Perturbed line, excluded from the fit.

TABLE 4. Line positions[a] (cm^{-1}) for the $B^2\Sigma^+$–$X^2\Sigma^+$ (010)Π–(000)Σ^+ band of SrOH. The table shows $\bar{\nu}_{obs}$, the measured wavenumbers (cm^{-1}) and the residuals, $\bar{\nu}_{obs} - \bar{\nu}_{calc}$

N	P_1		Q_1		R_1		P_2		Q_2		R_2	
2	16 777.025	0.001										
3	16 776.460	−0.002			16 779.832	−0.005			16 778.403	0.000	16 780.475	−0.002
4	16 775.900	−0.003			16 780.285	0.002			16 778.501	0.009	16 781.067	0.000
5	16 775.354	0.005			16 780.729	−0.004	16 775.996	0.002	16 778.588	0.001	16 781.645	−0.015[b]
6	16 774.793	−0.006			16 781.185	−0.002	16 775.585	−0.002	16 778.689	0.003	16 782.249	−0.007
7	16 774.251	−0.001			16 781.645	0.000			16 778.794	0.005	16 782.855	−0.002
8	16 773.706	−0.003			16 782.107	0.001	16 774.794	0.011[b]	16 778.902	0.005	16 783.456	−0.005
9	16 773.170	−0.001			16 782.569	−0.003	16 774.385	−0.003	16 779.018	0.008	16 784.061	−0.008
10	16 772.632	−0.004			16 783.036	−0.005	16 773.992	−0.004	16 779.133	0.006	16 784.677	−0.004
11	16 772.095	−0.010[b]			16 783.514	0.000	16 773.602	−0.005	16 779.256	0.007		
12	16 771.577	−0.001			16 783.988	−0.003	16 773.221	−0.002	16 779.387	0.012	16 785.938	0.022[b]
13	16 771.056	0.001			16 784.470	−0.001	16 772.841	−0.002	16 779.515	0.009	16 786.524	−0.016
14	16 770.533	−0.003			16 784.966	0.010	16 772.461	−0.005	16 779.651	0.009	16 787.158	−0.009
15	16 770.017	−0.004			16 785.442	−0.002	16 772.095	0.001[b]	16 779.799	0.017	16 787.790	−0.007
16	16 769.504	−0.005			16 785.938	0.002[b]	16 771.721	−0.004	16 779.942	0.016	16 788.456	0.024[c]
17	16 769.003	0.001			16 786.428	−0.003	16 771.351	−0.010	16 780.092	0.016[c]	16 789.072	0.002[c]
18	16 768.497	−0.001			16 786.931	0.001	16 770.992	−0.008[c]	16 780.248	0.019[c]	16 789.712	0.000[c]
19	16 768.004	0.005			16 787.431	−0.003	16 770.632	−0.011[c]	16 780.407	0.020[c]	16 790.338	−0.020[c]
20	16 767.508	0.005			16 787.938	−0.002	16 770.278	−0.012[c]	16 780.569	0.019[c]	16 791.003	−0.004[c]
21	16 767.015	0.003			16 788.456	0.005[b]	16 769.928	−0.013[c]	16 780.744	0.027[c]	16 791.655	−0.005[c]
22	16 766.525	0.001			16 788.970	0.005	16 769.581	−0.014[c]	16 780.917	0.028[c]	16 792.313	−0.003[c]
23	16 766.035	−0.005[b]	16 777.710	−0.001	16 789.487	0.004	16 769.241	−0.013[c]	16 781.090	0.025[c]	16 792.983	0.007[c]
24	16 765.564	0.004	16 777.749	−0.001	16 790.004	−0.001	16 768.906	−0.010[c]	16 781.276	0.030[c]	16 793.632	−0.008[c]
25	16 765.090	0.005	16 777.791	−0.002	16 790.533	0.003	16 768.569	−0.014[c]	16 781.460	0.029[c]	16 794.308	0.000[c]
26	16 764.614	0.001	16 777.838	−0.002	16 791.062	0.003	16 768.241	−0.012[c]	16 781.655	0.034[c]	16 794.968	−0.011[c]
27	16 764.148	0.003	16 777.891	−0.001	16 791.596	0.005	16 767.919	−0.008[c]	16 781.842	0.027[c]	16 795.644	−0.010[c]
28	16 763.682	0.001	16 777.946	−0.003	16 792.132	0.004	16 767.591	−0.015[c]	16 782.040	0.027[c]	16 796.321	−0.011[c]
29	16 763.225	0.005	16 778.008	−0.002	16 792.672	0.005	16 767.273	−0.014[c]	16 782.251	0.035[c]	16 796.997	−0.017[c]
30	16 762.765	0.001	16 778.074	−0.001	16 793.218	0.007	16 766.960	−0.013[c]	16 782.466	0.042[c]	16 797.686	−0.013[c]
31	16 762.316	0.004	16 778.145	0.000	16 793.763	0.005	16 766.642	−0.021[c]	16 782.670	0.034[c]	16 798.374	−0.014[c]
32	16 761.864	0.000	16 778.217	−0.003	16 794.308	−0.001[b]	16 766.332	−0.025[c]	16 782.878	0.026[c]	16 799.047	−0.033[c]
33	16 761.420	0.001	16 778.296	−0.003	16 794.866	0.003	16 766.035	−0.019[c]	16 783.090	0.017[c]	16 799.740	−0.036[c]
34	16 760.979	0.000	16 778.381	−0.001	16 795.422	0.001	16 765.726	−0.029[c]	16 783.312	0.014[c]	16 800.433	−0.043[c]
35	16 760.541	−0.001	16 778.470	0.000	16 795.988	0.006	16 765.424	−0.037[c]	16 783.534	0.006[c]	16 801.127	−0.052[c]
36	16 760.106	−0.004	16 778.560	−0.003	16 796.549	0.002	16 765.125	−0.045[c]	16 783.760	−0.002[c]	16 801.804	−0.081[c]
37	16 759.678	−0.003	16 778.657	−0.003	16 797.115	−0.001	16.764.826	−0.057[c]	16 783.987	−0.013[c]	16 802.499	−0.096[c]
38	16 759.258	0.002	16 778.761	0.000	16 797.686	−0.002[b]	16 764.526	−0.073[c]	16 784.193	−0.050[c]	16 803.171	−0.138[c]
39	16 758.836	0.000	16 778.866	−0.001	16 798.265	0.002	16 764.224	−0.096[c]	16 784.381	−0.110[c]	16 803.819	−0.207[c]
40	16 758.419	0.000	16 778.976	−0.002	16 798.838	−0.004	16 763.905	−0.140[c]	16 784.522	−0.220[c]		
41	16 758.004	−0.002	16 779.092	−0.001	16 799.426	0.001	16 763.559	−0.214[c]			16 805.823	0.353[c]
42	16 757.599	0.002	16 779.210	−0.002	16 800.010	−0.001			16 785.565	0.306[c]	16 806.443	0.246[c]
43	16 757.189	−0.003	16 779.333	−0.003	16 800.602	0.001	16 763.647	0.406[c]	16 785.776	0.252[c]	16 807.119	0.192[c]
44	16 756.791	0.000	16 779.464	0.000	16 801.190	−0.004	16 763.226	0.245[c]	16 786.010	0.217[c]	16 807.823	0.162[c]

Can. J. Chem. Downloaded from www.nrcresearchpress.com by 203.198.23.82 on 09/08/12
For personal use only.

TABLE 4 (*concluded*)

N	P_1		Q_1		R_1		P_2		Q_2		R_2	
45	16 756.393	−0.001	16 779.596	−0.001	16 801.803	0.013[b]	16 762.922	0.197[c]	16 786.268	0.202[c]	16 808.542	0.144[c]
46	16 756.001	0.000	16 779.733	−0.001	16 802.389	−0.001	16 762.642	0.169[c]			16 809.271	0.132[c]
47	16 755.609	−0.002	16 779.874	−0.001	16 802.991	−0.003	16 762.368	0.144[c]	16 786.884	0.258[c]	16 810.004	0.121[c]
48	16 755.224	−0.002	16 780.020	−0.001	16 803.604	0.003	16 762.111	0.132[c]	16 787.097	0.184[c]	16 810.742	0.112[c]
49	16 754.843	−0.002	16 780.173	0.001	16 804.205	−0.006	16 761.864	0.126[c]	16 787.393	0.189[c]	16 811.495	0.114[c]
50	16 754.464	−0.003	16 780.328	0.002	16 804.824	−0.001	16 761.615	0.114[c]			16 812.247	0.112[c]
51	16 754.092	−0.002	16 780.487	0.001	16 805.439	−0.003	16 761.380	0.112[c]			16 813.006	0.114[c]
52	16 753.723	−0.001	16 780.652	0.003	16 806.058	−0.004	16 761.148	0.109[c]			16 813.767	0.114[c]
53	16 753.357	−0.001	16 780.818	0.001	16 806.684	−0.002	16 760.919	0.106[c]			16 814.529	0.113[c]
54	16 753.000	0.003	16 780.990	0.000	16 807.312	−0.001	16 760.700	0.108[c]			16 815.299	0.116[c]
55	16 752.643	0.004	16 781.169	0.002	16 807.943	−0.001	16 760.490	0.116[c]				
56	16 752.287	0.002	16 781.347	−0.001	16 808.575	−0.003	16 760.276	0.116[c]			16 816.846	0.118[c]
57	16 751.937	0.002	16 781.536	0.002	16 809.217	0.001	16 760.061	0.111[c]			16 817.622	0.117[c]
58	16 751.590	0.000	16 781.725	0.001	16 809.850	−0.007	16 759.851	0.107[c]			16 818.403	0.118[c]
59	16 751.248	0.000	16 781.919	0.000	16 810.499	−0.002						
60	16 750.911	0.001	16 782.121	0.003	16 811.150	0.001	16 759.465	0.122[c]				
61	16 750.580	0.004	16 782.324	0.002	16 811.797	−0.003						
62	16 750.250	0.004	16 782.530	0.000	16 812.451	−0.003	16 759.080	0.123[c]				
63	16 749.922	0.002	16 782.742	0.000	16 813.112	0.000	16 758.902	0.132[c]				
64	16 749.602	0.004	16 782.960	0.001	16 813.767	−0.006[b]	16 758.718	0.131[c]				
65	16 749.285	0.005	16 783.180	0.000	16 814.435	−0.002						
66	16 748.972	0.005	16 783.406	0.000								
67	16 748.658	0.001	16 783.636	0.000								
68	16 748.348	−0.003	16 783.866	−0.005								
69	16 748.048	−0.001										

[a]Unless indicated otherwise, line positions have an assigned uncertainty of 0.004 cm^{-1}.
[b]Blended line with assigned uncertainty of 0.02 cm^{-1}.
[c]Perturbed line, excluded from the fit.

TABLE 5. Line positions[a] (cm^{-1}) for the $B^2\Sigma^+$–$X^2\Sigma^+$ $(02^00)\Sigma^+$–$(02^00)\Sigma^+$ band of SrOH. The table shows $\bar{\nu}_{obs}$, the measured wavenumbers (cm^{-1}) and the residuals, $\bar{\nu}_{obs} - \bar{\nu}_{calc}$

N	P_1		R_1		P_2		R_2	
1			16 446.105	−0.047[b]			16 446.350	−0.163[b]
2	16 444.135	−0.092[b]	16 446.516	−0.075[b]			16 446.907	−0.190[b]
3	16 443.616	−0.052[b]	16 446.994	−0.040[b]	16 443.883	−0.151[b]	16 447.454	−0.232[b]
4	16 433.085	−0.029[b]	16 447.459	−0.024[b]	16 443.431	−0.194[b]		
5	16 442.538	−0.027[b]	16 447.916	−0.020[b]	16 442.978	−0.244[b]		
6	16 441.992	−0.029[b]					16 449.059	−0.423[b]
7	16 441.453	−0.029[b]	16 448.866	0.009[b]			16 449.583	−0.508[b]
8			16 449.353	0.028[b]	16 441.809	−0.232[b]	16 450.057	−0.647[b]
9	16 440.401	−0.017[b]	16 449.796	−0.003[b]	16 441.144	−0.513[b]	16 452.328	1.005[b]
10	16 439.905	0.011[b]			16 440.614	−0.664[b]	16 452.738	0.792[b]
11	16 439.365	−0.010[b]	16 450.767	0.008[b]	16 441.862	0.958[b]	16 453.208	0.634[b]
12					16 441.328	0.798[b]		
13	16 438.355	0.003[b]	16 451.745	0.005[b]	16 440.809	0.637[b]		
14			16 452.224	−0.013[b]				
15	16 437.340	−0.009[b]	16 452.748	0.009				
16	16 436.833	−0.022[b]						
17	16 436.360	−0.006	16 453.769	0.011				
18			16 454.266	−0.009			16 457.306	0.200[b]
19	16 435.406	0.003	16 454.823	0.027			16 457.932	0.159[b]
20	16 434.887	−0.042	16 455.337	0.014	16 437.959	0.195[b]	16 458.622	0.178[b]
21	16 434.469	0.009	16 455.878	0.024	16 437.612	0.172[b]	16 459.348	0.228[b]
22	16 434.000	0.004	16 456.400	0.010	16 437.299	0.178[b]		
23	16 433.538	0.002			16 437.030	0.223[b]	16 460.605	0.119[b]
24	16 433.068	−0.014	16 457.461	−0.014			16 461.310	0.134[b]
25					16 436.339	0.145[b]		
26	16 432.175	−0.014	16 458.547	−0.033	16 435.980	0.086[b]	16 462.712	0.142[b]
27							16 463.385	0.111[b]
28	16 431.290	−0.026	16 459.708	0.005	16 435.441	0.131[b]	16 464.108	0.126[b]

Can. J. Chem. Downloaded from www.nrcresearchpress.com by 203.198.23.82 on 09/08/12
For personal use only.

TABLE 5 (*concluded*)

N	P_1		R_1		P_2		R_2	
29					16 435.115	0.089[b]		
30	16 430.470	0.008	16 460.846	0.001	16 434.898	0.152[b]	16 465.504	0.091[b]
31								
32	16 429.637	0.009	16 462.008	0.003	16 434.306	0.105[b]	16 466.903	0.041[b]
33								
34	16 428.816	0.002	16 463.205	0.022	16 433.756	0.080[b]	16 468.398	0.069[b]
35							16 469.139	0.070[b]
36	16 428.104	0.084	16 464.395	0.015	16 433.243	0.073[b]	16 469.875	0.062[b]
37			16 464.995	0.010	16 433.031	0.107[b]		
38	16 427.256	0.011	16 465.630	0.036	16 432.737	0.054[b]	16 471.341	0.025[b]
39	16 426.830	−0.035	16 466.256	0.048				
40	16 426.498	0.008	16 466.775	−0.052	16 432.233	0.017[b]	16 472.840	0.004[b]
41	16 426.157	0.038						
42	16 425.716	−0.038	16 468.001	−0.076	16 431.736	−0.031[b]	16 474.357	−0.016
43								
44	16 424.979	−0.059	16 469.355	0.011	16 431.323	−0.015	16 475.886	−0.041
45			16 469.995	0.010				
46	16 424.319	−0.022	16 470.552	−0.077	16 430.875	−0.053	16 477.422	−0.076
47	16 424.032	0.033					16 478.366	0.076
48	16 423.594	−0.069			16 430.483	−0.054		
49			16 472.605	0.016	16 430.387	0.039		
50								
51	16 422.714	0.032					16 481.530	0.030
52			16 474.629	0.042				
53					16 429.701	0.060		
54	16 421.794	0.049	16 475.954	0.014			16 483.994	0.043
55								
56	16 421.177	0.033			16 429.204	0.044	16 485.643	0.038
57								
58					16 428.912	0.050		
59			16 479.379	−0.016				
60							16 488.922	−0.039
61	16 419.688	−0.038						
62					16 428.266	−0.058	16 490.614	−0.050
63							16 491.490	−0.031
64					16 428.083	0.001	16 492.377	−0.005
65					16 427.957	−0.011		
66					16 427.882	0.023	16 494.121	0.005
67								
68					16 427.678	0.023		

[a]Unless indicated otherwise, line positions have an assigned uncertainty of 0.03 cm^{-1}.
[b]Perturbed line, excluded from the fit.

TABLE 6. Line positions[a] (cm^{-1}) for the $B^2\Sigma^+$–$X^2\Sigma^+$ $(02^20)\Delta$–$(02^20)\Delta$ band of SrOH. The table shows $\bar{\nu}_{obs}$, the measured wavenumbers (cm^{-1}), and the residuals, $\bar{\nu}_{obs} - \bar{\nu}_{calc}$

N	P_{1f}		P_{1e}		R_{1f}		R_{1e}	
3					16 449.424	−0.046	16 449.424	−0.046
4								
5	16 445.014	0.010	16 445.014	0.010	16 450.355	−0.017	16 450.355	−0.017
6								
7	16 433.909	−0.013	16 443.909	−0.013				
⋮								
18					16 456.715	0.019	16 456.775	0.079
19					16 457.243	0.027	16 457.282	0.067
20	16 437.350	−0.015	16 437.370	0.006			16 457.816	0.077
21	16 436.902	0.007	16 436.938	0.044			16 458.292	0.024
22			16 436.434	0.005				
23			16 435.999	0.031			16 459.341	0.000
24							16 459.871	−0.013
25			16 435.028	−0.034			16 460.429	−0.002

Can. J. Chem. Downloaded from www.nrcresearchpress.com by 203.198.23.82 on 09/08/12
For personal use only.

TABLE 6 (*concluded*)

N	P_{1f}		P_{1e}		R_{1f}		R_{1e}	
26			16 434.594	−0.023				
27			16 434.143	−0.033	16 461.534	−0.009	16 461.517	−0.024
28					16 462.101	−0.004		
29	16 433.316	0.002	16 433.301	−0.009	16 462.665	−0.007		
30	16 432.860	−0.029			16 463.274	0.030	16 463.234	−0.006
31	16 432.467	−0.002						
32	16 432.049	−0.005	16 432.056	0.008				
33								
34					16 465.552	−0.024		
35								
36	16 430.441	−0.004						
37							16 467.377	0.011
38					16 467.983	−0.001	16 467.971	−0.003
39			16 429.288	0.010				
40	16 428.923	0.007	16 428.892	−0.010				
41								
42					16 470.479	0.012		
43								
44	16 427.468	−0.002						
45								
46					16 473.008	−0.017		
47								
48	16 426.110	0.003					16 474.294	−0.011
49								
50			16 425.436	0.016	16 475.631	−0.028		
51								
52	16 424.817	−0.010						

N	P_{2f}		P_{2e}		R_{2f}		R_{2e}	
4					16 450.726	0.022	16 450.726	0.022
5					16 451.305	0.005	16 451.305	0.005
6	16 445.240	−0.012	16 445.240	−0.012				
7	16 444.867	0.011	16 444.867	0.011				
⋮								
19					16 460.147	0.000	16 460.142	−0.005
20					16 460.802	−0.012	16 460.800	−0.015
21	16 439.820	−0.012	16 439.847	0.014			16 461.465	−0.022
22	16 439.507	−0.002	16 439.484	−0.027			16 462.148	−0.015
23			16 439.186	−0.007				
24			16 438.874	−0.007				
⋮								
31							16 468.460	−0.002
32					16 469.151	−0.029	16 469.151	−0.034
33			16 436.303	0.010	16 469.846	−0.061	16 469.889	−0.024
34	16 436.034	0.011	16 436.040	0.010				
35	16 435.746	−0.018	16 435.777	0.005				
36								
37					16 472.859	−0.002		
38								
39	16 434.797	0.019			16 474.389	0.024	16 474.381	0.005
40							16 475.154	0.018
41	16 434.303	−0.012	16 434.396	0.065				
42			16 434.156	0.047				

[a]Line positions have an assigned uncertainty of 0.03 cm^{-1}.

$\tilde{B}^2\Sigma^+(010)\Pi \leftarrow \tilde{X}^2\Sigma^+(000)\Sigma^+$

In their analysis of the $\tilde{B}^2\Sigma^+(010)\Pi \leftarrow \tilde{X}^2\Sigma^+(010)\Pi$ transition, Nakagawa et al. (1) reported an anomalous ℓ-type doubling in the $\tilde{B}$ state whereby the F_1 spin manifold exhibited a much larger splitting than the corresponding F_2 levels. This effect was attributed to an electronic perturbation caused by the $\tilde{A}^2\Pi(010)$ $\mu^2\Sigma$ and $\kappa^2\Sigma$ vibronic states. Brazier and Bernath (2) have determined T_e = 14 674.332(2) cm^{-1} for $\tilde{A}^2\Pi(000)$, while for the $\tilde{B}^2\Sigma^+$ electronic state the (000) level lies at an energy of 16 377.505(1) cm^{-1} (1). Neglecting the spin-orbit and Renner–Teller effects in the $\tilde{A}^2\Pi$ state, the $\tilde{A}^2\Pi(010)$ polyad is located approximately 1700 cm^{-1} below the $\tilde{B}^2\Sigma^+(010)\Pi$ level, suggesting this perturbation to be a relatively long-range interaction. In the present work,

Can. J. Chem. Downloaded from www.nrcresearchpress.com by 203.198.23.82 on 09/08/12
For personal use only.

TABLE 7. Least-squares parameters[a] for the $B^2\Sigma^+$ and $X^2\Sigma^+$ states of SrOH

		$(01^10)^b$	$(01^10)^c$	$(02^00)^c$	$(02^20)^c$
$B^2\Sigma^+$	T_v		16778.341(1)	17148.577(2)	17181.280(2)
	B_v	0.25134(4)	0.2513132(12)	0.2506490(15)	0.2503788(14)
	10^7D_v	2.22(8)	2.2962(26)	2.3647(52)	2.3377(34)
	$10^{13}H_v$		[9.2]	9.2(10)	[9.2]
	γ_v	−0.1439(6)	−0.14047(6)	−0.143090(35)	−0.140194(23)
	$10^7\gamma_v^D$		[3.4]	3.41(8)	[3.4]
	10^4q_v	3.87(14)	−3.622(8)	−3.22(9)	
	$10^{10}q_v^D$		−7.1(22)	−118(22)	
$X^2\Sigma^+$	T_v	360 ± 3	363.689(2)	703.288(8)	733.547(6)
	B_v	0.24859(4)	0.2485815(13)	0.248164(9)	0.247972(11)
	10^7D_v	2.19(8)	2.2097(32)	2.094(36)	2.335(48)
	$10^{13}H_v$		[1.6]	[1.6]	[1.6]
	$10^3\gamma_v$	0.2(6)	2.409(15)	2.34(16)	3.11(18)
	10^4q_v	4.05(13)	−3.9503(46)	−4.9(7)	
	$10^{10}q_v^D$		6.0(13)	[−116]	

[a]All parameters are in cm^{-1} units; values in parentheses are one standard error, in units of the least significant digit of the corresponding parameter; values in square brackets indicate parameters constrained at fixed values in the least-squares fit; with the exception of H_v, which was determined as $1.58(27) \times 10^{-13}$ cm^{-1}, the constants for $X(000)$ were fixed to the values of ref. 20, $B_0 = 0.24919981(2)$, $D_0 = 2.1744(2) \times 10^{-7}$, and $\gamma_0 = 2.4275(4) \times 10^{-3}$ cm^{-1}.

[b]From Nakagawa et al. (1).

[c]This work.

Can. J. Chem. Downloaded from www.nrcresearchpress.com by 203.198.23.82 on 09/08/12
For personal use only.

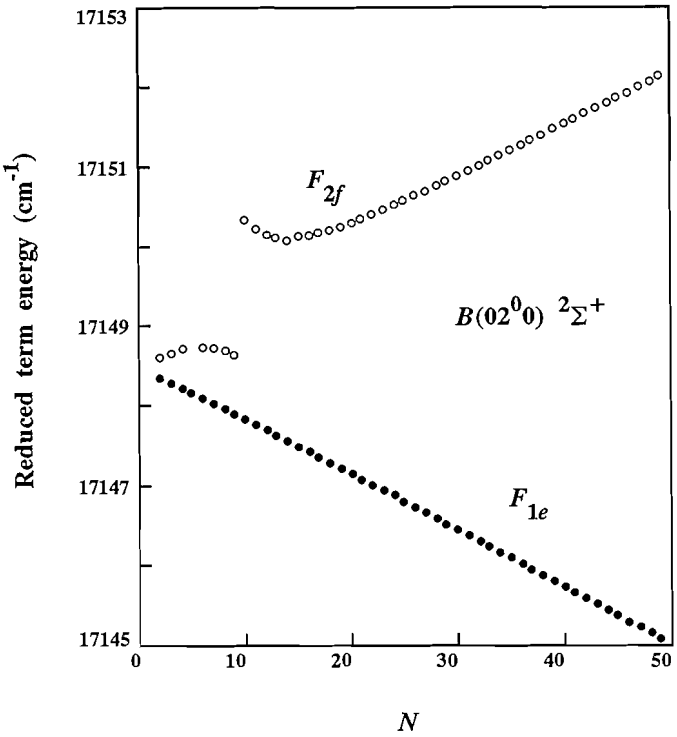

FIG. 2. Reduced term energy plot for the $\tilde{B}^2\Sigma^+(02^00)\Sigma^+$ state of SrOH showing a level crossing at $N \sim 10$ in the F_2 component. The vertical scale is expanded by substraction of $B_vN(N + 1) - D_vN^2(N + 1)^2$ from the term energies.

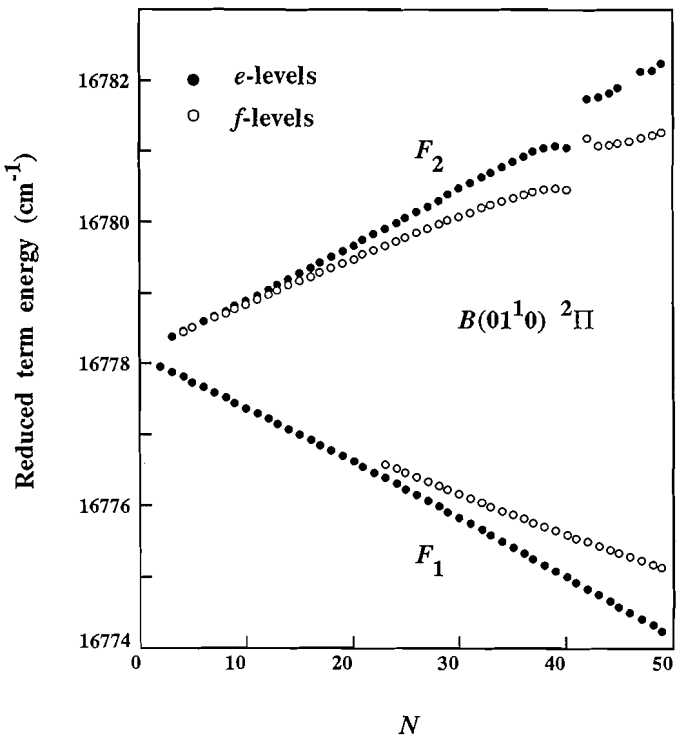

FIG. 3. Reduced term energy plot for the $\tilde{B}^2\Sigma^+(010)\Pi$ state of SrOH. The F_1 levels show no detectable perturbation, whereas the F_2 component shows evidence of a level crossing at $N \sim 41$. The vertical scale is expanded by subtraction of $B_vN(N + 1) - D_vN^2(N + 1)^2$ from the term energies.

we observe the $\tilde{B}^2\Sigma^+(010)\Pi$ level directly in excitation from $\tilde{X}^2\Sigma^+(000)\Sigma^+$ in a perpendicular-type transition. The plot in Fig. 3 of reduced rotational term energies for $\tilde{B}^2\Sigma^+(010)\Pi$ as a function of N indicates a level crossing in the F_2 manifold at $N \sim 41$. If the standard expressions for a $^2\Pi$ vibronic state are applied, all F_1 and F_2 levels up to $N = 16$ are well represented, giving $q_v = -3.622(8) \times 10^{-4}$ cm^{-1}, which is consistent with the sign and magnitude of the ground state value. Since the energy level shifts in the crossing region are of comparable magnitude to those in the perturbation of the $\tilde{B}^2\Sigma^+(02^00)\Sigma^+$ level, we expect the effects of this perturba-

Can. J. Chem. Downloaded from www.nrcresearchpress.com by 203.198.23.82 on 09/08/12
For personal use only.

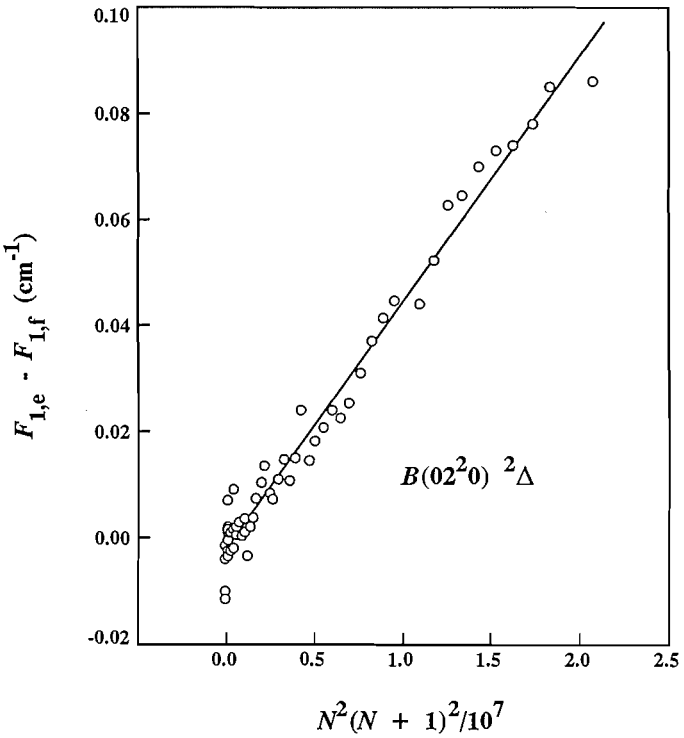

FIG. 4. Plot of e/f splitting in the F_1 levels of SrOH $\tilde{B}^2\Sigma^+(02^20)\Delta$.

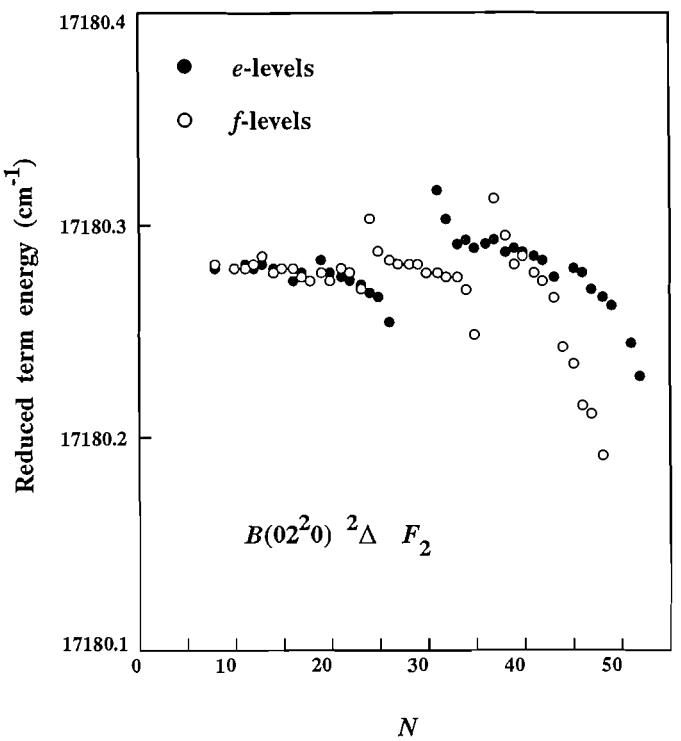

FIG. 5. Reduced term energy plot for the F_2 levels of SrOH $\tilde{B}^2\Sigma^+(02^20)\Delta$. The F_{2f} levels show clear indications of two level crossings at $N = 24$ and $N = 36$. In the F_{2e} levels, only one crossing at $N \sim 28$ is obvious. The negative deviation for $N > 40$ may be caused by extrapolation of the spin-rotation splitting rather than the effects of a perturbation. The vertical scale is expanded by subtraction of $B_vN(N+1) - D_vN^2(N+1)^2 - 1/2\ \gamma_v(N+1)$ from the term energies.

TABLE 8. Molecular constants (cm^{-1}) for the $B^2\Sigma^+$ and $X^2\Sigma^+$ states of SrOH

	$B^2\Sigma^+$	$X^2\Sigma^+$
α_2	1.05(7) × 10^{-3a}	7.3(4) × 10^{-4b}
γ_2	6.4(22) × 10^{-5a}	5.3(15) × 10^{-5b}
$\gamma_{\ell\ell}$	−6.76(5) × 10^{-5a}	−4.8(14) × 10^{-5b}
ω_2^0	399.785(2)^c	360.605(6)
x_{22}^0	−7.124(2)^c	−4.480(5)
g_{22}	8.1758(7)^c	7.5646(25)

[a]Calculated using B_{000} = 0.25224(2) cm^{-1} from Nakagawa et al. (1).
[b]Calculated using B_{000} from Anderson et al. (20)
[c]Calculated using T_e for $B^2\Sigma^+$ from Nakagawa et al. (1).

tion to extend over a considerable range of N, consistent with a perturbing level characterized by a similar B value. In the previous analysis (1) this perturbation was considered to be less extensive; only F_2 levels for $32 \leq N \leq 52$ were omitted from the fit. We believe the unequal e/f parity splittings in the F_1 and F_2 levels observed in the $\tilde{B}^2\Sigma^+(010)\Pi$–$\tilde{X}^2\Sigma^+(010)\Pi$ system are due to the level crossing occurring at $N = 41$ rather than a long-range interaction with the $\mu^2\Sigma$ and $\kappa^2\Sigma$ vibronic states of the $\tilde{A}^2\Pi(010)$ manifold. This is apparent for two reasons: first, ℓ-type doubling in the F_2 spin manifold of the $\tilde{B}^2\Sigma^+(01^10)^2\Pi$ state was observed by Nakagawa et al. (1) only as a splitting of the P_2 and R_2 branches at high N. Consequently, the ℓ-type splittings observed for the F_2 manifold are strongly influenced by the perturbing level. Second, a perturbation caused by interaction with the $\tilde{A}^2\Pi(010)\Sigma$ states would also affect the F_1 levels. We have found that the rotational term values of the F_1 spin manifold are well represented by the standard expression of eq. [3].

$\tilde{B}^2\Sigma^+(02^00)\Sigma^+ \rightarrow \tilde{X}^2\Sigma^+(02^00)\Sigma^+$ *and* $\tilde{B}^2\Sigma^+(02^20)\Delta \rightarrow \tilde{X}^2\Sigma^+(02^20)\Delta$

Having established the vibrational term energies of the upper vibrational levels, the origins of the resolved fluorescence transitions fix the position of the ground state $(02^20)\Delta$ and $(02^00)\Sigma^+$ levels. These levels are separated by 30.259 cm^{-1} (g_{22} = 7.5646(25) cm^{-1}). Despite the lower accuracy of the resolved fluorescence measurements, the effective ℓ-type doubling constant q_{eff} was determined to be 9.7(31) × 10^{-9} cm^{-1} for the $\tilde{X}^2\Sigma(02^20)\Delta$ state. Although poorly determined, this estimate is similar in magnitude to that of the $\tilde{B}$ state, as expected given the similar separations of the $^2\Sigma^+$ and $^2\Delta$ states.

Molecular constants

Vibrational–rotational interactions in linear triatomics, specifically the variation of the rotational constant B_v with increasing excitation of the degenerate bending mode, has been considered previously by Lide and Matsumura (22). Precise microwave measurements are reliably represented by:

$$[7] \quad B_v = \bar{B}_e - \alpha_2(v_2 + 1) + \gamma_{22}(v_2 + 1)^2 + \gamma_{ll}\ell^2$$

where $\bar{B}_e = B_e - 1/2\alpha_1 - 1/2\alpha_3$. Using the values of Nakagawa et al. (1) and Anderson et al. (20) for B_v of the (000) levels of the $\tilde{B}$ and $\tilde{X}$ states, respectively, α_2, γ_{22}, and γ_{ll} have been determined for both states, and are given in Table 8. The constant α_2, which represents the main influ-

Can. J. Chem. Downloaded from www.nrcresearchpress.com by 203.198.23.82 on 09/08/12
For personal use only.

ence of vibration on B_v for low v_2, is positive for both the $\tilde{B}$ and $\tilde{X}$ states. The ground state value, $\alpha_2 = 7.3(4) \times 10^{-4}$ cm^{-1}, is very similar to that for CaOH (footnote 2) (6.4×10^{-4} cm^{-1}), CsOH (24) (6.34×10^{-4} cm^{-1}), and ^{85}RbOH (23) (1.11×10^{-3} cm^{-1}). In a detailed account of vibration–rotation interactions, Lide amd Matsumura (22) have attributed the positive sign of α_2 in the alkali monohydroxides to a dominant contribution from the $(\alpha_2)_{anh}$ term. This is seen primarily as a result of the small mass of the hydrogen atom combined with a small force constant for the metal–oxygen bond. We expect this argument to be equally valid for SrOH. Owing to the similar magnitude but opposite signs of γ_2 and γ_{ll}, the rotational constant B_v should decrease approximately linearly with increasing v_2.

The vibrational term energies for the bending mode, referred to the (000) level, are given by (25):

$$[8] \quad G_0(0,v_2,0) = \omega_i^0 v_2 + x_{22}^0 v_2^2 + g_{22}\ell^2$$

where ω_2^0 and x_{22}^0 have their usual meanings. Estimates of these parameters for both electronic states are given in Table 8. In the approximation that neglects third and higher order anharmonic constants, x_{22}^0 can be taken as equal to x_{22}. A comparison of the values of x_{22} for the two states indicates the bending potential is considerably more anharmonic for the $\tilde{B}$ state.

Rotational ℓ-type doubling and ℓ-type resonance

The phenomena of ℓ-type doubling and ℓ-type resonance arise from the combination of rotational asymmetry and Coriolis interactions of the degenerate bending mode with the stretching vibrations. In the contact-transformed Hamiltonian, the principal matrix element responsible for these interactions in a signed case (b) basis is (26,[3] 27) as follows:

$$[9] \quad \langle v_1,v_2^l,v_3; N,\ell| H | v_1,v_2^{l\pm2},v_3; N,\ell \pm 2\rangle = 1/4\, q_v[(v_2 \mp \ell)(v_2 \pm \ell + 2)[N(N+1) - \ell(\ell \pm 1)][N(N+1) - (\ell \pm 1)(\ell \pm 2)]]^{1/2}$$

The ℓ-type doubling parameter q_v experiences a small variation with rotational and vibrational quantum number and accordingly the following substitution is required (28):

$$[10] \quad q_{vJ} = q_e + \Sigma\, q_{vi}(v_i + d_i/2) + q_v^D N(N+1)$$

Direct microwave observations of ℓ-type splittings in the $v_2 = 2$ vibrational level of HCN and DCN (29) have shown this treatment to be inadequate for highly precise measurements. In a case (b) basis, matrix elements of the type[4]

$$[11] \quad \langle v_1,v_2^l,v_3; N,\ell| H | v_1,v_2^{l\pm4},v_3; N,\ell \pm 4\rangle = \rho_v\{[N(N+1) - \ell(\ell \pm 1)][N(N+1) - (\ell \pm 1)(\ell \pm 2)][N(N+1) - (\ell \pm 2)(\ell \pm 3)][N(N+1) - (\ell \pm 3)(\ell \pm 4)]\}^{1/2}$$

must also be considered for levels with $v_2 > 1$. However, since the contributions from q_v^D and ρ_v to the ℓ-type doubling in (020) are highly correlated (29), the present fits were performed with ρ_v fixed at zero, as in the similar treatment for OCS (30).

For $v_2 = 1$ of Σ electronic states, the off-diagonal matrix element connects states with $\ell = 1$ and $\ell = -1$ in the signed basis. Taking Wang combinations of the appropriate case (b) functions (31),

$$[12] \quad |\eta|K|SNJ\pm\rangle = 2^{-1/2}\,[|\eta KSNJ\rangle \pm (-1)^{J+S-1}|\eta - KSNJ\rangle]$$

where η represents the vibrational quantum number, the interaction is diagonalized and is represented by q_v in eqs. [3 and 4]. The net effect is a removal of the e/f degeneracy associated with the Π vibrational level and is referred to as ℓ-type doubling (32). The magnitude of the splitting is dependent upon q_v, where according to Nielsen et al. (33, 34)

$$[13] \quad q_v = -\frac{2B_e^2}{\omega_2}\left[1 + 4\sum_i \frac{\xi_{2i}^2\omega_2^2}{\omega_i^2 - \omega_2^2}\right]$$

Using the estimates of α_1 and B_{000} of refs. 1 and 19, taking $\omega_2 = \omega_2^o$, and setting α_3(SrOH) = α_3(RbOH) (23), the experimental values of q_v of $-3.622(8) \times 10^{-4}$ and $-3.9503(46) \times 10^{-4}$ cm^{-1} for the $\tilde{B}$ and $\tilde{X}$ states lead to estimates of $4\Sigma_i\, \xi_{2i}^2\omega_2^2/(\omega_i^2 - \omega_2^2)$ of 0.12 and 0.14, respectively. These results can be compared with the typical value of 0.3 for this Coriolis term found by Townes and Schalow (35).

The $\ell = 0$ and $\ell = \pm 2$ components of the $v_2 = 2$ vibrational level also interact via the matrix element of eq. [9]. By convention such an interaction is referred to as the ℓ-type resonance to indicate the approximate degeneracy of the interacting levels. The magnitude of the ℓ-type resonance interaction is dependent on the separation of the (02^00) and (02^20) levels. In the $\tilde{A}^2\Sigma^+(020)$ vibrational level of N_2O^+, where the ℓ-type resonance is particularly strong (36) ($g_{22} = 1.39(9)$ cm^{-1}), an ℓ-type uncoupling is observed. For weaker interactions the net effect is primarily a splitting of the e and f parity levels in the Δ state. In SrOH, the $^2\Sigma^+$ and $^2\Delta$ components of the $v_2 = 2$ vibrational level were observed for the $\tilde{B}$ and $\tilde{X}$ electronic states enabling the off-diagonal matrix element to be evaluated directly. This involved removing the diagonal term q_{eff} of eqs. [5] and [6] and constructing the appropriate interaction matrix. In the parity basis of eq. [12], the interaction matrix takes the form:

$$[14] \quad e\text{-levels} \quad \begin{vmatrix} E_{F2}(^2\Delta) & 0 & 0 \\ 0 & E_{F1}(^2\Delta) & W_{20} \\ 0 & W_{20} & E(^2\Sigma^+) \end{vmatrix}$$

$$[15] \quad f\text{-levels} \quad \begin{vmatrix} E_{F2}(^2\Delta) & 0 & W_{20} \\ 0 & E_{F1}(^2\Delta) & 0 \\ W_{20} & 0 & E(^2\Sigma^+) \end{vmatrix}$$

where $W_{20} = [q_v + q_v^D N(N+1)]\{[N(N+1)][N(N+1) - 2]\}^{1/2}$. For the $\tilde{B}^2\Sigma^+$ state, q_v and q_v^D are found to be $-3.22(9) \times 10^{-4}$ and $-1.18(22) \times 10^{-8}$ cm^{-1}, respectively. The small difference of q_v from that for (010) yields an estimate of q_{22} in eq. [10] of $4.0(9) \times 10^{-5}$ cm^{-1}. The q_v^D parameter, however, is significantly larger in magnitude than that of the (010) level. As discussed earlier, however, q_v^D for (020) is an ef-

[3]Note the typographical errors in eq. 3a on p. 18. The equation should read:

$$\langle v,\ell \pm 2,N|H|v,\ell,N\rangle = 1/4q_v\,\{[(v+1)^2 - (\ell \pm 1)^2][N^2 - (\ell \pm 1)^2][(N+1)^2 - (\ell \pm 1)^2]\}^{1/2}$$

[4]A reviewer suggested this modified form of the equation listed in ref. 29.

fective parameter that absorbs the effect of the matrix elements connecting states with $\Delta\ell = \pm 4$. For the $\tilde{X}$ state the ℓ-type doubling constant was found to be $-4.9(7) \times 10^{-4}$ cm^{-1}, with the constant q_v^D fixed to the $\tilde{B}(020)$ value.

Perturbations

The effects of rotational perturbations in the $\tilde{B}^2\Sigma^+$ vibrational levels lead to a contamination of the purely physical meaning of the molecular constants. Although this is mitigated to some extent in the least-squares fits by the exclusion of lines in the crossing regions, only a full deperturbation analysis can properly take account of the perturbations. In our experiments, observations of the perturbing states are limited to a few weak additional rotational lines in the crossing regions of the $(010)\Pi$ and $(02^00)\Sigma$ states; consequently, such an approach is not yet feasible. Nevertheless, based on these additional lines we have estimated the vibronic energy of the perturbing states of the $(010)\Pi$ and $(02^00)\Sigma^+$ vibrational levels to be 16 800 ± 15 and 17 152 ± 1 cm^{-1}, respectively. The most recent theoretical calculations place the $^2\Delta$ electronic state at 20 221 cm^{-1} (37), suggesting the perturbing states must be excited vibrational levels of the $\tilde{A}^2\Pi$ electronic state. Preliminary investigations carried out in this laboratory have determined T_{ev} of the $\tilde{A}^2\Pi(010)\kappa\Sigma$–$\tilde{X}^2\Sigma^+(000)\Sigma^+$ and $\tilde{A}^2\Pi(100)\Pi_{1/2}$–$\tilde{X}^2\Sigma^+(000)\Sigma^+$ bands to be 15 190.861(1) and 15 084.656(1) cm^{-1}, respectively. Adopting the spin-orbit coupling constant obtained in ref. 2, and neglecting anharmonicity, we find $\omega_1 = 542.1$ and $\omega_2 = 382.8$ cm^{-1}. Given the similarity of $3\omega_2 + 1/2A_o = 1758.0$ cm^{-1} and $T_e(\tilde{B}^2\Sigma^+) - T_e(\tilde{A}^2\Pi) = 1703.17$ cm^{-1}, it seems likely that the unidentified perturbers of the $\tilde{B}(010)$ and $\tilde{B}(02^00)$ levels belong to the upper spin-orbit manifold of the $\tilde{A}(310)$ and $\tilde{A}(320)$ vibronic states.

Based on the vibrational constants determined in this work and those of ref. 1, the unperturbed $(03^10)\Pi$ and $(200)\Sigma^+$ vibrational levels of SrOH are expected to lie within 25 cm^{-1} of one another in both the $\tilde{B}$ and $\tilde{X}$ electronic states. We thus expect a strong $(03^10) \sim (200)$ Coriolis interaction, resulting in considerable mixing of the vibrational eigenfunctions. As a result of intensity borrowing, it is possible that this perturbation may be used to provide a convenient window to access the (030) vibrational levels. In particular, the $\tilde{B}^2\Sigma^+(200)\Sigma^+ \leftarrow \tilde{X}^2\Sigma^+(03^10)\Pi$ and $\tilde{B}^2\Sigma^+(030) \leftarrow \tilde{X}^2\Sigma^+$-$(000)\Sigma^+$ transitions are expected to have an appreciable oscillator strength.

Acknowledgment

Support for this work from the Natural Sciences and Engineering Research Council of Canada is gratefully acknowledged. P.I.P. thanks Dalhousie University for the award of a Sumner Graduate Scholarship. The authors also thank Mr. Minguang Li for many helpful discussions.

1. J. Nakagawa, R.F. Wormsbecher, and D.O. Harris. J. Mol. Spectrosc. **97**, 37 (1983).
2. C.R. Brazier and P.F. Bernath. J. Mol. Spectrosc. **114**, 163 (1985).
3. J.A. Coxon, M. Li, and P.I. Presunka. Mol. Phys. **76**, 1463 (1992).
4. J.A. Coxon, M. Li, and P.I. Presunka. J. Mol. Spectrosc. **150**, 33 (1991).
5. M. Li and J.A. Coxon. J. Chem. Phys. **97**, 8961 (1992).
6. P.F. Bernath and S. Kinsey-Nielsen. Chem. Phys. Lett. **105**, 663 (1984).
7. C.N. Jarman and P.F. Bernath. J. Chem. Phys. **97**, 1711 (1992).
8. Ch. Jungen and A.J. Merer. *In* Molecular spectroscopy: modern research. Vol. 2. Academic Press, New York. 1976.
9. R.N. Dixon and D.A. Ramsay. Can. J. Phys. **46**, 2619 (1968).
10. D.C. Frost, S.T. Lee, and C.A. McDowell. Chem. Phys. Lett. **23**, 472 (1973).
11. R.N. Dixon. Philos. Trans. R. Soc. London, A:**252**, 165 (1960).
12. P.S.H. Bolman, J.M. Brown, A. Carrington, I. Kopp, and D.A. Ramsay. Proc. R. Soc. London, A: **343**, 17 (1975).
13. S. Gernstenkorn and P. Luc. *In* Atlas du spectre d'absorption de la molécule d'iode. Centre National de la Recherche Scientifique, Paris. 1978.
14. S. Gernstenkorn and P. Luc. Rev. Phys. Appl. **14**, 791 (1979).
15. B.A. Palmer, R.A. Keller, and R. Engleman, Jr. Report LA-8251-MS, Los Alamos Scientific Laboratory, Los Alamos, N. Mex. July 1980.
16. L.R. Ramaley, S.C. Foster, and J.A. Coxon. Chem. Biomed. Environ. Instrum. **12**, 229 (1982).
17. G. Herzberg. Electronic spectra and electronic structure of polyatomic molecules. Van Nostrand Reinhold Company, New York. 1966.
18. I. Kopp and J.T. Hougen. Can. J. Phys. **45**, 2581 (1967).
19. R.S. Mulliken and A. Christy. Phys. Rev. **38**, 87 (1931).
20. M.A. Anderson, W.L. Barclay, Jr., and L.M. Ziurys. Chem. Phys. Lett. **196**, 166 (1992).
21. D.L. Albritton, A.L. Schmeltekopf, and R.N. Zare. Molecular spectroscopy: modern research. Vol. 2. Academic Press, New York. 1976.
22. D.R. Lide, Jr. and C. Matsumura. J. Chem. Phys. **50**, 3080 (1968).
23. C. Matsumura and D.R. Lide, Jr. J. Chem. Phys. **50**, 71 (1968).
24. D.R. Lide Jr. and R.L. Kuczkowski. J. Chem. Phys. **46**, 4768 (1967).
25. G. Herzberg. Infrared and Raman spectra of polyatomic molecules. D. Van Nostrand Company, Inc., New York. 1945.
26. M. Larzilliere and Ch. Jungen. Mol. Phys. **67**, 807 (1987).
27. Ch. Jungen, K.E. Hallin, and A.J. Merer. Mol. Phys. **40**, 65 (1980).
28. D.M. Jonas, X. Yang, and A.M. Wodtke. J. Chem. Phys. **97**, 2284 (1992).
29. A.G. Maki and D.R. Lide Jr. J. Chem. Phys. **47**, 3206 (1967).
30. B. Fabricant and J.S. Meunter. J. Mol. Spectrosc. **53**, 57 (1974).
31. M. Larzilliere, S. Abed, M. Carre, M.L. Gaillard, J. Lerme, and M. Broyer. Chem. Phys. Lett. **119**, 55 (1985).
32. G. Amat and H.H. Nielsen. J. Mol. Spectrosc. **23**, 359 (1967).
33. H.H. Nielsen. Phys. Rev. **77**, 132 (1950).
34. H.H. Nielsen, G. Amat, and M. Goldsmith. J. Chem. Phys. **26**, 1060 (1957).
35. C.H. Townes and A.L. Schalow. Microwave spectroscopy. McGraw–Hill Book Company Inc., New York. 1955.
36. M. Larzilliere, K. Gragueb, J. Lerme, and B. Koffend. Chem. Phys. Lett. **134**, 467 (1987).
37. J.M. Mestdagh and J.P. Visticot. Chem. Phys. **155**, 79 (1991).

Can. J. Chem. Downloaded from www.nrcresearchpress.com by 203.198.23.82 on 09/08/12
For personal use only.

Ab initio predictions of the zero field splittings and the singlet–triplet transition strengths for the $\tilde{a}^3A_2(T_1) \leftarrow \tilde{x}^1A_1(S_0)$, $n \rightarrow \pi^*$ transition of selenoformaldehyde

D.C. MOULE[1] AND L. CHANTRANUPONG
Department of Chemistry, Brock University, St Catharines, ON L2S 3A1, Canada

R.H. JUDGE
Department of Chemistry, University of Wisconsin – Parkside, Kenosha, WI 53141-2000, U.S.A.

AND

D.J. CLOUTHIER
Department of Chemistry, University of Kentucky, Lexington, KY 40506-0055, U.S.A.

Received January 29, 1993

This paper is dedicated to Professor Gerald W. King on the occasion of his 65th birthday

D.C. MOULE, L. CHANTRANUPONG, R.H. JUDGE, and D.J. CLOUTHIER. Can. J. Chem. **71**, 1706 (1993).

The energy levels of the lower valence and Rydberg states of selenoformaldehyde, CH_2Se, have been calculated by the SCF/CI method. Wavefunctions for the ROHF (restricted open shell Hartree–Fock) states were obtained with the Binnings–Curtis double-ζ basis set, augmented with Rydberg and polarization functions. Configuration interaction was applied to the parent configurations, PCMO (parent configuration molecular orbital). Oscillator strengths were evaluated for the allowed electric dipole transitions by the RPA (random phase approximation), and SOPPA (second-order polarization propagator approximation) methods. The spin-orbit contribution to the zero field splitting of the first triplet state, $^3A_2(n,\pi^*)$ as well as the oscillator strengths to the three spin components were calculated by perturbation theory. These calculations predict that the S_x, S_y, and S_z components are shifted by −96.091, −96.707, and +29.167 cm^{-1}, respectively, from their unperturbed position. The oscillator strengths for the three components f_x, f_y, and f_z of the $^3A_2(n,\pi^*) \leftarrow {}^1A_1$(g.s.) transition were calculated to be 3.45×10^{-7}, 1.15×10^{-7}, and 173.0×10^{-7}.

D.C. MOULE, L. CHANTRANUPONG, R.H. JUDGE et D.J. CLOUTHIER. Can. J. Chem. **71**, 1706 (1993).

Faisant appel à la méthode SCF/CI, on a calculé les niveaux d'énergie de la basse valence et des états de Rydberg du sélénoformaldéhyde, CH_2Se. On a obtenu les fonctions d'onde des états ROHF (couche ouverte restreinte de Hartree–Fock) en utilisant le double ensemble ζ de Binnings–Curtis de concert avec des fonctions de Rydberg et de polarisation. On a appliqué l'interaction de configuration aux configurations fondamentales, PCMO (orbitale moléculaire de la configuration fondamentale). Faisant appel aux méthodes de RPA (approximation aléatoire de la phase) et SOPPA (approximation du deuxième ordre de la polarisation du propagateur), on a évalué les forces de l'oscillateur pour les transitions électriques dipolaires permises. Utilisant la théorie de perturbation, on a calculé la contribution spin-orbite au couplage au dédoublement de champ zéro du premier état triplet, $^3A_2(n,\pi^*)$, ainsi que les forces d'oscillateur des composantes à trois spin. Ces calculs permettent de prédire que les composantes S_x, S_y et S_z sont déplacés respectivement de −96,091, −96,707 et +29,16 cm^{-1} par rapport à leur position non perturbée. On a calculé que les forces d'oscillateur des trois composantes f_x, f_y et f_z de la transition $^3A_2(n,\pi^*) \leftarrow {}^1A_1$(e.f.) sont respectivement $3{,}45 \times 10^{-7}$, $1{,}15 \times 10^{-7}$ et $173{,}0 \times 10^{-7}$.

[Traduit par la rédaction]

Introduction

The CH_2X molecules, where X = O, S, and Se, may be regarded as the molecular prototypes for correlating the spectral properties of the carbonyl, thiocarbonyl, and selenocarbonyl classes of molecules. The spectrum of formaldehyde, a stable molecule, has been exhaustively studied and has been the subject of several reviews (1, 2). Thioformaldehyde, on the other hand, is unstable and must be generated by pyrolysis or photolysis. As the substitution of sulphur for oxygen has the effect of lowering the excitation energies into more accessible regions of the spectrum, the lower systems of this molecule have recently received considerable attention (3). Like thioformaldehyde, selenoformaldehyde is unstable and must be synthesized by the technique of flash pyrolysis and subsequently detected in the effluent of a flow system. As a result of the experimental difficulties in handling this molecule, the spectroscopy is still not as well understood at this time as the other analogues.

Selenoformaldehyde was detected as a visible absorption spectrum by the long path length photographic technique (4) and at the same time by photoelectron spectroscopy (5). Shortly thereafter it was found as an emission in the cool flames of a F_2 and $(CH_3)_2Se_2$ mixture (6). Both the singlet $^1A_2(n-\pi^*)$ and the triplet $^3A_2(n-\pi^*)$ states are emissive and are accessible through laser-induced fluorescence (LIF) and laser-induced phosphorescence (LIP) spectroscopy. Excitation spectra of both systems have been studied under low resolution (7). In the case of the $S_0 \rightarrow S_1$ system, the 0_0^0 origin band has been observed as a moderately strong magnetic dipole band governed by a-type selection rules, whereas the first Herzberg–Teller band, 4_0^1, is a weak and extensive b-type perpendicular band. Both of these bands have been subjected to high-resolution rotational analyses (8). The bands of the $S_0 \rightarrow T_1$ singlet–triplet transition are very strong in the red end of the spectrum and the vibrational assignment did not present any great difficulty. The rotational analyses of these bands has proven to be more difficult. By analogy with the singlet-triplet bands of CH_2O and CH_2S, one expects prominent S and O branches characteristic of Hund's case (b) coupling in the excited state, in which the three spin

[1]Author to whom correspondence may be addressed.

Can. J. Chem. Downloaded from www.nrcresearchpress.com by 203.198.23.82 on 09/08/12
For personal use only.

TABLE 1. SCF energies[a] for selenoformaldehyde, CH_2Se, from SCF and CI calculations

State	Excitation	E(SCF) Expt.[b]	E(SCF) Opt.[c]	CI	SD + Q	C=Se	C—H	HCH	CSF's	Ref. 16	Expt.[d]
$^1A_1$	Ground state	0.000	0.000	0.000	0.000	1.721	1.075	114.8	2296	0.00	0.000
$^3A_2$	$5b_2$–$5b_1$ (n–π^*)	0.887	0.798	1.260	1.541	1.844	1.069	119.8	32903	1.62	1.509
$^1A_2$	$5b_2$–$5b_1$ (n–π^*)	0.927	0.957	1.458	1.737	1.866	1.069	119.9	20588	2.02	1.681
$^3A_1$	$4b_1$–$5b_1$ (π–π^*)	1.724	1.300	1.919	2.199	1.933	1.069	120.0	32452	1.42	
$^3B_1$	$11a_1$–$5b_1$ (σ–π^*)	5.106	4.176	4.640	4.919	2.174	1.065	141.3	32787	4.96	
$^3B_2$	$5b_2$–$12a_1$ (n–$5s$)	4.821	4.851	4.936	5.215	1.737	1.083	118.1	33697	5.46	
$^1B_2$	$5b_2$–$12a_1$ (n–$5s$)	4.956	4.990	5.056	5.336	1.731	1.081	117.4	21492	5.25	
$^1A_1$	$4b_1$–$5b_1$ (π–π^*)	1.921	1.434	5.394	5.673	1.947	1.069	120.4	21174	4.94	
$^3B_2$	$5b_2$–$13a_1$ (n–$5p_z$)	5.495	5.008	5.495	5.775	1.918	1.078	115.2	33697	5.86	
$^1B_1$	$11a_1$–$5b_1$ (σ–π^*)	5.095	5.098	5.528	5.808	2.118	1.065	146.7	20752	5.87	
$^1B_2$	$5b_2$–$13a_1$ (n–$5p_z$)	5.589	5.615	5.640	5.919	1.739	1.080	116.1	21492	5.48	
$^3A_2$	$5b_2$–$6b_1$ (n–$5p_x$)	5.878	5.878	5.948	6.228	1.714	1.077	117.4	32903	6.66	
$^3A_1$	$5b_2$–$6b_2$ (n–$5p_y$)	5.695	5.701	6.021	6.301	1.717	1.081	118.8	33522	6.83	
$^1A_1$	$5b_2$–$6b_2$ (n–$5p_y$)	5.747	5.755	6.125	6.404	1.719	1.080	118.9	21839	5.88	
$^1A_2$	$5b_2$–$6b_1$ (n–$5p_x$)	5.892	5.893	6.240	6.520	1.715	1.077	117.3	20588	5.98	
$^1A_1$	$5b_2$–$5b_1$ (n^2–π^{*2})	6.294	6.265	6.398	6.677	1.820	1.075	125.3	2251		
$^3B_1$	$4b_1$–$12a_1$ (π–$5s$)	6.489	6.260	6.620	6.899	1.875	1.084	115.3	31805	6.62	
$^1B_1$	$4b_1$–$12a_1$ (π–$5s$)	6.686	6.516	7.008	7.287	1.888	1.087	116.4	20080		
$^3B_1$	$4b_1$–$13a_1$ (π–$5p_z$)	7.246	6.913	7.275	7.554	1.923	1.080	114.9	31805		
$^1B_1$	$4b_1$–$13a_1$ (π–$5p_z$)	7.395	7.180	7.548	7.828	1.918	1.078	115.1	20080		
$^1A_2$	$4b_1$–$6b_2$ (π–$5p_y$)	7.438	7.473	8.154	8.433	1.839	1.082	118.6	19923		
$^3A_2$	$4b_1$–$6b_2$ (π–$5p_y$)	7.520	7.451	8.131	8.410	1.839	1.082	118.6	31833		

[a]In eV.
[b]r(C=Se) = 1.753 Å, r(C—H) = 1.090 Å, α(HCH) = 117.9° for the ground state (ref. 13).
[c]GS: SCF: −2436.592468549 au; opt. SCF: −2436.593752879 au; CI: −2436.706107485 au; SQ + D: −2436.716374986 au.
[d]From refs. 7, 8.

components of the nonrotating molecule are separated by energies small compared to the rotational intervals. However, at high resolution, the CH_2Se bands are found to have simple P-, Q-, and R-branch structure following $\Delta K = 0$ selection rules, with no evidence of spin splittings, despite a pronounced Zeeman effect indicating that the upper state has an appreciable magnetic moment.[2] Thus, the rotational structure suggests that the upper state is of singlet multiplicity whereas the magnetic effects are those of a triplet state. The most likely solution to this dilemma is to postulate that the triplet state of CH_2Se actually corresponds to Hund's case (ab) (9), in which two of the spin components are close together and the third is remote from them. If the observed transitions are to the remote level, then the rotational structure of the bands would be expected to be similar to that of a singlet–singlet transition in the absence of strong spin-rotation coupling between the three spin components. To our knowledge, the only type of molecule known to exhibit this type of spin splitting is carbon disulphide, in which the near-ultraviolet bands have been shown to result from a transition to one component of the $^3A_2$ state (10, 11). It is therefore of considerable interest to determine if selenoformaldehyde also has this type of anomalous triplet state energy level structure.

The purpose of this work is to evaluate the spin-orbit coupling between the $^3A_2(n$–$\pi^*)$ state and the other singlet and triplet states of CH_2Se and to calculate the zero field splittings (ZFS) between the three spin components of the nonrotating molecule. This information is intended to provide a starting point for attempts to more thoroughly understand the singlet–triplet bands. For this purpose, the relative strengths of the transitions to the three spin substates have also been estimated from perturbation theory.

[2]D.J. Clouthier, R.H. Judge, and D.C. Moule. To be published.

Method

The HF/SCF calculations were carried out with the GAMESS system of programs (12). The Dunning/Hay (DH) double-ζ basis set (13) was used for carbon: $(9s,5p)/[3s,2p]$ augmented by d polarization functions α_d = 0.1875, 0.75, and 3.00 and Rydberg $3s$, $3p$ orbitals with exponents α_s = 0.023, α_p = 0.021 for the total basis C: $(10s,6p,3d)/[4s,3p,3d]$. For hydrogen: $(3s)/[2s]$, the addition of p polarization functions with exponents α_p = 0.25, 1.0, and 4.0. gave H: $(3s,3p)/[2s,3p]$. The Binnings/Curtis (BC) double-ζ basis set (14) $(14s,11p,5d)/[6s,4p,1d]$ was used for the selenium atom supplemented with d polarization function α_d = 0.315 and Rydberg $5s$ and $5p$ orbitals with exponents α_s = 0.016 and α_p = 0.014 for the basis, Se: $(15s,12p,6d)/[7s,5p,2d]$ Thus this calculation employed a total of 87 basis functions with 34 shells and 42 electrons to give as the ground state electron configuration:

$$(1a_1)^2(2a_1)^2(3a_1)^2(1b_1)^2(1b_2)^2(4a_1)^2(5a_1)^2(2b_1)^2(6a_1)^2$$
$$(2b_2)^2(7a_1)^2(3b_1)^2(1a_2)^2(3b_2)^2(8a_1)^2(9a_1)^2(10a_1)^2(4b_2)^2$$
$$(11a_1)^2(4b_1)^2(5b_2)^2(12a_1)^0(5b_1)^0(13a_1)^0(6b_2)^0(6b_1)^0(14a_1)^0$$
$$(7b_2)^0(7b_1)^0(15a_1)^0 \ldots$$

where $5b_2$ and $12a_1$ are the HOMO and LUMO orbitals, respectively.

Buenker and Peyerimhoff (15) have shown that the parent configuration molecular orbital technique, CI(PCMO),

Can. J. Chem. Downloaded from www.nrcresearchpress.com by 203.198.23.82 on 09/08/12
For personal use only.

TABLE 2. Spin-orbit matrix elements[a,b] between the $^3A_2(n,\pi^*)$ triplet state of CH_2Se and adjacent singlet and triplet states. Spin-orbit contributions to the $^3A_2(n,\pi^*)$ zero field splitting of selenoformaldehyde from electronic states near or below the first ionization potential

				Fine structure contribution					
		SOC[c,d]		S_x		S_y		S_z	
Contributing State		(1)	(2)	(1)	(2)	(1)	(2)	(1)	(2)
$^1A_1$	Ground state	791.97	698.64					50.4642	39.2711
$^1A_1$	$(\pi-\pi^*)$	−603.02	−531.54					−10.9112	−8.4777
$^1A_1$	$(n^2-\pi^{*2})$	−363.02	−319.70					−3.1813	−2.4673
$^1A_1$	$(n-5p_y)$	−95.19	−83.74					−0.2310	−0.1788
$^3A_1$	$(n-5p_y)$	−93.34	−82.10	−0.2269	−0.1756	−0.2269	−0.1756		
$^3A_1$	$(\pi-\pi^*)$	820.25	723.14	−126.7755	−98.5343	−126.7755	−98.5343		
$^1B_2$	$(n-5s)$	67.22	59.29			−0.1476	−0.1149		
$^1B_2$	$(n-5p_z)$	62.85	55.48			−0.1119	−0.0872		
$^3B_2$	$(n-5s)$	68.85	60.72	−0.1599	−0.1244			−0.1599	−0.1244
$^3B_2$	$(n-5p_z)$	75.56	66.66	−0.1672	−0.1301			−0.1672	−0.1301
$^1B_1$	$(\sigma-\pi^*)$	−466.21	−454.97	−6.3155	−6.0147				
$^1B_1$	$(\pi-5s)$	2.48	2.19	−0.0001	−0.0001				
$^1B_1$	$(\pi-5p_z)$	−3.86	−3.41	−0.0002	−0.0002				
$^3B_1$	$(\sigma-\pi^*)$	−481.50	−427.20			−8.5095	−6.6840	−8.5095	−6.6840
$^3B_1$	$(\pi-5s)$	−1.47	−1.30			0.0000	0.0000	0.0000	0.0000
$^3B_1$	$(\pi-5p_z)$	3.10	2.73			−0.0002	−0.0002	−0.0002	−0.0002
	Total			−133.6454	−104.9794	−135.7717	−105.5962	27.3039	21.1942

[a]In cm^{-1}.
[b]CI (SD + Q) from Table 1.
[c]Model (1) Z_{eff} (Se) = 34.51.
[d]Model (2) Z_{eff} (Se) = 30.43.

is an excellent method for obtaining excitation energies in small polyatomic molecules. In this technique, the configuration interaction is applied to the SCF orbitals of the parent configuration. The details of this calculation are shown in Table 1 where the first column lists the ROHF/SCF open shell excitation energies of the parent configurations up to the 8.81 eV ionization limit (16) for the r_s ground state structure (17): C=Se = 1.753 Å, r(CH) = 1.090 Å, and α(HCH) = 117.9°. The second column lists excitation energies that were obtained for the fully optimized structural parameters found in columns 5–7. The corrections for the effects of electron correlation were made with the Graphical Unitary Group Approach (18), GUGA, which is available in the GAMESS package. For each state the parent configurations were used with all singles and doubles electron excitation. This active space consisted of 27 orbitals occupied by 12 electrons, with 15 core orbitals frozen. The CI excitation energy and the CI energy with the Davidson correction (19) (SD + Q), as well as the number of configuration state functions (CSF's), are given in Table 1.

The spin-orbit coupling constants were calculated at the MCSCF level with the $TRANST routine, which is incorporated in the GAMESS program. In this treatment, the Hamiltonian for spin-orbit coupling is given in terms of one-electron integrals while the need for two-electron terms is circumvented by use of a parameterized effective nuclear charge, Z_{eff}. Values of Z_{eff} for first and second row atoms of the Periodic Table have been recently calibrated by Koseki, Schmidt, and Gordon (20). Their procedure involves a calculation of the fine structure splittings between the $\Pi_{3/2}$ and $\Pi_{1/2}$ levels of AH molecules, where H is hydrogen and A the heavy atom. With the assumption that for hydrogen Z_{eff} = 1.0, they adjusted Z_{eff} for A until the experimental intervals were reproduced. In the case of Se, which lies in the third row of the Periodic Table, two separate values of the $\Pi_{3/2} - \Pi_{1/2}$ energy difference for SeH are available from electron detachment spectroscopy (21) and from electron spin resonance spectroscopy (22). The most recent estimate of the splitting (21) at -1815 ± 100 cm^{-1} required a Z_{eff} of 34.51 to reproduce the splitting, which is greater than Z_{true} = 34.0, whereas the second value (22) of -1600 ± 50 cm^{-1} yielded a Z_{eff} = 30.43. As Z_{eff} must be less than Z_{true}, the calibration favours the second observation. Table 2 gives the values of the spin-orbit coupling to the $^3A_2(n,\pi^*)$ T_1 triplet excited state and to the $^1A_1$ S_0 ground electronic state. The calculations were carried out with a fully optimized reaction space multiconfigurational self-consistent wavefunction (FORS/MCSCF) with 10 valence orbitals and 12 valence electrons. Planar structures were adopted for both states.

Since the $^3A_2(n,\pi^*)$ state is orbitally nondegenerate, the first nonzero spin-orbit contribution to the zero field splitting requires second-order perturbation theory. With the molecule oriented in the yz plane and the z axis directed along the C=Se bond, a consideration of the symmetry (23) of the orbital and spin wave functions shows that the perturbations between the S_z level of the $^3A_2(T_1)$ state and the other electronic states of $^1A_1$, $^3B_1$, and $^3B_2$ symmetry can be written as

$$[1]\quad \Delta E(S_z) = -\sum_m [\langle {}^1A_1, m \mid H_{SO} \mid {}^3A_2,T_1\rangle^2 [E_m({}^1A_1) - E({}^3A_2,T_1)]^{-1} + \langle {}^3B_1,m \mid H_{SO} \mid {}^3A_2,T_1\rangle^2 [E_m({}^3B_1) - E({}^3A_2,T_1)]^{-1} + \langle {}^3B_2,m \mid H_{SO} \mid {}^3A_2,T_1\rangle^2 [E_m({}^3B_2) - E({}^3A_2,T_1)]^{-1}]$$

where the sum is taken over the manifold of m states. Symmetry considerations likewise show that it is the electronically excited states of $^3A_1$, $^1B_1$, and $^3B_2$ symmetry that interact

Can. J. Chem. Downloaded from www.nrcresearchpress.com by 203.198.23.82 on 09/08/12
For personal use only.

TABLE 3. Oscillator strengths and electric dipole transition moments[a] for selenoformaldehyde[b] by random phase approximation (RPA) and by second-order polarization propagator (SOPPA) methods

State	Excitation	RPA				SOPPA			
		$f(v)$	$f(l)$	$M(v)$	$M(\ell)$	$f(v)$	$f(l)$	$M(v)$	$M(\ell)$
$^1A_1$	$4b_1$–$5b_1$ (π–π^*)	0.240	0.237	−1.085	−1.078	0.113	0.174	0.629	0.781
$^1A_1$	$5b_2$–$6b_2$ (n–$5p_y$)	0.014	0.007	−0.237	−0.164	0.063	0.153	0.463	0.721
$^1B_1$	$4b_1$–$13a_1$ (π–$5p_z$)	0.023	0.023	0.276	0.272	0.018	0.022	−0.223	−0.245
$^1B_1$	$11a_1$–$5b_1$ (σ–π^*)	0.010	0.008	0.203	0.188	0.002	0.009	0.082	0.145
$^1B_1$	$4b_1$–$12a_1$ (π–$5s$)	0.116	0.117	0.646	0.649	0.090	0.167	0.512	0.698
$^1B_2$	$5b_2$–$12a_1$ (n–$5s$)	0.060	0.060	−0.523	−0.522	0.059	0.081	0.481	0.560
$^1B_2$	$5b_2$–$13a_1$ (n–$5p_z$)	0.025	0.016	−0.329	−0.265	0.018	0.013	0.257	0.213
	Transitions to the x, y, and z spin components from eq. [2][c]								
$^3A_2$	$5b_2$–$5b_1$ (n–π^*) $-x$	4.05	3.45	−0.267	−0.247	0.62	1.97	−0.104	−0.187
$^3A_2$	$5b_2$–$5b_1$ (n–π^*) $-y$	1.33	1.15	−0.153	−0.143	1.01	1.13	0.133	0.141
$^3A_2$	$5b_2$–$5b_1$ (n–π^*) $-z$	179.5	173.0	1.780	1.748	68.70	110.8	−1.110	−1.399

[a]In au.
[b]r(C═Se) = 1.753 Å, r(C—H) = 1.090 Å, α(HCH) = 117.9°, CI(SD + Q), Z_{eff}(Se) = 30.43.
[c]Oscillator strengths are $f \times 10^{-7}$; transition moments are $M \times 10^{-2}$.

with the x component of the $^3A_2(n,\pi^*)$ state while the $^3A_1$, $^1B_2$, and $^3B_1$ states mix and perturb the y component. Expressions similar to eq. [1] have been constructed (23) for the energy shifts to these levels.

Oscillator strengths can be obtained for the transitions to the S_x, S_y, and S_z spin components from perturbation theory. For z-polarized light (C═Se bond direction), the transition moment to the S_z component can be obtained from the expression

$$[2]\quad M(^1A_1,S_0 \rightarrow {}^3A_2,T_1) = \sum_s \frac{\langle {}^1A_1,s\,|H_{SO}|\,{}^3A_2,T_1\rangle}{[E(^3A_2,T_1) - E(^1A_1,s)]} M(^1A_1,S_0 \rightarrow {}^1A_1,s) + \sum_t \frac{\langle {}^1A_1,S_0\,|H_{SO}|\,{}^3A_2,t\rangle}{[E(^1A_1,S_0) - E(^3A_2,t)]} M(^3A_2,t \rightarrow {}^3A_2,T_1)$$

where $\langle {}^1A_1,s|H_{so}|{}^3A_2,T_1\rangle$ is the spin-orbit matrix element between the $^3A_2(n,\pi^*)$ triplet and the adjacent ground and singlet excited states $^1A_1,s$. $E(^1A_1,S_0)$–$E(^3A_2,t)$ is the perturbation gap between the interacting states and $M(^1A_1,S_0 \rightarrow {}^1A_1,s)$ the transition moment between ground state and the excited singlet states. Thus, it is possible to interpret the first term as the mixing of the triplet S_z $^3A_2(n,\pi^*)$ wavefunction by the adjacent singlet excited states and a borrowing or stealing of their allowed electronic transition strength. In a similar way the second term is a perturbation of the ground state $^1A_1(S_0)$ by members of the triplet manifold of states. Thus the perturbation treatment requires (*a*) the spin-orbit matrix elements between the $^3A_2(n,\pi^*)$ and the $^1A_1$, $^1B_1$, and $^1B_2$ states as well as the elements between the $^1A_1$(g.s.) and the $^3A_2$, $^3B_1$, and $^3B_2$ states; (*b*) excitation energies for the manifolds of singlet and triplet electronic states; and (*c*) transition moments between the $^1A_1$(g.s.) and all of the allowed singlet states as well as those between the $^3A_2(n,\pi^*)$ state and the other triplet states of the molecule

Oscillator strengths were calculated from the RPAC group of programs (24). Oscillator strengths are sensitive to the quality of the electronic wavefunctions and are difficult to evaluate. The random phase approximation (RPA) and the second-order polarization propagator (SOPPA) methods were used to determine the transition strengths. Table 3 lists the transition moments and the oscillator strengths for both the velocity and the length approximations.

Results and discussion

As only the first two electronic transitions have been observed in the visible spectrum of selenoformaldehyde, it is difficult to obtain a complete calibration for this model calculation. In wavenumbers, the positions for the 0_0^0 transitions that result from $n \rightarrow \pi^*$ excitation, $^1A_1 \rightarrow {}^1A_2/{}^1A_1 \rightarrow {}^3A_2$, lie at 13 555/12 171 cm^{-1} or, in eV, 1.681/1.509. As the spectroscopic analysis has shown that the excited $^1A_2(S_1)$ and $^3A_2(T_1)$ states are pseudo-planar, the maximum in the Franck–Condon intensity profile should lie close to the origins of the two electronic transitions. Our results, in eV, which are tabulated in Table 1, give the following energies: ROHF (microwave geometry) 0.9027/0.887, with optimized C_{2V} structure 0.957/0.798, with CI 1.458/1.260, and with CI(SD + Q) 1.737/1.541. It is clear that the calculations at the ROHF level of approximation badly underestimate the transition energies and are not significantly changed by optimization of the structure. The CI corrections for correlations markedly improve the agreement while the CI(SD + Q) correction slightly overestimates the energies of the two transitions. Our value of 1580 cm^{-1} for the S_1–T_1 interval compares favourably with the 1387 cm^{-1} observed in the spectrum of selenoformaldehyde. The pattern of the lower excited states is different from that found by Collins et al. (16), who predicted that the $^3A_1(\pi,\pi^*)$ state should have the lowest energy, 1.42 eV, and be followed by the $^3A_2(n,\pi^*)$ and $^1A_2(n,\pi^*)$ states at 1.62 and 2.02 eV.

The transitions to the higher electronic states of selenoformaldehyde have not been observed. The calculations show the next singlet state, at 5.336 eV, is of Rydberg character $^1B_2(n,5s)$ and is followed by the intervalence $^1A_1(\pi,\pi^*)$ state at 5.673 eV. This latter state with a populated π^* orbital could have a nonplanar structure. The ordering of the valence states follows the pattern of CH_2O except that the states with π,π^* configurations are at much lower energies. Two

Can. J. Chem. Downloaded from www.nrcresearchpress.com by 203.198.23.82 on 09/08/12
For personal use only.

Can. J. Chem. Downloaded from www.nrcresearchpress.com by 203.198.23.82 on 09/08/12
For personal use only.

manifolds of Rydberg states are generated from the present basis set, namely, those that arise from an electron promotion from the $n(5b_2)$ orbital and those which are from the $\pi(4b_1)$ orbital. The order of the n–$5p$ Rydberg states is n–$5p_z$, n–$5p_y$, and n–$5p_x$, which differs from the order found for formaldehyde where the Rydberg $3p_y$ and $3p_z$ orbital energies are reversed.

The matrix elements for spin-orbit coupling between the $^3A_2(n,\pi^*)$ state and the adjacent singlet and triplet valence states are quite large. For example, with the $Z_{eff} = 30.43$, the coupling to the singlet $^1A_1(\pi,\pi^*)$ state is -531.54 cm^{-1} and, to the corresponding triplet state, 723.14 cm^{-1}. At 698.64 cm^{-1}, the matrix element coupling to the A_1 (g.s.) ground state is also appreciable. On the other hand, the coupling elements to the Rydberg states are much smaller, 59.29 and 55.48 cm^{-1} for the $^1B_2(n,5s)$ and $^1B_2(n,5p_z)$ states, respectively. In the case of the $^1B_1(\pi,5s)$ electronic state where the configuration contains neither $(n)^1$ nor $(\pi^*)^1$ orbitals, the matrix element connecting the $^3A_2(n,\pi^*)$ state is very small, 2.19 cm^{-1}.

The spin-orbit displacements to each of the fine structure levels were evaluated from eq. [1]. For this purpose, the matrix elements for models (1) and (2) were taken from the first two columns of Table 2 and were combined with the CI(SD + Q) excitation energies of Table 1, column 4, to give the fine structure contributions of Table 2. The $^3A_1(\pi,\pi^*)$ state was found to make the greatest contribution to the ZFS and has the effect of pushing the S_x and S_y components of the $^3A_2(n,\pi^*)$ state downwards from their unperturbed positions by -98.53 cm^{-1}. The S_z level, on the other hand, is displaced -8.48 cm^{-1} downwards by the $A_1(\pi,\pi^*)$ state and upwards 39.27 cm^{-1} by the $^1A_1$(g.s.) ground state. The displacement by the $^1A_1(n,5p_y)$ Rydberg state of -0.18 cm^{-1} is not a significant factor. Thus, while the S_z level is not appreciably shifted from its unperturbed position, the S_x and S_y levels are depressed to lower energies by about -100 cm^{-1}. The other valence interaction is with the singlet and triplet $B_1(\sigma,\pi^*)$ states. In this case, while the displacement of the x component by the singlet $^1B_1(\sigma,\pi^*)$ state is -6.01 cm^{-1}, the corresponding y and z displacements by the $^3B_1(\sigma,\pi^*)$ are -6.68 cm^{-1}. The effect of this interaction is to depress all three levels by about the same amount. The perturbations by the Rydberg states are small. Moreover, since the singlet and triplet Rydberg state have almost the same energies and their spin-orbit matrix elements are nearly equal, they interact and shift all three spin components by roughly the same extent. Thus, while the interactions with the higher Rydberg states uniformly shift the three components in a downwards direction they do not alter their relative positions.

The location of the $^3A_1(\pi,\pi^*)$ state is critical to the positioning of the S_X, S_Y, and S_Z components. From Table 2 it is clear that the interactions with this state account for a large part of the displacements of the x and y components. The $^3A_1$ (π,π^*) state is only $2.199 - 1.541 = 0.658$ eV or 5306 cm^{-1} above the $^3A_2(n,\pi^*)$. The difficulty here is that Collins et al. (16) calculate a separation of $1.42 - 1.62 = -0.20$ or -1613 cm^{-1} between these levels, but in their case the $^3A_2(\pi,\pi^*)$ state was found to lie below the $^3A_2(n,\pi^*)$ state and would result in an upward perturbation of the (n,π^*) states. For this reason we focused on the three major interacting states: $^1A_1$(g.s.), $^3A_2(n,\pi^*)$, and $^3A_1(\pi,\pi^*)$. As a better approximation, we repeated the previous calculations but used instead the experimentally determined molecular structure (8) of the zero point level of the companion $^1A_2(n,\pi^*)$ singlet state. In this final calculation we obtained, E(SD + Q): $^3A_2(n,\pi^*) = 1.497$, $^1A_2(n,\pi^*) = 1.694$, which are in excellent agreement with the observed electronic origins, 1.509 and 1.681 eV. This same calculation yielded a value of $^3A_1(\pi,\pi^*) = 2.284$ eV and the coupling constants between the $^3A_2(n,\pi^*)$ and $^1A_1$(g.s.), $^3A_1(\pi,\pi^*)$ states of 755.27 and 754.34 cm^{-1}. Combined with the energies of the previous calculation, we obtain: $\Delta E(S_x) = -96.091$, $\Delta E(S_y) = -96.707$, and $\Delta E(S_z) = 29.167$ cm^{-1} as our most reliable calculation for the spin-orbit contribution to the zero field splitting. As a test of the method we performed similar calculations on the $^3A_2(n,\pi^*)$ state of the sulphur analogue, CH_2S. With the (DH) molecular orbital basis set we obtain for the three spin-orbit components: $\Delta(S_x) = -7.5139$, $\Delta(S_y) = -7.4828$, and $\Delta(S_z) = 0.8541$ cm^{-1}. From these values it is possible to derive the spectroscopic constants for spin-orbit coupling: $D = -8.3525$ and $E = 0.0156$ cm^{-1}. These constants may be compared to the experimentally determined values for $v = 0$; $D = -4.078$ and $E = 0.0942$ cm^{-1} obtained from long-path absorption studies (25) and $v_3 = 1$; $D = -4.3474$ and $e = 0.0853$ cm^{-1} from high-resolution LIP spectroscopy (26). The agreement between the calculated and observed constants is not unreasonable since the contributions from the spin–spin coupling have not been incorporated into the model calculations. Inclusion of this effect would move D and E closer to their observed values.

Table 3 gives the results of the intensity calculations. It is clear by comparing the results of the different methods that it is difficult to obtain accurate values of the oscillator strength. As a case in point, the RPA method yields oscillator strengths for the velocity and length formalisms of $f(v) = 0.240$ and $f(\ell) = 0.237$ for the $\pi \rightarrow \pi^*$ transition, whereas the SOPPA method gives $f(v) = 0.113$ and $f(\ell) = 0.174$. Thus the oscillator strengths by the two methods are quite different. The value obtained for this intervalence $\pi \rightarrow \pi^*$ transition is, however, comparable with the $f_z = 0.222$ calculated for formaldehyde (23). The strength of the $n \rightarrow 5s$ Rydberg transition at 0.060 appears to be satisfactorily accounted for and is similar to the 0.017 strength in the corresponding $n \rightarrow 3s$ transition in formaldehyde.

It is clear, from eq. [2], that the strengths of the singlet–triplet transitions depend not only on the spin-orbit matrix elements and the perturbation energy gaps, but also on the magnitude of the electronic transition moments. Four sets of intensity calculations are presented in Table 3. These calculations used the matrix elements from model (2) and the CI(SD + Q) energies and the length and velocity approximation of the RPA and SOPPA methods. Of these, we believe the RPA(length) form to be the most reliable. This calculation gave for the oscillator strength to the spin components, $f_x = 3.45 \times 10^{-7}$, $f_y = 1.15 \times 10^{-7}$, and $f_z = 173.0 \times 10^{-7}$. It is clear from these numbers that 98.8% of the strength of the $^1A_1$(g.s.) $\rightarrow$ $^3A_2(n,\pi^*)$ transition is induced in the $A_1(z)$ polarized direction. This is a consequence of the $H_{SO}(a_2)$ spin-orbit coupling between the z spin component of the $^3A_2(n,\pi^*)$ state and the $^1A_1(\pi,\pi^*)$ state and the adjacent $\pi \rightarrow \pi^*$ transition of high strength. The only other contributor to this component is the $n \rightarrow 5p_y$ transition, which provides only about 0.5% of the intensity.

Can. J. Chem. Downloaded from www.nrcresearchpress.com by 203.198.23.82 on 09/08/12
For personal use only.

The calculated strength to the $B_2(y)$ spin component is low, (1.15×10^{-7}) and comes from the couplings to the lower Rydberg $^1B_2(n,5s)$ and $^1B_2(n,5p_z)$ states. While these states do have a partial valence character, and the spin-orbit coupling constants are of an intermediate size, their low oscillator strengths mitigate against intensity borrowing. Similarly, the transition to the x component obtains intensity from the $\sigma \rightarrow \pi^*$ intervalence transition but, again, the low oscillator strength of this system (0.008) works against this mechanism.

Summary

The valence and low-lying Rydberg electronic states of selenoformaldehyde have been calculated by ab initio methods. The orbital basis set for the calculation was of double-ζ quality and was augmented with polarization and Rydberg functions. These were used in an ROHF procedure to generate the parent configuration molecular orbitals, CI(PCMO). The four valence states $^1A_1$(g.s.), $^3A_2(n,\pi^*)$, $^1A_2(n,\pi^*)$, and $^3A_1(\pi,\pi^*)$ were found to lie at relatively low energies and were separated from the higher valence and Rydberg states. Intensities were calculated by the RPA and SOPPA techniques and were found to correlate with those of formaldehyde. The matrix elements for the spin-orbit coupling of the $^3A_2(n,\pi^*)$ state to the intervalence and Rydberg states that lie below the first ionization limit were evaluated. The couplings to the intervalence states were found to be large, 200–800 cm^{-1}, whereas those to the Rydberg states were typically 60–80 cm^{-1}. The positions of the lower valence states have a critical influence on the separations of the three spin components of the $^3A_2(n,\pi^*)$ state. As a result of their close proximity and their quite large spin-orbit matrix elements, the $^1A_1$(g.s.) and $^1A_1(\pi,\pi^*)$ states interact with and repel the $^3A_2(n,\pi^*)$ state. As they lie on either side of the $^3A_2(n,\pi^*)$ state, the z spin-orbit component is pushed upwards and downwards by nearly equal amounts, which results in a small shift from the unperturbed position. The other major interaction is a repulsion between the x and y components of the $^3A_2(n,\pi^*)$ state and the $^3A_1(\pi,\pi^*)$ state. This has the effect of depressing the levels downwards to give as the final result: $\Delta E(S_x) = -96.091$, $\Delta E(S_y) = -96.707$, and $\Delta E(S_z) = 29.167$ cm^{-1}.

Intensities were calculated by perturbation theory where the intensity induced into the singlet–triplet transition can be described as a borrowing or stealing of the oscillator strength from neighbouring states of the correct symmetry. It is the $\pi \rightarrow \pi^*$ state with an f value of 0.237 that provides the strength for the singlet–triplet transition. This highly allowed intervalence transition also determines the polarization. The RPA(1) method, which appears to be the most dependable of those tested, yields oscillator strengths for the three components: $f_x = 3.45 \times 10^{-7}$, $f_y = 1.15 \times 10^{-7}$, and $f_z = 173.0 \times 10^{-7}$.

The present calculations strongly support the notion that the T_1 state of selenoformaldehyde corresponds to Hund's case (ab), rather than case (b). In CH_2O and CH_2S, the spin splittings in the nonrotating molecule are small and the predominant transition is from the ground state to the S_z component, induced by coupling with the $^1A_1(\pi,\pi^*)$ state. In the rotating molecule, the spin-rotation coupling mixes the S_z, S_y, and S_x components so that the intensity is shared between the three components. Similarly, in CH_2Se, the calculations show that almost all of the singlet–triplet transition intensity is to the S_z component due to mixing with the (π,π^*) state. However, in this case the S_x and S_y components are calculated to be 125 cm^{-1} below S_z so that the spin uncoupling will not appreciably redistribute the intensity between the three components. In this case, the 0_0^0 band of the singlet–triplet transition should follow a-type selection rules and show rotational structure very similar to that of a singlet–singlet transition. It is doubtful if the transitions to the other two components will be observed in the room temperature laser-induced phosphorescence spectrum since they are predicted to be 50–100 times weaker.

Acknowledgments

D.C.M. and L.C. would like to thank the Natural Sciences and Engineering Research Council of Canada (NSERC) for financial assistance. D.J.C. acknowledges the support of the National Science Foundation under grant No. CHE-8914403. Helpful discussions with M.S. Gordon and S. Koseki are gratefully acknowledged.

1. (*a*) D.C. Moule and A.D. Walsh. Chem. Rev. **75**, 67 (1975); (*b*) D.J. Clouthier and D.A. Ramsay. Annu. Rev. Phys. Chem. **34**, 31 (1983).
2. R.P. Steer. Rev. Chem. Intermed. **4**, 1 (1981).
3. D.J. Clouthier and D.C. Moule. Top. Curr. Chem. **150**, 167 (1989).
4. R.H. Judge and D.C. Moule. J. Am. Chem. Soc. **106**, 5406 (1984).
5. H. Bock, S. Aygen, P. Rosmus, B. Solouki, and E. Weissflog. Chem. Ber. **117**, 187 (1984).
6. R.J. Glinski, E.A. Mishalanie, and J.W. Birks. J. Am. Chem. Soc. **108**, 531 (1986).
7. (*a*) D.J. Clouthier, R.H. Judge, and D.C. Moule. Chem. Phys. **114**, 417 (1987); (*b*) R.H. Judge, D.J. Clouthier, and D.C. Moule. J. Chem. Phys. **89**, 1807 (1988).
8. D.J. Clouthier, R.H. Judge, and D.C. Moule. J. Mol. Spectrosc. **141**, 175 (1990).
9. F. Creutzberg and J.T. Hougen. Can. J. Phys. **45**, 1363 (1967).
10. A.E. Douglas and E.R.V. Milton. J. Chem. Phys. **41**, 357 (1964).
11. J.T. Hougen. J. Chem. Phys. **41**, 363 (1964).
12. (*a*) M. Dupuis, D. Splanger, and J.J. Wendoloski. National resource for computations in chemistry. Software Catalog. University of California, Berkeley, Calif. 1980. Program QG01; (*b*) M.W. Schmidt, J.A. Boatz, K.K. Baldridge, S. Koseki, M.S. Gordon, S.T. Elbert, and B. Lam. QCPE Bull. **7**, 115 (1987); (*c*) M.W. Schmidt, K.K. Baldridge, J.A. Boatz, J.H. Jensen, S. Koseki, M.S. Gordon, K.A. Nguyen, T.L. Windus, S.T. Elbert, and B. Lam. QCPE Bull. **10**, 52 (1990).
13. T.H. Dunning, Jr. and P.J. Hay. *In* Methods of electronic structure theory. *Edited by* H.F. Schaefer III. Plenum Press, New York. 1977. Chap. 1. pp. 1–27.
14. R.C. Binning, Jr. and L.A. Curtiss. J. Comput. Chem. **11**, 1206 (1990).
15. R.J. Buenker and S.D. Peyerimhoff. J. Chem. Phys. **53**, 1368 (1970).
16. S. Collins, T.G. Back, and A. Rauk. J. Am. Chem. Soc. **107**, 6589 (1985).
17. R.D. Brown, P.D. Godfrey, D. McNaughton, and P.R. Taylor. J. Mol. Spectrosc. **120**, 292 (1986).
18. (*a*) B. Brooks and H.F. Schaefer. J. Chem. Phys. **70**, 5092 (1979); (*b*) B. Brooks, W.K. Laidig, P. Saxe, N. Handy, and H.F. Schaefer. Phys. Scr. **21**, 312 (1980).
19. E.R. Davidson. *In* The world of quantum chemistry. *Edited by* R. Daudel and B. Pullman. Reidel, Dordrecht. 1974. p. 17.
20. S. Koseki, M.W. Schmidt, and M.S. Gordon. J. Phys. Chem. Submitted.

21. K.C. Smyth and J.I. Brauman. J. Chem. Phys. **56**, 5993, (1972).
22. H.E. Radford. J. Chem. Phys. **40**, 2732 (1972).
23. S.R. Langhoff and E.R. Davidson. J. Chem. Phys. **64**, 4699 (1976).
24. T.D. Bouman and Aa. E. Hansen. RPAC molecular properties package, Version 9.0. Southern Illinois University at Edwardsville, Ill. 1991.
25. R.H. Judge, D.C. Moule, and G.W. King. J. Mol. Spectrosc. **81**, 37 (1980).
26. T. Suzuki, S. Saito, and E. Hirota. J. Chem. Phys. **79**, 1641 (1983).

Can. J. Chem. Downloaded from www.nrcresearchpress.com by 203.198.23.82 on 09/08/12
For personal use only.

Accurate *ab initio* relativistic Dirac–Fock–Coulomb calculations on heavy atoms using universal Gaussian basis set

A.B.F. Da Silva[1] and G.L. Malli
Department of Chemistry, Simon Fraser University, Burnaby, BC V5A 1S6, Canada

AND

Yasuyuki Ishikawa
Department of Chemistry and the Chemical Physics Program, University of Puerto Rico, P.O. Box 23346, U.P.R. Station, San Juan 00931, Puerto Rico

Received March 17, 1993

This paper is dedicated to Professor Gerald W. King on the occasion of his 65th birthday

A.B.F. Da Silva, G.L. Malli, and Yasuyuki Ishikawa. Can J. Chem. **71**, 1713 (1993).

A universal Gaussian basis set (UGBSII) is reported for *ab initio* relativistic Dirac–Fock calculations on atoms and molecules. The Dirac–Fock–Coulomb energies obtained with this universal Gaussian basis set are presented for the neutral heavy atoms Yb ($Z = 70$), W ($Z = 74$), Pb ($Z = 82$), Ra ($Z = 88$), and Pu ($Z = 94$). The total Dirac–Fock–Coulomb energies computed with the UGBSII, for all the systems, are in better agreement with the corresponding numerical finite-difference results than those obtained with our previous universal Gaussian basis set (UGBSI). The UGBSII represents a very accurate Gaussian basis set for relativistic Dirac–Fock atomic calculations.

A.B.F. Da Silva, G.L. Malli et Yasuyuki Ishikawa. Can J. Chem. **71**, 1713 (1993).

On rapporte un ensemble gaussien universel (UGBSII) pour des calculs *ab initio* Dirac–Fock relativistes sur des atomes et des molécules. On présente les énergies Dirac–Fock–Coulomb obtenues à l'aide de cet ensemble gaussien pour les atomes lourds neutres Yb ($Z = 70$), W ($Z = 74$), Pb ($Z = 82$), Ra ($Z = 88$) et Pu ($Z = 94$). Les énergies totales Dirac–Fock–Coulomb calculées pour tous les systèmes à l'aide de UGBSII sont en meilleur accord avec les résultats numériques correspondants de différences finies que ceux obtenus à l'aide de notre ensemble gaussien antérieur (UGBSI). L'ensemble UGBSII représente un ensemble gaussien très précis pour des calculs atomiques relativistes de Dirac–Fock.
[Traduit par la rédaction]

Introduction

Gaussian-type functions (GTFs) have been widely used in relativistic calculations during the last decade (1–7). This is basically due to three reasons: first, if the nucleus is represented by a finite body of uniform proton-charge distribution, the solutions of the radial Dirac equation can be represented by GTFs (8–10), and therefore, the GTFs are capable of reproducing the correct relativistic kinematics near the origin. Second, the multicenter integrals over the GTFs can be evaluated exactly by closed analytical formulas. Third, the basis sets of GTFs are less prone to near linear dependency than the basis sets of Slater-type functions (STFs). In particular, well-tempered and geometrical GTFs have been used for Dirac–Fock–Coulomb (DFC) and Dirac–Fock–Breit (DFB) atomic calculations (5, 7).

Recently, we have introduced universal Gaussian basis set (UGBS) for relativistic atomic and molecular calculations (11–13). The total DFC energies obtained with our previous universal Gaussian basis set (12, 13) (designated hereafter as UGBSI) for the neutral heavy atoms ($Z > 70$) are within about 30 millihartrees of the corresponding DFC energies obtained with the numerical-finite-difference Dirac–Fock program (14). In this paper we report a universal Gaussian basis set (hereafter referred to as UGBSII) which leads to the DFC energies for the heavy atoms Yb ($Z = 70$), W ($Z = 74$), Pb ($Z = 82$), Ra ($Z = 88$), and Pu ($Z = 94$) within 2 millihartrees or less of the corresponding results obtained with the numerical-finite-difference program (14).

[1]Permanent address: Departamento de Química e Física Molecular, Instituto de Física e Química de São Carlos, C.P. 369, 13560 São Carlos, SP, Brazil.

Computational

The relativistic universal Gaussian basis used in this work is generated by employing the integral discretization (ID) technique of the generator coordinate Hartree–Fock (GCHF) method (15, 16). In the GCHF method, the one-electron functions are chosen as integral transforms, viz.,

$$[1] \quad \psi_i(1) = \int \phi_i(1, \alpha) f_i(\alpha) d\alpha, \qquad i = 1, \ldots, n$$

where the ϕ_i, f_i, and α are the generator function, the weight function, and the generator coordinate, respectively. The application of the variational principle to the energy expectation value built with eq. [1] leads to the Griffin–Wheeler–Hartree–Fock (GWHF) equations:

$$[2] \quad \int [F(\alpha, \beta) - \varepsilon_i S(\alpha, \beta)] f_i(\beta) d\beta = 0, \qquad i = 1, \ldots, n$$

The integration of the GWHF equations is performed through integral discretization (ID) (15, 16), which is implemented through a relabelling of the generator coordinate space, α, viz.,

$$[3] \quad \Omega = \frac{\ln \alpha}{A}, \qquad A > 1$$

In the new generator coordinate space, Ω, an equally spaced N-point mesh, Ω_i, is chosen so that one can obtain an adequate numerical integration range for the relativistic $s_{1/2}$, $p_{1/2}$, $p_{3/2}$, $d_{3/2}$, $d_{5/2}$, $f_{5/2}$, and $f_{7/2}$ symmetries for several atoms. The integration range is characterized by a starting point, Ω_{min}, an increment, $\Delta\Omega$, and N (number of points). The same scaling parameter, $A = 6.0$, is used in all the calculations.

The exponents of the relativistic UGBSI and UGBSII used

Can. J. Chem. Downloaded from www.nrcresearchpress.com by 203.198.23.82 on 09/08/12
For personal use only.

TABLE 1. Starting exponents (α_{min}) of the universal Gaussian basis set UGBSI ($\Delta\Omega = 0.13$)

		Symmetry			
α_{min}	Ω_{min}	$s_{1/2}$	$p_{1/2}$ $p_{3/2}$	$d_{3/2}$ $d_{5/2}$	$f_{5/2}$ $f_{7/2}$
0.019063	−0.66	X			
0.041586	−0.53		X		
0.090718	−0.40			X	
0.197899	−0.27				X

TABLE 2. Starting exponents (α_{min}) of the universal Gaussian basis set UGBSII ($\Delta\Omega = 0.12$)

		Symmetry			
α_{min}	Ω_{min}	$s_{1/2}$	$p_{1/2}$ $p_{3/2}$	$d_{3/2}$ $d_{5/2}$	$f_{5/2}$ $f_{7/2}$
0.021494	−0.64	X			
0.044157	−0.52		X		
0.090718	−0.40			X	
0.186374	−0.28				X

TABLE 3. Total Dirac–Fock–Coulomb (E_{DFC}) energies (in hartrees) computed with the universal Gaussian basis sets UGBSI and UGBSII[a]

Atom	E_{DFC} (UGBSI)	E_{DFC} (UGBSII)	Finite-difference[b] (E_{DFC})
Yb	−14067.6609	−14067.6795	−14067.7
W	−16156.2234	−16156.2476	−16156.2484
Pb	−20913.6876	−20913.7165	−20913.7184
Ra	−25027.9732	−25028.0165	−25028.0165
Pu	−29656.4431	−29656.5111	−29656.5122

[a]The basis-set size is the same in both UGBSI and UGBSII for all the atoms, viz., 32*s* 30*p* 20*d* 15*f*.

[b]E_{DFC} computed by using the Oxford numerical-finite-difference Dirac–Fock program (14), except Yb, for which Desclaux's program (17) was used because the Oxford program (14) presents serious convergence problems for a few atomic systems, including Yb.

in this work are generated by using the following discretization parameters in eq [3]:

Symmetry	Ω_{min}	$\Delta\Omega$	N
UGBSI: $s_{1/2}$, $p_{1/2}$, $p_{3/2}$, $d_{3/2}$, $d_{5/2}$, $f_{5/2}$, and $f_{7/2}$	−0.66	0.13	32
UGBSII: $s_{1/2}$, $p_{1/2}$, $p_{3/2}$, $d_{3/2}$, $d_{5/2}$, $f_{5/2}$, and $f_{7/2}$	−0.64	0.12	32

We have used the same basis set size (32*s* 30*p* 20*d* 15*f*) of Gaussian exponents, in both UGBSI and UGBSII, for the $s_{1/2}$, $p_{1/2}$, $p_{3/2}$, $d_{3/2}$, $d_{5/2}$, $f_{5/2}$, and $f_{7/2}$ symmetries. The Dirac–Fock–Coulomb (DFC) self-consistent-field (SCF) calculations with these two sets of universal Gaussian basis functions are performed using the DFC SCF methodology described previously (5). In our calculations we employ the finite-nucleus model of uniform proton-charge distribution and the restricted kinetic balance condition (one-to-one correspondence between the basis functions of the large and small components) (5).

TABLE 4. Dirac–Fock–Coulomb (E_{DFC}) orbital energies (in hartrees) of Ra ($Z = 88$) computed with the universal Gaussian basis sets UGBSI and UGBSII

Orbital	E_{DFC} (UGBSI)	E_{DFC} (UGBSII)	Finite-difference[a] (E_{DFC})
$1s_{1/2}$	−3845.799	−3845.795	−3845.792
$2s_{1/2}$	−712.6593	−712.6557	−712.6550
$2p_{1/2}$	−685.0981	−685.0945	−685.0938
$2p_{3/2}$	−571.9385	−571.9348	−571.9352
$3s_{1/2}$	−179.6881	−179.6851	−179.6848
$3p_{1/2}$	−167.2364	−167.2339	−167.2334
$3p_{3/2}$	−141.1884	−141.1856	−141.1858
$3d_{3/2}$	−121.3193	−121.3161	−121.3161
$3d_{5/2}$	−115.9627	−115.9594	−115.9596
$4s_{1/2}$	−45.68291	−45.68215	−45.6820
$4p_{1/2}$	−40.11673	−40.11580	−40.1156
$4p_{3/2}$	−33.39925	−33.39827	−33.39853
$4d_{3/2}$	−24.42034	−24.41887	−24.41895
$4d_{5/2}$	−23.16195	−23.16049	−23.16080
$4f_{5/2}$	−11.35811	−11.35600	−11.35606
$4f_{7/2}$	−11.04869	−11.04660	−11.04671
$5s_{1/2}$	−10.00193	−10.00162	−10.00166
$5p_{1/2}$	−7.844003	−7.843692	−7.843758
$5p_{3/2}$	−6.373405	−6.373080	−6.373351
$5d_{3/2}$	−3.117968	−3.117490	−3.117740
$5d_{5/2}$	−2.903024	−2.902553	−2.902889
$6s_{1/2}$	−1.624580	−1.624478	−1.624626
$6p_{1/2}$	−0.9738995	−0.9737883	−0.9739604
$6p_{3/2}$	−0.7405934	−0.7404486	−0.7406612
$7s_{1/2}$	−0.1662212	−0.1661491	−0.1662282

[a]Numerical DFC orbital energies computed by using the Oxford numerical-finite-difference Dirac-Fock program (14).

Results and discussion

The Dirac–Fock–Coulomb (DFC) SCF calculations are performed on the heavy atoms: Yb ($Z = 70$), W ($Z = 74$), Pb ($Z = 82$), Ra ($Z = 88$), and Pu ($Z = 94$). The atomic masses used for Yb, W, Pb, Ra, and Pu are 173.04, 183.85, 207.19, 226.0, and 242.0, respectively. The speed of light used in our DFC SCF calculations is 137.0370 au. In Tables 1 and 2 are collected the starting exponent (α_{min}) and the corresponding Ω_{min} for each $s_{1/2}$, $p_{1/2}$, $p_{3/2}$, $d_{3/2}$, $d_{5/2}$, $f_{5/2}$, and $f_{7/2}$ symmetry of the UGBSI and UGBSII. The universal Gaussian exponents used in the 32*s* 30*p* 20*d* 15*f* UGBSI and UGBSII basis sets are generated using eq [3] and the parameters Ω_{min} and $\Delta\Omega$ in Tables 1 and 2. The results of the total DFC energies obtained with the universal Gaussian basis sets (UGBSI and UGBSII) are presented in Table 3.

It can be seen from Table 3 that the UGBSII yields total DFC energies within 2 millihartrees or less of the corresponding numerical-finite-difference values. However, the UGBSI yields total DFC energies that are within about 25–70 millihartrees of the corresponding numerical-finite-difference results. In particular, for the Ra (Z=88) atom, the total DFC energy obtained with the UGBSII is in excellent agreement with the corresponding numerical value computed with the numerical-finite-difference program (14). In this work we have investigated the best starting exponents (α_{min}) for each symmetry, since it was observed that the inclusion of diffuse functions (corresponding to low exponents) is as important as the addition of functions with higher exponents. In Tables 1 and 2, α_{min} represents for each $s_{1/2}$, $p_{1/2}$, $p_{3/2}$, $d_{3/2}$, $d_{5/2}$, $f_{5/2}$, and $f_{7/2}$ symmetry the best starting

Can. J. Chem. Downloaded from www.nrcresearchpress.com by 203.198.23.82 on 09/08/12
For personal use only.

exponent for all the atoms studied. It should be mentioned that the inclusion of additional higher exponent functions beyond the UGBS size given in Table 3 does not lead to substantial improvement in the total DFC energies computed with both the UGBSI and UGBSII.

Table 4 displays the DFC orbital energies for Ra (Z=88) obtained with the UGBSI and UGBSII. The last column in Table 4 shows the numerical-finite-difference DFC orbital energies computed with the numerical-finite-difference program (14). It can be seen from Table 4 that the DFC orbital energies of Ra obtained with the UGBSII are in better agreement with the corresponding numerical DFC orbital energies than those obtained with the UGBSI.

Conclusion

The universal Gaussian basis set (UGBSII) presented in this work yields Dirac–Fock–Coulomb energies, for the heavy atoms Yb (Z = 70), W (Z = 74), Pb (Z = 82), Ra (Z = 88), and Pu (Z = 94), within a few millihartrees or less as compared to the corresponding numerical-finite-difference values. The Dirac–Fock orbital energies obtained with the UGBSII for the Ra (Z = 88) atom are in very good agreement with the corresponding numerical Dirac–Fock orbital energies. In conclusion, it can be stated that the UGBSII is a very accurate basis set for relativistic Dirac–Fock atomic calculations, and could be useful in calculating spectroscopic states of atoms and molecules containing heavy atoms.

Acknowledgments

This work was supported by the Natural Sciences and Engineering Research Council of Canada (NSERC) to G.L. Malli (grant no. A3598), by the CNPq (Brazilian Agency) to A.B.F. Da Silva and G.L. Malli, and by the National Science Foundation to Y. Ishikawa (grant PHY-9008627). All support is gratefully acknowledged. Calculations reported in this work were performed on an IBM RISC/6000 workstation at Simon Fraser University.

1. G.L. Malli. Chem. Phys. Lett. **68**, 529 (1979).
2. P.J.C. Aerts and W.C. Nieuwpoort. Chem. Phys. Lett. **113**, 165 (1985).
3. S. Okada and O. Matsuoka. J. Chem. Phys. **91**, 4193 (1989).
4. Y. Ishikawa. Phys. Rev. A, **42**, 1142 (1990); Chem. Phys. Lett. **179**, 291 (1991).
5. Y. Ishikawa, H.M. Quiney, and G.L. Malli. Phys. Rev. A, **43**, 327 (1991).
6. F.A. Parpia, A.K. Mohanty, and E. Clementi. J. Phys. B, **25**, 1 (1992).
7. Y. Ishikawa, G.L. Malli, and A.J. Stacey. Chem. Phys. Lett. **188**, 145 (1992).
8. F.G. Werner and J.A. Wheeler. Phys. Rev. **109**, 126 (1958).
9. Y. Ishikawa, R. Baretty, and R.C. Binning, Jr. Chem. Phys. Lett. **121**, 130 (1985).
10. Y. Ishihawa and H.M. Quiney. Int. J. Quant. Chem. **S21**, 523 (1987).
11. G.L. Malli, A.B.F. Da Silva, and Y. Ishikawa. Can. J. Chem. **70**, 1822 (1992).
12. G.L. Malli, A.B.F. Da Silva, and Y. Ishikawa. Chem. Phys. Lett. **201**, 37 (1993).
13. A.B.F. Da Silva, G.L. Malli, and Y. Ishikawa. Chem. Phys. Lett. **203**, 201 (1993).
14. I.P. Grant, B.J. McKenzie, P.H. Norrington, D.F. Mayers, and N.C. Pyper. Comput. Phys. Commun. **21**, 207 (1980).
15. J.R. Mohallem, R.M. Dreizler, and M. Trsic. Int. J. Quant. Chem. **S20**, 45 (1986).
16. A.B.F. Da Silva, H.F.M. Da Costa, and M. Trsic. Mol. Phys. **68**, 433 (1989).
17. J.P. Desclaux. Comput. Phys. Commun. **9**, 31 (1975).

Can. J. Chem. Downloaded from www.nrcresearchpress.com by 203.198.23.82 on 09/08/12
For personal use only.

Diode laser spectrum and rovibrational analysis of the ν_6 band of vinyl fluoride

S. GIORGIANNI, P. STOPPA, M. PEDRALI, AND S. GHERSETTI[1]

Dipartimento di Chimica Fisica, Università di Venezia, D.D. 2137, I-30123 Venice, Italy

Received March 5, 1993

This paper is dedicated to Professor Gerald W. King on the occasion of his 65th birthday

S. GIORGIANNI, P. STOPPA, M. PEDRALI, and S. GHERSETTI. Can. J. Chem. **71**, 1716 (1993).

The vibration–rotation spectrum of CH_2=CHF has been investigated in the ν_6 band region around 1305 cm^{-1} at Doppler limited resolution using a tunable diode laser spectrometer. The measurements have been performed at low temperature (240 K) to decrease hot band interferences. This fundamental of symmetry species A' gives rise to an **a**/**b** hybrid band, which was mainly composed of **a**-type transitions. Both J and K structures have been resolved in the $^{Q}Q_K(J)$ subbranches and the rovibrational analysis in the P, Q, and R branches has led to the identification of more than 1000 lines with $J \leq 43$ and $K_a \leq 14$. The ν_6 band is affected by first-order **b**-type and second-order **a**-type Coriolis resonances with the $\nu_9 + \nu_{11}$ combination, and the perturbation effect has been found stronger for the $K'_a = 11$ level. About 870 transitions free of major resonance contributions were fitted using Watson's A-reduction Hamiltonian in the I^r representation, and a set of effective rotational and quartic centrifugal distortion constants was determined for the $v_6 = 1$ state of CH_2=CHF.

S. GIORGIANNI, P. STOPPA, M. PEDRALI et S. GHERSETTI. Can. J. Chem. **71**, 1716 (1993).

On a étudié le spectre de vibration–rotation du CH_2=CHF dans la région de la bande ν_6 à environ 1305 cm^{-1} à une résolution limitée de Doppler en utilisant un spectromètre au laser à diode adressable. On a effectué ces mesures à basse température (240 K) pour diminuer les interférences dues à la bande chaude. Cette vibration de symétrie des espèces A' donne une bande hybride **a**/**b** composée principalement de transitions de type **a**. On a résolu les structures J et K dans les sous branches $^{Q}Q_K(J)$ et l'analyse rotavibrationnelle dans les branches P, Q et R a permis d'identifier plus de 1000 lignes avec $J \leq 43$ et $K_a \leq 14$. La bande ν_6 est affectée par les résonances de Coriolis d'ordre un de type **b** et d'ordre deux de type **a** avec la combinaison $\nu_9 + \nu_{11}$ et on a trouvé un effet de perturbation plus grand pour le niveau $K'_a = 11$. Environ 870 transitions libres de toute contribution de résonance significative sont adjustées en utilisant l'Hamiltonien de réduction A de Watson dans la représentation I^r et on a déterminé un ensemble de constantes effectives de distorsion centrifuge quartique et rotationnelle pour l'état $v_6 = 1$ du CH_2=CHF.

[Traduit par la rédaction]

Introduction

In the last few years, there has been continued progress in spectroscopic studies of vinyl fluoride motivated, in part, by its potential importance in atmospheric chemistry. This compound, which plays a significant role in photochemical processes (1, 2), is mainly employed as a monomer for the production of synthetic resins such as polyvinyl fluoride, and its release is accidental. Knowledge of the rovibrational spectrum and determination of accurate spectroscopic parameters are essential for detecting trace gases of this molecule; for this purpose high-resolution measurements are the best source of information.

Recently, we began an infrared study, under high resolution, of small halogenated molecules containing the >C=C< group, and different investigations concerning selected bands of CH_2=CF_2 and CH_2=CHCl have already been carried out (3–5). In the present work the diode laser measurements have been extended to the ν_6 band of CH_2=CHF lying near 1305 cm^{-1}; little is known, on the other hand, of the vibrational behaviour of this compound, for which no high-resolution results are available to date.

Studies on low-resolution infrared spectra were performed much earlier (refs. 6–8 and references quoted therein), and all the fundamentals together with some combination bands seem to have been already characterized. The analysis of medium-resolution spectra in the region 800–1000 cm^{-1} led to establishment of a Coriolis interaction between the ν_8, ν_{10}, and ν_{11} modes and to a calculation of the related coupling constants (9). Microwave spectra were measured many years ago (10, 11) and, again, more recently (12). The effect of jet cooling on the complex ν_8, ν_{10} band system near 936 cm^{-1} has also been investigated using diode laser spectoscopy (13). The theoretical and experimental structures of this molecule were recently derived using *ab initio* calculations and a reanalysis of existing microwave data (14).

The present paper deals with the results of Doppler-limited measurements of the ν_6 band of CH_2=CHF using a tunable diode laser spectrometer, and the interpretation of the Coriolis interaction mechanism.

Experimental

The sample of CH_2=CHF (purity ≃ 99%) was obtained commercially from Peninsular Chemical Research, Inc. and was used without further purification. The high-resolution spectra were recorded in the range 1280–1333 cm^{-1} using the tunable diode laser at the University of Venice, a brief description of which is given here.

The arrangement of the spectrometer is mainly based on the SP-5000 assembly of Laser Analytics, Inc. The crystal diode is mounted in a closed-cycle cryogenic refrigerator and a temperature stabilizer maintains the required temperature in the range 10–70 K. The output frequency is coarsely controlled by changing the temperature of the diode, and the fine adjustment of the frequency is provided by a variable and precisely tunable current for the diode, producing different laser modes. A sweeping current is used to continuously scan a laser mode.

In the present version the spectrometer setup is in a triple-beam configuration, which allows simultaneous recording of the sample spectrum, the calibration lines, and the interference fringes from a 2.59-cm solid germanium etalon (FSR ≃ 0.0475 cm^{-1}). The instrument is interfaced to a 286 PC that provides data acquisition, storage, and conversion into transmittance of the spectra.

[1]Author to whom correspondence may be addressed.

Can. J. Chem. Downloaded from www.nrcresearchpress.com by 203.198.23.82 on 09/08/12
For personal use only.

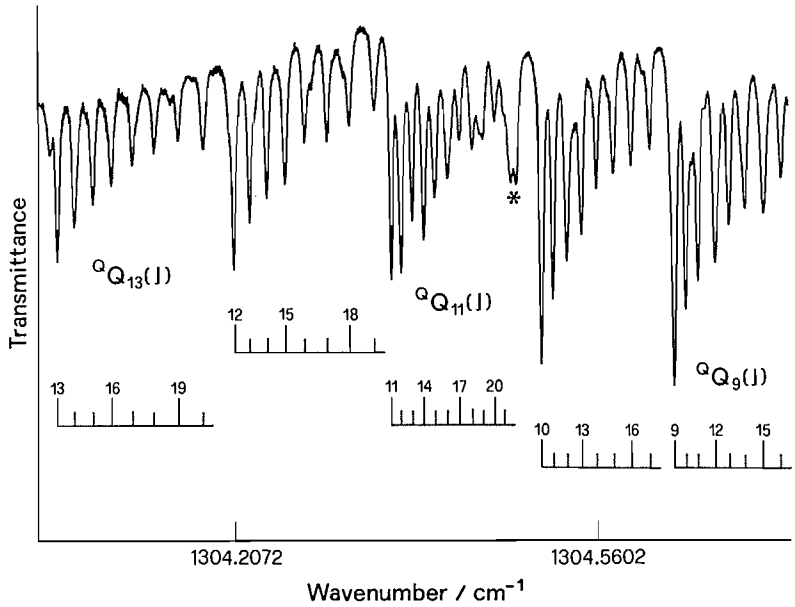

FIG. 1. A section of the central part of the Q-branch spectrum of the CH_2=CHF ν_6 band (T = 240 K, $P \simeq 1$ mbar, 49 cm cell) indicating the J assignment of the $^{Q}Q_9(J) - {}^{Q}Q_{13}(J)$ manifolds. Note the narrow spacings between the perturbed components in the $^{Q}Q_{11}(J)$ series and the unresolved peak marked by an asterisk including the transitions with J = 22–26.

The measurements were performed at pressures ranging from 1 to 3 mbar (1 bar = 100 kPa) with a 49 cm long absorption cell cooled to 240 K to reduce the interferences arising from hot bands. Absolute calibration of the spectra was based on the wavenumbers of well-known N_2O lines (15), and selected SO_2 transitions were measured on an FTIR spectrometer as described in ref. 16; the relative calibration was obtained using the germanium etalon patterns. The absolute wavenumber accuracy is estimated to be of the order of 0.001 cm^{-1} and the internal consistency within the same laser mode is better than 0.0005 cm^{-1}.

Analysis and perturbations

Vinyl fluoride is a planar molecule belonging to the symmetry point group C_s; the 12 fundamentals are distributed in the vibrational irreducible representation as 9 of species A' (ν_1–ν_9) and 3 of species A'' (ν_{10}–ν_{12}). The molecular symmetry plane contains the a and b axes, while the remaining c axis is perpendicular to it. Thus the A' vibrations will give rise to **a**/**b** hybrid bands though one of the components might be much weaker than the other, and the A'' modes will produce pure **c**-type bands. Since this molecule is a nearly prolate symmetric top (κ = −0.945) the structure of the absorptions would correspond to that of parallel (**a**-type) and perpendicular (**b**- and **c**-type) bands. The ν_6 vibration (≃1305 cm^{-1}), mainly due to the C=CH deformation mode, is of symmetry species A' and exhibits a predominant **a**-type envelope. Following the selection rules (ΔJ = 0, ±1; ΔK_a = 0; ΔK_c = ±1) several types of transitions are expected in the P, Q, and R branches, which are composed by even and odd subbands depending on ($K''_a + K''_c = J''$) or ($K''_a + K''_c = J'' + 1$), respectively.

A convenient starting point for the analysis of the spectrum is represented by the interpretation of the Q-branch features. The band center is dominated by a series of ^{Q}Q subbranches consisting of groups of lines that begin to show the fine structure as one moves away from the origin toward lower wavenumbers. The individual groups are defined by a K_a value and within each cluster the resolved J components progress from the most intense line ($J = K_a$) toward higher wavenumbers until they blend into the neighbouring block. As an example, a portion of the Q-branch spectrum containing the $^{Q}Q_9(J)$–$^{Q}Q_{13}(J)$ manifolds is depicted in Fig. 1, where the J assignment is also presented. As can be seen, the fine structure in the $^{Q}Q_{11}(J)$ cluster does not reflect a regular displacement and the observed irregularity indicates the existence of perturbations. In particular, unlike the behaviour in the other groups, the J components gradually shift toward lower wavenumbers with increasing J until they overlap for $J \simeq 22$, which means that the upper levels are depressed in energy by interaction effects; the wavenumbers of the more perturbed transitions (K_a = 10–12) are included in Table 3 (see later).

The analysis of the Q-branch data provided an approximate set of the ν_6 band parameters, which, when combined with the ground state constants from ref. 11, allowed prediction of a number of transitions in the P and R branches. From single subband analyses it appeared clear that significant deviations from the expected positions occur even for lines with different K_a values and not only for transitions with K_a = 11; the discrepancies become larger with increasing J, thus indicating a J-dependent resonance.

From symmetry considerations it follows that A' and A'' modes may interact through **a** as well as **b** Coriolis resonances, while vibrations having the same symmetry interact by a **c** Coriolis perturbation. In the range investigated the ν_6 vibration (≃1305 cm^{-1}) appears relatively isolated from other modes, with the exception of the $\nu_9 + \nu_{11}$ combination (A'') lying at about 1345 cm^{-1}. Although we have no direct observation for the latter band, it can couple with the fundamental mode via **a**- and **b**-type Coriolis resonances. In a first-order perturbation, the former involves rotational levels with the same J and K_a values while the latter links levels with the same J and with K_a values differing by ±1.

Assuming the same A and $\bar{B}$ values for the ground and the excited states, and considering a separation of about 40 cm^{-1}

Can. J. Chem. Downloaded from www.nrcresearchpress.com by 203.198.23.82 on 09/08/12
For personal use only.

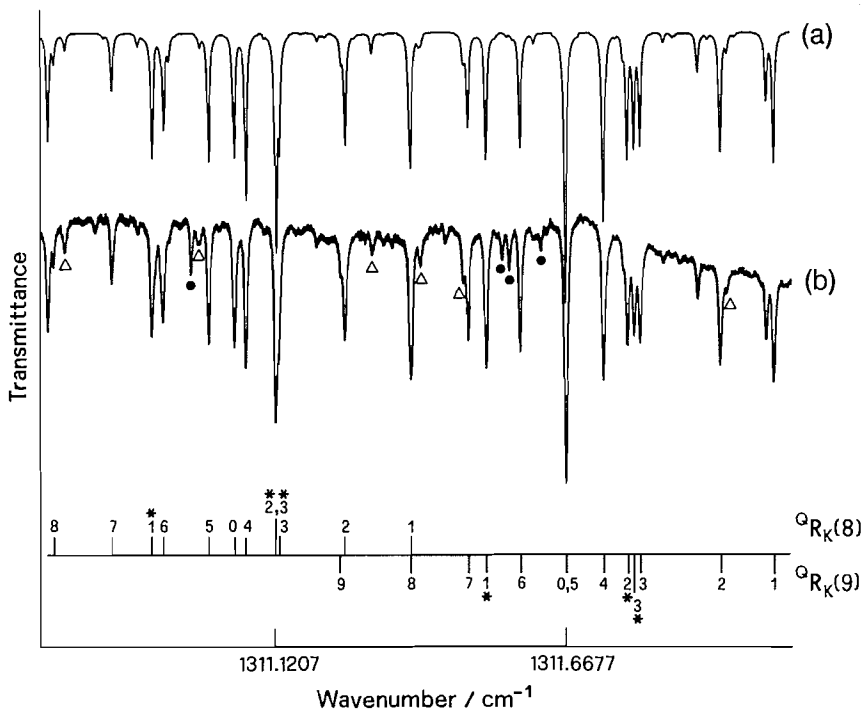

FIG. 2. A portion of the R-branch spectrum of the CH_2=CHF ν_6 band near 1311.5 cm^{-1} showing the K_a structure of the series $^{Q}R_K$ (8,9); asymmetry splitting is observed and transitions marked by an asterisk refer to the odd component. (*a*) Simulated spectrum. (*b*) Experimental spectrum (T = 240 K, $P \simeq$ 1.5 mbar, 49 cm cell); (△) lines due to the weak **b**-type component; (●) features very likely due to a different band.

between the ν_6 and the $\nu_9 + \nu_{11}$ vibrations, calculations in the prolate symmetric top limit indicate that the K_a levels of ν_6 come close to and cross the $(K_a - 1)$ levels of $\nu_9 + \nu_{11}$. In particular, from the reduced energy level scheme it appears that the K_a = 11 and 12 levels of ν_6 are just below and above the K_a = 10 and 11 levels of $\nu_9 + \nu_{11}$, respectively. These states are then expected to be most seriously influenced by a first-order **b** Coriolis resonance. Effects due to a first-order **a** Coriolis interaction seem to be of little significance, the energy levels with the same K_a value of the vibrations involved being widely spaced. Interestingly, a localized perturbation due to a second-order **a** Coriolis resonance with $\nu_9 + \nu_{11}$ is expected to occur for K_a = 7 and 8 levels of ν_6, which are slightly higher in energy than the K_a = 5 and 6 levels, respectively, of the former vibration. Since this interaction is of high order, it should produce only significant energy shifts under conditions of near-resonance.

The spectrum exhibits in most regions a structure similar to that observed in a parallel band of a symmetric top, and the $^{Q}P_K(J)$ and $^{Q}R_K(J)$ subbranches are composed of a series of transitions proceeding toward higher wavenumbers with decreasing K_a. A typical example is illustrated in Fig. 2, where a section of the R branch near 1311 cm^{-1} with the assignment of the K_a structure in the $^{Q}R_K(8,9)$ manifolds is reported. The effect of the asymmetry splitting can be seen in an irregular numbering of the lines with low K_a values; transitions with K_a = 1, 2 are widely split, with the even component lying on the higher wavenumber side. Lines arising from the **b**-type component are very weak and, since the identification in most of the cases becomes very difficult because of the overlap of the much stronger features from the **a**-type band, no rotational analysis has been attempted. Nevertheless, as can be observed in the upper trace of Fig. 2, the **b**-type characteristics appear well reproduced in the synthetic spectrum, generated with the molecular constants reported later.

Not surprisingly, when the J value increases the different subbands begin to run into one another and the fine structure becomes more difficult to identify; due to a larger asymmetry effect, the transitions with low K_a value give rise to spreading lines without exhibiting any regular pattern. A portion of the P branch near 1286 cm^{-1} showing the displacement of the K_a structure in the $^{Q}P_K(29,30)$ subbranches is illustrated in Fig. 3. As can be seen, the relatively small splitting for K_a = 6 increases strongly for K_a = 2 in $^{Q}P_K(30)$; in contrast to what was found in the R branch, the even component lies here at the lower wavenumber side. To show how well the determined parameters (see later) reproduce the observed characteristics, the wavenumbers of the assigned transitions occurring in the range of Fig. 3 are listed in Table 1, together with their residuals and the corresponding weights.

Results and discussion

The ground and excited rotational energy levels were computed employing the Watson's *A*-reduction Hamiltonian in the I^r representation,

$$\mathbf{H} = 1/2(B + C)\mathbf{P}^2 + [A - 1/2(B + C)]\mathbf{P}_a^2 - \Delta_J\mathbf{P}^4 - \Delta_{JK}\mathbf{P}^2\mathbf{P}_a^2 - \Delta_K\mathbf{P}_a^4 + \Phi_J\mathbf{P}^6 + \Phi_{JK}\mathbf{P}^4\mathbf{P}_a^2 + \Phi_{KJ}\mathbf{P}^2\mathbf{P}_a^4 + \Phi_K\mathbf{P}_a^6 + [1/2(B - C) - 2\delta_J\mathbf{P}^2 + 2\varphi_J\mathbf{P}^4](\mathbf{P}_b^2 - \mathbf{P}_c^2) + [(-\delta_K\mathbf{P}_a^2 + \varphi_{JK}\mathbf{P}^2\mathbf{P}_a^2 + \varphi_K\mathbf{P}_a^4), (\mathbf{P}_b^2 - \mathbf{P}_c^2)]_+$$

where $\mathbf{P}$, $\mathbf{P}_a$, $\mathbf{P}_b$, and $\mathbf{P}_c$ are the operators of the total angu-

Can. J. Chem. Downloaded from www.nrcresearchpress.com by 203.198.23.82 on 09/08/12
For personal use only.

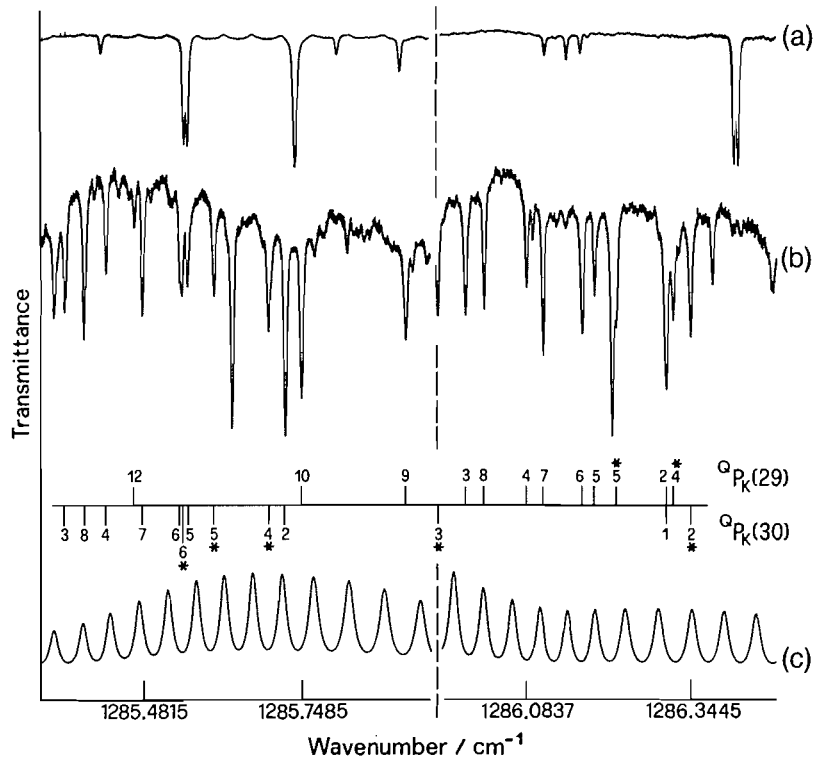

FIG. 3. Details of the P-branch spectrum of the CH_2=CHF ν_6 band around 1286 cm^{-1} exhibiting two consecutive laser modes. The K_a structure of the $^{Q}P_K(29,30)$ clusters is indicated; transitions marked by an asterisk belong to the odd component. (*a*) N_2O calibration lines; (*b*) experimental spectrum (T = 240 K, $P \simeq 3$ mbar, 49 cm cell); (*c*) germanium etalon patterns. Frequency scale is not precisely linear owing to nonlinear variation of diode laser emission frequency with injection current.

lar momentum and its components along the principal inertial axes.

The rovibrational analysis was performed according to commonly used procedures and the assignment of the structure was started, as previously mentioned, in the Q-branch region, where in most of the clusters regular absorption line patterns can be easily recognized. Preliminary line assignments were fitted by a least-squares routine, keeping the ground state constants fixed and refining the excited vibrational state parameters together with the band origin. Once the first set of upper state constants had been obtained, the analysis proceeded iteratively with additional identifications, revision of constants, and prediction of new transitions. However, such a standard procedure did not work well for all the assignments because of the perturbation effects, and even single subband fits for some K_a values yielded poor results.

From the present analysis about 1030 transitionos with $J \leq 43$ and $K_a \leq 14$ of the subbranches $^{e,o}P(0,-1)$, $^{e,o}R(0,1)$, and $^{e}Q(0,1)$ were identified. In absence of asymmetry splitting the assigned lines comprise only the set of even transitions; inclusion in the fit of the remaining odd transitions did not yield any substantial improvement in the molecular constants.

In the choice of the ground state parameters we preferred the set of Gerry (11) to the more recent one of Hayashi and Inagusa (12); the former was derived using the Watson *A*-reduction Hamiltonian, while the latter was obtained in the Watson *S*-reduction expression. In particular, the constants of ref. 11, computed from a set of transitions with J ($\leq$40) and K_a ($\leq$8) values much higher than those of ref. 12, also include the sextic coefficients, some of which, not significantly determined, are substantially fitting parameters. Noting that the J and K_a values reached in the present assignments are higher than those employed in ref. 11, we attempted to improve the sextic terms for the ground state by performing a simultaneous fit of the ν_6 combination differences and the available microwave data. Since the $^{Q}P_K(J)$ and $^{Q}R_K(J)$ even transitions reach the upper level for which $K'_a + K'_c = J'$, in order to also obtain combination differences with Q-branch lines, we considered the set of $^{Q}Q_K(J)$ odd transitions, which in this case are coincident with the assigned even ones because of the absence of asymmetry splitting. Unfortunately, the low number of combinations with $J > 40$ and $K_a > 8$ and the greater accuracy of the microwave transitions, weighted 10^4 times the infrared data, did not allow a better determination of the sextic coefficients than that of ref. 11; therefore, a substantial improvement in the uncertainty of the constants can be reached only when combinations with much higher J and K_a values are available.

The assigned transitions, with the exception of those considered more strongly perturbed, were employed to determine the spectroscopic parameters of the ν_6 vibration. Unit weight was given to lines appearing as single transitions, while blended or scarcely resolved features were given a weight factor of 0.1. In the refinement procedure the ground state parameters were kept fixed, and only the band origin and the excited state constants were allowed to change. The variation of the sextic distortion terms led to poorly determined values without any significant improvement in the standard deviation of the fit; on this basis, the sextic coefficients were constrained to their ground state values. The

Can. J. Chem. Downloaded from www.nrcresearchpress.com by 203.198.23.82 on 09/08/12
For personal use only.

Can. J. Chem. Downloaded from www.nrcresearchpress.com by 203.198.23.82 on 09/08/12
For personal use only.

TABLE 1. Assigned transitions in the range 1285.33–1286.38 cm^{-1} of the ν_6 band of CH_2=CHF

J'	K'_a	K'_c	J''	K''_a	K''_c	Obs./cm^{-1}[a]	O − C[b]	Weight
30	3	28	31	3	29	1285.3304	−0.0017	0.1
29	3	26	30	3	27	1285.3482	−0.0021	0.1
29	8	21	30	8	22	1285.3811 *	0.0005	0.1
29	4	25	30	4	26	1285.4193	−0.0019	0.1
28	12	16	29	12	17	1285.4668 *	0.0366	1.0
29	7	22	30	7	23	1285.4815 *	0.0042	1.0
29	6	23	30	6	24	1285.5453	−0.0013	0.1
29	6	24	30	6	25	1285.5491	−0.0011	0.1
29	5	24	30	5	25	1285.5574	−0.0010	1.0
29	5	25	30	5	26	1285.6041	0.0003	1.0
31	1	31	32	1	32	1285.6346	−0.0004	1.0
31	0	31	32	0	32	1285.6346	0.0003	1.0
29	4	26	30	4	27	1285.6962	0.0008	1.0
29	2	27	30	2	28	1285.7233	0.0000	1.0
30	1	29	31	1	30	1285.7233	0.0005	1.0
28	10	18	29	10	19	1285.7485 *	−0.0063	0.1
30	2	29	31	2	30	1285.7485	−0.0009	1.0
28	9	19	29	9	20	1285.8921	0.0004	1.0
27	13	14	28	13	15	1285.9005 *	0.0283	1.0
29	3	27	30	3	28	1285.9365	0.0004	1.0
28	3	25	29	3	26	1285.9816	0.0006	1.0
28	8	20	29	8	21	1286.0118	0.0014	1.0
28	4	24	29	4	25	1286.0837	0.0000	1.0
27	12	15	28	12	16	1286.0938 *	0.0350	1.0
28	7	21	29	7	22	1286.1126 *	0.0040	1.0
28	6	22	29	6	23	1286.1808	−0.0001	0.1
28	5	23	29	5	24	1286.2021	−0.0004	1.0
30	1	30	31	1	31	1286.2296	−0.0019	0.1
30	0	30	31	0	31	1286.2296	−0.0008	0.1
28	5	24	29	5	25	1286.2363	−0.0010	1.0
28	2	26	29	2	27	1286.3096	0.0013	0.1
29	1	28	30	1	29	1286.3096	−0.0017	0.1
28	4	25	29	4	26	1286.3193	−0.0002	1.0
29	2	28	30	2	29	1286.3445	−0.0003	1.0
27	10	17	28	10	18	1286.3775 *	−0.0066	1.0

[a]Lines marked by asterisk were not used in the fit.
[b]O − C is (Obs. − Calc.) in cm^{-1}.

TABLE 2. Molecular constants (cm^{-1}) for the ν_6 band of CH_2=CHF[a]

	Ground state[b]	$\upsilon_6 = 1$
ν_0		1305.19365(7)
A	2.1543135	2.1473633(35)
B	0.35480825	0.35576898(45)
C	0.30414493	0.30427618(36)
$\Delta_J \times 10^6$	0.2814	0.2852(2)
$\Delta_{JK} \times 10^5$	−0.2533	−0.2535(3)
$\Delta_K \times 10^4$	0.4434	0.4418(4)
$\delta_J \times 10^7$	0.5890	0.6037(14)
$\delta_K \times 10^5$	0.1189	0.1115(15)
$\sigma \times 10^3$		0.73
No. of data		867

$\Phi_J \times 10^{12} = -0.3$, $\Phi_{JK} \times 10^{11} = -0.2$, $\Phi_{KJ} \times 10^9 = -0.14$, $\Phi_K \times 10^8 = 0.12$, $\varphi_J \times 10^{12} = 0.21$, $\varphi_{JK} \times 10^{10} = -0.22$, $\varphi_K \times 10^8 = 0.13$[c]

[a]Uncertainties given are one standard deviation in units of the last digit quoted.
[b]Constants from ref. 11.
[c]Ground state sextic coefficients (11) fixed for the upper level.

effective constants for the ν_6 state, derived from the final fit of about 870 lines ($\sigma \simeq 7 \times 10^{-4}$ cm^{-1}), are reported in Table 2; the rotational and quartic centrifugal distortion parameters are reasonably close to their ground state values, and hence the transitions included in the fit do not seem to be much affected by perturbations.

Significant and systematic differences in the residuals occur for several lines of different subbands and this effect has been ascribed to the Coriolis resonance with the $\nu_9 + \nu_{11}$ state. In particular, the first-order **b** Coriolis perturbation becomes stronger near the crossing, where the $K'_a = 10$, 11 levels are depressed in energy and the $K'_a = 12$, 13, 14 levels are pushed up. It is worthy of note that within each subband the interaction effect becomes stronger as J increases and no crossing has been observed in the features identified. This behaviour can be clearly observed in Table 3, which reports the wavenumbers of the assigned transitions having the upper level with $K'_a = 10$, 11, and 12; the largest discrepancies between observed and calculated values occur for $K'_a = 11$ ($J' = 26$) and $K'_a = 12$ ($J' = 31$) with $\Delta_{max} = -0.204$ and 0.048 cm^{-1}, respectively. Besides, the positive residuals for the $K'_a = 7$, 8 levels with J' values higher than 21 and 29, respectively, are explained by the second-order **a** Coriolis

TABLE 3. Assigned transitions with K'_a = 10, 11, and 12 of the ν_6 band of CH_2=CHF

J'	K'_a	K'_c	J''	K''_a	K''_c	Obs./cm^{-1}[a]	O − C[b]	Weight
10	10	1	10	10	0	1304.5063	0.0006	1.0
11	10	1	12	10	2	1296.6007	−0.0005	1.0
11	10	2	11	10	1	1304.5178	−0.0001	1.0
11	10	1	10	10	0	1311.7769	0.0023	0.1
12	10	2	13	10	3	1295.9557	0.0011	1.0
12	10	3	12	10	2	1304.5316	0.0004	1.0
13	10	4	13	10	3	1304.5456	0.0000	1.0
13	10	3	12	10	2	1313.1221	0.0000	1.0
14	10	4	15	10	5	1294.6647	0.0002	1.0
14	10	5	14	10	4	1304.5602	−0.0009	1.0
14	10	4	13	10	3	1313.7976	−0.0001	1.0
15	10	5	16	10	6	1294.0221	0.0011	1.0
15	10	6	15	10	5	1304.5773	−0.0004	1.0
15	10	5	14	10	4	1314.4734	−0.0010	1.0
16	10	7	16	10	6	1304.5957	0.0002	1.0
16	10	6	15	10	5	1315.1511	−0.0011	1.0
17	10	7	18	10	8	1292.7366	−0.0008	1.0
17	10	8	17	10	7	1304.6125	−0.0020	1.0
18	10	8	19	10	9	1292.0957	−0.0015	1.0
19	10	9	18	10	8	1317.1923	−0.0008	0.1
20	10	10	21	10	11	1290.8177 *	−0.0023	1.0
20	10	10	19	10	9	1317.8732 *	−0.0027	1.0
21	10	11	22	10	12	1290.1802 *	−0.0028	1.0
21	10	11	20	10	10	1318.5573 *	−0.0026	1.0
22	10	12	23	10	13	1289.5436 *	−0.0035	1.0
22	10	12	21	10	11	1319.2422 *	−0.0029	1.0
24	10	14	25	10	15	1288.2737 *	−0.0049	1.0
24	10	14	23	10	13	1320.6155 *	−0.0038	1.0
25	10	15	26	10	16	1287.6414 *	−0.0046	1.0
25	10	15	24	10	14	1321.3045 *	−0.0038	1.0
26	10	16	25	10	15	1321.9927 *	−0.0059	1.0
27	10	17	28	10	18	1286.3775 *	−0.0066	1.0
27	10	17	26	10	16	1322.6876 *	−0.0026	0.1
28	10	18	29	10	19	1285.7485 *	−0.0063	0.1
29	10	19	30	10	20	1285.1176 *	−0.0090	1.0
29	10	19	28	10	18	1324.0702 *	−0.0071	0.1
30	10	20	31	10	21	1284.4898 *	−0.0097	1.0
30	10	20	29	10	19	1324.7644 *	−0.0085	1.0
31	10	21	32	10	22	1283.8632 *	−0.0103	1.0
31	10	21	30	10	20	1325.4613 *	−0.0085	1.0
32	10	22	33	10	23	1283.2377 *	−0.0110	1.0
33	10	23	32	10	22	1326.8553 *	−0.0123	1.0
34	10	24	35	10	25	1281.9906 *	−0.0118	1.0
34	10	24	33	10	23	1327.5555 *	−0.0131	1.0
35	10	25	34	10	24	1328.2568 *	−0.0142	1.0
36	10	26	37	10	27	1280.7442 *	−0.0166	1.0
36	10	26	35	10	25	1328.9580 *	−0.0168	0.1
38	10	28	37	10	27	1330.3684 *	−0.0182	1.0
39	10	29	38	10	28	1331.0747 *	−0.0200	1.0
11	11	0	12	11	1	1296.4440	0.0003	1.0
11	11	1	11	11	0	1304.3603	−0.0007	1.0
12	11	2	12	11	1	1304.3700 *	−0.0043	1.0
13	11	3	13	11	2	1304.3811 *	−0.0076	1.0
13	11	2	12	11	1	1312.9576 *	−0.0083	1.0
14	11	4	14	11	3	1304.3926 *	−0.0116	1.0
14	11	3	13	11	2	1313.6292 *	−0.0122	1.0
15	11	4	16	11	5	1293.8486 *	−0.0151	0.1
15	11	5	15	11	4	1304.4030 *	−0.0178	1.0
15	11	4	14	11	3	1314.3008 *	−0.0171	1.0
16	11	5	17	11	6	1293.2000 *	−0.0214	0.1
16	11	6	16	11	5	1304.4165 *	−0.0220	1.0
16	11	5	15	11	4	1314.9724 *	−0.0232	1.0
17	11	6	18	11	7	1292.5507 *	−0.0296	1.0

Can. J. Chem. Downloaded from www.nrcresearchpress.com by 203.198.23.82 on 09/08/12
For personal use only.

TABLE 3 (*concluded*)

J'	K'_a	K'_c	J''	K''_a	K''_c	Obs./cm^{-1}[a]	O − C[b]	Weight
17	11	7	17	11	6	1304.4274 *	−0.0300	1.0
17	11	6	16	11	5	1315.6443 *	−0.0302	1.0
18	11	8	18	11	7	1304.4396 *	−0.0378	1.0
19	11	9	19	11	8	1304.4497 *	−0.0489	0.1
20	11	9	21	11	10	1290.6047 *	−0.0587	1.0
20	11	10	20	11	9	1304.4613 *	−0.0596	1.0
21	11	10	22	11	11	1289.9528 *	−0.0739	1.0
21	11	11	21	11	10	1304.4713 *	−0.0730	0.1
21	11	10	20	11	9	1318.3289 *	−0.0729	1.0
22	11	11	23	11	12	1289.3016 *	−0.0894	1.0
22	11	12	22	11	11	1304.4772 *	−0.0917	0.1
23	11	13	23	11	12	1304.4818 *	−0.1129	0.1
23	11	12	22	11	11	1319.6608 *	−0.1117	1.0
24	11	13	25	11	14	1287.9862 *	−0.1369	1.0
24	11	14	24	11	13	1304.4818 *	−0.1398	0.1
24	11	13	23	11	12	1320.3228 *	−0.1369	1.0
25	11	15	25	11	14	1304.4818 *	−0.1678	0.1
26	11	15	27	11	16	1286.6553 *	−0.2043	1.0
26	11	16	26	11	15	1304.4772 *	−0.2017	0.1
26	11	15	25	11	14	1321.6335 *	−0.2042	1.0
12	12	1	12	12	0	1304.2072 *	0.0045	1.0
13	12	1	14	12	2	1294.9848 *	0.0059	1.0
13	12	2	13	12	1	1304.2233 *	0.0063	1.0
14	12	2	15	12	3	1294.3425 *	0.0080	1.0
14	12	3	14	12	2	1304.2400 *	0.0075	1.0
15	12	3	16	12	4	1293.7017 *	0.0105	1.0
15	12	4	15	12	3	1304.2580 *	0.0089	1.0
15	12	3	14	12	2	1314.1562 *	0.0090	0.1
16	12	4	17	12	5	1293.0597 *	0.0108	1.0
16	12	5	16	12	4	1304.2772 *	0.0104	1.0
16	12	4	15	12	3	1314.8343 *	0.0095	0.1
17	12	5	18	12	6	1292.4202 *	0.0123	1.0
17	12	6	17	12	5	1304.2983 *	0.0126	1.0
17	12	5	16	12	4	1315.5159 *	0.0123	1.0
18	12	7	18	12	6	1304.3198 *	0.0142	1.0
18	12	6	17	12	5	1316.1981 *	0.0146	1.0
19	12	7	20	12	8	1291.1445 *	0.0155	1.0
19	12	8	19	12	7	1304.3443 *	0.0176	1.0
19	12	7	18	12	6	1316.8811 *	0.0166	1.0
20	12	8	19	12	7	1317.5647 *	0.0180	1.0
21	12	9	22	12	10	1289.8759 *	0.0212	1.0
21	12	9	20	12	8	1318.2505 *	0.0205	1.0
22	12	10	23	12	11	1289.2432 *	0.0240	0.1
23	12	11	22	12	10	1319.6251 *	0.0250	1.0
24	12	12	25	12	13	1287.9792 *	0.0276	1.0
24	12	12	23	12	11	1320.3143 *	0.0274	1.0
26	12	14	27	12	15	1286.7218 *	0.0332	1.0
26	12	14	25	12	13	1321.6973 *	0.0333	1.0
27	12	15	28	12	16	1286.0938 *	0.0350	1.0
27	12	15	26	12	14	1322.3881 *	0.0339	0.1
28	12	16	29	12	17	1285.4668 *	0.0366	1.0
29	12	17	28	12	16	1323.7793 *	0.0410	0.1
31	12	19	32	12	20	1283.5991 *	0.0478	0.1

[a]Asterisk indicates perturbed transition not used in the fit.
[b]O–C is (Obs. − Calc.) in cm^{-1}.

resonance still with the $\nu_9 + \nu_{11}$ state; the major interaction effect ($\Delta \simeq 0.012$ cm^{-1}) is observed for $K'_a = 7$ ($J' = 35$). However, because of different resonances occurring in this region and their counteracting effects, further transitions with different K_a values exhibiting a regular structure can be actually perturbed.

A complete list of all the assigned transitions is reported in the Appendix.

In conclusion, the rovibrational analysis of the ν_6 band of CH_2=CHF has led to the assignment of many transitions up to high J and K_a values, and to the determination of a set of effective molecular parameters. The observed irregularities

Can. J. Chem. Downloaded from www.nrcresearchpress.com by 203.198.23.82 on 09/08/12
For personal use only.

in the rotational structure have been attributed to perturbations with the $\nu_9 + \nu_{11}$ vibration, and the interaction mechanisms are consistent with the first-order **b**-type and the second-order **a**-type Coriolis resonances; moreover, the sense of the residuals suggests a value of 1345 ± 1 cm^{-1} for the band origin of the perturber $\nu_9 + \nu_{11}$. The simulated spectra, considering the intensities of contributions of **a**- and **b**-type components to be about 85 and 15%, respectively, agree quite well with the observed characteristics (see Fig. 2); this is clear evidence of the good accuracy of the parameters obtained in the present analysis.

Acknowledgment

This work was supported in part by funds from the Ministero dell'Università e della Ricerca Scientifica e Tecnologica (MURST), Roma (40% and 60% programs).

1. W.A. Guillory and G.H. Andrews. J. Chem. Phys. **62**, 4667 (1975).
2. R.A. Perry, R. Atkinson, and J.N. Pitts, Jr. J. Chem. Phys. **67**, 458 (1977).
3. A. De Lorenzi, S. Giorgianni, A. Gambi, R. Visinoni, P. Stoppa, and S. Ghersetti. J. Mol. Spectrosc. **151**, 322 (1992).
4. S. Giorgianni, A. De Lorenzi, M. Pedrali, P. Stoppa, and S. Ghersetti. J. Mol. Spectrosc. **156**, 373 (1992).
5. R. Visinoni, S. Giorgianni, A. Gambi, A. De Lorenzi, and S. Ghersetti. J. Mol. Spectrosc. **157**, 382 (1993).
6. J.R. Scherer and W.J. Potts. J. Chem. Phys. **31**, 1691 (1959).
7. G.R. Smith and W.A. Guillory. J. Chem. Phys. **63**, 1311 (1975).
8. D.C. McKean. Spectrochim. Acta, Part A: **31A**, 1167 (1975).
9. R. Elst and A. Oskam. J. Mol. Spectrosc. **39**, 357 (1971).
10. H.W. Morgan and J.H. Goldstein. J. Chem. Phys. **30**, 1025 (1959).
11. M.C.L. Gerry. J. Mol. Spectrosc. **45**, 71 (1973).
12. M. Hayashi and T. Inagusa. J. Mol. Spectrosc. **138**, 135 (1989).
13. P.B. Davies and A.J. Morton-Jones. Appl. Phys. B: **B42**, 35 (1987).
14. B.J. Smith, D. Coffey, Jr., and L. Radom. J. Chem. Phys. **97**, 6113 (1992).
15. G. Guelachvili and K. Narahari Rao. Handbook of infrared standards. Academic Press, New York. 1986.
16. S. Giorgianni, P. Stoppa, A. De Lorenzi, and S. Ghersetti. J. Mol. Spectrosc. **154**, 265 (1992).

Can. J. Chem. Downloaded from www.nrcresearchpress.com by 203.198.23.82 on 09/08/12
For personal use only.

Appendix

TABLE A1. Complete list of assigned transitions of CH_2=CHF ν_6 band

J′	K'_a	K'_c	J″	K''_a	K''_c	Obs./cm^{-1} [a]	O-C [b]	W [c]	J′	K'_a	K'_c	J″	K''_a	K''_c	Obs./cm^{-1} [a]	O-C [b]	W [c]	J′	K'_a	K'_c	J″	K''_a	K''_c	Obs./cm^{-1} [a]	O-C [b]	W [c]
37	9	28	38	9	29	1280.2704	-0.0012	1.0	30	6	24	31	6	25	1284.9122	-0.0007	0.1	25	4	21	26	4	22	1288.0743	0.0025	0.1
40	1	40	41	1	41	1280.2839	-0.0012	1.0	30	5	25	31	5	26	1284.9122	-0.0013	0.1	26	1	25	27	1	26	1288.0743	0.0001	0.1
40	0	40	41	0	41	1280.2839	-0.0011	1.0	30	6	25	31	6	26	1284.9164	-0.0016	0.1	25	6	19	26	6	20	1288.0882	0.0005	1.0
37	8	29	38	8	30	1280.3834 *	0.0036	1.0	30	5	26	31	5	27	1284.9716	-0.0003	1.0	25	2	23	26	2	24	1288.0922	-0.0005	1.0
39	2	38	40	2	39	1280.4211	-0.0023	0.1	32	1	32	33	1	33	1285.0377	-0.0013	1.0	25	5	20	26	5	21	1288.1318	0.0004	1.0
39	1	38	40	1	39	1280.4211	0.0004	0.1	32	0	32	33	0	33	1285.0377	-0.0007	1.0	26	2	25	27	2	26	1288.1380	0.0003	1.0
37	6	32	38	6	33	1280.5226	-0.0009	1.0	30	4	27	31	4	28	1285.0738	-0.0002	1.0	25	5	21	26	5	22	1288.1472	0.0014	1.0
38	2	36	39	2	37	1280.5226	-0.0001	1.0	29	10	19	30	10	20	1285.1176 *	-0.0090	1.0	25	4	22	26	4	23	1288.2078	0.0003	1.0
37	3	34	38	3	35	1280.5401	0.0001	1.0	31	1	30	32	1	31	1285.1330	-0.0009	1.0	24	10	14	25	10	15	1288.2737 *	-0.0049	1.0
38	3	36	39	3	37	1280.5710	-0.0006	1.0	30	2	28	31	2	29	1285.1404	-0.0014	1.0	25	3	23	26	3	24	1288.3779	-0.0004	1.0
37	5	33	38	5	34	1280.6045	0.0002	1.0	31	2	30	32	2	31	1285.1536	-0.0014	1.0	24	9	15	25	9	16	1288.4183	0.0006	1.0
36	10	26	37	10	27	1280.7442 *	-0.0166	1.0	28	13	15	29	13	16	1285.2719 *	0.0281	1.0	24	8	16	25	8	17	1288.5407	0.0010	1.0
37	4	34	38	4	35	1280.8046	0.0006	1.0	30	3	28	31	3	29	1285.3304	-0.0017	0.1	23	9	14	24	9	15	1289.0541	0.0022	0.1
39	1	39	40	1	40	1280.8770	-0.0009	1.0	29	3	26	30	3	27	1285.3482	-0.0021	0.1	23	8	15	24	8	16	1289.1755	0.0010	1.0
39	0	39	40	0	40	1280.8770	-0.0008	1.0	29	8	21	30	8	22	1285.3811 *	0.0005	0.1	25	0	25	26	0	26	1289.2180	0.0022	0.1
36	9	27	37	9	28	1280.8908	-0.0009	1.0	29	4	25	30	4	26	1285.4193	-0.0019	0.1	25	1	25	26	1	26	1289.2209	0.0008	1.0
38	1	38	39	1	39	1281.4698	-0.0013	1.0	28	12	16	29	12	17	1285.4668 *	0.0366	1.0	23	3	20	24	3	21	1289.2284	0.0012	1.0
38	0	38	39	0	39	1281.4698	-0.0012	1.0	29	7	22	30	7	23	1285.4815 *	0.0042	1.0	22	12	10	23	12	11	1289.2432 *	0.0240	0.1
35	9	26	36	9	27	1281.5116	-0.0012	0.1	29	6	23	30	6	24	1285.5453	-0.0013	0.1	24	1	23	25	1	24	1289.2481	0.0006	1.0
35	4	31	36	4	32	1281.5116	-0.0025	0.1	29	6	24	30	6	25	1285.5491	-0.0011	0.1	23	7	16	24	7	17	1289.2828 *	0.0039	1.0
37	1	36	38	1	37	1281.5974	-0.0009	1.0	29	5	24	30	5	25	1285.5574	-0.0010	1.0	22	11	11	23	11	12	1289.3016 *	-0.0894	1.0
37	2	36	38	2	37	1281.6014	-0.0016	1.0	29	5	25	30	5	26	1285.6041	0.0003	1.0	23	2	21	24	2	22	1289.3135	0.0005	1.0
35	8	27	36	8	28	1281.6268 *	0.0031	1.0	31	1	31	32	1	32	1285.6346	-0.0004	1.0	24	2	23	25	2	24	1289.3405	0.0006	1.0
35	5	30	36	5	31	1281.6718	-0.0018	1.0	31	0	31	32	0	32	1285.6346	0.0003	1.0	23	6	17	24	6	18	1289.3630	0.0006	1.0
36	2	34	37	2	35	1281.6783	-0.0005	1.0	29	4	26	30	4	27	1285.6962	0.0008	1.0	23	4	19	24	4	20	1289.3924	0.0006	1.0
35	3	32	36	3	33	1281.7057	-0.0002	1.0	29	2	27	30	2	28	1285.7233	0.0000	1.0	23	5	18	24	5	19	1289.4170	0.0007	1.0
35	6	29	36	6	30	1281.7517	0.0014	0.1	30	1	29	31	1	30	1285.7233	0.0005	1.0	23	5	19	24	5	20	1289.4252	0.0015	1.0
36	3	34	37	3	35	1281.7517	-0.0003	0.1	28	10	18	29	10	19	1285.7485 *	-0.0063	0.1	23	4	20	24	4	21	1289.4785	0.0006	1.0
35	6	30	36	6	31	1281.7722	-0.0005	1.0	30	2	29	31	2	30	1285.7485	-0.0009	1.0	22	10	12	23	10	13	1289.5436 *	-0.0035	1.0
35	5	31	36	5	32	1281.8414	0.0006	1.0	28	9	19	29	9	20	1285.8921	0.0004	1.0	23	3	21	24	3	22	1289.6160	-0.0003	1.0
34	10	24	35	10	25	1281.9906 *	-0.0118	1.0	27	13	14	28	13	15	1285.9005 *	0.0283	1.0	22	9	13	23	9	14	1289.6872	0.0001	1.0
33	4	30	34	4	31	1283.2262	-0.0008	1.0	29	3	27	30	3	28	1285.9365	0.0004	1.0	22	8	14	23	8	15	1289.8135	0.0032	0.1
32	10	22	33	10	23	1283.2377 *	-0.0110	1.0	28	3	25	29	3	26	1285.9816	0.0006	1.0	24	0	24	25	0	25	1289.8135	-0.0001	0.1
35	1	35	36	1	36	1283.2531	-0.0002	1.0	28	8	20	29	8	21	1286.0118	0.0014	1.0	24	1	24	25	1	25	1289.8197	0.0004	1.0
35	0	35	36	0	36	1283.2531	0.0001	1.0	28	4	24	29	4	25	1286.0837	0.0000	1.0	23	1	22	24	1	23	1289.8353	0.0012	1.0
34	1	33	35	1	34	1283.3659	-0.0002	1.0	27	12	15	28	12	16	1286.0938 *	0.0350	1.0	21	12	9	22	12	10	1289.8759 *	0.0212	1.0
34	2	33	35	2	34	1283.3762	0.0001	1.0	28	7	21	29	7	22	1286.1126 *	0.0040	1.0	22	3	19	23	3	20	1289.8933	0.0011	1.0
32	9	23	33	9	24	1283.3824	-0.0005	1.0	28	6	22	29	6	23	1286.1808	-0.0001	0.1	22	7	15	23	7	16	1289.9187 *	0.0030	1.0
33	2	31	34	2	32	1283.4089	0.0001	1.0	28	5	23	29	5	24	1286.2021	-0.0004	1.0	22	2	20	23	2	21	1289.9342	0.0009	1.0
32	4	28	33	4	29	1283.4469	-0.0011	1.0	30	1	30	31	1	31	1286.2296	-0.0019	0.1	23	2	22	24	2	23	1289.9430	-0.0005	1.0
32	8	24	33	8	25	1283.5005 *	0.0030	0.1	30	0	30	31	0	31	1286.2296	-0.0008	0.1	21	11	10	22	11	11	1289.9528 *	-0.0739	1.0
32	3	29	33	3	30	1283.5005	0.0020	0.1	28	5	24	29	5	25	1286.2363	-0.0010	1.0	22	6	16	23	6	17	1290.0009	-0.0001	1.0
33	3	31	34	3	32	1283.5341	0.0006	1.0	28	2	26	29	2	27	1286.3096	0.0013	0.1	22	4	18	23	4	19	1290.0502	0.0009	1.0
31	12	19	32	12	20	1283.5991 *	0.0478	0.1	29	1	28	30	1	29	1286.3096	-0.0017	0.1	22	5	17	23	5	18	1290.0595	0.0006	1.0
32	7	25	33	7	26	1283.5991 *	0.0101	0.1	28	4	25	29	4	26	1286.3193	-0.0002	1.0	22	4	19	23	4	20	1290.1164	0.0004	1.0
32	5	27	33	5	28	1283.6196	-0.0010	1.0	29	2	28	30	2	29	1286.3445	-0.0003	1.0	21	10	11	22	10	12	1290.1802 *	-0.0028	1.0
32	6	26	33	6	27	1283.6455	-0.0014	1.0	27	10	17	28	10	18	1286.3775 *	-0.0066	1.0	22	3	20	23	3	21	1290.2398	0.0001	1.0
32	6	27	33	6	28	1283.6560	-0.0005	1.0	27	9	18	28	9	19	1286.5206	-0.0010	1.0	21	9	12	22	9	13	1290.3227	-0.0007	1.0

Can. J. Chem. Downloaded from www.nrcresearchpress.com by 203.198.23.82 on 09/08/12
For personal use only.

Appendix

TABLE A1. (*continued*)

J′	K'_a	K'_c	J″	K''_a	K''_c	Obs./cm^{-1}[a]		O-C[b]	W[c]
32	5	28	33	5	29	1283.7134		0.0001	1.0
32	4	29	33	4	30	1283.8393		-0.0005	1.0
34	1	34	35	1	35	1283.8481		0.0000	1.0
34	0	34	35	0	35	1283.8481		0.0003	1.0
31	10	21	32	10	22	1283.8632	*	-0.0103	1.0
33	1	32	34	1	33	1283.9553		-0.0001	1.0
33	2	32	34	2	33	1283.9682		-0.0002	1.0
32	2	30	33	2	31	1283.9849		-0.0005	1.0
31	9	22	32	9	23	1284.0076		-0.0009	1.0
31	4	27	32	4	28	1284.1013		-0.0011	1.0
31	3	28	32	3	29	1284.1068		-0.0022	1.0
31	8	23	32	8	24	1284.1263	*	0.0021	1.0
32	3	30	33	3	31	1284.1301		-0.0009	1.0
31	7	24	32	7	25	1284.2241	*	0.0066	0.1
31	5	26	32	5	27	1284.2670		-0.0006	1.0
31	6	25	32	6	26	1284.2787		-0.0010	1.0
31	6	26	32	6	27	1284.2859		-0.0008	1.0
31	5	27	32	5	28	1284.3417		0.0000	1.0
33	1	33	34	1	34	1284.4428		-0.0005	1.0
33	0	33	34	0	34	1284.4428		-0.0001	1.0
31	4	28	32	4	29	1284.4549		-0.0006	1.0
30	10	20	31	10	21	1284.4898	*	-0.0097	1.0
32	1	31	33	1	32	1284.5447		0.0000	1.0
31	2	29	32	2	30	1284.5620		-0.0008	1.0
32	2	31	33	2	32	1284.5620		0.0007	1.0
30	9	21	31	9	22	1284.6342		-0.0009	1.0
29	13	16	30	13	17	1284.6484	*	0.0319	1.0
30	3	27	31	3	28	1284.7271		0.0008	0.1
31	3	29	32	3	30	1284.7292		-0.0012	0.1
30	8	22	31	8	23	1284.7546	*	0.0027	1.0
30	4	26	31	4	27	1284.7603		-0.0002	1.0
30	7	23	31	7	24	1284.8529	*	0.0059	1.0
19	2	18	20	2	19	1292.3777		-0.0010	1.0
17	12	5	18	12	6	1292.4202	*	0.0123	1.0
18	7	11	19	7	12	1292.4726		0.0002	1.0
18	2	16	19	2	17	1292.4791		-0.0009	1.0
17	11	6	18	11	7	1292.5507	*	-0.0296	1.0
18	6	12	19	6	13	1292.5623		-0.0008	1.0
18	3	15	19	3	16	1292.5777		0.0000	1.0
18	5	13	19	5	14	1292.6322		-0.0004	1.0
18	4	14	19	4	15	1292.6644		-0.0005	1.0
18	4	15	19	4	16	1292.6839		-0.0008	1.0
17	10	7	18	10	8	1292.7366		-0.0008	1.0
18	3	16	19	3	17	1292.7620		0.0000	1.0
18	1	17	19	1	18	1292.7950		0.0003	1.0
19	0	19	20	0	20	1292.8028		-0.0004	1.0
19	1	19	20	1	20	1292.8241		0.0002	1.0
17	9	8	18	9	9	1292.8792		0.0003	1.0
18	2	17	19	2	18	1292.9923		-0.0011	1.0
17	8	9	18	8	10	1293.0042		-0.0004	1.0
16	12	4	17	12	5	1293.0597	*	0.0108	1.0
17	7	10	18	7	11	1293.1152		0.0013	1.0
17	2	15	18	2	16	1293.1333		0.0011	1.0
16	11	5	17	11	6	1293.2000	*	-0.0214	0.1
17	6	11	18	6	12	1293.2054		-0.0002	1.0
17	3	14	18	3	15	1293.2506		0.0006	1.0
17	5	12	18	5	13	1293.2778		0.0006	1.0
16	8	8	17	8	9	1293.6474		0.0009	1.0
15	12	3	16	12	4	1293.7017	*	0.0105	1.0
16	7	9	17	7	10	1293.7571		0.0008	1.0
16	2	14	17	2	15	1293.7901		0.0001	1.0
15	11	4	16	11	5	1293.8486	*	-0.0151	0.1
16	6	10	17	6	11	1293.8486		-0.0004	1.0
16	5	11	17	5	12	1293.9222		-0.0001	1.0
16	3	13	17	3	14	1293.9222		0.0012	0.1
16	4	12	17	4	13	1293.9674		0.0005	1.0
16	4	13	17	4	14	1293.9761		-0.0003	1.0
17	0	17	18	0	18	1293.9987		0.0004	1.0
16	1	15	17	1	16	1294.0092		0.0005	1.0
15	10	5	16	10	6	1294.0221		0.0011	1.0
17	1	17	18	1	18	1294.0317		0.0004	1.0
16	3	14	17	3	15	1294.0388		-0.0002	1.0
15	9	6	16	9	7	1294.1632		0.0002	1.0
16	2	15	17	2	16	1294.2305		-0.0003	1.0
15	8	7	16	8	8	1294.2898		0.0004	1.0
14	12	2	15	12	3	1294.3425	*	0.0080	1.0
15	7	8	16	7	9	1294.3994		-0.0003	1.0
15	2	13	16	2	14	1294.4531		0.0001	1.0
15	6	9	16	6	10	1294.4934		0.0002	1.0
15	5	10	16	5	11	1294.5690		0.0009	1.0
28	3	26	29	3	27	1286.5419		-0.0007	1.0
27	3	24	28	3	25	1286.6187		0.0005	1.0
27	8	19	28	8	20	1286.6430		0.0018	1.0
26	11	15	27	11	16	1286.6553	*	-0.2043	1.0
26	12	14	27	12	15	1286.7218	*	0.0332	1.0
27	7	20	28	7	21	1286.7457	*	0.0049	0.1
27	4	23	28	4	24	1286.7457		-0.0011	0.1
27	6	21	28	6	22	1286.8167		0.0009	1.0
29	1	29	30	1	30	1286.8275		-0.0008	0.1
29	0	29	30	0	30	1286.8275		0.0006	0.1
27	5	22	28	5	23	1286.8455		-0.0004	1.0
27	5	23	28	5	24	1286.8725		0.0003	1.0
27	2	25	28	2	26	1286.8983		0.0006	0.1
28	1	27	29	1	28	1286.8983		-0.0012	0.1
28	2	27	29	2	28	1286.9406		-0.0007	0.1
27	4	24	28	4	25	1286.9483		0.0020	0.1
27	1	26	28	1	27	1287.4881		0.0010	0.1
26	5	21	27	5	22	1287.4914		0.0026	0.1
26	2	24	27	2	25	1287.4914		-0.0008	0.1
26	5	22	27	5	23	1287.5090		0.0006	1.0
27	2	26	28	2	27	1287.5397		0.0008	1.0
26	4	23	27	4	24	1287.5760		0.0003	1.0
25	10	15	26	10	16	1287.6414	*	-0.0046	1.0
26	3	24	27	3	25	1287.7641		0.0005	1.0
25	9	16	26	9	17	1287.7852		0.0006	1.0
25	8	17	26	8	18	1287.9077		0.0019	0.1
25	3	22	26	3	23	1287.9109		-0.0005	0.1
24	12	12	25	12	13	1287.9792	*	0.0276	1.0
24	11	13	25	11	14	1287.9862	*	-0.1369	1.0
25	7	18	26	7	19	1288.0115	*	0.0035	1.0
27	1	27	28	1	28	1288.0223		-0.0010	0.1
27	0	27	28	0	28	1288.0223		0.0014	0.1
12	8	4	13	8	5	1296.2242		0.0002	1.0
12	7	5	13	7	6	1296.3350		-0.0005	1.0
13	0	13	14	0	14	1296.3878		0.0000	1.0
12	6	6	13	6	7	1296.4310		0.0000	1.0
11	11	0	12	11	1	1296.4440		0.0003	1.0
13	1	13	14	1	14	1296.4611		0.0007	1.0
12	2	10	13	2	11	1296.4683		0.0001	1.0
12	5	7	13	5	8	1296.5094		-0.0001	1.0
12	4	8	13	4	9	1296.5678		-0.0003	1.0
12	3	9	13	3	10	1296.5821		-0.0011	1.0
11	10	1	12	10	2	1296.6007		-0.0005	1.0
12	3	10	13	3	11	1296.6174		-0.0011	1.0
12	2	11	13	2	12	1296.7371		-0.0016	0.1
11	8	3	12	8	4	1296.8698		-0.0011	1.0
11	7	4	12	7	5	1296.9839		0.0013	0.1
12	0	12	13	0	13	1296.9864		-0.0005	1.0
12	1	12	13	1	13	1297.0711		-0.0003	1.0
11	6	5	12	6	6	1297.0778		-0.0008	1.0
11	2	9	12	2	10	1297.1460		0.0002	1.0
11	5	6	12	5	7	1297.1573		-0.0008	0.1
11	1	10	12	1	11	1297.1573		0.0013	0.1
11	4	7	12	4	8	1297.2191		0.0004	1.0
11	3	8	12	3	9	1297.2437		0.0002	1.0
11	3	9	12	3	10	1297.2674		-0.0002	1.0
11	2	10	12	2	11	1297.3739		0.0012	1.0
10	9	1	11	9	2	1297.3923		0.0009	1.0
10	8	2	11	8	3	1297.5198		0.0010	1.0
11	0	11	12	0	12	1297.5889		0.0010	1.0
10	7	3	11	7	4	1297.6297		-0.0011	1.0
11	1	11	12	1	12	1297.6836		-0.0006	1.0
10	6	4	11	6	5	1297.7266		-0.0006	1.0
10	5	5	11	5	6	1297.8063		-0.0011	0.1
10	1	9	11	1	10	1297.8063		0.0026	0.1
10	2	8	11	2	9	1297.8248		0.0003	1.0
10	4	6	11	4	7	1297.8702		0.0005	1.0
10	3	7	11	3	8	1297.9025		0.0004	1.0
10	3	8	11	3	9	1297.9186		0.0006	1.0
10	2	9	11	2	10	1298.0103		0.0008	1.0
9	9	0	10	9	1	1298.0409		0.0006	1.0
9	8	1	10	8	2	1298.1679		0.0002	1.0
10	0	10	11	0	11	1298.1931		0.0010	1.0
9	7	2	10	7	3	1298.2797		-0.0002	1.0
10	1	10	11	1	11	1298.2987		-0.0001	1.0
9	6	3	10	6	4	1298.3763		-0.0003	1.0
9	5	4	10	5	5	1298.4574		0.0000	1.0
9	1	8	10	1	9	1298.4574		0.0008	1.0
9	2	7	10	2	8	1298.5026		-0.0005	1.0
9	4	5	10	4	6	1298.5212		0.0001	1.0
22	2	21	23	2	22	1290.5501		0.0010	1.0
21	7	14	22	7	15	1290.5558	*	0.0023	1.0
21	3	18	22	3	19	1290.5606		-0.0002	1.0
21	2	19	22	2	20	1290.5606		0.0004	1.0
20	11	9	21	11	10	1290.6047	*	-0.0587	1.0
21	6	15	22	6	16	1290.6394		-0.0009	1.0
21	5	16	22	5	17	1290.7028		0.0010	0.1
21	4	17	22	4	18	1290.7028		-0.0024	0.1
20	10	10	21	10	11	1290.8177	*	-0.0023	1.0
21	3	19	22	3	20	1290.8664		0.0004	1.0
20	9	11	21	9	12	1290.9602		-0.0005	1.0
21	1	20	22	1	21	1291.0090		-0.0013	1.0
22	0	22	23	0	23	1291.0090		-0.0004	1.0
22	1	22	23	1	23	1291.0180		-0.0011	1.0
20	8	12	21	8	13	1291.0852		0.0001	1.0
19	12	7	20	12	8	1291.1445	*	0.0155	1.0
21	2	20	22	2	21	1291.1555		-0.0012	1.0
19	7	12	20	7	13	1291.8327		0.0009	1.0
19	2	17	20	2	18	1291.8327		-0.0011	1.0
19	3	16	20	3	17	1291.9032		-0.0015	1.0
19	6	13	20	6	14	1291.9197		-0.0016	1.0
19	5	14	20	5	15	1291.9880		-0.0005	1.0
19	4	15	20	4	16	1292.0118		-0.0010	1.0
19	4	16	20	4	17	1292.0397		-0.0008	1.0
18	10	8	19	10	9	1292.0957		-0.0015	1.0
19	3	17	20	3	18	1292.1269		-0.0003	1.0
19	1	18	20	1	19	1292.1957		-0.0002	1.0
20	0	20	21	0	21	1292.2051		-0.0003	1.0
20	1	20	21	1	21	1292.2220		0.0004	1.0
17	13	4	18	13	5	1292.2315	*	0.0112	1.0
18	9	9	19	9	10	1292.2379		-0.0006	1.0
18	8	10	19	8	11	1292.3634		-0.0004	1.0
5	3	2	6	3	3	1301.1829		0.0000	1.0
5	2	3	6	2	4	1301.1961		0.0001	1.0
5	2	4	6	2	5	1301.2305		-0.0006	1.0
5	0	5	6	0	6	1301.2915		-0.0001	1.0
5	1	5	6	1	6	1301.4034		0.0009	1.0
4	4	0	5	4	1	1301.7857		-0.0016	0.1
4	1	3	5	1	4	1301.7857		0.0011	1.0
4	3	1	5	3	2	1301.8380		-0.0006	1.0
4	2	2	5	2	3	1301.8618		0.0000	1.0
4	2	3	5	2	4	1301.8824		0.0002	1.0
4	0	4	5	0	5	1301.9302		-0.0001	1.0
4	1	4	5	1	5	1302.0294		0.0001	1.0
3	1	2	4	1	3	1302.4613		0.0010	1.0
3	3	0	4	3	1	1302.4950		0.0003	1.0
3	2	1	4	2	2	1302.5257		0.0008	1.0
3	2	2	4	2	3	1302.5361		0.0009	1.0
3	0	3	4	0	4	1302.5757		0.0009	1.0
3	1	3	4	1	4	1302.6582		0.0004	1.0
2	1	1	3	1	2	1303.1382		-0.0003	1.0
2	2	0	3	2	1	1303.1871		0.0012	0.1
2	0	2	3	0	3	1303.2242		-0.0001	1.0
2	1	2	3	1	3	1303.2875		-0.0005	1.0
18	14	5	18	14	4	1303.9316	*	0.0135	1.0
19	14	6	19	14	5	1303.9546	*	0.0155	1.0
20	14	7	20	14	6	1303.9786	*	0.0174	1.0
21	14	8	21	14	7	1304.0035	*	0.0190	1.0
22	14	9	22	14	8	1304.0293	*	0.0204	1.0
13	13	1	13	13	0	1304.0370	*	0.0063	1.0
14	13	2	14	13	1	1304.0536	*	0.0074	1.0
15	13	3	15	13	2	1304.0714	*	0.0087	1.0
16	13	4	16	13	3	1304.0900	*	0.0096	1.0
17	13	5	17	13	4	1304.1099	*	0.0107	1.0
18	13	6	18	13	5	1304.1309	*	0.0117	1.0
19	13	7	19	13	6	1304.1541	*	0.0139	1.0
20	13	8	20	13	7	1304.1779	*	0.0155	1.0
12	12	1	12	12	0	1304.2072	*	0.0045	1.0
13	12	2	13	12	1	1304.2233	*	0.0063	1.0
14	12	3	14	12	2	1304.2400	*	0.0075	1.0
15	12	4	15	12	3	1304.2580	*	0.0089	1.0
16	12	5	16	12	4	1304.2772	*	0.0104	1.0
17	12	6	17	12	5	1304.2983	*	0.0126	1.0
18	12	7	18	12	6	1304.3198	*	0.0142	1.0
19	12	8	19	12	7	1304.3443	*	0.0176	1.0
11	11	1	11	11	0	1304.3603		-0.0007	1.0
12	11	2	12	11	1	1304.3700	*	-0.0043	1.0
13	11	3	13	11	2	1304.3811	*	-0.0076	1.0
14	11	4	14	11	3	1304.3926	*	-0.0116	1.0
15	11	5	15	11	4	1304.4030	*	-0.0178	1.0

TABLE A1. (*continued*)

J′	K'_a	K'_c	J″	K''_a	K''_c	Obs./cm^{-1}[a]	O-C[b]	W[c]
15	3	12	16	3	13	1294.5907	0.0008	1.0
16	0	16	17	0	17	1294.5950	-0.0005	1.0
15	4	11	16	4	12	1294.6174	0.0001	1.0
15	4	12	16	4	13	1294.6248	0.0012	0.1
15	1	14	16	1	15	1294.6248	-0.0003	1.0
16	1	16	17	1	17	1294.6366	0.0000	1.0
14	10	4	15	10	5	1294.6647	0.0002	1.0
15	3	13	16	3	14	1294.6806	-0.0003	1.0
14	9	5	15	9	6	1294.8063	-0.0003	1.0
15	2	14	16	2	15	1294.8536	0.0001	1.0
14	8	6	15	8	7	1294.9337	0.0005	1.0
13	12	1	14	12	2	1294.9848 *	0.0059	1.0
14	7	7	15	7	8	1295.0447	0.0007	1.0
14	2	12	15	2	13	1295.1210	0.0001	1.0
14	6	8	15	6	9	1295.1379	-0.0004	1.0
15	0	15	16	0	16	1295.1925	-0.0001	1.0
13	9	4	14	9	5	1295.4513	0.0001	1.0
14	2	13	15	2	14	1295.4789	-0.0002	1.0
13	8	5	14	8	6	1295.5781	0.0000	1.0
13	7	6	14	7	7	1295.6896	0.0003	1.0
13	6	7	14	6	8	1295.7852	0.0010	1.0
13	2	11	14	2	12	1295.7925	-0.0004	0.1
14	0	14	15	0	15	1295.7925	0.0026	0.1
14	1	14	15	1	15	1295.8521	0.0011	1.0
13	5	8	14	5	9	1295.8627	0.0010	1.0
13	1	12	14	1	13	1295.8790	0.0012	1.0
13	4	9	14	4	10	1295.9213	0.0036	0.1
13	3	10	14	3	11	1295.9213	0.0003	0.1
12	10	2	13	10	3	1295.9557	0.0011	1.0
13	3	11	14	3	12	1295.9720	0.0011	1.0
12	9	3	13	9	4	1296.0990	0.0021	1.0
13	2	12	14	2	13	1296.1087	0.0012	1.0
13	8	6	13	8	5	1304.8153	0.0003	1.0
14	8	7	14	8	6	1304.8304	-0.0002	1.0
15	8	8	15	8	7	1304.8472	-0.0002	1.0
7	7	1	7	7	0	1304.8573	0.0000	1.0
8	7	2	8	7	1	1304.8671	0.0009	1.0
9	7	3	9	7	2	1304.8759	-0.0003	1.0
10	7	4	10	7	3	1304.8873	0.0000	1.0
11	7	5	11	7	4	1304.8993	-0.0002	1.0
12	7	6	12	7	5	1304.9137	0.0008	1.0
13	7	7	13	7	6	1304.9281	0.0006	1.0
6	6	1	6	6	0	1304.9473	0.0003	1.0
7	6	2	7	6	1	1304.9551	0.0004	1.0
8	6	3	8	6	2	1304.9634	-0.0002	1.0
9	6	4	9	6	3	1304.9744	0.0008	1.0
10	6	5	10	6	4	1304.9852	0.0004	1.0
11	6	6	11	6	5	1304.9981	0.0010	1.0
12	6	7	12	6	6	1305.0116	0.0010	1.0
5	5	1	5	5	0	1305.0236	0.0008	1.0
6	5	2	6	5	1	1305.0293	-0.0001	1.0
7	5	3	7	5	2	1305.0378	0.0006	1.0
8	5	4	8	5	3	1305.0459	-0.0002	1.0
9	5	5	9	5	4	1305.0569	0.0007	1.0
10	5	6	10	5	5	1305.0667	-0.0007	1.0
4	4	1	4	4	0	1305.0843	-0.0004	1.0
5	4	2	5	4	1	1305.0901	-0.0001	1.0
6	4	3	6	4	2	1305.0958	-0.0011	1.0
7	4	4	7	4	3	1305.1049	0.0002	1.0
8	4	5	8	4	4	1305.1139	0.0002	1.0
9	4	6	9	4	5	1305.1247	0.0009	1.0
3	1	3	2	1	2	1307.0911	0.0007	1.0
3	0	3	2	0	2	1307.1726	0.0000	1.0
3	1	2	2	1	1	1307.2467	-0.0006	1.0
4	1	4	3	1	3	1307.7256	0.0004	1.0
4	3	1	3	3	0	1307.7756	0.0003	1.0
4	2	3	3	2	2	1307.8097	0.0001	1.0
4	2	2	3	2	1	1307.8208	0.0001	1.0
4	0	4	3	0	3	1307.8292	0.0000	1.0
5	1	5	4	1	4	1308.3600	0.0004	1.0
5	4	1	4	4	0	1308.3878	0.0002	1.0
5	3	2	4	3	1	1308.4418	0.0004	1.0
5	2	4	4	2	3	1308.4726	0.0003	1.0
5	0	5	4	0	4	1308.4823	0.0000	1.0
5	2	3	4	2	2	1308.4948	0.0002	1.0
5	1	4	4	1	3	1308.6256	0.0006	1.0
6	5	1	5	5	0	1308.9869	0.0006	0.1
6	1	6	5	1	5	1308.9936	0.0003	1.0
6	4	2	5	4	1	1309.0545	0.0000	1.0
6	3	3	5	3	2	1309.1094	-0.0001	1.0
9	3	6	10	3	7	1298.5584	-0.0011	1.0
9	3	7	10	3	8	1298.5690	-0.0004	1.0
9	2	8	10	2	9	1298.6484	-0.0005	1.0
9	0	9	10	0	10	1298.8012	0.0008	1.0
8	8	0	9	8	1	1298.8171	-0.0005	1.0
9	1	9	10	1	10	1298.9155	0.0000	1.0
8	7	1	9	7	2	1298.9297	-0.0003	1.0
8	6	2	9	6	3	1299.0262	-0.0008	1.0
8	5	3	9	5	4	1299.1086	0.0003	1.0
8	1	7	9	1	8	1299.1136	-0.0007	1.0
8	4	4	9	4	5	1299.1731	0.0000	1.0
8	2	6	9	2	7	1299.1799	-0.0004	1.0
8	3	5	9	3	6	1299.2167	0.0007	1.0
8	3	6	9	3	7	1299.2213	-0.0005	1.0
8	2	7	9	2	8	1299.2903	-0.0005	1.0
8	0	8	9	0	9	1299.4143	0.0005	1.0
8	1	8	9	1	9	1299.5347	0.0006	1.0
7	7	0	8	7	1	1299.5809	-0.0001	1.0
7	6	1	8	6	2	1299.6782	0.0000	1.0
7	5	2	8	5	3	1299.7597	-0.0003	1.0
7	1	6	8	1	7	1299.7767	0.0004	1.0
6	5	1	7	5	2	1300.4119	-0.0006	1.0
6	1	5	7	1	6	1300.4422	-0.0001	1.0
6	4	2	7	4	3	1300.4781	-0.0007	1.0
6	3	3	7	3	4	1300.5275	0.0001	0.1
6	2	4	7	2	5	1300.5275	0.0003	0.1
6	2	5	7	2	6	1300.5817	-0.0003	1.0
6	0	6	7	0	7	1300.6592	0.0001	1.0
6	1	6	7	1	7	1300.7782	0.0005	1.0
5	5	0	6	5	1	1301.0652	-0.0007	1.0
5	1	4	6	1	5	1301.1118	0.0000	1.0
5	4	1	6	4	2	1301.1323	-0.0004	1.0
9	3	6	8	3	5	1311.1253	-0.0033	0.1
10	9	1	9	9	0	1311.2436	-0.0005	0.1
9	2	7	8	2	6	1311.2508	-0.0015	1.0
10	8	2	9	8	1	1311.3744	0.0033	0.1
9	1	8	8	1	7	1311.3744	-0.0001	1.0
10	7	3	9	7	2	1311.4839	0.0003	1.0
10	1	10	9	1	9	1311.5189	0.0010	1.0
10	6	4	9	6	3	1311.5824	0.0006	1.0
10	5	5	9	5	4	1311.6677	0.0015	0.1
10	0	10	9	0	9	1311.6677	0.0008	0.1
10	4	6	9	4	5	1311.7393	0.0011	1.0
11	10	1	10	10	0	1311.7769	0.0023	0.1
10	2	9	9	2	8	1311.7836	0.0006	1.0
10	3	8	9	3	7	1311.7964	0.0006	1.0
10	3	7	9	3	6	1311.8085	0.0007	1.0
11	9	2	10	9	1	1311.9171	0.0009	1.0
10	2	8	9	2	7	1311.9591	0.0012	1.0
11	8	3	10	8	2	1312.0436	0.0003	1.0
10	1	9	9	1	8	1312.0579	0.0003	1.0
11	1	11	10	1	10	1312.1458	0.0000	1.0
11	7	4	10	7	3	1312.1554	-0.0006	1.0
11	6	5	10	6	4	1312.2540	-0.0007	1.0
11	0	11	10	0	10	1312.2859	-0.0003	1.0
11	2	9	10	2	8	1312.6686	-0.0002	1.0
12	8	4	11	8	3	1312.7165	-0.0002	1.0
11	1	10	10	1	9	1312.7370	-0.0006	1.0
12	1	12	11	1	11	1312.7716	-0.0007	1.0
12	7	5	11	7	4	1312.8292	-0.0006	1.0
12	0	12	11	0	11	1312.9014	0.0003	1.0
12	6	6	11	6	5	1312.9286	-0.0004	1.0
13	11	2	12	11	1	1312.9576 *	-0.0083	1.0
12	5	7	11	5	6	1313.0151	-0.0002	1.0
12	4	8	11	4	7	1313.0905	-0.0008	1.0
12	2	11	11	2	10	1313.1010	-0.0007	1.0
13	10	3	12	10	2	1313.1221	0.0000	1.0
12	3	10	11	3	9	1313.1474	-0.0009	1.0
12	3	9	11	3	8	1313.1778	-0.0008	1.0
13	9	4	12	9	3	1313.2624	-0.0015	1.0
12	2	10	11	2	9	1313.3837	-0.0001	1.0
13	6	7	12	6	6	1313.6040	-0.0008	1.0
14	11	3	13	11	2	1313.6292 *	-0.0122	1.0
13	5	8	12	5	7	1313.6921	-0.0002	1.0
13	2	12	12	2	11	1313.7590	0.0000	1.0
13	4	9	12	4	8	1313.7702	-0.0010	1.0
14	10	4	13	10	3	1313.7976	-0.0001	1.0
13	3	11	12	3	10	1313.8263	0.0001	1.0
13	3	10	12	3	9	1313.8715	0.0001	1.0
14	9	5	13	9	4	1313.9396	0.0000	1.0
16	11	6	16	11	5	1304.4165 *	-0.0220	1.0
17	11	7	17	11	6	1304.4274 *	-0.0300	1.0
18	11	8	18	11	7	1304.4396 *	-0.0378	1.0
19	11	9	19	11	8	1304.4497 *	-0.0489	0.1
20	11	10	20	11	9	1304.4613 *	-0.0596	1.0
21	11	11	21	11	10	1304.4713 *	-0.0730	0.1
22	11	12	22	11	11	1304.4772 *	-0.0917	0.1
26	11	16	26	11	15	1304.4772 *	-0.2017	0.1
23	11	13	23	11	12	1304.4818 *	-0.1129	0.1
24	11	14	24	11	13	1304.4818 *	-0.1398	0.1
25	11	15	25	11	14	1304.4818 *	-0.1678	0.1
10	10	1	10	10	0	1304.5063	0.0006	1.0
11	10	2	11	10	1	1304.5178	-0.0001	1.0
12	10	3	12	10	2	1304.5316	0.0004	1.0
13	10	4	13	10	3	1304.5456	0.0000	1.0
14	10	5	14	10	4	1304.5602	-0.0009	1.0
15	10	6	15	10	5	1304.5773	-0.0004	1.0
16	10	7	16	10	6	1304.5957	0.0002	1.0
17	10	8	17	10	7	1304.6125	-0.0020	1.0
9	9	1	9	9	0	1304.6366	-0.0001	1.0
10	9	2	10	9	1	1304.6479	0.0002	1.0
11	9	3	11	9	2	1304.6593	-0.0006	1.0
12	9	4	12	9	3	1304.6746	0.0014	1.0
13	9	5	13	9	4	1304.6872	-0.0005	1.0
14	9	6	14	9	5	1304.7031	-0.0001	1.0
15	9	7	15	9	6	1304.7216	0.0017	1.0
16	9	8	16	9	7	1304.7388	0.0010	1.0
8	8	1	8	8	0	1304.7544	0.0005	1.0
9	8	2	9	8	1	1304.7636	-0.0003	1.0
10	8	3	10	8	2	1304.7759	0.0010	1.0
11	8	4	11	8	3	1304.7872	0.0001	1.0
12	8	5	12	8	4	1304.8010	0.0005	1.0
17	12	5	16	12	4	1315.5159 *	-0.0123	1.0
16	7	9	15	7	8	1315.5370	-0.0015	0.1
15	2	13	14	2	12	1315.5370	-0.0006	0.1
16	6	10	15	6	9	1315.6409	-0.0004	1.0
17	11	6	16	11	5	1315.6443 *	-0.0302	1.0
16	2	15	15	2	14	1315.7198	-0.0006	1.0
16	5	11	15	5	10	1315.7334	-0.0006	1.0
16	4	13	15	4	12	1315.8178	0.0000	1.0
16	4	12	15	4	11	1315.8272	0.0008	0.1
16	3	14	15	3	13	1315.8624	-0.0011	1.0
17	1	17	16	1	16	1315.8864	0.0004	1.0
17	0	17	16	0	16	1315.9472	0.0006	1.0
17	9	8	16	9	7	1315.9747	0.0006	1.0
16	3	13	15	3	12	1315.9876	0.0007	1.0
18	13	5	17	13	4	1316.0117 *	0.0135	1.0
16	1	15	15	1	14	1316.0634	0.0003	1.0
17	8	9	16	8	8	1316.1042	0.0010	1.0
18	12	6	17	12	5	1316.1981 *	0.0146	1.0
17	7	10	16	7	9	1316.2194	0.0002	1.0
16	2	14	15	2	13	1316.2538	-0.0001	1.0
17	6	11	16	6	10	1316.3229	-0.0004	1.0
17	2	16	16	2	15	1316.3706	0.0004	1.0
17	5	12	16	5	11	1316.4188	0.0003	1.0
17	4	14	16	4	13	1316.5061	0.0016	0.1
18	1	18	17	1	17	1316.5061	0.0004	0.1
17	4	13	16	4	12	1316.5174	-0.0003	1.0
17	3	15	16	3	14	1316.5422	-0.0005	1.0
18	0	18	17	0	17	1316.5558	0.0004	1.0
18	9	9	17	9	8	1316.6550	0.0002	1.0
17	3	14	16	3	13	1316.7076	0.0019	0.1
17	1	16	16	1	15	1316.7076	-0.0004	0.1
18	8	10	17	8	9	1316.7844	-0.0001	1.0
19	12	7	18	12	6	1316.8811 *	0.0166	1.0
18	7	11	17	7	10	1316.9030	0.0016	1.0
18	5	13	17	5	12	1317.1035	-0.0014	1.0
19	1	19	18	1	18	1317.1243	-0.0003	1.0
19	0	19	18	0	18	1317.1650	0.0001	1.0
18	4	15	17	4	14	1317.1923	-0.0005	1.0
19	10	9	18	10	8	1317.1923	-0.0008	0.1
18	4	14	17	4	13	1317.2123	-0.0003	1.0
18	3	16	17	3	15	1317.2213	-0.0001	1.0
19	9	10	18	9	9	1317.3365	-0.0003	1.0
18	1	17	17	1	16	1317.3452	-0.0001	1.0
20	13	7	19	13	6	1317.3769 *	0.0158	1.0
18	3	15	17	3	14	1317.4313	-0.0002	1.0
19	8	11	18	8	10	1317.4670	-0.0001	1.0
20	12	8	19	12	7	1317.5647 *	0.0180	1.0
19	7	12	18	7	11	1317.5857	0.0006	1.0

Can. J. Chem. Downloaded from www.nrcresearchpress.com by 203.198.23.82 on 09/08/12
For personal use only.

TABLE A1. (*continued*)

J′	K'_a	K'_c	J″	K''_a	K''_c	Obs./cm^{-1}[a]	O-C[b]	W[c]	J′	K'_a	K'_c	J″	K''_a	K''_c	Obs./cm^{-1}[a]	O-C[b]	W[c]	J′	K'_a	K'_c	J″	K''_a	K''_c	Obs./cm^{-1}[a]	O-C[b]	W[c]
6	0	6	5	0	5	1309.1319	0.0009	0.1	14	1	14	13	1	13	1314.0218	0.0004	1.0	20	1	20	19	1	19	1317.7419	−0.0009	1.0
6	2	5	5	2	4	1309.1345	−0.0007	0.1	14	8	6	13	8	5	1314.0674	0.0000	1.0	20	0	20	19	0	19	1317.7746	−0.0007	1.0
6	2	4	5	2	3	1309.1743	0.0001	1.0	13	1	12	12	1	11	1314.0850	−0.0002	1.0	19	5	14	18	5	13	1317.7916	−0.0019	0.1
6	1	5	5	1	4	1309.3135	−0.0003	1.0	13	2	11	12	2	10	1314.1010	−0.0002	1.0	20	10	10	19	10	9	1317.8732 *	−0.0027	1.0
7	6	1	6	6	0	1309.5708	−0.0004	1.0	14	0	14	13	0	13	1314.1217	−0.0004	1.0	19	4	16	18	4	15	1317.8822	−0.0007	1.0
7	1	7	6	1	6	1309.6256	−0.0006	1.0	15	12	3	14	12	2	1314.1562 *	0.0090	0.1	19	3	17	18	3	16	1317.8984	−0.0009	1.0
7	5	2	6	5	1	1309.6528	−0.0013	1.0	14	7	7	13	7	6	1314.1805	−0.0009	1.0	19	4	15	18	4	14	1317.9111	−0.0006	1.0
7	4	3	6	4	2	1309.7221	−0.0008	1.0	14	6	8	13	6	7	1314.2812	−0.0009	1.0	19	1	18	18	1	17	1317.9755	0.0003	1.0
7	3	4	6	3	3	1309.7772	−0.0027	0.1	15	11	4	14	11	3	1314.3008 *	−0.0171	1.0	20	9	11	19	9	10	1318.0199	−0.0001	1.0
7	0	7	6	0	6	1309.7772	0.0031	0.1	14	5	9	13	5	8	1314.3704	−0.0006	1.0	21	13	8	20	13	7	1318.0614 *	0.0171	1.0
7	2	6	6	2	5	1309.7969	−0.0010	1.0	14	2	13	13	2	12	1314.4144	−0.0003	1.0	20	8	12	19	8	11	1318.1513	0.0002	1.0
7	2	5	6	2	4	1309.8599	−0.0003	1.0	14	4	10	13	4	9	1314.4518	−0.0017	0.1	19	3	16	18	3	15	1318.1635	−0.0002	1.0
7	1	6	6	1	5	1310.0013	−0.0007	0.1	15	10	5	14	10	4	1314.4734	−0.0010	1.0	21	12	9	20	12	8	1318.2505 *	0.0205	1.0
8	7	1	7	7	0	1310.1416	−0.0009	1.0	14	3	12	13	3	11	1314.5044	−0.0005	1.0	20	7	13	19	7	12	1318.2713	0.0010	1.0
8	6	2	7	6	1	1310.2389	−0.0012	1.0	14	3	11	13	3	10	1314.5696	−0.0005	1.0	20	2	19	19	2	18	1318.3064	0.0003	1.0
8	1	8	7	1	7	1310.2581	0.0001	1.0	14	2	12	13	2	11	1314.8175	−0.0021	0.1	21	11	10	20	11	9	1318.3289 *	−0.0729	1.0
8	5	3	7	5	2	1310.3232	−0.0001	1.0	16	12	4	15	12	3	1314.8343 *	0.0095	0.1	21	1	21	20	1	20	1318.3610	0.0004	1.0
8	4	4	7	4	3	1310.3927	−0.0002	1.0	15	7	8	14	7	7	1314.8590	−0.0002	1.0	20	6	14	19	6	13	1318.3817	0.0022	0.1
8	0	8	7	0	7	1310.4111	−0.0002	1.0	15	6	9	14	6	8	1314.9600	−0.0009	1.0	19	2	17	18	2	16	1318.3852	0.0029	0.1
8	3	5	7	3	4	1310.4513	−0.0014	0.1	16	11	5	15	11	4	1314.9724 *	−0.0232	1.0	21	0	21	20	0	20	1318.3852	−0.0013	0.1
8	2	7	7	2	6	1310.4603	0.0001	1.0	15	5	10	14	5	9	1315.0503	−0.0013	1.0	20	5	15	19	5	14	1318.4833	−0.0012	0.1
8	2	6	7	2	5	1310.5527	−0.0002	1.0	15	2	14	14	2	13	1315.0675	−0.0010	1.0	22	14	8	21	14	7	1318.5496 *	0.0209	1.0
8	1	7	7	1	6	1310.6889	−0.0002	1.0	15	4	12	14	4	11	1315.1338	0.0007	0.1	21	10	11	20	10	10	1318.5573 *	−0.0026	1.0
9	8	1	8	8	0	1310.6993	−0.0008	1.0	15	4	11	14	4	10	1315.1370	−0.0015	0.1	20	4	17	19	4	16	1318.5752	0.0009	1.0
9	7	2	8	7	1	1310.8117	−0.0007	1.0	16	10	6	15	10	5	1315.1511	−0.0011	1.0	20	3	18	19	3	17	1318.5752	−0.0008	1.0
9	1	9	8	1	8	1310.8879	−0.0007	1.0	15	3	13	14	3	12	1315.1842	0.0001	1.0	20	1	19	19	1	18	1318.5989	0.0006	1.0
9	6	3	8	6	2	1310.9089	−0.0013	1.0	16	1	16	15	1	15	1315.2654	−0.0001	1.0	20	4	16	19	4	15	1318.6157	0.0004	1.0
9	5	4	8	5	3	1310.9931	−0.0009	1.0	15	3	12	14	3	11	1315.2744	−0.0007	1.0	21	9	12	20	9	11	1318.7053	0.0007	1.0
9	0	9	8	0	8	1311.0415	−0.0006	1.0	16	9	7	15	9	6	1315.2944	−0.0003	1.0	21	6	15	20	6	14	1319.0686	0.0002	1.0
9	4	5	8	4	4	1311.0634	−0.0012	1.0	16	0	16	15	0	15	1315.3377	−0.0007	1.0	20	2	18	19	2	17	1319.0829	0.0008	1.0
9	3	7	8	3	6	1311.1207	−0.0009	0.1	15	1	14	14	1	13	1315.4104	−0.0002	1.0	21	5	17	20	5	16	1319.1742	−0.0001	0.1
9	2	8	8	2	7	1311.1207	−0.0013	0.1	16	8	8	15	8	7	1315.4232	−0.0001	1.0	21	5	16	20	5	15	1319.1761	−0.0017	0.1
21	1	20	20	1	19	1319.2166	0.0011	1.0	26	6	20	25	6	19	1322.5396	−0.0026	0.1	33	1	33	32	1	32	1325.7624	0.0023	0.1
22	10	12	21	10	11	1319.2422 *	−0.0029	1.0	26	3	24	25	3	23	1322.5960	−0.0006	1.0	33	0	33	32	0	32	1325.7624	0.0011	0.1
21	3	19	20	3	18	1319.2511	−0.0002	1.0	25	3	22	24	3	21	1322.6184	−0.0012	1.0	31	8	23	30	8	22	1325.7761 *	0.0033	1.0
21	4	18	20	4	17	1319.2674	0.0003	1.0	26	5	22	25	5	21	1322.6657	0.0010	1.0	31	5	27	30	5	26	1326.1974	0.0006	1.0
21	4	17	20	4	16	1319.3241	−0.0002	1.0	28	1	28	27	1	27	1322.6777	0.0001	1.0	31	4	28	30	4	27	1326.1974	0.0005	1.0
22	9	13	21	9	12	1319.3912	0.0008	1.0	28	0	28	27	0	27	1322.6824	0.0002	1.0	30	3	27	29	3	26	1326.2483	−0.0002	1.0
23	13	10	22	13	9	1319.4340 *	0.0200	0.1	27	10	17	26	10	16	1322.6876 *	−0.0026	0.1	31	2	29	30	2	28	1326.2634	0.0002	1.0
22	8	14	21	8	13	1319.5244	0.0010	1.0	26	5	21	25	5	20	1322.6876	−0.0012	0.1	31	5	26	30	5	25	1326.3049	−0.0010	1.0
22	2	21	21	2	20	1319.5861	0.0006	1.0	26	4	23	25	4	22	1322.7393	−0.0006	1.0	32	9	23	31	9	22	1326.3252	0.0001	1.0
23	1	23	22	1	22	1319.5950	0.0001	1.0	27	2	26	26	2	25	1322.7484	−0.0004	1.0	34	1	34	33	1	33	1326.3790	0.0022	0.1
23	0	23	22	0	22	1319.6115	0.0004	1.0	27	9	18	26	9	17	1322.8397	−0.0004	1.0	34	0	34	33	0	33	1326.3790	0.0013	0.1
23	12	11	22	12	10	1319.6251 *	0.0250	1.0	27	1	26	26	1	25	1322.8653	−0.0001	1.0	32	8	24	31	8	23	1326.4792 *	0.0040	1.0
22	7	15	21	7	14	1319.6463 *	0.0010	0.1	28	13	15	27	13	14	1322.8880 *	0.0302	1.0	33	2	32	32	2	31	1326.5012	0.0014	1.0
21	3	18	20	3	17	1319.6463	0.0030	0.1	26	4	22	25	4	21	1322.9661	−0.0001	1.0	32	3	30	31	3	29	1326.5240	0.0013	1.0
23	11	12	22	11	11	1319.6608 *	−0.1117	1.0	27	8	19	26	8	18	1322.9807	0.0010	1.0	33	1	32	32	1	31	1326.5357	0.0011	1.0
22	6	16	21	6	15	1319.7588	−0.0004	1.0	27	7	20	26	7	19	1323.1164 *	0.0045	1.0	32	7	25	31	7	24	1326.6325 *	0.0086	0.1
21	2	19	20	2	18	1319.7761	0.0003	1.0	26	2	24	25	2	23	1323.1278	0.0002	1.0	32	6	27	31	6	26	1326.7745	0.0003	1.0
22	1	21	21	1	20	1319.8276	−0.0006	1.0	27	6	21	26	6	20	1323.2422	−0.0012	0.1	31	4	27	30	4	26	1326.7745	0.0009	1.0
22	5	17	21	5	16	1319.8731	−0.0007	1.0	27	3	25	26	3	24	1323.2587	0.0007	1.0	32	6	26	31	6	25	1326.7874	−0.0003	1.0
22	3	20	21	3	19	1319.9250	0.0002	1.0	29	1	29	28	1	28	1323.2962	0.0022	0.1	33	10	23	32	10	22	1326.8553 *	−0.0123	1.0
23	9	14	22	9	13	1320.0764	−0.0012	1.0	29	0	29	28	0	28	1323.2962	−0.0014	0.1	32	2	30	31	2	29	1326.8713	−0.0002	1.0
24	13	11	23	13	10	1320.1229 *	0.0224	1.0	26	3	23	25	3	22	1323.3591	0.0014	1.0	32	4	29	31	4	28	1326.8828	0.0003	1.0
23	8	15	22	8	14	1320.2118	0.0001	1.0	27	5	23	26	5	22	1323.3708	0.0025	0.1	32	5	28	31	5	27	1326.9066	0.0004	1.0
24	1	24	23	1	23	1320.2118	0.0001	1.0	28	2	27	27	2	26	1323.3773	0.0007	1.0	31	3	28	30	3	27	1326.9502	−0.0011	1.0
23	2	22	22	2	21	1320.2234	0.0014	1.0	27	5	22	26	5	21	1323.4026	0.0007	1.0	35	1	35	34	1	34	1326.9948	0.0012	1.0
24	0	24	23	0	23	1320.2234	−0.0010	1.0	28	1	27	27	1	26	1323.4743	0.0006	1.0	35	0	35	34	0	34	1326.9948	0.0005	1.0
24	12	12	23	12	11	1320.3143 *	0.0274	1.0	28	9	19	27	9	18	1323.5338	−0.0004	1.0	33	9	24	32	9	23	1327.0269	0.0004	1.0
24	11	13	23	11	12	1320.3228 *	−0.1369	1.0	29	13	16	28	13	15	1323.5830 *	0.0331	1.0	32	5	27	31	5	26	1327.0474	−0.0002	1.0
23	7	16	22	7	15	1320.3371 *	0.0018	1.0	28	8	20	27	8	19	1323.6770	0.0014	1.0	34	2	33	33	2	32	1327.1226	0.0003	1.0
22	3	19	21	3	18	1320.3877	−0.0001	1.0	27	4	23	26	4	22	1323.7165	0.0002	1.0	34	1	33	33	1	32	1327.1504	0.0003	1.0
23	1	22	22	1	21	1320.4377	0.0001	1.0	27	2	25	26	2	24	1323.7712	0.0001	1.0	33	3	31	32	3	30	1327.1678	0.0005	1.0
23	6	17	22	6	16	1320.4510	−0.0009	1.0	29	12	17	28	12	16	1323.7793 *	0.0410	0.1	33	8	25	32	8	24	1327.1825 *	0.0032	1.0
22	2	20	21	2	19	1320.4624	−0.0002	1.0	28	7	21	27	7	20	1323.8152 *	0.0047	1.0	33	7	26	32	7	25	1327.3423 *	0.0100	1.0
23	5	19	22	5	18	1320.5656	0.0010	1.0	30	1	30	29	1	29	1323.9132	0.0028	0.1	33	2	31	32	2	30	1327.4773	0.0005	1.0
23	5	18	22	5	17	1320.5732	0.0006	1.0	28	3	26	27	3	25	1323.9150	−0.0016	0.1	33	6	28	32	6	27	1327.4874	0.0005	1.0
23	3	21	22	3	20	1320.5970	0.0007	1.0	30	0	30	29	0	29	1323.9150	0.0018	0.1	33	6	27	32	6	26	1327.5052	−0.0005	1.0
24	10	14	23	10	13	1320.6155 *	−0.0038	1.0	28	6	22	27	6	21	1323.9448	−0.0021	0.1	32	4	28	31	4	27	1327.5446	−0.0001	1.0
23	4	20	22	4	19	1320.6554	0.0001	1.0	29	2	28	28	2	27	1324.0030	−0.0001	1.0	34	10	24	33	10	23	1327.5555 *	−0.0131	1.0
23	4	19	22	4	18	1320.7597	−0.0004	1.0	29	10	19	28	10	18	1324.0702 *	−0.0071	0.1	33	4	30	32	4	29	1327.5652	−0.0004	1.0
24	9	15	23	9	14	1320.7659	−0.0003	1.0	28	5	24	27	5	23	1324.0741	0.0005	1.0	33	5	29	32	5	28	1327.6122	−0.0037	0.1
24	7	17	23	7	16	1321.0293 *	0.0024	1.0	29	1	28	28	1	27	1324.0832	−0.0001	1.0	36	1	36	35	1	35	1327.6122	0.0018	0.1
24	1	23	23	1	22	1321.0459	0.0009	1.0	27	3	24	26	3	23	1324.0904	−0.0003	1.0	36	0	36	35	0	35	1327.6122	0.0012	0.1
23	3	20	22	3	19	1321.1344	0.0013	1.0	28	5	23	27	5	22	1324.1196	−0.0001	1.0	32	3	29	31	3	28	1327.6486	0.0041	0.1
24	6	18	23	6	17	1321.1461	−0.0005	0.1	28	4	25	27	4	24	1324.1271	0.0000	1.0	34	9	25	33	9	24	1327.7294	−0.0001	1.0
23	2	21	22	2	20	1321.1461	0.0042	0.1	29	9	20	28	9	19	1324.2294	−0.0003	1.0	35	2	34	34	2	33	1327.7441	−0.0003	1.0
24	5	20	23	5	19	1321.2612	−0.0015	0.1	30	13	17	29	13	16	1324.2776 *	0.0344	1.0	35	1	34	34	1	33	1327.7666	0.0000	1.0
24	3	22	23	3	21	1321.2654	−0.0002	1.0	29	8	21	28	8	20	1324.3754 *	0.0024	1.0	33	5	28	32	5	27	1327.7955	−0.0012	1.0
24	5	19	23	5	18	1321.2748	0.0003	1.0	28	2	26	27	2	25	1324.4059	0.0004	1.0	34	3	32	33	3	31	1327.8097	0.0002	1.0

Can. J. Chem. Downloaded from www.nrcresearchpress.com by 203.198.23.82 on 09/08/12
For personal use only.

TABLE A1. (*continued*)

J′	K'_a	K'_c	J″	K''_a	K''_c	Obs./cm^{-1} [a]		O-C [b]	W [c]
25	10	15	24	10	14	1321.3045	*	-0.0038	1.0
24	4	21	23	4	20	1321.3511		0.0009	1.0
26	1	26	25	1	25	1321.4445		-0.0003	1.0
26	0	26	25	0	25	1321.4533		0.0008	1.0
25	9	16	24	9	15	1321.4533		-0.0028	0.1
24	4	20	23	4	19	1321.4879		-0.0002	1.0
25	2	24	24	2	23	1321.4879		-0.0010	1.0
26	13	13	25	13	12	1321.5051	*	0.0282	1.0
25	8	17	24	8	16	1321.5923		-0.0004	1.0
26	11	15	25	11	14	1321.6335	*	-0.2042	1.0
25	1	24	24	1	23	1321.6521		0.0006	1.0
26	12	14	25	12	13	1321.6973	*	0.0333	1.0
25	7	18	24	7	17	1321.7238	*	0.0036	1.0
24	2	22	23	2	21	1321.8129		0.0001	1.0
25	6	19	24	6	18	1321.8420		-0.0013	1.0
24	3	21	23	3	20	1321.8777		0.0001	1.0
25	3	23	24	3	22	1321.9326		0.0002	1.0
25	5	21	24	5	20	1321.9643		0.0015	1.0
25	5	20	24	5	19	1321.9795		-0.0003	1.0
26	10	16	25	10	15	1321.9927	*	-0.0059	1.0
25	4	22	24	4	21	1322.0450		-0.0002	1.0
27	1	27	26	1	26	1322.0609		-0.0003	1.0
27	0	27	26	0	26	1322.0668		-0.0004	1.0
26	2	25	25	2	24	1322.1185		-0.0011	1.0
26	9	17	25	9	16	1322.1468		-0.0006	1.0
27	13	14	26	13	13	1322.1948	*	0.0280	1.0
25	4	21	24	4	20	1322.2219		-0.0015	1.0
26	1	25	25	1	24	1322.2569		-0.0012	1.0
26	8	18	25	8	17	1322.2851		-0.0003	1.0
27	12	15	26	12	14	1322.3881	*	0.0339	0.1
26	7	19	25	7	18	1322.4185	*	0.0033	1.0
25	2	23	24	2	22	1322.4745		-0.0003	1.0
36	9	27	35	9	26	1329.1403		0.0003	1.0
36	2	34	35	2	33	1329.2880		0.0002	1.0
39	1	39	38	1	38	1329.4626		0.0011	1.0
39	0	39	38	0	38	1329.4626		0.0008	1.0
36	4	33	35	4	32	1329.5975		0.0006	1.0
38	2	37	37	2	36	1329.6099		0.0009	1.0
38	1	37	37	1	36	1329.6208		0.0009	1.0
36	6	31	35	6	30	1329.6365		0.0006	1.0
35	3	32	34	3	31	1329.6627		0.0016	1.0
37	3	35	36	3	34	1329.7233		0.0008	1.0
36	5	32	35	5	31	1329.7450		0.0018	1.0
35	4	31	34	4	30	1329.8443		-0.0002	1.0
37	9	28	36	9	27	1329.8470		-0.0006	1.0
37	2	35	36	2	34	1329.8936		0.0007	1.0
37	8	29	36	8	28	1330.0179	*	0.0045	1.0
40	1	40	39	1	39	1330.0795		0.0008	1.0
40	0	40	39	0	39	1330.0795		0.0006	1.0
36	5	31	35	5	30	1330.0893		-0.0017	0.1
39	2	38	38	2	37	1330.2286		-0.0015	0.1
39	1	38	38	1	37	1330.2383		-0.0004	1.0
37	4	34	36	4	33	1330.2681		0.0006	1.0
36	3	33	35	3	32	1330.3119		0.0006	1.0
37	6	32	36	6	31	1330.3556		0.0001	1.0
28	4	24	27	4	23	1324.4733		0.0001	1.0
29	7	22	28	7	21	1324.5150	*	0.0041	1.0
31	1	31	30	1	30	1324.5275		0.0006	0.1
31	0	31	30	0	30	1324.5275		-0.0015	0.1
29	3	27	28	3	26	1324.5718		-0.0006	1.0
30	2	29	29	2	28	1324.6280		-0.0005	1.0
29	6	24	28	6	23	1324.6484		0.0001	0.1
29	6	23	28	6	22	1324.6506		-0.0023	0.1
30	1	29	29	1	28	1324.6951		0.0009	1.0
30	10	20	29	10	19	1324.7644	*	-0.0085	1.0
29	5	25	28	5	24	1324.7807		0.0005	1.0
29	4	26	28	4	25	1324.8187		-0.0002	0.1
28	3	25	27	3	24	1324.8187		0.0013	0.1
29	5	24	28	5	23	1324.8426		0.0001	1.0
30	9	21	29	9	20	1324.9264		-0.0003	1.0
29	2	27	28	2	26	1325.0312		-0.0004	1.0
30	8	22	29	8	21	1325.0752	*	0.0031	1.0
32	1	32	31	1	31	1325.1449		0.0014	0.1
32	0	32	31	0	31	1325.1449		-0.0002	0.1
30	3	28	29	3	27	1325.2253		0.0000	1.0
29	4	25	28	4	24	1325.2359		-0.0002	1.0
31	2	30	30	2	29	1325.2528		-0.0002	1.0
31	1	30	30	1	29	1325.3066		0.0001	1.0
30	6	24	29	6	23	1325.3587		-0.0029	0.1
31	10	21	30	10	20	1325.4613	*	-0.0085	1.0
30	5	26	29	5	25	1325.4900		0.0019	1.0
30	4	27	29	4	26	1325.5093		0.0004	1.0
29	3	26	28	3	25	1325.5376		0.0006	1.0
30	5	25	29	5	24	1325.5712		0.0001	1.0
31	9	22	30	9	21	1325.6264		0.0012	1.0
30	2	28	29	2	27	1325.6508		0.0004	1.0
32	13	19	31	13	18	1325.6739	*	0.0407	0.1
38	3	36	37	3	35	1330.3556		-0.0008	1.0
38	10	28	37	10	27	1330.3684	*	-0.0182	1.0
37	5	33	36	5	32	1330.4516		0.0011	1.0
38	2	36	37	2	35	1330.4997		0.0001	1.0
38	9	29	37	9	28	1330.5575		0.0006	1.0
41	1	41	40	1	40	1330.6970		0.0010	1.0
41	0	41	40	0	40	1330.6970		0.0009	1.0
38	8	30	37	8	29	1330.7315	*	0.0049	1.0
40	2	39	39	2	38	1330.8513		0.0002	1.0
40	1	39	39	1	38	1330.8576		-0.0003	1.0
37	5	32	36	5	31	1330.8686		-0.0024	0.1
38	4	35	37	4	34	1330.9357		0.0009	1.0
37	3	34	36	3	33	1330.9517		0.0010	1.0
39	3	37	38	3	36	1330.9859		-0.0027	0.1
38	6	33	37	6	32	1331.0747		-0.0018	0.1
39	10	29	38	10	28	1331.0747	*	-0.0200	1.0
39	2	37	38	2	36	1331.1082		0.0001	1.0
38	6	32	37	6	31	1331.1573		-0.0014	0.1
38	5	34	37	5	33	1331.1573		0.0011	0.1
39	9	30	38	9	29	1331.2687		0.0009	1.0
42	1	42	41	1	41	1331.3171		0.0038	0.1
42	0	42	41	0	41	1331.3171		0.0037	0.1
39	8	31	38	8	30	1331.4464	*	0.0047	1.0
34	8	26	33	8	25	1327.8881	*	0.0030	1.0
34	7	27	33	7	26	1328.0544	*	0.0116	0.1
34	2	32	33	2	31	1328.0797		-0.0008	1.0
34	6	29	33	6	28	1328.2004		-0.0011	1.0
34	6	28	33	6	27	1328.2281		0.0008	0.1
37	1	37	36	1	36	1328.2281		0.0007	0.1
37	0	37	36	0	36	1328.2281		0.0003	0.1
34	4	31	33	4	30	1328.2468		0.0010	1.0
35	10	25	34	10	24	1328.2568	*	-0.0142	1.0
33	4	29	32	4	28	1328.3141		-0.0007	1.0
34	5	30	33	5	29	1328.3266		0.0011	0.1
33	3	30	32	3	29	1328.3266		-0.0009	0.1
36	2	35	35	2	34	1328.3657		-0.0005	1.0
36	1	35	35	1	34	1328.3834		-0.0004	1.0
35	9	26	34	9	25	1328.4340		0.0001	1.0
35	3	33	34	3	32	1328.4499		0.0006	1.0
34	5	29	33	5	28	1328.5525		-0.0011	1.0
35	8	27	34	8	26	1328.5965	*	0.0038	1.0
35	2	33	34	2	32	1328.6846		0.0007	1.0
35	7	28	34	7	27	1328.7665	*	0.0109	0.1
38	1	38	37	1	37	1328.8451		0.0007	1.0
38	0	38	37	0	37	1328.8451		0.0004	1.0
35	6	30	34	6	29	1328.9181		0.0002	1.0
35	4	32	34	4	31	1328.9224		-0.0005	1.0
35	6	29	34	6	28	1328.9540		0.0010	1.0
36	10	26	35	10	25	1328.9580	*	-0.0168	0.1
37	2	36	36	2	35	1328.9878		0.0001	1.0
34	3	31	33	3	30	1329.0010		0.0012	0.1
37	1	36	36	1	35	1329.0010		-0.0006	0.1
35	5	31	34	5	30	1329.0335		-0.0013	1.0
34	4	30	33	4	29	1329.0810		-0.0010	1.0
36	3	34	35	3	33	1329.0870		0.0001	1.0
41	2	40	40	2	39	1331.4719		-0.0002	1.0
41	1	40	40	1	39	1331.4766		-0.0008	1.0
38	3	35	37	3	34	1331.5810		0.0009	1.0
39	4	36	38	4	35	1331.5989		0.0002	1.0
40	3	38	39	3	37	1331.6202		0.0007	1.0
40	2	38	39	2	37	1331.7172		-0.0012	1.0
39	6	34	38	6	33	1331.7985		0.0000	1.0
39	5	35	38	5	34	1331.8604		0.0005	1.0
43	1	43	42	1	42	1331.9306		-0.0001	1.0
43	0	43	42	0	42	1331.9306		-0.0002	1.0
38	4	34	37	4	33	1332.0912		0.0016	0.1
42	2	41	41	2	40	1332.0912		-0.0018	0.1
39	3	36	38	3	35	1332.2003		-0.0001	1.0
41	3	39	40	3	38	1332.2489		-0.0002	1.0
40	4	37	39	4	36	1332.2587		-0.0005	1.0
41	2	39	40	2	38	1332.3293		-0.0013	1.0
44	1	44	43	1	43	1332.5493		0.0011	0.1
44	0	44	43	0	43	1332.5493		0.0011	0.1
40	5	36	39	5	35	1332.5627		0.0013	1.0
41	9	32	40	9	31	1332.6952		0.0006	1.0
43	2	42	42	2	41	1332.7143		0.0004	0.1
43	1	42	42	1	41	1332.7143		-0.0028	0.1

[a] Asterisk indicates perturbed transition not used in the fit.
[b] O–C is (Obs.-Calc.) in cm^{-1}.
[c] *W* is weight.

Can. J. Chem. Downloaded from www.nrcresearchpress.com by 203.198.23.82 on 09/08/12
For personal use only.

Raman spectral studies of solutions at elevated temperatures and pressures. 13. Sodium formate – water

RICHARD J. BARTHOLOMEW AND DONALD E. IRISH[1]

Guelph–Waterloo Centre for Graduate Work in Chemistry, Department of Chemistry, University of Waterloo, Waterloo, ON N2L 3G1, Canada

Received March 16, 1993

This paper is dedicated to Professor Gerald W. King on the occasion of his 65th birthday

RICHARD J. BARTHOLOMEW and DONALD E. IRISH. Can. J. Chem. **71**, 1728 (1993).

Raman spectra of the formate anion in water (H_2O and D_2O) have been measured for four concentrations under ambient conditions and for two concentrations at temperatures ranging from 49 to 239°C and a pressure of 10 MPa. Five of the six fundamental modes of vibration are polarized. This result is inconsistent with C_{2v} symmetry. The Fermi resonance doublet clearly results from the interaction of $2\nu_5$ and ν_1. The latter mode decreases in frequency as the temperature rises, thus increasing the coupling and hence the intensity of the $2\nu_5$ component. The coupling constant, W, and the positions of the unperturbed bands $2\nu_5^0$ and ν_1^0 have been calculated. No evidence to support a bifurcated structure for the solvated anion was found.

RICHARD J. BARTHOLOMEW et DONALD E. IRISH. Can. J. Chem. 71, 1728 (1993).

On a mesuré le spectre Raman de l'anion formiate dans l'eau (H_2O et D_2O), à quatre concentrations dans les conditions ambiantes et à deux concentrations à des températures allant de 49 à 239°C et à une pression de 10 MPa. Cinq des six modes de vibration fondamentaux sont polarisés. Ce résultat n'est pas en accord avec une symétrie C_{2v}. Le doublet de la résonance de Fermi résulte clairement d'une interaction de $2\nu_5$ et de ν_1. La fréquence de ce dernier mode diminue lorsqu'on augmente la température; il en résulte un couplage plus important et, en conséquence, une plus grande intensité de la composante $2\nu_5$. On a calculé la constante de couplage, W, et les positions des bandes $2\nu_5^0$ et ν_1^0 non perturbées. On n'a trouvé aucune indication pouvant suggérer l'existence d'une structure bifurquée pour l'anion solvaté.

[Traduit par la rédaction]

Introduction

The formate anion is frequently viewed as being a symmetric (C_{2v} symmetry) resonance hybrid of two important canonical forms:

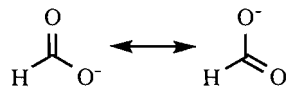

I **II**

In sodium formate crystal the formate anion lies on a C_2 axis and has C_{2v} symmetry; the C—O bond length is 124.6 pm and the O—C—O bond angle is 126.3°. The electron distribution suggests that structures of the types:

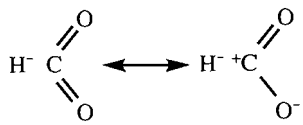

III **IV**

also contribute to the overall structure (1).

For solutions the traditional view of the symmetry of the formate ion (C_{2v}) has been challenged by Spinner (5, 6). He has argued that the ion exists not as a resonance hybrid but as two rapidly interconverting structures (**I** and **II**), undetectable on the NMR or X-ray time scales. Thus, he favours a C_s structure with two distinguishable vibrations, C—O and C=O. The evidence for this proposal rests largely on the number of polarized Raman bands. The vibrational representations for the two models are

$$C_s\colon \Gamma_{vib} = 5A' + A''$$

$$C_{2v}\colon \Gamma_{vib} = 3A_1 + 2B_1 + B_2$$

In both cases all modes are Raman active, but for C_s symmetry five bands are polarized, whereas for C_{2v} symmetry only three bands are polarized. Spinner observed five polarized bands (6). He suggested that medium effects and interionic forces are not responsible for this because they are not sufficiently strong and asymmetric for the two oxygen atoms to be in different environments.

In aqueous solution the water molecules near the formate anion can be expected to interact via hydrogen bonding and dipole–ion interactions and could conceivably introduce some distortion. Calculations (2–4) of the interaction between water and formate ion suggest that a bifurcated structure:

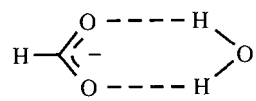

is more stable than a "traditional" linear hydrogen bond for a one-to-one interaction. It is dangerous, however, to extrapolate this result to infer the molecular arrangement of aqueous solutions. In fact, for dilute solutions Jorgensen and Gao (4) calculated a primary hydration number of 11 for the formate anion.

We felt the conclusions of Spinner (5, 6) were sufficiently radical that a further investigation was warranted. In particular, by raising the temperature, one can anticipate changing the forces between the anion and its surroundings; spectral changes might occur that could further elucidate the problem. In addition, from a practical point of view, it is now known that organic impurities in high-temperature fluids contribute to local corrosion in the tubes of boiler plants. Acetate, formate, and lactate ions have been identified (7).

[1]Author to whom correspondence may be addressed.

Can. J. Chem. Downloaded from www.nrcresearchpress.com by 203.198.23.82 on 09/08/12
For personal use only.

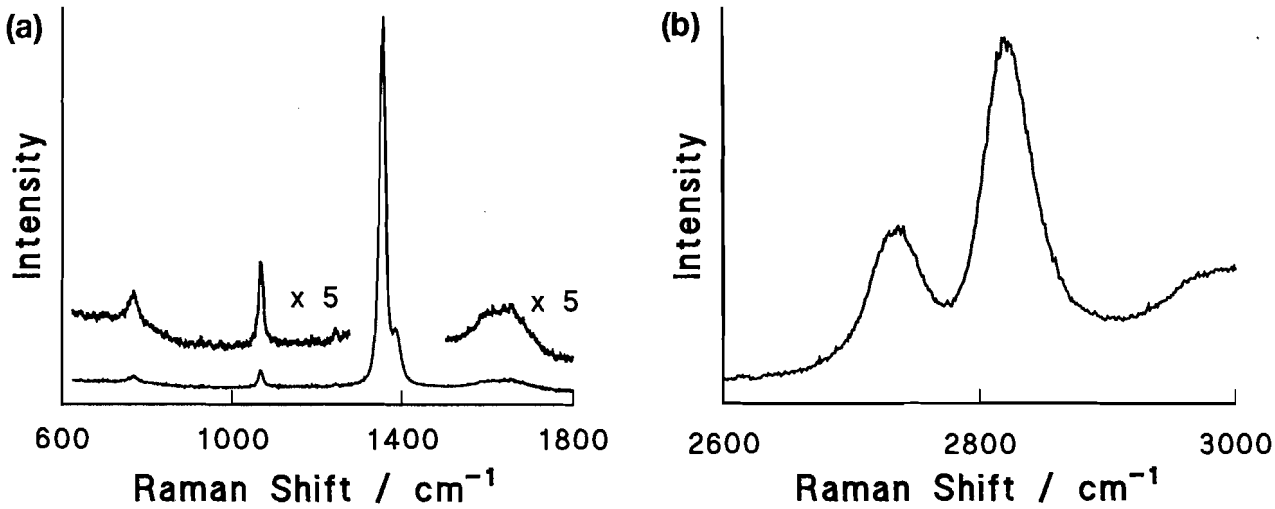

FIG. 1. Survey spectra of 5.6 *m* $NaHCOO/H_2O$ at room temperature. (The envelope at ca. 1600 cm^{-1} includes the 1638 cm^{-1} ν_2 bend of H_2O.)

Our interest in these technically important systems, as evident from our previous publications on Raman spectral studies of acetic acid (8) and acetate salts (9, 10) at elevated temperatures and pressures, was further motivation for this study of sodium formate in water. While several Raman spectral studies of aqueous formate have been conducted (5, 6, 11, 12), none, to our knowledge, has been performed at elevated temperatures and pressures. Our spectra were collected at various temperatures ranging from ambient to 239°C. Evidence of decomposition dictated the upper temperature limit.

Experimental

Sodium formate was supplied by Aldrich and had a stated purity of greater than 99%. No further purification was conducted. Sodium deuteroformate was obtained from M.S.D. Laboratories and had a stated purity of better than 99%. Again, no further purification was performed. Solutions were prepared on a molal scale (moles per kilogram of solvent). This is preferred for high-temperature work because the molal scale is independent of density. Either deionized Milli-Q water or D_2O (M.S.D. Laboratories 99.9% deuterium oxide) was used.

The construction and use of the high-pressure apparatus, capable of reaching pressures of 15 MPa, has been described previously (13). High temperatures were achieved with a furnace (13) connected to an LFE Corp. Series 128-10 temperature controller. The temperature was measured using a Chromel–Alumel thermocouple connected to a Fluke 8800a digital multimeter. Equilibration times were approximately 20–25 min at each temperature.

A Jarrell–Ash spectrometer with a 1.0-m Czerny–Turner scanning double monochromator with a digital cosecant stepping drive was used. The detector was a thermoelectrically cooled R.C.A. 31034 photomultiplier tube. Control of the monochromator and acquisition of spectral data were by an IBM PS/2 computer. Excitation was achieved by a Spectra-Physics model 165-08 laser operating at either 488.0 nm or 514.5 nm. The exciting wavelength sometimes had to be changed to avoid coincidence between laser plasma lines and vibrational bands of the sample. Powers, measured at the laser head with a Coherent model 210 power meter, ranged from 500 to 900 mW depending on the nature of the sample and the particular experiment. Late in the research some of the measurements were repeated at higher laser power, 1500 mW, using a Coherent Innova 305 laser. The mechanical slit width was set at 200μm. Depolarization measurements were made with a Polaroid analyser and a Karl Lambrecht polarization scrambler, mounted between the collection lens and the slits. For room temperature experiments, spectra were collected using melting point capillary tubes as sample cells.

Data manipulation was carried out on PCs with software written in our laboratory. The fitting of overlapping bands was performed using software based on the routine of Pitha and Jones (14) with modifications by Murphy and Bernstein (15). This routine approximates a Raman band as the product of Gaussian and Lorentzian contributions.

Results and discussion

Survey spectra (collected at room temperature) for solutions of 5.6 *m* $NaHCOO/H_2O$, 6.0 *m* $NaDCOO/D_2O$, and 5.3 *m* $NaHCOO/D_2O$ are shown in Figs. 1–3. Most of the bands are quite weak and thus study was limited to the stronger bands. This was especially necessary at elevated temperatures and pressures where the sample cells were much thicker and signals from weak bands were diminished.

The assignment of the aqueous formate anion spectrum is based on the study of Ito and Bernstein (12) and is given in Table 1. They assumed a C_{2v} symmetry. They did not report a Raman band for ν_4, the O—C—O asymmetric stretch (implied by C_{2v}); this is a weak band masked by $\nu_2(H_2O)$ but it is strong in the infrared. Spinner (5, 6) based his discussion on the assumption of C_s symmetry and the assignments implied by his analysis are given in parentheses in Table 1. He reported all six bands in the Raman spectrum. For the purposes of discussion we shall use Ito and Bernstein's assignment.

For 5.6 *m* $NaHCOO/H_2O$, the ν_4 band is extremely weak and broad and cannot be clearly distinguished from the scissoring band of H_2O. Spinner (6) assigned a frequency of ~1591 cm^{-1} to this vibration. For D_2O solvent the band is isolated and occurs at 1597 cm^{-1} (1587 cm^{-1} for $DCOO^-/D_2O$). On deuteration the C—H in-plane bend (ν_5), which is seen as a shoulder at 1381 cm^{-1} in Figs. 1 and 2, shifts to 1025 cm^{-1} (Fig. 3). The C—H out-of-plane bend (ν_6) at 1063 cm^{-1} appears to be the weak feature at 915 cm^{-1} (see Fig. 3) for the isotopomer.

The doublet at 2733 and 2819 cm^{-1} is attributed to a Fermi resonance. A characteristic Fermi resonance doublet occurs in this spectral region for aldehydes (16). It is believed to

Can. J. Chem. Downloaded from www.nrcresearchpress.com by 203.198.23.82 on 09/08/12
For personal use only.

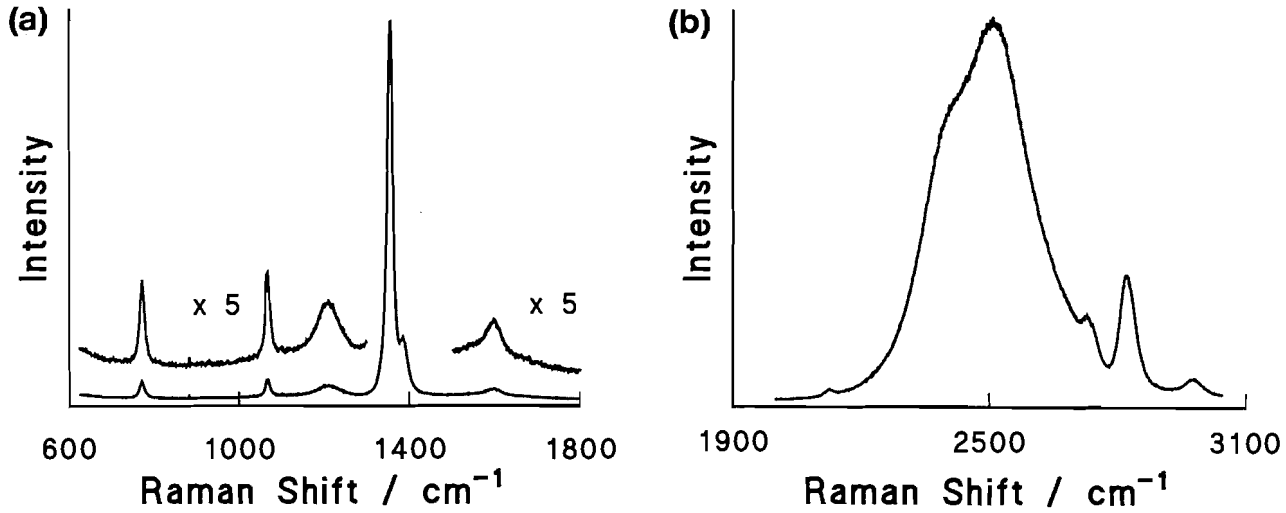

FIG. 2. Survey spectra of 5.9 *m* NaHCOO/D_2O at room temperature. (The band at 1202 cm^{-1} is ν_2 (D_2O).)

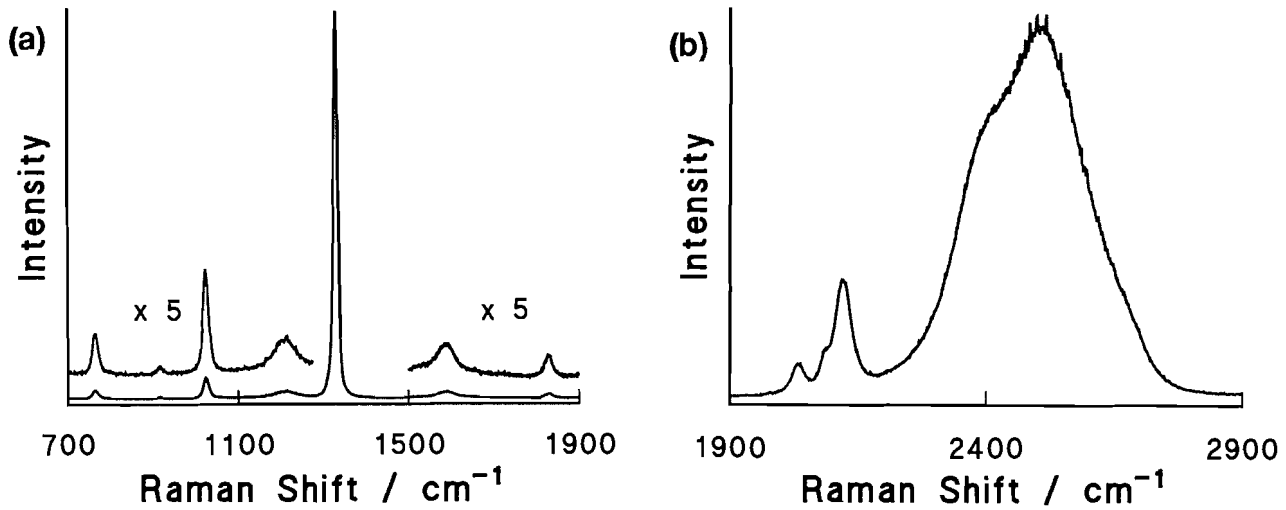

FIG. 3. Survey spectra of 6.0 *m* NaDCOO/D_2O at room temperature. (The band at 1202 cm^{-1} is ν_2 (D_2O); the band at 1829 cm^{-1} is tentatively assigned to $2\nu_6$.)

arise from interaction between the C—H stretch and the first overtone of the in-plane C—H bending vibration ($2 \times \nu_5$). The assignment also applies to the formate ion. On exchanging deuterium for hydrogen the doublet is shifted downward to 2028 and 2113 cm^{-1} and the resonance condition is maintained, indicating that both vibrations involve a C—H (or C—D) bond, thus excluding a resonance between $2\nu_2$ and ν_1.

Effect of concentration

Spectra were collected for solutions of NaHCOO in H_2O at concentrations of 9.5 *m*, 5.6 *m*, 2.7 *m*, and 1.3 *m*. Between 675 and 1800 cm^{-1} no significant changes in band positions or in band shapes occurred. Between 2900 and 3900 cm^{-1} (Fig. 4) the broad Raman band profile from the hydrogen-bonded O—H oscillators of water changes significantly. As the concentration rises, there is a decrease in the intensity of the broad shoulder (~3240 cm^{-1}) attributed to hydrogen bonding structure relative to the peak at 3400 cm^{-1}, an effect characteristic of "structure breakers" (17). A structure breaker is an ion that decreases the intermolecular coupling between water molecules. Common structure breakers include BF_4^- (17), I^- (17), and ClO_4^- (18).

Polarization studies

Polarization measurements were conducted on the fundamental vibrations and on the Fermi resonance doublet of the formate anion for several solutions that differed in concentration and solvent. An attempt to measure the parallel and perpendicular spectra at elevated temperatures and pressures, with sufficient quality, proved impractical. The solvent was changed to avoid the overlapping of solvent bands with bands of the formate anion: to measure ρ for ν_2, ν_3, ν_4, ν_5, and ν_6, D_2O was used as the solvent; to measure ρ for the Fermi resonance doublet, H_2O was used as the solvent. Polarization studies of neat CCl_4 were conducted to check the orientation of the polarization analyzer and the following average depolarization ratios were obtained:

$$\rho(216\ \text{cm}^{-1}) = 0.77;\ \rho(312\ \text{cm}^{-1}) = 0.78;$$

$$\rho(459\ \text{cm}^{-1}) = 0.03$$

These compare favourably with the theoretical values of 0.75, 0.75, and 0, respectively, and the values 0.758, 0.751, and 0.0039, respectively, reported by Murphy et al. (19). The depolarization ratios obtained from the various formate solutions are summarized in Table 2.

Can. J. Chem. Downloaded from www.nrcresearchpress.com by 203.198.23.82 on 09/08/12
For personal use only.

TABLE 1. Vibrational assignments for aqueous NaHCOO[a]

Assignment	Description	Position/cm^{-1}		
		5.6 m NaHCOO/H_2O	5.3 m NaHCOO/D_2O	6.0 m NaDCOO/D_2O
ν_3 (ν_5)	OCO scissoring	764	768	759
ν_6 (ν_6)	C—H out-of-plane bend	1063	1060	915
ν_2 (ν_4)	C—O sym. str. (C—O^- str.)	1350	1350	1324
ν_5 (ν_3)	C—H in-plane bend	1381	1379	1025
ν_4 (ν_2)	C—O asym. str. (C=O str.)	[b]	1597	1587
$2\nu_5$,[c] ν_1 ($2\nu_3$, ν_1)	Fermi resonance doublet	2733, 2819	2727, 2818	2028, 2113

[a]Assignments after ref. 12; the assignments of ref. 6 are presented in parentheses.
[b]Weak, partially masked by ν_2 (H_2O).
[c]Originally assigned to $\nu_2 + \nu_5$ in ref. 12.

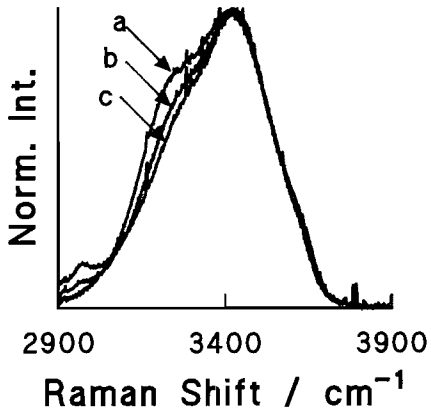

FIG. 4. Effect of $HCOO^-$ concentration on the shape of the OH stretching profile of water: (*a*) 0.63 *m*; (*b*) 2.7 *m*; (*c*) 9.5 *m*.

The results for 5.3 *m* NaHCOO/D_2O and 5.9 *m* NaHCOO/H_2O show that ν_2, ν_3, ν_4, ν_5, and both bands of the Fermi resonance doublet are polarized ($\rho < 0.75$) and ν_6 is depolarized. The depolarization ratios do not change significantly with increasing concentration. Because five of the six fundamentals are polarized, a formate ion in an aqueous environment appears not to have C_{2v} symmetry.

NaHCOO in H_2O at elevated temperatures and pressures

Spectra of 5.9 *m* NaHCOO/H_2O were collected at elevated temperatures and a pressure of 10 MPa in two separate sets of experiments. The first set included temperatures of 49, 100, 151, and 239°C and the second set included temperatures of 75, 127, 176, 198, and 225°C. The study concentrated on two spectral regions: 1250–1460 cm^{-1} and 2575–3025 cm^{-1}. Bands in the spectra were resolved into components by fitting Gaussian–Lorentzian product functions to the intensity envelope (15).

In the first region two bands were observed. The positions and relative intensities of these bands do not change significantly with increasing temperature; they remain centred at ~1348 and ~1381 cm^{-1}.

The spectral region from 2575 to 3025 cm^{-1} shows more interesting changes. The frequencies of the two bands of the Fermi resonance doublet decrease linearly with temperature (see Fig. 5). The data from the two sets of experiments were in agreement and were combined. A linear regression analysis of the combined data gave:

[1] $$\text{“}2\nu_5\text{”} = [-0.095(\pm 0.009)t + 2736(\pm 1.5)]\ \text{cm}^{-1}$$
$$r = -0.990$$

[2] $$\text{“}\nu_{\text{C—H str.}}\text{”} = [-0.088(\pm 0.009)t + 2822(\pm 1.5)]\ \text{cm}^{-1}$$
$$r = -0.994$$

where t is the temperature in Celsius and r is the correlation coefficient. The similarity of the slopes means the separation of the peaks is virtually independent of temperature.

The intensity of the $2\nu_5$ band increased with respect to the "C—H stretch" band. The temperature dependence of the intensity ratio is given by:

[3] $$\frac{I_{2\nu_5}}{I_{\nu_1}} = 1.12 \times 10^{-3}(\pm 4.8 \times 10^{-4})t + 0.408(\pm 0.077)$$
$$r = 0.909$$

If the wavefunctions involved in a Fermi resonance interaction are Ψ_i^0 and Ψ_n^0 and their eigenvalues are E_i^0 and E_n^0, the energies of the perturbed levels (20) are

[4] $$E = E_{\text{in}} \pm \tfrac{1}{2}\sqrt{\Delta^2 + 4W^2}$$

where $E_{\text{in}} = 0.5\,(E_i^0 + E_n^0)$; $\Delta = E_i^0 - E_n^0$ (separation of the unperturbed levels); W = Fermi coupling constant. By factoring out "hc", this expression can be rewritten in terms of wavenumbers (cm^{-1}):

[5] $$\nu = \nu_{\text{in}} \pm \tfrac{1}{2}\sqrt{\Delta^2 + 4W^2}$$

[6] $$X = \sqrt{\Delta^2 + 4W^2}$$

These equations can be used to calculate the unperturbed frequency of the C—H stretch, ν_1^0, in the following way:

[7] $$\nu_{2\nu_5} = \tfrac{1}{2}(\nu_1^0 + 2\nu_5^0) - \tfrac{1}{2}X$$

[8] $$\nu_{\text{C—H}} = \tfrac{1}{2}(\nu_1^0 + 2\nu_5^0) + \tfrac{1}{2}X$$

where $\nu_{2\nu_5}$ and $\nu_{\text{C—H}}$ represent the lower and upper fre-

Can. J. Chem. Downloaded from www.nrcresearchpress.com by 203.198.23.82 on 09/08/12
For personal use only.

TABLE 2. Summary of depolarization ratios

Band	5.3 m NaHCOO/D_2O	5.9 m NaHCOO/H_2O	12 m NaHCOO/D_2O	9.5 m NaHCOO/H_2O
ν_3, OCO scissoring	0.36	—	0.34	—
ν_6, C—H out-of-plane bend	0.75	—	0.78	—
ν_2, C—O sym. stretch	0.14	—	0.14	—
ν_5, C—H in-plane bend	0.56	—	0.52	—
ν_4, C—O asym. stretch	0.46	—	0.50	—
$2\nu_5$, ν_1	—	0.27, 0.28	—	0.26, 0.26

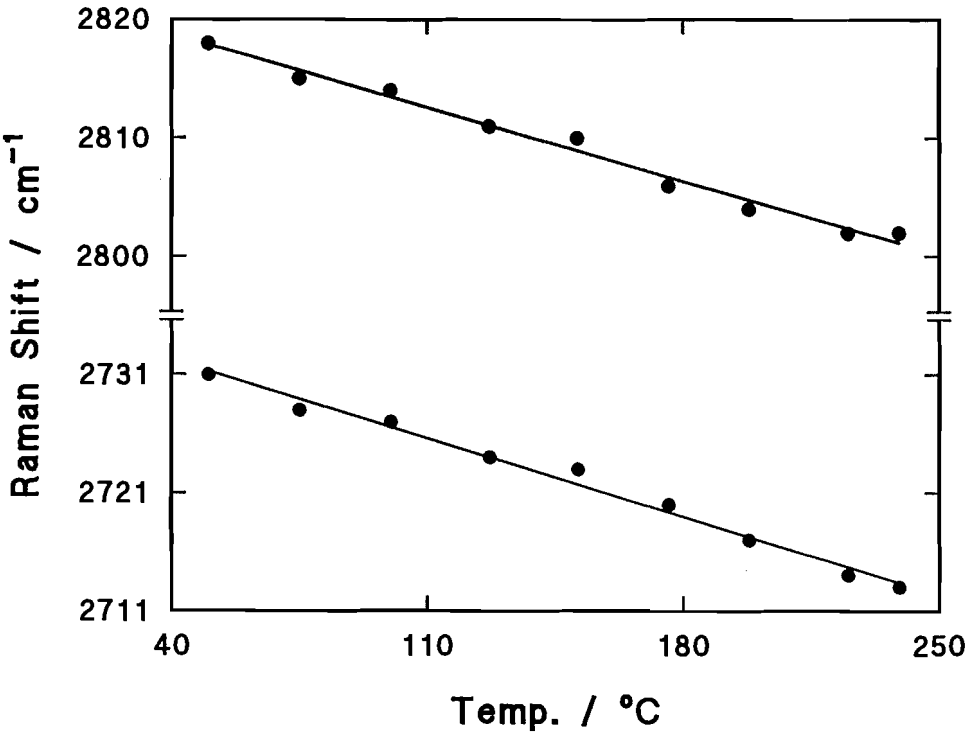

FIG. 5. Effect of temperature on the frequencies of the Fermi resonance doublet.

TABLE 3. Analysis of the Fermi resonance doublet, 5.9 *m*

Temperature/°C	ν_5^0/cm^{-1}	$2\nu_5^0$/cm^{-1}	Fermi doublet	ν_1^0/cm^{-1}	W/cm^{-1}	$\lvert\Delta\rvert$/cm^{-1}
49	1383	2766	2731, 2818	2783	42.7	17
75	1382	2764	2728, 2815	2779	42.9	15
100	1381	2762	2727, 2814	2779	42.7	17
127	1382	2764	2724, 2811	2771	43.4	7
151	1380	2760	2723, 2810	2773	43.0	13
176	1382	2764	2720, 2806	2762	43.0	5
198	1381	2762	2717, 2804	2759	43.5	3
225	1381	2762	2714, 2802	2754	43.8	8
239	1379	2758	2713, 2802	2757	44.5	1

quency bands of the Fermi resonance doublet, respectively, and $2\nu_5^0$ and ν_1^0 are the unperturbed frequencies, respectively. Adding these equations gives:

$$[9] \quad \nu_{2\nu_5} + \nu_{C—H} = \nu_1^0 + 2\nu_5^0$$

At 75°C, $\nu_{C—H}$ = 2815 cm^{-1}, $\nu_{2\nu_5}$ = 2728 cm^{-1}, ν_5^0 = 1382 cm^{-1}. In the absence of anharmonicity $2\nu_5^0$ is 2 × ν_5^0 = 2764 cm^{-1} and ν_1^0 is found to be 2779 cm^{-1}. This calculation was performed at each temperature and the values for ν_1^0, $2\nu_5^0$, Δ, and W are summarized in Table 3. The unperturbed frequency for ν_1^0 decreases with increasing temperature but ν_5^0, and therefore $2\nu_5^0$, remains virtually unchanged. As a consequence the two unperturbed frequencies shift closer together and the relative intensity of the low-frequency band of the doublet increases (as given by eq. [3]), as expected

Can. J. Chem. Downloaded from www.nrcresearchpress.com by 203.198.23.82 on 09/08/12
For personal use only.

from theory. At 239°C, $2\nu_5^0$ and ν_1^0 are virtually coincident but the relative intensity is not 1:1. We have no explanation for this, but anharmonicity in the $2\nu_5^0$ overtone may contribute to this discrepancy.

A similar set of experiments was conducted on 9.5 *m* $NaHCOO/H_2O$ using five different temperatures; consistent results were obtained.

Conclusions

The experiments and results presented above lead to several conclusions about the formate ion in aqueous solutions.

First, the results from the polarization studies do not support a C_{2v} symmetry for formate ion in aqueous solutions. However, the intensity from the C=O stretching band (implied by C_s symmetry) is weak (cf. the intensity of the C=O stretching band from acetone or other carbonyls); thus the intensity is more characteristic of the antisymmetric stretching mode of a $-CO_2$ group (C_{2v} symmetry) than of a C=O group (C_s symmetry). It is not clear whether the depolarization ratio results reflect the inherent symmetry of the formate ion, a lowering of symmetry because of solute–solvent interactions, or the limitations of the selection rules when applied to condensed phases. In the solid phase, where there are no solvent effects, most workers have assumed C_{2v} symmetry when interpreting their spectra (21–24). Spinner (5) has argued that when correct assignments are applied to Newman's (21) polarized infrared study of formate crystal a conclusion of C_{2v} symmetry cannot be correct. We favour an explanation involving aquation of formate anion, which perturbs the symmetry.

Second, a symmetrical bifurcated structure for the solvated anion is highly unlikely. This conclusion is based on a number of experiments that showed no change in the position of the C—O vibration (ν_2) with increasing concentration, with increasing temperature, or with changing the solvent from H_2O to D_2O. One would predict that the bifurcated structure would be perturbed and the resulting distortion would cause changes in band properties with changes in concentration, temperature, or solvent. The independence of the spectra from these variables suggests that the solvation structure is retained and is not the bifurcated structure.

Third, the components of the Fermi resonance doublet (band position and relative intensity) show a strong dependence on temperature. This results from the lowering of the frequency of the unperturbed C—H stretching mode, ν_1^0, with temperature.

Lastly, because of the changes in shape of the vibrational bands of water with addition of salt, formate can be considered a "structure breaking" ion.

Experiments at elevated temperatures, which show that a hydrogen–deuterium exchange reaction occurs at the H—C bond, have also been conducted on $HCOO^-/D_2O$. This reaction is still under study and the results will be published in a future paper.

Acknowledgements

This work was supported by grants from the Natural Sciences and Engineering Research Council of Canada. This research was stimulated by results found by Richard Visser, an undergraduate working in our laboratory.

1. P.L. Markila, S.J. Rettig, and J. Trotter. Acta. Crystallogr. Sect. B: Struct. Crystallogr. Cryst. Chem. **B31**, 2927 (1975).
2. G. Alagona, C. Ghio, and P. Kollman. J. Am. Chem. Soc. **105**, 5226 (1983).
3. K. Hermansson, G.C. Lie, and E. Clementi. Theor. Chim. Acta, **74**, 1 (1988).
4. W.L. Jorgensen and J. Gao. J. Phys. Chem. **90**, 2174 (1986).
5. E. Spinner. J. Chem. Soc. **B**, 879 (1967).
6. E. Spinner. Aust. J. Chem. **38**, 47 (1985).
7. W.A. Byers and G.B. Gockley. Organic impurity transport in PWR secondary systems. EPRI report NP-4099. 1985.
8. J. Semmler and D.E. Irish. J. Solution Chem. **17**, 805 (1988).
9. M.M. Yang, D.A. Crerar, and D.E. Irish. Geochim. Cosmochim. Acta, **53**, 319 (1989).
10. J. Semmler, D.E. Irish, and T. Ozeki. Geochim. Cosmochim. Acta, **54**, 947 (1990).
11. R. Fonteyne. Naturwissenschaften, **31**, 441 (1943).
12. K. Ito and H.J. Bernstein. Can. J. Chem. **34**, 170 (1956).
13. D.E. Irish, T. Jarv, and C.I. Ratcliffe. Appl. Spectrosc. **36**, 137 (1982).
14. J. Pitha and R.N. Jones. Can. J. Chem. **44**, 3031 (1966).
15. W.F. Murphy and H.J. Bernstein. J. Phys. Chem. **76**, 1147 (1972).
16. D. Lin-Vien, N.B. Colthup, W.G. Fateley, and J.G. Grasselli. *In* The handbook of infrared and Raman characteristic frequencies of organic molecules. Academic Press, San Diego, Calif. 1991. p. 122.
17. D.E. Irish and M.H. Brooker. Adv. Infrared Raman Spectrosc. **2**, 212 (1976).
18. C.I. Ratcliffe and D.E. Irish. Can. J. Chem. **62**, 1134 (1984).
19. W.F. Murphy, M.V. Evans, and P. Bender. J. Chem. Phys. **47**, 1836 (1967).
20. G. Herzberg. *In* Molecular spectra and molecular structure. II. Infrared and Raman spectra of polyatomic molecules. D. Van Nostrand Co. Inc., Princeton, N.J. 1945. p. 216.
21. R. Newman. J. Chem. Phys. **20**, 1663 (1952).
22. K.B. Harvey, B.A. Morrow, and H.F. Shurvell. Can. J. Chem. **41**, 1181 (1963).
23. T.L. Charlton and K.B. Harvey. Can. J. Chem. **44**, 2717 (1966).
24. I. Tajima, H. Takahashi, and K. Machida. Spectrochim. Acta, **37A**, 905 (1981).

Can. J. Chem. Downloaded from www.nrcresearchpress.com by 203.198.23.82 on 09/08/12
For personal use only.

An analysis of the $F'O_u^+$ ion-pair state of I_2 by a sequential three-photon excitation

FATEN S.M. ABD EL-HAMEED[1]

Department of Chemistry, McMaster University, Hamilton, ON L8S 4M1, Canada

Received March 1, 1993

This paper is dedicated to Professor Gerald W. King on the occasion of his 65th birthday

FATEN S.M. ABD EL-HAMEED. Can. J. Chem. **71**, 1734 (1993).

A three-photon absorption technique that utilizes a visible $B^3\Pi(O_u^+)$–$X^1\Sigma_g^+$ transition followed by two-photon absorption was applied to characterize the high-lying vibrational levels of the $F'O_u^+$ ion-pair state of I_2, which correlates with $I^-(^1S) + I^+(^1D)$ at the dissociation limit. The multiphoton spectrum was examined at high resolution using either a single tunable dye laser (3P1C), or two independently tunable pump and probe dye lasers (3P2C), operating in the blue–green region. The one-color spectrum excited by a single laser shows transitions that have not been assigned by previous workers; these rotational lines are interpreted as being due partly to 3P1C transitions to the $F'O_u^+$ ion-pair state, for which molecular constants are derived to be (for $v' = 60$–74, $J' = 3$–100):

$$Y_{00} = 58\ 150.76(1) \quad Y_{10} = 92.98(11) \quad Y_{20} = -1.305(37) \times 10^{-2}$$

$$Y_{01} = 0.017\ 657\ 8(25) \quad Y_{11} = -9.098(05) \times 10^{-5} \quad Y_{02} = -2.06 \times 10^{-9}$$

(all in cm^{-1} with one standard deviation in the last quoted digit in parentheses).

FATEN S.M. ABD EL-HAMEED. Can. J. Chem. **71**, 1734 (1993).

On a appliqué une technique d'absorption de trois photons qui utilise une transition visible $B^3\Pi(O_u^+)$–$X^1\Sigma_g^+$ suivie par l'absorption de deux photons pour caractériser les niveaux vibrationnels élevés de l'état paire d'ions $F'O_u^+$ du I_2 qui, à la limite de dissociation, est en corrélation avec $I^-(^1S) + I^+(^1D)$. On a examiné le spectre multiphoton à haute résolution utilisant soit un laser à colorant ajustable simple (3P1C) ou deux lasers ajustables indépendamment (3P2C) opérant dans la région du bleu–vert. Le spectre monocolore obtenu par excitation à l'aide d'un seul laser présente des transitions qui n'ont pas été attribuées antérieurement par d'autres chercheurs; on attribue en partie ces raies de rotation à des transitions 3P1C conduisant à l'état de paire d'ions $F'O_u^+$ pour lequel on a déterminé que les constantes moléculaires sont (pour $v' = 60$–74, $J' = 3$–100) :

$$Y_{00} = 58\ 150{,}76(1) \quad Y_{10} = 92{,}98(11) \quad Y_{20} = -1{,}305(37) \times 10^{-2}$$

$$Y_{01} = 0{,}017\ 657\ 8(25) \quad Y_{11} = -9{,}098(05) \times 10^{-5} \quad Y_{02} = -2{,}6 \times 10^{-9}$$

(toutes les données sont en cm^{-1} avec un écart type pour les valeurs entre parenthèses).

[Traduit par la rédaction]

Introduction

A large number of papers on the spectrum of diatomic iodine exist in the literature (1), but analysis of the higher electronic states tends still to be incomplete. There have been many problems in interpretating the existing spectroscopic data clearly and unambiguously (2).

Multiphoton absorption techniques using tunable laser beams have recently been introduced to clarify the assignment of the UV emission spectrum of molecular iodine. More than half of the 20 ion-pair states correlating with $I^-(^1S) + I^+(^3P, ^1D, ^1S)$ have been spectroscopically identified (3–8). Ishiwata et al. (9) reported an optical–optical double resonance (OODR) study of the $F'O_u^+$ state over the vibrational range $v' = 0$–38. Lehmann, Smolarek, and Goodman (10) observed under low resolution, using a single laser beam, seven multiphoton ionization (MPI) lines in the 19 500 cm^{-1} region of the spectrum, which they did not analyse.

In this paper we report a rotational analysis of the upper levels of the $F'O_u^+$ ion-pair state ($v' = 60$–74), which tends toward $I^-(^1S) + I^+(^1D)$ at the dissociation limit. Three types of double resonance signals induced by an overall three-photon process were detected and included in the analysis of the F' state: 3P1C denotes three-photon absorption from the probe laser only, 3P2C(1 + 2) corresponds to the excitation of I_2 to the appropriate $B(O_u^+)$ rovibronic level by the pump laser followed by two-photon simultaneous transition by the probe frequency to the upper F' state, and 3P2C (2 + 1) is a process involving absorption of one pump photon followed by a combination of the pump and probe laser pulses. The three-photon absorption scheme is shown in Fig. 1 as it applies to I_2. Furthermore, by combining our data with the data of Ishiwata et al. (9), we present Dunham coefficients for the state valid over the vibrational range $v' = 0$–74.

Experimental

The experimental setup used in the present work has been described in detail previously (11). Two independently tunable dye lasers were pumped by the divided output of a XeCl excimer laser developed from the model described by Kearsley *et al.* (12). This pump laser produce pulses of 15 ns duration and 1-MW peak power at a pulse repetition rate of 3 Hz.

In the 3P2C experiment, the I_2 molecules in the XO_g^+ ground state were excited to the BO_u^+ state by the broad-band pump laser (BDL, $\Delta\nu \sim 0.7\ cm^{-1}$). The narrow-band dye laser (NDL, $\Delta\nu - 0.1\ cm^{-1}$) was then used as a scanning probe to induce two-photon transitions to the high-lying states from the B-state rovibronic levels photo-selected by the BDL. In the 3P1C work, the NDL was used to excite the multiphoton spectra. The high-resolution spectra obtained by scanning the NDL were calibrated by simultaneously recording the single photon B–X LIF spectrum of I_2 (13), and the fixed BDL frequency in the 3P2C mode was determined precisely by photographing the laser output on a 1.5-m Bausch and lomb spectrograph calibrated against an Fe/Ne emission spectrum.

To achieve the necessary output power needed for the multiphoton absorption experiments while keeping the band width of the dye laser (NDL) constant, a passive external amplifier was used.

[1]Present address: Department of Chemistry, Faculty of Science, Ain Shams University, Cairo, Egypt.

Can. J. Chem. Downloaded from www.nrcresearchpress.com by 203.198.23.82 on 09/08/12
For personal use only.

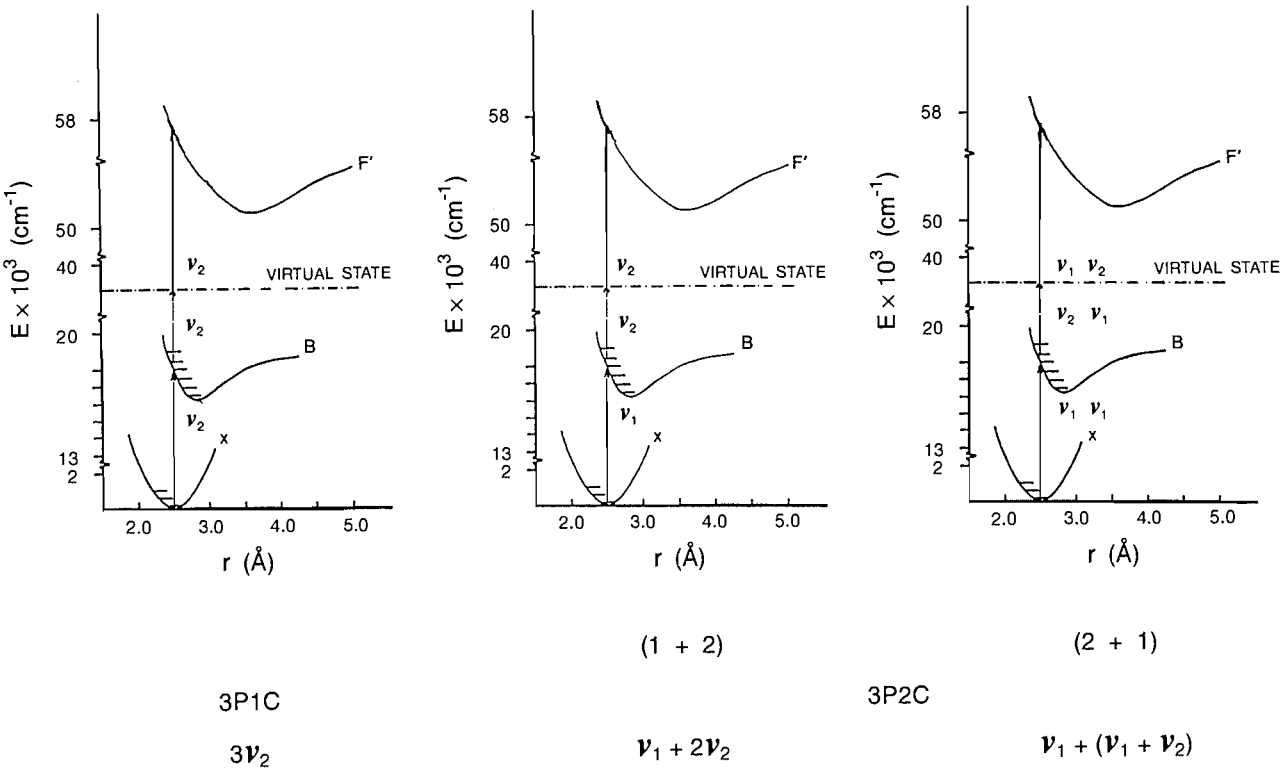

FIG. 1. The OODR experiment as it applies to iodine, where ν_1 and ν_2 are the pump and probe laser frequencies, respectively.

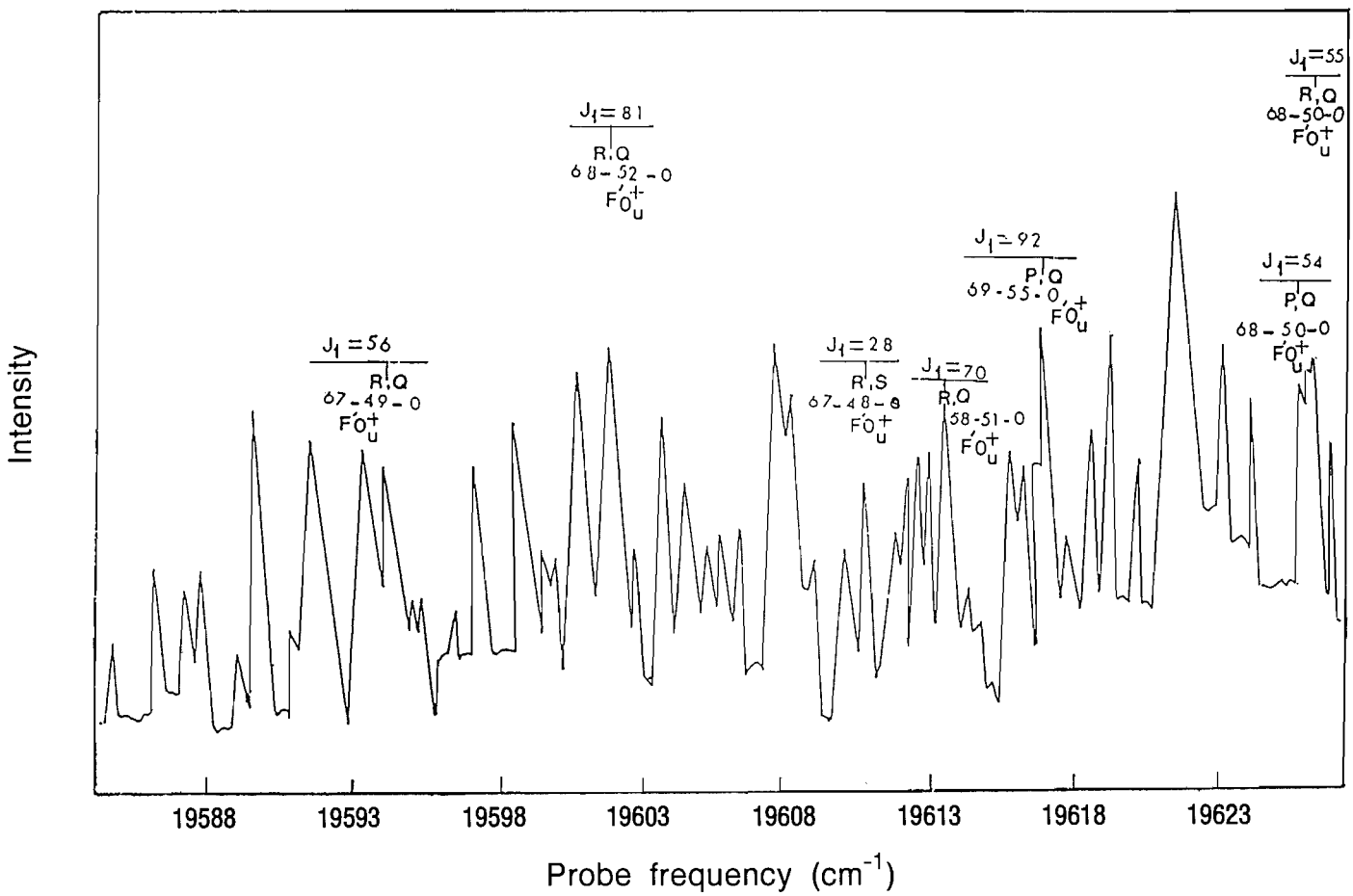

FIG. 2. High-resolution 3P1C spectrum of $^{127}I_2$.

Can. J. Chem. Downloaded from www.nrcresearchpress.com by 203.198.23.82 on 09/08/12
For personal use only.

Can. J. Chem. Downloaded from www.nrcresearchpress.com by 203.198.23.82 on 09/08/12
For personal use only.

TABLE 1. Comparison of OODR lines given in ref. 10 and those from this study for $^{127}I_2$ in the C-500 region

This study		Lehman et al. (10)	
Probe Frequency (cm^{-1})	Intensity	Frequency (cm^{-1})	Intensity
19 520.345	M	19 520.496	S
19 522.429	VS		
19 529.015	M	19 530.781	M
19 533.095	S		
19 533.921	S		
19 537.416	S		
19 538.701	S		
19 541.406	S		
19 541.701	S		
19 542.027	S		
19 544.290	S		
19 545.738	M		
		19 546.25	S
19 548.214	VS	19 548.125	S
19 550.361	VS		
19 551.271	S	19 551.875	S
19 552.496	S		
19 554.359	S		
19 555.281	S		
19 557.623	M		
19 566.025	S		
19 570.668	VS		
19 574.277	S		
19 575.121	M	19 575.781	VS
19 577.325	S	19 578.125	S
19 580.272	VS		
19 580.862	S		
19 581.511	M		

W = weak; VW = very weak; M = medium; S = strong; VS = very strong.

The amplification medium was a dye solution at the same concentration and flow rate as that of the oscillator. The amplifier cell was side-pumped by the excimer beam.

The excitation spectra were recorded by monitoring the filtered fluorescence at 250 nm with an electrothermally cooled PMT (EMI 9816 QB). The PMT anode output went to a fast preamplifier (Ortec 9305) and then to a two-channel boxcar integrator (Stanford Research Systems model SR- 250). The signal from the sample cell was processed through one channel while the other handled the signal from the calibration cell. Both channels were digitally recorded and stored using an on-line PDP-11 minicomputer. The data were later processed using peak-finding and interpolation routines.

Pure solid iodine (BDH 99.9%) was used without further purification and was sublimed into an evacuated quartz cell (3–4 Torr; 1 Torr = 133.3 Pa). The cell was then permanently sealed and used at room temperature.

Results and discussion

High-resolution one-color spectra

Under high resolution, a total of 65 3P1C lines were recorded for the F' state of the $^{127}I_2$ molecule over the 19 200–19 900 cm^{-1} energy region using C-500 laser dye in the NDL. Lehmann, Smolarek, and Goodman (10) scanned a very narrow energy region (19 500–19 580 cm^{-1}) during the course of a multiphoton ionization study (MPI) using a broadband laser ($\Delta\nu \sim 3$ cm^{-1}). Table 1 lists some of the strong peaks recorded during the course of this study as compared to those observed by Lehmann et al., only six of which appear to correlate with the strong features we recorded. No analysis for this portion of the spectrum was provided by Lehmann et al.; instead, they suggested that some high state(s) must be contributing to the resonance terms and that those features they observed may have resulted from four- or five-photon ionization. The multiphoton lines recorded in this study over the above-mentioned spectral region are most likely due to transitions to upper state(s) that lie about 58 000–59 000 cm^{-1} above the iodine ground state. The corresponding fluorescence, monitored at 250 nm, is from these levels to the X-state below its dissociation limit. These transitions would be strong according to the Franck–Condon principle. The pumped B–X transitions are nearly vertical transitions; therefore, a high population of the B-state levels is obtained. Vertical transitions from the B state would terminate on high levels of the F' state, due to the relative positions of the potential curves, and would be stronger, according to the Franck–Condon principle.

The apparently random frequency distribution of the observed 3P1C lines is due to two main constraints. To be allowed, transitions must satisfy two sets of selection rules such that the cross sections for both the first transition B–X and the second two-photon simultaneous transition out of the real intermediate state are nonzero. A further constraint on possible 3P1C transitions, resonance-enhanced through a real intermediate state, is that the resonance criterion:

$$[1] \quad 2\sigma_{21} = \sigma_{32}$$

must be fulfilled, where σ_{21} is the single-photon transition frequency and σ_{32} represents the frequency of the two-photon transition from the B state to the higher lying states. As a result, the high-resolution spectrum takes on a highly irregular appearance and classical methods of analysis are inapplicable.

The frequencies σ_{21} of the P and R lines of the B–X transition, in near resonance with each observed line frequency (3P1C), could be calculated from the constants given by Hutson et al. (14) and Tromp and LeRoy (15), respectively. A Fortran routine scanned over the ranges $v_1 = 0$–4 and $J_1 = 0$–150. About 10 possible resonance lines σ_{21} were found within ± 0.2 cm^{-1} of each 3P1C transition.

For each σ_{21}, the energy of the corresponding possible three-photon excited level (E_3) was calculated from:

$$[2] \quad E_3(v_3, J_3) = 3\sigma(3P1C) + E_1(v_1, J_1)$$

using a Fortran routine, where E_1 is the ground state term value relative to ($v_x = 0$, $J_x = 0$) and J_3 has the possible values ($J_2 + 2$), J_2, and ($J_2 - 2$) for a two-photon $\Delta\Omega = 0$ transition, O, Q, and S branches.

A Fortran program then separates those calculated E_3 values into groups of possible vibrational origins E_{30} for state 3 using an assumed B_3 value. It finds sets of lines for which a minimum number of E_{30} agree within 0.7 cm^{-1} and does a least-squares analysis on each set of lines. All these for all B_3 values are then sorted and separated into groups. Each group of origins so obtained represents a potential state 3 vibrational origin. The possible E_{30} values were then separated into progressions that could represent successive vibrational levels. After refinement of this preliminary analysis, the approximate vibrational spacing was found to be 92 cm^{-1} for the $^{127}I_2$ molecule.

TABLE 2. $^{127}I_2$ 3P1C lines and assignments

Line (cm^{-1})	v_3	v_2	v_1	J_3	J_2	J_1	Remarks
19 795.587	74	61	0	70	70	71	M
19 792.521	73	55	0	36	36	35	S
19 791.851	74	62	0	74	74	75	W
19 788.591	74	63	0	77	77	78	W
19 785.429	73	56	0	52	50	49	M
19 784.127	73	56	0	51	51	50	S
19 782.220	73	56	0	50	52	51	W
19 780.740	74	66	0	83	83	84	M
19 779.824	74	67	0	84	84	85	M
19 778.177	74	68	0	85	85	86	M
19 776.535	73	57	0	61	61	60	M
19 768.617	72	53	0	16	16	15	M
19 768.25	72	53	0	15	17	16	M
19 758.581	72	54	0	43	43	42	S
19 754.791	73	61	0	83	83	82	VS
19 751.685	73	62	0	86	86	85	VS
19 746.695	73	63	0	86	86	87	VS
19 740.068	72	56	0	67	67	66	S
19 724.560	71	53	0	48	48	47	S
19 723.252	71	53	0	45	45	46	W
19 722.601	71	53	0	47	49	48	VS
19 720.785	72	59	0	82	82	83	M
19 716.390	72	60	0	89	89	88	M
19 713.339	71	54	0	62	62	61	M
19 705.692	72	63	0	94	94	95	M
19 703.671	70	51	0	29	29	28	S
19 682.476	70	53	0	67	65	64	M
19 679.527	70	53	0	66	66	65	M
19 671.290	69	50	0	31	31	30	M
19 659.665	69	51	0	56	54	53	VS
19 657.581	69	51	0	55	55	54	VS
19 656.612	69	51	0	53	55	54	VS
19 653.828	70	56	0	87	87	88	VS
19 648.785	69	52	0	70	68	67	S
19 647.922	70	57	0	95	95	94	S
19 640.002	68	49	0	31	31	30	S
19 639.675	68	49	0	30	32	31	M
19 636.017	69	53	0	79	79	78	S
19 633.352	69	53	0	78	80	78	M
19 628.429	68	50	0	57	55	54	M
19 627.692	68	50	0	54	52	53	W
19 626.788	68	50	0	56	56	55	M
19 625.762	68	50	0	53	53	54	M
19 617.019	69	55	0	91	91	92	S
19 613.818	68	51	0	71	71	70	S
19 611.052	67	48	0	29	29	28	M
19 602.272	68	52	0	82	82	81	S
19 601.290	68	52	0	79	79	80	S
19 594.642	67	49	0	57	57	56	M
19 582.291	66	47	0	23	23	22	M
19 580.296	67	50	0	73	73	72	S
19 548.986	66	49	0	70	70	71	M
19 523.699	66	51	0	96	96	95	M
19 518.785	65	48	0	70	70	71	M
19 508.648	64	46	0	52	50	49	W
19 506.679	64	46	0	51	51	50	S
19 474.283	64	48	0	87	87	86	W
19 443.826	63	47	0	83	83	84	M
19 442.613	63	47	0	87	87	86	M
19 432.601	62	45	0	67	67	66	W
19 431.615	62	45	0	64	64	65	W
19 414.111	62	46	0	82	83	83	W
19 397.429	62	47	0	99	99	98	W
19 396.945	62	47	0	96	96	97	W
19 393.939	62	47	0	98	100	99	W
19 378.136	60	43	0	56	59	59	M

Can. J. Chem. Downloaded from www.nrcresearchpress.com by 203.198.23.82 on 09/08/12
For personal use only.

TABLE 3. Molecular constants (cm^{-1}) of the $F'O_u^+$ state relative to $v' = 60$ from analysis of the spectrum of the $^{127}I_2$ molecule

Constant	3P1C analysis	3P2C analysis	Combined analysis
$Y_{0,0}$	58 150.7(46)	58 150.99(7)	58 150.76(1)
$Y_{1,0}$	93.02(03)	92.99(56)	92.98(11)
$Y_{2,0}$	−0.014 00(35)	−0.016 12(57)	−0.013 05(37)
$Y_{0,1}$	0.017 5494(45)	0.017 4588(41)	0.017 6578(25)
$Y_{1,1} \times 10^5$	−9.606(19)	−8.369 7(75)	−9.098 0(05)
$Y_{0,2} \times 10^9$	−2.600	−2.600	−2.600
Red. χ^2	0.86	0.73	0.86

The numbers in parentheses correspond to one standard deviation in the last quoted digit.

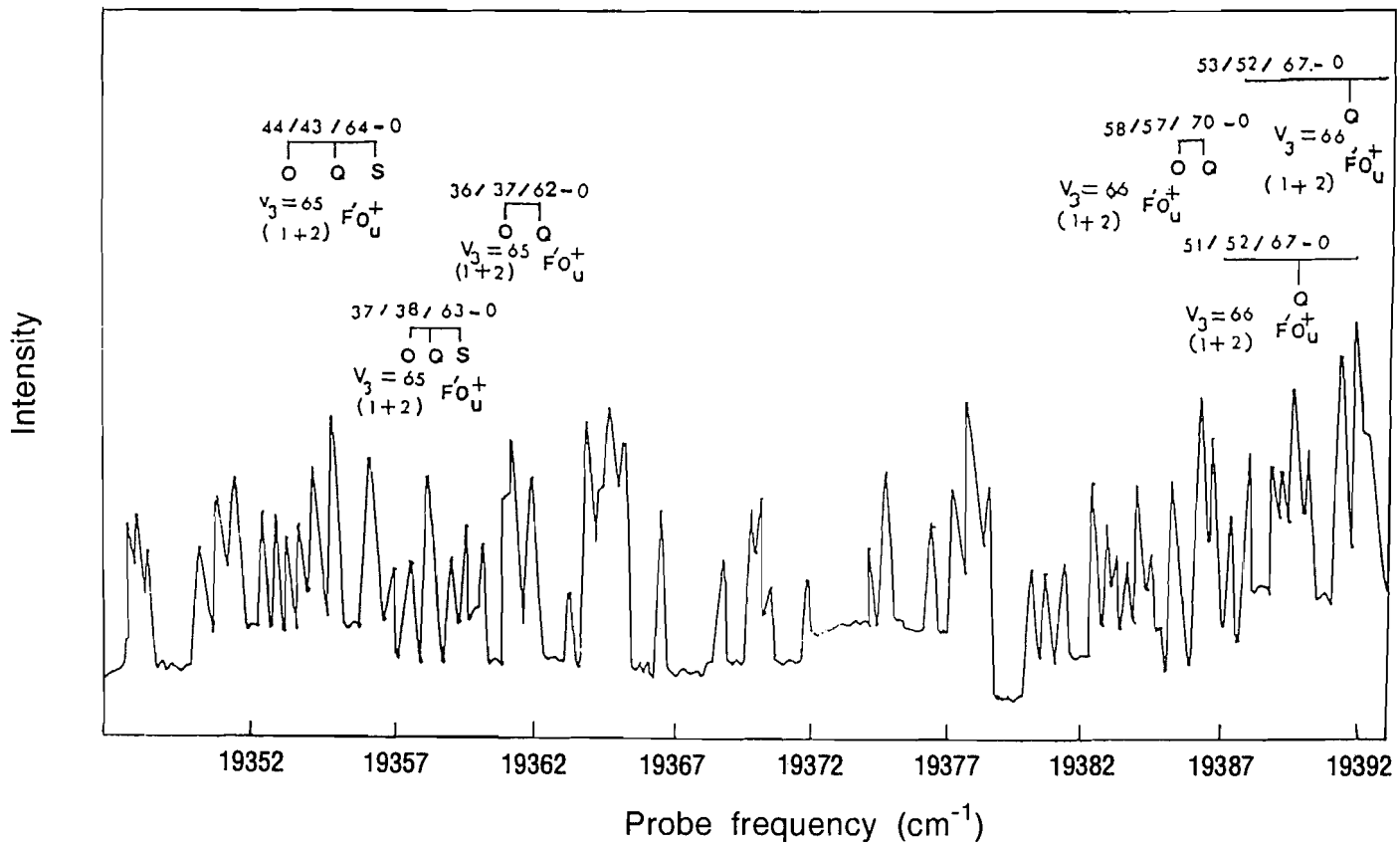

FIG. 3. 3P2C spectrum of $^{127}I_2$ molecule with the pump frequency set at 19 914.5 cm^{-1}.

Given the experimental 3P1C frequencies together with their possible assignments as pump lines and as members of the appropriate vibrational levels, a least-squares analysis was performed on the three-photon term values for each vibrational level and the rotational constants were determined.

A global least-squares fit with equal weightings was performed on all the rotational lines assigned to the $F'O_u^+$ state, using a multiple regression routine, to generate the Dunham coefficients for the upper state using:

$$[3] \quad E_3(v_3, J_3) = \Sigma_{m=0} \Sigma_{l=0} Y_{lm}(v_3 + 1/2)^l [J_3(J_3 + 1)]^m$$

for the $^{127}I_2$ isotope. Those derived molecular constants could be used to assign more 3P1C lines.

Three-photon transitions were observed for all the vibrational levels over the range $n = 0$–14, where n is an arbitrary number to be related later to the vibrational numbering. A list of 3P1C assignments for the normal molecule is given in Table 2. The molecular constants obtained from the 3P1C assignments are listed in Table 3. These parameters are given with respect to the lowest observed level ($v_3 = 60$). Figure 2 shows part of the spectrum recorded in the 19 600 cm^{-1} region for the normal isotope. The designation "R, Q" denotes an R-branch single photon B–X resonance transition from level J_1, followed by a two-photon Q-branch transition (hence $J_3 = J_1 - 1$). The figure also shows transitions to other systems (11).

Two-color spectra

With the analysis well underway, analysis of the observed 3P2C spectra was quite easy.

The two-photon-allowed rotational transitions from the pumped B state (by both (1 + 2) and (2 + 1) absorption pathways) follow the $\Delta J = 0, \pm 2$ selection rule. The ob-

Can. J. Chem. Downloaded from www.nrcresearchpress.com by 203.198.23.82 on 09/08/12
For personal use only.

TABLE 4. $^{127}I_2$ 3P2C lines and assignments

Pump (cm^{-1})	v_2	v_1	J_2	J_1	Probe (cm^{-1}) $J_3 = J_2 - 2$	$J_3 = J_2$	$J_3 = J_2 + 1$	v_3	Type
19 917.115	67	0	53	52		19 391.927	19 393.246	66	(I)
19 917.108	62	0	30	31	19 360.982	19 361.845		65	(I)
19 916.961	64	0	44	43	19 352.921	19 345.328	19 355.718	65	(I)
19 916.961	64	0	44	43	19 399.207	19 400.080		66	(I)
19 915.838	63	0	37	38	19 356.966	19 357.990	19 358.718	65	(I)
19 915.838	63	0	37	38		19 403.548		66	(I)
19 915.619	70	0	58	57	19 385.554	19 386.679		66	(I)
19 915.405	62	0	31	32	19 361.119	19 361.845		65	(I)
19 915.381	67	0	51	52		19 390.060		66	(I)
19 294.866	40	0	3	2		19 451.275		60	(I)
19 294.866	40	0	3	2		19 497.603		61	(I)
19 293.976	49	1	83	84	19 409.076	19 411.302		63	(I)
19 293.809	48	1	74	75		19 559.007		63	(II)
19 293.683	41	0	50	51	19 468.959	19 472.060		61	(I)
19 293.384	51	2	5	6		19 463.524		63	(II)
19 293.311	50	1	94	93		19 491.017		65	(I)
19 293.068	42	0	70	71		19 539.218		63	(II)
19 293.013	40	0	12	11		19 497.630		61	(I)
19 292.918	40	0	8	9		19 451.275		60	(I)
19 292.636	47	1	63	64		19 407.084		61	(I)
19 292.636	47	1	63	64		19 499.005		62	(II)
19 292.624	53	2	48	49	19 491.017	19 493.326		66	(I)
19 292.624	53	2	48	49	19 537.427	19 539.218		67	(I)
19 292.541	48	1	78	77		19 472.060		64	(I)
19 292.541	48	1	78	77		19 468.261		62	(II)
19 292.237	56	2	74	73		19 419.697		65	(I)
19 292.202	52	2	35	36		19 411.302		64	(I)
19 292.163	51	1	97	98		19 432.601		64	(I)
19 292.031	51	2	12	11		19 563.335		67	(I)
19 291.856	54	2	61	60		19 390.127	19 392.377	64	(I)
19 291.856	54	2	61	60	19 527.304	19 529.015	19 531.875	67	(I)
19 291.812	47	1	67	66		19 442.613		63	(I)
19 291.812	47	1	67	66		19 500.115		62	(II)
19 291.808	51	2	9	10		19 463.523		63	(II)
19 291.731	41	0	51	52		19 563.335		63	(I)
19 291.583	58	2	83	82		19 497.630	19 500.414	67	(I)
19 291.593	50	1	91	92		19 444.007		67	(I)
19 291.593	50	1	91	92		19 491.017		65	(I)
19 291.524	45	1	26	25	19 432.601	19 433.152		62	(I)
19 291.524	45	1	26	25		19 481.957		61	(II)
19 291.209	49	1	87	86		19 504.237		65	(I)
19 291.209	49	1	87	86		19 531.875		63	(II)

served OODR high J transitions could be assigned as triplets of lines, corresponding to $\Delta J = -2$ (O-branch), $\Delta J = 0$ (Q-branch), and $\Delta J = +2$ (S-branch). The upper state term values ($E_3(v_3, J_3)$) were calculated from eq. [4] for the (1 + 2) and from eq. [5] for the (2 + 1) transitions:

$$[4] \quad E_3(v_3, J_3) = 2\sigma(\text{NDL}) + E_2(v_2, J_2)$$

$$[5] \quad E_3(v_3, J_3) = \sigma(\text{NDL}) + \sigma(\text{BDL}) + E_2(v_2, J_2).$$

The approximate vibrational spacing was found to be 92 cm^{-1} for $^{127}I_2$.

All the observed 3P2C transitions, both (1 + 2) and (2 + 1), terminating in the F' state, were recorded using the pump and probe frequencies within the C-500 dye profile. Most of the observed OODR lines for the F' state were recorded pumping the 40–0 and 60–0 band regions of the B–X system. The intense 3P2C-observed lines resulted from pumping the higher J-lines falling within the bandhead region rather than the low J's. Figure 3 shows a sample spectrum recorded for this state in the 19 350 cm^{-1} region, pumping at 19 914.5 cm^{-1}. The 3P2C spectral lines were observed to arise not only from a σ(BDL) + 2σ(NDL) absorption process, (1 + 2), but also from a σ(BDL) + σ(BDL) + σ(NDL) transition sequence, (2 + 1). Two O, Q, and S triplets are shown in the figure for the (1 + 2) absorption mode corresponding to the $v_3 = 65$ vibrational level with the Q-lines at 19 355 and 19 358.5 cm^{-1}. The figure also shows some strong lines for the $v_3 = 66$ vibrational level in the (1 + 2) mode.

Transitions were recorded over the $n = 0$–8 vibrational range for the F' state. A summary of the 3P2C assignments is given in Table 4. The term values for state 3 calculated according to eqs. [4] and [5] are used to calculate the molecular constants for the state using a multivariate least-

Can. J. Chem. Downloaded from www.nrcresearchpress.com by 203.198.23.82 on 09/08/12
For personal use only.

TABLE 5. Dunham parameters of the $F'O_u^+$ state derived from amalgamation of this study with the work of ref. 9

Constant	Dunham coefficients (cm^{-1})	
	This study	Ref. 9
$Y_{0,0}$	51 705.528	51 706.237 0
$Y_{1,0}$	131.327(02)	131.000 410
$Y_{2,0}$	−0.549 80(73)	−0.516 270
$Y_{3,0}$	$5.450(68) \times 10^{-3}$	$4.264\ 0 \times 10^{-3}$
$Y_{4,0}$	$-6.232\ 4(66) \times 10^{-5}$	$-4.579\ 73 \times 10^{-5}$
$Y_{5,0}$	$3.62(5) \times 10^{-7}$	$2.831\ 837 \times 10^{-7}$
$Y_{0,1}$	0.021 948 99	0.021 948 99
$Y_{1,1}$	$-9.250\ 800 \times 10^{-5}$	$-9.250\ 800 \times 10^{-5}$
$Y_{2,1}$	$2.447\ 94(32) \times 10^{-7}$	8.359×10^{-7}
$Y_{3,1}$		-8.550×10^{-9}
$Y_{0,2}$	-2.600×10^{-9}	-2.632×10^{-9}
Red. χ^2	0.95	
Constants valid over:	v_3 = 0–74	0–38

Constants are relative to the ground state potential minumum, $Y_{0,2}$ constrained to its theoretical value -2.600×10^{-9}. The numbers in parentheses correspond to one standard deviation in the last quoted digit.

squares routine. The resulting molecular constants are listed in Table 3.

Spectral assignment of the $F'O_u^+$ state

Initial attempts to assign this state to a lower lying ion-pair state focused on the $DO_u^+(^3P_2)$, $F\ O_u^+(^3P_0)$, and $F'O_u^+(^1D)$ states. Previous work on both the D and F states (16) suggested that the vibrational spacing of these states would be much less than 92 cm^{-1} observed in this region of the spectrum. This leaves the F' state as a possible assignment for this upper state. Spectroscopic data for the low vibrational levels of the F' state were reported in refs. 9 and 17. As an initial step, the low v_3 data from ref. 9 were integrated into the analysis. Polynomial fits were made by letting the level designated as $n = 0$ take the values 58–62. The fits were judged by their standard deviations and also on how well the calculated values of $Y_{0,0}$ and $Y_{0,1}$ compared with the values obtained from the low v data. The fit that best represented the combination of both sets of data gave $n = v_3 - 60$. The results of this final fit are listed in Table 5.

The upper state of the analysed transitions was assigned as $F'O_u^+(^1D)$. The current study represents the first vibrational and rotational analysis of this ion-pair state in this energy region, as all previous work had been confined to low v analysis. This study also gives the first high-resolution 3P1C analysis for the iodine molecule in this energy region of the spectra. The MPI spectra recorded by Lehmann et al. (10), which they did not analyse, can be, in part, satisfactorily explained as resonance-enhanced 3P1C transitions to the $F'O_u^+$ state, see Table 2, and the rest of the lines from ref. 10 were assigned to three-photon states lying in the same energy region (11).

Acknowledgments

The author would like to express her gratitude to Professor G.W. King of the Chemistry Department at McMaster University, Hamilton, Ont., Canada, for suggesting the problem, in multiphoton laser spectroscopy, while supervising the author's doctoral study.

1. K.P. Huber and G. Herzberg. Molecular spectra and molecular structure IV. Constants of diatomic molecules. Van Nostrand, Princeton. 1979.
2. R.S. Mulliken. J. Chem. Phys. **55**, 288 (1971).
3. J. Tellinghuisen. J. Mol. Spectrosc. **94**, 231 (1982).
4. J.P. Perrot, M. Broyer, J. Chevaleyre, and B. Femelat. J. Mol. Spectrosc. **98**, 161 (1983).
5. J. Tellinghuisen. Chem. Phys. Lett. **99**, 373 (1983).
6. J.C.D. Brand, A.R. Hoy, A.K. Kalkan, and A.B. Yamashita. J. Mol. Spectrosc. **95**, 350 (1983).
7. G.W. King, I.M. Littlewood, and J.R. Robins. Chem. Phys. **56**, 145 (1981).
8. K.S. Viswanathan and J. Tellinghuisen. J. Mol. Spectrosc. **101**, 285 (1983).
9. T. Ishiwata, A. Tokunaga, T. Shinzawa, and I. Tanaka. J. Mol. Spectrosc. **117**, 89 (1986).
10. K.K. Lehmann, J.S. Smolarek, and L. Goodman. J. Chem. Phys. **69**, 1569 (1978).
11. F.S.M. Abd El-Hameed. Ph.D. Thesis, McMaster University, Hamilton, Ont., Canada. 1990.
12. A.J. Kearsley, A.J. Andrews, and C.E. Webb. Opt. Commun. **31**, 181 (1979).
13. S. Gersternkorn and P. Luc. Atlas du spectra d'absorption de la molecule d'iode entre 14 800 et 20 000 cm^{-1}. Éditions du CNRS, Paris. 1978.
14. J.M. Hutson, S. Gerstenkorn, P. Luc, and J. Sinzelle. J. Mol. Spectrosc. **96**, 266 (1982).
15. J.W. Tromp and R.J. LeRoy. J. Mol. Spectrosc. **109**, 352 (1985).
16. A.D. Williamson and R.N. Compton. Chem. Phys. Lett. **62**, 295 (1979).
17. T.D. McLean. Ph.D. Thesis, McMaster University, Hamilton, Ont., Canada, 1987.

Can. J. Chem. Downloaded from www.nrcresearchpress.com by 203.198.23.82 on 09/08/12
For personal use only.

Conformational preferences and barriers to internal rotation in fluorothioanisoles from long-range spin–spin couplings, photoelectron spectroscopy, and semiempirical molecular orbital calculations

DIETMAR CHMIELEWSKI, NICK HENRY WERSTIUK, AND TIMOTHY A. WILDMAN[1]

Department of Chemistry, McMaster University, 1280 Main Street West, Hamilton, ON L8S 4M1, Canada

Received June 15, 1993

This paper is dedicated to Professor Gerald W. King on the occasion of his 65th birthday

DIETMAR CHMIELEWSKI, NICK HENRY WERSTIUK, and TIMOTHY A. WILDMAN. Can. J. Chem. **71**, 1741 (1993).

The conformational preferences and barriers to internal rotation about the S—C(phenyl) bond have been investigated for thioanisole and its 2-fluoro, 2,6- and 3,5-difluoro, and 2,3,5,6-tetrafluoro derivatives. Measurements of long-range spin–spin couplings between the methyl carbon and the *para* ring proton indicate that the 2-fluoro and 3,5-difluoro compounds prefer conformations with all heavy atoms coplanar. The 2,6-difluoro and 2,3,5,6-tetrafluoro compounds prefer conformations in which the methyl carbon lies in or near the plane perpendicular to the aromatic ring. Semiempirical molecular orbital calculations with the MNDO method indicate that all of the molecules prefer perpendicular conformations while similar calculations with AM1 indicate that all prefer planar conformations. Apparently the conformational behaviour can be quite sensitive to subtle changes in intramolecular interactions, which may indicate improvements to these semiempirical methods. The NMR results have been used to derive an internally consistent set of rotational potentials. Synthetic photoelectron spectra derived from these potentials and the AM1 orbital energies are in good agreement with the experimental spectra.

DIETMAR CHMIELEWSKI, NICK HENRY WERSTIUK et TIMOTHY A. WILDMAN. Can. J. Chem. **71**, 1741 (1993).

On a examiné les préférences conformationnelles et les barrières à la rotation interne autour de la liaison S—C(phényle) dans le thioanisole et ses dérivés 2-fluoro-, 2,6- et 3,5-difluoro- et 2,3,5,6-tétrafluoro-. Des mesures des couplages spin–spin à longue distance entre le carbone du méthyle et le proton en *para* du cycle indiquent que, dans les conformations préférées des composés 2-fluoro- et 3,5-difluoro-, les atomes lourds sont coplanaires. Dans les conformations privilégiées des composés 2,6-difluoro- et 2,3,4,6-tétrafluoro- le carbone du groupe méthyle se trouve dans le, ou près du, plan perpendiculaire au noyau aromatique. Des calculs semiempiriques d'orbitales moléculaires avec la méthode MNDO indiquent que toutes les molécules préfèrent des conformations perpendiculaires alors que des calculs semblables à l'aide de la méthode AM1 indiquent que chacun préfère les conformations planaires. Il semble que le comportement conformationnel peut être très sensible à des changements subtils dans les interactions intramoléculaires; ceci peut indiquer des méthodes pour améliorer les méthodes semiempiriques. On a utilisé les résultats de la RMN pour développer un ensemble autocohérent de potentiels rotationnels. Les spectres photoélectroniques de synthèse derivés de ces potentiels et les énergies orbitalaires obtenues à l'aide de la méthode AM1 sont en bon accord avec les spectres expérimentaux.

[Traduit par la rédaction]

Can. J. Chem. Downloaded from www.nrcresearchpress.com by 203.198.23.82 on 09/08/12
For personal use only.

Introduction

The important role of molecular conformation in the determination of chemical reactivity and molecular recognition is abundantly clear. In addition to experimental probes, quantum mechanical models of molecular electronic structure are increasingly important means of assessing subtle changes in conformational preferences and internal motions. Confidence in the use of computational methods is largely based on their demonstrable success in reproducing certain empirical results.

In this article, the conformational behavior of the thiomethyl group in a number of fluorothioanisoles is reported. The aims of this investigation are (1) to develop a consistent picture of the conformational behaviour of these thioanisoles and (2) to examine the reliability of results from semiempirical methods for such molecules. Long-range NMR spin–spin coupling constants are used to examine conformational preferences and to derive barriers to internal rotation. These preferences and barriers are compared with those from semiempirical molecular orbital (MO) calculations. The resulting empirical and semiempirical potentials are used to derive synthetic photoelectron spectra for comparison with the experimental spectra. This comparison serves to test the consistency of the experimental and computational results and to illustrate the utility of photoelectron spectroscopy (PES) for the study of conformational behaviour in highly flexible molecules.

In thioanisole (1, 2), as in thiophenol (3, 4), the barrier to internal rotation about the S—C1(phenyl) bond is determined largely by conjugation between the sulphur 3*p*-orbital and the π-system. This interaction gives rise to a predominantly twofold barrier to internal rotation. Molecular orbital calculations indicate the presence of a relatively small fourfold component, but this has not yet been observed experimentally. If the dihedral angle about the S—C1 bond is denoted by ϕ = Me—S—C1—C2, where $\phi = 0°$ or 180° corresponds to a structure in which the methyl carbon is coplanar with the aromatic ring, such barriers have the form

$$[1a] \quad V(\phi) = V_2 \sin^2(\phi)$$

if planar conformations ($\phi = 0°$ or 180°) are energetically more stable or

$$[1b] \quad V(\phi) = V_2[1 - \sin^2(\phi)] = V_2 \cos^2(\phi)$$

if the perpendicular conformations ($\phi = 90°$ or 270°) are preferred. For a mono-*ortho*-substituted compound, the *syn* conformation is arbitrarily selected as $\phi = 0°$; thus the *anti* conformation corresponds to $\phi = 180°$.

[1]Author to whom correspondence may be addressed. Present address: 15 Danbury Street, Dundas, ON L9H 4P6, Canada.

Can. J. Chem. Downloaded from www.nrcresearchpress.com by 203.198.23.82 on 09/08/12
For personal use only.

It is well known that certain long-range spin–spin coupling constants between nuclei in the side chain and the aromatic ring of benzene derivatives have a simple conformational dependence (5–7). In particular, the coupling over six formal bonds between the methyl carbon and the *para* ring proton, $^6J_p^{C,H}$, has the form

$$[2] \quad {}^6J_p^{C,H} = {}^6J_{90}^{C,H}\langle\sin^2(\phi)\rangle$$

where $^6J_{90}^{C,H}$ is an empirical constant appropriate to the class of compounds under investigation (−0.56(2) Hz) (1) and ⟨...⟩ denotes an expectation value. Because $\langle\sin^2(\phi)\rangle$ and thus $^6J_p^{C,H}$ may be computed as a function of V_2 in eq. [1] for hindered internal rotation, comparison of the experimentally measured value of $^6J_p^{C,H}$ with tables of computed values provides an estimate of the barrier height in addition to information concerning the conformational preference. Clearly, the success of this method relies upon the constancy of $^6J_{90}^{C,H}$. INDO FPT calculations on 2-fluoroanisole indicate that a single *ortho* fluorine substituent changes $^6J_{90}^{C,H}$ by 0.01 Hz at most and the intrinsic effect of two fluorine substituents on $^5J^{C,C}$ is typically a reduction of less than 5% (7). According to these findings, the expected variation of $^6J_{90}^{C,H}$ within the present series of compounds is on the order of the estimated error.

Although conformational preferences have a profound influence on chemical reactivity, their knowledge provides only a partial description of the underlying conformational distribution. Empirical evidence can be derived from relatively slow methods, like NMR, that provide averages over the conformational potential energy hypersurface, or from fast methods, like PES, that examine all conformations on the hypersurface. In this work, empirical potentials from eq. [2] and semiempirical potentials from MO calculations have been used in conjunction with computed angle-dependent orbital energies to generate synthetic photoelectron spectra. A comparison of synthetic and experimental spectra has been performed to support the interpretation of the NMR data and to determine the utility of PES for the study of conformational distributions.

Experimental and computational method

The compounds examined in this study were prepared by standard methods. The fluorothioanisoles were obtained by methylation of the corresponding fluorothiophenols with dimethyl sulphate. The fluorothiophenols were synthesized from the corresponding fluoroanilines (Aldrich) by the xanthate method (8).

Precision bore, 5 mm o.d. NMR tubes, containing solutions of about 5 mol% of the fluorothioanisole in acetone-d_6 and TMS, were degassed by several freeze–pump–thaw cycles. ^{1}H and ^{13}C NMR spectra were recorded on a Bruker AM500 or AC300 spectrometer at a probe temperature of 303 K unless otherwise indicated. The DEPT pulse sequence (9) was used to obtain proton-coupled ^{13}C spectra of the methyls.

Photoelectron spectra were recorded on a noncommercial instrument described previously (10). Spectra were obtained by signal averaging of 20–30 scans. Argon was used as a calibration standard.

Semiempirical MO calculations were performed using the packages AMPAC 2.10 and MOPAC 5.00 on a Sun 3/60 workstation. AM1 parameters for sulphur were incorporated from ref. 11. Full geometry optimizations were performed for fixed values of the Me—S—C1—C2 torsion angle at 15° increments between 0° and 180°. Convergence criteria were tightened through use of the keyword "PRECISE." Synthetic photoelectron spectra were computed with the program PESPEC (12) on the basis of the calculated angular dependencies of the orbital energies and heats of formation.

TABLE 1. Long-range ^{13}C,^{1}H coupling constants for thioanisoles

Compound	$^6J_p^{C,H}$ (Hz)	$\langle\sin^2(\phi)\rangle$	Preferred conformation[a]
Thioanisole	−0.147(3)[b]	0.26(1)	0°
2-Fluoro	−0.18(3)	0.32(6)	180°
2,6-Difluoro	−0.42(3)	0.75(6)	90°
3,5-Difluoro	<−0.1	<0.18	0°
2,3,5,6-Tetrafluoro	−0.36(2)	0.64(4)	90°

[a]ϕ = 0° and 180° or ϕ = 90° and 270° are equivalent by symmetry, except for 2-fluorothioanisole.
[b]Reference 1.

Results and discussion

Conformational preferences on the basis of long-range ^{13}C,^{1}H couplings

The long-range ^{13}C,^{1}H couplings are listed in Table 1, along with values of $\langle\sin^2(\phi)\rangle$ derived under the assumption that $^6J_{90}^{C,H}$ is −0.56(2) Hz in eq. [2] (1). Free rotation corresponds to $\langle\sin^2(\phi)\rangle$ = 0.5. For a simple, twofold barrier, values smaller than 0.5 indicate that planar conformations are preferred (ϕ = 0° or 180°) while values greater than 0.5 indicate that the methyl carbon prefers to lie in the plane perpendicular to the ring plane (ϕ = 90° or 270°). Qualitatively, the numbers in Table 1 are evidence that thioanisole and its 2-fluoro and 3,5-difluoro derivatives prefer planar conformations. The 2,6-difluoro and 2,3,5,6-tetrafluoro derivatives on the other hand prefer perpendicular conformations. This behaviour might be attributable to repulsions between the methyl and *ortho* fluorine substituents. Of course, within the σ–π separation approximation, the electronegative *ortho* fluorine substituent is expected to withdraw electron density from the σ-framework and donate electron density to the π-system, thereby lowering the barrier to internal rotation. This effect is insufficient to explain the preference for a nonplanar conformation.

In light of the above discussion, the conformational preference of 2-fluorothioanisole points to the dominant effect. If repulsions are more important than the substituent effect on the barrier, 2-fluorothioanisole should prefer the planar *anti* conformer to allow conjugation between sulphur orbitals and the π-system while avoiding methyl–fluorine repulsion. In fact, the magnitude of $^4J_o^{C,F}$ is 2.37(2) Hz at 303 K, smaller than the values in the 2,6-difluoro (3.62 Hz) and 2,3,5,6-tetrafluoro (3.93 Hz) derivatives. Because this coupling has a large proximate contribution that decreases as the nuclei are separated, the magnitude is an indication of the distance between the coupled nuclei (7, 13). This suggests that the methyl carbon and fluorine nuclei are well separated in the preferred conformation of 2-fluorothioanisole. Moreover, from variable-temperature NMR experiments, the magnitude of $^4J_o^{C,F}$ decreases as the probe temperature decreases: $^4J_o^{C,F}$ in 2-fluorothioanisole is about 1.45 Hz at 220 K. Because a reduction in temperature sharpens the distribution of conformations about the minimum energy conformation, this observation further supports the notion that the carbon and fluorine nuclei are distant from one another in the preferred conformation.

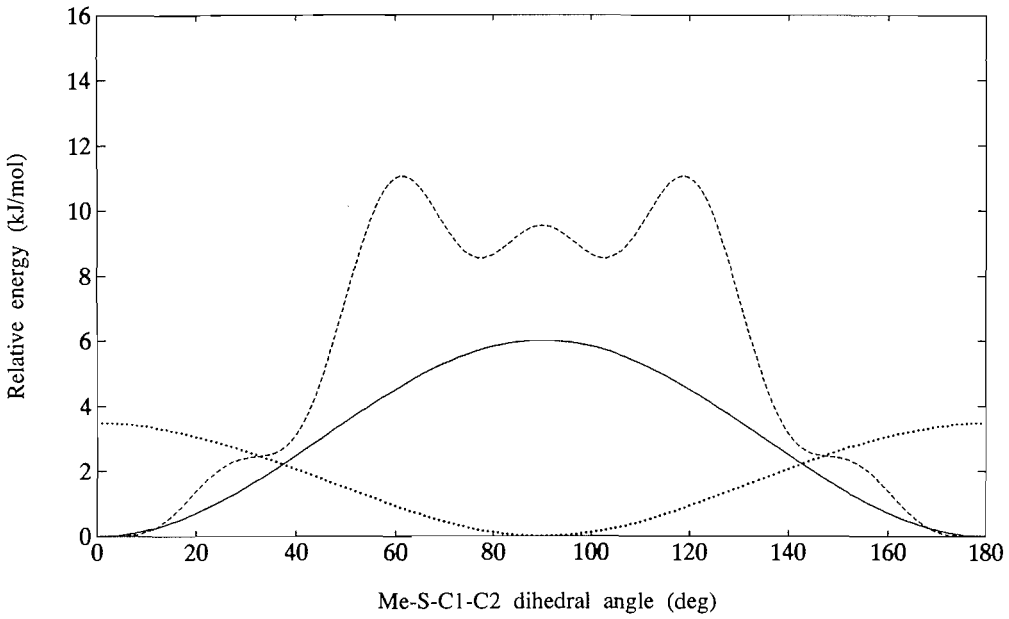

FIG. 1. Barriers to internal rotation about the exocyclic C1—S bond in thioanisole. Dotted (MNDO) and dashed (AM1) lines correspond to relative heats of formation from semiempirical computations. The solid line represents a purely twofold barrier derived from the observed value of $^6J_p^{C,H}$ in ref. 1.

TABLE 2. Barriers to internal rotation about the sulphur–phenyl bond in thioanisoles

Compound	V_2 (kJ mol^{-1}) MNDO[b]	AM1[c]	NMR	Preferred conformation[a]
Thioanisole	3.4	10.7	5.4[d]	0°
2-Fluoro	8.4	6.9	0	180°
2,6-Difluoro	14.8	2.3	6	90°
3,5-Difluoro	1.3	13.1	9	0°
2,3,5,6-Tetrafluoro	12.2	7.2	3	90°

[a]From $^6J_p^{C,H}$.
[b]Perpendicular conformations are preferred (ϕ = 90°).
[c]Planar conformations are preferred (ϕ = 0°).
[d]Reference 1.

Results of semiempirical MO calculations

The dependence of the relative energy on the Me—S—C1—C2 dihedral angle, ϕ, in thioanisole in shown in Fig. 1. A dotted line represents the relative heats of formation from MNDO (14) calculations. Barrier heights for all compounds are summarized in Table 2. For each molecule, the MNDO results indicate that the preferred conformer corresponds to a dihedral angle of about 90°. Even for 2-fluorothioanisole, for which the *anti* conformer is slightly lower in energy than the *syn*, both planar conformers are relative maxima. This finding is obviously contrary to the implications of the long-range $^{13}C,^1H$ couplings described in the preceding section: empirically, it is clear that thioanisole, 2-fluorothioanisole, and 3,5-difluorothioanisole prefer planar conformations. The pattern of the MNDO results may arise from the underestimation of resonance stabilization or the overestimation of steric repulsion in the MNDO model, which are recognized weaknesses (15). This deficiency was remedied by the modification of core repulsion functions (CRFs) in the AM1 method (15, 16), which generally appears to yield reliable estimates of heats of formation, geometries, and certain other properties at a fraction of the cost of ab initio computations (11).

The dashed line in Fig. 1 represents the relative heats of formation from calculations employing AM1. With the AM1 parametrization, all of the molecules prefer planar conformations, which is again at variance with the experimental results. However, the discrepancies now coincide with the presence of *ortho* fluorine substituents. This correspondence holds even in the case of a single *ortho* fluorine substituent: according to the AM1 results, 2-fluorothioanisole prefers the *syn* conformation (ϕ = 0°), but experimentally it prefers the *anti* conformation (ϕ = 180°), like 2-fluoroanisole (17). It seems that AM1 slightly underestimates the steric repulsions between the methyl and phenyl moieties or, alternatively, overestimates stabilization of the planar conformations through changes to the resonance integral parameters (11), leading to excessively high barriers in thioanisole and 3,5-difluorothioanisole and to incorrect conformational preferences in the 2-fluoro-, 2,6-difluoro-, and 2,3,5,6-tetrafluorothioanisoles.

Parenthetically, "hybrid calculations" that employed AM1 parameters for all atoms except sulphur and MNDO parameters for sulphur alone produced the correct conformational preferences for all compounds. Dewar describes the use of MNDO parameters within AM1 as "wholly unacceptable" (11), a view with which we concur.

It may be worthwhile to note that geometry-optimized, restricted Hartree–Fock (RHF) calculations with the STO-3G basis yield a twofold barrier of 14.85 kJ mol^{-1} for thiophenol, which is found to be preferentially planar (18). RHF computations with larger bases, even split-valence sets augmented by *d*-orbitals on heavy atoms, fail to reproduce the experimental preference. Inclusion of *d*-orbitals reduces the energy difference between the planar and perpendicular conformations but the latter remains the more stable. Of course, all such results refer to the gas phase while the present NMR experiments were performed on dilute solutions,

Can. J. Chem. Downloaded from www.nrcresearchpress.com by 203.198.23.82 on 09/08/12
For personal use only.

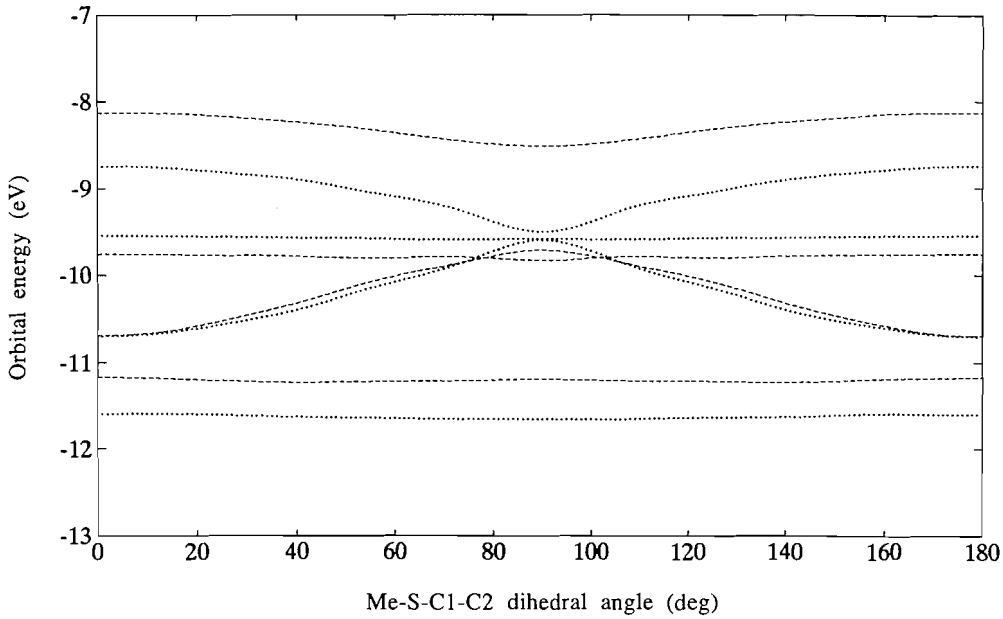

FIG. 2. Angle-dependent energies of the four highest occupied MOs of thioanisole from semiempirical calculations with MNDO (dotted lines) and AM1 (dashed lines) methods.

Can. J. Chem. Downloaded from www.nrcresearchpress.com by 203.198.23.82 on 09/08/12
For personal use only.

for which solvent effects could play a role. However, an earlier comparison of barriers in *para*-substituted thiophenols determined by NMR and by microwave spectroscopy provides evidence that solvents have little effect (3).

MNDO and AM1 orbital energies were computed as a function of dihedral angle ϕ at 15° intervals, as mentioned above. Representative results for thioanisole appear in Fig. 2. The continuity of these curves was established by monitoring the smooth change in composition of the various MOs from calculations with different ϕ-values. The most noticeable difference between the methods is the lower ionization energy of the highest occupied molecular orbital, the sulphur lone pair, with AM1.

Potentials from long-range C,H couplings

Given the inability of both semiempirical methods to provide a satisfactory description of the conformational behaviour of the fluorothioanisoles under study, the possibility of using the coupling $^6J_p^{C,H}$ to develop an internally consistent set of potentials was investigated. Strict additivity of components was assumed. From RHF calculations with the STO-3G basis, the potential for internal rotation about the sulphur–phenyl bond in thioanisole is (19)

$$[3] \quad V(\phi) = (5.8 \pm 0.2)\sin^2(\phi) + (2.4 \pm 0.2)\sin^2(2\phi) - (0.6 \pm 0.2)\sin^2(3\phi)$$

The fourfold and sixfold components give rise to shallow secondary minima at $\phi = 90°$ and 270°. The relative maxima are thus shifted from 90° and 270° to about 60°, 120°, 240°, and 300°. For the present purpose, truncation of eq. [3] after the first term will suffice. The twofold component is consistent with the values of $^6J_p^{C,H}$ in the present and previous work (1), and with other methods that yield barriers between 2.5 and 18.4 kJ mol^{-1} (20).

From $^6J_p^{C,H}$ in 2,6-difluorothioanisole, $\langle\sin^2\phi\rangle$ is 0.75, which is consistent with a twofold barrier of the form

$$[4] \quad V(\phi) = V_2\cos^2(\phi) = (5.9 \pm 1.2)\cos^2(\phi)$$

The barrier height, 5.9 ± 1.2 kJ mol^{-1}, is obtained from comparison of the measured $\langle\sin^2\phi\rangle$ with a table of values computed from

$$[5] \quad \langle\sin^2\phi\rangle = \frac{\int d\phi \sin^2\phi \exp[-V(\phi)/k_BT]}{\int d\phi \exp[-V(\phi)/k_BT]}$$

for various barrier heights. Equation [4] can be rewritten as

$$[6] \quad V(\phi) \approx 6 - 12\sin^2(\phi) + 6\sin^2(\phi)$$

where the last term corresponds to the (truncated) potential in thioanisole itself. Under the assumption of strict additivity of potential components, the two *ortho* fluorine substituents reduce the twofold component by 12 kJ mol^{-1}. One might infer that each *ortho* substituent reduces V_2 by 6 kJ mol^{-1}. That would imply that the twofold component of the barrier in 2-fluorothioanisole is close to zero while the onefold component is 6 kJ mol^{-1}:

$$[7] \quad V(\phi) \approx V_1\sin^2(\phi/2) - 6\sin^2(\phi) + 6\sin^2(\phi) = V_1\sin^2(\phi/2)$$

where the first two terms represent the one- and twofold components due to a single *ortho* fluorine substituent and the last term represents the potential in thioanisole itself. This presumption is consistent with the AM1 results above, which indicate a 4 kJ mol^{-1} decrease in the twofold component if a single *ortho* fluorine substituent is present. V_1 is 2.6 kJ mol^{-1} according to the AM1 energies and only −0.4 kJ mol^{-1} according to the MNDO energies.

From $^6J_p^{C,H}$ in 2,3,5,6-tetrafluorothioanisole, $\langle\sin^2\phi\rangle$ is 0.64 and the twofold potential is found to be

$$[8] \quad V(\phi) = (3.0 \pm 0.9)\cos^2(\phi) \approx 3 - 3\sin^2(\phi)$$

In comparison with the potential for the 2,6-difluoro derivative, the addition of the *meta* fluorine substituents makes nonplanar conformations less stable. By combining this po-

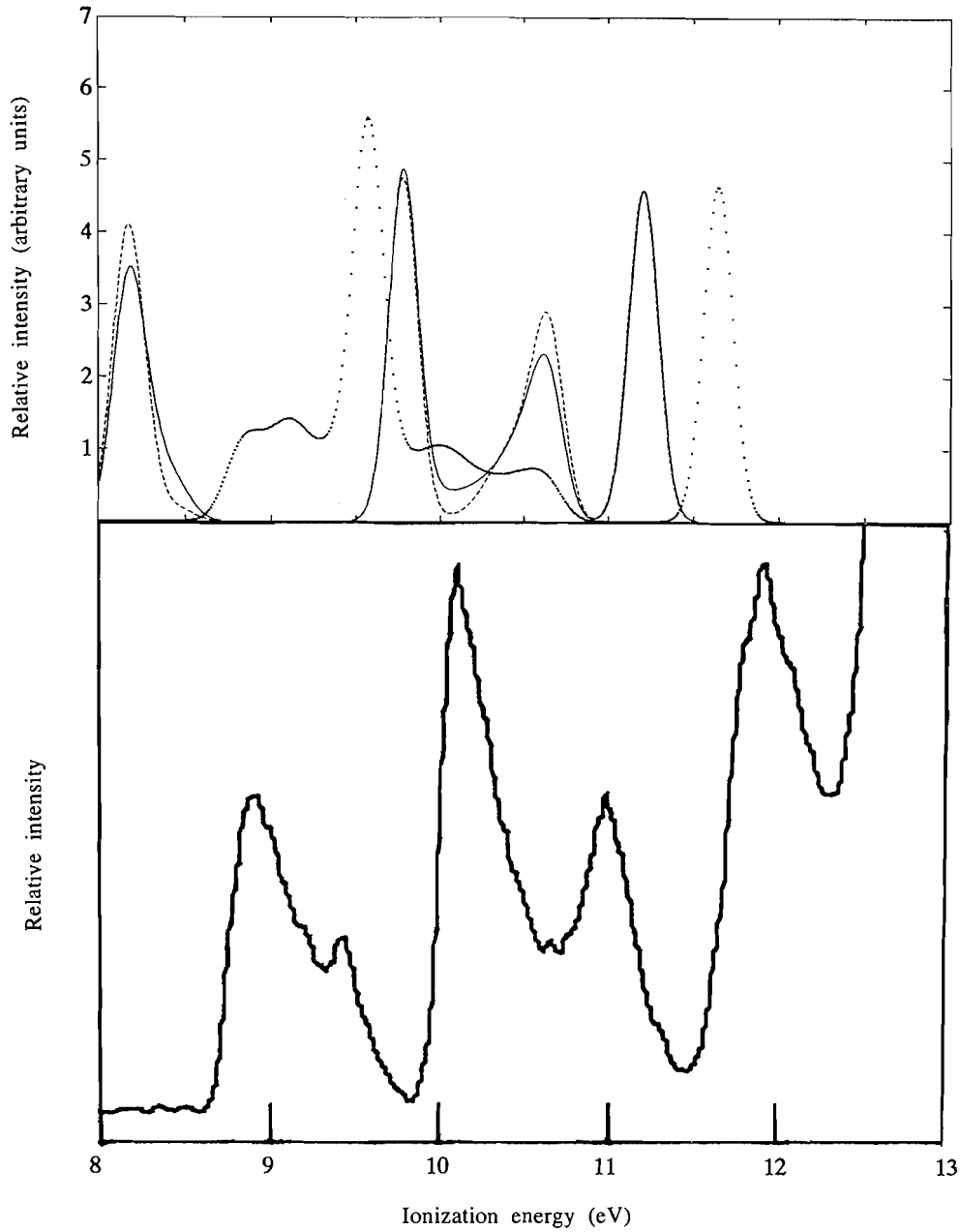

FIG. 3. The photoelectron spectrum of thioanisole. Synthetic spectra based on the MNDO (dotted line) and AM1 (dashed line) results appear in the upper panel. The solid line was obtained from the hindering potential derived from the NMR data and the AM1 orbital energies. The actual spectrum appears in the lower panel.

Can. J. Chem. Downloaded from www.nrcresearchpress.com by 203.198.23.82 on 09/08/12
For personal use only.

tential with those for thioanisole and 2,6-difluorothioanisole, the potential for 3,5-difluorothioanisole is

$$[9] \quad V(\phi) = 6\sin^2(\phi) + [3 - 3\sin^2(\phi)] - [6 - 12\sin^2(\phi) + 6\sin^2(\phi)] = -3 + 9\sin^2(\phi)$$

i.e., the *meta* fluorine substituents raise the twofold barrier by about 3 kJ mol^{-1} relative to thioanisole. It follows that ${}^6J_p^{C,H}$ for 3,5-difluorothioanisole, which is certainly less than 0.1 Hz in magnitude, should be smaller than that for thioanisole itself (−0.147 Hz), as found experimentally. Thus, all of these findings are internally consistent. Barriers are summarized in Table 2.

Photoelectron spectra

Synthetic photoelectron spectra were generated by a method given previously (12). Briefly, the angular dependencies of the conformational energy and orbital energies are expressed as Fourier series. The intensity of a spectral band at a given ionization energy is proportional to the thermal population density of conformations at the corresponding dihedral angle. Calculations were made for a sample temperature of 300 K. Because a proper calculation of the vibronic structure is beyond the available resources, the intensity distribution is convoluted with a Gaussian lineshape (FWHH = 0.2 eV) to approximate the Franck–Condon envelope.

Three sets of calculations were performed for each com-

Can. J. Chem. Downloaded from www.nrcresearchpress.com by 203.198.23.82 on 09/08/12
For personal use only.

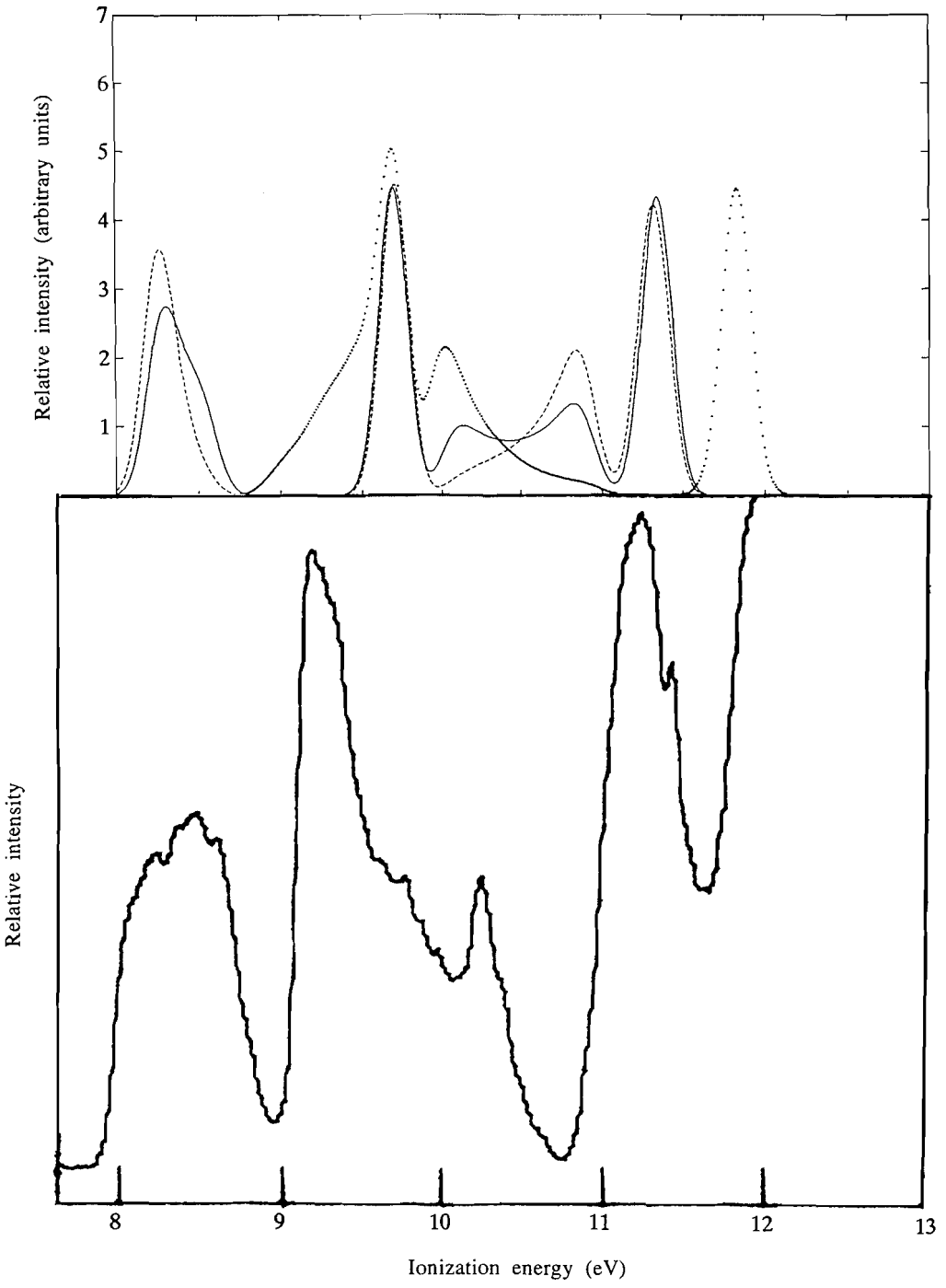

FIG. 4. The photoelectron spectrum of 2-fluorothioanisole. Synthetic spectra based on the MNDO (dotted line) and AM1 (dashed line) results appear in the upper panel. The solid line was obtained from the AM1 orbital energies and a purely onefold 6 kJ mol^{-1} barrier favouring the *anti* orientation. The actual spectrum appears in the lower panel.

pound: one in which the MNDO orbital energies and potentials were used to compute a synthetic spectrum (MNDO spectrum); one in which the AM1 results were used to compute a spectrum (AM1 spectrum); and one in which the AM1 orbital energies were used with the empirical potentials derived from $^6J_p^{C,H}$. Experimental and synthetic spectra appear in Figs. 3–7. For the synthetic spectra, dashed lines correspond to AM1 results, dotted lines correspond to MNDO results.

In comparison with the experimental spectra, it is apparent that the AM1 spectrum is a better reproduction if the molecule prefers a planar conformation, but the MNDO spectrum is better if the molecule prefers the perpendicular conformation. Because the angular dependencies of the orbital energies are quite similar, this observation merely reflects the fact that planar conformations are always preferred in the AM1 calculations and perpendicular ones are always preferred in the MNDO calculations, as described above. However, neither of these sets is consistent with the entire set of experimental spectra. Calculations that combine the internally consistent empirical potentials inferred from $^6J_p^{C,H}$ with the AM1 orbital energies yield a set of synthetic spec-

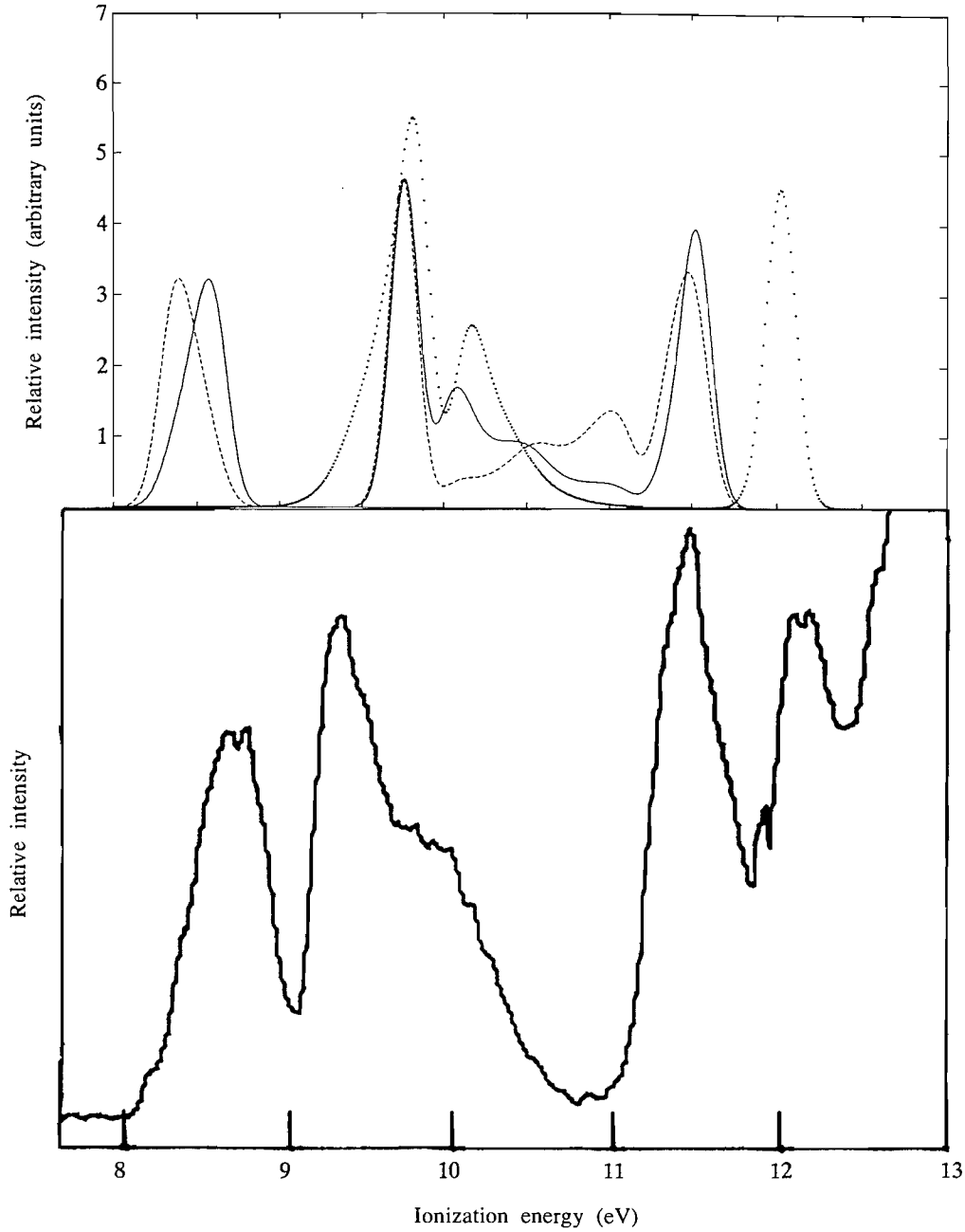

FIG. 5. The photoelectron spectrum of 2,6-difluorothioanisole. Synthetic spectra based on the MNDO (dotted line) and AM1 (dashed line) results appear in the upper panel. The solid line was obtained from the hindering potential derived from the NMR data and the AM1 orbital energies. The actual spectrum appears in the lower panel.

tra that is in good agreement with all of the experimental spectra. These synthetic spectra are plotted as solid lines in Figs. 3–7.

The synthetic spectra of thioanisole appear in Fig. 3. Clearly the spectrum based on the MNDO results bears little resemblance to the experimental one. This primarily reflects the method's incorrect description of the rotational potential. Both the spectrum based on the AM1 results and that based on the AM1 orbital energies with the potential derived from ${}^6J_p^{C,H}$ are better representations. Both also resemble the spectrum calculated previously on the basis of empirical data (21). The present calculations indicate strong temperature dependencies for the intensities of the high-energy shoulder on the lowest energy peak and the long, low-energy shoulder on the third peak, both shoulders being associated with nonplanar conformations. Such effects have been observed in the variable temperature photoelectron spectrum (22). Thus, the photoelectron spectrum does indicate that thioanisole prefers the planar conformation and the spectrum is not inconsistent with a twofold barrier of about 5 kJ mol^{-1}. Attempts to reproduce the experimental spectra more exactly are not warranted given the crudity of the present computational model and the available orbital energies.

For 2-fluorothioanisole, the breadth of the first and third peaks in Fig. 4 demonstrates that the methyl group can undergo a large amplitude libration about the planar minimum in the rotational potential because the twofold com-

Can. J. Chem. Downloaded from www.nrcresearchpress.com by 203.198.23.82 on 09/08/12
For personal use only.

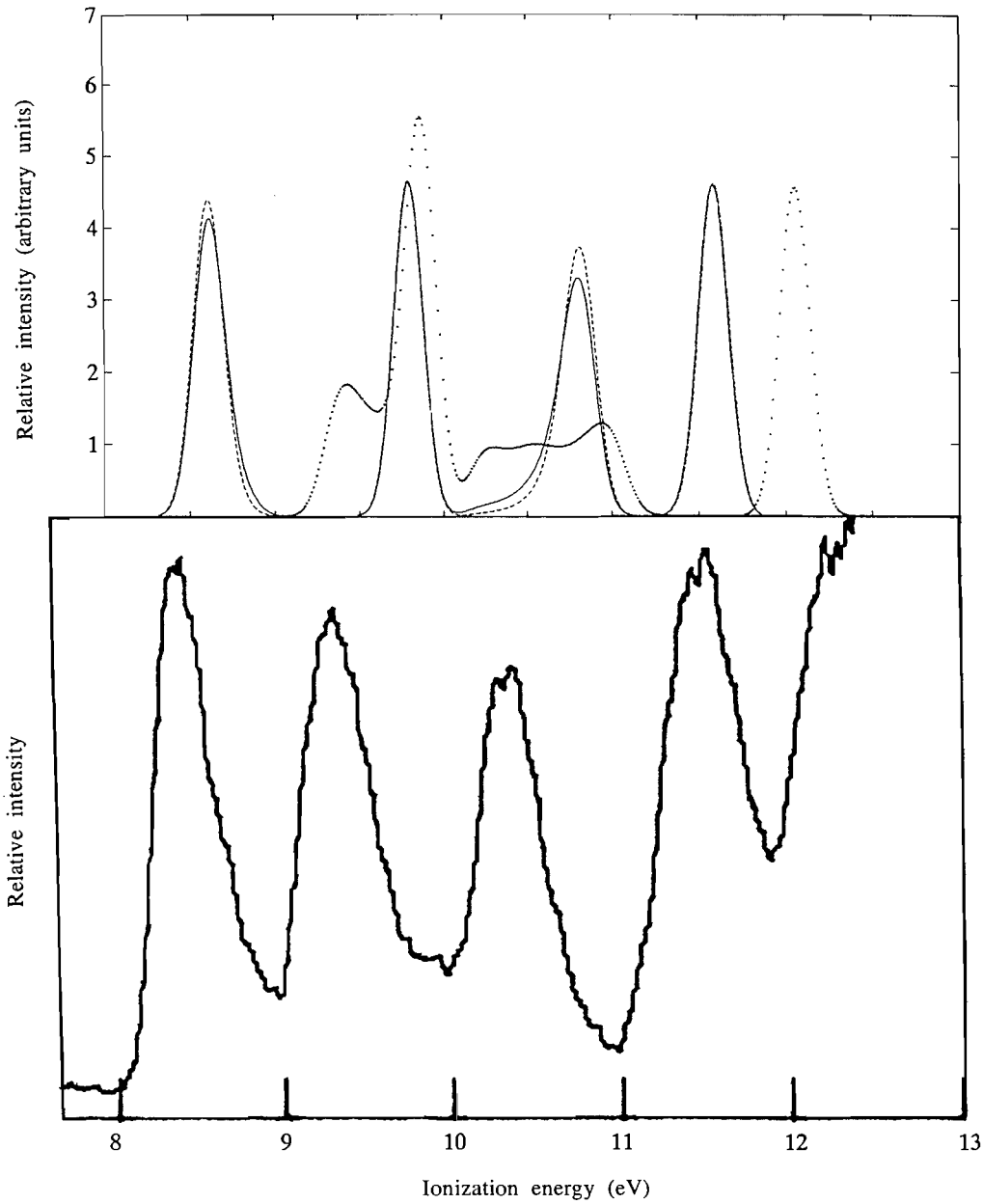

FIG. 6. The photoelectron spectrum of 3,5-difluorothioanisole. Synthetic spectra based on the MNDO (dotted line) and AM1 (dashed line) results appear in the upper panel. The solid line was obtained from the hindering potential derived from the NMR data and the AM1 orbital energies. The actual spectrum appears in the lower panel.

ponent of the potential is small. Because these orbital energies have relatively strong angular dependencies, this librational freedom is manifest in broadened peaks. The actual spectrum bears little similarity to the spectrum based on the MNDO results, but the other two synthetic spectra are reasonable facsimiles. With no twofold component to the barrier, the spectrum might be strongly dependent upon the *syn–anti* preference, but the computations give nearly identical spectra for both cases because of the near symmetry of the orbital energies about $\phi = 90°$. Thus, there is no strong evidence to support the preference for the *anti* orientation. The solid line in the upper panel of Fig. 4 was computed for a purely onefold barrier of 6 kJ mol^{-1}. As the height of the onefold component is increased in the calculations, the computed intensity in the 10.8 eV region increases relative to that in the 10.2 eV region. On this basis, the shape of the experimental spectrum suggests that the true barrier is of comparable or greater height.

The MNDO-based spectrum of 2,6-difluorothioanisole in Fig. 5 does not resemble the actual spectrum, despite the fact that the MNDO calculations reproduce the correct conformational preference. As for 2-fluorothioanisole, the first and third bands are indicative. The peak around 8.5 eV is somewhat narrower than the corresponding peak in Fig. 4, as found experimentally. The third band appears as a broad, high-energy shoulder in the 10–10.5 eV range. Unlike the corresponding band for 2-fluorothioanisole, this band is essentially featureless, as found experimentally. Notice that the intensity of the band *decreases* as the ionization energy increases. In the synthetic spectrum derived from the AM1

Can. J. Chem. Downloaded from www.nrcresearchpress.com by 203.198.23.82 on 09/08/12
For personal use only.

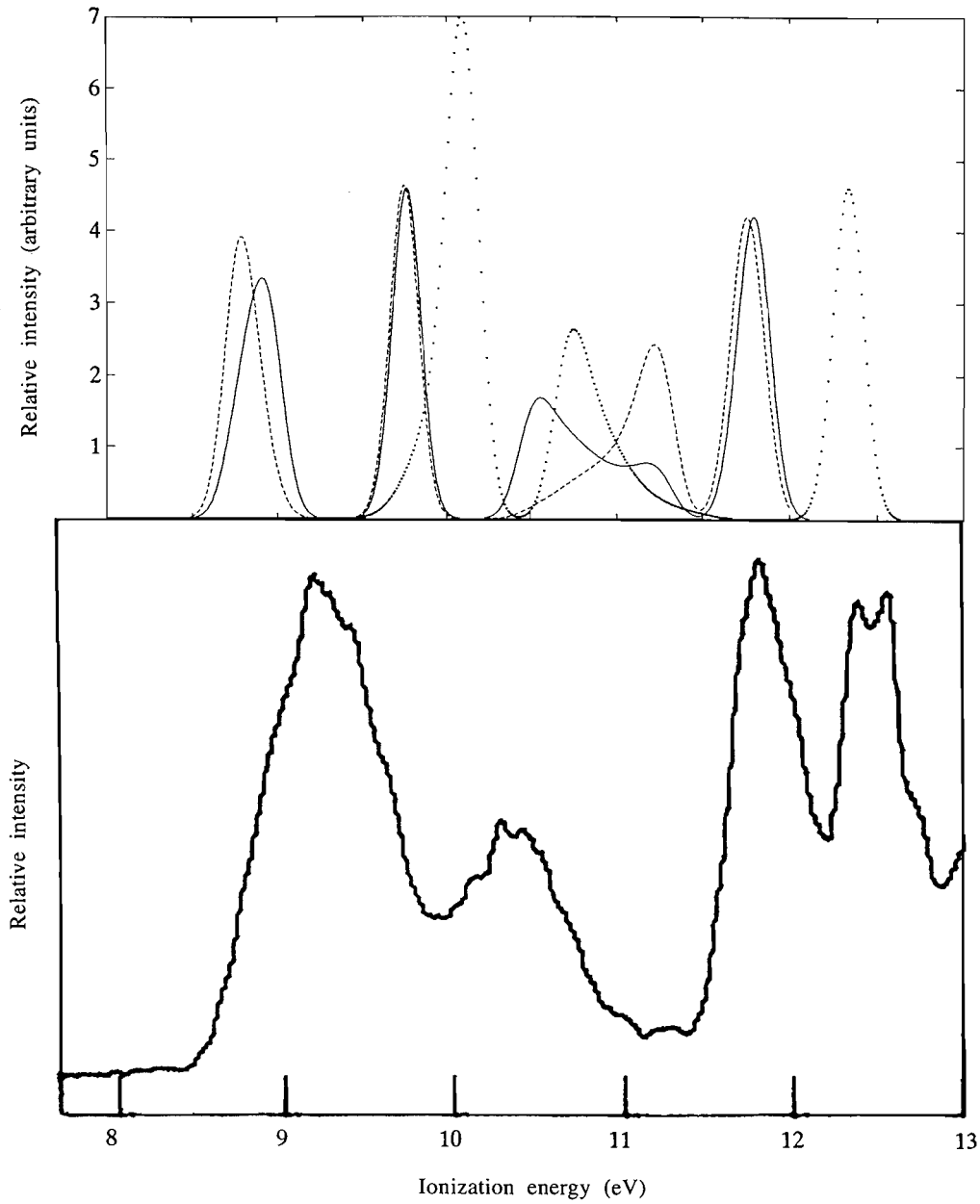

FIG. 7. The photoelectron spectrum of 2,3,5,6-tetrafluorothioanisole. Synthetic spectra based on the MNDO (dotted line) and AM1 (dashed line) results appear in the upper panel. The solid line was obtained from the hindering potential derived from the NMR data and the AM1 orbital energies. The actual spectrum appears in the lower panel.

results (dashed line in Fig. 5), which give the wrong conformational preference, the intensity increases with ionization energy because the conformations with the higher orbital energy have a lower thermal population. This feature provides strong evidence that 2,6-difluorothioanisole prefers conformations near $\phi = 90°$.

For the 3,5-difluoro derivative, both the AM1 and NMR potentials produce four relatively sharp, well-separated peaks, as shown in Fig. 6, despite the strong dependence of the first and third orbital energies on ϕ. The same pattern is found experimentally. This is consistent with a relatively high barrier and a preference for the planar conformation. According to the model, the low-energy shoulder of the third peak should grow as the temperature increases and nonplanar conformations become more abundant, but no attempt has been made in this laboratory to verify this prediction experimentally.

In the case of 2,3,5,6-tetrafluorothioanisole, the MNDO spectrum is somewhat similar to the actual spectrum in Fig. 7. According to the MNDO results, the two highest orbitals are nearly degenerate in the vicinity of $\phi = 90°$, giving rise to a single, intense peak in the spectrum. Both the barrier implied by the AM1 results and the barrier derived from ${}^6J_p^{C,H}$ yield spectra that are similar to the experimentally observed spectrum of 2,3,5,6-tetrafluorothioanisole, but neither method reproduces the intensity of the lowest energy peak because the two highest orbitals remain well separated in energy. The peak around 10.3 eV is more indicative. It is associated with the third highest occupied MO. Recall that the AM1 results indicate that the molecule prefers $\phi =$

Can. J. Chem. Downloaded from www.nrcresearchpress.com by 203.198.23.82 on 09/08/12
For personal use only.

0° but the NMR results suggest $\phi = 90°$. From the dashed and solid curves in the upper panel of Fig. 7, a peak at lower energy with a high-energy shoulder is consistent with a preference for the perpendicular conformation. This is the more likely description of the actual spectrum in the lower panel. While the conformational preference implied by the experimental photoelectron spectrum is disputable, it seems clear that, even if planar conformations are preferred as AM1 suggests, the barrier is low, i.e., less than about 7 kJ mol^{-1}. Given the approximations involved in the synthesis of the spectra, the observed spectrum is probably consistent with the NMR potential.

Summary and conclusions

In this article, $^6J_p^{C,H}$ and the MNDO and AM1 semiempirical MO methods were used to investigate the conformational preferences and barriers to internal rotation about the exocyclic C1—S bond in a series of fluorothioanisoles. The NMR results indicated that these compounds preferred planar conformations unless both *ortho* positions are occupied by fluorine substituents. *ortho* Fluorine substituents tended to lower the twofold component of the barrier to internal rotation while *meta* fluorines raised this component. Neither semiempirical method could accurately predict the conformational preferences for all of the compounds, despite their apparent similarity: MNDO indicated that $\phi = 90°$ was energetically more favourable than $\phi = 0°$ or 180° in every case while AM1 indicated the opposite. On the basis of the empirical (NMR) and semiempirical rotational potentials and the orbital energies from the AM1 calculations, synthetic photoelectron spectra were generated. A comparison of the synthetic spectra with experimental spectra supported the conclusions derived from the $^6J_p^{C,H}$ measurements. The photoelectron spectra were indeed sensitive to the subtle conformational behaviour of these highly flexible molecules. However, the complexity of the integral equation relating the potential and orbital energies to the observed spectrum represents a significant impediment to the use of PES for obtaining quantitative information of the kind available from NMR.

Acknowledgment

We thank Dr. Donald Hughes for assistance in acquiring some of the NMR spectra. Professor Michael Dewar kindly provided a copy of ref. 11 prior to publication. D.C. is grateful to the Deutscher Akademischer Austauschdienst for a Foreign Country Scholarship. This work was supported by grants from the Natural Sciences and Engineering Research Council of Canada to N.H.W. and to T.A.W. Finally, we thank Professor Gerald King for his dedication to the education of his fellow scientists in the art and science of molecular spectroscopy.

1. T. Schaefer and J.D. Baleja. Can. J. Chem. **64**, 1376 (1986).
2. T. Schaefer and J.D. Baleja. J. Magn. Reson. **60**, 131 (1984).
3. T. Schaefer and T.A. Wildman. Chem. Phys. Lett. **80**, 280 (1981).
4. T. Schaefer, J.D. Baleja, and G.H. Penner. Can. J. Chem. **63**, 2471 (1985).
5. W.J.E. Parr and T. Schaefer. Acc. Chem. Res. **13**, 400 (1980).
6. T. Schaefer, T.A. Wildman, and R. Sebastian. Can. J. Chem. **60**, 1924 (1982).
7. T. Schaefer, R. Laatikainen, T.A. Wildman, J. Peeling, G.H. Penner, J. Baleja, and K. Marat. Can. J. Chem. **62**, 1592 (1984); T. Schaefer and G.H. Penner. Can. J. Chem. **66**, 1635 (1988).
8. A.I. Vogel. Practical organic chemistry. 3rd ed. Longman, London. 1956.
9. D.M. Doddrell, D.T. Pegg, and M.R. Bendall. J. Magn. Reson. **48**, 323 (1982).
10. N.H. Werstiuk, D.N. Butler, and E. Shahid. Can. J. Chem. **65**, 760 (1986).
11. M.J.S. Dewar and Y.-C. Yuan. Inorg. Chem. **29**, 3881 (1990).
12. N.H. Werstiuk, G. Timmins, J. Ma, and T.A. Wildman. Can. J. Chem. **70**, 1971 (1992).
13. T. Schaefer, G.H. Penner, T.A. Wildman, and J. Peeling. Can. J. Chem. **63**, 2256 (1985).
14. M.J.S. Dewar and W. Thiel. J. Am. Chem. Soc. **99**, 4899 (1977).
15. M.J.S. Dewar, E.G. Zoebisch, E.F. Healy, and J.J.P. Stewart. J. Am. Chem. Soc. **107**, 3902 (1985).
16. M.J.S. Dewar and E.G. Zoebisch. J. Mol. Struct. (Theochem), **180**, 1 (1988).
17. T. Schaefer, S.R. Salman, T.A. Wildman, and G.H. Penner. Can. J. Chem. **63**, 782 (1985).
18. G.H. Penner. J. Mol. Struct. **168**, 335 (1988).
19. T. Schaefer and G.H. Penner. J. Mol. Struct. (Theochem), **152**, 179 (1987).
20. H. Lumbroso, Ch. Liegeois, L. Testaferri, and M. Tiecco. J. Mol. Struct. **144**, 121 (1986).
21. E. Honegger and E. Heilbronner. Chem. Phys. Lett. **81**, 615 (1981).
22. A. Schweig and N. Thon. Chem. Phys. Lett. **38**, 482 (1976).

Can. J. Chem. Downloaded from www.nrcresearchpress.com by 203.198.23.82 on 09/08/12
For personal use only.

Raman and infrared spectra, conformational stability, vibrational assignment, and *ab initio* calculations of *cis*-1,3-dichloropropene

J.R. DURIG,[1] T.G. COSTNER,[2] AND T.S. LITTLE

Department of Chemistry and Biochemistry, University of South Carolina, Columbia, SC 29208, U.S.A.

Received April 15, 1993

This paper is dedicated to Professor Gerald W. King on the occasion of his 65th birthday

J.R. DURIG, T.G. COSTNER, and T.S. LITTLE. Can. J. Chem. **71**, 1751 (1993).

The Raman (3200–10 cm^{-1}) and infrared (3200–20 cm^{-1}) spectra of gaseous and solid *cis*-1,3-dichloropropene, *cis*-ClHC=CHCH$_2$Cl, have been recorded. Additionally, the Raman spectrum of the liquid with qualitative depolarization data has also been obtained. These spectral data have been interpreted on the basis that the molecule exists predominantly in the *gauche* (allylic chlorine atom oriented *gauche* to the double bond) conformation in all physical phases. Some bands in the infrared spectrum of the gas could be due to a second higher energy conformer but the lack of corresponding Raman bands casts doubt on such an assignment. *Ab initio* Hartree–Fock gradient calculations employing the RHF/6-31G* basis set are consistent with two minima that correspond to the two equivalent *gauche* forms for the potential surface for the internal rotation about the C—C bond. These minima occur at dihedral angles, $\measuredangle_{dih}$ ClCCC, of 122° and 238° (0° corresponds to the *syn* conformation) and the *gauche* to *gauche* barrier at the 180° transition state, which corresponds to the *anti* structure, is 342 cm^{-1}. The barrier from the *gauche* minima to the *syn* (0°) structure, which is also a transition state, is 2425 cm^{-1}. Complete equilibrium geometries for the *gauche* structure have been determined with the RHF/3-21G*, RHF/6-31G*, and MP2/6-31G* basis sets. A normal coordinate analysis utilizing a harmonic force field calculation with the RHF/3-21G* basis set has been carried out for the *gauche* conformer. The results are discussed and compared with the corresponding quantities obtained for some similar molecules.

J.R. DURIG, T.G. COSTNER et T.S. LITTLE. Can. J. Chem. **71**, 1751 (1993).

On a mesuré les spectres Raman (3200–10 cm^{-1}) et infrarouges (3200–20 cm^{-1}) du *cis*-1,3-dichloropropène, *cis*-ClHC=CHCH$_2$Cl, à l'état gazeux et solide. On a aussi obtenu le spectre Raman du liquide avec des données sur la dépolarisation qualitative. On interprète ces données spectrales sur la base d'une molécule qui existerait principalement dans la conformation *gauche* (l'atome de chlore allylique *gauche* par rapport à la double liaison) dans toutes les phases physiques. Quelques bandes du spectre infrarouge à l'état gazeux pourraient être dues à un deuxième conformère d'énergie plus élevée; toutefois, le manque de bandes correspondantes dans le spectre Raman jette un doute sur une telle attribution. Des calculs *ab initio* de gradient de Hartree–Fock réalisés à l'aide d'ensembles de base RHF/6-31G* sont en accord avec la présence de deux minima qui correspondent aux deux formes *gauche* équivalentes pour la surface de potentiel de la rotation interne autour de la liaison C—C. Ces minima se présentent aux angles dièdres, $\measuredangle_{dih}$ ClCCC, de 122° et 238° (0° correspond à la conformation *syn*) et la barrière *gauche* à *gauche* de l'état de transition de 180°, qui correspond à la structure *anti*, se présente à 342 cm^{-1}. La barrière pour le passage du minima *gauche* à la structure *syn* (0°), qui est aussi un état de transition, se présente à 2425 cm^{-1}. Utilisant des ensembles de base RHF/3-21G*, RHF/6-31G* et MP2/6-31G*, on a déterminé les géométries d'équilibre complètes de la structure *gauche*. Faisant appel à un ensemble de base RHF/3-21G* et utilisant un calcul de champs de force harmonique, on a effectué une analyse en coordonnées normales du conformère *gauche*. On discute des résultats obtenus et on les compare aux quantités correspondantes obtenues pour quelques molécules similaires.

[Traduit par la rédaction]

Introduction

The vibrational and rotational spectra of the allyl halides have been of interest for a number of years (1–23). Our recent investigations have included the determination of the potential functions governing internal rotation about the C(sp^3)—C(sp^2) bonds of the parent 3-halopropenes and some substituted derivatives (24–32). Allyl fluoride (24–26), chloride (27), bromide (28, 31), and iodide (32) have been determined to exist as a mixture of *syn* and *gauche* conformers, and for the fluoride we have shown that the conformer that has the halogen atom *syn* to the double bond is the more stable rotamer (24–26). For 3-chloropropene, the value of the energy difference (27) was inferred to be less than 100 cm^{-1} (286 cal/mol) and the spectral data merely indicated a very slight preference for the *syn* conformer for the gaseous state. For allyl bromide (28, 31) and iodide (32) the *gauche* structure is thermodynamically preferred.

Most recently, we extended our studies of the 3-halopropene series to include an investigation of the far-infrared and Raman spectra of a number of simple alkenes for which one of the vinylic hydrogen atoms was substituted by a methyl group or halogen atom. For *trans*-1,3-dichloropropene (33) we showed that both the *syn* and *gauche* conformers are present in the vibrational spectra and that the *gauche* conformer is thermodynamically preferred by 342 cm^{-1}, which is consistent with the previously reported NMR (34) and molecular mechanics (35) results.

To provide similar data for the corresponding molecule with the chlorine atom substituted *cis* to the CH_2Cl moiety, we initiated an infrared and Raman spectroscopic study of *cis*-1,3-dichloropropene. Shen (36) reported the electron diffraction data for *cis*-1,3-dichloropropene and the results indicated that only one rotamer (*gauche*) was present. It was found that the torsional potential function could be approximated by a quartic double minimum function with transition states at the *syn* (0°) and *anti* (180°) positions. This study

[1]Author to whom correspondence may be addressed.

[2]Taken in part from the thesis of T.G. Costner which will be submitted to the Department of Chemistry and Biochemistry in partial fulfillment of the Ph.D. degree.

Can. J. Chem. Downloaded from www.nrcresearchpress.com by 203.198.23.82 on 09/08/12
For personal use only.

Can. J. Chem. Downloaded from www.nrcresearchpress.com by 203.198.23.82 on 09/08/12
For personal use only.

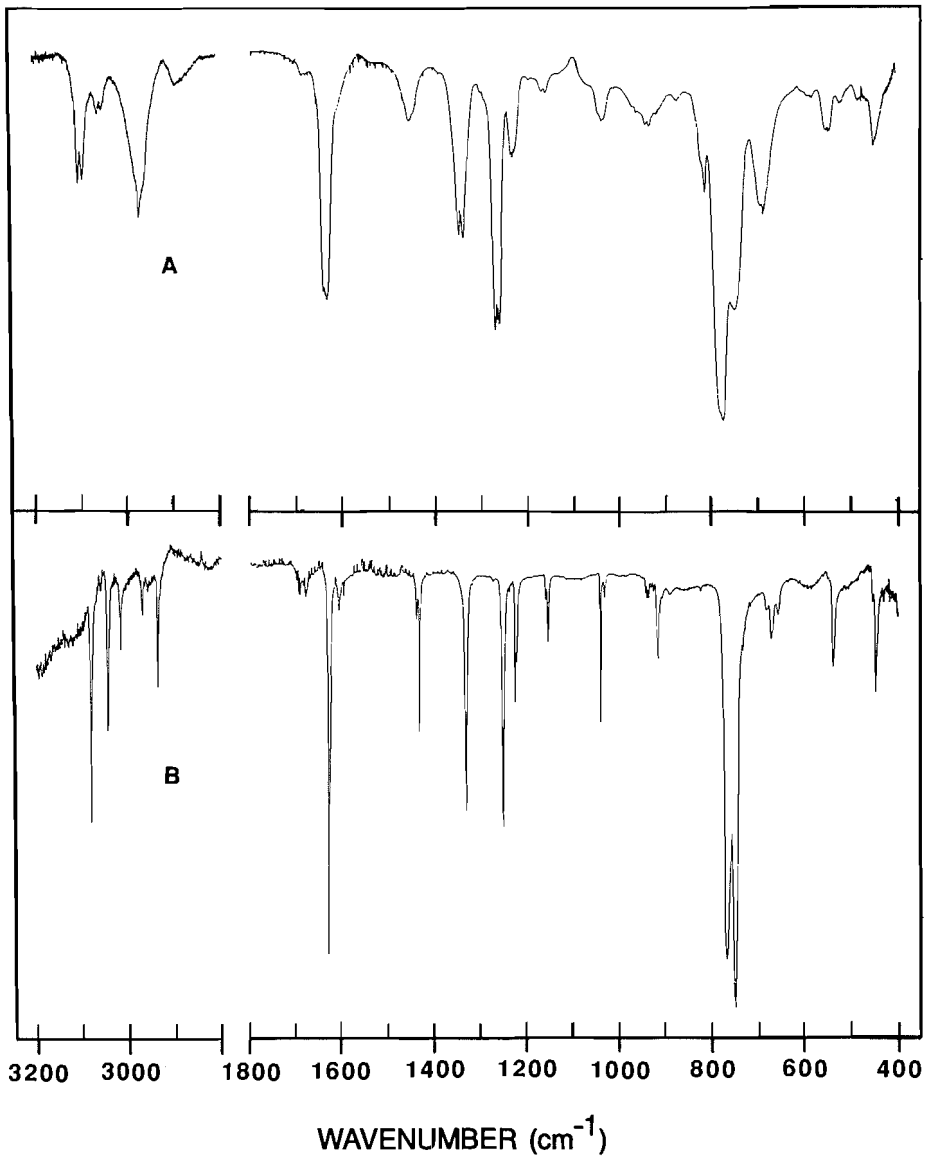

FIG. 1. Mid-infrared spectra of *cis*-1,3-dichloropropene: (*A*) gas and (*B*) annealed solid.

is in agreement with a previous NMR study (34) and molecular mechanics calculations (35) in which the authors found no evidence for a higher energy *syn* conformer. In each of these studies steric effects, arising from the two chlorine atoms eclipsing each other, were deemed to be the major cause for the nonexistence of a *syn* conformer.

Because an appreciable amount of a second higher energy conformer has been detected in the vibrational spectra of the 3-halopropenes (24–28, 31, 32) and *trans*-1,3-dichloropropene (33), the possibility remains that a small amount of it may exist for *cis*-1,3-dichloropropene. Therefore, we have undertaken the present spectroscopic study to carry out a conformational analysis, based on the previously unreported vibrational spectra, and to perform *ab initio* calculations for comparison with the results obtained from molecular mechanics calculations (35). The conformational stability, structural parameters, and torsional potential function are compared to the corresponding quantities for some related molecules.

Experimental

The sample of *cis*-1,3-dichloropropene was purchased from Columbia Organic Chemical Company (Columbia, S.C.) with a stated purity of >80%. Further purification was carried out with a low-temperature, low-pressure fractionation column. The sample was stored in the dark at Dry Ice temperature in an evacuated sample tube equipped with a greaseless stopcock.

The mid-infrared spectra (3200–400 cm^{-1}) of the gas and solid (Fig. 1) were recorded with a Digilab model FTS-14C Fourier transform interferometer equipped with a Ge/KBr beamsplitter, a Nichrome wire source, and a triglycine sulfate (TGS) detector. A KBr plate cooled with boiling liquid nitrogen was used as the sample substrate for the spectrum of the solid and a 12-cm cell equipped with CsI windows was used to contain the sample for obtaining the spectrum of the gas. The spectrum of the solid, at a resolution of 1 cm^{-1}, was obtained after several cycles of warming and cooling the sample until no changes were observed in the spectrum.

The far-infrared spectrum of the gas (Fig. 2) was recorded from the sample contained in a 1-m cell at a resolution of 0.10 cm^{-1} on a Nicolet model 200 SXV interferometer equipped with a vacuum bench and a liquid helium cooled germanium bolometer contain-

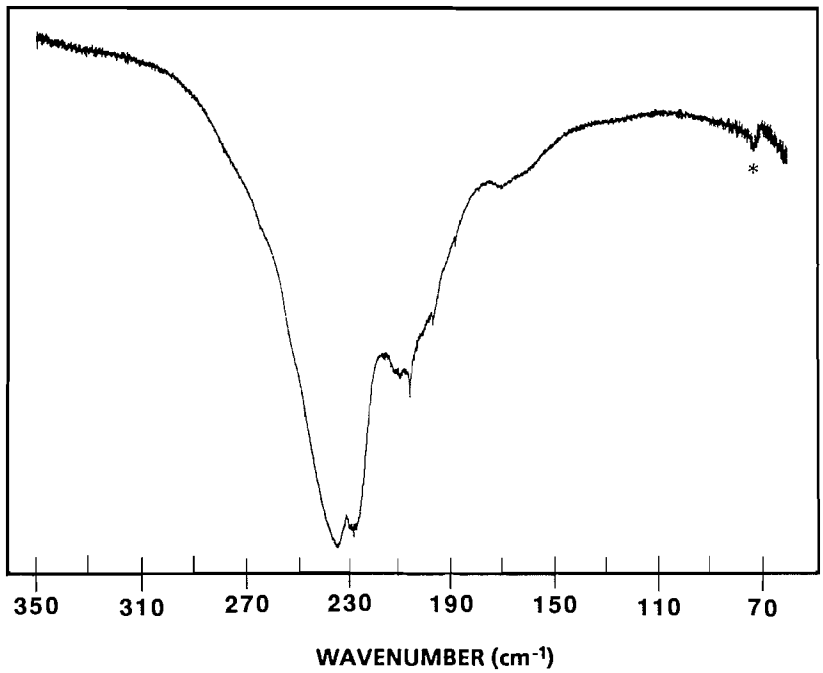

FIG. 2. Far-infrared spectrum of gaseous *cis*-1,3-dichloropropene. The asterisk (*) denotes absorption due to polyethylene.

Can. J. Chem. Downloaded from www.nrcresearchpress.com by 203.198.23.82 on 09/08/12
For personal use only.

ing a wedged sapphire filter and polyethylene windows. Interferograms for both the sample and empty reference cell were recorded 512 times, averaged, and transformed with a boxcar truncation function. Traces of water were removed by passing the gaseous sample through activated 3 Å molecular sieves using standard high-vacuum techniques.

The Raman spectra (Fig. 3) were recorded on a Cary model 82 spectrophotometer equipped with a Spectra-Physics model 171 argon ion laser operating on the 5145 Å line. The spectrum of the gas was recorded using a standard Cary multipass accessory and a laser power at the sample of 2 W. Reported frequencies are expected to be accurate to ± 2 cm^{-1}. The spectrum of the liquid was recorded from the sample sealed in a glass capillary. For the spectrum of the solid, the sample was deposited onto a blackened brass plate, held 15° from the normal, cooled by boiling liquid nitrogen, and contained in a cell fitted with quartz windows.

The FT–Raman spectrum of liquid *cis*-1,3-dichloropropene was recorded on a Bruker model IFS 66 interferometer equipped with a model FRA106 FT–Raman attachment. The excitation source was the 1.064 μm line from a CVI YAG-MAX model C-95 laser, giving a 2-mm beam with an optical noise of 4%. The Nd:YAG rod (65 mm long) was pumped by two 1.5-kW tungsten–halogen lamps. A liquid nitrogen cooled Ge detector was used to collect the spectrum. Detector cooling, laser warming, and stabilization for more than 30 min were allowed before data collection. These data were recorded by coaddition of 100 scans at 2 cm^{-1} resolution with a laser power of approximately 300 mW at the sample.

Vibrational assignment

The bands observed in the mid-infrared spectrum of gaseous *cis*-1,3-dichloropropene have hybrid contours. Furthermore, the Raman spectrum of the gas exhibits 14 *Q* branches, which persist in the corresponding spectrum of the solid. These spectral features are consistent with a conformer of C_1 symmetry in the fluid phases, i.e., the *gauche* form, and the persistence of this form in the solid. For this form, all 21 of the normal vibrational modes belong to the totally symmetric *A* species, which are expected to give rise to *Q* branches in the Raman spectra of the vapor and hybrid infrared band contours.

It has been shown that the number and position of hydrogen atoms bonded to substituted ethylenes can be characterized by group frequency correlations made from vibrational spectra (37). Our most recent studies of the 3-halopropenes (24–28, 31, 32) have shown a wide variation in the observed frequencies of the carbon–hydrogen and skeletal bending modes. The extent of mixing among the chosen set of symmetry coordinates for these vibrational modes is significantly influenced by the halogen substituent and the structural conformation.

A comparison of the observed vibrational spectra for *trans*-1,3-dichloropropene (33) with those for the *cis* molecule (Figs. 1–3) shows little sensitivity in the observed frequencies for the fundamentals associated with the -CH_2Cl moiety. The CH_2 antisymmetric stretch and CH_2 wag occur at the slightly higher frequencies of 3020 and 1264 cm^{-1} for the *cis* molecule, compared to 3005 and 1241 cm^{-1} for the *trans* molecule. These frequencies are only slightly different from the observed frequencies of 2999 and 1260 cm^{-1} for the corresponding vibrations of 3-chloropropene (27). The -CH_2 twist and rock both occur within 10 cm^{-1} of each other for the *cis* and *trans* dichloropropene molecules.

Of particular interest are the assignments of the two out-of-plane C—H bending modes of the vinyl group. Factors affecting the out-of-plane hydrogen deformation frequencies in olefins and their derivatives have been studied extensively (37). For a *cis*-disubstituted system, the out-of-plane hydrogen bends are either in-phase, with respect to the symmetry plane of the vinyl group, or out-of-phase. The out-of-phase, out-of-plane motion has little or no resultant dipole moment change and is expected to give rise to an infrared absorption of small intensity. This mode is assigned to the observed Raman frequency of 1036 cm^{-1} in the liquid phase. The calculated infrared intensity for this fun-

Can. J. Chem. Downloaded from www.nrcresearchpress.com by 203.198.23.82 on 09/08/12
For personal use only.

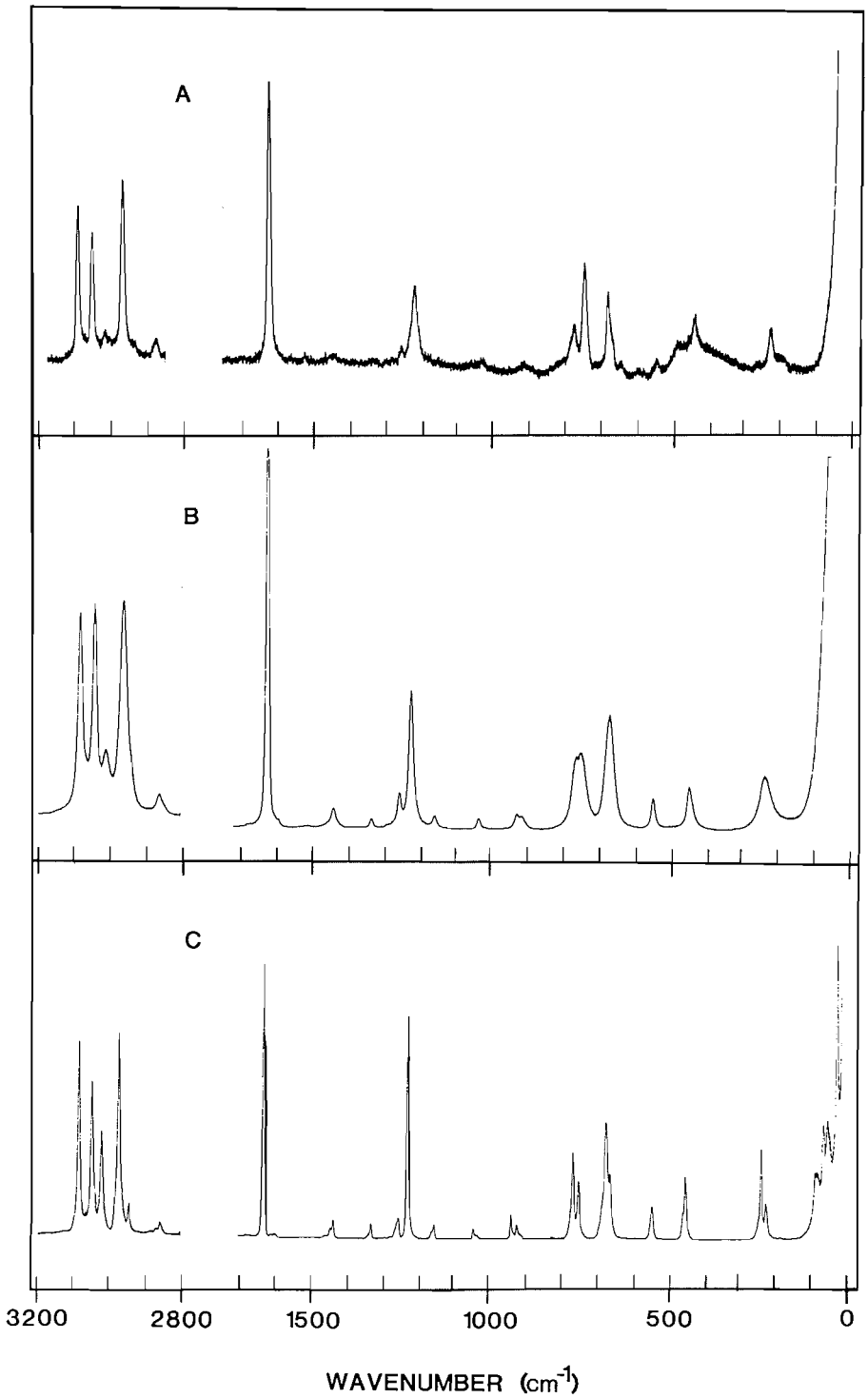

FIG. 3. Raman spectra of *cis*-1,3-dichloropropene: (*A*) gas; (*B*) liquid; and (*C*) annealed solid.

damental is small (see *Ab initio* calculations), but this mode is observed as an infrared band of moderate intensity. The in-phase, out-of-plane mode has been reported (37) to have a group frequency range of 675–730 cm^{-1} for *cis*-disubstituted ethylenes and is expected to give rise to a strong band in the infrared spectrum. This mode is assigned to the infrared band observed at 780 cm^{-1} and is calculated and observed to be the most intense feature in the infrared spectrum. The closely lying, and intense, absorption of one of the C—Cl stretching modes (751 cm^{-1}) would complicate these assignments in the absence of the normal coordinate analysis. From these results it is clear that the CH bend should be assigned to the higher frequency of 780 cm^{-1} and the C—Cl stretch to the frequency of 751 cm^{-1} in the infrared spectrum of the gas phase.

A review of the assignments for the skeletal bending modes of related molecules indicates considerable variation in the assigned frequency for a given vibration. For example, the CCC bending mode for allyl chloride (27) (3-chloropropene) is assigned to a band at 404 cm^{-1}, but for *trans*-1,3-

Can. J. Chem. Downloaded from www.nrcresearchpress.com by 203.198.23.82 on 09/08/12
For personal use only.

dichloropropene (33) this vibration occurs near 150 cm^{-1}. This variation in assignment is consistent with the change in potential energy distribution among a similar set of symmetry coordinates. The change in potential energy is directly related to the structural conformation and the type and position of the substituent on the vinyl group. The CCC and CCCl bending modes for *cis*-1,3-dichloropropene, which occur in the plane of the vinyl group, are extensively mixed (see *Ab initio* calculations). The calculated scaled frequency of 205 cm^{-1} has a potential energy distribution representing approximately 50% each of the symmetry coordinates corresponding to the CCC and CCCl bending modes. Similarly, the calculated scaled frequency of 541 cm^{-1} has its potential energy nearly equally distributed over four symmetry coordinates. Based on these results, it would be misleading to assign the CCC and CCCl bending modes to any one observed frequency such as the 550 and 200 cm^{-1} bands, respectively. For *trans*-1,3-dichloropropene, the symmetry coordinate corresponding to the CCC bend has its maximum potential energy distribution corresponding to the observed frequency of 328 cm^{-1} for the *gauche* conformer but at 150 cm^{-1} for the *syn* conformer. Thus, it is not very instructive to compare frequencies for these low-frequency bending modes between individual conformers or among similar molecules. A summary of the observed vibrational frequencies and approximate description of the vibrational modes is provided in Table 1.

Also included in Table 1 are several infrared bands that appear in the spectrum of the gas but are absent in all other spectra. The most prominent of these occur at 813, 585, 520, and 476 cm^{-1}. These bands become less pronounced or disappear in the infrared spectrum of the solid, which indicates that they could arise from fundamental modes of a higher energy conformation. Alternatively, they may arise from combination or difference bands of the *gauche* form. If a higher energy conformer exists, then, based on related molecules, this conformer would have a *syn* (allylic chlorine *syn* to the double bond) structure. Calculated frequencies for this form indicate that the 585 cm^{-1} band would correspond to an A' mode and should become pronounced in the Raman spectrum of the gas at higher temperatures. Spectra obtained at 55°C did not reveal any such feature. If this conformer exists, then it would lie at a considerably higher energy, >1 kcal/mol, than the *gauche* form and should become pronounced with a relatively small increase in temperature. Therefore, the absence of discrete Raman features that coincide with these infrared frequencies, casts doubt that they arise from a higher energy form.

Ab initio calculations

The LCAO-MO-SCF restricted Hartree–Fock calculations were performed with the GAUSSIAN-90 program (38) using Gaussian-type basis functions. The energy minima with respect to nuclear coordinates were obtained by the simultaneous relaxation of all of the geometric parameters using the gradient method of Pulay (39). The structural parameters, rotational constants, and dipole moments for the *gauche* conformer determined with the RHF/3-21G*, RHF/6-31G*, and MP2/6-31G* basis sets are given in Table 2, along with the structural parameters obtained for the *gauche* conformer from an earlier electron diffraction study (36).

Considering the results obtained from the calculations with both the RHF/3-21G* and RHF/6-31G* basis sets, the bond distances agree to within 0.008 Å except for the C—Cl* (Cl atom of the -CH_2Cl group) bond distance. This parameter is calculated to have a value of 1.821 Å with the RHF/3-21G* basis set but is predicted to be 0.021 Å shorter when calculated with the RHF/6-31G* basis set. The shorter C—Cl* bond distance is more consistent with the results from the electron diffraction study, where a value of 1.806 ± 0.003 Å is reported (36). The bond angles typically agree within ~1° between the two basis sets.

The structures were also calculated by employing the 6-31G* basis set with electron correlation at the MP2 level. The absolute values for the structures are quite different from those obtained using the basis sets with Hartree–Fock limits. The carbon–hydrogen bond lengths calculated with the 6-31G* basis set with electron correlation are ~0.01 Å longer than those calculated with Hartree–Fock limits and those determined from the electron diffraction study (36). The longer C—H distances should be closer to the actual values since the C—H distances of 1.078 Å for the -CH_2Cl group are certainly too short.

The heavy atom bond lengths predicted from the MP2/6-31G* calculation are in better agreement with the structural parameters obtained from the electron diffraction study (36) than those from the calculations using the RHF/3-21G* and RHF/6-31G* basis sets, except for the C—C and C—Cl* bond distances. Clearly, both of these bond distances are calculated with the MP2/6-31G* basis set to be entirely too short by at least 0.010 Å. The bond angles, on the other hand, are hardly effected by using the different basis sets and all are within the uncertainties reported in the electron diffraction study (36). It is difficult to ascertain the reliability of the calculated and experimentally determined bond angles. Uncertainties of greater than 1° are reported in the electron diffraction study (36) and the determination of the values and uncertainties is based, in part, on assumed values for the HCC angles. According to our experiences, however, the *ab initio* calculated bond angles are generally reliable to about 1° except for dihedral angles for the *gauche* conformers.

Potential surface scan

The optimized geometry for the *gauche* conformer obtained with the RHF/6-31G* basis set was utilized to estimate an asymmetric torsional potential surface by allowing the torsional dihedral angle, $\measuredangle_{dih}$ ClCCC, to change from 180° to 0°, in increments of 10°, with calculation of the energy at each point. This rough estimation did not provide any indication of a second conformer at the *syn* (0°) position, which is consistent with the previously reported electron diffraction and molecular mechanics results for *cis*-1,3-dichloropropene (35, 36). Calculations at the *gauche* minimum and at the *anti* (180°) transition state, by relaxing all of the geometric parameters, result in the potential function given in Fig. 4. From these optimizations with the RHF/6-31G* basis set, the total energies are −1034.871097 and −1034.869537 hartree (1 hartree = 219 474 cm^{-1}) for the *gauche* and *anti* (180°) positions, respectively. Since the 3-halopropenes and substituted derivatives typically have a minimum at the *syn* (0°) position in their corresponding potential functions, an optimization was attempted at the *syn* (0°) position by relaxing all of the geometric parameters. A minimum energy structure was not found. A subsequent calculation, treating the *syn* (0°) position as a transition state, converged on an optimized structure with a total energy of

TABLE 1. Observed[a] infrared and Raman frequencies for *cis*-1,3-dichloropropene

Infrared				Raman						Assignment	
Gas	Rel. int.	Solid	Rel. int.	Gas	Rel. int.	Liquid	Rel. int.	Solid	Rel. int.	ν_i	Approximate description[b,c]
3101 *R* 3096 *Q* 3091 *P*	s	3087	s	3098	s	3087	s	3078	s	ν_1	CH[†] stretch
3060 *R* 3054 ctr 3050 *P*	w	3050	s	3056	s	3046	s	3042	s	ν_2	CH[§] stretch
3022	vvw	3022	m	3020	w	3014	m	3014	s	ν_3	CH_2 antisymmetric stretch
2970 *Q*	s	2974	w	2972	s	2966	s	2966	s	ν_4	CH_2 symmetric stretch
2960 *P*	sh	2942	m								
		2942	s					2934	w		Combinations and overtones
2890	bd,w			2876	w	2865	w	2846	w		
1700	bd,w	1700	w								
1640 *R* 1636 *Q* 1631 *P*	vs	1630		1634	vs	1629	vs	1632	vs	ν_5	C=C stretch
1608	sh	1608	w								
1452 *R*		1440	w					1442	w		
1446 ctr 1442 *P*	m	1434	s	1450	bd,w	1442	w	1435	w	ν_6	CH_2 deformation
1362	sh										
1348 *R* 1342 *Q* 1338 *P*	s	1332	s			1336	w	1330	w	ν_7	CH[†] bend
1268 *R* 1264 *Q* 1258 *P*	vs	1252	s	1264	w	1259	w	1254	w	ν_8	CH_2 wag
1232 *R*		1226	s								
1228 *Q* 1224 *P*	m	1224	m	1228	s	1226	s	1228	s	ν_9	CH[§] bend
1193	vw										
1165 *R*		1162	sh					1160	sh		
1160 *Q* 1150 *P*	w	1156	m			1158	w	1154	w	ν_{10}	CH_2 twist
1035 ctr	bd,w	1040	ms	1030	vw	1036	w	1044	w	ν_{11}	CH[†] bend
		1032	w								
960 max	bd,w										
940 max		938	w			928	w	937	w	ν_{12}	C—C stretch
		917									
932 max	bd,w	914	m	915	bd,vw	912	w	922	vw	ν_{13}	CH_2 rock
								910	sh		
813 *Q*	sh,m										
784 *R* 780 ctr 778 *P*	vs	1768	vs	780	m	764	s	764	s	ν_{14}	CH[§] bend
751 ctr	vs	750	vs	752	s	750	s	749	s	ν_{15}	C—Cl stretch
693 *R*		684									
689 *Q*	s	672	m	686	s						
687 *Q*		658		676	sh	671	s	673	s	ν_{16}	C—Cl* stretch
684 *Q* 678 *P*								662	sh		
				652	w						
				602	vw						

Can. J. Chem. Downloaded from www.nrcresearchpress.com by 203.198.23.82 on 09/08/12
For personal use only.

TABLE 1 (*concluded*)

Infrared				Raman						Assignment	
Gas	Rel. int.	Solid	Rel. int.	Gas	Rel. int.	Liquid	Rel. int.	Solid	Rel. int.	ν_i	Approximate description[b,c]
588 *R* 585 min 580 *P*	w										
552 *R* 546 *Q* 544 *P*	w	539	m	550	w	549	m	543	m	ν_{17}	CCC/CCCl bend
520 ctr	bd,vw										
476	bd,w							456	sh		
446 ctr	m	447	m	444	m	448	m	450	m	ν_{18}	CCCl bend
235 *R* 231 ctr 227 *P*	m			232	m	236	m	238	s	ν_{19}	C—CCl* bend
209 *R* 205 *Q*	m			200	sh			226	m	ν_{20}	CCCl/CCC bend
										ν_{21}	Asymmetric torsion (not observed)
								85			
								65			
								53			
								29			Lattice modes

[a]Abbreviations used: s, strong; m, moderate; w, weak; v, very; bd, broad; sh, shoulder; p, polarized; dp, depolarized; *P*, *Q*, and *R* refer to the rotational–vibrational branches.
[b]The asterisk (*) denotes chlorine atom bonded to the sp^3 carbon.
[c]The (†) and (§) denote the hydrogen atom bonded to carbon-1 and carbon-2, respectively.

Can. J. Chem. Downloaded from www.nrcresearchpress.com by 203.198.23.82 on 09/08/12
For personal use only.

−1034.860048 hartree. Therefore, at this level of calculations, the *gauche* conformer is found to be the only stable conformer. The *gauche* to *gauche* barrier over the *anti* (180°) transition state and the *gauche* to *gauche* barrier over the *syn* (0°) transition state are found to be 342 and 2425 cm^{-1}, respectively.

Normal coordinate analysis

To obtain a more complete description of the molecular motions involved in the normal modes of *cis*-1,3-dichloropropene, and to aid in the vibrational assignment of the fundamentals, we carried out a normal coordinate analysis. The force field in Cartesian coordinates was calculated by the GAUSSIAN-90 program (38) with the RHF/3-21G* basis set. From previous studies (24), it was found that the differences in the values of force constants and frequencies are not significant when the smaller, as opposed to the larger, RHF/6-31G* basis set is used. These calculations were performed by using the Wilson FG matrix method (40). The following procedure was used to transform the force constants in Cartesian coordinates from the *ab initio* calculations to the required internal symmetry coordinates.

The Cartesian coordinates obtained for the optimized structure for the *gauche* conformer were input into a *G*-matrix program (41) with a complete set of 24 internal coordinates (Fig. 5). This set of 24 internal coordinates was used to form 21 symmetry coordinates together with three redundancies (Table 3). The *B*-matrix was used to convert the *ab initio* force field in Cartesian coordinates to the desired internal coordinates. The force fields for the *gauche* conformer are provided in Table 4. All diagonal elements of the force fields in internal coordinates were assigned scaling factors. Initially, all scaling factors were kept fixed at a value of 1.0 to produce pure *ab initio* calculated vibrational frequencies. Scaling factors of 0.9 for stretching coordinates, 0.8 for bending coordinates, and 1.0 for torsional coordinates were used to obtain the "fixed scaled" force field, resultant frequencies, and the potential energy distribution (P.E.D.), which are listed in Table 5. Even with these relatively crude scaling factors the predicted frequencies are in error by approximately 5%, which provides excellent support for the vibrational assignment.

Calculated Raman spectrum

A Raman spectrum for *cis*-1,3-dichloropropene was calculated (Fig. 6) using frequencies and scattering activities determined from the GAUSSIAN-90 program (38) using the RHF/3-21G* basis set. The GAUSSIAN-90 option to calculate the polarizability derivatives analytically was used. The Raman scattering cross sections, $\partial\sigma_j/\partial\Omega$, which are proportional to the Raman intensities, can be calculated from the scattering activities and the predicted frequencies for each normal mode using the relationship (42)

$$\frac{\partial\sigma_j}{\partial\Omega} = \left(\frac{2^4\pi^4}{45}\right)\left(\frac{(\nu_0 - \nu_j)^4}{1 - \exp\left[\frac{-hc\nu_j}{kT}\right]}\right)\left(\frac{h}{8\pi^2 c\nu_j}\right)S_j$$

where ν_0 is the exciting frequency, ν_j is the vibrational frequency of the jth normal mode, and S_j is the corresponding

TABLE 2. Structural parameters,[a] rotational constants, and dipole moments for *cis*-1,3-dichlorpropene

	gauche			Electron diffraction	
Parameter[b,c]	RHF/3-21G*	RHF/6-31G*	MP2/6-31G*	Model I[e]	Model II[f]
Cl*—C	1.821	1.800	1.794	1.805 ± 0.003	1.806 ± 0.003
Cl—C	1.744	1.736	1.729	1.726 ± 0.003	1.726 ± 0.003
C=C	1.311	1.315	1.337	1.341 ± 0.005	1.340 ± 0.005
C—C	1.495	1.495	1.487	1.508 ± 0.007	1.508 ± 0.007
H1—C	1.068	1.071	1.083	1.078 ± 0.010	1.078 ± 0.010
H2—C	1.073	1.076	1.087	1.078 ± 0.010	1.078 ± 0.010
H3—C	1.078	1.079	1.091	1.078 ± 0.010	1.078 ± 0.010
H4—C	1.074	1.076	1.089	1.078 ± 0.010	1.078 ± 0.010
∠ClCC	124.7	125.3	124.8	124.5 ± 1.6	124.6 ± 1.6
∠Cl*CC	109.9	110.7	110.6	111.9 ± 1.8	111.7 ± 1.8
∠CCC	126.3	126.9	126.0	125.6 ± 1.5	125.5 ± 1.5
∠H1CC	122.6	122.3	122.3	120 (assumed)	120 (assumed)
∠H2CC	117.7	116.8	116.9	120 (assumed)	120 (assumed)
∠H3CC	111.2	111.0	111.2	109 (assumed)	109 (assumed)
∠H4CC	112.6	112.5	111.6	109 (assumed)	109 (assumed)
Dihedral angle	123.6	122.5	118.3	132.7 ± 7.5	123 ± 5
A	8381	8817	8269		
B	1260	1233	1277		
C	1171	1149	1183		
μ_a	0.811	0.820	0.828		
μ_b	1.908	1.760	1.883		
μ_c	0.944	1.010	0.945		
μ_t	2.299	2.186	2.264		
$-(E + 1030)$[d]	0.065855	4.871097	5.547973		

[a]Bond lengths in Å, bond angles in degrees, rotational constants in MHz, and dipole moments in debye.
[b]For atom numbering see Fig. 5.
[c]The asterisk (*) denotes the chlorine atom bonded to the methylene carbon.
[d]SCF energy for *ab initio* calculations in hartree.
[e]Values are taken from ref. 36 (static model).
[f]Values are taken from ref. 36 (dynamic model).

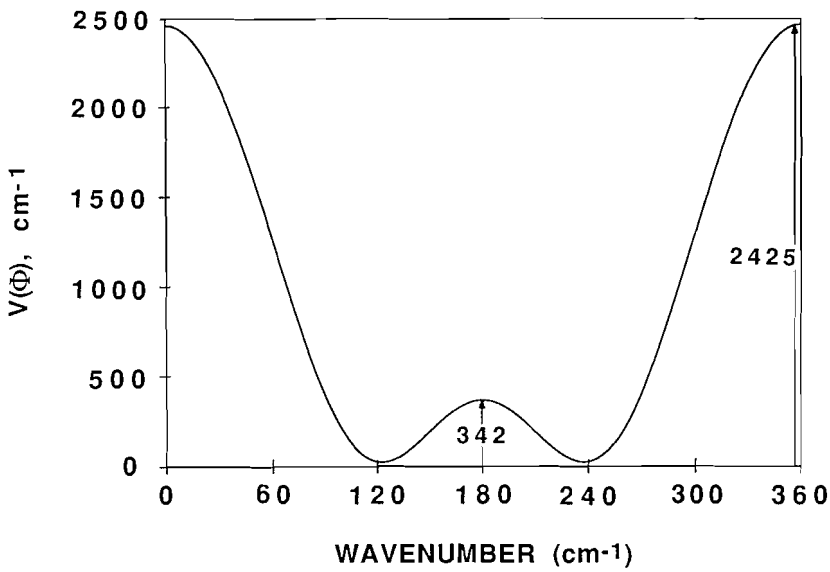

FIG. 4. The potential function governing internal rotation of *cis*-1,3-dichloropropene as determined by *ab initio* calculations with the RHF/6-31G* basis set. This potential surface was calculated by allowing for optimization at the transition states and at the *gauche* minimum by relaxing all of the geometric parameters.

Raman scattering activity. To obtain the polarized Raman scattering cross sections, the polarizabilities are incorporated into S_j by $S_j[(1 - \rho_j)/(1 + \rho_j)]$, where ρ_j is the depolarization of the jth normal mode. The Raman scattering cross sections and calculated frequencies are used together with a Lorentzian function to obtain the calculated spectrum. The predicted Raman spectrum for the *gauche* conformer of *cis*-1,3-dichloropropene, using scaled frequencies (Table 5), is

Can. J. Chem. Downloaded from www.nrcresearchpress.com by 203.198.23.82 on 09/08/12
For personal use only.

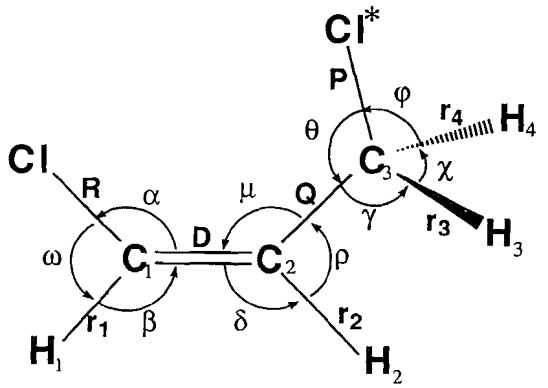

FIG. 5. Internal coordinates for *cis*-1,3-dichloropropene.

compared to the FT–Raman spectrum of the liquid phase (Fig. 6) and is remarkably similar, with the exception of the relative intensities of the C=C and C—Cl stretching modes, the C—C—Cl* bending mode, and the asymmetric torsional mode. In the 800–1300 cm^{-1} region, where the C—H bending motions occur and assignments are often difficult, the two spectra are very comparable. It should be noted that ν_{21}, the asymmetric torsional mode, was omitted from the calculated spectrum since its large calculated intensity interfered with the scaling of the vertical axis, and that the very weak band at ~330 cm^{-1} (Fig. 6) is due to an impurity arising from a small amount of *trans*-1,3-dichloropropene.

Discussion

From a careful inspection of the infrared spectra of the gas and the Raman spectra of the gas, liquid, and solid phases of *cis*-1,3-dichloropropene, it is clear that the conformer that persists in the spectrum of the annealed solid also predominates in the spectra of the gas and liquid phases. Possible spectral evidence to support the existence of a higher energy conformer was observed in the infrared spectrum of the gas, but was inconclusive since corresponding bands were not observed in the Raman spectrum of the gas. Therefore, we have interpreted all of the data on the basis that the *gauche* conformer is the only existing form of this molecule at ambient temperature. This conclusion is supported by *ab initio* calculations using the RHF/6-31G* basis set, which indicated that the *anti* (180°) and *syn* (0°) positions are transition states. This interpretation is in agreement with previous studies (34–36). For the *syn* conformer of 3-fluoropropene and 3-chloropropene, the nonbonded distance between the halogen atom and the vinylic hydrogen atom is near the sum of the van der Waals radii. Therefore, it is not surprising that when the hydrogen atom is substituted with a chlorine atom, steric forces predominate and this form of *cis*-1,3-dichloropropene is either unstable or occurs at a much higher energy than the *gauche* conformer. Additionally, the C—H bond on carbon-2 would eclipse the C—X bond on the CH_2X group in the *anti* position. This is why the struture corresponding to this conformer occurs as a transition state in the asymmetric potential functions of the 3-halopropenes.

The most pronounced spectral feature in the spectra of the gas or liquid, which disappears in the spectrum of the solid, is the infrared band observed at 813 cm^{-1} in the spectrum of the gas. If this intense band was due to a conformer peak, we would expect to observe more evidence throughout the vibrational spectrum for the existence of a *syn* conformer. However, it is possible that this infrared peak is a difference or combination band.

TABLE 3. Symmetry coordinates for *cis*-1,3-dichloropropene

Species	Description[a,b]	Symmetry coordinate[c]
	$CH^{\dagger}$ stretch	$S_1 = r_1$
	CH_2 antisymmetric stretch	$S_2 = r_3 - r_4$
	$CH^{\S}$ stretch	$S_3 = r_2$
	CH_2 symmetric stretch	$S_4 = r_3 + r_4$
	C=C stretch	$S_5 = D$
	CH_2 deformation	$S_6 = (\sqrt{6}+2)\chi - (\sqrt{6}-2)\theta - \gamma_1 - \gamma_2 - \phi_1 - \phi_2$
	$CH^{\dagger}$ bend	$S_7 = \omega - \beta$
	CH_2 wag	$S_8 = \phi_1 + \phi_2 - \gamma_1 - \gamma_2$
	$CH^{\S}$ bend	$S_9 = \delta - \rho$
	CH_2 twist	$S_{10} = \phi_1 - \phi_2 + \gamma_1 - \gamma_2$
	$CH^{\dagger}$ bend	$S_{11} = \xi$
	C—C stretch	$S_{12} = Q$
	CH_2 rock	$S_{13} = \gamma_1 - \gamma_2 - \phi_1 + \phi_2$
	$CH^{\S}$ bend	$S_{14} = \sigma$
	C—Cl stretch	$S_{15} = R$
	C—Cl* stretch	$S_{16} = P$
	C—C—Cl bend	$S_{17} = 2\alpha - \omega - \beta$
	C—C—Cl bend	$S_{18} = \pi$
	C—C—Cl* bend	$S_{19} = (\sqrt{6}-2)\chi - (\sqrt{6}+2)\theta + \gamma_1 + \gamma_2 + \phi_1 + \phi_2$
	C—C—C bend	$S_{20} = 2\mu - \rho - \delta$
	Torsion	$S_{21} = \tau$
	Redundancy	$S_{1R} = \alpha + \omega + \beta$
	Redundancy	$S_{2R} = \mu + \delta + \rho$
	Redundancy	$S_{3R} = \phi_1 + \phi_2 + \gamma_1 + \gamma_2 + \chi + \theta$

[a]The asterisk (*) denotes the chlorine atom bonded to the sp^3 carbon.
[b]The (†) and (§) denote the hydrogen atom bonded to carbon-1 and carbon-2, respectively.
[c]Not normalized.

Can. J. Chem. Downloaded from www.nrcresearchpress.com by 203.198.23.82 on 09/08/12
For personal use only.

TABLE 4. *Ab initio* harmonic force constants (mdyn/Å)

	r_1	r_2	r_3	r_4	D	Q	R	P	α	β	ω	δ
r_1	6.399	0.015	0.002	0.000	0.059	−0.013	0.081	0.004	−0.077	0.075	0.002	−0.016
r_2		6.195	0.009	−0.011	0.079	0.072	−0.019	0.016	0.028	−0.023	−0.005	0.072
r_3			6.004	0.050	−0.006	0.113	0.000	0.086	0.001	0.003	−0.004	−0.010
r_4				6.172	−0.051	0.053	0.004	0.056	−0.064	0.031	0.033	0.036
D					11.690	0.283	0.459	−0.034	0.243	0.044	−0.286	0.021
Q						5.038	0.015	0.295	0.011	0.010	−0.020	−0.269
R							3.891	0.028	0.294	−0.400	0.106	0.044
P								3.178	−0.004	0.009	−0.005	−0.019
α									0.738	−0.361	−0.377	−0.032
β										0.500	−0.139	0.002
ω											0.516	0.029
δ												0.507
μ												
ρ												
θ												
χ												
ϕ_1												
ϕ_2												
γ_1												
γ_2												
π												
σ												
ξ												
τ												

From the *ab initio* calculations with the RHF/STO-3G* basis set, the structure corresponding to the *syn* conformation occurs as a transition state in the potential surface governing internal rotation about the C—C bond. The structure corresponding to this transition state was optimized and frequencies and Raman scattering activities for the normal modes were calculated with the RHF/3-21G* basis set. A 5% population of the *syn* conformer was then added to the calculated Raman spectrum for the *gauche* form to obtain a calculated Raman spectrum for a mixed conformational system. Such a mixture would correspond to a conformational energy difference of approximately 600 cm^{-1} (1.7 kcal/mol). The only difference between this calculated spectrum and that of the pure *gauche* form (Fig. 6) was the presence of two very weak lines at 603 and 396 cm^{-1}. It is tempting to assign the weak line observed at 602 cm^{-1} in the Raman spectrum of the gas to the *syn* form, but this line did not appreciably increase in intensity as the temperature was increased. Therefore, if the *syn* conformer is present in ≤5% abundance it is likely that we would not have observed any evidence for its existence, and if present in >5% abundance more definitive evidence would probably have been observed.

The absence of an observed frequency for the asymmetric torsional mode of *cis*-1,3-dichloropropene precludes the estimation of the *gauche* to *gauche* barrier from experimental data, but comparisons to related molecules provide some information. The asymmetric torsional modes for the *gauche* conformers of the 3-halopropenes and substituted derivatives typically occur between 70 and 110 cm^{-1} and give rise to infrared bands having hybrid contours. The frequencies of these modes have been fairly well predicted by *ab initio* calculations using the RHF/3-21G* or RHF/STO-3G* basis sets. For example, the torsional mode for the *gauche* conformer of *trans*-1,3-dichloropropene (33) was predicted to occur at 87 cm^{-1} (RHF/3-21G*) and was observed in the far-infrared spectrum of the gas at 84.0 cm^{-1}. For *cis*-1,3-dichloropropene this mode is calculated to occur at 45 cm^{-1}, which seems too low when compared to the corresponding modes of some similar molecules. However, if the *gauche* to *gauche* barrier is as low as predicted by *ab initio* calculations (342 cm^{-1}), or estimated by the electron diffraction technique (~350 cm^{-1}) (36), then this would explain the considerably lower torsional frequency than those for 3-chloropropene (102 cm^{-1}) or *trans*-1,3-dichloropropene (84 cm^{-1}), which have *gauche* to *gauche* barriers of ~700 and ~400 cm^{-1}, respectively.

Another interaction affecting the torsional frequency is the extent of mixing of the torsional mode with other skeletal bending modes, which is present for 3-chloropropene (27) and *trans*-1,3-dichloropropene (33), but absent for *cis*-1,3-dichloropropene. Additionally, hyperconjugative interactions similar to those found in acetaldehyde (43) and fluoroacetyl chloride (44), both of which have the internal rotor bonded to an sp^2 carbon, may play a significant role in the ultimate value of this barrier. Further, for the *gauche* structure of *cis*-1,3-dichloropropene, one of the hydrogen atoms bonded to the sp^3 carbon eclipses the chlorine atom on the vinyl group, which would raise the total energy of the *gauche* structure relative to 3-chloropropene or *trans*-1,3-dichloropropene. For these latter two molecules the *gauche* structure results in two hydrogen atoms eclipsing each other and the nonbonded steric interactions would be minimal. This is evidenced by the change in the C—C—H_4 bond angle (RHF/6-31G*) between *cis*-1,3-dichloropropene (112.5°) and *trans*-1,3-dichloropropene (111.3°). Some steric repulsion exists for this structure of the *cis*-substituted molecule that would raise the energy of the *gauche* minima and, assuming the *gauche* to *gauche* transition state is approximately the same

Can. J. Chem. Downloaded from www.nrcresearchpress.com by 203.198.23.82 on 09/08/12
For personal use only.

for the *gauche* conformer of *cis*-1,3-dichloropropene

μ	ρ	θ	χ	ϕ_1	ϕ_2	γ_1	γ_2	π	σ	ξ	τ
0.022	−0.007	0.001	0.000	−0.001	0.000	−0.006	0.006	−0.001	−0.001	−0.001	0.001
−0.120	0.049	−0.028	−0.001	−0.006	0.004	0.031	−0.003	0.000	0.002	0.004	0.001
0.021	−0.011	−0.051	0.101	−0.009	−0.056	−0.074	0.087	0.015	−0.006	0.008	−0.006
−0.095	0.059	−0.038	0.096	−0.042	−0.009	0.052	−0.064	0.000	0.002	0.003	−0.001
0.298	−0.319	−0.008	−0.004	0.001	−0.015	0.016	0.007	0.006	0.009	0.004	0.003
0.213	0.056	0.161	−0.177	−0.186	−0.159	0.178	0.150	0.032	−0.024	0.019	−0.007
−0.011	−0.032	0.010	−0.015	−0.011	−0.023	0.037	−0.001	0.009	0.005	0.002	−0.005
0.055	−0.036	0.303	−0.258	0.291	0.251	−0.266	−0.260	−0.035	0.038	−0.015	0.009
0.119	−0.087	−0.022	0.004	−0.005	−0.003	0.042	−0.019	−0.004	0.005	−0.001	0.001
−0.031	0.028	0.014	−0.004	0.001	−0.001	−0.023	0.014	0.003	−0.002	0.000	0.000
−0.088	0.059	0.008	0.000	0.005	0.003	−0.019	0.004	0.002	−0.002	0.001	−0.001
−0.357	−0.150	0.010	0.010	0.018	0.011	−0.041	−0.004	0.002	0.002	0.006	−0.002
0.704	−0.347	0.029	−0.012	−0.021	−0.019	−0.019	0.040	0.001	−0.004	0.003	0.001
	0.497	−0.039	0.002	0.003	0.008	0.060	−0.036	−0.004	0.002	−0.002	0.000
		0.933	−0.185	−0.161	−0.168	−0.215	−0.185	−0.032	0.064	−0.001	−0.001
			0.595	−0.109	−0.114	−0.100	−0.094	−0.009	−0.005	−0.008	0.002
				0.738	−0.131	−0.167	−0.114	0.005	−0.005	0.003	−0.002
					0.722	−0.116	−0.160	0.001	0.001	0.003	0.000
						0.690	−0.148	−0.007	0.000	−0.006	0.002
							0.667	0.041	−0.053	0.009	−0.001
								0.707	0.328	0.368	−0.013
									0.592	0.181	0.003
										0.674	−0.013
											0.005

TABLE 5. Observed and calculated frequencies (cm^{-1}) for the gauche conformer of cis-1,3-dichloropropene

Species	Vib. no.	Fundamental[a]	Ab initio[b]	Fixed scaled[c]	IR int.[d]	Raman act.[d]	Obd[e]	P.E.D.
A	ν_1	CH† stretch	3423	3247	4.52	97.04	3098	$96S_1$
	ν_2	CH_2 antisymmetric stretch	3369	3196	0.85	17.02	3056	$66S_2,26S_3$
	ν_3	CH§ stretch	3353	3181	1.42	94.72	3020	$70S_3,25S_2$
	ν_4	CH_2 symmetric stretch	3287	3118	7.75	98.13	2972	$90S_4,10S_2$
	ν_5	C=C stretch	1853	1745	20.44	57.65	1634	$83S_5$
	ν_6	CH_2 deformation	1648	1474	9.22	12.98	1450	$96S_6$
	ν_7	CH† bend	1516	1358	24.12	0.64	1336*	$43S_7,45S_9$
	ν_8	CH_2 wag	1439	1285	38.82	5.13	1264	$77S_8,16S_7$
	ν_9	CH§ bend	1399	1259	7.42	48.04	1228	$28S_9,23S_7,18S_8,17S_{10}$
	ν_{10}	CH_2 twist	1328	1188	1.98	6.72	1158*	$70S_{10},16S_9,10S_7$
	ν_{11}	CH† bend	1152	1033	0.12	8.33	1030	$35S_{11},24S_{14},19S_{18},13S_{12}$
	ν_{12}	C—C stretch	1107	1017	2.82	3.69	928*	$38S_{12},15S_{13}$
	ν_{13}	CH_2 rock	1000	909	10.85	3.55	912*	$61S_{13},18S_{12},11S_{14}$
	ν_{14}	CH§ bend	869	786	113.01	15.51	780	$39S_{14},24S_{11},16S_{16}$
	ν_{15}	C—Cl stretch	799	740	76.44	9.72	752	$52S_{15},12S_{17}$
	ν_{16}	C—Cl* stretch	728	677	8.78	34.64	686	$46S_{16},19S_{15},16S_{11}$
	ν_{17}	CCC/CCCl bend	589	541	12.78	7.70	550	$28S_{17},23S_{15},22S_{20},16S_{16}$
	ν_{18}	C—C—Cl bend	500	453	8.38	7.50	444	$42S_{18},17S_{16},17S_{19},10S_{11}$
	ν_{19}	CCCl/CCC bend	261	235	4.78	6.71	238*	$56S_{19},25S_{18}$
	ν_{20}	C—C—C bend	229	205	2.59	2.19	200	$43S_{20},42S_{17}$
	ν_{21}	Torsion	45	45	2.68	2.67		$98S_{21}$

[a]See Fig. 5 for atom numbering. The (†) and (§) denote the hydrogen atom bonded to carbon-1 and carbon-2, respectively, and the asterisk (*) denotes the chlorine atom bonded to the sp^3 carbon.
[b]Calculated using the RHF/3-21G* basis set.
[c]Calculated using scaling factors of 0.9 for stretches, 0.8 for bends, and 1.0 for the torsion.
[d]Calculated infrared intensities and Raman activities in km/mol and $Å^4$/amu, respectively.
[e]Taken from the spectrum of the gas phase. Frequencies denoted with an asterisk (*) are taken from the spectrum of the liquid phase.

energy, would consequently lower the *gauche* to *gauche* barrier over the *anti* (180°) transition state.

The potential function governing internal rotation of the CH_2Cl top of *cis*-1,3-dichloropropene has been determined using the RHF/6-31G* basis set and is consistent with the *gauche* minima lying 342 and 2425 cm^{-1} lower in energy than the *anti* (180°) and *syn* (0°) transition states, respectively. This potential function is in fair agreement with that obtained from molecular mechanics (35) calculations where the *syn* and *anti* barriers are 2169 cm^{-1} (6.2 kcal/mol) and

Can. J. Chem. Downloaded from www.nrcresearchpress.com by 203.198.23.82 on 09/08/12
For personal use only.

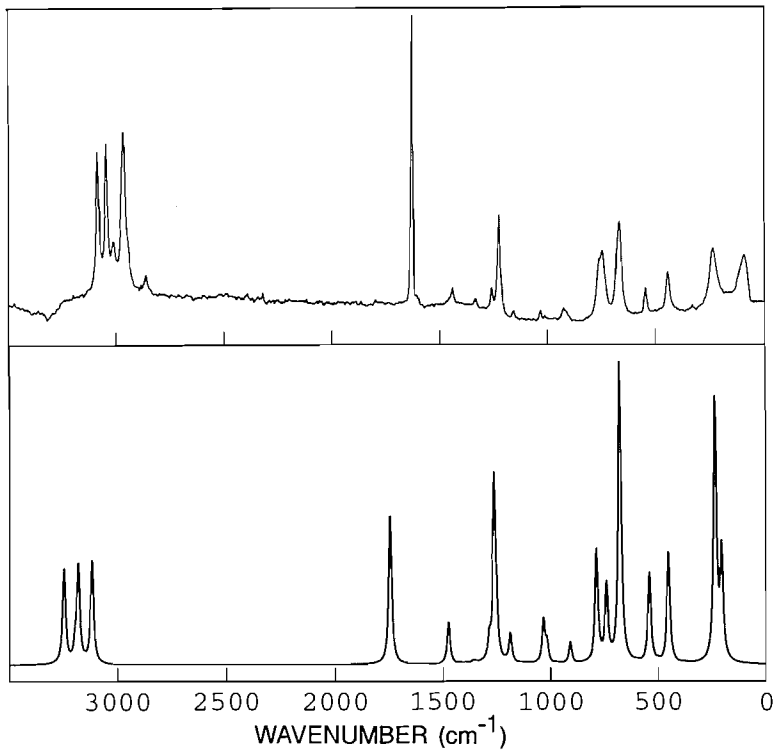

FIG. 6. Raman spectra of *cis*-1,3-dichloropropene: (top) FT–Raman spectrum of the liquid phase and (bottom) calculated at the RHF/3-21G* basis set.

804 cm^{-1} (2.3 kcal/mol), respectively. It could be argued that the *anti* barrier is overestimated by molecular mechanics calculations due to the fact that the value of 342 cm^{-1} (0.98 kcal/mol) obtained from *ab initio* calculations is much closer to the experimental value of 350 cm^{-1} (1.0 kcal/mol) obtained from the electron diffraction data (36).

The structural parameters calculated with the 6-31G* basis set with electron correlation at the MP2 level reasonably reproduce the values obtained from the electron diffraction results (36). The heavy atom bond distances calculated with this basis set are within 0.01 Å of the experimental values except for the C—C bond distance, which is calculated to be 0.021 Å longer as determined from the electron diffraction results (36). This value of 1.508 Å for the C—C distance is a little longer than one might expect when compared to the corresponding distance in some similar molecules, but the distance calculated with the MP2/6-31G* basis set (1.487 Å) is clearly too short by probably as much as 0.014 Å. On the other hand, the bond angles are very similar to those obtained experimentally (36). It is difficult to ascertain the reliability of the *ab initio* calculated bond angles since there were rather large uncertainties for several of the angles from the electron diffraction study (36) and some were assumed. As previously mentioned, *ab initio* calculated bond angles are generally reliable to about 1° except for dihedral angles for the *gauche* conformers. The *gauche* dihedral angle of 107.1°, from the molecular mechanics study (35), is clearly too small when compared to the *ab initio* (118.3°) and electron diffraction results (123° ± 5°).

The utility of using *ab initio* calculations with the RHF/3-21G* basis set to calculate the intensities of the Raman lines has been demonstrated. These results indicate that the Raman intensity data should be useful to improve vibrational assignments as well as for analytical identification purposes for these types of molecules. However, it is necessary to scale the calculated vibrational frequencies, which are then comparable to those obtained experimentally. Usually, the relative order of the vibrational fundamentals is correct. In the past, only Raman frequency data have been used for chemical information, but with high-speed inexpensive computers it should be possible to use both the frequency and intensity data from the Raman spectrum to obtain chemical information on a sample.

Acknowledgement

The authors gratefully acknowledge partial financial support of this study by the National Science Foundation by Grant OSR-9108772.

1. G.H. Griffith, L.A. Harrah, J.W. Clark, and J.R. Durig. J. Mol. Struct. **4**, 255 (1969).
2. B. Gross and M.T. Forel. J. Chem. Phys.**62**, 1163 (1965).
3. A.L. Verma. J. Mol. Spectrosc. **39**, 247 (1971).
4. P. Hornischer and H. Moser. Spectrochim. Acta, Part A: **28A**, 81 (1972).
5. B. Silvi and C. Sourisseau. J. Chem. Phys. **73**, 101 (1976).
6. B. Silvi and C. Sourisseau. Spectrochim. Acta, Part A: **31A**, 565 (1975).
7. E. Hirota. J. Mol. Spectrosc. **35**, 9 (1970).
8. E. Hirota. J. Chem. Phys. **42**, 2071 (1965).
9. P. Meakin, D.O. Harris and E. Hirota. J. Chem. Phys. **51**, 3775 (1969).
10. R.D. McLachlan and R.A. Nyquist. Spectrochim. Acta, Part A: **24A**, 103 (1968).
11. J. Luppi, M. Räsänen, J. Murto, and P. Pajunen. J. Mol. Struct. **245**, 307 (1991).
12. H.J.M. Bowen, A. Gilchrist, and L.E. Sutton. Trans. Faraday Soc. **51**, 1341 (1955).

Can. J. Chem. Downloaded from www.nrcresearchpress.com by 203.198.23.82 on 09/08/12
For personal use only.

13. S.H. Schei and Q. Shen. J. Mol. Struct. **81**, 269 (1982).
14. Y. Niide, M. Takano, T. Satoh, and Y. Sasada. J. Mol. Spectrosc. **63**, 108 (1976).
15. Y. Niide. J. Sci. Hiroshima Univ. Ser. A: Phys. Chem. **48**, 23 (1984).
16. A.A. Bothner-By and H. Gunther. Discuss. Faraday Soc. **34**, 127 (1962).
17. R.E. Rondeau and L.A. Harrah. J. Mol. Spectrosc. **21**, 332 (1966).
18. K. Radcliffe and J.L. Wood. Trans. Faraday Soc. **62**, 2038 (1966).
19. C. Sourisseau and B. Pasquier. J. Mol. Struct. **12**, 1 (1972).
20. A.A. Bothner-By, S. Castellano, S.J. Ebersole, and H. Gunther. J. Am. Chem. Soc. **88**, 2466 (1966).
21. A. Barnes, S. Holroyd, W. George, J. Goodfield, and W. Maddams. Spectrochim. Acta, Part A: **38A**, 1245 (1982).
22. S.H. Schei and Q. Shen. J. Mol. Struct. **128**, 161 (1985).
23. R. Stolevik and O. Thingstad. J. Mol. Struct. **106**, 333 (1984).
24. J.R. Durig, Mengzhang Zhen, and T.S. Little. J. Chem. Phys. **81**, 4259 (1984).
25. J.R. Durig, Mengzhang Zhen, H.L. Heusel, P.J. Joseph, P. Groner, and T.S. Little. J. Phys. Chem. **89**, 2877 (1985).
26. J.R. Durig, T.J. Geyer, T.S. Little, and D.T. Durig. J. Mol. Struct. **172**, 165 (1988).
27. J.R. Durig, D.T. Durig, M.R. Jalilian, Mengzhang Zhen, and T.S. Little. J. Mol. Struct. **194**, 259 (1989).
28. J.R. Durig and M.R. Jalilian. J. Phys. Chem. **84**, 3543 (1980).
29. D.T. Durig, T.S. Little, T.G. Costner, and J.R. Durig. J. Mol. Struct. **266**, 277 (1992).
30. D.T. Durig, G.A. Guirgis, and J.R. Durig. J. Raman Spectrosc. **23**, 37 (1992).
31. J.R. Durig, Q. Tang, and T.S. Little. J. Mol. Struct. **269**, 257 (1992).
32. J.R. Durig, Q. Tang, and T.S. Little. J. Raman Spectrosc. **23**, 653 (1992).
33. J.R. Durig, T.G. Costner, T.S. Little, and D.T. Durig. J. Phys. Chem. **96**, 7194 (1992).
34. R.J. Abraham and K. Parry. J. Chem. Soc. B, 724 (1971).
35. P.J. Stavnebrekk and R. Stolevik. J. Mol. Struct. **159**, 153 (1987).
36. Q. Shen. J. Mol. Struct. **75**, 303 (1981).
37. W.J. Potts and R.A. Nyquist. Spectrochim. Acta, **9**, 679 (1959).
38. M.J. Frisch, M. Head-Gordon, G.W. Trucks, J.B. Foresman, H.B. Schlegel, K. Raghavachari, M.A. Robb, J.S. Binkley, C. Gonzales, D.J. DeFrees, D.J. Fox, R.A. Whiteside, R. Seeger, C.F. Melius, J. Baker, R.L. Martin, L.R. Kahn, J.J.P. Stewart, S. Topiol, and J.A. Pople. Gaussian-90. Gaussian, Inc., Pittsburgh, Pa. 1990.
39. P. Pulay. Mol. Phys. **17**, 197 (1969).
40. E.B. Wilson, J.C. Decius, and P.C. Cross. Molecular vibrations. McGraw Hill, New York. 1955.
41. J.H. Schachtschneider. Vibrational analysis of polyatomic molecules. Parts V and VI. Technical Report Nos. 231 and 57, Shell Development Co., Houston, Tex. 1964 and 1965.
42. A. Anderson (*Editor*). The Raman effect. Vol. 1. Marcel Dekker, Inc., New York. 1971.
43. M. Baba, U. Nagashima, and I. Hanazaki. J. Chem. Phys. **83**, 3514 (1985).
44. J.R. Durig, H.V. Phan, J.A. Hardin, and T.S. Little. J. Chem. Phys. **90**, 6840 (1989).

Can. J. Chem. Downloaded from www.nrcresearchpress.com by 203.198.23.82 on 09/08/12
For personal use only.

Raman studies of cyanate: Fermi resonance, hydration and hydrolysis to urea

MURRAY H. BROOKER[1] AND NANPING WEN

Chemistry Department, Memorial University of Newfoundland, St. John's, NF A1B 3X7, Canada

Received March 24, 1993

This paper is dedicated to Professor Gerald W. King on the occasion of his 65th birthday

MURRAY H. BROOKER and NANPING WEN. Can. J. Chem. **71**, 1764 (1993).

Raman spectra were measured for potassium cyanate in the solid phase and as aqueous solutions in H_2O and D_2O for freshly prepared and for aged solutions. The results indicated that the assignment of the Fermi doublet, ν_1 and $2\nu_2$, for solid potassium cyanate was reversed from the assignment for the aqueous solution. The Fermi doublet has an associated pair of hot bands at 1191 and 1315 cm^{-1} which originate from the 638 cm^{-1} ν_2 state, 010. Assignment of the hot bands was confirmed by studies of solid potassium cyanate at liquid-N_2 temperature, room temperature, and at 473 K. Raman spectra of aged aqueous potassium cyanate revealed that the cyanate ion hydrolyzed slowly and spontaneously at room temperature (even without added ammonium) to produce urea and a carbamate, carbonate equilibrium mixture in parallel reactions. Hydrolysis of cyanate in aqueous ammonium chloride solution resulted in almost total conversion of cyanate to urea. The reaction was not reversible under ambient conditions. Differences in peak frequencies and half-widths were observed for the cyanate dissolved in H_2O compared to solutions in D_2O. The results provide evidence for strong hydrogen bonding of cyanate to water and are consistent with greater structure in the D_2O solution. Theoretical *ab initio* calculations indicated that the water molecules hydrogen bond well at both the oxygen and nitrogen atoms of cyanate although the hydrogen bond to nitrogen was found to be slightly stronger.

MURRAY H. BROOKER et NANPING WEN. Can. J. Chem. **71**, 1764 (1993).

On a mesuré les spectres Raman du cyanate de potassium en phase solide et en solutions aqueuses dans le H_2O et le D_2O pour des solutions fraîchement préparées ainsi que pour des solutions qui avaient vieillies. Les résultats obtenus indiquent que l'attribution du doublet de Fermi, ν_1 et $2\nu_2$, pour le cyanate de potassium à l'état solide doit être inversé par rapport à ce qui est observé en solution aqueuse. La doublet de Fermi est associé à une paire de bandes chaudes à 1191 et 1315 cm^{-1} qui ont leur origine dans l'état ν_2, 010, à 638 cm^{-1}. On a pu confirmer l'attribution des bandes chaudes par des études sur le cyanate de potassium solide à la température de l'azote liquide, à la température ambiante et à 473 K. Les spectres Raman des solutions aqueuses du cyanate de potassium qui ont vieillies révèlent que l'ion cyanate s'hydrolyse lentement et spontanément à la température ambiante (même sans addition d'ammonium) pour former de l'urée et un mélange à l'équilibre de carbamate/carbonate provenant de réactions parallèles. L'hydrolyse du cyanate en solution aqueuse de chlorure d'ammonium provoque une conversion presque globale du cyanate en urée. La réaction n'est pas réversible dans les conditions ambiantes. On a observé des différences dans les fréquences et les demi-largueurs des bandes du cyanate dissous dans le H_2O par rapport aux solutions dans le D_2O. Les résultats suggèrent qu'il existe de fortes liaisons hydrogènes entre le cyanate et l'eau et ils sont en accord avec la plus grande structure en solution dans le D_2O. Des calculs théoriques *ab initio* indiquent que les molécules d'eau forment aussi facilement des liaisons hydrogènes avec les atomes d'oxygène que d'azote du cyanate, même si l'on a trouvé que la liaison hydrogène avec l'azote est légèrement plus forte.

[Traduit par la réduction]

Can. J. Chem. Downloaded from www.nrcresearchpress.com by 203.198.23.82 on 09/08/12
For personal use only.

1. Introduction

Wöhler (1) first synthesized urea in 1828 by evaporation to dryness of a mixture of aqueous ammonium sulphate and potassium cyanate. It has long been supposed that the ammonium cyanate produced in the metathesis reaction rearranged into urea. The mechanism has been the subject of considerable interest since both ionic and molecular mechanisms have been proposed. The relative merits of each mechanism have been reviewed by Frost and Pearson (2) and Moelwyn Hughes (3). As part of a comprehensive study of aqueous solutions of small molecules which contain N, C, O, and H the Raman spectrum of KOCN has been measured for the solid and aqueous phases. The Raman spectrum of potassium cyanate has been studied previously in aqueous solutions by Goubeau (4), Pal and Sen Gupta (5), and Cleveland (6). Difficulties in making vibrational assignments were encountered due to the cyanate ion hydrolysis. Infrared studies of potassium cyanate have been carried out with solid and aqueous solution by Waddington (7), Williams (8), Maki and Decius (9), and Decius and Gordon (10). Although the basic assignments for the three expected fundamental vibrations of cyanate were well established the actual data and the vibrational assignments were inconsistent. The region of the ν_1 fundamental was found to be complicated by Fermi resonance with $2\nu_2$.

Isolated cyanate ion, written in either canonical form, O=C=N$^-$ or N≡C—O$^-$, has a linear configuration with $C_{\infty v}$ symmetry. The vibration representation is $\Gamma_{vib} = 2\,\Sigma^+ + \Pi$ with all the vibrational modes both infrared and Raman active. The isolated, unperturbed cyanate ion should have three fundamental vibration frequencies, the symmetric stretching frequency, $\nu_1(\Sigma^+)$ or ν_{CO}, a degenerate bending frequency, $\nu_2(\Pi)$ or ν_{OCN}, with two degrees of freedom at right angles, and an antisymmetric stretching vibration, $\nu_3(\Sigma^+)$ or ν_{CN}. One of the overtones, $2\nu_2$, is of particular importance to the Raman spectra of solid and aqueous potassium cyanate because it is known that a component of this state, $2\nu_2(\Sigma^+)$, is in resonance with the $\nu_1(\Sigma^+)$ fundamental to give rise to a pair of bands of nearly equal intensity. These two vibrational states are neither pure CO stretching, ν_{CO} or $\nu_1(\Sigma^+)$, nor pure OCN bending, $2\nu_{OCN}$ or $2\nu_2(\Sigma^+)$, but they are mixed states often referred to ambiguously as the $\nu_1 + 2\nu_2$ doublet. The Raman spectra in the region of the Fermi doublet were found to be sensitive to the environment about

[1]Author to whom correspondence may be addressed.

the cyanate ion. The Fermi doublet then served as an experimental probe to study the interaction of cyanate to water and heavy water.

It was interesting to observe that after the aqueous cyanate solution had stood a few days, new peaks were observed. Cleveland (6) and Williams (8) have reported evidence for hydrolysis and assigned the new infrared peaks to ammonium, carbonate and bicarbonate ions formed by the hydrolysis reaction (eqs. [1.1] and [1.2]).

[1.1] $KOCN + 3H_2O + \rightarrow KHCO_3 + NH_4OH$

[1.2] $2KOCN + 4H_2O \rightarrow K_2CO_3 + (NH_4)_2CO_3$

However, the present study on aged aqueous potassium cyanate revealed the presence of considerable urea, carbamate, and carbonate formed by hydrolysis (Eq. 2). Urea is formed even in the absence of added ammonium salts.

[2] $3OCN^- + 3H_2O \rightarrow H_2NCO_2^- + (NH_2)_2CO + CO_3^{2-}$

There was no evidence for the presence of bicarbonate or ammonium ions in the aged solutions although small quantities of these ions would be expected since aqueous carbamate has been shown to exist in equilibrium with ammonium, carbonate and bicarbonate (11). Addition of potassium cyanate to aqueous ammonium chloride resulted in a greater yield of urea.

2. Experimental

The spectroscopic measurements were carried out on a Coderg PHO Raman spectrometer after sample excitation with a INNOVA 70-4 argon ion laser operating at approximately 300 mW at the sample with the 488.0 nm wavelength line. The usual right angle scattering geometry was employed with the incident light vertically polarized and the scattered light analyzed with polaroid film to give the $I_{\parallel}$ $[x(zz)y]$ and $I_{\perp}$ $[x(zx)y]$ scattering geometries. A quarter-wave plate before the entrance slit served to compensate for the grating polarization preference. Raman wavenumber calibration was achieved with the plasma lines of the laser, but when required a narrow-bandpass interference filter was used to remove the unwanted plasma lines. The spectral slit widths of the double monochromator were set at 2.0 cm^{-1} which is sufficiently narrow to avoid the need for a slit correction to the bandshape. The Raman scattering light was detected with a PMT cooled to −30°C, integrated with a photon counter and processed with a home-built boxcar averager interfaced to the Memorial University VAX 8800 computer. The scan rate was 50 cm^{-1} min^{-1} and two data points were collected per wavenumber. Spectra were signal-averaged, and smoothed twice with a Savitsky-Golay three-point smoothing function. Curve resolution of overlapped bands and calculations of band half-width and intensity were achieved with a standard computer fitting program. The experimental spectrum was fit to a minimum number of bands synthesized with a Gaussian–Lorenzian product function.

All chemicals were reagent grade used without further purification. Potassium cyanate was obtained from BDH Chemical Ltd. All samples were sealed in quartz tubing (4 mm id, 5 mm od). Solid potassium cyanate was sealed under vacuum to prevent reaction with water vapour. Aqueous solutions were sealed under their own vapour pressure to avoid loss of ammonia and carbon dioxide gases which are decomposition products of carbamic acid. Ordinary aqueous solutions of potassium cyanate were prepared with distilled water. Deuterated aqueous solutions of potassium cyanate were prepared with deuterium oxide (99.9 atom % D, MSD Isotopes). Aqueous samples were routinely centrifuged for 5 min to settle dust particles. The Raman spectra of the fresh aqueous solution were obtained and the samples were then stored in a light-proof place. Additional Raman studies were made after suitable time intervals.

The Raman spectrum of solid potassium cyanate at 77 K was obtained on the copper cold tip of an evaporating liquid nitrogen cryostat. The high temperature study of solid potassium cyanate was performed on the powder sample sealed under vacuum in a quartz tube and heated in an insulated furnace with a proportional temperature controller. The temperature was monitored with a chromel–alumel thermocouple and the quoted temperature at the sample was constant and accurate to ±0.5°C.

Theoretical calculations with *ab initio* methods were performed at the Hartree Fock level with MUNGAUSS (12) to obtain minimum energies, optimized geometries and electron densities.

3. Result and discussion

The Raman spectra are shown (Fig. 1) for solid potassium cyanate and for freshly prepared and aged aqueous solutions of potassium cyanate in H_2O and D_2O for the region from 300 to 2400 cm^{-1}. The peak frequencies, half-widths and assignments of the observed Raman bands for potassium cyanate in the different conditions are collected in Tables 1 to 4. The antisymmetric stretching vibration, ν_3 (Σ^+) or ν_{CN}, appears at about 2170 cm^{-1}. The degenerate bending mode, $\nu_2(\Pi)$ or ν_{OCN}, occurs as a band of medium intensity in the 640 cm^{-1} region. In solid KOCN the degeneracy of ν_2 was removed, and two vibrational bands at 628 and 638 cm^{-1} were found due to the bending vibrations of the cyanate ion split by the local electric field of the crystal lattice. The shoulder at about 2185 cm^{-1} in the spectrum of solid KOCN also appears to be due to the effects of the crystal packing. $\nu_1(\Sigma^+)$ expected about 1245 cm^{-1} was found to be in Fermi resonance with $2\nu_2(\Sigma^+)$. Decius and co-workers (9, 10) have studied the Fermi resonance of $\nu_1 + 2\nu_2$ for cyanate in matrix isolation. The Fermi resonance pattern in cyanate strongly resembles that observed in the Raman spectrum of gaseous and aqueous carbon dioxide (13, 14).

Fermi resonance

The undisturbed symmetric stretching frequency, $\nu_1(\Sigma^+)$, would be expected at about 1245 cm^{-1}. However, the first harmonic of the bending mode, $2\nu_2(\Sigma^+)$, is very close in energy to the $\nu_1(\Sigma^+)$ and has a component with the same symmetry type, (Σ^+), with the result that vibrational coupling occurs (Fermi resonance). The overtone borrows intensity from the fundamental and appears as a fairly strong Raman band. In addition the two states repel each other and neither is found at the expected frequency (Fig. 2). The relative intensities and the separation of the peak maxima for the fundamental and the overtone depend on how closely the two undisturbed frequencies fall and may be calculated approximately with the expression (15).

$$[3] \qquad \nu^0 = \tfrac{1}{2}(\nu_a + \nu_b) \pm \tfrac{1}{2}(\nu_a - \nu_b)\frac{I_a - I_b}{I_a + I_b}$$

The two values of ν^0 are the unperturbed frequencies; ν_a and ν_b are the observed frequencies, and I_a and I_b are the associated band intensities.

For fresh ordinary aqueous cyanate (refer to curve *b* in Fig. 1), the two strong bands at 1310 and 1223 cm^{-1} are due to the Fermi doublet, ν_1 and $2\nu_2$. It is reasonable to associate the lower frequency component of the Fermi doublet with $2\nu_2$ because of the lower intensity and the higher frequency component with ν_1 because of its greater intensity i.e., $\nu_1^0 > 2\nu_2^0$. The Fermi doublet of solid cyanate (see curve *a* in Fig.

Can. J. Chem. Downloaded from www.nrcresearchpress.com by 203.198.23.82 on 09/08/12
For personal use only.

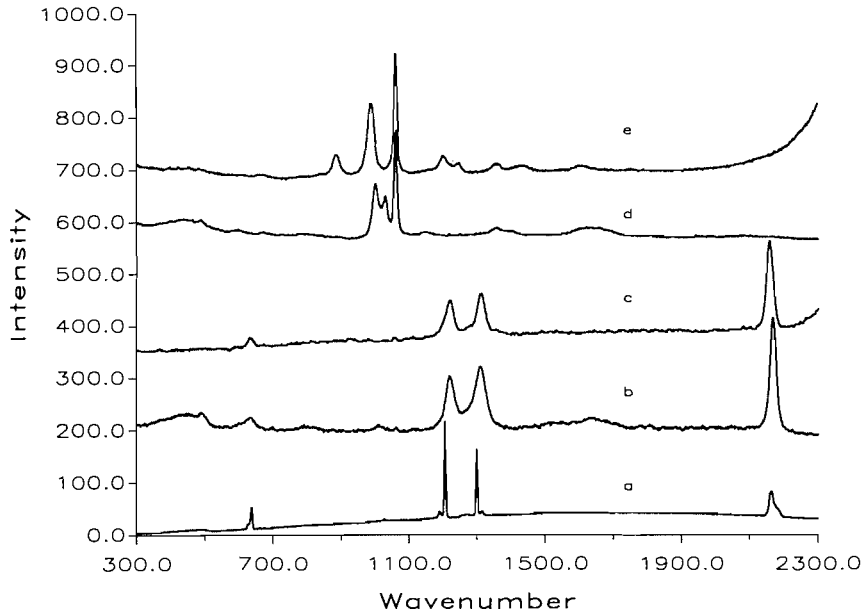

FIG. 1. Raman spectra of potassium cyanate in the states of solid (curve *a*), fresh ordinary aqueous (curve *b*), fresh deuterium aqueous (curve *c*), aged ordinary aqueous (curve *d*), and aged deuterium aqueous (curve *e*). The scale expansion of curves *c*, *d*, and *e* are times 0.5, 0.8, and 0.5, respectively. Spectra are off-set for clarity.

TABLE 1. Raman bands of solid potassium cyanate

Frequency[a] (cm^{-1})	$\Delta\nu_{1/2}$[b]	I[c]	Assignment	Reference
630.2	13.4	3.39×10^2	$\nu_2'(\Pi)$ or ν'_{OCN}	9
637.7	13.4	1.15×10^3	$\nu_2(\Pi)$ or ν_{OCN}	9
1190.9	11.7	3.42×10^2	hot band, (010) → (110)	This study
1206.6	4.8	1.99×10^3	$\nu_1(\Sigma^+)$ or ν_{CO}	9
1270.8			$2\nu_2$ of $O^{13}CN^-$	This study
1300.2	4.8	1.37×10^3	$2\nu_2(\Sigma^+)$	9
1315.0	10.4	2.49×10^2	hot band, (010) → (030)	This study
2110.8			ν_3 of $O^{13}CN^-$	9
2162.8	14.0	1.50×10^3	ν_3 or ν_{CN}	9
2180.5	18.1	6.05×10^2		This study
1244.8			ν_1^0	This study
1261.9			$2\nu_2^0$	This study

[a]Resolution is better than 0.5 cm^{-1}.
[b]Full width at half height.
[c]Integrated intensity.

TABLE 2. Raman bands of fresh aqueous potassium cyanate in H_2O

Frequency[a] (cm^{-1})	$\Delta\nu_{1/2}$[b]	I[c]	Assignment	Reference
631.8	25.3	1.21×10^3	$\nu_2(\Pi)$ or ν_{OCN}	This study
1223.2	40.1	4.34×10^3	$2\nu_2(\Sigma^+)$	This study
1309.6	48.4	6.20×10^3	$\nu_1(\Sigma^+)$ or ν_{CO}	This study
2167.9	23.9	5.76×10^3	$\nu_3(\Sigma^+)$ or ν_{CN}	This study
1274.0			ν_1^0	This study
1258.8			$2\nu_2^0$	This study

[a]Resolution is better than 0.5 cm^{-1}.
[b]Full width at half height.
[c]Integrated intensity.

TABLE 3. Raman bands of fresh aqueous potassium cyanate in D_2O

Frequency[a] (cm^{-1})	$\Delta\nu_{1/2}$[b]	I[c]	Assignment	Reference
637.3	25.1	1.21×10^3	$\nu_2(\Pi)$ or ν_{OCN}	This study
1222.0	40.0	10.7×10^3	$2\nu_2(\Sigma^+)$	This study
1313.2	39.2	10.4×10^3	$\nu_1(\Sigma^+)$ or ν_{CO}	This study
2159.5	20.5	12.8×10^3	$\nu_3(\Sigma^+)$ or ν_{CN}	This study
1268.3			ν_1^0	This study
1266.9			$2\nu_2^0$	This study

[a]Resolution is better than 0.5 cm^{-1}.
[b]Full width at half height.
[c]Integrated intensity.

Can. J. Chem. Downloaded from www.nrcresearchpress.com by 203.198.23.82 on 09/08/12
For personal use only.

TABLE 4. Raman bands of aged aqueous potassium cyanate in H_2O and D_2O

H_2O	D_2O	Assignment	Reference
563		ν_{12} (torsion about the C—N axis) of carbamate	24
683	700	$\nu_4(E')$ of carbonate	13,17
1003	889	$\nu_4(A_1)$ urea	23
1034		ν_5 (sym. NH_2 rock) of carbamate	24
1065	1064	$\nu_1(A_1')$ of carbonate	13,17
1155	991	$\nu_3(A_1)$ of urea	23
1380		$\nu_3(E')$ of carbonate	13
1405	1428	ν_3(C—N stretch) of carbamate	24
1597	1248	$\nu_2(A_1)$ of urea	23
1623	1202	ν_2 (NH_2 bend) of carbamate	24
1665	1612	$\nu_1(A_1)$ of urea	23

Can. J. Chem. Downloaded from www.nrcresearchpress.com by 203.198.23.82 on 09/08/12
For personal use only.

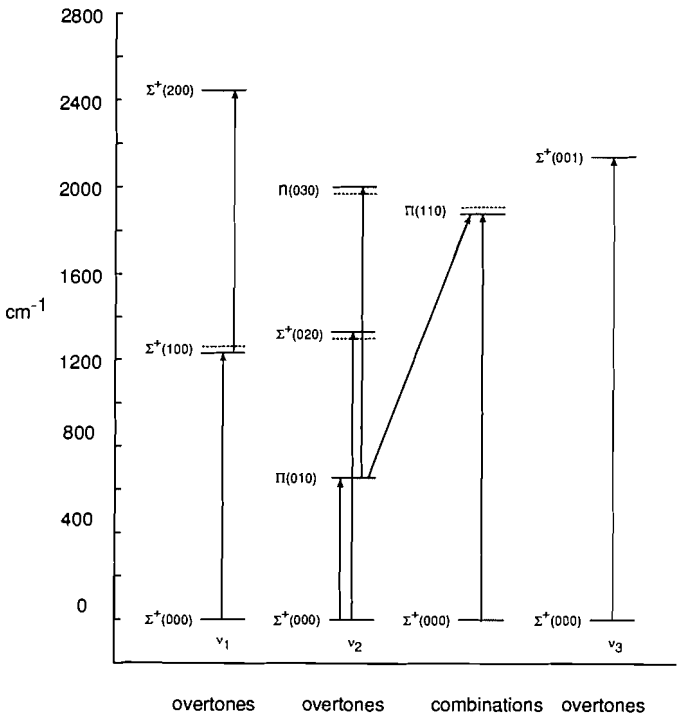

FIG. 2. Vibrational energy level diagram of the cyanate ion. The horizontal solid lines are at energies observed for the solid state, and the horizontal broken lines are at energies calculated for the undisturbed frequencies. The vertical arrows represent Raman transitions observed in this study.

1) appears at 1207 and 1300 cm^{-1}. When compared to the results for aqueous solution it can be seen that for solid KOCN the low frequency component of the Fermi doublet has become more intense and shifted to much lower frequency. Therefore, for solid KOCN the low frequency component has been associated with the ν_1. These result indicated that the assignment of the Fermi doublet, ν_1 and $2\nu_2$, for solid cyanate was reversed with respect to that for fresh aqueous cyanate. The unperturbed frequencies, ν_1^0 and $2\nu_2^0$, of cyanate in the states of solid, fresh ordinary aqueous and fresh deuterium aqueous were calculated from eq. [3] and the results listed in Tables 1, 2, and 3, respectively.

From Tables 1 and 2 it can be seen that the unperturbed frequency $2\nu_2^0$ of cyanate is very close to 1260 cm^{-1} in both solid and fresh ordinary aqueous states, but that the undisturbed frequency ν_1^0 shifts from 1245 cm^{-1} in the solid state to 1274 cm^{-1} in the fresh ordinary aqueous solution. Since the ν_2 mode remains near 635 cm^{-1} for solid and aqueous cyanate the change in the Fermi resonance pattern must be due to a frequency shift of the symmetric stretching mode. Strong interactions between cyanate ion and the water molecules appear to have a pronounced effect on the frequency of the ν_1 mode. The shift of ν_1^0 results in the inter-change of the assignment of the frequency sequence of the Fermi doublet from $\nu_1 > 2\nu_2$ for solid KOCN to $\nu_1 < 2\nu_2$ for aqueous OCN^-. In the case of fresh aqueous cyanate in deuterated water, the undisturbed frequencies ν_1^0 and $2\nu_2^0$ are about the same as for normal water and again the sequence of the Fermi doublet $\nu_1 < 2\nu_2$, is reversed from that found in solid potassium cyanate.

In addition to the intense Fermi doublet three additional bands appear in this region for solid KOCN at 1191, 1272, and 1315 cm^{-1}. The bands at 1191 and 1315 cm^{-1} have been assigned to a second Fermi doublet of hot bands (1191 cm^{-1}, (110) ← (010), and 1315 cm^{-1}, (030) ← (010)). A similar pair of hot bands were detected in the Raman spectrum of gaseous carbon dioxide (14). The appropriate transitions can be identified on the vibrational energy level diagram for the cyanate ion (Fig. 2). The hot bands originate from the 638 cm^{-1} ν_2 excited state of cyanate, (010), thermally populated at 295 K by a Boltzmann factor of $e^{-3.11} = 0.0446$. The assignment was confirmed by studies of solid KOCN at different temperatures. When the sample temperature was reduced to liquid-N_2 temperature, corresponding to a Boltzmann factor of $e^{-11.9} = 6.70 \times 10^{-6}$, the hot bands disappeared. However, when the sample temperature was raised to 473 K, corresponding to a Boltzmann factor of $e^{-1.94} = 0.144$, the intensities of the hot bands at 1191 and 1315 cm^{-1} obviously increased (Fig. 3). The cyanate ion isotopomer $O^{13}CN^-$ (about 1% abundance) can give rise to two Raman lines displaced to lower frequencies. One stands by itself at 1272 cm^{-1}, and the other apparently has not been resolved from the hot band at 1191 cm^{-1}. The Fermi resonance pair of hot bands have not been resolved from the broad bands of the ($\nu_1 + 2\nu_2$) pair in studies of the aqueous solutions of cyanate.

Hydration of cyanate

The differences between the spectrum of cyanate dissolved in normal and heavy water provides good evidence to indicate the presence of strong hydrogen bond interactions between cyanate and the water solvent. Identical peak positions and half-widths would be expected for aqueous cyanate dissolved in H_2O or D_2O in the absence of strong

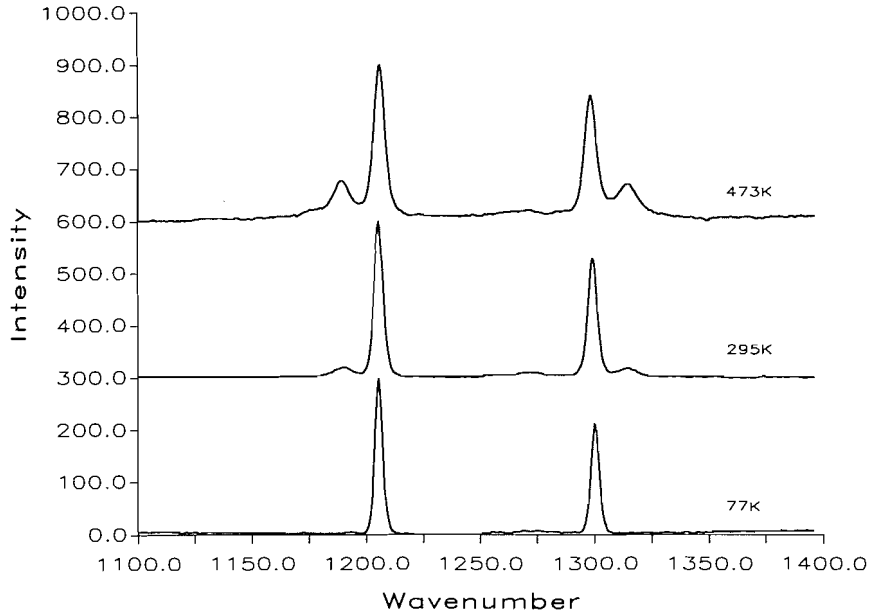

FIG. 3. Raman spectra of solid KOCN at different temperatures: (*a*) 473 K; (*b*) 295 K; (*c*) 77 K. Spectra are off-set for clarity.

interactions between the water and cyanate. In fact, there are significant differences (Tables 2 and 3). The unperturbed frequencies (ν_1^0) of aqueous cyanate were evaluated to be 1274 cm^{-1} in H_2O and 1268.3 cm^{-1} in D_2O. Although there is some uncertainty with these frequencies it is clear from the differences of the Fermi doublet for cyanate in H_2O and D_2O that there is a significant difference between the two systems. Furthermore, the $\nu_1(\Sigma^+)$ band at 1309.6 cm^{-1} was found to be significantly broader (half-width 48.4 cm^{-1}) in H_2O than the comparable band at 1313.2 cm^{-1} (half-width 39.2 cm^{-1}) in D_2O. The ν_3 mode of cyanate in H_2O was also considerably higher in frequency and broader (2167.9 cm^{-1}, half-width 23.9 cm^{-1}) than the comparable band in D_2O (2159.5 cm^{-1}, half-width 20.5 cm^{-1}). However, the most interesting difference was for the $\nu_2(\Pi)$ region were the peak position in D_2O was *higher* at (637.3 cm^{-1}) than in H_2O (631.8 cm^{-1}).

A qualitative explanation of the differences in the spectra of cyanate between water and heavy water can be developed from arguments based on differences in the zero point energies of vibrations which involve the motions of hydrogen (deuterium) in the hydrogen bond. Buckingham and Fan-Chen (16) have invoked similar arguments to explain differences in the physical properties of H_2O and D_2O. The decrease in frequency for the symmetric and antisymmetric modes of cyanate could be explained simply as a mass effect because the water, hydrogen-bonded to the O and/or N atoms would increase the apparent mass of these atoms (with D_2O more than H_2O). However, this explanation cannot explain the *increase* of the bending frequency for cyanate in D_2O compared to the H_2O solution and another explanation must be sought. When water hydrogen bonds to the cyanate at either the oxygen or nitrogen the O···H—O and O—H···N bonds tend to be linear hydrogen bonds. In the deuterium form the hydrogen bonds will have smaller thermal displacements perpendicular to the bond axis and will tend to be more linear, slightly shorter and stronger. In the case of the bending mode of cyanate in the deuterium solution the force constant will increase because the deuterium hydrogen-bond will provide a greater resistance to the bending motion. Similar arguments have been proposed to account for the unusual frequency shifts between the deuterium and protium solutions of carbonate and hydroxyborate (17, 18). In the *ab initio* calculations (described below) it was noted that the hydration of cyanate decreased the bond order of both the CN and the CO bonds. Hydrogen-bonding in deuterated solution may decrease the bond order more effectively than normal water with the result that the cyanate stretching force constants become slightly weaker in deuterium solution. This explanation is at least consistent with the experimental observations. Molecular dynamics models are not sensitive enough to probe such subtle differences and *ab initio* calculations treat hydrogen and deuterium as electronically equivalent (Born–Oppenheimer approximation).

In an effort to learn about the nature of the hydration of cyanate *ab initio* calculations have been performed to calculate optimum geometries and minimum energies for cyanate and cyanate hydrogen bonded to one and two water molecules. The results are collected in Table 5 for the 3-21G and 6-31G** basis sets. Since the 3-21G minimum basis set tended to over-emphasize the effect of hydrogen bonding the present discussion refers primarily to the results for the 6-31G** basis set. In all cases the cyanate retained a linear structure with the NCO angle of 180°. The *ab initio* calculations of free cyanate ion, cyanate ion bound to a water molecule through either the nitrogen or oxygen atom and cyanate ion bound to two water molecules through both nitrogen and oxygen atoms (refer to Table 4) gave a calculated bond order between C and N of about 2.6 and a bond order between C and O of about 1.5. The results were consistent with the deductions based on the Raman frequencies of the cyanate. Normally, a C=N double bond stretching vibration frequency is approximately 1650 cm^{-1}, and a C≡N triple bond stretching vibration frequency is close to 2250 cm^{-1}. The Raman spectrum of potassium cyanate indicated that the $\nu_3(\Sigma^+)$, i.e., ν_{CN}, was at about 2168 cm^{-1} which suggested a bond order of about 2.6 and not a full triple band. Similar arguments for the $\nu_1(\Sigma^+)$ suggested a bond

Can. J. Chem. Downloaded from www.nrcresearchpress.com by 203.198.23.82 on 09/08/12
For personal use only.

order of about 1.5 because the observed frequency of about 1260 cm^{-1} was about midway between the expected values for a single bond C—O (1000 cm^{-1}) and a double bond C=O (1600 cm^{-1}). The calculated optimum geometry for free cyanate resulted in approximately equal negative charge at the oxygen and nitrogen atoms (−0.74459 at N and −0.73462 at O, Table 5). It was also interesting to note that in all cases the sum of the CO and CN bond orders exceeded 4.0. Furthermore, as noted above, the total CO plus CN bond order decreased from 4.23 in free cyanate to 4.09 in cyanate hydrogen bonded to two water molecules. Apparently hydrogen bonding to water weakens the CO and CN bonds.

The results of the *ab initio* calculations indicated that relatively strong hydrogen bond interactions were possible for

TABLE 5. Results of *ab initio* calculations of free and hydrated cyanate

Structure	Parameter		Value 3-21G	Value 6-31G**
$\delta- \; \delta+ \; \delta-$ $N \equiv C = O$	Bond length (Å)	NC	1.168	1.167
		CO	1.238	1.216
	Bond order	NC	2.514	2.660
		CO	1.424	1.567
	Angle	NCO	180.0	180.0
	Atomic charge	N	−0.74641	−0.74459
		C	0.56487	0.47921
		O	−0.81846	−0.73462
	Energy (Hartree)		−166.232661	−167.195435
H_1-O_2 O_1 $\parallel$ C $\equiv$ N H_2	Bond length (Å)	NC	1.162	1.162
		CO_1	1.249	1.223
		O_1H_1	1.700	1.896
		H_1O_2	0.991	0.958
		O_2H_2	0.968	0.943
	Bond order	NC	2.568	2.696
		CO_1	1.294	1.458
		O_1H_1	0.148	0.085
		H_1O_2	0.671	0.789
		O_2H_2	0.863	0.899
	Angle	NCO_1	179.4	179.3
		CO_1H_1	121.8	113.4
		$O_1H_1O_2$	168.2	165.1
		$H_1O_2H_2$	105.0	102.8
	Atomic charge	N	−0.69622	−0.69783
		C	0.60062	0.49744
		O_1	−0.81109	−0.75346
		H_1	0.42439	0.39414
		O_2	−0.83408	−0.75446
		H_2	0.31638	0.31419
	Energy (Hartree)		−241.853783	−243.242308
O_2-H_2 H_1 N $\equiv$ C $\parallel$ O_1	Bond length (Å)	O_1C	1.227	1.208
		CN	1.166	1.166
		NH_1	1.748	1.916
		H_1O_2	0.933	0.962
		O_2H_2	0.968	0.943
	Bond order	O_1C	1.472	1.602
		CN	2.388	2.547
		NH_1	0.151	0.100
		H_1O_2	0.658	0.772
		O_2H_2	0.870	0.908
	Angle	O_1CN	180.0	180.0
		CNH_1	178.7	174.9
		NH_1O_2	165.5	164.1
		$H_1O_2H_2$	104.1	102.1
	Atomic charge	O_1	−0.78773	−0.71624
		C	0.67365	0.51985
		N	−0.79674	−0.75070
		H_1	0.44351	0.40567
		O_2	−0.83800	−0.75809
		H_2	0.30531	0.29951
	Energy (Hartree)		−241.854421	−243.244640

Can. J. Chem. Downloaded from www.nrcresearchpress.com by 203.198.23.82 on 09/08/12
For personal use only.

TABLE 5 (*concluded*)

Structure	Parameter		Value 3-21G	Value 6-31G**
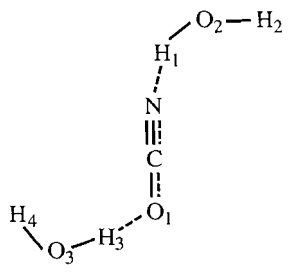	Bond length (Å)	O_1C	1.237	1.215
		CN	1.161	1.162
		NH_1	1.790	1.947
		H_1O_2	0.987	0.959
		O_2H_2	0.968	0.943
		O_1H_3	1.739	1.919
		H_3O_3	0.985	0.956
		O_3H_4	0.968	0.943
	Bond order	O_1C	1.344	1.495
		CN	2.449	2.592
		NH_1	0.134	0.089
		H_1O_2	0.676	0.781
		O_2H_2	0.865	0.906
		O_1H_3	0.131	0.075
		H_3O_3	0.689	0.797
		O_3H_4	0.859	0.899
	Angle	O_1CN	180.5	180.4
		CNH_1	176.8	176.4
		NH_1O_2	164.9	163.8
		$H_1O_2H_2$	104.5	102.5
		CO_1H_3	124.4	117.0
		$O_1H_3O_3$	167.8	165.7
		$H_3O_3H_4$	105.4	103.3
	Atomic charge	O_1	−0.78998	−0.72914
		C	0.70173	0.53551
		N	−0.75195	−0.71858
		H_1	0.43902	0.40251
		O_2	−0.82960	−0.75231
		H_2	0.31248	0.30281
		H_3	0.42128	0.39246
		O_3	−0.82501	−0.74788
		H_4	0.32202	0.31462
	Energy (Hartree)		−317.471049	−319.288961

both $NCO^- \cdots HOH$ and $OCN^- \cdots HOH$ conformers (Table 5). The minimum energies for the optimized geometries of $NCO^- \cdots HOH$ and $OCN^- \cdots HOH$ were −241.853783 and −241.854421 Hartree in 3-21G basis set, respectively (−243.242308 and −243.244640 Hartree in 6-31G** basis set). The hydrogen bond $OCN^- \cdots HOH$ with a bond order 0.151 in 3-21G basis set (0.100 in 6-31G** basis set) appeared slightly stronger than $NCO^- \cdots HOH$ with a bond order of 0.148 in 3-21G basis set (0.085 in 6-31G** basis set). Typical hydrogen bond lengths of about 1.9 Å were obtained for both the N···H (1.918 Å, in 6-31G**) and O···H (1.896 Å, in 6-31G**) hydrogen bonding configurations. The hydrogen bond angles O···H—OH and N···H—OH both tended to linear values of about 170°. The angle of attachment of the hydrogen bond to cyanate was markedly different for the two conformations. For the C—N···H interaction the bond angle was again close to linear (165°) whereas, for the C—O···H interaction the value was closer to trigonal (113°). These results were found to be consistent with a simple bonding model for cyanate that puts two lone pairs on the oxygen atom and one lone pair on the nitrogen. In solution it would seem very likely that the cyanate would have two water molecules of hydration at the oxygen and one at the nitrogen although this structure was not calculated. The results for cyanate hydrogen bonded simultaneously at both the oxygen and nitrogen ends gave similar hydrogen bond lengths and angles to those described above for the single water of hydration. Again the bond order of the N···H hydrogen bond was about 20% greater than for the O···H hydrogen bond which suggested a slight preference for cyanate hydration at the nitrogen. In summary the *ab initio* results indicated that cyanate has the excess charge distributed approximately equally well on the nitrogen and oxygen ends of the ion with the nitrogen slightly more negative.

The fact that the calculations indicated a stronger hydrogen bond from water to the N atom of cyanate than to the oxygen was consistent with the known stability of isocyanic acid (HNCO) compared to the cyanic acid isomer (NCOH) (19–21). It has been established from microwave studies (19) of isocyanic acid that the NCO angle was very close to 180° with a maximum error of 10° while the HNC angle was about 128°. Theoretical calculations have established isocyanic acid as the most stable isomer but these calculations indicated a small departure from linearity for the NCO angle (20, 21).

Cyanate hydrolysis

Since previous studies of aqueous cyanate (6, 8) described spectra that changed with time it seemed advisable to study the spectrum of a solution of potassium cyanate after different time intervals. It was found that the peaks which

Can. J. Chem. Downloaded from www.nrcresearchpress.com by 203.198.23.82 on 09/08/12
For personal use only.

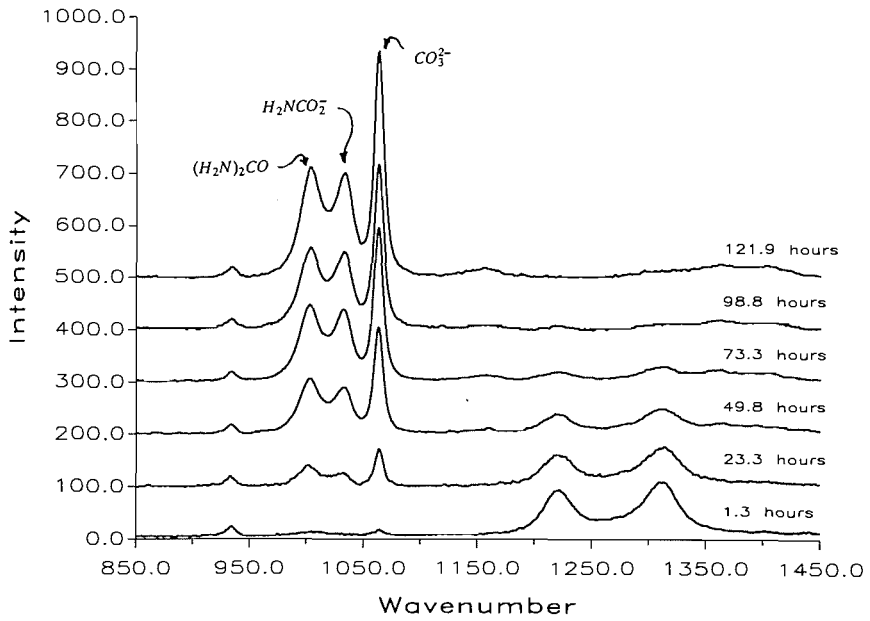

FIG. 4. Raman spectra of aged 2.0 M KOCN. The weak peak at 934 cm^{-1} is due to 0.1 M $NaClO_4$ added as an internal standard: (*a*) 1.3 h old; (*b*) 23.3 h old; (*c*) 49.8 h old; (*d*) 73.3 h old; (*e*) 98.8 h old; (*f*) 121.9 h old. Spectra are off-set for clarity.

were attributed to cyanate became less intense with time while new peaks which appeared at 1003, 1034, and 1065 cm^{-1} increased in intensity with the passage of time (Fig. 4). Cleveland (6) and Williams (8) suggested that the new peaks arose from the carbonate, bicarbonate, and ammonium, formed by hydrolysis of potassium cyanate (eqs. [1.1] and [1.2]). There can be no doubt that the new band at 1065 cm^{-1} was due ν_1 of carbonate since the frequency, half-width, and depolarization ratio were identical to that of a pure sodium carbonate solution. However, there was no evidence to suggest the presence of peaks due to bicarbonate or ammonium as suggested by Cleveland and Williams. The characteristic peaks for bicarbonate (13) and ammonium (22) are at 1017 and 1450 cm^{-1}. It was possible to identify the urea and carbamate ion as the source of the peaks at 1003 and 1034 cm^{-1} by comparison with spectra of known samples. The difference between our results and those of Cleveland and Williams can be accounted for by experimental differences in the sample control. In the present work the samples were maintained in sealed tubes which prevented the escape of gaseous ammonia. An aged sample (sealed) 2.0 M potassium cyanate aqueous solution had a pH value about 10 after hydrolysis was complete. At this pH there should be considerable ammonia but because of the presence of carbonate an equilibrium reaction results in carbamate formation. If open to the air the carbamate solution slowly loses ammonia and the solution becomes more acidic.

Wöhler (1) synthesized urea in 1828 by adding a solution of ammonium sulphate to a solution of potassium cyanate and evaporating the mixture to dryness. It has normally been supposed that ammonium cyanate was prepared in a metathesis reaction (eq. [4])

$$[4] \quad NH_4^+ + OCN^- \rightarrow NH_4OCN$$

followed by rearrangement of ammonium cyanate rearrange to form urea (eq. [5]).

$$[5] \quad NH_4OCN \rightarrow NH_2CONH_2$$

Raman spectrum of a similar mixture, 2.0 M ammonium chloride with 2.0 M potassium cyanate aqueous solution, was observed in region from 900 to 1800 cm^{-1} (curve *b* in Fig. 5). The very strong band at 1003 cm^{-1} was attributed to the $\nu_4(A_1)$ of urea and could be compared with the spectrum of pure aqueous urea (curve *a* in Fig. 5). The urea has been characterized not only by the 1003 cm^{-1} band but also by bands at 1155, 1597, and 1665 cm^{-1} bands (23). It is obvious that the urea is one of the hydrolysis products. The presence of carbonate was clearly indicated by characteristic peaks at 676 cm^{-1} $\nu_4(E')$, 1065 cm^{-1} $\nu_1(A_1')$ and a weak broad band at 1380 cm^{-1} $\nu_3(E')$. The band at 1034 cm^{-1} with medium intensity and overlapped with the 1003 cm^{-1} band has been attributed (11, 24) to carbamate ion, H_2NCOO^-. In a recent Raman investigation (11) of aqueous ammonium carbonate solutions it has been found that carbamate ion was a major equilibrium species but urea was not formed in this system.

$$[6] \quad CO_3^{2-} + NH_4^+ \rightleftarrows H_2NCOO^- + H_2O$$

The carbamate ion has been characterized by Raman bands at 563, 1034, and 1405 cm^{-1}. These additional characteristic frequencies of carbamate ion have also been detected in the Raman spectrum of aged ordinary aqueous cyanate (refer to curve *d* in Fig. 1).

According to our investigation, cyanate ion hydrolysis to form urea, carbamate, and carbonate slowly and spontaneously, even without added ammonium and at room temperature. In an open sample vessel the escape of ammonia would decrease the formation of urea and carbamate but the addition of ammonium (as in the Wöhler synthesis) can compensate for ammonia loss. The formation of urea occurs totally in solution and cannot be considered just a rearrangement of solid NH_4OCN. Further studies indicated that the hydrolysis of pure potassium cyanate was a very slow process (about 7 ~ 10 days at room temperature) while the reaction of ammonium and cyanate to urea was moderately

Can. J. Chem. Downloaded from www.nrcresearchpress.com by 203.198.23.82 on 09/08/12
For personal use only.

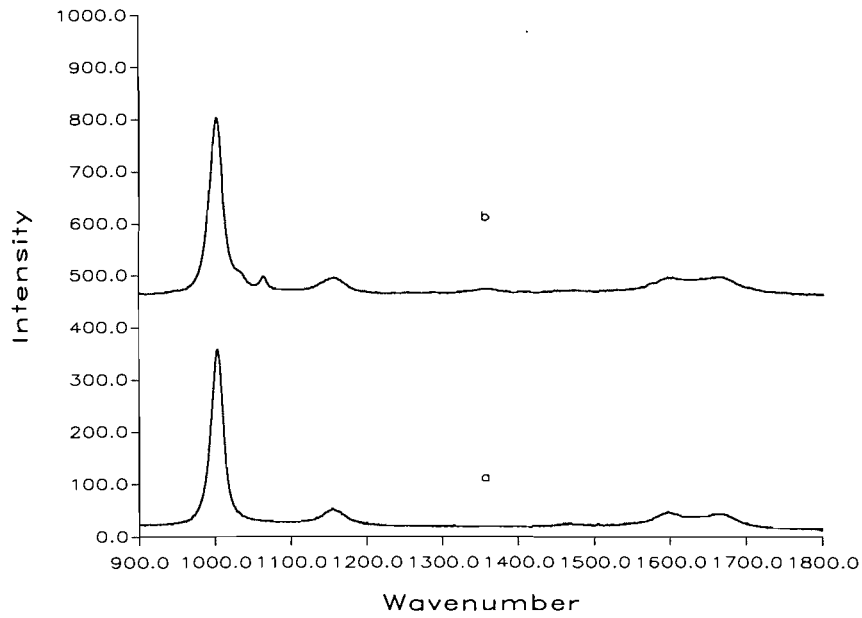

FIG. 5. Raman spectra of the aged solution from a solution which was 2.0 M NH_4Cl and 2.0 M KOCN (curve *b*) and 2.0 M urea made from pure urea dissolved in water (curve *a*). Spectra are off-set for clarity.

fast (about 2 ~ 3 days at room temperature). In an effort to determine if the reaction of cyanate proceeded by a direct nucleophilic attack of aqueous ammonia at the C of cyanate the hydrolysis was monitored for potassium cyanate dissolved in a 2.0 M ammonia solution. The rate and products of reaction for cyanate in ammonia solution were essentially identical to the reaction in pure water. The basic property of NCO^- should give rise to a small amount of isocyanic acid, HNCO (10^{-5} M) but here was no indication that the acid had a role in the reaction mechanism.

The possible hydrolysis processes might be as follows:

[7] $$OCN^- + 2H_2O \rightarrow CO_3^{2-} + NH_4^+$$

[8] $$CO_3^{2-} + NH_4^+ \rightleftarrows H_2NCOO^- + H_2O$$

[9] $$OCN^- + NH_4^+ \rightarrow H_2NCONH_2$$

The overall reaction can be written as:

[10] $$3OCN^- + 3H_2O \rightarrow H_2NCONH_2 + H_2NCOO^- + CO_3^{2-}$$

The molecular form of eq. [9] (as eq. [11]) cannot be excluded although Moelwyn Hughes (3) has suggested that the kinetic data were more consistent with an ionic mechanism.

[11] $$OCNH + NH_3 \rightarrow H_2NCONH_2$$

The formation of urea and the formation of carbamate were found to be independent parallel reactions. Studies of these systems as a function of concentration and temperature indicated that under normal aqueous conditions urea and carbamate were not in equilibrium and were not interconvertible. These facts do not appear to have been established previously. A detailed account of the rate process will be reported elsewhere.

4. Acknowledgments

This work was supported in part by a grant from the Natural Science and Engineering Research Council of Canada. One of the authors (N. Wen) gratefully acknowledges the support of a Memorial University of Newfoundland Graduate Student Fellowship. The authors thank Dr. R. Poirier for his support with the *ab initio* calculations.

1. F. Wöhler. Ann. Physik. Chem. **12**, 253 (1828).
2. A.A. Frost and R.G. Pearson. Kinetics and mechanisms. 2nd ed. Wiley, New York. 1963, p. 307.
3. E.A. Moelwyn Hughes. Chemical statics and kinetics of solutions. Academic Press, New York. 1971, p. 187.
4. J. Goubeau. Ber. Dtsch. Chem. Ges. **68**, 912 (1935).
5. N.N. Pal and P.N. Sen Gupta. Indian J. Phys. **5**, 612 (1930).
6. F.F. Cleveland. J. Am. Chem. Soc. **63**, 622 (1941).
7. T.C. Waddington. J. Chem. Soc. 4340 (1958).
8. D. Williams. J. Am. Chem. Soc. **62**, 2442 (1940).
9. A. Maki and J.C. Decius. J. Chem. Phys. **31**, 772 (1959).
10. J.C. Decius and D.J. Gordon. J. Chem. Phys. **47**, 1286 (1967).
11. M.H. Brooker, J. Hand, and N. Wen. Raman studies of aqueous carbamate, bicarbonate, carbonate equilibria: Proceedings of the International Conference on Raman Spectroscopy, XI, London, England. *Edited by* R.J.H. Clark and D.A. Long. Wiley, Chichester. 1988.
12. R.A. Poirier. MUNGAUSS. Department of Chemistry, Memorial University of Newfoundland, St. John's, Newfoundland, Canada.
13. A.R. Davis and B.G. Oliver. J. Solution Chem. **1**, 329 (1972).
14. G.R. Anderson. J. Phys. Chem. **81**, 273 (1977).
15. V.L. Strizhevskii. Opt. Spectrosc. **8**, 86 (1960) (English translation).
16. A.D. Buckingham and L. Fan-Chen. Int. Rev. Phys. Chem. **1**, 253 (1981).
17. M.H. Brooker. Hydrogen versus deuterium hydrogen bonds to hydrated carbonate ion: Proceedings of the International Conference on Raman Spectroscopy, XIII, Würzburg, Germany. *Edited by* W. Kiefer et al. Wiley. 1992.
18. M.H. Brooker and P.R. Tremaine. Geochim. Cosmochim. Acta, **56**, 2573 (1992).

Can. J. Chem. Downloaded from www.nrcresearchpress.com by 203.198.23.82 on 09/08/12
For personal use only.

19. W.H. Hocking, M.C.L. Gerry, and G. Winnewisser. Can. J. Phys. **53**, 1869 (1975).
20. D. Poppinger, L. Radom, and J.A. Pople. J. Am. Chem. Soc. **99**, 7806 (1977).
21. A.D. Buckingham, N.C. Handy, J.E. Rice, K. Somasundram, and C. Dijkgraaf. J. Comput. Chem. **7**, 283 (1986).
22. K. Mitsui and T. Ukaji. Research Reports of Ikutoku Tech. Univ. **B-1**, 89 (1976).
23. A. Yamaguchi, T. Miyazawa, T. Shimanouchi, and S. Mizushima. Spectrochim. Acta, **10**, 170 (1958).
24. D.L. Frasco. J. Chem. Phys. **41**, 2134 (1964).

Can. J. Chem. Downloaded from www.nrcresearchpress.com by 203.198.23.82 on 09/08/12
For personal use only.

1993 ALCAN Award Lecture
Chemical binding within and between inorganic rings; the design and synthesis of molecular conductors[1]

RICHARD T. OAKLEY
Department of Chemistry and Biochemistry, University of Guelph, Guelph, ON N1G 2W1, Canada

Received June 14, 1993

RICHARD T. OAKLEY. Can. J. Chem. **71**, 1775 (1993).

For a given number of skeletal atoms, the π-electron count of an unsaturated heterocycle can be modified by the incorporation of heteroatoms from different periodic groups. Sulfur and nitrogen are particularly effective in this regard, as their high electronegativity can stabilize electron-rich π-systems. A variety of aromatic, anti-aromatic, and radical systems can be prepared from admixtures of these elements. While the properties of these ring systems are interesting in their own right, the compounds are not without relevance in the design of new materials. The strong interannular interactions that are developed between these rings in the solid state makes them ideal candidates for the fabrication of molecular conductors. The origins and development of this area of research are the subjects of this presentation.

RICHARD T. OAKLEY. Can. J. Chem. **71**, 1775 (1993).

Pour une quantité donnée d'atome de squelette, le nombre d'électrons π contenus dans un hétérocycle insaturé peut être modifié par l'incorporation d'hétéroatomes de divers groupes périodiques. Les atomes de soufre et d'azote sont particulièrement utiles à ces fins car leur grande électronégativité permet de stabiliser des systèmes-π riches en électrons. On a préparé une variété de systèmes aromatiques, antiaromatiques et radicalaires par le mélange de ces éléments. Alors que les propriétés de ces systèmes cycliques présentent un intérêt inhérent à leur nature, ces composés ne sont toutefois pas sans intérêt pour la préparation de nouveaux matériaux. Les fortes interactions interannulaires qui se développent entre ces cycles à l'état solide en font des candidats idéaux pour la préparation de conducteurs moléculaires. Les origines et le développement de domaine de recherches font l'objet de cette présentation.

[Traduit par la rédaction]

Introduction

The present article continues a "tradition" initiated in 1992 by the Canadian Journal of Chemistry to provide a forum for the recipient of the annual ALCAN Award to summarize the highlights of the award lecture in a short monograph (1). Like my oral presentation at Sherbrooke, this account will focus more on recent events, but it is instructive (to me at least) to begin with a personal account of the historical origins of our research. This approach also provides me with an opportunity to identify and acknowledge the contributions of my students and collaborators.

The work to be described can be traced back to 1975, the year when superconductivity in $(SN)_x$ polymer was reported (2). As a graduate student working on phosphazene chemistry in Norman Paddock's laboratory at U.B.C., this discovery was of natural interest. My curiosity in structures containing conjugated SN units was further stimulated by an observation of my colleague Nick Westwood (then a postdoctoral fellow with Charles McDowell) that $(SN)_x$ could be vaporized to afford a species of formula $[S_3N_3]\cdot$ (3). At the time this radical represented one of the few known odd-electron species containing the $(SN)_x$ unit, and its generation from and reversion to the polymer were intriguing results that prompted many questions. Could new heterocycles, with unusual π-electron counts, be made? Might these serve as models for, or precursors to, novel polymeric systems? Within this context the isostructural (but not isoelectronic) replacement of —S= in $[S_3N_3]\cdot$ by either R_2P and (or) RC fragments represented an appealing synthetic challenge. The bottom row (compounds **7**–**10**) of the "family tree" illustrated in Scheme 1 were well-known (formally 6π-electron) compounds, and the potential for making 7π-electron radicals (**4**, **5**, and **6**) and 8π-electron anti-aromatic rings (**2** and **3**) seemed to provide an inspirational, if not logical, link to the ephemeral 9π-electron $[S_3N_3]\cdot$ species **1**.

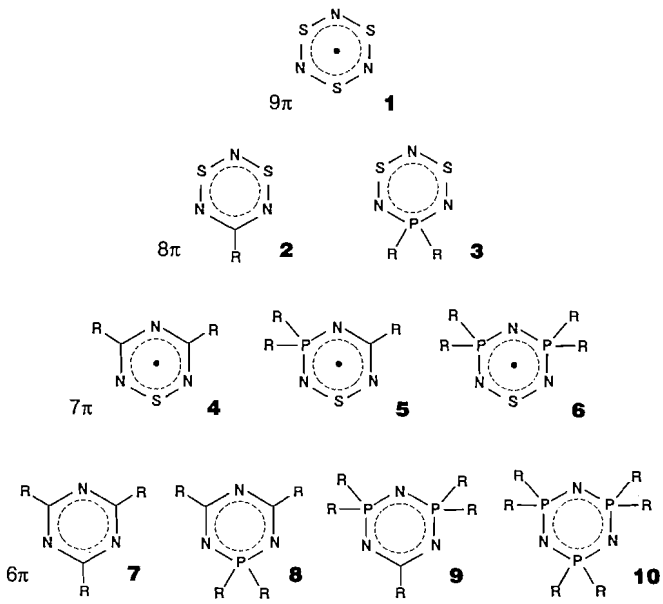

SCHEME 1

Some years later, first at the University of Calgary, and then at the University of Guelph, my students and I had the opportunity to develop these ideas. At first our work was driven by the desire to explore synthetic approaches to novel radical and anti-aromatic ring systems, and to study their chemical and structural stability. In more recent years the

[1]This article is based on the ALCAN Award Lecture delivered by Professor Oakley at the Annual Conference of the Canadian Society for Chemistry, Sherbrooke, Quebec, June, 1993.

Can. J. Chem. Downloaded from www.nrcresearchpress.com by 203.198.23.82 on 09/08/12
For personal use only.

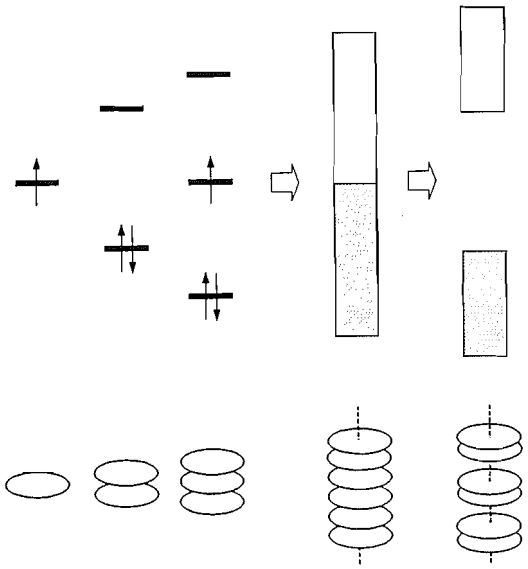

FIG. 1. Half-filled energy band associated with a uniformly spaced stack of π-radicals, and the energy gap arising from dimerization of the radicals.

work has evolved into the exploitation of the early results to fabricate molecules that, in the solid state, exhibit specific physical properties, notably electrical conductivity. These latter ideas were prompted by the early proposal of Robert Haddon that molecular conductors might be constructed from building blocks consisting of planar, neutral π-radicals (4). It is interesting that, while the design of molecular conductors from ionic radicals, in the form of charge transfer or Bechgaard salts (5), is now a well-developed field, the idea of using neutral radicals as plate-like building blocks has received relatively little attention. The dearth of results on these latter systems can perhaps be attributed, in part at least, to the experimental difficulty associated with preparing and characterizing any neutral radical. A second, and perhaps more difficult problem, has stemmed from the need to sculpt such radicals in a manner that obliges them to come together, in the solid state, in the stacked fashion illustrated in Fig. 1. The half-filled energy band, generated by the interaction of the unpaired π-electron on each molecular unit should, at first glance, afford a metallic ground state. Nature, however, is only partially impressed by this reasoning (vide infra), and both persistence and compromise have been necessary to achieve highly conductive materials.

The work described in this article represents a mélange of exploratory and targeted research in inorganic heterocyclic chemistry. I begin by outlining the results that emerged from our early pursuits of novel anti-aromatic and radical rings. In that way the chronological (but not necessarily logical) evolution towards the more directed work, to be described in later sections, can be better appreciated.

Aromatic and anti-aromatic rings

The possibility of observing aromatic/anti-aromatic effects in inorganic rings was first raised by Craig and Paddock who, in the late 1950s, mapped out (and later demonstrated) the physical and chemical consequences of cyclic π-delocalization in cyclophosphazenes (6). Similar ideas took root in cyclothiazene chemistry in the 1970s, with seminal papers by Gleiter (7) and Banister (8). The structural stability associated with aromatic $(4n+2)$ π-electron counts was recognized, and important examples of new aromatic systems, e.g., the binary rings $S_3N_3^-$ (9) and $S_4N_4^{2+}$ (10) and heterocyclic dithiatetrazocines $R_2C_2N_4S_2$ (11), were identified. The electron richness of these heterocycles, coupled with the differing electronegativities of their constituent atoms (S and N), leads to highly polarizable π-systems (12). In the early 1980s, soon after I began my NSERC University Research Fellowship at the University of Calgary, I explored the structural instabilities that these electronic features generate. The dramatic changes that accompany the protonation of S_4N_4 (13) and $S_3N_3^-$ (14), as well as the puckering of dithiatetrazocines in the presence of π-donor ligands ($R = NMe_2$), could all be interpreted in terms of severe localizations of anti-bonding π*-electron density (15).

Examples of anti-aromatic $(4n)$ π-electron rings were (predictably) more scarce. While still at Calgary, and in conjunction with Tris Chivers, Bill Laidlaw, and Neil Burford, I explored the synthesis and characterization of heterocyclic phosphadithiatriazines $R_2PN_3S_2$ **3**. The electronic structures of these rings are best described by an internal salt formulation but, to the extent that cyclic delocalization survives (through *d*-orbital involvement or hyperconjugation at phosphorus), they can be considered as anti-aromatic 8π-electron rings (16). Consistently they exhibit a low-energy π*–π* electronic absorption (a small HOMO–LUMO gap), and readily undergo cycloaddition reactions (with reverse electron demand) (17).

Hans Koenig, my first graduate student, continued to explore the relevance of aromatic concepts in inorganic rings by synthesizing and comparing the physical and chemical properties of the (deep blue) anti-aromatic 12π-benzodithiadiazine **11** and the (canary yellow) aromatic 14π-benzotrithiadiazepine **12** (18). The most appealing chemical finding related to their cycloaddition behaviour with norbornadiene (eqs. [1] and [2]). Both rings undergo a reversible cycloaddition with electron-rich olefins, but the equilibrium lies further to the right-hand side for addition to the *anti-aromatic* ring. Following the approach of Dewar, the two equilibrium constants for the addition can be converted into a *difference* in delocalization energies of ca. 5 kcal/mol, a value that is quite in keeping with the corresponding differences observed between classical aromatic and anti-aromatic annulenes of similar ring size. Later photoelectron and electron energy loss spectroscopic studies on these systems confirmed the expected trends in frontier orbital energies (19).

[1] 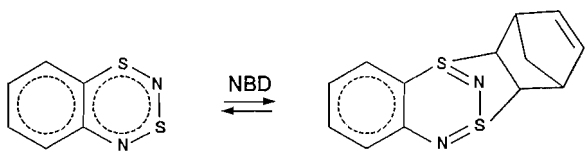

11

[2] 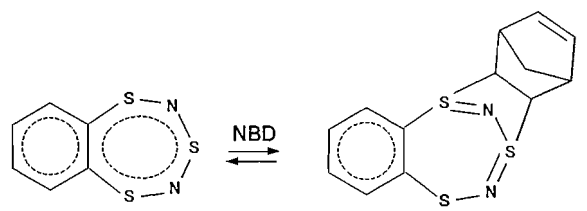

12

Can. J. Chem. Downloaded from www.nrcresearchpress.com by 203.198.23.82 on 09/08/12
For personal use only.

Can. J. Chem. Downloaded from www.nrcresearchpress.com by 203.198.23.82 on 09/08/12
For personal use only.

René Boeré, a NSERC postdoctoral fellow in my group, also pursued elusive anti-aromatic rings, most notably derivatives of the dithiatriazine RCN_3S_2 **2**. His approach, outlined in Scheme 2, required the use of persilylated amidines. These reagents, which are now widely used in much of our chemistry, are conveniently prepared by the Sanger reaction, i.e., the addition of $LiN(SiMe_3)_2$ to an aromatic nitrile (20). Persilylated amidines can be condensed with $S_3N_3Cl_3$ to produce the bicyclic derivatives **13** (21). In the case of R = phenyl, treatment of **13** with chlorine cleaves the -NSN- bridge, producing the dichlorodithiatriazine **14**. Reduction of **14** did not afford the monomeric 8π-electron ring **2** that we expected; eventual X-ray characterization of the isolated product revealed instead the dimeric system **15**, in which two CN_3S_2 rings are linked through two long (2.527 Å) S—S bonds (22). Evidently the monomer is sufficiently anti-aromatic that it dimerizes. Later computational work by my colleague John Goddard revealed a close energetic balance between the two spin states of the monomeric (gas phase) HCN_3S_2, the singlet being slightly favoured over the triplet by a Jahn–Teller distortion into C_s symmetry **16** (23). The proclivity for these rings to self-associate, however, was an exciting and important finding. The conversion of S—N π*-electrons to S—S σ-electrons encouraged us to pursue the design of other molecules that exhibit *inter*annular binding.

Neutral radical rings

Soon after my arrival at Guelph we started to look at neutral heterocyclic radicals. Our reasons were twofold. Firstly, my preoccupation with Scheme 1 required that we pursue 7π-radicals such as **4**, **5**, and **6**, and, secondly, we wished to explore the solid state structural ideas expounded by Robert Haddon (4). His neutral radical approach to molecular conductors required the use of odd-alternant hydrocarbons, i.e., ring systems capable of existing in a triad of oxidation states, neutral radical, aromatic ($4n$ + 2) cation, and anti-aromatic ($4n$) anion. While compounds such as **4** do not possess the fully nonbonding SOMO (singly occupied molecular orbital) that his model demanded, they had other features that made them attractive candidates for study. Pat Hayes (a research assistant), Robert Reed (an M.Sc. student), and René Boeré all contributed to this work, which involved the condensation of an imidoylamidine with sulfur dichloride to afford the cationic thiatriazine **17**. Reduction of the 6π-cations (typically with triphenylantimony) afforded the very stable 7π-radicals **4** (Scheme 3) (24), and further reduction with Na/NH_3(l) yielded the 8π-imides **18**, which were isolated, after protonation, as the corresponding imides **19** (25).

ESR studies on a series of thiatriazinyls revealed a spin density evenly spread over the three nitrogen centres; this distribution was, however, quite sensitive to the nature of the 3,5-substituents. The radicals associate, both in solution and the solid state; the crystal structure of the cofacial dimer **20** (R = Ph) exhibits a long (d(S—S) = 2.666 Å) interannular S—S bond. The corresponding selenatriazinyl radical dimerizes in a similar fashion, with a longer (d(Se—Se) = 2.792 Å) but stronger bond (26). Several conclusions related to molecular conductor design emerged from this work. In contrast to the 9π-radical $[S_3N_3]\cdot$, thiatriazinyls, with their lower π-electron counts, are very thermally stable. They also exhibit a triad of readily accessible oxidation states, a desirable feature for the efficient transfer of conduction electrons. The radicals associate but, unlike thiopyranyls, which dimerize through carbon (27), association of thiatriazinyls occurs at sulfur. However, while the dimerization is quite reversible, the interannular "bond" is still somewhat stronger, and more localized, than we desired. Moreover, the radicals are very electronegative, a feature that does not auger well for electron transport along a stacked array of radicals.

The characterization of the phosphorus-containing variants **5** (and also their selenium analogues) was pursued by Jim Bestari, who later became my first Ph.D. graduate. This was not an easy task, as the demands of selenium chemistry required some novel approaches to ring condensations. Likewise the simulation of the experimental ESR spectra required both persistence and patience. Once completed, however, the latter analyses echoed the earlier results on the phosphadithiatriazines **3**, in that the extent of electron delocalization across the phosphorus centres was minimal (28). The electronic structures of the compounds were, indeed, best represented by internal salt (zwitterionic) rather than delocalized formulations. In the solid state the sulfur-based compound forms a twisted (for steric reasons) cofacial dimer **21**, with a 2.481 Å S—S interannular bond (eq. [3]). By contrast, its selenium analogue associates not by an Se—Se linkage but rather via a long (1.99 Å) interannular Se—N bond (eq. [3]), to produce the dimer **22**, whose internal structural features resemble those of a 6π-cation/8π-anion pair.

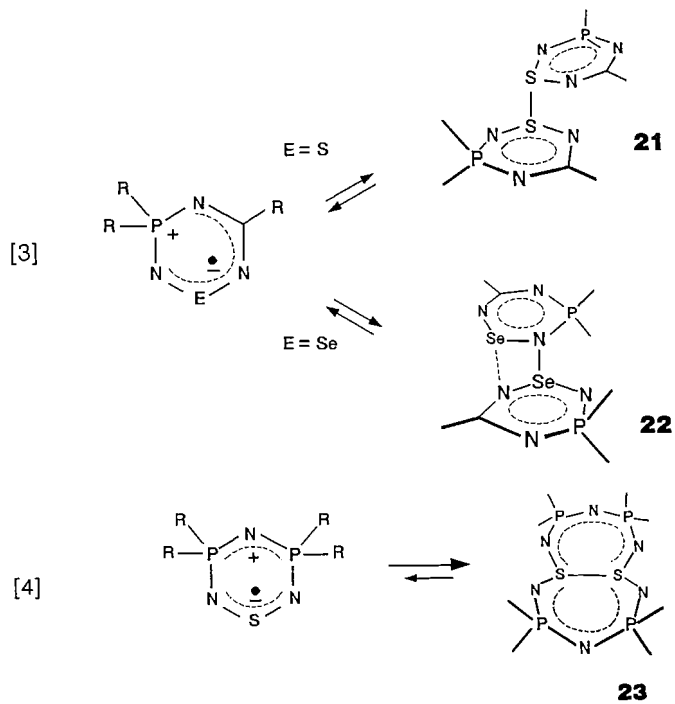

[3]

[4]

In the "purely inorganic" (non-carbon containing) radicals **6**, spin localization is even more pronounced. Spin density is now restricted to the NSN (or NSeN) fragment, and again an internal salt formulation applies. Interestingly, as Tris Chivers and his group established, the sulfur compound rearranges upon association to form the macrocyclic structure **23** (eq. [4]). This process remains reversible; the macrocycle and the radical coexist in equilibrium, albeit one that heavily favours the dimer. The mechanism of the bond exchange necessary to interconvert **6** and its dimer intrigued us and, insofar as these radicals are best depicted as

Can. J. Chem. Downloaded from www.nrcresearchpress.com by 203.198.23.82 on 09/08/12
For personal use only.

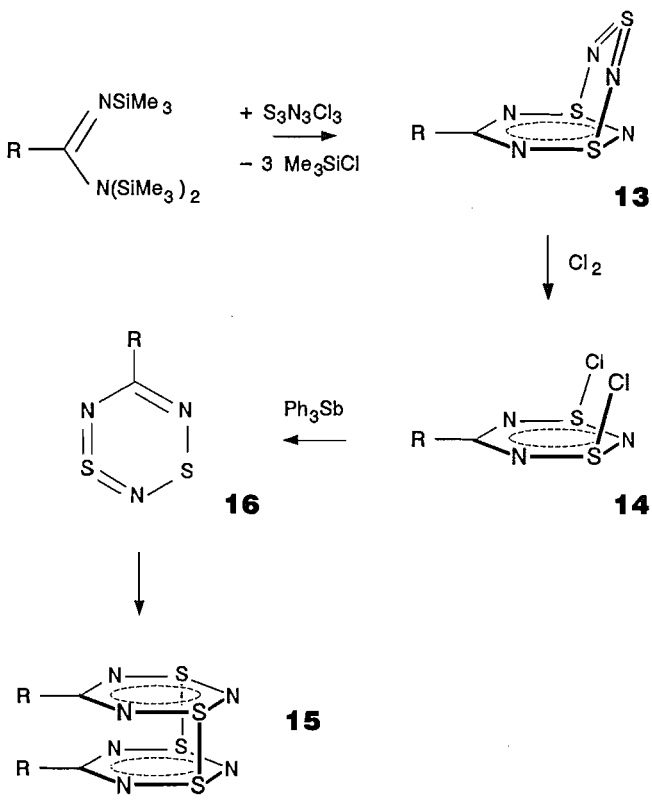

SCHEME 2

radical ion salts, we wondered whether simple acyclic sulfur diimide radical anions, i.e., $[RNSNR]^{-\cdot}$, might undergo a similar scrambling reaction based on the association and rearrangement of the resulting dimer. Jim Bestari set about exploring this possibility by studying the crossover reaction between radical anions of different sulfur diimides (29). The reaction (eq. [5]) worked surrprisingly well; the rearrangement required the addition of only catalytic amounts of reducing agent to the mixture of sulfur diimides. Moreover,

[5]

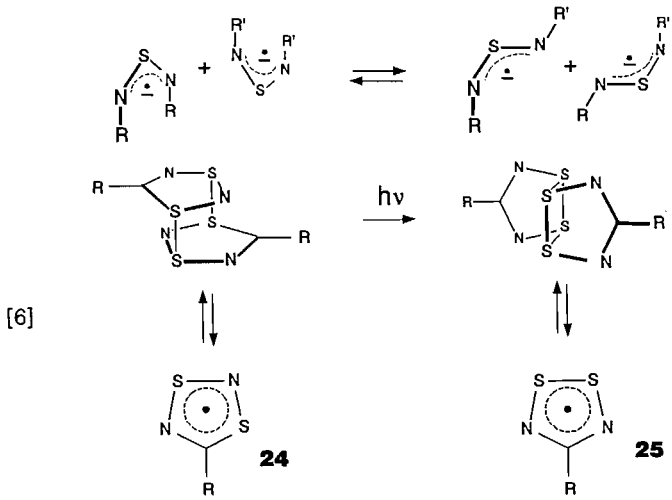

[6]

when relatively dissimilar R and R′ groups (e.g., Ar and Me_3Si) were employed, the equilibrium was shifted well to the right-hand side. The procedure thus afforded a simple preparative route to unsymmetrical sulfur diimides.

At the same time as we were investigating this radical rearrangement, Jack Passmore and his students at New Brunswick discovered a related reaction. By means of some elegant ESR experiments they observed that the 1,3,2,4-dithiadiazolyl radical **24** could be photochemically converted to its more stable 1,2,3,5-isomer **25** (30). The reaction was shown to be second order in radical, and an orbital symmetry analysis of the proposed mechanism, which involved the centrosymmetric association and rearrangement of the resulting dimer (eq. [6]), indicated that such a process should be photochemically allowed (31).

Pleasing though the identification of these radical rearrangements were, the recognition of such facile bimolecular pathways for structural change revealed a fundamental weakness of some heterocyclic frameworks based on catenated -S=N- units. These findings, coupled with results that we had obtained on the unimolecular rearrangements of closed-shell molecules (32, 33), reminded us that the design of molecular building blocks would require careful consideration of the kinetic and thermodynamic stability of the target molecules.

Neutral radical molecular conductors

By the end of the last decade, a wide variety of heterocyclic thiazyl radicals had been identified by ESR spectroscopy. As indicated earlier, some radical dimers had also been isolated and characterized by X-ray crystallography. The structural stability of some, and the propensity of others to rearrange, or decompose, had been recognized (34). Of the various candidates for applications in molecular materials, the thiatriazinyls that we had investigated early on showed some promise, but their dimerization constants were too high. Other systems, such as 1,3,2,4-dithiadiazolyls **24**, have been explored, but their tendency to rearrange has hampered structural characterization (35). The most promising candidates, certainly in our minds, were derivatives of the 1,2,3,5-dithiadiazolyl system **25** (this being the more stable of the two isomers noted above). These compounds have relatively high ionization potentials (36), and their exposed peripheries, replete with lone pairs, suggested to us that strong interannular interactions might be developed between adjacent rings in the solid state. Such attributes are vital for molecular metal design.

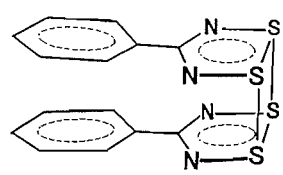

26

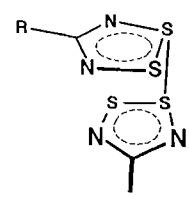

27

The first example (R = Ph) was fully characterized, both in solution and the solid state, by Arthur Banister's group at Durham in the early 1980s (37). While the crystal structure showed no indication of the stacked packing pattern alluded to in Fig. 1, the internal structural features of the dimer **26** were promising; the interannular S---S contact (mean value

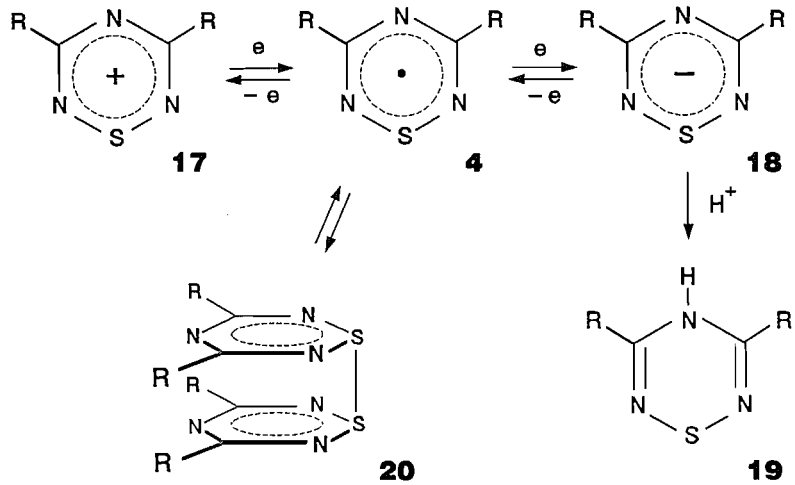

SCHEME 3

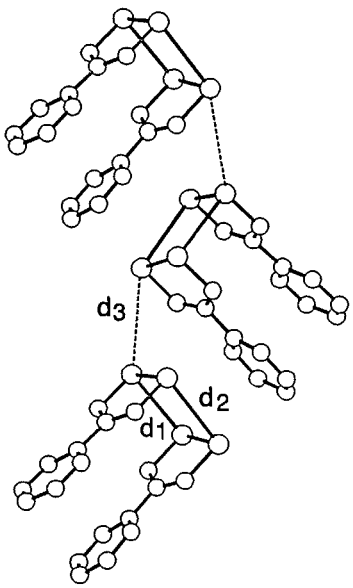

FIG. 2. Herring-bone stacking of $[PhCN_2Se_2]_2$ (d_1 = 3.160 Å, d_2 = 3.347 Å, and d_3 = 3.815 Å).

3.109 Å) was long, and the radical association enthalpy in solution was weak (38). Later structural work on related derivatives (R = CF_3 (39), NMe_2 (40), and Me (41)) revealed other dimerization modes, e.g., **27**, but afforded little encouragement that stacked structures were possible. Clearly, some modifications would be necessary if such rings were to be used as molecular building blocks. To this end a direct and flexible synthetic route was required, one which would also allow access to the corresponding selenium heterocycles.

[7] 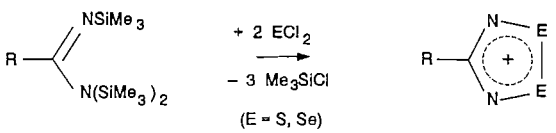

The time and effort invested in the synthesis of persilyated amidines now proved worthwhile. We found that the condensation of persilylated benzamidine with sulfur (or selenium) dichloride afforded, in excellent yield, the corresponding 4-phenyldithiadiazolium (or diselenadiazolium) chloride (eq. [7]). Reduction of the cations was a relatively straightforward task, and the radicals could be purified by vacuum sublimation (they are *surprisingly* thermally stable). The crystal structure of the selenium dimer $[PhCN_2Se_2]_2$ is illustrated in Fig. 2 (42). In contrast to its sulfur analogue, the packing pattern reveals a weak *inter*dimer Se---Se interaction that links dimers into infinite chains parallel to the z direction. The compound exhibits no measurable conductivity, but the observation that extended *inter*dimer interactions could be developed was enough to convince us to take a leap of faith. We therefore set about the design of new materials, a venture which has flourished thanks to a rewarding and enjoyable collaboration with Robert Haddon and his colleagues at AT&T Bell Laboratories.

Our architectural objective was simple enough in principle. We wished to design molecules, variations on the dithia- and diselenadiazolyl theme, with structural or electronic features incorporated into the exocyclic R-group that would promote the crystallization of uniformly spaced molecular stacks. Overlap of the π-SOMOs on adjacent rings should then afford a half-filled energy band. There is, however, a serious problem associated with this objective. As in any one-dimensional structure with a half-filled electronic band, the stacks are subject to a charge density wave (CDW) driven or Peierls instability (43), i.e., a tendency to dimerize (Fig. 1). This distortion, the solid state variant of a Jahn–Teller effect, opens up an energy gap at the Fermi level, and the materials slide into either semiconducting or insulating states, the final result depending on the magnitude of the residual band gap. It was into this trap that many of the early charge transfer salts first fell. The solution to the problem, the stabilization of highly conducting states, requires increasing the dimensionality of the overall structure; extended networks of lateral as well as longitudinal interannular contacts must be developed. There are at least two potential solutions to this problem. One is to compress the system, i.e., to apply physical pressure. The other is less direct, but sometimes more flexible; one applies "chemical pressure," i.e., the R-group is sculpted in such a way that the columnar stacks are packed as tightly as possible.

The control of molecular packing is still more of an art

Can. J. Chem. Downloaded from www.nrcresearchpress.com by 203.198.23.82 on 09/08/12
For personal use only.

Can. J. Chem. Downloaded from www.nrcresearchpress.com by 203.198.23.82 on 09/08/12
For personal use only.

form than a science (44), and many research groups are, with different goals in mind, pursuing the design of molecular systems that, when assembled within the demands of a crystal lattice, generate a specific supramolecular architecture. In our work we have adopted several design strategies. The primary objective has been to induce stacking, albeit of dimers. In those cases where stacking has been achieved we sought to make subtle molecular adjustments, in the hope of enhancing the lateral interactions noted above. The effects of replacing sulfur by selenium on both structure and transport properties have also been closely monitored.

One of our first architectural variations involved the placement of cyanophenyl (2-, 3-, and 4-), dicyanophenyl, or cyanofuryl substituents on the radical ring. This work was carried out largely by Robin Hicks at the start of his Ph.D. research (45, 46). The idea here was based on the well-known tendency of the nitrile group to influence packing. The structure of iodobenzonitrile, for example, consists of molecular ribbons held together by CN---I links (47). The necessary amidines were synthesized by the Sanger route, and the cations generated according to eq. [7]. Reduction and sublimation then afforded the radical dimers and, after some effort,[2] the crystal structures were established by X-ray crystallography. The results were mixed. Although the packing pattern of the 4-cyanophenyl compounds is ribbon-like, with CN---E (E = S, Se) contacts linking the molecular units, stacking of the dimers is not found. In the case of the 3,5-dicyanophenyl derivative (E = Se) stacking of dimers is observed, but the steric bulk of the organic ligand is such that the dimer columns are separated in pairs, with no extended lattice-wide network of interdimer Se---Se contacts (48). In the 3-cyanophenyl and 2-cyanophenyl derivatives, stacking is again observed, but now the dimer columns are linked by an extended array of lateral as well as longitudinal Se---Se interactions. The relative effects of longitudinal and lateral interactions are illustrated by the results of Extended Hückel band structure calculations on the crystal structures of the diselenadiazolyls shown in Fig. 3. The density of states for the 4-cyanophenyl compound reveals, as expected, a wide band gap, as only lateral contacts are available. In the 3,5-dicyanophenyl compound, where isolated pairs of stacks are observed, the band gap is diminished, as extended longitudinal contacts replace extended lateral interactions. In the 3-cyanophenyl derivative both types of interactions are present, and the combined effect leads to an overall decrease in the band gap. However, single crystal conductivity measurements on the 3-cyanophenyl derivative, which is the best of the three structures, reveal a room temperature conductivity of only 10^{-9} S cm^{-1}.

In the compounds outlined above, the size of the organic residue inevitably restricts the approach of the heterocyclic peripheries, and thus precludes low band gap materials. This limitation can be alleviated in several ways. One approach to increasing the solid state density of the radicals, and hence the number and magnitude of the interdimer contacts, involves the design of polyfunctional radicals, i.e., systems in which two or more radical centers are linked by a common bridging ligand. Steve Liblong (a NSERC postdoctoral fellow) and Kelly Young (a research assistant) helped start this

[2]Crystal growth by sublimation tends to produce twinned materials, especially when the packing pattern involves the columnar stacking that we desired.

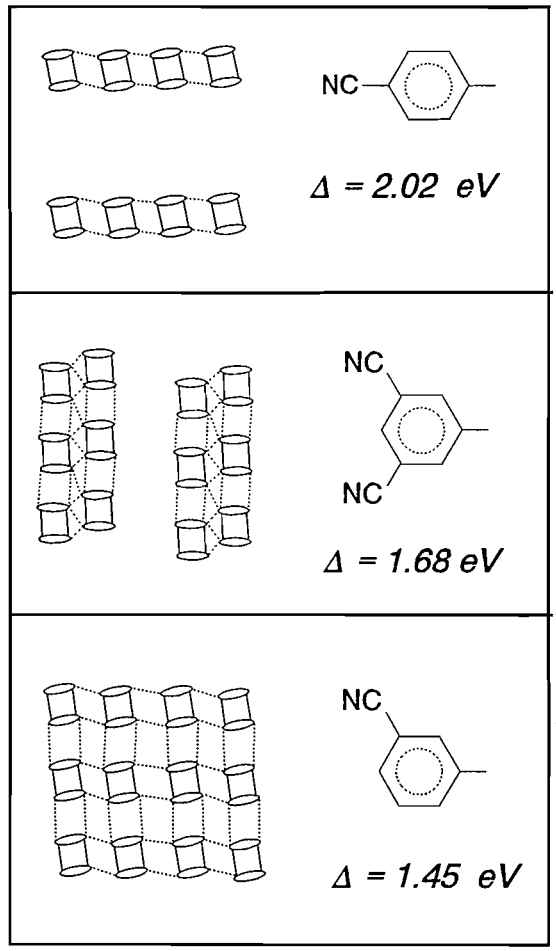

FIG. 3. Stacking patterns for selected monofunctional diselenadiazolyl dimers, and computed (EHMO) band gaps (Δ). In the 4-cyanophenyl compound, alternate layers are occupied by the organic ligand.

work, which was based initially on the 1,4- and 1,3-phenylene-bridged diradicals **28** and **29**. Purification and crystal growth of these materials required extremes in both temperature and pressure (vacuum), but we were eventually able to characterize both the sulfur and selenium derivatives of these two systems (E = S, Se). Figure 4 illustrates the herring-bone packing found in the 1,4-compounds (49). The structures are characterized by short intra- and interdimer S---S (or Se---Se) contacts that link consecutive ribs along the spine. There is also a series of short contacts that bind consecutive layers. Extended Hückel band structure calculations revealed a highly developed 2-dimensional electronic structure, and while the sulfur compound was found to be insulating, the selenium compound exhibited a pressed pellet conductivity near 10^{-2} S cm^{-1}.

Crystals belonging to the tetragonal space group $I4_1/a$ (the so-called α-phase) can be grown for the 1,3-derivatives of both sulfur and selenium (50). Within the unit cell there are fourfold pinwheel-like clusters of columnar stacks of diradicals that run parallel to the *y* axis. The stacks consist of molecular "plates" slightly offset from the ideal regular spacing sequence, i.e., a Peierls distortion. The plates do not, however, couple as discrete dimers, as do the 1,4-diradicals, but rather exhibit a subtle rocking, so as to produce a zigzag arrangement of short and long interannular contacts

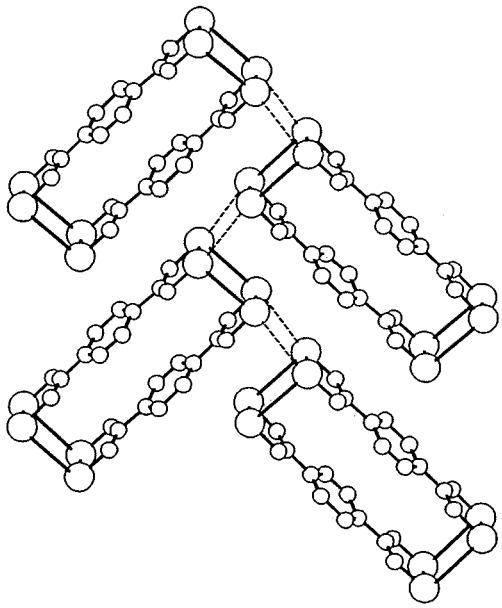

FIG. 4. Herring-bone stacking of the 1,4-benzene-bridged compounds **28** (E = S, Se). The mean intra- and interdimer E---E contacts are 3.121/3.275 Å (S/Se) and 3.500/3.578 Å (S/Se), respectively.

(Fig. 5). The selenium compound also forms a second, monoclinic phase (space group $P2_1/n$), when the material is sublimed at higher pressures and temperatures. This β-phase consists of discrete dimers that are not stacked; instead they interlock like links in a chain, with short interdimer contacts to either side as well as above and below (51). Overall, the structure possesses a weaker, but more 3-dimensional, network of interactions than is found in the α-phase.

Extensive magnetic and conductivity measurements have been performed on these 1,3-compounds. They are all essentially diamagnetic at room temperature, but the sulfur compound shows a large hysteretic increase in paramagnetism at elevated temperatures; the selenium compound (α-phase) shows a much smaller, but similar, effect. We have assigned this behaviour to the occurrence of phase kinks in the lattice, which serve to trap isolated spin-bearing rings. This phenomenon does not appear to serve as a source of carriers, as would be expected in most semiconductors. There is, for example, only a minor increase in conductivity of the sulfur compound associated with the paramagnetic "breakout". The results of variable temperature single crystal conductivity measurements on both phases of the 1,3-selenium compound are consistent with a conduction mechanism involving thermal activation of electrons. Experimental estimates for the band gaps of 0.55 and 0.77 eV have been derived for the α- and β-phases, respectively.

The unusual zigzag stacking found in the α-phase of the 1,3-derivatives prompted us to pursue molecular variants, including the furan-bridged and 5-cyanobenzene-bridged compounds **30** (46) and **31** (52). The former elected to crystallize in a totally different motif, one more reminiscent of the 1,4-derivatives **28**, and while the latter adopts a zigzag stacking arrangement, the lateral intercolumnar contacts are far less effective than those observed in the parent 1,3-derivatives, and the observed conductivities are correspondingly lower. As an offshoot to this work we were interested to see if quinoidal, as opposed to diradical, states might be observed for certain 1,4-phenylene-bridged systems. This possibility had been probed for the phenylene-bridged bis(1,3,2,4-dithiadiazolyls), for which a diradical dimer structure was found (53). Similarly, phenylene-bridged diradicals such as **32**, which are based on the PCN_3S skeleton **5** (Scheme 1), showed no indication, either in solution or the solid state, for the quinoidal structure **33** (54).

Determined to go beyond the diradical systems, Robin Hicks and Dietmar Kennepohl (a postdoctoral fellow) looked at the two triradical systems **34** and **35**. The 1,3,5-benzene-bridged compound was found to crystallize as girder-like

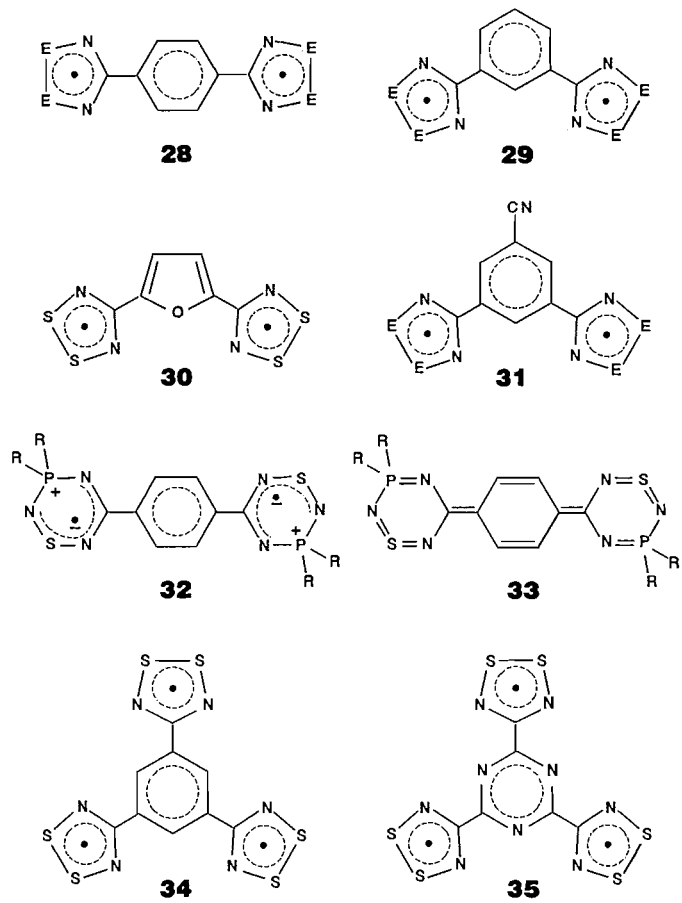

stacks (Fig. 6) with a bond alternation pattern reminiscent of the α-phase of the 1,3-compounds described earlier (55). The intercolumnar contacts were, however, even tighter. The minor molecular change on going from a benzene to a triazine bridge was intended to induce a general compression of the original structure. While, within two dimensions, our objective was achieved (57), the full crystal structure of **35** (space group $C2/c$) was quite different to that of **34** (space group $P2_1/c$); the change in space group, precipitated by a seemingly minor chemical modification, effectively eliminated the desired columnar stacking. Here, as elsewhere, we were chastened by Nature; the *a priori* prediction of crystal structures remains, at best, a sporting pastime.

Iodine doped radicals

We continue to design, prepare, and study neutral radicals. The derivatives characterized to date confirm that low band gap materials are possible, and the prospect of gener-

Can. J. Chem. Downloaded from www.nrcresearchpress.com by 203.198.23.82 on 09/08/12
For personal use only.

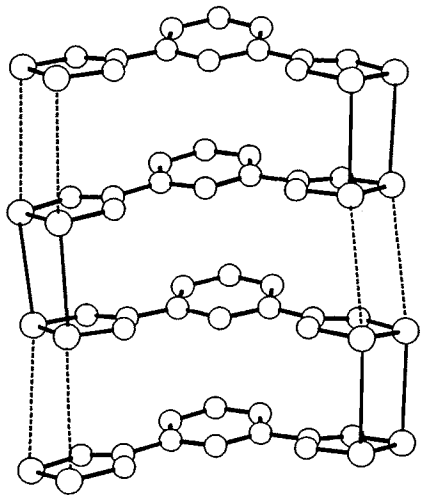

FIG. 5. Zigzag stacking of the 1,3-benzene-bridged compounds **29** (E = S, Se). The mean intra- and interdimer E---E contacts are 3.140/3.284 (S/Se) and 3.966/4.014 Å (S/Se), respectively.

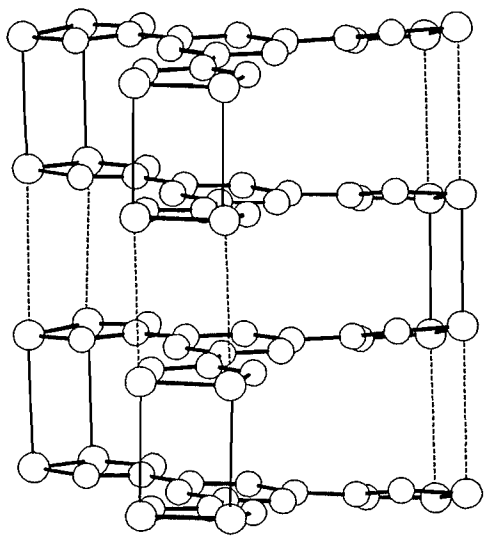

FIG. 6. Stacking of the 1,3,5-benzene-bridged triradical **34**. The mean intradimer and interdimer S---S contacts are 3.117 and 3.832 Å, respectively.

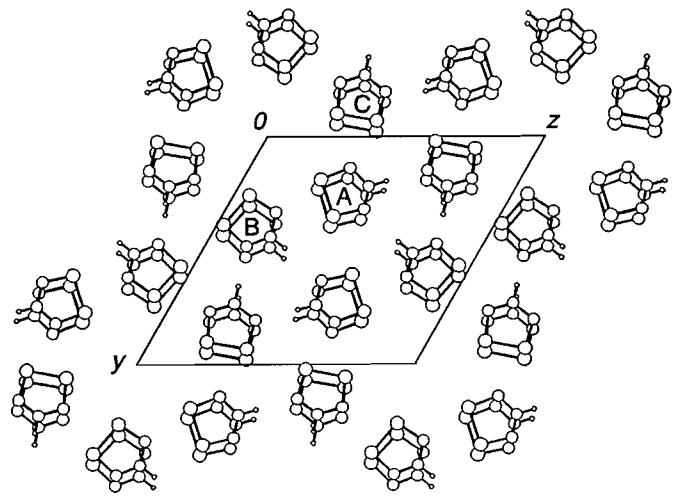

FIG. 7. Close-packed arrangement of molecular rings in the triclinic phase of $[HCN_2S_2]_2$. The three dimers in the asymmetric unit are labelled **A**, **B**, and **C**.

ating new variants remains as enticing as ever. A totally different lure, one which we resisted for a long time, involves *p*-type doping radicals, i.e., the removal of electrons from the half-filled energy band of Fig. 1 and the generation of a stable stack of uniformly spaced molecular plates.

This doping work began with an accidental finding, at a time when we were investigating the prototypal radicals $[HCN_2E_2]\cdot$ (E = S, Se) (57). Our original intent here was to incorporate the smallest possible ligand, a hydrogen atom, in the hope of generating high-density materials. The selenium derivative consists of dimers arranged in a slipped stack structure that exhibits very short *inter*dimer as well as *intra*dimer contacts, and the room temperature conductivity is 7×10^{-6} cm^{-1}. As a result of its relatively high vapour pressure and low thermal stability, however, this compound does not lend itself to detailed physical study.

Later work on the sulfur radical $[HCN_2S_2]^{\cdot}$ revealed that its dimer was dimorphic. When prepared by sublimation under an atmosphere of argon, the dimer grows as needles belonging to the monoclinic space group $P2_1/n$ (58); a second, triclinic phase, space group $P\bar{1}$ is generated when the sublimation is performed in vacuo. The structures of both modifications consist of stacked dimers, with three dimers per asymmetric unit. The triclinic phase exhibits, however, a rather unusual feature. Essentially, the structure consists of close-packed "tubes," each tube (with a 7.43 Å internal diameter) being built from a near-hexagonal merry-go-round composed of six dimers. This remarkable tubular structure invited a doping experiment, and we quickly set about trying to incorporate iodine into the lattice.

Robin Hicks and Dietmar Kennepohl started the doping experiments, and later were joined by two new graduate students, Noel George and Craig MacKinnon. After some effort we found that when the native radical and iodine are coevaporated in a sealed evacuated tube, lustrous silver-black rods of composition $[HCN_2S_2]_6[I]_{1.1}$ can be grown (59). Careful X-ray work revealed a crystal structure very similar to that of the parent material. The doped crystals belong to the hexagonal space group $P6_1$, and the structure again exhibits a close-packed arrangement of tubes, each tube being constructed from a pinwheel array of six HCN_2S_2 rings. The important structural differences between the doped and undoped phases can be understood with reference to Fig. 8, which illustrates the columnar motifs formed by the innermost sulfur atom of each HCN_2S_2 ring. In the undoped structure the dimers, each represented by a single sulfur atom per ring, form layers with a mean intradimer S---S distance of 3.104 Å and a mean interdimer S---S separation of 3.779 Å. In the doped structure the sulfur atoms lie on a sixfold screw axis, with a regular S---S separation (along the stack) of 3.352 Å. The iodines, which lie within the cavity in a spiral wrapped tightly about the 6_1 axis, are disordered. Examination of the physical properties of this compound has been hampered by its air sensitivity, but its conductivity, 10^2 S cm^{-1} along the needle axis, has been established.

The preparation of this highly conductive doped material, isolable as a discrete crystalline phase, was an exciting finding, and we are now pressing on to see if the idea is

Can. J. Chem. Downloaded from www.nrcresearchpress.com by 203.198.23.82 on 09/08/12
For personal use only.

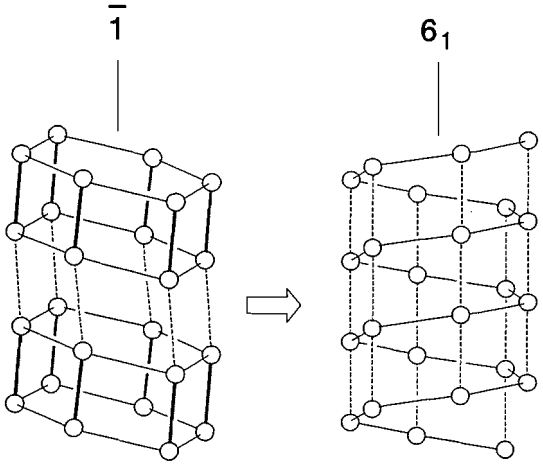

FIG. 8. Internal rearrangement of columnar cavities in $[HCN_2S_2]_2$ occasioned by iodine doping.

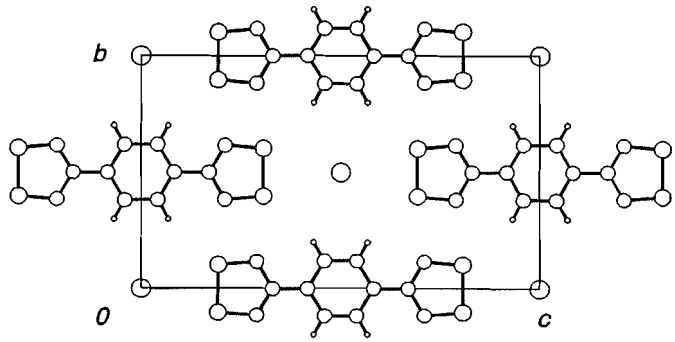

FIG. 9. Structure of $[1,4\text{-}(S_2N_2C)C_6H_4(CN_2S_2)][I]$. The iodines are disordered along x.

generally applicable. Fortunately, the synthetic approach appears not to be limited to volatile radicals. For example, coevaporation of the 1,4-phenylene-bridged bis(dithiadiazolyl) (**28**, E = S) and iodine affords air-stable needles of stoichiometry $[(S_2N_2C)C_6H_4(CN_2S_2)][I]$, formally the iodide salt of a radical cation. The room temperature crystal structure (space group *Immm*) consists of one-dimensional arrays of evenly spaced (3.415 Å) molecular plates, with interspersed columns of disordered iodines (Fig. 9). The single crystal conductivity at room temperature of this material is also 10^2 S cm^{-1} (60), but its stability in air has allowed more detailed physical studies. The conductivity is metallic at room temperature, but near 190 K a CDW-driven instability sets in, and the material becomes an insulator. Analysis of the CDW wavevector has provided a measure of the bandfilling, and hence the degree of charge transfer from radical to iodine. Based on this data, the material can be formulated as $[(S_2N_2C)C_6H_4(CN_2S_2)]^{0.5+}[I]^{0.5-}$.

Summary

The paradigms and prejudices that chemists use to explain and predict molecular structure have allowed the construction of exotic molecules, both large and small. One of the challenges for the future lies in the exploitation of this knowledge to fabricate molecules that will serve as building blocks for specific solid state (crystal) structures. The research described above has been so motivated. It began, however, not with attempts to address the final targeted objectives, but with exploratory work on the preparation and characterization of thiazyl and selenazyl heterocycles with novel electron counts. These rings are electron rich, and as such possess notoriously weak skeletal bonds. Stable variants can, however, be made, and *inter-* as well as *intra*-annular bonding is observed in many of these compounds. Methods for the conversion of these localized interannular *bonds* into more extensive and lattice-wide *bands* have been developed, and we have been able to generate single-component molecular solids with semiconductive properties. Preliminary results on the iodine doping of some of these systems indicate that highly conductive phases can be made, and we look forward with excitement to the discoveries that lie ahead. Basic research in molecular chemistry has opened a window of opportunity for the advancement of materials science.

Acknowledgements

I am grateful to the Canadian Society for Chemistry for selecting me as this year's recipient of the ALCAN Lecture award, and to ALCAN for its continuing support of chemical research in the Canadian academic community. The work described above has been sustained by grants from the Natural Sciences and Engineering Research Council of Canada and, in the early years, the Research Corporation. I thank both agencies for this funding. I am endebted to the past and present members of my research group, and to my colleagues and collaborators, most of whose names I have noted above, for their enthusiastic and invaluable support. Acknowledgement of the contributions of one individual is notably absent. Wally Cordes, at the University of Arkansas, has provided, amongst other things, the X-ray structural results for virtually every paper I have published in the past 17 years. For some of the samples that I have sent him in recent times, he may never forgive me. For the personal and professional enrichment that our collaboration has brought me, I can never repay him.

1. M.D. Fryzuk. Can. J. Chem. **70**, 2839 (1992).
2. R.L. Greene, G.B. Street, and L.J. Suter. Phys. Rev. Lett. **34**, 577 (1975).
3. W.M. Lau, N.P.C. Westwood, and M.H. Palmer. J. Am. Chem. Soc. **108**, 3229 (1986).
4. R.C. Haddon. Nature, **256**, 394 (1975).
5. J.R. Ferraro and J.M. Williams. Introduction to synthetic electrical conductors. Academic Press, New York. 1987.
6. (*a*) D.P. Craig and N.L. Paddock. Nature, **18**, 1052 (1958); (*b*) Non-Benzenoid Aromat. **2**, 273 (1972).
7. R.J. Gleiter. J. Chem. Soc. A, 3174 (1970).
8. A.J. Banister. Nature, **237**, 92 (1972); **239**, 69 (1972).
9. J. Bojes, T. Chivers, W.G. Laidlaw, and M. Trsic. J. Am. Chem. Soc. **101**, 4517 (1979).
10. R.J. Gillespie, D.R. Slim, and J.D. Tyrer. J. Chem. Soc. Chem. Commun. 253 (1977).
11. I. Ernest, W. Holick, G. Rihs, D. Schomburg, G. Shoham, D. Wenkert, and R.B. Woodward. J. Am. Chem. Soc. **103**, 1540 (1981).
12. R.T. Oakley. Prog. Inorg. Chem. **36**, 299 (1988).
13. A.W. Cordes, C.G. Marcellus, M.C. Noble, R.T. Oakley, and W.T. Pennington. J. Am. Chem. Soc. **105**, 6008 (1983).
14. C.G. Marcellus, R.T. Oakley, A.W. Cordes, and W.T. Pennington. Can. J. Chem. **62**, 1822 (1984).
15. R.T. Oakley. Can. J. Chem. **62**, 2763 (1984).

Can. J. Chem. Downloaded from www.nrcresearchpress.com by 203.198.23.82 on 09/08/12
For personal use only.

16. N. Burford, T. Chivers, A.W. Cordes, W.G. Laidlaw, M.C. Noble, R.T. Oakley, and P.N. Swepston. J. Am. Chem. Soc. **104**, 1282 (1982).
17. S.W. Liblong, R.T. Oakley, A.W. Cordes, and M.C. Noble. Can. J. Chem. **61**, 2062 (1983).
18. A.W. Cordes, M. Hojo, H. Koenig, M.C. Noble, R.T. Oakley, and W.T. Pennington. Inorg. Chem. **25**, 1137 (1986).
19. A.P. Hitchcock, R.S. DeWitte, J.M. Van Esbroeck, C.L. French, R.T. Oakley, and N.P.C. Westwood. J. Electron Spectrosc. Relat. Phenom. **57**, 165 (1991).
20. (*a*) A.R. Sanger. Inorg. Nucl. Chem. Lett. **9**, 351 (1973); (*b*) R.T. Boeré, R.T. Oakley, and R.W. Reed. J. Organomet. Chem. **331**, 161 (1987).
21. R.T. Boeré, A.W. Cordes, and R.T. Oakley. J. Chem. Soc. Chem. Commun. 929 (1985).
22. R.T. Boeré, C.L. French, R.T. Oakley, A.W. Cordes, J.A.J. Privett, S.L. Craig, and J.B. Graham. J. Am. Chem. Soc. **107**, 7710 (1985).
23. R.E. Hoffmeyer, W.-T. Chan, J.D. Goddard, and R.T. Oakley. Can. J. Chem. **66**, 2279 (1988).
24. P.J. Hayes, R.T. Oakley, A.W. Cordes, and W.T. Pennington. J. Am. Chem. Soc. **107**, 1346 (1985).
25. R.T. Boeré, A.W. Cordes, P.J. Hayes, R.T. Oakley, R.W. Reed, and W.T. Pennington. Inorg. Chem. **25**, 2445 (1986).
26. R.T. Oakley, R.W. Reed, A.W. Cordes, S.L. Craig, and J.B. Graham. J. Am. Chem. Soc. **109**, 7745 (1987).
27. Z.-i. Yoshida, Y. Shigeo, S. Toyanari, and K. Osanu. Tetrahedron Lett. **43**, 3999 (1971).
28. K. Bestari, A.W. Cordes, R.T. Oakley, and K.M. Young. J. Am. Chem. Soc. **112**, 2249 (1990).
29. K. Bestari, R.T. Oakley, and A.W. Cordes. Can. J. Chem. **69**, 94 (1991).
30. N. Burford, J. Passmore, and M.J. Schriver. J. Chem. Soc. Chem. Commun. 140 (1986).
31. W.V.F. Brooks, N. Burford, J. Passmore, M.J. Schriver, and L.H. Sutcliffe. J. Chem. Soc. Chem. Commun. 69 (1987).
32. K.T. Bestari, R.T. Boeré, and R.T. Oakley. J. Am. Chem. Soc. **111**, 1579 (1989).
33. (*a*) R.T. Boeré, A.W. Cordes, and R.T. Oakley. J. Am. Chem. Soc. **109**, 7781 (1987); (*b*) A.W. Cordes, S.W. Liblong, S.G. Phillips, and R.T. Oakley. Inorg. Chem. **28**, 4147 (1989).
34. A.W. Cordes, R.C. Haddon, and R.T. Oakley. *In* The chemistry of inorganic ring systems. *Edited by* R. Steudel. Elsevier, Amsterdam. 1992. p. 295.
35. A.J. Banister and J.M. Rawson. *In* The chemistry of inorganic ring systems. *Edited by* R. Steudel. Elsevier, Amsterdam. 1992. p. 323.
36. R.T. Boeré, R.T. Oakley, R.W. Reed, and N.P.C. Westwood. J. Am. Chem. Soc. **111**, 1180 (1989).
37. A. Vegas, A. Perez-Salazar, A.J. Banister, and R.G. Hey. J. Chem. Soc. Dalton Trans. 1812 (1980).
38. S.A. Fairhurst, K.M. Johnson, L. Sutcliffe, K.F. Preston, A.J. Banister, Z.V. Hauptman, and J. Passmore. J. Chem. Soc. Dalton Trans. 1465 (1986).
39. H.-U. Höfs, J.W. Bats, R. Gleiter, G. Hartmann, R. Mews, M. Eckert-Macksić, H. Oberhammer, and G.M. Sheldrick. Chem. Ber. **118**, 3781 (1985).
40. A.W. Cordes, J.D. Goddard, R.T. Oakley, and N.P.C. Westwood. J. Am. Chem. Soc. **111**, 6147 (1989).
41. A.J. Banister, M.I. Hansford, Z.V. Hauptman, S.T. Wait, and W. Clegg. J. Chem. Soc. Dalton Trans. 1705 (1989).
42. P. Del Bel Belluz, A.W. Cordes, E.M. Kristof, P.V. Kristof, S.W. Liblong, and R.T. Oakley. J. Am. Chem. Soc. **111**, 9276 (1989).
43. R.E. Peierls. Quantum theory of solids. Oxford Press, London. 1953. p. 108.
44. (*a*) G.R. Desiraju. Prog. Solid State Chem. **17**, 295 (1987); (*b*) G.M. Whitesides, J.P. Mathias, and C.T. Seto. Science, **254**, 1312 (1991).
45. A.W. Cordes, R.C. Haddon, R.G. Hicks, R.T. Oakley, and T.T.M. Palstra. Inorg. Chem. **31**, 1802 (1992).
46. A.W. Cordes, C.M. Chamchoumis, R.G. Hicks, R.T. Oakley, K.M. Young, and R.C. Haddon. Can. J. Chem. **70**, 919 (1992).
47. (*a*) E.O. Schlemper and D. Britton. Acta Crystallogr. **18**, 419 (1965); (*b*) R.B. Heiart and G.B. Carpenter. Acta Crystallogr. **9**, 889 (1956).
48. W.M. Davis, R.G. Hicks, R.T. Oakley, B. Zhao, and N.J. Taylor. Can. J. Chem. **71**, 180 (1993).
49. A.W. Cordes, R.C. Haddon, R.T. Oakley, L.F. Schneemeyer, J.A. Waszczak, K.M. Young, and N.M. Zimmerman. J. Am. Chem. Soc. **113**, 582 (1991).
50. M.P. Andrews, A.W. Cordes, D.C. Douglass, R.M. Fleming, S.H. Glarum, R.C. Haddon, P. Marsh, R.T. Oakley, T.T.M. Palstra, L.F. Schneemeyer, G.W. Trucks, R.R. Tycko, J.V. Waszcak, W.W. Warren, K.M. Young, and N.M. Zimmerman. J. Am. Chem. Soc. **113**, 3559 (1991).
51. A.W. Cordes, R.C. Haddon, R.G. Hicks, R.T. Oakley, T.T.M. Palstra, L.F. Schneemeyer, and J.V. Waszczak. J. Am. Chem. Soc. **114**, 1729 (1992).
52. A.W. Cordes, R.C. Haddon, R.G. Hicks, D.K. Kennepohl, R.T. Oakley, T.T.M. Palstra, L.F. Schneemeyer, S.R. Scott, and J.V. Waszczak. Chem. Mater. **5**, 820 (1993).
53. A.J. Banister, J.M. Rawson, W. Clegg, and S.L. Birkby. J. Chem. Soc. Dalton Trans. 1099 (1991).
54. K. Bestari, G. Ferguson, J.F. Gallagher, and R.T. Oakley. Inorg. Chem. **31**, 443 (1992).
55. A.W. Cordes, R.C. Haddon, R.G. Hicks, R.T. Oakley, T.T.M. Palstra, L.F. Schneemeyer, and J.V. Waszcak. J. Am. Chem. Soc. **114**, 5000 (1992).
56. A.W. Cordes, R.C. Haddon, R.G. Hicks, D.K. Kennepohl, R.T. Oakley, L.F. Schneemeyer, and J.V. Waszczak. Inorg. Chem. **32**, 1554 (1993).
57. A.W. Cordes, S.H. Glarum, R.C. Haddon, R. Hallford, R.G. Hicks, D.K. Kennepohl, R.T. Oakley, T.T.M. Palstra, and S.R. Scott. J. Chem. Soc. Chem. Commun. 1265 (1992).
58. A.W. Cordes, C.D. Bryan, W.M. Davis, R.H. de Laat, S.H. Glarum, J.D. Goddard, R.C. Haddon, R.G. Hicks, D.K. Kennepohl, R.T. Oakley, S.R. Scott, and N.P.C. Westwood. J. Am. Chem. Soc. **115**, 7232 (1993).
59. C.D. Bryan, A.W. Cordes, R.C. Haddon, S.H. Glarum, R.G. Hicks, D.K. Kennepohl, C.D. MacKinnon, R.T. Oakley, T.T.M. Palstra, A.S. Perel, L.F. Schneemeyer, S.R. Scott, and J.V. Waszczak. J. Am. Chem. Soc. Submitted.
60. C.D. Bryan, A.W. Cordes, R.M. Fleming, N.A. George, S.H. Glarum, R.C. Haddon, R.T. Oakley, T.T.M. Palstra, A.S. Perel, L.F. Schneemeyer, and J.V. Waszczak. Nature. In press.

Can. J. Chem. Downloaded from www.nrcresearchpress.com by 203.198.23.82 on 09/08/12
For personal use only.

Association of neutral red with micelles and its effect on the pK_a

ROBIN K. DUTTA AND SUBRAY N. BHAT[1]
Department of Chemistry, North-Eastern Hill University, Shillong-793003, India

Received June 22, 1992[2]

ROBIN K. DUTTA and SUBRAY N. BHAT. Can. J. Chem. **71**, 1785 (1993).

The interactions of neutral red with cationic surfactants, viz., *N*-hexadecylpyridinium chloride and alkyltrimethylammonium bromides; a nonionic surfactant, viz., Triton X100; and an anionic surfactant, viz., sodium dodecyl sulfate, were investigated spectroscopically. The equilibrium constants for the association of the indicator with the micelles were determined from the apparent association constants at constant pH at 298 K. The effects of the indicator–micelle association on the apparent pK_a of the indicator in aqueous surfactant solutions are discussed. It was shown that the apparent pK_a of the indicator in cationic surfactant solution can be predicted from knowledge of the indicator–micelle association constant.

ROBIN K. DUTTA et SUBRAY N. BHAT. Can. J. Chem. **71**, 1785 (1993).

Faisant appel à la spectroscopie, on a examiné les interactions entre le rouge neutre et des agents tensioactifs cationiques (le chlorure de *N*-hexadécylpyridinium et les bromures d'alkyltriméthylammonium), un agent tensioactif non ionique (le Triton X100) et un agent tensioactif anionique (le dodécylsulfate de sodium). En se basant sur les constantes apparentes d'association, à pH constant, à 298 K, on a déterminé les constantes d'équilibre pour l'association de l'indicateur avec les micelles. On discute des effets de l'association indicateur–micelle sur le pK_a apparent de l'indicateur dans des solutions aqueuses d'agent tensioactif. On a démontré que l'on peut prédire le pK_a apparent de l'indicateur dans la solution d'agent tensioactif cationique à partir d'une connaissance de la constante d'association indicateur–micelle.

[Traduit par la rédaction]

Can. J. Chem. Downloaded from www.nrcresearchpress.com by 203.198.23.82 on 09/08/12
For personal use only.

Introduction

Micelles are frequently employed in combination with acid–base indicators in analytical chemistry to shift the chemical equilibrium and pK_a of the indicator to a desired degree (1). The effect of micelles on the pK_a of an indicator is due to micellar catalysis of the acid dissociation reaction (2). The shifts in the pK_a have been attributed to an electrostatic potential at the micelle surface (3), to ion exchange between the micelle surface and the bulk aqueous phase (4), and to low interfacial effective dielectric constant, interfacial salt effect, and ion-pair formation between oppositely charged indicator species and monomeric surfactant head groups (5). Nevertheless, most of the indicator equilibria in micellar medium studied so far are cases in which the indicator species are completely incorporated into the micelles. Even recently, it was considered pointless to analyse the observed p$K_{a,app}$'s of indicators in which both the conjugate acid–base forms are not fully solubilized by the micelles (5*d*). The association constants of indicators with micelles may be quite informative about the pK_a shifts of such partly solubilized indicators, as any observation can be better understood with the help of equilibrium properties (3*b*). In the present paper we report the results of a systematic study of the preferential association of 3-amino-7-dimethylamino-2-methyl phenazinium chloride (neutral red), with micelles of cationic, nonionic, and anionic surfactants at constant pH, and the effect of such associations on the observed p$K_{a,app}$ of the indicator (6). The structures of neutral red in its base (NR) and acid (NR^+H) forms are shown in Scheme 1.

Experimental

Neutral red, a Sigma product, was recrystallized twice from a water–ethanol mixture and dried before use. *N*-Hexadecylpyridinium chloride (cetylpyridinium chloride, CPC) was obtained from Hexel Corporation, U.S.A. Hexadecyltrimethylammonium bromide (CTAB), dodecyltrimethylammonium bromide (DTAB), and Triton X100 ($(CH_3)_3CCH_2C(CH_3)_2C_6H_4(OCH_2CH_2)_{10}OH$, TX100) were Sigma products. Tetradecyltrimethylammonium bromide (TTAB) was obtained from Sisco Research Laboratories, India. All cationic surfactants were recrystallized from acetone. Sodium dodecyl sulfate (SDS), obtained from Aldrich, was first washed with ether and then recrystallized from ethanol and the recrystallized samples were dried in a vacuum desiccator. TX100 was used as such. Buffer constituents were of AR grade. Triply distilled water, prepared by adding $KMnO_4$ in the first distillation, was used as solvent.

The visible absorption spectra were recorded by a Hitachi-330 spectrophotometer using a matched pair of cells of 1-cm path length fitted in a thermostated cell holder. The pH of the solutions was measured using a Systronics Digital pH meter model-335. All the experiments were carried out at 298 (±0.1) K.

Results and discussion

p$K_{a,w}$ of neutral red

Neutral red, in aqueous solution, exists in two forms, viz., NR^+H and NR, which are in equilibrium with each other. NR, which has an absorption maximum at 450 nm, is yellow in color, whereas NR^+H, a red-colored product, is reported to have an absorption maximum between 535 and 545 nm (7). The position of the λ_{max} of NR^+H is dependent upon the constituents of the buffer. The variation of the λ_{max} of neutral red in different buffer media has been attributed to formation of dimers and higher aggregates of the dye where buffers are believed to influence the aggregation equilibrium differently (5*c*, 7). We have observed that in phthalate buffer of pH 4 (0.05 mol dm^{-3} potassium hydrogen phthalate) the λ_{max} is 538 nm, whereas in phosphate buffer, i.e., in the presence of 0.05 mol dm^{-3} KH_2PO_4 and 0.001 mol dm^{-3} HCl, it is 527 nm. The visible spectra of the acid–base titration of neutral red using phosphate buffer (0.05 mol dm^{-3} KH_2PO_4 with added NaOH or HCl) pass through a sharp isosbestic point at 477 nm, whereas such a sharp isosbestic point was not observed in phthalate buffer (0.05 mol dm^{-3} potassium hydrogen phthalate with added NaOH) medium.

[1]Author to whom correspondence may be addressed.
[2]Revision received June 1, 1993.

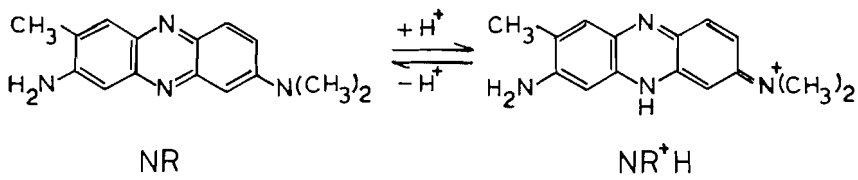

SCHEME 1

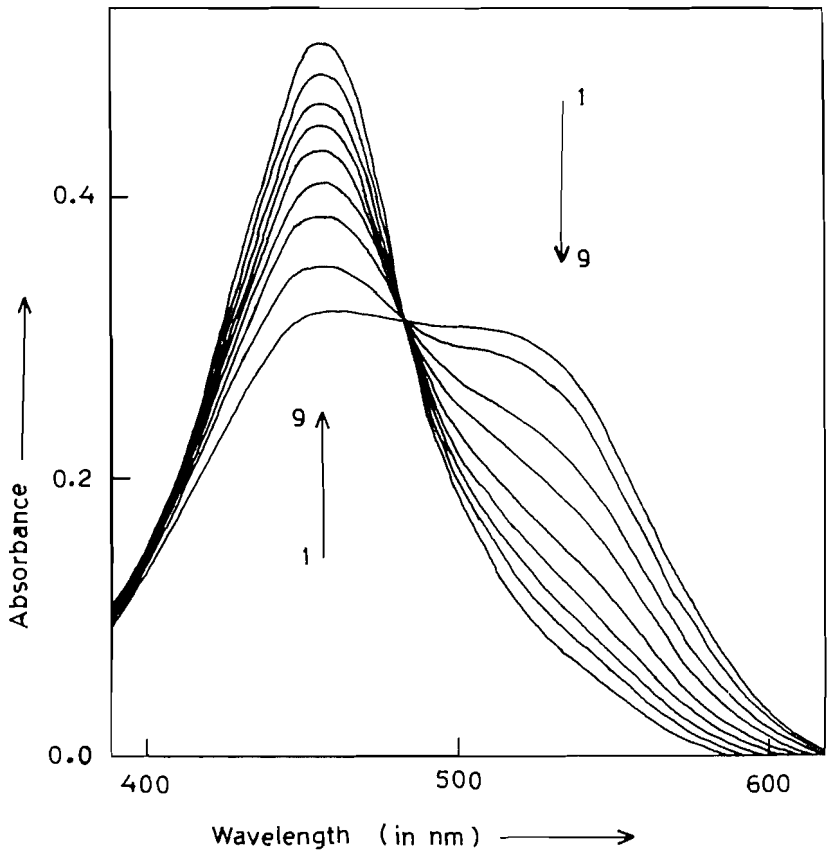

FIG. 1. Spectra of neutral red (4×10^{-5} mol dm^{-3}) at various concentrations of CPC at pH 7.25; concentrations of CPC $\times 10^{-4}$ mol dm^{-3}: 1 = 0.0, 2 = 1.2, 3 = 2.4, 4 = 3.6, 5 = 5.9, 6 = 9.5, 7 = 14.2, 8 = 24.1, and 9 = 114.9.

We feel that the absence of a clear isosbestic point in the spectra of neutral red, as reported by Drummond et al. (*5c*), was because these authors used more than one buffer system in the same experiment. The p$K_{a,w}$ of neutral red determined using KH_2PO_4 (0.05 mol dm^{-3}), NaOH, and HCl (for varying pH) was found to be 6.75 (±0.02), whereas the reported values vary from 6.5 to 7.4 (*5c*, 8).

Determination of K_{ass} *at constant pH*

The visible absorption spectra of neutral red in varying concentrations of CPC at pH 7.25 (0.05 mol dm^{-3} KH_2PO_4 + 0.036 mol dm^{-3} NaOH) are shown in Fig. 1. As the concentration of CPC was increased from 0 to 1.15×10^{-2} mol dm^{-3}, the absorption on the higher wavelength side (λ_{max} = 527 nm) decreased, whereas that on the lower wavelength side (λ_{max} = 460 nm) increased and a sharp isosbestic point was observed at 482 nm. The positions of the absorption maxima and the isosbestic point were not affected when the surfactant was changed from CPC to CTAB, TTAB, and DTAB. The presence of the isosbestic point indicates the existence of an equilibrium between the indicator species in aqueous and micellar pseudophases. The shift in the λ_{max} from 450 nm (in water) to 460 nm (in surfactant) is due to the association of the basic form of neutral red with the CPC micelles. The λ_{max} was found to be same in buffered micellar media of pH 7.25 (0.05 mol dm^{-3} KH_2PO_4 + 0.036 mol dm^{-3} NaOH), 7 (0.05 mol dm^{-3} KH_2PO_4 + 0.029 mol dm^{-3} NaOH), and 5.87 (0.05 mol dm^{-3} KH_2PO_4 + 0.0043 mol dm^{-3} NaOH). The effect of an increase in CPC concentration at constant pH is similar to that of an increase in pH of the aqueous indicator solution. It can be mentioned here that the pH of phosphate buffer solutions of pH 7.25, 7.00, and 5.87 (compositions as mentioned above) are unaffected on addition of cationic surfactants up to a concentration of ca. 0.02 mol dm^{-3}. This observation parallels that reported by Bunton and Minch (9).

The acid–base equilibrium of an indicator is represented by

$$[1] \quad A_w^z \overset{K_{a,w}}{\rightleftharpoons} B_w^{z-1} + H_w^+$$

where A_w^z and B_w^{z-1} are the acid and its conjugate base forms and $K_{a,w}$ is the acid dissociation constant of the indicator in

Can. J. Chem. Downloaded from www.nrcresearchpress.com by 203.198.23.82 on 09/08/12
For personal use only.

TABLE 1. Association constants of neutral red with surfactants at various pH, K_{ass}, and the equilibrium constants (independent of pH) K_s and K_e at 298 (±0.1) K

Surfactant	pH (±0.01)	The cmc of the surfactant in buffer medium (× mol dm^{-3})	K_{ass} (× mol dm^{-3})	K_s (× mol dm^{-3})	pK_e
CPC	7.25[a]	1.2×10^{-4}	3800 (±50)	5000	3.05
CPC	7.00[b]	1.7×10^{-4}	3060 (±50)	4990	3.05
CPC	5.87[c]	7.0×10^{-4}	580 (±20)	4980	3.05
CTAB	7.00[b]	7.0×10^{-5}	3630 (±50)	5920	2.98
TTAB	7.00[b]	7.0×10^{-4}	2440 (±50)	3980	3.15
DTAB	7.00[b]	7.0×10^{-3}	900 (±20)	1470	3.58
TX100	7.00[b]	5.0×10^{-4}	610 (±20)		
SDS	9.20[d]	7.4×10^{-4}	1400 (±50)		

[a]Buffer composition: 0.05 mol dm^{-3} KH_2PO_4 + 0.036 mol dm^{-3} NaOH.
[b]Buffer composition: 0.05 mol dm^{-3} KH_2PO_4 + 0.029 mol dm^{-3} NaOH.
[c]Buffer composition: 0.05 mol dm^{-3} KH_2PO_4 + 0.0043 mol dm^{-3} NaOH.
[d]Buffer composition: 0.01 mol dm^{-3} $Na_2B_4O_7$.

water. It follows from the definition of $K_{a,w}$ that at constant pH

$$[2] \quad [In_w] = [B_w^{z-1}](1 + [H_w^+]/K_{a,w}) = [A_w^z](1 + K_{a,w}/[H_w^+])$$

where $[In_w]$ is the total indicator concentration. In other words, it is possible to consider the total concentration of the indicator for an equilibrium study in buffered medium since the relative concentrations of the two indicator species remain the same irrespective of the total concentration at constant pH.

The expression of the association equilibrium of the indicator with the micelles can be simplified if eq. [2] holds in the micellar pseudophase. This would be so if the buffers were able to control the pH of the micellar surfaces, about which there have been differing reports in the literature (10, 11). Quina et al. (10) are of the opinion that buffers do not control the pH of the micellar surface. Frahm and Diekmann (11) observed that, within experimental uncertainties, the micellar surface potential is independent of the surfactant concentration (up to 10 times the critical micelle concentration). Nevertheless, in the present case, the intensity of the absorption band due to the acid form of the dye decreases with increase in concentration of the cationic surfactant and the band almost disappears at higher concentrations of surfactant (e.g., at and above ca. 1.15×10^{-2} mol dm^{-3} of CPC at a pH of 7.25; Fig. 1). This indicates that only NR is partitioned between the aqueous and micellar pseudophases, whereas NR^+H is largely in water. Therefore, for the present case, the total concentration of the indicator in the micellar pseudophase can be approximated to the total concentration of NR in the micellar pseudophase, i.e., we can consider a total indicator concentration term $[In_m]$ for the indicator in the micellar pseudophase.

Thus,

$$[3] \quad In_w + S_m \underset{\longleftarrow}{\overset{K_{ass}}{\longrightarrow}} In_m$$

or

$$[4] \quad K_{ass} = [In_m]/([In_w] \cdot [S_m])$$

where K_{ass} is the association constant of indicator with micelles at constant pH and $[S_m]$ is the micellized surfactant. In principle, eqs. [3] and [4] should be applicable for any indicator–micelle association interaction at any pH. However, in the presence of other types of molecular interactions, e.g., ion-pair formation between oppositely charged indicator species and monomeric surfactant, the equations are not applicable.

The association constants, K_{ass}, of indicator with micelles at constant pH were determined using Ketelaar's equation (12):

$$[5] \quad \frac{[In]_0}{(d-d_0)} = \frac{1}{(\epsilon_{ass}-\epsilon_0)} + \frac{1}{K_{ass}(\epsilon_{ass}-\epsilon_0)[S_m]_0}$$

where $[In]_0$ is the total concentration of the indicator, d and d_0 are the optical densities of the indicator in the presence and absence of the surfactant, respectively, ϵ_{ass} and ϵ_0 are the extinction coefficients of the indicator in the micelle-associated and free states, respectively, and $[S_m]_0$ is the total concentration of micellized surfactant, i.e., $[S_m]_0$ = (total concentration of surfactant − cmc) where cmc is the critical micelle concentration of the surfactant in the buffered medium, obtained from changes in absorbance of the indicator with addition of the surfactant.

The plots of $[In]_0/(d - d_0)$ *vs.* $(1/[S_m]_0)$ are quite linear, which suggests the validity of the assumption that the change in the ratio of acid to base forms of neutral red in the micellar pseudophase with change in surfactant concentration is within the experimental uncertainty. The K_{ass} values obtained from such plots are summarized in Table 1. It can be seen from the data that, in the case of CPC, K_{ass} increases with increase in pH of the medium. This can be attributed to the fact that at higher pH the concentration of the nonionic form of the indicator is high and it has preferential affinity towards the cationic micelles (rather than the cationic form). The value of K_{ass} of the indicator with CTAB (which has the same hydrocarbon chain length as CPC but a different head group) at constant pH 7 (0.05 mol dm^{-3} KH_2PO_4 + 0.029 mol dm^{-3} NaOH) was found to be higher than that with CPC. This indicates that the association of the indicator with cationic micelles not only depends on the hydrocarbon chain length but also on the head group of the surfactant. It is quite interesting to note that, as in the case

Can. J. Chem. Downloaded from www.nrcresearchpress.com by 203.198.23.82 on 09/08/12
For personal use only.

Can. J. Chem. Downloaded from www.nrcresearchpress.com by 203.198.23.82 on 09/08/12
For personal use only.

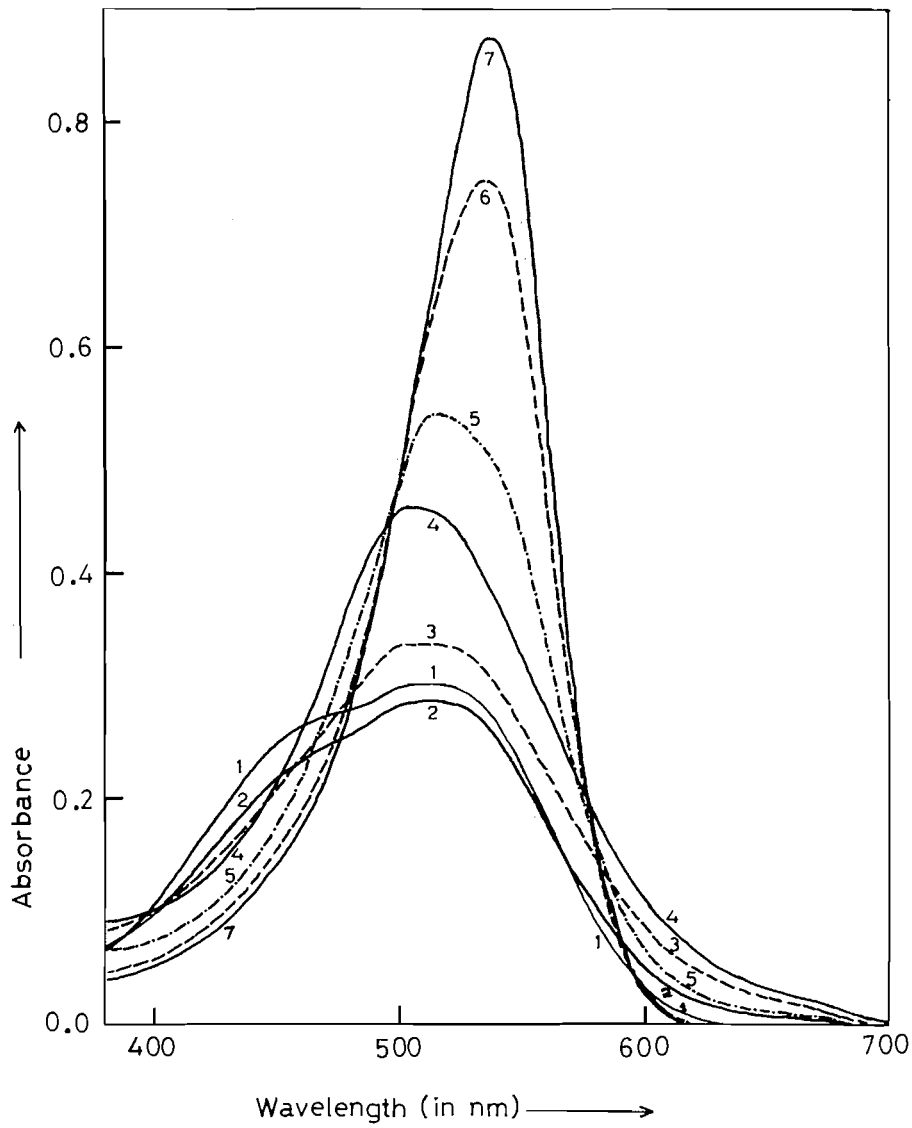

FIG. 2. Spectra of neutral red (3.2×10^{-5} mol dm^{-3}) at various concentrations of SDS at pH 7; concentrations of SDS $\times 10^4$ mol dm^{-3}: 1 = 0.0, 2 = 2.0, 3 = 2.8, 4 = 4.0, 5 = 8.0, 6 = 14.0, and 7 = 200.

of aqueous medium, the plot of the (log cmc) of CTAB, TTAB, and DTAB in buffered medium of pH 7 vs. hydrocarbon chain length is quite linear (13). This probably implies that even though the presence of the buffer components lowers the cmc, the process of micelle formation in the buffered medium is otherwise similar to that in pure water. The effect of surfactant counterions Cl^- or Br^- on K_{ass} cannot be inferred from the present study as the relatively large concentration of phosphate ion in the buffer solutions ensures that the counterion is mainly phosphate.

The spectra of neutral red (at constant pH 7) in varying amounts of TX100 are almost similar to those of neutral red in CPC and this indicates that the TX100 micelles associate with NR in preference to NR^+H. At higher concentrations of TX100, a weak shoulder at ca. 538 nm appears, which can be ascribed to a comparatively weaker but appreciable interaction of NR^+H with the micelles. The presence of an NR^+H–micelle association does not invalidate eqs. [3] and [4] as K_{ass} includes the associations of both species (i.e., NR and NR^+H) with micelles. The low K_{ass} of the indicator with TX100 (Table 1) suggests that the interaction is weak.

The spectra of neutral red in varying amounts of SDS at pH 7 are shown in Fig. 2. The lack of a single isosbestic point indicates the presence of more than one type of equilibrium between the indicator and the surfactant. At very low concentrations of SDS (i.e., below the cmc, the cmc in this buffer found, from surface tension measurements, to be ca. 7.4×10^{-4} mol dm^{-3}) the indicator absorbs in the high-wavelength region, ca. 580–680 nm. This absorbance has been attributed to the doubly protonated neutral red that is obtained in strong acidic medium of pH <1 in aqueous medium (7). Recently we showed that phenazinium dyes, which are generally protonated in highly acidic medium (below pH 1), can undergo protonation in submicellar anionic surfactant solutions even in neutral media, where the protonation is enforced by the strong hydrophobicity of the dye–surfactant ion pair (14). So, the absorption band above 580 nm can be attributed to doubly protonated neutral red in the dye–surfactant ion pair, viz., $NR^{2+}H_2 \cdot SDS^-$. At higher concentration of SDS (above the cmc) the λ_{max} was found to be 538 nm. The absorbance at this wavelength can be attributed to micelle-associated NR^+H. The determination of K_{ass}

Can. J. Chem. Downloaded from www.nrcresearchpress.com by 203.198.23.82 on 09/08/12
For personal use only.

of the indicator with SDS micelle at this pH was not possible due to the presence of more than one type of interaction. The spectral changes of the indicator with addition of SDS at pH 4.5 (acetate buffer) were almost similar to those at pH 7. However, at pH 9.2 (borate buffer), the spectral data (Fig. 3) show that there is no interaction (e.g., formation of $NR^{2+}H_2 \cdot SDS$) in the submicellar concentration range, whereas at higher concentration of surfactant (above the cmc) there is a clear isosbestic point at 466 nm, indicating the presence of an equilibrium. As the concentration of SDS is increased, the absorbance of the band on the higher wavelength side (λ_{max} = 538 nm) increases. Unlike the results obtained in CPC and TX100, the increase in intensities at higher wavelengths is much more comparable to the decrease in intensities of the 450-nm band (which shifts to 461 nm with increase in concentration of SDS). With the addition of more and more SDS, the anionic micelles associate with NR^+H in preference to NR. Therefore, the new band at λ_{max} = 538 nm can be ascribed to NR^+H_m. Absorption in the region of ca. 580–680 nm is absent above the cmc, possibly due to association of indicator with micelles, whereupon the protonated ion pairs are dissociated (Figs. 2 and 3). The shift of the 450-nm band of NR to 461 nm indicates that the conjugate base form, NR, is also associated (even though to a lesser extent than NR^+H) with the anionic micelles of SDS.

It has been seen that neutral red associates with cationic micelles only in the deprotonated form, NR. The association of the protonated form, NR^+H, is negligible compared to that of NR because of electrostatic repulsion between similar charges on the indicator and the micelle. Such behaviour is expected when the indicator is less hydrophobic (or more water soluble). Thus, substituting $[In_m]$ by $[B_m^{z-1}]$ in eq. [4] gives

$$[6] \quad K_{ass} = [B_m^{z-1}]/([In_w][S_m])$$

Now, we can examine the overall equilibrium constant, K_e, of neutral red in the cationic micellar medium (15):

$$[7] \quad NR^+H_w + S_m \overset{K_e}{\rightleftharpoons} NR_m + H_w^+$$

This equilibrium is the product of the partial equilibria [8] and [9]:

$$[8] \quad NR^+H_w \overset{K_{a,w}}{\rightleftharpoons} NR_w + H_w^+$$

and

$$[9] \quad NR_w + S_m \overset{K_s}{\rightleftharpoons} NR_m$$

where K_s is the pH-independent association constant of NR_w with similarly charged micelles (16) and is related to K_{ass} and K_e by

$$[10] \quad K_s = K_{ass}(1 + [H_w^+]/K_{a,w})$$

and

$$[11] \quad K_e = K_s \cdot K_{a,w}$$

A direct determination of K_s for the base form of neutral red is difficult as the indicator is unstable in strong basic medium, the condition required for the same. The equilibrium constants K_s and K_e calculated for neutral red with cationic micellar systems at various pH are included in Table 1. It can be seen from the table that K_s and K_e are independent of pH and are true thermodynamic quantities.

$pK_{a,app}$ of neutral red

The apparent dissociation constant, $K_{a,app}$ of an indicator in micellar solution is defined (9) as

$$[12] \quad K_{a,app} = \frac{[\text{total indicator in conjugate base form}]\,[H_w^+]}{[\text{total indicator in acid form}]}$$

For neutral red in cationic micellar medium:

$$[13] \quad K_{a,app} = ([NR_m] + [NR_w])\,[H_w^+]/[NR^+H_w]$$

or,

$$[14] \quad K_{a,app} = K_{a,w} + K_{ass} \cdot [S_m]\,([H_w^+] + K_{a,w})$$

or,

$$[15] \quad K_{a,app} = K_{a,w}(1 + K_s \cdot [S_m])$$

Thus, once the value of K_{ass} at (a suitable) fixed pH or the value of K_s is known, $K_{a,app}$ of the indicator at any concentration of the surfactant can be predicted. The $pK_{a,app}$ thus predicted for neutral red at various concentrations of CPC are shown in Fig. 4 along with the experimentally determined values. Here it can be mentioned that an error in the experimental $pK_{a,app}$ values is expected to be involved due to the variation in ionic strength of the medium, as the experimental values were determined using buffer (3*a*, 17). However, the variation in ionic strength of the medium (due to addition of NaOH) was within 0.04. It has been reported that when the ionic strength of the medium was varied from 0.1 to 0.5, the pK_a of neutral red altered by ca. 0.07 (18). Therefore the variation in the ionic strength or the interfacial salt effect is not likely to have any significant effect on the acid–base equilibria of neutral red in micellar medium (5*c*). The predicted $pK_{a,app}$, obtained from K_{ass} of different pH, were within the experimental error limit of ±0.1. The $pK_{a,app}$'s (predicted as well as observed) decrease with increase in concentration of CPC and finally level off. Our observations parallel those of Rychlovsky and Nemcova (19) who had observed such a trend in similar systems. The decrease in $pK_{a,app}$ with increase in concentration of CPC is expected from the fact that the higher the micelle concentration, the greater is the incorporation of NR into the micelles (in preference to that of NR^+H), which causes an increase in the relative concentration of the conjugate base form of the indicator at the expense of the acid form. It can be noted here that the predicted and observed pK_a values for the indicator in TTAB also agreed well with each other.

The acid–base equilibria of neutral red in aqueous nonionic and anionic surfactants were studied by Drummond et al. (5*c*). As both the base and conjugate acid forms of the indicator associate with nonionic micelles, such acid–base equilibria cannot be explained simply in terms of indicator–micelle association. In nonionic surfactants, considering partition of both forms of the indicator between the micellar pseudophase and aqueous phase, one can predict the $pK_{a,app}$. But for such predictions, the dissociation constant of the indicator in the micellar pseudophase is required. As in the case of nonionic micelles, both forms of the indicator associate with anionic micelles. Drummond et al. (5*c*) were of the opinion that ion-pair formation between NR^+H and the anionic headgroup of SDS, a "specific molecular interac-

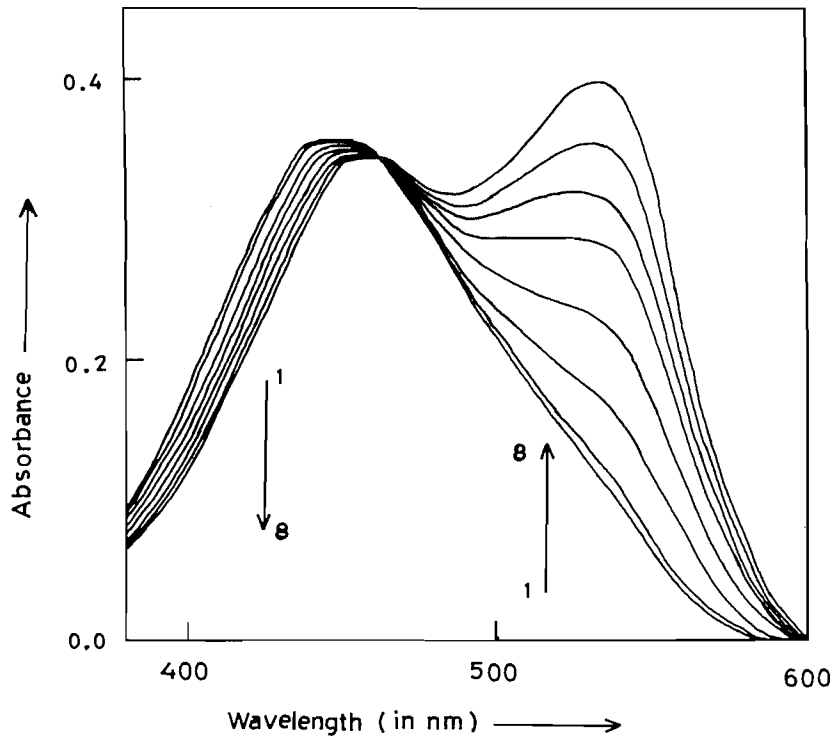

FIG. 3. Spectra of neutral red (4×10^{-5} mol dm^{-3}) at various concentrations of SDS at pH 9.2; concentrations of SDS $\times 10^4$ mol dm^{-3}: 1 = 0.0, 2 = 7.5, 3 = 10.0, 4 = 12.6, 5 = 17.6, 6 = 25.1, 7 = 50.2, and 8 = 251.0.

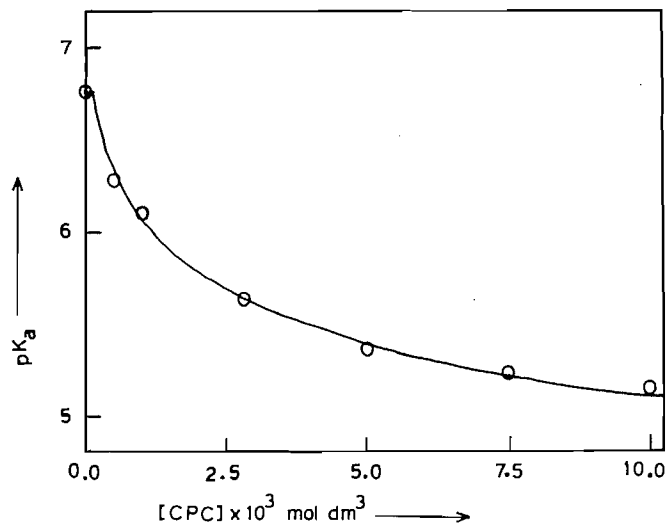

FIG. 4. Plot of predicted and observed $pK_{a,app}$ of neutral red in aqueous micellar medium of CPC *vs.* concentration of CPC; solid curve: predicted; O: observed.

tion," is one of the factors that affects the $pK_{a,app}$ of neutral red in SDS. Our observation indicates that the so-called specific molecular interaction is not simply an ion pair between NR^+H and SDS head groups but in fact $NR^{2+}H_2 \cdot SDS^-$, where the strong hydrophobicity of the hydrocarbon tail of the monomeric surfactant induces the second protonation.

Conclusion

The apparent association constants of neutral red with micelles at constant pH can be determined by the present method. The equilibrium constant for the association of the indicator with the cationic micelles can be determined from the apparent association constant. The apparent pK_a of the indicator in cationic micellar solutions can be predicted from the equilibrium constants.

Acknowledgement

One of the authors (R.K.D.) thanks North-Eastern Hill University and the University Grants Commission for the award of a senior research fellowship.

1. (*a*) M.E. Diaz-Garcia and A. Sanz-Medel. Talanta, **33**, 255 (1986); (*b*) E. Barni, P. Savarino, and G. Viscardi. Acc. Chem. Res. **24**, 98 (1991).
2. L.J. Cline Love, J.G. Habarta, and J.G. Dorsey. Anal. Chem. **56**, 1133 (1984).
3. (*a*) M.S. Fernandez and P. Formherz. J. Phys. Chem. **81**, 1755 (1977); (*b*) D.F. Evans and B.W. Ninham. J. Phys. Chem. **87**, 5025 (1983); (*c*) C. Dolcet and E. Rodenas. Can. J. Chem. **68**, 932 (1990); (*d*) M. Pesavento. J. Chem. Soc. Faraday Trans. **88**, 2035 (1992).
4. (*a*) C.A. Bunton, F. Nome, F.H. Quina, and L.S. Romsted. Acc. Chem. Res. **24**, 357 (1991); (*b*) L.S. Romsted. *In* Surfactants in solution. Vol. 2. *Edited by* K.L. Mittal and B. Lindman. Plenum Press, New York. 1985. p. 1015; (*c*) J. Phys. Chem. **89**, 5107 (1985); (*d*) J. Phys. Chem. **89**, 5113 (1985); (*e*) Z. He, P.J. O'Connor, L.S. Romsted, and D. Zanette. J. Phys. Chem. **93**, 4219 (1989); (*f*) C.A. Bunton, L.S. Romsted, and L. Sepulveda. J. Phys. Chem. **84**, 2611 (1980).
5. (*a*) C.J. Drummond, F. Grieser, and T.W. Healy. J. Chem. Soc. Faraday Trans. 1, **85**, 521 (1989); (*b*) J. Chem. Soc. Faraday Trans. 1, **85**, 537 (1989); (*c*) J. Chem. Soc. Faraday Trans. 1, **85**, 551 (1989); (*d*) J. Chem. Soc. Faraday Trans. 1, **85**, 561 (1989).
6. G.S. Hartley. Trans. Faraday Soc. **30**, 444 (1934).

Can. J. Chem. Downloaded from www.nrcresearchpress.com by 203.198.23.82 on 09/08/12
For personal use only.

7. N.V. Rao and R.L. Narayana. Indian J. Chem. **21A**, 995 (1982).
8. (*a*) R.G. Bates. Determination of pH, theory and practice. 1st ed. John Wiley and Sons Inc., New York. 1973. p. 156; (*b*) E. Baumgartner, R. Fernandez-Prini, and D. Turyn. J. Chem. Soc. Faraday Trans. 1, **70**, 1518 (1974).
9. C.A. Bunton and M.J. Minch. J. Phys. Chem. **78**, 1490 (1974).
10. F.H. Quina, M.J. Politi, I.M. Cuccovia, E. Baumgarten, S.M. Martins-Franchetti, and H. Chaimovich. J. Phys. Chem. **84**, 361 (1980).
11. J. Frahm and S. Diekmann. *In* Surfactants in solution. Vol. 2. *Edited by* K.L. Mittal and B. Lindman. Plenum Press, New York. 1985. p. 897.
12. J.A.A. Ketelaar, C. Van De Stolpe, and H.R. Gersmann. Recl. Trav. Chim. Pays-Bas, **70**, 499 (1952).
13. B. Lindman and H. Wennerstrom. Top. Curr. Chem. **87**, 8 (1980).
14. R.K. Dutta and S.N. Bhat. Bull. Chem. Soc. Jpn. **65**, 1089 (1992).
15. C.F. Hiskey and T.A. Downey. J. Phys. Chem. **58**, 835 (1954).
16. C.A. Bunton, G. Cerichelli, Y. Ihara, and L. Sepulveda. J. Am. Chem. Soc. **101**, 2429 (1979).
17. N. Funasaki. J. Phys. Chem. **83**, 1998 (1979).
18. R.G. Bates. Determination of pH, theory and practice. 1st ed. John Wiley and Sons Inc., New York. 1973. p. 150.
19. P. Rychlovsky and I. Nemcova. Talanta, **35**, 211 (1988).

Can. J. Chem. Downloaded from www.nrcresearchpress.com by 203.198.23.82 on 09/08/12
For personal use only.

X-ray crystal structure of [Ni(III)(cyclam)$(NO_3)_2$](ClO_4) and electron transfer reactions of the Ni(III)/Ni(II) couple

A. McAuley, T. Palmer, and T.W. Whitcombe
Department of Chemistry, University of Victoria, Victoria, BC V8W 3P6, Canada

Received March 19, 1993

A. McAuley, T. Palmer, and T.W. Whitcombe. Can. J. Chem. **71**, 1792 (1993).

The synthesis and crystal structure of [Ni(cyclam)$(NO_3)_2$](ClO_4) are described ($P1$, a = 8.347(4) Å, b = 15.960(7) Å, c = 7.656(3) Å, α = 90.33(6)°, β = 110.97(4)°, γ = 104.45(5)°, V = 917.0(7) Å^3, R = 0.0425, R_w = 0.0384). The crystal contains two unique Ni(III) cations within the unit cell, with a network of hydrogen bonding interactions linking one of the cations into a stacked configuration while the other cation contains a strong internal hydrogen bond. This provides an interesting inorganic example of multi-site cooperative binding involving a metal complex cation. By use of electron transfer data from known outer-sphere redox reagents, measurement of the cross-reactions with $[Ni(cyclam)]^{3+/2+}$ in 3 M nitrate media yielded a self-exchange rate constant of 1.4×10^5 M^{-1} s^{-1}. The structural data have been utilized to obtain a calculated estimate of the self-exchange rate constant (1.0×10^8 M^{-1} s^{-1}) for this couple. The relationship between these two values is explored. The lack of adiabaticity is reflected in a value ≈0.01 for κ_{el}, not only for this couple but also for other related cyclam complexes.

A. McAuley, T. Palmer et T.W. Whitcombe. Can. J. Chem. **71**, 1792 (1993).

On décrit la synthèse et la structure cristalline du [Ni(cyclame)$(NO_3)_2$](ClO_4) ($P1$, a = 8,347(4), b = 15,960(7) et c = 7,656(3) Å, α = 90,33(6), β = 110,97(4) et γ = 104,45(5)°, V = 917,0(7) Å^3, R = 0,0425 et R_w = 0,0384). Le cristal comporte deux cations Ni(III) indépendants dans la maille élémentaire avec un réseau d'interactions de liaisons hydrogènes liant un des cations dans une configuration empilée alors que l'autre cation est impliqué dans une forte liaison hydrogène interne. Ceci fournit un exemple inorganique intéressant d'une liaison coopérative à plusieurs centres impliquant un cation métallique complexe. Utilisant des données de transfert électronique obtenues à partir de réactifs rédox de sphère externe connue, des mesures de sections droites du $[Ni(cyclame)]^{3+/2+}$ dans un milieu de nitrate 3 M on fournit une constante de vitesse d'auto-échange de $1,4 \times 10^5$ M^{-1} s^{-1}. On a utilisé les données structurales pour obtenir une évaluation calculée de la constante de vitesse d'auto-échange ($1,0 \times 10^8$ M^{-1} s^{-1}) de ce couple. On étudie la relation entre ces deux valeurs. Le manque d'adiabicité se traduit par une valeur d'environ 0,01 pour κ_{el} tant pour ce couple que pour d'autre complexes de cyclames apparentés.

[Traduit par la rédaction]

Introduction

Although numerous Ni(II) macrocyclic complexes have been characterized structurally, there is a paucity of comparable data for complexes with higher valent nickel (1–6). This is, in part, due to the relative instability of the nickel(III) oxidation state which, in some instances, results in redox degradation of the complex before crystallization can occur. Nevertheless, a few examples of stable Ni(III) species have been reported (7–10, footnote 1) with ligands exhibiting a variety of ligand field strengths. With the growing awareness (11, 12) of the role that Ni(III) may play in the biological and catalytic reactions involving this metal ion (13), the investigation of the structural parameters of such systems is increasingly of interest.

In addition, the investigation of Ni(III) structures provides some of the parameters necessary for more detailed investigations of the electron transfer process during oxidation or reduction (14). *Ab initio* calculation of the Marcus-type self-exchange rate constants rely upon an exact knowledge of the bond lengths in both oxidation states. Attempts to rationalize measured self-exchange rate constants with the theoretically predicted values have met with varying degrees of success (14–18), although the Marcus–Sutin model has predicted rate data over many orders of magnitude to within a factor of 30.

In the present paper details are presented of the synthesis and crystal structure of the Ni(III) cation, [Ni(cyclam)-$(NO_3)_2]^+$, (cyclam = 1,4,8,11-tetraazacyclotetradecane) together with an investigation into the electron transfer reactions of $[Ni(cyclam)]^{3+}$ under conditions in which axial ligation by two nitrate ions would be ensured. The self-exchange rate for $[Ni(cyclam)(NO_3)_2]^{+/0}$ obtained from these measurements is compared with a value predicted based upon a Marcus–Sutin calculation (15). Similar calculations for the systems $[Ni(cyclam)(OH_2)_2]^{3+/2+}$, $[Ni(cyclam)Cl_2]^{+/0}$, $[Ni([9]aneN_3)_2]^{3+/2+}$ ([9]aneN$_3$ = 1,4,7-triazacyclononane), and a hypothetical square planar $[Ni(cyclam)]^{3+/2+}$ are provided for comparison along with their measured self-exchange rates.

Experimental

Synthesis

To a hot solution of 1.5 M nitric acid (≈20 mL), sufficient Ni(cyclam)$(ClO_4)_2$ was added to saturate the solution. The reaction mixture rapidly turned dark green and, upon cooling, yielded X-ray quality crystals of [Ni(cyclam)$(NO_3)_2$](ClO_4). Owing to the instability of the Ni(III) ion in solution, no further attempts were made to re-crystallize the compound. Analysis for Ni-$C_{10}H_{24}N_6O_{10}Cl$. Calcd.: Ni 12.2; C 24.98; H 5.02; N 17.41; O 33.16; Cl 7.35; found: Ni 12.3; C 25.16; H 5.00; N 17.52; O 35.45; Cl 6.96.

Crystallography

A dark green crystal was mounted inside a Lindemann tube using epoxy resin. An initial unit cell was obtained by Weissenberg and precession photography. The crystal was transferred to a Picker Four-circle Diffractometer and the unit cell refined using 27 reflections in the 2θ range, 24 to 50°. The data were collected using 200 steps of 0.01° in 2θ at 0.25 s per step. Background counting for 25 s was carried out before and after each reflection measure-

[1] A. McAuley and T.W. Whitcombe, unpublished results.

Can. J. Chem. Downloaded from www.nrcresearchpress.com by 203.198.23.82 on 09/08/12
For personal use only.

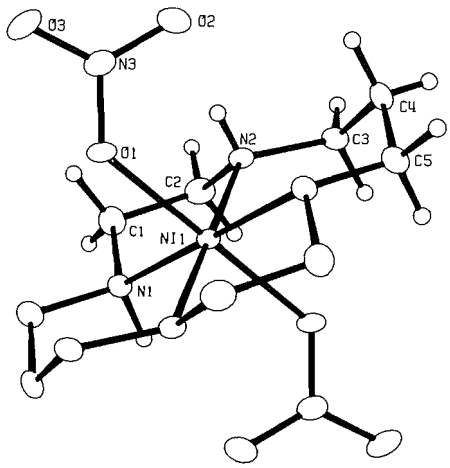

FIG. 1. ORTEP diagram of the $[Ni(cyclam)(NO_3)_2]^+$ cation at the cell origin. Atomic labelling scheme is as shown.

ment. Three standard reflections were measured at the beginning of every 50 reflections, with no significant decay being observed.

A total of 3212 reflections were obtained of which 2936 were within the limits $I > 2\sigma(I)$. Refinement was achieved through the use of MULTAN (19) to locate the two nickel atoms and the least squares difference maps generated with SHELX76 (20) to locate the remaining atoms. The atomic scattering factors and Ni *f*-curve were taken from the usual source (21). Absorption corrections were performed using a local modification of an existing program (22). The hydrogen atoms were locatable from the difference maps for this structure and were included in the final stages of refinement. Final values of $R = 0.0384$ and $R_w = 0.0425$ were obtained with all non-hydrogen atoms anisotropic. A final difference map gave a maximum residual electron density of 1.0 e/Å^3, with a maximum shift/e.s.d. of 0.150 for one of the non-coordinating oxygen atoms.

Experimental techniques

Cyclic voltammograms were obtained using a PAR 273 Potentiostat/Galvanostat connected to an IBM PC. The program "HEADSTART" (23) was used to control the instrument. A bridged cell was employed which consisted of one compartment containing the working and counter platinum electrodes and a second compartment containing the Ag/AgCl reference electrode, with the two compartments separated by a glass frit. The reference electrode compartment was filled with 2 M $HClO_4$ as the supporting electrolyte. The working cell contained either nitrate or perchlorate media. No correction was applied for the junction potential across the bridge since its effect was considered negligible.

Stopped-flow measurements were obtained with an Applied Photophysics DX-17MV instrument equipped with an Acorn computer. Details of measurements of observed electron transfer rates are provided are provided in Table 7. The $[Ni(cyclam)]^{3+}$ ion was generated immediately prior to the reaction by chemical oxidation using Co^{3+} as oxidant (24).

Ultraviolet/visible spectra were obtained using a Cary 5 NIR Spectrometer. Electron spin resonance spectra were obtained on a Varian E6S spectrometer. Microanalytical results were provided by Canadian Microanalytical Services, New Westminster, B.C.

Results and discussion

Crystallography

The asymmetric unit in this crystal was found to consist of two "half" molecules of the $[Ni(cyclam)(NO_3)_2]^+$ cation, together with a single perchlorate anion. One of the cations is shown in Fig. 1, together with the atomic labelling scheme. The ORTEP diagram of the remaining cation is included in the supplementary material.[2] The crystallographic data and associated fractional atomic coordinates, selected bond lengths, and selected angles for each ion are contained in Tables 1 to 4. Table 5 contains the mean planes calculated for both Ni cations together with pertinent atomic positions.

TABLE 1. Crystallographic parameters for $[Ni(cyclam)(NO_3)_2](ClO_4)$

Parameter	Value
Formula	$C_{10}H_{24}N_6O_{10}NiCl$
Molecular weight	482.49 g/mol
Space group	Triclinic, P1 (no. 2)
Unit cell	
a	8.347(4) Å
b	15.960(7) Å
c	7.656(3) Å
α	90.33(6)°
β	110.97(4)°
γ	104.45(5)°
Volume	917.0(7) Å^3
Z	2
Crystal size	0.309 × 0.368 × 0.535 mm
μ	12.46 cm^{-1}
Transmission range	0.627–0.731
ρ_{calc}	1.747 g/cm^3
ρ_{meas}	1.713 g/cm^3
Radiation	Mo K_α, 0.71069 Å
2θ	0.1–50.0°
No. of reflections	3212
$I > 2\sigma(I)$	2936
No. of parameters	352
Residual electron density	1.0 e/Å^3
Maximum final shift/e.s.d.	−0.150
R, R_w[a]	0.0384, 0.0425

[a] $R = \Sigma(|F_o| - |F_c|)/\Sigma|F_o|$, $R_w = [\Sigma(|F_o| - |F_c|)^2/\Sigma w(|F_o|)^2]^{1/2}$.

The nickel atom, Ni1, shown in Fig. 1, lies on a special position (0, 0, 0) at the corner of the unit cell, which is an inversion center and hence, the complete cation is generated by symmetry operators. The second nickel atom in the unit cell (Ni2) also occupies an inversion center at the special position ($\frac{1}{2}$, $\frac{1}{2}$, 0). The cation is labelled in a manner similar to that shown in Fig. 1, except a "1" has been added to the numbering scheme. The perchlorate ions do not occupy positions of site symmetry.

All of the atoms, including the hydrogen atoms, were locatable from the Fourier difference maps. This provides an

[2]Table of experimental crystallographic data, Tables S2-S8, containing fractional coordinates, bond lengths, bond angles, interatomic distances, and anisotropic temperature parameters for the complexes (10 pages), Table listing calculated and observed structure factors (13 pages), Figure S1 illustrating the alternate $[Ni(cyclam)(NO_3)_2]^+$ cation, and the calculations of the theoretical self-exchange rate constants (4 pages) have been deposited as supplementary data and may be purchased from The Depository of Unpublished Data, Document Delivery, CISTI, National Research Council Canada, Ottawa, Canada K1A 0S2.

Supplementary table of crystallographic parameters for $[Ni(cyclam)(NO_3)_2](ClO_4)$ (2 pages), bond angles (Table S2, 1 page), bond angles involving H atoms (Table S8, 1 page), have also been deposited with the Cambridge Crystallographic Data Centre and are available on request from the Director, Cambridge Crystallographic Data Centre, University Chemical Laboratory, 12 Union Road, Cambridge CB2 1EZ, U.K.

Can. J. Chem. Downloaded from www.nrcresearchpress.com by 203.198.23.82 on 09/08/12
For personal use only.

Can. J. Chem. Downloaded from www.nrcresearchpress.com by 203.198.23.82 on 09/08/12
For personal use only.

TABLE 2. Fractional atomic coordinates and equivalent temperature parameters for non-hydrogen atoms[a]

Atom	x/a	y/b	z/c	U_{eq}
Ni(1)	0	0	0	209(2)
N(1)	−1980(3)	553(2)	−871(3)	28(1)
N(2)	1182(3)	959(2)	2062(3)	27(1)
N(3)	934(3)	887(1)	−3215(3)	33(1)
O(1)	1439(3)	777(1)	−1455(3)	36(1)
O(2)	−666(3)	637(2)	−4202(3)	44(1)
O(3)	2077(3)	1228(2)	−3832(3)	53(1)
C(1)	−1749(4)	1171(2)	717(4)	35(1)
C(2)	190(4)	1636(2)	1578(4)	36(1)
C(3)	3127(4)	1339(2)	2661(4)	34(1)
C(4)	4133(4)	667(2)	3281(4)	38(1)
C(5)	3838(4)	4(2)	1688(4)	37(1)
Ni(2)	50000	50000	0	219(2)
N(11)	6550(3)	5851(2)	2195(4)	32(1)
N(12)	6332(3)	4178(2)	1280(4)	31(1)
N(13)	7571(3)	6049(2)	−1773(3)	35(1)
O(11)	6950(3)	5330(1)	−1221(3)	43(1)
O(12)	8994(3)	6184(2)	−1963(4)	54(1)
O(13)	6652(4)	6567(2)	−2216(5)	77(2)
C(11)	7437(4)	5358(2)	3708(4)	43(1)
C(12)	7974(4)	4694(2)	2815(5)	41(1)
C(13)	6721(4)	3553(2)	163(5)	42(1)
C(14)	5045(5)	3005(2)	−1344(6)	46(1)
C(15)	4207(5)	3531(2)	−2872(5)	44(1)
Cl(1)	15009(11)	72918(5)	37763(11)	432(3)
O(21)	2572(4)	7971(2)	3155(4)	58(1)
O(22)	−315(5)	7278(3)	2608(8)	119(2)
O(23)	1769(8)	7488(3)	5664(5)	117(3)
O(24)	1704(6)	6473(2)	3425(6)	101(2)

[a]Estimated standard deviations are given in parentheses. Coordinates are × 10″ where n = 5, 5, 4, 4, 4 for Ni, Cl, N, O, C. Temperature parameters are × 10″ where n = 4, 4, 3, 3, 3 for Ni, Cl, N, O, C.

opportunity for examination of the disposition of the protons within the macrocyclic ligand and to ascertain the extent of hydrogen bonding within the crystalline lattice.

The differing nature of the hydrogen bonding interactions leads to the identification of the two $[Ni(cyclam)(NO_3)_2]^+$ cations within the unit cell, as can be seen in Fig. 2. The chain of cations positioned at the unit cell origin is linked together by a series of interactions between the oxygen atoms of the bound NO_3^- anions and the protons attached to the nitrogens of the macrocyclic ligands. The distances for the intramolecular O—H (2.386 and 2.469 Å) and an intermolecular O—H (2.294 Å) interactions are consistent with reported distances for hydrogen bonding (25). The intermolecular bond, being slightly shorter, is presumed also to be the strongest interaction. Despite bifurcation of the hydrogen bonding to the proton, H2, it is involved in both of the shorter interactions, suggesting that O2 favours bonding with this proton.

The orientation of the nitrate ion is such that it is positioned to accommodate the interactions with all four points within the cell (Ni1 and the three protons). However, in describing the structure, the NO_3^- may be viewed as bisecting the six-membered chelating ring as opposed to bisecting the five-membered ring. This might be anticipated since this would minimize the interaction of the oxygen atoms with the carbon backbone of the ligand owing to the larger size of the chelating ring.

TABLE 3. Selected bond lengths for both $[Ni(cyclam)(NO_3)_2]^+$ cations[a]

Bond	Length	Bond	Length
O(1)—Ni(1)	2.110(2)	O(11)—Ni(2)	2.114(2)
N(1)—Ni(1)	1.975(2)	N(11)—Ni(2)	1.970(2)
N(2)—Ni(1)	1.978(2)	N(12)—Ni(2)	1.970(2)
N(3)—O(1)	1.287(3)	N(13)—O(11)	1.277(3)
N(3)—O(2)	1.233(3)	N(13)—O(12)	1.214(3)
N(3)—O(3)	1.223(3)	N(13)—O(13)	1.233(4)
C(1)—N(1)	1.487(4)	C(11)—N(11)	1.481(4)
C(2)—N(2)	1.491(4)	C(12)—N(12)	1.487(4)
C(3)—N(2)	1.501(4)	C(13)—N(12)	1.477(4)
C(2)—C(1)	1.495(5)	C(12)—C(11)	1.497(5)
C(4)—C(3)	1.501(4)	C(14)—C(13)	1.508(5)
C(5)—C(4)	1.520(4)	C(15)—C(14)	1.510(5)

[a]All distances are in angstroms (Å). Estimated standard deviations are given in parentheses.

The second series of cations in the unit cell do not display a similar network of interactions and, in fact, are positioned so as to minimize the spatial interactions of adjacent molecules. The mean plane described by $(Ni2)(N)_4$ is at an angle of 22.15° relative to the plane described by $(Ni1)(N)_4$ (see Table 5), which results in a twisting of this series of cations, as can be seen in Fig. 2. One consequence of this crystal packing is that the NO_3^- is free to orient in any direction relative to the macrocyclic ligand. In this second case, the nitrate ion is now positioned directly over one of the protons on the ligand nitrogen and at a "bond interaction" distance of only 2.003 Å. This is a short contact for this type of compound and is indicative of a moderately strong hydrogen bond, which might be maintained upon dissolution of the complex.

Other than the positioning of the nitrate moieties, there is very little structural difference between the two cations. The largest discrepancy in bond lengths is 0.010(5) Å (excluding the nitrate ion). Similarly, the internal angles are essentially the same, with only a slight difference observed (1.2(2)°) for the Ni—N—C angle in the six-membered ring. However, none of the structural differences is sufficiently significant to render either cation unique. In both cases, the macrocycle is in a *trans* III geometry, as might be anticipated, with a mean Ni—N bond length of 1.973(4) Å.

Comparison of the mean bond length for this Ni(III) complex with similar species (7–10, footnote 1) indicates that for an octahedral Ni(III) ion, the equatorial Ni—N distance has a mean value of 1.973 ± 0.006 Å. The corresponding Ni(II) ions give a mean value of 2.081 ± 0.026 Å, with an average change of 0.11 Å in the equatorial Ni—N bond length between the two oxidation states. Owing to the Jahn–Teller distortion exhibited by low spin d^7 ions, the decrease along the axial directions is only ≈0.05 Å, but very dependent upon the nature of the axial ligation.

An interesting comparison is provided by the square planar Ni(II) and Ni(III) ions in tetra-aza macrocyclic complexes. The former has been shown (26) to have a mean Ni—N distance of 1.945 ± 0.029 Å. In the only square planar Ni(III) complex (9) to have been characterized structurally, the Ni—N bond was found to be 1.84(1) Å. The change in bond length is ≈0.11 Å, suggesting that the contraction is independent of the coordination number of the nickel ion or de-

TABLE 4. Selected bond angles for both $[Ni(cyclam)(NO_3)_2]^+$ cations[a]

Bonds	Angle	Bonds	Angle
N(1)—Ni(1)—O(1)	93.6(1)	N(11)—Ni(2)—O(11)	90.2(1)
N(2)—Ni(1)—O(1)	86.1(1)	N(12)—Ni(2)—O(11)	84.8(1)
N(2)—Ni(1)—N(1)	86.3(1)	N(12)—Ni(2)—N(11)	86.6(1)
N(3)—O(1)—Ni(1)	129.0(2)	N(13)—O(11)—Ni(2)	130.1(2)
C(1)—N(1)—Ni(1)	107.2(2)	C(11)—N(11)—Ni(2)	107.1(2)
C(2)—N(2)—Ni(1)	107.7(2)	C(12)—N(12)—Ni(2)	107.2(2)
C(3)—N(2)—Ni(1)	118.5(2)	C(13)—N(12)—Ni(2)	119.7(2)
O(2)—N(3)—O(1)	118.9(2)	O(12)—N(13)—O(11)	119.5(3)
O(3)—N(3)—O(1)	117.9(2)	O(13)—N(13)—O(11)	118.8(2)
O(3)—N(3)—O(2)	123.1(2)	O(13)—N(13)—O(12)	121.5(3)

[a]All angles are given in degrees (°). Estimated standard deviations are in parentheses.

TABLE 5. Mean planes for the $Ni(cyclam)(NO_3)_2^+$ cations

Atom No.	X	Y	Z	P	ESD(P)
Ni1	0.0000	0.0000	0.0000	0.0000	0.0000
N1	−1.6345	0.9203	−0.6189	0.0000	0.0024
N2	0.0397	1.3274	1.4656	0.0000	0.0025
N1′	1.6345	−0.9203	0.6189	0.0000	0.0024
N2′	0.0397	−1.3274	−1.4656	0.0000	0.0025
		Sum of $P(I)$		0.0000	
Ni2	2.1822	7.7276	0.0000	5.9145	0.0000
C11	−2.6858	10.9858	2.6843	3.6671	0.0008
N3	1.3070	1.6120	−2.2855	3.0013	0.0025
O1	1.2904	1.3108	−1.0346	2.1010	0.0022
O2	0.3419	1.3000	−2.9873	2.6715	0.0024
O3	2.2946	2.1859	−2.7239	4.1482	0.0025
C1	−2.1226	1.7560	0.5100	−0.4022	0.0034
C2	−0.9258	2.4106	1.1335	0.3154	0.0033
C3	1.3478	1.9702	1.8918	0.8171	0.0032
C4	2.2854	0.7841	2.3325	0.4292	0.0034
C5	2.7399	−0.1211	1.1996	0.7728	0.0034
Ni2	2.1822	7.7276	0.0000	0.0000	0.0000
N11	2.5362	8.8772	1.5601	0.0000	0.0029
N12	3.2706	6.3602	0.9100	0.0000	0.0028
N11′	1.8282	6.5779	−1.5601	0.0000	0.0029
N12′	1.0938	9.0949	−0.9100	0.0000	0.0028
		Sum of $P(I)$		0.0000	
Ni1	0.0000	0.0000	0.0000	−4.5345	0.0000
C11	−2.6858	10.9858	2.6843	−4.0398	0.0009
N13	4.3965	9.4824	−1.2606	3.0046	0.0027
O11	4.0131	8.3293	−0.8978	2.1047	0.0025
O12	5.5824	9.7045	−1.3956	4.1171	0.0028
O13	3.5442	10.3160	−1.5751	2.7422	0.0035
C11	3.0577	8.0028	2.6360	−0.3645	0.0037
C12	4.0148	7.0436	2.0010	0.3647	0.0036
C13	4.1507	5.4787	0.1157	0.7649	0.0039
C14	3.3819	4.7460	−0.9555	0.3537	0.0042
C15	2.8916	5.6735	−2.0412	0.7669	0.0041
Direction cosines:					
Plane #1:	0.5567	0.6082	−0.5659		
Plane #2:	0.8206	0.3551	−0.4479		
Angle between planes:		22.15°			

pendent only upon the change in oxidation state, as might be anticipated. However, as pointed out by one of the referees, the nitrogen atom hybridization is sp^2 in the tervalent planar complex while it is sp^3 in the planar Ni(II) complex ions. The change in hybridization accounts for some of the bond length reduction observed. Nonetheless, the values are of interest in that they provide indications of potential overall changes in bond lengths accompanying such redox processes.

Can. J. Chem. Downloaded from www.nrcresearchpress.com by 203.198.23.82 on 09/08/12
For personal use only.

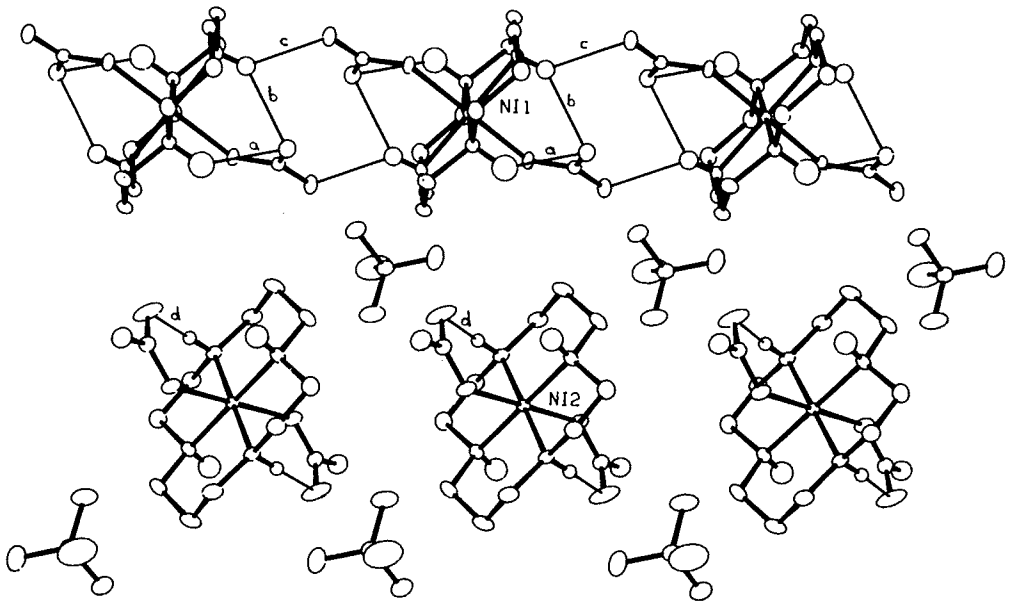

FIG. 2 ORTEP diagram illustrating the unit cell packing of the two $[Ni(cyclam)(NO_3)_2]^+$ cations and the hydrogen bonding interactions. These are indicated by the thin lines (*a*) H(1)···O(2) 2.469 Å, (*b*) H(2)···O(2) 2.386 Å, (*c*) H(2)···O(3) 2.294 Å, and (*d*) H(2A)···O(13) 2.003 Å.

TABLE 6. Electrochemical potential of $Ni(cyclam)^{3+/2+}$ in nitrate and perchlorate media

Ionic strength	$E_{1/2}$ *(nitrate)*	$E_{1/2}$ *(perchlorate)*
0.5	0.780	
1.0	0.761	0.806
1.5	0.738	
2.0	0.712[a]	0.798
2.5	0.710	
3.0	0.701	0.802
4.0		0.807

[a]Not used in calculations.

For both $[Ni(cyclam)(NO_3)_2]^+$ cations in the present structure, each Ni(III) ion is situated exactly in the plane as a result of space group symmetry. In the free state or in a hypothetical polymorph, where Ni would not sit on an inversion center, this constraint need not apply. However, the nickel atom would probably be close to the plane described by the four nitrogen donors.

Curiously, conventional drawings of the cyclam ring coordinated to a metal center usually depict the six-membered ring in a boat configuration with the apical carbon above the NiN_4 plane. This is not the case in these cations, since all of the carbon atoms in one-half of the molecule (split through the middle of the five-membered ring) lie either above or below the plane.

Electrochemistry

To investigate the extent of complexation of the $[Ni(cyclam)]^{3+}$ cation in aqueous nitrate media and to derive an approximate (or relative) equilibrium constant, the redox potentials for the complexed $Ni^{3+/2+}$ couple were measured by cyclic voltammetry in $H^+/NaNO_3$ media, at various ionic strengths (Table 6) resulting in an observed anion concentration dependent redox potential, $E^C_{1/2}$. For these experiments, the reference electrode was in a separate compartment, isolated by a fine glass frit, and was maintained in an electrolyte of constant composition and ionic strength. The advantage of this arrangement is that it eliminates any effects that changing the supporting electrolyte composition might have on the reference electrode potential. The disadvantage is that the presence of a junction potential across the frit prevents an accurate absolute determination of $E_{1/2}$ and only a relative value is obtained.

For the equation (27),

$$E^C_{1/2} = E^F_{1/2} + (RT/nF) \ln (K_{ox}/K_{red}) + (p - q)(RT/nF) \ln (x)$$

$E^F_{1/2}$ is the "free" (anion-independent) potential, K_{ox} and K_{red} are the stability constants of the oxidized and reduced complexes with the anion respectively, and $(p - q)$ represents the change in the number of anions coordinated. Only relative values are necessary since $E^F_{1/2}$ is available from a measurement of the redox potential in perchlorate media (the base line) under the same conditions. From the data, a mean value of 0.805 ± 0.004 V may be ascribed to $E^F_{1/2}$. A plot of $E^C_{1/2}$ for the nitrate complex versus ln $[NO_3^-]$ is linear, with a slope of −0.456 and an intercept of 0.754. Using the above value for $E^F_{1/2}$ results in $K_{ox}/K_{red} = 7.3$, and a value of −1.77 for $(p - q)$. Both of these results are consistent with expectations, since $(p - q)$ represents the change in coordination number accompanying the redox reaction and, in this case, corresponds to the complexation of two nitrate ions. The ratio of the equilibrium constants implies a value of ≈ 7 for K_{ox}. This is similar to the value of 7.8 calculated for the Ni(III) complex ion using the Eigen–Fuoss equation (28, 29) and an approximate value of ≈6 obtained by UV/Visible spectroscopy (30).

Kinetics studies

In order to investigate the electron transfer self-exchange reaction of the $[Ni(cyclam)(NO_3)_2]^{+/0}$ couple, the rate con-

Can. J. Chem. Downloaded from www.nrcresearchpress.com by 203.198.23.82 on 09/08/12
For personal use only.

TABLE 7. Observed rate constants[a] for the reaction of Ni(cyclam)$(NO_3)_2^{+/o}$ with Ni(sar)$^{3+/2+}$

	Rate constant where [Ni(sar)$^{2+}$] =			
[Ni(cyc)$^{2+}$]	2×10^{-4} M	5×10^{-4} M	7×10^{-4} M	10×10^{-4} M
2×10^{-4} M	17.8 ± 0.9	44.6 ± 3.0	59.0 ± 3.9	84.7 ± 5.8
5×10^{-4} M	21.0 ± 1.3	47.4 ± 1.5	62.0 ± 2.2	87.5 ± 0.8
7×10^{-4} M	22.1 ± 2.0	50.8 ± 1.6	68.0 ± 2.0	94.2 ± 1.8

[a]All rate constants are in units of s^{-1}. Temperature = 20.0 ± 0.1°C; ionic strength 3.0 M; $[H^+]$ = 0.1 M; λ = 380 nm.

Can. J. Chem. Downloaded from www.nrcresearchpress.com by 203.198.23.82 on 09/08/12
For personal use only.

stants were obtained for the cross-reaction with [Ni(sar)]$^{3+/2+}$ (sar = 3,5,10,13,16,19-hexaazabicyclo[6.6.6]icosane). The latter couple has recently been investigated[3] by CD and found to have an absolute self-exchange rate of 5300 M^{-1} s^{-1}, consistent with the values obtained for other $[NiN_6]^{3+/2+}$ couples (31). In addition, the position and intensity of the UV/Visible spectroscopic features for both $[Ni(sar)]^{2+}$ and $[Ni(sar)]^{3+}$ make it ideally suitable for study.

The presence of the ion, $[Ni(cyclam)(NO_3)_2]^+$, was ensured by the use of a large excess nitrate ion (I = 3.0 M H^+/$NaNO_3$). At the concentrations used in this study, with $K_{eq} \approx 7$, >98% of the Ni(III) ion is present as the di-nitrato complex. The Ni(III) ion was generated immediately prior to use in the stopped-flow instrument by the addition of aqueous Co^{3+}. Completion and stoichiometry of the oxidation were monitored on trial solutions by UV/Visible and EPR spectroscopy. The EPR spectra were consistent with a low-spin d^7 ion, with two axial oxygen donor ligands in a frozen matrix ($g_\parallel$ = 2.027, $g_\perp$ = 2.240).

The data obtained for the cross reaction of $[Ni(cyclam)(NO_3)_2]^+$ and $[Ni(sar)]^{2+}$ are presented in Table 7. The small driving force for the reaction (ΔE = 0.052 V) resulted in an equilibration between the two species, with the necessary recourse to concentration studies dependent on oxidant and reductant. A known excess concentration of both "Ni(II)(cyclam)$(NO_3)_2$" and Ni(II)(sar) was included in the reaction mixture, so that the equilibrium would be established as first-order in both directions. The rate law for this system

$$Ni(cyclam)(NO_3)_2^+ + Ni(sar)^{2+} \underset{k_{-1}}{\overset{k_1}{\rightleftharpoons}} Ni(cyclam)(NO_3)_2 + Ni(sar)^{3+}$$

$$\frac{d[Ni(III)]}{dt} = (k_1[Ni(sar)^{2+}] + k_{-1}[Ni(cyclam)(NO_3)_2]) \times [Ni(cyclam)(NO_3)_2^+]$$

is a function of both Ni(II) species, and the data yields values of $k_1 = (8.42 \pm 0.24) \times 10^4$ M^{-1} s^{-1} and $k_{-1} = (1.10 \pm 0.10) \times 10^4$ M^{-1} s^{-1}. Application of these values to a Marcus-type cross correlation, where K_{12} = 7.65 is obtained directly from k_1/k_{-1}, gives "forward" and "reverse" self-exchange rate constants of 1.38×10^5 and 1.36×10^5 M^{-1} s^{-1}, respectively, for the $[Ni(cyclam)(NO_3)_2]^{+/0}$ couple, under the experimental conditions employed.

[3]A.M. Sargeson, private communication.

An examination of the oxidation of $[Ni(cyclam)]^{2+}$ in 3.0 M $H^+/NaNO_3$ by $Co^{3+}_{(aq.)}$ was performed using stopped-flow techniques as part of this investigation. The relatively low pK_a of the $Co^{3+}_{(aq.)}$ ion usually results in the rate law having two terms, with an inverse hydrogen ion dependence resulting from the deprotonated species (32). In the present study, this behaviour was not observed. Rather, for $[Ni(cyclam)]^{2+}$ oxidation, a complex behaviour with a non-stoichiometric hydrogen ion dependence was obtained, where x = 0.5, k_a = 540,

$$k_{obs} = k_a + \frac{k_b K_H}{[H^+]^x}$$

and k_b = 1070 (assuming K_H to still be 2×10^{-3} M). A similar expression was found for the reaction using $[Ni(sar)]^{2+}$ with values of x = 0.1, k_a = 200, and $k_b = 1.7 \times 10^4$. These results are not simply a result of using 3 M ionic strength media, since the $[Ni(cyclam)]^{2+}$ oxidation was investigated in 3 M ClO_4^- media and the values obtained were within acceptable error limits of previous investigations (24). Since the deviation from the expression normally anticipated is common to both sets of data obtained in nitrate media, and the $[Ni(sar)]^{3+/2+}$ couple does not exhibit any equilibration with nitrate, the presumption is that the $Co^{3+}_{(aq.)}$ ion is associating with the supporting electrolyte. However, attempts to detect complex formation using UV/Visible spectroscopy were not successful. An alternate explanation may involve a nitrate-mediated electron transfer via a hydrogen-bonded species similar to that observed in the solid state. However, it is difficult to envisage the kinetic order observed arising from such a reaction pathway.

Calculation of self-exchange rates

The Marcus theory has been adapted (14, 15) to calculate, from first principles, the self-exchange rate constant of a redox couple. This requires a knowledge of the following parameters: the equilibrium constant (K_o) which is the work necessary to bring two ions together in solution and is based on the Debye–Huckel approach; the nuclear factor (κ_n) which may be calculated from the energies of reorganization for the inner- and outer-sphere nucleii based upon the equilibrium bond lengths and vibrational force constants; the electronic factor (κ_{el}) which arises from the overlap integral of the potential energy surfaces and is a measure of the adiabaticity of the reaction; a vibrational term (ν_n) which describes the vibrational interactions within the complex and the surrounding media, and provides the maximum limiting rate for the reorganization of the molecule. The resulting equation

TABLE 8. Calculated self-exchange rates for $Ni^{3+/2+}$ couples[a]

Redox couple	ΔG^*_{in}	ΔG^*_{out}	κ_N	ν_N	K_0	k_{11} (calcd)	k_{11} (obsd)
$Ni(cyc)^{3+/2+}$	12.3	23.6	4.5×10^{-7}	7.9×10^{12}	0.09	3.3×10^5	$(2 \times 10^3)^{b,c}$
$Ni(cyc)(OH_2)_2^{3+/2+}$	19.5	21.2	6.4×10^{-8}	9.3×10^{12}	0.15	8.7×10^4	2×10^{3c}
$Ni(cyc)Cl_2^{+/0}$	10.0	22.9	1.5×10^{-6}	6.4×10^{12}	0.42	4.2×10^6	3.4×10^{4d}
$Ni(cyc)(NO_3)_2^{+/0}$	9.9	17.9	1.7×10^{-5}	8.1×10^{12}	0.75	1.0×10^8	1.4×10^{5e}
$Ni([9]aneN_3)_2^{3+/2+}$	24.2	21.4	1.2×10^{-8}	9.6×10^{12}	0.15	1.7×10^4	6.0×10^{3d}

[a] ΔG^*_{in} and ΔG^*_{out} are given in kJ/mol. The units of ν_n are s^{-1}. The units of K_0 and M^{-1}. The rate constants are expressed in units of M^{-1} s^{-1} · cyc-cyclam or 1,4,8,11-tetraazacyclotetradecane. [9]aneN$_3$-1,4,7-triazacyclononane.

[b] The value shown is that evaluated from direct measurement of the self exchange rate for the "Ni(cyclam)$^{3+/2+}$" couple in aqueous solution. It is presented for both the square planar couple and the octahedral aquo couple. However, it is likely that it pertains to the $[Ni(cyclam)(OH_2)_2]^{3+/2+}$ self exchange.

[c] Reference 33.

[d] Reference 31.

[e] This work.

combines these parameters to give the self-exchange rate constant, k_{11}:

$$k_{11} = K_o \kappa_n \kappa_{el} \nu_n$$

It is not the intent of this paper to derive this expression in detail nor to expand upon the calculation of these values except where germane to the following discussion. Full details of the calculations have been included as supplementary material.

Table 8 contains the relevant data employed in the calculation of the self-exchange rate constants for the couples, $[Ni(cyclam)(OH_2)_2]^{3+/2+}$, $[Ni(cyclam)(Cl)_2]^{+/0}$, $[Ni(cyclam)(NO_3)_2]^{+/0}$, sq.pl./sq.pl. $[Ni(cyclam)]^{3+/2+}$, and $[Ni([9]aneN_3)_2]^{3+/2+}$. The last couple is included in order to provide a comparison with a known octahedral/octahedral system and to confirm the suitability of parameters used in other calculations. From the data presented in Table 8, it is apparent that the major contribution leading to the differentiation of the electron transfer rates originates with the nuclear term, κ_n. This is not surprising since this term reflects the relative magnitudes of the inner- and outer-sphere reorganization energies. While the latter is fairly constant (ΔG^*_{out}), reflecting the similarity in the ionic radii of these complexes, the inner-sphere reorganization energy (ΔG^*_{in}) is intimately dependent upon the changes in bond lengths and geometry that accompany the electron transfer reaction.

As may be seen from these tabulated rate constants, with the exception of $[Ni([9]aneN_3)_2]^{3+/2+}$, there is a significant discrepancy between the theoretical values and those obtained experimentally through a Marcus-type cross correlation. A feature is that the ratio of k_{obs} to k_{calc} is roughly constant not only for the postulated sq.pl./sq.pl. $[Ni(cyclam)]^{3+/2+}$ but also for the oct./oct. $[Ni(cyclam)(Cl)_2]^{+/0}$, $[Ni(cyclam)(NO_3)_2]^{+/0}$, and $[Ni(cyclam)(OH_2)_2]^{3+/2+}$ complexes, giving values of 0.006, 0.008, 0.0014, and 0.023, respectively. For the latter complexes, this implies strongly that there is a commonality of reaction mechanism amongst these three species.

The origin of the differences between the theoretical and observed self-exchange rate constants lies in the assumption that $\kappa_{el} = 1$ (i.e., the reactions observed are adiabatic). The axial ligands in the "Ni(cyclam)" complexes may not necessarily be constrained and, hence, these complexes do not represent ideal outer-sphere redox couples. Such an effect would serve to lower the adiabaticity. An average value of 0.01 for κ_{el}, as determined for the present complexes, would be consistent with κ_{el} found for other transition metal complexes (14–16) and would account for the discrepancy. It is of interest to note that the calculated and observed values for $[Ni([9]aneN_3)_2]^{3+/2+}$ agree remarkably well. In this complex the metal ion is constrained within an octahedral geometry by the facial tridentate macrocyclic ligand. It has been suggested that $[Ni([9]aneN_3)_3]^{3+/2+}$ is an adiabatic electron transfer reagent (31) and the present calculations appear to support that assertion.

Acknowledgements

We acknowledge the Natural Sciences and Engineering Research Council of Canada for operating support and equipment funding for the stopped-flow and UV/Visible spectrometers and the University of Victoria for their continued financial support of this research. We would also like to thank Mrs. Kathy Beveridge for her assistance with the X-ray crystallography and Dr. Donal Macartney for his helpful comments.

1. K. Henrick, P.D. Tasker, and L.F. Lindoy. Prog. Inorg. Chem. **33**, 1 (1985).
2. V.J. Thöm, C.G. Fox, J.C.A. Boeyens, and R.D. Hancock. J. Am. Chem. Soc. **106**, 5947 (1984).
3. B. Bosnich, R. Mason, P.J. Pauling, G.B. Robertson, and M.L. Tobe. J. Chem. Soc. Chem. Commun. 97 (1965).
4. E.K. Barefield, A. Bianchi, E.J. Billo, P.J. Connolly, P. Pauletti, J.S. Summers, and D.G. Van Derveer. Inorg. Chem. **25**, 4197 (1986).
5. L. Prasad, S.C. Nyburg, and A. McAuley. Acta Crystallogr. **C43**, 1038 (1987).
6. T.N. Margulis and L.J. Zompa. J. Chem. Soc. Chem. Commun. 430 (1979).
7. T. Ito, M. Sugimoto, K. Toriumi, and H. Ito. Chem. Lett. 1477 (1981).
8. T.J. Collins, T.R. Nichols, and E.S. Uffelman. J. Am. Chem. Soc. **113**, 4708 (1991).
9. K. Weighardt, W. Walz, B. Nuber, J. Weiss, A. Ozarowski, H. Stratemeier, and D. Reinen. Inorg. Chem. **25**, 1650 (1986).
10. M. Yamashita and H. Miyamae. Inorg. Chim. Acta, **156**, 71 (1989).
11. R. Cammack. Adv. Inorg. Chem. **32**, 297 (1988).
12. J.R. Lancaster, Jr. (*Editor*). Bioinorganic chemistry of nickel VCH, New York. 1988.

Can. J. Chem. Downloaded from www.nrcresearchpress.com by 203.198.23.82 on 09/08/12
For personal use only.

13. H. Toon, T.R. Wagler, K.J. O'Connor, and C.J. Burrow. J. Am. Chem. Soc. **112**, 4568 (1990).
14. N. Sutin. Prog. Inorg. Chem. **30**, 441 (1983).
15. N. Sutin. Acc. Chem. Res. **15**, 275 (1982).
16. B.S. Brunschwig, C. Creutz, D.H. Macartney, T.K. Sham, and N. Sutin. Faraday Discuss. Chem. Soc. **74**, 113 (1982).
17. A. McAuley and T.W. Whitcombe. Inorg. Chem. **27**, 3090 (1988).
18. H.J. Kuppers, A. Neves, C. Pomp, D. Ventur, K. Weighardt, B. Nuber, and J. Weiss. Inorg. Chem. **25**, 2400 (1986).
19. P. Main, L. Lessinger, M.M. Woolfson, G. Germain, and J.P. Declarecq. MULTAN77. Universities of York (UK) and Louvain (Belgium). 1977.
20. G.M. Sheldrick. SHELX76. University of Cambridge, UK. 1976.
21. International tables for X-ray crystallography. Vol. IV. Kynoch Press, Birmingham, UK. 1974.
22. P. Coppens, L. Leiserowitz, and D. Rabinovich. Modified by G.W. Bushnell, University of Victoria.
23. HEADSTART VO.1. Princeton Applied Research, Princeton, N.J. 1985.
24. J.-C. Brodovitch and A. McAuley. Inorg. Chem. **20**, 1667 (1981).
25. I. Olovson and P.-G. Jönsson. *In* The hydrogen bond. Vol. II. *Edited by* P. Shuster, G. Zundel, and C. Sandorfy. North Holland Publishing Company, New York, 1976.
26. A. McAuley, K. Beveridge, S. Subramanian, and T.W. Whitcombe. J. Chem. Soc. Dalton Trans. 1821 (1991).
27. W.E. Geiger. Prog. Inorg. Chem. **33**, 275 (1985).
28. M. Eigen. Z. Phys. Chem. (Frankfurt), **1**, 176 (1954).
29. R.M. Fuoss. J. Am. Chem. Soc. **80**, 5059 (1958).
30. R.I. Haines and A. McAuley. Inorg. Chem. **19**, 719 (1980).
31. A. McAuley, P.R. Norman, and O. Olubuyide. J. Chem. Soc. Dalton Trans. 1501 (1984).
32. G. Davies and B. Warnqvist. Coord. Chem. Rev. **5**, 349 (1970).
33. D.H. Macartney, A. McAuley, and T. Oswald. J. Chem. Soc. Chem. Commun. 274 (1982).

Can. J. Chem. Downloaded from www.nrcresearchpress.com by 203.198.23.82 on 09/08/12
For personal use only.

Abductive networks: generalization, pattern recognition, and prediction of chemical behavior

JOHN L.E. CAMPBELL AND KEITH E. JOHNSON[1]
Department of Chemistry, The University of Regina, Regina, SK S4S 0A2, Canada

Received February 16, 1993

JOHN L.E. CAMPBELL, and KEITH E. JOHNSON. Can. J. Chem. **71**, 1800 (1993).

Using commercially available software, it is possible to reduce numerical data to a mathematical representation called an abductive network (AN). In the current communication, we describe several simple examples which illustrate the interesting, and potentially useful properties of abductive networks. We show that when applied to the correlation of Kovats indices with molecular refractivities and dipole moments of substituted phenols, abductive networks more accurately predict Kovats indices than do counter-propagation neural networks or linear regression equations. When applied to the modeling of quantitative structure–activity relationships (QSAR) for local anesthetics, AN's are marginally superior to regression. AN's offer the advantage that correlations may be drawn between variables which are not easily related within a mathematical context.

JOHN L.E. CAMPBELL et KEITH E. JOHNSON. Can. J. Chem. **71**, 1800 (1993).

Utilisant un programme commercialement disponible, il est possible de réduire des données numériques en une représentation mathématique que l'on appelle un réseau abductif. Dans le présent travail, on décrit plusieurs exemples simples qui illustrent les propriétés intéressantes et potentiellement utiles des réseaux abductifs. On montre que lorsqu'on les applique à la corrélation des indices de Kovats avec les réfractivités moléculaires et les moments dipolaires de phénols substitués, les réseaux abductifs permettent de prédire les indices de Kovats avec plus de précision que les réseaux neurales de contre-propagation ou que les équations de régression linéaire. Lorsqu'on les applique à faire un modèle des relations quantitatives structure/activité des anesthésiques locaux, les réseaux abductifs ne sont que marginalement supérieurs à la régression. Les réseaux abductifs offrent l'avantage que les corrélations peuvent être développées entre des variables qui ne sont facilement reliées dans un contexte mathématique.

[Traduit par la rédaction]

Can. J. Chem. Downloaded from www.nrcresearchpress.com by 203.198.23.82 on 09/08/12
For personal use only.

A general description of the properties of neural networks has recently been presented by Jansson (1). As this author points out, research concerning practical applications of networks has been severely hampered, somewhat ironically, by its very proponents. Visions of thinking, learning machines uttered by some workers have certainly earned contempt from onlookers, and perhaps rightly so; such visions are terribly unrealistic at present. However, simple applications of network technology are currently not only possible, but successful as well. In the last year, several papers describing the use of networks in solving chemical problems have appeared in the literature (2, 3). Peterson has demonstrated the use of neural networks in the modelling and prediction of Kovats indices (used to characterize chromatographic retention behavior) for substituted phenols (2). It was shown that when linear regression analysis affords poor correlation, neural networks provide greater accuracy in modeling of Kovats indices. Schadmer et al. have reported the use of neural networks in correlating the process parameters for reactive ion etching, with the optical and mass spectra of the plasma (3). Research concerning neural networks has been underway for several decades (4, 5). In the past several years, a relatively new product of this research, called an abductive network (AN), has appeared (6). By means of examples, we demonstrate that AN's can accurately generalize and recognize patterns in data presented to them; if carefully generated, AN's can make accurate predictions based on as yet unseen data. In the current communication, we describe several simple examples in which AN's were synthesized using commercially available software (AIM[2]) and shown to be capable of accurately predicting chemical behavior. In experiments analogous to Peterson's, we find that abductive networks more accurately predict Kovats indices than do counter-propagation neural networks, or equations from linear regression.

The principles of neural network function and synthesis are well described in the literature (1, 4, 5). For a description of the principles of abductive networks, see Montgomery and Drake (6). In general, networks consist of an interconnected array of functional elements sometimes referred to as "nodes." A simple abductive network is illustrated in Fig. 1. Though they have the common task of cor-

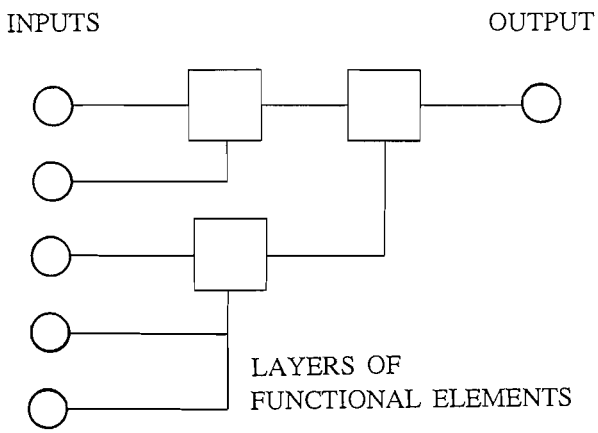

FIG. 1. A simple Abductive Network (AN) which correlates five input variables with a single output.

[1]Author to whom correspondence should be addressed.

[2]AIM stands for Abductory Induction Mechanism and is a registered trademark of AbTech Corporation, 700 Harris St., Charlottesville, VA 22901, U.S.A. The software is available directly from the manufacturer.

Can. J. Chem. Downloaded from www.nrcresearchpress.com by 203.198.23.82 on 09/08/12
For personal use only.

relating some set of input and output variables, the various networks differ in the nature and connectivity of their functional elements, and in the means by which the networks are synthesized. In general, the output of a functional element is a polynomial function of its input variables. The nodes of neural networks consist of linear-weighted sums of the input variables (1). Those of an abductive network, however, may also incorporate third degree polynomial functions in up to three input variables (6). The coefficients of the polynomial terms are "weighting" factors determined during synthesis. The algorithm by which AIM generates an abductive network is proprietary in nature and so for the purpose of this communication, suffice it to say that network synthesis is accomplished by "training" the network with a database of example inputs and outputs, and entails adjustment of the weighting factors until the network can calculate the database outputs with a minimum of error. If successful, the resulting network will have "learned" to model the contents of the database, *i.e.* to generate all the training set output values from the corresponding inputs. The AN is, effectively, an algebraic generalization of the data from which it was synthesized. A comparison of the performance of abductive networks with that of back-propagation neural networks, claims that the former is characterized by a considerably lower (*ca.* one order of magnitude) standard error (6). The abductive network was synthesized in less than 1% of the time required for training of the back-propagation network. As the name implies, the structure of a neural network is based on an analogy with neurons. The structure of an abductive network, on the other hand, is not limited to biological analogies (6), and is therefore expected to be more flexible.

The AIM algorithm incorporates automatic determination of optimum network structure and connectivity, an obvious advantage for the non-expert. This is accomplished by minimizing a modelling criterion called the *predicted squared error*, or PSE (6, 7):

$$\mathrm{PSE} = \mathrm{FSE} + \mathrm{CPM} \times (2K/N) \times s_p^2$$

FSE is the *fitting squared error* of a given network model with respect to the training data, K is the number of coefficients (proportional to network complexity), N is the number of training data, and s_p^2 is an *a priori* estimate of the variance. The *complexity penalty multiplier*, CPM, may be specified by the user, its default value being unity. As the complexity of the model increases, the FSE decreases (in the same way as increasing the number of variable parameters in regression leads to a better fit). However, as the model complexity increases, so does K, and hence the second term, the *complexity penalty* term, also increases. The level of complexity corresponding to the minimum PSE may therefore be varied through manipulation of the complexity penalty term, *e.g.* lowering the CPM has the effect of shifting the optimum PSE towards higher levels of network complexity. This is evident in Fig. 5 of ref. 6. In short, the CPM determines the degree of complexity which the AIM algorithm will allow in hypothesized networks; network synthesis terminates if increased complexity fails to improve model performance.

Synthesis of a network involves the recognition of patterns in the training data. In a sense the network is a generalization, or re-expression of patterns in the training data, and the structure of the network is dependent upon them. If the patterns have any real significance, as opposed to being coincidental, the network may be capable of correlating real physical quantities in a meaningful way. We should therefore suspect that if properly trained, the network may be capable of making accurate predictions from data to which it has not yet been exposed. Forcing the network to recognize real as opposed to spurious patterns may be accomplished through two means. Obviously, one should synthesize the network from data which are expected to have some real significance, *e.g.* inputs: mass, volume; output: density. Limiting the degree of complexity which the network is allowed to assume prevents overfitting to the data, while at the same time, allowing recognition of meaningful patterns.

As a simple example of pattern recognition by an AN, consider the numbers 0 through 127, which can each be expressed as a 7 bit binary number. A database was generated consisting of 128 data sets, each of which comprised 8 pieces of data: 7 input variables corresponding to each of 7 bits, and 1 output variable corresponding to the decimal equivalent. Thirty-two of the 128 sets were randomly selected as a basis for synthesis of an AN. Run on an 80286/287 (12 MHz) processor, such a synthesis takes about a minute, and the resulting network, when given *any* 7 bit integer, can correctly calculate the decimal equivalent. The network reduces to a weighted sum of 7 linear functions of the input variables, *i.e.* $\mathrm{DECIMAL} = \Sigma\ (c_{i1} + c_{i2} * \mathrm{BIT}_i)$ where $i = 1, 2, 3, \ldots 7$. One finds it difficult to argue that in synthesizing such a network, AIM has not *learned* to convert 7 bit binary numbers to their decimal equivalents, as simple and insignificant a task as this may be.

Peterson has shown that for modelling and prediction of Kovats indices based on solute molecular refractivity and dipole moment, a counter-propagation neural network (CPNN) is superior to multivariate linear regression (2). Kovats indices form the dependent variables in certain quantitative structure-chromatographic retention relationships (QSRR, 2). The Kovats index, I, may be written as $I = a\mathrm{MR} + b\mathrm{D}^2 + c$, where MR and D are the respective molecular refractivities and dipole moments of the solute; a, b, and c are constants particular to the column material. For a set of 20 phenols, Peterson has modeled Kovats indices for dimethylpolysiloxane (SE-30), (3-cyanopropyl)methylpolysiloxane (OV-225), and polyneopentyl glycol adipate (NGA) using multivariate linear regression (MLR), and by training CPNN's. The database from which the calculations were performed consisted of twenty sets of the inputs MR and D^2, and outputs I(SE-30), I(OV-225), and I(NGA), *i.e.* one set for each phenol; the I span the range *ca.* 1000–2700. For training of the CPNN, the I values were scaled so that all values lay in the range 0–0.5; in general, neural networks are incapable of handling large numbers. In each of twenty experiments (for a given Kovats index) 19 of the sets were used to train a network (or for MLR), and the result was then tested on the set which had been excluded. These "leave-one-out" calculations serve as a measure of the ability to predict Kovats indices from as yet unseen MR and D^2 data. Using data from ref. 2, we have repeated these calculations by synthesizing an analogous series of AN's. AN's were synthesized from unscaled data; AIM incorporates automatic input normalization. Our results for the AN, and Peterson's results for the CPNN and MLR treatments, are summarized in Table 1. The values tabulated are average root-mean-squared errors, *i.e.* the RMSE averaged over the

TABLE 1. Modeling of Kovats indices by abductive networks (AN), neural networks[a] (CPNN), and linear regression[a] (MLR)—results of leave-one-out calculations for 20 phenol data set; inputs: MR and D^2, outputs: I(SE-30), I(OV-225), and I(NGA)

	Training sets[b]		
Index	AN	CPNN	MLR
SE-30	49.3 (7.7)	8.7 (1.8)	106.7 (4.3)
OV-225	99.2 (7.5)	158.7 (22.1)	248.7 (14.7)
NGA	97.9 (10.8)	159.1 (27.3)	248.7 (13.7)
	Testing sets[c]		
Index	AN	CPNN	MLR
SE-30	66.0 (49.4)	64.1 (71.2)	119.8 (100.5)
OV-225	130.8 (123.5)	154.6 (162.9)	290.1 (268.7)
NGA	128.9 (118.7)	161.1 (175.0)	285.8 (266.0)

[a]Data from ref. 2.
[b]Average RMSE over 20, 19-phenol training sets.
[c]Average RMSE over 20, 1-phenol testing sets; standard deviations in parentheses.

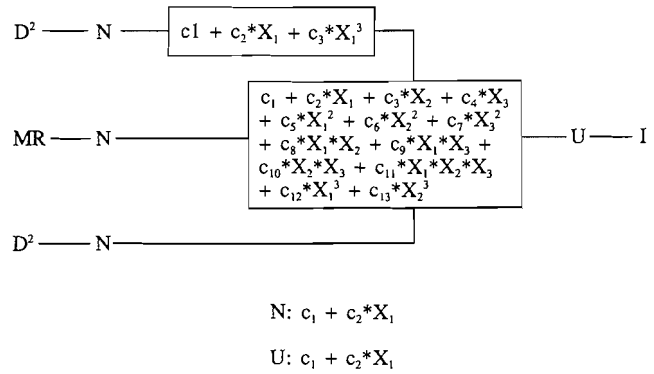

FIG. 2. Abductive network for correlation of I with MR and D^2, showing the forms of the functional elements: X_i's are inputs from previous layer, c_i's are weighting coefficients. N's and U's represent normalization and rescaling elements.

TABLE 2. Modeling of Kovats indices by abductive networks (AN), neural networks[a] (CPNN), and linear regression[a] (MLR)—results of leave-one-out calculations for 43 phenol data set; inputs: MR and I(SE-30), outputs: I(OV-225), and I(NGA)

	Training sets[b]		
Index	AN	CPNN	MLR
OV-225	67.7 (1.6)	14.3 (7.7)	68.4 (1.6)
NGA	81.8 (2.6)	16.1 (7.7)	82.6 (1.8)
	Testing sets[c]		
Index	AN	CPNN	MLR
OV-225	68.3 (70.2)	108.4 (137.6)	60.3 (51.3)
NGA	77.5 (72.7)	109.9 (119.0)	71.9 (64.4)

[a]Data from ref. 2.
[b]Average RMSE over 43, 42-phenol training sets.
[c]Average RMSE over 43, 1-phenol testing sets; standard deviations in parentheses.

number of observations in the data set, 20 in this case. The RMSE for each set was calculated from 19 observations in the case of training, and a single observation in the case of testing. It is clear from the testing sets of Table 1 that in predicting Kovats indices, the networks afford greater accuracy than linear regression. For OV-225 and NGA indices, the abductive network makes predictions which are significantly more accurate than those of the neural net; for all three indices, the AN predictions are associated with a significantly lower standard deviation than those of either the CPNN or MLR treatments. It is notable that for CPNN's, the quoted errors are those obtained for an optimized level of network complexity (see ref. 2); the abductive networks were synthesized using software default parameters. As described below, it is possible to improve performance of the SE-30 AN by restricting its complexity relative to the default limits. Synthesis of the AN's (60, twenty for each index) in batch mode took about 3 min on an 80486/33 PC and about 20 min on an 80286/287/12 PC. CPNN's described by Peterson consisted of at least 16 functional elements. In contrast, the corresponding abductive networks comprised, maximally, 6 elements, 4 of which serve to normalize and rescale the data (see Fig. 2). This may be owing to the AN's inclusion of nonlinear functional elements, *i.e.* inclusion of such terms may reduce the complexity required to model the data.

Peterson performed an analogous set of calculations for a 43-phenol data set in which the OV-225 and NGA indices were correlated with the inputs I(SE-30) and MR. In this case linear regression (MLR) was found to be considerably more accurate than CPNN modelling (2). The results of these calculations and those of an analogous series of AN experiments are summarized in Table 2. Though the CPNN is considerably less accurate than MLR, the AN treatment yields results comparable to, albeit not as good as, MLR. At any rate, considering both the 20- and 43-phenol experiments, it is clear that overall, the abductive network proves superior to either the neural network or linear regression treatments.

The ability of an AN to accurately *generalize* data from which it is synthesized, depends on the degree of complexity that the network is allowed to assume. The ability of the resulting network to make accurate predictions, however, will depend on whether or not its structure corresponds to some physically significant relation between input and output variables. By controlling its complexity, it may be possible to force the network to recognize real rather than spurious patterns, *i.e.* noise. We have repeated the leave-one-out calculations (as in Table 1) using three levels of complexity restrictions: (*A*) unrestricted, CPM = 0.01; (*B*) default, CPM = 1.0; (*C*) restricted relative to default, CPM = 1.5. The results of these experiments are summarized in Table 3. We observe that high accuracy in fitting of training data is associated with diminished accuracy in subsequent predictions; we suggest that networks most capable of prediction are those whose average RMSE's in training and testing are most similar. In other words, there is a trade-off between performance of the network on the data from which it was synthesized (*i.e.* generalization, recognition of meaningful patterns), and that on data to which it has not yet been exposed (*i.e.* predictive ability). Note that this is also evident in the data of Table 2, in which the most successful treatments (AN and MLR) have similar training/testing average RMSE's.

Can. J. Chem. Downloaded from www.nrcresearchpress.com by 203.198.23.82 on 09/08/12
For personal use only.

TABLE 3. Modeling of Kovats indices by abductive networks (AN), 20 phenol data set; inputs: MR and D^2, outputs: I(SE-30), I(OV-225), and I(NGA)

Index	Complexity level (CPM)		
	A (0.01)	B (1.0)	C (1.5)
	Training sets[a]		
SE-30	0.6 (0.2)	49.3 (7.7)	52.0 (5.1)
OV-225	1.5 (0.5)	99.2 (7.5)	111.9 (18.1)
NGA	1.5 (0.5)	97.9 (10.8)	109.1 (12.2)
	Testing sets[b]		
SE-30	117.9 (108.5)	66.0 (49.4)	58.8 (46.4)
OV-225	288.1 (266.7)	130.8 (123.5)	173.2 (165.8)
NGA	305.2 (258.9)	128.9 (118.7)	139.0 (106.4)

[a]Average RMSE over 20, 19-phenol training sets.
[b]Average RMSE over 20, 1-phenol testing sets; standard deviations in parentheses.

Of significant interest to pharmacological investigators, are the identification of quantitative structure–activity relationships (QSAR's). For example, several groups have attempted to relate the ability of compounds to act as local anaesthetics with molecular properties such as molecular polarizability α, ionization potential I, and van der Waals volume V_w (8). Correlations of the form log (MBC) = $a + b\beta$ have been investigated; MBC is the minimum concentration (mM) necessary for complete blocking of excitability, a and b are constants, and the parameter β is either α, V_w, or the product αI (8). We have performed a set of leave-one-out calculations for a set of 39 compounds using both linear regression, and AN's; data were taken from ref. 8; log (MBC) spans the range from −4.20 to 3.09. The results of these calculations are summarized in Table 4. It is seen that the AN yields marginally better results for both generalization and prediction of log (MBC). Notably, standard deviations for prediction by the AN are significantly smaller than for the linear regression equations. Abductive networks using all three quantities as input variables yield significantly lower prediction errors. Though it is reasonably straightforward to perform multivariate regression, this assumes that one has knowledge of the order of the equation with respect to each of the independent variables. The utility of the AN lies in the fact that one need not possess this knowledge, *i.e.* it is determined automatically during synthesis of the network. We must be careful to state that AIM generates functions/networks which *mimic* relationships amongst variables. Only in cases where these relationships may be written in terms of polynomial functions, *i.e.* AIM functional elements, can we say that AIM is capable of actually finding them. Synthesis of the AN is, effectively, a curve-fitting procedure which assumes no prior knowledge of the form of the equations!

As a general strategy for modelling with AN's, we suggest that leave-one-out calculations be performed using a series of allowed network complexities. In cases where many data sets are involved, leave-N-out calculations may be appropriate. Our results suggest that the optimum network is that for which the average RMSE for training and testing are the least different. The magnitude of the average RSME is a measure of the quality of the training data. Obviously it is desireable to train networks with the most reliable data, and so it would be useful to have some means of detecting

TABLE 4. Modeling of local anesthetic QSAR's by AN and linear regression—results of leave-one-out calculations for 39 compound data set—RMSE log (MBC)

Independent variable	Training[a]	
	AN	LR
α	0.32(0.01)	0.34(0.48)
V_w	0.55(0.03)	0.55(0.80)
αI	0.21(0.01)	0.24(0.34)
$\alpha, V_w, \alpha I$	0.13(0.003)	—
Independent variable	Testing[b]	
	AN	LR
α	0.29(0.18)	0.30(0.47)
V_w	0.38(0.42)	0.40(0.71)
αI	0.18(0.13)	0.20(0.33)
$\alpha, V_w, \alpha I$	0.15(0.12)	—

[a]RMSE averaged over 39, 38-compound training sets.
[b]RMSE averaged over 39, 1-compound testing sets; standard deviations in parentheses.

errors in potential training data. Minimizing such errors, in addition to minimizing RMSE's, should also reduce the tendency towards overfitting the network. It should be possible to detect errors in training data during the course of leave-one-out calculations. For example, consider such a set of calculations involving N data sets, and yielding N test results and their associated errors, from which may be calculated an *average absolute error* and corresponding standard deviation. Sets yielding errors which are widely divergent from the norm could then be excluded from further use on the basis of standard statistical tests: Q-tests, z-statistics *etc*. Such methods of detecting errors in training data have yet to be explored, and are probably deserving of some attention.

In conclusion, their ability to recognize patterns in numerical data leads us to envisage a wide variety of applications for network modelling. For example, the ability to synthesize an abductive network which successfully predicts correlations amongst training variables might be taken as confirmation of a real relationship between those variables. We have had some success in predicting the association constant for supramolecular complexes consisting of a macrocycle and a variety of substituted phenols, though the paucity of available data does not currently allow firm conclusions to be drawn (unpublished work). Here we attempted to correlate the association constant with the Hammet σ values of the phenol substituents. In conjunction with other techniques, such modelling might facilitate the design of molecules which have known differential association constants with a variety of receptors; this may have applications in the design of molecular devices. In principle, any model which may be generalized to a set of input and output parameters can be investigated with networks; logical variables, when given numeric values, and empirical data, may also be employed. The great power of networks lies in their ability to recognize relationships among variables which might otherwise remain hidden; these relationships need not have any mathematical foundation corresponding to a set of equations. For example, it may be

Can. J. Chem. Downloaded from www.nrcresearchpress.com by 203.198.23.82 on 09/08/12
For personal use only.

possible, using networks, to correlate experimentally observed primary and secondary protein structure, so as to predict the folding of proteins on the basis of amino acid sequence, and perhaps other descriptors. Though limited success has been achieved empirically in this area, a strictly theoretical treatment of the problem is daunting indeed; it is simply too complex (admittedly, this may change as contemporary computers become increasingly powerful). Through their ability to recognize patterns in data, networks may provide means of dealing with complex problems which are otherwise difficult or intractable. In the applications discussed here, abductive networks exhibit performance which is, on the whole, superior to that of neural networks or more standard regression techniques. It remains to be seen whether or not this applies more generally. The degree of complexity which can be accommodated by AN's is unclear. All of the examples discussed here involved single or double layer networks with fewer than ten functional elements; current software allows up to 9 layers and perhaps hundreds of nodes. Other work indicates that AN's are capable of modelling more complex systems of equations (9); further applications are necessary in order to evaluate the capabilities and limitations of abductive networks, and indeed, networks in general.

Can. J. Chem. Downloaded from www.nrcresearchpress.com by 203.198.23.82 on 09/08/12
For personal use only.

Acknowledgments

The authors wish to thank NSERC for assistance in the form of a scholarship to JLC. We also acknowledge useful comments from the reviewers.

1. P.A. Jannson. Anal. Chem. **63**, 357A (1991).
2. K.L. Peterson. Anal. Chem. **64**, 379 (1992) and references therein.
3. R. Schadmer, D. Angell, P.B. Chou, G.S. Oehrlein, and R.S. Jaffe. J. Electrochem. Soc. **139**, 907 (1992).
4. P.K. Simpson. Artificial neural systems. Pergamon Press, New York, N.Y. 1990.
5. M.C. McClelland and D.E. Rummelhart. Explorations in parallel distributed processing. MIT Press, Cambridge, Mass. 1988.
6. G.J. Montgomery and K.C. Drake. Proc. SPIE—Int. Soc. Opt. Eng. 1294, **56** (1990). Applications of Artificial Neural Networks Conference, April 16–20 1990, Orlando, Fla. U.S.A.
7. A.R. Barron. *In* Self-organizing methods in modeling: GMDH type algorithms. *Edited by* S.J. Farlow. Marcel-Dekker Inc., New York. 1984.
8. S.P. Gupta. Chem. Rev. **91**, 1109 (1991).
9. J.L. Campbell and K.E. Johnson. *In* Proceedings of The Eighth International Symposium on Molten Salts, St. Louis, Mo. May 17–22, 1992. *Edited by* G. Blomgren, R. Gale and H. Kojima. The Electrochemical Society Inc., Pennington, N.J. pp. 317–334.

Synthesis and characterization of 5,12-dimethyl-7,14-diphenyl-1,4,8,11-tetraazacyclotetradecane-4,11-diacetic acid and its transition metal complexes; crystal structure of the copper(II) complex of the macrocycle

LIQIN CHEN,[1] LAURENCE K. THOMPSON[1] AND JOHN N. BRIDSON
Department of Chemistry, Memorial University of Newfoundland, St. John's, NF A1B 3X7, Canada

AND

JIDE XU, SHISHENG NI, AND RUIPING GUO
Department of Chemistry, Anhui University, Hefei, Anhui, China 230039

Received April 20, 1993

LIQIN CHEN, LAURENCE K. THOMPSON, JOHN N. BRIDSON, JIDE XU, SHISHENG NI, and RUIPING GUO. Can. J. Chem. **71**, 1805 (1993).

The synthesis and characterization of a new 14-membered tetraazamacrocyclic ligand 5,12-dimethyl-7,14-diphenyl-1,4,8,11-tetraazacyclotetradecane-4,11-diacetic acid (H_2L^1) is reported. Cobalt(III), nickel(II), and copper(II) complexes with this ligand were prepared and characterized by infrared, electronic, and electron spin resonance (esr) spectra and in one case by X-ray crystallography. The complex $CuL^1 \cdot 2CH_3CH_2OH$ (**3**) crystallized in the triclinic system, space group $P\bar{1}$, with a = 8.440(2), b = 13.445(2), c = 7.523(1) Å, α = 99.30(1), β = 106.57(1), γ = 87.00(1)° and Z = 2 (R = 0.027, R_w = 0.028 for 2618 reflections). The complex shows a distorted *trans*-octahedral geometry with four amino nitrogens in a plane and two apical carboxylate oxygen donors.

LIQIN CHEN, LAURENCE K. THOMPSON, JOHN N. BRIDSON, JIDE XU, SHISHENG NI et RUIPING GUO. Can. J. Chem. **71**, 1805 (1993).

On rapporte la synthèse et la caractérisation d'un nouveau coordinat tétraazamacrocyclique à 14 chaînons, l'acide 5,12-diméthyl-7,14-diphényl-1,4,8,11-tétraazacyclotétradécane-4,11-diacétique (H_2L^1). On a préparé des complexes du cobalt(III), du nickel(II) et du cuivre(II) avec ce coordinat et on les a caractérisés par leurs spectres infrarouges, électroniques et de résonance paramagnétique électronique et, dans un cas, par diffraction des rayons x. Le complexe $CuL^1 \cdot 2CH_3CH_2OH$ (**3**) cristallise dans le système triclinique, groupe d'espace $P\bar{1}$, avec a = 8,440(2), b = 13,445(2) et c = 7,523(1) Å, α = 99,30(1), β = 106,57(1) et γ = 87,00(1)° et Z = 2 (R = 0,027 et R_w = 0,028 pour 2618 réflexions). Le complexe présente une géométrie *trans*-octaédrique déformée comportant quatre azotes aminés dans un plan et deux oxygènes carboxyliques donneurs en position apicale.

[Tradiut par la rédaction]

Introduction

There has been great interest in the coordination chemistry of polyaza macrocycles (1, 2). These ligands have been shown to be capable of producing generally strong ligand fields, but their inherent disadvantage is that they cannot completely "wrap up" the majority of transition metals, producing a completely filled coordination sphere. The solution to this would be either to increase the size and the number of donor atoms of the macrocycles or to append coordinating groups to the periphery of the macrocycle, which themselves may coordinate and thus increase the ligating ability of the macrocycles.

We are interested in the coordination chemistry of *N*-functionalized polyazamacrocycles and mixed oxygen–nitrogen donor macrocycles. Their specific complexation behaviour is clearly of interest in many areas such as the design of potential lanthanide ion selective reagents (3–5), the design of complexes to act as medical imaging agents (6), and for the treatment of heavy metal intoxication in the case of metal poisoning (7, 8). Our initial studies in this area have involved the synthesis and characterization of a series of *N*-acetic acid functionalized tetraazamacrocycles and mixed oxygen–nitrogen donor macrocycles and their coordination chemistry with transition metals, lanthanides, and actinides (9–14). The present paper describes the synthesis and characterization of 5,12-dimethyl-7,14-diphenyl-1,4,8,11-tetraazacyclotetradecane-4,11-diacetic acid (H_2L^1) (Fig. 1) and its metal complexes with Co(III), Ni(II), and Cu(II) salts.

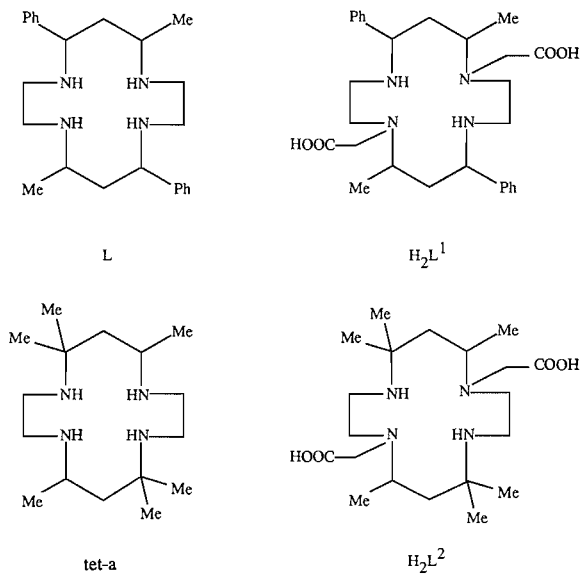

FIG. 1. Structures of the ligands.

Experimental section

All chemicals were analytical grade and were not purified further. The macrocycle *meso-meso*-5,12-dimethyl-7,14-diphenyl-

[1]Authors to whom correspondence should be addressed.

Can. J. Chem. Downloaded from www.nrcresearchpress.com by 203.198.23.82 on 09/08/12
For personal use only.

Can. J. Chem. Downloaded from www.nrcresearchpress.com by 203.198.23.82 on 09/08/12
For personal use only.

1,4,8,11-tetraazacyclotetradecane (L) was prepared as previously described (15). Proton NMR spectra were recorded with a JEOL FX90Q spectrometer. Infrared spectra were obtained with Nicolet 170Sx spectrometer. Electronic spectra were recorded as mull using a Cary 5E spectrometer. The esr spectra were recorded with a Bruker ESP 300 X-band spectrometer at room temperature and 77 K. Room temperature magnetic moments were measured using a Cahn 7600 Faraday magnetic balance. Microanalyses were performed by the Center of Structure and Elemental Analysis, China University of Science and Technology.

Synthesis of ligands and complexes

H_2L^1 (A)

To 16.70 g (0.12 mol) of bromoacetic acid in 100 mL dry methanol was added 6.72 g (0.12 mol) of KOH in 200 mL of dry methanol. L (19.0 g, 0.050 mol) in 100 mL dry methanol and 12.70 g (0.12 mol) of powered anhydrous sodium carbonate were then added, and the mixture was stirred at 60°C for 24 h. The reaction mixture was cooled, and the white precipitate of $NaHCO_3$ was filtered off. After nearly complete evaporation of the solvent on a rotary evaporator, the residue was dissolved in 50 mL water and the solution was filtered to remove any solid. The filtrate was acidified to pH 5 with dilute hydrochloric acid. The product H_2L^1 precipitated upon standing as a white powder, which was filtered off, washed with water and ethanol, and air dried. Yield 14.5 g (58%). It does not dissolve appreciably in common solvents. Anal. calcd. for $C_{28}H_{40}N_4O_4$: C 67.71, H 8.12, N 11.28; found: C 67.78, H 7.95, N 11.14. IR (KBr, cm^{-1}): 2660–2900 (NH_2^+); 1600 (COO^-).

$H_2L^1 \cdot 2HCl \cdot 4H_2O$ (B)

A (10.0 g, 0.020 mol) was dissolved in 20 mL dilute NaOH solution, then 20 mL concentrated HCl was added immediately and a white precipitate formed slowly. The mixture was stirred at room temperature for 6 h and filtered. The white solid was recrystallized from water to give colourless crystals 9.5 g (74%). Anal. calcd. for $C_{28}H_{40}N_4O_4 \cdot 2HCl \cdot 4H_2O$; C 52.41, H 7.85, N 8.73; found: C 52.72, H 7.47, N 8.75. IR (KBr, cm^{-1}): 3410 (OH); 2600–2900 (NH_2^+); 1730 (COOH). ^1H NMR (D_2O): (δ (relative intensity)): 0.95(6) (doublet, CH_3), 1.74 (4) (multiplet, C—CH_2—C), 2.66(8) (multiplet, CH_2—N), 3.09(4) (multiplet, C—CH—N), 3.80(4) (singlet, CH_2COOH), 7.42(10) (doublet, phenyl).

$NiL^1 \cdot 2H_2O$ (1) and $CoL^1Cl \cdot 4H_2O$ (2)

B (320 mg, 0.50 mmol) and $NiCl_2 \cdot 6H_2O$ (240 mg, 1.0 mmol) were dissolved in 20 mL water, and the pH was successively adjusted to 5 with NaOH. After refluxing for 2 h, violet crystals formed. These were collected and recrystallized from $EtOH/H_2O$ (1:1). Yield; 195 mg (66%). Anal. calcd. for $C_{28}H_{38}N_4O_4Ni \cdot 2H_2O$: C 57.06, H 7.18, N 9.51; found: C 56.95, H 7.29, N 9.29. IR (KBr, cm^{-1}): 3435 (OH); 3106 (NH); 1628 (COO^-). $CoL^1Cl \cdot 4H_2O$ (**2**) was prepared in a similar manner by using $CoCl_2 \cdot 6H_2O$ and was obtained as red crystals. Yield 53%. Anal. calcd. for $C_{28}H_{38}N_4O_4CoCl \cdot 4H_2O$: C 50.87, H 7.01, N 8.48; found: C 50.96, H 7.24, N 8.27. IR (KBr, cm^{-1}): 3463, 3398 (OH); 3103 (NH); 1648 (COO^-).

$CuL^1 \cdot 3H_2O$ (3)

B (320 mg, 0.50 mmol) and $CuSO_4 \cdot 5H_2O$ (125 mg, 0.50 mmol) were dissolved in 20 mL water and the pH was adjusted to 2, and warmed in an oil bath (80°C) for 2 h and filtered. The deep blue filtrate was placed in a refrigerator overnight. Blue crystals formed, which were filtered off, and air dried. Yield 175 mg (57%). Anal. calcd. for $C_{28}H_{38}N_4O_4Cu \cdot 3H_2O$: C 54.93, H 7.24, N 9.15; found: C 54.97, H 7.25, N 8.96. IR (KBr, cm^{-1}): 3394 (OH); 3132 (NH); 1612 (COO^{-1}).

$Cu_2L^1Cl_2$ (4)

B (320 mg, 0.50 mmol) and $CuCl_2 \cdot 2H_2O$ (205 mg, 1.2 mmol) were dissolved in 20 mL water and the pH was successively adjusted to 5 and filtered. The filtrate was heated in an oil bath (80°C) for 2 h. Deep green crystals formed, which were filtered off, and air dried. Yield 240 mg (69%). Anal. calcd. for $C_{28}H_{38}N_4O_4Cu_2Cl_2$: C 48.57, H 5.53, N 8.09; found: C 48.35, H 5.45, N 7.95. IR (KBr, cm^{-1}): 3160 (NH); 1640 (COO^-).

TABLE 1. Summary of crystal data, intensity collection, and structure refinement for $CuL^1 \cdot 2CH_3CH_2OH$ (3)[a]

Chemical formula	$CuC_{32}H_{50}N_4O_6$
Crystal colour	Blue
Formula weight	650.32
Crystal system	Triclinic
Space group	$P\bar{1}$
a (Å)	8.440(2)
b (Å)	13.445(2)
c (Å)	7.523(1)
α (°)	99.30(1)
β (°)	106.57(1)
γ (°)	87.00(1)
V (Å^3)	807.5(2)
T (°C)	−117(1)
λ (Å)	0.71069
ρ_{calcd} (g cm^{-3})	1.337
Z	1
Absorption coefficient μ (cm^{-1})	7.23
F_{000}	347
Reflections collected	3032
Reflections with $I > 2.00\sigma(I)$	2618
No. refined parameters	197
Goodness of fit	2.21
R	0.027
R_w	0.028

[a] $R = \Sigma||F_o| - |F_c||/\Sigma|F_o|, R_w = [(\Sigma w(|F_o| - |F_c|)^2/\Sigma w|F_o^2|)]^{1/2}$.

X-ray crystallographic analysis of $CuL^1 \cdot 2CH_2CH_2OH$ (3)

Blue crystals of **3** suitable for an X-ray structural determination were obtained by the vapour diffusion of ethyl ether into an ethanolic solution.

The data were collected at a temperature of −117(1)°C, on a Rigaku AFC6S diffractometer (MoKα radiation, graphite monochromator) in the ω–2θ scan mode to $2\theta_{max} = 50°$. Lorentz and polarization corrections were applied. The structure was solved by direct methods (16, 17) using the TEXSAN (18) crystallographic software package. Refined parameters were calculated by using anisotropic thermal parameters for non-hydrogen atoms and isotropic factors for all hydrogen atoms.

A summary of crystal data is given in Table 1. Atomic positional parameters are given in Table 2 and selected bonded distances and angles are given in Table 3. The full description of the structural determination, thermal parameters (Table S-1), hydrogen atom positional parameters (Table S-2), a full listing of bond distances and angles (Table S-3), observed and calculated structure factors ($10|F_o|$ and $10|F_c|$) (Table S-4), and least-squares planes data (Table S-5) are deposited as supplementary material.[2]

Result and discussion

The alkylation of *C-meso*-5,5,7,12,12,14-hexamethyl-1,4,8,11-tetraazacyclotetradecane (tet-a; Fig. 1) (9) and *C*-

[2]These tables may be purchased from: the Depository of Unpublished Data, Document Delivery, CISTI, National Research Council Canada, Ottawa, Canada K1A OS2.

Table S-3 (bond distances and bond angles for $CuL^1 \cdot 2CH_3CH_2OH$) has also been deposited with the Cambridge Crystallographic Data Centre and is available upon request from the Director, Cambridge Crystallographic Data Centre, University Chemical Laboratory, 12 Union Road, Cambridge, CB2 1EZ, U.K.

Can. J. Chem. Downloaded from www.nrcresearchpress.com by 203.198.23.82 on 09/08/12
For personal use only.

TABLE 2. Positional parameters and B(eq) values (esd's) for $CuL^1 \cdot 2CH_3CH_2OH$ (**3**)

atom	x	y	z	B(eq)
Cu(1)	1/2	1/2	1/2	0.96(1)
O(1)	0.4765(2)	0.5833(1)	0.7756(2)	1.43(5)
O(2)	0.6226(2)	0.6110(1)	1.0782(2)	1.84(5)
O(3)	0.7903(2)	0.3079(1)	0.1666(2)	2.16(6)
N(1)	0.3849(2)	0.3748(1)	0.5281(2)	1.07(5)
N(2)	0.7297(2)	0.4606(1)	0.6758(2)	1.01(5)
C(1)	0.4769(2)	0.2778(1)	0.5035(3)	1.22(7)
C(2)	0.6426(2)	0.2811(1)	0.6544(3)	1.33(7)
C(3)	0.7736(2)	0.3504(1)	0.6376(3)	1.25(7)
C(4)	0.8450(2)	0.5216(1)	0.6214(3)	1.32(7)
C(5)	0.7813(2)	0.6283(1)	0.6088(3)	1.28(7)
C(6)	0.7336(2)	0.4935(1)	0.8765(2)	1.33(7)
C(7)	0.6004(2)	0.5696(1)	0.9130(3)	1.24(7)
C(8)	0.3811(2)	0.1847(1)	0.5020(3)	1.38(7)
C(9)	0.3177(3)	0.1744(1)	0.6494(3)	1.94(8)
C(10)	0.2378(3)	0.0865(2)	0.6483(3)	2.45(9)
C(11)	0.2219(3)	0.0076(2)	0.5016(3)	2.39(8)
C(12)	0.2849(3)	0.0167(1)	0.3553(3)	2.20(8)
C(13)	0.3631(2)	0.1049(1)	0.3546(3)	1.77(7)
C(14)	0.9436(2)	0.3230(1)	0.7612(3)	1.73(7)
C(15)	0.7556(3)	0.2032(2)	0.1417(3)	2.22(8)
C(16)	0.9106(3)	0.1441(2)	0.1391(3)	3.1(1)

TABLE 3. Selected bond distances (Å) and angles (deg) for $CuL^1 \cdot 2CH_3CH_2OH$ (**3**)

Bond	Distance	Bonds	Angle
Cu(1)—O(1)	2.248(1)	O(1)—Cu(1)—O(1)′	180.00
Cu(1)—N(1)	2.056(2)	O(1)—Cu(1)—N(1)	92.25(5)
Cu(1)—N(2)	2.109(2)	O(1)—Cu(1)—N(1)′	87.75(5)
		O(1)—Cu(1)—N(2)	80.88(5)
		O(1)—Cu(1)—N(2)′	99.12(5)
		N(1)—Cu(1)—N(1)′	180.00
		N(1)—Cu(1)—N(2)	93.03(6)
		N(1)—Cu(1)—N(2)′	86.97(6)
		N(2)—Cu(1)—N(2)′	180.00

meso-2,4,4,11,13,13-hexamethyl-1,5,10,14- tetraazacyclooctadecane (12) and *C-meso*-2,2,4,13,13,15-hexamethyl-1,5,12,16-tetraazacyclodocosane (13) (analogues of tet-a) with a large excess of bromoacetic acid in alkaline methanol medium gave only the di-*N*-substituted product. It may be concluded that the reaction of a hexamethyltetraazamacrocycle (tet-a or its analogues) with an alkylating agent is stereospecific. In L the alkylation may take place in the 1- and 8-positions as the nitrogen atoms in these two positions are less sterically hindered than those in tet-a, since the phenyl group is less bulky than two methyl groups. By controlling the ratio of L and bromoacetic acid the di-*N*-substituted (H_2L^1) product can be prepared. We have found that the mono-*N*-substituted, tri-*N*-substituted, and per-*N*-substituted products also can be isolated by alkylation of L or H_2L^1 with bromoacetic acid by controlling the ratio of L (for mono- and per-*N*-substituted products) or H_2L^1 (for tri- and per-*N*-substituted products) and bromoacetic acid. The work on these three substituted ligands is in progress.[3]

[3]L. Chen, J. Xu, and S. Ni, unpublished results.

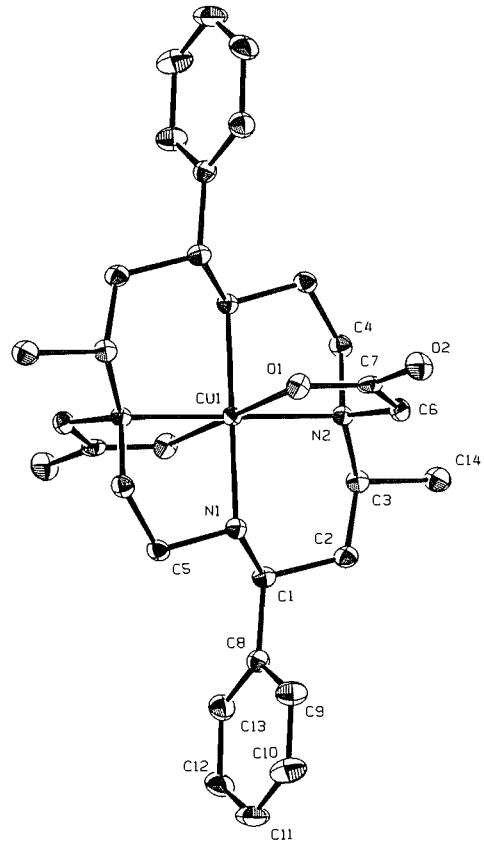

FIG. 2. Structural representation of CuL^1 (**3**) with hydrogen atoms omitted (40% probability thermal ellipsoids).

The difunctionalized ligand H_2L^1, in principal, occurs in several configurations arising from the presence of chirally substituted nitrogen centers. The existence of all these stereoisomers is possible. It has six potentially coordinating atoms. The metal complexes were studied in part in solution, but mainly by preparing some crystalline compounds.

Description of the structure of $CuL^1 \cdot 2CH_3CH_2OH$

The structure of CuL^1 (**3**) is illustrated in Fig. 2. The complex shows a distorted *trans*-octahedral geometry with four amino nitrogens in a plane and two apical carboxylate oxygen donors. The molecule has a centre of symmetry at Cu1 with the result that the phenyl, methyl, and carboxylate groups are each *trans*. The four nitrogens and the metal ion are exactly in a plane. The conformation of each six-membered chelate ring is that of a *chair* while the five-membered chelate rings are a twisted "envelope" with C5 and C4 as the flap. The five-membered chelate rings involving the carboxylates are close to planar. The benzene ring and five-membered carboxylate chelate ring have dihedral angles of 81.63 and 89.03°, respectively in relation to the N_4 mean plane. Cu—N (secondary) (2.109(2) Å) distances are longer than Cu—N (tertiary) (2.056(2) Å). This is probably due to the electron-attracting inductive effect of the appended carboxylate groups. The strongest distortion is due to the Jahn–Teller effect and leads to axial Cu—O bond lengths of 2.248(1) Å, which are much longer than those in related complexes of some tetraazamacrocyclic tetraacetates where carboxylate oxygens coordinate to copper in equatorial positions (Cu—O = 1.965(5)) (19); Cu—O = 1.957(7), 1.982(5) (20), but are slightly shorter than those

TABLE 4. Spectral and magnetic data

Compound	μ_{eff} (BM) (RT)	UV/VIS (nm)[a]	ESR[b]
$NiL^1 \cdot 2H_2O$ (**1**)	3.20	306, (345), 525, 850, 990	
$CoL^1Cl \cdot 4H_2O$ (**2**)	DIAM	307, 365, 512	
$CuL^1 \cdot 3H_2O$ (**3**)	1.87	318, 620	$g_1 = 2.04$ $g_2 = 2.09$ $g_3 = 2.19$
$Cu_2L^1Cl_2$ (**4**)	1.72	320, 605	$g_{av} = 2.10$

[a]Mull transmittance (shoulder).
[b]Solid (RT).

in the similar complex $[CuL^3]^{2-}$ (L^3 = 1,4,8,11-tetraazacyclotetradecane-*N*,*N'*,*N''*,*N'''*-tetraacetic acid), in which the copper ion also has a distorted *trans*-octahedral geometry with two Cu—O distances of 2.302(5) and 2.278(6) Å, respectively (21). It is also interesting to compare the structure of CuL^1 with the structure of NiL^2 (H_2L^2 = 5,5,7,12,12,14-hexamethyl-1,4,8,11-tetraazacyclotetradecane-*N*,*N''*-diacetic acid; Fig. 1) for which a *cis*-octahedral structure was found (9). This phenomenon is probably due to the fact that the two macrocycles prefer different basic conformations when they coordinate to metal ions (22). In CuL^1, the macrocycle is in the *trans*-III conformation according to the nomenclature of Bosnish *et al.* (23). In NiL^2, the coordination is achieved by folding the macrocycle, which allows both of the carboxylic oxygen atoms to coordinate in a *cis*-arrangement. Here the macrocycle is in the *cis*-V conformation (9, 23). Because two tertiary nitrogen donors are present in these two ligands, their relative stereochemistries are fixed so long as they remain coordinated to the metal, since the conjugate base pathway for inversion is no longer available. The two ethanol molecules in **3** are hydrogen-bonded to the two coordinated carboxyl oxygens (O(1)—O(3) = 2.722(2) Å). There are no other intermolecular contacts.

Spectroscopy and magnetism

H_2L^1 forms complexes with Co(III), Ni(II), Cu(II) with a metal-to-ligand ratio of 1:1 and also a 2:1 Cu(II) complex (**4**), which is insoluble in most solvents. The infrared spectra of **1**, **2**, and **3** are very similar in the range 4000–500 cm^{-1}, indicating the likelihood of a similar structural arrangement. Solid state, mull transmittance electronic spectra (Table 4) for all the complexes show a strong band at 306–320 nm which is associated with intraligand charge transfer. **1** exhibits *d–d* bands at 345, 525, 850, and 990 nm, which can be associated with a tetragonal arrangement involving a *trans*-N_4O_2 chromophore. The *d–d* bands for **2** at 365 and 512 nm can be associated with a similar geometrical arrangement around a cobalt(III) centre. Actually a preliminary structural study of **1** confirmed that it also has a *trans*-octahedral structure similar to **3**.[3] **3** exhibits a *d–d* band at 620 nm while **4** has a broad band at 605 nm.

Room temperature magnetic measurements (Table 4) show that **1** has a magnetic moment of 3.20 BM, indicating that the Ni(II) ion is in a high spin state. **2** is diamagnetic indicating the presence of a low spin Co(III) state. The formation of a cobalt(III) complex from a cobalt(II) salt is not considered unusual with ligands of this sort, especially since the reaction mixture was exposed to air. **3** has a magnetic moment of 1.87 BM suggesting the presence of a dilute Cu(II) centre. The magnetic moment for **4** is 1.72 BM per copper centre and is close to the spin-only value for copper(II), but much lower than that in **3**. The question as to whether any spin coupling occurs in this complex can only be answered with a variable temperature magnetic study, which has not, as yet, been carried out. The dinuclear nature of the complex is, however, evident both from the analytical data and the magnitude of the magnetic moment. Structurally, free carboxylate groups could provide a bridging medium for linking the copper centres in a polynuclear arrangement.

Powder esr spectra (Table 4) of **3** exhibit three peaks both at room temperature and 77 K indicating a rhombic distorted octahedral coordination sphere. In ethanolic solution, at room temperature, the esr spectrum is indicative of an axial species ($g_\perp = 2.05$, $g_\parallel = 2.12$) but in frozen solution it gives an uninformative spectrum with $g_{av} = 2.10$. Compound **4** exhibits a very broad, single resonance in the solid state at room temperature centred at $g = 2.10$ and an axial spectrum at 77 K with $g_\perp = 2.10$, $g_\parallel = 2.20$. Electron spin-resonance data for **4** appear normal for a copper(II) species suggesting that spin exchange in this system is very weak.

Acknowledgment

We thank the Natural Sciences and Engineering Research Council of Canada for funds to purchase the Rigaku AFC6S X-ray diffractometer.

1. G. Melson (*Editor*). Coordination chemistry of macrocyclic compounds. Plenum, New York. 1979.
2. P.V. Bernhardt and G.A. Lawrance. Coord. Chem. Rev. **104**, 297 (1990).
3. C.A. Chang and M.E. Rowland. Inorg. Chem. **22**, 3866 (1983).
4. C.A. Chang and V.O. Ochaya. Inorg. Chem. **25**, 355 (1986).
5. C.A. Chang, P.H.-L. Chang, V.K. Manchanda, and S.P. Kasprzyk. Inorg. Chem. **27**, 3786 (1988).
6. R.B. Lauffer. Chem. Rev. **87**, 901 (1987).
7. R.D. Hancock, M.S. Shaikjee, S.M. Dobson, and J.C.A. Boeyens. Inorg. Chim. Acta, **154**, 229 (1988).
8. R.D. Hancock, R. Bhavan, P.W. Wade, J.C.A. Boeyens, and S.M. Dobson. Inorg. Chem. **28**, 187 (1989).
9. J. Xu, S. Ni, and Y. Lin. Inorg. Chim. Acta, **111**, 61 (1986).
10. J. Xu, S. Ni, and Y. Lin. Inorg. Chem. **27**, 4651 (1988).
11. J. Xu, S. Ni, K. Cui, Z. Xu, and Y. Lin. Inorg. Chim. Acta, **171**, 239 (1990).
12. L. Chen, S. Ni, and J. Xu. Yingyong Huaxue, **8**, 7 (1991).
13. L. Chen, J. Xu, and S. Ni. Gaodeng Xuexiao Huaxue Xuebao, **12**, 444 (1991).
14. L. Chen, S. Ni, and J. Xu. Wuji Huaxue Xuebao, **7**, 138 (1991).
15. R.W. Hay and P.M. Gidney. J. Chem. Soc. Dalton Trans. 974 (1976).

Can. J. Chem. Downloaded from www.nrcresearchpress.com by 203.198.23.82 on 09/08/12
For personal use only.

16. C.J. Gilmore. J. Appl. Crystallogr. **17**, 42 (1984).
17. P.T. Beurskens. Dirdif: Technical report 1984/1, Crystallography Laboratory, Toernooiveld, 6525 Ed Nijmegen, Netherlands.
18. Texsan-Texray structure analysis package, Molecular Structure Corporation, 1985.
19. A. Riesen, M. Zehnder, and T.A. Kaden. Helv. Chim. Acta, **69**, 2067 (1986).
20. A. Riesen, M. Zehnder, and T.A. Kaden. Helv. Chim. Acta, **69**, 2074 (1986).
21. A. Riesen, M. Zehnder, and T.A. Kaden. Acta. Crystallogr. **C44**, 1740 (1988).
22. R.D. Hancock. Prog. Inorg. Chem. **37**, 187 (1989).
23. B. Bosnich, C.K. Poon, and M.L. Tobe. Inorg. Chem. **4**, 1102 (1965).

Can. J. Chem. Downloaded from www.nrcresearchpress.com by 203.198.23.82 on 09/08/12
For personal use only.

Molecular motion of guests trapped in N-methyl-1,3-diaminopropanecadmium(II) tetracyanonickelate(II) host lattices[1]

SHINICHI NISHIKIORI,[2] CHRISTOPHER I. RATCLIFFE,[3] AND JOHN A. RIPMEESTER
Steacie Institute for Molecular Sciences, National Research Council of Canada, Ottawa, ON K1A 0R6, Canada

Received April 20, 1993

SHINICHI NISHIKIORI, CHRISTOPHER I. RATCLIFFE, and JOHN A. RIPMEESTER. Can. J. Chem. **71**, 1810 (1993).

The molecular motion of guest molecules in Cd(*mtn*)Ni(CN)$_4$ · 0.5G clathrates (*mtn* = *N*-methyl-1,3-diaminopropane, G = toluene, nitrobenzene, dichloromethane, and chloroform) were studied by using CP/MAS ^{13}C and ^{2}H NMR techniques. At room temperature, application of ^{13}C CP/MAS NMR with dipolar dephasing showed the presence of large amplitude molecular motion in all cases. Temperature dependent ^{2}H NMR spectra for the toluene-d_8 clathrate shows that the methyl group rotated at all temperatures down to 77 K. Also, a 2-site in-plane reorientation process of the entire molecule is activated above 180 K, which goes over into axially symmetric in-plane rotation around 450 K. Severely restricted motions were also observed for the nitrobenzene and haloalkane guests. The rather complicated dynamic behaviour of the guest molecules at low and room temperatures can be attributed to the presence of static disorders which disappear at higher temperatures due to time averaging.

SHINICHI NISHIKIORI, CHRISTOPHER I. RATCLIFFE et JOHN A. RIPMEESTER. Can J. Chem. **71**, 1810 (1993).

Utilisant des techniques de rmn du ^{1}H et du ^{13}C en CP/MAS, on a étudié la mouvement moléculaire des molécules hôtes dans des clathrates de Cd(*mtn*)Ni(CN)$_4$ · 0,5G (*mtn* = *N*-méthyl-1,3-diaminopropane, G = toluène, nitrobenzène, dichlorométhane ou chloroforme). À la température ambiante, l'utilisation de la rmn par CP/MAS avec déphasage dipolaire démontre, dans tous les cas, la présence d'un mouvement moléculaire d'une grande amplitude. Le spectre rmn du ^{2}H en fonction de la température du clathrate du toluène-d_3 montre que le groupe méthyle subit une rotation à toutes les températures, jusqu'à 77 K. De plus, un processus de réorientation dans le plan, de la molécule dans son ensemble, impliquant deux sites est activé au-dessus de 180 K et il se transforme en rotation dans le plan, axialement symétrique, autour de 450 K. On a aussi observé des mouvements extrêmement restreints avec le nitrobenzène et les haloalcanes agissant comme hôtes. On peut attribuer le comportement dynamique relativement complexe des molécules hôtes à basse température et à température ambiante à la présence de désordres statiques qui disparaissent à des températures plus élevées à cause d'une moyenne provoquées par le temps.

[Traduit par la rédaction]

Introduction

In several recent reviews (1, 2) it was indicated that solid-state NMR techniques are playing an increasingly important role in the definition of structure and order in guest–host materials. The use of ^{13}C CP/MAS NMR, together with temperature-dependent ^{2}H NMR lineshape studies, is an especially powerful combination in tackling problems of this nature, and we apply these to several new systems generally related to the Hofmann clathrates.

In the continuing structural studies of Hofmann type clathrates, a series of clathrates Cd(*mtn*)Ni(CN)$_4$ · 0.5G (*mtn* = *N*-methyl-1,3-diaminopropane, G = guest molecule) was synthesized with a number of features significantly different from the Hofmann and related clathrates (3). The new clathrate host Cd(*mtn*)Ni(CN)$_4$ has a structure which is independent of the various possible organic guests, and which has been defined by X-ray diffraction for the cyclohexane clathrate (3). The molecules which can act as guest are defined by the size and shape of the cavity, a 7 Å × 7 Å × 5 Å rectangular box with a four-fold axis perpendicular to its square faces, which is relatively rigid due to a three-dimensional framework of bridging cyano groups (3). One expects that the dynamic state of the guest molecule will be determined primarily by the guest–cage interactions.

Host–guest systems may be viewed as simple models for molecular recognition and are important for throwing light on how the guest and its dynamics influence, and are influenced by the shape and symmetry of the host cavity it occupies. We have studied molecular motions in several *mtn* clathrates containing guest molecules of various shapes by NMR techniques. A study of the unusual behaviour of the cyclohexane – *mtn* clathrate was presented separately (4). Evidence was found for reorientation about the molecular three-fold axis, as well as inversion of the cyclohexane molecule, and the motional rates were obtained by simulation of the ^{2}H NMR lineshapes for intermediate motional rates. In this work we present results and appropriate motional models for guest molecules of lower symmetry than cyclohexane such as toluene, nitrobenzene, dichloromethane, and chloroform, which show the importance of the interaction of the symmetry of both the guest and the host cavity in determining the dynamics and the effects of disorder present in the host.

Experimental

The clathrates were prepared by the method reported in a previous paper (3) and analysed by X-ray powder diffraction. Deuteriated materials used in the preparations $C_6D_5CD_3$ and $C_6H_5CD_3$ (99.6 atom% D), $C_6D_5NO_2$ (99.6 atom% D), CD_2Cl_2 (99.8 atom% D), and $CDCl_3$ (99.8 atom% D) were purchased from MSD Isotopes.

^{13}C CP/MAS NMR spectra, some recorded with interrupted decoupling (5) of 40 μs, were obtained using a Bruker MSL 300 spectrometer and a Doty Scientific Inc. 5 mm MAS probe. Spinning rates were typically about 5 kHz. The ^{2}H NMR lineshapes were measured using a Bruker CXP 180 spectrometer at 27.63 MHz by means of a variable temperature N_2 gas-flow probe with a Bruker

[1]NRCC No. 37203.

[2]Permanent address: Department of Chemistry, College of Arts and Sciences, the University of Tokyo, Komaba, Meguro, Tokyo 153, Japan.

[3]Author to whom correspondence should be addressed.

Can. J. Chem. Downloaded from www.nrcresearchpress.com by 203.198.23.82 on 09/08/12
For personal use only.

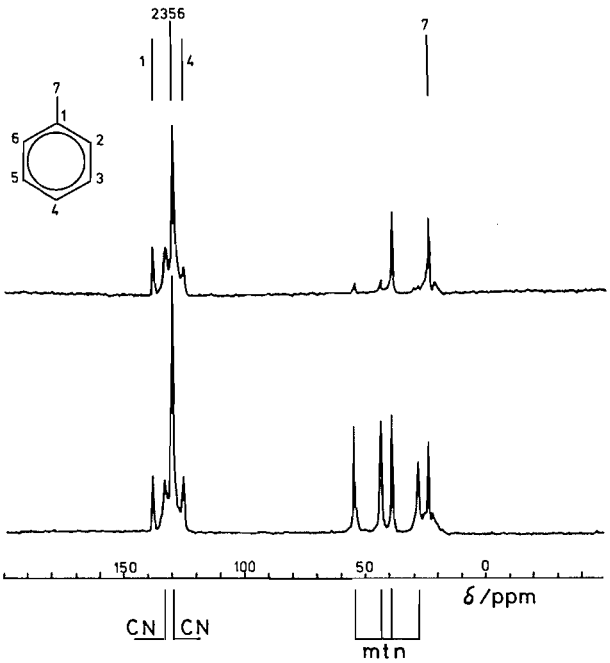

FIG. 1. ^{13}C CP/MAS NMR spectra of Cd(*mtn*)Ni(CN)$_4 \cdot 0.5C_6H_5CH_3$, with (top) and without (bottom) dipolar dephasing.

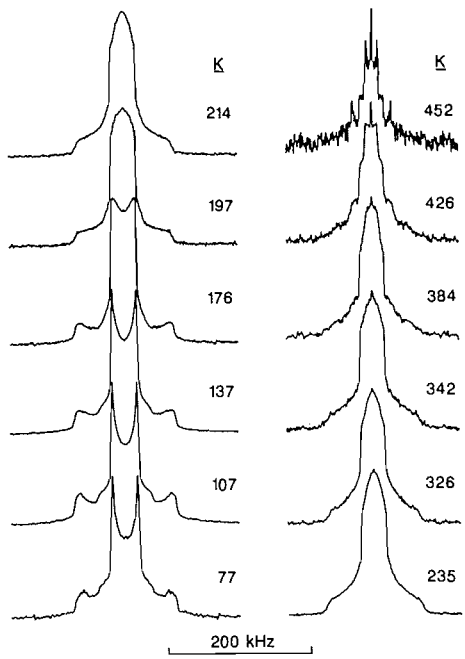

FIG. 2. ^2H NMR lineshapes of Cd(*mtn*)Ni(CN)$_4 \cdot 0.5C_6D_5CD_3$ as a function of temperature.

B-VT-1000 temperature controller. A phase alternated quadrupole echo pulse sequence (6) was used with a delay time of 35 μs between *X* and *Y* pulses of 2.6–3.0 μs. Dynamically averaged ^2H NMR lineshapes in the fast motion limit were calculated by using well-established methods (7, 8) as described previously (4).

Results and discussion

Toluene clathrate

The ^{13}C CP/MAS NMR spectra obtained for the host lattice of the toluene clathrate (Fig. 1) show lines at 128.9 and

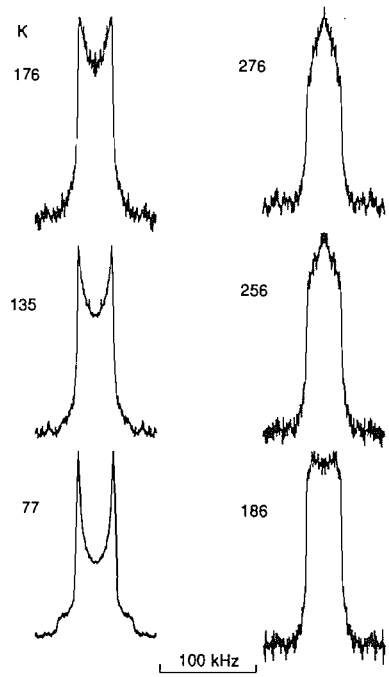

FIG. 3. ^2H NMR lineshapes of Cd(*mtn*)Ni(CN)$_4 \cdot 0.5C_6H_5CD_3$ as a function of temperature.

132.5 ppm for the ^{14}N quadrupole perturbed cyanide carbon, and at 28.5, 38.4, 43.5, and 54.7 ppm for the *N*-methyl-1,3-diaminopropane. The methyl and quaternary carbons show little loss of intensity in the dipolar dephased spectra, as expected. These features are the same as those for results previously obtained for the cyclohexane clathrate (4), and also for the other clathrates studied here.

On examining the toluene carbon lines with and without dipolar dephasing, it is clear that the lines due to the proton-bearing carbons (C2,3,4,5,6) have lost about half their intensity in the dephased spectrum, and that the methyl group intensity does not change at all. This is a clear indication that the whole toluene molecule is involved in some kind of large amplitude molecular motion.

To investigate this further, ^2H NMR lineshapes were examined for a sample prepared with perdeuteriated toluene as a function of temperature (Fig. 2) and for a sample deuteriated only on the methyl group (Fig. 3). At 77 K, the $C_6D_5CD_3$ lineshape consists of two overlapping powder doublets, the narrower component being an axially symmetric pattern ($\eta = 0$) with a quadrupole coupling constant, $\chi = 51$ kHz, the broader component having only general symmetry with $\chi = 180$ kHz and $\eta = 0.052$. Only the narrow component is present for the $C_6H_5CD_3$ clathrate. These values agree with reported values for neat toluene at 77 K, 52 kHz, $\eta = 0$, and 179.9 kHz, $\eta = 0.056$ (9), which correspond to the rotating methyl group C—D's and aromatic C—D's respectively. The motional state of the enclathrated and neat toluenes at 77 K therefore is identical.

Above 137 K, the lineshapes begin to change, and reach a limit at about 214 K. Again, it appears that there are two components to the lineshape of the $C_6D_5CD_3$ clathrate, so that the division of the C—D bonds into aromatic and methyl subgroups still seems to hold. The lack of apparent doublet splitting must be attributed to large asymmetry parameters, indicating the presence of non-axially symmetric motions.

Can. J. Chem. Downloaded from www.nrcresearchpress.com by 203.198.23.82 on 09/08/12
For personal use only.

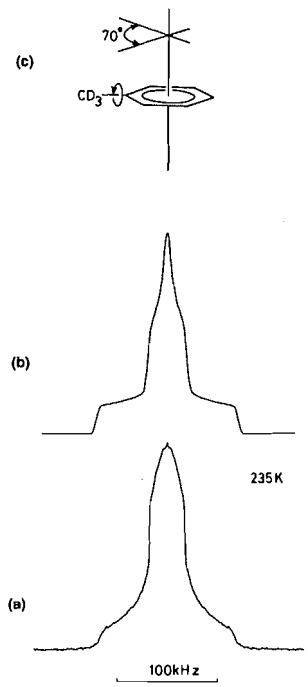

FIG. 4. (*a*) ^2H NMR lineshape of Cd(*mtn*)Ni(CN)$_4 \cdot 0.5C_6D_5CD_3$ at 235 K, (*b*) simulated lineshape for an in-plane motion of toluene-d_8 between two sites separated by 70° as shown in (*c*).

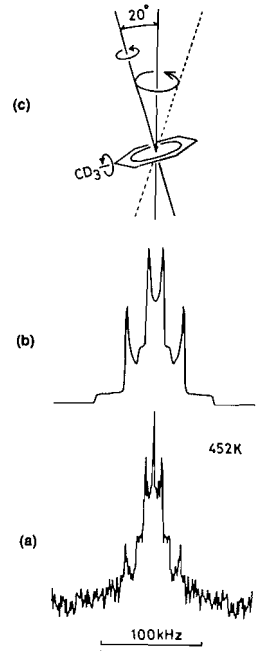

FIG. 5. (*a*) ^2H NMR lineshape of Cd(*mtn*)Ni(CN)$_4 \cdot 0.5C_6D_5CD_3$ at 425 K, (*b*) simulated lineshape for a toluene-d_8 molecule rotating as shown in (*c*).

If the motion is to preserve the equivalence of all the aromatic C—D's it must be an in-plane motion. Considering that the clathrate cage is a slightly flattened square box with the toluene molecule flat in the box, the following motions may be considered. From inspection of the structural information, the toluene molecule is restricted from performing a complete in-plane rotation by the *mtn* molecules which make up the sides of the box. The in-plane motion could be a large angle libration, with a broad potential well centered roughly on a diagonal of the square of the box, or a jumping between two sites with the potential wells displaced on either side of the diagonal. The simulation in Fig. 4 is for a two-site model, with the two sites 70° apart. The agreement with experiment is reasonable, but far from exact, and only a slight improvement could be achieved by allowing for a conical rotation of the out-of-plane axis (e.g. cone angle 12° with in-plane motion between the two sites 66° apart). Evidently, a more complex model is required. In fact, the appearance of the lineshapes of both $C_6D_5CD_3$ and $C_6H_5CD_3$ samples is more suggestive of a distribution of degrees of motional averaging. In this regard, there are a number of implications for the disorder of the toluene and the *mtn* groups which must be taken into account when the structure of the clathrate is considered. Since the toluene appears to have room to move only within one quarter of the square of the cavity, there must be orientational disorder of the long toluene axis throughout the crystal. This will give rise to a distribution of toluene sites when neighbouring toluene orientations are considered, and hence there will be a distribution of motional amplitudes and averaged lineshapes. Furthermore, there is also a disorder in the positions of the NH_2 and $NHCH_3$ groups of the *mtn* molecules of the host which must also contribute to the distribution of the reorientational potentials. These two groups could not be distinguished in the X-ray structural determination (10). There are also some obvious spin–lattice relaxation (T_1) effects on the appearance of the spectra, viz. in the 77 K spectrum of the $C_6D_5CD_3$ sample the broad C_6D_5 component is much weaker than the CD_3 line due to the latter group being in a state of relatively rapid motion and thus having a considerably shorter relaxation time. Spin–lattice relaxation time (T_1) measurements as a function of temperature (either ^1H or ^2H NMR) might be informative with respect to an average activation energy for the motion and the distribution of correlation times for the motions arising from the disorder. The latter may cause a skewed B.P.P. plot (11).

Between 348 and 452 K the lineshape becomes temperature dependent again, indicating the onset of a new motion. The motion reaches its fast limit above 452 K, and now the lineshape consists of two axially symmetric patterns with $\chi = 22$ and 75 kHz. The simplest explanation is that the toluene molecule has now become an axial rotor by overcoming the barriers to in-plane rotation. One might also speculate that the new motion might be closely associated with the onset of dynamic disorder of the *mtn* molecules. This would make the cavity much more symmetric on time average. The doublets are narrower than calculated for a simple in-plane rotation, however (see Table 1). Formally, agreement with experiment can be obtained by allowing the rotation axis to fluctuate over the surface of a cone, where the additional reduction in doublet splitting is equal to $0.5\ (3\cos^2\theta - 1)$, with θ the angle between the cone surface and the symmetry axis (Fig. 5). A close match between experiment and calculation is obtained with $\theta = 17°$ when the calculation is based on the 77 K spectral parameters (see Table 1).

Nitrobenzene clathrate

Figure 6 shows ^{13}C CP/MAS NMR spectra of nitrobenzene enclathrated in the Cd(*mtn*)Ni(CN)$_4$ host lattice obtained at room temperature. The C2,3,4,5,6 lines of the nitrobenzene overlap the cyano carbon peaks, however, it is possible to see that there is significant intensity even in the dipolar dephasing experiment, thus again suggesting the

Can. J. Chem. Downloaded from www.nrcresearchpress.com by 203.198.23.82 on 09/08/12
For personal use only.

TABLE 1. *mtn*-toluene ^2H lineshape parameters[a]

	Conditions	χ/kHz	η
Obsd	77 K	51	0
		180	0.052
		22	0
	452 K	75	0
Calcd	In-plane	25.5	0
	n-site, $n > 3$	85.32	0
	In-plane plus conical average[b]	22.21	0
		74.32	0

[a]In each case the top entry refers to the CD_3 group and the bottom entry to the C_6D_5 group.
[b]Conical averaging of out-of-plane axis, tilt angle = 17.05°.

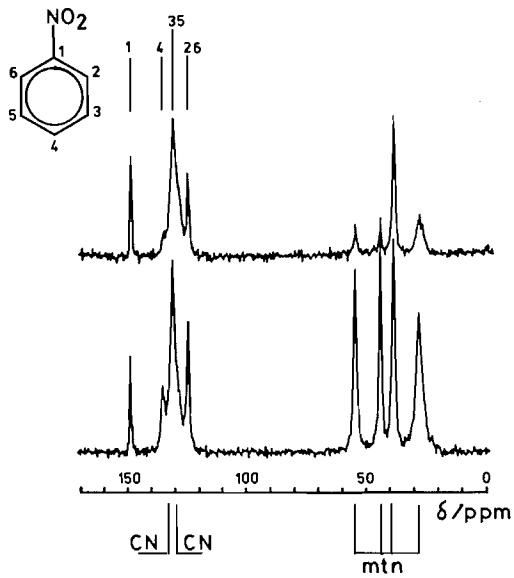

FIG. 6. ^{13}C CP/MAS NMR spectrum of Cd(*mtn*)$Ni(CN)_4 \cdot 0.5C_6H_5NO_2$ with (top) and without (bottom) dipolar dephasing.

presence of significant motional amplitudes of the nitrobenzene molecule. Examination of the ^2H NMR lineshapes (Fig. 7, Table 2) gives an indication that a slow motion sets in above 230 K. However, it does not appear to have reached the fast motion limit at the highest temperature of study, 420 K. This again is probably associated with disordering of both the guest orientations and the *mtn*'s $NH_2/NHCH_3$ groups. In fact, the nitrobenzene clathrate is problematical in that structural considerations (based on the framework of the cyclohexane clathrate) suggest that it cannot fit into the cavity without significant van der Waals' overlap with the host. Its structural similarity to the cyclohexane clathrate is based on a powder X-ray diffraction determination (10) of its unit cell parameters (a = 14.22 Å, c = 7.83 Å). Perhaps one should allow for a distortion of the structure, especially of the *mtn* groups which are important in forming the sides of the cavity, to allow for a better fit of the nitrobenzene. At 420 K the pattern is not very well defined but seems to indicate a large η, with one of the electric field gradient tensor components unchanged from the rigid lattice condition. This could be accounted for by two-fold flips of the nitrobenzene about the C—N axis, if the lineshape is attributed

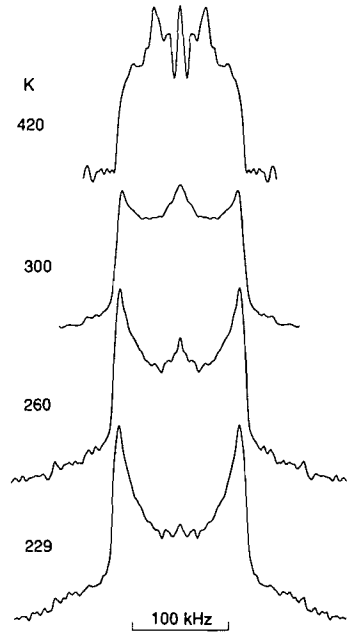

FIG. 7. ^2H NMR lineshape of Cd(*mtn*)$Ni(CN)_4 \cdot 0.5C_6D_5NO_2$ at several temperatures.

TABLE 2. ^2H NMR parameters for nitrobenzene, chloroform, and dichloromethane in *mtn* clathrates

Guest	T/K	χ/kHz	η
$C_6D_5NO_2$	77	182	0.048
	229	175.3	0.057
	420	123.4[a]	0.42[a]
$CDCl_3$	190	150.7	0
	299	144	0
	(77	167.8	0)[b]
CD_2Cl_2	254	67[a]	0
	299	61[a]	0
	346	56[a]	0
	(77	167.3	0)[b]

[a]Estimated average values for distribution.
[b]Values obtained for the pure guest materials at 77 K.

only to the C—D bonds off the flipping axis. The ^2H nucleus on the flipping axis may have a much longer relaxation time than the off-axis ones, thus making it much more difficult to observe. Alternatively, it could arise from a distribution of in-plane motions (for example, two sites 52° apart) similar to the toluene low temperature motion.

The amount of information obtainable is much more limited than for the toluene clathrate, however, the general picture is that nitrobenzene is much more restricted than toluene in the Cd(*mtn*)$Ni(CN)_4$ clathrate.

Chloroform clathrate

In the ^{13}C CP/MAS NMR spectrum, the chloroform line at 79.5 ppm retains about 28% of its intensity on applying the dipolar dephasing experiment, again indicating that appreciable molecular motion is likely. Figure 8*a* shows the ^2H NMR lineshape at room temperature. The lineshapes represent axially symmetric tensors, but their width, which

Can. J. Chem. Downloaded from www.nrcresearchpress.com by 203.198.23.82 on 09/08/12
For personal use only.

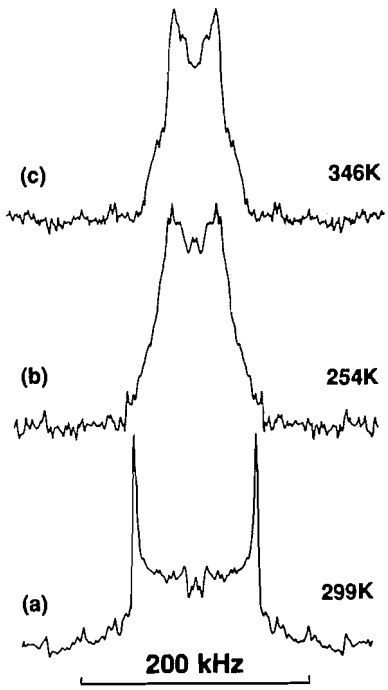

FIG. 8. ^{2}H NMR lineshapes of Cd(*mtn*)Ni(CN)$_4 \cdot 0.5CDCl_3$ at 299 K (*a*), and that of Cd(*mtn*)Ni(CN)$_4 \cdot 0.5CD_2Cl_2$ at 254 K (*b*) and at 346 K (*c*).

gradually decreases with increasing temperature, is significantly less than that of the static molecule determined from pure solid $CDCl_3$ at 77 K (see values of χ in Table 2). The natural orientation for the chloroform molecule is with its three-fold axis along the four-fold axis of the cavity, since this puts the least restriction on the three Cl atoms and allows the molecule to fit into the cavity. The molecule probably reorientates in the 12-fold potential around this axis: the fact that we see no effect of the quadrupolar Cl atoms on the ^{13}C spectrum suggests that the Cl's are self-decoupled because of motion. Such a motion alone would produce no narrowing of the ^{2}H spectrum since the C—D bond would be along the rotation axis. The observed small ^{2}H linewidth reduction could then arise through reorientation of the molecular three-fold axis over a cone about the four-fold axis of the cavity (e.g. cone angle of 17.9° at 299 K).

Dichloromethane clathrate

Again, some intensity is maintained in the dipolar dephased ^{13}C CP/MAS NMR spectrum of the guest, indicating that some molecular motion occurs. The ^{2}H NMR lines are considerably narrower than for the chloroform clathrate (Fig. 8*b*, *c*), and at room temperature the motion still appears to occur at an intermediate rate. As with the low temperature motion of the toluene clathrate, the lineshapes are not characteristic of a single tensor, and a distribution of motional amplitudes arising from the various orientational disorders present seems likely. However, at 346 K the lineshape is approaching that expected for an axially symmetric tensor (Table 2).

Note that tensors averaged to axial symmetry arise when n-fold ($n \geq 3$) reorientation occurs, and the reduction in linewidth is given by $(3 \cos^2 \theta - 1)/2$ where θ is the angle between the C—D bond and the rotation axis. With $\angle$ HCH = 112° this reduction factor is 0.031 for reorientation about the molecular two-fold axis (rotation 1), 0.5 for reorientation about the axis parallel to the Cl—Cl direction (rotation 2), and 0.531 for reorientation about the third orthogonal axis (rotation 3). For the static molecule χ = 167.3 kHz, measured in pure solid CD_2Cl_2 at 77 K. From this the reduced χ values for motions about the three axes are 5.2, 83.7, and 88.8 kHz, respectively. Clearly the first is much smaller than the observed values and this rules out n-fold reorientation about the molecular two-fold axis. Careful consideration of the structure and the ^{2}H NMR results then leads to the following self-consistent picture with regard to the location and orientation of the dichloromethane in the cavity. If the centre of mass of the CD_2Cl_2 is located at the centre of the cavity, then the H atoms can be rotated over a sphere and not come into contact with any of the host atoms. However, the Cl atoms will have severe van der Waals' overlap when they approach the top and bottom square faces of the cavity. This suggests that the preferred location for the Cl atoms is in the square plane in the middle of the cavity, and therefore the two H's are located on either side of this plane. There is then no overlap if the guest is rotated about the four-fold axis of the cavity (rotation 3). The H's could still rotate about the axis parallel to the Cl—Cl vector, but the rotation symmetry in the cavity is now reduced to two-fold, and 180° rotation has no averaging effect on the ^{2}H tensors. The observed χ are reduced by more than the factor of 0.531 expected for rotation 3. This can be accommodated by smaller amplitude motions about the other two axes.

Conclusion

For all of the Cd(*mtn*)Ni(CN)$_4$ clathrates considered, there is some degree of motional freedom, however, enclathration seems to impose rather severe limits on the motions so that these are spatially quite restricted. This is in agreement with the earlier statement that the cage should be seen as quite a rigid, anisotropic box. In the case of toluene and dichloromethane, the motions found should show marked effects of disorder in attempts to solve the structures by diffraction methods. One pattern which has emerged from the study is that the guest dynamics are very much influenced by the disorders present: the *mtn* groups which distort the potential away from true four-fold symmetry, and the guest orientations in neighbouring cages which may have substantial electrostatic effects. The high lattice symmetry apparent from diffraction is achieved only because of static disorder. In the NMR studies the effects of disorder on the lineshapes disappear only when reorientation rates become rapid enough so that even the local symmetries are high on time average.

Acknowledgment

S.N. thanks the Nishina Memorial Foundation for support during his visit to the National Research Council of Canada.

1. J.A. Ripmeester and C.I. Ratcliffe. *In* Inclusion compounds.Vol. 5. *Edited by* J.L. Atwood, J.E.D. Davies, and D.D. MacNicol. Oxford UniversityPress, Oxford. 1991.
2. J.A. Ripmeester and C.I. Ratcliffe. *In* Spectroscopic and computational studies of supramolecular systems. *Edited by* J.E.D. Davies. Kluwer, Dordrecht. 1992.
3. S. Nishikiori and T. Iwamoto. Chem. Lett. 1127 (1987).
4. S. Nishikiori, C.I. Ratcliffe, and J.A. Ripmeester. J. Phys. Chem. **94**, 8098 (1990).

Can. J. Chem. Downloaded from www.nrcresearchpress.com by 203.198.23.82 on 09/08/12
For personal use only.

5. S.J. Opella and M.H. Frey. J. Am. Chem. Soc. **101**, 5854 (1979).
6. J.H. Davis, K.R. Jeffrey, M. Bloom, M.I. Valic, and T.P. Higgs. Chem. Phys. Lett. **42**, 390 (1976).
7. R.J. Wittebort, E.T. Olejniczak, and R.G. Griffin. J. Chem. Phys. **86**, 5411 (1987).
8. M.S. Greenfield, A.D. Ronemus, R.L. Vold, R.R. Vold, P.D. Ellis, and T.E. Raidy. J. Magn. Reson. **72**, 89 (1987).
9. R.G. Barnes and J.W. Bloom. J. Chem. Phys. **57**, 3082 (1972).
10. S. Nishikiori, Y. Takahashi-Ebisudani, and T. Iwamoto. J. Inclusion Phenom. **9**, 10 (1990).
11. N. Bloembergen, E.M. Purcell, and R.V. Pound. Phys. Rev. **73**, 679 (1948).

Can. J. Chem. Downloaded from www.nrcresearchpress.com by 203.198.23.82 on 09/08/12
For personal use only.

Lignes monovariantes de l'isotherme 75°C du système quaternaire réciproque : H_3PO_4–K_2SO_4–H_2SO_4–K_3PO_4–H_2O

NÉJI BOURGUIBA[1] ET TAHAR JOUINI

Département de chimie, faculté des sciences de Tunis, Campus universitaire, 1060 Tunis, Tunisie

Reçu le 19 juillet 1993

NÉJI BOURGUIBA et TAHAR JOUINI. Can. J. Chem. **71**, 1816 (1993).

Toutes les lignes monovariantes de l'isotherme isobare (75°C, 1 atm) du système quaternaire H_3PO_4–K_2SO_4–H_2SO_4–K_3PO_4–H_2O sont étudiées. Elles ont été déterminées par analyse chimique de solutions correspondant à des mélanges situés dans les volumes tri-phasés. Les intersections de ces lignes, qui sont des points invariants quaternaires, ont été localisées en préparant des mélanges à l'intérieur des tétraèdres d'invariance quaternaires isothermes, et en analysant les solutions correspondantes en équilibre avec trois sels. Les composés qui se manifestent sont K_2SO_4, $K_2SO_4 \cdot KHSO_4$, $K_2SO_4 \cdot 7KHSO_4 \cdot H_2O$, $KHSO_4$, une solution solide de substitution $K_8(H_2PO_4)_{1+x}(HSO_4)_{7-x}$, $0 \leq x \leq 1$, $KH_2PO_4 \cdot KHSO_4$, $KH_5(PO_4)_2$, KH_2PO_4, $3K_2HPO_4 \cdot KH_2PO_4 \cdot 2H_2O$, K_2HPO_4 et $K_3PO_4 \cdot 3H_2O$. Les huit premiers sels possèdent des domaines à l'intérieur du prisme de Janecke. Par contre les nappes de cristallisation des trois derniers sont pratiquement confondues avec les courbes de solubilité du système ternaire limite K_3PO_4–H_3PO_4–H_2O. L'ensemble des résultats obtenus est discuté et interprété.

NÉJI BOURGUIBA and TAHAR JOUINI. Can. J. Chem. **71**, 1816 (1993).

The boundary curves and quaternary invariant points of the reciprocal system H_3PO_4–K_2SO_4–H_2SO_4–K_3PO_4–H_2O were investigated at 75°C and 1 atm by chemical analysis of solutions in equilibria, respectively, with two or three salts. Eleven compounds occur in this system. Only eight of them have crystallization areas inside Janecke's prism; these are K_2SO_4, $K_2SO_4 \cdot KHSO_4$, $K_2SO_4 \cdot 7KHSO_4 \cdot H_2O$, $KHSO_4$, $KH_2PO_4 \cdot KHSO_4$, $KH_5(PO_4)_2$, KH_2PO_4, and a solid solution $K_8(H_2PO_4)_{1+x}(HSO_4)_{7-x}$, $0 \leq x \leq 1$, of substitution type continuous between the two limiting compositions $KH_2PO_4 \cdot 7KHSO_4$ and $KH_2PO_4 \cdot 3KHSO_4$. The crystallization fields of $3K_2HPO_4 \cdot KH_2PO_4 \cdot 2H_2O$, K_2HPO_4, and $K_3PO_4 \cdot 3H_2O$ are very close to the solubility curves of the ternary system K_3PO_4–H_3PO_4–H_2O. Results are explained and discussed.

Introduction

Le procédé PENNZOIL (1), en vue de préparer HCl, permet l'obtention de $KHSO_4$ avec un coût presque nul :

$$H_2SO_4 + KCl \rightarrow KHSO_4 + HCl$$

$KHSO_4$ pourrait à son tour servir de point de départ pour préparer, par attaque de l'apatite naturelle, des engrais phosphopotassiques (2–8). Cette action produit un mélange hétérogène. Après dégagement des composés volatils (HF, SiF_4, CO_2...) et séparation de l'insoluble constitué surtout de phosphogypse, la solution aqueuse résultante contient essentiellement les ions H^+, K^+, PO_4^{3-} et SO_4^{2-}.

Toute application industrielle devra se baser sur l'étude du diagramme faisant intervenir ces ions en présence d'eau : H_3PO_4–K_2SO_4–H_2SO_4–K_3PO_4–H_2O. Il s'agit d'un système quaternaire réciproque caractérisé par la réaction de double décomposition :

$$2H_3PO_4 + 3K_2SO_4 \underset{\longleftarrow}{\overset{H_2O}{\longrightarrow}} 3H_2SO_4 + 2K_3PO_4$$

La température optimale de l'attaque sulfurique de l'apatite est comprise entre 70 et 80°C. Cela nous a incité à mener cette étude à 75°C.

Toutes les isothermes ternaires limitant ce système ont été établies à 75°C et décrites dans un travail antérieur (9).

Nous poursuivons, dans ce mémoire, l'investigation du système quaternaire réciproque H_3PO_4–K_2SO_4–H_2SO_4–K_3PO_4–H_2O en établissant les lignes monovariantes et les points invariants de l'isotherme 75°C et 1 atm (1 atm = 101,3 kPa).

1. Auteur à qui adresser toute correspondance.

Techniques expérimentales

Les techniques expérimentales relatives aux mesures de solubilité, à la mise à l'équilibre, aux produits utilisés et au mode de représentation ont été décrites dans une publication antérieure (9).

La détermination des caractéristiques des lignes monovariantes du système étudié a été réalisée au moyen de méthodes adaptées aux différents éléments à étudier :

(*a*) Les lignes monovariantes ont été définies au moyen de mélanges situés dans les volumes à trois phases où coexistent deux solides en présence d'une solution. Un tel volume est engendré par le triangle dont les deux sommets, représentant les solides concernés, restent fixes, le troisième relatif à la solution est mobile et décrit la ligne monovariante correspondante. À l'équilibre les solutions sont analysées et les phases solides identifiées.

(*b*) Les points invariants quaternaires ont été déterminés en préparant des mélanges à l'intérieur des tétraèdres d'invariance quaternaire isotherme, définis par les quatre points représentant respectivement les trois solides et la solution en équilibre. L'analyse de cette solution permet une localisation précise du point invariant.

(*c*) Les phases solides connues sont identifiées par leurs diffractogrammes X sur poudre. Celles inconnues sont d'abord caractérisées par les méthodes des ensembles (10) et des restes (11).

Les compositions limites de la solution solide $K_8(H_2PO_4)_{1+x}(HSO_4)_{7-x}$ ($KH_2PO_4 \cdot 7KHSO_4$ et $KH_2PO_4 \cdot 3KHSO_4$) ont été précédemment précisées par analyse chimique des cristaux correspondants (9).

Analyse bibliographique

Ce système n'a fait l'objet d'aucune étude à 75°C. Seule une étude à 25°C a été effectuée (12). Les phases solides signalées par l'auteur sont KH_2PO_4, $KH_2PO_4 \cdot KHSO_4$, $KH_2PO_4 \cdot 3KHSO_4$, $KHSO_4$, K_2SO_4, $K_2SO_4 \cdot 3KHSO_4$ (ou $K_2SO_4 \cdot 6KHSO_4$). Cette étude est incomplète dans le sens où les lignes de niveau d'eau constant et les ternaires limites font défaut. De plus la stoechiométrie de l'une des

Can. J. Chem. Downloaded from www.nrcresearchpress.com by 203.198.23.82 on 09/08/12
For personal use only.

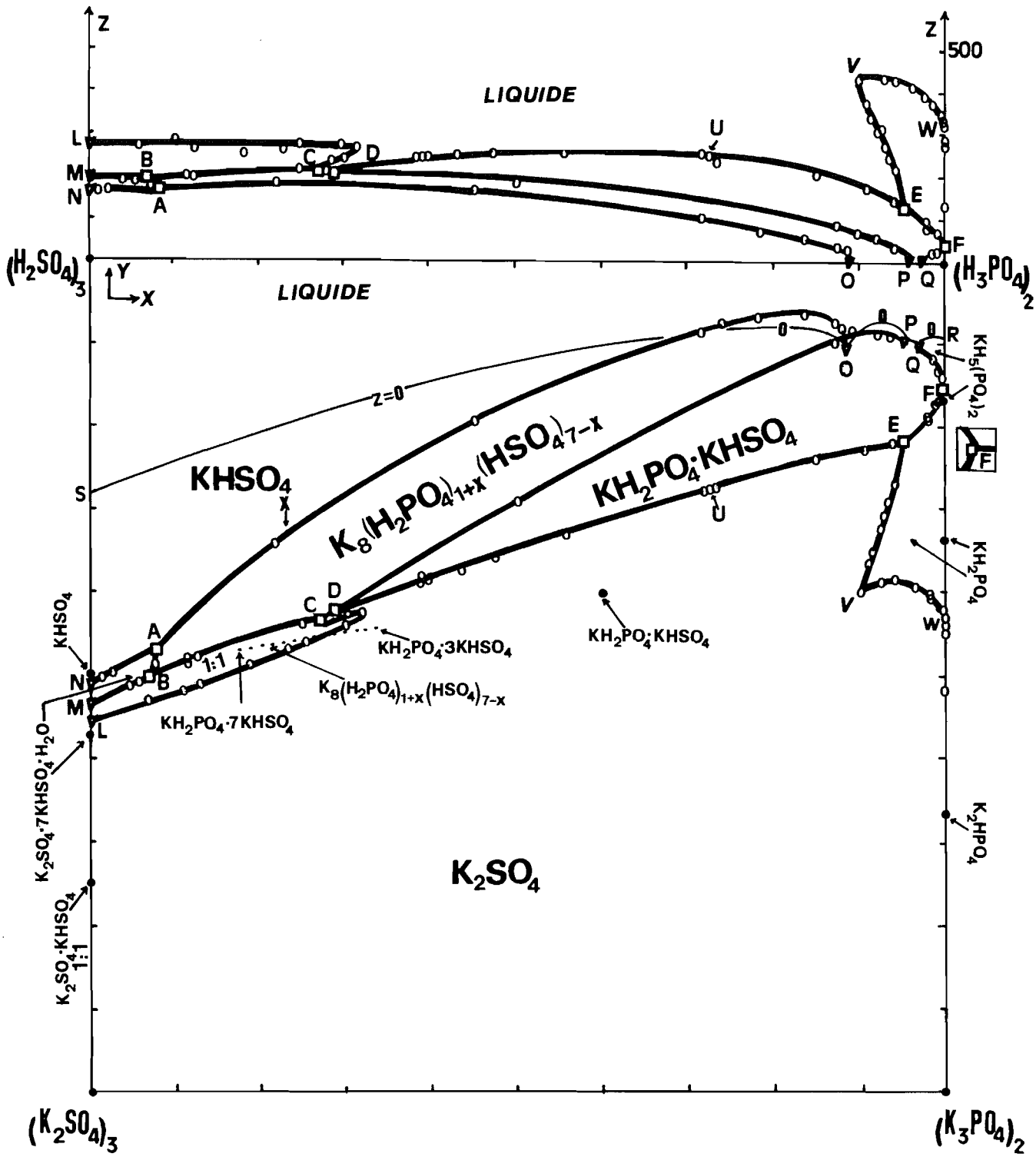

FIG. 1A. Projection sur les plans horizontal et frontal des lignes de deux sels de l'isotherme 75°C du système quaternaire réciproque H_3PO_4–K_2SO_4–H_2SO_4–K_3PO_4–H_2O. ○ : Point appartenant à une ligne monovariante, □ : invariant quaternaire isotherme, ▽ : invariant ternaire isotherme, (.....): solution solide.

phases solides fait l'objet d'un doute de la part de l'auteur ($K_2SO_4 \cdot 3KHSO_4$ ou $K_2SO_4 \cdot 6KHSO_4$), et a donné lieu à des résultats contradictoires dans la littérature (cf. la référence 13). Nous avons montré dans un travail antérieur (13), par une détermination structurale aux rayons X, que la formule exacte de ce sulfate acide est $K_2SO_4 \cdot 7KHSO_4 \cdot H_2O$. Une autre phase décrite, dans la référence 12, comme étant un composé défini ($KH_2PO_4 \cdot 3KHSO_4$) est en fait une solution solide de substitution, $K_8(H_2PO_4)_{1+x}(HSO_4)_{7-x}$, $0 \leq x \leq 1$, continue entre les deux compositions limites $KH_2PO_4 \cdot 7KHSO_4$ et $KH_2PO_4 \cdot 3KHSO_4$. Nous avons délimité, dans une publication antérieure (9), le domaine de cristallisation de cette phase, et indexé les diagrammes de poudre des composés limites.

Can. J. Chem. Downloaded from www.nrcresearchpress.com by 203.198.23.82 on 09/08/12
For personal use only.

TABLEAU 1. Lignes monovariantes du système quaternaire réciproque : H^+, K^+, PO_4^{3-}, SO_4^{2-}, H_2O–isotherme 75°C

Lignes	Phases solides en équilibre
NA	$KHSO_4 + K_2SO_4 \cdot 7KHSO_4 \cdot H_2O$
BC	$K_2SO_4 \cdot KHSO_4 + K_8(H_2PO_4)_{1+x}(HSO_4)_{7-x}$
BA	$K_2SO_4 \cdot 7KHSO_4 \cdot H_2O + KH_2PO_4 \cdot 7KHSO_4$
MB	$K_2SO_4 \cdot 7KHSO_4 \cdot H_2O + K_2SO_4 \cdot KHSO_4$
LC	$K_2SO_4 \cdot KHSO_4 + K_2SO_4$
CD	$K_2SO_4 + KH_2PO_4 \cdot 3KHSO_4$
AO	$KHSO_4 + KH_2PO_4 \cdot 7KHSO_4$
DP	$KH_2PO_4 \cdot KHSO_4 + KH_2PO_4 \cdot 3KHSO_4$
DE	$KH_2PO_4 \cdot KHSO_4 + K_2SO_4$
EVW	$K_2SO_4 + KH_2PO_4$
EF	$KH_2PO_4 + KH_2PO_4 \cdot KHSO_4$
QF	$KH_2PO_4 \cdot KHSO_4 + KH_5(PO_4)_2$

On relève également dans la littérature l'étude de quelques coupes isopléthiques :

K_2SO_4–H_3PO_4–H_2O partiellement effectuée à 20°C (14), pour des concentrations pondérales en P_2O_5 inférieures à 50%. Les phases solides observées sont K_2SO_4 et $KH_2PO_4 \cdot KHSO_4$.

K_2SO_4–KH_2PO_4–H_2O qui présente à 80°C deux branches de cristallisation relatives respectivement à K_2SO_4 et à KH_2PO_4 (15).

$KHSO_4$–H_3PO_4–H_2O et $KHSO_4$–KH_2PO_4–H_2O partiellement établies à 80°C (15).

Résultats expérimentaux

Toutes les isothermes 75°C des systèmes ternaires limitant le quaternaire considéré ont été, dans une première étape, déterminées (9).

Étude des lignes monovariantes du système quaternaire réciproque H^+, K^+, PO_4^{3-}, SO_4^{2-} et H_2O à 75°C et 1 atm

Douze lignes monovariantes ont été définies et cinq points invariants quaternaires isothermes ont été localisés. Les résultats sont résumés aux tableaux 1 et 2.

La figure 1*A* représente les projections, sur les plans horizontal et frontal des lignes de deux sels ainsi que la ligne SR de côte en eau $Z = 0$ qui représente les courbes de solubilité du système ternaire anhydre H_2SO_4–H_3PO_4–K_2SO_4–H_3PO_4 (9).

Les agrandissements de deux parties encombrées de la figure 1A sont représentés dans les figures 1B et 1C.

L'examen de ce diagramme suggère les observations suivantes :

1. Huit domaines d'existence, relatifs respectivement aux sels suivants, se manifestent à l'intérieur du prisme de Janecke : K_2SO_4, $K_2SO_4 \cdot KHSO_4$, $K_2SO_4 \cdot 7KHSO_4 \cdot H_2O$, $KHSO_4$ une solution solide de substitution $K_8(H_2PO_4)_{1+x}$-$(HSO_4)_{7-x}$, $0 \leq x \leq 1$, $KH_2PO_4 \cdot KHSO_4$, $KH_5(PO_4)_2$ et KH_2PO_4.

Les compositions limites de la solution solide continue, $KH_2PO_4 \cdot 7KHSO_4$ et $KH_2PO_4 \cdot 3KHSO_4$, ont été déterminées par analyse chimique des cristaux correspondants. Les paramètres de leurs mailles ainsi que les diagrammes de poudre indexés ont été fournis dans une publication antérieure (9).

2. Les domaines de $KHSO_4$, $KH_2PO_4 \cdot KHSO_4$, $K_8(H_2PO_4)_{1+x}$ $(HSO_4)_{7-x}$ et $KH_5(PO_4)_2$ sont délimités dans le carré de base respectivement par les branches SO, OP, PQ et QR, appartenant à la ligne de niveau $Z = 0$. Elles constituent les courbes de solubilité du système ternaire réciproque précédemment décrit (9).

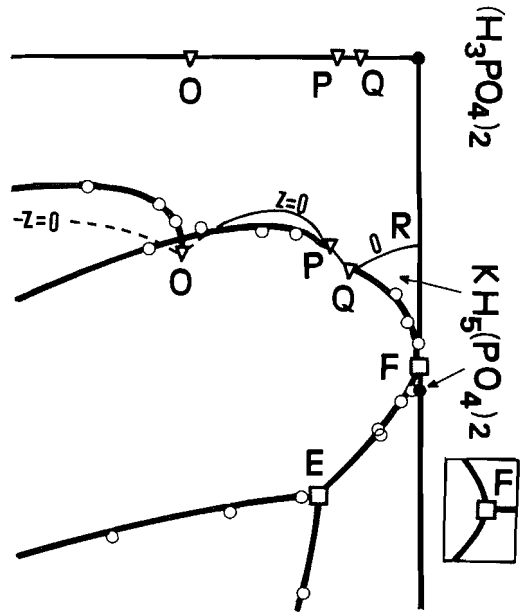

FIG. 1B. Agrandissement de la région acide de l'isotherme 75°C du système quaternaire réciproque H_3PO_4–K_2SO_4–H_2SO_4–K_3PO_4–H_2O.

3. (*a*) Les lignes de deux sels AB, AN, EVW et EF sont à saturation congruente; elles sont caractérisées par des équilibres du type

$$\text{liquide} \rightleftharpoons S_1 + S_2$$

S_1 et S_2 étant deux phases solides. Ces lignes ne peuvent être franchies par les chemins de cristallisation. En particulier l'évaporation de solutions leur appartenant provoque la précipitation de deux sels. Le chemin de cristallisation résultant suit cette ligne monovariante en s'éloignant du segment joignant les points représentatifs des deux sels qui coprécipitent.

(*b*) Les lignes de deux sels : BM, BC, CD, LC DE, FQ et DP sont à saturation non congruente; elles sont caractérisées par des équilibres du type

$$\text{liquide} + S_1 \overset{I}{\rightleftharpoons} S_2$$

De telles lignes peuvent être franchies par les chemins de cristallisation. C'est pourquoi certains auteurs les représentent par une ligne discontinue. En particulier l'évaporation de solutions leur appartenant provoque le déplacement de l'équilibre dans le sens *I* et le dépôt d'un seul sel (S_2). Le chemin de cristallisation résultant ne suit pas cette ligne, il se déplace sur la nappe de S_2. En projection son point représentatif s'éloigne de S_2 selon un segment de droite, dont le prolongement passe par S_2.

(*c*) La ligne AO est à saturation congruente entre A et X et non congruente au delà. Le point X est tel que la tangente en X à AO passe par le point représentatif de $KHSO_4$.

4. Les lignes de deux sels DE et EW, possèdent chacune un point, respectivement U et V, de côte en eau maximum, admettant par conséquent une tangente horizontale. Chacun de ces points doit être situé, sur la projection horizontale, à l'intersection de la ligne de deux sels correspondante et de

Can. J. Chem. Downloaded from www.nrcresearchpress.com by 203.198.23.82 on 09/08/12
For personal use only.

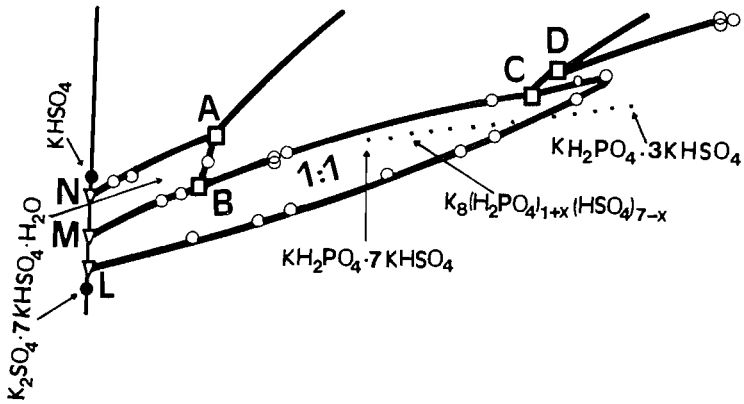

FIG. 1C. Agrandissement d'une région de l'isotherme 75°C du système quaternaire réciproque H_3PO_4–K_2SO_4–H_2SO_4–K_3PO_4–H_2O.

TABLEAU 2. Coordonnées des points représentatifs des invariants quaternaires du système quaternaire réciproque : H^+, K^+, PO_4^{3-}, SO_4^{2-}, H_2O–isotherme 75°C

Points invariants	Solution saturée							Phases solides en équilibre
	Coordonnées de Janecke			Composition pondérale				
	X	*Y*	*Z*	$\%K_2O$	$\%SO_3$	$\%P_2O_5$	$\%H_2O$	
A	7,70	52,78	174,6	22,89	38,00	1,88	37,23	$KHSO_4$ + $K_2SO_4 \cdot 7KHSO_4 \cdot H_2O$ + $KH_2PO_4 \cdot 7KHSO_4$
B	7,28	49,67	178,0	23,94	37,45	1,74	36,87	$K_2SO_4 \cdot KHSO_4$ + $K_2SO_4 \cdot 7KHSO_4 \cdot H_2O$ + $KH_2PO_4 \cdot 7KHSO_4$
C	27,42	56,34	210,8	20,75	29,30	6,55	43,40	K_2SO_4 + $K_2SO_4 \cdot KHSO_4$ + $KH_2PO_4 \cdot 3KHSO_4$
D	29,14	57,44	207,7	20,49	28,97	7,05	43,49	K_2SO_4 + $KH_2PO_4 \cdot KHSO_4$ + $KH_2PO_4 \cdot 3KHSO_4$
E	95,15	78,08	123,6	16,12	3,03	35,15	45,70	K_2SO_4 + $KH_2PO_4 \cdot KHSO_4$ + KH_2PO_4
F	100,0	84,58	40,62	15,84	0,00	51,61	32,55	$KH_2PO_4 \cdot KHSO_4$ + KH_2PO_4 + $KH_5(PO_4)_2$

la droite passant par les points représentatifs de ces deux sels : respectivement ($KH_2PO_4 \cdot KHSO_4$ et K_2SO_4) et (KH_2PO_4 et K_2SO_4).

5. Miscibilité des sulfates dans les solutions saturées en phosphates. Seuls les phosphates acides $KH_5(PO_4)_2$ et KH_2PO_4 possèdent des domaines à l'intérieur du prisme de Janecke.

Les lignes de deux sels faisant intervenir les autres phosphates du système ternaire K_3PO_4–H_3PO_4–H_2O :

$$K_3PO_4 \cdot 3H_2O + K_2SO_4,\ K_2HPO_4 + K_2SO_4,$$

$$3K_2HPO_4 \cdot KH_2PO_4 \cdot 2H_2O + K_2SO_4$$

ainsi que la ligne de deux sels (KH_2PO_4 + K_2SO_4) à partir du point W, sont confondues avec les courbes de solubilité du système ternaire K_3PO_4–H_3PO_4–H_2O. Elles se projettent par conséquent sur le côté K_3PO_4–H_3PO_4 du carré de base. Cela traduit l'insolublité de K_2SO_4 dans les solutions saturées en phosphates à partir de W, c'est-à-dire, au delà des rapports molaires $K_3PO_4/H_3PO_4 \geq 0.71$.

L'allure de la ligne E V W est révélatrice à cet égard : K_2SO_4 est soluble dans les solutions saturées en KH_2PO_4 de composition comprise entre les points E et V. À partir de V sa solubilité décroît pour s'annuler en W qui représente une solution pratiquement ternaire ne contenant pas d'ions SO_4^{2-}.

Un phénomène dans une certaine mesure similaire se manifeste dans le système quaternaire CaO–P_2O_5–SO_3–H_2O (16), où du fait de l'insolubilité des sulfates de calcium dans les solutions saturées en phosphates, les lignes de deux sels du système quaternaire sont confondues avec les courbes de solubilité du système ternaire CaO–P_2O_5–H_2O.

Notons également la particularité que présente $KH_2PO_4 \cdot KHSO_4$: insoluble en présence de KH_2PO_4 et $KH_5(PO_4)_2$ dans la solution représentée par le point F (en effet, F est pratiquement contenu dans le plan K_3PO_4–H_3PO_4–H_2O), il est cependant soluble dans les solutions monovariantes, contenant l'un ou l'autre de ces sels, représentées respectivement par les lignes FE et FQ qui sont situés à l'intérieur du prisme de Janecke.

Ces résultats sont appliqués à la fabrication d'engrais phosphopotassiques dans une publication (en préparation) où nous avons étudié les nappes du liquidus du système. Leur connaissance est en effet nécessaire à la délimitation précise

Can. J. Chem. Downloaded from www.nrcresearchpress.com by 203.198.23.82 on 09/08/12
For personal use only.

des domaines de solubilité des différents sels qui cristallisent dans ce diagramme.

1. Pennzoil. Phosphorus Potassium, **68**, 44 (1973).
2. E.K. Drechsel, J.B. Sardisco et J.R. Stewart, Jr. (Pennzoil United Inc.). U.S. Patent 3 697 246 (Cl. 71–34; C 05b), 10 Oct 1972; Appl. 81, 280, 16 Oct 1970.
3. E.K. Drechsel et J.B. Sardisco (Pennzoil Co.). U.S. Patent 3 726 660 (Cl. 71–37; C 05b), 10 Apr 1973; Appl. 136, 960, 23 Apr 1971.
4. E.K. Drechsel (Pennzoil Co.). U.S. Patent 3 840 640 (Cl. 423–167; C 22b, C 01f), 08 Oct 1974; Appl. 284, 045, 28 Aug 1972.
5. E.K. Drechsel, J.B. Sardisco et J.R. Stewart, Jr. (Pennzoil Co.). U.S. Patent 3 956 464 (Cl. 423–308; C 01B13/16), 11 May 1976; Appl. 81, 280, 16 Oct 1970.
6. H. Gabriel, L. Kacalski, U. Glabisz et Z. Trojanowski. pr. Nauk. Akad. Ekon. im. Oskara Langego Wroclawiu. 267 305 (1984).
7. L. Huanwei. Faming Zhuanli Shenqing Gongkai Shuomingshu CN 1, 045, 388 (Cl. C05F17/00), 19 Sep 1990; Appl. 89, 101, 314, 10 Mar 1989.
8. V.A. Khusnutdinov, T.G. Akhmetov, V.V. Shestakov et R. Kh. Khuziakhmetov. pr. Nauk. Akad. Ekon. im. Oskara Langego Wroclawiu. 526 122 (1990).
9. N. Bourguiba et T. Jouini. Can. J. Chem. **70**, 2197 (1992).
10. A. Chretien. Ann. Chim. **12**, 26 (1919).
11. F.A.H. Schreinemakers. Z. Phys. Chem. **11**, 76 (1893).
12. A.W. Frazier. J. Agric. Food Chem. **28**, 461 (1980).
13. N. Bourguiba et T. Jouini. C.R. Acad. Sci. Paris. Ser. II, **309**, 1643 (1989).
14. A.B. Bekturov, R.S. Erzhanova, V.I. Litvinenko et A.V. Ekshtelis. Izv. Akad. Nauk Kaz. SSR. Ser. Khim. **20**, 1 (1970).
15. V.N. Lamp et M.L. Chepelevetskii. Tr. Nauchn. Inst. Poudobr. i Insekto Fung N° 208 108 (1965).
16. A.N. Campbell et J.W. Coutts. Ind. Eng. Chem. **40**, 1295 (1948).

Can. J. Chem. Downloaded from www.nrcresearchpress.com by 203.198.23.82 on 09/08/12
For personal use only.

Preparation and nuclear magnetic resonance characterization of N-bonded complexes of platinum(II) with phosphorus-nitrogen rings containing three-coordinate chalcogens: X-ray structure of $[PtCl_2(PEt_3)]_2(Ph_4P_2N_4Se_2Et_2)$

TRISTRAM CHIVERS,[1] DANIEL D. DOXSEE, ROBERT W. HILTS, AND MASOOD PARVEZ
Department of Chemistry, The University of Calgary, Calgary, AB T2N 1N4, Canada

Received April 21, 1993

TRISTRAM CHIVERS, DANIEL D. DOXSEE, ROBERT W. HILTS, and MASOOD PARVEZ. Can J. Chem. **71**, 1821 (1993).

The reaction of 1,5-$Ph_4P_2N_4S_2Ph_2$ with $[PtCl_2(PEt_3)]_2$ in chloroform at 60°C produces the 1:1 adduct *trans*-$PtCl_2(PEt_3)(Ph_4P_2N_4S_2Ph_2)$ in which the platinum is attached to a nitrogen atom on the basis of ^{31}P nmr spectroscopy. By contrast, the corresponding reactions of 1,5-$Ph_4P_2N_4Se_2R_2$ (R = Me, Et, Ph) produce the 2:1 adducts $[PtCl_2(PEt_3)]_2(Ph_4P_2N_4Se_2R_2)$ (**7***a*, R = Me; **7***b*, R = Et; **7***c*, R = Ph) which have been characterized by ^1H, ^{31}P and ^{77}Se nmr spectroscopy and, in the case of **7***b*, by X-ray crystallography. Crystals of **7***b* are monoclinic, space group $C2/c$, with a = 27.803(7) Å, b = 12.378(7) Å, c = 15.752(8) Å, β = 115.49(2)°, V = 4893(3) Å^3, and Z = 4. The least-squares refinement with anisotropic thermal parameters for all non-hydrogen atoms converged at R = 0.037 and R_w = 0.022. The platinum centres in **7***b* are attached to distal nitrogen atoms of the disordered $P_2N_4Se_2$ ring. The reaction of the six-membered ring $Ph_4P_2N_3SPh$ with $[PtCl_2(PEt_3)]_2$ in dichloromethane at 23°C occurs in a regiospecific manner to give the 1:1 adduct $PtCl_2(PEt_3)(Ph_4P_2N_3SPh)$ in which, on the basis of ^{31}P nmr spectroscopy, the platinum is coordinated to a nitrogen atom between phosphorus and sulfur.

TRISTRAM CHIVERS, DANIEL D. DOXSEE, ROBERT W. HILTS et MASOOD PARVEZ. Can. J. Chem. **71**, 1821 (1993).

La réaction du 1,5-$Ph_4P_2N_4S_2Ph_2$ avec le $[PtCl_2(PEt_3)]_2$, dans le chloroforme à 60°C conduit à un adduit 1:1, le *trans*-$PtCl_2(PEt_3)(Ph_4P_2N_4S_2Ph_2)$, dans lequel le platine est attaché à l'atome d'azote d'après la rmn du ^{31}P. Par opposition, les réactions correspondantes des 1,5-$Ph_4P_2N_4Se_2R_2$ (R = Me, Et et Ph) conduisent à des adduits 2:1, les $[PtCl_2(PEt_3)]_2(Ph_4P_2N_4Se_2R_2)$ (**7***a*, R = Me; **7***b*, R = Et; **7***c*, R = Ph), qui ont été caractérisés par rmn du ^1H, du ^{31}P et du ^{77}Se et, dans le cas du composé **7***b*, par diffraction des rayons X. Les cristaux du composé **7***b* sont monocliniques, groupe d'espace $C2/c$, avec a = 27,803(7), b = 12,378(7) et c = 15,752(8) Å, β = 115,49(2)°, V = 4893(3) Å^3 et Z = 4. L'affinement par la méthode des moindres carrés pour les paramètres thermiques anisotropiques pour tous les atomes différents de l'hydrogène convergent à R = 0,037 et R_w = 0,022. Les centres de platine du composè **7***b* sont attachés aux atomes d'azote distales du cycle $P_2N_4Se_2$ désordonné. La réaction du cycle à six chainons $Ph_4P_2N_3SPh$ avec le $[PtCl_2(PEt_3)]$, dans le dichlorométhane à 23°C, se produit d'une facon régiospécifique pour donner l'adduit 1:1 $PtCl_2(PEt_3)(Ph_4P_2N_3SPh)$ dans lequel, d'après la rmn du ^{31}P, le platine est coordiné à un atome d'azote entre le phosphore et le soufre.

[Traduit par la rédaction]

Introduction

The coordination chemistry of unsaturated sulfur–nitrogen and selenium–nitrogen rings has been an active area of investigation recently (1). We have been particularly interested in exploring the range of metal complexes that can be formed by the folded $P_2N_4E_2$ rings **1** and **2** (2–4). The presence of the NPR_2 units in **1** and **2** provides a brace that serves to maintain the integrity of the ring and yields structural information through ^{31}P nmr spectroscopy. To date the following bonding modes have been established for **1** and **2**: η^1-N (2, 4), η^2-E,E′ (3–6) and η^2-E,N-μ,η^1-E′ (3, 4, 7). The combination of η^1-N and η^2-E,E′, i.e. μ^2,η^3-E,E′,N has also been observed for both **1** and **2** (2, 4). The $P_2N_4E_2$ ring can accommodate three (E = S) (2) or two (E = Se) (4) *N*-bonded $PtCl_2(PEt_3)$ groups. In addition, the organolithium derivatives $Li[Ph_4P_2N_4S_2R]$ form η^1-S bonded complexes with platinum(II) or palladium(II) (8).

The S,S′- and Se,Se′-diorgano derivatives of these eight-membered rings, **3** and **4**, are readily prepared (9, 10). The $P_2N_4E_2$ ring in **3** and **4** adopts a chair conformation with the two chalcogen atoms disposed on either side of the P_2N_4 plane and the exocyclic substituents on S or Se occupying axial positions (9, 10). These ring systems are potential precursors of hybrid inorganic polymers containing alternating PN and EN (E = S, Se) units. Polymers containing two PN and one SN groups in a repeating unit have been prepared from cyclic precursors (*six*-membered rings) (11, 12).

We report here the formation of platinum(II) complexes of **3** and **4**, which were prepared in order to compare the ligand behaviour of the open rings **3** and **4** with that of the corresponding folded rings **1** and **2** and, in particular, to determine (*a*) the site of coordination, (*b*) the effect of coordination on the structure of the $P_2N_4E_2$ ring, (*c*) the number of Pt(II) groups that can be attached to the $P_2N_4E_2$ ring, and (*d*) any differences between the coordinating ability of the sulfur and selenium systems. A platinum(II) complex of the related six-membered ring **5** was also characterized.

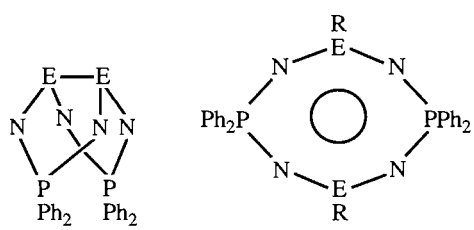

1, E = S
2, E = Se

3, E = S, R = Ph
4*a*, E = Se, R = Me
4*b*, E = Se, R = Et
4*c*, E = Se, R = Ph

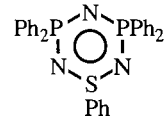

5

Experimental

Reagents and general procedures

Manipulations of air-sensitive reagents and products were per-

[1]Author to whom correspondence may be addressed.

Can. J. Chem. Downloaded from www.nrcresearchpress.com by 203.198.23.82 on 09/08/12
For personal use only.

Can. J. Chem. Downloaded from www.nrcresearchpress.com by 203.198.23.82 on 09/08/12
For personal use only.

formed under an atmosphere of prepurified nitrogen or argon using standard Schlenk or dry box techniques. Solvents (acetonitrile, chloroform, dichloromethane, hexanes, diethyl ether) were dried with the appropriate desiccant and purged with N_2 or argon. The compounds 1,5-$Ph_4P_2N_4Se_2R_2$ (R = Me, Et, Ph) (9), $Ph_4P_2N_3SPh$ (13), and $[PtCl_2(PEt_3)]_2$ (14) were prepared by the literature procedures. The compound 1,5-$Ph_4P_2N_4S_2Ph_2$ was obtained in 59% yield from $Ph_2PN_2(SiMe_3)_3$ and three molar equivalents of PhSCl by a modification of the literature method (10) in which acetonitrile was used as a solvent instead of CH_2Cl_2. The solubility of the Ph_2S_2 by-product in acetonitrile facilitates the purification of the product by obviating the need to wash it with n-pentane.

Instrumentation

^{31}P nmr spectra were obtained on a Bruker AM-400 MHz spectrometer operating at 161.978 MHz. ^{31}P chemical shifts are reported in ppm relative to external 85% H_3PO_4. Proton nmr spectra were recorded on a Bruker ACE-200 MHz spectrometer at 200.1 MHz. ^{77}Se nmr spectra were recorded at 76.311 MHz on the Bruker AM-400 instrument. The lock signal for the ^{31}P and ^{77}Se nmr spectra was provided by sealed D_2O inserts. ^{77}Se chemical shifts are referenced to external Ph_2Se_2 [$\delta^{77}Se$ + 461 ppm relative to $SeMe_2$ (0 ppm)]. Elemental analyses were performed by the microanalytical service within the Chemistry Department at The University of Calgary.

*Preparation of trans-[$PtCl_2(PEt_3)(Ph_4P_2N_4S_2Ph_2)$], **6***

A solution of 1,5-$Ph_4P_2N_4S_2Ph_2$ (0.200 g, 0.31 mmol) in $CHCl_3$ (20 mL) was added by cannula to a solution of $[PtCl_2(PEt_3)]_2$ (0.118 g, 0.154 mmol) in $CHCl_3$ (20 mL). The resulting pale yellow solution was heated at 60°C for 1 h and then stirred for 1 h at 23°C. The solvent was removed under vacuum and the yellow residue was recrystallized from chloroform – diethyl ether at −18°C to give **6** · Et_2O as pale yellow needles (0.107 g, 0.097 mmol, 31%). Anal. calcd. for $C_{46}H_{55}Cl_2N_4OP_3PtS_2$: C 50.09, H 5.03, N 5.08; found: C 50.83, H 4.44, N 5.71. ^1H nmr ($CDCl_3$), δ(ppm): 7.22–8.48 (m, PC_6H_5 and SC_6H_5, 30H), 3.34 (q, $O[CH_2CH_3]_2$, 4H, ^3J(H—H) = 7.5 Hz, 1.07 (t, $O(CH_2CH_3)_2$, 6H, ^3J(H—H) = 7.5 Hz), 1.51 (dq, PCH_2CH_3, 6H, ^2J(P—H) = 12 Hz, ^3J(H—H) = 7.5 Hz), 0.76 (dt, PCH_2CH_3, 9H, ^2J(P—H) = 17 Hz, ^3J(H—H) = 7.5 Hz). ^{31}P nmr (CH_2Cl_2), δ(ppm): 41.5 (dd, ^3J(P—P) = 5 Hz, ^4J(P—P) = 6 Hz, ^2J(Pt—P) = 30 Hz), 31.3 (d, ^4J(P—P) = 7 Hz), −1.4 (d, ^3J(P—P) = 5 Hz, ^1J(Pt—P) = 3696 Hz).

*Preparation of [$PtCl_2(PEt_3)]_2(Ph_4P_2N_4Se_2Me_2$), 7*a

A cold (−78°C) solution of $[PtCl_2(PEt_3)]_2$ (0.309 g, 0.402 mmol) in CH_2Cl_2 (15 mL) was added dropwise by cannula to a slurry of 1,5-$Ph_4P_2N_4Se_2Me_2$ (0.247 g, 0.402 mmol) in CH_2Cl_2 (15 mL) at −78°C. The mixture was allowed to reach room temperature and stirred for 45 min to give a yellow solution. The volume of the solution was reduced under vacuum to ca. 10 mL and the addition of hexanes (5 mL) produced a yellow precipitate of $[PtCl_2(PEt_3)]_2$ (1,5-$Ph_4P_2N_4Se_2Me_2$) (0.538 g, 0.389 mmol, 97%). Yellow crystals of **7***a* · CH_2Cl_2 were obtained from CH_2Cl_2 solutions layered with hexanes at 0°C. Anal. calcd. for $C_{39}H_{58}Cl_6N_4P_4Pt_2Se_2$: C 31.92, H 3.98, N 3.82; found: C 32.35, H 4.04, N 4.07. ^1H nmr (CD_2Cl_2, 23°C), δ(ppm): 7.1–8.4 (m, C_6H_5, 20H), 5.32 (s, CH_2Cl_2, 2H), 1.5–2.0 (m, CH_2CH_3, 12H), 0.6–1.2 (m, CH_2CH_3 and CH_3Se, 24H). ^{31}P nmr (CH_2Cl_2), δ(ppm): 44.3 (s, Ph_2P), −0.2 (s, Et_3P, ^1J(P—Pt) = 3620 Hz).

*Preparation of [$PtCl_2(PEt_3)]_2(Ph_4P_2N_4Se_2Et_2$), 7*b*, and [$PtCl_2(PEt_3)]_2(Ph_4P_2N_4Se_2Ph_2$), 7*c

Compounds **7***b* and **7***c* were obtained as yellow crystals in ca. 95% yield from $[PtCl_2(PEt_3)]_2$ and 1,5-$Ph_4P_2N_4Se_2Et_2$ or 1,5-$Ph_4P_2N_4Se_2Ph_2$, respectively, by a procedure similar to that described for the preparation of **7***a*. The products were recrystallized from CH_2Cl_2 solutions layered with hexanes at 0°C.

7*b*: Anal. calcd. for $C_{40}H_{60}Cl_4N_4P_4Pt_2Se_2$: C 34.05, H 4.30, N 3.97; found: C 33.59, H 4.43, N 3.89. ^1H nmr (CD_2Cl_2, 23°C), δ(ppm): 7.1–8.4 (m, C_6H_5, 20H), 1.5–1.9 (m, PCH_2CH_3 and $SeCH_2CH_3$, 16H), 0.7–1.2 (m, PCH_2CH_3) and $SeCH_2CH_3$, 24H). ^{31}P nmr (CH_2Cl_2), δ(ppm): 44.9 (s, Ph_2P), −0.6 (d, Et_3P, ^1J(P—Pt) = 3600 Hz, ^3J(P—P) = 3 Hz).

7*c*: Anal. calcd. for $C_{48}H_{60}Cl_4N_4P_4Pt_2Se_2$: C 38.26, H 4.01, N 3.71; found: C 37.38, H 4.08, N 3.63. ^1H nmr (CD_2Cl_2, 23°C), δ(ppm): 7.1–8.6 (m, PC_6H_5 and SeC_6H_5, 30H), 1.41 (q, CH_2CH_3, 12H), 0.74 (t, CH_2CH_3, 18H). ^{31}P nmr (CH_2Cl_2), δ(ppm): 43.3 (s, Ph_2P), −1.4 (d, Et_3P, ^1J(P—Pt) = 3646 Hz, ^3J(P—P) = 5 Hz).

Preparation of trans-[$PtCl_2(PEt_3)(Ph_4P_2N_3SPh)$], **8**

A solution of $[PtCl_2(PEt_3)]_2$ (0.200 g, 0.26 mmol) in CH_2Cl_2 (20 mL) at 23°C was added dropwise by cannula (10 min) to a solution of $Ph_4P_2N_3SPh$ (0.272 g, 0.52 mmol) in CH_2Cl_2 (20 mL) at 23°C. The resulting yellow solution was stirred for 1 h and then solvent was removed under vacuum. Recrystallization of the residue from diethyl ether at 23°C afforded yellow crystals of *trans*-[$PtCl_2(PEt_3)(Ph_4P_2N_3SPh)$] (0.211 g, 0.233 mmol, 45%). Anal. calcd. for $C_{36}H_{40}Cl_2N_3P_3PtS$: C 47.74, H 4.45, N 4.64; found: C 46.81, H 4.73, N 4.53. ^1H nmr ($CDCl_3$), δ(ppm): 6.85–8.3 (m, PC_6H_5 and SC_6H_5, 25H), 1.72 (dq, PCH_2CH_3, 6H, ^2J(P—H) = 12 Hz, ^3J(H—H) = 8 Hz), 0.98 (dt, PCH_2CH_3, 9H, ^3J(P—H) = 17 Hz, ^3J(H—H) = 8 Hz). ^{31}P nmr (CH_2Cl_2), δ(ppm): 20.5 (d, ^3J(P—P) = 10 Hz, ^2J(Pt—P) = 40 Hz), 10.0(s), 1.2 (d, ^3J(P—P) = 10 Hz, ^1J(Pt—P) = 3637 Hz).

X-ray crystallographic analysis of **7***b*

Yellow crystals of **7***b* were obtained from a CH_2Cl_2 solution layered with hexane. The crystal was attached to a glass fibre with epoxy. Pertinent crystallographic data are listed in Table 1.

The unit cell constants were determined from the setting angles of 25 reflections with $18.76° < 2\theta < 21.29°$. All measurements were made on a Rigaku AFC6S diffractometer with the ω–2θ scan technique and calculations were done using the teXsan programs (15). An empirical absorption correction using the program DIFABS

TABLE 1. Crystallographic parameters for $[PtCl_2(PEt_3)]_2$-$[Ph_4P_2N_4Se_2Et_2]$, **7***b*

Formula	$C_{40}H_{60}Cl_4P_4N_4Se_2Pt_2$
fw	1410.75
Crystal size (mm)	0.31 × 0.40 × 0.10
Space group[a]	*C*2/*c* (No. 15)
a (Å)	27.803(7)
b (Å)	12.378(7)
c (Å)	15.752(8)
β (°)	115.49(2)
V (Å^3)	4893(3)
Z	4
D_{calcd} (g/cm^3)	1.915
Radiation, Å	Mo K_α (λ = 0.71069 Å) Graphite monochromated
Temperature (K)	170(1)
F(000)	2720
Scan width (°)	1.31 + 0.35 tan θ
Scan speed (° min^{-1})	4.0
Maximum θ (°)	25
Octants	hk ± l
Unique reflections	4528
Observed reflections (>3.0 σ)	2302
μ (MoK_α) (cm^{-1})	75.59
Minimum-maximum absorption correct	0.75–0.90
Parameters refined	261
GOF	1.50
R, R_w[b]	0.037; 0.022

[a]Space group *Cc* or *C*2/*c* from systematic absences *hkl*: $h + k = 2n + 1$ and *h*0*l*: $l = 2n + 1$; the latter was indicated by the *E*-statistics and confirmed by successful refinement.

[b]$R = \Sigma(||F_o| - |F_c||)/\Sigma|F_o|$; $R_w = [\Sigma w(|F_o| - |F_c|)^2/\Sigma w|F_o|^2]^{1/2}$.

Can. J. Chem. Downloaded from www.nrcresearchpress.com by 203.198.23.82 on 09/08/12
For personal use only.

(16) was applied. The data were corrected for Lorentz and polarization effects.

The structure was solved by direct methods (17) and expanded using Fourier techniques (18). All non-H atoms, except the methylene carbon atom attached to Se which was disordered over two sites, were refined anisotropically and were allowed isotropic temperature factors; the Se atom was also disordered over two sites. All H atoms except those on the ethyl group attached to Se were included in the refinement at geometrically idealized positions. In the full-matrix least-squares refinement, the function minimized was $\Sigma w(|F_o| - |F_c|)^2$, where $w = 4F_o^2/\sigma^2(F_o^2)$. Conventional atomic scattering factors (19), corrected for anomalous dispersion (20), were used. Positional parameters are given in Table 2 and selected bond distances and bond angles are summarized in Table 3.

Hydrogen atom parameters, anisotropic thermal parameters, torsion angles, complete tables of bond lengths and bond angles, and structure factors have been deposited.[2]

Results and discussion

Synthesis and ^{31}P nmr characterization of **6**

The reaction of two molar equivalents of 1,5-$Ph_4P_2N_4S_2Ph_2$, **3**, with $[PtCl_2(PEt_3)]_2$ in chloroform at 60°C produces the 1:1 adduct **6** in about 30% yield. On the basis of the ^{31}P nmr spectra of the reaction mixture, the low yield of **6** is attributed to the equilibrium shown in reaction [1]. Unlike the selenium-containing rings **4***a–c*, a 2:1 adduct could not be obtained either by the reaction of **6** with $[PtCl_2(PEt_3)]_2$ or by treatment of **3** with an excess of $[PtCl_2(PEt_3)]_2$.

[1] $2Ph_4P_2N_4S_2Ph_2 + [PtCl_2(PEt_3)]_2 \rightleftharpoons 2trans\text{-}PtCl_2(PEt_3)(\eta^1\text{-}N\text{-}Ph_4P_2N_4S_2Ph_2)$

The composition and structure of **6** were established on the basis of the ^1H and ^{31}P nmr spectra. The ^{31}P nmr spectrum of **6** shows three equally intense resonances at −1.4, +31.3, and +41.5 ppm consistent with the proposed *N*-bonded structure. The resonance at −1.4 ppm is a doublet ($^3J(P_A—P_B)$ = 5 Hz) with platinum satellites ($^1J(Pt—P_A)$ = 3696 Hz) and is attributed to the PEt_3 ligand. The value of the $^{195}Pt—^{31}P$ coupling constant is typical for complexes of the type *trans*-$PtCl_2(PEt_3)L$, where L is an *N*-bonded unsaturated PNS ring (2, 21). The resonances at 31.3 and 41.5 Hz are assigned to the inequivalent ring phosphorus atoms P_C and P_B, respectively, which exhibit a mutual coupling of 7 Hz. The resonance at 41.5 ppm appears as a doublet of doublets and so is readily attributed to P_B.

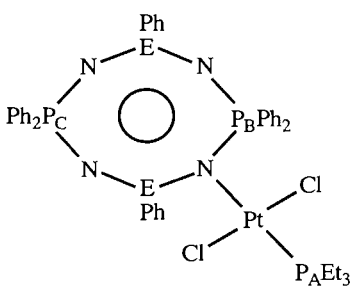

6

Synthesis and nmr characterization of 7a–c

In contrast to the behaviour of **3**, the reaction of two molar equivalents of **4***a–c* with the dimer $[PtCl_2(PEt_3)]_2$ yielded only the 2:1 adducts **7***a–c*. These adducts could be obtained as yellow, air-sensitive solids in essentially quantitative yields by using the stoichiometry shown in reaction [2].

[2] $Ph_4P_2N_4Se_2R_2 + [PtCl_2(PEt_3)]_2 \rightarrow [PtCl_2(PEt_3)]_2(Ph_4P_2N_4Se_2R_2)$

7*a*, R = Me; **7***b*, R = Et; **7***c*, R = Ph

The composition of the 2:1 adducts **7***a–c* was established by elemental analyses and by the integrated ^1H nmr spectra (see Experimental section). The ^{31}P nmr spectra of **7***a–c* all exhibit a singlet at 43–45 ppm (cf. $\delta(^{31}P)$ = 32–34 ppm for **4***a–c* (9)) for the heterocyclic phosphorus atoms in addition to a resonance at 0 to −2 ppm ($^1J(Pt—P)$ = 3600–3650 Hz) for the PEt_3 ligand. The $J(PEt_3—PPh_2)$ coupling of 3–5 Hz is observed (as a doublet) in the PEt_3 resonance of **7***b* and **7***c*, but it was not resolved in the case of **7***a*. Thus the ^{31}P nmr data rule out a structure for **7***a–c* in which the two $PtCl_2(PEt_3)$ groups are attached to nitrogen atoms which are bonded to the same phosphorus atom or a structure in which the platinum atoms are coordinated to selenium, but do not distinguish between "distal" or "vicinal" *N*-bonded arrangements (see Fig. 1). The ^{77}Se nmr spectrum of **7***a*, however, consists of a virtual triplet, centered at 944 ppm, characteristic of an AA'X spin system (where X is ^{77}Se (natural abundance = 7.7%) for the most abundant isotopomer and the phosphorus atoms (represented by A and A') are *magnetically inequivalent*). The "averaged" value of 40 Hz for $^2J(P—Se)$ obtained from the ^{77}Se nmr spectrum of **7***a* is smaller than the value of 86 Hz found for the ligands **4***a–c* (9*b*). These ^{77}Se nmr data rule out the "vicinal" *N*-bonded structure for **7***a* (see Fig. 1(*b*)), since this isomer should exhibit two resonances for the inequivalent selenium atoms. In support of the inference based on the ^{31}P nmr spectra of **7***a–c*, the Se-coordinated structure (an A_2X spin system, see Fig. 1(*c*)) which should give rise to a 1:2:1 triplet, may also be discounted on the basis of the ^{77}Se nmr data. Thus the ^{77}Se nmr spectrum of **7***a* is only consistent with the "distal" *N*-bonded structure (see Fig. 1(*a*)). This conclusion has been confirmed by an X-ray crystal structure determination of **7***b*.

X-ray crystal structure of $[PtCl_2(PEt_3)]_2(Ph_4P_2N_4Se_2Me_2)$, **7**b

The X-ray analysis of **7***b* establishes that the two $PtCl_2(PEt_3)$ groups are attached to opposite (distal) nitrogen atoms of the $P_2N_4Se_2$ ring with the PEt_3 ligands *trans* to nitrogen. An ORTEP drawing of the structure with the atomic numbering scheme is displayed in Fig. 2.

In the solid state, the complex lies on a twofold axis with the SeC_2H_5 group disordered in such a way that the Se and methylene carbon atoms lie over two sites (Se(1), Se(2) and C(191), C(192), respectively) with half-occupancy factors; the thermal parameters of the methyl carbon atom C(20) indicate a large degree of thermal motion. For clarity, Fig. 2 depicts one long chair conformation of the disordered $P_2N_4Se_2$ ring. There are three possible conformations of the $P_2N_4Se_2$

[2]Supplementary material mentioned in the text may be purchased from: The Depository of Unpublished Data, Document Delivery, CISTI, National Research Council Canada, Ottawa, Canada, K1A 0S2.

Tables of hydrogen atom parameters and bond lengths and angles have also been deposited with the Cambridge Crystallographic Data Centre and can be obtained on request from The Director, Cambridge Crystallographic Data Centre, University Chemical Laboratory, 12 Union Road, Cambridge, CB2 IEZ, U.K.

TABLE 2. Positional parameters and B(eq) for **7***b*

Atom[a]	x	y	z	B(eq)[b]
Pt(1)	0.34861(2)	0.11466(4)	0.71832(3)	2.91(2)
Se(1)′	0.45425(8)	0.13125(16)	0.66747(13)	2.31(8)
Se(2)′	0.42507(9)	0.27215(18)	0.63623(14)	2.9(1)
Cl(1)	0.2992(1)	0.2724(2)	0.6675(2)	4.2(1)
Cl(2)	0.4010(1)	−0.0347(2)	0.7781(2)	5.0(2)
P(1)	0.4609(1)	0.2571(3)	0.8348(2)	3.2(1)
P(2)	0.2723(1)	0.0280(2)	0.6862(2)	3.8(1)
N(1)	0.4182(3)	0.2034(6)	0.7373(5)	3.3(4)
N(2)	0.4788(4)	0.2250(8)	0.6334(6)	5.3(5)
C(1)	0.4414(4)	0.2173(8)	0.9258(7)	2.5(4)
C(2)	0.4745(4)	0.1529(8)	0.9980(7)	3.8(5)
C(3)	0.4620(5)	0.1265(11)	1.0735(7)	5.3(6)
C(4)	0.4172(5)	0.1648(10)	1.0741(7)	5.6(7)
C(5)	0.3827(5)	0.2267(10)	1.0021(8)	4.6(6)
C(6)	0.3953(4)	0.2545(8)	0.9291(7)	3.3(5)
C(7)	0.4555(4)	0.4036(9)	0.8268(7)	3.3(5)
C(8)	0.4955(6)	0.4690(11)	0.8843(9)	7.3(8)
C(9)	0.4901(7)	0.5800(11)	0.8766(10)	8(1)
C(10)	0.4448(6)	0.6239(12)	0.8112(10)	6.4(8)
C(11)	0.4065(6)	0.5652(13)	0.7571(13)	11(1)
C(12)	0.4118(6)	0.4498(12)	0.7619(11)	11(1)
C(13)	0.2748(4)	−0.1168(10)	0.6919(7)	5.0(6)
C(14)	0.2871(5)	−0.1699(9)	0.6165(8)	6.6(7)
C(15)	0.2408(5)	0.0660(9)	0.7605(10)	6.4(7)
C(16)	0.2755(6)	0.0394(11)	0.8625(8)	7.0(8)
C(17)	0.2236(5)	0.0582(9)	0.5643(8)	6.7(7)
C(18)	0.1682(6)	0.0063(12)	0.5349(12)	12(1)
C(191)′	0.3894(7)	0.1005(17)	0.5487(12)	4.6(7)
C(192)′	0.3658(7)	0.1999(14)	0.5288(11)	6.7(6)
C(20)	0.3726(7)	0.2117(15)	0.4516(11)	14(1)

[a]Primed atoms were disordered over two sites with equal site occupancy factors; C(191) and C(192) were allowed isotropic temperature factors.

[b]$B_{eq} = \frac{8}{3}\pi^2(U_{11}(aa^*)^2 + U_{22}(bb^*)^2 + U_{33}(bb^*)^2 + 2U_{12}aa^*bb^* \cos\gamma + 2U_{13}aa^*cc^* \cos\beta + 2U_{23}bb^*cc^* \cos\alpha)$.

Can. J. Chem. Downloaded from www.nrcresearchpress.com by 203.198.23.82 on 09/08/12
For personal use only.

ring which could contribute to the disordered structure, viz. boat–boat (BB), crown (CR), or long chair (LC) (see Fig. 3).[3] Three combinations of these ring conformations could give rise to the observed disorder. These are (*i*) equal contributions of BB and CR, (*ii*) equal contributions of two LC conformations, or (*iii*) equal contributions of BB, CR, and two LC conformations. Although it is not possible to distinguish between these alternatives on the basis of the crystallographic data, option (*ii*) (two LC conformations involved in a rotational disorder) seems the most likely explanation since the other combinations require equal contributions of energetically different species.

As a result of the disorder the P—N bond distances fall within the range 1.57(1)–1.65(1) Å with a mean value of 1.61 Å, and the Se—N bond distances vary from 1.56(1) to 1.99(1) with a mean value of 1.77 Å. These distances can be compared with the values of 1.605(3) and 1.773(1) Å found for the P—N and Se—N bonds, respectively, in the uncomplexed ligand 1,5-$Ph_4P_2N_4Se_2Me_2$, **4***a* (9). The geometry of the rest of the molecule is not affected by the disorder. The Pt—N bond length of 2.130(8) Å is indicative of a weak interaction. For comparison, the Pt—N bond length in $[PtCl_2(PEt_3)]_2(Ph_4P_2N_4Se_2)$, a closely related "distal" platinum(II) complex of **2** is 2.162(9) Å (4), while values of 2.02–2.03 Å are found for complexes of chelating, anionic Se—N ligands (22).

Preparation and ^{31}P nmr characterization of **8**

Investigations of the Lewis base properties of the six-membered ring **5** have shown that the interaction of the P_2N_3S ring with Lewis or Brønsted acids is not regiospecific. Whereas methylation occurs at a nitrogen between phosphorus and sulfur, protonation takes place at the unique nitrogen atom (23). Furthermore, the 1:1 boron trihalide adducts of **5** are mixtures of symmetrical and unsymmetrical *N*-bonded isomers and the formation of a 2:1 BCl_3 adduct is indicated on the basis of ^{31}P nmr investigations. It was of interest, therefore, to include an examination of the ligand behaviour of **5** towards platinum(II) in the current investigation.

The six-membered ring **5** reacts with $[PtCl_2(PEt_3)]_2$ in dichloromethane at room temperature to give the 1:1 adduct **8** in essentially quantitative yield according to the ^{31}P nmr spectrum of the reaction mixture. Attempts to attach a second platinum to the P_2N_3S ring by heating **8** with $[PtCl_2(PEt_3)]_2$ in boiling dichloromethane or chloroform were unsuccessful.

The composition of **8** was established by elemental analyses and the ^1H nmr spectrum (see Experimental section).

[3]This terminology for the conformation of eight-membered rings is taken from ref. 21.

TABLE 3. Selected bond lengths (Å) and bond angles (deg) for $[PtCl_2(PEt_3)]_2$-$[Ph_4P_2N_4Se_2Et_2]$, *7b*

Bond[a]	Length	Bond[a]	Length
Pt(1)-Cl(1)	2.323(3)	Pt(1)-Cl(2)	2.291(3)
Pt(1)-P(2)	2.231(3)	Pt(1)-N(1)	2.130(8)
Se(1)-N(1)	1.991(8)	Se(1)-N(2)	1.554(9)
Se(1)-C(191)	2.00(2)	Se(2)-N(1)	1.887(7)
Se(2)-N(2)	1.622(9)	Se(2)-C(192)	1.99(2)
P(1)-N(1)	1.625(7)	P(1)-N(2)′	1.580(9)
P(1)-C(1)	1.804(9)	P(1)-C(7)	1.82(1)
P(2)-C(13)	1.79(1)	P(2)-C(15)	1.80(1)
P(2)-C(17)	1.85(1)	Se(1)...Se(1)′	2.746(4)
Bonds	**Angle**	**Bonds**	**Angle**
Cl(1)-Pt(1)-Cl(2)	176.0(1)	Cl(1)-Pt(1)-P(2)	87.8(1)
Cl(1)-Pt(1)-N(1)	89.0(2)	Cl(2)-Pt(1)-P(2)	94.6(1)
Cl(2)-Pt(1)-N(1)	88.9(2)	P(2)-Pt(1)-N(1)	175.1(2)
N(1)-Se(1)-C(191)	97.9(6)	N(1)-Se(1)-N(2)	104.9(4)
N(1)-Se(2)-C(192)	99.6(5)	N(2)-Se(1)-C(191)	99.9(6)
N(1)-P(1)-N(2)	116.2(5)	N(1)-Se(2)-N(2)	106.9(4)
N(1)-P(1)-C(7)	109.7(5)	N(2)-Se(2)-C(192)	104.5(6)
N(2)-P(1)-C(7)	108.5(5)	N(1)-P(1)-C(1)	106.9(4)
Pt(1)-P(2)-C(13)	117.1(4)	N(2)-P(1)-C(1)	108.7(5)
Pt(1)-P(2)-C(17)	109.8(4)	Pt(1)-P(2)-C(15)	114.1(4)
Pt(1)-N(1)-Se(1)	109.5(4)	Pt(1)-N(1)-Se(2)	122.0(4)
Pt(1)-N(1)-P(1)	126.4(4)	Se(2)-N(1)-P(1)	108.3(4)
Se(1)-N(1)-P(1)	111.6(5)	Se(1)-N(2)-P(1)′	129.9(6)
Se(2)-N(2)-P(1)′	139.9(7)		

[a]Primed atoms are related to the unprimed atoms by the symmetry: $1 - x, y, 1\frac{1}{2} - z$.

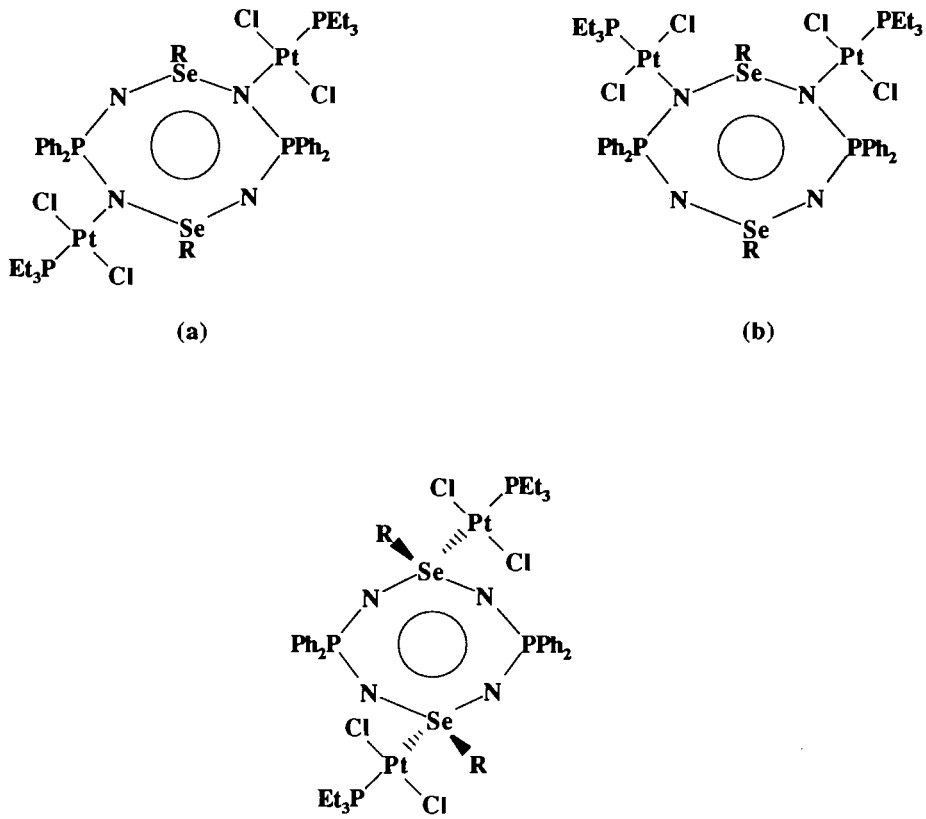

FIG. 1. Structural isomers of $[PtCl_2(PEt_3)]_2(Ph_4P_2N_4Se_2R_2)$: (*a*) *N*-bonded "distal", (*b*) *N*-bonded "vicinal", (*c*) Se-bonded.

Can. J. Chem. Downloaded from www.nrcresearchpress.com by 203.198.23.82 on 09/08/12
For personal use only.

Can. J. Chem. Downloaded from www.nrcresearchpress.com by 203.198.23.82 on 09/08/12
For personal use only.

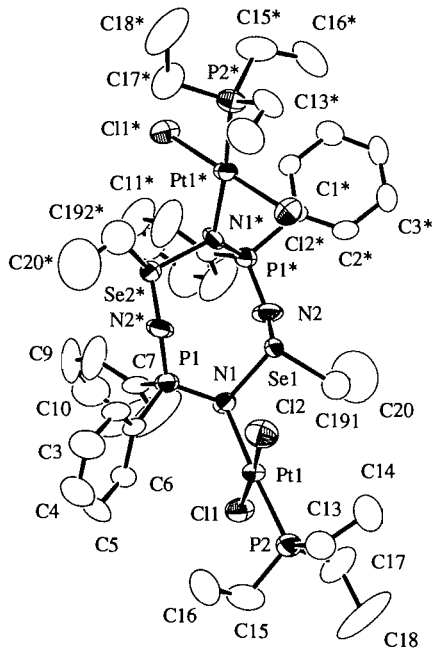

FIG. 2. ORTEP drawing for one long chair conformation of $[PtCl_2(PEt_3)]_2[Ph_4P_2N_4Se_2Et_2]$, *7b*, showing the atomic numbering scheme.

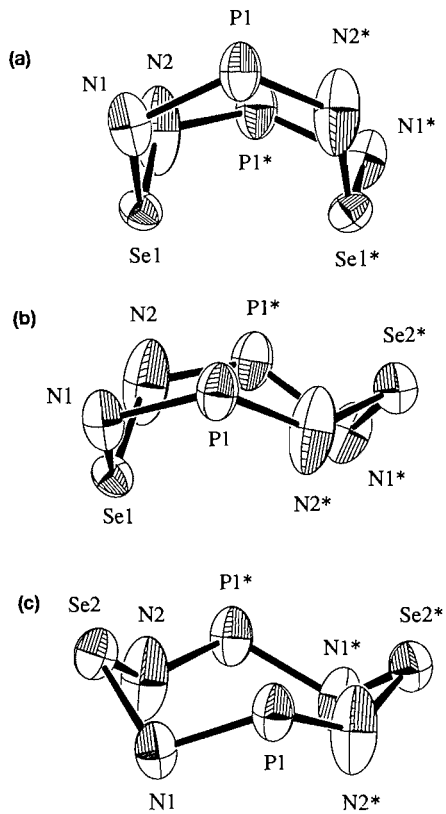

FIG. 3. ORTEP drawings of three conformations of the $P_2N_4Se_2$ ring in *7b*; (*a*) boat–boat (BB), (*b*) crown (CR), (*c*) long chair (LC). Only one of the LC conformations is shown.

The ^{31}P nmr spectrum of **8** is uniquely consistent with a structure in which the $PtCl_2(PEt_3)$ group is attached to one of the sulfur-bonded nitrogen atoms and the PEt_3 ligand is *trans* to nitrogen. Three equally intense resonances are observed at 1.2, 10.0, and 20.5 ppm. The resonance at 1.2 ppm, which appears as a doublet (^3J(P—P) = 10 Hz) with platinum satellites (^1J(Pt—P) = 3637 Hz), is readily attributed to the PEt_3 ligand, while the signals at 10.0 and 20.5 ppm are assigned to the inequivalent ring phosphorus atoms P_C and P_B, respectively. The former appears as a singlet while the latter is a doublet (^3J(P—P) = 10 Hz) with platinum satellites (^2J(Pt—P)~40 Hz). The two-bond coupling between the inequivalent heterocyclic phosphorus atoms, P_B and P_C, could not be resolved. In the *N*-methylated derivative of **5** this coupling is *ca.* 6 Hz, but it was not resolved in the unsymmetrical 1:1 adducts of **5** with BX_3 (X = Cl, F) (23).

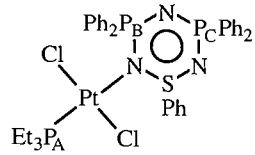

8

Previous studies of the interaction of PNS rings with electrophiles, have shown that the site of electrophilic attack is governed by electrostatic effects (24, 25). In the specific case of the P_2N_3S ring, however, the interaction with BCl_3 or methyl triflate is not regiospecific whereas protonation occurs exclusively at the unique nitrogen atom. It is possible, therefore, that the observed regiospecific adduct formation with the electrophile $PtCl_2(PEt_3)$ is controlled by steric effects.

Conclusions

The eight-membered rings 1,5-$Ph_4P_2N_4E_2R_2$ (E = S, Se) form either 1:1 (E = S) or 2:1 (E = Se) adducts with platinum(II). By contrast, the folded eight-membered ring $Ph_4P_2N_4S_2$ (**1**) forms the 1:1, 2:1, and 3:1 adducts $[PtCl_2(PEt_3)]_n(Ph_4P_2N_4S_2)$ (n = 1–3) (2). An X-ray structure of the 2:1 adduct of the open ring 1,5-$Ph_4P_2N_4Se_2Et_2$ (**4***b*) reveals features similar to those found for the corresponding adduct of the folded ring (4). In both cases the platinum atoms are attached to "distal" nitrogen sites of the $P_2N_4Se_2$ rings and the Pt—N distances are indicative of a weak interaction. The $P_2N_4Se_2$ ring in the 2:1 adduct of **4***b* exists as a mixture of at least two conformations but, as a result of the disorder, it is not possible to assess the effect of adduct formation on the geometrical parameters of the heterocyclic ring. In contrast to the behavior of Lewis and Brønsted acids, adduct formation between the six-membered ring $Ph_4P_2N_3SPh$ and platinum(II) occurs in a regiospecific manner to give the isomer in which the metal is attached to a nitrogen between the phosphorus and sulfur atoms.

Acknowledgements

We thank the Natural Sciences and Engineering Research Council of Canada for financial support. We are grateful to one of the reviewers for helpful comments on the crystallographic section of the manuscript.

1. P.F. Kelly, A.M.Z. Slawin, D.J. Williams, and J.D. Woollins. Chem. Soc. Rev. 246 (1992).
2. T. Chivers and R.W. Hilts. Inorg. Chem. **31**, 5272 (1992).
3. T. Chivers, M. Edwards, A. Meetsma, J.C. van de Grampel, and A. van der Lee. Inorg. Chem. **31**, 2156 (1992).

4. (*a*) T. Chivers, D.D. Doxsee, R.W. Hilts, A. Meetsma, M. Parvez, and J.C. van de Grampel. J. Chem. Soc. Chem. Commun. 1330 (1992); (*b*) T. Chivers, D.D. Doxsee, and R.W. Hilts. Inorg. Chem. **32**, 3244 (1993).
5. T. Chivers, K.S. Dhathathreyan, and T. Ziegler. J. Chem. Soc. Chem. Commun. 86 (1989).
6. T. Chivers, M. Cowie, M. Edwards, and R.W. Hilts. Inorg. Chem. **31**, 3349 (1992).
7. T. Chivers, M. Edwards, P.N. Kapoor, A. Meetsma, J.C. van de Grampel, and A. van der Lee. Inorg. Chem. **29**, 3068 (1992).
8. T. Chivers, M. Edwards, R.W. Hilts, A. Meetsma, and J.C. van de Grampel. J. Chem. Soc. Dalton Trans. 3053 (1992).
9. (*a*) T. Chivers, D.D. Doxsee, and J.F. Fait. J. Chem. Soc. Chem. Commun. 1703 (1989); (*b*) T. Chivers, D.D. Doxsee, J.F. Fait, and M. Parvez. Inorg. Chem. **32**, 2243 (1993).
10. T. Chivers, S.S. Kumaravel, A. Meetsma, J.C. van de Grampel, and A. van der Lee. Inorg. Chem. **29**, 4591 (1990).
11. M. Liang and I. Manners. J. Am. Chem. Soc. **113**, 4044 (1991).
12. J.A. Dodge, I. Manners, H.R. Allcock, G. Renner, and O. Nuyken. J. Am. Chem. Soc. **112**, 1268 (1990).
13. T. Chivers and M.N.S. Rao. Inorg. Chem. **23**, 3605 (1984).
14. J. Chatt and L.M. Venanzi. J. Chem. Soc. 2787 (1955).
15. teXsan: Crystal structure analysis packages, Molecular Structure Corporation. 1985 and 1992.
16. N. Walker and D. Stuart. Acta Crystallogr. **A39**, 158 (1983).
17. SAPI91: H.-F. Fan. Structure analysis programs with intelligent control. Rigaku Corporation, Tokyo, Japan. 1991.
18. DIRDIF92: P.T. Beurskens, G. Admiraal, G. Beurskens, W.P. Bosman, S. Garcia-Granda, R.O. Gould, J.M.M. Smits, and C. Smykalla. Technical Report of the Crystallography Laboratory, University of Nijmegen, The Netherlands. 1992.
19. D.T. Cromer and J.T. Waber. International tables for X-ray crystallography. Vol. IV. Kynoch Press, Birmingham, England. 1974.
20. J.A. Ibers and W.C. Hamilton. Acta Crystallogr. **17**, 781 (1964).
21. V.A. Palyulin, N.S. Zefirov, V.E. Shklover, and Yu.T. Struchkov. J. Mol. Struct. **70**, 65 (1981).
22. (*a*) P.F. Kelly, I.P. Parkin, A.M.Z. Slawin, D.J. Williams, and J.D. Woollins. Angew. Chem. Int. Ed. Engl. **28**, 1047 (1989); (*b*) C.A. O'Mahoney, I.P. Parkin, D.J. Williams, and J.D. Woollins. Polyhedron, **8**, 2215 (1989).
23. T. Chivers, J.F. Fait, and S.W. Liblong. Inorg. Chem. **28**, 2803 (1989).
24. T. Chivers, S.W. Liblong, J.F. Richardson, and T. Ziegler. Inorg. Chem. **27**, 860 (1988).
25. T. Chivers, S.W. Liblong, J.F. Richardson, and T. Ziegler. Inorg. Chem. **27**, 4344 (1988).

Can. J. Chem. Downloaded from www.nrcresearchpress.com by 203.198.23.82 on 09/08/12
For personal use only.

Light-induced change of the molecular charge in a spironaphthoxazine compound

PAUL RYS,[1] RUTH WEBER, AND QINGLAN WU

Department of Industrial and Engineering Chemistry, Swiss Federal Institute of Technology, ETH, ETH-Zentrum, CH-8092 Zürich, Switzerland

Received March 4, 1993

PAUL RYS, RUTH WEBER, and QINGLAN WU. Can. J. Chem. **71**, 1828 (1993).

To evaluate the experimental conditions for the light-induced change of the molecular charge, the dependence of the photochromic reaction behaviour of the indolino spiro naphthoxazine compound 1,3,3-trimethyl-spiro[2*H*-indol 2,3′-[3*H*]naphth[2,1-*b*]-[1,4]oxazine] on the pH value of the solution is investigated. In the absence of UV light an acid–base equilibrium between the spiro form and a protonated closed form is established. By irradiation under appropriate acidic conditions the spiro form can be transformed into an open cationic form through the merocyanine form. Between the two open forms an acid–base equilibrium is established. Except for the closed protonated form the structures are confirmed by mean of NMR. The kinetics of the thermal ring-closing reaction of both forms are investigated by flash photolysis. It is shown that the ring-closing reaction proceeds exclusively via the merocyanine form. The p*K* values determined for both equilibria give the pH range, in which the light-induced change of the molecular charge occurs.

PAUL RYS, RUTH WEBER et QINGLAN WU. Can. J. Chem. **71**, 1828 (1993).

Dans le but d'évaluer les conditions expérimentales conduisant à un changement induit par la lumière de la charge moléculaire, on a étudié la dépendance du comportement de la réaction photochromique du composé indoline spiro naphtoxazine, 1,3,3-triméthyl-spiro[2*H*-indole-2,3′-[3*H*]napht[2,1-*b*]-[1,4]oxazine], sur la valeur du pH de la solution. En l'absence de lumière UV, il s'établit un équilibre acide–base entre la forme spiro et une forme protonée fermée. Par irradiation dans des conditions acides appropriées, on peut transformer la forme spiro en une forme cationique ouverte par le biais de la forme mérocyanine. Il s'établit un équilibre acide–base entre les deux formes ouvertes. À l'exception de la forme protonée fermée, on a confirmé les structures par RMN. Faisant appel à la photolyse éclair, on a étudié la cinétique de la réaction thermique de fermeture de cycle des deux formes. Il est démontré que la réaction de fermeture de cycle se produit uniquement par le biais de la forme mérocyanine. Les valeurs de p*K*, déterminées pour les deux équilibres, fournissent les valeurs de pH dans lesquelles le changement de charge moléculaire induit par la lumière se produit.

[Traduit par la rédaction]

Introduction

Recently, the photochromic behaviour of indolinospiro-oxazine derivatives has been intensively investigated (1–6). This is mainly due to their rapid photoresponsive change of the molecular structure and the better photodurability as compared to the indolinospiropyran derivatives. The photochromism and the acid–base behaviour of indolinospiro compounds is summarized in Scheme 1.

By UV irradiation the C—O bond of the colourless spiroform A is cleaved and the coloured merocyanine form B is formed. The reverse reaction proceeds thermally or photochemically (5–11). In the case of spiropyran derivatives it has been established (12–18) that the zwitterionic B-form can be protonated to the cationic C-form. The same is expected for spirooxazine compounds.

Due to the different electronic structures and molecular geometries of the A-, the B-, and the C-forms, their physical and chemical properties, such as colour, polarity, charge, and their acidity and basicity are also different. The possibility to switch between the various forms and thus the various properties by turning the UV light on and off makes the spiro compounds interesting for practical purposes (6, 7). For optical data recording or regulation of light fluxes the interconversion between the spiro form A and the open form B is important. The merocyanine form B is obtained if the pH of the solution is in the range $pH > pK_1 > pK_2$. Most investigations dealing with the photochromism of spiro compounds have been carried out in this pH range (19–26). To obtain a light-induced change of the molecular charge the pH of the solution must be in the range $pK_1 < pH < pK_2$. Under these conditions the neutral spiro form A is transformed into the positively charged C-form by UV light. In the case of adsorbed spiropyran derivatives the light-induced change of the molecular charge can influence considerably the behaviour of the substrate, such as in polymer membranes (27, 28) or enzymes (29).

The present study aims at achieving a better understanding of the light-induced, reversible transformation of the A- into the C-form of the spironaphthoxazin compound 1,3,3-trimethyl-spiro[2*H*-indol 2,3′-[3*H*]naphth[2,1-*b*]-[1,4]-oxazine] **SP**.

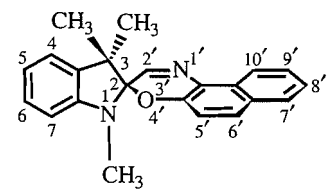

Compound **SP**

The structures of the various forms are investigated by ^1H NMR experiments. The acid–base equilibria described in Scheme 1 as well as the kinetics of the thermal decolouration of the B- and the C-forms are studied quantitatively in buffered 50% (v/v) ethanol–water solutions at various pH values.

Experimental

Synthesis

The spirooxazin **SP** was synthesized following a method described in the literature (30).

[1]Author to whom correspondence may be addressed.

Can. J. Chem. Downloaded from www.nrcresearchpress.com by 203.198.23.82 on 09/08/12
For personal use only.

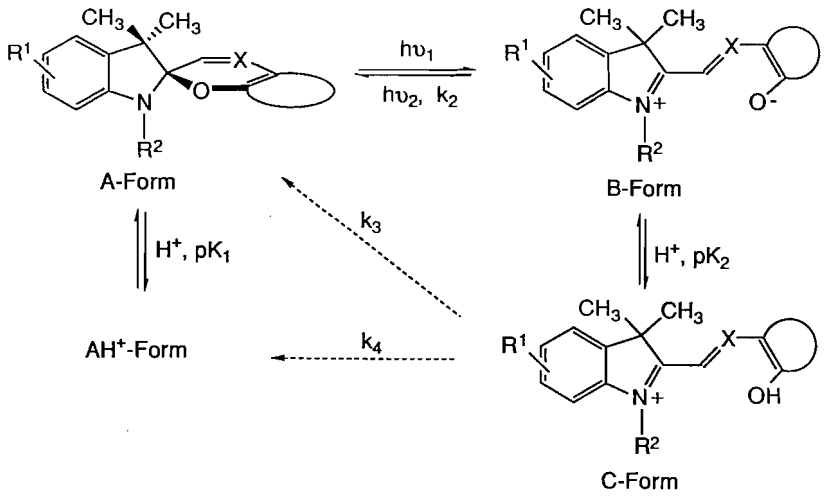

SCHEME 1. Photochromism of indolinospiro compounds under neutral and acidic conditions; X = CH: spiropyrane; X = N: spiroxazine; R_1, R_2: substituents.

TABLE 1. Buffer systems used to prepare the aqueous ethanolic solutions

Buffer system	pH range
0.01 M potassium hydrogen phthalate 0.01 M HCl	2.7–4.0
0.01 M potassium hydrogen phthalate 0.01 M NaOH	5.0
0.01 M potassium dihydrogen phosphate 0.01 M NaOH	6.0–8.0
0.005 M sodium bicarbonate 0.01 M NaOH	10.0

^1H NMR

The ^1H NMR spectra of the various forms of compound **SP** were determined in acetone-d_6 at −80°C on a Brucker AM300 WB. The concentration of the solution investigated was 0.03 M. After measuring the spectrum of the closed A-form, the NMR tube was transferred into a thermostated vessel and the solution was irradiated with UV light for 5 min. The spectrum of the B-form was measured immediately after irradiation. To obtain the spectrum of the C-form, 1–2 drops of 98% D_2SO_4 was added into the irradiated solution.

Kinetic studies and determination of pK_1 and pK_2

The kinetic studies and the determination of the dissociation constants of the AH^+- and the C-forms were carried out in buffered aqueous ethanolic solutions of compound **SP**. The buffer systems used to prepare the solutions are listed in Table 1, the various pH values were obtained according to 31.

The ionic strength of the buffer solutions was adjusted to 0.1 M by adding sodium chloride.

The spirooxazin compound **SP** was dissolved in ethanol and mixed with the buffer solutions in the ratio of 1:1 by volume. The concentration of compound **SP** in the final solution was $c = 2.317 \times 10^{-5}$ M.

The pH of the buffered ethanolic solutions was measured using a glass electrode. The values were corrected for solvent effects by subtracting 0.26 from the measured pH. The correction term was determined from a master curve obtained by measuring the pH of a set of standard solutions (32–35).

The dissociation constants pK_1 and pK_2 were determined from the pH dependence of the absorption of the AH^+-form at 350 nm and of the B- and C-forms at 620 nm and 530 nm, respectively.

The kinetics of the thermal ring-closing reactions and the VIS spectra of the irradiated solutions were studied using flash photolysis. The solutions were irradiated by a flash from a high-pressure mercury lamp. Immediately after irradiation, the absorption of the solutions was measured continuously at 530 and 620 nm.

Results and discussion

Photochromism and acid–base equilibria

The pH dependence of the UV spectra of compound **SP** in aqueous ethanolic solutions (1:1) before irradiation is shown in Fig. 1. Under slightly acidic conditions (curve 1) the spectrum of the colourless spiro form A with a maximum absorption at λ = 230 nm is obtained. With acidified solutions an additional peak appears at λ = 215 nm, the intensity of which increases with increasing acid concentration. This indicates the formation of a protonated form AH^+. The curves in Fig. 1 show three isobestic points at λ = 230, 260, and 290 nm, respectively. Thus, the total concentration of the A- and the AH^+-forms remains constant and an acid–base equilibrium is established between the two forms.

Figure 2 shows the VIS spectra of irradiated solutions of compound **SP** under neutral (curve 1) and acidic (curve 2) conditions, respectively. By irradiation of the neutral solution, the spiro form A is transformed into the merocyanine form B, which absorbs at λ_{max} = 620 nm. In ref. 6 the VIS spectrum of an irradiated solution of **SP** in pure ethanol at −75°C shows the maximum of absorption at 612 nm and a shoulder at 578 nm. A shoulder might be the explanation of the unsymmetrical shape of curve 1 in Fig. 2. As curve 2 in Fig. 2 shows, a new form is produced by irradiation of the acidic solution. In similar investigations with spiropyran derivatives (12–18) a protonated open structure is suggested for the form existing under the experimental conditions applied. The structure of the C-form in Scheme 1 with the long conjugated π-electron system may account for the maximum absorption at λ = 530 nm seen in Fig. 2.

To confirm the structure of the various forms suggested in Scheme 1, ^1H NMR spectra of neutral and acidic solutions before and after irradiation were measured. Since the thermal ring-opening reaction can be neglected at −80°C, the spectrum of the pure A-form is obtained at this temperature from the neutral solution. After irradiation, the peaks of the

Can. J. Chem. Downloaded from www.nrcresearchpress.com by 203.198.23.82 on 09/08/12
For personal use only.

A- and the B-forms coexist in the measured ^{1}H NMR spectrum. From the intensities of the signals an approximate conversion of about 40% can be estimated. In the spectrum of the acidified irradiated solution no peaks of the A- and the B-forms were found. This indicates a complete conversion to the C-form.

Due to the low solubility of compound **SP** in aqueous ethanol, the ^{1}H NMR spectra had to be measured in acetone-d_6. The protonated form AH^+, postulated from the results of the UV/VIS spectroscopy (Fig. 1), could not be found in this solvent. Thus, no information about the structure of the AH^+ form was available from NMR spectroscopy.

The significant peaks to distinguish between the spiro and the open structures of compound **SP** are those of the methyl groups at the C3 atom of the indolering. The existence and localization of the positive charge postulated for the open forms B and C can be discussed by means of the signals of the methyl group at the indole nitrogen atom. The chemical shifts measured in the spectra are listed in Table 2.

In the ^{1}H NMR spectrum of the neutral solution two singlets at 1.27 and 1.31 ppm, respectively, are seen for the two methyl groups at the C3 atom, which indicates that the two groups must be diastereotopic. This is in agreement with the unsymmetrical substitution of the spiro carbon. In the open merocyanine form, however, the two methyl groups become equivalent and therefore they are expected to show up as a single peak. Indeed this is the case with both the B- and the C-forms, as is shown in Table 2. Based on the NMR spectra, the postulated open structure of the C-form, which allows for the free rotation of the naphthol ring, could be confirmed.

The singlets of the methyl protons at the nitrogen atom of the indole ring are found at 2.73, 3.68, and 4.47 ppm for the A-, the B-, and the C-forms, respectively. The shift of the signal to lower magnetic fields indicates a decreasing electron density and thus an increasing positive charge at the indole nitrogen atom. The existence of a positive charge localized on the indole nitrogen in the C-form of compound **SP** can further be confirmed by the similarity of the chemical shifts of the peaks of the N-CH_3 protons of the C-form to those of the positively charged model compound 5-cyano-1,3,3-trimethyl-2-methylen-3*H*-indol.

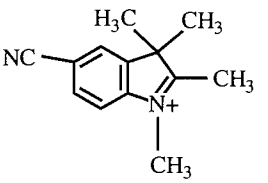

δ_{NCH_3} = 3.94 ppm (solv. CD_3CN)

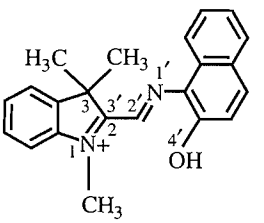

SP, C-Form

δ_{NCH_3} = 4.47 ppm (solv. CD_3COCD_3)

There are three positions in the B-form that can be protonated, namely, the indole nitrogen, the nitrogen N1′, and the oxygen O4′. Since the positive charge of the zwitterionic B-form is localized on the indole nitrogen and the difference of the chemical shifts of the proton at carbon C2′ in the B- and C-forms (Table 2) is very small, the protonation at one of the two nitrogen atoms can be excluded. Thus, the most probable position for a protonation of the B-form is the oxygen atom O4′, as suggested in Scheme 1.

According to the UV spectra in Fig. 1 an acid–base equilibrium between the spiroform A and a protonated form AH^+ is established under the experimental conditions applied. To determine the corresponding equilibrium constant K_1, the absorption of a number of buffered aqueous ethanolic solutions of compound **SP** was measured at λ = 350 nm. The results are shown in Table 3.

Using eq. [1]

$$[1] \quad pK = pH + \log \frac{A_{(\lambda)} - A_{M(\lambda)}}{A_{HM(\lambda)} - A_{(\lambda)}}$$

with pK: −log (acidity constant),

$A_{(\lambda)}$: measured absorption at the wavelength λ,

and the $A_{(\lambda)}$ values listed in Table 3, pK_1 = 2.26 ± 0.06 is obtained.

In Scheme 1 an acid–base equilibrium is also postulated between the open forms B and C of compound **SP**. The equilibrium is coupled to the kinetics of the thermal decolouration reactions of the two forms. By continuous absorption measurements at λ = 620 nm and λ = 530 nm the concentrations of the B- and the C-forms were measured as a function of time starting immediately after the irradiation of the solutions. For any solution investigated, the ratio of the absorption of the B-form and the C-form is constant over the reaction time, as shown in Fig. 3. Consequently, the acid–base equilibrium between the two forms is established during the decolouration reaction and eq. [1] can be used to determine pK_2. From the $A_{(\lambda)}$ values shown in Table 4, pK_2 = 4.00 ± 0.05 is obtained.

The coupling between the acid–base equilibrium and the thermal decoloration reactions

The continuously measured decrease of the absorption of the B- and C-forms of compound **SP** is shown in Fig. 4 for pH = 5.0. For all solutions investigated, the thermo decolouration of both forms is seen to be a first-order reaction, the kinetics of which can be described by eqs. [2] and [3].

$$[2] \quad -\frac{d[B]}{dt} = k_{Bexp}[B]$$

$$[3] \quad -\frac{d[C]}{dt} = k_{Cexp}[C]$$

with [B], [C]: concentrations of the B- and the C-forms and

Can. J. Chem. Downloaded from www.nrcresearchpress.com by 203.198.23.82 on 09/08/12
For personal use only.

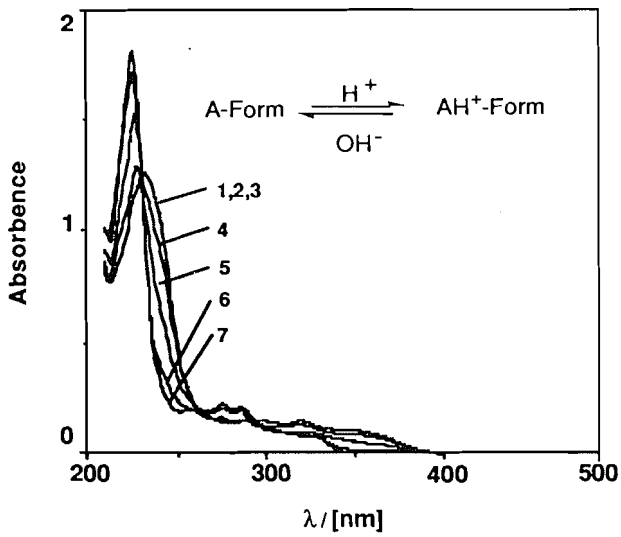

FIG. 1. UV/VIS spectra of 50% aqueous ethanolic solutions of compound **SP** in dependence on the pH value, T = 20°C; c = 2.317 × 10^{-5} M; no UV irradiation. 1: pH = 4.52; 2: pH = 3.88; 3: pH = 3.19; 4: pH = 2.67; 5: pH = 2.04; 6: pH = 1.44; 7: pH = 1.28.

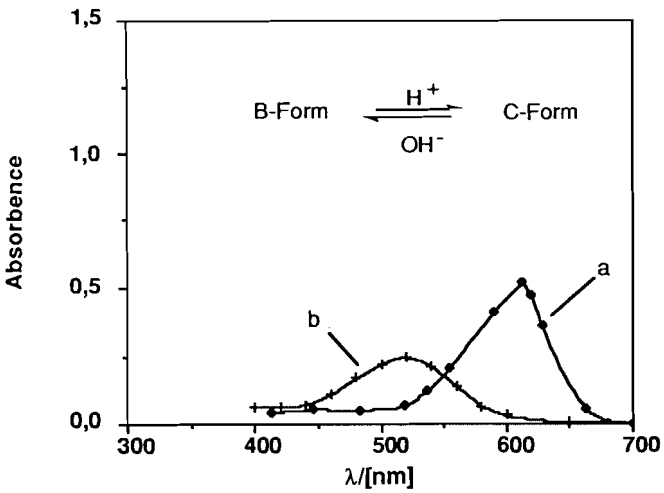

FIG. 2. VIS spectra of irradiated 50% aqueous ethanolic solutions of compound **SP** under neutral (a: pH = 7.0) and acidic (b: pH = 3.0) conditions, T = 20°C; c = 2.317 × 10^{-5} M.

TABLE 2. Chemical shifts of the essential peaks in the ^{1}H NMR spectra of the A-, B-, and C-forms of compound **SP** in acetone-d_6 at −80°C

Proton	Chemical shift (ppm)		
	A-form	B-form	C-form
$C(3)(CH_3)_2$	1.27; 1.31	1.86	2.06
$N(1)CH_3$	2.73	3.68	4.47
C(10′)-H	8.53	8.30	8.61
C(2′)-H	7.95	10.09	10.17

k_{Bexp}, k_{Cexp}: experimentally determined reaction rate constants.

The reaction rate constants calculated from the experimental results are listed in Table 4 together with the corresponding pH values of the solution.

TABLE 3. Absorption of compound **SP** at λ = 350 nm in dependence on the pH value of the solutions

pH	1.64	1.71	2.05	2.78	3.68	4.48	6.80
$A_{(350\ nm)}$	0.093	0.120	0.193	0.413	0.468	0.500	0.527

T = 20°C; solvent: ethanol/water = 1/1 (v/v); c = 2.18 × 10^{-4} M; A_M = 0.527; A_{HM} = 0.000.

For any chosen pH value of the solutions investigated, the reaction rate constants of the decolouration of the B- and the C-forms are equal within experimental error. With increasing pH, k_{Bexp} and k_{Cexp} increase, and for pH > 5 approach the constant value 0.152 ± 0.002 s^{-1}. Similar effects have been found for spiropyran derivatives (36). Scheme 1 outlines decolouration pathways considered, which are coupled to the acid–base equilibrium between the B- and the C-forms. Taking into account the first-order kinetics of the decolouration reactions, the change of the total concentration of the B- and the C-forms is described by eq. [4].

$$[4] \quad -\frac{d([B] + [C])}{dt} = k_2[B] + (k_3 + k_4)[C]$$

By introducing the equilibrium constant K_2

$$[5] \quad K_2 = \frac{[H^+][B]}{[C]}$$

into eq. [4] and eliminating the concentration of the C-form, eq. [6] is obtained.

$$[6] \quad \frac{d[B]}{dt} = -\frac{k_2K_2 + (k_3 + k_4)[H^+]}{K_2 + [H^+]}[B]$$

For a constant pH value, eq. [6] describes a first-order reaction with the overall reaction rate constant k_{Bcal}.

$$[7] \quad k_{Bcal} = \frac{k_2K_2 + (k_3 + k_4)[H^+]}{K_2 + [H^+]}$$

For the C-form, the same calculation leads to eqs. [8] and [9].

$$[8] \quad \frac{d[C]}{dt} = -\frac{k_2K_2 + (k_3 + k_4)[H^+]}{K_2 + [H^+]}[C]$$

$$[9] \quad k_{Ccal} = \frac{k_2K_2 + (k_3 + k_4)[H^+]}{K_2 + [H^+]}$$

Comparison of eqs. [7] and [9] shows, that k_{Bcal} and k_{Ccal} are identical for any chosen pH value. Furthermore, if $(k_3 + k_4) \ll k_2$ and $[H^+] < K_2$ then k_{Bcal} and k_{Ccal} approach the constant value k_2. Thus, eqs. [7] and [9] show qualitatively the same pH dependence of the reaction rate constants as the experimentally determined values listed in Table 3.

Introducing k_2 = 0.152 ± 0.002 s^{-1} into eq. [7] or [9], the expression [10] with the fit parameter $(k_3 + k_4)$ and K_2 is obtained.

$$[10] \quad k_{Ccal} = k_{Bcal} = k_{cal} = \frac{k_2K_2 + (k_3 + k_4)[H^+]}{K_2 + [H^+]}$$

Can. J. Chem. Downloaded from www.nrcresearchpress.com by 203.198.23.82 on 09/08/12
For personal use only.

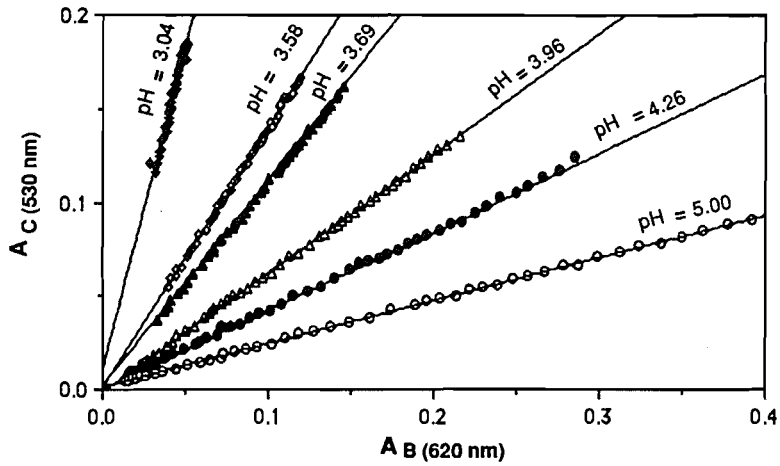

FIG. 3. Absorption $A_{B(530\ nm)}$ and $A_{C(620\ nm)}$ of compound **SP** during the thermal decolouration reaction.

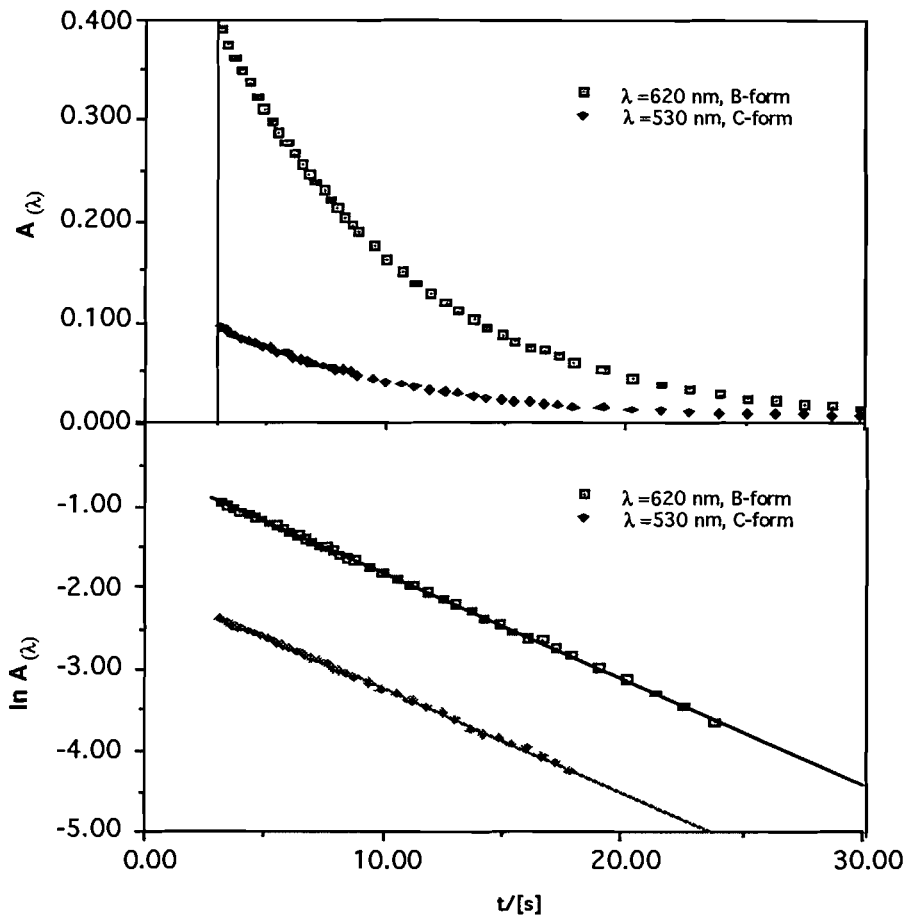

FIG. 4. Time dependence of the absorption ($A_{(\lambda)}$ and ln $A_{(\lambda)}$) of the B- and the C-forms of compound **SP** in the solution of pH = 5.0 during the decolouration reaction.

Using eq. [10], the best fit for the experimentally determined values k_{Bexp} and k_{Cexp} is obtained with $(k_3 + k_4) = 0$ and $pK_2 = 3.95$. In Fig. 5 the experimental results are presented together with the fitting curve. The fit parameter $pK_2 = 3.95$ and the experimentally determined value $pK_2 = 4.0 \pm 0.05$ are in good agreement within experimental error.

Since $(k_3 + k_4) = 0$, the direct decolouration from the C-form to the A- or AH^+-form as considered in Scheme 1 can be neglected. Thus, the ring closure of the C-form proceeds via the B-form. This is in agreement with the fact observed in the experiments, that the equilibrium between the B- and the C-forms is established during the decolouration and the reaction rate constants k_{Bexp} and k_{Cexp} are the same for both forms.

Conclusion

To study the light-induced change of the molecular charge, the pH dependence of the photochromic properties of the

Can. J. Chem. Downloaded from www.nrcresearchpress.com by 203.198.23.82 on 09/08/12
For personal use only.

TABLE 4. Reaction rate constants k_{Bexp} and k_{Cexp} and the absorption of the B- and the C-forms of compound **SP** in dependence on the pH value

pH	$A_{B(620\ nm)}$	$A_{C(530\ nm)}$	k_{Bexp} (s^{-1})	k_{Cexp} (s^{-1})
3.04	0.057	0.180	0.017	0.017
3.58	0.116	0.162	0.042	0.042
3.69	0.144	0.160	0.056	0.057
3.96	0.211	0.133	0.087	0.086
4.26	0.298	0.124	0.112	0.113
5.00	0.397	0.090	0.129	0.132
6.48	0.451	0.093	0.148	0.149
7.61	0.476	0.090	0.154	0.150
7.65	0.477	0.091	0.152	0.152
8.59	0.471	0.087	0.148	0.149
10.79	0.483	0.089	0.151	0.149

T = 20°C; solvent: ethanol/water = 1:1 (v/v); irradiated solution c = 2.317×10^{-5} M; I = 0.05 M.

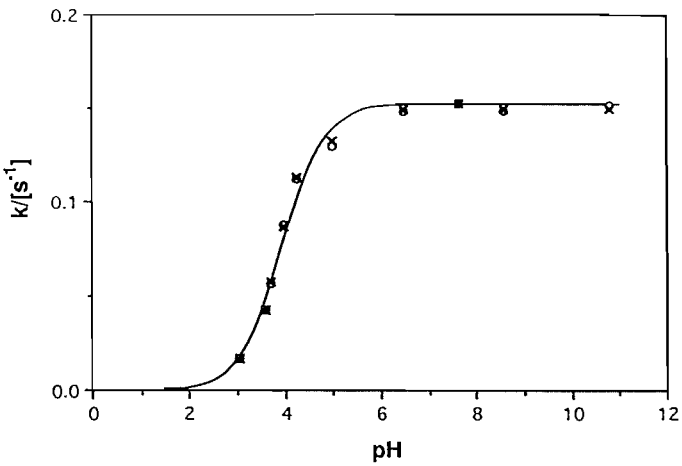

FIG. 5. Comparison of the calculated and experimentally determined reaction rate constants of the decolouration of the B- and the C-forms. o: k_{Bexp}; x: k_{Cexp}; —: k_{cal}.

spirooxazin compound **SP** in buffered aqueous ethanolic solutions was investigated. In the absence of UV light, the compound mainly existed in the uncharged spiroform A. By irradiation, the zwitterionic merocyanine form B was produced. In acidified solutions, an acid–base equilibrium between the spiroform A and AH^+ was established. By acidifying an irradiated solution, the merocyanine form B could be protonated. With the help of ^1H NMR measurements, the structure of the new form C was identified as a ring-open structure with the positive charge localized on the nitrogen atom of the indole ring. Furthermore, the existence of an acid–base equilibrium between the B- and the C-forms was confirmed by flash photolysis experiments. Results from the present studies would suggest that the ring closure of the C-form proceeds via the B-form. As the B-form undergoes decolouration, the equilibrium between the B- and the C-forms is shifted towards the formation of the B-form, thus compensates its disappearance.

The dissociation constants of the AH^+- and the C-forms were determined as $pK_1 = 2.3$ and $pK_2 = 4.0$, respectively. Thus, a light-induced transformation between the neutral spiroform A and the positively charged C-form could be achieved in the pH range $2.3 < pH < 4.0$.

1. N.Y.C. Chu. Can. J. Chem. **61**, 300 (1983).
2. S. Schneider, A. Mindl, and G. Elfinger. Ber Bunsen-Ges. Phys. Chem. **91**, 1222 (1987).
3. S. Aramaki and G.H. Atkinson. Chem. Phys. Lett. **170**, 181 (1990).
4. Q. Wu. Ph. D. Thesis, ETH Nr. 9520, Zürich (1991).
5. J.C. Crano, W.S. Kwak, and C.N. Welch. *In* Applied photochromic polymer systems. *Edited by* C.B. Mc Ardle. Chapman and Hall, New York. 1992.
6. N.Y.C. Chu. *In* Photochromism, molecules and systems. *Edited by* H. Dürr and H. Bonas-Laurent. Elsevier, Amsterdam. 1990. Chap. 10, p. 493, and references therein.
7. R.C. Bertelson. *In* Photochromism. *Edited by* G.H. Brown. Wiley–Interscience, New York. 1971. Chap. III, p. 45, and references therein.
8. M. Gehrtz, C. Bräuchle, and J. Voitländer. J. Am. Chem. Soc. **104**, 2094 (1982).
9. N.P. Ernsting. Chem. Phys. Lett. **159**, 526 (1989).
10. Y. Kalisky, T.E. Orlowski, and D.J. Williams. J. Phys. Chem. **87**, 5333 (1983).
11. C. Lenoble and R.S. Becker. J. Phys. Chem. **90**, 62 (1986).
12. T. Bercovici, R. Eiligman-Rim, and E. Fischer. Mol. Photochem **1**, 189 (1969).
13. L.S. Atabekyan and A.K. Chibisov. J. Photochem. **31**, 123 (1985).
14. I. Shimizu, H. Kokado, and E. Inoue. Bull. Chem. Soc. Jpn. **42**, 1726 (1969).
15. I.R. Bellobono, S. Calgari, A. Berlin, D. Nosari, and M.F. Perrone. Gazz. Chim. Ital. **110**, 613 (1980).
16. I.R. Bellobono, S. Giovavardi, B. Marcandalli, S. Calgari, and D. Nosari. Polym. Photochem. **4**, 59 (1984).
17. I.R. Bellobono, B. Marcandalli, E. Selli, and S. Calgari. Photogr. Sci. Eng. **28**, 162 (1984).
18. C.J. Drummond and D.N. Furlong. J. Chem. Soc. Faraday Trans. **86**, 3613 (1990).
19. D.A. Holden, H. Ringsdorf, V. Deblauwe, and G. Smets. J. Phys. Chem. **88**, 716 (1984).
20. C.B. McArdle and H.S. Blair. Colloid Polym. Sci. **262**, 481 (1984).
21. T. Shimidzu and M. Yoshikawa. J. Membr. Sci. **13**, 1 (1983).
22. S. Hayashida, H. Sato, and S. Sugawara. Polym. J. **18**, 227 (1986).
23. T. Seki and K. Ichimura. Macromolecules, **20**, 2959 (1987).
24. K. Namba and S. Suzuki. Chem. Lett. 947 (1975).
25. E. Ando, K. Moriyama, K. Arita, and K. Morimoto. Langmuir, **6**, 1451 (1990).
26. C.J. Drummond, D.N. Furlong, and G. Georgaklis. Chem. Soc. Faraday Trans. **86**, 3913 (1990).
27. J. Anzai, Y. Hasebe, A. Ueno, and T. Osa. Bull. Chem. Soc. Jpn. **61**, 2959 (1988).
28. S. Kato, M. Aizawa, and S. Suzuki. J. Membr. Sci. **1**, 289 (1976); J. Membr. Sci. **2**, 39 (1977); J. Membr. Sci. **3**, 289 (1977).
29. K. Namba and S. Suzuki. Chem. Lett. Jpn. 947 (1975).
30. E. Berman, R.E. Fex, and F.D. Thomson. J. Am. Chem. Soc. **81**, 5605 (1959).
31. Handbook of chemistry and physics. 64th ed. CRC Press, Boca Rota, Fla. 1983–1984.
32. H. Galster. *In* pH-Messung: Grundlagen, Methoden, Anwendungen, Geräte. VCH, Weinheim. 1990.
33. T. Mussini, A.K. Covington, P. Longhi, and S. Rondinini. Pure Appl. Chem. **57**, 805 (1985).
34. G. Bates, M. Paabo, and R.A. R. Robinson. J. Phys. Chem. **67**, 1833 (1963).
35. E.J. Gelsema, C.L. de Ligny, A.G. Remijnse, and H.A. Blijleven. Recl. Trav. Chim. Pays-Bas, **85**, 647 (1966).
36. T. Yamaguchi, T. Tamaki, Y. Kawanish, T. Seki, and M. Sakuragi. J. Chem. Soc. Chem. Commun. 867 (1990).

Can. J. Chem. Downloaded from www.nrcresearchpress.com by 203.198.23.82 on 09/08/12
For personal use only.

Solvatochromic parameters and solubilities in supercritical fluid systems

MARK L. O'NEILL[1] AND PEETER KRUUS
Department of Chemistry, Carleton University, Ottawa, ON K1S 5B6, Canada

AND

ROBERT C. BURK
Centre for Analytical and Environmental Chemistry, Carleton University, Ottawa, ON K1S 5B6, Canada

Received November 13, 1992[2]

MARK L. O'NEILL, PEETER KRUUS, and ROBERT C. BURK. Can. J. Chem. **71**, 1834 (1993).

Spectroscopic studies of the compound 2-nitroanisole in supercritical fluids CO_2 and N_2O show that π^* values vary linearly with density. The solubility trends in these single component supercritical fluid solvents qualitatively followed the trends in solvent power predicted from π^*. However, the relative solvent power predicted for CO_2 and N_2O based on π^* resulted in an opposite order to what was determined experimentally through solubility measurements. The π^* parameter may be of some use for solubility prediction if only a limited set of solute–solvent systems are considered. Measurements of π^*, especially those in binary supercritical fluid solvents, suggest that π^* could be a valuable tool for probing the solute-organized cybotactic region.

MARK L. O'NEILL, PEETER KRUUS et ROBERT C. BURK. Can. J. Chem. **71**, 1834 (1993).

Des études spectroscopique du 2-nitroanisole dans les liquides supercritiques CO_2 et N_2O présente des valeurs de π^* qui varient d'une façon linéaire avec la densité. Les variations de solubilité dans ces fluides supercritiques à un seul composant suivent qualitativement les tendances du pouvoir de solvant que l'on peut prédire à l'aide de π^*. Toutefois, les pouvoirs relatifs de solvant prédits pour le CO_2 et le N_2O sont opposés à ceux déterminés expérimentalement par les mesures de solubilité. Le paramètre π^* peut s'avérer utile pour prédire la solubilité si on ne considère qu'un ensemble limité de systèmes soluté–solvant. Les mesures de π^*, spécialement celles dans des solvants supercritiques binaires, suggèrent que π^* peut s'avérer un outil utile pour étudier la région cybotactique d'un soluté organisé.

[Traduit par la rédaction]

Can. J. Chem. Downloaded from www.nrcresearchpress.com by 203.198.23.82 on 09/08/12
For personal use only.

Introduction

The use of supercritical fluids (SCFs) in extraction technology has become more common over the past several years (1, 2). One of the advantages of SCFs over liquid solvents is that their high compressibilities allow for substantial and continuous changes in density and other physicochemical properties without changing the chemical nature of the solvent.

Theories of solvation for liquid state solvents are well established (3, 4), but extensions of these to supercritical fluids are often not available. The characterization of solute–solvent interactions through such things as shifts in the ultraviolet–visible absorption maxima of organochromophores (solvatochromic shifts) should make it possible to predict solubilities in fluid solvents, including SCFs. Solvatochromic shifts are indicative of the types of interactions between the solvent and the solute in the immediate vicinity of the solute, referred to as the solute's cybotactic region. The resulting changes in the physical properties of the supercritical fluid are reflected by changes in the solvatochromic parameter π^*.

Several groups have used the solvatochromic parameter π^* to predict solvent strength (5–9). Some studies have also examined the behaviour of π^* in SCF solvents (10, 11). The variability of solvent power through density in one-component SCF solutions makes it possible to test the validity of the linear free energy relations underlying the concept of solvatochromic shifts. Here the relation tested is that between the logarithm of the solubility and π^*.

Binary SCF solvents are often used in SCF extractions as they can improve the solvent power and selectivity. An organic cosolvent (i.e., the minor component of the solvent mixture) can have the ability to extend the range of the desirable characteristics of the fluid to much lower pressures while retaining the major advantages of SCFs (1). In binary solvent systems a preferential enrichment (clustering) by one of the solvent components in the cybotactic region of a compound is detectable by changes in π^*. It is of interest here to quantify this effect in both single and binary SCF solvents in order to accurately predict changes in the solvent power from π^* values.

Linear free energy relations

Linear free energy relationships for solutions are used to quantify solvent effects on many types of physicochemical properties. The shifts of $p\rightarrow\pi^*$ and $\pi\rightarrow\pi^*$ electronic transition energies of solute molecules due to interactions between solvent and solute molecules can be characterized by the general relationship (6):

$$[1] \quad XYZ = XYZ^0 + h(\delta_h^2) + s(\pi^* + d\delta) + a\alpha + b\beta$$

Here XYZ is some specific physical characteristic of the solute such as the position of maximum absorption in a UV–VIS or NMR spectrum, a free energy or heat of solution, or the logarithm of a solubility or some other equilibrium constant. XYZ^0 refers to the value of that given characteristic at given reference conditions. We will be concerned with the position of the maximum in the UV–VIS absorption peak, ν_{max}, and the logarithm of the solubility.

The latin alphabet coefficients in eq. [1] (a, b, d, h, s) correspond to properties of the solute, and the greek alphabetic symbols (α, β, δ, δ_h, π^*) to those of the solvent. The parameter $d\delta$ is a polarizability correction term for solvent type, which is zero when nonchlorinated and nonaromatic solvents are used. The α and b parameters refer to the hy-

[1]Author to whom correspondence may be addressed.
[2]Revision received June 18, 1993.

drogen-bond donor (HBD) acidities of the solvent and the solute, respectively, while β and *a* refer to their hydrogen-bond acceptor (HBA) basicities. The terms ($a\alpha$) and ($b\beta$) can also be reduced to zero if nonprotic solutes and solvents are employed. The *h* parameter, a differential cavity term, is a function of solute molecular size. From the Frank–Condon Principle, the change in molecular volume on going from the ground to excited state species of the solute is very small (12), and the overall contribution of $h(\delta_h^2)$ is negligible. For the purposes of this study, eq. [1] can therefore be reduced to the form

$$[2] \quad \nu_{max} = \nu^0_{max} + s\pi^*$$

In such cases, interactions between solute and solvent are restricted to nonspecific dispersion-type forces, and a linear relation between π^* and solvent strength is predicted (9). There are no further variables present that could explain any nonlinearity in this predicted linear relation.

The solute parameter *s* is a measure of the susceptibility of the solute to changes in solvent polarity. The value of *s* for a specific solute can be obtained using solvents of known π^* value, as *s* is the slope of a graph of the absorption maximum energy, π_{max}, versus π^*. To decrease errors due to instrument resolution and spectral anomalies, solutes with large *s* values should be employed. A negative *s* value is indicative of a solute that has an electronically excited state that is stabilized more than its ground state with increases in solvent π^* value, reducing the energy of the $p \rightarrow \pi^*$ or $\pi \rightarrow \pi^*$ transitions and thus reducing the energy of the absorption maximum.

In binary solvent mixtures, the cosolvent can show enrichment in the cybotactic region due to more favourable solute–cosolvent intermolecular interactions (13). This should be reflected in the solvatochromic shifts observed. In the specific case of a solute that has an excited electronic state of higher polarity than its ground state, small additions of a polar cosolvent to a less polar primary solvent should show relatively large changes in π^* due to greater interactions with the excited state species of the solute. Further incremental additions of cosolvent will affect π^* to a point, beyond which more additions will have minimal effect (i.e., π^* asymptotically approaches the value for pure cosolvent). This can be thought of as the cybotactic saturation point of the cosolvent about the solute.

The mole fraction of cosolvent in the cybotactic region (i.e., the local mole fraction) was estimated by Yonker et al. (8) by use of the following equation

$$[3] \quad \Delta\pi^* = \pi^*_m - \pi^*_c = \pi^*_m - (X_{12}\,\pi^*_1 + X_{32}\,\pi^*_3)$$

where π^*_m and π^*_c are the measured and calculated values for the binary mixture, X_{12} and X_{32} are the local mole fractions of cosolvent and primary solvent about the solute approximated by the bulk fluid values, and π^*_1 and π^*_3 are the solvatochromic parameters for the pure cosolvent and primary solvent.

Experimental

Materials and equipment

The solute chosen to be studied was 2-nitroanisole (**1**, Aldrich Gold Label, 99+%), due to its reasonable *s* value (−2.43 ± 0.20), absorption maximum position ($\nu_0 = 32.56 \times 10^{+3}$ cm^{-1}), and widespread use in many previous studies (2, 8, 9). The polyaromatic hydrocarbons chrysene (**2**), *meta*-terphenyl (**3**), and anthracene (**4**) were chosen for study mainly because of their physicochemical nature and the availability of their SCF solubility data (14, 15). All solids were recrystallized before use. The absorption maxima of **1–4** were determined in various pure solvents (pentane, hexane, cyclohexane, ethyl ether, acetone, ethyl acetate, tetrahydrofuran, dimethyl sulfoxide). All of the solvents used were spectro grade (ACS/Caledon, Anachemia, Fisher Scientific, Eastman–Kodak); their absorption spectra were measured versus air in the range 250–400 nm. Liquid solution spectra were run on a Perkin–Elmer Lambda 4B UV–VIS spectrophotometer using quartz cells of 1.00 cm path length with pure solvent as the reference.

Supercritical fluid solvents used were CO_2 (Air Products, 99.8% pure in the gas phase, dip tube) and N_2O (Air Products, 99.0+% pure in the gas phase). Tetrahydrofuran (THF) was used as a cosolvent in CO_2. Care should be taken in the handling of high-pressure N_2O, especially when using organic cosolvents, because of its strong oxidizing power.

A Milton–Roy UV–visible Critical Extraction Monitor (CEM) with a thermostatted high-pressure optical cell (6000 psi (1 psi = 6.89 kPa), 25–60°C, spectral bandwidth 3 nm) was used to obtain supercritical phase spectra of compound **1**. The CEM was first tested with liquid solutions and the results were compared to spectra obtained from the Lambda 4B. This comparison showed the CEM to have a systematic error of 260 cm^{-1}, which was corrected for in subsequent data.

A high-pressure Milton–Roy miniPump piston pump (type NSI-33R, model 920231) was used to pressurize the supercritical solvent. The system pressure was measured with an Alltech flow-through pressure gauge (0–6000 psig) to ±20 psig. The internal volume of the system was intentionally increased by approximately 50% to dampen the effect of the cycling of the pump. Flow of the solution through the cell was limited so that temperature equilibration to above the critical temperature (T_c) of the solution was obtained before it entered the cell space. The pressure drop downstream from the gauge to the cell was calculated to be negligible at the flow rates used. For all SCF spectra measured the temperature of the CEM cell was kept constant at 40.0 ± 0.5°C using the Milton–Roy CEM cell heater.

Procedure

Solutions were prepared in a high-pressure vessel of approximately 150 mL internal volume by first adding solute (approximately 12 mg of **1**), and then cosolvent if required. The vessel was then chilled in ice water and the desired solvent (CO_2 or N_2O) was condensed into it. The solutions were allowed to equilibrate at room temperature for a minimum of 12 h before use. The system was flushed with at least two system volumes of solution (approximately 10 mL solution) before measuring a spectrum.

The CEM is a single beam type spectrophotometer. Baselines of blank solutions were therefore tested initially before any solution spectra, and all SCF spectra were subsequently corrected for baseline variation. Spectral data from the CEM were obtained as digital readout. The most accurate method to get an absorption maximum was found to be a plot of the change in absorbance, over a 2.5 nm wavelength range, versus the mean wavelength. The differentiated data produce an intercept with the *x*-axis that designates the absorption maximum.

Spectroscopic measurement of CO_2 and N_2O solutions on the CEM were performed twice, with two separately prepared solutions, in alternating order, and of slightly different concentration of solute (80 and 110 ppm). The order of pressures and of solutions used was varied to ensure reproducibility in the experimental procedure and the data.

The apparatus setup and procedure used for measuring solubilities in SCF systems was taken from Burk *et al.* with only a few alterations (15). Solute solubilities were obtained by passing solvent at a given pressure through a 1/4-in. stainless steel tube, ca. 15 cm in length, packed with solute. Screens (10 μm mesh size) were placed inside end-fittings to prevent solid solute from being

Can. J. Chem. Downloaded from www.nrcresearchpress.com by 203.198.23.82 on 09/08/12
For personal use only.

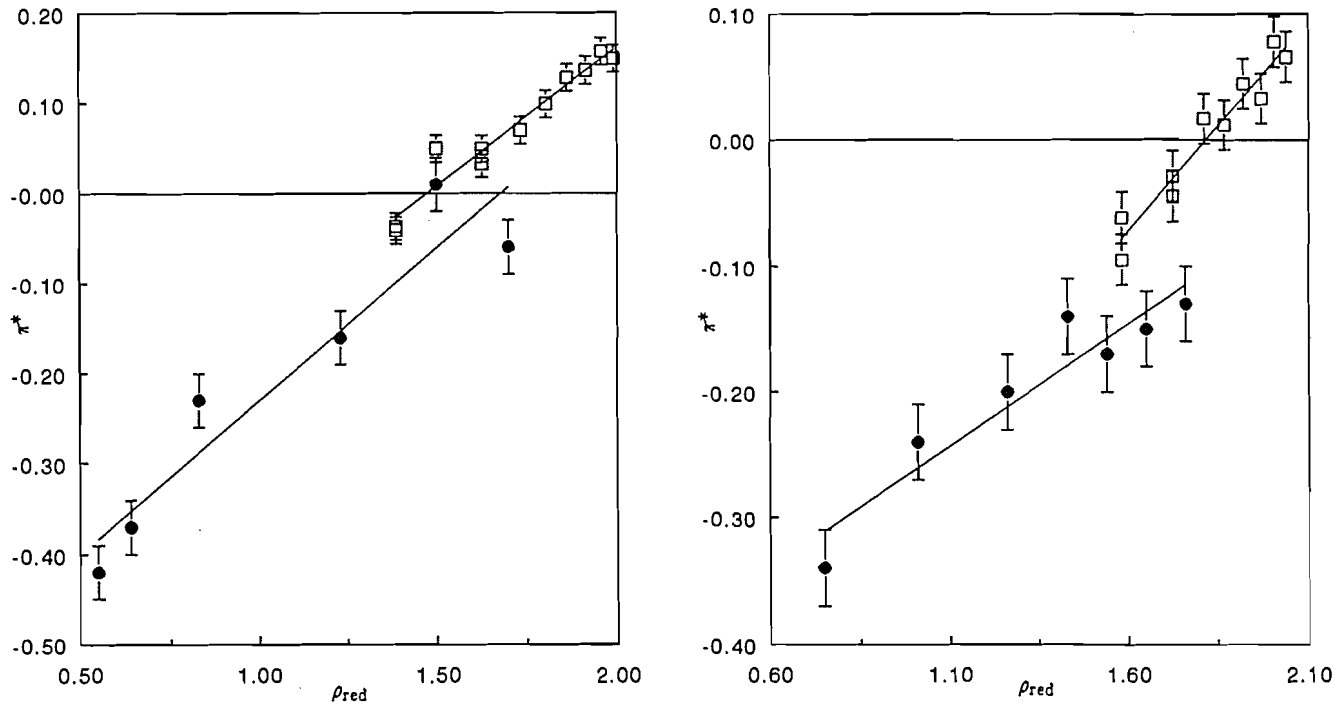

FIG. 1. (*a*) Solvatochromic parameter (π^*) values as a function of CO_2 reduced density (ρ_{red}) using 2-nitroanisole. Literature values (circles) from ref. 9 (33°C) are shown along with the experimentally determined values (squares) obtained at 40°C. (*b*) Solvatochromic parameter (π^*) values as a function of N_2O reduced density (ρ_{red}) using 2-nitroanisole. Literature values (circles) from ref. 9 (33°C) are shown along with the experimentally determined values (squares) obtained at 40°C.

Can. J. Chem. Downloaded from www.nrcresearchpress.com by 203.198.23.82 on 09/08/12
For personal use only.

pushed through. A restrictor made of 1/16-in. stainless steel tubing with a crimped end was used as the outlet. This was heated to prevent crystallization of solute during decompression. The solute was trapped in a gas-tight glass U-tube, which was cooled in ice water externally and packed with stainless steel balls to ensure that all solute was being collected. The glass tube was plugged with Pyrex wool near the end to trap any solid particulates that may get blown through. Flow rates of outgases were measured with a bubble flow meter to allow for back-calculations of solvent flow rates, and to ensure that the flow rates were slow enough to allow the solvent to become saturated with solute before deportment from the column. The trap was then rinsed, using spectro grade dichloromethane (Caledon), into a 10.00 mL volumetric flask. The quantitation of solutes was performed on a Varian Saturn II GC–MS, instrument.

Results and discussion

Solvatochromic shifts

Liquid solutions

A ν^0_{max} (intercept) of $(32.60 \pm 0.02) \times 10^{+3}$ cm^{-1} and an s value (slope) of (-2.42 ± 0.15) were determined from an ν_{max} versus π^* plot from measured spectra of **1** in various non-HBD (Handinson–Brobst–Thompson) liquid solvents. This compares reasonably well with the accepted values for **1** quoted in the experimental section. With both solute and solvent having only HBA character, the shifts in ν_{max} are free of hydrogen-bonding effects. The values of π^* used for various liquids were taken from ref. 7.

Varying the solute concentration from approximately 80 to 110 ppm showed no effect on the ν_{max} values of the liquid spectra measured. This eliminated the problem of attempting to keep the solution composition constant throughout the experiments with SCF solvents.

The UV–VIS spectra of **2–4** were also measured in several liquid solvents for the purpose of comparison of solvatochromic trends with solubility data. The solvents used provided a π^* range of −0.08 (hexane) – 1.0 (dimethyl sulfoxide). The s values proved to be very small and difficult to determine accurately due to the relatively inert behaviour of these of solutes towards changes in solvent type.

Supercritical fluid solutions

Figures 1*a* and 1*b* show the variation of π^* with reduced density (ρ_{red}) for CO_2 and N_2O, respectively. The values for π^* were obtained by correlation with the s value of **1** determined from liquid solution measurements. The densities and critical parameter values of the SCF solvents were calculated from the Handinson–Brobst–Thompson (HBT) equation of state, and commonly used mixing rules when required (4). The values determined for π^* indicate that CO_2 and N_2O should show similar solvent powers as nonpolar to slightly polar organic solvents. Both CO_2 and N_2O are assumed to have negligible hydrogen-bonding effects with **1** due to their essentially only HBA character at the densities used here (16).

The data in Figs. 1*a* and 1*b* also show that the π^* values obtained for CO_2 differ from previously reported data (2, 5, 9), even after correcting for systematic errors and allowing for a significant experimental uncertainty. Some of this error may be accounted for by the slightly different temperatures at which the data were obtained. Large discrepancies are commonly seen in the measured π^* values for solvents using various chromophores (12), and are attributed to solute-specific effects. However, the π^* values for CO_2 and N_2O from the literature were obtained using the same solute probe (2-nitroanisole). The errors in the calculated ρ values for all SCF mixtures from the HBT equation of state are assumed to be negligible compared to instrumental errors from the CEM.

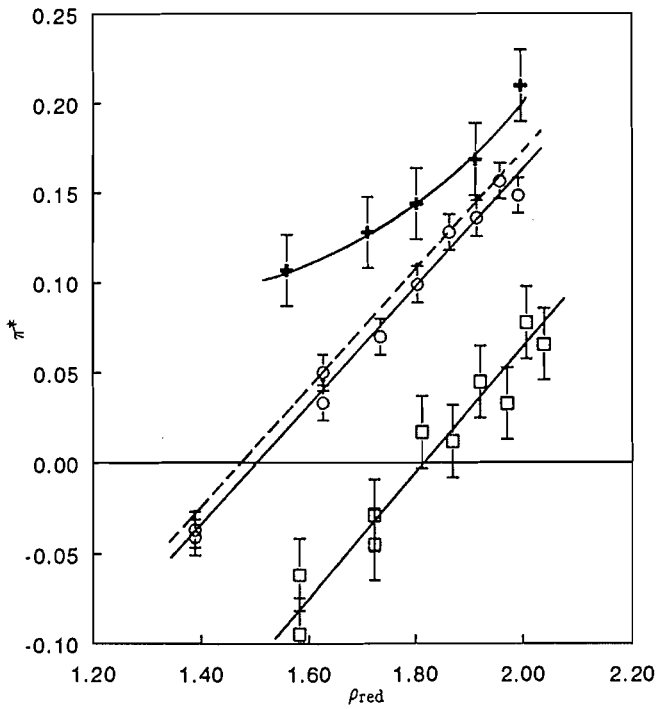

FIG. 2. Experimental π^* values for CO_2 (circles), N_2O (squares), and CO_2/2.0 mol% THF (crosses) versus reduced density (ρ_{red}) at 40°C using 2-nitroanisole. The dashed line corresponds to the calculated CO_2/THF π^* values based on a bulk mole fraction average.

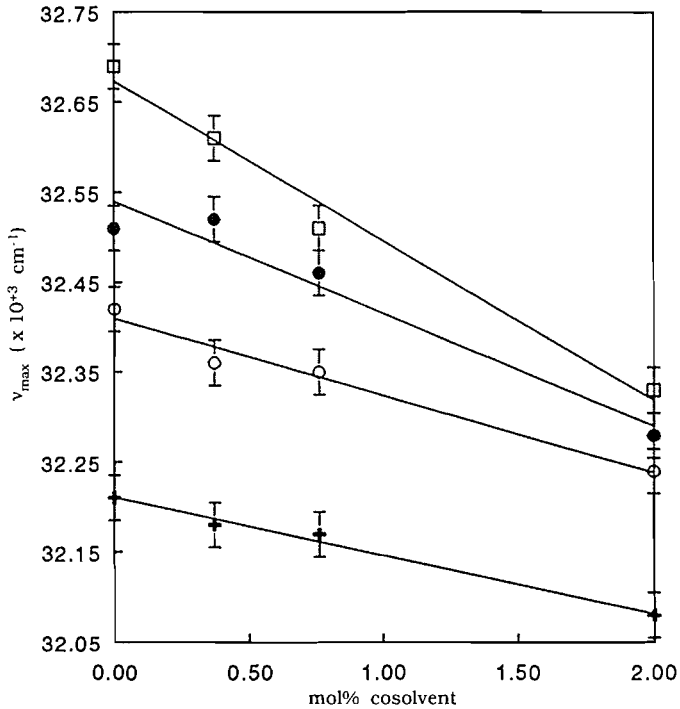

FIG. 3. Absorbance maxima energy (ν_{max}) for 2-nitroanisole versus mol% cosolvent at pressures of 103 bar (squares), 138 bar (filled circles), 173 bar (hollow circles), 310 bar (crosses). All values were obtained at 40°C.

It is worth noting that studies using Nile Red as a solute in SCF solutions produced inadequate resolution of solvent strength differences with pressure using π^* (17). There is, however, excellent correlation in the $\Delta\nu_{max}$ values obtained for the Nile Red data and the data reported here for **1** in liquid solutions (i.e., $\Delta\nu_{max} \simeq 1.5 \times 10^{+3}$ cm^{-1} with a $\Delta\pi^* \cong 1.1$ for both chromophores).

Figure 2 shows the variation of π^* with reduced density for CO_2, N_2O, and CO_2/2.0 mol% THF. THF was chosen as the cosolvent for CO_2 because of its low cutoff wavelength, and its physicochemical properties (i.e., HBA, non-HBD, polarity, and π^* value). It also proved to be miscible with CO_2 in the required composition range.

The positive slopes for both CO_2 and N_2O in Figs. 1*a* and 1*b*, respectively, are explained by the increase in the absolute number of solute–solvent interactions when density is increased. These π^* values indicate that CO_2 is the stronger solvent. This seems counterintuitive considering that N_2O has a small dipole moment (0.17 D). Assuming the polarizability of N_2O to be no larger than for CO_2, the stronger solvent power as measured spectroscopically must be a result of a larger degree of clustering of solvent molecules in the cybotactic region of the solute. The π^* values for N_2O may be affected to a certain degree by an increase in the number of unfavourable solvent–solvent interactions (increasing with density) that occur during nonspecific-type molecular interactions. This effect may be great enough in N_2O, as compared to CO_2, to effectively decrease clustering in the cybotactic region of **1**, destabilizing the electronic states of the solute.

Figure 2 shows that CO_2/THF has higher π^* values than CO_2. The variation in π^* with ρ also appears to be nonlinear. The increase in π^* values from the pure solvent values can be attributed to the contribution of stronger dipolar interactions between THF and the solute molecules. A nonlinear trend in values may be attributed to preferential clustering of the cosolvent molecules about the solute. When the experimentally determined data are compared to the calculated values based on a bulk mole fraction average, the largest amount of clustering is seen at lower pressures. Since solute–cosolvent effects dominate at lower densities where the fluid is more compressible, higher densities should produce a π^* trend that asymptotically approaches that of the calculated bulk fluid values. This is also suggested by the data in Fig. 2.

The effect of cosolvent concentration on the absorption maximum of the solute can be seen in Fig. 3. The largest changes in ν_{max} with respect to cosolvent mole fraction are seen at lower pressures due to the drastic effect pressure has on the bulk fluid density in this highly compressible region. The effect of pressure on ν_{max} is less pronounced as the amount of cosolvent is increased, and can be interpreted as a decrease in compressibility of the fluid in the solute cybotactic region due to preferential cosolvent clustering (18).

A local mole fraction cosolvent in the cybotactic region (X_{12}^{loc}) can be obtained from spectroscopic data based on a simple mole fraction average calculation:

$$[4] \quad X_{12}^{loc} = (\pi_m^* - \pi_3^*)/(\pi_1^* - \pi_3^*)$$

In Fig. 4, the X_{12}^{loc} calculated using eq. [4] are plotted versus pressure. These curves show definite trends in the reduction of X_{12}^{loc} with increasing pressure. The relative clustering (calculated X_{12}^{loc} versus the bulk fluid X_{12}) is much larger at lower pressures, and clearly shows the preferential clustering effect of the cosolvent. The results using eq. [4] are only

Can. J. Chem. Downloaded from www.nrcresearchpress.com by 203.198.23.82 on 09/08/12
For personal use only.

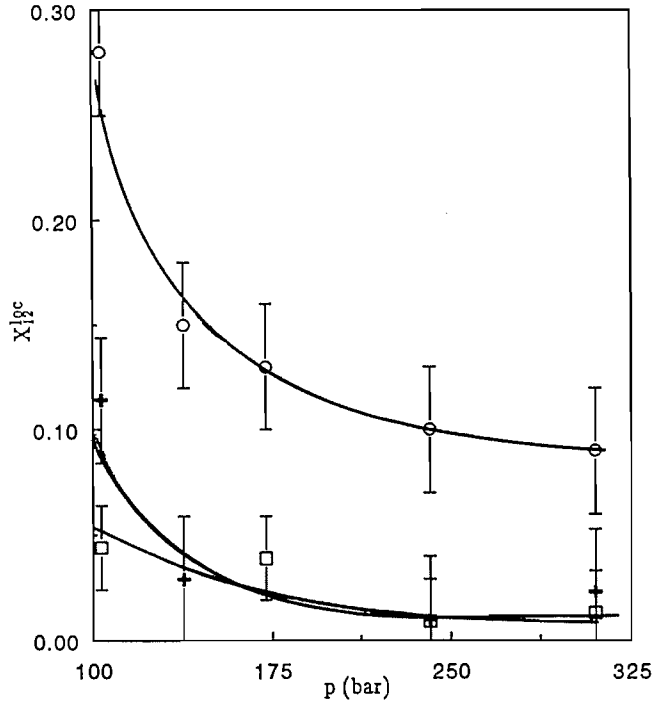

FIG. 4. Local cosolvent mole fraction (X_{12}^{loc}) versus pressure (p) at 40°C for various mol% cosolvent (squares, 0.37%; crosses, 0.76%; circles, 2.0%).

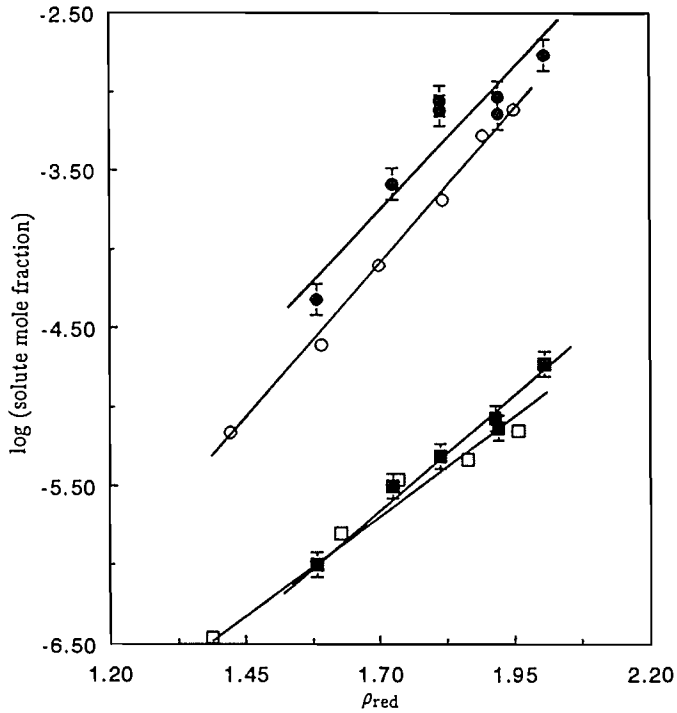

FIG. 5. Solute solubility in CO_2 (hollow symbols) and N_2O (filled symbols) versus reduced density (ρ_{red}) at a temperature of 40°C. The circular symbols correspond to *meta*-terphenyl, the square symbols to chrysene.

semiquantitative as errors produced from absorption values used to calculate π^* values are relatively large at such low cosolvent mole fractions. The determined X_{12}^{loc} values are, however, in agreement with more quantitative clustering data reported in ref. 18. Kim and Johnston report, at a bulk cosolvent concentration of 2.0 mol%, a reduction in the average cosolvent enrichment (cosolvents: acetone, methanol, ethanol, and *n*-octane) of the cybotactic region from about 14 mol% at 80 bar to only about 4 mol% at 300 bar (1 bar = 100 kPa).

Solvatochromic data provide information concerning the solute-organized cybotactic region of both single-component and binary-component SCF solvents (18, 19). The use of such solvatochromic parameters is, however, restricted to compounds that absorb light in the UV–visible spectrum. As well, π^* values themselves have proven to be somewhat solute specific.

Solubility

Predicting solvent power

Very little work has been done on the quantitative prediction of solvent power in SCF systems. The bulk of the quantification data on solubilities and increases in solvent power was done for systems that have specific solute–solvent interactions (e.g., H-bonding) (13, 20, 21). Much less success has been realized for the seemingly simpler systems possessing only nonspecific-type interactions (i.e., dispersion forces). There has been some use made of solvatochromic data for binary solvent systems, and there is a possibility that these could be of significant utility for solubility predictions (18).

The Hildebrand solubility parameter (δ_h) is the most commonly used parameter for the prediction of solubilities in liquids. Through empirical formula, it has been extended for use in the supercritical regime (22). Conceptually, it is a measure of the amount of energy necessary to create a cavity amongst solvent molecules for the solvation of a solute, better known as the cohesive energy density. As both δ_h and π^* vary linearly with fluid density in single-component SCF solvents, then δ_h also varies linearly with π^*. This indicates that for CO_2 and N_2O the number of solvent–solute interactions, which increases with increasing density, is the determining factor in predicting solvent power both for π^* and δ_h.

A comparison of π^* and δ_h data for CO_2/THF shows a similar, apparently nonlinear, trend to that seen in Fig. 2. The calculated δ_h values vary linearly with density as they are influenced solely by that parameter; preferential clustering is not considered. The π^* parameter therefore seems to be a more universal parameter for the prediction of solvent power, into which the strengths of nonspecific interactions are incorporated. This would be especially true for multicomponent SCF solvents.

It is generally not this easy to predict solubilities immediately from π^*, as solute character must also be considered. In our case, solute–solvent interactions may be considered identical when comparing solvatochromic and solubility data, due to the nature of **1**. It should be noted that π^* correlates well with a variety of other "solvent scales" when only restricted solvent–solute combinations are used (23), identical to the restrictions placed on the systems studied here.

Comparison to solubility data

The solubilities of **2** and **3** in both CO_2 and N_2O are plotted in Fig. 5 as the logarithm of the solute mole fraction versus solvent reduced density. Depicting the solubility in

Can. J. Chem. Downloaded from www.nrcresearchpress.com by 203.198.23.82 on 09/08/12
For personal use only.

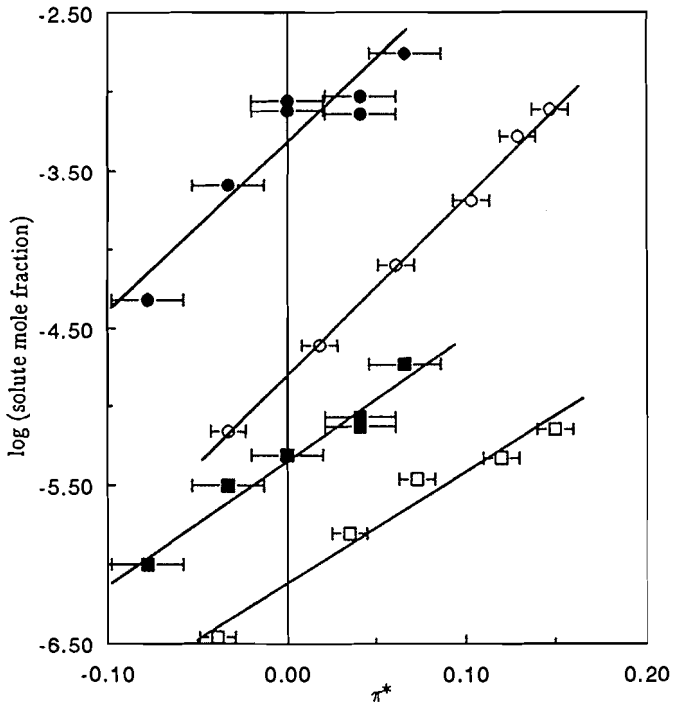

FIG. 6. Solute solubility in CO_2 (hollow symbols) and N_2O (filled symbols) versus the solvatochromic parameter (π^*) at a temperature of 40°C. The circular symbols correspond to *meta*-terphenyl, the square symbols to chrysene.

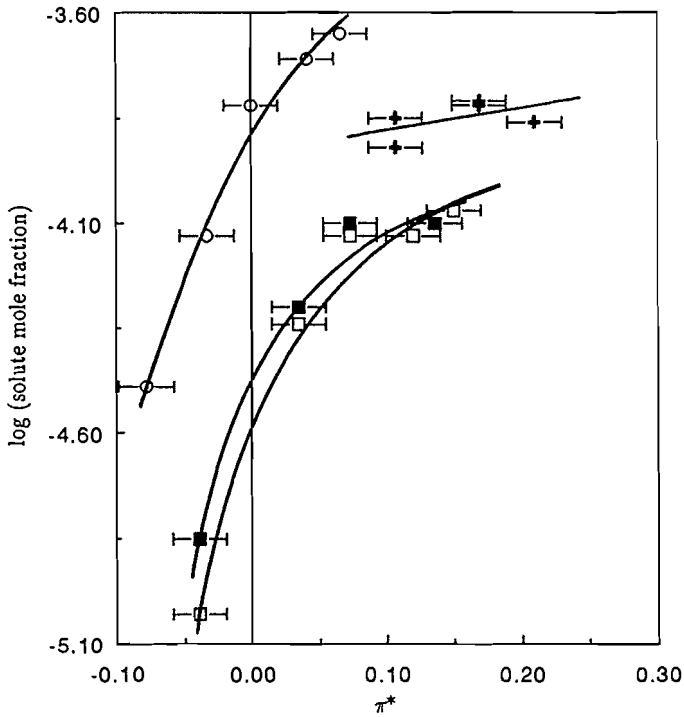

FIG. 8. Anthracene solubility versus solvatochromic parameter (π^*) in CO_2 for this study (hollow squares) at 40°C and from ref. 14 (solid squares) at 35°C; in N_2O (circles) and in CO_2/1.7 mol% THF (crosses), both at 40°C.

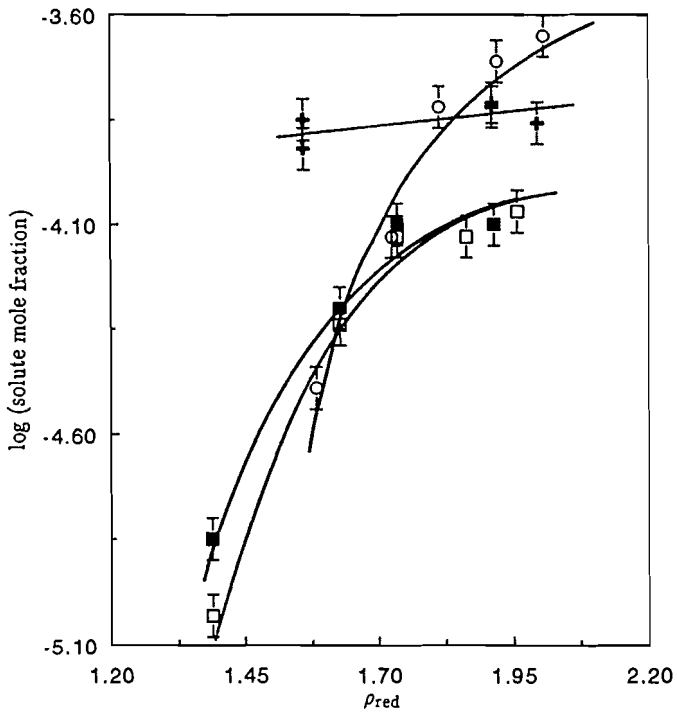

FIG. 7. Anthracene solubility versus reduced density (ρ_{red}) in CO_2 for this study (hollow squares) at 40°C and from ref. 14 (solid squares) at 35°C; in N_2O (circles) and in CO_2/1.7 mol% THF (crosses), both at 40°C.

its more common form as (the log of) the number of grams of solute per millilitre of solvent produces identical trends. The absolute solubilities of both **2** and **3** in CO_2 and N_2O are comparable, in agreement with a corresponding states concept. The major contribution to errors in solubility measurements was in the accurate determination of outgas flow rates from the heated restrictor, which could vary up to ±10% during a single measurement. For Figs. 6 and 8, however, the major contribution to experimental error in ν_{max} was found to be larger than that for solubilities, and thus are the only error estimates shown.

A serious problem arises in the prediction of absolute solvent strength, as trends appear to be reversed from that predicted through solvatochromic data. The discrepancy is shown graphically in the plot of solubility versus π^* (Fig. 6), which indicates that N_2O has greater solvating power than CO_2 at the same π^* value.

Figure 6 indicates the susceptibility of the solute to changes in solvent strength for **2** and **3**, as demonstrated by a consistent slope seen between the two solvents for each solute. Further experimentation may prove that the slopes of the solubility isotherms (logarithm of solubility versus π^*) are constant for a given solute, as are solute s values in solvatochromic data, in which case π^* would be quantitatively useful in predicting solubility trends in SCFs.

Comparison of the slopes of solubility isotherms to solute s values for **2**, **3**, and **4** was unsuccessful due to problems previously described in obtaining s values for such nonpolar substances. As well, experimentation to obtain solubility data for **1** was unsuccessful due to problems related to the use of liquid solutes.

For **4**, agreement with literature data is promising (15, 16). However, a definite nonlinear relationship is indicated be-

Can. J. Chem. Downloaded from www.nrcresearchpress.com by 203.198.23.82 on 09/08/12
For personal use only.

tween solubility and reduced density, and thus with π^* as well (Figs. 7 and 8). Although this deviates from theories of linear solvation energy relationships, comparisons of data trends will still be made. Solubility data for **4** in CO_2 and N_2O indicate the same trend of relative solubilities that was seen in **2** and **3**, and the same reversal of solvent strength when solubility is plotted versus π^*.

The most interesting result comes in the comparison of the binary solvent solubility data to the single-component SCF solvents in Fig. 8. The solubility is only slightly higher for **4** in the binary solvent than in CO_2, and lower than that for N_2O at higher densities. The rate of solubility increase with reduced density or π^* is also significantly lowered. These effects are the result of cybotactic saturation by the cosolvent, which reduces the effect of pressure on changes to the solvent strength. These trends were also seen in the solvatochromic data.

Although solvatochromic data prove to be inappropriate for the prediction of solvent power or absolute solubilities, they have shown promise of providing valuable information concerning the cybotactic region of the solute in both single and binary SCF solvents. These data may also prove to be an asset in the prediction of relative solubility trends for cases where there is limited data on a specific solute–solvent pair.

Acknowledgements

The authors are grateful to L.A. McMillen and D.A. Robertson for experimental assistance, to the Ontario Ministry of the Environment for use of some equipment, and to Natural Sciences and Engineering Research Council of Canada (NSERC) for their assistance through a postgraduate scholarship.

1. W.J. Schmitt and R.C. Reid. Fluid Phase Equilib. **32**, 77 (1986).
2. C.R. Yonker and R.D. Smith. Supercritical fluids extraction and chromatography. *Edited by* M.J. Comstock. American Chemical Society. 1988, pp. 160–178.
3. J.H. Hildebrand and R.L. Scott. The solubility of non-electrolytes. Dover Publications, New York. 1964.
4. J.M. Prausnitz, R.N. Lichtenthaler, and E.G. de Azevedo. Molecular thermodynamics of fluid phase equilibria. 2nd ed. Prentice–Hall, New Jersey. 1986.
5. S.L. Frye, C.R. Yonker, D.R. Kalkworf, and R.D. Smith. Supercritical fluids—chemistry and engineering principles and applications. *Edited by* M.E. Paulatis and T.G. Squires. American Chemical Society. 1987. pp. 29–41.
6. M.J. Kamlet, R.W. Taft, and J-L.M. Abboud. J. Am. Chem. Soc. **99**, 6027 (1977).
7. M.J. Kamlet, J-L.M. Abboud, M.H. Abraham, and R.W. Taft. J. Org. Chem. **48**, 2877 (1983).
8. M.J. Kamlet, R.M. Doherty, J-L.M. Abboud, M.H. Abraham, and R.W. Taft. CHEMTECH, 566 (1986).
9. (*a*) M.J. Kamlet, P.W. Carr, R.W. Taft, and M.H. Abraham. J. Am. Chem. Soc. **103**, 6062 (1981); (*b*) R.W. Taft, J-L.M. Abboud, and M.J. Kamlet. J. Am. Chem. Soc. **103**, 1080 (1981); (*c*) M.J. Kamlet and R.W. Taft. J. Am. Chem. Soc. **98**, 377 (1976); (*d*) R.W. Taft and M.J. Kamlet. J. Am. Chem. Soc. **98**, 2886 (1976).
10. C.R. Yonker and R.D. Smith. J. Phys. Chem. **92**, 8, 2374 (1988).
11. C.R. Yonker, S.L. Frye, D.R. Kalkworf, and R.D. Smith. J. Phys. Chem. **90**, 3022 (1986).
12. M.E. Sigman, S.M. Lindley, and J.E. Lefflar. J. Am. Chem. Soc. **107**, 1471 (1985).
13. J.M. Walsh, G.D. Ikonomou, and M.D. Donohue. Fluid Phase Equilib. **33**, 295 (1987).
14. E. Kosal and G.T. Holder. J. Chem. Eng. Data, **25**, 326 (1980).
15. R.C.B. Burk and P. Kruus. Can. J. Chem. Eng. **70**, 403 (1992).
16. Y. Ikushima, N. Saito, M. Aria, and K. Aria. Bull. Chem. Soc. Jpn. **64**, 2224 (1991).
17. J.F. Deye, T.A. Berger, and A.G. Anderson. Anal. Chem. **62**, 615 (1990).
18. S. Kim and K.P. Johnston. A.I.Ch.E.J. **33**, 1603 (1987).
19. S. Kim and K.P. Johnston. Ind. Eng. Chem. Res. **26**, 1206 (1987).
20. J.M. Dobbs, J.M. Wong, R.J. Lahiere, and K.P. Johnston. Ind. Eng. Chem. Res. **26**, 56 (1987).
21. K.P. Johnston, G.J. McFann, D.G. Peck, and R.M. Lement. Fluid Phase Equilib. **52**, 337 (1989).
22. J.C. Monin, D. Barth, M. Perrut, M. Espitalie, and B. Durand. Adv. Org. Geochem. **13**, 1079 (1987).
23. J.L. Abboud, M.J. Kamlet, and R.W. Taft. J. Am. Chem. Soc. **99**, 8325 (1977).

Can. J. Chem. Downloaded from www.nrcresearchpress.com by 203.198.23.82 on 09/08/12
For personal use only.

Studies on the $B_{AL}2$ mechanism for ester hydrolysis

JUDY E. DOUGLAS, GRANT CAMPBELL, AND DONALD C. WIGFIELD
The Ottawa–Carleton Chemistry Institute, Carleton University Campus, Ottawa, ON K1S 5B6, Canada

Received April 15, 1993

JUDY E. DOUGLAS, GRANT CAMPBELL, and DONALD C. WIGFIELD. Can. J. Chem. **71**, 1841 (1993).

The preparation and alkaline hydrolysis of ^{18}O-methyl 2,2-dimethylpropanoate and ^{18}O-methyl triphenylacetate are reported. From mass spectral analysis of the carboxylic acid products, it is concluded that the former substrate is hydrolyzed exclusively by the $B_{AC}2$ mechanism, whereas the latter substrate proceeds 95% by the $B_{AC}2$ mechanism and 5% by the $B_{AL}2$ mechanism. The balance between these two mechanisms is discussed.

JUDY E. DOUGLAS, GRANT CAMPBELL et DONALD C. WIGFIELD. Can. J. Chem. **71**, 1841 (1993).

On a réalisé la préparation et l'hydrolyse alcaline du 2,2-diméthylpropanoate de ^{18}O-méthyle et du triphénylacétate de ^{18}O-méthyle. En se basant sur l'analyse des spectres de masse des acides carboxyliques produits, on peut conclure que le premier substrat s'hydrolyse exclusivement par un mécanisme $B_{AC}2$ alors que le dernier substrat s'hydrolyse à 95% par le mécanisme $B_{AC}2$ et 5% par le mécanisme $B_{AL}2$. On discute de la balance entre ces deux mécanismes.
[Traduit par la rédaction]

Introduction

This paper examines a mechanistic question that is over 40 years old, which has never been properly resolved, and which has been largely ignored for the past 30 years. It was recognized in 1941 that esters could, in principal, be hydrolyzed by as many as eight possible mechanisms (1). Ingold, in his classic 1953 book, revised in 1969 (2), classified these using a convenient notation in which the common base-catalyzed mechanism:

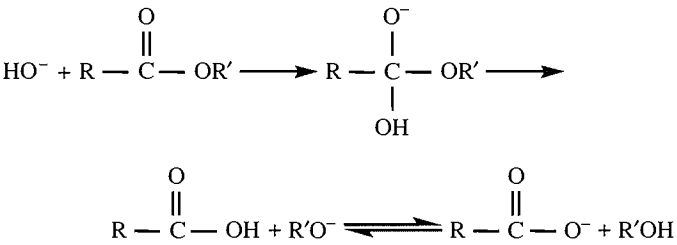

is referred to as $B_{AC}2$. In this notation, the letter B indicates that the reaction is base-catalyzed; the symbol "AC" indicates that acyl–oxygen bond breakage occurs; and the number 2 refers to the bimolecular nature of the reaction. Isotopic labelling studies and kinetics established (2) that in basic media most esters are hydrolyzed by this mechanism, and, indeed, most texts do not even mention the other possibilities. One of these possibilities, the $B_{AL}2$ mechanism, shown below,

is, however, at least on paper, a very reasonable mechanism and it is surprising to find that this mechanism has occurred so rarely. Ingold (2) noted both the rather special case of β-lactone hydrolysis (3), and also the transesterification work of Bunnett and co-workers in which a $B_{AL}2$-type mechanism leads to a different product (4), and states that "the generality of the $B_{AL}2$ mechanism . . . has been established . . . despite its usual eclipse by the $B_{AC}2$ mechanism . . ." However, *no* example of a $B_{AL}2$ hydrolysis of an actual ester was cited. Gould's view, in his 1959 book, was that the mechanism was "extremely rare; observed only for hydrolysis of β-lactones in the absence of both strong base and strong acid." (5). More recent texts have become more vague on the question of whether or not the mechanism can actually be observed, and tend to mention only the lactone and the methanolysis results (6).

In fact, there appears to be only one example in the entire chemical literature of an unambiguous $B_{AL}2$ hydrolysis[1] of an ester, and this dates from over 30 years ago. In 1962 Barclay, Hall, and Cooke presented isotopic analysis data on the hydrolysis of methyl 2,4,6-tri-*tert*-butylbenzoate, which unambiguously established that the mechanism of hydrolysis was $B_{AL}2$ (7). Evidently in this case the bulky *ortho* substituents rendered impossible the attack on the carbonyl to initiate the $B_{AC}2$ mechanism, and the $B_{AL}2$ mechanism, with attack on the relatively unhindered methyl group, occurred instead. Both *ortho tert*-butyl groups were apparently required in order to change the mechanism; it was reported that methyl 2-methyl-4,6-di-*tert*-butylbenzoate is hydrolyzed by a mixture of $B_{AL}2$ and $B_{AC}2$ mechanisms, and other hindered esters exclusively by $B_{AC}2$ (7). This important paper has not had the attention it perhaps deserves; it is not mentioned by Ingold (2), or in other texts (6), and has, in the past 15 years, been cited only twice. In contrast to this report, the hydrolysis of the closely related 2,4,6-triphenylbenzoate has been reported to proceed by the $B_{AC}2$ mechanism (9).

It is clear that the $B_{AL}2$ mechanism is an extraordinarily rare process. What is not so clear is whether this is because it has simply not been extensively looked for, and has been "eclipsed" by the $B_{AC}2$ mechanism, or whether it is, despite its attractiveness on paper, an intrinsically unfavourable mechanism. In an effort to find other examples of this mechanism, not involving the benzoate group, and to try to gain some further understanding of the balance between the $B_{AC}2$ and the $B_{AL}2$ mechanisms, we have investigated the hydrolysis of two more potential candidates — methyl 2,2-dimethylpropanoate (methyl trimethylacetate, methyl pivalate) and methyl triphenylacetate — both of which offer significant steric hindrance to attack on carbonyl ($B_{AC}2$), but little impediment to attack on the methyl group ($B_{AL}2$). Herein we report our findings.

[1]It should be noted, however, that several apparent examples of $B_{AL}2$ methanolysis have been reported; see, for example, refs. 4, 8.

Can. J. Chem. Downloaded from www.nrcresearchpress.com by 203.198.23.82 on 09/08/12
For personal use only.

Can. J. Chem. Downloaded from www.nrcresearchpress.com by 203.198.23.82 on 09/08/12
For personal use only.

Results

The most clearcut strategy for detection of the $B_{AL}2$ hydrolysis mechanism is by ^{18}O labelling of the methoxy group of the ester. Hydrolysis by the $B_{AL}2$ mechanism will lead to ^{18}O incorporation into the carboxylic acid product, whereas the $B_{AC}2$ mechanism will result in loss of the ^{18}O as $Me^{18}OH$. Unlike other oxygen labelling studies, this strategy does not suffer from oxygen exchange ambiguities.

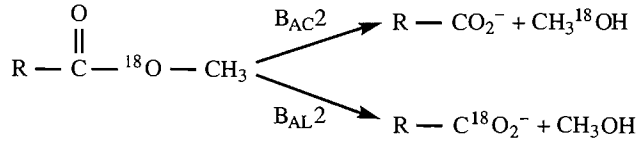

Hydrolysis of ^{18}O-methyl 2,2-dimethylpropanoate

Methyl 2,2-dimethylpropanoate may be prepared by methanolysis of the commercially available 2,2-dimethylpropanyl chloride. In view of the high cost of ^{18}O-labelled methanol, considerable effort was expended in order to maximize the conversion of the acid chloride to the ester with the minimum excess of labelled methanol. The maximization of conversion was important not only for reasons of cost; any acid chloride impurity in the ester sample for hydrolysis would give rise to unlabelled carboxylic acid, thus vitiating the mechanistic conclusion. It was found that conducting the reaction in dichloromethane with a pyridine catalyst, using a 20% molar excess of methanol over acid chloride, achieved the desired result.

To effect hydrolysis of methyl 2,2-dimethylpropanoate, it was found that a 1 M sodium hydroxide solution caused essentially complete hydrolysis at room temperature in 80 h. These conditions were therefore used to hydrolyze samples of the prepared ^{18}O-methyl 2,2-dimethylpropanoate; the resulting 2,2-dimethylpropanoic acid was converted to the TMS ester and analysed by mass spectrometry. The key peaks in the mass spectrum are those at m/z 159 and 161, corresponding to M − 15 (loss of methyl) in the unlabelled and labelled silyl ester, respectively. A small (M − 15) + 2 peak in these compounds occurs inevitably due to the isotopic composition of silicon, and thus the extent of labelling in the sample is estimated by the comparison of the 161:159 peak intensity ratios in the TMS esters of both the hydrolyzed sample and authentic unlabelled 2,2-dimethylpropanoic acid. In both cases this peak intensity ratio was 0.044, thus clearly showing that the hydrolyzed sample contained no detectible ^{18}O. It must therefore be concluded that the hydrolysis of methyl 2,2-dimethylpropanoate proceeds completely, within experimental detection limits, through the $B_{AC}2$ mechanism. Evidently the three methyl groups are insufficient to interfere with this normal mechanism of ester hydrolysis to an extent that would permit the $B_{AL}2$ mechanism to compete.

Hydrolysis of ^{18}O-methyl triphenylacetate

We next turned our attention to the more severely hindered methyl triphenylacetate system. In this case the acid chloride, triphenylacetyl chloride, was not commercially available and was prepared by thionyl chloride treatment of triphenylacetic acid. This was a very slow reaction and, in our hands, required two successive 6-h periods with the reaction under reflux, fresh thionyl chloride being used for the second reflux period. Conversion of this acid chloride to the desired methyl ester was also a difficult reaction, and was eventually managed by a 25-h reflux reaction in benzene, using a pyridine catalyst and an 18-fold excess of methanol over acid chloride. Once again, conditions were worked out on unlabelled materials, followed by preparation of the labelled ester using ^{18}O-methanol.

Hydrolysis of methyl triphenylacetate proved to be an extremely slow reaction, and one that we were not able to bring to completion. In our experience, heating with 1 M sodium hydroxide at 100°C for 287 h caused a conversion of only approximately 40%. This was sufficient, however, to allow mass spectral analysis of the isotopic content of the carboxylic acid product, since the molecular mass of the unconverted methyl ester is less than that of the TMS ester of the acid product and therefore its mass spectrum does not interfere with the mass spectral peaks of interest. As in the case of the 2,2-dimethylpropanoate series, the peaks on which the isotopic content is estimated are the M − 15 and the (M − 15) + 2 peaks of the TMS ester; in the triphenylacetate series these occur at m/z 345 and 347, respectively.

Comparison of the 345 and 347 mass spectral peaks of the TMS ester of authentic triphenylacetic acid and that produced through the hydrolyses of the ^{18}O-labelled ester showed a consistent small, but definite, enhancement of the 347 peak in the latter cases. This enhancement corresponds to the presence of 5% ^{18}O-labelled triphenylacetic acid to 95% unlabelled acid. This result indicates that once again the predominant mechanism of hydrolysis is $B_{AC}2$, but in this case 5% of the reaction has proceeded through the rare $B_{AL}2$ mechanism.[2]

Discussion

The notion that the $B_{AL}2$ mechanism is a reasonably accessible one, whose only reason for rare occurrence is its "eclipse" by the more usual $B_{AC}2$ mechanism, appears to be dispelled by the present results. In the case of hydrolysis of methyl triphenylacetate we have a reaction verging on impossible, yet which still proceeds 95% by the usual $B_{AC}2$ mechanism. The $B_{AL}2$ mechanism is not particularly impeded by any obvious steric factors, and yet, even under circumstances which practically bring the $B_{AC}2$ mechanism to a halt, it can only compete to the extent of about 5%. Clearly the $B_{AL}2$ mechanism must be intrinsically unfavourable and it is this reason why it has been so rarely observed. Only one case has ever been uncovered in which the $B_{AL}2$ mechanism predominates (7), and perhaps this one example, with the extraordinary steric hindrance of two *ortho tert*-butyl groups, is unique in its promotion of the $B_{AL}2$ mechanism.

The kinetic results on the hydrolysis of methyl 2,4,6-tri-*tert*-butylbenzoate reported by Barclay, Hall, and Cooke (7), together with our own results on the incomplete conversion of methyl triphenylacetate, allow a slightly deeper analysis of the problems surrounding the $B_{AL}2$ mechanism. Barclay et al. reported values of E_a and of $\log_{10}$ PZ of 25.07 kcal/mol and 10.93, respectively, and commented that the $\log_{10}$ PZ factor was over 100 times more favourable than other

[2]A referee pointed out that this experimental result, given the unusually harsh hydrolysis conditions (100°C, 287 h), could conceivably have resulted from a hydrolysis that was primarily a $B_{AL}2$ process, followed by loss of the ^{18}O in the carboxylic acid by exchange with solvent. To ensure that this exchange did not occur, triphenylacetic acid was subjected to these conditions using $H_2{}^{18}O$ as solvent. Subsequent mass spectral analysis showed no detectable ^{18}O incorporation into the acid.

Can. J. Chem. Downloaded from www.nrcresearchpress.com by 203.198.23.82 on 09/08/12
For personal use only.

reported values for alkaline hydrolyses of benzoic esters. While this is certainly true, it is not an unusual value for a second-order reaction in solution (10), and it is still a substantially negative factor on the rate, corresponding to an entropy of activation of over -100 J mol^{-1} K^{-1}. In fact, the free energy barrier to this reaction of approximately 120 kJ mol^{-1} at 100°C appears to be about two-thirds enthalpy and one-third entropy. Taking the concentrations, extent of conversion, and temperature of our partial conversion of methyl triphenylacetate, and assuming a second-order process, the free energy barrier is calculated to be approximately 135 kJ mol^{-1}.

Taking these values, and comparing them with those for alkaline hydrolyses of less hindered esters (10–12), it is evident that the increase of steric hindrance causes a steady increase in the energy of activation (11.5 kcal/mol for methyl acetate (11); 13.8 kcal/mol for ethyl benzoate (11); around 20 kcal/mol for a variety of 2,6-dimethylbenzoates (12); and the 25.07 kcal/mol value for methyl 2,4,6-tri-*tert*-butylbenzoate (7), which apparently proceeds by the $B_{AL}2$ mechanism). These values are partially compensated for by increasingly favourable pre-exponential factors, or entropies of activation, and, despite the change of mechanism, the $\log_{10}$ PZ factor reported by Barclay *et al.* is not out of line with this trend.

What is clear from these considerations is that, even when steric hindrance seriously impedes the $B_{AC}2$ mechanism, and increases the activation barrier to well over 100 kJ mol^{-1}, the $B_{AL}2$ route is just not available to take over the reaction. In that sense it is not merely "eclipsed" by the usual $B_{AC}2$ mechanism; it is a highly unfavourable reaction with an intrinsic energy barrier, regardless of steric hindrance, of at least 120–130 kJ mol^{-1}. For this improbable mechanism to be realized, two conditions apparently must be met: (*a*) this barrier must be overcome, which implies a slow reaction even at >100°C; and (*b*) the $B_{AC}2$ mechanism must, by some device, be made even more difficult and energy requiring. This is a tough requirement, and to find even one more example, beyond the one demonstrated by Barclay, Hall, and Cooke, may represent a substantial challenge.

Experimental

Infrared spectra were obtained on a Perkin–Elmer 1600 Series FTIR. Proton magnetic resonance spectra were obtained on a Varian XL-200 spectrometer; peak positions are recorded in ppm (δ) with respect to TMS. Mass spectra were obtained on a VG 7070E mass spectrometer.

^{18}O-Methyl trimethylacetate

A solution of trimethylacetyl chloride (0.211 g, 1.75 mmol), ^{18}O-methanol (85 μL, 2.10 mmol), and pyridine (4 drops) in dichloromethane (3 mL) was heated under reflux for 3 h. The resulting clear solution was diluted with dichloromethane (5 mL) and water (5 mL). The layers were separated, and the organic layer successively extracted with 1 M HCl solution (3 × 3 mL), water (1 × 3 mL), saturated $NaHCO_3$ solution (2 × 3 mL), and water (1 × 3 mL). The original organic layer, the first three extracts, and the last three extracts were each back-extracted with dichloromethane (2 × 3 mL). The combined organic extracts were dried over $MgSO_4$ and the solvent evaporated under reduced pressure to yield a clear liquid (0.169 g, 82% yield); bp 100°C (lit. (13) bp 100–102°C); ν_{max} (CH_2Cl_2): 1738 cm^{-1}; ^{1}H NMR ($CDCl_3$) δ: 1.70 (9H, s), and 3.70 ppm (3H, s).

Triphenylacetyl chloride

A suspension of triphenylacetic acid (1.0 g, 3.5 mmol) in thionyl chloride (20 mL) was heated under reflux for 6 h. The solution was evaporated under reduced pressure, fresh thionyl chloride was added, and the solution again heated under reflux for a further 6 h. The acid gradually dissolved to give a yellow solution. The thionyl chloride was evaporated under reduced pressure to give yellow crystals, IR analysis of which showed no detectable carboxylic acid remaining. The acid chloride, ν_{max} 1810 cm^{-1} ($CHCl_3$), was used directly for preparation of the methyl ester.

^{18}O-Methyl triphenylacetate

A solution of triphenylacetyl chloride (120 mg, 0.39 mmol), ^{18}O-methanol (300 mL, 7.06 mmol), and pyridine (5 drops) in benzene (5 mL) was heated under reflux for 25 h. The solution was then washed successively with 1 M HCl solution (3 × 5 mL), water (1 × 5 mL), saturated $NaHCO_3$ solution (2 × 5 mL), and water (2 × 5 mL), dried ($MgSO_4$), and evaporated to give flaky white crystals, mp 185–186°C (lit. (13) mp 186°C); ν_{max}: 1733 cm^{-1} ($CHCl_3$); ^{1}H NMR ($CDCl_3$) δ: 3.79 (3H, s) and 7.27 ppm (15 H, s).

Base hydrolysis of ^{18}O-methyl trimethylacetate

A solution of ^{18}O-methyl trimethylacetate (0.167 g, 1.44 mmol) in 1.0 M NaOH solution (20 mL) was kept at room temperature for 80 h. The resulting clear solution was acidified to approximately pH 3 by the careful addition of 1.0 M HCl solution, and then extracted with dichloromethane (3 × 3 mL). The combined extracts were dried ($MgSO_4$) and evaporated under reduced pressure to yield white crystals whose IR spectra showed the complete replacement of the peak at 1738 cm^{-1} (ester) by one at 1701 cm^{-1} (carboxylic acid). The mass spectrum of the TMS ester, prepared by addition of 20 μL of 20% Trisyl BSA in pyridine to 1 mg of carboxylic acid, was identical to that from authentic trimethylacetic acid, and showed no measurable enhancement of the m/z 161:159 ratio.

Base hydrolysis of ^{18}O-methyl triphenylacetate

A solution of ^{18}O-methyl triphenylacetate (36 mg, 0.12 mmol) in a mixture of dioxane (6 mL) and 1.0 M NaOH solution (5 mL) was heated under reflux in the presence of a boiling chip for 287 h in a system protected with a drying tube containing NaOH pellets. Periodic additions of dioxane were made to maintain the 11 mL volume. The resulting solution was carefully acidified to approximately pH 3 using 1.0 M HCl solution. Water (5 mL) and chloroform (5 mL) were added, the organic layer removed, and the aqueous layer extracted with further portions of chloroform (3 × 5 mL). The combined organic extracts were washed with water (1 × 10 mL), dried ($MgSO_4$), and evaporated, to yield a white powder, whose IR spectrum showed the presence of both ester (1733 cm^{-1}) and carboxylic acid (1697 cm^{-1}). Studies on mixtures of ester and acid of known proportion showed that this hydrolysis mixture consisted of 60% ester and 40% acid. GC – mass spectrometry of the TMS ester of the acid, prepared as described above, showed an enhancement of the m/z 347:345 ratio consistent with the presence of 5% ± 1% ^{18}O-labelled triphenylacetic acid to 95% unlabelled acid.

Acknowledgments

We wish to thank Dr. Clem Kazakoff for the mass spectral and the GC–MS determinations. We also wish to acknowledge the financial support of this work by the Natural Sciences and Engineering Research Council of Canada.

1. J.N.E. Day and C.K. Ingold. Trans. Faraday Soc. **37**, 686 (1941).
2. C.K. Ingold. Structure and mechanism in organic chemistry. 2nd ed. Cornell University Press, Ithaca, N.Y. 1969. pp. 1128–1144.
3. W.A. Cowdrey, E.D. Hughes, C.K. Ingold, S. Masterman, and A.D. Scott. J. Chem. Soc. 1252 (especially p. 1264) (1937).
4. J.F. Bunnett, M.M. Robison, and F.C. Pennington. J. Am. Chem. Soc. **72**, 2378 (1950).

5. E.S. Gould. Mechanism and structure in organic chemistry. Holt, Rinehart and Winston, New York. 1959. pp. 314–318.
6. N.S. Isaacs. Physical organic chemistry. Longman Group, Harlow, U.K. 1987. p. 483.
7. L.R.C. Barclay, N.D. Hall, and G.A. Cooke. Can. J. Chem. **40**, 1981 (1962).
8. F.C. Chang and N.F. Wood. Tetrahedon Lett. 2969 (1964).
9. C.A. Bunton, A.E. Comyns, J. Graham, and J.R. Quayle. J. Chem. Soc. 3817 (1955).
10. H. Maskill. The physical basis of organic chemistry. Oxford University Press, Oxford. 1985. pp. 216–267.
11. W.B.S. Newling and C.N. Hinshelwood. J. Chem. Soc. 1357 (1936).
12. H.L. Goering, T. Rubin, and M.S. Newman. J. Am. Chem. Soc. **76**, 787 (1954).
13. Dictionary of organic compounds. 5th ed. Chapman and Hall, New York. 1982.

Can. J. Chem. Downloaded from www.nrcresearchpress.com by 203.198.23.82 on 09/08/12
For personal use only.

Novel [2.2]paracyclophane derivatives via charge-transfer complexation

ASHRAF A. ALY, ALAA A. HASSAN, AND ABOUL-FETOUH E. MOURAD[1]
Chemistry Department, Faculty of Science, El-Minia University, El-Minia, A.R. Egypt

Received March 8, 1993

ASHRAF A. ALY, ALAA A. HASSAN, and ABOUL-FETOUH E. MOURAD. Can. J. Chem. **71**, 1845 (1993).

The transannular electronic interactions in [2.2]paracyclophanes affect the selectivity of the tricyanovinylation reaction with tetracyanoethylene (TCNE). In addition to the normal *N*-tricyanovinyl product, 4-amino[2.2]paracyclophane reacts with TCNE to give oxaziridine derivatives. In the case of reaction with 4-*N*-methylamino[2.2]paracyclophane, the unusual *N*-tricyanovinylated product as well as 4-(*N*-carbonitrile-*N*-methyl)amino[2.2]paracyclophane was isolated. The reaction of 2,3-dichloro-5,6-dicyano-1,4-benzoquinone (DDQ) with 4-amino[2.2]paracyclophane results in formation of 2-cyano-3-(4-[2.2]paracyclophanyl)amino-5,6-dichloro-1,4-benzoquinone.

ASHRAF A. ALY, ALAA A. HASSAN et ABOUL-FETOUH E. MOURAD. Can. J. Chem. **71**, 1845 (1993).

Les interactions électroniques transannulaires des [2.2]paracyclophanes affectent la sélectivité de la réaction de tricyanovinylation du tétracyanoéthylène (TCNE). En plus du produit *N*-tricyanovinyle normal, la réaction du 4-amino[2.2]paracyclophane avec le TCNE fournit des derivés oxaziridines. Dans le cas de la réaction avec le 4-*N*-méthylamino[2.2]paracyclophane, on a isolé le dérivé inhabituel *N*-tricyanovinylé ainsi que le 4-(*N*-carbonitrile-*N*-méthyl)amino[2.2]paracyclophane. La réaction de la 2,3-dichloro-5,6-dicyano-1,4-benzoquinone (DDQ) avec le 4-amino[2.2]paracyclophane conduit à la formation de la 2-cyano-3-(4-[2.2]paracyclophanyl)amino-5,6-dichloro-1,4-benzoquinone.

[Traduit par la rédaction]

Can. J. Chem. Downloaded from www.nrcresearchpress.com by 203.198.23.82 on 09/08/12
For personal use only.

Introduction

As part of a program designed to synthesize heterocyclics via charge-transfer (CT) complexation between heterocyclic compounds as electron donors and electron-deficient compounds as electron acceptors, we recently reported the synthesis of some interesting heterocyclic systems such as pyrazolopyrimidines (1), indanopyrazolopyrimidines (2), and pyrazoloquinazolines (3) via CT-complexation between pyrazole derivatives and tetracyanoethylene (TCNE), 2-(dicyanomethylen)indane-1,3-dione ((CNIND), as well as 2,3-dichloro-5,6-dicyano-1,4-benzoquinone (DDQ), respectively.

One of the reasons for the continuing interest in the reactivity of [2.2]paracyclophane derivatives (4) is that their chemical behaviour differs considerably from that of classical aromatic systems (5–9).

In the present investigation, we turned our attention to 4-amino[2.2]paracyclophane (**1**) and its *N*-methyl derivative **5** as electron donors, aiming to shed more light on the impact of the transannular electronic interactions existing in the [2.2]paracyclophane nucleus on its behaviour towards TCNE and DDQ as π-acceptors. This aim can in principal be achieved by comparing the behaviour of the phane system with that of model compounds such as 2,5-dimethylaniline. 2,5-Dimethylaniline reacts with TCNE to give mainly the *N*-tricyanovinyl derivative (ca. 95%) (10). The attack of TCNE on the nitrogen atom of the free amino group is more favourable than on the carbon atom in the *para*-position, since the amino group is the more nucleophilic center.

Results and discussion

Interaction between 4-amino[2.2]paracyclophane (**1**) and TCNE in absolute ethyl acetate results in the formation of 4-*N*-tricyanovinyl-amino[2.2]paracyclophane (**2**), i.e., the expected product, 2-(4-[2.2]paracyclophanyl)-3,3-dicyanooxaziridine (**3**), and tetracyanoethane (**4**) (Fig. 1). It is worth noting that **3** is the first oxaziridine derivative formed by CT-complexation between TCNE and the primary aromatic amine. Figure 2 illustrates a plausible mechanism for its formation. This sequence shows initial formation of a CT-complex that absorbs at 620 nm followed by elimination of malononitrile, then addition of an H_2O molecule to the C=N bond followed by dehydrogenation by another molecule of TCNE, affording the oxaziridine derivative **3** and tetracyanoethane (**4**). The enhancement of formation of **2** and **3** may be explained as due to the transannular electronic interactions in 4-amino[2.2]paracyclophane (**1**), which tend to increase the nucleophilic character of the amino group through the donation of π-electrons from the unsubstituted half of **1** to the aminosubstituted half.

It has been reported that tertiary and secondary aromatic amines are tricyanovinylated at the *para*-position on reaction with TCNE (10). Using 4-*N*-methylamino[2.2]paracyclophane (**5**) as a secondary aromatic amine, the reaction with TCNE gave the unexpected *N*-tricyanovinylation product **6** as well as 4-(*N*-carbonitrile-*N*-methyl)amino[2.2]paracyclophane (**7**). The mechanism of formation of **7** is illustrated in Fig. 3, which indicates initial formation of a CT-complex (absorbing at 610 nm), followed by formation of *N*-tricyanovinylated intermediate **6**. Hydrolysis of **6** and elimination of one molecule of malononitrile from **14** results in formation of **7**. The formation of *N*-tricyanovinyl derivative **6** can be attributed to the effect of the transannular electronic interactions (see Fig. 4), which play an important role in increasing the electron-donating character of the nitrogen atom so that the electronic factor predominates with respect to the steric one. The structure of **6** is confirmed by the disappearance of the NH proton (IR, ^{1}H NMR spectra, cf. Experimental). (The NH proton in **5** appears as a multiplet at $\delta = 2.70–2.61$ ppm and ν(NH) ≈ 3325 cm^{-1} (11).)

The participation of moist air in formation of compounds **3** and **7** as illustrated in the proposed mechanism, in Figs. 2 and 3, was confirmed by adding both donors **1** and **5** to TCNE under nitrogen and dry conditions. Only stable CT-complexes were formed, which dissociate into their com-

[1]Author to whom correspondence may be addressed.

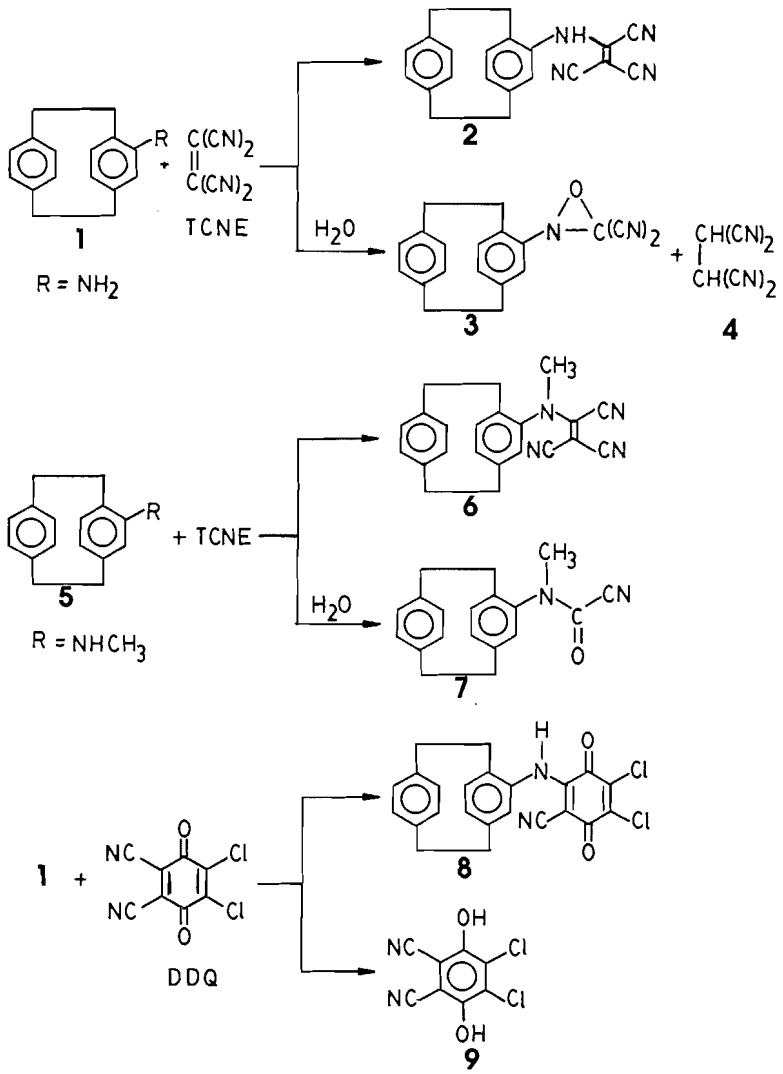

FIG. 1. Interaction of **1** and **5** with π-acceptors.

ponents after time and do not follow the given sequence of chemical reaction.

Addition of DDQ to **1** results in formation of a CT-complex (absorbing at 580 nm), accompanied by elimination of HCN, giving rise to the reaction product **8** in addition to DDQ-H_2 (**9**), as shown in Fig. 1. The proposed mechanism of formation of **8** and **9** is given in Fig.5.

In conclusion, the transannular electronic interaction existing in [2.2]paracyclophanylamines tends to change the mode of reaction with π-acceptors significantly as compared to normal aromatic amines; consequently, interesting and unexpected reaction products were obtained that cannot be easily prepared by conventional synthetic methods.

Experimental

Melting points are uncorrected. UV/vis: Perkin–Elmer Lambda 2 spectrophotometer. IR: Nicolet 320 FT-IR(KBr). ^{1}H and ^{13}C NMR: Bruker WM 400 (400.1 MHz). MS: Finigan 8430 at 70 eV. Elemental analyses: microanalytical unit at Cairo University.

Electron acceptors

Tetracyanoëthylene (Aldrich) was recrystallized from chlorobenzene and sublimed. 2,3-Dichloro-5,6-dicyano-1,4-benzoquinone (Aldrich) was recrystallized from benzene–chloroform (2:3).

Electron donors

4-Amino[2.2]paracyclophane (**1**) and 4-*N*-methylamino[2.2]-paracyclophane (**5**) were prepared according to refs. 12 and 11, respectively.

Reaction of 4-amino[2.2]paracyclophane (1) with TCNE

A solution of **1** (0.223 g, 0.001 mol) in 10 mL of absolute ethyl acetate was added to a solution of TCNE (0.256 g, 0.002 mol) in 10 mL of absolute ethyl acetate and the reaction mixture was stirred for 48 h at room temperature. On concentration and chromatography on thin-layer plates (Merck Silica Gel 60 PF 254) using toluene – ethyl acetate (1:1), two zones were well separated. The first zone contained compound **2** and the second zone contained compound **3**. The base line of the tlc rechromatographed using toluene – ethyl acetate (1:2) contained the tetracyanoethane (**4**).

2: Yellow crystals, yield 41%, mp 204–206°C (toluene). IR (KBr), $\bar{\nu}$: 3445 (NH); 3100 (Ar-CH); 2900–2800 (Ali-CH); 2235, 2212 (CN); 1645 (Ar-C=C) cm^{-1}. ^{1}H NMR ($CDCl_3$), δ: 7.80 (s, br, 1H, NH), 6.75–6.48 (m, 6H, Ar-H), 6.18 (d, 1H, Ar-H), 3.45–2.70 (m, 8H, CH_2). ^{13}C NMR, δ: 142.60, 139.56, 138.78, 136.67, 134.62, 134.48, 134.22, 133.84, 132.13 (Ar-C=C, Ali C=C); 111.62, 111.36, 109.33 (CN); 35.08, 34.65, 34.43, 32.36 (CH_2). MS (70 eV), *m/z* (%): 324 [M^+] (16), 297 (6), 193 (10), 104 (100), 103 (16). Anal. calcd. for $C_{21}H_{16}N_4$ (324.38): C 77.76, H 4.97, N 17.27; found: C 77.60, H 4.95, N 17.30.

3: Yellow crystals, yield 31%, mp 289–291°C (toluene). IR

Can. J. Chem. Downloaded from www.nrcresearchpress.com by 203.198.23.82 on 09/08/12
For personal use only.

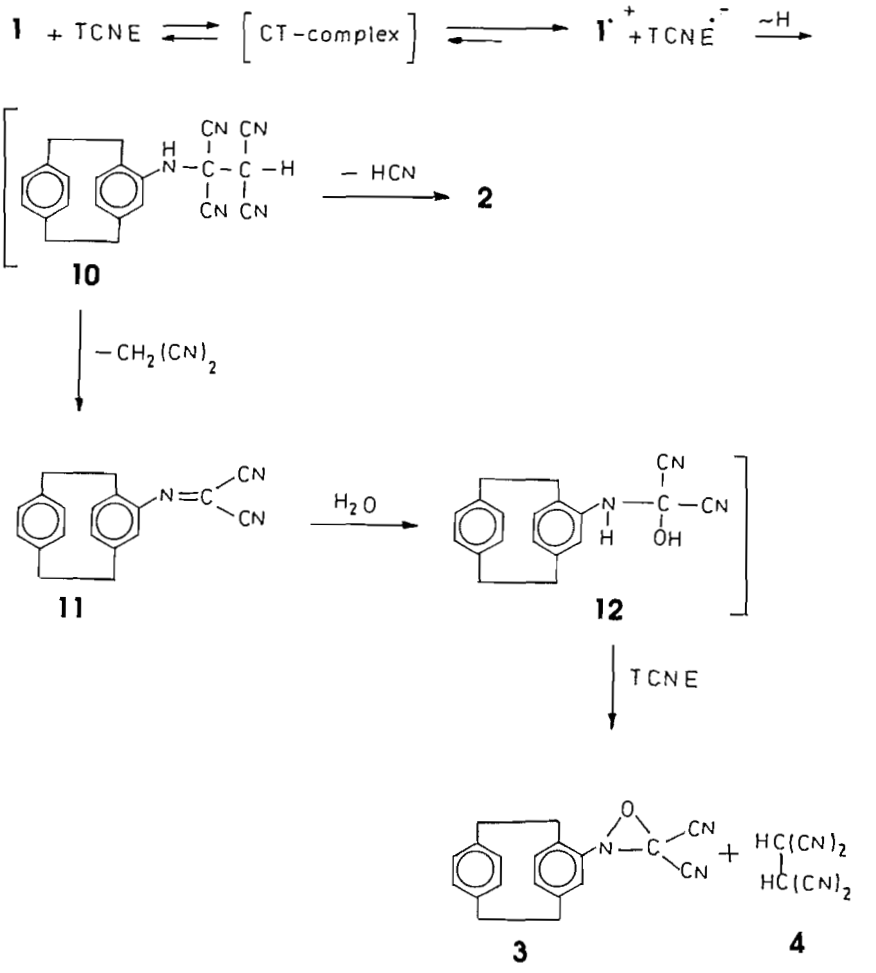

FIG. 2. Proposed mechanism for formation of **2** and **3**.

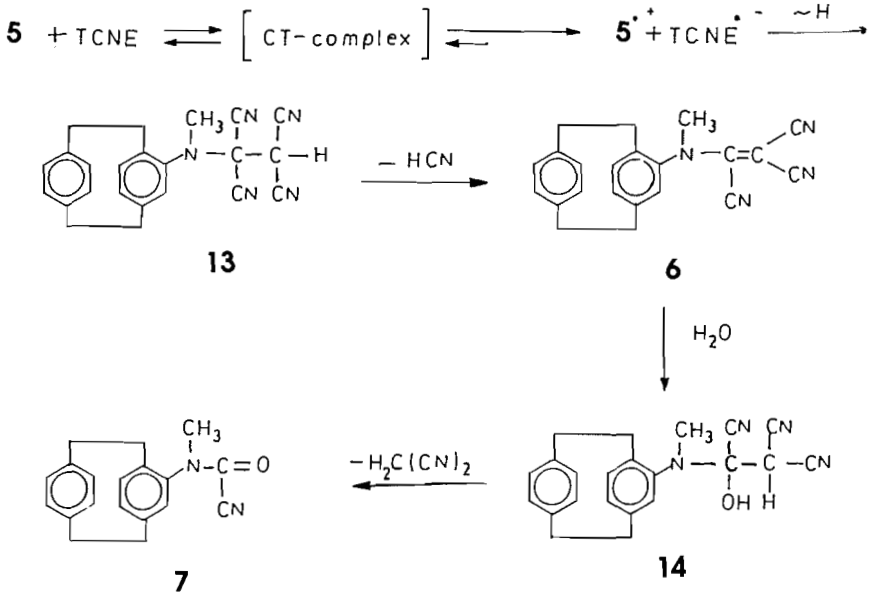

FIG. 3. Proposed mechanism for formation of **6** and **7**.

(KBr), $\bar{\nu}$: 3162, 3138 (Ar-CH); 2961, 2935 (Ali-CH); 2241, 2225 (CN) cm^{-1}. ^1H NMR ($CDCl_3$), δ: 7.00–6.30 (m, 7H, Ar-H), 3.30–2.85 (m, 8H, CH_2). MS (70 eV), *m/z* (%): 301 (8) [M^+], 265 (68), 197 (10), 195 (22), 161 (100), 119 (82), 104 (72). Anal. calcd. for $C_{19}H_{15}N_3O$ (301.35): C 75.73, H 5.02, N 13.94; found: C 75.53, H 4.90, N 13.90.

4: The structure of TCNE-H_2 was established from comparison of its IR spectrum (which shows characteristic strong C—H ab-

Can. J. Chem. Downloaded from www.nrcresearchpress.com by 203.198.23.82 on 09/08/12
For personal use only.

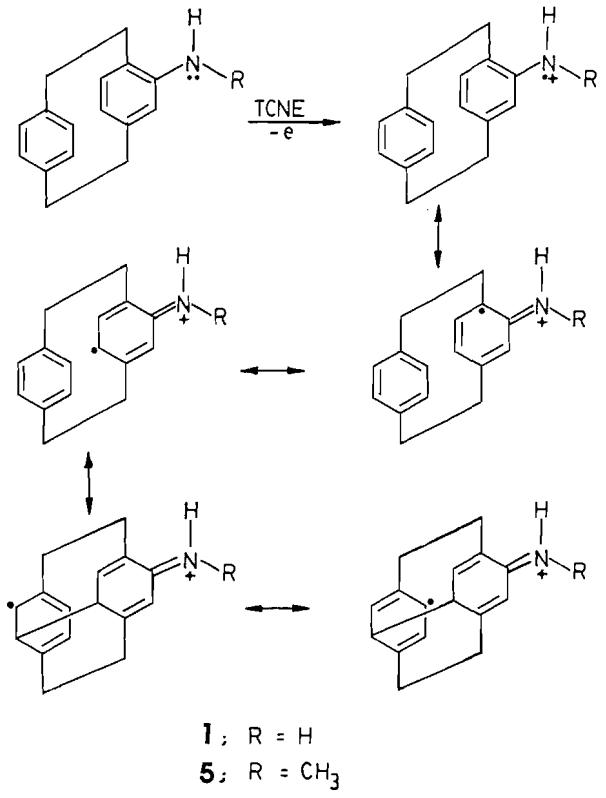

FIG. 4. Transannular electronic interactions in compounds **1** and **5**.

sorption at 2900 cm^{-1} and weak cyano absorption at 2260 cm^{-1}) and melting point with those of an authentic sample prepared according to ref. 13.

The reaction of 4-N-methylamino[2.2]paracyclophane (5) with TCNE

A solution of **5** (0.337 g, 0.001 mol) in absolute ethyl acetate (10 mL) was added to a solution of TCNE (0.256 g, 0.002 mol) in 10 mL of absolute ethyl acetate and the reaction mixture was stirred for 3 days at room temperature. The colour of the reaction mixture changed from blue to red after 48 h. Concentration of the mixture under reduced pressure and chromatography on thin-layer plates of Silica Gel 60 PF 254 using toluene – ethyl acetate (10:1) as eluent afforded two zones containing compounds **6** and **7** that were rechromatographed by successive elution with toluene.

6: Pink crystals, yield 28%, mp >360°C (ether – pet. ether). IR (KBr), $\bar{\nu}$: 2964–2926 (Ali-CH); 2213 (CN); 1597 (Ar-C=C) cm^{-1}. ^1H NMR ($CDCl_3$), δ: 6.90–6.50 (m, 7H, Ar-H), 3.80–2.80 (m, 8H, CH_2), 2.40 (s, 3H, $\geq$ N (CH_3)). MS (70 eV), *m/z* (%): 339 (10) [M^+], 338 (38), 324 (8), 234 (100), 208 (38), 104 (50). Anal. calcd. for $C_{22}H_{18}N_4$ (338.41): C 78.08, H 5.36, N 16.56; found: C 77.90, H 5.30, N 16.40.

7: Colourless crystals, yield 34%, mp 201–203°C (ethanol). IR (KBr), $\bar{\nu}$: 2958–2853 (Ali-CH); 2240 (CN); 1695 (CO) cm^{-1}. ^1H NMR ($CDCl_3$), δ: 6.80–6.36 (m, 7H, Ar-H), 3.20–2.90 (m, 8H, CH_2), 2.43 (s, 3H, $\geq$N (CH_3)). ^{13}C NMR, δ: 191.57 (CO), 139.53, 139.26, 136.48, 135.19, 133.35, 132.65, 130.92 (Ar-CH), 126.78 (C=N). MS (70 eV), *m/z* (%): 290 (90) [M^+], 263 (4), 186 (30), 185 (78), 104 (100). Anal. calcd. for $C_{19}H_{18}N_2O$ (290.36): C 78.60, H 6.25, N 9.65; found: C 78.45, H 6.20, N 9.60.

Reaction of 4-amino[2.2]paracyclophane (1) with DDQ

To a solution of DDQ (0.454 g, 0.002 mol) in 10 mL of absolute ethyl acetate, a solution of **1** (0.223 g, 0.001 mol) in 10 mL

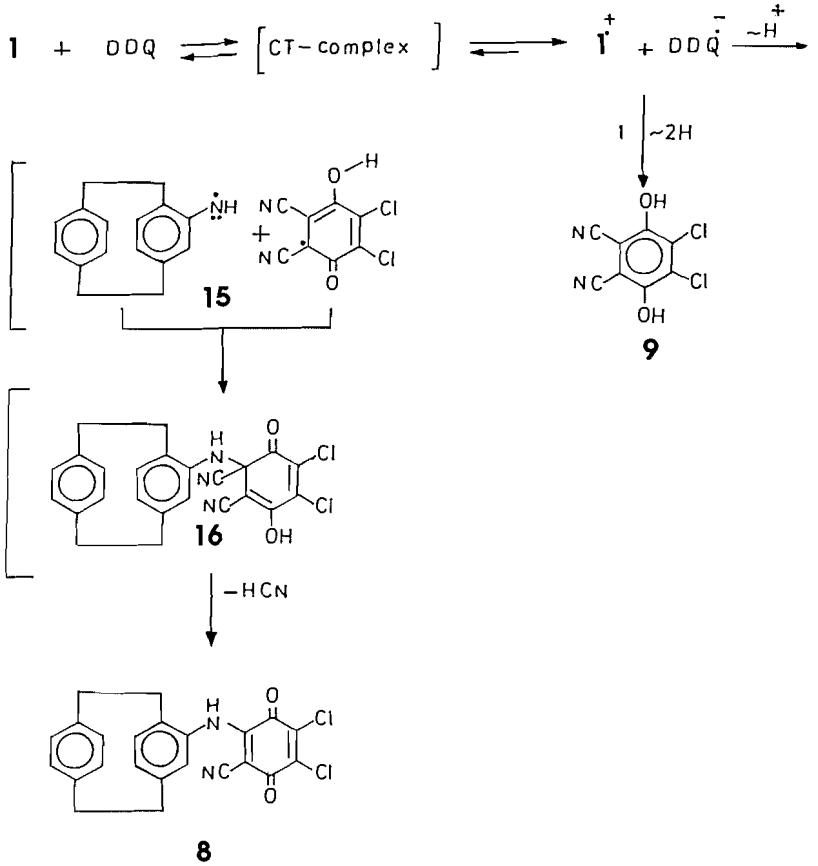

FIG. 5. Proposed mechanism for formation of **8** and **9**.

Can. J. Chem. Downloaded from www.nrcresearchpress.com by 203.198.23.82 on 09/08/12
For personal use only.

of absolute ethyl acetate was added. The reaction mixture was stirred for 72 h at room temperature. The colour of the reaction mixture changed spontaneously from blue to reddish brown. The solution was concentrated under reduced pressure and applied on chromatographic plates using toluene – ethyl acetate (1:1) as eluent. Two zones were well separated; the fastest migrating zone contained compound **8**, the slowest migrating zone (which is always characterized by quenching all indicator fluorescence upon exposure to 254-nm UV light) contained compound **9**.

8: Orange crystals, yield 47%, mp >360°C (ethanol). IR(KBr), $\bar{\nu}$: 3423 cm^{-1} (NH); 3009 (Ar-CH); 2931–2858 (Ali-CH); 2230 (CN); 1632 (Ar-C=C). ^1H NMR ($CDCl_3$), δ: 7.73 (s, br, 1H, NH), 7.10–6.20 (m, 8H, Ar-H), 3.80–2.60 (m, 8H, CH_2). MS (70 eV), *m/z*(%): 424 (100) [M^+], 423 (26), 422 (68), 396 (48), 364 (84), 337 (58), 104 (12). Anal. calcd. for $C_{23}H_{16}N_2O_2Cl_2$ (423.30): C 65.26, H 3.81, N 6.62; found: C 65.35, H 3.80, N 6.60.

9: Was identified by comparing its physical properties with that of an authentic sample.

Acknowledgement

The authors are deeply indepted to Prof. Dr. H. Hopf, Institute of Organic Chemistry, Braunschweig University, for valuable discussions and for measuring the spectra, and to the Alexander von Humboldt Foundation for donation of the Perkin–Elmer Lambda 2 spectrophotometer.

1. A.A. Hassan, Y.R. Ibrahim, N.K. Mohamed, and A.E. Mourad. J. Prakt. Chem. **332**, 1049 (1990).
2. A.A. Hassan, Y.R. Ibrahim, N.K. Mohamed, and A.E. Mourad. Liebigs Ann. Chem. 71 (1991).
3. Y.R. Ibrahim, A.A. Hassan, N.K. Mohamed, and A.E. Mourad. Arch. Pharm. (Weinheim), **325**, 389 (1992).
4. P.M. Keehn and S.M. Rosenfeld (*Editors*). The Cyclophanes. Vols. I, II. Academic Press, New York. 1983; C.F. H. Hopf. Naturwissenschaften, **70**, 349 (1983).
5. D.J. Cram and R.H. Bauer. J. Am. Chem. Soc. **81**, 5971 (1959).
6. M. Sheehan and D.J. Cram. J. Am. Chem. Soc. **91**, 3553 (1969).
7. E. Langer and H.L. Lehner. Tetrahedron, **29**, 375 (1973).
8. L.A. Singer and D.J. Cram. J. Am. Chem. Soc. **85**, 1080 (1963).
9. H.J. Reich and D.J. Cram. J. Am. Chem. Soc. **91**, 3534 (1969).
10. Z. Rappoport and E. Shohamy. Israel J. Chem. **6**, 865 (1968).
11. H. Hopf, W. Grahn, D.G. Barrett, A. Gerdes, J. Hilmer, J. Hucker, Y. Okamoto, and Y. Kaida. Chem. Ber. **123**, 841 (1990).
12. D.J. Cram and N.L. Allinger. J. Am. Chem. Soc. **77**, 6289 (1955).
13. W.J. Middleton, R.E. Heckert, E.L. Little, and C.G. Krespan. J. Am. Chem. Soc. **80**, 2783 (1958).

Can. J. Chem. Downloaded from www.nrcresearchpress.com by 203.198.23.82 on 09/08/12
For personal use only.

Electrocatalytic hydrogenation of ketones and of α- and β-diketones on Raney metal electrodes

AMOY KAM CHEONG, YVON BOLDUC, AND JEAN LESSARD[1]

Laboratoire d'électrochimie et d'électrocatalyse, Département de chimie, Université de Sherbrooke, Sherbrooke, QC J1K 2R1, Canada

Received February 1, 1993

AMOY KAM CHEONG, YVON BOLDUC, and JEAN LESSARD. Can. J. Chem. **71**, 1850 (1993).

The electrocatalytic hydrogenation (ECH) of various ketones was investigated at codeposited Raney metal electrodes in aqueous methanol. The influence of different parameters (pH, supporting electrolyte, and water percentage) on the ECH of cyclohexanone and acetophenone was studied. The relative ease of electrohydrogenation of a variety of monoketones was determined in competitive electrolyses. The ECH of α- and β-diketones was carried out and different products were obtained selectively by the right choice of catalytic material and electrolysis conditions. The diastereoselectivity of the formation of diols was also determined.

AMOY KAM CHEONG, YVON BOLDUC et JEAN LESSARD. Can. J. Chem. **71**, 1850 (1993).

Nous avons étudié l'hydrogénation électrocatalytique (HEC) de plusieurs cétones sur des électrodes codéposées de métaux de Raney en milieu méthanol–eau. L'étude de l'influence de plusieurs paramètres (pH, électrolyte-support et pourcentage d'eau) sur l'HEC de la cyclohexanone et de l'acétophénone a été effectuée. Nous avons comparé la facilité relative de l'électrohydrogénation de différentes monocétones lors d'électrolyses compétitives. Lors de l'HEC d'α- et β-dicétones, différents produits ont été obtenus sélectivement, selon le choix du catalyseur et des conditions d'électrolyse. La diastéréosélectivité lors de la formation des diols a aussi été déterminée.

Can. J. Chem. Downloaded from www.nrcresearchpress.com by 203.198.23.82 on 09/08/12
For personal use only.

Introduction

Electrocatalytic hydrogenations (ECH) have been known since the beginning of the century (1–3). They involve the electrochemical reduction of water (eq. [1]) at the surface of a metal electrode M. The chemisorbed hydrogen M(H) thus formed reacts with the adsorbed organic substrate M(Y=Z) (eq. [3]), this step being the same as in catalytic hydrogenation. A competing reaction is the formation of molecular hydrogen

[1] $H_2O + e^- \rightarrow M(H) + OH^-$

[2] $Y = Z + M \rightarrow M(Y{=}Z)$

[3] $2M(H) + M(Y = Z) \rightarrow M(YH\text{-}ZH)$

[4] $M(YH\text{-}ZH) \rightarrow YH\text{-}ZH + M$

[5] $M(H) + e^- + H_2O \rightarrow H_2 + M + OH^-$

[6] $2M(H) \rightarrow H_2 + M$

(eq. [5] and (or) [6]). The efficiency of ECH will depend on the competition arising between reactions [3] and [5] and (or) [6]. This competition depends on the substrate, the electrode material and surface, and, for a given substrate and electrode, on the electrolysis conditions. Electrocatalytic hydrogenations are very clean since only hydrogenation and hydrogen evolution are involved. In ECH, the current efficiency of the hydrogenation reflects the competition between these two processes. Raney metal based electrodes have proven to be very efficient for the ECH of various substrates (4–13).

Compared to catalytic hydrogenation, ECH presents several advantages: the kinetic barrier relative to the splitting of gaseous hydrogen is bypassed, elevated temperatures and pressures of hydrogen are avoided, and poisoning of the catalyst is diminished due to the cathodic potential applied (5, 14). ECH is advantageous when compared to electrohydrogenation by direct electronation–protonation. The formation of chemisorbed hydrogen by electrolysis of water takes place at a less negative potential than the direct electroreduction of most organic substrates, hence the lower energy required. Furthermore, side reactions such as dimerization (resulting in pinacols, for example, during reduction of ketones) can be avoided. As a consequence, much work is being done on the application of this electroorganic technique.

This paper reports the results of a study of the ECH of various ketones on Raney metal electrodes and in aqueous methanol. First we describe the influence of different conditions of electrolysis on the electrohydrogenation of cyclohexanone and acetophenone, and on the chemoselectivity of the competitive electrohydrogenations of pairs of ketones (cyclohexanone, acetophenone, benzylacetone, and 2-octanone). We also report the results of the ECH of two α-diketones (benzil and 1-phenyl-1,2-propanedione) and of two β-diketones (1,3-diphenyl-1,3-propanedione and 2,4-pentanedione).

Results and discussion

The catalytic electrodes consisted of Raney nickel (RaNi) or Raney cobalt (RaCo) or Devarda copper (DeCu) particles embedded in a nickel matrix. The preparation of such electrodes has been described elsewhere (6–9). Prior to the electrocatalytic hydrogenation, that is, before adding the organic substrate, electrolysis of water was carried out at a constant current so that the cathode material was saturated with adsorbed hydrogen. The potential was then brought to a more positive value until the current reached zero (no hydrogen evolution) and was maintained at that value during the electrohydrogenation. This potential varied with the pH of the medium. In alkaline solutions it was about −1 V (vs. SCE), and in neutral or slightly acidic media it was about −0.65 V (vs. SCE). The addition of the substrate (1 or 2 mmol) caused an increase in current that gradually diminished during the electrolysis. The latter was stopped after the

[1]Author to whom correspondence may be addressed.

TABLE 1. ECH of cyclohexanone on RaNi in different conditions[a]

Entry	Supporting electrolyte	$CH_3OH:H_2O$	pH	$-E^b$ (V vs. ECS)	Chemical yield[c] (%)	Current efficiency (%)
1	KOH 0.14 M	93:7	>13	1.03	85	99
2	NaOH 0.14 M	93:7	>13	1.02	100	100
3	Bu_4NOH 0.1 M	93:7	>13	1.08	99.5	98
4	Bu_4NCl 0.1 M	93:7	8–12[d]	0.99	93	92
5	H_3BO_3/NaCl[e]	93:7	5–7[d]	0.68	81	103[f]
6	CH_3COOH/ CH_3COONa[g]	93:7	~7	0.64	0[h]	0[h]
7	KOH 0.14 M	99:1	>13	1.04	100	100
8	KOH 0.14 M	85:15	>13	1.03	99	87

[a]The electrolyses were carried out in methanol:water mixtures (w/w), at room temperature, and were stopped after a charge corresponding to two moles of electrons per mole of ketones was passed. The electrodes contained about 1 g of Raney alloy before leaching.
[b]All potentials shown correspond to a zero current before the addition of the substrate.
[c]Product analysis was carried out by vpc, and the mass balance was 85–100%.
[d]Initial and final pH are indicated.
[e]H_3BO_3 0.1 M; NaCl 0.1 M.
[f]This current efficiency higher than 100% is due to chemisorbed hydrogen formed during the leaching process and the electrolysis of water carried out prior to the addition of the organic substrate.
[g]CH_3COOH 0.54 M; CH_3COONa 0.37 M.
[h]Hydrogen evolution was the sole electrochemical process.

TABLE 2. ECH of cyclohexanone on RaCo in different conditions[a]

Entry	Supporting electrolyte	$-E^b$ (V vs. ECS)	Chemical yield[c] (%)	Current efficiency (%)
1	KOH	0.99	27	21
2	NaOH	1.04	75	55
3	Bu_4NOH	1.05	46	42
4	H_3BO_3/NaCl	0.74	25	22
5	CH_3COOH/CH_3COONa	0.63	0[d]	0[d]

[a,b,c]Same as in Table 1. The percentage of water is 7. The supporting electrolyte concentrations and the pH were the same as those indicated in Table 1.
[d]Hydrogen evolution was the sole electrochemical process.

theoretical charge required for complete hydrogenation of the organic substrate was passed: 2 F for 1 mol of monoketone and 4 F for 1 mol of diketone. It is noteworthy that though there was no hydrogen evolution in the absence of the organic substrate at the zero current potential, hydrogen evolution did occur in the presence of the substrate, which in some cases resulted in low or even zero current efficiency of electrohydrogenation.

We investigated the influence of the electrode material, the pH of the solution, the supporting electrolyte, and the percentage of water in the solvent mixture on the ECH of cyclohexanone and of acetophenone. In all the experiments, only one product was observed in each case: cyclohexanol and 1-phenylethanol, respectively. ECH of cyclohexanone was performed on RaNi (Table 1) and on RaCo (Table 2) and was more efficient on RaNi than on RaCo, as shown by the chemical yields and current efficiencies, which are much higher on RaNi. Attempts to electrohydrogenate cyclohexanone on DeCu were unsuccessful, hydrogen evolution being the sole electrochemical process occurring. Thus, the activity of Raney metals in the ECH of cyclohexanone is the same as in catalytic hydrogenation in general: RaNi > RaCo > DeCu (15). Acetophenone was electrohydrogenated on all three types of electrode materials (Tables 3–5). Again, the yields and current efficiencies were higher on RaNi (Table 3). But, with this substrate, the electrohydrogenations were more efficient on DeCu (Table 5) than on RaCo (Table 4). Thus the relative efficiencies of RaCo and DeCu electrodes in electrocatalytic hydrogenations are not only related to the catalytic material itself but depend also on the type of substrate.

On RaNi, in very alkaline media, ECH of cyclohexanone led to excellent chemical yields and current efficiencies (Table 1, entries 1–3, 7, and 8), the best results being obtained with NaOH (entry 2). Satisfactory results were obtained in less alkaline media (entries 4 and 5). However, when an acetate buffer was used, no hydrogenation took place (entry 6), hydrogen evolution being the sole electrochemical process observed. This can be explained by the strong adsorption of the acetic acid, which would prevent the adsorption of cyclohexanone (or displace it), thus inhibiting its hydrogenation. In contrast, the ECH of acetophenone was very efficient in the acetate buffer (Table 3, entry 2). Because of the presence of the phenyl ring, acetophenone would be more strongly adsorbed than cyclohexanone and would be more able to displace the acetic acid adsorbed on RaNi

Can. J. Chem. Downloaded from www.nrcresearchpress.com by 203.198.23.82 on 09/08/12
For personal use only.

TABLE 3. ECH of acetophenone on RaNi[a]

Entry	Supporting electrolyte	$-E$ (V vs. ECS)	Chemical yield (%)	Current efficiency (%)
1	KOH	1.03	97	90
2	CH_3COOH/CH_3COONa	0.63	98	93
3	$H_3BO_3/NaCl$	0.75	100	100

[a]The electrolysis conditions are the same as in Table 2.

TABLE 4. ECH of acetophenone on RaCo[a]

Entry	Supporting electrolyte	$-E$ (V vs. ECS)	Chemical yield (%)	Current efficiency (%)
1	KOH	1.02	5	8
2	NaOH	1.02	15	17
3	$H_3BO_3/NaCl$	0.74	33	32

[a]The electrolysis conditions are the same as in Table 2.

TABLE 5. ECH of acetophenone on DeCu[a]

Entry	Supporting electrolyte	$-E$ (V vs. ECS)	Chemical yield (%)	Current efficiency (%)
1	KOH	1.04	43	51
2	$H_3BO_3/NaCl$	0.71	55	59

[a]The electrolysis conditions are the same as in Table 2.

TABLE 6. Competitive ECHs between pairs of ketones at RaCo electrodes in basic medium[a]

Entry	Substrates	Reduction ratio[b]
1	Cyclohexanone:2-octanone	30:70
2	Cyclohexanone:acetophenone	36:64
3	Cyclohexanone:benzylacetone	91:9
4	2-Octanone:acetophenone	29:71[c]
5	Acetophenone:benzylacetone	100:0

[a]Equimolar amounts of both substrates were simultaneously added to the solution (0.3 M Bu_4NOH in methanol:water 80:20).

[b]Products were analyzed and ratios were determined by vpc after a charge corresponding to 0.5 mole of electrons per mole of ketone.

[c]After a charge corresponding to 2 moles of electrons per mole of ketone.

and react with chemisorbed hydrogen. Furthermore, a carbonyl group conjugated with a phenyl ring is probably more reactive towards chemisorbed hydrogen (see Table 6 and discussion below). The fact (*i*) that acetophenone was not electrohydrogenated in the acetate buffer on the less active RaCo and DeCu electrodes (hydrogen evolution being the sole electrochemical reaction occurring) and (*ii*) that the zero current potential was the same on all three electrodes (−0.62 to −0.65 V vs. SCE) strongly suggests that the electrohydrogenation on RaNi electrodes does not proceed by direct electroreduction of protonated acetophenone.

Although chloride ions are known to poison Raney nickel during catalytic hydrogenation (16), electrohydrogenation in the $H_3BO_3/NaCl$ medium was successful on all three electrodes (see Tables 1–5). The adsorption of chloride ions is probably prevented when the catalyst is submitted to a cathodic potential (9). In fact, the ECH of acetophenone in $H_3BO_3/NaCl$ was more efficient than in the alkaline medium on all three electrodes (Tables 3–5). The ECH of cyclohexanone on RaNi was as efficient in $H_3BO_3/NaCl$ as in the alkaline media (Table 1) but, on the RaCo electrode, the ECH was more efficient in the NaOH medium (Table 2). The effect of varying the water percentage in methanol had little effect, as shown in entries 1, 7, and 8 of Table 1.

Experiments were carried out to study the relative ease of ECH of pairs of monoketones on RaCo electrodes in alkaline medium and the results are shown in Table 6. In each case, equimolar amounts of both substrates were added to the electrolytic solution, and the charge necessary to reduce one-fourth of the total molar quantity of ketones (0.5 mol of electrons for 1 mol of ketone) was passed. The relative ease of ECH is in the order acetophenone > 2-octanone > cyclohexanone ≫ benzylacetone. Acetophenone is more easily electrohydrogenated than 2-octanone because of conjugation of the carbonyl group with the phenyl ring. Direct electroreduction of unprotonated acetophenone at −1.0 V vs. SCE is much less probable than its electrocatalytic hydrogenation. The difference between 2-octanone and cyclohexanone (entry 1) is most probably of steric origin, the approach of the carbonyl group of cyclohexanone to the surface of the catalyst being more sterically hindered due to the axial hydrogens of the ring. A phenyl ring one carbon away from the carbonyl group hinders the hydrogenation (entries 3 and 5). The less efficient electrohydrogenation of benzylacetone could be accounted for by: steric hindrance to adsorption of the carbonyl group by the phenyl group, and (or) preferential adsorption of the phenyl ring rendering more difficult the approach of the carbonyl to the catalyst surface, and (or) partial poisoning of the catalyst surface due to the strong adsorption of the product, 1-phenyl-2-propanol. It is worth noting that the ECH of benzophenone was unsuccessful in all media and on all three electrodes. This can be attributed to the strong adsorption of the product, benzhydrol, preventing the adsorption of benzophenone. The current dropped to zero after the passage of a few coulombs only.

Reduction of α-diketones

ECH of benzil occurred with good yields on all three of catalytic electrodes (Table 7). On RaNi, the hydrogenations gave hydrobenzoins, of which the *meso* form was predominant. In the acetate buffer medium, the relative percentages of *meso* and *threo* isomers were constant throughout the electrolysis. In the KOH medium, the *meso* isomer alone was present at the beginning of the electrolysis and the *threo* form appeared later, with its percentage increasing gradually. Following this observation, we studied the behavior of *meso*

Can. J. Chem. Downloaded from www.nrcresearchpress.com by 203.198.23.82 on 09/08/12
For personal use only.

TABLE 7. ECH of benzil[a]

Entry	Electrode	pH[b]	$-E$ (V vs. ECS)	Product(s)	Chemical yield (%)	Current efficiency (%)
1	RaNi	Alkaline	1.01	Hydrobenzoins[c] (*meso*/*threo* = 76/24)	99	92
2		Neutral	0.61	Hydrobenzoins (*meso*/*threo* = 69/31)	84	56
3	RaCo	Alkaline	0.87	Benzoin	—[d]	—[d]
4		Neutral	0.61	Benzoin[e]	83	81
5	DeCu	Neutral	0.59	Benzoin	84	76

[a]The electrolysis conditions were the same as in Table 2 except that electrolyses were stopped at a charge corresponding to 4 moles of electrons per mole of substrate.
[b]Alkaline: KOH 0.14 M; neutral: CH_3COOH 0.54 M, CH_3COONa 0.37 M.
[c]The *meso* isomer was formed at the beginning then isomerized to the *threo* form (see text).
[d]Benzoin was reoxidised into benzil so the yield was not determined (see text).
[e]A small amount of hydrobenzoin was obtained.

TABLE 8. Isomerization of mesohydrobenzoin in alkaline medium[a]

Entry	Conditions	Isomerization
1	Absence of electrode	None (30 h)
2	RaNi not saturated with hydrogen, open circuit	None (37 h)
3	RaNi saturated with hydrogen, open circuit	47% (87.5 h)
4	RaNi saturated with hydrogen and cathodic potential applied	58% (60 h)
5	RaCo saturated with hydrogen and cathodic potential applied	None (44 h)
6	Threohydrobenzoin: RaNi saturated with hydrogen and cathodic potential applied	26% (26 h)

[a]KOH 0.14 M in CH_3OH:H_2O 93:7 (w/w).

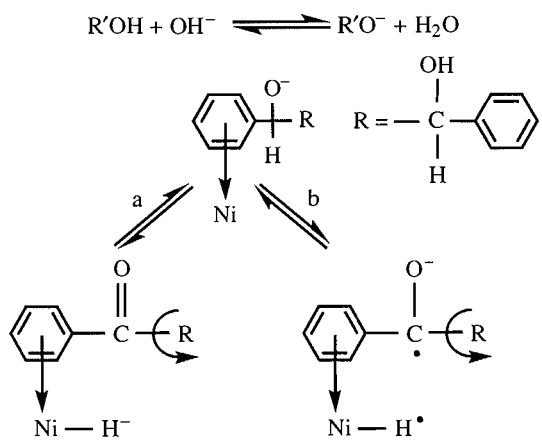

SCHEME 1

hydrobenzoin in alkaline medium (Table 8). Isomerization to the *threo* form was found to occur only in the presence of a RaNi electrode charged with chemisorbed hydrogen (entries 3 and 4). Furthermore, the isomerization was faster when the RaNi electrode was polarized (entry 4). We also observed the isomerization of *threo* hydrobenzoin into the *meso* form under the conditions of entry 4, up to 26% after 26 h (see entry 6). In the absence of a RaNi electrode (entry 1) or in the presence of a RaNi electrode from which chemisorbed hydrogen was removed by heating under vacuum (entry 2), there was no isomerization. There was no isomerization either in the presence of a RaCo electrode charged with hydrogen and polarized (entry 5). We propose a dehydrogenation–hydrogenation mechanism that involves the conjugate base of hydrobenzoin generated in the alkaline medium (Scheme 1). The alkoxide anion can undergo dehydrogenation either by losing a hydride anion (path a) or a hydrogen atom (path b). A simple rotation along the C—R axis followed by addition of hydride (path a) or of a hydrogen atom (path b) gives the *threo* isomer. The RaCo catalyst, which is known to be less active than RaNi, would not be active enough to dehydrogenate the alkoxide ion. The RaNi catalyst would be deactivated by removing the chemisorbed hydrogen, most probably because of the formation of oxides since the RaNi was in contact with air for a few minutes after the chemisorbed hydrogen has been removed. It is quite conceivable that a polarized catalyst could be more active in the dehydrogenation–hydrogenation process involving path b, that is, hydrogen atoms. The loss of a hydride ion should be more difficult on a negatively charged catalyst, so we favor path b over path a. The loss of a hydrogen atom from hydrobenzoin to form a neutral radical would be more difficult than from the conjugate base to form a radical anion (ketyl radical) since the *meso* → *threo* isomerization was not observed in a neutral medium. Vara Prasad *et al.* (17, 18) also proposed a dehydrogenation–hydrogenation pathway analogous to path b of Scheme 1 as one of the possible mechanism for the isomerization of allylic alcohols into aldehydes through the enol form on Raney nickel.

Can. J. Chem. Downloaded from www.nrcresearchpress.com by 203.198.23.82 on 09/08/12
For personal use only.

TABLE 9. ECH of 1-phenyl-1,2-propanedione[a]

Entry	Electrode	Medium	$-E$ (V vs. ECS)	Products	Chemical yield (%)	Current efficiency (%)
1	RaNi	Neutral[b]	0.76	Diols (94%) *erythro/threo* = 84/16 Ketols[d] (6%) **1/2** = 68/32	83	80
2		Neutral[c]	0.63	Diols (53%) *erythro/threo* = 73/27 Ketols[d] (47%) **1/2** = 95/5	75	68
3	RaCo	Neutral[b]	0.76	Ketols[d] **1/2** = 83/17	66	63
4	DeCu	Neutral[b]	0.78	Ketols[d] **1/2** = 85/15	78	63

[a]The electrolysis conditions are the same as in Table 7.
[b]The supporting electrolyte was H_3BO_3/NaCl.
[c]The supporting electrolyte was CH_3COOH/CH_3COONa.
[d]Ketol **1**: $PhCH(OH)COCH_3$; ketol **2**: $PHCOCH(OH)CH_3$.

On RaCo and DeCu, which are less active catalysts for hydrogenation, only one carbonyl group of benzil was reduced, giving benzoin (Table 7, entries 3–5). In alkaline medium (entry 3), we observed that the benzoin formed was oxidized back into benzil so the yield was not calculated. Benzoin is known to be easily oxidized (19, 20). Using pure benzoin, we showed that its oxidation (dehydrogenation) required both the presence of the catalyst and basic conditions. Raney metals are known to catalyse not only hydrogenations but also dehydrogenations and we assume that benzoin is dehydrogenated on the surface of the metal (eq. [7]) and that this process is much more rapid in an alkaline medium than in a neutral one. In the absence of RaCo or DeCu, in alkaline medium, some oxidation of benzoin to benzil did take place but at a much slower rate. This oxidation can only be explained by the presence in the electrolyte of traces of oxidizing agents, even if the experiments were performed under a nitrogen or argon atmosphere.

$$\text{[7]}\quad \underset{\text{Ph-C(=O)-CH(OH)-Ph}}{\text{O OH}} + \text{M} \xrightarrow{\text{OH}^-} \underset{\text{Ph-C(=O)-C(=O)-Ph}}{\text{O O}} + 2\,\text{MH}_{ads}$$

We have also studied the ECH of biacetyl. The study in alkaline solutions was precluded because of rapid aldol condensation. In neutral solutions, ECH mainly gave acetoin on both RaNi and RaCo electrodes. No hydrogenation occurred on DeCu electrodes, hydrogen evolution again being the sole electrochemical process observed.

1-Phenyl-1,2-propanedione was also subject to an aldol condensation in alkaline solutions. ECH of this diketone was therefore carried out in neutral media only (Table 9). On RaNi, two different electrolytes were used: H_3BO_3/NaCl (entry 1) and the acetate buffer (entry 2). As with cyclohexanone and acetophenone, the ECH of 1-phenyl-1,2-propanedione was more efficient in the boric acid medium (94% of diols, 6% of ketols, current efficiency of 80%) than in the acetate buffer (53% of diols, 47% of ketols, current efficiency of 68%). The *erythro* isomer of the diols was predominant and, of the two ketols **1** and **2**, ketol **1**, corresponding to the hydrogenation of the more reactive conjugated carbonyl, largely predominated. On the less active RaCo and DeCu electrodes, the electrohydrogenations were carried out only in the boric acid medium and stopped at the ketols, with ketol **1** again predominating (entries 3 and 4).

Reduction of β-diketones

Tables 10 and 11 show the results concerning the ECH of 1,3-diphenyl-1,3-propanedione and of 2,4-pentanedione, respectively. In the alkaline medium (KOH 0.14 M), these 1,3-diketones ($pK_a \sim 9$ (21)) should exist as their conjugate base, the conjugated enolate. In the neutral medium, the enol form most probably predominates. The percentage of enol form in pure diphenylpropanedione can be up to 100% (22). The enol form content is 80% in pure pentanedione and 83% in its solution in absolute alcohol (23).

On RaNi, the ECH of 1,3-diphenyl-1,3-propanedione (Table 10) yielded a mixture of 1,3-diphenyl-1,3-propanediols (**4**) and 1,3-diphenyl-1-propanol (**3**). In the alkaline medium, the monoalcohol **3** was the major product (72%, entry 2). On RaCo (entry 3), the ECH in the alkaline medium was much less efficient than on RaNi but the sole product obtained was the monoalcohol **3**. On DeCu, there was no electrohydrogenation at all, only hydrogen evolution occurred. The monoalcohol **3** most probably comes from the ECH of chalcone resulting from the dehydration of the intermediate β-hydroxyketone (Scheme 2), a relatively easy process either in an acidic or a basic medium (24). The relative proportions of diols **4** and monoalcohol **3** depend on the relative rates of hydrogenation and dehydration of the intermediate β-hydroxyketone (Scheme 2). In the alkaline medium, the hydrogenation would be faster than the dehydration whereas in the boric acid medium, the hydrogenation would be slower than the dehydration. On RaCo, which is less active than RaNi, hydrogenation of the β-hydroxyketone would be slower than its dehydration.

ECH of 2,4-pentanedione occurred on RaNi only and was very inefficient, hydrogen evolution being faster than electrohydrogenation (Table 11). In this case, the rate of dehydration of the intermediate β-hydroxyketones was slower than

Can. J. Chem. Downloaded from www.nrcresearchpress.com by 203.198.23.82 on 09/08/12
For personal use only.

TABLE 10. ECH of 1,3-diphenyl-1,3-propanedione[a]

Entry	Electrode	Medium[b]	$-E$ (V vs. ECS)	Conversion (%)	Yield of products[c] (%)	Current efficiency (%)
1	RaNi	Alkaline	1.02	100	**3**: 17 **4**: 83	92
2	RaNi	Neutral	0.73	85	**3**: 72 **4**: 13	93
3	RaCo	Alkaline	1.03	15	**3**: 15	20

[a]The electrolysis conditions were the same as in Table 7.
[b]Alkaline: KOH; neutral: H_3BO_3/NaCl.
[c]**3**: Monoalcohol; **4**: diols (*RS*:*RR* + *SS* ~ 50:50).

TABLE 11. ECH of 2,4-pentanedione[a]

Electrode	Medium[b]	$-E$ (V vs. ECS)	Conversion introdiols[c] (%)	Current efficiency (%)
RaNi	Alkaline	1.03	21	28
RaNi	Neutral	0.74	20	19

[a]The electrolysis conditions are the same as in Table 7.
[b]Alkaline: KOH; neutral: H_3BO_3/NaCl.
[c]Mixture of *RS* and *RR* + *SS* diastereomers (60:40).

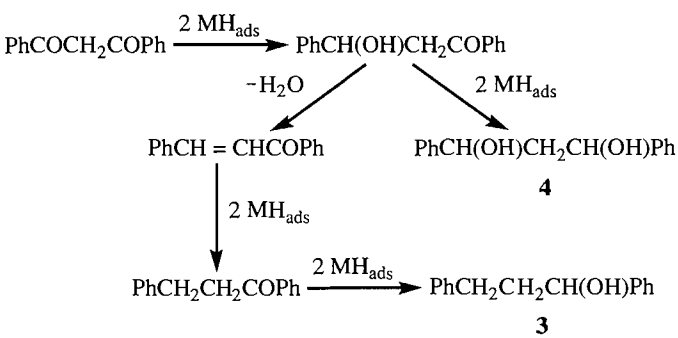

SCHEME 2

its hydrogenation and only the diols were obtained. With both β-diketones studied, there was little diastereoselectivity for diol formation. The ratio *RS*:*RR* + *SS* was about 50:50 with the diphenylpropanedione and about 60:40 with the pentanedione.

Conclusion

Generally, electroreduction of ketones takes place at quite negative potentials, i.e., from −1.2 to −2.2 V (vs. ECS) for cyclohexanone and from −1 to −1.6 V (vs. ECS) for acetophenone (25). In the case of α-diketones, the reported potentials are about −1 and −2 V (vs. ECS) for the reduction of the first and second carbonyl group, respectively. Thus the reduction at Raney metal electrodes requires less energy (−0.7 to −1.0 V vs. ECS). Furthermore, no pinacol was detected. These are two advantages of ECH over electroreduction. By the right choice of electrode material and conditions of electrolysis, the ECH of benzil gave selectively either benzoin or hydrobenzoin, showing that chemoselective reductions of one carbonyl of α-diketones can be carried out by ECH.

The diastereoselectivity observed for the diol formation in the ECH of α-diketones and β-diketones was comparable to that encountered in catalytic hydrogenations. In the literature, Raney nickel powder has been modified by optically active tartaric acid (26–32) and used in catalytic hydrogenations or in electrocatalytic hydrogenations of various monoketones and diketones. We modified our codeposited RaNi electrodes with the reported procedure and used these modified electrodes for the ECH of benzil. The *threo* hydrobenzoin isolated from the mixture of the *threo* and *meso* forms had an optical yield of 7.3%. When tartaric acid was added to the electrolytic solution and the ECH carried out with a modified RaNi electrode, the optical yield increased to 22%.

Experimental

Vapor phase chromatographic analyses were performed on a Hewlett Packard 5710A chromatograph equipped with a flame ionization detector, an HP 3390A integrator, and a DB-5 fused capillary column 30 m long. NMR spectra were recorded on a Bruker WM250 spectrometer coupled with an Aspect 2000 computer. The mass spectra were recorded on a VG ZAB-1F spectrometer. IR spectra were recorded on a Perkin–Elmer 781 spectrometer. Optical rotations were measured with a Perkin–Elmer 141MC polarimeter.

The products were all commercially available: cyclohexanone from Anachemia; acetophenone and 2,4-pentanedione from Fisher; benzylacetone, 2-octanone, benzil, 1-phenyl-1,2-propanedione, and 1,3-diphenyl-1,3-propanedione from Aldrich. The authentic products of electrohydrogenation were purchased: cyclohexanol, 2-octanol, 2,4-pentanediol, benzoin, hydrobenzoin and 1-phenyl-1,2-propanediol from Aldrich; 1-phenylethanol from Fluka; and 4-phenyl-2-butanol from Lancaster Synthesis. Distilled water and commercial methanol (BDH Assured ACS) were used for the solutions.

The Raney metal electrodes were prepared following the detailed procedure described earlier (6–9). Leaching (or activation) of the electrodes was performed in a 30% NaOH solution at 70°C during 6h, then at room temperature overnight.

The electrolyses were carried out with a PAR 173 potentiostat connected to an ECS 410 coulometer and a Dynascan Corporation 2830 multimeter. A two-compartment H-type cell, having a Nafion 324 (E.I. du Pont de Nemours) membrane or a fine glass frit as separator, was used. The counter-electrode was a graphite rod (7 mm) or a platinum plate (3 cm^2). A Cole Parmer saturated calomel electrode placed in a separate compartment was used to monitor the cathode potential.

The solutions were prepared by dissolving the supporting electrolyte in the methanol:water (w/w) mixture. The pH was measured with a Sargent Welch 6000 pH meter and a Cole Parmer glass

Can. J. Chem. Downloaded from www.nrcresearchpress.com by 203.198.23.82 on 09/08/12
For personal use only.

electrode that was calibrated beforehand with commercial aqueous buffer solutions. It should be noted here that the real values of pH (if calibration had been made with buffers prepared in methanol:water solvents) should be higher; for example the calculated value for the acetate buffer in methanol is 7.1 compared to a measured value of 6.5 in methanol:water. The solution was poured into the cell (125 mL in each compartment) and deaerated. The activated cathode, the anode, and the reference electrode were immersed. Electrolysis of water was carried out at a constant current (100 mA) for a passage of 440 C, after which the potential was shifted to a more positive value until the current reached zero. One (or two) mmoles of substrate was then added, which induced an increase in the current. A charge equivalent to 2 F/mol of organic substrate (in the case of monoketones) or 4 F/mol (in the case of diketones) was passed. Aliquots were extracted with ether after the addition of saturated NaCl solution, and analyzed by vpc, with comparison with authentic samples. Yields and mass balance were determined by the internal standard method using authentic samples. In the case of 1,3-diphenyl-1,3-propanedione, mass spectrometry, IR, and ^{1}H NMR spectra were consistent with the structure of the products, and the distribution of diastereomers was determined by ^{1}H NMR.

Acknowledgments

We acknowledge the financial support from the Natural Sciences and Engineering Research Council of Canada, the Fonds pour la formation de chercheurs et l'aide à la recherche (FCAR) du Québec, the Ministère de l'énergie et des ressources du Québec, and the Ministère des Relations internationales du Québec.

1. S. Fokin. Z. Elektrochem. **12**, 749 (1906).
2. M.P. Breteau. Bull. Soc. Chim. Fr. Ser. 4, **9**, 764 (1911).
3. F. Fichter and R. Stocker. Chem. Ber. **47**, 2015 (1914).
4. X. de Hemptinne and J.C. Jungers. Z. Phys. Chem. N.F. **15**, 137 (1958).
5. X. de Hemptinne. Mem. Cl. Sci. Acad. R. Belg. Sci. Collect. 8, **32**, 5 (1961).
6. G. Belot, S. Desjardins, and J. Lessard. Tetrahedron Lett. **25**, 5347 (1984).
7. A. Cyr, P. Huot, G. Belot, and J. Lessard. Electrochim. Acta, **35**, 147 (1990).
8. A. Velin-Prikidanovics, and J. Lessard. J. Appl. Electrochem. **20**, 527 (1990).
9. D. Robin, M. Comtois, A. Martel, R. Lemieux, A. Kamcheong, G. Belot, and J. Lessard. Can. J. Chem. **68**, 1218 (1990).
10. T. Chiba, M. Okimoto, H. Nagai, and Y. Takata. Bull. Chem. Soc. Jpn. **56**, 719 (1983).
11. M. Fujihira, A. Yokosawa, H. Kinishita, and T. Osa. Chem. Lett. 1089 (1982).
12. K. Park, P.N. Pintauro, M.M. Baizer, and K. Nobe. J. Electrochem. Soc. **132**, 1850 (1985).
13. G.J. Yusem and P.N. Pintauro. J. Am. Chem. Soc. **69**, 399 (1992).
14. I.V. Kirilyus and M.A. Zhuk. Sov. Electrochem. **8**, 967 (1972).
15. R.L. Augustine. Catalytic hydrogenation. Marcel Dekker Inc., New York. 1965. p. 26.
16. J.N. Pattison and E.F. Degering. J. Am. Chem. Soc. **73**, 611 (1951).
17. J.V.N. Vara Prasad, A.G. Samuelson, and C.N. Pillai. J. Catal. **71**, 1 (1982).
18. J.V.N. Vara Prasad, and C.N. Pillai. J. Catal. **88**, 418 (1984).
19. B.A. Marshall and W.A. Waters. J. Chem. Soc. 1579 (1961).
20. S. Patai and I. Shenfield. J. Chem. Soc. 366 (1966).
21. E.S. Gould. Mechanism and structure in organic chemistry. Holt, Rinehart and Winston Inc., New York. 1965. p. 367.
22. H. Gilman. Organic chemistry: an advanced treatise. J. Wiley and Sons, New York. 1953. p. 1041.
23. G.W. Wheland. Advanced organic chemistry. J. Wiley and Sons, New York. 1960. p. 685.
24. L. Cazaux, G. Chassaing, and P. Maroni. C.R. Acad. Sci. Ser. C, **278**, 1305 (1974).
25. L. Meites and P. Zuman. CRC handbook series in organic electrochemistry. CRC Press Inc., Cleveland, Ohio.
26. T. Osawa. Chem. Lett. 1609 (1985).
27. S. Murakami, T. Harada, and A. Tai. Bull. Chem. Soc. Jpn. **53**, 1356 (1980).
28. K. Ito, T. Harada, and A. Tai. Bull. Chem. Soc. Jpn. **53**, 3367 (1980).
29. A. Tai, T. Harada, Y. Hiraki, and S. Murakami. Bull. Chem. Soc. Jpn. **56**, 1414 (1983).
30. T. Osawa and T. Harada. Bull. Chem. Soc. Jpn. **57**, 1518 (1984).
31. A. Tai, T. Kikukawa, T. Sugimura, Y. Inoue, T. Osawa, and S. Fujii. J. Chem. Soc. 795 (1991).
32. M.D. Baturova, T.I. Kuznetsova, A.A. Vendenyapin, and E.I. Klabunovskii. Izv. Akad. Nauk S.S.S.R. **12**, 2694 (1987).

Can. J. Chem. Downloaded from www.nrcresearchpress.com by 203.198.23.82 on 09/08/12
For personal use only.

4-Acylamino-4*H*-1,2,4-triazoles and related structures: new investigations of their chemical and physicochemical properties associated with their particular exocyclic amide function

BERNARD PIROTTE,[1] PASCAL DE TULLIO, BERNARD MASEREEL, MARC SCHYNTS, AND JACQUES DELARGE
Laboratoire de chimie Pharmaceutique, Institut de pharmacie, 3, rue Fusch, Université de Liège, B-4000, Belgium

LÉON DUPONT
Laboratoire de cristallographie, Institut de physique, Sart Tilman, Université de Liège, B-4000, Belgium

AND

LÉOPOLD THUNUS
Laboratoire de chimie Analytique, Institut de pharmacie, 3, rue Fusch, Université de Liège, B-4000, Belgium

Received November 17, 1992[2]

BERNARD PIROTTE, PASCAL DE TULLIO, BERNARD MASEREEL, MARC SCHYNTS, JACQUES DELARGE, LÉON DUPONT, and LÉOPOLD THUNUS. Can. J. Chem. **71**, 1857 (1993).

The acido-basic behavior of 4-acylamino-4*H*-1,2,4-triazoles and of the related structures, 4-acylamino-4*H*-1,2,4-triazolium salts, 4-acylamino-1,2,4-triazoline-3-thiones, and 4-acylamino-1,2,4-triazolin-3-ones, has been compared. Among the triazolium salts examined, the 1-carboxymethyl-4-phenylacetylamino derivative has been selected as a particular triazolium salt bearing two acidic centres, a carboxylic acid group and an exocyclic amide group. This compound has been isolated in three different ionic forms corresponding to different protonation and deprotonation states of the molecule. For these compounds, IR, NMR, and X-ray data were compared and the preferential localization site of the labile proton on the betainic intermediate structure has been discussed. Taking into account that deprotonation of the amide function of 4-acylamino-4*H*-1,2,4-triazolium salts may introduce a negative pole in the proximity of the strong electrophilic carbon atom in the 2-position of the ring, reactivity of different triazolium salts toward the nucleophilic addition of the hydride ion has been compared. In particular, 4-acylamino-4*H*-1,2,4-triazolium salts free of alkyl substituent on the amide nitrogen failed to give the corresponding 4-acylamino-Δ2-1,2,4-triazolines after reaction with the hydride ion, while, under the same conditions, the 4-*N*-methyl derivatives were transformed into this unusual ring system in good yields. In this case, no decrease of reactivity toward the nucleophilic agent was observed since, as a result of the N-alkylation, no deprotonation of the amide group can occur in these alkaline experimental conditions.

BERNARD PIROTTE, PASCAL DE TULLIO, BERNARD MASEREEL, MARC SCHYNTS, JACQUES DELARGE, LÉON DUPONT et LÉOPOLD THUNUS. Can. J. Chem. **71**, 1857 (1993).

Le comportement acido-basique de 4-acylamino-4*H*-1,2,4-triazoles et de structures associées, à savoir, les sels de 4-acylamino-4*H*-1,2,4-triazolium, les 4-acylamino-1,2,4-triazoline-3-thiones et les 4-acylamino-4*H*-1,2,4-triazolin-3-ones, a été comparé. Parmi les sels de triazolium examinés, le 1-carboxyméthyl-4-phénylacétylamino-4*H*-1,2,4-triazolium a été sélectionné en raison de la présence sur la molécule de deux groupements acides, une fonction acide carboxylique et une fonction amide exocyclique. Ce composé a été isolé sous trois formes ioniques différentes correspondant à trois états de protonation et de déprotonation différents de la molécule. Pour ces composés, les données IR, RMN et cristallographiques ont été comparées, et le site de localisation préférentiel du proton labile sur la structure bétaïnique intermédiaire a été discuté. Tenant compte du fait que la déprotonation de la fonction amide des sels de 4-acylamino-4*H*-1,2,4-triazolium est susceptible d'introduire un pôle négatif à proximité de l'atome de carbone fortement électrophile en position 2 du cycle, la réactivité de différents sels de triazolium vis-à-vis de l'addition nucléophile de l'ion hydrure a été comparée. En particulier, les sels de 4-acylamino-4*H*-1,2,4-triazolium ne possédant pas de substituant alkyle sur l'azote amide ne permirent pas d'obtenir les 4-acylamino-Δ2-1,2,4-triazolines correspondantes après réaction avec l'ion hydrure, tandis que, dans les mêmes conditions, les dérivés 4-*N*-méthylés furent transformés en cet hétérocycle avec de bons rendements. Dans ce cas, il n'y a pas de diminution de la réactivité vis-à-vis de l'agent nucléophile puisque, en raison de la N-alkylation, la déprotonation du groupe amide ne peut avoir lieu dans ces conditions expérimentales alcalines.

Can. J. Chem. Downloaded from www.nrcresearchpress.com by 203.198.23.82 on 09/08/12
For personal use only.

Introduction

Although the synthesis of 4-amino-4*H*-1,2,4-triazole was described much earlier (1), little has appeared in the literature on 4-acylamino derivatives and related structures, i.e., 4-acylamino-4*H*-1,2,4-triazolium salts, 4-acylamino-1,2,4-triazoline-3-thiones, and 4-acylamino-1,2,4-triazolin-3-ones.

The chemistry of 4-amino-4*H*-1,2,4-triazolium salts has been explored by Becker and Timpe and co-workers (2–11). Moreover, the synthesis of some 4-acylaminotriazolin-3-ones and -thiones free of an alkyl substituent on the (N)-2 position have also been reported (12–18). The present work describes unknown aspects of the chemistry and physicochemical properties of 4-acylamino-4*H*-1,2,4-triazoles and related triazolium salts, triazolinethiones, and triazolinones. Acidity of the exocyclic amide function of the different classes of compounds is of particular interest since some of these products have been selected as potential bioactive molecules (18–22). In fact, their bioavailability and (or) interaction with their biological targets will depend upon their ionic and stereoelectronic nature at physiological pH.

In addition, the present work describes a new synthetic pathway to the very unstable 4-amino- and 4-*N*-methyl-*N*-acylamino-Δ2-1,2,4-triazolines via borohydride reduction of the corresponding 4-amino- and 4-*N*-methyl-*N*-acylamino-

[1]Author to whom correspondence may be addressed.
[2]Revision received June 14, 1993.

Can. J. Chem. Downloaded from www.nrcresearchpress.com by 203.198.23.82 on 09/08/12
For personal use only.

4*H*-1,2,4-triazolium salts. The behavior of triazolinethiones to oxidation in presence of a peracid is also reported.

Results and discussion

*(a) 4-Acylamino-4*H*-1,2,4-triazoles*

4-Phenylacetylamino-4*H*-1,2,4-triazole (**2**) was obtained from acylation of 4-amino-4*H*-1,2,4-triazole (**1**) with phenylacetyl chloride as previously described (Scheme 1) (19). This model compound exhibits the amphoteric character of 4-acylamino-4*H*-1,2,4-triazoles. In spite of the acylation of the exocyclic amino group, one of the ring nitrogens conserves a pronounced basic character as demonstrated by the easy alkylation of this position to give the corresponding 4-acylamino-4*H*-1,2,4-triazolium salts. Moreover, a stable and crystallizable hydrochloride salt **3** was isolated from the reaction of **2** with hydrochloric acid.

On the other hand, the acidity of the exocyclic amide proton of **2** may be compared to some extent to that of dihydrazides (23), and the sodium salt **4** was isolated from the reaction of **2** with a stoichiometric amount of sodium hydroxide in methanolic solution.

IR and NMR spectra of compounds **2**, **3**, and **4** are in accordance with expected electronic effects associated with their different ionic nature. Table 1 reports, for **2**, **3**, and **4**, the IR amide carbonyl absorption wavelength and the chemical shifts in DMSO-d_6 of the different protons of each molecule.

The high IR absorption band assigned to the amide carbonyl band of **3** is in accordance with those observed for 1-alkyl-4-acylamino-4*H*-1,2,4-triazolium salts (5) (see also compounds **10**, **11***a*, *b*, and **14**). The carbonyl absorption band at 1580 cm^{-1} for **4** associated to a strong one at 1365 cm^{-1} is typical of an anionic amide group and has been observed for the zwitterionic compounds **5**, **8**, **9**, and **13**. These values can be compared to some extent to the symmetric and asymmetric C—O bands near 1600 and 1400 cm^{-1} for salts of carboxylic acids.

For compound **3** the NMR data reflect that protonation of the triazole ring logically induces a strong deshielding, in particular, of the two ring hydrogens (3-H and 5-H). In contrast, the negative charge located on the exocyclic amide group of **4** induces a marked shielding of the overall protons and especially of the methylene hydrogens as a result of their proximity to the anionic group.

Of particular interest is the reaction of **2** with diazomethane which does not lead to the exocyclic N-methylation, as expected by analogy with carboxylic acids, but to the formation of the 1-methyl-1,2,4-triazolium derivative via alkylation of the ring nitrogen. Figure 1 illustrates the probable reaction mechanism and presents the ring nitrogen as the main nucleophilic center of the deprotonated molecule. Further confirmation of the low reactivity of the anionic amide group is given by the fact that zwitterionic compounds like **5**, **9**, or **13** do not react with CH_3I or $(CH_3)_2SO_4$ under various conditions; moreover, compound **11***a* fails to react with diazomethane.

*(b) 4-Acylamino-1-alkyl-4*H*-1,2,4-triazolium salts*

Becker and Timpe reported access to 4-acylamino-1-alkyl-4*H*-1,2,4-triazolium salts via two different pathways: alkylation of 4-acylamino-4*H*-1,2,4-triazoles (i.e., **9** via **2**) or acylation of 1-alkyl-4-amino-4*H*-1,2,4-triazolium salts (i.e., **13** via **12**) (5). These two processes were used to obtain various 4-acylamino-1-alkyl-4*H*-1,2,4-triazolium salts of therapeutic interest, for which detailed synthetic procedures have been described in part in a previous report (19).

The present report investigates in more details the interesting acido-basic behavior of the 4-acetyl and the 4-phenylacetylaminotriazolium derivatives.

Alkylation of **2** with bromoacetic acid in nitromethane did not permit direct isolation of the carboxylic acid derivative of structure **10** (as the bromide). The crude product obtained crystallized in cold water to give a solid (**6**), which was identified as a mixed salt containing equal amounts of the carboxylic acid **10**, as the bromide, and of the betaine **7**.

Direct isolation of the acid **10** was accomplished via catalytic deprotection of the tert-butyl ester **9** in nitromethane with gaseous HCl. This interesting triazolium salt has been isolated in three different protonated forms. The sparingly soluble betaine **7** was isolated in methanolic solution after exact neutralization of the carboxylic proton of the mixed salt **6** (19). A crystallographic study of betaine **7** reveals the establishment of a strong hydrogen bond between the amide group and the carboxylic group of a neighbouring molecule (24).

As expected from the stronger acidic character of the exocyclic amide proton of 4-acylaminotriazolium salts compared to 4-acylaminotriazoles, compound **7** reacts with weak bases, i.e., sodium hydrogen carbonate, to give the corresponding sodium salt **8**, which has been isolated as the dihydrate and characterized by X-ray crystallography (25).

NMR data of **7**, **8**, and **10** are in accordance with expected electronic effects associated with their different ionic nature (see Table 2). The successive deprotonations logically induce a progressive shielding of the different hydrogen atoms as expected from the increasing electronic density that results from the increasing global negative charge of the molecule.

Chemical shift data for the mixed salt **6** appear to be intermediate in value between those of the acid hydrochloride **10** and the betaine **7**. Thus, in accordance with the rapid proton exchange existing between the two species in solution, the NMR spectrum of **6** corresponds to an average picture of the two chemical entities.

Examination of the NMR chemical shifts of a series of 4-acylaminotriazolium salts (Table 2) led us to the conclusion that the betaine **7**, which can adopt two tautomeric forms **7***a* and **7***b* in solution (Fig. 2), seems to exist mainly as the **7***b* tautomer.

Indeed, the chemical shifts obtained in DMSO-d_6 on compound **7** (see Table 2) resemble those of compound **9** for which the presence of a negative charge exclusively located on the exocyclic amide function induces a marked shielding of the (Ph)-methylene and 3-H protons, but exerts a lower influence on the (N)-methylene protons (compare **11***a* with **9** and **10** with **7**). The chemical shift of the (N)-methylene protons of **7** (5.10 ppm) cannot be compared to that reported for the same protons of **18** (4.62 ppm) for which the N-methylation of the exocyclic amide moiety directs the negative charge exclusively on to the carboxylate group. Therefore, according to these data, predominance of the **7***a* tautomer in solution, which would result in the localization of the negative charge mainly on the carboxylate moiety, seems to be less probable.

Observation in solution (NMR data) that the amide function of **10** appears to be the first deprotonation site has not

Can. J. Chem. Downloaded from www.nrcresearchpress.com by 203.198.23.82 on 09/08/12
For personal use only.

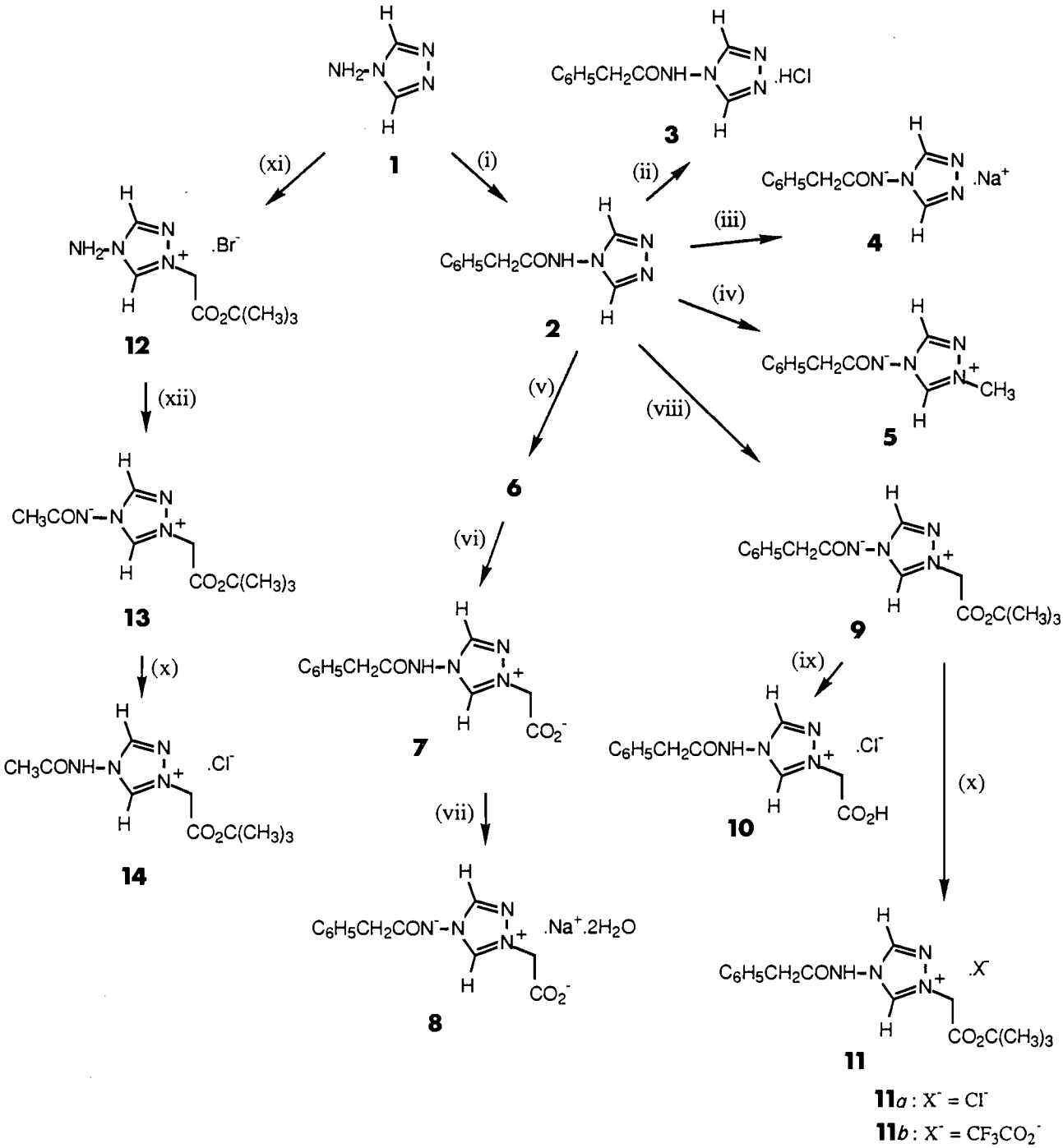

Reagents: (i) $C_6H_5CH_2COCl$, pyridine, dioxane. (ii) HCl. (iii) NaOH, MeOH. (iv) CH_2N_2, MeOH, ether. (v) $BrCH_2CO_2H$, CH_3NO_2, Δ. (vi) NaOH, MeOH. (vii) $NaHCO_3$, H_2O. (viii) 1. $BrCH_2CO_2C(CH_3)_3$, CH_3NO_2, Δ. 2. $NaHCO_3$. (ix) HCl, CH_3NO_2, 90°C. (x) HX, CH_2Cl_2, room t°. (xi) $BrCH_2CO_2C(CH_3)_3$, CH_3NO_2, Δ. (xii) 1. Ac_2O. 2. $NaHCO_3$.

SCHEME 1

been fully confirmed in the solid state (X-ray data). In fact, the crystal structures of **7** (24) and **8** (25) indicate, for the carboxylic function, atomic distances *d*(C—O) of 1.263 and 1.232 Å for **7**, and 1.248 and 1.246 Å for **8**. As a result, **8** clearly exhibits the carboxylate ion geometry (twofold *d*(C—O) near 1.25 Å (26)). But, for compound **7**, even if the distances *d*(C—O) do not correspond to the pure carboxylate ion geometry, they are far from those reported for

TABLE 1. IR absorption wavelength (cm^{-1}) of the amide carbonyl bond and ^1H NMR chemical shifts (δ, ppm) in DMSO-d_6 (HMDS) for compounds **2**, **3**, and **4**

	C=O	Ph-CH_2-CO	C_6H_5	3-H + 5-H
Hydrochloride **3**	1730	3.67	7.30	9.20
Neutral **2**	1692	3.60	7.30	8.58
Sodium salt **4**	1580	3.20	7.15	8.45

a pure carboxylic acid (*d*(C—O) near 1.31 Å; *d*(C=O) near 1.21 Å). In addition, bond lengths and angles reported for the amide function of **7** (*d*(C—O) = 1.222 Å; *d*(C—N) = 1.351 Å; N—C—O = 122.9°) and of **8** (*d*(C—O) = 1.264 Å; *d*(C—N) = 1.319 Å; N—C—O = 126.0°) may be compared, to some extent, to those reported for dihydrazides and their anionic salts (i.e., $CH_3CONHNHCOCH_3$: *d*(C—O) = 1.220 Å; *d*(C—N) = 1.340 Å; N—C—O = 122.3° (27); $CH_3CONHN^-COCF_2NO_2 \cdot NH_2NH_3^+$: *d*(C—O) = 1.249 Å; *d*(C—N) = 1.324 Å; N—C—O = 130.3° (28)). Thus, for these two chemical classes, deprotonation of the amide function results in the lengthening of the C—O bond associated with the contraction of the C—N bond, and in a significant increase of the N—C—O bond angle. Therefore, in accordance with the X-ray data, betaine **7** in the solid state does not show a clear deformation of the amide function that could be explained by a significant deprotonation.

Moreover, in accordance with the expected pK_a values attributable to the two acidic groups of **10**, the carboxylic function logically exhibits the strongest acidic character and must be the first deprotonation site. In fact, the pK_a value of this function, according to the presence of a quaternary nitrogen in the α-position of the carboxylic group, could be estimated as not far from those of amino-acid hydrochlorides (pK_a = 2–2.5).

The pK_a values attributed to the exocyclic amide function of different 4-acylaminotriazolium salts have been determined (see Table 3). These results, in fact, indicate a strong acidic character for this function, which appears to be equal to, or, in some cases, higher than conventional carboxylic acids (pK_a = 4–4.5), but lower than amino-acid hydrochlorides. However, this observation explains the ability of weak bases (i.e., $NaHCO_3$) to deprotonate 4-acylaminotriazolium salts.

The esters **14** and **11***a* logically exhibit a stronger acidic character since the first deprotonation for **21** and **7** leads to the formation of a carboxylate anion group expected to be a lower electron-withdrawing group than the ester function.

The specific chemical reactivity of the 4-acylamino-4*H*-1,2,4-triazolium salts is essentially confined to the 5-position of the molecule (11), which exhibits a considerable electrophilic character. We have compared the reactivity toward nucleophilic addition of different 4-acylamino-4*H*-1,2,4-triazolium salts with or without an alkyl substituant on the exocyclic amide nitrogen. In fact, it may be expected that deprotonation of the exocyclic amide group in slight alkaline conditions, which therefore introduces a delocalized negative charge on this position, increases the electron density at the 5-position of the ring and, as a result, may decrease its susceptibility to nucleophilic addition.

The strong electrophilic character of the carbon atom in this position was exploited for the transformation of 4-(*acyl*)amino-4*H*-1,2,4-triazolium salts into their corresponding 4-(*acyl*)amino-1,2,4-triazoline-3-thiones by heating the former in pyridine (or a mixture of pyridine and triethylamine) in presence of elemental sulfur (Scheme 2) (19). The basic solvent catalyses the deprotonation of the slightly acidic hydrogen atom in the 5-position to give an ylide or a carbene intermediate able to react with the sulfur atom (7, 10). The *N*-methyl derivatives reacted comparably with sulfur in pyridine (Scheme 2), but the reaction conditions were found to be milder in this case (15 min at 50°C instead of 1 h at reflux (19)). This result could be explained by the higher reactivity of the *N*-methyl derivatives **22** (R′ = CH_3) since alkyl substitution of the amide nitrogen prevents the deprotonation of this position by the basic solvent. As a result, no decrease of the electrophilic character of the 5-position can be accomplished by the proximity of an electron-donor anionic amide group.

The ring opening of azolium salts (29), and in particular of 4-acylaminotriazolium salts (4–7), in aqueous alkaline solution has already been studied. It results from the nucleophilic addition of the hydroxide ion to the strong electrophilic iminium moiety of the ring. Susceptibility of this moiety to hydride addition has also been studied for a long time for different azolium salts, i.e., for thiazolium (30, 31) and oxazolinium (32, 33) salts, to give the corresponding thiazolidines and oxazolidines, respectively. However, no comparable studies have been conducted on the 4-amino-4-*H*-1,2,4-triazolium derivatives.

We have observed that the hydrophilic water soluble 4-aminotriazolium derivative **12** can be reduced in aqueous solution with sodium borohydride into the corresponding hydrophobic Δ2-triazoline **30** (Scheme 3). As expected, the NMR spectrum of **30** shows a strong shielding of most of the protons of the molecule since the positive charge on the ring, and its aromatic character, has disappeared after hydride addition (i.e., the 3-H hydrogen atom is found at 9.15 ppm in **12** and at 6.65 ppm in **30**). Under the same reduction conditions the 4-acylaminotriazolium salts such as **9** and **13** do not react with sodium borohydride. Whatever the conditions employed, the starting material was recovered unchanged even in the presence of a large excess of sodium borohydride.

In contrast, the corresponding N-CH_3 derivatives **31** readily react with sodium borohydride to give the corresponding 4-acylamino-Δ2-1,2,4-triazolines **32** (Scheme 4). The chemical structure of these unusual triazolines has been confirmed by NMR, IR, mass spectroscopy, and elemental analysis.

As observed with **30**, hydride addition on the 4-acylaminotriazolium salt **31** is responsible for a strong shielding of most protons, and comparable chemical shifts are found on the two NMR spectra (i.e., 3-*H*, N-CH_2-N, N-CH_2-CO). In addition, differentiation of the methylene protons is observed and might result from restricted free rotation at the N—N bond as a probable result of steric hindrance between the methyl radical linked to the exocyclic tertiary amide nitrogen and the ring methylene moiety.

Addition of CF_3COOD to the NMR sample doesn't modify the spectrum. As a result, compounds **32***a–b* do not exhibit a net basic character (no significative deshielding of any protons indicating protonation of a basic position) and appear to be stable in the presence of a strong acid.

Can. J. Chem. Downloaded from www.nrcresearchpress.com by 203.198.23.82 on 09/08/12
For personal use only.

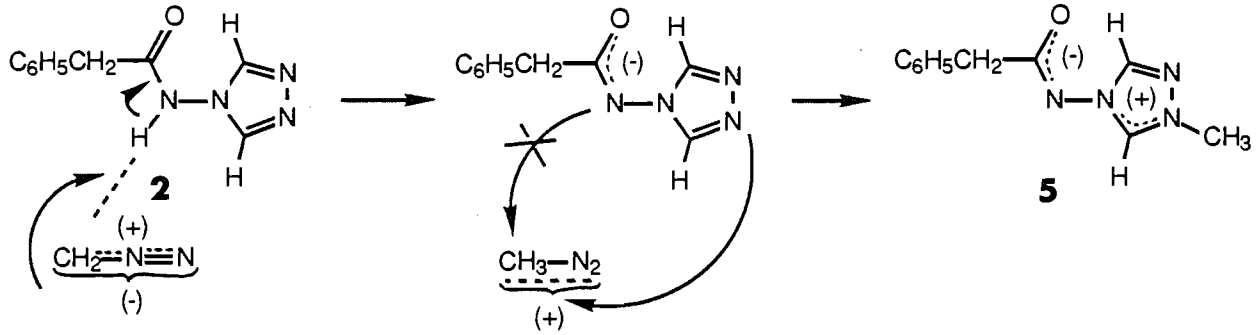

FIG. 1. Probable reaction mechanism between 4-phenylacetylamino-4*H*-1,2,4-triazole and diazomethane suggesting the ring nitrogen atom as the main nucleophilic centre of the deprotonated molecule.

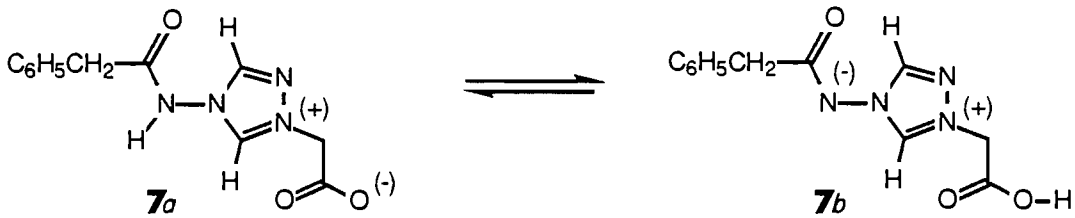

FIG. 2. Tautomer equilibrium for the betaine **7**.

TABLE 2. ^{1}H NMR chemical shifts (δ, ppm) in DMSO-d_6 (HMDS) for the different 4-acylamino-4*H*-1,2,4-triazolium salts studied

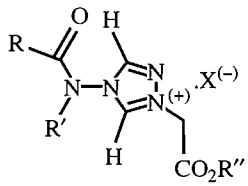

Compound no.	R	N-R′	CO_2R''	X^-	$C(CH_3)_3$	CH_3CO	$Ph-CH_2$	$N-CH_2-CO$	C_6H_5	3-H	5-H	$N-CH_3$
15[a]	CH_3	NH	CO_2H	$CF_3CO_2^-$	—	2.05	—	5.41	—	9.45	10.50	—
16[a]	CH_3	NCH_3	CO_2H	ClO_4^-	—	2.17	—	5.40	—	9.51	10.52	3.50
14	CH_3	NH	$CO_2C(CH_3)_3$	Cl^-	1.37	2.10	—	5.40	—	9.50	10.65	—
17[a]	CH_3	NCH_3	$CO_2C(CH_3)_3$	Br^-	1.40	2.15	—	5.43	—	9.62	10.65	3.50
18[a]	CH_3	NCH_3	CO_2^-	—	—	2.05	—	4.62	—	9.41	10.52	3.45
13[b]	CH_3	N^-	$CO_2C(CH_3)_3$	—	1.35	1.70	—	5.10	—	8.95	10.55	—
10	$C_6H_5CH_2$	NH	CO_2H	Cl^-	—	—	3.75	5.38	7.30	9.52	10.65	—
6[a]	$C_6H_5CH_2$	NH	CO_2^-/CO_2H	1/2 Br^-	—	—	3.56	5.25	7.26	9.30	10.58	—
7[a]	$C_6H_5CH_2$	NH	CO_2^-	—	—	—	3.37	5.10	7.20	9.05	10.51	—
8	$C_6H_5CH_2$	N^-	CO_2^-	—	—	—	3.30	4.53	7.20	8.88	10.20	—
11[a]	$C_6H_5CH_2$	NH	$CO_2C(CH_3)_3$	Cl^-	1.35	—	3.75	5.37	7.25	9.52	10.65	—
11[b]	$C_6H_5CH_2$	NH	$CO_2C(CH_3)_3$	$CF_3CO_2^-$	1.35	—	3.65	5.30	7.23	9.45	10.55	—
9[a]	$C_6H_5CH_2$	N^-	$CO_2C(CH_3)_3$	—	1.35	—	3.25	5.10	7.20	9.03	10.60	—
19[a]	$C_6H_5CH_2$	NCH_3	CO_2H	Br^-	—	—	3.82	5.40	7.20	9.58	10.64	3.53
20[b]	$C_6H_5CH_2$	NCH_3	$CO_2C(CH_3)_3$	Br^-	1.40	—	3.85	5.45	7.25	9.62	10.70	3.60

[a]Reference 19.
[b]Reference 20.

(c) 4-Acylamino-2-alkyl-1,2,4-triazoline-3-thiones and -3-ones

As explained above, the triazolinethiones may be obtained via treatment of the corresponding triazolium salts with sulfur in pyridine (or a mixture of pyridine and triethylamine). Different triazolinethiones have also been prepared via acylation of the amine intermediate **27** (19). They were eventually transformed into the corresponding carboxylic acids after removal of the *tert*-butyl protecting group (19). The pK_a values for the exocyclic amide function of the former have been compared to those of the corresponding triazolium salts. These values were logically found to be higher for triazolinethiones than for triazolium salts (compare Tables 3 and 4) since the electron-withdrawing effect of an ar-

Can. J. Chem. Downloaded from www.nrcresearchpress.com by 203.198.23.82 on 09/08/12
For personal use only.

TABLE 3. Dissociation constants of 4-acylamino-4*H*-1,2,4-triazolium salts (expressed as pK_a)

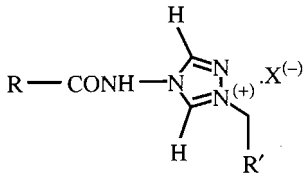

Compound no.	R	R′	X^-	pK_a
21	CH_3	COO^-	—	4.84
14	CH_3	$COOC(CH_3)_3$	Cl^-	4.32
7	$C_6H_5CH_2$	COO^-	—	4.21[a]
11[a]	$C_6H_5CH_2$	$COOC(CH_3)_3$	Cl^-	3.72

[a]Reference 19.

omatic cationic ring is expected to be more pronounced than those of a non-aromatic and non-cationic ring.

The pK_a values of the exocyclic amide group of the corresponding 4-acylaminotriazolinones have also been determined (see Table 4). These compounds were synthesized via alkaline hydrolysis into **29** of the *S*-methylthiouronium derivative **28**, resulting from treatment of **27** with methyl iodide (19), and acylation of the exocyclic amino group of **29** (19) (see Scheme 2). Direct transformation of the triazolinethiones into the triazolinones via treatment of **25**, **26**, or **27** with hydrogen peroxide in acetic acid or with *meta*-chloroperoxybenzoic acid was unsuccessful, although this process was earlier reported for different thiono compounds (34, 35). Surprisingly, the corresponding triazolium salts have been isolated in good yields under these oxidative conditions (Scheme 2).

We observe that the pK_a values of the exocyclic amide function are approximately 0.8–1.0 pH units lower for triazolinethiones than for the corresponding triazolinones. It can be concluded that the electron-withdrawing effect on the amide function is significantly more pronounced for the triazolinethione ring. These results are consistent with the experimental NMR chemical shifts (19), which, to some extent, reflects the different electron-withdrawing impact of the two ring systems (see Table 4). In fact, the overall protons of all the triazolinethiones were found to be more deshielded than those of the triazolinones. Moreover, a slight difference (0.3 pH units) exists between the acetyl and the phenylacetyl derivatives as a result of expected electron-withdrawing effects.

The second pK_a values for the carboxylic acids (**33**, **34**, **35**, and **37**) are found to be 0.5–0.7 pH unit higher than those of the corresponding esters (**25**, **26**, **36**, and **38**) because of the lower electron-withdrawing effect of the carboxylate function (resulting from the first neutralization) compared to the ester function.

In conclusion, the acido-basic character of potential bioactive molecules may influence not only their interaction with biological targets (recognition by specific enzymes or receptors, charge distribution compatibility, interaction with active site amino-acids of target enzymes, . . .), but also their bioavailability (absorption, plasma half life, elimination, . . .).

Therefore, since the 4-amino-4*H*-1,2,4-triazole ring system has been extensively explored in medicinal chemistry and will find new applications in the future, the present results are important for predictive behavior of 4-acylamino-1,2,4-triazoles and related structures in biological systems. In particular, in spite of an apparent similarity, 4-acylamino-4*H*-1,2,4-triazolium salts and their 4-*N*-alkyl-acylamino analogs are expected to exert very different biological responses with regard to their different reactivity and charge distribution at physiological pH.

Moreover, the strong acid character of 4-acylaminotriazolium salts, which is comparable in some cases with that of carboxylic acids, may help the design of bioactive molecules for which a deprotonated form at the neutral pH contributes to their biological activity. In contrast, if a negative charge on the molecule could be unfavorable (i.e., for its recognition by a specific target), it would be preferable to examine (4-acylamino)triazolinones rather than (4-acylamino)triazolinethiones, even if these two ring systems appear to be very similar. In fact, some of these thiono derivatives, which are stronger acids, could exist in a partial ionic form at physiological pH.

Experimental

Melting points were determined in a Büchi–Tottoli cappilary melting point apparatus and are uncorrected. Infrared spectra were recorded on a Perkin–Elmer 297 spectrophotometer. The ^1H NMR spectra were taken on either a Brucker AW-80 (80 MHz) or a Brucker AM-400 (400 MHz) instrument in DMSO-d_6 or in $CDCl_3$. The ^{13}C NMR spectra were recorded on a Brucker AM-400 instrument. Chemical shifts are expressed in ppm downfield from internal HMDS (for DMSO-d_6) or TMS (for $CDCl_3$). ^1H NMR data are tabulated in the following order: chemical shift, multiplicity, number of protons, attribution. Elemental analyses were realized on a Heraeus Micro U instrument. Mass spectra were recorded on a LKB-GC 9000S mass spectrometer or a KRATOS MS-80 RFA mass spectrometer (FAB technique). The syntheses of compounds **1**, **2**, **6**, **7**, **9**, **12**, **13**, **21**, **25–29**, **31**, and **33–38** has been described elsewhere (19, 20). For the other compounds, their preparation was realized as follows.

Synthesis

*4-Phenylacetylamino-4*H*-1,2,4-triazole hydrochloride* **3**

To a solution of 4-phenylacetylamino-4*H*-1,2,4-triazole **2** (19) (1.0 g, 4.95 mmol) in ethanol (10 mL) was added aqueous 5 N HCl (1.0 mL). The solvents were removed under reduced pressure. The resulting solid was crystallized from a 1:3 mixture of methanol–acetone (90%): mp 131–133°C; IR and ^1H NMR (DMSO-d_6, HMDS, 80 MHz), see Table 1. Anal. calcd. for $C_{10}H_{10}N_4O \cdot HCl$: C 50.32, H 4.64, N 23.47; found: C 50.14, H 4.77, N 23.29.

*4-Phenylacetylamino-4*H*-1,2,4-triazole sodium salt* **4**

A solution of 4-phenylacetylamino-4*H*-1,2,4-triazole **2** (1.0 g, 4.95 mmol) in methanol (20 mL) was mixed with a solution of sodium hydroxide (0.2 g, 5.0 mmol) in methanol (10 mL). Addition of diethyl ether (100 mL) gave rise to the precipitation of **4**, which was filtered, washed with a 1:3 mixture of methanol – diethyl ether, and dried under vacuum (very hygroscopic) (80%): mp 210–215°C; IR and ^1H NMR (DMSO-d_6, HMDS, 80 MHz), see Table 1.

*1-Methyl-4-phenylacetylimino-4*H*-1,2,4-triazolium inner salt* **5**

To a solution of 4-phenylacetylamino-4*H*-1,2,4-triazole **2** (1.0 g, 4.95 mmol) in methanol (40 mL) was added an ethereal solution of diazomethane until a slight yellow color persisted. The solvents were removed under reduced pressure and the residue was dissolved in dichloromethane (20 mL). The residual insoluble material was removed by filtration and the filtrate, diluted with petroleum ether (40–60°C) (40 mL), yielded the crystalline **5**, which

Can. J. Chem. Downloaded from www.nrcresearchpress.com by 203.198.23.82 on 09/08/12
For personal use only.

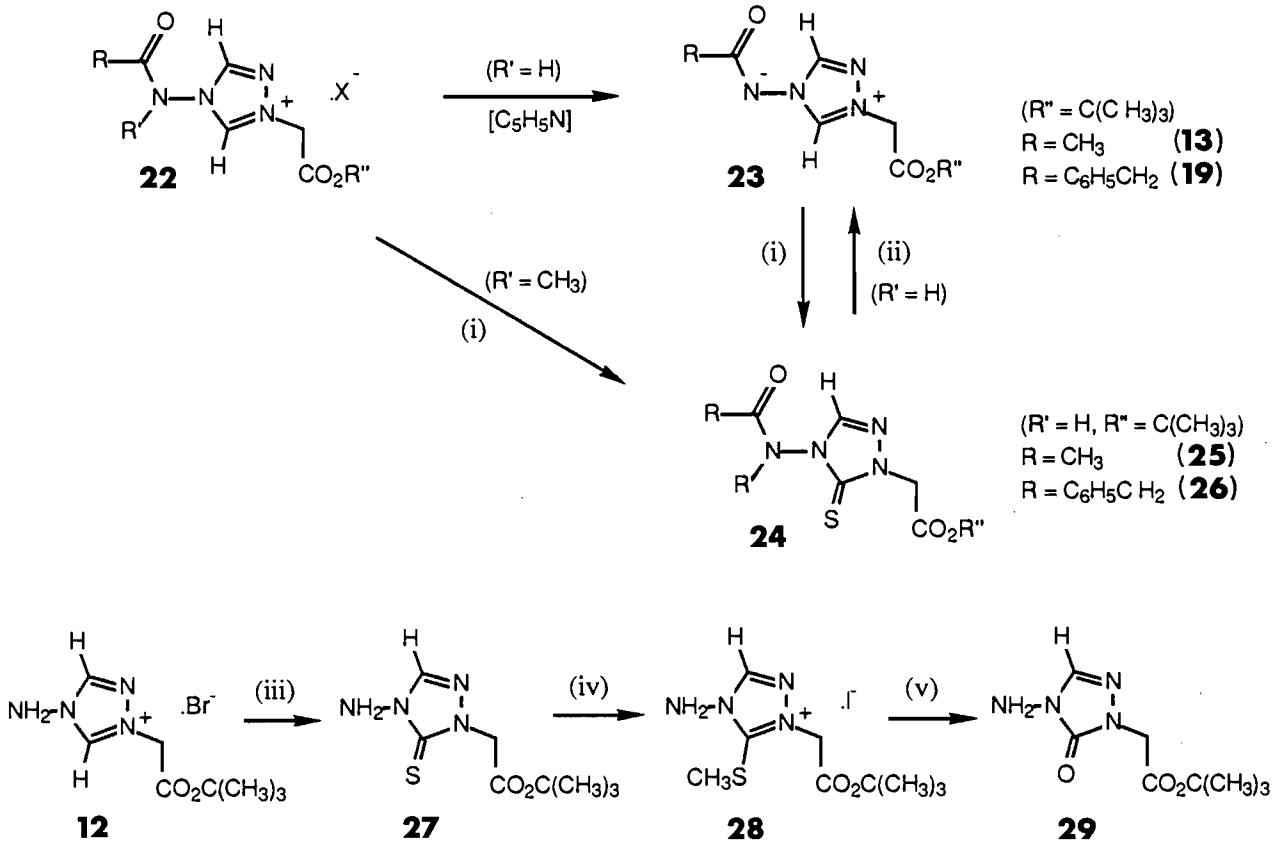

Reagents: (i) C_5H_5N, S_8, Δ. (ii) H_2O_2, HOAc. (iii) C_5H_5N, $N(C_2H_5)_3$, S_8, Δ. (iv) CH_3I. (v) NaOH, H_2O.

SCHEME 2

was filtered, washed with petroleum ether (40–60°C), and dried (75%), mp 149–151°C; IR, ν_{max}: 1585 (C—O asym.), 1525 (C=N), 1510 (C=N), and 1360 (C—O sym.) cm^{-1}; ^1H NMR (DMSO-d_6, HMDS, 80 MHz) δ: 3.25 (s, 2H, CH_2), 3.85 (s, 3H, CH_3), 7.15 (m, 5H, C_6H_5), 8.90 (s, 1H, 3-H), 10.28 (s, 1H, 5-H). Anal. calcd. for $C_{11}H_{12}N_4O$: C 61.10, H 5.59, N 25.91; found: C 60.99, H 5.72, N 25.83.

Sodium (4-phenylacetylimino-4H-1,2,4-triazolio)acetate dihydrate ***8***

To a solution of (4-phenylacetylamino-4*H*-1,2,4-triazolio)acetate **7** (19) (0.5 g, 1.92 mmol) in water (50 mL) was added a solution of sodium hydrogen carbonate (0.1612 g, 1.92 mmol) in water (5 mL). After 15 min at room temperature, the solvent was removed under reduced pressure and the solid residue so obtained was dissolved in methanol (50 mL). Traces of insoluble material were removed by filtration. Addition of diethyl ether (100 mL) to the filtrate gave rise to the precipitation of the crystalline **8**, which was filtered, washed with methanol – diethyl ether (1:2), and dried (90%); mp 105–110°C (dec.); IR, ν_{max}: 1635 (C—O carboxylate asym.) 1580 (C—O amide asym.), and 1380 (C—O sym.) cm^{-1}; ^1H NMR (DMSO-d_6, HMDS, 80 MHz), see Table 2. Anal. calcd. for $C_{12}H_{11}N_4O_3Na \cdot 2H_2O$: C 45.29, H 4.75, N 17.60; found: C 45.38, H 4.80, N 17.52.

1-Carboxymethyl-4-phenylacetylamino-4H-1,2,4-triazolium chloride ***10***

Into a solution of 1-*tert*-butoxycarbonylmethyl-4-phenylacetylimino-4*H*-1,2,4-triazolium inner salt **9** (19) (1.0 g, 3.16 mmol) in hot nitromethane (20 mL) was passed anhydrous HCl during 15 min. The solution was warmed 2 h at 90°C, after which time the solvent was removed under reduced pressure. The residue was dispersed in CH_2Cl_2 (50 mL) and the insoluble material was filtered and recrystallized in hot nitromethane. The compound crystallizes with one solvent molecule (85%); mp 162–165°C; IR, ν_{max}: 1745 (C=O carboxylic acid) and 1715 (C=O amide) cm^{-1}; ^1H NMR (DMSO-d_6, HMDS, 80 MHz), see Table 2 except δ 4.35 (s, 3H, CH_3NO_2). Anal. calcd. for $C_{12}H_{13}N_4O_3Cl \cdot CH_3NO_2$: C 43.64, H 4.51, N 19.58; found: C 43.54, H 4.70, N 19.49.

1-Tert-Butoxycarbonylmethyl-4-phenylacetylimino-4H-1,2,4-triazolium inner salt ***9***

To a solution of *tert*-butyl (4-phenylacetylamino-2,3-dihydro-3-thioxo-4*H*-1,2,4-triazol-2-yl)acetate **26** (19) (2.0 g, 8.68 mmol) in acetic acid (20 mL) was added a 30% solution of hydrogen peroxide in water (2.4 mL). After stirring for 15 min at room temperature, the solution was concentrated under reduced pressure, and the solid residue so obtained was dissolved in water (80 mL). The insoluble material was filtered and the filtrate was adjusted to pH 7.0 with sodium hydrogen carbonate. The solution was extracted three times with chloroform (120 mL). The combined organic layers were dried over anhydrous magnesium sulfate and filtered. The filtrate was concentrated under reduced pressure and the residue was purified by dissolution in chloroform (40 mL) followed by addition of petroleum ether (40–60°C) (160 mL) yielding the crystalline **9**, which was filtered, washed with petroleum ether (40–60°C), and dried (65%); mp 184–186°C; IR and NMR spectra identical with the compound obtained after direct alkylation of **2** (20).

4-Acetylimino-1-tert-butoxycarbonylmethyl-4H-1,2,4-triazolium inner salt ***13***

Compound **13** was obtained as described for **9** (see above) starting from (4-acetylamino-2,3-dihydro-3-thioxo-4*H*-1,2,4-tria-

Can. J. Chem. Downloaded from www.nrcresearchpress.com by 203.198.23.82 on 09/08/12
For personal use only.

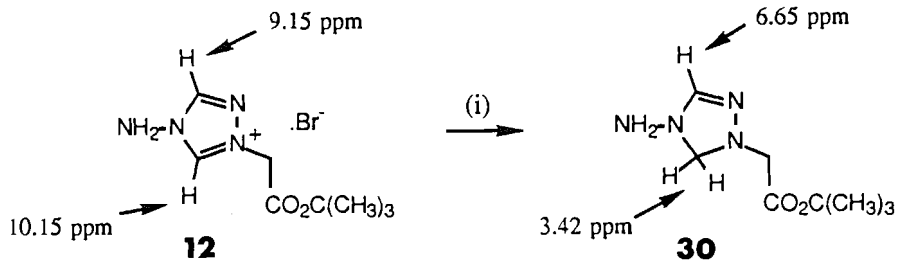

Reagents: (i) $NaBH_4$, H_2O, 0°C

SCHEME 3

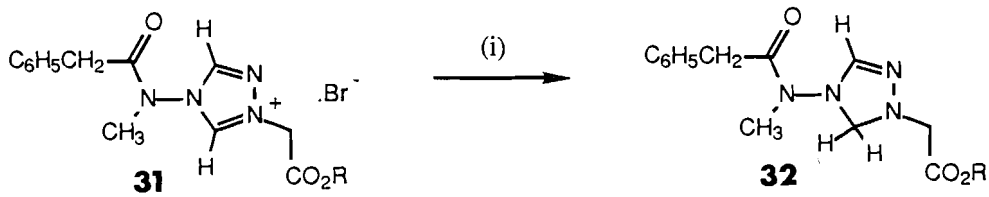

31*a*: R = H
31*b*: R = $C(CH_3)_3$

32*a*: R = H
32*b*: R = $C(CH_3)_3$

Reagent : (i) $NaBH_4$, H_2O

SCHEME 4

zol-2-yl)acetate **25** (19) (75%); mp 172–174°C (lit. (19); mp 174–175°C); IR and NMR spectra identical with the compound obtained after acetylation of **12** (19).

1-tert-*Butoxycarbonylmethyl-4-phenylacetylamino-4*H-*1,2,4-triazolium chloride* ***11***a

Into a solution of 1-*tert*-butoxycarbonylmethyl-4-phenylacetylimino-4*H*-1,2,4-triazolium inner salt **9** (19) (1.0 g, 3.16 mmol) in dichloromethane (20 mL) was passed anhydrous HCl during 5 min at room temperature. Addition of diethyl ether (80 mL) gave rise to the precipitation of the crystalline **11***a*, which was filtered, washed with diethyl ether, and dried (95%); mp 161–163°C; IR, ν_{max}: 1755 (C=O ester), 1697 (C=O amide), and 1234 (C—O ester) cm^{-1}; ^1H NMR (DMSO-d_6, HMDS, 80 MHz), see Table 2. Anal. calcd. for $C_{16}H_{21}N_4O_3Cl$: C 54.47, H 6.00, N 15.88; found: C 54.07, H 6.48, N 15.63.

1-tert-*Butoxycarbonylmethyl-4-phenylacetylamino-4*H-*1,2,4-triazolium trifluoroacetate* ***11***b

Compound **11***b* was obtained as described for **11***a* (see above) except that anhydrous HCl was replaced with trifluoroacetic acid (1.1 molar equivalent) (80%); mp 148–152°C; IR, ν_{max}: 1750 (C=O ester), 1705 (C=O amide), 1630 (C—O carboxylate asym.), and 1425 (C—O carboxylate sym.) cm^{-1}; ^1H NMR (DMSO-d_6, HMDS, 80 MHz), see Table 2. Anal. calcd. for $C_{18}H_{21}N_4O_5F_3$: C 50.23, H 4.92, N 13.02; found: C 50.58, H 5.15, N 12.88.

4-Acetylamino-1-tert-*butoxycarbonylmethyl-4*H-*1,2,4-triazolium chloride* ***14***

Compound **14** was obtained as described for **11***a* (see above) starting from 4-acetylimino-1-*tert*-butoxycarbonyl-4*H*-1,2,4-triazolium inner salt **13** (85%); mp 161–163°C; IR, ν_{max}: 1742 (C=O ester), 1719 (C=O amide), and 1251 (C—O ester) cm^{-1}; ^1H NMR (DMSO-d_6, HMDS, 80 MHz), see Table 2. Anal. calcd. for $C_{10}H_{17}N_4O_3Cl$: C 43.40, H 6.19, N 20.25; found: C 43.66, H 6.25, N 20.30.

tert-*Butyl [4-amino-Δ2-1,2,4-triazolin-1-yl]acetate* ***30***

A solution of 4-amino-1-*tert*-butoxycarbonylmethyl-4*H*-1,2,4-triazolium bromide **12** (19) (1.0 g, 3.58 mmol) in water (10 mL), and chloroform (40 mL), were kept in an ice bath during the dropwise addition of a freshly prepared aqueous solution of sodium borohydride (0.5 g in 5 mL) under vigourous stirring. After complete addition, the organic layer was separated. The aqueous phase was extracted once with chloroform (20 mL), and the combined organic layers were dried over anhydrous magnesium sulfate. After filtration and removal of the solvent under reduced pressure, the final product was isolated as an oil (92%); IR, ν_{max}: 3430 (N—H), 3349 (N—H), 2979 (C—H aliph.), 2934 (C—H aliph.), 1739 (C=O ester), and 1156 (C—O ester) cm^{-1}; ^1H NMR (DMSO-d_6, HMDS, 80 MHz) δ: 1.30 (s, 9H, $C(CH_3)_3$), 3.42 (s, 2H, N-CH_2-N), 4.00 (s, 2H, N-CH_2-CO), 4.10 (br s, 2H, NH_2), 6.65 (s, 1H, 3-H); after addition of CF_3COOD, δ: 1.35 (s, 9H, $C(CH_3)_3$), 5.05 (s, 2H, N-CH_2-CO), 8.25 (s, 1H), 8.90 (s, 1H).

*[4-(*N*-Methyl-*N*-phenylacetylamino)-Δ2-1,2,4-triazolin-1-yl]acetic acid* ***32***a

To a solution of 1-carboxymethyl-4-(*N*-methyl-*N*-phenylacetylamino)-4*H*-1,2,4-triazolium bromide **31***a* (19) (0.3 g, 0.76 mmol) in water (3 mL) was added dropwise a solution of sodium borohydride (0.15 g) in water (1.5 mL). After 5 min at room temperature, the solution was adjusted to pH 3 with 0.1 N HCl and then extracted (×3) with chloroform (20 mL). The combined organic layers were dried over anhydrous magnesium sulfate. After filtration and removal of the solvent under reduced pressure, the residue was dissolved in ethyl acetate (5 mL). Insoluble material was removed by filtration, and the filtrate, mixed with petroleum ether

Can. J. Chem. Downloaded from www.nrcresearchpress.com by 203.198.23.82 on 09/08/12
For personal use only.

TABLE 4. Dissociation constants (expressed as pK_a: pK_{a_1} for CO_2H; pK_{a_2} for CONH), and selected ^1H NMR data (DMSO-d_6, HMDS, δ ppm) for the 4-acylamino-1,2,4-triazoline-3-thiones and 4-acylamino-1,2,4-triazolin-3-ones

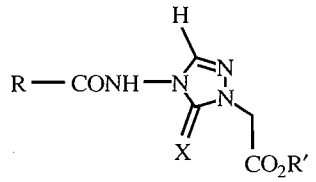

Compound no.	R	R′	X	pK_{a_1}	pK_{a_2}	N-CH_2-CO	5-H	N-H
33	CH_3	H	S	3.10	8.54	4.75	8.58	11.30
25	CH_3	$C(CH_3)_3$	S	—	8.03	4.75	8.60	11.25
34	$C_6H_5CH_2$	H	S	3.37	8.44[a]	4.77	8.60	11.60
26	$C_6H_5CH_2$	$C(CH_3)_3$	S	—	7.76	4.75	8.60	11.65
35	CH_3	H	O	3.46	9.55	4.35	7.98	10.82
36	CH_3	$C(CH_3)_3$	O	—	8.87	4.32	7.98	10.80
37	$C_6H_5CH_2$	H	O	3.50	9.25[a]	4.35	8.02	11.10
38	$C_6H_5CH_2$	$C(CH_3)_3$	O	—	8.56	4.30	8.00	11.10

[a]Reference 19.

(40–60°C) (20 mL), gave rise to the precipitation of the crystalline **32***a* (57%); mp 124–127°C; IR, ν_{max}: 1714 (C=O carboxylic acid), 1664 (C=O amide), and 1609 (C=N) cm^{-1}; ^1H NMR (DMSO-d_6, HMDS, 80 MHz) δ: 2.90 (s, 3H, N-CH_3), 3.45 (m, 1H, H_a of N-CH_2-N), 3.70 (s, 2H, Ph-CH_2), 3.80 (m, 1H, H_b of N-CH_2-N), 4.02 (m, 1H, H_a of N-CH_2-CO), 4.41 (m, 1H, H_b of N-CH_2-CO), 6.90 (s, 1H, 3-H), 7.15 (m, 5H, C_6H_5); MS (FAB) *m/z*: 277 [MH^+], 275 [$MH^+ - H_2$, hydride abstraction]. Anal. calcd. for $C_{13}H_{16}N_4O_3$: C 56.51, H 5.81, N 20.28; found: C 56.10, H 6.07, N 20.70.

tert-*Butyl* [*4-(N-methyl-*N*-phenylacetylamino)-Δ2-1,2,4-triazolin-1-yl*]*acetate* ***32***b

To a solution of 1-*tert*-butoxycarbonylmethyl-4-(*N*-methyl-*N*-phenylacetylamino)-4*H*-1,2,4-triazolium bromide **31***b* (20) (0.3 g, 0.68 mmol) in water (4 mL) was added dropwise a solution of sodium borohydride (0.15 g) in water (1.5 mL). After 5 min at room temperature, the oily precipitate was extracted (×3) with chloroform (20 mL). The combined organic layers were dried over anhydrous magnesium sulfate, filtered, and concentrated under reduced pressure to give **32***b* as an oil (85%); IR, ν_{max}: 2978 (C—H aliph.), 2932 (C—H aliph.), 1738 (C=O ester), 1674 (C=O amide), 1604 (C=N), and 1230 (C—O ester) cm^{-1}; ^1H NMR (DMSO-d_6, HMDS, 80 MHz) δ: 1.30 (s, 9H, $C(CH_3)_3$), 2.87 (s, 3H, N-CH_3), 3.42 (m, 1H, H_a of N-CH_2-N), 3.70 (s, 2H, Ph-CH_2), 3.75 (m, 1H, H_b of N-CH_2-N), 4.00 (m, 1H, H_a of N-CH_2-CO), 4.38 (m, 1H, H_b of N-CH_2-CO), 6.90 (s, 1H, 3-H), 7.15 (m, 5H, C_6H_5); ^1H NMR ($CDCl_3$, TMS, 400 MHz) δ: 1.50 (s, 9H, $C(CH_3)_3$), 3.10 (s, 3H, N-CH_3), 3.64 (d, 1H, H_a of N-CH_2-N, J = 17.2 Hz), 3.81 (s, 2H, Ph-CH_2), 3.89 (d, 1H, H_b of N-CH_2-N), 4.17 (d, 1H, H_a of N-CH_2-CO, J = 2.0 Hz), 4.47 (d, 1H, H_b of N-CH_2-CO), 6.40 (s, 1H, 3-H), 7.29 (m, 5H, C_6H_5); ^{13}C NMR ($CDCl_3$, TMS, 400 MHz) δ: 28.08 (s, 3C, 3 × *C*H_3), 30.06 (s, 1C, N-*C*H_3), 40.48 (s, 1C, Ph-*C*H_2), 56.07 (s, 1C, N-*C*H_2-CO), 70.47 (s, 1C, N-*C*H_2-N), 81.93 (s, 1C, *C*$(CH_3)_3$), 126.82 (s, 1C, *C* arom., *para*), 128.64 (s, 2C, *C* arom., *meta*), 129.02 (s, 2C, *C* arom., *ortho*), 134.86 (s, 1C, *C* arom., subst.), 141.63 (s, 1C, *C*=N), 168.27 (s, 1C, *C*=O), 173.82 (s, 1C, *C*=O); MS *m/z* (RI %): 332 (3) [M^+], 276 (4) [$M^+ - CH_2$=$C(CH_3)_2$], 231 (7) [$M^+ - COOC(CH_3)_3$], 184 (13) [$M^+ - PhCH_2CONCH_3$], 149 (15) [$PhCH_2CONHCH_3^+$], 128 (33) [$M^+ - PhCH_2CONCH_3 - CH_2$=$C(CH_3)_2$].

Determination of dissociation constants

The pK_a values of the triazole derivatives were determined on a Metrohm 670 Titroprocessor using a Metrohm 665 Dosimat and a Metrohm 6.0204.100 combined pH glass electrode. The pK_a values of the water soluble carboxylic acids were established, either in water, or in a 1:1:3 mixture of dimethylformamide, methanol, and water. The resulting ΔpK_a values calculated for the different carboxylic acids were used to correct the experimental values obtained in the same 1:1:3 solvent mixture for the corresponding sparingly water soluble *tert*-butyl esters.

Monotonic titration

Monotonic titration: Increment: 2 μL; rate for the volume of increment: 10 mL/min; maximum drift for measurement: 10 mV/min; delay time for measurement acquisition: 52 s; output for each increment: pH; output for each increment: total vol.

Method applied to water soluble products

The product (2.5×10^{-5} mol), dissolved in water (1 mL), was introduced in a micro titration cell. 1.0 N NaOH was added in a monotonic titration mode using a 2-μL step addition. The pH was determined at all steps and the titration curve was established. The equivalent point was automatically calculated. Three points just before and after the half-neutralization point were chosen. For each point, the pH and the added volume of NaOH were introduced in an appropriate calculation program from which the pK_a values were obtained taking into account the activity of the ions in solution. The mean of the six results with the standard deviation was calculated.

Method applied to water insoluble products

The above experimental conditions and calculation procedure were applied to the sparingly water soluble products except that the samples (2.5×10^{-5} mol) were dissolved in a dimethylformamide (0.2 mL) – methanol (0.2 mL) – water (0.6 mL) mixture.

Acknowledgements

We thank Mrs. M-L. Pirard for technical assistance and Dr. M. Schuerch for help in the English editing. We thank the Fonds National de la Recherche Scientifique (F.N.R.S.) for financial support. During this work, B.P. was senior research assistant of the F.N.R.S.

1. C.F.H. Allen and A. Bell. Org. Synth. Coll. Vol. **3**, 96 (1955).
2. H.G.O. Becker, H. Böttcher, T. Röthling, and H.-J. Timpe. Wiss. Z. Tech. Hochsch. Chem. "Carl Schorlemmer" Leuna-Merseburg, **8**, 22 (1966).
3. H.G.O. Becker, K. Heimburger, and H.-J. Timpe. Wiss. Z. Tech Hochsch. Chem. "Carl Schorlemmer" Leuna-Merseburg, **8**, 11 (1966).

Can. J. Chem. Downloaded from www.nrcresearchpress.com by 203.198.23.82 on 09/08/12
For personal use only.

4. H.G.O. Becker and H.-J. Timpe. J. Prakt. Chem. **311**, 9 (1969).
5. H.G.O. Becker, N. Sander, and H.-J. Timpe. J. Prakt. Chem. **311**, 897 (1969).
6. H.G.O. Becker and H.-J. Timpe. J. Prakt. Chem. **312**, 1112 (1970).
7. H.G.O. Becker, K. Heimburger, and H.-J. Timpe. J. Prakt. Chem. **313**, 795 (1971).
8. H.-J. Timpe. Z. Chem. **11**, 340 (1971).
9. H.-J. Timpe and H.G.O. Becker. J. Prakt. Chem. **314**, 325 (1972).
10. H.G.O. Becker, D. Nagel, and H.-J. Timpe. J. Prakt. Chem. **315**, 97 (1973).
11. H.-J. Timpe. Adv. Heterocycl. Chem. **17**, 213 (1974).
12. F.L. Scott, T.M. Lambe, and R.N. Butler. Tetrahedron Lett. **20**, 1729 (1971).
13. R.N. Butler, T.M. Lambe, and F.L. Scott. J. Chem. Soc. Perkin Trans. 1, 269 (1972).
14. O. Tsunge, M. Yoshida, and S. Kanemasa. J. Org. Chem. **39**, 1226 (1974).
15. K.T. Potts and R.M. Huseby. J. Org. Chem. **31**, 3528 (1966).
16. R. Milcent and C. Redeuilh. J. Heterocycl. Chem. **17**, 1691 (1980).
17. F. Malbec, R. Milcent, and G. Barbier. J. Heterocycl. Chem. **21**, 1689 (1984).
18. N.F. Eweiss, A.A. Bahajaj, and E.A. Elsherbini. J. Heterocycl. Chem. **23**, 1451 (1986).
19. B. Pirotte, G. Dive, J. Delarge, B. Masereel, L. Dupont, L. Thunus, M. Schynts, J. Coyette, and J.M. Frère. Eur. J. Med. Chem. **27**, 193 (1992).
20. A.-C. Vilain, B. Pirotte, I. Vergely, N. Boggetto, B. Masereel, M. Schynts, J. Delarge, and M. Reboud-Ravaux. J. Pharm. Pharmacol. **45**, 466 (1993).
21. T. George, D.V. Mehta, R. Tahibramani, J. David, and P.K. Talwalker. J. Med. Chem. **14**, 335 (1971).
22. H. Emilsson, K. Luthman, and H. Selander. Eur. J. Med. Chem. **21**, 235 (1986).
23. S. Patai. The chemistry of the hydrazo, azo and azoxy group. Part 1. John Wiley and Sons, New York. 1975.
24. L. Dupont, O. Dideberg, B. Pirotte, and J. Delarge. Acta Crystallogr. Sect. C: Cryst. Struct. Commun. **C45**, 1928 (1989).
25. L. Dupont, S. Englebert, O. Dideberg, B. Pirotte, and J. Delarge. Acta Crystallogr. Part C: Cryst. Struct. Commun. **C47**, 1079 (1991).
26. F.H. Allen, O. Kennard, D.G. Watson, L. Brammer, A.G. Orpen, and R. Taylor. J. Chem. Soc. Perkin Trans. 2, S1 (1987).
27. R. Shintani. Acta Crystallogr. **13**, 609 (1960).
28. A.N. Chekhlov. I.V. Martynov, and V.K. Brel. Dokl. Akad. Nauk SSSR, **292**, 149 (1987).
29. J.W. Bunting. Adv. Heterocycl. Chem. **25**, 1 (1979).
30. G.M. Clarke and P. Sykes. J. Chem. Soc. (C), 1269 (1967).
31. G.M. Clarke and P. Sykes. J. Chem. Soc. (C), 1411 (1967).
32. A.I. Meyers and E.D. Mihelich. Angew. Chem. Int. Ed. Engl. **15**, 270 (1976).
33. I.C. Nordin. J. Heterocyl. Chem. **3**, 531 (1966).
34. W. Walter, J. Voss, and J. Curts. Justus Liebigs Ann. Chem. **695**, 77 (1966).
35. W. Walter and J. Voss. Justus Liebigs Ann. Chem. **695**, 87 (1966).

Can. J. Chem. Downloaded from www.nrcresearchpress.com by 203.198.23.82 on 09/08/12
For personal use only.

Palladium(0)-catalyzed conversion of vinyl trifluoromethanesulfonates into α,β-unsaturated nitriles

EDWARD PIERS[1] AND FRASER F. FLEMING

Department of Chemistry, University of British Columbia, 2036 Main Mall, University Campus, Vancouver, BC V6T 1Z1, Canada

Received March 31, 1993

EDWARD PIERS and FRASER F. FLEMING. Can. J. Chem. **71**, 1867 (1993).

Treatment (benzene, room temperature) of each of the vinyl trifluoromethanesulfonates **16–23** with dry lithium cyanide in the presence of catalytic amounts of tetrakis(triphenylphosphine)palladium(0) and the crown ether 12-crown-4 provides good to excellent yields of the corresponding α,β-unsaturated nitriles **24–31**.

EDWARD PIERS et FRASER F. FLEMING. Can. J. Chem. **71**, 1867 (1993).

Le traitement (benzène, température ambiante) de chacun des trifluorométhanesulfonates de vinyle **16–23** par du cyanure de lithium sec, en présence de quantités catalytiques de tétrakis(triphénylphosphine)palladium(0) et d'éther 12-couronne-4 conduit à d'excellents rendements des nitriles α,β-insaturés correspondants, **24–31**.

[Traduit par la rédaction]

Introduction

In connection with projects directed toward the total synthesis of natural products, we required a method for the conversion of unsymmetrically substituted cyclic ketones (see general formula **1**) into the corresponding α,β-unsaturated nitriles **2**. One-carbon homologations of ketones into unsaturated nitriles have traditionally been accomplished via a two-step method involving conversion of the carbonyl substrate into a cyanohydrin derivative **3**, followed by subjection of the latter species to a suitable elimination procedure (1–6). However, if this type of process is applied to unsymmetrically substituted ketones, the product usually consists of a mixture of the two possible positional isomers **2** and **4** (1, 4–6).

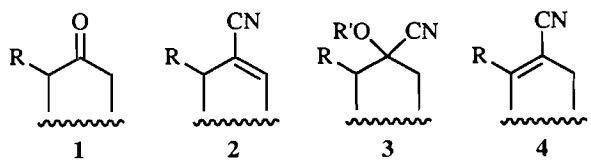

1 **2** **3** **4**

A number of methods for the transformation of vinyl halides into α,β-unsaturated nitriles have been developed (7–10, and citations therein). With respect to the present work, the reports by Yamamura and Murahashi (7) and Prochazka and Siroky (10) are particularly pertinent. These groups showed that treatment of vinyl halides with potassium cyanide in the presence of catalytic amounts of tetrakis(triphenylphosphine)palladium(0) and the crown ether 18-crown-6 in hot benzene provides, efficiently, the corresponding vinyl nitriles. For example, (*E*)-1-bromo-1-hexene (**5**) was converted into the nitrile **6** in high yield (7) (eq. [1]).

It is now well known, primarily from the important studies by Stille and co-workers (11–13), that vinyl trifluoromethanesulfonates (triflates) participate effectively in palladium(0)-catalyzed cross-coupling processes. Therefore, since the conversion of ketones into vinyl triflates is usually achieved easily and efficiently (14), we were attracted by the possibility of effecting the desired conversion of **1** into **2** via the intermediacy of vinyl triflates **7**, as shown in general terms in eq. [2]. We report in this paper the details of a study (15) that showed that, under carefully defined conditions, α,β-unsaturated nitriles can be derived, cleanly and efficiently, from vinyl triflates.[2]

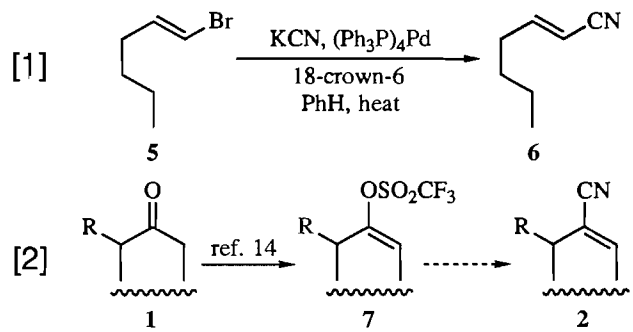

Results and discussion

*(a) Preparation of the vinyl triflates **16–23***

The structural formulas of the ketones **8–15**[3] employed in this study are shown in Chart 1. Collectively, these substances exhibit various ring sizes and an interesting assortment of functional groups.

The effective method of McMurry and Scott (14) was employed to convert the ketones **8–15** into the corresponding vinyl triflates **16–23**, respectively (see Chart 1). The results of these transformations are summarized in Table 1. In general, the reactions proceeded in good-to-excellent yields (66–84%) and the crude products were conveniently purified by flash chromatography on silica gel (21).

*(b) Conversion of the vinyl triflates **16–23** into the α,β-unsaturated nitriles **24–31** (Chart 1, Table 1)*

Exploratory studies involved attempts to convert the vinyl triflate **16** into the unsaturated nitrile **24**. Initially, conditions similar to those employed by Yamamura and Murahashi (7) for the transformation of vinyl halides into nitriles were

[1]Author to whom correspondence may be addressed.

[2]For a recent report describing the Ni(0)- and Pd(0)-mediated conversion of aryl triflates into benzonitrile derivatives, see ref. 16.

[3]Substances **8**, **11**, and **15** are commercially available, while the remaining ketones were prepared during the course of other studies in our laboratory (compounds **9** and **10**, ref. 17; compounds **12–14**, refs. 18–20, respectively).

Can. J. Chem. Downloaded from www.nrcresearchpress.com by 203.198.23.82 on 09/08/12
For personal use only.

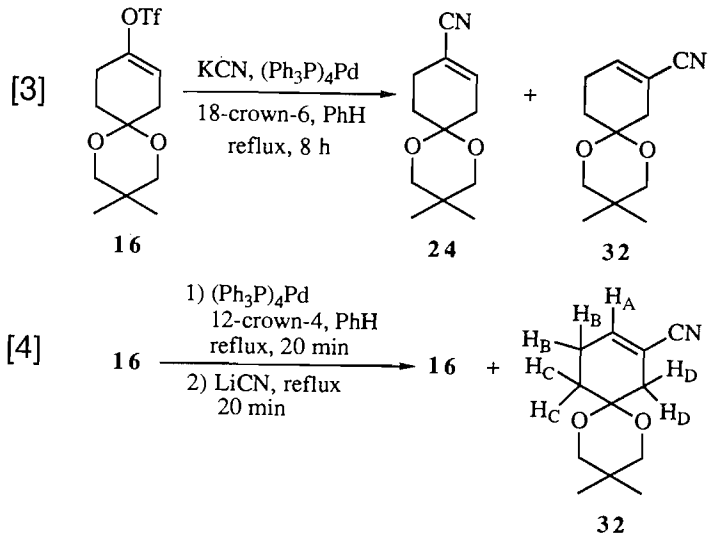

TABLE 1. Conversion of ketones into α,β-unsaturated nitriles

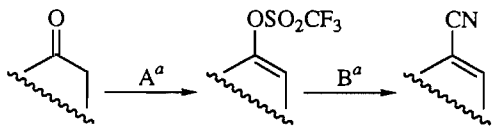

Entry	Ketone	Vinyl triflate (yield, %)[b]	Reaction time for B (h)	Nitrile (yield, %)[b]
1	**8**	**16** (75)	2	**24** (80)
2	**9**	**17** (80)	2	**25** (89)
3	**10**	**18** (76)	2.5	**26** (87)
4	**11**	**19** (66)	3	**27** (78)
5	**12**	**20** (73)	2	**28** (85)
6	**13**	**21** (84)	20	**29** (76)[c]
7	**14**	**22** (72)	2	**30** (78)
8	**15**	**23** (82)[d]	4	**31** (59)[e]

[a]A: (*i*-Pr)$_2$NLi (1.15 equiv.), THF, −78°C, 2 h; PhN(SO$_2$CF$_3$)$_2$ (1.1 equiv.), −78°C → room temperature. B: LiCN (2 equiv.), $(Ph_3P)_4Pd$ (0.07 equiv.), 12-crown-4 (0.07 equiv.), PhH, room temperature.

[b]Yield of chromatographically purified and, where appropriate, distilled product.

[c]An additional amount (0.07 equiv.) of $(Ph_3P)_4Pd$ was added after a reaction time of 6.5 h.

[d]Compound **23** was obtained by treatment of **15** with KH in THF (room temperature), followed by addition of PhN(SO$_2$CF$_3$)$_2$.

[e]Additional amounts (0.07 equiv.) of $(Ph_3P)_4Pd$ were added after reaction times of 1, 2, and 3 h.

examined. However, when **16** was treated (benzene, reflux, 8 h) with potassium cyanide in the presence of $(Ph_3P)_4Pd$ and 18-crown-6, a mixture of two products was obtained. Analyses of the mixture by gas–liquid chromatography (glc) and ^{1}H nmr spectroscopy showed that the two components were present in a ratio of about 5:1. Furthermore, although the two substances were inseparable by column chromatography on silica gel, comparison of the ^{1}H nmr spectrum with spectra of pure samples of **24** and **32** (*vide infra*) showed that the two products were **24** and **32**, respectively (eq. [3]).

The formation of the unsaturated nitrile **32** was unexpected. Subsequent attempts to maximize the formation of this substance did not lead to synthetically useful results but did provide a means of obtaining, in very low yield, a sample of pure **32** for characterization purposes. Thus, a benzene solution of $(Ph_3P)_4Pd$ (0.07 equiv.), 12-crown-4 (0.35 equiv.), and the enol triflate **16** (1.0 equiv.) was refluxed for 20 min. The resultant dark brown solution was treated with dry lithium cyanide (5.5 equiv.) and reflux was continued for a further 20 min. Work-up and flash chromatography of the crude material gave recovered vinyl triflate **16** (85%) and a small amount (15% based on recovered **16**) of the nitrile **32** (eq. [4]).

The infrared (ir) spectrum of **32** showed the expected absorptions (2217, 1638 cm^{-1}) for the unsaturated nitrile function. The ^{1}H nmr spectrum exhibited the following signals: δ 0.98, 1.00 (s, s, 3H each), 1.93 (t, 2H, J = 6 Hz, H_C), 2.29–2.36 (m, 2H, H_B), 2.55–2.59 (m, 2H, H_D), 3.48–3.56 (m, 4H, ketal methylene protons), 6.59–6.63 (m, 1H, H_A). The signal assignments were confirmed by suitable decoupling experiments. Thus, irradiation at δ 2.33 (H_B) changed the triplet at 1.93 (H_C) to a singlet, sharpened the multiplet at 2.55–2.59 (H_D) to a broad singlet ($w_{1/2}$ = 4 Hz), and simplified the signal due to H_A (6.59–6.63) to a triplet (J = 2 Hz); irradiation at δ 2.57 (H_D) simplified the multiplet at 2.29–2.36 (H_B) and changed the multiplet at 6.59–6.63 (H_A) to a triplet (J = 4 Hz); irradiation at δ 6.61 (H_A) sharpened the multiplet at 2.29–2.36 (H_B) and changed the multiplet at 2.55–2.59 (H_D) to a triplet (J = 2 Hz).

Further evidence for the structure of **32** was derived from a nuclear Overhauser enhancement (nOe) difference experiment and two SINEPT (22) experiments. Thus, in the nOe experiment, irradiation of the olefinic proton resonance (H_A, δ 6.61) caused signal enhancement at 2.29–2.36 (H_B) but not at 2.55–2.59 (H_D). In the two SINEPT experiments, both optimized for a $^3J_{C-H}$ of 7 Hz, irradiation of the signal at δ 3.48–3.56 (ketal methylene hydrogens) gave strong polarization transfer through three-bond coupling to the quaternary ketal carbon (δ 95.3), while irradiation at δ 6.61 (H_A) gave strong polarization transfer through three-bond coupling to the nitrile carbon (δ 118.9) but not to the quaternary ketal carbon. These observations are entirely consistent with structure **32**.

Experiments aimed at suppressing the formation of the "undesired" α,β-unsaturated nitrile **32** examined the use of a number of different solvents (*N*,*N*-dimethylformamide, hexamethylphosphoramide, THF, benzene) at different

Can. J. Chem. Downloaded from www.nrcresearchpress.com by 203.198.23.82 on 09/08/12
For personal use only.

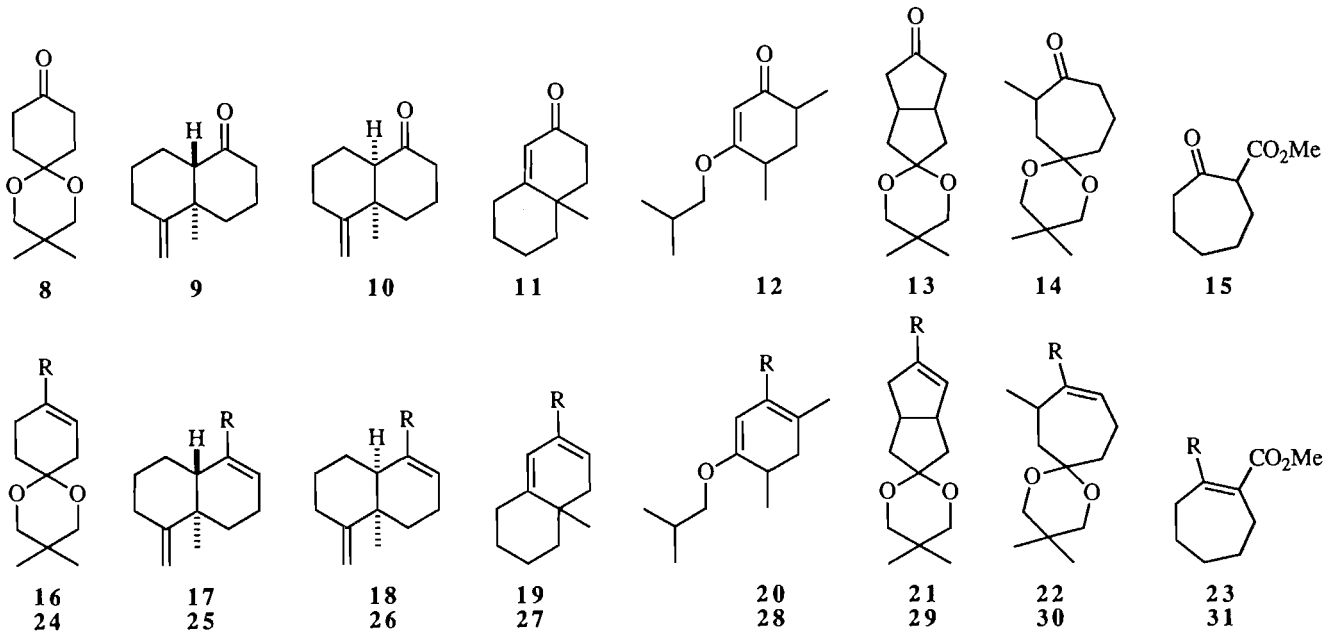

CHART 1

temperatures. Eventually it was found that treatment of **16** with KCN, 18-crown-6, and $(Ph_3P)_4Pd$ in benzene at room temperature for 4 h gave a mixture of starting material and the desired nitrile **24** in a ratio of ~ 3:1, respectively. Only a trace of **32** could be detected. A longer reaction time (47 h) led to almost complete consumption of the vinyl triflate **16** and produced **24** and **32** in a ratio of about 17:1, respectively.

The latter results were encouraging and led to the discovery that, at room temperature in benzene, reaction of the vinyl triflate **16** with lithium cyanide in the presence of $(Ph_3P)_4Pd$ and 12-crown-4 produced only the unsaturated nitrile **24**. After extensive experimentation, during which the reaction temperature and the relative concentrations of reagents and catalysts were varied, the conversion of **16** into **24** was found to proceed cleanly and efficiently (80%) using *dry* LiCN (2 equiv.), $(Ph_3P)_4Pd$ (0.07 equiv.), and 12-crown-4 (0.07 equiv.) in benzene (~5.5 mL per mmol of **16**) at room temperature. Under these conditions, complete conversion of **16** into **24** was achieved within 2 h (eq. [5]).

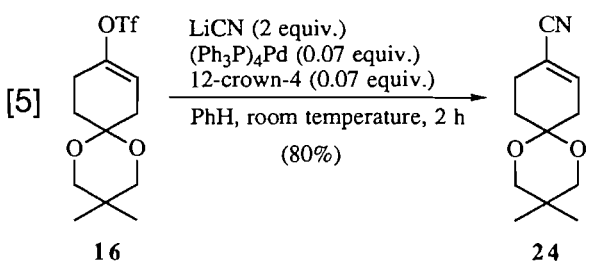

The spectral data derived from compound **24** are fully consistent with the assigned structure. Data obtained from nmr spectroscopy, including ^1H nmr decoupling and nOe experiments and two SINEPT (22) experiments, provided conclusive evidence for the substitution pattern on the cyclohexene ring (see experimental for details).

The generality of this new method for the conversion of vinyl triflates into α,β-unsaturated nitriles was demonstrated, at least to some degree, by transformation of substrates **17–23** into the corresponding products **25–31** (see Chart 1 and Table 1). For most of these cases (Table 1, entries 1–5, 7) the procedure developed for the acquisition of **24** from **16** (eq. [5]) worked well. These processes were efficient (78–89% yields) and were complete within reaction times of 2–3 h at room temperature. On the other hand, the reactions involving triflates **21** and **23** (Table 1, entries 6, 8) were somewhat sluggish. In these cases, an acceptable rate of conversion of substrate into product could be achieved by adding additional amounts of the catalyst $(Ph_3P)_4Pd$ to the reaction mixtures at appropriate times, as summarized in Table 1.

The method is compatible with the presence of a variety of functional groups. Thus, collectively, the substrates **16–23** contain ketal, alkene, conjugated diene, enol ether, and ester functions.

Each of the α,β-unsaturated nitriles listed in Table 1 exhibit spectra in full accord with the structural assignment. Appropriate ^1H nmr nOe difference experiments and, for the nitriles **24–26**, SINEPT (22) experiments, provided corroborative evidence for the structures of the nitrile products.

(c) Mechanistic considerations

On the basis of proposals for reaction pathways related to Pd(0)-catalyzed cross-coupling of vinyl triflates with organostannanes (11, 12, 23) and taking into account the recent important mechanistic studies of Stang *et al.* (24, 25) on related Pt(0)-mediated processes, it is reasonable to propose that the Pd(0)-catalyzed conversion of vinyl triflates into nitriles proceeds via the catalytic cycle shown in general terms in Scheme 1. Oxidative addition of palladium(0) to the C—O bond of the vinyl triflate provides the ionic (11, 24) palladium(II) species **33**. Reaction of **33** with cyanide ion (derived from the LiCN · 12-crown-4 complex), would produce

Can. J. Chem. Downloaded from www.nrcresearchpress.com by 203.198.23.82 on 09/08/12
For personal use only.

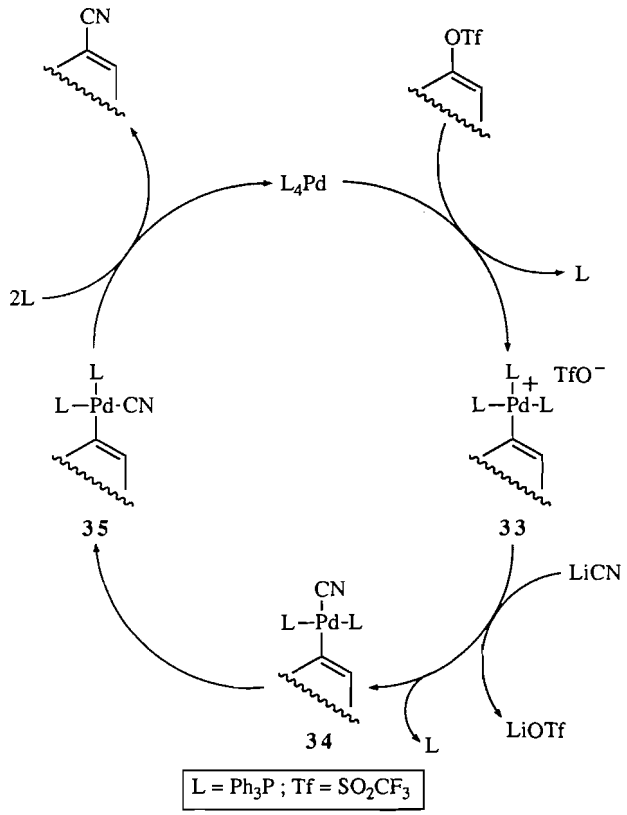

SCHEME 1

the *trans* palladium(II) cyanide **34**. Isomerization of **34** to the *cis* isomer **35**, followed by a (rapid) reductive elimination process would provide the α,β-unsaturated nitrile product.

Conclusion

The work described in this paper culminated in a synthetically effective method for the conversion of vinyl triflates into the corresponding α,β-unsaturated nitriles. Since vinyl triflates are readily available from ketones via a variety of methods (14) and since α,β-unsaturated nitriles are versatile synthetic intermediates, the chemistry developed in this study should prove to be useful in the area of organic synthesis.

Experimental

General information

Distillation temperatures, which refer to short-path (Kugelrohr) distillations, and melting points are uncorrected. Proton nuclear magnetic resonance (^{1}H nmr) spectra were recorded on $CDCl_3$ solutions and signal positions (δ values) are given relative to the resonance of Me_4Si. Carbon nuclear magnetic resonance (^{13}C nmr) spectra were taken on $CDCl_3$ solutions and resonances were measured relative to that of $CDCl_3$ (δ 77.0). Signals with negative intensities in an attached proton test (APT) are so indicated by (−ve) following the chemical shift. Flash chromatography (21) was carried out with 230–400 mesh silica gel (E. Merck). Thin-layer chromatography (tlc) was performed on commercial aluminum-backed silica gel plates. Gas–liquid chromatography (glc) was carried out with instruments equipped with 25 m × 0.21 mm fused silica columns coated with cross-linked SE-54. Reagents and solvents were purified and dried using standard methods. Aqueous NH_4Cl–NH_4OH (pH 8) refers to a solution prepared by addition of ~50 mL of aqueous NH_3 (30%) to ~950 mL of saturated aqueous NH_4Cl.

Note: All reactions were carried out under an atmosphere of dry argon in flame- or oven-dried glassware.

General procedure for the preparation of vinyl triflates

A solution of the ketone (1.0 equiv.) in dry THF (0.45 mL per mmol of ketone) was added, dropwise, to a cold (−78°C), stirred solution of lithium diisopropylamide (1.15 equiv.) in dry THF (3.4 mL per mmol of ketone). After the solution had been stirred at −78°C for 2 h, *N*-phenyltrifluoromethanesulfonimide (1.10 equiv.) was added as a finely powdered solid, the solution was warmed to room temperature, and stirring was continued for a further period of time (specified as reaction time in the descriptions below). Work-up and purification of the crude product as described provided the desired vinyl triflate.

*Vinyl triflate **16***

The ketone **8** (5.0 g, 25.3 mmol) was converted into the vinyl triflate **16** (reaction time 16 h). The entire reaction mixture was filtered through a short column (5.5 × 5 cm) of Florisil (elution with petroleum ether, ~250 mL). Concentration of the combined filtrate and flash chromatography of the residual material on silica gel (5.5 × 15 cm column, 9:1 petroleum ether – Et_2O) afforded 6.22 g (75%) of the vinyl triflate **16** as a white solid. Recrystallization (hexane–Et_2O) gave white, plate-like crystals (mp 24–25°C) that displayed ir (KBr): 3076, 1695, 1206, 1142 cm^{-1}; ^{1}H nmr (400 MHz) δ: 0.96 (s, 3H), 1.02 (s, 3H), 2.11 (t, 2H, J = 6 Hz), 2.40–2.47 (m, 2H), 2.50–2.56 (m, 2H), 3.50 (d, 2H, J = 10 Hz), 3.56 (d, 2H, J = 10 Hz), 5.62 (t, 1H, J = 4 Hz). Exact Mass calcd. for $C_{12}H_{17}F_3O_5S$: 330.0749; found: 330.0740.

*Vinyl triflate **17***

The ketone **9** (2.47 g, 13.9 mmol) was transformed into the vinyl triflate **17** (reaction time 2 h). Concentration (reduced pressure) of the entire reaction mixture, followed by flash chromatography (4.5 × 15 cm silica gel column, 9:1 petroleum ether – Et_2O) of the residual material and distillation (81–86°C/0.3 Torr (1 Torr = 133.3 Pa)) of the acquired oil, produced 3.44 g (80%) of **17**. This colorless oil exhibited ir (neat): 3088, 1681, 1645, 1208, 1144; ^{1}H nmr (400 MHz) δ: 1.03 (s, 3H), 1.29–1.67 (m, 4H), 1.73–1.80 (m, 1H), 1.84–1.98 (m, 2H), 2.17–2.24 (dd, 1H, J = 14, 4 Hz), 2.26–2.36 (m, 2H), 2.46 (td, 1H, J = 14, 4 Hz), 4.64 (br s, 1H), 4.72 (br s, 1H), 5.70–5.74 (m, 1H). Exact Mass calcd. for $C_{13}H_{17}F_3O_3S$: 310.0850; found: 310.0845.

*Vinyl triflate **18***

This substance was derived from the ketone **10** (719 mg, 4.04 mmol) (reaction time 1 h). Aqueous NH_4Cl–NH_4OH (pH 8) (10 mL) was added to the reaction mixture and the mixture was extracted three times with Et_2O. The combined organic extracts were washed with brine until the aqueous phase was neutral (pH paper) and then were dried ($MgSO_4$) and concentrated. Flash chromatography (4.5 × 15 cm silica gel column, petroleum ether) of the crude material, followed by distillation (128–134°C/0.3 Torr) of the oil thus obtained, gave 950 mg (76%) of the vinyl triflate **18**, a colorless oil that displayed ir (neat): 3092, 1687, 1638, 1208, 1145 cm^{-1}; ^{1}H (400 MHz) δ: 1.12–1.18 (m, 1H), 1.20 (s, 3H), 1.28–1.40 (m, 1H), 1.46–1.57 (m, 1H), 1.68–1.77 (m, 1H), 1.93–2.09 (m, 3H), 2.16–2.33 (m, 4H), 4.79 (s, 1H), 4.82 (s, 1H), 5.57 (t, 1H, J = 4 Hz). Exact Mass calcd. for $C_{13}H_{17}F_3O_3S$: 310.0850; found: 310.0843.

*Vinyl triflate **19***

This material was obtained from the enone **11** (300 mg, 1.83 mmol) (reaction time 1 h). Removal of the solvent (reduced pressure) from the reaction mixture, followed by flash chromatography (2.7 × 15 cm silica gel column, petroleum ether) of the remaining material and distillation (90–95°C/0.3 Torr) of the acquired liquid gave 356 mg (66%) of the vinyl triflate **19**, a colorless oil that showed ir (neat): 1658, 1612, 1210, 1143 cm^{-1}; ^{1}H nmr (400 MHz) δ: 1.04 (s, 3H), 1.25–1.37 (m, 2H), 1.47–1.60 (m, 1H), 1.63–1.74 (m, 2H), 1.77–1.85 (m, 1H), 2.14 (dd, 1H, J = 16, 8 Hz), 2.23–2.30 (m, 2H), 2.35 (br d, J = 16 Hz), 5.48 (s,

Can. J. Chem. Downloaded from www.nrcresearchpress.com by 203.198.23.82 on 09/08/12
For personal use only.

Can. J. Chem. Downloaded from www.nrcresearchpress.com by 203.198.23.82 on 09/08/12
For personal use only.

1H), 5.52–5.57 (m, 1H). Exact Mass calcd. for $C_{12}H_{15}F_3O_3S$: 296.0694; found: 296.0686.

Vinyl triflate 20

The ketone **12** (1.0 g, 5.1 mmol) was converted into the vinyl triflate **20** (reaction time 16 h). Concentration (reduced pressure) of the reaction mixture, followed by flash chromatography of the crude product on silica gel (4.5 × 15 cm column, petroleum ether) gave an oil that, upon distillation (84–88°C/0.3 Torr), produced 1.21 g (73%) of **20**, a colorless oil that exhibited ir (neat): 1681, 1624, 1208, 1143 cm^{-1}; ^1H nmr (400 MHz) δ: 0.97 (d, 6H, J = 6 Hz), 1.08 (d, 3H, J = 7 Hz), 1.80 (s, 3H), 1.96–2.05 (m, 2H), 2.53 (dd, 1H, J = 16, 7 Hz), 2.40 (br hextet, 1H, J = 7 Hz), 3.39–3.54 (m, 2H), 4.78 (s, 1H). Exact Mass calcd. for $C_{13}H_{19}F_3O_4S$: 328.0956; found: 328.0949.

Vinyl triflate 21

This material was derived from the ketal ketone **13** (624 mg, 2.79 mmol) (reaction time 2 h). The entire reaction mixture was passed through a short column (5 × 4 cm) of silica gel (elution with Et_2O, 250 mL). Concentration of the combined eluate and flash chromatography (3.8 × 15 cm silica gel column, 17:3 petroleum ether – Et_2O) of the residual oil provided 835 mg (84%) of the vinyl triflate **21** as a white solid. Recrystallization (hexane–Et_2O) afforded white crystals (mp 80.0–81.5°C) that displayed ir (KBr): 3092, 1662, 1206, 1143 cm^{-1}; ^1H nmr (400 MHz) δ: 0.95 (s, 3H), 0.98 (s, 3H), 1.65–1.75 (m, 2H), 2.24–2.42 (m, 3H), 2.77–2.90 (m, 2H), 3.17–3.26 (br m, 1H), 3.46 (s, 2H), 3.48 (s, 2H), 5.59 (br s, 1H). Exact Mass calcd. for $C_{14}H_{19}F_3O_5S$: 356.0905; found: 356.0912.

Vinyl triflate 22

The ketone **14** (1.0 g, 4.42 mmol) was transformed into the vinyl triflate **22** (reaction time 2.5 h). Concentration (reduced pressure) of the reaction mixture, flash chromatography (4.5 × 15 cm column of silica gel, 9:1 petroleum ether – Et_2O) of the remaining material, and distillation (90–94°C/0.3 Torr) of the acquired oil afforded 1.15 g (72%) of the vinyl triflate **22**, a colorless oil that displayed ir (neat): 1674, 1210, 1144 cm^{-1}; ^1H nmr (400 MHz) δ: 0.95 (s, 3H), 0.99 (s, 3H), 1.22 (d, 3H J = 7 Hz), 1.92–2.22 (m, 6H), 2.81–2.91 (m, 1H), 3.45–3.52 (m, 4H), 5.88 (br t, 1H, J = 6 Hz). Exact Mass calcd. for $C_{14}H_{21}F_3O_5S$: 358.1061; found: 358.1065.

Vinyl triflate 23

To a well-stirred suspension of potassium hydride (~380 mg, ~9.5 mmol) in dry THF (16 mL) at room temperature was added a solution of the keto ester **15** (800 mg, 4.71 mmol) in dry THF (2 mL). The mixture was stirred for 1 h and then powdered $PhN(SO_2CF_3)_2$ (2.02 g, 5.65 mmol) was added in one portion. Stirring was continued for 16 h. Water was added and the mixture was extracted three times with Et_2O. The combined extracts were washed (brine), dried ($MgSO_4$), and concentrated. Flash chromatography (3.8 × 15 cm silica gel column, 4:1 petroleum ether – Et_2O) of the residual oil and distillation (75–78°C/0.3 Torr) of the acquired oil produced 1.17 g (82%) of the vinyl triflate **23**, a colorless oil that showed ir (neat): 1733, 1655, 1211, 1145 cm^{-1}; ^1H nmr (400 MHz) δ: 1.63–1.83 (m, 6H), 2.51–2.56 (m, 2H), 2.58–2.63 (m, 2H), 3.81 (s, 3H). Exact Mass calcd. for $C_{10}H_{13}F_3O_5S$: 302.0436; found: 302.0440.

General procedure for the preparation of α,β-unsaturated nitriles

Lithium cyanide, obtained from Morton Thiokol Inc. (Alfa Products), was dried at 40–50°C under reduced pressure (vacuum pump) for 2 h.

To a sample of dry lithium cyanide (2.0 equiv.) were added tetrakis(triphenylphosphine)palladium(0) (0.07 equiv.) and neat 12-crown-4 (0.07 equiv.). A solution of the vinyl triflate (1.0 equiv.) in dry benzene (5.6 mL per mmol of vinyl triflate) was added. The resultant mixture was stirred at room temperature until the reaction was determined to have reached completion (analyses by glc or tlc). In those cases in which the reaction was sluggish, additional amounts of $(Ph_3P)_4Pd$ (0.07 equiv.) were added periodically until the reaction was complete or nearly complete. Water (~1.5 mL per mmol of vinyl triflate used) was added and the mixture was stirred vigorously until no further effervescence occurred. The aqueous layer was separated and extracted three times with Et_2O. The combined organic extracts were washed (brine), dried ($MgSO_4$), and concentrated. Flash chromatography of the crude product on silica gel, along with distillation or crystallization, provided the desired product.

α,β-Unsaturated nitrile 24

The vinyl triflate **16** (4.81 g, 14.5 mmol) was converted into the nitrile **24** (reaction time 2 h). Flash chromatography (7.5 × 15 cm silica gel column, 7:3 petroleum ether – Et_2O) of the crude product gave 2.4 g (80%) of **24** as a white solid. Recrystallization (petroleum ether) provided white flakes (mp 72–73°C) that displayed ir (KBr): 2211, 1642, 1114 cm^{-1}; ^1H nmr (400 MHz) δ: 0.94 (s, 3H), 1.03 (s, 3H), 2.01 (t, 2H, J = 6 Hz), 2.32–2.39 (m, 2H), 2.50–2.55 (m, 2H), 3.47 (d, 2H, J = 11 Hz), 3.57 (d, 2H, J = 11 Hz), 6.44–6.48 (m, 1H). In decoupling experiments, irradiation at δ 2.32–2.39 (allylic protons vicinal to CN) changed the signals at 2.01, 2.50–2.55, and 6.44–6.48 to a singlet, a doublet (J = 4 Hz), and a triplet (J = 4 Hz), respectively; irradiation at δ 2.50–2.55 simplified the multiplet at 2.32–2.39 to a broad triplet (J = 6 Hz) and collapsed the signal at 6.44–6.48 to a broad singlet. In a nOe difference experiment, irradiation at δ 6.44–6.48 caused signal enhancement at 2.50–2.55; ^{13}C nmr (75.3 MHz) δ: 22.5 (−ve), 22.7 (−ve), 25.3, 26.8, 30.2, 35.4, 70.3, 95.3, 111.9, 119.0, 141.3 (−ve). In SINEPT experiments optimized for a $^3J_{C-H}$ of 7 Hz, irradiation at δ 3.52 (both pairs of OCH_2 hydrogens) gave strong polarization transfer through three-bond coupling to the quaternary ketal carbon (δ 95.3) and the ketal CH_2O carbon (δ 70.3), while irradiation at δ 6.46 (olefinic proton) gave strong polarization transfer through three-bond coupling to the quaternary ketal carbon (δ 95.3) and the nitrile carbon (δ 119.0). Exact Mass calcd. for $C_{12}H_{17}NO_2$: 207.1260; found: 207.1258.

α,β-Unsaturated nitrile 25

This substance was obtained from the vinyl triflate **17** (805 mg, 2.6 mmol) (reaction time 2 h). Flash chromatography (3.5 × 15 cm column of silica gel, 9:1 petroleum ether – Et_2O) of the crude product and distillation (120–126°C/0.3 Torr) of the acquired oil provided 432 mg (89%) of **25**, a colorless oil that showed ir (neat): 3086, 3035, 2213, 1641 cm^{-1}; ^1H nmr (400 MHz) δ: 0.95 (s, 3H), 1.34–1.67 (m, 3H), 1.80 (dd, 1H, J = 12, 4 Hz), 1.91–2.07 (m, 3H), 2.18–2.52 (m, 4H), 4.61 (s, 1H), 4.73 (s, 1H), 6.61–6.65 (m, 1H). In a nOe difference experiment, irradiation at δ 6.63 caused an increase in the intensity of the signal at 2.27–2.38 (allylic CH_2 protons); ^{13}C nmr (75.3 MHz) δ: 16.6 (−ve), 24.2, 25.2, 27.2, 31.5, 32.0, 37.4, 44.0 (−ve), 105.7, 115.7, 118.4, 144.8 (−ve), 154.8. In a SINEPT experiment optimized for a $^3J_{C-H}$ of 7 Hz, irradiation at 6.63 gave strong polarization transfer through three-bond coupling to the nitrile carbon (δ 118.4) and the tertiary angular carbon (δ 44.0). Exact Mass calcd. for $C_{13}H_{17}N$: 187.1361; found: 187.1362.

α,β-Unsaturated nitrile 26

The vinyl triflate **18** (35 mg, 0.113 mmol) was converted into the nitrile **26** in a reaction time of 2.5 h. Flash chromatography (0.7 × 8 cm silica gel column, 9:1 petroleum ether – Et_2O) of the crude product and distillation (103–110°C/0.3 Torr) of this material provided 18.4 mg (87%) of **26**, a colorless oil that displayed ir (neat): 3088, 3034, 2216, 1636 cm^{-1}; ^1H nmr (400 MHz) δ: 1.14 (s, 3H), 1.18–1.26 (m, 1H), 1.36–1.73 (m, 3H), 1.98–2.11 (m, 3H), 2.16–2.39 (m, 4H), 4.79 (s, 1H), 4.81 (s, 1H), 6.57 (t, 1H, J = 4 Hz); ^{13}C nmr (75.3 MHz) δ: 23.9, 24.3 (−ve), 25.6, 28.5, 29.3, 32.9, 37.3, 44.2 (−ve), 108.3, 117.2, 119.5, 143.8 (−ve). Irradiation at δ 6.57 in a SINEPT experiment optimized for a $^3J_{C-H}$ of 7 Hz gave a strong polarization transfer through three-bond coupling to the nitrile carbon (δ 119.5) and to the tertiary angular

carbon (δ 44.2). Exact Mass calcd. for $C_{13}H_{17}N$: 187.1361; found: 187.1355.

α,β-Unsaturated nitrile 27

This material was obtained from the vinyl triflate **19** (183 mg, 0.62 mmol) in a reaction time of 3 h. Flash chromatography (1.8 × 15 cm column of silica gel, 19:1 petroleum ether – Et_2O) of the crude product and distillation (100–103°C/0.3 Torr) of the acquired liquid provided 83.6 mg (78%) of the nitrile **27**, a colorless oil that showed ir (neat): 3047, 2221, 1640 cm^{-1}; ^1H nmr (400 MHz) δ: 0.98 (s, 3H), 1.22–1.36 (m, 1H), 1.46–1.75 (m, 4H), 1.78–1.86 (m, 1H), 2.15–2.28 (m, 4H), 5.57 (s, 1H), 6.48 (t, 1H, J = 5 Hz). Exact Mass calcd. for $C_{12}H_{15}N$: 173.1204; found: 173.1205.

α,β-Unsaturated nitrile 28

The vinyl triflate **20** (197 mg, 0.60 mmol) was converted into the nitrile **28** in a reaction time of 2 h. Flash chromatography (1.8 × 15 cm column of silica gel, 19:1 petroleum ether – Et_2O) of the crude product and distillation (113–118°C/0.3 Torr) of the acquired liquid provided 105 mg (85%) of the nitrile **28**, a colorless oil that exhibited ir (neat): 3082, 2217, 1641, 1604 cm^{-1}; ^1H nmr (400 MHz) δ: 0.97 (d, 6H, J = 6 Hz), 1.03 (d, 3H, J = 7 Hz), 1.95–2.11 (m, 2H), 2.07 (s, 3H), 2.40 (hextet, 1H, J = 7 Hz), 2.54 (dd, 1H, J = 20, 7 Hz), 3.40–3.55 (m, 2H), 4.85 (s, 1H). Exact Mass calcd. for $C_{13}H_{19}NO$: 205.1467; found: 205.1467.

α,β-Unsaturated nitrile 29

This material was derived from the vinyl triflate **21** (160 mg, 0.453 mmol). After a reaction time of 6.5 h, an additional amount of $(Ph_3P)_4Pd$ (0.07 equiv.) was added to the reaction mixture. The total reaction time was 20 h. Flash chromatography (1.8 × 15 cm silica gel column, 4:1 petroleum ether – Et_2O) of the crude material gave 80 mg (76%) of the nitrile **29** as a white solid. Recrystallization (petroleum ether) provided white flakes (mp 58–59°C) that displayed ir (KBr): 3064, 2216, 1615, 1116 cm^{-1}; ^1H nmr (400 MHz) δ: 0.97 (s, 6H), 1.65 (dd, 1H, J = 13, 8 Hz), 1.76 (dd, 1H, J = 13, 6 Hz), 2.24–2.45 (m, 3H), 2.80–2.93 (m, 2H), 3.30–3.38 (m, 1H), 3.41–3.52 (m, 4H), 6.49–6.53 (m, 1H). In a nOe difference experiment, irradiation at δ 6.51 caused enhancement of the resonance at 3.30–3.38 (angular allylic hydrogen). Exact Mass calcd. for $C_{14}H_{19}NO_2$: 233.1416; found: 233.1415.

α,β-Unsaturated nitrile 30

This substance was obtained from the vinyl triflate **22** (206 mg, 0.574 mmol) in a reaction time of 2 h. Flash chromatography (1.8 × 15 cm silica gel column, 7:3 petroleum ether – Et_2O) of the crude product and distillation (75–78°C/0.3 Torr) of the acquired oil provided 105 mg (78%) of the nitrile **30**, a colorless oil that showed ir (neat): 3035, 2213, 1625, 1120 cm^{-1}; ^1H nmr (400 MHz) δ: 0.95 (s, 3H), 0.98 (s, 3H), 1.26 (d, 3H, J = 7 Hz), 1.47–1.60 (m, 2H), 2.11–2.35 (m, 4H), 2.58–2.69 (m, 1H), 3.41–3.48 (m, 4H), 6.72–6.79 (m, 1H). In a nOe difference experiment, irradiation at δ 6.75 caused enhancement of the signal at 2.20–2.35. Exact Mass calcd. for $C_{14}H_{21}NO_2$: 235.1572; found: 235.1572.

α,β-Unsaturated nitrile 31

This material was derived from the vinyl triflate **23** (55.4 mg, 0.183 mmol). After reaction times of 1, 2, and 3 h, additional amounts of $(Ph_3P)_4Pd$ (0.07 equiv.) were added to the reaction mixture. The total reaction time was 4 h. Flash chromatography (0.7 × 15 cm silica gel column, 7:3 petroleum ether – Et_2O) of the crude product, followed by distillation (125–131°C/0.3 Torr) of the acquired oil, afforded 19.2 mg (59%) of the nitrile **31**, a colorless oil that displayed ir (neat): 2216, 1722, 1107 cm^{-1}; ^1H nmr (400 MHz) δ: 1.54–1.69 (m, 4H), 1.80–1.88 (m, 2H), 2.59–2.69 (m, 4H), 3.85 (s, 3H). Exact Mass calcd. for $C_{10}H_{13}NO_2$: 179.0946; found: 179.0945.

Acknowledgement

We are grateful to the Natural Sciences and Engineering Research Council of Canada for financial support and to the University of British Columbia for a Killam Predoctoral Fellowship (to F.F.F.).

1. A.J. Fatiadi. *In* The chemistry of the cyano group. *Edited by* Z. Rappoport. John Wiley and Sons, Inc., New York. 1970. pp. 1079–1091, 1109.
2. J.E. Baldwin, D.H.R. Barton, I. Dainis, and J.L.C. Pereira. J. Chem. Soc. (C), 2283 (1968).
3. M.R. Short. J. Org. Chem. **37**, 2201 (1972).
4. T. Holm. Acta Chem. Scand. **18**, 1577 (1964).
5. S. Takahashi, T. Kusumi, and H. Kakisawa. Chem. Lett. 515 (1979).
6. M. Oda, A. Yamamuro, and T. Watanabe. Chem. Lett. 1427 (1979).
7. K. Yamamura and S.-I. Murahashi. Chem. Lett. 4429 (1977).
8. Y. Sakakibara, N. Yadani, I. Ibuki, M. Sakai, and N. Uchino. Chem. Lett. 1565 (1982).
9. T. Funabiki, H. Hosomi, S. Yoshida, and K. Tarama. J. Am. Chem. Soc. **104**, 1560 (1982).
10. M. Prochazka and M. Siroky. Collect. Czech. Chem. Commun. **48**, 1765 (1983).
11. W.J. Scott and J.K. Stille. J. Am. Chem. Soc. **108**, 3033 (1986).
12. J.K. Stille. Angew. Chem. Int. Ed. Engl. **25**, 508 (1986).
13. W.J. Scott, G.T. Crisp, and J.K. Stille. Org. Synth. **68**, 116 (1990).
14. J.E. McMurry and W.J. Scott. Tetrahedron Lett. **24**, 979 (1983); W.J. Scott and J.E. McMurry. Acc. Chem. Res. **21**, 47 (1988).
15. E. Piers and F.F. Fleming. J. Chem. Soc. Chem. Commun. 756 (1989).
16. K. Takagi and Y. Sakakibara. Chem. Lett. 1957 (1989).
17. E. Piers and B.W.A. Yeung. J. Org. Chem. **49**, 4567 (1984). E. Piers, B.W.A. Yeung, and F.F. Fleming. Can. J. Chem. **71**, 280 (1993).
18. E. Piers and M. Winter. Liebigs Ann. Chem. 973 (1982).
19. E. Piers and V. Karunaratne. Can. J. Chem. **67**, 160 (1989).
20. E. Piers and R.W. Friesen. Can. J. Chem. **70**, 1204 (1992).
21. W.C. Still, M. Kahn, and A. Mitra. J. Org. Chem. **43**, 2923 (1978).
22. A.J. Bax. J. Magn. Reson. **57**, 314 (1984).
23. V. Farina and B. Krishnan. J. Am. Chem. Soc. **113**, 9585 (1991).
24. P.J. Stang, M.H. Kowalski, M.D. Schiavelli, and D. Longford. J. Am. Chem. Soc. **111**, 3347 (1989).
25. P.J. Stang and M.H. Kowalski. J. Am. Chem. Soc. **111**, 3356 (1989).

Can. J. Chem. Downloaded from www.nrcresearchpress.com by 203.198.23.82 on 09/08/12
For personal use only.

X-ray structures of adducts of 1,2,5-triphenylphosphole with dimethyl acetylenedicarboxylate: a confirmation, a revision, and a new structure[1]

MARTIN B. HOCKING[2] AND FRANCIES W. VAN DER VOORT MAARSCHALK
Department of Chemistry, University of Victoria, Victoria, BC V8W 3P6, Canada

Received October 1, 1992[3]

MARTIN B. HOCKING and FRANCIES W. VAN DER VOORT MAARSCHALK. Can. J. Chem. **71**, 1873 (1993).

Dimethyl acetylenedicarboxylate was reacted with 1,2,5-triphenylphosphole under mild conditions, and four products isolated. Regardless of conditions used, every preparation gave low yields of dimethyl 3,6-diphenylphthalate coincident with loss of the phosphorus bridge. NMR data and X-ray crystal structures are provided for a yellow, and a red, 2:1 adduct. The yellow adduct, tetramethyl 1,6,7-triphenyl-6-phospha(V)-tricyclo[7.3.1.$0^{1,9}$]nona-3,5,7-triene-2,3,4,5-tetracarboxylate **6**, crystallized in the triclinic space group $P\bar{1}$ (No. 2) with two molecules in the unit cell. Refinement (a = 11.259(1) Å, b = 12.947(3) Å, c = 13.784(3) Å, α = 112.25(2)°, β = 103.44(1)°, and γ = 101.80(1)°) converged at R = 0.0453 (R_w = 0.0453) for 537 parameters using 2880 reflections with $I > 2\sigma(I)$. The red adduct, trimethyl 1,2,5-triphenylphosphoranylidene-4-methoxycyclopent-2-ene-5-one-2,3,4-tricarboxylate, an exocyclic phosphorane **8**, crystallized in the monoclinic space group $P2_1/c$ (No. 14) with four molecules in the unit cell. Refinement of this structure (a = 13.233(5) Å, b = 15.712(5) Å, c = 17.191(7) Å, α = 90°, β = 110.35(4)°, and γ = 90°) converged at R = 0.0916 (R_w = 0.0937) for 400 parameters using 2052 reflections with $I > 2.5\sigma(I)$. Small amounts of a white or buff amorphous material, which could represent a polymeric product from the lost phosphorus bridge, were also obtained. Thermal rearrangement of the yellow adduct gave a colourless 6,5,3 tricyclic isomer **11**, possibly via the isomeric cyclopropyl derivative **15** or the nine-membered phosphonin **7**. The structure of **11** was confirmed by mild oxidation of the colourless rearrangement product to its P-oxide. This product, tetramethyl 2,3,6-triphenyl-2-phosphatricyclo[6.1.$0^{1,8}$.$0^{5,9}$]-2-oxonona-3,6-diene-1,7,8,9-tetracarboxylate **12**, was also colourless. It crystallized in the orthorhombic space group $Pbc2_1$ (No. 29) with four pairs of molecules in the unit cell. Refinement of this structure (a = 8.918(1) Å, b = 22.605(4) Å, and c = 30.169(6) Å) converged at R = 0.0747 (R_w = 0.0757) for 321 parameters using 3255 reflections with $I \geq 3\sigma(I)$. Unequivocal structures for these adducts and derivatives finally confirms, and establishes further understanding of, the complex reactions of the triphenylphosphole with dimethyl acetylenedicarboxylate.

MARTIN B. HOCKING et FRANCIES W. VAN DER VOORT MAARSCHALK. Can. J. Chem. **71**, 1873 (1993).

On a fait réagir l'acétylènedicarboxylate de diméthyle avec le 1,2,5-triphénylphosphole dans des conditions douces et on a isolé quatre produits. Quelles que soient les conditions utilisées, chaque préparation a conduit à de faibles rendements de 3,6-diphénylphtalate de diméthyle qui résulte de la perte du pont phosphoré. On rapporte les données RMN et les structures cristallines déterminées par diffraction des rayons X d'un adduit jaune et d'un adduit 2 : 1 qui est rouge. Les cristaux de l'adduit jaune, le 1,6,7-triphényl-6-phospha(V)-tricyclo[7.3.1.$0^{1,9}$]nona-3,5,7-trième-2,3,4,5-tétracarboxylate de tétraméthyle; **6**, sont tricliniques, groupe d'espace $P\bar{1}$ (No. 2) avec a = 11,259(1), b = 12,947(3) et c = 13,784(3) Å, α = 112,25(2)°, β = 103,44(1)° et γ = 101,80(1)° et deux molécules par motif. L'affinement de 537 paramètres provenant de 2880 réflexions avec $I > 2\sigma(I)$ converge à R = 0,0453 (R_w = 0,0453). Les cristaux de l'adduit rouge, le phosphorane exocyclique **8**, le 1,2,5-triphénylphosphoranylidène-4-méthoxycyclopent-2-èn-5-one-2,3,4-tricarboxylate de triméthyle, sont monocliniques, groupe d'espace $P2_1/c$ (No. 14) avec a = 13,233(5), b = 15,712(5) et c = 17,191(7) Å, α = 90°, β = 110,35(4)° et γ = 90° et quatre molécules par motif. L'affinement de 400 paramètres provenant de 2052 réflexions avec $I > 2\sigma(I)$ converge à R = 0,0916 (R_w = 0,0937). On a aussi isolé de faibles quantités d'un produit amorphe blanc ou coquille d'oeuf qui correspond peut-être à un polymère provenant de la perte du pont phosphoré. La transposition thermique de l'adduit jaune conduit à un isomère 6,5,3 tricyclique incolore, **11**, qui pourrait se former par le biais du dérivé cyclopropyle isomère **15** ou de la phosphonine à neuf chainons **7**. On a confirmé la structure du composé **11** par une oxydation douce du produit de réarrangement incolore en son P-oxyde. Les cristaux de ce produit, le 2,3,6-triphényl-2-phosphatricyclo[6.1.$0^{1,8}$.$0^{5,9}$]-2-oxonona-3,6-diène-1,7,8,9-tétracarboxylate de tétraméthyle, **12**, sont incolores et orthorhombiques, groupe d'espace $Pbc2_1$ (No. 29) avec a = 8,918(1), b = 22,605(4) et c = 30,169(6) Å et quatre paires de molécules par motif. L'affinement de 321 paramètres provenant de 3255 réflexions avec $I > 2\sigma(I)$ converge à R = 0,0747 (R_w = 0,0757). La détermination univoque des structures de ces adduits et de leurs dérivés élargit et confirme notre compréhension des réactions complexes du triphénylphosphole avec l'acétylènedicarboxylate de diméthyle.

[Traduit par la rédaction]

Introduction

The first reactions of 1,2,5-triphenylphosphole, **1** with dimethyl acetylenedicarboxylate gave only dimethyl 3,6-diphenylphthalate **3**, a cycloaddition occurring with concomitant extrusion of the phosphorus-containing group (1). Loss of the Ph—P bridge probably occurred via a reverse Diels–Alder reaction causing loss of an appropriate fragment in the manner first proposed by Alder and Rickert, and confirmed by Cope and others (2, 3). While this reaction provided a useful component of the structure confirmation for the first synthesis of this phosphole it was not particularly valuable synthetically (4). More potentially useful was the reaction conducted under inert atmosphere and room temperature conditions, when Hughes and Uaboonkul isolated the phthalate ester **3** as obtained earlier and, in addition, two adducts that retained the phosphorus moiety (5). They assigned the spiro-biphosphole structure **4** to the yel-

[1]Presented at the 11th Lakeland Heterocyclic Symposium, Grasmere, U.K., May 6–10th, 1993.

[2]Author to whom correspondence may be addressed.

[3]Revision received May 10, 1993.

Can. J. Chem. Downloaded from www.nrcresearchpress.com by 203.198.23.82 on 09/08/12
For personal use only.

TABLE 1. Selected ^{1}H NMR spectral data for phosphole adducts in deuteriochloroform

Compound	Ester methyls δ, ppm	Methine δ, ppm	Methine J, Hz	Vinyl proton(s) δ, ppm	Vinyl proton(s) J, Hz
Yellow 2:1 adduct, **6**	3.41 3.44 3.63 3.86	3.52 dd (cyclopropyl)	9.9 (P,H) 3.3 (H,H)	7.39	3.3 (H,H)
Rearranged yellow adduct, **11**	2.89 3.68 3.75 3.82	4.92 d (methine)	8.4 (H,H)	6.41 dd[b]	8.4 (P,H) 8.4 (H,H)
Oxide of rearrangement product, **12**	2.98 3.69 3.75 3.85	4.72 dd (methine)	1.8 (P,H)[a] 8.2	6.86 dd	8.2 (H,H) 30.8 (P,H)
Red 2:1 adduct, **8**	3.16 3.25 3.62 3.71				

[a]Uncertain assignment.
[b]Overlapping. Appears as triplet. ^{31}P decoupling reduces to doublet.

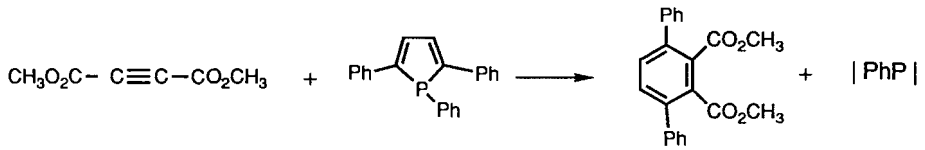

1 2 3

low 2:1 (ester to phosphole) adduct. An additional red crystalline product (mp 218–220°C (dec.)) was isolated and established to be a 4:1 adduct but without structural assignment (5). They also found that the yellow spiro-biphosphole could be rearranged thermally in chloroform to a colourless isomer initially formulated as **5**, and smoothly converted this to its P-oxide.

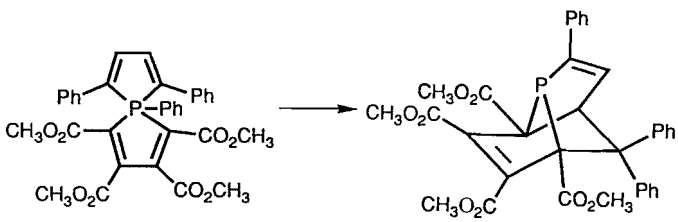

4 5

Later spectroscopic and synthetic tests by Waite and Tebby led to structural reassignments of the yellow 2:1 adduct to the tricyclic, ester-stabilized, alkylidene phosphorane structure **6**, and of its colourless rearrangement product to the phosphonin, a nine-membered cyclic phosphine **7** (6). These workers, who used freshly redistilled dimethyl acetylenedicarboxylate in their reactions, did not obtain any of the initially reported red adduct from their preparations.

With the current availability of higher frequency and pulsed NMR techniques not accessible to either of the previous groups, we sought to reexamine the well-reasoned though rather unusual structures assigned to the yellow 2:1 adduct and its colourless rearrangement product, and in addition to attempt to determine the structure of the red 4:1 adduct reported by the first group.

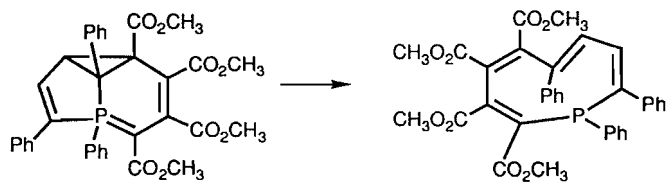

6 7

Results and discussion

Primary products

Reaction of 1,2,5-triphenylphosphole with dimethyl acetylenedicarboxylate at room temperature gave 6–10% yields of the colourless dimethyl 3,6-diphenylphthalate **3**, much lower than the 71% obtained under severe conditions (1, 2) but similar to the 9% previously obtained under mild conditions (5). This product was not examined further.

The yellow 2:1 acetylene ester:phosphole adduct was obtained in 31–35% yields, similar to that reported from the first preparation (5), and regardless of whether the reaction was conducted with neat reactants or in benzene, or whether or not freshly distilled ester or an inert atmosphere was used. Varied reaction conditions did, however, affect the yields of

Can. J. Chem. Downloaded from www.nrcresearchpress.com by 203.198.23.82 on 09/08/12
For personal use only.

TABLE 2. Selected ^{13}C NMR spectral data for phosphole adducts in deuteriochloroform

Compound	Quaternary C δ, ppm	Quaternary C J, Hz	Methine δ, ppm	Methine J, Hz	Ester methyls δ, ppm	Ester carbonyls δ, ppm
Yellow 2:1 adduct, **6**	34.8	83.0 (P,C)	34.5	7.8	50.5	165.7
	49.5	3.5 (P,C)			51.4	166.0
					52.3	166.6
					52.6	168.4
Rearranged yellow adduct, **11**	40.0	38.5 (P,C)			51.6	163.6
	49.5	20.5 (P,C)			51.9	166.2
	47.6	38.5 (P,C)			52.7	167.1
	53.0	—			53.1	168.8
Oxide of rearrangement product, **12**	45.5	75.1 (P,C)			52.0	163.2
	52.3	3.4 (P,C)	51.7	13.1	52.1	165.0[a]
	53.9	3.3 (P,C)			52.9	166.1
					53.3	167.5
Red 2:1 adduct, **8**	29.7				51.3	157.5[b]
					51.6	162.4
					52.3	166.0
					52.6	167.9

[a]Doublet. $J_{P,C}$ = 4.8 Hz.
[b]Doublet. $J_{P,C}$ = 13.1 Hz.

TABLE 3. Coupled and decoupled ^{31}P NMR spectral data for phosphole adducts

Compound	Shift, ppm (^1H decoupled)	Coupling constants, Hz (^1H coupled)		
Yellow 2:1 adduct, **6**	34.7	d,[a]	29.9	
Rearranged yellow adduct, **11**	−34.8	Quartet[b]	8.4	
Oxide of rearrangement product, **12**	12.6	d triplet[c]	12.7	(P,H_1)
			12.7	(P,H_2)
			30.8	(P,H_3)
Red 2:1 adduct, **8**	15.9			

[a]With some fine structure, several couplings in 3.3–3.6 Hz range.
[b]Apparent. Spacing 8.4, 8.4, 8.1 Hz; relative intensities 2.7:7.0:7.0:2.9.
[c]Overlapping. Appears as quintet of relative intensities 2:4:3:4:2.

other products, as discussed later. Elemental analysis confirmed that a 2:1 adduct had been obtained, and that this sample had crystallized almost mole for mole with acetone. Melting point and spectroscopic properties of this product were essentially in agreement with those previously reported (Tables 1–3).

However, despite the detailed analysis of high-frequency proton and phosphorus NMR spectra and decoupling experiments together with various pulsed NMR techniques, it was still not possible to unequivocally assign a structure to the yellow adduct.

An X-ray structure determination on a suitable single crystal of the yellow 2:1 adduct gave confirmation that structure 6, previously assigned by Waite and Tebby (6), was the correct assignment (Tables 4–8). Figure 1 gives an ORTEP representation of the molecular structure, including the resolved hydrogen atoms. Noteworthy in this rigid framework of fused six, five, and three-membered rings is the strain imposed on the C4—P—C1 and the P—C1—C2 bonds, which are each compressed to about 12° less than the normal sp^2 bond angles. The internal angles of the cyclopropane are all very close to the expected 60°. Bonds from the cyclopropane ring fusion to the rest of the molecule show little evidence of strain, except for an expansion of the C4—C5—C6 angle of about 12° from the normal sp^3. Carbon–carbon bond lengths correspond quite closely to those expected for isolated single and double bonds and show negligible evidence of any electron delocalization. The shortened phosphorane carbon to phosphorus bond, the presence of which had been previously demonstrated by protonation (6), is also clearly evident from this structure determination.

The yield of red adduct varied widely with reaction conditions, unlike the yield insensitivity found for the preparation of yellow adduct **6**. About 6.5% of a red crystalline adduct was obtained from room temperature reactions using neat reagents whether the acetylene ester was used as supplied, or was redistilled just before use. Conducting the reaction in benzene caused the isolated yield to drop to 0.4%. The red product obtained here, however, melted at 198–201°C without decomposition, rather than the 218–220°C (dec.) previously reported for a red adduct (5). It also was a 2:1 product (acetylene ester:phosphole), from NMR spectra and the X-ray crystal structure, rather than the 4:1 ad-

Can. J. Chem. Downloaded from www.nrcresearchpress.com by 203.198.23.82 on 09/08/12
For personal use only.

TABLE 4. Experimental crystallographic data measured at 20°C

Parameters	Yellow adduct, **6**	Red adduct, **8**	Colourless P-oxide, **12**
Crystal dimensions, mm	0.27 × 0.22 × 0.19	0.13 × 0.21 × 0.95	0.08 × 0.21 × 0.72
Molecular formula · Method used	$C_{34}H_{29}O_8P$ Elemental analysis Molecular ion from mass spectrum	$C_{34}H_{29}O_8P$ Molecular ion from mass spectrum	$C_{34}H_{29}O_9P$ Molecular ion from mass spectrum
Crystal system	Triclinic	Monoclinic	Orthorhombic
Space group	$P\bar{1}$ (no. 2) centrosymmetric	$P2_1/c$ (No. 14) centrosymmetric	$Pbc2_1$ (No. 29) noncentrosymmetric
Unit/ cell: *a*	11.259(1) Å	13.233(5) Å	8.918(1) Å
b	12.947(3) Å	15.712(5) Å	22.605(4) Å
c	13.784(3) Å	17.191(7) Å	30.169(6) Å
α	112.25(2)°	90.0°	90.0°
β	103.44(1)°	110.35(4)°	90.0°
γ	101.80(1)°	90.0°	90.0°
Cell volume, Å^3	1710.5	3351.2	6081.7
Z, molecules/cell	2	4	4 (pairs)
Asymmetric unit	1 molecule	1 molecule	2 molecules
Density: Calculated, g cm^{-3}	1.271	1.297	1.338
Measured, g cm^{-3} (by flotation)	1.260	1.263	1.340
Diffractometer	Nonius + PDP11	Picker 4-circle + PDP11/10	Nonius + PDP11
Radiation	Zr-filtered Mo K_α λ = 0.71069 Å	Zr-filtered Mo K_α λ = 0.71069 Å	Ni-filtered Cu K_α λ = 1.542 Å
Intensity measurements Number	2θ = 0.1°–45° 2880, $I > 2\sigma(I)$	2θ = 12°–36° 2052, $I > 2.5\sigma(I)$	2θ = 0°–130° 3255, $I > 3\sigma(I)$
Refinement method	SHELX-76, least squares[b]	SHELX-76, least squares[b]	SHELX-76, least squares[b]
Final *R* value	0.0453	0.0916	0.0747
Finally R_w	0.0453	0.0937	0.0757
Absorption coefficient μ, cm^{-1}	0.86	0.92	12.50

duct reported previously. At no time was the 4:1 adduct observed, despite the testing of a variety of reaction conditions and recovery techniques.

As with the yellow 2:1 adduct, it was possible to discern many of the principal structural features of the red adduct from the high-frequency NMR data (Tables 1–3), but it was still not possible to derive an unequivocal structure entirely from this information. An X-ray crystal structure determination established that this adduct was also a phosphorane, a phosphacyclopentadienylidene bonded to the α position of a stabilizing conjugated cyclopentenone, **8** (Fig. 2, and Tables 9–12). In this adduct the phosphole ring remains intact, as found previously in ylide preparations related to the testing of 1,2,5-triphenylphosphole as a phosphine for Wittig reactions (7). Carbon–carbon single bonds of the cyclopentenone involved in electron delocalization are foreshortened by about 0.1 Å as compared to the 1.53 and 1.57 Å of the single bonds not so involved (Table 6). The carbon–carbon single bonds in both the starting phosphole

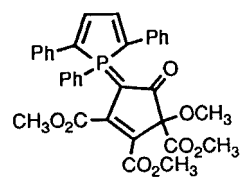

8

and the red adduct also are similarly foreshortened. However, there is no significant change in the lengths of the carbon–carbon single and double bonds in the phosphole ring of the adduct as compared to the starting phosphole, these being 1.38 and 1.47 Å, and 1.35 and 1.44 Å (8), respectively. All the sp^2 carbons of both five-membered rings have bond angles somewhat compressed from a normal noncyclic sp^2 carbon, the most pronounced being the compression for the P—C4—C3 angle, with a value of 106°. But

Can. J. Chem. Downloaded from www.nrcresearchpress.com by 203.198.23.82 on 09/08/12
For personal use only.

Can. J. Chem. Downloaded from www.nrcresearchpress.com by 203.198.23.82 on 09/08/12
For personal use only.

TABLE 5. Fractional atomic coordinates and temperature parameters for all non-hydrogen atoms of the yellow 2:1 adduct **6**[a,b]

Atom	x/a	y/b	z/c	U_{eq}[c]
P(1)	34422(9)	32733(8)	18764(7)	320(4)
O(1)	6092(2)	4721(2)	3500(2)	46(1)
O(2)	5981(3)	4116(2)	4809(2)	55(1)
O(3)	5361(2)	1581(2)	3676(2)	50(1)
O(4)	4269(2)	1997(2)	4869(2)	53(1)
O(5)	2696(2)	−139(2)	2842(2)	51(1)
O(6)	690(3)	−277(2)	1978(2)	61(2)
O(7)	443(2)	2181(2)	3366(2)	55(1)
O(8)	−911(2)	1502(2)	1628(2)	51(1)
C(1)	3311(3)	1975(3)	665(3)	36(2)
C(2)	2099(4)	1226(3)	246(3)	40(2)
C(3)	1151(4)	1604(3)	748(3)	39(2)
C(4)	1736(3)	2858(3)	1667(3)	33(2)
C(5)	1353(3)	1832(3)	1955(3)	34(2)
C(6)	2365(3)	1492(3)	2583(3)	32(2)
C(7)	3612(3)	2224(3)	3199(3)	33(2)
C(8)	4230(3)	3258(3)	3123(3)	33(2)
C(9)	5484(3)	4051(3)	3903(3)	38(2)
C(10)	7298(5)	5630(5)	4265(5)	72(3)
C(11)	4428(3)	1937(3)	4024(3)	37(2)
C(12)	6250(7)	1349(8)	4458(7)	91(4)
C(13)	1822(4)	299(3)	2451(3)	41(2)
C(14)	2189(6)	−1313(4)	2727(6)	71(3)
C(15)	160(4)	1788(3)	2265(3)	40(2)
C(16)	−636(6)	2255(7)	3760(5)	86(4)
C(21)	3874(3)	4594(3)	1729(3)	33(2)
C(22)	4236(4)	5713(3)	2623(3)	43(2)
C(23)	4394(4)	6685(4)	2422(4)	55(2)
C(24)	4196(4)	6573(4)	1359(4)	59(3)
C(25)	3814(4)	5479(4)	477(4)	56(2)
C(26)	3658(4)	4487(4)	653(3)	47(2)
C(31)	4417(4)	1756(3)	321(3)	37(2)
C(32)	4237(4)	795(4)	−681(3)	47(2)
C(33)	5282(5)	571(4)	−987(4)	56(3)
C(34)	6518(5)	1298(4)	−300(4)	58(3)
C(35)	6709(4)	2258(4)	675(4)	53(2)
C(36)	5679(4)	2490(4)	981(3)	44(2)
C(41)	1070(3)	3767(3)	1821(3)	39(2)
C(42)	248(4)	3771(4)	910(4)	54(2)
C(43)	−358(5)	4617(5)	1050(6)	81(4)
C(44)	−136(6)	5462(6)	2082(7)	93(4)
C(45)	691(7)	5484(5)	2988(6)	89(4)
C(46)	1305(4)	4635(4)	2878(4)	58(2)
O(50)	472(4)	1989(4)	6188(3)	116(3)
C(51)	1347(5)	1607(4)	6391(5)	79(3)
C(52)	1766(7)	960(6)	5457(6)	124(5)
C(53)	1909(8)	1744(9)	7527(6)	153(6)

[a]Estimated standard deviations are given in parentheses. Coordinates × 10^n where n = 5,4,4,4, for P,O,N,C Temperature parameters × 10^n where n = 4,3,3,3, for P,O,N,C.

[b]Hydrogen data have been deposited. See footnote 4.

[c]U_{eq} = the equivalent isotropic temperature parameter. $U_{eq} = 1/3\,\Sigma_i\Sigma_j U_{ij} a_i * a_j * (a_i \cdot a_j)$. $T = \exp - (8\pi^2 U_{iso} \sin^2 \theta/\lambda^2)$.

TABLE 6. Interatomic distances for all skeletal atoms for crystal structure of yellow adduct **6** (Å)[a]

Atoms	Distance	Atoms	Distance
C(1)—P(1)	1.815(3)	C(6)—C(5)	1.509(5)
C(4)—P(1)	1.807(4)	C(15)—C(5)	1.499(6)
C(8)—P(1)	1.750(4)	C(7)—C(6)	1.372(4)
C(21)—P(1)	1.781(4)	C(13)—C(6)	1.464(6)
C(2)—C(1)	1.343(5)	C(8)—C(7)	1.431(5)
C(31)—C(1)	1.473(6)	C(11)—C(7)	1.501(6)
C(3)—C(2)	1.469(6)	C(9)—C(8)	1.439(4)
C(4)—C(3)	1.514(4)	C(51)—O(50)	1.212(9)
C(5)—C(3)	1.527(6)	C(52)—C(51)	1.486(10)
C(5)—C(4)	1.534(6)	C(53)—C(51)	1.472(11)
C(41)—C(4)	1.495(6)		

[a]Estimated standard deviations are given in parentheses. Mean phenyl carbon – carbon distance and standard deviation was 1.380(7) Å, range 1.352 – 1.401(5–12) Å. Mean carbon–oxygen distances and standard deviations were C=O, 1.203(5); (CO)—O, 1.343(5); and O—CH_3, 1.448(8) Å.

none of the angles are significantly different from the expectation for a cyclopentane or cyclopentadiene.

A further product was isolated from these reactions that contained only 4 moles of dimethyl acetylenedicarboxylate and no phosphole or fragment thereof. This product, like the red adduct isolated here, was not observed previously from these reactions. Yields of 0.7–1.8% were obtained, the lowest recoveries being achieved in those reactions which started with freshly redistilled acetylene ester. This suggested that the isolated product may well have been present as an impurity in the starting ester, a suspicion confirmed by literature references to this occurrence (9–12). Our detailed NMR studies of this tetramer of dimethyl acetylenedicarboxylate, a cyclopropenyl derivative of oxynorbornadiene, **9**, are in accord with the published structure. We are further examining some evidence of isomerism observed in some of the high-frequency NMR spectra of this compound.

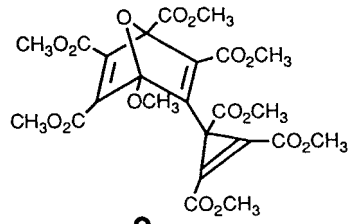

9

A white, or off-white, highly insoluble material **10** was also isolated from some of these reactions. It was not possible to fully characterize this amorphous powder because of the small amounts obtained, low solubility, and its intractibility, but later we speculate briefly on the possible nature of this material.

Secondary products

The yellow 2:1 adduct **6** was rearranged by the previous group to a colourless isomer formulated as **5**, in 23% yield, by boiling a chloroform solution of the yellow adduct under reflux for 4 h (5). Repetition of this procedure confirmed that the low yield was the result of poor conversion of starting material rather than diversion of starting material to other products via side reactions. We therefore tested the use of a higher boiling solvent, 1,2-dichloroethane for this procedure. At the 22° higher temperatures much improved yields of 72–88% of the purified rearrangement product were obtained. Most improvement was obtained with short-term (5 h) reflux, or with longer refluxing times under nitrogen. The melting point and other physical properties of this rearranged material were in good agreement with the previously published data (5, 6).

Significant changes were evident in the proton NMR of the rearrangement product as compared to that of the yellow adduct **6** (Tables 1–3). Neither of the methine protons

TABLE 7. Bond angles for all skeletal atoms of yellow adduct **6** (deg)[a]

Atoms	Angle	Atoms	Angle
C(4)—P(1)—C(1)	95.0(2)	C(15)—C(5)—C(3)	114.7(3)
C(8)—P(1)—C(1)	111.8(2)	C(15)—C(5)—C(4)	111.6(3)
C(8)—P(1)—C(4)	107.0(2)	C(15)—C(5)—C(6)	116.1(4)
C(21)—P(1)—C(1)	112.9(2)	C(7)—C(6)—C(5)	123.6(3)
C(21)—P(1)—C(4)	107.7(2)	C(13)—C(6)—C(5)	110.7(3)
C(21)—P(1)—C(8)	119.3(1)	C(13)—C(6)—C(7)	125.7(4)
C(2)—C(1)—P(1)	108.3(3)	C(8)—C(7)—C(6)	125.6(4)
C(31)—C(1)—P(1)	123.9(2)	C(11)—C(7)—C(6)	118.8(4)
C(31)—C(1)—C(2)	127.4(3)	C(11)—C(7)—C(8)	115.7(3)
C(3)—C(2)—C(1)	118.6(3)	C(7)—C(8)—P(1)	112.5(2)
C(4)—C(3)—C(2)	111.2(3)	C(9)—C(8)—P(1)	125.3(3)
C(5)—C(3)—C(2)	118.9(4)	C(9)—C(8)—C(7)	121.2(4)
C(5)—C(3)—C(4)	60.6(2)	C(22)—C(21)—P(1)	122.4(3)
C(3)—C(4)—P(1)	105.9(3)	C(26)—C(21)—P(1)	117.6(2)
C(5)—C(4)—P(1)	109.9(3)	C(32)—C(31)—C(1)	121.1(3)
C(5)—C(4)—C(3)	60.1(2)	C(36)—C(31)—C(1)	121.4(3)
C(41)—C(4)—P(1)	119.8(2)	C(42)—C(41)—C(4)	120.4(3)
C(41)—C(4)—C(3)	124.1(3)	C(46)—C(41)—C(4)	120.3(4)
C(41)—C(4)—C(5)	122.6(3)	C(52)—C(51)—O(50)	118.1(6)
C(4)—C(5)—C(3)	59.3(2)	C(53)—C(51)—O(50)	119.4(7)
C(6)—C(5)—C(3)	121.8(3)	C(53)—C(51)—C(52)	122.4(7)
C(6)—C(5)—C(4)	121.0(3)		

[a]Estimated standard deviations are given in parentheses. Mean phenyl carbon – carbon–carbon bond angle and standard deviation was 120.0(5)°, range 117.5°–121.4(3–7)°. Range of carbon–oxygen–carbon, and carbon–carbon–oxygen bond angles was 110.7°–125.2(3–4)°.

TABLE 8. Intermolecular distances of less than 3.4 Å from the crystal structure of yellow adduct **6**[a]

Atoms	Distance	Sym	T_x	T_y	T_z
C(9)···O(2)	3.358	−1	1	1	1
C(22)···O(4)	3.327	−1	1	1	1
C(23)···O(4)	3.262	−1	1	1	1
C(3)···O(6)	3.376	−1	0	0	0
C(10)···O(7)	3.368	−1	1	1	1
C(34)···O(8)	3.331	1	1	0	0
C(35)···O(8)	3.205	1	1	0	0
C(2)···O(8)	3.238	−1	0	0	0
C(25)···O(25)	3.487	−1	1	1	0
C(33)···O(31)	3.521	−1	1	0	0

[a]The symmetry positions are for the second atom. They are defined: 1 = x, y, z, A negative symmetry position denotes inversion. The translations (T) are applied finally.

was at high enough field to be assignable as a cyclopropyl hydrogen, and the higher field methine was now only proton coupled (and not to phosphorus). One of the methoxyls had also shifted ca. 0.5 ppm upfield. But again, despite detailed NMR studies, the structure could not be completely assigned with confidence. Even the quite reasonable assumption that there was no longer a cyclopropyl moiety in the rearranged product, from the loss of the resonance at the appropriate shift for cyclopropyl hydrogen in the ^{1}H NMR spectrum, would have turned out to be wrong, as will be seen shortly.

When checking the decoupled ^{31}P NMR spectrum of the rearranged product **5** after it had stood for a few days in deuteriochloroform, two ^{31}P resonances were noted, the new one probably that of the P oxide. A portion of the rearranged adduct was therefore oxidized and this product, the oxide of the rearrangement product, **12**, was purified and crystallized for X-ray work to ensure molecular stability of the crystal during data collection. The proton NMR spectrum of the oxide gave very similar methoxyl and methine shifts to those of the rearranged yellow adduct, except that the methine now showed a small coupling to phosphorus (Table 1). There was, however, a nearly 0.5 ppm downfield shift of the vinyl proton, explained by its proximity to the newly formed phosphoryl group, plus a sharply increased coupling of this proton to phosphorus, from 8 to 31 Hz. The same number and types of carbons were present in the two compounds from the ^{13}C NMR spectra. The only changes observed were in the P—C coupling constants, which were anticipated from the change in phosphorus oxidation state. The IR spectra of the two compounds were also very similar. For these reasons it is thought that the oxidation of the rearranged adduct under mild conditions only oxidized the phosphorus of the rearrangement product **11** and did not introduce any further skeletal rearrangements.

Two enantiomers of the oxide **12** crystallized together in the unit cell, so that the X-ray structure determination required resolution of the atom locations of both enantiomers (Fig. 3, Tables 13–16). The continued presence of a cyclopropyl component in the oxide **12** was unexpected. Although this product is still a fusion of six, five, and three-membered rings, as found in the yellow adduct **6**, quite complex steps are necessary to obtain the new bond locations. In the oxidized product **12** phosphorus is a component of only the six-membered ring rather than common to both the five and the six-membered rings, and the cyclopropyl no longer has any hydrogen substituents. Bond angles in the cyclopropane are all normal. Only the bond angles C3—C4—C5 and C4—C5—C6, C4—C3—C8, and C3—C8—C7 show any significant distortions caused by the

Can. J. Chem. Downloaded from www.nrcresearchpress.com by 203.198.23.82 on 09/08/12
For personal use only.

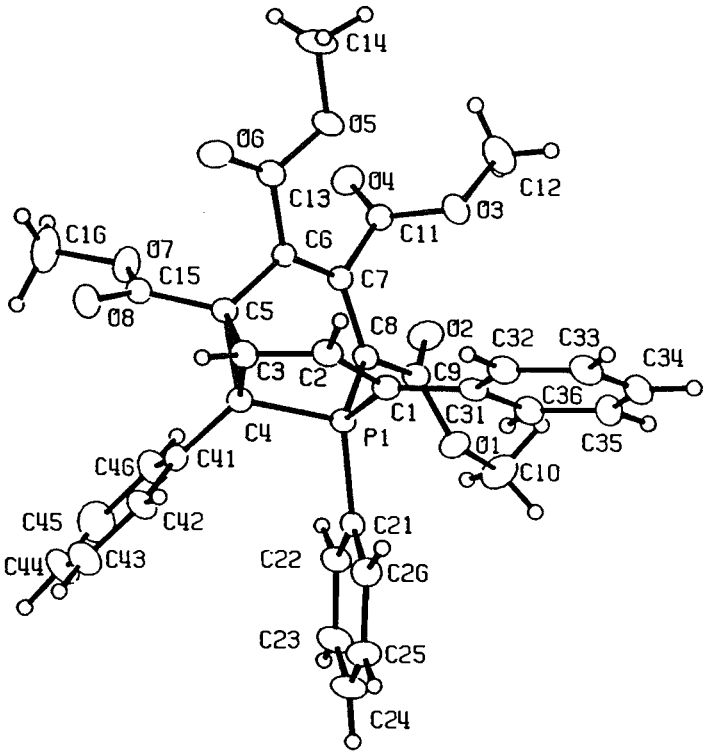

FIG. 1. ORTEP drawing of the crystal structure of the yellow 2:1 adduct **6**.

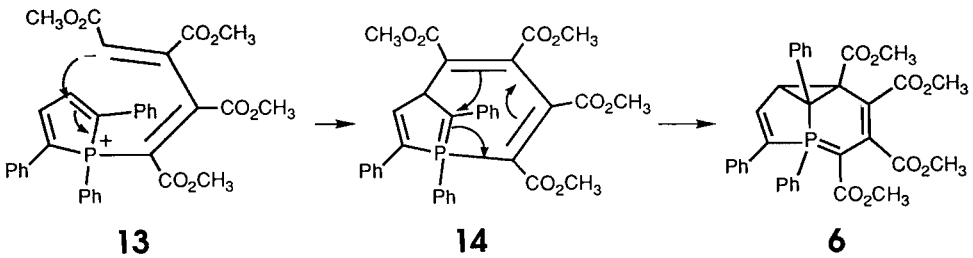

SCHEME 1. Proposed pathway to the yellow 2:1 adduct **6**.

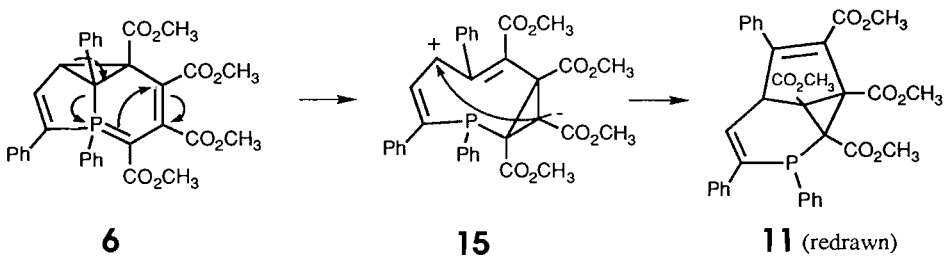

SCHEME 2. Possible pathway to the colourless rearrangement product **11**.

strained ring fusions. The first three are compressed 5°–8° from the normal and the last expanded to about the same extent. Bond lengths are all unremarkable.

Reaction and rearrangement pathways

The likely steps involved in the formation of the yellow 2:1 adduct **6** of dimethyl acetylenedicarboxylate to the phosphole **2** can be plausibly outlined as shown in Scheme 1. Provision of polar versus nonpolar conditions (neat reagents versus reaction in benzene) made a negligible difference to the yield, suggesting that none of the rates of the individual steps of initial formation of the zwitterion **13**, ring closure to structure **14** nor the following electrocyclic rearrangement to the product **6**, are overwhelmingly rate-determining. Our experimental observations are completely in accord with this reaction path, which is very similar to that previously proposed for this reaction by Waite and Tebby (6).

Scheme 2 gives a suggested pathway for rearrangement of adduct **6** to the colourless isomer **11**. It involves intermediate formation of a cyclopropane, which is retained in the final product. The carbocation formed is secondary and

Can. J. Chem. Downloaded from www.nrcresearchpress.com by 203.198.23.82 on 09/08/12
For personal use only.

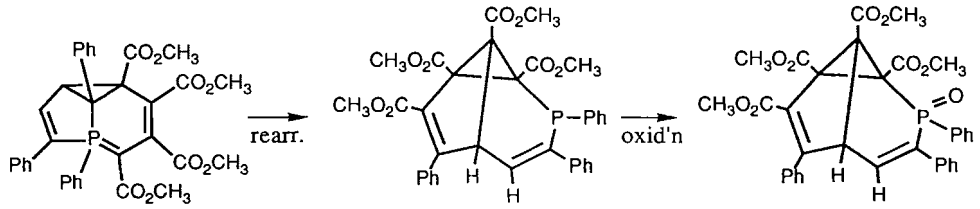

6 11 12

allylically stabilized and the anionic center required is stabilized via the adjacent carbonyl.

While it is possible to involve the *cis, cis, trans, cis* phosphonin **7** proposed by Waite and Tebby (6) in the pathway to the observed product **11**, this would require an additional step to reach structure **15**. Support is given to this possibility, however, from atom and electronic proximities noted from molecular models of this geometry as well as from the facile formation of the dihydrophosphindole oxide **17** from the *cis, cis, cis, trans* phosphonin oxide **16** (13). The presence of two benzo groups in the phosphonin prevents formation of the phosphindole (14).

A possible pathway to the red 2:1 adduct **8** from the acetylene ester plus phosphole is given in Scheme 3. Support for this suggestion is given by the pathway proposed for the related phosphorane product **20**, probably formed via similar steps from the acetylene ester and triphenylphosphine (15, 16). The structure of this final product was confirmed by an X-ray single crystal determination on the

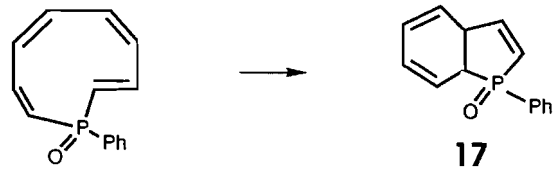

16 17

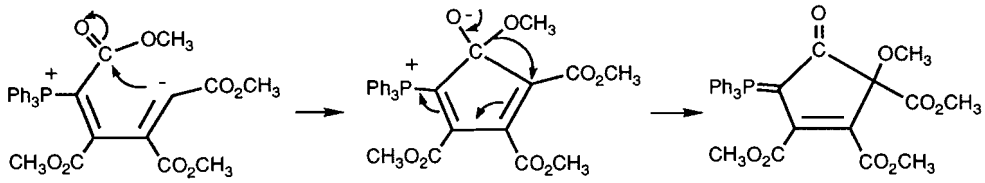

18 19 20

related compound **21** prepared from tri-*p*-tolylphosphine and the acetylene ester, which is also analogous to the red adduct **8** (17).

An equally plausible outcome from intermediate **18** on paper could have been the phosphole **22**, from direct closure of the zwitterion. As far as we are aware, however, compound **22** has not been isolated from any reaction of the acetylene ester with triphenylphosphine. It has at least been implicated in this reaction by the observed formation of another stable product, compound **23**, via migration of a phenyl group of intermediate **22** (18).

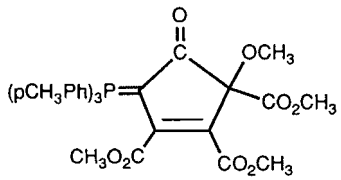

21

Compound **4**, analogous to **22**, was proposed as the structure of an adduct from the reaction of 1,2,5-triphenylphosphole with the acetylene ester. But we now know that it is not likely that spiro-biphosphole **4** forms from this interaction, even as an intermediate, since it would be difficult to sketch a plausible pathway from the spiro product to any of the adducts yet isolated from this reaction.

It should be mentioned here by way of a further precedent for the structure assigned to the red adduct that structure **25** has been proposed for a yellow 2:1 adduct of dimethyl acetylenedicarboxylate with the phosphindole **24**

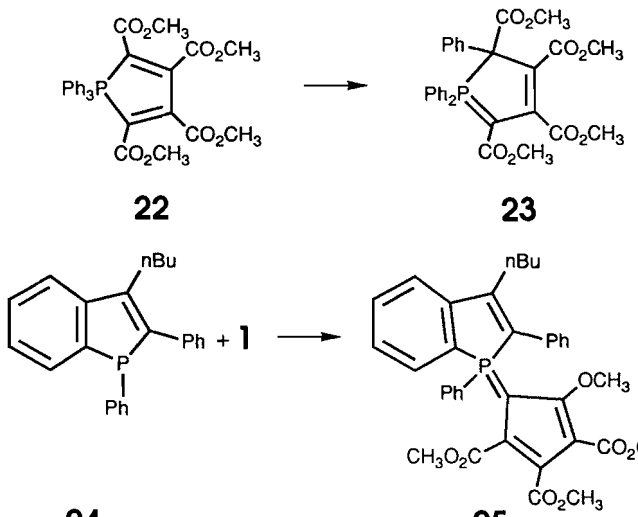

22 23

24 25

Can. J. Chem. Downloaded from www.nrcresearchpress.com by 203.198.23.82 on 09/08/12
For personal use only.

Can. J. Chem. Downloaded from www.nrcresearchpress.com by 203.198.23.82 on 09/08/12
For personal use only.

TABLE 9. Fractional atomic coordinates and temperature parameters of all non-hydrogen atoms of red 2:1 adduct **8**[a]

Atom	x/a	y/b	z/c	U_{eq}
P(1)	73782(23)	19558(17)	7314(17)	442(12)
C(1)	8667(9)	1424(7)	1238(7)	54(5)
C(2)	8679(10)	1215(7)	2016(7)	63(6)
C(3)	7705(10)	1450(7)	2229(7)	64(6)
C(4)	6901(9)	1866(7)	1615(6)	51(5)
C(21)	6504(8)	1294(7)	−82(7)	52(5)
C(22)	5618(9)	1674(8)	−726(7)	64(5)
C(23)	4879(10)	1143(8)	−1296(8)	76(6)
C(24)	5023(11)	272(10)	−1231(8)	76(7)
C(25)	5907(11)	−107(8)	−614(8)	70(6)
C(26)	6657(10)	414(7)	−30(7)	62(6)
C(31)	5854(9)	2142(7)	1603(7)	50(5)
C(32)	5236(10)	2721(7)	983(8)	68(6)
C(33)	4214(11)	2977(9)	975(9)	85(7)
C(34)	3800(12)	2652(10)	1547(11)	96(8)
C(35)	4427(13)	2066(11)	2157(9)	93(8)
C(36)	5454(10)	1804(7)	2172(7)	61(6)
C(41)	9491(9)	1321(7)	865(8)	59(6)
C(42)	9222(10)	1472(7)	18(7)	57(5)
C(43)	10060(11)	1378(8)	−336(8)	75(6)
C(44)	11087(12)	1139(9)	159(9)	86(8)
C(45)	11333(10)	989(8)	1008(9)	79(7)
C(46)	10542(10)	1078(8)	1386(8)	73(6)
C(5)	7504(8)	2998(6)	438(5)	41(4)
C(6)	7799(8)	3716(7)	961(6)	41(4)
C(7)	7871(8)	4442(7)	544(7)	51(5)
C(8)	7615(9)	4247(7)	−361(6)	46(5)
C(9)	7419(8)	3252(7)	−383(7)	45(5)
C(10)	9388(10)	4022(9)	−353(9)	88(7)
C(11)	6583(11)	4623(7)	−925(7)	52(6)
C(12)	4652(11)	4786(10)	−1159(10)	117(8)
C(13)	8139(10)	5268(8)	921(8)	62(6)
C(14)	8279(13)	6767(7)	714(10)	110(9)
C(15)	8026(10)	3681(7)	1862(7)	47(5)
C(16)	7260(11)	3921(8)	2935(7)	84(7)
O(1)	7264(6)	2840(4)	−1026(4)	56(3)
O(2)	8387(7)	4469(5)	−708(5)	66(4)
O(3)	5774(7)	4479(5)	−641(5)	81(4)
O(4)	6441(7)	4997(6)	−1545(6)	92(5)
O(5)	7985(7)	5907(5)	375(5)	75(4)
O(6)	8506(8)	5397(5)	1659(6)	94(5)
O(7)	7187(7)	3978(5)	2059(4)	65(4)
O(8)	8821(7)	3398(5)	2354(5)	75(4)
C(51)	1244(20)	3765(17)	2010(16)	211(10)′
C(52)	1330(27)	3412(19)	2919(22)	313(16)′
O(53)	2082(23)	4336(17)	2376(19)	399(15)′

[a]Estimated standard deviations are given in parentheses. Coordinates × 10[n] where n = 5,4,4,4, for P,O,N,C. Temperature parameters × 10[n] where n = 4,3,3,3, for P,O,N,C.

[b]U_{eq} = the equivalent isotropic temperature parameter. $U_{eq} = 1/3\ \Sigma_i\Sigma_j U_{ij} a_i * a_j * (a_i \cdot a_j)$. Primed values indicate that U_{iso} is given. $T = \exp - (8\pi^2 U_{iso} \sin^2 \theta/\lambda^2)$.

TABLE 10. Interatomic distances for all skeletal atoms from the crystal structure of the red adduct **8** (Å)[a]

Atoms	Distance	Atoms	Distance
C(1)—P(1)	1.826(11)	C(9)—C(5)	1.434(16)
C(4)—P(1)	1.843(13)	C(7)—C(6)	1.368(16)
C(21)—P(1)	1.802(10)	C(15)—C(6)	1.472(15)
C(5)—P(1)	1.738(10)	C(8)—C(7)	1.503(16)
C(2)—C(1)	1.371(18)	C(13)—C(7)	1.440(17)
C(41)—C(1)	1.454(20)	C(9)—C(8)	1.582(15)
C(3)—C(2)	1.504(20)	C(11)—C(8)	1.495(15)
C(4)—C(3)	1.375(14)	O(2)—C(8)	1.395(16)
C(31)—C(4)	1.445(18)	O(1)—C(9)	1.236(14)
C(6)—C(5)	1.411(14)		

[a]Estimated standard deviations are given in parentheses. Mean phenyl carbon – carbon distance and standard deviation was 1.405(19) Å, range 1.370–1.446(14–23) Å. Mean carbon–oxygen distances and standard deviations were C=O, 1.188(15); (CO)—O, 1.345(17); and O—CH_3, 1.488(15) Å.

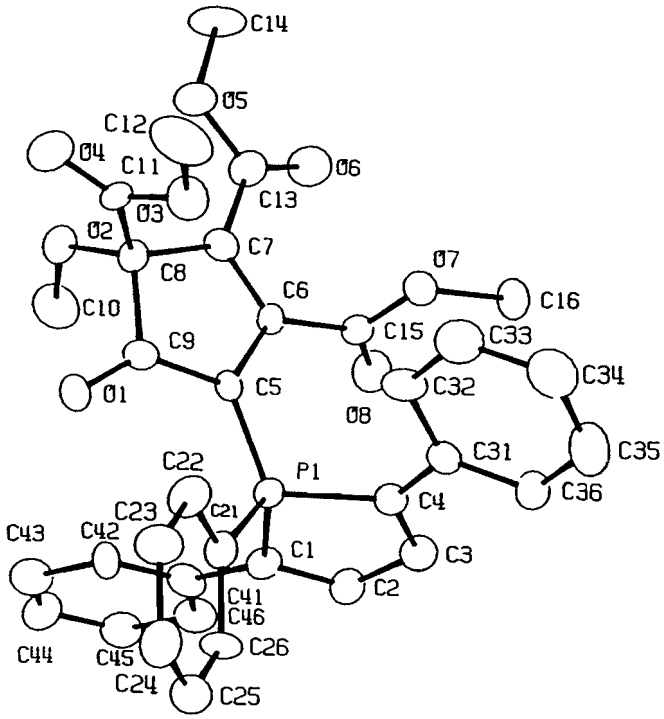

FIG. 2. ORTEP drawing of the crystal structure of the red 2:1 adduct **8**.

(19). It was suggested that the observed loss of the atom of oxygen in the formation of **25** occurred via an intermediate oxirane rearrangement product.

Finally, a brief speculation on the nature of the white or buff, highly insoluble, amorphous powder that was also isolated from some of the phosphole – acetylene ester reactions. This is quite possibly poly(phenylphosphinidene), $(C_6H_5P)_n$, or an oxidized version of this, $(C_6H_5P)_n(C_6H_5PO)_m$, formed from the 1:1 acetylene adduct that lost the phosphorus bridge to yield dimethyl 3,6-diphenylphthalate. Or it could be a copolymer of the phosphorus fragment with some incorporation of acetylene ester $(C_6H_5P)_n(CH_3O_2C\text{-}C{\equiv}C\text{-}CO_2CH_3)_m$, since the NMR shows the presence of ester methyl. In the absence of sufficient material for full characterization of this product these possibilities could not be better established. However, support for these suggestions is obtained from the reported isolation of poly(phenylphosphinidene oxide) from an analogous reaction of pentaphenylphosphole oxide with benzyne (20).

Experimental

Infrared spectra were obtained on KBr pellets scanned on a Perkin Elmer model 1330 instrument calibrated with polystyrene film.

TABLE 11. Bond angles for all skeletal atoms of the red adduct **8** (deg)[a]

Atoms	Angle	Atoms	Angle
C(4)—P(1)—C(1)	95.9(5)	C(26)—C(21)—P(1)	118.8(7)
C(21)—P(1)—C(1)	110.3(5)	C(6)—C(5)—P(1)	127.0(8)
C(21)—P(1)—C(4)	106.4(5)	C(9)—C(5)—P(1)	124.5(8)
C(5)—P(1)—C(1)	113.7(5)	C(9)—C(5)—C(6)	108.3(9)
C(5)—P(1)—C(4)	114.0(5)	C(7)—C(6)—C(5)	112.7(9)
C(5)—P(1)—C(21)	114.8(5)	C(15)—C(6)—C(5)	123.4(10)
C(2)—C(1)—P(1)	105.5(9)	C(15)—C(6)—C(7)	123.8(10)
C(41)—C(1)—P(1)	124.0(9)	C(8)—C(7)—C(6)	109.9(9)
C(41)—C(1)—C(2)	130.4(10)	C(13)—C(7)—C(6)	124.5(11)
C(3)—C(2)—C(1)	117.3(10)	C(13)—C(7)—C(8)	125.5(11)
C(4)—C(3)—C(2)	115.4(11)	C(9)—C(8)—C(7)	101.7(9)
C(3)—C(4)—P(1)	105.9(10)	C(11)—C(8)—C(7)	114.6(10)
C(31)—C(4)—P(1)	124.5(8)	C(11)—C(8)—C(9)	105.6(8)
C(31)—C(4)—C(3)	129.5(12)	C(8)—C(9)—C(5)	107.2(9)
C(22)—C(21)—P(1)	119.4(9)		

[a]Estimated standard deviations are given in parentheses. Mean phenyl carbon – carbon–carbon bond angle and standard deviation was 120.0(12)°, range 117.1°–122.9(9–16)°. Range of carbon–oxygen–carbon and carbon–carbon–oxygen bond angles was 105.3°–124.9(8–14)°.

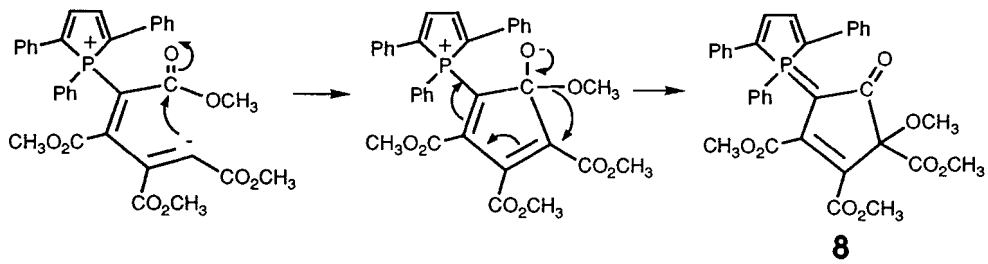

8

SCHEME 3. Pathway to the red 2:1 adduct **8** from 1,2,5-triphenylphosphole and dimethyl acetylenedicarboxylate.

TABLE 12. Intermolecular distances of less than 3.4 Å from the crystal structure of the red adduct **8** (Å)[a]

Atoms	Distance	Sym	T_x	T_y	T_z
O(53)···C(2)	3.399	2	1	0	0
O(53)···C(3)	3.383	2	1	0	0
O(1)···C(36)	3.238	−2	0	1	0
O(6)···C(46)	3.329	2	2	0	0
O(7)···C(12)	3.078	−1	1	1	0
O(1)···C(16)	3.292	−2	0	1	0
O(53)···O(2)	3.300	−1	1	1	0
O(53)···O(4)	2.983	−1	1	1	0
O(52)···O(8)	3.118	1	−1	0	0

[a]The symmetry positions are for the second atom. They are defined: $2 = -x, \frac{1}{2} + y, \frac{1}{2} - z$, A negative symmetry position denotes inversion. The translations (T) are applied finally.

Where useful, absorptions have been noted thus: s = strong, m = medium, w = weak, b = broad. UV spectra were obtained on a Philips PU 8740 UV/VIS spectrophotometer. Routine NMR spectra were recorded on a Perkin Elmer R-12 60 MHz instrument using solutions in deuteriochloroform at room temperature, unless otherwise specified. More detailed NMR experiments were performed on a Bruker WM 250 instrument, or, particularly for optimum resolution of coupled ^{31}P spectra, at 145.78 MHz on a Bruker AMX 360 spectrometer. Decoupling, nuclear Overhauser effect, or DEPT experiments were conducted wherever necessary to aid in assignments. Melting points were conducted on a Reichert type 7905 hot stage microscope or on a Gallenkamp model MF-370 Kofler aluminum block apparatus and are uncorrected. Mass spectra were determined on a Finnigan 3300 GC/MS system. Elemental analysis was by Canadian Microanalytical Service Ltd., Vancouver.

Reaction of 1,2,5-triphenylphosphole with neat dimethyl acetylenedicarboxylate

The finely ground phosphole (2.04 g; 6.52 mmol) was placed in a 100 mL round bottom flask fitted with a septum and flushed with oxygen-free nitrogen for 10 min. Dimethyl acetylenedicarboxylate (as supplied, Aldrich), 20 mL (163 mmol), was added via a syringe, with stirring. The initially yellow solution became red during 1 h, and then gradually turned dark brown.

After stirring the reaction mixture for 2 days at room temperature under nitrogen, it was filtered to recover 207 mg of white crystals, mp 183–186°C, identified as dimethyl 3,6-diphenylphthalate **3** by melting point and ^1H NMR (60 MHz), 7.5–7.0 ppm (multiplet, 12H), 3.6 (singlet, 6H). Filtration of the mother liquor after standing a further 2 days, no longer under nitrogen, gave a further 1.43 g of orange crystals. A portion of this recrystallized from ethanol, ethanol–chloroform, and then 100% ethanol gave 0.56 g of yellow crystals, mp 159–161°C without decomposition. This was identified from the X-ray structure determination as tetramethyl 1,6,7-triphenyl-6-phospha(V)tricyclo[7.3.1.$0^{1,9}$]nona-3,5,7-triene-2,3,4,5-tetracarboxylate, the yellow adduct **6**. ^1H NMR (250 MHz) ppm: aromatic plus one vinyl proton 6.6–7.5 (16H), ester methyl resonances at 3.41 (3H), 3.44 (3H), 3.63 (3H), 3.86 (3H), and one methine resonance as a doublet of doublets centered at 3.52 ppm. ^{13}C NMR (250 MHz) ppm: carbonyl carbons 168.4, 166.6, 166.0, 165.7; ester methyl carbons, 52.6, 52.3, 51.4, 50.5; methine carbon doublet centered at 34.5, J_{PC} 7.8 Hz; quaternary carbons, doublet centered at 34.8, J_{PC} 83.0 Hz; 49.5, J_{PC} 3.5 Hz; peak positions (relative intensities) for aromatic and olefinic carbons, some overlap and some coupled to phosphorus 146.1

Can. J. Chem. Downloaded from www.nrcresearchpress.com by 203.198.23.82 on 09/08/12
For personal use only.

Can. J. Chem. Downloaded from www.nrcresearchpress.com by 203.198.23.82 on 09/08/12
For personal use only.

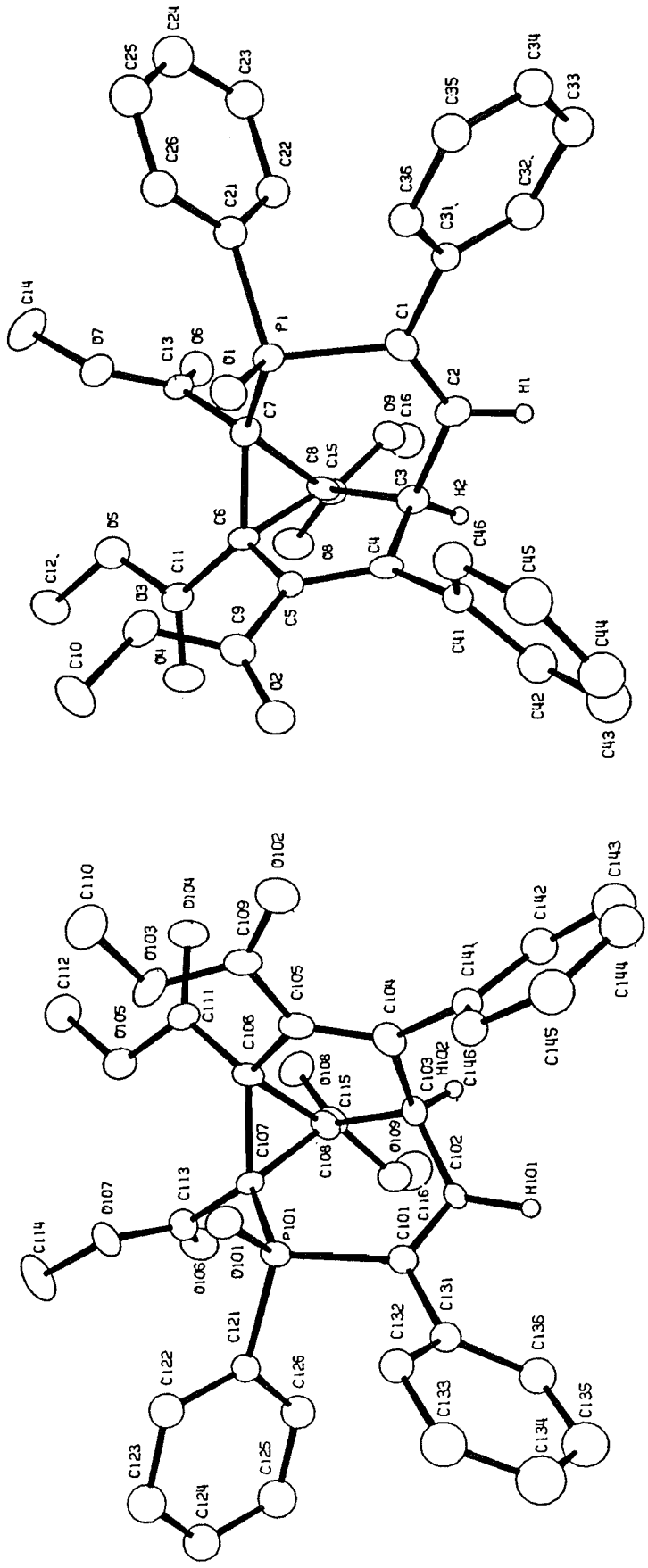

FIG. 3. ORTEP drawings of the two enantiomers of the oxide of the rearrangement product **12**.

Can. J. Chem. Downloaded from www.nrcresearchpress.com by 203.198.23.82 on 09/08/12
For personal use only.

TABLE 13. Fractional atomic coordinates and temperature parameters for the two enantiomers of the oxide of the rearrangement product **12**[a]

Atom	x/a	y/b	z/c	U_{eq}[b]
P(1)	19170(1)	10300(1)	0(1)	331(8)
P(101)	30634(30)	−24677(11)	−26720(9)	306(7)
O(1)	1116(8)	932(3)	413(2)	45(2)
O(2)	−291(9)	−939(3)	482(3)	52(2)
O(3)	−1599(9)	−138(3)	263(3)	51(2)
O(4)	−1461(9)	−595(3)	−680(3)	53(2)
O(5)	−1702(9)	325(3)	−899(2)	48(2)
O(6)	842(8)	1196(4)	−1187(2)	47(2)
O(7)	−649(9)	1433(3)	−608(3)	48(2)
O(8)	1093(9)	−136(3)	−1419(3)	53(2)
O(9)	3350(8)	260(3)	−1324(2)	40(2)
C(1)	3892(11)	756(5)	0(3)	37(2)
C(2)	4244(13)	258(4)	−208(3)	40(2)
C(3)	3120(12)	−146(4)	−414(3)	34(2)
C(4)	2236(11)	−436(4)	−39(3)	33(2)
C(5)	756(10)	−288(4)	−52(3)	27(2)
C(6)	391(11)	74(4)	−455(3)	30(2)
C(7)	1138(11)	684(4)	−490(3)	33(2)
C(8)	1914(12)	145(4)	−690(3)	32(2)
C(9)	−403(12)	−500(5)	256(3)	39(2)
C(10)	−2870(13)	−325(6)	547(4)	57(3)
C(11)	−1011(12)	−110(5)	−691(3)	38(2)
C(12)	−3080(15)	164(6)	−1143(5)	65(3)
C(13)	446(12)	1126(4)	−817(3)	31(2)
C(14)	−1459(16)	1875(6)	−891(5)	76(3)
C(15)	2056(12)	85(4)	−1186(3)	34(2)
C(16)	3656(14)	173(5)	−1794(4)	53(2)
C(21)	2192(12)	1826(5)	−137(4)	43(2)′
C(22)	3134(13)	1983(5)	−472(4)	46(2)′
C(23)	3364(14)	2601(6)	−567(4)	58(3)′
C(24)	2567(15)	3002(6)	−304(5)	71(3)′
C(25)	1669(15)	2835(6)	35(5)	69(3)′
C(26)	1460(13)	2230(5)	131(4)	49(3)′
C(31)	5003(11)	1123(4)	256(3)	29(2)′
C(32)	6436(14)	1184(5)	91(4)	54(3)′
C(33)	7549(14)	1518(6)	343(4)	60(3)′
C(34)	7071(13)	1795(5)	740(4)	52(3)′
C(35)	5638(14)	1740(5)	901(4)	51(3)′
C(36)	4579(12)	1403(5)	639(4)	41(2)′
C(41)	2975(12)	−755(4)	329(3)	34(2)′
C(42)	3651(14)	−1322(6)	232(4)	57(3)′
C(43)	4300(16)	−1643(6)	574(5)	68(3)′
C(44)	4257(16)	−1427(6)	994(5)	71(3)′
C(45)	3741(16)	−862(7)	1092(5)	77(3)′
C(46)	3069(14)	−504(5)	748(4)	52(3)′
H(1)	530(5)	7(3)	−21(3)	5(1)′
H(2)	371(5)	−36(3)	−63(3)	5(1)′
O(101)	3992(8)	−2400(3)	−3070(2)	43(2)
O(102)	5128(10)	−453(4)	−3161(3)	69(2)
O(103)	6435(9)	−1251(4)	−2962(3)	58(2)
O(104)	6387(10)	−768(3)	−2011(3)	58(2)
O(105)	6684(8)	−1715(4)	−1780(3)	54(2)
O(106)	4317(9)	−2621(3)	−1495(3)	55(2)
O(107)	5733(8)	−2812(3)	−2085(2)	46(2)
O(108)	3908(8)	−1276(4)	−1244(3)	55(2)
O(109)	1642(8)	−1696(3)	−1333(2)	44(2)
C(101)	1174(11)	−2199(4)	−2699(3)	34(2)
C(102)	766(11)	−1698(4)	−2486(3)	31(2)
C(103)	1848(11)	−1288(4)	−2250(3)	34(2)
C(104)	2675(12)	−961(5)	−2613(3)	40(2)
C(105)	4122(12)	−1102(4)	−2615(3)	38(2)
C(106)	4578(12)	−1481(4)	−2221(3)	34(2)
C(107)	3885(10)	−2113(4)	−2175(3)	30(2)
C(108)	3090(12)	−1578(4)	−1972(3)	35(2)
C(109)	5248(13)	−891(5)	−2946(4)	44(2)
C(110)	7621(15)	−1077(7)	−3270(5)	79(3)
C(111)	5948(12)	−1281(4)	−1995(4)	38(2)
C(112)	7972(14)	−1537(6)	−1518(4)	60(3)
C(113)	4660(12)	−2536(5)	−1875(3)	39(2)
C(114)	6599(16)	−3231(6)	−1824(5)	76(3)
C(115)	2990(13)	−1508(4)	−1475(4)	40(2)
C(116)	1345(15)	−1597(6)	−870(4)	61(3)
C(121)	2804(11)	−3223(4)	−2507(3)	35(2)′
C(122)	3717(13)	−3650(5)	−2710(4)	51(3)′
C(123)	3439(15)	−4263(6)	−2600(5)	62(3)′
C(124)	2357(14)	−4406(6)	−2305(4)	58(3)′
C(125)	1472(15)	−3985(6)	−2087(4)	65(3)′
C(126)	1722(13)	−3388(5)	−2191(4)	51(3)′
C(131)	150(11)	−2545(5)	−2985(3)	36(2)′
C(132)	742(12)	−2807(5)	−3365(4)	44(2)′
C(133)	−282(16)	−3125(6)	−3655(5)	74(3)′
C(134)	−1830(18)	−3119(7)	−3569(6)	90(4)′
C(135)	−2373(16)	−2839(7)	−3207(5)	80(3)′
C(136)	−1407(14)	−2561(5)	−2886(4)	53(3)′
C(141)	1793(12)	−607(4)	−2940(3)	37(2)′
C(142)	1091(13)	−93(5)	−2794(4)	52(3)′
C(143)	347(15)	269(6)	−3113(5)	70(3)′
C(144)	216(15)	89(6)	−3548(5)	68(3)′
C(145)	806(16)	−442(6)	−3681(5)	73(3)′
C(146)	1667(13)	−784(5)	−3377(4)	47(3)′
H(101)	−39(5)	−160(4)	−252(3)	6(1)′
H(102)	135(5)	−103(3)	−209(3)	4(1)′

[a]Estimated standard deviations are given in parentheses. Coordinates × 10^n where n = 5,4,4,4, for P,O,N,C Temperature parameters × 10^n where n = 4,3,3,3, for P,O,N,C.

[b]U_{eq} = the equivalent isotropic temperature parameter. $U_{eq} = 1/3\ \Sigma_i\Sigma_j U_{ij} a_i * a_j * (a_i \cdot a_j)$. Primed values indicate that U_{iso} is given. $T = \exp - (8\pi^2 U_{iso} \sin^2 \theta/\lambda^2)$.

(3.8), 145.7 (3.7), 133.0 (12.6), 132.8 (9.2), 131.8 (2.7), 131.4 (1.9), 131.2 (2.2), 131.0 (1.5), 130.1 (5.8), 129.5 (6.9), 129.12 (17.5), 129.05 (10.2), 128.6 (7.4), 128.2 (13.4), 128.0 (14.7), 126.9 (9.6), 126.8 (7.4), 120.0 (1.3), 118.5 (1.2). A combined total of 1.203 g of **6** was recrystallized twice more from acetone and dried in vacuo for an analytical sample. Anal. (adduct cocrystallized with 0.74-mol of acetone, determined by integrated 60 MHz ^{1}H NMR) calcd. for $C_{34}H_{29}PO_8 \cdot 0.74\ C_3H_6O$: C 68.02, H 5.27, P 4.84%; found: C 67.87, H 5.16, P 3.77%. Mass spectrum, methane CI, 200°C probe temp. (relative intensity), calcd. for $C_{34}H_{29}O_8P$: 596; found: M + 1, 597(100); M + 29, 625(15); M + 41, 637(6).

Further recrystallizations of the yellow adduct **6** from acetone and 95% ethanol produced X-ray quality crystals, mp 167–169°C. UV (95% EtOH) λ_{max} nm (log ϵ): 202 (4.77), 225 (4.47), 269 (4.27), 349 (4.00), 392 (3.78). IR (KBr) cm^{-1}: 3060w, 2950w, 1735s, 1700w, 1680m, 1650s, 1635m, 1500m, 1430m, 1340m, 1310m, 1280m, 1235s, 1210s, 1140m, 1110m, 1065w, 760m, 700m, 695m.

The residual mother liquors were combined and chromatographed on 40–140 mesh silica gel (Bakersil, 128 g) in a 4 cm diameter column. Rechromatography of combined similar fractions (from TLC tests) on Davisil 62 silica gel (60–200 mesh) enabled a further 99 mg of yellow crystals of **3** and a total of 255 mg of red crystals of impure adduct **8** to be recovered. Recrystallization of the red adduct twice more from acetone gave pure material, mp 198–201°C.

TABLE 14. Interatomic distances for all skeletal atoms of the two enantiomers of the oxide of the rearrangement product **12** (Å)[a]

Atoms	Distance	Atoms	Distance
O(1)—P(1)	1.454(7)	C(11)—C(6)	1.497(14)
C(1)—P(1)	1.867(10)	C(8)—C(7)	1.526(14)
C(7)—P(1)	1.810(9)	C(13)—C(7)	1.534(13)
C(21)—P(1)	1.862(11)	C(15)—C(8)	1.509(13)
O(101)—P(101)	1.467(7)	C(102)—C(101)	1.352(13)
C(101)—P(101)	1.793(10)	C(131)—C(101)	1.480(14)
C(107)—P(101)	1.850(10)	C(103)—C(102)	1.517(14)
C(121)—P(101)	1.794(10)	C(104)—C(103)	1.514(14)
C(2)—C(1)	1.328(14)	C(108)—C(103)	1.535(14)
C(31)—C(1)	1.505(14)	C(105)—C(104)	1.330(15)
C(3)—C(2)	1.489(15)	C(141)—C(104)	1.493(14)
C(4)—C(3)	1.527(14)	C(106)—C(105)	1.519(14)
C(8)—C(3)	1.511(14)	C(109)—C(105)	1.496(15)
C(5)—C(4)	1.363(13)	C(107)—C(106)	1.563(13)
C(41)—C(4)	1.479(14)	C(108)—C(106)	1.541(15)
C(6)—C(5)	1.502(13)	C(111)—C(106)	1.470(14)
C(9)—C(5)	1.469(14)	C(108)—C(107)	1.530(13)
C(7)—C(6)	1.535(13)	C(113)—C(107)	1.489(14)
C(8)—C(6)	1.541(14)	C(115)—C(108)	1.510(14)

[a]Estimated standard deviations are given in parentheses. Mean phenyl carbon – carbon distance and standard deviation was 1.402(18) Å, range 1.351–1.461(15–23) Å. Mean carbon–oxygen distances and standard deviations were C=O, 1.199(13); (CO)—O, 1.330(13); and O—CH_3, 1.466(15) Å.

Recrystallization of pure red compound **8** from 95% ethanol gave X-ray quality crystals, mp 198–199°C without decomposition. UV (95% EtOH) λ_{max} nm (log ϵ): 203 (4.74), 224 (4.37), 273 (4.09), 384 (4.27). IR (KBr) cm^{-1}: 3060w, 2950w, 1750s, 1690m, 1645m, 1545m, 1495w, 1435w, 1350m, 1330m, 1235s, 1210s, 1180s, 1160m, 1115m, 1055w, 760m, 750m, 690m, 580w. ^1H NMR (250 MHz) ppm: aromatic 7.9–7.09 (17H), methoxyl hydrogen resonances at 3.71 (3H), 3.62 (3H), 3.25 (3H), 3.16 (3H). ^{13}C NMR (250 MHz) ppm: carbonyl carbons 167.9, 166.0, 162.4, 157.6, ester methyl carbons 52.6, 52.3, 51.6, 51.3; quaternary carbon 29.7; peak positions (relative intensities) for aromatic and olefinic carbons, some overlap and some coupled to phosphorus 137.1 (3.2), 136.8 (3.6), 136.7 (3.6), 136.4 (3.3), 136.3 (1.4), 134.9 (1.1), 134.7 (1.4), 134.0 (4.4), 133.4 (2.2), 133.3 (6.4), 133.1 (6.0), 131.3 (1.7), 131.23 (1.9), 131.16 (1.6), 129.9 (7.9), 129.8 (8.0), 129.5 (7.2), 129.3 (9.0), 129.1 (17.7), 128.3 (0.8), 127.4 (6.6), 127.3 (7.6), 127 (7.2), 126.9 (6.4), 117.4 (1.3), 116.0 (1.2), 114.2 (0.6), 109.9 (0.7), 109.7 (0.7). Mass spectrum, methane CI, 350°C probe temp., calcd. for $C_{34}H_{29}O_8P$: 596; found: M + 1, 597. Recrystallization several times from toluene gave what appeared to be a different polymorph of the same compound, mp 251–252°C, and an identical 250 MHz ^1H NMR, identified to be trimethyl 1,2,5-triphenylphosphoranylidene-4-methoxycyclopent-2-ene-5-one-2,3,4-tricarboxylate, **8**, from the X-ray determination.

An off-white powder identified as **10** (11.8 mg; mp 185°C) was also isolated. UV (95% EtOH) λ_{max} nm: 202, 219, 257, 368; molecular weight and hence extinction coefficients not known. IR (KBr) cm^{-1}: 3060, 3010, 2960, 1740, 1590, 1500, 1460, 1435, 1360, 1290, 1250, 1200, 1180, 1110, 1000, 1055, 910, 700, 520. ^1H NMR (250 MHz), high intensity peak positions, ppm (intensity): 7.26 (19), 7.10 (1.7), 4.90 (1.2), 4.12 (1.4), 4.06 (1.6), 3.98 (10.4, 3H), 3.96 (10.4, 3H), 3.82 (10.3, 3H), 3.65 (10.1, 3H), 3.59 (10.6, 3H), 3.39 (10.2, 3H), 3.28 (1.2), 3.21 (1.1), 2.16 (1.3). ^{31}P NMR (250 MHz): +55.77 ppm.

From the column fractions a total of 0.41 g of an acetylene tetramer was also isolated, identified as tetramethyl 4-methoxy-5[1,2,3-tris (methoxycarbonyl)-2-cyclopropen-1-yl]-7-oxabicyclo[2,2,1]hepta-2,5-diene-1,2,3,6-tetracarboxylate **9**, via comparison of the physical properties with published values (refs. 9–12). IR (KBr) cm^{-1}: 3000w, 2960m, 2850w, 1875m, 1755s, 1735s, 1720s, 1620m, 1435s, 1350s, 1335s, 1295s, 1275s, 1205s, 1140s, 1060s, 1003m, 980m, 965m, 905w, 770w, 720w. ^1H NMR (60 MHz) ppm: 3.89 (12H), 3.78 (3H), 3.75 (3H), 3.67 (3H), 3.61 (3H); in acetone-d_6 (60 MHz): 3.86 (3H), 3.78 (6H), 3.76 (3H), 3.7 (3H), 3.66 (3H), 3.6 (3H), 3.54 (3H). ^1H NMR in $CDCl_3$ (250 MHz) each integrating for 3H: 3.87, 3.85, 3.84, 3.83, 3.74, 3.70, 3.63, and 3.56 ppm.

Reaction of 1,2,5-triphenylphosphole with dimethyl acetylenedicarboxylate in benzene

A solution of 2.3 g (6.52 mmol) of the finely ground phosphole was made up under oxygen-free nitrogen in 50 mL of benzene dried over Molecular Sieve 4A by gentle warming in a water bath. After cooling the solution to room temperature, dimethyl acetylenedicarboxylate (Aldrich), 20 mL (163 mmol), was added to the solution all at once via a syringe. The initially yellow solution changed to deep red within minutes and then turned dark brown.

After stirring the solution for 2 days at room temperature, the reaction mixture was filtered to give 1.10 g of yellow solid, mp 163–165°C, which was identified as the previously isolated yellow adduct **6**. Further impure **6** (0.395 g) was obtained in a second crop, which when recrystallized yielded a further 0.26 g of pure material, mp 159–163°C.

The volume of the mother liquor was reduced and the solution was allowed to crystallize further to yield white needles (0.29 g), mp 186–189°C, ^1H NMR (60 MHz) ppm: 7.5–7.0 (12H), 3.6 (6H). This was identified as dimethyl 3,6-diphenylphthalate **3** from the NMR spectrum.

The collected mother liquors were reduced in volume and the residue was taken up in a minimum volume of chloroform, chromatographed on silica gel (Merck 70–230 mesh, 120 g) in a 2.5 cm diameter column, and eluted with chloroform. Selected fractions were crystallized from acetone to yield a further 0.15 g of impure yellow adduct **6** and 18 mg of the red adduct **8**. A quantity of the acetylene tetramer **9** (0.313 g) was also isolated, mp 89–91°C, and ^1H NMR was identical to that of the previously isolated material.

A small amount of off-white powder **10** (110 mg) was also obtained. UV (95%EtOH) λ_{max} nm: 202, 219, 257, 368, again molecular weight unknown. IR (KBr) cm^{-1}: 3060w, 3010m, 2960w, 1740s, 1710s, 1590s, 1500s, 1460s, 1435s, 1360m, 1290s, 1250s, 1200s, 1180s, 1110m, 1065m, 1055w, 1010m, 910m, 700m, 695m, 520m. ^1H and ^{31}P NMR spectra were identical to those of **10** isolated from the 1,2,5-triphenylphosphole reaction with neat DMADC. This was not further characterized.

The last fraction of the previous column was reduced in volume and chromatographed on silica gel (Merck 70–230 mesh, 160 g) in a 2.5 cm diameter column. Crystallization of combined similar fractions from CCl_4 enabled recovery of 0.299 g of a tan powder, UV (95% EtOH) λ_{max} nm: 200, 219, 261 (molecular weight unknown). IR (KBr) cm^{-1}: 3400br, 3055w, 2950w, 1725m, 1650br, 1440w, 1385m, 1220 broad, 1140m, 1065m, 1050w, 750w, 700w, 560w, which also could not be identified.

Reaction of phosphole 2 with neat freshly distilled acetylene ester

The acetylene ester (20 mL) was distilled under reduced pressure (2 Torr; 1 Torr = 133.3 Pa) in an inert atmosphere to recover a sharp cut of 15 mL of the pure material. The residual viscous oil from the distillation was dissolved in 95% ethanol and allowed to crystallize to yield 2.13 g of clear crystals, identified by IR as the tetramer of the acetylene ester, **9**.

The distilled acetylene ester (15 mL, 122 mmol) was added all at once via syringe to 4.01 g (1.28 mmol) of finely ground 1,2,5-triphenylphosphole, in a flask that had been previously flushed with oxygen-free nitrogen. The mixture was allowed to react at room temperature, with occasional mixing, for several days. Toluene

Can. J. Chem. Downloaded from www.nrcresearchpress.com by 203.198.23.82 on 09/08/12
For personal use only.

TABLE 15. Bond angles for all skeletal atoms of the two enantiomers of the oxide of the rearrangement product **12** (deg)[a]

Atoms	Angle	Atoms	Angle
C(1)—P(1)—O(1)	114.4(4)	C(22)—C(21)—P(1)	119.9(8)
C(7)—P(1)—O(1)	116.5(4)	C(26)—C(21)—P(1)	116.5(8)
C(7)—P(1)—C(1)	102.6(5)	C(32)—C(31)—C(1)	118.7(9)
C(21)—P(1)—O(1)	113.8(4)	C(36)—C(31)—C(1)	120.3(9)
C(21)—P(1)—C(1)	101.3(5)	C(42)—C(41)—C(4)	117.8(9)
C(21)—P(1)—C(7)	106.6(4)	C(46)—C(41)—C(4)	120.8(9)
C(101)—P(101)—O(101)	117.3(5)	C(102)—C(101)—P(101)	121.0(8)
C(107)—P(101)—O(101)	113.2(4)	C(131)—C(101)—P(101)	115.3(7)
C(107)—P(101)—C(101)	105.2(4)	C(131)—C(101)—C(102)	123.6(9)
C(121)—P(101)—O(101)	113.5(4)	C(103)—C(102)—C(101)	124.4(9)
C(121)—P(101)—C(101)	102.3(5)	C(104)—C(103)—C(102)	105.5(8)
C(121)—P(101)—C(107)	103.9(4)	C(108)—C(103)—C(102)	117.0(8)
C(2)—C(1)—P(1)	120.3(8)	C(108)—C(103)—C(104)	104.6(8)
C(31)—C(1)—P(1)	116.0(7)	C(105)—C(104)—C(103)	111.0(9)
C(31)—C(1)—C(2)	123.7(9)	C(141)—C(104)—C(103)	118.9(9)
C(3)—C(2)—C(1)	123.9(10)	C(141)—C(104)—C(105)	129.6(10)
C(4)—C(3)—C(2)	107.6(8)	C(106)—C(105)—C(104)	113.1(9)
C(8)—C(3)—C(2)	116.3(8)	C(109)—C(105)—C(104)	125.3(10)
C(8)—C(3)—C(4)	103.2(8)	C(109)—C(105)—C(106)	121.5(9)
C(5)—C(4)—C(3)	111.9(8)	C(107)—C(106)—C(105)	118.5(8)
C(41)—C(4)—C(3)	122.4(9)	C(108)—C(106)—C(105)	103.3(8)
C(41)—C(4)—C(5)	124.9(9)	C(108)—C(106)—C(107)	59.1(6)
C(6)—C(5)—C(4)	111.5(8)	C(111)—C(106)—C(105)	114.4(8)
C(9)—C(5)—C(4)	125.7(9)	C(111)—C(106)—C(107)	124.6(8)
C(9)—C(5)—C(6)	122.4(8)	C(111)—C(106)—C(108)	122.2(8)
C(7)—C(6)—C(5)	116.8(8)	C(106)—C(107)—P(101)	118.8(7)
C(8)—C(6)—C(5)	103.8(8)	C(108)—C(107)—P(101)	119.0(7)
C(8)—C(6)—C(7)	59.5(6)	C(108)—C(107)—C(106)	59.7(6)
C(11)—C(6)—C(5)	114.5(8)	C(113)—C(107)—P(101)	113.4(7)
C(11)—C(6)—C(7)	125.4(8)	C(113)—C(107)—C(106)	117.2(8)
C(11)—C(6)—C(8)	123.1(8)	C(113)—C(107)—C(108)	118.6(8)
C(6)—C(7)—P(1)	119.9(6)	C(106)—C(108)—C(103)	107.2(8)
C(8)—C(7)—P(1)	119.6(7)	C(107)—C(108)—C(103)	116.9(8)
C(8)—C(7)—C(6)	60.4(6)	C(107)—C(108)—C(106)	61.2(6)
C(13)—C(7)—P(1)	113.4(7)	C(115)—C(108)—C(103)	117.0(9)
C(13)—C(7)—C(6)	117.1(8)	C(115)—C(108)—C(106)	121.3(9)
C(13)—C(7)—C(8)	116.7(8)	C(115)—C(108)—C(107)	120.5(8)
C(6)—C(8)—C(3)	109.2(8)	C(122)—C(121)—P(101)	117.3(8)
C(7)—C(8)—C(3)	116.8(8)	C(126)—C(121)—P(101)	121.9(8)
C(7)—C(8)—C(6)	60.1(6)	C(132)—C(131)—C(101)	118.0(9)
C(15)—C(8)—C(3)	116.7(8)	C(136)—C(131)—C(101)	119.6(9)
C(15)—C(8)—C(6)	121.4(8)	C(142)—C(141)—C(104)	118.4(9)
C(15)—C(8)—C(7)	120.2(8)	C(146)—C(141)—C(104)	121.2(9)

[a]Estimated standard deviations are given in parentheses. Mean phenyl carbon – carbon–carbon bond angle and standard deviation was 119.9(12)°, range 116.8°–123.5(10–15)°. Range of carbon–oxygen–carbon and carbon–carbon–oxygen bond angles was 105.5°–125.9(8–10)°.

Can. J. Chem. Downloaded from www.nrcresearchpress.com by 203.198.23.82 on 09/08/12
For personal use only.

(100 mL) was added and the mixture filtered to yield 2.63 g of yellow crystals, mp 162–165°C, which was confirmed to be the yellow adduct **6**. A second crop of crystals, which were red (0.76 g), mp 197–199°C, was obtained on cooling the mother liquor. This was identified as the red adduct **8**.

The filtrate from the red crystals was then chromatographed on Merck Kieselgel 60 (70–230 mesh ASTM) using diethyl ether as eluent. The first 100 mL fraction yielded 120 mg of clear crystals of the acetylene tetramer **9**, identified by IR. Evaporation of the second 100 mL fraction gave colourless crystals, 279 mg, mp 187–191°C, identified by IR as dimethyl 3,6-diphenylphthalate **3**. The third 100 mL fraction yielded 0.881 g of red crystals of **8**, mp 193–199°C. This fraction was combined with the red adduct **8** recovered by crystallization (0.76 g) and recrystallized from 10 mL of toluene to yield 0.312 g of pure material, mp 197–199°C.

Rearrangement of the yellow adduct ***6***

(a) By literature method

The adduct **6** (112 mg) was dissolved in 50 mL of chloroform and refluxed for 3 h according to the published method (5). The solvent was removed under reduced pressure and the residue crystallized from 95% ethanol to yield 79 mg of yellow crystals, mp and mixture mp with starting material 163–165°C, and confirmed by ^{1}H NMR. A second crop of 27.5 mg of impure yellow crystals was mostly the rearrangement product **11** by ^{1}H NMR. The samples were combined (107 mg) in 50 mL of 1,2-dichloroethane and refluxed for 5 h. Crystallization of the evaporation residue as before gave 98 mg of colourless crystals of the rearrangement product **11**, mp 183–185.5°C. This was identified as tetramethyl 2,3,6-triphenyl-2-phospha(III)tricyclo[6.5.0^{1,8}.0^{5,9}]-nona-3,6-diene-1,7,8,9-tetracarboxylate, compound **11**, via an X-ray structure

TABLE 16. Intermolecular distances of less than 3.4 Å from the crystal structure of the two enantiomers of the oxide of the rearrangement product, **12** (Å)[a]

Atoms	Distance	Sym	T_x	T_y	T_z
C(133)···O(2)	3.355	3	0	−1	−1
C(25)···O(2)	3.318	4	0	0	0
C(112)···O(4)	3.344	1	1	0	0
C(114)···O(6)	3.254	4	1	−1	0
C(32)···O(7)	3.395	1	1	0	0
C(33)···O(7)	3.295	1	1	0	0
C(12)···O(9)	3.238	1	−1	0	0
O(104)···C(12)	3.394	1	1	0	0
O(106)···C(14)	3.334	4	0	−1	0
C(124)···O(104)	3.394	4	1	−1	0
C(112)···O(109)	3.340	1	1	0	0

[a]The symmetry positions are for the second atom. They are defined: $2 = -x, -y, \frac{1}{2} + z$; $3 = x, \frac{1}{2} - y, \frac{1}{2} + z$; $4 = -x, \frac{1}{2} + y, z$. A negative symmetry position denotes inversion. The translations (T) are applied finally.

determination carried out on crystals of the oxide of this compound produced under mild conditions (see below).

(b) By improved modification

A solution of the yellow adduct **6** (1.013 g) in 100 mL of 1,2-dichloroethane was boiled under reflux for 12 h. Progress of the reaction was followed by thin-layer chromatography (Polygram silica gel G, UV 254) using 5% acetone – 95% toluene for development. When the reaction was complete colourless crystals of the rearrangement product **11** (0.731 g) were isolated as described above, mp 210–213°C. UV (95% EtOH) λ_{max} nm (log ε): 201 (4.80), 248 (4.39). IR (KBr) cm^{-1}: 3030w, 3010w, 2955w, 2840w, 1750–1710s, 1640w, 1600w, 1485w, 1430s, 1375w, 1320m, 1230s, 1200s, 1120w, 1105w, 1060w, 945w, 850w, 815w, 760m, 700m, 640w, 520w. ^{1}H NMR (360 MHz) ppm: aromatic/olefinic protons 7.54–6.9; triplet centered at 6.4, J_{PH} 8.83, J_{HH} 8.76; doublet centered at 4.85, J_{HH} 8.45; ester methyl protons 3.82, 3.75, 3.68, 2.89. ^{13}C NMR (360 MHz) ppm: carbonyl carbons 168.8, 167.1, 166.2, and 163.6; primary carbon (CH) 53 (DEPT 90°); quaternary carbon 47.6 J_{PC} 38.5 Hz; quaternary carbon 49.5, J_{PC} 20.5 Hz; quaternary carbon 40, J_{PC} 2.6 Hz (DEPT 135°); ester methyl carbons 51.6, 51.9, 52.7, 53.1, peak positions (relative intensities) for aromatic and olefinic carbons, some overlap and some coupled to phosphorus 152.2 (1.3), 145.5 (1.0), 145.3 (1.3), 141.0 (1.1), 140.9 (1.2), 136.8 (0.55), 133.9 (2.1), 132.7 (1.1), 132.6 (1.1), 129.7 (2.9), 129.6 (3.0), 129.5 (4.7), 128.8 (5.9), 128.2 (0.76), 128.1 (1.2), 128.0 (13.1), 127.9 (10.8), 127.8 (10.8), 127.7 (4.2), 127.6 (2.7), 127.32 (5.8), 127.25 (5.9), 126.6 (4.8). Decoupled ^{31}P NMR, ppm: −34.8 SR (standard reference) 85% ortho phosphoric acid. Mass spectrum (relative intensity) calcd. for $C_{34}H_{29}O_8P$: 596, ^{13}C satellite 597(38); found: methane negative ion CI (probe temp. 280°C): M^-, 596(100); (M^-) + 1, 597(37); methane CI (probe temp. >350°C), M + 1, 597.

Oxidation of the rearranged yellow adduct

The rearranged yellow adduct **11** (0.602 g) was dissolved in 50 mL of a 30:70 mixture of ethyl acetate and 95% ethanol, then 3.5 mL of 30% hydrogen peroxide was added. The mixture was refluxed for 7 h after which 25 mL of water was added and the organic solvent removed from the mixture by evaporation under reduced pressure. The residual aqueous phase was extracted with chloroform (3 × 50 mL), and the combined chloroform extracts were reduced in volume and ethyl acetate added. Colourless crystals of the oxide of the rearrangement product (0.312 g, mp 251–254°C), for which structure **12** was established later, were obtained from this solution. UV (95%EtOH) λ_{max} nm (log ε): 202 (4.66), 268 (4.18). IR (KBr) cm^{-1}: 3030m, 3010m, 2955w, 2840w, 1750–1705s, 1640m, 1600w, 1485w, 1430s, 1375m, 1320w, 1250–1230s, 1200s, 1120m, 1105w, 1060m, 945m, 850w, 815w, 760s, 700s, 640w, 520m. ^{1}H NMR (360 and 250 MHz) ppm: aromatic/olefinic protons 8.2–6.85; doublet of doublets centered at 4.72, J_{HH} 8.20 Hz, J_{PH} 1.82 Hz; methyl ester protons 3.86, 3.75, 3.69, 2.99. ^{13}C NMR given in next preparation. ^{31}P–^{1}H coupled NMR (360 MHz): appears as a doublet of triplets J_{PH1} 12.9 Hz, J_{PH2} 12.9 Hz, J_{PH3} 30.8 Hz. Decoupled ^{31}P NMR 12.6 ppm, standard reference 85% ortho phosphoric acid. Mass spectrum (relative intensity) calcd. for $C_{34}H_{29}O_9P$: 612, ^{13}C satellite 613(38); found: methane negative ion CI (probe temp. 350°C) M^-, 612(100); (M^-) + 1,613(39).

*X-ray quality crystals from the oxide of the rearranged yellow adduct, **12***

The title compound **12** (0.312 g) was crystallized from 20 mL of warm ethyl acetate to yield 0.219 g of colourless crystals, mp 252–254°C, too small for X-ray. X-ray quality crystals of the product were obtained from a low-recovery recrystallization from ethyl acetate, mp 252–254°C, on which an X-ray structure determination established that this was tetramethyl 2,3,6-triphenyl-2-phosphatricyclo[6.1.0^{1,8}.0^{5,9}]-2-oxonona-3,6-diene-1,7,8,9-tetracarboxylate, compound **12**. ^{13}C NMR (360 MHz) ppm: carbonyl carbons 167.5, 166.1, 163.2, 165.0, J_{PC} 4.8 Hz; methine carbon 51.7, J_{PC} 13.1 Hz; tertiary carbons at 53.9, J_{PC} 3.3 Hz; 52.4, J_{PC} 3.3 Hz; 52.3; 45.5, J_{PC} 75.1 Hz; ester methyl carbons at 53.3, 52.9, 52.1, and 52.0; peak positions (relative intensities) for aromatic and olefinic carbons, some overlap and some coupled to phosphorus 156.6 (1.3), 145.8 (3.1), 140.9 (1.2), 139.9 (1.0), 137.2 (1.3), 137.1 (1.2), 133.3 (2.3), 132.8 (1.2), 131.6 (1.3), 131.49 (2.9), 131.47 (2.9), 130.3 (1.0), 129.82 (0.7), 129.76 (0.7), 129.6 (1.0), 129.4 (1.0), 128.9 (4.8), 128.1 (16.0), 127.8 (5.0), 127.6 (1.0), 126.9 (5.7), 126.8 (5.0).

*Effect of alcoholic carbonate on oxide of rearrangement product, **12***

A small sample of the oxide of the rearrangement product, **12**, was dissolved in 10 mL of 95% EtOH and 0.5 g of K_2CO_3 was added. During warming the solution colour changed from the initial colourless to purplish pink. Crystallization from ethyl acetate after removal of the potassium carbonate produced white crystals with different NMR properties than the starting material: decoupled ^{31}P NMR (250 MHz) ppm: 19.8, SR 85% ortho phosphoric acid; ^{1}H NMR (250 MHz) ppm: aromatic and olefinic protons, 7.52–7.09; aromatic or olefinic proton centered at 6.57 (possible doublet of doublets), J_1 34.55 Hz, J_2 3.69 Hz; methine proton centered at 4.34, J 21.162 Hz; ester methyl protons at 3.77, 3.66, 3.55, and 2.98.

X-ray crystallography

The crystals of all three compounds gave well-defined extinctions between crossed polars. Crystals were mounted in glass Lindemann tubes, and Weissenberg and precision photography using Cu K_α radiation was used to determine unit cells and space groups, in all cases at 20°C. The experimental parameters and crystal data for all three compounds are given in Table 4. In all cases scattering factors for uncharged atoms were used (21). Supplementary material, (Tables S1–S8), including complete bond length and angle data and hydrogen atom fractional atomic coordinates where determined, anisotropic temperature parameters, and observed and calculated structure factors for all three crystals, has been deposited.[4]

[4]This supplementary material can be purchased from: The Depository of Unpublished Data, Document Delivery, CISTI, National Research Council Canada, Ottawa, ON K1A OS2, Canada.

Tables of hydrogen atom coordinates and bond lengths and angles have also been deposited with the Cambridge Crystallographic Data Centre, and can be obtained on request from The Director, Cambridge Crystallographic Data Centre, University Chemical Laboratory, 12 Union Road, Cambridge, CB2 1EZ, U.K.

Can. J. Chem. Downloaded from www.nrcresearchpress.com by 203.198.23.82 on 09/08/12
For personal use only.

Can. J. Chem. Downloaded from www.nrcresearchpress.com by 203.198.23.82 on 09/08/12
For personal use only.

Data collection and processing for yellow adduct ***6***

The crystal was found to be triclinic, space group $P\bar{1}$ (No. 2), and approximate unit cell dimensions were established. The unit cell and matrix were refined using 25 2θ measurements in the range 24–41°, each measured in both the positive and negative directions. Intensity measurements were made in the 2θ range, 0.1°–45° from $hkl = -11,0,-13$ to 11,12,12. Three standard orientation reflections 0,0,9; 6,0,0; and 0,8,0 were measured every 400 reflections. The standard intensity reflections were 5,2,−4; 6,−1,−2; and 5,−5,0, also measured every 3600 seconds of X-ray time. The measurements were corrected for absorption, using an empirical absorption correction on the Nonius ($\mu = 0.86$ cm^{-1}), then the EMPABS program[5] was run on the mainframe computer. The phase problem was solved by direct methods. All atoms, including H, were found for the main molecule. Methyl hydrogens on acetone were calculated using AFIX in the SHELX program.[6] The refinements converged with a maximum shift/e.s.d. (non-H) of 0.04 and the final difference map had a maximum of 0.21 e Å^{-3} and a minimum of 0.12 e Å^{-3}, indicating that nothing had been missed. The final residuals were $R = 0.0453$, $R_w = 0.0453$, for 537 parameters and 2880 independent observations. Results are given in Tables 5–8.

X-ray data collection and processing for the red 2:1 adduct ***8***

This crystal was monoclinic, space group $P2_1/c$(No. 14), and approximate unit cell dimensions were established. The unit cell and matrix were refined using 20 2θ measurements in the range 12°–36°, each measured in both the positive and negative directions. Intensity measurements were made in the 2θ range, 0.1°–45° from $hkl = -14,0,0$ to 14,15,18 at 20°C. The scanning was in 200 steps of 0.01° in 2θ counting for 0.25 s/step with background counting for 25 s at each end of the scan. Three standard orientation and intensity reflections 0,6,0; 0,0,6; and 6,0,0 were measured before every 50 reflections and were corrected for absorption using ABSB02 ($\mu = 0.98$ cm^{-1}) as an absorption correction.[7]

The phase problem was solved by MULTAN.[8] Phosphorus and all carbon and oxygen atoms were found for the main molecule and for the cocrystallized ethanol. Ethanol was slightly disordered. Distance C52-O53 was DFIX'd at 2.15. The poor ethanol angle was not resolvable by crystallography, and this kept the *R*-value high. The refinement converged with a maximum shift/e.s.d.(non-H) of 0.128 (ethanol) and 0.023 otherwise. The final difference map had a maximum of 0.67 e Å^{-3} and a minimum of 0.15 e Å^{-3}, and indicated that nothing had been missed. The final residuals were $R = 0.0916$, $R_w = 0.0937$, for 400 parameters and 2052 independent observations. Results are given in Tables 9–12.

X-ray data collection and processing for the oxide of the rearrangement product ***12***

This crystal was orthorhombic, space group $Pbc2_1$ (No. 29). Approximate unit cell dimensions and other data are given in Table 4. The unit and cell matrix were refined using 25 2θ measurements in the range 40°–64°, each measured in both the positive and negative directions. Intensity measurements were made in the 2θ range, 0°–130° from $hkl = 0,0,0$ to 9,26,35 at 20°C. Three standard orientation reflections 4,0,0; 0,0,16; and 0,12,0 were measured before every 400 reflections. The standard intensity reflections were the same three reflections, also measured every 3600 seconds of X-ray time, approximately every 50 reflections. The measurements were corrected for absorption using an empirical absorption correction, on the Nonius ($\mu = 12.5$ cm^{-1}), then the EMPABS program (22) was run on the mainframe computer. The phase problem was solved by SHELXS Patterson methods. Because two molecules made up the asymmetric unit, all carbons could not be made anisotropic due to the SHELX-76 limitations on the number of parameters, so the six phenyl rings were left isotropic. Only four hydrogens were sought and refined (those on C2, C3, C102, and C103). We did not look for or calculate phenyl or methyl hydrogens. The refinements converged with a maximum shift/e.s.d. of 0.07, including the four located hydrogens. The final difference map had a maximum of 0.61 e Å^{-3} and a minimum of 0.22 e Å^{-3}, and indicated that nothing had been missed. The final residuals were $R = 0.0747$, $R_w = 0.0757$, for 321 parameters and 3255 independent observations. Results are given in Tables 13–16.

Summary

As has been found with the reaction of dimethyl acetylenedicarboxylate with *N*-substituted pyrroles (23) and with furans (e.g., refs. 24, 25), the adducts of this ester with 1,2,5-triphenylphosphole are complex and similarly varied. We found few, if any, direct equivalencies in mode of reaction to the phosphorus heterocycle as compared to those observed for the nitrogen and oxygen heterocycles. The X-ray structure component of this work unequivocally confirms the cyclopropane-containing structure **6** for the yellow 2:1 adduct of the acetylene ester, formerly deduced solely from derivatives and spectroscopically. We also correct the various previously assigned structures of the thermal rearrangement product of this yellow adduct to structure **11** and that of its oxide to **12**, which both still contain cyclopropyl moieties. Finally, we isolated for the first time a red 2:1 adduct of the acetylene ester to phosphole and have established its structure to be the cyclopent-3-enone stabilized phosphorane **8**. In this product the phosphole ring remains intact, the only example among the adducts isolated. Preparation, isolation, and full characterization of the several products of the reaction of acetylene ester with the phosphole under different conditions as described here should also dispel the impression given by the literature (e.g., ref. 19) that these two compounds do not react under normal conditions.

Acknowledgements

The authors thank K. Beveridge for the X-ray crystal structures, M.J. Gallagher and the University of New South Wales for provision of facilities to assemble this paper, and the Government of British Columbia and the University of Victoria for financial support of the experimental work.

[5]An empirical absorption correction program for the Nonius diffractometer. The absorption correction is measured as a function of χ for a conveniently placed reflection, and the experimental curve is used to correct other reflections. For details see ref. 22 and the Nonius CAD4 manual.

[6]G.M. Sheldrick and E. Egert. A program for crystal structure determination. Anorganisch-Chemisches Institut der Universitat Gottingen, Tammannstr. 4, 3400 Gottingen, Germany.

[7]P. Coppens, L. Leiserowitz, and D. Rabinovich. A program for the correction of crystallographic data for absorption. Modified to deal with the axis system on the University of Victoria Picker Diffractometer by G. Bushnell.

[8]P. Coppens, L. Leiserowitz, and D. Rabinovich. A system of computer programs for the automatic solution of crystal structures from X-ray diffraction data.

1. I.G.M. Campbell, R.C. Cookson, and M.B. Hocking. Chem. Ind. (London), 359 (1962).
2. K. Alder and H.F. Rickert. Annalen, **524**, 180 (1936).
3. A.C. Cope, A.C. Haven, Jr., F.L. Ramp, and E.R. Trumbull. J. Am. Chem. Soc. **74**, 4867 (1952).
4. I.G.M. Campbell, R.C. Cookson, M.B. Hocking, and A.N. Hughes. J. Chem. Soc. 2184 (1965).
5. A.N. Hughes and S. Uaboonkul. Tetrahedron, **24**, 3437 (1968).
6. N.E. Waite and J.C. Tebby. J. Chem. Soc. (C), 386 (1970).
7. M.B. Hocking. Can. J. Chem. **44**, 1581 (1966).
8. W.P. Ozbirn, R.A. Jacobsen, and J.C. Clardy. Chem. Commun. 1062 (1971).

9. E. Winterfeldt and G. Giesler. Angew. Chem. Int. Ed. Engl. **5**, 579 (1966).
10. R. Gericke and E. Winterfeldt. Tetrahedron, **27**, 4109 (1971).
11. J.C. Kauer and H.E. Simmons. J. Org. Chem. **33**, 2720 (1968).
12. E. LeGoff and R.B. LaCount. Tetrahedron Lett. 2333 (1967).
13. L.D. Quin, N.S. Rao, R.J. Topping, and A.T. McPhail. J. Am. Chem. Soc. **108**, 4519 (1986).
14. L.D. Quin, E.D. Middlemas, and N.S. Rao. J. Org. Chem. **47**, 905 (1982).
15. N.E. Waite, D.W. Allen, and J.C. Tebby. Phosphorus, **1**, 139 (1971).
16. N.E. Waite, J.C. Tebby, R.S. Ward, M.A. Shaw, and D.H. Williams. J. Chem. Soc. (C), 1620 (1971).
17. O. Kennard, W.D.S. Motherwell, and J.C. Coppola. J. Chem. Soc. (C), 2461 (1971).
18. N.E. Waite, J.C. Tebby, R.S. Ward, and D.H. Williams. J. Chem. Soc. (C), 1100 (1969).
19. A.N. Hughes, K. Amornraksa, S. Phisithkul, and V. Reutrakul. J. Heterocycl. Chem. **13**, 65 (1976).
20. J.K. Stille, J.L. Eichelberger, J. Higgins, and M.E. Freeburger. J. Am. Chem. Soc. **94**, 4761 (1972).
21. D.T. Cromer and J.T. Waber. *In* International tables for X-ray crystallography. Vol. IV. *Edited by* J.A. Ibers and W.C. Hamilton. Kynoch Press, Birmingham. 1974.
22. A.C.T. North, D.C. Phillips, and F.S. Mathews. Acta. Crystallogr. Sect. A: Cryst. Phys. Diffr. Theor. Gen. Crystallogr. **A24**, 351 (1968).
23. R.M. Acheson and N.F. Elmore. Adv. Heterocycl. Chem. **23**, 264 (1978).
24. A.W. McCulloch, D.G. Smith, and A.G. McInnes. Can. J. Chem. **51**, 4125 (1973).
25. J.D. Slee and E. LeGoff. J. Org. Chem. **35**, 3897 (1970).

Can. J. Chem. Downloaded from www.nrcresearchpress.com by 203.198.23.82 on 09/08/12
For personal use only.

Order–disorder transitions in adamantane derivatives: vibrational spectroscopic and ^{13}C NMR studies of 1-chloroadamantane

YINING HUANG, RALPH M. PAROLI, D.F.R. GILSON,[1] AND I.S. BUTLER[1]

Department of Chemistry, McGill University, 801 Sherbrooke St., West, Montreal, QC H3A 2K6, Canada

Received January 19, 1993

YINING HUANG, RALPH M. PAROLI, D.F.R. GILSON, and I.S. BUTLER. Can. J. Chem. **71**, 1890 (1993).

The order–disorder behaviour of 1-chloroadamantane (1-$C_{10}H_{15}Cl$) has been investigated by differential scanning calorimetry, and variable-temperature vibrational and ^{13}C NMR spectroscopy. The factor group splittings in the vibrational spectra are in accord with the known crystal structures of the two phases. The ^{13}C spin-lattice relaxation times and dipolar dephasing measurements have been analysed to give the barriers to rotation in both phases and to determine the nature of the rotations in each phase. In the ordered phase, the motion is limited to rotation about the molecular axis. In the disordered phase, additional motions occur about axes through the tertiary carbon atoms.

YINING HUANG, RALPH M. PAROLI, D.F.R. GILSON et I.S. BUTLER. Can. J. Chem. **71**, 1890 (1993).

Faisant appel à la calorimétrie à balayage différentielle, à la RMN du ^{13}C et à la spectroscopie vibrationnelle à température variable, on a étudié le comportement ordre–désordre du 1-chloroadamantane (1-$C_{10}H_{15}Cl$). Les dédoublements des facteurs de groupe des spectres de vibration sont en accord avec les structures cristallines connues des deux phases. On a analysé les temps de relaxation spin-réseau du ^{13}C et les mesures de déphasage dipolaire pour obtenir les barrières à la rotation dans les deux phases et pour déterminer la nature des rotations dans chaque phase. Dans la phase ordonnée, la mouvement se limite à une rotation autour de l'axe moléculaire. Dans la phase désordonnée, des mouvements additionnels se produisent autour des axes des atomes de carbone tertiaires.

[Traduit par la rédaction]

Can. J. Chem. Downloaded from www.nrcresearchpress.com by 203.198.23.82 on 09/08/12
For personal use only.

Introduction

Adamantane and many of its derivatives possess orientationally disordered structures (1–3) in which the high-temperature phases are usually characterized by extensive molecular motions about one or more axes and, in some cases, translational diffusion (4–11). Interpretations of the mechanisms of the transition to the ordered phase are hindered by the lack of information on the crystal structure of the low-temperature ordered phase and the molecular dynamics associated with the transition. The 1-haloadamantanes, although they have the same molecular symmetry, exhibit marked differences in their phase transition behaviour (2, 3). 1-Fluoroadamantane displays one solid–solid phase transition, but this phase change is not of the order–disorder type (3–5) and both phases are orientationally disordered. On the other hand, 1-chloro- and 1-bromoadamantane have disordered high-temperature phases and undergo one and two phase transformations, respectively, with the lowest temperature phases being ordered. The 1-iodo compound also has a single phase transition but overall molecular tumbling in the high-temperature phase does not occur and the molecules only undergo a 12-fold uniaxial rotation (6).

1-Chloroadamantane, where the melting and transition temperatures are 442.5 and 244.2 K with transition entropies of 11.01 and 24.61 J K^{-1} mol^{-1}, respectively (2), is one of few compounds for which the crystal structures of both the ordered and disordered phases have been reported (7, 8). The low entropy of fusion indicates that the high-temperature phase is disordered, and, in common with most singly substituted adamantane derivatives, the structure is face-centred cubic, space group $Fm3m$, with four molecules per unit cell. The ordered phase is monoclinic, space group $P2_1/c$, also with four molecules per unit cell.

Although 1-chloroadamantane has been investigated by several different experimental methods, the molecular dynamics remain unclear, especially for the disordered phase (9–11). On the basis of proton NMR studies, Virlet et al. (6) concluded that the motion in phase I of 1-bromoadamantane is a fast endospherical reorientation. Using the same technique, Ursu *et al.* (9, 11) suggested that the motion in phase I for both 1-chloro- and 1-bromoadamantane is a combination of a rotation about the molecular C_3 axis and a jump reorientation of this axis in the lattice, but did not specify about which crystallographic axes this reorientation of the C_3 axis is taking place. In the low-temperature phase, only one barrier was indicated by proton T_1 measurements and a C_3 uniaxial rotation was assumed to be responsible for the relaxation (9).

The results of an incoherent quasi-elastic neutron scattering study have suggested that there are two types of motion occurring in the high-temperature phase of 1-chloroadamantane: tumbling of the molecular C_3 axis among six fourfold crystallographic axes along the [100] directions, and a uniaxial rotation about the molecular threefold axis (10). The barrier to molecular tumbling is about twice that of uniaxial rotation. Incoherent neutron scattering studies have been widely used to provide models of the molecular motions in plastic crystals. Since the timescale of neutron scattering is fast, this technique is particularly useful for characterizing motions on the timescale of 10^{-11} to 10^{-13} s. However, this method offers little information about the slower motions in the disordered phases. NMR spectroscopic methods, however, are more sensitive to the presence of slow motions and can be used to detect such motions in both disordered and ordered phases, determine the barriers to motions, and identify the nature of the reorientations.

The factor group method (12), by which the splittings of vibrational peaks can be correlated with the changes in symmetry that occur at the phase transition, provides an indirect method of obtaining structural information. In the present work, we have examined the FT-IR and Raman spectra of the two different phases of 1-chloroadamantane and measured ^{13}C spin-lattice relaxation times and dipolar dephasing times. The dipolar dephasing technique has been

[1]Authors to whom correspondence may be addressed.

Can. J. Chem. Downloaded from www.nrcresearchpress.com by 203.198.23.82 on 09/08/12
For personal use only.

widely used to obtain chemical structural information and to assign the resonance signals. Although it is well known (13, 14) that molecular motion has a great impact on the dephasing of carbon signals, especially for methylene and methine carbons, this method has not been widely used in the study of molecular motions. However, the technique can be readily used to identify the motions existing in orientationally disordered crystals, such as 1-substituted adamantane derivatives (15).

Experimental

1-Chloroadamantane (1-$C_{10}H_{15}Cl$, Alfa products, 98%) was purified by repeated slow vacuum sublimation (21°C, 10^{-3} Torr; 1 Torr = 133.3 Pa). The purified material was analyzed by gas chromatography and was greater than 99.5% pure.

Differential scanning calorimetry (DSC) measurements were performed on a Perkin–Elmer DSC-7 calorimeter, calibrated for both temperature and enthalpy scales using the phase and melting transitions of cyclohexane (Aldrich Chemical Co, "Gold" grade), at a scanning rate of 2.5 K min^{-1}.

The IR spectra (1 cm^{-1} resolution) were recorded on an Analect AQS-18 FT-IR spectrometer equipped with a DTGS detector. The spectra were obtained using KBr pellets, which were allowed to relax for at least 1 month prior to use. The Raman spectra (1–2 cm^{-1} resolution) were acquired on a Instruments S.A. spectrometer with a Jobin Ramanor U-1000 double monochromator using the 514.5-nm line of a Spectra Physics model 164 argon-ion laser (~250 mW power at the sample) as the excitation source. The samples were sealed in glass capillary tubes and mounted on the cold finger of a cryostat by using indium foil as the conducting junction. The temperature was controlled, for both the IR and Raman studies, by a Cryodyne Cryocooler model 21 cryostat (Cryogenics Technology Inc.) and was measured with a silicon diode temperature sensor attached to a Cryophysics model 4052 controller.

The ^{13}C spin-lattice relaxation and dipolar dephasing time measurements were performed on a Chemagnetics M100 spectrometer operating at 25.2 MHz. The samples were packed in a bullet-type zirconia rotor (9.5 mm diameter). The sample temperature was regulated to within ±2 K by a Chemagnetics RKC REX-C1000 temperature controller. The ^{13}C spin-lattice relaxation times were measured by the standard inversion–recovery pulse sequence, using seven or more τ values and a delay of at least 5 times T_1. The 90° pulse widths were between 5 and 6 μs. The number of transients required to obtain good signal-to-noise ratios were 32 and 128 for the disordered and ordered phases, respectively. A nonlinear, three-parameter-fit program was used to calculate the T_1 values. The spinning speed of the sample was between 3 and 4 kHz.

The pulse sequence used for the dipolar dephasing experiment was that proposed by Bodenhausen et al. (16) and described by Alemany et al. (14). The contact time for cross polarization was 4 ms for phase II of 1-chloroadamantane but, due to the extensive motion occurring in the high-temperature phase, the carbon spins were difficult to polarize and a 20 ms contact time was necessary.

Results and discussion

The DSC results were obtained for both cooling and heating directions and the transition was observed at 240 and 245 K, with enthalpy and entropy of transition of 5.35 kJ mol^{-1} and 22.0 J K^{-1} mol^{-1}, respectively. The results are in reasonable agreement with those previously reported (2) except for the small hysteresis in transition temperature. The latter is consistent with the relatively low entropy of transition (17).

Typical vibrational spectra are shown in Figs. 1 and 2. In the infrared spectrum, the broad C—H stretching region displayed considerable splitting when the sample was cooled

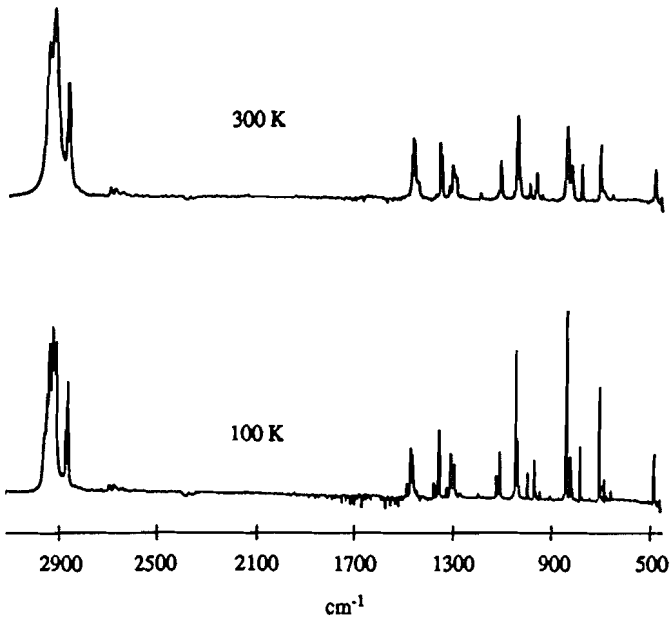

FIG. 1. Infrared spectra of phases I and II of 1-chloroadamantane.

from phase I to the ordered phase II. In the remaining regions of the spectrum, nearly all the peaks split into doublets. The notable exceptions were those at 1343 and 1350 cm^{-1}, the CH_2 wag and CCH deformation, respectively, which collapse to a single peak in phase II. The relative intensities of some of the peaks also change at the transition, with the CCC bending and CC stretching (1036 cm^{-1}), CH_2 wagging and CCH deformation (1459, 1346 cm^{-1}), and C—Cl stretch (828 cm^{-1}) modes showing the most pronounced effects. In the Raman spectra, most of the peaks exhibited the same splitting into two components and the most obvious changes in intensity occurred for the C—C—Cl bend at 215 cm^{-1}, and the C—C—C bend and C—C stretch at 1104 cm^{-1}.

The vibrational representation for the free 1-chloroadamantane molecule transforms as $\Gamma_{vib} = 16a_1 + 8a_2 + 24e$, where the a_1 and e modes are both IR and Raman active and the a_2 modes are inactive in both the IR and Raman spectra. Thus, there should be a total of 40 IR/Raman active modes, and a total of 29 Raman and 26 IR bands were observed, Table 1. Coincidence of the fundamentals in the infrared and Raman spectra of phase II confirms that the unit cell is not centrosymmetric. Moreover, since the space group of the ordered phase is $P2_1/c$, the $C_{10}H_{15}Cl$ molecule, with molecular symmetry C_{3v}, can only occupy sites with C_1 symmetry in the C_{2h} factor group and all the vibrational modes should split into four components, with the a_g and b_g modes being active in the Raman and the a_u and b_u modes being active in the infrared spectra. The correlation diagram is given in Fig. 3. Since no peak in either spectrum was split into more than a doublet, the observed splittings are in agreement with the factor group predictions.

The spin-lattice relaxation times of the three different protonated carbons, C_β, C_δ, and C_γ, were measured with respect to temperature in both the disordered and ordered phases. Figure 4 shows the temperature dependences of the T_1 values in each phase. In phase I, the T_1 values for all three carbons decreased with decreasing temperature and started approaching a minimum just before the transition tempera-

Can. J. Chem. Downloaded from www.nrcresearchpress.com by 203.198.23.82 on 09/08/12
For personal use only.

TABLE 1. Vibrational frequencies (cm^{-1}) for 1-chloroadamantane

Phase I (190 K)		Phase II (300 K)		
Raman	IR	Raman	IR	Assignments
2960s				
2954s		2954s		a_1 CH str.
	2947sh			
2940s,sh	2939s		2934vs	
2927vs	2928vs	2927vs		
2920vs	2920sh	2920sh		a_1,e
	2915vs			
2910sh	2906vs	2910sh	2908vs	CH_2 antisymmetric str.
2902vs	2900vs	2900s		
2887m				
2870s,sh				a_1,e
	2861vs			CH_2
2855s	2855s	2855s	2854s	sym. str.
1476vw		1477vw		
	1459w		1460m	a_1,e
	1451w		1450m	CH_2 def.
1440sh			1440sh	
1439s	1434sh	1439s		
1380vw		1380vw		
1370vw	1367w	1370vw		a_1,e
			1352vw	CH_2 wag and CCH def.
			1350m	
	1346m		1343m	
1320vw	1318vw	1320vw		
	1314vw		1313vw	a_1,e CH def.
1300w	1298m	1298br,w	1299br,w	
1290w	1287w			
1280w	1282m			e
1266s			1268vw	
1265sh		1264s		C—C str.
	1257vw			
1191vs			1190vw	e
1186s	1186vw	1186s		CH def
1110vw	1113w			
1104s	1105w	1103br,s		
1100sh	1099m		1102w	
1035w	1035s	1036w,br	1036m	
1030w				a_1,e
	1026m			
			1000vw	CCC bend and C—C str.
990sh				
988sm	984w	985s	985s	
960vs	955w	958s	953w	
950w	950sh			
933m	931vw	932vw		a_1 C—Cl str.
828m	825vs	829m,br		
			827m	
810w	810w	810w,br	809w	
806vw	806w			a_1,e
	801w,sh			CH_2 antisymmetric def.
772vs	770sh	772vs	767m	
	768m			

TABLE 1 (*concluded*)

Phase I (190 K)		Phase II (300 K)		Assignments
Raman	IR	Raman	IR	
693s	690s	694s	691m	a_1,e
			680sh	
673w	670vw			C—C—C
			650vw	
645w	643vw	645w	645vw	bending
476m	474w	479m,br		e
453w		455w		C—Cl
			477w	bend
404w		404br,w		
360w				Skeletal
355w				modes
339vs		339s,br		
330s				
221m				C—C—Cl
215m		215m		str.
83vw				
65w				Skeletal
64w				modes
60sh				

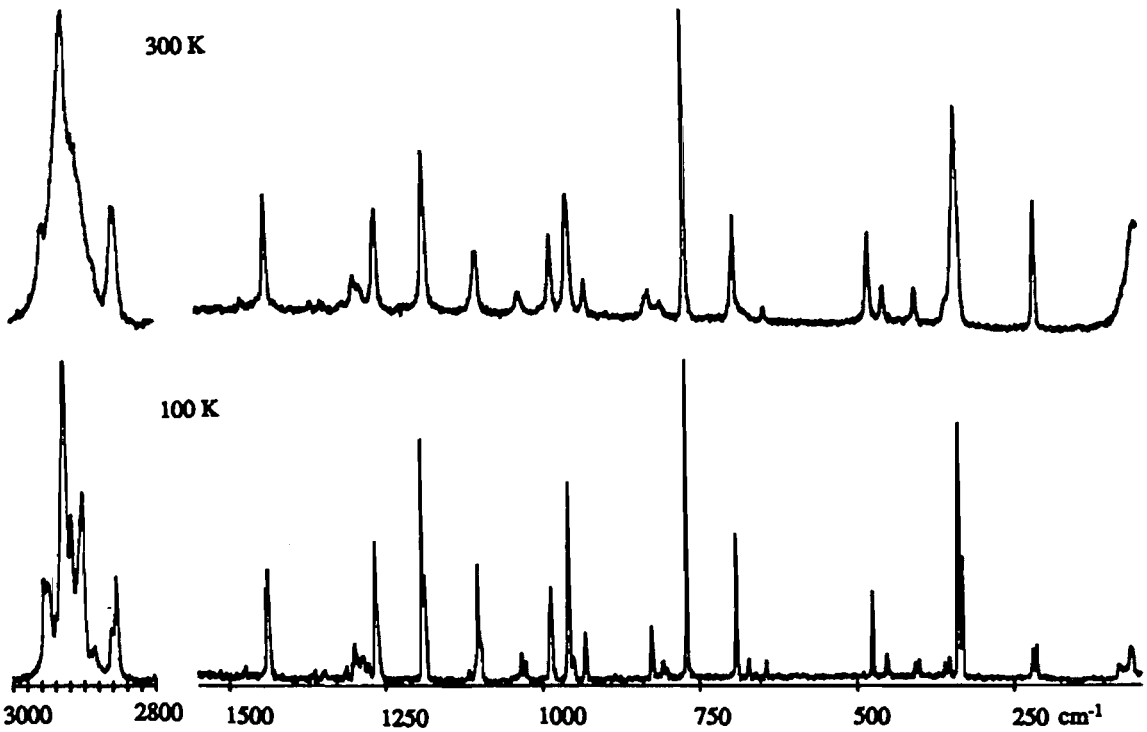

FIG. 2. Raman spectra of phases I and II of 1-chloroadamantane.

ture. The dominant relaxation mechanism of the methylene and methine carbons is the dipole–dipole interaction between the ^{13}C nuclei and their attached protons, and T_1 is given by eq. [1].

$$[1] \quad 1/T_1 = (3\gamma_H^2 \gamma_{C2} h^2/10 r_{CH}^6) \Sigma A_i f(\omega_H,\omega_C,\tau_i)$$

where

$$f(\omega_H,\omega_C,\tau_i) = \tau_i/[1 + (\omega_H - \omega_C)^2\tau^2] + 3\tau_i/[1 + \omega_{C2}\tau^2] + 6\tau_i/[1 + (\omega_H + \omega_C)^2\tau^2]$$

and the A_i terms are constants related to the changes in the second moments that result from the different motions. In a completely rigid lattice, or in the case of fast isotropic rotation, the ratio of the T_1 values for the methine and meth-

Can. J. Chem. Downloaded from www.nrcresearchpress.com by 203.198.23.82 on 09/08/12
For personal use only.

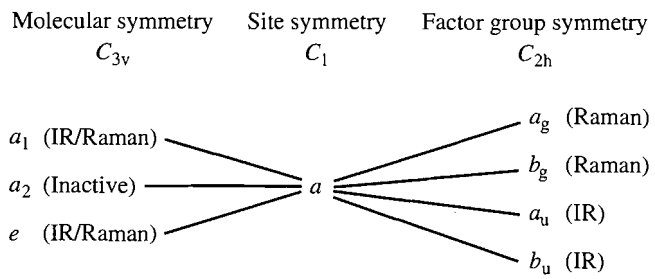

FIG. 3. Correlation diagram for the ordered phase of 1-chloroadamantane.

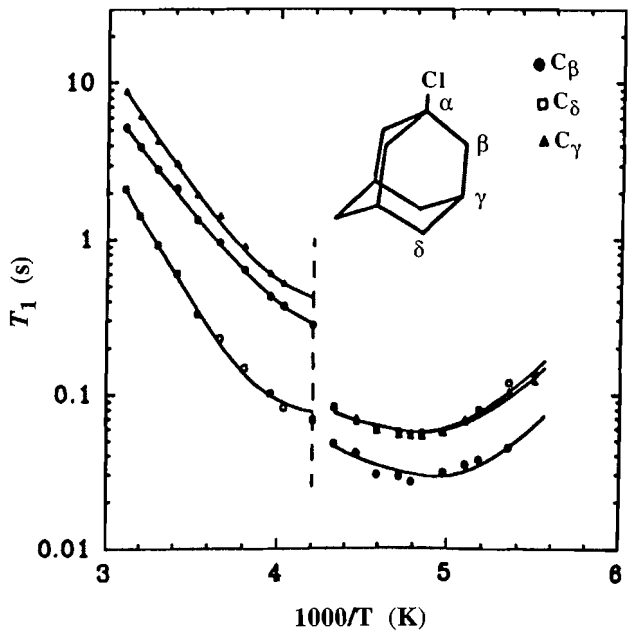

FIG. 4. ^{13}C spin-lattice relaxation times in 1-chloroadamantane.

TABLE 2. Activation energies (kJ mol^{-1}) from the temperature dependences of the ^{13}C T_1 values in 1-chloroadamantane

Carbon[a]	Phase I	Phase II
C(β)	25.8 ± 0.7	22.4 ± 1.1
C(γ)	26.7 ± 0.7	20.7 ± 1.2
C(δ)	32.1 ± 0.6	21.0 ± 1.2
Average	28.2	21.4
^1H[b]	28.6	23.8

[a]Peak assignments are from ref. 18.
[b]From ref. 9.

ylene carbons of 1-chloroadamantane should be 2:1, or close to it. In the disordered phase I of 1-chloroadamantane, however, the order of T_1 was $C_\gamma > C_\beta > C_\delta$ and the average ratios $T_1(\gamma)/T_1(\beta)$ and $T_1(\gamma)/T_1(\delta)$ were 1.5 and 5.9, respectively. These results are almost exactly the same as those observed for phase I of 1-bromoadamantane (15), indicating that the motions modulating the relaxation process in phase I of both compounds are the same, and are not due to isotropic rotation. Furthermore, this motion may be different from that in the disordered phase of 1-fluoroadamantane since the ratios of T_1 $(\gamma)/T_1(\beta)$ and $T_1(\gamma)/T_1(\delta)$ are different, although the T_1 order for the three protonated carbons is the same. According to the neutron scattering results (10), the tumbling motion for 1-chloroadamantane in phase I is the reorientation of the molecular axis among six fourfold crystallographic [100] directions, while the molecular axis of the 1-fluoro derivative tumbles between the eight [111] directions (5). A uniaxial rotation about the molecular axis also occurs in phase I of both compounds. This fast C_3 rotation is not the dominant cause of the overall relaxation process since the combined jumps of the C—Cl axis among the six crystallographic [100] directions should average the intramolecular dipolar interaction close to zero, which is close to isotropic reorientation. If it dominated relaxation, then the order of the T_1 values would be $C_\gamma > C_\beta \approx C_\delta$, which is not the case, and, therefore, an additional motion must contribute to the relaxation. The change in second moment is reciprocally related to the T_1 minimum for each carbon, and calculations show that the second moment changes on going from a rigid lattice to a 120° jump about a C_3' axis (along the C_γ—H directions) yield the order of the T_1 minima: $C_\gamma > C_\beta > C_\delta$, which is qualitatively consistent with the experimental observations.

The activation energies for rotation for each carbon in phase I are given in Table 2. The transition to phase II occurred before the minima in T_1 were reached and, therefore, separation of the motions into the uniaxial and tumbling contributions was not possible. However, the average value is in good agreement with that obtained from ^1H NMR spin-lattice relaxation time measurements (8), but the barrier is much higher than those obtained in the neutron scattering study (9) for molecular tumbling among the [100] directions (10.28 kJ mol^{-1}) and for C_3 rotation (21.41 kJ mol^{-1}). Since the NMR experiment has a slower timescale than does neutron scattering, it is not surprising that the two techniques are sensitive to different motions. The activation energy for the possible C_3' rotation for 1-chloroadamantane is smaller than that for the same motion in the 1-bromo analogue (33.0 kJ mol^{-1}).

At the transition, all three carbons showed obvious discontinuities in their T_1 values. In phase II, the relaxation times have the relation: $T_1(\delta) \approx T_1(\gamma) \approx 2T_1$ (β) (average $T_1(\delta)/T_1(\beta) = 1.95$, $T_1(\gamma)/T_1(\beta) = 1.91$). These results indicate that the dominant motion in the ordered phase has changed to a rotation about the molecular threefold axis. Since phase II is ordered, the rotation about the C—Cl axis must be the 120° jump between crystallographically equivalent sites, without introducing any disorder. A calculation of the change of second moment from the rigid lattice to C_3 rotation yields the following T_1 minima relation: $1.6\,T_1(\beta) \approx T_1(\delta) \approx T_1(\gamma)$, which is consistent with the experimental observations. By fitting the T_1 curve for each carbon, the barrier to motion was obtained, and the resulting values are listed in Table 2. The values are in good agreement with that obtained by proton T_1 measurements (8).

At the transition from phase I to phase II, the molecular tumbling is restricted, leaving rotation about the C_3 axis as the only motion responsible for relaxation. This is confirmed by the dipolar dephasing time measurements, which determine how fast a polarized carbon loses its magnetization after proton spin locking is terminated. The decay rate of the carbon signal intensity depends on the dipole–dipole interactions between the proton and carbon spins. Generally, for a molecule in a rigid lattice, dephasing is most rapid

Can. J. Chem. Downloaded from www.nrcresearchpress.com by 203.198.23.82 on 09/08/12
For personal use only.

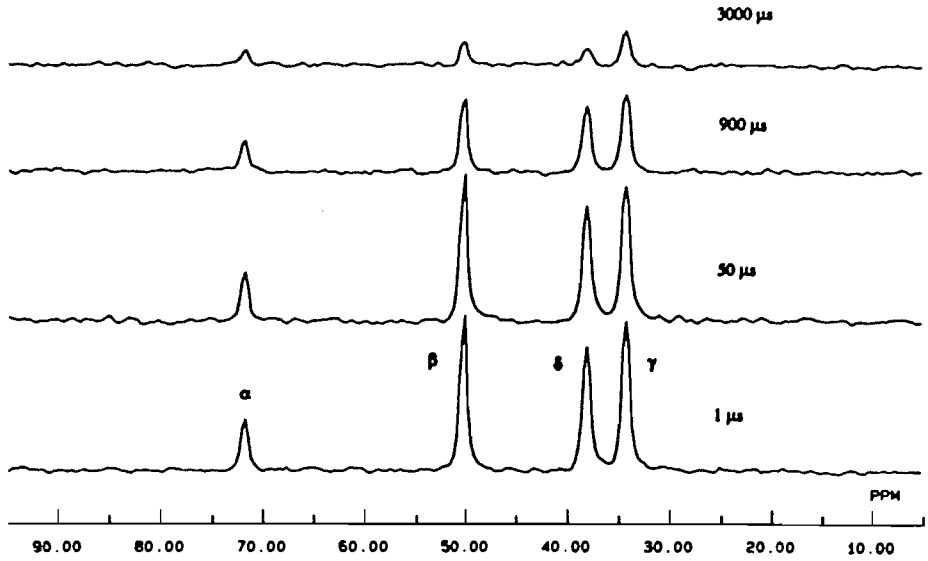

FIG. 5. Dipolar dephased spectra of phase I.

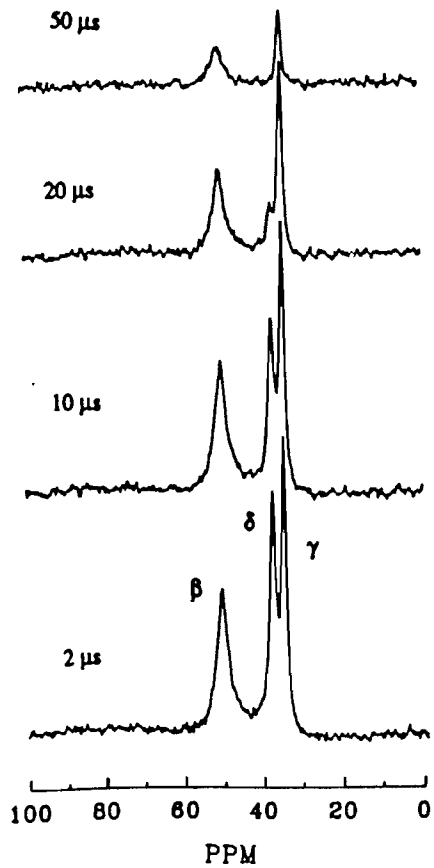

FIG. 6. Dipolar dephased spectra of phase II.

for those carbons having directly bonded protons, such as CH and CH_2 groups, while nonprotonated carbons retain phase coherence for longer times, because there is only a small effective dipolar interaction from neighboring groups. Methyl carbons usually experience a moderate degree of C—H dipolar coupling because the internal motion tends to weaken the dipolar interactions. The decrease in signal intensity during the dephasing time is characterized by a constant T'_2. Alemany et al. (14) have shown that fast decays, due to strong $^{13}C-^{1}H$ dipolar coupling, follow a second-order exponential decay (Gaussian decay):

$$[2] \quad I_G = I_{OG} \exp(-t_{dd}^2 / 2T_{2G}'^2)$$

where I_{OG} is the signal intensity at zero time and T'_{2G} is the Gaussian decay constant. Slow decays (weak dipolar interactions) can be fitted by a first-order exponential decay (Lorentzian decay):

$$[3] \quad I_L = I_{OL} \exp(-t_{dd}/T'_{2L})$$

Sometimes, the experimental data may be resolved into multicomponent decays, such as a two-component Gaussian–Lorentzian decay, described by eq. [4].

$$[4] \quad I = I_{OG} \exp(-t_{dd}^2/2T_{2G}'^2) + I_{OL} \exp(-t_{dd}/T'_{2L})$$

If rapid molecular reorientation occurs in the crystal lattice, then the rate of signal decay is diminished as the motion attenuates the effective $^{13}C-^{1}H$ dipolar interaction. This can be used to assign the motions occurring in different phases of the orientationally disordered solids. Figures 5 and 6 show the dipolar dephased spectra for different delay times, and Figs. 7 and 8 show the dependence of the intensities on the delay time, for 1-chloroadamantane in phases I and II, respectively. In the disordered phase, the intensities of all the α, β, γ, and δ carbons decayed very slowly and followed a Lorentzian decay. The decay constants for each carbon are given in Table 3. Although the β, γ, and δ carbons have directly attached protons, they decayed as slowly as the nonprotonated α-carbon, with similar Lorentzian decay constants, indicating that the motion modulates the three types of C—H vectors in a similar manner.

The intensities of the β, γ, and δ carbons in phase II decayed much faster than they did in phase I, indicating that the freedom of motion is drastically reduced. The relaxations of the β and γ carbons contain both Gaussian and Lorentzian components, suggesting that the motion still weakens the dipolar interaction but to a much lesser extent than in phase I. In particular, the decay of the signal for C_δ is much faster than for the other two carbons, Table 2, im-

Can. J. Chem. Downloaded from www.nrcresearchpress.com by 203.198.23.82 on 09/08/12
For personal use only.

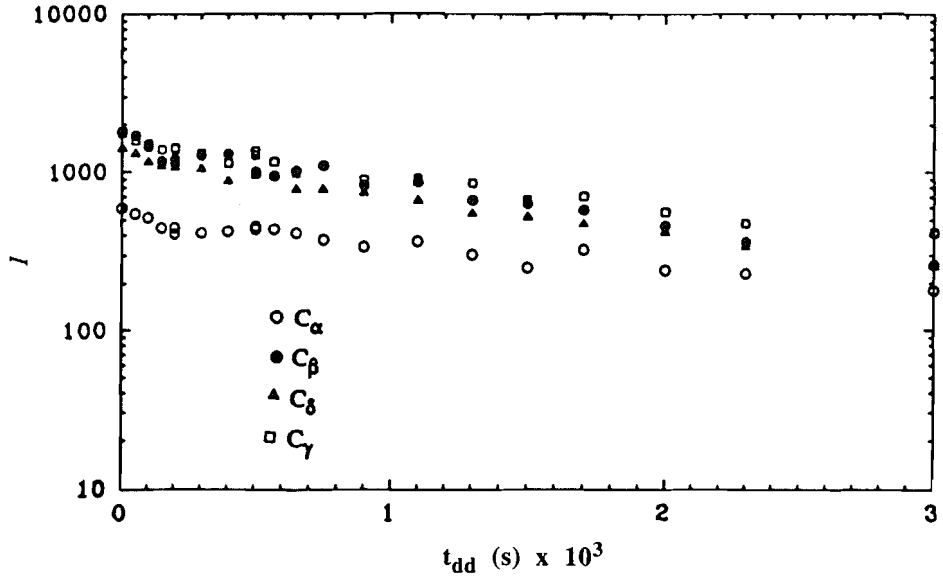

FIG. 7. Intensities (arbitrary units) of the dipolar dephased signal versus delay time for carbon spins in phase I of 1-chloroadamantane at 283 K. Rotational echoes occur at multiples of the spinning speed.

TABLE 3. Dipolar dephasing constants (T_2', s) for 1-chloroadamantane[a]

Phase		α	β	γ	δ
I	$T_{2L'}$	2.9×10^{-3}	1.7×10^{-3}	2.1×10^{-3}	1.8×10^{-3}
II	$T_{2G'}$	—	1.4×10^{-5}	1.9×10^{-5}	1.0×10^{-5}
	I_{G0}	—	486	1029	1924
	$T_{2L'}$	—	7.1×10^{-5}	5.1×10^{-5}	—
	I_{L0}	—	658	1461	—

[a]Measured at 283 and 263 K for phases I and II, respectively.

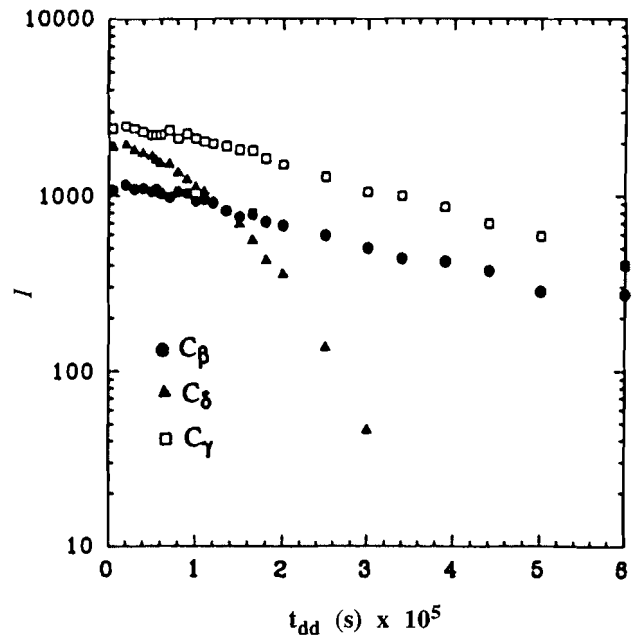

FIG. 8. Intensities (arbitrary units) of the dipolar dephased signals versus delay time for phase II of 1-chloroadamantane at 263 K.

plying that the dipolar interaction for this carbon is still strong, and was fitted to a Gaussian decay only. The protons in the axial positions on C_δ lie parallel to the axis of rotation and, therefore, no reduction in dipolar coupling occurs as a result of the rotation. Figures 7 and 8 show clearly that, after a delay time of 50 ms, the C_δ signal has completely disappeared in phase II, but remains unchanged in phase I.

The ^{13}C spin-lattice relaxation and dipolar dephasing time behaviour of 1-chloroadamantane in phases I and II is very similar to that of phases I and III of the 1-bromo compound and we conclude that the rotational motions in these two compounds are the same, but different from the fluoroadamantane case.

Acknowledgments

This work was supported by grants from the Natural Sciences and Engineering Research Council of Canada (NSERC) and the Fonds pour la formation de chercheurs et l'aide à la recherche (FCAR) (Quebec). Y.H. acknowledges the award of a Graduate Fellowship from McGill University.

1. N.G. Parsonage and L.A. Staveley. Disorder in crystals. Clarendon Press, Oxford. 1978.
2. T. Clark, T. Mc. O. Knox, and M.A. McKervey. J. Chem. Soc. Faraday Trans. 1, **73**, 1224 (1977).

Can. J. Chem. Downloaded from www.nrcresearchpress.com by 203.198.23.82 on 09/08/12
For personal use only.

3. P. Zielinski and M. Foulon. *In* Dynamics of molecular crystals. *Edited by* J. Lascombe. Elsevier Science Publishers, Amsterdam. 1987.
4. N.T. Kawai, D.F.R. Gilson, and I.S. Butler. Can. J. Chem. **69**, 1758 (1991).
5. R. Decressain, J.P. Amoureux, L. Carpentier, and J.B. Nagy. Mol. Phys. **73**, 553 (1991).
6. J. Virlet, L. Quiroga, B. Boucher, J.P. Amoureux, and M. Castelain. Mol. Phys. **48**, 1289 (1983).
7. M. Foulon, T. Belgrand, C. Gors, and M. More. Acta Crystallogr. Sect. B: Struct. Sci. **B45**, 404 (1989).
8. J.P. Amoureux, M. Bee, and J.L. Sauvajol. Mol. Phys. **45**, 709 (1982).
9. I. Ursu, R. Grosescu, M. Lupu, and E. Cornilesu. Rev. Roum. Phys. **28**, 789 (1983).
10. M. Bee and J.P. Amoureux. Mol. Phys. **48**, 63 (1983).
11. I. Ursu, R. Grosescu, M. Lupu, and E. Cornilesu. Rev. Roum. Phys. **28**, 253 (1983).
12. W.G. Fateley, F.R. Dollish, N.T. McDevitt, and F.F. Bentley. Infrared and Raman selection rules for molecular and lattice vibrations: the correlation method. Wiley–Interscience, New York. 1972.
13. M. Alla and E. Lippmaa. Chem. Phys. Lett. **37**, 260 (1976).
14. L.B. Alemany, D.M. Grant, T.G. Alger, and R.J. Pugmire. J. Am. Chem. Soc. **105**, 6697 (1983).
15. Y. Huang, D.F.R. Gilson, I.S. Butler, and F. Morin. J. Phys. Chem. **95**, 2151 (1991).
16. G. Bodenhausen, R.E. Stark, R.E. Ruben, and R.G. Griffin. Chem. Phys. Lett. **67**, 424 (1979).
17. N.T. Kawai, D.F.R. Gilson, and I.S. Butler. J. Phys. Chem. **96**, 8556 (1992).
18. T. Pehk, E. Lippmaa, V.V. Sevostjanova, M.M. Krayuschkin, and A.I. Tarasova. Org. Magn. Reson. **3**, 783 (1971).

Can. J. Chem. Downloaded from www.nrcresearchpress.com by 203.198.23.82 on 09/08/12
For personal use only.

Absorption and magnetic circular dichroism spectra of nitrogen homologues of magnesium and zinc phthalocyanine

EDWARD A. OUGH AND MARTIN J. STILLMAN[1]
Department of Chemistry, The University of Western Ontario, London, ON N6A 5B7, Canada

AND

KATHERINE A.M. CREBER
Department of Chemistry and Chemical Engineering, Royal Military College, Kingston, ON K7K 5L0, Canada

Received April 7, 1993

Can. J. Chem. Downloaded from www.nrcresearchpress.com by 203.198.23.82 on 09/08/12
For personal use only.

EDWARD A. OUGH, MARTIN J. STILLMAN, and KATHERINE A.M. CREBER. Can. J. Chem. **71**, 1898 (1993).

Absorption and magnetic circular dichroism (MCD) spectra are reported for the metallophthalocyanine-*N*-isologs: magnesium-3,4-pyridinoporphrazine ($MgPcN_4(-2)$), zinc-3,4-pyridinoporphyrazine ($ZnPcN_4(-2)$), and zinc-3,4-pyridazinoporphyrazine ($ZnPcN_8(-2)$). Band deconvolution calculations, which couple both the absorption and the MCD spectra, are reported for each complex. The presence of the peripherally fused pyridine rings in $MgPN_4(-2)$ and $ZnPcN_4(-2)$ reduces the molecular symmetry and splits the degenerate Q band into its x and y components with zero field splitting parameters (ΔQ_{xy}) of 224 and 279 cm^{-1}, respectively. Band fitting results for $ZnPcN_8(-2)$ show that with the fused pyridazine rings the degeneracy in the ^1E_g excited state is retained and the MCD envelope in the region of the Q_{00} transition can be described by an MCD A term. Comparison of the fitted band energies with the results reported for ZnPc(−2) (T. Nyokong, Z. Gasyna, and M.J. Stillman. Inorg. Chem. **26**, 1087 (1987)) and MgPc(−2) (E.A. Ough, T. Nyokong, K.A.M. Creber, and M.J. Stillman. Inorg. Chem. **27**, 2725 (1988)) shows that as the number of nitrogens substituted increases from 0 to 8, the Q band blue shifts from 671 nm in ZnPc(−2) to 664 nm in $ZnPcN_4(-2)$ (midpoint between the x and y components) to 654 nm in $ZnPcN_8(-2)$ and from 672 nm in MgPc(−2) to 666 nm in $MgPcN_4(-2)$ (midpoint). These results demonstrate that chemical modification (symmetric and asymmetric) of the peripherally fused benzene rings influences both the energy and the symmetry of the states that form the inner 18-π-electron system.

EDWARD A. OUGH, MARTIN J. STILLMAN et KATHERINE A.M. CREBER. Can. J. Chem. **71**, 1898 (1993).

On a déterminé les spectres d'absorption et de dichroïsme circulaire magnétique (DCM) des *N*-isologues suivants de métallonaphthalocyanines : magnésium-3,4-pyridinoporphrazine ($MgPcN_4(-2)$), zinc-3,4-pyridinoporphrazine ($ZnPcN_4(-2)$) et zinc-3,4-pyridazinoporphrazine ($ZnPcN_8(-2)$). Pour chacun des complexes, on a effectué des calculs de déconvolution de bande qui permettent de coupler les spectres d'absorption et de DCM. La présence de noyaux pyridines condensés d'une façon périphérique dans de $MgPcN_4(-2)$ et dans le $ZnPcN_4(-2)$ réduit la symétrie moléculaire et dédouble la bande Q dégénérée en ses composants x et y avec des paramètres de couplage de champ zéro (ΔQ_{xy}) de 224 et 279 cm^{-1} respectivement. Un ajustement des bandes du $ZnPcN_8(-2)$ montre qu'avec les cycles pyridazines condensés la dégénérescence de l'état excité ^1E_g est conservée et que l'enveloppe du DCM dans la région de la transition Q_{00} peut être décrite par un terme A du DCM. Une comparaison des énergies des bandes ajustées avec les résultats rapportés pour le ZnPc(−2) (T. Nyokong, Z. Casyna et M.J. Stillman. Inorg. Chem. **26**, 1087 (1987)) et pour le MgPc(−2) (E.A. Ough, T. Nyokong, K.A.M. Creber et M.J. Stillman. Inorg. Chem. **27**, 2725 (1988)) montre que lorsque le nombre d'atomes d'azote substitués augmente de 0 à 8, la bande Q se déplace de 671 nm dans le ZnPc(−2) à 664 nm dans le $ZnPcN_4(-2)$ (point moyen entre les composantes x et y) et à 672 nm dans le $ZnPcN_8(-2)$, et de 672 nm dans le MgPc(−2) à 666 nm dans le $MgPcN_4(-2)$ (point moyen). Ces résultats démontrent que la modification chimique (symétrique et asymétrique) des noyaux benzéniques condensés en périphérie influence à la fois l'énergie et la symétrie des états qui forment le système interne de 18-électrons-π.

[Traduit par la rédaction]

Introduction

In recent years there has been considerable effort to examine how changes to the 18-π-electron, 16-membered, polyene aromatic ring of porphin affect its chemical, electrochemical, photochemical, and spectroscopic properties (1–3). Amongst the molecules examined have been tetraazatetrabenzoporphyrins, the phthalocyanines. Introduction of the 4-fold symmetry axis from both the bridging aza groups and the peripherally fused benzenes leads to dramatically changed chemical and optical properties of phthalocyanines when compared to unsubstituted porphyrins (1–8). Despite the magnitude of these molecular changes, metallophthalocyanines are symmetric molecules and exhibit a characteristic optical spectrum that is dominated by allowed π–π* transitions to a number of singlet excited states between 800 and 250 nm. Each of these states is doubly degenerate, which allows the technique of magnetic circular dichroism (MCD) to probe their electronic composition through measurement of the transition energy, molar absorptivity, and angular momentum (1, 2, 9). The MCD spectrum has, in the past, provided exquisite detail about the electronic structure of both porphyrins and phthalocyanines (1, 2, 6–11). However, few data have been reported for phthalocyanines in which peripheral substitution reduces the molecular symmetry below C_{4v}. Such molecules exhibit spectral properties midway between symmetric phthalocyanines and the unsymmetric chlorophylls.

Substitution at the periphery of both phthalocyanines and porphyrins offers a means of tuning the redox chemistry (1–3), linking the macrocycles into polymeric networks, and, in the case of the phthalocyanines, increasing their solubility (3–5). While studies of the chemical and physical properties of porphyrins have been aided by their solubility in a wide variety of solvents, similar studies of phthalocyanines

[1]Author to whom correspondence may be addressed.

Can. J. Chem. Downloaded from www.nrcresearchpress.com by 203.198.23.82 on 09/08/12
For personal use only.

have been hindered by their limited solubility in these solvents. The solubility of phthalocyanines can be enhanced by the choice of the central metal, by the addition of axial ligands to form soluble five- and six-coordinate MPc complexes, and by chemical modification of the peripherally fused benzene rings. Group I and II metallophthalocyanines exhibit high solubilities in a wide range of spectroscopic and electrochemically useful solvents. While axial ligands do enhance the solubility of many metallophthalocyanines, the bound ligand or excess free ligand greatly reduces the transparency in the 200–300 nm region. In tetrasulphonated phthalocyanines the sulphate groups enhance the solubility of the phthalocyanine but severe aggregation makes interpretation of the spectroscopic data difficult (1).

Analysis of optical and magnetic data obtained from nonsymmetric species is difficult because the effect of the distortion on the states involved must be determined. The MCD experiment is an ideal tool in that it provides, directly from solutions at room temperature, values for the angular momentum in the specific state. If new orbitals or new vibronic couplings become allowed as a result of the geometric distortions then the angular momentum will not be conserved. Apart from modifications to the ring itself, the free base phthalocyanine (H_2Pc) offers the most significant reduction in symmetry that has been readily studied (1). The optical spectrum is characterized by two major bands in the Q region, at 650 and 697 nm (1, 6, 7). The reduction from D_{4h} to D_{2h} symmetry breaks the degeneracy of the $e_g(\pi^*)$ orbitals and the MCD spectra clearly identify the split Q_x (negative B term in the MCD spectrum) and Q_y (positive B term in the MCD spectrum) components (1, 6, 7). Unsymmetric peripheral substitution in protoporphyrin IX removes the degeneracy of the E_g excited states through rhombic distortion of the molecule (8). The zero field splitting parameters for metalloporphyrins can be measured from MCD and absorption spectra, but the compression of the electronic transitions into a narrow spectral range makes accurate determination of these parameters difficult. The intense, narrow, and relatively isolated Q_{00} transition (1) in metallophthalocyanines can be used to study rhombic distortions and to determine zero field splitting parameters. The MCD technique provides unambiguous assignment criteria that can be used to calculate the extent of the splitting induced by the reduction in symmetry. A simplified molecular orbital diagram based on Gouterman's four-orbital calculations (9), which identifies the one-electron transitions that give rise to the first five allowed transitions in symmetric, closed-shell metallophthalocyanines (1, 10, 11), is shown in Fig. 1. Each of the resulting excited states are orbitally degenerate and positive A terms will be observed in the MCD spectrum.

In the late 1950s and early 1960s cobalt and nickel salts were reacted in a urea melt with cinchomeronic acid (3,4-dicarboxypyridine) to form phthalocyanine derivatives where the peripherally fused benzene rings were replaced with fused pyridines (12–16). Absorption spectra of various metal-3,4-pyridinoporphrazines (metallophthalocyanine-*N*-isologs; $MPcN_4(-2)$) indicated the presence of two overlapping bands where a single degenerate Q band was normally situated (12, 14). During its synthesis, $MPcN_4(-2)$ can be formed as one or more of the four possible structural isomers displayed in Fig. 2. Because three isomers have reduced symmetries it is reasonable to assume that the two overlapping bands occur either from a mixture of structural isomers or from a single structural isomer exhibiting significant rhombic distortion.

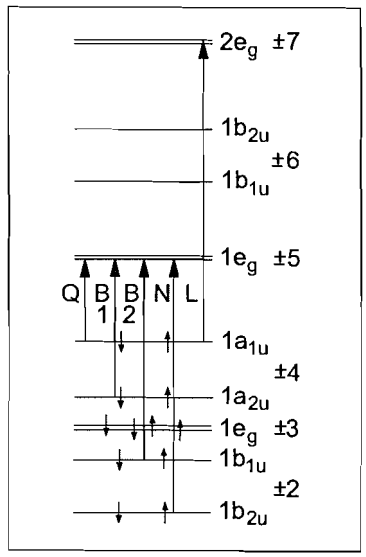

FIG. 1. Selected molecular orbitals of the phthalocyanines with D_{4h} symmetry. The order of the orbitals has been adapted from ref. 9.

In this paper, we report absorption and MCD spectra for $MgPcN_4(-2)$, $ZnPcN_4(-2)$, and the symmetric D_{4h} zinc-tetra-3,4-pyridizoporphrazine ($ZnPcN_8(-2)$). Deconvolution calculations are used to obtain band centre energies and the method of moments has been used to obtain the magnetic moments of the transitions that contribute to the observed spectral envelopes, especially the in Q region between 500 and 700 nm.

Experimental section

Materials and methods

$MgPcN_4(-2)$ was prepared by heating 1.0 g $MgCl_2$ (BDH), 1.0 g urea (BDH), 3.0 g 3,4-pyridine dicarboxylic acid (Aldrich), and 0.03 g ammonium molybdate (BDH) together at 160°C for 20 mins. $ZnPcN_4(-2)$ was prepared using the above method by replacing $MgCl_2$ with $ZnCl_2$. Both complexes were purified by literature methods (12, 14–16). The first step in the preparation of $ZnPcN_8(-2)$ was the oxidation of phthalazine (Aldrich) to 4,5-dicarboxypyridazine using potassium permanganate (BDH). The 4,5-dicarboxypyridazine (3.0 g) was heated with 1.0 g $ZnCl_2$, 1.0 g urea, and 0.03 g ammonium molybdate at 160°C for 20 mins. The purification method used for $ZnPcN_4(-2)$ was used to purify $ZnPcN_8(-2)$. Dimethylacetamide (DMA; BDH), dimethyl sulphoxide (DMSO; BDH), isopropanol (iPrOH; BDH), and tetrabutylammonium cyanide (TBACN; Aldrich) were used without purification.

Spectroscopic methods

All spectra were recorded as either DMA, DMSO, or iPrOH solutions at concentrations of approximately 10^{-6} mol L^{-1} which gave maximum absorbances of 1.0–1.5 in the Q-band region. Absorption spectra were recorded using a Cary model 219 spectrophotometer and digitized on an IBM S9001 computer. MCD spectra were recorded at room temperature using a Jasco J500 C spectropolarimeter controlled by a IBM S9001 computer using the computer program CDSCAN5 (17), with a field of 5.5 T provided by an Oxford Instruments SM2 superconducting magnet. The MCD signal intensity was calibrated using aqueous cobalt (II) sulphate ($\Delta\epsilon_M(510\text{ nm}) = -1.9 \times 10^{-2}$ L mol^{-1} cm^{-1} T^{-1}).

Can. J. Chem. Downloaded from www.nrcresearchpress.com by 203.198.23.82 on 09/08/12
For personal use only.

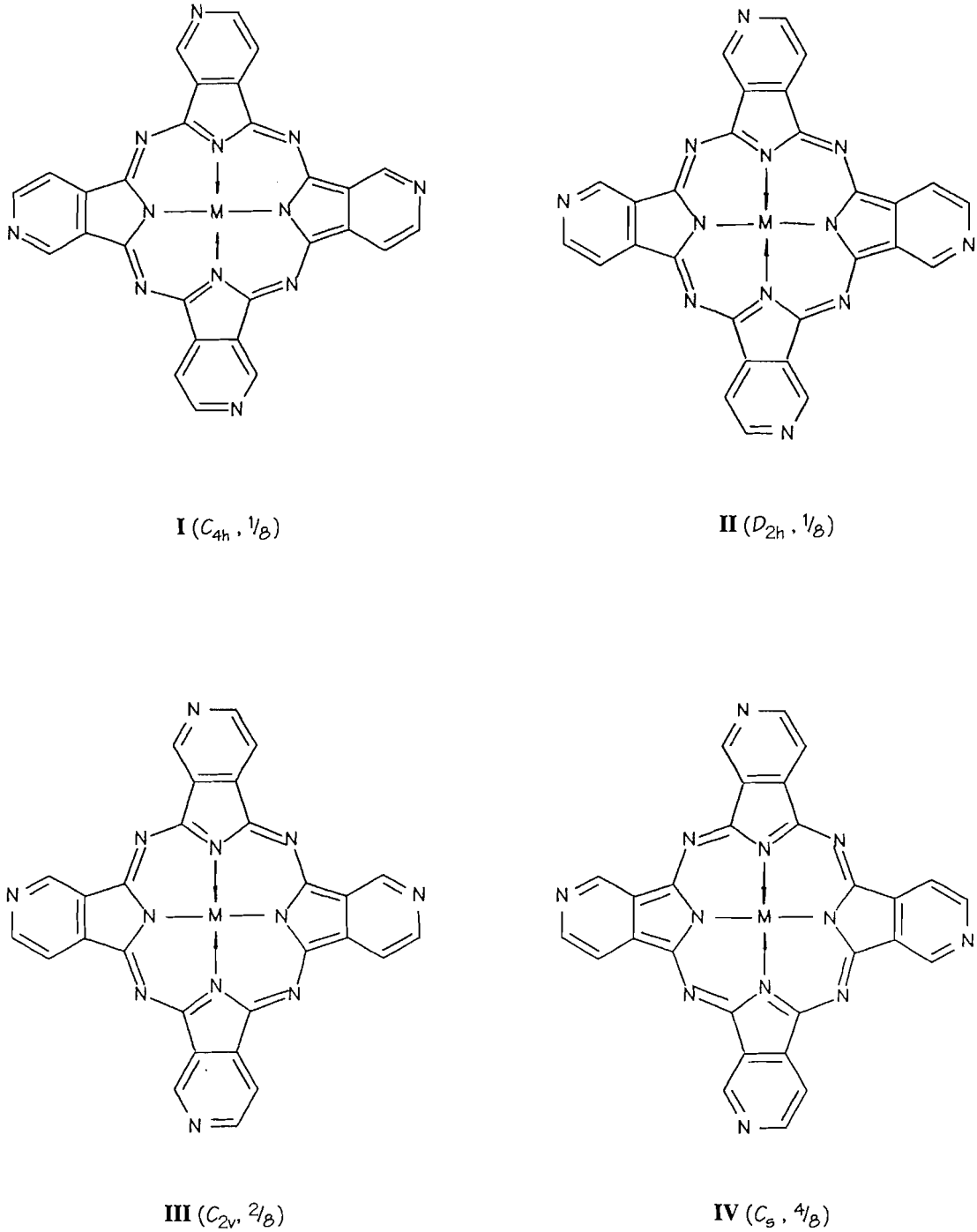

FIG. 2. The four structural isomers of $MPcN_4(-2)$. The symmetry group of each isomer is listed below the isomer and in parentheses, the statistical fraction formed during the reaction.

Data analysis

As in our previous work, Gaussian band shapes were used to fit the absorption and MCD spectra. A Simplex routine was used to fit the MCD spectra and a least-squares minimization routine based on second derivatives was used to fit the absorption data (18*a*). The database management program Spectra Manager (18*b*) was used to manipulate the spectral data.

Results

Spectral data

The room temperature absorption and MCD data for $MgPcN_4(-2)$, $ZnPcN_4(-2)$, $TBA[(CN)ZnPcN_4(-2)]$, and $ZnPcN_8(-2)$ are shown in Figs. 3, 5, 6, and 7. The observed band maxima are tabulated in Table 1. The results of deconvolution calculations for $MgPcN_4(-2)$ and $TBA[(CN)ZnPcN_4(-2)]$ in the visible region are shown in Figs. 4 and 8, and for $MgPcN_4(-2)$, $ZnPcN_4(-2)$, and $ZnPcN_8(-2)$ in the 300–500 nm region as Figs. 9, 10*a*, and 10*b*. The fitting parameters are tabulated in Tables 2–4. Common features in the absorption spectra of symmetric metallophthalocyanines are (*i*) an intense, narrow *Q* band located near 670 nm, which is associated with a positive MCD *A* term; (*ii*) a series of weak overlapping bands to the blue side of the *Q* band

TABLE 1. Observed maxima in the absorption spectra of the $MPcN_{4,8}(-2)$ complexes

$MPcN_{4,8}$	λ/nm					
$ZnPcN_8$/DMSO	655	594		569	381	
$MgPcN_4$/DMA	671	662[a]		603	369	
$ZnPcN_4$/DMA	672	664[a]		602	380	
$[(CN)ZnPcN_4]^-$/iPrOH	671	660	627	601	389	312

[a]Shoulder.

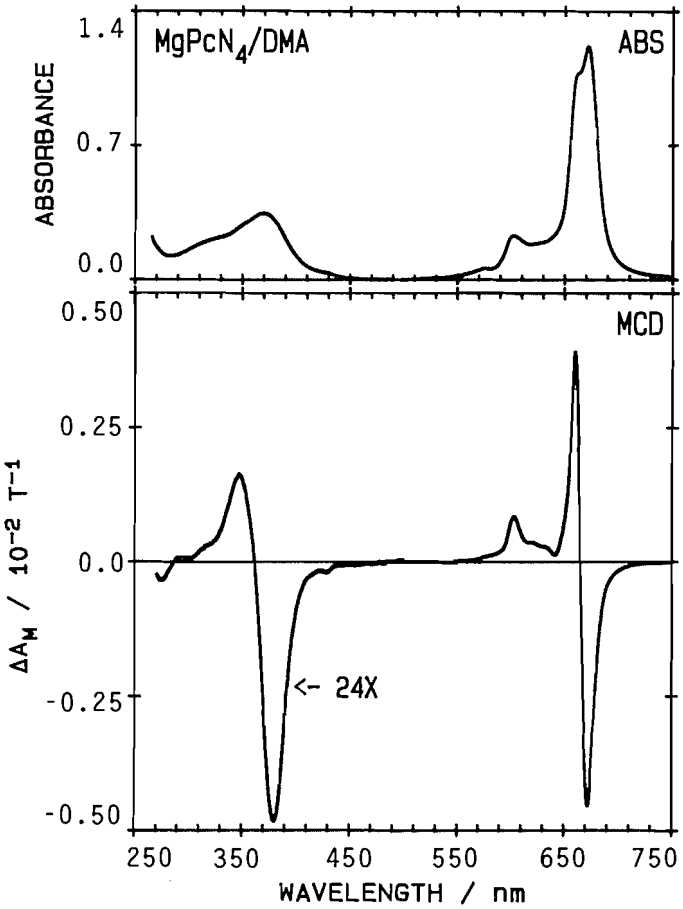

FIG. 3. Absorption and magnetic circular dichroism (MCD) spectra for $MgPcN_4(-2)$ in DMA. Spectra were measured in 1-cm path length square UV cells or 1-cm path length cylindrical MCD cells.

assigned as a combination of several vibrational progressions, Q_{vib}; (*iii*) a "window" region between 580 and 450 nm; and finally, (*iv*) between 400 and 250 nm, a region of more intense, broader bands that essentially overlap to the solvent cutoff at 250 nm (1). MCD *A* terms are measured under each of the major absorption bands (1, 10, 11, 19–22).

The absorption and MCD spectra for $MgPcN_4(-2)$ shown in Fig. 3 essentially exhibit these features. Although the split *Q* band envelope observed between 650 and 680 nm is associated with a derivative-shaped MCD envelope, the results of band deconvolution calculations, shown as Fig. 4, *conclusively show that the two components are polarized in the* x *and* y *directions*. We can then unambiguously assign the band as arising from the *Q* state where the degenerate components split as a result of the molecular geometry.

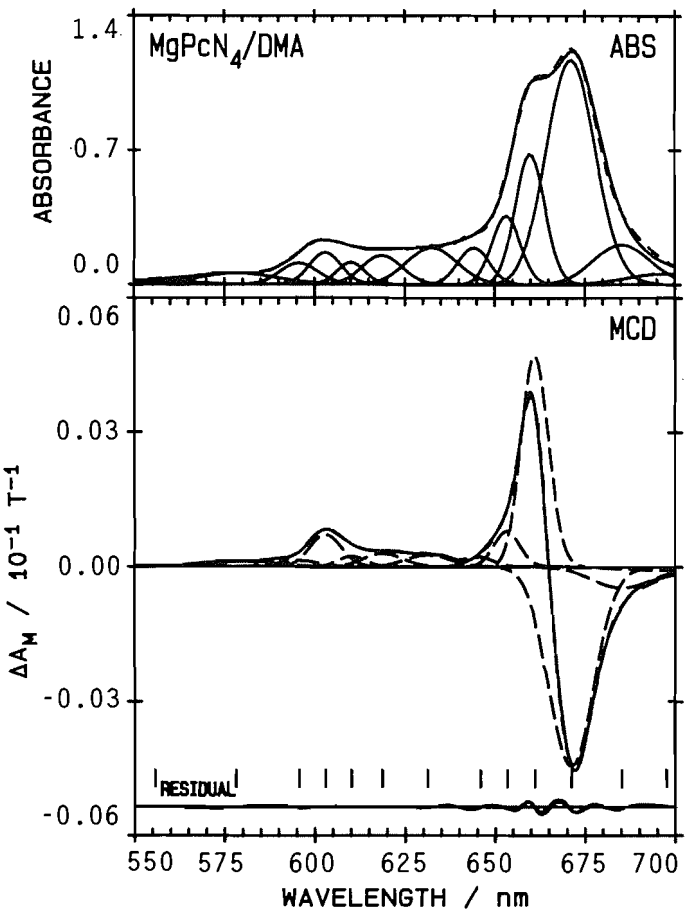

FIG. 4. Results of a band analysis for $MgPcN_4(-2)$ in DMA in the visible region (bands 1–13). (Top) Absorption: (——) experimental data; (----) fitted data; (——) individual bands. (Bottom) MCD (——) experimental data; (---) fitted data; (---) B terms.

Molecular aggregation can be ruled out as the cause of this splitting, since aggregation causes extensive broadening in the *Q* region (1). The apparent derivative shape of the MCD spectral envelope between 625 and 700 nm can be accounted for by two overlapping oppositely signed *B* terms separated by 224 cm^{-1}. With the exception of the *Q* band, the remainder of both the absorption and MCD spectra bear close similarities to those of unsubstituted diamagnetic main group phthalocyanines (1). The *B* region in main group phthalocyanines is difficult to assign in the absence of deconvolution data as the bands are significantly overlapped. We describe later the fits obtained for the *B* region; suffice to say that because the *Q* band region required MCD *B* terms, no degenerate states will be found and the entire MCD spectrum is dominated by *B* terms. The molecular symmetry must be less than D_{4h}.

The *Q* region absorption and MCD spectra of $ZnPcN_4(-2)$ and TBA[$(CN)ZnPcN_4(-2)$], shown in Figs. 5 and 6, respectively, closely resemble those of $MgPcN_4(-2)$. Both complexes exhibit a split *Q* band in the absorption spectrum and deconvolution of the $ZnPcN_4(-2)$ spectrum in the *Q* region (not shown) fits these two bands to two overlapping, oppositely signed, MCD *B* terms separated by 279 cm^{-1}, Table 3. The spectral envelope exhibited by TBA[$(CN)ZnPcN_4(-2)$] in the *B* region is consistent with the spectra

Can. J. Chem. Downloaded from www.nrcresearchpress.com by 203.198.23.82 on 09/08/12
For personal use only.

TABLE 2. Band fitting parameters[a] for Mg(II)$PcN_4(-2)$ in DMA[e]

Band no.	ν cm^{-1}	λ nm	$\Delta\nu$ cm^{-1}	D_0/C^b (10^{-5})	Band type	$\langle\Delta A_M\rangle_0{}^c$ (10^{-5})	$\mathcal{B}_0/C^d$ (10^{-7})	$\mathcal{B}_0/D_0$ (10^{-3})
1	14 334	698	522	1.83	*B*	−2.74	−1.80	−9.84
2	14 593	685	414	4.07	*B*	−15.48	−10.15	−24.94
3	14 902	671	323	17.01	*B*	−112.9	−74.07	−43.54
4	15 126	661	204	6.69	*B*	74.59	48.91	73.11
5	15 308	653	200	3.35	*B*	12.12	7.95	23.73
6	15 483	646	200	2.00	*B*	3.32	2.17	10.85
7	15 843	631	358	3.29	*B*	7.14	4.68	14.22
8	16 162	619	333	2.03	*B*	7.33	4.81	23.69
9	16 389	610	243	1.14	*B*	4.17	2.74	24.04
10	16 585	603	282	1.82	*B*	14.51	9.51	52.25
11	16 788	596	344	1.49	*B*	3.58	2.35	15.77
12	17 295	578	754	1.71	*B*	5.96	3.91	22.87
13	17 997	556	699	0.56	*B*	0.352	0.231	4.13
14	22 214	450	1861	0.17	*B*	−0.139	−0.091	−5.35
15	23 395	427	1255	0.97	*B*	−0.332	−0.218	−2.25
16	24 867	402	1637	3.28	*B*	−0.868	−0.569	−1.73
17	26 311	380	1568	10.07	*B*	−13.93	−9.13	−9.07
18	27 359	366	1511	7.16	*B*	−0.335	−0.220	−0.307
19	28 595	350	1912	10.07	*B*	5.11	3.35	3.33
20	30 084	332	1761	5.61	*B*	0.985	0.646	1.15
21	31 254	320	1728	4.51	*B*	0.524	0.343	0.761
22	32 613	307	1970	5.70	*B*	0.226	0.148	0.260
23	34 233	292	1786	3.46	*B*	0.201	0.132	0.382
24	35 761	280	1762	2.92	*B*	−0.416	−0.273	−0.935
25	37 107	270	1708	3.59	*B*	−0.940	−0.616	−1.72
26	38 138	262	1391	4.36	*B*	−3.81	−2.50	−5.73

[a]Statistics are as follows. *B*-band region: $\lambda_{260-500\ nm}$, $\chi^2 = 1.37 \times 10^{-3}$, $\Sigma(\Delta A)^2 = 4.09 \times 10^{-7}$. *Q*-band region: $\lambda_{500-700\ nm}$, $\chi^2 = 4.51 \times 10^{-4}$, $\Sigma(\Delta A)^2 = 2.38 \times 10^{-4}$.

[b]$D_0 = \langle A\rangle_0/326.6$ where the units of D_0 (dipole strength) are D^2 (D: Debye units).

[c]$\langle\Delta A_M\rangle_0$ is the zeroth moment of the MCD. When fitting with a *B* term, the program calculates $\langle\Delta A_M\rangle_0$. The Faraday term value of $\mathcal{B}_0$ is calculated directly from the moments as follows: $\mathcal{B}_0 = \langle\Delta A_M\rangle_0/152.5$; $A_1 = \langle\Delta A_M\rangle_1/152.5$.

[d]The units of $\mathcal{B}_0$ are D^2/cm^{-2}.

[e]The concentration (*C*) of the solute is not known.

of other phthalocyanines where cyanide is an axial ligand (1, 19, 20). In these data, we find that the lowest energy *B* band, *B*1, red shifts out of the main envelope and two bands are clearly seen. In symmetric metallophthalocyanines this region can be fit with two *A* terms (1, 10, 11). We will see in Fig. 10*b*, that two sets of oppositely signed *B* terms fill the MCD envelope adequately.

The absorption and MCD spectra of $ZnPcN_8(-2)$ are displayed in Fig. 7. The predominant spectral feature is the single intense absorbance band centred on 654 nm. The MCD spectrum in this region exhibits the symmetric derivative shape expected for a degenerate excited state. It is interesting that, as with some other MPc species, there is greater resolution in the MCD spectrum in the Q_{vib} region. In particular, a common feature of Q_{vib} envelopes, the positive MCD band at 600 nm, is more pronounced than is usually found. The results from spectral deconvolution of the *Q* region are presented in Fig. 8 and demonstrate that the 654-nm band can only be fit to an MCD *A* term (a residual *B* term is necessary because of field-induced mixing between this state and all other states). The absorption band maxima recorded from all the absorption spectra are listed in Table 1. In the absence of a strongly coordinated axial ligand we observe, Fig. 10*b*, that the *B*1 and *B*2 bands collapse to a single broad band centred on 380 nm as seen for ZnPc(−2) in DMA (19).

Spectral envelope deconvolution calculations

As with our previous analyses of the spectral data for ZnPc(−2) (10), MgPc(−2) (11), and MgPc(−1) (21), exact band positions can be determined through the use of deconvolution techniques. The deconvolution calculations were carried out on coupled pairs of absorption and MCD spectra (1, 18*a*). In the pairing of the fitting to associated absorption and MCD spectra we aim to place the same number of bands, with similar band centre and band width parameters, in both spectra. Although several band shapes are possible for these calculations, we feel that the Gaussian shape is satisfactory in accurately reproducing the absorption and MCD spectral envelopes of the experimental data. This is a compromise, but the previously reported spectral fits (10, 11, 21) and the data presented here do show placement of bands where one would expect them and the resultant fit forms reasonable envelopes in *both* the absorption and MCD spectra. The most significant constraint on the fitting is the requirement to place bands in both the absorption and MCD envelopes at the same energy and with similar band width values. While we aim for identical band widths, we have found that in general the MCD bands must be fitted with narrower bands than in the associated absorption band. This effect is not so pronounced when low temperature spectral data are used (J. Mack and M.J. Stillman, unpublished data). In fits of many other metallophthalocyanines, the band width

Can. J. Chem. Downloaded from www.nrcresearchpress.com by 203.198.23.82 on 09/08/12
For personal use only.

TABLE 3. Band fitting parameters[a] for $Zn(II)PcN_4$ (−2) in DMA[e]

Band no.	ν cm^{-1}	λ nm	$\Delta\nu$ cm^{-1}	$D_0/C^{b,e}$ (10^{-5})	Band type	$\langle\Delta A_M\rangle_0^c$ (10^{-5})	$\mathcal{B}_0/C^{d,e}$ (10^{-7})	$\mathcal{B}_0/D_0$ (10^{-3})
1	14 334	698	521	0.54	*B*	−2.55	−1.67	−30.97
2	14 667	682	323	1.04	*B*	−5.30	−3.48	−30.42
3	14 910	671	318	5.98	*B*	−55.82	−36.60	−61.21
4	15 189	658	278	3.88	*B*	41.42	+27.16	70.00
5	15 433	648	266	1.06	*B*	2.88	1.89	17.82
6	15 621	640	229	0.52	*B*	1.22	0.80	15.38
7	15 843	631	358	0.97	*B*	3.24	2.13	21.90
8	16 162	619	333	0.78	*B*	2.60	1.70	21.86
9	16 389	610	243	0.41	*B*	1.82	1.19	29.11
10	16 585	603	281	0.66	*B*	6.66	4.37	66.17
11	16 788	596	344	0.68	*B*	2.24	1.47	21.60
12	17 294	578	754	0.48	*B*	2.48	1.63	33.88
13	17 997	556	699	0.26	*B*	0.20	0.13	5.04
14	24 242	413	1638	1.12	*B*	−0.92	−0.60	−5.37
15	25 660	390	1744	2.46	*B*	−2.07	−1.36	−5.53
16	26 662	375	1449	2.54	*B*	−2.69	−1.76	−6.93
17	27 547	363	1549	3.87	*B*	0.133	0.09	0.23
18	28 738	348	1564	4.07	*B*	0.923	0.61	1.49
19	29 990	333	1655	4.06	*B*	0.475	0.31	0.77
20	31 314	319	1736	3.74	*B*	0.272	0.18	0.48
21	32 769	305	1837	3.83	*B*	0.032	0.02	0.06
22	34 288	292	1814	3.58	*B*	0.002	0.0	0.0
23	35 686	280	1663	3.19	*B*	−0.385	−0.25	−0.79
24	37 112	269	1774	4.93	*B*	−0.183	−0.12	−0.24
25	38 352	261	1267	5.13	*B*	0.123	0.08	0.17

[a]Statistics are as follows. *B*-band region: $\lambda_{260-500\ nm}$, $\chi^2 = 8.09 \times 10^{-6}$, $\Sigma(\Delta A)^2 = 5.66 \times 10^{-8}$. *Q*-band region: $\lambda_{500-700\ nm}$, $\chi^2 = 2.89 \times 10^{-4}$, $\Sigma(\Delta A)^2 = 5.31 \times 10^{-5}$.
[b–c]Parameters as for Table 2.

TABLE 4. Band fitting parameters[a] for $Zn(II)PcN_8$ (−2) in DMSO

Band no.	ν cm^{-1}	λ nm	$\Delta\nu$ cm^{-1}	$D_0/C^{b,e}$ (10^{-5})	Band type	$\langle\Delta A_M\rangle_n^{c,f}$ (10^{-5})	$\mathcal{B}_0(\mathcal{A}_1)/C^{d,e}$ (10^{-7})	$\mathcal{B}_0(\mathcal{A}_1)/D_0$ (10^{-3})	μ
1	13 253	755	759	0.25	*B*	−0.879	−0.576	−23.04	
2	14 190	705	782	0.57	*B*	−0.893	−0.586	−10.28	
3	14 850	673	546	1.17	*B*	−6.33	−4.15	−35.47	
4	15 282	654	350	3.94	*A*	3469.	2275.	5.77[g]	5.39
					B	−1.05	−0.686	−1.74	
5	15 648	639	307	0.24	*B*	0.648	0.425	17.71	
6	15 964	626	507	0.96	*B*	1.67	1.09	11.35	
7	16 405	610	491	0.66	*B*	1.73	1.13	17.12	
8	16 836	594	507	0.69	*B*	3.91	2.56	37.10	
9	17 244	580	503	0.34	*B*	0.765	0.501	14.74	
10	17 784	562	754	0.60	*B*	2.21	1.45	24.17	
11	18 718	534	1198	0.39	*B*	0.707	0.464	11.90	
12	20 003	500	1247	0.19	*B*	−0.084	−0.055	−9.00	
13	22 350	447	1786	0.71	*B*	−0.965	−0.633	−8.92	
14	23 687	422	1823	1.71	*B*	−1.29	−0.844	−4.94	
15	25 306	395	1946	2.78	*B*	−0.178	−0.117	−0.421	
16	26 909	372	2028	2.89	*B*	0.977	0.640	2.21	
17	28 649	349	2012	2.35	*B*	0.446	0.293	1.25	
18	30 110	332	1610	1.24	*B*	−0.076	−0.050	−0.403	
19	31 287	320	1718	1.46	*B*	−0.192	−0.126	−0.863	
20	32 781	305	2014	2.46	*B*	−0.852	−0.558	−2.27	
21	34 325	291	1780	1.98	*B*	0.117	0.077	0.389	
22	35 626	281	1659	1.73	*B*	0.367	0.241	1.39	
23	36 937	271	1785	1.74	*B*	−4.04	−2.65	−15.23	

[a]Statistics are as follows. *B*-band region: $\lambda_{260-500\ nm}$, $\chi^2 = 1.33 \times 10^{-5}$, $\Sigma(\Delta A)^2 = 9.22 \times 10^{-9}$. *Q*-band region: $\lambda_{500-800\ nm}$, $\chi^2 = 1.34 \times 10^{-4}$, $\Sigma(\Delta A)^2 = 3.22 \times 10^{-3}$.
[b–c]Parameters as for Table 2.
[f]$n = 0$ for $\mathcal{B}_0$ terms; $n = 1$ for $\mathcal{A}_1$ terms.
[g]$\mathcal{A}_1/D_0$ value = 5.77; $\mathcal{B}_0/D_0$ values with units 10^{-3}.

Can. J. Chem. Downloaded from www.nrcresearchpress.com by 203.198.23.82 on 09/08/12
For personal use only.

Can. J. Chem. Downloaded from www.nrcresearchpress.com by 203.198.23.82 on 09/08/12
For personal use only.

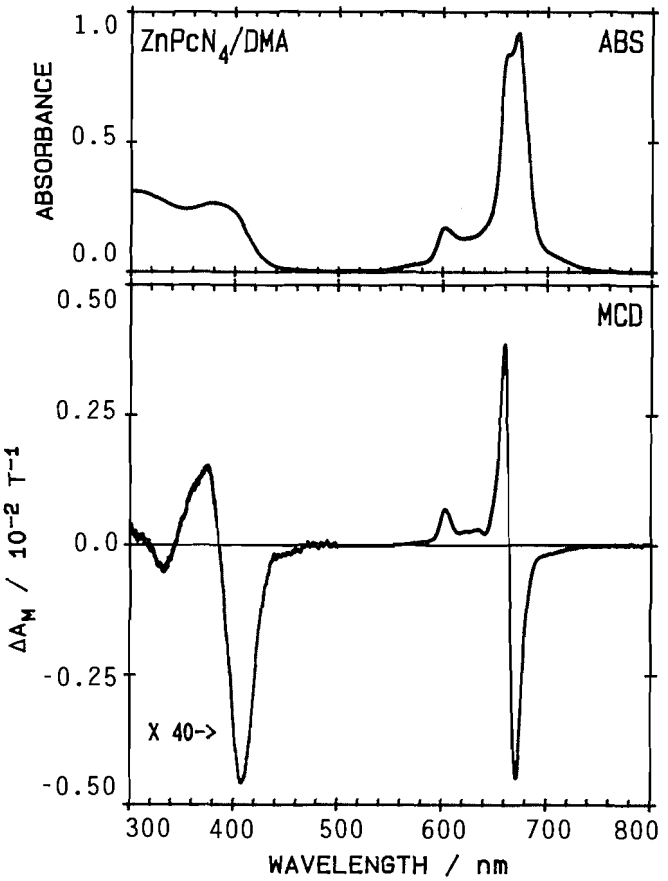

FIG. 5. Absorption and magnetic circular dichroism (MCD) spectra for $ZnPcN_4(-2)$ in DMA.

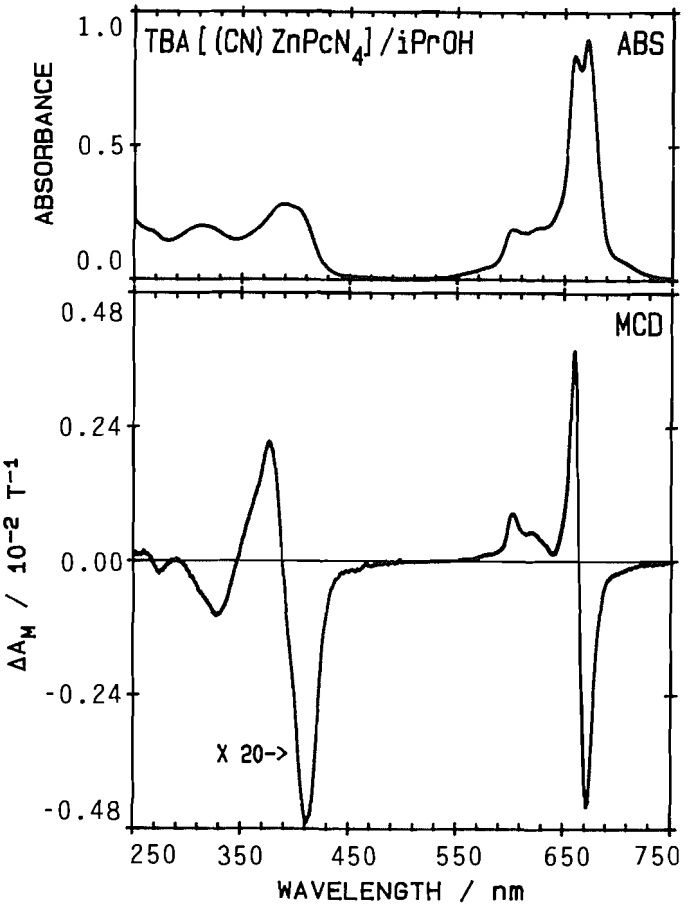

FIG. 6. Absorption and magnetic circular dichroism (MCD) spectra for TBA[(CN)$ZnPcN_4(-2)$] in iPrOH.

of the MCD *Q* band *A* term is as much as 30–40% narrower than the corresponding absorption band. Several reasons can be suggested for the discrepancy with the data described here. Amongst them, minor fractions of impurities will tend to broaden the absorption band more than the MCD band, leading to the incorporation of spurious bands to the red of the *Q* band maximum (see especially Fig. 8), and the effect of a zero field splitting induced by the solvent is most likely.

The absorption and MCD spectral fits for $MgPcN_4(-2)$, $ZnPcN_4(-2)$, and $ZnPcN_8(-2)$ are divided into the 500–800 nm (*Q*) and 250–500 nm (*B*) regions. Deconvolution of the *Q* region for both $MgPcN_4(-2)$ (Fig. 4) and $ZnPcN_4(-2)$ (not shown) required 13 bands to fill the absorption and the MCD spectral envelopes. Each absorption band was fitted with MCD *B* terms; therefore, the electronic states in these complexes are nondegenerate. Included in the MCD plots is the residual, which is the difference between the experiment and fitted envelopes. The random shape of the MCD residuals indicates that there is little systematic error in the fitted MCD envelope. The greatest noise occurs in the 650–700 nm region where two *B* terms were fit to the two overlapping absorption bands. Attempts to fit one or two MCD *A* terms in this region did not significantly reduce the residual noise or enhance the quality of the spectral fit. The bands at 671 nm (14 902 cm^{-1}) and 661 nm (15 126 cm^{-1}), for $MgPcN_4(-2)$, and at 671 nm (14 910 cm^{-1}) and 658 nm (15 189 cm^{-1}), for $ZnPcN_4(-2)$, have been assigned as the zero field split *x* and *y* components of the *Q* band, as in the D_{2h} $H_2Pc(-2)$ (1, 6, 7).

The *B* region (250–450 nm) of the phthalocyanine-*N*-isologs is complicated by the presence of several overlapping bands of relatively equal intensity. Twelve and eleven bands are required to fit this spectral region for $MgPcN_4(-2)$ (Fig. 9) and $ZnPcN_4(-2)$ (Fig. 10*a*). When the absorption spectrum has the complexity that the *B* region displays, the MCD spectrum provides the necessary and critical information that allows sensible fits to be obtained. Since the absorption bands in the *B* region were fit to MCD *B* terms, the spectral envelope in this region is dominated by transitions to nondegenerate states as well. The residuals show little systematic noise, a result that indicates a satisfactory fit of the MCD spectra. The fitting parameters for $MgPcN_4(-2)$ and $ZnPcN_4(-2)$ are summarized in Tables 2 and 3.

Deconvolution results for the 500–800 nm (*Q*) and the 290–500 nm (*B*) regions of $ZnPcN_8(-2)$ are plotted in Figs. 8 and 10*b*. In the *Q* region, a coupled pair of *A* and *B* term was used to fit the band centred on 654 nm (15 282 cm^{-1}). The quality of the MCD spectrum between 300 and 500 nm is low because of the limited solubility of $ZnPcN_8(-2)$ in DMSO. The poor quality makes the fit of this region (Fig. 10*b*) difficult. The fitting parameters for $ZnPcN_8(-2)$ are summarized in Table 4.

Moments analysis of the Q band region

Before we describe application of the method of moments, we need to summarize the origin of the MCD spectral intensity. The MCD spectrum arises from a combination

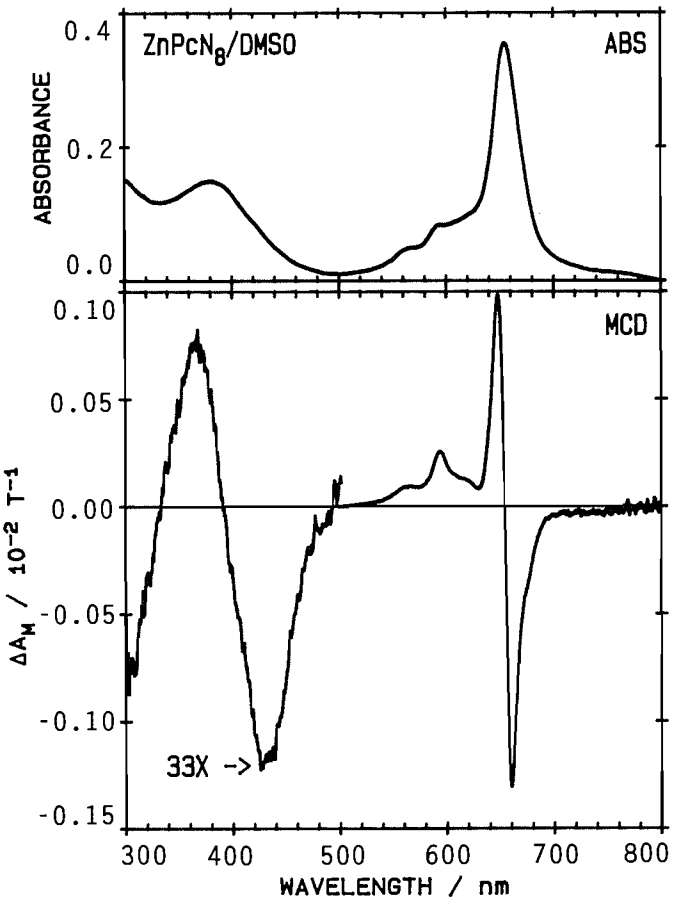

FIG. 7. Absorption and magnetic circular dichroism (MCD) spectra for $ZnPcN_8(-2)$ in DMSO.

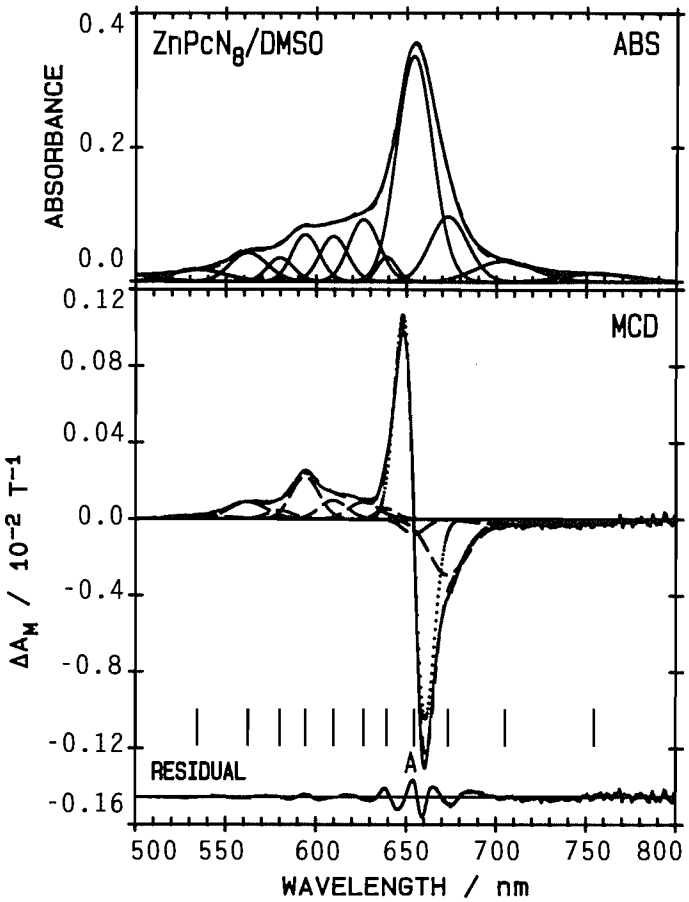

FIG. 8. Results of a band analysis for $ZnPcN_8(-2)$ in DMA in the visible region (bands 1–11). (Top) Absorption: (——) experimental data; (----) fitted data; (——) individual bands. (Bottom) MCD (——) experimental data; (---) fitted data; (.....) A terms; (---) B terms. The band center of the *A* term is labeled.

of three spectral features (22, 23), namely, (*i*) *A* terms, (*ii*) *B* terms, and (*iii*) a *C* term. Intensity at a single wavelength

$$\Delta A = 326.6\ \mu_B\ Bcl[\mathcal{A}_1(-\partial f/\partial\epsilon) + (\mathcal{B}_0 + \mathcal{C}_0/kT)f]$$

where $\Delta A = A_L - A_R$ for the absorption of left and right circularly polarized light, respectively. *B* is the magnetic field intensity (tesla) in the direction of the optical axis (*z*); *c* and *l* are the concentration and cell path length, respectively; ϵ is the energy at this point of the MCD lineshape, and μ_B is the Bohr magneton with units $cm^{-1}\ T^{-1}$. The Faraday parameters $\mathcal{A}_1$, $\mathcal{B}_0$, and $\mathcal{C}_0$ are defined according to Piepho and Schatz (23), and are used with the dipole strength, D_0, which is calculated from the absorption spectrum according to $A = 326.6clD_0f$, the line shape for the *A* term, $(-\partial f/\partial\epsilon)$, is the derivative of the lineshape, *f*, that defines the shape of the *B* and *C* terms. Each term can be either positive or negative in sign. Only the *C* term is necessarily temperature dependent. *f* is chosen here to be the Gaussian lineshape. For a full description of current usage of these symbols, see the book by Piepho and Schatz (23).

Theoretical analysis for the $^1A_{1g} \rightarrow {}^1E_u$, electronic transitions for D_{4h} metallophthalocyanines (and metalloporphyrins) relates the magnetic moment of the excited state M_{jj} to the magnitude of the $\mathcal{A}_1$ term. However, calculation of $\mathcal{A}_1$ is necessarily difficult because of the presence of matrix elements involving the electric dipole operator in addition to the magnetic dipole operator (23). Evaluation of $\mathcal{A}_1/D_0$ overcomes this restriction as D_0 involves the same electric dipole moment matrix elements. Thus the value of $\mathcal{A}_1/D_0$ simply reports the value of the measured orbital angular momentum of the excited state in terms of $i\langle e_x|L_z|e_y\rangle$.

While the deconvolution provides a good estimate of $\mathcal{A}_1$, $\mathcal{B}_0$, $\mathcal{C}_0$, and D_0, the most valuable contribution is in pairing absorption and MCD bands to obtain accurate band centres and polarization information. Errors introduced by a poor match of the lineshape and irregularities introduced by vibronic effects effectively reduce the accuracy of the magnitudes calculated. We can extract the values of the Faraday $\mathcal{A}_1$, $\mathcal{B}_0$, and $\mathcal{C}_0$ parameters by using the Method of Moments (22, 23). The method involves integration over the complete absorption and MCD lineshape. Because the technique is applicable only to isolated transitions, the *Q* band of phthalocyanines is an ideal case. For diamagnetic, symmetric molecules the ground state will be orbitally nondegenerate so $\mathcal{C}_0$ must equal 0. Transitions from the ground to the excited state will be characterized by *A* and *B* terms in the MCD spectrum. The magnitude of the *A* term depends on the orbital angular momentum of the excited state.

The results of a moments analysis for the *Q* region (500–750 nm) of $MgPcN_4(-2)$, $ZnPcN_4(-2)$, and $ZnPcN_8(-2)$ and the previously reported results for (im)ZnPc(−2), (CN^-)-ZnPc(−2) (10, 19), and $(im)_2MgPc(-2)$ (11) are listed in Table 5. The moments calculations were carried out using

Can. J. Chem. Downloaded from www.nrcresearchpress.com by 203.198.23.82 on 09/08/12
For personal use only.

Can. J. Chem. Downloaded from www.nrcresearchpress.com by 203.198.23.82 on 09/08/12
For personal use only.

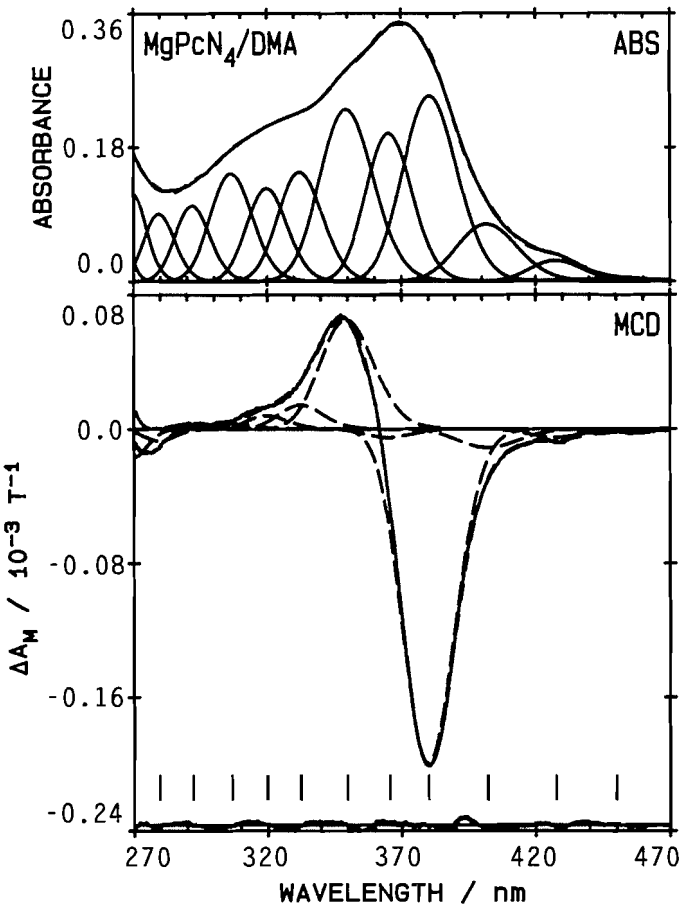

FIG. 9. Results of a band analysis for $MgPcN_4(-2)$ in DMA in the ultraviolet region (bands 14–24). (Top) Absorption: (——) experimental data; (----) fitted data; (——) individual bands. (Bottom) MCD (——) experimental data; (---) fitted data; (---) *B* terms.

the program TNMOMET4 (T. Nyokong and M.J. Stillman, unpublished program) on the well-resolved and isolated *Q* bands.

Discussion

The majority of experimental and theoretical studies of phthalocyanines have been performed on symmetric phthalocyanine molecules with D_{4h} metal or D_{2h} free base symmetry (1, 6, 7). The rich ultraviolet–visible (250–800 nm) spectrum observed for phthalocyanines originates from molecular orbitals within the aromatic 18-π-electron system and from overlapping orbitals on the central metal (1). Reported absorption maxima for the Q_{00} transition in octasubstituted phthalocyanines (1, 24, 25) indicate a distinct perturbation of the core π system. Clearly, peripheral substitution influences the transition energies and the redox potentials of the 18-π-electron system. Asymmetric peripheral substitution is expected to reduce the molecular symmetry that defines the π system, which will be manifested by a splitting of degenerate states. The studies reported here describe the effect of introducing one and two nitrogen atoms into the fused benzene rings. Reduction of the tetragonal (D_{4h}) symmetry by the introduction of fused pyridine rings and its restoration through the introduction of fused pyridazine rings was monitored by absorption and MCD spectroscopy.

Assignment of the Q_{00} band in $MgPcN_4(-2)$ and $ZnPcN_4(-2)$

Used alone, absorption spectroscopy is not sufficient to probe the electronic structure of porphyrins and phthalocyanines. MCD spectroscopy has proven invaluable in the studies of phthalocyanines (1, 2) and porphyrins (8, 26). The MCD technique is sensitive to the symmetry, spin degeneracy, and orbital degeneracy within a molecule (1, 8, 26, 27).

The spectral envelopes of $MgPcN_4(-2)$ (Fig. 3) and $ZnPcN_4(-2)$ (Figs. 5 and 6) exhibit significant zero field splitting of the *Q* band. Spectral deconvolution of the *Q* region requires two MCD *B* terms here, which suggests that the asymmetry of the peripheral groups imparts a rhombic distortion on the inner 18-π-electron system. Before definitely assigning these two bands as the *x* and *y* components of the zero field split *Q* band, the possibility that these bands arise from different structural isomers needs to be addressed.

The structural isomers of $MPcN_4(-2)$

The four structural isomers of the $MPcN_4(-2)$ molecule are shown in Fig. 2. Only the isomer with C_{4h} symmetry will have degenerate excited states (28). Based on a statistical analysis, the relative abundance of the four structural isomers (**I, II, III,** and **IV**) is predicted to be 1:1:2:4. If the four isomers are synthesized in the predicted ratio, the observed absorption and MCD spectra represent the weighted spectral intensity of individual isomers. Assuming that all four isomers are present in solution, we can use the electronic spectra to determine whether the isomers have similar or different transition energies. When the isomers have different transition energies, the bands in the *Q* region should be broadened and the spectral envelope should be less resolved than the same region in $MgPc(-2)$ (11) and $ZnPc(-2)$ (1, 11, 20, 21). Aside from the split bands in the region of the Q_{00} transition, the *Q* region of $MgPcN_4(-2)$ and $ZnPcN_4(-2)$ displays the spectral sharpness and clarity seen in the unsubstituted phthalocyanines.

If all four isomers are present and their transition energies are similar, we should be able to determine if peripheral substituents distort the D_{4h} symmetry of the 18-π-electron system. If D_{4h} symmetry is maintained, the shape of the 500–700 nm (*Q* region) spectral envelope should resemble the same region in unsubstituted metallophthalocyanines. The split *Q* band in $MgPcN_4(-2)$ and $ZnPcN_4(-2)$ is not seen in the room temperature spectra of $MgPc(-2)$ (11) or $ZnPc(-2)$ (10). A reduction from tetragonal symmetry in isomers **II–IV** is expected to broaden the Q_{00} band and introduce high- and low-energy shoulders. The sharpness of the split *Q* bands in $MPcN_4(-2)$ and the absence of shoulders indicates that only one structural isomer is present.

Although there is limited information on the mechanism for the formation of phthalocyanines and their derivatives (29), analysis of the absorption and MCD spectra of $MPcN_4(-2)$ indicates that the pyridine rings in 3,4-pyridocarboxylic acid influence the template synthesis of $MPcN_4(-2)$. Since the spectral fits of $MgPcN_4(-2)$ (Fig. 4) and $ZnPcN_4(-2)$ (Fig. 7) were unable to place a MCD *A* term in the *Q* region, isomer **I** cannot be the synthesis product. If the precursor molecules are required to be aligned in an ordered arrangement, isomer **IV** is also ruled out as the product. The synthesis of isomers **II** and **III** can be explained by

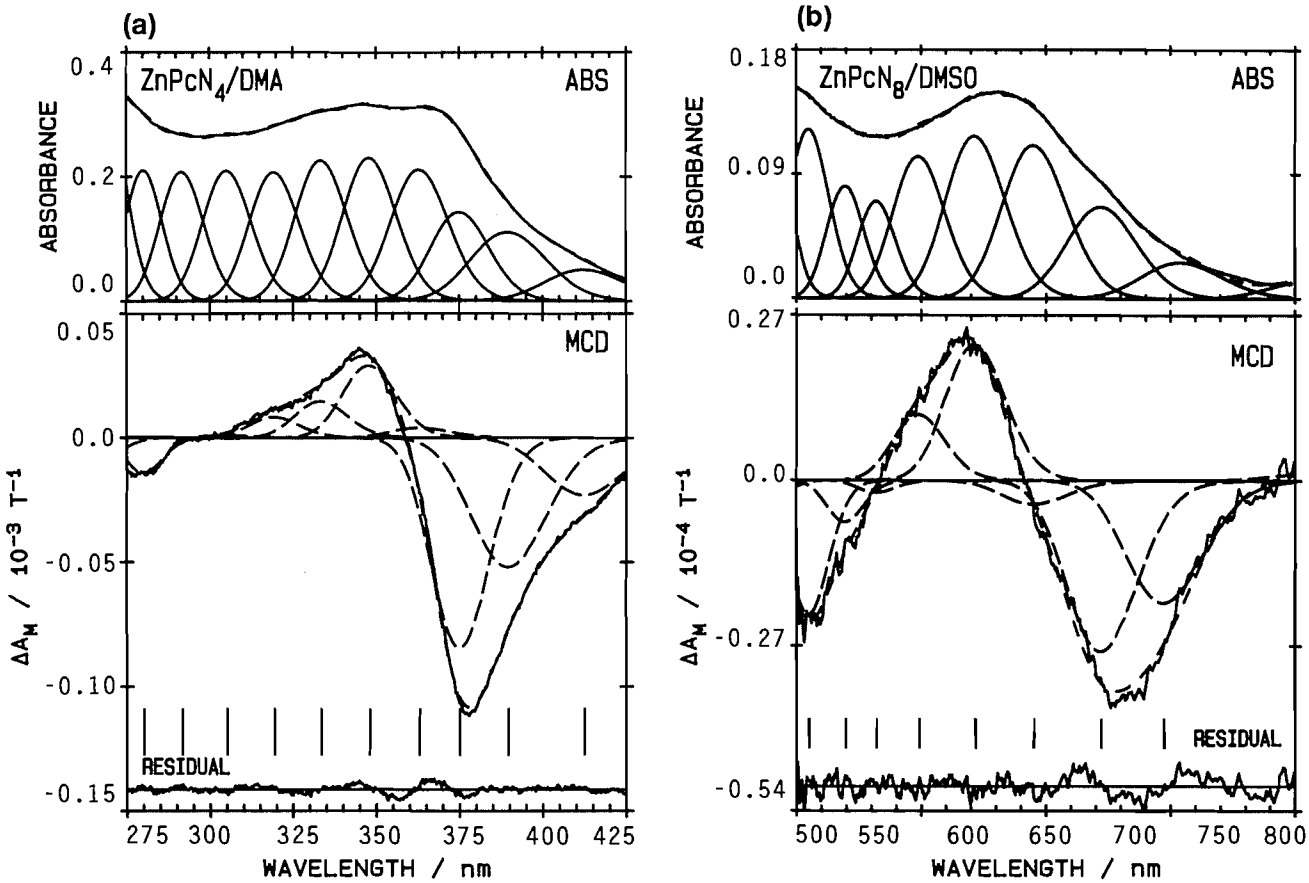

FIG. 10. (*a*) Results of a band analysis for $ZnPcN_4(-2)$ in DMA in the ultraviolet region (bands 14–23). (Top) Absorption: (——) experimental data; (----) fitted data; (——) individual bands. (Bottom) MCD (——) experimental data; (---) fitted data; (---) *B* terms. (*b*) Results of a band analysis for $ZnPcN_8(-2)$ in DMA in the ultraviolet region (bands 12–19). (Top) Absorption: (——) experimental data; (----) fitted data; (——) individual bands. (Bottom) MCD (——) experimental data; (---) fitted data; (---) *B* terms.

Can. J. Chem. Downloaded from www.nrcresearchpress.com by 203.198.23.82 on 09/08/12
For personal use only.

mechanisms that require the precursor molecules to arrange in a specific orientation. There is, however, a difference in the number of steps required to form the products. Isomer **III** is synthesized in a two-step reaction, where two precursor molecules react to form an intermediate complex and then two intermediate complexes react to form isomer **III**, while isomer **II** forms via a template reaction of four precursor molecules. Since phthalocyanines form by concerted template reactions (29) and since isomer **III** does not form by a true template reaction, we assign isomer **II** as the synthesis product.

Zero field splitting of the excited states in $MPcN_4(-2)$

The absorption spectrum of FePc · HCl (30) exhibits the split *Q* band similar to that observed in the spectra of $MgPcN_4(-2)$ and $ZnPcN_4(-2)$. The origin of the split *Q* band in FePc · HCl is attributed to ring protonation that lowers the molecular symmetry from D_{4h} to C_s (30). We suggest that a simple rhombic distortion of the D_{4h} 18-π-electron system occurs in $MPcN_4(-2)$. The single degenerate *Q* band in the spectra of D_{4h} $ZnPcN_8(-2)$ (Fig. 8) supports the rhombic distortion of the *Q* band excited state in $MPcN_4(-2)$.

Comparison of the deconvolution data for $ZnPc(-2)$, $ZnPcN_4(-2)$, $ZnPcN_8(-2)$, $MgPc(-2)$, and $MgPcN_4(-2)$

The spectral fits for (im)ZnPc(−2) (10), $ZnPcN_4(-2)$ and $ZnPcN_8(-2)$, $(im)_2MgPc(-2)$ (11), and $MgPcN_4(-2)$ are presented as energy level diagrams in Fig. 11. The fitted band centre energies in the *Q* region are plotted in Fig. 12. A blue shift in band centre energies occurs as the nitrogen content of the peripherally fused rings is increased. There is a shift from 14 906 cm^{-1} in (im)ZnPc(−2), to 15 050 cm^{-1} in $ZnPcN_4(-2)$ (this is the midpoint between the 14 910 cm^{-1} (−) and 15 189 cm^{-1} (+) MCD bands), to 15 282 cm^{-1} in $ZnPcN_4(-2)$, and from 14 874 cm^{-1} in $(im)_2MgPc(-2)$, to 15 014 cm^{-1} in $MgPcN_4(-2)$ (midpoint between the (14 902 cm^{-1} (−) and 15 126 cm^{-1} (+) bands). If the blue shift is related to the number of nitrogen atoms included in the fused rings, then the energy of the Q_{00} transition, or the average energy for the split *x* and *y* components for $ZnPcN_4(-2)$, should be midway between the band centre energies for ZnPc(−2) (10) and for $ZnPcN_8(-2)$. The midpoint between the *Q* bands for (im)ZnPc(−2) and for $ZnPcN_8(-2)$ occurs at 15 094 cm^{-1}, which is very close to the midpoint (15 050 cm^{-1}) of the Q_x and Q_y bands for $ZnPcN_4(-2)$. The zero field splitting of the *Q* band in $ZnPcN_4(-2)$ is 279 cm^{-1} and in $MgPcN_4(-2)$ it is 224 cm^{-1}. The larger rhombic distortion in $ZnPcN_4(-2)$ may be due to a small displacement of the zinc ion out of the plane of the $PcN_4(-2)$ ring.

Moments analysis

The isolation of the *Q* band (Q_{00} + Q_{vib} transitions) from other ring transitions in $MPcN_{4,8}(-2)$ complexes allows the use of the MCD spectral results to determine the angular

TABLE 5. Values calculated from a moments analysis of the complete Q band region in the absorption and MCD spectra of the $MPcN_{4,8}$ complexes

$MPcN_{4,8}$	ν^a cm^{-1}	$D_0{}^b$ 10^{-4}	$\langle \Delta A_M \rangle_1{}^c$ 10^{-4}	$\mathcal{A}_1{}^d$ 10^{-4}	$\mathcal{A}_1/D_0{}^e$	$\langle \Delta A_M \rangle_0{}^f$ 10^{-4}	$\langle \mathcal{B}_0/D_0 \rangle^g$ 10^{-4}
$ZnPcN_4$ (DMA)	15 271	2.48	1780	11.7	4.72	0.36	9.5
$[(CN)ZnPcN_4]^-$	15 378	1.95	1070	7.04	3.61	0.15	5.0
$MgPcN_4$ (DMA)	15 343	2.72	1270	8.30	3.06	0.06	1.4
$ZnPcN_8$ (DMSO)	15 682	0.97	446	2.93	3.02	0.06	4.1
$(im)_2MgPc$ (11)	15 173				2.54		
(im)ZnPc (10)	15 289	31.2*	12410*	81.6	1.51		
(CN^-)ZnPc (10)	15 252	36.4*	19770*	129.0	3.55		

[a]Calculated by setting $\langle A \rangle_1 = 0$; see ref. 23, eq. 7.3.4.

[b]Calculated from $\langle A \rangle_0 = 326.6\, D_0 cl$ (ref. 23, eq. A.4.19); the concentrations have not been included in the moments calculations of either absorption or MCD data; however, the parameter of interest, $\mathcal{A}_1/D_0$ factors out both c and l. The units of the dipole strength, D_0 are D^2 (D = Debye units). Note that the data for (im)ZnPc and (CN^-)ZnPc (*) are in $\Delta\epsilon$ and $\Delta\epsilon_M$ units.

[c]$\langle \Delta A_M \rangle_1 = \int \Delta A(\epsilon - \bar{\epsilon}) d\epsilon$; with units of μ_B, tesla, and cm^{-1}; ref. 23, eq. A.4.16.

[d]$\mathcal{A}_1 = \langle \Delta A_M \rangle_1 / 326.6\ \mu_B$ and has units of D^2.

[e]$\mathcal{A}_1/D_0 = \langle \Delta A_M \rangle_1 / (\mu_B \langle A \rangle_0)$; $\mu_B = 0.4669\ cm^{-1}\ T^{-1}$.

[f]$\langle \Delta A_M \rangle_0 = \int \Delta A d\epsilon$.

[g]$B_0/D_0 = \langle \Delta A_M \rangle_0 / (\mu_B \langle A \rangle_0)$; $\mu_B = 0.4669\ cm^{-1}\ T^{-1}$; B_0 has the units of D^2/cm^{-2}.

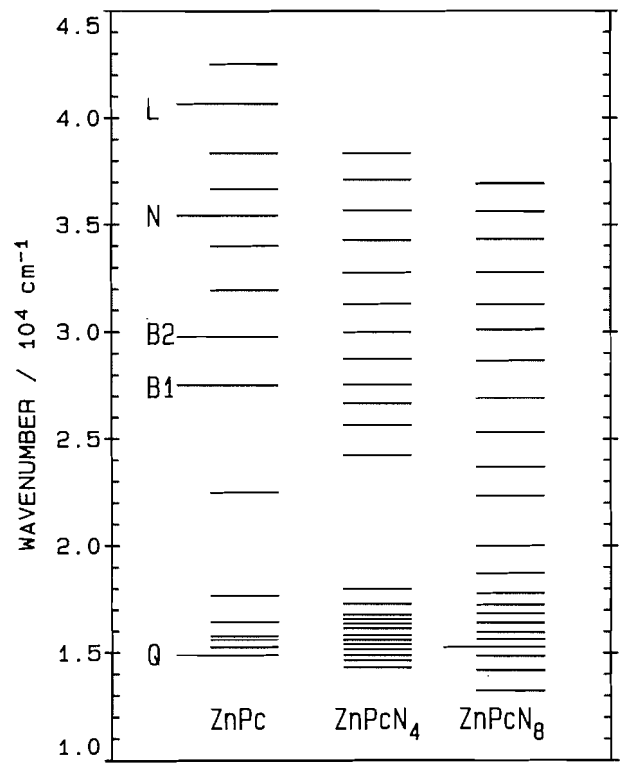

FIG. 11. Comparison of the energy levels, between 12 000 cm^{-1} and 40 000 cm^{-1}, of (im)ZnPc(−2) (ref. 10), $ZnPcN_4(-2)$, and $ZnPcN_8(-2)$ calculated by band deconvolution of the absorption and MCD spectra.

momentum of the excited state. Since the Q band is generally isolated from the charge transfer bands of transition metal phthalocyanines, it is possible to compare the magnetic moments of a wide range of substituted and unsubstituted metallophthalocyanines.

The $\mathcal{A}_1/D_0$ values for $MgPcN_4(-2)$ (3.06) and $ZnPcN_4(-2)$ (4.72 and 3.65) are consistently above the mid-range values previously reported: 1.3–3.55 for LZnPc(−2) (19); 2.49–2.78 for $L_2MgPc(-2)$ (11); and 2.7–3.11 for $L_2Fe(II)Pc(-2)$. Because of the large zero field splittings, 279 cm^{-1} in $ZnPcN_4(-2)$ and 224 cm^{-1} in $MgPcN_4(-2)$, the $\mathcal{A}_1/D_0$ values for the $MPcN_4(-2)$ complexes were predicted to be below those for more symmetrical D_{4h} MPc complexes, which inherently have smaller zero field splitting values. This prediction is based on the inverse relationship between the MCD intensity and the energy separation between the zero field split excited states (23). The moments data reported here are the first for peripherally substituted phthalocyanines. The blue shift in the band centres calculated from the first moment of the absorption $\langle A \rangle_1$, suggests an explanation for the unexpected values for $\mathcal{A}_1/D_0$. The presence of the peripheral nitrogens increases the size of the aromatic ring current that is responsible for the angular momentum. Unlike the case where substitution at the periphery extends the delocalization, which would then result in a red shift for the Q band, these nitrogens interact differently with the ground and excited states. We would have expected the $\mathcal{A}_1/D_0$ value for $ZnPcN_8$ to be the largest; however, it is clear from the fits (Fig. 8) that the dipole strength obtained by integration will be much too large because of extra bands to the red of the band maximum.

Conclusions

Absorption and MCD spectra are reported for the metallophthalocyanine-*N*-isologs: $ZnPcN_4(-2)$, $MgPcN_4(-2)$, and $ZnPcN_8(-2)$. Qualitative analysis of the spectra of $ZnPcN_4(-2)$ and $MgPcN_4(-2)$ indicated that only one of the four structural isomers of $MPcN_4(-2)$ is formed during synthesis. The isomer with D_{2h} symmetry is tentatively assigned as the synthesis product. Quantitative analysis of the spectral results for $ZnPcN_4(-2)$ and $MgPcN_4(-2)$ yielded zero field splitting parameters (ΔQ_{xy}) of 279 and 224 cm^{-1} and band center energies (midpoint between the Q_x and Q_y bands) of 664 nm (15 050 cm^{-1}) and 666 nm (15 014 cm^{-1}), respectively. No appreciable zero field splitting was observed in the spectra of $ZnPcN_8(-2)$ and spectral deconvolution placed the degenerate Q band at 654 nm (15 282 cm^{-1}). Spectral band deconvolution showed a blue shift in the band center energy of the Q band as the nitrogen content of the fused peripheral rings was increased. The first moments re-

Can. J. Chem. Downloaded from www.nrcresearchpress.com by 203.198.23.82 on 09/08/12
For personal use only.

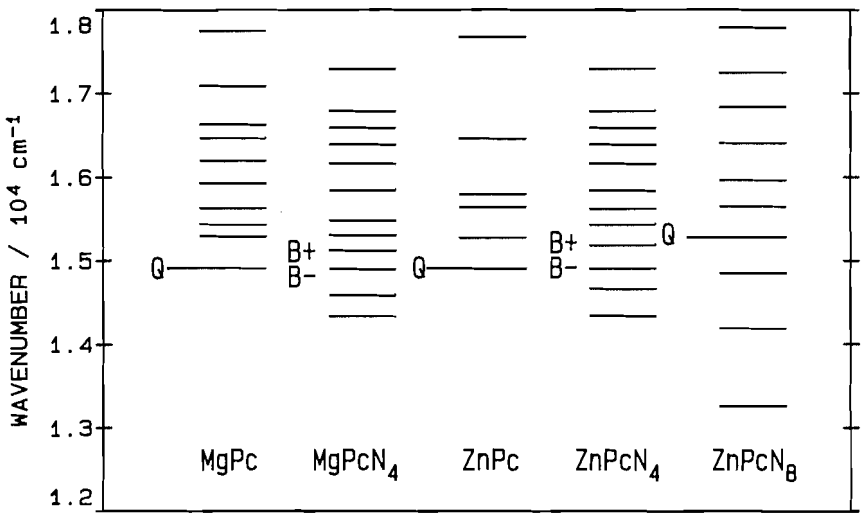

FIG. 12. Comparison of the energy levels, between 12 000 cm^{-1} and 18 000 cm^{-1}, of $(im)_2MgPc(-2)$ (ref. 11), $MgPcN_4(-2)$, (im)ZnPc(−2) (ref. 10), $ZnPcN_4(-2)$, and $ZnPcN_8(-2)$ calculated by band deconvolution of the absorption and MCD spectra.

sults reported for peripherally substituted phthalocyanines suggest that addition of electronegative groups to the periphery of the ring increases the angular momentum of the first excited state.

Acknowledgements

We gratefully acknowledge financial support from the Natural Sciences and Engineering Research Council of Canada (NSERC) in the form of operating and equipment grants. M.J.S. is a member of the Centre for Chemical Physics and the Photochemistry Unit at the University of Western Ontario. This is publication No. 495 of the Photochemistry Unit.

1. M.J. Stillman and T.N. Nyokong. *In* Phthalocyanines: properties and applications. Vol. 1. *Edited by* C.C. Leznoff and A.B.P. Lever. VCH Publications, New York. 1989. Chap. 3. pp. 133–289.
2. M.J. Stillman. *In* Phthalocyanines: properties and applications. Vol. 3. *Edited by* C.C. Leznoff and A.B.P. Lever. VCH Publications, New York. 1993. Chap. 5. pp. 227–296.
3. A.B.P. Lever, E.R. Milaeva, and G. Speier. *In* Phthalocyanines: properties and applications. Vol. 3. *Edited by* C.C. Leznoff and A.B.P. Lever. VCH Publications, New York. 1993. Chap. 1. pp. 1–70.
4. W.A. Nevin, W. Liu, M. Melnik, and A.B.P. Lever. J. Electrochem. **213**, 217 (1986).
5. A.B.P. Lever, M.R. Hempstead, C.C. Leznoff, W. Liu, M. Melnik, W.A. Nevin, and P. Seymour. Pure Appl. Chem. **58**, 1467 (1986).
6. K.A. Martin. M.Sc. Thesis, The University of Western Ontario, London, Ontario, Canada, 1979.
7. K.A. Martin, and M.J. Stillman. Can J. Chem. **57**, 1111 (1979).
8. Y.A. Sharonov. Sov. Sci. Rev. Sect. D: Physicochem. Biol. Rev. Vol. **10**(3), *Edited by* V.P. Skulachev. Harwood Academic Publishers, London. 1991.
9. M. Gouterman. *In* The porphyrins. Vol. III, Part A. Physical chemistry. *Edited by* D. Dolphin. Academic Press, New York. 1989. pp. 1–165.
10. T. Nyokong, Z. Gasyna, and M.J. Stillman. Inorg. Chem. **26**, 1087 (1987).
11. E.A. Ough, T. Nyokong, K.A.M. Creber, and M.J. Stillman. Inorg. Chem. **27**, 2725 (1988).
12. M. Yokote and F. Fukumatsu. Koka (Industrial Chemistry), **61**, 994 (1958).
13. N. Fukada. Nika (Japanese Journal of Chemistry), **78**, 1348 (1957).
14. M. Yokote, F. Shibamiya, and S. Shoji. Koka (Industrial Chemistry), **67**, 166 (1964).
15. M. Yokote and F. Shibamiya. Koka (Industrial Chemistry), **62**, 224 (1959).
16. M. Yokote, F. Shibamiya, and H. Yokomizo. Yogokto, **29**, 340 (1969).
17. Z. Gasyna, W.R. Browett, T. Nyokong, R. Kitchenham, and M.J. Stillman. Chemom. Intell. Lab. Syst. **5**, 233 (1989).
18. (*a*) W.R. Browett and M.J. Stillman. Comput. Chem. **11**, 241 (1987); (*b*) Comput. Chem. **11**, 73 (1987).
19. T.N. Nyokong. Ph.D. Thesis, The University of Western Ontario, London, Ontario, Canada, 1986.
20. M.J. Stillman and A.J. Thomson. J. Chem. Soc. Faraday Trans. 2, **70**, 790 (1974).
21. E.A. Ough, Z. Gasyna, and M.J. Stillman. Inorg. Chem. **30**, 2301 (1991).
22. P.J. Stephens, W. Suetaka, and P.N. Schatz. J. Chem. Phys. **44**, 4595 (1966).
23. S.B. Piepho and P.N. Schatz. Group theory in spectroscopy, with applications to magnetic circular dichroism. John Wiley and Sons, New York. 1983.
24. D. Wohrle and V. Schmidt. J. Chem. Soc. Dalton Trans. 549 (1988).
25. N. Kobayashi and A.B.P. Lever. J. Am. Chem. Soc. **109**, 7433 (1987).
26. S. Radzki, J. Mack, and M.J. Stillman. New. J. Chem. **16**, 583 (1992).
27. J.H. Dawson and D.M. Dooley. *In* Iron porphyrins. Part 3. *Edited by* A.B.P. Lever and H. Gray. VCH Publishers, New York. 1988.
28. F.A. Cotton. Chemical applications of group theory. Wiley–Interscience, New York. 1971.
29. C.H. Yang and C. Chang. J. Chem. Soc. Dalton Trans. 2539 (1982).
30. J.G. Jones and M.V. Twigg. J. Chem. Soc. (A), 1546 (1970).

Can. J. Chem. Downloaded from www.nrcresearchpress.com by 203.198.23.82 on 09/08/12
For personal use only.

A new synthesis of *in situ* cyclopropanones and the observation of a thermal cyclopropanone–dienol rearrangement

C. BLACK, P. LARIO, A.P. MASTERS, T.S. SORENSEN,[1] AND F. SUN
The Department of Chemistry, University of Calgary, Calgary, AB T2N 1N4, Canada

Received April 15, 1993

C. BLACK, P. LARIO, A.P. MASTERS, T.S. SORENSEN, and F. SUN. Can. J. Chem. **71**, 1910 (1993).

A new *in situ* low-temperature synthesis of cyclopropanones from α,α′-dibromo ketones is described. The synthetic procedure is particularly well suited to NMR tube-scale experiments, which then easily allows one to spectroscopically characterize low-temperature solutions of these unstable molecules. Nine systems were studied, seven of which give high yields of the cyclopropanones at −78°C or, in one case, −93°C. The major rearrangement pathway of these cyclopropanones leads to an α,β-unsaturated ketone. The mechanism of this reaction has been studied in some detail, including deuterium isotope studies, and the direct observation of enols, silyl enol ethers, and dimers. The rearrangement reaction is postulated to involve the intermediacy of an oxyallyl, the transfer of a hydrogen from the *anti*-alkyl substituent of this oxyallyl to the oxyallyl oxygen atom, which leads to an enol, and then finally tautomerization of the enol to the ketone. The thermal stability of the cyclopropanones is directly related to the ease of this rearrangement and, in two cases studied here, the rearrangement takes place rapidly even at −95°C and the cyclopropanones could not be observed. There is a remarkably strong correlation between cyclopropanone structure and reactivity, with the main structural factor being the external angles of the cyclopropanone substituents.

C. BLACK, P. LARIO, A.P. MASTERS, T.S. SORENSEN et F. SUN. Can. J. Chem. **71**, 1910 (1993).

On décrit une nouvelle synthèse *in situ* et à basse température des cyclopropanones à partir d'α,α′-dibromocétones. La méthode de synthèse est particulièrement adaptée à des études dans des tubes de RMN; cette particularité permet d'obtenir facilement une caractérisation spectroscopique à basse température de solutions de ces espèces instables. On a étudié neuf systèmes, dont sept qui donne d'excellents rendements en cyclopropanones à −78°C ou, dans un cas, à −93°C. La voie réactionnelle du réarrangement principal de ces cyclopropanones conduit à une cétone α,β-insaturée. On a étudié en détail le mécanisme de cette réaction, incluant des études d'effet isotopique du deutérium ainsi que l'observation directe d'énols, d'éthers énoliques silylés et de dimères. On suggère que la réaction de réarrangement implique un oxyallyle comme intermédiaire, le transfert d'un hydrogène à partie du substituant alkyle *anti* de cet oxyallyle vers l'atome d'oxygène de l'oxyallyle, qui conduit à un énol, et finalement une tautomérisation de l'énol en cétone. La stabilité thermique des cyclopropanones est directement reliée à la facilité de ce réarrangement et, dans deux cas étudiés ici, ce réarrangement se produit tellement rapidement même à −95°C que les cyclopropanones n'ont pu être observées. Il existe une forte corrélation importante entre la structure de la cyclopropanone et la réactivité, le facteur structural principal étant les angles externes des substituants de la cyclopropanone.

[Traduit par la rédaction]

Can. J. Chem. Downloaded from www.nrcresearchpress.com by 203.198.23.82 on 09/08/12
For personal use only.

Turro and co-workers pioneered the first preparations (as *in situ* solution species) of several simple cyclopropanones, using the cycloaddition of a diazoalkane to a ketone (1). Subsequently, cyclopropanones have been made by other methods, notably by the rearrangement of allene oxides (2), from hindered α-bromo ketones (3), and from the electrochemical reductive debromination of α,α′-dibromo ketones (4). Classic studies by Loftfield have also implicated cyclopropanones as unseen intermediates in the "normal" Favorski rearrangement (5).

In this paper, we describe a relatively simple *in situ* preparation of cyclopropanones from α,α′-dibromo ketones, using an organometallic reagent for the reductive elimination. The initial work involved the carbonyl anion of manganese ($Mn(CO)_5^-$), but further experimentation has shown that an isoelectronic chromium salt is considerably more reactive, as well as being cheaper and more conveniently prepared. This anion, $Cr(CO)_4NO^-$, as the PPN^+ salt, is quite soluble in THF or methylene chloride, even at −95°C. Furthermore, most of the dibromides react immediately with the reagent at −78°C (or −95°C) to produce very high *in situ* yields of the corresponding cyclopropanone, together with $Cr(CO)_4NOBr$ and PPN^+Br^-. However, the method is apparently limited to tri- or tetra-substituted cyclopropanones.

Because all of the cyclopropanones in this study are unstable at ambient temperature, this synthetic procedure works well for conducting NMR tube-scale reactions at low temperatures, since CD_2Cl_2 can be used as solvent, the chromium by-product produces only one ^{13}C peak, and the PPN^+ peaks are at intermediate chemical shifts in the ^{13}C NMR and low field in the ^1H NMR, relative to the cyclopropanone peaks.

The synthetic method has some advantages over the diazoalkane–ketene or allene oxide reactions in that some bicyclo[*n*,1,0]cyclopropanones are accessible.

Because of very distinctive thermal stability differences between various cyclopropanones, this study has evolved to include the following (**1–9**). Attempts were made to directly observe and characterize (*in situ* ^1H and ^{13}C NMR) all of these examples. This group of cyclopropanones was shown to experimentally encompass a range of very different thermal stabilities, which we have qualitatively correlated with the external angles θ and ϕ, as shown in structure **A**.

Results and discussion

The NMR spectrum of a typical cyclopropanone preparation is shown in Fig. 1 to illustrate both the high yield in the reaction and to show the typical quality of the ^1H NMR spectra obtained in most cases. Only cyclopropanones **1** and **2** have been previously reported (1).

In characterizing the cyclopropanones, there are a number of distinct NMR spectral differences compared to the

[1]Author to whom correspondence may be addressed.

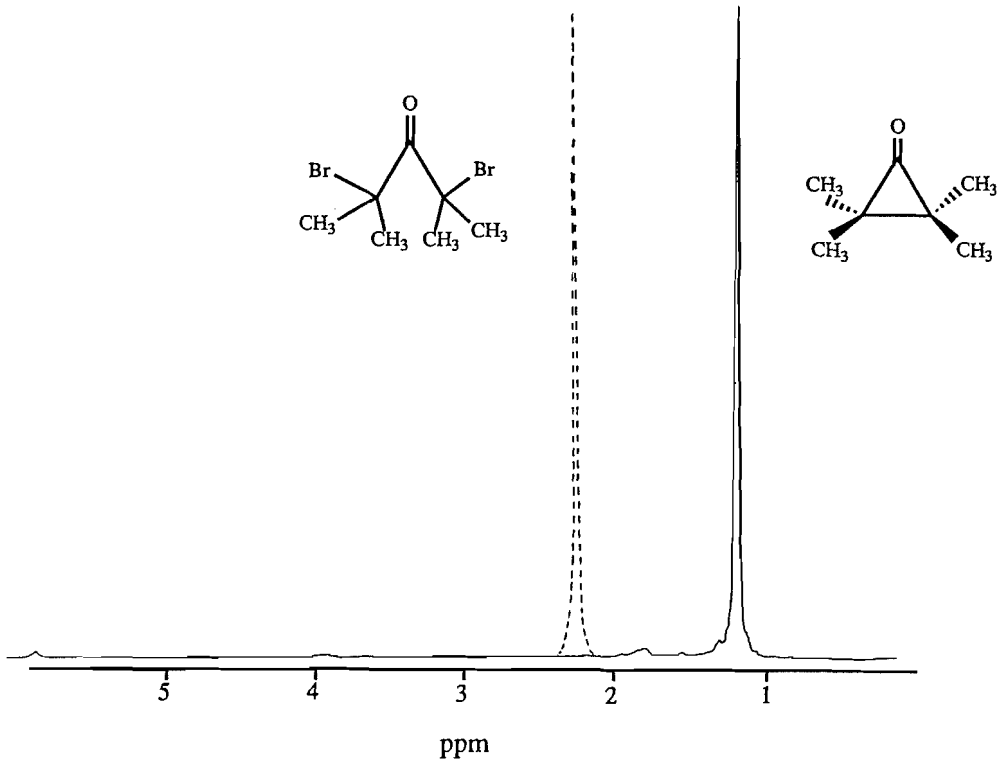

FIG. 1. 200 MHz ^{1}H NMR spectrum of tetramethylcyclopropanone **1** at −80°C in CD_2Cl_2, with the original peak for the dibromoketone starting material sketched in. The peaks for the PPN^+ cation (δ 7–8) are not shown. Small base-line peaks are from solvents carried through from the $PPN^+Cr(CO)_4NO^-$ preparation.

Can. J. Chem. Downloaded from www.nrcresearchpress.com by 203.198.23.82 on 09/08/12
For personal use only.

starting dibromo ketones, e.g., CH_3 ^{1}H signals are about 1 ppm higher field (see Fig. 1), and in the ^{13}C NMR spectra the —C=O peak moves considerably downfield (in the range δ ~ 230 ppm) and there is of course a large change in the α and α′ carbons.

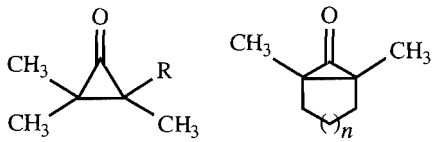

1 R = CH_3
2 R = H

3 *n* = 1
4 *n* = 2
5 *n* = 3

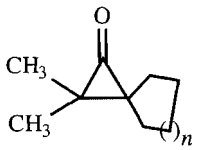

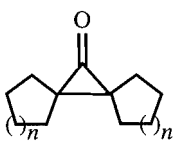

6 *n* = 1
7 *n* = 2

8 *n* = 1
9 *n* = 2

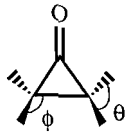

A

Since it was not possible to obtain analytical data on the cyclopropanones, we also verified the cyclopropanone formation in several cases (**1**, **2**, and **9**) by preparing the corresponding [3+4] furan cycloaddition adduct, as originally described by Fort (6), and used repeatedly by later researchers. Furthermore, the distinctive IR carbonyl stretching frequency was measured in several instances, so we believe that there is no question about the identity of the cyclopropanones reported here.

TABLE 1. Approximate thermal stability of cyclopropanones **1–9**

Cyclopropanone	Approximate $t_{1/2}$ (min)	Temperature (°C)
1	30	−10
2	30	−40
3	<2	−78
	<5	−95
4	10	−10
5	30	0
6	30	−70
7	10	20
8	<2	−78
9	10	20

Cyclopropanones **1, 2, 4, 5, 7**, and **9** were easily prepared and observed at −78°C. Their approximate thermal stabilities are shown in Table 1. Cyclopropanone **6** was marginally stable at −78°C, but could be studied at −93°C. Cyclopropanones **3** and **8** could not be observed, even at −95°C (the freezing point of the solvent). From attempts to prepare **8** at −78°C, where furan or cyclopentadiene was initially present in the solvent, we were able to obtain the

corresponding [3+4] cycloadducts (no $AlCl_3$ needed). This result constitutes reasonable evidence that **8** was formed as at least a transient species. Other evidence (see later) also indicates that **3** and **8** are formed at −78°C but rearrange on a time scale faster even than the dibromo ketone addition time (ca. 2 min).

One can see from the Table 1 comparisons that even small structural changes result in large changes in thermal stability. Largely because **8** could not be directly observed, the synthesis of the unsymmetrical cyclopropanone **6** was undertaken. Comparing the stability of **1** and **6**, and projecting this stability difference to **8**, one can easily understand why **8** was not directly observed. A discussion of why **3** and **8** are so unstable will be presented later.

Nature of the cyclopropanone thermal rearrangement reactions

Before discussing this topic in detail, there are two generalizations that one can make: (1) the more thermally stable the cyclopropanone, the "cleaner" the rearrangement process; and (2) the more concentrated the solution, the "cleaner" the rearrangement, i.e., there appear to be bimolecular steps involved.

The major monomeric product in all cases is an α,β-unsaturated ketone, e.g., ketone **10** is formed from **1**, and the yields of this ketone product are reasonably good in the case of **4, 5, 7**, and **9**, and less so for **1, 2**, and **6**. Furthermore, in the case of the bicyclic cyclopropanones **4** and **5** (and indirectly implied for **3**, see later), the α,β-unsaturation is *exclusively* in the exocyclic position, e.g., **4** → **11**. In the case of the unsymmetrical cyclopropanones **6** and **7**, one observes both α,β-unsaturated ketones, e.g., **7** → **12** and **13**. However, cyclopropanone **2** gives ketone **14** as the only monomeric product.

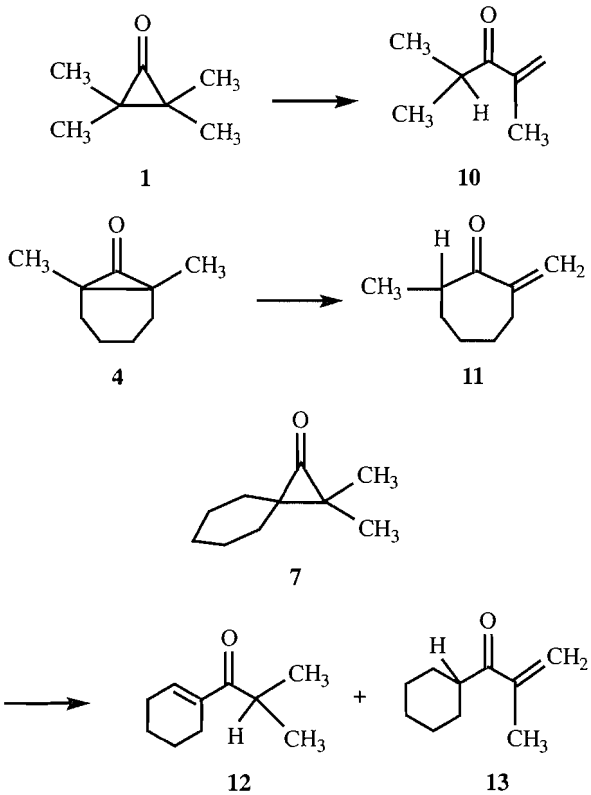

Ratio **12/13** = ca. 2:1

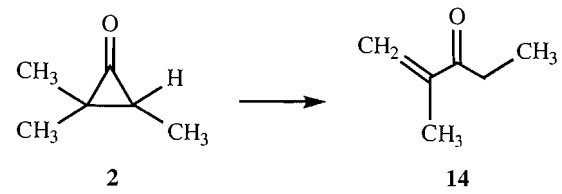

The rearrangement of **1** to **10** has been previously observed and a suggested mechanism (*4a*) involved a direct hydrogen shift from the *syn*-methyl of the oxyallyl equilibrium partner of **1**, as shown in eq. [1]. It seems clear to us that an oxyallyl must indeed be the reactive intermediate but that a hydrogen on an *anti*-methyl group is the one that is shifted (i.e., in order to explain the results for the bicyclic cases). There is in fact a considerable amount of evidence from our work that the ketone product arises by way of the corresponding enol (dienol) **15**, i.e., eq. [2]. The evidence for this enol intermediate can be summarized as follows:

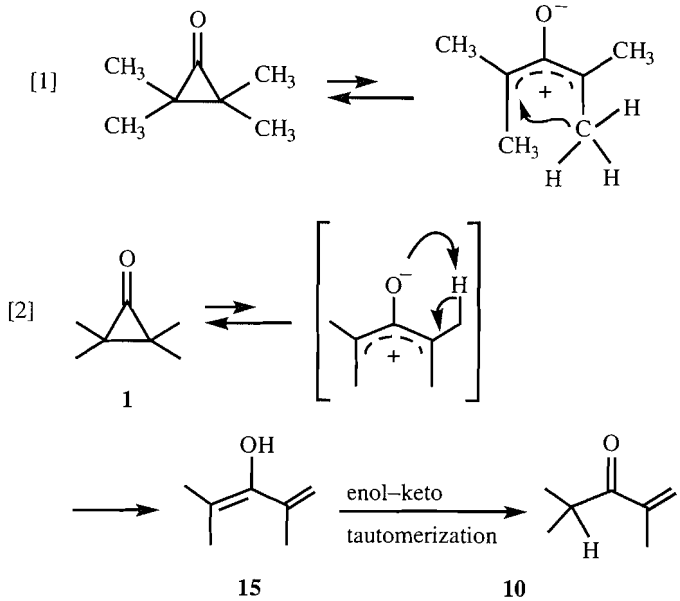

1. In the case of the cyclopropanone rearrangements of **1** and **2**, one can see an extra pair of $=CH_2$ proton peaks in the ^1H NMR spectrum (in addition to those from the α,β-unsaturated ketone), which appear during the rearrangement and have disappeared by the end of the reaction, i.e., they arise from a transient species. Their chemical shift position is considerably upfield from those of the corresponding ketone peaks, indicating the absence of a conjugated carbonyl group. The position of these peaks can be compared with those of the silyl enol ether **23** (see later), which has $=CH_2$ peaks at δ 4.99 and 4.67. We suggest therefore that the transient peaks referred to above originate from the enols **15** and **16**. Enol **15** has previously been described in pioneering work by Hoffmann and Schmidt (7), and a comparison of ^1H NMR data (δ 4.77 and 4.92 in CCl_4 solvent) indicates a close fit. Furthermore, in enol **16**, the proton on the enol double bond is assigned to a quartet at δ 4.02, very similar in chemical shift to that reported (8) for the simple enol **17**. Unfortunately, one cannot unambiguously locate the -OH signal. The high-field CH_3 region of the ^1H NMR spectra of the rearranging **1** and **2** contain a large number of peaks. However, for **1**, three of these have intensity changes appropriate for the transient existence of enol **15** and their

Can. J. Chem. Downloaded from www.nrcresearchpress.com by 203.198.23.82 on 09/08/12
For personal use only.

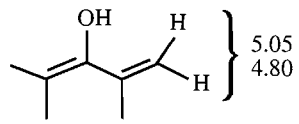

15

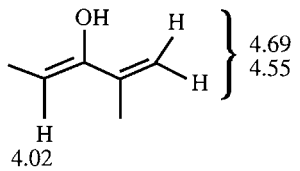

16

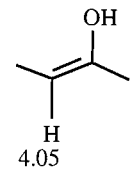

17

chemical shift positions also agree well with those reported (7). For enol **16**, a peak at δ 1.81 can be assigned to the enol.

2. Both the hexadeutero and dodecadeuterocyclopropanones **18** and **19** were prepared and characterized by ^1H, ^2H, and ^{13}C NMR spectroscopy. As one perhaps expects, **18** shows a sizeable (ca. 4) isotope effect in favoring ketone **20** as the major ketone rearrangement product (the overall reaction yield, as with **1**, is mediocre). However, a majority of the product from reaction of the deuterated side of the molecule is a d_5 species, **21**, in which a proton occupies the methine position, i.e., an intermolecular crossover has occurred. This result clearly rules out any mechanism in which a deuterium shift directly produces the ketone.

However, an enol intermediate would probably tautomerize by a bimolecular mechanism, so the appearance of

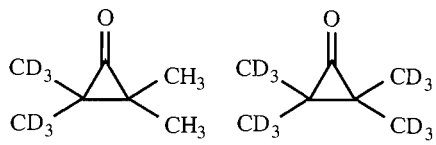

18 19

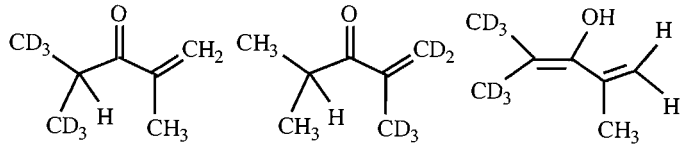

20 21 22

ketone **21** is not unexpected, given the dominant presence of enol **22** in the solution as a source of methine hydrogen for this bimolecular ketonization process. In the work of Hoffmann and Schmidt (7), rather large isotope effects were observed for the ketonization of enol **15**-OD compared to **15**, and the operation of such an effect in our case would further enhance the specific formation of ketone **21**.

The perdeutero ketone **19** was prepared because we wanted to see if there was any evidence for a kinetic isotope effect in the formation of an enol, which in turn could provide evidence on whether the C—H(D) bond-breaking step shown in eq. [2] is a rate-limiting step. In this case, however, we were unable to observe the formation of any rearranged ketone. As previously noted, one sees a number of other NMR peaks (besides those for **10**) due to competing decomposition pathways for **1**. In the case of **19**, it appears that the formation of the α,β-unsaturated ketone has been slowed down to such an extent that *only* competing processes are occurring. Nevertheless, the presence of a sizeable kinetic isotope effect in forming **10** is not ruled out.

3. The presence of an enolate intermediate can be directly implied in the cyclohexyl case **3**. At −78°C, with addition of the dibromo ketone to the $Cr(CO)_4NO^-$ solution over a 2-min period, one observes a ca. 1.5–2:1 stoichiometry ($Cr(CO)_4NO^-$: dibromo ketone). Conducting the reaction in the presence of TMS-Cl, one obtains a modest isolated yield of the silyl enol ether **23**. Both the 1.5–2:1 stoichiometry and the trapping of this silyl ether are consistent with the following mechanism (eq. [3]):

[3]

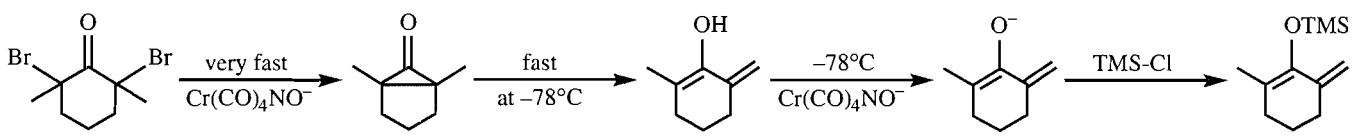

3 23

+ $Cr(CO)_4NOBr$ + $Cr(CO)_4NOH$

Thus, the chromium reagent is also a moderately strong base (9) in addition to the reductive debromination capability. If, as in this case, the cyclopropanone → enol transformation takes place on a time scale faster than the dibromo ketone can be added, then there is "excess" chromium reagent present for a second reaction with the enol to form the enolate. In the "normal" reactions, all of the $Cr(CO)_4NO^-$ has been consumed in a 1:1 reaction with dibromo ketone before *any* enol is formed. A related silyl enol ether **24** can also be trapped in the case of the reactive cyclopropanone **8**, again with approximate 2:1 stoichiometry.

4. The accumulation of an enol intermediate at any time in the overall rearrangement of the cyclopropanone is likely to induce side reactions. Thus, it is known that putative oxyallyl species rapidly react with nucleophiles (4*a*, 10). It is quite conceivable that an enol will serve this purpose, which

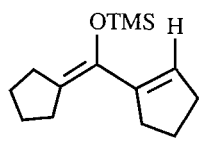

24

could then lead to the formation of dimeric products. In the overall transformation:

$$\text{cyclopropanone} \xleftarrow{\rightarrow (a)} [\text{oxyallyl}] \xrightarrow{(b)} \text{enol} \xrightarrow{(c)} \text{ketone}$$

it seems a reasonable assumption that step c will have a similar rate (for a given temperature) in all cases. The ac-

Can. J. Chem. Downloaded from www.nrcresearchpress.com by 203.198.23.82 on 09/08/12
For personal use only.

cumulation of enol in the reaction depends therefore on the ratio of steps a–b/step c. In the case of cyclopropanones **4, 5, 7**, and **9**, in which near-ambient temperatures are involved for steps a–b, the c process can be assumed to be fast, there is thus no accumulation of enol, and good yields of the α,β-unsaturated ketone are formed (the latter *is not* likely to be reactive in the presence of an oxyallyl intermediate). In the case of cyclopropanones **1** and **2**, steps (a)–(b) are faster, hence lower temperatures are needed for the NMR study; step (c) is consequently slower at this lower temperature, and observable enol accumulates. This enol, in addition to tautomerizing, can also react with the oxyallyl intermediate itself in those situations where the reaction is ongoing, i.e., unreacted cyclopropanone is also still present. Also, the yields of the ketone are higher when the solutions are more concentrated, consistent with a mechanism in which an enol intermediate is tautomerized by a *bimolecular* process, whereas earlier steps leading to the enol appear experimentally to be first order (or pseudo-first order).

5. In the case of cyclopropanones **3** and **8**, we have already noted that the rearrangements are very fast at −78°C. Although only small amounts of monomeric α,β-unsaturated ketones are formed in these cases, one can in fact isolate reasonable yields of dimeric products from the reaction, compound **25** from **3** and **26** from **8**. Both were fully characterized by a range of 2D NMR techniques. In the case of

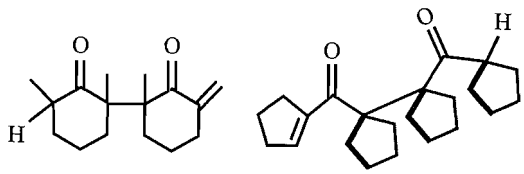

25 **26**

(two stereoisomers in a ca. 10:1 ratio)

25, one again notes the presence of the exocyclic $=CH_2$ functionality and there was no evidence that a corresponding endocyclic dimer was present in the product mixture. These particular dimeric products can be rationalized as a carbon alkylation of an oxyallyl intermediate by the corresponding enol (or enolate), i.e., as discussed in the previous section.

Mechanism of the original cyclopropanone formation

The accumulated evidence from studies of the Favorski reaction can be interpreted in terms of initial oxyallyl formation from a bromo enolate intermediate (11). There is good evidence that our reactions proceed in a similar manner, i.e., eq. [4].

[4]

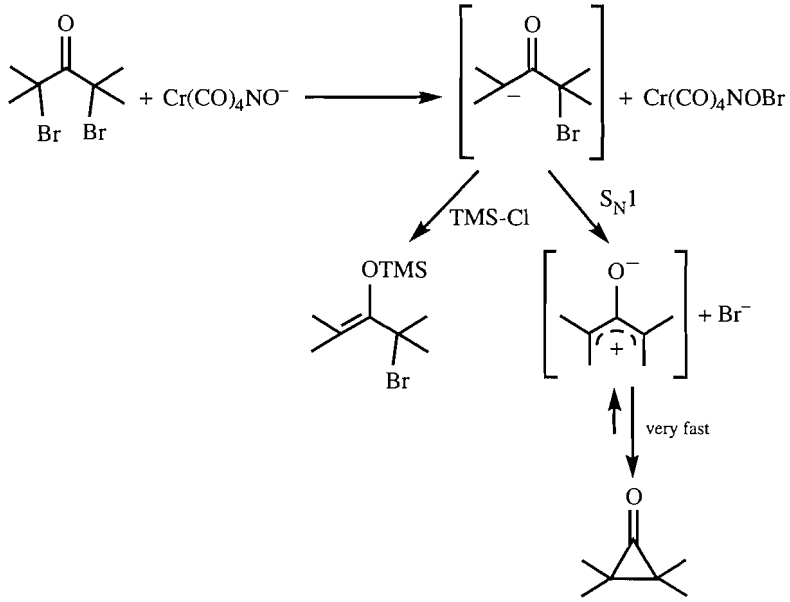

Thus, in the case of primary and secondary centers on the α and α′ ketone positions, we see essentially no cyclopropanone formation, presumably because other reactions compete with a slower S_N1 loss of Br^-. Indeed, when these primary and secondary systems are reacted with $Cr(CO)_4NO^-$ in the presence of TMS-Cl, good yields of the corresponding α′-bromosilylenol ethers were isolated.[2] However, in the tertiary cases, only cyclopropanones were observed (loss of Br^- faster than any trapping of the bromo enolate).

The subsequent disrotatory closure (12) of an oxyallyl to a cyclopropanone is expected to be very rapid, with almost no activation barrier (theoretical calculations) (13).

It might be argued that a bromo enolate intermediate could also form an allene oxide via nucleophilic attack by the enolate oxygen (allene oxides are known to rearrange to cyclopropanones (2). However, one might expect such a reaction to actually be enhanced in the primary and secondary dibromo ketones, contrary to what one observes in the TMS-Cl trapping reactions, assuming one can use these reactions as a measure of the bromo enolate lifetime.

Cyclopropanone stabilities

All of the early work of Turro (1) involved *in situ* solution formation of cyclopropanones, which in most cases ap-

[2]A.P. Masters, T.S. Sorensen, and F. Sun. Unpublished results.

Can. J. Chem. Downloaded from www.nrcresearchpress.com by 203.198.23.82 on 09/08/12
For personal use only.

peared to polymerize at ambient temperatures. Pazos and Greene (3) and later Crandall et al. (*2a*) isolated stable cyclopropanones, the *tert*-butyl-substituted derivatives **27** and **28**. The general assumption would be that the bulky *t*Bu groups hinder "polymerization", but it should also be noted that these two examples have *no* β-hydrogens of the type shown in structure **B**, which are being transferred (rearranged) in our cyclopropanone systems, so the stability of **27** and **28** may also be due to this absence.

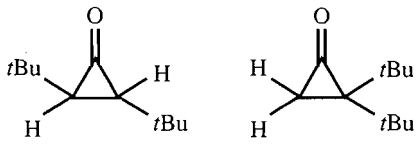

27 **28**

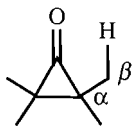

B

In assessing the wide range of thermal stabilities exhibited by the cyclopropanones **1–9**, one needs to look both at the cyclopropanones themselves and at the stability of the oxyallyl partner, which is almost certainly the reactive form. In support of this assumption, Cordes and Berson recently determined (14) a forward E_a for a cyclopropanone $\rightleftarrows$ oxyallyl reaction of about 16–18 kcal/mol, and while this number will vary greatly in different systems and in different solvents, it is still a relatively low barrier. In addition, recent high-level *ab initio* calculations show fairly small ground-state energy differences between some cyclopropanones and the corresponding oxyallyl partner (15).

The important steric factors in determining the thermal stability of the cyclopropanones, as intimated in the Introduction, are the angles θ and ϕ in structure **A**. Thus, X-ray structures of unconstrained cyclopropane rings show, not unexpectedly, that both of these angles are larger than the tetrahedral sp^3 angle. A search of the Cambridge data file (16) for subunit **C** gives $\theta_{av.} = 113.3°$, $\phi_{av.} \sim 118°$ (34 structures). One can see that cyclopropanones **3** and **8** involve ϕ and θ angles that are, respectively, too small, and one sees dramatic stability increases (Table 1) when only one more carbon atom is included in these external rings, i.e., **3** vs. **4** and **8** vs. **9**. The corresponding oxyallyl partners have to some extent opposite steric problems; thus a six-membered oxyallyl should be quite "favorable" in a relative sense, but a seven-membered ring less so, as shown in eq. [5].

Given these steric constraints, one expects the equilibrium constant for [oxyallyl]/[cyclopropanone] to be increased in the case of **3** and **8**, and, since more oxyallyl means more reactivity, these cyclopropanones are very unstable.

In summary, we have developed a high-yield cyclopropanone synthesis that can be used at temperatures as low as −95°C and is suitable for *in situ* NMR monitoring. This has allowed for the preparation of bicyclic cyclopropanones. Cyclopropanones are very reactive molecules, and one major rearrangement route is isomerization to an α,β-unsaturated ketone. We have shown by a variety of means that this rearrangement probably involves an enol intermediate, in which a β-hydrogen from the *anti*-alkyl substituent in an oxyallyl intermediate is transferred to oxygen. In ring systems, this leads to an exocyclic double bond. We have also rationalized why various cyclopropanones exhibit very different thermal stabilities.

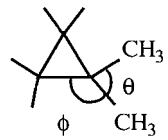

C

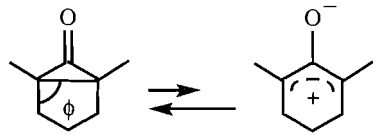

3, ϕ too small favorable sp^2 bond angle

[5]

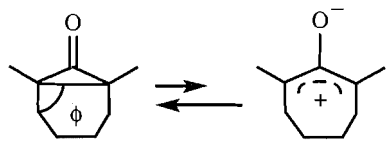

4, ϕ larger slightly more steric strain

Experimental

Gas chromatography was performed on a Hewlett–Packard model 5890A, with either a 10 m 0V1 530 μ or a packed 3% 0V1 (8 ft × 2 mm i.d.) column. NMR spectroscopy was carried out on a Varian XL-200, Bruker ACE-200, or, where noted, Bruker AM-400 (δ values in $CDCl_3$, *J* in hertz). For ^1H NMR, s = singlet, d = doublet, t = triplet, q = quartet, m = multiplet, b = broad. For ^{13}C {^1H} NMR, q = quaternary, multiplicities were determined from DEPT 90 or 135 spectra. Mass spectra were determined with a Kratos MS-90 (peak intensities in parentheses), a VG Micromass 7070F, or a Hewlett Packard 5971A mass spectrometer. Infrared spectra were determined on a Nicolet 5-DX or a Mattson model 4030, both FT instruments, peaks being reported as very strong (vs), strong (s), medium (m), or weak (w).

Preparation of the dibromo ketones

All of the dibromo ketones were prepared by direct bromination of the corresponding ketone, and only one of these is unreported. In general, these dibromides are not very stable and should be stored in a freezer.

trans-*2,8-Dibromo-2,8-dimethylcyclooctanone*

Bromine (1.1 mL) was added dropwise with stirring to a solution of *trans*-2,8-dimethylcyclooctanone (17) (1.47 g, 9.54 mmol) in 15 mL chloroform and 0.3 mL 48% HBr. The reaction was then heated to reflux for 20 h, cooled, diluted with 30 mL chloroform, and then washed successively with 10% $NaHSO_3$, 10% Na_2CO_3, and water. After drying ($MgSO_4$) and solvent removal, a crude oil residue was obtained, 2.09 g. In hexane, crystals of the title compound were obtained (0.91 g), which could be recrystallized from the same solvent, mp 38–40°C. ^1H NMR (200 MHz): 2.45–2.75 (m, 4 H); 2.17 (s, 6 H); 1.6–1.9 (m, 4 H); 1.31 (m, 2 H). ^{13}C NMR: 202.5 (Cq); 71.2 (Cq × 2); 43.2 (CH_2 × 2); 34.0 (CH_3 × 2); 25.3 (CH_2 × 2); 21.1 (CH_2). MS, *m/z*: 312 (3), 233 (10), 151 (100). Exact Mass calcd. for $C_{10}H_{16}O_{79}Br_2$: 309.9563; found: 309.9587.

An attempt was made to prepare the dibromide of dicycloheptyl ketone but, although the monobromo ketone is easily obtained, attempts to introduce a second bromine resulted in an intractable mixture. The dicycloheptyl ketone was prepared by a procedure

Can. J. Chem. Downloaded from www.nrcresearchpress.com by 203.198.23.82 on 09/08/12
For personal use only.

Can. J. Chem. Downloaded from www.nrcresearchpress.com by 203.198.23.82 on 09/08/12
For personal use only.

identical to that used for the known dicyclohexyl ketone (18). ^{1}H NMR (200 MHz): 2.55–2.75 (m, 2 H); 1.9–0.8 (m, ca. 24 H). ^{13}C NMR: 198.4 (Cq); 51.0 (CH × 2); 30.2, 28.3, 26.8 (all CH_2 × 2). MS, *m/z*: 222, 125, 97 (100), 55.

General procedure for in situ *cyclopropanone preparation*

The salt $PPN^+Cr(CO)_4NO^-$ was prepared as described (9). Reactions were carried out in 10-mL oven-dried Schlenk tubes fitted with a septum and magnetic stirrer, and generally cooled to −78°C. The chromium salt can be weighed and transferred to the Schlenk tube in air. After nitrogen purging, the solvent was added and stirring commenced. The dibromide solution was added by syringe, the rate of addition normally being about 2 min, but occasionally faster or slower addition rates were used. Methylene chloride was normally used as the solvent, about 1–2 mL used to dissolve the chromium salt and a similar volume used for the dibromo ketone solution (0.2–0.4 mmol scale). In most cases, a slight molar excess of chromium salt was weighed out (ca. 5%). The deep red color of the salt serves as an indicator for the reaction, and in some cases, i.e., **3** and **8**, the continued addition of the dibromide solution was halted when the deep red color of the salt had "prematurely" disappeared. After completion of the reaction, most work-ups involved the addition of a 3× volume of pentane or hexane. These were added slowly so that no appreciable warming took place. A precipitate (PPN^+Br^-) forms at this stage. Eventually, the solution was allowed to slowly warm to 20°C ($Cr(CO)_4NOBr$ decomposes to insoluble material) and the mixture was then filtered through Celite to leave an essentially inorganics-free solution.

For the NMR studies, 10–25 mg of the dibromide were generally used, and a total of ca. 0.5 mL of CD_2Cl_2 was used as solvent. The reactions were conducted in the 5 mm NMR tube by adding the requisite amount of the dry chromium salt. The tube was then cooled and kept at −78°C while purging with nitrogen. About 0.4 mL of solvent was added to dissolve the salt. The dibromide in ca. 0.1 mL of solvent was then added by syringe to the top of the salt solution and the tube stoppered and mixed at −78°C by shaking. NMR peaks were referenced relative to $CDHCl_2$ = 5.32 and $^{13}CD_2Cl_2$ = 53.8.

2,2,3,3-Tetramethylcyclopropanone ***1***. IR: 1839, 1820 cm^{-1}. The ^{1}H NMR spectrum of a typical preparation is shown in Fig. 1. ^{1}H NMR: 1.17 (s, 12 H), reported (1) 1.19. ^{13}C NMR: 229.8 (C=O); 24.4 (Cq × 2); 16.6 (CH_3 × 4).

2,2,3-Trimethylcyclopropanone ***2***. IR: 1850, 1813 cm^{-1}. ^{1}H NMR: 1.91 (qt, J = 7.5, 1 H); 1.31 (s, 3 H); 1.08 (d, J = 7.5, 3 H); 1.06 (s, 3H). This data is at some variance with that reported (1). 1.4–1.1 (m, 1 H); 1.36 (s, 3H); 1.22 (d, J = 5); 1.12 (s, 3 H). ^{13}C NMR: 226.7 (C=O); 25.1 (CH); 23.2 (Cq); 21.8, 13.9, 7.8 (all CH_3).

cis-*1,6-Dimethylbicyclo[4.1.0]heptan-7-one* ***4***. ^{1}H NMR: 1.76 (m, 2 H); 1.35–1.55 (m, 4 H); 1.15–1.22 (m, 4 H); 1.14 (s, 6 H). ^{13}C NMR: 232.1 (C=O); 27.6 (CH_2 × 2); 23.9 (Cq); 21.7 (CH_2 × 2); 16.1 (CH_3 × 2).

cis-*1,7-Dimethylbicyclo[5.1.0]octan-8-one* ***5***. ^{1}H NMR: 1.7–1.8 (m, 5 H); 1.47–1.55 (m, 5 H); 1.18 (s, 6 H). ^{13}C NMR: 228.2 (C=O); 33.6 (CH_2); 31.1 (b, CH_2 × 2); 28.7 (Cq); 26.7 (CH_2 × 2); 14.8 (CH_3 × 2). The peak at 31.1 is quite broad, a likely indication of some slow conformational interchange process.

2,2-Dimethylspiro[2.4]heptan-1-one ***6***. ^{1}H NMR: 1.45–1.7 (m, 6 H); 1.75–1.95 (m, 2 H); 1.13 (s, 6 H). ^{13}C NMR: 230.4 (C=O); 33.8 (Cq); 28.8 (CH_2 × 2); 27.2 (CH_2 × 2); 22.7 (Cq); 16.4 (CH_3 × 2).

2,2-Dimethylspiro[2.5]octan-1-one ***7***. IR: 1823 cm^{-1}. ^{1}H NMR: 1.3–1.7 (m, 10 H); 1.21 (s, 6 H). ^{13}C NMR: 228.2 (C=O); 31.3 (Cq); 27.4 (CH_2 × 2); 25.9 (Cq); 25.6 (CH_2 × 2); 25.2 (CH_2); 16.3 (CH_3 × 2). Changes in the profile of the broad ^{1}H cyclohexyl proton peaks with temperature may indicate a mixture of two chair conformational isomers.

Dispiro[5.0.5.1]tridecan-13-one ***9***. IR: 1829, 1813 cm^{-1}. ^{1}H NMR: 1.66 (bs, ca. 10 H); 1.56 (m, ca. 4 H); 1.37 (bs, ca. 6 H). ^{13}C NMR: 227.1 (C=O); 32.6 (Cq × 2); 26.7 (CH_2 × 4); 25.5 (CH_2 × 2); 25.2 (CH_2 × 4).

2,2-Dimethyl-3,3-dimethyl-d_6*-cyclopropanone* ***18***. ^{1}H NMR: 1.15 (s, 6 H). ^{13}C NMR: 229.5 (C=O); 24.18 (Cq, next to CH_3); 23.96 (Cq, next to CD_3); 16.5 (CH_3 × 2); 15.8 (heptet, J = 19, CD_3 × 2).

2,2,3,3-Tetramethyl-d_{12}*-cyclopropanone* ***19***. ^{2}H NMR: 1.13 (s, 12 ^{2}H). ^{13}C NMR: 229.6 (C=O); 23.6 (Cq × 2); 15.5 (heptet, J = 20, CD_3 × 4).

Furan and cyclopentadiene trapping reactions

From cyclopropanone ***9***

A standard procedure was used to prepare the cyclopropanone **9** at −78°C (0.34 mmol of the $Cr(CO)_4NO^-$ and 0.28 mmol of the dibromide). The reaction mixture was then diluted with 7:1 pentane:furan at −78°C, followed by the addition of 0.020 g anhydrous $AlCl_3$. The mixture was vigorously stirred for 15 min at −78°C. Warming and work-up (flash chromatography, CH_2Cl_2) of the reaction led to 0.0312 (43%) of the pure crystalline adduct, *2,2,4,4-bis(pentamethylene)-8-oxabicyclo[3.2.1]hept-6-en-3-one*, mp 78–79°C. ^{1}H NMR: 6.355 (2 H); 4.907 (2 H); 2.10 (2 H); 1.0–1.9 (m, 19 H). ^{13}C NMR: 217.09 (q); 133.45 (CH × 2); 81.39 (CH × 2); 55.3 (q × 2); 33.72 (CH_2 × 2); 29.62 (CH_2 × 2); 25.69 (CH_2 × 2); 21.46 (CH_2 × 2); 21.26 (CH_2 × 2). Anal. calcd. for $C_{17}H_{24}O$: C 78.42, H 9.29; found: C, 78.02, H 9.23.

From cyclopropanones ***1*** *and* ***2***

Using an identical procedure to that described for **9**, the known furan adducts of **1** and **2** were prepared (1).

From presumed cyclopropanone ***8***

The reactions were carried out in the standard way except that a four-fold excess of either cyclopentadiene or furan was mixed with the CH_2Cl_2 solvent used to dissolve the chromium salt. The cyclopentadiene adduct has been reported (19). The furan adduct, *2,2,4,4-bis(tetramethylene)-8-oxabicyclo[3.2.1]hept-6-en-3-one*, was separated by preparative TLC using CH_2Cl_2 as eluant. ^{1}H NMR (400 MHz): 6.321 (2 H); 4.480 (2 H); 2.563 (m, 2 H); 2.18 (m, 2 H); 2.08 (m, 2 H); 1.5–1.85 (m, 8 H); 1.07 (m, 2 H). ^{13}C NMR (100 MHz): 216.1 (q); 133.9 (CH × 2); 84.9 (CH × 2); 61.0 (q × 2); 38.2 (CH_2 × 2); 31.2 (CH_2 × 2); 26.2 (CH_2 × 2); 25.8 (CH_2 × 2). MS, *m/z*: 232 (M^+), 164, 136 (100), 135, 107, 96. Exact Mass calcd. for $C_{15}H_{20}O_2$: 232.1463; found: 232.1462.

Formation of enols from ***1*** *and* ***2***

The cyclopropanones were prepared in 5 mm NMR tubes and the ^{1}H NMR spectra were carefully monitored while gradually warming the solutions. In the case of **1**, peaks assigned to the enol began slowly building up at about 240 K. On reaching ambient temperature, these peaks had disappeared. In addition to the peaks reported in the text, there are CH_3 peaks at 1.86 (bs), 1.64 (bs), and 1.62 (s), which are assigned to the enol (7). In the case of **2**, enol peaks started appearing at 220 K, and in addition to the peaks reported in the text, there is a CH_3 peak at 1.81 (s), which can be assigned to the enol.

α,β-Unsaturated ketones

The ketones from **1** and **2**, 2,4-dimethylpent-1-en-3-one, **10**, and 2-methylpent-1-en-3-one, **14**, respectively, were characterized by ^{1}H NMR comparison to the known compounds. The ketone from **4**, *2-methylene-7-methylcycloheptanone*, **11**, was isolated by preparative GC (oil). ^{1}H NMR (200 MHz): 5.99 (m, 1 H); 5.26 (m, 1 H); 2.9–1.2 (m, 9 H); 1.10 (d, J = 6.5, 3 H). ^{13}C NMR (100 MHz): 204.8 (Cq); 148.3 (Cq); 122.3 (CH_2); 45.2 (CH); 34.5 (CH_2); 33.4 (CH_2), 30.6 (CH_2), 30.1 (CH_2), 17.2 (CH_3). MS *m/z*: 138, 110, 95 (100), 82, 81, 68, 67. Exact Mass calcd. for $C_9H_{14}O$: 138.1044; found: 138.1044. The ketone from **5**, *2-methylene-8-methylcyclooctanone*, was also isolated by preparative GC (oil). ^{1}H NMR (200 MHz): 5.78 (m, 1 H); 5.20 (bs, 1 H); 2.80–3.00 (m, 1 H); 2.75–2.40 (m, 2 H); 1.9–1.2 (m, 8 H); 1.08 (d, J = 6.5, 3 H). ^{13}C NMR (100 MHz): 209.8 (Cq); 149.6 (Cq); 121.1 (CH_2); 41.1 (CH); 37.7 (CH_2); 31.8 (CH_2); 30.9 (CH_2); 25.7 (CH_2); 25.5

Can. J. Chem. Downloaded from www.nrcresearchpress.com by 203.198.23.82 on 09/08/12
For personal use only.

(CH_2); 17.3 (CH_3). MS, *m/z*: 152, 124, 109, 96, 95, 82, 81, 67 (100). Exact Mass calcd. for $C_{10}H_{16}O$: 152.1201; found: 152.1195. The known ketone from **9**, cyclohexyl 1-cyclohexenyl ketone, was isolated in 96% yield (flash chromatography, CH_2Cl_2) as an oil. ^1H NMR (400 MHz): 6.88 (quintet, $J \sim 2$, 1 H); 2.96 (t, t, $J = 11.2$, 3.3, 1 H); 2.24 (m, 4 H); 1.55–1.9 (m, 9 H); 1.1–1.5 (m, 5 H). Reported (20): 6.83 (1 H). ^{13}C NMR (100 MHz): 205.01 (q); 138.75 (CH); 138.12 (q); 44.15 (CH); 29.73 ($CH_2 \times 2$); 26.06 (CH_2); 25.92 ($CH_2 \times 2$); 23.35 (CH_2); 22.04 (CH_2); 21.61 (CH_2). MS, *m/z*: 222 (M^+), 192 (66), 163 (38), 109 (100). Reported (20): 192 (21), 163 (3), 109 (100). From **7**, a mixture of isopropyl 1-cyclohexenyl ketone (21), **12**, and cyclohexyl isopropenyl ketone (22), **13**, (ca. 2:1) was produced in good yield. ^1H NMR for **12** (400 MHz, CD_2Cl_2): 0.99 (d, $J = 6.5$); 2.09 (bs); 2.21 (bs); 3.28 (heptet, $J = 6.5$); 6.93 (bs); the remaining peaks are overlapped with **13**. GC–MS, *m/z*: 152 (M^+), 109 (100), 99, 81, 79. For **13**, ^1H NMR (400 MHz, CD_2Cl_2): 1.78 (s); 3.02 (poorly resolved multiplet); 5.80 and 5.97 (both bs); the remaining peaks are overlapped with **12**. GC–MS, *m/z*: 152 (M^+), 110, 83, 69 (100), 55, 41. From **6**, the two monomeric ketones were produced in poor yield and from the GC–MS, most of the material is a dimer. For the known isopropyl 1-cyclopentenyl ketone (21), ^1H NMR (400 MHz, CD_2Cl_2): 5.82 and 5.97 (both bs). GC–MS, *m/z*: 138 (M^+), 95 (100), 67. For the known (22) cyclopentyl isopropenyl ketone, ^1H NMR (400 MHz, CD_2Cl_2): 6.77 (bs). GC–MS, *m/z*: 138 (M^+), 97, 69 (100).

Preparation of the deuterated derivatives

Acetone-d_6 (≥99.8% *d*) was converted to 2,4-dimethylpentan-3-ol-d_6 or -d_{12} by way of the isopropyl alcohol, bromide, Grignard reagent, and reaction of the latter with either 2-methylpropanal or ethyl formate. The alcohol was oxidized to the ketone using Jones reagent, care being taken during the ketone isolation (fractional distillation of the excess solvent) because of the volatility of the ketone. The ketone was brominated using the same procedure as for the h_{12} compound. Based on the mass and ^1H NMR spectra at intermediate stages in the synthesis, there was no loss of deuterium content over the course of the overall synthesis.

*Rearrangements of deuterated cyclopropanones **18** and **19***

From **18**, the α,β-unsaturated ketone (a mixture of isotopomers **20** and **21**) was obtained by preparative GC. ^1H NMR (400 MHz): 5.95 (relative area 1.0); 5.78 (area 0.97); 3.28 (bs) and 3.32 (center of a heptet) with combined area 1.11; 1.88 (area 3.0); 1.12 (d, $J = 6.5$, area 2.1). ^2H NMR (61.42 MHz): 5.92 and 5.76 (both bs, relative areas both ca. 0.3); 1.81 (bs, relative area 1.0); 1.07 (bs, relative area 7.7). The lack of a methine deuterium (^2H NMR) and the absence of a "singlet" at ca. 1.1 (^1H NMR) rule out the presence of significant amounts (<10%) of the two other possible isotopomers. The peaks at 3.28 and 3.32 in the ^1H NMR spectrum are a direct measure of the ratio **20/21** and a careful integration of these gave a 4:1 ratio for **20/21**. Obviously, in a quantitative reaction, one should get isotopomer mixtures in which the protium and deuterium content will be equal when averaged over all isotopomers. However, for our actual case, it appears that the enol in which a deuterium has migrated is more likely to undergo one of the side reactions.

For reactions involving the perdeutero species **19**, a 1:1 mixture of **19** and **1** was used for a competitive rearrangement rate study, employing the ^{13}C quaternary NMR signals, 23.6 vs. 24.4, for monitoring purposes. Disappointingly, both peaks decreased at about the same rate. However, in the ^2H NMR spectrum of the final crude reaction mixture, there were no detectable ^2H peaks characteristic of the rearranged perdeutero ketone, whereas the ^1H NMR spectrum showed rearranged ketone **10** in >50% yield.

*Trimethylchlorosilane (TMS-Cl) trapping reactions involving enolates from rearrangement of presumed cyclopropanones **3** and **8***

These were conducted at −78°C by including 50% molar excess of TMS-Cl in the methylene chloride solvent (there is no reaction between the chromium salt and TMS-Cl at −78°C) used to dissolve the $Cr(CO)_4NO^-$ salt. The dibromo ketone solution was added until the deep red color of the salt had disappeared (a precipitate is present), which generally meant that only slightly more than one half of the dibromo ketone solution (calculated on a 1:1 molar basis) was actually added. Silyl enol ether **23**, *1-trimethylsilyloxy-2-methyl-6-methylene-1-cyclohexene*, was obtained as an oil from **3**, after the usual work-up followed by a rapid preparative TLC using 1:1 hexane–CH_2Cl_2 as eluant. ^1H NMR (400 MHz): 4.992 and 4.668 (1 H each, exomethylene protons); ca. 2.38 (m, 2 H); ca. 2.14 (m, 2 H); ca. 1.66 (m, 2 H); 1.542 (s, 3 H); 0.078 (s, 9 H). Exact Mass calcd. for $C_{11}H_{20}OSi$: 196.1283; found: 196.1291. Interestingly, the hydrolysis product is the endocyclic ketone. In the case of **8**, the crude silyl enol ether **24**, *1-[1'-cyclopentene]-1-trimethylsiloxy-2,2-tetramethyleneethene*, was not purified, but could be characterized from the ^1H and ^{13}C NMR spectra and the Exact Mass. ^1H NMR (200 MHz): 5.71 (s, 1 H); 1.3–2.7 (m, ca. 14 H); 0.17 (s, 9 H). ^{13}C NMR (50 MHz): 141.6 (Cq); 139.6 (Cq); 127.7 (CH); 126.0 (Cq); 34.1, 32.2, 31.1, 30.2, 27.5, 26.0, 23.7 (all CH_2); 0.61 ($CH_3 \times 3$). MS, *m/z*: 236 (70, M^+), 208 (82), 180 (72), 167 (50), 75 (72), 73 (100). Exact Mass calcd. for $C_{14}H_{24}OSi$ (from GC–MS): 236.1597; found: 236.1586.

*Dimer **25***

The yield of this dimer, *3-methylene-1,1',3'-trimethyldicyclohexan-2,2'-dione*, was optimized by the very rapid addition of the dimbromo ketone to the chromium salt solution (ca. 60% yield). The crude material contains a ca. of 10:1 mixture of two diastereomers of **25**. On silica gel/CH_2Cl_2 flash chromatography, there is some resolution of this pair, the major isomer being obtained from the first fractions in ca. 95% purity (^1H NMR) as an oil that solidifies. ^1H NMR (400 MHz): 5.124 (t, d, $J = 2.3$, 0.9, 1 H); 5.773 (t, $J = 2.3$, 1 H); 2.9–3.1 (1); 2.5–2.9 (3 H); 1.4–2.15 (9 H); 1.174 (d, $J = 0.75$, 3 H); 1.011 (d, $J = 0.72$, 3 H); 0.964 (d, $J = 6.4$, 3 H). ^{13}C NMR (100 MHz): 216.3 (q); 207.0 (q); 145.9 (q); 120 (CH_2); 49.8 (q); 41.6 (CH); 36.9, 35.5, 35.4, 32.6, 22.0, 21.6 (all CH_2); 18.9, 18.5, 14.9 (all CH_3). One quaternary carbon is unassigned. MS (for **25**), *m/z*: 248 (M^+), 151, 126, 124 (100). Exact Mass calcd. for $C_{16}H_{24}O_2$: 248.1776; found: 248.1782. The minor disastereomer (400 MHz) shows peaks at 5.65 and 5.09 for the exomethylene protons; 1.14 (3 H); 1.12 (3 H); 1.055 (d, $J = 7$, 3 H). The detailed NMR splittings observed for this minor isomer (i.e., like the major isomer, both quaternary methyls are finely resolved doublets with $J \sim 0.7$ Hz) clearly identify this material as a diastereomer of the **25** structure.

*Dimer **26***

The yield of this dimer was maximized with slow addition of the dibromo ketone to the chromium salt. After work-up and flash chromatography (CH_2Cl_2), an 86% yield of a pale yellow oil was obtained (0.55 mmol scale). IR: 1694, 1648 cm^{-1} (both strong). ^1H NMR (400 MHz): 6.243 (quintet, $J = 2.2$, 1 H); 3.050 (quintet, $J = 7.8$, 1 H); 2.616 (m, 2 H); 2.519 (m, 2 H); 2.346 (m, 2 H); 2.18 (m, 2 H); 1.838 (quintet, $J = 7.8$, 4 H); 1.5–1.9 (m, 18 H). ^{13}C NMR: 218.7 (q); 206.5 (q); 144.5 (q); 136.6 (CH); 67.2 (q); 66.0 (q); 47.4 (CH); 35.2 (CH_2); 34.2 (CH_2); 33.8 ($CH_2 \times 2$); 33.2 ($CH_2 \times 2$); 32.6 ($CH_2 \times 2$); 26.7 ($CH_2 \times 2$); 26.0 ($CH_2 \times 2$); 25.7 ($CH_2 \times 2$); 22.3 (CH_2). MS, *m/z*: 328 (M^+), 232 (21), 191 (19), 136 (27), 135 (24), 97 (83), 95 (100). The spectroscopic data establish that two carbonyls are present, one α,β-unsaturated. The molecule has twofold symmetry involving 12 methylene carbons (six sets of two). This data establishes the structure as *4-cyclopentyl-1-(1-cyclopentene)-2,2,3,3-bis-tetramethylenediylbutane-1,4-dione*, **26**. Exact Mass calcd. for $C_{22}H_{32}O_2$: 328.24023; found: 328.2386. COSY and HETCOR 2D-spectra allowed a partial assignment of the ^1H and ^{13}C NMR spectra, for example, the cyclopentene and outer cyclopentane rings can be verified by the connectivity of the carbon skeleton.

Acknowledgements

We thank the Natural Sciences and Engineering Research Council of Canada for generous financial support.

1. N.J. Turro. Acc. Chem. Res. **2**, 25 (1969), and reference contained in this review.
2. (*a*) J.K. Crandall, W.W. Conover, J.B. Komin, and W.H. Machleder. J. Org. Chem. **39**, 1723 (1974); (*b*) T.H. Chan and B.S. Ong. Tetrahedron, **36**, 2269 (1980).
3. J.F. Pazos and F.D. Greene. J. Am. Chem. Soc. **89**, 1030 (1967).
4. (*a*) J.P. Dirlam, L. Eberson, and J. Casanova. J. Am. Chem. Soc. **94**, 240 (1970); (*b*) W.J.M. van Tilborg, R. Plomp, R. de Ruiter, and C.J. Smith. Recl. Trav. Chim. Pays-Bas, **99**, 206 (1980).
5. R.B. Loftfield. J. Am. Chem. Soc. **73**, 4707 (1951).
6. A.W. Fort. J. Am. Chem. Soc. **84**, 4979 (1962).
7. (*a*) H.M.R. Hoffmann and E.A. Schmidt. J. Am. Chem. Soc. **94**, 1374 (1972); (*b*) E.A. Schmidt and H.M.R. Hoffmann. J. Am. Chem. Soc. **94**, 7832 (1972).
8. S.H. Bergens and B. Bosnich. J. Am. Chem. Soc. **113**, 958 (1991).
9. D.R. Mantell and W.L. Gladfelter. J. Organomet. Chem. **347**, 333 (1988).
10. A.J. Fry and G.S. Ginsburg. J. Am. Chem. Soc. **101**, 3927 (1979).
11. F.J. Bordwell and J. Almy. J. Org. Chem. **38**, 575 (1973), and earlier articles in this series.
12. B. Föhlisch, E. Gehrlach, J.J. Stezowski, P. Kollat, E. Martin, and W. Gottstein. Chem. Ber. **119**, 1661 (1986).
13. L.J. Schaad, A. Hess, Jr., and R. Zahradnik. J. Org. Chem. **46**, 1909 (1981).
14. M.H.J. Cordes and J.A. Berson. J. Am. Chem. Soc. **114**, 11010 (1992).
15. (*a*) M.B. Coolidge, K. Yamashita, K. Morokuma, and W.T. Borden. J. Am. Chem. Soc. **112**, 1751 (1990); (*b*) A. Ichimura, P.M. Lahti, and A. Matlin. J. Am. Chem. Soc. **112**, 2868 (1990).
16. F.H. Allen, O. Kennard, and R. Taylor. Cambridge Structural Database. Acc. Chem. Res. **16**, 146 (1983).
17. W.C. Still and I. Galynker. Tetrahedron, **37**, 3981 (1981).
18. J.L.E. Erickson, F.E. Collins, Jr., and B.L. Owen. J. Org. Chem. **31**, 480 (1966).
19. H.M.R. Hoffmann, V. Eggert, U. Gibbels, K. Giesel, O. Koch, L. Reinhard, and J. Rabe. Tetrahedron, **44**, 3899 (1988).
20. S. Tsuyoshi, I. Masayuki, T. Ohara, and K. Yamakawa. Bull. Chem. Soc. Jpn. **60**, 1839 (1987).
21. J. Moskal and A.M. van Leusen. Tetrahedron Lett. 2585 (1984).
22. G.A. Russell and G. Hamprecht. J. Org. Chem. **35**, 3007 (1970).

Can. J. Chem. Downloaded from www.nrcresearchpress.com by 203.198.23.82 on 09/08/12
For personal use only.

Inhibitors of *endo*-α-mannosidase. Part I.[1] Derivatives of 3-*O*-(α-D-glucopyranosyl)-D-mannopyranose

ULRIKE SPOHR[2] AND MIMI BACH
Chembiomed Ltd., Edmonton, and Department of Chemistry, University of Alberta, Edmonton, AB T6G 2G2, Canada

AND

ROBERT G. SPIRO
Departments of Biological Chemistry and Medicine, Harvard Medical School, and the Elliott P. Joslin Research Laboratory, Boston, MA 02215, U.S.A.

Received June 10, 1993

Can. J. Chem. Downloaded from www.nrcresearchpress.com by 203.198.23.82 on 09/08/12
For personal use only.

ULRIKE SPOHR, MIMI BACH, and ROBERT G. SPIRO. Can. J. Chem. **71**, 1919 (1993).

Golgi membrane *endo*-α-D-mannosidase releases the disaccharide αDGlc(1→3)DMan (**34**) from the $GlcMan_9GlcNAc_2$ oligosaccharide of immature *N*-linked glycoproteins. To convert the hydrolysis product **34** into a potent inhibitor of the enzyme, chemical modifications at the 1- and 2-positions of the mannose unit of **34** were performed. These include replacement of OH-1 by hydrogen (**6**), fluorine (**12**), and *p*-nitrophenoxy (**5**). Two potent inhibitors resulted, as reported recently, when both OH-1 and OH-2 of **34** were replaced by a double bond (glucal derivative **8**) or replaced by hydrogen (1,2-dideoxy **9**). **9** proved 40 times stronger as an inhibitor than 1-deoxy **6**. However, further modifications at the 4- and 6-positions of **9**, namely deoxygenation, methylation, and replacement of OH-6 by an amino group, were now found to largely abolish the activity, demonstrating that OH-4 and OH-6 of **9** are involved in H-bonding with the enzyme.

ULRIKE SPOHR, MIMI BACH et ROBERT G. SPIRO. Can. J. Chem. **71**, 1919 (1993).

Sous l'influence de l'*endo*-α-D-mannosidase de la membrane de Golgi, l'oligosaccharide $GlcMan_9GlcNAc_2$ de glycoprotéines immatures liées par l'azote fournit le disaccharide αDGlc(1→3)DMan (**34**). Dans le but de transformer le produit d'hydrolyse **34** en un inhibiteur puissant de l'enzyme, on a effectué des modifications chimiques aux positions 1 et 2 de l'unité mannose du composé **34**. Celles-ci comprennent le remplacement du OH-1 par un hydrogène (**6**), un fluor (**12**) ou un groupe *p*-nitrophénoxy (**5**). Tels que rapportés récemment, deux inhibiteurs puissants sont obtenus lorsque les groupes hydroxyles en positions 1 *et* 2 du composé **34** sont tous les deux remplacés par une double liaison (dérivé glucal **8**) ou par des hydrogènes (dérivé 1,2-didésoxy, **9**). Le composé **9** s'avère 40 fois plus puissant comme inhibiteur que le dérivé 1-désoxy, **6**. Toutefois, on a maintenant trouvé que d'autres modifications dans les positions 4 et 6 du composé **9**, soit la désoxygénation, la méthylation et le remplacement du OH-6 par un groupe aminé, ont pour effet d'éliminer l'activité; ces résultats démontrent que les groupes OH-4 et OH-6 du composé **9** sont impliqués dans la liaison hydrogène avec l'enzyme.

[Traduit par la rédaction]

Introduction

During the biosynthesis of asparagine-linked glycoproteins, an oligosaccharide of the type $Glc_3Man_9GlcNAc_2$ is assembled on dolichyl pyrophosphate and transferred *en bloc* to the asparagine residues of the polypeptide chains (1–4) (Fig. 1). The immature protein-bound oligosaccharide is then subjected to a sequence of trimming reactions involving various glycohydrolases before transformation into complex type or high-mannose type side chains. The trimming sequence is initiated in the rough endoplasmic reticulum by the stepwise removal of the glucose units, catalyzed by at least two glucosidases, namely I and II, and leading to *N*-linked $Man_9GlcNAc_2$, which is further processed by the action of mannosidase I and, after GlcNAc transfer, by that of mannosidase II.

Recently, Lubas and Spiro (5, 6) discovered a novel glycoprotein-processing glycosidase present in the Golgi membranes from rat liver. The natural substrate of this *endo*-α-D-mannosidase was found to be incompletely deglucosylated $GlcMan_9GlcNAc_2$, which it converts into $Man_8GlcNAc_2$ with the release of αDGlc(1→3)DMan (Fig. 1). It was shown that the *endo*-mannosidase provides an alternative pathway during the blockage of trimming glucosidases by inhibitors (7, 8) and also in the glycoprotein processing by glucosidase II deficient mutant cells (9, 10). That glucosidase absence or inhibition leads only to a partial blockage of complex oligosaccharide synthesis has been observed in several instances (11, see also refs. 3–10 of ref. 10). This has been accounted for by the deglucosylation effected by *endo*-mannosidase, although the then prevailing di- and triglucosylated species $Glc_3Man_9GlcNAc_2$ and $Glc_2Man_9GlcNAc_2$ constitute weaker substrates than $GlcMan_9GlcNAc_2$ (6). It was therefore desirable to develop potent inhibitors of *endo*-mannosidase to achieve a more complete blockage of oligosaccharide formation and an extensive chemical and biological study was undertaken. The biological results of this investigation were recently disclosed (12).

We now wish to report on the syntheses of a series of these inhibitors derived from the hydrolytic product of the enzyme, namely αDGlc(1→3)DMan (**34**), by modification of substituents of the mannose unit, while two accompanying papers describe the syntheses and properties of disaccharidic congeners of 1-deoxymannojirimycin (13, 14).

Some of the biological data reported recently (12) are summarized in Table 1. The most potent inhibitor resulted when the mannose unit of **34** was replaced by 1-deoxymannojirimycin (1,5-dideoxy-1,5-imino-D-mannitol) to produce **35** (13), which was found to inhibit the cleavage of

[1]For Parts II and III, see refs. 13 and 14.
[2]Author to whom correspondence may be addressed.

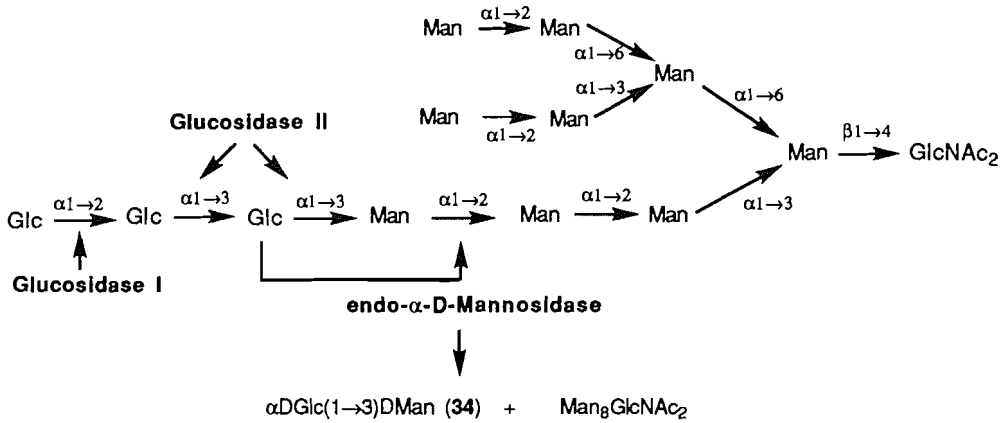

FIG. 1. $Glc_3Man_9GlcNAc_2$ as transferred from dolichylpyrophosphate to asparagine residues of the polypeptide chain. Cleavage sites for deglucosylating trimming enzymes and reaction products of *endo*-mannosidase.

TABLE 1. The effect of chemical modification of the mannose unit of αDGlc(1→3)DMan (**34**) on the activity as inhibitor of *endo*-mannosidase (12)

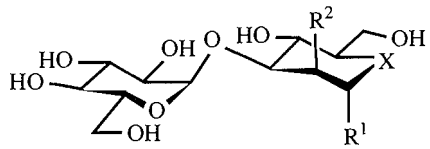

Compound	R^1	R^2	X	Relative potency[a]
34	OH	OH	O	0.8
6	H	OH	O	1.1
9	H	H	O	45
8	Double bond		O	74
35	H	OH	NH	100
36	H	H	NH	0.6

[a]% Potency relative to **35**.

$GlcMan_9GlcNAc$ at IC_{50} = 1.7 μmol in vitro. In accordance with previous observations with 1,5-dideoxy-1,5-iminoalditols (15), **35** proved to be 90 times stronger as an inhibitor than its 5-oxygen analogue **6** (Table 1), which is derived from αDGlc(1→3)DMan (**34**) by deoxygenation at the 1-position. An inhibitor almost equally as strong as **35** was obtained when the OH-1 and OH-2 groups of **34** were replaced by a double bond to give the glucal derivative **8**. Glycals have been found in several cases (16) to serve as *pseudo*-substrates of some glycosidases to form, under hydroxylation, a 2-deoxyhexose derivative. Remarkably, also the saturation product of glucal **8**, namely **9**, resulting from deoxygenation at the 2-position of anhydromannitol **6**, proved a very potent inhibitor. In contrast, deoxygenation at the 2-position of aza analogue **35** to give 1,2-dideoxy **36** (13) essentially abolished activity. Apparently, the interaction of NH-5 of **35** with the protein induces a different conformational change in the catalytic region of the protein than when O-5 is at its place. Further modifications of the anhydrohexitol unit of 1,2-dideoxy **9** are also reported in this communication.

Discussion

With the aim to convert the product of the hydrolytic action of *endo*-α-D-mannosidase, namely αDGlc(1→3)DMan (**34**), into a potent inhibitor for the enzyme, structural modifications at the 1- and 2-positions of the mannose unit of **34** were performed.

The nitrophenyl aglycon was introduced by melting octaacetate **1**[3] with *p*-nitrophenol and zinc chloride (17) (Scheme 1) to produce **3** in 38% yield. The α-configuration of the new linkage was confirmed by the coupling constant $J_{C1,H1}$ 175.8 Hz for C-1 in the C–H coupled ^{13}C NMR spectrum (18). Zemplen deacetylation of **3** then provided **5** in 95% yield; **5** proved an even weaker inhibitor than **27** (12).

Deoxygenation at the 1-position of **27** was achieved by reductive debromination of bromide **2**[3] with tributyltin hydride to give crystalline **4** in 65% yield. Zemplen deacetylation of **4** led to **6** in quantitative yield. The ^1H and ^{13}C NMR data are presented in Tables 2 and 3 and are in agreement with the structural assignments.

To prepare the mannosyl fluoride **12**, the blocked disaccharide **10**[3] was treated with diethylaminosulfur trifluoride in dichloromethane at −30°C (19) to give the α-fluoride **11** in 83% yield. The α-configuration followed from the coupling constants $J_{C1,H1}$ 185.0 Hz, $J_{C1,F}$ 225.1, and $J_{H1,F}$ 49.0 Hz in the ^{13}C and ^1H NMR spectra. Catalytic hydrogenation over 5% palladium-on-carbon provided **12** in 91% yield. **12** was found 3 times as strong an inhibitor as 1-deoxy **6** (12).

Since glycals proved to be potent inhibitors of some glycosidases (16), 3-*O*-(α-D-glucopyranosyl)-D-glucal (**8**) was prepared by the action of zinc and acetic acid on bromide **2** to provide hexaacetate **7** in 65% yield followed by Zemplen deacetylation (96% yield). Glucal **8** was then saturated to the 1,2-dideoxy derivative **9** by catalytic hydrogenation.

When the strong inhibitory properties of the 1,2-dideoxy disaccharide **9** became known (12), further modifications at the 4- and 6-positions of the hexitol unit of **9** were undertaken (Scheme 2). As a common intermediate, the disaccharide **16** was prepared: 1,5-Anhydrohexitol **13** (20) was converted into the *p*-methoxybenzylidene acetal **14** in 83% yield; **14** was glucosylated with bromide **15** (21) under halide ion catalyzed conditions (21) to afford **16** in 56% yield. **16** was also deblocked to **9** (Scheme 1) by catalytic hydro-

[3]U. Spohr, M. Bach, S.E.H. Moore, and R.G. Spiro. Manuscript in preparation.

Can. J. Chem. Downloaded from www.nrcresearchpress.com by 203.198.23.82 on 09/08/12
For personal use only.

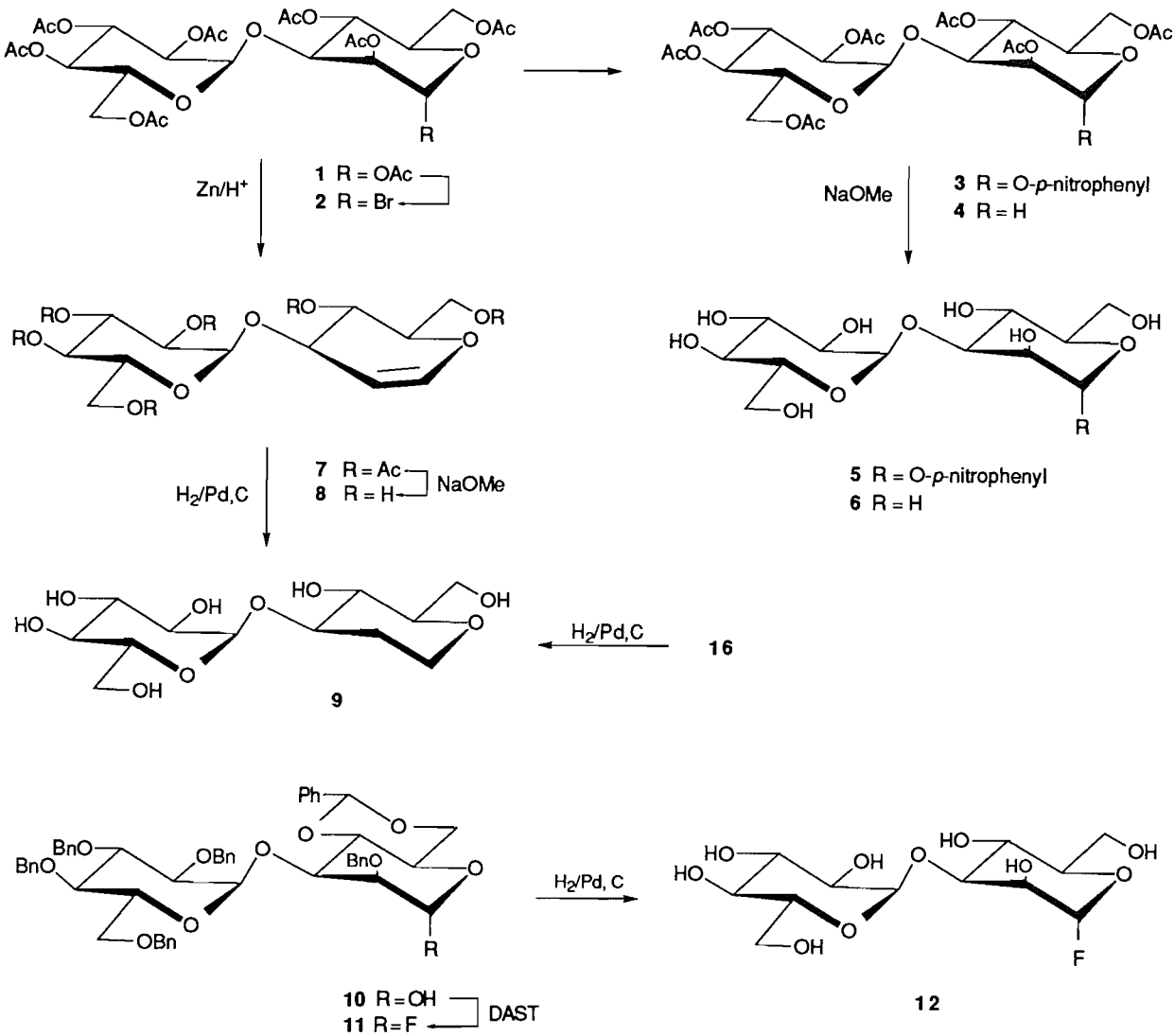

SCHEME 1

genolysis. Reductive cleavage of the *p*-methoxybenzylidene ring of **16** (Scheme 2) was performed with sodium cyanoborohydride and trimethylsilyl chloride as electrophile (22) and provided the 6-hydroxy compound **17** in 74% yield as well as the 4-hydroxy isomer **27** in 8.8% yield.

17 was methylated to **19** (83% yield) using methyl iodide and sodium hydride. Mesylation of **17** with methanesulfonyl chloride led to mesylate **18** (91% yield), which showed the characteristic downfield shifts of H-6A and H-6B in the ^{1}H NMR spectrum. The mesyloxy group in **18** was substituted by iodide to form **20** (65% yield), which was reduced with tributyltin hydride to give **21** (54% yield). Partial loss of the *p*-methoxybenzyl group occurred during the reduction and the 6-deoxy-4-hydroxy derivative **22** was also isolated in 30% yield. The mesyloxy group of **18** was easily replaced by azide to provide **23** in quantitative yield. Catalytic hydrogenation over 5% palladium-on-carbon of the 6-*O*-methyl, 6-deoxy, and 6-azido-6-deoxy derivatives **19**, **21**, and **23** led to the deblocked disaccharides **24**, **25**, and **26**. The 6-amino-6-deoxy compound **26** was obtained only 90% homogeneous.

To liberate the 4-position of intermediate **16**, the reductive cleavage of the *p*-methoxybenzylidene ring was undertaken using sodium cyanoborohydride in the presence of trifluoroacetic acid (22). The desired 4-hydroxy compound **27** was isolated in 54% yield, as well as 15% of the regio isomer **17**. Proof for the structural assignment of **27** was obtained from the ^{1}H NMR spectrum of the acetate **28** in which the downfield shift of H-4 could be observed. **27** was then methylated in the usual way to **29** (87% yield). For deoxygenation of the 4-position of **27** the Barton–McCombie procedure (23) was applied and the intermediate methyl xanthate (**30**) was reduced to 4-deoxy **31** (73% yield from **27**). Catalytic hydrogenolysis then provided 4-*O*-methyl **32** and 4-deoxy **33** in high yields.

The ^{1}H and ^{13}C NMR data are reported in Tables 2 and 3 and fully support the various structural assignments. Conformational preferences about the interglycosidic torsion angles ϕ/ψ of 1-deoxy **6** and 1,2-dideoxy **9** were determined at near $-50°/-10°$ (13) by HSEA calculations (24). Observed and theoretical nuclear Overhauser enhancements calculated for the low-energy conformer of **9** at $\phi/\psi = -45°/-15°$ are reported in Table 4. Nonbonded interactions between H-1′ and H-3, as well as H-2e and H-5′, were found

Can. J. Chem. Downloaded from www.nrcresearchpress.com by 203.198.23.82 on 09/08/12
For personal use only.

TABLE 2. ^{1}H NMR chemical shifts (δ, ppm) and coupling constants (Hz) for αDGlc(1b→3a)DMan derived disaccharides[a]

	1-*p*-Nitrophenyl **5**	1-Fluoro **12**	1-Deoxy **6**	Glucal **8**	1,2-Dideoxy **9**	Derivatives of **9**				
						4-Deoxy **33**	4-OMe[d] **32**	6-Deoxy **25**	6-OMe[e] **24**	6-Amino **26**
a-unit										
H-1e($J_{1e,2e}$)	5.76 (1.8)	5.63 (1.7)[b]	3.90	6.43 (6.0)	3.96 (1.0)	4.04 (1.0)	3.97 (1.0)	3.91 (1.0)	3.94 (1.0)	4.00 (1.0)
H-1a($J_{1e,1a}$)	—	—	3.65 (12.5)	—	3.53 (12.5)	3.52 (12.0)	3.52 (12.0)	3.52 (12.0)	3.51 (11.7)	3.54 (12.0)
H-2e($J_{2e,3}$)	4.31 (3.0)	4.28 (2.5)	4.15	4.94 (2.5)	2.15 (5.5)	2.01 (5.0)	2.08 (4.8)	2.15 (5.0)	2.15 (5.0)	2.16 (5.0)
H-2a($J_{2a,2e}$)	—	—	—	—	1.76 (13.0)	1.63 (12.0)	1.76 (13.0)	1.76 (13.0)	1.75 (13.0)	1.78 (13.0)
H-3($J_{3,4}$)	4.18 (9.5)	3.95	3.74	4.27	3.75 (9.5)	3.94 (11.0)	3.87 (9.0)	3.71	3.74	3.76
H-4($J_{4,5}$)	3.96 (9.5)	*	3.78 (9.2)	3.98	3.48 (9.5)	1.26 (12.0)[c]	3.27	3.26	3.44	3.40
H-5($J_{5,6}$)	3.68 (2.5)	*	3.35 (2.0)	3.86	3.33 (2.2)	3.60	3.34 (2.2)	3.36 (6.5)	3.41	3.48
H-6($J_{6,6'}$)	3.90-	*	3.90 (12.5)	3.89-	3.89 (12.5)	*	3.88	1.27	3.75 (11.0)	3.48 (13.2)
H-6′($J_{5,6'}$)	3.72 (5.0)	*	3.70 (6.0)	3.72	3.71 (5.5)	*	3.74 (5.5)	—	3.61	3.09 (8.5)
αDGlc b-unit										
H-1($J_{1,2}$)	5.33 (3.7)	5.26 (3.7)	5.25 (3.7)	5.22 (3.5)	5.21 (3.7)	5.11 (3.8)	5.19 (3.8)	5.21 (3.8)	5.21 (3.8)	5.21 (3.8)
H-2($J_{2,3}$)	3.59 (10.0)	3.56 (10.0)	3.55 (9.7)	3.55 (9.5)	3.54 (10.0)	3.53 (10.0)	3.56 (10.0)	3.53 (10.0)	3.53 (10.0)	3.54 (10.0)
H-3($J_{3,4}$)	3.78 (9.5)	3.77 (9.5)	3.79 (9.5)	3.69 (9.5)	3.75 (9.5)	3.72	3.74 (9.0)	3.72	3.72	3.71
H-4($J_{4,5}$)	3.44 (9.5)	3.42 (9.5)	3.42 (9.5)	3.41 (9.5)	3.40 (9.5)	3.40	3.43 (9.5)	3.40	3.40	3.40
H-5	3.85	3.82	3.85	3.76	3.83	3.81	3.82	3.81	3.81	3.82
H-6	3.77	*	*	*	*	*	*	*	*	*
H-6′	*	*	3.75	*	*	*	*	*	*	*

[a]Measured at 360 MHz and 295 K using 0.03 M solutions in D_2O with acetone as internal standard at 2.225 ppm. The assignments were based on homonuclear shift correlated 2-D experiments (COSY)
[b]$J_{H1,F}$ 50.0 Hz.
[c]H-4e 2.06 ppm.
[d]MeO 3.59 ppm.
[e]MeO 3.38 ppm.
*Could not be assigned.

TABLE 3. ^{13}C NMR chemical shifts (δ, ppm) for αDGlc(1b→3a)DMan derived disaccharides[a]

	1-*p*-Nitrophenyl **5**	1-Fluoro **12**	1-Deoxy **6**	Glucal **8**	1,2-Dideoxy **9**	Derivatives of **9**				
						4-Deoxy **33**	4-OMe[f] **32**	6-Deoxy **25**	6-OMe[g] **24**	6-Amino **26**
a-unit										
C-1	98.48	108.49[d]	70.66	145.45	66.07	66.55	65.96	65.99	66.09	66.34
C-2	70.29[b]	69.18[e]	69.81[b]	99.45	33.13	33.65	33.21	33.32	33.07	33.05
C-3	79.09	78.49	82.21[c]	76.02	81.05[b]	74.12	79.25[b]	81.14	81.36	81.02
C-4	66.52	66.00	67.48[b]	67.80	71.10	33.65	80.42[b]	76.60[b]	71.22	72.72
C-5	74.64	75.82	81.37[c]	79.06	81.58[b]	77.65	81.29[b]	77.23[b]	79.49	76.72
C-6	61.34[c]	61.36	61.97	60.65	61.86	65.22	61.47[c]	18.09	72.44	41.70
αDGlc b-unit										
C-1	101.46	101.38	101.22	101.88	100.62	97.19	100.45	100.53	100.57	100.62
C-2	72.63	72.57	72.61	72.23	72.50	72.01	72.19	72.51	72.49	72.43
C-3	73.71	73.64	73.65	73.76	73.75	73.90	73.66	73.77	73.75	73.73
C-4	70.47[b]	70.40	70.43	70.49	70.46	70.47	70.55	70.47	70.46	70.45
C-5	73.28	73.23	73.13	73.05	72.90	72.80	72.90	72.89	72.90	72.87
C-6	61.45[c]	61.36	61.35	61.40	61.38	61.40	61.42[c]	61.38	61.38	61.40

[a]0.05 M solutions in D_2O with dioxane as internal reference at 67.4 ppm were measured at 75 MHz and 295 K. The assignments were made by inspection and are tentative.
[b,c]The corresponding assignments of the chemical shifts are tentative and may be reversed.
[d]$J_{C1,F}$ 221.4 Hz, $J_{C1,H1}$ 183.6 Hz.
[e]$J_{C2,F}$ 37.0 Hz.
[f]CH_3O 60.82 ppm.
[g]CH_3O 59.34 ppm.

to be similar to those determined for inhibitor 1-deoxy-3-*O*-(α-D-glucopyranosyl)-mannojirimycin (**35**) (13), suggesting that both inhibitors show similar conformational preferences.

Both monodeoxygenation (**33**, **25**) and mono-*O*-methylation (**32**, **24**) at the 4- and 6-positions of **9** essentially abolished the activities (Fig. 2), indicating that these hydroxyl groups are involved in polar interactions with the enzyme,

Can. J. Chem. Downloaded from www.nrcresearchpress.com by 203.198.23.82 on 09/08/12
For personal use only.

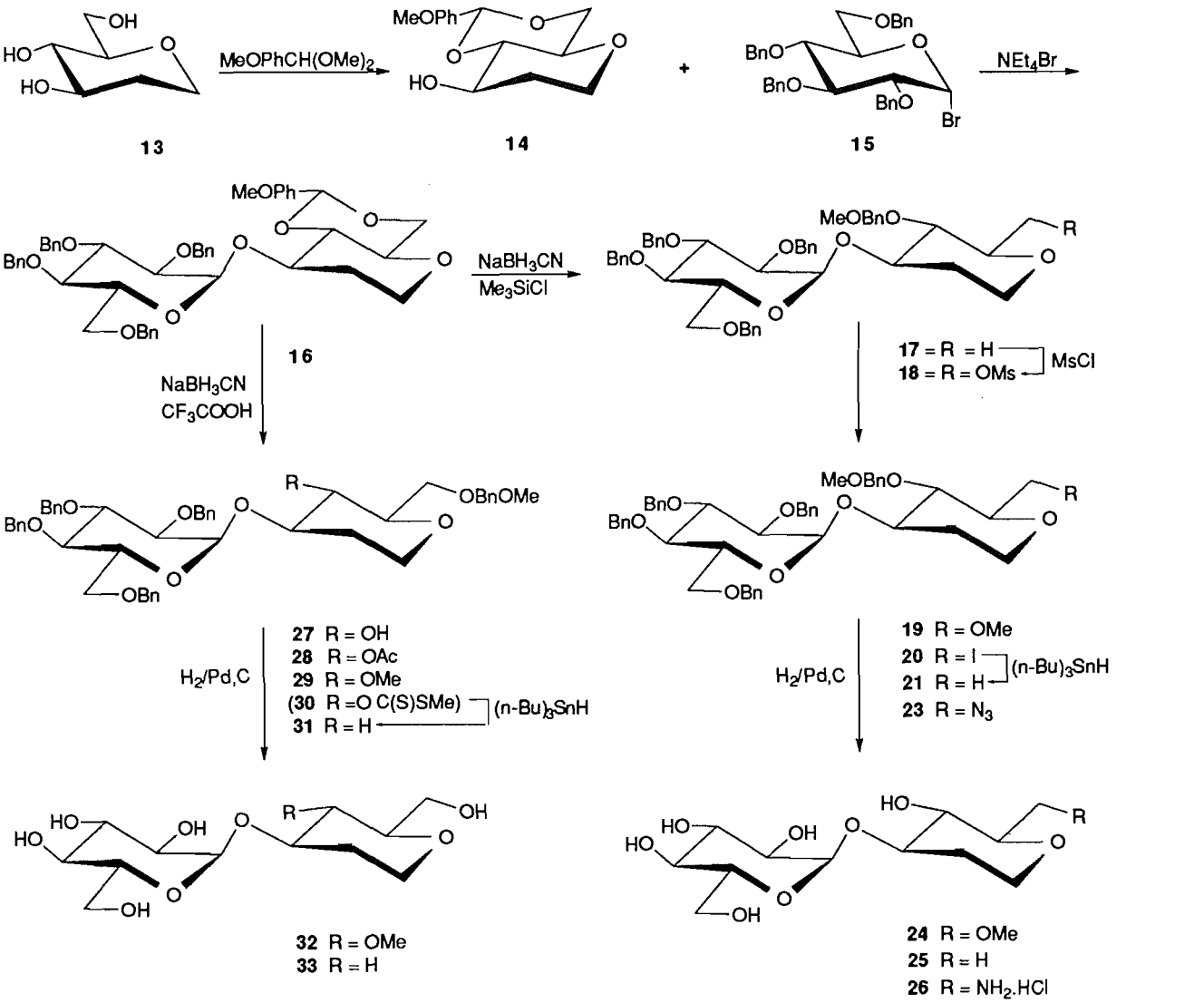

SCHEME 2

TABLE 4. Intra- and interunit nuclear Overhauser enhancements for compound **9**[a]

Proton saturated	Signal enhanced	% Enhancement	Relative NOE values	
			Observed	Calculated
H-1′	H-2′	17.7	0.54	0.60
	H-3	15.2	0.46	0.37
H-2e	H-1e	2.9	0.07	0.02
	H-1a	2.6	0.06	0.08
	H-2a	26.4	0.65	0.54
	H-3	9.0	0.22	0.16
	H-5′			0.20

[a]See ref. 13 for experimental details.

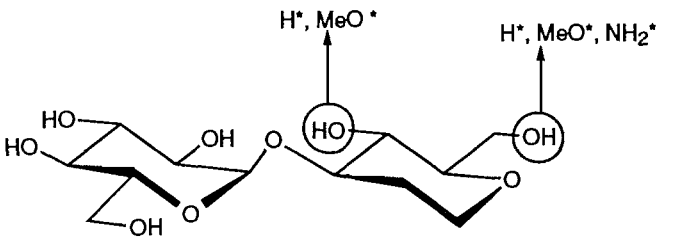

FIG. 2. The effect of chemical modifications of **9** on the activities as inhibitors of *endo*-mannosidase. *Denotes <2% activity of **9**[4].

as was found for the complexation of the NH-5 analogue **35** (12, 14). In the case of the OH-6 group, its polar interaction cannot be substituted by that of an amino group, since 6-amino congener **26** was also found inactive. Similar observations were made in combining site studies with the lectin IV of *Griffonia simplicifolia* when essential hydroxyl groups of the Lewis b tetrasaccharide could not be substituted for by amino groups (25).

Experimental

General methods

The ^{1}H NMR spectra were measured at 300 MHz and 360 MHz (Bruker AM 300 and WM 360) with tetramethylsilane as internal

[4]R.G. Spiro, unpublished results.

Can. J. Chem. Downloaded from www.nrcresearchpress.com by 203.198.23.82 on 09/08/12
For personal use only.

Can. J. Chem. Downloaded from www.nrcresearchpress.com by 203.198.23.82 on 09/08/12
For personal use only.

standard for $CDCl_3$ solutions. Reference standard for D_2O solutions was acetone (2.225 ppm). The ^{13}C NMR spectra were recorded at 75 MHz with dioxane (67.4 ppm) as reference for D_2O solutions and the $CDCl_3$ signal (77.0 ppm) as reference in $CDCl_3$ solutions. Optical rotations were measured at room temperature (23 ± 1°C) in a 1-dm cell on a Perkin–Elmer 241 polarimeter. Thin-layer chromatography (TLC) was performed on precoated plates of silica gel (60-F254, E. Merck, Darmstadt) and visualized by spraying with 5% sulfuric acid in ethanol followed by heating. For column chromatography silica gel 60 (230–400 mesh, E. Merck, Darmstadt) and distilled solvents were used. Solvents and reagents were purified and dried according to standard procedures. Melting points are uncorrected.

p-*Nitrophenyl 2,4,6-tri*-O-*acetyl-3*-O-*(2,3,4,6-tetra*-O-*acetyl-α-*D*-glucopyranosyl)-α-*D*-mannopyranoside (3)*

A mixture of octaacetate **1** (161.0 mg, 0.24 mmol),[3] *p*-nitrophenol (92.6 mg, 0.67 mmol), and zinc chloride (4 mg) was heated with magnetic stirring in an oil bath at 160°C for 35 min. The melt was allowed to reach room temperature and was dissolved in dichloromethane. A TLC check indicated that ~40% of the starting material was still left. The solution was washed with aqueous 1 N sodium hydroxide until colorless and then with water until neutral, followed by drying and evaporation. The resultant material was chromatographed on a column of silica gel (hexane–dichloromethane – ethyl acetate, 3:2:2) to provide **3** (67.4 mg, 38%) as an amorphous solid; $[\alpha]_D$ +1.3 (*c* 0.5, chloroform). ^1H NMR ($CDCl_3$) δ: 8.22 and 7.2 (2d, each 2H, Ph), 5.64 (d, 1H, $J_{1,2}$ 1.5 Hz, H-1), 5.45 (dd, $J_{2,3}$ 3.5 Hz, H-2), 5.39 (t, 1H, $J_{3,4} \sim J_{4,5}$ 9.5 Hz, H-4), 5.38 (t, 1H, $J_{2',3'} \sim J_{3',4'}$ 10.0 Hz, H-3′), 5.34 (d, 1H, $J_{1',2'}$ 4.0 Hz, H-1′), 5.05 (t, 1H, $J_{4',5'}$ 10.0 Hz, H-4′), 4.79 (dd, 1H, H-2′), 4.41 (dd, 1H, H-3), 4.28 (dd, 1H, $J_{6A',6B'}$ 12.5 Hz, $J_{6A',5'}$ 4.5 Hz, H-6A′), 4.22–3.97 (m, 4H, H-6A, H-6B, H-6B′, H-5′), 3.86 (ddd, 1H, $J_{5,6A}$ 2.5 Hz, $J_{5,6B}$ 5.5 Hz, H-5), 2.30, 2.09, 2.01, 2.00 (4s, each 3H, $4CH_3CO$), 2.06 (s, 9H, $3CH_3CO$); ^{13}C NMR ($CDCl_3$) δ: 170.50, 170.41, 170.31, 169.70, 169.59 (CH_3CO), 159.91, 143.19, 125.82, 123.01 (aromatic C), 96.69, 95.58 (C-1, C-1′, $J_{C,H}$ 175.77 Hz, 174.94 Hz), 72.20 (C-3), 70.76 (C-2′), 69.96, 69.79, 69.06 (C-2, C-3′, C-5), 68.33, 68.08 (C-4′, C-4), 67.60 (C-5′), 61.88 (C-6, C-6′), 20.73, 20.56 (CH_3CO). Anal. calcd. for $C_{32}H_{39}NO_{20}$: C 50.73, H 5.19, N 1.85; found: C 50.70, H 5.30, N 1.95.

2,4,6-Tri-O-*acetyl-1,5-anhydro-3*-O-*(2,3,4,6-tetra*-O-*acetyl-α-*D*-glucopyranosyl)-*D*-mannitol (4)*

Bromide **2** (135.1 mg, 0.19 mmol),[3] tributyltin hydride (231 μL, 0.86 mmol), and 2,2′-azobis(isobutyronitrile) (7.85 mg) in toluene (5.7 mL) were heated for 1 h at 80°C. The solvent was evaporated and the resultant material was applied to a column of silica gel (hexane – ethyl acetate, 1:1) to give **4** (75.4 mg, 65%) as a solid; mp 156–157°C (ethanol); $[\alpha]_D$ +40.8 (*c* 0.5, chloroform). ^1H NMR ($CDCl_3$) δ: 5.36 (t, 1H, $J_{3',4'} \sim J_{3',2'}$ 10.0 Hz, H-3′), 5.28 (t, overlapped, H-4), 5.27 (overlapped, H-2), 5.26 (d, 1H, $J_{1',2'}$ 4.0 Hz, H-1′), 5.04 (t, 1H, $J_{4',5'}$ 10.0 Hz, H-4′), 4.76 (dd, 1H, H-2′), 4.30–4.02 (m, 6H, H-6A′, H-6B′, H-5′, H-6A, H-6B, and H-1A at 4.09, $J_{1,2}$ 1.5 Hz), 3.95 (dd, 1H, $J_{2,3}$ 3.5 Hz, $J_{3,4}$ 9.5 Hz, H-3), 3.61 (bd, $J_{1A,1B}$ 13.0 Hz, H-1B), 3.47 (ddd, 1H, $J_{5,6A}$ 5.5 Hz, $J_{5,6B}$ 2.5 Hz, H-5), 2.25, 2.10, 2.09, 2.0 (4s, each 3H, $4CH_3CO$), 2.08 (s, 9H, $3CH_3CO$). ^{13}C NMR ($CDCl_3$) δ: 170.78, 170.72, 170.59, 170.50, 169.77 (CH_3CO), 96.48 (C-1′), 76.85, 75.36, 70.80 (C-2′), 69.78 (C-3′), 69.15, 68.40, 68.19, 68.19, 68.12, 62.70 and 61.81 (C-6, C-6′) and 20.97, 20.79, 20.64, 20.59 (CH_3CO). Anal. calcd. for $C_{26}H_{36}O_{17}$: C 50.32, H 5.85; found: C 50.31, H 5.71.

p-*Nitrophenyl 3*-O-*(α-*D*-glucopyranosyl)-α-*D*-mannopyranoside (5)*

Heptaacetate **3** (51.9 mg, 0.068 mmol) was deacetylated in methanolic 0.25 N sodium methoxide (3 mL) for 1 h. The solution was made neutral with Amberlite IRC 50 (H^+) and evaporated. The resultant material was passed through a column of Sephadex LH 20 (ethanol–water, 1:1) to provide **5** (30.0 mg, 95%) as a white solid; $[\alpha]_D$ +157.5 (*c* 0.5, water). The ^1H and ^{13}C NMR data are reported in Tables 2 and 3.

1,5-Anhydro-3-O-*(α-*D*-glucopyranosyl)-*D*-mannitol (6)*

Heptaacetate **4** (50 mg, 0.081 mmol) was deacetylated in methanolic 0.15 N sodium methoxide for 1 h. The solution was neutralized with Amberlite IRC 50 (H^+) and evaporated. The material was passed through a column of Sephadex LH 20 (ethanol–water, 1:1) to provide **6** (26 mg, quant.) as a white powder; $[\alpha]_D$ +60 (*c* 0.5, water). The ^1H and ^{13}C NMR data are reported in Tables 2 and 3.

4,6-Di-O-*acetyl-1,5-anhydro-2-deoxy-3*-O-*(2,3,4,6-tetra*-O-*acetyl-α-*D*-glucopyranosyl)-*D*-*arabino*-hex-1-enitol (7)*

A mixture of bromide **2** (0.13 mmol) and sodium acetate (20 mg) in 50% acetic acid (0.5 mL) was added at −10°C to a mixture of zinc (180 mg) and copper sulfate (18 mg) in 50% acetic acid (0.5 mL). The temperature was raised to 0°C and the reaction mixture was stirred for 5 h. It was diluted with dichloromethane, filtered, and the filtrate was washed with water, aqueous saturated sodium hydrogen carbonate, and water, followed by drying and evaporation. The crude product was purified on a column of silica gel (hexane – ethyl acetate, 2:1, 1:1) to provide **7** (47 mg, 65%) as a white solid; mp 125.5–126.5°C (ethanol); $[\alpha]_D$ +54 (*c* 0.3, chloroform). ^1H NMR ($CDCl_3$) δ: 6.46 (dd, 1H, $J_{1,2}$ 6.0 Hz, $J_{1,3} \sim$ 1 Hz, H-1), 5.43 (t, 1H, $J_{3',4'} \sim J_{2',3'}$ 9.5 Hz, H-3′), 5.29 (d, 1H, $J_{1',2'}$ 3.5 Hz, H-1′), 5.16 (dd, 1H, *J* 6.5 Hz, 5.5 Hz, H-4), 5.06 (t, 1H, $J_{4',5'}$ 9.5 Hz, H-4′), 4.85 (dd, 1H, H-2′), 4.82 (dd, 1H, $J_{2,3}$ 3.5 Hz, H-2), 4.36 (dd, 1H, $J_{6A,6B}$ 13.0 Hz, $J_{6A,5}$ 6.5 Hz, H-6A), 4.27–4.0 (m, 6H, H-6B, H-6A′, H-6B′, H-5′, and H-3 at 4.23, H-5 at 4.04), 2.11, 2.10, 2.09, 2.08, 2.04, 2.01 (6s, each 3H, $6CH_3CO$). ^{13}C NMR ($CDCl_3$) δ: 170.51, 170.33, 169.88, 169.49 (CH_3CO), 145.08 (C-1), 99.90 (C-2), 95.81 (C-1′), 74.20, 71.18 (C-3, C-5), 70.51 (C-2′), 69.81 (C-3′), 68.46, 68.31 (C-4, C-4′), 67.75 (C-5′), 61.86, 61.44 (C-6, C-6′), 20.74, 20.64, 20.56 (CH_3CO). Anal. calcd. for $C_{24}H_{32}O_{15}$: C 51.42, H 5.75, found: C 51.76, H 5.93.

1,5-Anhydro-2-deoxy-3-O-*(α-*D*-glucopyranosyl)-*D*-*arabino*-hex-1-enitol (8)*

Hexaacetate **7** (130 mg, 0.23 mmol) was deacetylated in methanolic 0.09 N sodium methoxide (1.1 mL) for 1.5 h. The solution was made neutral with Amberlite IRC 50 (H^+) and evaporated. The reaction product was purified on a column of Iatrobeads® (chloroform–methanol–water, 65:30:2) followed by gel filtration on a column of Sephadex LH 20 (ethanol–water, 1:1) to provide the title compound **8** (68.8 mg, 96%) as a white solid; $[\alpha]_D$ +46.4 (*c* 0.2, water). The ^1H and ^{13}C NMR data are reported in Tables 2 and 3.

1,5-Anhydro-2-deoxy-3-O-*(α-*D*-glucopyranosyl)-*D*-*arabino*-hexitol (9)*

(*a*) A mixture of glucal **8** (46 mg, 0.149 mmol) and 5% palladium-on-carbon (42 mg) in methanol (4 mL) was hydrogenated in the hydrogen stream for 1 h. Filtration, solvent evaporation, and gel filtration on a column of Sephadex LH 20 (ethanol–water, 1:1) provided **9** (45.2 mg, 98%) as a white solid, $[\alpha]_D$ +89.8 (*c* 0.2, water). The ^1H and ^{13}C NMR data are reported in Tables 2 and 3.

(*b*) A mixture of **16** (110 mg, 0.14 mmol) and 5% palladium-on-carbon (110 mg) in methanol (6 mL) was hydrogenated in the hydrogen stream for 2.5 h. Usual processing and gel filtration provided a product identical to **9** (43.5 mg, 101%).

2-O-*Benzyl-4,6*-O-*benzylidene-3*-O-*(2,3,4,6-tetra*-O-*benzyl-α-*D*-glucopyranosyl)-α-*D*-mannopyranosyl fluoride (11)*

Diethylaminosulfur trifluoride (50 μL, 0.38 mmol) was added to a stirred solution of **10** (201 mg, 0.228 mmol)[3] in dichloromethane (1 mL) at −30°C. Stirring was continued for 30 min at −30°C and 25 min at room temperature. The mixture was cooled down again to −30°C and methanol (1.5 mL) was added to quench the reaction. The remainder obtained on solvent evaporation was dissolved in dichloromethane, and the organic solution was washed

Can. J. Chem. Downloaded from www.nrcresearchpress.com by 203.198.23.82 on 09/08/12
For personal use only.

with aqueous saturated sodium hydrogen carbonate and water, dried, and evaporated. The resultant product was purified on a column of silica gel (hexane – ethyl acetate, 6:1) and obtained as a syrup (168 mg, 83%), $[\alpha]_D$ +47.4 (*c* 0.5, chloroform). ^{1}H NMR ($CDCl_3$) δ: 7.5–6.9 (m, 30H, 6Ph), 5.53 (d, 1H, $J_{1',2'}$ 3.5 Hz, H-1'), 5.52 (dd, 1H, $J_{1,2} \sim 1$ Hz, $J_{1,F}$ 49.0 Hz, H-1), 5.45 (s, 1H, C*H*Ph), 3.53 (dd, 1H, $J_{2',3'}$ 9.5 Hz, H-2'); ^{13}C NMR ($CDCl_3$) δ: 106.91 ($J_{C,F}$ 225.1 Hz, $J_{C,H}$ 185.0 Hz, C-1), 102.47 (*C*HPh), 97.0 (C-1'). Anal. calcd . for $C_{54}H_{55}FO_{10}$: C 73.45, H 6.28; found: C 73.33, H 6.27.

*3-O-(α-D-Glucopyranosyl)-α-D-mannopyranosyl fluoride (**12**)*

11 (147.8 mg, 0.167 mmol) in 95% ethanol (12 mL) was hydrogenated in the presence of 5% palladium-on-carbon (140 mg) at atmospheric pressure for 1 h. The catalyst was removed by filtration and the solvent evaporated. Gel filtration of the product on a column of Sephadex LH 20 (ethanol–water, 1:1) and lyophilization of an aqueous solution provided title compound **12** (52.4 mg, 91%) as a white solid; $[\alpha]_D$ +89.7 (*c* 0.53, water). The ^{1}H and ^{13}C NMR data are reported in Tables 2 and 3.

*1,5-Anhydro-2-deoxy-4,6-*O*-p-methoxybenzylidene-D-*arabino*-hexitol (**14**)*

A solution of 1,5-anhydro-2-deoxy-D-*arabino*-hexitol (**13**) (835 mg, 5.63 mmol) (20), *p*-methoxybenzaldehyde dimethyl acetal (1.3 mL, 7.63 mmol), and *p*-toluenesulfonic acid monohydrate (300 mg) in acetonitrile (24 mL) was kept overnight. It was neutralized with triethylamine and the material obtained on evaporation applied to a column of silica gel (hexane – ethyl acetate, 2:1) to provide **13** (1.25 g, 83%) as a solid; mp 113.5–115°C (dichloromethane, ether, hexane); $[\alpha]_D$ −34 (*c* 0.4, chloroform). ^{1}H NMR ($CDCl_3$) δ: 7.42 and 6.9 (2d, each 2H, Ph), 5.53 (s, 1H, C*H*Ph) 4.26 (dd, 1H, $J_{6a,6e}$ 10.5 Hz, $J_{5,6e}$ 4.5 Hz, H-6e), 4.00 (ddd, 1H, $J_{1e,1a}$ 11.5 Hz, $J_{1e,2a}$ 5.0 Hz, $J_{1e,2e}$ 1.5 Hz, H-1e), 3.89 (ddd, 1H, $J_{2ax,3}$ 10.5 Hz, $J_{2e,3}$ 5.5 Hz, $J_{3,4}$ 8.0 Hz, H-3), 3.81 (s, 3H, CH_3O), 3.69 (t, 1H, $J_{6a,5}$ 10.0 Hz, H-6a), 3.58 (dt, 1H, $J_{1a,2a}$ 12.5 Hz, $J_{1a,2e}$ 2.5 Hz, H-1a), 3.43 (t, 1H, $J_{4,5}$ 8.5 Hz, H-4), 3.33 (dt, 1H, H-5), 2.04 (m, 1H, $J_{2e,2a}$ 13.5 Hz, H-2e), 1.82 (m, 1H, H-2a). Anal. calcd. for $C_{14}H_{18}O_5$: C 63.15, H 6.81; found: C 62.89, H 6.94.

*1,5-Anhydro-2-deoxy-4,6-*O*-p-methoxybenzylidene-3-*O*-(2,3,4,6-tetra-*O*-benzyl-α-D-glucopyranosyl)-D-*arabino*-hexitol (**16**)*

A solution of 2,3,4,6-tetra-*O*-benzyl-α-D-glucopyranosyl bromide (**15**) (21) (13.5 mmol) in dichloromethane (14 mL) was transferred into a mixture of alcohol **14** (1.2 g, 4.51 mmol), tetraethylammonium bromide (2.1 g, 10.0 mmol), *N,N*-dimethylformamide (2.5 mL), Hünig's base (2.8 mL, 16.1 mmol), and 4 Å molecular sieves (powdered, 5 g) in dichloromethane (3 mL). The mixture was concentrated in a stream of nitrogen and kept stirring for 60 h. Then the reaction was quenched by the addition of moist pyridine (1 mL) and after 1 h it was diluted with dichloromethane and filtered through a pad of Celite. The solution was washed with saturated aqueous sodium hydrogen carbonate and water, followed by drying and evaporation. Purification was achieved by column chromatography on silica gel (hexane – ethyl acetate, 5:1, 4:1, containing 0.05% triethylamine) to provide solid **16** (1.98 g, 56%); mp 124–126°C (dichloromethane, ether, hexane); $[\alpha]_D$ +28 (*c* 0.3, chloroform, 0.1% triethylamine). ^{1}H NMR ($CDCl_3$) δ: 7.40–6.80 (m, 24H, 5Ph), 5.49 (s, 1H, C*H*PhOMe), 5.46 (d, 1H, $J_{1',2'}$ 3.5 Hz, H-1'), 5.05–4.31 (4ABq, 8H, 4CH_2Ph), 4.24 (dd, 1H, $J_{6a,6e}$ 10.0 Hz, $J_{6e,5}$ 5.0 Hz, H-6e), 4.07 (q, 1H, H-3), 3.96 (2H, m, H-1A, t, $J_{2',3'}$ 10.0 Hz, $J_{3',4'}$ 9.0 Hz, H-3'), 3.87 (td, 1H, $J_{4',5'}$ 10.0 Hz, H-5'), 3.76 (s, 3H, CH_3O), 3.73 (t, overlapped, $J_{3,4} \sim J_{4,5}$ 9.0 Hz, H-4), 3.69 (t, H-6A, overlapped by H-6A', H-6B'). 3.56 (t, 1H, H-4'), ~ 3.54 (H-1B), 3.48 (dd, 1H, H-2'), 3.37 (dt, 1H, $J_{5,6a}$ 10.0 Hz, H-5), 1.95 (m, 2H, H-2A, H-2B). Anal. calcd. for $C_{48}H_{52}O_{10}$: C 73.08, H 6.64; found: C 72.84, H 6.59.

*1,5-Anhydro-2-deoxy-4-*O*-p-methoxybenzyl-3-*O*-(2,3,4,6-tetra-O-benzyl-α-D-glucopyranosyl)-D-*arabino*-hexitol (**17**)*

Trimethylsilyl chloride (560 μL, 4.4 mmol) was added dropwise to a stirred mixture of **16** (580 mg, 0.74 mmol), sodium cyanoborohydride (280 mg, 4.46 mmol), and 4 Å molecular sieves (0.5 g) in acetonitrile (15 mL) at ice-bath temperature. After 6 h at room temperature, it was poured into aqueous saturated sodium hydrogen carbonate and extracted with dichloromethane. The organic solution was washed with water, dried, and evaporated. Subsequent column chromatography on silica gel (hexane – ethyl acetate, 4:1 to 1:1 containing 0.05% triethylamine) provided as a minor component the 4-hydroxy compound **27** (50.9 mg, 8.8%) followed by the major product **17** (430 mg, 74%); $[\alpha]_D$ +47 (*c* 0.6, chloroform, 0.1% triethylamine). ^{1}H NMR ($CDCl_3$) δ: 7.40–6.80 (m, 24H, 5Ph), 5.12 (d, 1H, $J_{1',2'}$ 3.5 Hz, H-1'), 5.01–4.44 (5ABq, 10H, 4CH_2Ph, CH_2PhOMe), 4.05 (t, 1H, $J_{2',3'}$ 9.5 Hz, $J_{3',4'}$ 9.0 Hz, H-3'), 3.94 (m, 1H, $J_{5',4'}$ 10.0 Hz, H-5'), 3.85 (ddd, 1H, $J_{1A,1B}$ 11.5 Hz, $J_{1A,2a}$ 4.0 Hz, $J_{1A,2e} \sim 1$ Hz, H-1A), 3.76 (s, 3H, CH_3O), 3.72 (dd, 1H, $J_{6A',6B'}$ 10.5 Hz, $J_{6A',5'}$ 4.0 Hz, H-6A'), 3.63 (overlapped, H-4'), 3.57 (dd, 1H, H-2'), 3.36 (t, 1H, $J_{3,4} \sim J_{4,5}$ 9.0 Hz, H-4), 3.36 (dt, H-1B), 3.22 (ddd, 1H, $J_{5,6B}$ 2.5 Hz, H-5), 2.19 (m, 1H, $J_{2e,2a}$ 13.0 Hz, H-2e), 1.71 (dq, 1H, $J_{2a,1B} \sim J_{2a,3} \sim$ 12.5 Hz, H-2a). Anal. calcd. for $C_{48}H_{54}O_{10}$: C 72.89, H 6.88; found: C 72.60, H 7.09.

*1,5-Anhydro-2-deoxy-6-*O*-methanesulfonyl-4-*O*-p-methoxybenzyl-3-*O*-(2,3,4,6-tetra-*O*-benzyl-α-D-glucopyranosyl)-D-*arabino*-hexitol (**18**)*

Methanesulfonyl chloride (53 μL, 0.69 mmol) was added dropwise to a stirred solution of **17** (273 mg, 0.35 mmol) in pyridine (6 mL) at ice-bath temperature. After 2 h at this temperature, the mixture was poured into ice-water, followed by extraction with dichloromethane and washing of the organic solution with saturated aqueous sodium hydrogen carbonate, drying, and evaporation. Purification of the crude product on a column of silica gel (hexane – ethyl acetate, 4:1, 3:1, 2:1, containing 0.05% triethylamine) afforded mesylate **18** (273 mg, 91%) as a tough syrup; $[\alpha]_D$ +49 (*c* 0.6, chloroform, 0.05% triethylamine). ^{1}H NMR ($CDCl_3$) δ: 7.40–6.80 (m, 24H, 5Ph), 5.09 (d, 1H, $J_{1',2'}$ 3.5 Hz, H-1'), 5.07–4.43 (5ABq, 10H, 4CH_2Ph, CH_2PhOMe), 4.38 (dd, 1H, $J_{6A,6B}$ 10.5 Hz, $J_{6A,5}$ 1.5 Hz, H-6A), 4.28 (dd, 1H, $J_{6B,5}$ 4.5 Hz, H-6B), 4.05 (t, 1H, $J_{2',3'}$ 9.5 Hz, $J_{3',4'}$ 9.0 Hz, H-3'), 3.93 (m, 1H, $J_{4',5'}$ 10.0 Hz, H-5'), 3.86 (ddd, 1H, $J_{1A,1B}$ 11.5 Hz, $J_{1A,2a}$ 4.0 Hz, $J_{1A,2e}$ 1.0 Hz, H-1A), 3.77 (s, 3H, CH_3O), 3.71 (dd, overlapped, $J_{6A',5'}$ 4.5 Hz, H-6A'), 3.63 (t, overlapped, H-4'), 3.57 (dd, 1H, H-2'), 3.36 (m, 3H, with H-5, H-1B), 3.01 (s, 3H, CH_3O), 2.21 (m, 1H, $J_{2e,2a}$ 13.5 Hz, $J_{2e,3}$ 4.5 Hz, H-2e), 1.72 (dq, 1H, $J_{2a,1B} \sim J_{2a,3} \sim$ 12.0 Hz, H-2a). Anal. calcd. for $C_{49}H_{56}O_{12}S$: C 67.72, H 6.50; found: C 67.74, H 6.53.

*1,5-Anhydro-2-deoxy-4-*O*-p-methoxybenzyl-6-*O*-methyl-3-*O*-(2,3,4,6-tetra-*O*-benzyl-α-D-glucopyranosyl)-D-*arabino*-hexitol (**19**)*

Sodium hydride (80% oily suspension, 30 mg, 1 mmol) was added to a solution of **17** (143 mg, 0.18 mmol) in *N,N*-dimethylformamide (3 mL) at ice-bath temperature. After 20 min, this was followed by the addition of methyl iodide (50 μL, 0.54 mmol). After 2 h, the reaction was quenched by the dropwise addition of methanol. It was diluted with dichloromethane, washed with water, dried, and evaporated. Column chromatography on silica gel (hexane – ethyl acetate, 2:1, containing 0.05% triethylamine) provided **19** (120 mg, 83%) as a tough (*very* viscous) syrup; $[\alpha]_D$ +34 (*c* 0.3, chloroform, 0.05% triethylamine). ^{1}H NMR ($CDCl_3$) δ: 7.40–6.78 (m, 24H, 5Ph), 5.12 (d, 1H, $J_{1',2'}$ 3.5 Hz, H-1'), 5.04–4.42 (5ABq, 10H, 4CH_2Ph, CH_2PhOMe), 4.04 (t, 1H, $J_{2',3'}$ 9.5 Hz, $J_{3',4'}$ 9.0 Hz, H-3'), 3.93 (ddd, 1H, $J_{4',5'}$ 10.0 Hz, $J_{5',6A'}$ 4.0 Hz, $J_{5',6B'}$ 1.7 Hz, H-5'), 3.88 (ddd, 1H, $J_{1A,1B}$ 11.5 Hz, $J_{1A,2a}$ 5.0 Hz, $J_{1A,2e}$ 1.0 Hz, H-1A), 3.76 (s, 3H, CH_3O), 3.72 (dd, overlapped, $J_{6A',6B'}$ 10.5 Hz, H-6A'), 3.63 (t, overlapped, H-4'),

Can. J. Chem. Downloaded from www.nrcresearchpress.com by 203.198.23.82 on 09/08/12
For personal use only.

3.56 (overlapped, H-2′), 3.33 (s, 3H, CH_3O), 3.26 (overlapped, H-1B), 2.16 (m, 1H, $J_{2e,2a}$ 13.0 Hz, $J_{2e,3}$ 4.5 Hz, H-2e), 1.74 (dq, 1H, $J_{2a,1B} \sim J_{2a,3}$ 12.5 Hz, H-2a). Anal. calcd. for $C_{49}H_{56}O_{10}$:C 73.11, H 7.01; found: C 73.04, H 7.02.

*1,5-Anhydro-2,6-dideoxy-6-iodo-4-*O-p-*methoxybenzyl-3-*O-*(2,3,4,6-tetra-*O-*benzyl-α-D-glucopyranosyl)-D-*arabino-*hexitol (20)*

A stirred mixture of **18** (173 mg, 0.20 mmol) and potassium iodide (200 mg) in *N,N*-dimethylformamide (7 mL) was heated at 95–100°C for 13 h. It was diluted with dichloromethane, washed with water, dried, and evaporated. Column chromatography on silica gel (hexane – ethyl acetate, 5:1, 4:1, containing 0.05% triethylamine) provided the title compound **20** (116 mg, 65%) as a crystallizing syrup; $[\alpha]_D$ +46 (*c* 0.3, chloroform, 0.03% triethylamine). ^{1}H NMR ($CDCl_3$) δ: 7.40–6.75 (m, 24H, 5Ph), 5.15–4.35 (5ABq, 10H, 4CH_2Ph, CH_2PhOMe), 5.07 (d, 1H, $J_{1',2'}$ 3.5 Hz, H-1′), 4.06 (t, 1H, $J_{2',3'}$ 9.5 Hz, $J_{3',4'}$ 9.0 Hz, H-3′), 3.95 (m, overlapped, H-5′), 3.91 (ddd, overlapped, $J_{1A,1B}$ 12.5 Hz, $J_{1A,2a}$ 5.0 Hz, $J_{1A,2e}$ 1.0 Hz, H-1A), 3.77 (s, 3H, CH_3O), 3.73 (dd, overlapped, $J_{6A',6B'}$ 10.5 Hz, $J_{6A',5'}$ 4.0 Hz, H-6A′), 3.66 (t, 1H, $J_{4',5'}$ 9.5 Hz, H-4′), 3.62 (dd, overlapped, $J_{5',6B'}$ 1.8 Hz, H-6B′), 3.57 (dd, 1H, H-2′), 3.46 (dd, 1H, $J_{6A,6B}$ 11.0 Hz, $J_{5,6A}$ 3.0 Hz, H-6A), 3.39 (overlapped, H-1B), 3.37 (dd, 1H, $J_{5,6B}$ 5.5 Hz, H-6B), 3.30 (t, 1H, $J_{3,4} \sim J_{4,5}$ 8.5 Hz, H-4), 2.91 (m, 1H, H-5), 2.22 (m, 1H, $J_{2e,2a}$ 12.5 Hz, $J_{2e,3}$ 4.5 Hz, H-2e), 1.76 (dq, 1H, $J_{2a,3} \sim J_{2a,1B}$ 12.5 Hz, H-2a).

*1,5-Anhydro-2,6-dideoxy-4-*O-p-*methoxybenzyl-3-*O-*(2,3,4,6-tetra-*O-*benzyl-α-D-glucopyranosyl)-D-*arabino-*hexitol (21)* *and 1,5-anhydro-2,6-dideoxy-3-*O-*(2,3,4,6-tetra-*O-*benzyl-α-D-glucopyranosyl)-D-*arabino-*hexitol (22)*

The iodo compound **20** (116 mg, 0.13 mmol), tributyltin hydride (150 μL, 0.56 mmol), and 2,2′-azobis(isobutyronitrile) (10 mg) in toluene (3 mL) were heated at 83°C for 30 min. Evaporation and subsequent column chromatography on silica gel (hexane – ethyl acetate, 4:1, 3:1 containing 0.05% triethylamine) provided in the first fraction **21** (54 mg, 54%) as a solid; $[\alpha]_D$ +35 (*c* 0.3, chloroform, 0.03% triethylamine). ^{1}H NMR ($CDCl_3$) δ: 7.40–6.77 (m, 24H, 5Ph), 5.12 (d, 1H, $J_{1',2'}$ 3.5 Hz, H-1′), 5.06–4.44 (5ABq, 10H, 4CH_2Ph, CH_2PhOMe), 4.05 (t, 1H, $J_{2',3'}$ 9.5 Hz, $J_{3',4'}$ 9.0 Hz, H-3′), 3.94 (m, 1H, $J_{4',5'}$ 9.5 Hz, H-5′), 3.79 (overlapped, H-1A), 3.76 (s, 3H, CH_3O), 3.73 (dd, overlapped, $J_{6A',6B'}$ 10.5 Hz, $J_{6A',5'}$ 3.5 Hz, H-6A′), 3.64 (t, overlapped, H-4′), 3.61 (overlapped, H-6B′), 3.56 (dd, 1H, H-2′), 3.31 (dt, $J_{1B,2a}$ 12.5 Hz, H-1B), 3.26 (m, H-5), 2.17 (m, 1H, $J_{2e,2a}$ 12.5 Hz, $J_{2e,3}$ 5.0 Hz, H-2e), 1.73 (dt, 1H, $J_{2a,3}$ 12.5 Hz, H-2a), 1.23 (d, 3H, $J_{5,6}$ 6.5 Hz, H_3-6). Continued elution provided **22** (25 mg, 30%) as a syrup; $[\alpha]_D$ +31 (*c* 0.1, chloroform). ^{1}H NMR ($CDCl_3$) δ: 7.40–7.10 (m, 20H, 4Ph), 4.94 (d, 1H, $J_{1',2'}$ 3.5 Hz, H-1′), 4.96–4.43 (4ABq, 8H, 4CH_2Ph), 4.01 (t, 1H, $J_{2',3'}$ 9.5 Hz, $J_{3',4'}$ 9.0 Hz, H-3′), 3.93 (ddd, 1H, $J_{4',5'}$ 10.0 Hz, $J_{5',6A'}$ 4.0 Hz, $J_{5',6B'}$ 1.5 Hz, H-5′), 3.86 (ddd, 1H, $J_{1A,1B}$ 12.0 Hz, $J_{1A,2a}$ 4.5 Hz, $J_{1A,2e}$ 1.0 Hz, H-1A), 3.69 (dd, 1H, $J_{6A',6B'}$ 10.5 Hz, H-6A′), 3.60 (overlapped, H-4′), 3.59 (dd, overlapped, H-6B′), 3.54 (dd, 1H, H-2′),~3.42 (m, overlapped, H-3), 3.40 (dt, $J_{1B,2a}$ 12.5 Hz, $J_{1B,2e}$ 2.0 Hz, H-1B), 3.26 (m, 1H, H-5), 3.19 (t, 1H, $J_{3,4} \sim J_{4,5}$ 9.0 Hz, H-4), 1.98 (m, 1H, $J_{2e,2a}$ 12.5 Hz, $J_{2e,3}$ 5.0 Hz, H-2e), 1.74 (dq, 1H, $J_{2a,3}$ 12.0 Hz, H-2a), 1.29 (d, 3H, $J_{5,6}$ 6.5 Hz, H_3-6).

*1,5-Anhydro-6-azido-2,6-dideoxy-4-*O-p-*methoxybenzyl-3-*O-*(2,3,4,6-tetra-*O-*benzyl-α-D-glucopyranosyl)-D-*arabino-*hexitol (23)*

A mixture of mesylate **18** (90 mg, 0.10 mmol) and sodium azide (90 mg, 1.38 mmol) in *N,N*-dimethylformamide (3 mL) was heated at 105°C for 2 h. It was poured into water, extracted with dichloromethane, and the organic solution was washed with water, dried, and evaporated. Column chromatography on silica gel (hexane – ethyl acetate, 4:1, 3:1, containing 0.05% triethylamine) provided azide **23** (84 mg, 99%) as a syrup; $[\alpha]_D$ +75 (*c* 0.3, chloroform, 0.03% triethylamine). ^{1}H NMR ($CDCl_3$) δ: 7.40–6.75 (m, 24H, 5Ph), 5.10 (d, 1H, $J_{1',2'}$ 3.5 Hz, H-1′), 5.06–4.43 (5ABq, 10H, 4CH_2Ph, CH_2PhOMe), 4.05 (t, 1H, $J_{2',3'}$ 9.5 Hz, $J_{3',4'}$ 9.0 Hz, H-3′), 3.94 (m, 1H, $J_{4',5'}$ 10.0 Hz, H-5′), 3.87 (ddd, 1H, $J_{1A,1B}$ 11.5 Hz, $J_{1A,2a}$ 4.5 Hz, $J_{1A,2e}$ 1.0 Hz, H-1A), 3.75 (s, 3H, CH_3O), 3.64 (overlapped, H-4′), 3.57 (dd, 1H, H-2′), 2.20 (m, 1H, $J_{2e,2a}$ 13.0 Hz, $J_{2e,3}$ 4.5 Hz, H-2e), 1.74 (dq, 1H, $J_{2a,1B} \sim J_{2a,3}$ 12.5 Hz, H-2a). Anal. calcd. for $C_{48}H_{53}N_3O_9$: C 70.66, H 6.55, N 5.15; found: C 70.97, H 6.81, N 4.83.

*1,5-Anhydro-2-deoxy-3-*O-*(α-D-glucopyranosyl)-6-*O-*methyl-D-*arabino-*hexitol (24)*

19 (95 mg, 0.12 mmol) and 5% palladium-on-carbon (95 mg) in methanol (5 mL) were hydrogenated in the hydrogen stream for 3 h. Work-up and gel filtration as described for **9** provided **24** (39.7 mg, 104%) as a white solid after freeze-drying an aqueous solution; $[\alpha]_D$ +105 (*c* 0.3, water). The ^{1}H and ^{13}C NMR data are reported in Tables 2 and 3.

*1,5-Anhydro-2,6-dideoxy-3-*O-*(α-D-glucopyranosyl)-D-*arabino-*hexitol (25)*

A mixture of **21** (54 mg, 0.07 mmol) and 5% palladium-on-carbon (55 mg) in methanol (4 mL) was hydrogenated in the hydrogen stream for 2.5 h. Usual processing and gel filtration provided **25** (21 mg, 102%) as a white solid after freeze-drying its aqueous solution; $[\alpha]_D$ +99 (*c* 0.3, water). The ^{1}H NMR spectrum indicated the presence of ~7% triethylamine in the compound. The ^{1}H and ^{13}C NMR data are reported in Tables 2 and 3.

*6-Amino-1,5-anhydro-2,6-dideoxy-3-*O-*(α-D-glucopyranosyl)-D-*arabino-*hexitol-hydrochloride (26)*

A mixture of azide **23** (65 mg, 0.08 mmol), 5% palladium-on-carbon (45 mg), and triethylamine (40 μL) in methanol (4 mL) was hydrogenated for 2 h in the hydrogen stream. The material obtained on filtration and evaporation was passed through a short column of silica gel (dichloromethane – 12% methanol). The product, 5% palladium-on-carbon (60 mg) and methanolic 0.12 N hydrochloric acid (700 μL, 0.084 mmol) in methanol (4 mL) were hydrogenated in the hydrogen stream for 2 h. Usual work-up and gel filtration as described for **9** provided **26** (18 mg, 66%) as a white solid after freeze-drying an aqueous solution. The ^{1}H NMR spectrum indicated only 90% homogeneity. The ^{1}H and ^{13}C NMR data are reported in Tables 2 and 3.

*1,5-Anhydro-2-deoxy-6-*O-p-*methoxybenzyl-3-*O-*(2,3,4,6-tetra-*O-*benzyl-α-D-glucopyranosyl)-D-*arabino-*hexitol (27)*

Trifluoroacetic acid (440 μL, 5.71 mmol) was added to a stirred mixture of **16** (750 mg, 0.95 mmol), sodium cyanoborohydride (358 mg, 5.70 mmol), and 4 Å molecular sieves (0.5 g) in *N,N*-dimethylformamide (20 mL) at 0°C. The mixture was kept at room temperature for 4 days and three more additions of trifluoroacetic acid (440 μL each time) were made. Then, the mixture was poured into aqueous saturated sodium hydrogen carbonate and extracted with dichloromethane, followed by washing of the organic solution with water, drying, and evaporation. The remainder was purified by column chromatography (hexane – ethyl acetate, 4:1 to 1:1, containing 0.05% triethylamine) to provide **27** (406 mg, 54%) as a crystallizing syrup; $[\alpha]_D$ +29 (*c* 1.8, chloroform, 0.05% triethylamine). ^{1}H NMR ($CDCl_3$) δ: 7.40–6.80 (m, 24H, 5Ph), 5.01 (d, 1H, $J_{1',2'}$ 3.5 Hz, H-1′), 4.96–4.43 (4ABq, 1s, 10H, 4CH_2Ph, CH_2PhOMe), 4.00 (t, 1H, $J_{2',3'}$ 10.0 Hz, $J_{3',4'}$ 9.0 Hz, H-3′), 3.93 (2m, 2H, H-1A, H-5′), 3.78 (s, 3H, CH_3O), 3.73 (dd, 1H, $J_{6A,6B}$ 10.5 Hz, $J_{6A,5}$ 2.5 Hz, H-6A), 3.69 (dd, 1H, $J_{6A',6B'}$ 10.0 Hz, $J_{6A',5'}$ 4.0 Hz, H-6A′), 3.59 (H-4′), 3.55 (dd, H-2′), 3.41 (dt, overlapped, H-1B), 3.38 (H-5), 1.97 (td, 1H, $J_{2e,2a}$ 13.5 Hz, H-2e), 1.75 (m, H-2a). Anal. calcd. for $C_{48}H_{54}O_{10}$: C 72.89, H 6.88; found: C 72.89, H 6.96. Continued elution of the column provided the isomer **17** (113 mg, 15%).

An analytical sample of **27** (10 mg, 0.13 mmol) was acetylated conventionally with pyridine – acetic anhydride to provide *4-*O-*acetyl-1,5-anhydro-2-deoxy-6-*O-p-*methoxybenzyl-3-*O-*(2,3,4,6-tetra-*O-*benzyl-α-D-glucopyranosyl)-D-*arabino-*hexitol (28)*, which

Can. J. Chem. Downloaded from www.nrcresearchpress.com by 203.198.23.82 on 09/08/12
For personal use only.

was characterized by ^{1}H NMR spectroscopy. ^{1}H NMR ($CDCl_3$) δ: 7.40–6.85 (m, 24H, 5Ph), 4.95 (d, 1H, $J_{1',2'}$ 3.5 Hz, H-1′), 4.91 (overlapped, $J_{3,4} \sim J_{4,5}$ 9.5 Hz, H-4), 4.92–4.42 (4ABq, 1s, 10H, 4CH_2Ph, CH_2PhOMe), 3.97 (t, 1H, $J_{2',3'}$ 9.5 Hz, $J_{3',4'}$ 9.0 Hz, H-3′), 3.93 (overlapped, H-1A), 3.88 (m, 1H, $J_{4',5'}$ 10.0 Hz, H-5′), 3.79 (s, 3H, CH_3O), 3.68 (dd, 1H, $J_{6A',6B'}$ 10.5 Hz, $J_{6A',5'}$ 4.0 Hz, H-6A′), ~3.65 (H-3), 3.59 (dd, 1H, $J_{6B',5'}$ 1.5 Hz, H-6B′), 3.57 (t, 1H, H-4′), 3.48 (dd, 1H, H-2′), 3.46 (m, H-5, H-6), 3.38 (m, H-1B), 2.15 (m, 1H, $J_{2a,2e}$ 13.5 Hz, H-2e), 1.80 (m, 1H, H-2a), 1.74 (s, 3H, CH_3CO).

*1,5-Anhydro-2-deoxy-6-*O-p-*methoxybenzyl-4-*O-*methyl-3-*O-*(2,3,4,6-tetra-*O-*benzyl-α-D-glucopyranosyl)-D-*arabino-*hexitol (29)*

Sodium hydride (80% oily suspension, 30 mg, 1 mmol) was added at ice-bath temperature to a solution of **27** (150 mg, 0.19 mmol) in *N,N*-dimethylformamide (2 mL). After 20 min, methyl iodide (50 μL, 0.54 mmol) was added. After 2 h, the reaction was quenched by the addition of methanol. The mixture was diluted with dichloromethane, followed by washing with water, drying, and evaporation of the organic solution. The remainder on evaporation was applied to a column of silica gel (hexane – ethyl acetate, 3:1, containing 0.05% triethylamine to provide **29** (133 mg, 87%) of a crystallizing syrup, $[\alpha]_D$ +49 (*c* 0.4, chloroform, 0.02% triethylamine). ^{1}H NMR ($CDCl_3$) δ: 7.40–6.85 (m, 24H, 5Ph), 5.15 (d, 1H, $J_{1',2'}$ 3.5 Hz, H-1′), 5.01–4.43 (5ABq, 10H, 4CH_2Ph, CH_2PhOMe), 4.00 (t, 1H, $J_{2',3'}$ 9.5 Hz, $J_{3',4'}$ 9.0 Hz, H-3′), 3.90 (m, H-5′), 3.87 (m, H-1A), 3.76 (s, 3H, CH_3O), 3.71 (dd, 1H, $J_{6A',6B'}$ 10.5 Hz, $J_{6A',5'}$ 4.3 Hz, H-6A′), 3.56 (dd, overlapped, H-2′), 3.42 (s, 3H, CH_3O), 3.33 (dt, $J_{1A,1B} \sim J_{1B,2a} \sim$ 13.5 Hz, H-1B), 3.24 (m, 1H, H-5), 2.08 (m, 1H, H-2e), 1.74 (m, 1H, H-2a). Anal. calcd. for $C_{49}H_{56}O_{10}$: C 73.11, H 7.01; found: C 73.30, H 7.00.

*1,5-Anhydro-2,4-dideoxy-6-*O-p-*methoxybenzyl-3-*O-*(2,3,4,6-tetra-*O-*benzyl-α-D-glucopyranosyl)-D-*threo-*hexitol (31)*

A mixture of **27** (270 mg, 0.34 mmol), sodium hydride (80% oily suspension, 50 mg, 1.67 mmol), and 3 crystals of imidazole in tetrahydrofuran (7 mL) was stirred for 30 min. Then carbon disulfide (205 μL, 3.41 mmol) was added, followed by the addition of methyl iodide (85 μL, 1.37 mmol), after 30 min. The mixture was stirred for another 30 min and then diluted with dichloromethane, and the organic solution was washed with aqueous sodium hydrogen carbonate, water, dried, and evaporated. The yellowish solid (**30**) was reduced with tributyltin hydride (400 μL, 1.49 mmol) in toluene (6 mL) at reflux temperature for 4 h. Evaporation and column chromatography on silica gel (hexane – ethyl acetate, 4:1, 3:1, containing 0.05% triethylamine) provided **31** (194 mg, 73%) as a crystallizing syrup. $[\alpha]_D$ +40 (*c* 0.3, chloroform, 0.03% triethylamine). ^{1}H NMR ($CDCl_3$) δ: 7.40–6.85 (m, 24H, 5Ph), 5.01–4.43 (5ABq, 10H, 4CH_2Ph, CH_2PhOMe), 4.89 (d, 1H, $J_{1',2'}$ 3.5 Hz, H-1′), 4.01 (m, H-1A), 3.98 (t, 1H, $J_{2',3'}$ 9.5 Hz, $J_{3',4'}$ 9.0 Hz, H-3′), 3.84 (m, 1H, H-5′), 3.79 (s, 3H, CH_3O), 3.71 (dd, overlapped, $J_{6A',6B'}$ 10.5 Hz, $J_{6A',5'}$ 3.8 Hz, H-6A′), 3.62 (dd, 1H, $J_{6B',5'}$ 2.0 Hz, H-6B′), 3.61 (t, 1H, $J_{4',5'}$ 9.5 Hz, H-4′), 3.55 (dd, 1H, H-2′), 3.38 (overlapped, H-1B), 1.89 (m, 1H, H-4e), 1.85 (m, 1H, H-2e), 1.69 (dq, 1H, $J_{2a,2e} \sim J_{2a,1a} \sim J_{2a,3} \sim$ 12.5 Hz, $J_{2a,1e}$ 4.5 Hz, H-2a), 1.33 (q, 1H, $J_{4a,4e} \sim J_{3,4a} \sim J_{5,4a} \sim$ 12.0 Hz, H-4a). Anal. calcd. for $C_{48}H_{54}O_9$: C 74.40, H 7.02; found: C 73.97, H 7.01.

*1,5-Anhydro-2-deoxy-3-*O-*(α-D-glucopyranosyl)-4-*O-*methyl-D-*arabino-*hexitol (32)*

A mixture of **29** (120 mg, 0.15 mmol) and 5% palladium-on-carbon (120 mg) in methanol (7 mL) was hydrogenated for 3 h in the hydrogen stream. Processing and gel filtration as described for **9** provided **32** (48.5 mg, 100%) as a white solid after freeze-drying an aqueous solution; $[\alpha]_D$ +116 (*c* 0.5, water). The ^{1}H and ^{13}C NMR data are reported in Tables 2 and 3.

*1,5-Anhydro-2,4-dideoxy-3-*O-*(α-D-glucopyranosyl)-D-*threo-*hexitol (33)*

A mixture of **31** (164 mg, 0.21 mmol) and 5% palladium-on-carbon (160 mg) in methanol (7 mL) was hydrogenated in the hydrogen stream for 2.5 h. Usual processing and gel filtration as described for **9** provided **33** (56.7 mg, 91%) as a white solid after freeze-drying an aqueous solution; $[\alpha]_D$ +146 (*c* 0.4, water). The ^{1}H and ^{13}C NMR data are reported in Tables 2 and 3.

Acknowledgements

Dr. Frank M. Unger's support of this project at Chembiomed Ltd. is gratefully acknowledged. We are deeply indebted to Professor R.U. Lemieux, Department of Chemistry, University of Alberta, thanks to whom the completion of the project and the preparation of this paper were possible. We thank Mrs. B. Jamieson-Hinz for the preparation of starting materials. The biological part of this work was supported by Grant DK17477 from the National Institutes of Health (to R.G.S.).

1. A.D. Elbein. Annu. Rev. Plant Physiol. **30**, 239 (1979).
2. S.C. Hubbard and R.J. Ivatt. Annu. Rev. Biochem. **50**, 555 (1981).
3. R.G. Spiro and M.J. Spiro. Philos. Trans. R. Soc. London, B: **300**, 117 (1982).
4. R. Kornfeld and S. Kornfeld. Annu. Rev. Biochem. **54**, 631 (1985).
5. W.A. Lubas and R.G. Spiro. J. Biol. Chem. **262**, 3775 (1987).
6. W.A. Lubas and R.G. Spiro. J. Biol. Chem. **263**, 3990 (1988).
7. S.E.H. Moore and R.G. Spiro. J. Biol. Chem. **265**, 13104 (1990).
8. C. Rabouille and R.G. Spiro. J. Biol. Chem. **267**, 11573 (1992).
9. K. Fujimoto and R. Kornfeld. J. Biol. Chem. **266**, 3571 (1991).
10. S.E.H. Moore and R.G. Spiro. J. Biol. Chem. **267**, 8443 (1992).
11. A. Tan, L. van den Broek, S. van Boeckel, H. Ploegh, and J. Bolscher. J. Biol. Chem. **266**, 14504 (1991).
12. S. Hiraizumi, U. Spohr, and R.G. Spiro. J. Biol. Chem. **268**, 9927 (1993).
13. U. Spohr, M. Bach, and R.G. Spiro. Can. J. Chem. **71**, 1928 (1993).
14. U. Spohr and M. Bach. Can. J. Chem. **71**, 1943 (1993).
15. U. Fuhrmann, E. Bause, and H. Ploegh. Biochim. Biophys. Acta, **825**, 95 (1985).
16. G. Legler. Adv. Carbohydr. Chem. Biochem. **48**, 319 (1990).
17. J. Conchie and G.A. Levvy. Methods Carbohydr. Chem. **2**, 345 (1963).
18. K. Bock and C. Pedersen. J. Chem. Soc. Perkin Trans. 2, 293 (1974).
19. G.H. Posner and R.S. Haines. Tetrahedron Lett. **26**, 5 (1985).
20. A.B. Foster, M. Stacey, and S.V. Vardheim. Acta Chem. Scand. **12**, 1819 (1958).
21. R.U. Lemieux, K.B. Hendriks, R.V. Stick, and K. James. J. Am. Chem. Soc. **97**, 4056 (1975).
22. R. Johansson and B. Samuelsson. J. Chem. Soc. Perkin Trans. 1, 2371 (1984).
23. D.H.R. Barton and S.W. McCombie. J. Chem. Soc. Perkin 1, 1574 (1975).
24. H. Thøgersen, R.U. Lemieux, K. Bock, and B. Meyer. Can. J. Chem. **60**, 44 (1982).
25. R.U. Lemieux, R. Szweda, E. Paszkiewicz-Hnatiw, and U. Spohr. Carbohydr. Res. **205**, c12 (1990).

Inhibitors of *endo*-α-mannosidase. Part II.[1] 1-Deoxy-3-*O*-(α-D-glucopyranosyl)-mannojirimycin and congeners modified in the mannojirimycin unit

ULRIKE SPOHR[2] AND MIMI BACH
Chembiomed Ltd., Edmonton, and Department of Chemistry, University of Alberta, Edmonton, AB T6G 2G2, Canada

AND

ROBERT G. SPIRO
Departments of Biological Chemistry and Medicine, Harvard Medical School, and the Elliott P. Joslin Research Laboratory, Boston, MA 02215, U.S.A.

Received June 10, 1993

ULRIKE SPOHR, MIMI BACH, and ROBERT G. SPIRO. Can. J. Chem. **71**, 1928 (1993).

The syntheses of 1-deoxy-3-*O*-(α-D-glucopyranosyl)-mannojirimycin (**9**) and its 2-deoxy, 2-*O*-methyl, 4-deoxy, 4-*O*-methyl, 6-deoxy, 6-*O*-methyl, *N*-methyl, and *N*-propyl congeners are described. Since **9** was previously shown to effectively inhibit *endo*-α-D-mannosidase, a glycoprotein-processing hydrolase, these chemical modifications were designed to assist in the assessment of intermolecular hydrogen bonds of the inhibitor–enzyme complex. The previously reported data require that all hydroxyl groups of the deoxymannojirimycin unit of **9**, namely, OH-2, OH-4, OH-6, and also the NH-5 group, interact with charged and polar groupings of the enzyme, since deoxygenations and alkylations abolished or significantly reduced activities. Conformational analysis of **9** and some of its congeners based on NMR chemical shifts, experimental and theoretical nuclear Overhauser enhancements, and HSEA calculations were performed. The chemical modifications of the glucose unit of **9** are described in the accompanying paper.

ULRIKE SPOHR, MIMI BACH et ROBERT G. SPIRO. Can. J. Chem. **71**, 1928 (1993).

On décrit la synthèse de la 1-désoxy-3-*O*-(α-D-glucopyranosyl)mannojirimycine (**9**) et de ses dérivés 2-désoxy, 2-*O*-méthyle, 4-désoxy, 4-*O*-méthyle, 6-désoxy, 6-*O*-méthyle, *N*-méthyle et *N*-propyle. Puisqu'il a été démontré antérieurement que le composé **9** inhibe d'une façon efficace l'*endo*-α-D-mannosidase, une hydrolase conduisant à des glycoprotéines, les modifications chimiques réalisées avaient pour but d'aide à évaluer les liaisons hydrogènes impliquées dans le complexe inhibiteur–enzyme. Les données rapportées antérieurement (les désoxygénations et les alkylations éliminent ou réduisent fortement les activités) suggèrent que tous les groupes hydroxyles de l'unité désoxymannojirimycine du composé **9**, soit les groupes OH en 2, 4 et 6 ainsi que le groupe NH en 5, interagissent avec les groupes chargés et polaires de l'enzyme. En se basant sur les déplacements chimiques en RMN, sur des effets d'Overhauser nucléaire expérimentaux et théoriques ainsi que sur des calculs HSEA, on a réalisé une analyse conformationnelle du composé **9** et de quelques-uns de ses dérivés. Les modifications chimiques de l'unité glucose du composé **9** sont décrites dans une publication adjointe.

[Traduit par la rédaction]

Introduction

The disaccharide 1-deoxy-3-*O*-(α-D-glucopyranosyl)-mannojirimycin (**9**) has been shown to strongly inhibit the action of *endo*-α-D-mannosidase (1), a glycoprotein-processing hydrolase that releases αDGlc(1→3)DMan from incompletely deglucosylated $GlcMan_9GlcNAc_2$ oligosaccharide of immature *N*-linked glycoproteins (2, 3). Although deoxymannojirimycin itself is known to be a strong *exo*-mannosidase inhibitor (4), it was found inactive towards *endo*-mannosidase (3). Apparently, the glucose unit is required for the recognition both of substrates and inhibitors (3) by the enzyme.

It was of interest to further investigate the involvement of the various substituents of inhibitor **9** in the complexation reaction with the enzyme by studying the effect of chemical modifications on the inhibitory properties, thus gaining insights into the topography recognized by the hydrolase. It is to be noted in this regard that extensive protein–oligosaccharide binding studies have been performed with numerous lectins (5–9), monoclonal antibodies (10–12), and enzymes such as amyloglucosidase (13–15) and glycosyltransferases (16–18). The results indicated that in these cases the acceptor protein recognizes only part of the oligosaccharide surface while leaving a considerable portion of the ligand in contact with water. This was confirmed for the complexation of the Lewis b tetrasaccharide by the lectin IV of *Griffonia simplicifolia* (5, 6) by the X-ray crystal structure of the complex (19).

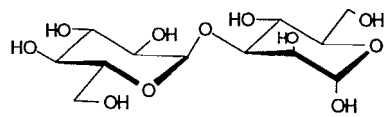

αDGlc(1→3)DMan

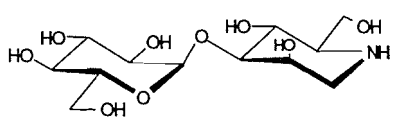

9

The approach developed by Lemieux and co-workers (5, 6) for protein–oligosaccharide binding studies, namely, the use of all monodeoxy and mono-*O*-methyl congeners of the parent compound for the appreciation of intermolecular hydrogen bonds, was applied in this investigation, and the bi-

[1]For Parts I and III, see refs. 37 and 32.
[2]Author to whom correspondence may be addressed.

Can. J. Chem. Downloaded from www.nrcresearchpress.com by 203.198.23.82 on 09/08/12
For personal use only.

Can. J. Chem. Downloaded from www.nrcresearchpress.com by 203.198.23.82 on 09/08/12
For personal use only.

ological results were recently published (1). The present communication reports on the syntheses and properties of **9** and its congeners modified in the 1-deoxymannojirimycin unit.

Discussion

Synthesis

For the synthesis of 1-deoxy-3-*O*-(α-D-glucopyranosyl)-mannojirimycin (**9**) (Scheme 1), the 1-deoxymannojirimycin derivative **1** reported by Fleet et al. (20) was used as the starting material. Diol **1** was protected at the 6-position either by selective acetylation with acetyl chloride at −78°C to provide **2** (75% yield) or by conversion of **1** into the oxazolidone derivative **13** (91% yield) by treatment with sodium methoxide. The ^{1}H NMR spectrum of acetate **2** showed very broad signals and duplication of the acetyl signal due to the hindered rotation of the *N*-benzyloxycarbonyl grouping about the N—C amide bond at room temperature. The ^{13}C NMR spectrum also displayed signal duplications. The 3-hydroxyl group of acetate **2** proved to be of very low reactivity in comparison to OH-3 of oxazolidone derivative **13**. No glucosidation of **2** was achieved under halide ion catalyzed conditions using bromide **14** (21). Therefore, the glucosidation was carried out with chloride **3** (22) and mediated by silver trifluoromethanesulfonate at −10°C to produce an α:β-mixture of **4** and **5** in the ratio 3.5:1. Repeated column chromatography provided the α-anomer **4** in 66% and the β-anomer **5** in 19% yield. An easier separation of the anomers was achieved after deacetylation of the anomeric mixture of **4** and **5** with triethylamine in aqueous methanol for 7 days to provide the anomers **6** and **7**. Under these conditions oxazolidone formation could be avoided. The anomeric assignments for **6** and **7** followed from the coupling constants $J_{C1',H1'}$ 168.0 Hz for **6** and $J_{C1',H1'}$ 160.5 Hz for **7** in the C–H coupled ^{13}C NMR spectrum (23). **6** was hydrogenolyzed in the presence of 5% palladium-on-carbon and 1 equivalent of hydrochloric acid to afford the target compound **9**. The ^{1}H and ^{13}C NMR data are presented in Tables 1 and 2 and are in full agreement with the structural assignment.

In contrast to acetate **2**, oxazolidone derivative **13** could be glucosylated with bromide **14** under halide ion catalysis, leading to **15** (60% yield). **15** was also obtained by treatment of **4** with sodium methoxide (81% yield). **15** was hydrogenolyzed to the oxazolidone derivative **16**, which showed the CO signal at 160.66 ppm in the ^{13}C NMR spectrum. Saponification of the cyclic carbamate in **15** with ethanolic potassium hydroxide provided **17**, the debenzylation of which also led to **9**.

6-*O*-Methyl congener **10** was prepared from the 6-hydroxy disaccharide **6** by treatment with methyl iodide and silver oxide in toluene (**8**, 91% yield) followed by hydrogenolytic debenzylation.

Disaccharide **9** was converted into the *N*-methyl and *N*-propyl derivatives **11** and **12** in high yields by reductive amination using formaldehyde in the presence of palladium/hydrogen and propionaldehyde in the presence of sodium cyanoborohydride (24).

The synthesis of the 6-deoxy congener **21** is outlined in Scheme 2. Although the 6-position of disaccharide **6** could be methylated under mild conditions to give **8** (Scheme 1), the benzyloxycarbonyl group proved unsuitable in attempts to halogenate or mesylate this position. Therefore this group was replaced by a benzyl group by treating amine **17** (Scheme 2) with benzyl bromide in the presence of potassium carbonate to produce **18** in 94% yield. Mesylation of **18** with methanesulfonyl chloride in pyridine at temperatures as low as −20°C produced a mixture of presumably the 6-*O*-methanesulfonyl ester and the 6-chloro-6-deoxy derivative **19** while a complete conversion into **19** (80% yield) was achieved on heating at 50°C for 1 h. **19** was then reduced with tributyltin hydride to the 6-deoxy derivative **20** (63% yield), which was debenzylated by catalytic hydrogenation over 5% palladium-on-carbon to afford **21** in high yield.

The syntheses leading to the 2-*O*-methyl and 2-deoxy congeners of **9**, namely, **36** and **37**, are presented in Scheme 3. The 4-*O*-benzyl-*N*-benzyloxycarbonyl-2-*O*-methyl derivative of 1-deoxymannojirimycin (**28**) was synthesized in a reaction sequence analogous to the one developed by Fleet et al. for the preparation of the 2,4-di-*O*-benzyl derivative **1** (20). Conventional methylation of 6-azido-3-*O*-benzyl-6-deoxy-1,2-*O*-isopropylidene-α-D-glucofuranose (25) gave the 5-*O*-methyl ether **22**, which was methanolyzed to the methyl glycosides **23** in high yield. Conversion into the trifluoromethanesulfonyl ester (intermediate **24**) followed by reduction of the azido group with triphenylphosphine, cyclization with inversion of configuration at C-2 (intermediate **25**), and *N*-benzyloxycarbonylation led to the bicyclic furanoside **26** in 68% yield. **26** was hydrolyzed to the reducing sugar (intermediate **27**) with subsequent reduction using sodium borohydride to produce **28** in 51% yield. The synthesis of the corresponding 1,2-dideoxy fagomine derivative **29** was reported by Fleet and Smith (26).

Both **28** and **29** were converted into the oxazolidones **30** and **31** in high yields by treatment with sodium methoxide. Glucosylation of **30** and **31** with bromide **14** under halide ion catalyzed conditions led to the α-linked disaccharides **32** and **33**, which were isolated in yields of 67 and 65%, respectively. Saponification of **32** and **33** using ethanolic potassium hydroxide to give **34** and **35** was followed by catalytic hydrogenolysis and provided the 2-*O*-methyl and 2-deoxy disaccharides **36** and **37** in high yields.

In the synthesis of the 4-*O*-methyl and 4-deoxy congeners of **9**, namely, **52** and **53** (Scheme 4), the 4-*O*-allyl disaccharide **45** served as an intermediate for both structures. The synthesis started from 3-*O*-allyl-1,2-*O*-isopropylidene-6-*O*-*p*-toluenesulfonyl-α-D-glucofuranose (27), which was converted conventionally into the methyl glycosides **38** by azide replacement, benzylation, and methanolysis. 1-Deoxymannojirimycin derivative **43** was then prepared from **38** as reported for **1** (20) and applied to the preparation of **28** via triflate **39**, which was reduced and cyclized with inversion of configuration at C-2 followed by *N*-benzyloxycarbonylation to give **41** (55%). Hydrolysis of the glycoside and subsequent reduction with sodium borohydride led to **43** (59% yield) from which **44** was obtained by treatment with sodium methoxide. Halide-ion catalyzed α-glucosidation of **44** with **14** provided disaccharide **45** in 61% yield. The 4-position of **45** was then liberated by isomerization of the allyl group to a 1-propenyl group with tris(triphenylphosphine)-rhodium(I)chloride (28), which was hydrolyzed using mercuric chloride to give alcohol **46** in 94% yield. **46** was converted into the 4-*O*-methyl derivative **47** with methyl iodide and sodium hydride (88% yield). For conversion into the 4-deoxy derivative **49**, the methyl xanthate **48** was prepared from **46** using sodium hydride, carbon disulfide, and

Can. J. Chem. Downloaded from www.nrcresearchpress.com by 203.198.23.82 on 09/08/12
For personal use only.

SCHEME 1

Can. J. Chem. Downloaded from www.nrcresearchpress.com by 203.198.23.82 on 09/08/12
For personal use only.

TABLE 1. ^{1}H NMR chemical shifts (δ, ppm) and coupling constants (Hz) for αDGlc(1→3)-1-DMJ (**9**) and related structures[a]

		Derivatives of **9**								
	9	2-Deoxy **37**	2-OMe **36**	4-Deoxy- **53**	4-OMe **52**	6-Deoxy **21**	6-OMe **10**	*N*-Me **11**	*N*-Propyl **12**[d]	*N*,6-*O*-Carbonyl **16**
1-DMJ unit										
H-1 ($J_{1,2}$)	3.42 (2.5)	3.47 (2.5)	3.75	3.46 (3.5)	3.38 (2.5)	3.36 (3.0)	3.42 (3.0)	3.53 (3.0)	3.51 (2.5)	3.73
H-1′ ($J_{1',1}$)	3.29 (13.5)	3.13 (13.0)	3.20 (13.5)	3.22 (13.5)	3.23 (13.5)	3.25 (13.5)	3.29 (13.5)	3.48 (13.5)	3.44 (13.5)	3.27 (14.5)
H-2 ($J_{1',2}$)	4.45 (<1)	2.40 (3.0)[b]	4.09 (<1)	4.34 (<1)	4.38 (<1)	4.42 (<1)	4.47 (<1)	4.41 (1)	4.43	4.32 (1.5)
H-3 ($J_{3,4}$)	3.81 (10.0)	3.83	3.85 (10.0)	4.03 (11.5)	3.89	3.76 (9.5)	3.82 (10.0)	3.84 (10.0)	3.81 (10.0)	3.74 (9.5)
H-4 ($J_{4,5}$)	4.08 (10.0)	3.78 (10.0)	4.01 (10.0)	1.87 (12.5)[c]	3.77	3.87 (9.5)	4.11 (10.0)	4.18 (10.0)	4.18 (10.0)	3.94 (9.5)
H-5 ($J_{5,6}$)	3.21 (3.0)	3.19 (4.0)	3.23 (3.0)	3.38 (3.5)	3.21 (2.5)	3.15 (6.5)	3.34 (3.2)	3.13 (<1)	3.21 (1.0)	3.78 (8.5)
H-6 ($J_{6,6'}$)	4.00 (12.5)	3.93 (0)	3.99 (12.5)	3.82 (12.5)	3.99 (12.5)	1.44	3.83	4.13 (13.5)	4.11 (13.5)	4.75 (8.5)
H-6′ ($J_{5,6'}$)	3.89 (6.7)	3.93 (4.0)	3.86 (6.5)	3.69 (7.2)	3.89	—	3.80 (6.5)	4.01 (2.7)	4.00 (2.0)	4.39 (4.5)
CH_3	—	—	3.46	—	3.59	—	3.45	2.99	0.98	—
αDGlc unit										
H-1 ($J_{1,2}$)	5.25 (4.0)	5.21 (3.5)	5.23 (3.5)	5.11 (3.5)	5.21 (3.5)	5.26 (3.5)	5.26 (3.7)	5.25 (3.5)	5.25 (4.0)	5.23 (3.7)
H-2 ($J_{2,3}$)	3.58 (10.0)	3.56 (10.0)	3.57 (10.0)	3.56 (9.5)	3.59	3.57 (9.5)	3.59 (10.0)	3.55 (10.0)	3.58 (9.5)	3.56 (10.0)
H-3 ($J_{3,4}$)	3.78 (9.5)	3.71 (9.5)	3.75 (9.0)	3.72 (9.0)	3.78 (9.0)	3.77 (9.0)	3.79	3.76 (9.0)	3.77 (9.0)	3.78 (9.5)
H-4 ($J_{4,5}$)	3.43 (9.5)	3.41 (9.0)	3.44 (9.5)	3.42 (9.5)	3.43 (9.5)	3.42 (9.5)	3.44	3.43 (9.5)	3.42 (9.0)	3.43 (9.5)
H-5 ($J_{5,6}$)	3.81	3.84 (9.5)	3.75	3.76	3.83	3.80	3.82	3.80	3.80	3.83
H-6	3.86	*	*	*	*	*	*	*	*	3.85
H-6′	*	*	*	*	*	*	*	*	*	*

[a]Measured at 360 MHz and 295 K using 0.03 M solutions in D_2O with acetone as internal standard at 2.225 ppm. The assignments were based on homonuclear shift-correlated 2-D experiments (COSY).

[b]H-2a 1.87 ppm. $J_{2a,2e}$ 14.5 Hz, $J_{2a,1}$ 4.5 Hz, $J_{2a,1'}$ 13.0 Hz.

[c]H-4e 2.11 ppm, $J_{4a,4e}$ 13.5 Hz, $J_{4e,5}$ 3.5 Hz, $J_{4e,3}$ 4.5 Hz.

[d]CH_3CH_2 1.74, CH_2O 3.26 ppm, J 7.5 Hz.

*Could not be assigned.

TABLE 2. ^{13}C NMR chemical shifts (δ, ppm) for αDGlc(1→3)-1-DMJ (**9**) and related structures[a]

		Derivatives of **9**								
	9	2-Deoxy **37**	2-OMe **36**	4-Deoxy **53**	4-OMe **52**	6-Deoxy **21**	6-OMe **10**	*N*-Me **11**	*N*-Propyl **12**	*N*-6-*O*-Carbonyl **16**[c]
1-DMJ unit										
C-1	48.44	42.45	43.57	48.77	48.02	48.45	48.27	54.74	55.41[b]	46.28
C-2	66.37[b]	28.64	76.21	65.34	66.79	66.77	66.52[b]	66.41[b]	66.31[c]	69.80[b]
C-3	81.67	79.59	81.09	73.66	79.36	80.67	80.86	80.89	80.82	82.28
C-4	67.24[b]	69.36	66.08	24.82	76.26	70.51	66.02[b]	68.66[b]	66.31[c]	68.97[b]
C-5	61.12	60.83	61.08	57.68	60.44[b]	56.32	59.67[c]	64.92[b]	65.32[c]	58.59
C-6	59.31	58.49	58.82	62.10	58.62	15.33	69.08	59.38	55.49[b]	67.53
CH_3	—	—	57.90	—	61.53[b]	—	59.27[c]	41.79	10.68[d]	—
αDGlc unit										
C-1	101.50	100.86	101.89	97.78	101.11	101.38	101.45	101.44	101.42	101.48
C-2	72.49	72.36	72.44	72.01	72.15	72.46	72.45	72.43	72.43	72.59
C-3	73.57	73.63	73.56	73.57	73.42	73.57	73.54	73.56	73.54	73.62
C-4	70.35	70.41	70.32	70.35	70.47	70.37	70.35	70.35	70.35	70.37
C-5	73.27	73.15	73.47	73.15	73.31	73.31	73.32	73.35	73.35	73.21
C-6	61.34	61.42	61.36	61.37	61.40	61.38	61.36	61.38	61.37	61.34

[a]0.05 M solutions in D_2O with dioxane as internal reference at 67.4 ppm were measured at 75 MHz and 295 K. The assignments were made by inspection and are tentative.
[b,c]The assignments are tentative and may be reversed.
[d]NCH_2 54.94, CH_2 16.39 ppm.
[e]CO 160.66 ppm.

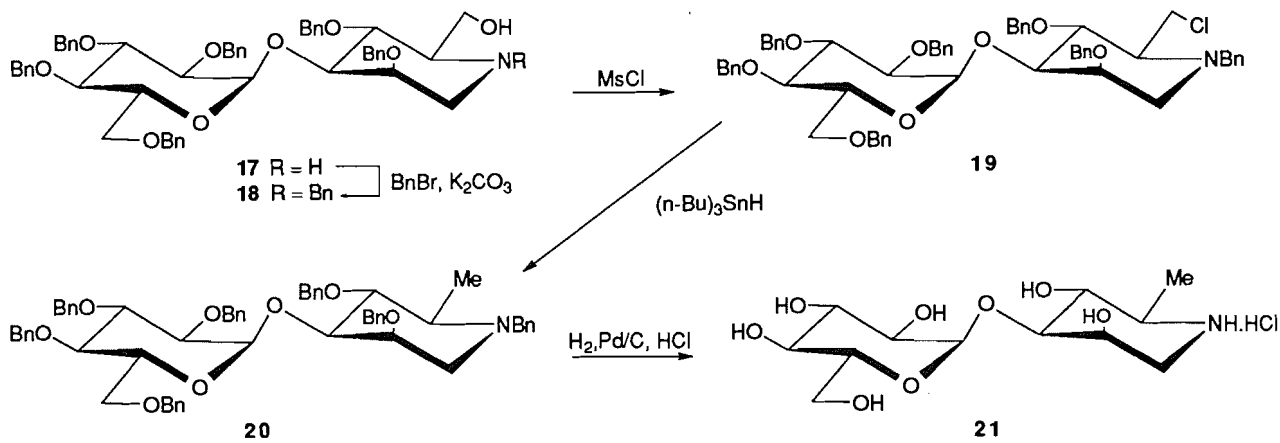

SCHEME 2

methyl iodide (29). This intermediate was reduced with tributyltin hydride to provide **49** in 79% yield. Saponification of the cyclic carbamate in **47** and **49** followed by catalytic hydrogenolysis of the benzyl groups then led to the 4-*O*-methyl and 4-deoxy disaccharides **52** and **53** in high yields.

NMR and conformational studies

The ^1H and ^{13}C NMR parameters for αDGlc(1→3)-1-DMJ (**9**) are reported in Tables 1 and 2 together with those for structural modifications involving changes of the 1-DMJ unit. The data are in full accord with the structural assignments. The ^1H NMR vicinal coupling constants of both units are typical for the $^4C_1$ conformation of pyranoid rings. Some flattening, though, in the DMJ-piperidine ring of the bicyclic derivative **16** may be expected.

HSEA calculations (30) predict for **9** a conformational preference with minimum energy at $\phi/\psi = -50°/-10°$. In this conformer, H-1′ is found at a close distance across the glycosidic linkage to H-3 (2.40 Å) and to O-4 (2.74 Å), while H-5′ is in nonbonded interaction to H-2 (2.27 Å). The nonbonded interaction of H-1′ to O-4 accounts for the intermediate deshielding of 0.14 ppm with respect to the chemical shift of H-1′ in the 4-deoxy congener **53** (31). NOE experiments with irradiation of H-1′ of **9** resulted in a strong intraunit enhancement of H-2′ and interunit enhancement to H-3 (Table 3, Fig. 1). Irradiation of H-2 caused an interunit NOE to H-5′, the signal of which, however, overlapped with the also enhanced H-3 signal. Relative theoretical NOE values were derived for the low-energy conformer of $\phi/\psi = -45°/-15°$ ($E = -1.7$) and provided a better agreement with the experimental data than those derived for the minimum energy conformer of $\phi/\psi = -50°/-10°$ ($E = -1.8$), particularly, with respect to the internuclear distance between H-2 and H-5′.

4-Deoxy congener **53** allowed additional NOE experi-

Can. J. Chem. Downloaded from www.nrcresearchpress.com by 203.198.23.82 on 09/08/12
For personal use only.

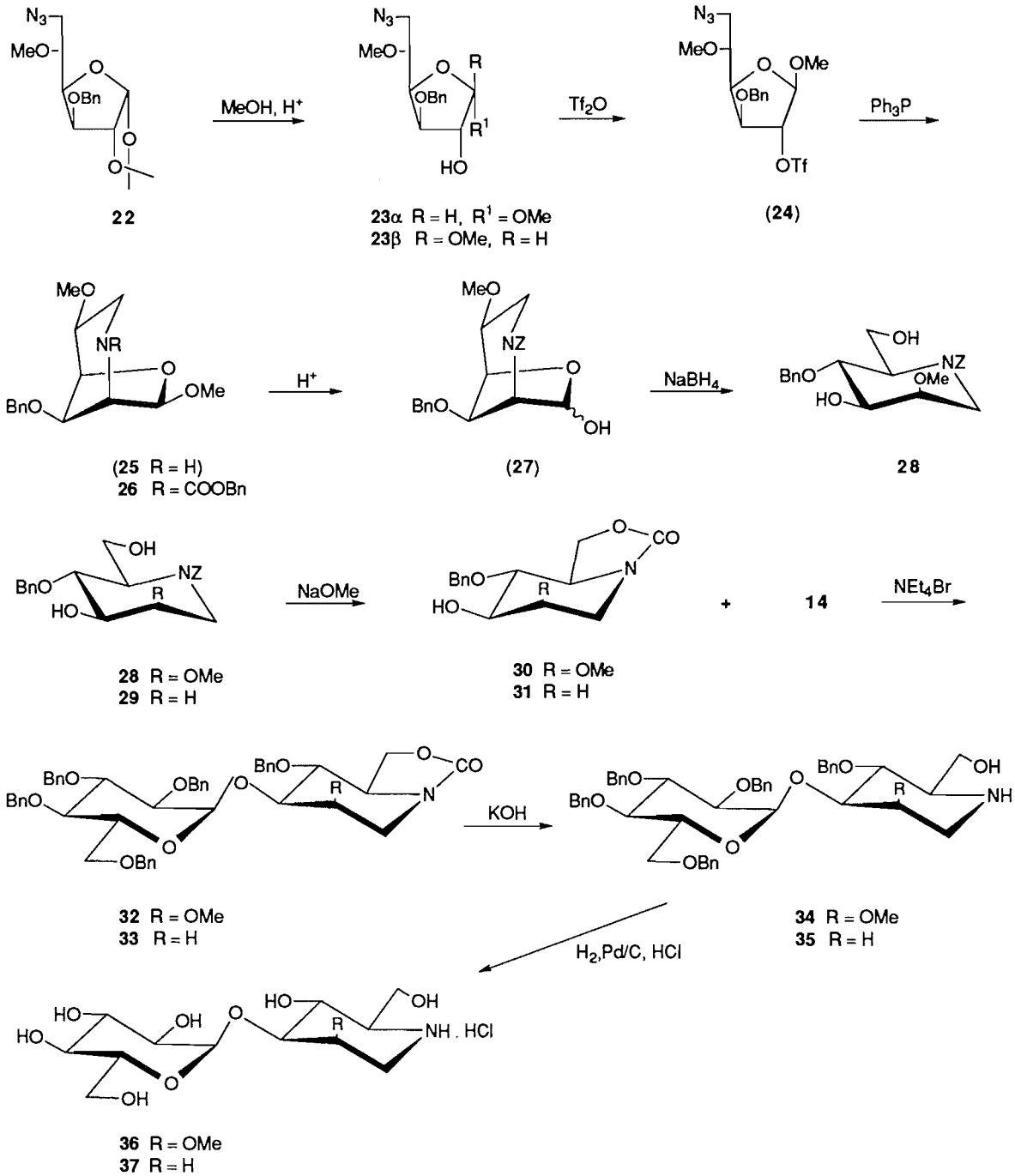

SCHEME 3

ments, since not only H-1′ and H-2, but also H-3 and H-4e provided well-separated signals in the ^{1}H NMR spectrum. HSEA calculations indicate somewhat more flexibility about the glycosidic bond and predict an energy minimum for conformations of $\phi/\psi = -55°$, $-50°/-25°$, $-20°$ ($E = -1.9$) in which H-1′ is in interunit nonbonded interaction to H-3 and H-4e, and H-5′ to H-2. Indeed, irradiation of H-1′ resulted in enhancements of H-3 and H-4e (Table 3), and, conversely, irradiation of H-3 and H-4e caused signal enhancements of H-1′ and also a smaller enhancement of H-5′ in the case of H-3. H-5′ was also enhanced when the H-2 signal was saturated. A reasonably good agreement of the experimental NOE data with the theoretical values was achieved when those were derived for the low-energy conformer of $\phi/\psi = -45°/-25°$ ($E = -1.7$), which appears to approximately represent the average internuclear proton distances of the conformers in equilibrium.

HSEA calculations for the 2-deoxy congener **37** indicate

Can. J. Chem. Downloaded from www.nrcresearchpress.com by 203.198.23.82 on 09/08/12
For personal use only.

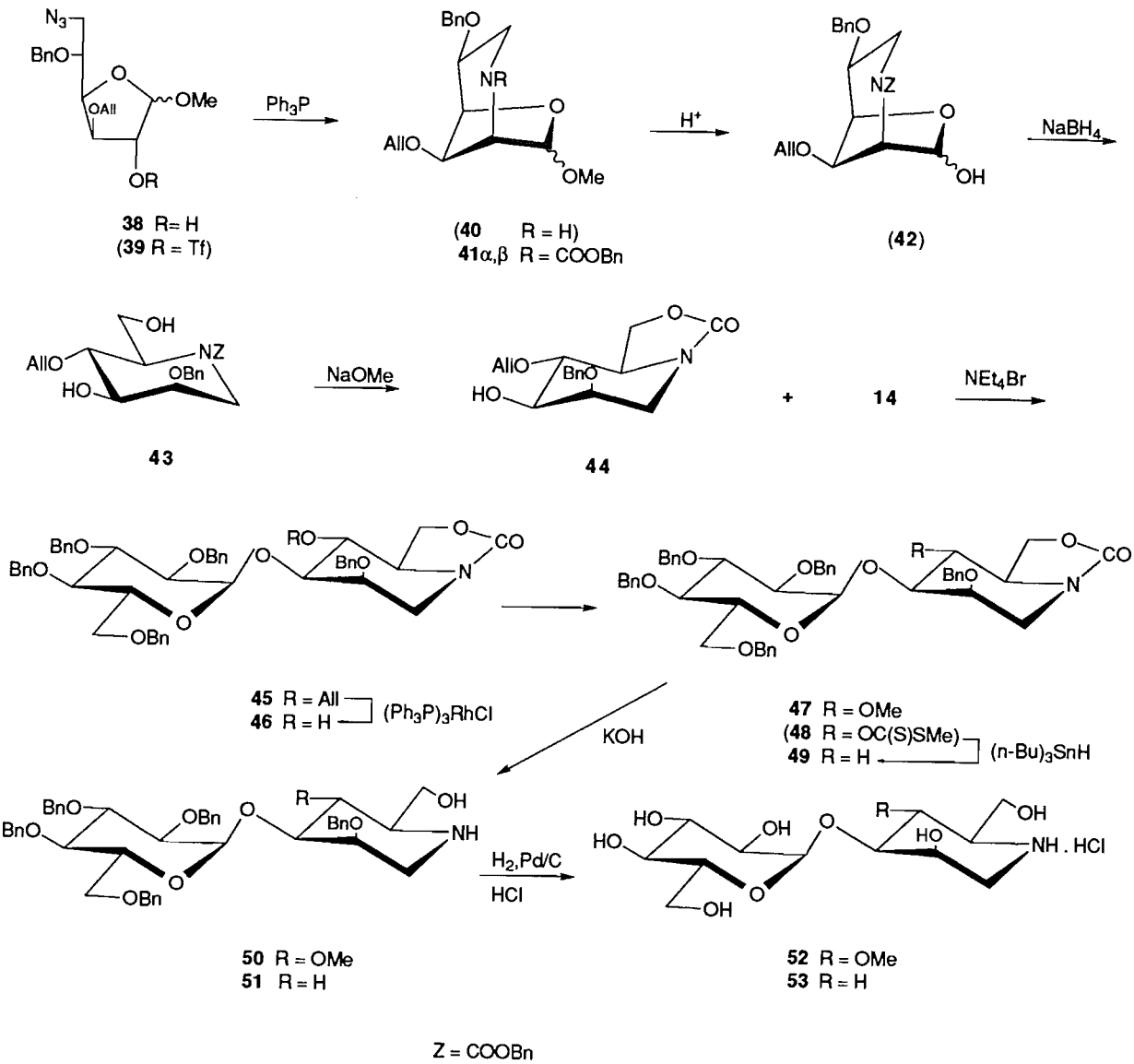

SCHEME 4

that the conformational preference of the parent compound **9** also applies to **35**, since in contrast to O-4, the axial O-2 of **9** is not involved in interunit nonbonded interactions. In fact, since none of the structural modifications, except deoxygenation of the 4-position, had marked effects on the ^1H and ^{13}C NMR chemical shift of the glucose unit (Tables 1 and 2), the interglycosidic conformational properties of **9** appear maintained in these congeners.

The biological data of this investigation (1) are discussed in the succeeding paper (32), which reports the syntheses of congeners of **9** modified in the glucose unit.

Experimental

Theoretical methods

Conformational preferences about the glycosidic torsion angles were calculated using the HSEA program (30). The calculations were done in 5° steps for the ϕ and ψ angles. The atomic coordinates were derived from neutron diffraction studies of methyl α-D-glucopyranoside and methyl α-D-mannopyranoside (33) with ω-angles of −60° and 180°, respectively. The deoxy functions were generated by bond modifications of methyl α-D-mannopyranoside using a C—H bond length of 1.10 Å. The internuclear distances provided by the HSEA calculations for a specific conformer (Table 3) were used for the determination of the theoretical nuclear Overhauser enhancements. The computer program developed by Helmut Beierbeck was used for this purpose (34).

NMR spectroscopy

The ^1H NMR spectra were measured at 300 MHz and 360 MHz (Bruker AM 300 and WM 360) with tetramethylsilane as internal standard for $CDCl_3$ solutions. Reference standard for D_2O solutions was acetone (2.225 ppm). The ^{13}C NMR spectra were recorded at 75 MHz with dioxane (67.4 ppm) as reference for D_2O solutions and the $CDCl_3$ signal (77.0 ppm) as reference in $CDCl_3$ solutions. The steady-state NOE experiments were performed at 298 K and 360 MHz with 0.05 M solutions in D_2O. Irradiation time was 5 s and the saturation of signals was achieved by multiple frequency irradiation per signal (35, 36).

General methods

Optical rotations were measured at room temperature (23 ± 1°C) in a 1-dm cell on a Perkin–Elmer 241 polarimeter. Thin-layer chromatography was performed on precoated plates of silica gel (60-F254, E. Merck, Darmstadt) and visualized by spraying with 5% sulfuric acid in ethanol followed by heating. For column chroma-

Can. J. Chem. Downloaded from www.nrcresearchpress.com by 203.198.23.82 on 09/08/12
For personal use only.

TABLE 3. Intra- and interunit nuclear Overhauser enhancements for compounds **9** and **53**[a]

Compound	Proton saturated	Signal enhanced	% Enhancement	Relative NOE values	
				Observed	Calculated
9[b]	H-1′	H-2′	16.3	0.54	0.59
		H-3	13.7	0.46	0.39
	H-2	H-1e	4.3	0.20	0.11
		H-1a	4.1	0.19	0.15
		H-3	} 12.6	} 0.60	0.34
		H-5′			0.40
53[c]	H-1′	H-2′	16.5	0.57	0.61
		H-3	8.5	0.29	0.25
		H-4e	3.9	0.13	0.13
	H-2	H-1e	4.2	0.24	0.13
		H-1a	3.8	0.22	0.18
		H-3	5.8	0.33	0.34
		H-5	3.8	0.22	0.34
	H-3	H-1a	3.6	0.12	0.08
		H-2	7.2	0.24	0.31
		H-4e	3.0	0.10	0.10
		H-5	6.1	0.20	0.15
		H-1′	10.3	0.34	0.32
		H-5′	1.4	0.05	0.05
	H-4e	H-3	4.2	0.08	0.11
		H-4a	29.4	0.59	0.55
		H-5	6.8	0.14	0.12
		H-6	2.5	0.05	0.04
		H-1′	7.1	0.14	0.18

[a]The experimental data are the mean of two measurements. Minor calculated or negative NOE values are not listed.
[b]The calculated NOE values were derived for the low-energy conformer of $\phi/\psi = -45°/-15°$.
[c]The calculated NOE values were derived for the low-energy conformer of $\phi/\psi = -45°/-25°$.

Can. J. Chem. Downloaded from www.nrcresearchpress.com by 203.198.23.82 on 09/08/12
For personal use only.

tography silica gel 60 (230–400 mesh, E. Merck, Darmstadt) and distilled solvents were used. Solvents and reagents were purified and dried according to standard procedures. Melting points are uncorrected.

6-O-Acetyl-2,4-di-O-benzyl-N-benzyloxycarbonyl-1,5-dideoxy-1,5-imino-D-mannitol (2)

Acetyl chloride (82 μL, 1.15 mmol) was added to a solution of diol **1** (20) (304 mg, 0.64 mmol) in dichloromethane (20 mL) and pyridine (200 μL, 2.5 mmol) at −78°C. After 1 h at this temperature, more acetyl chloride (25 μL, 0.35 mmol) was added. The reaction mixture was kept for another hour at −78°C. Then the excess of reagent was quenched by the addition of methanol (50 μL). The solution was diluted with dichloromethane, washed with water, dried, and evaporated. The crude product was purified on a column of silica gel (hexane – ethyl acetate, 3:1, 2:1) yielding crystallizing acetate **2** (249 mg, 75%). The analytical sample was recrystallized from ether – hexane; mp 69–71°C; $[\alpha]_D$ −19 (*c* 0.6, chloroform). ^{1}H NMR ($CDCl_3$, signals broad, mixture of two rotamers in the ratio ~3:2) δ: 7.4–7.1 (m, 15H, 3Ph), 5.2–5.02 (m, 2H, $COOCH_2Ph$), 4.13 (d, 1H, *J* 11.5 Hz, 1 CH_2Ph), 4.12 (d, 1H, *J* 11.5 Hz, 1 CH_2Ph), 3.86–3.6 (m, 2H, H-1, H-1′), 3.18–3.00 (m, 1H, H-5), 2.35–2.26 (m, 1H, OH), 1.92 and 1.77 (2s, 3H, CH_3CO). ^{13}C NMR ($CDCl_3$, δ for minor rotamer in parentheses) δ: 75.98 (74.81) (C-4),[3] 72.20 (C-2)$^+$, 71.35 (2 CH_2Ph), 68.04 (C-3)$^+$, 67.34 ($COOCH_2Ph$), 61.09 (C-6), 52.18 (51.41) (C-5), (37.43), 36.88 (C-1). Anal. calcd. for $C_{30}H_{33}O_7$: C 69.35, H 6.40, N 2.70; found: 69.55, H 6.58, N 2.66.

2,3,4,6-Tetra-O-benzyl-α-D-glucopyranosyl chloride (3) (22)

Oxalyl chloride (160 μL, 1.83 mmol) was added to a stirred solution of 2,3,4,6-tetra-*O*-benzyl-D-glucopyranose (740 mg, 1.37 mmol) and *N*,*N*-dimethylformamide (150 μL, 2.11 mmol) in dichloromethane (15 mL). The mixture was stirred for 20 min and then poured into ice-water. The organic solution was washed with ice-water, dried, and evaporated to provide chloride **3** (quant.) as a syrup.

6-O-Acetyl-2,4-di-O-benzyl-N-benzyloxycarbonyl-1,5-dideoxy-1,5-imino-3-O-(2,3,4,6-tetra-O-benzyl-α-D-glucopyranosyl)-D-mannitol (4) and -β-D-glucopyranosyl)-D-mannitol (5)

A solution of chloride **3** (7.92 mmol) in dichloromethane (12 mL) was added at −78°C to a stirred mixture of alcohol **2** (2.0 g, 3.85 mmol), silver trifluoromethanesulfonate (2.31 g, 8.99 mmol), *sym*-collidine (418 μL, 3.16 mmol), and 4 Å molecular sieves (1.5 g) in dichloromethane (5.0 mL). The temperature was gradually raised to −10°C and after 2 h at this temperature, *sym*-collidine (630 μL, 4.97 mmol) was added. The mixture was filtered through Celite, the organic solution was washed with aqueous saturated sodium hydrogen carbonate and water, followed by evaporation. Two column chromatographic separations on silica gel (hexane – ethyl

[3]Tentative assignments are marked with +.

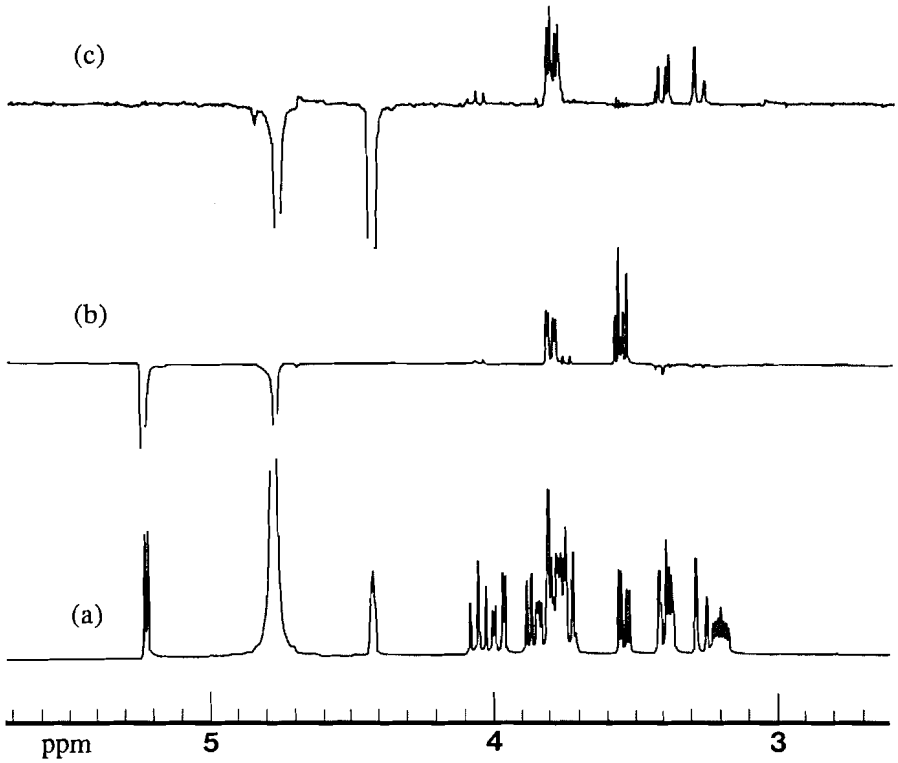

FIG. 1. NOE difference spectra for disaccharide **9**; (*a*) reference spectrum; (*b*) irradiation of H-1′; (*c*) irradiation of H-2.

acetate, 6:1, 5:1) provided the β-isomer **5** (0.774 g, 19%) as a tough syrup; $[\alpha]_D$ +5 (*c* 0.2, chloroform). ^{1}H NMR ($CDCl_3$, broad, mixture of two rotamers in the ratio 3:2) δ: 7.4–7.0 (m, 35H, 7Ph), 5.2–3.1 (complex m, 29H), 1.89 and 1.81 (2s, 3H, CH_3CO). Anal. calcd. for $C_{64}H_{67}NO_{12}$: C 73.76, H 6.48, N 1.34; found: C 74.18, H 7.06, N 1.34. Continued elution of the column provided the α-isomer **4** (2.64 g, 66%) as a tough syrup; $[\alpha]_D$ +33 (*c* 0.4, chloroform). ^{1}H NMR ($CDCl_3$, broad, mixture of two rotamers in the ratio 3:2) δ: 7.40–7.00 (m, 35H, 7Ph), 5.2–2.95 (complex m, 29H), 1.83 and 1.76 (2s, 3H, CH_3CO). Anal. calcd. for $C_{64}H_{67}NO_{12}$: C 73.76, H 6.48, N 1.34; found: C 73.62, H 6.44, N 1.34.

*2,4-Di-*O*-benzyl-N-benzyloxycarbonyl-1,5-dideoxy-1,5-imino-3-*O*-(2,3,4,6-tetra-*O*-benzyl-α-D-glucopyranosyl)-D-mannitol (6) and -β-D-glucopyranosyl)-D-mannitol (7)*

(*a*) A solution of compound **4** (1.37 g, 1.31 mmol) in methanol (48 mL), triethylamine (20 mL), and water (9.6 mL) was kept at room temperature for 7 days. It was evaporated and the crude product purified on a column of silica gel (hexane – ethyl acetate, 4:1 to 2:1) to provide, in the first fraction, acetate **4** (0.179 g, 13%). Further development gave compound **6** (0.894 g, 68%) as a tough syrup; $[\alpha]_D$ +14.6 (*c* 0.2, chloroform). ^{1}H NMR ($CDCl_3$, broad, mixture of two rotamers) δ: 7.4–6.95 (m, 35H, 7Ph), 5.17–2.83 (complex m, 30H). ^{13}C NMR ($CDCl_3$, δ for minor rotamer in parentheses) δ: 156.10 (CO), 99.24 ($J_{C,H}$ 168.0 Hz, C-1′), 59.14 (C-6), 53.82 (53.34) (C-5), (39.19) 38.63 (C-1). Anal. calcd. for $C_{62}H_{65}NO_{11}$: C 74.45, H 6.55, N 1.40; found: C 74.44, H 6.56, N 1.37.

(*b*) An anomeric mixture of compounds **4** and **5** (415 mg, 0.40 mmol) was deacetylated as described under (*a*). Chromatographic separation on a column of silica gel (hexane – ethyl acetate, 4:1, 3:1) provided, in the first main fraction, the α-isomer **6** (230 mg, 58%). Continued elution provided the β-isomer **7** (51 mg, 13%) as a tough syrup; $[\alpha]_D$ −10.4 (*c* 0.2, chloroform). ^{1}H NMR ($CDCl_3$, mixture of two rotamers, broad) δ: 7.4–7.0 (m, 35H, 7Ph), 5.0–3.1 (complex m, 30H). ^{13}C NMR ($CDCl_3$, δ for minor isomer in parentheses) δ: 156.1 (CO), 105.68 ($J_{C,H}$ 160.5, C-1′), 59.68 (59.53) (C-6), 54.83 (54.50) (C-5), (39.49) 39.04 (C-1). Anal. calcd. for $C_{62}H_{65}NO_{11}$: C 74.45, H 6.55, N 1.40; found: C 74.53, H 6.54, N 1.40.

*2,4-Di-*O*-benzyl-N-benzyloxycarbonyl-1,5-dideoxy-1,5-imino-6-*O*-methyl-3-*O*-(2,3,4,6-tetra-*O*-benzyl-α-D-glucopyranosyl)-D-mannitol (8)*

Methyl iodide (172 μL, 2.76 mmol) was added to a stirred mixture of **6** (150 mg, 0.15 mmol) and silver oxide (320 mg, 1.38 mmol) in toluene (5 mL) at 0°C. After 3 h, the temperature was raised to room temperature and stirring continued for 5 days. More methyl iodide (120 μL, 1.93 mmol) was added, followed by stirring for another day. The solids were removed by filtration and the solvent was evaporated. The remainder was applied to a column of silica gel (hexane–dichloromethane – ethyl acetate, 5:1:1) to provide **8** (137.6 mg, 91%) as a tough syrup; $[\alpha]_D$ +37 (*c* 0.5, chloroform). ^{1}H NMR ($CDCl_3$, broad, mixture of two rotamers) δ: 7.4–7.0 (m, 35H, 7Ph), 5.2–2.9 (complex m, 32H), 3.11 and 3.04 (2s, 3H, CH_3O). Anal. calcd. for $C_{63}H_{67}NO_{11}$: C 74.61, H 6.66, N 1.38; found: C 74.66, H 6.56, N 1.45.

*1,5-Dideoxy-3-*O*-(α-D-glucopyranosyl)-1,5-imino-D-mannitol-hydrochloride (9)*

A mixture of compound **6** (369 mg, 0.37 mmol), 5% palladium-on-carbon (370 mg), methanolic 0.12 N hydrochloric acid (3.8 mL, 0.46 mmol), and methanol (20 mL) was hydrogenated in a hydrogen stream for 1.5 h. The catalyst was removed by filtration and it was codistilled a few times with water. The product was passed through a column of Sephadex LH 20 (ethanol–water, 1:1) and obtained as a white, hygroscopic solid (125 mg, 96%) after freeze-drying its aqueous solution; $[\alpha]_D$ +62.5 (*c* 0.24, water). The ^{1}H and ^{13}C NMR data are reported in Tables 1 and 2. Likewise, **17** can be debenzylated to **9**.

*1,5-Dideoxy-3-*O*-(α-D-glucopyranosyl)-1,5-imino-6-*O*-methyl-D-mannitol-hydrochloride (10)*

A mixture of **8** (159 mg, 0.157 mmol), 5% palladium-on-carbon (112 mg), and methanolic 0.12 N hydrochloric acid (1.65 mL,

Can. J. Chem. Downloaded from www.nrcresearchpress.com by 203.198.23.82 on 09/08/12
For personal use only.

Can. J. Chem. Downloaded from www.nrcresearchpress.com by 203.198.23.82 on 09/08/12
For personal use only.

0.19 mmol) in methanol (7 mL) was hydrogenated in the hydrogen stream for 2 h. Further processing as described for the preparation of **9** provided the title compound **10** (59 mg, 100%) as a white solid; $[\alpha]_D$ +75.2 (*c* 0.5, water). The ^{1}H and ^{13}C NMR data are reported in Tables 1 and 2.

*1,5-Dideoxy-3-*O*-(α-D-glucopyranosyl)-1,5-imino-*N*-methyl-D-mannitol-hydrochloride (**11**)*

A mixture of **9** (30.8 mg, 0.085 mmol), palladium black (8 mg), methanolic 0.1 N sodium methoxide (851.5 μL), and 37% formaldehyde solution (40 μL, 0.49 mmol) in methanol (2.2 mL) was hydrogenated in the hydrogen stream for 1 day. Then more palladium black (5 mg) and 37% formaldehyde solution (40 μL, 0.49 mmol) were added and hydrogenation continued for another day. The catalyst was removed by filtration and the solution neutralized with methanolic 0.12 N hydrochloric acid (710 μL, 0.085 mmol). It was evaporated and the remainder applied to a column of Sephadex LH 20 (ethanol–water, 1:1). Freeze-drying an aqueous solution of the resultant material provided **11** (27.7 mg, 87%) as a solid; $[\alpha]_D$ +64 (*c* 0.5, water). The ^{1}H and ^{13}C NMR data are reported in Tables 1 and 2.

*1,5-Dideoxy-3-*O*-(α-D-glucopyranosyl)-1,5-imino-*N*-n-propyl-D-mannitol-hydrochloride (**12**)*

Sodium cyanoborohydride (12.8 mg, 0.20 mmol) was added to a stirred mixture of **9** (49.6 mg, 0.14 mmol) and propionaldehyde (56.6 μL, 0.79 mmol) in methanol (2 mL) at room temperature. After 2 h, the solvent was evaporated to provide a milky residue which was applied to a column of Iatrobeads® (chloroform–methanol–water, 65:35:8). The resultant material was dissolved in methanol (1 mL) and methanolic 0.12 N hydrochloric acid solution (1.15 mL, 0.14 mmol) was added, followed by evaporation and codistillation with water. Subsequent gel filtration on a column of Sephadex LH 20 (ethanol–water, 1:1) provided **12** (51 mg, 101%) as a white solid; $[\alpha]_D$ +51.4 (*c* 0.5, water). The ^{1}H and ^{13}C NMR data are reported in Tables 1 and 2.

*2,4-Di-*O*-benzyl-*N*,6-*O*-carbonyl-1,5-dideoxy-1,5-imino-D-mannitol (**13**)*

A solution of **1** (300 mg, 0.63 mmol) in methanolic 0.5 N sodium methoxide (3 mL) was kept at room temperature for 15 h. The solution was made neutral with Amberlite IRC 50 (H^+), filtered, and evaporated. The resulting product was applied to a column of silica gel (dichloromethane – ethyl acetate 4:1, 3:1) to provide **13** (210 mg, 91%) as a white foam; $[\alpha]_D$ +5.9 (*c* 0.4, chloroform). IR ($CHCl_3$): 1755 (CO) cm^{-1}. ^{1}H NMR ($CDCl_3$) δ: 7.40–7.25 (m, 10H, 2Ph), 5.03, 4.86, 4.61, 4.37 (2ABq, each 2H, $J_{A,B}$ 11.5 Hz, 2CH_2Ph), 4.33 (dd, 1H, $J_{6A,6B}$ 8.5 Hz, $J_{6A,5}$ 7.2 Hz, H-6A), 4.26 (dd, 1H, $J_{1A,1B}$ 14.0 Hz, $J_{1A,2}$ 2.5 Hz, H-1A), 4.03 (dd, 1H, $J_{6B,5}$ 3.0 Hz, H-6B), 3.83 (m, 1H, H-2), 3.70 (bdd, 1H, H-3), 3.59 (t, 1H, $J_{4,5} \sim J_{3,4}$ 9.0 Hz, H-4), 3.51 (m, 1H, H-5), 2.92 (dd, 1H, $J_{1B,2}$ 1.5 Hz, H-1B), 2.48 (bs, 1H, OH). Anal. calcd. for $C_{21}H_{23}NO_5$: C 68.28, H 6.28, N 3.79; found: C 67.98, H 6.21, N 3.77.

*2,3,4,6-Tetra-*O*-benzyl-α-D-glucopyranosyl bromide (**14**) (21)*

Oxalyl bromide (200 μL, ~1.85 mmol) was added to a stirred solution of 2,3,4,6-tetra-*O*-benzyl-D-glucopyranose (800 mg, 1.48 mmol) in dichloromethane (10 mL) and *N,N*-dimethylformamide (500 μL, 7.0 mmol). After 20 min at room temperature, the mixture was poured into ice-water and the organic solution was washed twice with ice-cold water, dried, and evaporated to provide **14** (quant.) as a syrup.

*2,4-Di-*O*-benzyl-*N*,6-*O*-carbonyl-1,5-dideoxy-1,5-imino-3-*O*-(2,3,4,6-tetra-*O*-benzyl-α-D-glucopyranosyl)-D-mannitol (**15**)*

(*a*) A solution of bromide **14** (1.48 mmol) in dichloromethane (2 mL) was transferred into a mixture of alcohol **13** (190 mg, 0.51 mmol), tetraethylammonium bromide (220 mg, 1.05 mmol), *N,N*-dimethylformamide (700 μL), and 4 Å molecular sieves (powdered, 0.5 g) in dichloromethane (1.5 mL). After stirring for 4 days, the reaction was quenched by the addition of methanol (300 μL) and stirring continued for 1 h. The mixture was diluted with dichloromethane, filtered through a pad of Celite, and the solution washed with aqueous sodium bicarbonate and water, followed by drying and evaporation. Purification was achieved by two column chromatographic separations on silica gel (hexane – ethyl acetate, 4:1 to 1:1 and hexane–dichloromethane – ethyl acetate, 5:2:1) to provide **15** (276 mg, 60%) as a slowly crystallizing syrup; $[\alpha]_D$ +15.6 (*c* 0.4, chloroform). ^{1}H NMR ($CDCl_3$) δ: 7.4–7.1 (m, 30H, 6Ph), 5.05 (d, 1H, $J_{1',2'}$ 3.5 Hz, H-1′), 4.24 (t, 1H, $J_{5,6A} \sim J_{6A,6B}$ 8.5 Hz, H-6A), 4.15 (dd, 1H, $J_{1A,1B}$ 14.5 Hz, $J_{1A,2}$ 2.2 Hz, H-1A), 3.82 (dd, 1H, $J_{6B,5}$ 3.5 Hz, H-6B), 2.78 (bd, 1H, $J_{1B,2} < 1$ Hz, H-1B). ^{13}C NMR ($CDCl_3$) δ: 157.5 (CO), 100.29 (C-1′), 65.76 (C-6), 57.45 (C-5), 40.82 (C-1). Anal. calcd. for $C_{55}H_{57}NO_{10}$: C 74.05, H 6.44, N 1.57; found: C 74.36, H 6.68, N 1.63.

(*b*) A solution of **4** (190 mg, 0.18 mmol) in methanolic 0.5 N sodium methoxide (1.1 mL) was kept at room temperature for 20 h. The solution was made neutral with Amberlite IRC 50 (H^+), filtered, and evaporated. Chromatographic purification of the remainder on a column of silica gel (hexane – ethyl acetate, 2:1, 1:1) provided a product identical to **15** (132 mg, 81%).

*N,6-O-Carbonyl-1,5-dideoxy-3-*O*-(α-D-glucopyranosyl)-1,5-imino-D-mannitol (**16**)*

A mixture of **15** (125 mg, 0.140 mmol) and 5% palladium-on-carbon (70 mg) in 95% ethanol (4 mL) was hydrogenated in a hydrogen stream for 1.5 h. The catalyst was removed by filtration, followed by evaporation of the solvent. Freeze-drying an aqueous solution provided **16** (50 mg, 102%) as a white solid; $[\alpha]_D$ +70.5 (*c* 0.4, water). The ^{1}H and ^{13}C NMR data are reported in Tables 1 and 2.

*2,4-Di-*O*-benzyl-1,5-dideoxy-1,5-imino-3-*O*-(2,3,4,6-tetra-*O*-benzyl-α-D-glucopyranosyl)-D-mannitol (**17**)*

A mixture of **15** (527 mg, 0.59 mmol) in 5% potassium hydroxide in 90% ethanol (15 mL) was heated at 80°C for 4 h. It was neutralized with acetic acid, followed by solvent removal. The material was taken up in dichloromethane and the solution was washed with a little water, dried, and evaporated to provide **17** as a tough syrup (488 mg, 95%). An analytical sample was purified by column chromatography on silica gel (dichloromethane – 3% methanol). ^{1}H NMR ($CDCl_3$) δ: 7.40–7.10 (m, 30H, 6Ph), 5.00 (bs, 1H, H-1′), 4.04 (overlapped, H-3′), 3.88 (m, H-2), 3.53 (dd, 1H, $J_{2',1'}$ 3.5 Hz, $J_{2',3'}$ 9.5 Hz, H-2′), 3.12 (dd, 1H, $J_{1A,1B}$ 13.5 Hz, $J_{1A,2}$ 4.0 Hz, H-1A), 2.59 (bd, 1H, H-1B).

*N-Benzyl-2,4-di-*O*-benzyl-1,5-dideoxy-1,5-imino-3-*O*-(2,3,4,6-tetra-*O*-benzyl-α-D-glucopyranosyl)-D-mannitol (**18**)*

A mixture of **17** (461 mg, 0.53 mmol), potassium carbonate (50 mg, 0.36 mmol), and benzyl bromide (166 μL, 1.40 mmol) in *N,N*-dimethylformamide (5 mL) was stirred for 2 h at 18°C. The solids were removed by filtration and the solution was concentrated. Column chromatography of the crude product on silica gel (hexane – ethyl acetate, 4:1) provided **18** (480 mg, 94%); $[\alpha]_D$ +38 (*c* 1.3, chloroform). ^{13}C NMR ($CDCl_3$) δ: 98.97 (C-1′), 60.89 (C-5), 58.54, 58.22 (C-1, C-6), 46.63 (NCH_2Ph). Anal. calcd. for $C_{61}H_{65}NO_9$: C 76.62, H 6.85, N 1.47; found: C 76.38, H 6.93, N 1.55.

*N-Benzyl-2,4-di-*O*-benzyl-6-chloro-1,5,6-trideoxy-1,5-imino-3-*O*-(2,3,4,6-tetra-*O*-benzyl-α-D-glucopyranosyl)-D-mannitol (**19**)*

Methanesulfonyl chloride (50 μL, 0.65 mmol) was added to a solution of **18** (336 mg, 0.35 mmol) in pyridine (5 mL). After 40 min at 22°C, the mixture was heated at 50°C for 1 h. Then it was poured into ice-water and extracted with dichloromethane, followed by washing of the organic solution with water, drying, and evaporation. The resultant material was applied to a column of silica gel (hexane – ethyl acetate, 4:1) to provide **19** (275 mg, 80%) as a tough syrup; $[\alpha]_D$ +31 (*c* 0.7, chloroform). ^{1}H NMR ($CDCl_3$, broad signals) δ: 7.45–7.05 (m, 35H, 7Ph), 4.90 (overlapped, H-1′), 4.11 (m, 1H, $J_{4',5'}$ 9.5 Hz, H-5′), 4.03 (overlapped, H-3′),

Can. J. Chem. Downloaded from www.nrcresearchpress.com by 203.198.23.82 on 09/08/12
For personal use only.

3.88 (overlapped, H-2), 3.60 (t, 1H, $J_{3',4'}$ 9.5 Hz, H-4'), 3.49 (dd, 1H, $J_{1',2'}$ 3.5 Hz, $J_{2',3'}$ 9.5 Hz, H-2'), 3.36 (dd, 1H, $J_{6A',6B'}$ 10.5 Hz, $J_{6A',5'}$ 3.0 Hz, H-6A'), 3.22 (bd, 1H, H-6B'), 2.99 (dd, 1H, $J_{1A,2}$ 6.5 Hz, $J_{1A,1B}$ 12.5 Hz, H-1A), 2.26 (bd, 1H, H-1B). ^{13}C NMR ($CDCl_3$) δ: 98.51 (C-1'), 57.49 (C-1), 47.51 (NCH_2Ph), 42.02 (C-6). Anal. calcd. for $C_{61}H_{64}ClNO_8$: C 75.17, H 6.62, Cl 3.64, N 1.44; found: C 75.07, H 6.60, Cl 4.19, N 1.51.

N-Benzyl-2,4-di-O-benzyl-1,5,6-trideoxy-1,5-imino-3-O-(2,3,4,6-tetra-O-benzyl-α-D-glucopyranosyl)-D-mannitol (20)

The chloro compound **19** (254 mg, 0.26 mmol), tributyltin hydride (420 μL, 1.56 mmol), and 2,2'-azobis(isobutyronitrile) (15 mg) in toluene (10 mL) were heated at 95–100°C for 3 h. Evaporation, followed by two column chromatographic purifications on silica gel (toluene – ethyl acetate, 20:1, hexane – ethyl acetate, 6:1) provided **20** (155 mg, 63%); $[\alpha]_D$ +11.3 (*c* 0.2, chloroform). ^{1}H NMR ($CDCl_3$, signals broad) δ: 7.40–7.05 (m, 35H, 7Ph), 5.03 (bs, 1H, H-1'), ~4.09 (m, overlapped, H-3'), 3.50 (dd, 1H, $J_{1',2'}$ 3.5 Hz, $J_{2',3'}$ 9.5 Hz, H-2'), 3.40 (bdd, 1H, $J_{6A',6B'}$ 10.5 Hz, H-6A'), 3.29 (bd, 1H, H-6B'), 1.30 (bd, 3H, $J_{5,6}$ 5.5 Hz, H_3-6). Anal. calcd. for $C_{61}H_{65}NO_8$: C 77.93, H 6.97, N 1.49; found: C 77.93, H 6.82, N 1.46.

1,5,6-Trideoxy-3-O-(α-D-glucopyranosyl)-1,5-imino-D-mannitol-hydrochloride (21)

A mixture of **20** (143 mg, 0.15 mmol), 5% palladium-on-carbon (143 mg), and methanolic 0.12 N hydrochloric acid (1.5 mL, 0.18 mmol) in methanol (5 mL) was hydrogenated in the hydrogen stream for 2 h. Usual processing followed by gel filtration (Sephadex LH 20, ethanol–water, 1:1) provided **21** (52 mg, 99%) as a white powder after freeze-drying an aqueous solution; $[\alpha]_D$ +71 (*c* 0.4, water). The ^{1}H and ^{13}C NMR data are reported in Tables 1 and 2.

6-Azido-3-O-benzyl-6-deoxy-5-O-methyl-1,2-O-isopropylidene-α-D-glucofuranose (22)

Sodium hydride (50% oily suspension, 4.81 g, 0.1 mol) was added slowly to a stirring solution of 6-azido-3-*O*-benzyl-6-deoxy-1,2-*O*-isopropylidene-α-D-glucofuranose (25) (26 g, 0.077 mol) at ice-bath temperature. After 20 min, methyl iodide (9 mL, 0.097 mol) was added and stirring continued for 30 min at ice-bath temperature, then another 30 min at room temperature. The reaction was quenched by the careful addition of methanol at 0°C, followed by evaporation of the solvent. The remainder was taken up in dichloromethane and the organic solution was washed with water, dried, and concentrated. Column chromatographic purification of the crude product on silica gel (hexane – ethyl acetate, 7.5:1) provided **22** (24.2 g, 89%) as an oil; $[\alpha]_D$ −65 (*c* 0.9, chloroform). ^{1}H NMR ($CDCl_3$) δ: 7.45–7.25 (m, 5H, Ph), 5.88 (d, 1H, $J_{1,2}$ 4.0 Hz, H-1), 4.69 and 4.55 (ABq, 2H, $J_{A,B}$ 11.5 Hz, CH_2Ph), 4.61 (d, 1H, H-2), 4.19 (dd, 1H, $J_{3,4}$ 2.8 Hz, $J_{4,5}$ 8.5 Hz, H-4), 4.08 (d, 1H, H-3), 3.74 (m, 1H, H-5), 3.68 (dd, 1H, $J_{6,6'}$ 12.5 Hz, $J_{6,5}$ 2.5 Hz, H-6), 3.40 (s, 3H, CH_3O), 3.38 (dd, 1H, $J_{5,6'}$ 4.5 Hz, H-6'), 1.50 and 1.32 (2s, each 3H, $(CH_3)_2C$). Anal. calcd. for $C_{17}H_{23}N_3O_5$: C 58.44, H 6.63, N 12.03; found: C 58.40, H 6.63, N 11.87.

Methyl 6-azido-3-O-benzyl-6-deoxy-5-O-methyl-α- and -β-D-glucofuranoside (23α, 23β)

A solution of **22** (24 g, 0.068 mol) in methanolic 1 N hydrochloric acid (220 mL) was kept overnight at room temperature. It was neutralized with sodium hydrogen carbonate and evaporated. The remainder was taken up in dichloromethane, followed by washing of the organic solution with water, drying, and evaporation. Column chromatographic purification on silica gel (hexane – ethyl acetate, 3.5:1) provided in the first fraction the α-anomer **23α** (5.24 g, 24%) as an oil; $[\alpha]_D$ +41.4 (*c* 0.4, chloroform). ^{1}H NMR ($CDCl_3$) δ: 7.40–7.25 (m, 5H, Ph), 5.01 (d, 1H, $J_{1,2}$ 4.5 Hz, H-1), 4.74 and 4.58 (ABq, 2H, $J_{A,B}$ 11.5 Hz, CH_2Ph), 4.23 (m, 1H, H-2), 4.21 (dd, 1H, $J_{3,4}$ 4.5 Hz, $J_{4,5}$ 7.5 Hz, H-4), 4.03 (dd, 1H, $J_{2,3}$ 2.2 Hz, H-3), 3.70 (m, 1H, H-5), 3.64 (dd, 1H, $J_{5,6A}$ 2.5 Hz, $J_{6A,6B}$ 13.0 Hz, H-6A), 3.49 and 3.40 (2s, each 3H, $2CH_3O$), 3.37 (dd, 1H, $J_{5,6B}$ 4.5 Hz, H-6B), 2.84 (d, 1H, $J_{2,OH}$ 5.5 Hz, OH). Anal. calcd. for $C_{15}H_{21}N_3O_5$: C 55.72, H 6.55, N 12.99; found: C 55.65, H 6.59, N 12.82. Continued elution provided an α,β mixture of **23** (3.31 g, 15%) and finally the pure β anomer **23β** (10.9 g, 49%, total yield 88%) as an oil; $[\alpha]_D$ −71 (*c* 0.4, chloroform). ^{1}H NMR ($CDCl_3$) δ: 7.40–7.25 (m, 5H, Ph), 4.80 (bs, 1H, $J_{1,2}$ ~ 1 Hz, H-1), 4.67 and 4.62 (ABq, 2H, $J_{A,B}$ 12.0 Hz, CH_2Ph), 4.30 (dd, 1H, $J_{3,4}$ 4.7 Hz, $J_{4,5}$ 8.5 Hz, H-4), 4.20 (bs, 1H, H-2), 3.97 (dd, 1H, $J_{2,3}$ 1.6 Hz, H-3), 3.76 (m, 1H, H-5), 3.73 (dd, 1H, $J_{6A,6B}$ 13.0 Hz, $J_{5,6A}$ 2.5 Hz, H-6A), 3.40 (dd, overlapped, $J_{5,6B}$ 4.5 Hz, H-6B), 3.394 and 3.390 (2s, each 3H, $2CH_3O$), 1.67 (d, 1H, $J_{2,OH}$ 3.5 Hz, OH). Anal. calcd. for $C_{15}H_{21}N_3O_5$: C 55.72, H 6.55, N 12.99; found: C 55.73; H 6.27, N 12.88.

Methyl 3-O-benzyl-N-benzyloxycarbonyl-2,6-dideoxy-2,6-imino-5-O-methyl-β-D-glucofuranoside (26)

Trifluoromethanesulfonic anhydride (4.1 mL, 24.4 mmol) was added at −50°C to a stirred solution of **23β** (5.34 g, 16.5 mmol) and pyridine (6 mL, 74.2 mmol) in dichloromethane (100 mL). After 1 h, another portion of the anhydride (1.5 mL, 8.9 mmol) was added and stirring continued for 30 more min at −50°C. The mixture was poured into ice-water, followed by extraction with dichloromethane, washing of the organic solution with water, drying, and evaporation. The remainder (**24**) was taken up in dichloromethane (51 mL) and reduced with triphenylphosphine (5 g, 19 mmol) by refluxing for 2 h. The mixture was allowed to reach room temperature and a solution of saturated aqueous potassium carbonate (10 mL) was added, followed by vigorous stirring overnight. The organic layer was separated, washed with water and evaporated. The resulting product (**25**) was taken up in ether (63 mL). Saturated aqueous sodium hydrogen carbonate (42 mL) and benzyl chloroformate (3.25 mL, 22.8 mmol) were added with vigorous stirring. After 30 min, the organic layer was separated, washed with water, dried, and evaporated. The crude product was applied to a column of silica gel and eluted with hexane-ethyl acetate, 3:1, 2:1 to afford pure **26** (4.6 g, 68%) as a tough syrup; $[\alpha]_D$ −68 (*c* 0.5, chloroform). ^{1}H NMR ($CDCl_3$, duplication of signals due to rotamers, a:b ~ 4:1) δ: 7.40–7.15 (m, 10H, 2Ph), 5.10 (d, overlapped, $J_{1,2}$ 3.0 Hz, H-1a), 5.05 (d, 1H, $J_{1,2}$ 3.0 Hz, H-1b), 4.89 (t, 1H,$J_{2,3}$ 3.5 Hz, H-2a), 4.68 (t, overlapped, $J_{2,3}$ 3.5 Hz, H-2b), 4.46 (dd, 1H, *J* 7.0 and 12.5 Hz, H-5b), 4.40 (overlapped, H-4a), 4.39 (overlapped, H-4b), 4.29 (dd, 1H, *J* 7.0 and 12.0 Hz, H-5a), 4.07 (dd, 1H, H-3a), 3.98 (dd, 1H, H-3b), 3.68–3.60 (m, H-6a, H-6b), 3.494, 3.489 (2s, each 3H, CH_3O-a, CH_3O-b), 3.37, 3.34 (2s, each 3H, CH_3O-a, CH_3O-b), 3.36–3.26 (m, 2H, H-6'a, H-6'b). Anal. calcd. for $C_{23}H_{27}NO_6$: C 66.81, H 6.58, N 3.39; found: C 66.82, H 6.78, N 3.37.

4-O-Benzyl-N-benzyloxycarbonyl-1,5-dideoxy-1,5-imino-2-O-methyl-D-mannitol (28)

A mixture of **26** (2.1 g, 5.07 mmol), dioxane (21.5 mL), trifluoroacetic acid (11 mL), and water (11 mL) was stirred for 3.5 h. Then a solution of sodium acetate (3.6 g) in water (53 mL) was added. The product was extracted with dichloromethane, followed by drying and evaporation of the organic solution. The resultant material (**27**) was dissolved in 95% ethanol (25 mL) and a suspension of sodium borohydride (600 mg, 15.9 mmol) in 50% ethanol (4 mL) was added at 0°C. After stirring for 30 min at room temperature, the reaction was quenched by the addition of ammonium chloride followed by evaporation. The remainder was extracted with dichloromethane, the organic solution was washed with a little water, dried, and evaporated. The reaction product was purified on a column of silica gel (dichloromethane – ethyl acetate, 1:1, 1:2, 1:3, 0:1) to afford **28** (1.044 g, 51%); $[\alpha]_D$ −36 (*c* 0.7, chloroform). Anal. calcd. for $C_{22}H_{27}NO_6$: C 65.82, H 6.78, N 3.49; found: 65.06, H 6.84, N 3.43.

Can. J. Chem. Downloaded from www.nrcresearchpress.com by 203.198.23.82 on 09/08/12
For personal use only.

4-O-Benzyl-N,6-O-carbonyl-1,5-dideoxy-1,5-imino-2-O-methyl-D-mannitol (30)

A solution of **28** (520 mg, 1.30 mmol) in methanolic 0.5 N sodium methoxide (4 mL) was kept for 2 h at room temperature. The solution was deionized with Amberlite IRC 50 (H^+), filtered, and evaporated. The remainder was applied to a column of silica gel (dichloromethane – ethyl acetate, 1:1) to afford pure **30** (308 mg, 81%) as a solid; mp 99.5–100.5°C (dichloromethane, ether, hexane); $[\alpha]_D$ +40 (*c* 0.3, chloroform). IR ($CHCl_3$): 1754 (CO) cm^{-1}. ^1H NMR ($CDCl_3$) δ: 7.40–7.20 (m, 5H, Ph), 5.01 and 4.65 (ABq, 2H, $J_{A,B}$ 11.5 Hz, CH_2Ph), 4.30 (dd, 1H, $J_{6A,6B}$ 9.0 Hz, $J_{6A,5}$ 7.5 Hz, H-6A), 4.17 (dd, 1H, $J_{1A,1B}$ 14.5 Hz, $J_{1A,2}$ 2.0 Hz, H-1A), 3.96 (dd, 1H, $J_{6B,5}$ 3.0 Hz, H-6B), 3.68 (unres. m, 1H, H-3), 3.60 (bs, 1H, H-2), 3.54 (t, 1H, $J_{3,4} \sim J_{4,5}$ 9.5 Hz, H-4), 3.49 (m, H-5), 3.44 (s, 3H, CH_3O), 2.84 (dd, 1H, $J_{1B,2}$ 1.5 Hz, H-1B), 2.56 (bd, 1H, OH). Anal. calcd. for $C_{15}H_{19}NO_5$: C 61.42, H 6.53, N 4.78; found: C 61.17, H 6.55, N 4.75.

*4-O-Benzyl-N,6-O-carbonyl-1,2,5-trideoxy-1,5-imino-D-*arabino*-hexitol (31)*

A solution of **29** (26) (360 mg, 0.97 mmol) in methanolic 0.5 N sodium methoxide (3.5 mL) was kept at room temperature for 1.5 h. The solution was neutralized with Amberlite IRC 50 (H^+), filtered, and evaporated. Column chromatography on silica gel (dichloromethane – ethyl acetate, 1:1) afforded **31** (227 mg, 89%) as a white solid; $[\alpha]_D$ +76 (*c* 0.3, chloroform). IR ($CHCl_3$): 1794 (CO) cm^{-1}. ^1H NMR ($CDCl_3$) δ: 7.40–7.25 (m, 5H, Ph), 4.88 and 4.67 (ABq, 2H, $J_{A,B}$ 11.5 Hz, CH_2Ph), 4.29 (dd, 1H, $J_{6A,6B}$ 8.5 Hz, $J_{6A,5}$ 7.5 Hz, H-6A), 3.89 (dd, $J_{5,6B}$ 5.5 Hz, H-6B), 3.82 (ddd, 1H, $J_{1e,1a}$ 13.5 Hz, $J_{1e,2a}$ 5.5 Hz, $J_{1e,2e}$ 1.5 Hz, H-1e), 3.68 (ddd, 1H, $J_{2a,3}$ 11.5 Hz, $J_{2e,3}$ 4.5 Hz, $J_{3,4}$ 9.0 Hz, H-3), 3.50 (ddd, 1H, $J_{4,5}$ 9.0 Hz, H-5), 3.15 (t, 1H, H-4), 2.93 (bs, 1H, OH), 2.85 (dt, $J_{1a,2a}$ 13.5 Hz, $J_{1a,2e}$ 3.5 Hz, H-1a), 1.95 (m, 1H, $J_{2e,2a}$ 13.0 Hz, H-2e), 1.56 (dq, 1H, H-2a). Anal. calcd. for $C_{14}H_{17}NO_4$: C 63.87, H 6.51, N 5.32; found: C 63.88, H 6.53, N 5.26.

*4-O-Benzyl-N,6-O-carbonyl-1,5-dideoxy-1,5-imino-2-O-methyl-3-O-(2,3,4,6-tetra-O-benzyl-α-D-glucopyranosyl)-D-*mannitol *(32)*

A solution of bromide **14** (2.58 mmol) in dichloromethane (4 mL) was transferred into a mixture of **30** (202 mg, 0.69 mmol), tetraethylammonium bromide (300 mg, 1.43 mmol), *N,N*-dimethylformamide (0.7 mL), and 4 Å molecular sieves (powdered, 0.7 g) in dichloromethane (2 mL). After stirring for 3 days, the mixture was processed as described for the preparation of **15** with subsequent column chromatography on silica gel (hexane – ethyl acetate, 4:1 to 1:1) to afford crystalline **32** (377 mg, 67%); mp 114–115°C (dichloromethane, ether, hexane); $[\alpha]_D$ +72 (*c* 0.3, chloroform). ^1H NMR ($CDCl_3$) δ: 7.35–7.10 (m, 25H, 5Ph), 5.14–4.43 (5ABq, 10H, $5CH_2Ph$), 4.96 (d, 1H, $J_{1',2'}$ 3.5 Hz, H-1'), 4.24 (t, 1H, $J_{6A,6B}$ 8.8 Hz, $J_{6A,5}$ 8.0 Hz, H-6A), 4.10 (overlapped, H-3'), 4.06 (dd, 1H, $J_{1A,1B}$ 14.5 Hz, $J_{1A,2}$ 2.5 Hz, H-1A), 3.84 (bs, 1H, H-2), 3.79 (dd, 1H, $J_{6B,5}$ 3.0 Hz, H-6B), 3.56 (dd, 1H, $J_{2',3'}$ 9.5 Hz, H-2'), 3.49 (m, 2H, H-3, H-5), 3.28 (s, 3H, CH_3O), 2.71 (bd, 1H, $J_{1B,2} < 1$ Hz, H-1B). ^{13}C NMR ($CDCl_3$) δ: 157.81 (CO), 100.37 (C-1'), 65.77 (C-6), 57.27 (C-5), 56.43 (CH_3O), 40.05 (C-1). Anal. calcd. for $C_{49}H_{53}NO_{10}$: C 72.13, H 6.55, N 1.72; found: C 71.78, H 6.68, N 1.76.

*4-O-Benzyl-N,6-O-carbonyl-1,2,5-trideoxy-1,5-imino-3-O-(2,3,4,6-tetra-O-benzyl-α-D-glucopyranosyl)-D-*arabino*-hexitol (33)*

A solution of bromide **14** (2.5 mmol) in dichloromethane (5 mL) was transferred into a mixture of **31** (197 mg, 0.75 mmol), tetraethylammonium bromide (300 mg, 1.43 mmol), *N,N*-dimethylformamide (0.7 mL), and 4 Å molecular sieves (powdered, 0.7 g), in dichloromethane (2 mL). After stirring for 3 days, the mixture was processed as described for **15** with subsequent column chromatography on silica gel (hexane – dichloromethane – ethyl acetate, 4:4:1, 3:5:1, 2:5:1.5) to provide **33** (379 mg, 65%) as a solid. The analytical sample was recrystallized from ethanol; mp 113–114°C, $[\alpha]_D$ +89 (*c* 0.8, chloroform). ^1H NMR ($CDCl_3$) δ: 7.40–7.15 (m, 25H, 5Ph), 5.08 (d, 1H, $J_{1',2'}$ 3.5 Hz, H-1'), 5.06–4.43 (5ABq, 10H, $5CH_2Ph$), 4.23 (t, 1H, $J_{6A,6B} \sim J_{6A,5}$ 8.0 Hz, H-6A), 4.02 (t, 1H, $J_{2',3'}$ 9.5 Hz, $J_{3',4'}$ 9.0 Hz, H-3'), 3.90 (m, 1H, H-5'), 3.76 (bdd, 1H, $J_{1e,1a}$ 13.5 Hz, $J_{1e,2a}$ 4.5 Hz, $J_{1e,2e} \sim 1$ Hz, H-1e), 3.71 (dd, overlapped, H-6B), ~3.63 (overlapped, H-4'), 3.57 (dd, 1H, H-2'), 3.49 (m, 1H, H-5), 3.22 (t, 1H, $J_{3,4} \sim J_{4,5}$ 9.0 Hz, H-4), 2.78 (dt, 1H, $J_{1a,2a}$ 13.5 Hz, $J_{1a,2e}$ 2.5 Hz, H-1a), 2.25 (m, 1H, $J_{2e,2a}$ 13.0 Hz, H-2e), 1.57 (dq, 1H, H-2a). ^{13}C NMR ($CDCl_3$) δ: 156.67 (CO), 99.64 (C-1'), 65.84 (C-6), 57.17 (C-5), 38.72 (C-1), 31.10 (C-2). Anal. calcd. for $C_{48}H_{51}NO_9$: C 73.36, H 6.54, N 1.78; found: C 73.11, H 6.35, N 1.82.

4-O-Benzyl-1,5-dideoxy-1,5-imino-2-O-methyl-3-O-(2,3,4,6-tetra-O-benzyl-α-D-glucopyranosyl)-D-mannitol (34)

A mixture of **32** (334 mg, 0.41 mmol) in 5% potassium hydroxide in 90% ethanol (10 mL) was heated at 65°C for 4 h. It was processed as described for **17** followed by column chromatography on silica gel (dichloromethane – 5% methanol) to afford **34** (295 mg, 91%); $[\alpha]_D$ +35 (*c* 0.7, chloroform). ^1H NMR ($CDCl_3$, broad signals) δ: 7.35–7.10 (m, 25H, 5Ph), 4.98 (overlapped, H-1'), 4.15 (overlapped, H-5'), 4.09 (t, overlapped, $J_{2',3'}$ 9.5 Hz, $J_{3',4'}$ 9.0 Hz, H-3'), 3.54 (dd, overlapped, H-2'), 3.27 (s, 3H, CH_3O), 3.15 (bd, 1H, $J_{1A,1B}$ 13.0 Hz, H-1A), 2.48 (H-1B).

*4-O-Benzyl-1,2,5-trideoxy-1,5-imino-3-O-(2,3,4,6-tetra-O-benzyl-α-D-glucopyranosyl)-D-*arabino*-hexitol (35)*

A mixture of **33** (306 mg, 0.39 mmol) and potassium hydroxide (0.5 g) in 90% ethanol (10 mL) was heated at 68°C for 1 h. It was processed as described for **17** followed by column chromatography on silica gel (dichloromethane – 5% methanol) to provide **35** (245 mg, 83%); $[\alpha]_D$ +58 (*c* 1.0, chloroform). ^1H NMR ($CDCl_3$) δ: 7.40–7.10 (m, 25H, 5Ph), 5.12–4.42 (5ABq, 10H, $5CH_2Ph$), 5.08 (d, 1H, $J_{1',2'}$ 3.5 Hz, H-1'), 4.04 (t, 1H, $J_{2',3'}$ 9.5 Hz, $J_{3',4'}$ 9.0 Hz, H-3'), 3.93 (m, 1H, H-5'), 3.72 (overlapped, H-6'), 3.63 (overlapped, H-4'), 3.55 (dd, 1H, H-2'), 3.02 (m, 1H, $J_{1e,1a}$ 12.5 Hz, H-1e), 2.61 (dt, 1H, $J_{1a,2a}$ 13.0 Hz, $J_{1a,2e}$ 1.5 Hz, H-1a), 2.23 (m, 1H, $J_{2a,2e}$ 13.5 Hz, H-2e), 1.59 (dq, 1H, H-2a).

1,5-Dideoxy-3-O-(α-D-glucopyranosyl)-1,5-imino-2-O-methyl-D-mannitol-hydrochloride (36)

A mixture of **34** (140 mg, 0.19 mmol), 5% palladium-on-carbon (145 mg), and methanolic 0.12 N hydrochloric acid (2 mL, 0.24 mmol) in methanol (3 mL) was hydrogenated in the hydrogen stream for 2 h. Usual processing followed by gel filtration as described for **9** provided **36** (68 mg, 98%) as a solid after freeze-drying an aqueous solution; $[\alpha]_D$ +73 (*c* 0.4, water). The ^1H and ^{13}C NMR data are reported in Tables 1 and 2.

*1,2,5-Trideoxy-3-O-(α-D-glucopyranosyl)-1,5-imino-D-*arabino*-hexitol-hydrochloride (37)*

A mixture of **35** (242 mg, 0.32 mmol), 5% palladium-on-carbon (240 mg), and methanolic 0.12 N hydrochloric acid (3.34 mL, 0.40 mmol) was hydrogenated in the hydrogen stream for 2 h. Usual work-up and gel filtration as described for **9** provided **37** (104 mg, 94%) as a white solid after freeze-drying an aqueous solution. The ^1H and ^{13}C NMR data are reported in Tables 1 and 2.

Methyl-3-O-allyl-6-azido-5-O-benzyl-6-deoxy-α- and -β-D-glucofuranoside (38)

The title compound was prepared conventionally from 3-*O*-allyl-1,2-*O*-isopropylidene-6-*O*-*p*-toluenesulfonyl-α-D-glucofuranose (27). Replacement of the *p*-toluenesulfonyloxy group by azide, benzylation of the 5-position, and subsequent methanolysis as described for **23** provided the title compound as an oil. **38** proved labile on storage. α-Anomer: ^1H NMR ($CDCl_3$) δ: 7.35–7.20 (m, 5H, Ph), 5.87 (m, 1H, $CH_2{=}CH$), 5.28 and 5.17 (2m, 2H, $CH_2{=}CH$), 5.02 (d, 1H, $J_{1,2}$ 4.5 Hz, H-1), 4.71 and 4.59 (ABq, 2H, $J_{A,B}$ 11.5 Hz, CH_2Ph), 4.26 (dd, 1H, $J_{3,4}$ 4.0 Hz, H-4), 4.22–4.15 (m, 2H, H-2, $1CH_2CH{=}CH_2$), 4.00–3.92 (m, 3H, H-3, H-5, $1CH_2CH{=}CH_2$), 3.62 (dd, 1H, $J_{6A,6B}$ 13.5 Hz, $J_{6A,5}$ 2.5 Hz, H-6A),

Can. J. Chem. Downloaded from www.nrcresearchpress.com by 203.198.23.82 on 09/08/12
For personal use only.

3.49 (s, 3H, CH_3O), 3.41 (dd, 1H, $J_{5,6B}$ 5.0 Hz, H-6B). β-Anomer: ^{1}H NMR ($CDCl_3$) δ: 7.40–7.20 (m, 5H, Ph), 5.88 (m, 1H, CH_2=C*H*), 5.27 and 5.18 (2m, 2H, CH_2=CH), 4.82 (d, 1H, $J_{1,2} \sim 1$ Hz, H-1), 4.72 and 4.60 (ABq, 2H, $J_{A,B}$ 11.0 Hz, CH_2Ph), 4.37 (dd, 1H, $J_{3,4}$ 5.2 Hz, $J_{4,5}$ 8.5 Hz, H-4), 4.21 (bs, 1H, H-2), 4.11 and 4.03 (2m, 2H, CH_2CH=CH_2), 4.02 (m, overlapped, H-5), 3.92 (dd, 1H, $J_{3,2}$ 1.2 Hz, H-3), 3.69 (dd, 1H, $J_{6A,6B}$ 13.0 Hz, $J_{6A,5}$ 2.5 Hz, H-6A), 3.42 (dd, 1H, $J_{6B,5}$ 4.5 Hz, H-6B), 3.40 (s, 3H, CH_3O).

*Methyl 3-*O*-allyl-5-*O*-benzyl-*N*-benzyloxycarbonyl-2,6-dideoxy-2,6-imino-α- and -β-*D*-glucofuranoside (**41**α,β)*

Trifluoromethanesulfonic anhydride (2.6 mL, 15.45 mmol) was added at −50 to −40°C to a solution of **38** (3.66 g, 10.5 mmol) and pyridine (3.6 mL, 44.5 mmol) in dichloromethane (70 mL). After 40 min at this temperature, it was processed as described for **26**. The resultant material (**39**) was dissolved in dichloromethane (40 mL) and reduced with triphenylphosphine (3.3 g, 12.6 mmol) for 20 min at room temperature and then for 2 h at reflux temperature. The mixture was allowed to reach room temperature and was vigorously stirred after the addition of saturated aqueous potassium carbonate (10 mL). After 12 h, the organic layer was separated, washed with water, and evaporated. A mixture of the resulting product (**40**), saturated aqueous sodium hydrogen carbonate (30 mL), and benzylchloroformate (2 mL, 14.0 mmol) in ether (45 mL) was vigorously stirred for 20 min. The organic layer was separated, washed with water, and evaporated, followed by column chromatography on silica gel (hexane – ethyl acetate, 3:1) to provide in the first fraction the α-anomer **41**α (330 mg, 7.2%); $[\alpha]_D$ +40 (*c* 0.9, chloroform). ^{1}H NMR ($CDCl_3$, mixture of two rotamers) δ: 7.40–7.15 (m, 10H, 2Ph), 5.83–5.66 (m, 1H, CH_2=C*H*), 4.27 (dd, overlapped, $J_{5,6}$ 6.5 Hz, H-6), 3.37 (s, 3H, CH_3O), 3.01–2.90 (m, H-6′). Anal. calcd. for $C_{25}H_{29}NO_6$: C 68.32, H 6.65, N 3.19; found: C 68.46, H 6.64, N 3.25. Continued elution afforded the β-anomer **41**β (2.21 g, 48%); $[\alpha]_D$ −132 (*c* 0.9, chloroform). ^{1}H NMR ($CDCl_3$, mixture of two rotamers) δ: 5.85–5.66 (m, CH_2=C*H*), 5.10 (d, 1H, $J_{1,2}$ 3.0 Hz, H-1a), 5.06 (d, 1H, $J_{1,2}$ 3.0 Hz, H-1b), 4.78 (t, 1H, $J_{2,3}$ 3.5 Hz, H-2a), 4.41 (dd, H-4a, H-4b), 4.38 (dd, $J_{5,6}$ 7.5 Hz, H-6b), 4.18 (dd, 1H, $J_{5,6}$ 7.0 Hz, $J_{6,6'}$ 12.5 Hz, H-6a), 4.00 (dd, 1H, $J_{3,4}$ 5.7 Hz, H-3a), 3.91 (overlapped, $J_{3,4}$ 5.5 Hz, $J_{2,3}$ 3.5 Hz, H-3b), 3.84–3.76 (m, H-5a, H-5b), 3.50 (s, 3H, CH_3O), 3.40 (H-6′a), 3.37 (H-6′b). Anal. calcd. for $C_{25}H_{29}NO_6$: C 68.32, H 6.65, N 3.19; found: C 68.35, H 6.79, N 3.20.

*4-*O*-Allyl-2-*O*-benzyl-*N*-benzyloxycarbonyl-1,5-dideoxy-1,5-imino-D-mannitol (**43**)*

50% Trifluoroacetic acid (25 mL) was added at ice-bath temperature to a solution of **41**β (2.45 g, 5.57 mmol) in dioxane (25 mL). After 4 h at room temperature, a solution of sodium acetate (4.1 g) in water (60 mL) was added. The product was extracted with dichloromethane, followed by drying and evaporation of the organic solution. The remainder was dissolved in 95% ethanol (41 mL) and a suspension of sodium borohydride (720 mg, 19 mmol) in 50% ethanol (6 mL) was added at ice-bath temperature. After 30 min at room temperature, it was worked up as described for **28** with subsequent column chromatography on silica gel (dichloromethane – ethyl acetate, 3:1, 2:1, 1:1) to afford **43** (1.40 g, 59%) as a syrup, $[\alpha]_D$ −22 (*c* 1.8, chloroform). Anal. calcd. for $C_{24}H_{29}NO_6$: C 67.43, H 6.84, N 3.28; found: C 67.57, H 6.92, N 3.30.

*4-*O*-Allyl-2-*O*-benzyl-*N*,6-*O*-carbonyl-1,5-dideoxy-1,5-imino-D-mannitol (**44**)*

A solution of **43** (1.74 g, 4.07 mmol) in methanolic 0.5 N sodium methoxide (13 mL) was kept at room temperature for 5 h. The solution was made neutral with Amberlite IRC 50 (H^+), filtered, and evaporated. The resultant solid material was purified on a column of silica gel (dichloromethane – ethyl acetate, 3:1, 2:1) to provide **44** (1.15 g, 89%). The analytical sample was recrystallized from dichloromethane, ether, hexane; mp 119.5–120.5°C; $[\alpha]_D$ −49 (*c* 0.4, chloroform). IR ($CHCl_3$): 1760 (CO) cm^{-1}. ^{1}H NMR ($CDCl_3$) δ: 7.40–7.25 (m, 5H, Ph), 5.90 (m, 1H, CH_2=C*H*), 5.26 and 5.19 (2m, 2H, CH_2=CH), 4.84 and 4.36 (ABq, 2H, $J_{A,B}$ 10.5 Hz, CH_2Ph), 4.46 and 4.12 (2m, 2H, CH_2=CH-CH_2), 4.43 (dd, overlapped, 1H, $J_{5,6A}$ 7.5 Hz, H-6A), 4.25 (dd, 1H, $J_{1A,1B}$ 14.5 Hz, $J_{1A,2}$ 2.5 Hz, H-1A), 4.22 (dd, 1H, $J_{6A,6B}$ 8.5 Hz, $J_{5,6B}$ 2.5 Hz, H-6B), 3.81 (m, 1H, H-2), 3.62 (bdd, 1H, $J_{2,3}$ 3.0 Hz, $J_{3,4}$ 8.5 Hz, H-3), 3.49 (m, 2H, H-4, H-5), 2.90 (dd, 1H, $J_{1B,2}$ 1.0 Hz, H-1B). Anal. calcd. for $C_{17}H_{21}NO_5$: C 63.94, H 6.63, N 4.39; found: C 64.10, H 6.60, N 4.40.

*4-*O*-Allyl-2-*O*-benzyl-*N*,6-*O*-carbonyl-1,5-dideoxy-1,5-imino-3-*O*-(2,3,4,6-tetra-*O*-benzyl-α-D-glucopyranosyl)-D-mannitol (**45**)*

A solution of bromide **14** (8.3 mmol) in dichloromethane (15 mL) was added to a mixture of **44** (0.99 g, 3.10 mmol), tetraethylammonium bromide (1.2 g, 5.7 mmol), *N*,*N*-dimethylformamide (2.7 mL), and 4 Å molecular sieves (powdered, 3 g) in dichloromethane (4 mL). After stirring for 3 days, more bromide (2.9 mmol) was added and stirring continued for 2 more days. Usual processing as described for **15** was followed by two column chromatographic purifications on silica gel (hexane – ethyl acetate, 4:1 to 1:2 and hexane–dichloromethane – ethyl acetate, 5:2:1) to provide pure **45** (1.6 g, 61%) as a white foam, $[\alpha]_D$ −1.3, $[\alpha]_{365}$ −32.9 (*c* 0.5, chloroform). ^{1}H NMR ($CDCl_3$) δ: 7.40–7.15 (m, 25H, 5Ph), 5.73 (m, 1H, CH_2=C*H*), 5.13 and 5.05 (2m, 2H, CH_2=CH), 5.04 (d, 1H, $J_{1',2'}$ 3.5 Hz, H-1′), 4.40 (t, 1H, $J_{6A,6B} \sim J_{5,6A}$ 8.5 Hz, H-6A), 4.19 (dd, 1H, $J_{6B,5}$ 3.5 Hz, H-6B), 4.16 (overlapped, dd, 1H, $J_{1A,1B}$ 14.5 Hz, $J_{1A,2}$ 2.5 Hz, H-1A), 2.79 (bd, 1H, H-1B). ^{13}C NMR ($CDCl_3$) δ: 157.63 (CO), 134.79 (CH_2=*C*H), 116.56 (*C*H_2=CH), 99.96 (C-1′), 65.62 (C-6), 57.32 (C-5), 40.63 (C-1). Anal. calcd. for $C_{51}H_{55}NO_{10}$: C 72.75, H 6.58, N 1.66; found: C 72.65, H 6.70, N 1.69.

*2-*O*-Benzyl-*N*,6-*O*-carbonyl-1,5-dideoxy-1,5-imino-3-*O*-(2,3,4,6-tetra-*O*-benzyl-α-D-glucopyranosyl)-D-mannitol (**46**)*

A mixture of **45** (1.2 g, 1.43 mmol), tris(triphenylphosphine)-rhodium(I)chloride (89 mg, 0.096 mmol), 1,4-diazabicyclo[2.2.2]-octane (40 mg, 0.36 mmol), 95% ethanol (84 mL), toluene (36 mL), and water (12 mL) was boiled under reflux for 10 h with stirring. The solvent was removed and the residue dissolved in acetone (116 mL) containing mercuric oxide (24 mg). A solution of mercuric chloride (3.2 g) in acetone–water (9:1, 72 mL) was added and the mixture stirred for 30 min. After solvent removal, the residue was taken up in dichloromethane, the solution washed with aqueous saturated potassium bromide and water, followed by evaporation. Chromatography on a column of silica gel (hexane – ethyl acetate, 2:1, 1:1, 1:2) gave alcohol **46** (1.07 g, 94%) as a white foam; $[\alpha]_D$ 0, $[\alpha]_{365}$ −6.4 (*c* 0.4, chloroform). ^{1}H NMR ($CDCl_3$) δ: 7.40–7.15 (m, 25H, 5Ph), 4.91 (d, 1H, $J_{1',2'}$ 3.5 Hz, H-1′), 4.39 (t, 1H, $J_{6A,6B} \sim J_{6A,5}$ 8.5 Hz, H-6A), 4.27 (dd, 1H, $J_{5,6B}$ 3.5 Hz, H-6B), 4.20 (dd, 1H, $J_{1A,1B}$ 14.5 Hz, $J_{1A,2}$ 2.0 Hz, H-1A), 4.04 (t, 1H, $J_{2',3'}$ 9.5 Hz, $J_{3',4'}$ 9.0 Hz, H-3′), 4.02 (t, 1H, $J_{3,4} \sim J_{4,5}$ 9.0 Hz, H-4), 3.91 (m, 1H, H-5′), 3.88 (m, 1H, H-2), 3.59–3.49 (m, 4H, H-5, H-2′, H-4′, H-6A′), 3.45 (dd, 1H, $J_{6A',6B'}$ 10.5 Hz, $J_{5',6B'}$ 2.0 Hz, H-6B′), 3.34 (dd, 1H, $J_{2,3}$ 2.5 Hz, H-3), 2.86 (bd, 1H, H-1B). ^{13}C NMR ($CDCl_3$) δ: 157.60 (CO), 100.41 (C-1′), 65.10 (C-6), 57.26 (C-5), 41.01 (C-1). Anal. calcd. for $C_{48}H_{51}NO_{10}$: C 71.89, H 6.41, N 1.75; found: C 71.48, H 6.37, N 1.79.

*2-*O*-Benzyl-*N*,6-*O*-carbonyl-1,5-dideoxy-1,5-imino-4-*O*-methyl-3-*O*-(2,3,4,6-tetra-*O*-benzyl-α-D-glucopyranosyl)-D-mannitol (**47**)*

To a solution of **46** (300 mg, 0.37 mmol) in *N*,*N*-dimethylformamide (1.2 mL), sodium hydride (80% oily suspension, 22 mg, 0.73 mmol) was added at ice-bath temperature with stirring. After 15 min, methyl iodide (45 μL, 0.72 mmol) was added and stirring was continued for 30 min at 0°C and then for 1.5 h at room temperature. The reaction was quenched by a few drops of methanol.

Can. J. Chem. Downloaded from www.nrcresearchpress.com by 203.198.23.82 on 09/08/12
For personal use only.

It was diluted with dichloromethane, washed with water, dried, and evaporated. The resultant material was applied to a column of silica gel (hexane – ethyl acetate, 2:1, 1:1) to afford **47** (305 mg, 88%); $[\alpha]_D$ −6.3 (*c* 0.3, chloroform). ^{1}H NMR ($CDCl_3$) δ: 7.40–7.15 (m, 25H, 5Ph), 5.08 (d, 1H, $J_{1',2'}$ 3.5 Hz, H-1′), 4.40 (t, 1H, $J_{5,6A} \sim J_{6A,6B}$ 8.5 Hz, H-6A), 4.17 (overlapped dd, 1H, $J_{5,6B}$ 3.0 Hz, H-6B), 4.14 (dd, 1H, $J_{1A,1B}$ 14.5 Hz, $J_{1A,2}$ 2.5 Hz, H-1A), 4.02 (overlapped, H-2), 3.52 (s, overlapped, CH_3O), 2.76 (bd, 1H, H-1B). ^{13}C NMR ($CDCl_3$) δ: 157.61 (CO), 99.86 (C-1′), 65.65 (C-6), 61.52 (CH_3O), 57.45 (C-5), 40.60 (C-1). Anal. calcd. for $C_{49}H_{53}NO_{10}$: C 72.13, H 6.55, N 1.72; found: C 72.04, H 6.62, N 1.73.

*2-O-Benzyl-N,6-O-carbonyl-1,4,5-trideoxy-1,5-imino-3-O-(2,3,4,6-tetra-O-benzyl-α-D-glucopyranosyl)-D-*lyxo*-hexitol (49)*

Sodium hydride (80% suspension, 52 mg, 1.73 mmol) was added to a solution of **46** (350 mg, 0.44 mmol) and a crystal of imidazole in tetrahydrofuran (5 mL). After 30 min, carbon disulfide (400 μL, 6.65 mmol) was added and, after another 30 min, methyl iodide (110 μL, 1.77 mmol). The mixture was kept stirring for 30 min, was diluted with dichloromethane, followed by washing of the organic solution with water, drying, and evaporation. The resultant yellowish solid (**48**) was taken up in toluene (5 mL) and reduced with tributyltin hydride (350 μL, 1.30 mmol) at reflux temperature for 4 h. The product obtained on evaporation was purified on a column of silica gel (hexane–dichloromethane – ethyl acetate, 5:1:0.5, 5:1:1) to provide pure **49** (270 mg, 79%); $[\alpha]_D$ +7.2 (*c* 0.4, chloroform. ^{1}H NMR ($CDCl_3$) δ: 7.40–7.10 (m, 25H, 5Ph), 4.89 (d, 1H, $J_{1',2'}$ 3.5 Hz, H-1′), 4.38 (t, 1H, $J_{6A,6B} \sim J_{6A,5}$ 8.5 Hz, H-6A), 4.15 (dd, 1H, $J_{1A,1B}$ 14.5 Hz, $J_{1A,2}$ 2.5 Hz, H-1A), 4.01 (t, 1H, $J_{2',3'}$ 9.5 Hz, $J_{3',4'}$ 8.5 Hz, H-3′), 3.97 (dd, 1H, $J_{6B,5}$ 4.5 Hz, H-6B), 3.83 (m, 1H, $J_{5',4'}$ 9.5 Hz, H-5′), 3.77 (m, 1H, H-2), 3.72 (m, 1H, H-5), 3.63 (m, 1H, H-3), 3.60–3.49 (m, 4H, H-4′, H-6A′, H-6B′ and H-2′ at 3.57), 2.75 (bd, 1H, H-1B), 2.13 (q, 1H, $J_{4a,4e} \sim J_{3,4a} \sim J_{4a,5}$ 11 Hz, H-4a), 1.75 (m, 1H, H-4e). ^{13}C NMR ($CDCl_3$) δ: 157.54 (CO), 95.97 (C-1′), 66.84 (C-6), 52.63 (C-5), 42.07 (C-1), 29.47 (C-4). Anal. calcd. for $C_{48}H_{51}NO_9$: C 73.36, H 6.54, N 1.78; found: C 73.06, H 6.49, N 1.84.

2-O-Benzyl-1,5-dideoxy-1,5-imino-4-O-methyl-3-O-(2,3,4,6-tetra-O-benzyl-α-D-glucopyranosyl)-D-mannitol (50)

A mixture of **47** (245 mg, 0.30 mmol) and potassium hydroxide (500 mg) in 90% ethanol (10 mL) was heated at 75°C for 4 h. The mixture was processed in the usual way and the resulting product purified on a column of silica gel (dichloromethane – 5–7% methanol) to provide **50** (175 mg, 74%) as a tough syrup; $[\alpha]_D$ +31 (*c* 0.7, chloroform). ^{1}H NMR ($CDCl_3$) δ: 7.35–7.15 (m, 25H, 5Ph), 5.09 (bs, 1H, H-1′), 3.56 (dd, overlapped, $J_{1',2'}$ 3.5 Hz, $J_{2',3'}$ 9.5 Hz, H-2′), 3.45 (s, 3H, CH_3O), 3.08 (dd, 1H, $J_{1A,1B}$ 14.0 Hz, H-1A), 2.54 (bd, 1H, H-1B).

*2-O-Benzyl-1,4,5-trideoxy-1,5-imino-3-O-(2,3,4,6-tetra-O-benzyl-α-D-glucopyranosyl)-D-*lyxo*-hexitol (51)*

A mixture of **49** (278 mg, 0.35 mmol) and potassium hydroxide (500 mg) in 90% ethanol (10 mL) was heated at 70°C for 10 h. Usual work-up with subsequent column chromatography on silica gel (dichloromethane – 4–6% methanol) provided **51** (239 mg, 89%) as a tough syrup; $[\alpha]_D$ +52 (*c* 0.5, chloroform). ^{1}H NMR ($CDCl_3$) δ: 7.40–7.10 (m, 25H, 5Ph), 4.88 (bs, overlapped, H-1′), 3.96 (t, 1H, $J_{3',4'} \sim J_{2',3'} \sim 9$ Hz, H-3′), 3.58 (dd, overlapped, H-2′).

1,5-Dideoxy-3-O-(α-D-glucopyranosyl)-1,5-imino-4-O-methyl-D-mannitol-hydrochloride (52)

A mixture of **50** (140 mg, 0.18 mmol), 5% palladium-on-carbon (140 mg), and methanolic 0.12 N hydrochloric acid (1.7 mL, 0.20 mmol) in methanol (4 mL) was hydrogenated in the hydrogen stream for 3 h. Usual work-up and gel filtration as described for **9** provided **52** (52.5 mg, 79%) as a white solid after freeze-drying an aqueous solution; $[\alpha]_D$ +92 (*c* 0.4, water). The ^{1}H and ^{13}C NMR data are reported in Tables 1 and 2.

*1,4,5-Trideoxy-3-O-(α-D-glucopyranosyl)-1,5-imino-D-*lyxo*-hexitol (53)*

A mixture of **51** (235 mg, 0.31 mmol), 5% palladium-on-carbon (235 mg), and methanolic 0.12 N hydrochloric acid (2.9 mL, 0.35 mmol) in methanol (5 mL) was hydrogenated in the hydrogen stream for 2.5 h. Usual work-up and gel filtration as described for **9** provided **53** (107 mg, 100%) as a white solid after freeze-drying an aqueous solution; $[\alpha]_D$ +106 (*c* 0.3, water). The ^{1}H and ^{13}C NMR data are reported in Tables 1 and 2.

Acknowledgements

Dr. Frank M. Unger's support of this project at Chembiomed Ltd. is gratefully acknowledged. We are deeply indebted to Professor R.U. Lemieux, Department of Chemistry, University of Alberta, who made possible the completion of the project and the preparation of this paper. We thank Mrs. B. Jamieson-Hinz for the preparation of starting materials and Dr. H. Beierbeck for his help with the calculation of theoretical nuclear Overhauser enhancements. The biological part of this work was supported by Grant DK17477 from the National Institutes of Health (to R.G.S.).

1. S. Hiraizumi, U. Spohr, and R.G. Spiro. J. Biol. Chem. **268**, 9927 (1993).
2. W.A. Lubas and R.G. Spiro. J. Biol. Chem. **262**, 3775 (1987).
3. W.A. Lubas and R.G. Spiro. J. Biol. Chem. **263**, 3990 (1988).
4. U. Fuhrmann, E. Bause, and H. Ploegh. Biochim. Biophys. Acta, **825**, 95 (1985).
5. U. Spohr, O. Hindsgaul, and R.U. Lemieux. Can. J. Chem. **63**, 2644 (1985).
6. P.V. Nikrad, H. Beierbeck, and R.U. Lemieux. Can. J. Chem. **70**, 241 (1992).
7. O. Hindsgaul, D.P. Khare, M. Bach, and R.U. Lemieux. Can. J. Chem. **63**, 2653 (1985).
8. U. Spohr, E. Paszkiewicz-Hnatiw, N. Morishima, and R.U. Lemieux. Can. J. Chem. **70**, 254 (1992).
9. R. Cromer, U. Spohr, D.P. Khare, J. LePendu, and R.U. Lemieux. Can. J. Chem. **70**, 1511 (1992).
10. U. Spohr, N. Morishima, O. Hindsgaul, and R.U. Lemieux. Can. J. Chem. **63**, 2659 (1985).
11. R.U. Lemieux, A.P. Venot, U. Spohr, P. Bird, G. Mandal, N. Morishima, and D.R. Bundle. Can. J. Chem. **63**, 2664 (1985).
12. R.U. Lemieux, O. Hindsgaul, P. Bird, S. Narasimhan, and W.W. Young, Jr. Carbohydr. Res. **178**, 293 (1988).
13. K. Bock and H. Pedersen. Acta Chem. Scand. Ser. B: **B41**, 617 (1987).
14. K. Adelhorst, K. Bock, H. Pedersen, and S. Refn. Acta Chem. Scand. Ser. B: **B42**, 196 (1988).
15. M. Palcic, T. Skrydstrup, K. Bock, N. Le, and R.U. Lemieux. Carbohydr. Res. In press.
16. D.P. Khare, O. Hindsgaul, and R.U. Lemieux. Carbohydr. Res. **136**, 285 (1985).
17. H. Paulsen, F. Reck, and I. Brockhausen. Carbohydr. Res. **236**, 39 (1992).
18. K.B. Wlasichuk, M.A. Kashem, P.V. Nikrad, P. Bird, C. Jiang, and A.P. Venot. J. Biol. Chem. **268**, 13971 (1993).
19. L.T.J. Delbaere, M. Vandonselaar, L. Prasad, J.W. Quail, J.R. Pearlstone, M.R. Carpenter, L.B. Smillie, P.V. Nikrad, U. Spohr, and R.U. Lemieux. Can. J. Chem. **68**, 1116 (1990); L.T.J. Delbaere, M. Vandonselaar, L. Prasad, J.W. Quail, K.S. Wilson, and Z. Dauter. J. Mol. Biol. **230**, 950 (1993).
20. G.W. Fleet, N.G. Ramsden, and D.R. Witty. Tetrahedron, **45**, 327 (1989).
21. R.U. Lemieux, K.B. Hendricks, R.V. Stick, and K. James. J. Am. Chem. Soc. **97**, 4056 (1975).

22. P.W. Austin, F.E. Hardy, J.G. Buchanan, and J. Baddiley. J. Chem. Soc. 2128 (1964).
23. K. Bock and C. Pedersen. J. Chem. Soc. Perkin Trans. 2, 293 (1974).
24. R.C. Bernotas and B. Ganem. Biochem. J. **270**, 539 (1990).
25. H. Saeki and E. Ohki. Chem. Pharm. Bull. **16**, 2476 (1968).
26. G.W.J. Fleet and P.W. Smith. Tetrahedron Lett. **26**, 1469 (1985).
27. A.B. Smith III, R.A. Rivero, K.J. Hale, and H.A. Vaccaro. J. Am. Chem. Soc. **113**, 2092 (1991).
28. E.J. Corey and J.W. Suggs. J. Org. Chem. **38**, 3224 (1973).
29. D.H. Barton and S.W. McCombie. J. Chem. Soc. Perkin Trans. 1, 1574 (1975).
30. H. Thøgersen, R.U. Lemieux, K. Bock, and B. Meyer. Can. J. Chem. **60**, 44 (1982).
31. R.U. Lemieux and K. Bock. Arch. Biochem. Biophys. **221**, 125 (1983).
32. U. Spohr and M. Bach. Can. J. Chem. **71**, 1943 (1993).
33. G.A. Jeffrey, R.K. McMullan, and S. Takagi. Acta Crystallogr. Sect. B: Struct. Crystallogr. Cryst. Chem. **B33**, 728 (1977).
34. H. Kawaki, H. Beierbeck, and G. Kotovych. J. Biomol. Struct. Dyn. **3**, 161 (1985).
35. D. Neuhaus. J. Magn. Reson. **53**, 109 (1983).
36. M. Kinns and J.K.M. Sanders. J. Magn. Reson. **56**, 518 (1984).
37. U. Spohr, R.G. Spiro, and M. Bach. Can. J. Chem. **71**, 1919 (1993).

Can. J. Chem. Downloaded from www.nrcresearchpress.com by 203.198.23.82 on 09/08/12
For personal use only.

Inhibitors of *endo*-α-mannosidase. Part III.[1] Congeners of 1-deoxy-3-*O*-(α-D-glucopyranosyl)-mannojirimycin modified in the glucose unit

ULRIKE SPOHR[2] AND MIMI BACH

Chembiomed Ltd., Edmonton, and Department of Chemistry, University of Alberta, Edmonton, AB T6G 2G2, Canada

Received June 10, 1993

ULRIKE SPOHR and MIMI BACH. Can. J. Chem. **71**, 1943 (1993).

The syntheses of congeners of 1-deoxy-3-*O*-(α-D-glucopyranosyl)-mannojirimycin (**1**), a strong inhibitor of the glycoprotein-processing *endo*-mannosidase, are described. The chemical modifications of **1** involved all monodeoxygenations and mono-*O*-methylations of the glucose unit and the replacement of this unit by D-galactose, D-xylose, and 2-chloro-2-deoxy-D-glucose. As reported previously, none of the modifications of **1**, including deoxygenations and *O*- and *N*-methylations of the deoxymannojirimycin unit, improved the inhibitory properties, but demonstrated the high specificity in the recognition of **1** by the enzyme and allowed the assignment of intermolecular hydrogen bonds of the inhibitor · enzyme complex. Essential for complex formation were found NH-5, OH-2, OH-4, and OH-6 of the DMJ unit, as well as OH-3′, OH-4′, and CH_2-6′ of the glucose unit. The residual activities on deoxygenating the OH-2′ and OH-6′ groups of **1** suggest their involvement at the periphery of the binding site.

ULRIKE SPOHR et MIMI BACH. Can. J. Chem. **71**, 1943 (1993).

On décrit la synthèse de congénères de la 1-désoxy-3-*O*-(α-D-glucopyranosyl)mannojirimycine (**1**), un inhibiteur puissant de l'*endo*-mannosidase qui peut agir sur les glycoprotéines. Les modifications chimiques de **1** impliquent toutes des monodésoxygénations et des mono-*O*-méthylations de l'unité glucose et le remplacement de cette unité par du D-galactose, du D-xylose et du 2-chloro-2-désoxy-D-glucose. Comme il a été rapporté antérieurement, aucune des modifications du composé **1**, y compris les désoxygénations et les *O*- et *N*-méthylations de l'unité désoxymannojirimycine, n'améliore les propriétés inhibitrices; toutefois, ces modifications ont permis de démontrer la grande spécificité de la reconnaissance du composé **1** par l'enzyme et ont permis d'attribuer les liaisons hydrogènes intramoléculaires du complexe inhibiteur · enzyme. On a trouvé que les unités NH-5, OH-2, OH-4 et OH-6 de l'unité DMJ ainsi que les unités OH-3′, OH-4′ et CH_2-6′ de l'unité glucose sont essentielles à la formation de complexes. Les activités résiduelles observées lors de la désoxygénation des groupes OH-2′ et OH-6′ du composé **1** suggèrent qu'ils sont impliqués à la périphérie du site de liaison.

[Traduit par la rédaction]

Introduction

The glycoprotein-processing *endo*-α-D-mannosidase discovered by Spiro and Lubas (1, 2) releases the disaccharide αDGlc(1→3)DMan from immature *N*-linked glycoproteins containing the incompletely deglucosylated polymannose oligosaccharide $GlcMan_9GlcNAc_2$ with the formation of $Man_8GlcNAc_2$. The action of the enzyme was effectively inhibited by the disaccharide 1-deoxy-3-*O*-(α-D-glucopyranosyl)-mannojirimycin (**1**) (3).

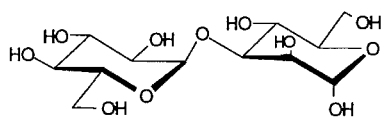

αDGlc(1→3)DMan

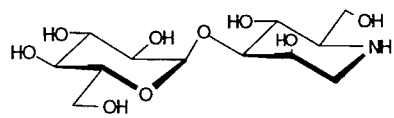

1

In the search for inhibitors with even greater potencies or better bioavailability all substituents of **1** were chemically modified, mainly by monodeoxygenation and mono-*O*-methylation and the effects of alteration on the inhibitory potencies observed, thus allowing for the assessment of intermolecular hydrogen bonds of the oligosaccharide · enzyme complex as demonstrated by Lemieux and coworkers (4, 5) for the complexation of oligosaccharides by lectins. The biological data of this investigation were published recently (3). While the chemical modifications of the deoxymannojirimycin unit of **1** are reported in the accompanying paper (6), the syntheses and properties of congeners of **1** modified in the glucose unit are described in this communication.

Discussion

Synthesis

The syntheses of congeners of αDGlc(1→3)-1-DMJ (**1**) (6) modified in the glucose unit are outlined in Schemes 1 and 2. The 1-deoxymannojirimycin derivative **2** (6, 7), which has a free hydroxyl group at the 3-position, was used as the glycosyl acceptor. The chloro sugars **3** (2-*O*-methyl), **5** (3-deoxy) (8), **6** (4-deoxy), **10** (4-*O*-methyl), **11** (galactosyl) (9), **12** (6-deoxy), **13** (xylosyl) (10), **50** (3-*O*-methyl), and **51** (6-*O*-acetyl) (11) were prepared from the corresponding hemiacetals by treatment with oxalyl chloride and *N*,*N*-dimethylformamide (12, 13). These precursors were de-

[1]For Parts I and II, see refs. 27 and 5.

[2]Author to whom correspondence may be addressed.

Can. J. Chem. Downloaded from www.nrcresearchpress.com by 203.198.23.82 on 09/08/12
For personal use only.

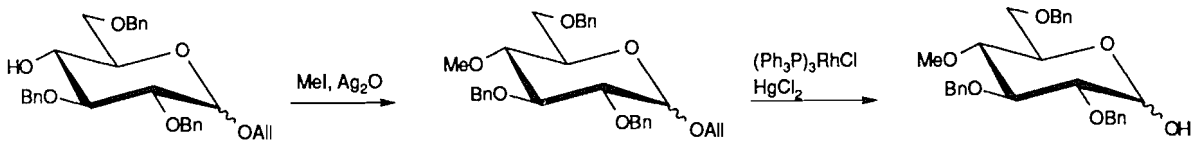

7 8 9

scribed in the literature (14–19), except for 4-*O*-methyl **9**, which was synthesized from an anomeric mixture of **7** (20) by conventional methylation with methyl iodide and sodium hydride to give **8**, followed by deallylation (**9**).

The 2-chloro-2-deoxy and 2-deoxy chlorides **4** (21) and **49** (22) were prepared from 3,4,6-tri-*O*-benzyl-D-glucal as reported.

Since the glycosyl acceptor **2** was of low reactivity (6), all glycosidation reactions were promoted by silver trifluoromethanesulfonate in the presence of *sym*-collidine and 4 Å molecular sieves in dichloromethane at low temperature. Usually, an α:β mixture was produced with a ratio varying from 3:1 to 0.9:1 in a combined yield of 93–66%. Higher α:β ratios were observed for couplings employing galactosyl chloride **11**, 2-*O*-methyl, 3-*O*-methyl, and 4-*O*-methyl chlorides **3**, **50**, and **10** than for those employing 3-deoxy, 4-deoxy, 6-deoxy, and 2-chloro-2-deoxy halides **5, 6, 12,** and **4**. However, in the preparation of the 2′-deoxy disaccharide **52** (73% yield) (Scheme 2), no significant amount of the β-isomer was detected as this was likely to be instable under the reaction conditions. In most of the cases, the anomers could be separated by column chromatography, except for the 4′-*O*-methyl, 6′-deoxy, and xylosyl disaccharides **22, 26**, and **28**, which were isolated as anomeric mixtures, but could be separated readily after deacetylation.

The ^{1}H NMR spectra of the coupling products were broad and showed duplications of the acetyl signals due to the restricted rotation of the benzyloxycarbonyl group about the C—N amide bond (6). Signal duplication was also observed in the ^{13}C NMR spectra. For unambiguous identification, both α- and β-anomers were isolated and characterized. To ascertain the anomeric configurations, C—H coupled ^{13}C NMR spectra were recorded for all β-anomers and some α-anomers. The C-1′ coupling constants $J_{C1',H1'}$ for the β-anomers were found in the range 158.0–162.3 Hz and those for the α-anomers from 166.2 to 171.8 Hz, in agreement with earlier observations (23).

Deacetylations of α-anomers **14, 16, 18, 20, 24**, and the α,β-mixtures **22** + **23**, **26** + **27**, **28** + **29** (Scheme 1) were carried out with triethylamine in aqueous methanol for several days at room temperature to provide the alcohols **30–40** in overall yields of 75% as well as some unreacted starting acetate. A different approach was employed for the 2′-deoxy, 3′-*O*-methyl, and 6′-*O*-acetyl disaccharides **52, 53**, and **55** (Scheme 2). Treatment with methanolic sodium methoxide produced the oxazolidone derivatives **57, 58**, and **59** in high yields (6). 6′-OH disaccharide **59** was converted into the 6′-*O*-methyl derivative **60** (91% yield) by reaction with methyl iodide and silver oxide in toluene. The cyclic carbamates in **57, 58**, and **60** were readily saponified with alcoholic alkali (6) to afford the secondary amines **61, 62**, and **63** in an overall yield of 80% from the benzyloxycarbonyl precursors **52, 53**, and **55**. Catalytic hydrogenation over 5% palladium-on-carbon in the presence of 1 equivalent of hydrochloric acid provided the disaccharides **41–48** (Scheme 1) and **64–66** (Scheme 2) after gel filtration in high yields.

The ^{1}H and ^{13}C NMR data of all deblocked compounds are presented in Tables 1 and 2 and fully confirm the structural assignments. The ^{1}H NMR coupling constants are in agreement with the $^4C_1$ conformation of the pyranose rings. Comparison of the ^{1}H NMR chemical shifts of the DMJ unit of all congeners with those of the parent compound **1** shows that modification of the glucose unit has only minor effects on these shifts, indicating that the conformational preferences about the interglycosidic torsion angles are similar in all compounds. Conformational analysis based on HSEA calculations and nuclear Overhauser enhancements predicted a conformational preference of Φ/Ψ near −50°/−10° (6).

The recognition of αDGlc(1→3)-1-DMJ (1) by endo-*mannosidase*

While αDGlc(1→3)-1-DMJ (**1**) proved a strong inhibitor of the cleavage of $Glc Man_9 GlcNAc$ by *endo*-mannosidase with IC_{50} = 1.7 μmol, modifications of its substituents either led to essentially inactive or weaker compounds, as reported recently (3) and summarized in Fig. 1.

The data require that both OH-3′ and OH-4′ of the glucose unit are involved in strong polar interactions deep in the combining site, since deoxygenation at these positions to give **43** and **44** and *O*-methylation to give **65** and **45** abolished the activity. The polar interaction undergone by equatorial OH-4′ of **1** can be maintained by an axial OH-4′, since galactosyl congener **46** retained substantial activity (17%). That the CH_2-6′ grouping of the glucose unit is essential for providing the required complementarity for complex formation, is indicated by the inactivity displayed by the xylosyl derivative **48**, which has the CH_2OH-6′ grouping replaced by hydrogen. Although OH-6′ can be substituted for by hydrogen to give 6′-deoxy **47** while still retaining 17% activity, *O*-methylation led to inactive **66** for steric reasons. It is therefore expected that OH-6′ is hydrogen bonded to amino acids near the periphery of the binding site (4). Also, OH-2′ of this unit must be located at the periphery of the binding site and possibly interact with water, since deoxygenation (**64**), *O*-methylation (**41**), and chlorination (**42**) produced active, albeit weaker, inhibitors.

Equally intimate as the acceptance of the glucose unit of **1** is the binding of the DMJ unit. While *N*-methylation of **1** produced an inhibitor with a residual activity of around 10%, *N*-*n*-propylation led to an inactive compound, indicating a strong steric interference to binding. It has been observed that *N*-alkylation of 5-deoxy-5-imino sugar analogues may or may not increase the inhibitory properties (24–26). Deoxygenation or *O*-methylation at the 2-, 4-, and 6-positions of **1** virtually abolished the activity, although a marginal activity was detected for 4-deoxy and 4-*O*-methyl congeners. The strong

Can. J. Chem. Downloaded from www.nrcresearchpress.com by 203.198.23.82 on 09/08/12
For personal use only.

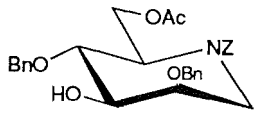

2

+

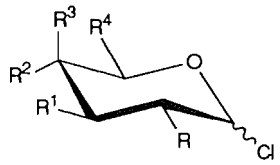

AgOTf →

	R	R^1	R^2	R^3	R^4
3	***OMe***	OBn	OBn	H	CH_2OBn
4	***Cl***	OBn	OBn	H	CH_2OBn
5	OBn	***H***	OBn	H	CH_2OBn
6	OBn	OBn	***H***	H	CH_2OBn
10	OBn	OBn	***OMe***	H	CH_2OBn
11	OBn	OBn	***H***	***OBn***	CH_2OBn
12	OBn	OBn	OBn	H	***CH_3***
13	OBn	OBn	OBn	H	***H***

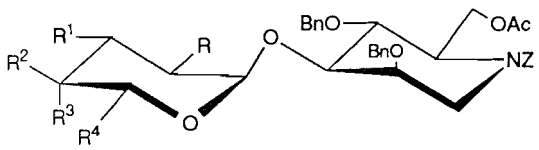

+

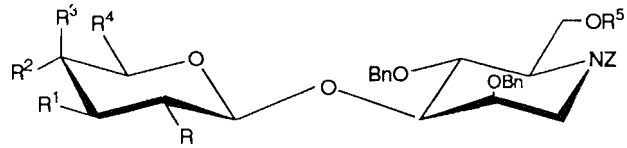

	R	R^1	R^2	R^3	R^4
14	***OMe***	OBn	OBn	H	CH_2OBn
16	***Cl***	OBn	OBn	H	CH_2OBn
18	OBn	***H***	OBn	H	CH_2OBn
20	OBn	OBn	***H***	H	CH_2OBn
(22	OBn	OBn	***OMe***	H	CH_2OBn)
24	OBn	OBn	***H***	***OBn***	CH_2OBn
(26	OBn	OBn	OBn	H	***CH_3***)
(28	OBn	OBn	OBn	H	***H***)

	R	R^1	R^2	R^3	R^4	R^5
15	***OMe***	OBn	OBn	H	CH_2OBn	Ac
17	***Cl***	OBn	OBn	H	CH_2OBn	Ac
19	OBn	***H***	OBn	H	CH_2OBn	Ac
21	OBn	OBn	***H***	H	CH_2OBn	Ac
(23	OBn	OBn	***OMe***	CH_2OBn	Ac)	
25	OBn	OBn	***H***	***OBn***	CH_2OBn	Ac
(27	OBn	OBn	OBn	H	***CH_3***	Ac)
(29	OBn	OBn	OBn	H	***H***	Ac)

↓ NEt_3 (23, 27, 29)

35	OBn	OBn	***OMe***	H	CH_2OBn	H
38	OBn	OBn	OBn	H	***CH_3***	H
40	OBn	OBn	OBn	H	***H***	H

↓ NEt_3

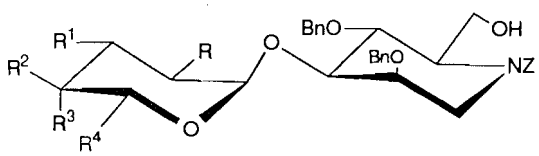

H_2, Pd/C, HCl →

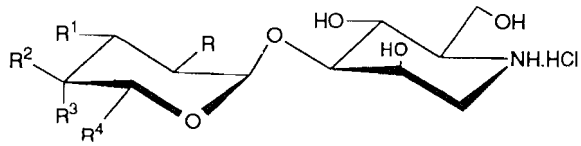

	R	R^1	R^2	R^3	R^4
30	***OMe***	OBn	OBn	H	CH_2OBn
31	***Cl***	OBn	OBn	H	CH_2OBn
32	OBn	***H***	OBn	H	CH_2OBn
33	OBn	OBn	***H***	H	CH_2OBn
34	OBn	OBn	***OMe***	H	CH_2OBn
36	OBn	OBn	***H***	***OBn***	CH_2OBn
37	OBn	OBn	OBn	H	***CH_3***
39	OBn	OBn	OBn	H	***H***

	R	R^1	R^2	R^3	R^4
41	***OMe***	OH	OH	H	CH_2OH
42	***Cl***	OH	OH	H	CH_2OH
43	OH	***H***	OH	H	CH_2OH
44	OH	OH	***H***	H	CH_2OH
45	OH	OH	***OMe***	H	CH_2OH
46	OH	OH	***H***	***OH***	CH_2OH
47	OH	OH	OH	H	***CH_3***
48	OH	OH	OH	H	***H***

Z = COOBn

SCHEME 1

Can. J. Chem. Downloaded from www.nrcresearchpress.com by 203.198.23.82 on 09/08/12
For personal use only.

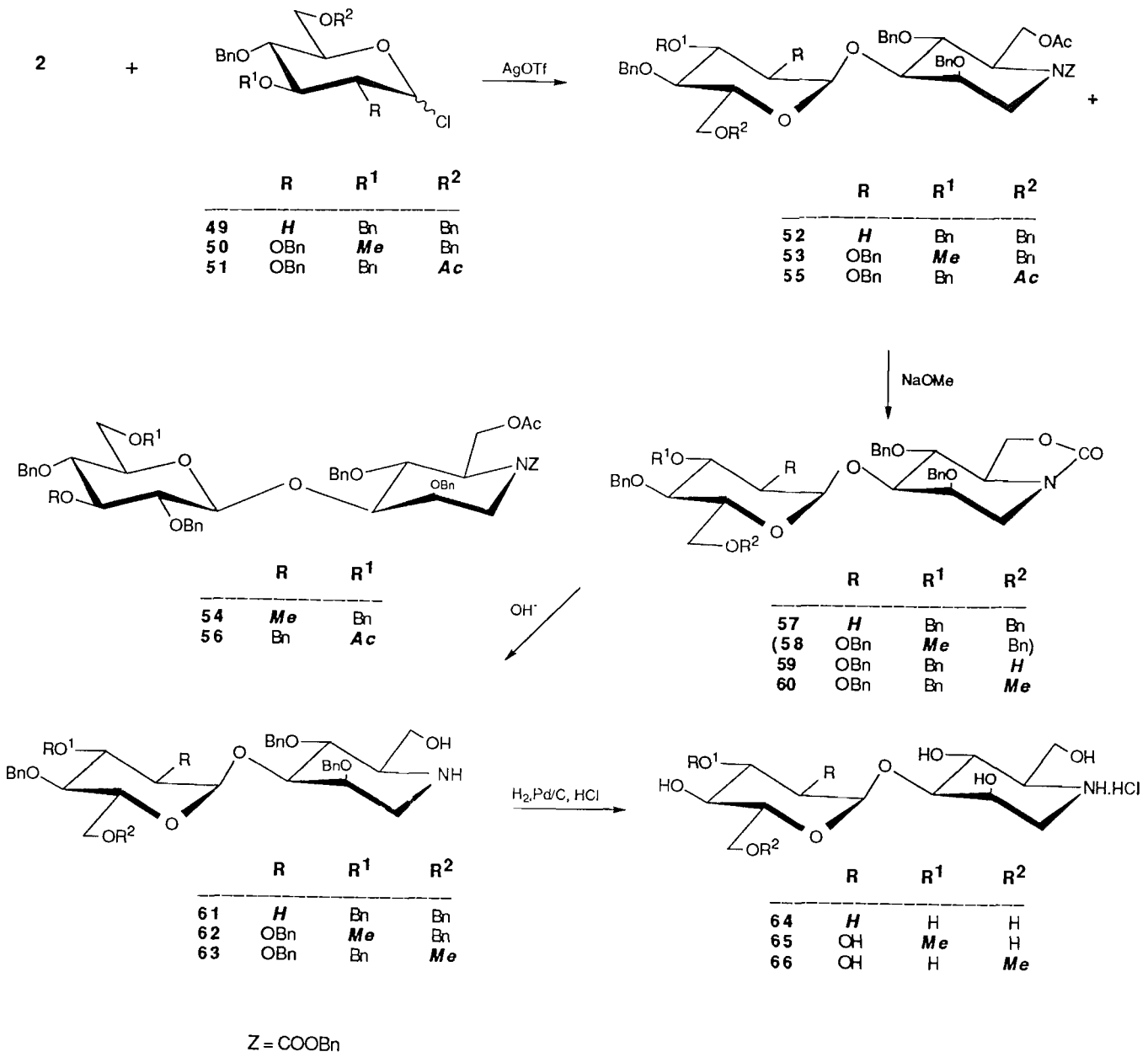

	R	R^1	R^2
49	*H*	Bn	Bn
50	OBn	*Me*	Bn
51	OBn	Bn	*Ac*

	R	R^1	R^2
52	*H*	Bn	Bn
53	OBn	*Me*	Bn
55	OBn	Bn	*Ac*

	R	R^1
54	*Me*	Bn
56	Bn	*Ac*

	R	R^1	R^2
57	*H*	Bn	Bn
(58	OBn	*Me*	Bn)
59	OBn	Bn	*H*
60	OBn	Bn	*Me*

	R	R^1	R^2
61	*H*	Bn	Bn
62	OBn	*Me*	Bn
63	OBn	Bn	*Me*

	R	R^1	R^2
64	*H*	H	H
65	OH	*Me*	H
66	OH	H	*Me*

SCHEME 2

inhibitory properties towards glycosidases of glycosylamines, 5-amino-5-deoxyhexopyranoses, and 1,5-dideoxy-1,5-iminohexitols have been ascribed to the formation of an ion pair at the catalytic site of the protonated inhibitor and a negatively charged group of the protein likely involved in catalysis (27). In the case of the *endo*-mannosidase, the thus adjusted conformation of the catalytic site requires that all three hydroxyl groups of the DMJ unit of **1** are available for interaction with polar or charged groups of the protein. It is interesting that the active site adjusts differently in the complexation of the neutral O-5 analogue of **1**, namely, αDGlc(1→3)-1,5-anhydro-D-mannitol (3, 28), in which case the replacement of OH-2 by hydrogen increased the activity 40-fold.

Besides these polar interactions, it is to be expected that the complex is stabilized by hydrophobic interactions between nonpolar side chains of the protein and nonpolar patches on the sides of the pyranose rings, such as the α-side of the DMJ unit with CH-1, CH-2, CH-3, and CH-5.

Further synthetic and biological studies of the substrate specificity of *endo*-mannosidase are the subject of a different communication.[3]

Experimental

General methods

The ^{1}H NMR spectra were measured at 300 MHz and 360 MHz (Bruker AM 300 and WM 360) with tetramethylsilane as internal standard for $CDCl_3$ solutions. Reference standard for D_2O solutions was acetone (2.225 ppm). The ^{13}C NMR spectra were recorded at 75 MHz with dioxane (67.4 ppm) as reference for D_2O solutions and the $CDCl_3$ signal (77.0 ppm) as reference in $CDCl_3$

[3]U. Spohr, M. Bach, S.E.H. Moore, and R.G. Spiro. Manuscript in preparation.

Can. J. Chem. Downloaded from www.nrcresearchpress.com by 203.198.23.82 on 09/08/12
For personal use only.

Can. J. Chem. Downloaded from www.nrcresearchpress.com by 203.198.23.82 on 09/08/12
For personal use only.

TABLE 1. ^{1}H NMR chemical shifts (δ, ppm) and coupling constants (Hz) for αDGlc(1→3)-1-DMJ (**1**) and related structures[a]

	Derivatives of **1**											
	1	2′-Deoxy **64**	2′-OMe **41**	2′-Chloro-2′-deoxy **42**	3′-Deoxy **43**	3′-OMe **65**	4′-Deoxy **44**	4′-OMe **45**	4′-Epi **46**	6′-Deoxy **47**	6′-OMe **66**	5′-Dehydroxy-methylene **48**
1-DMJ unit												
H-1 ($J_{1,2}$)	3.42 (2.5)	3.38 (3.0)	3.40 (3.0)	3.38 (2.7)	3.45 (3.5)	3.44 (3.0)	3.44 (3.0)	3.42 (3.0)	3.44 (3.0)	3.42 (3.5)	3.41 (3.0)	3.42 (3.0)
H-1′ ($J_{1',1}$)	3.29 (13.5)	3.25 (13.5)	3.26 (13.5)	3.24 (13.5)	3.32 (13.5)	3.30 (13.5)	3.30 (13.5)	3.29 (13.5)	3.29 (13.5)	3.30 (13.5)	3.29 (13.5)	3.28 (13.5)
H-2 ($J_{1',2}$)	4.45 (<1)	4.38 (<1)	4.41 (<1)	4.41 (<1)	4.49 (<1)	4.45 (<1)	4.46 (1.0)	4.41 (<1)	4.48 (<1)	4.39 (<1)	4.41 (<1)	4.43 (<1)
H-3 ($J_{3,4}$)	3.81 (10.0)	3.75	3.80 (10.0)	3.81 (10.0)	3.85 (10.0)	3.81 (10.0)	3.80 (9.5)	3.79 (9.5)	3.82	3.78 (9.5)	3.77 (10.0)	3.78 (10.0)
H-4 ($J_{4,5}$)	4.08 (10.0)	3.97 (10.0)	4.05 (10.0)	4.05 (10.0)	4.09 (10.0)	4.09 (10.0)	4.08 (9.5)	4.06 (9.5)	4.06 (10.0)	4.07 (10.0)	4.07 (10.0)	4.08 (10.0)
H-5 ($J_{5,6}$)	3.21 (3.0)	3.17 (3.5)	3.18 (3.0)	3.15 (3.5)	3.25 (3.0)	3.24 (3.5)	3.24 (3.0)	3.25 (3.0)	3.23 (3.5)	3.21 (3.0)	3.22 (3.0)	3.21 (3.0)
H-6 ($J_{6,6'}$)	4.00 (12.5)	3.97	4.00 (12.5)	3.99 (12.5)	4.02 (12.5)	4.02 (13.0)	4.02 (12.5)	4.01 (12.0)	4.00	4.00 (12.5)	4.05 (13.0)	4.01 (13.5)
H-6′ ($J_{5,6'}$)	3.89 (6.7)	3.88 (6.5)	3.87 (6.5)	3.86 (6.5)	3.89 (6.5)	3.89 (6.2)	3.89 (6.5)	3.89 (6.0)	3.89 (6.5)	3.89 (6.5)	3.88 (6.0)	3.88 (6.0)
αDGlc unit												
H-1 ($J_{1,2}$)	5.25 (4.0)	5.27 (3.5)	5.46 (4.0)	5.34 (2.5)	5.15 (3.5)	5.23 (3.5)	5.28 (4.0)	5.23 (3.5)	5.27 (3.5)	5.18 (4.0)	5.23 (3.5)	5.22 (3.5)
H-2 ($J_{2,3}$)	3.58 (10.0)	1.72 (12.0)[b]	3.32 (9.5)	3.92	3.84 (11.5)	3.62 (9.5)	3.50 (10.0)	3.61 (9.5)	3.85 (10.0)	3.58 (10.0)	3.56 (10.0)	3.56 (9.5)
H-3 ($J_{3,4}$)	3.78 (9.5)	3.98 (9.0)	3.77 (9.5)	3.91 (9.5)	1.84 (11.5)[d]	3.54 (9.0)	4.01 (12.0)	3.87 (9.5)	3.94	3.72 (9.5)	3.79 (9.5)	3.71
H-4 ($J_{4,5}$)	3.43 (9.5)	3.38 (9.5)	3.43 (9.5)	3.49 (9.5)	3.67	3.49 (9.0)	1.46 (12.0)[e]	3.26 (9.5)	4.01	3.18 (9.5)	3.43 (9.5)	3.75–3.61[f]
H-5 ($J_{5,6}$)	3.81	3.76	3.78	3.91	3.75	3.83	4.10 (3.1)	3.81	4.10 (6.0)	3.89 (6.5)	3.90 (2.5)	
H-6 ($J_{6,6'}$)	3.86	*	3.84[c]	*	3.85	3.77[c]	3.68 (12.5)	3.81[c]	3.74 (0)	1.27	3.70 (11.0)	—
H-6′ ($J_{5,6'}$)	*	*	3.78[c]	3.77[c]	*	3.75	3.60 (6.5)	3.86[c]	3.74 (6.0)	—	3.68 (4.5)	—
CH_3O	—	—	3.50	—	—	3.62	—	3.59	—	—	3.39	—

[a]0.03 M solutions in D_2O with acetone as internal reference at 2.225 ppm were measured at 360 MHz and 295 K.
[b]H-2eq 2.29 ppm, $J_{2eq,2ax}$ 13.5 Hz, $J_{1,2eq}$ <1 Hz.
[c]Expected to be within ± 0.03 ppm.
[d]H-3eq 2.19 ppm, $J_{3eq,3ax}$ 11.5 Hz, $J_{3eq,4} \sim J_{2,3eq}$ 4.5 Hz.
[e]H-4eq 2.02 ppm, $J_{4eq,4ax}$ 12.7 Hz, $J_{3,4eq}$ 5.0 Hz, $J_{4eq,5}$ 2.0 Hz.
[f]H-5′ 3.75–3.61 ppm.
*Could not be assigned.

Can. J. Chem. Downloaded from www.nrcresearchpress.com by 203.198.23.82 on 09/08/12
For personal use only.

TABLE 2. ^{13}C NMR chemical shifts (δ, ppm) for αDGlc(1→3)-1-DMJ (**1**) and related structures[a]

	Derivatives of **1**										
	1	2′-Deoxy **64**	2′-OMe **41**	2′-Chloro-2′-deoxy **42**	3′-Deoxy **43**	3′-OMe **65**	4′-Deoxy **44**	4′-OMe **45**	4′-Epi **46**	6′-Deoxy **47**	6′-OMe **66**	5′-Dehydroxy-methylene **48**
1-DMJ unit												
C-1	48.44	48.37	48.34	48.28	48.31	48.30	48.26	48.32	48.35	48.31	48.28	48.35
C-2	66.37[b]	65.91[b]	66.06[b]	65.88[b]	65.95[b]	65.89[b]	65.91[b]	65.98[b]	66.21[b]	65.80[b]	66.64[b]	66.01[b]
C-3	81.67	80.53	81.22[c]	81.27	80.79	81.13	81.16	81.26	81.42	81.33	81.30	81.03
C-4	67.24[b]	66.40[b]	66.79[b]	66.29[b]	66.61[b]	66.55[b]	66.63[b]	66.70[b]	66.92[b]	66.67[b]	67.40[b]	66.73[b]
C-5	61.12	61.17	61.33	61.24	61.12	60.97	61.08	60.95	61.12	61.07	61.08	61.08
C-6	59.31	58.83	58.96	58.81	58.82	58.78	58.83	58.92	59.31	58.79	58.83	58.87
αDGlc unit												
C-1	101.50	100.92	98.61	101.06	100.30	101.55	102.27	101.35	101.71	101.49	101.53	101.60
C-2	72.49	37.59	80.87[c]	61.24	67.56	72.02	74.28	72.47[c]	69.43	72.72	72.39	72.48
C-3	73.57	68.82	72.57	73.56[c]	35.15	83.41	67.78	73.37[c]	70.07	73.32	73.44	73.74
C-4	70.35	71.81	70.40	71.12	65.03	69.78	34.92	80.10	70.07	75.75	70.39	70.11
C-5	73.27	73.80	73.08	73.47[c]	74.11	73.39	70.37	72.32[c]	72.39	69.30	72.01	62.63
C-6	61.34	61.51	61.35	61.26	61.42	61.23	64.44	61.08	62.05	17.35	71.79	—
CH_3O	—	—	58.36	—	—	61.08	—	60.95	—	—	59.49	—

[a]0.05 M solutions in D_2O with dioxane as internal reference at 67.4 ppm were measured at 75 MHz and 295 K. The assignments were made by inspection and are tentative.
[b,c] assignments are tentative and may be reversed.

solutions. Optical rotations were measured at room temperature (23 ± 1°C) in a 1-dm cell on a Perkin–Elmer 241 polarimeter. Thin-layer chromatography was performed on precoated plates of silica gel (60-F254, E. Merck, Darmstadt) and visualized by spraying with 5% sulfuric acid in ethanol followed by heating. For column chromatography silica gel 60 (230–400 mesh, E. Merck, Darmstadt) and distilled solvents were used. Solvents and reagents were purified and dried according to standard procedures. Melting points are uncorrected.

3,4,6-Tri-O-*benzyl-2*-O-*methyl-α,β-D-glucopyranosyl chloride (3)*

Oxalyl chloride (97 μL, 1.11 mmol) was added to a stirred solution of 3,4,6-tri-*O*-benzyl-2-*O*-methyl-D-glucopyranose (14) (385 mg, 0.83 mmol) and *N,N*-dimethylformamide (91 μL, 1.28 mmol) in dichloromethane (9 mL). The mixture was stirred for 20 min and then poured into ice-water. The organic solution was washed with ice-water, dried, and evaporated to provide chloride **3** (quant.) as a syrup. ^1H NMR ($CDCl_3$, α:β = 1:2.2) δ: 7.4–7.05 (m, 15H, 3Ph), 6.26 (d, $J_{1\alpha,2}$ 4.0 Hz, H-1α), 5.09 (d, $J_{1\beta,2}$ 8.5 Hz, H-1β), 4.08 (m, $J_{4,5}$ 10.0 Hz, H-5α), 3.96 (t, $J_{2,3} \sim J_{3,4}$ 9.5 Hz, H-3α), 3.67 (s, CH_3O-β), 3.54 (s, CH_3O-α).

2,4,6-Tri-O-*benzyl-3-deoxy-α-D*-ribo-*hexopyranosyl chloride (5) (8)*

2,4,6-Tri-*O*-benzyl-3-deoxy-D-*ribo*-hexopyranose (15) (251 mg, 0.58 mmol) was converted into chloride **5** just prior to use as reported for the preparation of **3**. ^1H NMR ($CDCl_3$, α:β = 3:1) δ: 7.45–7.20 (m, 15H, 3Ph), 6.19 (bd, 1H, $J_{1,2}$ 3.5 Hz, $J_{1,3eq} < 1$ Hz, H-1), 5.21 (d, $J_{1,2}$ 8.0 Hz, H-1β), 3.97 (ddd, $J_{4,5}$ 10.0 Hz, $J_{5,6}$ 3.5 Hz, $J_{5,6'}$ 2.5 Hz, H-5), 3.77 (dd, 1H, $J_{6,6'}$ 11.0 Hz, H-6), 3.67 (dt, overlapped, $J_{2,3eq} \sim 4.5$ Hz, H-2), 3.64 (H-6′), 2.35 (btd, 1H, $J_{3eq,3ax}$ 12.0 Hz, $J_{3eq,4} \sim 4.5$ Hz, H-3eq), 1.97 (q, 1H, $J_{3ax,4} \sim J_{2,3ax} \sim 11.5$ Hz, H-3ax).

2,3,6-Tri-O-*benzyl-4-deoxy-α-D*-xylo-*hexopyranosyl chloride (6)*

2,3,6-Tri-*O*-benzyl-4-deoxy-D-*xylo*-hexopyranose (16) (392.6 mg, 0.90 mmol) was converted into chloride **6** just prior to use as reported for the preparation of **3**. ^1H NMR ($CDCl_3$) δ: 7.40–7.20 (m, 15H, 3Ph), 6.09 (d, 1H, $J_{1,2}$ 3.5 Hz, H-1), 4.76 and 4.66 (ABq, 2H, $J_{A,B}$ 12.0 Hz, CH_2Ph), 4.74 and 4.70 (ABq, 2H, $J_{A,B}$ 12.0 Hz, CH_2Ph), 4.52 (s, 2H, CH_2Ph), 4.25 (m, 1H, H-5), 3.98 (ddd, 1H, $J_{2,3}$ 9.3 Hz, $J_{3,4eq}$ 5.0 Hz, $J_{3,4ax}$ 11.0 Hz, H-3), 3.61 (dd, 1H, H-2), 3.47 (d, 2H, $J_{6,5}$ 4.5 Hz, 2H-6), 2.10 (ddd, 1H, $J_{4eq,5}$ 2.0 Hz, $J_{4eq,4ax}$ 13.0 Hz, H-4eq), 1.61 (q, 1H, H-4ax).

Allyl 2,3,6-tri-O-*benzyl-4*-O-*methyl-α,β-D-glucopyranoside (8)*

Sodium hydride (528 mg, 22 mmol) was added to a stirred solution of allyl, 2,3,6-tri-*O*-benzyl-α,β-D-glucopyranoside (**7**, 5.51 g, 11.2 mmol) in *N,N*-dimethylformamide (70 mL) at ice-bath temperature. After 20 min, methyl iodide (1.37 mL, 22 mmol) was added and stirring continued for 4 h at room temperature. The excess of reagents was quenched by the addition of methanol (1 mL). The mixture was diluted with dichloromethane, poured into ice-water, and the aqueous layer was extracted with dichloromethane. The combined organic solutions were washed with water, dried, and evaporated to leave the title compound **8** (5.7 g, quant.) as an oil. The analytical sample was purified by column chromatography on silica gel (hexane–chloroform – ethyl acetate, 20:1:1). Evaporation of the first fraction provided the α-anomer, which was characterized; $[\alpha]_D$ +57 (*c* 1.0, chloroform). ^1H NMR ($CDCl_3$) δ: 7.4–7.2 (m, 15H, 3Ph), 5.93 (m, 1H, CH_2=C*H*), 5.31 and 5.20 (2m, 2H, CH_2=CH), 4.94 and 4.79 (ABq, 2H, $J_{A,B}$ 11.0 Hz, CH_2Ph), 4.81 (d, 1H, $J_{1,2}$ 3.5 Hz, H-1), 4.76 and 4.63 (ABq, 2H, $J_{A,B}$ 12.5 Hz, CH_2Ph), 4.63 and 4.50 (ABq, 2H, $J_{A,B}$ 12.5 Hz, CH_2Ph), 4.16 and 4.01 (2m, 2H, CH_2=CH-CH_2), 3.89 (t, 1H, $J_{2,3} \sim J_{3,4}$ 9.5 Hz, H-3), 3.72–3.61 (m, 3H, H-6, H-6′, H-5), 3.51 (dd, 1H, H-2), 3.46 (s, 3H, CH_3O), 3.34 (t, 1H, $J_{4,5}$ 9.0 Hz, H-4). Anal. calcd. for $C_{31}H_{36}O_6$: C 73.79, H 7.19; found: C 73.70, H 7.33.

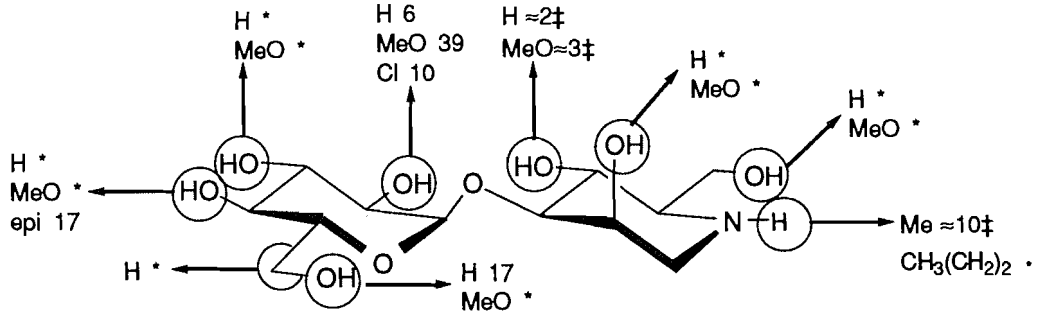

FIG. 1. The effect of chemical modification of **1** on the activity as inhibitor of *endo*-mannosidase in relative potencies (percentage of potency of **1**). ‡Approximate rel. potencies based on IC_{50} values as derived from inhibition data obtained for two inhibitor concentrations (3). *Denotes inactivity (rel. potency < 1).

Can. J. Chem. Downloaded from www.nrcresearchpress.com by 203.198.23.82 on 09/08/12
For personal use only.

2,3,6-Tri-O-benzyl-4-O-methyl-D-glucopyranose (9)

A mixture of crude **8** (5.7 g, 11.3 mmol), tris(triphenylphosphine)rhodium(I) chloride (805 mg, 0.87 mmol), 1,8-diazabicyclo[2.2.2]octane (342 mg, 3.05 mmol), and 95% ethanol–toluene–water (7:3:1, 77 mL) was boiled under reflux for 5 h. The solvent was evaporated and the remainder was taken up in acetone (70 mL) containing mercuric oxide (294 mg). A solution of mercuric chloride (14.4 g) in acetone–water (9:1, 50 mL) was added and the mixture stirred for 30 min. After solvent removal, the residue was taken up in dichloromethane, the solution washed with aqueous saturated potassium bromide and water, and the organic solution concentrated. Purification on a column of silica gel (hexane – ethyl acetate, 3:1) provided **9** (2.32 g, 44%) as a solid. The analytical sample was recrystallized from ether/hexane; mp 91–92°C; $[\alpha]_D$ +39 (*c* 0.3, chloroform). ^{1}H-nmr ($CDCl_3$, α:β = 1:0.6) δ: 7.42–7.24 (m, 15H, 3Ph), 5.20 (d, $J_{1\alpha,2}$ 3.5 Hz, H-1α), 5.03–3.97 (m, 3CH_2Ph, H-1β), 3.93 (ddd, $J_{4,5}$ 10.0 Hz, $J_{5,6}$ 2.5 Hz, $J_{5,6'}$ 3.5 Hz, H-5α), 3.85 (t, 1H, $J_{3,4}$ 9.5 Hz, H-3α), 3.72 (dd, $J_{6,6'}$ 11.0 Hz, $J_{6,5}$ 2.0 Hz, H-6β), 3.69 (dd, $J_{6,6'}$ 11.0 Hz, H-6α), 3.67 (H-6′β), 3.64 (dd, H-6′α), 3.54 (t, overlapped by H-2α, $J_{2,3} \sim J_{3,4}$ 9.0 Hz, H-3β), 3.53 (dd, H-2α), 3.47 (s, CH_3O-α), 3.465 (s, CH_3O-β), 3.43 (ddd, H-5β), 3.33 (dd, $J_{1\beta,2}$ 7.8 Hz, H-2β), 3.33 (t, H-4α), 3.27 (t, $J_{4,5}$ 9.5 Hz, H-4β). Anal. calcd. for $C_{28}H_{32}O_6$: C 72.39, H 6.94; found: C 71.78, H 6.92.

2,3,6-Tri-O-benzyl-4-O-methyl-α,β-D-glucopyranosyl chloride (10)

9 (550 mg, 1.18 mmol) was converted into **10** as described for the preparation of **3**. ^{1}H NMR ($CDCl_3$, α:β = 3:1) δ: 7.4–7.15 (m, 15H, 3Ph), 6.01 (d, 1H, $J_{1,2}$ 3.5 Hz, H-1), 3.95 (m, 1H, $J_{4,5}$ 10.0 Hz, H-5), 3.89 (t, $J_{2,3} \sim J_{3,4}$ 9.5 Hz, H-3), 3.46 (s, CH_3O), 3.41 (t, 1H, H-4).

2,3,4-Tri-O-benzyl-6-deoxy-α,β-D-glucopyranosyl chloride (12)

2,3,4-Tri-*O*-benzyl-6-deoxy-D-glucopyranose (17) (552.2 mg, 1.27 mmol) was converted into chloride **12** just prior to use as described for the preparation of **3**. ^{1}H NMR ($CDCl_3$, α:β = 2.2:1) δ: 7.45–7.2 (m, 15H, 3Ph), 5.98 (d, $J_{1\alpha,2}$ 4.0 Hz, H-1α), 5.19 (d, $J_{1\beta,2}$ 8.0 Hz, H-1β), 5.00–4.61 (m, 6H, 3CH_2Ph), 4.07 (m, H-5α), 4.00 (t, $J_{2,3} \sim J_{3,4}$ 9.0 Hz, H-3α), 3.69 (dd, H-2α), 3.60 (m, H-2β, H-3β), 3.49 (m, H-5β), 3.29 (t, $J_{4,5} \sim J_{3,4}$ 9.0 Hz, H-4β), 3.18 (t, $J_{4,5}$ 9.5 Hz, H-4α), 1.35 (d, $J_{5,6}$ 6.0 Hz, H_3-6β), 1.28 (d, $J_{5,6}$ 6.0 Hz, H_3-6α).

6-O-Acetyl-2,4-di-O-benzyl-N-benzyloxycarbonyl-1,5-dideoxy-1,5-imino-3-O-(3,4,6-tri-O-benzyl-2-O-methyl-α-D-glucopyranosyl)-D-mannitol (14) and -β-D-glucopyranosyl)-D-mannitol (15)

A solution of chloride **3** (0.82 mmol) in dichloromethane (5 mL) was added at −78°C to a stirred mixture of **2** (7) (210 mg, 0.40 mmol), silver trifluoromethanesulfonate (220 mg, 0.86 mmol), *sym*-collidine (43.9 μL, 0.33 mmol), and 4 Å molecular sieves (500 mg) in dichloromethane (1.5 mL). The temperature was gradually raised to 0°C and after 7 h the reaction was quenched by the addition of *sym*-collidine (75 μL, 0.57 mmol). The mixture was filtered through Celite, the organic solution washed with aqueous saturated sodium hydrogen carbonate and water, followed by evaporation. Column chromatography on silica gel (hexane – ethyl acetate, 5:1, 4:1) provided in the first main fraction the β-isomer **15** (90.1 mg, 23%); $[\alpha]_D$ −17.8 (*c* 0.5, chloroform). ^{1}H NMR ($CDCl_3$, broad, mixture of two rotamers in the ratio 3:2) δ: 7.40–7.00 (m, 30H, 6Ph), 5.20–3.0 (complex m, 30H), 3.58 (s, 3H, CH_3O), 1.91 and 1.82 (2s, 3H, CH_3CO). ^{13}C NMR ($CDCl_3$, δ minor rotamer in parentheses) δ: 170.62 (CH_3CO), 156.23 (OCO), 104.72 ($J_{C,H}$ 160.6 Hz, C-1′), 61.40 (61.21) (C-6), 60.59 (CH_3O), 52.97 (52.35) (C-5), (38.37) 37.83 (C-1), (20.74) 20.57 (CH_3CO). Evaporation of the second main fraction provided **14** (200 mg, 51%); $[\alpha]_D$ +34.1 (*c* 0.3, chloroform). ^{1}H NMR ($CDCl_3$, broad, mixture of two rotamers in the ratio 3:2) δ: 7.40–7.00 (m, 30H, 6Ph), 5.2–3.0 (complex m, 30H), 3.34 (s, 3H, CH_3O), 1.94 and 1.85 (2s, 3H, CH_3CO).

6-O-Acetyl-2,4-di-O-benzyl-N-benzyloxycarbonyl-1,5-dideoxy-1,5-imino-3-O-(3,4,6-tri-O-benzyl-2-chloro-2-deoxy-α-D-glucopyranosyl)-D-mannitol (16) and -β-D-glucopyranosyl)-D-mannitol (17)

A solution of chloride **4** (21) (0.60 mmol) in dichloromethane (2 mL) was added at −65°C to a stirred mixture of **2** (186 mg, 0.19 mmol), silver trifluoromethanesulfonate (165.9 mg, 0.65 mmol), *sym*-collidine (31 μL, 0.23 mmol), and 4 Å molecular sieves (800 mg) in dichloromethane (1.5 mL). The temperature was allowed to gradually rise to −20°C within 3 h. More *sym*-collidine (40 μL, 0.30 mmol) was added and, after 1 h at room temperature, the mixture was processed in the usual way. Column purification on silica gel (hexane – ethyl acetate, 5:1) provided, according to the ^{1}H NMR spectrum, an α:β mixture (231 mg, 67%) in the ratio 0.9:1. Separation of the anomers was achieved by repeated column chromatography on silica gel 60H (for thin-layer chromatography, E. Merck, Darmstadt) using hexane–chloroform – ethyl acetate, 14:14:1. Evaporation of the earlier fractions provided the α-anomer **16** (87.8 mg, 25%) as a syrup; $[\alpha]_D$ +45.6 (*c* 0.5, chloroform). ^{1}H NMR ($CDCl_3$, broad, mixture of two rotamers in the ratio 3:2) δ: 7.4–7.0 (m, 30H, 6Ph), 5.3–2.95 (complex m, 27H), 1.93 and 1.86 (2s, 3H, CH_3CO). ^{13}C NMR ($CDCl_3$, δ minor rotamer in parentheses) δ: 170.56 (CH_3CO), 156.09 (CO), 99.62 ($J_{C,H}$ 168.7 Hz, C-1′), 61.80 (61.66) (C-6), 60.21 (C-2), 52.51 (51.83) (C-5), (38.12), 37.49 (C-1), (20.74) 20.62 (CH_3CO). Anal. calcd. for $C_{57}H_{60}ClNO_{11}$: C 70.54, H 6.23, Cl 3.65, N 1.44; found: C 70.14, H 6.46, Cl 3.98, H 6.46. Continued development eluted the β-anomer **17** (75 mg, 22%) as a syrup; $[\alpha]_D$ −10.8 (*c* 0.5, chloroform). ^{1}H NMR ($CDCl_3$, broad, mixture of two rotamers in the ratio 3:2) δ: 7.4–7.1 (m, 30H, 6Ph), 5.25–3.25 (complex m, 27H), 1.93 and 1.82 (2s, 3H, CH_3CO). ^{13}C nmr ($CDCl_3$, δ minor rotamer in parentheses) δ: 156.19 (CO), 101.88 (C-1′), 61.73 (C-2′), 61.50 (61.31) (C-6), 52.87 (52.16) (C-5), (38.08) 37.56 (C-1), (20.79) 20.61 (CH_3CO). Anal. calcd. for $C_{57}H_{60}ClNO_{11}$: C 70.54,

Can. J. Chem. Downloaded from www.nrcresearchpress.com by 203.198.23.82 on 09/08/12
For personal use only.

H 6.23, N 1.44; found: C 70.34, H 6.15, N 1.39. A second batch of α,β-mixture (42 mg) was separated by thin-layer chromatography (Whatman, silica gel 150A PLK5F, hexane–chloroform – ethyl acetate, 14:14:1, fourfold development). Elution of the higher zone provided the α-anomer **16** and elution of the lower zone the β-anomer **17** in slightly higher yields.

6-O-Acetyl-2,4-di-O-benzyl-N-benzyloxycarbonyl-1,5-dideoxy-1,5-imino-3-O-(2,4,6-tri-O-benzyl-3-deoxy-α-D-ribo-hexopyranosyl)-D-mannitol (18) and -β-D-ribo-hexopyranosyl)-D-mannitol (19)

A solution of chloride **5** (0.57 mmol) in dichloromethane (3 mL) was added at −78°C to a stirred mixture of **2** (166.8 mg, 0.32 mmol), silver trifluoromethanesulfonate (164 mg, 0.64 mmol), *sym*-collidine (30 μL, 0.23 mmol), and 4 Å molecular sieves (1 g) in dichloromethane (1.5 mL). Within 2 h the temperature was raised to −30°C and more *sym*-collidine (35 μL, 0.26 mmol) was added. After 1 h at room temperature, it was worked up in the usual way. Chromatographic separation on a column of silica gel (hexane – ethyl acetate, 5:1) provided in the earlier fractions the β-anomer **19** (121.2 mg, 40%) as a syrup; $[\alpha]_D$ +10 (*c* 0.6, chloroform). ^{1}H NMR ($CDCl_3$, broad, mixture of two rotamers in the ratio 3:2) δ: 7.4 –7.05 (m, 30H, 6Ph), 5.24–3.15 (complex m, 26H), 2.46 (dt, 1H, $J_{3ax',3eq'}$ 13.0 Hz, $J_{2',3eq'} \sim J_{3eq',4'} \sim$ 4.5 Hz, H-3eq′), 1.92 and 1.82 (2s, 3H, CH_3CO), 1.51 (q, 1H, $J_{2',3ax'} \sim J_{3ax',4'} \sim$ 12 Hz, H-3ax′). ^{13}C NMR ($CDCl_3$, δ minor rotamer in parentheses) δ: 170.8 (CH_3CO), 156.1 (CO), 106.8 ($J_{C,H}$ 161.7 Hz, C-1′), 61.44 (61.25) (C-6), 53.12 (52.48) (C-5), (38.50) 37.94 (C-1), 35.06 (C-3′), (20.81), 20.62 (CH_3CO). Anal. calcd. for $C_{57}H_{61}NO_{11}$: C 73.14, H 6.57, N 1.50; found: C 73.28, H 6.47, N 1.51. Continued elution provided the α-anomer **18** (140.0 mg, 47%) as a syrup; $[\alpha]_D$ +47 (*c* 0.5, chloroform). ^{1}H NMR ($CDCl_3$, broad, mixture of two rotamers in the ratio 3:2) δ: 7.4–7.1 (m, 30H, 6Ph), 5.2–3.03 (complex m, 26H), 2.32 (m, 1H, $J_{3eq',3ax'}$ 13.0 Hz, H-3eq′), 1.85 and 1.74 (2s, 3H, CH_3CO), 1.75 (q, 1H, $J_{2',3ax'} \sim J_{4',3ax'} \sim$ 12 Hz, H-3ax′). ^{13}C NMR ($CDCl_3$, δ minor rotamer in parentheses) δ: 170.5 (CH_3CO), 156.1 (CO), 96.48 ($J_{C,H}$ 166.2 Hz, C-1′), 61.96 (61.78) (C-6), 52.56 (51.94) (C-5), (38.10) 37.52 (C-1), 29.73 (C-3′), (20.68) 20.50 (CH_3CO). Anal. calcd. for $C_{57}H_{61}NO_{11}$: C 73.14, H 6.57, N 1.50; found: C 73.20, H 6.38, N 1.17.

6-O-Acetyl-2,4-di-O-benzyl-N-benzyloxycarbonyl-1,5-dideoxy-1,5-imino-3-O-(2,3,6-tri-O-benzyl-4-deoxy-α-D-xylo-hexopyranosyl)-D-mannitol (20) and -β-D-xylo-hexopyranosyl)-D-mannitol (21)

A solution of chloride **6** (0.90 mmol) in dichloromethane (4 mL) was added at −65°C to a stirred mixture of **2** (234.7 mg, 0.45 mmol), silver trifluoromethanesulfonate (256 mg, 1.0 mmol), *sym*-collidine (47.5 μL, 0.36 mmol), and 4 Å molecular sieves (1 g) in dichloromethane (2 mL). Within 2 h, the temperature was raised to −55°C. More *sym*-collidine (60 μL, 0.48 mmol) was added. After 1 h at room temperature, the mixture was worked up in the usual way, followed by column chromatography on silica gel (hexane – ethyl acetate, 5:1) to provide an anomeric mixture of **20** and **21**. A second chromatographic purification (carbon tetrachloride – ethyl acetate, 8:1) provided the α-anomer **20** (230.7 mg, 55%) as a syrup; $[\alpha]_D$ +54 (*c* 0.4, chloroform). ^{1}H NMR ($CDCl_3$, broad, mixture of two rotamers in the ratio 3:2) δ: 7.4–7.1 (m, 30H, 6Ph), 5.2–3.0 (complex m, 26H), 1.95 (unresolv. ddd, 1H, $J_{4eq',4ax'}$ 13.0 Hz, H-4eq′), 1.82 and 1.73 (2s, 3H, CH_3CO), 1.55 (q, 1H, H-4ax′). Anal. calcd. for $C_{57}H_{61}NO_{11}$: C 73.14, H 6.57, N 1.50; found: C 73.21, H 6.65, N 1.54. Continued development of the column eluted the β-anomer **21** (153.6 mg, 36%) as a syrup; $[\alpha]_D$ −19.8 (*c* 0.4, chloroform). ^{1}H NMR ($CDCl_3$, broad, mixture of two rotamers in the ratio 3:2) δ: 7.4–7.05 (m, 30H, 6Ph), 5.2–3.1 (complex m, 26H), 2.05 (unresolv. ddd, 1H $J_{4eq',4ax'}$ 12.5 Hz, H-4eq′), 1.89 and 1.80 (2s, 3H, CH_3CO), 1.38 (q, 1H, $J_{3',4ax'} \sim J_{4ax',5'} \sim$ 12 Hz, H-4ax′); ^{13}C NMR ($CDCl_3$, δ minor rotamer in parentheses) δ: 105.14 ($J_{C,H}$ 161.1 Hz, C-1′), 61.41 (61.22) (C-6), 53.04 (52.35) (C-5), (38.44) 37.89 (C-1), 33.76 (C-4′), 20.61 (CH_3CO). Anal. calcd. for $C_{57}H_{61}NO_{11}$: C 73.14, H 6.57, N 1.50; found: C 72.94, H 6.64, N 1.51.

6-O-Acetyl-2,4-di-O-benzyl-N-benzyloxycarbonyl-1,5-dideoxy-1,5-imino-3-O-(2,3,6-tri-O-benzyl-4-O-methyl-α-D-glucopyranosyl)-D-mannitol (22) and -β-D-glucopyranosyl)-D-mannitol (23)

A solution of chloride **10** (1.18 mmol) in dichloromethane (7 mL) was added to a stirred mixture of **2** (253 mg, 0.49 mmol), silver trifluoromethanesulfonate (380 mg, 1.48 mmol), *sym*-collidine (51 μL, 0.39 mmol), and 4 Å molecular sieves (500 mg) in dichloromethane (2.0 mL) at 0°C. Stirring was continued for 2.5 h. Then more *sym*-collidine (150 μL, 1.14 mmol) was added, followed by conventional work-up. Chromatographic isolation of the product on a column of silica gel (hexane – ethyl acetate 5:1, 4:1, 3:1) provided a 2.5:1 mixture of **22** and **23** (310 mg, 66%). This mixture was not further characterized, but was deacetylated.

6-O-Acetyl-2,4-di-O-benzyl-N-benzyloxycarbonyl-1,5-dideoxy-1,5-imino-3-O-(2,3,4,6-tetra-O-benzyl-α-D-galactopyranosyl)-D-mannitol (24) and -β-D-galactopyranosyl)-D-mannitol (25)

A solution of chloride **11** (9) (0.94 mmol) in dichloromethane (6.5 mL) was added to a stirred mixture of **2** (265 mg, 0.51 mmol), silver trifluoromethanesulfonate (310 mg, 1.20 mmol), *sym*-collidine (55 μL, 0.42 mmol), and 4 Å molecular sieves (500 mg) in dichloromethane (1.5 mL) at −78°C. The temperature was gradually raised to 0°C and, after 7 h, *sym*-collidine (180 μL, 1.36 mmol) and methanol (200 μL) were added. The mixture was processed in the usual way and the product mixture purified on a column of silica gel (hexane – ethyl acetate, 5:1). Evaporation of the first main fraction provided **24** (357.9 mg, 67%) as a tough syrup; $[\alpha]_D$ +38.5 (*c* 1.0, chloroform). ^{1}H NMR ($CDCl_3$, broad, mixture of two rotamers in the ratio 3:2) δ: 7.4–7.0 (m, 35H, 7Ph), 5.2–3.0 (complex m, 29H), 1.82 and 1.73 (2s, 3H, CH_3CO). Anal. calcd. for $C_{64}H_{67}NO_{12}$: C 73.76, H 6.48, N 1.34; found: C 73.60, H 6.49, N 1.41. Continued elution of the column furnished the β-anomer **25** (38.8 mg, 7.3%) as a tough syrup; $[\alpha]_D$ −18.9 (*c* 0.3, chloroform). ^{1}H NMR ($CDCl_3$, broad, mixture of two rotamers in the ratio 3:2) δ: 7.4–7.0 (m, 35H, 7Ph), 5.2–3.1 (complex m, 29H), 1.82 and 1.73 (2s, 3H, CH_3CO). ^{13}C NMR ($CDCl_3$, δ minor rotamer in parentheses) δ: 170.4 (CH_3CO), 156.22 (CO), 104.83 ($J_{C,H}$ 160.7 Hz, C-1′), 61.22 (C-6), 52.85 (52.21) (C-5), (37.82) 37.35 (C-1), 20.62 (CH_3CO).

6-O-Acetyl-2,4-di-O-benzyl-N-benzyloxycarbonyl-1,5-dideoxy-1,5-imino-3-O-(2,3,4-tri-O-benzyl-6-deoxy-α-D-glucopyranosyl)-D-mannitol (26) and -β-D-glucopyranosyl)-D-mannitol (27)

A solution of chloride **12** (1.25 mmol) in dichloromethane (2 mL) was added at −40°C to a stirred mixture of alcohol **2** (287 mg, 0.55 mmol), silver trifluoromethanesulfonate (360 mg, 1.40 mmol), *sym*-collidine (58 μL, 0.44 mmol), and 4 Å molecular sieves (300 mg) in dichloromethane (1 mL). After 1 h at this temperature, the temperature was allowed to reach 0°C within 3 h. The reaction was quenched by the addition of *sym*-collidine (150 μL, 1.14 mmol) followed by usual work-up. Column chromatography on silica gel (hexane – ethyl acetate, 6:1) provided the anomeric mixture of **26** and **27** (464 mg, 90%), which was not further characterized, but deacetylated.

6-O-Acetyl-2,4-di-O-benzyl-N-benzyloxycarbonyl-1,5-dideoxy-1,5-imino-3-O-(2,3,4-tri-O-benzyl-α-D-xylopyranosyl)-D-mannitol (28) and -β-D-xylopyranosyl)-D-mannitol (29)

Chloride **13** (10) was prepared from 2,3,4-tri-*O*-benzyl-D-xylopyranose (18) as described for **3**. A solution of **13** (0.72 mmol) in dichloromethane (4.5 mL) was transferred into a stirred mixture of **2** (263 mg, 0.51 mmol), silver trifluoromethanesulfonate (334 mg, 1.3 mmol), *sym*-collidine (55 μL, 0.42 mmol), and 4 Å molecular sieves (0.5 g) in dichloromethane (1 mL) at −78°C. The mixture was allowed to reach 0°C within 4.5 h and more *sym*-col-

Can. J. Chem. Downloaded from www.nrcresearchpress.com by 203.198.23.82 on 09/08/12
For personal use only.

lidine (100 μL, 0.76 mmol) was added. It was processed as described for the preparation of **14**, followed by chromatography on a column of silica gel (hexane – ethyl acetate, 5:1, 4:1), which provided a 2:1 mixture of the anomers **28** and **29** (432.5 mg, 93%) according to the ^{1}H NMR spectrum. This mixture was not further characterized but deacetylated.

*2,4-Di-*O*-benzyl-*N*-benzyloxycarbonyl-1,5-dideoxy-1,5-imino-3-*O*-(3,4,6-tri-*O*-benzyl-2-*O*-methyl-α-D-glucopyranosyl)-D-mannitol (**30**)*

A solution of **14** (193 mg, 0.20 mmol) in methanol (5 mL), triethylamine (2 mL), and water (1 mL) was kept at room temperature for 4 days. It was evaporated to dryness and the resultant material was applied to a column of silica gel (hexane–dichloromethane – ethyl acetate, 5:1:1, 4:1:1) to provide the title compound **30** (144 mg, 78%) as a tough syrup; $[\alpha]_D$ +44.2 (*c* 0.2, chloroform). ^{1}H NMR ($CDCl_3$, broad, mixture of rotamers) δ: 7.4–7.0 (m, 30H, 6Ph), 5.20–2.90 (complex m, 31H), 3.42 (s, 3H, CH_3O). Anal. calcd. for $C_{56}H_{61}NO_{11}$: C 72.79, H 6.65, N 1.52; found: C 73.05, H 6.68, N 1.45.

*2,4-Di-*O*-benzyl-*N*-benzyloxycarbonyl-1,5-dideoxy-1,5-imino-3-*O*-(3,4,6-tri-*O*-benzyl-2-chloro-2-deoxy-α-D-glucopyranosyl)-D-mannitol (**31**)*

A mixture of **16** (60 mg, 0.065 mmol), methanol (1.43 mL), triethylamine (572 μL), and water (286 μL) was kept at room temperature for 3 days. Evaporation, followed by column chromatography on silica gel (hexane – ethyl acetate, 2:1), provided syrupy **31** (54.6 mg, 95%); $[\alpha]_D$ +69 (*c* 0.5, chloroform). ^{1}H NMR ($CDCl_3$, broad, mixture of rotamers) δ: 7.4–7.0 (m, 30H, 6Ph), 5.15–2.9 (complex m, 28H). ^{13}C NMR ($CDCl_3$) δ: 99.25 (C-1′), 60.44 (C-6, C-2′), 55.59 (C-5), 38.0 (C-1). Anal. calcd. for $C_{55}H_{58}ClNO_{10}$: C 71.15, H 6.30, N 1.51; found: C 70.95, H 6.51, N 1.36.

*2,4-Di-*O*-benzyl-*N*-benzyloxycarbonyl-1,5-dideoxy-1,5-imino-3-*O*-(2,4,6-tri-*O*-benzyl-3-deoxy-α-D-*ribo*-hexopyranosyl)-D-mannitol (**32**)*

A mixture of **18** (121 mg, 0.13 mmol), methanol (3.2 mL), triethylamine (1.28 mL), and water (0.64 mL) was stirred at room temperature for 5 days. Evaporation and column chromatography on silica gel (hexane – ethyl acetate, 3:1) provided **32** (88.5 mg, 77%) as a tough syrup; $[\alpha]_D$ +36 (*c* 0.5, chloroform). ^{1}H NMR ($CDCl_3$, broad, mixture of rotamers) δ: 7.43–7.05 (m, 30H, 6Ph), 5.2–2.9 (complex m, 27H), 2.30 (m, 1H, H-3eq′), 1.71 (q, 1H, $J_{3ax',3eq'} \sim J_{2',3ax'} \sim J_{3ax',4'} \sim 12$ Hz, H-3ax′). ^{13}C NMR ($CDCl_3$, δ minor rotamer in parentheses) δ: 156.10 (CO), 97.52 ($J_{C,H}$ 167.9 Hz, C-1′), 58.93 (C-6), 53.70 (53.26) (C-5), (39.19) 38.60 (C-1), 29.74 (C-3′). Anal. calcd. for $C_{55}H_{59}NO_{10}$: C 73.89, H 6.65, N 1.57; found: C 73.92, H 6.75, N 1.55.

*2,4-Di-*O*-benzyl-*N*-benzyloxycarbonyl-1,5-dideoxy-1,5-imino-3-*O*-(2,3,6-tri-*O*-benzyl-4-deoxy-α-D-*xylo*-hexopyranosyl)-D-mannitol (**33**)*

A solution of **20** (230.6 mg, 0.25 mmol) in methanol (6.1 mL), triethylamine (2.43 mL), and water (1.2 mL) was kept at room temperature for 6 days. The material resulting on evaporation was applied to a column of silica gel (hexane – ethyl acetate, 3:1) to provide syrupy **33** (172 mg, 78%); $[\alpha]_D$ +44 (*c* 0.5, chloroform). ^{1}H NMR ($CDCl_3$, broad, mixture of rotamers) δ: 7.4–7.05 (m, 30H, 6Ph), 5.2–2.9 (complex m, 27H), 2.01 (ddd, 1H, $J_{4ax',4eq'}$ 13.0 Hz, $J_{3',4eq'}$ 5.0 Hz, $J_{4eq',5'}$ 2.0 Hz, H-4eq′), 1.62 (q, 1H, H-4ax′). ^{13}C NMR ($CDCl_3$, δ minor rotamer in parentheses) δ: 156.06 (CO), 99.71 ($J_{C,H}$ 166.9 Hz, C-1′), 58.06 (C-6), 53.90 (53.46) (C-5), (39.38) 38.75 (C-1), 33.09 (C-4′). Anal. calcd. for $C_{55}H_{59}NO_{10}$: C 73.89, H 6.65, N 1.57; found: C 73.70, H 6.65, N 1.62.

*2,4-Di-*O*-benzyl-*N*-benzyloxycarbonyl-1,5-dideoxy-1,5-imino-3-*O*-(2,3,6-tri-*O*-benzyl-4-*O*-methyl-α-D-glucopyranosyl)-D-mannitol (**34**) and -β-D-glucopyranosyl)-D-mannitol (**35**)*

An anomeric mixture of compounds **22** and **23** (295 mg, 0.31 mmol) in methanol (7.5 mL), triethylamine (3 mL), and water (1.5 mL) was kept for 7 days at room temperature. It was evaporated and the resultant material applied to a column of silica gel (hexane–dichloromethane – ethyl acetate, 4:1:1) to provide in the first fraction starting material **22** and **23** (58 mg, 20%). Evaporation of the second fraction gave α-isomer **34** (145.1 mg, 51%); $[\alpha]_D$ −3 (*c* 0.5, chloroform). ^{1}H NMR ($CDCl_3$, broad, mixture of two rotamers) δ: 7.45–7.10 (m, 30H, 6Ph), 5.2–2.84 (complex m, 31H), 3.37 (s, 3H CH_3O). ^{13}C NMR ($CDCl_3$, δ minor rotamer in parentheses) δ: 156.10 (CO), 99.28 ($J_{C,H}$ 168.5 Hz, C-1′), 60.42 (CH_3O), 59.12 (C-6), 53.87 (53.39) (C-5), (39.22) 38.65 (C-1). Anal. calcd. for $C_{56}H_{61}NO_{11}$: C 72.79, H 6.65, N 1.52; found: C 72.59, H 6.70, N 1.47. Continued elution of the column provided the β-isomer **35** (58.8 mg, 21%); $[\alpha]_D$ −6 (*c* 0.8, chloroform). ^{1}H NMR ($CDCl_3$, broad, mixture of two rotamers) δ: 7.4–7.0 (m, 30H, 6Ph), 5.2–3.0 (complex m, 31H), 3.40 (s, CH_3O). ^{13}C NMR ($CDCl_3$, δ minor rotamer in parentheses) δ: 156.0 (CO), 105.61 ($J_{C,H}$ 158.0 Hz, C-1′), 60.64 (CH_3O), 59.71 (C-6), 54.85 (54.53) (C-5), (39.41) 38.98 (C-1).

*2,4-Di-*O*-benzyl-*N*-benzyloxycarbonyl-1,5-dideoxy-1,5-imino-3-*O*-(2,3,4,6-tetra-*O*-benzyl-α-D-galactopyranosyl)-D-mannitol (**36**)*

A solution of acetate **24** (225 mg, 0.22 mmol) in methanol (5 mL), triethylamine (2 mL), and water (1 mL) was kept for 6 days at room temperature. It was evaporated and the resultant material applied to a column of silica gel (hexane–dichloromethane – ethyl acetate, 5:1:1). Evaporation of the first main fraction provided starting material **24** (51.8 mg, 23%). Continued elution gave **36** (138.4 mg, 64%) as a tough syrup; $[\alpha]_D$ +22.7 ^{1}H NMR ($CDCl_3$, broad, mixture of rotamers) δ: 7.4–7.0 (m, 35H, 7Ph), 5.15–2.90 (complex m, 29H). Anal. calcd. for $C_{62}H_{65}NO_{11}$: C 74.45, H 6.55, N 1.40; found: C 74.50, H 6.57, N 1.35.

*2,4-Di-*O*-benzyl-*N*-benzyloxycarbonyl-1,5-dideoxy-1,5-imino-3-*O*-(2,3,4-tri-*O*-benzyl-6-deoxy-α-D-glucopyranosyl)-D-mannitol (**37**) and -β-D-glucopyranosyl)-D-mannitol (**38**)*

An anomeric mixture of compounds **26** and **27** (450 mg, 0.48 mmol), triethylamine (4.7 mL), water (2.3 mL), and methanol (11.8 mL) was kept at room temperature for 5 days. It was evaporated and the resultant material applied to a column of silica gel (hexane – ethyl acetate, 3:1) to provide in the first main fraction α-anomer **37** (197 mg, 46%) as a syrup; $[\alpha]_D$ +33.4 (*c* 0.5, chloroform). ^{1}H NMR ($CDCl_3$, broad, mixture of two rotamers) δ: 7.50–7.10 (m, 30H, 6Ph), 5.2–3.0 (complex m, 26H), 0.87 (d, 3H, $J_{5',6'}$ 6.2 Hz, H_3-6′). ^{13}C NMR (δ minor rotamer in parentheses) δ: 156.13 (CO), 98.95 ($J_{C,H}$ 171.8 Hz, C-1′), 59.25 (C-6), 53.94 (53.47) (C-5), (39.35) 38.76 (C-1), 17.45 (C-6′). Anal. calcd. for $C_{55}H_{59}NO_{10}$: C 73.89, H 6.65, N 1.57; found: C 73.88, H 6.39, N 1.57. Continued development eluted the syrupy β-isomer **38** (122.1 mg, 28%); $[\alpha]_D$ −16.5 (*c* 0.6, chloroform). ^{1}H NMR ($CDCl_3$, broad, mixture of two rotamers) δ: 7.45–7.05 (m, 30H, 6Ph), 5.2–2.8 (m, 26H), 1.13 (d, 3H, $J_{5',6'}$ 6.0 Hz, H_3-6′). ^{13}C NMR (δ minor rotamer in parentheses) δ: 156.28 (CO), 105.47 ($J_{C,H}$ 162.3 Hz, C-1′), (58.67) 58.44 (C-6), 54.51 (54.29) (C-5), 39.32 (38.84) (C-1), 17.72 (C-6′).

*2,4-Di-*O*-benzyl-*N*-benzyloxycarbonyl-1,5-dideoxy-1,5-imino-3-*O*-(2,3,4-tri-*O*-benzyl-α-D-xylopyranosyl)-D-mannitol (**39**) and -β-D-xylopyranosyl)-D-mannitol (**40**)*

A solution of the anomeric mixture of **28** and **29** (433 mg, 0.47 mmol) in methanol (10 mL), triethylamine (4 mL), and water (2 mL) was kept at room temperature for 7 days. It was evaporated and the product mixture separated on a column of silica gel (hexane–dichloromethane – ethyl acetate, 5:1:1 to 2:1:1) to provide in the first main fraction the α-anomer **39** (193 mg, 47%) as a tough syrup; $[\alpha]_D$ +22.6 (*c* 0.2, chloroform). ^{1}H NMR ($CDCl_3$, broad, mixture of two rotamers) δ: 7.40–7.10 (m, 30H, 6Ph), 5.20–3.0 (complex m, 27H). Anal. calcd. for $C_{54}H_{57}NO_{10}$: C 73.70, H 6.53, N 1.59; found: C 73.85, H 6.44, N 1.59. Continued development of the column eluted the β-anomer **40** (100.2 mg, 24%); $[\alpha]_D$ −22.1 (*c* 0.3, chloroform). ^{1}H NMR ($CDCl_3$, broad, mixture

Can. J. Chem. Downloaded from www.nrcresearchpress.com by 203.198.23.82 on 09/08/12
For personal use only.

of two rotamers) δ: 7.40–7.10 (m, 30H, 6Ph), 5.10–2.60 (complex m, 27H). ^{13}C NMR ($CDCl_3$, δ minor rotamer in parentheses) δ: 156.25 (CO), 106.46 ($J_{C,H}$ 161.5 Hz, C-1′) (58.87) 58.55 (C-6), 54.69 (C-5), (39.19) 38.64 (C-1). Anal. calcd. for $C_{54}H_{57}NO_{10}$: C 73.70, H 6.53, N 1.59; found: C 73.49, H 6.50, N 1.54.

*1,5-Dideoxy-1,5-imino-3-*O*-(2-*O*-methyl-α-D-glucopyranosyl)-D-mannitol-hydrochloride (**41**)*

A mixture of **30** (131 mg, 0.14 mmol), 5% palladium-on-carbon (130 mg), and methanolic 0.12 N hydrochloric acid (1.3 mL, 0.156 mmol) in methanol (7 mL) was hydrogenated in a hydrogen stream for 2 h. Removal of the catalyst by filtration, evaporation, and gel filtration (Sephadex LH 20, ethanol–water, 1:1) provided **41** (50.9 mg, 96%) as a white solid after freeze-drying its aqueous solution; $[\alpha]_D$ +83.3 (*c* 0.2, water). The ^1H and ^{13}C NMR data are reported in Tables 1 and 2.

*3-O-(2-Chloro-2-deoxy-α-D-glucopyranosyl)-1,5-dideoxy-1,5-imino-D-mannitol-hydrochloride (**42**)*

A mixture of **31** (32 mg, 0.034 mmol), 5% palladium-on-carbon (30 mg), and methanolic 0.12 N hydrochloric acid (0.3 mL, 0.036 mmol) in methanol (4.5 mL) was hydrogenated in a hydrogen stream for 4 h. Removal of the catalyst by filtration, evaporation, and gel filtration (Sephadex LH 20, ethanol–water, 1:1) provided **42** (10.9 mg, 83%) as a white solid after lyophilization of an aqueous solution; $[\alpha]_D$ +48.5 (*c* 0.4, water). The ^1H and ^{13}C NMR data are reported in Tables 1 and 2.

*1,5-Dideoxy-3-*O*-(3-deoxy-α-D-*ribo*-hexopyranosyl)-1,5-imino-D-mannitol-hydrochloride (**43**)*

Compound **32** (93 mg, 0.104 mmol), 5% palladium-on-carbon (90 mg), and 0.12 N methanolic hydrochloric acid (1 mL, 0.12 mmol) in methanol (12 mL) were hydrogenated in the hydrogen stream for 1.5 h. Usual processing followed by gel filtration (Sephadex LH 20, ethanol–water, 1:1) provided **43** (32.4 mg, 90%) as a white solid; $[\alpha]_D$ +70.3 (*c* 0.3, water). The ^1H and ^{13}C NMR data are reported in Tables 1 and 2.

*1,5-Dideoxy-3-*O*-(4-deoxy-α-D-*xylo*-hexopyranosyl)-1,5-imino-D-mannitol-hydrochloride (**44**)*

A mixture of compound **33** (163.6 mg, 0.183 mmol), 5% palladium-on-carbon (150 mg), and methanolic 0.12 N hydrochloric acid (1.7 mL, 0.20 mmol) in methanol (18 mL) was hydrogenated in the hydrogen stream for 2.5 h. The catalyst was removed by filtration, followed by evaporation. Gel filtration of the resultant material on a column of Sephadex LH 20 (ethanol–water, 1:1) afforded the title compound **44** (45.6 mg, 72%) as a slightly yellowish powder; $[\alpha]_D$ +77.3 (*c* 0.3, water). The ^1H and ^{13}C NMR data are reported in Tables 1 and 2.

*1,5-Dideoxy-1,5-imino-3-*O*-(4-*O*-methyl-α-D-glucopyranosyl)-D-mannitol-hydrochloride (**45**)*

A mixture of **34** (114.3 mg, 0.12 mmol), 5% palladium-on-carbon (110 mg), and methanolic 0.12 N hydrochloric acid (1.13 mL, 0.14 mmol) in methanol (6 mL) was hydrogenated in the hydrogen stream for 2 h. The catalyst was removed by filtration and the solvent evaporated. The resultant material was passed through a column of Iatrobeads® (chloroform–methanol–water, 65:35:8) followed by gel filtration (Sephadex LH 20, ethanol–water, 1:1) to provide **45** (46.5 mg, 100%) as a solid; $[\alpha]_D$ +81 (*c* 0.4, water). The ^1H and ^{13}C NMR data are reported in Tables 1 and 2.

*1,5-Dideoxy-3-*O*-(α-D-galactopyranosyl)-1,5-imino-D-mannitol-hydrochloride (**46**)*

A mixture of **36** (128 mg, 0.128 mmol), 5% palladium-on-carbon (128 mg), and methanolic 0.12 N hydrochloric acid (1.1 mL, 0.13 mmol) in methanol (7 mL) was hydrogenated in a hydrogen stream for 3 h. The catalyst was removed by filtration, followed by evaporation. The resultant material was subjected to gel filtration (Sephadex LH 20, ethanol–water, 1:1) to provide, after freeze-drying an aqueous solution, title compound **46** (42.5 mg, 92%); $[\alpha]_D$ +91.6 (*c* 0.2, water). The ^1H and ^{13}C NMR data are reported in Tables 1 and 2.

*1,5-Dideoxy-3-*O*-(6-deoxy-α-D-glucopyranosyl)-1,5-imino-D-mannitol-hydrochloride (**47**)*

A mixture of **37** (183.1 mg, 0.21 mmol), 5% palladium-on-carbon (140 mg), and methanolic 0.12 N hydrochloric acid (1.87 mL, 0.224 mmol) in methanol (10 mL) was hydrogenated in the hydrogen stream for 2 h. The catalyst was removed by filtration and the solvent evaporated. The resultant material was passed through a column of Iatrobeads® (chloroform–methanol–water, 65:35:8) followed by gel filtration (Sephadex LH 20, ethanol–water, 1:1) to provide **47** (60.5 mg, 85%) as a white solid, $[\alpha]_D$ +64.4 (*c* 0.5, water). The ^1H and ^{13}C NMR data are reported in Tables 1 and 2.

*1,5-Dideoxy-1,5-imino-3-*O*-(α-D-xylopyranosyl)-D-mannitol-hydrochloride (**48**)*

A mixture of compound **39** (170 mg, 0.19 mmol), 5% palladium-on-carbon (170 mg), methanolic 0.12 N hydrochloric acid (1.6 mL, 0.19 mmol), and methanol (10 mL) was hydrogenated in a hydrogen stream for 3 h. The catalyst was removed by filtration, followed by evaporation and codistillation with water. The product was passed through a column of Sephadex LH 20 (ethanol–water, 1:1) to provide, after freeze-drying an aqueous solution, the title compound **48** (59.6 mg, 93%) as a white solid, $[\alpha]_D$ +63 (*c* 0.3, water). The ^1H and ^{13}C NMR data are reported in Tables 1 and 2.

*3,4,6-Tri-*O*-benzyl-2-deoxy-α-D-*arabino*-hexopyranosyl chloride (**49**) (22)*

49 was prepared just prior to use according to ref. 22 and characterized by ^1H NMR spectroscopy. ^1H NMR ($CDCl_3$) δ: 7.4–7.1 (m, 15H, 3Ph), 6.30 (d, 1H, $J_{1,2ax}$ 3.3 Hz, $J_{1,2eq}$ ~ 1 Hz, H-1), 4.16 (ddd, 1H, $J_{2ax,3}$ 11.0 Hz, $J_{2eq,3}$ 4.5 Hz, $J_{3,4}$ 9.5 Hz, H-3), 4.06 (ddd, 1H, $J_{4,5}$ 9.5 Hz, $J_{5,6}$ 3.7 Hz, $J_{5,6'}$ 1.8 Hz, H-5), 3.81 (dd, 1H, $J_{6,6'}$ 11.0 Hz, H-6), 3.71 (t, 1H, H-4), 3.65 (dd, 1H, H-6′), 2.51 (ddd, 1H, $J_{2eq,2ax}$ 13.5 Hz, H-2eq), 3.73 (ddd, 1H, H-2ax).

*2,4,6-Tri-*O*-benzyl-3-*O*-methyl-α,β-D-glucopyranosyl chloride (**50**)*

2,4,6-Tri-*O*-benzyl-3-*O*-methyl-D-glucopyranose (15) (550 mg, 1.18 mmol) was converted into chloride **50** as described for the preparation of **3**. ^1H NMR ($CDCl_3$, α:β = 2:1) δ: 7.4–7.1 (m, 15H, 3Ph), 5.99 (d, $J_{1\alpha,2}$ 3.5 Hz, H-1α), 5.13 (d, $J_{1\beta,2}$ 8.5 Hz, H-1β), 4.00 (m, $J_{4,5}$ 10.0 Hz, H-5α) 3.64 (s, CH_3O-α), 3.62 (s, CH_3O-β).

*6-O-Acetyl-2,3,4-tri-*O*-benzyl-α,β-D-glucopyranosyl chloride (**51**) (11)*

6-*O*-Acetyl-2,3,4-tri-*O*-benzyl-D-glucopyranose (19) (68 mg, 0.138 mmol) was converted into **51** as described for the preparation of chloride **3**. ^1H NMR ($CDCl_3$, α:β = 1.5:1) δ: 7.4–7.1 (m, 15H, 3Ph), 5.99 (d, $J_{1\alpha,2}$ 3.5 Hz, H-1α), 5.20 (d,$J_{1\beta,2}$ 8.0 Hz, H-1β), 4.33 (dd, $J_{6,6'}$ 12.0 Hz, $J_{5,6}$ ~ 1 Hz, H-6β), 4.25 (d, $J_{6,5}$ 3.2 Hz, 2H-6α), 4.18 (dd, $J_{5,6'}$ 4.5 Hz, H-6′β), 4.12 (dt, $J_{4,5}$ 10.0 Hz, H-5α), 4.04 (t, 1H, $J_{3,4}$ ~ $J_{2,3}$ 9.2 Hz, H-3α), 3.68 (dd, H-2α), 3.51 (dd, H-4α), 2.04, 2.00 (2s, CH_3CO-β, CH_3CO-α).

*6-O-Acetyl-2,4-di-*O*-benzyl-N-benzyloxycarbonyl-1,5-dideoxy-1,5-imino-3-*O*-(3,4,6-tri-*O*-benzyl-2-deoxy-α-D-*arabino*-hexopyranosyl)-D-mannitol (**52**)*

A solution of chloride **49** (0.73 mmol) in dichloromethane (1 mL) was added at −65°C to a stirred mixture of **2** (145 mg, 0.28 mmol), silver trifluoromethanesulfonate (188.3 mg, 0.73 mmol), *sym*-collidine (34.9 μL, 0.26 mmol), and 4 Å molecular sieves (400 mg) in dichloromethane (2 mL). After 1.5 h at this temperature, triethylamine (80 μL, 0.61 mmol) was added and stirring continued for 30 min at room temperature. Usual work-up was followed by chromatography on a column of silica gel to afford **52** (189.3 mg, 73%) as a syrup; $[\alpha]_D$ +26.2 (*c* 0.5, chloroform). ^1H NMR ($CDCl_3$, broad, mixture of two rotamers in the ratio 3:2) δ: 7.4–7.05 (m,

30H, 6Ph), 5.2–3.0 (complex m, 26H), 2.04 (ddd, 1H, $J_{2eq',2ax'}$ 13.5 Hz, $J_{2eq',3'}$ 4.5 Hz, H-2eq'), 1.94 and 1.85 (2s, 3H, CH_3CO), 1.67 (ddd, 1H, $J_{2ax',1'}$ 3.3 Hz, $J_{2ax',3'}$ 12.0 Hz, H-2ax'). Anal. calcd. for $C_{57}H_{61}NO_{11}$: C 73.14, H 6.57, N 1.50; found: C 73.32, H 7.01, N 1.59.

*6-O-Acetyl-2,4-di-O-benzyl-N-benzyloxycarbonyl-1,5-dideoxy-1,5-imino-3-O-(2,4,6-tri-O-benzyl-3-O-methyl-α-D-glucopyranosyl)-D-mannitol (**53**) and -β-D-glucopyranosyl)-D-mannitol (**54**)*

A solution of chloride **50** (1.18 mmol) in dichloromethane was added to a stirred mixture of **2** (276 mg, 0.53 mmol), silver trifluoromethanesulfonate (335 mg, 1.30 mmol), *sym*-collidine (56 μL, 0.42 mmol), and 4 Å molecular sieves (500 mg) in dichloromethane (2 mL) at −40°C. The mixture was gradually allowed to reach 0°C and, after 10 h, more *sym*-collidine (100 μL, 0.76 mmol) was added. Conventional work-up was followed by chromatography of the crude product on a column of silica gel (hexane–ethyl acetate, 5:1, 4:1, 3:1) to provide in the first main fraction the β-isomer **54** (111.1 mg, 22%); $[\alpha]_D$ −4.7 (*c* 0.7, chloroform). ^{1}H NMR (broad, mixture of two rotamers in the ratio 3:2) δ: 7.4–7.0 (m, 30H, 6Ph), 5.2–3.1 (complex m, 30H), 3.58 (s, 3H, CH_3O), 1.88 and 1.79 (2s, 3H, CH_3CO). ^{13}C NMR ($CDCl_3$, δ minor rotamer in parentheses) δ: 156.0 (CO), 104.86 ($J_{C,H}$ 160.9 Hz, C-1'), 61.35, 61.21 (CH_3O, C-6), 53.07 (52.44) (C-5), 38.40 (37.85) (C-1), 20.58 (CH_3CO). Continued elution gave **53** (277.4 mg, 54%); $[\alpha]_D$ +48.4 (*c* 0.7, chloroform). ^{1}H NMR ($CDCl_3$, broad, mixture of two rotamers in the ratio 3:2) δ: 7.4–7.0 (m, 30H, 6Ph), 5.2–3.0 (complex m, 30H), 3.65 (s, 3H, CH_3O), 1.82 and 1.74 (2s, 3H, CH_3CO). Anal. calcd. for $C_{58}H_{63}NO_{12}$: C 72.11, H 6.57, N 1.45; found: C 72.49, H 6.38, N 1.42.

*6-O-Acetyl-3-O-(6-O-acetyl-2,3,4-tri-O-benzyl-α- and -β-D-glucopyranosyl)-2,4-di-O-benzyl-N-benzyloxycarbonyl-1,5-dideoxy-1,5-imino-D-mannitol (**55** and **56**)*

A solution of chloride **51** (0.13 mmol) in dichloromethane (1.5 mL) was transferred into a stirred mixture of **2** (34 mg, 0.065 mmol), silver trifluoromethanesulfonate (43 mg, 0.17 mmol), *sym*-collidine (7.1 μL, 0.054 mmol), and 4 Å molecular sieves (100 mg) in dichloromethane (0.3 mL) at 0°C. After 1 h at this temperature, more *sym*-collidine (10 μL, 0.076 mmol) was added and the reaction mixture was processed as usual. The resultant material was applied to a column of silica gel (hexane – ethyl acetate, 5:1, 4:1) to provide in the first main fraction the β-anomer **56** (14.0 mg, 22%) as a tough syrup; $[\alpha]_D$ −18.9 (*c* 0.3, chloroform). ^{1}H NMR ($CDCl_3$, broad, mixture of two rotamers) δ: 7.4–7.0 (m, 30H, 6Ph). 5.2–3.1 (complex m, 27H), 1.98 (s, 3H, CH_3CO-6') 1.92 and 1.82 (2s, 3H, CH_3CO-6). ^{13}C NMR ($CDCl_3$, δ minor rotamer in parentheses) δ: 170.57 (CH_3CO), 156.40 (OCO), 104.91 ($J_{C,H}$ 161.5 Hz, C-1'), 62.51 (C-6'), 61.20 (61.04) (C-6), 52.90 (52.20) (C-5), 38.37 (37.84) (C-1), 20.77, 20.57 (CH_3CO). Continued elution of the column afforded **55** (40 mg, 62%) as a tough syrup; $[\alpha]_D$ +19.5 (*c* 0.2, chloroform). ^{1}H NMR (broad, mixture of two rotamers) δ: 7.4–7.1 (m, 30H, 6Ph), 5.2–3.0 (complex m, 27H), 1.91 (s, 3H, CH_3CO-6'), 1.83 and 1.75 (2s, 3H, CH_3CO-6). Anal. calcd. for $C_{59}H_{63}NO_{13}$: C 71.28, H 6.39, N 1.41; found: C 71.44, H 6.42, N 1.44.

*2,4-Di-O-benzyl-N,6-O-carbonyl-1,5-dideoxy-1,5-imino-3-O-(3,4,6-tri-O-benzyl-2-deoxy-α-D-*arabino*-hexopyranosyl)-D-mannitol (**57**)*

A solution of **52** (156.6 mg, 0.167 mmol) in methanolic 0.5 N sodium methoxide (1 mL) was kept at room temperature for 3.5 h. The remainder on evaporation was taken up in dichloromethane and the solution washed with water until neutral, followed by evaporation. Column chromatography provided the title compound **57** (108.4 mg, 83%) as a syrup; $[\alpha]_D$ +15 (*c* 0.5, chloroform). ^{1}H NMR ($CDCl_3$) δ: 7.4–7.1 (m, 25H, 5Ph), 5.22 (bd, 1H, $J_{1',2ax'}$ 3.0 Hz, $J_{1',2eq'}$ ~ 1 Hz, H-1'), 4.97–4.37 (m, 10H, 5CH_2Ph), 4.28 (t, 1H, $J_{5,6A}$ ~ $J_{6A,6B}$ ~ 8.5 Hz, H-6A), 4.06 (dd, 1H, $J_{1A,1B}$ 14.0 Hz, $J_{1A,2}$ 2.0 Hz, H-1A), 4.01 (m, 1H, H-3'), 3.88 (overlapped, H-2), 2.71 (bd, 1H, H-1B), 2.25 (bdd, 1H, $J_{2eq',2ax'}$ 13.0 Hz, $J_{2eq',3'}$ 11.0 Hz, H-2eq') 1.72 (ddd, 1H, $J_{2ax',3'}$ 11.0 Hz, H-2ax'). ^{13}C NMR ($CDCl_3$) δ: 157.7 (CO), 100.03 ($J_{C,H}$ 169.4 Hz, C-1'), 65.58 (C-6), 57.53 (C-5), 41.12 (C-1), 35.77 (C-2'). Anal. calcd. for $C_{48}H_{51}NO_9$: C 73.35, H 6.54, N 1.78; found: C 73.46, H 6.88, N 1.64.

*2,4-Di-O-benzyl-N-6-O-carbonyl-1,5-dideoxy-1,5-imino-3-O-(2,3,4-tri-O-benzyl-α-D-glucopyranosyl)-D-mannitol (**59**)*

A solution of **55** (400 mg, 0.40 mmol) in methanolic 0.5 N sodium methoxide (4 mL) was kept at room temperature for 15 h. It was diluted with dichloromethane and the solution was washed with 1% hydrochloric acid and water. The product obtained on evaporation was purified on a column of silica gel (dichloromethane – ethyl acetate, 1:2) to provide **59** (294.9 mg, 91%) as a white foam; $[\alpha]_D$ +33.6 (*c* 0.3, chloroform). ^{1}H NMR ($CDCl_3$) δ: 7.4–7.0 (m, 25H, 5Ph), 4.99 (d, 1H, $J_{1',2'}$ 3.5 Hz, H-1'), 4.20 (dd, overlapped, 1H, $J_{1A,1B}$ 14.5 Hz, $J_{1A,2}$ 2.5 Hz, H-1A), 3.94 (bs, 1H, H-2), 3.46 (dd, 1H, $J_{2',3'}$ 10.0 Hz, H-2'), 2.82 (dd, 1H, $J_{1B,2}$ < 1 Hz, H-1B). ^{13}C NMR ($CDCl_3$) δ: 156.76 (CO), 100.21 (C-1'), 65.77 (C-6), 61.98 (C-6'), 57.47 (C-5), 40.93 (C-1). Anal. calcd. for $C_{48}H_{51}NO_{10}$: C 71.89, H 6.41, N 1.75; found: C 71.68, H 6.36, N 1.60.

*2,4-Di-O-benzyl-N-6-O-carbonyl-1,5-dideoxy-1,5-imino-3-O-(2,3,4-tri-O-benzyl-6-O-methyl-α-D-glucopyranosyl)-D-mannitol (**60**)*

A mixture of **59** (258 mg, 0.32 mmol), silver oxide (410 mg, 1.77 mmol), and methyl iodide (300 μL, 4.82 mmol) in toluene (6.3 mL) was stirred in the dark for 17 h. More methyl iodide (200 μL, 3.21 mmol) was added and stirring continued for another 4 h. Filtration and evaporation of the solvent left a crystalline residue, which was passed through a column of silica gel (dichloromethane – ethyl acetate, 1:1, 1:2) to give **60** (240.3 mg, 91%) as a white solid; $[\alpha]_D$ +22 (*c* 0.3, chloroform). ^{1}H NMR ($CDCl_3$) δ: 7.4–7.0 (m, 25H, 5Ph), 4.99 (d, 1H, $J_{1',2'}$ 3.5 Hz, H-1'), 4.21 (dd, 1H, $J_{1A,1B}$ 14.5 Hz, $J_{1A,2}$ 2.5 Hz, H-1A), 4.01 (m, 1H, H-2), 3.50 (overlapped, H-2'), 3.27 (s, 3H, CH_3O), 2.82 (dd, 1H, $J_{1B,2}$ < 1 Hz, H-1B). Anal. calcd. for $C_{49}H_{53}NO_{10}$: C 72.13, H 6.55, N 1.72; found: C 72.21, H 6.26, N 1.67.

*2,4-Di-O-benzyl-1,5-dideoxy-1,5-imino-3-O-(3,4,6-tri-O-benzyl-2-deoxy-α-D-*arabino*-hexopyranosyl)-D-mannitol (**61**)*

57 (85.5 mg, 0.109 mmol) in a 0.5 N potassium hydroxide solution in 90% ethanol (9.5 mL) was heated at 60°C for 3 h. It was neutralized with acetic acid, followed by solvent removal. The material was taken up in dichloromethane, and the solution was washed with a little water and evaporated. Chromatographic purification on a column of silica gel (dichloromethane – 3% methanol) afforded **61** (73.6 mg, 89%) as a syrup; $[\alpha]_D$ +20.6 (*c* 0.5, chloroform). ^{1}H NMR ($CDCl_3$) δ: 7.45–7.10 (m, 30H, 5Ph), 5.26 (unresolv. dd, 1H, $J_{1',2ax'}$ 3.0 Hz, $J_{1',2eq'}$ ~ 1 Hz, H-1'), 4.02 (ddd, 1H, $J_{3',4'}$ 9.0 Hz, $J_{2ax',3'}$ 11.5 Hz, $J_{2eq',3'}$ 4.5 Hz, H-3'), 3.89 (dt, 1H, $J_{4',5'}$ 9.5 Hz, H-5'), 3.54 (overlapped, H-4'), 3.06 (dd, 1H, $J_{1A,2}$ 2.5 Hz, $J_{1A,1B}$ 14.2 Hz, H-1A), 2.55 (m, 1H, H-5), 2.47 (d, 1H, $J_{1B,2}$ < 1 Hz, H-1B), 2.25 (dd, 1H, $J_{2eq',2ax'}$ 13.0 Hz, H-2eq'), 1.71 (ddd, 1H, H-2ax'). ^{13}C NMR ($CDCl_3$) δ: 99.69 (C-1'), 62.57, 61.66 (C-5, C-6), 46.57 (C-1), 35.82 (C-2'). Anal. calcd. for $C_{47}H_{51}NO_8$: C 74.28, H 7.03, N 1.84; found: C 74.26, H 7.14, N 1.75.

*2,4-Di-O-benzyl-1,5-dideoxy-1,5-imino-3-O-(2,4,6-tri-O-benzyl-3-O-methyl-α-D-glucopyranosyl)-D-mannitol (**62**)*

A solution of **53** (230 mg, 0.24 mmol) in methanolic 0.5 N sodium methoxide (2 mL) was left at room temperature for 17 h. The solvent was evaporated and the remainder (**58**) was taken up in 0.5 N sodium hydroxide in 90% ethanol (4 mL) and heated at 70°C for 30 h. It was neutralized with acetic acid, followed by evaporation. The resultant material was taken up in dichloromethane and the solution washed with a little water, followed by drying and

Can. J. Chem. Downloaded from www.nrcresearchpress.com by 203.198.23.82 on 09/08/12
For personal use only.

Can. J. Chem. Downloaded from www.nrcresearchpress.com by 203.198.23.82 on 09/08/12
For personal use only.

evaporation of the organic solution. Chromatographic purification of the crude product on a column of silica gel (dichloromethane – 3% methanol) afforded **62** (163.5 mg, 87%) as a tough syrup; $[\alpha]_D$ +31.3 (*c* 0.2, chloroform). ^{1}H NMR ($CDCl_3$) δ: 7.4–7.1 (m, 25H, 5Ph), 4.02 (unres. ddd, 1H, $J_{4',5'}$ 10.0 Hz, H-5′), 3.82 (unres. m, 1H, H-2), 3.63 (s, 3H, CH_3O), 3.03 (dd, 1H, $J_{1A,1B}$ 14.5 Hz, $J_{1A,2}$ 4.5 Hz, H-1A), 2.64 (m, 1H, H-5), 2.52 (bd, 1H, H-1B). Anal. calcd. for $C_{48}H_{53}NO_9$: C 73.17, H 6.78, N 1.78; found: C 72.84, H 6.98, N 1.71.

*2,4-Di-*O*-benzyl-1,5-dideoxy-1,5-imino-3-*O*-(2,3,4-tri-*O*-benzyl-6-*O*-methyl-α-*D*-glucopyranosyl)-*D*-mannitol (**63**)*

Compound **60** (220 mg, 0.27 mmol) in 0.9 N potassium hydroxide solution in 90% ethanol (5 mL) was heated at 60°C for 7 h. The mixture was neutralized with glacial acetic acid and evaporated to dryness. The remainder was taken up in dichloromethane, followed by washing of the organic solution with a little water, drying, and evaporation. Column chromatography on silica gel (dichloromethane – 3–5% methanol) provided syrupy **63** (190 mg, 89%); $[\alpha]_D$ +44 (*c* 0.2, chloroform). ^{1}H NMR ($CDCl_3$) δ: 7.4–7.15 (m, 25H, 5Ph), 4.01 (m, 2H, H-3′, H-5′), 3.81 (m, 1H, H-2), 3.48 (dd, $J_{1',2'}$ 3.5 Hz, $J_{2',3'}$ 9.5 Hz, H-2′), 3.22 (s, 3H, CH_3O), 3.08 (dd, 1H, $J_{1A,1B}$ 14.5 Hz, $J_{1A,2}$ 5.0 Hz, H-1A), 2.69 (m, 1H, H-5), 2.58 (dd, 1H, $J_{1B,2}$ 1.8 Hz, H-1B).

*1,5-Dideoxy-3-*O*-(2-deoxy-α-*D*-*arabino*-hexopyranosyl)-1,5-imino-*D*-mannitol (**64**)*

Compound **61** (55.4 mg, 0.073 mmol), 5% palladium-on-carbon (50 mg), and methanolic 0.12 N hydrochloric acid (759 μL, 0.09 mmol) in methanol (6 mL) were hydrogenated in the hydrogen stream for 2 h. The excess of acid was neutralized by a minimal amount of triethylamine to avoid hydrolysis of the glycosidic linkage. Usual processing and gel filtration provided **64** (22.2 mg, 88%) as a solid after lyophilization of an aqueous solution; $[\alpha]_D$ +53 (*c* 0.3, water). The ^{1}H and ^{13}C NMR data are reported in Tables 1 and 2.

*1,5-Dideoxy-1,5-imino-3-*O*-(3-*O*-methyl-α-*D*-glucopyranosyl)-*D*-mannitol-hydrochloride (**65**)*

A mixture of **62** (140 mg, 0.18 mmol), 5% palladium-on-carbon (140 mg), and methanolic 0.12 N hydrochloric acid (1.9 mL, 0.23 mmol) in methanol (7 mL) was hydrogenated in a hydrogen stream for 2 h. Usual processing provided **65** (64.3 mg, 96%) as a white solid; $[\alpha]_D$ +72 (*c* 0.2, water). The ^{1}H and ^{13}C NMR data are reported in Tables 1 and 2.

*1,5-Dideoxy-1,5-imino-3-*O*-(6-*O*-methyl-α-*D*-glucopyranosyl)-*D*-mannitol-hydrochloride (**66**)*

Compound **63** (190 mg, 0.24 mmol), 5% palladium-on-carbon (190 mg), and 0.12 N methanolic hydrochloric acid (2.5 mL, 0.3 mmol) in methanol (8 mL) were hydrogenated in the hydrogen stream for 2 h. Usual processing followed by gel-filtration (Sephadex LH 20, ethanol–water, 1:1) provided **66** (82.9 mg, 92%) as a white solid; $[\alpha]_D$ +67.8 (*c* 0.2, water). The ^{1}H and ^{13}C NMR data are reported in Tables 1 and 2.

Acknowledgements

Dr. Frank M. Unger's support of this project at Chembiomed Ltd. is gratefully acknowledged. We are deeply indebted to Professor R.U. Lemieux, Department of Chemistry, University of Alberta, thanks to whom the completion of the project and the preparation of this paper were possible. We thank Mrs. B. Jamieson-Hinz for the preparation of starting materials.

1. W.A. Lubas and R.G. Spiro. J. Biol. Chem. **262**, 3775 (1987).
2. W.A. Lubas and R.G. Spiro. J. Biol. Chem. **263**, 3990 (1988).
3. S. Hiraizumi, U. Spohr, and R.G. Spiro. J. Biol. Chem. **268**, 9927 (1993).
4. P.V. Nikrad, H. Beierbeck, and R.U. Lemieux. Can. J. Chem. **70**, 241 (1992).
5. R.U. Lemieux, M.-H. Du, U. Spohr, S. Acharya, and A. Surolia. Can. J. Chem. In press.
6. U. Spohr, M. Bach, and R.G. Spiro. Can. J. Chem. **71**, 1928 (1993).
7. G.W. Fleet, N.G. Ramsden, and D.R. Witty. Tetrahedron, **45**, 327 (1989).
8. K. Bock and H. Pedersen. Acta Chem. Scand. Ser. B: **B41**, 617 (1987).
9. P.W. Austin, F.E. Hardy, J.G. Buchanan, and J. Baddiley. J. Chem. Soc. 1419 (1965).
10. M. Nishizawa, Y. Kan, and H. Yamada. Chem. Pharm. Bull. **37**, 565 (1989).
11. P. Kovac, V. Sklenar, and C.P.J. Glaudemans. Carbohydr. Res. **175**, 201 (1988).
12. H.H. Bossard, R. Mory, M. Schmid, and H. Zollinger. Helv. Chim. Acta, **42**, 1653 (1959).
13. T. Iversen and D.R. Bundle. Carbohydr. Res. **103**, 29 (1982).
14. V.K. Srivastava and C. Schuerch. Tetrahedron Lett. **35**, 3269 (1979).
15. K. Yoshimoto and Y. Tsuda. Chem. Pharm. Bull. **31**, 4335 (1983).
16. J. Kihlberg, T. Frejd, K. Jansson, S. Kitzing, and G. Magnusson. Carbohydr. Res. **185**, 171 (1989).
17. S. Koto, N. Morishima, Y. Mori, H. Tanaka, S. Hayashi, Y. Iwai, and S. Zen. Bull. Chem. Soc. Jpn. **60**, 2301 (1987).
18. S. Tejima, R.K. Ness, R.L. Kaufman, and H.G. Fletcher, Jr. Carbohydr. Res. **7**, 485 (1968).
19. M. Hoch, E. Heinz, and R.R. Schmidt. Carbohydr. Res. **191**, 21 (1989).
20. F. Sugawara, H. Nakayama, G.A. Strobel, and T. Ogawa. Agric. Biol. Chem. **50**, 2251 (1986).
21. P. Boullanger and G. Descotes. Carbohydr. Res. **51**, 55 (1976).
22. J.-M. Lancelin, L. Morin-Allory, and P. Sinay. J. Chem. Soc. Chem. Commun. 335 (1984).
23. K. Bock and C. Pedersen. J. Chem. Soc. Perkin Trans. 2, 293 (1974).
24. A. Tan, L. van den Broek, S. van Boeckel, H. Ploegh, and J. Bolscher. J. Biol. Chem. **266**, 14504 (1991).
25. H. Hettkamp, G. Legler, and E. Bause. Eur. J. Biochem. **142**, 85 (1984).
26. J. Schweden, G. Legler, and E. Bause. Eur. J. Biochem. **157**, 563 (1986).
27. G. Legler. Adv. Carbohydr. Chem. Biochem. **48**, 319 (1990).
28. U. Spohr, M. Bach, and R.G. Spiro. Can. J. Chem. **71**, 1919 (1993).

The synthesis of the isomeric components of San Jose scale pheromone — an illustration of a stereospecific synthesis of trisubstituted alkenes

MARGOT ALDERDICE, CLAUDE SPINO,[1] AND LARRY WEILER[2]

Department of Chemistry, University of British Columbia, 2036 Main Mall, Vancouver, BC V6T 1Z1, Canada

Received April 14, 1993

MARGOT ALDERDICE, CLAUDE SPINO, and LARRY WEILER. Can. J. Chem. **71**, 1955 (1993).

The three isomeric components of the San Jose scale pheromone, **5**–**7**, have been synthesized from a common β-keto ester intermediate. A study of the alkylation of the dianion of methyl acetoacetate with a series of alkylating agents with the same carbon skeleton has been carried out. The trisubstituted alkenes in **5** and **6** have been synthesized stereospecifically via a copper-catalyzed coupling of a methyl Grignard reagent with the *E* or *Z* enol phosphate from the alkylated β-keto ester. In the case of the *Z* enol derivative, the coupling reaction was carried out on the diethyl- and diphenylphosphates, and the enol triflate. The diethyl enol phosphate gave the highest stereoselectivity. The synthetic pheromones were attractive to San Jose scale in the field.

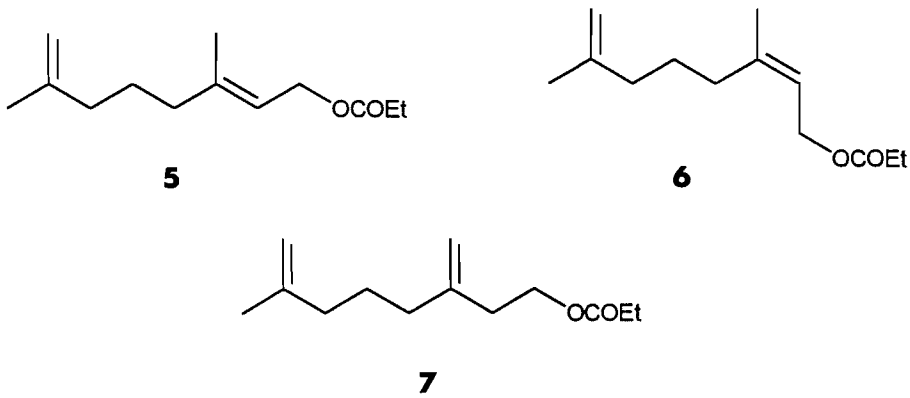

5 **6** **7**

MARGOT ALDERDICE, CLAUDE SPINO et LARRY WEILER. Can. J. Chem. **71**, 1955 (1993).

Utilisant un β-céto ester commun comme intermédiaire, on a synthétisé les trois isomères **5**–**7** de la phéromone du pou de San José. On a réalisé une étude de l'alkylation du dianion de l'acétoacétate de méthyle par une série d'agents d'alcoylation ayant le même squelette carboné. On a synthétisé les alcènes trisubstitués **5** et **6** d'une manière stéréospécifique en faisant appel à un couplage catalysé par le cuivre d'un méthyl magnésien avec le phosphate d'énol *E* ou *Z* obtenu à partir du β-céto ester alcoylé. Dans le cas du dérivé énolique *Z*, on a réalisé la réaction de couplage sur les phosphates énoliques diéthylé et de diphénylé et sur le triflate énolique. Le phosphate énolique diéthylique donne la meilleure stéréosélectivité. Dans les champs, les phéromones de synthèse attirent le pou de San José.

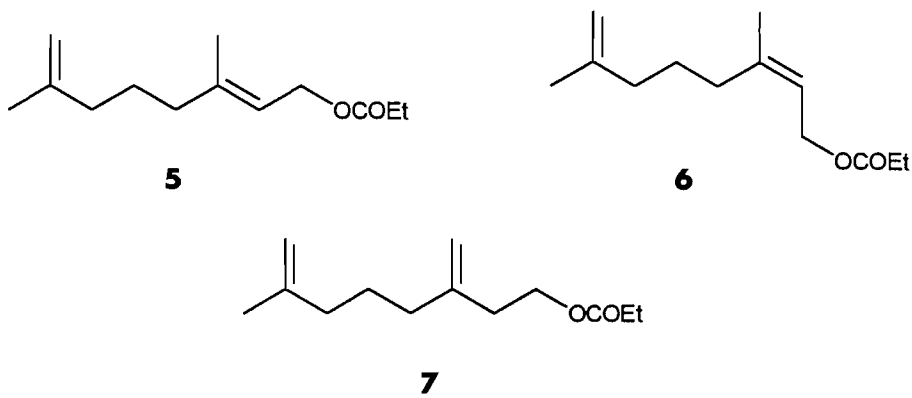

5 **6** **7**

[Traduit par la rédaction]

Introduction

The ability to introduce alkenes with control of the position and geometry of the double bond has led to significant advances in the synthesis of natural and unnatural products for several decades (1). Those methods which allow one to control the regio- and stereochemistry of the double bond often have the most widespread utility. The synthesis of tri- and tetrasubstituted alkenes is usually more challenging than that of disubstituted alkenes.

3,3-Dimethylacrylate esters undergo regioselective deprotonation (2), and subsequent alkylation of the derived lithium carbanions usually occurs at the α-carbon, although the copper enolate of the dianion from the corresponding acid was found to react with allylic halides at the γ-carbon (3).

[1]Present address: Department of Chemistry, University of Victoria, P.O. Box 3055, Victoria, BC, V8W 3P6, Canada.

[2]Author to whom correspondence may be addressed.

Can. J. Chem. Downloaded from www.nrcresearchpress.com by 203.198.23.82 on 09/08/12
For personal use only.

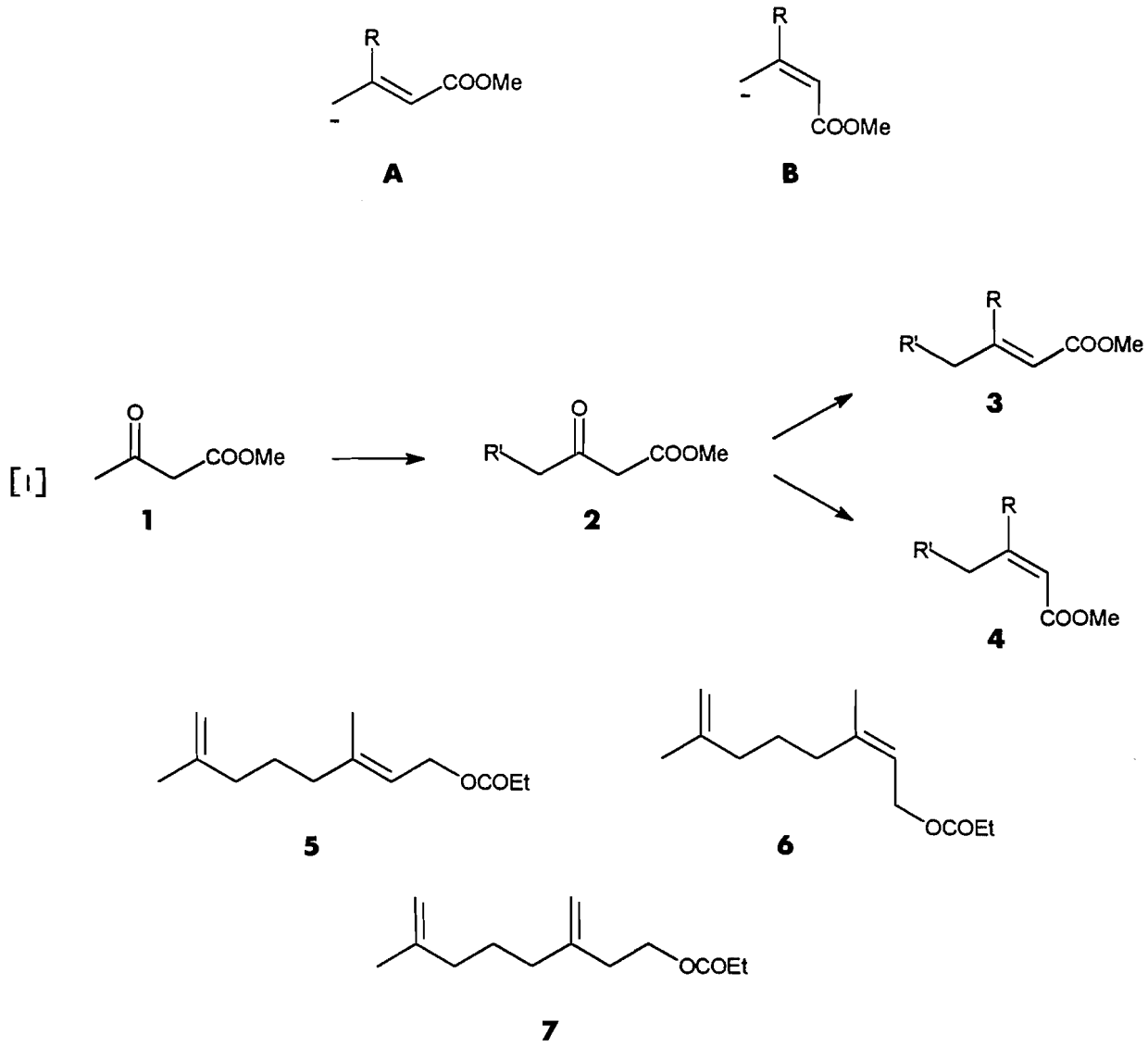

A general method to directly alkylate the carbanion corresponding to synthons **A** or **B** has not been reported to date. The Horner-Wadsworth-Emmons reaction has proven useful in the synthesis of molecules of structure **3** in which the group R is "smaller" than the $R'CH_2$ (4) group. The conjugate addition of cuprates to alkynes (5) has provided a highly stereoselective route to compounds of the type **3** (6). A recent very promising method utilizes the stereospecific conjugate addition of a stannyl cuprate to propargyl esters to give either the (*E*)- or (*Z*)-3-stannyl-2-alkenoate depending on the reaction conditions (7). Subsequent coupling of the vinyl stannane or halogenation followed by coupling gives the (*E*)- or (*Z*)-trisubstituted alkene (8).

A few years ago we developed a method for the stereospecific synthesis of the trisubstituted alkenes **3** or **4** (9). This, in combination with the dianion alkylation of β-keto esters such as **1** (10), led to a method to introduce the units **A** or **B** into a synthetic intermediate via the pathway outlined in eq. [1]. In this paper we report the application of this methodology to the synthesis of the three components of the San Jose scale pheromone.

The San Jose scale, *Quadraspidiotus pernicious*, is a widespread insect pest that attacks fruit and ornamental trees. San Jose scale is a particularly serious pest in the apple orchards of the southern Okanagan Valley of British Columbia. The insect is controlled by heavy pruning, and extensive spraying of dormant oil and organophosphates. By optimizing the timing of the organophosphate sprays, which are targeted at the mature male stage of the insect (11), the amount of spray required for control can be reduced significantly. The female scale produces a mixture of three compounds that are highly attractive to the male species. The structures of the three compounds, **5**–**7**, were solved by spectroscopic methods (12) and confirmed by synthesis (13).

Following the preliminary communication of our work (14), two other syntheses of these compounds were reported (15). The first of these syntheses involved a regioselective allylic chlorination of the propionate esters of geraniol or nerol followed by reduction of the allylic halide to give **5** or **6** as shown in eq. [2] (15*a*). The second method relied on the photochemical isomerization of the conjugated ester shown in eq. [3] to a mixture of the β,γ-unsaturated esters in which the desired disubstituted alkene was the major component and it was converted into **7** (15*b*).

Can. J. Chem. Downloaded from www.nrcresearchpress.com by 203.198.23.82 on 09/08/12
For personal use only.

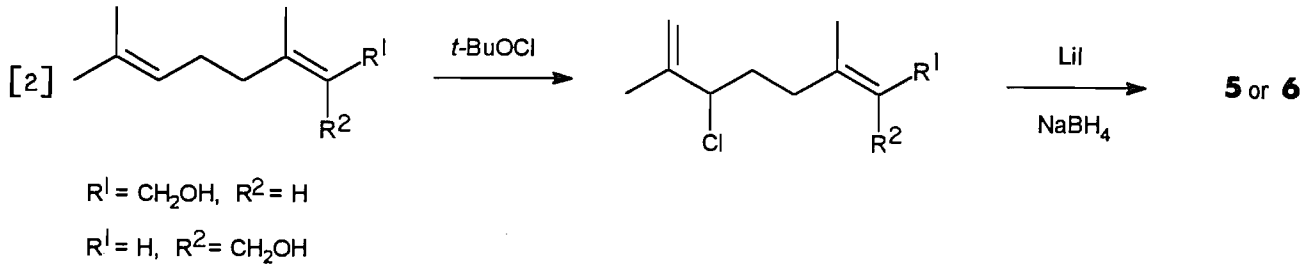

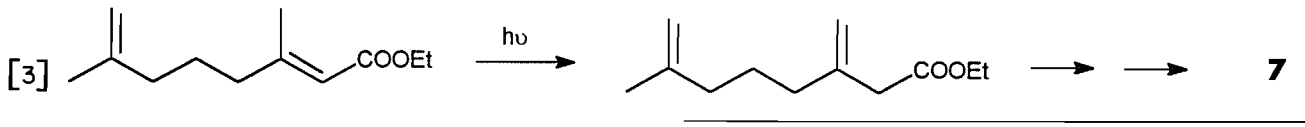

TABLE 1. Alkylation of the dianion from methyl acetoacetate (**8**) with alkylating agents **9**[a]

Entry	**9**, X =	Yield of **10**[b] (%)
1	Br	70
2	I	65
3	$PhSO_3$	62
4	TsO	56
5	TfO	45
6	$MeSO_3$	40

[a]All alkylations were carried out by adding **9** to the solution of the dianion in THF at 0°C.
[b]Yield of distilled product **10**.

TABLE 2. Copper-catalyzed Grignard coupling with enol derivatives **11**[a]

Entry	**11**, R =	Yield of **12**[b]	*E*:*Z*
a	$PO(OPh)_2$	78%	90:10
b	$PO(OEt)_2$	70%	98:2
c	OTf	82%	88:12

[a]Coupling reactions were carried out by adding the enol derivative **11** to a solution of MeCu and MeMgCl in THF at −25°C.
[b]Yield of distilled or chromatographed product **12**.

Results and discussion

We sought a method to prepare all three of the San Jose scale pheromone components from a common intermediate. An obvious choice for this intermediate is the β-keto ester **10**, which would be readily available from the dianion **8** of methyl acetoacetate and an alkylating agent derived from 3-methyl-3-buten-1-ol (**9**, X = OH). This provided an opportunity to evaluate the utility of various alkylating agents in the reaction with the dianion of methyl acetoacetate. Table 1 contains the results of a study of leaving groups in this alkylation. The highest yields are obtained with halides, although the aryl sulfonates are usually easier to prepare and purify. Thus, we found the benzenesulfonate to be best for the large scale preparation of **10**. In the case of hindered alkylating agents we have found that the triflate is the best leaving group (16).

The β-keto ester **10** was converted into the *Z*-enol phosphates and enol triflate **11**. These reactions were very stereoselective. The enol derivative **11***b* was obtained in excellent yield and the greater than 99% *Z* as determined by GC. The stereochemistry of the olefin was proven by ^1H NMR. Next we undertook a study of the coupling reaction of these enol derivatives with the methyl Grignard reagent in the presence of a copper catalyst (17). The diphenyl phosphate and triflate gave a higher yield of **12**, but with a lower stereoselectivity (Table 2). Because of the difficulty in separating the geometric isomers of **12**, experimentally we found the diethyl phosphate coupling to be the most satisfactory to carry out in this case.

The *E*-alkene **12** was then converted into the *E* pheromone **5** by reduction and esterification in greater than 80% yield for the two steps. This compound had identical spectroscopic properties and biological activity to the natural pheromone.

By altering the reaction conditions, we are able to cleanly prepare the *E*-enol phosphate **13**. This stereoselectivity takes advantage of the fact that in ether solvents the metal cation enolates are tight ion pairs and in these solvents exist as the coordinated complex **15**, whereas in more polar solvents, such as HMPA and organic cationic counterions, the enolate is free and exists in the W-conformation **16** in which the negatively charged oxygens are distant from each other (18). In each case the O-alkylating agent traps the enolate before any conformational isomerization. Thus **16** gives **13** in good yield with no trace of any *Z*-enol phosphate **11***b* in the crude reaction mixture as determined by GC. The copper-catalyzed Grignard coupling of **13** then gives **14** in good yield and excellent stereoselectivity. Ester **14** was reduced and esterified to give the pheromone **6**, which was identical to the naturally occurring compound.

The synthesis of the third component of the pheromone mixture, alkene **7**, presented a different problem if we were to use the β-keto ester **10** as starting material. Due to the acidity of the α-methylene protons, Wittig reactions and their variations proceed in low yield on enolizable β-keto esters. We had shown that trimethylsilylmethylmagnesium chlo-

Can. J. Chem. Downloaded from www.nrcresearchpress.com by 203.198.23.82 on 09/08/12
For personal use only.

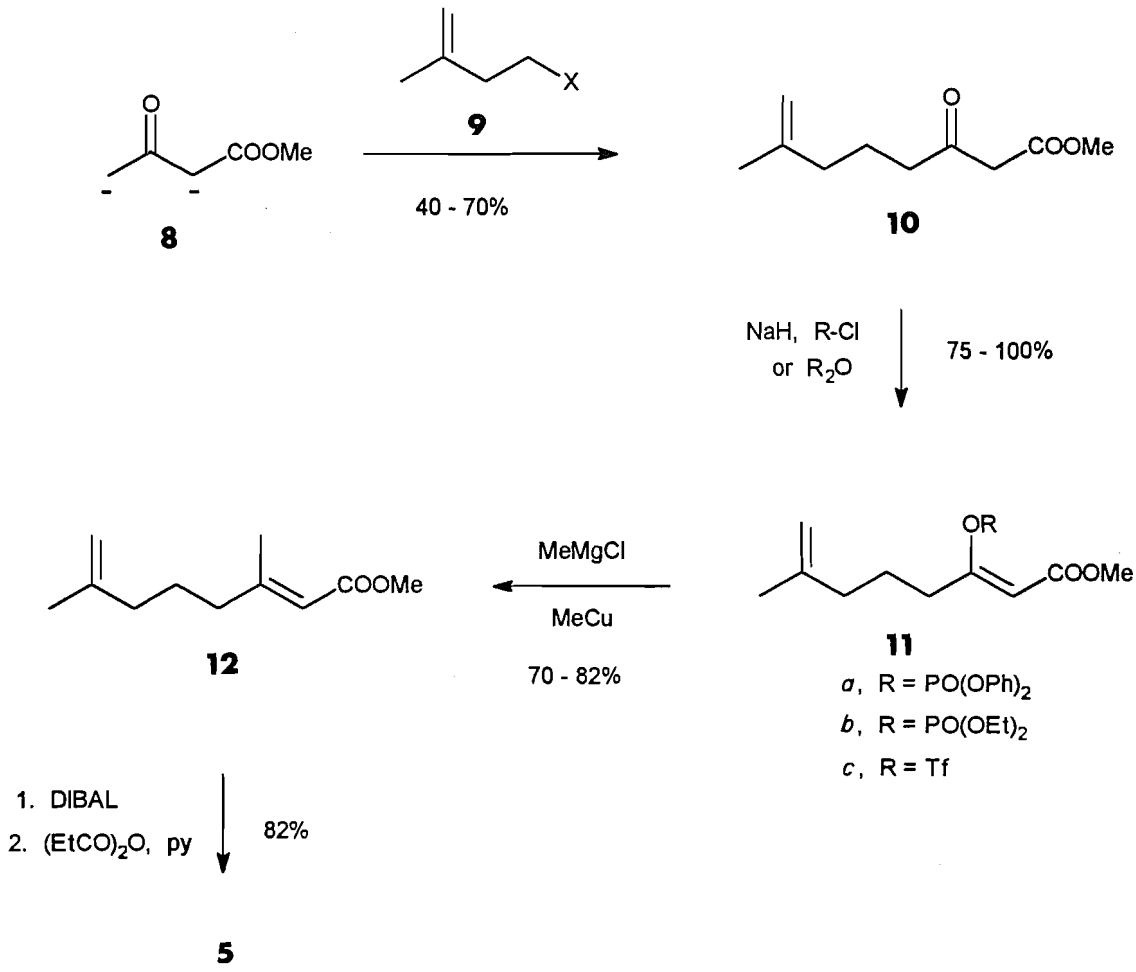

ride in the presence of nickel(II) added cleanly to enol phosphates of β-keto esters (19). Indeed the addition of these reagents to **11***b* or **13** gave the corresponding allyl silanes **17** and **18**, respectively. Treatment of these allyl silanes with a variety of protic and Lewis acids gave the cyclized compound **19** as the only isolable product. If the reaction was allowed to continue for longer periods of time **19** did slowly isomerize to the endocyclic isomers. Thus electrophilic attack on the terminal disubstituted alkene is faster than attack on the conjugated alkene, and the deactivating effect of the ester must be greater than the activating effect of the allylic trimethylsilyl group (20).

This problem was eventually solved by reducing the ester and then carrying out an olefination reaction. Ester reduction was achieved in two ways. The first involved formation of the monoanion of the β-keto ester **10** and reduction of this monoanion with DIBAL (21) to **20**. In the second method, the ketone carbonyl was converted into its silyl enol ether. The ester was then reduced and the enol ether hydrolyzed during work-up to give **20**. In our hands the latter route, although longer, consistently gave better yields of **20**. The keto alcohol **20** was then esterified and treated with the modified Tebbe reagent (22) to give **7**, which was identical in spectroscopic properties and biological activity to the third component of the San Jose scale pheromone.

Thus we have illustrated the utility of the methodology to stereoselectively introduce the units **A**, **B**, or **C** into a molecule using the alkylation of the dianion of a β-keto ester. The three synthetic components **5**–**7** were used to monitor San Jose scale in the Okanagan Valley. All three isomers were active in the field and the *E* isomer **5** was the most attractive of the three at the same release rates (23).

Experimental section

General procedures

Kugelrohr distillations were performed with a Büchi Kugelrohr apparatus. Infrared spectra were recorded in chloroform solution on a Perkin–Elmer model 710 spectrophotometer, and were calibrated with the 1601 cm^{-1} band of polystyrene. Proton nuclear magnetic resonance spectra were recorded on a Varian T-60 (60 MHz) and a Bruker WP-80 (80 MHz). Chemical shifts are reported on the δ scale, with $CDCl_3$ as solvent and tetramethylsilane as internal standard. The multiplicity, coupling constants (if determined), and integrated peak areas are given in parentheses after each signal. Low-resolution mass spectra were recorded on a Kratos-AEI MS-50, and high-resolution mass measurements were determined on a Kratos-AEI MS-9 or MS-50. Both instruments were operated at an ionization potential of 70 eV. Elemental analyses were performed by Mr. Peter Borda, Microanalysis Laboratory, University of British Columbia.

Silica gel $PF_{254+366}$ (E. Merck) was used for both analytical and preparative thin-layer chromatography, while flash chromatography (24) was carried out using Silica Gel 60, 230–400 mesh ASTM (E. Merck). All mixed solvent systems are expressed in ratios by volume.

The petroleum ether used was of the boiling range 30–60°C. Dry solvents were prepared as follows: diethyl ether and tetrahydrofuran by distillation from lithium aluminium hydride or sodium–

Can. J. Chem. Downloaded from www.nrcresearchpress.com by 203.198.23.82 on 09/08/12
For personal use only.

Can. J. Chem. Downloaded from www.nrcresearchpress.com by 203.198.23.82 on 09/08/12
For personal use only.

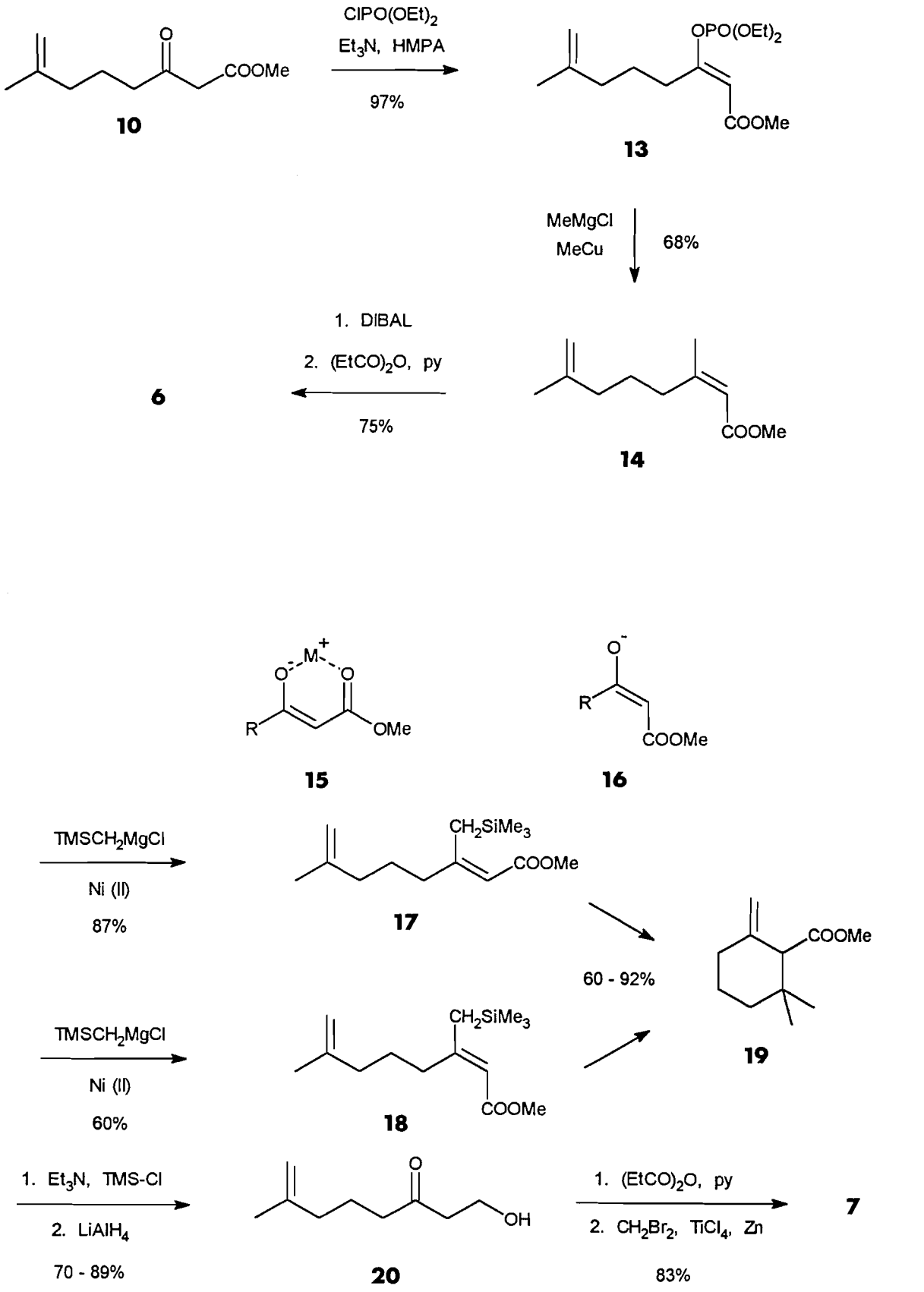

benzophenone; dichloromethane by distillation from phosphorus pentoxide; and acetone by distillation from Drierite. *n*-Butyllithium and diisobutylaluminium hydride solutions were obtained from Aldrich. The *n*-BuLi solutions were standardized by titration against 0.1 M *tert*-butanol solution using 1,10-phenanthroline as indicator (25). Sodium hydride (Aldrich) was weighed as a 60% dispersion in mineral oil and washed with ether or petroleum ether to remove the oil prior to use. All reactions were run under a dry nitrogen at-

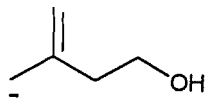

c

mosphere and organic extracts were dried with anhydrous magnesium sulfate.

*4-Bromo-2-methyl-1-butene (**9**a)*

This compound was prepared from 1.4 g (16 mmol) of 3-methyl-3-buten-1-ol in 42% distilled yield according to the procedure of Bhanot and Dutta (26) to give a colourless oil; bp 105°C/760 Torr (1 Torr = 133.3 Pa) (lit. (26) bp 105–107°C/760 Torr); ^{1}H NMR (60 MHz) δ: 1.76 (bs, 3H), 2.53 (t, J = 7 Hz, 2H), 3.43 (t, J = 7 Hz, 2H), and 4.7–5.0 (m, 2H).

*4-Iodo-2-methyl-1-butene (**9**b)*

A solution of 10.0 g (42 mmol) of the tosylate **9***d* (see below) was dissolved in 160 mL of a dry acetone-saturated solution of NaI. This solution was stirred at room temperature overnight. Then the solid salts were filtered off and the precipitate was washed several times with acetone. The acetone was evaporated under reduced pressure. The resulting oil was dissolved in 100 mL of ether and washed with 2 × 50 mL of 10% aqueous $Na_2S_2O_3$. The aqueous layers were extracted with 3 × 50 mL of ether. The ether layers were combined, dried, and the solvents were removed under reduced pressure to yield 5.9 g (72%) of a crude product, which was one spot by TLC and was suitable for the subsequent dianion alkylation. This material was a pale orange oil that gradually darkened on standing; ^{1}H NMR (60 MHz) δ: 1.70 (bs, 3H), 2.57 (t, J = 7 Hz, 2H), 3.23 (t, J = 7 Hz, 2H), and 4.77 (bd, J = 4 Hz, 2H); HRMS calcd. for C_5H_9I: 195.9749; found: 195.9753.

*3-Methyl-3-butenyl-1-benzenesulfonate (**9**c)*

A solution of 8.00 g (93 mmol) of 3-methyl-3-buten-1-ol in 100 mL of CH_2Cl_2 was flushed with N_2 and cooled in an ice bath. Pyridine (14.7 g, 15.0 mL, 0.186 mol) and benzenesulfonyl chloride (16.4 g, 11.8 mL, 0.093 mol) were added, and the resulting solution was stirred at 0°C for 4 h. The reaction mixture was then diluted with cold ether and acidified with cold 1 M HCl. The organic layer was separated, washed with cold saturated aqueous $NaHCO_3$ solution, cold brine, dried, filtered, and concentrated to give a quantitative yield (21.0 g) of the benzenesulphonate **9***c* as a yellow oil. The benzenesulfonate is relatively unstable and is best stored at 0°C or lower. The material darkens quickly at room temperature and should be used as soon as possible. ^{1}H NMR (60 MHz) δ: 1.60 (bs, 3H), 2.32 (t, J = 7 Hz, 2H), 4.13 (t, J = 7 Hz, 2H), 4.68 (bd, 2H), and 7.25–7.9 (m. 5H); HRMS calcd. for $C_{11}H_{14}O_3S$: 226.0664; found: 226.0671.

*3-Methyl-3-butenyl-1-p-toluenesulfonate (**9**d)*

This material was prepared from 2.0 g (23 mmol) of 3-methyl-3-buten-1-ol in 97% crude yield according to the procedure of Trost and Kunz (27) to give **9***d* as a yellow oil that was used directly in the dianion alkylation or to prepare the iodide **9***b* above.

*3-Methyl-3-butenyl-1-trifluoromethanesulfonate (**9**e)*

To a solution of 73 μL (0.91 mmol) of pyridine in 1 mL of CH_2Cl_2 at −40 to −50°C was added 140 μL (0.82 mmol) of freshly purified trifluoromethanesulfonic anhydride with stirring. A white precipitate formed immediately and after 5 min a solution of 71 mg (0.82 mmol) of 3-methyl-3-buten-1-ol was added to the mixture. The mixture was stirred at −40 to −50°C for 15 min, The precipitate was filtered off and washed with cold hexane. The filtrates were combined and the solvents removed under reduced pressure while maintaining the temperature below 0°C. The residue was dissolved in cold hexane (−20°C), and filtered. The solvent was removed from the filtrate while maintaining the temperature below 0°C to yield 165 mg (92%) of the triflate **9***e* as a pink oil that was used directly in the dianion step.

*3-Methyl-3-butenyl-1-methanesulfonate (**9**f)*

To a solution of 0.67 mL (4.8 mmol) of triethylamine in 10 mL of ether at 0°C was added a solution of 0.30 g (3.5 mmol) of 3-methyl-3-buten-1-ol in 10 mL of ether. After stirring at 0°C for 5 min, 0.27 mL (3.5 mmol) of methanesulfonyl chloride was added to the reaction, and the mixture was stirred at 0°C for 1 h and then warmed to room temperature. The reaction was quenched with 1 M HCl, and the organic phase was washed with 2 × 10 mL of 1 M HCl, 2 × 10 mL of saturated $NaHCO_3$, once with saturated brine, and dried. The solvent was removed under reduced pressure to yield 0.57 g (quantitative) of the mesylate **9***f* as a colourless oil that could be used directly in the dianion alkylation. A small amount was purified by chromatography using petroleum ether – ethyl acetate (6:1) to give pure **9***f* as a colourless oil; ^{1}H NMR (60 MHz) δ: 1.65 (bs, 3H), 2.45 (t, J = 7 Hz, 2H), 3.01 (s, 3H), 4.35 (t, J = 7 Hz, 2H), and 4.78 (bd, 2H); HRMS calcd. for $C_6H_{12}O_3S$: 164.0507; found: 164.0500.

*Methyl 7-methyl-3-oxo-7-octenoate (**10**)*

The dianion of methyl acetoacetate was prepared by using the following general procedure (10). Sodium hydride (60% by weight in oil, 1.12 equiv.) was weighed into a flask, washed under a N_2 atmosphere with ether, and resuspended in dry tetrahydrofuran. The flask was sealed, flushed with N_2, and cooled in an ice bath. Methyl acetoacetate (1.00 equiv.) was syringed dropwise into the NaH suspension, and the resulting monoanion was stirred at 0°C for 15 min, before the *n*-butyllithium (2.0 M in hexane, 1.12 equiv.) was syringed dropwise into the cooled reaction mixture. The resulting orange dianion solution was stirred at 0°C for 15 min. In the case of the triflate **9***e*, the dianion solution was cooled to −40°C for the addition of the alkylating agent. The alkylating agent (0.80 equiv.) dissolved in minimum dry THF was then syringed dropwise into the flask. No immediate change occurred, but within 5 min the reaction mixture became a lighter orange and was more difficult to stir due to the abundant formation of precipitate. The suspension was stirred for 1 h at 0°C, warmed to room temperature and stirred for a further 2 h.

The reaction mixture was diluted with ether and acidified with 1 M HCl. The organic layer was separated, washed with saturated aqueous $NaHCO_3$ solution, brine, dried, filtered, and concentrated to give the crude β-keto ester. This material was distilled at 0.3 Torr and the distillate boiling from 74–76°C was collected to give the desired product **10**. The yields of pure distilled product are given in Table 1. The β-keto ester **10** is a colourless oil; IR ν_{max}: 900, 1660, 1715, and 1745 cm^{-1}; ^{1}H NMR (80 MHz) δ: 1.70 (bs, 3H), 1.6–2.2 (m, 4H), 2.52 (t, J = 7 Hz, 2H), 3.45 (s, 2H), 3.73 (s, 3H), and 4.65 (m, 2H); MS m/z (relative intensity): 41 (57), 43 (87), 55 (77), 59 (42), 68 (56), 69 (58), 74 (100), 101 (37), 111 (35), 116 (75), 117 (34), 129 (37), 166 (18) and 184 (24). Anal. calcd. for $C_{10}H_{16}O_3$: C 65.19, H 8.75; found: C 65.16, H 8.80.

*Methyl (2Z)-3-(diethylphosphoryloxy)-7-methyl-2,7-octadienoate (**11**a)*

Sodium hydride (60% by weight in oil, 0.238 g, 5.97 mmol) was weighed into a flask, washed under a N_2 atmosphere with 15 mL of ether, and resuspended in 20 mL of fresh ether. The flask was flushed with N_2 and cooled in an ice bath. The β-keto ester **10** (1.00 g, 5.43 mmol) dissolved in 5 mL of ether was added dropwise to the NaH suspension. The resulting monoanion was stirred at 0°C for 15 min before diethyl chlorophosphate (0.984 g, 0.82 mL, 5.70 mmol) was syringed dropwise into the cooled reaction mixture. Within 30 min a thick white precipitate had formed (NaCl) and stirring was continued overnight at room temperature.

The reaction mixture was quenched with saturated aqueous NH_4Cl solution and then acidified with 1 M HCl. The organic layer was separated, washed with saturated aqueous $NaHCO_3$ solution, washed with brine, dried, filtered, and concentrated to give 1.74 g (100%) of the crude enol phosphate, which was suitable for the coupling reaction. The product was >99% *Z* by GC analysis. This material was purified by column chromatography using pe-

Can. J. Chem. Downloaded from www.nrcresearchpress.com by 203.198.23.82 on 09/08/12
For personal use only.

troleum ether – ethyl acetate (1:1) to give 1.30 g (75%) of the enol phosphate **11***a* as a pale yellow oil; IR ν_{max}: 990, 1020, 1270, 1420, 1670, and 1725 cm^{-1}; ^1H NMR (80 MHz) δ: 1.35 (dt, J = 1 and 7 Hz, 6H), 1.70 (bs, 3H), 1.6–2 (m, 2H), 2–2.3 (m, 2H), 2.43 (bt, J = 7 Hz, 2H), 3.67 (s, 3H), 4.25 (q, J = 7 Hz, 4H), 4.70 (bs, 2H), and 5.41 (s, 1H); MS m/z (relative intensity): 41 (22), 79 (29), 81 (22), 99 (80), 127 (55), 134 (42), 155 (100), 164 (10), 166 (30), 177 (9), 192 (21), 220 (25), 252 (12), 289 (6), 320 (2). Anal. calcd. for $C_{14}H_{25}O_6P$: C 52.50, H 7.87; found: C 52.57, H 7.90.

*Methyl (2Z)-3-(diphenylphosphoryloxy)-7-methyl-2,7-octadienoate (**11**b)*

This compound was prepared following the same method as for **11***a* using 0.24 g (6.0 mmol) of NaH (60% by weight), 1.0 g (5.4 mmol) of ester **10**, and 1.5 g (5.6 mmol) of diphenyl chlorophosphate to quantitatively yield the enol phosphate **11***b*, which was used in the coupling reaction. A small sample of this material was purified by column chromatography using petroleum ether – ethyl acetate (4:1) to give pure **11***b* as a colourless oil; IR ν_{max}: 1020, 1625, 1685, and 1725 cm^{-1}; ^1H NMR (60 MHz) δ: 1.65 (bs, 3H), 2 (m, 4H), 2.51 (bt, J = 7 Hz, 2H), 3.72 (s, 3H), 4.74 (bs, 2H), 5.64 (s, 1H), and 7.2–7.7 (m, 10H); HRMS calcd. for $C_{22}H_{25}O_6P$: 416.1389; found: 416.1395.

*Methyl (2Z)-3-(trifluoromethylsulfonyloxy)-7-methyl-2,7-octadienoate (**11**c)*

The β-keto ester **10** (1.00 g, 5.43 mmol) in 50 mL of dry THF was added to 0.24 g (6.0 mmol) of NaH (60% by weight) and cooled to −78°C. Then 1.55 g (5.50 mmol) of Tf_2O was slowly added and the reaction mixture was allowed to warm to room temperature over several hours. The reaction mixture was quenched with saturated aqueous NH_4Cl solution and then acidified with 1 M HCl. The organic layer was separated, washed with saturated aqueous $NaHCO_3$ solution, washed with brine, dried, filtered, and concentrated to give 1.7 g (ca. 100%) of the crude enol triflate **11***c*, which was suitable for the coupling reaction. A small amount of this material was purified by thin-layer chromatography using petroleum ether – ethyl acetate (9:1) to give pure **11***c* as a colourless oil; IR ν_{max}: 1630, 1665, and 1735 cm^{-1}; ^1H NMR (60 MHz) δ: 1.68 (bs, 3H), 2 (m, 4H), 2.51 (bt, J = 7 Hz, 2H), 3.70 (s, 3H), 4.65 (bs, 2H), and 5.52 (s, 1H); HRMS calcd. for $C_{11}H_{15}O_5F_3S$: 316.0592; found: 316.0587.

Preparation of the stock methylmagnesium chloride solution

Magnesium turnings (9.37 g, 0.385 mol) were weighed into a 500-mL, three-necked, round-bottom flask, equipped with a Dry Ice condenser and gas bubbling frit. The apparatus was sealed, flushed with N_2, and dried with a hot air gun. Dry THF (250 mL) was syringed into the flask, the condenser was cooled, and methyl chloride was bubbled into the stirred suspension. The Grignard reaction commenced immediately and was so vigorous that an ice bath was required to keep the reaction under control. As the reaction slowed, more methyl chloride was bubbled into solution. This procedure was repeated until all the magnesium had reacted (about 2 h). The resulting solution (with a fine black suspension) was cannulated into a stoppered, N_2 flushed bottle, and then titrated.

The titration was carried out as a back-titration. A 1 mL aliquot of the Grignard reagent was quenched with 50 mL of 0.05 M HCl. The resulting solution was titrated to a phenolphthalein endpoint using 0.1 M NaOH to give the total base concentration.

*Methyl (2E)-3,7-dimethyl-2,7-octadienoate (**12**)*

*(a) From the enol phosphate **11**a*

Purified cuprous iodide (28) (3.57 g, 0.019 mol) and 100 mL of THF were added to a 250-mL flask, which was equipped with an internal thermometer. The flask was flushed with N_2 and cooled to 0°C. Methyllithium (1.25 M in ether, 15 mL, 0.019 mol) was syringed dropwise into the stirred white suspension while keeping the internal temperature below 10°C. The resulting yellow MeCu suspension was stirred at 0°C for 10 min and then cooled to −30°C. Methylmagnesium chloride (1.3 M in THF, 24 mL, 0.031 mol) was syringed dropwise into the flask while maintaining the internal temperature below −25°C. The resulting clear, tan-coloured solution was stirred at −30°C for 15 min before a THF solution of the enol phosphate **11***a* (2.0 g, 6.2 mmol) was syringed into the flask. The resulting deep maroon solution was stirred for 3 h at −25°C.

The reaction mixture was quenched by pouring it quickly into a stirred, ice-cold mixture of NH_4Cl in aqueous NH_4OH. The organic layer was diluted with ether and washed with NH_4Cl in aqueous NH_4OH until these washes were no longer blue. The ethereal layer was washed with brine, dried, and the solvents removed under reduced pressure to give 1.05 g (92%) of the crude product as yellow oil that was purified by flash column chromatography using petroleum ether – ethyl acetate (19:1) to give 0.795 g (70%) of the ester **12**. The ratio of E:Z was determined by GC to be 98:2. The ester is a colourless oil, bp (Kugelrohr distillation) 65°C/0.1 Torr; IR ν_{max}: 1150, 1445, 1655, and 1715 cm^{-1}; ^1H NMR (80 MHz) δ: 1.70 (bs, 3H), 1.5–1.8 (m, 2H), 1.9–2.3 (m, 4H), 2.16 (d, J = 1 Hz, 3H), 3.68 (s, 3H), 4.70 (bs, 2H), and 5.65 (m, 1H); MS m/z (relative intensity): 41 (100), 55 (35), 59 (25), 67 (67), 68 (75), 69 (50), 81 (25), 82 (23), 83 (35), 95 (55), 108 (40), 114 (38), 122 (20), 123 (24), 124 (24), 125 (20), 135 (15), 139 (40), 150 (8), 167 (12), 182 (7). Anal. calcd. for $C_{11}H_{18}O_2$: C 72.49, H 9.95; found: C 72.56, H 9.90.

*(b) From the enol phosphate **11**b*

In the same manner as above, using 1.5 g (3.6 mmol) of the diphenyl phosphate **11***b*, 0.51 g (78%) of chromatographed ester **12** was obtained. The ratio of E:Z was 90:10 as determined by GC.

*(c) From the enol triflate **11**c*

In the same manner as above, using 1.2 g (3.8 mmol) of the triflate **11***c*, 0.57 g (82%) of chromatographed ester **12** was obtained. The ratio of E:Z was 88:12 as determined by GC.

(2E)-3,7-Dimethyl-2,7-octadien-1-ol

The α,β-unsaturated ester **12** (1.364 g, 7.48 mmol) was dissolved in 30 mL of ether, flushed with N_2, and cooled to 0°C. As diisobutylaluminium hydride (1 M in hexane, 18.7 mL, 1.87 mmol) was syringed into the flask, the reaction mixture became yellow, but the colour faded as all the DIBAL was added. Stirring was continued for 2 h at 0°C. The reaction was quenched at 0°C with saturated aqueous NH_4Cl solution and allowed to stir at this temperature for 1 h. The aluminum salts solidified into a sticky solid top layer, which was broken up and poured into a separatory funnel along with the aqueous and organic layers. This mixture was acidified with 1 M HCl and was shaken until the solid had dissolved. The ethereal layer was separated, washed several times with brine, dried, and the solvents were removed under reduced pressure to give 1.13 g (98%) of the alcohol as a yellow oil. The crude material was purified by column chromatography using petroleum ether – ethyl acetate (4:1) to give 0.96 g (84%) of the alcohol, which was shown to be 96% pure by GC. IR$_{\nu_{max}}$: 900, 995, 1660, 1680, 3475, and 3625 cm^{-1}; ^1H NMR (80 MHz) δ: 1.2–1.7 (m, 2H), 1.67 (bs, 3H), 1.70 (bs, 3H), 1.8–2.2 (m, 4H), 4.14 (d, J = 7 Hz, 2H), 4.67 (bs, 2H), and 5.65 (t, J = 7 Hz, 1H); MS m/z (relative intensity): 41 (100), 43 (37), 53 (27), 55 (46), 67 (36), 68 (65), 69 (75), 71 (40), 81 (40), 83 (34), 93 (17), 95 (35), 107 (10), 109 (14), 121 (18), 123 (11), 136 (14), 139 (2), 154 (1). Anal. calcd. for $C_{10}H_{18}O$: C 77.87, H 11.76; found: C 77.76, H 11.64.

E *Pheromone **5***

The above E alcohol (1.43 g, 9.27 mmol) and a catalytic amount of 4-dimethylaminopyridine (10 mg) were dissolved in 50 mL of ether under N_2. Propionic anhydride (1.33 g, 1.31 mL, 0.010 mol) and pyridine (1.46 g, 1.49 mL, 0.019 mol) were syringed into the reaction mixture, which was stirred at room temperature for 24 h. The reaction mixture was washed with 1 M HCl to remove pyridine. The organic layer was separated, washed with saturated aqueous $NaHCO_3$ solution and brine, dried, and the solvents were removed under reduced pressure to give 1.94 g (100%) of product

Can. J. Chem. Downloaded from www.nrcresearchpress.com by 203.198.23.82 on 09/08/12
For personal use only.

Can. J. Chem. Downloaded from www.nrcresearchpress.com by 203.198.23.82 on 09/08/12
For personal use only.

as a light yellow liquid. The crude material was Kugelrohr distilled at 85–90°C/0.05 Torr to give 1.87 g (96%) of the desired propionate **5** as a colourless oil; $IR_{\nu_{max}}$: 1195, 1660, 1680, and 1730 cm^{-1}; ^1H NMR (80 MHz) δ: 1.12 (t, J = 7 Hz, 3H), 1.2–1.7 (m, 2H), 1.70 (bs, 6H), 1.8–2.2 (m, 4H), 2.32 (q, J = 7 Hz, 2H), 4.6–4.8 (m, 4H), and 5.33 (t, J = 7 Hz, 1H); MS m/z (relative intensity): 53 (40), 55 (60), 57 (100), 68 (100), 69 (60), 79 (56), 80 (56), 81 (90), 93 (64), 94 (25), 95 (30), 96 (56), 97 (24), 107 (50), 108 (25), 109 (25), 121 (80), 136 (71), 139 (5), 154 (20), 195 (0.5), 210 (0.5). Anal. calcd. for $C_{13}H_{22}O_2$: C 74.24, H 10.54; found: C 74.00, H 10.65.

*Methyl (2E)-3-(diethylphosphoryloxy)-7-methyl-2,7-octadienoate (**13**)*

4-Dimethylaminopyridine (0.146 g, 1.2 mmol), triethylamine (1.21 g, 1.67 mL, 12.0 mmol), HMPA (2.15 g, 2.09 mL, 12.0 mmol), and the β-keto ester **10** (2.00 g, 10.9 mmol) were added to a flask. The resulting yellow solution was stirred for 30 min at 0°C and then cooled to −20°C. Diethyl chlorophosphate (2.07 g, 12.0 mmol) was added dropwise to the cooled solution and a heavy precipitate began to form immediately. The yellow-orange paste was warmed to room temperature and stirred at this temperature for 4 h. The reaction mixture was diluted with ether and acidified with 1 M HCl. The ethereal extracts were washed with saturated aqueous $CuSO_4$ to remove HMPA, dried and concentrated to give 3.39 g (97%) of product as an orange oil that was suitable for the Grignard coupling step. This material was >99% *E* by GC analysis and a small sample was purified by column chromatography using petroleum ether – ethyl acetate (1:1) to give a pure sample of enol phosphate **13** as a colourless oil; $IR_{\nu_{max}}$: 960, 1030, 1285, 1440, 1650, and 1720 cm^{-1}; ^1H NMR (80 MHz) δ: 1.35 (dt, J = 1 and 7 Hz, 6H), 1.73 (bs, 3H), 1.6–2 (m, 2H), 2–2.3 (m, 2H), 2.79 (bt, J = 7 Hz, 2H), 3.70 (s, 3H), 4.2 (m, J = 7 Hz, 4H), 4.70 (bs, 2H), and 5.85 (d, J = 1 Hz, 1H); MS m/z (relative intensity): 55 (15), 79 (20), 91 (26), 99 (72), 107 (20), 127 (51), 134 (42), 152 (10), 155 (100), 164 (15), 166 (30), 177 (5), 192 (16), 205 (4), 220 (23), 234 (9), 252 (12), 260 (5), 288 (4), 289 (3), 320 (3). Anal. calcd. for $C_{14}H_{25}O_6P$: C 52.50, H 7.87; found: C 52.38, H 7.90.

*Methyl (2Z)-3,7-dimethyl-2,7-octadienoate (**14**)*

This reaction was carried out following the same procedure as in the synthesis of **12** from **11***a* using cuprous iodide (8.91 g, 0.047 mol), methyllithium (1.7 M in ether, 27.5 mL, 0.047 mol), methylmagnesium chloride (1.5 M in THF, 52 mL, 0.078 mol), and the *E* enol phosphate **13** (5.0 g, 0.016 mol). The reaction was worked up to give 2.69 g (95%) of crude ester, which was purified by column chromatography to yield 1.94 g (68%) of a faint yellow oil in which the ratio of *E*:*Z* was determined by GC to be 97:3; bp (Kugelrohr distillation) 60°C/0.2 Torr; $IR_{\nu_{max}}$: 1180, 1440, 1650, and 1710 cm^{-1}; ^1H NMR (80 MHz) δ: 1.73 (bs, 3H), 1.5–1.8 (m, 2H), 1.89 (d, J = 1 Hz, 3H), 1.9–2.3 (m, 4H), 3.65 (s, 3H), 4.68 (bs, 2H), and 5.62 (bs, 1H); MS m/z (relative intensity): 41 (80), 53 (21), 55 (30), 59 (16), 67 (46), 68 (75), 82 (27), 83 (73), 95 (50), 108 (22), 109 (25), 114 (100), 122 (20), 123 (33), 135 (8), 139 (30), 150 (13), 167 (7), 182 (9). Anal. calcd. $C_{11}H_{18}O_2$: C 72.49, H 9.95; found: C 72.70, H 10.10.

(2Z)-3,7-Dimethyl-2,7-octadien-1-ol

This alcohol was produced by reduction of the α,β-unsaturated ester **14** (2.00 g, 0.011 mol) with diisobutylaluminium hydride (1 M in hexane, 27.5 mL, 0.0275 mol) according to the same procedure as for the ester **12** above. The reaction, on work-up, yielded 1.74 g (>100%) of crude alcohol, which was purified by chromatography using petroleum ether – ethyl acetate (4:1) to yield 1.40 g (82%) of the desired *Z* alcohol, which was greater than 90% *Z* by GC and was distilled (Kugelrohr) at 64°C/0.2 Torr; $IR_{\nu_{max}}$: 895, 985, 1650, 1670, 3450, and 3625 cm^{-1}; ^1H NMR (80 MHz) δ: 1.2–1.7 (m, 2H), 1.75 (bs, 6H), 1.8–2.2 (m, 4H), 4.12 (d, J = 6 Hz, 2H), 4.68 (bs, 2H), and 5.40 (t, J = 6 Hz, 1H); MS m/z (relative intensity): 41 (100), 43 (30), 53 (27), 55 (50), 56 (25), 67 (32), 68 (40), 69 (50), 71 (30), 81 (34), 83 (27), 93 (14), 95 (17), 107 (7), 109 (9), 121 (13), 123 (8), 136 (9), 139 (3), 154 (2). Anal. calcd. for $C_{10}H_{18}O$: C 77.87, H 11.76; found: C 77.57, H 11.89.

*Z Pheromone **6***

The above *Z* alcohol (0.90 g, 5.8 mmol) was esterified with a catalytic amount of 4-dimethylaminopyridine (10 mg), propionic anhydride (0.83 g, 0.82 mL, 6.4 mmol), and pyridine (0.93 g, 0.95 mL, 0.012 mol) as above for **5** to yield, after chromatography, 1.13 g (92%) of a colourless oil that distilled (Kugelrohr) at 60°C/0.02 Torr; $IR_{\nu_{max}}$: 1105, 1665, 1687, and 1725 cm^{-1}; ^1H NMR (80 MHz) δ: 1.12 (t, J = 7 Hz, 3H), 1.2–1.7 (m, 2H), 1.72 (bs, 3H), 1.74 (bs, 3H), 2.1 (bq, J = 7 Hz, 4H), 2.25 (q, J = 7 Hz, 2H), 4.5–4.7 (m, 4H), and 5.35 (bt, J = 7 Hz, 1H); MS m/z (relative intensity): 41 (98), 43 (20), 53 (38), 55 (70), 57 (100), 67 (62), 68 (91), 69 (78), 79 (49), 80 (52), 81 (99), 93 (66), 94 (25), 95 (42), 96 (54), 97 (23), 98 (41), 107 (47), 108 (23), 109 (28), 121 (74), 136 (76), 154 (20), 196 (1), 210 (1). Anal. calcd. for $C_{13}H_{22}O_2$: C 74.24, H 10.54; found: C 74.45, H 10.61.

*Methyl (2Z)-3-(trimethylsilylmethyl)-7-methyl-2,7-octadienoate (**17**)*

The Grignard reagent was prepared from magnesium turnings (0.304 g, 0.0124 mol) and trimethylsilylmethyl chloride (1.66 g, 0.014 mol) in 20 mL of dry ether. This solution was cannulated into a clean flask under N_2 to remove any unreacted magnesium and then treated with 0.08 g (0.31 mmol) of nickel(II) acetylacetonate. Then 2.00 g (6.2 mmol) of the enol phosphate **11***b* was slowly added to the Grignard solution. After 0.5 h and 1.5 h, additional portions of the $Ni(acac)_2$ catalyst were added (0.08 g each time). The reaction was stirred overnight and quenched with 20 mL of dilute HCl. The aqueous phase was extracted with 3 × 20 mL of ether. The extracts were combined, washed with brine, dried, and the solvents removed under reduced pressure to yield 1.6 g of a crude product that was purified by column chromatography using petroleum ether – ethyl acetate (40:1) to give 1.37 g (87%) of a pale yellow oil; $IR_{\nu_{max}}$: 1620 and 1710 cm^{-1}; ^1H NMR (60 MHz) δ: 0.05 (s, 9H), 1.2–1.7 (m, 2H), 1.75 (bs, 3H), 1.8–2.2 (m, 4H), 2.45 (s, 2H), 3.65 (s, 3H), 4.7 (bs, 2H), and 5.65 (bs, 1H).

*Methyl (2E)-3-(trimethylsilylmethyl)-7-methyl-2,7-octadienoate (**18**)*

This compound was prepared in the same way as **17** using magnesium turnings (0.10 g, 4.0 mmol), trimethylsilylmethyl chloride (0.55 g, 5.0 mmol), 0.08 g (0.31 mmol) of nickel(II) acetylacetonate (0.03 g × 3), and the enol phosphate **13** (0.68 g, 2.1 mmol) to yield, after chromatography, 0.32 g (60%) of the *E* ester **18**; $IR_{\nu_{max}}$: 1635 and 1715 cm^{-1}; ^1H NMR (60 MHz) δ: 0.08 (s, 9H), 1.2–1.7 (m, 2H), 1.75 (bs, 3H), 1.8–2.2 (m, 2H), 2.15 (s, 2H), 2.6 (m, 2H), 3.62 (s, 3H), 4.65 (bs, 2H), and 5.6 (bs, 1H).

*Methyl 2,2 dimethyl-6-methylenecyclohexanecarboxylate (**19**)*

This compound was prepared with a variety of Lewis acid and acid catalysts on **17** or **18** using procedures established earlier in our laboratory (19). The product **19** was isolated in 64–92% yield and had spectroscopic and chromatographic properties identical to the compound prepared earlier (19).

*3-Oxo-7-methyl-7-octen-1-ol (**20**)*

*(a) Directly from the β-keto ester **10***

A solution 0.160 g (0.87 mmol) of the ester **10** in 20 mL of dry ether was added to 42 mg of NaH (60% oil, 1.0 mmol), which had been washed with dry petroleum ether at 0°C. The monoanion was stirred at 0°C for 10 min and then treated with 2.6 mL of a 1 M DIBAL solution in hexane. This reaction was allowed to warm to room temperature with stirring for 1 h. The reaction was quenched with saturated aqueous NH_4Cl and filtered through Celite. The aqueous phase was extracted with 3 × 30 mL of ether. The extracts were combined washed with brine, dried, and the solvents evaporated to give 167 mg of a crude product that was purified by column chromatography using petroleum ether – ethyl acetate (3:2) to give 94 mg (70%) of **20** as a colourless oil; $IR_{\nu_{max}}$: 895, 1060, 1650, 1705, and 3575 cm^{-1}; ^1H NMR (80 MHz) δ: 1.5–2.2 (m,

4H), 1.75 (bs, 3H), 2.47 (t, J = 7 Hz, 2H), 2.70 (t, J = 6 Hz, 2H), 3.87 (t, J = 6Hz, 2H), and 4.7 (bs, 2H); HRMS m/z calcd. for $C_9H_{16}O_2$: 156.1150; found: 156.1143.

(b) Via the enol silyl ether

The β-keto ester **10** (0.250 g, 1.36 mmol) was dissolved in 25 mL of dry ether and then 0.20 mL (1.4 mmol) of triethylamine was added and the solution was stirred for 10 min before 0.17 mL (1.36 mmol) of trimethylsilyl chloride was added. A thick, white precipitate formed immediately and the reaction was stirred overnight. The reaction mixture was filtered through Florisil and the column was washed with 25 mL of dry ether. The solvents were removed under reduced pressure to give 0.34 g (97%) of the silyl enol ether, which was used directly in the next step; ^{1}H NMR (60 MHz) δ: 0.4 (s, 9H), 1.8 (bs, 3H), 1.4–2.3 (m, 4H), 2.8 (t, J = 7 Hz, 2H), 3.75 (s, 3H), 4.7 (bs, 2H), and 5.15 (bs, 1H). This enol ether (0.163 g, 0.64 mmol) was dissolved in 1 mL of dry ether and added to a solution of 25 mg (0.64 mmol) of $LiAlH_4$ in 2 mL of dry ether at 0°C. The reaction was stirred at 0°C for 0.5 h and allowed to warm to room temperature for 0.5 h. The reaction was quenched with 1 M HCl and extracted with 3 × 10 mL of ether. The extracts were combined, washed with brine, dried, and the solvents removed to yield 101 mg of a pale yellow oil that was purified as above to yield 89 mg (89%) of the alcohol **20**.

Pheromone 7

A solution of the alcohol **20** (1.20 g, 7.68 mmol), 1.10 g (8.45 mmol) of propionic anhydride, 1.22 g (15.4 mmol) of pyridine, and a catalytic amount of DMAP were dissolved in 75 mL of ether and stirred overnight. The reaction mixture was washed with 1 M HCl, saturated aqueous $NaHCO_3$, and brine, then dried and the solvents removed under reduced pressure to yield 1.62 g (99%) of crude propionate ester. The crude ester was purified by column chromatography using petroleum ether – ethyl acetate (9:1) to give 1.46 g (90%) of pure keto ester; $IR_{\nu_{max}}$: 900, 1190, 1650, 1725, and 1740 cm^{-1}; ^{1}H NMR (80 MHz) δ: 1.14 (t, J = 7 Hz, 3H), 1.4–2.05 (m, 4H), 1.70 (bs, 3H), 2.38 (five-line pattern, 4H), 2.75 (t, J = 7 Hz, 2H), 4.35 (t, J = 7 Hz, 2H), and 4.7 (m, 2H); HRMS m/z calcd. for $C_{12}H_{20}O_3$: 212.1412; found: 212.1422.

To a stirred slurry of zinc dust (11.5 g, 0.176 mol) and dibromomethane (4.04 mL, 0.056 mol) in 100 mL of THF at −40°C was added 4.6 mL (0.042 mol) of $TiCl_4$ over 0.5 h in a well-vented fume-hood. The reaction was vigorous and copious amounts of a green gas evolved. After the addition of the $TiCl_4$, the reaction mixture was a gray slurry and was stirred at −40°C for 2 h and then at 0°C for at least 24 h before use. This solution of the active methylene complex could be stored in the freezer for up to 2 weeks.

A solution of 101 mg (0.48 mmol) of the above keto propionate in 3 mL of dry CH_2Cl_2 was treated with 3 × 3 mL of the above active methylene complex. The reaction was followed by TLC after each addition; the solution turned black immediately after each addition and then slowly cleared until after the final addition when the solution remained black. The reaction mixture was poured into a mixture of saturated aqueous $NaHCO_3$ and ether, and stirred until the ether layer became clear. The ether layer was removed, washed with brine, dried, and the solvents removed under reduced pressure to yield 90 mg of crude product, which was purified by column chromatography on Florisil using petroleum ether – ethyl acetate (19:1) to give 77 mg (83%) of **7** as a colourless oil; $IR_{\nu_{max}}$: 890, 1190, 1645, and 1730 cm^{-1}; ^{1}H NMR (80 MHz) δ: 1.12 (t, J = 7 Hz, 3H), 1.5–1.8 (m, 2H), 1.72 (bs, 3H), 1.85–2.5 (m, 8H), 4.20 (t, J = 7 Hz, 2H), 4.70 (bs, 2H), and 4.83 (bs, 2H); HRMS m/z calcd. for $C_{13}H_{22}O_2$: 210.1620; found: 210.1622.

Acknowledgment

We are grateful to the British Columbia Science Council and the Natural Sciences and Engineering Research Council of Canada for financial support of this work.

1. (*a*) S. Patai. The chemistry of alkenes. Interscience Publishers, London. 1970; (*b*) B.E. Maryanoff and A.B. Reitz. Chem. Rev. **89**, 863 (1989); (*c*) J.E. McMurry. Chem. Rev. **89**, 1513 (1989).
2. F.L. Harris and L. Weiler. Tetrahedron Lett. **25**, 1333 (1984).
3. J.A. Katzenellenbogen and A. Crumrie. J. Am. Chem. Soc. **98**, 4925 (1976).
4. D.R. Williams and J.M. McGill. J. Org. Chem. **55**, 3457 (1990).
5. E.J. Corey and J.A. Katzenllenbogen. J. Am. Chem. Soc. **91**, 1851 (1969).
6. A.B. Smith, J.W. Leahy, I. Noda, S.W. Remiszewski, N.J. Liverton, and R. Zibuck. J. Am. Chem. Soc. **114**, 2995 (1992).
7. (*a*) E. Piers, T. Wong, and K.A. Ellis. Can. J. Chem. **70**, 2058 (1992); (*b*) E. Piers, H.E. Morton, and J.M. Chong. Can. J. Chem. **65**, 78 (1987).
8. (*a*) E. Piers and J. Roberge. Tetrahedron Lett. **33**, 6923 (1992); (*b*) D.A. Evans, J.R. Gage, and J.L. Leighton. J. Am. Chem. Soc. **114**, 9434 (1992).
9. F.W. Sum and L. Weiler. Can. J. Chem. **57**, 1431 (1979).
10. S.N. Huckin and L. Weiler. J. Am. Chem. Soc. **96**, 1082 (1974).
11. R.S. Downing and D.M. Logan. Can. Entomol. **109**, 1249 (1977).
12. M.J. Gieselmann, R.E. Rice, R.A. Jones, and W.L. Roelofs. J. Chem. Ecol. **5**, 891 (1979).
13. (*a*) R.J. Anderson, H.R. Chin, K. Gill, and C.A. Hendrick. J. Chem. Ecol. **5**, 919 (1979); (*b*) R.J. Anderson, M.J. Gieselmann, H.R. Chin, K.G. Adams, C.A. Hendrick, R.E. Rice, and W.L. Roelofs. J. Chem. Ecol. **7**, 695 (1981).
14. M. Alderdice, C. Spino, and L. Weiler. Tetrahedron Lett. **25**, 1643 (1984).
15. (*a*) L. Novak, L. Poppe, and C. Szantay. Synthesis, 939 (1985); (*b*) D.A. Lombardo and A.C. Weedon. Tetrahedron Lett. **27**, 5555 (1986).
16. R.J. Armstrong and L. Weiler. Can. J. Chem. **64**, 584 (1986).
17. J. Drouin, F. Leyendecker, and J.M. Conia. Nouv. J. Chim. **2**, 267 (1978).
18. C. Cambillau, G. Bram, J. Corest, C. Riche, and C. Pascard-Billy. Tetrahedron, **34**, 2675 (1978).
19. R.J. Armstrong and L. Weiler. Can. J. Chem. **61**, 2530 (1983).
20. I. Fleming and D. Higgins. J. Chem. Soc. Perkin Trans. 1, 3327 (1992), and references therein.
21. E.J. Corey and D.E. Cane. J. Org. Chem. **36**, 3070 (1971).
22. K. Takai, Y. Hotta, K. Oshima, and H. Nozaki. Tetrahedron Lett. 2417 (1978).
23. N.P. Angerilli and D.M. Logan. Can. Entomol. **118**, 767 (1986).
24. W.C. Still, M. Kahn, and A. Mitra. J. Org. Chem. **43**, 2923 (1978).
25. S.C. Watson and J.F. Eastham. J. Organomet. Chem. **9**, 165 (1967).
26. O.S. Bhanot and P.C. Dutta. J. Chem. Soc. C, 2583 (1968).
27. B.M. Trost and R.A. Kunz. J. Am. Chem. Soc. **97**, 7152 (1975).
28. G.B. Kauffman and L.A. Tetter. Inorg. Synth. **7**, 9 (1963).

Can. J. Chem. Downloaded from www.nrcresearchpress.com by 203.198.23.82 on 09/08/12
For personal use only.

A flash photolytic investigation of the photosolvolysis of α-(2,6-dimethoxyphenyl)vinyl chloride. Characterization of the 2,6-dimethoxyacetophenone keto–enol system

YVONNE CHIANG, ROBERT ELIASON,[1] JOEL JONES,[2] AND A. JERRY KRESGE[3]
Department of Chemistry, University of Toronto, Toronto, ON M5S 1A1, Canada

AND

KEVIN L. EVANS AND RICHARD D. GANDOUR
Department of Chemistry, Louisiana State University, Baton Rouge, LA 70803-1804, U.S.A.

Received April 2, 1993

YVONNE CHIANG, ROBERT ELIASON, JOEL JONES, A. JERRY KRESGE, KEVIN L. EVANS, and RICHARD D. GANDOUR. Can. J. Chem. **71**, 1964 (1993).

Photosolvolysis of α-(2,6-dimethoxyphenyl)vinyl chloride in trifluoroethanol solution at 25°C was found to produce the α-(2,6-dimethoxyphenyl)vinyl cation as a transient species with the lifetime τ = 1 μs. Addition of water reduced this lifetime markedly, until, at compositions greater than 80% water, it was too short to measure (τ < 20 ns); extrapolation of the data suggests τ = 9 ns in pure water. Hydration of this cation gave the much longer lived enol of 2,6-dimethoxyacetophenone, whose rates of ketonization were measured in dilute perchloric acid and sodium hydroxide solutions. These data, when combined with rates of enolization of the ketone determined by iodine scavenging, give pK_E = 6.98 for the keto–enol equilibrium constant in the 2,6-dimethoxyacetophenone system, pK_a^E = 10.72 for the acidity constant of the enol ionizing as an oxygen acid, and pK_a^K = 17.70 for the acidity constant of the ketone ionizing as a carbon acid; these constants refer to wholly aqueous solution at 25°C and ionic strength = 0.10 M.

YVONNE CHIANG, ROBERT ELIASON, JOEL JONES, A. JERRY KRESGE, KEVIN L. EVANS et RICHARD D. GANDOUR. Can. J. Chem. **71**, 1964 (1993).

On a trouvé que la photosolvolyse du chlorure de α-(2,6-diméthoxyphényl)vinyle en solution dans le trifluoroéthanol, à 25°C, conduit au cation α-(2,6-diméthoxyphényl)vinyle comme espèce transitoire dont le temps de vie, τ = 1 μS. L'addition d'eau au milieu réactionnel réduit ce temps de vie d'une façon importante jusqu'à des compositions en eau supérieures à 80% alors que les temps de vie deviennent trop courts pour être mesurés (τ < 20 ns); l'extrapolation des données suggère que τ = 9 ns dans l'eau pure. L'hydratation de ce cation conduit à l'énol de la 2,6-diméthoxyacétophénone dont la longueur de vie est beaucoup plus longue et dont on a mesuré les vitesses de cétonisation dans des solutions diluées d'acide perchlorique et d'hydroxyde de sodium. Lorsqu'on combine ces données avec les vitesses d'énolisation de la cétone telles que déterminées par piégeage d'iode, elles fournissent des valeurs de pK_E = 6,98 pour la constante d'équilibre céto–énolique du système 2,6-diméthoxyacétophénone, de pK_a^E = 10,72 pour la constante d'acidité de l'énol s'ionisant sous la forme d'une oxyacide et de pK_a^K = 17,70 pour la constante d'acidité de la cétone s'ionisant sous la forme d'une acide carboné; ces constantes se réfèrent à des solutions entièrement aqueuses, à 25°C et à une force ionique de 0.10 M.

[Traduit par la rédaction]

Vinyl cations have been observed as short-lived transient species formed by flash photolytic photosolvolysis of vinyl halides or photohydration of acetylenes in organic solvents such as acetonitrile (1, 2), acetic acid (2), and trifluoroethanol (3). There is evidence that they are formed by these reactions in aqueous solution as well, for their enol hydration products, eq. [1], have been observed as transients in

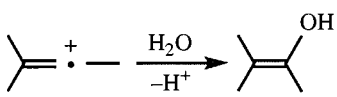

this medium; the ions themselves, however, have not been seen in this solvent, presumably because none of the systems examined so far give vinyl cations with sufficiently long lifetimes to allow detection by the methods that have been employed.

We have investigated the flash photolysis of α-(2,6-dimethoxyphenyl)vinyl chloride, **1**, in the hope that the stabilizing effect of the two *ortho* methoxyl groups in the vinyl cation formed from this substrate, **2**, eq. [2], coupled with the steric hindrance that these groups might provide to attack of water at the cationic center, would be sufficient to permit observation of this ion in wholly aqueous solution. This hope, unfortunately, was not realized: we were able to see this ion in trifluoroethanol solution and also in trifluoroethanol–water mixtures up to a water content of 80%; above this point, however, the lifetime of the ion became less than 20 ns, which is the limit of detection of our system.

[2]

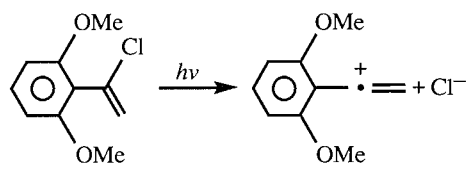

1 **2**

Although we did not see this ion in wholly aqueous solution, we could observe its enol hydration product, **3**, in this medium. We therefore studied the ketonization of this enol, eq. [3], and the results we obtained, in combination with information on enolization of the corresponding ketone, 2,6-dimethoxyacetophenone, **4**, have allowed us to characterize this keto–enol system. These results are of special interest

[1]On leave from the Department of Chemistry, Southwest State University, Marshall, MN 56258, U.S.A.

[2]On leave from Instituto de Quimica, Universidade Federal do Rio de Janeiro, Rio de Janeiro, Brazil.

[3]Author to whom correspondence may be addressed.

Can. J. Chem. Downloaded from www.nrcresearchpress.com by 203.198.23.82 on 09/08/12
For personal use only.

[3] 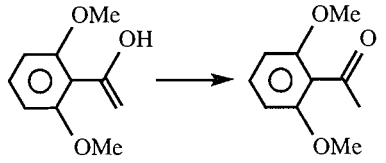

3 4

in connection with corresponding information on the 2,4,6-trimethylacetophenone, **5**, keto–enol system, eq. [4] (*4b*), and also on the hydrolysis of methyl α-(2,6-dimethoxyphenyl)vinyl ether, (**6**), eq. [5] (*5*).

[4] 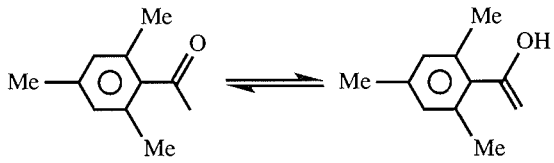

5

[5] 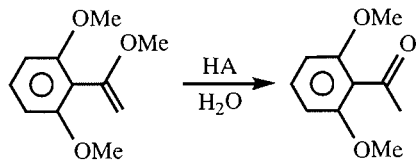

6

Experimental section

Materials

α-(2,6-Dimethoxyphenyl)vinyl chloride was prepared by treating 2,6-dimethoxyacetophenone with phosphorus pentachloride under conditions that prevent chlorination of the benzene ring (*6*). All other materials were best available commercial grades and were used as received.

Kinetics

Flash photolysis was performed using a conventional flash lamp system for the slower reactions and a laser system for the faster ones. Details of the conventional system have already been published (*7*). The laser system used a Lumonics Ex-510 excimer laser operating at λ = 248 nm for excitation and a pulsed Oriel model 66002 Xenon-arc lamp as monitoring light source. The monitoring light, after leaving the sample, was passed through an Oriel model 77250 monochrometer and onto a Hamamatsu 1P28 photomultiplier whose output was fed into a Tektronix model SCD1000 transient digitizer. Data analysis was performed with a Tektronix PEP 301 computer using Enzfitter software (Elsevier-BIOSOFT) for fitting to exponential functions. Reaction mixtures were contained in quartz cuvettes placed in a brass holder whose temperature was controlled at 25.0 ± 0.1°C by water circulating from a constant temperature bath.

Rates of enolization of 2,6-dimethoxyacetophenone were determined by iodine scavenging in the presence of iodide ion using the absorbance of I_3^- to monitor the reaction. Absorbance measurements were made with a Cary model 118C spectrometer whose cell compartment was thermostatted at 25.0 ± 0.1°C. Iodine concentrations in the reaction mixtures were 3×10^{-5} M; iodide ion concentrations, 7×10^{-4} M; and 2,6-dimethoxyacetophenone concentrations, 7×10^{-4} M. Reactions were followed to about 1% completion and zero-order rates of change of absorbance with time, $\Delta A/\Delta t$, were converted into observed first-order rate constants, k_{obs}, according to eq. [6]. In this expression K_{I_3} (= 1.5×10^{-3} M) (*8*) is the equilibrium

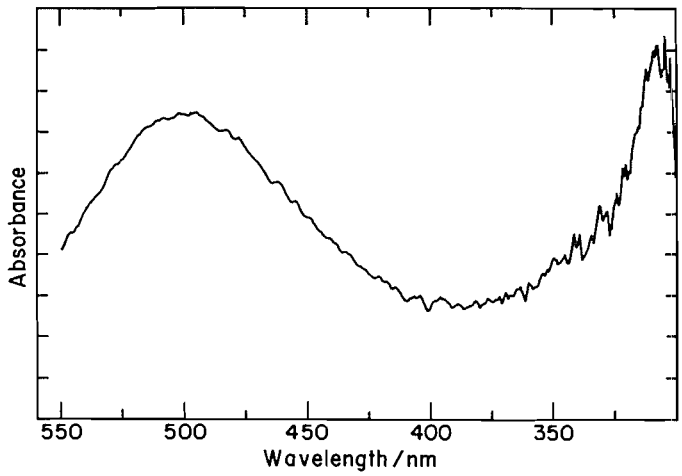

FIG. 1. Absorption spectrum of the shorter lived of the two transients produced upon flash photolysis of α-(2,6-dimethoxyphenyl)vinyl chloride in trifluoroethanol solution.

$$[6] \quad k_{obs} = (\Delta A/\Delta t)(1 + K_{I_3}/[I_3^-])/\epsilon_{351}[S]$$

constant for dissociation of I_3^- into I_2 and I^-, ϵ_{351} (= 2.6×10^4 M^{-1} cm^{-1}) (*8*) is the extinction coefficient of I_3^- at λ = 351 nm, the wavelength at which the measurements were made, and [S] is the concentration of 2,6-dimethoxyacetophenone.

Results

The UV spectrum of α-(2,6-dimethoxyphenyl)vinyl chloride dissolved in water consists of an absorption maximum at λ = 280 nm, plus strong end absorption at low wavelengths with a shoulder at λ = 240 nm. Upon irradiation of an aqueous solution with a few pulses from our conventional flash photolysis apparatus, these spectral features move to lower wavelengths and give a spectrum similar to that of an authentic sample of 2,6-dimethoxyacetophenone, with λ_{max} = 265 nm and a shoulder at λ = 220 nm. This shows that photolysis of α-(2,6-dimethoxyphenyl)vinyl chloride in aqueous solution gives 2,6-dimethoxyacetophenone as an ultimate reaction product. Flash photolytic examination of this transformation shows that it occurs via short-lived vinyl cation and enol intermediates.

Vinyl cation

Flash photolysis of α-(2,6-dimethoxyphenyl)vinyl chloride dissolved in trifluoroethanol produces a transient species with absorption maxima at λ = 300 and 500 nm (Fig. 1) and a lifetime of τ ≅ 1 μs. Degassing the solution has no effect on this lifetime, but addition of chloride ion or water shortens it markedly. This behavior indicates that this transient is the α-(2,6-dimethoxyphenyl)vinyl cation, **2**, formed as expected according to eq. [2]. In the absence of added reagents, the lifetime of this ion is governed by its reaction with the solvent to give the corresponding trifluoroethyl vinyl ether, and also by its reaction with chloride ion produced by the photoionization to regenerate the starting material. Addition of chloride ion to the photolysis solution speeds up the latter reaction, shortening the lifetime of the vinyl cation. Water has a similar lifetime-shortening effect through its reaction with the cation to give enol according to eq. [1].

Decay of this transient absorbance attributed to the vinyl

Can. J. Chem. Downloaded from www.nrcresearchpress.com by 203.198.23.82 on 09/08/12
For personal use only.

Can. J. Chem. Downloaded from www.nrcresearchpress.com by 203.198.23.82 on 09/08/12
For personal use only.

TABLE 1. Rates of reaction of the α-(2,6-dimethoxyphenyl)vinyl cation in trifluoroethanol–water mixtures at 25°C[a]

% Trifluoroethanol	$k/10^6\ s^{-1}$
100	1.18,[b] 1.58
100[c]	1.18
100[d]	3.31
80	5.83
60	9.33
40	15.7
20	49.8

[a]Monitored at λ = 500 nm unless otherwise indicated.
[b]Monitored at λ = 340 nm.
[c]Solution degassed.
[d]With 0.004 M NaCl.

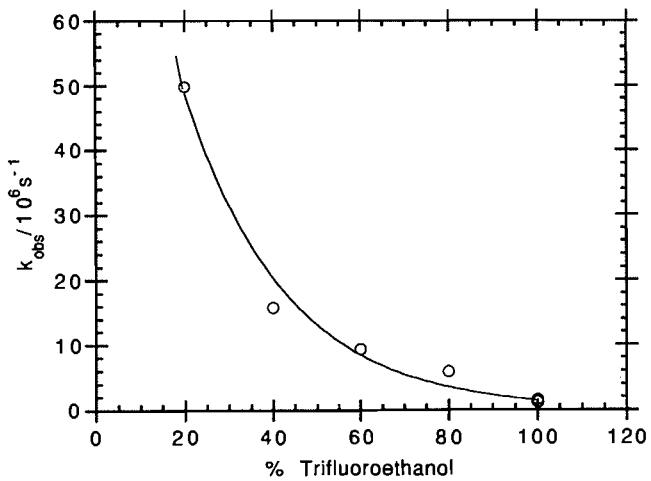

FIG. 2. Relationship between solvent composition and rates of decay of the α-(2,6-dimethoxyphenyl)vinyl cation in trifluoroethanol–water mixtures.

cation conformed to the first-order rate law, and first-order rate constants were determined in trifluoroethanol–water mixtures of increasing water content. The data are summarized in Table 1 and are displayed in Fig. 2. It may be seen that the rate of reaction increases markedly with water content, especially in the more water-rich mixtures, suggesting an exponential dependence of rate upon water content. As Fig. 3 shows, there is a reasonably good linear relationship between the logarithms of observed rate constants and percent trifluoroethanol, $\log(k_{obs}/s^{-1}) = 8.07 - 0.0190$ (% TFE), which allows extrapolation to a wholly aqueous solvent. The result of this extrapolation, $k_{obs} = (1.2 \pm 0.3) \times 10^8\ s^{-1}$, gives $\tau = 9$ ns as the lifetime of the α-(2,6-dimethoxyphenyl)vinyl cation in aqueous solution. This is shorter, by about a factor of two, than the shortest excitation pulse available from our flash photolysis apparatus, and that renders this ion unobservable in wholly aqueous solution with our equipment.

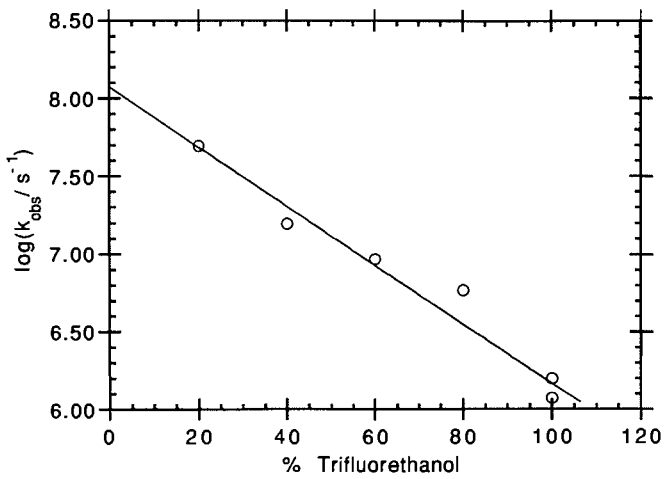

FIG. 3. Logarithmic relationship between solvent composition and rates of decay of the α-(2,6-dimethoxyphenyl)vinyl cation in trifluoroethanol–water mixtures.

The relationship of Fig. 3 gives $k = (1.5 \pm 0.2) \times 10^6\ s^{-1}$ as the rate constant for decay of the present vinyl cation in 100% trifluoroethanol solution; this is similar to $k = 1.3 \times 10^6\ s^{-1}$ reported for reaction of the α-(*p*-methoxyphenyl)-vinyl cation in the same solvent (3).

Enol

This very rapid reaction of the α-(2,6-dimethoxyphenyl)-vinyl cation in wholly aqueous solution appeared as an instantaneous rise in absorbance at lower wavelengths, in the vicinity of λ = 300 nm, where the enol is expected to absorb. This rise, which took place within the excitation pulse, was then followed by an additional further increase in absorbance as the enol was converted to the still more strongly absorbing ketone. This latter absorbance change is similar to that observed in the hydrolysis of the vinyl ether analog of this enol, ethyl α-(2,6-dimethoxyphenyl)vinyl ether, (5) **6**, which gives the same ketone as its reaction product (eq. [5]).

Rates of ketonization of the enol were measured in dilute perchloric acid and sodium hydroxide solutions; these data are summarized in Tables 2 and 3. As Fig. 4 shows, observed first-order rate constants determined in perchloric acid solutions proved to be accurately proportional to acid concentration. This is the behavior expected for enol ketonization; it represents rate-determining protonation of the enol on its β-carbon atom followed by rapid removal of the oxygen-bound proton of the ketone conjugate acid thus formed, eq. [7] (9). Linear least-squares analysis of the data gave $k^K_{H^+} = 120\ M^{-1}\ s^{-1}$ as the hydronium-ion catalytic coefficient for this ketonization reaction.

Ketonization was also catalyzed by sodium hydroxide but, as Fig. 5 demonstrates, observed first-order rate constants

[7] 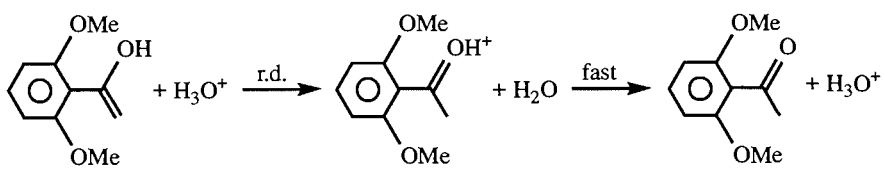

TABLE 2. Rates of ketonization of 2,6-dimethoxyacetophenone enol in aqueous perchloric acid solutions at 25°C[a]

$[HClO_4]/10^{-2}$ M	k_{obs}/s^{-1}
10.0	13.2, 13.3, 12.9
8.00	11.2, 10.7, 11.1, 11.2
5.00	7.01, 7.33, 6.93, 7.15
3.00	4.22, 5.17, 4.67, 5.05
1.00	2.57, 2.26, 2.48, 2.65

$k_{obs}/s^{-1} = 1.22 \pm 0.12 + (120 \pm 2)[HClO_4]$

[a]Ionic strength = 0.10 M.

TABLE 3. Rates of ketonization of 2,6-dimethoxyacetophenone enol in aqueous sodium hydroxide solutions at 25°C[a]

$[NaOH]10^{-3}$ M	$k_{obs}/10^2 s^{-1}$
10.0	28.7, 30.2, 26.9
2.00	24.9, 25.4
1.00	19.3, 18.9, 17.2
0.600	13.1, 13.0, 13.6
0.400	9.78, 10.5, 9.07
0.200	5.25, 4.35. 3.79

$k_{obs} = k_0' K_a^E[HO^-]/(K_a^E[HO^-] + 1.59 \times 10^{-14})$[b]
$k_0' = (3.21 \pm 0.11) \times 10^3\ s^{-1}$
$K_a^E = (1.91 \pm 0.19) \times 10^{-11}$ M
$pK_a^E = 10.72 \pm 0.04$

[a]Ionic strength = 0.10 M.
[b]See eq. [9]; $1.59 \times 10^{-14} = K_w/f_{H^+}f_{HO^-}$ using values of the activity coefficients f_{H^+} and f_{HO^-} for ionic strength = 0.10 M recommended by Bates (10).

were proportional to hydroxide-ion concentration only at low basicity; at progressively higher basicities this proportionality gave way to saturation of catalysis, and rate constants approached a constant value. This again is as expected for enol ketonization; it represents reaction through the much more reactive enolate ion under conditions where the initial state shifts from enol at low basicity to enolate at high basicity, as shown in eq. [8] (9). The rate law that applies in this situation is given as eq. [9], in which k_0' is the rate

[8] 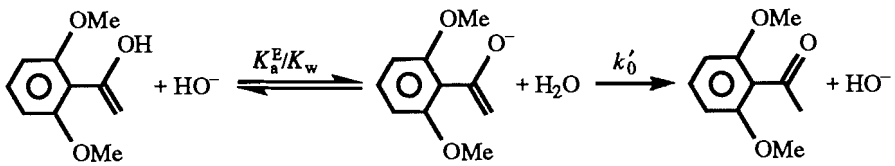

[9] $k_{obs} = k_0' K_a^E[HO^-]/(K_a^E[HO^-] + K_W)$

constant for carbon protonation of the enolate ion by water, K_a^E is the acidity constant of the enol, and K_W is the autoprotolysis constant of water. Nonlinear least-squares fitting of the data to this expression gave $k_0' = 3.21 \times 10^2\ s^{-1}$ and $K_a^E = 1.91 \times 10^{-11}$, $pK_a^E = 10.72$; the latter is a concentration dissociation constant that applies at the ionic strength of the measurements (0.10 M).

Enolization

Rates of enolization of 2,6-dimethoxyacetophenone were measured in dilute perchloric acid solutions; the data are summarized in Table 4. Observed first-order rate constants proved to be proportional to acid concentration, as expected for enolization of a ketone (9), and linear least-squares analysis of the data gave $k_{H^+}^E = 1.26 \times 10^{-5}\ M^{-1}\ s^{-1}$ as the hydronium-ion catalytic coefficient for this enolization reaction.

Discussion

The amount of enol tautomer in equilibrium with a simple ketone, such as 2,6-dimethoxyacetophenone, in aqueous solution is generally very small, and it is consequently often difficult to evaluate keto–enol equilibrium constants in such systems by direct determination of enol concentration. An equilibrium constant, however, can also be evaluated as the ratio of rate constants for the reaction in the forward and reverse directions, and the hydronium-ion catalytic coefficients determined here for the enolization of 2,6-dimethoxyacetophenone and ketonization of its enol may therefore be used to determine the keto–enol equilibrium constant for this system: $K_E = k_{H^+}^E/k_{H^+}^K = (1.05 \pm 0.06) \times 10^{-7}$, $pK_E = 6.98 \pm 0.02$.

This enolization reaction plus the acid dissociation of the enol, whose equilibrium constant was determined here by the ketonization rate measurements in sodium hydroxide solutions, form two legs of a thermodynamic cycle whose third member is ionization of the ketone as a carbon acid, eq. [10]. The equilibrium constant for this carbon acid ionization,

[10] 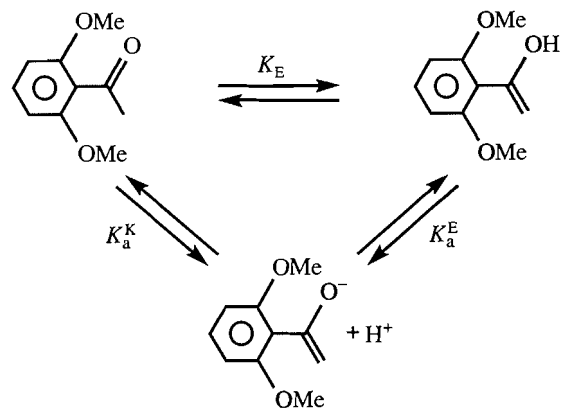

K_a^K, may therefore be evaluated as the product of the equilibrium constants for the other two reactions: $K_a^K = K_E K_a^E = (2.00 \pm 0.23) \times 10^{-18}$, $pK_a^K = 17.70 \pm 0.05$.

It is interesting that this equilibrium constant, as well as those for the other two reactions of the scheme shown in eq. [10], are quite similar to the corresponding values for

Can. J. Chem. Downloaded from www.nrcresearchpress.com by 203.198.23.82 on 09/08/12
For personal use only.

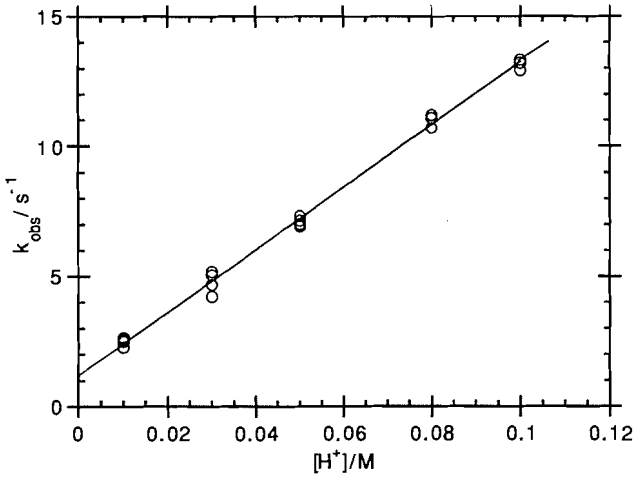

FIG. 4. Relationship between perchloric acid concentration and rates of ketonization of 2,6-dimethoxyacetophenone enol in aqueous solution at 25°C.

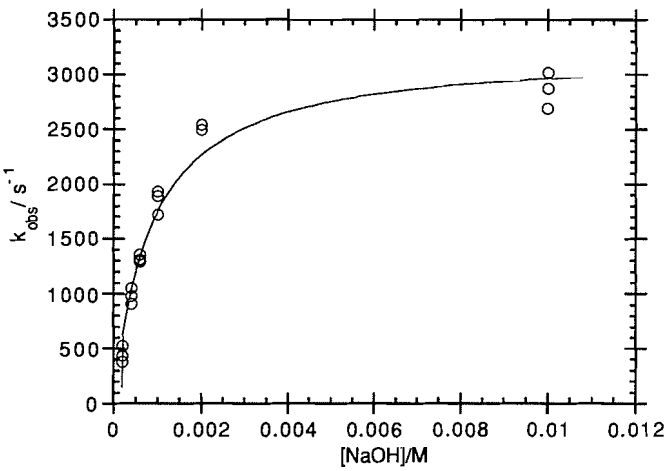

FIG. 5. Relationship between sodium hydroxide concentration and rates of ketonization of 2,6-dimethoxyacetophenone enol in aqueous solution at 25°C.

TABLE 4. Rates of enolization of 2,6-dimethoxyacetophenone in aqueous perchloric acid solutions at 25°C[a]

$[HClO_4]/10^{-2}$ M	$k_{obs}/10^{-7}$ s^{-1}
10.5	14.0, 15.5, 14.9, 14.9, 12.3
8.36	9.43, 11.8, 10.5, 10.5, 11.0, 11.4
6.27	9.08, 8.51, 8.54, 7.30, 7.43
4.18	7.75, 7.67, 7.22, 5.38, 5.81
2.09	3.86, 3.53, 2.72, 2.36, 2.88

$k_{obs}/s^{-1} = (6.99 \pm 4.76) \times 10^{-8} + (1.26 \pm 0.07) \times 10^{-5}$ $[HClO_4]$

[a]Ionic strength = 0.10 M.

the 2,4,6-trimethylacetophenone (**5**) keto–enol system: the numbers, listed in Table 5, show hardly any differences at all. There are, on the other hand, significant differences between these two ketones and the parent, unsubstituted acetophenone, values for whose reactions are also listed in Table 5.

The largest difference occurs in the pK_E values: the keto–enol equilibrium constants for the substituted ketones are an order of magnitude greater than that for acetophenone. This difference may be understood by making a further comparison with acetaldehyde, which has no aromatic substituent and for which $pK_E = 6.23$ (7). There is thus a marked decrease in keto–enol equilibrium constant upon introduction of a phenyl substituent; this can be attributed to a difference in stabilization of the keto and enol forms produced by conjugation with the phenyl group. Conjugation of phenyl with the carbonyl group of the keto isomer is strong because the carbonyl carbon atom bears a partial positive charge, whereas conjugation with the neutral double bond of the enol is considerably weaker. The keto isomer is thus stabilized relative to the enol form, and the keto–enol equilibrium constant is decreased. *Ortho* substituents, such as those in 2,6-dimethoxyacetophenone and 2,4,6-trimethylacetophenone, inhibit this conjugation and shift the equilibrium constant back toward that of the acetaldehyde system.

It is significant that most of this increase in keto–enol equilibrium constant upon introduction of *ortho* substituents appears as a decrease in the rate of ketonization and that rates of enolization are hardly affected: the data of Table 5 show $k^K_{H^+}$ values for 2,6-dimethoxyacetophenone and 2,4,6-trimethylacetophenone that are an order of magnitude less than those for acetophenone but $k^E_{H^+}$ values that are virtually the same. This is consistent with little conjugative effect on the stability of the enol isomer and a stronger effect on both the keto isomer and the transition state of the reaction. The effect on the transition state and the keto isomer might, in fact, be expected to be of similar strength because both species have partial positive charges in positions where charge can be delocalized into the phenyl group; this similarity of conjugative effect on ketone and transition state is attested to by the fact that a Yukawa–Tsuno correlation of rates of acid-catalyzed enolization of ring-substituted acetophenones gives a resonance ρ value that is vanishingly small (12).

There are also differences in pK^E_a and pK^K_a values between acetophenone and *ortho*-substituted derivatives, but these are smaller than the differences in pK_E. The slightly weaker acidity of the enols of 2,6-dimethoxyacetophenone and 2,4,6-trimethylacetophenone may be attributed to the electron-supplying nature of their methoxyl and methyl groups, which will tend to destabilize the enolate ions. This effect, however, is overwhelmed in the carbon acid ionization of the ketones, for here 2,6-dimethoxyacetophenone and 2,4,6-trimethylacetophenone are stronger acids than acetophenone. This inversion of relative acidity can be ascribed to the conjugative effects discussed above, which destabilize the substituted ketones relative to the parent acetophenone.

The acid-catalyzed ketonization of enols bears a close mechanistic resemblance to the acid-catalyzed hydrolysis of vinyl ethers: both reactions occur by rate-determining proton transfer from the catalysts to the β-carbon atom of the substrate, and mechanistic differences occur only after this step (9, 13). The effects of structure on reactivity for the two reactions might therefore be expected to be similar, and this, in fact, is the case: hydronium-ion catalytic coefficients for enol ketonization have been found to parallel those for methyl vinyl ether hydrolysis over a wide range of structural vari-

Can. J. Chem. Downloaded from www.nrcresearchpress.com by 203.198.23.82 on 09/08/12
For personal use only.

TABLE 5. Comparison of related keto–enol systems[a]

Parameter	2,6-Dimethoxy-acetophenone	2,4,6-Trimethyl-acetophenone[b]	Acetophenone[c]
pK_E^E	6.98	6.92	7.96
pK_a^E	10.72	10.69	10.34
pK_a^K	17.70	17.61	18.31
$k_{H^+}^E/10^{-5}\ M^{-1}\ s^{-1}$	1.26	1.30	1.21
$k_{H^+}^K/10^3\ M^{-1}\ s^{-1}$	0.120	0.109	1.25

[a]Ionic strength = 0.10 M; equilibrium constants are concentration quotients at this ionic strength.
[b]Reference 4*b*.
[c]Reference 11.

ation spanning five orders of magnitude in reactivity, with the ketonisation reactions consistently 10–100 times faster than the hydrolyses (9). A comparison of the two reactions can be made for the present system, for the hydronium-ion catalytic coefficient has recently been measured for the hydrolysis of methyl α-(2,6-dimethoxyphenyl)vinyl ether, **6** (5). This comparison shows the present enol to be 42 times more reactive than the vinyl ether, which is nicely consistent with previous experience.

Acknowledgement

We are grateful to Conselho Nacional de Desenvolvimento Cientifico e Tecnologico for a fellowship to J.J. and to the Natural Sciences and Engineering Research Council of Canada, the Petroleum Research Fund, administered by the American Chemical Society, and the U.S. National Institutes of Health and National Science Foundation for financial support of this work.

1. W. Schnabel, I. Naito, T. Kitamura, S. Kobayashi, and H. Taniguchi. Tetrahedron, **36**, 3229 (1980); S. Kobayashi, T. Kitamura, H. Taniguchi, and W. Schnabel. Chem. Lett. 2101 (1983); S. Kobayashi, Q.Q. Zhu, and W. Schnabel. Z. Naturforsch. B: Chem. Sci. **43**, 825 (1988).
2. F.I.M. van Ginkel, R.J. Wisser, C.A.G.O. Varma, and G. Lodder. J. Photochem. **30**, 453 (1985).
3. R.A. McClelland, F. Cozens, and S. Steenken. Tetrahedron Lett. **31**, 2821 (1990).
4. (*a*) Y. Chiang, A.J. Kresge, M. Capponi, and J. Wirz. Helv. Chim. Acta, **69**, 1331 (1986); (*b*) A.J. Kresge and N.P. Schepp. J. Chem. Soc. Chem. Commun. 1548 (1989).
5. J. Jones and A.J. Kresge. Can. J. Chem. **71**, 38 (1993).
6. K.L. Evans, P. Prince, E.T. Huang, K.R. Boss, and R.D. Gandour. Tetrahedron Lett. **31**, 6753 (1990).
7. Y. Chiang, M. Hojatti, J.R. Keeffe, A.J. Kresge, N.P. Schepp, and J. Wirz. J. Am. Chem. Soc. **109**, 4000 (1987).
8. E.T. Harper and M.L. Bender. J. Am. Chem. Soc. **87**, 5625 (1965).
9. J.R. Keeffe and A.J. Kresge. *In* The chemistry of enols. *Edited by* Z. Rappoport. Wiley, New York. 1990. Chap. 7.
10. R.G. Bates. Determination of pH. Theory and practise. Wiley, New York. 1973. p. 49.
11. Y. Chiang, A.J. Kresge, and J. Wirz. J. Am. Chem. Soc. **106**, 6392 (1984); J. R. Keeffe, A.J. Kresge, and J. Toullec. Can. J. Chem. **64**, 1224 (1986).
12. J.-E. Dubois, M. El-Alaoui, and J. Toullec. J. Am. Chem. Soc. **103**, 5393 (1981).
13. A.J. Kresge. Acc. Chem. Res. **20**, 365 (1987).

Can. J. Chem. Downloaded from www.nrcresearchpress.com by 203.198.23.82 on 09/08/12
For personal use only.

Colorimetric studies of the reduction of Fe^{3+} by coal

RONALD R. MARTIN[1] AND JINJIANG LI

Department of Chemistry, University of Western Ontario, London, ON N6A 5B7, Canada

AND

J. ANTHONY MACPHEE

CANMET Energy Research Laboratory, Canada Department of Energy Mines & Resources, Ottawa, ON K1A 0R6, Canada

Received April 1, 1993

RONALD R. MARTIN, JINJIANG LI, and J. ANTHONY MACPHEE. Can. J. Chem. **71**, 1970 (1993).

The reduction of Fe^{3+} by coal surfaces has been followed colorimetrically. The kinetics of the reaction in coals with a relatively high O/C ratio are sensitive to mild air oxidation, those having a low O/C ratio are relatively insensitive.

RONALD R. MARTIN, JINJIANG LI et J. ANTHONY MACPHEE. Can. J. Chem. **71**, 1970 (1993).

On a fait appel à une méthode colorimétrique pour suivre la réduction du Fe^{3+} par des surfaces de charbon. Les cinétiques des réactions dans les charbons, avec un rapport relativement élevé de O/C, sont sensibles à une oxydation douce par l'air alors que celles avec un faible rapport O/C sont relativement insensibles.

[Traduit par la rédaction]

Introduction

Coal confronts chemists with formidable analytical problems. Defined as a rock consisting of more than 65% carbon by weight and constructed largely from plant material metamorphosed by time, temperature, and pressure in the earth's crust, it is essentially a non-repeating polymer of immense complexity. It remains a puzzle to organic and inorganic chemists alike since it is known to include in its structure virtually all the naturally occurring elements in the periodic table. It remains as the focus of intense study both because it is an interesting problem in its own right and because of its industrial importance. The value of coal increases significantly if it can be used to make coke for steel production. The coking properties of a given coal are usually inferred from optical reflectance data while thermal coal is usually valued on the basis of the degree of oxidation of the material. Both the coking and thermal properties of coal deteriorate more or less rapidly after mining for reasons that, while clearly related to air oxidation (so-called low-temperature oxidation), are poorly understood. The oxygen content is normally obtained from difference measurements and is generally regarded as being the least accurate value obtained in normal coal analysis. Surface-sensitive techniques usually yield O/C ratios that are higher than those obtained from bulk analysis. A simple chemical analysis that would be reflective of the O/C ratio would find wide utility in coal characterization.

Coal research is often frustrated by the variability of the parent material from mine to mine and often within a given coal seam. A series of coal samples representative of North American coal has been prepared as part of the Argonne Premium Coal Sample Program for use by researchers to insure a common set of starting materials. These samples, from which the coal samples used in this study were drawn, are described in detail elsewhere (1).

$Ba(OH)_2$ has been used as an indicator of ion-exchange sites, which could then be identified using scanning electron microscopy (2). Iron salts have been used to stain coal surfaces as an aid in optical and electron microscopy (3). We suggest that the development of blue colours on the coal surfaces following exposure to $Fe^{3+}/Fe(CN)_6^{3-}$ solutions results from oxidation of the coal surface by Fe^{3+} with the subsequent formation of a charge-transfer complex (prussian blue) $Fe^{2+}/Fe^{3+}(CN)_6^{3-}$. Since this complex absorbs strongly in the visible region the reaction can be followed by colorimetry of appropriate coal slurries. The kinetics of the Fe^{3+} reduction are a direct measure of the reactivity of individual coals with these reagents and may provide a means of predicting coal quality in specific industrial uses.

Experimental

Five 100 mesh Argonne Premium coal samples, Pocahontas, Stockton, Illinois no. 6, Wyodak, and North Dakota, chosen to give a wide range of O/C ratios (Table 1), were exposed with rapid stirring to 0.6 M $FeCl_3$ solutions having a pH of 2.6 at 30°C. The resulting slurry contained 3 g of coal per 100 mL. Approximately 1 mL of solution was withdrawn from the slurry at appropriate time intervals using a syringe fitted with a 0.8 μm filter. This solution was added to 10 mL 0.3 M $K_3Fe(CN)_6$, which served as an indicator due to the formation of $Fe^{2+}/Fe^{3+}(CN)_3^{3-}$ (prussian blue.) The progress of the reaction was followed by UV–VIS spectroscopy using the strong absorption line at 700 nm. The procedure was repeated with the same set of coal samples after they had been exposed to air at 105°C for 5 days, and with fresh coals that had been demineralized by soaking overnight in concentrated HCl.

A single sample was prepared by adding $K_3Fe(CN)_6$ directly to the coal–$FeCl_3$ slurry. The coal was withdrawn and the infrared spectrum of both fresh and exposed coal was obtained on KBr discs. In addition, X-ray photoelectron spectra (XPS) were obtained from coal surfaces after exposure to $FeCl_3$.

Results and discussion

The sample prepared by adding $K_3Fe(CN)_6$ directly to the coal–$FeCl_3$ slurry showed only minimal reduction of the Fe^{3+}. Since the $K_3Fe(CN)_6$ clearly acted as an inhibitor to the Fe(III) reduction we suggest that it adsorbed on the coal surface, blocking the reduction sites against further reaction. The IR

[1]Author to whom correspondence may be addressed.

Can. J. Chem. Downloaded from www.nrcresearchpress.com by 203.198.23.82 on 09/08/12
For personal use only.

TABLE 1. Fe^{3+} reduction rate 0–5 min

Coal	O/C	Rate fresh $\times 10^{-5}$ mol L^{-1} min^{-1}	Rate oxidized $\times 10^{-5}$ mol L^{-1} min^{-1}
Pocahontas (POC)	0.038	0.4	0.5
Stockton (WV)	0.10	1.3	0.73
Illinois no. 6 (IL)	0.14	4.3	3.9
Wyodak (WY)	0.26	5.3	2.6
North Dakota (ND)	0.29	8.0	0.9

TABLE 2. Fe^{3+} reduction rate 5–25 min

Coal	O/C	Rate fresh $\times 10^{-5}$ mol L^{-1} min^{-1}	Rate oxidized $\times 10^{-5}$ mol L^{-1} min^{-1}
Pocahontas (POC)	0.038	0.3	0.2
Stockton (WV)	0.10	0.3	0.2
Illinois no. 6 (IL)	0.14	0.9	0.6
Wyodak (WY)	0.26	1.0	Not observed
North Dakota (ND)	0.29	0	Not observed

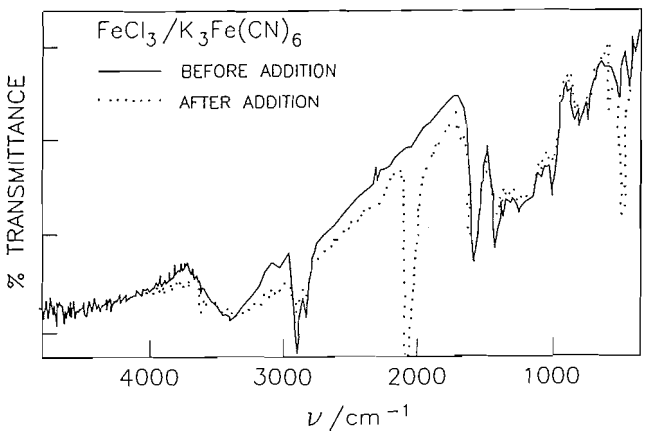

FIG. 1. IR spectrum of coal before and after exposure to $FeCl_3$/$K_3Fe(CN)_6$ solution.

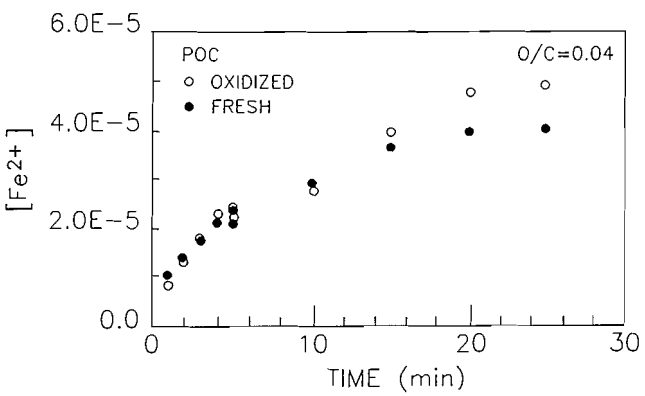

FIG. 2. $[Fe^{2+}]$ vs. time for Pocahontas coal before and after oxidation in air at 105°C.

spectra from this coal and untreated material are shown in Fig. 1. The intense absorption at around 2100 cm^{-1}, the C≡N vibration, in the treated sample that is resistant to reaction with Fe^{3+}, is consistent with the suggestion that CN^-

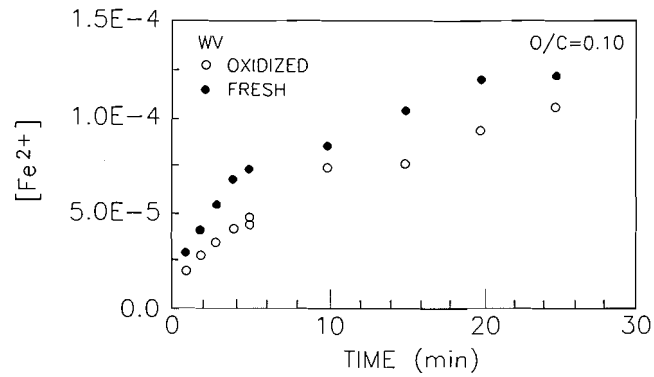

FIG. 3. $[Fe^{2+}]$ vs. time for Stockton coal before and after oxidation in air at 105°C.

adsorbs, possibly as $Fe(CN)^{3-}$, on active sites on the coal surface inhibiting reduction of Fe^{3+} species in the bulk slurry.

The XPS spectrum shows several iron species including Fe_3O_4 (708.3 eV), Fe_2O_3 (711.1 eV), and FeO (709.5 eV). These results, coupled with the formation of prussian blue, would account for the suite of colours observed by Salehi and Hamilton (3).

The other results obtained are recorded in Tables 1 and 2 and are displayed in Figs. 2–6. The kinetics of Fe^{3+} reduction in this system cannot be fixed with certainty for several reasons. The first is purely mechanical: separation of the solution from the slurry requires rapid withdrawal of material through a fine mesh and therefore easily clogs the filter. Secondly, although a large excess of Fe^{3+} is used, thus ensuring pseudo-zero-order kinetics for iron, the nature and distribution of the reactive surface species (i.e., the concentration) is unknown and probably varies rapidly during the course of reaction. Finally, the possibility that Fe^{2+} is oxidized back to Fe^{3+} cannot be rigorously excluded. Nevertheless, the following analysis, which is meant to assess the relative reactivities of the coals studied, is internally consistent.

The two coals having the highest O/C ratios, Figs. 5 and

Can. J. Chem. Downloaded from www.nrcresearchpress.com by 203.198.23.82 on 09/08/12
For personal use only.

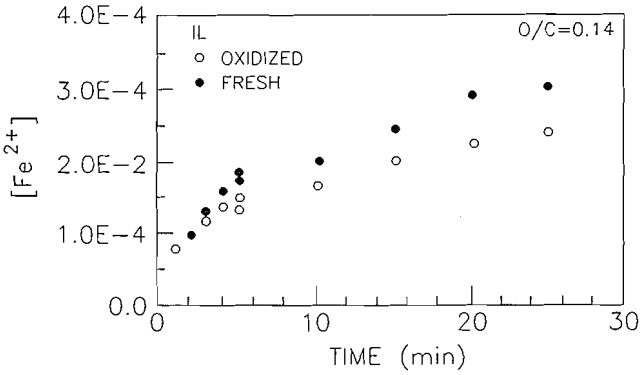

FIG. 4. $[Fe^{2+}]$ vs. time for Illinois no. 6 coal before and after oxidation in air at 105°C.

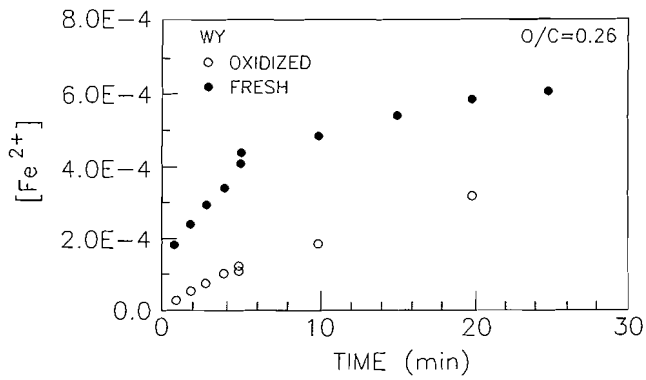

FIG. 5. $[Fe^{2+}]$ vs. time for Wyodak coal before and after oxidation in air at 105°C.

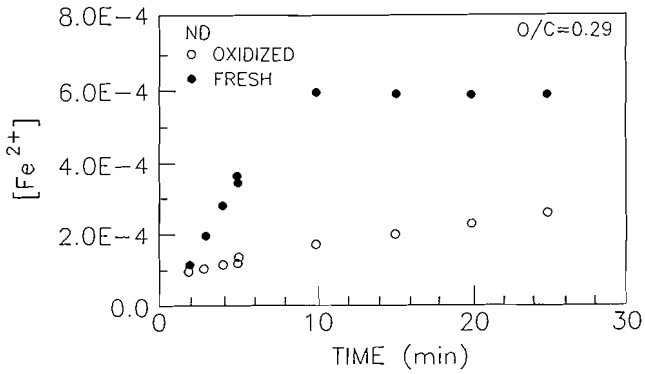

FIG. 6. $[Fe^{2+}]$ vs. time for North Dakota before and after oxidation in air at 105°C.

6, show two distinct reaction regimes, an initial fast reaction that appears to be close to completion after 5 min followed by a relatively slow reaction. These regions become progressively less distinct as the O/C ratio falls, Figs. 4, 3, and 2, and the fast reaction appears to be completely absent in the coal of lowest O/C, Pocahontas, Fig. 2. The fast reaction is probably due to reactive oxygen functional groups, which are more abundant in the coals of highest O/C ratio, while the slow reaction originates from less reactive oxygen species and (or) basic nitrogen groups (4). In an attempt to quantify these results, reaction rates (shown in Figs. 2–6) for the various coals were compared by taking the slope of the $[Fe^{2+}]$ vs. time plot between 2 and 4 min to avoid either forcing the data through the origin or biasing the results to later times in the reaction sequence. A second reaction rate was determined by taking the slope between 10 and 20 min. These data, together with the names and O/C ratios of the coals used are recorded in Tables 1 and 2. This relatively simple approach was chosen because a more sophisticated treatment is precluded by the scatter of the data and uncertainty about the concentration of the surface-reactive material, which can only be inferred from the O/C ratio. We refer to the two time regions as the fast and slow reactions, respectively, although this description is most appropriate for the North Dakota and Wyodak coals (Figs. 5 and 6). The lowest O/C coals, Pocahontas (Fig. 2), may well present a single continuous reaction while Stokton and Illinois (Figs. 3 and 4) appear to represent an intermediate case. The reaction rate for both regions is a clear function of the O/C ratio of the parent coal.

After air oxidation, the initial fast reaction is absent in the coals having the highest O/C ratio and appears to be much reduced in coals with intermediate O/C ratios (Figs. 2–6). There is little or no change in the initial reaction rate in the coal with the lowest O/C values. The slower reaction, i.e., that estimated from the slope after 10 min, appears to extend continuously into the "pre 5-min" region for the coals of highest O/C ratio after air oxidation (Figs. 5 and 6); for this reason we have chosen to describe this reaction simply as "not observed" in Table 2. The intermediate O/C coals (Figs. 3 and 4) still show a second process, while the lowest O/C material (Fig. 2) shows essentially one process. Thus the reactive sites may be divided into two classes, those sensitive to both air oxidation and oxidation by Fe^{3+} and those sensitive to oxidation by Fe^{3+} only. The standard reduction potential for the quinone/hydroquinone system is −0.7 V while that for Fe^{3+}/Fe^{2+} is 0.77; although the concentration of surface species is unknown, it is clear that oxygen-based organic functional groups are capable of reducing Fe^{3+} and that a continuous series of reactive sites having structures similar to the quinone system could be responsible for the behaviour we observe.

Mineral matter has been shown to be capable of reducing Fe^{3+}; however, there is no charge in kinetics after demineralization with concentrated HCl. Consequently, we do not believe that indwelling minerals play a significant role in iron reduction.

Conclusions

Fe^{3+} oxidizes coal and the reaction kinetics can be followed colorimetrically using $K_3Fe(CN)_6$ as an indicator. The formation of various iron oxides and $Fe^{2+}/Fe^{3+}(CN)_6^{3-}$ on the coal surface is responsible for the colours observed by Salehi and Hamilton (3) after treating coal with these reagents. Fresh coal having a relatively high O/C appears to exhibit two oxidation processes of differing kinetics. The differences between the two rates appear to be absent in coals having low O/C ratios and are more pronounced in coals with high O/C ratios. In any case the rates are a smooth function of the O/C ratio of the parent coal. Mild air oxidation effectively eliminates the first, more rapid, reaction, allowing

Can. J. Chem. Downloaded from www.nrcresearchpress.com by 203.198.23.82 on 09/08/12
For personal use only.

the active species to be divided into two types, those oxidized by Fe^{3+} and air oxidation and those oxidized by Fe^{3+} only. The coal may thus be viewed as containing a series of functional groups of varying oxidation potential. The kinetics of Fe^{3+} oxidation of coal may provide a direct measure of coal quality in industrial applications.

1. K.S. Vorres. Energy Fuels, **4**, 420 (1990).
2. J.F. Corcoran and J.F. Stephens. Fuel, **66**, 1306 (1987).
3. M.R. Salehi and L.H. Hamilton. Fuel, **67**, 296 (1988).
4. S. Wallace, N. Taylor, D. Mills, and K.D. Bartle. Fuel, **70**, 121 (1991).

Can. J. Chem. Downloaded from www.nrcresearchpress.com by 203.198.23.82 on 09/08/12
For personal use only.

Robert Chênevert, René Gagnon, Daniel Chamberland, and Michel Simard. Crystalline complexes of 18-crown-6 with methyl sulfonates. Can. J. Chem. **71**, 1225 (1993).

We regret that the name of Robert Chênevert was misspelled in both the Table of Contents and the Cumulative Author Index of the August issue.

Can. J. Chem. Downloaded from www.nrcresearchpress.com by 203.198.23.82 on 09/08/12
For personal use only.

In situ Fourier transform infrared spectroelectrochemical studies of the oxidation of some octaethylporphyrin complexes

A. Scott Hinman[1] and Temitayo Olorunyolemi
Department of Chemistry, The University of Calgary, Calgary, AB T2N 1N4, Canada

Received June 1, 1993

A. Scott Hinman and Temitayo Olorunyolemi. Can. J. Chem. **71**, 1975 (1993).

The oxidations of OEPNi(II), OEPCu(II), OEPFe(III)Cl, OEPMn(III)ClO_4, OEPAg(II), OEPCo(II), and OEPZn(II) (OEP = 2,3,7,8,12,13,17,18-octaethylporphyrin dianion) have been studied by in situ FTIR reflectance spectroelectrochemistry in dibromomethane. One-electron oxidation of the porphyrin ring to produce a π-cation radical results in the appearance of a strong new absorbance band near 1550 cm^{-1}. Other features typical of π-cation radical formation are a strong absorbance increase near 1470 cm^{-1}, and absorbance decreases near 1270 and 1018 cm^{-1}. Oxidation of the metal centre, as observed for OEPCo(II) in the presence of CH_3CN, and for OEPAg(II), results in considerably less perturbation of the vibrational spectra of the complexes. For OEPCo(II) in dry dibromomethane, initial oxidation at the porphyrin ligand is followed by a second oxidation at the metal centre. This order is reversed when acetonitrile is added to solution. Production of porphyrin π-dications was observed for OEPCu(II) and OEPNi(II). This results in a shift of the 1550 cm^{-1} π-cation radical marker band to higher energy, and a strong absorbance increase near 1380 cm^{-1}. Unusual spectral changes observed on one-electron oxidation of OEPZn(II) are suggested to result from the formation of a dimer.

A. Scott Hinman et Temitayo Olorunyolemi. Can. J. Chem. **71**, 1975 (1993).

Faisant appel à la spectroélectrochimie par FTIR à réflectance in situ, on a étudié les oxydations du OEPNi(II), OEPCu(II), OEPFe(III)Cl, OEPMn(III)ClO_4, OEPAg(II), OEPCo(II) et OEPZn(II) (OEP = le dianion 2,3,7,8,12,13,17,18-octaéthylporphyrine) dans le dibromométhane. L'oxydation du noyau porphyrine par un électron conduisant à un radical π-cationique donne lieu à l'apparition d'une forte bande d'absorption près de 1550 cm^{-1}. D'autres caractéristiques typiques de la formation d'un radical π-cationique sont la forte augmentation de l'absorption près de 1470 cm^{-1} et une diminution de l'absorption près de 1270 et 1018 cm^{-1}. L'oxydation du centre métallique observé avec le OEPCo(II) en présence de CH_3CN et avec le OEPAg(II) provoque beaucoup moins de perturbation dans les spectres de vibration des complexes. Avec le OEPCo(II) dans le dibromométhane sec, l'oxydation initiale du coordinat porphyrine est suivie par une deuxième oxydation du centre métallique. Cet ordre en inversé lorsqu'on ajoute de l'acétonitrile à la solution. On a observé la formation de dications-π de la porphyrine avec le OEPCu(II) et le OEPNi(II). Dans ces cas, on observe un déplacement de la bande typique des radicaux π-cationiques de 1550 cm^{-1} vers des énergies plus élevées et une forte augmentation de l'absorption vers 1380 cm^{-1}. Des changements spectraux inhabituels observés lors de l'oxydation du OEPZn(II) par un électron suggèrent qu'il y aurait formation d'un dimère.

[Traduit par la rédaction]

Can. J. Chem. Downloaded from www.nrcresearchpress.com by 203.198.23.82 on 09/08/12
For personal use only.

Introduction

One-electron oxidation of a metalloporphyrin complex may result in loss of an electron from the porphyrin ring, to form a π-cation radical, or from the central metal atom of the complex. Since both types of process have been implicated in the biological action of heme-proteins, porphyrin chemists have directed considerable attention to the problem of identifying the oxidation site within the complex, and a number of criteria have been developed in this regard (1).

While infrared spectroscopy has been suggested to provide the simplest criteria for identifying the oxidation site within the complex (2), it has not yet been widely exploited for this purpose. Goff, Reed, and co-workers (3) were the first to investigate the applicability of infrared spectra to determining the site of oxidation in metalloporphyrins. These workers isolated a number of metalloporphyrin complexes following one-electron oxidation of the porphyrin ring. In the case of 5,10,15,20-tetraphenylporphyrin (TPP) complexes a strong new band at ca. 1280 cm^{-1} was observed in the solid state infrared spectra of the oxidized products, and this band was suggested to be diagnostic of π-cation radical formation. Similarly, a band near 1550 cm^{-1} was suggested as a diagnostic criterion for porphyrin ring oxidation in 2,3,7,8,12,13,17,18-octaethylporphyrin (OEP) complexes.

This laboratory was the first to apply in situ Fourier transform infrared reflectance spectroelectrochemistry to observe changes to the vibrational spectra of metalloporphyrins accompanying electrochemical oxidation of the porphyrin ring (4, 5). In this technique, infrared radiation passes through a thin layer of solution (10–100 μm) onto a polished Pt electrode, and is reflected back to the detector. The intensity of the infrared radiation is determined prior to and following electrolysis of the thin layer of solution. Because replacing the solution in the thin-layer cavity requires repositioning of the electrode, it is difficult to precisely determine a background spectrum in the absence of electroactive species. The technique is thus not well suited to determining individual spectra of the electroactive species prior to and following electrolysis. On the other hand, the difference in absorbance resulting from electrolysis of the thin layer of solution is readily measurable. This is determined by rationing the energy spectrum obtained following electrolysis to that obtained prior to electrolysis and taking the logarithm. No repositioning of the electrode or cell assembly is required in obtaining these spectra.

In a series of studies (4–7), we have investigated the application of in situ FTIR reflectance spectroelectrochemistry to studies of the one-electron oxidation of metal–tetraphenylporphyrin complexes in a variety of solvents or solvent mixtures. In addition to facilitating identification of the oxidation site within the complexes (4, 5), the tech-

[1]Author to whom correspondence may be addressed.

Can. J. Chem. Downloaded from www.nrcresearchpress.com by 203.198.23.82 on 09/08/12
For personal use only.

nique has proven useful for observing axial coordination changes accompanying the oxidation (4), and for characterizing products of irreversible homogeneous reactions following the electron transfer (7).

In situ FTIR spectroelectrochemistry is now, in our view, well established as a technique for identifying the oxidation site within tetraphenylporphyrin complexes, but considerably less work in this regard has been done with octaethylporphyrins. As noted above, Goff, Reed, and co-workers (3) observed a band near 1550 cm^{-1} in the infrared spectra of some solid isolated iron and zinc octaethylporphyrin π-cation radicals and suggested that this band might serve as a marker for oxidation of the porphyrin ring. Kadish et al. (8) similarly observed a band near 1550 cm^{-1} in an electrochemically generated iridium octaethylporphyrin π-cation radical by in situ FTIR transmission spectroelectrochemistry.

Because the octaethylporphyrin complexes are the second most commonly studied class of synthetic metalloporphyrins, following the tetraphenylporphyrins, and since they are structurally more similar to naturally occurring metalloporphyrins, we have utilized in situ FTIR reflectance spectroelectrochemistry to examine the infrared difference spectra associated with the oxidation of a variety of octaethylporphyrin complexes including Ag, Co, Cu, Fe, Mn, Ni, and Zn. Our results are reported here.

Experimental

Metalloporphyrins

Octaethylporphyrin ($OEPH_2$) and its Co(II), Cu(II), Fe(III)Cl, Mn(III)Cl, and Zn(II) complexes were obtained from Aldrich and used as received. OEPAg(II) was prepared by refluxing Ag(I)-CF_3CO_2 with $OEPH_2$ for ca. 30 min according to the method of Adler *et al.* (9), and purified chromatographically on an alumina column using methylene chloride as eluent. The electronic absorbance spectrum of the purified product was identical to that reported in the literature (10).

OEPMn(III)Cl was converted to $OEPMn(III)ClO_4$ by precipitation from methanol to which a small quantity of dilute aqueous perchloric acid had been added. The procedure is identical to that previously reported for the preparation of perchlorato(tetraphenylporphinato)manganese(III) ($TPPMnClO_4$) (11). The presence of perchlorate in the product was confirmed by the appearance of a strong band at 1146 cm^{-1} in the infrared spectrum (KBr disk). The product was further characterized by elemental analysis, which gave satisfactory results assuming the presence of one water molecule per porphyrin unit. (Calculated for $OEPMnClO_4 \cdot H_2O$: C 61.67%, H 6.03%, N 7.99%, found: C 62.09%, H 5.98%, N 7.90%.) The presence of water was similarly indicated in crystalline $TPPMnClO_4$ prepared by the same method (11).

Solvents and supporting electrolyte

Tetra-*n*-butylammonium hexafluorophosphate was used as supporting electrolyte in all electrochemical and spectroelectrochemical experiments. This was prepared, purified, and dried as previously reported (5). Dibromomethane (Aldrich) was used as solvent throughout. This was shaken with activated alumina, distilled from P_2O_5, and stored in the dark over CaH_2 prior to use. Acetonitrile was refluxed over CaH_2 and distilled prior to use.

Spectroscopy, electrochemistry, and spectroelectrochemistry

A Hi Tek model DT2101 potentiostat operating in conjunction with a Hi Tek PPRI waveform generator was utilized for potential control in all cyclic voltammetric and UV–visible spectroelectrochemical experiments. Control of electrode potential in in situ FTIR reflectance spectroelectrochemistry was accomplished with either the Hi Tek potentiostat or a PAR model 174 polarographic analyzer. A home-built saturated calomel reference electrode (SCE) was utilized as reference electrode throughout.

Conventional cyclic voltammetry utilized a two-compartment three-electrode cell, which has been described previously (7). The cell utilized for in situ FTIR reflectance spectroelectrochemistry and time-resolved thin-layer UV–visible reflectance spectroelectrochemistry has similarly been described in detail (6), the only modification being the inclusion of a stray light deflector to prevent light reflected from the front surface of the window from reaching the detector. The cell was fitted with a CaF_2 window for infrared measurements, and a quartz window for UV–visible measurements. A Pt disc, polished to a mirror finish, was utilized as working electrode in both cases.

A Nicolet 8000 FTIR spectrometer fitted with a narrow-range MCT detector was utilized for in situ FTIR reflectance spectroelectrochemistry. The methodology, instrumentation, and optical configuration were as described in previous publications (4–6). Infrared difference spectra are reported as the difference between absorbance of the thin-layer solution resulting from switching the potential from a base potential, $E1$, at which no oxidation occurs, and a second potential, $E2$, chosen to facilitate the desired oxidation.

The instrument employed for time-resolved thin-layer UV–visible reflectance spectroelectrochemistry employed a Rofin–Sinar RSO 6101 spinning-grating monochromator. Its construction and implementation have been described in detail in a previous publication (12).

Absolute infrared absorbance spectra of all of the unoxidized porphyrins were determined in dibromomethane. Either a Mattson 4030 Galaxy series FTIR spectrometer or a Nicolet 5DX FTIR spectrometer was used. Saturated solutions were used in a 0.2-mm pathlength cell fitted with KBr windows.

Results and discussion

Comparison of metal vs. ligand oxidation: OEPAg(II) and OEPCo(II)

OEPAg(II) and OEPCo(II) are both well known to be subject to oxidation at the metal centre as well as at the porphyrin ligand. As such, these complexes provided an opportunity to compare directly the changes to the vibrational spectrum of the complexes arising from metal-centred oxidation with those due to oxidation at the porphyrin ligand.

Cyclic voltammetry of OEPCo(II) in CH_2Br_2/0.1 M $TBAPF_6$ indicates the presence of three clean reversible one-electron oxidations with half-wave potentials of 0.69, 0.98, and 1.29 V vs. SCE, respectively. In dry dichloromethane containing perchlorate as counterion, the first oxidation has been shown to result in loss of an electron from the porphyrin ring to form the $OEP^{\cdot}Co(II)^{+}$ π-cation radical, while the second oxidation is metal centred, forming the $OEP^{\cdot}Co(III)^{2+}$ doubly charged species (13, 14).

Figure 1 illustrates in situ infrared difference spectra associated with the first two oxidations of OEPCo(II) in CH_2Br_2 containing 0.1 M $TBAPF_6$. A strong absorption band of the CH_2Br_2 solvent removes most of the incident radiation in a narrow range around 1200 cm^{-1}, accounting for the high noise level in this region of the spectra.

Loss of one electron from OEPCo(II) (Fig. 1*a*) results in major perturbation of the vibrational spectrum of the porphyrin ligand, as evidenced by major appearance features (absorbance increases) at 1587, 1562, and 1471 cm^{-1}, and major disappearance features (absorbance decreases) at 1272 and 1018 cm^{-1}. By way of contrast, the first oxidation of TPPCo(II), which is well established as a metal-centred process (4, 5, 15, 16) has been shown to result in only very slight changes to the vibrational spectrum of the porphyrin

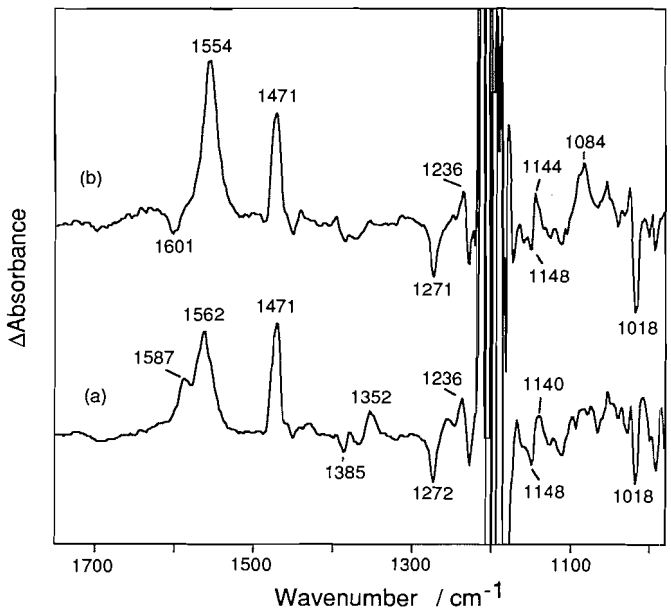

FIG. 1. In situ FTIR difference spectra for (*a*) one- and (*b*) two-electron oxidation of OEPCo(II) in CH_2Br_2 containing 0.1 M $TBAPF_6$. In *a*, *E*1 = 0.50 V and *E*2 = 0.85 V vs. SCE. In *b*, *E*1 = 0.50 V and *E*2 = 1.25 V vs. SCE.

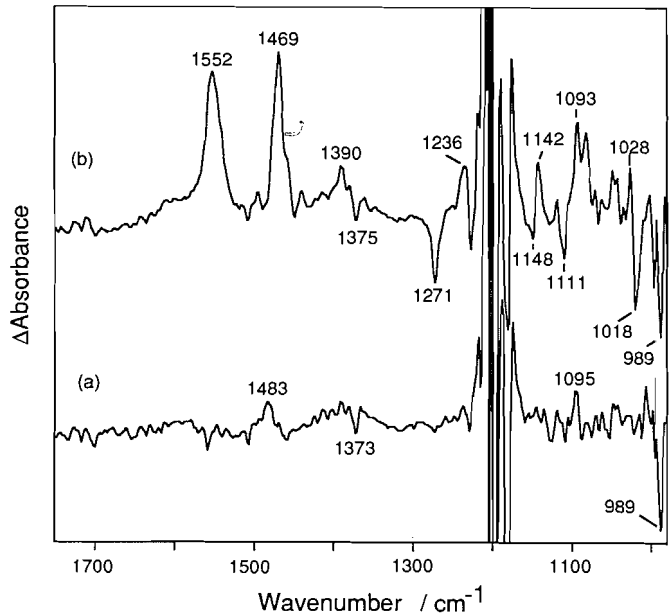

FIG. 2. In situ FTIR difference spectra for (*a*) one- and (*b*) two-electron oxidation of OEPCo(II) 1.44 mM in CH_2Br_2 containing 0.1 M $TBAPF_6$ and 0.01 M CH_3CN. In *a*, *E*1 = 0.40 V and *E*2 = 0.80 V vs. SCE. In *b*, *E*1 = 0.40 V and *E*2 = 1.20 V vs. SCE.

(4, 5). The observations in the present case thus support the conclusions (13, 14) of previous workers that one-electron oxidation of OEPCo(II) in dry noncoordinating media is porphyrin ligand centred. This is further supported by the appearance of a strong new absorption band at 1562 cm^{-1} in the oxidized complex. New absorbance bands in this region of the spectrum were previously suggested to be diagnostic of porphyrin ring oxidation (3).

Removal of a second electron from OEPCo(II) (Fig. 1*b*) results in collapse of the 1587 and 1562 cm^{-1} bands of the singly oxidized product into a single band at 1554 cm^{-1}. In other respects the difference spectra observed on one and two-electron oxidation are very similar. In dry noncoordinating media, the second oxidation of OEPCo(II) is metal centred (13, 14), and a similar situation is expected to pertain in the present case. An alternate assignment of the difference spectra of Fig. 1*b* as arising from formation of the $OEPCo(II)^{2+}$ π-dication rather than the $OEP^{\cdot}Co(III)^{2+}$ π-cation radical is inconsistent with observations of difference spectra arising from formation of other OEP π-dications (vide infra). In these cases, a strong new absorption band near 1385 cm^{-1} is observed, and a band near 1550 cm^{-1} due to the corresponding π-cation radical is observed to shift to higher wavenumber rather than to lower wavenumber, as in the present case.

When dry CH_3CN is added to CH_2Br_2/0.1 M $TBAPF_6$ solutions of OEPCo(II), the half-wave potential for the first oxidation shifts negatively, indicating that complexation of CH_3CN is involved in the electrode process. For a solution containing 1.44 mM porphyrin and 0.01 M CH_3CN, the first oxidation occurred with a half-wave potential of 0.560 V vs. SCE. Subsequent reversible oxidations were observed at half-wave potentials of 0.94 and 1.29 V vs. SCE. The number of coordinating CH_3CN species and the magnitude of the relevant binding constants are currently under investigation.

Figure 2 illustrates in situ infrared difference spectra observed on one and two-electron oxidation of OEPCo(II) in the presence of excess CH_3CN. In contrast to observations in the absence of CH_3CN, one-electron oxidation (Fig. 2*a*) results in very little perturbation of the vibrational spectrum of the porphyrin, suggesting that oxidation is associated with the metal centre rather than the porphyrin ligand. Removal of a second electron (Fig. 2*b*) produces a difference spectrum very similar to that observed in Fig. 1*b* for formation of $OEP^{\cdot}Co(III)^{2+}$ in the absence of CH_3CN. In conjunction with the observation of a strong band at 1552 cm^{-1}, this clearly indicates a porphyrin ring-centred oxidation to produce a π-cation radical species. Thus, addition of CH_3CN results in a reversal of the order of oxidation of the metal and porphyrin ring redox sites, with the first electron now being derived from the metal and the second from the porphyrin ring. Previous workers similarly indicated that the order of oxidation for the two sites in OEPCo(II) is reversed in the presence of H_2O or CH_3OH (14), as well as in the presence of Cl^-, Br^-, or $SbCl_6^-$ (13).

OEPAg(II) undergoes two reversible one-electron oxidations in CH_2Br_2/0.1 M $TBAPF_6$ with half-wave potentials of 0.44 and 1.54 V vs. SCE. The first oxidation was established by a variety of techniques as a metal-centred process producing the $OEPAg(III)^+$ cation (10, 17–19). The second oxidation results in removal of an electron from the porphyrin ring to produce the $OEP^{\cdot}Ag(III)^{2+}$ π-cation radical (10).

Figure 3 shows in situ FTIR difference spectra observed on one- and two-electron oxidation of OEPAg(II). Removal of the first electron from the complex (Fig. 3*a*) results in somewhat greater perturbation of the porphyrin vibrational spectrum than was observed for metal oxidation of OEPCo(II) in the presence of CH_3CN (Fig. 2*a*), but considerably less than observed for ring-centred oxidations of the cobalt–por-

Can. J. Chem. Downloaded from www.nrcresearchpress.com by 203.198.23.82 on 09/08/12
For personal use only.

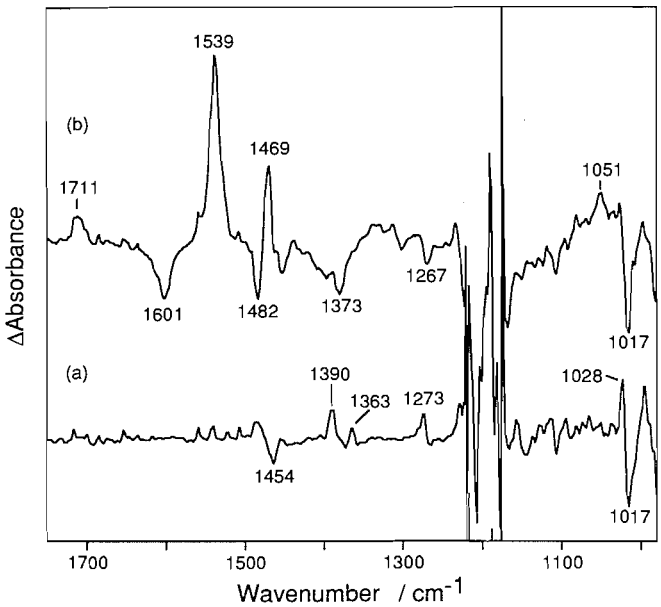

FIG. 3. In situ FTIR difference spectra for (*a*) one- and (*b*) two-electron oxidation of OEPAg(II) in CH_2Br_2 containing 0.1 M $TBAPF_6$. In *a*, $E1 = 0.30$ V and $E2 = 0.60$ V vs. SCE. In *b*, $E1 = 0.30$ V and $E2 = 1.65$ V vs. SCE.

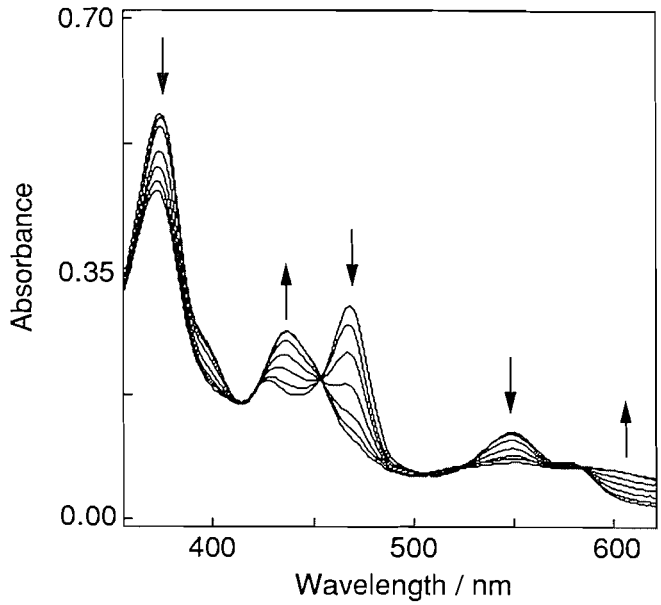

FIG. 4. Time-resolved UV–visible thin-layer spectroelectrochemistry observed during the one-electron oxidation of $OEPMnClO_4$ (1.0 mM) in CH_2Br_2 containing 0.1 M $TBAPF_6$. Spectra were recorded at 10.6 s intervals during a potential step from 1.0 to 1.3 V vs. SCE.

TABLE 1. Half-wave potentials[a] (V vs. SCE) for oxidation of OEP complexes

Complex	Metal oxidation	Ligand oxidation	Additional oxidation
OEPNi(II)		0.77	1.42
OEPCu(II)		0.75	1.35
OEPFe(III)Cl		0.99	1.47
$OEPMn(III)ClO_4$		1.19	1.52
OEPAg(II)	0.44	1.54	
OEPZn(II)		0.71	1.04
OEPCo(II)	0.98	0.69	1.29
OEPCo(II) + CH_3CN[b]	0.560	0.94	1.29

[a]All measurements in CH_2Br_2 containing 0.1 M $TBAPF_6$.
[b][OEPCo(II)] = 1.44 mM, [CH_3CN] = 0.01 M.

phyrin adducts. In particular, no strong new absorbance near 1550 cm^{-1} is found. Removal of a second electron from OEPAg(II) (Fig. 3*b*) results in far more substantial changes to the porphyrin spectrum, and causes the appearance of a strong new absorption at 1539 cm^{-1}. These observations are clearly consistent with the first electron deriving from the Ag(II) metal centre, and the second electron being removed from the porphyrin ring.

Similarities in difference spectra observed on ring oxidation in OEP complexes

To provide a comparison of the infrared difference spectra for formation of a greater variety of OEP π-cation radicals, the oxidations of OEPCu(II), OEPNi(II), OEPFe(III)Cl, and $OEPMn(III)ClO_4$ were investigated. Cyclic voltammetry in CH_2Br_2 indicates that all of these complexes undergo two reversible oxidations with half-wave potentials as indicated in Table 1. Table 1 also includes potentials for oxidation of the Co(II) and Ag(II) complexes (vide supra) as well as for OEPZn(II) (vide infra).

The one-electron oxidation products of OEPCu(II) (19–21), OEPNi(II) (21), and OEPFe(III)Cl (21–23) have all been previously characterized as porphyrin π-cation radicals. Because $OEPMn(III)ClO_4$ has not, to our knowledge, been previously investigated, we monitored the oxidation of this compound by visible as well as infrared spectroelectrochemistry. Figure 4 illustrates the spectral changes accompanying one-electron oxidation of this compound as observed by time-resolved thin-layer UV–visible reflectance spectroelectrochemistry. The oxidation is accompanied by well-defined isosbestic points, indicating the reversible nature of the redox couple. The spectrum of the final oxidation product displays a broad, featureless absorbance in the 500–620 nm region. This is typical of porphyrin π-cation radicals, but is not characteristic of species where electron abstraction has occurred at the metal centre (1). As such, the spectral changes indicate that the one-electron oxidation product may be formulated as the $OEP^{\cdot}Mn(III)ClO_4^+$ π-cation radical.

Prior to investigating the difference spectra observed on oxidation of the OEP complexes, the infrared spectra of all unoxidized species were first measured in CH_2Br_2. Table 2 lists the strong and medium intensity infrared absorptions in the 1800–1000 cm^{-1} region for all species investigated in this study. The porphyrin core vibrational modes ν_{38}–ν_{44} and ethyl substituent vibrational modes for OEPNi(II) were assigned in accordance with a recent detailed analysis by Li et al. (24). Because our measurements were done on solution species, while those of Li et al. were based on KBr disc spectra, some small differences in band position are evident. The assignments for bands of other complexes were made on the basis of their proximity to those of OEPNi(II).

In situ FTIR difference spectra for one-electron oxidation of OEPNi(II), OEPCu(II), OEPFe(III)Cl, and $OEPMn(III)ClO_4$ are presented in Figs. 5*a*, 6*a*, 7, and 8, respectively. In comparing these among themselves, and with the spectra

Can. J. Chem. Downloaded from www.nrcresearchpress.com by 203.198.23.82 on 09/08/12
For personal use only.

TABLE 2. Infrared band positions (cm^{-1}) of OEP complexes

Assignment[a]	OEPNi	OEPCu	$OEPMnClO_4$	OEPFeCl	OEPCo	OEPAg	OEPZn
Combination	1693		1694	1701	1691		1709
ν_{38}, $\nu(C_\beta-C_\beta)$	1601	1602	1602		1601	1601	1601
	1558				1564		
ν_{39}, $\nu(C_\alpha-C_m)_{sym}$	1489	1484	1481		1485	1482 1474	1480
Ethyl CH_2 scissors	1462 1450	1465 1452	1464 1451	1468 1453	1462 1450	1464 1451	1464 1451
ν_{40}, ν(Pyr quarter ring)	1389	1380	1391		1385		
Ethyl CH_2 wag	1375		1373	1375 1362	1375	1373	1373
ν_{41}, $\nu(\text{Pyr half-ring})_{sym}$		1348					
Ethyl CH_2 twist	1271	1272	1269	1269	1271	1267	1267
ν_{42}, $\delta(C_m-H)$	1231						1238
ν_{43}, $\nu(C_\beta-C_1)$	1147	1148	1148	1146	1148	1148	1146
ν_{44}, $\nu(\text{Pyr half-ring})_{asym}$	1133						
	1113	1113	1113	1111	1111	1107	1109
	1057	1058	1057	1057	1057	1057	1057
Ethyl $\nu(C_1-C_2)$	1018	1018	1020	1017	1018	1017	1015

[a]Notation and definition of local coordinates may be found in ref. 24. Bands to which no assignment is made were not reported in ref. 24. C_α and C_β denote the α and β carbons of the pyrrole subunits, C_m denotes the porphyrin *meso* carbon, and C_1 and C_2 denote ethyl carbons.

Can. J. Chem. Downloaded from www.nrcresearchpress.com by 203.198.23.82 on 09/08/12
For personal use only.

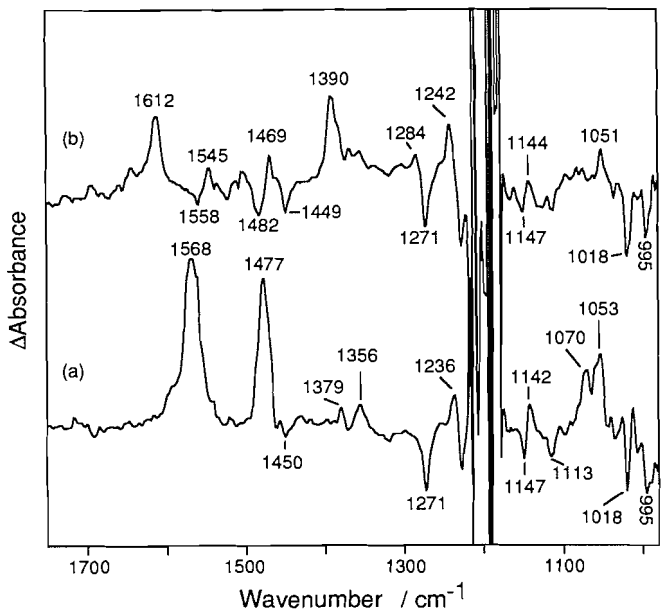

FIG. 5. In situ FTIR difference spectra for (*a*) one- and (*b*) two-electron oxidation of OEPNi(II) in CH_2Br_2 containing 0.1 M $TBAPF_6$. In *a*, *E*1 = 0.65 V and *E*2 = 1.00 V vs. SCE. In *b*, *E*1 = 0.65 V and *E*2 = 1.65 V vs. SCE.

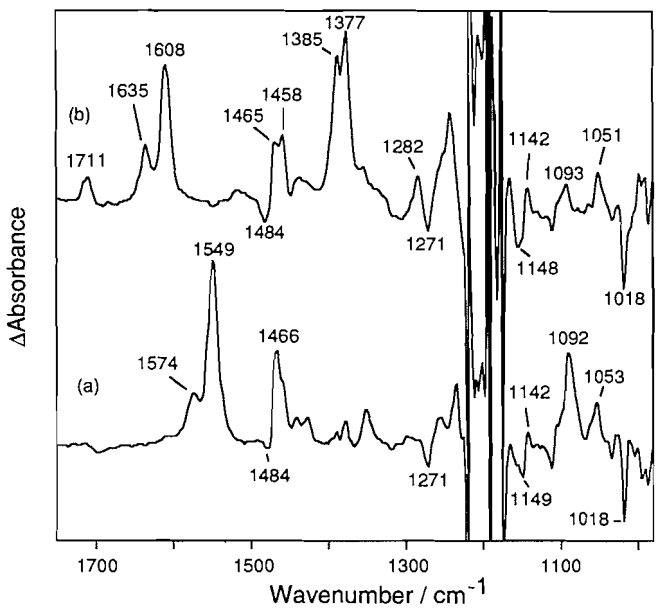

FIG. 6. In situ FTIR difference spectra for (*a*) one- and (*b*) two-electron oxidation of OEPCu(II) in CH_2Br_2 containing 0.1 M $TBAPF_6$. In *a*, *E*1 = 0.60 V and *E*2 = 0.90 V vs. SCE. In *b*, *E*1 = 0.60 V and *E*2 = 1.65 V vs. SCE.

discussed previously for oxidation of the porphyrin ring in Ag and Co OEP complexes (Figs. 1–3), there are several features common to all, or at least the majority, of the cases studied. These are indicated in Table 3.

The most notable feature common to all spectra is the presence of at least one strong new absorption band in the region 1537–1589 cm^{-1}. This is in accordance with the suggestion of previous workers (3) of a 1550 cm^{-1} marker band for OEP π-cation radical formation.

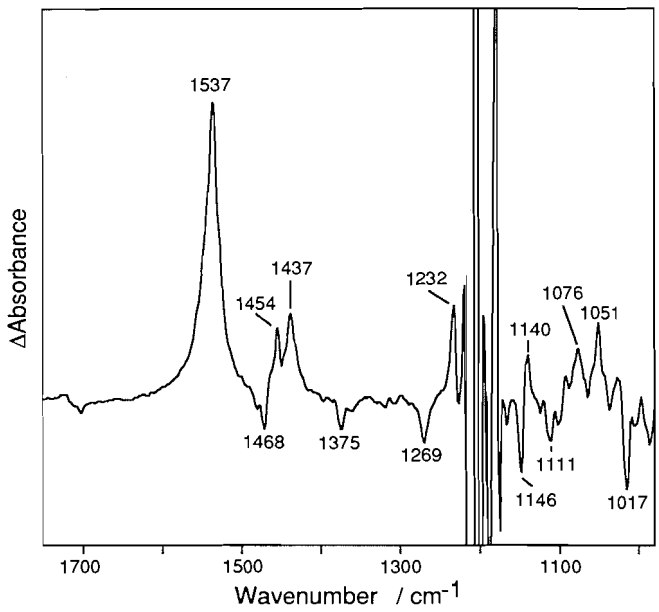

FIG. 7. In situ FTIR difference spectra for one-electron oxidation of OEPFe(III)Cl in CH_2Br_2 containing 0.1 M $TBAPF_6$. $E1$ = 0.85 V and $E2$ = 1.25 V vs. SCE.

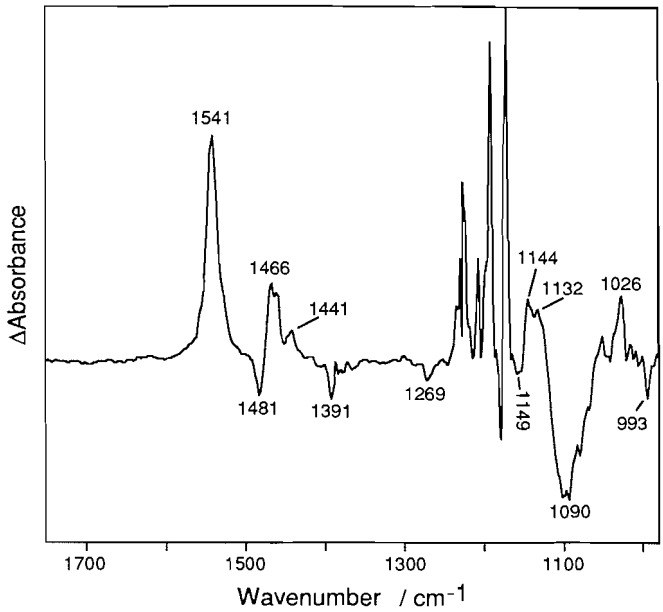

FIG. 8. In situ FTIR difference spectra for one-electron oxidation of $OEPMn(III)ClO_4$ in CH_2Br_2 containing 0.1 M $TBAPF_6$. $E1$ = 1.00 V and $E2$ = 1.35 V vs. SCE.

Also apparent is the presence of one or more strong appearance bands near 1470 cm^{-1}. In most of these cases, especially for OEPAg(III) (Fig. 3*b*), OEPCu(II) (Fig. 6*a*), OEPFe(III)Cl (Fig. 7), and $OEPMn(III)ClO_4$ (Fig. 8), this feature occurs in conjunction with a disappearance feature at higher wavenumber, as apparent in Table 3. For the Ag, Cu, and Mn complexes, this disappearance coincides with ν_{39} as indicated in Table 2. The appearance of a 1470 cm^{-1} band for these cases in the difference spectra is thus suggested to result from a shift to lower energy and increase in intensity of ν_{39} of the parent compound as a result of porphyrin ring oxidation. For OEPFe(III)Cl, the disappearance at 1468 cm^{-1} coincides more closely with that expected for the ethyl CH_2 scissors mode, as indicated in Table 2. However, the similarity in this region of the difference spectrum for OEPFe(III)Cl and those obtained for the other complexes suggests the same band is responsible in all cases.

In most of the difference spectra, as indicated in Table 3, there is evidence of a disappearance feature near 1147 cm^{-1} that coincides with ν_{43} from Table 2. This usually appears in conjunction with an appearance feature with a lower energy of approximately 5 cm^{-1}, suggesting that ν_{43} of the unoxidized complexes shifts to lower energy on removal of an electron from the porphyrin ring.

Also apparent in most cases are disappearance features near 1380, 1270, and 1018 cm^{-1}. The 1380 cm^{-1} band lies close to the positions expected for either the ν_{40} porphyrin core vibrational mode, or the ethyl CH_2 wagging mode, as indicated in Table 2. The disappearance at 1270 cm^{-1} coincides with a band observed in all the solution spectra of the unoxidized porphyrins studied here, and which was assigned by Li et al. (24) to CH_2 twisting in the ethyl substituents for OEPNi(II). In an earlier study by Abe et al. (25), a band at 1268 cm^{-1} in the solid state infrared spectrum of OEPNi(II) was assigned as the ν_{42} porphyrin core vibrational mode. The disappearance near 1018 cm^{-1} coincides with the C_1–C_2 stretching mode of the ethyl groups indicated in Table 2. While the difference spectra clearly indicate a loss in absorbance of these bands, they do not provide clear insight as to whether a shift in band position also occurs.

Metalloporphyrins are believed to possess two nearly degenerate highest occupied molecular orbitals (HOMOs), designated a_{1u} and a_{2u} (26). The pyrrole C_β–C_β interaction is anti-bonding in the a_{1u} orbital, but bonding in the a_{2u} orbital. In resonance Raman studies (21, 27), it was observed that bands thought to possess appreciable C_β–C_β stretching character shift to higher energy on oxidation of the porphyrin ring in OEP complexes, but to lower energy in TPP complexes. This led to the suggestion that, in general, oxidation results in loss of an electron from the a_{1u} orbital for OEP complexes, and from the a_{2u} orbital in TPP complexes (21).

The infrared spectrum of OEPNi(II) displays a band at 1601 cm^{-1}, which has been assigned as arising from the ν_{38} porphyrin core vibrational mode (24). This mode is thought to be primarily C_β–C_β stretching in character. As indicated in Table 2, all of the OEP complexes except OEPFe(III)Cl display an infrared band at this position. In accordance with the suggestion (21) that oxidation of the porphyrin ring in OEP complexes is associated with loss of an electron from the a_{1u} orbital, a shift to higher wavenumber would be anticipated to be evident in the difference spectra obtained on oxidation of the complexes in this study. A disappearance coincident with this band is observed in the difference spectra obtained for formation of $OEP^{\cdot}Ag(III)^+$ (Fig. 3*b*) and $OEP^{\cdot}Co(III)^{2+}$ (Fig. 1*b*), but no shift to higher wavenumber is apparent. In the rest of the cases investigated, no perturbation of this band is observed at all. Shifts in band positions that are observed do not provide clear insight as to the ground state configuration of the π-cation radical complexes. Thus, at present, in situ FTIR spectroelectrochemistry does not appear to have the same utility for assigning

Can. J. Chem. Downloaded from www.nrcresearchpress.com by 203.198.23.82 on 09/08/12
For personal use only.

TABLE 3. Positions (cm^{-1}) of appearance (a) and disappearance (d) bands in the infrared difference spectra of OEP π-cation radials

OEPNi(II)	1568a	1477a		1271d	1147d 1142a	1018d
OEPCu(II)	1574a 1549a	1484d		1271d	1149d	1018d
OEPFe(III)Cl	1537a	1468d 1454a	1375d	1269d	1146d 1140a	1017d
$OEPMnClO_4$	1541a	1481d 1466a 1457a	1391d	1269d	1149d 1144a	
OEPAg(III)	1539a	1469a	1373d	1267d		1017d
OEPCo(II)	1587a 1562a	1485d 1471a		1271d	1148d 1140a	1018d
OEPCo(III)	1554a	1485d 1471a		1271d	1148d 1144a	1018d
OEPCo(III) + CH_3CN	1552a	1469a	1375d	1271d	1148d	1018d

ground state configurations in porphyrin π-cation radicals as does resonance Raman spectroscopy.

The in situ FTIR difference spectrum observed for oxidation of $OEPMn(III)ClO_4$ shown in Fig. 8 displays a strong disappearance feature at 1090 cm^{-1} that was not observed on oxidation of any of the other OEP complexes investigated. This frequency corresponds to that observed for free solution perchlorate in dibromomethane solutions containing tetra-*n*-butyl ammonium perchlorate (4). The disappearance is accompanied by strong absorption at 1132 cm^{-1}, and a weaker one at 1051 cm^{-1}. Bands at these positions are typical of coordinated perchlorate (4). These features in the difference spectrum indicate that the perchlorate anion in $OEPMn(III)ClO_4$ dissociates, at least partially, on dissolution in CH_2Br_2. The binding constant is enhanced on oxidation to the π-cation radical, resulting in a loss of absorbance due to free perchlorate and an increase of absorbance bands due to coordinated perchlorate. Enhanced coordination of perchlorate has similarly been indicated in the in situ FTIR difference spectra observed on oxidation of the porphyrin ring in several TPP complexes (4).

In situ FTIR difference spectra observed on formation of OEP π-dications

For OEPCu(II) and OEPNi(II), we were able to observe reproducible difference spectra associated with removal of a second electron from the complexes. The spectral changes were reversible, as indicated by a return of the difference spectra to a flat baseline when the applied potential was returned to its base value, *E*1. We were not able to observe reproducible and spectrally reversible behavior for removal of a second electron from OEPFe(III)Cl or $OEPMn(III)ClO_4$.

Figure 6*b* illustrates the difference spectra observed on removal of a second electron from OEPCu(II). The product in this case was previously characterized as the $OEPCu(II)^{2+}$ π-dication (10). In comparing the spectrum with that in Fig. 6*a* for one-electron oxidation, it is evident that the 1549 π-cation radical marker band shifts to 1608 cm^{-1} on removal of a second electron from the porphyrin ring. Also apparent are major appearance features at 1385 and 1377 cm^{-1}. By way of contrast, removal of an electron from the metal centre in $OEP^{\cdot}Co(II)^{+}$ results in a shift of the π-cation radical marker band to lower energy, as apparent in Fig. 1, and produces no major new appearance features in the region near 1380 cm^{-1}.

The in situ FTIR difference spectrum observed on removal of a second electron from OEPNi(II) is illustrated in Fig. 5*b*. Similar to the changes observed for the second oxidation of OEPCu(II), loss of the second electron from OEPNi(II) results in a shift to higher energy of the 1568 cm^{-1} π-cation radical marker band (Fig. 5a) to 1612 cm^{-1}, and the observation of a major appearance feature at 1390 cm^{-1}. The product of the second oxidation of OEPNi(II) does not appear to have been conclusively identified, and Ni(III) porphyrin complexes are known (28). However, the similarity of the difference spectrum to that observed for the second oxidation OEPCu(II) suggests that, at least under the present conditions, the second electron from OEPNi(II) is derived from the porphyrin ring producing the $OEPNi(II)^{2+}$ π-dication.

Unusual difference spectrum observed for oxidation of OEPZn(II)

Figure 9 illustrates the in situ FTIR difference spectrum observed on removal of a single electron from OEPZn(II). The spectrum does possess an appearance band at 1535 cm^{-1}, but in other respects is considerably different from the spectra observed on one-electron oxidation of the porphyrin ring for the other OEP complexes in this study. In particular, very intense appearance features are observed at 1427, 1342, 1269, 1097, and 1007 cm^{-1} that do not appear to be typical of simple π-cation radical formation. Fuhrhop et al. (29, 30) suggested that the $OEP^{\cdot}Zn(II)$ π-cation radical formed by chemical oxidation of OEPZn(II) exists in equilibrium with a diamagnetic π–π dimer. As one possibility, the dimer was suggested to involve multicentred face-to-face overlap of the half-filled π-orbitals of two π-cation radicals. The visible spectrum of one-electron oxidized OEPZn(II) observed under our conditions by time-resolved UV–visible thin-layer reflectance spectroelectrochemistry appears identical to that reported by Fuhrhop et al. (29) for solutions of the dimer. Dimer formation thus appears to provide a plausible expla-

Can. J. Chem. Downloaded from www.nrcresearchpress.com by 203.198.23.82 on 09/08/12
For personal use only.

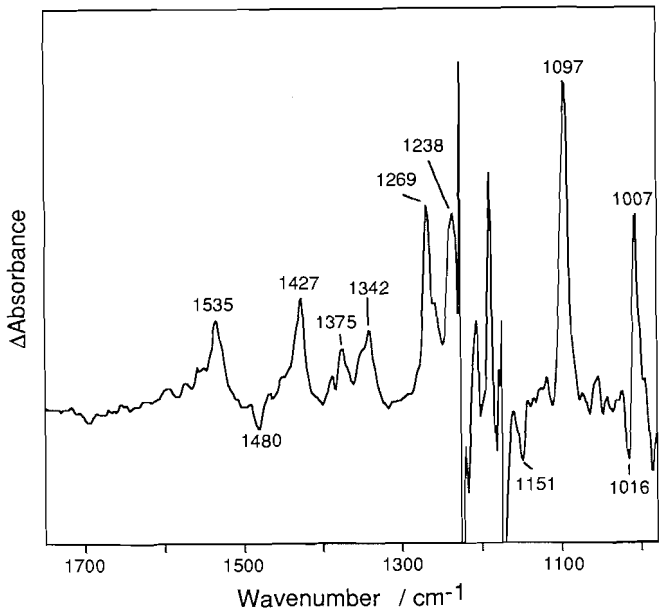

FIG. 9. In situ FTIR difference spectra for one-electron oxidation of OEPZn(II) in CH_2Br_2 containing 0.1 M $TBAPF_6$. $E1$ = 0.60 V and $E2$ = 0.90 V vs. SCE.

nation for the unusual infrared spectral changes observed on one-electron oxidation of OEPZn(II).

Acknowledgements

The authors are grateful to the Natural Sciences and Engineering Research Council of Canada for financial support of this work.

1. J.-H. Fuhrhop. Struct. Bonding (Berlin), **18**, 1 (1974).
2. P. Gans, G. Buisson, E. Duee, J. Marchon, B.S. Erler, W.F. Scholz, and C.A. Reed. J. Am. Chem. Soc. **108**, 1223 (1986).
3. E.T. Shimomura, M.A. Phillipi, H.M. Goff, W.F. Scholz, and C.A. Reed. J. Am. Chem. Soc. **103**, 6778 (1981).
4. A.S. Hinman, B.J. Pavelich, and K.M. McGarty. Can. J. Chem. **66**, 1589 (1988).
5. D.H. Jones and A.S. Hinman. J. Chem. Soc. Dalton Trans. 1504 (1992).
6. A.S. Hinman and B.J. Pavelich. Can. J. Chem. **65**, 919 (1987).
7. A.S. Hinman, B.J. Pavelich, A.E. Kondo, and S. Pons. J. Electroanal. Chem. Interfacial Electrochem. **234**, 145 (1987).
8. K.M. Kadish, X.H. Mu, and X.Q. Lin. Electroanalysis, **1**, 35 (1989).
9. A.D. Acler, F.R. Longo, F. Kampas, and J. Kim. J. Inorg. Nucl. Chem. **32**, 2443 (1970).
10. A. Antipas, D. Dolphin, M. Gouterman, and E.C. Johnson. J. Am. Chem. Soc. **100**, 7705 (1978).
11. A.S. Hinman, K. McGarty, C. Tang, and B.J. Pavelich. Can. J. Chem. **67**, 545 (1988).
12. D.H. Jones and A.S. Hinman. Can. J. Chem. **68**, 2234 (1990).
13. Z. Gasyna and M.J. Stillman. Inorg. Chem. **29**, 5101 (1990).
14. A. Salehi, W.A. Oertling, G.T. Babcock, and C.K. Chang. J. Am. Chem. Soc. **108**, 5630 (1986).
15. Z. Gasyna, W.R. Browett, and M.J. Stillman. Inorg. Chem. **23**, 382 (1984).
16. K.M. Kadish. *In* Progress in inorganic chemistry. Vol. **34**. *Edited by* S.J. Lippard. John Wiley, New York. 1986. pp. 437–605.
17. D. Karweik, N. Winograd, D.G. Davis, and K.M. Kadish. J. Am. Chem. Soc. **96**, 591 (1974).
18. A. McCragh, C.B. Storm, and W.S. Koski. J. Am. Chem. Soc. **87**, 1470 (1965).
19. G.M. Godzeila and H.M. Goff. J. Am. Chem. Soc. **108**, 2237 (1986).
20. W.R. Browett and M.J. Stillman. Inorg. Chim. Acta, **49**, 69 (1981).
21. R.S. Czernuszewicz, K.A. Macor, X.-Y. Li, J.R. Kincaid, and T.G. Spiro. J. Am. Chem. Soc. **111**, 3860 (1989).
22. M.A. Phillipi, E.T. Shimomura, and H.M. Goff. Inorg. Chem. **20**, 1332 (1981).
23. W.R. Scheidt, H. Song, K.J. Haller, M.K. Safo, R.D. Orosz, C.A. Reed, P.G. Debrunner, and C.E. Schulz. Inorg. Chem. **31**, 941 (1992).
24. X.-Y. Li, R.S. Czernuszewicz, J.R. Kincaid, P. Stein, and T.G. Spiro. J. Phys. Chem. **94**, 47 (1990).
25. M. Abe, T. Kitagawa, and Y. Kyogoku. J. Chem. Phys. **69**, 4526 (1978).
26. M. Gouterman. *In* The porphyrins. Vol. III. *Edited by* D. Dolphin. Academic Press, New York. 1979. pp. 1–165.
27. W.A. Oertling, A. Salehi, C.K. Chang, and G.T. Babcock. J. Phys. Chem. **93**, 1311 (1989).
28. D. Chang, T. Malinski, A. Ulman, and K.M. Kadish. Inorg. Chem. **23**, 817 (1984).
29. J.-H. Fuhrhop, P. Wasser, D. Riesner, and D. Mauzerall. J. Am. Chem. Soc. **94**, 7996 (1972).
30. J.-H. Fuhrhop and D. Mauzerall. J. Am. Chem. Soc. **91**, 4174 (1969).

Can. J. Chem. Downloaded from www.nrcresearchpress.com by 203.198.23.82 on 09/08/12
For personal use only.

Benzo-9-crown-3 ether: X-ray crystal structure, NMR studies in solution and the solid phase, and *ab initio* calculations of isotropic ^{13}C chemical shifts using LORG with a D95V basis set

G.W. BUCHANAN,[1] A.B. DRIEGA, A. MOGHIMI, AND C. BENSIMON
Ottawa–Carleton Chemistry Institute, Department of Chemistry, Carleton University, Ottawa, ON K1S 5B6, Canada

AND

R.A. KIRBY AND T.D. BOUMAN[2]
Department of Chemistry, Southern Illinois University at Edwardsville, Edwardsville, IL 62026, U.S.A.

Received April 15, 1993

G.W. BUCHANAN, A.B. DRIEGA, A. MOGHIMI, C. BENSIMON, R.A. KIRBY, and T.D. BOUMAN. Can. J. Chem. **71**, 1983 (1993).

Using the X-ray crystal geometry as input, the ^{13}C NMR chemical shifts of benzo-9-crown-3 ether have been calculated via *ab initio* methods using a localized orbital local origin (LORG) approach. Reasonable agreement is found between the calculated values for an isolated molecule in the gas phase and those obtained in the ^{13}C CPMAS NMR spectrum. Solid phase ^{13}C spectra of the C7,10-d_4 derivative confirm the existence of a 7.9 ppm shift difference between these sites in the solid, whereas in solution they are conformationally averaged to one resonance. The effects of C—H bond length variation on calculated ^{13}C shifts have been explored.

G.W. BUCHANAN, A.B. DRIEGA, A. MOGHIMI, C. BENSIMON, R.A. KIRBY et T.D. BOUMAN. Can. J. Chem. **71**, 1983 (1993).

Utilisant la géométrie déterminée par diffraction des rayons X comme donnée et faisant appel à des méthodes *ab initio* impliquant une approche d'orbitale localisée à l'origine locale, on a calculé les déplacements chimiques de la RMN du ^{13}C de l'éther benzo-9-couronne-3. On a obtenu un accord raisonnable entre les valeurs calculées pour une molécule isolée en phase gazeuse et celles obtenue par RMN CPMAS du ^{13}C. Le spectre RMN du ^{13}C en phase solide du dérivé C7,10-d_4 confirme l'existence d'un déplacement chimique de 7,9 ppm entre ces sites dans le solide alors que, en solution, la moyenne conformationnelle les fait apparaître comme une seule résonance. On a examiné les effets de la variation de la longueur des liaisons sur les déplacements chimiques calculés du ^{13}C.

[Traduit par la rédaction]

Can. J. Chem. Downloaded from www.nrcresearchpress.com by 203.198.23.82 on 09/08/12
For personal use only.

Introduction

The study of crown ether conformations in solution and in the solid phase has become an area of considerable recent research activity. In several cases correlations have been presented between experimentally observed ^{13}C NMR chemical shifts in the solid and X-ray crystallographic structural features. The benz-annelated crown ether systems that have been examined via these techniques to date are 30-crown-10 (1), 24-crown-8 (1), 15-crown-5 (1, 2), 14-crown-4 (3), 13-crown-4 (4), and 12-crown-4 (5). In no case, however, have there been any theoretical calculations of the ^{13}C shifts for the particular system under study, a situation arising mainly from the complexity of the molecules examined. This complexity has made the number of basis functions in a reasonable basis set representation of the molecule so large that NMR chemical shift calculations could not be done using available computing facilities.

In the present work we report the X-ray crystallographic structure of 2,3-benzo-1,4,7-trioxacyclonona-2-ene (benzo-9-crown-3) **1**, as well as its ^{13}C NMR spectrum in the solid phase and ^1H and ^{13}C spectra in solution. The relative simplicity of this molecule has permitted an *ab initio* calculation of its ^{13}C chemical shifts via the LORG (6–8) method, using as input for the calculations the geometry for C and O atoms obtained from the X-ray crystal structure.

Since the X-ray derived C—H bond lengths show a large range (0.06 Å), these bond lengths cannot be used as input for the LORG calculations. Rather, plausible proton positions have been determined via geometry optimization and used as input for LORG.

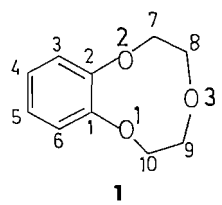

1

FIG. 1. Structure and numbering scheme for benzo-9-crown-3 ether (**1**).

The synthesis of **1**-7,10-d_4 has been carried out and its solid phase ^{13}C spectrum obtained to check that the large shift difference calculated between these two carbons (8.5 ppm) is consistent with experiment.

Results and discussion

Figure 1 contains numbering scheme used for **1**. Its ORTEP diagram is presented in Fig. 2 while the solid phase ^{13}C CPMAS spectrum is shown in Fig. 3. Figure 4*a* contains the normal ^{13}C CPMAS spectrum of the C7,10-d_4 derivative of **1**, while the dipolar dephased spectrum of this molecule is shown in Fig. 4*b*. Bond lengths and angles are collected in Table 1 while the torsional angles for ring skeletal atoms are provided in Table 2. ^{13}C NMR chemical shifts are in Table 3. Crystallographic data are presented in Table 4 and the atomic parameters in Table 5. In Table 6 are presented LORG

[1]Author to whom correspondence may be addressed.
[2]Deceased, April 12, 1992.

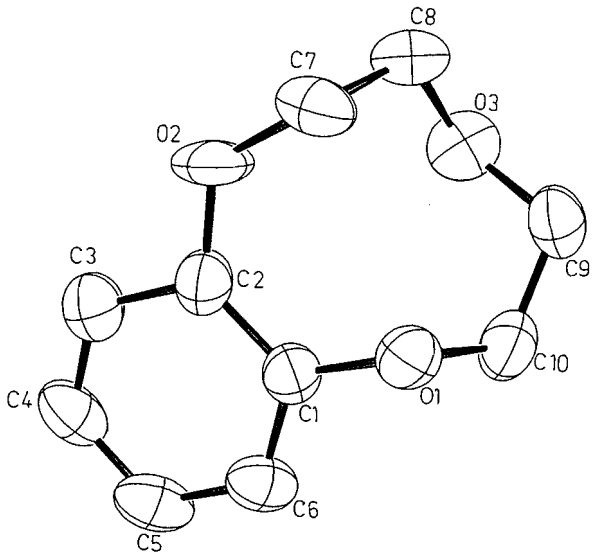

FIG. 2. ORTEP plot for **1**.

calculated isotropic ^{13}C shifts for ethane as a function of C—H bond length.

(a) Solution ^{13}C and ^{1}H NMR spectra

In the 400 MHz ^{1}H NMR spectrum of **1**, multiplets observed for both the ether and aromatic protons are characteristic of AA'BB' spin systems, as has been reported (9) for the dimer of **1**, dibenzo-18-crown-6, **2**. Data for the ethereal protons of **1**, as determined via iterative analysis, are as follows: δ_A = 4.334 ppm, δ_B = 3.895 ppm, $J_{AA'}$ = −10.91 Hz, $J_{BB'}$ = −11.01 Hz, J_{AB} = $J_{A'B'}$ = 6.17 Hz, $J_{A'B}$ = $J_{AB'}$ = 2.69 Hz. The magnitude of these coupling constants is consistent with a situation in which there is rapid conversion between rotamers in which the oxygen atoms are *gauche* to one another (9). This observation is also consistent with the X-ray data for **1**, where the O2—C7—C8—O3 and O3—C9—C10—O1 angles are 63.3° and 66.7°, respectively.

Assignments of the aliphatic protons of **1** were made via results from a NOESY experiment. A weak cross peak was noted between the resonance centered at 4.34 ppm and the aromatic proton resonance. Such a cross peak could only arise from relaxation between the *ortho* aromatic protons and the protons on C7,10 of **1**. No such correlation was found for the aliphatic multiplet centered at 3.89 ppm, since this arises from the more distant (from the aromatic ring) C8,9 site. With the NOESY results in hand, a $^{1}H^{13}C$ HETCOR experiment furnished the ^{13}C assignments of **1** in solution. These assignments were confirmed by comparison of spectra for **1**-d_4.

The solution ^{13}C spectrum of **1** is independent of temperature (apart from minor chemical shift changes) over the range 300–173 K. Hence the conformational interconversions in the nine-membered ring must remain fast on the NMR timescale at all accessible temperatures.

(b) Solid phase ^{13}C NMR spectrum

In the solid phase, the ^{13}C NMR spectral multiplicity will reflect the asymmetric unit in the crystal if no unusual crystal packing effects or nonequivalent molecules in the unit cell are present (1). For **1**, neither of these complicating phenomena is present in the crystal structure and one thus expects to see 10 distinct resonances in the ^{13}C CPMAS spectrum. The experimental ^{13}C CPMAS spectrum is shown in Fig. 3 and there are indeed 10 clearly resolved lines with the expected relative intensities based on the X-ray crystallographic structure.

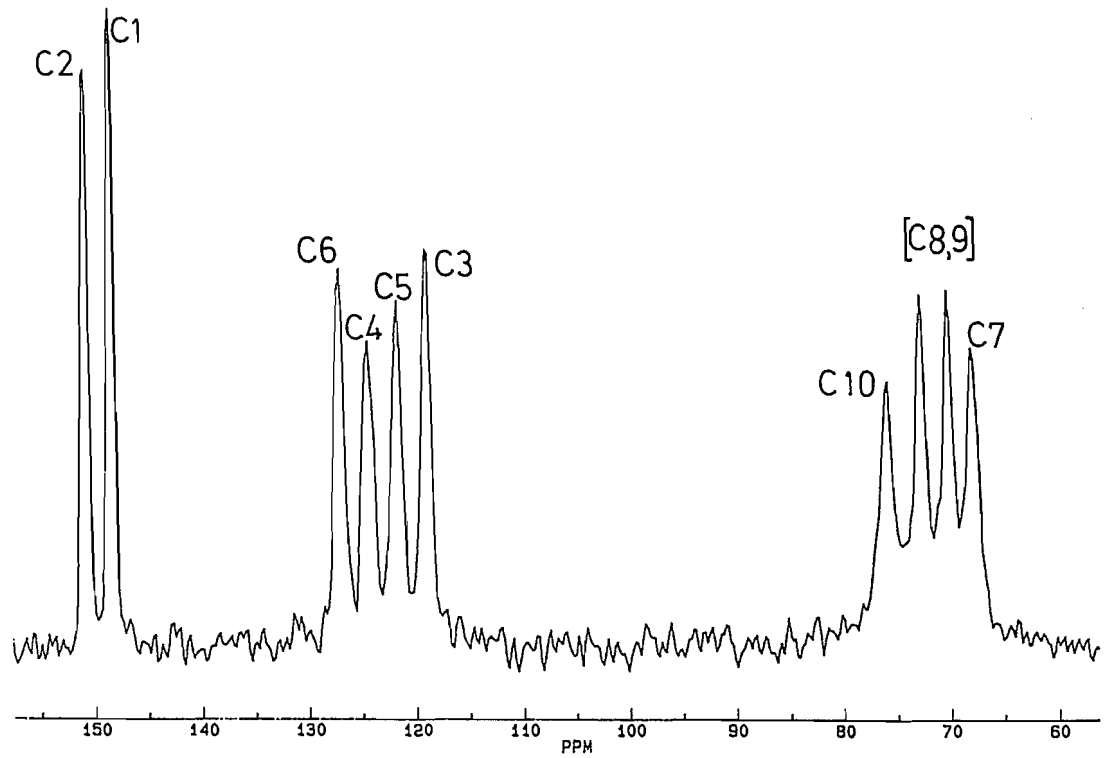

FIG. 3. 45.3 MHz ^{13}C CPMAS NMR spectrum of **1**.

Can. J. Chem. Downloaded from www.nrcresearchpress.com by 203.198.23.82 on 09/08/12
For personal use only.

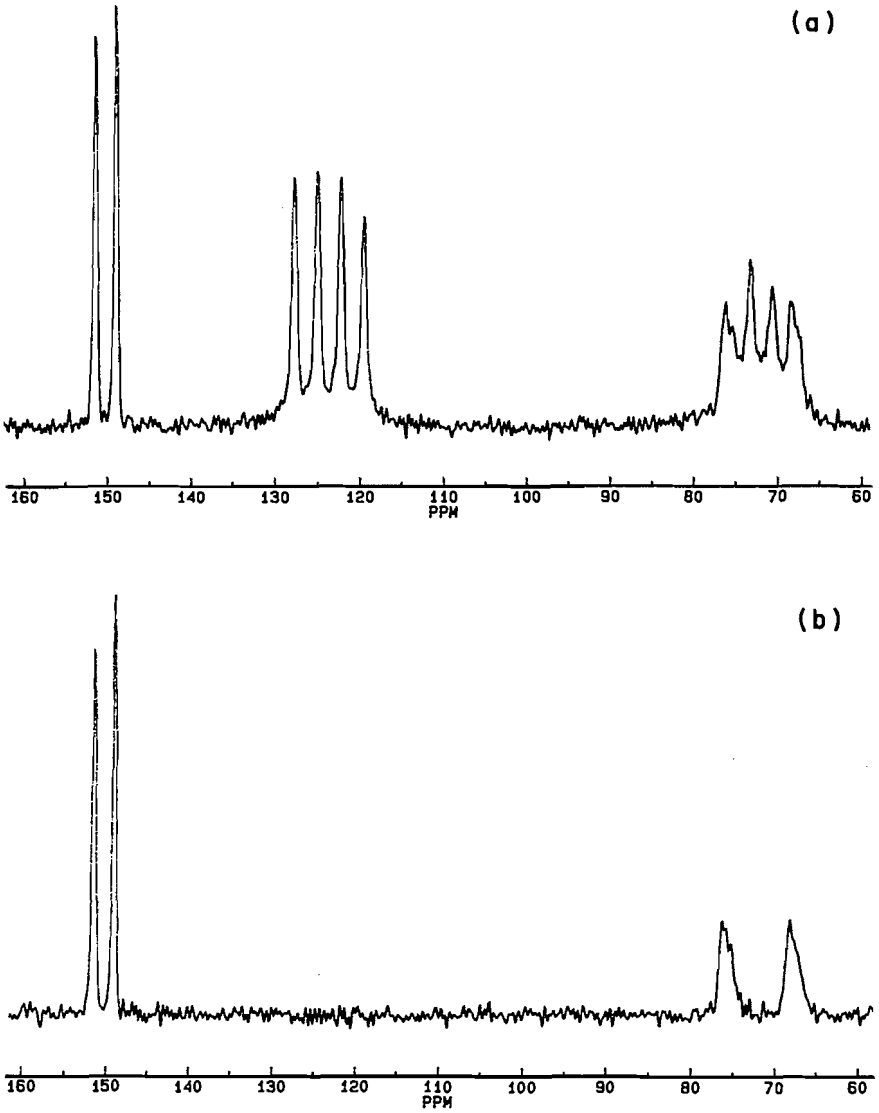

FIG. 4. (*a*) Normal and (*b*) dipolar dephased ^{13}C CPMAS NMR spectra of **1**-C7,10-d_4.

(c) Ab initio *calculations: agreement between theory and experiment*

It has been demonstrated (10) that calculated ^{13}C shieldings are very sensitive to C—H bond lengths, i.e., a decrease of 2 ppm per 0.01 Å increase in the length of the C—H bond for the CH_4 molecule. Accordingly, the X-ray derived C—H bond lengths for **1** (Table 1), which show a range of 0.06 Å, are not of sufficient accuracy for use as input for the LORG calculations. The LORG calculations for **1** were carried out using the X-ray data only for the C and O atoms and plausible proton positions were determined via geometry optimization using the MOPAC (11) routine.

It is known (12) that the MNDO Hamiltonian produces C—H bond lengths that are within 0.014 Å of experimental values and bond angles which are within 2.8° of experiment. We assume that the present optimized H positions for **1** are within these approximate ranges of true experimental values. To test the variation of LORG calculated ^{13}C shifts as a function of C—H bond length at the D95V basis set, ethane has been examined. The results in Table 6 indicate a variance of only 1.37 ppm when all six C—H bonds are shortened by 0.01 Å. For the shortening of a single C—H bond, the isotropic ^{13}C shift changes by only 0.38 ppm at the bonded carbon and 0.08 ppm at the neighbouring site. Hence it appears that the use of plausible proton positions will not compromise the overall validity of the calculated ^{13}C shieldings for **1**.

(i) Aromatic carbons

The LORG calculations for **1** indicate, for the carbons bearing oxygen, that C2 should be deshielded relative to C1 by 2.9 ppm (i.e., 152.9 vs. 150.0). The observed difference between these sites is 2.3 ppm (151.0 vs. 148.7), in excellent agreement with the theory. The X-ray data indicate that the torsional angle for the C7—O2—C2—C3 network is 170.3°, while that for the corresponding C10—O1—C1—C6 network is 79.9°. As a result of the C7—O2—C2—C3 geometry, one of the lone pairs of electrons on O2 occupies an orbital that is nearly perpendicular to the plane of the aromatic ring. This geometry is optimal for conjugative electron release by oxygen. Hence C2 is expected to be deshielded relative to C1 because of the enhanced double-bond character of the O2—C2 bond relative to the O1—C1 bond.

The LORG calculations predict, for the nonoxygenated aromatic carbons, a range of shifts of 11 ppm (i.e., 126.9–

Can. J. Chem. Downloaded from www.nrcresearchpress.com by 203.198.23.82 on 09/08/12
For personal use only.

Can. J. Chem. Downloaded from www.nrcresearchpress.com by 203.198.23.82 on 09/08/12
For personal use only.

TABLE 1. (*a*) Bond distances in angstroms for **1**

O(1)—C(1)	1.387(11)	C(8)—H(8B)	1.124
O(1)—C(10)	1.443(12)	C(9)—C(10)	1.475(13)
O(2)—C(2)	1.326(11)	C(9)—H(9A)	1.084
O(2)—C(7)	1.429(11)	C(9)—H(9B)	1.140
O(3)—C(8)	1.409(11)	C(3)—C(4)	1.326(14)
O(3)—C(9)	1.425(11)	C(3)—H(3)	1.124
C(1)—C(2)	1.369(13)	C(5)—C(4)	1.384(15)
C(1)—C(6)	1.354(13)	C(5)—H(5)	1.147
C(2)—C(3)	1.396(14)	C(7)—H(7A)	1.084
C(6)—C(5)	1.385(14)	C(7)—H(7B)	1.112
C(6)—H(6)	1.110	C(10)—H(10A)	1.093
C(8)—C(7)	1.494(13)	C(10)—H(10B)	1.091
C(8)—H(8A)	1.128	C(4)—H(4)	1.097

(*b*) Bond angles in degrees

C(1)—O(1)—C(10)	115.4(6)	H(9A)—C(9)—H(9B)	104.9
C(2)—O(2)—C(7)	124.4(7)	C(2)—C(3)—C(4)	120.6(8)
C(8)—O(3)—C(9)	115.3(7)	C(2)—C(3)—H(3)	123.3
O(1)—C(1)—C(2)	122.6(8)	C(4)—C(3)—H(3)	116.0
O(1)—C(1)—C(6)	119.2(8)	C(6)—C(5)—C(4)	118.3(8)
C(2)—C(1)—C(6)	118.0(8)	C(6)—C(5)—H(5)	118.1
O(2)—C(2)—C(1)	127.5(9)	C(4)—C(5)—H(5)	123.6
O(2)—C(2)—C(3)	112.1(8)	O(2)—C(7)—C(8)	109.6(7)
C(1)—C(2)—C(3)	120.4(8)	O(2)—C(7)—H(7A)	114.7
C(1)—C(6)—C(5)	122.2(8)	O(2)—C(7)—H(7B)	112.3
C(1)—C(6)—H(6)	118.1	C(8)—C(7)—H(7A)	105.1
C(5)—C(6)—H(6)	119.6	C(8)—C(7)—H(7B)	107.8
O(3)—C(8)—C(7)	116.6(6)	H(7A)—C(7)—H(7B)	106.8
O(3)—C(8)—H(8A)	109.6	O(1)—C(10)—C(9)	110.0(7)
O(3)—C(8)—H(8B)	109.7	O(1)—C(10)—H(10A)	112.4
C(7)—C(8)—H(8A)	109.9	O(1)—C(10)—H(10B)	112.3
C(7)—C(8)—H(8B)	107.1	C(9)—C(10)—H(10A)	108.3
H(8A)—C(8)—H(8B)	103.1	C(9)—C(10)—H(10B)	105.9
O(3)—C(9)—C(10)	108.6(7)	H(10A)—C(10)—H(10B)	107.7
O(3)—C(9)—H(9A)	110.2	C(3)—C(4)—C(5)	120.3(8)
O(3)—C(9)—H(9B)	108.3	C(3)—C(4)—H(4)	126.5
C(10)—C(9)—H(9A)	115.3	C(5)—C(4)—H(4)	113.2
C(10)—C(9)—H(9B)	109.3		

TABLE 2. Torsion angles for **1**

C10—O1—C1—C2	−105.0(9)	C10—O1—C1—C6	79.9(8)
C1—O1—C10—C9	111.9(9)	C7—O2—C2—C1	−10.5(5)
C7—O2—C2—C3	170.3(10)	C2—O2—C7—C8	98.4(8)
C9—O3—C8—C7	−73.4(7)	C8—O3—C9—C10	108.7(9)
O1—C1—C2—O2	4.4(4)	O1—C1—C2—C3	−176.4(11)
C6—C1—C2—O2	179.5(12)	C6—C1—C2—C3	−1.3(5)
O1—C1—C6—C5	177.6(11)	C2—C1—C6—C5	2.3(5)
O2—C2—C3—C4	178.4(12)	C1—C2—C3—C4	−0.9(5)
C2—C3—C4—C5	2.1(5)	C3—C4—C5—C6	−1.1(5)
C4—C5—C6—C1	−1.2(5)	O2—C7—C8—O3	−63.3(6)
O3—C9—C10—O1	−66.7(6)		

137.9 ppm). The observed range in solid **1** is 8.2 ppm (i.e., 119.0–127.2). Since our calculations are for an isolated molecule in the gas phase and the size of the molecule limits our basis set representation, we regard this agreement with experimental solid phase ^{13}C shift data as satisfactory. It is interesting to note that the theoretical calculations have C3 being shielded relative to its counterpart C6, and C5 being shielded relative to C4. Such results are consistent with more effective conjugative electron release from the lone pairs on O2 vs. O1. Thus enhanced partial negative charge is built up at C3 over C6 and at C5 over C4. This resonance model for the stereochemical dependence of the *ortho* ^{13}C shielding effect in oxygenated aromatic systems is consistent with recent anisotropic ^{13}C shift tensor results for 1,4-dimethoxybenzene (13).

^{13}C shieldings in aromatic systems have been correlated

Can. J. Chem. Downloaded from www.nrcresearchpress.com by 203.198.23.82 on 09/08/12
For personal use only.

TABLE 3. Observed and calculated ^{13}C chemical shifts (δ_C from TMS $\mp$ 0.1)

	1 (solution)[a]	**1** (solid)	**1** (calculated)[c]	($\delta_{calcd} - \delta_{obsd}$)
C1	151.4	148.7	150.0	1.3
C2	151.4	151.0	152.9	1.9
C3	122.9	119.0	126.9	7.9
C4	123.9	124.6	136.8	12.2
C5	123.9	121.8	134.4	12.6
C6	122.9	127.2	137.9	10.7
C7	74.0	68.2	61.9	−6.3
C8	72.3	(72.9)[b]	69.6	−3.3
C9	72.3	(70.4)[b]	69.7	−0.7
C10	74.0	76.1	70.1	−6.0

[a]0.1 M in $CDCl_3$.
[b]Assignments may be interchanged.
[c]*Ab initio* using LORG method (6–8).

TABLE 4. Crystallographic data

Formula	$C_{10}H_{12}O_3$
fw	180.20
Crystal system	Orthorhombic
Space group	*P cab*
a, Å	8.5351(18)
b, Å	25.005(5)
c, Å	8.2679(16)
V, Å^3	1764.5(6)
Z (molecules/cell)	8
D_C, g cm^{-3}	1.357
Crystal dimensions, mm^3	0.20 × 0.20 × 0.20
Radiation (λ, Å)	Mo Kα_1 (0.70932 Å)
Octant meas'd	$0 \rightarrow h$, $0 \rightarrow k$, $0 \rightarrow l$
Max 2Θ	47.0
No. of unique reflections	1312
No. of obsvd reflections	627
($I/\sigma(I)$ ratio)	2.5
Avg. std, fluctuations, %	0.11
Abs coeff., mm^{-1}	0.05
R	0.080
R_w	0.040
S (GOF)	3.21

TABLE 5. Atomic parameters and B_{iso}

Atom	*x*	*y*	*z*	B_{iso}[a]
O1	0.1561(8)	0.65243(21)	0.2289(6)	4.1(3)
O2	−0.0707(7)	0.57272(21)	0.3402(8)	5.8(4)
O3	0.2696(8)	0.55548(22)	0.3649(7)	5.0(3)
C1	0.0406(10)	0.6616(4)	0.3436(10)	3.6(5)
C2	−0.0656(11)	0.6233(4)	0.3881(11)	4.0(5)
C3	−0.1851(11)	0.6354(4)	0.4974(12)	4.8(5)
C4	−0.1963(11)	0.6839(4)	0.5614(10)	4.9(5)
C5	−0.0925(11)	0.7237(3)	0.5166(11)	4.7(5)
C6	0.0240(11)	0.7133(3)	0.4061(11)	4.1(5)
C7	0.0214(11)	0.5511(3)	0.2116(11)	4.5(5)
C8	0.1617(12)	0.5234(3)	0.2798(11)	4.6(5)
C9	0.3640(10)	0.5897(4)	0.2673(10)	4.5(5)
C10	0.3123(11)	0.6454(4)	0.2921(11)	4.6(5)

[a]ESDs refer to the last digit printed. B_{iso} is the mean of the principal axes of the thermal ellipsoid.

TABLE 6. Isotropic ^{13}C shieldings of ethane as a function of C—H bond length as calculated by LORG using a D95V basis set

Atom	Bond length (Å)	Calculated ^{13}C shielding[a]
C1	1.090	185.77
C2	1.090	185.77
C1	1.089	186.15
C2	1.090	185.85
C1	1.088	186.53
C2	1.090	185.92
C1	1.087	186.91
C2	1.090	186.00
C1	1.087	186.99
C2	1.089	186.37
C1	1.087	187.07
C2	1.088	186.76
C1	1.087	187.14
C2	1.087	187.14

[a]Absolute scale; TMS calculated herein to be at 198.62 ppm.

with both π and σ charge densities as well as mobile bond order terms (14), so that, of course, caution must be exercised when using any electron density argument to rationalize ^{13}C shieldings.

(ii) Aliphatic carbons

With respect to the four crown ether carbons, the range of shifts calculated spans 8.2 ppm (i.e., 61.9–70.1) while that observed is 7.9 ppm (68.2–76.1). The calculations predict that C8 and C9, being most remote from the aromatic ring, will have a negligible shift difference. In contrast, a difference of 8.2 ppm is calculated for C7 vs. C10, with C7 the more shielded of this pair. Experimentally, C8 and C9 are separated by 2.5 ppm, while C7 and C10 differ by 7.9 ppm. The dipolar dephased ^{13}C CPMAS spectrum (Fig. 4*b*) of **1**, which has been selectively deuterated at C7,10, shows only carbons bearing no protons. Hence the appearance of lines at 68.5 and 76.2 ppm confirms these as arising from C7 and C10. No experimental method is presently available, however, to distinguish between C7 and C10 resonances.

It remains to isolate the origin of the substantial shielding differences between C7 and C10. Anisole represents a convenient model for examining the effects of aryl-O—C geometry on the aliphatic carbon ^{13}C shielding. In Fig. 5 the calculated total shielding for the methyl group of anisole is depicted as a function of the CH_3—O—C—C torsional angle. For a torsional angle of 79.9°, i.e., the same as that for C10—O1—C1—C6 of **1**, the total shielding is calculated to be 136.8 ppm. In contrast, for a torsional angle of 170.3°, i.e., the same as that for C7—O2—C2—C3 of **1**, the total shielding is calculated to be 143.0 ppm. Thus using anisole as a model for the LORG calculations, the prediction is that C7 of **1** will be more shielded than C10 of **1** by 6.2 ppm. The present calculations for anisole are in good agreement with results reported earlier (13), in which the isotropic ^{13}C chemical shift of a perpendicular CH_3 of anisole was calculated to be 7 ppm downfield from the case of a planar CH_3 group. The LORG calculations on **1** itself predict that C7 will be shielded by 8.2 ppm relative to C10, in substantially better agreement with the experimental difference of 7.9 ppm.

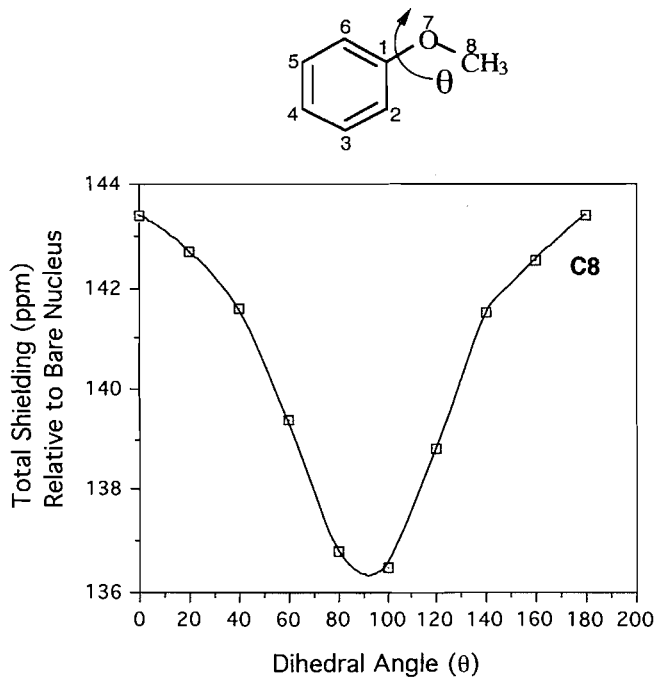

FIG. 5. LORG calculation of angular dependence of total ^{13}C shielding for the methyl group of anisole.

Conclusions

This work illustrates that satisfactory agreement between *ab initio* LORG calculated ^{13}C NMR chemical shifts at a D95V basis set level and solid phase experimental results is possible for medium molecular weight materials, provided that X-ray data for the solids are available. With more powerful computing capabilities becoming available, one can anticipate extension of studies of this nature to molecules of increasing complexity.

Experimental

Materials

The syntheses of **1** and its 7,10-d_4 analog have been described elsewhere (15).

Spectra

The solid phase ^{13}C NMR spectrum of **1** was recorded on a Bruker CXP-180 spectrometer at 45.3 MHz under conditions described previously (3). The dipolar dephasing experiments were carried out with a delay of 40 μs.

Solution NMR spectra were obtained using a Bruker AMX 400 spectrometer. The ^1H spectra were obtained at 400.14 MHz using sweep widths of 4 kHz and 32 K data points. Pulse angles were 45° with a recycle time of 1 s. The ^{13}C spectra were obtained at 100.62 MHz under conditions of complete ^1H noise decoupling. Sweep width was normally 10 kHz with 32 K data points employed. Pulse angles were 30° with an acquisition time of 1.6 s and a pulse delay of 1 s. Samples for both ^1H and ^{13}C NMR were contained in 5-mm tubes at a concentration of 0.1 M in $CDCl_3$ solution.

Crystallographic measurements and structure solution and refinement

A single crystal of **1** was hand-picked, mounted on a glass capillary, and measured on a Rigaku diffractometer. Accurate cell parameters and intensity data were obtained at room temperature using graphite-monochromated MoKα radiation. Crystal data are provided in Table 4. The space group *Pcab* was uniquely defined based on systematic absences and the data were corrected in the usual fashion for Lorentz and polarization effects (16). The structure was solved using direct methods. All atoms were refined anisotropically except hydrogens, which were calculated. Weights based on counting statistics were used and all calculations were performed using the NRCVAX crystallographic software package (17). Bond lengths and angles are presented in Table 1, while torsional angles involving ring skeletal atoms are given in Table 2. Details of the crystallographic data are presented in Table 4 and refined coordinates for C and O atoms are listed in Table 5. Available as Supplementary Material are structure factor tables and tables of anisotropic temperature factors, all torsional angles, and H atomic parameters.[3]

Computations

Calculations were done at SIUE using the experimental geometry for **1** obtained by X-ray analysis for the heavy atoms and MOPAC (11) optimized positions for the H atoms. A Silicon Graphics 4D/310S computer was employed for all calculations with shielding constants calculated using the RPAC molecular properties program (18). Molecular wavefunctions used in the RPAC program were calculated using the Gaussian 90 (19) set of programs.

Computed shift values for **1** were obtained by calculating shielding constants for the atoms in **1** and finding the difference between these and the carbon of TMS (198.62 ppm from the bare nucleus). The D95V basis set (20) was used to calculate the molecular wavefunction of **1** and the D95V coefficients and exponents were used to represent the carbon and hydrogen atoms in the TMS calculation. The silicon atom of TMS, however, was represented with D95 coefficients and exponents since the D95V basis set does not represent the silicon atom. The geometry used for the TMS calculation was determined from the MOPAC (11) geometry optimization routine. It should be noted that the TMS value calculated herein differs from the accepted value of 186.0 ppm calculated previously (21, 22).

For anisole, the shielding constants were obtained from D95V basis set utilization with geometries also obtained from MOPAC (11). Bond lengths and bond angles were optimized at each dihedral angle for which shielding constants were calculated. The NOSORT localization scheme was used in the RPAC (17) program for the calculation of shielding constants in **1**, anisole, and TMS.

Acknowledgements

G.W.B. thanks the Natural Sciences and Engineering Research Council of Canada (NSERC) for continuing support via Operating Grants. R.A.K. acknowledges the support of NSERC for the award of a Postdoctoral Fellowship. T.D.B. was funded by the U.S. National Science Foundation, Grant no. CHE-9007809. We thank Dr. C.I. Ratcliffe and Dr. J.A. Ripmeester of the National Research Council of Canada for access to the solid phase NMR facilities.

1. P.S. Belton, S.F. Tanner, K.M. Wright, M.P. Payne, M.R. Truter, and J.N. Wingfield. J. Chem. Soc. Perkin Trans. 2, 1307 (1985).
2. G.W. Buchanan, S. Mathias, Y. Lear, and C. Bensimon. Can. J. Chem. **69**, 404 (1991).
3. G.W. Buchanan, R.A. Kirby, and J.P. Charland. J. Am. Chem. Soc. **110**, 2477 (1988).

[3]These tables can be purchased from: The Depository of Unpublished Data, Document Delivery, CISTI, National Research Council Canada, Ottawa, ON K1A 0S2, Canada.

The table of H atomic parameters has also been deposited with the Cambridge Crystallographic Data Centre, and can be obtained on request from The Director, Cambridge Crystallographic Data Centre, University Chemical Laboratory, 12 Union Road, Cambridge, CB2 1EZ, U.K.

Can. J. Chem. Downloaded from www.nrcresearchpress.com by 203.198.23.82 on 09/08/12
For personal use only.

4. G.W. Buchanan, R.A. Kirby, and J.P. Charland. Can. J. Chem. **68**, 49 (1990).
5. G.W. Buchanan, R.A. Kirby, J.P. Charland, and C.I. Ratcliffe. J. Org. Chem. **56**, 203 (1991).
6. Aa.E. Hansen and T.D. Bouman. J. Am. Chem. Soc. **107**, 4828 (1985).
7. Aa.E. Hansen and T.D. Bouman. J. Chem. Phys. **82**, 5035 (1985).
8. T.D. Bouman and Aa.E. Hansen. Chem. Phys. Lett. **149**, 510 (1988).
9. D. Live and S.I. Chan. J. Am. Chem. Soc. **98**, 3769 (1976).
10. M. Schindler and W. Kutzelnigg. J. Am. Chem. Soc. **105**, 1360 (1983).
11. J.J.P. Stewart. QCPE No. 455 (1983); Version 5.0 (1989).
12. W. Thiel. Tetrahedron, **44**, 7393 (1988).
13. C.M. Carter, J.C. Facelli, D.W. Alderman, D.M. Grant, N.K. Dalley, and B.E. Wilson. J. Chem. Soc. Faraday Trans. **84**, 3673 (1988).
14. A.J. Jones, T.D. Alger, D.M. Grant, and W.M. Litchman. J. Am. Chem. Soc. **92**, 2386 (1970).
15. G.W. Buchanan, A.B. Driega, A. Moghimi, C. Bensimon, and K. Bourque. Can. J. Chem. **71**, 951 (1993).
16. D.F. Grant and E.J. Gabe. J. Appl. Crystallogr. **11**, 114 (1978).
17. E.J. Gabe, F.L. Lee, and Y. Lepage. J. Appl. Crystallogr. **22**, 384 (1989).
18. T.D. Bouman and Aa.E. Hansen. RPAC Molecular Properties Package, Southern Illinois University at Edwardsville, 1990.
19. M.J. Frisch, M. Head-Gordon, G.W. Trucks, J.B. Forsman, H.B. Schlegel, K. Raghavachari, M.A. Robb, J.S. Binkley, G. Gonzalez, R.J. Defrees, D.J. Fox, R.A. Whiteside, R. Seeger, C.F. Melius, J. Baker, R.L. Martin, L.R. Kahn, J.J.P. Stewart, S. Topial, and J.A. Pople. Gaussian Inc., Pittsburgh, Pa. 1990.
20. T.H. Dunning, Jr. J. Chem. Phys. **53**, 2823 (1970).
21. A.K. Jameson and C.J. Jameson. Chem. Phys. Lett. **134**, 461 (1987).
22. W.T. Raynes, R. McVay, and S.J. Wright. J. Chem. Soc. Faraday Trans. 2, **85**, 759 (1989).

Can. J. Chem. Downloaded from www.nrcresearchpress.com by 203.198.23.82 on 09/08/12
For personal use only.

Hammett ρσ correlation for reactions of lactoperoxidase compound II with phenols

HONGCHANG ZHANG AND H. BRIAN DUNFORD[1]
Department of Chemistry, University of Alberta, Edmonton, AB T6G 2G2, Canada

Received August 31, 1992[2]

HONGCHANG ZHANG and H. BRIAN DUNFORD. Can. J. Chem. **71**, 1990 (1993).

A stopped-flow kinetic study shows that the reaction rates of lactoperoxidase compound II with substituted phenols are greatly dependent upon the substituent on the benzene ring. Of the 15 phenols studied, it has been possible to relate the reaction rate constants with the ionization constants of 11 phenols by a linear Hammett free-energy relationship: (log $(k_X/k_H) = \rho\sigma$) at pH 7.0 and 25.0°C. The 11 *m*-and *p*-substituted phenols yield a ρ value of -2.7 ± 0.2. The data do not correlate with σ^+ values using the Brown–Okamoto equation. These results can be explained by a mechanism in which the substrate simultaneously gives an electron and a proton to lactoperoxidase compound II, and they indicate that the active site is accessible to substrate. To explain the abnormal behavior of the four phenols that do not fit the Hammett plot we used Hansch hydrophobic factors π for all of the substituents. The resultant best-fit equation: log $(k_X/k_H) = \rho\sigma + r\pi + c$ yielded the values $\rho = -2.1 \pm 0.5$, $r = 0.4 \pm 0.1$, and $c = -0.2 \pm 0.1$. The rates of reduction of lactoperoxidase compound II by *p*-iodophenol have been studied from pH 6.5 to 11.2. The kinetics are influenced by an acid group of pK_E 9.5 in the active site of lactoperoxidase compound II and by the ionization of the substrate (pK_S 9.0). The acidic form of lactoperoxidase compound II and the electrically neutral, unionized form of phenol are the reactive species. A reanalysis of data on reactions of horseradish peroxidase compounds I and II with substituted phenols using more recent σ values yielded Hammett ρ values of -5.5 ± 0.3 and -4.5 ± 0.2.

HONGCHANG ZHANG et H. BRIAN DUNFORD. Can. J. Chem. **71**, 1990 (1993).

Une étude cinétique par flux stoppé montre que les vitesses de réaction du composé II de la lactoperoxydase avec les phénols substitués dépend beaucoup du substituant présent sur le noyau benzénique. Des 15 phénols étudiés, il a été possible d'établir une corrélation linéaire d'énergie libre de Hammett entre la vitesse de réaction et les constantes d'ionisation de 11 phénols : (log $(k_X/k_H) = \sigma\rho$) à un pH = 7,0 et à 25,0°C. La valeur de ρ pour les 11 phénols *m*- et *p*-substitués est égale à $-2,7 \pm 0,2$. Il n'existe pas de corrélation entre les données et les valeurs de σ^+ de l'équation de Brown–Okamoto. Ces résultats peuvent être expliqués par un mécanisme dans lequel le substrat donne simultanément un électron et un proton au composé II de la lactoperoxydase et ils indiquent que le site actif est accessible au substrat. Afin d'expliquer le comportement anormal des quatre phénols qui ne donnent pas de corrélation de Hammett, on a fait appel aux facteurs hydrophobes π de Hansch pour tous les substituants. L'équation résultante qui fournit la meilleure corrélation, $\log(k_X/k_H) = \rho\sigma + r\chi + c$, conduit à des valeurs de $\rho = -2,1 \pm 0,5$, $r = 0,4 \pm 0,1$ et $c = -0,2 \pm 0,1$. On a étudié les vitesses de réduction du composé II de la lactoperoxydase par le *p*-iodophénol à des pH allant de 6,5 à 11,2. Les vitesses sont influencés par un groupe acide de pK_E 9,5 dans le site actif du composé II de la lactoperoxydase et par l'ionisation du substrat (pK_S 9,0). Les espèces réactives sont la forme acide du composé II de la lactoperoxydase et la forme non ionisée et électriquement neutre du phénol. Une nouvelle analyse des données relatives aux réactions des composés I et II de la peroxydase du raifort avec les phénols substitués faisant appel à des valeurs plus récentes de σ conduit à des valeurs respectives de ρ de Hammett de $-5,5 \pm 0,3$ et $-4,5 \pm 0,2$.

[Traduit par la rédaction]

Introduction

The reactions of phenols (and other organic substrates) with lactoperoxidase may be summarized as follows (1–3):

[1] $\text{LPO} + \text{H}_2\text{O}_2 \rightarrow \text{LPO-I} + \text{H}_2\text{O}$

[2] $\text{LPO-I} + \text{AH}_2 \rightarrow \text{LPO-II} + \cdot\text{AH}$

[3] $\text{LPO-II} + \text{AH}_2 \rightarrow \text{LPO} + \cdot\text{AH}$

[4] $2 \cdot \text{AH} \rightarrow \text{A}_2\text{H}_2 \text{ or } \text{A} + \text{AH}_2$

where lactoperoxidase and its two oxidized intermediates, compounds I and II, are represented by LPO, LPO-I, and LPO-II, the phenols by AH_2, and their free radical product by $\cdot$AH. Because of their ability either to scavenge free radicals or to react directly with oxidant (4), phenols are widely used as antioxidants. An example of physiological significance is the fat-soluble α-tocopherol (Vitamin E) (5). *p*-Methoxyphenol exhibits action against malignant melanomas (6). It has been suggested that peroxidases could be used commercially to remove phenol contaminants from water supplies (7–9).

In this study, 15 phenols are reacted with LPO-II to gain information on the mechanism of their reactions and to determine whether there is any linear free-energy correlation in their relative reactivities. In one case the pH–rate profile is obtained.

Materials and methods

Lactoperoxidase (EC 1.11.1.7, donor-H_2O_2 oxidoreductase) was purchased from Sigma. The RZ (A_{412}/A_{280}) of the sample used in experiments was 0.70–0.85 and its concentration was determined by using a molar absorptivity of $1.12 \times 10^5\ \text{M}^{-1}\ \text{cm}^{-1}$ at 412 nm (10). LPO-II (λ_{max} 430 nm) (11) was obtained after mixing 2 μM LPO with 4 μM H_2O_2. It did not exhibit significant decay over a period of 6 min. Hydrogen peroxide was obtained as a 30% solution from Fisher; the concentrations of diluted stock solutions were determined by the peroxidase assay (12).

Solutions of all substrates were prepared each day by dissolving a weighed amount of the compound in an appropriate volume of water (deionized in a Milli-Q water purification system) to make fresh stock solutions of about 10 mM. The solutions were stored in bottles wrapped in aluminum foil and placed in ice to prevent photochemical reactions. The substrate solutions for each experiment were then made by diluting portions of the stock solution to

[1]Author to whom correspondence may be addressed.
[2]Revision received August 6, 1993.

Can. J. Chem. Downloaded from www.nrcresearchpress.com by 203.198.23.82 on 09/08/12
For personal use only.

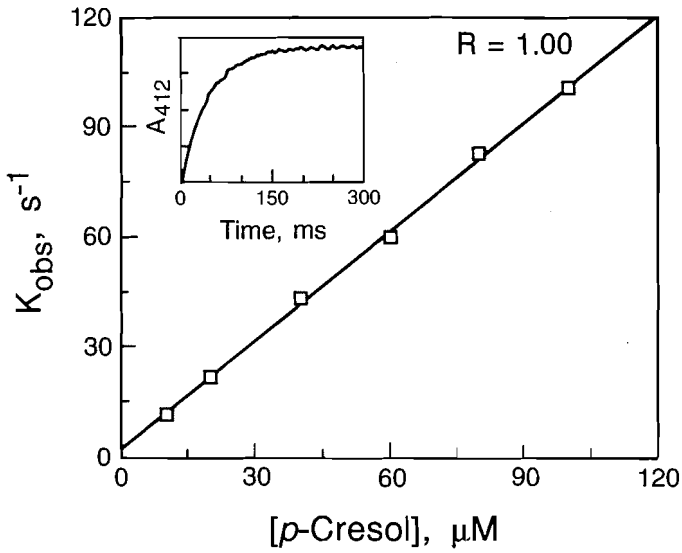

FIG. 1. Linear plot of pseudo-first-order constant versus [*p*-cresol] for the reaction between LPO-II and *p*-cresol. pH 7.0; ionic strength 0.11 M; temperature 25.0°C; [LPO-II] 1.0 μM. The inset shows an example of a first-order exponential trace (20 μM *p*-cresol) from which k_{obs} was obtained.

give a desired range of concentrations, using phosphate buffer of pH 7.0 (0.025 M, ionic strength μ = 0.11). In the case of *p*-iodophenol, buffers in the range of pH 6.5–11.2 were used in the determination of the pH–rate profile. At least a 10-fold excess of substrate over the enzyme was always used so that the reaction occurred by a pseudo-first-order process. Stock buffer solutions used for both enzyme and substrate were made up to ionic strength μ = 0.11 M by adding sufficient KNO_3 to 0.025 M buffer. For solutions of pH 6.0–7.0, citrate–phosphate buffers were used. Phosphate buffers were used between pH 7.0 and 9.0, and carbonate buffers were used above pH 9.0.

Kinetic measurements were made on a Photal (formerly Union Giken) stopped-flow spectrophotometer model RA-601. The 1-cm cells were thermostated at 25.0°C for all the experiments. One of the drive syringes of the stopped-flow spectrophotometer was filled with LPO-II solution, freshly prepared prior to the experiment, and the other syringe was filled with substrate. The reaction was then followed by monitoring the appearance of the native LPO at 412 nm. Each result quoted in this paper is an average of 10–20 experimental values.

Spectra of native LPO in the presence of each of the 15 phenols used in this study were examined in the Soret region and also in the region around 280 nm, where the aromatic amino acid residues absorb, in a search for indicators of possible different binding sites for different phenols.

Results

Pseudo-first-order traces were observed when the substrate concentration was 10 times larger, or more, than that of LPO-II. An example is shown in the inset to Fig. 1. The apparent second-order rate constant, k_{app}, was found to be related to the observed pseudo-first-order rate constant, k_{obs}, by the expression:

$$[5] \quad k_{obs} = k_{app}[S] + k_0$$

where [S] is the concentration of substrate. Thus k_{app} was determined from the slope of the plot of k_{obs} against substrate concentration. Figure 1 is an example, where k_{app} is 1.13×10^6 M^{-1} s^{-1}. The intercept k_0 is close to, but not equal to, zero in Fig. 1, which can be explained by the small autodecay of LPO-II (15). Second-order rate constants determined in this study for 15 *meta*- and (or) *para*-substituted phenols reacting with LPO-II at pH 7.0 are listed in Table 1 with corresponding literature values for Hammett σ (13), Brown–Okamoto σ^+ (14), and Hansch π (13) parameters.

Hammett plot

A Hammett plot (16) according to eq. [6]

$$[6] \quad \log (k_X/k_H) = \rho\sigma$$

is shown in Fig. 2. A rate constant, k_H, of 1.40×10^6 M^{-1} s^{-1} for unsubstituted phenol reacting with LPO-II is used as reference; k_X is the rate constant for the substituted phenol. The value of ρ, the Hammett reaction constant or susceptibility factor, is -2.7 ± 0.2, from the slope of the linear plot in Fig. 2. The electronic substituent constant σ depends on the nature and position of the substituent group. It can be seen that four of the phenols, labelled with asterisks in Table 1 and as open squares in Fig. 2, do not fit the plot. For these four phenols at least, something else, in addition to the electronic substituent effect, must also affect the reaction rate constant.

Possible role of a hydrophobic factor

By analyzing the data in Table 1, we found that not only electronic factors (σ constants) but also the hydrophobic properties (π constants) of the substituents appear to play a role in the activity of phenols. The reaction rate constants are increased by substituents that are electron donating or are hydrophobic, but they are decreased by substituents that are electron withdrawing or are hydrophilic. This is well illustrated in comparisons of phenol with *p*-hydroxybenzoic acid and *p*-hydroxybenzaldehyde with *p*-hydroxyphenol.

Quantitative analysis of structural effects was conducted for all 15 phenols by using an extended eq. [7], which covers both electronic and hydrophobic effects:

$$[7] \quad \log (k_X/k_H) = \rho\sigma + r\pi + c$$

In eq. [7], π is the Hansch hydrophobic parameter, r is its coefficient, and c is a constant. The term $\rho\sigma$ has the same meaning as in the Hammett relation.

Multiple linear regression of the experimental data yielded the following equation:

$$[8] \quad \log (k_X/k_H) = -(2.1 \pm 0.5)\sigma + (0.4 \pm 0.1)\pi - (0.2 \pm 0.1)$$

Figure 3, a logarithmic plot of the measured values of k_X/k_H against their calculated values from eq. [8], shows that the four phenols that do not fit the simple Hammett plot fit the extended equation better. The standard deviation of all points from the multiple linear regression analysis is 0.17.

Attempted Brown–Okamoto plot

An attempted plot according to the Brown–Okamoto equation (14):

$$[9] \quad \log (k_X/k_H) = Q\sigma^+$$

is shown in Fig. 4 for the eight phenols for which σ^+ values are available. Q is the reaction constant, which depends on the reaction and the conditions under which it occurs. It is obvious that there is not a linear correlation.

Can. J. Chem. Downloaded from www.nrcresearchpress.com by 203.198.23.82 on 09/08/12
For personal use only.

TABLE 1. Rate constants for the reactions of LPO-II with *m*- and *p*-substituted phenols at 25°C, pH 7.0, and ionic strength 0.11 M; Hammett σ values,[a] Brown–Okamoto σ^+ values,[b] and Hansch π values[a]

Substituent	$k_{app}(M^{-1} s^{-1})$	σ	π	σ^+
p-COO^-*	$(9.70 \pm 0.10) \times 10^3$	0.00	−4.36*	0.421
p-CHO	$(3.20 \pm 0.04) \times 10^4$	0.42	−0.65	
m-CHO	$(1.45 \pm 0.05) \times 10^5$	0.35	−0.65	
p-Cl*	$(1.12 \pm 0.03) \times 10^6$	0.23	0.71*	0.114
m-Coumaric acid	$(1.72 \pm 0.08) \times 10^5$	0.19	−0.22	
p-I*	$(1.66 \pm 0.01) \times 10^6$	0.18	1.12*	0.135
m-OC_2H_5*	$(3.80 \pm 0.20) \times 10^6$	0.10	0.38*	
p-Coumaric acid	$(2.44 \pm 0.04) \times 10^5$	0.03	−0.22	
H	$(1.40 \pm 0.02) \times 10^6$	0.00	0.0	0.00
m-CH_3	$(1.09 \pm 0.05) \times 10^6$	−0.07	0.56	−0.066
m, *p*-$(CH_3)_2$	$(1.91 \pm 0.05) \times 10^6$	−0.083	1.12	
p-CH_3	$(1.10 \pm 0.10) \times 10^6$	−0.17	0.56	−0.311
p-OC_2H_5	$(1.90 \pm 0.10) \times 10^6$	−0.24	0.38	
p-OCH_3	$(2.40 \pm 0.06) \times 10^6$	−0.13[c]	−0.02	−0.778
p-OH	$(1.16 \pm 0.07) \times 10^7$	−0.37	−0.67	−0.92

[a]Reference 13.
[b]Reference 14.
[c]Reference 30.

pH dependence

A log k_{app} versus pH plot is shown in Fig. 5 for the reaction of *p*-iodophenol with LPO-II. The reaction mechanism that is used to fit the experimental data is

$$\begin{array}{ccccc} & \text{HE-II} & + & \text{HS} & \xrightarrow{k} \text{products} \\ [10] & K_E \downarrow\uparrow H^+ & & K_S \downarrow\uparrow H^+ & \\ & \text{E-II} & & \text{S} & \end{array}$$

where HE is the protonated form of LPO-II and HS is unionized *p*-iodophenol. Equation [10] leads to:

$$[11] \quad k_{app} = \frac{k}{\left[1 + \frac{K_E}{[H^+]}\right]\left[1 + \frac{K_S}{[H^+]}\right]}$$

where k_{app} is the experimentally determined pH-dependent second-order rate constant and k is defined in eq. [10]. K_E and K_S are acid dissociation constants of LPO-II and substrate, respectively. A best fit to the experimental data was obtained using a nonlinear least-squares program in which k, K_E, and K_S are adjustable parameters. From the fit, $k = (1.9 \pm 0.2) \times 10^6\ M^{-1}\ s^{-1}$, $pK_E = 9.5 \pm 0.4$, and $pK_S = 9.0 \pm 0.3$, which are in agreement with reported values for pK_E of 9.7 (17) and pK_S of 9.3 (18). The best-fit line is shown in Fig. 5 as the solid line. If one simplifies eq. [11] by setting either equilibrium constant K equal to zero, and allows the nonlinear least-squares program to adjust the remaining single K to its best-fit value, a value of $pK_a = 8.9$ is obtained. The best-fit curve in this case is shown as a dashed line in Fig. 5, which is not a satisfactory fit.

Discussion

The Hammett plot in Fig. 2 shows a reasonable correlation of log (k_X/k_H) versus σ values of 11 phenols. Thus, for those 11 phenols, the electron-donating or -withdrawing effect of *meta* and *para*-substituents is sufficient to explain the relative reactivities. Electron-donating groups (negative σ values) enhance the reaction rate and the converse is also true. From Fig. 2, it can be seen that four points do not fit the Hammett plot. The observed values of k_X for *p*-Cl, *p*-I, and *m*-OC_2H_5 substituted phenols are 10 times greater and that for *p*-COO^- is 100 times less than those predicted by the linear correlation for the other substituted phenols. For those four phenols deviating from the Hammett plot for LPO-II,

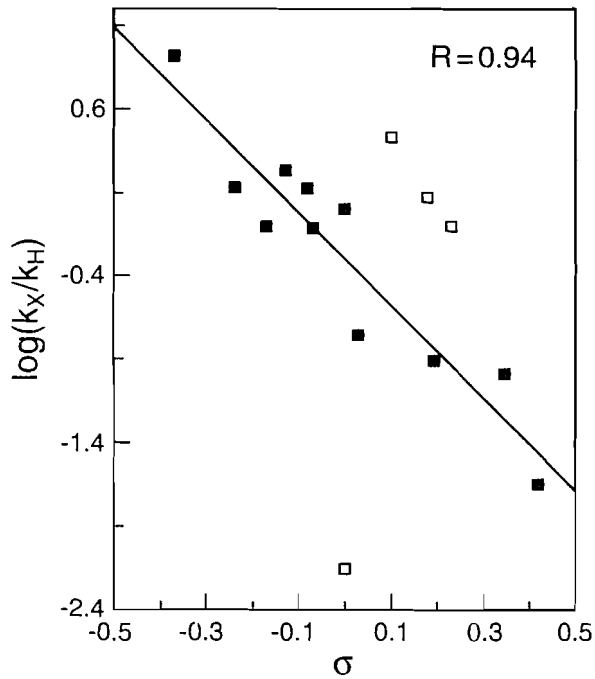

FIG. 2. Hammett plot for reactions of LPO-II with 15 phenols at 25°C, pH 7.0, and ionic strength 0.11 M. The slope yields $\rho = -2.7 \pm 0.2$ with a correlation coefficient, R, of 0.94 for the 11 phenols denoted by solid squares. The four phenols with large deviations, indicated by open squares, were not included in the linear least-squares analysis.

Can. J. Chem. Downloaded from www.nrcresearchpress.com by 203.198.23.82 on 09/08/12
For personal use only.

Can. J. Chem. Downloaded from www.nrcresearchpress.com by 203.198.23.82 on 09/08/12
For personal use only.

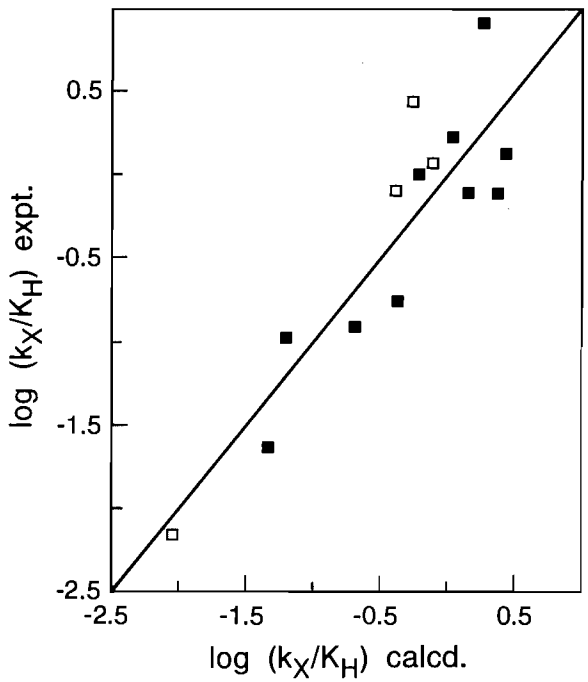

FIG. 3. Logarithmic plot of the experimentally measured values of k_X/k_H against the calculated values from eq. [8]. It can be seen that phenols denoted by open squares, which correspond to the open squares in Fig. 2, correlate better with the other phenols because of inclusion of hydrophobic factors for all phenols. The standard deviation of all 15 phenols from the multiple linear regression analysis of eq [8] is 0.17.

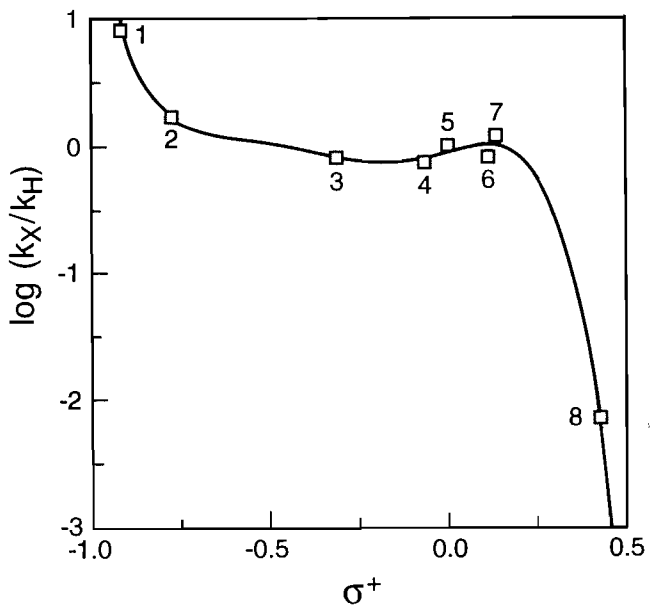

FIG. 4. Brown–Okamoto plot for the rate constants of LPO-II reduction by various substituted phenols at pH 7.0, ionic strength 0.11 M, and temperature 25°C. Substituent: (1) *p*-OH, (2) *p*-OCH_3, (3) *p*-CH_3, (4) *m*-CH_3, (5) H, (6) *p*-Cl, (7) *p*-I, (8) *p*-COO^-.

introduction of Hansch π parameters accounts for their anomalously high (or low) reactivities. *p*-COO^- is a strongly hydrophilic group; this will interfere with the accessibility of *p*-COO^- substituted phenol to the active site of LPO-II,

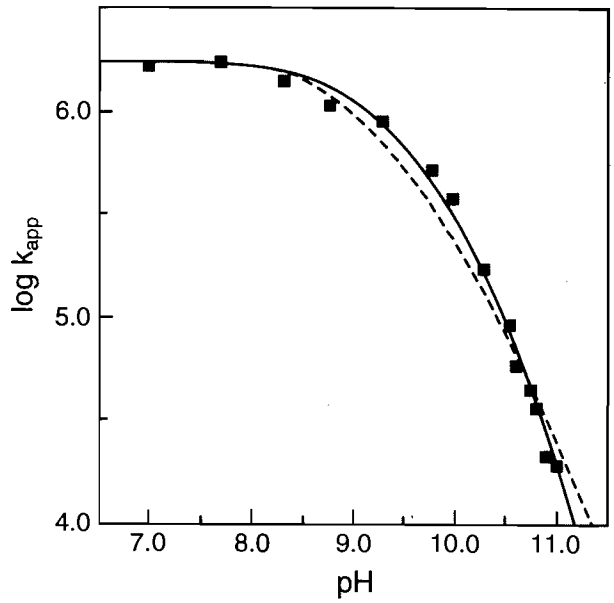

FIG. 5. pH–rate profile for the reaction of LPO-II with *p*-iodophenol at 25°C and ionic strength 0.11 M. Experimental (solid squares), best-fit curve with two *K*'s (solid line), best-fit curve with single *K* (dashed line). The fit is obviously better with the inclusion of two ionization constants.

so the reaction rate is slowed. However, *p*-Cl, *p*-I, and *m*-OC_2H_5 are hydrophobic groups that will promote binding to a hydrophobic region in the active site of LPO-II. Therefore their reaction rates are increased. There is no logical reason to apply Hansch π values selectively. No pattern of different spectral properties for the native enzyme–phenol complexes was observed for the four phenols that do not fit the simple Hammett equation. Therefore the extended equation including hydrophobic factors was applied to all the data.

We have reanalysed the data of Job and Dunford (19) for the reactions of HRP-I with phenols, using the σ values of Hansch and Leo (13), which were published three years after the original HRP-I publication. The result is a value of ρ of -5.5 ± 0.3 compared to the original value of -6.94. We regard the new value as more accurate. Because of their enhancement of luminescence of the HRP–luminol reaction (20), the reactions of three more phenols with HRP-I have been studied (21) and they are more reactive than predicted by the Hammett correlation. These are phenols with the substituents *p*-phenyl, *p*-I, and *p*-Cl, which all have high hydrophobic π values.

We have also reanalysed the data for the Hammett correlation of HRP-II–phenol reactivities. The originally published ρ value was -4.6 (22). Since then another study of HRP-II reactions with phenols has been completed (23), which is generally in agreement with the earlier data (22). An exception is the rate of reaction of *p*-Cl phenol and we have reason to believe the newer value is more accurate. Using only σ values of Hansch and Leo where possible, we obtain an identical ρ value of -4.5 ± 0.2 by inclusion of data for 20 of 23 phenols from refs. 22 and 23. Of the remaining three phenols, two are exceptionally unreactive phenols (*p*-NH_2 and *p*-COO^- substituents) and we note that they are hydrophilic. The other is more reactive (*m*-Cl substituent). The phenolic luminescence enhancers, with *p*-phenyl, *p*-I, and *p*-Cl substituents, are also more reactive with HRP-II than

Can. J. Chem. Downloaded from www.nrcresearchpress.com by 203.198.23.82 on 09/08/12
For personal use only.

predicted by the Hammett correlation (23). All four of the latter phenols are hydrophobic. Therefore the trend for both HRP-I and HRP-II reactions is the same as for LPO-II: most phenols fit a Hammett correlation well, and, for the few exceptions, strongly hydrophilic substituents retard the reaction and hydrophobic groups enhance it.

A recent study showed that the rate constants for phenols reacting with prostaglandin H synthase (PGHS) compound II also fit a Hammett plot, with $\rho = -2.0$ at 4°C (24). There were dual effects of phenols on the cyclooxygenase activity of PGHS, with small concentrations of phenols enhancing cyclooxygenase activity and large concentrations causing inhibition. Both electronic and hydrophobic effects are evident. Multiple linear regression analysis according to eq. [7] led to ρ values of -2.2 (stimulation) and -2.6 (inhibition) at 25°C (24).

The pH–rate profile for the reaction of LPO-II with *p*-iodophenol (Fig. 4) is not the same as that reported by Hodgson and Jones (20) for the reaction between the same substrate and horseradish peroxidase compound II (HRP-II), where the pH dependence of log k_{app} above pH 8.0 is linear with a slope of -1. In our case, with increasing pH, the plot of log k_{app} versus pH has a slope that changes from zero to increasingly negative values, as LPO-II and phenol each lose a proton. By inclusion of ionization constants for both LPO-II and phenol, the excellent fit shown by the solid line in Fig. 4 is obtained. If one postulates that only a single ionization is affecting the kinetics, the fit to the experimental data is not as good, as shown by the dashed line in Fig. 4. The data are entirely consistent with a protonated form of LPO-II reacting with the un-ionized *p*-iodophenol. The phenoxide ion appears to be unreactive (22).

Brewster et al. (25) used semiempirical molecular orbital methods to calculate several properties of substrate molecules and compared them with rates of reaction of HRP-II. They did not make a choice between a hydrogen atom versus an electron transfer mechanism. Sakurada et al. (23) showed that the HRP-II reaction rates with phenols correlate HOMO and LUMO energy levels well.

Our major conclusion, applicable to substrates such as phenols and aromatic amines (23, 26) that react via a normal peroxidatic cycle, native peroxidase → compound I → compound II → native peroxidase, is the following. The Hammett $\rho\sigma$ correlations, in themselves providing a rationale for the rates of most phenols and aromatic amines, indicate that these substrates react by hydrogen atom transfer: an electron and a proton are transferred simultaneously from the reducing substrate to the enzyme. Hydrophobicity (or hydrophilicity) can account, at least qualitatively, for most deviations from the Hammett correlations. The hydrogen atom transfer mechanism is in accord with the proton balance for conversions of compound I to II and compound II to native enzyme (27). The same mechanism explains the results obtained with enols. Schematic representations of the mechanisms for enols and phenols (28, 29) and aromatic amines (26) have been published, which show that the active sites of compounds I and II are accessible to substrate.

1. P. George. Biochem. J. **54**, 267 (1953).
2. I. Yamazaki and H. Souzu. Arch. Biochem. Biophys. **86**, 294 (1960).
3. M. Nakamura, I. Yamazaki, T. Kotami, and S. Ohtaki. J. Biol. Chem. **260**, 13546 (1985).
4. J.A. Howard. Rubber Chem. Technol. **47**, 976 (1974).
5. G.W. Burton, T. Doba, E.J. Gabe, L. Hughes, F.L. Lee, L. Prasad, and K.U. Ingold. J. Am. Chem. Soc. **107**, 7053 (1985).
6. P.A. Riley, B. Sawyer, and M.A. Wolff. J. Invest. Dermatol. **64**, 86 (1975).
7. A.M. Klibanov, T.U. Tu, and K.P. Scott. Science, **221**, 259 (1983).
8. S.W. Maloney, J. Manem, J. Mallevialle, and F. Fiessinger. Water Sci. Technol. **17**, 273 (1985).
9. R. Carmichael, P.M. Fedoruk, and M.A. Pickard. Biotechnol. Lett. **7**, 389 (1985).
10. K.-G. Paul and P.-I. Ohlsson. *In* The lactoperoxidase system. *Edited by* K.M. Pruitt and Y.O. Tenovuo. Marcel Dekker, New York. 1985. pp. 15–30.
11. H. Jenzer, W. Jones, and H. Kohler. J. Biol. Chem. **261**, 15550 (1986).
12. M.L. Cotton and H.B. Dunford. Can. J. Chem. **51**, 582 (1973).
13. C. Hansch and A. Leo. Substituent constants for correlation analysis in chemistry and biology. John Wiley & Sons, New York. 1979. pp. 49–52.
14. H.C. Brown and Y. Okamoto. J. Am. Chem. Soc. **80**, 4979 (1958).
15. D.M. Kardel, H.B. Dunford, and S. Alexandre. Eur. J. Biochem. **194**, 259 (1990).
16. L.P. Hammett. Physical organic chemistry. McGraw–Hill, New York. 1940. pp. 184–199.
17. E.P. Sarjeant and B. Dempsey. Ionisation constants of organic acids in aqueous solution. Pergamon Press, Oxford. 1979. p. 195.
18. R.J. Maguire and H.B. Dunford. Can. J. Chem. **51**, 1721 (1973).
19. D. Job and H.B. Dunford. Eur. J. Biochem. **66**, 607 (1976).
20. G.H.G. Thorpe, L.J. Kricka, S.B. Moseley, and T.P. Whitehead. Clin. Chem. **31**, 1335 (1985).
21. M. Hodgson and P. Jones. J. Biolumin. Chemilumin. **3**, 21 (1989).
22. H.B. Dunford and A.J. Adeniran. Arch. Biochem. Biophys. **251**, 536 (1986).
23. J. Sakurada, R. Sekiguchi, K. Sato, and T. Hosoya. Biochemistry, **29**, 4093 (1990).
24. Y. Hsuanyu and H.B. Dunford. J. Biol. Chem. **267**, 17649 (1992).
25. M.E. Brewster, D.R. Doerge, M.J. Huang, J.J. Kaminski, E. Pop, and N. Bodor. Tetrahedron, **47**, 7525 (1991).
26. J. Huang and H.B. Dunford. Can. J. Chem. **68**, 2159 (1990).
27. H. Yamada and I. Yamazaki. Arch. Biochem. Biophys. **165**, 728 (1974).
28. C. Bohne, I.D. MacDonald, and H.B. Dunford. J. Biol. Chem. **262**, 3572 (1987).
29. H.B. Dunford. *In* Peroxidases in chemistry and biology. Vol. II. *Edited by* J. Everse, K.E. Everse, and M.B. Grisham. CRC Press, Boca Raton, Fla. 1991. Chap. 1, pp. 1–24.
30. A.I. Biggs and R.A. Robinson. J. Chem. Soc. 388 (1961).

Global and internal molecular dynamics of poly(acrylamide-*co*-allyl 2-acetamido-2-deoxy-D-glucopyranoside) glycopolymers from ^{13}C NMR relaxation studies[1]

RENÉ ROY,[2] FRANÇOIS D. TROPPER, AND ANTONY J. WILLIAMS[2,3]
Chemistry Department, University of Ottawa, Ottawa, ON K1N 6N5, Canada

AND

JEAN-ROBERT BRISSON
Division of Biological Sciences, National Research Council of Canada, Ottawa, ON K1A 0R6, Canada

Received May 17, 1993

RENÉ ROY, FRANÇOIS D. TROPPER, ANTONY J. WILLIAMS, and JEAN-ROBERT BRISSON. Can. J. Chem. **71**, 1995 (1993).

^{13}C spin-lattice and spin–spin relaxation times and nuclear Overhauser enhancements have been used to examine the molecular dynamics of the α- (**1**) and β- (**2**) anomeric forms of poly(acrylamide-*co*-allyl 2-acetamido-2-deoxy-D-glucopyranoside) glycopolymers. The timescale of motions and the spatial restriction of these motions were determined by using various forms of the "model-free" approach. It is shown that the motions of the C—H vectors of the polymer backbone may be described by a scaled Lorentzian spectral density function, giving rise to an effective correlation time for overall tumbling. The temperature dependence of this correlation time suggests that the overall motion is dependent on viscosity. The overall motion of the polymer molecules is shown to be anisotropic in nature by including the spin–spin relaxation data in the analysis. The *N*-acetyl methyl and sugar hydroxymethyl (C_6) groups exhibit internal motions. The activation energies associated with these internal motions are derived. The difference in relaxation rates between the α and β anomeric forms, though small, suggests that the motions of the sugar ring may be different for the two systems. This conclusion is supported by potential energy contour map calculations, which indicate that the β anomer (**2**) has almost twice the conformational flexibility of the α anomer (**1**).

RENÉ ROY, FRANÇOIS D. TROPPER, ANTONY J. WILLIAMS et JEAN-ROBERT BRISSON. Can. J. Chem. **71**, 1995 (1993).

On a utilisé les temps de relaxation spin-réseau et spin–spin en RMN du ^{13}C ainsi que des expériences d'effets Overhauser nucléaires pour étudier la dynamique moléculaire des formes anomères α (**1**) et β (**2**) des glycopolymères poly(acrylamide-*co*-2-acetamido-2-désoxy-D-glucopyranoside d'allyle). On a déterminé l'ordre de grandeur des vitesses des mouvements et de la restriction spaciale de ces mouvements en faisant appel à diverses formes de l'approche ⟨⟨non-modèlisée⟩⟩. On a montré que l'on peut décrire les mouvement des vecteurs C—H de la structure de polymère par une fonction de Lorentz de densité spectrale qui donne lieu à une corrélation efficace du temps de renversement global. La relation entre la température et ce temps de corrélation suggère que le mouvement global dépend de la viscosité. En incluant les données de relaxation spin–spin dans l'analyse, on montre que le mouvement global de la molécule est naturellement anisotrope. Les groupes *N*-acétylméthyle et hydrométhyle (C_6) du sucre présentent des mouvements internes. On a déduit les énergies d'activation associées à ces mouvements internes. Les différences dans les vitesses de relaxation entre les formes anomères α et β, même si elles sont faibles, suggérent que les mouvements du cycle du sucre peuvent être différents pour les deux systèmes. Cette conclusion est en accord avec les calculs des cartes de contour de l'énergie potentielle qui indiquent que la flexibilité de l'anomère β (**2**) est deux fois plus grandes que celle de l'anomère α (**1**).

[Traduit par la rédaction]

Introduction

Water-soluble glycopolymers (1)[4] have attracted considerable interest since their first appearance (2), and have demonstrated a number of useful bio- and immuno-chemical properties (3). Glycopolymers containing sialic acid have recently been shown to be inhibitors of host cell adherences by human influenza viruses (4). They also constitute valuable tools as coating antigens in enzyme-linked immunosorbent assays (ELISA). In this technique, the water-soluble glycopolymers are adsorbed by hydrophobic interactions to the surface of the plastic (polyvinyl chloride or polystyrene) microtiter plates. The carbohydrate portions of the polymers are then freely exposed to the aqueous surroundings and thus are accessible for bindings to antibodies and lectins.

In ongoing research (1, 5), directed at studies of molecular recognition between multivalent carbohydrates and lectins as models in cellular interactions, we have demonstrated the relative binding of pairs of anomers of *N*-acetylglucosaminides towards wheat germ agglutinin.[5] This lectin has been well characterized by X-ray data and binding experiments using serological methods (6). Wheat germ agglutinin is a dimeric, carbohydrate-free protein composed of two identical subunits and presenting primary and secondary binding sites, each of which possesses three subsites. Our glycopolymers were designed to provide directed access to the inner and (or) outer subsites by carefully controlling the length of the spacer arms between the carbohydrate ligands and the polymer backbone. In these studies, we observed that the α anomer of the poly(acrylamide-*co*-allyl 2-acetamido-2-deoxy-α-D-glucopyranoside) (**1**) showed higher binding properties (higher affinities) than its homologous β anomer

[1]Presented at the XVIth International Carbohydrate Symposium, Paris, France, July 5–10, 1992.

[2]Authors to whom correspondence may be addressed.

[3]Present address: Eastman-Kodak Limited, Analytical Technology Division, Building 82, Kodak Park, Rochester, NY 14650-2132, U.S.A.

[4]The term "glycopolymer" is introduced here. It is suggested as a replacement for "pseudopolysaccharide" inadequately utilised previously. The term has been chosen in analogy to glycoproteins and glycolipids. In the present context, it is used to indicate water-soluble polymers bearing covalently bound carbohydrate. However, the new term should be equally well applicable to insoluble polymers such as those used in affinity chromatography.

[5]R. Roy, F.D. Tropper, and A. Romanowska. Unpublished results.

Can. J. Chem. Downloaded from www.nrcresearchpress.com by 203.198.23.82 on 09/08/12
For personal use only.

Can. J. Chem. Downloaded from www.nrcresearchpress.com by 203.198.23.82 on 09/08/12
For personal use only.

(**2**) (see Fig. 1). This behaviour is seemingly contradictory to what one might anticipate on the basis of overall carbohydrate mobility and accessibility within the glycopolymers, even for an outer binding subsite. To probe and, hopefully, to correlate the physical properties of these glycopolymers with their ligand properties, we have examined their motional properties by ^{13}C NMR relaxation measurements and examined their conformational flexibilities by potential energy calculations using MM2 computations taking *exo*-anomeric effects into consideration.

Experimental

Preparation of compounds

Materials and methods

All reagents were obtained from Aldrich. Solvents were obtained from various sources but were all of reagent grade, and used without further purification. Polymers were dialysed using cellulose tubing (obtained from Sigma) having a molecular weight cutoff of 12 kDa. Lyophilizations were performed using a Virtis model 24 freeze dryer. Polymer molecular weight estimations were measured on a Waters HPLC model 625LC equipped with a Waters 991 diode array detector using a TSK G4000 SWXL column (7.5 mm × 30 cm). A phosphate buffer (0.1 M, pH 7.0) was used as eluant at a flow rate of 1 mL/min. Poly(acrylic acid) with molecular weights of 50, 90, 150, and 200 kDa with M_n/M_w of 7 ± 3 were used as standards (Polyscience Inc., Warrington, Pa.) after transformation into polyacrylamide using usual carbodiimide (EDC) activation and quenching with ammonia.

Preparation of allyl 2-acetamido-2-deoxy-D-glucopyranosides

Allyl 2-acetamido-2-deoxy-D-glucopyranosides in both the α and β anomeric configurations were prepared according to previously published procedures (7) with only slight modifications (2c). All physical data were in good agreement.

Copolymer preparation

*(i) Poly(acrylamide-*co*-allyl 2-acetamido-2-deoxy-α-D-glucopyranoside), **1**:* 0.50 g (7.03 mmol) of acrylamide, 1.00 g (3.83 mmol) of allyl 2-acetamido-2-deoxy-α-D-glucopyranoside, and 10 mg (0.4 mol%) of ammonium persulfate ($(NH_4)_2S_2O_8$) were boiled in 10 mL of deoxygenated water for 10 min under a nitrogen atmosphere. The viscous solution was allowed to cool to room temperature after which it was exhaustively dialysed against distilled water. Lyophilization of this solution gave 1.00 g of a white, spongy solid. The incorporated monomer ratio was determined as 1:5.1 glycoside to acrylamide units by ^1H NMR. Elemental analysis gave C 45.41, H 6.98, N 12.38, corresponding to a monomer incorporation ratio of 1:5.3 with a retained water content of 10.3% by weight.[6]

[6]The monomer incorporations calculated by elemental analysis should be established using $(C_3H_5NO)_x(C_{11}H_{19}NO_6)_y(H_2O)_n$ as the general structure of the copolymer obtained after freeze-drying since polyacrylamides are known to strongly retain some water of hydration. By setting up three equations for percent C, H, and N in addition to $x + y + n = 1$, four simultaneous equations with three unknowns can be solved and verified algebraically:

$$\%\ \text{Element} = \frac{\text{am}_{\text{element}} \times \sum_{x,y,n} E_{\text{mu}} \times M_{\text{mu}}}{\text{Mol. Wt. of the average repeating unit}}$$

where

$\text{am}_{\text{element}}$ = atomic mass of the element

E_{mu} = number of elements per monomer unit

M_{mu} = molar fraction of each monomer unit (x,y,n)

(For example, for % C: $\%C = 12.0115\,(3x + 11y)/(71.0794x + 261.2772y + 18.0152n)$). Note that this method has the distinct advantage that the water content (variable from batch to batch) in the polymers can be calculated and taken into consideration during serological studies.

*(ii) Poly(acrylamide-*co*-allyl 2-acetamido-2-deoxy-β-D-glucopyranoside), **2**:* 0.78 g (2.99 mol) of allyl 2-acetamido-2-deoxy-β-D-glucopyranoside, 0.39 g (5.49 mmol) of acrylamide, and 8 mg (0.4 mol%) of ammonium persulfate were boiled in 8 mL of deoxygenated water under a nitrogen atmosphere for 12 min. The polymer was processed as above and 0.54 g of material was obtained. The incorporated monomer ratio was determined as 1:5.0 by ^1H NMR.

NMR spectroscopy

Polymer characterization

Proton NMR spectra were obtained at 300 MHz using a Varian XL-300 spectrometer. Monomer incorporations in the glycopolymers were determined by comparison of the integrations of the glycoside resonances (2.3–4.5 ppm; 9H) to the backbone methylene and methine resonances (1.0–2.6 ppm; 3H) after correction for the *N*-acetyl methyl resonance at 2.0 ppm (3H).

^{13}C NMR measurements

All spectra were obtained on solutions of the appropriate polymer dissolved in D_2O (50 mg/mL) allowing measurements to be made under conditions of internal lock. The samples were contained in sealed 5-mm NMR tubes and were degassed using a number of freeze–thaw cycles to remove dissolved oxygen and other gases.

^{13}C NMR spectra were obtained at four different magnetic field strengths corresponding to resonance frequencies of 50.29, 75.43, 100.62, and 125.73 MHz. The spectrometer systems used were a Varian Gemini-200, Varian XL-300, Bruker AM-400, and Bruker AM-500, respectively. Averaging of >2000 scans gave a good signal-to-noise ratio at all fields.

T_1 relaxation times were determined at each of these fields using the fast inversion–recovery technique (8) (FIRFT) with a pulse repetition time of $>3T_1$, where T_1 was the estimated value for the methyl group. A suitable number of dummy scans were used to generate a steady-state magnetization. Between 12 and 15 τ-values were generally used to characterize the relaxation decay, and the intensities of the peaks were fitted to a three-parameter exponential function using spectrometer system software. T_1's of all resolved protonated carbons were measured simultaneously using a selection of carefully chosen τ-values to characterize each of the different relaxation rates. All relaxation rates measured were accurate to better than 5% at each magnetic field.

Nuclear Overhauser enhancements (nOe's) were determined at 75.43 and 100.62 MHz using a direct comparison of gated decoupled and fully decoupled spectra. A relaxation delay of 10 times the T_1 of the methyl group was used between scans and a 90° pulse was used prior to acquisition of the spectrum. The individual spectra were acquired in blocks of eight scans to average out possible temperature inhomogeneities during the experiment.

Spin–spin relaxation times were obtained at 30°C at a resonance frequency of 75.43 MHz by measurement of the half-height linewidth rather than the spin-echo determination and using an inhomogeneity contribution of 1 Hz (based on the natural line width of a reference sample of acetone). Due to the number of types of backbone methylene and methine resonances, linewidths were only determined for the sugar resonances (C_1–C_6) and for the *N*-acetyl methyl group.

The experimental temperature was determined at each magnetic field, under decoupling conditions to correct for decoupler heating effects, using a calibrated copper–constantan thermocouple. The uncertainty in temperature is estimated to be ±1°C. Heating effects due to decoupling were partly circumvented by using the WALTZ composite decoupling mode.

Viscosity measurements

Temperature dependence of viscosity

Viscosities were measured as a function of temperature over the range 20–60°C using an Ostwald viscometer. The viscometer was suspended in a thermostated water bath that controlled the temper-

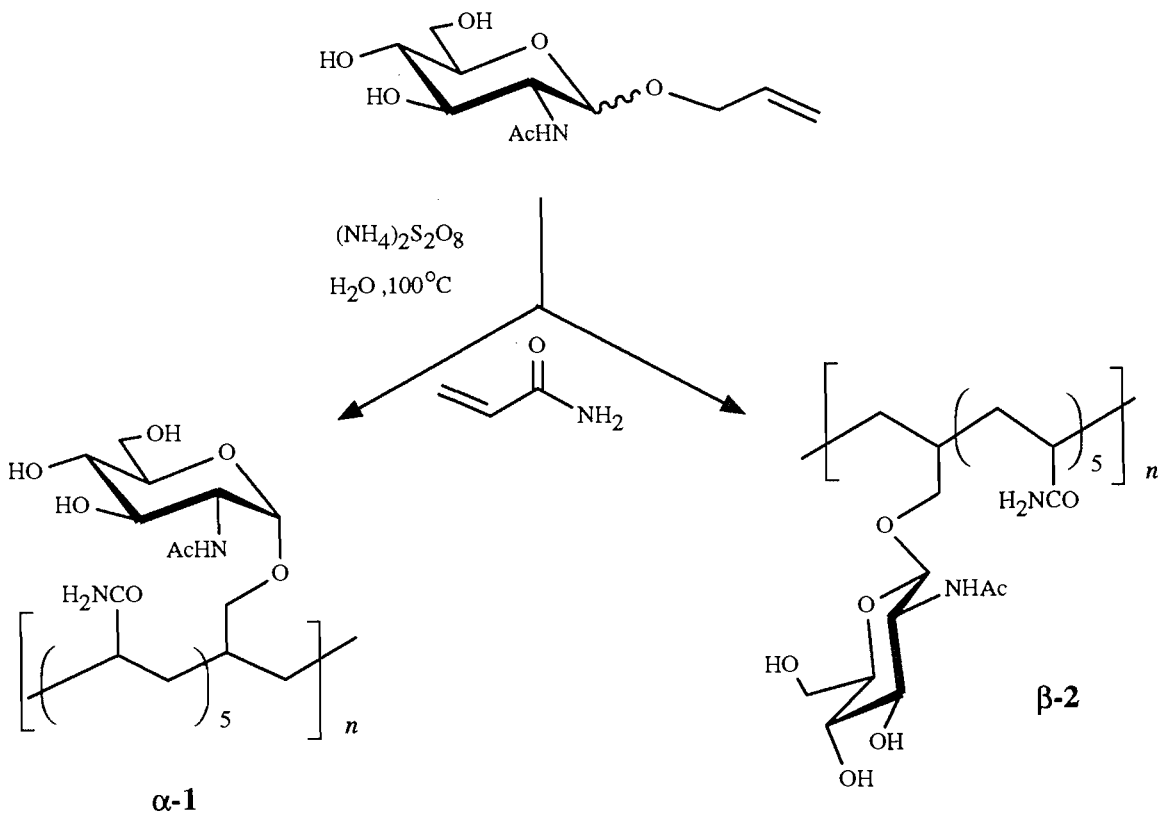

FIG. 1. Polymerization of allyl 2-acetamido-2-deoxy-α/β-D-glucopyranoside to give the α- (**1**) and β- (**2**) poly(acrylamide-*co*-allyl 2-acetamido-2-deoxy-D-glucopyranosides).

Can. J. Chem. Downloaded from www.nrcresearchpress.com by 203.198.23.82 on 09/08/12
For personal use only.

ature to ±0.2°C. The temperature of the bath was measured with an electronic thermometer using a Cr–Al thermocouple. Distilled water was used as the calibrating liquid. Flow times were measured twice, to within ±0.1 s, for each liquid and at each temperature. The densities of both the water and the polymer solution were identical within experimental error.

Molecular weight determination of polymer by viscosity measurements and HPLC

The viscosity average molecular weight of the α-glycopolymer was calculated from the measured intrinsic and specific viscosities in H_2O at 25.0°C as described by Flory (9). Flow times, relative to water, for 10.0-mL samples were measured using the equipment described above for seven twofold dilutions of a stock polymer solution originally prepared by dissolving 332.0 mg of lyophilized polymer (containing 10.3% of H_2O by weight) in 20.0 mL of H_2O. Extrapolation to infinite dilution gave values of 40.3 and 40.4 for intrinsic and specific viscosities (correlation coefficients >0.995). The viscosity is related to the Mark–Houinik expression (9, 10) $\eta = KM^a$. Assuming similar behavior for the glycopolymer **1** and simple polyacrylamide in a "good" solvent such as water, values of 5.6×10^{-3} and 0.80 were used for K and **a**, respectively, as suggested by Molyneux (10). This method gave a molecular weight average of 66.4 kDa for the glycopolymer.

Relative mobility through agarose gel gave an average molecular weight of 50–80 kDa (1). The glycopolymers **1** and **2** had retention times between 7 and 12 min, centred at 10.0 min in gel permeation chromatography over a TSK G4000 SWXL column relative to polyacrylamide with 50 kDa as molecular weight centred at 11.2 min on the same column. The 90 kDa polyacrylamide had a retention time of 8.4 min, thus confirming the above viscometry measurements and justifying the **a** and K values used for the Mark–Houinik equation.

Using the calculated intrinsic viscosity, the partial specific volume of the polymer in solution was calculated to be 16.1 $cm^3\ g^{-1}$. Therefore, the volume occupied by an average polymer molecule in a random-coil arrangement is 1.57×10^{-24} m^3.

Molecular mechanics calculations

The starting geometry of the backbone repeating unit around the carbohydrate portion was built using ALCHEMY (Tripos Associates, Inc.). It was then submitted to a complete refinement of bond lengths and valence and torsion angles through MM2(87) computations (QCPE). The coordinates for the glucosaminide units were obtained from MM2(87) minimizations of the crystal structures (11, 12).

The conformational analyses for the α (**1**) and β (**2**) glycopolymers were performed using the Potential for Oligosaccharides (PFOS) approach, which included the partitioned contributions arising from van der Waals interactions, and torsional and *exo*-anomeric potentials (13). Rotational barriers of 1.0 and 0.5 kcal/mol were used for φ and ψ, respectively. No electrostatic contributions were considered. The pyranose ring geometry was treated as invariant, and hydroxylic hydrogen atoms were not taken into account. The angles for the glycosidic bond were defined as φ = (H1—C1—O1—C6′) and ψ = (C1—O1—C6′—C3′). The glycosidic bond angle C—O—C was set at 117°. Potential energy maps were generated for φ and ψ under the following conditions. For a setting of the torsional angles φ and ψ, the amide group was allowed to rotate over the whole angular range in increments of 20°. All other torsion angles were allowed to adopt staggered orientations of −60°, 180°, and 60°, except for the C1′—C2′—C3′—C4′—C5′ orientation, which was kept in the *trans* position. The glycosidic torsional angles φ and ψ were stepped in increments of 20° over the whole angular range and the minimum energy for each grid point upon rotation of all other torsional angles was plotted. This allowed the calculations to simulate a flexible structure where all pendant groups can adopt minimum energy conformations. Calculations were repeated for other staggered orientations of the

backbone C1′—C2′—C3′—C4′—C5′ and no expansion of the allowable conformational space for ϕ and ψ was observed. All calculations were performed on a Micro VAX 3500.

Theory

It is assumed that the ^{13}C nuclei examined here are relaxed solely by dipolar interactions with attached proton(s). The general expressions for T_1, T_2, and nOe are given by (14)

$$[1] \quad \frac{1}{T_1} = R_1 = \frac{N_i}{20}\left[\frac{\mu_0\gamma_H\gamma_C h}{8\pi^2 r_{C-H}^3}\right]^2 \times (J(\omega_H - \omega_C) + 3J(\omega_C) + 6J(\omega_H + \omega_C))$$

$$[2] \quad \frac{1}{T_2} = R_2 = \frac{N_i}{40}\left[\frac{\mu_0\gamma_H\gamma_C h}{8\pi^2 r_{C-H}^3}\right]^2 \times (4J(0) + J(\omega_H - \omega_C) + 3J(\omega_C) + 6J(\omega_H) + 6J(\omega_H + \omega_C))$$

$$[3] \quad \eta = \frac{1}{20}\gamma_H^3\gamma_C\left[\frac{\mu_0 h}{8\pi^2 r_{C-H}^3}\right]^2 (N_i T_{1i}) \times (6J(\omega_H + \omega_C) - J(\omega_H - \omega_C))$$

where T_1, T_2, and η are the spin-lattice and spin–spin relaxation times and nOe for a specific carbon in the molecule. μ_0 is the permeability of a vacuum, γ_H and γ_C represent the magnetogyric ratios of the proton and carbon nuclei respectively, and r_{C-H} denotes the C—H bond length (vide infra). The $J(\omega)$'s are spectral densities, N_i is the number of protons directly attached to carbon i, ω_H and ω_C are the Larmor frequencies of the protons and carbons at a given magnetic field, and all other constants have their usual meanings.

The motions of polymers are inherently complex and the interpretation of NMR measurements for such systems is often not unique. For polymers undergoing internal or segmental motions as well as overall reorientational motion, there are many motional processes, which may necessitate analyzing the data in terms of an empirical distribution of correlation times (15). Since analyses have proven useful for the analysis of relaxation data in recent years, a certain preference has been given to the utilization of the "model-free" approach of Lipari and Szabo (16) (equivalent in spectral density form to the "two-step" model suggested by Wennerstrom et al. (17)). A number of authors have applied this model-free approach to the molecular dynamics of a number of biologically related systems (18–21). In particular, and in relation to this work, the model has been adapted to examine both the internal and overall motions of a number of saccharides (22–24).

Lipari and Szabo (16) derived a simple form for the spectral density function for a nonrigid molecule undergoing overall and internal motions. For a ^{13}C–^1H vector attached to an isotropically reorienting molecule, the spectral density function is given by

$$[4] \quad J(\omega) = S^2\left[\frac{2\tau_c}{1 + \omega^2\tau_c^2}\right] + (1 - S^2)\left[\frac{2\tau}{1 + \omega^2\tau^2}\right]$$

where

$$[5] \quad 1/\tau = 1/\tau_c + 1/\tau_{eff}$$

Here, τ_c is the correlation time, which describes the overall isotropic motion of the whole molecule, S is a generalized order parameter, and τ_{eff} is an effective correlation time for reorientation of the ^{13}C–^1H vector being examined. This equation is valid if $\tau_c >> \tau_{eff}$ and only if the overall motion is isotropic. The order parameter S describes the spatial restriction of the internal motions and may vary between 1, when the motion at that carbon is completely restricted, and zero, the limit of completely unrestricted motion. When $S^2 = 1$, eq. [4] reduces to the rigid isotropic case ($J(\omega) = 2\tau_c/(1 + \omega^2\tau_c^2)$).

The effective correlation time τ_{eff} provides a limit for the timescale describing the internal motions and is defined as the area of the internal motion correlation function. This effective correlation time holds no specific value unless it is interpreted in the framework of an appropriate model.

Equation [4] assumes that the internal motions of the C—H vectors are independent of the overall motion of the molecule. If the internal motions are assumed to be within the extreme narrowing regime, then $\omega^2\tau^2 << 1$ and

$$[6] \quad J(\omega) = S^2\left[\frac{2\tau_c}{1 + \omega^2\tau_c^2}\right] + (1 - S^2)2\tau$$

If the internal motions are assumed to be *much* more rapid than the overall motion, then with $\tau << \tau_c$ we obtain

$$[7] \quad J(\omega) = S^2\left[\frac{2\tau_c}{1 + \omega^2\tau_c^2}\right]$$

The restriction of extreme narrowing to the internal motions is not required by the theory and may well be inapplicable, especially for the relaxation data obtained at the higher field strengths.

For the case where the overall motion cannot be described by a single isotropic correlation time, the anisotropic motional spectral density function is given by

$$[8] \quad J(\omega) = 2\left[\frac{AS^2\tau_1}{1 + (\omega\tau_1)^2}\right] + \left[\frac{(1 - A)S^2\tau_2}{1 + (\omega\tau_2)^2}\right] + \left[\frac{A(1 - S^2)\tau'}{1 + (\omega\tau')^2}\right] + \left[\frac{(1 - A)(1 - S^2)\tau''}{1 + (\omega\tau'')^2}\right]$$

where

$$[9] \quad (\tau')^{-1} = \tau_{eff}^{-1} + \tau_1^{-1}$$

$$[10] \quad (\tau'')^{-1} = \tau_{eff}^{-1} + \tau_2^{-1}$$

For a nucleus rigidly attached to an anisotropically reorienting backbone on a macromolecule, $S^2 = 1$ and eq. [8] simplifies to

$$[11] \quad J(\omega) = A\left[\frac{2\tau_1}{1 + \omega^2\tau_1^2}\right] + (1 - A)\left[\frac{2\tau_2}{1 + \omega^2\tau_2^2}\right]$$

When $\tau_1 = \tau_2$ or $A = 1$ then the spectral density for the rigid isotropic case is recovered.

Results and discussion

Assignments

The natural abundance ^{13}C NMR spectrum of both the α- and β-glycopolymers is dominated by backbone resonances due to the methine and methylene groups (see (Fig. 2). This range of chemical shifts for the backbone resonances is presumably due to the variety of substituted methines (R^1R^2CHX, X = $CONH_2$, CH_2OR) in combination with the

Can. J. Chem. Downloaded from www.nrcresearchpress.com by 203.198.23.82 on 09/08/12
For personal use only.

Can. J. Chem. Downloaded from www.nrcresearchpress.com by 203.198.23.82 on 09/08/12
For personal use only.

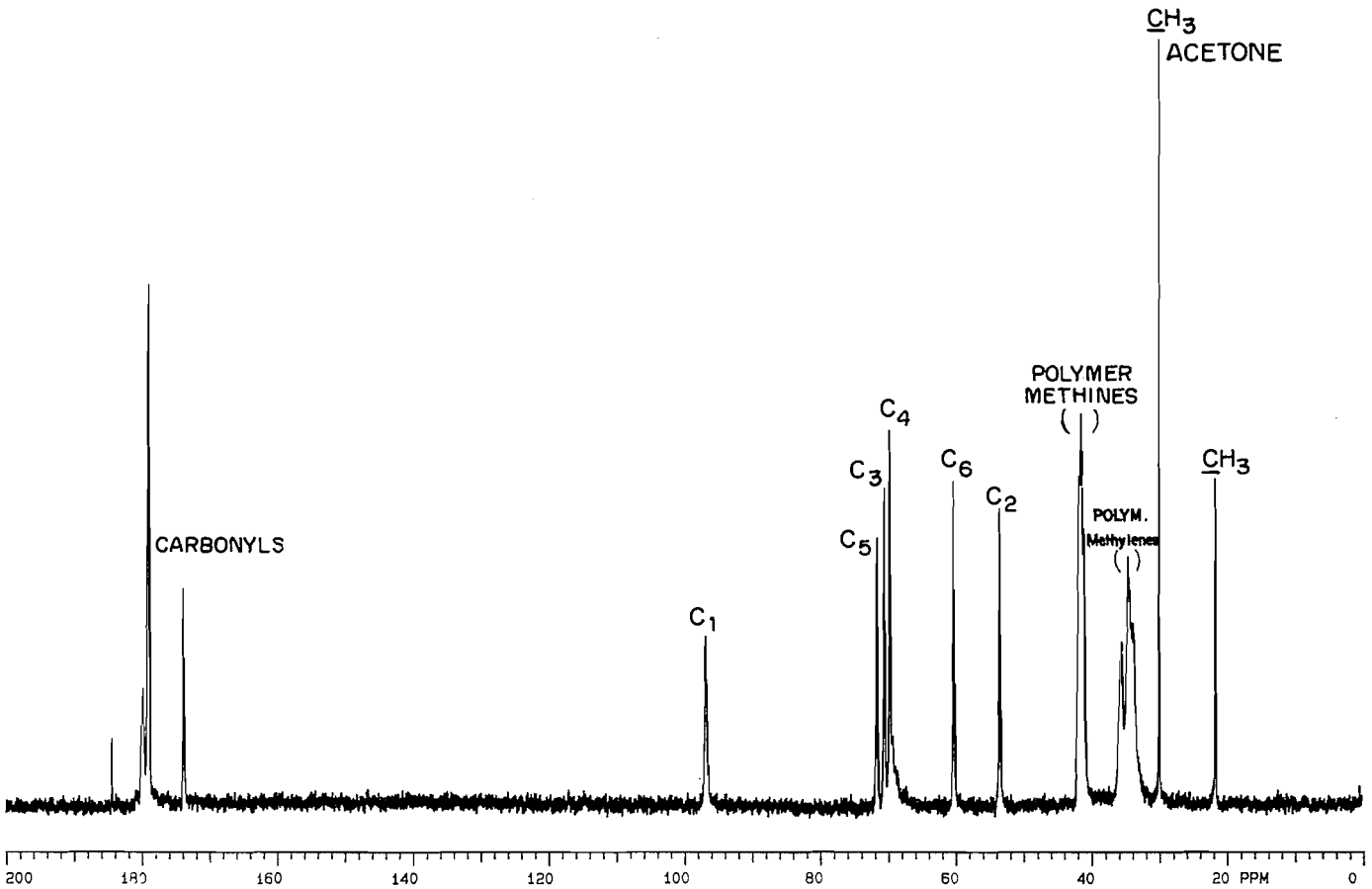

FIG. 2. The assigned ^{13}C NMR spectrum of poly(acrylamide-*co*-allyl 2-acetamido-2-deoxy-α-D-glucopyranoside) α-**1** at 75.43 MHz. Internal acetone was used as the reference for this spectrum.

TABLE 1. ^{13}C relaxation times of the α-glycopolymer (**1**) as a function of temperature and resonance frequency

ω(MHz)	Temperature (°C)	Methine[a]	NT_1(s)[e](±STD)[f] methylene[a]	Sugar[b]	Hydroxymethyl[c]	Methyl[d]
50.29	30	0.145 (0.006)	0.152 (0.004)	0.155 (0.004)	0.188 (0.003)	2.445 (0.056)
	20	0.193 (0.005)	0.202 (0.006)	0.202 (0.006)	0.250 (0.003)	2.502 (0.064)
	30	0.199 (0.004)	0.214 (0.003)	0.211 (0.005)	0.260 (0.004)	2.703 (0.043)
75.43	48.8	0.228 (0.005)	0.238 (0.004)	0.239 (0.007)	0.312 (0.004)	2.835 (0.051)
	58.1	0.246 (0.005)	0.264 (0.005)	0.248 (0.009)	0.328 (0.005)	2.949 (0.039)
	67.4	0.268 (0.003)	0.282 (0.004)	0.269 (0.009)	0.352 (0.005)	3.273 (0.075)
100.62	30	0.244 (0.009)	0.264 (0.004)	0.291 (0.007)	0.320 (0.005)	3.312 (0.062)
125.73	30	0.323 (0.007)	0.354 (0.006)	0.328 (0.007)	0.376 (0.006)	3.399 (0.078)

[a]Polymer backbone resonances.
[b]C_1–C_5 sugar resonances.
[c]Hydroxymethyl (C_6) attached to sugar ring.
[d]*N*-Acetyl methyl group.
[e]*N* is the number of directly attached protons.
[f]Standard deviation errors are given in parentheses.

atactic nature of the polymer. Different head-to-head, head-to-tail, and tail-to-tail polymerization combinations might also play a role to some extent. The singlet to lowest frequency is due to the *N*-acetyl methyl group. The sugar methine and hydroxymethyl resonances are to low field of the bulk chain (between 50 and 100 ppm), and are assigned according to Roy et al. (25). A number of carbonyl resonances are also observed at ca. 180 ppm.

Qualitative analysis of relaxation parameters of the α-glycopolymer (1)

Spin-lattice relaxation times and nOe values were measured for all resolvable peaks. Table 1 gives the spin-lattice relaxation times (NT_1), obtained for the α-glycopolymer (**1**) as a function of temperature and magnetic field strength. The magnetization relaxation curves were all single exponential in nature for all fields. The relaxation times for the groups

Can. J. Chem. Downloaded from www.nrcresearchpress.com by 203.198.23.82 on 09/08/12
For personal use only.

of resolvable methylene and methine groups within the backbone are all within error, and an average value for both types of carbon was thus used for further analysis. A similar approach was taken for analysis of the methine sugar resonances. No attempt was made to measure accurate values of the carbonyl T_1's due to the possible contributions of chemical shift anisotropy to the relaxation.

The T_1 data obtained show several interesting features. If the sugar ring (C_1–C_5) and attached hydroxymethyl group (C_6) were experiencing the same motions, then NT_1 should be identical. However, at each magnetic field $NT_1(CH_2OH) > NT_1$(sugar). This suggests that the hydroxymethyl group has added mobility over the sugar. This can be imagined to be the spinning of the -CH_2OH group, similar to the C_3 rotation of a methyl group about its axis, though probably more restricted. A similar observation for the relative NT_1's can be made for the polymer backbone methylene groups compared to the methine segments. In this case the methylene groups have slightly more mobility than the CH groups, as shown by a longer NT_1 value. Since the methylene and methine NT_1 values are averages of all possible configurations of these groups, it would be expected that the added freedom of the methylene group attached to the sugar moiety may increase NT_1 to such an extent that the average value may have a bias to the motions of the side-chain methylenes.

Quantitative analysis of relaxation parameters for the α-glycopolymer (1)

To calculate accurate correlation times from the relaxation data using any of the equations given above, an accurate value of the C—H bond length is required. Consultation of the literature shows that for alkyl chains the bond length used varies between 1.09 (26) and 1.11 Å (27). For the ring-carbon atoms in sucrose, the C—H bond length is 1.10 Å by neutron diffraction (28). However, the effective bond length is influenced by vibrational motions, and Brown and Levy (28) estimated a bond length of 1.11 Å from their neutron diffraction data. Using a correction suggested by Henry and Szabo (29) based on the combined effect of harmonic and anharmonic C—H stretching force constants, McCain and Markley (22) showed that the best estimate for the r_{C-H} bond length is 1.12 Å.

The overall contribution to the relaxation of the carbon nuclei will be from distant protons as well as directly attached protons. By using crystal structure data, and including all the hydrogen atoms in sucrose except those in the hydroxyl groups, McCain andl Markley (22) calculated an extra contribution to the relaxation of the ring-carbon atoms from distant protons. This added contribution, equivalent to an extra 5% C—H dipolar relaxation, can be estimated as an apparent r_{C-H} bond length of 1.11 Å. For internal consistency, this bond length has been adopted for all C—H bonds for the data analyses made in this work. Other values of r_{C-H} have been used to examine errors in the fits (vide infra).

Polyacrylamide is known to exist in solution as random-coil polymers (30). Lipari and Szabo (16) suggested that for polymers in such a random-coil conformation, the macromolecule would be expected to deviate from a sphere, and that the data for such systems should be analysed using the double-exponential correlation function given by eq. [8].

The information regarding the overall anisotropic motion of the polymer is extracted from the backbone carbons. Assuming the anisotropic form of the spectral density function (eq. [11]), the relaxation data for the different carbon atoms within the polymer backbone should be describable by a global parameter τ_1, and a pair of (A, τ_2) parameters corresponding to the methine and methylene carbons. The complete set of parameters that reproduces the data gives a global minimum in the error.

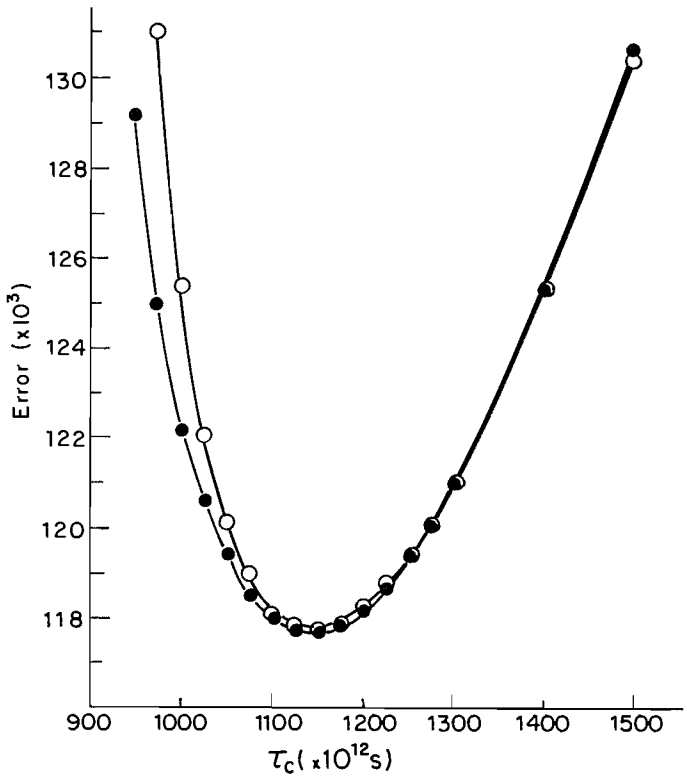

FIG. 3. The representation of the error minimization using the error function (see text) as a funcction of τ_1.

The approach taken here is to choose a value of τ_1 from the experimental ^{13}C R_1 values obtained at the different magnetic field strengths and calculate values of τ_2 and A using an iterative fit to the multifrequency relaxation data. Since the errors for the nOe data are larger than for the rate data, ±20% compared to ±5%, only the relaxation rate data were used to calculate the motional parameters. The values of τ_1, τ_2, and A that minimize the error function (26)

$$[12] \quad \text{error} = \frac{(R_{obs} - R_{calc})^2}{(R_{obs})^2}$$

are then chosen as the best values for the whole molecule. In this function R_{obs} and R_{calc} are the observed and calculated relaxation rates, respectively. Using these values as global constants allows τ_{eff} and S^2 values describing internal motions to be calculated for the remaining carbons in the molecule, i.e., for the sugar resonances (C_1–C_6) and the *N*-acetyl methyl.

Figure 3 illustrates the result of the minimization procedure obtained by fitting the multifrequency relaxation data for the polymer backbone methylene groups. Two curves are evident, corresponding to the minimized errors obtained using r_{C-H} bond lengths of 1.098 and 1.110 Å in the dipolar interaction constant. Note that for the narrow range of corre-

TABLE 2. Viscosity of the α-glycopolymer (**1**) as a function of temperature

Temperature (°C)	Viscosity (cP)
23.0	3.43
30.0	2.95
44.3	2.22
56.8	1.75

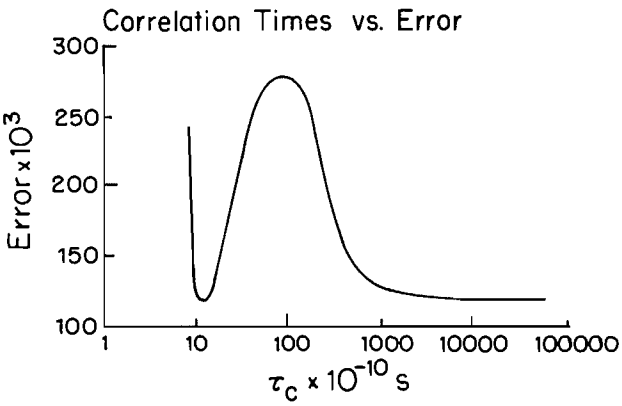

FIG. 4. The representation of the error minimization using the error function as a function τ_1 over a range of 1 ns to 10 μs.

TABLE 3. Internal motion correlation times and order parameters for the α-glycopolymer (**1**)[a]

Carbon[b]	τ_{eff} (ps)	S^2
Sugar (C1–C5)	13.6 ± 74.5	0.625 ± 0.092
Hydroxymethyl (C6)	48.1 ± 22.5	0.472
Methyl (N-Ac)	9.9 ± 2.0	

[a]Data fitted using eqs. [12] and [4] with τ_e = 1.15 ns.
[b]See Table 1 for assignments.

lation times examined, there is only one minimum for the different values of r_{C-H} corresponding to τ_1 = 1.15 ± 0.02 ns. A similar fit to the methine relaxation data gives the same overall correlation time within error. It is obvious that the motions may be sufficiently described by the single correlation time τ_1 since the error in τ_2 makes the parameter meaningless. In this case eq. [11] may be reduced to the same functional form as eq. [7] with S^2 replaced by A.

The question remains as to whether this calculated correlation time of 1.15 ns is appropriate for the expected dimensions of the polymer as derived from the viscosity measurements. For a sphere rotating in a medium of viscosity η, the Debye theory (31) gives the following expression for τ_c:

$$[13] \quad \tau_c = fV\eta/kT$$

where V is the volume of a sphere (calculated earlier to be 1.57×10^{-24} m^3) (32) and f is the microviscosity factor. Assuming that the randomly coiled polymer molecules may be approximated as tumbling spheres (9, 10, 30), and using a typical value for the microviscosity factor (33) of 0.16, the correlation time for overall tumbling of a polymer sphere at 30°C, using the viscosity given in Table 2, is 1 μs. This correlation time is far outside the range that spin-lattice relaxation and nOe measurements can probe, and only spin–spin relaxation can provide confirmation of such a timescale of motion due to the presence of the zero-frequency spectral density component $J(0)$ in eq. [2]. However, due to the problem of many overlapping methylene and methine backbone resonances in the ^{13}C spectrum, attempts to correlate the spin–spin relaxation time, or its associated linewidth, with a correlation time of this magnitude is not possible.

Figure 4 illustrates the error function, eq. [12], as a function of τ_1 over a range up to and including 1 μs. It is obvious that at large values of τ_1 a plateau is reached where the error is almost equivalent to that obtained for the first minimum (error values; 0.1197 cf. 0.1177). At long τ_1, the values of τ_2 and A that are extracted become highly insensitive to the magnitude of τ_1; for example, with τ_1 = 200 ns, τ_2 = 1225 ps and A = 0.365, while for τ_1 = 2000 ns, τ_2 = 1254 ps and A = 0.359. Since τ_1 correlation times of this magnitude will have only a negligible effect on the spin-lattice relaxation times and nOe's, the contribution of this timescale of motion to spin-lattice relaxation may be ignored. Measurements of molecular motions of a timescale of 200–2000 ns would be possible via $T1\rho$. However, spectrometer limitations did not allow these determinations to be made as contributors to the relaxation. As a result, the overall motions may be described by a function of the form given in eq. [7], where S^2 is replaced by $(1 - A)$. Using this function returns us to the situation where the overall correlation time is 1.15 ns.

The spin-lattice relaxation times of the sugar ring carbons are identical within the experimental error limits, and it is correct to assume that the reorientational motion of the sugar fragment is isotropic. Table 3 lists the S^2 and τ_{eff} values obtained for the remainder of the molecule using eq. [4]. The values of the parameters are listed for an r_{C-H} bond length of 1.110 Å. It is obvious that, within error, an effective internal or "fast" correlation time cannot be extracted from the data obtained for the sugar ring carbons, while both the hydroxymethyl group and the *N*-acetyl methyl group have associated fast correlation times.

McCain and Markley (22, 23) examined the internal motions in sucrose while Kovacs et al. (24) probed the internal motions in sucrose and a disaccharide methyl 3-*O*-(α-D-rhamnopyranosyl)-α-D-glucopyranoside. Both groups of workers analysed the relaxation data of the sugar rings in terms of a "reduced" spectral density, equivalent in functional form to eq. [7], where the fast motions were assumed to be vibrations or torsional oscillations. The normal Lorentzian spectral density is premultiplied by a so-called "amplitude factor," equivalent to our S^2 parameter, which indicates the importance of vibrational motions to the relaxation. As the vibrational motions increase in importance, then the amplitude factor decreases.

For sucrose, amplitude factors of 0.89 and 0.94 have been obtained (22, 24). These values were in different solvent systems with different viscosities and H-bonding capabilities, and a slight change in the amplitude factor would be expected. The overall correlation time was also shown to be viscosity dependent by McCain and Markley (22, 23).

For our system, the S^2 parameter obtained can be thought of as being equivalent to the A parameter that is associated with the backbone motions since no internal motions can be

Can. J. Chem. Downloaded from www.nrcresearchpress.com by 203.198.23.82 on 09/08/12
For personal use only.

Can. J. Chem. Downloaded from www.nrcresearchpress.com by 203.198.23.82 on 09/08/12
For personal use only.

detected for the sugar. The value of A found for the sugar agrees, within error, with those values obtained for the backbone. This observation does not preclude the fact that librational motions may also be contributing to the relaxation of the ring, but rather than their contribution to the overall relaxation is small and this contribution is rendered undetectable, within error, by the added complication of anisotropic overall motion.

The hydroxymethyl group attached to the sugar has a smaller order parameter than the sugar ring, as well as an associated τ_{eff} correlation time (48 ± 22 ps). Rotation of the CH_2OH fragment relative to the ring would be expected to contribute to the relaxation, while librational motion of the ring itself, if it occurs, would be superimposed on this rotation.

McCain and Markley (23) attempted to detect the internal motions of the three hydroxymethyl groups in aqueous sucrose. Their studies failed to detect a rotational motion of the hydroxymethyl group, and again the relaxation of this group was expressed in terms of torsional librations and overall motion, the conclusion previously derived for the ring-carbon atoms (22). Their data showed that the motional amplitudes for the three hydroxymethyl groups of sucrose are similar and that none of them rotates freely, supporting the known existence of intramolecular hydrogen bonds within sucrose (23).

The internal motion of the -CH_2OH group detected in this work is indicative that the fragment may not be suffering intramolecular H-bonding as exists in the sucrose molecule. By relaxing this constraint, the fragment would be expected to rotate. The motions are still obviously restricted, however, as shown by the magnitude of the S^2 parameter.

The observation that the polymer backbone methine and methylene resonances as well as the sugar resonances can, within error, be described by the same values of τ_c and A suggests that the polymer network, including the saccharide side chain, is being relaxed by anisotropic tumbling. The similarity between the T_1 values for the sugar carbons was earlier accepted to be an indication of isotropic overall tumbling. The errors present for the T_1 values of the sugar resonances may be disguising the presence of anisotropic motion. The freer motions of the N-acetyl methyl and hydroxymethyl groups are superimposed upon the overall molecular tumbling. The hydroxymethyl group may suffer intermolecular hydrogen bonding with water, thereby restricting its rotation, while the methyl group would be expected to have less hindrance to its internal rotation.

Using eq. [4], an effective correlation time of ca. 10 ps can be calculated for the N-acetyl methyl group. If symmetric rotation occurs about the methyl group axis, then S^2 is given (17) by

$$[14] \quad S^2 = S^2_{axis}(3\cos^2\beta - 1) = 0.111\, S^2_{axis}$$

where β is the angle between the axis of the methyl group and the C—H bond. The angle β is taken to be 70.5°, assuming perfect tetrahedral geometry (17). The maximum value of S^2 is thus 0.111 if these assumptions are correct. Since S^2 is 0.023 for this system, the indications are that the relaxation of the methyl group cannot be described by methyl group rotation alone but by another superimposed motion, possibly the motion of the -NH-C=O side chain attached to the sugar.

TABLE 4. Experimental and calculated nOe's for the α-glycopolymer (**1**)

	ω(MHz):			
	η_{exp}		η_{calcd}	
Carbon[a]	75.43	100.62	75.43	100.62
Methine[b]	0.79	0.29	0.53	0.39
Methylene[b]	0.81	0.28	0.53	0.39
Sugar[b] (C_1–C_5)	0.73	0.21	0.53	0.39
Hydroxymethyl[c] (C_6)	0.86	0.53	0.71	0.63
Methyl[c] (N-Ac)	0.98	1.07	1.31	1.34

[a]See Table 1 for assignments.
[b]Calculated using τ_c = 1.15 ns.
[c]Calculated using τ_c = 1.15 ns.

Nuclear Overhauser enhancements

Nuclear Overhauser enhancements are inherently difficult to measure with the same degree of accuracy as spin-lattice relaxation times. Table 4 lists the experimental and calculated nOe's obtained at 75.4 and 100.6 MHz for the α polymer (**1**). The calculated nOe's were obtained using the global parameter τ_c = 1.15 ns and the individual pairs of S^2 and τ_{eff} parameters for the hydroxymethyl and methyl groups in eq. [4]. For the methine, methylene, and sugar ring carbons, the nOe's were calculated using the "reduced" form of the spectral density (eq. [7]).

It is important to note that the nOe is a ratio of spectral density terms, and is therefore unaffected by the S^2 parameter as a pre-multiplier. By using the "reduced" form of the spectral density only the dependence of the nOe on correlation time is probed. This is the reason that the calculated values for the methine, methylene, and sugar carbons are identical, even though the S^2 parameters used from Table 3 vary slightly. At both field strengths, the experimental nOe's for these carbon atoms are very similar, in accordance with the suggestion of the relaxation being brought about by only overall motion.

The agreement between observed and calculated nOe's at both field strengths is quite good, normally within about 25%. Estimates of the overall correlation time can be determined by averaging the observed nOe's at both field strengths for the backbone and sugar carbons. At 75.4 MHz the average nOe is 0.77, corresponding to τ_c = 0.82 ns. At 100.6 MHz the average nOe is 0.26, corresponding to τ_c = 1.75 ns. The average of these parameters is 1.28 ± 0.46 ns, in fairly good agreement with the overall correlation time of 1.15 ± 0.02 ns obtained from the spin-lattice relaxation rate data.

The observed nOe's for the hydroxymethyl and methyl groups are in fairly good agreement with those calculated, again within 25%. An indication of the possible errors in the magnitude of the errors in nOe can be established by consideration of the values calculated using the various pairs of error parameters of S^2 and τ_{eff} determined from fitting of the relaxation rate data. For the methyl group, nOe's of between 1.13 and 1.51, a change of approximately 25%, can be calculated using minimum τ_{eff}/maximum S^2 and maximum τ_{eff}/minimum S^2 parameters, respectively. In any case, the theoretical ordering of the nOe's at each magnetic field is observed experimentally; sugar ≈ polymer(methylene ≈ methine) < hydroxymethyl < N-acetyl methyl.

Can. J. Chem. Downloaded from www.nrcresearchpress.com by 203.198.23.82 on 09/08/12
For personal use only.

Spin–spin relaxation times

As discussed earlier, it is probable that the larger of the correlation times describing the anisotropic tumbling is of such a magnitude that the spin-lattice relaxation times and nOe's would not be affected. Due to the zero-frequency spectral density contribution to spin–spin relaxation, the half-height linewidths may provide information regarding the magnitude of this parameter.

Since the polymer backbone resonances exhibit approximately the same T_1 and nOe behaviour as the sugar resonances, it could be expected that the T_2 relaxation for these carbons will also be similar. This is not necessarily a safe assumption, however, since the saccharide side chain may exhibit some wobbling motion relative to the more restricted motions of the backbone. The overlap of the polymer backbone methine and methylene groups of resonances circumvents their use for examination of the behaviour of the T_2 relaxation of the backbone.

The sugar resonances (C_1–C_6) are well resolved. Examination of the 300 MHz ^{13}C spectrum (see Fig. 2) shows that C_1 is a factor of two broader than the other carbons within the sugar ring. This is presumably due to slight differences in the shift of C_1 brought about by the atactic nature of the polymer. The linewidth for C_1 increases by a factor of ca. three between the different resonance frequencies of 75 and 100 MHz, and observation of distinct fine structure at a resonance frequency of 125 MHz verifies this suggestion. Similar increases in linewidth are observed for the *N*-acetyl methyl group.

At 75.3 MHz resonance frequency the average linewidth for C_2–C_5 is 10.7 ± 1 Hz while at 100.6 MHz the linewidth is 11.3 ± 1 Hz. Using the spectral density defined by eq. [11] and fixing τ_2 = 1150 ps and A = 0.333, gives τ_1 = 21 and 23.5 ns at 75 and 100 MHz, respectively. The linewidths at these frequencies for C_6 are 9.3 and 9.5 Hz, which gives τ_1 = 18 and 19.5 ns when using eq. [8] with τ_2 = 1150 ps, A = 0.333, τ_{eff} = 48 ps, and S^2 = 0.472. These values of τ_1 for C_2–C_6 are in excellent agreement with each other, and give an average of 20.5 ns for τ_1. This timescale is not *necessarily* the second timescale associated with the anisotropic tumbling of the polymer networrk, but may be some average correlation time describing overall tumbling as well as wobbling of the saccharide side chain.

Activation energies of motions by variable temperature

T_1 *measurements*

Spin-lattice relaxation times for the α polymer (**1**) measured as a function of temperature, from 20 to 64°C in increments of ca. 10°C, are given in Table 1. It was assumed that both the overall and internal motions could be described by a normal Arrhenius activation energy, while the S^2 and A parameters were assumed to be temperature independent. Other workers (23) have suggested that S^2 may be temperature dependent, but this dependence is expected to be small.

The activation energy for overall motions was obtained by application of the "reduced" spectral density to the backbone methine and methylene and the sugar methine carbon relaxation data. Relaxation times were calculated for each of these groups by fixing S^2 and changing τ_c to give the observed experimental relaxation times. A linear fit of these calculated τ_c values as a function of $1/T$ allowed the activation energy to be obtained (see Table 5).

TABLE 5. Activation energies for overall and internal motions in the α-glycopolymer (**1**)[a]

Carbon	E_a (τ) (kJ mol^{-1})	τ_{eff} (ps)
Methine[b]	16.9 ± 0.9	—
Methylene[b]	15.5 ± 0.7	—
Sugar (C_1–C_5)[b]	17.6 ± 0.7	—
Hydroxymethyl (C_6)[c]	47.8 ± 20.6	24.6 ± 6.7
Methyl (N-Ac)[c]	4.2 ± 1.4	11.2 ± 0.4

[a]See text for details of calculations.
[b]Activation energies calculated using τ_1 = 1.15 ns.
[c]Activation energies calculated using τ_1 = 1.15 ns, E_a (τ_1) = 16.7 kJ mol^{-1}, and S_2 parameters given in Table 3.

The activation energy associated with the overall tumbling correlation time is $\langle E_a(\tau_c)\rangle_{av}$ = 16.7 ± 1.1 kJ mol^{-1}. If this activation energy is associated with the overall motion, then it should be related to the activated energy associated with viscosity (32). Table 2 lists the viscosities of the α-glycopolymer (**1**) as a function of temperature. According to the Debye equation (31) the overall correlation time is proportional to η/T and the activation energy obtained from the slope of a plot of $\ln(\eta/T)$ against $1/T$ should therefore be associated with the tumbling of the molecule. From the viscosity data given in Table 2, a value of $E_a(\eta/T)$ = 18.7 ± 0.2 kJ mol^{-1} is obtained, while a value of $E_a(\eta)$ = 16.1 ± 0.1 kJ mol^{-1} is obtained from a plot of $\ln(\eta)$ against $1/T$. The activation energy associated with overall tumbling agrees well with both of these viscosity related activation energies.

Using the value $\langle E_a(\tau_c)\rangle_{av}$ = 16.7 kJ mol^{-1} as a fixed parameter, and using the values of τ_c and S^2 given in Table 3, the correlation times and activation energies associated with the internal motions of the methyl and hydroxymethyl groups were calculated. For both groups the correlation times, τ_{eff}^{301K}, were within error of those determined by fitting of the magnetic field dependent relaxation data. For the methyl group the value obtained was τ_{eff}^{301K} = 11.2 ± 0.4 ps compared with 9.9 ± 2.0 ps, while for the hydroxymethyl group τ_{eff}^{301K} = 24.6 ± 6.7 ps compared with 48.1 ± 22.5 ps.

$E_a(\tau)$ for the methyl group (*N*-acetyl) is small (see Table 5). As discussed above, the rotation of the methyl group is probably superimposed on some other motion(s) due to the magnitude of the S^2 parameter. The activation energy is therefore characterizing a number of motions, and no further meaningful information can be gleaned from its magnitude.

$E_a(\tau)$ for the hydroxymethyl group (C_6) of **1** is quite large (47.8 kJ mol^{-1}), and has a large error associated with it (±20.6 kJ mol^{-1}). Due to the nature of the hydroxymethyl group, the activation energy may also be characterizing the change in hydrogen-bonding as a function of temperature as well as an internal barrier to rotation. The authors are unaware of any literature data referring to this rotation.

Comparison of relaxation times in the α- (1) and β- (2) glycopolymers

Table 6 lists the relaxation times obtained for the α- and β-glycopolymers at a temperature of 30°C and 300 MHz resonance frequency. Examination of these data shows that the T_1 values for the β polymer are all greater than those obtained for the α polymer. These differences could be due to a number of minor factors, including slightly different mo-

TABLE 6. ^{13}C relaxation times (s) for the α- and β-glycopolymers at 30°C and 75.43 MHz[a]

Carbon[b]	α Polymer (**1**)	β Polymer (**2**)
Methine	0.199 (0.004)	0.201 (0.005)
Methylene	0.107 (0.003)	0.114 (0.009)
Sugar (C_1–C_5)	0.211 (0.005)	0.238 (0.005)
Hydroxymethyl (C_6)	0.130 (0.004)	0.139 (0.006)
Methyl (N-Ac)	0.901 (0.043)	0.889 (0.064)

[a]Errors given in parentheses.
[b]See Table 1 for assignments.

lecular weights and therefore different viscosities or different motions in the two polymers. An alternative possibility could be differential retention of water in the polymers after lyophilization, thereby affecting the weight of actual polymer dissolved in the solutions, and therefore again affecting the viscosities.

It is to be expected that the overall motion would be more affected by a change in viscosity than would the internal motions (32). The overall motion contribution to the relaxation times for the different carbon nuclei in the molecule will therefore be affected and the T_1's will change. Assuming this argument, the observed T_1's suggest that the β polymer (**2**) has a faster overall motion than the α polymer (**1**). This observation does *not* preclude differences in internal motion as well.

The internal motions are of particular interest and the configuration at the anomeric center may affect the motions of the sugar unit. A suitable comparison to probe differences in internal motions is to observe the differences in motion between the backbone and the sugar itself.

Assuming a 5% error in the T_1 values, the ratio of the methine T_1's to the methylene T_1's is the same for both anomers. To establish a level of error comparison, the ratios of T_1(sugar, C_1–C_5) to T_1(hydroxymethyl, C_6) were calculated. These ratios are 1.62 and 1.71 for the α and β anomers, respectively, agreeing to within <5%. Repeating this process for the methine and methylene resonances of the backbone shows an agreement to better than 2%. However, relating the sugar T_1's to the backbone T_1's (methine and methylene) by this method suggests a difference of ca. 8% between the two anomers. There are some possible sources of error involved with this analysis, but the results are *suggestive* that the motions of the sugar ring in the α anomer are more restricted than those obtained for the β anomer.

This restriction of motion can be explained in terms of a change in the motion of the ring relative to the side chain. The earlier discussion suggested that the relaxation of the ring carbons could be influenced by a librational process and by some wobbling of the sugar ring relative to the backbone. For the α polymer (**1**) the proximity to the backbone (see Fig. 1) may lead to additional H-bonding between the sugar hydroxyl groups and protons on the backbone, thereby affecting the extent of motion of the ring. This behaviour is exposed by the difference in T_1's between the two anomers. However, since there are two contributions to the spin-lattice relaxation, the overall difference in the relaxation between the two polymers would be expected to be small. For the sugar ring in the α polymer the relaxation is ca. 65%:35% slow motions to fast motions (vide supra).

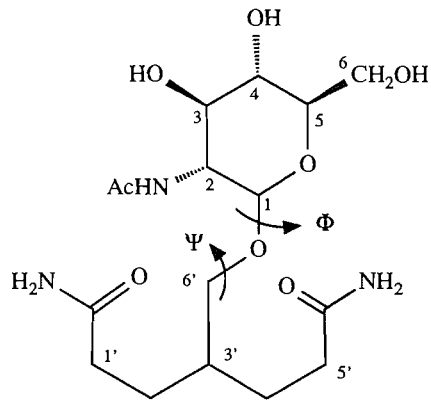

1 R = α-GlcNAc
2 R = β-GlcNAc

FIG. 5. The structures used for the potential energy calculations.

Comparison of the conformational flexibility of the α- (1) and β- (2) glycopolymers by molecular mechanics calculations

To evaluate whether there is a difference in the conformational flexibility of the two polymers, **1** and **2**, the ϕ,ψ energetically allowable conformational space was explored with the use of potential energy calculations. A suitable structure was constructed (vide supra) that could reproduce all the degrees of freedom present in the glycopolymer (Fig. 5) near the vicinity of the glycosidic bond. The potential energy as a function of ϕ and ψ, where the molecule is allowed to adopt a minimum energy conformation for each setting of the glycosidic torsion angles, is shown in Figs. 6 and 7 for the α and β forms of the glycopolymers.

Comparison of these figures immediately indicates that the β anomer has far greater conformational flexibility than the α anomer. The β anomer samples a total ϕ angular displacement of ca. 270° while the β anomer is restricted in motion, allowing sampling of a ϕ range of only 100°.

This observation of the different conformational flexibilities of the different anomers supports the observation of different spin-lattice relaxation behaviour, and the approach of comparing the relaxation times of the sugar rings relative to the backbone is shown to be valid.

Conclusion

The objective of this study was to examine the molecular motions and relative conformational flexibilities of the α (**1**) and β (**2**) anomeric forms of poly(acrylamide-*co*-alkenyl *O*-glycosides) to determine whether NMR relaxation measurements could offer any information regarding the overall and internal motions in these types of systems. This study indicates the importance of determining all relaxation parameters for polymers, T_1, T_2, and nOe, to allow all timescales of motion to be examined. The faster motions are readily accessible by T_1 and nOe measurements, though only the T_2 determinations provide information regarding much slower overall motions. The applicability of the model-free approach in its various forms to the analysis of ^{13}C relaxation data has been illustrated fully.

The derived global dynamic parameters of the polymer

Can. J. Chem. Downloaded from www.nrcresearchpress.com by 203.198.23.82 on 09/08/12
For personal use only.

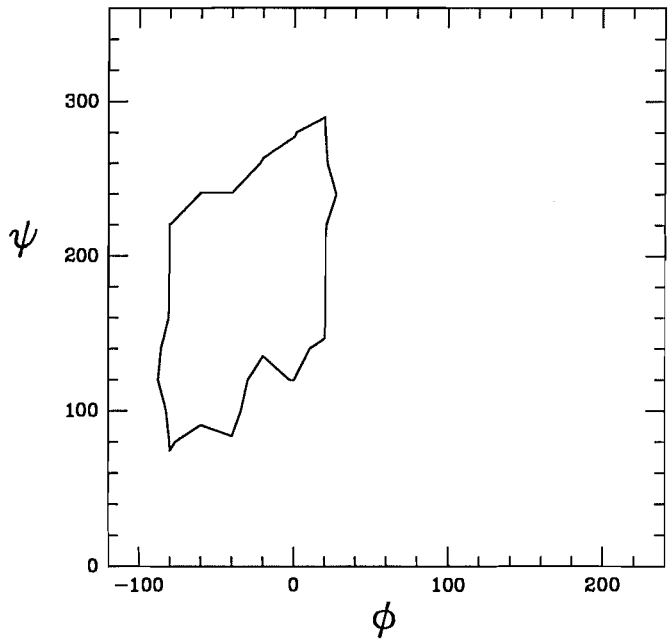

FIG. 6. The potential energy contour map for the α-glycopolymer (**1**). The 10 kcal/mol level with respect to the global minimum is shown.

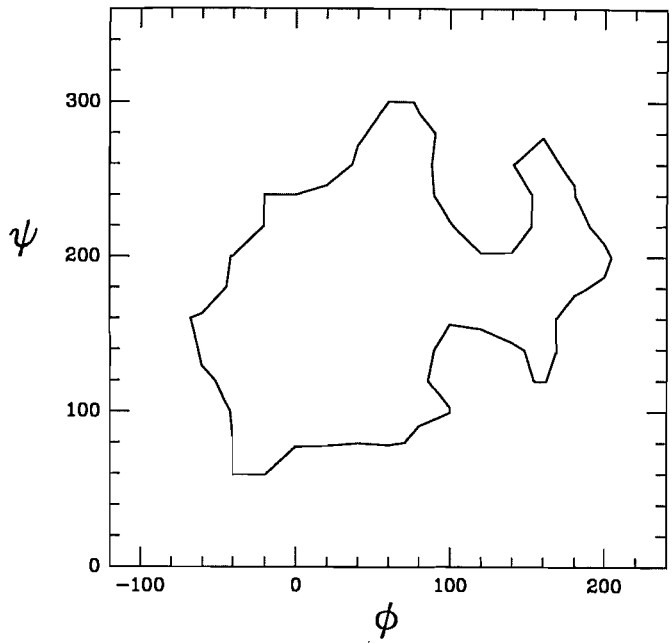

FIG. 7. The potential energy map for the β-glycopolymer (**2**). The 10 kcal/mol level with respect to the global minimum is shown.

molecules suggest anisotropic motion that supports a random-coil arrangement for this macromolecule in solution. These motions are characterized by a correlation time of the order of 1.15 ns, which appears to probe the viscosity of the surroundings as shown by similarity of the temperature dependences of the viscosities and the overall motion.

Internal motions of the *N*-acetyl methyl and sugar hydroxymethyl groups are evident in the relaxation data, and their associated activation energies have been obtained. The spin-lattice relaxation and nOe data for the sugar ring support an overall tumbling correlation time of 1.15 ns, but the spin–spin relaxation data suggest that a slower motion, of the order of 20 ns, is affecting the relaxation. This may characterize the rate of wobbling of the sugar and supporting side chain relative to the backbone.

The *small* change in the relaxation rates for the sugar ring *suggests* that the motions of the α anomer (**1**) are slightly more restricted than those of the β anomer (**2**). This observation is supported by the results of molecular mechanics calculations, which indicate that the β anomer has greater conformational flexibility than the α anomer.

The data obtained for the α- and β-glycopolymers, and the derived information regarding the motions, suggest that the better binding properties of the α-glycopolymer (**1**), in spite of lower overall mobility and perhaps lower accessibility of the sugar moiety than the β-glycopolymer (**2**), might be associated with other geometrical constraints.

Acknowledgements

The authors would like to thank Barbara Blackwell of Agriculture Canada and Jacques Bornais and Michael Guiver of the National Research Council of Canada (Ottawa) for access to their NMR facilities as well as invaluable technical assistance. F. Tropper is grateful to the Natural Sciences and Engineering Research Council of Canada for a postgraduate scholarship.

1. R. Roy, F.D. Tropper, and A. Romanowska. Bioconjugate Chem. **3**, 256 (1992).
2. (*a*) V. Horejši, P. Smolek, and J. Kocourek. Biochem. Biophys. Acta, **568**, 293 (1978); (*b*) R. Roy and F.D. Tropper. J. Chem. Soc. Chem. Commun. 1058 (1988); (*c*) Glycoconjugate J. **5**, 203 (1988); (*d*) A.Y. Chernyak, A.B. Levinsky, and N.K. Kochetkov. Bioorg. Khim. **14**, 1047 (1988); (*e*) A.Y. Chernyak, G.V.M. Sharma, L.O. Kononov, P.R. Krishna, A.V. Rao, and N.K. Kochetkov. Glycoconjugate J. **8**, 82 (1991); (*f*) P. Kosma, J. Gass, G. Schulz, R. Christian, and F.M. Unger. Carbohydr. Res. **167**, 39 (1987); (*g*) S.-I. Nishimura, K. Matsuoka, T. Furuike, S. Ishii, K. Kurita, and K.M. Nishimura. Macromolecules, **24**, 4236 (1991); (*h*) S.A. Cartlidge, R. Duncan, J.B. Lloyd, P. Kopečková-Rejmanová, and J. Kopeček. J. Controlled Release, **4**, 265 (1987); (*i*) K. Kobayashi, H. Sumimoto, A. Kobayashi, and T. Akaike. J. Macromol. Sci. Chem. **A25**, 655 (1988); (*j*) E. Kallin, H. Lönn, T. Norberg, and M. Elofsson. J. Carbohydr. Chem. **8**, 597 (1989).
3. (*a*) N.K. Kochetkov. Pure Appl. Chem. **56**, 923 (1984); (*b*) A.Y. Chernyak, A. Weintraub, T. Norberg, and E. Kallin. Glycoconjugate J. **7**, 111 (1990); (*c*) A.Y. Chernyak, L.O. Kononov, and N.K. Kochetkov. Carbohydr. Res. **216**, 381 (1991); (*d*) A. Rozalski, L. Brade, H.-M. Kuhn, H. Brade, P. Kosma, B.J. Appelmelk, S. Kusumoto, and H. Paulsen. Carbohydr. Res. **193**, 257 (1989).
4. (*a*) R. Roy, C.A. Laferrière, A. Gamian, and H.J. Jennings. J. Carbohydr. Chem. **6**, 161 (1987); (*b*) R. Roy and C.A. Laferrière. Carbohydr. Res. **177**, C1 (1988); (*c*) M.N. Matrosovich, L.V. Mochalova, V.P. Marinina, N.E. Byramova, and N.V. Bovin. FEBS Lett. **272**, 209 (1990); (*d*) A. Gamian, M. Chomik, C.A. Laferrière, and R. Roy. Can. J. Microbiol. **37**, 233 (1991); (*e*) A. Spaltenstein and G.M. Whitesides. J. Am. Chem. Soc. **113**, 686 (1991); (*f*) N.E. Byramova, L.V. Mochalova, I.M. Belyanchikov, M.N. Matrosovich, and N.V. Bovin. J. Carbohydr. Chem. **10**, 691 (1991).
5. R. Roy, F.D. Tropper, A. Romanoswka, M. Letellier, L. Cousineau, S.J. Meunier, and J. Boratynski. Glycoconjugate J. **8**, 75 (1991).

Can. J. Chem. Downloaded from www.nrcresearchpress.com by 203.198.23.82 on 09/08/12
For personal use only.

6. J.J. Goldstein and R.D. Poretz. *In* The lectins. Properties, functions and applications in biology and medicine. *Edited by* I.E. Liener, N. Sharon, and I.J. Goldstein. Academic Press, Fla. 1986. pp. 103–115.
7. R.T. Lee and Y.C. Lee. Carbohydr. Res. **37**, 193 (1974).
8. D. Canet, G.C. Levy, and I.R. Peat. J. Magn. Reson. **18**, 199 (1975).
9. P.J. Flory. *In* Principles of polymer chemistry. Cornell University Press, Ithaca, N.Y. 1953. pp. 308–314.
10. P. Molyneux. *In* Water soluble synthetic polymers: properties and behaviour. Vol. 1. CRC Press, Boca Raton, Fla. 1985. p. 90.
11. G.A. Jeffrey and S. Takagi. Acta Crystallogr. Sect. B: Struct. Crystallogr. Cryst. Chem. **B33**, 738 (1977).
12. G.M. Brown and H.A. Levy. Acta Crystallogr. Sect. B: Struct. Crystallogr. Cryst. Chem. **B35**, 656 (1979).
13. I. Tvaroska and S. Perez. Carbohydr. Res. **149**, 389 (1986).
14. H. Walderhaug, O. Soderman, and P. Stilbs. J. Phys. Chem. **88**, 1655 (1984).
15. R.M. Fuoss and J.C. Kirkwood. J. Am. Chem. Soc. **63**, 385 (1941); K.S. Cole and R.H. Cole. J. Chem. Phys. **9**, 341 (1941); R.H. Cole and D.W. Davidson. J. Chem. Phys. **18**, 1417 (1950).
16. (*a*) G. Lipari and A. Szabo. J. Am. Chem. Soc. **104**, 4546 (1982); (*b*) J. Am. Chem. Soc. **104**, 4559 (1982).
17. H. Wennerstrom, B. Lindman, O. Soderman, T. Drakenberg, and J.B. Rosenholm. J. Am. Chem. Soc. **101**, 6860 (1979).
18. G.D. Henry, J.H. Weiner, and B.D. Sykes. Biochemistry, **25**, 590 (1986).
19. L.T. Hughes, J.S. Cohen, A. Szabo, C. Niu, and S. Matsuura. Biochemistry, **23**, 4390 (1984).
20. P.G. Schmidt, H. Sierzputowska-Gracz, and P.F. Agris. Biochemistry, **26**, 8529 (1987).
21. J.L. Dimiroli, H. Lam-Tanh, F. Toma, and S. Fermandjian. Biochemistry, **23**, 3173 (1984).
22. D.C. McCain and J.L. Markley. J. Am. Chem. Soc. **108**, 4259 (1986).
23. D.C. McCain and J.L. Markley. J. Magn. Reson. **73**, 244 (1987).
24. H. Kovacs, S. Bagley, and J. Kovalewski. J. Magn. Reson. **85**, 530 (1989).
25. R. Roy, F.D. Tropper, and A.J. Williams. Magn. Reson. Chem. **29**, 852 (1991).
26. M. Monduzzi, A. Ceglie, B. Lindman, and O. Soderman. J. Colloid Interface Sci. **136**, 113 (1989).
27. Z. Gao, R.E. Wasylishen, and J.C.T. Kwak. J. Phys. Chem. **94**, 773 (1990).
28. G.M. Brown and H.A. Levy. Acta Crystallogr. Sect. B: Struct. Crystallogr. Cryst. Chem. **B29**, 790 (1973).
29. E.R. Henry and A. Szabo. J. Chem. Phys. **82**, 4753 (1985).
30. E.A. Bekturov and Z.K. Bakauora. *In* Synthetic water soluble polymers in solution. Hüthig & Wepf Verlag, Basel, Heidelberg, New York. 1986. pp. 127–135.
31. A. Gierer and K. Wirtz. Z. Naturforsch. A: Astrophys. Phys. Phys. Chem. **8**, 532 (1953).
32. K.J. Laidler and J.H. Meiser. *In* Physical chemistry. Benjamin Cummings, Menlo Park, Calif. 1982. pp. 867–871.
33. L.M. Bull, D.G. Gillies, S.J. Matthews, L.H. Sutcliffe, and A.J. Williams. Magn. Reson. Chem. **29**, 273 (1991).

Can. J. Chem. Downloaded from www.nrcresearchpress.com by 203.198.23.82 on 09/08/12
For personal use only.

Styrylbenzodiazinones 1. Synthèse, structure et propriétés photophysiques

LOUIS CAZAUX,[1] MOURAD FAHER, CLAUDE PICARD et PIERRE TISNÈS

Synthèse et physicochimie organique, Unité de recherche associée au Centre national de la recherche scientifique, n° 471, Université Paul Sabatier, 118 route de Narbonne, 31062 Toulouse Cédex, France

Reçu le 25 février 1993

LOUIS CAZAUX, MOURAD FAHER, CLAUDE PICARD et PIERRE TISNÈS. Can. J. Chem. **71**, 2007 (1993).

Plusieurs dérivés 3-styryliques de la 1,4-benzodiazine-2-one et de la 1-méthyl-1,4-benzodiazine-2-one ont été préparés. Une étude structurale de ces composés a été réalisée par RMN ^1H et ^{13}C ainsi que par modélisation moléculaire. L'isomérie rotationnelle autour de la liaison reliant les groupes imine et vinyle de ces *E* styrylbenzodiazinones est discutée; le rotamère s-*cis* est le rotamère prédominant. Enfin, les propriétés photophysiques de ces colorants fluorescents sont décrites.

LOUIS CAZAUX, MOURAD FAHER, CLAUDE PICARD, and PIERRE TISNÈS. Can. J. Chem. **71**, 2007 (1993).

Several 3-styryl derivatives of 1,4-benzodiazine-2-one and of 1-methyl-1,4-benzodiazine-2-one were prepared. A structural study of these compounds by ^1H and ^{13}C NMR and by molecular modelling was carried out. The rotational isomerism around the bond connecting the imine and vinyl groups in these *E* styrylbenzodiazinones is discussed. The s-*cis* rotamer is shown to be the predominant isomer. The photophysical properties of these fluorescent dyes are reported.

Can. J. Chem. Downloaded from www.nrcresearchpress.com by 203.198.23.82 on 09/08/12
For personal use only.

Les colorants fluorescents couvrent un vaste champ d'applications, soit en tant que traceurs, soit dans le domaine de l'électronique (colorants laser, concentrateurs solaires, capteurs de fibres optiques . . .) ou bien dans les domaines de l'immunologie, de la biochimie, de la biologie cellulaire et de la neurochimie. Bien évidemment ce sont les propriétés spectrales développées par ces molécules organiques qui régissent leur domaine d'utilisation; il est donc primordial de pouvoir disposer de plusieurs classes de colorants fluorescents. Nous nous sommes ainsi intéressés aux styrylbenzodiazinones qui sont des analogues structuraux des styrylbenzoxazinones dont les propriétés de fluorescence ont été montrées récemment (1). Ces styrylbenzoxazinones font partie des rares composés qui émettent au-delà de 520 nm avec un effet de Stokes important et un rendement quantique élevé, autant de caractéristiques essentielles pour une bonne sonde biologique. Toutefois leur nature lactone peut les rendre vulnérables aux estérases de certains milieux biologiques. Aussi, la substitution d'un cycle lactone par un cycle lactame dans les styrylbenzodiazinones devrait entraîner une plus grande résistance de ces molécules aux estérases et fournir une possibilité supplémentaire de substitution sur l'azote lactamique, par exemple pour en modifier la lipophilie.

Les quelques styrylbenzodiazinones connues (2, 3) n'ayant pas fait l'objet d'étude de leurs propriétés physicochimiques, nous nous proposons dans ce mémoire d'en synthétiser deux séries et d'analyser leurs propriétés structurales et photophysiques. Dans un autre mémoire (4) nous nous sommes intéressés plus particulièrement à deux chromo et fluoroionophores dérivés de ces styrylbenzodiazinones et comportant un motif éther couronne, le mono aza-15-c-5.

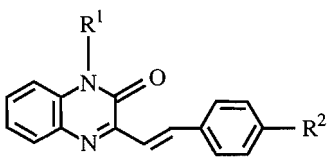

$R^1 = H$	$R^2 = H$		**1**
		CHO	**2**
		$C(OCH_3)_2$	**3**
		$N(CH_3)_2$	**4**
$R^1 = CH_3$	$R^2 = CH_3$		**5**
		CF_3	**6**
		CHO	**7**
		$N(CH_3)_2$	**8**

[1]Auteur à qui adresser toute correspondence.

Les propriétés photophysiques des dérivés styryliques dépendant fortement de la polarité des substituants aux extrémités du système, nous avons synthétisé les composés **1–8** répartis en deux séries.

La synthèse et l'étude structurale de ces huit styrylbenzodiazinones ont nécessité la préparation des benzodiazinones suivantes :

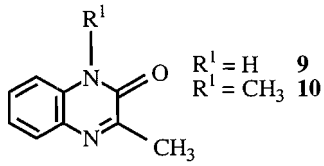

$R^1 = H$ **9**
$R^1 = CH_3$ **10**

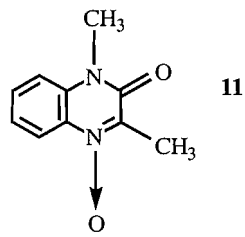

11

Résultats

Synthèse

Les benzodiazinones précurseurs **9** et **10** ont été obtenues avec de bons rendements par chauffage à reflux de l'orthophénylènediamine en présence de pyruvate d'éthyle dans l'éthanol (**9**) suivie d'une méthylation par le paratoluène sulfonate de méthyle dans le diméthylformamide en présence de carbonate de potassium (**10**). Les styrylbenzodiazinones s'obtiennent par condensation des benzodiazinones précurseurs avec des aldéhydes aromatiques selon la méthode de Badr *et al.* (3) utilisant comme base la pipéridine en présence ou non de pyridine.

À côté de cette méthode, il nous a paru intéressant d'en étudier deux autres : la méthode à l'anhydride acétique utisée pour préparer les styrylbenzoxazinones à partir des benzoxazinones (1*a*, 1*b*) et la méthode au diisopropylamidure de lithium (DAL).

Méthode à la pipéridine

Elle donne en général de bons rendements mais doit être utilisée de préférence avec des composés de point de fusion peu élevé ($F < 120°C$); en effet l'emploi de pyridine comme solvant avec les composés de point de fusion élevé diminue sensiblement le rendement. Dans le premier cas un chauffage de 15–20 min suffit alors que dans le second le temps de réaction doit être porté à 6–8 h.

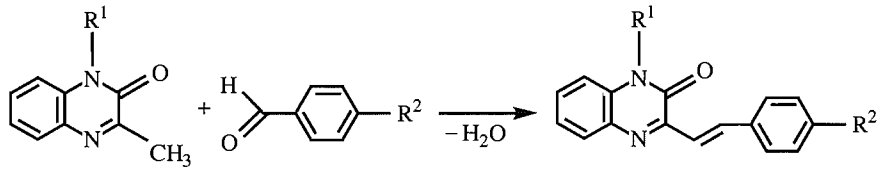

TABLEAU 1. Caractéristiques RMN ^{1}H des styrylbenzodiazinones **1–8** dans $CDCl_3$ (δ (ppm), *J* (Hz))

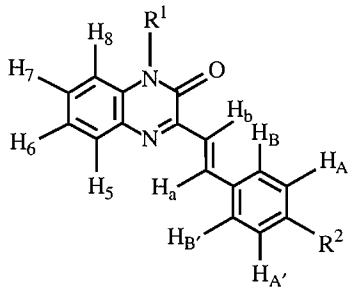

Composé	δ_a	δ_b	J_{ab}	$\delta_{A,A'}$	$\delta_{B,B'}$	$J_{AB,A'B'}$
1[a,b]	8,58	8,13	16,3	—	—	—
2[a,b]	8,13	7,64	16,2	7,43	7,79	7,4
3[a,c]	8,17	7,43	16,3	7,38	7,82	9,2
4[d]	8,15	7,58	16,0	6,73	7,62	9,0
5[d]	8,06	7,66	16,0	7,16	7,54	8,0
6[a]	8,10	7,79	16,2	7,58	7,81	8,5
7[a]	8,20	7,89	16,2	7,83	7,90	7,9
8[d]	8,07	7,56	16,3	6,69	7,58	9,0

[a]200 MHz.
[b]DMSO-d_6.
[c]$CDCl_3$ + CD_3OD.
[d]80 MHz.

TABLEAU 2. Analyse RMN ^{1}H de la partie benzodiazinone des composés **6–10** à 200 MHz dans $CDCl_3$ (δ (ppm), *J* (Hz))

Composé	δ_5	δ_6	δ_7	δ_8	$J_{5,6}$	$J_{5,7}$	$J_{6,7}$	$J_{6,8}$	$J_{7,8}$
6	7,87	7,37	7,54	7,30	8,0	1,6	7,3	1,15	8,4
7	7,93	7,39	7,57	7,34	7,9	1,55	7,3	1,2	8,3
8	7,85	7,30	7,47	7,35	7,8	1,5	7,6	1,5	8,2
9	7,82	7,34	7,50	7,30	8,0	1,5	7,5	1,5	8,0
10	7,78	7,31	7,51	7,27	7,8	1,55	7,8	1,55	8,3

Méthode à l'anhydride acétique

L'aldéhyde en léger excès (10%) est mélangé à la benzodiazinone et à l'anhydride acétique et l'ensemble est porté au reflux de l'anhydride (140°C) pendant plusieurs heures. En série benzoxazinone (1*b*) un aldéhyde comportant un substituant *para* électrodonneur donne un faible rendement, tandis qu'avec un substituant électroattracteur les rendements peuvent atteindre 70–80%, ce qui semble assez évident à première vue.

Méthode au DAL

Elle est basée sur la formation de carbanion de type allylique sur le méthyle proche de la fonction imine. Cette méthode a été utilisée avec succès par Meyers dans le cas des méthyl oxazolines pour l'obtention des 2-alcényl oxazolines (5). La formation du carbanion et la condensation avec l'aldéhyde s'opèrent à −78°C dans le THF.

Une comparaison des trois méthodes de synthèse des styrylbenzodiazinones a d'abord été réalisée sur le composé **8**. On note des rendements compris entre 20 (Ac_2O) et 45% (pipéridine). La méthode au DAL (41%) conduit à un rendement proche de celle à la pipéridine; l'utilisation de *N*,*N*,*N*′,*N*′-tétraméthyléthylènediamine (TMEDA) pour dissocier la paire d'ions par chélation du lithium n'a pas amélioré le rendement.[2]

On constate, de plus, que la synthèse des styrylbenzodiazinones par la voie de l'anhydride acétique dépend moins fortement du caractère électroattracteur ou électrodonneur du substituant R^2 que celle des styrylbenzoxazinones. En effet, les composés **2**, **4**, **5** et **8** sont obtenus par cette méthode avec des rendements respectifs de 39, 12, 3 et 20%. La méthode au DAL semble par contre pratiquement indépendante de ce facteur puisque les composés **5**, **6** et **8** à substituants Me, CF_3 et NMe_2 présentent le même rendement voisin de 40%; tout comme celle à la pipéridine : **7** (48%) et **8** (45%)

En résumé, la méthode à la pipéridine, quoique nous ayant donné des rendements inférieurs à ceux annoncés par Badr et al. (3), se révèle très intéressante pour les styrylbenzodiazinones issues de benzodiazinones à faible point de fusion comme **10**; celle au DAL peut lui être dans chaque cas substituée avec succès, la méthode à l'anhydride acétique étant réservée aux composés à substituants électrodonneurs et dont la benzodiazinone de départ, peu soluble dans le THF, a un point de fusion élevé. Quoi qu'il en soit les rendements en produits isolés ne dépassent pas 50%.

Analyse structurale

La nature styrylique des styrylbenzodiazinones pose deux problèmes structuraux: (*i*) configuration *Z* ou *E* des substituants de la liaison styrylique, (*ii*) conformation s-*cis* ou s-*trans* de cette liaison par rapport à la fonction imine de la partie benzodiazinone. Si par la seule RMN ^{1}H on peut facilement résoudre le premier problème (configuration *E* de cette liaison), le deuxième (isomérie rotationnelle) sera abordé conjointement par RMN, mécanique moléculaire et spectrofluorimétrie (durée de vie des états excités). Il est à noter que le problème d'isomérie s-*cis*, s-*trans* dans les systèmes styryliques a fait récemment l'objet d'une mise au point (7).

RMN ^{1}H

Les caractéristiques RMN ^{1}H des benzodiazinones et styrylbenzodiazinones étudiées sont reportées dans les tableaux 1 et 2 dans $CDCl_3$ sauf exceptions signalées.

La préparation de la nitrone **11**, forme *N*-oxyde du composé **10**, et l'examen comparé des spectres RMN ^{1}H de ces deux composés nous ont permis d'assigner de manière univoque les signaux RMN du motif benzodiazinone. Le passage de **10** à **11** se traduit par le déplacement à champ faible

[2]L'utilisation du THF comme solvant pourrait expliquer ce résultat (6).

Can. J. Chem. Downloaded from www.nrcresearchpress.com by 203.198.23.82 on 09/08/12
For personal use only.

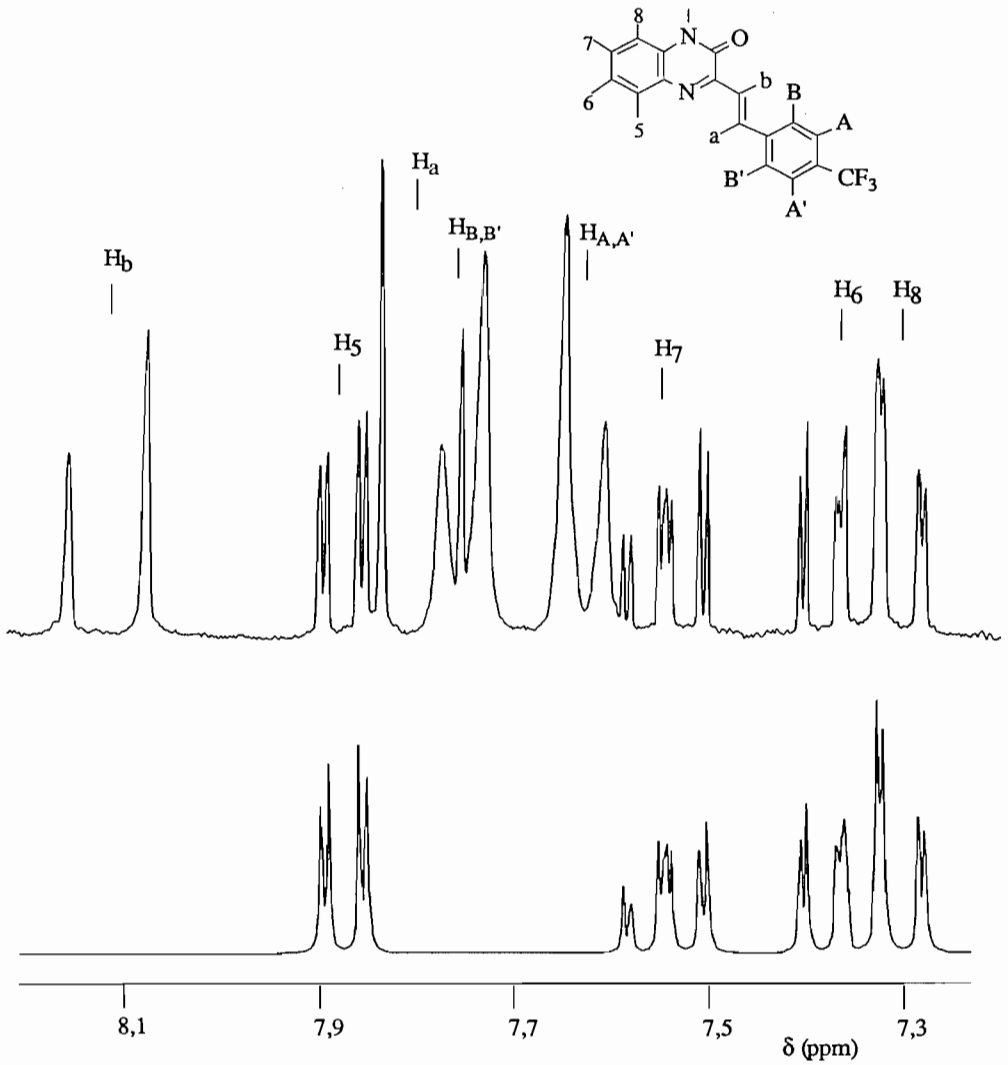

FIG 1. Spectres expérimental et simulé pour la partie benzodiazinone du composé **6** à 200 MHz dans $CDCl_3$.

($\Delta\delta$ = 0,71 ppm) du signal d'un des protons aromatiques, signal qui a été attribué au proton H-5. En effet, dans **11**, le proton H-5, en *péri* de la fonction *N*-oxyde est le plus déblindé (8,49 ppm) et présente deux constantes de couplage de 8 et 2 Hz avec les protons en *ortho* et *méta*. Il est à noter qu'un déblindage du même ordre de grandeur ($\Delta\delta$ = 0,4–0,6 ppm) pour ce même type de proton a été observé dans la série des quinoxalines et de leurs formes *N*-oxydes (8). L'analyse des spectres ^1H à 200 MHz de **9** et **10** et leurs simulations avec le programme LAOCOON 3 nous a alors permis de déduire les paramètres rassemblés dans le tableau 2.

L'analyse détaillée des spectres de **6**, **7** et **8** à 200 MHz permettra une généralisation aux autres styrylbenzodiazinones des deux séries étudiées. À titre d'exemple le spectre du composé **6** (Fig. 1) montre au premier abord un système AB attribué aux protons H_a et H_b de la liaison styrylique avec une constante de couplage de 16 Hz qui indique une configuration *E*. Le système AA′BB′ de la partie trifluorométhylbenzène donne deux doublets avec une constante J_{AB} = 8,5 Hz. La largeur à mi-hauteur du signal des protons H_B et $H_{B'}$ (W = 3,0 Hz) est supérieure à celle du signal de H_A et $H_{A'}$ (W = 2,0 Hz) du fait du couplage de H_B et $H_{B'}$ avec le proton éthylénique H_a, ce dernier étant lui-même élargi (W = 1,5 Hz) par rapport à H_b (W = 1,0 Hz). On en déduit les déplacements suivants pour le système AA′BB′ : $\delta_{A,A'}$ = 7,58 ppm et $\delta_{B,B'}$ = 7,81 ppm. Les protons aromatiques de la partie benzodiazinone présentent des déplacements chimiques et des constantes de couplage très proches de ceux du précurseur **10**.

RMN ^{13}C

Les attributions sont effectuées sur la base des valeurs calculées (9) à partir des tables d'incréments[3] et des spectres corrélés ^1H-^{13}C pour les composés **7**, **9** et **10**. D'autre part (*i*) les carbones c et d (notation des schémas du tableau 3) présentent des signaux d'intensité double par rapport aux autres carbones tertiaires; (*ii*) les carbones b, e, h, i, j, o sont quaternaires et leur attribution a été établie à partir des spectres *J* modulé et des spectres enregistrés sans découplage des protons, les carbones o et j en position α d'un atome d'azote ne pouvant pas être distingués; (*iii*) les carbones quaternaires i et h des groupes carbonyle et imine ont été différenciés par enregistrement des spectres ^{13}C couplés ^1H à 62,9 MHz. Les carbones des groupes imine et carbonyle

[3]La partie des carbones f→p est simulée par le groupe vinyle.

Can. J. Chem. Downloaded from www.nrcresearchpress.com by 203.198.23.82 on 09/08/12
For personal use only.

TABLEAU 3. Caractéristiques RMN ^{13}C (δ (ppm)) des benzodiazinones **9–11** et styrylbenzodiazinones **1–8** dans $CDCl_3$ à 50,32 MHz

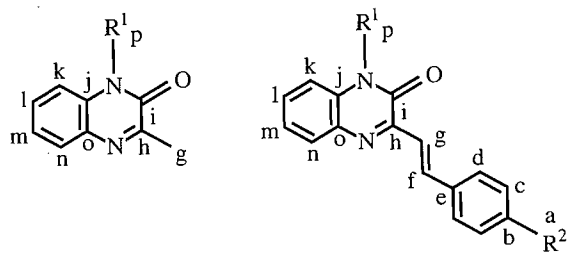

Composé	Carbone															
	a	b	c	d	e	f	g	h	i	j(o)	k	l	m	n	o(j)	p
1[a]	—	129,3	127,6	128,9	135,9	137,0	121,9	152,5	154,7	131,6	115,2	129,7	123,4	128,3	132,3	—
2[a]	192,4	136,0	129,7	128,1	141,6	135,4	125,1	152,5	154,6	131,7	115,2	130,2	123,5	128,4	132,2	—
3[b]	103,7	139,9	127,9	128,3	137,5	138,7	124,9	153,9	156,6	132,1	116,0	130,7	122,6	129,2	133,8	—
4	40,4	151,1	112,3	129,8	125,0	139,4	116,5	153,6	156,3	130,3	115,2	128,9	124,3	128,4	133,5	—
5	21,4	139,4	129,5	127,9	133,7	138,1	121,1	152,5	155,0	132,8	113,5	129,8	123,7	129,7	133,4	29,1
6	124,1	130,5	125,7	128,0	139,8	136,2	124,7	151,7	155,0	133,1	113,7	130,3	124,0	130,1	133,3	29,2
7	191,6	136,5	130,2	128,4	142,3	137,0	125,3	151,7	155,0	133,1	113,8	130,6	124,2	130,1	133,2	29,4
8	40,2	151,2	112,0	129,6	124,6	138,7	117,1	153,0	155,2	132,7	113,6	129,4	123,7	128,7	133,7	29,2
9[a]	—	—	—	—	—	—	20,5	159,2	154,9	131,7	115,2	129,2	123,0	127,8	131,9	—
10	—	—	—	—	—	—	21,5	158,2	155,0	132,5	113,5	129,4	123,4	129,3	133,1	28,9
11	—	—	—	—	—	—	12,3	140,0	156,6	132,4	114,2	131,7	123,6	120,6	130,6	29,3

[a]DMSO-d_6.
[b]$CDCl_3$ + CD_3OD.

présentent des constantes de couplage avec les protons du groupe méthyle en position 3 de 7,2 et 2,7 Hz respectivement dans le cas des benzodiazinones et de 5,6 et 2.8 Hz dans le cas des styrylbenzodiazinones (couplage avec le proton vinylique); (*iv*) les déplacements chimiques des carbones a, b et c du composé fluoré **6** ont été attribués en tenant compte des couplages avec le fluor (^1J = 272 Hz, ^2J = 37 Hz et ^3J = 3,8 Hz).

De l'analyse du tableau 2, il ressort que les carbones h du type imine subissent un blindage du fait de la conjugaison du système styrylique. Par contre, les autres carbones sp^2 du motif benzodiazinone conservent des déplacements chimiques pratiquement identiques à ceux correspondants des benzodiazinones **9** et **10** et ceci quelle que soit la nature du substituant R^2.

En vue d'une éventuelle mise en évidence d'une isomérie rotationnelle s-*cis*, s-*trans* autour de la liaison N , l'examen des déplacements chimiques des carbones f et g de la liaison styrylique conduit à remarquer que leur différence (Δδ en ppm) traduit bien l'effet des substituants R^2 sur la polarisation de la liaison styrylique dans les deux séries étudiées (9) soit : R^2 = CHO (10,3 et 11,7), CF_3 (11,5), $CH(OCH_3)_2$ (13,8), H (15,1), CH_3 (17,0) et $N(CH_3)_2$ (22,9 et 21,6). Compte tenu de ce large effet du substituant il paraît difficile de déceler l'influence de la structure s-*cis* ou s-*trans* sur le déplacement chimique en RMN ^{13}C.

Mécanique moléculaire

Le problème de l'isomérie rotationnelle autour de la liaison N de systèmes styryliques a déjà été étudié par mécanique moléculaire avec le programme MACROMODEL pour les 1-(2-naphtyl)2-pyrazin-2-yl éthylène (10). Dans la présente étude le même programme dans sa version V 3.5 X est utilisé avec les champs de force MM2* et MM3* (11). Pour vérifier la validité de ces deux champs de force deux tests ont été réalisés. Un premier test a été effectué sur les isomères s-*cis* et s-*trans* du butadiène et de l'acroléine. Des valeurs de 2,6 et 1,75 kcal/mol (exp : 2,5 (12)) ont été trouvées respectivement avec MM2* et MM3* pour le butadiène; 1,6 et 1,86 kcal/mol (exp : 1,7 (13)) pour l'acroléine. Ces résultats confirment ceux obtenus par Pettersson et coll. (14) indiquant que MM2* est la méthode de choix pour le calcul des énergies conformationnelles sur les hydrocarbures et les composés oxygénés et azotés. Un deuxième test a été réalisé sur les angles de torsion («tilts») autour de la liaison C—Ar des *Z* (φ_1) et *E*(φ_2) stilbènes. Avec MM2* et MM3* on obtient respectivement des angles φ_1 de 47° et 42° et φ_2 de 31° et 18° pour des valeurs expérimentales déterminées par diffraction électronique de 43° ± 10 (15) et 32°2 (16). Nos résultats peuvent ainsi compléter ceux discutés récemment par Hohlneicher *et al.* (17). Avec les deux champs de force nous trouvons que la forme *E* est la plus stable de 2,6 (MM2*) ou 2,0 (MM3*) kcal/mol.

Compte tenu de ces résultats encourageants nous avons abordé l'analyse de l'isomérie rotationnelle autour de la liaison N de la styrylbenzodiazinone **8**. Pour cela nous avons calculé l'énergie conformationnelle de la configuration *E* à chaque rotation d'un angle θ = 30° suivie d'une minimisation effectuée grâce à l'algorithme PRCG jusqu'à un RMS < 0,008 (Fig. 2).

Il apparaît clairement que c'est la forme s-*cis* qui est d'énergie minimale avec un minimum (MM3*) ou deux minima (MM2*) très rapprochés (0 ± 30°). La forme s-*trans* oscille également entre deux minima à 180 ± 26° (MM2*). La différence d'énergie entre les deux formes est de 0,7 kcal/mol (MM2*) ou 1,5 kcal/mol (MM3*). Les barrières à la rotation sont respectivement de 2,6 (MM2*) et 3,9 (MM3*) kcal/mol.

Can. J. Chem. Downloaded from www.nrcresearchpress.com by 203.198.23.82 on 09/08/12
For personal use only.

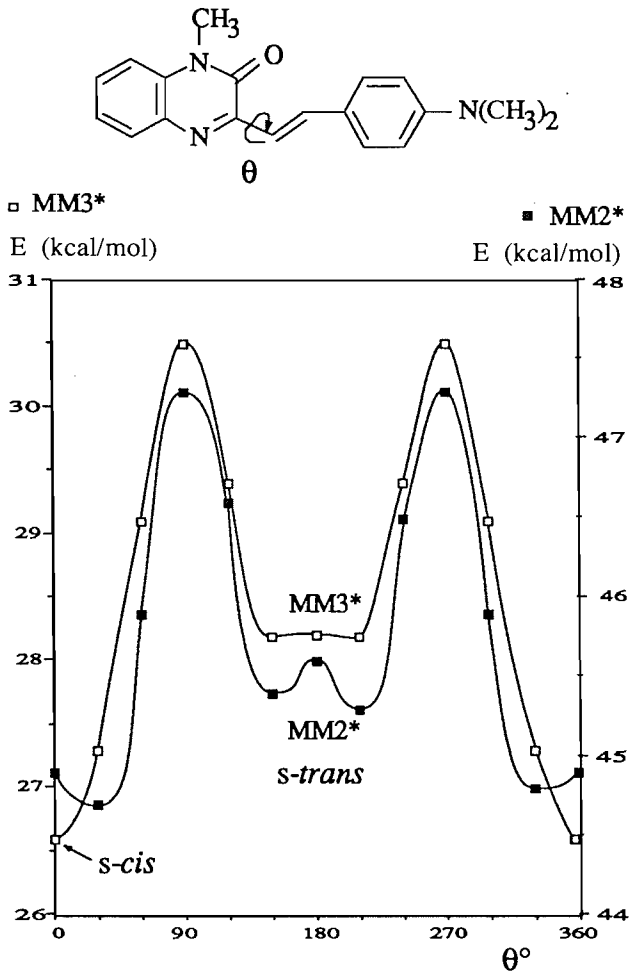

FIG 2. Variation de l'énergie conformationnelle de la styrylbenzodiazinone **8** (conformation *E*) en fonction de l'angle de torsion θ autour de la liaison N–Ph.

Propriétés photophysiques

Les propriétés photophysiques des deux séries de styrylbenzodiazinones étudiées sont rassemblées dans le tableau 4. Nous y avons également reporté celles des trois dérivés styryliques d'aminobenzoxazinones suivants (18) :

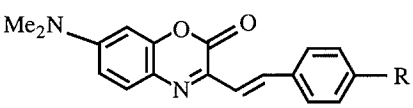

R = NMe_2	BOZ-NMe_2
R = H	BOZ-H
R = CHO	BOZ-CHO (DFSBO)

Les dérivés styryliques **1–8** présentent des absorptions à 382,5–456 nm ($CHCl_3$), 381,5–440,5 nm (CH_3CN) et 389–448 (EtOH). Les émissions de fluorescence correspondantes sont : 456–568 nm ($CHCl_3$), 454,5–604 nm (CH_3CN) et 453–631,5 nm (EtOH). Les deux composés **4** et **8** à groupement diméthylamino émettent comme prévu aux plus fortes longueurs d'onde dans le rouge; par contre, le composé **5** méthyl substitué émet aux plus faibles longueurs d'onde.

Cette classification se retrouve au niveau des déplacements de Stokes $\bar{\nu}_{abs} - \bar{\nu}_{em} = 10^7 (1/\lambda^{abs}_{max} - 1/\lambda^{em}_{max})$ (en cm^{-1}) qui peuvent être reliés linéairement à $\Delta f = (\epsilon - 1)/(2\epsilon + 1) - (n^2 - 1)/(2n^2 + 1)$ (19); la pente de la droite étant proportionnelle[4] au carré de la différence entre le moment dipolaire dans l'état excité et dans l'état fondamental $(\mu_e - \mu_f)$ soit $s = 2 (\mu_e - \mu_f)^2/hca^3$.

À partir des mesures (tableau 4) réalisées en solvant aprotique (chloroforme et acétonitrile) nous pouvons ainsi déterminer la pente de la droite relative à la corrélation : déplacement de Stokes en fonction[5] de Δf. On observe des pentes faibles ($(4 \pm 0,5) \times 10^3$) pour les composés **2**, **6** et **7** à substituant R^2 électroattracteur, presque nulle ($0,5 \times 10^3$) pour **5** ($R^2 = CH_3$) et très fortes ($11,5 \times 10^3$) pour **4** et **8** à substituant diméthylamino fortement électrodonneur.

En comparant ces valeurs aux pentes des styrylbenzoxazinones correspondantes (18) : $7,4 \times 10^3$ (BOZ-CHO), $4,4 \times 10^3$ (BOZ-H) et $7,3 \times 10^3$ (BOZ-NMe_2) on note une variabilité du déplacement de Stokes avec la polarité du solvant plus importante dans le cas des styrylbenzodiazinones et donc de plus grandes variations entre moments dipolaires de l'état excité et de l'état fondamental, soit 31,5 D ($R^2 = NMe_2$), 18,5 D (R = CHO ou CF_3) et 5,6 D (R^2 = Me). Le fort déplacement solvatochromique et donc l'important moment dipolaire à l'état excité observés pour **4** et **8**, supérieurs à ceux de BOZ-NMe_2, seraient dus vraisemblablement comme pour ce dernier (1*g*) à l'existence d'un état TICT (twisted intramolecular charge transfer state) fluorescent formé par torsion de la simple liaison N–Ph sous excitation. Le substituant diméthylamino fortement électrodonneur entraîne donc le plus grand déplacement de Stokes et le plus grand transfert de charge, mais il s'accompagne par contre d'un rendement quantique peu élevé ($\phi_f \sim 0.20$).

D'autre part, on observe que la méthylation sur l'atome d'azote lactamique n'entraîne qu'une faible variation sur les propriétés photophysiques des styrylbenzodiazinones (comparaison de **2** et **7**, **4** et **8**).

Cette comparaison avec les styrylbenzoxazinones peut se poursuivre sur la question de savoir si les styrylbenzodiazinones peuvent être considérées comme des benzodiazinones substituées ou comme des chromophores de type stilbène substitués. Pour les styrylbenzoxazinones la première proposition a été démontrée (18) notamment en considérant que le substituant en *para* sur le groupe phényle n'était pas impliqué dans le transfert de charge photoinduit; en effet le maximum d'émission de BOZ-H n'est pas intermédiaire de ceux de BOZ-NMe_2 et de BOZ-CHO dans les solvants étudiés (respectivement 542, 627 et 558 nm dans le chloroforme). Avec les styrylbenzodiazinones les valeurs correspondantes dans $CHCl_3$ sont respectivement 456, 568 et 462 nm. Elles conduisent donc à une conclusion analogue à celle des styrylbenzoxazinones.

Enfin, la durée de vie (τ) des états excités de la styrylbenzodiazinone **8** a été mesurée dans le chloroforme (tableau 5) et les constantes radiatives (k_r) et non radiatives (k_{nr}) ont été calculées selon les formules classiques $k_r = \phi/\tau$ et $k_{nr} = (1 - \phi)/\tau$. Le meilleur accord pour la fonction de décroissance de fluorescence est obtenu par l'utilisation de deux exponentielles. Les deux durées de vie différentes reflètent des constantes de vitesse radiatives différentes plutôt que des rendements quantiques différents (7).

[4] *h* est la constante de Planck, *c* la vitesse de la lumière et *a* le rayon en Å de la cavité sphérique selon Onsager.

[5] Δf = 0,148 ($CHCl_3$), 0,304 (CH_3CN).

Can. J. Chem. Downloaded from www.nrcresearchpress.com by 203.198.23.82 on 09/08/12
For personal use only.

Can. J. Chem. Downloaded from www.nrcresearchpress.com by 203.198.23.82 on 09/08/12
For personal use only.

TABLEAU 4. Caractéristiques photophysiques des styrylbenzodiazinones **1–8** et des styrylbenzoxazinones BOZ-H, BOZ-NMe_2 et BOZ-CHO (DFSBO)

Composé	Solvant	λ_{max}^{abs} (nm)	λ_{max}^{em} (nm)	déplacement de Stokes (cm^{-1})	Φ_f[a]
1	$CHCl_3$	382,5	456	4215	—
	CH_3CN	381,5	—	—	—
	EtOH	390	454	3615	—
2	$CHCl_3$	389	462	4060	0,04
	CH_3CN	389	477,5	4760	0,09
	EtOH	394,5	481,5	4580	0,08
3	EtOH	398	465	3620	0,06
4	$CHCl_3$	456	568	4325	0,18
	CH_3CN	440,5	603,5	6130	—
	EtOH	446	604	5865	—
5	$CHCl_3$	394	459	3595	0,04
	CH_3CN	389,5	454,5	3670	—
	EtOH	392	453	3435	—
6	$CHCl_3$	389 339	456,5	3800	0,06
	CH_3CN	387 329	462	4195	0,06
	EtOH	389 336,5	460	3970	0,07
7	$CHCl_3$	397,5	465	3650	—
	CH_3CN	393	470	4170	—
	EtOH	395	471	4085	—
8	$CHCl_3$	452,5	563,5	4355	0,20
	CH_3CN	440	604	6170	—
	EtOH	448	631,5	6485	—
BOZ-NMe_2[b]	$CHCl_3$	497	627	4170	0,52
	CH_3CN	489	650	5065	0,21
	EtOH	494	666	5230	0,016
BOZ-H[b]	$CHCl_3$	467	542	2965	0,81
	CH_3CN	463	567	3960	0,54
	EtOH	466	574	4035	0,55
BOZ-CHO[c] (DFSBO)	$CHCl_3$	488	558	2570	0,85
	EtOH	488	590	3540	0,58

[a]Les rendements quantiques des composés **2–6** ont été déterminés par rapport au sulfate de quinine, celui de **8** par rapport au DFSBO.
[b]Selon la référence 18.
[c]Selon la référence 1*c*.

Discussion

On a vu que, par leurs propriétés photophysiques, les styrylbenzodiazinones se rapprochent plus des benzodiazinones que des dérivés du stilbène. À l'instar des styrylbenzoxazinones, on peut donc considérer que le transfert électronique responsable de ces propriétés pourrait impliquer le carbonyle et l'atome d'azote hétérocyclique comme groupes électroattracteurs et comme groupe électrodonneur non plus le groupe diméthylamino de la partie benzo inexistant dans les styrylbenzodiazinones étudiées ici mais l'atome d'azote du groupe amide que l'on sait être fortement polarisé.

La nature styrylique des composés étudiés intervient cependant au niveau de la possibilité d'existence d'une isomérie rotationnelle autour de la liaison N .

En particulier, deux rotamères sont souvent observés dans les diaryléthylènes (7) et même dans les styrylbenzoxazinones (18) où la fonction de décroissance de fluorescence ne peut s'expliquer que par une décroissance à double exponentielle. L'équilibre suivant est alors proposé dans la série des BOZ.

L'apparition d'un second rotamère serait favorisée dans les solvants non polaires ou dans les solvants visqueux. Ce qui, d'après les auteurs, indiquerait qu'un des rotamères de forme s-*trans* serait stabilisé par liaison hydrogène comme déjà postulé pour le DFSBO (20).

TABLEAU 5. Durées de vie (τ) et constantes radiatives (k_r) et non radiatives (k_{nr}) du composé **8** dans le chloroforme

Formes %	τ (ns) ± 20%	ϕ_f	k_r (ns^{-1})	k_{nr} (ns^{-1})
70	0,5	0,20	0,28	1,72
30	4,2		0,014	0,22

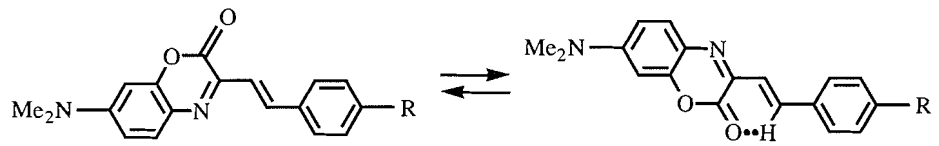

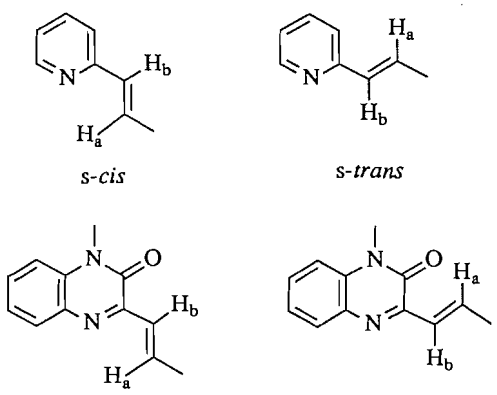

SCHÉMA 1

Toutefois, peu de démonstrations de l'isomérie rotationnelle dans les *E* 1,2 diaryléthylènes ont été faites par RMN (7). Il est cependant à noter que les molécules de type éthylène disubstitué par un noyau pyridine ont leur protons éthyléniques H_a et H_b (schéma 1) dans un environnement tel que leurs déplacements chimiques sont très sensibles à l'anisotropie de cycle et aux effets magnétiques et électriques de l'atome d'azote, particulièrement H_a dans la forme s-*cis*. Ainsi Coletta *et al.* (22) ont déterminé que dans $CDCl_3$ la forme s-*cis* est préférentielle avec δH_a = 7,62 ppm (styryl-2 pyridine) ou 7,69 ppm (1,2-di[pyridyl(2)]éthylène) alors qu'après calcul une valeur de 7,8 ppm serait attendue pour le même proton dans cette forme et une valeur de 7,2 ppm pour H_b dans la forme s-*trans*.

Le proton H_a dans les styrylbenzodiazinones (tableau 1) résonne dans le chloroforme deutérié en moyenne à 8,12 ppm; le proton H_b à 7,70 ppm. Ce résultat serait donc plutôt en faveur de la forme s-*cis*. Toutefois on ne peut exclure la forme s-*trans* car H_a dans s-*trans* pourrait être déblindé par participation à une éventuelle liaison H C=O···H_a (*vide infra*).

La préférence de la forme s-*cis* est trouvée dans la détermination des énergies conformationnelles des styrylbenzodiazinones par mécanique moléculaire. On a vu effectivement que la forme s-*cis* du composé **8** était plus stable que sa forme s-*trans* de 0,7 ou 1,5 kcal/mol selon le champ de force utilisé. La différence d'énergie entre les deux formes est donc suffisamment basse pour que l'existence de 10–30% de forme s-*trans* soit plausible. L'intervention dans cette forme d'une interaction C=O···H_a attractive comme suggéré par Mialocq et Meyer (20) pour les styrylbenzoxazinones ne peut pas être démontrée par mécanique moléculaire.[6] Une différence d'énergie ≤ 1,6 kcal/mol entre formes s-*cis* et s-*trans* et une barrière à la rotation autour de la liaison N=C inférieure à 4 kcal/mol laissent la possibilité d'avoir une ou deux formes indifféremment selon le substituant R^2 et le type de solvant; la forme s-*cis* demeurant majoritaire.

Pour la styrylbenzodiazinone **8** dans le chloroforme une détermination des durées de vies de fluorescence nous a montré que la fonction de décroissance de fluorescence s'interprétait par deux exponentielles montrant l'existence de deux populations en proportion 70 : 30.[7] D'après ce qui précède la configuration s-*cis* devrait être la forme majoritaire, les rotamères dans l'état excité singulet étant différents et ne s'interconvertissant pas (7).

Conclusion

Au cours de ce travail nous avons montré que les styrylbenzodiazinones synthétisées présentaient dans le chloroforme une configuration *E* au niveau de la liaison styrylique. De plus, l'isomérie s-*cis* s-*trans* autour de la liaison N=C, rendue possible par une barrière à la rotation peu élevée, est à l'avantage de la forme s-*cis* de moindre énergie à l'état gazeux ou dans un solvant aprotique peu polaire. Les propriétés photophysiques de ces composés sont proches de celles des styrylbenzoxazinones et diffèrent peu dans les deux séries étudiées. On note cependant pour les dérivés diméthylaminés des déplacements de Stokes supérieurs à celui de BOZ-NMe_2 mais dont l'origine est vraisemblablement la même. De même, dans les deux cas, la durée de vie des états excités est analogue, leur analyse par une décroissance de fluorescence de type double exponentielle supportant l'existence de l'isomérie s-*cis* s-*trans* précitée.

Même si les rendements quantiques de fluorescence des styrylbenzodiazinones étudiées sont relativement faibles, les déplacements de Stokes élevés, leur nature lactame et la possibilité de substitution sur l'azote lactamique confèrent à ces composés un intérêt au plan fondamental voire appliqué. En effet, la facilité de greffage d'éthers couronnes de type notamment aza-15-couronne-5 en prise directe sur le système conjugué peut entraîner des modifications spectrales exploitables, par exemple, pour le dosage sélectif de cations métalliques.

Partie expérimentale

Les points de fusion (*F*) ont été déterminés au banc Köfler. Les spectres infra-rouges ont été enregistrés à l'aide d'un spectrophotomètre Perkin–Elmer 883 (dans des pastilles de KBr) et les spectres RMN ^1H et ^{13}C sur les appareils Brüker AC 80, AC 200 ou AC 250 (avec le TMS comme référence interne, les déplacements chimiques étant exprimés en ppm). Pour une description détaillée des

[6]Le résultat de la figure 2 irait plutôt à l'encontre de la liaison H mais MM2* ne tient pas compte de manière très précise des énergies de liaison H et les inclut généralement dans la composante électrostatique de l'énergie totale (21). Cependant, vu le très faible caractère acide du proton éthylénique, si cette liaison existe, elle doit être très faible.

[7]En supposant que le principe de non équilibration des rotamères excités s'applique aux styrylbenzodiazinones comme aux *trans*-1,2-diaryléthylènes (7), la barrière d'interconversion dans l'état excité est alors remarquablement plus haute que celle de l'état fondamental. Dans ces conditions on peut assimiler abondance relative des espèces excitées et proportion des populations à l'état fondamental.

Can. J. Chem. Downloaded from www.nrcresearchpress.com by 203.198.23.82 on 09/08/12
For personal use only.

Can. J. Chem. Downloaded from www.nrcresearchpress.com by 203.198.23.82 on 09/08/12
For personal use only.

spectres RMN ^1H, il faut se reporter aux tableaux 1 et 2 et pour les spectres RMN ^{13}C au tableau 3. Les spectres de masse ont été effectués sur un appareil Nermag R 10-10C (mode d'ionisation : DCI/NH_3). Les analyses centésimales ont été réalisées au service commun de microanalyse élémentaire UPS-INP à Toulouse. Les spectres d'absorption ont été effectués sur un spectrophotomètre Perkin–Elmer Lambda 17 et les spectres d'émission sur un spectrofluorimètre Perkin–Elmer LS-3B ou Aminco SPF 500 C interfacé à un microcalculateur. Les rendements quantiques de fluorescence ont été mesurés en prenant comme standarts le sulfate de quinine (ϕ_f = 0,54 dans H_2SO_4 0,1 N), la coumarine **6** (ϕ_f = 0,78 dans l'éthanol (23)), le DFSBO (ϕ_f = 0,76 dans le chloroforme, ϕ_f = 0,60 dans l'éthanol (1*c*)). Les relevés des déclins de fluorescence sont effectués sur une chaîne de mesure Edinburg Instrument modèle 199. Les détails de conception de cet appareillage et les techniques de déconvolution qui conduisent aux durées de vies ont été déjà décrites (24). Les séparations par chromatographie liquide (CPL) sont réalisées sur colonne de silice Merck Kieselgel 60 (70–230 μm ATM). La pureté des produits a été vérifiée par chromatographie sur couche mince (CCM) sur plaque de gel de silice Merck 60 F 254 prête à l'emploi. Les calculs de mécanique quantique ont été effectués sur une station Silicon Graphics Iris 4D-30 à l'aide du programme MACROMODEL V 3.5 X.

*3-Styryl-1,4-benzodiazine-2-one : **1***

Une solution de 5,4 mmol (0,864 g) de composé **9** et 6,4 mmol (0,678 g) de benzaldéhyde fraîchement distillé dans 5 mL de pyridine est portée à reflux pendant 8 h en présence de cinq gouttes de pipéridine. Après refroidissement la pyridine est éliminée sous vide et le solide résiduel est purifié par CPL (éluant dichlorométhane/acétate d'éthyle 75/25). Une recristallisation dans le dioxane fournit 0,620 g de **1**. Rdt 46%, fines aiguilles jaunes, *F* = 254°C (litt. (3*a*) 252°C); IR : 3438 (NH), 1657 (C=O), 1626 (C=N), 1595 (C=C) cm^{-1}; UV (chloroforme) : λ_{max} = 382,5 nm (ϵ = 21 000 M^{-1} cm^{-1}); RMN ^1H (DMSO-d_6) : 7,70–8,63 (m, 11H, arom. et vinyl), 12,4 (s, 1H, NH); SM : *m/e* 249 $[M+H]^+$, 100%. Anal. calc. pour $C_{16}H_{12}N_2O$: C 77,40, H 4,87, N 11,28; trouvée : C 77,35, H 4,90, N 11,25.

*3-(4-Formylstyryl)-1,4-benzodiazine-2-one : **2***

On chauffe durant 5 h, au bain d'huile, à 140°C, 4 mmol (0,640 g) de composé **9** et 4,4 mmol (0,590 g) d'aldéhyde téréphtalique dans 2 mL d'anhydride acétique. Le milieu réactionnel est ensuite dilué avec de l'eau et évaporé à sec sous vide. L'opération est répétée plusieurs fois de façon à éliminer l'acide acétique formé et l'excès d'anhydride acétique. Le résidu ainsi obtenu est partagé entre l'eau et l'excès d'anhydride acétique. Le résidu solide de la phase organique est ensuite traité par un petit volume d'acétone. Après filtration et recristallisation dans l'éthanol on obtient 0,430 g de **2**. Rdt 39%, cristaux jaune clair, *F* = 247°C; IR : 3436 (NH), 1700 (C=O aldéhyde), 1660 (C=O amide), 1625 (C=N), 1598 (C=C) cm^{-1}; UV (chloroforme) : λ_{max} = 389 nm (ϵ = 20 200 M^{-1} cm^{-1}); RMN ^1H (DMSO-d_6) : 7,24-8,19 (m, 10H, arom, et vinyl), 10,04 (s, 1H, CHO), 12,50 (s, 1H, NH); SM : *m/e* 277 $[M+H]^+$, 100%. Anal. calc. pour $C_{17}H_{12}N_2O_2$: C 73,90, H 4,38, N 10,14; trouvée : C 73,75, H 4,32, N 10,07.

*3-(4-Diméthoxyméthylstyryl)-1,4-benzodiazine-2-one : **3***

À 276 mg (1 mmol) de composé **2** dissous dans 50 mL d'un mélange chloroforme/méthanol (50/50), on ajoute 7 μL de chlorure de thionyle (0,1 mmol). Aprés 1 nuit d'agitation à température ambiante et évaporation des solvants sous pression réduite on obtient 320 mg de **3**. Rdt 100%, huile jaune; IR (entre lames de KBr) : 3440 (NH), 1660 (C=O), 1625 (C=N) cm^{-1}; UV (éthanol) : λ_{max} = 398 nm (ϵ = 9500 M^{-1} cm^{-1}); RMN ^1H ($CDCl_3$/CD_3OD) : 3,35 (s, 6H, CH_3), 5,38 (s, 1H, CH), 7,25–8,18 (m, 10H, arom. et vinyl). Anal. calc. pour $C_{19}H_{18}N_2O_3$: C 70,79, H 5,63, N 8,69; trouvée : C 71,05, H 5,75, N 8,49.

*3-(4-Diméthylaminostyryl)-1,4-benzodiazine-2-one : **4***

Ce composé a été obtenu par condensation dans l'anhydride acétique entre le *p*-diméthylaminobenzaldéhyde et la benzodiazine-2-one **9** suivant le mode opératoire décrit pour le composé **2**. La recristallisation est effectuée dans le toluène. Rdt 12%, cristaux rouges, *F* = 257°C (litt. (3*a*) 256°C); IR : 3438 (NH), 1665 (C=O), 1625 (C=N), 1600 (C=C) cm^{-1}; UV (chloroforme) : λ_{max} = 456 nm (ϵ = 30 000 M^{-1} cm^{-1}); RMN ^1H ($CDCl_3$) : 3,03 (s, 6H, $N(CH_3)_2$), 6,50 (s, 1H, NH), 6,70–8,20 (m, 10H, arom. et vinyl). Anal. calc. pour $C_{18}H_{17}N_3O$: C 74,21, H 5,88, N 14,42; trouvée : C 74,20, H 5,80, N 14,49.

*1-Méthyl-3-(4-méthylstyryl)-1,4-benzodiazine-2-one : **5***

À une solution de 5,88 mmol de diisopropylamidure de lithium (préparée à partir de quantités équimolaires de *n*-butyllithium et de diisopropylamine, 0°C, THF) dans 20 mL de THF anhydre, refroidie à −78°C et sous atmosphère d'argon, on additionne goutte à goutte 1 g (5,75 mmol) de **10** dissous dans 3 mL de THF. Après 1 h d'agitation on obtient une solution noire à laquelle on ajoute 0,690 g (5,75 mmol) de 4-méthyl benzaldéhyde. Après 1 heure d'agitation à −78°C on traite le milieu réactionnel avec 2 mL de méthanol et on le laisse revenir à température ambiante. À la solution orangée on ajoute alors 20 mL d'eau saturée en chlorure d'ammonium. La phase organique est séparée, la phase aqueuse est extraite avec du chloroforme. Les phases organiques combinées sont lavées avec une solution à 10% de bisulfite de sodium, puis avec de l'eau saturée en chlorure de sodium et séchées ($MgSO_4$). Après évaporation des solvants, le résidu est traité par un petit volume d'acétone. Après filtration et recristallisation dans de l'éthanol on obtient 0,60 g de **5**. Rdt 38%, cristaux jaunes, *F* = 150°C (litt. (3*b*) *F* 149–150°C); IR : 1647 (C=O), 1625 (C=N), 1598 (C=C) cm^{-1}; UV (chloroforme) : λ_{max} = 394 nm (ϵ = 19 400 M^{-1} cm^{-1}); RMN ^1H ($CDCl_3$) : 2,35 (s, 3H, Ar-CH_3), 3,66 (s, 3H, N-CH_3), 7,11–8,22 (m, 10H, arom. et vinyl). Anal. calc. pour $C_{18}H_{16}N_2O$: C 78,24, H 5,84, N 10,14; trouvée : C 78,22, H 5,80, N 10,05.

5 a également été préparé par la méthode à l'anhydride acétique (voir préparation de **2**) avec un rendement de 3%.

*1-Méthyl-3-(4-trifluorométhylstyryl)-1,4-benzodiazine-2-one : **6***

6 a été préparé par condensation entre la benzodiazine-2-one **10** et le 4-trifluorométhyl benzaldéhyde en présence de DAL suivant le mode opératoire décrit pour le composé **5**. La recristallisation est effectuée dans le toluène. Rdt 39%, cristaux jaunes, *F* = 156°C; IR : 1656 (C=O), 1625 (C=N), 1603 (C=C) cm^{-1}; UV (chloroforme) : λ_{max} = 389 nm (ϵ = 20 600 M^{-1} cm^{-1}); RMN ^1H ($CDCl_3$) : 3,67 (s, 3H, N-CH_3), 7,28–8,18 (m, 10H, arom. et vinyl); RMN ^{19}F ($CDCl_3$, référence : CF_3COOH) : 12,86 ppm; SM : *m/e* 331 $[M+H]^+$, 100%. Anal. calc. pour $C_{18}H_{13}F_3N_2O$: C 65,45, H 3,97, N 8,48; trouvée : C 65,54, H 3,84, N 8,36.

*1-Méthyl-3-(4-formylstyryl)-1,4-benzodiazine-2-one : **7***

On a chauffé 500 mg (2,87 mmol) de benzodiazine-2-one **10** et 460 mg (3,44 mmol) d'aldéhyde téréphtalique pendant 20 min à 170°C en présence de 5 gouttes de pipéridine. On réalise une purification par CPL (éluant dichlorométhane/acétate d'éthyle 95/05). On obtient ainsi 400 mg de **7**. Rdt 48%, cristaux jaunes, *F* = 187°C; IR : 1689 (C=O aldéhyde), 1647 (C=O amide), 1628 (épaulement, C=N), 1600 (C=C) cm^{-1}; UV (chloroforme) : λ_{max} = 397,5 nm (ϵ = 28 100 M^{-1} cm^{-1}); RMN ^1H ($CDCl_3$) : 3,76 (s, 3H, N-CH_3), 7,30–8,24 (m, 10H, arom. et vinyl), 10,02 (1H, s, CHO); SM : *m/e* 291 $[M + H]^+$, 100%. Anal. calc. pour $C_{18}H_{14}N_2O_2$: C 74,47,H 4,86, N 9,65; trouvée : C 74,25,H 4,79, N 9,66.

*1-méthyl-3-(4-diméthylaminostyryl)-1,4-benzodiazine-2-one : **8***

8 a été préparé à partir de la benzodiazine-2-one **10** et du *p*-diméthylaminobenzaldéhyde par la méthode au DAL (cf. mode opératoire de **5**) avec un rendement de 41%, par la méthode à la pipéridine (cf. mode opératoire de **7**) avec un rendement de 45%, par la méthode à l'anhydride acétique (cf. modc opératoire de **2**) avec un rendement de 20%. **8** est cristallisé dans l'éthanol et purifié par recristallisation dans le benzène. Cristaux rouge vif, *F* = 198°C (litt. (3*b*) *F* 197–198°C); IR : 1651 (C=O), 1625 (C=N)

cm^{-1}; UV (chloroforme) λ_{max} = 452,5 nm (ϵ = 32 000 M^{-1} cm^{-1}); RMN ^1H ($CDCl_3$) : 2,99 (s, 6H, $N(CH_3)_2$), 3,68 (s, 3H, N-CH_3), 6,60-8,14 (m, 10H, arom. et vinyl.); SM : *m/e* 306 $[M + H]^+$, 100%. Anal. calc. pour $C_{19}H_{19}F_3N_3O$: C 74,73, H 6,27, N 13,76; trouvée : C 74,93, H 6,39, N 13,70.

*3-Méthyl-1,4-benzodiazine-2-one : **9***

Une solution d'orthophénylène diamine dans l'éthanol est chauffée au reflux en présence de pyruvate d'éthyle (1,05 équivalent) pendant 3 à 4 h. Après refroidissement de la solution, le précipité est filtré et recristallisé dans l'éthanol. Rdt 100%, aiguilles blanches, *F* = 242°C (litt. (25) *F* 245°C).

*1,3-Diméthyl-1,4-benzodiazine-2-one : **10***

À une suspension de 0,60 g (3,75 mmol) de **9** et de 0,83 g (6 mmol) de carbonate de potassium dans le DMF (7 mL) maintenue à 135°C, on ajoute goutte à goutte 1,40 g (7,50 mmol) de paratoluène sulfonate de méthyle dissous dans 5 mL de DMF. Après l'addition on laisse le mélange 20 min à 135°C avant retour à température ambiante. Le précipité est filtré, lavé au DMF et purifié par CPL (éluant dichlorométhane/acétate d'éthyle 50/50). On obtient ainsi 0,392 g de **10**. Rdt 60%, *F* = 85°C (litt. (26) *F* 85–86°C).

*1,3-Diméthyl-4-oxyde-1,4-benzodiazine-2-one : **11***

On a chauffé 1 g (5,75 mmol) de **10** dans 7 mL d'acide acétique et 2,4 mL de peroxyde d'hydrogène à 30% dans l'eau à 65°C pendant 4 h 30. Après refroidissement, la solution est diluée avec de l'eau et concentrée sous vide. Le résidu est neutralisé avec du bicarbonate de sodium et extrait au dichlorométhane. Une purification par CPL (éluant dichlorométhane/acétate d'éthyle 50/50) fournit 0,22 g de **11**. Rdt 20%, cristaux oranges, *F* = 201°C; IR : 1639 (C=O), 1630 (ép, C=N), 1590 (C=C), 1223 (N → O) cm^{-1}; RMN ^1H ($CDCl_3$) : 2,60 (s, 3H, CH_3), 3,73 (s, 3H, NCH_3), 7,36–7,43 (m, 2H, H_6 et H_8), 7,62–7,71 (m, 1H, H_7), 8,46–8,51 (dd, 1H, H_5). Anal. calc. pour $C_{10}H_{10}F_3N_2O_2$: C 63,15, H 5,30, N 14,73; trouvée : C 62,98, H 5,14, N 14,63.

Remerciements

Les auteurs remercient A. Lopez (UPR CNRS 8221, Toulouse) pour la mesure des durées de vie de fluorescence, ainsi que le Centre National de la Recherche Scientifique et la Direction de la Recherche et des Études Doctorales pour leur soutien financier.

1. (*a*)M.T. Le Bris. J. Heterocycl. Chem. **21**, 551 (1984), (*b*) J. Heterocycl. Chem. **22**, 1275 (1985); (*c*) M.T. Le Bris, J. Mugnier, J. Bourson et B. Valeur. Chem. Phys. Lett. **106**, 124 (1984); (*d*) F. Dupuy, C. Rulliere, M.T. Le Bris et B. Valeur. Opt. Commun. **51**, 36 (1984); (*e*) J. Mugnier, Y. Dordet, J. Pouget, M.T. Le Bris et B. Valeur. Sol. Energy Mater. **15**, 65 (1987); (*f*) M. Monsigny, P. Midoux, M.T. Le Bris, A.C. Roche et B. Valeur. Biol. Cell. **67**, 193 (1989); (*g*) S. Fery-Forgues, M.T. Le Bris, J.P. Guetté et B. Valeur. J. Phys. Chem. **92**, 6233 (1988).
2. A.H. Cook et C.A. Perry. J. Chem. Soc. 394 (1943).
3. (*a*) M.Z.A. Badr, G.M. El-Naggar, H.A.H. El-Sherief, A.E. Abdel-Rahman et M.F. Aly. Bull. Chem. Soc. Jpn. **56**, 326 (1983); (*b*) M.Z.A. Badr, G.M. El-Naggar, H.A.H. El-Sherief et S.A. Mahgoub. Bull. Chem. Soc. Jpn. **57**, 1653 (1984).
4. L. Cazaux, M. Faher, C. Picard et P. Tisnès. Can. J. Chem. **71**, 1236 (1993).
5. A.I. Meyers, R.K. Smith et C.E. Whitten. J. Org. Chem. **44**, 2250 (1979).
6. D.B. Collum. Acc. Chem. Res. **25**, 448 (1992).
7. U. Mazzucato et F. Momicchioli. Chem. Rev. **91**, 1679 (1991).
8. S.N. Bannore, J.L. Bose, A.A. Thakar et M.S. Wadia. Indian J. Chem. **13**, 609 (1975).
9. J.B. Stothers. *Dans* Carbon-13 NMR spectroscopy. Academic Press, New York et Londres. 1972. pp. 196–205.
10. S.C. Shim et M.S. Kim. J. Chem. Soc. Perkin Trans. 2, 1897 (1989).
11. (*a*) N.L. Allinger. J. Am. Chem. Soc. **99**, 8127 (1977); (*b*) N.L. Allinger, Y.H. Yuh et J.H. Lii. J. Am. Chem. Soc. **111**, 8551 (1989); (*c*) N.L. Allinger, F. Li, L. Yan et J.C. Tai. J. Comput. Chem. **11**, 868 (1990).
12. L.A. Carreira. J. Chem. Phys. **62**, 3851 (1975).
13. C.E. Blom et A. Bauder. Chem. Phys. Lett. **88**, 55 (1982).
14. K. Gundertofte, J. Palm, I. Pettersson et A. Stamvik. J. Comput. Chem. **12**, 200 (1991).
15. T. Kobayashi, K. Yokota et S. Nagakura. Bull. Chem. Soc. Jpn. **48**, 412 (1975).
16. M. Traetteberg, E.B. Frantsen, F.C. Mijlhoff et A. Hoekstra. J. Mol. Struct. **26**, 57 (1975).
17. G. Hohlneicher, M. Müller, M. Demmer, J. Lex, J.H. Penn, L.-X. Gan et P.D. Loesel. J. Am. Chem. Soc. **110**, 4483 (1988).
18. S. Fery-Forgues, M.T. Le Bris, J.C. Mialocq, J. Pouget, W. Rettig et B. Valeur. J. Phys. Chem. **96**, 701 (1992).
19. (*a*) E. Lippert. Z. Naturforsch. A: Astrophys. Phys. Phys. Chem. **10a**, 541 (1955); (*b*) Z. Electrochem. **61**, 962 (1957); (*c*) N. Mataga, Y. Kaifu et M. Koizumi. Bull. Chem. Soc. Jpn. **29**, 465 (1956).
20. J.C. Mialocq et M. Meyer. Laser Chem. **10**, 277 (1990).
21. N.L. Allinger, R.A. Kok et M.R. Imam. J. Comput. Chem. **9**, 591 (1988).
22. F. Coletta, A. Gambaro et L. Pasimeni. Gazz. Chim. Ital. **103**, 265 (1973).
23. G.A. Reynolds et K.H. Drexhage. Opt. Commun. **13**, 222 (1975).
24. E. Perochon, A. Lopez et J.F. Tocanne. Biochemistry, **31**, 7672 (1992).
25. D.C. Morrison. J. Am. Chem. Soc. **76**, 4483 (1954).
26. G.W.H. Cheeseman. J. Chem. Soc. 1804 (1955).

Can. J. Chem. Downloaded from www.nrcresearchpress.com by 203.198.23.82 on 09/08/12
For personal use only.

A mechanistic study of the carbocation route from tetrahydrodicyclopentadiene to the adamantane ring

ROGER P. KIRCHEN, TED S. SORENSEN,[1] AND STEVEN M. WHITWORTH
The Department of Chemistry, University of Calgary, Calgary, AB T2N 1N4, Canada

Received March 24, 1993

ROGER P. KIRCHEN, TED S. SORENSEN, and STEVEN M. WHITWORTH. Can. J. Chem. **71**, 2016 (1993).

The energy profile for the transformation of the *endo*-tetrahydrodicyclopentadienyl cation **A** into the 1-adamantyl cation **R** has been probed by means of six separate experiments employing superacid techniques. Of the approximately 14 cations between **A** and **R**, required as *intermediates* for the above transformation, it can be shown that only one of these is capable of direct observation. This cation, the tricyclo[5.2.1.$0^{3,8}$]dec-3-yl (homobrendyl) cation **J**, is characterized in detail in one of the six experiments. The rate of the rearrangement of **J** into the 1-adamantyl cation has been measured. Cation **J** also undergoes a degenerate rearrangement, the dynamics of which can be probed using NMR line-broadening and selective inversion–recovery experiments. The relationship between the *exo* and *endo* tetrahydrodicyclopentadienyl cations **D** and **A** has been studied. Only **A** is directly observable, even though in some experiments direct precursors of **D** were used as cation sources. Several experimental probes were made in an attempt to detect the presence of a small equilibrium concentration of **D**, without success, and a rationale is provided for the much greater stability of **A** vs. **D**. The remaining four experiments involved the addition of neutral precursors to superacid solutions, but the initially formed (expected) cations could not be observed, only cations **A**, **J**, or **R** being observed instead. These "partitioning"-type experiments prove whether the corresponding left-hand or right-hand transition-state barriers are the lower in energy. In the case of starting with transient cation intermediate **E**, only observable cation **J** is obtained, showing that the barrier between **B** and **E** is the high point on the overall carbocation reaction profile.

ROGER P. KIRCHEN, TED S. SORENSEN et STEVEN M. WHITWORTH. Can. J. Chem. **71**, 2016 (1993).

En se basant sur six expériences séparées faisant appel à des techniques de superacide, on a étudié le profil d'énergie de la transformation du cation *endo*-tétrahydrodicyclopentadiényle **A** en cation 1-adamantyle **R**. Des 14 cations requis comme intermédiaires pour la transformation de **A** en **R**, on peut montrer qu'un seul peut être observé directement. On a caractérisé en détail ce cation, **J**, le cation tricyclo[5.2.1.$0^{3,8}$]déc-3-yle (homobrendyle), au cours de l'une des six expériences. On a mesuré la vitesse de réarrangement du cation **J** en cation 1-adamantyle. Le cation **J** subit aussi un réarrangement dégénéré dont on a examiné la dynamique par des expériences d'élargissement des raies de RMN et par récupération d'inversion sélective. On a étudié la relation entre les cations *exo* et *endo* tétrahydrodicyclopentadiényles **D** et **A**. Seul le cation **A** peut être observé directement, même si dans quelques expériences on a utilisé des précurseurs directs de **D** comme sources. Dans le but de détecter la présence d'un faible quantité de **D** à équilibre, on a développé sans succès plusieurs sondes expérimentales; on présente une rationalisation de la stabilité beaucoup plus grande de **A** par rapport à **D**. Les quatre dernières expériences impliquent l'addition de précurseurs neutres à des solutions de superacides; lorsque les cations formés (attendus) initialement n'ont pu être observés, seuls les cations **A**, **J** ou **R** ont été observés. Ces expériences de «partition» ont permis de déterminer si les barrières «gauche» ou «droite» correspondantes sont d'énergie plus basse. Dans le cas où le cation transitoire intermédiaire est le **E**, le seul cation observable est le **J**; ce résultat démontre que la barrière entre les cations **B** et **E** est un maximum sur le profil réactionnel global du carbocation.

[Traduit par la rédaction]

Introduction

Adamantane **1** is produced commercially by the rearrangement of tetrahydrodicyclopentadiene **2** using strong Lewis acid catalysts and a hydride transfer initiator. The reactive intermediates in this process are carbocations, and the overall reaction is "driven" by the thermodynamic stability

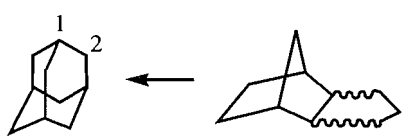

1 **2**

of the adamantane ring. At any given time in the reaction process, *most of the organic material exists as neutral $C_{10}H_{16}$ hydrocarbons* and only a small proportion is in the form of $C_{10}H_{15}^{+}$ cations.

By way of contrast, one can also prepare the adamantane skeleton by converting all of the starting skeleton **2** to an observable carbocation, and this has also been shown to rearrange to the 1-adamantyl cation (1, 2). In this case, *almost all of the organic material exists as $C_{10}H_{15}^{+}$ carbocations*, with negligible amounts of neutral hydrocarbons present at any given time.

Because of these key characteristics, the above reactions exhibit different behavior, yet one knows that the underlying rearrangement mechanisms should be reasonably similar in each case. These differences can be summarized as follows:

1. Excluding three- and four-membered rings and other high-energy geometries,[2] there are a total of 19 neutral tri-

[1]Author to whom correspondence may be addressed.

[2]The number of hydrocarbon skeletons included in "adamantaneland" involves some arbitrary decisions, since a theoretical connectivity surface for $C_{10}H_{16}$ contains several other skeletons, even excluding three- and four-membered rings. These systems all involve steric strain of variable severity ("inverted" bridgeheads, severe bond angle "distortions") and range from plausible synthetic possibilities to "impossible" structures.

Can. J. Chem. Downloaded from www.nrcresearchpress.com by 203.198.23.82 on 09/08/12
For personal use only.

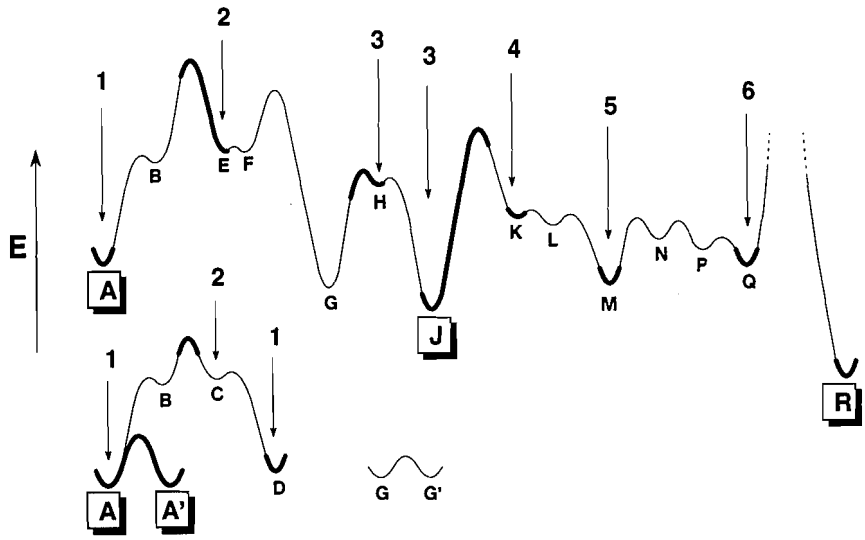

FIG. 1. Qualitative picture of the overall energy profile deduced for the rearrangement of the *endo*-tetrahydrodicyclopentadienyl cation **A** to the 1-adamantyl cation **R** (see Fig. 2 for the structures of the cations). The numbers 1–6 refer to individual experiments carried out in this work to probe various sections of the profile. Heavy lines indicate that either attempts were made to generate the cation concerned or that barriers for various transition states were determined (either directly or from closely related systems). Cations that can be directly observed are highlighted. In addition to our superacid work, several of the cationic transformations were previously probed by solvolysis studies, e.g., **H** → **J** and **P** → **Q**. The separate profile shown in the lower left involves a major diversion prior to the rate-determining step, including a degenerate rearrangement of **A** itself. A degenerate rearrangement of **G** is shown next to this (the barrier is based on a model system) because this is important in understanding how one can probe the profile in the **G**–**H**–**J** region. The **Q** → **R** transformation is an intermolecular process and the hypothetical intramolecular shift is known to be very high in energy (>25 kcal/mol), hence the open-ended profile.

Can. J. Chem. Downloaded from www.nrcresearchpress.com by 203.198.23.82 on 09/08/12
For personal use only.

cyclic $C_{10}H_{16}$ isomers (known as "adamantaneland"). All have now been synthesized, mainly through the recent efforts of Ganter and co-workers (3). Only seven of the hydrocarbons are considered to be on the most direct pathway from **2** to **1** (the Whitlock–Siefkin (W–S) mechanism) (4), although most of the others are also convertible to adamantane using acid catalysis. In all cases, those hydrocarbons considered as intermediates in the **2** → **1** reaction have been independently studied in the isomerization process (5) and the general outline of the W–S mechanism is firmly established.

2. In contrast to the rich chemistry of $C_{10}H_{16}$ neutral compounds, the carbocation from **2** rearranges to the 1-adamantyl cation with *no detectable intermediates*. Nevertheless, observable carbocation studies are inherently better for gauging the magnitude of transition-state barriers and other specifics of carbocation rearrangements and in this paper we have looked in detail at this carbocation route. From our work, it turns out that under the normal low-temperature methods used to prepare and study solution carbocations, *only one carbocation* (i.e., other than the tertiary carbocations from **1** or **2**) among the 14 or so intermediate carbocations that are part of the W–S mechanism is capable of direct observation.

This paper reports on the characterization and rearrangement behavior of this key species, on further attempts to form other observable carbocations that are on the W–S route, and on studies in which the partitioning reactions of high-energy transient carbocations are investigated. From this, and various older studies of simple 2-norbornyl cations, one can piece together a reasonably complete unified "picture" of the complex energy surface whereby the tertiary cation from **2** is transformed into the 1-adamantyl cation. With appropriate modifications, much of this work is directly relevant to the Lewis acid catalyzed rearrangement route and provides one with a more complete understanding of the process than is given by the more qualitative W–S mechanistic formulations.

Results and discussion

Figure 1 shows the overall energy profile for the rearrangement of cations **A** or **D** (from *endo*- or *exo*-**2**) into the 1-adamantyl cation **R** as determined in this work. The actual reaction scheme corresponding to this energy profile is shown in Fig. 2 and follows the general lines of the W–S mechanism, but is elaborated in considerably more detail. In Fig. 1, various parts of the overall profile are specifically identified by means of a heavy line and an accompanying arrow and number. These provide a point of reference for the six sets of experiments that were performed in this work in order to determine this data. In order not to clutter Fig. 1, no quantitative (ΔH-ΔG-ΔS) or ($\Delta H^{\neq}$, $\Delta G^{\neq}$, $\Delta S^{\neq}$) data are shown, but are provided when discussing each case.

The key new observable intermediate, mentioned in the Introduction, is **J**, the tricyclo[5.2.1.$0^{3,8}$]dec-3-yl (homobrendyl) cation,[3] and this cation, highlighted with a circle in Fig. 2, occupies a central position in the overall rearrangement. The *observable* cations **A**, **J**, and **R** (all tertiary carbocations) are indicated in Figs. 1 and 2 in accented type.

[3]The systematic name and numbering. For ease of description, the numbering scheme used for cations **A** and **J** in the following discussion is non-systematic and is based on the usual 2-norbornyl cation labelling scheme. The experimental description of the neutral precursors again uses systematic numbering.

Can. J. Chem. Downloaded from www.nrcresearchpress.com by 203.198.23.82 on 09/08/12
For personal use only.

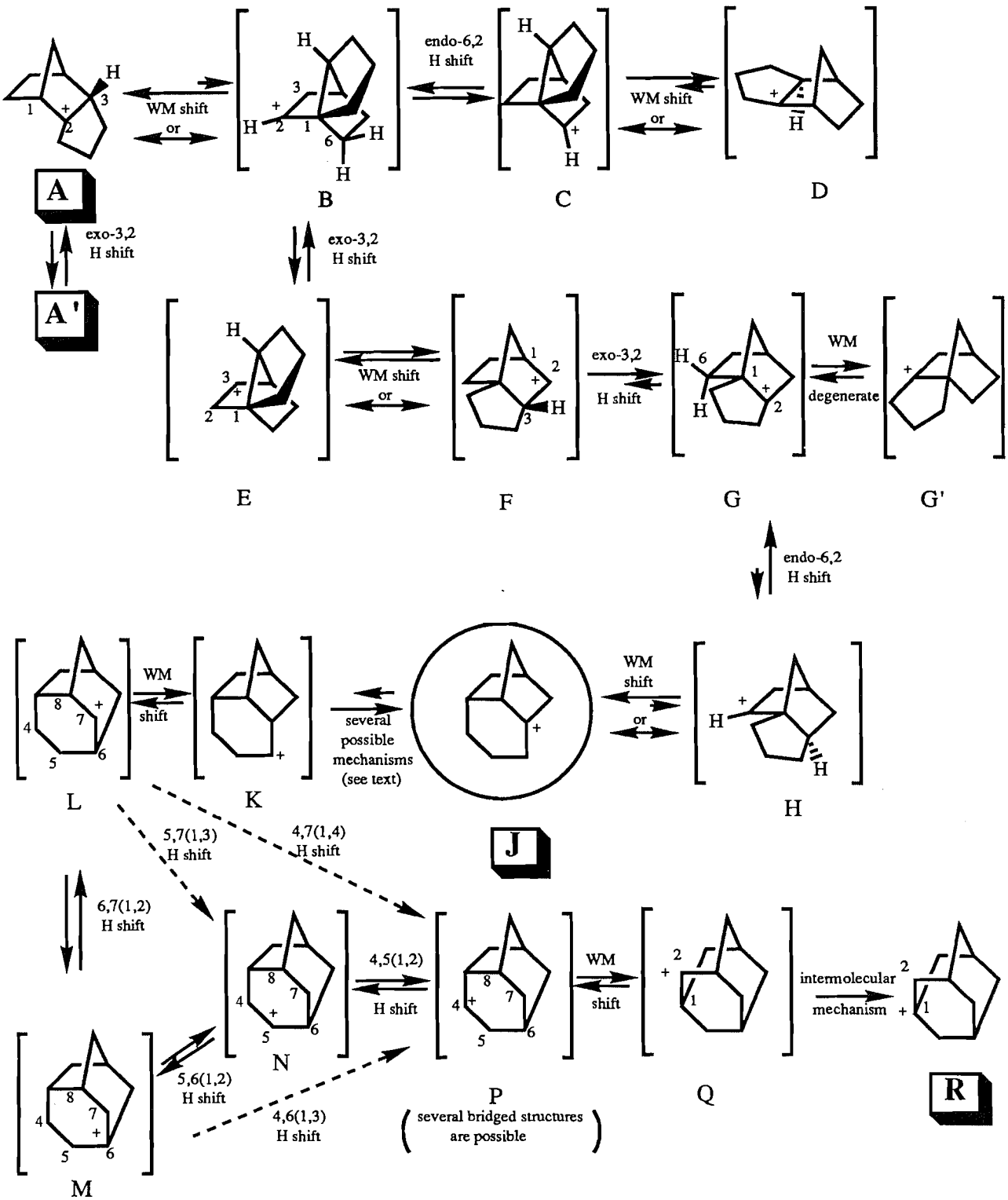

FIG. 2. Detailed reaction scheme corresponding to the energy profile shown in Fig. 1. As explained in the text, it is uncertain whether "pairs" of 2-norbornyl-type cations, e.g., **A**–**B**, **C**–**D**, **E**–**F**, **G**–**H**, separated by a "formal" C6—C1 → C6—C2 Wagner–Meerwein rearrangement are in fact distinct species, as defined in the context of existing for at least one vibration. The 7-protoadamantyl cation **L** may be a carbon-bridged species, as also may be the case for the 4-protoadamantyl cation **P** (see text). The three directly observable cations in this sequence are highlighted.

There are three other tertiary carbocations shown in Figs. 1 and 2, i.e., **D**, **G**, and **M**, but these turn out to be not directly observable, as we will show, because of a combination of unfavorable thermodynamics and low barriers connecting them to the more stable **A**, **J**, and **R**, respectively.

Each of the experimental regions 1–6, shown in Fig. 1, will now be treated in order.

Can. J. Chem. Downloaded from www.nrcresearchpress.com by 203.198.23.82 on 09/08/12
For personal use only.

Region 1 of Fig. 1

Cations **A** and **D** (Fig. 2) are tertiary 2-norbornyl cations, with an *endo* (**A**) or *exo* (**D**) trimethylene bridge. However, when one prepares cations from logical precursors of both **A** and **D**, only a single ion appears to be formed. This cation (the stereochemistry undefined) was originally prepared by Olah and co-workers in 1964 (1) and shown to rearrange to the 1-adamantyl cation **R**. In 1985, a full paper appeared (2), in which the cation was assigned the **A** structure. Our laboratory also studied this cation briefly a number of years ago (^{13}C NMR), but with recent advances in NMR spectroscopy we have now undertaken a more complete study.

Cation A

In Figs. 1 and 2, cation **A** is shown to be involved in three processes: (1) a degenerate rearrangement involving an *exo*-3,2-hydride shift, (2) an irreversible rearrangement to the 1-adamantyl cation, and (3) a reaction sequence shown as **A** $\rightleftarrows$ **[B]** $\rightleftarrows$ **[C]** $\rightleftarrows$ **D**, with transition states much lower than that for the rearrangement to the 1-adamantyl cation. The fact that organic precursors of **D**, when added to SbF_5–SO_2ClF at −135°C, produce only **A**, allows one to set a maximum possible lifetime ($t_{1/2}$) for **D** of ca. 20 min at −135°C (a generous estimate of the carbocation preparation time and time involved in the NMR measurement). Using the Eyring equation, this translates into a maximum possible $\Delta G^{\neq}$ of 10 kcal/mol for the barrier separating **A** and **D** (measured from the **D** side). This maximum $\Delta G^{\neq}$ estimate is reasonably in line with measured barriers of ca. 11 kcal/mol for this same overall rearrangement mechanism involving a number of different polymethyl-2-norbornyl cations (6). Since this **D** → **A** barrier is much lower than that for the 1-adamantyl cation formation from **A**, one expects to form an equilibrium mixture of the tertiary cations **A** and **D**. Since it was already apparent from the earlier NMR results that no detectable **D** was in fact present in these cation **A** solutions, the present study involved only a more stringent search for a small equilibrium population of **D** and a more complete characterization of the ^{1}H NMR spectrum of **A**.

The "ordinary" ^{13}C NMR spectrum of **A** at low temperatures (e.g., −100°C) shows no detectable peaks due to any other cation and, from S/N estimations, **D** cannot be present in amounts exceeding 2–3%. A search for a possibly even smaller equilibrium population of **D** was carried out in two ways: (1) a conventional NMR search employing high S/N conditions and (2) a search for possible line-broadening in the peaks of **A** that might be caused by the dynamic exchange of **A** with a small equilibrium population of **D** (7, 8). This latter experiment necessitates some estimate of the probable barrier so that one covers the appropriate temperature range, and based on the measured <10 kcal/mol (**D** → **A**), and values of 11 kcal/mol for model systems, we chose the range of 11–14 kcal/mol (**A** → **D**) as a reasonable estimate. In neither case could we obtain any evidence for the existence of **D**. One can put a lower limit on the possible equilibrium population of **D** using both methods, ca. 1% for method (1), at −100°C, $\Delta\Delta G > 3$ kcal/mol, and ca. 0.4% for method (2) at −20 to −60°C, $\Delta\Delta G > 2.5$ kcal/mol. In Fig. 1, much of the energy profile for the **A**–**B**–**C**–**D** interconversion is left as a light line to indicate that no quantitative data on barrier heights were directly obtained, but we emphasize that the overall mechanism shown in Fig. 2 has considerable precedent from the studies on methyl-substituted 2-norbornyl cations.

In the *exo* and *endo* hydrocarbons **2***a* and **2***b*, the *exo* isomer is actually the more stable (K = 100, $\Delta\Delta G$ = 2.7 kcal/mol, at 25°C) (5). Why then is the *exo* cation **D** so unstable relative to the *endo* cation **A**?

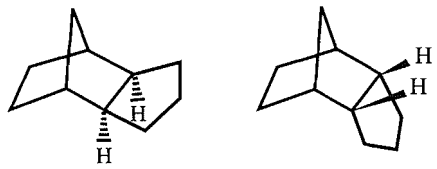

2a **2b**

Semi-empirical MO calculations (MNDO) provide no guide here. For the fully optimized structures, the calculated energies are ΔH = 202.1 kcal/mol for **D** and 203.0 for **A**, i.e., giving **D** > **A** in stability. The calculated **A**–**D** energy difference of 0.9 kcal/mol is thus in the same direction as that found for the hydrocarbons **2a** and **2b** and likely reflects some steric factor favoring the *exo* isomer in each case.

We believe that the greater stability of the *endo* isomer **A**(vs. **D**) is the result of a stabilizing "partial bridging" that is sterically much more favorable in **A**. This "partial bridging" has been observed in simple tertiary 2-methyl-2-norbornyl cations (6*a*) and others (9), and also shows up in the X-ray structure of a 1,2-dimethyl-2-norbornyl derivative (10). For our purposes, this partial C2–C6 bridging can be described as a "back-lobe" interaction of the C—*exo*-H6 bond with the carbocation *p*-orbital and, in the two ions **A** and **D**, the directionality of the C^+ orbital is likely to be much more favorable in the **A** case. This "back-lobe" interaction results in an abnormally low-field ^{1}H NMR shift for the *exo*-H6 proton, as shown in the ^{1}H data for a number of 2-methyl-2-norbornyl cations. The previously reported (1) ^{1}H NMR spectrum of **A** was not well resolved and the *exo*-H6 proton shift could not be identified. At 400 MHz, however, the cation **A** ^{1}H shifts are mostly assignable (Table 1), with the aid of a COSY spectrum, and in Table 2 we have collected the δ *exo*-H6 shifts for several of the model systems and for **A**, and there is a close similarity. It is unfortunate that the corresponding *exo*-H6 chemical shift for cation **D** has been impossible to obtain since one would expect a much higher field value. In conclusion, we suggest that the experimental >3 kcal/mol stability of **A** over **D** is mostly a result of this partial C2–C6 bridging delocalization.

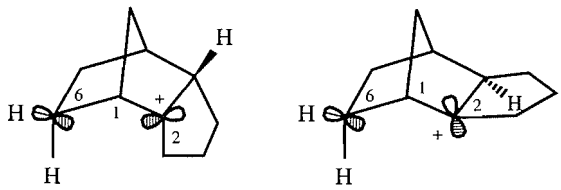

A **D**

The degenerate *exo*-3,2-hydride shift observed in cation **A** (shown in Figs. 1 and 2) is essentially irrelevant to the 1-adamantyl cation rearrangement picture except for isotopic labelling schemes. Olah et al. obtained an estimate of $\Delta G^{\neq}$ = 7.2 kcal/mol for the barrier (2). Using ^{13}C NMR line-broadening data, and simulating this in the usual way, we obtained a similar value of $\Delta G^{\neq}$ = 7.2 kcal/mol, $\Delta H^{\neq}$ = 8 kcal/mol, $\Delta S^{\neq}$ = +3 eu. The ^{13}C NMR assignments are

TABLE 1. ^{1}H NMR spectra of cations **A** and **J**

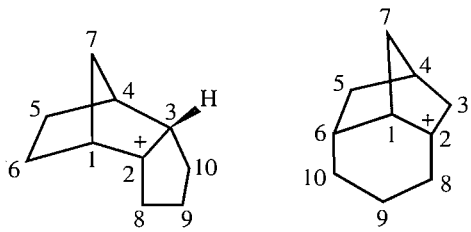

Position[a]										
Cation **A**										
H1	H3	H4	H5*exo*	H5*endo*	H6*exo*	H6*endo*	H7*syn*	H7*anti*	H8 H9 H10	
4.74[b]	3.44[c]	3.12[b]	1.8–2.0[h]	1.46[d]	3.5–3.7[g,h]	1.46[d]	2.18[f]	2.28[f]	2.9–3.1(2H)[e] 2.45–2.67(4H)[e]	
Cation **J**										
H1	H3*exo*	H3*endo*	H4	H5*exo*	H5*endo*	H6	H7	H8	H9	H10
5.32[c]	3.05–3.2	3.3–3.5	3.22[c]	2.10[j]	1.24[k]	5.22[c]	2.05[i] 1.98[i]	3.60[c] 3.3–3.5	3.05–3.2 3.38[c]	1.76

[a]In ppm relative to $CHDCl_2$ = 5.30.
[b]180 K.
[c]Broad singlet.
[d]Fast exchange averaged position at 232 K, d, J = 10.
[e]Averaged values at 323 K.
[f]AB spectrum, J = 11.5, the assignment based on W-coupling (COSY) with H5*endo*—H6*endo* averaged peak (232 K).
[g]Exact position slightly obscured by H8 protons.
[h]At 232 K: under fast exchange H5*exo*—H6*exo* is found at 2.73, J = 10.
[i]AB spectrum, J = 12.
[j]Multiplet.
[k]Two doublets, J = 13, 6.5.

TABLE 2. Chemical shifts for the H-6 protons in tertiary 2-norbornyl cations

Cation	δ*exo*-H6	δ*endo*-H6
2-Methyl-2-norbornyl[a]	3.56	1.71
2,4-Dimethyl-2-norbornyl (6*e*)	3.68	1.70
2,3,3-Trimethyl-2-norbornyl (6*d*)	3.70	~1.9
A	3.5–3.7	~1.4

[a]Determined very accurately using the h_1d_9-CD_3 cation, which produces "singlets" for all of the protons, see ref. 39.

listed in Table 3. The *exo*-3,2-hydride shift barrier found for **A** is similar to that observed in other tertiary 2-norbornyl cations (6*c*, 11).

Finally,the rate for the cation **A** → **R** rearrangement was measured at 20°C by conventional kinetic methods (monitoring by ^{1}H NMR spectroscopy) using 1:1 SbF_5–FSO_3H solution. The reaction follows simple first-order kinetics, giving $\Delta G^{\neq}$ = 22 ± 1 kcal/mol. This value is consistent with qualitative data obtained by Olah et al., but differs from another measurement made in sulfur dioxide solvent in being somewhat larger (1). The magnitude of this barrier, as previously mentioned, makes the **A**–**B**–**C**–**D** group, with mutual interconnecting barriers half this size, completely able to equilibrate before conversion to the 1-adamantyl cation **R**. A similar kinetic result is found in the Lewis acid catalyzed rearrangements, although in this case, as previously mentioned, the *endo* hydrocarbon **2***b* is initially converted almost completely to the *exo* isomer **2***a*, i.e., completely opposite to the cation behavior.

The measured barrier of 22 ± 1 kcal/mol is obviously the highest point in the overall energy profile from **A** to **R**, but it tells one very little about the actual position of this barrier since one has numerous transition states spanning this structural change. The next experiment, however, clears up this point.

Region 2 of Fig. 1

The formulation of the secondary cations **E** and **F** (Fig. 2) as distinct species is questionable since the evidence is now overwhelming that the 2-norbornyl cation itself is a symmetrically bridged structure (single minimum) (12). However, this need not absolutely be the case for **E** and **F** since no natural symmetry exists in these cations, and Bentley et al. have described an example where a secondary 2-norbornyl cation was not symmetrical (13). To leave the matter open, we show a very small barrier between **E** and **F** (a somewhat similar problem ensues when considering cations such as **A** and **B** (or **C** and **D**), where it is also possible that **B** or **C** do not represent energy minima, although MINDO/3 and MNDO optimizations of these do not "fall-back" to the tertiary ions).

The tricyclic hydrocarbon corresponding to cations **B**, **C**, or **E** has been synthesized by Holm and co-workers (15), Jäggi and Ganter (3*d*), and Tobe et al. (16*a*). A small sam-

Can. J. Chem. Downloaded from www.nrcresearchpress.com by 203.198.23.82 on 09/08/12
For personal use only.

TABLE 3. ^{13}C NMR spectra of cations **A** and **J**

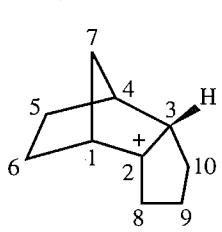

A

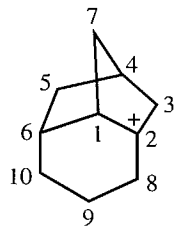

J

	Position[a]									
Carbon	1	2	3	4	5	6	7	8	9	10
Cation **A**	69.6[b]	310.3[c]	79.6[b]	47.8[b]	25.9	38.9	45.7	41.9	28.3	21.2
Cation **J**	90.6[b]	289.9[c]	57.3	48.6[b]	28.7	87.0[b]	39.9	46.0	53.2	27.7

[a]A wide range of temperatures were used to characterize the line-broadening. Data for **A** are at 153 K (22.63 MHz), for **J** at 210 K (100.61 MHz).
[b]CH.
[c]Quaternary.

Can. J. Chem. Downloaded from www.nrcresearchpress.com by 203.198.23.82 on 09/08/12
For personal use only.

ple of a mixture of the isomeric acids **3***a* and **3***b* in a ca. 2:1 ratio was made available to us. The mixture was converted to the corresponding chlorides using a modified Hunsdiecker

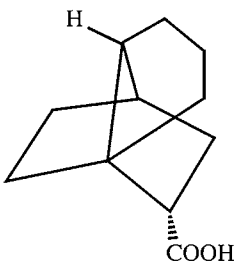

3a

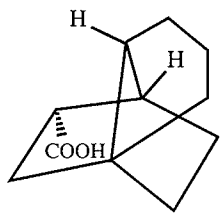

3b

reaction. On treatment with SbF_5 in SO_2ClF at −135°C, these two chlorides should lead to the instantaneous production of cations **C** and **E**, respectively (see Figs. 1 and 2). In fact, cations **A** and **J** (see subsequent discussion) were the products observed and were produced in the same ratios as present in the chloride precursors, i.e., transient ion **C** → **A** and transient ion **E** → **J**. Given the previous discussion concerning the Region 1 experiment, the transformation **C** → **A** is anticipated, even though **D** is the first tertiary ion that one would expect to produce.

More significant is the observation that **E** is transformed into cation **J**. From the non-observation of **E** under these low-temperature conditions, the barrier for **E** → **J** is placed at <11 kcal/mol. Also, since **E** does *not go backwards* to **A**, the overall barrier for the **A** → **R** reaction is established as the barrier immediately to the left of **E**, i.e., the *exo*-3,2-hydride shift. This barrier from **A** actually consists of two parts, a ΔG contribution for a secondary-tertiary cation energy difference and a $\Delta G^{\neq}$ component for the *exo*-3,2-hydride shift. The measured $\Delta G^{\neq}$ for **A** → **R** (see previous section) is 22±1 kcal/mol. An independent estimate for $\Delta G^{\neq}$ for the 3,2-hydride shift in 2-norbornyl cation is ca. 11 kcal/mol (14), leaving 11 kcal/mol for the energy difference between **A** and **B**. The latter seems a little large, so it is probable that the former is somewhat larger than 11 kcal/mol.

To summarize to this point, starting with cation **A**: (1) the degenerate rearrangement to **A** is very fast ($\Delta G^{\neq}$ = 7.2 kcal/mol) but somewhat irrelevant; (2) an **A** ⇄ **D** equilibrium must exist, but the low population of **D** precludes any direct detection of **D**; (3) the overall rearrangement barrier for **A** → **R** involves a combined ΔG value from **A** ⇄ [**B**] and a $\Delta G^{\neq}$ contribution for [**B**] → [**E**].

Schleyer et al. (15) have previously shown that hydrocarbon **4** occupies a pivotal dividing point for the neutral hydrocarbon studies, i.e., **4** gives both **2** and **1** using Lewis acid catalysis, together with at least one other "adamantane-land" hydrocarbon. One can be specific about why **4** occupies this "watershed" position in the acid-catalysis process, i.e., hydride abstractions from ○ hydrogens in structure **4** will ultimately give **2**, while those from ⊘ will ultimately produce **1**. Also, as originally postulated by Schleyer et al., abstraction of □ hydrogens could be responsible for an

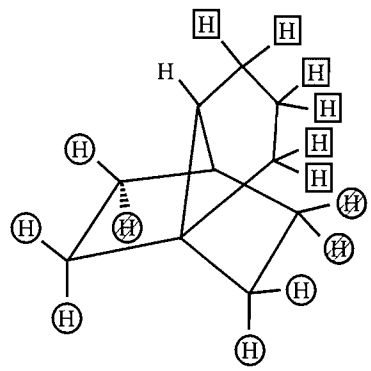

4

"aberrant" pathway. This has been confirmed by Ghatak and Ganter, using functionalized derivatives (16*b*). Formation of this "aberrant" cation by a cation–cation rearrangement (i.e., an intramolecular hydride shift) is a less likely process, and this illustrates why the overall rearrangement is a simpler process at the "observable" carbocation level.

Region 3 of Fig. 1

The very low temperature formation of **J** from **E** (previous section) implies that no "nearer" intermediates more stable than **J** are present in the system (see Fig. 1) and that all cation–cation transition state barriers between **E** and **J** are

Can. J. Chem. Downloaded from www.nrcresearchpress.com by 203.198.23.82 on 09/08/12
For personal use only.

less than 11 kcal/mol. In particular, the tertiary carbocation **G** is a required part of the W–S mechanism and **G** precedes **J** in the overall carbocation progression. It is clear therefore that **G** is not observable under stable carbocation preparation and observation conditions. In this section we now look at cation **J** in detail. The initial impetus was to verify the structure of the then unknown ion produced from **E** (see previous section) and, secondly, to understand the nature of a degenerate rearrangement that was detected when we prepared an authentic sample of **J** and looked in detail at the NMR spectrum. It turns out that an understanding of this rearrangement ultimately allows for an exploration of the energy surface "backwards" from **J** to **G**.

Cation **J**, previously unreported, was prepared from the corresponding alcohol **5** and was characterized by both ^{13}C and ^{1}H NMR spectroscopy (Tables 1 and 3). A combination of 1D and 2D techniques allows one to assign all of the peaks (a necessity for understanding the degenerate rearrangement).

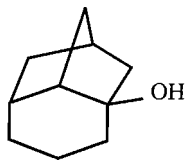

5

The degenerate rearrangement in **J** is characterized by a noticeable line-broadening of six of the ten ^{13}C peaks as one warms the cation solution to −40°C. This is the maximum temperature for which the ^{13}C data for **J** could be obtained because the irreversible rearrangement to the 1-adamantyl cation **R** is becoming fairly rapid at this temperature. The six peaks that are line-broadened are those shown in structure **J** *without* a dark circle. The line-broadening in **J** could be accounted for if the H6 proton were to reversibly migrate to C2 (see eq. [1]), but this seems a very unlikely process for steric reasons. Further insights were provided by looking at the ^{1}H 2-D NOESY exchange spectrum, where one sees qualitatively the exchange of H5*exo*–H3*exo*, H5*endo*–H3*endo*, and the H8–H10 protons. These results are expected based on the ^{13}C spectral observations, but there is also qualitative evidence from this NOESY spectrum for the *further exchange* of H6 and H1, i.e., a process *not* simply related to a symmetry plane through C4-C7-C1-C9, as shown in dark circles in structure **J** of eq. [1]. On the basis of the ^{13}C NMR line-broadening data, the rate of the symmetrization process can be determined by simulation of the experimental data in the usual way. The exchange of H1 and H6 was also quantified using spin-inversion transfer procedures. Since the chemical shift difference of these two protons is only 0.096 ppm, we used a 400 MHz field and a Dante pulse train (17) for the selective 180° pulse. A typical sequence is shown in Fig. 3, using varying delay times prior to the final "reading" pulse. Experiments in which both H1 and H6 were separately irradiated at a number of temperatures were carried out and analyzed to give both T_1 and the rate constants for the exchange process (18). Within experimental error, the latter values are the same as those obtained from the ^{13}C line-broadening results, $\Delta G^{\neq} = 12.5 \pm 0.5$ kcal/mol.

With reference to Figs. 1 and 2, the degenerate rearrangement observed in **J** can be uniquely rationalized by the following mechanism (eq. [1]):

[1]

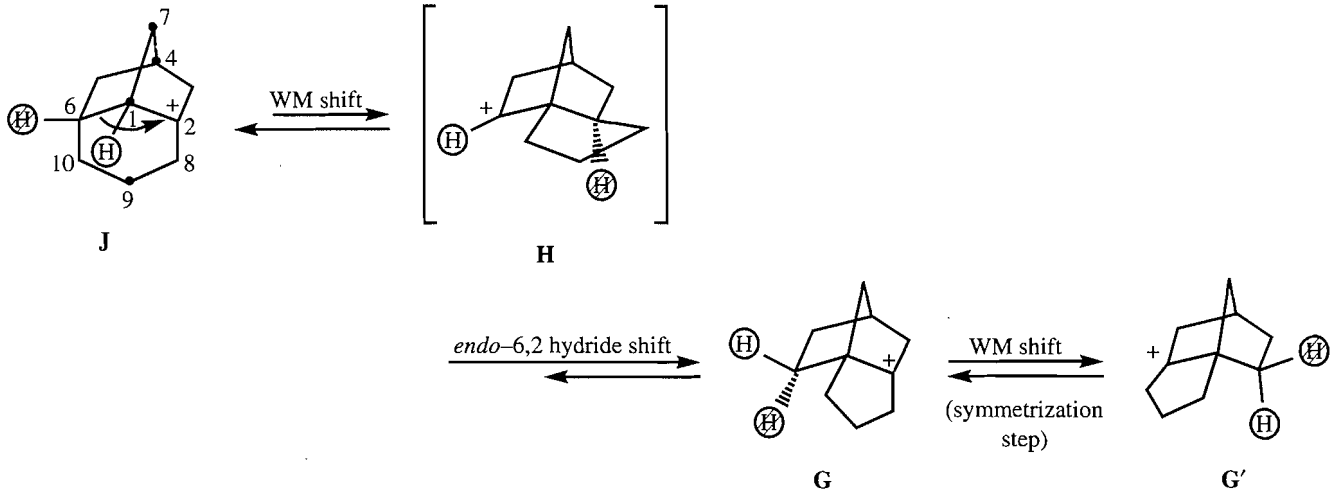

J **H** **G** **G′**

As stated previously, the existence of secondary cations such as **H** is not proven, and the reaction could proceed from **J** to **G** by direct migration of H6 to H1. However, we will consider for this discussion that **H** occupies a shallow potential well minimum (see Fig. 1). The symmetrization process observed in the NMR spectrum of **J** actually takes place via a small equilibrium population of **G** (undetectable in a direct sense by NMR). The degenerate rearrangement **G** ⇄ **G′** exchanges the three pairs of carbons referred to previously and the H6 and H1 protons of **J** (which have transformed to H6 *exo* and *endo* (**G**-labelling) in the actual exchange process undergone by **G**). Based on the NMR S/N level observed for **J**, the maximum possible **G** population is 2%, giving ΔG (**J**–**G**) ⩾ 1.7 kcal/mol at −60°C. Cation **G** is closely related structurally to the well-known 1,2-dimethyl-2-norbornyl cation (19), for which both solvolysis data and observable ion measurements show a very small barrier for the degenerate WM shift ($\Delta G^{\neq} \leq 3$ kcal/mol). A similar small barrier has been incorporated into Fig. 1 for the **G** ⇄ **G′** process. It has also been shown in the Lewis acid

Can. J. Chem. Downloaded from www.nrcresearchpress.com by 203.198.23.82 on 09/08/12
For personal use only.

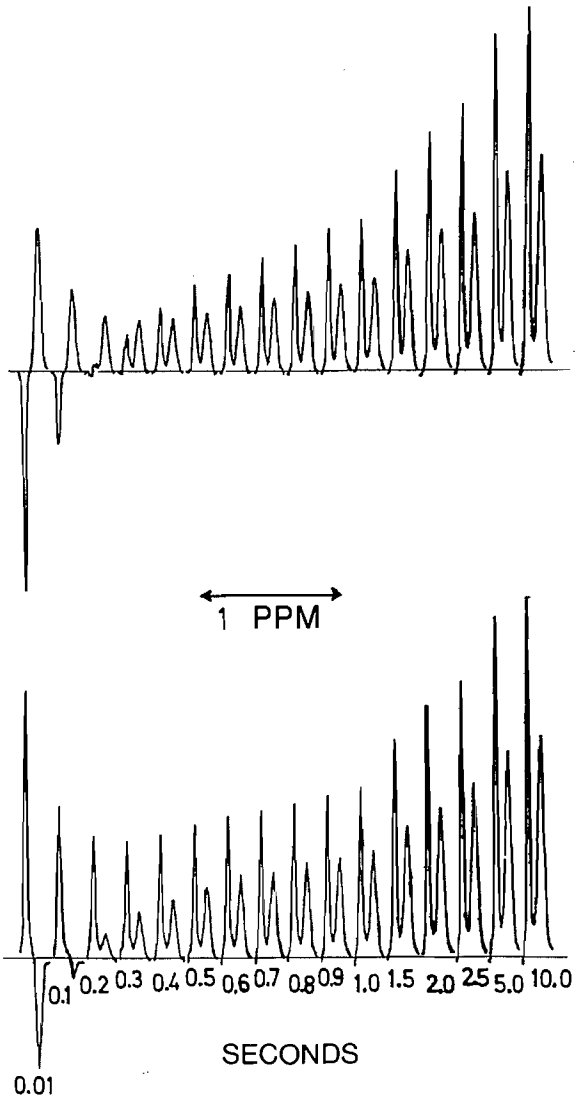

FIG. 3. The 400 MHz ^{1}H NMR spectra showing only the H1–H6 protons of cation **J**. Each of the 16 plots involves a different delay time in the spin inversion transfer experiment. The spectra illustrate the selectivity of the DANTE pulse since the two exchanging protons are separated by only 0.1 ppm. The solution temperature is 223 K.

catalyzed rearrangement of one of the hydrocarbons corresponding to **G**, using a ^{13}C labelled compound (20*a*) or with deuterated analogs involving both neutral **G** hydrocarbons (20*b,c,d*), that the degenerate **G** $\rightleftarrows$ **G′** process must take place here as well. Also relevant to this discussion is the fact that the **H** cation skeleton (as the alkene) is the synthetic precursor of the cation **J** skeleton (the alcohol **5**), via a facile acid-catalyzed rearrangement (21), thereby showing that the **H** $\rightarrow$ **J** barrier is also small.

The rate of the irreversible rearrangement of **J** into **R** was obtained by conventional kinetic measurements using ^{13}C NMR peak areas. The reaction is first order and gives $\Delta G^{\neq} = 18 \pm 0.5$ kcal/mol.

All of these data are shown qualitatively in Fig. 1, but the experiments described here show that **G** is $\geqslant$1.7 kcal/mol less stable than **J**, the barrier from **G** to **J** is $\leq$11 kcal/mol (see previous data on Region 2 of Fig. 1), and the barrier from **J** to **G** is 12.5 kcal/mol (the degenerate rearrangement data on J). The difference between $\geqslant$11 kcal/mol and 12.5 kcal/mol, i.e., $\geqslant$1.5 kcal/mol for the **J–G** energy difference, is quite consistent with the independently determined $\geqslant$1.7 kcal/mol (see above). Finally, although **J** is structurally distant from **R**, the 18 kcal/mol barrier for this rearrangement occurs between **J** and **K**, as shown in the next section.

Before proceeding to this section, it is worth noting that cation **J** itself is of some interest. The low-field nature of H6 in the ^{1}H NMR spectrum suggests that the partial C2–C6 bonding, discussed earlier for **A**, is also present in **J**. It seems probable from the structure of **J** that the cation center would be substantially nonplanar, and MNDO calculations are in agreement with this assessment, the dihedral angles being about 160°. Interestingly, cation **J** was originally regarded by Whitlock and Siefkin as *the* high energy "bottle-neck" in the acid-catalyzed rearrangement of **1** to **2**, principally on the basis of the expected nonplanarity (and hence instability) of the C^+ center in **J**. Clearly this nonplanarity is not a particularly destabilizing effect. In particular, as we have shown, cation **J** is $\geqslant$1.7 kcal/mol more stable than **G**, even though the calculated (MNDO) C^+ dihedral angles in **G** are much closer to a planar structure (average dihedral angles of ca. 173°). However, like the semi-empirical computations involving cations **A** and **D**, those involving **G** and **J** are at odds with the experimental energies, $\Delta\Delta E_{\text{calc. MNDO}}$ **G** > **J** by 4.5 kcal/mol, $\Delta\Delta G_{\text{exp.}}$ **J** > **G** by $\geqslant$1.7 kcal/mol, so the calculated geometries of **G** and **J** should be regarded with some suspicion. Elegant studies by Ganter and co-workers (20*b,c,d*) have shown that the neutral hydrocarbon of **J** is more stable than either of the hydrocarbons related to **G**.

Region 4 of Fig. 1

Cation **J** is still some structural "distance" from **R** and is confronted at one stage in the pathway by a relatively high barrier of 18 kcal/mol (previous section). We suspected that this barrier probably involved the transformation of **J** into **K**, and this was confirmed by starting with the mesylate **6**, a logical precursor of **K**, which on addition to 1:1 FSO_3H–SbF_5 in SO_2ClF at −100°C gives only the 1-adamantyl cation **R**; i.e., **K** is on the other side of the 18 kcal/mol barrier. It is not entirely clear how one proceeds from **J** to **K**

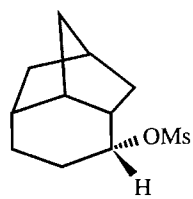

6

since the direct 1,2-hydride shift suffers from a poor overlap angle between either of the two possible migrating methylene protons (circled in **J**, below) and the C^+ center. An alternative to a direct shift could proceed by way of two separate steps, an *exo*-1,2-hydride shift from the other side of the cation, followed by a 1,3-hydride shift, as shown in eq. [2] (the number description of hydride shifts is generic and does not refer to the actual carbon–hydrogen skeletons involved):

[2] 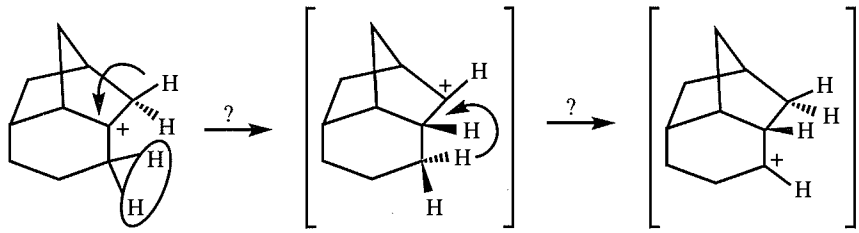

J H K

The observed barrier of 18 kcal/mol for **J** → [**K**] is actually only about 2–4 kcal/mol larger than that observed for a number of other carbocation transformations where a stable tertiary species proceeds to a secondary carbocation intermediate via a 1,2-hydride shift; for example, the transformation of the 1-ethylcyclopentyl cation to the 1-methylcyclohexyl cation involves a barrier of 15.4 kcal/mol (22). In this model case the 1,2-hydride shift presumably involves a favorable overlap angle, so, for the **J** → [**K**] case, the somewhat larger $\Delta G^{\neq}$ value is consistent with either a more difficult direct 1,2-hydride shift or the combination of a 1,2 and 1,3-hydride shift as shown in eq. [2]. However, for simplicity we have shown the transformation in Fig. 1 as a direct 1,2-hydride shift.

Region 5 of Fig. 1

The previous experiment shows that there are no barriers greater than ca. 11 kcal/mol, between cations **K** and **R**, i.e., no other cations than **R** are observed when the transient **K** is produced at −100°C. The step between **K** and **L** (Fig. 1) is a Wagner–Meerwein shift between secondary cations and is expected to have a very small barrier. Cation **L** is the 7-protoadamantyl skeleton but, in order to reach **R**, the 4-protoadamantyl cation **P** is a required intermediate. A direct 1,4-hydride shift could conceivably be involved in this process, i.e., **L** → **P**, in which case the tertiary 6-protoadamantyl cation **M** need not be involved. If this were so, it seemed possible that the 6-protoadamantyl cation (coincidentally the most stable of the tertiary protoadamantyl cations) (23) might be experimentally observable as a non-direct-pathway species. However, addition of the alcohol **7** to 1:1 FSO_3H–SbF_5 in SO_2ClF at −100°C yields only the 1-adamantyl cation **R**. Since the hydride shift connecting **L** to **M** is favorably aligned, and since 1,2-hydride shifts generally have lower barriers than 1,3- or 1,4-shifts, it therefore seems very probable that **M** would lie on the direct path from **A** to **R**.

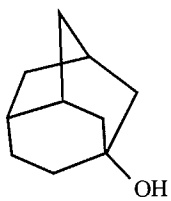

7

The conversion of **M** to **P** can again be a direct process (a 1,3-hydride shift) or it might involve the 5-protoadamantyl cation **N** if two 1,2-hydride shifts were involved. We have no direct evidence on this point, although the latter may be a lower energy pathway, given that 1,3-hydride shifts generally have a somewhat higher barrier than 1,2-shifts. Both possibilities are presented in Fig. 2, while Fig. 1 for simplicity shows only the 1,2-hydride shift pathways. Any attempts to generate transient cations **L**, **N**, or **P** would be uninformative since one already knows that no observable ions, save **R**, will be produced. However, some deuterium-labelled versions of these cations would offer useful information; for example, a transiently produced 6-deutero-**L** cation might allow one to distinguish between a 1,2-hydride shift mechanism, giving a transient **M**, and those involving a direct 1,3- or 1,4-hydride shift. In Fig. 1, all 1,2-hydride shifts involving secondary cations **L** or **N** are shown with very low barriers, since model systems like the cyclopentyl cation have, experimentally (24), very low 1,2-hydride shift barriers, ≤3 kcal/mol.

Region 6 of Fig. 1

Solvolysis work on the 4-protoadamantyl system shows that cations **P** and **Q** are connected by a very low barrier (a Wagner–Meerwein shift) (25). *Ab initio* calculations are also consistent with this conclusion (26).

The conversion of the secondary adamantyl cation **Q** to the tertiary cation **R**, the final product, is known to involve intermolecular hydride shifts (27) and, at least in sulfuric acid carbonylation studies (28), the rearrangement is clearly a second-order rate process. We have had an ongoing interest in characterizing the 2-adamantyl cation **P** as an observable species. One approach has involved an attempt to prepare very dilute solutions of the cation at very low temperatures in the hope that bimolecular processes could be slowed down to such an extent that one might be able to observe **P** by NMR spectroscopy. However, even at a projected 10 μg **Q**/0.5 mL (1.5×10^{-4} M) solution level, the NMR spectra at −120°C show only the 1-adamantyl cation **R**. In other studies, 2-deuteroadamantan-2-ol **8** was used as a potential precursor to **Q**. In 1:1 FSO_3H–SbF_5/SO_2ClF, the alcohol is protonated at low temperatures and only slowly solvolyzes to the

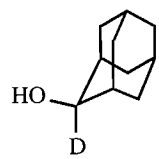

8

cation (hence low initial concentrations of **Q** would be expected). However, the 1-adamantyl cation **R** is still the only simple carbocation observed, although at intermediate times in the reaction there is a clear indication in the ^1H and ^2H NMR spectra for the presence of mono-functionalized 1-adamantyl cation peaks, which we believe are formed from a hydride transfer to a transient 2-adamantyl cation from a tertiary C-H position in the starting protonated alcohol. This mono-functionalized carbocation can then rereact with the

Can. J. Chem. Downloaded from www.nrcresearchpress.com by 203.198.23.82 on 09/08/12
For personal use only.

Can. J. Chem. Downloaded from www.nrcresearchpress.com by 203.198.23.82 on 09/08/12
For personal use only.

just-formed adamantane to form the 1-adamantyl cation **R** and regenerate the protonated alcohol; i.e., the latter acts as a chain hydride transfer agent. Alternatively, the adamantane can serve as a hydride transfer chain carrier by itself reacting with the transient 2-adamantyl cation. Whitlock and Siefkin even reported (4) that preformed 1-adamantyl cations will undergo subsequent intermolecular hydride transfer.

All rearrangement steps up to **Q** in Figs. 1 and 2 have been regarded as unimolecular transformations. However, in light of the bimolecular [**Q**] → **R** rearrangement, is this justified? The overall barrier for **A** → **R** and the subsidiary **J** → **R** both appear to follow first-order kinetics and the rate is not noticeably concentration dependent. Thus, these barriers themselves do not involve bimolecular reactions. Furthermore, in many studies of rearrangements in tertiary 2-norbornyl cations, bimolecular reactions have not been observed, and cations **A–B–C–D–E–F–G–H–I–J–K** in Figs. 1 and 2 all have this ring system in part. In fact, it is quite possible that the adamantane ring skeleton is an unique system in allowing bimolecular hydride transfers. For example, the Whitlock–Siefkin work involving hydride transfers in preformed 1-adamantyl cation is most easily explained if one postulates the existence of transient adamantane dications. Of all the ring systems in Figs. 1 and 2, the adamantane skeleton would appear to be the most feasible, and perhaps only, candidate for a reasonably low energy (di-tertiary) dication intermediate.

Comparison of the cation–cation route with the Lewis acid catalysis route

The W–S mechanism is divisible into two kinds of carbocation rearrangement steps: (1) those involving WM shifts which interconvert members of "adamantaneland" and (2) those that involve "moving" the C^+ center from one position to another within a given skeleton.

In terms of Figs. 1 and 2, the transformations **B–C**, **B–E**, **F–G–H**, **J–K**, **L–M–N–P**, and **Q–R** are in the latter category, while **A–B**, **C–D**, **E–F**, **H–J**, **K–L**, and **P–Q** are in the former. Category 1 steps are not likely to be much affected by reaction conditions, whereas those in category 2 most certainly are. In the Lewis acid catalyzed reactions it seems likely that virtually all of the category 2 steps will involve *intermolecular hydride transfers*, particularly if this process can circumvent a "difficult" unimolecular process, whereas for the cations, as previously mentioned, only the **Q–R** transformation appears to be bimolecular. An examination of Figs. 1 and 2 shows that the cation–cation barriers for **A** → **R** or **J** → **R** do indeed involve several difficult unimolecular hydride shifts, e.g., **B** → **E** or **J** → **K**, which can thus be short-circuited in the Lewis acid catalysis route. On the surface, it might appear somewhat remarkable that the Lewis acid catalyzed formation of adamantane from tetrahydrodicyclopentadiene is about as fast as, or even faster than, the carbocation route, but one can now see the reasons for this.

A second distinction between carbocation studies and the Lewis acid catalyzed rearrangements involves secondary and tertiary carbocations. Since these are very different in energy, we cannot hope to directly observe those hydrocarbon skeletons with a secondary carbocation functionality. As it turns out, of course, we do not even directly observe several of the tertiary carbocation systems either. With neutral hydrocarbons, differences in stability between various "adamantaneland" skeletons is the determining factor, and since these involve reasonably small energy differences, one expects to pick up the appearance of many more of the rearrangement intermediates in such reactions.

Conclusions

For the rearrangement of the observable *endo*-tetrahydrodicyclopentadiene cation **A** into the observable 1-adamantyl cation **R**, the reaction mechanism energy profile has been mapped out for much of the route. A new cationic intermediate has been found and it is also shown that the three other tertiary cations on or near the rearrangement route are not observable under superacid conditions. In fact no other ions in the whole rearrangement pathway will be observable under the present preparation techniques (even in the whole "adamantaneland", there may be no further observable cations (29)). The highest barrier occurs early in the overall reaction and the experimental $\Delta G^{\neq}$ value for this can be correlated with values for the combined secondary–tertiary energy difference in 2-norbornyl cations and the transition state for an *exo*-3,2-hydride shift.

Experimental

NMR spectra were obtained on a Bruker WH-90, AM-400, or on a Varian XL-200 spectrometer. Deuterochloroform was used as a solvent for all neutral compounds. Carbon multiplicities were determined by off-resonance decoupling or by DEPT-90 and 135 sequences. Carbocation preparations for NMR measurement purposes were made up directly in the NMR tube. Several procedures were used: (*a*) for work on the WH-90 spectrometer, 10-mm tubes were used, and a small volume of $CFCl_3$ was used to dissolve the organic precursor prior to the addition to the acid solution. The ^{19}F peak of SO_2ClF was used as the lock and $^{13}CFCl_3$ was used as the internal reference, δ = 117.9; (*b*) for work on the XL-200 or AM-400 spectrometers, a small volume of CD_2Cl_2 was used as organic solvent and as a ^2H lock. Spectra were referenced relative to $^{13}CD_2Cl_2$ = δ 53.8. Proton (^1H) NMR spectra were run using the latter procedure, where the internal $CHDCl_2$ reference was taken as δ 5.32. The inversion-transfer experiments were performed at 400 MHz using 16 delay times for each run, as illustrated in Fig. 3. The kinetic analysis for this process is given in ref. 30. HETCOR, COSY, NOESY, and INADEQUATE spectra were obtained at 400 MHz. Semi-empirical molecular orbital calculations were carried out at the MINDO/3 or MNDO level with full optimization of all geometric parameters (31).

8-exo-*Hydroxy*-exo-*tricyclo[5.2.1.0^{2,6}]decane* (32), *8*-endo-*hydroxy*-exo-*tricyclo[5.2.1.0^{2,6}]decane* (33), and *8*-exo-*chloro*-exo-*tricyclo[5.2.1.0^{2,6}]decane* (34) were prepared as described in the literature.

2-exo-*Hydroxy*-endo-*tricyclo[5.2.1.0^{2,6}]decane* and 2-endo-*hydroxy*-exo-*tricyclo[5.2.1.0^{2,6}]decane* were prepared as described by Takaishi et al. (35).

Identification of cation A by quenching

8-exo-Chloro-*exo*-tricyclo[5.2.1.0^{2,6}]decane (10.7 mg) in 50 μL of CD_2Cl_2 was added to 0.5 mL of a 1:4 mixture of FSO_3H–SbF_5 in SO_2ClF, contained in a 5-mm NMR tube, at −78°C and with stirring. After verifying the presence of cation **A**, the cold solution (−78°C) was quenched by cautiously pouring it into ambient aqueous K_2CO_3 with stirring (fumehood). The aqueous solution was extracted with ether; dried, and, after ether removal, the residue was taken up in a small volume of methylene chloride, filtered through a pad of silica gel, and the solvent removed. A comparison of GLC retention times and ^1H NMR spectra with authentic material confirmed the quench product as 2-*exo*-hydroxy-*endo*-tricyclo-[5.2.1.0^{2,6}]decane.

Can. J. Chem. Downloaded from www.nrcresearchpress.com by 203.198.23.82 on 09/08/12
For personal use only.

Attempts to prepare cation ***D***

Both 8-*exo*-chloro-*exo*-tricyclo[5.2.1.$0^{2,6}$]decane and 2-*endo*-hydroxy-*exo*-tricyclo-[5.2.1.$0^{2,6}$]decane were used as organic precursors. The former is expected to rapidly rearrange to the tertiary cation system by way of an *endo*-6,2-hydride shift, and one would therefore initially expect **D** to be formed. From the alcohol, **D** should be formed directly. In both cases, carbocation preparation and measurement were carried out at ca. −135°C, but the ^{1}H NMR spectra failed to show any peaks other than those for cation **A**.

Mixture of endo-*7-chloro- and* endo-*9-chlorotricyclo[4.2.2.*$0^{1,6}$*]decane*

A small sample of the mixed *endo*-carboxylic acids **3***a* and **3***b* was a gift from K. Holm and L. Skattebøl, University of Oslo, Norway (15). Initially it was believed that the two acids were the *endo*-7 and *exo*-7 isomers, and so this mixture was converted to what was expected to be the *endo*- and *exo*-7 chloro derivative. However, the acid is actually a mixture of the *endo*-7 (**3***b*) and *endo*-9 (**3***a*) isomers and so the chlorides were later reassigned the title structures. To a solution of 0.697 g (0.39 mmol) of the mixed acid and 2.46 g (1.84 mmol) of *N*-chlorosuccinimide in 3 mL of a 3:1 mixture of DMF and glacial acetic acid, and under an argon atmosphere, was added 1.65 g (0.62 mmol) of lead tetraacetate (36). Provision was made for monitoring evolved gas volumes and the mixture was slowly heated with an oil bath. At ca. 55°C, the reaction was strongly initiated and gas evolution (180 mL) was complete after 3 min. The semisolid mixture was extracted twice with pentane, water was added to dissolve the precipitate, and the aqueous mixture was extracted twice with pentane. The combined pentane extracts were washed successively with dilute perchloric acid, sodium carbonate solution, and water, dried over $MgSO_4$, and most of the pentane removed. Column chromatography on neutral alumina, activity 1, using a pentane eluent led to the isolation of several fractions of a mixture of two chlorides with resolved GLC peaks. Distinctive ^{1}H NMR peaks were observed at δ 4.18 and 4.26 (both broad doublets, *J* ca. 4 Hz). For the carbocation work, a fraction containing a 3:2 ratio of the two chlorides was used, along with a preparation temperature of ca. −135°C (using SbF_5 in 3:1 SO_2ClF–SO_2F_2). One sees only cations **A** and **J**, in a ca. 3:2 ratio. The 9-chloro isomer is expected to initially form tertiary cation **D**, so this experiment represents a third precursor of **D** that fails to give this cation.

Tricyclo[5.2.1.$0^{3,8}$*]decan-3-ol* was prepared as described by Corey and Glass (21). A definitive assignment of all of the ^{13}C peaks was desired as an aid in characterizing the corresponding cation **J**. To unambiguously assign these, a 2D ^{13}C INADEQUATE spectrum was obtained. ^{1}H NMR, δ: 2.21 (bs, H1), 2.13 (m, H7), 1.70 (d, *J* = 4, H8), 1.73–1.83 (2H, H9 and H4). 1.65–1.3 (complex, 9H), 1.22 (d, *J* = 9.5, H9), 0.84 (d, m, *J* = 12, H10 *endo*). ^{13}C NMR, δ: 37.0 (C1), 44.7 (C2), 77.0 (C3), 35.8 (C4), 18.5 (C5), 26.3 (C6), 34.0 (C7), 49.9 (C8), 39.6 (C9), 31.3 (C10).

Tricyclo[5.2.1.$0^{3,8}$*]decan-4-one* and *tricyclo[5.2.1.*$0^{4,8}$*]decan-3-one* were prepared as a mixture, as described (37) by Majerski and Janjatovic and were separated by preparative HPLC. The first-named ketone was reduced with lithium aluminum hydride to a single oily alcohol, *tricyclo[5.2.1.*$0^{3,8}$*]decan-4-ol*, most probably of the 1*R**3*R**4*S**7*S**8*R** stereochemistry. ^{1}H NMR, δ: 3.6–3.8 (m, 1H), remaining peaks from 2.3–0.8, including a fully resolved peak at 0.88 (d, t, *J* = 12, 3, 1H). ^{13}C NMR, δ: 70.5 (CH), 42.6 (CH), 41.7 (CH), 40.8 (CH_2), 36.7 (CH), 33.6 (CH_2), 32.7 (CH), 28.8 (CH_2), 25.8 (CH_2), 23.6 (CH_2). The crude alcohol was converted to the *mesylate*, ^{1}H NMR, δ: 4.82 (m, 1H), 2.98 (s, 3H), 2.42 (m, 1H), 2.20 (m, 1H), 2.04 (m, 1H), 1.96 (m, 1H), 1.2–1.9 (complex), 0.94 (d, *J* = 12, 1H). ^{13}C NMR, δ: 83.2 (CH), 43.0 (CH), 40.9 (CH_2), 39.6 (CH), 38.7 (CH_3), 36.8 (CH), 33.4 (CH_2), 32.2 (CH), 29.6 (CH_2), 25.6 (CH_2), 21.5 (CH_2). Addition of the mesylate to 1:1 FSO_3H–SbF_5 in SO_2ClF at −100°C yielded only the 1-adamantyl cation **R**.

Tricyclo[4.3.1.$0^{3,8}$*]decan-6-ol* was prepared as described (38), ^{13}C NMR, δ: 71.3 (q), 48.1 (CH_2), 41.2 (CH_2), 41.0 (CH_2), 36.6 (CH_2), 36.4 (CH_2), 35.9 (CH), 34.9 (CH), 33.3 (CH), 24.2 (CH_2). Addition of the alcohol to 1:1 FSO_3H–SbF_5 in SO_2ClF at −100°C yielded only the 1-adamantyl cation **R**.

Tricyclo[3.3.1.$1^{3,7}$*]decan-2-ol-2*-d was prepared by reducing the ketone with $LiAlD_4$.

Acknowledgements

We thank Christian Falkenberg-Anderson and Susan Ranson for help in some of the synthetic work. We are grateful to Professor L. Skattebøl and Dr. K. Holm, University of Oslo, Norway, for a small sample of the mixed acids **3***a* and **3***b*. The Natural Sciences and Engineering Research Council of Canada is thanked for the generous funding of this research.

1. P. von R. Schleyer, R.C. Fort, Jr., W.E. Watts, M.B. Comisarow, and G.A. Olah. J. Am. Chem. Soc. **86**, 4195 (1964).
2. G.A. Olah, G.K.S. Prakash, J.G. Shih, V.V. Krishnamurthy, G.C. Mateescu, G. Liang, G. Sipos, V. Buss, T.M. Gund, and P. von R. Schleyer. J. Am. Chem. Soc. **107**, 2764 (1985).
3. (*a*) B. Ernst and C. Ganter. Helv. Chim. Acta, **61**, 1107 (1978); (*b*) F.J. Jäggi, P. Buchs, and C. Ganter. Helv. Chim. Acta, **63**, 872 (1980); (*c*) F.J. Jäggi and C. Ganter. Helv. Chim. Acta, **63**, 2087 (1980); (*d*) Helv. Chim. Acta, **63**, 214 (1980); (*e*) H.-R. Känel, H.-G. Capraro, and C. Ganter. Helv. Chim. Acta, **65**, 1032 (1982); (*f*) H.-R. Känel and C. Ganter. Helv. Chim. Acta, **68**, 1226 (1985).
4. H.W. Whitlock, Jr. and M.W. Siefkin. J. Am. Chem. Soc. **90**, 4929 (1968).
5. P. von R. Schleyer. *In* Cage hydrocarbons. *Edited by* G.A. Olah. John Wiley and Sons, Inc., New York. 1990. Chap. 1.
6. (*a*) E. Huang, K. Ranganayakulu, and T.S. Sorensen. J. Am. Chem. Soc. **94**, 1780 (1972); (*b*) J. Am. Chem. Soc. **94**, 1778 (1972); (*c*) A.J. Jones, E. Huang, R. Haseltine, and T.S. Sorensen. J. Am. Chem. Soc. **97**, 1133 (1975); (*d*) R. Haseltine, E. Huang, K. Ranganayakulu, and T.S. Sorensen. Can. J. Chem. **53**, 1056 (1976); (*e*) R. Haseltine, E. Huang, K. Ranganayakulu, T.S. Sorensen, and N. Wong. Can. J. Chem. **53**, 1876 (1975).
7. F.A.L. Anet and V.J. Basus. J. Magn. Reson. **32**, 339 (1978).
8. N. Okazawa and T.S. Sorensen. Can. J. Chem. **56**, 2737 (1978).
9. D.G. Farnum and A.D. Wolf. J. Am. Chem. Soc. **96**, 5166 (1974); **96**, 5175 (1974).
10. T. Laube. Angew. Chem. Int. Ed. Engl. **26**, 56 (1987).
11. R.P. Haseltine and T.S. Sorensen. Can. J. Chem. **53**, 1067 (1975).
12. G.A. Olah, G.K.S. Prakash, and M. Saunders. Acc. Chem. Res. **16**, 440 (1983).
13. T.W. Bentley, B. Goer, and W. Kirmse. J. Org. Chem. **53**, 3066 (1988).
14. G.A. Olah, A.M. White, J.R. DeMember, A. Commeyras, and C.Y. Lui. J. Am. Chem. Soc. **92**, 4627 (1970).
15. P. von R. Schleyer, P. Grubmuller, W.F. Maier, O. Vostrowsky, L. Skattebøl, and K.H. Holm. Tetrahedron. Lett. **21**, 921 (1980).
16. (*a*) Y. Tobe, K. Terashima, Y. Sakai, and Y. Odaira. J. Am. Chem. Soc. **103**, 2307 (1981); (*b*) K.L. Ghatak and C. Ganter. Helv. Chim. Acta, **71**, 124 (1988).
17. G.A. Morris and R. Freeman. J. Magn. Reson. **29**, 433 (1978).
18. S. Forsén and R.A. Hoffman. J. Chem. Phys. **39**, 2892 (1963).
19. G.A. Olah, J.R. DeMember, C.Y. Lui, and R.D. Porter. J. Am. Chem. Soc. **93**, 1442 (1971).
20. (*a*) M. Farcasiu, E.W. Hagaman, E. Wenkert, and P. von R. Schleyer. Tetrahedron Lett. **22**, 1501 (1981); (*b*) F.J. Jäggi and C. Ganter. Helv. Chim. Acta, **63**, 886 (1980); (*c*) A.M.

Klester, F.J. Jäggi, and C. Ganter. Helv. Chim. Acta, **63**, 1294 (1980); (*d*) A.M. Klester and C. Ganter. Helv. Chim. Acta, **66**, 1200 (1983).
21. E.J. Corey and R.S. Glass. J. Am. Chem. Soc. **89**, 2600 (1967).
22. R.P. Kirchen, T.S. Sorensen, and K.E. Wagstaff. J. Am. Chem. Soc. **100**, 5134 (1978).
23. (*a*) A. Karim, M.A. McKervey, E.M. Engler, and P. von R. Schleyer. Tetrahedron Lett. 3987 (1971); (*b*) A. Karim and M.A. McKervey. J. Chem. Soc. Perkin Trans. 1, 2475 (1974).
24. G.A. Olah and A.M. White. J. Am. Chem. Soc. **91**, 3954 (1969).
25. (*a*) D. Lenoir, R.E. Hall, and P. von R. Schleyer. J. Am. Chem. Soc. **96**, 2138 (1974), and earlier references; (*b*) J.E. Nordlander, J.E. Haky, and J.P. Landino. J. Am. Chem. Soc. **102**, 7487 (1980); (*c*) J.E. Nordlander and J.E. Haky. J. Org. Chem. **45**, 4780 (1980); (*d*) A.D. Allen and T.T. Tidwell. J. Am. Chem. Soc. **104**, 3145 (1982); (*e*) J.A. Bone, J.R. Pritt, and M.C. Whiting. J. Chem. Soc. Perkin Trans. **2**, 1447 (1975).
26. R. Dutler, A. Rauk, S.M. Whitworth, and T.S. Sorensen. J. Am. Chem. Soc. **113**, 411 (1991).
27. P. Vogel, M. Saunders, W. Thielecke, and P. von R. Schleyer. Tetrahedron Lett. 1429 (1971).
28. P. von R. Schleyer, L.K.M. Lam, D.J. Raber, J.L. Fry, M.A. McKervey, J.R. Alford, B.D. Cuddy, V.G. Keizer, H.W. Geluk, and J.L.M.A. Schlatmann. J. Am. Chem. Soc. **92**, 5246 (1970).
29. T.S. Sorensen and S.M. Whitworth. *In* Cage hydrocarbons. *Edited by* G.A. Olah. John Wiley and Sons, Inc., New York. 1990. Chap. 2.
30. R. Freeman. A handbook of nuclear magnetic resonance. Longman Scientific and Technical, Essex, England. 1987. pp. 198–202.
31. M.J.S. Dewar and J.J.P. Stewart. QCPE publication 455, Department of Chemistry, Indiana University, Bloomington, Ind.
32. B.A. Dawson and J.B. Stothers. Org. Magn. Reson. **21**, 217 (1983).
33. P. von R. Schleyer and M.M. Donaldson. J. Am. Chem. Soc. **78**, 5702 (1956).
34. P. Wilder, Jr. and G.T. Youngblood. J. Am. Chem. Soc. **78**, 5706 (1956).
35. N. Takaishi, H. Takahashi, O. Yamashita, and Y. Inamoto. J. Org. Chem. **51**, 4862 (1986).
36. K.B. Becker, M. Geisel, C.A. Grob, and F. Kuhnen. Synthesis, 493 (1973).
37. Z. Majerski and J. Janjatović. Tetrahedron Lett. 3977 (1979).
38. A. Karim and M.A. McKervey. J. Chem. Soc. Perkin Trans. **1**, 2477 (1974).
39. K. Ranganayakulu and T.S. Sorensen. J. Org. Chem. **49**, 4310 (1984).

Can. J. Chem. Downloaded from www.nrcresearchpress.com by 203.198.23.82 on 09/08/12
For personal use only.

Local and framework stereochemical markers in vibrational circular dichroism: 1,2- and 2,3-dimethylaziridines

DANYA YANG, THOMAS EGGIMANN, HAL WIESER, AND ARVI RAUK[1]
Department of Chemistry, The University of Calgary, Calgary, AB T2N 1N4, Canada

AND

GENNADII SHUSTOV
Institute of Chemical Physics, Russian Academy of Sciences, 117977 Moscow, Russia

Received July 6, 1993

DANYA YANG, THOMAS EGGIMANN, HAL WIESER, ARVI RAUK, and GENNADII SHUSTOV. Can. J. Chem. **71**, 2028 (1993).

The vibrational circular dichroism (VCD) spectra of 2,3-dimethylaziridine **1** and 1,2-dimethylaziridine **2** were measured experimentally and interpreted with the help of *ab initio* Vibronic Coupling Theory (VCT) both in the common origin (CO) and distributed origin (DO) gauge. The absolute magnitudes of the VCD intensities by the VCT-CO method in the mid-IR range are closer to the experimental measurement. Both VCT-DO and VCT-CO methods, however, predict the same signs for almost all VCD bands. In general, both VCT-DO and VCT-CO methods predict VCD and IR spectra that are both in good agreement with the experimental spectra. The VCT method together with the 6-31G*$^{(0.3)}$ basis set can be employed with confidence in determining the absolute configuration of a chiral molecule. The theoretical and experimental VCD spectra of **1** and **2** were compared with the VCD spectra of the isostructural 2,3-dimethyloxirane and -thiirane. One of the Me rocking motions, in the wave number range 1050–1150 cm^{-1}, was found to serve as a possible marker for the stereochemistry of the molecular skeleton. Two other modes were identified whose Cotton effects (CEs) are characteristic of the *local* asymmetry, and for which chirality rules were proposed. The first is a methyne vibration, ‖CH, which is expected to have a (−) CE at a three-ring centre with (*R*) absolute configuration. The second is an umbrella motion of a methyl group, which is expected to have a (+) CE when attached to a three-ring centre with (*R*) absolute configuration.

DANYA YANG, THOMAS EGGIMANN, HAL WIESER, ARVI RAUK et GENNADII SHUSTOV. Can. J. Chem. **71**, 2028 (1993).

On a déterminé les spectres VCD expérimentaux des 2,3-diméthylaziridine (**1**) et 1,2-diméthylaziridine (**2**) et on les a interprétés à l'aide de la théorie *ab initio* du couplage vibronique (VCT) avec origine commune (CO) ou distribution d'origine (DO). Les amplitudes absolues des intensités des spectres VCD obtenues par la méthode VCT-DO pour la plage de l'infrarouge moyen se rapprochent le plus des valeurs expérimentales. Toutefois, les deux méthodes, VCT-DO et VCT-CO, prédisent les mêmes signes pour toutes les bandes VCD. En général, les méthodes VCT-DO et VCT-CO prédisent des spectres IR et VCD qui sont en accord avec les données expérimentales. On peut donc utiliser en toute confiance la méthode VCD de concert avec un ensemble 6-31G*$^{(0.3)}$ pour déterminer la configuration absolue d'une molécule chirale. On a comparé les spectres VCD expérimentaux et théoriques des composés **1** et **2** avec le spectre VCD des 2,3-diméthyloxirane et -thiirane isostructurales. On a trouvé que l'un des mouvements de balancement du méthyle, dans la région de nombre d'onde de 1050 à 1150 cm^{-1} peut éventuellement servir de marqueur pour la stéréochimie du squelette moléculaire. On a aussi identifié deux autres modes dont les effets Cotton (EC) sont caractéristiques d'une asymétrie *locale* et pour lesquels on propose des règles de chiralité. Le premier est une vibration méthyne, ‖CH, qui devrait posséder un EC négatif et un configuration absolue (*R*) lorsqu'il est attaché à un centre à trois cycles. Le deuxième est un mouvement de parapluie d'un groupe méthyle pour lequel on attend un effet Cotton positif avec une configuration absolue (*R*) lorsqu'il est attaché à un centre à trois cycles.

[Traduit par la rédaction]

Introduction

Vibrational circular dichroism (VCD) has become a powerful spectroscopic tool for probing absolute configurations and conformation of chiral molecules in solution and in the gas phase. The observed VCD bands have to be interpreted using suitable and reliable theoretical models. The magnetic field perturbation (MFP) theory (1), the vibronic coupling theory (VCT) (2), and the localized molecular orbital (LMO) theory (3) are based on *ab initio* quantum chemical formulations, and their reliability has been established by direct comparisons of theoretical predictions to the experimental data. We have applied the VCT method to calculate a series of small ring molecules, for which experimental data are available and *ab initio* calculations of VCD intensities are possible. The VCT method along with a modest-sized basis set, designated 6-31G*$^{(0.3)}$ (4), has proved to be successful in producing the correct patterns of most VCD bands of substituted oxiranes (5, 6) and thiiranes (6, 7), and of 2-methylaziridine (8). In the latter case, the analysis was complicated by the existence of inversional (at N) diastereomers. The inverted configuration at N resulted in the prediction of opposite handedness in many of the VCD bands, and the ensuing partial cancellation of the VCD spectrum was proffered as an explanation for the very weak experimental VCD spectrum. To explore the relative roles of the heteroatom configuration and the skeletal asymmetry as defined by the σ framework of the molecule, we have synthesized two dimethyl aziridines, which have the same skeletal configuration but which differ in the position of the N atom. In this paper, we present the experimental and theoretical VCD spectra of (2*S*,3*S*)-2,3-dimethylaziridine (**1**) and (1*R*,2*R*)-1,2-dimethylaziridine (**2**), and provide an analysis of the spectroscopic implications by the VCT/6-31G*$^{(0.3)}$ method. The VCD and IR (9) spectra of another substituted aziridine, 2-methylaziridine, were reported earlier.

In the VCT method (2), the individual electric and mag-

[1]Author to whom correspondence may be addressed.

Can. J. Chem. Downloaded from www.nrcresearchpress.com by 203.198.23.82 on 09/08/12
For personal use only.

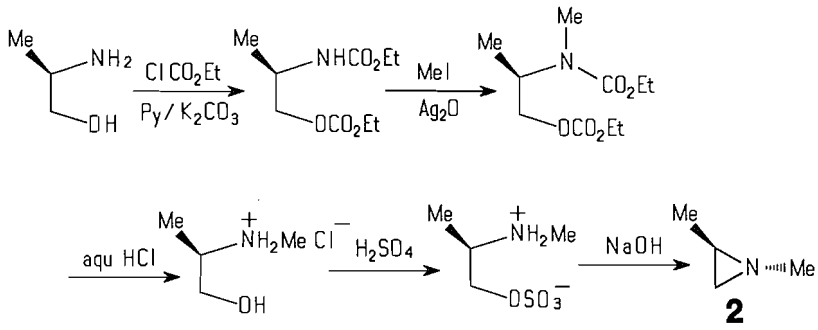

SCHEME 1

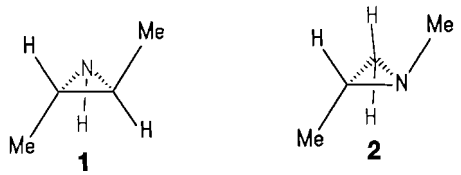

netic dipole transition moments are, respectively,

$$[1]\quad (\mu)^j_{00,01} = e\left(\frac{\hbar}{2\omega_j}\right)^{1/2}\left[\sum_n^{\text{atoms}} Z_n \mathbf{S}^j_n - 2\sum_n^{\text{atoms}}\sum_i^{\text{electrons}} \left\langle \Psi_0 \left| \mathbf{r}_i \frac{\partial}{\partial \mathbf{R}_n} \right| \Psi_0 \right\rangle \mathbf{S}^j_n\right]$$

and

$$[2]\quad (\mathbf{m})^j_{01,00} = \frac{e}{2c}\left(\frac{\hbar\omega_j}{2}\right)^{1/2}\left[i\sum_n^{\text{atoms}} Z_n\left(\mathbf{R}^0_n \times \mathbf{S}^j_n\right) + \frac{2\hbar}{m_e}\sum_n^{\text{atoms}}\sum_i^{\text{electrons}}\sum_e^{\text{ex}} \langle \Psi_0|\mathbf{r}_i \times \mathbf{p}_i|\Psi_e\rangle \left\langle \Psi_e \left| \frac{\partial}{\partial \mathbf{R}_n} \right| \Psi_0 \right\rangle \mathbf{S}^j_n \frac{1}{E_e - E_0}\right]$$

where Z_n is the bare nuclear charge of atom n with positional vector $\boldsymbol{R}_n$ and displacement vector $\boldsymbol{S}^j_n = (\partial \boldsymbol{R}_n/\partial Q_j)$ during a normal vibrational mode Q_j, $\boldsymbol{r}_i$ and $\boldsymbol{p}_i$ are the position and momentum of the ith electron, ω_j is the frequency of the jth normal mode, and $E_e - E_0$ is the vertical electronic excitation energy. The electronic wavefunctions are denoted Ψ_0 and Ψ_e. The energy difference and all matrix elements are evaluated at the equilibrium geometry of the ground state. The subscript (00,01) signifies that the transition is between the $v = 0$ and $v = 1$ vibrational levels of the ground electronic state of the molecule. The VCT rotational strength is the imaginary part of the scalar product of $(\mu)^j_{00,01}$ and $(\boldsymbol{m})^j_{01,00}$, eqs. [1] and [2], respectively.

The VCT formalism has been implemented at the *ab initio* level of theory in both the common origin (CO) (10) and the distributed origin (DO) (6, 11) gauges. In the CO gauge, all transition moments are calculated in the same coordinate system, i.e., the same origin gauge. In the distributed origin gauge, the magnetic transition moments corresponding to each atom are calculated by using different origin gauges for different atoms.

Experimental and computational details

Synthesis

(2R,3R)-2,3-Dimethylaziridine, bp 74–75°C, $[a]^{20}_D$ −101.6 (*c* 1.7 heptane) was synthesized according to ref. 12. Synthesis of *(2R)-1,2-dimethylaziridine* followed Scheme 1.

Ethyl chloroformate (8.68 g, 0.08 mol) was added dropwise to (2*R*)-2-aminopropanol (2.5 g, 0.022 mol) and K_2CO_3 (5.53 g, 0.04 mol) in 30 mL absolute pyridine with cooling (0°C) and stirring. After 8 h at 20°C, the precipitate was filtered off and the solvent was evaporated in vacuo. The product was extracted from the residue with ether and, after removal of ether, was dissolved in DMF (70 mL).

Silver(I) oxide (15.5 g, 0.066 mol) and methyl iodide (37.8 g, 0.266 mol) were successively added to the resulting solution with cooling (10°C) and stirring. After 20 h of stirring at 20°C, the precipitate was filtered off and the solution was mixed with ether (300 mL). The resulting solution was decanted from the dark residue, washed by water and brine, and was dried ($MgSO_4$). After removal of the solvent in vacuo, the residue (dark red oil, 3.6 g) was dissolved in aqueous 50% H_2SO_4 (8.4 mL). After about 7 mL of H_2O had been distilled from the mixture (at 20 Torr; 1 Torr = 133.3 Pa), the residue was dissolved in MeOH (15 mL) and precipitated by ether. The solid sulfate (3.4 g) was placed in a distilling flask and a cold solution of NaOH (4 g, 0.1 mol) in H_2O (16 mL) was added. The mixture was heated and 40 mL of distillate (bp 40–100°C) was collected. The distillate was cooled and saturated with KOH (pellets); the organic layer was separated and dried (KOH pellets), and twice distilled over the fresh KOH pellets, providing (2*R*)-1,2-dimethylaziridine (0.2 g, bp 42–44°C (lit. (13); bp 42–44°C), $[\alpha]^{20}_D$ −46.1 (*c* 0.9 CCl_4). ^{1}H NMR spectrum in $CDCl_3$ (200 MHz) δ, ppm (*J*, Hz): 1.12 d (H_A, $^3J^{cis}$ = 6.1), 1.15 (Me, ^3J = 5.0), 1.25 m (H_C), 1.45 d (H_B, $^3J^{trans}$ = 3.3), 2.29 (MeN).

Measurement

The absorption spectrum was measured with a Nicolet 8000 FT-IR spectrometer and, for VCD, a linear polarizer, a ZnSe photoelastic modulator (Hinds International), a f/1 ZnSe focusing lens, and the necessary electronic equipment were added to the instrument as described elsewhere (14). A narrow band MCT detector cooled with liquid nitrogen was used for all experiments. The interferometer was operated at an effective resolution of 4 cm^{-1}, coadding 50 scans and 20 000 scans for the absorption and VCD spectra, respectively.

Solutions of (2*R*)-1,2-dimethylaziridine (0.969 M and 1.67 M (VCD), and 0.969 M (IR)) and (2*S*,3*S*)-2,3-dimethylaziridine (0.87 M (VCD and IR)) in carbon tetrachloride were prepared to record absorption and VCD spectra. Neat CCl_4 was utilized to subtract the VCD background. The sample cell had KBr windows and a path length of 0.1 mm.

Computations

All calculations were done with the 6-31G*$^{(0.3)}$ basis set (a modification of the conventional 6-31G* basis set in which the *d*

Can. J. Chem. Downloaded from www.nrcresearchpress.com by 203.198.23.82 on 09/08/12
For personal use only.

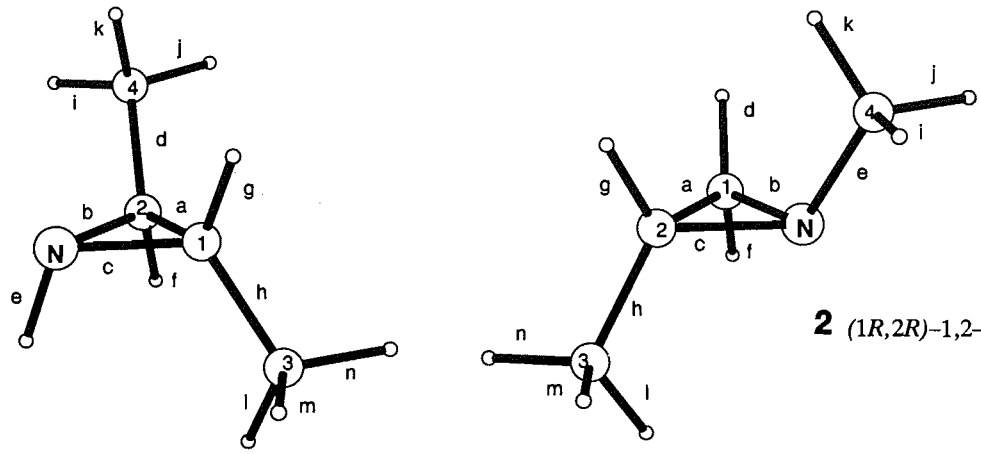

FIG. 1. RHF/6-31G*(0.3) structures of (2*S*,3*S*)-2,3-dimethylaziridine **1** and (1*R*,2*R*)-1,2-dimethylaziridine **2**. See Table 1 for parameter values.

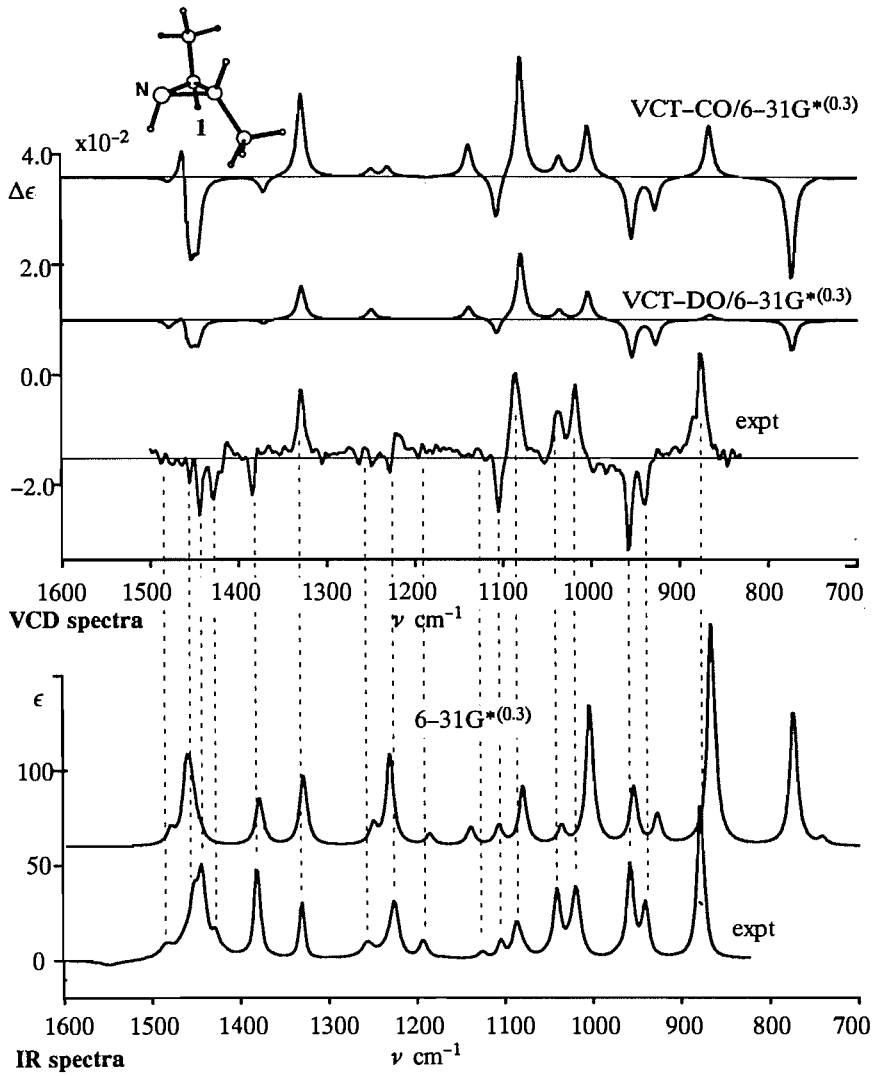

FIG. 2. Theoretically simulated and experimental VCD and IR spectra of (2*S*,3*S*)-2,3-dimethylaziridine **1** in the region 700–1600 cm^{-1}.

orbital exponent of the C and N basis sets is set to 0.3 from the usual value of 0.8), at the corresponding optimized geometries. The optimized geometry, *ab initio* quantum mechanical force field, and Cartesian displacement vectors for the normal modes were obtained using the GAUSSIAN90 program (15). The VCT intensities, which were evaluated both in a common origin (CO) gauge and a distributed origin (DO) gauge (6, 11), were obtained using the program, VCT90 (6, 16). The centre of the molecular mass was

Can. J. Chem. Downloaded from www.nrcresearchpress.com by 203.198.23.82 on 09/08/12
For personal use only.

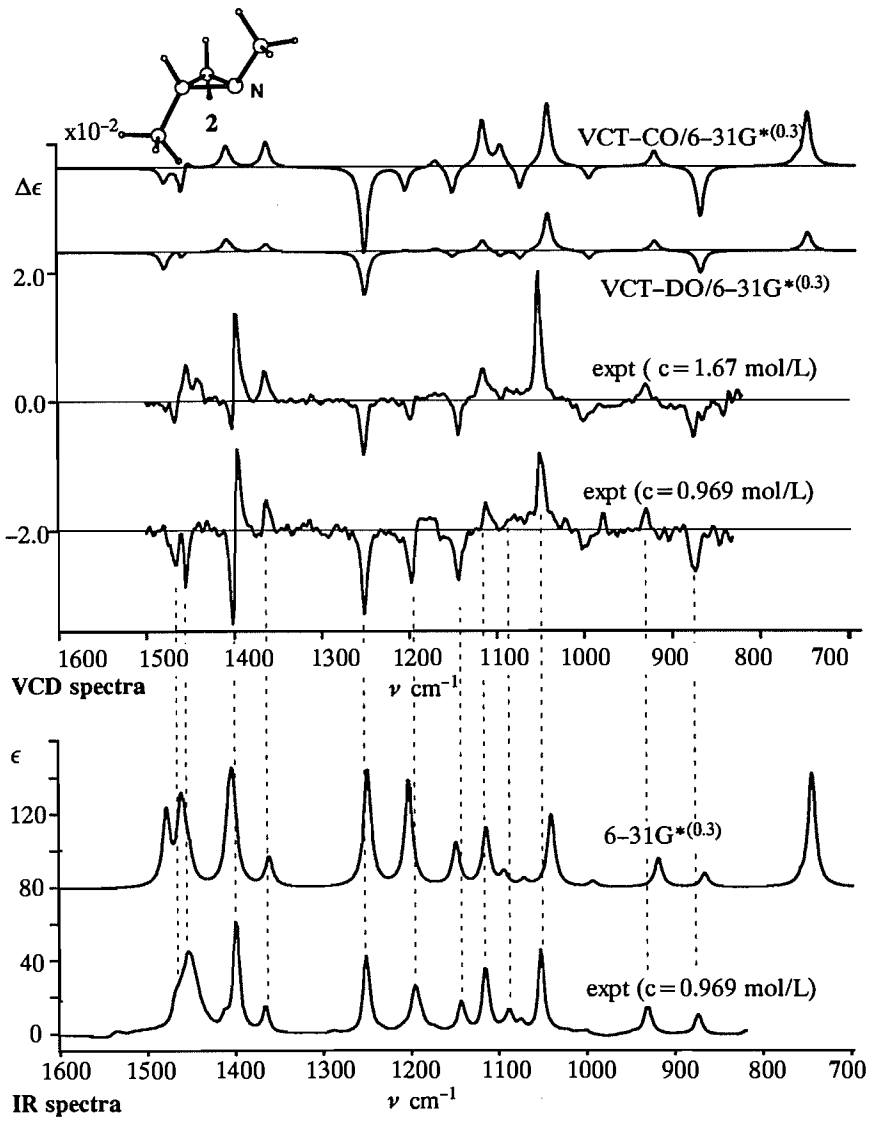

FIG. 3. Theoretically simulated and experimental VCD and IR spectra of (1*R*,2*R*)-1,2-dimethylaziridine **2** in the region 700–1600 cm^{-1}.

chosen as the common origin in the CO gauge, and the nuclear positions were used as origins in the DO gauge. The electronic ground state in eqs. [1] and [2] is approximated by the Hartree–Fock (SCF) determinantal wave function, and the excited states involved in the summation in eq. [2] are approximated as singlet-spin-adapted singly excited configurations derived from the Hartree–Fock wave function.

The theoretical results are displayed as simulated spectra using Lorentzian line shapes with 10 cm^{-1} band width (full width at half height) in Figs. 2 and 3. The *ab initio* harmonic frequencies were uniformly scaled by 0.9 to compensate for systematic errors in the computation of force constants at the Hartree–Fock level (17) and to make comparison with the experimental spectra easier. The assignments of the vibrational modes in Tables 2 and 3 were from computer animation of normal modes based on the 6-31G*$^{(0.3)}$ force fields, and only the major group motions are identified, in decreasing order of their apparent involvement. The nature of the vibrations is particularly complex in the range 800–1400 cm^{-1} for the two molecules discussed here, and the assignments listed in Tables 2 and 3 are only approximate. The notations used in assigning vibrational modes are: ⊥ = perpendicular to df or gh plane; ∥ = parallel to df or gh plane (Fig. 1); str = stretch; def = deformation; umb = umbrella motion; scis = scissor. Wherever available, the experimental frequencies are mentioned in the discussion below.

Results and discussion

The 6-31G*$^{(0.3)}$ geometries of (2*S*,3*S*)-2,3-dimethylaziridine **1** and (1*R*,2*R*)-1,2-dimethylaziridine **2** are shown in Fig. 1. In the latter case, the structure of the *cis* diastereomer, (1*S*,2*R*)-**2**, was also determined. Since this diastereomer was found to be 10.6 kJ mol^{-1} less stable (MP2/6-31G*$^{(0.3)}$//RHF/6-31G*$^{(0.3)}$), it will have no spectroscopic consequences and was not considered further. Complete details of the structures in terms of parameters defined in Fig. 1 are listed in Table 1. Partial experimental data of 2-methylaziridine deduced from MW studies (18) are also given in Table 1 for comparison. Neither complete experimental nor theoretical structures of the two molecules have previously been reported. The lengths of ring C—C and C—N bonds in **1** are close to those of the corresponding bonds in 2-methylaziridine. The ring C—N bonds in **2** are notice-

Can. J. Chem. Downloaded from www.nrcresearchpress.com by 203.198.23.82 on 09/08/12
For personal use only.

Can. J. Chem. Downloaded from www.nrcresearchpress.com by 203.198.23.82 on 09/08/12
For personal use only.

TABLE 1. RHF/6-31G*(0.3) geometries of aziridines **1** and **2**

Parameter[a]	Expt.[b]	**1** calcd.	**2** calcd.
a	1.480[c]	1.483	1.489
b	1.488[c]	1.479	1.467
c	1.488[c]	1.478	1.464
d	1.517	1.512	1.083
e	1.010	1.008	1.459
f		1.084	1.080
g		1.082	1.085
h		1.514	1.512
i		1.091	1.089
j		1.092	1.089
k		1.089	1.097
l		1.091	1.089
m		1.091	1.091
n		1.091	1.092
ab		59.9	59.4
ac		59.9	59.6
ad	120.5	123.2	117.9
af		115.2	120.2
ag		116.7	114.9
ah		121.9	123.0
bc		60.2	61.1
bd		116.8	117.5
be		111.0	116.8
bf		115.4	115.3
ce		110.8	117.3
cg		111.9	115.2
ch		120.5	117.8
df		115.0	115.1
di (ei)		110.7	109.3
dj (ej)		110.9	109.3
dk (ek)		110.4	113.0
gh	116.7[c]	114.6	115.0
hl		111.1	110.4
hm		110.9	110.8
hn		110.8	110.8
adi (bei)		150.2	−155.6
adj (bej)		−89.7	85.9
adk (bek)		30.7	−34.9
ahl		28.2	−31.8
ahm		148.4	−151.5
ahn		−91.8	88.5

[a]See Fig. 1 for a definition of the parameters: the letters denote bonds, e.g., a is the length (Å), ab is the bond angle (°), and abc is the diheral angle (°); notations in parentheses are for **2**.
[b]2-Methylaziridine, ref. 18.
[c]Assumed from aziridine.

ably shorter (Table 1, Fig. 1). The N—CH_3 bond in **2** is also shorter than the ring C—N bonds in the two molecules.

(2S,3S)-2,3-Dimethylaziridine ***1***

The vibrational properties of this molecule are summarized in Table 2. The experimental and the simulated IR and VCD spectra in the range of 700–1600 cm^{-1} are shown in Fig. 2. Qualitatively, the similarities between the experimental and the simulated IR and VCD spectra are striking, especially the VCD spectrum calculated by the VCT-CO method.

For the IR spectra, the band at 879 cm^{-1}, which is due to the symmetric C—N stretching motion, is both observed and calculated to be the strongest band in the range of 700–1600 cm^{-1}. The VCD feature at this band is correctly reproduced by the VCT-CO method, but underestimated by the VCT-DO method. There is a noticeable inconsistency between the simulated and the experimental IR spectra near 1030 cm^{-1}, where two bands with about equal absorption intensities show up in the experimental spectrum. Of these two bands, the one at 1041 cm^{-1} (an asymmetric C—CH_3 stretching mode) is calculated to be too weak, and the one at 1020 cm^{-1} (a mixed mode of ‖NH and -CH_3 rocking) is calculated to be too intense. The VCD features of these two bands are, however, reproduced reasonably well, especially by the VCT-CO method. The simulated VCD spectrum by the VCT-CO method is generally in better agreement with the experiment, and the VCT-DO method underestimates the magnitudes of the VCD intensities for most of the bands in the experimental range for this molecule. The band at 1226 cm^{-1} appears as a very weak negative VCD, but is calculated as a weak positive VCD by both VCT-CO and VCT-DO methods, and this is the only noticeable inconsistency between the theoretical VCD predictions and the experimental measurements for this molecule. The four -CH_3 deformation modes with closely spaced theoretical frequencies between 1462 and 1446 cm^{-1} are calculated to be almost equally strong in the VCD spectrum. Correspondingly, only three frequencies are observed, at 1454, 1444, and 1430 cm^{-1}. Of these four -CH_3 deformation bands, the highest frequency band is calculated to have positive rotatory strength, and the other three are calculated to have negative rotatory strengths (which appear as a broad negative peak in the simulated VCD spectra). Three negative VCD bands are observed in the experimental VCD spectrum in this range; a positive VCD band, however, is not observed. It is possible that a mode with a positive rotatory strength is buried under other negative bands, and that the calculated frequencies are in error.

(1R,2R)-1,2-Dimethylaziridine ***2***

The vibrational properties of this molecule are summarized in Table 3. The simulated IR spectrum bears remarkable resemblance to the experimental IR spectrum (Fig. 3). The only noteworthy difference between the two is the region near 1450 cm^{-1}, where the four nearly degenerate -CH_3 deformation modes yield a broad absorption band in the experimental IR spectrum, while in the simulated IR spectrum the four are split into two bands. The sum of the four absorptions is, however, close to the experimental observation.

Two experimental VCD spectra (measured at different concentrations) are available for **2** (Fig. 3). Some of the band appearances in the two experimental VCD spectra differ considerably, which may be caused by strong underlying absorptions at these bands. The absolute magnitudes calculated by the VCT-CO method are generally closer to the experimental observations than those calculated by the VCT-DO method. All distinguishable signs and intensities of the VCD bands in the range of 800–1380 cm^{-1} in the experimental VCD spectra are reproduced well in the simulated VCD spectrum by the VCT-CO method. The VCT-DO calculations reproduce the signs of the VCD bands but underestimate the VCD intensities overall. One possible error is the calculated negative rotatory strength at 1076 cm^{-1}, which is due to mode ν_{13} (a mixed mode of -CH_2 wagging and -CH_3 rocking), where no clear negative VCD band appears in either experimental VCD spectrum. The band at

TABLE 2. VCT/6-31G*(0.3) vibrational properties of (2*S*, 3*S*)-2,3-dimethylaziridine **1**

	Frequency cm^{-1}			R^b		
	Calcd.[d]	Expt.[e]	D^b	CO	DO	Assignments[c]
1	182		0.7	−0.6	−0.4	CH_3 torsion
2	201		5.9	−2.1	−1.4	CH_3 torsion
3	233		15.7	2.1	1.5	⊥CH_3 group
4	270		3.3	0.4	−1.4	∥CH_3 group
5	417		20.7	5.6	1.6	∥CH_3 group
6	437		76.5	−8.0	−1.7	⊥CH_3 group
7	741		6.6	2.3	−0.7	asym CN str
8	773		117.4	−85.0	−25.1	ring CC str, sym CN
9	866	879	175.1	39.4	3.9	sym CN str, ring CC str
10	927	941	21.9	−22.0	−16.8	∥CH, CH_3 rocks, ⊥NH
11	954	958	40.8	−42.2	−25.3	⊥CH, ⊥NH, CH_3 rock
12	1004	1020	94.6	33.5	18.0	∥NH, CH_3 rock
13	1036	1041	11.8	11.8	5.6	C-CH_3 str, asym CN
14	1079	1087	36.8	73.6	39.9	CH_3 rock, ⊥NH
15	1107	1105	11.7	−25.9	−9.3	⊥f,[f] CH_3 rock
16	1139	1126	10.8	18.6	7.1	⊥g[g]
17	1185	1192	6.4	−0.8	−0.1	⊥NH, sym C-CH_3 str, ∥f,[f] ⊥g[g]
18	1230	1226	50.1	5.0	0.6	∥NH, ⊥f,[f] ∥g[g]
19	1249	1255	10.5	3.8	5.1	⊥NH, ∥CH, ring breath
20	1328	1330	35.7	41.3	16.5	∥CH
21	1372		0.9	−7.3	−1.9	sym CH_3 umb
22	1379	1382	22.9	−0.5	0.0	asym CH_3 umb
23	1446	1430	4.5	−26.5	−9.2	CH_3 def
24	1454	1444	10.7	−25.5	−6.8	CH_2 def
25	1458	1454	24.0	−19.6	−6.8	CH_3 def
26	1462		20.7	29.9	6.3	CH_3 def
27	1479	1483	6.3	−1.8	−3.1	ring breath, CH_3 def
28	2817		41.5	−2.3	−2.3	CH_3 sym str (C^3)
29	2822		35.4	1.0	1.8	CH_3 sym str (C^4)
30	2887		23.1	10.8	16.8	CH_3 asym str (C^3)
31	2888		32.2	−16.5	−21.8	CH_3 asym str (C^4)
32	2890		42.3	7.9	7.8	CH_3 asym str (C^3)
33	2903		3.1	−0.7	−0.9	CH_3 asym (C^4), CH (C^2) str
34	2922		40.0	−12.0	−20.7	CH str (C^2), CH_3 asym str (C^4)
35	2936		64.9	13.6	19.0	CH str (C^1)
36	3310		2.3	1.0	0.8	NH str

[a]In units of 10^{-40} esu^2 cm^2.
[b]In units of 10^{-44} esu^2 cm^2.
[c]Superscript numbers are indices of atoms (see Fig. 1).
[d]Uniformly scaled by 0.9
[e]Tentative assignments by measuring peak positions in Fig. 2.
[f]Bond f (see Fig. 1).
[g]Bond g (see Fig. 1).

1090 cm^{-1}, which is due to mode ν_{14} (a mixed mode of -CH_2 wagging and -CH_3 rocking), is calculated to have oppositely signed rotatory strength by the VCT-CO and VCT-DO methods. It is again difficult to judge which is correct since the experimental feature at this position is not clear. The relative intensities of the three moderately strong negative VCD bands at 1144, 1196, and 1251 cm^{-1} in the simulated VCD spectrum are closer to those of the corresponding bands in the experimental spectrum recorded at the higher concentration. The appearance of the VCD feature at the band of 1053 cm^{-1} is different in the two experimental VCD spectra; while a very strong positive VCD band appears in the higher concentration spectrum, the absolute intensity of this band is much smaller in the more dilute VCD spectrum. The VCD feature at this band in the higher concentration VCD spectrum may be misleading because the absorption at this band is strong, which may mistakenly yield strong absorption in the VCD spectrum. The calculated magnitude of this VCD band by the VCT-CO method is closer to the observed one in the lower concentration spectrum.

The experimental spectra in the range of 1350–1500 cm^{-1} yield a few uncertainties, which may be largely caused by the strong absorptions in this range. The four -CH_3 deformation modes near 1450 cm^{-1} yield two distinguishable negative VCD bands in the simulated VCD spectra. While the lower concentration experimental VCD spectrum supports the calculations for these four modes, the higher concentration VCD spectrum gives totally different appearance in this range. The prominent bisignate feature near 1400 cm^{-1} in the lower concentration VCD spectrum is doubtful, since the corresponding feature in the higher concentration VCD spectrum has a different appearance, that of a stronger positive VCD and much weaker negative VCD. There is only one observable absorption band corresponding to the above-

Can. J. Chem. Downloaded from www.nrcresearchpress.com by 203.198.23.82 on 09/08/12
For personal use only.

TABLE 3. VCT/6-31G*(0.3) vibrational properties of (1*R*, 2*R*)-1,2-dimethylaziridine **2**

	Frequency cm^{-1}			R^b		
	Calcd.[d]	Expt.[e]	D^a	CO	DO	Assignments[c]
1	182		0.5	−1.0	−0.7	CH_3 torsion
2	202		9.4	−3.0	−1.3	CH_3 torsion
3	235		15.5	1.6	0.2	⊥CH_3 group (C^3), C^4NC^1 bend
4	291		57.3	0.1	3.6	∥CH_3 group (C^3), C^4NC^2 bend
5	405		15.0	−3.7	−0.4	∥CH_3 group (C^3), C^4NC^2 bend
6	425		3.3	−2.6	−2.1	⊥CH_3 group (C^3), C^4NC^1 bend
7	744		108.1	40.2	13.9	ring sym CN str, ring CC str
8	757		4.2	3.8	0.0	ring asym CN str, C—CH_3 str
9	866	874	11.1	−32.5	−14.0	CH_2 twist, ⊥CH, ring def
10	918	931	22.0	9.4	5.9	C—CH_3 str, N—CH_3 str
11	993	1000	3.9	−7.3	−4.3	CH_2 twist, ∥CH, CH_3 rock (C^3)
12	1040	1053	49.2	33.7	20.1	C—CH_3 str, ⊥CH, CH_2 wag
13	1071	1076	4.1	−12.7	−4.2	CH_2 wag CH_3 rock
14	1094	1090	8.4	10.3	−2.8	CH_2 wag, CH_3 rock
15	1114	1116	36.3	22.9	5.3	CH_3 rock, ⊥d, ⊥CH
16	1148	1144	26.2	−13.4	−2.8	CH_3 rock, ⊥CH, CH_2 twist
17	1167	1173	0.3	3.7	1.3	CH_3, CH_2 rocks
18	1202	1196	62.3	−10.7	0.6	⊥CH, CH_3 rock (C^4), CH_2 twist
19	1249	1251	65.8	−38.4	−19.2	∥CH, ring breath
20	1362	1367	14.9	10.3	3.0	CH_3 umb (C^3)
21	1402	1400	44.8	1.3	1.5	CH_3 umb (C^4)
22	1408		27.1	7.8	4.0	CH_2 scis, ∥ CH, CH_3 umb
23	1453		9.9	5.3	0.8	CH_3 def (C^3)
24	1459	1454	20.4	−16.1	−4.4	CH_3def
25	1462		4.7	16.4	5.4	CH_3def
26	1462		20.3	−10.3	−1.8	CH_3 def (C^4)
27	1479	1469	34.6	−5.6	−6.4	CH_2 scis, ring breath
28	2782		79.6	−5.5	−6.0	CH_3 sym str (C^4)
29	2822		40.4	2.1	2.5	CH_3 sym str (C^3)
30	2872		61.2	5.2	4.4	CH_3 asym str (C^4)
31	2888		40.5	−2.6	−3.3	CH_3 asym str (C^3)
32	2897		13.7	6.3	7.1	CH, sym CH_2, CH_3 asym (C^3) str
33	2903		24.0	−14.2	−20.6	sym CH_2, CH, CH_3 asym (C^3) str
34	2907		36.7	9.2	13.9	CH_3 asym str (C^4)
35	2918		57.0	8.4	11.6	CH, CH_3 asym (C^3) str
36	2992		25.7	−2.0	−2.7	asym CH_2 str

[a]In units of 10^{-40} esu^2 cm^2.
[b]In units of 10^{-44} esu^2 cm^2.
[c]Superscript numbers are indices of atoms (see Fig. 1).
[d]Uniformly scaled by 0.9.
[e]Tentative assignments by measuring peak positions in Fig. 3.

mentioned two VCD bands. Two calculated frequencies, 1402 and 1408 cm^{-1} (modes ν_{21} and ν_{22}) are close to the observed frequency, 1400 cm^{-1}. The calculated VCD intensities at these two bands are much weaker and both positive.

Local and global stereochemistry

As stated in the introduction, the two dimethyl aziridines, **1** and **2**, have the same skeletal symmetry. One might expect that the Cotton effects (CEs) of *skeletal* vibrations, that is to say, normal modes that are composed of many strongly coupled local motions, should reflect the *global* stereochemistry and have the same sign, characteristic of the absolute handedness of the molecular skeleton (the *global* environment). On the other hand, as suggested by the stereochemical labels, (2*S*,3*S*) and (1*R*,2*R*), respectively, some regions of the molecule have different *local* symmetry. For instance, the environments of the methyne bond (CH) in **2** and both CH bonds in **1** are essentially, although not exactly, antipodal, as are the environments of the C—Me groups. If localized motions can be identified, the corresponding CEs should have opposite signs, and be characteristic of the absolute handedness of the *local* environment. The experimental VCD spectra of **1** and **2** are reproduced in Fig. 4b, together with the VCD spectra of (2*S*,3*S*)-2,3-dimethylthiirane (**7**) and (2*S*,3*S*)-2,3-dimethyloxirane (**4**), both of which also have the same *global* chirality. VCT-CO/6-31G*(0.3) simulated VCD spectra are also available for the four compounds, and these are reproduced in Fig. 4*a*. A cursory glance reveals little similarity between the four sets of spectra, experimental or theoretical. However, some commonality is readily adduced upon inspection of the descriptions of the normal modes as given in Tables 2 and 3 and in corresponding tables of refs. 4 and 7. These mode descriptions were derived from the theoretical calculations. Features that are most similar in the four compounds, as judged by the mode descriptions and correlation of theoret-

Can. J. Chem. Downloaded from www.nrcresearchpress.com by 203.198.23.82 on 09/08/12
For personal use only.

Can. J. Chem. Downloaded from www.nrcresearchpress.com by 203.198.23.82 on 09/08/12
For personal use only.

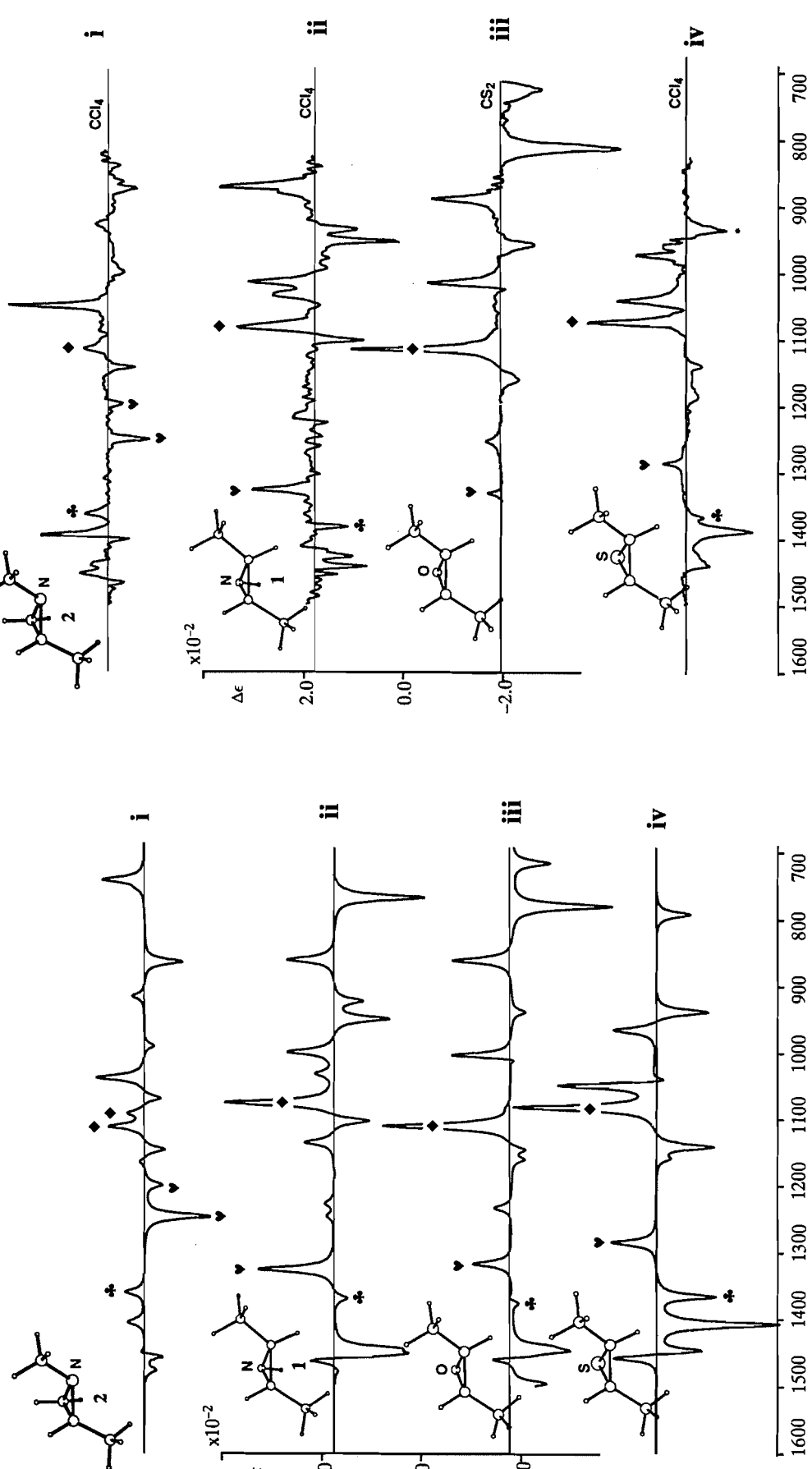

FIG. 4. (*a*) Theoretical VCT-CO/6-31G*$^{(0.3)}$ and (*b*) experimental VCD spectra of (1*R*,2*R*)-1,2-dimethylaziridine **2** (**i**), (2*S*,3*S*)-2,3-dimethylaziridine **1** (**ii**), (2*S*,3*S*)-2,3-dimethyloxirane (**iii**), (2*S*,3*S*)-2,3-dimethylthiirane (**iv**), in the region 700–1600 cm^{-1}.

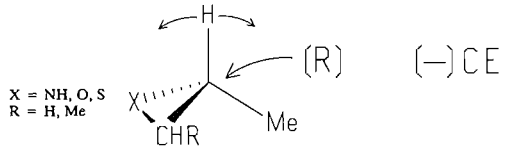

SCHEME 2. Chiral rule for ‖CH mode.

ical and experimental frequencies and intensities, are marked by common symbols in Fig. 4.

The strongest VCD feature in the spectra of each of the 2,3-dimethyl heterocycles is a methyl rock (◆), which has mixed into it CH and some ring CC stretching component. In the O and S compounds both the *a* and *b* symmetry modes have a (+) CE, the *a* symmetry mode being stronger in the oxirane, while both modes are moderately strong in the thiirane, the *b* symmetry mode dominating. The corresponding mode, also with (+) CE, is mixed with a wag of the NH bond in **1**. In **2**, the corresponding rock of the Me groups is mixed with perpendicular motions (wags) of the CH and CH_2 protons, and appears in two modes, both with (+) CE. This prominent feature would appear to be characteristic of the skeletal chirality. In principal, there are four combinations of the methyl rocking motions that should contribute to the fundamental vibrations of the molecule in the region 1050–1150 cm^{-1}. These are almost invariably mixed with other modes, participating in truly skeletal vibrations. The particular combination that gives rise to the prominent VCD feature (◆) corresponds to a rocking motion about an axis more or less in the plane of the exocyclic substituents (e.g., the gh plane, Fig. 1).

Several other features also appear to persist with the same sign in each of the four compounds. However, analysis of the composition yields little similarity in terms of local motions and these are unlikely to prove to be as reliable indicators of skeletal chirality as the Me rocks.

In the three-ring molecules, two types of motions of the CH (methyne) bonds are observed, either perpendicular to the plane formed by the exocyclic bonds (⊥), or in the plane of these bonds (‖). When not coupled by symmetry, these motions are in some cases highly localized. Modes in the four compounds where the dominant component is ‖CH are labelled with ♥ in Fig. 4. These correspond to modes of *b* symmetry in the C_2 compounds and are coupled in the same "antisymmetric" fashion in **1**. In each case (in the C_2 compounds) the mode has a moderately strong (+) CE. The "handedness" of the methyne environment ((*S*) absolute configuration) is the same in each of the compounds, except **2**. In **2**, the ‖CH motion occurs in an antipodal environment ((*R*) absolute configuration) and appears with (−) CE. It is of interest that the same ‖CH mode may be identified in 2-methyloxirane (mode 13, Tables 4 and 5 of ref. 4), 2-methylthiirane (calcd. frequency 1146 cm^{-1}, Table 6 of ref. 7), and 2-methylaziridine (mode 13 of both *cis* and *trans* forms, ref. 8). In each case, the calculated (VCT-CO/60-31G*$^{(0.3)}$) CE is consistent with the chiral rule shown in Scheme 2. Thus, the "‖CH" motion of a methyne attached to a chiral centre with (*R*) absolute configuration is expected to display a (−) CE, and vice versa. The ‖CH mode is readily identified in the experimental VCD spectra of all compounds except 2-methylthiirane where it is overlapped with two other vibrational modes and displays a weak CE in the region (near 1160 cm^{-1}) that is inconsistent with the rule.

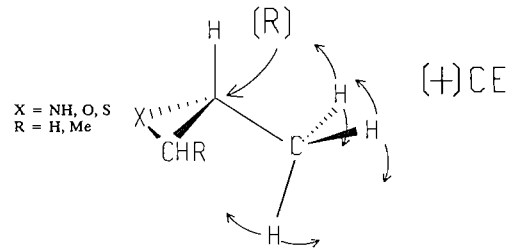

SCHEME 3. Chiral rule for Me umb mode.

The individual methyl groups also may function as a probe for the *local* chirality. In each of the 2,3-dimethyl heterocycles of Fig. 4, the methyl groups are attached to a centre with the same chirality ((*S*) absolute configuration), whereas in the 1,2-dimethyl aziridine 2, the C-Me group "sees" the antipodal environment ((*R*), as shown in Scheme 2). The umbrella motions are marked with ♣ in Fig. 4. In **2**, the umbrella motions of the two methyl groups are well separated from each other and other fundamental vibrations, the C-Me umbrella motion appearing at 1367 cm^{-1}, with (+) CE. In **1**, the in- and out-of-phase Me umbrella vibrations are only separated by 5 cm^{-1}, with the in-phase (sym) combination having the larger, and (−) CE. In the case of the dimethyloxirane, relatively small rotatory strengths of opposite sign are calculated for the umbrella modes of a and b symmetry with the larger corresponding to the b symmetry mode. In the dimethyl thiirane, the two umbrella modes are also calculated to have oppositely signed CEs, with the a symmetry mode having the much larger value. *In each case*, and in the case of the corresponding monomethyl heterocycles, the calculated and observed CE in the Me umbrella region is consistent with the Me umb chirality rule as shown in Scheme 3. The umbrella motion at a centre of (*R*) absolute chirality has a (+) CE, and vice versa.

Conclusions

In summary, for the two aziridines discussed above, VCT-CO calculations predict generally stronger VCD in mid-IR range and VCT-DO calculations predict generally stronger VCD in the C—H stretching range. This pattern is similar to that observed for the oxiranes (5) and thiiranes (7). The absolute magnitudes of the VCD intensities by the VCT-CO method in the mid-IR range are closer to the experimental measurement. Both VCT-DO and VCT-CO methods, however, predict the same signs for almost all VCD bands. In general, both VCT-DO and VCT-CO methods predict VCD and IR spectra that are both in good agreement with the experimental spectra. The VCT method together with the 6-31G*$^{(0.3)}$ basis set can be employed with confidence in determining the absolute configuration of a chiral molecule.

The theoretical and experimental VCD spectra of **1** and **2** were compared with the VCD spectra of the isostructural 2,3-dimethyloxirane and -thiirane. One of the Me rocking motions, in the wave number range 1050–1150 cm^{-1}, was found to have a similar description in each of the compounds and give rise to a strong VCD band whose sign may serve as a marker for the skeletal stereochemistry. Two other modes were identified whose CE are characteristic of the local asymmetry, and for which chirality rules could be proposed. The first is a methyne vibration, ‖CH, which is expected to have a (−) CE at a three-ring centre with (*R*)

Can. J. Chem. Downloaded from www.nrcresearchpress.com by 203.198.23.82 on 09/08/12
For personal use only.

absolute configuration (Scheme 2). The second is an umbrella motion of a methyl group, which is expected to have a (+) CE when attached to a three-ring centre with (*R*) absolute configuration (Scheme 3).

Acknowledgment

Financial support in the form of a grant from the Natural Sciences and Engineering Research Council of Canada (NSERC) is gratefully acknowledged.

1. P.J. Stephens. J. Phys. Chem. **89**, 748 (1985).
2. L.A. Nafie and T.B. Freedman. J. Phys. Chem. **78**, 7108 (1983).
3. (*a*) L.A. Nafie and T.H. Walnut. Chem. Phys. Lett. **49**, 441 (1977); (*b*) T.H. Walnut and L.A. Nafie. J. Chem. Phys. **67**, 1501 (1977); (*c*) L.A. Nafie and P.L. Polavarapu. J. Chem. Phys. **75**, 2935 (1981).
4. A. Rauk and D. Yang. J. Phys. Chem. **96**, 437 (1992).
5. S.T. Pickard, H.E. Smith, T.M. Black, P.L. Polavarapu, T.M. Black, A. Rauk, and D. Yang. J. Am. Chem. Soc. **114**, 6850 (1992).
6. D. Yang and A. Rauk. J. Chem. Phys. **97**, 6517 (1992).
7. P.L. Polavarapu, S.T. Pickard, H.E. Smith, T.M. Black, A. Rauk, and D. Yang. J. Am. Chem. Soc. **113**, 9748 (1991).
8. A. Rauk, T. Eggimann, H. Wieser, G.V. Shustov, and D. Yang. Can. J. Chem. In press.
9. A. Rauk, T. Eggimann, H. Wieser, and D. Yang. Can. J. Chem. **70**, 464 (1992).
10. (*a*) R. Dutler. Ph. D. Dissertation, The University of Calgary, 1988; (*b*) R. Dutler and A. Rauk. J. Am. Chem. Soc. **111**, 6957 (1989).
11. P.J. Stephens. J. Phys. Chem. **91**, 1712 (1987).
12. G.V. Shustov, A.V. Kachanov, V.A. Korneev, R.G. Kostyanovsky, and A. Rauk. J. Am. Chem. Soc. In press.
13. Yu. Minoura, M. Takebayashi, and Ch. C. Price. J. Am. Chem. Soc. **81**, 4689 (1959).
14. R.A. Shaw, H. Wieser, R. Dutler, and A. Rauk. J. Am. Chem. Soc. **112**, 5401 (1990).
15. M.J. Frisch, M. Head-Gordon, G.W. Trucks, J.B. Foresman, H.B. Schlegel, K. Raghavachari, M.A. Robb, J.S. Binkley, C. Gonzalez, D.J. Defrees, D.J. Fox, R.A. Whiteside, R. Seeger, L.R. Martin, J. Baker, L.R. Martin, L.R. Kahn, J.J. Stewart, S. Topiol, and J.A. Pople. GAUSSIAN 90, Gaussian, Inc., Pittsburgh, Pa. 1990. The version at the University of Calgary was modified to write extra information to the Read-Write file for VCD calculations.
16. D. Yang. Ph. D. Dissertation, The University of Calgary, 1992.
17. J.A. Pople, H.B. Schlegel, R. Krishnan, D.J. DeFrees, J.S. Binkley, M.J. Frisch, R.A. Whiteside, R.F. Hout, and W.J. Hehre. Int. J. Quantum Chem. Symp. **15**, 269 (1981).
18. Y.S. Li, M.D. Harmony, D. Hayes, and E.L. Beeson, Jr. J. Chem. Phys. **47**, 4514 (1967).

Can. J. Chem. Downloaded from www.nrcresearchpress.com by 203.198.23.82 on 09/08/12
For personal use only.

Activity coefficients and standard Gibbs free energies of transfer of NaCl and KCl from water to aqueous solution of 2-butoxyethanol by EMF studies

YVONNE MACPHERSON AND R. PALEPU[1]

Department of Chemistry, University College of Cape Breton, Sydney, NS B1P 6L2, Canada

Received April 8, 1993

YVONNE MACPHERSON and R. PALEPU. Can. J. Chem. **71**, 2038 (1993).

From the emf measurements of the cell Na- or K-glass electrode|2-butoxyethanol, H_2O, NaCl or KCl|Cl ion-selective electrode, the standard potentials were determined at 298 K for five different compositions of the solvent. From the emf data the mean activity coefficients of NaCl and KCl were calculated and fitted to an empirical equation. The standard Gibbs free energies of transfer of NaCl and KCl from water to mixtures of water and 2-butoxyethanol were calculated from the cell potential.

YVONNE MACPHERSON et R. PALEPU. Can. J. Chem. **71**, 2038 (1993).

Utilisant des fém mesurées à 298 K pour la cellule électrode de verre de Na ou de K|2-butoxyéthanol, H_2O, NaCl ou KCl|électrode à membrane sélective à l'ion Cl, on a déterminé les potentiels standard pour cinq compositions différentes de solvant. À partir des données de fém, on a calculé les coefficients moyens d'activité du NaCl et du KCl et on les a ajusté dans une équation empirique. Utilisant le potentiel de la cellule, on a calculé les énergies libres standard de transfert de Gibbs du NaCl et du KCl de l'eau vers des mélanges d'eau et de 2-butoxyéthanol.

[Traduit par la rédaction]

Can. J. Chem. Downloaded from www.nrcresearchpress.com by 203.198.23.82 on 09/08/12
For personal use only.

Introduction

The solution properties of aqueous mixtures of 2-butoxyethanol (B.E.) have received considerable attention in the literature (1–5). It is well established that 2-butoxyethanol forms microaggregates in a very dilute aqueous solution and is used as a cosurfactant in microemulsions (6). In the systems of water, 2-butoxyethanol, and NaCl or KCl a phase separation occurs at certain compositions of the system. To calculate the enthalpy of this process the data on activity coefficients of NaCl and KCl are required. Mean activity coefficients of these electrolytes are also required to calculate the counterion binding of various micelles in 2-butoxyethanol + water systems by the standard calibration method (7). The value of counterion binding is an important quantity in understanding the role of 2-butoxyethanol in microemulsions.

The use of ion-selective electrodes (I.S.E.) to study the thermodynamic properties of solutions is simple and safe compared to the classical amalgam cells. Ion-selective electrodes were recently used to determine the activity coefficients of alkali-metal halides in various binary mixtures of alcohols with water (8–10). This paper reports the determination of the activity coefficients of NaCl and KCl in binary mixtures of aqueous 2-butoxyethanol solutions at 298 K.

Experimental

The experimental cell can be represented as

Anion (Cl^-)-responsive I.S.E.	MCl H_2O + B.E.	Cation (M^+)-responsive I.S.E.

A Ross sodium electrode (84-11), Corning monovalent cation glass electrode (Catalogue no. 416220), and an Orion solid state chloride electrode (94-17) were used in the present investigation. Analytical reagent grades of sodium and potassium chloride of either Merck or B.D.H. chemicals were used without further purification. The crystals were dried prior to use. Concentration changes in the emf cell were made by adding a weighed quantity of sodium or potassium chloride directly to the cell containing the electrodes in either pure water or a binary solution of 2-butoxyethanol and H_2O. Thus electrodes remained in the same cell throughout a particular run. The cell was kept in a thermostatted water bath at 25.00 ± 0.05°C. The cell solutions were stirred by an air-driven magnetic stirrer. The cell potentials were measured with an Orion research microprocessor ion analyzer/901 and this arrangement allowed the emf to be read to ±0.1 mV. All solutions were made with NANO pure water and 2-butoxyethanol (Aldrich) of stated purity better than 99+%. The electrode system was periodically tested by determining the activity coefficients of aqueous NaCl or KCl over the concentration range 0.05–0.5 mol kg^{-1}. The activity coefficients of electrolytes in the mixed solvents were determined only after the values obtained for the activity coefficients of NaCl and KCl in water agreed with the values reported in the N.B.S. tables (11). The electrodes were stored in 0.1 M MCl solution when not in use.

Results and discussion

The emf, E, of the cell applied in this work is given by

$$[1] \quad E = E^0 + 0.1183 \log m\gamma_{\pm}$$

where E is the standard electrode potential of the M^+ (I.S.E.) and chloride (I.S.E.), and $\gamma_{\pm}$ is the mean ionic coefficient of MCl of molality m. The standard emf E^0 in eq. [1] was obtained in the following manner. Introducing the Debye–Hückel expression (12) for the rational activity coefficient in eq. [1] yields the equation:

$$[2] \quad E' = E - 0.1183 \log m + \frac{0.1183\, A \sqrt{C}}{1 + B\, a \sqrt{C}} + 0.1183 \log (1 + 0.002\, \bar{M}m)$$

where the last term represents the difference between the rational and molal mean activity coefficients, A and B are the values of the Debye–Hückel constants for each solvent composition, a is the ionic size parameter in A^0, and $\bar{M}$ is the average molecular mass of the solvent mixture. The molarity C in eq. [2] was obtained from the molality (m) and the density of solution. The values of E^0 were obtained by extrapolation of E' to zero ionic strength, $m = 0$. The E' val-

[1]Author to whom correspondence may be addressed.

Can. J. Chem. Downloaded from www.nrcresearchpress.com by 203.198.23.82 on 09/08/12
For personal use only.

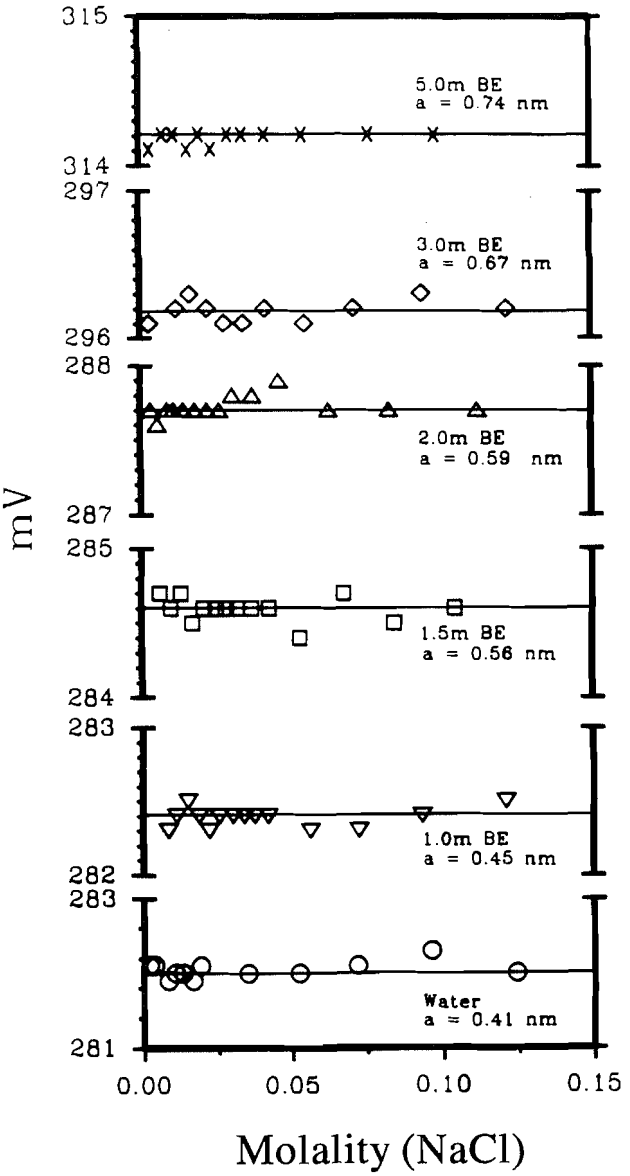

FIG. 1. E' as a function of m for NaCl in different compositions of the B.E. + H_2O system. The corresponding value of the ionic diameter as indicated (eq. [2]).

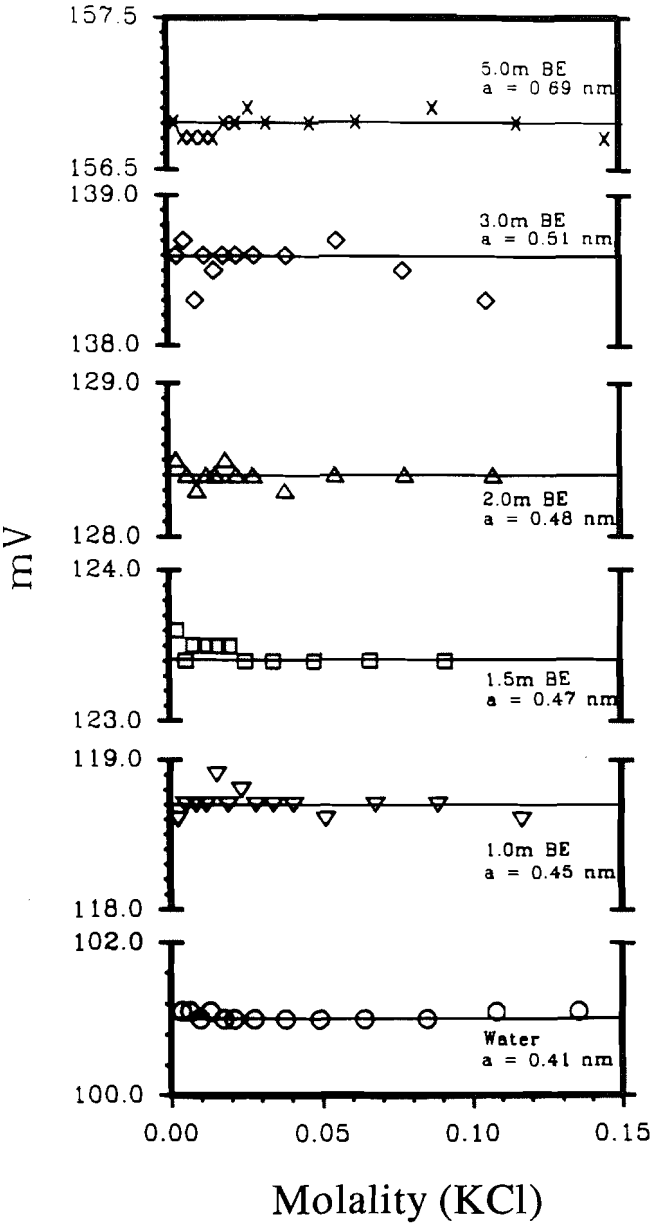

FIG. 2. E' as a function of m for KCl in different compositions of the B.E. + H_2O system. The corresponding value of the ionic diameter as indicated.

ues of the solution and the magnitude of the ion size parameter were determined by the method described by Harned (13, 14). In this procedure, E' in eq. [2] was solved for various values of a. The values used ranged from 0.40 to 0.75 nm. The E' values were plotted against the molality. The proper value gives a zero slope for such a curve. These curves also give the values of E^0, the standard electrode potentials. The results are illustrated in Figs. 1 and 2. The constants used in eq. [2] for the evaluation of E^0 are given in Table 1.

The mean molal activity coefficient values of NaCl and KCl were computed from experimental data according to eq. [1]. These values were fitted by the method of least squares to the empirical equation (15).

$$[3]\quad \log \gamma_A = \log \gamma_A^0 + m_B\,[B_{10} + B_{11}\,m_A^{1/2} + B_{12}\,m_A + B_{13}\,m_A^{3/2}] + m_B^2\,[B_{20} + B_{21}\,m_A^{1/2}]$$

TABLE 1. Constants of equation [2]

Molarity of B.E.	Dielectric constant	A	B	$\bar{M}$
1.0	70.66	0.5972	0.3466	19.7929
1.5	66.98	0.6469	0.3559	20.6562
2.0	63.99	0.6929	0.3642	21.5042
3.0	56.34	0.8386	0.3881	23.1569
5.0	42.93	1.2611	0.4446	26.2982

where γ_A and γ_A^0 represent the activity coefficients of MCl with and without 2-butoxyethanol and A stands for the electrolyte and B for 2-butoxyethanol. The activity coefficient (γ_A^0) values for the pure electrolyte at various molalities were

TABLE 2. Parameters of equation [3]

	Parameter						
	$10^3 \cdot B_{10}$	$10^2 \cdot B_{11}$	$10^1 \cdot B_{12}$	$10^3 \cdot B_{20}$	$10^2 \cdot B_{13}$	$10^5 \cdot B_{21}$	$10^3 \cdot \sigma^a$
NaCl	0.1189	−5.3348	1.2798	−0.7448	−7.8951	434.9	2.2
KCl	4.3130	−9.6992	1.7060	−1.3991	−1.3091	−7.042	1.7

[a]σ = standard deviation.

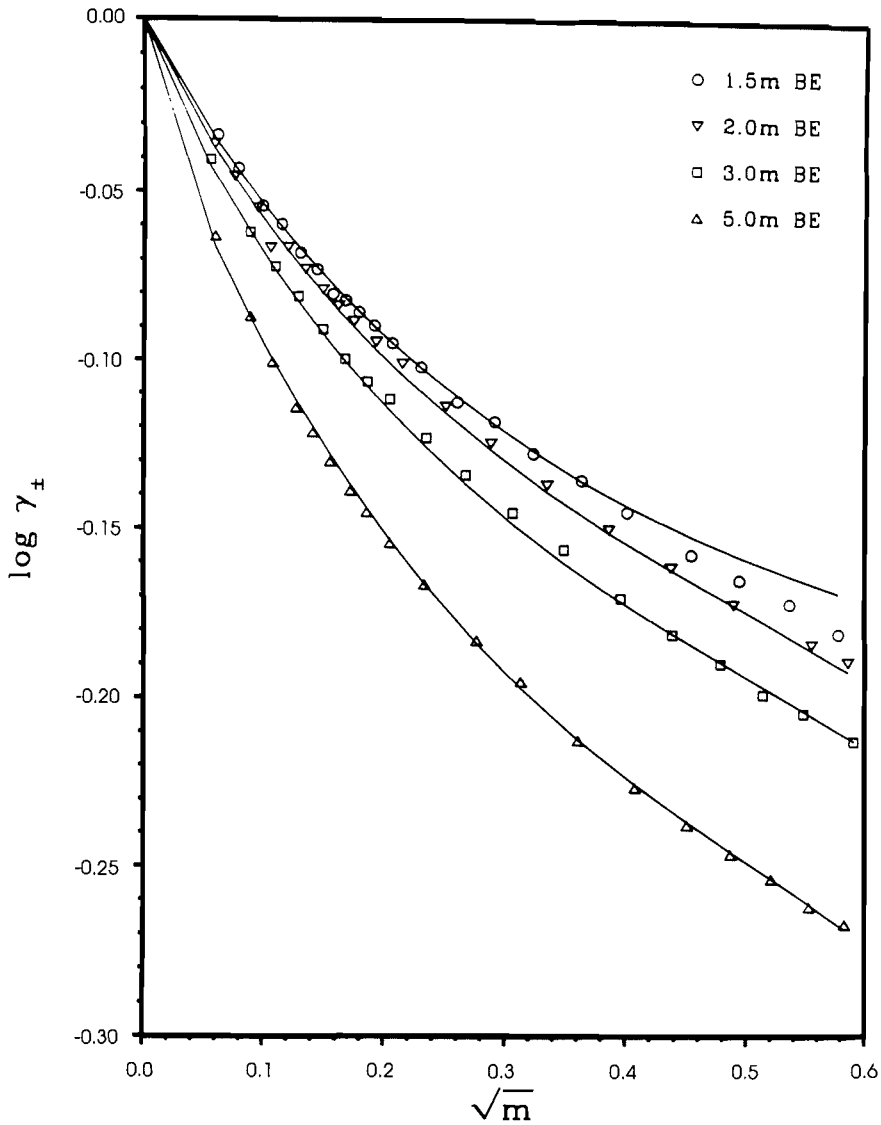

FIG. 3. The mean molal activity coefficients of NaCl in B.E. + H_2O systems as a function of $\sqrt{m}$. The curve for 1.0 *m* B.E. is not included for clarity purposes.

calculated using Pitzer's treatment (16). The values of the parameters for the above equation are presented in Table 2. The mean activity coefficient values of NaCl and KCl are plotted against $\sqrt{m}$ (Figs. 3 and 4) and the continuous curves were generated with the aid of the parameters in Table 2. It is obvious that eq. [3] expresses adequately the results within the experimental errors. The activity coefficient values decrease with the values of the dielectric constant of the media, leading to an increase in the short-range interactions.

The standard free energies of monovalent salt in a mixed solvent are given by:

[4] $\Delta G^0_{t(m)} = F \cdot \Delta E^0_{t(m)}$

where F is Faraday's constant and

[5] $\Delta E^0_{t(m)} = [E^0_{(B.E.+H_2O)} - E^0_{H_2O}]$

The calculated values of $\Delta G^0_{t(m)}$ at various binary mixtures

Can. J. Chem. Downloaded from www.nrcresearchpress.com by 203.198.23.82 on 09/08/12
For personal use only.

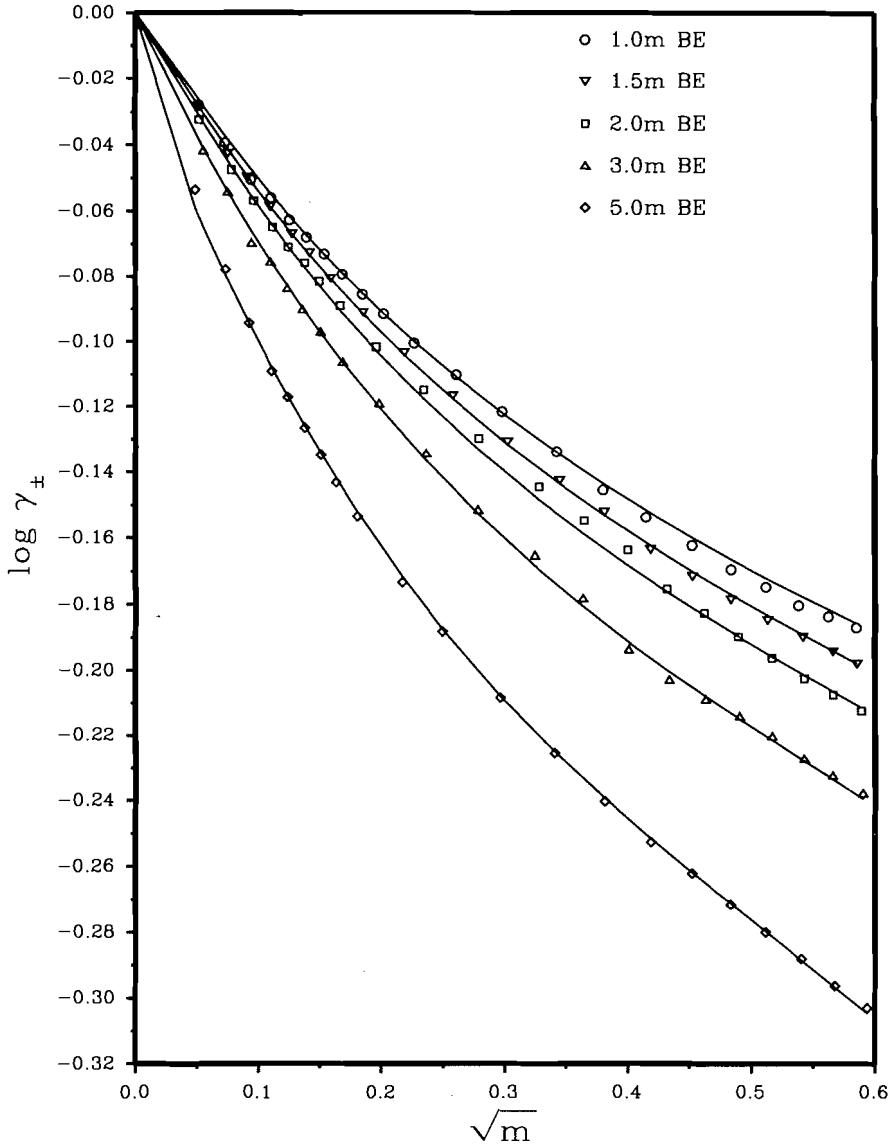

FIG. 4. The mean molal activity coefficients of KCl in B.E. + H_2O systems as a function of $\sqrt{m}$.

of 2-butoxyethanol are presented in Table 3. The free energies of transfer of the ion are the difference between the free energies of solvation of the ion in the different solvent mixtures. The values of $\Delta G^0_{t(m)}$ are found to be dependent on the 2-butoxyethanol content in the solvent mixture. This dependency may be due to the change in the solvation of Na^+, K^+, and Cl^- ions by the presence of 2-butoxyethanol molecules in the mixture. Some water molecules in the primary shell might be substituted by 2-butoxyethanol molecules or the microaggregates. The change in the nature of the solvation process is currently under investigation using viscosity, ultrasonic velocity, and spectroscopic measurements.

Conclusions

Ion-selective electrodes were proven to be valuable in the determination of mean activity coefficient values of NaCl and KCl at various concentrations of 2-butoxyethanol in water, and the data were fitted into an empirical equation. This process allows one to obtain the values of $\gamma_{\pm}$ at various concentrations. The Gibbs free energies of transfer were calculated and found to be very small.

TABLE 3. Gibbs free energies of transfer of NaCl and KCl from $H_2O \rightarrow$ B.E. + water mixtures

Molality of B.E.	$\Delta G^0_{t(m)}$ [a] (kJ mol^{-1})	
	NaCl	KCl
1.0	0.05	1.71
1.5	0.21	2.16
2.0	0.55	2.64
3.0	1.37	3.63
5.0	3.11	5.38

[a]Estimated error in $\Delta G^0_{t(m)}$ is about ±0.01 kJ.

Acknowledgements

The financial support by the Natural Sciences and Engineering Research Council of Canada (NSERC) and the committee for the Evaluation of Research Proposals of U.C.C.B. is greatly appreciated. Y.M. wishes to acknowl-

Can. J. Chem. Downloaded from www.nrcresearchpress.com by 203.198.23.82 on 09/08/12
For personal use only.

edge the award of an undergraduate Summer Research Fellowship (1988) by NSERC.

1. M. Manabe and M. Koda. Bull. Chem. Soc. Jpn. **19**, 1599 (1978).
2. J.E. Desnoyers. Pure Appl. Chem. **54**, 1469 (1982).
3. F. Quirion and J.E. Desnoyers. J. Colloid Interface Sci. **115**, 176 (1987).
4. J.E. Desnoyers, F. Quirion, D. Hetu, and G. Perron. Can. J. Chem. Eng. **61**, 672 (1983).
5. A. Roux, D. Hetu, G. Perron, and J.E. Desnoyers. J. Solution Chem. **13**, 1 (1984).
6. I.D. Robb. *In* Microemulsions. Plenum, New York. 1982.
7. C. Botre, V.K. Crescenzi, and A. Mele. J. Phys. Chem. **63**, 650 (1959).
8. De-Ying Chu, Quian Zhang, and Rui-Lin Liu. J. Chem. Soc. Faraday Trans. 1, 83, 635 (1987).
9. L. Malahlas and O. Popovych. J. Chem. Eng. Data, **27**, 105 (1982).
10. K. Covington and J.M. Thain. J. Chem. Soc. Faraday Trans. 1, **71**, 78 (1975).
11. R.N. Goldgerg and R.L. Nuttall. J. Phys. Chem. Ref. Data, **7**, 263 (1978).
12. E. Hückel. Phys. Z. **26**, 93 (1925).
13. H.S. Harned. J. Am. Chem. Soc. **60**, 336 (1938).
14. H.D. Crockford, S.B. Knight, and H.A. Staton. J. Am. Chem. Soc. **72**, 2164 (1950).
15. M.Y. Spink and E.E. Schrier. J. Chem. Thermodyn. **2**, 821 (1970).
16. Hee-Talk Kim and W.J. Federick, Jr. J. Chem. Eng. Data, **33**, 177 (1988).

Can. J. Chem. Downloaded from www.nrcresearchpress.com by 203.198.23.82 on 09/08/12
For personal use only.

Metal-thiolate chemistry: The structure of the first adamantane-type cation, $[(\mu\text{-SPh})_6(HgPPh_3)_4]^{2+}$

JAGADESE J. VITTAL, PHILIP A.W. DEAN, AND NICHOLAS C. PAYNE[1]
Department of Chemistry, University of Western Ontario, London, ON N6A 5B7, Canada

Received June 18, 1993

JAGADESE J. VITTAL, PHILIP A. W. DEAN, and NICHOLAS C. PAYNE. Can. J. Chem. **71**, 2043 (1993).

The compound $[(\mu\text{-}SC_6H_5)_6\{HgP(C_6H_5)_3\}_4][ClO_4]_2$ crystallizes in the triclinic space group $P\bar{1}$ as a bis(chloroform) solvate with cell dimensions a = 15.799(4), b = 26.813(5), c = 15.040(5) Å, α = 96.35(2), β = 114.52(2), γ = 100.45(2)° and two formula units per cell. The crystal and molecular structures of this salt were solved by X-ray diffraction techniques using 9898 counter data with $I > 2.5\sigma(I)$ recorded at −50(2)°C. Refinement of 477 variables by full-matrix least-squares converged at an agreement factor R = 0.046. The cation has adamantane-type stereochemistry with a $(\mu\text{-SPh})_6Hg_4$ cage and four terminal triphenylphosphine ligands. The S—C_α vectors of the bridging SC_6H_5 groups adopt the configuration [aae, aae, aee, aee] with the minimum number of two 1,3-axial, axial substituent interactions. There is a significant flattening of the two Hg_3S_3 rings with two axial substituents into an envelope conformation; each has two torsion angles less than 25°, instead of the ideal values of ±60° in adamantane. One perchlorate ion is doubly solvated by chloroform molecules in an unusual, weakly hydrogen bonded, $[ClO_4 \cdot 2HCCl_3]^-$ complex.

JAGADESE J. VITTAL, PHILIP A.W. DEAN et NICHOLAS C. PAYNE. Can. J. Chem. **71**, 2043 (1993).

Le composé $[(\mu\text{-}SC_6H_5)_6\{HgP(C_6H_5)_3\}_4][ClO_4]_2$ cristallise dans le groupe d'espace triclinique $P\bar{1}$ sous la forme d'un composé solvaté par deux molécules de chloroforme, avec a = 15,799(4), b = 26,813(5) et$c$ = 15,040(5) Å, α = 96,35(2), β = 114,52(2) et γ = 100,45(2)° et deux formules unitaires par motif. On a résolu les structures moléculaires et cristallines par des techniques de diffraction des rayons x utilisant 9898 données avec $I > 2{,}5\ \sigma(I)$ enregistrées à −50(2)°C. On a affiné 477 variables par la méthode des moindres carrés jusqu'à une valeur de R = 0,046. Le cation posséde une stéréochimie semblable à celle de l'adamantane avec une cage de $(\mu\text{-}SC_6H_5)_6Hg_4$ et quatre triphénylphosphine comme coordinats terminaux. Les vecteurs S—C_α des groupes SC_6H_5 agissant comme ponts adoptent la configuration [aae, aae, aee, aee] avec le nombre minimal d'interactions 1,3-axiale, axiale entre les substituants. On observe un aplatissement notable des deux noyaux Hg_3S_3 avec deux substituants axiaux dans une conformation enveloppe; chacun présente deux angles de torsion inférieurs à 25° par rapport aux valeurs idéales de ±60° dans l'adamantane. Un ion perchlorate est doublement solvaté par des molécules de chloroforme et il forme un complexe inhabituel avec une faible liaison hydrogène, $[ClO_4 \cdot 2HCCl_3]$.

[Traduit par la rédaction]

Introduction

In the chemistry of metal-thiolates, a frequently encountered structural unit is the adamantane-type tetranuclear cluster with a $(\mu\text{-SR})_6M_4$ core (1–3). More than twenty such compounds have been characterized by X-ray structure analyses to date (4–24, footnote 2) with metal atoms M = Mn(II), Fe(II), Co(II), Zn(II), Cu(II), and Cd(II). In most cases the cluster is an anion; in no case is it a cation. Five of these are complexes of the Group 12 atoms Zn and Cd. By contrast, the structural chemistry of the Hg congener is undeveloped, though the nature of the $(\mu\text{-SR})_6Hg_4$ cage is of interest in connection with the mercury-binding site of metallothioneins (25). Previously, some of us have reported (26) the synthesis of various complex cations of formula $[(\mu\text{-SR})_6(HgPR'_3)_4]^{2+}$, and their characterization in solution by multinuclear magnetic resonance spectroscopy. Kunkely and Vogler (27) have described the electronic and photoluminescence spectra of the species with R = R′ = phenyl.

We present here an account of our studies of the compound $[(\mu\text{-SPh})_6(HgPPh_3)_4](ClO_4)_2 \cdot 2CHCl_3$, **1** which is unique in two ways: as the first example of a cationic thiolate cluster complex with the adamantane-type stereochemistry, and as the first case of a $(\mu\text{-SR})_6Hg_4$ cage characterized by X-ray crystallography.

[1]To whom correspondence should be addressed.
[2]I.G. Dance, Personal Communication.

Experimental

General procedures

The salt $[(\mu\text{-SPh})_6(HgPPh_3)_4](ClO_4)_2$ was synthesized as reported earlier (26), and solvated crystals of a quality suitable for diffraction experiments were grown by diffusing diethyl ether into a chloroform solution at 5°C.

X-ray crystallography

Crystals of $[(\mu\text{-SPh})_6(HgPPh_3)_4](ClO_4)_2 \cdot 2CHCl_3$ are colorless, transparent, and fairly stable in air, though they show a tendency to decompose on prolonged exposure to X-radiation. Precession and Weissenberg photographs were taken to establish the space group and to obtain preliminary cell dimensions. The crystal density was measured by the neutral buoyancy method in mixtures of carbon tetrachloride and 1,2-dibromoethane. Data collection was carried out on an Enraf-Nonius CAD4F diffractometer (28) at a reduced temperature of −50(2)° to retard decomposition. Intensity data were recorded in ω–2θ scan mode at variable scan speeds within a maximum time per datum of 50 s. Static background estimates were made at scan extensions on each side. Standard reflections were monitored every 180 min of X-ray exposure time. Lorentz, polarization, and decay corrections were applied using the NRCVAX programs (29) running on a Sun 3/80 workstation. A Gaussian absorption correction (30) was applied to the data, which were then averaged to yield 15 282 unique data with $I > 0$ for structure solution and refinement. Crystal and experimental data are summarized in Table 1.

The structure was solved by a combination of MULTAN (31) and difference Fourier syntheses, and refined by full-matrix least-squares techniques on F using the SHELX76 software (32) running on a CDC Cyber 2000 computer. Scattering factors for Hg

Can. J. Chem. Downloaded from www.nrcresearchpress.com by 203.198.23.82 on 09/08/12
For personal use only.

TABLE 1. Summary of X-ray structure determination: crystal data for $[(\mu\text{-}SC_6H_5)_6\{HgP(C_6H_5)_3\}_4][ClO_4]_2 \cdot 2CHCl_3$

Formula	$C_{110}H_{92}Cl_8O_8P_4S_6Hg_4$	
Formula weight	1970.44	
Crystal system, space group	triclinic, $P\bar{1}$	
Cell dimensions (Å, deg)	a = 15.799(4)	b = 26.813(5)
	c = 15.040(5)	α = 96.35(2)
	β = 114.52(2)	γ = 100.45(2)
Cell volume (Å^3), Z	5576(3), 2	
Temperature, °C	−50(2)	
Density, g cm^{-3}, obsd, calcd.	1.75(2), 1.753	
F(000) electrons	1428	
Experimental details		
Radiation, wavelength (Å)	Mo(K$\bar{\alpha}$), 0.71073	
Monochromator	Graphite	
Scan type and width (deg)	$\omega - 2\theta$, 0.70 + 0.35 tan θ	
Maximum time per datum (s)	50	
No. of data, time (h)	16820, 182	
No. of unique data ($I > 0$)	15282	
Absorption coefficient (cm^{-1})	59.0	
Refinement details		
No. of observ. data ($I \geq 2.5\sigma(I)$)	9898	
No. of variables	477	
Extinction coefficient	$8.8(9) \times 10^{-5}$	
Final model; R and R_1	0.0464, 0.0495	

were taken from the International tables (33). In the refinement, all Hg, P, and S atoms were assigned anisotropic thermal parameters. The phenyl ring carbon atoms were constrained to regular hexagonal geometry with C—C = 1.392 Å and allotted isotropic thermal parameters. All phenyl hydrogen atoms were located successfully by difference Fourier methods, placed in calculated positions (C—H = 0.95 Å), and included in the structure factor calculations. Some disorder was present. One of the perchlorate anions showed a 60:40 occupancy of two orientations related approximately by a 60° rotation about one Cl—O bond. It was modelled by refining rigid groups of T_d symmetry and a Cl—O bond length of 1.42 Å. The phenyl ring on S (34) had large C atom thermal parameters and was accompanied by significant residual electron density in a difference Fourier synthesis. A disorder model using rigid groups could not be formulated, so individual anisotropic thermal parameters were assigned. The resulting model is the best we could achieve, with C—C bond lengths ranging from 1.32(3) to 1.42(3) Å. The chloroform solvent molecules were refined with a restrained geometry, Cl—C—Cl 110° and H—C—Cl 108°, varying an overall C—Cl bond length to a final value of 1.715(3) Å. A secondary extinction correction was applied to the data. An analysis of variance suggested that the weighting scheme was appropriate. With three reflections omitted, refinement converged at agreement factors $R = \Sigma(||F_o| - |F_c||)/\Sigma(|F_o|) = 0.046$ and $R_1 = (\Sigma w(|F_o| - |F_c|)^2/\Sigma w F_o^2)^{1/2} = 0.050$.

Selected experimental details of the X-ray determination are given in Table 1. Final positional parameters for **1** are given in Table 2, supplementary experimental details, hydrogen atom parameters and anisotropic thermal parameters have been deposited as Tables S1, S2, and S3.[3]

[3]Copies of supplementary experimental details, hydrogen atom parameters, anisotropic thermal parameters, selected non-bonded contacts, supplementary dimensions, and structure amplitudes may be purchased from the Depository of Unpublished Data, CISTI, National Research Council of Canada, Ottawa, ON K1A 0S2, Canada.

Results and discussion

The synthesis of the Hg salt $[(\mu\text{-}SC_6H_5)_6\{HgP(C_6H_5)_3\}_4][ClO_4]_2$ has been described previously (26).

The crystal structure consists of well-separated complex cations, perchlorate anions, and $[ClO_4 \cdot 2CHCl_3]^-$ anionic complexes, Fig. 1. The closest cation–anion and anion–anion distances of approach, and complex dimensions, are given in Table S4. The doubly solvated perchlorate ion appears to be unprecedented in the literature. In essence the anion is bracketed in linear fashion (H1. . .Cl(1) 3.08, Cl(1). . .H2 2.94 Å, H1. . .Cl(1). . .H2 176°) by the hydrogen atoms of two chloroform molecules (C(1)—H1. . .Cl(1) 168, (C(2)—H2. . .Cl(1) 179°). The O. . .H distances range from 2.38 to 2.55 Å, slightly less than the sum of van der Waals radii, 2.70 Å, with C—H. . .O angles varying remarkably little from 148 to 152°. A search of the Cambridge Structural Database (CSD) (34) found 19 entries containing at least one perchlorate anion and one chloroform molecule. Of these, only three studies (35–37) reported coordinates for the hydrogen atom, two of which (36, 37) proved to contain a $[ClO_4 \cdot CHCl_3]^-$ anion–solvent complex of closely similar geometry. Dimensions from these two studies are included in Table S4. Although the pK_a of chloroform is only 24.1 (38), we characterize this interaction as weak, bifurcated hydrogen bonding, similar, for example, to that observed in $MgSO_4 \cdot 4H_2O$ (39).

The cage skeleton of the cation in **1** is depicted in Fig. 2. The mercury atoms, each with a terminal triphenylphosphine ligand, are located at the vertices of a tetrahedron, with phenylthiolate ligands bridging the six edges. Thus each face of the tetrahedron is composed of a six-membered $Hg_3(\mu\text{-}S)_3$ ring in approximate chair conformation, to give an adamantane-like stereochemistry. Isomerism can occur in such a cage due to the difference between the lone pair and phenyl substituents upon the sulphur atoms. The phenyl groups are po-

Can. J. Chem. Downloaded from www.nrcresearchpress.com by 203.198.23.82 on 09/08/12
For personal use only.

TABLE 2. Atomic positional ($\times 10^4$) and thermal ($\times 10^3$) parameters

Atom	x	y	z	U or U_{eq} (Å^2)[a]
Hg(1)	−983.0(4)	3280.4(2)	1232.8(4)	29.7(2)
Hg(2)	1006.1(4)	3358.9(2)	4265.1(4)	29.5(2)
Hg(3)	−1696.1(4)	2225.4(2)	2996.4(4)	32.7(2)
Hg(4)	489.0(4)	2053.9(2)	2031.3(4)	31.2(2)
P(1)	−1644.8(25)	3662.6(13)	−274.5(24)	32.6(14)
P(2)	2369.9(24)	3964.3(13)	5776.2(25)	31.9(14)
P(3)	−3114.6(23)	1745.2(13)	3139.4(26)	32.1(14)
P(4)	1324.4(24)	1500.1(13)	1423.1(26)	33.3(14)
S(12)	106.0(23)	3872.8(12)	2954.3(24)	32.2(13)
S(13)	−2098.5(23)	2941.9(12)	2024.6(24)	31.8(13)
S(14)	−700.1(24)	2412.5(13)	665.6(25)	35.1(14)
S(23)	−170.8(23)	2735.1(12)	4617.8(24)	31.3(13)
S(24)	1727.6(23)	2839.8(12)	3354.0(24)	31.9(13)
S(34)	−532.7(24)	1699.7(13)	2865.1(26)	37.8(14)
C(121)	1099(6)	4255(3)	2854(6)	31(3)
C(122)	1475(6)	4770(3)	3364(6)	48(4)
C(123)	2259(6)	5073(3)	3309(6)	68(5)
C(124)	2668(6)	4862(3)	2745(6)	65(5)
C(125)	2292(6)	4347(3)	2236(6)	57(4)
C(126)	1508(6)	4043(3)	2290(6)	43(4)
C(131)	−3238(6)	2681(2)	983(7)	36(3)
C(132)	−3827(6)	3016(2)	649(7)	54(4)
C(133)	−4697(6)	2841(2)	−211(7)	64(5)
C(134)	−4977(6)	2332(2)	−737(7)	66(5)
C(135)	−4388(6)	1997(2)	−403(7)	50(4)
C(136)	−3519(6)	2172(2)	457(7)	45(4)
C(141)	−90(4)	2548(3)	−77(6)	35(3)
C(142)	−629(4)	2419(3)	−1111(6)	42(4)
C(143)	−185(4)	2516(3)	−1724(6)	62(5)
C(144)	798(4)	2743(3)	−1305(6)	58(4)
C(145)	1336(4)	2872(3)	−271(6)	56(4)
C(146)	892(4)	2775(3)	343(6)	43(4)
C(231)	−493(6)	3188(3)	5316(5)	33(3)
C(232)	−1175(6)	3460(3)	4867(5)	48(4)
C(233)	−1386(6)	3807(3)	5455(5)	56(4)
C(234)	−915(6)	3883(3)	6492(5)	50(4)
C(235)	−233(6)	3611(3)	6941(5)	56(4)
C(236)	−22(6)	3264(3)	6352(5)	49(4)
C(241)	2477(5)	2575(3)	4349(6)	27(3)
C(242)	3443(5)	2839(3)	4865(6)	40(4)
C(243)	4062(5)	2666(3)	5668(6)	48(4)
C(244)	3714(5)	2229(3)	5955(6)	49(4)
C(245)	2748(5)	1964(3)	5439(6)	41(4)
C(246)	2129(5)	2137(3)	4635(6)	35(3)
C(341)	−1169(9)	1057(6)	2240(13)	50(7)
C(342)	−1579(10)	891(6)	1204(13)	59(8)
C(343)	−2033(11)	361(7)	809(16)	84(9)
C(344)	−2163(15)	23(8)	1344(24)	124(18)
C(345)	−1767(15)	192(8)	2324(22)	112(16)
C(346)	−1269(11)	687(7)	2821(13)	65(8)
C(431)	528(6)	1040(3)	270(6)	33(3)
C(432)	−316(6)	1156(3)	−359(6)	45(4)
C(433)	−921(6)	828(3)	−1282(6)	60(4)
C(434)	−683(6)	385(3)	−1577(6)	53(4)
C(435)	161(6)	269(3)	−948(6)	55(4)
C(436)	766(6)	596(3)	−25(6)	46(4)
C(11)	−2454(5)	4042(3)	−190(5)	35(3)
C(12)	−2389(5)	4223(3)	746(5)	34(3)
C(13)	−2990(5)	4525(3)	836(5)	50(4)
C(14)	−3656(5)	4647(3)	−10(5)	54(4)
C(15)	−3721(5)	4466(3)	−946(5)	72(5)
C(16)	−3120(5)	4164(3)	−1036(5)	69(5)
C(21)	−716(5)	4065(3)	−485(6)	29(3)
C(22)	−864(5)	4473(3)	−980(6)	45(4)

Can. J. Chem. Downloaded from www.nrcresearchpress.com by 203.198.23.82 on 09/08/12
For personal use only.

TABLE 2 (*continued*)

Atom	*x*	*y*	*z*	*U* or U_{eq} (Å^2)[a]
C(23)	−142(5)	4743(3)	−1176(6)	52(4)
C(24)	728(5)	4604(3)	−877(6)	57(4)
C(25)	875(5)	4195(3)	−383(6)	59(4)
C(26)	153(5)	3925(3)	−187(6)	40(4)
C(31)	−2356(6)	3166(3)	−1410(5)	28(3)
C(32)	−3020(6)	2752(3)	−1394(5)	49(4)
C(33)	−3553(6)	2355(3)	−2236(5)	53(4)
C(34)	−3422(6)	2371(3)	−3093(5)	65(5)
C(35)	−2758(6)	2785(3)	−3109(5)	60(4)
C(36)	−2225(6)	3183(3)	−2267(5)	46(4)
C(41)	3474(6)	4080(3)	5645(5)	40(3)
C(42)	4327(6)	4013(3)	6362(5)	44(4)
C(43)	5134(6)	4068(3)	6187(5)	57(4)
C(44)	5088(6)	4189(3)	5294(5)	59(4)
C(45)	4234(6)	4256(3)	4577(5)	49(4)
C(46)	3427(6)	4202(3)	4753(3)	41(4)
C(51)	2627(6)	3712(3)	6901(5)	28(3)
C(52)	2527(6)	3181(3)	6841(5)	45(4)
C(53)	2750(6)	2980(3)	7702(5)	57(4)
C(54)	3072(6)	3309(3)	8623(5)	57(4)
C(55)	3171(6)	3840(3)	8683(5)	68(5)
C(56)	2949(6)	4041(3)	7822(5)	53(4)
C(61)	2135(4)	4589(3)	6020(6)	32(3)
C(62)	2847(4)	5050(3)	6350(6)	40(4)
C(63)	2651(4)	5517(3)	6603(6)	44(4)
C(64)	1744(4)	5522(3)	6525(6)	49(4)
C(65)	1032(4)	5060(3)	6195(6)	52(4)
C(66)	1228(4)	4594(3)	5942(6)	45(4)
C(71)	−4003(6)	1336(3)	1944(6)	27(3)
C(72)	−4947(6)	1380(3)	1508(6)	47(4)
C(73)	−5596(6)	1077(3)	573(6)	53(4)
C(74)	−5301(6)	731(3)	73(6)	47(4)
C(75)	−4357(6)	688(3)	508(6)	49(4)
C(76)	−3708(6)	990(3)	1444(6)	41(4)
C(81)	−2791(6)	1346(4)	4061(6)	37(3)
C(82)	−3168(6)	811(4)	3819(6)	71(5)
C(83)	−2891(6)	520(4)	4555(6)	85(6)
C(84)	−2235(6)	764(4)	5532(6)	82(6)
C(85)	−1858(6)	1299(4)	5773(6)	85(6)
C(86)	−2135(6)	1590(4)	5038(6)	62(5)
C(91)	−3713(6)	2172(2)	3538(6)	30(3)
C(92)	−4292(6)	1995(2)	3984(6)	45(4)
C(93)	−4762(6)	2323(2)	4275(6)	53(4)
C(94)	−4653(6)	2828(2)	4119(6)	63(5)
C(95)	−4074(6)	3005(2)	3673(6)	62(4)
C(96)	−3603(6)	2677(2)	3382(6)	55(4)
C(101)	2253(5)	1879(3)	1189(5)	33(3)
C(102)	2346(5)	1745(3)	320(5)	43(4)
C(103)	3048(5)	2059(3)	153(5)	55(4)
C(104)	3656(5)	2506(3)	855(5)	52(4)
C(105)	3562(5)	2640(3)	1725(5)	52(4)
C(106)	2860(5)	2327(3)	1892(5)	47(4)
C(111)	1916(5)	1159(3)	2379(7)	35(3)
C(112)	1441(5)	977(3)	2924(7)	46(4)
C(113)	1894(5)	744(3)	3714(7)	61(4)
C(114)	2821(5)	692(3)	3960(7)	74(5)
C(115)	3296(5)	874(3)	3414(7)	86(6)
C(116)	2843(5)	1107(3)	2624(7)	65(5)
Cl(1)	6554(2)	9089(1)	2814(3)	60(2)
O(1)	6253(2)	9529(1)	2475(3)	89(2)
O(2)	7355(2)	9250(1)	3773(3)	89(2)
O(3)	6821(2)	8828(1)	2134(3)	89(2)
O(4)	5789(2)	8748(1)	2875(3)	89(2)

Can. J. Chem. Downloaded from www.nrcresearchpress.com by 203.198.23.82 on 09/08/12
For personal use only.

TABLE 2 (*concluded*)

Atom	x	y	z	U or U_{eq} (Å^2)[a]
Cl(2)[b]	4628(6)	4133(3)	1697(6)	57(1)
O(5)	3613(6)	3987(3)	1128(6)	86(2)
O(6)	4994(6)	4641(3)	1613(6)	86(2)
O(7)	5037(6)	3780(3)	1331(6)	86(2)
O(8)	4869(6)	4125(3)	2715(6)	86(2)
Cl(2)′	4582(9)	4192(5)	1733(9)	57(1)
O(5)′	3617(9)	3920(5)	1078(9)	86(2)
O(6)′	5019(9)	4430(5)	1178(9)	86(2)
O(7)′	5099(9)	3840(5)	2209(9)	86(2)
O(8)′	4593(9)	4579(5)	2466(9)	86(2)
Cl(3)	9429(4)	8349(2)	4169(4)	150(4)
Cl(4)	9238(5)	8705(3)	2412(4)	173(5)
Cl(5)	9876(5)	9425(2)	4220(5)	196(5)
C(1)	9155(3)	8828(2)	3512(3)	73(5)
Cl(6)	3223(4)	8909(2)	1381(5)	160(5)
Cl(7)	4119(5)	9983(2)	1949(5)	150(4)
Cl(8)	3977(7)	9428(3)	3394(5)	281(9)
C(2)	4107(4)	9399(2)	2314(4)	127(8)

[a]Anisotropic thermal parameters are given in the form of isotropic equivalent parameter defined as $U_{eq} = (1/3)\,\Sigma_i\Sigma_j U_{ij} \cdot a_i^* \cdot a_j^* \cdot a_i \cdot a_j$.

[b]Cl(2) through O(8) have multiplicity 0.6, Cl(2)′ through O(8)′ multiplicity 0.4.

TABLE 3. Selected distances (Å) and angles (deg)

Atoms	Distance	Atoms	Distance
Hg(1)–P(1)	2.494(3)	Hg(2)–P(2)	2.509(3)
Hg(3)–P(3)	2.478(3)	Hg(4)–P(4)	2.489(3)
Hg(1)–S(12)	2.567(3)	Hg(1)–S(13)	2.598(3)
Hg(1)–S(14)	2.568(3)	Hg(2)–S(12)	2.606(3)
Hg(2)–S(23)	2.534(3)	Hg(2)–S(24)	2.562(3)
Hg(3)–S(13)	2.554(3)	Hg(3)–S(23)	2.610(3)
Hg(3)–S(34)	2.566(3)	Hg(4)–S(14)	2.562(3)
Hg(4)–S(24)	2.564(3)	Hg(4)–S(34)	2.543(3)
P(1)–C(11)	1.807(8)	P(1)–C(21)	1.817(9)
P(1)–C(31)	1.820(9)	P(2)–C(41)	1.811(9)
P(2)–C(51)	1.808(9)	P(2)–C(61)	1.810(8)
P(3)–C(71)	1.821(8)	P(3)–C(81)	1.807(10)
P(3)–C(91)	1.809(8)	P(4)–C(101)	1.809(9)
P(4)–C(111)	1.806(9)	P(4)–C(431)	1.807(9)
S(12)–C(121)	1.784(9)	S(13)–C(131)	1.773(9)
S(14)–C(141)	1.778(9)	S(23)–C(231)	1.795(9)
S(24)–C(241)	1.794(8)	S(34)–C(341)	1.760(14)

Bonds	Angle	Bonds	Angle
S(12)—Hg(1)—S(13)	85.75(10)	S(12)—Hg(1)—S(14)	123.03(10)
S(13)—Hg(1)—S(14)	98.50(10)	S(12)—Hg(2)—S(23)	110.63(10)
S(12)—Hg(2)—S(24)	102.55(10)	S(23)—Hg(2)—S(24)	109.07(10)
S(13)—Hg(3)—S(23)	101.64(10)	S(13)—Hg(3)—S(34)	122.42(10)
S(23)—Hg(3)—S(34)	82.02(10)	S(14)—Hg(4)—S(24)	106.57(10)
S(14)—Hg(4)—S(34)	101.03(11)	S(24)—Hg(4)—S(34)	103.12(11)
P(1)—Hg(1)—S(12)	120.12(11)	P(1)—Hg(1)—S(13)	118.95(11)
P(1)—Hg(1)—S(14)	107.06(11)	P(2)—Hg(2)—S(12)	110.75(11)
P(2)—Hg(2)—S(23)	115.23(11)	P(2)—Hg(2)—S(24)	107.78(11)
P(3)—Hg(3)—S(13)	111.18(11)	P(3)—Hg(3)—S(23)	119.14(11)
P(3)—Hg(3)—S(34)	116.46(11)	P(4)—Hg(4)—S(14)	114.00(11)
P(4)—Hg(4)—S(24)	109.69(11)	P(4)—Hg(4)—S(34)	121.04(11)
Hg(1)—S(12)—Hg(2)	111.90(12)	Hg(1)—S(13)—Hg(3)	116.96(12)
Hg(1)—S(14)—Hg(4)	116.33(13)	Hg(2)—S(23)—Hg(3)	112.76(12)
Hg(2)—S(24)—Hg(4)	113.06(12)	Hg(3)—S(34)—Hg(4)	116.25(13)

Can. J. Chem. Downloaded from www.nrcresearchpress.com by 203.198.23.82 on 09/08/12
For personal use only.

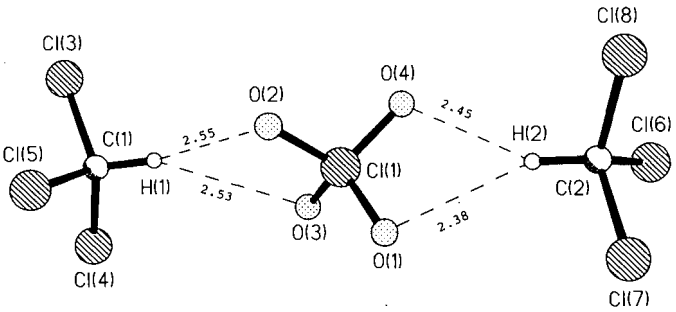

FIG. 1. A view of the $[ClO_4 \cdot 2CHCl_3]^-$ assembly.

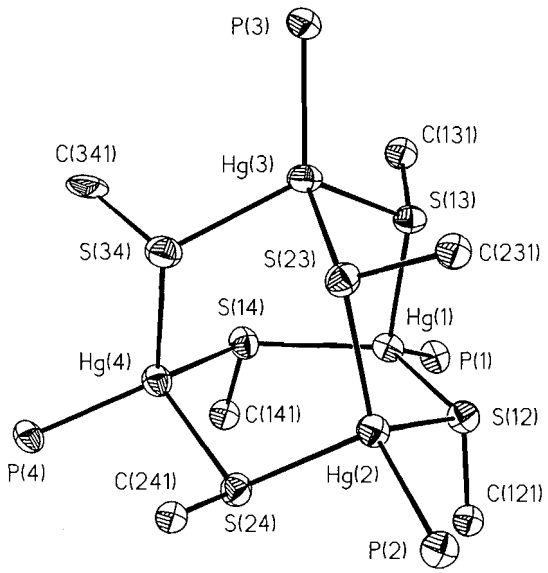

FIG. 2. The adamantane-like skeleton of the cation. Thermal ellipsoids are drawn at the 50% probability level.

sitioned either axially (a) or equatorially (e) in each ring (1). However, where two rings share a common edge formed by a bridging thiolate ligand, the adoption of an axial disposition with respect to one ring, *ipso facto* defines this group as equatorially disposed with respect to the other; there are thus always six axial and six equatorial substituents.

The four geometric isomers of $Hg_4(\mu\text{-}SR)_6$ that are possible (40) differ in the number of energetically disfavored 1,3-axial,axial substituent–substituent non-bonded interactions (3). The cation in **1** adopts the stereochemistry of isomer III, [aee, aee, aae, aae]. This isomer has only two axial–axial pairs of interactions, and occurs in twelve of the twenty one reported $(\mu\text{-}SR)_6M_4$ cages (3–24, footnote 2). Isomer III has point symmetry C_1 and can exist in enantiomeric forms. Both enantiomers are present in the crystal lattice, since **1** crystallizes in the centrosymmetric space group $P\bar{1}$.

Selected interatomic distances and angles for **1** are given in Table 3, the remainder have been deposited as Table S5. The non-bonded Hg. . .Hg distances range from 4.276 to 4.392 and the S. . .S values from 3.397 to 4.227 Å. The Hg—S distances range from 2.534(3) to 2.610(3) Å, and around the Hg atoms the S—Hg—S angles vary particularly widely, from 82.0(1) to 123.0(1)°, the S—Hg—P angles less so, from 107.1(1) to 121.0(1)°. The Hg—S—Hg angles also differ, ranging from 111.9(1) to 117.0(1)°.

TABLE 4. Torsion angles in degrees for Hg_3S_3 rings

	Atom 1	Atom 2	Atom 3	Atom 4	Angle[a]
Ring 1	S(13)	Hg(1)	S(12)	Hg(2)	73.14(15)
	S(23)	Hg(2)	S(12)	Hg(1)	−66.25(16)
aee	S(12)	Hg(2)	S(23)	Hg(3)	44.44(16)
	S(13)	Hg(3)	S(23)	Hg(2)	−43.68(16)
	S(23)	Hg(3)	S(13)	Hg(1)	73.18(15)
	S(12)	Hg(1)	S(13)	Hg(3)	−84.20(14)
Ring 2	S(14)	Hg(1)	S(12)	Hg(2)	−24.24(21)
	S(24)	Hg(2)	S(12)	Hg(1)	49.96(16)
aae	S(12)	Hg(2)	S(24)	Hg(4)	−76.67(14)
	S(14)	Hg(4)	S(24)	Hg(2)	66.17(15)
	S(24)	Hg(4)	S(14)	Hg(1)	−30.60(19)
	S(12)	Hg(1)	S(14)	Hg(4)	13.70(22)
Ring 3	S(13)	Hg(3)	S(34)	Hg(4)	13.25(20)
	S(14)	Hg(4)	S(34)	Hg(3)	−36.59(16)
aae	S(34)	Hg(4)	S(14)	Hg(1)	76.82(17)
	S(13)	Hg(1)	S(14)	Hg(4)	−76.74(17)
	S(14)	Hg(1)	S(13)	Hg(3)	38.59(15)
	S(34)	Hg(3)	S(13)	Hg(1)	−14.70(19)
Ring 4	S(23)	Hg(3)	S(34)	Hg(4)	−85.51(15)
	S(24)	Hg(4)	S(34)	Hg(3)	73.52(16)
aee	S(34)	Hg(4)	S(24)	Hg(2)	−39.75(15)
	S(23)	Hg(2)	S(24)	Hg(4)	40.66(15)
	S(24)	Hg(2)	S(23)	Hg(3)	−67.65(16)
	S(34)	Hg(3)	S(23)	Hg(2)	77.91(15)

[a]An angle is positive if, when viewed from atom 2 to atom 3, a clockwise rotation superimposes the bond from atom 1 to atom 2 upon that from atom 3 to atom 4.

Moreover, an inspection of the torsion angles in Table 4 shows that the ideal chair conformation of the two Hg_3S_3 rings bearing aae substituents is flattened into one better described as an envelope. Thus in this cationic mercury complex there are significant deviations from ideal adamantane-type stereochemistry.

The Hg—P distances vary from 2.478(3) to 2.509(3) Å, values significantly shorter than those of 2.527(4) and 2.547(4) Å observed in the $[Hg(PMe_2Ph)_4]^+$ cation (41). There is good agreement between P—C and S—C bond lengths, with mean values of 1.811(5) and 1.780(13) Å, respectively.

The structural chemistry of mercury thiolates shows a fascinating variety of assemblies containing both common Hg(II) coordination geometries, linear and tetrahedral. Bridging thiolate ligands are common, with a wide range of Hg—S distances. A search of the CSD (34) yielded thirteen entries describing a total of fifteen structures with $(\mu_2\text{-}SR)$ ligands (42–52). The structures of the complexes and geometries of the Hg—S—Hg bridges are summarised in Table 5. The prevalent structural feature is the infinite —(—Hg—SR—)$_n$— chain (42–46), cross-linked into sheets or three-dimensional networks. With dithiolate ligands, an infinite chain of $[Hg_2(SCH_2CH_2S)_3]^{2-}$ dianions is formed by 1,2-dithiolatoethane (47), while *trans*-1,2-dithiolatocyclohexane forms a dinuclear complex with Hg_2S_2 core (48). $Hg(SCH_2CH_2CH_2CH_3)_2$ crystallizes with two HgS_4 tetrahedra linked by edge and corner sharing into helical chains (49), and the $[Hg_2(SCH_3)_6]^{2-}$ ion forms a centrosymmetric, doubly bridged dimer (50). Hg_3S_8 cores are known (47, 51), as are eight-membered Hg_4S_4 rings (43, 52). The cation in **1** consists of four HgS_3P tetrahedra, each interlinked by $(\mu_2\text{-}SR)$ ligands

Can. J. Chem. Downloaded from www.nrcresearchpress.com by 203.198.23.82 on 09/08/12
For personal use only.

Can. J. Chem. Downloaded from www.nrcresearchpress.com by 203.198.23.82 on 09/08/12
For personal use only.

TABLE 5. Selected details of structures containing Hg—S—Hg bridges

Compound	Reference	Description	Hg—S	S_{br}—Hg—S_{br}	Hg—S—Hg	Hg...Hg
$(CH_3COO)Hg(SPh)$	42	Two chains	2.403(3) 2.410(3) 2.481(3) 2.445(3)	162.4(1) 143.7(1)	98.1(1) 98.4(1)	3.689 3.676
$(CH_3COO)Hg(SMe)$	43	Chain	2.387(5) 2.405(5)	159.0(2)	96.8(2)	3.583
(Cl)Hg(S-*i*-propyl)	44	Chain	2.378(6) 2.537(6)	178.2(2) 119.5(2)	93.5(2)	3.582
$Hg_2(p\text{-}SC_6H_4NO_2)^+$	45	Chain	2.488(6) 2.474(5)	—	94.5(2)	3.644
$(CH_3COO)Hg(SEt)C_5H_5N$	46	Chain	2.414(4) 2.452(4)	150.0(1)	98.4(1)	3.683(1)
$(CH_3COO)Hg(SMe)C_5H_5N$	43	Chain	2.471(5) 2.432(5)	143.0(2)	98.9(2)	3.683(1)
$(CH_3COO)Hg(SMe)C_6H_7N$	46	Two chains	2.471(7) 2.459(7) 2.414(7) 2.473(6)	141.3(2) 136.1(2)	108.6(3) 106.8(2)	3.967(2) 3.960(2)
$Hg(SCH_2CH_2CH_2CH_3)_2$	49	Two HgS_4 units linked into helical chains	2.549(5) 2.628(5) 2.482(5) 2.522(5) 2.500(5) 2.524(5) 2.535(5) 2.584(4)	Ranging from 94.3(2) to 122.2(1)	85.7(2) 103.0(2) 106.8(2) 101.5(2)	3.521(2) 3.892(2) 3.965(1)
$Hg_2(SCH_2CH_2S)_3^{2-}$	47	Chain	2.674(1) 2.722(1)	94.2(1)	85.8	3.674(1)
$(CH_3Hg)_2(S_2C_6H_{10})$	48	Hg_2S_2 core	2.363(4) 2.857(3)	84.0(1)	100.6(1)	3.859(1)
$[Hg_2(SCH_3)_6]^{2-}$	50	Hg_2S_6 core	2.629(2) 2.706(2)	94.27(5)	85.73(5)	3.631
$[Hg_2(SCH_2CH_2S)_3]^{2-}$	51	Hg_3S_8 core	2.563(2) 2.545(2) 2.864(2) 2.852(2)	101.1(3) 116.0(1) 115.0(1) 107.6(1)	84.4 84.9	3.652(1)
$[Hg_3(S_2\text{-}o\text{-xyl})_4]^{2-}$	52	Hg_3S_8 core	2.631 2.543 2.945 2.451	130.7	86.3 94.2	3.708(1) 3.792(1)
$(^tBuS)_4Cl_4Hg_2(C_6H_7N)_2$	43	Hg_4S_4 ring	2.505(8) 2.501(8) 2.379(8) 2.395(8)	130.9(2) 158.1(3)	102.5(3) 103.8(3)	3.810(3) 3.852(2)
$Cl_4Hg_4(C_4H_{10}NS)_4$	53	Hg_4S_4 ring	2.415(1) 2.414(1) 2.487(1) 2.504(1)	163.6(1) 130.0(1)	95.9(1) 93.1(1)	3.640
1	This work	Adamantane -like	Ranging from 2.543(3) to 2.509(3)	82.0(1) to 122.4(1)	111.9(1) to 117.0(1)	4.276 to 4.392

at three corners. The major differences between **1** and other structures containing (μ_2-SR) ligands are the much larger Hg—S—Hg angles and the greater Hg. . .Hg separations in the adamantane-like structure.

We have noted that the isomer of $[(\mu\text{-}SC_6H_5)_6\{HgP(C_6H_5)_3\}_4]^+$ found in the solid state, isomer III, is that with the smallest number of 1,3-axial, axial phenyl non-bonded interactions. In an earlier study of related Cd and Zn selenolate complex anions (24), we suggested that the skeleton distorts to minimise the unfavourable repulsive interactions between axially disposed substituents. The presence of bulky triphenylphosphine ligands on the Hg atoms apparently magnifies this distortion. Further studies are planned to explore this hypothesis.

Acknowledgments

We thank the Natural Sciences and Engineering Research Council of Canada for financial support of this work, in the form of operating grants to P.A.W.D. and N.C.P., and the Academic Development Fund, U.W.O., for funds to upgrade the X-ray diffractometer low-temperature equipment.

1. I.G. Dance. Polyhedron, **5**, 1037 (1986).
2. P.J. Blower and J.R. Dilworth. Coord. Chem. Rev. **76**, 121 (1987).
3. P.A.W. Dean and J.J. Vittal. *In* Metallothioneins. Synthesis, structure and properties of metallothioneins, phytochelatins and metal-thiolate complexes. *Edited by* M.J. Stillman, C.F. Shaw and K.T. Suzuki. VCH Publishers, New York. 1992. Chap. 14. p. 346–386.
4. P.A.W. Dean, J.J. Vittal, and N.C. Payne. Inorg. Chem. **26**, 1683 (1987).
5. T. Costa, J.R. Dorfman, K.S. Hagen, and R.H. Holm. Inorg. Chem. **22**, 4091 (1983).
6. K.S. Hagen, D.W. Stephan, and R.H. Holm. Inorg. Chem. **21**, 3928 (1982).
7. K.S. Hagen and R.H. Holm. Inorg. Chem. **23**, 418 (1984).
8. D. Coucouvanis, M. Kanatzidis, E. Simhon, and N.C. Baenziger. J. Am. Chem. Soc. **104**, 1874 (1982).
9. M.A. Whitener, J.K. Bashkin, K.S. Hagen, J.-J. Girerd, E. Gamp, N. Edelstein, and R.H. Holm. J. Am. Chem. Soc. **108**, 5607 (1986).
10. (*a*) I.G. Dance. J. Am. Chem. Soc. **101**, 6264 (1979); (*b*) I.G. Dance and J.C. Calabrese. J. Chem. Soc. Chem. Commun. 762 (1975).
11. D. Fenske, J. Meyer, and K. Merzweiler. Z. Naturforsch. **42**, 1207 (1987).
12. J.L. Hencher, M.A. Khan, F.F. Said, and D.G. Tuck. Polyhedron, **4**, 1263 (1985).
13. J.L. Hencher, M.A. Khan, F.F. Said, and D.G. Tuck. Inorg. Nucl. Chem. Lett. **17**, 287 (1981).
14. I.G. Dance. Inorg. Chem. **20**, 2155 (1981).
15. I.G. Dance. J. Am. Chem. Soc. **102**, 3445 (1980).
16. K.S. Hagen and R.H. Holm. Inorg. Chem. **22**, 3171 (1983).
17. I.G. Dance, G.A. Bowmaker, G.R. Clark, and J.K. Seadon. Polyhedron, **2**, 1031 (1983).
18. D. Coucouvanis, C.N. Murphy, and S.K. Kanodia. Inorg. Chem. **19**, 2993 (1980).
19. J.R. Nicholson, I.L. Abrahams, W. Clegg, and C.D. Garner. Inorg. Chem. **24**, 1092 (1985).
20. G. Henkel, P. Betz, and B. Krebs. Angew. Chem. Int. Ed. Engl. **26**, 145 (1987).
21. J. Zhao, D. Adcock, W.T. Pennington, and J.W. Kolis. Inorg. Chem. **29**, 4358 (1991).
22. W. Tremel, B. Krebs, K. Greiwe, W. Simon, H.-O. Stephan, and G. Henkel. Z. Naturforsch, **47**b, 1580 (1992).
23. P.A.W. Dean, J.J. Vittal, and Y. Wu. Can. J. Chem. **70**, 779 (1992).
24. J.J. Vittal, P.A.W. Dean, and N.C. Payne. Can. J. Chem. **70**, 792 (1992).
25. M.J. Stillman. *In* Metallothioneins. Synthesis, structure and properties of metallothioneins, phytochelatins and metal-thiolate complexes. *Edited by* M.J. Stillman, C.F. Shaw, and K.T. Suzuki. VCH Publishers, New York. 1992. Chap. 4. p 105ff and references therein.
26. P.A.W. Dean, J.J. Vittal, and M.H. Trattner. Inorg. Chem. **26**, 4245 (1987).
27. H. Kunkely and A. Vogler. Chem. Phys. Lett. **164**, 621 (1989).
28. Enraf-Nonius CAD4F Users Manual, Version 5; Enraf-Nonius: Delft, The Netherlands. 1982.
29. E.J. Gabe, Y. Le Page, J-P. Charland, and F.L. Lee. J. Appl. Crystallogr. **22**, 384 (1989).
30. Enraf-Nonius Structure Determination Package, SDP-PLUS, Version 3.0, 1985.
31. P. Main et al. Multan 82 Manual. Department of Physics, University of York, York, England. 1982.
32. Shelx-76. Program for Crystal Structure Determination. G.M. Sheldrick, University of Cambridge, England. 1976.
33. International Tables for X-ray Crystallography. (*a*) Volume A. D Reidel Publishing Co., Boston, 1983; (*b*) Volume IV. Kynoch Press, Birmingham, England. 1974.
34. Cambridge Structural Database, CSD Version 5, Cambridge Crystallographic Data Centre, Cambridge, U.K. October 1992.
35. P.K. Coughlin and S.J. Lippard. J. Am. Chem. Soc. **106**, 2328 (1984).
36. R. Uson, L.A. Oro, J. Gimeno, M.A. Ciriano, J.A. Cabeza, A. Tiripicchio, and M. Tiripicchio Camellini. J. Chem. Soc. Dalton Trans. 323 (1983).
37. I.R. Butler, W.R. Cullen, and S.J. Rettig. Organometallics, **5**, 1320 (1986).
38. A.C. Lin, Y. Chiang, D.H. Dahlberg, and A.J. Kresge. J. Am. Chem. Soc. **105**, 5380 (1983).
39. W. Baur. Acta Crystallogr. **17**, 863 (1964).
40. J.J. Vittal. J. Chem. Educ. **69**, 955 (1992).
41. F.A. Cotton, S.A. Duraj, and W.J. Roth. Acta Crystallogr. Sect. C: **41**, 881 (1985).
42. C. Stålhandske and F. Zintl. Acta Crystallogr. Sect. C: **42**, 1731 (1986).
43. A.J. Canty, C.L. Raston, and A.H. White. Aust. J. Chem. **31**, 677 (1978).
44. P. Biscarini, E. Forest, and G. Pradella. J. Chem. Soc. Dalton Trans. 953 (1984).
45. K. Brodersen and A. Knorr. Z. Naturforsch. Teil B, **45**, 1193 (1990).
46. A.J. Canty, C.L. Raston, and A.H. White. Aust. J. Chem. **32**, 311 (1979).
47. G. Henkel, P. Betz, and B. Krebs. J. Chem. Soc. Chem. Commun. 1498 (1985).
48. N.W. Alcock, P.A. Lampe, and P. Moore. J. Chem. Soc. Dalton Trans. 953 (1984).
49. C. Stålhandske and F. Zintl. Acta Crystallogr. Sect. C: **43**, 863 (1987).
50. G.A. Bowmaker, I.G. Dance, B.C. Dobson, and D.A. Rogers. Aust. J. Chem. **37**, 1607 (1984).
51. G. Henkel, P. Betz, and B. Krebs. Inorg. Chim. Acta, **134**, 195 (1987).
52. I. Casals, P. Gonzalez-Duarte, W. Clegg, C. Foces-Foces, F.H. Cano, M. Martinez-Ripoll, M. Gomez, and X. Solans. J. Chem. Soc. Dalton Trans. 2511 (1991).

Can. J. Chem. Downloaded from www.nrcresearchpress.com by 203.198.23.82 on 09/08/12
For personal use only.

Limiting quantum yield measurements for the disappearance of 1-propanol and propanal: an oxidative reaction study employing a TiO_2 based photoreactor

GIUSEPPE P. LEPORE, BHUVAN C. PANT, AND COOPER H. LANGFORD[1]

Department of Chemistry, University of Calgary, 2500 University Drive N. W., Calgary, AB T2N 1N4, Canada

Received March 30, 1993

GIUSEPPE P. LEPORE, BHUVAN C. PANT, and COOPER H. LANGFORD. Can. J. Chem. **71**, 2051 (1993).

Relative initial quantum yields ($\Phi'_{0\ dis}$) for the disappearance of 1-propanol and propanal were estimated based on total light intensity entering the reaction vessels. Two types of photocatalytic reactor geometries were compared, a commercial prototype flow reactor with immobilized TiO_2 and a conventional reactor with TiO_2 dispersion. A maximum relative quantum yield, $\Phi'_{lim} \approx 1$, was extrapolated for pure propanol and propanal in both geometries. The high quantum yields were attributed to efficient competition of substrate oxidation with electron–hole recombination, at high surface coverage. Propanal was identified as the primary intermediate generated from 1-propanol in both reactor systems, but yields of propanal were systematically 10 times lower than 1-propanol loss, indicating that there was an effective pathway for propanal oxidation on the surface prior to desorption. The inhibition of 1-propanol reaction caused by accumulation of product arises because both reactant and product compete for active sites on the photocatalyst surface. These propositions were confirmed by introducing propanal into the feed. The relative quantum yields converge to unity for pure substrates, suggesting that they are true yields. That is to say, absorption by TiO_2 of light entering the reactor is efficient in these geometries.

GIUSEPPE P. LEPORE, BHUVAN C. PANT et COOPER H. LANGFORD. Can J. Chem. **71**, 2051 (1993).

En se basant sur l'intensité totale de la lumière entrant dans les récipients réactionnels, on a évalué les rendements quantiques relatifs initiaux ($\Phi'_{0\ dis}$) de disparition du 1-propanol et du propanal. On a comparé deux types de géométries pour les réacteurs photocatalytiques, un prototype commercial d'un réacteur à écoulement avec du TiO_2 immobilisé et un réacteur conventionnel avec une dispersion de TiO_2. Pour chacune des géométries, on a pu extrapoler un rendement quantique relatif maximal, $\Phi'_{lim} \approx 1$, pour le propanol pur ainsi que pour le propanal. On attribue les valeurs élevées des rendements quantiques à une compétition efficace, à une couverture élevée de la surface, de l'oxydation du substrat avec la recombinaison électron–trou. Pour chacun des réacteurs, on a identifié le propanal comme intermédiaire primaire généré par le 1-propanol, mais les rendements en propanal sont systématiquement 10 fois plus lents que les pertes du 1-propanol; ces observations indiquent que, avant la désorption, il existe à la surface une voie efficace pour l'oxydation du propanal. L'inhibition de la réaction du 1-propanol avec accumulation de produits a été attribuée à une compétition entre le réactif et le produit pour les sites actifs présents à la surface du photocatalyseur. Ces propositions sont confirmées par l'introduction de propanal dans la source. La convergence des rendements quantiques relatifs vers l'unité pour les substances pures suggère que ces valeurs correspondent au rendement quantique vrai, c'est-à-dire que, pour ces géométries, l'absorption par le TiO_2 de la lumière entrant dans le réacteur est efficace.

[Traduit par la rédaction]

Can. J. Chem. Downloaded from www.nrcresearchpress.com by 203.198.23.82 on 09/08/12
For personal use only.

Introduction

This work studies the band gap excitation of TiO_2 in the photochemical destruction of organic wastes. References 1–13 cover this topic. Photochemical activation excites an electron from a valence band to a conduction band, leaving a vacancy ("hole") in the valence band. The electron–hole pair may then migrate to and be trapped at the surface of the semiconductor. The holes in the valence band and the electrons in the conduction band can then oxidize or reduce the adsorbed species, surface groups, or the semiconductor itself. When there are no suitable hole or electron scavengers at the surface, carrier recombination dominates (and can occur within a few nanoseconds) and the energy absorbed will dissipate energy as heat (13–15). Since interfacial charge transfer can occur in less than 10 ps (15, 37), it can compete effectively with recombination.

In an aqueous medium, water is the dominant adsorbate. The primary product of interfacial electron transfer is often an adsorbed hydroxyl radical (16, 17). Moreover, this radical can be detected directly by spin trapping and electron paramagnetic resonance (18–20). Hydroxyl radicals are often assumed to be active in the photocatalytic degradation of many contaminants by initiating reactions of organic compounds. Since electron transfer rates are expected to correlate with the over-potential according to the Levich equation (21–23), an adsorbed organic molecule may capture holes from TiO_2 faster than water. Recent studies clearly indicated that reaction takes place on the TiO_2 surface rather than in the solution (7, 24–26). However, the distinction between a surface-bound hydroxyl radical and a trapped hole may be little more than semantic (35).

In the past six years, there have been studies to immobilize TiO_2 on various supports. Serpone et al. have bound titanium dioxide onto glass beads (27) and Matthews successfully immobilized TiO_2 onto the interior of glass (28) and Teflon (29) tubing, woven glass mesh (30), and sand (31). The fibre glass mesh has been used in a commercial prototype photoreactor.[2] To understand TiO_2 reactions, one must first answer the following questions. Does electron–hole recombination in TiO_2 limit its efficiency as a catalyst? Or, is substrate conversion controlled by mass transport, adsorption and the relative rates of primary intermediates compete with substrate desorption? What is the relation of the mechanism on the titanium dioxide surface to that indicated by intermediates observed after desorption into the liquid bulk? This paper will address these issues by examining a small prototype photoreactor from Nutech Envi-

[1]Author to whom correspondence may be addressed.

[2]Nutech Environmental, a division of Nutech Energy Systems, Inc., 511 McCormick Blvd., London, ON N5W 4C8, Canada.

Can. J. Chem. Downloaded from www.nrcresearchpress.com by 203.198.23.82 on 09/08/12
For personal use only.

ronmental[2] and a dispersion of TiO_2 in a reactor of similar geometry.

We choose to focus on a parameter related to quantum yield rather than on rate constant, since it deals with efficiency more directly. The choice of 1-propanol is to bias results toward maximum quantum yield, which in turn will shed better light on electron–hole recombination.

Experimental

Chemicals

Anhydrous 1-propanol 99+%, propionaldehyde (propanal) 99+%, 1,10-phenanthroline 99+% and propionic acid 99+% gold label were purchased from Aldrich. Titanium dioxide, Degussa P-25, was a gift from Degussa. Ferric chloride (J.T. Baker Co.) and potassium oxalate (Fisher) were laboratory grade reagents. These reagents required no further purification and their solutions were prepared in doubly deionized distilled water.

Instruments

A Perkin–Elmer Sigma 2 gas chromatograph combined with a Chromosorb 101 packed column (Chromatographic Specialties Inc.) and a flame ionization detector, interfaced with a Sigma 10 data station, was used to quantitatively monitor reactant and product concentrations. The operating conditions were as follows: column temperature (isothermal) 140°C, injection port temperature 180°C, detector temperature 200°C, and the carrier gas was prepurified nitrogen at a flow rate of 30 mL/min. Product qualitative analysis used a Hewlett–Packard GC–MSD (5890 gas chromatograph – 5970 mass selective detector) interfaced with a 9000/216 data station. The analyses were conducted by temperature programming: initial temperature, 70°C, temperature increment, 1°C/min; final temperature, 120°C. The injection port was set to 150°C and the detector zone, 250°C. The column was a Hewlett-Packard Pona capillary, crossed-linked methyl silicon gum (50 m × 0.2 m × 0.5 μm film thickness). The flow rate of the prepurified helium was 8 mL/min. The MSD was set to scan 20–500 amu.

A Hewlett–Packard diode array spectrophotometer (model HP8452) was used to determine absorbance during the chemical actinometry experiments. Surface area analysis was conducted with a Micrometrics instrument at low temperature using N_2 adsorption.

Photocatalytic reactors

In this work we use two geometries: Reactor I, a control system that contains TiO_2 suspensions (Fig. 1*a*), and Reactor II, a commercial prototype flow photoreactor (courtesy of Nutech Environmental[2]), which incorporates a TiO_2 film that is firmly bound to a fiberglass mesh (Fig. 1*b*).

Reactor I: The reaction vessel was a stainless steel tray (2.0 cm high × 4.5 cm wide × 38.0 cm long). It has two grooves, each at the end of the layout to accommodate a 20-W, tubular, low-pressure mercury fluorescent lamp (Phillips Electronics Ltd., "TL" 44 D25/09N) (Fig. 1*a*). According to the manufacturer's specification, the lamp emits radiation between 320 and 390 nm with a maximum intensity at 350 nm. The depth of the reaction vessel was 1.75 cm from the lamp, providing a maximum volume of 300 mL. However, the solution was set at 250 mL, a level well below the lamp. The 250 mL solution was thoroughly mixed by three stirring bars positioned at different locations along the tray. During illumination experiments the entire reactor was placed inside a wooden box which had a nonreflecting interior. The photoactive catalyst for this system was a finely dispersed white powder of titanium dioxide (Degussa P-25). Its B.E.T. (Brunauer–Emmett–Teller) surface area was confirmed to be 55.7 ± 0.5 m^2/g. An appropriate catalyst loading was determined experimentally by studying the conversion of a 0.010 M 1-propanol solution. A catalyst density of 0.3 g/L proved to be an effective quantity for this reactor. The conversion of 1-propanol was found to be insensitive to further increase of semiconductor loading. This insensitivity comes from the reaction geometry, which permits essentially total light absorption. Samples of these finely dispersed particles were taken by removing 2.00 mL aliquots after various exposure times and then centrifuging for 20 min at 4750 rpm. A portion of the centrifuged liquid was withdrawn with a Pasteur pipette and transferred to 2-mL sealed vials that were refrigerated for later analysis.

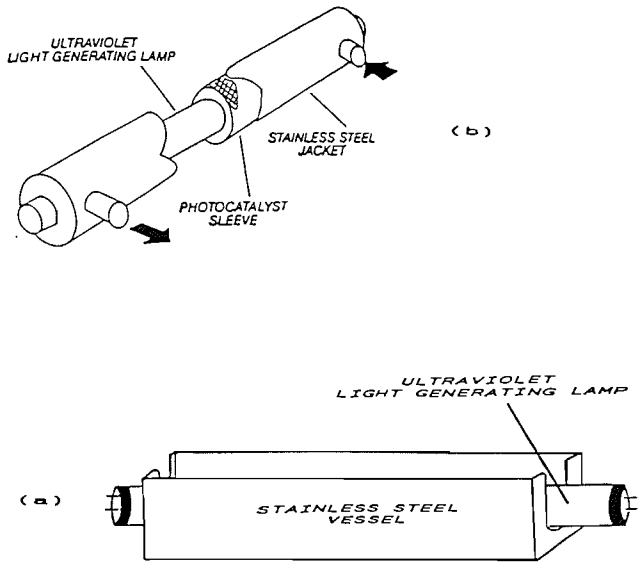

FIG. 1. Two photoreactor geometries examined in this investigation: (*a*) Reactor I, which employed a TiO_2 suspension and (*b*) Reactor II, a commercial prototype photoreactor that incorporates immobilized TiO_2.

Reactor II: The prototype flow reactor was fabricated from a stainless steel jacket (34 cm long by 2.3 cm inner radius), which accommodated a lamp and a photocatalytic mesh (Fig. 1*b*). An identical lamp to that in Reactor I (Phillips Electronics Ltd., "TL" 44 D25/09N, 20 W) was arranged coaxially within the jacket. Encircling the lamp was a fiberglass mesh (30 cm in length by 45 cm in width and an average 95 μm thick) coated with a firmly bonded layer of anatase titanium dioxide made via a sol–gel method.[2] The bound titanium dioxide layer had a B.E.T. surface area of 8.20 ± 1.48 m^2/g in comparison to the bare fiberglass mesh area of 6.56 ± 0.78 m^2/g. Its estimated coverage thickness was ≈2 μm and the catalyst loading on the fibers was calculated to be roughly 1 g/L, taking 20 as the number of perforations per cm^2 and each opening having an average area of 4×10^{-2} cm^2.

The total volume of solution circulated in the reactor was 750 mL. The reactor itself, excluding a reservoir, had a dead volume of 410 mL. The liquid was recirculated with an oscillating pump (Gormann–Rupp Industries Inc.) with a flow rate of 150 mL/min from a 1-L reservoir. The perforations and configuration of the mesh in the reactor create turbulent mixing that ensures good contact between the reactants and the photocatalyst.[2] A magnetic stirring bar was placed in the reservoir. To assure proper mixing and aeration, the outflow from the reactor entered the reservoir a few centimetres above the surface of the bulk solution. Materials in contact with the solution were stainless steel, polypropylene (pump valve housings), glass, and Tygon tubing.

Stock solutions were prepared in 2-L volumetric flasks to simplify comparison between dark controls and the photocatalytic experiments. Samples were taken by removing 1.00 mL aliquots from the reservoir after different exposure times. These aliquots were then placed into 2-mL sealed vials and refrigerated for later analysis. After every run the reactor was left on and flushed several times with water and the effluent was monitored until no residual organ-

Can. J. Chem. Downloaded from www.nrcresearchpress.com by 203.198.23.82 on 09/08/12
For personal use only.

ics could be detected. The reactor was then rinsed with an another 4 L of water.

In both reactors, the lamps were warmed up for 10 min prior to photolysis. Furthermore, the solution in the reactor was in constant contact with air to ensure complete O_2 (gas–liquid) equilibration. Parallel dark experiments (controls) were performed to monitor the possibility of substrate loss and susceptibility to air oxidation. Substrate losses encountered during dark experiments were subtracted from losses measured in the photocatalysis study. As well, the bulk solution was monitored for pH and temperature changes in both reactors.

Quantum yield measurements

The quantum yield is the ratio of the amount in moles of product formed or reactant consumed to the amount in einsteins of energy absorbed. An elementary reaction that is completely energy efficient will have a quantum yield of unity. Thus, the quantum yield is the best parameter to indicate the efficiency of a photocatalyst. Unfortunately, quantum yield is not easily measured in heterogeneous photochemical reactions, since the amount of light absorbed by a catalyst cannot be measured in a reliable manner. Several authors (41, 42) have recently overcome this obstacle. Sciavello et al. (41) used photon flux to measure the amount of reflected and absorbed light at the entrance and exit of the light-tight photoreactor, which contained a selection of commercially available titanium dioxide preparations. Lepore et al. (42) evaluated true quantum yields for essentially transparent, suspended P-25 TiO_2 particles (diameter $\approx$ 124 nm) under monochromatic irradiation at 313 nm. The absorbed light intensity was calculated from the incident photon intensity and the known absorbance of TiO_2 at 313 nm.

In this paper we discuss a parameter (Φ') that reduces to the quantum yield Φ if, by using a sufficiently concentrated chemical actinometer, all the light entering the reactor is absorbed by the photocatalyst TiO_2 (5, 10, 43, 44). Trott, Henwood, and Langford (38) described this approach and recognized that the values obtained must be less than or equal to the true quantum yield since it assigns the maximum possible value to the denominator. This parameter was introduced as a tool for the comparison of relative efficiencies of some photodegradations under sunlight illumination.

A well-established chemical actinometer, potassium ferrioxalate, was selected for its sensitivity, ease of use, and wide spectral range (200–546 nm). The actinometry procedure was taken from the literature (34) and, since both reactors employed equivalent light sources, comparison of the two reactors was simplified. A 0.006 M actinometer concentration used for the two geometries was sufficient to absorb all entering light. This was confirmed by the insensitivity of light intensity to changes in actinometer concentrations. The duration of irradiation was chosen to limit the conversion of ferrioxalate to less than 15% to avoid secondary photo-processes. The static design of Reactor I accommodated an actinometer volume of 250 mL, which was continuously stirred and illuminated for 60 s. However, for the recirculating system (Reactor II) the flow rate (150 mL/min) and irradiation time (5 min) were selected for maximum light exposure of the 750 mL solution.

The quantity of Fe^{2+} formed upon irradiation was spectrophotometrically determined by the complexation of ferrous ions with 1,10-phenanthroline (phen) to form the red $[Fe(phen)_3]^{2+}$ moiety, which has an absorption maxima at λ = 510 nm (ϵ = 1.11 $\times$ 10^4 M^{-1} cm^{-1}). The reported quantum yield $\phi_{Fe^{2+}}$ for the production of Fe^{2+} is 1.21 at 350 nm.

Results

The radiant intensity inside Reactor II was determined to be 1.30 $\times$ 10^{18} photons per second either with or without the TiO_2 bound mesh. This value represents the maximum photon absorption rate for the anchored photocatalyst during photoreaction. The actual absorption of photons by the TiO_2 might be lower in both systems, especially in Reactor II, because of the low catalyst loading.

The light intensity in the static system (Reactor I) in the absence of the photocatalyst suspension was 1.60 $\times$ 10^{18} photons per second. The photon fluxes agreed within 4%, each time the chemical actinometer was employed in either system. Furthermore, the lamps could be interchanged between reactors. The difference in light intensities between the two reactor geometries may be due to the shadowing of the lamp ends in Reactor II.

Weak dependence of measured light intensity on actinometer concentration was seen in the commercial photoreactor. Since theoretical and mechanistic interest focuses on measurement of true quantum yields (Φ), the value quoted is in the concentration-independent region. Because variation of actinometer concentration has little effect on changes in the depth of light penetration around the TiO_2 bonded mesh, Φ' must closely approach the true quantum yield. The only reason for such weak dependence is absorption by the mesh of all photons reaching the mesh. We note below that the overall results support this view. It is important to interpretation of Φ' that in Reactor II no appreciable difference was observed for the ferrioxalate actinometer in the absence or presence of the immobilized TiO_2 mesh.

Relative values of Φ' given below for various propanol and propanal concentrations remain significant in any case since the variations of nonabsorbing substrate concentrations do not affect the efficiency of light absorption by TiO_2. The quantity Φ' is a lower limit to the true quantum yield as explained above. The relative quantum yield (Φ') is calculated from eqs. [1] and [2]

$$[1] \quad \Phi' = \frac{C_p}{I}$$

$$[2] \quad \Phi'_{dis} = \frac{(C_0 - C_i)}{I}$$

where Φ'_0 is the relative initial quantum yield (intercept at t = 0); Φ', the quantum yield of product formed, Φ'_{dis}, the quantum yield of the sum of products formed or the disappearance of the reactant; C_p represents moles of individual product formed (1°, 2°, 3° . . . etc.); C_0, initial moles of reactant; C_i, moles of reactant remaining in the ith irradiated sample; and I, the intensity, in einsteins, of light entering the reactor.

The difference in system geometry and dead volumes between the two reactors determines the amount of light delivered to the reaction zone in each. In Reactor II, several experiments were performed with 1-propanol and propanal separately as a function of substrate concentration, while in Reactor I only 1-propanol was investigated for reasons given below. In both reactors the solutions were well aerated so that oxygen could be an efficient acceptor for conduction band electrons. Prior to photocatalysis, blank experiments were conducted under illumination in the absence of TiO_2 for each substrate, for a duration of 70 min. Since none of these compounds absorb light above 300 nm, any change in their respective concentrations would be due to evaporation, thermal decomposition, or air oxidation. Furthermore, parallel dark experiments were also carried out in the presence of TiO_2 for a period of 70 min. The blank and dark samples

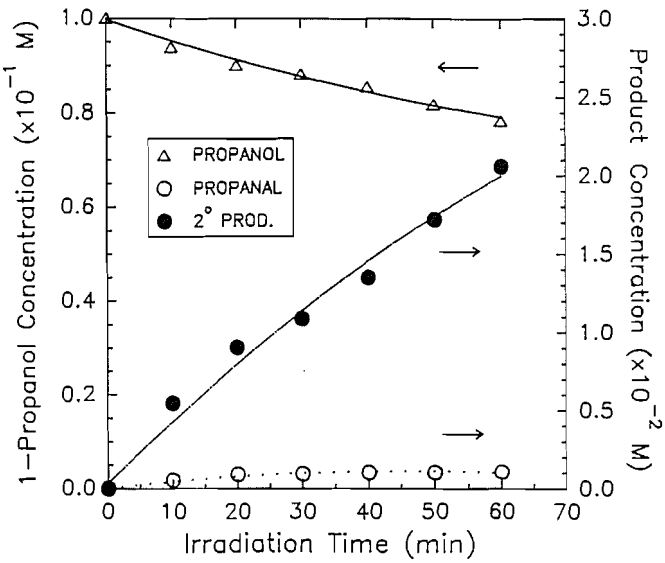

FIG. 2. The photocatalytic conversion of 1-propanol (open triangles) employing Reactor I. The measured concentration of 1-propanol remaining is delineated on the left vertical axis ($\times 10^{-1}$ M). Concentrations of generated products, propanol (open circles) and 2° prod. (filled circles), are represented on the right vertical axis ($\times 10^{-2}$ M).

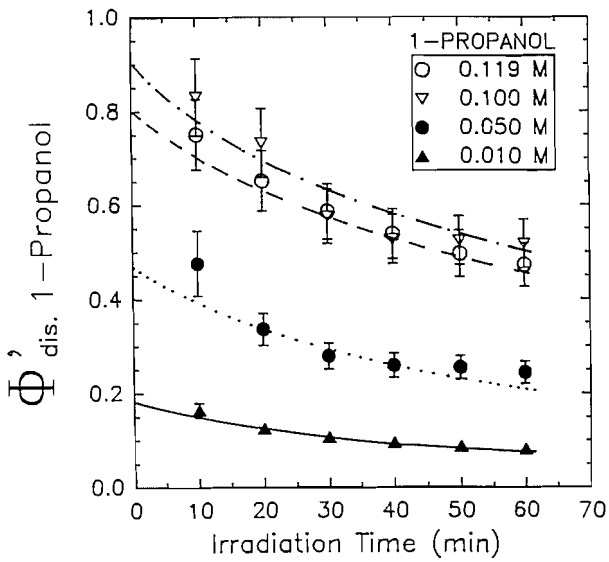

FIG. 3. Quantum yields of disappearance of 1-propanol (Φ'_{dis}) in Reactor I measured as a function of illumination time at four different reactant concentrations: 0.010 M (filled triangles), 0.050 M (filled circles), 0.100 M (inverted open triangles), 0.119 M (open circles).

were analyzed several times by GC–MSD, and under these circumstances only some evaporation could be demonstrated as a loss mechanism.

Significant losses were observed in Reactor I under blank conditions for propanal solutions. This confined the investigation to 1-propanol, since it is less volatile and it is also possible to monitor its oxidation intermediates. All photocatalysis results were corrected for small substrate losses from the blank controls. In all cases, as discussed below, the apparent quantum yields exhibited distinct decreases with increasing illumination time. This behavior is not simply a reflection of substrate loss since it becomes significant at low conversion. One major contributor to the decline in quantum yields is reactant–product competition for active surface sites. However, quantitative discussion is limited in most cases to values of Φ' extrapolated to time zero (Φ'_0), a parameter that eliminates the need for blank correction and the influence of product buildup, and thus makes interpretation more straightforward.

Reaction temperatures were monitored throughout this study, and were found not to exceed 30°C for either system. It has been documented that reaction rates are influenced by the solution temperature (32, 33). Moreover, Harvey et al. (33) reported that activation energies (277–313 K temperature range) for rutile TiO_2 are insensitive to reaction conditions, but are influenced by changes in excitation wavelengths. This insensitivity implicates processes within the photocatalyst instead of in the photocatalysed reaction. The contribution of thermal decomposition proved to be insignificant: in an experiment in which a 0.062 M 1-propanol solution (in the presence of TiO_2) was maintained at 35°C for 90 min in the dark, no intermediates were detected. The pH was also monitored (initial pH 5.5) but no significant change was observed. Prior to illumination, substrate solutions were thoroughly mixed for 5 min in the reactors.

Experiments using Reactor I

A typical experiment using the dispersion of P-25 TiO_2 is shown in Fig. 2. An initial concentration of 0.100 M 1-propanol was illuminated for a duration of 60 min. Over this time span the propanol concentration decreased by about 20%. The slight upward curvature indicates declining apparent quantum yield. Notice that measurable propanal produced never exceeds 20% of 1-propanol consumed; this curve was corrected for losses averaged over three dark controls. At longer irradiation times (>90 min) propanal concentration decreased almost to zero. If propanal is the primary intermediate, it is not efficiently desorbed. The flat propanal curve suggests an **A** → **B** → **C** sequence. On this assumption, the curve for secondary intermediate(s) (2° prod.) is calculated. Quantitative analysis performed with GC–MSD revealed that the 2° prod. includes a small amount of propionic acid and ethane; however, all further stages of oxidation to CO_2 may contribute.

The reaction sequence (**A** → **B** → **C**) was confirmed by an independent study of propanal in a closed system that revealed clearly the presence of propionic acid. In the series of experiments with initial 1-propanol concentration ranging from 0.030 to 0.119 M, secondary intermediate(s) occur in greater quantity than propanal. It seems that further photolysis of propanal is relatively rapid compared to desorption. This phenomenon was also observed for Reactor II, which implies that propanal is adsorbed more strongly than the alcohol. Contributions due to propanal evaporation would be inconsistent with this interpretation, since results were corrected for losses.

Relative quantum yields for 1-propanol disappearance (Φ'_{dis}) were calculated for the full range of the alcohol concentrations (0.010–0.119 M) and plotted versus irradiation time (Fig. 3). The individual curves displayed a high apparent yield (>0.2) at time zero, which falls with continued illumination. Yields of propanal found in the solution are

Can. J. Chem. Downloaded from www.nrcresearchpress.com by 203.198.23.82 on 09/08/12
For personal use only.

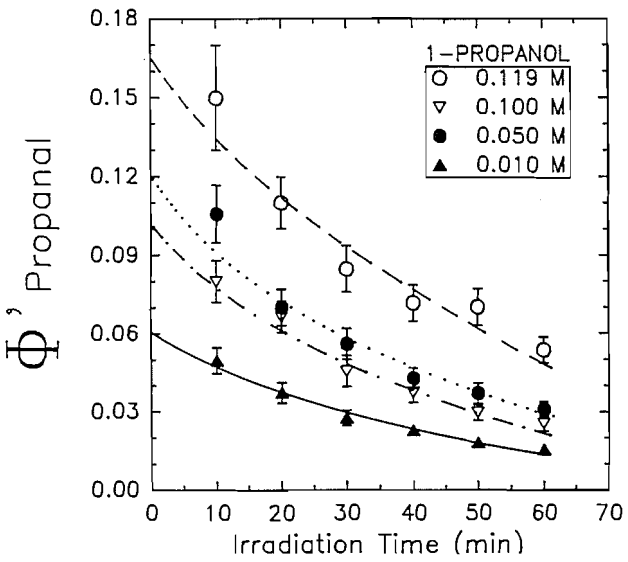

FIG. 4. Quantum yield for the production of propanal (Φ′) plotted as a function of irradiation time in Reactor I. Four distinct curves were obtained, each corresponding to an initial 1-propanol concentration: 0.010 M (filled triangles), 0.050 M (filled circles), 0.100 M (inverted open triangles), 0.119 M (open circles).

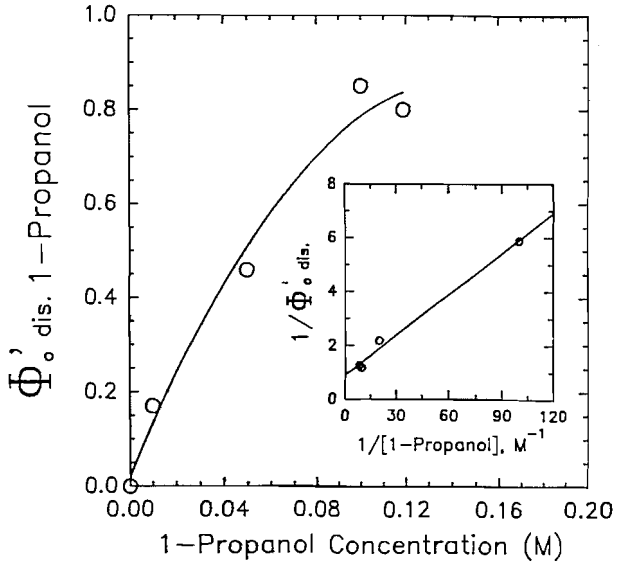

FIG. 5. A concentration dependence plot; initial quantum yields of disappearance of 1-propanol ($\Phi'_{0\ dis}$). The inset represents the double reciprocal plot of $\Phi'_{0\ dis}$ vs. propanol concentration, for the evaluation of limiting quantum yield conversion and apparent binding constant for the reactant.

illustrated in Fig. 4. The apparent quantum yields of observable propanal are all low (<0.2). The intermediate (propanal) decreases with prolonged exposure to irradiation in a way comparable to the reactant, 1-propanol. The changes are more pronounced at higher total concentration, which corresponds to higher surface coverage. This suggests that propanal is retained on the surface long enough to be efficiently oxidized in competition with its desorption into solution.

Langmuir–Hinshelwood kinetics (L–H) have often been applied to TiO_2 photocatalysis (eq. [3]). This expression represents surface unimolecular reactions that arise from light excitation of TiO_2 in cases where the reactant is more strongly adsorbed than the intermediate(s) (which may be minimal or absent). The above results imply strong adsorption of intermediates. Relative quantum yields for 1-propanol disappearance were extrapolated to time zero $\Phi'_{0\ dis}$, where there is no product accumulation. There, Langmuir–Hinshelwood kinetics may apply. The solvent (water) may adsorb competitively but its concentration is much greater than that of the solute and remains essentially constant. Thus water has been omitted from the expression. Its competitive effect enters into the equilibrium adsorption–desorption coefficient, K (binding constant).

$$[3] \quad \Phi'_{0\ dis} = \frac{\Phi'_{lim}\, K[C_0]}{1 + K[C_0]}$$

In eq. [3], Φ'_{lim} is the limiting quantum yield of conversion at high surface coverage. The Φ'_{lim} is a function of the competition between interfacial electron transfer and carrier recombination. Equation [3] can be transformed into a linear expression (eq. [4]), where the intercept gives the limiting quantum yield and the slope allows calculation of K.

$$[4] \quad \frac{1}{\Phi'_{0\ dis}} = \frac{1}{\Phi'_{lim}} + \frac{1}{\Phi'_{lim}\, K[C_0]}$$

Figure 5 shows the linearized plot of initial quantum yields for the disappearance of 1-propanol ($\Phi'_{0\ dis}$) as a function of initial reactant concentration. The limiting yield is extrapolated to neat (infinite) 1-propanol levels, and is determined from the best-fit straight line to be about one. This is in agreement with an aspect of earlier work by Ergeton and King (39), for *pure* isopropanol. These authors reported a maximum unit quantum yield under unfiltered uv light, which decreased at 335 nm (filtered light) by about one half and at 404 nm (filtered light) by approximately one third. However, extrapolation to pure substrate levels does not imply that this is the critical concentration for attaining such a maximum quantum yield. The important factor in reaching Φ'_{lim} is complete surface coverage of the photocatalyst, which may well occur at lower substrate concentration as our results suggest.

The slope of the best-fit linearized plot in Fig. 5 gave an approximate equilibrium binding constant of 18 M^{-1}. The limiting value of unity for $\Phi'_{0\ dis}$ suggests that this parameter is in fact the true quantum yield, since a true yield above one is unlikely and Φ′ is always less than Φ. The photocatalyst, TiO_2, appears to absorb all the photons in this reactor configuration.

Experiments using Reactor II

The next stage of this investigation was to evaluate the change of geometry imposed by the commercial prototype photoreactor and to further investigate the points suggested by the study in Reactor I. In a typical experiment (Fig. 6), the photolysis of 0.0615 M 1-propanol solution for a period of 70 min in the presence of an immobilized TiO_2 resulted in a decline in the initial concentration of alcohol, with low production of propanal. The calculated secondary component was once again the major observed product in the system.

The apparent $\Phi'_{0\ dis}$ values for various initial 1-propanol concentrations in the reservoir were obtained by extrapolation. The data were then treated with the modified L–H

Can. J. Chem. Downloaded from www.nrcresearchpress.com by 203.198.23.82 on 09/08/12
For personal use only.

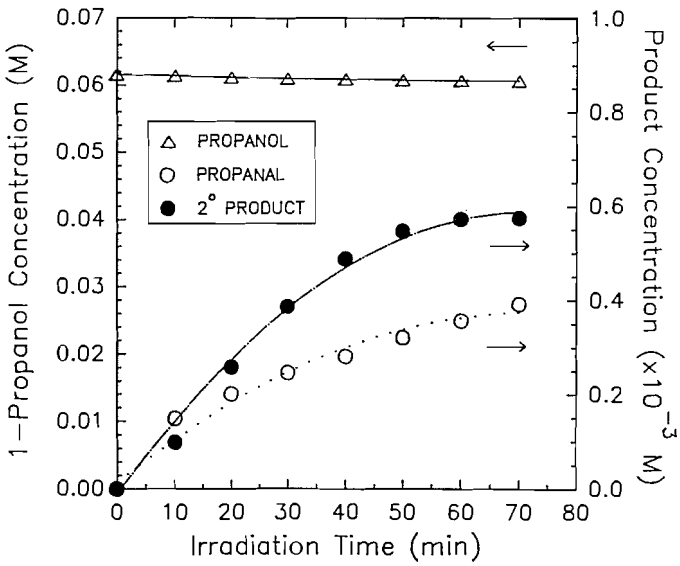

FIG. 6. The photocatalytic oxidation of 1-propanol (open triangles) in a prototype photoreactor (Reactor II) is represented on the left vertical axis. Product accumulation, propanal (open circles) and 2° prod. (filled circles), is delineated on the right vertical axis ($\times 10^{-3}$ M).

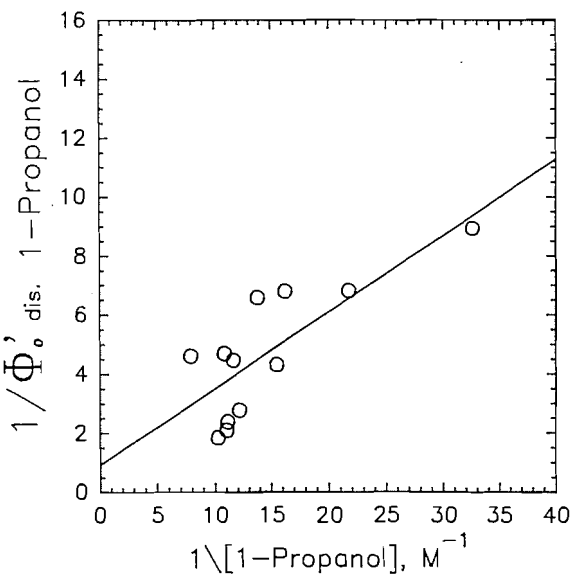

FIG. 7. Double reciprocal plot of initial quantum yields of disappearance ($\Phi'_{0\,dis}$) vs. initial 1-propanol concentration for the estimation of limiting quantum yield and apparent binding constant (Reactor II).

expression (double reciprocal plot) to estimate the Φ_{lim} and the equilibrium binding constant (Fig. 7). The best-fit double reciprocal plot gave an approximate limiting quantum yield near unity with a binding constant of 3.6 M^{-1} for 1-propanol. The high noise in Fig. 7 is characteristic of the high reactant concentrations required, which made it difficult to measure the loss of 1-propanol. The data are consistent with earlier results, indicating a limiting yield of one. Since three experiments imply a limiting yield near one using objective linear least-squares fitting techniques, we must comment on the precision of the limits. The standard deviation of the intercepts ranges from 17% in the best case (propanal) to over 100% in the worst case (propanol on the mesh). However, these overstate the uncertainty of the estimation of the intercept. The slope/intercept fitting uses all data points equally; the intercepts are most strongly determined by the *few points* at the highest concentrations and these do not support such large variation in intercept. Certainly, the higher points are not consistent with an intercept much below one. Only deviations from values greater than one could be large. We would need to view the present results as mainly qualitative, indicating large yields. Our confidence in the assignment of values near one depends on a supplementary confirming study. Lepore et al. (42) developed a separation of dispersion of Degussa P-25 TiO_2, which produced dispersions that are transparent in the visible with definable absorption at 313 nm. It was possible to measure precise and well-defined quantum yields for these dispersions using conventional spectrophotometric absorption techniques. As reported in detail (42), we can confirm unit limiting quantum yield with an uncertainty of less than 10%. We do not believe that particle size segregation is a critical factor and we propose to interpret the indications of the present study at face value.

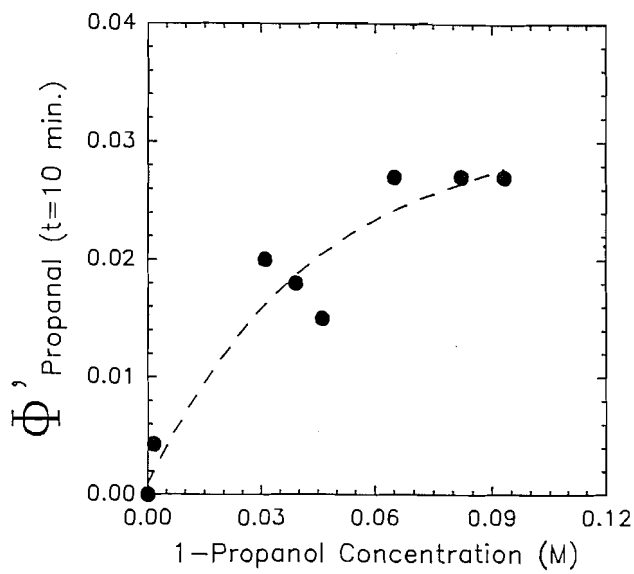

FIG. 8. A plot of quantum yield for the production of propanal (Φ') vs. initial reactant concentration (1-propanol). The Φ' were measured at an illumination time of 10 min (Reactor II).

The significant differences between the results for the particle dispersion (Reactor I) and the TiO_2 film on a glass mesh (Reactor II) are the lower apparent K in the second case and the reduced ratio of propanal produced to 1-propanol consumed in the TiO_2 film reactor. The consecutive accumulation of propanal (Φ') from the photocatalytic oxidation of 1-propanol was measured at an illumination time of 10 min (Fig. 8). The curve manifests a relative maximum quantum yield for the production of propanal at elevated alcohol concentrations. This optimum production of propanal (Φ') in the bulk solution is approximately 20 times lower than the consumption of 1-propanol.

To investigate the suggestion that propanal adsorbs strongly and can subsequently be efficiently oxidized, propanal was introduced into the feed in the next series of experiments. As noted above, a parallel experiment was not feasible in Re-

Can. J. Chem. Downloaded from www.nrcresearchpress.com by 203.198.23.82 on 09/08/12
For personal use only.

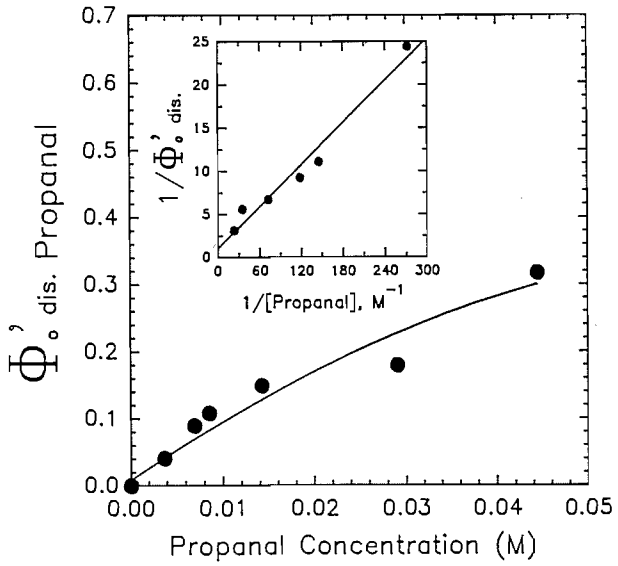

FIG. 9. Initial quantum yields of propanal disappearance plotted against initial propanal concentration, employing Reactor II. The inset figure depicts a double reciprocal plot of $\Phi'_{0\ dis}$ vs. initial reactant concentration.

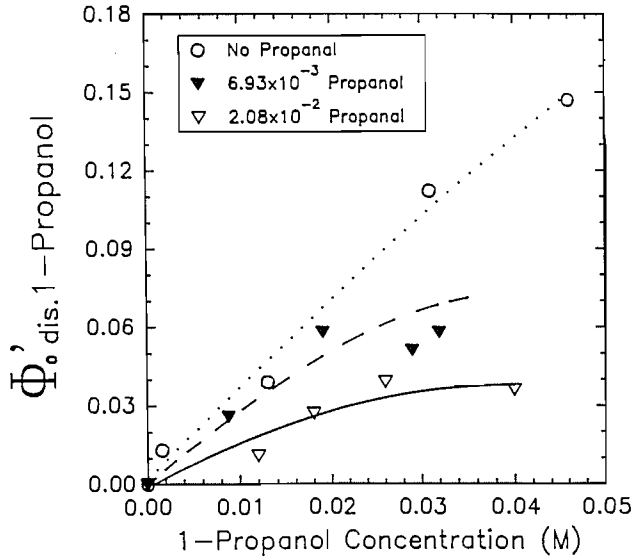

FIG. 10. Two-component mixture to exemplify reactant–product competition (Reactor II). Propanal concentration was maintained constant while concentration of 1-propanol was varied. The $\Phi'_{0\ dis}$ of the alcohol were extrapolated and plotted against initial 1-propanol concentration. The figure displays three curves: no propanal present (open circles), 6.93×10^{-3} M propanal (inverted filled triangles), and 2.08×10^{-2} M propanal (inverted open triangles).

actor I. A plot with less scattering was obtained as a result of good conversion at lower total propanal concentration (Fig. 9). A double reciprocal plot of the data (Fig. 9, inset) revealed once again a best-fit extrapolated Φ_{lim} of ≈ 1.0 with an equilibrium binding constant $K = 13\ M^{-1}$. This value is 3.8 times greater than the binding constant of 1-propanol, which confirms that propanal is more strongly adsorbed than 1-propanol over the immobilized metal oxide. This result provides a background for direct propanol–propanal competition experiments. Equation [3] may be written in a general form (eq. [5]) to accommodate several competitive adsorbates: C_0, C_1, . . . C_n; other symbols have meanings parallel to those given for eq. [3].

$$[5] \quad \Phi'_{0\ dis} = \frac{\Phi'_{lim} K[C_0]}{1 + K[C_0] + K_1[C_1] + \ldots K_n[C_n]}$$

Ideally, we would wish to evaluate directly the competition for 1-propanol offered by propanal generated as an intermediate on the surface of the metal oxide. Unfortunately, data for reaction of propanal introduced in solution do not give direct access to this information, since the equilibrium for adsorption from solution includes diffusional transport to the surface, which causes the dependence on bulk concentration. As a second best, mainly suggestive, experiment, we establish competition between 1-propanol and propanal, both from the solution.

Two-component mixtures were fed into the reactor with propanal concentration maintained constant and that of 1-propanol varied. The individual solutions were illuminated for a period of 70 min and $\Phi'_{0\ dis}$ values for 1-propanol were estimated by extrapolating to time zero. These $\Phi'_{0\ dis}$ values were plotted against initial 1-propanol concentration (Fig. 10). Three curves are presented in Fig. 10: one curve depicts a solution containing exclusively 1-propanol (dotted curve), the other two curves represent two-component mixtures, which contained 6.93×10^{-3} M (broken lines) and 2.08×10^{-2} M propanal (solid curve). The data clearly illustrate propanal inhibition of 1-propanol photocatalytic oxidation, which is qualitatively consistent with the relative K values obtained above.

Discussion

The first consequence of this investigation was to demonstrate, by employing different reactor geometries, that high quantum yields on TiO_2 surfaces can be obtained. Our related results (42) add additional "geometries". If the quantum yields for electron–hole pair separation (surface carrier trapping) following band-gap excitation can reach unity, then it is plausible to capture most, if not all, of these surface reactive species with suitable scavengers. For reaction quantum yields to reach unity over the surface of the semiconductor oxide, substrate reactions must occur quite rapidly. As earlier picosecond transient spectroscopy indicated (15, 37), interfacial electron transfer can compete effectively with electron–hole recombination. However, colloidal particles of TiO_2 were used in these investigations. The reaction sequence on larger particles (with a space charge layer) is more complex. The transit times for diffusion of minority carriers to the surface of large particles are longer and consequently may make recombination effects important in competition with surface trapping (36). With TiO_2 bound to supports there should be no significant difference from the TiO_2 dispersions, with the exception of extremely small colloidal dispersions (36). Thus a low limiting quantum yield for conversion of a readily oxidizable substrate in the fixed TiO_2 geometry would reveal the contributions of recombination events.

The assumption that the reactor geometries used here lead to a TiO_2 photon absorption of 100% implies that Φ approaches a limit of 1.0 in both systems. Any failure of light absorption by the photocatalyst causes Φ' to fall below the

Can. J. Chem. Downloaded from www.nrcresearchpress.com by 203.198.23.82 on 09/08/12
For personal use only.

TABLE 1. Quantum yield disappearance for 1-propanol and propanal

Concentration (M) at $t = 0$	$K(M^{-1})$ Reactor I	Φ'_0 dis Reactor I	$K(M^{-1})$ Reactor II	Φ'_0 dis Reactor II
High propanol	18	≈1.0	3.6	≈1.0
High propanal	—	—	13	≈1.0
Propanol (0.02 M)	18	0.33	3.6	0.08
Propanal (0.02 M)	—	—	13	0.19
Propanol (0.001 M)	18	0.018	3.6	0.0036
Propanal (0.001 M)	—	—	13	0.013

true quantum yield (Φ). Conversely, if Φ' exceeds unity, the implication of a "current doubling" type of mechanistic route (25) must not be overlooked. This could arise if conduction band electrons scavenged by molecular oxygen give rise to superoxide radical anions ($O_2^{\cdot -}$) that disproportionate to hydroxyl radicals (·OH). This could lead to a maximal Φ of two. However, it is more likely that superoxide intermediates contribute the second oxidative equivalent required in two-electron overall organic oxidations. The common convergence on 1.0, along with the relative insensitivity of measured intensity to changing concentrations of actinometer solution in actinometry experiments, favours the conclusion that all the photons in the reactive zones of these two reactor configurations are absorbed by TiO_2. Of course, many photons can be initially reflected and scattered but ultimately absorbed.

The extrapolated limiting quantum yield of 1 reflects conditions of high surface coverage, no longer comparable to conditions encountered at typical trace contamination levels of 10^{-6} to 10^{-3} M often studied in the literature. At the Φ_{lim} value, diffusion and mass transfer effects are minimized and high apparent substrate binding constants are no longer crucial for optimum conversion (under the assumption that product accumulation is negligible). Therefore, photo-processes become rate determining.

We now consider differences between the two reactors. When quantum yields for low-level contaminants are assessed, all of the photochemical and mass transfer factors contribute to the observed Φ'. An estimate of $\Phi'_{0\,dis}$ at different substrate concentrations has been tabulated (Table 1) for both reactor geometries. The data show that at 0.02 M, Reactor I (dispersion) is about 4 times more efficient than Reactor II (stationary TiO_2). This reflects substrate coverage on TiO_2 and the number of active sites available for conversion. It is well documented that the surface of TiO_2 is readily hydroxylated when in contact with moisture (45–49), where both molecular and dissociated water is bound to the surface. Most researchers report coverages of 7–10 OH^-/nm^2 at room temperature (46–49). Since OH^- groups and water are the most abundant sites on the surface of the photocatalyst, adsorption of propanol may well occur through these sites (i.e., H bonding). If we then compare the density of surface sites of the slurry reactor to that of the stationary TiO_2 Reactor II, we find that 1.7×10^{20} OH^- sites are available in the dispersed phase (Reactor I) and 1.7×10^{19} sites on the stationary TiO_2 in Reactor II. On a per site basis, Reactor II may be more efficient, but the final calculation of the balance of factors is complex.

It has been reported that reaction quantum efficiency may vary with illumination levels (I) (10, 39, 40) and inversely with wavelength. For light intensities above 1 sun, the quantum efficiency can change as a function of $I^{-0.5}$ to $I^{-1.0}$ for high photon fluxes. At lower intensities, the quantum efficiency is constant and the reaction rate is catalyst dependent. This dependency reflects the competitive rate of carrier recombination to that of interfacial charge transfer. In this investigation the lamp intensities exceeded 1 sun; however, the high scavenger concentrations employed compete effectively with the recombination process. The generated reactive surface species were all captured by the adsorbed substrate. Therefore, quantum efficiency dependence on light intensities (I) is not seen in this study as would be the case at low surface coverage.

The next significant observation is that the quantum yield for the production of the observed primary intermediate is always found to be an order of magnitude smaller than the quantum yield for alcohol consumption. This indicates that propanal reacts further on the surface prior to desorption. This conclusion is consistent with the observation that apparent quantum yield for alcohol consumption decreases beyond $t = 0$, especially in the context of the result that the binding constant for propanal is larger than that for 1-propanol. The efficiency of any particular step of a photocatalytic oxidation sequence is determined by the relative adsorption of the particular substrate and its immediate product and their relative reactivity. The single L–H treatment assumes weak product adsorption. In the present case, it can be applied only to the time limit $t = 0$, before buildup of any intermediate(s).

It is unfortunate that the most intriguing question is not readily addressable. It would be of great interest to measure the relative rate of oxidation of 1-propanol, propanal, and water on the surface. All of the present observations are consistent with either the hypothesis that all three rates are very rapid and similar or that all three are proportional to their respective electrochemical over-potentials. At present, we are only able to show qualitative agreement with a two-component L–H model (Fig. 10) when feeds include both 1-propanol and propanal. The noise level in our experiments proved too high to permit quantitative evaluation of Φ_{lim} values in two-feed component competition experiments.

Conclusion

This work establishes that interfacial electron transfer involving organic substrates on the titanium dioxide surface can compete efficiently with "carrier recombination." All holes are surface trapped and available. A recent paper (35) makes the point that a trapped hole at the TiO_2–water interface may be only semantically distinguished from an adsorbed hydroxyl radical. From this point of view, carrier recombination is the back reaction of an adsorbed hydroxyl radical with

Can. J. Chem. Downloaded from www.nrcresearchpress.com by 203.198.23.82 on 09/08/12
For personal use only.

surface-trapped electrons (Ti^{3+} sites). If so, our conclusion can be reexpressed as the proposition that adsorbed hydroxyl radicals react more rapidly with alcohol and aldehyde substrates than with surface-trapped electrons (Ti^{3+} centres). The central point for the development of TiO_2 photocatalytic systems for organic oxidation is that the conclusion for alcohol and aldehyde substrates is likely to be generalized to many organic substrates. Thus, the aim should be to design systems that appropriately control adsorption–desorption. As well, mass transport will be critical at low substrate concentrations.

The results contain one warning for TiO_2 photocatalytic studies that have diagnosed reaction pathways from intermediates found in solutions. These intermediates may be arising on inefficient pathways, while the intermediates of the most efficient pathways may never be significantly released. For example, in some qualitative runs on methanol oxidation, we were unable to detect any methanal.

Acknowledgments

Much of this investigation was performed at Concordia University (Chemistry and Biochemistry Department). We would like to thank the Concordia Ecotoxicology Laboratories, Dr. P. Anderson for providing access to instruments and Mr. B. Sjiariel for carrying out the B.E.T. surface area measurements. A substantial portion of the work on the dispersion reactor was performed by Mr. D. Palacios as his undergraduate project at Concordia. The collaboration of Nutech Environmental, especially through Dr. H. Al-Ekabi, has been very valuable. This study was supported by grants from the Natural Sciences and Engineering Research Council of Canada (NSERC), the Fonds pour la formation de chercheurs et l'aide à la recherche (FCAR) du Québec, and the Ministère d'enseignement supérieur et de la science (MESS) du Québec.

1. J.H. Carey, J. Lawrence, and H.M. Tosine. Bull. Environ. Contam. Toxicol. **16**, 697 (1976).
2. A. Mills. Chem. Soc. Rev. **18**, 285 (1989).
3. R.W. Matthews. J. Chem. Soc. Faraday Trans. 1, **80**, 457 (1984).
4. K. Harada, T. Hisanaga, and K. Tanaka. New J. Chem. **11**, 597 (1987).
5. C. Kormann, D.W. Bahnemann, and M.R. Hoffmann. Environ. Sci. Technol. **22**, 798 (1988).
6. Y. Xu, P.E. Menassa, and C.H. Langford. Chemosphere, **17**, 1971 (1988).
7. G.P. Lepore and C.H. Langford. Water Pollut. Res. J. Can. **24**, 537 (1989).
8. H. Al-Ekabi, N. Serpone, E. Pelizzetti, C. Minero, M.-A. Fox, and R.B. Draper. Langmuir, **5**, 250 (1989).
9. D.F. Ollis. Photocatalysis and environment. *Edited by* M. Schiavello. Kluwer Academic Publishers, The Netherlands. 1989. p. 663.
10. K. Okamato, Y. Yamamoto, H. Tanaka, and A. Itaya. Bull. Chem. Soc. Jpn. **58**, 2023 (1985).
11. J. Doménech and J. Peral. Sol. Energy, **41**, 55 (1988).
12. C.D. Jaeger and A. Bard. J. Phys. Chem. **83**, 3146 (1987).
13. J.J. Kasinski, L.A. Gomez-Jahn, K.J. Faran, S.M. Gracewski, and R.J.D. Miller. J. Chem. Phys. **90**, 1253 (1989).
14. G. Rothenburger, J. Moser, M. Grätzel, N. Serpone, and D.K. Sharma. J. Am. Chem. Soc. **107**, 8054 (1985).
15. C. Arbour, D.K. Sharma, and C.H. Langford. J. Phys. Chem. **94**, 331 (1990).
16. H. Tanaka, M. Tanaka, and A. Itaya. Bull. Chem. Soc. Jpn. **58**, 2015 (1985).
17. J. Cunningham and S. Srijaran. J. Photochem. Photobiol. A, **42**, 329 (1988).
18. E.M. Ceresa, L. Burlamacchi, and M. Visca. J. Mater. Sci. **18**, 289 (1983).
19. C.D. Jaeger and A.J. Bard. J. Phys. Chem. **83**, 3146 (1979).
20. J.R. Bolton. Symp. Proc. Advanced oxidation processes for the treatment of contaminated water and air. Toronto, Canada. 1990. Session 2. Waste water Technology Centre of Environment Canada.
21. V.G. Levich. Adv. Electrochem. Electrochem. Eng. **4**, 249 (1966).
22. V.G. Levich. Physical chemistry; an advanced treatise. Vol. 9B. *Edited by* H. Eyring, D. Henderson, and W. Jost. Academic Press, New York. 1970. Chap. 12.
23. R.R. Dogonadze. Reactions of molecules at electrodes. *Edited by* N.S. Hush. Wiley–Interscience, New York. 1971. Chap. 3.
24. M.-A. Fox, R.B. Draper, M. Dulay, and K. O'Shea. Photochemical conversion and storage of solar energy. *Edited by* E. Pelizetti and M. Schiavello. Kluwer Academic Publishers, The Netherlands. 1991. p. 277.
25. S. Yamagata, S. Nakabayashi, K.-M. Spancier, and A. Fujishima. Bull. Chem. Soc. Jpn. **61**, 3429 (1988).
26. S. Yamagata, R. Baba, and A. Fujishima. Bull. Chem. Soc. Jpn. **62**, 1004 (1989).
27. N. Serpone, E. Borgarello, R. Harris, P. Cahill, M. Borgarello, and E. Pelizzetti. Sol. Energy Mater. **14**, 121 (1986).
28. R.W. Matthews. Australian Patent Application: Canberra, Australia. 7/22/86.
29. R.W. Matthews, M. Abdullah, and G.K.-C. Low. Anal. Chim. Acta, **223**, 171 (1990).
30. R.W. Matthews. Sol. Energy Mater. **38**, 405 (1987).
31. R.W. Matthews. Water Res. **25**, 1169 (1991).
32. P.E. Menassa, M.K.S. Mak, and C.H. Langford. Environ. Technol. Lett. **9**, 825 (1988).
33. P.R. Harvey, R. Rudham, and S. Ward. J. Chem. Soc. Faraday Trans. 1, **79**, 1381 (1983).
34. A.J. Gordon and R.A. Ford. The chemist's companion: a handbook of practical data, techniques, and references. John Wiley & Sons Inc., New York. 1972 p. 349.
35. D. Lawless, N. Serpone, and D. Meisel. J. Phys. Chem. **95**, 5166 (1991).
36. R. Memming. Top. Curr. Chem. **143**, 79 (1988).
37. P.V. Kamat and N.M. Dimitrijevic. Sol. Energy, **44**, 83 (1990).
38. T. Trott, R.W. Henwood, and C.H. Langford. Environ. Sci. Technol. **6**, 367 (1972).
39. T.A. Egerton and C. King. J. Oil. Colour Chem. Assoc. **62**, 386 (1979).
40. J.-C. D'Oliveira, G. Al-Sayyed, and P. Pichat. Environ. Sci. Technol. **24**, 990 (1990).
41. M. Schiavello, V. Augugiaro, and L. Palmisano. J. Catal. **127**, 332 (1991).
42. G.P. Lepore, C.H. Langford, J. Vĭchová, and A. Vlcek, Jr. J. Photochem. Photobiol. 1993. In press.
43. J.-M. Herrman, and P. Pichat. J. Chem. Soc. Faraday Trans. 1, **76**, 1136 (1980).
44. V. Augugiaro, L. Palmisano, A. Sclafani, C. Minero, and E. Pelizzetti. Toxicol. Environ. Chem. **16**, 89 (1988).
45. J. Augustynski. Struct. Bonding (Berlin), **69**, 1–61 (1988).
46. Y. Suda and T. Morimoto. Langmuir, **3**, 786 (1987).
47. K. Tanaka and J.M. White. J. Phys. Chem. **86**, 4708 (1982).
48. K. Morishige, F. Kanno, S. Ogawara and S. Sasaki. J. Phys. Chem. **89**, 4404 (1985).
49. C. Doremieux-Morin, M.A. Enriquez, and J. Fraissard. J. Colloid Interface Sci. **95**, 502 (1983).

Can. J. Chem. Downloaded from www.nrcresearchpress.com by 203.198.23.82 on 09/08/12
For personal use only.

Preparation and structure of oxo-rhenium(V) complexes with 7-azaindole

ANNE-MARIE LEBUIS AND ANDRÉ L. BEAUCHAMP[1]

Département de chimie, Université de Montréal, C.P. 6128, Succ. A, Montréal, QC H3C 3J7, Canada

Received March 17, 1993

ANNE-MARIE LEBUIS and ANDRÉ L. BEAUCHAMP. Can. J. Chem. **71**, 2060 (1993).

Four Re(V) oxo compounds were obtained from 7-azaindole (Haza) and $ReOCl_3(PPh_3)_2$: the oxo-bridged dimer $Re_2O_3Cl_4(Haza)_4$ (**1**), the oxo–ethoxo monomers $ReO(OEt)Cl_2(Haza)_2$ (**2**) and $ReO(OEt)Cl_2(Haza)(PPh_3)$ (**3**), and the dioxo $[ReO_2(Haza)_4]Cl$ salt (**4***a*). $[ReO_2(Haza)_4]I$ (**4***b*) was also prepared from $ReO_2I(PPh_3)_2$. The $ReO(OEt)Cl_2(Haza)_2$ complex was shown by X-ray diffraction ($C2/c$, a = 16.292, b = 9.395, c = 12.104 Å, β = 101.47°, R = 0.041) to consist of individual molecules of the *trans–trans* isomer in which azaindole is N7-bonded. Crystals of $[ReO_2(Haza)_4]Cl \cdot 4H_2O \cdot \frac{1}{2}CHCl_3$ ($C2/m$, a = 15.422, b = 13.055, c = 9.086 Å, β = 91.13°, R = 0.059) contain well separated Cl^- anions and *trans*-dioxo cations. The N7-bonded azaindole ligands are held parallel to the O=Re=O direction by intramolecular N1—H···O hydrogen bonds, but the relative orientation of the four ligands cannot be determined because of disorder. Characteristic Re—oxygen vibrations are observed in infrared for each type of compounds. The ^1H and ^{13}C NMR spectra are discussed in relation with the azaindole binding mode.

ANNE-MARIE LEBUIS et ANDRÉ L. BEAUCHAMP. Can. J. Chem. **71**, 2060 (1993).

Quatre composés oxo du Re(V) ont été obtenus par réaction du 7-azaindole (Haza) avec $ReOCl_3(PPh_3)_2$: le dimère à pont oxo $Re_2O_3Cl_4(Haza)_4$ (**1**), les monomères oxo-éthoxo $ReO(OEt)Cl_2(Haza)_2$ (**2**) et $ReO(OEt)Cl_2(Haza)(PPh_3)$ (**3**), et le sel dioxo $[ReO_2(Haza)_4]Cl$ (**4***a*). $[ReO_2(Haza)_4]I$ (**4***b*) a aussi été obtenu à partir de $ReO_2I(PPh_3)_2$. La diffraction des rayons X a montré que $ReO(OEt)Cl_2(Haza)_2$ ($C2/c$, a = 16,292, b = 9,395, c = 12,104 Å, β = 101,47°, R = 0,041) renferme le monomère *trans–trans*, où l'azaindole est lié par N7. Les cristaux de $[ReO_2(Haza)_4]Cl \cdot 4H_2O \cdot \frac{1}{2}CHCl_3$ ($C2/m$, a = 15,422, b = 13,055, c = 9,086 Å, β = 91,13°, R = 0,059) contiennent des anions Cl^- et des cations *trans*-dioxo. Les ligands azaindoles liés par N7 sont retenus en position parallèle à la direction O=Re=O par des liaisons hydrogène N1—H···O intramoléculaires, mais l'orientation relative des quatre ligands ne peut pas être déterminée à cause du désordre. Des vibrations Re—O caractéristiques sont observées en infrarouge pour chaque type de composés. On discute des spectres RMN ^1H et ^{13}C en relation avec le mode de coordination de l'azaindole.

Introduction

In many of the complexes formed by 7-azaindole[2] (Haza) (**I**), the monoanion plays a bidentate bridging role in dinuclear molecules (1–5) or units of higher nuclearity (2). As the neutral form, where N7 is the only donor atom available, the ligand behaves somewhat like pyridine (6, 8, footnote 3). However, the hydrogen-bonding ability of the N1—H bond, directed on the same side as the N7 lone pair, combined with ring rigidity and general hydrophobic surface, can favour interesting molecular architectures (9, 10).

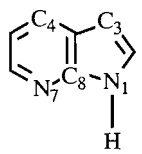

I

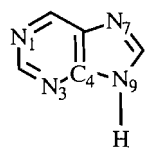

II

The present paper reports on oxo-Re(V) complexes with neutral azaindole, which are being considered as potential precursors to metal-metal bonded Re(III) dimers of the "paddle-wheel" type (1, 11, footnote 4). This ligand serves as a simplified and less reactive model for purines (**II**), having only two endocyclic nitrogens oriented similarly to N3 and N9 of purines.

Our efforts were first directed toward oxo-Re(V) compounds of the types known to form with pyridines (13–16). In recent years, oxo complexes of various metals, including mono and dioxo complexes of Re(V) with pyridine and related ligands, have attracted increasing attention in connection with electron (17) and oxo (18) transfer reactions. These compounds exhibit interesting electrochemical (19) and excited-state emission properties (20), which can be used for various applications (21).

In the present study, four new oxo-rhenium(V) compounds were prepared with azaindole and the crystal structures of two of them were determined.

Experimental

Reactants and methods

PPh_3, $KReO_4$, and 7-azaindole were used as received from Aldrich. $ReOCl_3(PPh_3)_2$ and $ReO_2I(PPh_3)_2$ were synthesized according to literature methods (22, 23). Solvents were dried over Na and distilled under argon before use, except for spectrograde methanol and absolute ethanol, which were used as received.

Infrared spectra were recorded as KBr or CsI pellets on a Perkin-Elmer 783 spectrophotometer. Nuclear magnetic resonance spectra were run in $CDCl_3$ (Cambridge Isotopes) or CD_2Cl_2 (Merck, Sharp & Dohme or Aldrich). ^1H spectra were recorded on a Varian VXR 300 MHz spectrometer and referenced to residual solvent signals ($CHCl_3$, δ 7.265; CH_2Cl_2, δ 5.320 ppm). ^{13}C and ^{31}P spectra were also recorded on this instrument at 121.42 and 75.43 MHz, respectively. The ^{31}P spectrum was referenced to external D_3PO_4 (δ 0 ppm) and the ^{13}C spectrum to the residual solvent signal ($CDCl_3$, δ 76.94, CD_2Cl_2; δ 53.79 ppm). The ^{13}C CP-MAS spectrum of **1** was recorded on the same instrument and referenced to the aromatic carbons of hexamethylbenzene (δ 132.1 ppm). Other conditions: relaxation delay, 50 s; spinning rate, 4.5 kHz; side-band suppression routine used. The solution ^{13}C spectrum of **4***b* was recorded at 100.62 MHz on the Bruker WH-400 spectrophotometer of the Centre Régional de RMN Haut Champ located at the Université de Montréal.

[1]Author to whom correspondence may be addressed.

[2]1*H*-Pyrrolo[2,3-*b*] pyridine.

[3]F. Allaire and A.L. Beauchamp. In preparation.

[4]A.M. Lebuis and A.L. Beauchamp. Inorg. Chem. Acta. In press.

Can. J. Chem. Downloaded from www.nrcresearchpress.com by 203.198.23.82 on 09/08/12
For personal use only.

Can. J. Chem. Downloaded from www.nrcresearchpress.com by 203.198.23.82 on 09/08/12
For personal use only.

Preparative work

Compounds **1** and **2** are sensitive to moisture and readily hydrolyse in wet solvents. Preparations were done in a Schlenk system. Compounds **3** and **4***a*,*b* could be filtered in open air, although **3** is sensitive in solution.

*$Re_2O_3Cl_4(Haza)_4$, **1***

$ReOCl_3(PPh_3)_2$ (0.81 g, 0.98 mmol) and a 50% excess of Haza (0.36 g, 3.05 mmol) were mixed in toluene at room temperature and two drops of deionized water were added. Stirring was maintained for 3 h, after which time the solution had become brownish and a light green solid had deposited. This solid was filtered, washed with toluene and diethyl ether, and then dried under vacuum. This product crystallized with 1/2 toluene molecule, as indicated by the ^{13}C CP-MAS NMR spectrum (see below) and elemental analysis. Anal. Calcd. for $C_{31.5}H_{28}Cl_4N_8O_3Re_2$: C 35.01, H 2.61, N 10.37; found: C 35.14, H 2.48, N 10.02. Yield: 0.42 g, 79%. IR (cm^{-1}): 966 ν(Re=O), 677 ν(Re—O—Re). The product obtained by recrystallization from CH_2Cl_2 is toluene-free, as evidenced from the ^1H NMR spectrum. Crystals suitable for X-ray work could not be grown.

*$ReO(OEt)Cl_2(Haza)_2$, **2***

Compound **1** (0.150 g, 0.139 mmol) was refluxed in ethanol. After 24 h, the solution had turned blue. After 48 h, the mixture was reduced to half volume and a blue product deposited. The solid was filtered, dried under vacuum, and redissolved in CH_2Cl_2. Slow evaporation to 1/10 volume yielded a homogeneous sample of blue crystals. One of these crystals was used for the X-ray diffraction study described hereafter. Yield: 0.124 g, 81%. IR (cm^{-1}): 955 ν(Re=O), 915 δ(O—CH_2).

*$ReO(OEt)Cl_2(Haza)(PPh_3)$, **3***

$ReOCl_3(PPh_3)_2$ (0.83 g, 1 mmol) and Haza (0.29 g, 2.5 mmol) were refluxed in absolute ethanol (100 mL) for 25 min. The bright blue precipitate was filtered, and washed with ethanol (15 mL) and diethyl ether (15 mL). Anal. Calcd. for $C_{27}H_{26}Cl_2N_2O_2PRe$: C 46.42, H 3.75, N 4.01, Cl 10.15; found: C 46.17, H 3.38, N 3.91, Cl 10.14. Yield: 0.41 g, 59%. IR (cm^{-1}): 941 ν(Re=O), 906 δ(O—CH_2). ^{31}P NMR (ppm): −7.47 (s). The dark brown filtrate yielded 0.11 g of **4***a*.

*$[ReO_2(Haza)_4]Cl$, **4**a*

$ReOCl_3(PPh_3)_2$ (0.84 g, 1.01 mmol) and Haza (0.71 g, 6.0 mmol) were mixed at room temperature in toluene (50 mL) and eight drops of deionized water were added. After 3 h, a light brown solid was filtered and washed with toluene. This raw material contained a small amount of PPh_3. Recrystallisation from methanol/toluene gave a pure orange powder. Yield: 0.56 g. IR (cm^{-1}): 794 ν(O=Re=O). Recrystallization from $CHCl_3$ in open air yielded orange platelets of the $CHCl_3$–water solvate (**4***a*′) studied by X-ray diffraction (see below).

This product was also obtained from **1** (0.72 g, 0.70 mmol) by refluxing with 4 equivalents (0.34 g) of Haza in absolute ethanol (40 mL). The solution turned very dark brown rapidly, volume was reduced to 15 mL, and diethyl ether (100 mL) was added to precipitate the dark brown solid. The product was isolated by filtration and washed with small amounts of methanol and acetone to afford the orange salt. Yield: 0.36 g.

*$[ReO_2(Haza)_4]I$, **4**b*

The method used was adapted from Brewer and Gray (14). $ReO_2I(PPh_3)_2$ (0.90 g, 1.04 mmol) was stirred at room temperature with Haza (1.17 g, 9.9 mmol) in methanol. The solution turned orange immediately. The mixture was refluxed for 20 min, after which time the solution had become dark orange. Toluene (50 mL) was added and the volume was reduced by half. The orange powder was filtered off, washed with toluene and hexane, and dried under vacuum. The compound is solvent-free, as evidenced from the ^1H NMR spectrum, which contains only the Haza signals observed for the Cl^- salt. Yield: 0.67 g. IR (cm^{-1}): 795 ν(O=Re=O).

Crystallographic measurements and structure resolution

X-ray work on both compounds was carried out on an Enraf-Nonius CAD-4 diffractometer with graphite-monochromatized MoK$\bar{\alpha}$ radiation. The reduced cell was determined from 25 centred reflections ($20° \leq 2\theta \leq 25°$) and checked with long-exposure axial photographs along the three axes. C-centred monoclinic cells were indicated by the Niggli coefficients and confirmed by axial photographs about the new axes. Final cell parameters were obtained by least-squares fit on the settings of the 25 reflections. Crystallographic data and conditions of data collection for both structures are summarized in Table 1. During data collection, orientation was monitored every 200 measurements and intensity was checked every hour with standard reflections.

*$ReO(OEt)Cl_2(Haza)_2$ (**2**)*

A total of 3091 $\bar{h}\bar{k}l$, $\bar{h}k\bar{l}$ and $h\bar{k}\bar{l}$, and $hk\bar{l}$ reflections with $h + k = 2n$ were measured. Averaging the $k/\bar{k}$ pairs yielded 1602 unique hkl and $\bar{h}kl$ reflections, of which 1279 with $I \geq 3.0\sigma(I)$ were retained for structure determination and refinement. The data were corrected for the effects of Lorentz, polarization, and absorption (Gaussian integration).

Space groups $C2/c$ and Cc were consistent with the monoclinic Laue symmetry and systematic absences (hkl, $h + k \neq 2n$; $h0l$, $l \neq 2n$). The structure was solved in the centric $C2/c$ space group by the heavy-atom method. Re was positioned from a Patterson map. All other non-hydrogen atoms were located by successive ΔF maps. The C_2H_5 group was found to be disordered, C(11) and C(12) occupying symmetry-related positions off the twofold axis.

Refinement was done on $|F_0|$ by full-matrix least-squares procedures. The function minimized was $\Sigma w(|F_0| - |F_c|)^2$, with weights $w = 1/(\sigma^2(|F_0|) + 0.0016|F_0|^2)$. Refinement was anisotropic for all non-hydrogen atoms, except C(12). Hydrogen atoms were introduced at idealized positions (C—H = 0.95 Å, N—H = 0.85 Å, U_{iso} = 0.075 Å^2). Their parameters were not refined, but the coordinates were recalculated after each cycle. The final residuals were $R = 0.041$, $R_w = 0.048$ and $S = 1.44$ for 119 parameters refined. The general background in final ΔF synthesis was below ± 0.48 e/Å^3, with five low residuals of $\pm|0.62 - 0.82|$ e/Å^3 near Re.

Attempts were made to refine the structure in the non-centric Cc space group. Refinement was extremely unstable with very high correlation coefficients and the ethoxo group remained disordered. Thus, the above $C2/c$ model was retained.

*$[ReO_2(Haza)_4]Cl \cdot 4H_2O \cdot \frac{1}{2}CHCl_3$ (**4**a′)*

A whole sphere of data was measured, providing 6291 reflections with $h + k = 2n$. Space groups $C2$, Cm, and $C2/m$ were consistent with Laue symmetry and the lack of systematic absences besides hkl, $h + k \neq 2n$. The data set was corrected for absorption (Gaussian integration) and the hkl and $hk\bar{l}$ octants were used to solve the structure. After the space group was identified as $C2/m$, equivalent reflections were averaged, yielding 1684 unique hkl and $hk\bar{l}$ reflections, of which 1245 with $I \geq 3.0\sigma(I)$ were retained for final refinement. The data were corrected for the effects of Lorentz and polarization.

Solving this structure was extremely laborious. The centrosymmetric $C2/m$ space group was considered first. The Patterson map indicated that two Re atoms occupied an equipoint with $2/m$ site symmetry and the origin ($2a$) (24) was arbitrarily chosen. A ΔF map revealed clear features for the apical oxygen (equipoint $4g$, twofold axis) and for two independent N7-coordinated azaindole ligands in general positions. These units, repeated by $2/m$ site symmetry, generated a *trans*-ReO_2N_4 coordination. However, the azaindole units, perpendicular to the mirror plane, had to be disordered over two orientations, with the five-membered rings directed above and below the plane, respectively. A new ΔF map phased on this model showed a number of residual peaks, in a pocket along the b axis ($y \sim 0.5$), surrounded by complex cations. None of these peaks were high enough to correspond to full occupancy by Cl^- and short inter-peak distances indicated extensive disordering. After testing a large number of combinations, two main

Can. J. Chem. Downloaded from www.nrcresearchpress.com by 203.198.23.82 on 09/08/12
For personal use only.

TABLE 1. Crystallographic data for $ReO(OEt)Cl_2(Haza)_2$ (**2**) and $[ReO_2(Haza)_4]Cl \cdot 4H_2O \cdot \frac{1}{2}CHCl_3$ (**4***a*′)

Compound	**2**	**4***a*′
Formula	$C_{16}H_{17}N_4O_2Cl_2Re$	$C_{28.5}H_{32.5}N_8O_6Cl_{2.5}Re$
Formula weight	554.45	857.96
Space group	$C2/c$	$C2/m$
a, Å	16.292(4)	15.422(4)
b, Å	9.395(4)	13.055(11)
c, Å	12.104(3)	9.086(1)
β, deg	101.47(2)	91.13(2)
V, Å^3	1816(1)	1829(2)
D_{calcd} g cm^{-3}	2.028	1.558
Z	4	2
λ, Å	0.71069	0.71069
μ, cm^{-1}	71.0	36.0
Crystal size, mm (faces)	$20\bar{1}/\bar{2}0\bar{1}$, 0.052 $11\bar{1}/\bar{1}\bar{1}1$, 0.22 $\bar{1}11/1\bar{1}\bar{1}$, 0.22 $10\bar{1}/\bar{1}01$, 0.22	$100/\bar{1}00$, 0.053 $\bar{1}\bar{1}0/110$, 0.198 $001/00\bar{1}$, 0.304
Transmission range	0.32–0.69	0.40–0.83
Scan	ω	ω/2θ
$2\theta_{max}$, deg	50	50
Number of unique reflections	1602	1684
Number of observed reflections	1279	1245
Rejection criterion, $I/\sigma(I)$	3.0	3.0
R^a	0.041	0.059
$R_w{}^a$	0.048	0.077
R_{int}	0.065 (3091)	0.064 (6291)
Goodness-of-fit, S^a	1.44	2.06
Number of parameters	119	113
Residual on final ΔF map, e/Å^3		
Maximum	0.62–0.82 (Re)	0.71 ($CHCl_3$)
General background	±0.48	±0.62

$^aR = \Sigma||F_o| - |F_c||/\Sigma|F_o|$; $R_w = [\Sigma w(|F_o| - |F_c|)^2/\Sigma w|F_o|^2]^{1/2}$; $S = [\Sigma w(|F_o| - |F_c|)^2/(N - V)]^{1/2}$.

patterns (Fig. S-2)[5] could be unravelled. In pattern *a*, water W(3) is present along with a $CHCl_3$ molecule and an extra water molecule occupying the C/W site, symmetry equivalent to the $CHCl_3$ carbon. In pattern *b*, the Cl^- ion is part of an infinite chain containing water molecules W(1), W(2), and W(3).

A number of attempts were made to solve the structure in space groups $C2$, Cm and even $C1$. $C1$ led to the same disordered structure, described with more parameters and giving extremely unstable refinement of highly correlated variables. Thus, the centrosymmetric $C2/m$ model is retained as the best interpretation of our results.

Refinement was done on $|F_o|$ with weights $w = 1/(\sigma^2(|F_o|) + 0.0016|F_o|^2)$. Only Re was refined anisotropically. All azaindole atoms were assigned half occupancies, as required by space group symmetry. In order to provide one Cl^- ion per Re atom, the two $Cl^-/H_2O/CHCl_3$ patterns *a* and *b* must have equal populations. Appropriate occupancy factors were assigned and the nitrogen scattering curve was used for the C/W position statistically occupied by a water oxygen and the $CHCl_3$ carbon. The coordinates and temperature factors of all non-hydrogen atoms were refined. Residuals in the ΔF map indicated that W(3) was slightly off the twofold axis: it was moved away from the axis and its three coordinates were refined. The final agreement factors were $R = 0.059$, $R_w = 0.077$, $S = 2.06$ for 113 parameters refined. The residuals in the final ΔF synthesis were below ±0.7 e/Å^3.

Considering the severe crystallographic problems encountered, the refined model is totally satisfactory. The only anomaly is the rather small temperature factor found for W(3). This may result from some protonated $[ReO(OH)(Haza)_4]^{2+}$ cations occupying the $[ReO_2(Haza)_4]^+$ site in the lattice. The W(3) site could then be occupied occasionally by the extra Cl^- ion needed to balance the charge for each such protonated species present. The O(1)—W(3) distance of ~2.8 Å is on the short side of the range for a O—H···Cl hydrogen bond (25), but the actual O(1)—Cl distance could well be greater than indicated by the refined W(3) position, defined primarily by water occupying the site most of the time. No evidence was provided from spectroscopic data for the presence of the protonated complex in the non-recrystallized material, but the ^1H NMR spectrum on a CD_2Cl_2 solution of the crystals showed a small amount of an additional species as well as the $CHCl_3$ found in the structure. This new species could not be identified, but it does not correspond to free neutral or protonated azaindole. Thus, the presence of coordinated azaindole signals would be consistent with the above assumption.

[5]The supplementary material includes a table of infrared frequencies and the following crystallographic material: diagram of the disorder in the $Cl^-/H_2O/CHCl_3$ region of **4***a*′, unit cell of **2** and probable short-range non-disordered structure of **4***a*′, lists of observed and calculated structure factor amplitudes, anisotropic thermal parameters, hydrogen coordinates, distances and angles in the ligands, and atom-to-plane distances for the structures (28 pages). A complete set of data may be purchased from: The Depository of Unpublished Data, Document Delivery, CISTI, National Research Council Canada, Ottawa, ON K1A 0S2, Canada.

Stereo view of the unit cell, hydrogen atom coordinates, and distances and angles in the azaindole ligand for $ReO(OEt)Cl_2(Haza)_2$, **2**, and distances and angles in the azaindole ligand and chloroform molecule for $[ReO_2(Haza)_4]Cl \cdot 4H_2O \cdot \frac{1}{2}CHCl_3$, **4***a* have also been deposited with the Cambridge Crystallographic Data Centre and can be obtained on request from the Director, Cambridge Crystallographic Data Centre, University Chemical Laboratory, 12 Union Road, Cambridge, CB2 1EZ, U.K.

TABLE 2. Final atomic coordinates (× 10^3, Re, Cl × 10^4) and equivalent isotropic temperature factors (× 10^3) for $ReO(OEt)Cl_2(Haza)_2$ (**2**)

Atom	*x*	*y*	*z*	U_{eq}
Re	0	1954(1)	2500	38
Cl	177(2)	2084(4)	569(2)	61
O(1)	0	14(1)	250	54
O(2)	0	392(1)	250	47
N(1)	145(1)	4(1)	435(1)	56
N(7)	133(1)	201(1)	304(1)	44
C(2)	212(1)	−64(2)	501(1)	76
C(3)	285(1)	−6(2)	490(1)	78
C(4)	310(1)	209(2)	366(1)	71
C(5)	266(1)	301(2)	290(1)	70
C(6)	180(1)	297(1)	260(1)	53
C(8)	176(1)	109(1)	379(1)	47
C(9)	264(1)	106(1)	411(1)	58
C(11)[a]	4(2)	528(3)	298(3)	98
C(12)[a]	−27(2)	644(3)	225(3)	77[b]

[a]Occupancy factors: 0.50.
[b]Isotropic temperature factor.

All calculations were done with the NRCVAX package (26). The refined coordinates for both structures are listed in Tables 2 and 3, respectively.[5]

Discussion

The light green oxo-bridged dimer $Re_2O_3Cl_4(Haza)_4$ (**1**) was obtained from $ReOCl_3(PPh_3)_2$ and excess azaindole in moist toluene. By the same method, Johnson, Taha, and Wilkinson (13) isolated the pyridine analog, which was shown to be the *cis*-dichloro-*cis*-pyridine isomer (**III**) (27). The same stereoisomer is likely obtained here, since the *trans-trans* isomer observed with 1-methylimidazole gives a dark blue solid.[6]

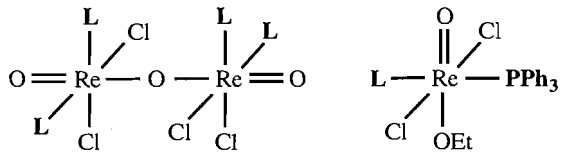

III

IV

The blue oxo-ethoxo monomer $ReO(OEt)Cl_2(Haza)_2$ (**2**) was prepared by refluxing **1** in ethanol, a method used by Johnson, Taha, and Wilkinson (13) for pyridine. The crystal structure (Fig. 1) confirmed the *trans-trans* stereochemistry. When Haza was refluxed with $ReOCl_3(PPh_3)_2$ in absolute ethanol, a new type of ethoxo complex $ReO(OEt)Cl_2(Haza)(PPh_3)$ (**3**) was obtained, in which only one phosphine was displaced. The ethoxo group is undoubtedly *trans* to the oxo group, as in **2** and all related octahedral Re(V) systems (15, 29, 30). Because of steric effect, the *trans-trans* structure **IV** is preferred for this complex.

The *trans*-dioxo salt $[ReO_2py_4]Cl$ was prepared from $ReOCl_3(PPh_3)_2$ and neat pyridine containing a little water (31). To obtain $[ReO_2(Haza)_4]Cl$ (**4***a*), six equivalents of the ligand, which is a solid, were reacted in moist toluene. As the Cl^- salt deteriorates slowly, the corresponding iodide (**4***b*) was also prepared from $ReO_2I(PPh_3)_2$, as described recently for pyridines by Brewer and Gray (14).

Infrared spectroscopy

The infrared spectrum of 7-azaindole has been discussed elsewhere (1, 9, 10). Complexation via N7 does not greatly change the azaindole bands (Table S-9)[5]. Owing to differences in hydrogen bonding, the ν(N—H) vibrations are sharper and shifted from 2900 to 3300–3430 cm^{-1}, whereas the γ(N—H) mode is displaced from 850 cm^{-1} to the 550 cm^{-1} region (9). Characteristic changes previously attributed to N7 coordination (9, 10) are generally observed here. The spectrum of **3** shows extra features due to PPh_3, namely a strong doublet at 738/745 cm^{-1} and a series of characteristic peaks near 500 cm^{-1} (32). Well-defined bands near 1374, 1115, and 1078 cm^{-1} correspond to the ethoxo group.

In **4***a* and **4***b*, the *trans*-dioxo unit shows a single $\nu_{as}(O{=}Re{=}O)$ band at 795 cm^{-1}, halfway between those found for $[ReO_2(CN)_4]^{3-}$ (775 cm^{-1}) (34) and other N-donor ligands (~815 cm^{-1}) (33–35). The terminal ν(Re=O) bands in the ethoxo compounds are found at 955 cm^{-1} for **2** and 941 cm^{-1} for **3**, whereas a strong band characteristic of the Re—O—Et unit appears near 910 cm^{-1}, as with $ReO(OEt)X_2(PPh_3)_2$ (33). For **1**, the terminal Re=O and asymmetric Re—O—Re stretching modes (966 and 677 cm^{-1}, respectively) show greater separation than for the corresponding pyridine and ethylenediamine compounds (935 and 730 cm^{-1}, respectively). The weak $\nu_{as}(ReO_2)$ mode near 800 cm^{-1}, mentioned by Jezowska-Trzebiatowska et al. (34) for the latter compounds, would be masked here by the very strong γ(C—H) azaindole bands at 790–800 cm^{-1}.

Crystal structure of $ReO(OEt)Cl_2(Haza)_2$, 2

The crystals contain roughly octahedral molecules of the *trans-trans* isomer (Fig. 1), in which the neutral azaindole ligand is coordinated via N(7). The same stereoisomer was found in the analogous pyridine compound (36). Selected distances and angles are given in Table 4.

The Re—Cl (2.414(3) Å) and Re—N distances (2.136(8) Å) are similar to those found for $ReO(OEt)Cl_2(py)_2$ (mean values 2.404 and 2.138 Å, respectively) (36). The Re=O(1) distance of 1.702(11) Å, although slightly longer than those found in the pyridine analogue (1.684(7) Å) and various oxo-Re(V) complexes (mean 1.691 Å, σ = 0.025) (37), compares well with those reported for the $ReO(OEt)X_2(PPh_3)_2$ series (X = I, 1.699(4); Cl, 1.678(6); Br, 1.715(9) Å) (15, 29, 30) and $ReO(OEt)(Ph_2PNPh_2Se)_2$ (1.70(2) Å) (38). The Re—O(2) distance of 1.845(10) Å, shorter than in the above compounds (1.880(6)–1.896(6) Å), indicates some multiple bond character, as discussed by other workers (15, 39).

The octahedron is only slightly distorted. Re, O(1), and O(2), all situated on the crystallographic twofold axis, define a perfectly linear unit. N(7) and Cl are slightly displaced away from the Re=O(1) bond, thereby making the O(1)—Re—Cl(N) angles 1–3° greater than 90°, with a corresponding reduction of the O(2)—Re—Cl(N) angles. The ethoxo group is disordered over two equally populated orientations about the axis, with positions for C(11) and C(12) being resolved. This type of disorder has also been observed for the phosphine analogues $ReO(OEt)X_2(PPh_3)_2$ (X = Cl, Br) (29, 30). A broad range (138–176°) is found in the literature for the Re—O—Et angle (15, 29, 30, 36): our Re—O(2)—C(11) angle (155.9(15)°) lies in the middle of this range.

[6]C. Pearson and A.L. Beauchamp. Acta Crystallogr. In press.

Can. J. Chem. Downloaded from www.nrcresearchpress.com by 203.198.23.82 on 09/08/12
For personal use only.

TABLE 3. Final atomic coordinates and isotropic temperature factors ($\times 10^3$) for $[ReO_2(Haza)_4]Cl \cdot 4H_2O \cdot \frac{1}{2}CHCl_3$ (**4***a'*)

Atom	*x*	*y*	*z*	U_{eq}	Occupancy
Re	0	0	0	56[a]	1.000
Cl(0)	212(1)	−464(1)	215(2)	71(6)	0.250
Cl(1)	205(2)	590(3)	199(3)	60(9)	0.125
Cl(2)	38(2)	614(2)	279(3)	61(7)	0.125
Cl(3)	113(2)	451(2)	395(3)	80(9)	0.125
O(1)	2(4)	136(1)	11(6)	57(5)	0.500
W(1)	48(2)	−365(2)	139(3)	30(6)	0.250
W(2)	53(1)	−527(2)	365(2)	26(6)	0.250
W(3)	0(1)	350(1)	−26(2)	6(3)	0.375
C/W[b]	104(2)	521(3)	223(3)	40(9)	0.250
N(11)	59(2)	170(2)	−254(3)	78(11)	0.500
C(21)	94(2)	226(3)	−381(3)	77(8)	0.500
C(31)	123(2)	163(3)	−487(4)	85(10)	0.500
C(41)	124(2)	−32(2)	−509(4)	81(12)	0.500
C(51)	100(2)	−123(4)	−425(4)	83(11)	0.500
C(61)	65(2)	−125(4)	−282(3)	44(8)	0.500
N(71)	50(1)	−21(2)	−223(2)	44(5)	0.500
C(81)	71(1)	69(2)	−300(2)	30(6)	0.500
C(91)	111(2)	62(3)	−448(3)	52(7)	0.500
N(12)	152(1)	−163(2)	125(2)	55(6)	0.500
C(22)	224(2)	−221(2)	185(3)	76(8)	0.500
C(32)	291(2)	−160(2)	214(4)	79(9)	0.500
C(42)	303(2)	36(2)	182(3)	66(10)	0.500
C(52)	263(2)	127(3)	138(3)	77(9)	0.500
C(62)	174(2)	113(3)	94(3)	43(7)	0.500
N(72)	132(1)	22(2)	81(1)	34(4)	0.500
C(82)	178(2)	−59(2)	126(3)	41(6)	0.500
C(92)	266(2)	−61(3)	175(3)	64(8)	0.500

[a]U_{eq}, anisotropic tensor elements ($\times 10^4$): U_{11} = 337(6), U_{22} = 995(12), U_{33} = 350(6), $U_{12} = U_{23} = 0$ (by symmetry), U_{13} = 15(4).
[b]Described with scattering curve of N.

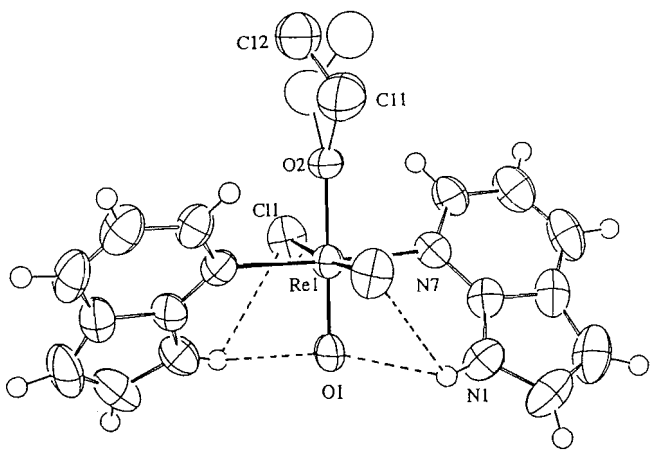

FIG. 1. Structure of the $ReO(OEt)Cl_2(Haza)_2$ molecule (**2**). The O(1)=Re—O(2) unit lies on a crystallographic twofold axis. The ethyl group is disordered over two equally populated orientations (second orientation shown as hollow spheres, ethyl hydrogens omitted). Azaindole atoms are labelled as in **I**. Ellipsoids correspond to 50% probability. Dashed lines represent possible hydrogen bonding interactions.

This is one of the few known complexes in which the 7-azaindole ligand is not disordered. The distances and angles are normal (40) and the two-ring system is planar within 0.02 Å (1.3σ)[5]. The plane of the ligand is roughly a bisector of the O(1)—Re—Cl angle (O(1)—Re— N(7)—C(8) torsion angle = −38.1(8)°). The same ligand orientation observed for the pyridine analogue has been ascribed to minimum intramolecular contacts with Cl, O(1), and alkoxo hydrogens (36). In the present case, the N(1)—H group is close enough to Cl and O(1) to form an intramolecular hydrogen bond (Table 4, Fig. 1), but the interaction is probably weak, especially with oxygen, since the Re=O unit is known not to be very nucleophilic in these systems.

A view of the unit cell is provided in Figure S-1.[5] The molecules are packed individually, and interact via normal van der Waals contacts and a weak intermolecular N(1)—H···Cl bond (Table 4).

Crystal structure of $[ReO_2(Haza)_4]Cl \cdot 4H_2O \cdot \frac{1}{2}CHCl_3$, **4**a'

Despite the severe crystallographic problems encountered, the presence of the *trans*-$[ReO_2(Haza)_4]^+$ cation containing N7-bonded azaindole is decisively established. However, the relative orientations of the ligands could not be determined from the X-ray results. Since the site occupied by Re has crystallographic $2/m$ (C_{2h}) symmetry, each azaindole ligand appeared in the electron density map as two overlapping images with the five-membered ring oriented either up (*u*) or down (*d*). The two most likely rotamers, shown in Fig. 2, correspond to *uudd* and *udud* ligand sequences about the O=Re=O axis, respectively.

Selected distances and angles corresponding to the patterns of Fig. 2 are listed in Table 5. In both cases, the *cis* N—Re—N angles remain within 90 ± 3° and the O—Re—N

Can. J. Chem. Downloaded from www.nrcresearchpress.com by 203.198.23.82 on 09/08/12
For personal use only.

Can. J. Chem. Downloaded from www.nrcresearchpress.com by 203.198.23.82 on 09/08/12
For personal use only.

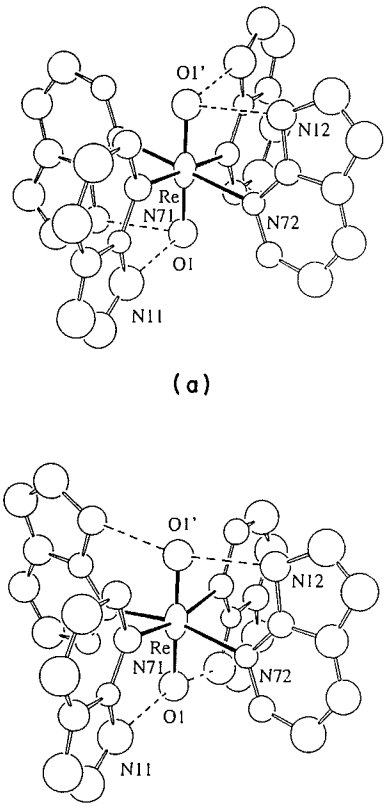

FIG. 2. Structure of the $[ReO_2(Haza)_4]^+$ cation in **4***a*′. The two most likely rotamers, whose geometry is described in Table 5, are represented: *uudd* (*a*), *udud* (*b*). Ellipsoids correspond to 50% probability. In the symbols used for the azaindole ligands, the first digit represents the position in the ring, as given in **I**, whereas the second digit is used to differentiate between the two independent ligands. Dashed lines represent hydrogen bonds.

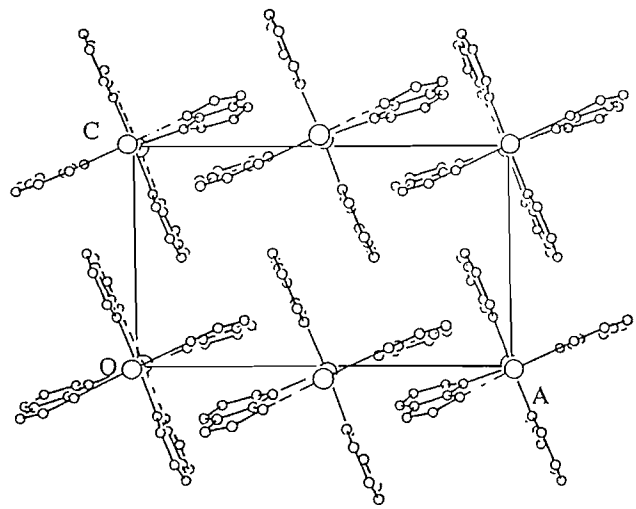

FIG. 3. Packing of the cations in **4***a*′ down the *b* axis, showing the parallel orientation of the azaindole ligands of the windmill-shaped cations. Cl^- and solvent molecules are omitted for simplicity. Ellipsoids correspond to 50% probability. Dashed lines represent hydrogen bonds.

angles range from 80 to 100°. The *trans* N—Re—N angles are 180° (by symmetry) and 165° in the *uudd* and *udud* rotamers, respectively, whereas the O=Re=O angles are always 180°. Thus, both geometries are reasonable. The Re=O(1) distance of 1.782(12) Å is comparable with those found for other $[ReO_2L_4]^+$ compounds, whereas the Re—N distances (mean 2.18 Å) seem to be slightly longer (31, 41–43).

Details on the geometry of coordinated azaindole are given in the supplementary material.[5] The distances and angles do not greatly differ from those of the free molecule (40). The rings are planar and aligned with the O=Re=O direction, as a result of a short intramolecular N1—H · · · O(1) hydrogen bond (~2.6 Å) to oxo groups (Table 5).

Figure 3 gives a projection of the unit cell down the *b* axis, along the O=Re=O bonds. The windmill-shaped cations are oriented so as to make the "vanes" of adjacent cations parallel. By repeating this pattern in the *b* direction, the O=Re=O units remain aligned and exactly above one another. They are separated by pockets containing the disordered Cl^- ions and lattice water and $CHCl_3$ molecules. A short-range ordered pattern consistent with the disorder observed is given in Fig. S-3.[5]

Nuclear magnetic resonance spectroscopy

^1H NMR data for all compounds are given in Table 6. Assignments are based on earlier work on CH_3Hg^+ compounds (10). The close H4 and H6 signals could be identified from their coupling constants to H5: ^3J(H5—H6) (~4.8 Hz) is smaller than ^3J(H4—H5) (~7.8 Hz) and it increases slightly when N7 is methylated (44) or metallated (10). ^{13}C NMR results are given in Table 7. The chloride **4***a* decomposed during acquisition, but the spectrum is not expected to be very different from that of the iodide **4***b*. Compounds **1** and **2** were not soluble enough to give good ^{13}C solution spectra. However, the solid-state CP-MAS spectrum of **1** could be recorded on the toluene solvate. For **3**, the strongest signals were easily assigned to the PPh_3 ligand (28). The ethoxo signals in both the ^1H and ^{13}C spectra occur at positions similar to those of *fac*-$(CO)_3$(dppe)Re(OEt) (12).

All compounds show only one set of azaindole signals in both types of spectra. This does not provide stereochemical information on the oxo-bridged dimer **1**, since both *cis-cis* and *trans-trans* stereochemistries about Re would make the four ligands equivalent in a species where the rotation barrier about the Re—O—Re axis is low. Similarly, rotamers cannot be identified for the *trans*-dioxo cation **4**, because fast rotation should take place about the Re—N7 bond.

The spectra are consistent with the ligand being bound to Re via N7 in all compounds. The N1—H proton produces a broad signal at low field. Coupling with this proton is always detected for the H2 and H3 signals, although the multiplet is not well resolved in some cases. Most of the solution ^{13}C signals for $ReO(OEt)Cl_2(Haza)(PPh_3)$ (**3**) and $[ReO_2(Haza)_4]I$ (**4***b*) follow the trends observed earlier for the N7-bonded $[CH_3Hg(Haza)]^+$ ion (10): substantial shifts upfield for C8 and downfield for C2, C4, and C9, lesser downfield shifts for C3 and C5. The spectrum of the oxo-bridged dimer $Re_2O_3Cl_4(Haza)_4$ (**1**) was obtained in the solid state and intermolecular interactions probably contribute to shifting some signals by 1–2 ppm, namely those of the well exposed C3 and C4 carbons.

Most of the ^1H resonances, together with the ^{13}C signal of C6, show large variations among the different Re compounds and differ from the CH_3Hg^+ model. In the case of $[CH_3Hg(Haza)]^+$ (10), H4 was the most affected by com-

TABLE 4. Selected distances and angles in $ReO(OEt)Cl_2(Haza)_2$ (**2**)

Atoms	Distance	Atoms	Distance
Re—Cl	2.414(3)	Re—N(7)	2.136(8)
Re—O(1)	1.702(11)	Re—O(2)	1.845(10)
O(2)—C(11)	1.40(3)		

Bonds	Angle	Bonds	Angle
O(1)—Re—O(2)	180.0[a]	Cl—Re—Cl[b]	174.21(10)
O(1)—Re—N(7)	91.4(3)	Cl—Re—N(7)[b]	90.7(2)
O(1)—Re—Cl	92.9(2)	Cl—Re—N(7)	89.2(2)
O(2)—Re—N(7)	88.6(3)	N(7)—Re—Cl[b]	90.7(2)
O(2)—Re—Cl	87.1(2)	N(7)—Re—N(7)[b]	177.2(3)
Re—O(2)—C(11)	155.9(15)		

	Distance		Angle
A—H···B	A—B	H—B	A—H—B
N(1)—H···O(1)	2.915(9)	2.41	118
N(1)—H···Cl(1)[b]	3.289(10)	2.80	117
N(1)—H···Cl(1)[c]	3.416(10)	2.80	130

[a]Fixed by symmetry
[b]$-x, y, 1/2 - z$
[c]$x, -y, 1/2 + z$

TABLE 5. Selected distances and angles in $[ReO_2(Haza)_4]Cl \cdot 4H_2O \cdot \frac{1}{2}CHCl_3$ (**4***a*′)

Atoms	Distance (Å)	Atoms	Distance
Re–O(1)	1.782(12)	Re–N(71)	2.193(15)
Re–N(72)	2.168(14)		

Rotamer uudd		Rotamer udud	
Bonds	Angle (deg)	Bonds	Angle (deg)
O(1)—Re—O(1)[b]	180.0	O(1)—Re—O(1)[b]	180.0
O(1)—Re—N(71)	99.6(15)	O(1)—Re—N(71)	99.6(15)
O(1)—Re—N(71)[b]	80.4(15)	O(1)—Re—N(71)[c]	94.7(15)
O(1)—Re—N(72)[a]	95.4(15)	O(1)—Re—N(72)	80.3(15)
O(1)—Re—N(72)[c]	84.6(15)	O(1)—Re—N(72)[c]	84.6(15)
N(71)—Re—N(71)[b]	180.0	N(71)—Re—N(71)[c]	165.7(7)
N(72)[a]—Re—N(72)[c]	180.0	N(72)—Re—N(72)[c]	164.8(6)
N(71)—Re—N(72)[a]	87.4(6)	N(71)—Re—N(72)	89.3(6)
N(71)—Re—N(72)[c]	92.6(6)	N(71)—Re—N(72)[c]	92.6(6)
N(71)[b]—Re—N(72)[c]	87.4(6)	N(71)[c]—Re—N(72)[c]	89.3(6)
N(71)[b]—Re—N(72)[a]	92.6(6)	N(71)[c]—Re—N(72)	92.6(6)

Distances involving hydrogen bonds

Atoms	Distance (Å)	Atoms	Distance (Å)
O(1)—N(11)	2.61(6)	Cl(0)—W(2)	2.93(3)
O(1)—N(11)[c]	2.47(6)	Cl(0)—W(1)	2.90(3)
O(1)—N(12)[a]	2.54(6)	W(1)—W(1)[e]	2.90(3)
O(1)—N(12)[b]	2.68(6)	W(1)—W(2)	2.94(3)
O(1)—W(3)	2.81(2)	W(3)—C/W[d]	2.88(4)
O(1)—W(1)	3.27(3)	W(2)—W(2)[f]	3.07(3)
		W(2)—W(2)[e]	2.99(3)

[a]$x, -y, z$
[b]$-x, -y, -z$
[c]$-x, y, -z$
[d]$-x, 1 - y, -z$
[e]$-x, y, 1 - z$
[f]$-x, -1 - y, 1 - z$.

Can. J. Chem. Downloaded from www.nrcresearchpress.com by 203.198.23.82 on 09/08/12
For personal use only.

TABLE 6. ^{1}H nuclear magnetic resonance data[a]

	Haza[d]	$Re_2O_3Cl_4$-(Haza)$_4$[d] **1**	ReO(OEt)-Cl_2(Haza)$_2$[d,f] **2**	ReO(OEt)Cl_2-(PPh_3)(Haza)[d,g] **3**	Haza[b,c]	[ReO_2-(Haza)$_4$]Cl[b] **4***a*	[ReO_2-(Haza)$_4$]I[b] **4***b*
H1	12.70	12.384 (−0.32)	10.439 (−2.26)	10.340 (−2.36)		12.160	12.183
H2	7.523	7.653 (0.13)	7.481 (−0.04)	7.384 (−0.14)	7.36	7.635 (0.27)	7.661 (0.30)
H3	6.588	6.785 (0.19)	6.698 (0.11)	6.639 (0.05)	6.45	6.413 (−0.04)	6.431 (−0.02)
H4	8.059	8.486 (0.43)	8.036 (−0.02)	8.085 (0.02)	7.92	7.679 (−0.24)	7.691 (−0.23)
H5	7.169	7.436 (0.27)	7.358 (0.19)	7.298[h] (0.13)	7.03	7.049 (0.02)	7.076 (0.05)
H6	8.443	8.337 (−0.10)	8.533 (0.09)	8.452[h] (0.01)	8.32	9.075 (0.75)	9.071 (0.75)
^3J(H2—H3)	3.5	3.5	3.5	3.5	3.5	3.5	3.4
^3J(H2—H1)	[e]	[e]	2.5	2.6	[e]	2.4	2.5
^4J(H3—H1)	[e]	[e]	2.1	2.1	[e]	1.9	2.0
^3J(H4—H5)	7.8	7.8	7.8	7.8	7.7	7.7	7.5
^4J(H4—H6)	1.5	1.2	0.8	1.7	1.5	1.0	[e]
^3J(H5—H6)	4.8	5.9	5.9	5.8	4.8	5.9	5.9

[a]δ in ppm (vs TMS), J in Hz, Δδ values from free Haza within parentheses.
[b]In $CDCl_3$.
[c]Data from Cox and Sankar (44).
[d]In CD_2Cl_2.
[e]Not resolved.
[f]Ethoxy group: CH_2, 3.364 (q); CH_3, 0.985 (t) ppm; ^3J(H—H), 7.0 Hz.
[g]Ethoxy group: CH_2, 3.100 (q); CH_3, 0.604 ppm (t); ^3J(H—H), 7.0 Hz; PPh_3 7.51 (m) and 7.81 ppm (m).
[h]Coupling is also observed to P of PPh_3 ligand: ^4J(H6—^{31}P), 1.7 Hz; ^5J(H5—^{31}P), 1.0 Hz.

TABLE 7. ^{13}C nuclear magnetic resonance spectra[a]

	Haza[b,c]	$Re_2O_3Cl_4$(Haza)$_4$[d,e]	ReO(OEt)Cl_2(PPh_3)(Haza)[h]	[ReO_2(Haza)$_4$]I[c]
C2	125.5	129.3 (3.8)	130.4 (4.9)	127.8 (2.4)
C3	100.5	103.5 (3.5)	101.9 (1.4)	101.2 (0.7)
C4	124.0	134.4 (10.3)	131.1 (7.1)	131.7 (7.8)
C5	115.6	115.9 (0.3)	116.1 (0.5)	115.7 (0.1)
C6	142.1	137.6 (−4.5)	133.2 (−8.9)	142.8 (0.7)
C8	148.9	148.8 (−0.1)	145.6 (−3.3)	146.8 (−2.1)
C9	120.7	124.9 (4.2)	126.1 (5.4)	123.6 (2.9)
CH_2			67.4	
CH_3			15.9	
C_{meta}			128.6[f]	
$C_{ipso,para}$			131.5[i]	
C_{ortho}			135.0[g]	

[a]δ in ppm (vs. TMS), Δδ values from free Haza within parentheses.
[b]From Cox and Sankar (44).
[c]In $CDCl_3$.
[d]Solid-state CP-MAS spectrum.
[e]Toluene resonances: 23.4 (CH_3), 121.9, 127.9 ppm.
[f]J_{C-P} 10.5 Hz.
[g]J_{C-P} 9.6 Hz.
[h]In CD_2Cl_2.
[i]Two components 0.03 ppm apart.

Can. J. Chem. Downloaded from www.nrcresearchpress.com by 203.198.23.82 on 09/08/12
For personal use only.

plexation, being shifted downfield by 0.47 ppm. A similar displacement is found here with the oxo-bridged dimer **1**, but the *trans*-dioxo complex **4** shows an upfield shift of 0.23 ppm, whereas the signal is barely displaced for the ethoxo complexes **2** and **3**. The C6 and H6 signals in the *trans*-dioxo cation **4** are much more deshielded than in the other compounds. The crystal structure of **4***a* (Fig. 2) shows that the four azaindole rings are parallel to the O=Re=O axis, bringing C6—H6 just above the Re=O bond. The downfield shifts on these resonances could be connected with the ligands being aligned with the O=Re=O unit, but it is difficult to decide which of Re=O anisotropy or particular backbonding is responsible for the observed deshielding.

Concluding remarks

7-Azaindole forms oxo-Re(V) compounds of the types known for pyridine, together with a mixed azaindole/PPh_3 species of a type isolated so far only when the nitrogen donor is part of a chelating agent (7). Binding occurs via N7 in all cases, but the presence of the N1—H bond, roughly parallel to the lone pair, introduces interesting structural features by making certain conformations more favoured. The $[ReO_2(Haza)_4]^+$ ion is particularly interesting, since strong hydrogen bonding to the oxo groups keeps the four ligands parallel to the O=Re=O axis. Rotation about the Re—N7 bond is likely to occur in solution, exchanging the direction of individual ligands, but the molecule probably spends most of its time in one of the possible "windmill" arrangements. In the solid state, the compound shows an interesting packing pattern with the O=Re=O directions of all molecules aligned along a crystallographic axis. Thus, this compound could be particularly suitable for studying optical properties, namely, the effect this particular configuration has on excited-state properties of the cation. Hydroxyl groups are known to quench luminescence for such systems and water molecules are hydrogen-bonded to the Re=O groups in the present dioxo complexes. Solid-state effects have been noted for guest/host complexes involving ReO_2^+ type molecules and clays (21). Because of disorder, the rotamer(s) present in the crystal could not be formally identified. Salts with various anions failed to provide suitable material for crystallographic studies so far, but work is underway to circumvent these difficulties.

Acknowledgments

We wish to thank M. Simard and F. Bélanger-Gariépy for assistance in collecting the X-ray data, and S. Bélanger for supplying $ReO_2I(PPh_3)_2$.

1. F. Allaire and A.L. Beauchamp. Inorg. Chim. Acta, **156**, 241 (1989).
2. S.M. Peng and Y.N. Lin. Acta Crystallogr. Sect. C: **42**, 1725 (1986); S.M. Peng and C.H. Lai. J. Chin. Chem. Soc. (Taipei), **35**, 325 (1988).
3. J.J.H. Edema, S. Gambarotta, A. Meetsma, F. Van Bolhuis, A.L. Spek, and W.J.J. Smeets. Inorg. Chem. **29**, 2147 (1990).
4. L.A. Oro, M.A. Ciriano, and B.E. Villarrova, J. Chem. Soc. Dalton Trans. 1891 (1985).
5. F.A. Cotton, D.G. Lay, and M. Millar. Inorg. Chem. **17**, 186 (1978).
6. F.A. Cotton and T.R. Felthouse. Inorg. Chem. **20**, 600 (1981).
7. V. Bertolasi, M. Sacerdoti, G. Gilli, and U. Mazzi. Acta Crystallogr. Sect. B: **38**, 426 (1982).
8. W.S. Sheldrick. Z. Naturforsch. **37B**, 653 (1982).
9. J. Poitras and A.L. Beauchamp. Can. J. Chem. **70**, 2846 (1992).
10. N. Dufour, A.M. Lebuis, M.C. Corbeil, A.L. Beauchamp, P. Dufour, Y. Dartiguenave, and M. Dartiguenave. Can. J. Chem. **70**, 2914 (1992).
11. F. Allaire. Ph.D. Thesis, Université de Montréal, Montréal, Que. 1987.
12. S.K. Mandal, D.M. Ho, and M. Orchin. Inorg. Chem. **30**, 2244 (1991).
13. N.P. Johnson, F.I.M. Taha, and G. Wilkinson. J. Chem. Soc. 2614 (1964).
14. J.C. Brewer and H.B. Gray. Inorg. Chem. **28**, 3334 (1989).
15. G.F. Ciani, G. D'Alfonso, P.F. Romiti, A. Sironi, and M. Freni. Inorg. Chim. Acta, **72**, 29 (1983).
16. M.S. Ram and J.T. Hupp, Inorg. Chem. **30**, 130 (1991).
17. J.T. Meyer, J. Electrochem. Soc. **131**, 221c (1984).
18. R.H. Holm. Chem. Rev. **87**, 1401 (1987).
19. D.W. Pipes and T.J. Meyer. Inorg. Chem. **25**, 3256 (1986); M.S. Ram, C.S. Johnson, R.L. Blackbourn, and J.T. Hupp. Inorg. Chem. **29**, 238 (1990); G.N. Holder and L.A. Bottomley. Inorg. Chim. Acta, **194**, 133 (1992).
20. J.R. Winkler and H.B. Gray. J. Am. Chem. Soc. **105**, 1373 (1983); H.H. Thorpe, J. Van Houten, and H.B. Gray. Inorg. Chem. **28**, 889 (1989); J.R. Winkler and H.B. Gray. Inorg. Chem. **24**, 346 (1985).
21. M.D. Newsham, E.P. Giannelis, T.J. Pinnavaia, and D.G. Nocera. J. Am. Chem. Soc. **110**, 3885 (1992); H.H. Thorp, C.V. Kumar, N.J. Turro, and H.B. Gray. J. Am. Chem. Soc. **111**, 4364 (1989); H.H. Thorp, N.J. Turro, and H.B. Gray. New J. Chem. **15**, 601 (1991).
22. G.W. Parshall, L.W. Shive, and F.A. Cotton. Inorg. Synth. **17**, 110 (1977).
23. M. Freni, D. Giusto, P. Romiti, and G. Minghetti. Gazz. Chim. Ital. **99**, 286 (1969).
24. International tables for crystallography. Vol. A. Reidel, Dordrecht. 1983.
25. G.H. Stout and L.H. Jensen, X-ray structure determination, a practical guide. MacMillan, London. 1968, p. 303.
26. J. Gabe, Y. Le Page, J.P. Charland, and F.L. Lee. J. Appl. Crystallogr. **22**, 384 (1989).
27. C.J.L. Lock and G. Turner. Can. J. Chem. **56**, 179 (1978).
28. M.A. Dewey, D.A. Knight, D.P. Klein, A.M. Arif, and J.A. Gladysz. Inorg. Chem. **30**, 4995 (1991); W.E. Buhro, S. Georgiou, J.M. Fernández, A.T. Patton, C.E. Strouse, and J.A. Gladysz. Organometallics, **5**, 956 (1986); A.W. Verstuyft, D.A. Redfield, L.W. Cary, and J.H. Nelson. Inorg. Chem. **15**, 1128 (1976).
29. R. Graziani, U. Casellato, R. Rossi, and A. Marchi. J. Crystallogr. Spectrosc. Res. **15**, 573 (1985).
30. A.M. Lebuis, C. Roux, and A.L. Beauchamp. Acta Crystallogr. Sect. C:**49**, 33 (1993).
31. C. Calvo, N. Krishnamachari, and C.J.L. Lock. J. Cryst. Molec. Struct. **1**, 161 (1971).
32. G.B. Deacon and J.H.S. Green. Spectrochim. Acta, **24A**, 845 (1968).
33. N.P. Johnson, C.J.L. Lock, and G. Wilkinson. J. Chem. Soc. 1054 (1964).
34. B. Jezowska-Trzebiatowska, J. Hanuza, and M. Baluka. Spectrochim. Acta, **27A**, 1753 (1971).
35. D. Parker and P.S. Roy. Inorg. Chem. **27**, 4127 (1988).
36. C.J.L. Lock and G. Turner. Can. J. Chem. **55**, 333 (1977).
37. J.M. Mayer. Inorg. Chem. **27**, 3899 (1988).
38. R. Rossi, A. Marchi, L. Marvelli, M. Peruzzini, U. Casellato, and R. Graziani. J. Chem. Soc. Dalton Trans. 435 (1992).

Can. J. Chem. Downloaded from www.nrcresearchpress.com by 203.198.23.82 on 09/08/12
For personal use only.

39. W.A. Nugent and J.M. Mayer. Metal–ligand multiple bonds. Wiley, New York. 1989.
40. P. Dufour, Y. Dartiguenave, M. Dartiguenave, N. Dufour, A.M. Lebuis, F. Bélanger-Gariépy, and A.L. Beauchamp. Can. J. Chem. **68**, 193 (1990).
41. C.J.L. Lock and G. Turner. Acta Crystallogr. Sect. B:**34**, 923 (1978).
42. V.S. Sergienko, M.A. Porai-Koshits, and T.S. Khodaskova. J. Struct. Chem. **15**, 250 (1974).
43. S.A. Luna, C. Bolzati, A. Duatti, G.L. Zucchini, G. Bandoli, and F. Refosco. Inorg. Chem. **31**, 2595 (1992).
44. R.H. Cox and S. Sankar. Org. Magn. Reson. **14**, 150 (1980).

Can. J. Chem. Downloaded from www.nrcresearchpress.com by 203.198.23.82 on 09/08/12
For personal use only.

Non-stoichiometric chloride salts of dioxotetrakis(imidazole)rhenium(V) cations

ANNE-MARIE LEBUIS, JIM M.C. YOUNG, AND ANDRÉ L. BEAUCHAMP[1]

Département de chimie, Université de Montréal, C.P. 6128, Succ. A, Montréal, QC H3C 3J7, Canada

Received June 21, 1993

ANNE-MARIE LEBUIS, JIM M.C. YOUNG, and ANDRÉ L. BEAUCHAMP. Can. J. Chem. **71**, 2070 (1993).

Orange $[ReO_2L_4]Cl$ salts were prepared with L = imidazole and 2-methylimidazole. The presence of a strong Re=O stretching band in the infrared spectra near 785 cm^{-1} is consistent with a *trans*-dioxo octahedral structure. With 1,2-dimethylimidazole, red-violet solids were obtained, which were studied by X-ray diffraction. Form I (from methanol): cubic, $Ia\bar{3}d$, a = 25.205 Å, R = 0.032, 986 observed reflections; form II (from ethanol–dichloromethane): cubic, $Ia\bar{3}d$, a = 25.520 Å, R = 0.056, 766 observed reflections. Both materials are non-stoichiometric, containing *trans*-$[ReO_2L_4]^+$ and protonated *trans*-$[ReO(OH)L_4]^{2+}$ in an approximate ratio of 3:1 for I and 2:1 for II. In both cases, the unit cell contains 1 "normal" Cl^- ion and 2/3 H_2O per complex. In form I, the additional charge of $[ReO(OH)L_4]^{2+}$ is balanced by an extra Cl^- ion partly occupying the unit cell origin, where it is replaced by disordered methanol the rest of the time. In form II, ReO_4^- and CH_2Cl_2 play the corresponding roles. In the infrared spectra, besides the characteristic band for the dioxo species, both forms show an extra peak at ~932 cm^{-1} originating from the protonated species, whereas form II shows an additional band at 907 cm^{-1} for uncoordinated ReO_4^-. The ^1H and ^{13}C NMR spectra of both forms in D_2O are identical to those of the pure $[ReO_2L_4]^+$ salt, indicating that the protonated species is strongly acidic.

ANNE-MARIE LEBUIS, JIM M.C. YOUNG et ANDRÉ L. BEAUCHAMP. Can. J. Chem. **71**, 2070 (1993).

Les sels orangés $[ReO_2L_4]Cl$ ont été préparés pour L = imidazole et 2-méthylimidazole. La présence d'une bande forte vers 785 cm^{-1} dans les spectres infrarouges pour l'élongation Re=O est en accord avec la structure octaédrique *trans*-dioxo. Avec le 1,2-diméthylimidazole, des solides rouge violet ont été obtenus et étudiés par diffraction des rayons X. Forme I (obtenue du méthanol) : cubique, $Ia\bar{3}d$, a = 25,205 Å, R = 0,032, 986 réflexions observées; forme II (éthanol–dichlorométhane) : cubique, $Ia\bar{3}d$, a = 25,520 Å, R = 0,056, 766 réflexions observées. Les deux solides sont non-stoechiométriques et contiennent l'ion *trans*-$[ReO_2L_4]^+$ et l'espèce protonée *trans*-$[ReO(OH)L_4]^{2+}$ dans un rapport approximatif de 3 : 1 pour I et de 2 : 1 pour II. Dans les deux cas, la maille renferme 1 ion Cl^- «normal» et 2/3 H_2O par complexe. Dans la forme I, la charge additionnelle de $[ReO(OH)L_4]^{2+}$ est équilibrée par un ion Cl^- supplémentaire occupant partiellement l'origine de la maille, où il est remplacé le reste du temps par du méthanol désordonné. Dans la forme II, ces rôles sont joués par ReO_4^- et CH_2Cl_2 respectivement. Dans les spectres infrarouges, en plus de la bande caractéristique de l'espèce dioxo, les deux formes présentent une bande vers 932 cm^{-1} provenant de l'espèce protonée, alors que la forme II possède une bande supplémentaire à 907 cm^{-1} pour l'ion ReO_4^- non-coordonné. Les spectres RMN ^1H et ^{13}C des deux formes dans D_2O sont identiques à celui du sel dioxo $[ReO_2L_4]^+$ pur, ce qui indique que l'espèce protonée est fortement acide.

Can. J. Chem. Downloaded from www.nrcresearchpress.com by 203.198.23.82 on 09/08/12
For personal use only.

Introduction

Dioxo complexes of Re(V) have recently drawn considerable interest, partly because of their potential applications in catalysis (1, 2). Electrochemical and photophysical properties of numerous compounds containing the $[ReO_2]^+$ core have been studied (3–6). In this regard, imidazoles (Scheme 1) are an interesting family of ligands, since it has been shown that rigidity is a prime factor in the control of the emission properties of $[ReO_2L_4]^+$ cations (7). Another potential use for Re(V) oxo complexes is as radiopharmaceuticals, since the β-emitter ^{186}Re and ^{188}Re nuclei have been proposed for use in radiotherapy (8–10). Combining the $[ReO_2]^+$ core with ligands such as imidazoles, which are themselves of biological importance, seemed to be a promising route to follow. The imidazole ring is naturally present in the body as part of histidine and its structural analogy to purines makes it a potentially valuable part of drugs aimed at DNA. With Ru(III), for instance, imidazole-containing complexes have been proposed as tumour targeting agents (11, 12). The photochemistry of $[ReO_2L_4]^+$ complexes in the presence of DNA has also been studied in an attempt to identify the site of interaction (13).

We describe here the preparation and characterization of $[ReO_2L_4]Cl$ complexes with three imidazoles. Orange compounds of the type known for other N-heterocyclic ligands (4, 14, 15) were isolated with imidazole and its 2-methyl derivative. On the other hand, our experiments yielded red-violet solids with 1,2-dimethylimidazole. These materials were examined carefully by X-ray diffraction and found to be non-stoichiometric phases containing some protonated $[ReO(OH)L_4]^{2+}$ species.

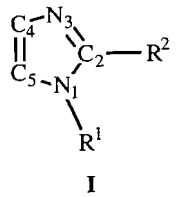

R^1	R^2	
H	H	ImH
H	CH_3	2-MeImH
CH_3	CH_3	1,2-Me_2Im

I

SCHEME 1

Experimental

Reactants and methods

PPh_3, $KReO_4$, and the ligands were used as received from Aldrich. $ReOCl_3(PPh_3)_2$ was prepared according to the literature method (16). Toluene was dried over Na and distilled under argon before use. All other solvents were used as received.

IR spectra were recorded as KBr or CsI pellets on a Perkin–Elmer 783 spectrophotometer. The NMR spectra were generally run in D_2O (Cambridge Isotopes). ^1H NMR spectra were recorded on a Varian VXR 300 MHz spectrometer and referenced to the residual solvent signal (δ 4.80 ppm). ^{13}C spectra were run on the same instrument at 75.43 MHz (dioxane signal at 66.56 ppm as internal reference) (17). Spectra of the complexes were obtained at near

[1]Author to whom correspondence may be addressed.

Can. J. Chem. Downloaded from www.nrcresearchpress.com by 203.198.23.82 on 09/08/12
For personal use only.

saturation. The ^{13}C CP-MAS spectrum was recorded on the same instrument and was referenced to the aromatic carbon signal of hexamethylbenzene (δ 132.1 ppm). Other conditions: relaxation delay, 10 s; spinning rate, 3.9 kHz; side-band suppression routine used.

Preparative work

Method 1

The method originally described by Johnson et al. (15) for pyridine was applied using a lower excess of ligand. $ReOCl_3(PPh_3)_2$ (1.00 g, 1.2 mmol) in ethanol (20 mL, not dried) was refluxed (2 h) with 6 equivalents of the imidazole ligand. Solvent was partly evaporated and CH_2Cl_2 was added to precipitate the product. With imidazole, a dark brown powder (0.58 g, 83%) of $[ReO_2(ImH)_4]Cl \cdot 2H_2O$ was obtained. IR: 790 cm^{-1} ν_{as}(O═Re═O). Anal. calcd. for $C_{12}H_{20}ClN_8O_4Re$: C 25.65, H 3.59, N 19.94; found: C 25.60, H 3.48, N 19.97. With 2-MeImH, the product was prepared as an orange oil, which was not further studied since better samples of the same complex were obtained by method 2. In the case of 1,2-Me_2Im, the crystals obtained (0.70 g) were red-violet and found by X-ray diffraction (see below, form II) to contain both $[ReO_2L_4]^+$ (IR: 781 cm^{-1} ν_{as}(O═Re═O)) and $[ReO(OH)L_4]^{2+}$ (IR: 931 cm^{-1} ν(Re═O)).

Method 2

$ReOCl_3(PPh_3)_2$ (0.41 g, 0.49 mmol) and 6 equivalents of ligand were stirred under nitrogen in 40 mL of toluene to which 4 drops of distilled water had been added. After 1–4 h, depending on the ligand, an orange sludge formed, which was filtered and washed with benzene to eliminate traces of PPh_3. Although this procedure led to oxo-bridged $[OReCl_2L_2]_2O$ dimers with pyridine (18), dioxo salts were isolated here. With ImH, recrystallization from methanol gave 0.22 g (83%) of a brown microcrystalline powder showing the same IR and NMR spectra as the compound isolated by method 1. With 2-MeImH, 0.20 g (68%) of an orange microcrystalline material of composition $[ReO_2(2\text{-MeImH})_4]Cl \cdot H_2O$ was obtained. IR: 780 cm^{-1} ν_{as}(O═Re═O). Anal. calcd. for $C_{16}H_{26}ClO_3N_8Re$: C 32.02, H 4.37, N 18.67, Cl 5.91; found: C 32.52, H 3.88, N 18.50, Cl 6.06. Again, 1,2-Me_2Im gave red-violet crystals (0.22 g), whose structure determined by X-ray diffraction (form I, see below) showed the presence of $[ReO_2L_4]^+$ and $[ReO(OH)L_4]^{2+}$.

Method 3

This procedure is a variation of a method initially proposed by Chakravorty (19) for pyridine complexes. $KReO_4$ (4.2 g) and KI (5.9 g) in concentrated HCl (50–70 mL) were heated to dryness until no purple vapours formed. The ligand (8 equivalents) was added as an aqueous solution (20 mL) and the mixture was refluxed for 2 h. Ethanol (150 mL) was then added and the mixture was filtered to remove the precipitated KCl. The filtrate was concentrated to afford a dark red-brown solution, from which crystals precipitated upon standing. The ImH compound was obtained in good yield (5.8 g, 71%). In contrast with the above methods, the 1,2-Me_2Im complex was orange and no protonated cations were present. IR: 795 cm^{-1} ν_{as}(O═Re═O). However, the sample also contained some $KReO_4$ (identified from the X-ray powder pattern and IR band at 907 cm^{-1}) that could not be easily removed.

Crystallographic measurements and structure resolutions

Two varieties of red-violet crystals obtained with 1,2-Me_2Im were studied. In both cases, the X-ray work was carried out on an Enraf–Nonius CAD-4 diffractometer, using graphite-monochromatized CuKα̅ radiation. The reduced cells were determined from 25 centred reflections found by the search routine of the CAD-4 software. The metrically rhombohedral reduced cells ($a = b = c$, $\alpha = 109.45°$) were checked with long-exposure axial photographs along the three axes and then converted to the I-centred cubic cell indicated by the Niggli matrix. Axial photographs on these new cells showed the presence of Laue mirror planes perpendicular to each of the three axes. A limited data collection showed equivalence in the *hkl/klh/lhk/lkh/hlk/khl* group as expected for *m3m* Laue symmetry. The cell parameters obtained by least-squares fit on the settings of the 25 reflections ($20° \leq 2\theta \leq 25°$) are given in Table 1. Intensity data were collected following the usual procedure (20). Orientation was monitored every 200 measurements and intensity was checked every hour with standard reflections.

Crystal I had the following dimensions (mm) between the indicated pairs of faces: 0.129 (101–$\bar{1}0\bar{1}$) × 0.175 ($\bar{1}10$–$1\bar{1}0$) × 0.243 (110–$\bar{1}\bar{1}0$). A whole octant (7222 reflections) was collected. The data were corrected for absorption (Gaussian integration, 10 × 10 × 10 grid, transmission range: 0.19–0.39). Inspection of the full data set confirmed the *m3m* Laue symmetry. The averaged data set consisted of 1252 unique reflections, of which 986 with $I \geq 3.0\ \sigma(I)$ were retained for structure determination. The systematic absences (*hkl* $h + k + l$ odd, *Okl* k odd, *hhl* $2h + l$ odd, and all cyclic permutations) unambiguously identified $Ia\bar{3}d$ (No. 230) (21) as the space group. The data were finally corrected for the effects of Lorentz and polarization.

Work on crystal II was originally undertaken as a check on the results with crystal I. The cell edges were found to be ~1% longer, but the same steps as above led again to space group $Ia\bar{3}d$. A minimum data set (*hkl*, $h + k + l$ *even*, $h \leq k \leq l$) was collected. The data set consisted of 1322 unique reflections, of which 766 with $I \geq 3.0\ \sigma(I)$ were retained for structure determination. The specimen used was a roughly spherical fragment of mean radius 0.11 mm without well-defined faces and no absorption correction could be applied.

The structures were solved by the heavy-atom method. Refinement was done on $|F|$ by full-matrix least-squares procedures. The function minimized was $\Sigma w(|F_o| - |F_c|)^2$, with weights $w = 1/(\sigma^2(F_o) + k F_o^2)$, where $k = 0.0001$ for I and 0.001 for II. The Patterson map calculated for crystal I indicated that special positions *24c* and *24d* (21) were occupied by Re and Cl, but could not distinguish between the two possible distributions. The ΔF map calculated with one of the models failed to reveal any chemically reasonable fragment. With the other model (Re on *24c* and Cl on *24d*), the Re-bonded oxygen (*48g*) and the non-hydrogen atoms in the 1,2-Me_2Im ligand (general position) were located. The next ΔF map showed residual electron density in two regions. A peak of 5 e $Å^{-3}$ at (1/8, 1/8, 1/8) was obviously due to a water molecule hydrogen bonded to Re═O groups. A stronger peak (9 e $Å^{-3}$) at the origin was too far from already identified units to be covalently or hydrogen bonded. Among various models considered, partial occupancy by Cl^- turned out to best fit the data. This extra Cl^- ion would balance the charge of either H_3O^+ ions replacing some water molecules at (1/8, 1/8, 1/8) or oxo-protonated $[ReO(OH)(1,2\text{-}Me_2Im)_4]^{2+}$ cations randomly replacing $[ReO_2(1,2\text{-}Me_2Im)_4]^+$ in the crystal. The latter model was retained since it allowed us to interpret unexplained features in the infrared spectra. A Cl(2) atom was positioned at (0, 0, 0) (*16a*) and assigned an isotropic temperature factor of 0.05 $Å^2$ (mean of U_{iso} for ligand atoms). The known atoms were refined anisotropically, and the occupancy factor for Cl(2), whose coordinates were fixed by symmetry, was included in the refinement. Occupancy converged to 0.35: this value was retained for the rest of the refinement. In the subsequent ΔF map, the water region was found to contain two close, but resolved, residuals: one peak W(2) of 2.5 e $Å^{-3}$ at (0.10, 0.10, 0.10) (*32e*) and the W(1) counterpart of 5 e $Å^{-3}$ at (0.125, 0.125, 0.125) (*16b*). With U_{iso} fixed at 0.05 $Å^2$ as above, the position of W(2) and the occupancy factors of W(1) and W(2) were allowed to refine. The converged values were 0.57 and 0.15, respectively. When equipoint multiplicities are taken into account, this corresponds to a roughly 2:1 ratio between the water populations on the W(1) (16 × 0.57 = 9.1) and the W(2) sites (32 × 0.15 = 4.8). These values were normalized to 0.65 and 0.17 to provide a whole water molecule in this region and were fixed for the rest of the interpretation. The question concerning the species present 65% of the time near the origin, when Cl(2) is absent, was answered by the next ΔF map. A peak of 4.1 e $Å^{-3}$ remained at

TABLE 1. Crystallographic data for the two 1,2-Me_2Im compounds

	$\{0.77[ReO_2(1,2\text{-}Me_2Im)_4]Cl \cdot 0.23[ReO(OH)(1,2\text{-}Me_2Im)_4]Cl_2\} \cdot 0.66\ H_2O \cdot 0.43\ MeOH$	$\{0.64[ReO_2(1,2\text{-}Me_2Im)_4]Cl \cdot 0.36[ReO(OH)(1,2\text{-}Me_2Im)_4]Cl(ReO_4)\} \cdot 0.66\ H_2O \cdot 0.31\ CH_2Cl_2$
Crystal	I	II
Formula	$ReCl_{1.23}O_{3.09}N_8C_{20.43}H_{35.27}$	$Re_{1.36}Cl_{1.62}O_{4.77}N_8C_{20.31}H_{33.95}$
Formula weight	672.24	777.33
Crystal system	Cubic	Cubic
Space group	$Ia\bar{3}d$	$Ia\bar{3}d$
a, Å	25.205(3)	25.520(3)
V, Å^3	16012(3)	16620(5)
T, K	293	293
D_{calc}, g cm^{-3}	1.673	1.864
Z	24	24
Radiation	CuKα	CuKα
λ, Å	1.54178	1.54178
μ, cm^{-1}	100.5	129.8
Scan	ω	ω
$2\theta_{max}$, deg	140	140
Standards (number, fluctuation)	5, ±0.7%	7, ±0.6%
R_{av}, %	4.2	
No. unique reflections	1252	1322
No. observed reflections	986	766
Rejection criterion, $I/\sigma(I)$	<3.0	3.0
R,[a] %	3.2	5.6
R_w,[a] %	4.1	5.6
Goodness-of-fit, S[a]	2.53	2.67
No. parameters varied (v)	80	82
Residual on final ΔF map, e/Å^3		
maximum	1.2	2.8
general background	≤ ±0.71	≤ ±0.98

[a] $R = \Sigma\,||F_o| - |F_c||/\Sigma|F_o|$; $R_w = [\Sigma w(|F_o| - |F_c|)^2/\Sigma w|F_o|^2]^{1/2}$; $S = [\Sigma w(|F_o| - |F_c|)^2/(n - v)]^{1/2}$.

(0.03, 0.03, 0.03), too close to Cl(2) to be present simultaneously, but close enough (1.6 Å) to the symmetry-related site at (−0.03, −0.03, −0.03) to define a methanol molecule with the CH_3 and OH groups statistically interchanged by disorder across the origin. This site (MET) was described with the scattering curve of nitrogen and occupancy was fixed to 0.65. The eight hydrogens on the 1,2-Me_2Im ligand were also visible in the ΔF map. They were fixed at idealized positions (C—H = 1.0 Å) with temperature factors 0.01 Å^2 greater than those of the corresponding carbons. The fractional hydrogens of lattice methanol were not found in the ΔF map and were neglected. In the final cycles, all adjustable coordinates of all non-hydrogen atoms were refined and temperature factors were anisotropic, except for the disordered atoms Cl(2)/MET and W(1)/W(2), which were kept isotropic. The final residuals were $R = 0.032$ and $R_w = 0.041$. The general background in the final ΔF map was below ±0.7 e Å^{-3}, except for a peak of 1.2 e Å^{-3} at (0.04, 0.04, 0.04), in the disordered Cl(2)–methanol region.

Form II belongs to the same space group. Again, the two starting points indicated by the Patterson map were tested and the above distribution of Re(1) and Cl(1) on *24c* and *24d*, respectively, proved to be correct. The coordinates obtained above for O(1) and the non-hydrogen atoms in 1,2-MeIm were then introduced. In the ΔF map, electron density was present near (1/8, 1/8, 1/8) for water molecules but, near the origin, a very high residual (18 e Å^{-3}) was found at (0.03, 0.03, 0.03). It was assigned to the Re atom of a fractional ReO_4^- ion, since it was surrounded by a tetrahedron of smaller peaks, assigned to oxygen, at ~1.65 Å: O(20) on the threefold axis (*32e*) and O(21) in general position. This interpretation was supported by the presence of an unexplained peak corresponding to uncoordinated ReO_4^- in the infrared spectrum. Hence, substitution of $[ReO_2(1,2\text{-}MeIm)_4]^+$ by $[ReO(OH)(1,2\text{-}MeIm)_4]^{2+}$ was again taking place and, in this case, the extra anion required for each protonated species present was not Cl^-, but ReO_4^-. Using the same strategy as above, U_{iso} factors of 0.05 Å^2 were assigned to W(1), W(2), and Re(2), and their positions and occupancies were adjusted, while the rest of the structure was refined anisotropically. Occupancy of Re(2) converged to 0.27. Fixed occupancies of 0.27 were then used for Re(2), O(20), and O(21). The refined occupancies of W(1) and W(2) (0.41 and 0.24) were normalized to 0.46 and 0.27, respectively, as above. Therefore, the amount of W(2) corresponds to the number of extra anions present. Occupancies of W(1) and W(2) were fixed for the rest of the interpretation. After refining this model, the ΔF map contained three residual peaks of 2.8, 1.6, and 1.0 e Å^{-3} near the ReO_4^- ion. They could be assembled into a CH_2Cl_2 molecule disordered over six orientations with Cl(3) lying on the threefold axis. Occupancies were fixed at 0.23 for Cl(3) and 0.08 for C(10) and Cl(2), assuming that the region around the origin is fully occupied by either ReO_4^- or CH_2Cl_2. Attempts to refine all parameters in this region led to high instability, because of the proximity of the disordered atoms. In the final model, Cl(2) and C(10) were fixed at the positions found in the ΔF map. All other adjustable coordinates of all non-hydrogen atoms were refined and temperature factors were anisotropic, except for the disordered atoms ReO_4/CH_2Cl_2 and W(1)/W(2), which were kept isotropic. The position of O(20) was also fixed, since refinement displaced it towards the origin making the Re—O distance too small. Hydrogens were not visible in the ΔF map. The final agreement factors were $R = 0.056$ and $R_w = 0.056$. The general background in the final ΔF map was below ±0.98 e Å^{-3}, except for a peak of 2.8 e Å^{-3} at origin. This peak could be an artefact due to our fixing O(20), but the possibility that a small amount of Cl^- (or ReO_4^-) is present at this site cannot be ruled out. No attempts were made, however, to introduce a third contributor to this disordered region.

Can. J. Chem. Downloaded from www.nrcresearchpress.com by 203.198.23.82 on 09/08/12
For personal use only.

TABLE 2. Final atomic coordinates and equivalent isotropic temperature factors

	Equipoint	x	y	z	B_{eq}	Occupancy
Form I						
Re(1)	*24c*	0.0000	0.2500	0.1250	2.73	1.00
Cl(1)	*24d*	0.0000	0.2500	0.3750	4.48	1.00
Cl(2)	*16a*	0.0000	0.0000	0.0000	4.76(18)[a]	0.35
O(1)	*48g*	0.0494(1)	0.2006	0.1250	3.3	1.00
N(1)	*96h*	−0.0760(2)	0.1600(2)	0.0025(2)	3.5	1.00
N(3)	*96h*	−0.0461(2)	0.2081(2)	0.0673(2)	3.1	1.00
C(2)	*96h*	−0.0325(2)	0.1790(2)	0.0256(2)	3.3	1.00
C(4)	*96h*	−0.1010(2)	0.2067(2)	0.0700(2)	3.4	1.00
C(5)	*96h*	−0.1193(2)	0.1774(3)	0.0296(2)	3.9	1.00
C(11)	*96h*	−0.0768(3)	0.1265(3)	−0.0443(3)	5.4	1.00
C(21)	*96h*	0.0219(3)	0.1683(4)	0.0064(3)	5.4	1.00
W(1)	*16b*	0.1250	0.1250	0.1250	7.6(5)[a]	0.65
W(2)	*32e*	0.1048(10)	0.1048	0.1048	4.6(9)[a]	0.17
MET	*32e*	0.0192(3)	0.0192	0.0192	4.0(3)[a]	0.65
Form II						
Re(1)	*24c*	0.00000	0.25000	0.12500	3.08	1.00
Re(2)	*32e*	0.02856(12)	0.02856	0.02856	4.60(12)[a]	0.27
Cl(1)	*24d*	0.0000	0.7500	0.1250	5.4	1.00
Cl(2)	*96h*	−0.0125[b]	−0.0367[b]	−0.0034[b]	9.1(22)[a]	0.08
Cl(3)	*32e*	0.0381(5)	0.0381	0.0381	1.6(4)[a]	0.23
O(1)	*48g*	0.0478(4)	0.2022	0.1250	3.6	1.00
O(20)	*32e*	0.0101[b]	0.0101	0.0101	4.0(14)[a]	0.27
O(21)	*96h*	−0.0097(19)	0.0703(19)	0.0556(19)	5.5(13)[a]	0.27
N(1)	*96h*	0.0739(5)	0.3369(5)	0.0025(6)	4.6	1.00
N(3)	*96h*	0.0449(5)	0.2934(5)	0.0688(4)	3.5	1.00
C(2)	*96h*	0.0296(6)	0.3171(6)	0.0250(6)	3.9	1.00
C(4)	*96h*	0.0998(5)	0.2947(6)	0.0714(6)	3.6	1.00
C(5)	*96h*	0.1195(7)	0.3216(7)	0.0311(6)	4.6	1.00
C(10)	*96h*	0.0037[b]	0.0252[b]	−0.0149[b]	6.3(20)[a]	0.08
C(11)	*96h*	0.0750(7)	0.3669(8)	−0.0491(7)	6.7(12)	1.00
C(21)	*96h*	−0.0244(6)	0.3256(6)	0.0035(7)	5.4	1.00
W(1)	*16b*	0.1250	0.1250	0.1250	8.5(19)[a]	0.46
W(2)	*32e*	0.1103(19)	0.1103	0.1103	10.6(34)[a]	0.27

[a]Isotropic temperature factor.
[b]Fixed at position found in ΔF map and not refined (see text).

All calculations were done with the NRCVAX system (22). The refined coordinates are listed in Table 2.[2]

Discussion

Three methods were applied to prepare $[ReO_2L_4]Cl$ with imidazole derivatives. For ImH and 2-MeImH, reacting $ReOCl_3(PPh_3)_2$ with 6 equivalents of ligand in ethanol led to the expected $[ReO_2L_4]^+$ ion. Thus, the very large ligand excess originally used to prepare the pyridine analogue (15) can be reduced without loss of efficiency, as noted in the case with 7-azaindole (23). The same ImH and 2-MeImH compounds were isolated from the reaction of $ReOCl_3(PPh_3)_2$ with 6 equivalents of ligand in moist toluene. With pyridine and azaindole, this method led to the oxo-bridged dimer $\{ORECl_2L_2\}_2O$, but dioxo monomers were isolated here and sample crystallinity was better than with the first method.

The two above methods, when applied to 1,2-Me_2Im, led to a red-violet, instead of orange, material. Under the microscope, it was clear that colour variability was not due to a mixture of two types of solids, since the samples were homogeneous both in colour and crystal morphology. Colour was eventually explained when X-ray work (see below) became available, showing that both materials were non-stoichiometric phases containing some protonated $[ReO(OH)L_4]^{2+}$ species together with the normal $[ReO_2L_4]^+$ unit. The protonation-free $[ReO_2L_4]^+$ salt could be prepared via a $KReO_4$/KI/HCl mixture by a method described by Chakravorty (19) for pyridine, but some $KReO_4$ impurity remained.

Infrared spectroscopy

Tables of infrared frequencies for the various complexes are given as supplementary material.[2] Assignments for the

[2]The supplementary material includes lists of observed and calculated structure factor amplitudes, anisotropic thermal parameters, hydrogen coordinates, distances and angles in form II, and atom-to-plane distances for both structures, as well as a table of infrared frequencies (22 pages). Complete set of data may be purchased from: The Depository of Unpublished Data, Document Delivery, CISTI, National Research Council Canada, Ottawa, ON K1A OS2 Canada.

The tables of hydrogen coordinates (forms I and II) and of distances and angles in form II (2 pages) have also been deposited with the Cambridge Crystallographic Data Centre, and can be obtained on request from The Director, Cambridge Crystallographic Data Centre, University Chemical Laboratory, 12 Union Road, Cambridge, CB2 1EZ, U.K.

Can. J. Chem. Downloaded from www.nrcresearchpress.com by 203.198.23.82 on 09/08/12
For personal use only.

TABLE 3. ^{1}H NMR data of $[ReO_2L_4]^+$ cations in D_2O[a]

	L = ImH		L = 2-MeImH		L = 1,2-Me_2Im	
	Free	Complex	Free	Complex	Free	Complex[e]
H2	7.75	7.76[b] (+0.01)				
H4	7.11	7.06[b] (−0.05)	6.92	6.80[c] (−0.12)	6.79	6.74[d] (−0.06)
H5	7.11	7.28[b] (+0.17)	6.92	7.08[c] (+0.16)	6.94	7.06[d] (+0.12)
CH_3(N1)					3.53	3.69 (+0.16)
CH_3(C2)			2.31	2.21 (−0.10)	2.27	2.23 (−0.04)

[a]In ppm, Δδ vs. free ligand within parentheses.
[b]Doublet of doublets with unresolved central component, $^3J_{45} \sim {}^4J_{25} \sim {}^4J_{24} \sim 1.4$ Hz.
[c]Doublet, $^3J_{45} = 1.3$ Hz.
[d]Doublet, $^3J_{45} = 1.6$ Hz.
[e]Signals of 1,2-Me_2ImH$^+$ present in aged solutions: H4/H5, 7.27/7.25; 1-CH_3, 3.75; 2-CH_3, 2.58; $^3J_{45}$, 2.2 Hz.

ImH system are based on earlier studies (24–28). Tentative assignments for the methylated ligands and their complexes are discussed elsewhere (29).

Metal coordination introduces characteristic shifts on a number of vibrations. Except for N—H bands in ImH and 2-MeImH, these changes are relatively small and they will not be described in detail here. However, a large shift in the interference-free 340–420 cm^{-1} region of the 2-methylated derivatives is worth mentioning: bands at 418 cm^{-1} in 1,2-Me_2Im and 345 cm^{-1} in 2-MeImH are displaced to higher frequency by ~50 cm^{-1} in the complexes. Since these bands likely originate for the δ(C—CH_3) mode, they probably reflect steric effects on the methyl group next to the coordination site.

The Re–oxygen stretching modes are usually easy to identify in the infrared spectra. The strong ν_{as}(O=Re=O) band, observed at ~820 cm^{-1} for the pyridine and ethylenediamine analogues (30), is clearly shifted below 800 cm^{-1} in the imidazole complexes, but assignment is not straightforward, since the ligands also show strong γ(C—H) bands in this region. Furthermore, the γ(N—H) mode of free ImH at ~950 cm^{-1} is known to move to the 700–850 cm^{-1} range in various complexes (29, 31, 32), mainly because of changes in hydrogen bonding. From comparisons within the present set of $[ReO_2L_4]^+$ compounds and with complexes of other metals, the ν(O=Re=O) mode was assigned to the strong component in the 780–795 cm^{-1} range. Similar values were found for the *trans*-ReO_2 units with 7-azaindole (23) and a tetraaza macrocyclic ligand (cyclam) (33). In the non-stoichiometric phases with 1,2-Me_2Im, besides the normal $[ReO_2L_4]_2^+$ band at 781 cm^{-1}, the red-violet crystals give a broader feature at 932 cm^{-1} for the ν(Re=O) mode of $[ReO(OH)L_4]^{2+}$. The similar band for the protonated species was observed at 981 cm^{-1} for ethylenediamine (30) and 969 cm^{-1} for cyclam (33). Also present in the sample obtained by method 1 (form II) is a band at 907 cm^{-1}, due to uncoordinated ReO_4^- acting as the counterion for the $[ReO(OH)L_4]^{2+}$ formed.

NMR spectroscopy

^{1}H and ^{13}C data obtained on D_2O solutions are collected in Tables 3 and 4, respectively. Assignments are based on previous studies (34–36). For free ImH and 2-MeImH, the N—H proton participates in a fast tautomeric exchange between the two nitrogens, leading to averaged signals for H4/H5 and C4/C5. Fast exchange does not take place in the complexes and individual resonances are observed.

The ^{13}C chemical shifts for the ring carbons are assigned in the order C2 > C4 > C5 reported by Henderson et al. (36) for $(NH_3)_5$Co(III)–imidazoles complexes. This same order has also been noted for acetone solutions of the Ni(II) complexes $[RNi(imidazoles)]^+$, where R = 7-amino-4-methyl-5-aza-3-hepten-2-one (37). C2 is found to be shifted ~2 ppm downfield by coordination, as noted for these two systems. The separation between C4 and C5 is greater in the present complexes. The displacements on C4 and C5 upon coordination (Table 4) are different for 1,2-Me_2Im when compared with ImH and 2-MeImH, but it should be remembered that these Δδ values are calculated from the averaged C4/C5 signal for the latter two ligands. If the chemical shifts for uncoordinated ImH and 2-MeImH are taken from spectra in the solid state (29, 38), where fast tautomeric exchange does not take place, similar shift patterns are noted for the three compounds: all ring signals are moved downfield and all methyl signals upfield.

The ligand ^{1}H chemical shifts are highly solvent-sensitive: they can vary by as much as 1 ppm by going from a protic solvent to an aromatic one (29). Since the ^{1}H studies on the above Co(III) and Ni(II) compounds were conducted in DMSO and acetone, respectively, comparisons with these systems are less straightforward. In all our compounds, the H4 and H5 resonances are closer together. From the Δδ values (Table 3), H5 seems to be the most affected by complexation, showing a downfield shift of ~0.16 ppm, whereas H4 shows smaller upfield shifts. Again, these comparisons are made with respect to the averaged H4/H5 signals for ImH and 2-MeImH.

Both types of spectra for the non-stoichiometric 1,2-Me_2Im materials were identical to those of the nonprotonated form, indicating that the $[ReO(OH)(1,2\text{-}Me_2Im)_4]^{2+}$ ion is acidic enough to be dissociated in water. Complex decomposition eventually occurred, since aged water solutions showed extra signals for $[1,2\text{-}Me_2ImH]^+$ (pK_a ~7) (34). A ^{13}C CP-MAS

Can. J. Chem. Downloaded from www.nrcresearchpress.com by 203.198.23.82 on 09/08/12
For personal use only.

TABLE 4. ^{13}C NMR data of $[ReO_2L_4]^+$ cations in D_2O[a]

	L = ImH		L = 2-MeImH		L = 1,2-Me_2Im		
							Non-stoichiometric
	Free	Complex	Free	Complex	Free	Complex	Form II[b]
C2	136.0	137.3 (+1.3) (+1.0)[c]	145.9	148.6 (+2.7) (+3.4)[c]	146.2	148.9 (+2.7)	150.6
C4	121.8	128.1 (+6.3) (+1.3)[c]	121.3	130.6 (+9.3) (+4.5)[c]	125.0	129.6 (+4.6)	128.9
C5	121.8	118.5 (−3.3) (+3.2)[c]	121.3	117.0 (−4.3) (+0.7)[c]	121.5	122.0 (+0.5)	124.8
1-CH_3					33.3	32.3 (−1.0)	35.1
2-CH_3			12.4	11.5 (−0.9) (−3.0)[c]	11.3	10.2 (−1.1)	13.2

[a]In ppm, Δδ relative to free ligand within parentheses.
[b]CP-MAS spectrum.
[c]Δδ value with respect with respect to solid-state signals. ImH: C2, 136.3; C4, 126.8; C, 115.3 ppm (38). 2-MeImH: C2, 145.2; C4, 126.1; C5, 116.3; 2-CH_3 14.5 ppm (29).

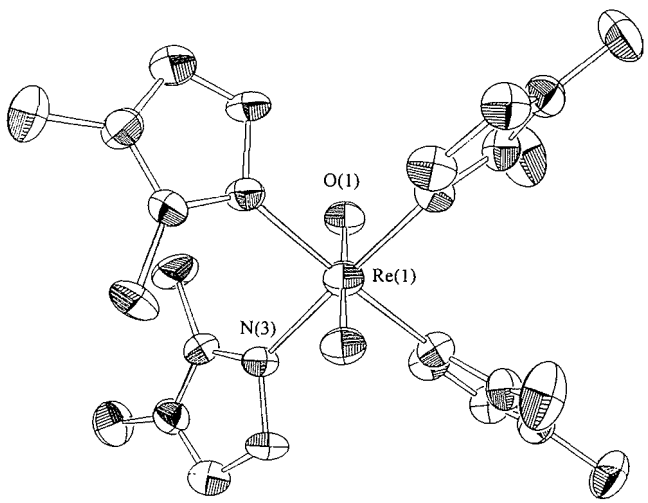

FIG. 1. ORTEP drawing of the *trans*-$[ReO_2(1,2\text{-}Me_2Im)_4]^+$ cation. Local symmetry at Re is *222* (D_2), the twofold axes lying along the O=Re=O bonds and bisecting the N—Re—N angles, respectively. Ellipsoids correspond to 50% probability. Hydrogens are omitted.

spectrum of form II was also recorded (Table 4) as an attempt to detect the presence of both neutral and protonated species. No splitting was observed and the δ values are in agreement with the solution data. Protonation of a remote Re=O group seems not to affect appreciably the ligand carbon resonances.

Crystal structures of the red-violet 1,2-dimethylimidazole compounds

The two types of crystals can be regarded as isostructural, the major building units being *trans*-$[ReO_2(1,2\text{-}Me_2Im)_4]^+$ cations and Cl^- anions. The cation (Fig. 1) occupies a site with crystallographic *222* (D_2) symmetry. The O=Re=O unit, lying on a crystallographic twofold axis, is perfectly linear. Selected distances and angles are listed in Table 5. The less accurate results from crystal II (Table S-4)[2] are not significantly different. The Re–ligand distances are normal (39–42). The steric effect of the imidazole 2-methyl group renders the Re(1)—N(3)—C(2) angle ~10° greater than Re(1)—N(3)—C(4) and displaces N(3) from the ReN_4 plane by 0.075 Å, producing a small tetrahedral distortion. The geometry of the imidazole itself is not affected (43*a*).[3]

Although the major Re species is *trans*-$[ReO_2(1,2\text{-}Me_2Im)_4]^+$, a significant number of these cations are found to be protonated. Besides the 24 $ReO_2(1,2\text{-}Me_2Im)_4$ units and the 24 "normal" Cl^- anions, there are 5.6 additional Cl^- in the unit cell of I and 8.6 ReO_4^- ions in that of II. As each such additional anion requires the presence of a protonated cation, the extent of protonation is 23% in I and 36% in II. Differences in Re–oxygen distances are expected between the O=Re—OH (33, 44) and the O=Re=O units, but since only 11% of the bonds in I and 18% in II are actually Re—OH, the extent of substitution is too small to produce a detectable variation of the average bond length or an elongated thermal ellipsoid (Fig. 1).

The structure shows interesting packing features. In Fig. 2, Re=O bonds in three $ReO_2(1,2\text{-}Me_2Im)_4$ units related by the threefold axis are directed toward a water molecule, with which they form hydrogen bonds. Our crystallographic results indicate that the occupancy in the W(1)/W(2) region is correlated with the number of extra anions near the origin and, consequently, with the extent of protonation of the $ReO_2(1,2\text{-}Me_2Im)_4$ unit. When the Re=O groups are not protonated, the water molecule occupies the W(1) site (*32* symmetry), at the intersection of the crystallographic twofold axes along O=Re=O. The W(1)—H···O(1) bonds

[3]The distances (not given in the paper) were calculated from the coordinates retrieved from the Cambridge Crystallographic Database of Organics and Organometallics (Refcode DIZZIV), ref. 43*b*.

Can. J. Chem. Downloaded from www.nrcresearchpress.com by 203.198.23.82 on 09/08/12
For personal use only.

TABLE 5. Distances and angles in form I

Bond lengths (Å)			
Re(1)—O(1)	1.761(5)	Re(1)—N(3)	2.140(4)
N(1)—C(2)	1.331(7)	N(1)—C(5)	1.359(8)
N(1)—C(11)	1.451(8)	N(3)—C(2)	1.325(7)
N(3)—C(4)	1.384(7)	C(2)—C(21)	1.480(9)
C(4)—C(5)	1.338(9)	MET–MET[d]	1.65(2)
Bond angles (deg)			
O(1)—Re(1)—O(1)[a]	180.0[f]	O(1)—Re(1)—N(3)	92.01(12)
O(1)—Re(1)—N(3)[a]	87.99(12)	O(1)—Re(1)—N(3)[b]	92.01(12)
O(1)—Re(1)—N(3)[c]	87.99(12)	N(3)—Re(1)—N(3)[a]	94.46(16)
N(3)—Re(1)—N(3)[b]	175.98(18)	N(3)—Re(1)—N(3)[c]	85.68(16)
N(3)[a]—Re(1)—N(3)[b]	85.68(16)	C(2)—N(1)—C(5)	108.8(5)
C(2)—N(1)—C(11)	125.2(5)	C(5)—N(1)—C(11)	125.9(5)
Re(1)—N(3)—C(2)	132.1(4)	Re(1)—N(3)—C(4)	121.4(4)
C(2)—N(3)—C(4)	106.5(4)	N(1)—C(2)—N(3)	109.5(5)
N(1)—C(2)—C(21)	123.6(5)	N(3)—C(2)—C(21)	126.9(5)
N(3)—C(4)—C(5)	108.7(5)		
Hydrogen bonds (Å)			
O(1)—W(1)	2.69(1)	O(1)—W(1)—O(1)[e]	120[f]
O(1)—W(2)	2.85(2)	O(1)—W(2)—O(1)[e]	110.0(8)

[a] $-x, 1/2-y, z$.
[b] $1/4-y, 1/4-x, 1/4-z$.
[c] $1/4+y, 1/4+x, 1/4-z$.
[d] $-x, -y, -z$, O—C distance in methanol solvent.
[e] y, z, x.
[f] Fixed by symmetry.

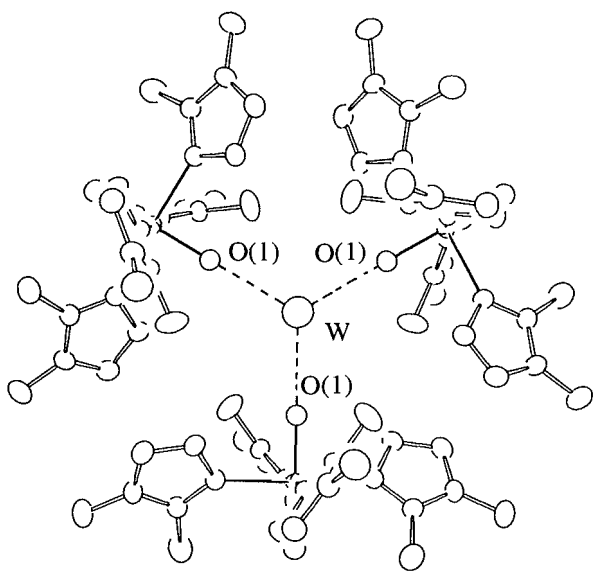

FIG. 2. Projection down the threefold axis showing water molecule W(1) with three hydrogen-bonded $[ReO_2(1,2\text{-}Me_2Im)_4]^+$ cations.

are moderately strong (2.69 Å) and the O(1)—W(1)—O(1) angles very favourable (120°). The two hydrogens in water molecule W(1) are obviously unable to form three hydrogen bonds at a time, so that the molecule is disordered over three orientations about the threefold axis. On the other hand, when one of the three Re=O groups in Fig. 2 is protonated, the water molecule remains on the threefold axis, but it no longer lies along the O=Re=O direction, probably to better accept the hydrogen bond from the bent Re—OH group. The O(1)—W(2) distance is then 2.85 Å and W(2) lies 0.88 Å above the plane through the three O(1) atoms.

Figure 3 shows the $0 < z < 1/4$ slice of the unit cell projected down the c axis. The "normal" Cl^- ion has an interesting environment, consisting only of imidazole C-H and $-CH_3$ hydrogens. This type of cation–anion interaction is probably restricted to N-methylated imidazoles, since ligands with N-H groups would impose a different pattern of interionic interactions. The pocket near the unit cell origin is extensively disordered. It contains the extra anion, or a solvent molecule when the anion is absent. Since the distances and angles involving the $ReO_2(1,2\text{-}Me_2Im)_4$ unit, Cl(1), W(2), and W(3) are essentially the same in both structures, the slightly greater cell edge found for II reflects the greater size of this pocket at origin: it is reasonable to assume that 0.54 ReO_4^- and 0.46 CH_2Cl_2 in form II take more space than 0.65 CH_3OH and 0.35 Cl^- ion form I.

Concluding remarks

Pure chloride salts of $[ReO_2L_4]^+$ were obtained with ImH and 2-MeImH. The fact that under similar conditions 1,2-Me_2Im led to a non-stoichiometric phase containing substantial amounts of $[ReO(OH)L_4]^{2+}$ can be related to four features of molecular packing: (*a*) the complex cations and water molecules form an efficient hydrogen-bonding framework, in which each water molecule interacts with three oxo or hydroxo groups; (*b*) the very high symmetry of the crystal allows both ends of the O-Re-O unit to participate in hydrogen bonding without forcing the Re-OH end to adopt a particular direction; (*c*) the structure contains a pocket near the origin, which can accommodate either the extra counter-anion or a solvent molecule; (*d*) since the ligand is devoid of hydrogen-bond donors, the environment of the "normal"

Can. J. Chem. Downloaded from www.nrcresearchpress.com by 203.198.23.82 on 09/08/12
For personal use only.

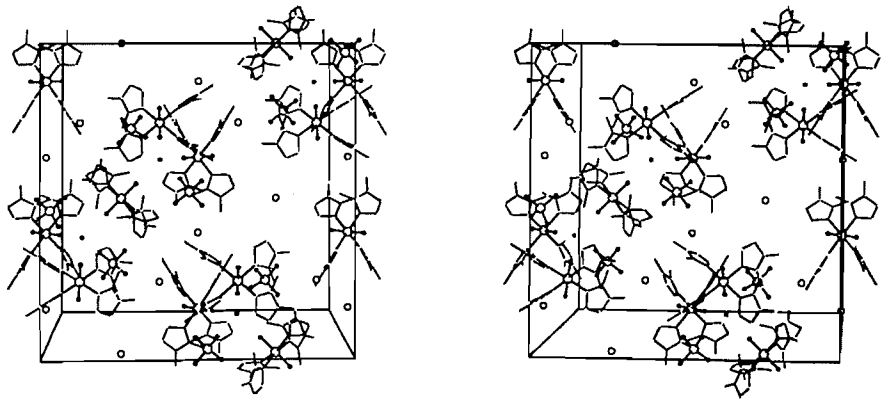

FIG. 3. Stereoview of the unit cell of form II down the c axis ($0 < z < 1/4$). Hydrogens are omitted for clarity. The isolated spheres are Cl^- ions (large) or water molecules (small). The tetrahedral ReO_4^- anion showed near the origin corresponds to one of two disordered orientations of this anion.

Cl^- counterion consists of ring or methyl C-H hydrogens only. For non-N1-methylated imidazoles, hydrogen bonding with the N1-H groups should impose a totally different architecture, in which such favourable conditions could hardly be achieved, so that more conventional stoichiometric materials, protonated or not depending on pH, will probably be isolated.

Chloride salts of various $[ReO_2L_4]^+$ cations have been found to show some instability (19). With 7-azaindole, replacing Cl^- by I^- improved stability (23), but this does not seem to be the case with pyridines (14). For cyclam, the iodide of the monoprotonated complex decomposed during recrystallization and X-ray diffraction work had to be done on the ReO_4^- salt (33). Brewer and Gray (14) noted that salts with larger noncoordinating counter-anions made the compound more resistant to ligand loss. Work is underway to obtain complexes with a variety of imidazoles with other counter-anions, in order to study their acid–base and optical properties.

Acknowledgments

We wish to thank M. Simard and F. Bélanger-Gariépy for assistance in collecting the X-ray data, C. Roux for preparing some of the samples, and S. Bélanger for valuable discussions.

1. J.T. Meyer. J. Electrochem. Soc. **131**, 221c (1984).
2. R.H. Holm. Chem. Rev. **87**, 1401 (1987).
3. D.W. Pipes and T.J. Meyer. Inorg. Chem. **25**, 3256 (1986).
4. M.S. Ram, C.S. Johnson, R.L. Blackbourn, and J.T. Hupp. Inorg. Chem. **29**, 238 (1990).
5. W. Liu, T.W. Welch, and H.H. Thorp. Inorg. Chem. **31**, 4044 (1992).
6. M.S. Ram, L.M. Jones, H.J. Ward, Y.H. Wong, C.S. Johnson, P. Subramanian, and J.T. Hupp. Inorg. Chem. **30**, 2928 (1991).
7. J.R. Winkler and H.B. Gray. Inorg. Chem. **24**, 346 (1985).
8. J. Singh, A.K. Powell, S.E.M. Clarke, and P.J. Blower. J. Chem. Soc. Chem. Commun. 1115 (1991).
9. E. Deutsch, K. Lisbon, J.L. Vanderheyden, A.L. Ketring, and H.R. Maxon. Nucl. Med. Biol. **13**, 465 (1986).
10. E. Deutsch, K. Lisbon, and J.L. Vanderheyden. *In* Technetium and rhenium in chemistry and nuclear medicine. *Edited by* N. Nicolini, G. Pandoli, and U. Mazzi. Raven Press, New York, and Cortina International, Verona. 1990. p. 13.
11. B.K. Keppler, D. Wehe, H. Endres, and W. Rupp. Inorg. Chem. **26**, 844 (1987).
12. B.K. Keppler, W. Rupp, U.M. Juhl, H. Endres, R. Neibl, and W. Balzer. Inorg. Chem. **26**, 4366 (1987).
13. H.H. Thorp, N.J. Turro, and H.B. Gray. New J. Chem. **15**, 601 (1991).
14. J.C. Brewer and H.B. Gray. Inorg. Chem. **28**, 3334 (1989).
15. N.P. Johnson, C.J.L. Lock, and G. Wilkinson. J. Chem. Soc. 1054 (1964).
16. G.W. Parshall, L.W. Shive, and F.A. Cotton. Inorg. Synth. **17**, 110 (1977).
17. R.E. Hoffman and D.B. Davies. Magn. Reson. Chem. **26**, 523 (1988).
18. N.P. Johnson, F.I.M. Taha, and G. Wilkinson. J. Chem. Soc. 2614 (1964).
19. M.C. Chakravorty. J. Indian Chem. Soc. **47**, 827 (1970).
20. F. Bélanger-Gariépy and A.L. Beauchamp. J. Am. Chem. Soc. **102**, 3461 (1980).
21. International tables for crystallography. Vol. A. Reidel, Dordrecht. 1983.
22. E.J. Gabe, Y. Le Page, J.P. Charland, and F.L. Lee. NRCVAX, an interactive program system for structure analysis. J. Appl. Crystallogr. **22**, 384 (1989).
23. A.M. Lebuis and A.L. Beauchamp. Can. J. Chem. **71**, 2060 (1993).
24. C. Perchard, A.M. Bellocq, and A. Novak. J. Chim. Phys. **62**, 1344 (1965).
25. A.M. Bellocq, C. Perchard, A. Novak, and M.L. Josien. J. Chim. Phys. **62**, 1334 (1965).
26. M. Cordes and J.L. Walter. Spectrochim. Acta, **24A**, 237 (1968).
27. J.B. Hodgson, G.C. Percy, and D.A. Thornton. J. Mol. Struct. **66**, 75 (1980).
28. C. Perchard and A. Novak. Spectrochim. Acta, **23A**, 1953 (1967).
29. G. Levasseur. M.Sc. Thesis, Université de Montréal, Montréal (1990).
30. B. Jezowska-Trzebiatowska, J. Hanuza, and M. Baluka. Spectrochim. Acta, **27A**, 1753 (1971).
31. C. Perchard and A. Novak. J. Chim. Phys. **65**, 1964 (1968).
32. J.B. Hodgson, G.C. Percy, and D.A. Thornton. J. Mol. Struct. **66**, 81 (1980).
33. B.W. Tsang, J. Reibenspies, and A.E. Martell. Inorg. Chem. **32**, 988 (1993).
34. M.R. Grimmett. Comprehensive heterocyclic chemistry. Vol. 5. *Edited by* A.R. Katritzki and C.W. Rees. Pergamon Press, Oxford. 1984. Chap. 4.06.
35. Y. Takeuchi, H.J.C. Yeh, K.L. Kirk, and L.A. Cohen. J. Org. Chem. **39**, 357 (1974).

Can. J. Chem. Downloaded from www.nrcresearchpress.com by 203.198.23.82 on 09/08/12
For personal use only.

36. W.W. Henderson, R.E. Shepherd, and J. Abola. Inorg. Chem. **25**, 3157 (1986).
37. J.P. Costes, G. Commenges, and J.P. Laurent. Inorg. Chim. Acta, **134**, 237 (1987).
38. J. Elguero, A. Fruchier, and V. Pellegrin. J. Chem. Soc. Chem. Commun. 1207 (1981).
39. C. Calvo, N. Krishnamachari, and C.J.L. Lock. J. Cryst. Mol. Struct. **1**, 161 (1971).
40. C.J.L. Lock and G. Turner. Acta Crystallogr. Sect. B: Struct. Crystallogr. Cryst. Chem. **B34**, 923 (1978).
41. V.S. Sergienko, M.A. Porai-Koshits, and T.S. Khodaskova. J. Struct. Chem. **15**, 250 (1974).
42. S.A. Luna, C. Bolzati, A. Duatti, G.L. Zucchini, G. Bandoli, and F. Refosco. Inorg. Chem. **31**, 2595 (1992).
43. (*a*) K.D. Karlin, R.W. Cruse, J.W. McKown, J.C. Hayes, P.L. Dahlstrom, and J. Zubieta. Trans. Met. Chem. (London), **9**, 404 (1984); (*b*) F.H. Allen, O. Kennard, and R. Taylor. Acc. Chem. Res. **16**, 146 (1983).
44. W. Purcell, A. Roodt, S.S. Basson, and J.G. Leipoldt. Trans. Met. Chem. (London), **14**, 5 (1989).

Can. J. Chem. Downloaded from www.nrcresearchpress.com by 203.198.23.82 on 09/08/12
For personal use only.

A simple apparatus for the study of experimental fractal structures in gaseous dielectric breakdown

J. LOGAN, J. TREURNIET, AND A.D.O. BAWAGAN[1]
Ottawa–Carleton Chemistry Institute, Carleton University, Ottawa, ON K1S 5B6, Canada

S. RIZZETTO AND J.M. BRAUN
Ontario Hydro Research Division, 800 Kipling Ave., Toronto, ON M8Z 5S4, Canada

AND

B.D. AGUDA
Department of Chemistry, University of Waterloo, Waterloo, ON N2L 3G1, Canada

Received June 14, 1993

J. LOGAN, J. TREURNIET, A.D.O. BAWAGAN, S. RIZZETTO, J.M. BRAUN, and B.D. AGUDA. Can. J. Chem. **71**, 2079 (1993).

An apparatus for the study of the discharge patterns generated in gaseous dielectric breakdown is described. The discharge patterns are imaged using a fast optical imaging system (≈ 40 ns exposure time) and are found to be fractals. The experimental fractal dimension obtained using a +17 kV pulse in air at atmospheric pressure is $D_{expt} \approx 1.8 \pm 0.1$, which is in very good agreement with previous studies.

J. LOGAN, J. TREURNIET, A.D.O. BAWAGAN, S. RIZZETTO, J.M. BRAUN et B.D. AGUDA. Can. J. Chem. **71**, 2079 (1993).

On décrit un appareil permettant d'étudier les patrons de décharge générés lors de décharges diélectriques gazeuses. On obtient l'image des patrons de décharge en faisant appel à un système d'imagerie optique rapide (≈ 40 ns de temps d'exposition) et on a trouvé qu'ils sont de nature fractale. La dimension fractale expérimentale obtenue en utilisant une pulsation de +17 kV, dans l'air, à la pression atmosphérique, $D_{exp} \approx 1{,}8 \pm 0{,}1$, est en très bon accord avec les valeurs obtenues antérieurement.

[Traduit par la rédaction]

1. Introduction

A high-voltage discharge generates a "tree-like" or branched pattern, which is commonly described as a random structure. Recent studies (1, 2), however, have indicated that these tree-like structures can be described as a fractal or self-similar pattern (3) in what is now known as the dielectric breakdown (DB) model (1). For a fractal structure in two dimensions the total length $N(r)$ of all branches inside a circle of radius, r, is related as follows:

[1] $$N(r) \approx r^D$$

Clearly, a plot of log N versus log r will yield a linear relationship characterized by a slope equal to D, or what is referred to as the fractal dimension or the Hausdorff dimension (3, 4).

A significant amount of theoretical work has led to an understanding of a wide range of physical phenomena characterized by some stochastic feature in one way or another. Several reviews are available in the literature (5). In particular, the qualitative description of dielectric breakdown of gases in terms of fractals has paved the way to a systematic study of such structures. By extension of these pioneering studies (1) to other chemical systems, the determination and elucidation of various fractal parameters in dielectric breakdown are now feasible.

Our interest in the description of dielectric breakdown of gases in terms of fractals stems from practical and fundamental reasons. An understanding of dielectric breakdown is motivated by an urgent need for *quantitative* models of gas insulating systems (6), which are essential components of electrical power delivery installations. The economic importance of proper design of gas insulating systems can therefore not be overemphasized. Of more basic interest is the introduction of a new mathematical language (i.e., the language of fractals) that allows us to study such seemingly disparate chemical processes (5) as diffusion-limited aggregation, electrodeposition, soot formation, and dielectric breakdown. The language of fractals in itself has brought significant understanding of "old problems" such as turbulence and phase transitions (7). It is foreseeable that the language of fractals will also provide the necessary descriptive tools that would allow us to unravel many more very complex phenomena such as, for example, electron–electron

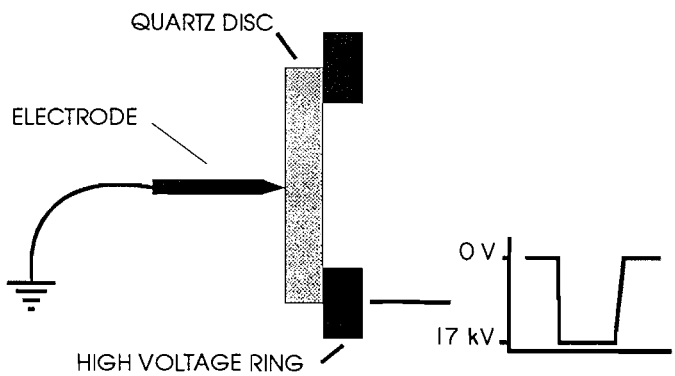

FIG. 1. Basic schematic for the generation of a surface-leader discharge. A positive high voltage is effectively introduced to the electrode by "grounding" the electrode. As the thyratron (see Fig. 2) switches on, the normally grounded ring goes negative. This produces a potential between the electrode and the ring that is of *positive* polarity.

[1]Author to whom correspondence may be addressed.

Can. J. Chem. Downloaded from www.nrcresearchpress.com by 203.198.23.82 on 09/08/12
For personal use only.

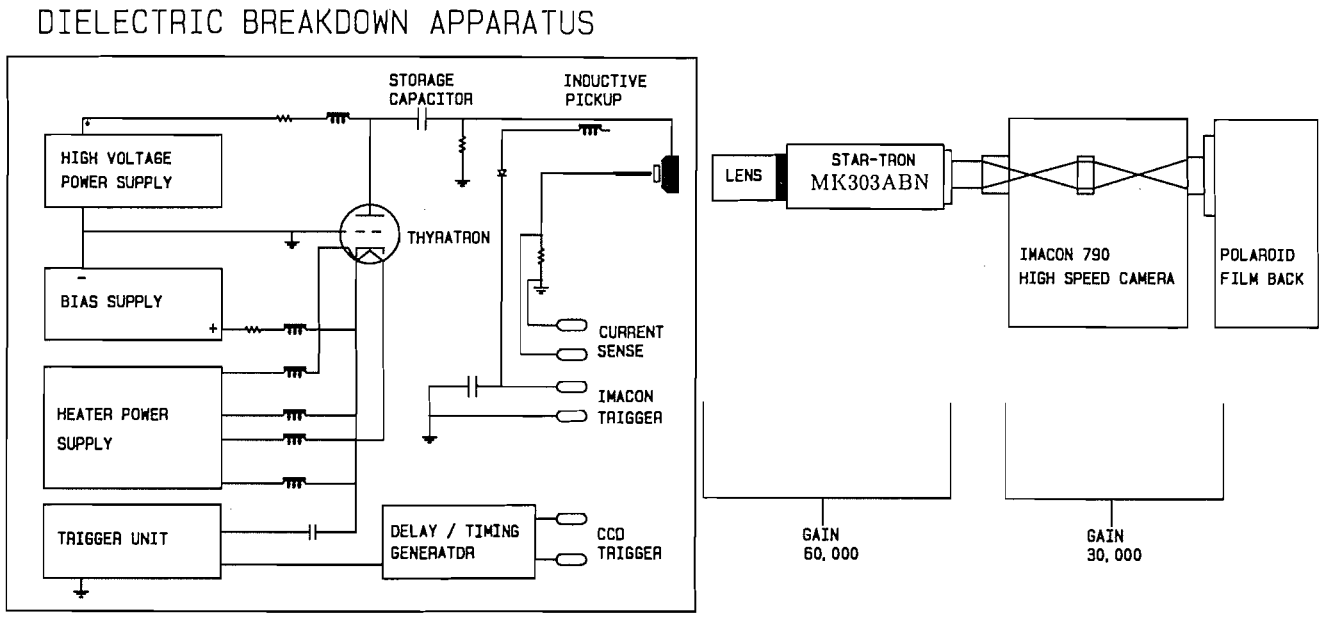

FIG. 2. Schematic of the dielectric breakdown apparatus (Carleton University) and the optical imaging system (Ontario Hydro Research Division). See text for details.

Can. J. Chem. Downloaded from www.nrcresearchpress.com by 203.198.23.82 on 09/08/12
For personal use only.

many–body interactions (8). However, the more immediate goal of the present investigation is to provide a "phenomenological link" between microscopic gas phase information (e.g., photoionization cross sections, reaction rates, thermal relaxation rates, etc.) and the macroscopic structures generated in a surface-leader discharge. Although at first glance this may appear as a daunting task, recent theoretical investigations (9), indicate that the language of fractals has made small but significant advances.

In the present paper we describe an apparatus for the generation of experimental fractals using a high-voltage discharge. The general schematic of the instrument and representative experimental fractal images are presented. A significant advantage of the present experiment compared to that conducted by Niemeyer et al. (1) is the capability to produce time-resolved images of the dielectric breakdown in the nanosecond range. The result is unprecedented since earlier published results (1) dealt with dielectric breakdown images that are time-integrated photographs in the microsecond range. The central result of the present work is to show that the time development of the dielectric breakdown is also a fractal, as revealed by an analysis of each single frame.

Computer-generated fractal images based on the DB model of Niemeyer et al. (1) are also presented. The DB model treats the growths of the dielectric breakdown patterns as a random process with the growth probability directly proportional ($\eta = 1$) to the local electric fields. The DB model is actually very general ($\eta \geq 0$) and can be applied to other problems by varying η. For example, as $\eta \sim 0$ the Eden model is recovered (1).

2. Description of apparatus

The gaseous dielectric breakdown experiment is shown schematically in Fig. 1. A positive high-voltage pulse (+17 kV, 1 μs width) is introduced to a sharp stainless steel electrode that is located in the center of a quartz disc (2 mm thick). The positive input voltage is referenced relative to a stainless steel ring (20 mm inner radius) situated at the rim of the quartz disc. The leader[2] surface discharge that results is observed from the back side of the quartz disc. The arrangement is very similar to the arrangement introduced by Niemeyer et al. (1) except that the present experiments are conducted in air at atmospheric pressure as opposed to high pressure SF_6. To a good approximation, this arrangement produces an equipotential channel system growing in a plane. The growth is therefore two-dimensional even though the electric field lines are three-dimensional (1).

The details of the high-voltage electronics and fast optical imaging system are shown in Fig. 2. The high-voltage electronics and breakdown apparatus were fabricated at Carleton University whereas the fast optical imaging system was provided by the Ontario Hydro Research Division. The fast high-voltage pulse is generated using a stable high-voltage DC supply (Brandenburg 25-P), a storage capacitor (1300 pF), and a grounded grid thyratron (EG&G HY-1102). The low impedance and stable switching ability of the thyratron allow the reproducible production of fast high-voltage pulses ($t_{rise} \approx 30$ ns). A bias supply and a heater are attached to the thyratron to maintain stable and consistent switching capability. The dielectricc breakdown apparatus can be triggered in two ways. First, a hand-held trigger is used with a delay/timing generator. This mode is used when a slow optical device like a charge-coupled device (CCD) camera (exposure time ≥5 ms) is employed to photograph the discharge patterns. Second, an inductive pickup device is used when a fast optical device like the IMACON streak camera (exposure time ≤1 μs) is employed to photograph the discharge patterns. The whole apparatus is housed and shielded in a mobile 19.5-in. electronics rack.

The fast optical imaging system is composed of several optical devices coupled together to achieve the maximum possible gain (Fig. 2). Because of the small exposure times necessary to ob-

[2]The microscopic processes involved in a surface discharge are called streamers and leaders (9, 10). The initial process involves the formation of streamers, which have very low optical luminosity, followed by the leader discharge, which is of higher luminosity. The final stage is referred to as the "spark-over," which is characterized by extreme brightness and sometimes a "sonic boom." The current experiments are concerned only with the streamer and leader processes (i.e., pre-breakdown).

Can. J. Chem. Downloaded from www.nrcresearchpress.com by 203.198.23.82 on 09/08/12
For personal use only.

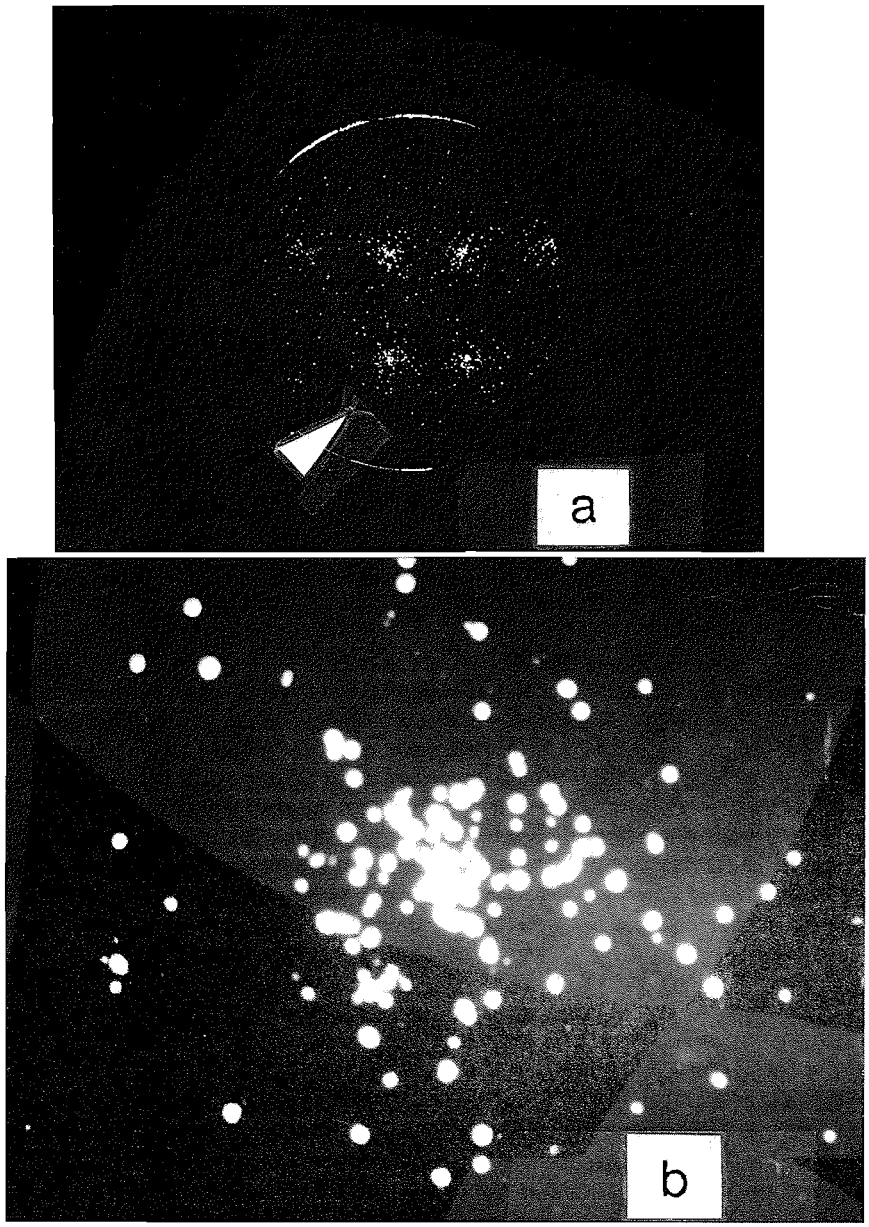

FIG. 3. (*a*) Time-resolved IMACON images generated by a fast +17 kV pulse. Exposure time is ≈40 ns per frame. See text for details. (*b*) Expanded view of a selected frame (indicated by arrow) of the IMACON image.

serve the streamer-leader discharge and the low visible photon flux generated during the pre-breakdown period, a total gain of $\geq 10^5$ was necessary. A macro lens (Canon) is attached to the back end of the quartz disc (Fig. 1) and after this an image intensifier (Star-Tron MK 303ABN) operated at maximum gain (≈60 000) was used. The image generated by the Star-Tron MK 303ABN is then photographed using a streak camera (IMACON 790 with IMACON 50/40 Intensifier) operated in framing mode with an exposure time of 40 ns per frame. The IMACON camera is triggered by inductive pickup from the dielectric breakdown apparatus. A total of 6–8 frames are generated for each single discharge and these frames are permanently recorded on Polaroid 612 film (20 000 ASA). The interframe time difference is ~160 ns, thus giving a total time record of 1600 ns for 8 frames (i.e., for each discharge).

3. Results and discussion

3.1 Characteristics of high-voltage pulse

An oscilloscope trace of the high-voltage pulse (+17 kV) generated using our apparatus was obtained. The estimated rise time (10% to 90%) is approximately 30 ns and the pulse duration is 1–3 μs. The variation in the pulse duration is due to the stochastic nature of the discharge. The current is dissipated from the quartz disc whenever the streamer–leader discharge reaches the rim of the disc (i.e., at "spark-over"). Careful shielding and high-voltage protection were necessary to generate reproducible fast high-voltage pulses. In practice, 2 min were made to elapse between discharges to allow the dielectric breakdown apparatus and the fast optical imaging system to stabilize. In the present application, it is also important to prevent the resulting discharge from overloading the optical imaging system. The dielectric breakdown apparatus was carefully calibrated to determine the spark-over conditions and to set the high voltage slightly *below* this value. The optimum condition was obtained for +17 kV. Changes in the thickness of the quartz disc will clearly change this optimum high voltage.

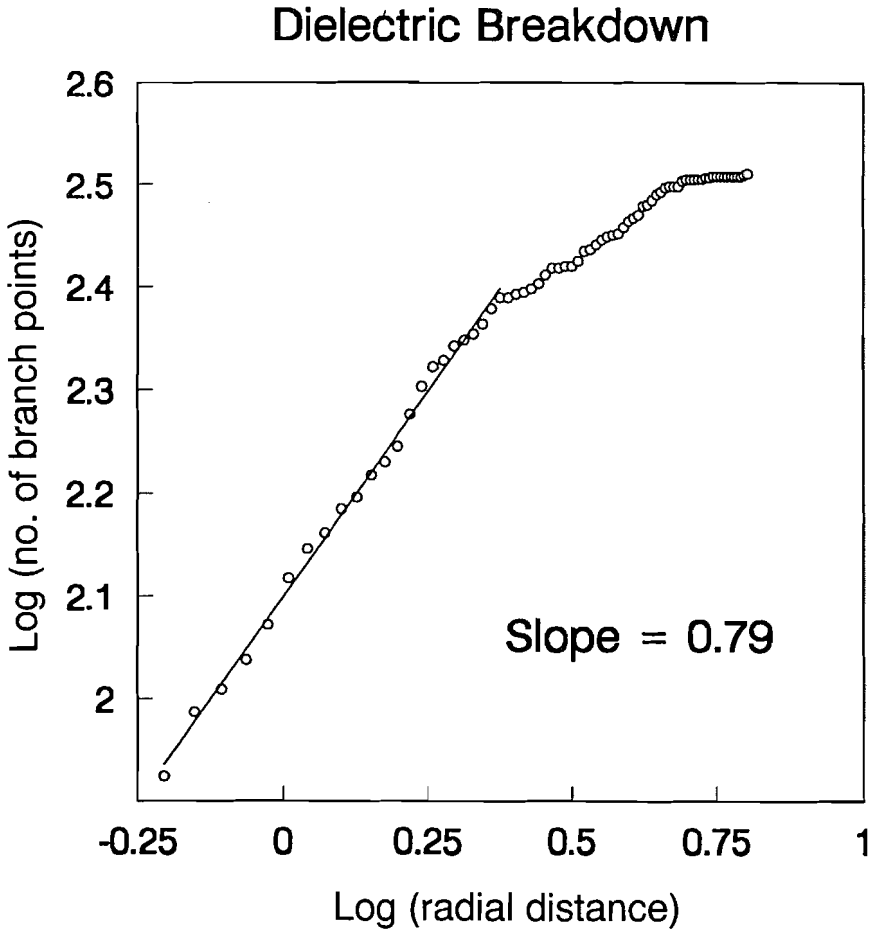

FIG. 4. Experimental fractal dimension of the time-resolved dielectric breakdown images. The number of branch points $b(r)$ occurring within a radial distance r is plotted in logarithmic scale. The experimental fractal dimension obtained from the slope is $D_{expt} \approx 1.8 \pm 0.1$. The estimated uncertainty corresponds to statistical limits and does not include systematic errors.

3.2 Experimental fractal patterns

An example of the IMACON images obtained from the dielectric breakdown apparatus is shown in Fig. 3*a*. One of the frames (indicated by an arrow) is enlarged and shown in Fig. 3*b*. The images obtained in the present experiment have an exposure time of 40 ns, in stark contrast to the images obtained by Niemeyer et al. (1), which are *time-integrated* and are equivalent to ≈1 μs exposure time. The resulting images were analyzed using a PC-based digitizer (Sigmascan JS-2). Each point on the IMACON image was digitized[3] and the radial distance from the electrode point was calculated. A log–log plot of the number of points, $b(r)$, as a function of the radial distance, r, is shown in Fig. 4. The linear relation obtained at $-0.5 \leq \ln r \leq 1.0$ clearly indicates that the time-resolved dielectric breakdown images are indeed *fractal images*. The points in the IMACON images (Fig. 3) are interpreted as the branch points, $b(r)$, of the surface-leader discharge. This is very plausible, especially in consideration of the detailed microscopic mechanism of streamer–leader formation. Spectroscopic studies by Gallimberti et al. (10) revealed that the brightest (in the visible range) region of the streamer–leader is the *tip* of the growing streamer–leader formation. The tip is essentially the growth point for new streamers and may be considered a branch point. It can then be argued that the number of branch points $b(r)$ at large enough values of r is proportional to the number of branches, which in turn is related to $N(r)$ (1):

$$[2] \quad b(r) \approx \frac{dN(r)}{dr} \approx r^{D-1}$$

and the slope of log b versus log r would then be equal to $D - 1$. Equation [2] involves several assumptions and a more rigorous derivation is presented elsewhere.[5] This result, which was originally derived by Niemeyer et al. (1), requires further theoretical investigation and is beyond the scope of the present study. Nevertheless it should be noted that the main result of the present work is to illustrate the fractal nature of the dielectric breakdown images at short exposure times (see Fig. 4). The calculated slope for the IMACON images is ≈0.8 (see Fig. 4) which gives an experimental fractal dimension, $D_{expt} \approx 1.8 \pm 0.1$,[4] based on eq. [2]. This experimental value is in very close agreement with the fractal dimension ($D_{theor} = 1.75$) predicted and also observed experimentally by Niemeyer and co-workers (1, 11) using time-

[3]Some faint points may not be visible in Fig. 3.

[4]The estimated error limits are statistical errors based on several discharge patterns and do not include systematic errors.

[5]J. Treurniet, D. McKay, B.D. Aguda, and A.D.O. Bawagan. To be published.

Can. J. Chem. Downloaded from www.nrcresearchpress.com by 203.198.23.82 on 09/08/12
For personal use only.

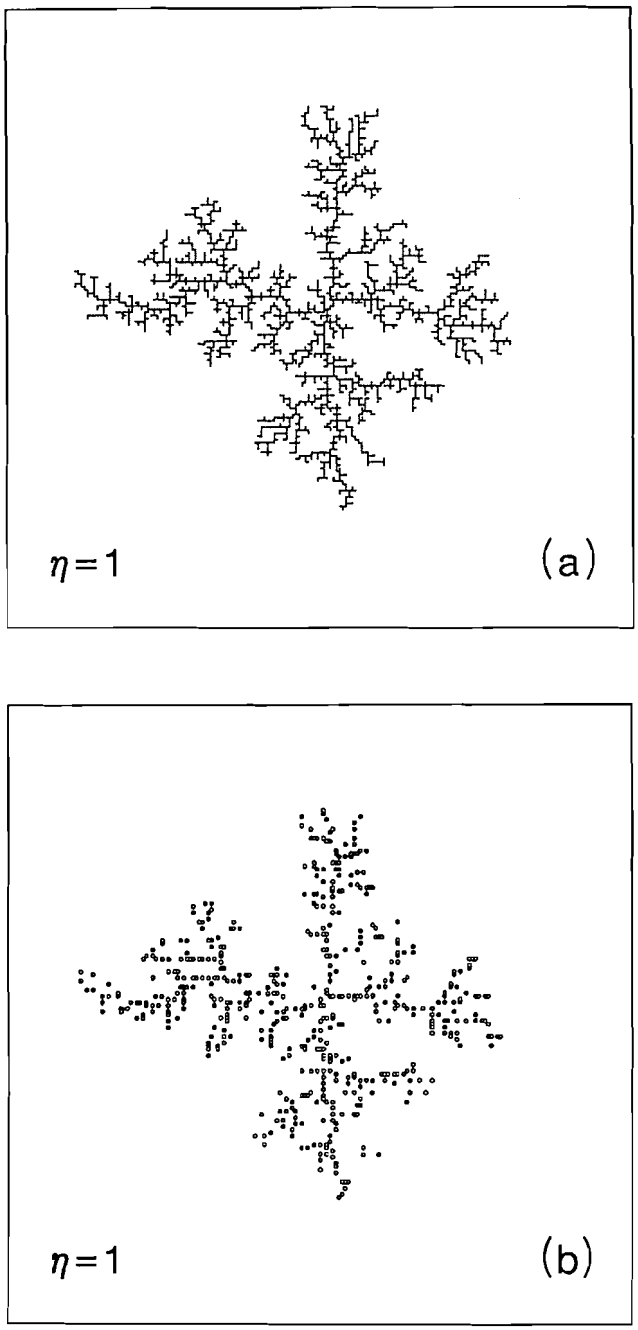

FIG. 5. Computer simulation of the dielectric breakdown images using the DB model of Niemeyer et al. (1). (*a*) Simulation of dielectric breakdown using $\eta = 1$ and 2270 points. Further details, see footnote 5. (*b*) Reproduction of Fig. 5*a* but displaying only the branch points (open circles). The exact relationship between dielectric breakdown IMACON images (Fig. 3) and the simulated branch points is currently under detailed investigation; however, some similarity can be noted.

integrated DB images. Using the theoretical stochastic model proposed by Niemeyer et al. (1), we have also developed a computer program to simulate the dielectric breakdown phenomenon and the results are shown in Fig. 5. We obtain a theoretical fractal dimension of $D_{\text{theor}} = 1.76 \pm 0.03$ based on five simulations reproducing the earlier results of Niemeyer et al. (1). Further analysis of the experimental fractals and the details of the computer simulation will be reported in a separate paper.[5] It should be noted that each frame in Fig. 3*a* corresponds to a 40 ns time slice of a single growing discharge. By summing each of the frames a "time-integrated image" with branched structure is recovered[5] that is analogous to that obtained in previous time-integrated studies (1, 11).

4. Conclusions

In summary, we have developed a dielectric breakdown apparatus coupled to a fast optical imaging system capable of producing *short exposure time* images (~40 ns) of the streamer–leader discharge pattern produced by a +17 kV pulse in air at atmospheric pressure. Preliminary analyses reveal that these images are fractals, which can be characterized by a fractal dimension of $D_{\text{expt}} \approx 1.8 \pm 0.1$. This is in close agreement with previous experimental and theoretical studies (1) of gaseous dielectric breakdown. Future experiments will involve more accurate measurements of the experimental fractal dimensions as well as the fractal dimensions for high-voltage discharges in different chemical environments.

Acknowledgements

We would like to thank D. McKay for assistance in the computer simulation diagrams. This work was funded by the Natural Sciences and Engineering Research Council (NSERC) of Canada.

1. L. Niemeyer, L. Pietronero, and H.J. Wiesman. Phys. Rev. Lett. **52**, 1033 (1984); Phys. Rev. Lett. **57**, 650 (1986).
2. Y. Sawada, S. Ohta, M. Yamazaki, and H. Honjo. Phys. Rev. A, **26**, 3557 (1982).
3. B. Mandelbrot. Fractals: form, chance and dimension. Freeman, San Francisco, Calif. 1977.
4. F. Hausdorff. Math. Ann. **79**, 157 (1919); H.E. Stanley. J. Phys. A, **10**, L211 (1977).
5. H.E. Stanley and N. Ostrowsky (*Editors*). Growth and form. Martinus Nijhoff, Dordrecht. 1985; L. Pietronero and E. Tosatti (*Editors*). Fractals in physics. North Holland, Amsterdam. 1986; P. Meakin. *In* Phase transitions and critical phenomena. Vol. 12. *Edited by* C. Domb and J. Lebowitz. Academic Press, New York. 1988.
6. L. Niemeyer. *In* Gaseous dielectrics. Vol. VI. *Edited by* L.G. Christophorou and I. Sauers. Plenum Press, New York. 1991.
7. B.B. Mandelbrot. Lect. Notes Phys., **12**, 333 (1972).
8. A.D.O. Bawagan, B.J. Olsson, K.H. Tan, J.M. Chen, and B.X. Yang. Chem. Phys. **164**, 283 (1992); S.J. Desjardins, A.D.O. Bawagan, and K.H. Tan. Chem. Phys. Lett. **196**, 261 (1992).
9. L. Pietronero and H.J. Wiesman. Z. Phys. B: Condens. Matter, **70**, 87 (1988).
10. I. Gallimberti. J. Phys. (Paris), **40**, C7-193 (1979); I. Gallimberti, J.K. Hepworth, and R.C. Klewe. J. Phys. D, **7**, 880 (1974).
11. N. Femia, L. Niemeyer, and V. Tucci. J. Phys. D, **26**, 619 (1993).

Can. J. Chem. Downloaded from www.nrcresearchpress.com by 203.198.23.82 on 09/08/12
For personal use only.

Isotope effects in nucleophilic substitution reactions. IX. The effect of bond strength on substituent effects on the structure of S_N2 transition states

KENNETH CHARLES WESTAWAY
Chemistry Department, Laurentian University, Sudbury, ON P3E 2C6, Canada

Received January 4, 1993[1]

KENNETH CHARLES WESTAWAY. Can. J. Chem. **71**, 2084 (1993).

The effects of substituents on the structure of S_N2 transition states suggested by kinetic isotope effects and Hammett ρ values are often different and, moreover, often do not agree with substituent effects predicted by current theories whether the change in substituent is made in the nucleophile, in the leaving group, or at the α-carbon. The importance of the strength of the reacting bonds in determining the effects of substituents on transition-state structure is investigated. A bond strength hypothesis that suggests there will be a significant change in the weaker reacting bond but little or no change in the stronger reacting bond in an S_N2 transition state when a substituent in the nucleophile, the substrate, or the leaving group is altered in an S_N2 reaction, predicts a high percentage of the experimental results.

KENNETH CHARLES WESTAWAY. Can. J. Chem. **71**, 2084 (1993).

Les effets des substituants sur la structure des états de transition S_N2 suggérés par les effets isotopiques cinétiques et par les valeurs ρ de Hammett sont souvent différents et, de plus, ils ne sont pas en accord avec les effets de substituants prédits par les théories actuelles que le changement de substituant soit fait dans le nucléophile, le groupe partant ou au niveau du carbone α. On a étudié l'importance de la force des liaisons qui réagissent pour évaluer les effets de substituants sur la structure de l'état de transition. Une hypothèse de force de liaison qui suggère que, pour un état de transition S_N2 dans lequel on modifie le nucléophile, le substrat ou le groupe partant, on observera un changement important si la liaison réagissante est faible mais peu ou pas de changement avec une liaison réagissant plus forte permet de prédire un fort pourcentage des résultats expérimentaux.

[Traduit par la rédaction]

Introduction

Chemists have been trying to determine and rationalize the effects of substituents on the structure of S_N2 transition states, eq. [1], for some time (1–10). The most useful tools for determining substituent effects on transition-state structure are kinetic isotope effects and linear free energy relationships. For example, Westaway and co-workers (11, 12) used these techniques to model the transition states of two different series of S_N2 reactions in some detail and were able to show how substituents in the leaving group, and at the α-carbon, alter the lengths of both the nucleophile–α-carbon and the α-carbon – leaving group bonds in S_N2 transition states. In spite of (*i*) these and other studies that have determined substituent effects experimentally (1, 2, 6–25), (*ii*) several theoretical studies (26–31), and (*iii*) several semi-empirical methods that have attempted to describe how substituents affect transition-state structure by altering the vibrational modes of the transition-state (32, 33) or the energy surface for the reaction (9, 34–37), the effects of substituents on the structure of S_N2 transition states are not well understood.

[1] $$Nu:^- + -\overset{|}{\underset{|}{C}}-L \longrightarrow [Nu^{\delta-} \cdots \overset{|}{\underset{|}{C}} \cdots L^{\delta-}]^{\ddagger -} \longrightarrow Nu-\overset{|}{\underset{|}{C}}- + L:^-$$

One of the problems in determining substituent effects on transition-state structure is that most of the studies have only indicated how a substituent affects one of the reacting bonds in the S_N2 transition state and give no information about the behaviour of the other reacting bond (2, 6, 7). Thus, one does not know how the total transition state is altered when a substituent is changed. An even greater problem is that the effects of substituents on the structure of S_N2 transition states found in similar systems are not the same. Finally, the theories that are most commonly used to predict substituent effects on transition-state structure (9, 32–37) often fail to predict the substituent effects suggested by experimental data when they are tested in detail (11, 12).

It is important that the systems used to assess substituent effects on the transition-state structure of S_N2 reactions are chosen carefully. In fact, we have only considered systems in which the *meta* or *para* substituent on a benzene ring that is bonded to the α-carbon or to the nucleophilic atom of the nucleophile or leaving group of an S_N2 reaction has been changed. This ensures that the observed substituent effects are the result of the electronic effects of the substituents and eliminates systems in which the structural change(s) in the transition state might be the result of other influences, for example, differences in the steric requirements of the two reactions or changes in solvation of the transition states.

Kinetic isotope effects and Hammett ρ values are widely used to deduce the structure of the S_N2 transition state. A larger heavy-atom leaving group kinetic isotope effect indicates a longer α-carbon – leaving group bond in the transition state (38), a larger Hammett $|\rho|$ value found by changing a substituent in the nucleophile (leaving group) is indicative of a shorter nucleophile–α-carbon (longer α-carbon – leaving group) transition-state bond[2] (12, 42), and the

[1]Revision received August 13, 1993.

[2]Hoz et al. (39) used the results of calculations on homolytic cleavage reactions to question the use of Hammett ρ values to determine transition-state structure. However, many workers are currently using linear free energy relationships such as ρ values to indicate differences in transition-state structure (40, 41). Although there is no experimental proof to show which position is correct, the author believes that ρ values found in closely related systems like those used in this study (vide infra) are related to transition-state structure. It is worth noting that ρ values have only been used in five out of the 37 reaction series used to test the bond strength hypothesis and, in two of the five systems, the changes in transition-state structure suggested by the ρ values have been confirmed by kinetic isotope effects (11, 12).

Can. J. Chem. Downloaded from www.nrcresearchpress.com by 203.198.23.82 on 09/08/12
For personal use only.

TABLE 1. The change in the nucleophile–α-carbon and α-carbon – leaving group transition-state bonds based on the change found in the isotope effects and Hammett ρ values when a substituent was changed in an S_N2 reaction

Change in transition-state structure predicted from isotope effects and (or) ρ values	The effect of changing to a better nucleophile[a]	The effect of adding a more electron-donating group to the α-carbon[b]	The effect of changing to a better leaving group[c]
A longer Nu--C_α bond	2	3	4
A shorter Nu--C_α bond	2	3	4
No change in the Nu--C_α bond	0	0	0
A longer C_α--L bond	0	5	0
A shorter C_α--L bond	4	1	0
No change in the C_α--L bond	3	5	1

[a]When a better nucleophile is used in an S_N2 reaction, the Nu--C_α bond is shorter in two reaction series and longer in two others. In the seven reaction series where the length of the C_α--L bond was determined, the C_α--L bond was shorter in four reaction series and did not change in three other reaction series when a better nucleophile is used.

[b]When a more electron-donating substituent is added to the phenyl group on the α-carbon of an S_N2 reaction, the Nu--C_α bond is longer in three reaction series and shorter in three others. When the C_α--L bond was monitored and a more electron-donating substituent was on the phenyl group on the α-carbon, the C_α--L bond was longer in five reaction series, shorter in one series, and did not change significantly in five other reaction series.

[c]When a better leaving group is used in an S_N2 reaction, the Nu--C_α bond is shorter in four reaction series and longer in four others. When the C_α--L bond was monitored, the C_α--L bond did not change significantly when a better leaving group was present.

Can. J. Chem. Downloaded from www.nrcresearchpress.com by 203.198.23.82 on 09/08/12
For personal use only.

transition state is tighter with a shorter nucleophile – leaving group distance when a smaller secondary α-deuterium kinetic isotope effect is observed (11, 12). When the experimental kinetic isotope effects and Hammett ρ values found in suitable series of S_N2 reactions (1, 2, 6–25) are interpreted in the above manner, one can deduce, Table 1, how the α-carbon–nucleophile and (or) α-carbon – leaving group transition-state bonds change when a substituent is altered in an S_N2 reaction.

In spite of the precautions taken in choosing the reaction systems for Table 1, it is clear that the substituent effects indicated by experimental data are not consistent. For example, changing to a better nucleophile leads to a longer C_α--Nu bond in two cases and to a shorter C_α--Nu transition-state bond in two other series of S_N2 reactions. The same problem is observed when one examines how changing to a better nucleophile affects the C_α--L bond length in the S_N2 transition state. The C_α--L bond becomes shorter in four of the seven suitable S_N2 reaction systems but does not change appreciably in the three other S_N2 reaction systems when a better nucleophile is used.

The changes that are found in the C_α--Nu and C_α--L transition-state bonds when a more electron-donating group is added to the α-carbon of the substrate are even more varied, Table 1. The C_α--Nu bond shortens in three of the suitable systems and lengthens in the other three suitable series of S_N2 reactions. The same difficulty is observed with the substituent effect on the C_α--L bond. When the 11 suitable reaction series in the literature are analyzed, a longer C_α--L bond is found in five systems, a shorter C_α--L bond is found in one system, and the C_α--L bond length does not change significantly in the five remaining series of S_N2 reactions when a more electron-donating group is added to the α-carbon.

Finally, the same problem is observed when a better leaving group is used in an S_N2 reaction. Changing to a better leaving group, Table 1, leads to a transition state with a longer C_α--Nu bond in half of the eight suitable systems and to a shorter C_α--Nu bond in the other four reaction series.

The marked variations in substituent effects found experimentally and the fact that less than 50% of the substituent effects shown in Table 1 are predicted by the simple application of Thornton's Reacting Bond Rule (32) or Harris and Kurz's extention of this rule (33) and the More O'Ferrall – Jencks energy surface method (35, 36), clearly indicate that some other factor(s) must play a role in determining how changes in substituents affect the structure of S_N2 transition states.

The substituent effects we found in one study (11) indicated that the major effect of changing the structure of the reactants in an S_N2 reaction was observed in the weakest reacting bond in the transition state and that little or no change occurred in the stronger reacting bond. A qualitative rationale for this behaviour is possible. Changing a substituent in the nucleophile, the substrate, or the leaving group of an S_N2 reaction changes the free energy of the transition state (32). This change in free energy will alter the lengths of the weak reacting bonds, i.e., the partially formed nucleophile–α-carbon and α-carbon – leaving group bonds. However, the greatest change in bond length should be observed in the weakest bond because the curvature of the potential energy surface for a weak bond is smaller (16). Thus, in an S_N2 transition state, the greatest change in structure would occur in the weakest transition-state bond and one would expect to see a greater change in the length of the weakest reacting bond and very little or no change in the length of the stronger reacting bond in the S_N2 transition state when the structure of the nucleophile, the substrate, or the leaving group is varied in an S_N2 reaction. In fact, this is what is observed in many S_N2 reactions (vide infra).

Explanation of the theory

Once the idea that the relative strengths of the two reacting bonds in an S_N2 transition state would determine the substituent effect on transition-state structure was accepted, a simple method for determining the strong and the weak reacting bonds in the transition state had to be adopted so that one could test the "bond strength" hypothesis, i.e., demonstrate that only the weak bond changes significantly when a substituent is altered. Unfortunately, it is impossible to measure the strength of the partially formed and partially broken bonds in a transition state. The best one can do is to assume that the relative strengths of the transition-state bonds

TABLE 2. The infrared stretching frequencies of several different types of bonds that are commonly used in the study of substituent effects in S_N2 reactions

Bond	$1/\lambda$ (cm^{-1})[a]	Reference	$\mu(\times 10^{23})$	Force constant (mD/Å)
C—OPh	1172	44	1.138	5.55
C—OH	1033	45	1.138	4.31
C—OTs/OTf	970	47	1.138	3.80
C—N^+	975	[c]	1.073	3.62
C—OCH_3	929	48	1.138	3.49
C—CN	920	49	0.996	2.99
C—Cl	732	50	1.489	2.83
C—SPh	722	51	1.449	2.68
C—$\overset{+}{O}H_2$	778	46	1.138	2.45[b]
C—SR	690	47	1.449	2.45
C—Br	611	52	1.732	2.29
C—I	533	52	1.820	1.83

[a]These stretching frequencies are for methyl compounds. The corresponding frequencies for the benzyl compounds are within a few percent of those quoted for the methyl substrates and do not affect the relative bond strengths significantly. Changing the *para* substituent on a benzene ring only causes small changes in the stretching frequencies (12).

[b]Based on a theoretical calculation at the 6-31G* and 6-31+G(d) levels.

[c]K.C. Westaway. Unpublished results.

Can. J. Chem. Downloaded from www.nrcresearchpress.com by 203.198.23.82 on 09/08/12
For personal use only.

are related to the strengths of the corresponding bonds in the reactant and in the product of the S_N2 reaction.[3]

The next problem was to choose a simple and rapid method of *estimating* the relative strengths of the appropriate bonds in the reactant and product. Although the strengths of the reacting bonds could be obtained from enthalpy measurements on stable molecules, they were *estimated* from the infrared stretching frequency (43). Equation [2],

$$[2] \quad k = 4\pi^2 c^2 \mu(1/\lambda)^2$$

where c is the speed of light and μ is the reduced mass calculated from the masses of the two atoms in the bond, was used to convert the wavenumber of the infrared stretching vibration ($1/\lambda$) into the force constant (k) for the bond. This method was chosen because the force constant is related to the curvature of the reaction coordinate surface, i.e., to the strength of the bond. Many of the α-carbon – leaving group stretching frequencies for methyl compounds are available in the literature and, since changing the alkyl group does not appear to alter the wavenumber of the stretching vibration significantly, this approach provides a rapid and simple method of *estimating*[5] the relative strengths of the reacting bonds in most S_N2 transition states. The infrared stretching frequencies, the reduced masses, and the force constants (approximate bond strengths) for some of the reacting bonds in methyl compounds are given in Table 2.

Testing the bond strength hypothesis

Once a method of estimating the relative strengths of the reacting bonds in an S_N2 transition state had been chosen, the importance of bond strength in determining the substituent effects on transition-state structure could be tested against the experimental results. The most useful tools for determining substituent effects on transition-state structure are kinetic isotope effects and linear free energy relationships. Unfortunately, there are only a few reactions for which one knows how a change in substituent affects the structure of both the nucleophile–α-carbon *and* the α-carbon – leaving group bond in an S_N2 transition state and can test the bond strength hypothesis completely. In the cases in which only one of the reacting bonds was monitored, one can say only that the substituent effects on transition-state structure are consistent with the bond strength hypothesis. The relationship between the strength of the reacting bonds and substituent effects on transition-state structure is examined in the following sections.

Systems in which a substituent on the α-carbon is changed

One of the few systems for which the changes in the nucleophile–α-carbon and the α-carbon – leaving group transition-state bonds were determined in a series of S_N2 reactions is the reactions between *para*-substituted thiophenoxide ions and *para*-substituted benzyl chlorides in methanol at 20°C (12), eq. [3].

[3] 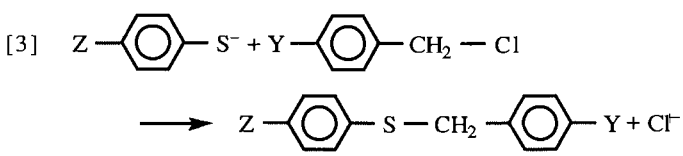

The results obtained for this system of S_N2 reactions are

[3]Theoretical calculations of the transition states for the series of S_N2 reactions, $Nu^- + CH_3—L \rightarrow Nu—CH_3 + L^-$, where $Nu^- = F^-$, Cl^-, OH^-, SH^-, SCH_3^-, and NH_2^- and $L = F^-$ and Cl^- at the 6-31+G* level[4] have shown that the Nu--C_α and C_α--L transition-state bonds are 35.4 ± 14.5% longer than the corresponding bonds in the reactants and products. Because the bonds are lengthened by roughly the same percentage in going to the transition state, a reasonable *estimate* of the relative strengths of the reacting bonds in *most* S_N2 transition states can be obtained from the strengths of their ground-state bonds. This approach would obviously fail when the transition state is very reactant-like or product-like, i.e., where the reacting bonds are very different in the transition state.

[4]R.A. Poirier and K.C. Westaway. Unpublished results.

[5]These force constants are approximate because off-diagonal force constants involving the methyl group have not been considered. The error caused by ignoring the off-diagonal force constants will probably not change the relative bond strengths for a reaction.

TABLE 3. The relative chlorine and secondary α-deuterium kinetic isotope effects, Hammett ρ values, and transition-state structures for the S_N2 reactions between *para*-substituted thiophenoxide ions and *para*-substituted benzyl chlorides in methanol – lithium methoxide at 20°C

para Substituent (Y) on the substrate	k^{35}/k^{37}	$(k_H/k_D)_\alpha$[a]	Hammett ρ found by changing (Z) on the nucleophile	Relative transition-state structure
CH_3O	1.01012	1.126[a]	−0.283[b]	S--------C-----Cl
CH_3	1.00963	1.096	−0.434	S------C-----Cl
H	1.00976	1.056	−0.500	S-----C-----Cl
Cl	1.01013	1.046	−0.720	S----C-----Cl
NO_2	1.00950	1.039	−0.961	S---C-----Cl

[a]Work in our laboratory has shown that the secondary α-deuterium kinetic isotope effect in S_N2 reactions is different when the reacting sodium thiophenoxide is an ion pair and when it is a free thiophenoxide ion. All of these isotope effects were measured at thiophenoxide ion concentrations where only one form of the nucleophile is present.
[b]At 0°C (see ref. 12).

TABLE 4. The chlorine leaving group kinetic isotope effects in the S_N2 reactions of several *para*-substituted benzyl chlorides with nucleophiles forming strong bonds to the α-carbon

	Chlorine kinetic isotope effects k^{35}/k^{37}[a]		
	Nucleophile		
para Substituent on the substrate	CH_3O^-	CN^-	$S_2O_3^{2-}$
MeO	1.0088	—	—
Me	1.0078	1.0079[b]	1.0074
H	1.0080	1.0072[b]	1.0064
Cl	1.0081	1.0060[b]	1.0058
NO_2	1.0076	1.0057	1.0058
Change in the isotope effect	0.0012	0.0022	0.0016

[a]The error in each isotope effect is ±0.00015.
[b]These reactions were originally thought to occur partially by a carbocation mechanism. Subsequent research by the original authors has shown them to be S_N2 reactions (53, 54).

shown in Table 3. The chlorine kinetic isotope effects measured by Grimsrud (12, 22) remain effectively constant when the *para* substituent on the benzene ring on the α-carbon is altered from methoxy to nitro, i.e., the standard deviation for the average chlorine isotope effect is only 0.00029 for all the substituents and, more important, there is no trend in isotope effect with electron-withdrawing power of the substituent. Thus, it appears that there is little or no change in the α-carbon – leaving group transition-state bond when the substituent on the α-carbon is altered. However, the secondary α-deuterium kinetic isotope effects decrease regularly as a more electron-withdrawing substituent is placed in the *para* position of the benzene ring on the α-carbon. This indicates that the transition state is tighter, i.e., the nucleophile – leaving group distance is shorter when a more electron-withdrawing substituent is on the α-carbon. Since the α-carbon – leaving group bond is virtually the same for all the substituents, the nucleophile–α-carbon bond must be shorter in the transition state with a more electron-withdrawing substituent. This conclusion is confirmed by the Hammett ρ values found by changing the substituent on the nucleophile. The Hammett ρ value increases in a regular fashion from −0.26 (estimated at 20°C), when the substituent on the substrate is methoxy, to −0.96, when the substituent on the substrate is nitro. A larger (more negative) ρ value indicates that there is a greater change in charge on the sulfur atom in going from the reactant to the transition state. This means the sulfur–α-carbon bond is more fully formed (significantly shorter) in the transition state with a more electron-withdrawing substituent. Since the sulfur–carbon bond is weaker than the α-carbon–chlorine bond, the major change in the structure of the transition state is observed in the weaker reacting bond and there is little or no change in the stronger carbon–chlorine transition-state bond in this series of S_N2 reactions. Both these changes in transition state structure are predicted by the bond strength hypothesis.

Leaving group kinetic isotope effects have been measured in several other S_N2 reactions of *para*-substituted benzyl chlorides. Grimsrud (22) and Hill and Fry (14) measured the chlorine kinetic isotope effects in the S_N2 reactions between several different nucleophiles and a series of *para*-substituted benzyl chlorides in methanol at 20°C and in 80% aqueous dioxane at 30°C, respectively. An examination of the observed kinetic isotope effects in Tables 4 and 5 shows that there are two different kinds of behaviour. In the S_N2 reactions where the nucleophile is methoxide ion, cyanide ion, and thiosulfate ion, Table 4, the chlorine kinetic isotope effect always decreases when a more electron-withdrawing substituent is placed on the benzene ring on the α-carbon of the substrate. For example, when the substi-

Can. J. Chem. Downloaded from www.nrcresearchpress.com by 203.198.23.82 on 09/08/12
For personal use only.

TABLE 5. The chlorine leaving group kinetic isotope effects in the S_N2 reactions between several *para*-substituted benzyl chlorides and nucleophiles that form weak bonds to the α-carbon

para Substituent on the substrate	Chlorine kinetic isotope effect k^{35}/k^{37}[a]			
	Nucleophile			
	H_2O[b]	I^-	*n*-BuS^-	PhS^-
MeO	—	—	—	1.01012
Me	1.0075	1.01028	1.00926	1.00963
H	1.0078	—	1.00952	1.00976
Cl	1.0078	1.01005	1.00947	1.01013
NO_2	1.0076	1.01008	1.00917	1.00950
Average isotope effect	1.0077 ±0.00015	1.01014 ±0.000125	1.00936 ±0.00017	1.00983 ±0.00029

[a]The error in the individual isotope effect is ±0.00015.
[b]These reactions were originally thought to occur partially by a carbocation mechanism. Subsequent research by the original authors has shown them to be S_N2 reactions (53, 54).

TABLE 6. The secondary α-deuterium kinetic isotope effects, Grunwald–Winstein "*m*" values, and selectivity for the solvolysis of *para*-substituted benzyl tosylates in 70% aqueous ethanol at 25°C

para Substituent	$(k_H/k_D)/\alpha-D$	*m*	k_{EtOH}/k_{H_2O}
CH_3		0.89	1.52
H	1.074	0.74	1.82
Cl		0.69	3.13
NO_2	1.005	0.48	4.30

tuent is altered, the magnitude of the kinetic isotope effect decreases by 0.0012 when methoxide ion is the nucleophile, by 0.0016 when thiosulfate ion is the nucleophile, and by 0.0022 when cyanide ion is the nucleophile. Since the average error in each chlorine isotope effect is approximately 0.00015, a decrease of between 0.0012 and 0.0022 means there is a significant change in these isotope effects and thus in the α-carbon–chlorine transition-state bond lengths when the substituent on the substrate is varied.

The chlorine kinetic isotope effects (Table 5) found for the S_N2 reactions between other nucleophiles and a series of *para*-substituted benzyl chlorides, on the other hand, are effectively constant and do not change with substituent in a regular way when a more electron-withdrawing group is added to the substrate. For example, when the nucleophile is water, the chlorine kinetic isotope effect only changes by 0.0003 when the substituent changes from *para*-methyl to *para*-nitro and there is no trend in the isotope effects with electron-withdrawing power of the substituent. In fact, the average kinetic isotope effect for all the substituents is 1.0077 with a standard deviation of 0.00015, which is the error in the individual isotope effect. The same behaviour is observed with the isotope effects found for the S_N2 reaction with iodide ion. Here, the isotope effect changes by only 0.0002 and the standard deviation on the average isotope effect is only 0.00013. The same behaviour is observed in the S_N2 reactions where *n*-butylthiolate ion is the nucleophile. In this case, the maximum difference in the isotope effect is 0.00035 and the standard deviation on the average isotope effect is only 0.00017. Finally, the maximum difference in the chlorine isotope effects in the reactions using thiophenoxide ion as the nucleophile is only 0.0006, the standard deviation of the average isotope effect is 0.00029, and there is no clear trend in isotope effect as a more electron-withdrawing substituent is added to the benzene ring on the α-carbon.

All of these seemingly contradictory results are predicted by the bond strength hypothesis. When the nucleophile is methoxide ion, cyanide ion, or thiosulfate ion, a stronger carbon–oxygen, carbon–carbon, or carbon–sulfur[6] bond, respectively, forms and a weaker carbon–chlorine bond is broken. Thus, changing the substituent on the benzene ring should lead to the change in the chlorine isotope effect (the length of the weaker carbon–chlorine transition-state bond) that is observed.

When the nucleophiles are iodide ion, water, *n*-butylthiolate ion, and thiophenoxide ion, the nucleophile–α-carbon bond that forms in the S_N2 reaction is weaker than the carbon–chlorine bond that is broken, i.e., the carbon–iodine, the carbon–O^+, and the carbon–sulfur bonds are all weaker than the carbon–chlorine bond. The bond strength hypothesis predicts that the nucleophile–α-carbon bond will change significantly but that there will be little or no change in the stronger carbon–chlorine bond (chlorine isotope effect) when the substituent on the benzene ring of the substate is altered. Thus, the apparent differences between the two types of substituent effects on the chlorine isotope effects in these S_N2 reactions of *para*-substituted benzyl chlorides are all consistent with, and rationalized by, the bond strength hypothesis. It is worth noting that these results are not predicted by the straightforward application of the other methods that predict how substituents alter transition-state structure (9, 32–37).

Harris et al. (8) also investigated the effect of changing the substituent in the substrate on the solvolysis of *para*-substituted benzyl tosylates in 70% aqueous ethanol. The smaller secondary α-deuterium kinetic isotope effects and Grunwald–

[6]The C_α—S bond in solid 4-nitrobenzylthiosulfate absorbs at 723 cm^{-1} whereas the C_α—Cl bond in solid 4-nitrobenzyl chloride absorbs at 701 cm^{-1}. Thus, the C_α—S bond in the thiosulfate (k = 2.69 mD/Å) is stronger than the C_α—Cl bond (k = 2.60 mD/Å) in the chloride.

Can. J. Chem. Downloaded from www.nrcresearchpress.com by 203.198.23.82 on 09/08/12
For personal use only.

TABLE 7. The Hammett ρ values found by changing the *para* substituent on the nucleophile and on the leaving group in the S_N2 reactions between *para*-substituted *N,N*-dimethylanilines and benzyl benzenesulfonates in acetone at 35°C

para Substituent (Y) on the nucleophile	Hammett ρ value found by changing the substituent on the leaving group
MeO	2.09
Me	2.13
H	2.10

para Substituent (Z) on the leaving group	Hammett ρ value found by changing the substituent on the nucleophile
Me	−3.63
H	−2.59
Cl	−2.34
NO_2	−1.63

Winstein "*m*" values found with a more electron-withdrawing substituent, Table 6, show that the transition state is tighter when a more electron-withdrawing substituent is present. The greater selectivity found with the more electron-withdrawing substituent indicates that the nucleophile–α-carbon transition-state bond is shorter in the reaction with the more electron-withdrawing substituent. Thus the weaker O^+—C_α bond shortens when the substituent is more electron withdrawing, as the bond strength hypothesis suggests. Unfortunately, there is no information to suggest how the stronger O—C_α bond (55) is altered with a change in substituent.

Systems in which the nucleophile is changed

Yamataka and Ando (10, 15–17) determined the rate constants for several S_N2 reactions between *para*-substituted *N,N*-dimethylanilines and benzyl benzenesulfonates, eq. [4].

[4] 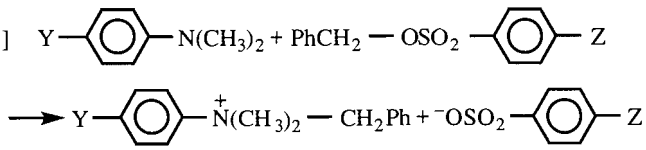

The data collected by these workers enabled us to calculate the Hammett ρ values for a change in substituent at both the nucleophile and the leaving group, Table 7. The Hammett ρ values found by changing the substituent on the leaving group in the reactions involving different nucleophiles range from 2.09 to 2.13, with an average value of 2.11 ± 0.02, when the nucleophile is changed from *para*-methoxy-*N,N*-dimethylaniline to *N,N*-dimethylaniline. The effectively constant Hammett ρ values suggest that the α-carbon – leaving group bond does not change significantly when the structure of the nucleophile is altered. This is exactly what the bond strength hypothesis predicts because the α-carbon – leaving group (C—O) bond is the stronger reacting bond in the S_N2 transition state.

The Hammett ρ values found when the substituent on the nucleophile is varied change markedly, from −3.63 when the leaving group is tosylate to −1.63 when the leaving group is *meta*-nitrobenzenesulfonate, Table 7. This is also consistent with the bond strength hypothesis because these ρ values indicate that the length of the weaker α-carbon–nucleophile (nitrogen–carbon) reacting bond is altered when the structure of the leaving group is varied. Thus, the bond strength hypothesis predicts the effect on both transition-state reacting bonds whether the substituent change is made in the nucleophile or in the leaving group.

Lee et al. (25) have determined the secondary incoming group (nucleophile) deuterium kinetic isotope effects, i.e., when deuterium replaces hydrogen in the N—H bonds of aniline or benzylamine in S_N2 reactions with benzyl, methyl, and ethyl benzenesulfonates in acetonitrile at 30°C. When a better nucleophile is used in these reactions, Table 8, the secondary deuterium isotope effect decreases (is more inverse) for two of the reactions but increases in the other two reactions. Since a more inverse isotope effect indicates a shorter Nu--C_α transition-state bond, changing to a better nucleophile leads to a transition state with a shorter C_α--Nu bond in the reactions between the benzyl benzenesulfonates and aniline or benzylamine but to a transition state with a longer Nu--C_α bond in the methyl and ethyl benzenesulfonate S_N2 reactions. Although the changes in transition-state structure are different in these reactions, all the changes are consistent with the bond strength hypothesis because the weaker C—N^+ bond changes in all four reactions. It would, of course, be of interest to determine how the stronger C—O bond is affected by the change in nucleophile.

The effect of changing to a better leaving group

The transition states for the S_N2 reactions between *para*-substituted thiophenoxide ions and *para*-substituted phenylbenzyldimethylammonium ions in DMF, eq. [5], have also been modeled in some detail (11).

[5] 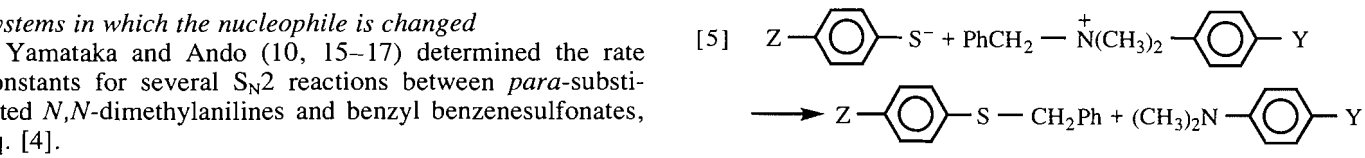

The nitrogen kinetic isotope effects, Table 9, are the same or increase very slightly when a better leaving group is used, i.e., when the substituent Y is more electron withdrawing. This means that the C_α--N transition-state bond length does not change or increases very slightly when a better leaving group is used. The smaller secondary α-deuterium kinetic isotope effects observed with the better leaving group, Table 9, indicate that the transition state is tighter, i.e., the nucleophile – leaving group distance is shorter, when a better leaving group is present. Since the C_α--N transition-state bond length does not change or increases slightly with a better leaving group, changing to a better leaving group must lead to a significant shortening of the nucleophile–α-carbon bond in the transition state (11). The shorter S--C_α transition-state bond with a better leaving group is confirmed by the Hammett ρ values found by changing the substituent on the nucleophile. The larger (more negative) ρ value found with the best leaving group indicates that there is a greater change in the charge on the sulfur atom in going to the transition state and that the nucleophile–α-carbon bond is more fully formed (shorter) in the transition state with a better leaving group.

Can. J. Chem. Downloaded from www.nrcresearchpress.com by 203.198.23.82 on 09/08/12
For personal use only.

Can. J. Chem. Downloaded from www.nrcresearchpress.com by 203.198.23.82 on 09/08/12
For personal use only.

TABLE 8. The secondary incoming group (nucleophile) deuterium kinetic isotope effect found by changing to a better nucleophile in the S_N2 reactions of *para*-substituted anilines and benzylamines with benzyl, methyl, and ethyl *para*-substituted benzenesulfonates in acetonitrile at 30°C

Substituent on the nucleophile	*para* Substituent on the leaving group	$(k_H/k_D)^a$
Benzyl *para*-substituted benzenesulfonates with *para*-substituted aniline/aniline-*N*,*N*-d_2		
m-NO_2	NO_2	0.951
p-CH_3O	NO_2	0.898
m-NO_2	CH_3	0.973
p-CH_3O	CH_3	0.955
Benzyl *para*-substituted benzenesulfonates with *para*-substituted benzylamine/benzylamine-*N*,*N*-d_2		
m-NO_2	NO_2	0.953
p-CH_3O	NO_2	0.940
m-NO_2	CH_3	0.966
p-CH_3O	CH_3	0.952
Methyl *para*-substituted benzenesulfonates with *para*-substituted aniline/aniline-*N*,*N*-d_2		
m-NO_2	NO_2	0.968 ± 0.009[b]
p-CH_3O	NO_2	0.984 ± 0.007[b]
m-NO_2	CH_3	0.963 ± 0.009[b]
p-CH_3O	CH_3	0.978 ± 0.008[b]
Ethyl *para*-substituted benzenesulfonates with *para*-substituted aniline/aniline-*N*,*N*-d_2		
m-NO_2	NO_2	0.858[b]
p-CH_3O	NO_2	0.869[b]
m-NO_2	CH_3	0.851[b]
p-CH_3O	CH_3	0.862[b]

[a]The original authors did not give error limits for most of these isotope effects. They imply that the error is less than 1%.
[b]At 65°C.

TABLE 9. The nitrogen and secondary α-deuterium kinetic isotope effects, Hammett ρ values, and transition-state structures found when the leaving group was changed in the S_N2 reaction between *para*-substituted phenylbenzyldimethylammonium ions and thiophenoxide ions in DMF at 0°C

para Substituent (Y) on the leaving group	k^{14}/k^{15a}	$(k_H/k_D)_\alpha{}^b$	Hammett ρ value (nucleophile)[c]	Relative transition-state structure
OCH_3	1.0197	1.207	−1.54	S--------C-----N
H	1.0200	1.179	−1.70	S-------C-----N
Cl	1.0202	1.151	−1.83	S------C-----N

[a]The error in the individual isotope effects ranges from 0.00034 to 0.0009.
[b]The errors in these isotope effects range from 0.007 to 0.020. Work in our laboratory has shown that the secondary α-deuterium kinetic isotope effect in S_N2 reactions is different when the reacting sodium thiophenoxide is an ion pair and when it is a free thiophenoxide ion. All of these isotope effects were measured at thiophenoxide ion concentrations where only one form of the nucleophile is present.
[c]The error in the ρ values is between 0.016 and 0.047.

Thus, changing to a better leaving group in this S_N2 reaction shortens the weaker C_α--S transition-state bond significantly but does not alter the length of the stronger C_α--N transition-state bond appreciably. Both these effects are predicted by the bond strength hypothesis.

A second series of S_N2 reactions in which the leaving group was altered was investigated by Lewis and Vanderpool (23). Hammett ρ values were calculated from the rate constants observed when the substituent on the nucleophile (a series of *para*-substituted thiophenoxide ions) was changed in the

TABLE 10. The secondary incoming group (nucleophile) deuterium kinetic isotope effect found by changing to a better leaving group in the S_N2 reactions of *para*-substituted anilines and benzylamines with benzyl, methyl, and ethyl *para*-substituted benzenesulfonates in acetonitrile at 30°C

Substituent on the nucleophile	*para* Substituent on the leaving group	(k_H/k_D)[a]
Benzyl *para*-substituted benzenesulfonates with *para*-substituted aniline/aniline-*N*,*N*-d_2		
p-CH_3O	CH_3	0.955
p-CH_3O	NO_2	0.898
m-NO_2	CH_3	0.973
m-NO_2	NO_2	0.951
Benzyl *para*-substituted benzenesulfonates with *para*-substituted benzylamine/benzylamine-*N*,*N*-d_2		
p-CH_3O	CH_3	0.952
p-CH_3O	NO_2	0.940
m-NO_2	CH_3	0.966
m-NO_2	NO_2	0.953
Methyl *para*-substituted benzenesulfonates with *para*-substituted aniline/aniline-*N*,*N*-d_2		
p-CH_3O	CH_3	0.978 ± 0.008[b]
p-CH_3O	NO_2	0.984 ± 0.007[b]
m-NO_2	CH_3	0.963 ± 0.009[b]
m-NO_2	NO_2	0.968 ± 0.009[b]
Ethyl *para*-substituted benzenesulfonates with *para*-substituted aniline/aniline-*N*,*N*-d_2		
p-CH_3O	CH_3	0.862[b]
p-CH_3O	NO_2	0.869[b]
m-NO_2	CH_3	0.851[b]
m-NO_2	NO_2	0.858[b]

[a]The original authors did not give error limits for most of these isotope effects. They imply that the error is less than 1%.
[b]At 65°C.

S_N2 reactions of methyl mesylate and methyl triflate in sulfolane at 42°C. These Hammett ρ values, which indicate the relative lengths of the nucleophile–α-carbon transition-state bonds for these reactions, changed from −3.23 when the leaving group was tosylate ion to −2.91 when the leaving group was triflate ion. Thus, the length of the weaker nucleophile–α-carbon (S--C_α) reacting bond is altered when the leaving group is changed in these S_N2 reactions. Although there is no information concerning the behaviour of the stronger carbon–oxygen reacting bond in these reactions, the changes that are observed in the weaker bond are consistent with the bond strength hypothesis.

Lee et al. (25) measured the secondary incoming group (nucleophile) deuterium kinetic isotope effects in the S_N2 reactions between benzyl, methyl, and ethyl benzenesulfonates and various *para*-substituted anilines and benzylamines deuterated at the N-H hydrogens. The results in Table 10 show that changing to a better leaving group leads to a more inverse isotope effect (a shorter nucleophile–α-carbon transition-state bond) in the benzyl benzenesulfonate reactions, but to a longer Nu--C_α bond when the substrates are methyl and ethyl benzenesulfonates. Although the substituent effects are different for the four reactions, they are all consistent with the predictions of the bond strength hypothesis because the weaker N^+--C_α transition-state bond changes in all four reactions when the leaving group is altered. It is worth noting that the weaker N^+--C_α transition-state bond changes in these reactions whether the nucleophile, Table 8, or the leaving group is changed, Table 10. This is not predicted by the usual methods for predicting substituent effects on S_N2 reactions (32, 35–37).

The effect of changing the solvent

Although a change in solvent is not, strictly speaking, a substituent effect, it seemed likely that a change in solvent might be viewed in the same way as a substituent effect. Certainly, a change in solvent alters the free energy of the transition state just as does a change in substituent. The effect of this change in free energy should again be found primarily in the weakest reacting bond in the S_N2 transition state. In fact, it appears that the results obtained in reactions for which the solvent has been changed are consistent with the predictions of the bond strength hypothesis.

Graczyk, Taylor, and Turnquist (7) reported that the chlorine kinetic isotope effects in the S_N2 reaction between *n*-butyl chloride and thiophenoxide ion, eq. [6],

[6] $C_6H_5S^- + CH_3CH_2CH_2CH_2—Cl \rightarrow C_6H_5S—CH_2CH_2CH_2CH_3 + Cl^-$

Can. J. Chem. Downloaded from www.nrcresearchpress.com by 203.198.23.82 on 09/08/12
For personal use only.

TABLE 11. The chlorine leaving group kinetic isotope effects and rate constants for the S_N2 reactions between thiophenoxide ion and *n*-butyl chloride in various solvents at 20°C

Solvent	k^{35}/k^{37}	Rate constant (L mol^{-1} s^{-1})
DMSO	1.00964	2.6×10^{-2}
DMF	1.00953	4.1×10^{-2}
Tetraglyme	1.00942	1.1×10^{-2}
Diglyme	1.00949	3.5×10^{-3}
n-Propanol	1.00931	6.2×10^{-5}
Methanol	1.00930	2.2×10^{-5}
Average isotope effect	1.00945 ± 0.00013[a]	

[a]The average error on the individual isotope effects is ±0.00015.

TABLE 12. The sulfur kinetic isotope effects and rate constants for the S_N2 reactions between ethoxide ion and trimethylsulfonium ion in various ethanol–DMSO mixtures at 60°C

Mol% DMSO	k^{32}/k^{34a}	Rate constant (L mol^{-1} s^{-1})
0	1.0095	2.90×10^{-3}
17	1.0075	4.38×10^{-3}
25	1.0071	5.67×10^{-3}
35	1.0066	9.73×10^{-3}
55	1.0040	14.80×10^{-3}
65	1.0035	31.10×10^{-3}

[a]The individual errors in the isotope effects are <0.0009.

did not change significantly when the solvent was altered over a very wide range of solvents, i.e., from the dipolar aprotic solvents, DMSO and DMF, to the less polar aprotic solvents diglyme and tetraglyme, to polar, protic solvents such as methanol and 1-propanol. In fact, the chlorine leaving group kinetic isotope effects found in these different solvents, Table 11, are the same within experimental error, i.e., the isotope effects range from a high of 1.00964 to a low of 1.00930 (only change by 0.0003) with an average isotope effect of 1.00944 ± 0.00012 when the solvent changes from DMSO to methanol and the rate constant changes by more than 1000. It is worth noting that the very small decrease in the isotope effects in going from the dipolar aprotic to the protic solvents may be the result of hydrogen bonding to the developing chloride ion in the S_N2 transition state (56, 57). However, since all of the isotope effects are within one standard deviation of the average isotope effect in all of the solvents, one must conclude that there is little or no change in the α-carbon–chlorine transition-state bond when the solvent is changed in this S_N2 reaction.[7] This is what one would expect if the bond strength hypothesis was important in determining how a change in solvent affects the structure of the S_N2 transition state, i.e., the stronger α-carbon–chlorine bond is not altered significantly even when the solvent is changed over a wide range and the rate is altered by more than 1000. Unfortunately, we do not know how the change in solvent affects the weaker sulfur–α-carbon transition-state bond in this reaction and the bond strength hypothesis cannot be tested completely. All that can be said is that the experimental results are consistent with the bond strength hypothesis.

Saunders and co-workers (61) obtained completely different results when they investigated how a change in solvent affected the transition-state structure of an S_N2 reaction. These workers measured the sulfur leaving group kinetic isotope effects in the S_N2 reactions between ethoxide ion and trimethylsulfonium ion in various ethanol – dimethyl sulfoxide mixtures at 60°C, eq. [7].

[7] $$C_2H_5O^- + CH_3{-}\overset{+}{S}(CH_3)_2 \rightarrow C_2H_5O{-}CH_3 + S(CH_3)_2$$

The sulfur kinetic isotope effect, Table 12, decreases significantly from 1.0095 to 1.0035 when the solvent is changed from 0 to 65 mol% DMSO. This means that changing the solvent changes the length of the α-carbon – leaving group (C--S) transition-state bond markedly. This different response to a change in solvent is consistent with the bond strength hypothesis because the carbon–S^+ bond is considerably weaker than the carbon–oxygen bond. Since the different experimental results are both consistent with the predictions based on the bond strength hypothesis, the bond strength hypothesis may be useful for predicting how a change in solvent will affect the structure of an S_N2 transition state.

Conclusion

Analysis of the 37 sets of experimental data that were suitable for testing the bond strength hypothesis led to the results shown in Table 13. First, it is important to note that the substituent effects in all three systems in which the effects of substituents were determined for both the nucleophile–α-carbon and α-carbon – leaving group transition-state bonds are predicted by the bond strength hypothesis.

The results also show that 30 out of 37, or 81% of the systems studied are consistent with the predictions based on the bond strength hypothesis. The weaker bond changes significantly in 8 out of 11 or 73% of the suitable systems when the structure of the nucleophile is varied. In the systems where the substituent on the substrate is altered, 12 out of 16 or 75% of the cases are consistent with the predictions based on the relative strengths of the reacting bonds. The weakest reacting bond changes in 8 out of 8 or 100% of the systems when the structure of the leaving group is altered. Finally, 100% or 2 out of 2 sets of experimental results found when the solvent is changed are consistent with the predictions based on the bond strength hypothesis. Because over 80% of the substituent effects found in suitable S_N2 reactions are predicted by the bond strength hypothesis, it appears that the strength of the reacting bonds plays an

[7]Calculations by McLennan et al. (58) have suggested that chlorine leaving group kinetic isotope effects can be levelled by hydrogen bonding to the developing chloride ion in an S_N1 reaction. Levelling becomes significant when the C_α--Cl bond order is ≤0.5 and the H--Cl bond order is fairly large, i.e., $0.3(1 - n)$ where "n" is the C_α--Cl transition-state bond order. However, since there is less C_α--Cl bond rupture in S_N2 transition states than in S_N1 transition states (59, 60) and since theoretical calculations[4] suggest the C_α--Cl bond order is approximately 0.65 in the S_N2 transition state, levelling should not be important even if the H--Cl bond order is as large as $0.3(1 - n)$. In any case, even if one argues that the chlorine isotope effect in the protic solvents is levelled, the isotope effects in all the aprotic solvents are, within experimental error, the same.

Can. J. Chem. Downloaded from www.nrcresearchpress.com by 203.198.23.82 on 09/08/12
For personal use only.

TABLE 13. The percentages of the substituent effects on the structure of S_N2 transition states that are consistent with the bond strength hypothesis

Nucleophile	Substrate	Results predicted for a change in Leaving group	Solvent	Total
8/11	12/16	8/8	2/2	30/37
73%	75%	100%	100%	81%

important role in determining substituent effects on the structure of the transition state.

Both Thornton (32) and Jencks (36) suggest that the curvature of the reaction coordinate surface, which is related to the force constant (the strength) of a reacting bond, will influence the effect of a change in substituent on the structure of a transition state. However, the More O'Ferrall – Jencks method does not indicate how to adjust for the strength of the reacting bonds. It is worth noting that Thornton (32) suggested that bond strength *might* be considered in cases where a substituent is changed at the α-carbon of the substrate. In fact, if one (*i*) considers that these substituent effects are completely determined by the effect of the substituent change on only the strongest bond of the S_N2 transition state as Thornton suggested *might* be necessary, and (*ii*) assumes that the parallel and perpendicular vibrations are equally important in determining the change in transition-state structure, Thornton's Reacting Bond Rule correctly predicts (*i*) that the weakest bond, but not the strongest bond, will change when a substituent is altered *and* (*ii*) the correct change in the weakest transition state bond, Table 4.

Thus, Thornton's Rule does predict the experimental substituent effects in systems where the substituent in the substrate is altered *if* one considers (*i*) the relative strengths of the reacting bonds in the S_N2 transition state and (*ii*) that the perpendicular and parallel vibrations are equally important in determining the substituent effect on transition-state structure.

In spite of the fact that Thornton's Rule predicts how a change in substituent alters the structure of an S_N2 transition state when the change in substituent is at the α-carbon, Thornton's Rule fails to predict most of the changes that are observed in transition-state structure when the substituent is changed in the nucleophile or the leaving group. Unfortunately, taking account of the relative strengths of the two reacting bonds or changing the relative importance of the parallel and perpendicular effects in the More O'Ferrall – Jencks energy surface method does not solve this problem.

The important observations, however, are (*i*) that the substituent effects based on experimental evidence are often different in similar reactions, (*ii*) that none of the methods available for predicting substituent effects consistently predicts the changes in the isotope effects and Hammett ρ values that are observed experimentally, and (*iii*) that the above analysis suggests that the strength of the reacting bonds plays an important role in determining substituent effects on the structure of S_N2 transition states.

Possible exceptions to the bond strength hypothesis

Although the agreement between the substituent effects based on experimental evidence and the predictions based on the bond strength hypothesis is high enough to suggest that the relative strengths of the reacting bonds should be considered when one is trying to determine how changing a substituent affects the structure of an S_N2 transition state, there are several reactions for which the experimental results do not agree with the predictions based on the bond strength hypothesis. These discrepancies may arise for the following reasons.

The relative strengths of the reacting bonds in an S_N2 transition state obviously cannot be measured. The relative strengths of the reacting bonds in S_N2 transition states were estimated from the infrared stretching frequencies of stable bonds in the reactants and products. One could only expect to obtain good estimates of the relative strengths of the reacting bonds in S_N2 transition states from the force constants of stable bonds if the two reacting bonds in the transition state had the same, or almost the same, bond order. In these circumstances, the bond strength hypothesis would be expected to be successful in indicating which transition-state bond will change when a substituent is altered in an S_N2 reaction. In fact, the success of the bond strength hypothesis in predicting the substituent effects in S_N2 transition states suggests that the reacting bonds in most S_N2 transition states have similar bond orders.

However, if one reacting bond were much shorter and stronger than the other reacting bond in a product-like or reactant-like transition state, the ground-state bond strengths would not give a good estimate of the relative strengths of the two reacting bonds in the S_N2 transition state and the bond strength hypothesis might fail to predict the substituent effect correctly. The bond strength hypothesis would also be expected to fail in reactions in which the strengths of the reacting bonds were equal or almost equal. In this instance, one would probably find that both of the reacting bonds would change when a substituent was changed. The rule would also be expected to fail in reactions where changing the structure of one of the reactants changed the relative strengths of the two reacting bonds in the S_N2 transition state, for example, if the substituent change was sufficient to change the nucleophile–α-carbon bond from the weakest bond to the strongest bond in the S_N2 transition state.

Although some reactions would be expected to violate the predictions of the bond strength hypothesis, the ability of this approach to rationalize many of the substituent effects that are not predicted by the simple theories suggests that this approach is valid. Because some substituent effects are not predicted by the bond strength hypothesis, other factor(s) may play a role in determining how substituents affect the structure of S_N2 transition states.

Acknowledgements

The author gratefully acknowledges the financial support provided by the Natural Sciences and Engineering Research Council of Canada.

1. R.F. Hudson and G. Klopman. J. Chem. Soc. 1062 (1962).
2. F.P. Ballistreri, E. Maccarone, and A. Mamo. J. Org. Chem. **41**, 3364 (1976).

Can. J. Chem. Downloaded from www.nrcresearchpress.com by 203.198.23.82 on 09/08/12
For personal use only.

3. E.F.C. Ko and A.J. Parker. J. Am. Chem. Soc. **90**, 6447 (1968).
4. K.M. Koshy and R.E. Robertson. J. Am. Chem. Soc. **96**, 914 (1974).
5. V.J. Shiner, Jr., M.W. Rapp, and H.R. Pinnick, Jr. J. Am. Chem. Soc. **92**, 232 (1970).
6. M.P. Friedberger and E.R. Thornton. J. Am. Chem. Soc. **98**, 2861 (1976).
7. D.G. Graczyk, J.W. Taylor, and C.R. Turnquist. J. Am. Chem. Soc. **100**, 7333 (1978).
8. J.M. Harris, S.G. Shafer, J.R. Moffatt, and A.R. Becker. J. Am. Chem. Soc. **101**, 3295 (1979).
9. P.R. Young and W.P. Jencks. J. Am. Chem. Soc. **101**, 3288 (1979).
10. T. Ando, H. Tanabe, and H. Yamataka. J. Am. Chem. Soc. **106**, 2084 (1984).
11. K.C. Westaway and S.F. Ali. Can. J. Chem. **57**, 1354 (1979).
12. K.C. Westaway and Z. Waszczylo. Can. J. Chem. **60**, 2500 (1982).
13. E. Buncel and C. Chuaqui. J. Org. Chem. **45**, 2825 (1980).
14. J.W. Hill and A. Fry. J. Am. Chem. Soc. **84**, 2763 (1962).
15. H. Yamataka and T. Ando. Tetrahedron Lett. 4805 (1982).
16. H. Yamataka and T. Ando. J. Am. Chem. Soc. **101**, 266 (1979).
17. H. Yamataka and T. Ando. Tetrahedron Lett. 1059 (1975).
18. S.D. Yoh. Taehan Hwahakhoe Chi **19**, 449 (1975).
19. S.D. Yoh. Taehan Hwahakhoe Chi **19**, 240 (1975).
20. S.D. Yoh. Taehan Hwahakhoe Chi **19**, 116 (1975).
21. E.P. Grimsrud and J.W. Taylor. J. Am. Chem. Soc. **92**, 739 (1970).
22. E.P. Grimsrud. PhD. Dissertation, University of Wisconsin, Madison. 1971.
23. E.S. Lewis and S.H. Vanderpool. J. Am. Chem. Soc. **100**, 6421 (1978).
24. P.S. Radhakrishnamarti and G.P. Panigrahi. Bull. Chem. Soc. Jpn. **43**, 81 (1970).
25. I. Lee, H.J. Koh, B.-S. Lee, D.S. Sohn, and B.C. Lee. J. Chem. Soc. Perkin Trans. 2, 1741 (1991).
26. R.F.W. Bader, A.J. Duke, and R.R. Messer. J. Am. Chem. Soc. **95**, 7715 (1973).
27. S. Wolfe and D.J. Mitchell. J. Am. Chem. Soc. **103**, 7692 (1981).
28. S. Wolfe, D. Mitchell, and H.B. Schlegel. J. Am. Chem. Soc. **103**, 7694 (1981).
29. Z. Shi and R.J. Boyd. J. Am. Chem. Soc. **113**, 1072 (1991).
30. Z. Shi and R.J. Boyd. J. Am. Chem. Soc. **113**, 2434 (1991).
31. Z. Shi and R.J. Boyd. Can. J. Chem. **70**, 450 (1992).
32. E.R. Thornton. J. Am. Chem. Soc. **89**, 2915 (1969).
33. J.C. Harris and J.L. Kurz. J. Am. Chem. Soc. **92**, 349 (1970).
34. G.S. Hammond. J. Am. Chem. Soc. **77**, 334 (1955).
35. R.A. More O'Ferrall. J. Chem. Soc. B, 274 (1970).
36. W.P. Jencks. Chem. Rev. **72**, 705 (1972).
37. S. Shaik and A. Pross. J. Am. Chem. Soc. **103**, 3702 (1981).
38. W.H. Saunders, Jr. Chim. Scr. **8**, 27 (1975).
39. S. Hoz, H. Basch, and M. Goldberg. J. Am. Chem. Soc. **114**, 4364 (1992).
40. D. Stefanidis and W.P. Jencks. J. Am. Chem. Soc. **115**, 6045 (1993).
41. I. Lee, W.H. Lee, and H.W. Lee. J. Phys. Org. Chem. **3**, 545 (1990).
42. K.C. Westaway and S.F. Ali. Can. J. Chem. **57**, 1089 (1979).
43. K.B. Wiberg. *In* Physical organic chemistry. J. Wiley and Sons, New York. 1964. p. 142.
44. J.H.S. Green. Spectrochim. Acta, **18**, 39 (1962).
45. M. Falk and E. Whalley. J. Chem. Phys. **34**, 1554 (1961).
46. M. Esseffar, E. El Mouhtadi, V. Lopez, and M. Yanez. 3rd European Symposium on Organic Reactivity, Goteborg, Sweden, July 7, 1991. Poster 31.
47. C.J. Pouchert. *In* The Aldrich library of infrared spectra. 2nd ed. Aldrich Chemical Co., Milwaukee, Wis. 1978.
48. K. Hamada and H. Morishita. Z. Phys. Chem. Neue Folge, **97**, 295 (1975).
49. D.E. Milligan and M.E. Jacox. J. Mol. Spectrosc. **8**, 126 (1962).
50. R.C. Williams and J.W. Taylor. J. Am. Chem. Soc. **95**, 1710 (1973).
51. J.H.S. Green. Spectrochim. Acta, **24**, 1627 (1968).
52. R.E. Kagarise. Spectrochim. Acta, **19**, 1979 (1963).
53. L.B. Sims, A. Fry, L.T. Netherton, J.C. Wilson, K.D. Reppond, and S.W. Crook. J. Am. Chem. Soc. **94**, 1364 (1972).
54. L. Melander and W.H. Saunders, Jr. *In* Reaction rates of isotopic molecules. Wiley–Interscience, New York. 1980. p. 244.
55. J. Rodgers, D.A. Femec, and R.L. Schowen. J. Am. Chem. Soc. **104**, 3263 (1982).
56. E.R. Thornton. *In* Solvolysis mechanisms. Ronald Press, New York. 1964. pp. 199–206.
57. G.W. Burton, L.B. Sims, J.C. Wilson, and A. Fry. J. Am. Chem. Soc. **99**, 3371 (1977).
58. D.J. McLennan, A.R. Stein, and B. Dobson. Can. J. Chem. **64**, 1201 (1986).
59. J. Bigeleisen and M. Wolfsberg. J. Chem. Phys. **22**, 1264 (1954).
60. D.G. Graczyk and J.W. Taylor. J. Am. Chem. Soc. **96**, 3255 (1974).
61. R.T. Hargreaves, A.M. Katz, and W.H. Saunders, Jr. J. Am. Chem. Soc. **98**, 2614 (1976).

Can. J. Chem. Downloaded from www.nrcresearchpress.com by 203.198.23.82 on 09/08/12
For personal use only.

Synthesis and physicochemical properties of bolaamphiphiles from dimeric acid

MA PILAR BOSCH[1] AND JOSÉ LUIS PARRA

Departamento de Tensioactivos, Centro de Investigación y Desarrollo – Consejo Superior de Investigaciones Científicas, C/ Jorge Girona Salgado 18–26, 08034 Barcelona, Spain

AND

FRANCISCO SÁNCHEZ-BAEZA

Departamento Química Orgánica Biológica, Centro de Investigación y Desarrollo – Consejo Superior de Investigaciones Científicas, C/ Jorge Girona Salgado 18–26, 08034 Barcelona, Spain

Received March 31, 1993

MA PILAR BOSCH, JOSÉ LUIS PARRA, and FRANCISCO SÁNCHEZ-BAEZA. Can. J. Chem. **71**, 2095 (1993).

The physicochemical behaviour of bolaamphiphile derivatives with an anionic, a cationic, or a non-ionic polar group and their mixtures is studied mainly by surface tension measurements, quasi-elastic light-scattering studies, ^{1}H NMR spectroscopy, and surface monolayers. Bolaamphiphiles are synthesized by classical methods from a non-expensive mixture of α,ω-dicarboxylic acids, obtained by thermal Diels–Alder type cyclization of methyl 10-*E*,12-*E* linoleate, obtained from tall oil. The anionic and cationic bolaamphiphiles synthesized are water soluble and form stable monolayers when they are compressed. The anionic and the cationic bolaamphiphiles with an iodide atom as counter-anion show a behaviour between liquid-condensed and liquid-expanded. The other synthesized cationic bolaamphiphiles and the (1 : 1) mixtures of anionic–cationic bolaamphiphiles behave as liquid-condensed.

MA PILAR BOSCH, JOSÉ LUIS PARRA et FRANCISCO SÁNCHEZ-BAEZA. Can. J. Chem. **71**, 2095 (1993).

Le comportement physico-chimique des dérivés bolaanfifiliques avec les groups polaires anionique, cationique ou non-ionique et leurs mélanges ont été étudiée par la mesure de la tension superficielle, diffusion quasi-élastique de la lumière, spectroscopie ^{1}H RMN et formation de couches monomoléculaires superficielles. Les composés bolaanfifiliques ont été synthetisés suivant des méthodes classiques utilisant une mélange des acides α,ω-dicarboxyliques pas chers, obtenu suivant la reaction de cyclisation thermique de Diels–Alder de l'ester méthylique de l'acid 10-*E*,12-*E* linoléique, obtenu à partir de l'huile de graisse. Les composés bolaanfifiliques anioniques et cationiques présentent solubilité dans l'eau et forment des couches monomoléculaires stables quand ils sont comprimés. Les composés bolaanfifiliques anionique et cationique avec un atome d'iode comme contre-ion présentent un comportement entre liquide condensé et liquide expandu. Les autres composés bolaanfifiliques synthetisés et leurs melánges (1 : 1) anionique–cationique présentent un comportement comme liquide condensé.

Can. J. Chem. Downloaded from www.nrcresearchpress.com by 203.198.23.82 on 09/08/12
For personal use only.

Introduction

The chemistry beyond the molecule, supramolecular chemistry (1), is the designed chemistry of the intermolecular bond, just as molecular chemistry is that of the covalent bond. It is a highly interdisciplinary field of science covering the chemical, physical, and biological features of compounds held together and organized by means of intermolecular (non-covalent) binding interactions.

During recent decades much work has been done to study properties and functions of biomembranes (2–9), Langmuir–Blodgett films (10), and vesicles (11, 12). They are different membrane models, but each of them allows the investigation, of only certain features of the properties of natural membranes (2, 13, 14). Vesicles constitute a model for the first "membrane material" that appeared on Earth before any form of life (15, 16). One of the interesting questions that has been raised is whether it is possible to develop new materials that simulate natural supramolecular systems in that their functioning is determined by self-tridimensional organization (1).

Bipolar lipids or *bolaform* molecules contain two polar head groups of equal or different polarity, connected by one or more hydrocarbon chains, which aggregate in aqueous media (5, 17). We wonder about the effect of different head groups on the aggregation properties of these compounds. A non-expensive mixture of α,ω-dicarboxylic acids **2** (dimeric acid or DA), obtained by thermal Diels–Alder type cyclization of methyl 10-*E*,12-*E* linoleate **1** obtained from tall oil (18), was used as starting material, followed by hydrogenation and saponification reactions. A dianionic bolaamphiphile with sodium sulphate as head group **3**, dicationic bolaamphiphiles *N,N,N*-trimethylethanaminium and di-*N,N,N*-trimethyl-*N'*-methylethanaminium with iodide **6** and **10**, respectively, chloride **7**, or bicarbonate **8** as counterion head groups, and, as non-ionic bolaamphiphiles, a digluconamide **9**, a di-*N*-[(2-(dimethylamino)ethyl **4**, and a di-*N*-[(2-methylamino)ethyl]aminomethyl **5** with neutral head groups were synthesized.

Physicochemical properties were studied by surface tension measurements, ^{1}H NMR spectroscopy, quasi-elastic light-scattering, and surface monolayers.

Results and discussion

Synthesis

As shown in Fig. 1, activation of the acid groups of dimeric acid, DA **2**, with thionyl chloride (19) and reaction with the amine, followed by quaternization reaction and ion exchange, gives the cationic acid amides, DAC-I **6**, DAC-Cl **7**, DAC-CO_3 **8**, and DAC-NMe_2I **10** with yields of 81, 88, 86, and 74%, respectively. The dianionic bolaamphiphile with sulphate as head groups (DAS **3**) was obtained with 65% yield and the non-ionic bolaamphiphiles DAC-NMe_2 **4**, DAC-NHMe **5**, and DAG **9** were obtained after activation of the acid group by the acid chloride or the mixed anhydride (19) with yields of 87, 95, and 64%, respectively. These yields are in agreement with those described for related compounds in the literature (19).

[1]Author to whom correspondence may be addressed.

Can. J. Chem. Downloaded from www.nrcresearchpress.com by 203.198.23.82 on 09/08/12
For personal use only.

FIG. 1. Scheme of synthesized compounds.

TABLE 1. Surface tension and transition temperature measurements

Compound	γ_L (mN/m)	Critical micelle concentration (M)	T_c (K)
DAS **3**	38	1.92×10^{-3}	≤r.t.
DAC-I **6**	34	2.02×10^{-5}	333
DAC-Cl **7**	40	3.2×10^{-3}	343
DAC-CO_3 **8**	33	3.5×10^{-4}	333
DAC-NMe_2 **4**	32	5.4×10^{-4}	—
DAG **9**	—	—	343

All products gave satisfactory spectra (IR, NMR, FAB/MS) and elemental analyses.

The infrared spectra of the cationic **6, 7, 8**, and **10** and non-ionic bolaamphiphiles **4, 5**, and **9** contained amide bands around 1645 (amide I st) and 1630 (amide II st) cm^{-1}, showing that the coupling reaction between the activated dimeric acid and the amines was accomplished. For the anionic bolaamphiphile **3** the strong signal at 1240 cm^{-1} shows the presence of the sulphate groups.

The ^1H NMR spectra of the intermediate and the end products are in agreement with the expected chemical shifts. The mass spectra obtained contain molecular weight recognition as well as sequence information. Sometimes $[M^+ + H]$ or $[M^+ + Na]$ are the more characteristic peaks. For the dicationic bolaamphiphiles the loss of one or two counterions $[M^+ - X]$ or $[M^+ - XH]$ are the more characteristic signals. The FAB/MS spectra of the synthesized compounds indicate an E_2 Hofmann elimination for DAC-I **6**, DAC-Cl **7**, and DAC-CO_3 **8**, with a lower value of elimination for the compound with iodide as counter-anion. Like results are given in the literature (20) from 2-halopentanes to 1-pentene; the chloride and iodide derivatives show a 37% and 20% of elimination reaction, respectively. The bolaamphiphile **7** with chloride as counter-anion decomposes when heated over 353 K, as shown by heating and TLC control studies and by the ^1H NMR study at different temperatures. The spectrum at 353 K has broader signals and has no fine structure, contrary to the behaviour observed for the cationic bolaamphiphile **6** with iodide as counter-anion.

Physicochemical properties

In Table 1 the surface tension values, γ_L, and the critical micelle concentration (cmc) for some of the synthesized products are given. The lowest value of the cmc, 2×10^{-5} M, corresponds to the cationic surfactant **6** with the iodide atom as counterion. The iodide atom is the bulkiest counterion used and has the bulkiest hydration sphere. Thus it is able to aggregate with fewer molecules to reach the cmc value than are the other bolaamphiphiles. In aqueous solution, the iodide derivative **6** forms a laminar liquid crystalline gel phase from a concentration of 4.3 to 20%. At lower concentration it becomes a fluid phase. The presence of the amide hydrogen bond facilitates a high water solubility and the change of the position of one methyl group may affect the solubility in aqueous solutions. Bolaamphiphiles **4** and **8** (DAC-NMe_2 and DAC-CO_3) and **3** and **7** (DAS and DAC-Cl) have cmc values of the same order, 5.4×10^{-4} M, 3.5×10^{-4} M, 1.92×10^{-3} M, and 3.2×10^{-3} M, respectively. DAG **9**, DAC-NHMe **5**, and DAC-NMe_2I **10** are water-insoluble and

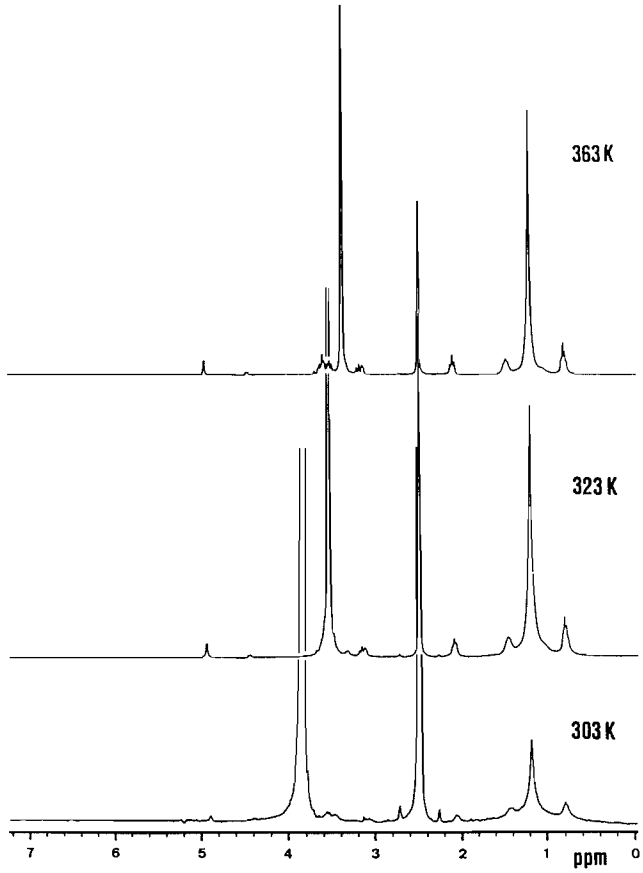

FIG. 2. NMR study of the behaviour of DAG **9** with temperature.

DAC-NMe_2 **4** presents low water solubility. Transition temperature values, also included in Table 1, will be discussed in the next paragraph.

^1H NMR studies

In the dispersed state, amphiphiles in water may produce well-defined high-resolution spectra due in part to the fact that the magnetic field heterogeneity effects that are present with coarse aggregates are averaged out when the phase consists of finer particles. This principle has been used for studying molecular interactions in biomembranes. Lipid–water systems sometimes give only slightly broadened spectra, because of the considerable mobility of various groups.

As previously described, surfactants give rise to a variety of phases depending upon the relative concentrations of the components and upon the temperature. Investigations of the state of water molecules, their motion, diffusion, mobility of the alkyl chains, and binding of small ions in the various phases have been undertaken by use of NMR. Lineshape, relaxation time data have been used in attempts to understand these systems, particularly for biological systems and micellar solutions (21). Abrupt changes in apparent NMR linewidths are usually observed at phase transitions and may in part be caused by variations in relaxation times resulting from differential freedom of motion (22).

A study of the NMR shifts and linewidths of the protons that build up the hydrophobic and hydrophilic moieties was carried out for all the synthesized compounds, at temperatures from 303 to 363 K. As shown in Fig. 2, the behav-

Can. J. Chem. Downloaded from www.nrcresearchpress.com by 203.198.23.82 on 09/08/12
For personal use only.

Can. J. Chem. Downloaded from www.nrcresearchpress.com by 203.198.23.82 on 09/08/12
For personal use only.

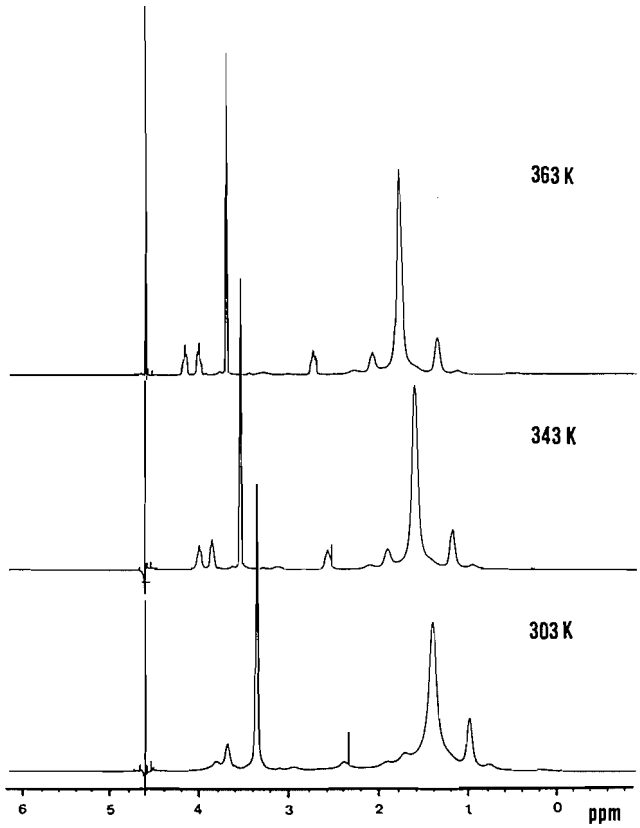

FIG. 3. NMR study of the behaviour of DAC-I **6** with temperature.

iour of the non-ionic bolaamphiphile DAG **9** in the NMR study at different temperatures shows narrow signals with increase of temperature, with linewidths of the hydrophobic part from 17.7 to 6.5 Hz (303–363 K, respectively). The signal sharpness at elevated temperature (363 K) shows that the methylene group bound to the amide nitrogen atom at δ 3.18 ppm is not involved in hydrogen bonding. At low temperature (303–343 K) the signal is broadened and no splitting remains. Also, the signals of the hydrocarbon chains broaden, and the mobility in the gel state of the hydrophobic moiety is greatly reduced. The HDO signal is affected with a downfield shift of 0.33 ppm from 303 to 363 K. DAG molecules may be organized as bilayers because the absorptions of the hydrophobic and hydrophilic moieties have a small linewidth; this indicates mobility and long relaxation times. Examination of the linewidths of the hydrophobic and hydrophilic parts shows that the transition temperature is around 343 K.

In the case of the cationic bolaamphiphile DAC-I **6**, as shown in Fig. 3, the ^{1}H NMR spectrum at 303 K shows the hydrophobic and hydrophilic moieties completely solidified. There is a bilayer highly packed with low water content. At 323 K (spectrum not shown in Fig. 3) the graph obtained is consistent with the presence of a bilayer structure that may even be packed. However, at 343 K the polar head groups have enough mobility because more defined peaks are observed in the range 3.6–4.0 ppm. At 363 K the second transition to liquid crystal is not accomplished. This indicates a bilayer structure with strong interactions because the hydrophobic absorption is broader than 15 Hz. The transition temperature is around 333 K and the mobility increases with the temperature. With heating, the absorption of the trimethylammonium polar group, the hydrocarbon chains, and the methyl end groups from the hydrocarbon chains is shifted upfield 0.54, 0.58, and 0.57 ppm, respectively. Another interesting fact is that the signal due to the CH_2 α to the nitrogen amide group is broader (59 Hz) than at 363 K, that a fine splitting is observed (13 Hz), and no gel structure is present. The CH_2 α to the trimethylammonium signal at 303 K has disappeared with the heating and a fine splitting is observed. Also, the CH_2 α and β to the carbon atom of the amide group present the same behaviour, showing that the amide proton is not involved in any hydrogen bond.

DAS **3**, DAC-Cl **7**, DAC-CO_3 **8**, and DAC-NH_2 **4** are structured as micelles from 303 to 363 K. The mobility of the hydrophobic part increases with the temperature, showing normal micelle behaviour. The transition temperatures studied by NMR for these compounds are lower than room temperature, 333 and 343 K, respectively, as shown in Table 1. From NMR spectra obtained for these compounds, it can be deduced that the signal due to the CH_2 α to the nitrogen amide bond does not present the broadness of the absorption on cooling, and no gel structure was seen.

Surface monolayers

Pressure–area isotherms (23, 24) of some bolaamphiphilic film monolayers spread on water surfaces were measured. Bolaform amphiphiles and aqueous surfaces may have different positions and conformations: both the hydrophobic and the hydrophilic moieties may lie on the water surface or head groups may lie on the water surface and the hydrophobic chain be turned out from the surface. When a monolayer is compressed, the head groups may remain on the aqueous surface or one of them may be lifted from the water surface (3). As shown in Table 2, the monolayer buildup by dimeric acid derivatives **3**, **6**, **7**, **8**, and their mixtures **3** + **6**, **3** + **7**, **3** + **8** collapses at low pressure values of 45–53 mN/m. This is a normal behaviour for bolaform monolayers on water, showing their apparent instability. The unusually large molecular area for compound DAC-I **6** of 116 Å^2/mol was unexpected, taking into account that the van der Waals diameter of chloride and iodide anions are 4.2 and 4.6 Å, respectively. Iodide, like ClO_4^-, is also known as a chaotropic anion (25), which tightly binds to the trimethylammonium head group. However, in the case of the chloride anion, this may remain in the water bulk phase not so tightly bound to the trimethylammonium head group. In fact, if we design these dimeric acid derivatives by molecular models according to Stuart and Briegleb, it is possible to appreciate that formation of a hydrogen bond could take place between the two amide groups of the two chains with the two polar head groups, building a macrocycle of 18 carbon atoms and a distance for the hydrogen bond of 2.51 Å. This peculiar molecular arrangement of DAC-I could be explained if we consider that the formation of a macrocycle and the chaotropic effect of iodide anion may force the cyclohexane ring to lie on the water surface. However, in the case of the bolaamphiphilic compound **7** with chloride as counteranion, the cyclohexane ring may remain vertical to the water surface, occupying less surface area per molecule. This would agree with the values of 116 and 62 Å^2/molecule obtained for compounds DAC-I **6** and DAC-Cl **7**, respectively. As shown in Table 2, the κ_{35} and K values show the behaviour

TABLE 2. Studies with the surface film balance

Compound(s)	Collapse point (mN/m)	Å²/molecule	κ_{35} (m/mN)	K (mN/m)	Behaviour
3	45	100	1.11×10^{-2}	90.3	Between liquid condensed and liquid expanded
6	46	116	1.07×10^{-2}	94	Between liquid condensed and liquid expanded
7	45	62	9.8×10^{-3}	102	Liquid condensed
8	48	78	8.5×10^{-3}	117	Liquid condensed
3+6	53	215	6.2×10^{-3}	162	Liquid condensed
3+7	49	161	6.7×10^{-3}	148	Liquid condensed
3+8	53	164	7×10^{-3}	139	Liquid condensed

of the molecules on the water surface. Values of κ_{35} below 100 may indicate behaviour between liquid-condensed and liquid-expanded, e.g., **3** and **6**; at values above these, the molecules may behave as liquid-condensed, e.g., **7, 8** and their mixtures **3** + **6**, and **3** + **7**, and **3** + **8**. The mixtures of cationic bolaamphiphiles **6, 7**, and **8** with anionic bolaamphiphile **3** may possess stability because one cationic compound may pack on the water surface close to an anionic compound, building a lipid layer on the water surface with values of the molecular surface area as shown.

Light-scattering studies

From the physicochemical point of view it is useful to study certain aspects of the molecular arrangement of the synthesized compounds by quasi-elastic light-scattering measurements. The results, for average size, obtained for DAC-I **6**, DAC-CO_3 **7**, and DAC-Cl **8** were 141.9, 31.7, and 15.7 nm, respectively. For the anionic disulphate bolaamphiphile DAS **3** the average mean size measured was 61 nm. From the results obtained for the synthesized compounds, the possible formation of micelles or small unilamellar vesicles must be considered. However, experiments carried out on all the bolaamphiphiles synthesized to investigate their entrapping availability using pyranine dye were unsuccessful. Nevertheless, TEM and image analysis studies carried out on sonicated dispersions of all the synthesized compounds permit us to establish different molecular associations based on open bilayer structures; their tridimensional arrangement depends on the type of polarity and the nature of the counterion of each bolaamphiphile (26).

Conclusions

1. For the first time the following bolaamphiphiles were synthesized:
   Anionic: DAS 3
   Non-ionic: DAG **9**, DAC-NMe_2 **4**, DAC-NMeH **5**
   Cationic: DAC-I **6**, DAC-Cl **7**, DAC-CO_3 **8**, DAC-NMe_2I **10**
2. The structural organization of the synthesized compounds was measured by light-scattering studies (from 15.7 to 142 nm), the critical micelle concentration ($2 \times 10^{-5} - 2 \times 10^{-3}$ M), and the static surface tension γ_L (32–40 mN/m).
3. The transition temperature was measured for each lipid.
4. The size of the counterion controls the organisation of the lipid: DAC-I **6** and DAG **9** are structured as bilayer structures; DAS **3**, DAC-Cl **7**, and DAC-CO_3 **8** are structured as micelles.
5. The synthesized bolaamphiphiles build stable surface monolayers. The dianionic bolaamphiphile **3** and the cationic bolaamphiphile **6** with I as counter-anion show behaviour between liquid-condensed and liquid-expanded. The other dicationic bolaamphiphiles **7, 8**, and their mixtures with the dianionic bolaamphiphile **3** behave as liquid-condensed.

Experimental

Commercial dimeric acid, Versadyme **2**, is a nonexpensive α,ω-dicarboxylic acid of appropriate chain length for the formation of vesicle membranes, supplied by Henkel S.A. Barcelona. Its spectra (^{1}H NMR, MS, IR) and elemental analysis were in agreement with the structure **2**. No attempts were made to separate the isomers.

The bolaamphiphiles were characterized by elemental (Carlo Erba 1108) and group analyses. Melting points were determined on a Kofler hot stage and are uncorrected. IR spectra were recorded on a Shimadzu IR-435 infrared spectrophotometer. The ^{1}H NMR spectra were run in a Bruker WP 80SY or Varian Unity Instrument of 300 MHz; the solvent used is specified in the description of each compound. Chemical shifts are reported in ppm downfield from HDO or DMSO signals. FAB-mass spectra (positive ion) were measured with an Auto Spec-Q instrument fitted with an atom gun of Cs. Ions produced were extracted and accelerated with a potential of 25 kV. Samples (≤0.1 mg) were dispersed in DMSO–glycerol used as probe matrix.

Synthesis

Dimeric sulphate 3

Dimeric acid **2** was converted to the dimeric alcohol by $LiAlH_4$ reduction (27). Dimeric alcohol (28) (2 g; 3.73 mmol) in diethyl ether (4 mL) was stirred at 273 K. Then chlorosulfonic acid (0.5 mL; 7.53 mmol) was added with care. The mixture was stirred during 3 h, followed by addition of ice, neutralization with a saturated solution of Na_2CO_3, and extraction with ether (3 × 20 mL). The aqueous solution was saturated with Na_2SO_4 and extracted with *n*-butanol (3 × 20 mL). The two organic phases were dried over Na_2SO_4 and evaporated to dryness, 2.15 g. Crystallization from methanol–ether gave white crystals of dimeric disulphate **3**, 1.81 g (65%) mp 166–168°C. IR ν: 1240 (SO_4^{2-}) cm^{-1}. ^{1}H NMR (DMSO, 300 MHz), δ: 0.85 (t, 3H each, $-CH_3$), 1.2 (s, 32H each, $-CH_2-$, -CH-), 3.65 (t, 2H each, $-CH_2O-$). FAB/MS (Mol. wt. 741.05): 764 [M^+ + Na], 93%; 661 [$M^+ - SO_3$], 100%. Anal. calcd. for $C_{36}H_{70}O_8S_2Na_2 \cdot 2H_2O$: C 55.63, H 9.61, S 8.25; found: C 56.02, H 9.49, S 8.37.

Dimeric di-N,N,N-trimethylethanaminium iodide 6

Dimeric di-acyloylchloride prepared from dimeric acid **2** (4.06 g; 7.19 mmol) and thionylchloride (1.32 mL; 18.29 mmol) was dissolved in 42 mL dry toluene. N,N-Dimethylethylenediamine (1.56 mL; 14.38 mmol) in 10 mL dry toluene was added dropwise to the stirred solution at room temperature and stirring was

Can. J. Chem. Downloaded from www.nrcresearchpress.com by 203.198.23.82 on 09/08/12
For personal use only.

Can. J. Chem. Downloaded from www.nrcresearchpress.com by 203.198.23.82 on 09/08/12
For personal use only.

continued for 1 h. The solution was then extracted with sodium carbonate (0.5 M), washed with water, dried over Na_2SO_4, and evaporated to dryness. The residual oil (4.40 g) was dissolved in a mixture of 40 mL CH_3NO_2 and 15 mL $CHCl_3$. Iodomethane (2.5 mL) was added and the mixture was stirred at room temperature for 3 h. The solvent was evaporated and the residue (6.06 g) was recrystallized from acetone, 5.76 g, yield 81%, mp 112–114°C. IR ν: 3350 (NH), 1650 (amide I), 1540 (amide II) cm^{-1}. ^1H NMR ($CDCl_3$, 300 MHz) δ: 0.84 (t, 3H each, $-CH_3$), 1.26 (s, 32H each, $-CH_2-$, -CH-), 1.56 (s, 2H each, $-CH_2-CH_2-CONH-$), 2.19 (br, 2H each, $-CH_2-CONH-$), 3.18 (s, 9H each, $-N^+(CH_3)_3$), 3.5 (br, 2H each, $-CONH-CH_2-$), 3.66 (br, 2H each, $-CH_2N^+-$), 7.7 (s, 1H each, -CONH-). FAB/MS (Mol. wt. 989.09): 863 [$M^+ - I + H$], 20%; 676 [$M^+ - 2I - (NC_3H_9)$, 25%; 615 [$M^+ - 2I - 2(NC_3H_{10})$], 100%. Anal. calcd. for $C_{46}H_{94}N_4O_2I_2$: C 55.86, H 9.58, N 5.66; found: C 55.91, H 9.69, N 5.50.

*Dimeric di-*N,N,N*-trimethylethanaminium chloride* **7**

Dimeric di-*N,N,N*-trimethylethanaminium iodide 6 (0.4 g; 0.40 mmol) was chromatographed three times on an ion-exchange resin (Dowex 1 × 2); affording 0.270 g of dimeric di-*N,N,N*-trimethylethanaminium chloride **7**. Yield 84%. IR ν: 3450 (NH), 1660 (amide I), 1560 (amide II) cm^{-1}. ^1H NMR (D_2O, 300 MHz) δ: 0.71 (bd, 3H each, $-CH_3$), 1.19 (s, 32H each, $-CH_2$, -CH-), 1.48 (bd, 2H each, $-CH_2CH_2CO-$), 2.18 (bd, 2H each, $-CH_2CH_2CONH-$), 2.14 (bd, 2H each, $-CH_2CONH-$), 3.1 (s, 9H each, $-N^+(CH_3)_3$), 3.38 (bd, 2H each, $-CH_2N^+-$), 3.56 (bd, 2H each, $-CH_2NH-$), 7.7 (s, 1H each, -CONH-). FAB/MS (Mol. wt. 806.18): 771 [$M^+ - ClH$], 100%; 677 [$M^+ - 2Cl - NC_3H_9 + H$], 8%; 617 [$M^+ - 2Cl - 2(NC_3H_9) + H$], 53%. Anal. calcd. for $C_{46}H_{94}N_4O_2Cl_2$: C 68.53, H 11.75, N 6.95, Cl 8.80; found: C 68.02, H 12.04, N 6.69, Cl 8.47.

*Dimeric di-*N,N,N*-trimethylethanaminium bicarbonate* **8**

Dimeric di-*N,N,N*-trimethylethanaminium iodide **6** (0.4 g; 0.4 mmol) was chromatographed three times on an ion-exchange resin (Dowex 1 × 2); affording 0.35 g of dimeric di-*N,N,N*-trimethylethanaminium bicarbonate **8**, yield after recrystallization 0.28 g (82%). IR ν: 3450 (NH), 1660 (amide I), 1560 (amide II) cm^{-1}. ^1H NMR (D_2O, 300 MHz) δ: 0.77 (bd, 3H each, $-CH_3$), 1.19 (s, 32H each, $-CH_2-$), 1.48 (s, 2H each, $-CH_2CH_2CONH-$), 2.14 (bd, 2H each, $-CH_2CONH-$), 3.1 (s, 9H each, $-N^+(CH_3)_3-$), 3.38 (bd, 2H each, $-CH_2N^+-$), 3.56 (bd, 2H each, $-CH_2NH-$), 7.7 (s, 1H each, -CONH-). FAB/MS (Mol. wt. 985.48): 674 [$M^+ - 2CO_3H - NCH_3H_9$], 14%; 615 [$M^+ - 2CO_3H - 2NC_3H_{10}$], 100%. Anal. calcd. for $C_{48}H_{96}N_4O_8$: C 67.23, H 11.3, N 6.53; found: C 67.06, H 11.57, N 6.77.

*Dimeric di-(*D*-glucopyranos-2-yl-carbamoyl)* **9**

Dimeric acid **2** (4.03 g; 7.09 mmol) in 115 mL DMF at 0°C was mixed under argon with 2.34 mL (21.28 mmol) *N*-methylmorpholine and 2.32 mL (17.75 mmol) isobutyl chloroformate. This mixture was stirred for 30 min at −15°C to yield the mixed anhydride. Then, 4.06 g (18.88 mmol) of 2-amino-2-deoxy-D-glucose hydrochloride and 4.0 mL (30 mmol) of triethylamine in 20 mL ethanol were added, and the mixture was stirred another 2 h. The solution was then cooled to room temperature. Colorless salts were removed by filtration and the solvents by evaporation. The residue (10.62 g) was recrystallized 3 times from methanol–ether. Yield 4.02 g (64%). IR ν: 3350 (NH), 1645 (amide I), 1545 (amide II) cm^{-1}. ^1H NMR (DMSO, 300 MHz) δ: 0.84 (t, 3H each, $-CH_3$), 1.22 (s, 32H each, $-CH_2-$, -CH-), 1.42 (bd, 2H each, $-CH_2CH_2-CONH-$), 2.2 (bd, 2H each, $-CH_2CONH-$), 3.0–3.7 (m, 6H each, 2,6 CH glucose), 4.4 (d, J = 8 Hz, 1H each, 1β-H glucose), 4.9 (d, J = 3 Hz, 1α-H), 7.5 (d, J = 9 Hz, D_2O inactive NH, 1H each, -CONH). FAB/MS (Mol. wt. 886.4): 887 [$M^+ + H$], 82%; 553 [$M^+ - 2(C_6H_{12}O_5N) + Na$], 20%; 369 [$(C_6H_{12}O_5N) + C_{11}H_{20}O + Na$], 100%. Anal. calcd. for $C_{48}H_{90}O_{12}N_2$: C 64.96, H 10.24, N 3.15; found: C 64.88, H 10.3, N 3.2.

*Dimeric di-*N,N,N*-trimethyl-*N'*-methylethanaminium iodide,* **10**

Dimeric di-acyloylchloride prepared from dimeric acid **2** (4.04 g; 7.16 mmol) and thionylchloride (1.28 mL; 17.64 mmol) was dissolved in 42 mL dry toluene. *N,N'*-Dimethylethylenediamine (1.54 mL; 14.28 mmol) in 10 mL dry toluene was added dropwise to the stirred solution at room temperature and stirring was continued for 1 h. The solution was then extracted with sodium carbonate (0.5 M), washed with water, dried over Na_2SO_4, and evaporated to dryness. The residual oil 4.74 g was dissolved in a mixture of 40 mL CH_3NO_2 and 15 mL $CHCl_3$, 2.5 mL of iodomethane was added, and the mixture was stirred at room temperature for 3 h. The solvent was evaporated and the residue (5.05 g) was recrystallized, yield 74%. IR ν: 1650 cm^{-1}. ^1H NMR ($CDCl_3$, 300 MHz) δ: 0.88 (t, 3H each, $-CH_3$), 1.22 (s, 32H each, $-CH_2-$,-CH-), 1.54 (s, 2H each, $-CH_2-CH_2-CONH-$), 2.2 (s, 3H each, CH_3-N-), 2.25 (br, 2H each, $-CH_2-CONH-$), 3.1 (s, 9H each, $-N^+(CH_3)_3$), 3.4 (br, 2H each, $-CH_2-N^+-$), 3.5 (br, 2H each, -CONMe-CH_2-); FAB/MS (Mol. wt. 1017.3): 706 [$M^+ - 2I - NC_3H_9 + 2H$], 15%; 617 [$M^+ - 2I - N(CH_3)_3 - (CH_2)_2N(CH_3)_3$], 100%; 586 [$M^+ - 2I - 2N(CH_3)_3 - N(CH_3)(CH_2)_2 - 2H$], 60%. Anal. calcd. for $C_{48}H_{98}N_4O_2I_2$: C 56.67, H 9.72, N 5.51; found: C 56.39, H 9.51, N 5.20.

Physicochemical properties

A Du Noüy ring tensiometer Krüss K12 with a platinum–iridium ring was used for surface tension measurements (γ_L). Aqueous solutions were allowed to equilibrate at 298 K until stabilization of surface tension readings. Critical micelle concentration (cmc) were determined from the γ_L–log C curves.

^1H NMR studies

^1H NMR spectra were recorded on a Varian Unity instrument (300 MHz). The solution was made from 10 mg of the bolaamphiphiles in 1 mL of D_2O (99.9% D) for water-soluble or from DMSO + D_2O for water-insoluble solutes. The NMR spectra were measured at six different temperatures. The line widths of the CH_2 band at 1.3 ppm were measured; 1024 scans were accumulated each time.

Surface monolayers

Monolayers were prepared at the air–water interface of a rectangular trough of poly(tetrafluoroethylene) on a Langmuir film balance, Lauda FW 2 (29). The compounds were spread as dilute solutions (0.4–0.6 mg/mL) in chloroform or in chloroform–methanol (4:1) if the compound was insufficiently soluble in chloroform. When a mixture of two compounds was measured, one of them was used as a matrix. Then an equimolar solution (1:1) was mixed and spread on the water surface. The films were allowed to rest for 2 min before compression by a movable barrier at a constant rate of 0.1 nm^2/(molecule.min). Doubly distilled water was filtered by a Milli-Q standard system. The subphase was pure water. The temperature of the subphase was 292 K, and was constant within 0.05 K. Air temperature was constant within 3 K. Each experiment was measured at least twice until reproducible.

Light-scattering studies

Dynamic light-scattering measurements were made on a Malvern-4700 instrument at 298 K with a scattering angle of 90°. Doubly distilled water was filtered by a Milli Q standard system. The samples were prepared by dissolution of bolaamphiphile (0.35%) and NaCl (0.1 M) in 2 mL water. Previously, the water was filtered three times through a Millipore 0.22 μm membrane. The solutions were centrifuged for 1 h at 5000 rpm.

Acknowledgments

We are grateful to Henkel Ibérica S.A. for supplying us the starting material; to Dr. J. Rivera from the Lab. Espectrometría de Masses, Dep. Química Ambiental (CID–CSIC) for carrying out the FAB/MS spectra of the isolated compounds; and to A. Pascual and M^a A. Pes for assistance in the experimental work. This research was supported in part

by a grant from Generalitat de Catalunya, CIRIT (Grant EE92/1-111) at the Institut for Organic Chemistry in Berlin (Germany).

1. J.M. Lehn. Angew. Chem. Int. Ed. Engl. **29**, 1304 (1990).
2. A. Gulik, V. Luzzati, M. de Rosa, and A. Gambacorta. J. Mol. Biol. **182**, 131 (1985).
3. J.H. Fuhrhop, H.H. David, J. Mathieu, V. Liman, H.J. Winter, and E. Boekema. J. Am. Chem. Soc. **108**, 1785 (1986).
4. J.H. Fuhrhop and J. Mathieu. J. Chem. Soc. Chem. Commun. 144 (1983).
5. J.H. Fuhrhop and D. Fritsch. Acc. Chem. Res. **19**, 130 (1986).
6. J.H. Fuhrhop, V. Liman, and V. Koesling. J. Am. Chem. Soc. **110**, 6840 (1988).
7. J.H. Fuhrhop, H. Hungerbühler, and V. Siggel. Langmuir, **6**, 1295 (1990).
8. J.H. Fuhrhop, M. Krull, A. Shulz, and D. Möbius. Langmuir, **6**, 497 (1990).
9. J.H. Fuhrhop, P. Schnieder, E. Boekema, and W. Helfrich. J. Am. Chem. Soc. **110**, 2861 (1988).
10. S. Palacin, M. Blanchard-Desce, J.M. Lehn, and A. Barraud. Thin Solid Films, **178**, 387 (1989).
11. P. Lo Nostro, G. Briganti, and S.H. Chen. J. Colloid Interface Sci. **142**, 214 (1991).
12. J. Fendler. Acc. Chem. Res. **13**, 7 (1980).
13. L. Gros, H. Ringsdorf, and H. Schupp. Angew. Chem. Int. Ed. Engl. **20**, 305 (1981).
14. F.M. Menger, J.J. Lee, P. Aikens, and S. Vavis. J. Colloid Interface Sci. **129**, 185 (1989).
15. A. Kotik, K. Janacek, and J. Korita. Biophysical chemistry of membranes. John Wiley, New York. 1988. p. 2.
16. H. Yanagawa, Y. Ogawa, K. Kojima, and M. Ito. Origin Life Evol. Biosphere, **18**, 179 (1988).
17. J.H. Fuhrhop and R. Bach. Monolayer lipid membranes from bolaamphiphiles. Advances in supramolecular chemistry. JAI Press, Greenwich, Conn. 1992. pp. 25–63.
18. J.H. Fuhrhop, W. Kaufmann, and F. Schambil. Langmuir, **1**, 387 (1985).
19. J.H. Fuhrhop and H. Tank. Chem. Phys. Lipids, **43**, 193 (1987).
20. W.H. Saunders, Jr., S.R. Fahrenholltz, E.A. Caress, J.P. Lowe, and M. Schreiber. J. Am. Chem. Soc. **87**, 3401 (1965).
21. J.H. Fuhrhop, S. Svenson, C. Boeltcher, E. Rössler, and H.M. Vieth. J. Am. Chem. Soc. **112**, 4307 (1990).
22. C.L. Khetrapal, A.C. Kunwar, A.S. Tracey, and P. Diehl. NMR:Basic Princ. Prog. **9**, Lyotropic liquid crystals. Springer Verlag, Berlin. 1975.
23. G.L. Gaines, Jr. Insoluble monolayers at liquid gas interfaces. John Wiley and Sons, New York. 1966.
24. W.D. Harkins. The physical chemistry of surface films. Reinhold Publishing Corporation, New York. 1952.
25. T. Pigor and R. Lawaczek. Z. Naturforsch. C: Biosci. **83C**, 307 (1983).
26. P. Bosch, J.L. Parra, and A. de la Maza. J. Electron. Microsc. Submitted.
27. J.E. McMurry. Org. Synth. **VI**, 781 (1988).
28. D. Jerchel, H. Becker, and M.K. Varahamuti. Z. Naturforsch. B: Anorg. Chem. Org. Chem. Biochem. Biophys. Biol. **11B**, 681 (1956).
29. F.B. Padley. The lipid handbook. *Edited by* Frank D. Gunstone, John L. Harwood, and F.B. Padley. Chapman and Hall, London. 1986. pp. 338–342.

Can. J. Chem. Downloaded from www.nrcresearchpress.com by 203.198.23.82 on 09/08/12
For personal use only.

Hydrophilic analogs of (*R*,*R*)-diaminocyclohexane dichloroplatinum (DACH) and the influence of relative stereochemistry on antitumor activity

STEPHEN HANESSIAN[1] AND JIANGUO WANG

Department of Chemistry, Université de Montréal, Box 6128, Station A, Montréal, QC H3C 3J7, Canada

Received June 3, 1993

STEPHEN HANESSIAN and JIANGUO WANG. Can. J. Chem. **71**, 2102 (1993).

A series of analogs of (*R*,*R*)-1,2-diaminocyclohexane dichloroplatinum(II) (DACH) containing stereochemically defined hydroxy groups and appropriate acidic leaving groups were synthesized and tested as antitumor agents. The (1α,2β,3α,4β)-1,4-dihydroxy-2,3-diaminocyclohexane analog showed the highest potency against P388 leukemia in mice. The results indicate that increasing the hydrophilicity of the platinum complex to a certain extent could improve the antitumor activity of the drug. It is also likely that the stereochemical disposition of the substituents on the cyclohexane ring affects the antitumor activity.

STEPHEN HANESSIAN et JIANGUO WANG. Can. J. Chem. **71**, 2102 (1993).

Des analogues du (*R*,*R*)-1,2-diaminocyclohexane dichloroplatine(II) (DACH) qui contiennent des groupes hydroxy et des groupes partant acides ont été synthétisés en vue d'obtenir des substances antitumorales. L'analogue (1α,2β,3α,4β)-1,4-dihydroxy-2,3-diaminocyclohexane s'est avéré être le plus actif contre la leucémie P388 chez la souris. Les résultats indiquent que l'augmentation de l'hydrophilicité de ces complexes pourrait aider à l'amélioration de l'activité antitumorale. Il est aussi possible que l'activité puisse dépendre sur la stéréochimie des substituants sur le noyau cyclohexanique.

[Traduit par la rédaction]

Can. J. Chem. Downloaded from www.nrcresearchpress.com by 203.198.23.82 on 09/08/12
For personal use only.

In spite of the multitude of structural analogs of the antitumor agent *cis*-diamine dichloroplatinum(II) (cisplatin) (1) only a few are presently used in clinical practice (2). Of these, *trans*-1,2-diaminocyclohexane dichloroplatinum(II) (DACH) and its variants with different anionic counterparts appear to be the most effective (3) (Fig. 1). Since the molecule is chiral, the relevance of stereochemical issues has been addressed by a number of investigators (4). In spite of conflicting views (5), the consensus is that the (*R*,*R*) isomer is generally more active than the (*S*,*S*) isomer (6), although activity has also been demonstrated with the (*R*,*S*) isomer (7). With regard to the stereochemistry of the complexes, the *trans* isomer is more active than the *cis* isomer (8). As in the case of the parent cisplatin, the antitumor activity of DACH is accompanied by some toxicity. The emergence of resistance, and low water solubility that can affect the pharmacokinetics, are additional features that must be improved in the quest for a more effective analog. An obvious choice for platinum II complexes that can increase water solubility in this series is the introduction of hydrophilic groups such as the hydroxyl group into the molecule. Witiak and co-workers (9) as well as other groups (10) have reported on the synthesis and antitumor activity of a series of 4-mono- and 4,5-dihydroxy 1,2-diaminocyclohexane dichloroplatinum derivatives. Although these derivatives are sparingly soluble in water, the monohydroxy analogs are more active than the dihydroxy analogs. This enhanced potency was attributed to subtle differences in crystalline structure, thus affecting drug dissolution and bio-availability (9).

As part of a program aimed at the discovery of novel cisplatin-type antitumor agents with improved solubility, bioavailability, and efficacy, we have prepared acyclic (11) and heterocyclic (12) hydroxylated vicinal *trans* diamino platinum complexes. In addition to exhibiting potent antitumor activity in vitro as well as in vivo, these derivatives are also quite water soluble compared to cisplatin or related analogs.

[1]Author to whom correspondence may be addressed.

We now report on the synthesis of diastereomeric 3,6-dihydroxy-1,2-diaminocyclohexane dichloroplatinum derivatives, in addition to other anionic analogs, as well as their *O*-methyl variants. The intended structures shown in Fig. 1 were patterned after DACH where a *trans* relationship exists between the vicinal diamino groups with a relative (*R*,*R*) configuration. An important symmetry element in the design of the dihydroxy derivatives was to ensure a C_2 symmetrical relationship in an all-*trans* structure such as in **2**, and to assess the influence of stereochemical changes as in **3**. Since the 4,5-dihydroxy and the 4-hydroxy analogs of **1** showed differences in their biological activity (9) and they were sparingly soluble in water, it was of interest to assess the behavior of analogs **2** and **3**.

Scheme 1 illustrates the synthetic route to two diastereomeric 1,4-dihydroxy-2,3-diaminocyclohexanes, corresponding to **2** and **3** (R = H), respectively. 1,3-Cyclohexadiene **4** was transformed into the (±)*trans*-2-cyclohexene-1,4-diol **5** according to a known procedure (13). Epoxidation and protection of the resulting epoxide as the tetrahydropyranyl ether gave **8** in excellent overall yield. Alternatively, formation of the THP ether **6** followed by epoxidation led to the same epoxide **8**. Treatment of the epoxide **8** with ammonium azide, formed in situ from sodium azide and ammonium chloride in aqueous methoxyethanol (14) led to the mixture of stereoisomeric monoazido derivatives **9** in excellent yield. Although epoxides of cyclohexane derivatives are subject to predominant diaxial opening (15), some diequatorial opening is not uncommon, which is the origin of the contaminating stereoisomer in **9**. Treatment of the isomeric hydroxy azide derivative **9** with triphenylphosphine in refluxing toluene led to a single aziridine derivative **10** in 94% yield. Opening of the aziridino group with ammonium azide as for **8** gave a mixture of two amino azides that could be separated by preparative HPLC into the *cis-trans-cis* isomer **11** and the *trans-trans-trans* isomer **12** (5:1 ratio respectively). The preponderance of **11** can be explained by the known preference for diaxial opening (16), which was also

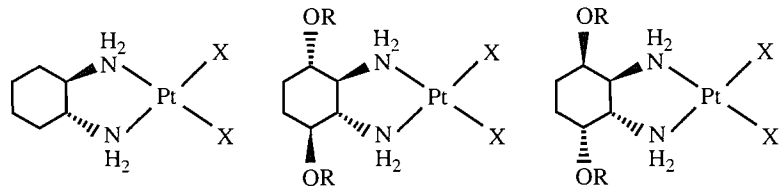

1 (DACH) **2** **3**

X = Cl, dicarboxylate, etc R = H, Me

FIG. 1

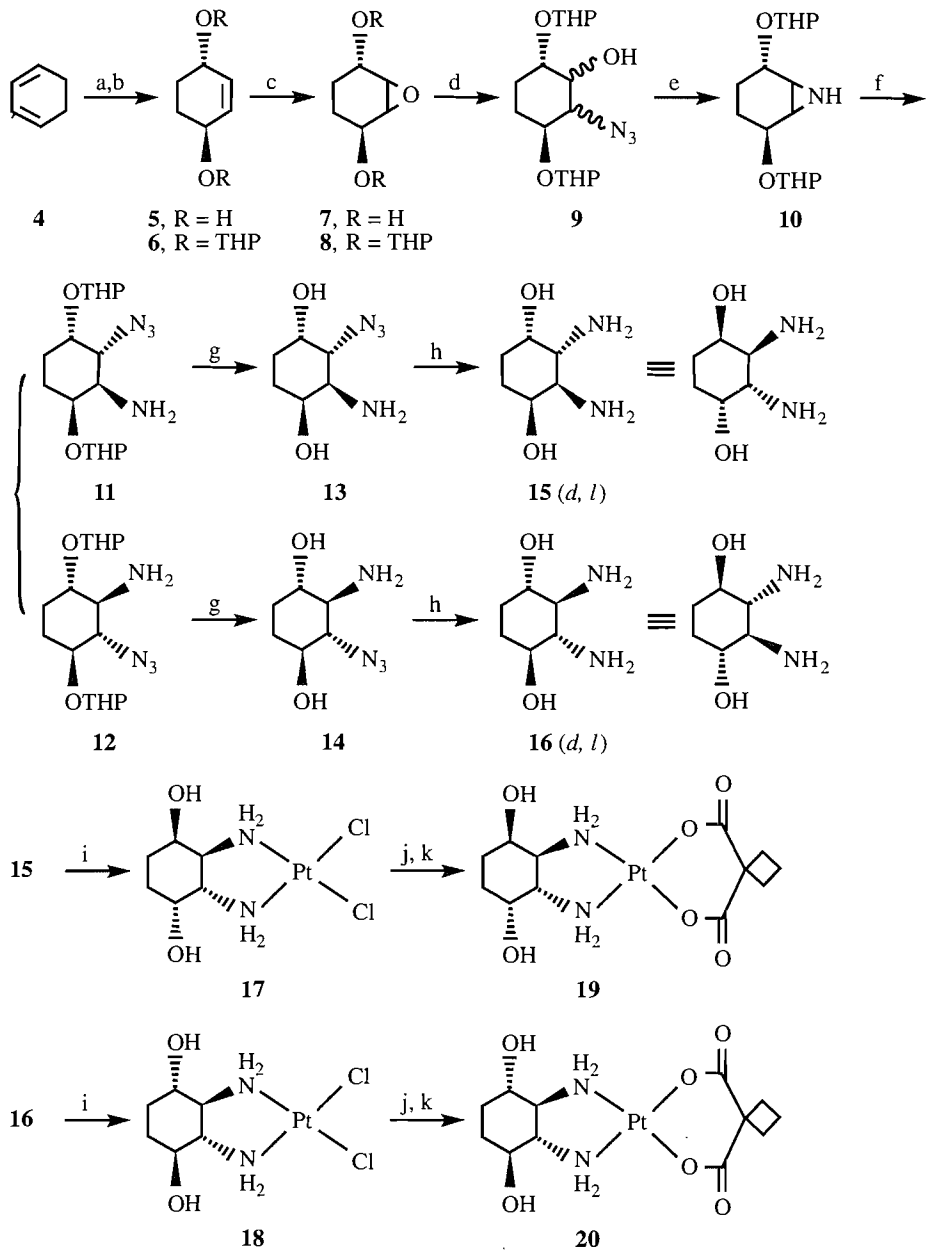

Reagents: (a) ref. 13; (b) dihydropyran, PPTS; (c) from **5**: (*i*) *m*-CPBA, CH_2Cl_2; (*ii*) dihydropyran, PPTS; from **6**: *m*-CPBA, CH_2Cl_2; (d) NaN_3, NH_4Cl, $MeOCH_2CH_2OH$; (e) Ph_3P, toluene; (f) NaN_3, NH_4Cl, $MeCH_2CH_2OH$; (g) Dowex-50 × 8(H^+), MeOH; (h) Pd/C (10%), H_2, MeOH; (i) K_2PtCl_4; H_2O; (j) $AgNO_3$; (k) dipotassium cyclobutane-1,1-dicarboxylate

SCHEME 1

Can. J. Chem. Downloaded from www.nrcresearchpress.com by 203.198.23.82 on 09/08/12
For personal use only.

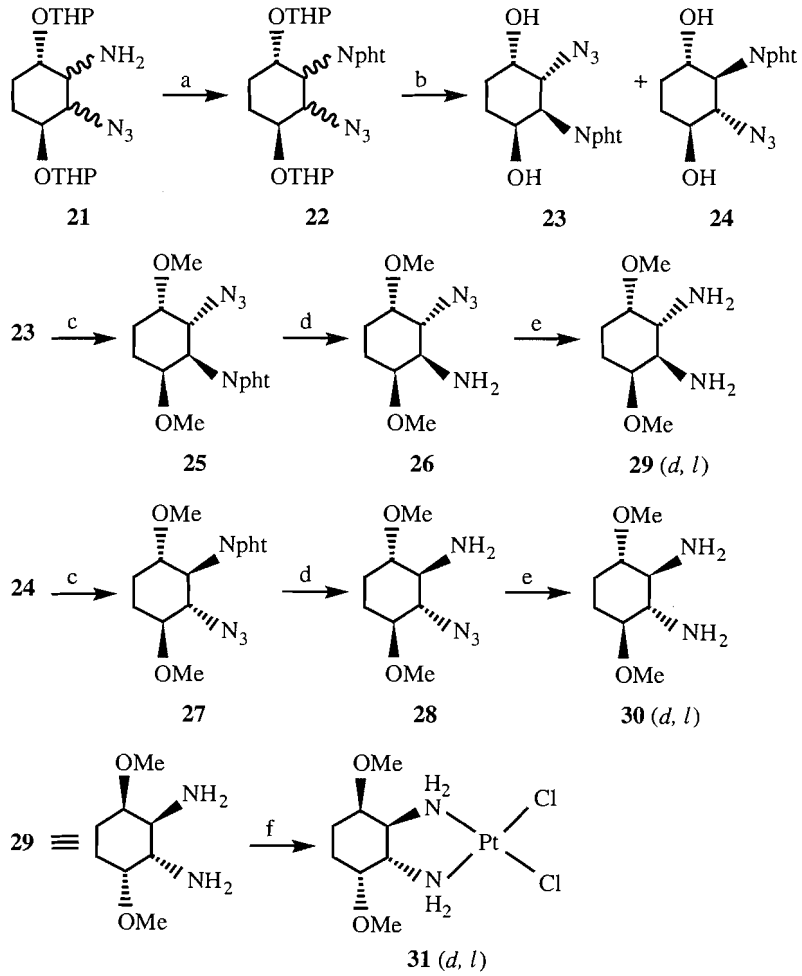

Reagents: (a) *N*-(ethoxycarbonyl) phthalimide, THF; (b) PPTS, EtOH; (c) KH, CH_3I, 18-crown-6, THF; (d) $NH_2NH_2 \cdot H_2O$, 95% EtOH; (e) Pd/C (10%), H_2, MeOH–H_2O; (f) K_2PtCl_4, H_2O

SCHEME 2

corroborated by ^1H NMR studies on **13** and its derivatives. The C_2 symmetrical analog **12** was the product of diequatorial opening as in the case of the epoxide **8**. Removal of the THP protective group from **11** and **12** led to **13** and **14**, respectively, which were transformed into the corresponding diamines **15** and **16** by catalytic hydrogenation. An alternative procedure was to use **11** and **12** as a mixture, and to separate **13** and **14** by column chromatography. Treatment of these diamines with dipotassium tetrachloroplatinate in aqueous solution gave the desired complexes **17** and **18** as pale yellow crystalline compounds. In view of the known influence of the anionic counterparts of cisplatinum complexes of vicinal diamines (17) on solubility and biological activity, we deemed it necessary to prepare the cyclobutane 1,1-dicarboxylate derivatives of **15** and **16** by adaptations of known procedures (18). Thus, the complexes **17** and **18** were individually transformed into the corresponding dinitrates and these were treated with dipotassium cyclobutane 1,1-dicarboxylate to give the corresponding complexes **19** and **20**, respectively. A single crystal X-ray analysis of **17** hydrate unequivocally confirmed its structure (19).

To assess the possible influence of polar vs. steric effects, we had envisaged the synthesis of the *O*-methyl derivatives of **17** and **18**, respectively. In view of the conditions of the methylation procedure, it was necessary to avoid the presence of a free amino group as in **11** or **12**. Consequently, a mixture of **11** and **12** (designated as **21**) was converted into a mixture of isomeric mono-*N*-phthalimido derivatives **22** (Scheme 2).

After cleavage of the THP group, it was possible to separate the diastereomeric diols **23** and **24** by column chromatography. As expected, the original 5:1 ratio present in the amino azides **11, 12** was retained. Methylation with potassium hydride and methyl iodide in the presence of 18-crown-6 led to the respective dimethyl ethers **25** and **27**, which upon hydrazinolysis led to **26** and **28**, respectively. Catalytic hydrogenation led to **29** and **30**, respectively. A yellow crystalline complex **31** was isolated from **29**, but the product from **30** was amorphous.

Biological results and discussion

The antitumor activities of the complexes **17, 18, 19, 20**, and **31** against P388 Leukemia were tested in vivo. BDF_1 mice (6 or 3 mice/group) were subjected to intraperitoneal transplants of 10^6 P388 tumor cell/mouse, and samples were administered i.p. in 0.2% Klucel brand methyl cellulose in water on days 1, 5, 9. Analysis of antitumor activity was

Can. J. Chem. Downloaded from www.nrcresearchpress.com by 203.198.23.82 on 09/08/12
For personal use only.

Can. J. Chem. Downloaded from www.nrcresearchpress.com by 203.198.23.82 on 09/08/12
For personal use only.

carried out according to the NCI protocol by comparing the median survival time (MST) of the treated groups vs. the untreated control groups. Increases in lifespan were expressed as % ILS, defined as the MST in a drug-treated group divided by the MST of the placebo-treated control group.

Preliminary data indicated that compound **18** had comparatively the highest antitumor activity with a % ILS value obtained with optimal ip dose (25 mg/kg) of 209, and an excellent MST (median survival time) of 34 days post tumor inoculation. Cisplatin showed a % ILS of 150 at 2 mg/kg with an MST of 27.5 days. Complexes **17, 20, 19**, and **31** showed very weak antitumor activity against P388 with poor survival ratios. It is thus possible that the stereochemistry of the dihydroxy cyclohexyldiamine platinum isomers may have a influence on their antitumor activities. Complex **18**, which contains a *trans-trans-trans* arrangement of substituents, was found to be significantly more active than the *cis-trans-cis* isomer **17**. The results of antitumor testing also showed that the complexes with hydroxyl group substituents (e.g., **17, 18**) were substantially more active than the complexes of the corresponding *O*-methyl ethers (e.g., **30, 31**). It seems that increasing the hydrophilicity of the DACH platinum complex to a certain extent could improve the antitumor activity of the drug.

Experimental

Melting points (mp) were determined on a Buchi melting point apparatus and they are uncorrected. Proton magnetic resonance (^{1}H NMR) spectra were determined on either a 300 MHz Varian or a 400 MHz Bruker spectrometer in deuterated chloroform, dimethyl sulfoxide-d_6, methanol-d_4, or deuterium oxide (D_2O) with $CHCl_3$ (δ_{ppm} = 7.265), Me_4Si (δ_{ppm} = 0.00), or dioxane (δ_{ppm} = 67.40 for ^{13}C) as references. Coupling constants are expressed in hertz (Hz). The abbreviations used for the description of the peaks are as follows: s, singlet; d, doublet; dd, doublet of doublets; dt, doublet of triplets; t, triplet; q, quartet; m, multiplet; br, broad. ^{13}C NMR spectra were recorded on a Varian VRX 300 at 75 MHz. Low-resolution mass spectra were determined on a VG Micro Mass 1212 mass spectrometer by using desorption chemical ionization (DCI), or by fast atom bombardment (FAB). High-resolution mass spectra were determined on a Kratos MS-50 TCTA mass spectrometer by using electron impact (EI) at 70 eV or by the fast atom bombardment (FAB) techniques. Infrared spectra (IR) were recorded on a Perkin–Elmer 781 infrared spectrophotometer. The spectra of solids were recorded as Nujol mulls. Liquid samples were determined as films between sodium chloride plates. Combustion analyses were performed by Guelph Laboratories Ltd, Guelph, Ontario. Flash chromatography was done according to the procedure of Still et al. (20) using Kieselgel 60 silica gel. Preparative HPLC was performed on a Waters Associates Prep LC/System 500 liquid chromatograph using Prep PAK-500/silica cartridge (5.7 × 30 cm) containing 325 g of silica gel.

(d,l)-trans-*1,4-Bis[(tetrahydropyran-2-yl)oxy]cyclohex-2-ene (6)*

A suspension of *trans*-2-cyclohexene-1,4-diol **5** (114 mg, 1 mmol) and dihydropyran (0.56 mL, 6 mmol) in dry CH_2Cl_2 (5 mL) containing a catalytic quantity of pyridinium *p*-toluenesulfonate (PPTS) was stirred for 7 h at room temperature. The reaction mixture was diluted with 20 mL ether, then washed with half-saturated brine (2 × 5 mL), dried with Na_2SO_4, and evaporated to give a colorless syrup, which was applied to a silica gel column. Elution with EtOAc/hexane (1:1), then concentration, gave **6** (242 mg, 83%) as a mixture of THP ethers: IR (film): 3030, 2940, 2870 cm^{-1}; ^{1}H NMR (400 MHz, $CDCl_3$) δ: 1.55–2.15 (m, 16H), 3.48–3.52 (m, 2H), 3.88–3.94 (m, 2H), 4.25–4.29 (m, 2H), 4.75–4.84 (m, 2H), 5.83–5.89 (m, 2H); MS *m/e*: 282 $(M)^+$; HRMS calcd. for $C_{16}H_{26}O_4$: 282.1832; found: 282.1812.

(d,l)-trans-*7-Oxabicyclo[4.1.0]heptane-2,5-diol (7)*

To a cold suspension of *trans*-2-cyclohexane-1,4-diol **5** (580 mg, 5 mmol) in 50 mL of dry CH_2Cl_2 was added dropwise a solution of 3-chloroperoxybenzoic acid (*m*-CPBA) (1.1 g, 5.1 mmol) at 0°C. The mixture was stirred at 0°C for 1 day, then a few drops of dimethyl sulfide were added to decompose the excess hydroperoxide. The solution was neutralized with triethylamine and evaporated to dryness. Purification by flash chromatography gave product **7** (0.64 g, 97%) as hygroscopic crystals: IR (Nujol) 3300 (br, OH) cm^{-1}; ^{1}H NMR (400 MHz, $CDCl_3$) δ: 1.24–1.38 (m, 2H, H-5,6), 1.73–1.82 (m, 2H, H-5,6), 3.28–3.39 (m, 2H, H-2,3), 4.07 (m, 2H, H-1,4); ^{13}C NMR (75 MHz, $CDCl_3$) δ: 23.98, 28.46, 55.90, 59.25, 64.97, 67.21; MS *m/e*: 131 $(M + 1)^+$.

(d,l)-trans-*2,5-Bis[(tetrahydropyran-2-yl)oxy]-7-oxabicyclo[4.1.0]heptane (8)*

Method A

To a suspension of epoxide **7** (7.50 g, 57.7 mmol) in 500 mL of dry CH_2Cl_2 was added dihydropyran (21 mL, 225 mmol) followed by PPTS (720 mg, 2.9 mmol). The mixture was stirred at room temperature for 1 day, then washed with half-saturated NaCl, dried with Na_2SO_4, and evaporated to give a syrup, which was applied to a silica gel column. Elution with hexane–EtOAc (5:1, then 1:2) gave the THP ether isomers **8** (14.30 g, 83%) as a syrup that was crystallized at 5°C overnight.

Method B

To a cold (0°C) solution of compound **6** (240 mg, 0.85 mmol) in 5 mL of dry CH_2Cl_2 was added a solution of *m*-CPBA (190 mg, 1.08 mmol) in 5 mL of dry CH_2Cl_2. The mixture was allowed to warm to room temperature and stirred for 1 day, then diluted with 10 mL of CH_2Cl_2, washed with 10% of sodium sulfite, saturated $NaHCO_3$, water, and brine, dried with Na_2SO_4, and evaporated to give a syrup that was applied to a silica gel column. Elution with EtOAc–hexane (1:3) gave the epoxide **8** (100 mg, 40%): mp 69–70°C; ^{1}H NMR (300 MHz, $CDCl_3$) δ: 1.15–2.00 (m, 16H), 3.13–3.34 (m, 1H), 3.38–3.40 (m, 1H), 3.48–3.53 (m, 2H), 3.83–3.98 (m, 3H), 4.02–4.10 (m, 1H), 4.68–4.89 (m, 2H); ^{13}C NMR (75 MHz, $CDCl_3$) δ: 19.15, 19.23, 19.29, 19.55, 20.08, 20.34, 21.73, 22.01, 25.14, 25.24, 26.14, 26.25, 28.08, 28.15, 30.61, 30.77, 53.21, 53.33, 55.31, 57.13, 57.29, 57.48, 61.99, 62.06, 62.32, 62.38, 62.71, 69.36, 69.73, 69.77, 71.70, 72.07, 72.45, 72.67, 97.03, 97.10, 97.20, 97.59, 97.67, 98.19; MS *m/e*: 299 $(M + 1)^+$; HRMS calcd. for $C_{16}H_{26}O_5$: 298.1781; found: 298.1779.

(d,l)-*(1α,2β,3α,6β)-2-Azido-3,6-bis(tetrahydropyran-2-yloxy)cyclohexanol and* (d,l)-*(1α,2β,3β,6α)-2-azido-3,6-bis(tetrahydropyran-2-yloxy)-cyclohexanol (9)*

To a solution of the epoxide **8** (1.0 g, 3.35 mmol) in 30 mL of 2-methoxyethanol–water (14:1) was added NaN_3 (1.30 g, 20 mmol) and NH_4Cl (0.54 g, 10 mmol). The mixture was heated at 90°C for 1 day and evaporated to give a residue that was applied to a short silica gel column (25 × 50 mm). Elution with EtOAc–hexane (1:1) gave a colorless syrup (1.10 g, 94%) that was the mixture of azide derivatives **9**: IR (film): 3430 (br, OH), 2105 (N_3) cm^{-1}; ^{1}H NMR (400 MHz, $CDCl_3$) δ: 1.33–1.90 (m, 16H), 3.54 (m, 3H), 3.85–4.17 (m, 5H), 4.50–4.80 (m, 2H); ^{13}C NMR (75 MHz, $CDCl_3$) δ: 18.52, 18.70, 19.44, 19.58, 19.79, 20.98, 21.04, 24.12, 24.47, 24.75, 24.94, 25.09, 25.22, 25.47, 25.62, 30.45, 30.62, 30.71, 30.75, 31.40, 61.48, 61.76, 62.64, 62.77, 63.14, 63.76, 63.91, 64.20, 64.89, 64.97, 69.27, 69.49, 69.67, 69.87, 71.55, 71.61, 76.14, 100.10, 100.27, 100.67; MS *m/e*: 342 $(M + 1)^+$, 341 $(M)^+$.

(d,l)-trans-*2,5-Bis(tetrahydropyran-2-yloxy)-7-azabicyclo[4,1,0]heptane (10)*

To a solution of the mixture of azide derivatives **9** (0.766 mg, 2.24 mmol) in 20 mL of dry toluene was added triphenylphosphine (710 mg, 2.7 mmol). The mixture was stirred at 105°C for 1 day, then evaporated to give a syrup that was applied to a silica gel column. Elution with EtOAc–hexane (3:1), then EtOAc, in the presence of 1% triethylamine gave the THP ether isomers **10** as a

Can. J. Chem. Downloaded from www.nrcresearchpress.com by 203.198.23.82 on 09/08/12
For personal use only.

syrup (630 mg, 94%) that crystallized after cooling in the refrigerator: mp 93–94°C, IR (film) 3300 (NH) cm^{-1}; ^1H NMR (300 MHz, $CDCl_3$) δ: 1.11–1.97 (m, 32H), 2.31–2.34 (m, 1H), 2.49–2.53 (m, 2H), 2.58–2.60 (m, 1H), 3.48–3.55 (m, 4H), 3.87–4.01 (m, 6H), 4.03–4.09 (m, 1H), 4.12–4.18 (m, 1H), 4.68–4.75 (m, 2H), 4.67–4.69 (m, 1H), 4.73–4.75 (m, 1H), 4.78–4.80 (m, 1H), 4.89–4.92 (m, 1H); ^{13}C NMR (75 MHz, $CDCl_3$) δ: 19.42, 19.48, 19.66, 19.73, 19.87, 20.37, 20.64, 22.11, 25.22, 25.30, 30.80, 30.86, 30.99, 31.96, 32.12, 34.15, 34.22, 36.01, 36.19, 36.29, 36.35, 62.41, 62.48, 62.75, 62.99, 71.55, 72.64, 96.67, 97.41, 97.75, 97.88, 98.05, 98.12; MS *m/e*: 298 $(M + 1)^+$. Anal. calcd. for $C_{16}H_{27}NO_4$: C 64.62, H 9.15, N 4.70; found: C 64.39, H 8.94, N 4.57.

(d,l)-*(1α,2β,3β,6α)-2-Azido-3,6-bis(tetrahydropyran-2-yloxy)cyclohexylamine* ***(11)*** *and* (d,l)-*(1β,2α,3β,6α)-2-azido-3,6-bis(tetrahydropyran-2-yloxy)cyclohexylamine* ***(12)***

A mixture of **10** (1.0 g, 3.36 mmol), NaN_3 (1.31 g, 20.1 mmol), and NH_4Cl (540 mg, 10.10 mmol) in 2-methoxyethanol and water (8:1) was stirred at 90°C for 18 h. Evaporation gave a residue that was extracted with EtOAc three times. After removal of the solvent the resulting syrup was purified on a silica gel column. Elution with EtOAc in the presence of 1% triethylamine gave a mixture of two isomers (1.0 g, 86%) that was separated by a preparative HPLC (Prep LC/System 500) liquid chromatograph (CH_2Cl_2/MeOH 40:1), to give the *trans-trans-trans* isomer **12** and the *cis-trans-cis* isomer **11** (ratio 1:5) as a syrup: ^1H NMR (300 MHz, $CDCl_3$) (mixture of **11** and **12**) δ: 1.5–1.9 (m, 16H), 3.4–3.6 (m, 4H), 3.85–4.30 (m, 4H), 4.56–4.88 (m, 2H); **11**: IR (film): 3380, 3320 (NH), 2105 (N_3) cm^{-1}; MS *m/e*: 341 $(M + 1)^+$; HRMS calcd. for $C_{16}H_{28}N_4O_4$: 340.2112; found: 340.2128; **12**: IR (film) 3380, 3300 (NH), 2100 (N_3) cm^{-1}; MS *m/e* 341 $(M + 1)^+$; HRMS calcd for $C_{16}H_{29}N_4O_4$ $(M + H)^+$: 341.2191; found: 341.2161.

(d,l)-*(1α,2α,3β,4β)-2-Amino-3-azidocyclohexane-1,4-diol* ***(13)***

A solution of **11** (115 mg, 0.34 mmol) in 10 mL of methanol was treated with 1.2 mL of Dowex 50w (H^+). The mixture was stirred vigorously at room temperature overnight. The resin was filtered and washed with MeOH and EtOAc three times, then eluted with 0.5 M NH_4OH aqueous solution. The eluant was evaporated to give a foam, which was dried over P_2O_5 under vacuum to afford the product **13** (58 mg, quant.) as a white powder: IR (film): 3350, 3280 (br), 2110 (N_3), 1560 cm^{-1}; ^1H NMR (300 MHz, D_2O) δ: 1.46 (m, 4H, H-5,6), 3.00 (dd, 1H, J = 2.6 Hz, 10.8 Hz, H-2), 3.53 (dd, 1H, J = 2.3 Hz, 10.8 Hz, H-3), 3.93 (s, 1H, H-1), 4.12 (s, 1H, H-4); ^{13}C NMR (75 MHz, D_2O) δ: 24.83, 24.92, 48.86, 51.39, 62.86, 66.56; MS *m/e*: 173 $(M + 1)^+$.

(d,l)-*(1α,2β,3α,4β)-2-Amino-3-azidocylohexane-1,4-diol* ***(14)***

This compound was prepared from **12** in 94% yield following the same procedure that was used for the preparation of **13**: IR (film): 3350, 3280 (br), 2105 (N_3), 1580 cm^{-1}; ^1H NMR (300 MHz, D_2O) δ: 1.17–1.29 (m, 2H, Hax-5,6), 1.73–1.80 (m, 2H, Heq-5,6), 2.47 (t, 1H, J = 10.3 Hz, H-2), 3.04 (t, 1H, J = 10.1 Hz, H-3), 3.33 (dt, 1H, J = 3.9 Hz, 10.2 Hz, H-1), 3.45 (dt, 1H, J = 3.8 Hz, 10.1 Hz, H-4); ^{13}C NMR (75 MHz, D_2O) δ: 30.10, 58.37, 71.62, 72.80, 73.27; MS *m/e* 173 $(M + 1)^+$; HRMS calcd. for $C_6H_{13}N_4O_2$: 173.1040; found: 173.1033.

(d,l)-*(1α,2α,3β,4β)-2,3-Diaminocyclohexane-1,4-diol* ***(15)***

To a solution of **13** (300 mg, 1.74 mmol) in 30 mL of MeOH and H_2O (1:1) was added 10% Pd/C (120 mg) suspended in 2 mL of methanol. The mixture was hydrogenated under atmospheric pressure overnight. The catalyst was removed by filtration through Celite, and the filtrate was evaporated to dryness to give the product **15** (226 mg, 89%) as a white solid: IR (film): 3500–3000 (br), 1560 cm^{-1}; ^1H NMR (300 MHz, D_2O) δ: 1.48–1.66 (m, 4H, H-5,6), 2.72 (s, 2H, H-2,3), 3.86 (s, 2H, H-1,4); MS *m/e*: 147 $(M + 1)^+$; HRMS calcd. for $C_6H_{14}N_2O_2$: 146.1056; found: 146.1057.

(d,l)-*(1α,2β,3α,4β)-2,3-Diaminocyclohexane-1,4-diol* ***(16)***

Compound **16** was prepared from **14** in 88% yield following the same procedure used for the preparation of **15**: IR (film): 3500–3000 (br), 1560 cm^{-1}; ^1H NMR (300 MHz, D_2O) δ: 1.16–1.23 (m, 2H, Hax-5,6), 1.71–1.77 (m, 2H, Heq-5,6), 2.19 (dd, 2H, J = 2.6 Hz, 6.7 Hz, H-2,3), 3.16 (ddd, 2H, J = 3.4 Hz, 6.8 Hz, 10.5 Hz, H-1,4); MS *m/e*: 147 $(M + 1)^+$; HRMS calcd. for $C_6H_{11}NO_2$ $(-NH_3)$: 129.0790; found: 129.0815.

(d,l)-*[SP-4-2-(1β,2α,3α,6β)]-dichloro(3,6-dihydroxycyclohexane-1,2-diamine*-N,N′*) platinum* ***(17)***

Potassium tetrachloroplatinate(II) (570 mg, 1.37 mmol) was dissolved in 6.7 mL of distilled water and insoluble material was filtered. To the dark red filtrate was added a solution of diamine **15** (200 mg, 1.37 mmol) in 3 mL of deionized water. The mixture was stirred manually until it became homogeneous, and the solution was left standing in the dark at room temperature. Yellow crystals began to appear after 3 h. When the original red color of the solution became yellow or orange yellow, the crystals were filtered, washed with cold water four times, and dried over P_2O_5 under vacuum in the absence of light to afford **17** (303 mg, 53%) as bright yellow crystals: mp 270°C (darkening), >290°C (dec.); IR (Nujol): 3420 (br), 3270, 3220, 3130, 1620, 1560 cm^{-1}; ^1H NMR (300 MHz, DMSO-d_6) δ: 1.30–1.40 (m, 2H, Hax-4,5), 1.53–1.66 (m, 2H, Heq-4,5), 2.78 (m, 2H, H-1,2), 3.91–3.98 (m, 2H, H-3,6), 5.10 (d, 1H, J = 3.3 Hz, OH), 5.28 (d, 1H, J = 3.3 Hz, OH), 5.12 (br s, 1H, NH), 5.60 (br s, 1H, NH), 6.07 (br s, 1H, NH), 6.25 (br s, 1H, NH); ^{13}C NMR (75 MHz, DMSO-d_6) δ: 23.4, 23.6, 57.2, 57.4, 64.1, 64.6; MS *m/e*: 414 $(M + 2)^+$, 413 $(M + 1)^+$, 412 $(M)^+$, 411 $(M - 1)^+$, 410 $(M - 2)^+$. Anal. calcd. for $C_6H_{14}Cl_2N_2O_2Pt$: C 17.48, H 3.42, N 6.80, Cl 17.20; found: C 17.34, H 3.51, N 6.53, Cl 16.82.

(d,l)-*[SP-4-2-(1β,2α,3α,6β)]-dichloro(3,6-dihydroxycyclohexane-1,2-diamine*-N,N′*) platinum* ***(18)***

The platinum complex **18** was prepared from the diamine **16** in 67% yield following the same procedure that was used for preparation of **17**: mp 275°C (darkening), >303°C (dec.); IR (Nujol): 3480, 3400 (br, OH), 3250, 3200, 3120 (NH), 1580 cm^{-1}; ^1H NMR (300 MHz, DMSO-d_6) δ: 0.99–1.06 (m, 2H, Hax-4,5), 1.57–1.62 (m, 2H, Heq-4,5), 2.14–2.19 (m, 2H, H-1,2), 3.32–3.39 (m, 2H, H-3,6), 4.83 (d, 2H, J = 4.6 Hz, OH), 5.01–5.06 (m, 2H, NH_2), 5.28–5.34 (m, 2H, NH_2); ^{13}C NMR (75 MHz, DMSO-d_6) δ: 31.15, 67.10, 70.71; MS *m/e*: 414 $(M + 2)^+$, 413 $(M + 1)^+$, 412 $(M)^+$. Anal. calcd. for $C_6H_{14}Cl_2N_2O_2Pt$: C 17.48, H 3.42, N 6.80, Cl 17.20; found: C 17.39, H 3.54, N 6.71, Cl 17.29. The solubility of **18** in water was > 1.2 mg/mL.

(d,l)-*[SP-4-2-(1β,2α,3β,6β)]-Cyclobutane-1,1-dicarboxylato(3,6-dihydroxycyclohexane-1,2-diamine*-N,N′*) platinum* ***(19)***

A suspension of **15** (100 mg, 0.24 mmol) in 25 mL of deionized water was heated until it dissolved. To this solution was added a solution of silver nitrate (82 mg, 0.48 mmol) in 5 mL of deionized water. The reaction mixture was stirred in the dark at room temperature for 20 h. The resulting white precipitate was filtered through Celite and washed with deionized water. The filtrate was concentrated to ca. 6 mL, then transferred into a solution of dipotassium cyclobutane-1,1-dicarboxylate (54 mg, 0.24 mmol) in 0.5 mL of deionized water. The mixture was stirred manually, and the clear solution was left standing in the dark. Crystals began to form after 2 days and they were filtered after 7 days, washed with deionized water, and dried over P_2O_5 under vacuum to afford **19** (77 mg, 66%, as white crystals); mp 260–265°C (dec.); IR (Nujol): 3440 (br, OH), 3270, 3240, 3180, 3100 (NH), 1660 (C=O), 1615 cm^{-1}; ^1H NMR (300 MHz, DMSO-d_6) δ: 1.25–1.28 (m, 2H, Hax-4,5), 1.52–1.55 (m, 2H, Heq-4,5), 1.58–1.69 (m, 2H, cyclobutane H-3), 1.58–1.69 (m, 2H, H-1,2), 2.63–2.71 (m, 4H, cyclobutane H-2,4), 3.81 (m, 2H, H-3,6), 4.48–4.55 (m, 2H, NH_2), 4.97 (d, 2H, J = 3.7 Hz, OH), 5.89–5.93 (m, 2H, NH_2); ^{13}C NMR (75 MHz, DMSO-d_6) δ: 15.21, 25.88, 30.38, 55.62, 60.15, 66.53, 177.53; MS *m/e*: 484 $(M + 1)^+$, 483 $(M)^+$, 482 $(M - 1)^+$; HRMS (FAB) calcd. for $C_{12}H_{21}N_2O_6Pt$: 484.1048; found:

Can. J. Chem. Downloaded from www.nrcresearchpress.com by 203.198.23.82 on 09/08/12
For personal use only.

484.1100. Anal. calcd. for $C_{12}H_{20}N_2O_6Pt \cdot H_2O$: C 28.74, H 4.42, N 5.59; found: C 28.35, H 4.67, N 5.41.

(d,l)-*[SP-4-2-(1α,2β,3α,6β)]-Cyclobutane-1,1-dicarboxylato(3,6-dihydroxycyclohexane-1,2-diamine*-N,N′*) platinum (**20**)*

The carboplatinum complex **20** was prepared from **16** in 52% yield following the same procedure that was used for the preparation of **19**: mp 250–255°C (dec.); IR (Nujol): 3520 (br, OH), 3270, 3210, 3100 (NH), 1640, 1610 cm^{-1}; ^1H NMR (300 MHz, DMSO-d_6) δ: 1.01–1.12 (m, 2H, Hax-4,5), 1.58–1.68 (m, 4H, Heq-4,5 and cyclobutane H-3), 2.02–2.09 (m, 2H, H-1,2), 2.67–2.75 (m, 4H, cyclobutane H-2,4), 3.28–3.32 (m, 2H, H-3,6), 4.83 (d, 2H, J = 4.8 Hz, OH), 5.27–5.32 (m, 2H, NH_2), 5.68–5.72 (m, 2H, NH_2); ^{13}C NMR (75 MHz, DMSO-d_6) δ: 15.09, 30.22, 31.49, 55.52, 66.54, 70.81, 177.44; MS *m/e*: 484 $(M + 1)^+$, 483 $(M)^+$; HRMS (FAB) calcd. for $C_{12}H_{21}N_2O_6Pt$: 484.1048; found: 484.1063. Anal. calcd. for $C_{12}H_{20}N_2O_6Pt \cdot H_2O$: C 28.74, H 4.42, N 5.59; found: C 28.51, H 4.34, N 5.28.

(d,l)-N-*2-Azido-3,6-bis(tetrahydropyran-2-yloxy)cyclohexyl-phthalimide (**22**)*

To a cold solution of *N*-(ethoxycarbonyl)phthalimide (1.05 g, 5 mmol) in 2 mL of dry THF was added a solution of **21** (mixture of **11** and **12**) (1.70 g, 5 mmol) in 2 mL of dry THF, followed by 1 mL of triethylamine at 0°C. The mixture was stirred at room temperature for 1 h, and then heated at reflux for 2 days. After removal of the solvent, the remaining syrup was dissolved in EtOAc, washed with 10% HCl, water, saturated $NaHCO_3$, water and brine, dried (Na_2SO_4), and evaporated to give a syrup, which was applied to a silica gel column. Elution with EtOAc–hexane (1:2) gave **22** (1.35 g, 58%) as a mixture of the THP isomers, which was used for the next reaction without further purification: IR (film): 2105 (N_3), 1800, 1775, 1720 (C=O) cms^{-1}; ^1H NMR (300 MHz, $CDCl_3$) δ: 0.85–2.05 (m, 16H), 2.91–3.10 (m, 1H), 3.40–3.85 (m, 2H), 3.89–3.97 (m, 1H), 4.08–4.28 (m, 2H), 4.35–4.50 (m, 1H), 4.60–4.68 (m, 1H), 4.84–4.93 (m, 2H), 7.70–7.76 (m, 2H, ArH), 7.85–7.89 (m, 2H, ArH); MS *m/e*: 471 $(M + 1)^+$.

(d,l)-*(1α,2α,3β,4β)-2-Azido-3-phthalimidocyclohexane-1,4-diol (**23**) and* (d,l)-*(1β,2α,3β,4α)-2-azido-3-phthalimidocyclohexane-1,4-diol (**24**)*

To a solution of **22** (1.34 g, 2.85 mmol) in 60 mL of 100% EtOH was added PPTS (0.1 g, 0.4 mmol). The reaction mixture was stirred at 55–60°C for 1 day. After removal of the solvent, the mixture was separated by flash chromatography with EtOAc–hexane (1:1) to give **23** (100 mg, 12%) and its isomer **24** (480 mg, 56%) as white crystals. For **23**: mp 174–175°C; IR (film): 3450 (br, OH), 2260, 2110 (N_3), 1780, 1720 (C=O) cm^{-1}; ^1H NMR (300 MHz, CD_3OD) δ: 1.62–1.76 (m, 2H, Hax-5,6), 2.00–2.07 (m, 2H, Heq-5,6), 4.08–4.09 (m, 1H, H-1), 4.31–4.32 (m, 1H, H-4), 4.53 (dd, 1H, J = 2.6 Hz, 12.0 Hz, H-2), 4.84 (dd, 1H, J = 2.8 Hz, 12.0 Hz, H-3), 7.79–7.88 (m, 4H, ArH); MS *m/e*: 303 $(M + 1)^+$: Anal. calcd. for $C_{14}H_{14}N_4O_4$: C 55.62, H 4.67, N 18.54; found: C 55.68, H 5.08, N 18.27. For **24**: mp 161–163°C; IR (film): 3480 (OH), 3410 (OH), 2260, 2105 (N_3), 1780, 1720 (C=O) cm^{-1}; ^1H NMR (300 MHz, CD_3OD) δ: 1.38–1.64 (m, 2H, Hax-5,6), 1.98–2.05 (m, 2H, Heq-5,6), 3.55 (ddd, 1H, J = 4.3 Hz, 9.3 Hz, 10.8 Hz, H-4), 3.80 (dd, 1H, J = 10.1 Hz, 11.3 Hz, H-2), 4.02 (dd, 1H, J = 9.3 Hz, 11.3 Hz, H-3), 4.31 (dt, 1H, J = 4.2 Hz, 10.4 Hz, H-1), 7.81–7.90 (m, 4H, ArH); ^{13}C NMR (75 MHz, CD_3OD) δ: 31.33, 31.48, 59.73, 66.83, 68.80, 74.16, 124.09, 124.39, 135.53, 135.62, 169.74, 170.13; MS *m/e*: 303 $(M + 1)^+$. Anal. calcd. for $C_{14}H_{14}N_4O_4$: C 55.62, H 4.67, N 18.54; found: C 56.07, H 4.84, N 18.87.

(d,l)-N-*[(1β,2α,3α,6β)-2-Azido-3,6-dimethoxycyclohexyl] phthalimide (**25**)*

To a cold solution of **23** (800 mg, 2.65 mmol) in 40 mL of dry THF was added methyl iodide (1.0 mL, 16.0 mmol), 18-crown-6 ether (catalytic), followed by potassium hydride (35% in oil) (730 mg, 6.37 mmol) suspended in 2 mL of THF. The mixture was stirred at 0°C for 5 h with the exclusion of moisture and the resulting precipitate was filtered and washed with 400 mL of ether. The filtrate was washed with cold water and brine, dried (Na_2SO_4), and evaporated to give a syrup that was purified by flash chromatography. Elution with EtOAc–hexane (1:1) gave **25** (0.63 g, 72%) as a syrup that crystallized on standing: mp 123–124°C; IR (film): 2105 (N_3), 1775, 1720 (C=O) cm^{-1}; ^1H NMR (300 MHz, $CDCl_3$) δ: 1.65–1.94 (m, 4H, H-4,5), 3.22 (s, 3H, OCH_3), 3.44 (s, 3H, OCH_3), 3.65 (m, 1H, H-3), 3.88 (m, 1H, H-6), 4.60 (dd, 1H, J = 2.9 Hz, 12.3 Hz, H-2), 4.85 (dd, 1H, J = 2.9 Hz, 12.3 Hz, H-1), 7.73 (m, 2H, ArH), 7.87 (m, 2H, ArH); MS *m/e*: 331 $(M + 1)^+$. Anal. calcd. for $C_{16}H_{18}N_4O_4$: C 58.17, H 5.49, N 16.96, found: C 57.98, H 5.11, N 16.71.

(d,l)-N-*[(1β,2α,3β,6α)-2-Azido-3,6-dimethoxycyclohexyl] phthalimide (**27**)*

Compound **27** was prepared from **24** in 57% yield following the same procedure that was used for the preparation of **25**: IR (film): 2105 (N_3), 1775, 1715 (C=O) cm^{-1}; ^1H NMR (300 MHz, $CDCl_3$) δ: 1.18–1.48 (m, 2H, Hax-4,5), 2.21–2.31 (m, 2H, Heq-4,5), 3.23 (s, 3H, OCH_3), 3.25 (ddd, 1H, J = 4.2 Hz, 9.3 Hz, 11.0 Hz, H-3), 3.49 (s, 3H, OCH_3), 3.36–3.45 (m, 2H, H-2,6), 4.16 (dd, 1H, J = 9.3 Hz, 11.3 Hz, H-1), 7.73–7.78 (m, 2H, ArH), 7.87 (m, 2H, ArH); MS *m/e*: 331 $(M + 1)^+$. Anal. calcd. for $C_{16}H_{18}N_4O_4$: C 58.17, H 5.49, N 16.96; found: C 57.99, H 5.19, N 16.86.

(d,l)-*(1β,2α,3α,6β)-3,6-Dimethoxy-2-azidocyclohexylamine (**26**)*

To a solution of compound **25** (620 mg, 1.88 mmol) in 30 mL of 95% EtOH and THF (2:1) was added hydrazine monohydrate (4.5 mL, 93 mmol). The reaction mixture was stirred at room temperature for 2 days and the resulting white precipitate was filtered and washed with ethanol. After concentration of the filtrate, excess 10% HCl was added and the resulting precipitate was filtered. The pH of the filtrate was adjusted with KOH to pH > 13 and the solution was extracted with ether. The extracts were dried (Na_2SO_4) and evaporated to give a syrup that was purified by flash chromatography, eluting with CH_2Cl_2–MeOH (15:1), to give compound **26** (262 mg, 70%) as a colorless syrup: IR (film): 3390, 3320 (NH), 2105 (N_3), 1580 cm^{-1}; ^1H NMR (300 MHz, D_2O) δ: 1.32–1.46 (m, 2H, Hax-4,5), 1.60–1.75 (m, 2H, Heq-4,5), 2.88 (m, 1H, H-1), 3.16 (s, 3H, OCH_3), 3.19 (s, 3H, OCH_3), 3.43 (m, 2H, H-2,6), 3.67 (m, 1H, H-3); MS *m/e*: 201 $(M + 1)^+$.

(d,l)-*(1β,2α,3β,6α)-3,6-Dimethoxy-2-azidocyclohexylamine (**28**)*

Compound **28** was prepared from **27** in 65% yield following the same procedure that was used for the preparation of **26**: IR (film): 3390, 3320 (NH), 2105 (N_3), 1580 cm^{-1}; ^1H NMR (300 MHz, D_2O) δ: 0.90–1.13 (m, 2H, Hax-4,5), 1.98–2.10 (m, 2H, Heq-4,5), 2.41 (t, 1H, J = 10.1 Hz, H-1), 2.95 (dt, 1H, J = 4.4 Hz, 10.6 Hz, H-6), 3.01 (t, 1H, J = 10.1 Hz, H-2), 3.17 (dt, 1H, J = 4.6 Hz, 10.9 Hz, H-3), 3.21 (s, 3H, OCH_3), 3.28 (s, 3H, OCH_3); MS *m/e*: 201 $(M + 1)^+$.

(d,l)-*(1β,2α,3α,6β)-3,6-Dimethoxycyclohexane-1,2-diamine (**29**)*

To a solution of azide **26** (260 mg, 1.3 mmol) in 15 mL of MeOH and deionized water (1:1) was added 10% Pd/C (100 mg) suspended in 2 mL of MeOH. After stirring under an atmosphere of hydrogen at room temperature overnight, the catalyst was removed by filtration through Celite and the filtrate was evaporated to give the diamine **29** (147 mg, 65%) as a syrup: ^1H NMR (300 MHz, D_2O) δ: 1.55 (m, 2H, H-4,5), 1.90 (m, 2H, H-4,5), 2.86 (m, 2H, H-1,2), 3.38 (s, 6H, OCH_3), 3.62 (m, 2H, H-3,6); MS *m/e*: 175 $(M + 1)^+$; HRMS calcd. for $C_8H_{18}N_2O_2$: 174.1369; found: 174.1352.

(d,l)-*(1α,2β,3α,6β)-3,6-Dimethoxycyclohexane-1,2-diamine (**30**)*

The diamine **30** was prepared from **28** in 60% yield following the same procedure that was used for the preparation of **29**: ^1H NMR (300 MHz, D_2O) δ: 1.20 (m, 2H, H-4,5), 2.25 (m, 2H, H-4,5), 2.59 (m, 2H, H-1,2), 3.13 (m, 2H, H-3,6), 3.43 (s, 6H, OCH_3);

MS *m/e*: 175 $(M + 1)^+$; HRMS calcd. for $C_8H_{18}N_2O_2$: 174.1369; found: 174.1366.

(d,l)-*[SP-4-2-(1β,2α,3α,6β)]-Dichloro(3,6-dimethoxycyclohexane-1,2-diamine-*N,N′*) platinum (31)*

Potassium tetrachloroplatinate(II) (310 mg, 0.75 mmol) was dissolved in 3.5 mL of deionized water and the insoluble material was filtered. To this dark red filtrate was added a solution of diamine **29** (130 mg, 0.75 mmol) in 2 mL of deionized water. The mixture was stirred manually until homogeneous and the solution was left standing in the dark at room temperature. Crystallization began after 3 h. When the original red color of the solution became yellow or orange yellow, the crystals were filtered, washed with cold water several times, and dried over P_2O_5 under vacuum in the absence of light to afford the platinum complex **31** (250 mg, 76%) as bright yellow crystals: IR (Nujol): 3280, 3260, 3220, 3180, 3105 (NH) cm^{-1}; ^1H NMR (300 MHz, DMSO-d_6) δ: 1.13–1.26 (m, 2H, Hax-4,5), 1.54–1.65 (m, 2H, Heq-4,5), 2.54–2.57 (m, 2H, H-1,2), 3.21 (s, 6H, OCH_3), 3.45–3.47 (m, 2H, H-3,6), 4.18–4.23 (m, 2H, NH), 5.53–5.66 (m, 2H, NH); ^{13}C NMR (75 MHz, DMSO-d_6) δ: 20.44, 56.61, 60.52, 76.10; MS *m/e*: 441 $(M + 1)^+$, 440 $(M)^+$, 439 $(M - 1)^+$; HRMS (FAB) calcd. for $C_8H_{18}Cl_2N_2O_2Pt$: 439.0395; found: 439.0442. Anal. calcd. for $C_8H_{18}Cl_2N_2O_2Pt$: C 21.82, H 4.12, N 6.36, Cl 16.11; found: C 21.68, H 3.80, N 6.13, Cl 15.78.

Acknowledgments

We wish to thank the National Cancer Institute (NCI) (Canada) and the Natural Sciences and Engineering Research Council of Canada for financial support. Biological tests were carried out at Lederle Laboratories, Pearl River, N.Y. We thank Dr. S. Lang for his support.

1. P.C. Hydes and M.J.H. Russell. Cancer Metastasis Rev. **7**, 67 (1988); I.H. Krakoff. *In* Platinum and other metal coordination compounds in cancer chemotherapy. *Edited by* M. Nicolini. Martinus Nijhoff Publishing, Boston. 1988. pp. 351–354; T.A. Connors, M. Jones, W.C.J. Ross, P.D. Braddock, A.R. Khokhar, and M.L. Tobel. Chem. Biol. Interact. **5**, 415 (1972); M.J. Cleare and J.D. Hoeschele. Bioinorg. Chem. **2**, 187 (1973); G.R. Gale, E.M. Walker, L.M. Atkins, A.B. Smith, and S.J. Meischen. Res. Commun. Chem. Pathol. Pharmacol. **7**, 529 (1974); H. Ridway, L.M. Hall, R.J. Speer, D.P. Stewart, G.R. Edwards, and J.H. Hill. Wadley Med. Bull. **6**, 11 (1976); B. Rosenberg, L. Van Camp, J.E. Trosko, and V.H. Mansour. Nature, **222**, 385 (1969).
2. J.C. Dabrowiak and W.T. Bradner. Prog. Med. Chem. **24**, 129 (1987).
3. M.J. Cleare and J.D. Hoeschele. Platinum Met. Rev. **17**, 2 (1973); L.S. Hollis, A.R. Amundsen, and E.W. Stern. J. Am. Chem. Soc. **107**, 274 (1985); P. Schwartz, S.J. Meischen, G.R. Gale, L.M. Atkins, A.B. Smith, and E.M. Walker. Cancer Treat. Rep. **61**, 1519 (1977).
4. Y. Kidani, K. Inagaki, R. Saito, and S. Tsukagoshi. J. Clin. Hematol. Oncol. **7**, 197 (1977); G. Mathe, Y. Kidani, M. Noji, R. Maral, C. Bourut, and E. Chenu. Cancer Lett. **27**, 135 (1985).
5. M. Gulloti, A. Pasini, R. Ugo, S. Filippeschi, L. Marmonti, and F. Spreafico. Inorg. Chim. Acta, **91**, 223 (1984); Y. Kidani, K. Inagaki, M. Iigo, A. Hoshi, and K. Kuretani. J. Med. Chem. **21**, 1315 (1978); M. Noji, K. Okamoto, Y. Kidani, and T. Tashiro. J. Med. Chem. **24**, 508 (1981); Y. Kidani, M. Noji, and T. Tashiro. Gann, **71**, 637 (1980); A. Pasini, A. Velcich, and A. Mariani. Chem. Biol. Interact. **42**, 311 (1982).
6. J.H. Burchenal, K. Kalaher, T. O'Toole, and J. Chisholm. Cancer Res. **37**, 3455 (1977); M.A. Bruck, R. Bau, M. Noji, K. Inagaki, and Y. Kidani. Inorg. Chim. Acta, **92**, 279 (1984).
7. J.F. Vollano, S. Al-Baker, J.C. Dabrowiak, and J.E. Schurig. J. Med. Chem. **30**, 716 (1987).
8. M. Noji, K. Okamoto, Y. Kidani, and T. Tashiro. J. Med. Chem. **24**, 508 (1981); K. Inagaki and Y. Kidani. Inorg. Chem. **25**, 1 (1986); K. Okamoto, M. Noji, T. Tashiro, and Y. Kidani. Chem. Pharm. Bull. **29**, 929 (1981).
9. D.T. Witiak, D.P. Rotella, J.A. Filppi, and J. Gallucci. J. Med. Chem. **30**, 1327 (1987); D.T. Witiak, D.P. Rotella, Y. Wei, J.A. Filppi, and J. Gallucci. J. Med. Chem. **32**, 214 (1989).
10. T. Tsubomura, S. Yano, K. Kobayashi, T. Sakurai, and S. Yoshikawa. J. Chem. Soc. Chem. Commun. 459 (1986); M. Noji, K. Chisaki, J. Hirose, T. Kato, and Y. Kidani. Chem. Pharm. Bull. **34**, 2321 (1986).
11. S. Hanessian, J.-Y. Gauthier, K. Okamoto, T. Theophanides, and A. Beauchamp. Can. J. Chem. **71**, 880 (1993).
12. S. Hanessian and J. Wang. Can. J. Chem. **71**, 886 (1993).
13. J.-E. Backvall, S.E. Bystrom, and R.E. Nordberg. J. Org. Chem. **49**, 4619 (1984).
14. R.D. Guthrie and D. Murphy. J. Chem. Soc. 5288 (1963); K. Ponsold. Chem. Ber. **97**, 3524 (1963).
15. F.H. Newth. Q. Rev. Chem. Soc. **13**, 30 (1959).
16. F.H. Newth and R.F. Homer. J. Chem. Soc. 989 (1953).
17. J.P. Macquet and J.L. Butour. J. Natl. Cancer Inst. **70**, 899 (1983).
18. T.A. Connors, M. Jones, W.C.J. Ross, P.D. Braddock, A.R. Khokhar, and M.L. Tobel. Chem. Biol. Interact. **5**, 415 (1972); B. Lippert, C.J.L. Lock, B. Rosenberg, and M. Zvagulis. Inorg. Chem. **16**, 1525 (1977); R.C. Harrison and C.A. McAuliffe. Inorg. Chim. Acta, **46**, L15–16 (1980); T. Totani, K. Aono, M. Komura, and Y. Adachi. Chem. Lett. 429 (1986).
19. J. Wang, Y.L. Bennani, F. Bélanger-Gariépy, and S. Hanessian. Acta Crystallogr. Sect. C: Cryst. Struct. Commun. **C47**, 1067 (1991).
20. W.C. Still, M. Kahn, and A. Mitra. J. Org. Chem. **43**, 2923 (1978).

Can. J. Chem. Downloaded from www.nrcresearchpress.com by 203.198.23.82 on 09/08/12
For personal use only.

The tetrahedral intermediate from the hydration of *N*-methylformanilide

J. PETER GUTHRIE,[1] JONATHAN BARKER, PATRICIA A. CULLIMORE, JINQIAO LU, AND DAVID C. PIKE
Department of Chemistry, University of Western Ontario, London, ON N6A 5B7, Canada

Received May 14, 1993

J. PETER GUTHRIE, JONATHAN BARKER, PATRICIA A. CULLIMORE, JINQIAO LU, and DAVID C. PIKE. Can. J. Chem. **71**, 2109 (1993).

Heats of hydrolysis of *N*-methylformanilide dimethyl acetal have been measured in basic solution. The heat of formation of *N*-methylformanilide was obtained by determining the equilibrium constant in aqueous solution for its formation from formic acid and *N*-methylaniline as a function of temperature: $\Delta H_f^0(l) = -33.78 \pm 1.85$ kcal/mol. These data permit the calculation of the heat of formation of *N*-methylformanilide dimethyl acetal, $\Delta H_f^0(l) = -72.95 \pm 1.85$ kcal/mol. The free energy of formation of the tetrahedral intermediate in the hydrolysis of *N*-methylformanilide was calculated by methods we have previously reported. Consideration of the energetics of the intermediates and the known rates of reaction leads to the conclusion that the rate-determining step for alkaline hydrolysis is cleavage of the C—N bond.

J. PETER GUTHRIE, JONATHAN BARKER, PATRICIA A. CULLIMORE, JINQIAO LU et DAVID C. PIKE. Can. J. Chem. **71**, 2109 (1993).

Opérant en solution basique, on a mesuré les chaleurs d'hydrolyse l'acétal diméthylique de la *N*-méthylformanilide. On a obtenu la chaleur de formation de la *N*-méthylformanilide en déterminant la constante d'équilibre en fonction de la température (en solution aqueuse) pour sa formation à partir de l'acide formique et la *N*-méthylaniline: $\Delta H_f^0(l) = -33{,}78 \pm 1{,}85$ kcal/mol. Ces données permettent de calculer la chaleur de formation de l'acétal diméthylique de la *N*-méthylformanilide, $\Delta H_f^0(l) = -72{,}95 \pm 1{,}85$ kcal/mol. Utilisant des méthodes décrites antérieurement, on a calculé l'énergie libre de formation de l'intermédiaire tétraédrique impliqué dans l'hydrolyse de la *N*-méthylformanilide. Une considération des énergies des intermédiaires et des constantes de vitesse connues mène à la conclusion que l'étape qui détermine la vitesse de la réaction de l'hydrolyse alcaline est le clivage de la liaison C—N.

[Traduit par la rédaction]

Can. J. Chem. Downloaded from www.nrcresearchpress.com by 203.198.23.82 on 09/08/12
For personal use only.

Introduction

Slebocka-Tilk et al. (1) recently studied ^{18}O exchange accompanying hydrolysis of anilides in acid. Brown, Guthrie, and co-workers (2) showed that this can be explained in terms of a detailed mechanism including the proton transfer steps interconverting different protonation states of the tetrahedral intermediates. Neither proton transfer nor bond rotation were rate determining, although proton transfers were concerted with the heavy atom bond-making and -breaking steps. To test this interpretation it would be desirable to have energies of the tetrahedral species on the reaction path for hydrolysis of these amides. We have undertaken to determine these energies for intermediates derived from *N*-methylformanilide by our thermochemical method (3).

Results

The first anilide derivative that we studied was *N*-methylformanilide dimethyl acetal, which will permit determination of the free energy of *N*-methylformanilide hydrate. This compound was chosen for reasons of experimental convenience, because the formanilide acetal is relatively stable to thermal decomposition, and so can be purified and studied relatively conveniently.

Base-catalyzed hydrolysis could be studied in 50% DMSO – water; in 90% DMSO – water the hydrolysis was too slow for calorimetry, while the acetal was too insoluble in water to permit measurement of the heat of reaction. Alternatively, hydrolysis could be studied in 50% methanol – water. Experimental results, heats of reaction and solution, are summarized in Table 1. The directly measured heat of hydrolysis refers to the process:

[1] $HC(OMe)_2N(Me)Ph\ (l) + H_2O\ (soln) \rightleftharpoons x[HCON(Me)Ph\ (soln) + 2MeOH\ (soln)] + (1 - x)[HCOOMe\ (soln) + PhNHMe\ (soln) + MeOH\ (soln)]$

It should be remembered that HCOOMe (soln) will actually be sodium formate plus methanol, the products of the rapid alkaline hydrolysis of methyl formate. The heat of reaction for process [1] must be converted, by combining with heats of solution, to the hypothetical reaction with all species in their standard states (process [2]) in order to allow convenient calculation of the standard enthalpy of formation.

[2] $HC(OMe)_2N(Me)Ph\ (l) + H_2O\ (l) \rightleftharpoons x[HCON(Me)Ph\ (l) + 2MeOH\ (l)] + (1 - x)[HCOOMe\ (l) + PhNHMe\ (l) + MeOH\ (l)]$

The stoichiometry of the hydrolysis, x, must also be known, and was determined by experiments using DMSO-d_6:D_2O or CD_3OD:D_2O as solvent. The products in both cases were >95% *N*-methylformanilide and <5% methyl formate by nmr analysis. Thus in base, $x = 1.0$, and the hydrolysis can be written.

[3] $HC(OMe)_2N(Me)Ph\ (l) + H_2O\ (l) \rightleftharpoons HCON(Me)Ph\ (l) + 2MeOH\ (l)$

To obtain a heat of formation for *N*-methylformanilide we determined the heat of reaction for process [4].

[4] $HCOOH(aq) + PhNHMe(aq) \rightleftharpoons HCON(Me)Ph(aq)\ (+ H_2O(l))$

[1]Author to whom correspondence may be addressed.

Can. J. Chem. Downloaded from www.nrcresearchpress.com by 203.198.23.82 on 09/08/12
For personal use only.

TABLE 1. Experimental heats of reaction and solution[a]

	Heat of reaction or solution
N-Methylformanilide dimethyl acetal	-4.09 ± 0.12[b]
	-4.49 ± 0.48[c]
N-Methylformanilide	$+2.33 \pm 0.06$[b]
	$+2.15 \pm 0.05$[c]
	$+0.20 \pm 0.06$[d]
Water	$+0.307 \pm 0.016$[b]
	-0.31 ± 0.02[c]
Methanol	$+0.094 \pm 0.021$[b]
	-0.26 ± 0.02[c]
Formic acid	-14.28 ± 0.20[b]
Methyl formate	-12.11 ± 0.37[b]
N-Methylaniline	$+2.13 \pm 0.02$[b]
	$+0.33 \pm 0.11$[d]

[a]At 25°C.
[b]In 50% DMSO, 50% water, with 0.1 N tetraethylammonium hydroxide.
[c]In 50% methanol, 50% water, with 0.1 N NaOH.
[d]In aqueous solution, pH 8.0 phosphate buffer, ionic strength 0.1 M.

TABLE 2. Transamidation[a]

Temperature	K[b]
24.90	2.41 ± 0.16
35.00	2.33 ± 0.34
45.90	2.40 ± 0.18

$\Delta H_{reaction}$[c] $= -0.06 \pm 0.31$ kcal/mol

[a]In aqueous solution, initial concentrations were 24.83 mM PhNHMe, 200.2 mM NH_2OH, and either 10.04 mM *N*-methylformanilide or 9.8 mM formohydroxamic acid, at ionic strength 1.0 (KCl). Suitable scaling corrections were made for the small differences in initial amide concentrations.
[b]Equilibrium constant for the reaction: HCONHOH + PhNHMe $\rightleftharpoons$ HCON(Me)Ph + NH_2OH. The standard state for all species is 1 M aqueous solution.
[c]From a van't Hoff plot of ln K vs. $1/T$.

This was done by van't Hoff analysis of the equilibrium constants at 25, 35, and 45°C for processes [5] and [6].

[5] HCONHOH(aq) + PhNHMe(aq) $\rightleftharpoons$ HCON(Me)Ph(aq) + NH_2OH(aq)

[6] HCOOH(aq) + NH_3OH^+(aq) $\rightleftharpoons$ HCONHOH(aq) + H^+(aq)

The equilibrium constant for the formation of *N*-methylformanilide from formohydroxamic acid and *N*-methylaniline, process [5], was determined by the method of Fersht and Requenna (4), which is based on determining the initial changes in concentration of formohydroxamic acid for process [5] under pseudo-first-order conditions for *N*-methylaniline and hydroxylamine, starting with either formohydroxamic acid or *N*-methylformanilide. Equilibration was slow at 25°C, with a pseudo-first-order rate constant for approach to equilibrium between formohydroxamic acid and *N*-methylformanilide of 1.7×10^{-3} h^{-1} at pH 6.12, 0.20 M total hydroxylamine, 0.025 M *N*-methylaniline. The equilibrium constants at the three temperatures are found in Table 2. From a van't Hoff plot we obtain an enthalpy of reaction of -0.06 ± 0.31 kcal/mol. At 25°C,

$$K = [HCON(Me)Ph][NH_2OH]/[HCONHOH][PhNHMe] = 2.41 \pm 0.16$$

TABLE 3. Formation of formohydroxamic acid[a]

Temperature	$10^4 K$[b]	
24.90	5.09[c]	5.02[d]
35.00	5.39[c]	5.20[d]
45.20	5.65[c]	5.49[d]

$\Delta H_{reaction}$[e] $= 0.97 \pm 0.04$ kcal/mol

[a]In aqueous solution, solutions contained 2.00 M HCOOH, 0.90 M $NH_2OH \cdot HCl$, and 0.1 MHCl, or 1.98 M HCOOH, 0.88 M $NH_2OH \cdot HCl$, 20.2 mM formohydroxamic acid, and 0.12 M HCl. These solutions were calculated to end with identical concentrations of all species.
[b]Equilibrium constant for the reaction: HCOOH + NH_3OH^+ $\rightleftharpoons$ HCONHOH + H^+ ($+H_2O$). [H^+] was taken as 10^{-pH}. pH was 0.906 for reactions starting with no formohydroxamic acid and 0.930 for reactions starting with 0.0202 formohydroxamic acid. The standard state of water was the pure liquid; for all other species the standard state was 1 M aqueous solution. K is then dimensionless.
[c]Initial formohydroxamic acid concentration was zero.
[d]Initial formohydroxamic acid concentration was 0.0202 M.
[e]From a van't Hoff plot of ln K vs. $1/T$.

The next step was to determine the enthalpy of reaction for formation of formohydroxamic acid according to reaction [6]. The apparent equilibrium constant for the formation of formohydroxamic acid was measured at 25, 35, and 45°C, following the method of Fersht and Requenna (4), which is based on determination of the final equilibrium concentration of formohydroxamic acid for solutions 2 M in formic acid, 0.1 M in HCl, and 0.9 M in hydroxylammonium. The equilibrium constant data are found in Table 3. These data led to a heat of reaction of $+0.97 \pm 0.04$ kcal/mol.

At 25°C Fersht and Requenna (4) derived a value for the equilibrium constant:

$$K = [HCONHOH]/[NH_2OH][HCOOH] = 934 \pm 37\ M^{-1}$$

From the heats of reaction for processes [5] and [6], the heat of formation data in Table 4, and heats of solution for *N*-methylaniline and *N*-methylformanilide, we can calculate the heat of formation of formohydroxamic acid in aqueous solution, and thence the heat of formation of *N*-methylformanilide in aqueous solution. This calculation required a heat of formation of *N*-methylaniline in aqueous solution, which was unexpectedly difficult to determine because of the low solubility of *N*-methylaniline, and in particular the slow dissolution of this compound. The pure liquid was injected into pH 8 phosphate buffer (ionic strength 0.1 M) and the temperature change was recorded. Immediately after determining the heat of solution, a sample was

Can. J. Chem. Downloaded from www.nrcresearchpress.com by 203.198.23.82 on 09/08/12
For personal use only.

removed, taking care to avoid contamination by undissolved amine, and the concentration of dissolved amine was determined by uv spectroscopy. This allowed determination of the heat of solution as 0.33 ± 0.11 kcal/mol. The heat of solution of *N*-methylformanilide was readily determined as 0.20 ± 0.06 kcal/mol. With these values in hand we are finally able to calculate the heat of formation of liquid *N*-methylformanilide as −33.71 ± 1.84 kcal/mol. The principal source of error in this estimate is the uncertainty in the heat of formation of *N*-methylaniline. This means that the absolute values we derive have substantial errors, but values of heats or free energies of reaction for processes involving *N*-methylaniline will have smaller errors.

A second estimate of the heat of formation of *N*-methylformanilide is possible starting with the equilibrium constant for amide formation from formic acid and *N*-methylaniline, process [4]. This allows calculation of the free energy of formation of *N*-methylformanilide in aqueous solution. Now we use the free energy of transfer to calculate the free energy of formation of *N*-methylformanilide as the gas. The free energy of transfer is available from the solubility, measured in this work as 0.26 M, and the vapor pressure, estimated (5) from the vapor pressure at 8 Torr (1 Torr = 133.3 Pa), using the heat of vaporization estimated (5) from the available vapor pressure data (6–9), an estimated heat capacity of vaporization (10), and a method based on that of Prausnitz (5, 11). We then used the standard entropy of *N*-methylformanilide to calculate the heat of formation of the gaseous anilide. The entropy was estimated using a disproportionation reaction, assuming that there is no entropy change except that due to symmetry numbers for the process:

[7] $HCON(Me)_2 + HN(Me)Ph \rightleftharpoons HCON(Me)Ph + HN(Me)_2$

The standard entropy of *N,N*-dimethylformamide was calculated from the vibrational frequencies (12), moments of inertia and reduced moments of inertia calculated from the MM2 geometry, and values for the rotational barriers from ref. 12; the rotational barrier used for the amide bond was that for formamide (12). These data lead to S_{tr} = 38.78, S_{rot} = 25.55, S_{vib} = 4.04, S_{hr} = 6.28, and $S^0(g)$ = 74.65 cal deg^{-1} mol^{-1}. The standard entropy of gaseous dimethylamine is 65.24 (13).

Finally, from the heat of vaporization, estimated as already described, we were able to estimate a heat of formation for liquid *N*-methylformanilide as −34.87 ± 1.93 kcal/mol, which is within the uncertainty limits of the other value. This confirms the internal consistency of our calculations.

Heats of formation of *N*-methylformanilide and *N*-methylformanilide dimethyl acetal are found in Table 4, which includes thermodynamic data for all compounds discussed in this paper.

With the enthalpy of formation of *N*-methylformanilide dimethyl acetal in hand, we proceed to calculate the free energy of formation of this compound in aqueous solution. First we require the heat of vaporization. This was estimated from the boiling point at reduced pressure, as previously described (5). Next we needed the standard entropy of the molecule in the gas phase. This was estimated by Benson's bond and group additivity schemes (14, 15); to apply group additivity it was necessary to estimate values for $[CH(O)_2(N)]$ (estimated from the bond additivity contributions as [C—H] + 0.5(2[C—O] + [C—N])), and for $[N(C_B)(C)_2]$ (taken as approximately $[N(C)_3]$). These two estimates were in good agreement. Finally, we needed a free energy of transfer. This cannot be measured because of the rapid hydrolysis of the amide acetal in aqueous solution (16), and so must be estimated. We did so using a method which we reported recently (17), making use of group additivity modified by a Taft $\rho^*-\Sigma\sigma^*$ correlation to allow for "Distant Polar Interactions" (18). The free energy of transfer requires contributions for each structural feature, and ρ^* values for each non-aliphatic group to allow for the effect of other polar substituents on the solvation of that group. ρ^* for ether oxygen is known (17) but we required a value for ρ^* for N(Me)Ph. To determine this we prepared $CF_3CH_2N(CH_3)Ph$ and determined its free energy of transfer. Since the ρ^* for F is known, the only thing required to calculate the free energy of transfer is ρ^* for N(Me)Ph, which was found to be 1.10, which is slightly larger than the value, 0.872, for aliphatic N. The free energy of transfer of *N*-methylformanilide dimethyl acetal can now be calculated as 2.48 kcal/mol. The free energy of formation of *N*-methylformanilide dimethyl acetal can now be calculated as −2.18 kcal/mol. The results of all of these calculations are found in Table 4.

The quantity of interest is the free energy of formation of the corresponding carbonyl hydrate, $HC(OH)_2N(Me)Ph$. This is calculated by our usual method (3) using the hypothetical hydrolysis process:

[8] $HC(OMe)_2N(Me)Ph + 2H_2O \rightleftharpoons HC(OH)_2N(Me)Ph + 2MeOH$

for which we estimate the free energy change, allowing for electronic, steric, and symmetry effects (19). When this is done we obtain the value found in Table 4.

Discussion

We are now going to use the free energies of formation of the tetrahedral intermediates to analyze the kinetic data for hydrolysis of *N*-methylformanilide. In doing this we will consistently report free energies or log *K* values to two decimal points. In terms of absolute values based on thermochemical data this is too many significant figures, as the associated uncertainty limits will show. However, giving this many digits provides guard figures to prevent accumulation of roundoff error, and allows calculation of differences in energy that may be, and often are, considerably more accurate than the absolute free energy values.

It is now possible to calculate the equilibrium constant for addition of water to *N*-methyl formanilide, process [9], from the

[9] $HCO\text{-}N(Me)Ph + H_2O \rightleftharpoons HC(OH)_2\text{-}N(Me)Ph$

free energies of formation of each of the species involved. The value so calculated is log K_{H_2O} = −10.22 ± 3.26, based on the pure liquid standard state for water. By estimating the pK_a of this covalent hydrate we can calculate the equilibrium constant for the addition of hydroxide, as log K_{OH^-} = −8.19 ± 3.41. From the intrinsic barrier for addition of hydroxide to carbonyl compounds, $\hat{G}$ = 8.7 kcal/mol (20), we can estimate the free energy of activation of OH^- addition as 17.61 kcal/mol relative to separate starting materials. This estimate allows for the partial desolvation of hydroxide when it diffuses into contact with the carbonyl carbon (20). The

TABLE 4. Thermodynamic values for compounds discussed in this paper[a]

(a) Compounds for which free energies of formation have been reported

Compound	ΔH_f(l)	ΔG_f(aq)
H_2O	−68.32 ± 0.01	−56.69[b]
HCOOH	101.60 ± 0.10	−88.83[c]
MeOH	−57.02 ± 0.07	−41.88[b]
HCOOMe	−92.28 ± 0.14	−73.38[d]

(*b*) Compounds for which free energies of formation were calculated in this work

Compound	ΔH_f(g)	S^0(g)	ΔG_f(g)	ΔH_{vap}	ΔH_f(l)	ΔG_t	ΔG_f(aq)
HN(Me)Ph	20.06 ± 1.50[e]	81.60 ± 3.00[f]	47.27 ± 1.74[h]	12.07 ± 1.01[g]	7.99 ± 1.80[h,i]	−2.61 ± 0.50[j]	44.65 ± 1.81[h]
HCON(Me)Ph	−18.07 ± 1.88[h]	92.39 ± 3.00[k]	13.63 ± 1.88[h]	16.80 ± 0.44[l]	−34.87 ± 1.93[m]	−5.70 ± 0.50[n]	7.93 ± 1.81[h]
	−16.90 ± 1.89[h]	92.39 ± 3.00[k]	14.85 ± 2.09[h]	16.80 ± 0.44[l]	−33.71 ± 1.84[o]	−5.70 ± 0.50[n]	9.10 ± 2.15[h]
$HC(OMe)_2N(Me)Ph$	−53.94 ± 2.07	137.65 ± 3.00[p]	0.30 ± 2.26[h]	16.91 ± 1.00[q]	−70.85 ± 1.82[r]	−2.55 ± 1.00[s]	−2.25 ± 2.47[h]
HC(OMe)(OH)N(Me)Ph							−19.05 ± 3.27[t]
$HC(OH)_2N(Me)Ph$							−34.80 ± 3.91[t]

(*c*) Compounds for which the heat of formation in aqueous solution was needed

Compound	ΔH_f(l)	$\Delta H_{solution}$	ΔH_f(aq)
NH_2OH			−23.49 ± 0.02[b]
NH_3OH^+			−32.79 ± 0.02[b]
HCOOH	−101.60 ± 0.02[b]	−0.16 ± 0.02[b]	−101.76 ± 0.02[b]
HCONHOH			−65.13 ± 0.16[u]
PhNHMe	7.99 ± 1.80[h,i]	0.33 ± 0.11[v]	8.32 ± 1.81[h]
HCO-N(Me)Ph	−33.78 ± 1.85[o]	0.20 ± 0.06[v]	−33.56 ± 1.84[h]

[a]All at 25°C; enthalpies and free energies are in kcal/mol, entropies are in cal deg^{-1} mol^{-1}, standard states are the ideal gas at 1 atm and 1 M aqueous solution with an infinitely dilute reference state. Unless otherwise noted, enthalpies of formation are from ref. 47, entropies are from ref. 48, free energies of formation in the gas phase are calculated from the corresponding enthalpies of formation and the standard entropies, and free energies of formation in aqueous solution are calculated from the corresponding free energies of formation in the gas and free energies of transfer.

[b]Reference 49, standard state is the pure liquid.

[c]Reference 50.

[d]Reference 51.

[e]Estimated starting from the value for HN(Et)Ph given in Pedley et al. (47), 13.46 ± 1.41 kcal/mol. This was adjusted for removal of CH_2 using Benson's (15) group contribution value for [CH2(N)(O)] = −6.6; the error was taken as 0.5. Thus we obtained ΔH_f^0(g) = 20.06 ± 1.73 kcal/mol for HN(Me)Ph; Vriens and Hill give 20.4 (52).

[f]Reference 52.

[g]Estimated starting from the value for HN(Et)Ph, given in Pedley et al. (47) as 12.50 ± 1.00 kcal/mol. This was adjusted for removal of CH_2 using a group contribution (53) for [CH2(N)(O)] = 0.43 ± 0.13. This led to ΔH_{vap} = 12.07 ± 1.41 kcal/mol. Vriens and Hill give 12.7 (52).

[h]Calculated from other values in this table.

[i]Vriens and Hill give 7.7 (52).

[j]Calculated from the solubility, measured in this work, and the vapor pressure at 25°C (52).

[k]Estimated by disproportionation as described in the text.

[l]Calculated from boiling point data. For *N*-methylformanilide the following values were available: bp (°C), *p* (Torr), derived heat of vaporization (kcal/mol); 118., 8., 16.99 (this work); 134., 20., 16.66 (ref. 6: Beil, 12, H, 234); 142., 20., 17.34 (ibid); 253., 716., 17.00 (ibid); 244., 760., 16.22 (ibid); 251., 760., 16.69 (ibid); 132., 22., 16.31 (ref. 7: Beil, 12, II, 136); 121., 8., 17.25 (ibid); 123., 13., 16.54 (ref. 8: Beil, 12, III, 454); 95., 4., 16.13 (ibid); 152., 40., 16.74 (ref. 9: Beil, 12, IV, 370); 130., 15., 16.87 (ibid); 95.5, 1.5, 17.72 (ibid); average 16.80 ± 0.44.

[m]Calculated from equilibrium constants and other data as described in the text.

[n]Calculated from the solubility, measured in this work, and the vapor pressure, estimated as described in the text.

[o]Calculated from heats of formohydroxamic acid formation and transamidation as described in the text.

[p]Estimated by group additivity as described in the text.

[q]Calculated from boiling point data: bp 87°C at 1.5 Torr leads to ΔH_{vap} = 16.91 kcal/mol.

[r]Calculated from the heat of hydrolysis as described in the text.

[s]Estimated as described in the text.

[t]Calculated using ΔG^0 values for hypothetical hydrolysis reactions as described in the text.

[u]Calculated from the heat of reaction as described in the text.

[v]This work.

value so estimated is significantly less than the observed value, 22.56 kcal/mol (30).

When we plot log k_{HO^-} vs. log K_{HO^-} we find that most carbonyl compounds fall approximately on a single curved line (21) but *N*-methylformanilide does not; see Fig. 1. The assumption that all carbonyl compounds would fall on one curve is equivalent to assuming that the addition step is always rate determining, which is not always the case, as has been recently shown for amides (22). If we estimate the rate constant for expulsion of *N*-methylaniline, assuming the mechanism proposed (22) for expulsion of dimethylamine in base-catalyzed hydrolysis of *N,N*-dimethyltoluamide, we obtain a good match to the observed rate constant.

First we estimate pK_a values leading to the anionic zwitterion, $HC(O^-)_2$–N^+H(Me)Ph, as previously described (22). These estimates require σ* values for N(Me)Ph and NH^+(Me)Ph; in the absence of data allowing better estimates, we use the values for NHPh and NH_2^+Ph (2), 1.19 and 4.07, respectively. The pK_a values that we estimated are given in Scheme 1. We carried out similar estimates for the

Can. J. Chem. Downloaded from www.nrcresearchpress.com by 203.198.23.82 on 09/08/12
For personal use only.

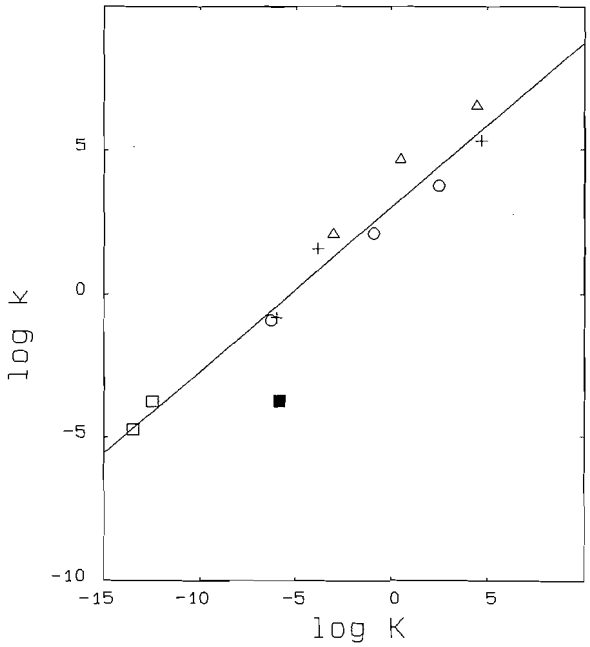

FIG. 1. Rate equilibrium correlation for the reaction of hydroxide with RCOZ, where the carbonyl compound can be *N*-methylformanilide (■), an amide (□), an ester (○), a thioester (⁺), or an aldehyde or ketone (△).

tetrahedral intermediates derived from *N,N*-dimethylformamide; these values are given in Scheme 2. Other pK_a values were needed in order to estimate the energies of "corner intermediates" for the application of Multidimensional Marcus Theory (23). These pK_a values are given in Table 5.

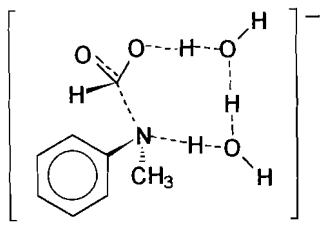

Multidimensional Marcus Theory (23) is an extension of our treatment of concerted reactions (20, 23*b*) to higher numbers of reaction coordinate dimensions. We have written computer programs (23*a*) to find the lowest transition state on the energy hypersurface. The position of the transition state on the hypersurface tells whether a reaction is stepwise, with essentially only one reaction coordinate changing in the transition state, or concerted, with two or more reaction coordinates changing in the transition state.

From the pK_a values estimated above we calculate the equilibrium constant for converting the anionic hydroxide adduct to the anionic zwitterion as log $K = -8.02$. From the equilibrium constants for overall reaction with hydroxide, addition of hydroxide, and anionic zwitterion formation, we can calculate the equilibrium constant for breakdown of the anionic zwitterion to products as log $K = 23.15$.

To calculate a rate constant for this breakdown process [10], we need the intrinsic barrier. For the addition of

[10] H-C(O^-)$_2$–N^+H(Me)Ph ⇌ H-COO^-, NH(Me)Ph

aniline, we can deduce an intrinsic barrier from data for the

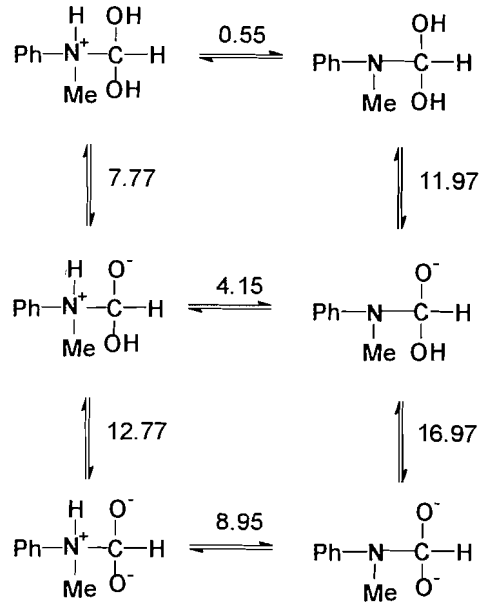

SCHEME 1. pK_a values for tetrahedral intermediates from *N*-methylformanilide.

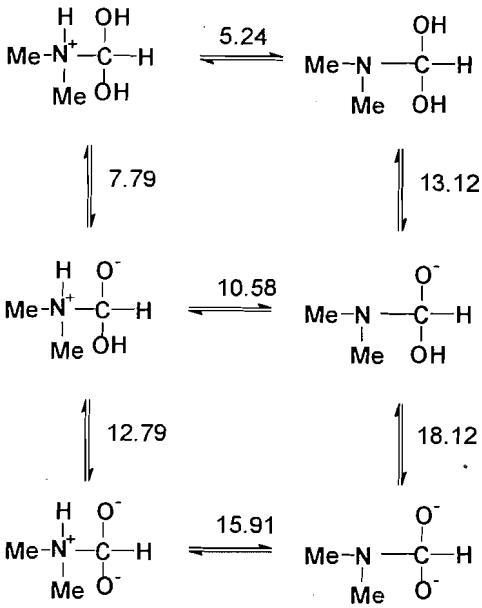

SCHEME 2. pK_a values for tetrahedral intermediates from *N,N*-dimethylformamide.

reaction of aniline with *p*-chlorobenzaldehyde (24). The rate constant for addition leading to the zwitterionic tetrahedral intermediate, process [11], is 60 M^{-1} s^{-1}. The equilibrium

[11] *p*ClPh-CHO + NH_2Ph ⇌ *p*ClPh-CH(O^-)(N^+H_2Ph)

constant for addition to give the neutral carbinolamine is 0.0089 M^{-1}. We estimate the pK_a for the NH^+ in the protonated carbinolamine, dissociation process [12], as follows: beginning

[12] *p*ClPh-CH(OH)(N^+H_2Ph)

⇌ *p*ClPh-CH(OH)(NHPh) + H^+

Can. J. Chem. Downloaded from www.nrcresearchpress.com by 203.198.23.82 on 09/08/12
For personal use only.

Can. J. Chem. Downloaded from www.nrcresearchpress.com by 203.198.23.82 on 09/08/12
For personal use only.

TABLE 5. pK_a values[a]

	pK_a
(*a*) Ammonium ions	
$NMe_2H_2^+$	10.64[b]
$PhNH_2Me^+$	4.85[b]
(*b*) Amines	
NMe_2H	36.[c]
NMe_2H	41.97[d]
$PhNH_2$	27.7[e]
PhN(Me)H	27.7[c]
PhN(Me)H	30.6[f]
(*c*) Carboxylic acids	
HCOOH	3.77[b]
(*d*) Protonated carbonyl compounds	
$HC(OH)_2^+$	−8.8[g]
NMe_2-CH=OH^+	−1.5[h]
PhN(Me)-CH=OH^+	−0.58[i]
*p*ClPh-CH=OH^+	−4.73[j]
(*e*) Tetrahedral intermediates	
$(NMe_2H^+)CH(OH)_2$	5.17[k,l]
$(NMe_2H^+)CH(OH)_2$	7.79[k,m]
$(NMe_2H^+)CH(OH)(O^-)$	12.38[k,n]
$(NMe_2H^+)CH(OH)(O^-)$	14.30[k,o]
$(NMe_2)CH(OH)_2$	12.72[k]
$(NMe_2)CH(OH)(O^-)$	19.23[k]
$(NMe_2H^+)CH(O^-)_2$	19.59[k]
$HC(OH)(NMe_2)(OH_2^+)$	−3.86[k,l]
$HC(OH)(NMe_2)(OH_2^+)$	8.83[k,m]
$HC(O^-)(NMe_2)(OH_2^+)$	−0.20[k]
$(PhN(Me)H^+)CH(OH)_2$	1.68[k,l]
$(PhN(Me)H^+)CH(OH)_2$	7.77[k,m]
$(PhN(Me)H^+)CH(OH)(O^-)$	6.50[k,n]
$(PhN(Me)H^+)CH(OH)(O^-)$	14.28[k,o]
$PhN(Me)CH(OH)_2$	11.97[k]
$PhN(Me)CH(OH)(O^-)$	18.48[k]
$PhN(Me)H^+CH(O^-)_2$	11.33[k]
$HC(OH)(NPhMe)(OH_2^+)$	−4.37[k,l]
$HC(OH)(NPhMe)(OH_2^+)$	8.08[k,m]
$HC(O^-)(NPhMe)(OH_2^+)$	−0.70[k]
$(PhNH_2^+)CH(OH)(p\text{ClPh})$	1.66[k,l]
$(PhNH_2^+)CH(OH)(p\text{ClPh})$	9.23[k,m]
$(PhNH)CH(OH)(p\text{ClPh})$	14.81[k]
$(PhNH)CH(O^-)(p\text{ClPh})$	7.24[k]

[a]All at 25°C, in aqueous solution unless otherwise noted.
[b]Reference 25.
[c]Reference 54.
[d]Estimated, after ref. 55, from the pK_a of dimethylammonium ion in water using a plot of the pK_a of ammonium ions in water against the pK_a of the corresponding amines in DMSO.
[e]Reference 56; this value is for aniline and is assumed to be approximately correct for *N*-methylaniline as well.
[f]Reference 55.
[g]Reference 36.
[h]Reference 57.
[i]Estimated from the pK_a for protonated DMF assuming the effect of replacing methyl by phenyl is the same as in *N*-methylacetamide (pK_{BH^+} = −0.42 (58)) and acetanilide (pK_{BH^+} = −0.99 (58)).
[j]Taken as the pK_{BH^+} of benzoic acid, since *p*-chlorobenzaldehyde and benzoic acid are half protonated at the same concentration of sulfuric acid (59).
[k]Estimated using the correlation equations reported in ref. 36, except that for oxonium ions we constrained the line to pass through the pK_{BH^+} for ethanol reported by Lee and Demchuk (60), and we now use $\sigma^*(H) = 0.0$ for oxonium ions. The σ^* values were from ref. 26 except for: PhN(Me)- (assumed to be the same as PhNH-, $\sigma^* = 1.19$ (2), H_2O^+-, $\sigma^* = 5.1$ (36), Me_2N-, $\sigma^* = 0.62$ (62).
[l]Dissociation from nitrogen to give the neutral species.
[m]Dissociation from oxygen to give the zwitterion.
[n]Dissociation from nitrogen to give the anion.
[o]Dissociation from oxygen to give the anionic zwitterion.

with *N*-methylanilinium ion, pK_a 4.85 (25), the effect of replacing methyl by benzyl is taken from the difference in pK_a between dimethylammonium, 10.64 (25), and benzylmethylammonium, 9.58 (25), this gives 3.97 for *N*-benzylanilinium ion. The effect of the *p*-chloro is taken from a Hammett correlation for benzylamines (26), $\Delta pK_a = 0.25$. The effect of the carbinolamine OH is taken as the average value recommended by Hine, $\Delta pK_a = 1.88$ (27). These corrections lead to a pK_a of 1.66 for the NH of the protonated carbinolamine. The pK_a for dissociation of the OH in the protonated carbinolamine, dissociation process[13], is estimated

[13] $p\text{ClPh-CH(OH)}(N^+H_2Ph) \rightleftharpoons p\text{ClPh-CH}(O^-)(N^+H_2Ph) + H^+$

as follows: beginning with hydroxymethylanilinium ion, pK_a 9.58 (28), the effect of replacing CH_2 by CHPh is taken from the difference in pK_a between methanol, 15.54 (25), and benzyl alcohol, 15.44 (25); this gives a pK_a for Ph-NH_2^+-CH(Ph) of 9.48. The effect of the *p*-chloro is taken from a Hammett correlation for benzylamines (26), leading to a pK_a for OH dissociation of the protonated carbinolamine of 9.23. The two pK_a values lead to a zwitterion content, $pK_z = 7.57$, and an

[14] $K_2 = [p\text{ClPh-CH}(O^-)(N^+H_2Ph)]/[p\text{CLPh-CH(OH)(NHPh)}]$

equilibrium constant for addition of aniline to *p*-chlorobenzaldehyde to give the zwitterionic carbinolamine of 2.39×10^{-10} M^{-1}. With rate and equilibrium constants for the rate-determining step in place, we may calculate the intrinsic barrier as 6.05 kcal/mol, using a work term calculated using only simple encounter with no favorable or unfavorable interactions (29). We will use this value for *N*-methylaniline as well. The zwitterionic tetrahedral intermediate formed from aniline and *p*-chlorobenzaldehyde has a very short lifetime, because it is so high in energy, and it will undergo a rapid water-mediated proton switch to give the neutral tetrahedral intermediate. When we apply Multidimensional Marcus Theory we find that the rate-determining step for addition of aniline is essentially pure C—N bond formation; the water-mediated proton switch is after the transition state.

With this intrinsic barrier, we see that the anionic zwitterion will probably have no lifetime, breaking down to products as fast as it is formed. This implies that the rate-determining step will be the water-mediated proton switch converting the anionic tetrahedral intermediate into the anionic zwitterion. We can estimate the rate constant for the breakdown of the anionic intermediate, by way of the anionic zwitterion, using Multidimensional Marcus Theory (23). The overall free energy of activation is predicted to be 21.47 kcal/mol relative to starting materials, and the tran-

sition state is predicted to be essentially proton transfer, with no C—N bond breaking.

In applying Multidimensional Marcus Theory we must estimate the free energies of formation of the various "corner intermediates" that would arise from the various stepwise processes that must occur to get from starting material to products. The energies of these corner intermediates are given in Table 6.

Comparison of the predicted transition state energies for hydroxide addition, 17.45 kcal/mol, and for breakdown by way of the anionic zwitterion, 20.08 kcal/mol (both relative to the separated starting materials), clearly shows that the second process is expected to be slower and rate determining. The relative activation energies for these processes, which both depend on the free energy of the anionic tetrahedral intermediate, should be more reliable than the absolute values. Error analysis suggests that the free energy of hydration of *N*-methylformanilide has an uncertainty of ±2.4 kcal/mol, and there will be an additional uncertainty from the Multidimensional Marcus Theory calculations. The observed free energy of activation is 22.56 kcal/mol (30). The detailed reaction coordinate diagram that we are now able to draw is shown in Fig. 2, based on the mechanism shown in Scheme 3.

For the base-catalyzed hydrolysis of acetanilides and formanilides, there is a consensus that the C—N cleavage process is rate limiting (31–33). Deslongchamps et al. (34) report extensive ^{18}O exchange accompanying hydrolysis of *N*-methylformanilide by aqueous KOH at 90°C.

Anilides are known (30–33) to hydrolyse in base by two paths, one first order and one second order in base. We will now do Multidimensional Marcus calculations for the latter path. We start with the encounter complex of hydroxide and the monoanionic form of the tetrahedral intermediate, and end with the encounter complex of formate ion, aniline, and hydroxide. This allows for the possibility of general base and (or) general acid-catalyzed breakdown of the intermediate, with hydroxide as possible general base, and water as possible general acid. The result is that the reaction is predicted to have a transition state with the dianion completely formed, and in the process of cleaving the C—N bond, and negligible transfer of proton from water to nitrogen. The predicted free energy of activation (relative to separate starting materials) is 18.90 kcal/mol. The observed value is 21.68 kcal/mol (30).

We must now look briefly at the case of *N,N*-dimethylformamide, for which hydroxide-catalyzed hydrolysis was assumed in our earlier papers (35, 36) to have rate-limiting addition of hydroxide, with the mechanism in process [15]. When we

$$[15]\quad HCO\text{-}NMe_2 + HO^- \rightleftharpoons HC(O^-)(OH)\text{-}NMe_2 \rightleftharpoons HC(O^-)_2\text{-}N^+HMe_2 \rightleftharpoons HCOO^- + NHMe_2$$

estimate the equilibrium constant for anionic zwitterion formation in this case, following the same pattern as above, we find that because of the greater basicity of the nitrogen the proton-switch equilibrium actually favors the anionic zwitterion. For loss of dimethylamine we deduced a barrier of 10.5 kcal/mol, based on the rate and equilibrium constants for addition reactions of dimethylamine (22). When we apply Multidimensional Marcus Theory to the breakdown of the

TABLE 6. Corner intermediates[a]

(*a*) Addition of hydroxide to *N*-methylformanilide		
$PhN(Me)CHO,H_2O,HO^-$	00	2.01[b]
$PhN(Me)CHO,HO^-,H_2O$	10	9.52[c]
$PhN(Me)CH(O^-)(OH_2^+),HO^-$	01	24.66[d]
$PhN(Me)CH(O^-)(OH),H_2O$	11	7.98[e]
(*b*) Expulsion of *N*-methylaniline by way of the anionic zwitterion		
$PhN(Me)CH(O^-)(OH),H_2O,H_2O$	0000	7.98[f]
$PhN(Me)CH(O^-)_2,H_3O^+,H_2O$	1000	27.94[g]
$PhN(Me)CH(O^-)(OH),HO^-,H_3O^+$	0100	24.27[h]
$PhNH^+(Me)CH(O^-)(OH),H_2O,HO^-$	0010	19.20[i]
$PhN(Me)^-,CH(=O)(OH),H_2O,H_2O$	0001	25.71[j]
$PhN(Me)CH(O^-)_2,H_2O,H_3O^+$	1100	30.57[k]
$PhNH^+(Me)CH(O^-)_2,H_3O^+,HO^-$	1010	28.53[l]
$PhN(Me)^-,CH(=O)(O^-),H_3O^+,H_2O$	1001	58.13[m]
$PhNH^+(Me)CH(O^-)(OH),HO^-,H_2O$	0110	19.08[n]
$PhN(Me)^-,CH(=O)(OH),HO^-,H_3O^+$	0101	27.57[o]
$PhNH(Me),CH(=O)(OH),H_2O,HO^-$	0011	13.77[p]
$PhNH^+(Me)CH(O^-)_2,H_2O,H_2O$	1110	17.76[q]
$PhN(Me)^-,CH(=O)(O^-),H_2O,H_3O^+$	1101	23.77[f]
$PhN(Me)^-,CH(=O)(O^-),H_3O^+,HO^-$	1011	12.01[g]
$PhNH(Me),CH(=O)(OH),HO^-,H_2O$	0111	3.99[f]
$PhNH(Me),CH(=O)(O^-),H_2O,H$	1111	−6.58[u]
(*c*) Addition of hydroxide to *N,N*-dimethylformamide		
Me_2NCHO,H_2O,HO^-	00	2.01[b]
Me_2NCHO,HO^-,H_2O	10	9.52[c]
$Me_2NCH(O^-)(OH_2^+),HO^-$	01	33.70[d]
$Me_2NCH(O^-)(OH),H_2O$	11	17.56[e]
(*d*) Expulsion of dimethylamine by way of the anionic zwitterion		
$Me_2NCH(O^-)(OH),H_2O,H_2O$	0000	17.56[f]
$Me_2NCH(O^-)_2,H_3O^+,H_2O$	1000	37.91[g]
$Me_2NCH(O^-)(OH),HO^-,H_3O^+$	0100	31.47[h]
$Me_2NH^+CH(O^-)(OH),H_2O,HO^-$	0010	20.18[i]
$Me_2N^-,CH(=O)(OH),H_2O,H_2O$	0001	45.84[j]
$Me_2NCH(O^-)_2,H_2O,H_3O^+$	1100	40.77[k]
$Me_2NH^+CH(O^-),H_3O^+,HO^-$	1010	27.80[l]
$Me_2N^-,CH(=O)(O^-),H_3O^+,H_2O$	1001	73.78[m]
$Me_2NH^+CH(O^-)(OH),HO^-,H_2O$	0110	19.65[n]
$Me_2N^-,CH(=O)(OH),HO^-,H_3O^+$	0101	39.63[o]
$Me_2NH,CH(=O)(OH),H_2O,HO^-$	0011	20.63[p]
$Me_2NH^+CH(O^-)_2,H_2O,H_2O$	1110	17.07[q]
$Me_2N^-,CH(=O)(O^-),H_2O,H_3O^+$	1101	39.37[r]
$Me_2NH,CH(=O)(O^-),H_3O^+,HO^-$	1011	18.87[s]
$Me_2NH,CH(=O)(OH),HO^-,H_2O$	0111	8.31[t]
$Me_2NH,CH(=O)(O^-),H_2O,H_2O$	1111	−1.86[u]
(*e*) Acid-catalyzed hydration of *N*-methylformanilide		
$H_2O,H_2O,CH(NMePh)=O,H_3O^+$	000	3.04[v]
$H_3O^+,HO^+,CH(NMePh)=O,H_3O^+$	100	19.71[w]
$H_2O,H_2O^+CH(NMePh)(O^-),H_3O^+$	010	17.43[x]
$H_2O,H_2O,CH(NMePh)=OH^+,H_2O$	001	2.83[y]
$H_3O^+,HOCH(NMePh)(O^-),H_3O^+$	110	25.86[z]
$H_3O^+,HO^-,CH(NMePh)=OH^+,H_2O$	101	18.85[aa]
$H_2O,H_2O^+CH(NMePh)(OH),H_2O$	011	16.72[ab]
$H_3O^+,HOCH(NMePh)(OH),H_2O$	111	14.25[ac]
(*f*) Breakdown of the *N*-protonated tetrahedral intermediate from *N*-methylformanilide		
$H_2O,CH(OH)_2(NMePh),H_3O^+$	000	12.63[ad]
$H_2O,CH(OH)_2(NMePhH^+),H_2O$	100	8.45[ae]
$H_2O,CH(OH)_2^+,NMePh^+,H_3O^+$	010	52.80[af]
$H_3O^+,CH(O^-)(OH)(NMePh),H_3O^+$	001	23.64[ag]

Can. J. Chem. Downloaded from www.nrcresearchpress.com by 203.198.23.82 on 09/08/12
For personal use only.

Can. J. Chem. Downloaded from www.nrcresearchpress.com by 203.198.23.82 on 09/08/12
For personal use only.

TABLE 6 (*continued*)

$H_2O,CH(OH)_2^+,NHMePh,H_2O$	110	19.02[ah]
$H_3O^+,CH(O^-)(OH)(NHMePh^+),H_2O$	101	17.29[ai]
$H_3O^+,O{=}CHOH,NMePh^-,H_3O^+$	011	46.54[aj]
$H_3O^+,O{=}CHOH,NHMePh,H_2O$	111	12.10[ak]
(*g*) Breakdown of the dianionic tetrahedral intermediate from *N*-methylformanilide		
$HO^-,(HO)CH(O^-)(NMePh),H_2O$	000	12.02[al]
$H_2O,CH(O^-)_2(NMePh),H_2O$	100	14.10[am]
$HO^-,(HO)CHO,NMePh^-,H_2O$	010	24.73[an]
$HO^-,(HO)CH(O^-)(NMePhH^+),HO^-$	001	21.93[ao]
$H_2O,HCOO^-,NMePh^+,H_2O$	110	11.74[ap]
$H_2O,CH(O^-)_2(NMePhH^+),HO^-$	101	41.36[aq]
$HO^-,HCOOH,NMePhH,HO^-$	011	10.62[ar]
$H_2O,HCOO^-,NMePhH,HO^-$	111	0.79[as]
(*h*) Addition of aniline to *p*-chlorobenzaldehyde		
$ArCHO,PhNH_2,H_2O,H_2O$	0000	2.42[at]
$ArCHO,PhNH^-,H_3O^+,H_2O$	1000	31.83[au]
$ArCH(O^-)(NH_2^+Ph),H_2O,H_2O$	0100	13.14[av]
$ArCHO,PhNH_2,HO^-,H_3O^+$	0010	24.72[aw]
$ArCHOH^+,PhNH_2,H_2O,HO^-$	0001	21.69[ax]
$ArCH(O^-)NHPh,H_3O^+,H_2O$	1100	23.88[ay]
$ArCHO,PhNH^-,H_2O,H_3O^+$	1010	43.72[az]
$ArCHOH^+,PhNH^-,H_3O^+,HO^-$	1001	29.11[ba]
$ArCH(O^-)(NH_2^+Ph),HO^-,H_3O^+$	0110	22.72[bb]
$ArCH(OH)(NH_2^+Ph),H_2O,HO^+$	0101	8.57[bc]
$ArCHOH^+,PhNH_2,HO^-,H_2O$	0011	32.94[bd]
$ArCH(O^-)(NHPh),H_2O,H_3O^+$	1110	0.60[be]
$ArCH(OH)(NHPh),H_3O^+,HO^-$	1101	18.55[bf]
$ArCHOH^+,PhNH^-,H_2O,H_2O$	1011	46.73[bg]
$ArCH(OH)(NH_2^+Ph),HO^-,H_2O$	0111	5.36[bh]
$ArCH(OH)NHPh,H_2O,H_2O$	1111	2.80[bi]

[a]All in aqueous solution at 25°C. Standard states are 1 M ideal solutions with an infinitely dilute reference state, except for water for which the standard state is the pure liquid at unit activity. For the formation of encounter complexes with neither stabilizing nor destabilizing interactions we follow Hine (29) and estimate the equilibrium constant as $0.0085n$, where n is the number of equivalent positions in which one reactant could be found in a water lattice relative to the other reactant; we assume a diamond lattice as in ice as an approximation to the short-range order in water. Species other than water that are separated by a comma are in an encounter complex; water molecules are included where appropriate so that all species in a set have the same composition. Hydrogen bond energies are calculated using the equation of Stahl and Jencks (48); because we explicitly correct for encounter, we extract the pure hydrogen bonding contribution from the Stahl and Jencks result, which gives the overall equilibrium that includes both encounter and hydrogen bonding. Electrostatic interactions are calculated relative to the ion pair interaction; the net energy for ion pair formation in water is 0.1 kcal/mol (61), which is the sum of encounter and electrostatics. Since encounter is 2.42 kcal/mol, electrostatics must be −2.32 kcal/mol. For the various species involved we made approximate estimates using a single interatomic distance, assumed the same for all, bonding or not, and a standard geometry based on a regular pentagon for cyclic arrays of atoms. Since electrostatic interactions are small in water, such crude calculations do not introduce large errors.

[b]Encounter is assumed to have four possible locations for hydroxide relative to the amide.

[c]Encounter is assumed to have two possible locations for hydroxide relative to the amide, and loss of one hydrogen-bonded water at a cost of 7.1 kcal/mol.

[d]Encounter is assumed to have two possible locations for the hydroxide relative to the amide, the energy of the zwitterion relative to the neutral form of the intermediate is calculated from pK_a values in Table 5, and the hydrogen bond energy is calculated as described.

[e]Based on a pK_a value in Table 5.

[f]Based on hydration and pK_a.

[g]Based on hydration, pK_a values, encounter with one position for the hydronium ion, and the hydrogen bond energy for H_3O^+ hydrogen bonded to the dianionic tetrahedral intermediate.

[h]Based on hydration, pK_a values, pK_w, encounter (three ways for hydronium hydroxide to form, one way for this to form a cyclic complex with the tetrahedral intermediate), hydrogen bonds between HO^- and H_3O^+ and HO^- and the monoanionic tetrahedral intermediate, and the ion pairing between H_3O^+ and HO^-.

[i]Based on hydration, pK_a values, encounter (one place for hydroxide next to the ammonium ion), hydrogen bonding between HO^- and ammonium ion, and electrostatic interactions between HO^- and the zwitterion.

[j]Based on hydrolysis, pK_a values, encounter (two ways for the amide ion to be next to formic acid), desolvation of the amide ion (difference in pK_a between water and DMSO).

[k]Based on hydration, pK_a values, encounter (one way for the hydronium to be next to the intermediate with a cyclic array of hydrogen bonds), and ion pairing.

[l]Based on hydration, pK_a values, pK_w, encounter (three ways for hydronium hydroxide to form, one way for this to form a cyclic complex with the tetrahedral intermediate), hydrogen bonding of H_3O^+ and HO^-, H_3O^+ with the oxyanion, and HO^- with the ammonium ion, and electrostatic interactions.

[m]Based on hydrolysis, pK_a values, encounter (two ways for the amide ion to be next to formate ion, one way for hydronium ion to be next to this with a cyclic array of hydrogen bonds), electrostatic interactions (essentially ion pairing), hydrogen bonding of H_3O^+ and formate ion, and desolvation of the amide ion (estimated as described above).

[n]Based on hydration, pK_a values, encounter (one way for HO^- to be next to the intermediate and give a cyclic hydrogen bond array), electrostatic interactions of HO^- with the zwitterion, and hydrogen bonding of HO^- with the hydroxyl of the intermediate.

[o]Based on hydrolysis, pK_a values, pK_w, encounter (three ways for hydronium hydroxide to form, one way for it to bind to the tetrahedral intermediate), electrostatic interactions in the ion triple, amide ion, H_3O^+, HO^-, and hydrogen bonding of HO^- with the hydroxyl of the intermediate, of HO^- with H_3O^+, and of H_3O^+ with the amide ion.

[p]Based on hydrolysis, encounter (two ways for the amine to encounter formic acid, one way for HO^- to bind with a cyclic hydrogen bonding array), and hydrogen bonding of HO^- and the amine.

[q]Based on hydration and pK_a values.

[r]Based on hydrolysis, pK_a values, encounter (two ways for the amine to encounter formate ion, one way for H_3O^+ to bind with a cyclic hydrogen bonding array), electrostatic interactions of H_3O^+ with the two anions, and hydrogen bonding of H_3O^+ with the amine.

[s]Based on hydrolysis, pK_a values, pK_w, encounter (two ways for the amine to encounter formate ion, three ways for hydronium hydroxide to form an ion pair, one way for this ion pair to bind with a cyclic hydrogen bonding array), electrostatic interactions of H_3O^+ with the two anions, and hydrogen bonding of H_3O^+ with formate ion and with HO^- and of HO^- with the amine.

[t]Based on hydrolysis, encounter of HO^- with formic acid (two ways this could happen), and hydrogen bonding between formic acid and HO^-.

[u]Based on hydrolysis and pK_a values.

[v]Based on encounter (two ways for hydronium to encounter the amide) and hydrogen bonding of H_3O^+ to the amide carbonyl.

[w]Based on encounter (two ways for hydronium to encounter the amide, three ways for the hydronium hydroxide pair to form, two ways for this ion pair to encounter the amide), electrostatic interactions, hydrogen bonding of H_3O^+ to the amide carbonyl and of H_3O^+ to HO^-, and desolvation of the HO^-.

[x]Based on hydration of the amide, pK_a values, encounter of H_3O^+ with the tetrahedral intermediate (two mechanistically significant positions), electrostatic interactions, and hydrogen bonding of H_3O^+ to the anionic end of the zwitterion.

[y]Based on the pK_a value for the amide.

[z]Based on hydration, pK_a values, encounter (three ways for hydronium to encounter the new OH, two mechanistically significant ways for hydronium to encounter the new oxyanion), and hydrogen bonding of H_3O^+ to the anion of the tetrahedral intermediate and of H_3O^+ to the hydroxyl of this intermediate.

[aa]Based on pK_a values, encounter (three ways for the hydronium hydroxide pair to form, two ways for this ion pair to encounter the amide), hydrogen bonding of H_3O^+ to HO^-, and desolvation of the HO^-.

[ab]Based on hydration and the pK_a value.

Can. J. Chem. Downloaded from www.nrcresearchpress.com by 203.198.23.82 on 09/08/12
For personal use only.

TABLE 6 (*continued*)

[ac]Based on hydration and encounter (three ways for hydronium to encounter the new OH).

[ad]Based on hydration, encounter (one way for hydronium to encounter the nitrogen of the tetrahedral intermediate), and hydrogen bonding of H_3O^+ to this nitrogen.

[ae]Based on hydration and the pK_a value.

[af]Based on hydrolysis pK_a values, encounter (two ways for amide ion to encounter formic acidium ion, one way for hydronium ion to encounter the amide ion), electrostatic interactions of amide ion with H_3O^+ and formic acidium ion, hydrogen bonding of H_3O^+ and the amide ion, and desolvation of the amide ion.

[ag]Based on hydration, pK_a values, encounter (three ways for H_3O^+ to encounter the oxyanion of the tetrahedral intermediate, one way for H_3O^+ to encounter the nitrogen of the intermediate), hydrogen bonding between H_3O^+ and the oxyanion of the tetrahedral intermediate and H_3O^+ to the nitrogen of the intermediate, and electrostatic interactions.

[ah]Based on hydrolysis, the pK_a value, and encounter (two ways for amine to encounter formic acidium ion).

[ai]Based on hydration, pK_a values, encounter (three ways for H_3O^+ to encounter the oxyanion of the tetrahedral intermediate), hydrogen bonding of H_3O^+ to the oxyanion of the tetrahedral intermediate, and electrostatic interactions.

[aj]Based on hydrolysis, pK_a values, encounter (two ways for the amide ion to encounter formic acid, two ways for H_3O^+ to encounter the carbonyl of formic acid, one way for H_3O^+ to encounter the amide ion), hydrogen bonding between H_3O^+ and the carbonyl of formic acid and H_3O^+ and the amide ion, electrostatic interactions, and desolvation of the amide ion.

[ak]Based on hydrolysis, encounter (two ways for H_3O^+ to encounter the carbonyl of formic acid, one way for the amine to encounter formic acid), and hydrogen bonding of H_3O^+ to the carbonyl of formic acid.

[al]Based on hydration, pK_a values, encounter (three ways HO^- can encounter the hydroxyl of the tetrahedral intermediate), hydrogen bonding between HO^- and the hydroxyl of the tetrahedral intermediate, and electrostatic repulsion between the negative charges.

[am]Based on hydration and pK_a values.

[an]Based on hydrolysis, pK_a values, encounter (two ways HO^- can encounter formic acid and two ways the amide ion can encounter formic acid), hydrogen bonding between HO^- and formic acid, electrostatic interactions, and desolvation of the amide ion.

[ao]Based on hydration, pK_a values, encounter (three ways HO^- can encounter the hydroxyl of the tetrahedral intermediate, one way HO^- can encounter the ammonium of the tetrahedral intermediate), hydrogen bonding between HO^- and the hydroxyl of the tetrahedral intermediate and HO^- and the ammonium of the tetrahedral intermediate, and electrostatic interactions.

[ap]Based on hydrolysis, pK_a values, encounter (two ways the amide ion can encounter formate ion), electrostatic repulsion between the anions, and desolvation of the amide ion.

[aq]Based on hydration, pK_a values, encounter (one way HO^- can encounter the ammonium ion of the tetrahedral intermediate), hydrogen bonding between HO^- and the ammonium ion of the tetrahedral intermediate, and electrostatic interactions.

[ar]Based on hydrolysis, pK_a values, encounter (two ways HO^- can encounter formic acid, two ways the amine can encounter formic acid, one way the HO^- can encounter the amine), hydrogen bonding of HO^- with formic acid and of HO^- with the amine, and electrostatic repulsion between the two HO^- ions.

[as]Based on hydrolysis, pK_a values, encounter (two ways the amine can encounter formate ion, one way HO^- can encounter the amine), hydrogen bonding between HO^- and the amine, and electrostatic repulsion between HO^- and formate ion.

[at]Based on encounter (two ways aniline can encounter an aldehyde).

[au]Based on pK_a values, encounter (three ways hydronium ion can encounter anilide ion, and two ways this complex can encounter an aldehyde), hydrogen bonding between H_3O^+ and anilide, ion pairing, and partial desolvation of anilide ion.

[av]Based on addition and pK_a values.

[aw]Based on pK_a values, encounter (three ways hydronium hydroxide can form, two ways aniline can encounter an aldehyde, and two ways the hydronium hydroxide pair can form a cyclic hydrogen-bonded complex with the amine aldehyde pair), hydrogen bonding of H_3O^+ with HO^- and with aldehyde and of HO^- with aniline, and ion pairing.

[ax]Based on pK_a values, encounter (two ways HO^- can encounter protonated aldehyde, and two ways aniline can encounter aldehyde), hydrogen bonding of HO^- and protonated aldehyde, and ion pairing.

TABLE 6 (*concluded*)

[ay]Based on addition, pK_a values, encounter (two ways H_3O^+ can encounter the tetrahedral intermediate oxyanion and form a cyclic hydrogen bond array), hydrogen bonding of H_3O^+ and the tetrahedral intermediate oxyanion, and ion pairing.

[az]Based on pK_a values, encounter (two ways anilide can encounter the aldehyde and two ways H_3O^+ can encounter the carbonyl oxygen), hydrogen bonding of H_3O^+ to aldehyde, ion pairing, and partial desolvation of the anilide.

[ba]Based on pK_a values, encounter (three ways H_3O^+ and HO^- can encounter, two ways anilide can encounter protonated aldehyde, and two ways the two pairs can meet and form a cyclic hydrogen-bonded array), hydrogen bonding of H_3O^+ to HO^- and to anilide and of HO^- to protonated aldehyde, electrostatic interactions in the ion quartet, and partial desolvation of the anilide.

[bb]Based on addition, pK_a values, encounter (three ways the H_3O^+ and HO^- can encounter, and two ways this pair can form a cyclic hydrogen-bonded array with the zwitterion), hydrogen bonding of H_3O^+ with HO^- and the oxyanion and of HO^- with the ammonium ion, and electrostatic interactions in the ion quartet.

[bc]Based on addition, pK_a values, encounter (two ways HO^- can encounter the hydroxyl of the tetrahedral intermediate), hydrogen bonding of HO^- with this hydroxyl, and ion pairing.

[bd]Based on pK_a values, encounter (two ways aniline can encounter protonated aldehyde, and two ways hydroxide can encounter aniline in this complex), hydrogen bonding of HO^- and aniline, and ion pairing.

[be]Based on addition, pK_a values, encounter (two ways H_3O^+ can encounter the oxyanion of the tetrahedral intermediate and form a cyclic hydrogen-bonded array), hydrogen bonding of H_3O^+ to the oxyanion of the tetrahedral intermediate, and ion pairing.

[bf]Based on addition, pK_a values, encounter (three ways H_3O^+ and HO^- can encounter, and two ways this pair can encounter the tetrahedral intermediate), hydrogen bonding of H_3O^+ to HO^- and to the amine and of HO^- to the hydroxyl, and ion pairing.

[bg]Based on pK_a values, encounter (two ways anilide can encounter protonated aldehyde), ion pairing, and partial desolvation of the anilide.

[bh]Based on addition, pK_a values, encounter (two ways HO^- can encounter the ammonium of the tetrahedral intermediate), hydrogen bonding of HO^- and the ammonium of the tetrahedral intermediate, and ion pairing.

[bi]Based on addition.

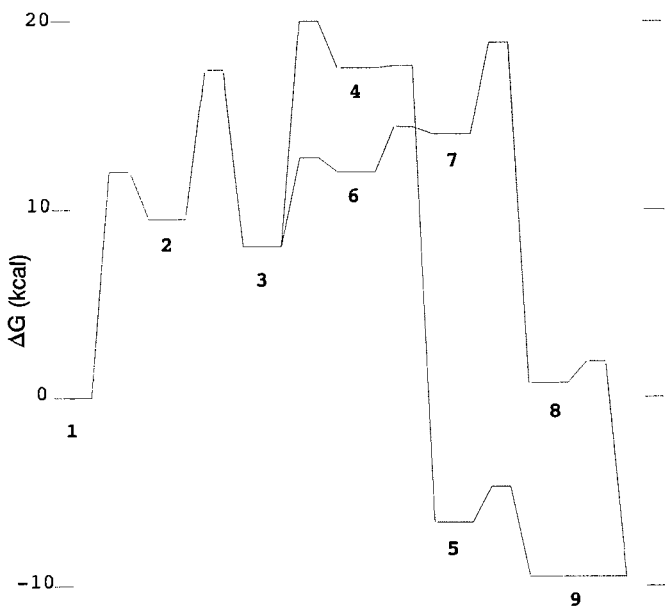

FIG. 2. Reaction coordinate diagram for the alkaline hydrolysis of *N*-methylformanilide. Species are identified in Scheme 3.

Can. J. Chem. Downloaded from www.nrcresearchpress.com by 203.198.23.82 on 09/08/12
For personal use only.

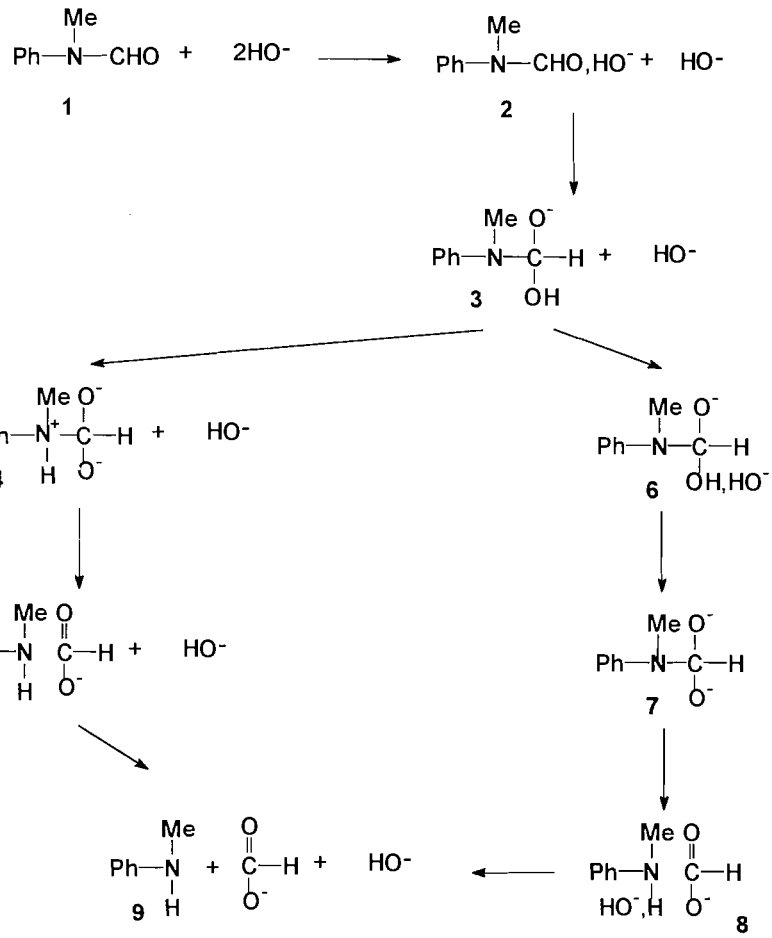

SCHEME 3. Mechanism for alkaline hydrolysis of *N*-methylformanilide.

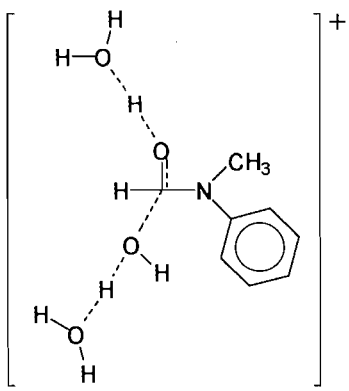

anionic intermediate to products by way of the anionic zwitterion, we obtain a predicted free energy of activation of 4.35 kcal/mol relative to the anionic intermediate or 21.91 kcal/mol relative to starting materials. This transition state is lower in energy than that for hydroxide addition, predicted to be 22.8 kcal/mol relative to starting materials; the observed transition state is at 22.56 kcal/mol relative to starting materials. The agreement is satisfactory, and we predict relatively little exchange, which is in accord with what is known. The detailed reaction coordinate diagram for this reaction is shown in Fig. 3, based on the mechanism, shown in Scheme 4.

We return to *N*-methylformanilide to discuss the rate of acid-catalyzed hydrolysis. We assume a general mecha-

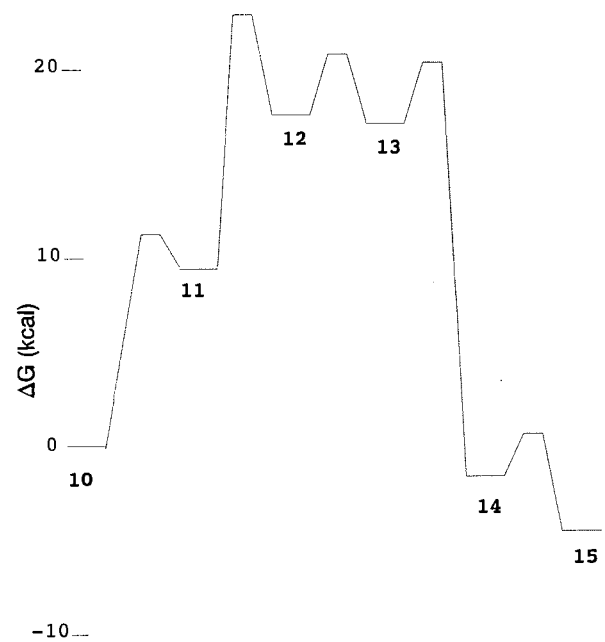

FIG. 3. Reaction coordinate diagram for the alkaline hydrolysis of *N*,*N*-dimethylformamide. Species are identified in Scheme 4.

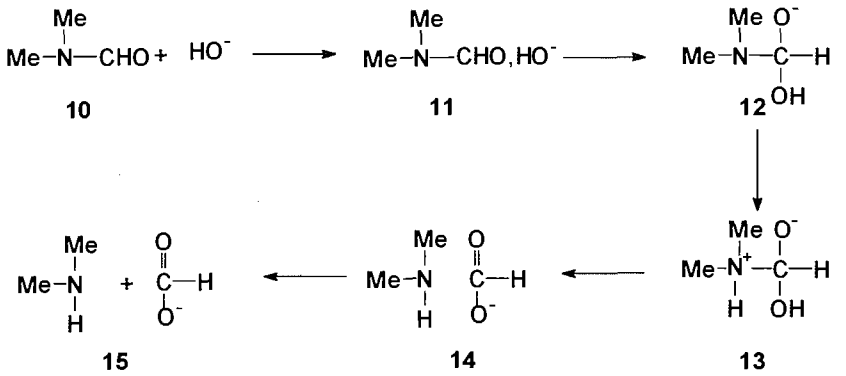

SCHEME 4. Mechanism for alkaline hydrolysis of *N*,*N*-dimethylformamide.

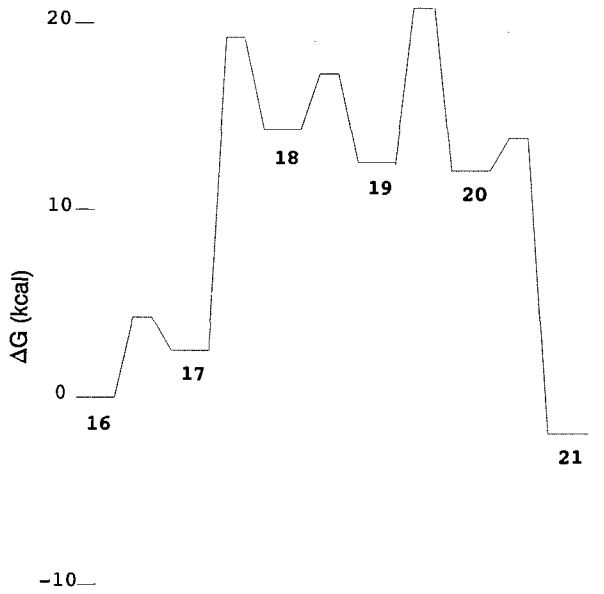

FIG. 4. Reaction coordinate diagram for the acid hydrolysis of *N*-methylformanilide. Species are identified in Scheme 5.

nism for this addition starting with the hydrogen-bonded complex of hydronium ion and the amide oxygen, and proceeding through possibly concerted proton transfer from hydronium to amide oxygen, addition of water, and loss of proton from this water to a second water molecule. We use Multidimensional Marcus Theory to predict which steps will have occurred before, or be occurring at the transition state. The calculated free energy of activation is 19.76 kcal/mol (relative to separate starting materials), and the transition state has almost complete proton transfer from hydronium to carbonyl oxygen, but only a small extent of proton transfer from the nucleophilic water to the general base water. Breakdown of the *N*-protonated tetrahedral intermediate is similarly predicted to have a free energy of activation of 20.88 kcal/mol relative to anilide plus hydronium ion. These results would predict ^{18}O exchange accompanying acid-catalyzed exchange of *N*-methylformanilide, which is contrary to observation. Brown and co-workers have studied the kinetics of acid-catalyzed hydrolysis and accompanying ^{18}O exchange of acetanilide (2) and *N*-methylformanilide.[2] For *N*-methylformanilide they found no detectable exchange. From the rate constants for hydrolysis of acetanilide at 72°C, taken as 3.41×10^{-6} M^{-1} s^{-1} (based on kinetics in dilute HCl (2), and at 25°C, taken as 2.81×10^{-6} s^{-1} (based on a rate constant at 1.42 M HCl, the pK_{BH^+} and H_A for HCl solutions (37)) we calculate the rate factor, $k_{72°C}/k_{25°C}$, to be 121. We assume the same rate factor for *N*-methylformanilide, and from the rate constant at 72°C, 2.18×10^{-2} M^{-1} s^{-1} (based on kinetics in dilute HCl[2]), we estimate a rate constant at 25°C of 1.80×10^{-4} M^{-1} s^{-1}, leading to a value of 22.57 kcal/mol for $\Delta G^{\ddagger}$. Again we observe that the calculated value is about 2 kcal too low. The difference between the energies of the transition states for reversion to starting material and cleavage to products was only 1.12 kcal/mol, by contrast to the situation in base, where the predicted difference was 2.6 kcal/mol. Furthermore, in acid the transition state for cleavage involves C—N bond breaking, and therefore its energy is dependent upon the intrinsic barrier for C—N bond breaking involving *N*-methylaniline. We were forced to use a barrier based on aniline for lack of suitable information for reactions of *N*-methylaniline. If the intrinsic barrier for *N*-methylaniline were a few kcal/mol smaller, the relative heights of the transition states would be correct. Since methanol/methoxide has a smaller intrinsic barrier for addition to a carbonyl than water/hydroxide (20), this is not impossible. In any case the prediction of ^{18}O exchange in acid is much weaker than the prediction of ^{18}O exchange in base. When the uncertainties in the energy levels are considered, all we can really say is that in acid ^{18}O exchange might be observable but would be of modest importance at best. The calculations depend on imperfectly known terms for encounter, hydrogen bonding, electrostatic interactions, and p*K*a's of various reaction intermediates. The detailed reaction coordinate diagram for this reaction is given in Fig. 4, based on the mechanism shown in Scheme 5.

In general, although the agreement between predicted and observed free energies of activation is within the experimental uncertainty in the energy levels of the tetrahedral intermediates, the predicted values are consistently low by a bit over 2 kcal. This suggests that our tetrahedral intermediate free energies are too low by a similar amount.

Experimental

Materials

N-Methylaniline (Aldrich) was redistilled before use: bp 84–85°C, 15 Torr. *N*-Methylformanilide was prepared by the Organic Synthesis (38) procedure, bp 117–119°C, 8 Torr; ^1H nmr (60 MHz,

[2]R.S. Brown, personal communication.

Can. J. Chem. Downloaded from www.nrcresearchpress.com by 203.198.23.82 on 09/08/12
For personal use only.

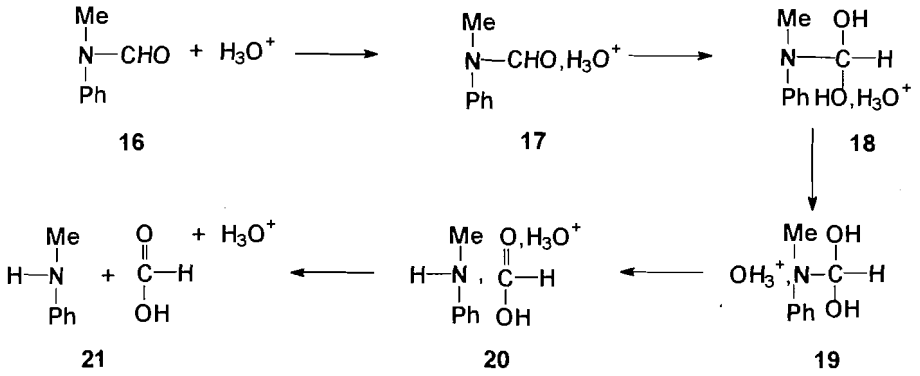

SCHEME 5. Mechanism for acid hydrolysis of *N*-methylformanilide.

$CDCl_3$) δ: 3.30 (s, 3H, NCH_3), 7.28 (m, 5H, aromatic H), 8.44 (s, 1H, formyl H).

N-*Methylformanilide dimethyl acetal*

A mixture of *N*-methyl formanilide (11.1 g, 82.5 mmol), trimethyloxonium tetrafluoroborate (39) (12.2 g, 82.5 mmol), and dry methylene chloride (100 mL) in a 500-mL three-necked flask was stirred at room temperature under a dry nitrogen atmosphere. After 3 h all of the trimethyloxonium tetrafluoroborate had dissolved and a 60 MHz ^{1}H nmr spectrum indicated that all the formanilide had been converted to oxonium salt. The reaction mixture was then cooled in a Dry Ice – acetone bath and a solution of sodium (1.9 g, 82.6 mmol) in anhydrous methanol was added dropwise over 30 min. The contents of the flask were then allowed to warm to room temperature and the solution separated from solid by centrifugation. Solvent was removed by flash distillation at 40 Torr using a 10°C water bath and the residue was stored in a freezer under a dry nitrogen atmosphere. The residue was purified by distillation, yielding 10 mL of a clear colourless liquid with bp 86–88°C at 3 Torr. This was redistilled for calorimetry, bp 86–88°C at 1.5 Torr, 70–71°C at 0.6 Torr, 63–64°C at 0.5 Torr; ^{1}H nmr (200 MHz, $CDCl_3$) δ: 2.86 (s, 3H, NCH_3), 3.32 (s, 6H, OCH_3), 5.36 (s, 1H, formyl H), 6.87 (m, 3H, aromatic H), 7.24 (m, 2H, aromatic H).

Formohydroxamic acid was prepared by the method of Bernhard et al. (40): mp 75–77°C, (lit. (40) mp 77.5°C; (4) mp 75–77°C). Hydroxylamine hydrochloride (Aldrich), potassium chloride (Baker), and potassium hydroxide (BDH) were used without further purification.

N-*Methyl*-N-*(2,2,2-trifluoroethyl)-aniline*

N-Methyl-*N*-phenyltrifluoroacetamide was prepared by the literature method (41); mp 26–27°C, satisfactory nmr. The amide was reduced, following Gribble et al. (42), by sodium borohydride – trifluoroacetic acid in dry THF, to give *N*-methyl-*N*-trifluoroethylaniline, bp 90°C at 19.5 Torr (lit. (42) bp 54°C at 0.4 Torr).

Methods

The calorimeter was modified to increase the stability of the base line and permit accurate determination of heats of reaction for slow reactions. A box was constructed surrounding the Dewar flask (20 cm × 20 cm × 40 cm). This box contains a coil for cooling water made of copper tubing surrounding, 2 cm away from, and up to the height of the Dewar flask. In a lower corner of the box is a coil of 1 ft of Nichrome wire (total resistance of wire 3 ohms) connected to a Powerstat variable transformer. One upper corner contains a small fan and in a second upper corner is a thermometer (24–30°C) with a Thermo-Watch detector (L6-1000) attached. A Powerstat is plugged into the Thermo-Watch and set at 8% of full voltage. Thus the internal air temperature of the box is regulated and routinely maintained at 24.00 ± 0.03°C. Cables connected to the solvent heating coil, the thermistor, and the solvent stirrer pass through holes in the box; a door allows access to the sample injection hole in the lid of the Dewar.

This modification has eliminated the influence of the variable room temperature on the temperature of the solution in the calorimeter. The temperature vs. time trace is now consistently a straight line instead of often being a curve. At the beginning of a set of measurements with a batch of solvent the temperature can be set slightly below 24°C so that there is a slow increase in the temperature vs. time trace. The calorimeter can be calibrated by passing a known amount of current through a heating resistor, and heats of reaction or heats of solution of samples can be measured with a gradual but quite explicable decrease in slope of the temperature vs. time trace.

Initial attempts at measuring the heat of hydrolysis of *N*-methylformanilide dimethyl acetal in 0.1 N sodium hydroxide in water were unsuccessful because the acetal was very slow to dissolve and the temperature vs. time trace did not return to its pre-injection slope until about 1.5 h after injection. An attempt was made to increase the solubility by using 0.1 N tetraethylammonium hydroxide in 90% DMSO, 10% water. There was no change in slope of the temperature vs. time trace upon injection of acetal. There was simply a very small instantaneous displacement of the line toward a lower temperature. This displacement presumably reflects the heat of solution. When the reaction solvent was 0.1 N sodium hydroxide in 50% DMSO, 50% water, reaction occurred but took appreciable time to occur. The temperature vs. time trace had returned to the pre-injection slope after about 20 min. The deflection was measured as the distance between the pre- and post-injection lines at the time of injection. We presume that at this solvent composition the solubility and the rate of reaction are adequate, although time is required for dissolution.

The solubility of *N*-methylformanilide in pH 7 aqueous phosphate buffer, ionic strength 0.1 M, was determined by ^{1}H nmr spectroscopy, integrating the signals from the *N*-methyl relative to the signal from 0.098 M *tert*-butyl alcohol added as an internal standard. There were two *N*-methyl singlets in a ratio of 6:1 attributed to the geometrical isomers of the amide. The same solubility was determined by integrating the formyl proton relative to the *tert*-butyl alcohol.

N-Methylformanilide dimethyl acetal used for calorimetry in aqueous methanol was found to contain 5 mol% of methanol and methyl formate; thus it had a purity of 97 mass percent.

Heat of reaction for amide formation and transamidation

The equilibrium constant for the reaction of *N*-methylaniline with formohydroxamic acid to give *N*-methylformanilide and hydroxylamine was studied at 25, 35, and 45°C in order to determine the heat of reaction. The procedure of Fersht and Requenna was used; because the reactions are slow and there seem to be side reactions, the initial changes in concentration of *N*-methylformanilide and formohydroxamic acid, for reactions starting with no *N*-methylformanilide and no formohydroxamic acid, respectively, were used to determine the equilibrium constant (4). In all cases the formohydroxamic acid concentration was determined by the ferric

Can. J. Chem. Downloaded from www.nrcresearchpress.com by 203.198.23.82 on 09/08/12
For personal use only.

Can. J. Chem. Downloaded from www.nrcresearchpress.com by 203.198.23.82 on 09/08/12
For personal use only.

hydroxamate assay, as described below. The initial slope of absorbance vs. time was determined for each solution. Points taken at short times deviated from the line, presumably because of the delay for temperature equilibration within an ampoule; these points were discarded, as were points at long times when deviations from the initial slope became severe. The results are found in Table 2.

The formation of formohydroxamic acid was studied at 25, 35, and 45°C in order to determine the heat of reaction. At each temperature the equilibrium was approached from both directions. The procedure of Fersht and Requenna (4) was followed. Each initial solution was sealed in an ampoule and thermostatted for a suitable period until equilibrium was attained. This required 17 h at 45.9°C, 33 h at 35°C, and 62 h at 24.9°C. An ampoule was cooled to room temperature, opened, and 500 μL added to 2.0 mL of ferric chloride solution (20% by mass in 1.4 M HCl) contained in a 1.000-cm uv cell. The absorbance of the ferric hydroxamate solution was read 2.0 min after adding the ferric chloride solution. Absorbance readings were calibrated by performing the same analysis using a standard solution of formohydroxamic acid in water. The results are found in Table 3. Our conditions closely match those reported by Fersht and Requenna, and our results are in good agreement at 25°C as to the extent of formohydroxamic acid formation. The apparent equilibrium constant is K_{app} = [CHONHOH][H^+]/[NH_3OH^+][HCOOH]: Fersht reports (4) $K_{app} = 4.47 \times 10^{-3}$ [H^+]; we find $K_{app} = 4.11 \times 10^{-3}$[$H^+$] (starting with no formohydroxamic acid) and $K_{app} = 4.29 \times 10^{-3}$ [H^+] (starting with 0.0202 M formohydroxamic acid). However, Fersht reports a final pH of 0.75, which was used to calculate an effective [H^+] = 10^{-pH} in calculating the final equilibrium constant. We obtain a pH of 0.91 or 0.93, calibrating our meter against 0.1 N HCl, taken as pH 1.1 (43). It seems clear that there are serious deviations from ideality, because the expected H^+ concentration, using a pK_a for formic acid (25) corrected for the effect of 1 M ionic strength using the Davies equation (44), is 0.107, and the activity coefficient for H^+, estimated using the Davies equation, is 0.699. Thus one would have expected pH = $-\log a_{H^+}$ = 1.13. The solvent, with 2 M formic acid, is no longer water, and this must be perturbing the activity coefficients. Acidity function studies (45) led to an H_0 value of 1.54 for 2 M formic acid. Taken at face value, this suggests that the effective pK_a of formic acid has become more acidic in this mixed solvent. This would increase the concentration of H^+, but only modestly; the HCl contribution would still dominate. To use a pK_a value for hydroxylammonium ion based on aqueous solution, even though it was determined at 1 M ionic strength, to calculate the concentration of free hydroxylamine, seems optimistic. Unfortunately we do not see a better way to extract the true equilibrium constant from these results. Rather than confuse the literature we will use Fersht's value for the equilibrium constant for formohydroxamic acid formation at 25°C.

Measurement of free energy of transfer for N-*methyl*-N-*(2,2,2-trifluoroethyl)-aniline*

The solubility was determined by measuring the concentration of a saturated solution in 0.1 N NaOH, by determining the uv absorbance at 243 nm, $\epsilon = 1.48 \times 10^4$ M^{-1} cm^{-1}. The value obtained was 6.89×10^{-4} M. The vapor pressure was determined using a semimicro ebulliometer (46); the values obtained were: bp(°C)/*p*(Torr); 77.8/10.7; 90.0/19.5; 104.2/36.0; 111.4/48.3; 119.0/61.3; 124.8/82.0; 130.0/101.8; 135.0/121.5; 140.0/143.5. These data were transformed to $\log_{10} p$, $1/T$(K), and fitted to $\log_{10} p = 2624/T + 8.505$; this allows extrapolation to give the vapor pressure at 25°C as 0.504 Torr.

Acknowledgments

We thank the Natural Sciences and Engineering Research Council of Canada for financial support of this work. We thank Professor R.A. McClelland for kindly providing a sample of *N*-methylformanilide dimethyl acetal for our initial experiments. We thank Professor R.S. Brown for providing rate constants for hydrolysis and exchange of *N*-methylformanilide in advance of publication.

1. H. Slebocka-Tilk, R.S. Brown, and J. Olekszyk. J. Am. Chem. Soc. **109**, 4620 (1987).
2. A.J. Bennet, H. Slebocka-Tilk, R.S. Brown, J.P. Guthrie, and A. Jodhan. J. Am. Chem. Soc. **112**, 8497 (1990).
3. J.P. Guthrie. Acc. Chem. Res. **16**, 122 (1983).
4. A.R. Fersht and Y. Requenna. J. Am. Chem. Soc. **93**, 3499 (1971).
5. J.P. Guthrie. Can. J. Chem. **64**, 635 (1986).
6. Beilstein. Handbuch der organischen chemie. Vol. 12. p. 234.
7. Beilstein. Handbuch der organischen chemie. Vol. 12 II. p. 136.
8. Beilstein. Handbuch der organischen chemie. Vol. 12 III. p. 454.
9. Beilstein. Handbuch der organischen chemie. Vol. 12 IV. p. 370.
10. J.P. Guthrie and K.F. Taylor. Can. J. Chem. **62**, 363 (1983).
11. D.S. Adams, H.A. Massaldi, and J.M. Prausnitz. Ind. Eng. Chem. Fundam. **13**, 259 (1977).
12. J.-H. Lii and N.L. Allinger. J. Comput. Chem. **12**, 186 (1991).
13. D.R. Stull, E.F. Westrum, Jr., and G.C. Sinke. The chemical thermodynamics of organic compounds. Wiley, New York. 1967.
14. S.W. Benson and J.H. Buss. J. Chem. Phys. **19**, 546 (1958).
15. S.W. Benson. Thermochemical kinetics. 2nd ed. Wiley, New York. 1976.
16. R.A. McClelland. J. Am. Chem. Soc. **100**, 1844 (1978).
17. J.P. Guthrie. Can. J. Chem. **69**, 1893 (1991).
18. J. Hine and P.K. Mookerjee. J. Org. Chem. **40**, 292 (1975).
19. J.P. Guthrie. Can. J. Chem. **53**, 898 (1975).
20. J.P. Guthrie. J. Am. Chem. Soc. **113**, 3941 (1991).
21. J.P. Guthrie. J. Am. Chem. Soc. **100**, 5892 (1978).
22. H. Slebocka-Tilk, A.J. Bennet, J.W. Keillor, R.S. Brown, J.P. Guthrie, and A. Jodhan. J. Am. Chem. Soc. **112**, 8507 (1990).
23. (*a*) J.P. Guthrie. Submitted; (*b*) Can. J. Chem. **68**, 1643 (1990).
24. E.H. Cordes and W.P. Jencks. J. Am. Chem. Soc. **84**, 826 (1962), **84**, 832 (1962).
25. W.P. Jencks and J. Regenstein. *In* C.R.C. Handbook of Biochemistry. 1st ed. *Edited by* H.A. Sober. The Chemical Rubber Co., Cleveland, Ohio, 1968. pp. J150–J189.
26. D.D. Perrin, B. Dempsey, and E.P. Serjeant. pK_a prediction for organic acids and bases. Chapman and Hall, London. 1981.
27. J. Hine, J.C. Craig, J.G. Underwood, and F.A. Via. J. Am. Chem. Soc. **92**, 5194 (1970).
28. W.R. Adams and R.G. Kallen. J. Am. Chem. Soc. **98**, 7777 (1976).
29. J. Hine. J. Am. Chem. Soc. **93**, 3701 (1971).
30. S.S. Biechler and R.W. Taft. J. Am. Chem. Soc. **79**, 4927 (1957).
31. M.L. Bender and R.J. Thomas. J. Am. Chem. Soc. **83**, 4183 (1961).
32. J. Kavalek, F. Krampera, and V. Sterba. Collect. Czech. Chem. Commun. **41**, 1685 (1976).
33. K. Bowden and K. Bromley. J. Chem. Soc., Perkin Trans. **2**, 2103 (1990).
34. P. Deslongchamps, P. Gerval, U.O. Cheriyan, A. Guida, and R.J. Taillefer. Nouv. J. Chim. **2**, 631 (1978).
35. J.P. Guthrie. J. Am. Chem. Soc. **96**, 3608 (1974).
36. J.P. Guthrie. J. Am. Chem. Soc. **100**, 5892 (1978).
37. J.W. Barnett and C.J. O'Connor. J. Chem. Soc. Perkin Trans. 2, 220 (1973).
38. L.F. Fieser. Org. Synth. Collect. Vol. **3**, 590 (1955).
39. T.J. Curphey. Org. Synth. **51**, 142 (1971).
40. S.A. Bernhard, Y. Shalitin, and Z.H. Tasjian. J. Am. Chem. Soc. **86**, 4406 (1964).

41. E.J. Bourne, S.H. Henry, and C.E.W. Tatlow. J. Chem. Soc. 4017 (1952).
42. G.W. Gribble, C.F. Nutaitis, and R.M. Leese. Heterocycles, **22**, 379 (1984).
43. R.G. Bates. Determination of pH, theory and practice. Wiley, New York. 1973.
44. C.W. Davies. J. Chem. Soc. 2093 (1938).
45. R. Stewart and T. Mathews. Can. J. Chem. **38**, 602 (1960).
46. S.R. Hoover, H. John, and E.F. Mellon. Anal. Chem. **25**, 1940 (1953).
47. J.B. Pedley, R.D. Naylor, and S.P. Kirby. Thermochemical data of organic compounds. 2nd ed. Chapman and Hall, London. 1986.
48. N. Stahl and W.P. Jencks. J. Am. Chem. Soc. **108**, 4196 (1986).
49. D.D. Wagman, W.H. Evans, V.B. Parker, R.H. Schurm, I. Halow, S.M. Bailey, K.L. Churney, and R.L. Nuttall. J. Phys. Chem. Ref. Data, **11**, Supplement 2, (1982).
50. J.P. Guthrie. J. Am. Chem. Soc. **95**, 6999 (1973).
51. J.P. Guthrie. Can. J. Chem. **70**, 1042 (1992).
52. G.N. Vriens and A.G. Hill. Ind. Eng. Chem. **44**, 2732 (1952).
53. J.P. Guthrie and K.F. Taylor. Can. J. Chem. **61**, 602 (1983).
54. J.P. Guthrie. *In* Applications of biochemical systems in organic chemistry. *Edited by* J.B. Jones, C.J. Sih, and D. Perlman. Wiley–Interscience, New York. 1976. p. 676.
55. F.G. Bordwell and D.J. Algrim. J. Am. Chem. Soc. **110**, 2964 (1988).
56. R. Stewart. The proton: applications to organic chemistry. Academic Press, New York. 1985. p. 70.
57. A. Bagno and G. Scorrano. J. Am. Chem. Soc. **110**, 4577 (1988).
58. R. Stewart. The proton: applications to organic chemistry. Academic Press, New York. 1985. pp. 112–113.
59. R. Stewart. The proton: applications to organic chemistry. Academic Press, New York. 1985. p. 118.
60. D.G. Lee and K.J. Demchuk. Can. J. Chem. **65**, 1769 (1987).
61. M.H. Abraham. J. Chem. Soc. Perkin Trans. 2, 1893 (1973).
62. C.D. Ritchie and W.F. Sager. Prog. Phys. Org. Chem. **2**, 323 (1965).

Can. J. Chem. Downloaded from www.nrcresearchpress.com by 203.198.23.82 on 09/08/12
For personal use only.

Energetics of acetic acid enol in aqueous solution. A new method for thermodynamic estimation

J. Peter Guthrie
Department of Chemistry, University of Western Ontario, London, ON N6A 5B7, Canada

Received May 26, 1993

J. Peter Guthrie. Can. J. Chem. **71**, 2123 (1993).

A new disproportionation calculation allows the estimation of the free energy of formation of the enol of acetic acid as 65 ± 2 kcal/mol. The value of pK_E derived from this free energy, $pK_E = 21 \pm 2$, is in satisfactory agreement with information from the literature about rates of exchange. Analysis of the data on rates of exchange of the C-H protons of acetic acid using Marcus theory allows an independent estimate of the enol content. Exchange in acid and in base lead to internally consistent estimates, $pK_E = 19.3 \pm 2.2$, which are within the combined uncertainties of the values from the thermodynamic estimate.

J. Peter Guthrie. Can. J. Chem. **71**, 2123 (1993).

Un nouveau calcul de dismutation permet d'évaluer que l'énergie libre de formation de l'énol de l'acide acétique est égale à 65 ± 2 kcal/mol. La valeur du pK_E, 21,2 ± 2, que l'on peut obtenir à partir de cette énergie libre est en bon accord avec l'information disponible dans la littérature au sujet des vitesses d'échange. L'analyse des données sur les vitesses d'échange des protons C-H de l'acide acétique réalisée à l'aide de la théorie de Marcus permet une évaluation indépendante de la quantité d'énol. Les échanges en milieux acide et basique conduisent à des évaluations autocohérentes, $pK_E = 19{,}3 \pm 2{,}2$, qui sont à l'intérieur des limites des incertitudes combinées des valeurs obtenues par des évaluations thermodynamiques.

[Traduit par la rédaction]

Can. J. Chem. Downloaded from www.nrcresearchpress.com by 203.198.23.82 on 09/08/12
For personal use only.

Introduction

Accurate values for the enol contents of simple aldehydes and ketones have been determined by Kresge and Wirz (1–4). Recently Kresge also determined the enol content of mandelic acid (5).

The techniques used to generate the enol appear to require the presence of the α-hydroxyl group, and will not easily be generalized to give the simplest carboxylic acid enol, that of acetic acid. The enol content of mandelic acid is very small, so that indirect methods for determining the enol content are difficult at best. Accordingly, it seemed of interest to devise ways to estimate the enol content of very simple carboxylic acids, as a possible guide to experimentation. I wish to report such a method, based on a novel application of the idea of disproportionation. It is also possible to calculate the enol content from exchange data, by making use of Marcus theory (6–8). This procedure leads to results consistent with those of the disproportionation assumption.

Results and discussion

Disproportionation

The basis of this approach is the assumption that the free energy change for process [1] will be approximately zero.

[1] $CH_2{=}CX_2 + 2\ Ph\text{-}OH \rightleftharpoons CH_2{=}C(OH)_2 + 2\ Ph\text{-}X$

This assumption is only plausible if X has an electronegativity very similar to that of oxygen, so that all interactions on the left-hand side of the equation are closely balanced by the analogous interactions on the right-hand side. In effect this limits X to being F or Cl, which have electronegativities similar to O, and are also similar in size.

The basis of this assumption can be tested by seeing how well the available data support the related assumption, that the free energy change for process [2] will be approximately zero.

[2] $CH_2{=}CXR + Ph\text{-}OH \rightleftharpoons CH_2{=}C(OH)R + Ph\text{-}X$

Data are available for R=H, X=Cl, F, and for R=CH_3, X=Cl; all thermodynamic data are given in Table 1. For each case we have calculated the free energy of formation of $CH_2{=}C(OH)R$ assuming that the change in free energy for process [2] is zero, and have compared this with the known free energy of formation. The results, Table 2, show that within about 2 kcal/mol the assumption for process [2] appears to be valid; the most serious discrepancy is for acetone enol, for which the corresponding chloro compound has a large uncertainty in ΔG_f^0(aq). This encourages one to look at the results of applying the same procedure to process [1] and thus predicting the free energy of formation for $CH_2{=}C(OH)_2$. When this is done, Table 2, we obtain two quite similar estimates, leading to a predicted value of −65 ± 2 kcal/mol for the free energy of formation of the enol of acetic acid in aqueous solution. This value, combined with the free energy of formation in aqueous solution of acetic acid itself, −94.35 kcal/mol (9), leads to a free energy change for the enolization shown in process [3] of +29 ± 2 kcal/mol, or to a $pK_E = 21$.

[3] $CH_3\text{-}COOH \rightleftharpoons CH_2{=}C(OH)_2$

There might be a geminal effect (anomeric effect) that, if substantial, would invalidate the disproportionation assumptions. This can be tested by comparison of the situation in process [4] for which geminal effects are known (10–12) with that in process [5].

[4] $CH_2X_2 + CH_4 \rightleftharpoons 2\ CH_3X$

[5] $CH_2{=}CX_2 + CH_2{=}CH_2 \rightleftharpoons 2\ CH_2{=}CHX$

Free energies of formation are available for both processes for X = Cl or F, and for process [4] with X = OCH_3; the values are given in Table 1.

For process [4], $\Delta G^0 = +9.3 \pm 2.7$ kcal/mol for X = F, -1.12 ± 0.44 for X = Cl, and $+9.33 \pm 0.37$ for X = OCH_3. For process [5], $\Delta G^0 = -3.39 \pm 1.26$ kcal/mol for X = F and -0.83 ± 0.61 for X = Cl.

Can. J. Chem. Downloaded from www.nrcresearchpress.com by 203.198.23.82 on 09/08/12
For personal use only.

TABLE 1. Thermodynamic data for compounds discussed in this paper[a]

(*a*) Compounds for which the free energy of formation in aqueous solution has not been reported

Compound	ΔH_f^0(g)	S^0(g)	ΔG_f^0(g)	ΔG_t	ΔG_f^0(aq)
Fluoromethane	−56.8 ± 2.	54.25 ± 0.3	−51.07	1.68 ± 0.5	−49.39 ± 2.06
Chloromethane	−19.57 ± 0.12	56.04 ± 0.3	−13.98	1.34 ± 0.1	−12.64 ± 0.18
Difluoromethane	−108.08 ± 0.22	58.94 ± 0.3	−101.45	1.48 ± 0.5	−99.97 ± 0.55
Dichloromethane	−22.85 ± 0.29	64.59 ± 0.3	−16.51	0.49 ± 0.1	−16.02 ± 0.32
Fluoroethene	−33.17 ± 0.41	60.39 ± 0.3[b]	−29.17	1.81 ± 0.1	−27.36 ± 0.43
Chloroethene	8.91 ± 0.31	63.08 ± 0.3	12.82	1.31 ± 0.1	14.13 ± 0.34
1,1-Difluoroethene	−80.07 ± 1.08	63.38 ± 0.3	−74.36	3.53 ± 0.1	−70.83 ± 1.08
1,1-Dichloroethene	0.62 ± 0.31	68.85 ± 0.3	6.10	3.49 ± 0.1[c]	9.59 ± 0.34
2-Chloro-1-propene	−5.02 ± 2.25	70.84 ± 0.3[d]	6.28	1.31 ± 1.0[e]	7.59 ± 2.46
Fluorobenzene	−27.72 ± 0.33	72.33 ± 0.3	−16.35	1.07 ± 0.1	−15.28 ± 0.36
Chlorobenzene	12.43 ± 0.31	74.92 ± 0.3	23.73	0.78 ± 0.1	24.50 ± 0.34

(*b*) Compounds for which the free energy of formation in aqueous solution has been reported[f]

Compound	ΔG_f^0(aq)	Compound	ΔG_f^0(aq)
Methane	−8.14 ± 0.16	Ethenol	−24.84 ± 0.21
Ethene	19.50 ± 0.16	1-Propen-2-ol	−27.02 ± 0.21
Acetic acid	−94.35 ± 0.38	Phenol	−12.60 ± 0.25
Dimethyl ether	−27.00 ± 0.18	Dimethoxymethane	−55.19 ± 0.23

[a]All at 25°C, enthalpies and free energies are in kcal/mol, entropies are in cal deg^{-1} mol^{-1}, standard states are the ideal gas at 1 atm and 1 M aqueous solution with an infinitely dilute reference state. Unless otherwise noted, enthalpies of formation are from ref. 36, and entropies are from ref. 37. Unless otherwise noted, free energies of transfer are calculated from solubilities from ref. 38, and vapor pressures from ref. 39. Free energies of formation are calculated from other values in the table.

[b]Reference 40.

[c]Calculated using a vapor pressure estimated by extrapolation from data in ref. 41.

[d]Reference 42.

[e]Estimated by additivity, assuming that the methyl increment from chloroethene to 2-chloropropene will be the same as from ethene to propene.

[f]All from ref. 9.

TABLE 2. Free energy changes (kcal/mol) for isodesmic reactions

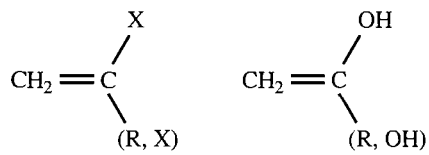

	Prediction[a]	Observed value[b]	Difference
Fluoroethene	−24.67 ± 0.61	−24.84 ± 0.21	0.17
Chloroethene	−22.98 ± 0.54	−24.84 ± 0.21	1.86
2-Chloro-1-propene	−29.52 ± 2.50	−27.02 ± 0.21	−2.50
1,1-Difluoroethene	−65.46 ± 0.62		
1,1-Dichloroethene	−64.62 ± 0.60		

[a]Based on disproportionation as described in the text, using free energy of formation values in Table I. Errors are calculated using the experimental errors in free energy values with no contribution for the uncertainty in the assumed free energy change of zero for the disproportionation reaction.

[b]From Table 1.

The message seems to be that there can be important geminal effects stabilizing CX_2 for sp^3 carbon when X is F or OCH_3, but that such effects are much smaller and *destabilizing* for sp^2 carbon. Furthermore, the difference between the destabilizing effect for F and Cl is only 2.56 ± 1.40 kcal/mol whereas the difference between the effects at sp^3 carbon for F and Cl was 10.4 ± 2.7 kcal/mol.

Thus it seems quite reasonable to expect *small* perturbations from this sort of interaction for process [1] where the *number* of electronegative substituents remains the same. Since the two examples of process [1], X = Cl and X = F, led to very similar estimates of the free energy of formation of $CH_2{=}C(OH)_2$ it seems likely that this is justified.

There have been various molecular orbital calculations addressing the question of the enol content (in the gas phase) of acetic acid, but the calculations for the most part were not

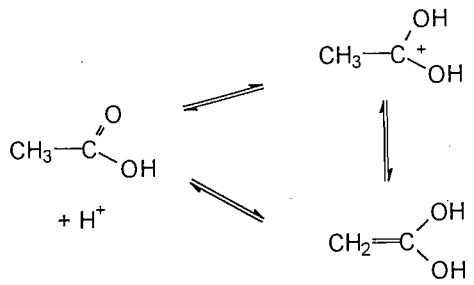

SCHEME 1

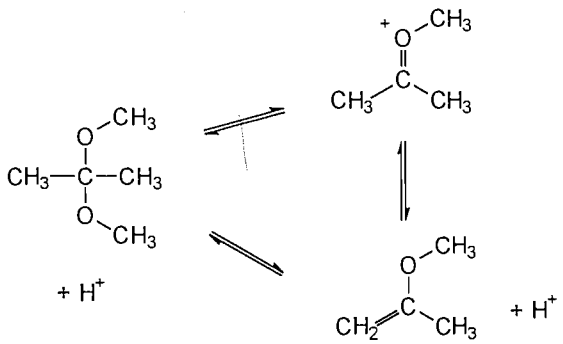

SCHEME 2

at a level that compels belief. Only ΔE was calculated but, assuming that the entropy change is small (13), these values can be translated into pK_E as follows: Nguyen and Hegarty (14), pK_E = 20.5 (STO-3G) (at this level, pK_E for acetaldehyde is predicted to be 13.5 (46), where the experimental value (gas phase) is 6.66 (15)); Heinrich et al. (16), pK_E = 26 (6-31G*) (at this level pK_E for acetone is predicted to be 12.3 (16) where the experimental value is 7.69 (gas phase) (15); Andraos et al. (17), pK_E = 18.8 (3-21G) (at this level pK_E for acetaldehyde is predicted to be 6.2 (13), experimental 6.66 (15). Unfortunately, this good result is the consequence of fortuitous cancellation of errors because "better" calculations, even MP4SDTQ/6-31G**//6-31G**, lead to poorer agreement (13). The best theoretical estimate so far, including zero point corrections, leads to pK_E = 10.9 (18), which differs significantly from the experimentally derived value of 6.66 (15). Apeloig et al. (13) have suggested that the experimental value may be in error because of the necessarily indirect way it is calculated. If this is so, and pK_E is really 10.9 for acetaldehyde, then the 3-21G calculations are in error, and are likely to be so for acetic acid as well. At the MP4/6-31G** level, calculations give good results for heats of isodesmic reactions of saturated molecules (19) and thus may be used to calculate heats of formation, given suitable reference values. Such calculations are distinctly less satisfactory for unsaturated molecules, for which higher level CI corrections are essential (19). Thus none of the calculations of the enol content reported to date can be expected to lead to "thermochemical" precision, i.e., ±1 kcal/mol.

To convert a gas phase value of ΔE into a solution phase ΔG requires the entropies (which can generally be estimated with useful accuracy) and the free energies of transfer. Unfortunately there is as yet no experimental basis for estimating free energies of transfer. Direct determination is impossible for such reactive species. Indirect calculation requires free energies of formation in both gas and aqueous solution. If one attempts to calculate group additivity terms for free energies of transfer, there are data (15) allowing evaluation of [CdH(O)] = 2.2 or 6.1 kcal/mol, and [Cd(C)(O)] = 1.8 or −2.8 kcal/mol. In either case the uncertainty in the average value is 2 kcal or greater. This presumably reflects uncertainties in the gas phase values, because free energies of transfer are generally predicted quite well by group additivity (44). From Keefe and Kresge's analysis of enthalpy data in the gas phase and in solution (43), there is a difference of 2.7 kcal in the double bond stabilization effect of OH between gas phase and solution, which must be reflected in the free energy of transfer. At the present time estimation of free energies of transfer will have uncertainties of at least 2–3 kcal/mol.

Exchange data

Our value for the enol content of acetic acid can be compared with other information from the literature bearing on the question of the enol content of acetic acid. The rate constant for acid-catalyzed exchange is known. Data permitting evaluation of the intrinsic barrier are available. We will then use Marcus theory to evaluate the equilibrium constant.

From the rate constants for deuterium exchange into acetic acid at higher temperatures, Bok and Geib (20) reported a rate constant for acid-catalyzed exchange: $\log k_{H^+} = -9.98$ (k in $M^{-1}\ s^{-1}$). Estimation of the solvent deuterium kinetic isotope effect by the method of Schowen (21–23) leads to a kinetic isotope effect of 0.69, and a revised estimate of the rate constant of $\log k_{H^+} = -10.14$. The rate-determining step is presumably deprotonation at carbon of acetic acidium ion, for which the pK_a is −6.56 (24, 25); see Scheme 1. The rate constant for deprotonation of acetic acidium ion by solvent water is then $\log k = -3.58$.

Now we must calculate the intrinsic barrier for this sort of C-protonation/deprotonation. We will use the set of reactions shown in Scheme 2. The rate constant for protonation of 2-methoxypropene is known, 970 $M^{-1}\ s^{-1}$ (26). The equilibrium constant for oxocation formation from 2,2-dimethoxypropane can be calculated from the rate constant for hydrolysis of acetone dimethyl acetal, 2950 $M^{-1}\ s^{-1}$,[1] and the rate constant for trapping of the cation by methanol, $1.08 \times 10^6\ M^{-1}\ s^{-1}$, (27), as 0.0027. Free energies of formation of 2,2-dimethoxypropane, 2-methoxypropene, and methanol (9) are available, which allows calculation of the equilibrium constant for conversion of 2,2-dimethoxypropane to 2-methoxypropene plus methanol as $\log K$ (M) = −2.79. This is substantially less favorable than the corresponding equilibrium constant for conversion of acetophenone dimethyl acetal to its enol ether, $\log K$ (M) = −1.22 (45). It is then possible to calculate the equilibrium constant for C-protonation of 2-methoxypropene as 1.7 M^{-1}. With rate and equilibrium constants for protonation of 2-methoxypropene in hand we will be able to calculate an intrinsic barrier once we allow for the work term for the protonation reaction. The "work term" in Marcus theory is the energy cost of bringing reactants together in an encounter complex. We follow Hine (28) and estimate the work terms for bringing two species together with the reactive atom of one species

[1] J. Barker, unpublished observations in this laboratory.

Can. J. Chem. Downloaded from www.nrcresearchpress.com by 203.198.23.82 on 09/08/12
For personal use only.

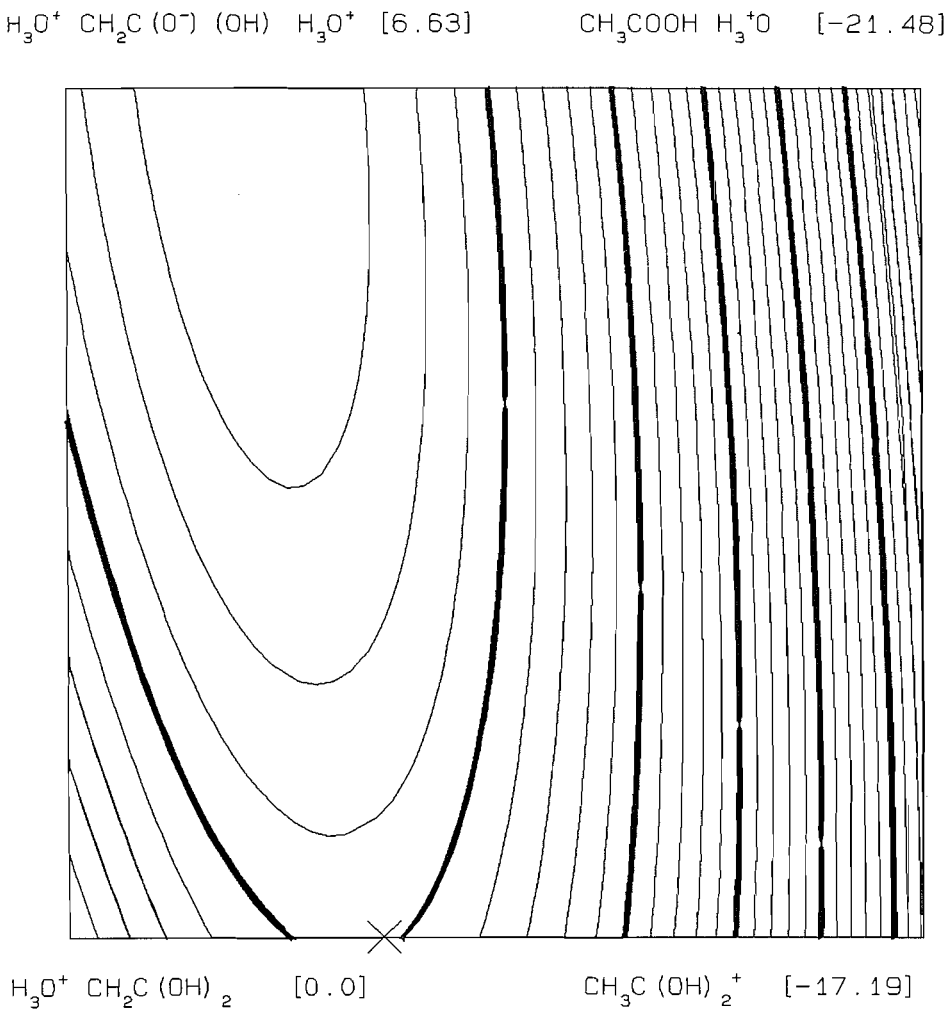

FIG. 1. Energy surface for protonation of acetic acid enol. Calculated using intrinsic barriers of 1 kcal/mol for oxygen to oxygen proton transfer and 12.3 kcal/mol for oxygen to carbon proton transfer. Contours are every kilocalorie with heavier contours every 5 kcal.

at either of two positions corresponding to the two lobes of the *p*-orbital of the other species, and with no net attraction or repulsion, as $K_{complex} = 0.017$ M. This assumes that there is hydrogen bonding of H_3O^+ to the π-cloud of the enol or enol ether, similar to the hydrogen bond of H_3O^+ to water. Given this assumed work term, the intrinsic barrier is 12.3 kcal/mol.

This barrier is expected to apply, at least approximately, to related reactions such as protonation of acetone enol or acetic acid enol. Now we can calculate the equilibrium constant for deprotonation at carbon of acetic acidium ion, and thence the equilibrium constant for enolization of acetic acid. To assess the sensitivity of the result to the value of the intrinsic barrier we assign an uncertainty of ±2 kcal/mol to this barrier. The value for the enolization equilibrium calculated as just described is $pK_E = 17.4 \pm 3$, in satisfactory agreement with the thermodynamic estimate. This analysis implies that protonation of the enol of acetic acid is much faster (log k (M^{-1} s^{-1}) is predicted to be 7.2) than protonation of ketene dimethyl acetal (log k (M^{-1} s^{-1}) was observed to be 5.86 (29)), because of the greater stability of acetic acidium ion relative to acetic acid enol than of methyl dimethoxymethylcarbenium ion relative to ketene dimethyl acetal. This is despite the expectation that methyl dimethoxymethylcarbenium ion will have at least a short lifetime, while acetic acidium ion will have no lifetime at all; it will lose a proton to water in less time than required for a vibration. Nonetheless an analysis using two-dimensional Marcus theory (6–8, 30, 31) suggests that the transition state for protonation of acetic acid enol is along the C-protonation edge: see Fig. 1.

We can also extract an estimate of the enol content from data for exchange catalyzed by OD^-. To do this we must consider the effect of ionization equilibria. Scheme 3 shows the various ionization and enolization processes possible for acetic acid. We assume that pK_1^0 will be 6.6 (5), the same as for mandelic acid enol, based on the very small substituent effect upon the pK_a of phenol by either *o*-phenyl or *o*-hydroxyl (32). We assume that substituent effects on the pK_a of a phenol are a suitable model for substituent effects on the pK_a of a carboxylic acid enol. Because this will not be exact we assign an uncertainty of ±1 to pK_1^0. pK_2^0 is estimated to be 11.6 ± 1.5 by applying Pauling's rules (33). Given these values and $pK_a^K = 4.76$ (32), K_1^C, K_2^E, and K_2^C are all calculable from K_1^E, and vice versa. The rate constant for the reaction of OD^- with CH_3COO^- is log $k = -8.25$ (20). Estimation of the solvent deuterium isotope effect for this process by the method of Schowen (21–23) using the frac-

Can. J. Chem. Downloaded from www.nrcresearchpress.com by 203.198.23.82 on 09/08/12
For personal use only.

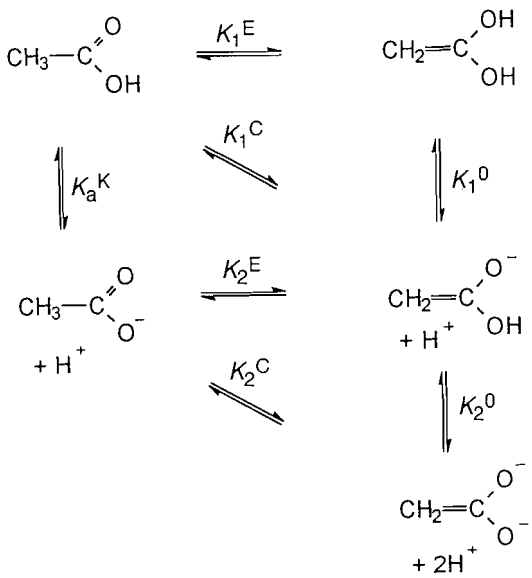

SCHEME 3

tionation factors for hydroxide ion and its solvating waters from Gold and Grist (34) leads to a kinetic isotope effect of 0.46, and a revised estimate of the rate constant of log $k = -8.59$. The intrinsic barrier for removal of the α-hydrogen from an aldehyde or ketone by hydroxide ion is 10.7 kcal/mol (35). This value is based on a work term calculated by assuming that the hydroxide must be partially desolvated, losing one hydrogen bond to water, in order to make contact with the hydrogen to be removed. Applying this value to the reaction with acetate leads to an equilibrium constant of log $K = 17.6 \pm 2.2$ or a $pK_2^E = 20.0 \pm 2.7$. Thence we can calculate $pK_1^E = 18.2 \pm 2.8$, in excellent agreement with the value derived from acid-catalyzed exchange of acetic acid.

The procedure that we have employed for estimation of free energies of formation by disproportionation seems to lead to reasonable answers, and could be employed to predict the free energies of formation of additional, currently interesting, enol intermediates if only there were thermodynamic data available for the corresponding halogen compounds. Since the latter are stable species there is no impediment, other than the work involved, in gathering these data, and this may prove to be the easiest way to get usefully accurate values for the corresponding enols. Exchange data provide an alternative general method, but represent a very large experimental effort.

After completing this work we learned that a kinetic determination of the pK_a of ethyl acetate[2] led to a value completely consistent with the enol contents reported here.

Acknowledgments

We thank the Natural Sciences and Engineering Research Council of Canada for financial support of this work. We thank Dr. T.L. Amyes for communicating results prior to publication.

1. Y. Chiang, A.J. Kresge, and J. Wirz. J. Am. Chem. Soc. **106**, 6392 (1984).
2. Y. Chiang, A.J. Kresge, M. Capponi, and J. Wirz. Helv. Chim. Acta, **69**, 1331 (1986).

[2]T.L. Amyes and J.P. Richard, unpublished results.

3. Y. Chiang, A.J. Kresge, J.A. Santaballa, and J. Wirz. J. Am. Chem. Soc. **110**, 5506 (1988).
4. Y. Chiang, A.J. Kresge, Y.S. Tang, and J. Wirz. J. Am. Chem. Soc. **106**, 460 (1984).
5. Y. Chiang, A.J. Kresge, P. Pruszynski, N.P. Schepp, and J. Wirz. Angew. Chem. Int. Ed. Engl. **29**, 792 (1990).
6. A.O. Cohen and R.A. Marcus. J. Phys. Chem. **65**, 1951 (1968).
7. R.A. Marcus. J. Am. Chem. Soc. **91**, 7224 (1969).
8. R.A. Marcus. Annu. Rev. Phys. Chem. **15**, 155 (1964).
9. J.P. Guthrie. Can. J. Chem. **70**, 1042 (1992).
10. R.A. More O'Ferrall and B.A. Murray. J. Chem. Soc. Chem. Commun. 1098 (1988).
11. M.P. Harcourt and R.A. More O'Ferrall. J. Chem. Soc. Chem. Commun. 823 (1987).
12. M.P. Harcourt and R.A. More O'Ferrall. Bull. Soc. Chim. Fr. 407 (1988).
13. Y. Apeloig, D. Arad, and Z. Rappoport. J. Am. Chem. Soc. **112**, 9131 (1990).
14. M.T. Nguyen and A.F. Hegarty. J. Am. Chem. Soc. **106**, 1552 (1984).
15. J.P. Guthrie. *In* The chemistry of enols. *Edited by* Z. Rappoport. Wiley, Chichester. 1990. pp. 75–93.
16. N. Heinrich, W. Koch, G. Frenking, and H. Schwarz. J. Am. Chem. Soc. **108**, 593 (1986).
17. J. Andraos, A.J. Kresge, M.R. Peterson, and I.G. Csizmadia. J. Am. Chem. Soc. **78**, 155 (1991).
18. Y. Apeloig. *In* The chemistry of enols. *Edited by* Z. Rappoport. Wiley, Chichester. 1990. pp. 1–74.
19. M. Sana and G. Leroy. J. Mol. Struct. (Theochem), **226**, 307 (1991).
20. L.D.K. Bok and K.H. Geib. Z. Phys. Chem. Abt. A: **183**, 353 (1939).
21. R.L. Schowen. Prog. Phys. Org. Chem. **9**, 275 (1972).
22. R.L. Schowen. *In* Isotope effects on enzyme catalyzed reactions. *Edited by* W.W. Cleland, M.H. O'Leary, and D.B. Northrup. University Park Press, Baltimore, Md. 1977.
23. K.B.J. Schowen. *In* Transition states of biochemical processes. *Edited by* R.D. Gandour and R.L. Schowen. Plenum Press, New York. 1978.
24. N.C. Deno, C.U. Pittman, and M.J. Wisotsky. J. Am. Chem. Soc. **86**, 4370 (1964).
25. J.P. Guthrie. Can. J. Chem. **65**, 1951 (1987).
26. P. Salomaa, A. Kankaanpera, and M. Lajunen. Acta. Chem. Scand. **20**, 1790 (1966).
27. T.L. Amyes and W.P. Jencks. J. Am. Chem. Soc. **111**, 7888 (1989).
28. J. Hine. J. Am. Chem. Soc. **93**, 3701 (1971).
29. A. Kresge and M. Leibovitch. J. Am. Chem. Soc. **114**, 3099 (1992).
30. J.P. Guthrie and D.C. Pike. Can. J. Chem. **65**, 1951 (1987).
31. J.P. Guthrie. Can. J. Chem. **68**, 1643 (1990).
32. W.P. Jencks and J. Regenstein. *In* Handbook of biochemistry and molecular biology. Vol. 1. *Edited by* G. Fassman. Chemical Rubber Company, Cleveland, Ohio. 1976. pp. 305–451.
33. L. Pauling. General chemistry. W.H. Freeman, San Francisco. 1947.
34. V. Gold and S. Grist. J. Chem. Soc. Perkin Trans. 2, 89 (1972).
35. J.P. Guthrie. J. Am. Chem. Soc. **113**, 7249 (1991).
36. J.B. Pedley, R.D. Naylor, and S.P. Kirby. Thermochemical data of organic compounds. Chapman and Hall, London. 1986.
37. D.R. Stull, E.F. Westrum, and G.C. Sinke. The chemical thermodynamics of organic compounds. Wiley, New York. 1967.
38. A.L. Horvath. Halogenated hydrocarbons: solubility–miscibility with water. Dekker, New York. 1982.

Can. J. Chem. Downloaded from www.nrcresearchpress.com by 203.198.23.82 on 09/08/12
For personal use only.

39. R.R. Dreisbach. Adv. Chem. Ser. **29**, (1961).
40. R.M. Joshi. J. Polym. Sci. A-2 **8**, 679 (1970).
41. R.C. Weast (*Editor*). Handbook of chemistry and physics. Chemical Rubber Co., Cleveland, Ohio. 1967.
42. J. Lielmezs and H. Aleman. Thermochim. Acta, **10**, 333 (1974).
43. J. Hine and P.K. Mookerjee. J. Org. Chem. **40**, 292 (1975).
44. J.R. Keeffe and A.J. Kresge. J. Phys. Org. Chem. **5**, 575 (1992).
45. J. Toullec and M. El-Alaoui. J. Org. Chem. **51**, 4054 (1986).
46. W.J. Bouma, D. Poppinger, and L. Radom. J. Am. Chem. Soc. **99**, 6443 (1977).

Can. J. Chem. Downloaded from www.nrcresearchpress.com by 203.198.23.82 on 09/08/12
For personal use only.

Structural studies of organoboron compounds LIX.[1] Reaction of two sterically hindered *N,N'*-dihydroxyaminals with phenylboronic acid, and the crystal and molecular structures of the resulting 1,3,5-trioxa-6,8-diaza-2,4-diboracyclooctanes and one of the adducts

WOLFGANG KLIEGEL AND GOTTFRIED LUBKOWITZ

Institut für Pharmazeutische Chemie der Technischen Universität Braunschweig, Beethovenstrasse 55, 38106 Braunschweig, Germany

AND

STEVEN J. RETTIG AND JAMES TROTTER[2]

Department of Chemistry, University of British Columbia, 2036 Main Mall, Vancouver, BC V6T 1Z1, Canada

Received June 30, 1993

WOLFGANG KLIEGEL, GOTTFRIED LUBKOWITZ, STEVEN J. RETTIG, and JAMES TROTTER. Can. J. Chem. **71**, 2129 (1993).

The syntheses of the sterically hindered *N,N'*-dihydroxyaminals; *N,N'*-bis(1-ethoxycarbonyl-1-methylethyl)-*N,N'*-dihydroxymethanediamine, **1***b*, and *N,N'*-bis(1,1-dimethylethyl)-*N,N'*-dihydroxymethanediamine, **1***c*, and their reactions with phenylboronic acid to yield the 1,3,5-trioxa-6,8-diaza-2,4-diboracyclooctanes **3** and **4**, respectively, are described. Crystals of **1***b* are tetragonal, a = 18.413(1), c = 9.867(2) Å, Z = 8, space group $I4_1$; those of **3** are monoclinic, a = 20.420(4), b = 8.272(4), c = 17.851(5) Å, β = 117.34(1)°, Z = 4, space group $C2/c$; and those of **4** are monoclinic, a = 9.493(4), b = 16.202(4), c = 14.783(3) Å, β = 101.90(2)°, Z = 4, space group $P2_1/c$. The structures were solved by direct methods and were refined by full-matrix least-squares procedures to R = 0.034, 0.039, and 0.040 (R_w = 0.035, 0.034, and 0.036) for 1550, 1438, and 2187 reflections with $I \geq 3\sigma(F^2)$, respectively. In the solid state, both **3** and **4** exhibit transannular N···B interactions. In **3** there are two identical (by symmetry) interactions with N···B = 2.433(3) Å that have estimated bond orders of 0.06, while the single transannular interaction in **4** has N—B = 1.953(3) Å and a bond order of about 0.3. The intermediate-strength transannular interaction in **4** is the first to be reported for this type of molecule.

WOLFGANG KLIEGEL, GOTTFRIED LUBKOWITZ, STEVEN J. RETTIG et JAMES TROTTER. Can. J. Chem. **71**, 2129 (1993).

On décrit la synthèse des *N,N'*-dihydroxyaminals stériquement empechés : *N,N'*-bis(1-éthoxycarbonyl-1-méthyléthyl)-*N,N'*-dihydroxyméthanediamine (**1***b*) et *N,N'*-bis(1,1-diméthyléthyl)-*N,N'*-dihydroxyméthanediamine (**1***c*) et leurs réactions avec l'acide phénylboronique qui conduisent aux 1,3,5-trioxa-6,8-diaza-2,4-diboracyclooctanes **3** et **4** respectivement. Les cristaux du composé **1***b* sont tétragonale, groupe d'espace $I4_1$, avec a = 18,413(1) et c = 9,867(2) Å et Z = 8; ceux du composé **3** sont monocliniques, groupe d'espace $C2/c$, avec a = 20,420(4), b = 8,272(4) et c = 17,851(5) Å, β = 117,34(1)°, Z = 4 et ceux du composé **4** sont monocliniques, groupe d'espace $P2_1/c$, avec a = 9,493(4), b = 16,202(4) et c = 14,783(3) Å, β = 101,90(2)', Z = 4. On a résolu les structures par des méthodes directes et on les a affinées par la méthode des moindres carrés jusqu'à des valeurs de R = 0,034, 0,039 et 0,040 (R_w = 0,035, 0,034 et 0,036) pour respectivement 1550, 1438 et 2187 réflexions avec $I \geq 3\sigma(F^2)$. À l'état solide, les composés **3** et **4** présentent tous les deux des interactions transannulaires B···N. Dans le composé **3**, il existe deux interactions identiques (par symétrie) avec B···N = 2,433(3) Å dont l'indice de liaison est évaluée à 0,06 alors que pour la seule interaction transannulaire du composé **4** N—B = 1,953(3) Å et que son indice de liaison est égale à environ 0,3. La force intermédiaire de l'interaction transannulaire observée dans le composé **4** est la première de ce type à être rapportée pour ce genre de molécules.

[Traduit par la rédaction]

Introduction

The reaction of the sterically hindered *N,N'*-bis(α-cyanoalkyl) substituted *N,N'*-dihydroxyaminal **1***a* (R = CMe_2CN) with phenylboronic acid gives the eight-membered heterocycle **2**, the structure of which has been established by an X-ray crystallographic analysis (1). As noted earlier (1, 2), the features of the molecular geometry of **2** are consistent with at least one weak transannular N···B interaction with an estimated bond order of about 0.05. It was of interest to investigate what effects on the transannular N—B bond formation would result from an enhanced basicity of the ring nitrogen atom without any major changes in the steric environment about the nitrogen atom. Varying the *N*-substitution from α-cyanoalkyl to α-alkoxycarbonyl and then to simple alkyl should distinctly increase the basicity (3). We have therefore synthesized the *N,N'*-dihydroxyaminal **1***b* (R = CMe_2COOEt), a compound not previously reported in the literature, and also the bis-*tert*-butyl derivative **1***c* (R = CMe_3) (4). The condensation reaction with phenylboronic acid gave crystalline compounds in both cases that show the elemental composition of heterocyclooctanes analogous to **2**. The infrared and ^1H nmr spectra of the products provide additional support for this formulation. The ^{11}B nmr spectrum of compound **3** (obtained from **1***b*) in $CDCl_3$ solution gives one broad signal having the same chemical shift value of $\delta(Et_2OBF_3)$ = 28.7 ppm that was reported for compound **2** (1). A broad singlet appears in the ^{11}B nmr spectrum of compound **4** at 23.3 ppm, similar to the value of ~22 ppm reported for the *N*-methyl derivative **5** (5). The bicyclic structure of **5** in the solid state has been established by an X-ray analysis (6). In each case the appearance of only one ^{11}B nmr signal for both boron nuclei is probably indicative of either a fluxional process in solution by which the two

[1]Previous paper in this series ref. 18.

[2]Author to whom correspondence may be addressed.

Can. J. Chem. Downloaded from www.nrcresearchpress.com by 203.198.23.82 on 09/08/12
For personal use only.

Can. J. Chem. Downloaded from www.nrcresearchpress.com by 203.198.23.82 on 09/08/12
For personal use only.

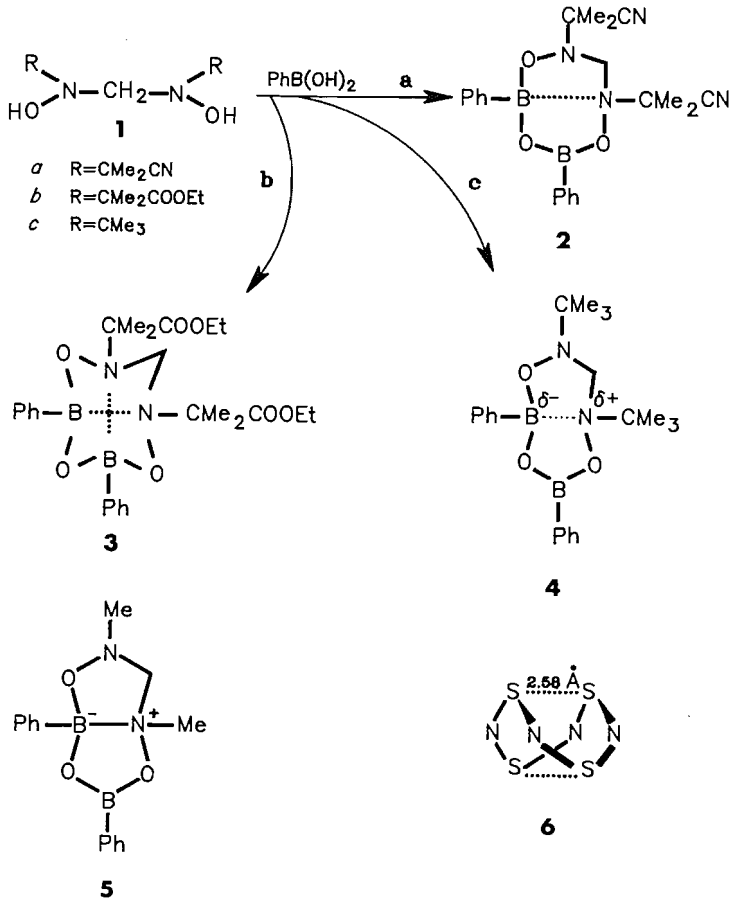

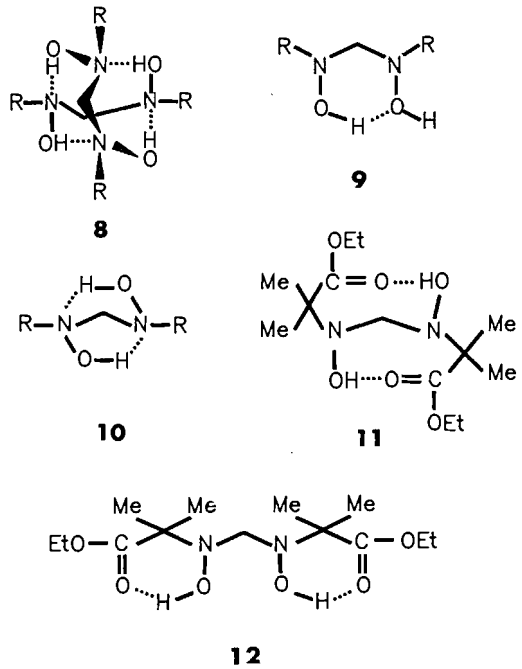

N···B coordinative bonds exchange, or of an essentially symmetric ring system having two equivalent boron atoms (1, 5, 6). To provide detailed structural information on the transannular N···B interactions in the solid state and to establish the crystal and molecular structures of both compounds, **3** and **4**, X-ray analyses were undertaken.

An X-ray analysis of the crystalline adduct **1***b* was also performed to clarify the molecular structure and, in particular, the nature of the hydrogen bonding in the crystal. It had been found that the *N*-methyl derivative **1** (R = Me) possesses a highly symmetric hydrogen-bonded dimeric structure of the type **8** in the solid state (7). Although intramolecular hydrogen bridging like that in **9** or **10** can be excluded from consideration, compound **1***b*, being somewhat less basic at the aminal nitrogen centres, might possibly form intramolecular O—H···O=C hydrogen bonds such as those in **11** or **12**. The synthesis of **1***b* started with the *N*-alkylation of (*Z*)-benzaldoxime with ethyl 2-bromo-2-methylpropionate to give the corresponding nitrone, which was then hydroxylaminolyzed to *N*-(1-ethoxycarbonyl-1-methylethyl)-hydroxylamine. This hydroxylamine derivative and formaldehyde were condensed to the aminal **1***b*. To elucidate the structure of **1***b* and to assess structural changes after its condensation with phenylboronic acid, we prepared single crystals for an X-ray analysis.

Experimental

*N,N′-Bis(1-ethoxycarbonyl-1-methylethyl)-N,N′-dihydroxymethanediamine, 1*b*, and its precursor compounds*

(*Z*)-Benzaldoxime (12.1 g, 100 mmol) and ethyl 2-bromo-2-methylpropionate (21.5 g, 110 mol) were reacted together with sodium (2.30 g, 100 mmol) following the prescribed method (8), yielding 19.5 g (83%) of colorless needles of *1-ethoxycarbonyl-1-methylethyl-N-(phenylmethylene)amine N-oxide*, mp 62°C (from ether – petroleum ether). Infrared (KBr): 1740 (C=O) cm^{-1}; ^1H nmr (90 MHz, $CDCl_3$ TMS) δ (ppm): 1.29 (t, J = 7 Hz, CH_2CH_3), 1.83 (s, $C(CH_3)_2$), 4.20 (q, J = 7 Hz, CH_2CH_3), 7.25–7.43

Can. J. Chem. Downloaded from www.nrcresearchpress.com by 203.198.23.82 on 09/08/12
For personal use only.

(m, 3 aromatic H), 7.44 (s, N=CH), 8.12–8.30 (m, 2 aromatic H). Anal. calcd. for $C_{13}H_{17}NO_3$: C 66.36, H 7.28, N 5.95; found: C 66.12, H 7.33, N 5.86.

1-Ethoxycarbonyl-1-methylethyl-*N*-(phenylmethylene)amine *N*-oxide (1.18 g, 5.00 mmol) and hydroxylamine hydrochloride (0.35 g, 5.0 mmol) were reacted according to the literature (9) to yield 0.43 g (58%) of a colorless oil, N-*(1-ethoxycarbonyl-1-methylethyl)hydroxylamine*. This material was not further purified. Infrared (film): 3500–3100 (br, O-H, N-H), 1740 (C=O) cm^{-1}; ^1H nmr (90 MHz, $CDCl_3$–TMS) δ(ppm): 1.28 (t, J = 7 Hz, CH_2CH_3), 1.33 (s, $C(CH_3)_2$), 4.16 (q, J = 7 Hz, CH_2CH_3), 5.55 (s, br, exchangeable, NHOH). Anal. calcd. for $C_6H_{13}NO_3$: C 48.97, H 8.90, N 9.52; found: C 49.10, H 9.15, N 9.56.

N-(1-Ethoxycarbonyl-1-methylethyl)hydroxylamine (1.18 g, 8.00 mmol) was dissolved in 10 mL of ethanol (99%). After the addition of formaldehyde solution (aqueous, 35%, 5 mmol) the mixture was stirred for 1 h at 40°C. Cooling of the partially evaporated solution gave 0.80 g (65%) of colorless crystals of **1***b*, mp 58°C (from benzene – petroleum ether). Infrared (KBr): 3210 (O-H), 1740 and 1715 (C=O) cm^{-1}; ^1H nmr (90 MHz, d_6-benzene–TMS) δ(ppm): 1.05 (t, J = 7 Hz, 2 CH_2CH_3), 1.51 (s, 2 $C(CH_3)_2$), 4.01 (q, J = 7 Hz, 2 CH_2CH_3), 4.07 (s, N-CH_2-N), 9.31 (s, br, exchangeable, 2 OH). Mass spectrum (EI, 70 eV) *m/z*: 159 (36%, $H_2C{=}N(O)C(CH_3)_2COOC_2H_5$), 87 (36%, $H_2C{=}N(OH)$-$C(CH_3)_2$), 74 (100%, $(CH_3)_2CNHOH$), 59 (27%). Anal. calcd. for $C_{13}H_{26}N_2O_6$: C 50.97, H 8.55, N 9.14; found: C 51.03, H 8.64, N 9.09. Crystals suitable for X-ray analysis were obtained by very slow recrystallization from benzene – petroleum ether.

N,N'-*Bis(1,1-dimethylethyl)*-N,N'-*dihydroxymethanediamine,* ***1****c*

N-tert-Butylhydroxylamine (8.90 g, 100 mmol) and formaldehyde (5.29 g of 35% aqueous solution, 50.0 mol) were reacted according to the literature (4). Yield: 5.73 g (60%), mp 101°C (from ethanol) (lit. (4) mp 100–101°C). Infrared (KBr): 3190 (O-H) cm^{-1}; ^1H nmr (90 MHz, d_6-benzene–TMS) δ(ppm): 1.20 (s, 2 $C(CH_3)_2$), 3.70 (s, N-CH_2-N), 9.84 (s, br, exchangeable, 2 OH). Mass spectrum (EI, 70 eV) *m/z*: 102 (72%, $H_2C{=}N(OH)C(CH_3)_3$), 74 (24%, $(CH_3)_2CNHOH$), 57 (100%, $C(CH_3)_3$). Anal. calcd. for $C_9H_{22}N_2O_2$; C 56.81, H 11.65, N 14.72; found: C 56.80, H 11.75, N 14.69.

6,8-Bis(1-ethoxycarbonyl-1-methylethyl)-2,4-diphenyl-1,3,5-trioxa-6,8-diaza-2,4-diboracyclooctane, ***3***

1*b* (0.61 g, 2.0 mmol) and phenylboronic acid (0.49 g, 4.0 mmol) were dissolved (or suspended) in 15 mL of benzene and refluxed for 1 h under continuous removal of reaction water in a Dean Stark trap. The solvent was distilled off, and the residue recrystallized from toluene – petroleum ether. Yield: 0.68 g (69%) of colorless crystals, mp 103–105°C. Infrared (KBr): 1740 (C=O), 1600 (C=C) cm^{-1}; ^1H nmr (90 MHz, $CDCl_3$–TMS) δ (ppm): 1.21 (t, J = 7 Hz, 2 CH_2CH_3), 1.33 (s, 2 $C(CH_3)_2$), 4.11 (s, N-CH_2-N), 4.13 (q, J = 7 Hz, 2 CH_2CH_3), 7.18–7.45 (m, 6 aromatic H), 7.70–7.88 (m, 4 aromatic H); ^{11}B nmr (64.2 MHz, $CDCl_3$–Et_2OBF_3) δ (ppm): 28.7 ($w_{1/2}$ = 685 Hz). Mass spectrum (EI, 70 eV, 90°C) *m/z*: 496 (8%, M^+), 423 (44%, $M^+ - COOC_2H_5$), 264 (100%, $M^+ - H_2C{=}N(O)C(CH_3)_2COOC_2H_5 - COOC_2H_5$), 236 (4%, $M^+ - ONC(CH_3)_2COOC_2H_5 - (CH_3)_2COOC_2H_5$), 105 (4%, C_6H_5BOH). Anal. calcd. for $C_{25}H_{34}B_2N_2O_7$: C 60.52, H 6.91, B 4.36, N 5.65; found: C 60.43, H 6.95, B 4.51, N 5.66. Crystals suitable for X-ray analysis were obtained by repeated recrystallization from toluene – petroleum ether.

6,8-Bis(1,1-dimethylethyl)-2,4-diphenyl-1,3,5-trioxa-6,8-diaza-2,4-diboracyclooctane, ***4***

1*c* (0.95 g, 5.0 mmol) and phenylboronic acid (1.22 g, 10.0 mmol) were reacted in 20 mL of benzene as described for compound **3** (above). Yield: 1.80 g (95%) of colorless crystals, mp 118–119°C (from toluene – petroleum ether). Infrared (KBr): 1605 (C=C) cm^{-1}; ^1H nmr (90 MHz, $CDCl_3$–TMS) δ (ppm): 1.15 (s, 2 $C(CH_3)_2$), 3.63 (s, N-CH_2-N), 7.18–7.38 (m, 6 aromatic H), 7.75–7.92 (m, 4 aromatic H); ^{11}B nmr (64.2 MHz, $CDCl_3$–Et_2OBF_3) δ (ppm): 23.3 ($w_{1/2}$ = 640 Hz). Mass spectrum (EI, 70 eV, 90°C) *m/z*: 380 (28%, M^+), 365 (28%, $M^+ - CH_3$), 264 (100%, $M^+ - H_2C{=}N(O)C_4H_9 - CH_3$), 236 (66%, $M^+ - C_4H_9NO - C_4H_9$), 105 (19%, C_6H_5BOH), 77 (15%, C_6H_5), 56 (74%, $H_2C{=}C(CH_3)_2$). Anal. calcd. for $C_{21}H_{30}B_2N_2O_3$: C 66.36, H 7.96, B 5.69, N 7.37; found: C 66.21, H 8.05, B 5.86, N 7.18. Crystals suitable for X-ray analysis were obtained by recrystallization from toluene – petroleum ether.

X-ray crystallographic analyses of ***1****b*, ***3****, and* ***4***

Crystallographic data for **1***b*, **3**, and **4** appear in Table 1. The final unit-cell parameters were obtained by least squares on the setting angles for 25 reflections with 2θ = 91.2°–113.2°, 20.6°–33.4°, and 25.1°–34.7°, respectively. The intensities of three standard reflections, measured every 200 reflections throughout the data collections, showed only small random fluctuations in each case. The data were processed,[3] corrected for Lorentz and polarization effects, and absorption (empirical, based on azimuthal scans for three reflections).

The structures were solved by direct methods, the coordinates of the non-hydrogen atoms being determined from *E*-maps or from subsequent difference Fourier syntheses. The structure analysis of **3** was initiated in the centrosymmetric space group $C2/c$ on the basis of the *E*-statistics, this choice being confirmed by the subsequent successful solution and refinement of the structure. In the structure of **1***b* there are two crystallographically independent molecules, each having exact C_2 symmetry. Molecules of **3** are also situated on a crystallographic C_2 axis. The thermal parameters and geometry involving the ethyl ester atoms C(13) and C(14) of one of the independent molecules of **1***b* suggest libration about the C(9)—C(12) bond, but not of such amplitude as to necessitate the use of a disordered model. Furthermore, the nearly isotropic cross section of the thermal motion of these atoms (viewed along the one small eigenvector) would lead to difficulties in producing a reasonable disordered model. Non-hydrogen atoms were refined with anisotropic thermal parameters. The carbon-bound hydrogen atoms were fixed in idealized positions (C—H = 0.98 Å, B_H = 1.2 $B_{\text{bonded atom}}$, methyl groups staggered) and the O-H hydrogen atoms of **1***b* were refined with isotropic thermal parameters. Corrections for secondary extinction were applied for all three structures, the final values of the extinction coefficients being $6.67(11) \times 10^{-6}$ for **1***b*, $1.06(3) \times 10^{-6}$ for **3**, and $1.12(4) \times 10^{-6}$ for **4**. Neutral atom scattering factors for all atoms and anomalous dispersion corrections for the non-hydrogen atoms were taken from the *International tables for X-ray crystallography* (10). A parallel refinement of the mirror-image structure of **1***b* gave slightly higher residuals, the R and R_w factor ratios being 1.003 and 1.002, respectively. Final atomic coordinates and equivalent isotropic thermal parameters, bond lengths, and bond angles appear in Tables 2–4, respectively. The structure of **1***b* is shown in Fig. 1, and the structures of **3** and **4** are shown in Fig. 2. Hydrogen atom parameters, anisotropic thermal parameters, torsion angles, intermolecular contacts, least-squares planes, and measured and calculated structure factor amplitudes for the three structures are included as supplementary material.[4]

[3] TEXSAN/TEXRAY structure analysis package (Version 5.1), Molecular Structure Corp. 1985.

[4] Supplementary material mentioned in the text may be purchased from: The Depository of Unpublished Data, Document Delivery, CISTI, National Research Council Canada, Ottawa, Canada K1A 0S2.

Tables of hydrogen atom coordinates and bond lengths and angles involving hydrogen atoms have also been deposited with the Cambridge Crystallographic Data Centre and can be obtained on request from The Director, Cambridge Crystallographic Data Centre, University Chemical Laboratory, 12 Union Road, Cambridge CB2 1EZ, U.K.

Can. J. Chem. Downloaded from www.nrcresearchpress.com by 203.198.23.82 on 09/08/12
For personal use only.

TABLE 1. Crystallographic data[a]

Compound	**1***b*	**3**	**4**
Formula	$C_{13}H_{26}N_2O_6$	$C_{25}H_{34}B_2N_2O_7$	$C_{21}H_{30}B_2N_2O_3$
fw	306.36	496.17	380.10
Crystal system	Tetragonal	Monoclinic	Monoclinic
Space group	$I4_1$	$C2/c$	$P2_1/c$
a, Å	18.413 (1)	20.420 (4)	9.493 (4)
b, Å	18.413 (1)	8.272 (4)	16.202 (4)
c, Å	9.867 (2)	17.851 (5)	14.783 (3)
β°	90	117.34 (1)	101.90 (2)
V, Å^3	3345.4 (6)	2678 (1)	2225 (2)
Z	8	4	4
ρ_{calc}, g/cm^3	1.216	1.230	1.135
F(000)	1328	1056	816
Radiation	Cu-K_α	Mo-K_α	Mo-K_α
μ, cm^{-1}	7.66	0.82	0.69
Crystal size, mm	0.35 × 0.40 × 0.45	0.30 × 0.30 × 0.35	0.25 × 0.30 × 0.45
Transmission factors (relative)	0.96–1.00	0.96–1.00	0.92–1.00
Scan type	ω–2θ	ω–2θ	ω–2θ
Scan range, deg in ω	1.21 + 0.20 tan θ	1.05 + 0.35 tan θ	1.21 + 0.35 tan θ
Scan speed, deg/min	32	16	32
Data collected	$+h$, $+k$, $+l$	$+h$, $+k$, $\pm l$	$+h$, $+k$, $\pm l$
$2\theta_{max}$, deg	155	55	55
Crystal decay	Negligible	Negligible	Negligible
Total reflections	1836	3389	5612
Total unique reflections	1726	3079	5109
R_{merge}	0.018	0.022	0.043
Reflections with $I \geq 3\sigma(I)$	1550	1438	2187
No. of variables	199	165	254
R	0.034	0.039	0.040
R_w	0.035	0.034	0.036
gof	3.37	1.82	2.34
Max Δ/σ (final cycle)	0.02	0.01	0.01
Residual density e/Å^3	−0.14 to 0.16	−0.16 to 0.17	−0.15 to 0.13

[a]Temperature 294 K, Rigaku AFC6S diffractometer, Cu-K_α (λ = 1.54178 Å) or Mo-K_α (λ = 0.71069 Å) radiation, graphite monochromator, takeoff angle 6.0°, aperture 6.0 × 6.0 mm at a distance of 285 mm from the crystal, stationary background counts at each end of the scan (scan/background time ratio 2:1, up to 8 rescans), $\sigma^2(F^2) = [S^2(C + 4B)]/Lp^2$ (S = scan rate, C = scan count, B = normalized background count), function minimized $\Sigma w(|F_o| - |F_c|)^2$ where $w = 4F_o^2/\sigma^2(F_o^2)$, $R = \Sigma||F_o| - |F_c||/\Sigma|F_o|$, $R_w = (\Sigma w(|F_o| - |F_c|)^2/\Sigma w|F_o|^2)^{1/2}$, and gof = $[\Sigma w(|F_o| - |F_c|)^2/(m - n)]^{1/2}$. Values given for R, R_w, and gof are based on those reflections with $I \geq 3\sigma(I)$.

Results and discussion

The X-ray analyses confirm the postulated cyclooctane skeletons for **3** and **4**. Both of these compounds have the cyclic pyroboronate structure found previously for **2** (1) that features an eight-membered ring having a distorted boat-boat ("saddle") conformation, typical for medium-sized heterocyclic rings with stabilizing transannular interactions (11). The transannular N···B interactions are effective to different extents in **3** and **4**. In the symmetric ring system of **3** the two N···B distances are equal (2.433(3) Å) with an estimated N—B bond order of 0.06 (empirical, corrected for hybridization and electronegativity effects). Both N···B interactions in **3** are slightly stronger than the single transannular N···B interaction in **2** (2.475(3) Å, N—B bond order 0.05) (1, 2), probably reflecting the increased basicity at the nitrogen centres of **3**. In compound **4**, possessing even more basic nitrogen centres, one of the N···B distances (N(2)—B(1) = 1.953(3) Å, bond order 0.29) approaches a transannular N—B bond as observed in the bicyclo[3.3.0]octane skeleton of compound **5** (mean 1.733 Å, bond order 0.62) (2, 6).

Steric factors (ring strain in particular) may be responsible for the lengthening of the N···B distance for the second donor–acceptor pair in **4** to N(1)—B(2) = 2.897(3) Å. This effect is even more pronounced in compound **5** (6), having a shorter mean N—B bond of 1.733 Å and an even longer mean nonbonded N···B distance of 3.083 Å. The substantial difference between the transannular N(2)···B(1) distances in **4** and **5** (1.953(3) and mean 1.733 Å, respectively) clearly demonstrates a steric impediment to the Lewis basicity at the nitrogen centres in **4**. The inductive (+*I*) effect of the *N-tert*-butyl substituents in **4** should induce an increased basicity compared to the *N*-methyl groups in **5**, leading to a stronger coordinative N—B interaction in **4**.

Including the transannular N···B interactions, compound **3** possesses a tricyclo[3.3.0.0^{3,7}]octane skeleton that corresponds roughly to the D_{2d} dinoradamantane ring system (12). The ring system of **3** is more similar to the D_{2d} "cradle" structures of S_4N_4, **6** (13), As_4S_4 (14), P_4S_4 (15), or N_4Se_4 (16). The bond order of the transannular S···S interaction in **6** has been estimated to be 0.4–0.5 (13*d*) and can be described as a $^3p_\sigma$–$^3p_\sigma$ bond (13*e*), different in nature from the N···B interaction in **3**.

Structural parameters for the N···B interactions in compounds **2–5** are compiled in Table 5. The degree of pyramidalization of the trigonal planar boronate group in its

TABLE 2. Final atomic coordinates (fractional) and B_{eq} (Å^2)[a]

Atom	x	y	z	B_{eq}
		1*b*		
O(1)	0.60325(10)	0.00317(10)	0.2559	4.3
O(2)	0.61500(9)	0.16040(10)	0.3365(3)	4.8
O(3)	0.70261(10)	0.13839(12)	0.1859(3)	6.0
O(4)	0.49346(11)	0.10254(11)	0.4660(3)	5.1
O(5)	0.39926(15)	0.19461(13)	0.6755(3)	7.7
O(6)	0.4423(2)	0.1025(2)	0.7986(3)	8.0
N(1)	0.54357(10)	0.04784(10)	0.2066(3)	3.6
N(2)	0.45086(11)	0.04256(11)	0.5136(3)	4.1
C(1)	1/2	0	0.1198(4)	3.9
C(2)	0.57792(13)	0.10882(13)	0.1285(3)	3.9
C(3)	0.52034(14)	0.16800(14)	0.1123(4)	4.6
C(4)	0.6084(2)	0.0877(2)	−0.0090(4)	5.5
C(5)	0.63993(13)	0.13654(13)	0.2180(4)	4.2
C(6)	0.6679(2)	0.1811(2)	0.4375(4)	5.3
C(7)	0.6296(2)	0.2170(2)	0.5485(5)	7.9
C(8)	1/2	0	0.6003(4)	4.7
C(9)	0.38688(14)	0.07524(15)	0.5836(3)	4.3
C(10)	0.3405(2)	0.0152(2)	0.6457(4)	5.5
C(11)	0.3418(2)	0.1160(2)	0.4779(4)	5.6
C(12)	0.4135(2)	0.1246(2)	0.6987(4)	5.1
C(13)	0.4226(3)	0.2454(3)	0.7797(7)	11.3
C(14)	0.3742(4)	0.2875(4)	0.8267(9)	17.1
		3		
O(1)	0.40778(7)	0.3961(2)	0.20015(8)	3.1
O(2)	1/2	0.1884(2)	1/4	3.3
O(3)	0.29173(9)	0.6248(2)	0.25198(10)	4.8
O(4)	0.37902(8)	0.7760(2)	0.24354(10)	4.2
N(1)	0.45947(9)	0.4747(2)	0.27736(10)	2.9
C(1)	1/2	0.5859(4)	1/4	3.1
C(2)	0.41930(12)	0.5342(3)	0.32277(13)	3.0
C(3)	0.38951(14)	0.3864(3)	0.3486(2)	4.5
C(4)	0.47423(13)	0.6248(3)	0.40097(14)	4.0
C(5)	0.35453(13)	0.6464(3)	0.26828(13)	3.3
C(6)	0.32402(15)	0.8947(3)	0.1914(2)	5.1
C(7)	0.2873(2)	0.8431(4)	0.1020(2)	7.4
C(8)	0.40971(12)	0.2003(3)	0.09296(13)	3.3
C(9)	0.43851(14)	0.0634(3)	0.07426(14)	4.4
C(10)	0.4070(2)	−0.0026(3)	−0.0058(2)	5.3
C(11)	0.3458(2)	0.0671(4)	−0.0694(2)	5.2
C(12)	0.31667(14)	0.2035(4)	−0.0533(2)	5.3
C(13)	0.34839(13)	0.2699(3)	0.02707(15)	4.5
B(1)	0.44468(15)	0.2704(3)	0.1838(2)	3.1
		4		
O(1)	0.3886(2)	0.17826(9)	0.36237(10)	3.8
O(2)	0.1132(2)	0.11046(9)	0.20333(11)	4.1
O(3)	0.1455(2)	0.12896(9)	0.36310(11)	4.2
N(1)	0.3979(2)	0.11278(11)	0.29597(12)	3.5
N(2)	0.2017(2)	0.18440(11)	0.21770(13)	3.6
C(1)	0.3462(2)	0.15542(14)	0.2091(2)	3.8
C(2)	0.5478(3)	0.08116(14)	0.3123(2)	4.0
C(3)	0.6608(3)	0.1468(2)	0.3072(2)	6.3
C(4)	0.5494(3)	0.0149(2)	0.2397(2)	6.0
C(5)	0.5765(3)	0.0416(2)	0.4076(2)	6.0
C(6)	0.1329(3)	0.24603(14)	0.1450(2)	4.1
C(7)	0.2144(3)	0.3273(2)	0.1628(2)	5.4
C(8)	−0.0217(3)	0.2591(2)	0.1558(2)	6.0
C(9)	0.1368(3)	0.2142(2)	0.0490(2)	5.9
C(10)	0.2066(3)	0.27999(14)	0.3960(2)	3.8
C(11)	0.3032(3)	0.3464(2)	0.4063(2)	4.5
C(12)	0.2795(3)	0.4181(2)	0.4517(2)	5.4

Can. J. Chem. Downloaded from www.nrcresearchpress.com by 203.198.23.82 on 09/08/12
For personal use only.

TABLE 2 (*concluded*)

Atom	*x*	*y*	*z*	B_{eq}
C(13)	0.1592(4)	0.4257(2)	0.4881(2)	6.2
C(14)	0.0616(3)	0.3623(2)	0.4790(2)	6.6
C(15)	0.0849(3)	0.2907(2)	0.4331(2)	5.4
C(16)	0.0109(3)	0.00035(15)	0.2927(2)	4.3
C(17)	−0.0546(3)	−0.0423(2)	0.2144(2)	5.6
C(18)	−0.1295(3)	−0.1154(2)	0.2213(3)	7.2
C(19)	−0.1394(4)	−0.1446(2)	0.3065(4)	7.8
C(20)	−0.0766(4)	−0.1035(2)	0.3848(3)	7.4
C(21)	−0.0013(3)	−0.0318(2)	0.3774(2)	5.7
B(1)	0.2387(3)	0.1954(2)	0.3521(2)	3.9
B(2)	0.0956(3)	0.0819(2)	0.2889(2)	3.9

[a] $B_{eq} = (8/3)\pi^2\Sigma\Sigma U_{ij}a_i * a_j * (a_i \cdot a_j)$.

TABLE 3. Bond lengths (Å) with estimated standard deviations

Atom	Atom	Distance	Atom	Atom	Distance
			1*b*		
O(1)	N(1)	1.456(3)	O(4)	N(2)	1.434(3)
O(2)	C(5)	1.331(3)	O(5)	C(12)	1.336(4)
O(2)	C(6)	1.445(3)	O(5)	C(13)	1.455(5)
O(3)	C(5)	1.197(3)	O(6)	C(12)	1.190(4)
N(1)	C(1)	1.468(3)	N(2)	C(8)	1.472(3)
N(1)	C(2)	1.502(3)	N(2)	C(9)	1.492(3)
C(2)	C(3)	1.529(4)	C(9)	C(10)	1.526(4)
C(2)	C(4)	1.519(4)	C(9)	C(11)	1.529(4)
C(2)	C(5)	1.531(4)	C(9)	C(12)	1.535(4)
C(6)	C(7)	1.461(5)	C(13)	C(14)	1.268(7)
			3		
O(1)	N(1)	1.449(2)	C(2)	C(5)	1.541(3)
O(1)	B(1)	1.391(3)	C(6)	C(7)	1.480(4)
O(2)	B(1)	1.381(3)	C(8)	C(9)	1.386(3)
O(3)	C(5)	1.191(2)	C(8)	C(13)	1.389(3)
O(4)	C(5)	1.340(3)	C(8)	B(1)	1.554(3)
O(4)	C(6)	1.460(3)	C(9)	C(10)	1.383(3)
N(1)	C(1)	1.463(2)	C(10)	C(11)	1.370(3)
N(1)	C(2)	1.478(3)	C(11)	C(12)	1.366(4)
C(2)	C(3)	1.528(3)	C(12)	C(13)	1.388(3)
C(2)	C(4)	1.526(3)			
			4		
O(1)	N(1)	1.461(2)	C(6)	C(9)	1.518(3)
O(1)	B(1)	1.426(3)	C(10)	C(11)	1.402(3)
O(2)	N(2)	1.454(2)	C(10)	C(15)	1.388(3)
O(2)	B(2)	1.390(3)	C(10)	B(1)	1.574(4)
O(3)	B(1)	1.424(3)	C(11)	C(12)	1.383(3)
O(3)	B(2)	1.339(3)	C(12)	C(13)	1.365(4)
N(1)	C(1)	1.452(3)	C(13)	C(14)	1.371(4)
N(1)	C(2)	1.485(3)	C(14)	C(15)	1.383(4)
N(2)	C(1)	1.480(3)	C(16)	C(17)	1.380(3)
N(2)	C(6)	1.513(3)	C(16)	C(21)	1.384(3)
N(2)	B(1)	1.953(3)	C(16)	B(2)	1.553(4)
C(2)	C(3)	1.522(3)	C(17)	C(18)	1.396(4)
C(2)	C(4)	1.520(3)	C(18)	C(19)	1.367(5)
C(2)	C(5)	1.520(3)	C(19)	C(20)	1.361(5)
C(6)	C(7)	1.522(3)	C(20)	C(21)	1.380(4)
C(6)	C(8)	1.524(3)			

Can. J. Chem. Downloaded from www.nrcresearchpress.com by 203.198.23.82 on 09/08/12
For personal use only.

TABLE 4. Bond angles (deg) with estimated standard deviations[a]

Atom	Atom	Atom	Angle	Atom	Atom	Atom	Angle
			1*b*				
C(5)	O(2)	C(6)	117.4(2)	C(12)	O(5)	C(13)	116.2(3)
O(1)	N(1)	C(1)	105.6(1)	O(4)	N(2)	C(8)	105.3(2)
O(1)	N(1)	C(2)	106.0(2)	O(4)	N(2)	C(9)	105.8(2)
C(1)	N(1)	C(2)	112.3(2)	C(8)	N(2)	C(9)	115.5(2)
N(1)	C(1)	N(1)′	108.6(3)	N(2)	C(8)	N(2)′	108.9(3)
N(1)	C(2)	C(3)	107.1(2)	N(2)	C(9)	C(10)	109.6(2)
N(1)	C(2)	C(4)	115.0(2)	N(2)	C(9)	C(11)	108.1(2)
N(1)	C(2)	C(5)	105.5(2)	N(2)	C(9)	C(12)	109.2(2)
C(3)	C(2)	C(4)	110.2(2)	C(10)	C(9)	C(11)	109.0(2)
C(3)	C(2)	C(5)	109.9(2)	C(10)	C(9)	C(12)	108.1(2)
C(4)	C(2)	C(5)	109.0(2)	C(11)	C(9)	C(12)	112.8(2)
O(2)	C(5)	O(3)	123.8(3)	O(5)	C(12)	O(6)	124.0(3)
O(2)	C(5)	C(2)	111.1(2)	O(5)	C(12)	C(9)	112.5(3)
O(3)	C(5)	C(2)	125.1(3)	O(6)	C(12)	C(9)	123.6(3)
O(2)	C(6)	C(7)	108.1(2)	O(5)	C(13)	C(14)	116.4(5)
			3				
N(1)	O(1)	B(1)	107.9(2)	O(3)	C(5)	C(2)	125.4(2)
B(1)	O(2)	B(1)″	121.1(3)	O(4)	C(5)	C(2)	110.3(2)
C(5)	O(4)	C(6)	117.0(2)	O(4)	C(6)	C(7)	110.7(2)
O(1)	N(1)	C(1)	104.0(1)	C(9)	C(8)	C(13)	116.9(2)
O(1)	N(1)	C(2)	109.0(1)	C(9)	C(8)	B(1)	120.9(2)
C(1)	N(1)	C(2)	121.0(2)	C(13)	C(8)	B(1)	122.2(2)
N(1)	C(1)	N(1)″	102.1(2)	C(8)	C(9)	C(10)	121.6(2)
N(1)	C(2)	C(3)	107.3(2)	C(9)	C(10)	C(11)	120.3(3)
N(1)	C(2)	C(4)	107.8(2)	C(10)	C(11)	C(12)	119.6(2)
N(1)	C(2)	C(5)	112.7(2)	C(11)	C(12)	C(13)	120.1(3)
C(3)	C(2)	C(4)	110.1(2)	C(8)	C(13)	C(12)	121.5(2)
C(3)	C(2)	C(5)	109.1(2)	O(1)	B(1)	O(2)	119.8(2)
C(4)	C(2)	C(5)	109.8(2)	O(1)	B(1)	C(8)	117.7(2)
O(3)	C(5)	O(4)	124.2(2)	O(2)	B(1)	C(8)	120.9(2)
			4				
N(1)	O(1)	B(1)	105.5(2)	C(11)	C(10)	C(15)	116.1(2)
N(2)	O(2)	B(2)	108.4(2)	C(11)	C(10)	B(1)	122.4(2)
B(1)	O(3)	B(2)	117.4(2)	C(15)	C(10)	B(1)	121.4(2)
O(1)	N(1)	C(1)	101.1(2)	C(10)	C(11)	C(12)	121.9(2)
O(1)	N(1)	C(2)	109.3(2)	C(11)	C(12)	C(13)	120.0(3)
C(1)	N(1)	C(2)	116.5(2)	C(12)	C(13)	C(14)	119.8(3)
O(2)	N(2)	C(1)	104.1(2)	C(13)	C(14)	C(15)	120.2(3)
O(2)	N(2)	C(6)	106.8(2)	C(10)	C(15)	C(14)	121.9(3)
O(2)	N(2)	B(1)	101.6(1)	C(17)	C(16)	C(21)	117.6(2)
C(1)	N(2)	C(6)	114.8(2)	C(17)	C(16)	B(2)	122.9(3)
C(1)	N(2)	B(1)	98.1(2)	C(21)	C(16)	B(2)	119.5(3)
C(6)	N(2)	B(1)	128.6(2)	C(16)	C(17)	C(18)	120.8(3)
N(1)	C(1)	N(2)	103.0(2)	C(17)	C(18)	C(19)	119.6(3)
N(1)	C(2)	C(3)	114.3(2)	C(18)	C(19)	C(20)	120.8(3)
N(1)	C(2)	C(4)	106.1(2)	C(19)	C(20)	C(21)	119.2(3)
N(1)	C(2)	C(5)	106.1(2)	C(16)	C(21)	C(20)	121.9(3)
C(3)	C(2)	C(4)	110.4(2)	O(1)	B(1)	O(3)	118.1(2)
C(3)	C(2)	C(5)	110.3(2)	O(1)	B(1)	N(2)	93.3(2)
C(4)	C(2)	C(5)	109.3(2)	O(1)	B(1)	C(10)	113.5(2)
N(2)	C(6)	C(7)	108.5(2)	O(3)	B(1)	N(2)	93.6(2)
N(2)	C(6)	C(8)	107.5(2)	O(3)	B(1)	C(10)	115.7(2)
N(2)	C(6)	C(9)	110.5(2)	N(2)	B(1)	C(10)	119.3(2)
C(7)	C(6)	C(8)	109.2(2)	O(2)	B(2)	O(3)	117.8(2)
C(7)	C(6)	C(9)	110.3(2)	O(2)	B(2)	C(16)	118.4(3)
C(8)	C(6)	C(9)	110.8(2)	O(3)	B(2)	C(16)	123.6(3)

[a]Here and elsewhere in this report, the symbols ′ and ″ refer to the symmetry operations: $1 - x, -y, z$ and $1 - x, y, 1/2 - z$, respectively.

Can. J. Chem. Downloaded from www.nrcresearchpress.com by 203.198.23.82 on 09/08/12
For personal use only.

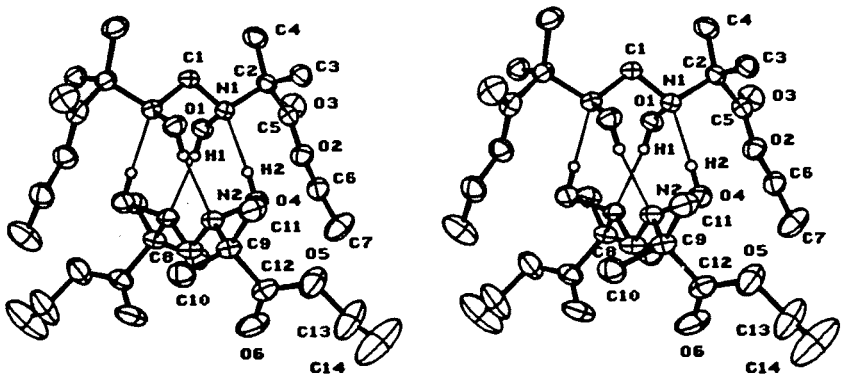

FIG. 1. Stereoview of the hydrogen-bonded of dimer of **1***b*; 33% probability thermal ellipsoids are shown for the non-hydrogen atoms. Hydrogen bonds are represented by fine lines.

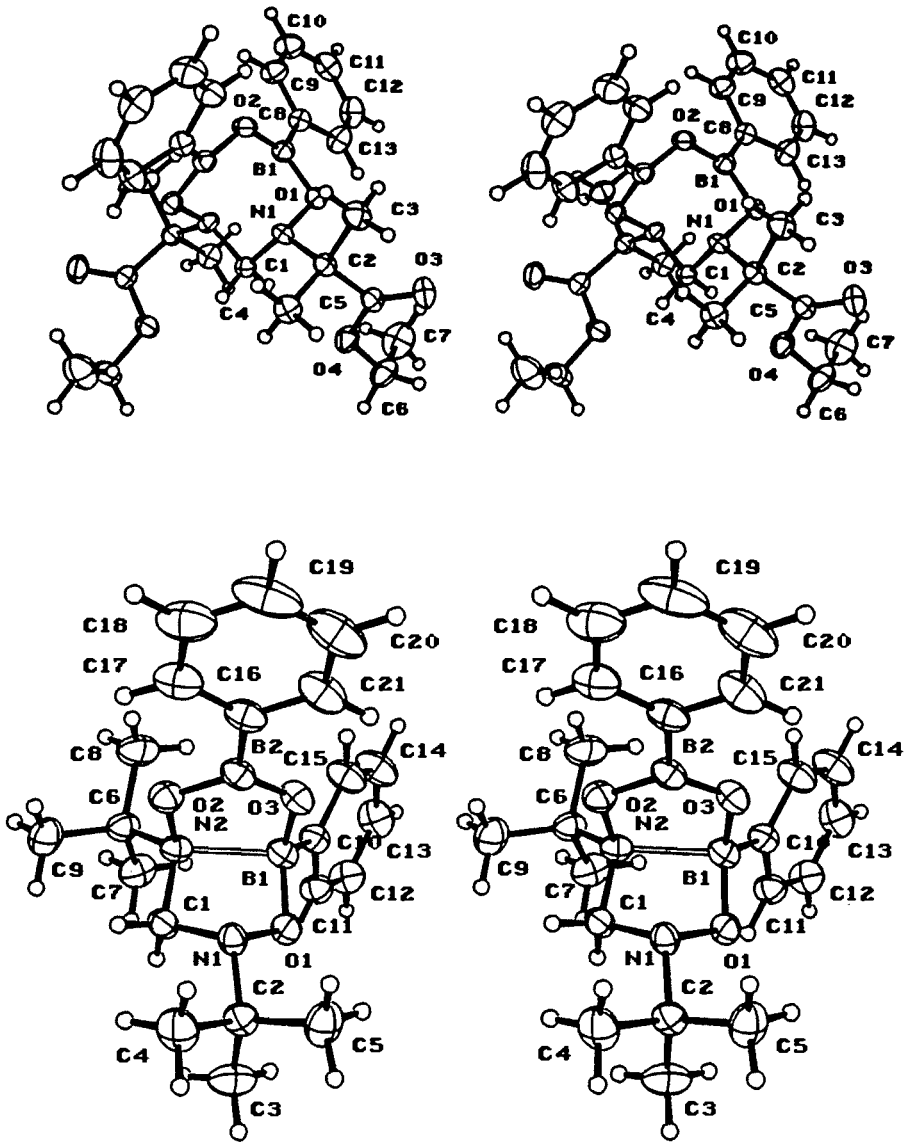

FIG. 2. Stereoviews of **3** (top) and **4** (bottom); 33% probability thermal ellipsoids are shown for the non-hydrogen atoms.

transition to a tetrahedral geometry (2) can be assessed by both the displacement of the boron atom from the O_2C plane towards the nitrogen atom (ΔB) and the "tetrahedral character" (THC) proposed recently by Toyota and Oki (17). The transition to tetrahedral geometry is just beginning in compound **2** (1), is slightly more pronounced for the two iden-

Can. J. Chem. Downloaded from www.nrcresearchpress.com by 203.198.23.82 on 09/08/12
For personal use only.

TABLE 5. Structural parameters for the N—B interactions in compounds **2–5**.

Compound	**2**	**3**	**4**	**5**[a]
N—B, Å	2.475(3)	2.433(3)	1.953(3)	1.733
N—B, bond order[b]	0.05	0.06	0.29	0.62
ΔB,[c] Å	0.098(2)	0.108(3)	0.305(3)	0.360
THC,[d] %	4.9	5.1	40.3	53.3

[a]Values averaged for the two independent molecules.
[b]Empirical, corrected for electronegativity and σ-hydridization effects.
[c]Displacement of the boron atom from the OOC plane.
[d]"Tetrahedral character" as defined in ref. 17.

Can. J. Chem. Downloaded from www.nrcresearchpress.com by 203.198.23.82 on 09/08/12
For personal use only.

tical transannular interactions in **3**, and is quite marked in the case of **4**. The THC value and the N—B distance in **5** are similar to those in other sterically hindered systems (Ref. 17, and references therein). The intermediate-strength interaction in **3** is unprecedented in systems of this type.

As discussed earlier (1), the difference between the two transannular N···B contacts in **2** and **5** is reflected by the C—N bonds of the aminal function. The C—N bond length increases with increasing positive charge: the $^{+}$N—C and C—N distances in the $^{+}$N—C—N moieties are 1.467(2) and 1.454(3) Å in **2** (1), 1.480(3) and 1.452(3) Å in **4**, and mean values of 1.475 and 1.447 Å (1.479 and 1.452 Å corrected for libration) in **5** (6). In compound **3**, where the two nitrogen atoms are involved in identical weak interactions, the symmetry-equivalent $^{\delta+}$N—C distances are 1.463(2) Å. The N—O bonds at the nitrogen atoms with higher positive charge are shorter than the other N—O bonds in **2** (1.446(2) vs. 1.452(2) Å), **4** (1.454(2) vs. 1.461(2) Å), and **5** (mean 1.447 vs. 1.459 Å), while both N—O distances in **3** are 1.449(2) Å.

Like **2** and **5**, compounds **3** and **4** each have the same configuration at both nitrogen centres (the (6*R*,8*R*) enantiomers are depicted in Fig. 2, or, if the boron centres are also considered tetracoordinate, the (2*S*,4*S*,6*R*,8*R*) enantiomers).[5] The centrosymmetric crystals of **3** and **4** each contain equal numbers of (2*S*,4*S*,6*R*,8*R*) and (2*R*,4*R*,6*S*,8*S*) enantiomers. Structures **3** and **4** are both consistent with the EI mass spectra, which show a fragmentation pattern very similar to those of compounds **2** (1) and **5** (5), the parent peak showing an elimination product **7** having the oxime pyroboronate complex structure previously postulated for this type of fragment (refs. 1, 5, and references therein). This fragment is identical in the mass spectra of both **3** and **4**.

The X-ray analysis of the *N*,*N*′-dihydroxyaminal **1***b* shows that, like the *N*-methyl derivative (**1**, R = Me) (7), the solid state structure of **1***b* consists of hydrogen-bonded dimeric pairs of enantiomers.[6] The *N*-(1-ethoxycarbonyl-1-methylethyl) substituents are found in an antiperiplanar orientation with respect to the adjacent geminal nitrogen substituents. The *N*-hydroxy groups are both in *trans-gauche* positions. The dimer (Fig. 1) has exact C_2 symmetry with the twofold axis passing through the central carbon atoms (C(1) and C(8)) of each of the two crystallographically independent molecules. Four intermolecular N—O—H···N bridges form a dimeric unit of the type **8** in the solid state (N(1)—O(1)—H(1)···N(2)(1 − *x*, −*y*, *z*) and N(2)—O(4)—H(2)···N(1), H···N = 2.00(4) and 2.03(4) Å, O···N = 2.858(3) and 2.901(3) Å, O—H···N = 172(3)° and 165(3)°, respectively). The C_2 symmetry of the **1***b* dimer is lower than the S_4 symmetry observed for the **1** (R = Me) dimer, presumably as an effect of crystal packing and (or) the greater complexity of the *N*-substituent in the present case. The N—O distances in the two independent half-molecules of **1***b* (N(1)—O(1) = 1.456(3) and N(2)—O(4) = 1.434(3) Å) differ significantly. Differences in the hydrogen bonding, conformation, and thermal motion are likely responsible for this observation. The remainder of the corresponding bond distances in the two independent half-molecules are in good agreement. On the basis of the structure analysis, the intramolecular hydrogen-bridging structures **9–12** can be excluded from consideration, at least for the solid state.

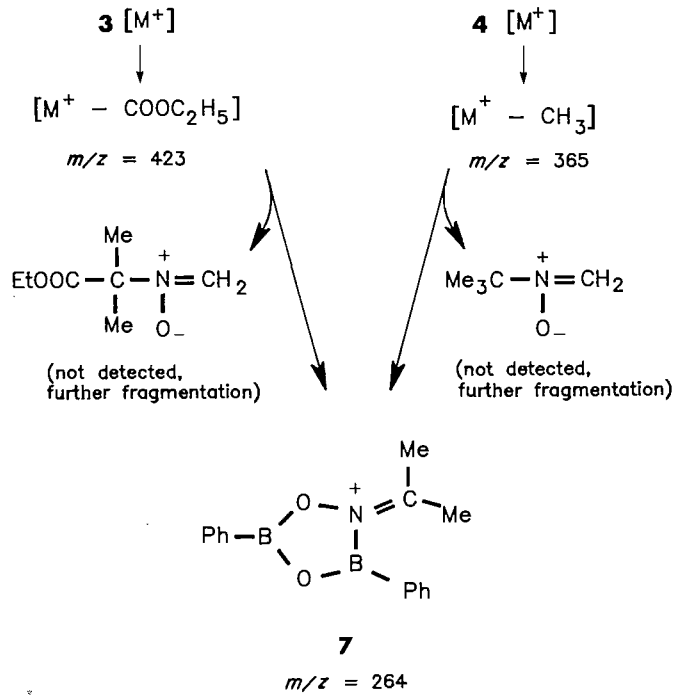

Mass spectral fragmentation of **3** and **4** (selected common fragments)

The N—C—N angle at the aminal carbon atom in dimeric **1***b* is somewhat compressed (108.6(3)° and 108.9(3)°)

[5]Designations refer to systematic, not crystallographic, numbering. The nitrogen atoms are in positions 6 and 8 and the boron atoms in positions 2 and 4.

[6]Because of the conformational differences between the two enantiomeric molecules comprising the dimer in the solid state, they are not true mirror images of one another but do have opposite configurations at the chiral centres. It is a reasonable assumption that in solution, or in the liquid and gaseous states, the enantiomers exist as true mirror images.

compared to the corresponding angle of 110.9(2)° in **1** (R = Me) (7). This corresponds to the slightly "elongated" overall structure of the **1***b* dimer and is further supported by the longer hydrogen bonds in **1***b* (O···N = 2.858(3) and 2.901(3) Å) relative to those in dimeric **1** (R = Me) (O···N = 2.775(3) Å) (7). An even greater angular compression occurs for the N—C—N bond angle in complex **3** (102.1(2)°), a phenomenon already noted for the bicyclic complex **5** (102.4(2)° and 102.6(2)°) (6) and assumed to be a result of the transannular coordinative bond forces. Similar angular compressions are also observed at the (N)C—N—O moieties, which show angles of 105.3(2)° and 105.6(1)° in dimeric **1***b* and an even smaller angle of 104.0(1)° in the phenylboronate complex **3**. Unlike the asymmetric bicyclo-[3.3.0]octane-type complex **5** (6), the aminal C—N bonds in the symmetric complex **3** are equal (1.463(2) Å) and not significantly different from those in dimeric **1***b* (mean C—N = 1.470(2) Å). Unlike compound **5** (6), the N—C(C) bonds of the *N*-alkyl substituents in **3** are shortened by an average of 0.019 Å relative to those in **1***b* (N(1)—C(2) = 1.478(3) Å in **3**, mean of N(1)—C(2) and N(2)—C(9) = 1.497(5) Å in **1***b*). This is most likely due to a combination of steric (packing) and electronic effects.

The *trans-gauche* conformation of the $RN(O)CH_2N(O)R$ moiety in **1***b* is retained after the condensation with phenylboronic acid, the two symmetry-related N—C—N—R torsion angles being −168.0(2)° and 166.4(2)° for the two independent molecules of **1***b* and 170.4(2)° for **3**. The configurations at the four nitrogen centres in the dimer **1***b* (Fig. 1) are *S* at N(1) and N(1′), *R* at N(2) and N(2′).

Acknowledgments

We thank the Natural Sciences and Engineering Research Council of Canada and the Fonds der Chemischen Industrie, Frankfurt am Main, for financial support. We are grateful to the Chemische Institute der Technischen Universität Braunschweig for running the ^{11}B nmr and mass spectra.

1. W. Kliegel, G. Lubkowitz, S.J. Rettig, and J. Trotter. Can. J. Chem. **69**, 1217 (1991).
2. S.J. Rettig, J. Trotter, W. Kliegel, and G. Lubkowitz. Mol. Cryst. Liq. Cryst. **219**, 101 (1992).
3. D.D. Perrin, B. Dempsey, and E.P. Serjeant. pK_a prediction for organic acids and bases. Chapman and Hall, London. 1981.
4. G. Zinner and U. Dybowski. Arch. Pharm. (Weinheim), **304**, 877 (1971).
5. W. Kliegel. J. Organomet. Chem. **253**, 9 (1983).
6. W. Kliegel, S.J. Rettig, and J. Trotter. Can. J. Chem. **62**, 515 (1984).
7. W. Kliegel, S.J. Rettig, and J. Trotter. Can. J. Chem. **67**, 1959 (1989).
8. T. Polonski and A. Chimiak. J. Org. Chem. **41**, 2092 (1976).
9. H.-H. Lau and U. Schöllkopf. Liebigs Ann. Chem. 1378 (1981).
10. International tables for X-ray crystallography. Vol. IV. Kynoch Press. Birmingham, U.K. (present distributor Kluwer Academic Publishers, Dordrecht, The Netherlands). 1974. pp. 99–102 and 149.
11. R.S. Glass. (*Editor*). Conformational analysis of medium-size heterocycles. VCH Publishers, Weinheim. 1988.
12. (*a*) P.K. Freeman, V.N.M. Rao, and G.E. Bigam. J. Chem. Soc. Chem. Commun. 511 (1965); (*b*) M. Nakazai, K. Naemura, H. Harada, and H. Narutaki. J. Org. Chem. **47**, 3470 (1982); (*c*) H.M.R. Hoffmann, A.M. El-Khawaga, and H.-H. Oehlerking. Chem. Ber. **124**, 2147 (1991).
13. (*a*) C.S. Lu and J. Donohue. J. Am. Chem. Soc. **66**, 818 (1944); (*b*) I. Lindquist. J. Inorg. Nucl. Chem. **6**, 159 (1958); (*c*) B.D. Sharma and J. Donohue. Acta Crystallogr. **16**, 891 (1963); (*d*) J.B. Mason. J. Chem. Soc. Sect. A, 1567 (1969); (*e*) R. Gleiter. J. Chem. Soc. Sect. A, 3174 (1970); (*f*) M.L. De Lucia and P. Coppens. Inorg. Chem. **17**, 2336 (1978); (*g*) R.H. Findley, M.H. Palmer, A.J. Downs, R.G. Egdell, and R. Evans. Inorg. Chem. **19**, 1307 (1980); (*h*) R. Gleiter. Angew. Chem. **93**, 442 (1981) (Angew. Chem. Int. Ed. Engl. **20**, 444 (1981)).
14. (*a*) T. Ito, N. Morimoto, and R. Sadanaga. Acta Crystallogr. **5**, 775 (1952); (*b*) D.E.J. Mullen and W. Nowacki. Z. Kristallogr. **136**, 48 (1972); (*c*) T.J. Bastow and H.J. Whitfield. J. Chem. Soc. Dalton Trans. 1739 (1973).
15. P.C. Minshall and G.M. Sheldrick. Acta Crystallogr. Sect. B: Struct. Crystallogr. Cryst. Chem. **B34**, 1326 (1978).
16. H. Bärnighausen, T. von Volkman, and J. Jander. Angew. Chem. **77**, 96 (1965).
17. S. Toyota and M. Oki. Bull. Chem. Soc. Jpn. **65**, 1832 (1992).
18. W. Kliegel, G. Lubkowitz, S.J. Rettig, and J. Trotter. Can. J. Chem. **71**, 919 (1993).

Can. J. Chem. Downloaded from www.nrcresearchpress.com by 203.198.23.82 on 09/08/12
For personal use only.

Catalysis of the deprotonation of β-keto esters by cyclodextrins

OSWALD S. TEE,[1] N. RANI IYENGAR, AND BRYAN K. TAKASAKI

Department of Chemistry and Biochemistry, Sir George Williams Campus, Concordia University, Montreal, QC H3G 1M8, Canada

Received April 26, 1993

OSWALD S. TEE, N. RANI IYENGAR, and BRYAN K. TAKASAKI. Can. J. Chem. **71**, 2139 (1993).

The rates of deprotonation of several β-keto esters in basic aqueous solution are elevated by α- and β-cyclodextrin (α- and β-CD). In most cases saturation kinetics are observed that indicate fairly strong binding of the esters to the CDs (K_d = 0.22–11 mM); catalytic ratios (k_c/k_u) are in the range 1.9–17. For esters of the form RCO-CH_2COOEt with both α- and β-CD the values of K_d and k_c/k_u show little sensitivity to the acyl group, RCO (R = Me, Et, Pr, i-Pr), and for 2-carboethoxycyclopentanone, a cyclic analogue, these parameters are similar. In contrast, for R-$COCH_2$CO-OR′ (R = Me or Et; R′ = Me, Et, allyl) there is a marked dependence of the parameters on the alkoxyl group, OR′. These results suggest that the β-keto esters studied bind to the CDs with their alkoxyl groups in the CD cavity and that the catalysis ensues from the complexes thus formed. Variations in two other kinetic parameters, $k_2 = k_c/K_d$ (substrate selectivity) and $K_{TS} = k_u/k_2$ (apparent constant for dissociation of CD from the transition state) support this interpretation. Apparent second-order rate constants for the reaction of the esters with neutral CD ($k_2 = k_c/K_d$) are 1900–360 000 M^{-1} s^{-1} (at pH ≈ 10), whereas for hydroxide ion attack on ethyl acetoacetate k_{OH} = 5500 M^{-1} s^{-1}. Assuming the pK_as of the CDs are 12.2 and 12.3, deprotonation of the esters by the CD anions has rate constants of 10^5 to 5 × 10^7 M^{-1} s^{-1}. Thus, binding of the β-keto esters in the CD cavities, adjacent to a basic oxyanion site, enhances the reactivity of the CD anions towards these weak carbon acids *by at least 2–4 orders of magnitude*.

OSWALD S. TEE, N. RANI IYENGAR et BRYAN K. TAKASAKI. Can. J. Chem. **71**, 2139 (1993).

Lés vitesses de déprotonation de plusieurs β-cétoesters en solutions aqueuses basiques sont augmentées par la présence d'α- ou de β-cyclodextrine (α- et β-CD). Dans la plupart des cas, on observe des cinétiques de saturation qui indiquent la présence d'une forte liaison des esters sur les CD (K_d = 0,022–11 mM); les rapports catalytiques (k_c/k_u) sont de l'ordre de 1,9 à 17. Pour des esters de la forme RCO-CH_2COOEt avec des CD tant α que β, les valeurs de K_d et de k_c/k_u ne présentent qu'une faible sensibilité à la nature du groupe acyle, RCO (R = Me, Et, Pr, i-Pr); pour le 2-carboéthoxycyclopentanone, un analogue cyclique, ces paramètres sont semblables. Par ailleurs, pour les esters du type R-$COCH_2$CO-OR′ (R = Me ou Et; R′ = Me, Et ou allyle), il existe une dépendance marquée des paramètres sur la nature du groupe alcoxyle, OR′. Ces résultats suggèrent que les β-cétoesters se lient par leurs groupes alcoxyles à la cavité des CD et que la catalyse découle de la formation de ces complexes. Les variations dans deux autres paramètres cinétiques, $k_2 = k_c/K_d$ (sélectivité du substrat) et $K_{TS} = k_u/k_2$ (constante apparente de la dissociation de la CD de l'état de transition) sont en accord avec cette interprétation. Les constantes apparentes de vitesse du deuxième ordre pour la réaction des esters avec de la CD neutre ($k_2 = k_c/K_d$) varient de 1900 à 360 000 M^{-1} s^{-1} (à un pH ≈ 10), alors que pour l'attaque de l'ion hydroxyde sur l'acétoacétate d'éthyle k_{OH} = 5500 M^{-1} s^{-1}. Faisant l'hypothèse que les pK_a des CD sont respectivement de 12,2 et 12,3, les constantes de vitesse de déprotonation des esters par les anions CD varient de 10^5 à 5 × 10^7 M^{-1} s^{-1}. La liaison des β-cétoesters dans les cavités des CD, dans une position adjacente à un site oxyanion basique, augmente donc la réactivité des anions CD vis-à-vis de ces faibles acides carbonés par *au moins 2 à 4 puissances de 10*.

[Traduit par la rédaction]

Introduction

Cyclodextrins (CDs) are cyclic oligomers of glucose that form guest–host complexes with many species in solution (and in the solid phase), most notably with organic guests (1, 2). Because of such complexation, CDs can have significant effects on the rates and products of organic reactions. Of special interest, they can function as catalysts in various kinds of reactions (1), although most attention has been paid to the hydrolysis of esters of various kinds, photochemical reactions, and various biomimetic reactions (1–11).

Recently, we have studied the effects of α- and β-cyclodextrin on the cleavage of certain aryl alkanoate esters in basic solution (7). Generally speaking, in this reaction an ionized secondary hydroxyl group of the CD host functions as a nucleophile towards the guest ester and acyl transfer occurs (1, 5–10). However, with some benzoate esters the CD anion acts as a general base that assists the nucleophilic attack of water (11) so that true catalysis takes place. Accordingly, we speculated that CD anions may also function as simple basic catalysts in the deprotonation of acidic organic substrates included in their cavities and we found two examples in the literature (12*a*,*b*) to support this speculation. Daffe and Fastrez (12*a*) studied the deprotonation and hydrolysis of some oxazolones in basic media containing CDs. Subsequently, in a paper that was primarily concerned with catalysis by amylose, Cheng et al. (12*b*) noted that CDs catalyze the deprotonation of some β-keto esters in basic aqueous DMSO.[2]

β-Keto esters appeared to be excellent choices for further study of this type of catalysis for several reasons. Firstly, a wide variety of such esters are available or accessible. Secondly, formation of their enolate anions gives rise to a strong absorption band in the uv region (12*b*, 13). Thirdly, purely aliphatic β-keto esters might serve as useful probes of the effects on reactivity of the inclusion of alkyl chains in the

[1]Author to whom correspondence may be addressed.

[2]A referee has pointed out that Breslow and co-workers (12*c*) studied catalysis of the deprotonation of a phenacyl alcohol by cyclodextrin phosphate anions.

Can. J. Chem. Downloaded from www.nrcresearchpress.com by 203.198.23.82 on 09/08/12
For personal use only.

Can. J. Chem. Downloaded from www.nrcresearchpress.com by 203.198.23.82 on 09/08/12
For personal use only.

hydrophobic cavities of CDs (6, 7*b–d*, 10, 14, 15).[3] Fourthly, it should be possible to study the effects of complexation by CDs on the various processes involved in keto–enol tautomerism.

We hereby report an initial study of the deprotonation of some β-keto esters (**1**, **2**, **3**) in the presence of α- and β-cyclodextrin (α-CD and β-CD)[4] in basic aqueous solution. The results have been summarized in two reviews (6).

1: $R\text{-}COCH_2COOEt$ (R = Me, Et, Pr, i–Pr)

2: $R\text{–}COCH_2COO\text{–}R'$ (R = Me or Et; R′ = Me, Et, allyl)

3:

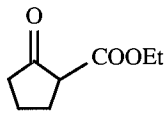

Results and discussion

All of the β-keto esters **1**, **2**, and **3** showed significant catalysis of deprotonation in the presence of added α- or β-CD.[4] For the two methyl esters the rate increases were linear with [CD] over the concentration range studied (0–5 mM), but all the others exhibited saturation-type kinetics, indicative of 1:1 binding of the substrates with the CDs (1, 6, 7). Therefore, the majority of the results are consistent with the reactions in eqs. [1*a*] and [1*b*]:

[1a] $S \xrightarrow{k_u}$ product

[1b] $S + CD \underset{K_d}{\rightleftharpoons} S \cdot CD \xrightarrow{k_c}$ product + CD

For the condition $[CD] \gg [S \cdot CD] < [S]_0$, the variation of the observed rate constant with [CD] is given by:

[2] $$k^{obsd} = (k_u K_d + k_c[CD])/(K_d + [CD])$$

Appropriate analysis of the rate data affords the constants k_c and K_d, with k_u fixed at the experimental value (1, 6, 7, 8*a*).

A derived value is $k_2 = k_c/K_d$, the apparent second-order rate constant for the reaction of S with CD; it is analogous to k_{cat}/K_M for enzymes (16). It is a useful measure of reactivity since it reflects the Gibbs energy difference between S + CD and the reaction transition state, regardless of the mode of binding of S to CD in the S · CD complex (6, 7). Viewed in other terms, k_2 is a measure of the selectivity of the CD for different substrates.

We also advocate (6) the use of another quantity:

[3] $$K_{TS} = \frac{[TS] \cdot [CD]}{[TS \cdot CD]} = \frac{k_u K_d}{k_c} = \frac{k_u}{k_2}$$

which is the apparent dissociation constant of the transition state of the catalyzed reaction (*symbolised* as TS · CD) into the transition state of the normal reaction (TS) and the catalyst, (here a CD). It provides a useful measure of the stabilization of the transition state by the catalyst (6). The derivation of eq. [3], which was originally due to Kurz (17), follows from the application of transition-state theory to k_u and k_c (or k_2). His approach has been adopted and elaborated on by enzymologists (18), but ignored by most physical organic chemists except for its recent usage for some reactions showing metal ion catalysis (19). We have shown that values of K_{TS} are useful parameters for discussing various reactions mediated by cyclodextrins, as well as by other catalysts (6). In particular, by looking at the variation of K_{TS} with structure one may be able to distinguish between different modes of transition-state binding, as distinct from the substrate binding, which is reflected in K_d.

First, we studied the deprotonation of some ethyl acylacetates ($RCOCH_2COOEt$, **1**) in basic solution and found that all gave saturation kinetics (eq. [2]) with added CD. Analysis of the results gave the constants k_u, k_c, and K_d in Table 1 and the derived quantities k_c/k_u, k_2, and K_{TS} in Table 2. For both α- and β-CD the dissociation constants (K_d) vary little with the acyl group, RCO (1.1–3.5 mM for α-CD; 2.4–11 mM for β-CD). Similarly, the catalytic ratios (k_c/k_u) are not particularly sensitive to the acyl group, although they are larger for α-CD (6.7–12) than for β-CD (1.9–4.9). Furthermore, the rate constants k_2 fall within narrow ranges: 18 000–51 000 M^{-1} s^{-1} for α-CD; 3300–7700 M^{-1} s^{-1} for β-CD. In a similar way, the values of K_{TS}, which are considered to reflect binding to the CD in the transition state (6), show remarkably little sensitivity to the acyl group: 0.26–0.40 (α-CD); 1.2–2.3 mM (β-CD). Note also that the greater catalysis (larger k_c/k_u and larger k_2) found for α-CD is largely due to more transition-state stabilization (lower K_{TS} values).

We have also studied the cyclic ester, 2-carboethoxycyclopentanone (**3**). This substrate has less conformational freedom and a more hindered acidic hydrogen than **1** but with α-CD it behaves just like the esters **1** (Table 1), although its reactivity is somewhat lower and its binding to the CD is weaker. In contrast, with β-CD the rate of deprotonation of **3** increases linearly with [CD], indicating very weak or insignificant binding. From the linear increase the second-order rate constant (k_2) is only 760 M^{-1} s^{-1}, so that **3** reacts with β-CD 5–10 times more slowly than the esters **1**. Correspondingly, its value of K_{TS} is 3–6 times larger than those for **1**.

Our more limited results[5] for β-keto esters with structural variation in the alkoxyl group (**2**) are also summarized in Tables 1 and 2. The two methyl esters do not show saturation kinetics, only linear increases of k^{obsd} for [CD] = 0–5 mM, and so binding of these esters to α-CD must be weak or nonexistent. In contrast, the ethyl esters do show saturation and stronger catalysis; the allyl ester binds more strongly and is more reactive still. Overall, the values of k_2 for $MeCOCH_2COOR'$ increase dramatically from 1.87×10^3 to 3.57×10^5 M^{-1} s^{-1} and the transition state dissociation constants decrease significantly (K_{TS} = 5.8, 0.40, 0.026 mM). Thus, as the reactivity increases by a factor of 200 the transition-state stabilization increases in direct pro-

[3]The binding of aliphatic compounds by CDs has been studied, though not in the same detail as that of aromatic compounds (1, 2, 6, 10), probably for practical reasons (lack of suitable chromophores, etc.). For example, while the binding of alcohols (10, 15) and of various detergents (14) has been documented, the effect of CDs on the reactivity of purely aliphatic substrates has received relatively little attention (1, 5–7).

[4]α-Cyclodextrin (cyclohexaamylose, α-CD) has six glucose units joined in a torus whereas β-cyclodextrin (cycloheptaamylose, β-CD) has seven such units. Thus, the sizes of their cavities differ in width, but not in depth (1).

[5]Various larger esters were tried unsuccessfully, as a result of their low solubility in water.

TABLE 1. Observed constants for the deprotonation of β-keto esters in the presence of α- and β-cyclodextrins in basic aqueous solution[a]

Substrate	pH	k_u, s^{-1}	k_c, s^{-1}	K_d, mM	cc
(*a*) With α-CD:					
$MeCOCH_2COOEt$	10.16	7.36	54.4 ± 1.7	2.94 ± 0.24	0.9997
$MeCOCH_2COOEt$[b]	10.62	14.9	110 ± 4	3.14 ± 0.25	0.9995
$EtCOCH_2COOEt$	10.04	9.32	61.9 ± 1.2	1.74 ± 0.11	0.9996
$PrCOCH_2COOEt$	10.25	7.42	87.4 ± 1.4	3.46 ± 0.12	0.9999
i-$PrCOCH_2COOEt$	10.08	12.8	58.5 ± 0.7	1.14 ± 0.06	0.9997
3	10.02	5.95	101 ± 7	10.0 ± 1.0	0.9997
$MeCOCH_2COOMe$	10.75	10.8	—[c]	—[c]	0.9882
$MeCOCH_2COOallyl$	10.75	9.18	71.8 ± 0.57	0.215 ± 0.015	0.9999
$EtCOCH_2COOMe$	10.02	10.3	—[c]	—[c]	0.9979
(*b*) With β-CD:					
$MeCOCH_2COOEt$	10.16	7.36	21.1 ± 1.3	6.34 ± 0.91	0.9990
$EtCOCH_2COOEt$	10.04	9.32	18.1 ± 0.4	2.36 ± 0.27	0.9995
$PrCOCH_2COOEt$	9.96	7.99	38.9 ± 4.1	11.0 ± 2.0	0.9992
i-$PrCOCH_2COOEt$	10.08	12.8	36.7 ± 2.0	6.61 ± 0.86	0.9995
3	10.08	5.59	—[c]	—[c]	0.9983

[a]At 25°C; cc is the correlation coefficient for the fit of eq. [2] to the data or for the linear variation of k^{obsd} with [CD].
[b]Reverse reaction. Solution of anion in 0.01 M NaOH quenched in a carbonate buffer.
[c]Saturation kinetics were not observed. The increase of k^{obsd} with [CD] was linear, with the slope equal to k_2 given in Table 2.

TABLE 2. Derived constants for the deprotonation of β-keto esters in the presence of α- and β-cyclodextrins in basic solution[a]

Substrate	CD	K_d, mM	k_c/k_u	k_2, $M^{-1}\,s^{-1}$	K_{TS}, mM
(*a*) R-$COCH_2COOEt$ (**1**)					
Me-	α	2.94	7.4	18 000	0.40
Me-[b]	α	3.14	7.4	35 000	0.42
Et-	α	1.74	6.6	35 600	0.26
Pr-	α	3.46	11.8	25 300	0.29
i-Pr-[c]	α	1.14	4.6	51 300	0.25
3	α	10.0	17.0	10 100	0.59
Me-	β	6.34	2.9	3330	2.2
Et-	β	2.36	1.9	7670	1.2
Pr-	β	11.0	4.9	3540	2.2
i-Pr-	β	6.61	2.9	5550	2.3
3	β	—[d]	—[d]	75 9	7.4
(*b*) $MeCOCH_2COO$-R′ (**2**, R = Me)					
-Me	α	—[d]	—[d]	1870	5.8
-Et	α	2.94	7.4	18 500	0.40
-Allyl	α	0.215	8.4	357 000	0.026
(*c*) $EtCOCH_2COOR'$ (**2**, R = Et)					
-Me	α	—[d]	—[d]	2670	3.9
-Et	α	1.74	6.6	35 600	0.26

[a]As in Table 1. Some of the values in this table (and Table 1) differ slightly from those summarized in ref. 6 because in the present work more significant figures were carried before rounding. Values of k_2 are the apparent second-order rate constants for reaction of neutral ester with the CD.
[b]As in Table 1.
[c]The entry for this compound in Table IV of ref. 6*a* was incorrect due to a transcription error.
[d]See footnote *c* of Table 1.

portion. The two esters $EtCOCH_2COOR'$ (R′ = Me and Et) show similar behaviour.

The variation of K_d values with the alkoxyl group of the ester (OR′ of **2**) and their relative invariance with changes in the acyl group (RCO in **1**) both suggest that the β-keto esters bind to CDs through the ester group rather than through their acyl moieties. Likewise, the sensitivity of the various kinetic parameters to OR′ and their insensitivity to RCO, as well as the similar behaviour of the cyclic ester **3**, all support CD-catalyzed deprotonation through a transition state in which the ester group is bound (**4** → **5**) and not through one involving acyl group binding (**6** → **7**). Thus, the present results provide an example where the modes of initial-state and transition-state binding of a catalyst are the same. In general this need not be the case and in many instances it is not (6, 7).

The high values of the second-order rate constants (k_2), up to $3.6 \times 10^5\ M^{-1}\,s^{-1}$, for the apparent reaction of neutral CDs with the β-keto esters are quite remarkable when compared to the rate constant for deprotonation of ethyl acetoacetate by hydroxide ion: $k_{OH} = 5500\ M^{-1}\,s^{-1}$ (see below). If one makes allowance for the experimental pHs and the pK_as of α-CD and β-CD (12.2 and 12.3) (20) the actual second-order rate constants for reaction of the CD anions range from 1.3×10^5 to $4.7 \times 10^7\ M^{-1}\,s^{-1}$. So, the CD anions are much more reactive than expected, given that their intrinsic reactivity should be less than that of OH^-. Thus, binding of the β-keto esters to the CDs greatly enhances the reactivity of the CD anions towards these weak carbon acids, *by at least 2–4 orders of magnitude.*

For background purposes, and as a test of our experimental method, we also studied the deprotonation of ethyl ace-

Can. J. Chem. Downloaded from www.nrcresearchpress.com by 203.198.23.82 on 09/08/12
For personal use only.

toacetate as a function of $[OH^-]$. At pHs near the pK_a of this ester ($\approx$ 10.7) (21) the reaction should be considered as an equilibration of the keto form, the enolate, and the enol (eq. [4]) and so the observed rate constant should have the form of eq. [5].

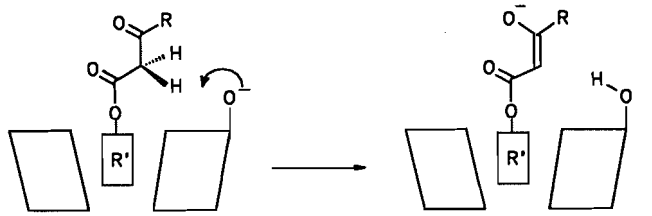

4 5

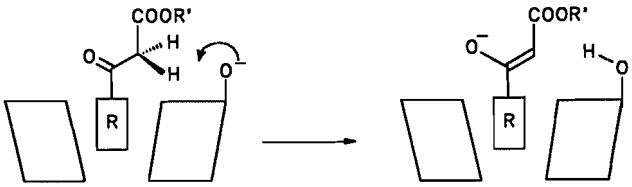

6 7

[4] $$\text{keto} + OH^- \underset{k_w}{\overset{k_{OH}}{\rightleftharpoons}} \text{enolate}^- \underset{H^+}{\overset{K_E}{\rightleftharpoons}} \text{enol}$$

[5] $$k^{obsd} = k_f + k_d = k_{OH}[OH^-] + k_w K_E/(K_E + [H^+])$$

However, experiments were carried out at pH > 10.5 > $pK_E \approx 9$ (21)[6] so that in the present case $K_E > [H^+]$, which means that the amount of enol is negligible and eq. [5] simplifies to:

[6] $$k^{obsd} = k_{OH}[OH^+] + k_w$$

The observed data show this a good linear dependence on hydroxide ion (cc = 0.9979) and they afford values of k_{OH} = 5460 M^{-1} s^{-1} and k_w = 6.43 s^{-1}, from which $K_a = k_{OH} K_w/k_w = 1.34 \times 10^{-11}$ M and so pK_a = 10.87, taking pK_w as 13.80 (for I = 1.0 M) (22). These values are in close agreement with those from temperature-jump studies of the enolization of ethyl acetoacetate in basic solution, carried out under slightly different conditions (21); literature values of the pK_a range from 10.64–10.90 (21). Our values differ somewhat from the very recent values of Bunting and Kanter,[6] obtained from a more detailed stopped-flow study, and with the ionic strength fixed at 0.1 M: k_{OH} = 3700 M^{-1} s^{-1}; k_w = 1.4 s^{-1}; pK_a = 10.57. Regardless of these differences, we feel our results for the β-keto esters in Tables 1 and 2 provide a useful overview of an interesting cyclodextrin-catalyzed deprotonation reaction.

Summary

In basic solution, α- and β-cyclodextrin catalyze the deprotonation of some β-keto esters of the form $RCOCH_2COOR'$ to their enolates. We propose that the catalysis arises from binding of the ester in the CD cavity and basic attack by an ionized (secondary) hydroxyl group since the reactivity of the CD anions is much greater than expected for oxyanions of $pK_a \approx 12$. Because both values of K_d and K_{TS} (and other kinetic parameters) are much more sensitive to the nature of the alkyl of the alkoxyl group (OR′) than that of the acyl group (RCO) we conclude that both substrate binding and transition-state binding involve inclusion to some extent of the ester alkoxyl (**4** → **5**). Presumably, with other substituents, better suited to binding in the CD cavity in the transition state, one could find even stronger catalysis. However, more detailed studies will probably require the use of mixed solvent systems, such as aqueous DMSO (12*b*), since the solubility of larger β-keto esters in water is very low.

Experimental

The β-keto esters were obtained from Aldrich. Any samples that were of inferior grades or were discoloured were distilled before use. While some of the esters gave perfectly acceptable kinetics results, other did not. Several larger esters were tried but due to their low solubility in water the experiments were unsuccessful.

Overall, the general quality of the kinetics was not high. This was for three reasons: (*i*) the "infinity" readings, taken after 10 half-lives, were often not stable, tending to rise with time; (*ii*) some of the catalyzed rates are high, approaching the limits of the stopped-flow equipment used; (*iii*) some of the esters have low solubility in water and so it is difficult to ensure that all of the substrate is in solution. The origin of reason (*i*) is not clear: it is not due to ester hydrolysis, which is much slower than deprotonation (13); it may be related to (*iii*). Another possibility is that in aqueous solution a fraction of the ester molecules are hydrated at the β-keto group ($RC(OH)_2CH_2COOR'$) so that when the ester is mixed with strong base some hydrate anion is formed rapidly which then converts slowly to the enolate.

Kinetics were measured using an Aminco DW2a uv–vis spectrophotometer, with an Aminco–Morrow stopped-flow accessory, interfaced to a microcomputer (23). The observation chamber was kept at 25°C by water circulation from a thermostat. In one syringe of the apparatus was a dilute solution (0.2–0.4 mM) of the β-keto ester in aqueous solution containing twice the desired [CD] (= 0, 1, 2, 3, 4, 5 mM) while the other syringe contained a sodium bicarbonate/carbonate buffer (0.02 M). These two solutions were mixed (1:1) in the stopped-flow apparatus. The total ionic strength was 1.0 M, maintained with NaCl, in the final, mixed solution. Most of the reaction pHs were nominally 10, chosen to ensure a reasonable production of the enolate while keeping the rate of reaction not too fast. In some instances higher pHs were necessary (see Table 1). Deprotonation was monitored by the appearance of the β-keto ester anion in the region 270–290 nm (13). The reverse reaction may also be followed (Table 1, second entry). Absorbance readings were taken for 10 half-lives, and whenever possible those covering 3–4 half-lives were analyzed for first-order behaviour, in the normal way (7). In cases where the infinity readings were not stable (vide supra), values were estimated by the Kezdy–Swinbourne method (24).

Saturation behaviour was analyzed in terms of eq. [2] by non-linear fitting of k_c and K_d, keeping k_u fixed at the experimental value, and using in-house computer software based on the Marquardt algorithm (25).

Acknowledgement

This work was supported by an operating grant from the Natural Sciences and Engineering Research Council of Canada. We thank Professor J.W. Bunting (University of Toronto) for providing results prior to publication.

[6]J.W. Bunting and J.P. Kanter, unpublished results.

1. M.L. Bender and M. Komiyama. Cyclodextrin chemistry. Springer-Verlag, New York. 1978; J. Szejtli. Cyclodextrins

Can. J. Chem. Downloaded from www.nrcresearchpress.com by 203.198.23.82 on 09/08/12
For personal use only.

and their inclusion complexes. Akademiai Kiado, Budapest. 1982.
2. W. Saenger. Angew. Chem. Int. Ed. Engl. **19**, 344 (1980); J.L. Atwood, J.E.D. Davies, and D.D. MacNicol. Inclusion compounds. Vols. 2 and 3. Academic Press, London. 1984; J.F. Stoddart and R. Zarzycki. Recl. Trav. Chim. Pays-Bas, **107**, 515 (1988).
3. I. Tabushi. Acc. Chem. Res. **15**, 66 (1982); R. Breslow. Science, **218**, 532 (1982); Acc. Chem. Res. **13**, 170 (1980); Adv. Enzymol. **58**, 1 (1986); Ann. N.Y. Acad. Sci. **471**, 60 (1986).
4. V. Ramamurthy. Tetrahedron, **42**, 5785 (1986); V. Ramamurthy and D.F. Eaton. Acc. Chem. Res. **21**, 300 (1988).
5. J.H. Fendler and E.J. Fendler. Catalysis in micellar and macromolecular systems. Academic Press, New York. 1975.
6. O.S. Tee. Carbohydr. Res. **192**, 181 (1989); Adv. Phys. Org. Chem. In press.
7. (*a*) O.S. Tee and B.K. Takasaki. Can. J. Chem. **63**, 3540 (1985); (*b*) O.S. Tee and X.-X. Du. J. Org. Chem. **53**, 1837 (1988); (*c*) O.S. Tee, C. Mazza, and X.-X. Du. J. Org. Chem. **55**, 3603 (1990); (*d*) O.S. Tee and X.-X. Du. J. Am. Chem. Soc. **114**, 620 (1992); (*e*) O.S. Tee and J.J. Hoeven. J. Am. Chem. Soc. **111**, 8318 (1989); O.S. Tee, M. Bozzi, J.J. Hoeven, and T.A. Gadosy. J. Am. Chem. Soc. **115**, 8990 (1993); (*f*) O.S. Tee and M. Bozzi. J. Am. Chem. Soc. **112**, 7815 (1990).
8. (*a*) R.L. VanEtten, J.F. Sebastian, G.A. Clowes, and M.L. Bender. J. Am. Chem. Soc. **89**, 3242 (1967); (*b*) R.L. VanEtten, G.A. Clowes, J.F. Sebastian, and M.L. Bender. J. Am. Chem. Soc. **89**, 3253 (1967); (*c*) M. Komiyama and M.L. Bender. J. Am. Chem. Soc. **100**, 4576 (1978); Bull. Chem. Soc. Jpn. **53**, 1073 (1980).
9. R. Breslow, G. Trainor, and A. Ueno. J. Am. Chem. Soc. **105**, 2739 (1983).
10. T. Matsui, T. Nishioka, and T. Fujita. Topics Curr. Chem. **128**, 61 (1985).
11. M. Komiyama and S. Inoue. Chem. Lett. 1101 (1979); Bull. Chem. Soc. Jpn. **53**, 3334 (1980); M. Komiyama and H. Hirai. Chem. Lett. 1251 (1980).
12. (*a*) V. Daffe and J. Fastrez. J. Chem. Soc. Perkin Trans. 2, 789 (1983); (*b*) X. Cheng, X. Jiang, J. Gu, and Y. Shen. Acta Chimica Sinica (Engl. Ed.) 84 (1985); (*c*) B. Siegel, A. Pinter, and R. Breslow. J. Am. Chem. Soc. **99**, 2309 (1977).
13. R.F. Pratt and T.C. Bruice. J. Am. Chem. Soc. **92**, 5956 (1970).
14. I. Satake, T. Ikenoue, T. Takeshita, K. Hayakawa, and T. Meda. Bull. Chem. Soc. Jpn. **58**, 2746 (1985); I. Satake, S. Yoshida, K. Hayakawa, T. Meda, and Y. Kusumoto. Bull. Chem. Soc. Jpn. **59**, 3991 (1986); R. Palepu and V.C. Reinsborough. Can. J. Chem. **66**, 325 (1988); R. Palepu, J.E. Richardson, and V.C. Reinsborough. Langmuir, **5**, 218 (1989); K. Ono, M. Tokuda, and K. Murakami. Polymer Reprints, Jpn. **28**, 1302 (1979).
15. Y. Matsui and K. Mochida. Bull. Chem. Soc. Jpn. **52**, 2808 (1979).
16. A. Fersht. Enzyme structure and mechanism. 2nd ed. W.H. Freeman, New York. 1985.
17. J.L. Kurz. J. Am. Chem. Soc. **85**, 987 (1963); Acc. Chem. Res. **3**, 1 (1972).
18. R. Wolfenden. Acc. Chem. Res. **5**, 10 (1972); G.E. Lienhard. Science, **180**, 149 (1973); W.P. Jencks. Adv. Enzymol. **43**, 219 (1975); R.L. Schowen. *In* Transition states in biochemical processes. *Edited by* R.D. Gandour and R.L. Schowen. Plenum Publishing, New York. 1978; J. Kraut. Science, **242**, 533 (1988).
19. E.J. Dunn and E. Buncel. Can. J. Chem. **67**, 1440 (1989); M.J. Pregel, E.J. Dunn, and E. Buncel. Can. J. Chem. **68**, 1846 (1990); G. Ercolani and L. Mandolini. J. Am. Chem. Soc. **112**, 423 (1990); R. Cacciapagli, A.R. van Doorn, L. Mandolini, D.N. Reinhoudt, and W. Verboom. J. Am. Chem. Soc. **114**, 2611 (1992).
20. R.I. Gelb, L.M. Schwartz, J.J. Bradshaw, and D.A. Laufer. Bioorg. Chem. **9**, 299 (1980); R.I. Gelb, L.M. Schwartz, and D.A. Laufer. Bioorg. Chem. **11**, 274 (1982).
21. P. Alcais and R. Brouillard. J. Chem. Soc. Perkin Trans. 2, 1214 (1972); R. Brouillard and J.-E. Dubois. J. Org. Chem. **39**, 1137 (1974).
22. R. Fischer and J. Bye. Bull. Soc. Chim. Fr. 2920 (1964).
23. O.S. Tee, N.R. Iyengar, and J.M. Bennett. J. Org. Chem. **51**, 2585 (1986).
24. E. Swinbourne. Analysis of kinetic data. Nelson, London. 1971.
25. P.R. Bevington. Data reduction and error analysis for the physical sciences. McGraw–Hill, New York. 1969; N.R. Draper and H. Smith. Applied regression. 2nd ed. Wiley, New York. 1981.

Can. J. Chem. Downloaded from www.nrcresearchpress.com by 203.198.23.82 on 09/08/12
For personal use only.

Substituent effects on azo coupling of indoles

HASSAN A. ALBAR
Department of Chemistry, Faculty of Science, King Abdulaziz University, Jeddah 21413, Saudi Arabia

AND

AHMAD S. SHAWALI[1] AND MAGDA A. ABDALIAH
Department of Chemistry, Faculty of Science, University of Cairo, Giza, Egypt

Received March 10, 1993

HASSAN A. ALBAR, AHMAD S. SHAWALI, and MAGDA A. ABDALIAH. Can. J. Chem. **71**, 2144 (1993).

The kinetics of the azo coupling of eight *para*-substituted benzenediazonium tetrafluoroborates **2***a–h* with indole and its 1-, 2-,and 3-methyl derivatives **1***a–d*, respectively, were studied in acetonitrile at 25°C under pseudo-first-order conditions. The relation k_1(obs) = k_2[diazonium salt] was found applicable in all cases. The logarithms of the rate constants k_2 for each reaction series were correlated by the Hammett equation. A plot of the values of the reaction constant, ρ, obtained against the acidity constants pK_a of **1***a–d* gave a straight line: ρ = 2.97 − 0.15 pK_a. These results indicate that the azo-coupling reactions of indoles **1***a–d* follow one general mechanism involving rate-limiting initial electrophilic attack at the 3-position for all four compounds, contrary to the previous conclusion of Jackson and Lynch that the final deprotonation step is rate limiting.

HASSAN A. ALBAR, AHMAD S. SHAWALI et MAGDA A. ABDALIAH. Can. J. Chem. **71**, 2144 (1993).

Opérant dans l'acétonitrile, à 25°C, dans des conditions de pseudo premier ordre, on a étudié la cinétique du couplage azo de huit tétrafluoroborates de benzènediazonium *para*-substitués, **2***a–h*, avec l'indole et ses dérivés 1-, 2- et 3-méthylés, **1***a–d*. On a trouvé que, dans tous les cas, la relation k_1(obs) = k_2 [sel de diazonium] peut s'appliquer. L'équation de Hammett permet d'établir une corrélation entre les logarithmes des constantes de vitesse k_2 de chaque série de réactions. Une courbe des valeurs de la constante de la réaction, ρ, en fonction des constantes d'acidité, pK_a, des composés **1***a–d* donne une ligne droite, ρ = 2,97 − 0,15 pK_a. Ces résultats indiquent que les réactions de couplage azo des indoles **1***a–d* se produisent par un mécanisme général impliquant une attaque électrophile initiale limitant la vitesse qui se produit en position 3 de chacun de ces composés; ce mécanisme est en désaccord avec les conclusions proposées antérieurement par Jackson et Lynch selon lesquelles la déprotonation finale serait l'état limite.

[Traduit par la rédaction]

Introduction

The mechanism of azo-coupling reactions of indole and its 1-, 2-, and 3-methyl derivatives **1***a–d* has been studied by several investigators (Scheme 1) (1–5). However, little is known about the substituent effects on the reaction rate. So far only Challis and Rzepa (3) have reported the rates of azo coupling of **1***c* with a series of five *para*-substituted benzenediazonium ions in aqueous dioxane. Here, we wish to report the results of our kinetic investigation of the azo-coupling reactions of **1***a–d* each with a series of eight *p*-substituted benzenediazonium tetrafluoroborates **2***a–h* in dry acetonitrile at 25°C (Chart 1). The goal of this study is the determination of the Hammett reaction constants (ρ) for the four reaction series in question under similar conditions and the correlation of the values of these constants with the acidity constants, p*K*a, of **1***a–d* (6–9). The knowledge of such data is necessary to support or to invalidate the recently reported mechanism for the reaction of **1***d* with *p*-nitrobenzenediazonium ion **2***h* in acetonitrile (Scheme 1) (4), and to cast light on the rate-limiting step in the reactions studied.

Results and discussion

Coupling of indole and its 1- and 2-methyl derivatives **1***a–c* each with the diazonium salts **2** in dry acetonitrile at 25°C yielded the corresponding 3-arylazoindole derivatives **3–5**, respectively (Scheme 1). 3-Methyl indole **1***d* couples with **2** under similar conditions to give 2-arylazo-3-methylindoles **6** (Scheme 1). The structures of the new products **3–6** (each *a–g*) were corroborated by their elemental analyses and spectral (^{1}H NMR and UV) data (Tables 1–4). Furthermore, the mass spectra of the products **3–6** were consistent with their assigned structures. Thus, each of the products **4–6** showed, in addition to the molecular ion ($M^{\cdot+}$) peak, two characteristic peaks at *m/e* 158 and 130. Such peaks correspond to the fragments ($M^{\cdot+}$ − Ar) and ($M^{\cdot+}$ − Ar − N_2), respectively. The mass spectra of the products **3** showed the peaks of the latter fragments at *m/e* 144 and 116, respectively. It is worth noting that the base peak in the spectra of the products **3–5** corresponds to the fragment ($M^{\cdot+}$ − Ar − N_2), whereas for the products **6** it corresponds to the molecular ion species ($M^{\cdot+}$). This observation suggests that the radical cation of 2-arylazo-3-methylindole **6** is more stabilized than that of the corresponding 3-arylazoindoles **3–5**.

The kinetics of the reactions of **1***a–d* each with tenfold excess or more of **2***a–h* in dry acetonitrile at 25°C were followed by the rate of appearance of the corresponding azoindole derivatives at their characteristic wavelengths (Table 5). In all cases good first-order plots of log(D_∞ − D_t) against time, *t*, were obtained. The pseudo-first-order rate constants, k_1 (obs), were calculated from the slopes of such plots by using the least-squares method. The plots of k_1 (obs) against [diazonium salt] were, in each case, linear, indicating that the azo-coupling reactions of the indoles **1***a–d* follow the equation

$$k_1(\text{obs}) = k_2\,[\text{diazonium salt}]$$

Table 6 lists the k_2 values, calculated by the least-squares method, from the slopes of such plots. The correlation coefficients were in the range 0.986–0.990.

[1]Author to whom correspondence may be addressed.

Can. J. Chem. Downloaded from www.nrcresearchpress.com by 203.198.23.82 on 09/08/12
For personal use only.

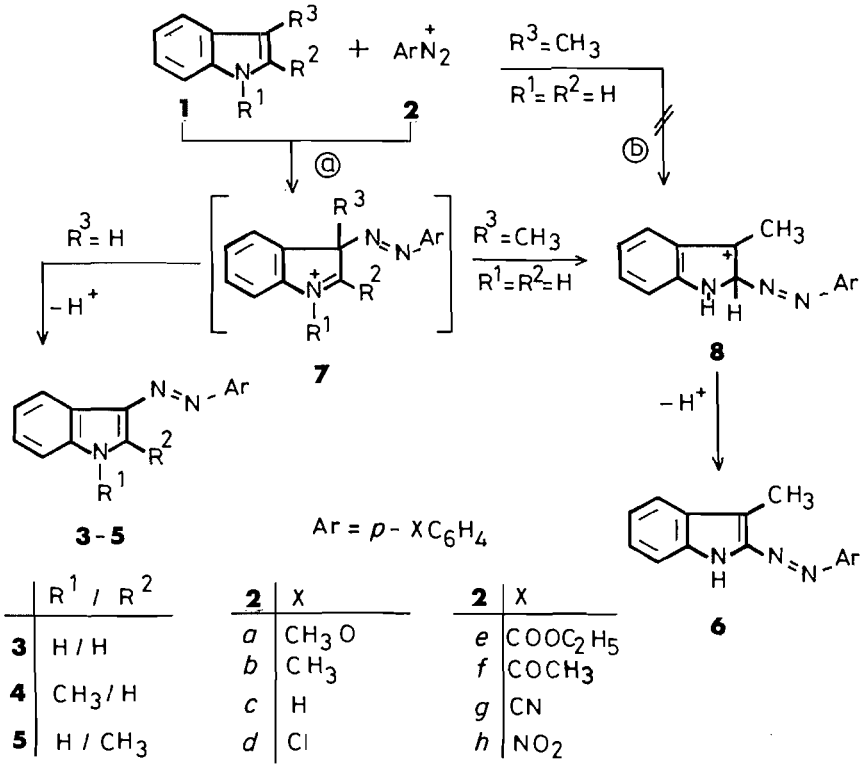

	R^1 / R^2
3	H / H
4	CH_3 / H
5	H / CH_3

2	X
a	CH_3O
b	CH_3
c	H
d	Cl

2	X
e	$COOC_2H_5$
f	$COCH_3$
g	CN
h	NO_2

SCHEME 1

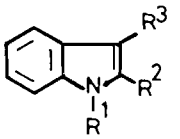

1

a, $R^1 = R^2 = R^3 = H$
b, $R^1 = CH_3$; $R^2 = R^3 = H$
c, $R^1 = R^3 = H$, $R^2 = CH_3$
d, $R^1 = R^2 = H$, $R^3 = CH_3$

$p\text{-}XC_6H_4N_2^+BF_4^-$

2

2	X
a	CH_3O
b	CH_3
c	H
d	Cl

2	X
e	$COOC_2H_5$
f	$COCH_3$
g	CN
h	NO_2

CHART 1

The results in Table 6 show that the azo-coupling reactions of **1***a–d* are affected by the substituent present in the diazonium salt, the reaction being retarded by electron-donating and enhanced by electron-withdrawing substituents. Figure 1 shows the plots of log k_2 values against the Hammett substituent constant σ (10). As shown, the relations are linear, following the equation: $\log (k/k_0)_2 = \rho\sigma$. The results of such correlations are summarized in Table 7. The lower susceptibility to substituent effects (ρ = 3.0) found in this work for the diazo coupling to 2-methylindole **1***c* in acetonitrile as compared to that (ρ = 3.3) reported for the same reaction in 20% (v/v) aqueous dioxane at pH 4.0 (3) seems to be due to solvent effects. It has been reported that in polar aprotic solvents the diazo-coupling reactions proceed faster than in protic solvents (13) and thus ρ decreases in the former solvents.

An examination of these data shows that the sensitivity of the reactions of **1***a–d* each with **2***a–h* decreases in the order: **1***d* > **1***a* > **1***b* > **1***c*. This is opposite to the order of the pK_a values reported for **1***a–d* (6–9), that is, the azo coupling with the less basic **1***d* is much more susceptible to polar requirements than the reaction of the stronger base **1***c*. This can also be seen by the excellent linear plot of the ρ values versus the pK_a values of the indoles studied, **1***a–d* (Fig. 2). The equation of the regression line is $\rho = 2.97 - 0.15\ pK_a$, with $r = 0.998$; $s = \pm 0.016$ and $S_\rho = \pm 0.005$.

This correlation seems to indicate that the nucleophilicity of the indoles studied, **1***a–d*, towards the diazonium cation is closely related to their pK_a values. In fact the plots of the log k_2 values of the reactions of **1***a–d* with a given diazonium salt against the pK_a values were linear in all cases examined. A similar relationship between the reactivity of

Can. J. Chem. Downloaded from www.nrcresearchpress.com by 203.198.23.82 on 09/08/12
For personal use only.

TABLE 1. 3-Arylazoindoles **3***a–h*

Compound no.	Melting point, °C (Lit mp)	Molecular formula	Anal. found (calcd.), % C	H	N	IR, ν cm^{-1} NH, N=N, (C=O or C≡N)	^{1}H NMR, δ^a ppm
3*a*	133–135	$C_{15}H_{13}N_3O$	71.5 (71.70)	5.1 (5.22)	16.6 (16.72)	3383,1460	3.10(3H,s,CH_3O), 8.50(1H,s,NH)
3*b*	170–172	$C_{15}H_{13}N_3$	76.1 (76.58)	5.6 (5.57)	17.6 (17.85)	3380,1460	2.44(3H,s,CH_3), 8.51(1H,s,NH)
3*c*	132–135	$C_{14}H_{11}N_3$	76.1 (76.01)	5.3 (5.01)	18.7 (18.98)	3385,1460	8.58(1H,s,NH)
3*d*	161–164	$C_{14}H_{10}ClN_3$	65.7 (65.75)	3.7 (3.94)	16.1 (16.42)	3396,1465	8.58(1H,s,NH)
3*e*	183–184	$C_{17}H_{15}N_3O_2$	69.3 (69.61)	5.1 (5.16)	14.2 (14.32)	3225,1465, (1695)	1.45(3H,t,CH_3), 4.41(2H,q,CH_2), 8.71(1H,s,NH)
3*f*	188–189	$C_{16}H_{13}N_3O$	72.8 (72.99)	4.8 (4.98)	15.7 (15.95)	3358,1463, (1672)	2.67(3H,s, CH_3CO), 8.78 (1H,s,NH)
3*g*	209–210	$C_{15}H_{10}N_4$	72.9 (73.17)	3.8 (4.09)	22.4 (22.74)	3285,1469, (2215)	8.74(1H,s,NH)
3*h*	196–199 (195–197)(4)	$C_{14}H_{10}N_4O_2$	63.2 (63.16)	3.8 (3.79)	20.9 (21.03)	3290,1468	8.88(1H,s,NH)

[a]All ^{1}H NMR spectra of **3***a–h* revealed an aromatic proton multiplet in the region 7.00–8.18 ppm.

TABLE 2. 3-Arylazo-1-methylindoles **4***a–h*

Compound no.	Melting point, °C (Lit. mp)	Molecular formula	Anal. found (calcd.) % C	H	N	IR-cm^{-1} N=N (=O or C≡N)	^{1}H NMR δ^a ppm
4*a*	111–112	$C_{16}H_{15}N_3O$	72.3 (72.43)	5.4 (5.70)	15.6 (15.84)	1465	3.88(3H,s, N-CH_3),3.90 (3H,s,CH_3O)
4*b*	148–149	$C_{16}H_{15}N_3$	76.8 (77.08)	5.8 (6.06)	16.5 (16.85)	1465	2.40(3H,s,CH_3) 3.89(3H,s,N-CH_3)
4*c*	90–92	$C_{15}H_{13}N_3$	76.7 (76.57)	5.5 (5.57)	18.0 (17.86)	1465	3.88(3H,s,N-CH_3)
4*d*	124–126	$C_{15}H_{12}ClN_3$	67.3 (66.80)	4.6 (4.48)	15.4 (15.58)	1465	3.88(3H,s,N-CH_3)
4*e*	168–171	$C_{18}H_{17}N_3O_2$	70.8 (70.34)	5.7 (5.58)	13.4 (13.67)	1465 (1710)	1.24(3H,t,CH_3), 3.88(3H,s, N-CH_3),4.40(2H, q,CH_2)
4*f*	140–142	$C_{17}H_{15}N_3O$	73.4 (73.63)	5.2 (5.45)	14.9 (15.15)	1465 (1680)	2.66(3H,s, $COCH_3$),3.90 (3H,s,N-CH_3)
4*g*	172–174	$C_{16}H_{12}N_4$	73.6 (73.82)	4.5 (4.65)	21.2 (21.52)	1465 (2220)	3.90(3H,s,N-CH_3)
4*h*	188–191 (188–191)(4)	$C_{15}H_{12}N_4O_2$	64.2 (64.28)	4.60 (4.32)	20.2 (19.99)	1465	3.92(3H,s,N-CH_3)

[a]All ^{1}H NMR spectra of **4***a–h* revealed an aromatic proton multiplet in the region 7.00–8.54 ppm.

phenols was found in the coupling reaction of *p*-substituted phenols with diazobenzene-4-sulfonic acid (11).

Evidently, on the basis of (*i*) the similarity between protonation of **1***a–d* and the initial step in their azo-coupling reactions and (*ii*) the fact that the basicity pattern of **1***a–d* has been shown to be consistent with the concept of preferred protonation at the 3-position (6–9), it is not unreasonable to conclude that the azo-coupling reactions of the indoles **1***a–d* proceed in all cases by initial electrophilic attack of the diazonium cation at the 3-position as outlined in Scheme 1.

Can. J. Chem. Downloaded from www.nrcresearchpress.com by 203.198.23.82 on 09/08/12
For personal use only.

TABLE 3. 3-Arylazo-2-methylindoles **5***a–h*

Compound no.	Melting point, °C (Lit. mp)	Molecular formula	Anal. found (calcd.), %			IR, ν cm^{-1} NH, N=N (C=O or C≡N)	^{1}H NMR, δ^a ppm
			C	H	N		
5*a*	137–139	$C_{16}H_{15}N_3O$	72.0 (72.43)	5.4 (5.70)	15.9 (15.84)	3260,1465	2.83(3H,s,2-CH_3), 3.89(3H,s,CH_3O), 8.22(1H,s,NH)
5*b*	180–181	$C_{16}H_{15}N_3$	77.1 (77.08)	6.2 (6.06)	16.6 (16.85)	3210,1465	2.41(3H,s,CH_3), 2.81(3H,s,2-CH_3), 8.2(1H,s,NH)
5*c*	122–123	$C_{15}H_{13}N_3$	76.5 (76.57)	5.2 (5.57)	17.5 (17.86)	3310,1465	2.86(3H,s,2-CH_3), 8.26(1H,s,NH)
5*d*	162–163	$C_{15}H_{12}ClN_3$	66.8 (66.80)	4.4 (4.48)	14.9 (15.58)	3250,1465	2.82(3H,s,2-CH_3), 8.29(1H,s,NH)
5*e*	221–222	$C_{18}H_{17}N_3O_2$	70.0 (70.34)	5.6 (5.58)	13.4 (13.67)	3270,1465, (1695)	1.43(3H,t,CH_3), 2.88(3H,s,2-CH_3), 4.42(2H,q,CH_2), 8.43(1H,s,NH)
5*f*	179–180	$C_{17}H_{15}N_3O$	73.0 (73.63)	5.4 (5.45)	14.8 (15.15)	3200,1465, (1675)	2.67(3H,s, CH_3CO),2.88 (3H,s,2-CH_3), 8.47(1H,s,NH)
5*g*	226–227	$C_{16}H_{12}N_4$	73.6 (73.82)	4.7 (4.65)	21.4 (21.52)	3315,1465, (2220)	2.88(3H,s,2-CH_3), 8.49(1H,s,NH)
5*h*	229–230 (228–230)(4)	$C_{15}H_{12}N_4O_2$	64.6 (64.28)	4.5 (4.32)	20.0 (19.99)	3300,1465	2.89(3H,s,2-CH_3), 8.54(1H,s,NH)

[a]All ^{1}H NMR spectra of **5***a–h*revealed an aromatic proton in the region 7.00–8.54 ppm.

TABLE 4. 2-Arylazo-3-methylindoles, **6***a–h*

Compound no.	Melting point, °C (Lit. mp)	Molecular formula	Anal. found (calcd.), %			IR, ν cm^{-1} NH, N=N (C=O or C≡N)	^{1}H NMR, δ^a ppm
			C	H	N		
6*a*	146–147	$C_{16}H_{15}N_3O$	72.3 (72.43)	5.8 (5.70)	15.7 (15.84)	3318,1465	2.71(3H,s,3-CH_3), 3.9(3H,s,CH_3), 8.85(1H,s,NH)
6*b*	168–170	$C_{16}H_{15}N_3$	76.9 (77.08)	6.0 (6.06)	16.5 (16.85)	3320,1465	2.24(3H,s,CH_3), 2.72(3H,s,3-CH_3), 8.86(1H,s,NH)
6*c*	111–112	$C_{15}H_{13}N_3$	76.2 (76.57)	5.5 (5.57)	17.7 (17.86)	3320,1465	2.74(3H,s,3-CH_3), 8.88(1H,s,NH)
6*d*	149–150	$C_{15}H_{12}ClN_3$	66.7 (66.80)	4.3 (4.48)	15.3 (15.58)	3325,1465	2.73(3H,s,3-CH_3), 8.85(1H,s,NH)
6*e*	194–196	$C_{18}H_{17}N_3O_2$	70.2 (70.34)	5.4 (5.58)	13.4 (13.67)	3318,1468, (1700)	1.44(3H,t,CH_3), 2.76(3H,s,3-CH_3), 4.21(2H,q,CH_2), 8.88(1H,s,NH)
6*f*	228–229	$C_{17}H_{15}N_3O$	73.4 (73.63)	5.2 (5.45)	15.0 (15.15)	3315,1465, (1675)	2.67(3H,s,CH_3), 2.77(3H,s,3-CH_3), 8.88(1H,s,NH)
6*g*	186–187	$C_{16}H_{12}N_4$	73.7 (73.82)	4.5 (4.65)	21.1 (21.52)	3390,1465, (2220)	2.75(3H,s,3-CH_3), 8.85(1H,s,NH)
6*h*	218–219 (217–220)(4)	$C_{15}H_{12}N_4O_2$	64.1 (64.28)	4.1 (4.32)	19.8 (19.99)	3330,1465	2.76(3H,s,3-CH_3), 8.87(1H,s,NH)

[a]All ^{1}H NMR spectra of **6***a–h*revealed an aromatic proton in the region 7.00–8.37 ppm.

Can. J. Chem. Downloaded from www.nrcresearchpress.com by 203.198.23.82 on 09/08/12
For personal use only.

TABLE 5. Characteristic electronic absorption maxima of 3-arylazo indoles **3–5** (*a–h*) and 2-arylazoindoles **6***a–h* in acetonitrile

Compound no.	λ_{max}(log ϵ), nm			
	3	4	5	6
a	361 (4.47)	363 (4.46)	365 (4.51)	389 (4.56)
b	364 (4.53)	386 (4.47)	370 (4.53)	390 (4.53)
c	365 (4.45)	369 (4.45)	372 (4.50)	392 (4.49)
d	372 (4.49)	368 (4.44)	380 (4.44)	394 (4.54)
e	405 (4.51)	382 (4.45)	382 (4.50)	394 (4.50)
f	378 (4.46)	387 (4.50)	372 (4.48)	395 (4.49)
g	375 (4.49)	386 (4.44)	387 (4.54)	396 (4.57)
h	419 (4.44)	421 (4.48)	432 (4.48)	426 (4.48)

TABLE 6. Second-order rate constants (k_2) of azo-coupling reactions of **1***a–d* each with **2***a–h* in acetonitrile at 25°C[a]

2	10^2k_2 (**1***a*)	10^2k_2(**1***b*)	k_2(**1***c*)	10^2k_2(**1***d*)
a	0.0249	0.246	0.250	0.004
b	0.0562	0.580	0.620	0.011
c	0.224	2.57	1.92	0.048
d	1.437	11.75	15.14	0.310
e	8.551	64.57	37.16	2.400
f	12.83	158.50	56.23	3.00
g	46.90	372.00	177.80	9.70
h	124.05	660.70	427.00	30.20

[a]k_2 in L mol^{-1} s^{-1}.

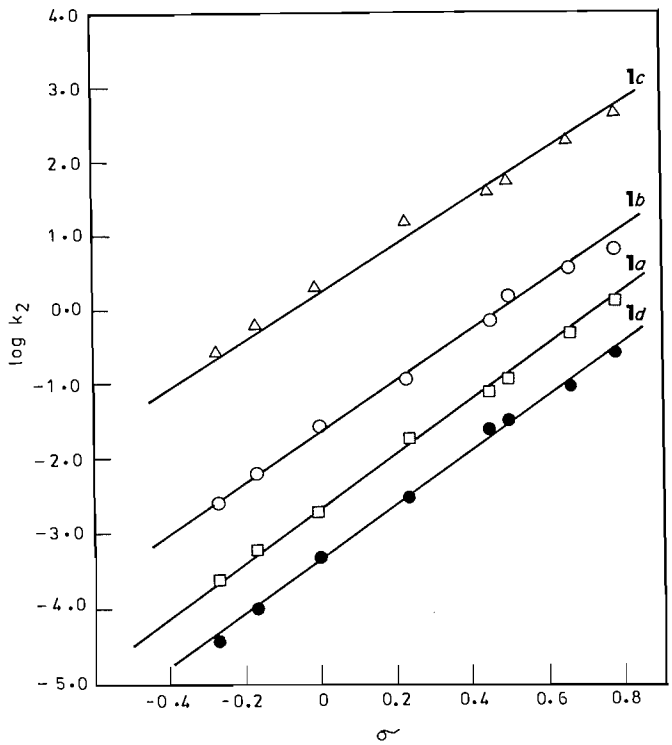

FIG. 1. Correlations of the second-order rate constants of the azo-coupling reactions of indoles **1***a–d* with *p*-substituted benzenediazonium ions **2***a–h* in acetonitrile at 25°C with the Hammett substituent constants σ.

Furthermore, the close similarity of the ρ value for 3-methylindole to those for indole and 1- and 2-methylindoles implies that the initial step must be the rate-limiting step for the reaction of all four compounds. This conflicts with the claim of Jackson and Lynch (4) that H^+-expulsion from the 2-position is rate limiting for diazo coupling of 3-methylindole **1***d*. The fact that ρ values correlate with the indole pK_a values also implies a common rate-limiting step for all four substrates **1***a–d*. This finding was also evident in Jackson and Lynch's study (4) but they chose to ignore its consequence in favour of a small positive isotope effect (ca. 2) for reactions with 2-[$^2H_1$]-3-methylindole.

Experimental

Melting points are uncorrected. UV spectra were determined with a Cary-17 spectrophotometer. ^{1}H NMR spectra were determined with a Varian 90 MHz instrument with tetramethylsilane as internal reference. Mass spectra were measured with a Varian CH5-D instrument by an electron impact, direct-insertion probe at 70 eV and 50 mA. IR spectra were recorded on a Unicam SP 200 grating spectrophotometer. Acetonitrile was distilled over anhydrous phosphorus pentoxide under nitrogen, the fraction of bp 82°C being collected. Elemental analyses were carried out using a Technicon CHN auto-analyser at the University of Wales, College of Cardiff.

Indole, 2-methylindole, and 3-methylindole were Aldrich reagents and were crystallized from light petroleum ether (60–80°C) before use in the kinetic experiments: indole, mp 51–52°C; 2-methylindole, mp 61°C; and 3-methylindole, mp 94–95°C. 1-Methylindole was prepared by methylation of indole using a literature procedure (4).

The diazonium salts **2** were prepared according to a previously described method (12) using amyl nitrite instead of *tert*-butyl nitrite. The purity of the salts was checked by ^{1}H NMR analyses (12).

Kinetics

The reactions were carried out in 1-cm ground-glass stoppered, fused-silica, absorption cells. The reactions were followed by rate of appearance of the azoindole absorption maximum (Table 5). Stock solutions of the diazonium tetrafluoroborate **2***a–h*, usually 10^{-2} M, were prepared in acetonitrile. Stock indole solutions, usually 10^{-3} M, were also prepared in the same solvent. Appropriate concentrations of the diazonium salts **2** and indole **1** were prepared by dilution of the stock solutions with acetonitrile. All indole concentrations were 5×10^{-5} M. All solutions were thermostated at 25 ± 0.1°C.

Reactions were followed up to 95% completion under pseudo-first-order conditions in which at least a tenfold excess of the diazonium salt over indole was used. Duplicate or triplicate runs were performed for each concentration and readings taken in any kinetic run cover a range of 96% transmittance. The pseudo-first-order

Can. J. Chem. Downloaded from www.nrcresearchpress.com by 203.198.23.82 on 09/08/12
For personal use only.

TABLE 7. Results of linear free energy correlations of the second-order rate constants of azo coupling of indoles **1***a–d* with diazonium salts **2***a–h* in acetonitrile at 25°C[a]

Rx series	$\log k_2 = \rho\sigma + \log k_0$	r	$+S_{est.}$	$+S_\rho$	pK_a
1*a* + **2***a–h*	$\log k_2 = 3.52\sigma - 2.651$	0.999	0.001	0.002	−3.63
1*b* + **2***a–h*	$\log k_2 = 3.34\sigma - 1.654$	0.997	0.010	0.018	−2.32
1*c* + **2***a–h*	$\log k_2 = 3.00\sigma + 0.288$	0.997	0.047	0.084	−0.28
1*d* + **2***a–h*	$\log k_2 = 3.65\sigma - 3.351$	0.999	0.055	0.034	−4.55

[a]Abbreviations: r = correlation coefficient; $S_{est.}$ = deviation; S_ρ = error estimate in ρ; pK_a = acidity constant of indole.

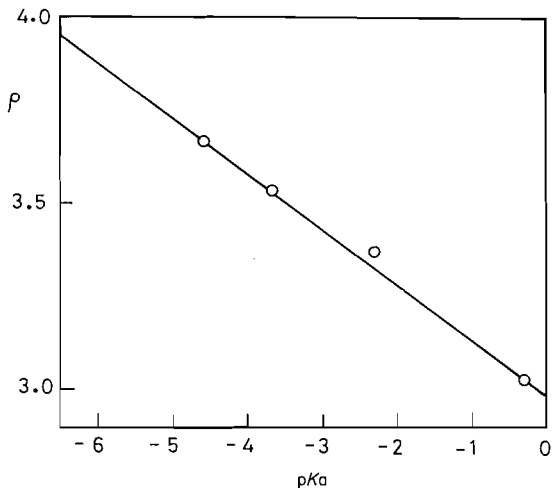

FIG. 2. Correlation of the reaction constants (ρ) of the azo-coupling reactions of indoles **1***a–d* with their acidity constants (pK_a).

rate constants, k_1(obs), were calculated from log $(D_\infty - D_t)$ against time, t, data using the least-squares method. D_t and D_∞ are the absorbance values of the reaction mixture at time, t, and infinite time, respectively. The average deviation from the mean value of the rate constant in duplicate or triplicate experiments was ±5% or less.

Isolation of products

To a solution of the appropriate indole **1** (0.001 mol) in acetonitrile (20 mL) was added a solution of the appropriate diazonium tetrafluoroborate (0.01 mol) in the same solvent (10 mL), with stirring, at room temperature. After 36 h, the solvent was evaporated under reduced pressure, the crude oil left was triturated with an ethanol–water mixture, and the solid formed was collected and crystallized from aqueous ethanol. The physical constants of azo-coupling products **3–6** are listed in Tables 1–4 together with their spectral data.

1. W. Madelong and R.C. Howarth. J. Chem. Soc. 670 (1944).
2. J.H. Binks and O.H. Ridd. J. Chem. Soc. 2398 (1957).
3. B.C. Challis and H.S. Rzepa. J. Chem. Soc. Perkin Trans. 2, 1209 (1975).
4. A.H. Jackson and P.P. Lynch. J. Chem. Soc. Perkin Trans. 2, 1483 (1987).
5. T.F. Spande and G.G. Gleaver. J. Am. Chem. Soc. **95**, 3400 (1973).
6. B.C. Challis and C.P. Millar. J. Chem. Soc. Perkin Trans. 2, 1116 (1972).
7. R.L. Hinman and C.P. Bauman. J. Org. Chem. **29**, 2437 (1964).
8. R.L. Hinman and E.B. Whippe. J. Am. Chem. Soc. **84**, 2534 (1962).
9. R.L. Hinman and J. Lang. J. Am. Chem. Soc. **86**, 3796 (1964).
10. C. Hansch and A.J. Leo. Substituent constants for correlation analysis in chemistry. Wiley, New York. 1979.
11. Y. Hashida, I. Shimoda, S. Sekiguchi, and K. Matsui. Kogyo Kagaku Zasshi, **74**, 73 (1971); Chem. Abstr. **74**, 127512b (1971).
12. M.P. Doyle and W.J. Bryker. J. Org. Chem. **44**, 1572 (1979).
13. Y. Hashida, H. Ishida, S. Sekiguchi, and K. Matsui. Bull. Chem. Soc. Jpn. **47**, 1224 (1974).

Can. J. Chem. Downloaded from www.nrcresearchpress.com by 203.198.23.82 on 09/08/12
For personal use only.

Electrostriction volumes of α-amino acids from density measurements in water and in aqueous HCl and NaOH solutions at 25°C

M. ABBATE, G. CASTRONUOVO,[1] V. ELIA, AND S. PUZZIELLO

Department of Chemistry, University Federico II of Naples, Via Mezzocannone, 4, 80134 Naples, Italy

Received October 24, 1991[2]

M. ABBATE, G. CASTRONUOVO, V. ELIA, and S. PUZZIELLO. Can. J. Chem. **71**, 2150 (1993).

The values of the limiting partial molar volumes, $\bar{V}^0$, for some α-amino acids bearing alkyl chains, in pure water and in aqueous solutions of hydrochloric acid and sodium hydroxide, have been obtained from density measurements. From these data it is possible to determine the volume change, ΔV_{zw}, due to the formation of the amphionic molecule from the corresponding neutral molecule.

M. ABBATE, G. CASTRONUOVO, V. ELIA et S. PUZZIELLO. Can. J. Chem. **71**, 2150 (1993).

Faisant appel à des mesures de densités et opérant dans de l'eau pure et dans des solutions aqueuses d'acide chlorhydrique et d'hydroxyde de sodium, on a déterminé les valeurs des volumes molaires partiels limites, $\bar{V}^0$, de quelques acides α-amineés portant des chaînes alkyles. À partir de ces données, il est possible de déterminer le changement de volume, ΔV_{zw}, accompagnant la formation de la molécule amphionique à partir de la molécule neutre correspondante.

[Traduit par la rédaction]

Introduction

The thermodynamic properties of α-amino acids in aqueous solutions have attracted the attention of many authors for the role played by these substances in determining the properties of proteins. In recent years, a considerable amount of thermodynamic data concerning amino acids (1), studied either calorimetrically (2–4) or volumetrically (5–7), has appeared in the literature. That permits the testing of simple additivity schemes for the prediction of the properties of molecules or biochemical systems (8–17).

Many approaches proposed to predict partial molar volumes assume that the contributions of the various groups present in a molecule are additive. However, to caution against the danger of such a simple treatment, Leslie and Lilley (18) studied isomeric species that differed only in the disposition of the groups on the backbone of some amino acid amides. Significant differences were found that led to doubts about simple atom or large group additivity. Even a change in the residue sequences for two dipeptides causes a volume difference of almost 2.5 $cm^3\ mol^{-1}$. The difficulties in reproducing the experimental values of $\bar{V}^0$ for amino acids and peptides were largely due to the dependence of the group contributions on the series from which they were derived. That has led some authors (6) to the conclusion that it is impossible to estimate the values of the group contributions when two functional groups are present simultaneously in a compound. In the case of α-amino acids, these difficulties are compounded because of the extreme preximity of the amino and carboxylate groups.

Many authors (12–17) have been concerned with the problem of determining the volume change, ΔV_{zw}, relative to the formation of the zwitterion from uncharged species:

[1] $\quad A \rightarrow A^{+/-}$

where $A^{+/-}$ represents the zwitterionic form $R(COO^-NH_3^+)$. Unfortunately, this determination cannot be accomplished experimentally, as equilibrium [1] is largely shifted to the right. Several methods have been proposed to calculate ΔV_{zw} that are dependent on the way the volume of the hypothetical neutral form in solution is calculated. Usually, the volume of the latter is evaluated from group contribution approaches or from the relations:

(*i*) $\quad \bar{V}^0$ (neutral amino acid) $\equiv \bar{V}^0$ (corresponding hydroxyamide)

(*ii*) $\quad \bar{V}^0$ (neutral amino acid) = $\bar{V}^0$ (glycolamide) + $\bar{V}^0$ (real amino acid) − $\bar{V}^0$ (real glycine)

Alhuwalia et al. (14) obtained the contribution of the neutral molecule by comparing the $\bar{V}^0$ of selected molecules regardless of whether they were mono-, or bifunctional. Cabani et al. (8) calculated $\bar{V}^0$ values from a group contribution approach using only hydrocarbons and monofunctional compounds. The main conclusion of this work was that ΔV_{zw} for α-amino acids is practically independent of the nature of the alkyl group, and that the average value of -14.7 ± 0.8 $cm^3\ mol^{-1}$ is due to reaction [1]. ΔV_{zw} greatly depends, instead, on the distance between the two charges, reaching the maximum value of -18.5 ± 0.4 when four or more $-CH_2-$ groups separate them.

In the present paper we report the densities, in pure water and in aqueous solutions of hydrochloric acid and sodium hydroxide, of some α-amino acids bearing alkyl chains of increasing length and branching: glycine, L-α-alanine, D-α-aminobutyric acid, D-valine, L-norvaline, L-leucine, L-isoleucine, and L-norleucine. The aim is to gain more direct information on the electrostriction volume for reaction [1]. That will be accomplished through the determination of limiting volumetric contributions to the total volume of the α-amino acids in the protonated, deprotonated, and zwitterionic forms.

Experimental

The α-aminoacids (glycine, L-α-alanine, D-α-aminobutyric acid, D-valine, L-norvaline, L-leucine, L-isoleucine, and L-norleucine) were Sigma products. Their purity was checked by several methods, as already described in ref. 2. Solutions were prepared by weighing the dried solutes and the bidistilled water, which was filtered on a Millipore membrane. Solutions were prepared by dissolving the solutes in a weighed quantity of the various solvents (pure water; (HCl or NaOH 1 mol L^{-1})). Densities of solutions were

[1]Author to whom correspondence may be addressed.

[2]Revision received June 14, 1993.

Can. J. Chem. Downloaded from www.nrcresearchpress.com by 203.198.23.82 on 09/08/12
For personal use only.

Can. J. Chem. Downloaded from www.nrcresearchpress.com by 203.198.23.82 on 09/08/12
For personal use only.

measured using an Anton Paar densimeter (DMA 620), at 25 ± 0.005°C. The data were obtained from the difference between the measured frequency of the solution and that of the respective solvent. The densimeter was calibrated using dry air and bidistilled water. Hydrochloric acid and sodium hydroxide solutions were prepared using a Normex (Carlo Erba), having care to use the same stock for all measurements of each system.

Thermodynamic relations

The excess Gibbs free energy of a system containing a single nonelectrolytic solute, x, and a solvent, s, is given by:

$$[2]\quad G^E(m_x) = G(m_x) - G^{id}(m_x) = G(m_x) - G_s^0 - m_x \bar{G}_x^0 - RTm_x(\ln m_x - 1)$$

where $G^E(m_x)$ is the excess free energy, $G(m_x)$ is the free energy of the solution, G_x^0 the standard free energy of 1 kg of solvent, $\bar{G}_x^0$ the limiting partial molar energy of the solute, and m_x the molality. In the case of the first derivative of the free energy with respect to the pressure, namely the volume, the term $RTm_x(\ln m_x - 1)$ is null.

According to the McMillan–Mayer solution theory, a thermodynamic excess property is usually expressed as a polynomial in the solute molality (19–21), and then the excess volume is given by

$$[3]\quad V^E(m_x) = V(m_x) - (V_s^0 + m_x\bar{V}_x^0) = v_{xx}m_x^2 + v_{xxx}m_x^3 + \text{higher terms}$$

where V_s^0 is the volume of 1 kg of solvent (pure water or aqueous solutions of 1 M hydrochloric acid or sodium hydroxide), $\bar{V}_x^0$ is the standard state partial molar volume of the solute, and v_{xx} and v_{xxx} are the second and third coefficients of the virial expansion of the excess volume.

Densities, d, were used to calculate the volume of the solution containing 1 kg of solvent (pure water or aqueous solutions of hydrochloric acid or sodium hydroxide) as follows:

$$[4]\quad V(m_x) = (1000 + m_xM_x)/d$$

where M_x is the molar mass of the solute.

The following three cases were examined, where the volumes of solutions containing m_x moles of amino acid per kg of solvent were calculated by means of eq. [4].

(a) Hydrochloric acid 1 mol L^{-1} as solvent

In this solvent the zwitterion is forced to assume a proton, according to the following reaction:

$$[5]\quad A^{+/-} + H^+ \rightarrow A^+$$

where A^+ is the protonated form $R(COOH\ NH_3^+)$ of the amino acid. Then, the volume of this solution is described by the following relation:

$$[6]\quad V = \Sigma_i n_i\bar{V}_i = n^s_{H_2O}\bar{V}_{H_2O} + n_{H^+}\bar{V}_{H^+} + n_{Cl^-}\bar{V}_{Cl^-} + n_{A^+}\bar{V}_{A^+}$$
$$= [n^s_{H_2O}\bar{V}_{H_2O} + n_{Cl^-}(\bar{V}_{H^+} + \bar{V}_{Cl^-})] + mA^+(\bar{V}_{A^+} - \bar{V}_{H^+})$$
$$= V_{(solvent)} + m_{A^+}(\bar{V}_{A^+} - \bar{V}_{H^+})$$

where $n^s_{H_2O}$ is the number of water molecules present in the solvent. The value of the difference, $V'(m)$, between the volume of the solution and that of the solvent is

$$[7]\quad V'(m) = m_{A^+}(\bar{V}_{A^+} - \bar{V}_{H^+}) = V^*m_{A^+} + b_vm_A^2 + \ldots$$

where V^* is the difference of two limiting values

$$V^* = \bar{V}^0_{A^+} - \bar{V}^0_{H^+}$$

and b_v is a constant depending on the volumetric cross coefficients.

(b) Sodium hydroxide 1 mol L^{-1} as solvent

In this solvent the amino acid is in the A^- form, according to:

$$[8]\quad A^{+/-} + OH^- = A^- + H_2O$$

where A^- is the deprotonated form $R(COO^-\ NH_2)$. The volume of the solution is then:

$$[9]\quad V = \Sigma_i n_i\bar{V}_i = n_{H_2O}\bar{V}_{H_2O} + n_{Na^+}\bar{V}_{Na^+} + n_{OH^-}\bar{V}_{OH^-} + m_{A^-}\bar{V}_{A^-}$$
$$= (n^s_{H_2O} + m_{A^-}\bar{V}_{H_2O} + n_{Na^+}\bar{V}_{Na^+} + (n_{Na^+} - m_{A^-})\bar{V}_{OH^-} + m_{A^-}\bar{V}_{A^-}$$
$$= [n^s_{H_2O}\bar{V}_{H_2O} + n_{Na^+}(\bar{V}_{Na^+} + \bar{V}_{OH^-})] + m_{A^-}(\bar{V}_{A^-} + \bar{V}_{H_2O} - \bar{V}_{OH^-})$$
$$= V_{(solvent)} + m_{A^-}(\bar{V}_{A^-} + \bar{V}_{H_2O} - \bar{V}_{OH^-})$$

The value of $V'(m)$ is in this case:

$$[10]\quad V'(m) = m_{A^-}(\bar{V}_{A^-} + \bar{V}_{H_2O} - \bar{V}_{OH^-}) = V^*m_{A^-} + b_vm^2_{A^-} + \ldots$$

The values of the coefficient of the interpolating polynomial are

$$V^* = \bar{V}^0_{A^-} + \bar{V}^0_{H_2O} - \bar{V}^0_{OH^-}$$

and b_v, which is again a constant depending on the volumetric cross coefficients. Then, solutions containing amino acid species are multicomponent solutions, because of the necessity of taking into account the H^+ and OH^- species reacting with the amino acid, during the preparation of the solutions.

(c) Pure water

In this case the solutions are binary ones, since they contain only zwitterionic species.

The value of $V'(m)$ is:

$$[11]\quad V'(m_x) = V(m_x) - V_w = V^*m + b_vm^2 + \text{higher terms}$$

As in the two preceding cases, the parameters of Eq. [11] have the usual meaning of limiting partial molar volume and interaction self-coefficients of the amino acid in the zwitterionic $A^{+/-}$ form.

Equations [7], [10], and [11] were interpolated by means of a least-squares procedure, choosing the polynomial of highest degree whose coefficients were larger than their own 95% confidence limits. For all of the systems studied, only two parameters (V^*, b_v) were necessary to represent the data adequately, underlining that Debye–Hückel corrections are not necessary.

Results and discussion

In Table 1, the V^* values are reported for solutions of all the amino acids studied in the three solvents employed. The values of $V_{A+/-}$ measured in water are in good agreement with the literature data. They fall in the 95% confidence indexes of the mean values reported by Cabani et al. (8). Up to now there are no data in the literature obtained in solvents other than pure water.

The V^* values obtained in the three solvents were interpolated as a function of the number of carbon atoms. The three relations were found to be linear and with the same mean slope, 15.7 ± 0.3 $cm^3\ mol^{-1}$, which is within the limits of variability reported in the literature, 14.8 ± 0.5 to 15.8 ± 0.6 (8). Intercepts and slopes of the three straight lines are reported in Table 2. The very similar values of the slopes indicate that the contribution of an added CH_2 can be considered the same regardless of the solvent and of the charge of the functional groups. To evaluate the influence of the different solvents on the hydration of the alkyl chain, measurements of limiting volumetric properties in the same three

Can. J. Chem. Downloaded from www.nrcresearchpress.com by 203.198.23.82 on 09/08/12
For personal use only.

TABLE 1. Values of V^* for the α-amino acids reported below in pure water and in aqueous solutions of hydrochloric acid and sodium hydroxide, 1 mol L^{-1}, at 25°C[a]

Amino acid	V*(H_2O) (cm^3 mol^{-1})	V*(HCl) (cm^3 mol^{-1})	V*(NaOH) (cm^3 mol^{-1})	Concentration range (mol kg^{-1})
Glycine	43.13(0.27)	49.77(0.16)	66.38(0.07)	0.26–0.02
L-α-Alanine	60.65(0.10)	68.86(0.23)	83.76(0.16)	1.0 –0.06
D-α-Aminobutyric acid	75.47(0.06)	83.60(0.30)	97.91(0.07)	0.26–0.05
D-Valine	90.48(0.02)	98.87(0.13)	113.11(0.28)	0.25–0.05
L-Norvaline	91.56(0.06)	98.15(0.21)	114.57(0.23)	0.15–0.03
L-Leucine	107.26(0.05)	116.79(0.35)	131.53(0.45)	0.15–0.025
L-Isoleucine	105.60(0.05)	117.64(0.55)	127.27(0.14)	0.15–0.03
L-Norleucine	107.57(0.07)	112.30(0.76)	129.69(0.30)	0.13–0.02

[a]Values in parentheses are the 95% confidence limits. The number of experimental data for each system varies from a maximum of 28 for L-isoleucine in HCl to a minimum of 12 for L-leucine in water.

TABLE 2. Parameters of the straight lines interpolating V* as a function of the number of carbon atoms for α-amino acids and alcohols at 25°C

Substances	Intercept[a]	Slope[a]
Amino acids (H_2O)	28.1(0.8)	15.7(0.2)
Amino acids (HCl)	34.8(1.7)	16.1(0.5)
Amino acids (NaOH)	52.0(1.5)	15.5(0.4)
Alcohols[b]	23.4(0.9)	15.4(0.3)
Average		15.7(0.3)

[a]Units are cm^3 mol^{-1}.
[b]The data for alcohols are fitted all together, regardless of the solvent used. Values in parentheses are the 68% confidence limits.

solvents were made using typical hydrophobic solutes, namely, alcohols bearing the same alkyl chains as those present in the amino acids studied. The alcoholic -OH group is not appreciably influenced by the pH changes on going from HCl to NaOH solutions. In these cases, where no reactions occur between solutes and solvent, the extrapolated values really give the partial molal volumes at infinite dilution of the solutes in the proper solvent. In Table 3 the $\bar{V}^0$ values determined in the three solvents are reported for methanol, ethanol, *n*-propanol, i-propanol, *n*-butanol, i-butanol, and *s*-butanol. It must be emphasized that these values were evaluated with the sole aim of obtaining an approximate $\bar{V}^0_{CH_2}$ value, to check whether large variations occur in the different solvents. The trends of $\bar{V}^0$ as a function of the number of carbon atoms in the three solvents were found to be linear, almost coincident, and with the same slope. This is a clear indication of an unaltered hydration of the alkyl chain. In Table 2, the parameters of the interpolating line are reported: they were evaluated by fitting all the data together, regardless of the solvent used and of some discrepancies concerning *n*- and i-butanol. The value of the slope (about 16 cm^3 mol^{-1}), which represents the contribution of a CH_2 to $\bar{V}^0_x$, is the same as that obtained for the α-amino acids in the three solvents. It is in good agreement with the values reported by other authors and obtained for aliphatic hydrocarbons and other neutral molecules.

Here we want to propose a method through which it is possible to deduce the value of the electrostriction volume ΔV_{zw} from the V^* values obtained for the amino acids in the three solvents. This method postulates the identity between the sum of the limiting volumes of the two species bearing one charge and the sum of the volumes of the zwitterionic and neutral forms:

$$\bar{V}^0_{A^+} + \bar{V}^0_{A^-} = \bar{V}^0_{A} + \bar{V}^0_{A^{+/-}}$$

Hence, the overall intramolecular interactions between charged and uncharged functional groups (right side of the relation) are considered to be equivalent to those between two charged groups (left side). Therefore, the following scheme holds:

$$V^*(\mathrm{HCl}) + V^*(\mathrm{NaOH}) - 2V^*(H_2O) = \bar{V}^0_{A^+} + \bar{V}^0_{A^-} - \bar{V}^0_{A^{+/-}} - \bar{V}^0_{A^{+/-}} + \bar{V}^0_{H_2O} - \bar{V}^0_{H^+} - \bar{V}^0_{OH^-}$$

Taking into account the postulated identity, it follows:

$$\begin{aligned}\bar{V}^0_{A} + \bar{V}^0_{A^{+/-}} - \bar{V}^0_{A^{+/-}} - \bar{V}^0_{A^{+/-}} - \Delta V_w &= \bar{V}^0_{A} - \bar{V}^0_{A^{+/-}} - \Delta V_w \\ &= -\Delta V_{zw} - \Delta V_w \\ &= 34.8 + 52.0 - 2 \times 28.1 \\ &= 30.6\end{aligned}$$

where ΔV_w is the volume change upon dissociation of one mole of water (22): its value, -22.2 cm^3 mol^{-1}, is assumed to be the same in the three solvents used. Then, ΔV_{zw} is -8.4 ± 3.0 cm^3 mol^{-1}, where the standard deviation is computed from those on the intercepts, assuming that on ΔV_w to be ± 0.2 cm^3 mol^{-1}. Because of the large error in ΔV_{zw}, this value can be assumed to be constant within the series of α-amino acids studied. Other approaches reported in the literature lead to ΔV_{zw} values that seem to be affected by a smaller error. However, the errors in the starting quantities are neglected in computing the derived result. In the group contribution approach, for instance, the various terms are considered unaffected by errors. On the other hand, comparison of the ΔV_{zw} values obtained by different methods (8) demonstrates the great variability of the derived results. In fact, differences of 2–4 cm^3 mol^{-1} are not unusual.

To test the reliability of our approach, we have applied it to the literature data concerning densities of hydrochloride and sodium salts of α,ω-amino acids. Using our notation we have: \

TABLE 3. Values of $\bar{V}^0$ for the alcohols reported below, in water and in aqueous solutions of hydrochloric acid and sodium hydroxide, 1 mol L^{-1}, at 25°C[a]

Alcohol	$\bar{V}^0(H_2O)$ (cm^3 mol^{-1})	$\bar{V}^0(HCl)$ (cm^3 mol^{-1})	$\bar{V}^0(NaOH)$ (cm^3 mol^{-1})	Concentration range (mol kg^{-1})
Methanol	38.2[b]	38.0(0.1)	37.7(0.1)	0.64–0.11
Ethanol	55.10[b]	54.0(0.1)	53.9(0.1)	0.66–0.12
n-Propanol	70.70[b]	70.1(0.1)	69.8(0.2)	0.54–0.11
i-Propanol	71.3(0.1)	71.2(0.2)	70.5(0.3)	0.5 –0.04
n-Butanol	85.6(0.1)	85.4(0.1)	80.9(0.3)	0.6 –0.02
i-Butanol	85.5(0.1)	85.1(0.2)	82.0(0.2)	0.5 –0.03
s-Butanol	85.1(0.1)	85.1(0.2)	84.8(0.2)	0.6 –0.03

[a]Values in parentheses are the 95% confidence limits. The number of experimental data for each system varies from a maximum of 17 for *n*-butanol in water, to a minimum of 10 for i-butanol in water.

[b]Ref. 24.

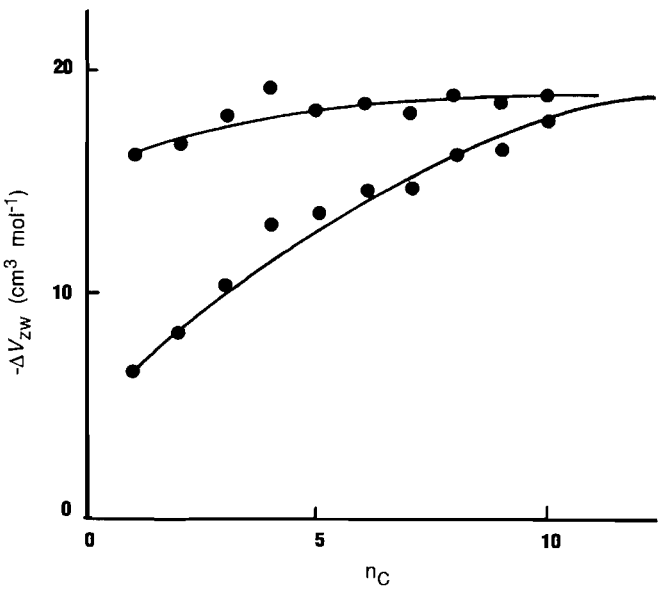

FIG. 1. ΔV_{zw} values for several α,ω-amino acids reported as a function of the number of carbon atoms of the alkyl chain, n_C. The values falling on the upper curve are from ref. 8. The values falling on the lower curve are obtained by the reelaboration of the data reported in ref. 15.

$$\bar{V}^0_{(\text{hydrochloride})} = \bar{V}^0_{A^+} + \bar{V}^0_{Cl^-}$$

$$\bar{V}^0_{(\text{sodium salt})} = \bar{V}^0_{A^-} + \bar{V}^0_{Na^+}$$

Then:

$$\bar{V}^0_{(\text{hydrochloride})} + \bar{V}^0_{(\text{sodium salt})} - 2\,\bar{V}^0_{A^{+/-}} = \bar{V}^0_{A^+} + \bar{V}^0_{A^-} + \bar{V}^0_{A^{+/-}} - \bar{V}^0_{A^{+/-}} + \bar{V}^0_{Cl^-} + \bar{V}^0_{Na^+} = \bar{V}^0_{A} + \bar{V}^0_{A^{+/-}} - \bar{V}^0_{A^{+/-}} - \bar{V}^0_{A^{+/-}} + \bar{V}^0_{NaCl} = \bar{V}^0_{A} - \bar{V}^0_{A^{+/-}} + \bar{V}^0_{NaCl} = -\Delta V_{zw} + \bar{V}^0_{NaCl}$$

where $\bar{V}^0_{NaCl}$ is 16.6 cm^3 mol^{-1} (23). For these substances, we find that ΔV_{zw} is largely dependent on the alkyl chain length. In Fig. 1 the ΔV_{zw} for α,ω-amino acids are reported as a function of the number of carbon atoms, n_C, constituting the alkyl chain. The lower curve describes the values obtained reelaborating the data of Shahidi and Farrell (15, 17) through our approach. The values increase almost linearly up to 6-aminohexanoic acid and then they tend slowly to a plateau. The upper curve describes the ΔV_{zw} data obtained by Cabani et al. (8) through a group contribution approach. A linear regression on the double reciprocal plot of $(\Delta V_{zw})^{-1}$ vs. $(n_C)^{-1}$ gave a value of -19.6 ± 1.3 in the first case, and a value of -19.2 ± 0.3 in the second case, in agreement with the reported mean value of -18.5 ± 0.4 cm^3 mol^{-1} (8). As can be seen, the two curves converge when the number of CH_2 groups separating the charges is larger than six or seven, while they greatly diverge for the shortest α,ω-amino acids: this is a strong indication that our model takes intramolecular interactions partially into account, an effect that becomes less important when the two functional groups are well separated. Moreover, as a further test, the Shahidi and Farrell data for glycine (15) were used to calculate ΔV_{zw}. It is found to be -7.2 cm^3 mol^{-1}, while using our data a value of -7.8 cm^3 mol^{-1} is obtained. The very good agreement between the two values underlines the validity of the proposed experimental procedure in the three solvents.

As a conclusion, the difference of about 6 cm^3 mol^{-1} between the presently determined value for ΔV_{zw} (-8.4 ± 3.0 cm^3 mol^{-1}) and that reported in the literature (-14.7 ± 0.8 cm^3 mol^{-1}) for α-amino acids (8) could be attributed to two reasons: (*i*) hydroxyamide may not be a good model of neutral amino acids, and (or) (*ii*) the group contribution approach cannot account for the different intramolecular interactions when the charges are extremely close, as in α-amino acids.

1. T.H. Lilley. *In* The chemistry and biochemistry of the amino acids. *Edited by* G.C. Barrett. Chapman and Hall, London. 1985. Chap. 21, and references therein cited.
2. G. Barone, G. Castronuovo, V. Elia, and S. Puzziello. J. Solution Chem. **18**, 1105 (1989).
3. G. Castronuovo, V. Elia, and M. Magliulo. Can. J. Chem. **69**, 794 (1991).
4. G. Castronuovo, V. Elia, C. Giancola, and S. Puzziello. J. Solution Chem. **19**, 855 (1990).
5. C. Jolicoeur, B. Riedl, D. Desrochers, L.L. Lemelin, R. Zamojska, and O. Enea. J. Solution Chem. **15**, 109 (1986).
6. A.K. Mishra and J.C. Ahluwalia. J. Phys. Chem. **88**, 86 (1984).
7. G. Di Paola and B. Belleau. Can. J. Chem. **56**, 1827 (1978).
8. S. Cabani, G. Conti, E. Matteoli, and M.R. Tinè. J. Chem. Soc. Faraday Trans. 1, **77**, 2377 (1981).

Can. J. Chem. Downloaded from www.nrcresearchpress.com by 203.198.23.82 on 09/08/12
For personal use only.

9. S. Cabani, G. Conti, E. Matteoli, and M.R. Tinè. J. Chem. Soc. Faraday Trans. 1, **77**, 2385 (1981).
10. F.J. Millero, A. Lo Surdo, and C. Shin. J. Phys. Chem. **82**, 784 (1978).
11. C. Jolicoeur and J. Boileau. Can. J. Chem. **56**, 2707 (1978).
12. F. Shahidi and D.G. Farrell. J. Chem. Soc. Faraday Trans. 1, **77**, 963 (1981).
13. F. Shahidi. J. Solution Chem. **12**, 295 (1983).
14. J.C. Ahluwalia, C. Ostigui, G. Perron, and J.E. Desnoyers. Can. J. Chem. **55**, 3364 (1977).
15. F. Shahidi and D.G. Farrell. J. Chem. Soc. Faraday Trans. 1, **74**, 858 (1978).
16. R. Zana. J. Phys. Chem. **81**, 1817 (1977).
17. F. Shahidi. J. Chem. Soc. Faraday Trans. 1, **76**, 101 (1980).
18. T.E. Leslie and T.H. Lilley. Biopolymers, **24**, 695 (1985).
19. W.G. McMillan and J.E. Mayer. J. Chem. Phys. **13**, 276 (1945).
20. H.L. Friedman. J. Chem. Phys. **32**, 135 (1960).
21. J.J. Kozak, W.S. Knight, and W. Kauzmann. J. Chem. Phys. **48**, 675 (1968).
22. G.C. Allred and E.M. Woolley. J. Chem. Thermodyn. **13**, 147 (1981).
23. F.J. Millero. *In* Water and aqueous solutions: structure, thermodynamics, and transport processes. *Edited by* C.A. Horne. Wiley–Interscience, New York, 1972.
24. G. Perron and J.E. Desnoyers. J. Chem. Thermodyn. **13**, 1105 (1981).

Can. J. Chem. Downloaded from www.nrcresearchpress.com by 203.198.23.82 on 09/08/12
For personal use only.

Kinetics and mechanism of the oxidation of oxalate ion by tris(acetylacetonato)-manganese(III) and its hydrolytic derivatives in aqueous perchlorate media

SUBRATA MUKHOPADHYAY, SWAPAN CHAUDHURI, RINA DAS, AND RUPENDRANATH BANERJEE[1]
Department of Chemistry, Jadavpur University, Calcutta 700 032, India

Received April 12, 1993

SUBRATA MUKHOPADHYAY, SWAPAN CHAUDHURI, RINA DAS, and RUPENDRANATH BANERJEE. Can. J. Chem. **71**, 2155 (1993).

In the pH range 6.6–8.6, $[MnL_2(H_2O)_2]^+$ and $[MnL_2(H_2O)(OH)]$ (HL = acetylacetone) oxidize oxalate ion (ox^{2-}) to CO_2 through the inner-sphere intermediates $[MnL_2(ox)]^-$ and $[MnL_2(OH)(ox')]^{2-}$, where ox′ is a half-bonded (unidentate) oxalate ion. Their rate constants of decomposition are 1.0×10^{-4} s^{-1} and 11.2×10^{-2} M^{-1} s^{-1} at 30°C and at I = 1.0 M ($NaClO_4$). Decomposition of these mixed complexes produces free radicals, presumably CO_2^-, which is further oxidized to CO_2 by another Mn(III) in a fast step. At pH 4.2, $[Mn(ox)_3]^{3-}$ is produced quantitatively when $[ox]_0 \geq 0.12$ M, which has been characterized spectrally, and its unimolecular decomposition rate constant k ($= 2.7 \times 10^{-4}$ s^{-1} at 30°C and I = 1.0 M) compares well with that reported earlier (2.44×10^{-4} s^{-1} at 25°C and I = 1.0 M).

SUBRATA MUKHOPADHYAY, SWAPAN CHAUDHURI, RINA DAS et RUPENDRANATH BANERJEE. Can. J. Chem. **71**, 2155 (1993).

Dans la plage de pH allant de 6,6 à 8,6, les entités $[MnL_2(H_2O)_2]^+$ et $[MnL_2(H_2O)(OH)]$ (HL = acétylacétone) oxydent l'ion oxalate (ox^{2-}) en CO_2 par le biais d'intermédiaires de sphère interne $[MnL_2(ox)]^-$ et $[MnL_2(OH)(ox')]^{2-}$, dans lequel ox′ est un ion oxalate à demi lié (monocoordiné). Leurs constantes de vitesse de décomposition sont respectivement $1{,}0 \times 10^{-4}$ s^{-1} et $11{,}2 \times 10^{-2}$ M^{-1} s^{-1}, à 30°C et à I = 1,0 M ($NaClO_4$). La décomposition de ces complexes mixtes fournit des radicaux libres, probablement de CO_2^-, qui sont oxydés en CO_2 par un autre Mn(III) dans une étape rapide. À un pH de 4,2 et une $[ox]_0 \geq 0{,}12$ M, il y a formation de $[Mn(ox)_3]^{3-}$ avec un rendement quantitatif; ce composé a été caractérisé par spectroscopie et sa constante de vitesse de décomposition unimoléculaire, $k = 2{,}7 \times 10^{-4}$ s^{-1}, à 30°C et I = 1,0 M, se compare bien avec celle rapportée antérieurement $k = 2{,}44 \times 10^{-4}$ s^{-1}, à 25°C et I = 1,0 M.

[Traduit par la rédaction]

Introduction

The oxidation of oxalate ion and its conjugate acids by higher valent manganese species has been a subject of kinetic study for more than a century (1–14). Thus, the involvement of oxalatomanganese(III) species in such reactions has been established, but the detailed mechanism is still not clear. Tris(acetylacetonato)manganese(III), $[MnL_3]$, is a well-characterized Mn(III) complex. The complex and its hydrolytic derivatives $[MnL_2(H_2O)_2]^+$ and $[MnL_2(H_2O)(OH)]$ oxidize glyoxylate (gox^-) (15), thiosulfate (16), hypophosphite (17), and sulfur(IV) (18) through inner-sphere adducts. Whether oxalate, which has some structural resemblance to glyoxylate, reacts similarly is an interesting question, particularly because it is known that (*trans*-1,2-cyclohexanediaminetetraacetato)manganate(III) ion, $[Mn(cdta)]^-$, oxidizes oxalate by an outer-sphere process (19) although $[Mn(cdta)]^-$ and (ethylenediaminetetraacetato)manganate(III), $[Mn(edta)]^-$ react with a variety of reductants such as S(IV), N_3^-, H_2O_2, V(IV), NO_2^-, etc., through an inner-sphere mechanism (20–24).

Experimental

Materials

Preparation of the Mn(III) complex and the standard $NaClO_4$ solution and purification of acetylacetone and N_2 gas have been described elsewhere (18, 25–27).

Oxalic acid dihydrate (G.R., E. Merck) solutions were prepared by direct weighing. All other chemicals, including acrylonitrile, were of reagent grade and were used as received.

Instrumentation has been described earlier (15–18).

Product analyses and stoichiometry

Analyses were carried out after all Mn(III) had reacted under kinetic conditions. Free acetylacetone was determined colourimetrically at 510 nm using *o*-phenylenediamine as the colour-forming reagent (28). We verified that neither Mn^{2+} nor oxalate interferes in this determination. Carbon dioxide was qualitatively detected by passing purified (Chromus scrubbed) dinitrogen through the reaction mixture and passing the outcoming gas through a narrow, long, absorber tube containing lime water (29). We verified that acetylacetone does not interfere with the detection procedure. Unreacted oxalate was determined gravimetrically by adding hot $CaCl_2$ solution to precipitate excess oxalate as $CaC_2O_4 \cdot H_2O$, which was weighed as $CaCO_3$ (30).

Kinetic measurements

Disappearance of Mn(III) in the presence of excess oxalate (at least 10 times the amount of Mn(III)) was generally followed at 560 nm with a 1-cm quartz cell in a thermostated (±0.1°C) cell housing.

Between absorbance measurements the cells with the kinetic mixtures were kept outside the light path to minimize any possible photoreaction (31). Ionic strength in most of the kinetic runs was 1.0 M, maintained by $NaClO_4$. No external buffer was used during the entire study to avoid any possible complexation with Mn(III) and because pH drift during the reactions was at most 0.05. Under the conditions the observed pseudo-first-order rate constants (k_0) were obtained from log(absorbance) against time plots, which were linear for as much as two half-lives. A built-in linear least-squares program of a Casio (Model fx 3600 P) calculator was used for evaluating the slopes of such straight lines. The individual rate constants and the equilibrium constants were evaluated by graphical solution of the appropriate rate law or by numerical analyses, e.g., Gauss's method of solving a set of linear observation equations (32). Associated errors were estimated using standard formulas (33).

Results and discussion

Spectral observations and stoichiometry

Immediate spectral changes are observable on adding oxalate to a solution of the Mn(III) complex in excess acetylacetone (0.1–1.0 M) in the pH range 4.0–7.0. In the pH range 4.0–6.5 a cherry-red colour appears, the equilibrium

[1]Author to whom correspondence may be addressed.

Can. J. Chem. Downloaded from www.nrcresearchpress.com by 203.198.23.82 on 09/08/12
For personal use only.

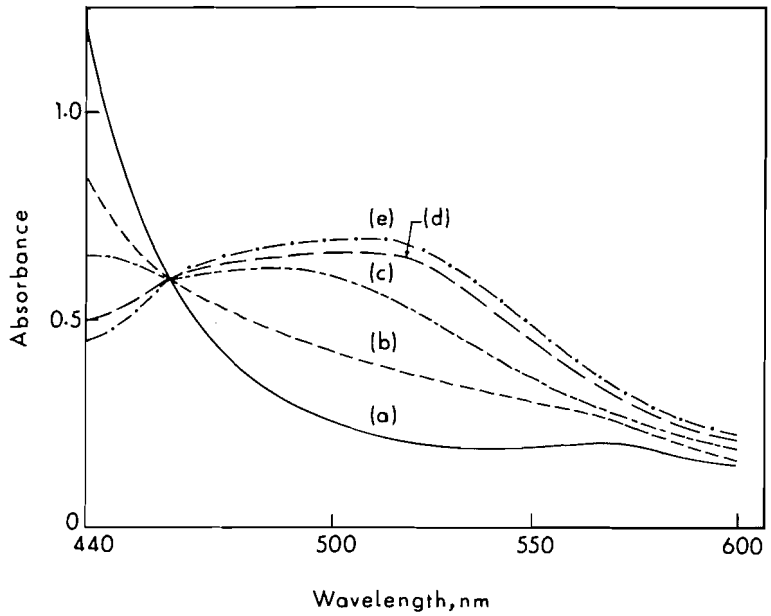

FIG. 1. Spectrum of (*a*) 2 mM of the manganese(III) complex in 0.5 M $[L]_0$ at pH 4.2 at 30°C. The spectra (*b*), (*c*), (*d*), and (*e*) resulted immediately on mixing 0.02, 0.04, 0.08, and 0.12 M $[ox]_0$, respectively, with the complex solution (*a*) under the same conditions. No further change in spectra results on increasing $[ox]_0$; spectrum (*e*) is identical to that reported for $[Mn(ox)_3]^{3-}$.

intensity of which, at a fixed pH, increases with increasing oxalate concentrations. At pH 4.2 and $[L]_0$ (total acetylacetone concentration) 0.5 M, the maximum colour intensity is observed when $[ox]_0 \geq 0.12$ M (Fig. 1). Under such conditions the solution spectrum is identical to one reported earlier for $[Mn(ox)_3]^{3-}$ (5, 6). Evidently all Mn(III)–L complexes are transformed to $[Mn(ox)_3]^{3-}$ quantitatively under such conditions. Mixed ligand complexes, viz. $[MnL_2(ox)]^-$ and $[MnL(ox)_2]^{2-}$, are also possible, along with $[Mn(ox)_3]^{3-}$, through equilibria [1]–[3] at higher pH and lower $[ox]_0$ (total oxalate concentration).

$$[1] \quad [MnL_3] + Hox^- \rightleftharpoons [MnL_2(ox)]^- + HL$$

$$[2] \quad [MnL_2(ox)]^- + Hox^- \rightleftharpoons [MnL(ox)_2]^{2-} + HL$$

$$[3] \quad [MnL(ox)_2]^{2-} + Hox^- \rightleftharpoons [Mn(ox)_3]^{3-} + HL$$

The intensity of the cherry-red colour decreases with increase in pH as $[Mn(ox)_3]^{3-}$ decreases. Above pH 6.5, the cherry-red colour disappears and $[Mn(ox)_3]^{3-}$ is practically absent as indicated by the spectral changes, which are completely different from Fig. 1, but analogous to the spectral changes observed for $[MnL_3]$–gox^- mixtures in the range pH 5.5–7.5 (15). Spectral changes above pH 6.5 are thus interpreted in terms of equilibria [4]–[6], which are analogous to those assigned for the $[MnL_3]$–gox^- system and are fully consistent with the kinetic observations expressed later.

$$[4] \quad [MnL_3] + H^+ + 2H_2O \overset{K_1}{\rightleftharpoons} [MnL_2(H_2O)_2]^+ + LH$$

$$[5] \quad [MnL_2(H_2O)_2]^+ \overset{K_h}{\rightleftharpoons} [MnL_2(H_2O)(OH)] + H^+$$

$$[6] \quad [MnL_2(H_2O)_2]^+ + ox^{2-} \overset{K_c}{\rightleftharpoons} [MnL_2(ox)]^- + 2H_2O$$

All the reaction mixtures discussed above, eventually decay slowly to a final absorbance of less than 0.02 at 560 nm. In this process, under kinetic conditions, very nearly two moles of Mn(III) are consumed per mole of oxalate oxidized to CO_2 under both aerobic and anaerobic conditions; no acetylacetone is consumed within the limit of experimental uncertainty. Five stoichiometric measurements were made in the following ranges of reagent concentrations: $[Mn(III)]_0 = 0.002$–0.004 M; $[ox]_0 = 0.004$–0.005 M; $[L]_0 = 0.05$–0.1 M; pH 6.0–8.0. The average value of $|\Delta[Mn(III)]|/|\Delta[ox]|$ was found to be 2.06 ± 0.11. This is represented in the stoichiometric equation [7].

$$[7] \quad 2Mn(III) + C_2O_4^{2-} \rightarrow 2Mn(II) + 2CO_2$$

The slow decrease in absorbance of the reaction mixture follows first-order kinetics for at least two half-lives but curves towards lower rate constants at longer times if the reaction mixture is not deoxygenated. Therefore, rate constants under aerobic conditions were determined from the initial linear portions (~two half-lives) of the reaction. In completely deoxygenated solutions, the first-order plots proved to be linear for at least 90% completion of the reaction. Moreover, k_0 values obtained from such plots are within 5% of the k_0 values obtained under aerobic conditions. The following changes in the reaction conditions had, within experimental error, no detectable influence on the values of k_0: a fivefold variation (1–5 mM) in complex concentration, addition of excess $Mn(ClO_4)_2$ up to 0.02 M (see later), and a variation in the monitoring wavelength in the range 500–650 nm. Polymerization occurs over the entire experimental range when 6% acrylonitrile is added to the reaction mixture. A free radical mechanism is thus indicated although no epr signals were received. Duplicate runs reproduced individual k_0 values within 4% and some representative values are summarized in Table 1. Under all experimental conditions the autodecomposition of the complex was negligible.

At pH 4.2, $[L]_0 = 0.5$ M and $[ox]_0 \geq 0.12$ M; $k_0 =$

Can. J. Chem. Downloaded from www.nrcresearchpress.com by 203.198.23.82 on 09/08/12
For personal use only.

TABLE 1. Some representative first-order rate constants for the reaction of Mn(III)–L complexes under different conditions[a]

pH	$[L]_0$ (M)	$[ox]_0$ (M)	$10^4 k_0$ (s^{-1}) 20°C	30°C	40°C
6.6	0.5	0.08	1.60	2.0	2.60
7.0	0.5	0.08	1.60	2.0	2.75
7.6	0.5	0.08	1.65	2.05	2.90
8.0	0.5	0.08	1.70	2.20	3.0
8.4	0.5	0.08	2.05	2.65	3.50
8.6	0.5	0.08	2.30	3.0	4.20
7.0	0.1	0.08	1.70	2.40	3.40
7.0	0.2	0.08	1.60	2.20	3.10
7.0	1.0	0.08	1.45	1.65	2.10
8.0	0.1	0.15	2.90	5.00	9.90
8.0	1.0	0.20	1.90	2.40	3.60
8.0	0.5	0.02	0.74	0.80	0.94
8.0	0.5	0.04	1.20	1.35	1.70
8.0	0.5	0.15	2.20	3.15	4.70
8.0	0.5	0.25	2.50	3.90	6.25
6.8	0.7	0.08	1.55	1.90	2.45

[a][complex] = 2.0 mM; I = 1.0 M.

$(2.7 \pm 0.2) \times 10^{-4}$ s^{-1} at 30°C and I = 1.0 M, and is in very good agreement with the reported rate constant (2.44×10^{-4} s^{-1} at 25°C and I = 1.0 M) for the redox decomposition of $[Mn(ox)_3]^{3-}$. The reaction path at lower pH, therefore, appears to be equilibrium [8]:

$$[8] \quad Mn(III) + 3Hox^- \overset{\text{fast}}{\rightleftharpoons} [Mn(ox)_3]^{3-} + 3HL \xrightarrow{\text{slow}} \text{Products}$$

We have not attempted an evaluation of the kinetic activity of mixed ligand complexes possible for pH ≤ 6.5 for want of equilibrium data on this unstable complex system. Moreover, kinetic analysis of such complex systems may lead to erroneous mechanistic conclusions because the precision achievable in k_0 values may not be enough to distinguish even between an $[ox]_0^2$ and an $[ox]_0^3$ path, for example.

In the pH range 6.6–8.6 k_0 against $[ox]_0$ plots follow saturation kinetics and $1/k_0$ against $1/[ox]_0$ plots are found to be linear ($r > 0.98$), which strongly suggests $[MnL_2(ox)]^-$ to be a kinetically active species. This kinetic observation and also the observed spectral behaviour in this pH range are explicable by the following scheme, with the rapid preequilibrium steps [4]–[6].

$$[9] \quad [MnL_2(ox)]^- \xrightarrow{k_c} Mn(II) + CO_2 + CO_2^- + 2L^-$$

$$[10] \quad [MnL_2(H_2O)(OH)] + ox^{2-} \xrightarrow{k_h} Mn(II) + CO_2 + CO_2^- + 2L^-$$

$$[11] \quad L^- + H^+ \overset{K_2}{\rightleftharpoons} LH$$

$$[12] \quad Mn(III) + CO_2^- \xrightarrow{\text{fast}} Mn(II) + CO_2$$

Selected values of the known equilibrium constants are summarized in Table 2. The radical CO_2^- being quickly oxidized by a second Mn(III), this scheme is comparable to that proposed earlier for the reaction of glyoxylate with these Mn(III) complexes; step [10] is necessary to explain the observed dependence of k_0 on pH. According to this scheme, the rate law derived is

$$[13] \quad k_0 = \frac{2(k_c K_c K_1[H^+] + k_h K_h K_1)[ox]_0}{([HL] + K_c K_1[H^+][ox]_0)}$$

In deriving eq. [13] it was assumed that $(K_1[H^+] + K_1K_h)$ is negligible compared to $([HL] + K_cK_1[H^+][ox]_0)$ under the reaction conditions.

K_c was evaluated from the linear plots ($r \geq 0.98$) of $1/k_0$ against $1/[ox]_0$ at every temperature. Using these K_c values, plots of $k_0([HL] + K_cK_1[H^+][ox]_0)$ against $[H^+]$ at any fixed $[ox]_0$ and temperature were found to be good straight lines (Fig. 2, $r > 0.98$), slopes and intercepts of which yielded the rate constants k_c and k_h. Equation [13] was also solved numerically following Gauss's method using the kinetically estimated K_c values at each temperature, (giving equal weight to all the observations), and the rate constants k_c and k_h thus evaluated agree nicely (within 3%) with the graphically evaluated values. The rate constants thus obtained, along with their activation parameters, are given in Table 3. They reproduce all k_0 values within 2–7%.

The proposed production of CO_2^- (or $C_2O_4^-$) by the intramolecular one-electron oxidation of oxalate by Mn(III) is a well-established process. Since CO_2^- is known to be a very strong reductant (34), it can rapidly reduce another Mn(III). But CO_2^- may also initiate other reactions, e.g., [14]–[16] under aerobic conditions (14, 35–37).

$$[14] \quad CO_2^- + O_2 \rightarrow CO_2 + O_2^-$$

$$[15] \quad O_2^- + Mn(III) \rightarrow Mn(II) + O_2$$

$$[16] \quad Mn(II) + O_2^- + 2H^+ \rightleftharpoons Mn(III) + H_2O_2$$

The overall effect of reactions [14] and [15] is same as reaction [12] and they should not affect kinetics and stoichiometric results. But equilibrium [16] might affect both kinetics and stoichiometry if the equilibrium is significantly displaced to the right. Probably such is the case under our conditions, only when [Mn(III)] is low, e.g., after two half-lives. Consequently, any effect of equilibrium [16] on the measured stoichiometry is hidden within the experimental uncertainties and the kinetics are affected only after at least 75% of the reaction is over. Hence, added Mn(II) does not affect k_0 that were measured from the first two half-lives. We have also verified that the Mn(III)–L complexes are reduced by

TABLE 2. Selected literature values of the equilibrium constants

Equilibrium	Value	Reference
K_1	1.16×10^5	[a]
K_2	8.62×10^8 M^{-1}	[b]
K_h	5.0×10^{-8} M	[c]

[a]T = 30°C; I = 0.2 M. See ref. 25. Values of K_1 at 20°C and 40°C were calculated to be 1.22×10^5 and 1.08×10^5, respectively, from this reference.
[b]T = 30°C; I = 1.0 M. See ref. 42. Values of K_2 at 20°C and 40°C were calculated to be 1.14×10^9 and 6.49×10^8 M^{-1}, respectively, from this reference.
[c]At 25°C. See refs. 25 and 27. Temperature dependence of K_h is not known.

Can. J. Chem. Downloaded from www.nrcresearchpress.com by 203.198.23.82 on 09/08/12
For personal use only.

Can. J. Chem. Downloaded from www.nrcresearchpress.com by 203.198.23.82 on 09/08/12
For personal use only.

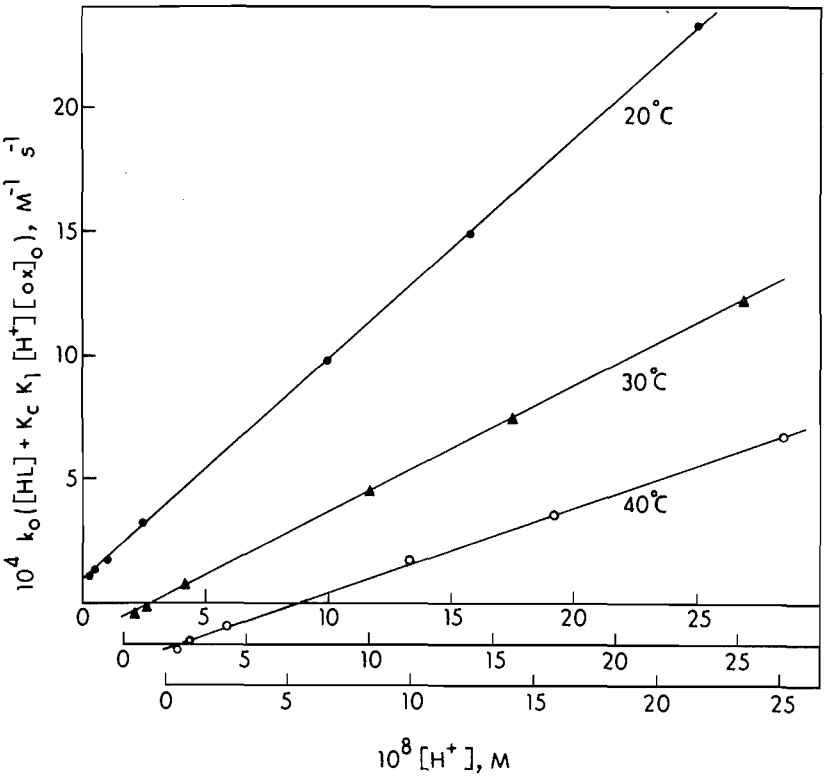

FIG. 2. Evaluation of rate constants k_c and k_h: plots of $k_0([HL] + K_c K_1[H^+][ox]_0)$ against $[H^+]$ at different temperatures. $[ox]_0$ = 0.08 M; I = 1.0 M ($NaClO_4$).

TABLE 3. Rate constants and activation parameters for the reaction of oxalate with Mn(III)–L complexes at I = 1.0 M ($NaClO_4$)[a]

T(°C)	$10^4\ k_c$ (s^{-1})	$10^2\ k_h$ ($M^{-1}\ s^{-1}$)	K_c[b] (M^{-1})
20	0.80 ± 0.04	8.5 ± 0.2	5750 ± 400
30	1.0 ± 0.04	11.3 ± 0.3	2750 ± 200
40	1.3 ± 0.04	16.1 ± 0.3	1550 ± 130
$\Delta H^{\neq}$ (kJ mol^{-1})	16 ± 2	22 ± 3	
$\Delta S^{\neq}$ (J K^{-1} mol^{-1})	−270 ± 30	190 ± 25	

[a]These k_c, k_h, and K_c values are obtained from the graphical solution of eq. [13]. The K_1 and K_h values (see Table 2) used to calculate the rate constants, k_c and k_h, are known under conditions somewhat different from those used in the kinetic studies. However, we found that the choice of K_1 and K_h is not particularly telling on the values of rate constants, e.g., a 15% change in K_1 changes k_1 by no more than 1%, but a simultaneous 15% change in both K_1 and K_h has a stronger effect; k_h then changes by 15%.
[b]ΔH = −50 ± 5 kJ mol^{-1}; ΔS = −100 ± 15 J K^{-1} mol^{-1}.

H_2O_2 at a moderate rate. Involvement of equilibrium [16] in the present system is therefore a distinct possibility.

Mechanism

A moderate $\Delta H^{\ddagger}$ and highly negative $\Delta S^{\ddagger}$ for both k_c and k_h paths dictate the formation of a compact transition state indicative of an inner-sphere mechanism. The high K_c values justify the postulation of the inner-sphere adduct $[MnL_2(ox)]^-$. This K_c value is higher than the formation constant of $[MnL_2(gox)]$ (15) from $[MnL_2(H_2O)_2]^+$ and gox^- and reflects the general tendency of binegative oxalate ion to form a more stable complex than by the uninegative glyoxylate ion with Mn(III). Macartney and Sutin, and Pelizzetti, observed that in oxidation reactions of Mn(III) the aqua path should be much more important than the hydroxo path for a given outer-sphere reductant (38). Since this is not the case in the present system, an inner-sphere mechanism probably is operative also for the k_h path via the plausible intermediate $[MnL_2(OH)(ox')]$, where ox′ represents unidentate oxalate ion. Unidentate behaviour of the oxalate ion is well known (39).

Mn(III)–L species do not prefer outer-sphere pathways, probably due to their weakly oxidizing nature (16), and oxidize oxalate ion via an inner-sphere pathway. Nevertheless, such a path is also not available for $[MnL_3]$ due to its coordinately saturated, pseudo-aromatic, stable chelate ring structure (40). Although $[MnL_3]$ is kinetically labile (estimated ligand exchange rate 1 s^{-1} at 25°C in MeCN) (40), the equilibrium constant for reaction [17] is only ~0.4, thus

$[MnL_2(ox)]^-$ is formed almost exclusively through reaction [6] for

[17] $[MnL_3] + ox^{2-} \rightleftharpoons [MnL_2(ox)]^- + L^-$

which the equilibrium constant K_c is of the order 10^3 M^{-1}. Probably for these reasons $[MnL_3]$ is inactive towards oxalate. In contrast to these Mn(III) species, the anionic complex $[Mn(cdta)]^-$ oxidizes oxalate through an outer-sphere path, probably because of its greater oxidizing power (41) than the Mn(III)–L complexes.

An interesting comparison may arise for the difference in redox behaviour of glyoxylate and oxalate towards the Mn(III) complexes. The gox^- anion catalytically reduces Mn(III). Neutral $gox^{\cdot}$ radical formed by the rate-determining inner-sphere oxidation of gox^- by Mn(III) is not further oxidized by a second Mn(III); rather, the radical is reduced back to gox^- by acetylacetone. In the present investigation, CO_2^- radical anion is quickly reoxidized by a second Mn(III), and the $[L]_0$ content before and after the reaction remains unaltered. This probably indicates that the neutral $gox^{\cdot}$ radical is a weaker reducing agent than the anionic radical species CO_2^-, which is known to be a very powerful reducing agent (34) and hence directly reduces Mn(III).

Acknowledgments

The award of a senior research fellowship to S.M. and a research associateship to R.D. by the Council of Scientific and Industrial Research (New Delhi) is gratefully acknowledged.

1. A.V. Harcourt and W. Esson. Philos. Trans. R. Soc. (London), **156**, 193 (1866); **157**, 117 (1867).
2. R.W. Money and C.W. Davies. Trans. Faraday Soc. **28**, 609 (1932).
3. H.F. Launer. J. Am. Chem. Soc. **54**, 2597 (1932); **55**, 865 (1933).
4. H.F. Launer and D.M. Yost. J. Am. Chem. Soc. **56**, 2571 (1934).
5. G.H. Cartledge and N.P. Ericks. J. Am. Chem. Soc. **58**, 2065 (1936).
6. H. Taube. J. Am. Chem. Soc. (*a*) **69**, 1418 (1947); (*b*) **70**, 1216 (1948); (*c*) **70**, 3928 (1948).
7. J.M. Malcolm and R.M. Noyes. J. Am. Chem. Soc. **74**, 2769 (1952), and refs. therein.
8. S.J. Adler and R.M. Noyes. J. Am. Chem. Soc. **77**, 2036 (1955).
9. T. Ernst, M. Wawrzenczyk, and M. Wronska. Z. Phys. Chem. (Leipzig), **261**, 306 (1980).
10. J.S. Reckley and K. Showalter. J. Am. Chem. Soc. **103**, 7012 (1981).
11. T.J. Jones and R.M. Noyes. J. Phys. Chem. **87**, 4686 (1983).
12. N. Ganapathisubramanian. J. Phys. Chem. **92**, 414 (1988).
13. R.T. Powell, T. Oskin, and N. Canapathisubramanian. J. Phys. Chem. **93**, 2718 (1989).
14. M. Kimura, M. Ohoto, and K. Tsukahara. Bull. Chem. Soc. Jpn. **63**, 151 (1990).
15. R. Banerjee, R. Das, and A.K. Chakraburtty. J. Chem. Soc. Dalton Trans. 3277 (1990).
16. R. Banerjee, R. Das, and A.K. Chakraburtty. J. Chem. Soc. Dalton Trans. 987 (1991).
17. R. Banerjee, R. Das, and A.K. Chakraburtty. Transition Met. Chem. **17**, 277 (1992).
18. S. Mukhopadhyay and R. Banerjee. J. Chem. Soc. Dalton Trans. 933 (1993).
19. M.A. Suwyn and R.E. Hamm. Inorg. Chem. **6**, 142 (1967).
20. V.M. Bobba, G. Giraudi, and E. Mentasti. Transition Met. Chem. **13**, 256 (1988).
21. M.A. Suwyn and R.E. Hamm. Inorg. Chem. **6**, 2150 (1967).
22. T.E. Jones and R.E. Hamm. Inorg. Chem. **13**, 1940 (1974).
23. D.J. Boone, E.H. Randall, and J.P. Hunt. Inorg. Chem. **11**, 1060 (1972).
24. T.E. Jones and R.E. Hamm. Inorg. Chem. **14**, 1027 (1975).
25. G.H. Cartledge. J. Am. Chem. Soc. **74**, 6015 (1952).
26. R.G. Charles and B.E. Bryant. Inorg. Synth. **7**, 183 (1966).
27. G.H. Cartledge. J. Am. Chem. Soc. **73**, 4416 (1951).
28. A. Agett and A.L. Odell. J. Chem. Soc. A, 1820 (1966).
29. R. Banerjee, K. Das, A. Das, and S. Dasgupta. Inorg. Chem. **28**, 585 (1989).
30. A.I. Vogel. Quantitative inorganic analysis. 3rd ed. ELBS, London. 1961. Chap. 5.
31. A. Harriman. Coord. Chem. Rev. **28**, 147 (1979), and refs. cited therein.
32. H. Margenau and G.M. Murphy. The mathematics of physics and chemistry. 2nd ed. D. Van Nostrand, New Jersey. 1956. Chap. 13.
33. A.C. Norris. Computational chemistry. John Wiley, New York. 1981. Chap. 3.
34. H.A. Schwartz, C. Creutz, and N. Sutin. Inorg. Chem. **24**, 433 (1985).
35. G.V. Buxton, R.M. Sellers, and D.R. McCracken. J. Chem. Soc. Faraday Trans. 1, **72**, 1464 (1976).
36. N. Getoff, F. Schworer, V.M. Markovic, K. Sehested, and S.O. Nielsen. J. Phys. Chem. **75**, 749 (1971).
37. M. Kimura, H. Ishiguro, and K. Tsukahara. J. Phys. Chem. **94**, 4106 (1990).
38. (*a*) D.H. Macartney and N. Sutin. Inorg. Chem. **24**, 3403 (1985); (*b*) E. Pelizzetti. J. Chem. Soc. Dalton Trans. 484 (1980).
39. B.S. Maritz and R. van Eldik. Inorg. Chim. Acta, **17**, 21 (1976).
40. H. Kido and K. Saito. J. Am. Chem. Soc. **110**, 3187 (1988).
41. R.E. Hamm and M.A. Suwyn. Inorg. Chem. **6**, 139 (1967).
42. J.O. Liljenzin and J.J. Stary. J. Inorg. Nucl. Chem. **32**, 1357 (1970).

Can. J. Chem. Downloaded from www.nrcresearchpress.com by 203.198.23.82 on 09/08/12
For personal use only.

Evaluation of organic compounds as new cathode active materials in primary cell systems

R. UDHAYAN[1] AND DEVENDRA P. BHATT
Central Electrochemical Research Institute, Karaikudi 623 006, India

Received January 18, 1993

R. UDHAYAN and DEVENDRA P. BHATT. Can. J. Chem. **71**, 2160 (1993).

The performance characteristics of magnesium/trichloroisocyanuric acid (Mg/TCIA) and magnesium/trichloromelamine (Mg/TCM) cells have been reported in this paper. These cells show higher open circuit (>2.5 V) and working voltages (>2.0 V) than known primary organic cells such as magnesium/*meta*-dinitrobenzene (OCV: 1.5 V; CCV: 1.0 V). The capacity, energy density, and coulombic efficiency of these cells are calculated using the galvanostatic technique and the results are compared with magnesium/dichloroisocyanuric acid (Mg/DCIA) cell.

R. UDHAYAN et DEVENDRA P. BHATT. Can. J. Chem. **71**, 2160 (1993).

On a examiné la performance des cellules magnésium/acide trichloroisocyanurique (Mg/ATCI) et magnésium/trichloromelamine (Mg/TCM). Ces cellules des voltages en circuit ouvert (>2,5 V) et de travail (>2,0 V) plus élevés que ceux obtenus avec des cellules organiques primaires connues comme magnésium/*méta*-dinitrobenzène (OCV: 1,5 V; CCV: 1,0 V). On a calculé la capacité, la densité d'énergie et l'efficacité coulombique de ces cellules en faisant appel à la technique galvanostatique et on a comparé les résultats avec ceux obtenus avec la cellule magnésium/acide dichloroisocyanurique (Mg/ADCI).

[Traduit par la rédaction]

Introduction

In the development of modern battery devices, magnesium-organic batteries have received much attention in recent years because of their high energy density and voltage stability. A series of organic depolarisers have been coupled with magnesium or zinc; among them aromatic nitrocompounds, e.g. *meta*-dinitrobenzene has dominated others because of its multielectron transfer property during electrochemical reduction (1–4). Nitro compounds have the following limitations: very low cathode potential, low power density, high solubility, and high toxicity. Halogens, on the other hand, have long been considered attractive materials for cathodes in battery devices because of their high electrode potential and high specific capacity (5). However, their corrosive nature and handling problems make them difficult ingredients in battery devices. To circumvent these problems, halogen-containing compounds (e.g. *N*-halogen organic compounds) have been used as attractive depolarisers in our recent series of publications (6–10). The present investigation demonstrates the electrochemical characteristics of magnesium cells with trichloroisocyanuric acid (TCIA) and trichloromelamine (TCM) as cathode depolarisers. The cells are activated using 2.0 M magnesium perchlorate solution and the performance characteristics have been evaluated and compared with Mg/DCIA cells.

Experimental details

The experimental details are similar as described elsewhere (6–8).

Results and discussion

Organic compounds used in battery devices are well known for their relatively low conductivity (4, 11), thus heterogeneous electrode reaction takes place primarily at the surface. Supplementary conducting materials which occupy critically desired space and contribute nothing coulometrically is typically required for the preparation of the cathode blends. The case is similar with *N*-halogen organic compounds chosen for this study. We have therefore decided to add a well-known conductor such as acetylene black to prepare our cathode mixes. We then subjected Mg/TCIA cells to a constant current drain of 25 mA to determine their actual capacities with varying amounts of acetylene black. The working voltage of the cell increases with increasing amount of acetylene black. Cell capacities using 10, 20, 30, 40 and 50% acetylene black are 31, 100, 176, 225, and 244 Ah (kg of TCIA)$^{-1}$, respectively. These results are further confirmed by voltage–current measurements. The observed linearity is indicative of the fact that the polarisation is ohmic in nature (Fig. 1). The internal resistance of the cell is 9.72, 6.24, 4.02, 3.41, and 3.00 mΩ for 10, 20, 30, 40, and 50% acetylene black, respectively. The capacity has been found to be maximum in 50% acetylene black at which concentration the internal resistance of acetylene black seems to be the lowest and the water retention property of acetylene black seems to be the highest. The internal resistance of a Mg/TCM cell using 50% acetylene black is found to be 7.34 mΩ. However, for cells with greater than 50% acetylene black, there is negligible difference in cell capacity and internal resistance. Thus 50% is considered an effective and optimum amount of acetylene black for Mg/TCIA and Mg/TCM cells.

The half cell potentials of TCIA and TCM cathodes have been measured separately at various current drains. The open circuit potentials (OCP) of TCIA and TCM are observed to be 1150 and 1030 mV (vs. Ag/AgCl), respectively. These figures are significantly higher than other organic depolarisers, e.g. OCP of *meta*-dinitrobenzene is 120 mV (vs. Ag/AgCl) (6). The higher observed potential of TCIA and TCM cathodes can be attributed to the presence of loosely attached chlorine (i.e. an electron-attracting group) in the ring of the organic compounds.

The electrochemical reactions of TCIA and TCM cells are represented by

[1]Present address: Keiyro Commercial (P) Ltd., No. 173, 5th Cross, IV "B" Block, Koramangala, Bangalore 560 034.

Can. J. Chem. Downloaded from www.nrcresearchpress.com by 203.198.23.82 on 09/08/12
For personal use only.

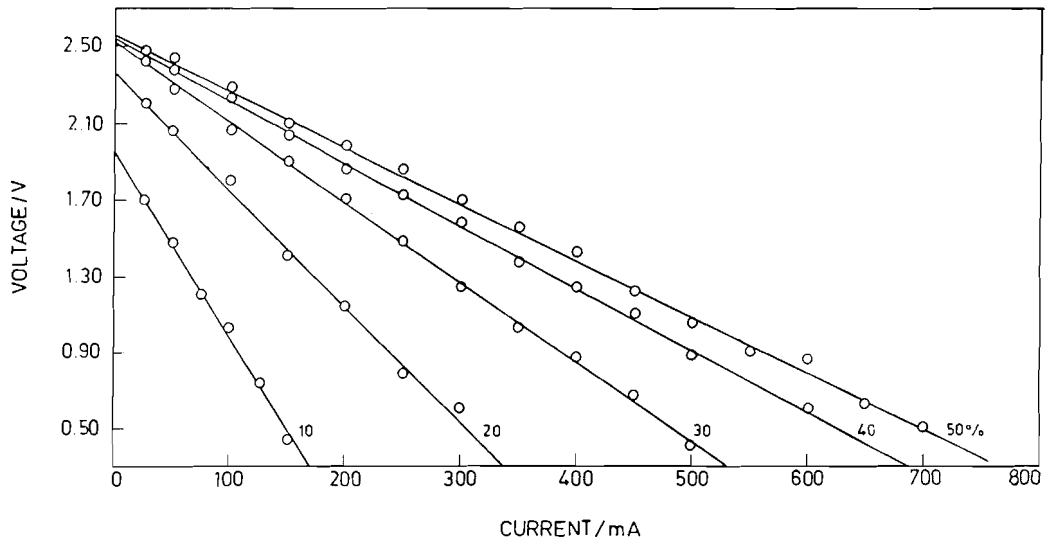

FIG. 1. Voltage–current relationship of Mg/TCIA cell with different percentages of acetylene black.

TABLE 1. Comparative evaluation of Mg/TCIA, TCM, DCIA organic cells (current drain: 25 mA)

Organic cell system	OCV (V)	IR (mΩ)	Capacity (Ah kg^{-1})	Energy density (Wh kg^{-1})	Utilisation efficiency (%)
Mg/TCIA	2.67	3.00	244	488	35.2
Mg/TCM	2.51	7.34	25	43	6.2
Mg/DCIA	2.45	3.65	180	371	43.0

TCIA cathode:

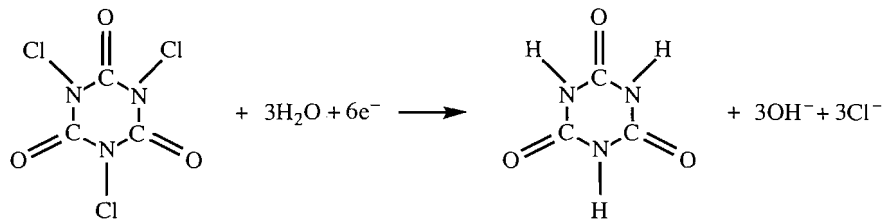

TCM cathode:

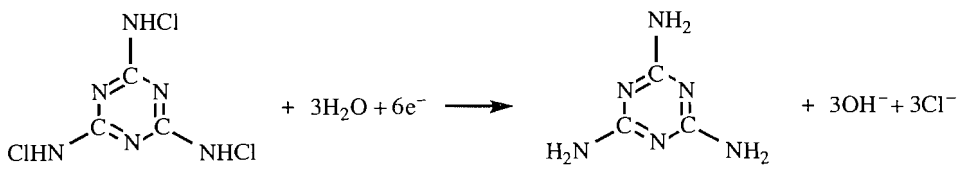

The discharge characteristics of Mg/TCIA and Mg/TCM cells are studied galvanostatically under continuous discharge at various current drains (Fig. 2). The open circuit voltage (OCV) of the cells are 2.67 and 2.51 V for Mg/TCIA and Mg/TCM systems, respectively. The closed circuit voltage (CCV) of Mg/TCIA cells are found to be in the range 2.52–1.90 V when the current drain is varied from 10 to 250 mA. Similarly, in the case of Mg/TCM cells, the CCV at 10, 25, and 50 mA current drains are found to be 2.22, 2.01, and 1.64 V, respectively. It is noticed that a further increase in current drain of Mg/TCM system results in the loss of cell capacity due to an increase in cathode polarisation.

The capacity and energy density of the Mg/TCIA cell systems are shown in Fig. 3. The coulombic efficiency at discharge rates of 10, 25, 50, 75, 100, 125, 150, 200, and 250 mA is found to be 43.4, 35.2, 32.5, 30.8, 28.9, 27.2, 23.6, 19.3, and 12.0%, respectively. The capacity, energy density, and coulombic efficiency for Mg/TCM cells at 10,

Can. J. Chem. Downloaded from www.nrcresearchpress.com by 203.198.23.82 on 09/08/12
For personal use only.

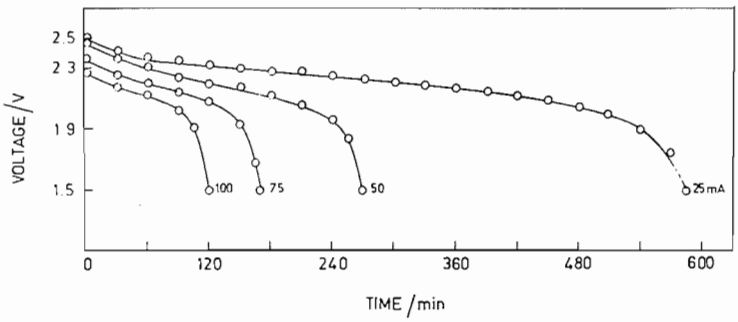

FIG. 2. Effect of current drain on the cell voltage of Mg/TCIA cell.

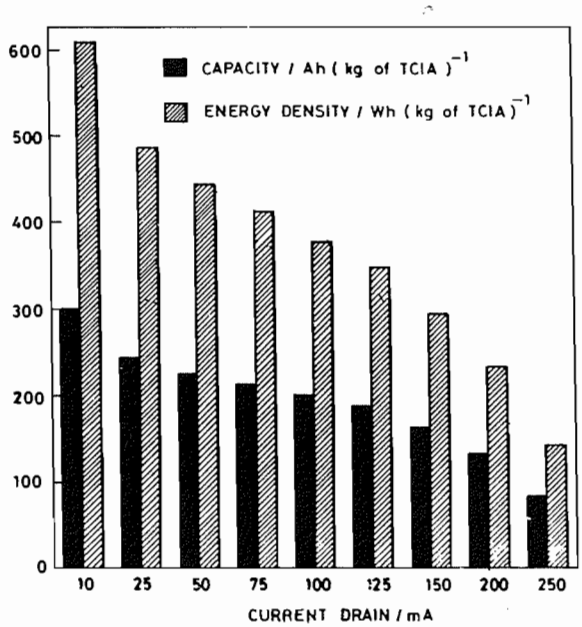

FIG. 3. Experimental histogram of Mg/TCIA cell showing the variation of battery parameters with current drain.

25, and 50 mA are 50, 25, and 17 Ah (kg of TCM)$^{-1}$; 93, 43, and 27 Wh (kg of TCM)$^{-1}$; 7.1, 6.2, and 2.4%, respectively. It is also evident from Fig. 3, that an increase in current drain from 10 to 250 mA brings about a gradual decrease in cell capacity and energy density. These characteristics reveal that a cell can perform more efficiently at lower current drains and also indicate that this cell can find application wherever higher energy density and voltages are basic requirements. Capacity measurements have been carried out on the Mg/DCIA cell system (8) and various battery parameters are compared in Table 1.

The lowest capacity observed in TCM is explained by extensive conjugation of the double bond in between N and —CNHCl, in addition to the electron-donating property of —NHCl group by which the entire —NHCl bond is tightened towards the cyclic ring and hence leads to a maximum stability of the compound. In this case, the electron-donating property of —NHCl is expected to dominate over the electron-withdrawing property of —NCl in TCIA. The maximum stability of TCM could also be attributed to the strong basicity owing to the presence of three nitrogen atoms in the form of N and —NHCl wherein the positive charge on the lone pair of electron on nitrogen atom is comparatively more intact. Hence, a change from —NHCl to —NH_2 is difficult and therefore less capacity is realised in TCM-based cells.

In the case of TCIA, the release of Cl is expected to be relatively easier in comparison with TCM primarily due to a loose bonding between N and Cl in the former compound. This is mainly attributed to the field effect caused by the influence of ion pairs of the electrons of the two atoms, viz. Cl and O, through space interactions which change the vibrational frequency of both atoms (or groups). In this case, an electrostatic repulsion takes place between the nonbonding electrons of oxygen and chlorine, causing a change in the hybridisation state of —CO group and enabling it to repel from the plane of the double bond. Moreover, the three N atoms (—NCl) have positive charge due to the adjacent presence of a highly electrophilic carbonyl group. Hence, the —NCl group can be easily reduced when compared to TCM (—NHCl). Because of these reasons, TCIA cells have realised higher capacity than the TCM-based systems. The presence of one additional —NCl reducible group in TCIA, compared with two additional —NCl groups in DCIA might account for the maximum capacity of cells using the former compound.

Conclusions

A concentration of 50% acetylene black is found to be optimum for TCIA and TCM cathodes. The OCP of TCIA and TCM cathodes are found to be 1150 and 1030 mV (vs. Ag/AgCl), respectively. Similarly, the open circuit (>2.5 V) and working voltages (>2.0 V) are much higher in comparison with known Mg/*meta*-dinitrobenzene cell systems (i.e., OCV: 1.5; CCV: 1.0 V). These type of new cell systems can also find application wherever higher energy density and voltages are considered basic factors for the application. These organic depolarisers are non-toxic (7) and are thus acceptable materials in the battery industry. The meterological department uses Mg/Cu_2Cl_2 system to monitor climatic conditions. Because of their higher voltage and higher capacity, Mg/*N*-halogen organic systems are useful materials or substitutes in Mg/AgCl (or $PbCl_2$, Cu_2Cl_2) cells for the appropriate applications.

Acknowledgement

The authors are grateful to Professor G.V. Subba Rao, Director, CECRI, Karaikudi for his support.

1. C.K. Morehouse and R. Glicksman. J. Electrochem. Soc. **105**, 299 (1958); **105**, 306 (1958).
2. C.K. Morehouse and R. Glicksman. U.S. Patent 2,880,122, 1959.

Can. J. Chem. Downloaded from www.nrcresearchpress.com by 203.198.23.82 on 09/08/12
For personal use only.

3. J.C. Pawlak. Organic depolarisers primary batteries, Technical Report, ECOM-2753, Progress Report I. 1976.
4. N.C. Cahoon. Primary batteries. Vol. II. Wiley, New York. 1976.
5. P.L. Howard. J. Electrochem. Soc. **99**, 206c (1952).
6. R. Udhayan. Ph.D. Thesis, Madurai Kamaraj University, Madurai, India. 1991.
7. D.P. Bhatt and R. Udhayan. Indian Pat. 749/DEL/91.
8. D.P. Bhatt, S. Karthikeyan, and R. Udhayan. J. Electrochem. Soc. **139**, 3019 (1992).
9. R. Udhayan and D.P. Bhatt. J. Power Sources, **39**, 323 (1992).
10. R. Udhayan and D.P. Bhatt. J. Appl. Electrochem. 1, 23, 393 (1993).
11. F. Gutman and L.E. Lyons. Organic semi-conductors. Wiley, New York. 1967.

Can. J. Chem. Downloaded from www.nrcresearchpress.com by 203.198.23.82 on 09/08/12
For personal use only.

Kinetics and mechanism of oxidation of hydroxylamine by hexachloroiridate(IV) ion in buffer solutions

MS. REKHA, ADITYA PRAKASH, AND RAJ N. MEHROTRA[1]
Department of Chemistry, University of Jodhpur, Jodhpur 342 005, India

Received June 23, 1993

MS. REKHA, ADITYA PRAKASH, and RAJ N. MEHROTRA. Can. J. Chem. **71**, 2164 (1993).

The oxidation of hydroxylammonium ion by $[IrCl_6]^{2-}$ ion in acetic acid – acetate buffer solutions, studied by stopped flow, has the stoichiometric ratio $\Delta[IrCl_6]^{2-}/\Delta[NH_2OH] = 1$. The oxidation involves the species $[IrCl_6]^{2-}$ and NH_3OH^+ although spectral analysis of the spent reaction mixture indicates $[IrCl_5(OH_2)]^{2-}$ to be the main product (almost to the extent of 80%). This anomaly arises because of the aquation of the reduced product $[IrCl_6]^{3-}$. The rate is retarded both by H^+ and Cl^- ions and the plots of k_2^{-1} against respective concentrations are linear. The proposed mechanism is given by reactions [*i*]–[*v*].

$$[i] \quad NH_3OH^+Cl^- \underset{}{\overset{K_{ipd}}{\rightleftharpoons}} NH_3OH^+ + Cl^-$$

$$[ii] \quad IrCl_6^{2-} + NH_3OH^+ \underset{k_{-1}}{\overset{k_1}{\rightleftharpoons}} [IrCl_6(NH_2OH)]^{2-} + H^+$$

$$[iii] \quad [IrCl_6 \cdot NH_2OH]^{2-} \underset{k_{-et}}{\overset{k_{et}}{\rightleftharpoons}} [IrCl_6^{3-} \ldots NH_2OH^{\cdot +}]$$

$$[iv] \quad [IrCl_6^{3-} \ldots NH_2OH^{\cdot +}] \underset{k_{-d}}{\overset{k_d}{\rightleftharpoons}} [IrCl_6]^{3-} + NH_2OH^{\cdot +}$$

$$[v] \quad 2NH_2OH^{\cdot +} \xrightarrow{\text{fast}} N_2 + 2H_2O + 2H^+$$

The values of the rate constants at 25°C are as follows: $k_1 = 147$ dm^3 mol^{-1} s^{-1} and $10^2 k_{et}K_{ia} = 2.8$ s^{-1}. The related activation parameters are $\Delta H^{\ddagger}_{k_1} = 29 \pm 2$ kJ mol^{-1}, and $\Delta S^{\ddagger}_{k_1} = -115 \pm 6$ J K^{-1} mol^{-1} and, $\Delta H^{\ddagger}_{k_{et}K_{os}} = 15 \pm 2$ kJ mol^{-1} and $\Delta H^{\ddagger}_{k_{et}K_{os}} = -233 \pm 3$ J K^{-1} mol^{-1}, respectively. The value of K_{ipd} is 2.91 ± 0.03 mol dm^{-3} and that of K_{ipa} ($= 1/K_{ipd}$) is 0.344 ± 0.004 dm^3 mol^{-1}; both values are almost independent of temperature.

MS. REKHA, ADITYA PRAKASH et RAJ N. MEHROTRA. Can. J. Chem. **71**, 2164 (1993).

L'oxydation de l'ion hydroxyammonium par l'ion $[IrCl_6]^{2-}$ dans des solutions tamponnées d'acétate et d'acide acétique a été étudiéc par la technique du flux stoppé a un rapport stoechiométrique $\Delta [IrCl_6]^{2-}/\Delta[NH_2OH] = 1$. L'oxydation implique les espèces $[IrCl_6]^{2-}$ et NH_3OH^+ même si l'analyse spectrale du mélange réactionnel résiduel indique que le produit principal de la réaction (pratiquement 80%) est l'ion $[IrCl_5(OH_2)]^{2-}$. Cette anomalie est due à l'aquation du produit réduit, le $[IrCl_6]^{3-}$. La vitesse de la réaction est retardée par les ions H^+ ainsi que Cl^- et les courbe de k_2^{-1} en fonction des concentrations sont linéaires. Le mécanisme proposés est représenté par les équations (*i*)–(*v*) :

$$[i] \quad NH_3OH^+Cl^- \underset{}{\overset{K_{ipd}}{\rightleftharpoons}} NH_3OH^+ + Cl^-$$

$$[ii] \quad IrCl_6^{2-} + NH_3OH^+ \underset{k_{-1}}{\overset{k_1}{\rightleftharpoons}} [IrCl_6(NH_2OH)]^{2-} + H^+$$

$$[iii] \quad [IrCl_6 \cdot NH_2OH]^{2-} \underset{k_{-et}}{\overset{k_{et}}{\rightleftharpoons}} [IrCl_6^{3-} \ldots NH_2OH^{\cdot +}]$$

$$[iv] \quad [IrCl_6^{3-} \ldots NH_2OH^{\cdot +}] \underset{k_{-d}}{\overset{k_d}{\rightleftharpoons}} [IrCl_6]^{3-} + NH_2OH^{\cdot +}$$

$$[v] \quad 2NH_2OH^{\cdot +} \xrightarrow{\text{rapide}} N_2 + 2H_2O + 2H^+$$

Les valeurs des constantes de vitesse à 25°C sont : $k_1 = 147$ dm^3 mol^{-1} s^{-1} et $10^2 k_{et}K_{ia} = 2.8$ s^{-1}. Les paramètres d'activation apparentés sont respectivement $\Delta H^{\ddagger}_{k_1} = 29 \pm 2$ kJ mol^{-1} et $\Delta S^{\ddagger}_{k_1} = -115 \pm 6$ J K^{-1} mol^{-1} et $\Delta H^{\ddagger}_{k_{et}K_{os}} = 15 \pm 2$ kJ mol^{-1} et $\Delta S^{\ddagger}_{k_{et}K_{os}} = -233 \pm 3$ J K^{-1} mol^{-1}. La valeur de K_{ipd} est égale à $2,91 \pm 0,03$ mol dm^{-3} et celle de K_{ipa} ($= 1/K_{ipd}$) est égale à $0,344 \pm 0,004$ mol dm^{-3}; les deux valeurs sont pratiquement indépendantes de la température.

[Traduit par la rédaction]

Introduction

Hydroxylamine is an intermediate in the enzymatic oxidation of ammonia to nitrite and (or) nitrate or in the reverse reduction of these ions to ammonia (1). This and the fact that it acts both as an oxidizing and reducing agent with transition metals and their complexes has stimulated a keen interest in investigating its redox and ligand properties (2). Amongst several oxidations, the oxidation by hexachloroiridate(IV) ion in the presence of perchloric acid has been studied (3). The rate, studied in low $[HClO_4]$ (0.01–0.15 mol dm^{-3}), showed an inverse dependence on $[H^+]$, and k_{obs} $[H^+]$ was constant. The simple two-step mechanism considered the formation of an $[IrCl_6(NH_2OH)]^{2-}$ complex in an equi-

[1]Author to whom correspondence may be addressed. Reprints are not available.

Can. J. Chem. Downloaded from www.nrcresearchpress.com by 203.198.23.82 on 09/08/12
For personal use only.

librium step prior to its disproportionation to $[IrCl_6]^{3-}$ and NHOH' free radical in the rate-determining step. The rate was found to become complex at $[HClO_4] > 0.15$ mol dm^{-3} and the reason was attributed to the probable formation of $[HIrCl_6]^-$. However, $[IrCl_6]^{2-}$ is considered to have a negligible base strength and is therefore unlikely to be protonated (4). The interesting feature was the detection and estimation of $[IrCl_5(OH_2)]^{2-}$ (<10%) in the spent reaction mixtures but no explanation for its probable formation was given.

The redox chemistry of NH_2OH with transition metals in solution is complicated. A variety of oxidation products, viz., N_2, N_2O, NO, NO_2, NO_2^-, or NO_3^-, depending on the fate of the $H_2NO\cdot$ radical that undergoes reactions [1]–[3], are formed under different conditions (2). Reaction [3] is the dimerization of $HNO\cdot$ to hyponitrous acid (5), which exists in *cis* and *trans* forms. The *trans* form, more stable than the *cis* form, decomposes into N_2O (6). In the case of strong oxidants such as Mn^{3+}(aq) and Ag^{2+}(aq) (7), the free radical is oxidized to NO_3^- by excess oxidant. The formation of the $H_2NO\cdot$ radical in oxidations by one-electron oxidants has been demonstrated by esr spectroscopy (8).

[1] $NH_2O\cdot \rightarrow 0.5N_2 + H_2O$

[2] $H_2NO\cdot \rightarrow HNO + H^+ + e^-$

[3] $2HNO \rightarrow H_2N_2O_2 \rightarrow N_2O + H_2O$

This study was, therefore, undertaken in the pH range 3.42–5.23 (acetic acid – sodium acetate buffer) to check if NH_2OH, which could be easily produced as a result of increased dissociation of NH_3OH^+ at such low $[H^+]$, happened to be reactive and whether $[IrCl_5(OH_2)]^-$ is the reactive Ir(IV) entity in view of the fact that $[IrCl_5(OH_2)]^{2-}$ was reported to be one of the oxidation products (3). We were further inclined to investigate whether the reaction proceeded through an Ir(IV)–hydroxylamine complex, and the same could be substantiated by a rapid-scan technique that might help to characterize its character as an *outer* or *inner* sphere. Preliminary studies indicated that the rates are retarded by H^+ and Cl^- ions; retardation by the latter ion was observed for the first time in an Ir(IV) oxidation although an acceleration of the rate in hydrazine oxidations by Ir(IV) (9) and $[Fe(CN)_6]^{3-}$ (10) was reported without any explanation being given.

Experimental

Fresh solutions of Ir(IV), using either H_2IrCl_6 (Soekawa Chemicals) or $Na_2IrCl_6\cdot 6H_2O$ (JM), were standardized spectrophotometrically (Shimadzu 240 Graphicord) using $\epsilon_{488} = 4050$ dm^3 mol^{-1} cm^{-1} (11) and were used within a few hours. Solutions of hexachloroiridate(III) (JM) were similarly prepared and standardized using $\epsilon_{358} = 74$ dm^3 mol^{-1} cm^{-1}) (12). However, we could more closely reproduce the ϵ_{460} literature value of 2080 dm^3 mol^{-1} cm^{-1} (12), more often, in a given sample in which ϵ_{488} showed considerable variation from the literature value of 4075 ± 25 dm^3 mol^{-1} (see Spectrophotometry section).

Solutions of hydroxylamine hydrochloride (E. Merck, puriss), prepared in distilled water purged with nitrogen, were standardized bromometrically (13). Solutions of lithium and sodium perchlorate were prepared by neutralizing lithium hydroxide (G.F. Smith) and sodium carbonate (E. Merck, GR) by perchloric acid. The solutions were cooled, the pH was adjusted to 7, and the concentration was determined by evaporating the water from weighed aliquots and drying to a constant weight. The buffer solutions of desired pH values were prepared by mixing solutions of sodium acetate (E. Merck, GR) and E. Merck's GR acetic acid (14) ($[CH_3COO^-] = 0.06$ mol dm^{-3}) and the pH was checked with a pH meter. While adjusting the ionic strength (I), CH_3COONa was assumed to be completely ionized.

One of the reviewers has drawn our attention to the catalysis by trace levels of Cu^{2+} ion (15); moreover, addition of Fe^{2+} at the level of 10^{-4} mol dm^{-3} is stated to accelerate the rates by more than a factor of 1000. Although the samples were not purified and were used as received, we feel in the light of observed linear correlations between the respective rate and concentration that these samples did not contain any Cu^{2+} or Fe^{2+} ions as impurity, at least at levels that could affect the rates.

Twice-distilled water, once from alkaline permanganate from an all-glass still, was purged with nitrogen before use.

Spectrophotometry

The uv–visible spectra of the various solutions, described below, were recorded using an HP8452 diode array spectrophotometer having a band width of 2 nm and using an integration time of 1 s. The reference in each case was a water solution having the other constituents of the same concentration. Although the spectra were recorded between 190 and 820 nm, the spectra in each of the various figures are shown over the relevant range of wavelength. The $[IrCl_6]^{2-}$ sample was about 3–4 months old.

A 25 mL stock solution of Ir(IV) was prepared by weighing 0.044 g (0.00314 mol dm^{-3}) of a $Na_2IrCl_6\cdot 6H_2O$ (JM) sample in $[HClO_4] = 1$ mol dm^{-3}. The spectrum of the diluted solution (1.57×10^{-4} mol dm^{-3}) in 3 mol dm^{-3} perchloric acid showed an absorbance of 0.497 and 0.263 at 488 (λ_{max}) and 460 (λ_{min}) nm, respectively, from which $\epsilon_{488} = 3163$ and $\epsilon_{460} = 1678$ dm^3 mol^{-1} cm^{-1} were calculated. These values, smaller than those obtained for a solution similarly diluted with chlorine-saturated perchloric acid of the same concentration (see below), indicate that the sample had some $[IrCl_6]^{3-}$ as the impurity. The fact that the characteristic peak of $[IrCl_6]^{3-}$ at 358 nm was not observed could well be due to its relatively small concentration present as impurity and to the small value of ϵ_{358}, 74 dm^3 mol^{-1} cm^{-1} (12*b*). The absorbance of the solution deteriorated slightly after 24 h.

The visible spectrum of a similarly diluted stock solution in chlorine-saturated perchloric acid (3 mol dm^{-3}) is shown in Fig. 1. The reference solution was 3 mol dm^{-3} perchloric acid saturated with chlorine. The absorbance at 488 and 460 nm was 0.554 and 0.328, respectively, giving $\epsilon_{488} = 3525$ against 4050 and $\epsilon_{460} = 2086$ against 2080 dm^3 mol^{-1} cm^{-1} (12*a*). The increase in the absorbance at both wave lengths could be ascribed to the oxidation of $[IrCl_6]^{3-}$, present as an impurity, by chlorine. The extent of $[IrCl_6]^{3-}$ present as impurity, calculated on the basis of the amount of the sample weighed and calculated on the basis of the ϵ_{488} value, is about 13%.

The $\epsilon_{460} = 2086$ dm^3 mol^{-1} cm^{-1}, closer to the literature value, was obtained more often, whereas a significant difference in the ϵ_{488} value existed in the same sample, for which we have no explanation at the moment. One of the reviewers felt that hydrolysis of Ir(IV) chloride could be the probable reason for the discrepancy. Although it was not investigated by us, the fact that the acidic $[IrCl_6]^{2-}$ solutions were spectrophotometrically shown to be stable for at least 7 days (4) negates such a possibility.

Next, the reaction mixture ($10^4[IrCl_6^{2-}] = 3.14$, $10^4[NH_3OH^+] = 4$, and $[HClO_4] = 1$ mol dm^{-3}) was left overnight for completion as the reaction was slow at this $[H^+]$ value. The spectrum of a twice-diluted reaction mixture in $[HClO_4] = 3$ mol dm^{-3} had a peak at 342 nm and an absorbance = 0.0227. The peak probably corresponds to $[IrCl_5(OH_2)]^{2-}$, which has a λ_{max} at 347 nm (12*a*). The peak at 358 nm corresponding to $[IrCl_6]^{3-}$ was not obtained. This indicates that the expected $[IrCl_6]^{3-}$ was aquated and converted to $[IrCl_5(OH_2)]^{2-}$, since the specific rate of aquation of $[IrCl_6]^{3-}$ is ca. 400 times that of $[IrCl_6]^{2-}$ at 50°C (11).

The spectral characters of $[IrCl_6]^{3-}$ and $[IrCl_5(OH_2)]^{2-}$ are very similar, making it difficult to distinguish one from the other. The spectra of the corresponding Ir(IV) species are, however, differ-

Can. J. Chem. Downloaded from www.nrcresearchpress.com by 203.198.23.82 on 09/08/12
For personal use only.

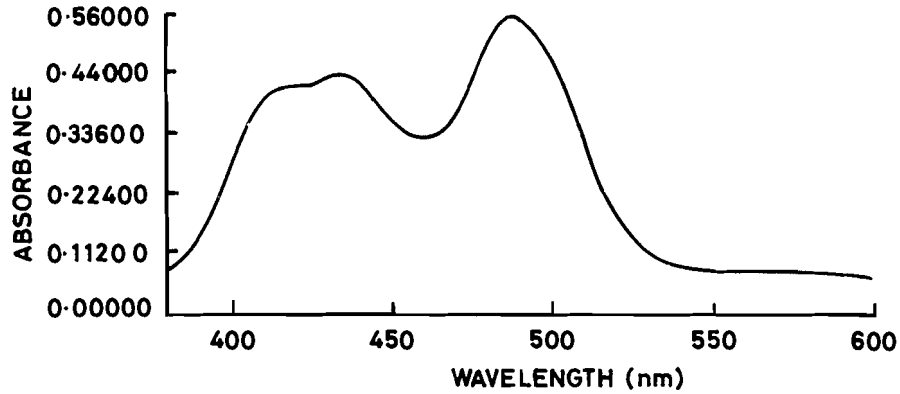

FIG. 1. The visible spectrum of 10^4[Ir(IV)] = 1.57 mol dm^{-3} treated with a calculated volume of chlorine-saturated perchloric acid to give a solution in 3 mol dm^{-3} perchloric acid. The reference solution was 3 mol dm^{-3} chlorine-saturated perchloric acid.

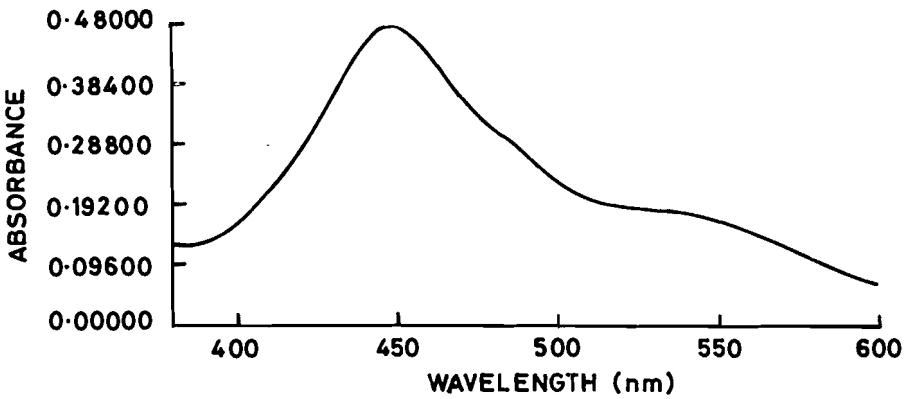

FIG. 2. The spectrum of the spent reaction mixture diluted with an equal volume of chlorine-saturated perchloric acid. The initial concentrations present in the diluted reaction mixture were $10^4[IrCl_6^{3-}]$ = 1.57 and $[HClO_4]$ = 3 mol dm^{-3}, along with unreacted hydroxylamine.

Can. J. Chem. Downloaded from www.nrcresearchpress.com by 203.198.23.82 on 09/08/12
For personal use only.

ent. Since Ir(III) complexes are rapidly and quantitatively oxidized to the corresponding Ir(IV) complexes by chlorine (11), the spent reaction mixture was oxidized with perchloric acid saturated with chlorine. The details are given below.

The spent reaction mixture was twice diluted with chlorine-saturated perchloric acid ($\simeq$ 3 mol dm^{-3}). The reference was a solution of the same perchloric acid of the same strength. The spectrum of this solution, Fig. 2, showed a peak absorbance of 0.477 at 448 nm, which is same as the known λ_{max} at 450 nm for $[IrCl_5(OH_2)]^-$ (12). Using ϵ_{450} = 3320 dm^3 mol^{-1} cm^{-1}, the $[IrCl_5(OH_2)^-]$ was calculated to be 1.44 × 10^{-4} mol dm^{-3}, indicating that it is present to the extent of almost 92% of the initial $[IrCl_6^{2-}]$. And this includes the conversion of 13% of $[IrCl_6]^{3-}$ present as impurity in the sample.

Rapid scan of the reaction mixture

The successive rapid-scan spectra of the reaction mixture, recorded using 482 nm as the central wavelength on an Union–Giken RA-415 stopped-flow spectrophotometer with an interval (the time lapsing between the two consecutive scans) of zero time and a gate time (time taken to complete the scan) of 2 ms, are shown in Fig. 3. The reference was a spent reaction mixture allowed to remain in the mixing cell of the stopped-flow instrument for a period much greater than 9 half-lives of the reaction. The scan (–O–O–O–) corresponds to pure $[IrCl_6]^{2-}$. It is to be noted that the absorbance of the scan recorded after 4 ms of mixing was greater than that of the pure solution. The absorbance of the successive scans, recorded at time intervals of 8, 12, 16, 20, 26, and 32 ms, decreased and tended to reach a saturation value. That the gradual decrease in the absorbance, indicative of the formation of new species believed to be an *outer*-sphere complex, is not due to the decrease of $[IrCl_6^{2-}]$ used in oxidizing of hydroxylamine during the period of measurement is supported by the rate constant at much higher $[NH_3OH^+]$. The equilibrium for the complex formation is probably attained in about 32 ms when the absorbance assumes a constant value.

Kinetic measurements

The kinetics were studied in acetate buffer under pseudo-first-order conditions ($[NH_2OH] \geqq 10[IrCl_6^{2-}]$) at constant ionic strength (I) maintained with $NaClO_4$. The solutions of NH_3OH^+ in the desired buffer and of Ir(IV), taken separately in the stock cylinders of the Union–Giken RA-401 stopped-flow spectrophotometer, were brought to thermal equilibrium at the desired temperature (±0.1°C). The temperature was maintained by circulating water from a Haake D8G refrigerated circulatory water bath. The instrument has a dead time of about 0.5 ms for a 2 mm flow cell. The rate was followed in terms of disappearance of $[IrCl_6]^{2-}$ at 488 nm, at which wavelength other components of the reaction mixture are transparent. The averaged volt–time curves, at least from 10–12 runs, were analysed for the values of the pseudo-first-order rate constant, k_{obs}, by an in-built program in the computer used for collecting the data. The reproducibility was within ±5%.

Test for free radical

The reactant solutions were purged with nitrogen and 1 mL of acrylonitrile was added to each solution. No polymerization of the monomer was noted over ca. 5–10 min. However, a curdy white

Can. J. Chem. Downloaded from www.nrcresearchpress.com by 203.198.23.82 on 09/08/12
For personal use only.

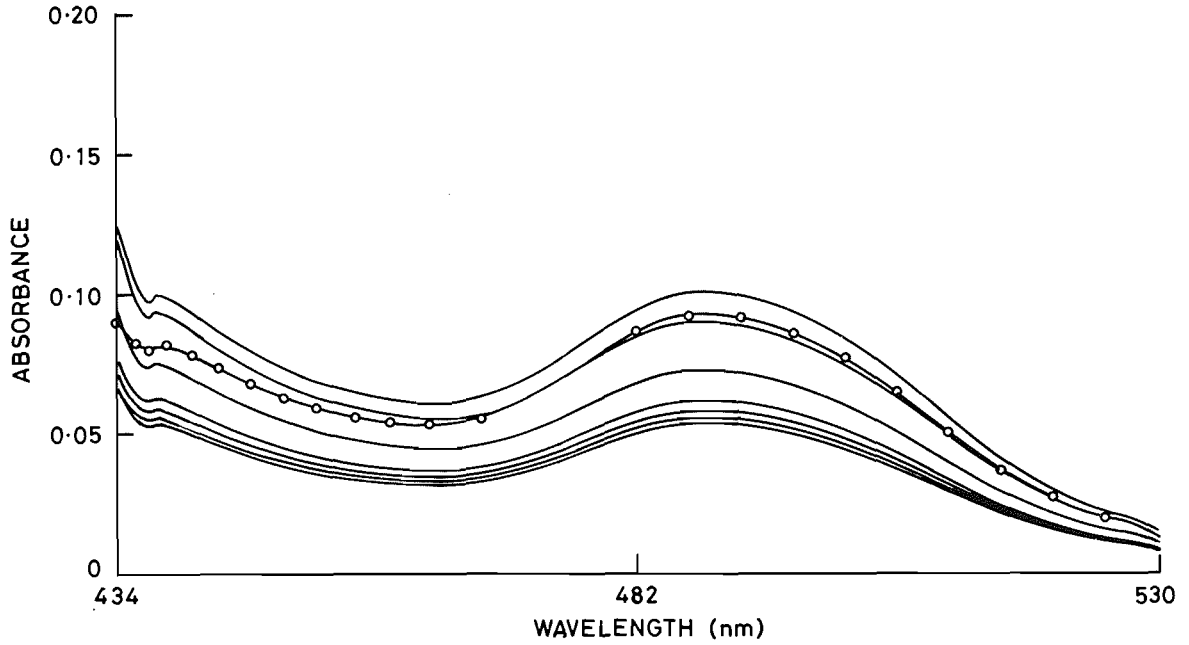

FIG. 3. The rapid-scan spectrum of the reaction mixture having $10^5[IrCl_6^{2-}] = 2.5$, $10^5[NH_3OH^+] = 5.0$ mol dm^{-3}, pH 4.27, and 20°C. The spectrum (–○–○–○–) corresponds to pure $[IrCl_6]^{2-}$ solution of the same concentration (absorbance = 0.0925, hence calculated ϵ = 3700 dm^3 mol^{-1} cm^{-1}). The solid line spectra, top to bottom, were recorded at the beginning of 4, 8, 12, 16, 20, 26, and 32 ms after mixing.

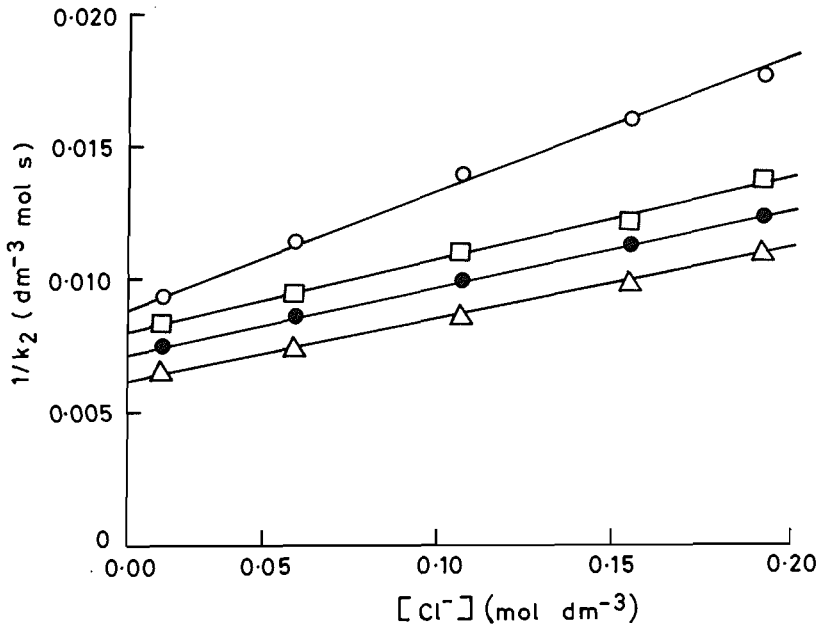

FIG. 4. Plots of k_2^{-1} vs. $[Cl^-]$ at temperatures 25°C (○), 30°C (□), 35°C (●) and 40°C (△). ($10^4[Ir(IV)] = 1.0$, $10^3[NH_3OH^+] = 1.0$, $[Na^+] = 0.4$, and $I = 0.4$ mol dm^{-3}).

precipitate appeared on mixing the two solutions, indicating the formation of a free radical in the reaction mixture.

Results

Stoichiometry

The stoichiometry is dependent upon the concentrations of the reactants. The $\Delta[IrCl_6^{2-}]/\Delta[NH_3OH^+]$ increased from 1.03 ± 0.04 to 2.13 ± 0.07 with decreasing $[NH_3OH^+]$ (Table S1[2]). The results could be expressed by the stoichiometric equations [4] and [5] under the two conditions.

[4] $$2[IrCl_6]^{2-} + 2NH_3OH^+ \rightarrow 2[IrCl_6]^{3-} + N_2 + 2H_2O + 4H^+$$

[5] $$4[IrCl_6]^{2-} + 2NH_3OH^+ \rightarrow 4[IrCl_6]^{3-} + N_2O + H_2O + 6H^+$$

TABLE 1. The effect of variation of pH on the rate constant k_2 (= $k_{obs}/[NH_2OH]$) at different temperatures[a]

	k_2(dm^3 mol^{-1} s^{-1})							
	25°C		30°C		35°C		40°C	
pH	Obsd.	Calcd.	Obsd.	Calcd.	Obsd.	Calcd.	Obsd.	Calcd.
3.42	49.1	49.3	55.9	55.9	63.7	63.3	70.9	70.9
3.72	74.3	73.5	83.3	84.0	97.1	97.1	111	110
4.27	113	115	132	131	152	159	185	182
4.45	124	124	141	143	172	172	200	196
4.80	135	137	154	156	188	192	222	217
4.99	139	140	159	161	201	196	232	227
5.23	145	143	164	164	213	204	244	232

[a]$10^4[IrCl_6^{2-}] = 1.0$, $10^3[NH_2OH] = 1.0$, $I = 0.3$ mol dm^{-3}.

A variable stoichiometry as a function of excess [oxidant] is known for one-electron oxidants (8, 9, and 16). Since the primary interest in the kinetics is the characterization of the initial product, the rates were measured in excess of $[NH_3OH^+]$, limiting the study represented by eq. [4].

Kinetic measurements were made over a broad range of [Ir(IV)] to confirm first-order dependence in [Ir(IV)]. The rate increased proportionately with $[NH_3OH^+]$ at different pH, and the plots of k_{obs} vs. $[NH_3OH^+]$ were linear, passing through the origin. The slope ($k_{obs}/[NH_3OH^+]$ of the plot is taken as the measure of k_2, the second-order rate constant. The k_{obs} was unaffected by the outside addition of $[IrCl_6]^{3-}$ (Table S2[2]). It was noted that changing the ratio of CH_3COOH and CH_3COO^- in the buffer did not affect the rate. The k_{obs} was independent of $[LiClO_4]$ but increased by 23% when $NaClO_4$ was increased by almost fivefold (Table S3[2]). The increase in the rate is, perhaps, due to medium effects of the sodium ion. The medium effect is an important factor in redox and substitution reactions (17), and is usually not so marked for intramolecular redox reactions (18).

The effect of $[Cl^-]$ on k_{obs} (Table S4[2]), was studied at constant $[Na^+] = 0.4$ mol dm^{-3}, being the sum total concentrations of NaCl, $NaClO_4$, and CH_3COONa present in the reaction mixture, to avoid variations in the rate due to the medium effects of the ion by using mixtures of NaCl and $NaClO_4$. Since the ionic strength and $[Na^+]$ are constant and $[ClO_4^-]$ has no effect on the rate, the decrease in the rate is considered to be due to chloride ions. At the suggestion of one of the referees, the effect of $[Cl^-]$ on the rate was briefly checked using mixtures of LiCl and $LiClO_4$. These results confirmed that the inhibition of the rate was due to the Cl^- ions. The linear plots of k_2^{-1} against $[Cl^-]$ have intercepts on the rate ordinate at each temperatures (Fig. 4). The data in Tables S1–S4 are presented as supplementary material.[2]

Dependence on pH

The effect of pH variation on the rate at different temperatures is given in Table 1. The values of k_2 increase with the pH. The plots of k_2^{-1} vs. $[H^+]$ are linear with positive intercepts on the rate ordinate at different temperatures (Fig. 5).

Thus the empirical rate law for the dependence of both $[H^+]$ and $[Cl^-]$ is expressed by eq. [6].

$$[6] \qquad k_2 = \frac{a}{b[X] + d}$$

where X represents H^+ and Cl^- ions.

Discussion

The evidence, provided by the inertness of $[IrCl_6]^{2-}$ to substitution,[3] the stoichiometry, the induced polymerization of acrylonitrile, and the empirical rate law, can be simply explained by an *outer*-sphere mechanism in which the intermediate $NH_2OH^{\cdot+}$ is not oxidized further by the deficient Ir(IV) present in the reaction mixture. The lack of rate dependence on [Ir(III)] indicates that it does not appear on the product side of any equilibrium involved, either at the rate-determining step or at any step preceding it.

The rate is retarded by both Cl^- and H^+ ions in an identical manner. It suggests the existence of equilibria in which these ions appear on the product side. For chloride ion, such an equilibrium could be as in eq. [7]:

$$[7] \qquad [IrCl_6]^{2-} + NH_3OH^+ \rightleftharpoons [IrCl_5(NH_3OH)] + Cl^-$$

However, the formation of an *inner*-sphere complex, $[IrCl_5(NH_3OH)]$, is considered improbable because $[IrCl_6]^{2-}$ is substitution inert (19). The retarding effect of Cl^- ion could therefore be attributed to either of the equilibria shown in eqs. [8] and [9] where $NH_3OH^+Cl^-$ is an ion-pair. These two equilibria offer scope for proposing two different mechanisms, each leading to a rate law that is consistent with the empirical rate law in eq. [6]. The mechanism based on equilibrium [8] will be discussed in detail whereas the mechanism based on equilibrium [9], in which $[IrCl_5(OH_2)]^-$ would react with NH_3OH^+ as in reaction [13], is less likely, in view of the fact that the spectra of freshly prepared solutions and those aged for 24 h are the same, indicating that

[2]Tables of supplementary data (Tables S1–S4) can be purchased from: The Depository of Unpublished Data, Document Delivery, CISTI, National Research Council Canada, Ottawa, ON K1A OS2, Canada.

[3]It means that substitution is not complete in less than 1 min. See ref. 10. Hence the formation of such an *inner*-sphere complex for a reaction taking place on the stopped-flow time scale is simply inadmissible.

Can. J. Chem. Downloaded from www.nrcresearchpress.com by 203.198.23.82 on 09/08/12
For personal use only.

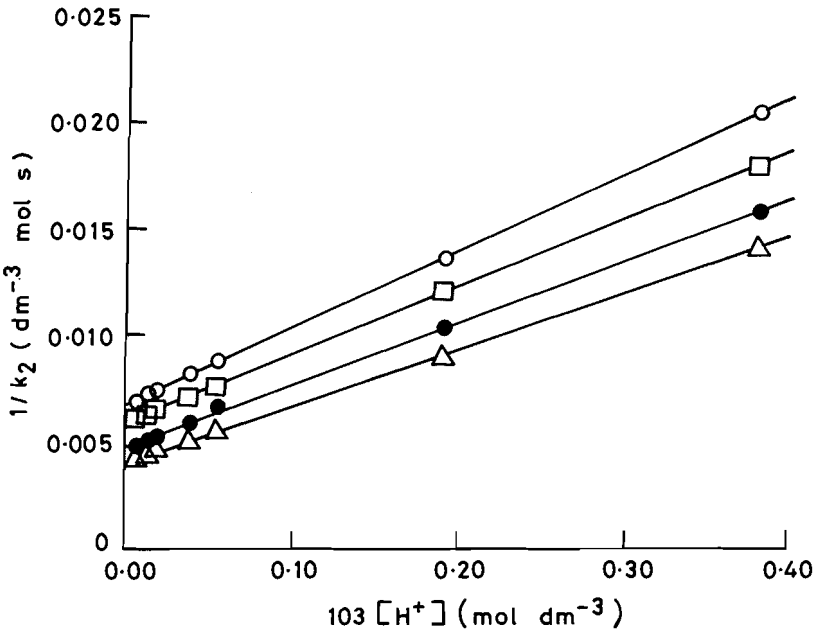

FIG. 5. Plots of k_2^{-1} vs. $[H^+]$ at 25°C (○), 30°C (□), 35°C (●), and 40°C (△). (10^4[Ir(IV)] = 1.0, 10^3[NH_3OH^+] = 1.0, and I = 0.3 mol dm^{-3}).

no species other than $[IrCl_6]^{2-}$ was initially present in the solution.

[8] $NH_3OH^+Cl^- \rightleftharpoons NH_3OH^+ + Cl^-$

[9] $[IrCl_6]^{2-} + H_2O \rightleftharpoons [IrCl_5(OH_2)]^- + Cl^-$

With support from the rapid-scan spectrum for the formation of an *outer*-sphere complex, the following mechanism is postulated. It might be mentioned that a chloride-bridged intermediate $[IrCl_5ClSO_3]^{4-}$, analogous to a cyanide-bridged intermediate $[Fe(CN)_5CNSO_3]^{5-}$ (19), was suggested in the Ir(IV) oxidation of sulphite ion (4). The formation of the intermediate was confirmed in a recent reinvestigation of the reaction (20). The formation of an *outer*-sphere complex is further probable on the basis of the analogy that the sulfur atom in SO_3^{2-} and the nitrogen atom in NH_2OH each have an s^2 pair of unshared electrons, and $[IrCl_6]^{2-}$ and $[Fe(CN)_6]^{3-}$ each have one unpaired d electron.

[8] $NH_3OH^+Cl^- \overset{K_{ipd}}{\rightleftharpoons} NH_3OH^+ + Cl^-$

[13] $[IrCl_6]^{2-} + NH_3OH^+ \underset{k_{-1}}{\overset{k_1}{\rightleftharpoons}} [IrCl_6NH_2OH]^{2-} + H^+$

[14] $[IrCl_6NH_2OH]^{2-} \underset{k_{-et}}{\overset{k_{et}}{\rightleftharpoons}} [IrCl_6^{3-}\ldots NH_2OH^{\cdot+}]$

[15] $[IrCl_6^{3-}\ldots NH_2OH^{\cdot+}] \underset{k_{-d}}{\overset{k_d}{\rightleftharpoons}} [IrCl_6]^{3-} + NH_2OH^{\cdot+}$

[16] $2NH_2OH^{\cdot+} \xrightarrow{\text{fast}} N_2 + 2H_2O + 2H^+$

where K_{ipd} is the equilibrium constant for the dissociation of the $NH_3OH^+Cl^-$ ion pair, K_{os} ($= k_1/k_{-1}$) is the equilibrium constant for the formation of the outer-sphere complex $[IrCl_6NH_2OH]^{2-}$, k_{et} is the rate constant for the electron transfer within the outer-sphere complex, and k_d is the rate constant for the dissociation of the product after the electron transfer. Reaction [16], with an excess of Ir(IV), is replaced by the reactions [16*a*] and [16*b*], leading to the formation of N_2O, and thus explaining the high stoichiometric ratio with excess of Ir(IV).

[16*a*] $NH_2OH^{\cdot+} + Ir(IV) \rightarrow Ir(III) + 2H^+ + HNO$

[16*b*] $2HNO \rightarrow N_2O + H_2O$

From the application of the steady-state treatment, one obtains:

$$[17]\quad [IrCl_6^{3-}\ldots NH_2OH^{\cdot+}] = \frac{k_{et}[IrCl_6NH_2OH]^{2-}}{k_{-et} + k_d}$$

$$[18]\quad [IrCl_6NH_2OH]^{2-} = \frac{k_1[IrCl_6]^{2-}\,[NH_3OH^+]}{k_{-1}[H^+] + k_{et}}$$

$$[19]\quad [NH_3OH^+] = \frac{K_{ipd}[NH_2OH\cdot HCl]_0}{K_{ipd} + [Cl^-]}$$

With the assumption that $k_d \gg k_{-et}$, the k_{obs} is expressed by eq. [20].

$$[20]\quad k_{obs} = \frac{K_{ipd}k_{et}k_1[NH_2OH\cdot HCl]_0}{(k_{-1}[H^+] + k_{et})(K_{ipd} + [Cl^-])}$$

Equation [20] can be rearranged to eq. [21] where $[NH_2OH\cdot HCl]_0/k_{obs} = k_2^{-1}$.

$$[21]\quad \frac{1}{k_2} = \frac{(k_{-1}(H^+) + k_{et})}{k_1k_{et}} + \frac{(k_{-1}[H^+] + k_{et})[Cl^-]}{K_{ipd}k_1k_{et}}$$

Equation [21] is consistent with the linear plots between k_2^{-1} and $[Cl^-]$, Fig. 4, at the different temperatures investigated. The estimated values of K_{ipd}, at different temperatures, from the intercepts and slopes of these plots are given in Table 2. It is interesting to note that the K_{ipd} values, 2.91 ± 0.03 mol dm^{-3}, are almost independent of temper-

Can. J. Chem. Downloaded from www.nrcresearchpress.com by 203.198.23.82 on 09/08/12
For personal use only.

TABLE 2. The values of the rate constants k_1 and $k_{et}K_{os}$ and the equilibrium constant K_{ipd} at different temperatures, and the respective activation parameters.

	Temperature (°C)			
	25	30	35	40
k_1 (dm^3 mol^{-1} s^{-1})	147	168	209	249
$10^2 k_{et}K_{os}$ (s^{-1})	2.80	3.18	3.46	3.77
K_{ipd} (mol dm^{-3})	2.94	2.92	2.91	2.87
K_{ipa} (dm^3 mol^{-1})	0.340	0.342	0.344	0.348
$\Delta H^{\ddagger}_{k_1} = 29 \pm 2$ kJ mol^{-1}		$\Delta H^{\ddagger}_{k_{et}K_{os}} = 15 \pm 2$ kJ mol^{-1}		
$\Delta S^{\ddagger}_{k_1} = -115 \pm 6$ J K^{-1} mol^{-1}		$\Delta S^{\ddagger}_{k_{et}K_{os}} = -233 \pm 3$ J K^{-1} mol^{-1}		

ature. This could be rationalized if the ΔH_{ipd} has a small value. The value of K_{ipd} ($= 1/K_{ipa}$) was computed from the Fuoss equation (21) using 1.40 and 1.81 Å as the radii of NH_3OH^+ and Cl^- ions, respectively.

Again, in the absence of $[Cl^-]$ eq. [20] can be written as eq. [22], which explains the dependence of the rate on $[H^+]$.

$$[22] \qquad k_{obs} = \frac{k_{et}k_1[NH_2OH \cdot HCl]_0}{k_{-1}[H^+] + k_{et}}$$

Equation [22] can be rearranged to eq. [23] $k_1/k_{-1} = K_{os}$, which is consistent with the plots of k_2^{-1} vs. $[H^+]$ (Fig. 5).

$$[23] \qquad \frac{[NH_2OH \cdot HCl]_0}{k_{obs}} = \frac{1}{k_2} = \frac{[H^+]}{k_{et}K_{os}} + \frac{1}{k_1}$$

The computed values of k_1 and $k_{et}K_{os}$ are given in Table 2 together with the associated activation and thermodynamic parameters. In conclusion, NH_3OH^+ rather than NH_2OH is the reactive hydroxylamine species and the skeleton mechanism proposed by Sen Gupta et al. (3) is confirmed. However, it must be noted that the retardation in the rate by H^+ is due to reaction [13] and is not due to the dissociation $NH_3OH^+ \rightleftharpoons NH_2OH + H^+$. Thus the mechanism of the oxidation of hydroxylamine by $[IrCl_6]^{2-}$ is different from its oxidation by isostructural $[PtCl_6]^{2-}$ studied in the same pH range (22).

Acknowledgments

The authors thank the Department of Science and Technology for the grant to purchase the stopped-flow instrument and the Council of Scientific and Industrial Research, New Delhi, for financial support of the research work. Thanks are also due to the referees and Professor D.M. Stanbury for the constructive suggestions.

1. M.N. Hughes. The inorganic chemistry of biological processes. 2nd. ed. Wiley, New York. 1981. pp. 204–211.
2. K. Wieghardt. *In* Advances in inorganic and bioinorganic mechanisms. Vol. 3. Academic Press, New York. 1984. p. 213.
3. P.K. Sen, S. Maiti, and K.K. Sen Gupta. Indian J. Chem. **19A**, 865 (1980).
4. E.L. Stapp and D.W. Carlyle. Inorg. Chem. **13**, 834 (1974).
5. M.N. Hughes and G. Stedman. J. Chem. Soc. 2824 (1963).
6. J.R. Buchholz and R.E. Powell. J. Am. Chem. Soc. **85**, 509 (1963); **87**, 2350 (1965).
7. D.S. Honig, K. Kustin, and J.F. Martin. Inorg. Chem. **11**, 1895 (1972).
8. (*a*) J.Q. Adams and J.R. Thomas. J. Chem. Phys. **39**, 1904 (1963); (*b*) J.Q. Adams, S.W. Nicksic, and J.R. Thomas. J. Chem. Phys. **45**, 654 (1965); (*c*) R. Stone and W.A. Waters. Proc. Chem. Soc. London, 253 (1962); (*d*) C.J. Gutch and W.A. Waters. J. Chem. Soc. 751 (1965).
9. D.F.C. Morris and T.J. Ritter. J. Chem. Soc. Dalton Trans. 216 (1980).
10. V.K. Jindal, M.C. Agrawal, and S.P. Mushran. Z. Naturforsch. B: Inorg. Chem. Org. Chem. Biochem. Biophys. Biol. **25B**, 188 (1970).
11. I.A. Poulsen and C.S. Garner. J. Am. Chem. Soc. **84**, 2032 (1962).
12. (*a*) C.K. Jørgensen. Acta Chem. Scand. **11**, 151 (1957); (*b*) A.G. Sykes and R.N.F. Thorneley. J. Chem. Soc. (A), 232 (1970).
13. A.I. Vogel. A textbook of quantitative inorganic analysis. Longmans, London. 1961. p. 391.
14. A.I. Vogel. A textbook of quantitative inorganic analysis. 4th ed. Longmans, London. 1986. p. 45.
15. D.M. Stanbury. Adv. Inorg. Chem. **33**, 69 (1989).
16. W.A. Waters and I.R. Wilson. J. Chem. Soc. (A), 534 (1966).
17. (*a*) D.L. Toppen and R.G. Linck. Inorg. Chem. **10**, 2635 (1971); (*b*) C. Lavalee and T.W. Newton. Inorg. Chem. **11**, 2616 (1972).
18. Z. Amjad, A. McAuley, and U.D. Gomwalk. J. Chem. Soc. Dalton Trans. 82 (1977).
19. J.M. Lancaster and R.S. Murray. J. Chem. Soc. (A), 2755 (1971).
20. R. Sarala and D.M. Stanbury. Inorg. Chem. **29**, 3456 (1990).
21. R.M. Fuoss. J. Am. Chem. Soc. **80**, 5059 (1958).
22. K.K. Sen Gupta and P.K. Sen. J. Inorg. Nucl. Chem. **39**, 1651 (1977).

Can. J. Chem. Downloaded from www.nrcresearchpress.com by 203.198.23.82 on 09/08/12
For personal use only.

Complexation of aqueous iodine by 18-crown-6

WARREN HIRSCH,[1] JONATHAN GREENMAN, AND RICHARD PIZER
Department of Chemistry, Brooklyn College of The City University of New York, Brooklyn, NY 11210, U.S.A.

Received June 1, 1993

WARREN HIRSCH, JONATHAN GREENMAN, and RICHARD PIZER. Can. J. Chem. **71**, 2171 (1993).

The reaction of 18-crown-6 with aqueous iodine has been monitored by UV and visible spectrophotometry. The stability constant for the reaction has been determined as well as the spectra for the pure aqueous complex. This stability constant has been related to other equilibrium constants for the complexation of molecular iodine. The relation appears to predict correctly the stability constant for the iodine–water charge-transfer complex.

WARREN HIRSCH, JONATHAN GREENMAN et RICHARD PIZER. Can. J. Chem. **71**, 2171 (1993).

Faisant appel à la spectrophotométrie UV–visible, on a suivi la réaction de l'éther 18-couronne-6 avec l'iode aqueux. On a déterminé la constante de stabilité pour cette réaction ainsi que le spectre du complexe pur en solution aqueuse. On a établi une corrélation entre cette constante de stabilité et d'autres constantes d'équilibre pour la complexation de l'iode moléculaire. La relation semble prédire correctement la constante de stabilité pour le complexe de transfert de charge iode–eau.

[Traduit par la rédaction]

Can. J. Chem. Downloaded from www.nrcresearchpress.com by 203.198.23.82 on 09/08/12
For personal use only.

Introduction

Crown ethers are cyclic ethers known for their ability to form inclusion complexes with cations and neutral molecules. 18-Crown-6 contains 12 carbon atoms and 6 oxygen atoms within its ring. However, the cavity has a diameter of 260–320 pm and is not large enough to accommodate an iodine molecule with a covalent diameter of 530 pm (1). Moreover, the van der Waals diameter of 390 pm for an iodine atom makes it unlikely that even a single iodine atom may be accommodated. Nevertheless, crown ether – iodine complexes have been observed in solutions of methylene chloride, cyclohexane, and carbon tetrachloride (2, 3). These are presumed to be charge-transfer-type complexes, without inclusion, in which the lone pairs of electrons on the oxygen atoms of the crown ethers are donated to vacant $b_{2\sigma u}$ molecular orbitals of iodine (2).

Charge-transfer complexes involving I_2 and a donor molecule with nonbonding electrons have been the subject of extensive research. Their absorption spectra are characterized by the appearance of a strong band in the near-ultraviolet region, at about 250–300 nm, and a blue shift of the I_2 visible peak (3–5). Aqueous I_2 solutions exhibit the characteristic UV spectrum (6). In the present work, the visible peak is blue—shifted by the addition of 18-crown-6 and the charge-transfer band grows in intensity. This indicates the formation of a complex between the ether and I_2 in aqueous solution. Both the UV charge transfer and visible spectra of the pure complex as well as its stability constant have been determined.

Experimental section

18-Crown-6 (Aldrich) was used without further purification. It was stored in a freezer with the sealed reagent bottle inside a larger sealed bottle. Iodine (Fisher Reagent Grade), which had been resublimed, was dissolved in distilled, deionized water. Concentrations were checked by titration with standard sodium thiosulfate (Baker). During spectrophotometry, weighed samples of the solid crown were added directly to 2.7×10^{-4} M aqueous iodine in the quartz cuvette. Since crown concentrations were kept low, volume changes due to mixing were negligible. Absorption spectra were obtained with a Perkin–Elmer Lambda Three spectrophotometer, which was driven by an IBM compatible computer using Perkin–Elmer software. Experiments were performed at 25 ± 1°C.

Scans in the ultraviolet and visible regions were obtained in separate experiments, using separate crown additions. This helped insure reproducibility of the stability constants obtained from each type of scan. Furthermore, it was found that the aqueous iodine solutions containing the higher crown concentrations would form a black precipitate upon standing for several hours. Therefore, it was desirable to complete the scans as quickly as possible to minimize the chance of the latter reaction interfering with the data obtained from the complex in solution. Performing UV and visible scans separately facilitated this end.

Results

The data from the absorption spectra in aqueous solution are characteristic of charge transfer spectra. The visible spectrum (Fig. 1) shows a noticeable blue shift. The maximum absorption for pure I_2 (aq) occurs at 449 nm. The absorbance maximum for the spectrum calculated for the complex using eq. [1] (below) occurs at 422 nm. At the same time, the UV absorbance in the charge-transfer region (Fig. 2) shows about a threefold increase in going from pure I_2(aq) to the calculated spectrum of the complex.

The formation constant for the reaction between I_2 (aq) and 18-crown-6, as well as the spectrum of the pure complex were determined by use of the equation

$$[1] \quad (A - A_0)/F_D = K_{DA}(A - A_\infty)$$

where A is the absorbance, F_D is the total concentration of the added crown ether (donor), A_0 is the initial absorbance of aqueous I_2 (aq) with no crown added, A_∞ is the absorbance of the pure complex (after the addition of "infinite" crown), and K_{DA} is the formation constant of the complex. Equation [1] is a form of the Ketelar equation (7). It may be derived from the conservation equations for iodine-containing species and crown-containing species with the proviso that the concentration of the crown is much greater than the initial concentration of iodine. (A large excess of crown was, in fact, used during the experiments.) In addition, the equilibrium expression for the formation of the crown ether – iodine complex in aqueous solution (see eq. [4] below), and Beer's law are used in the derivation. The Beer's law expression assumes that both I_2(aq) and the complex ab-

[1]Author to whom correspondence may be addressed.

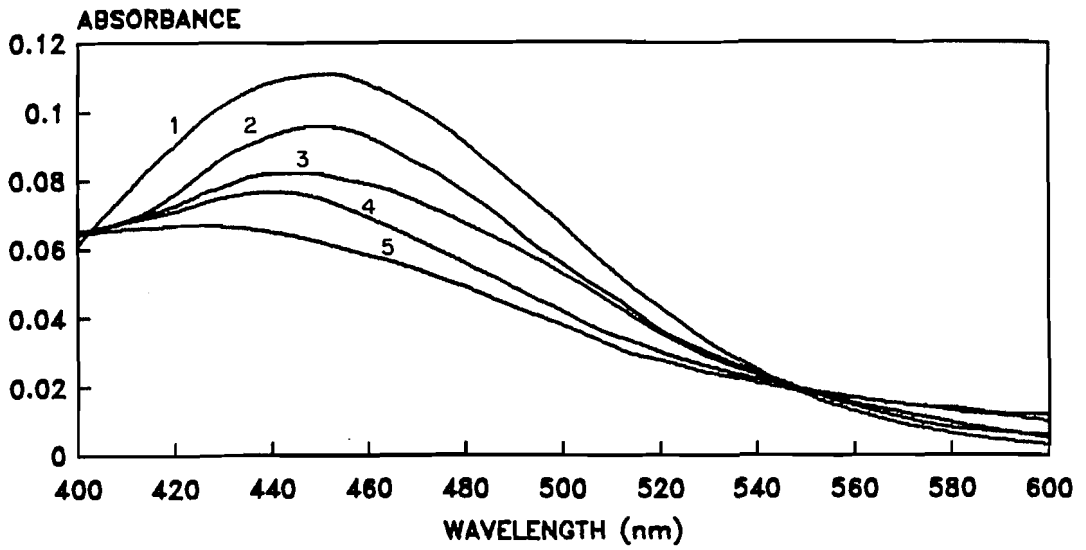

FIG. 1. Addition of 18-crown-6 to iodine (aq), visible data. (1) Pure 2.7×10^{-4} M I_2 (aq); (2) 0.048 M 18-C-6; (3) 0.18 M 18-C-6; (4) 0.31 M 18-C-6; (5) pure complex.

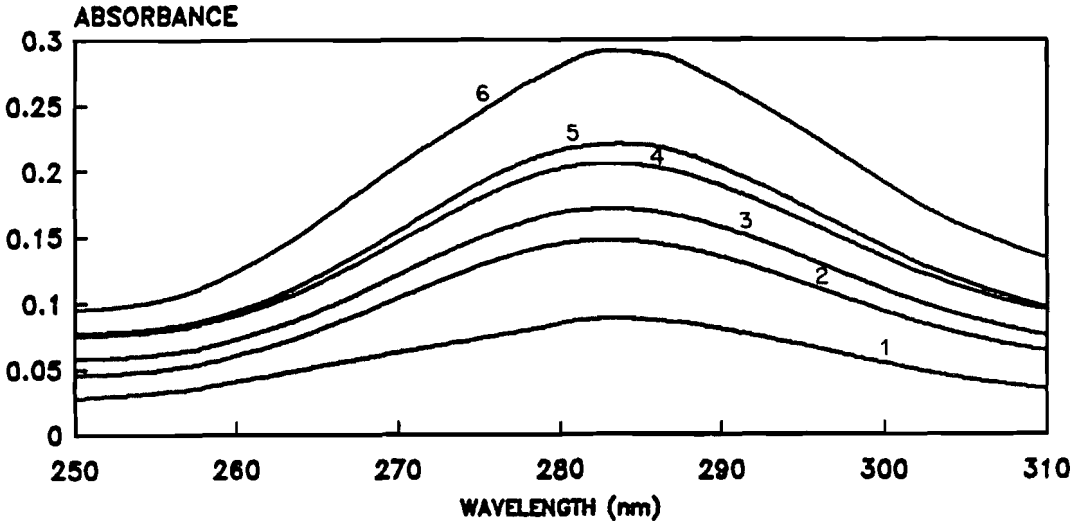

FIG. 2. Addition of 18-crown-6 to iodine (aq), ultraviolet data. (1) Pure 2.7×10^{-4} M (aq); (2) 0.0369 M 18-C-6; (3) 0.0781 M 18-C-6; (4) 0.132 M 18-C-6; (5) 0.170 M 18-C-6; (6) pure complex.

sorb. This assumption is valid since the absorption bands for I_2(aq) and the complex overlapped in both the visible and the ultraviolet.

The average results of linear least-square plots of eq. [1] in the visible region were 11.2 ± 1.7 $(mol/L)^{-1}$ at 25 ± 1°C. The average results of linear least-square plots for results in the ultraviolet charge-transfer region using separate solutions in separate experiments were 10.2 ± 0.9 $(mol/L)^{-1}$ at 25 ± 1°C. The results are nearly equal, within experimental error, so that reproducibility is demonstrated. The average of the two results, giving equal weight to each, is 10.7 ± 1.3 $(mol/L)^{-1}$ at 25 ± 1°C. This equilibrium constant can be directly related to other equilibrium constants for molecular iodine complexation as discussed below.

The reaction of I_2 with crown ether donor (D) in aqueous solution may occur in two different ways. In the first, molecular iodine in water reacts directly with D (the nature of aqueous D will be discussed later), forming a charge-transfer complex as represented in eq. [2], below. In the second, a charge-transfer complex first forms between molecular iodine and excess water. This complex, in turn, reacts with D forming a second charge-transfer complex (DI_2) accompanied by deaquation. These equilibria are indicated by eqs. [3] and [4], below.

[2] $I_2 + D \rightleftarrows DI_2$

[3] $I_2 + H_2O \rightleftarrows I_2 \ldots H_2O$

[4] $I_2 \ldots H_2O + D \rightleftarrows DI_2 + H_2O$

The relationship among the equilibrium constants for these reactions is given by:

[5] $K_2 = K_3K_4$

If the literature value (2) for the formation of the crown ether – iodine complex in the inert solvent cyclohexane at

Can. J. Chem. Downloaded from www.nrcresearchpress.com by 203.198.23.82 on 09/08/12
For personal use only.

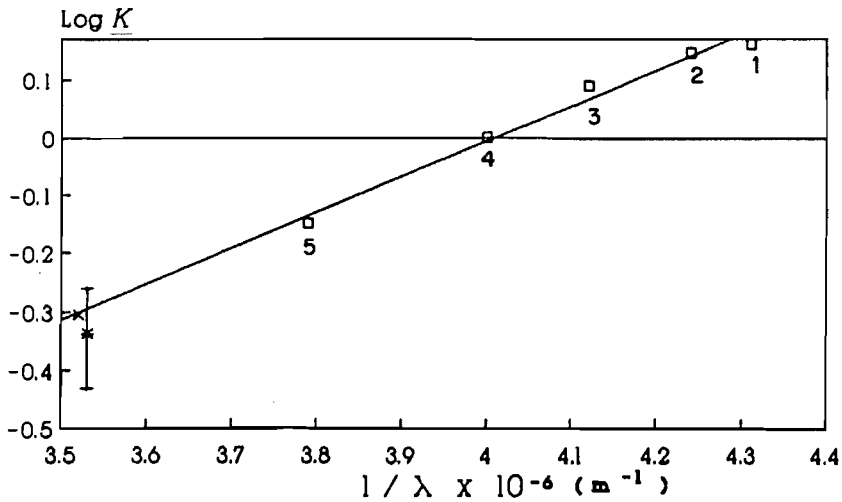

FIG. 3. Log K vs. $1/\lambda$. (1) Methanol; (2) *tert*-butanol; (3) ethanol; (4) ethyl ether; (5) dioxane; (*) water (eq. [5]) × 18-C-6.

25°C (4.93 ± 0.33) is substituted for K_2 and the above value of 10.7 ± 1.3 is substituted for K_4 (assuming that the huge excess of water drives eq. [3] almost to completion, so that eq. [4] is the principal reaction in the current experiments), one obtains the value of 0.46 ± 0.09 for K_3, the formation constant of the charge-transfer complex between iodine and water. To assess whether this value is reasonable, a semiempirical plot of log K vs. $1/\lambda_{max}$ was constructed (Fig. 3) using literature values for the formation constants and charge-transfer band maximum wavelengths for several compounds of the form R-O-R′ (8–11). The plot is well correlated (r = 0.991) and the value for water calculated from eq. [5] fits well, within experimental error.

The motivation for such a plot stems from the idea that after the formation of a contact pair between the donor and acceptor molecules, the electron from the donor can be placed in a vacant MO of the acceptor, upon the absorption of a UV photon. The promotion of the electron may hence be viewed as resulting in an excited state of a very weak van der Waals complex, represented by D + A, below. Therefore, with D in excess, so that its concentration is essentially constant, a Boltzmann distribution may be applied. Hence,

$$[6] \quad UV + D + A \overset{K'}{\rightleftharpoons} DA$$

and

$$[7] \quad K' = [DA]/[D][A] = \exp(-hc/\lambda_{max}\, kT)$$

In logarithmic form,

$$[8] \quad \log K' = -hc/\lambda_{max}\, kT$$

Therefore, for a group of similar donors with the same acceptor, the plot in Fig. 3 seems justified.

It is interesting to note that the plot in Fig. 3 does not immediately seem to predict the literature value of the stability constant for the crown ether – iodine complex (2), 4.93 ± 0.33. When the reciprocal of the wavelength of maximum absorbance for the pure complex from the present work (Fig. 2) is used as the abscissa in Fig. 3 the predicted value for K obtained from the ordinate is 0.45 ± 0.12. However, if this value is multiplied by a statistical factor of 6, accounting for the six oxygens in the crown, one obtains 2.7 ± 1.2 for the predicted stability constant, which is a bit closer to the above literature value. In fact, another reference (3) lists the formation constant for the complex of 18-crown-6 with iodine in a carbon tetrachloride medium at 25°C as 2.8 ± 0.8. This seems to support the contention of the author of ref. 2 that cooperative action of oxygen atoms in the formation of the 18-crown-6 complex with iodine is not an important effect. On the other hand, the literature value for the stability constant in 1,3-dioxane fits the plot well (9). De Maine (9) concluded, by similar statistical considerations, that the two oxygens might well act cooperatively to form the iodine adduct. Figure 3 and eqs. [6]–[8] seem to support this assertion, since the action of two oxygen atoms together should indeed affect the maximum wavelength, whereas oxygen atoms acting independently, as in the crown ether case, should not.

The possibility exists, particularly in cases where the guest is too large to form an inclusion complex with the host, that "sandwich"-type complexes having a guest to host ratio of 1:2 may occur (12). The linear least-square plots of eq. [1], which assumes 1:1 stoichiometry, were well correlated. It is therefore likely that the complex in solution is indeed of the latter type.

A black precipitate was mentioned in the experimental section. The precipitate was air dried, collected, and analysed by titration with standard sodium thiosulfate and by pyrolysis. It was composed of 20.4% carbon, 3.6% hydrogen, 15.6% oxygen, and 58.6% iodine by mass. From this composition, one may surmise the formula for the non-stoichiometric complex

$$C_{12}H_{24}O_6I_{3.3}\cdot H_2O$$

In this formula, the ratio of iodine atoms to crown is greater than two, precluding a "sandwich" complex in the solid. More likely is the possibility that, besides 18C6–I_2, 18C6–$I^+I_3^-$ may occur. The existence of mixed halogen oxidation states in charge-transfer complexes is well established (13).

1. C.J. Pedersen. Science, **241**, 536 (1988).
2. H.P. Hopkins, Jr., D.V. Jahagirdar, and J.W. Windler III. J. Phys. Chem. **82**, 1254 (1979).
3. L.J. Andrews and R.M. Keefer. J. Org. Chem. **52**, 2960 (1987).

Can. J. Chem. Downloaded from www.nrcresearchpress.com by 203.198.23.82 on 09/08/12
For personal use only.

4. H.A. Benesi and J.H. Hildebrand. J. Am. Chem. Soc. **71**, 2703 (1949).
5. R.S. Mulliken and W.B. Person. Molecular complexes—A lecture and reprint volume. Wiley, New York. 1969.
6. N.J. Rose and R.S. Drago. J. Am. Chem. Soc. **81**, 6138 (1959).
7. J.A. Ketelar. Recl. Trav. Chim. Pays-Bas, **71**, 1104 (1952).
8. A.D. Awtrey and R.E. Connick. J. Am. Chem. Soc. **73**, 1842(1951).
9. P.A.D. De Maine. J. Chem. Phys. **26**, 1199 (1957).
10. A.F. Garito and B.B. Wayland. J. Phys. Chem. **71**, 4062 (1967).
11. M. Tamres, Sr., O.P. Brandon, and S. Searles, Jr. J. Am. Chem. Soc.**82**, 2129 (1960); **82**, 2134 (1960).
12. C.J. Pedersen. J. Am. Chem. Soc. **92**, 386 (1970).
13. F.A. Cotton and G. Wilkinson. Advanced inorganic chemistry: a comprehensive text. 5th ed. Wiley, New York. 1988. pp. 549–551.

Can. J. Chem. Downloaded from www.nrcresearchpress.com by 203.198.23.82 on 09/08/12
For personal use only.

Properties of some alkali fluoride–chloride salt mixtures I. Primary crystallization and density measurements

N. RAJAGOPALAN, J.B. BELAWADI, AND UTPAL SEN[1]
Central Electrochemical Research Institute, Karalkudi 623 006, Tamilnadu, India

Received May 12, 1992[2]

N. RAJAGOPALAN, J.B. BELAWADI, and UTPAL SEN. Can. J. Chem. **71**, 2175 (1993).

The primary crystallization and density of the fluoride–chloride salt systems (*i*) NaF–LiCl and (*ii*) NaF–(LiCl + KCl) eutectic were determined experimentally using thermal analysis and the Archimedean technique, respectively. The corresponding liquidus curves for the two systems were constructed and compared. Molar volume and excess volume functions were computed from density data at different compositions and temperatures. The positive values of the excess volumes correspond to volume expansion that increases with temperature for both systems. The results suggest that as far as the primary crystallization and density behaviours are concerned, it is possible to replace the component, pure LiCl, in the fluoride–chloride salt system by the eutectic mixture of (LiCl + KCl) for the system's use as a potential electrolyte for aluminium electrolysis.

N. RAJAGOPALAN, J.B. BELAWADI et UTPAL SEN. Can. J. Chem. **71**, 2175 (1993).

Faisant appel à l'analyse thermique et à la technique d'Archimède, on a déterminé respectivement la cristallisation primaire et la densité des systèmes eutectiques de sels de fluorure–chlorure : (*i*) NaF–LiCl et (*ii*) NaF–(LiCl + KCl). On a construit les courbes liquides correspondantes pour les deux systèmes et on les a comparés. En se basant sur des données de densités à différentes compositions et à différentes températures, on a calculé les fonctions de volume molaire et de volume en excès. La valeur positive des volumes en excès correspond à une expansion de volume qui augmente avec la température dans les deux systèmes. Les résultats suggèrent que, en autant que la cristallisation primaire et les comportements de la densité sont concernés, il est possible de remplacer le composant LiCl pur du système de sel fluorure–chlorure par le mélange eutectique du (LiCl + KCl) pour l'utilisation du système comme électrolyte potentiel pour l'électrolyse de l'aluminium.

[Traduit par la rédaction]

Can. J. Chem. Downloaded from www.nrcresearchpress.com by 203.198.23.82 on 09/08/12
For personal use only.

I. Introduction

Considering the melting point of metallic aluminium (933 K), the most suitable temperature for Al electrolysis could be expected to be around 973 K. However, to date the commercial Hall–Heroult process for Al electrolysis is still being operated in the temperature range of around 1223–1243 K. The main reason for these high operational temperatures is the high melting point of the bath, which can, however, be reduced with use of suitable additive salts. But the decrease in temperature as well as the presence of many of such additives also brings down the solubility of alumina in the cryolite-based bath electrolyte. One way to avoid the problem of alumina solubility in the bath electrolyte may be to use consumable composite anodes consisting of a paste made of carbon and alumina (1). In this suggested alternative process, cryolite (mp 1285 K) need not be the electrolyte and instead a mixture of NaF and LiCl has been suggested, where the temperature of electrolysis could be around 973–998 K (1). Study of the various physico-chemical properties of such a fluoride–chloride system is therefore important. However, from the viewpoint of commercial application, LiCl is an expensive chemical and any suitable replacement would be welcome.

In the present work the primary crystallization and density of different compositions of two series of fluoride–chloride salt mixtures viz., (*i*) NaF–LiCl and (*ii*) NaF–(LiCl + KCl) eutectic, were studied and a comparative study was made, keeping in view their commercial applications. Fluoride–chloride salt systems also have potentiality for applications in solar thermal energy utilization systems (2). Density data of the bath electrolyte are important in connection with easy separation and collection of the molten metal from the bath electrolyte, whereas molar volume data are important for the estimation of suitability of the systems for their potential use as energy storage materials.

The density readings were used for the determination of different volume functions such as average molar volume (V_M) and molar excess volume (V^E) and the results are discussed in the light of the existing theory and concepts of molten salt mixtures.

II. Experimental

II.1 Thermal analysis

The primary freezing points of the salt mixtures were determined by the thermal analysis method. A vertical muffle furnace, a variable speed strip chart Y–t recorder, and a constant current generator were used. The accuracy of the detection of temperature change is 0.13 K. A Chromel–Alumel thermocouple was used for the temperature measurements. Details of the procedure followed may be found elsewhere (3).

II.2 Density apparatus

The density of the liquid mixtures was determined by employing the Archimedean technique (4, 5). The procedure consisted of measuring the loss of weight of an inert bob (sinker) in the melt. The density of the melt can be given as

$$[1] \qquad \rho_L = (W_I - W_F)/V_B$$

where ρ_L is the density of the liquid, W_I and W_F are the weights of the bob before and after dipping in the melt, respectively, and V_B is the volume of the bob at the measurement temperature.

A conical-shaped bob made of platinum with a hook for the suspension wire attachment was used in the density experiments. The bob was suspended from one arm of a balance by a thin Pt wire (0.25 mm diameter). The volume of the bob was around 1 cm^3. Graphite crucibles (4 cm diameter and 6 cm high) were used in the present experiments to contain the molten salts. The salt mixture

[1]Author to whom correspondence may be addressed.
[2]Revision received June 4, 1993.

Can. J. Chem. Downloaded from www.nrcresearchpress.com by 203.198.23.82 on 09/08/12
For personal use only.

was melted in a separate furnace and then carefully poured into the graphite crucible to maintain a preset liquid level. The crucible containing the melt was then placed on a steel rod that slides through a tight seal at the bottom of a tubular furnace having a 10 cm constant temperature zone. The vertical movement of the crucible inside the furnace was accomplished by attaching the supporting steel rod to a laboratory jack below the furnace. Initially the crucible with the melt was placed beneath the bob and the crucible was then raised to a predetermined height. The temperature of the melt was measured using a Chromel–Alumel thermocouple placed adjacent to the crucible within the furnace.

To obtain accurate density values of the molten salt systems at elevated temperatures using the Archimedean method, a number of corrections were necessary (5). The main corrections involve the surface tension of the liquid, the cubical expansion of the bob material, and also the buoyancy due to the atmosphere if the readings are not taken in vacuum. These corrections require a lot of calculations involving a number of accurate physical parameters for the materials used in the density measuring process. Moreover, accurate values of the bob volume at the different experimental temperatures are essential for ensuring accurate density measurements.

Usually the bob volume was determined at room temperature by weighing first in air and then in deionized water and was then corrected to the operating temperature using the thermal expansion coefficient values for the materials of which the sinker bob is made (5, 6). We have, however, simplified the correction procedure by calibrating the measurements against a standard salt mixture with known density at different temperatures, which in this case was an eutectic mixture of KCl and NaCl (mp 931 K). A calibration curve was drawn of the weight loss of the platinum bob when dipped into the standard melt against different temperatures. The density (ρ) versus temperature curve of the same system was also drawn from the literature data (7). Now, if it can be assumed that the bob volume at a particular temperature would not change during the course of the experiments, the density of any experimental liquid (ρ_L) may be determined using the following equation:

$$[2] \quad \frac{\text{Weight loss in the experimental liquid}}{\text{Weight loss in the standard liquid}} = \frac{\rho_L}{\rho_{std}}$$

It would be assumed that the effect due to the surface tension of the standard molten salt mixture would not be significantly different from that due to the surface tension of the experimental liquid.

Analytical reagent grade NaF was used. LiCl and KCl, both analytical grade, were dried at about 400°C before use. LiCl is highly hygroscopic and was handled inside a dry box. Weighing was, however, done outside the dry box in a closed vessel. One of the major sources of error in this procedure for density measurement is bubble formation on the bob surface during the actual experiment. This is normally attributed to traces of moisture in the melt (6), and is more likely to occur when hygroscopic salts are involved. The premelting in our case helped to avoid the problem to a large extent. However, the bob was made to move up and down before each measurement. The melt was kept at a constant temperature for at least an hour before each measurement and at the time of recording the weight of the bob immersed into the melt, the temperature reading was also noted. For each preset temperature at least two readings were taken and the average value was used for density calculations. With each particular composition density readings were taken at about eight to ten different temperatures. Care was taken to note the salt deposition on the top portion of the suspension wire. No significant salt deposition was observed. Thermal analysis and density experiments were carried out under N_2 atmosphere.

To check the validity of the present density measurements, we measured the densities of the pure components at different temperatures. The differences between our results and the literature values (7) lie within the experimental error limits.

III. Results

III.1 Primary crystallization

From the experimental readings of the primary crystallization points obtained by thermal analysis of various salt mixtures of known composition, the corresponding liquidus curves for both salt systems were constructed. The plotting was done on the same graph sheet for comparison (Fig. 1). We have the mixture of NaF and LiCl as a true binary system. But the three-component mixture of NaF, LiCl, and KCl was converted to a quasibinary system by keeping the amount of LiCl and KCl in the mixture always in the eutectic proportion of LiCl (58.5 mol %) and KCl (41.5 mol %) (mp 634 K). The (LiCl + KCl) eutectic mixture was treated as a single component. Temperature–composition phase diagrams of binary fluoride–chloride salt systems having a common cation, such as NaF–NaCl, show only one minimum whereas binary systems with different cations, such as KF–NaCl, are known to have liquidus curves showing more than one minimum and maximum (8). The liquidus curve for the NaF–LiCl system (Fig. 1) apparently has two minima (at $x_{NaF} \approx 0.25$ and $x_{NaF} \approx 0.7$) and a rather flat maximum (at $x_{NaF} \approx 0.45$). This kind of liquidus curve may indicate eutectic as well as compound formation with congruent or incongruent melting point (9–11). The maximum observed in the liquidus curve of the NaF–LiCl system does not appear to be well defined, which may mean that the compound formed would be rather unstable (9).

The other system, viz., NaF–(LiCl + KCl), consists of three cations and two anions. The liquidus plot of the corresponding quasibinary system (Fig. 1) does not show any minimum. Addition of eutectic (LiCl + KCl) to NaF decreases the primary crystallization temperature throughout the composition range. The rate of decrease apparently has two breaks at $x_{NaF} \approx 0.75$ and $x_{NaF} \approx 0.3$ and is smallest in the range between them. This kind of liquidus curve for purely binary systems may indicate simple monotectic or partially miscible solid solution with peritectic formations (9). Further studies are necessary to make this information more clear. Nevertheless, the present data may be sufficient to give an approximate idea of the primary crystallization behaviour of the molten salt systems and, from the comparison (Fig. 1), it can be seen that up to the composition $x_{NaF} \approx 0.7$ the liquidus temperature for both systems stays below or near the melting point of metallic aluminum (933 K). This might suggest that as far as the primary crystallization of the mixture is concerned, LiCl can be replaced by the eutectic mixture of LiCl (58.5) and KCl (41.5) as the electrolyte for metal extraction, and the optimum bath composition in these systems may be around the 1:1 mixture of the fluoride–chloride salts.

III.2 Density

Experimental density (ρ) values at different temperatures corresponding to the various mixtures containing different proportions of (*i*) NaF and LiCl and (*ii*) NaF and (LiCl + KCl) eutectic determined using eq. [1] have been presented in Tables S1(*a*) and S1(*b*) respectively.[3]

[3]Tables of experimental density values (Tables S1(*a*) and S1(*b*)), the constants *C* and *D* of eq. [5] and the corresponding standard deviation (S_D) (Table S2), and the expansivity at 1000 K (Table S3) may be purchased from: The Depository of Unpublished Data, Document Delivery, CISTI, National Research Council Canada, Ottawa, Canada K1A OS2.

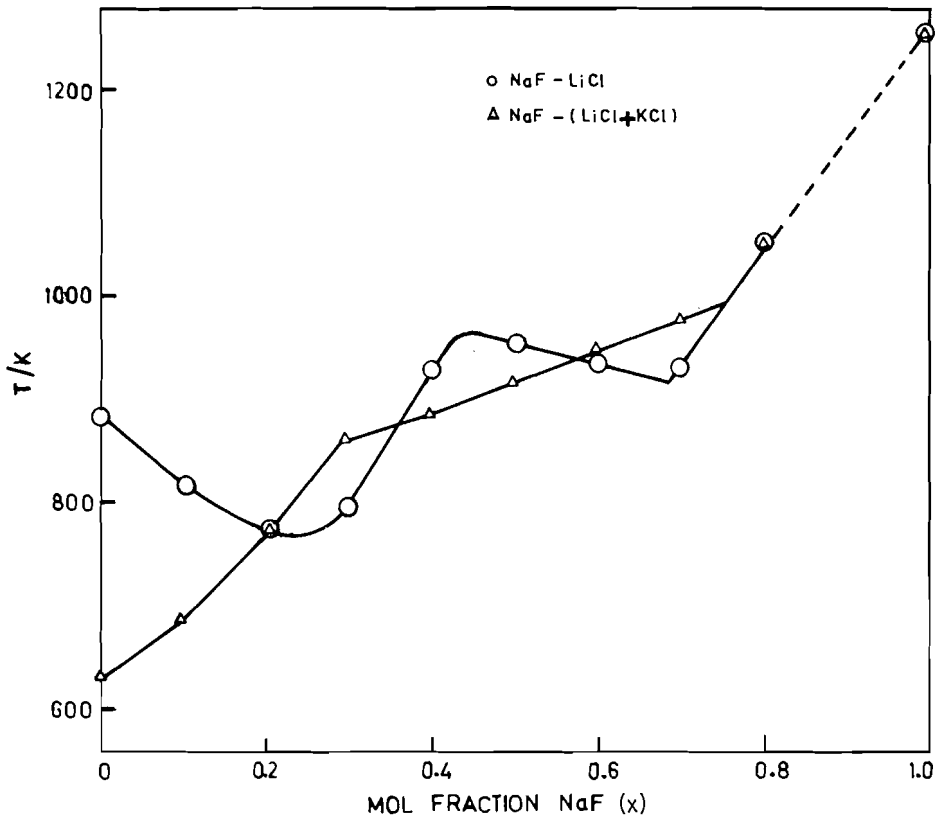

FIG. 1. Fusibility diagram of the two fluoride–chloride systems; ○ NaF–LiCl; △ NaF–(LiCl + KCl).

III.3 Molar volume

From the straight-line plots of density (ρ) vs. temperature (T/K), densities at some rounded temperatures such as 1000, 1050, 1150, and 1250 K have been determined for each composition of the salt mixtures. From such values the corresponding average molar volumes (V_M) have been calculated by using the equation:

$$[3] \quad V_M = M_{AV}/\rho$$

where $M_{AV} = \Sigma M_i x_i$, M_i and x_i being the molar weight and the mol fraction of the individual components, and ρ is the density of the mixture.

In Figs. 2 and 3 the values of V_M obtained from eq. [3] at different temperatures have been plotted against composition for the two salt systems. Since 1000 K may be the nearest temperature of cell operation suggested for the alternative method for aluminum electrolysis as mentioned above (1), a comparison of the variation of the average molar volumes (V_M) with composition (x) in both salt systems at 1000 K is shown in Fig. 4. It can be seen from Fig. 2–4 that the average molar volumes (V_M) for both systems seem to have a maximum at the composition where the mol fraction of NaF is around 0.1 ($x = 0.1$), which means that the corresponding density values at this particular composition are at the maximum for the particular system.

For a given composition the measured densities were found to decrease linearly with increasing temperature. Accordingly, the results were fitted to the linear expression

$$[4] \quad \rho = A + BT$$

where A and B are constants and T is the absolute temperature in degrees Kelvin. The coefficients A and B were determined by the least-squares method. These data are presented in Table 1, which also includes the corresponding standard deviations (S_D).

The average molar volume (V_M) for different compositions increases with temperature. The experimental density data[3] were used to determine the corresponding average molar volumes (V_M), which were then fitted to the linear expression

$$[5] \quad V_M = C + DT$$

where C and D are constants. Table S2 lists the constants C and D along with the corresponding standard deviation (S_D) for the two fluoride–chloride salt systems.[3] Gutierrez and Toguri (12) determined density and molar volume of the ternary systems $PbCl_2$–KCl–NaCl and $PbCl_2$–KCl–LiCl. They fitted their density and molar volume data to linear temperature equations. The constants A, B and C, D did not indicate any regular trends with respect to composition. Similar observations may be made from the results of the present work.

III.4 Expansivity

The coefficient of thermal expansion or expansivity α is given by

$$[6] \quad \alpha = \frac{1}{V}\left(\frac{\partial V}{\partial T}\right)_P$$

Since $V_M = M_{AV}/\rho$ it may be shown that

Can. J. Chem. Downloaded from www.nrcresearchpress.com by 203.198.23.82 on 09/08/12
For personal use only.

Can. J. Chem. Downloaded from www.nrcresearchpress.com by 203.198.23.82 on 09/08/12
For personal use only.

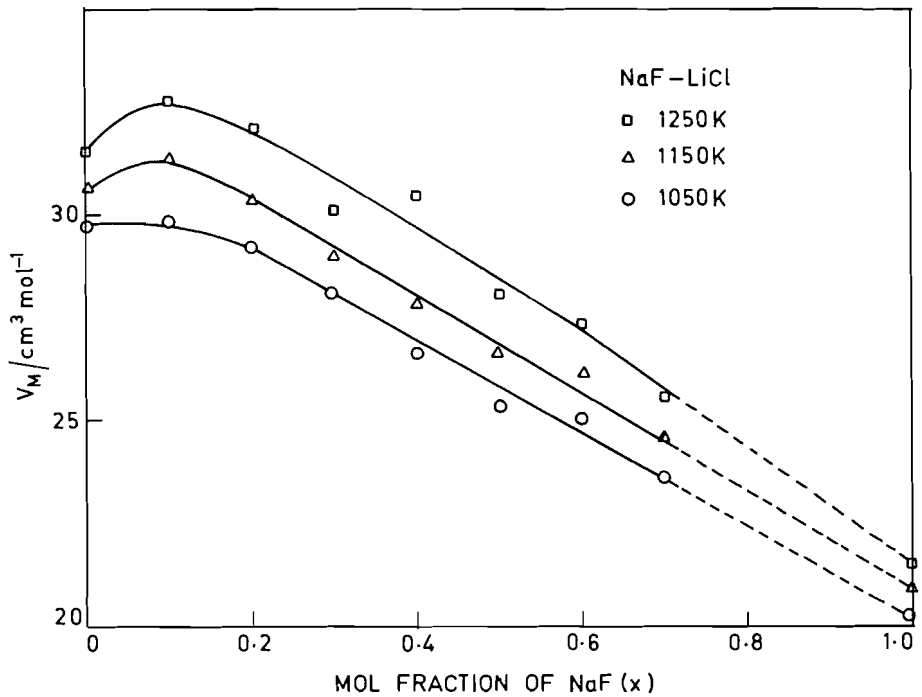

FIG. 2. Variation of average molar volume (V_M) with composition at different temperatures for the NaF–LiCl system; ○ 1050 K; △ 1150 K; □ 1250 K.

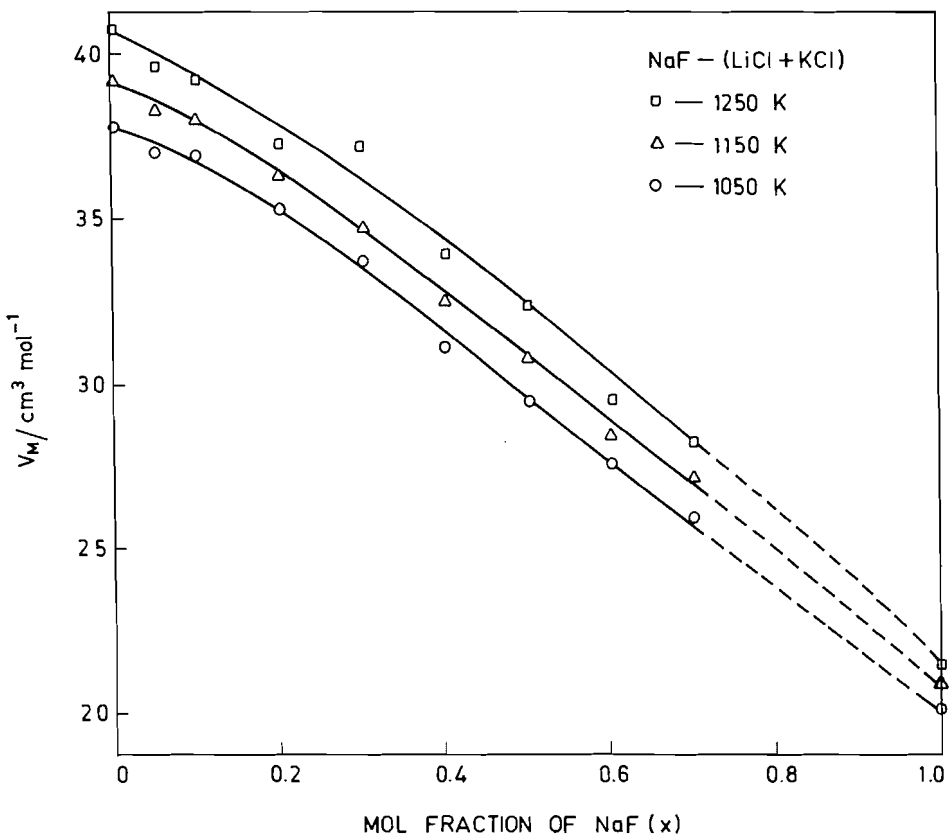

FIG. 3. Variation of average molar volume (V_M) with composition at different temperatures for the NaF–(LiCl + KCl) eutectic system; ○ 1050 K; △ 1150 K; □ 1250 K.

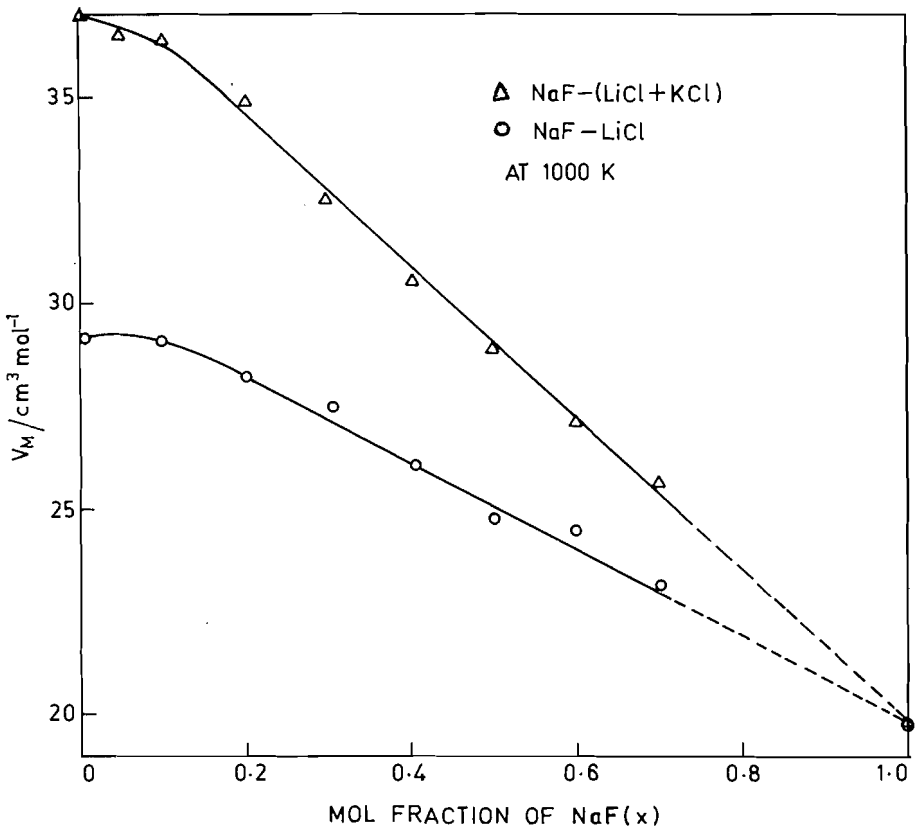

FIG. 4. A comparison of the variation of average molar volume (V_M) with composition for the two fluoride–chloride systems at 1000 K; O NaF–LiCl; Δ NaF–(LiCl + KCl).

$$[7] \quad \alpha = -\frac{1}{\rho}\left(\frac{\partial \rho}{\partial T}\right)_P$$

Substituting $\rho = A + BT$ in the above equation one obtains

$$[8] \quad \alpha = \frac{-B}{A + BT}$$

From the results of this study, it is observed that the density decreases with increasing temperature and α is positive.

Table S3 lists the values of α at 1000 K for the two systems (3). Carmichael and Flengas (13) determined α values for the $MnCl_2$–NaCl–CsCl system at different compositions and plotted them against the corresponding mol fraction of $MnCl_2$. They found that α values exhibited some maxima and minima before approaching the values of the pure individual components. Somewhat similar behaviour but no regular trends are, however, observed with respect to the variation of α values with composition in the present work.

III.5 Molar excess volume

Although the use of direct methods for measuring molar excess volume (V^E) may now be standard practice in the study of liquids at room temperature, nearly all V^E values for fused salts have been derived from density measurements using the following equation

$$[9] \quad V^E = V_M - \sum V_i^0 x_i$$

where V_i^0 and x_i are the molar volume and the mol fraction of each individual pure component in the mixture.

This procedure involves the subtraction of two nearly equal quantities. At least three densities have to be measured for any binary system to obtain an excess volume, which magnifies the error due to uncertainty in the temperature measurements. Any inaccuracy in the data for either of the pure components will give rise to systematic errors in the V^E values for all the mixtures. Very few attempts of direct measurements of V^E for molten salts have been reported in the literature (14, 15), and these were confined to low-melting salt systems such as molten nitrate salt mixtures, and as such they may not be suitable for high-melting fluoride–chloride salt systems. In the present work V^E values have been generated from the density data.

From the smooth plots of V_M vs. composition, the values of V_M at the rounded temperatures were obtained by interpolation and such values were utilised to obtain the corresponding molar excess volume (V^E) function by using eq. [9]. Density values for the individual pure components NaF, LiCl, and KCl were obtained from the literature (14, 15). It was assumed that the use of literature values of the densities of the pure components would not introduce any significant error. Some extrapolation had to be done beyond the actual recommended limits to generate liquid density values (from literature data) to cover the entire temperature range of interest to us (7, 16). The present temperature range, 1000 – 1250 K, would fairly represent the range between the lowest possible temperature of aluminum electrolysis to the temperature of operation of the only commercially viable conventional Hall–Heroult cells for aluminium electrolysis (17).

From analysis of the experimental data of the present work

Can. J. Chem. Downloaded from www.nrcresearchpress.com by 203.198.23.82 on 09/08/12
For personal use only.

TABLE 1. The constants (A and B) of the temperature equation ($\rho = A + BT$) of densities and the corresponding standard deviations (S_D) of the two molten salt systems.

Mol fraction of NaF x	Mixture I NaF – LiCl			Mixture II NaF – (LiCl + KCl eutectic)		
	A (g cm^{-3})	-10^4B (g cm^{-3} K^{-1})	10^3S_D (g cm^{-3})	A (g cm^{-3})	-10^4B (g cm^{-3} K^{-1})	10^3S_D (g cm^{-3})
0	1.8842[a]	4.328[a]	—	2.0292[b]	5.275[b]	—
0.05	—	—	—	1.9969	4.841	0.99
0.1	2.0706	6.176	1.92	1.9158	4.218	0.59
0.2	2.0451	5.610	0.61	1.9179	3.979	1.93
0.3	2.0578	5.207	2.05	2.0209	4.797	1.05
0.4	2.1923	5.957	0.47	2.0801	4.655	2.37
0.5	2.5269	8.176	0.66	2.4363	7.419	0.87
0.6	2.3969	6.795	1.39	2.3450	5.912	1.47
0.7	2.4909	6.707	0.99	2.5127	7.090	4.06
1.0	2.7550[a]	6.360[a]	—	2.7550[a]	6.360[a]	—

[a]Reference 16.
[b]Reference 7.

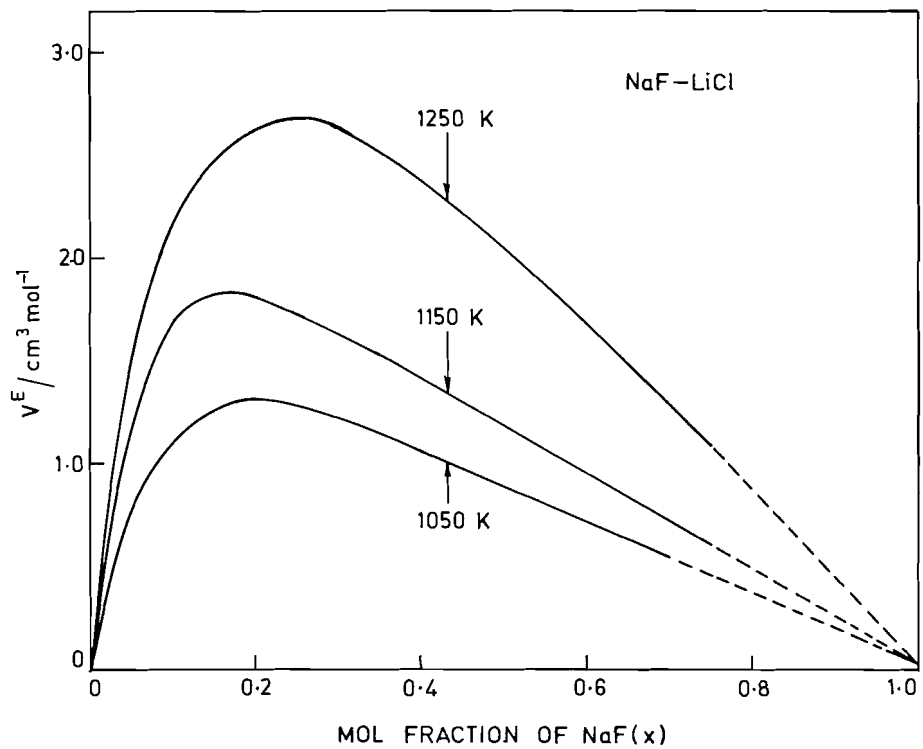

FIG. 5. Variation of molar excess volume (V^E) with composition at different temperatures for the NaF–LiCl system.

involving molten mixtures of (*i*) NaF – LiCl and (*ii*) NaF – (LiCl + KCl) eutectic it has been found that an uncertainty of about 0.4% in the experimental density readings could cause an uncertainty of about 0.08 cm^3 in the corresponding molar volume (V_M) data. This might introduce an error of as much as twice the magnitude in the calculated values of molar excess volume (V^E).

Figures 5 and 6 show the plots of the molar excess volume (V^E) with respect to composition (x) at some rounded temperatures for the two salt systems. V^E values are always positive and the value apparently reaches a maximum when the mol fraction of NaF approximates 0.3 ($x \approx 0.3$) for both salt systems at all temperatures. Similar detailed studies of molar excess volume functions at different temperatures have perhaps not been reported for high-temperature molten salt systems.

We also expressed the excess molar volume data at different temperatures as a function of composition by fitting them to the polynomial expansion (18)

$$[10] \quad V^E = x(1 - x)(a + bx + cx^2 + dx^3 + ex^4 + fx^5)$$

where x is the mol fraction of NaF and a, b, c, d, e, and f are the coefficients of the polynomial. The details of the calculations are shown in Table 2.

Can. J. Chem. Downloaded from www.nrcresearchpress.com by 203.198.23.82 on 09/08/12
For personal use only.

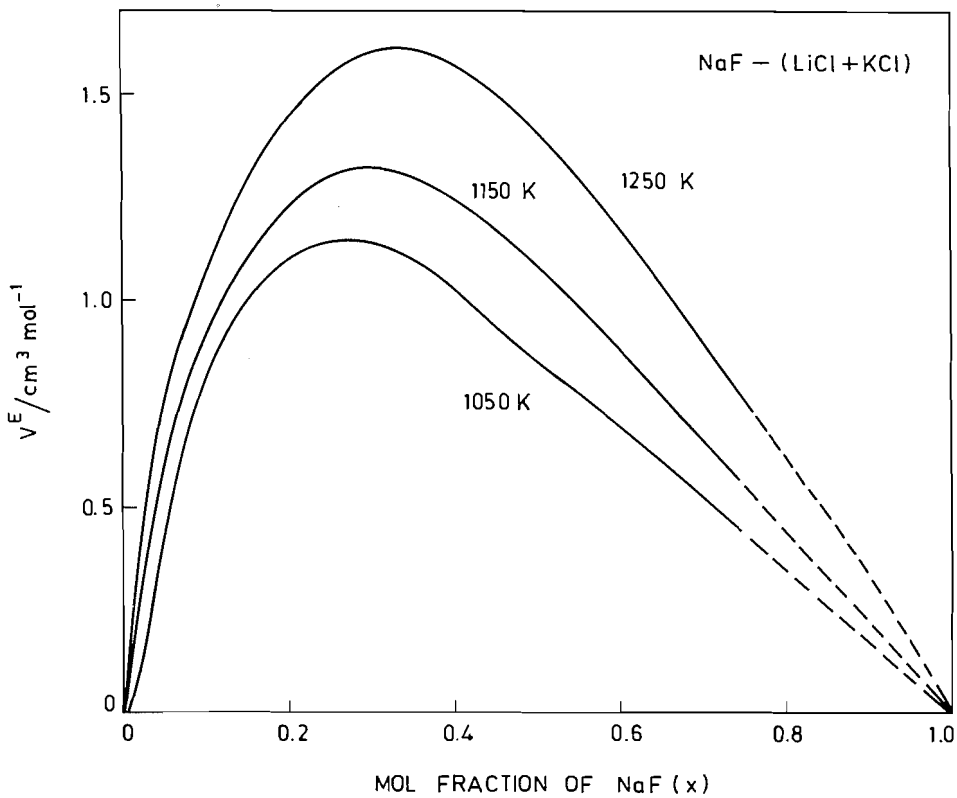

FIG. 6. Variation of molar excess volume (V^E) with composition at different temperatures for the NaF–(LiCl + KCl) eutectic system.

TABLE 2. The constants for the polynomial fitting of molar excess volumes (V_E) with respect to composition (x, mol fraction of NaF) for the two molten salt systems at different temperatures

$V_E = x(1 - x)(a + bx + cx^2 + dx^3 + ex^4 + fx^5)$

Mixture I = NaF – LiCl. Mixture II = NaF – (LiCl + KCl eutectic).

Temperature (K)	Mixture	a	b	c	d	e	f
1000	I	12.91	−27.91	−58.63	335.46	−477.86	222.93
	II	10.89	−7.79	−166.50	633.82	−892.13	444.88
	I	15.08	−25.46	−107.51	450.72	−580.05	253.85
1050	II	11.29	−7.04	−163.95	643.38	−947.71	496.11
	I	36.51	−242.98	840.27	−1558.77	−1465.11	−545.84
1150	II	16.00	−80.49	292.09	−598.17	601.01	−230.91
	I	48.33	−368.64	1560.81	−3439.02	3685.64	−1514.43
1250	II	24.44	−235.28	1366.64	−3813.21	4927.22	−2381.74

IV. Discussion

Grjotheim et al. (18) recalled that there is no *a priori* reason to expect that the mixing of two salts proceeds without volume change. For the same reason, the mixing of spheres of unequal size does not yield an additive volume. They also noted that when the two salts are very similar, the volume change, as expected, is usually observed to be small. Therefore, a rational way of presenting the excess volume results is by the deviation from additivity. Nevertheless, molar excess volume is often identified with nonideality in the mixing of the components. In the present work the positive values of V^E for all the compositions in the systems increase with increasing temperature (See Figs. 5 and 6). This may suggest that the so-called nonideality in mixing has in general a tendency to increase with temperature.

When a mixing of any two salt components introduces some nonideality (i.e., $V^E \neq 0$) it may be expected that at 50 mol% composition of the binary system (i.e., 0.5 mol fraction) the introduced nonideality would reach a maximum unless there are some complex formations. In the present case, however, the maximum positive value of V^E is reached when the mol fraction of NaF is well below 0.5. Significant differences in the behaviour of alkali fluoride–chloride systems from that of other halide–halide systems were observed earlier (13, 19, 20).

The positive excess volume is normally attributed to purely Coulombic interactions between ions in the molten salt systems (21). For such systems a second-order theory, based on the conformal solution theory, has been advanced by Reiss, Katz, and Kleppa (21). According to such a concept, V^E

Can. J. Chem. Downloaded from www.nrcresearchpress.com by 203.198.23.82 on 09/08/12
For personal use only.

would be a function of the ionic distances in the melt system. The function is rather simple in the case of a binary salt mixture with a common anion or cation (15). The present fluoride–chloride systems are, however, more complicated and involve a number of ions. Further work is necessary to test the applicability of the above concept in molten salt mixtures containing different cations and anions.

V. Conclusion

1. Though the presence of different cations in alkali metal fluoride–chloride salt systems introduces, among other things, some unstable compound formation, the liquidus temperatures for both of the systems studied in this work are around or below the melting temperature of Al metal (at least up to $x_{NaF} = 0.7$).

2. The density values for both systems in the temperature range from 1000 to 1200 K remain close to each other.

It may therefore be concluded that as far as the primary crystallization and density behaviour are concerned, it may be possible to replace the pure LiCl component in the fluoride–chloride salt system by a eutectic mixture of (LiCl + KCl) without decreasing the capability of the system as an electrolyte for aluminium electrolysis.

Acknowledgment

The authors thank their colleagues at the Electropyrometallurgy Division for their interest in the work.

1. A.P. Ratvik, T.M. Latier, G. Mamantov, S.S. Roberts, and J.Y. Josefowiez. J. Electrochem. Soc. **134**, 321 (1987).
2. Y. Marcus. Molten salt technology. *Edited by* D.G. Lovering. Plenum, New York. 1982. Chap. 10.
3. J.B. Belawadi, N. Rajagopalan, P.S. Desikan, and U. Sen. J. Appl. Electrochem. **12**, 501 (1982).
4. J.D. MacKenzie. Rev. Sci. Instrum. **27**, 297 (1956).
5. L.D. Lucas. Physico-chemical measurements in metal research. Part 2. *In* Techniques of metal research. Vol. IV. Volume Editor: R.A. Rapp. Series Editor: R.F. Bunshah. Interscience, New York. 1970. Chap. 7B.
6. A.K. Mishra. J. Electrochem. Soc. **135**, 2780 (1988).
7. E.R. Van Artsdalen and I.S. Yaffe. J. Phys. Chem. **59**, 118 (1955).
8. G.J. Jauz, R.P.T. Tomkin, and C.B. Allen. J. Phys. Chem. Ref. Data, **8**, 125 (1979).
9. S.T. Bowden. The phase rule and phase reactions. McMillan, London. 1950. pp. 172–183.
10. N.F. Rhines. Phase diagrams in metallurgy. McGraw–Hill, New York. 1956. pp. 34–56.
11. H.C. Yeh. Phase diagrams in refractive materials. Vol. 6–1. *Edited by* A.M. Alper. Academic Press, New York. 1970. pp. 169–197.
12. A. Gutierrez and J.M. Toguri. J. Chem. Eng. Data, **27**, 109 (1982).
13. N.R. Carmichael and S.N. Flengas. J. Electrochem. Soc. **126**, 2098 (1979).
14. B.F. Powers, J.L. Katz, and O.J. Kleppa. J. Phys. Chem. **66**, 103 (1962).
15. B. Cleaver and B.C.J. Neil. Trans. Faraday Soc. **65**, 2860 (1969).
16. G.J. Jane, G.L. Gardner, U. Krebs, and R.P.T. Tomkins. J. Phys. Chem. Ref. Data, **3**, 9 (1974).
17. K. Grjotheim, C. Krohn, M. Malinovsky, K. Matiasovsky, and J. Thonstad. Aluminium electrolysis. 2nd ed. Aluminium Verlag, Dusseldorf, Germany. 1982. pp. 382–384.
18. K. Grjotheim, J.L. Holm, B. Lillebuen, and H.A. Oye. Trans. Faraday Soc. **67**, 640 (1971).
19. J.L. Holm. Acta Chem. Scand. **25**, 3609 (1971).
20. O.J. Kleppa. *In* Molten salt chemistry. Ser. C, Vol. 202. *Edited by* G. Mamantov and R. Marassi. D. Reidel, Holland. 1987. p. 89.
21. H. Reiss, J.L. Katz, and O.J. Kleppa. J. Chem. Phys. **36**, 144 (1962).

Can. J. Chem. Downloaded from www.nrcresearchpress.com by 203.198.23.82 on 09/08/12
For personal use only.

Topological investigations of aniline and substituted anilines in binary solutions containing methylene bromide

V.K. SHARMA,[1] PREM PAUL SINGH, SANJEEV MAKEN, AND B. SINGH
Department of Chemistry, Maharshi Dayanand University, Rohtak-124 001, India

Received April 21, 1993

V.K. SHARMA, PREM PAUL SINGH, SANJEEV MAKEN, and B. SINGH. Can. J. Chem. **71**, 2183 (1993).

Molar excess volumes and molar excess enthalpies for various (i + j) binary methylene bromide (i) + aniline or *N*-methyl aniline and + *N*,*N*-dimethyl aniline (j) mixtures have been determined as a function of composition at 308.15 K. The data have been analysed in terms of the graph-theoretical approach and Sanchez and Lacombe theory. The graph-theoretical analyses of V^E data suggest that aniline, *N*-methyl aniline, and *N*,*N*-dimethyl aniline exist as equilibrium mixtures of monomer and dimer and that these mixtures contain 1:1 molecular complexes. The IR studies lend further credence to the nature and extent of interaction along with support for the proposed structure of molecular species in these mixtures.

V.K. SHARMA, PREM PAUL SINGH, SANJEEV MAKEN et B. SINGH. Can. J. Chem. **71**, 2183 (1993).

Opérant à 308,15 K, on a déterminé les volumes molaires en excès et les enthalpies molaires en excès de divers mélanges binaires (i + j) de bromure de méthylène (i) + aniline (ou de *N*-méthylaniline et *N*,*N*-diméthylaniline) (j) en fonction de la composition. On a analysé les données en fonction de l'approche théorique des graphes ainsi que de la théorie de Sanchez et Lacombe. L'analyse des données de V^E par le théorie des graphes suggère que, dans ces mélanges, l'aniline, la *N*-méthylaniline et la *N*,*N*-diméthylaniline existent sous la forme de mélanges à l'équilibre de monomères et de dimères et que ces mélanges contiennent de complexes moléculaires 1:1. Des études infrarouges apportent un certain support à la nature, au degré d'interactions et à la structure des espèces moléculaires présentes dans ces mélanges.
[Traduit par la rédaction]

Introduction

Aniline and substituted anilines are known to be associated (1, 2) in the pure state through hydrogen bonding and electron donor–acceptor interactions. Bellamy and Williams (3) have shown that aniline in the pure state exists as a monomer; Wolff and Mathias (4) and Kreglewski and Wilhoit (5) favor the associated structure of aniline and suggest that only one of the hydrogens of its NH_2 group is free to form a hydrogen bond and the other hydrogen atom is involved in weak interactions with the π-electron cloud of the aniline molecule. The addition of a compound like methylene bromide to aniline and substituted anilines may tend either to rupture or enhance the self-association of the latter components. As the state of association of aniline and substituted anilines in pure as well as in binary solutions may or may not be the same, it follows that thermodynamic equilibrium properties of aniline or substituted anilines + methylene bromide mixtures may provide valuable insight into the state of aggregation of these compounds and the nature of the species present in these mixtures.

Experimental

Aniline (A) (E. Merck, AR Grade), methylene bromide (MB), *N*-methyl aniline (MA), and *N*,*N*-dimethyl aniline (DMA) (Fluka, Purris quality) were purified by standard methods (6, 7). The purities were then checked by measuring their densities at 298.15 ± 0.01 K and these agreed to $\pm 5 \times 10^{-5}$ gm cm^{-3} with their corresponding literature values (8–10) (the density of MB at 298.15 K was calculated from the density versus temperature data (11)).

Molar excess volumes V^E, for the various (i + j) mixtures were determined at 308.15 K in a V-shaped dilatometer that has been described elsewhere (12). The temperature of the water thermostat was controlled to ±0.01 K by means of a toluene regulator and the uncertainty in the measured V^E values was about 0.5%.

Molar excess enthalpies, H^E, for the various binary mixtures were measured at 308.15 K in a flow microcalorimeter (LKB Broma, Sweden) in a manner described elsewhere (13) and the uncertainty in the measured H^E values was ca. 1%.

Samples for IR spectroscopic studies were prepared by mixing i and j in a 1:1 (w/w) ratio and their IR spectra were recorded on a Beckmann IR spectrophotometer (model 4250) using sodium chloride optics.

Results

The measured V^E and H^E data for MB(i) + A or MA or DMA (j) binary mixtures (recorded in Tables 1 and 2) were expressed as

$$[1] \qquad X^E(X = V \text{ or } H) = x_i (1 - x_i) \sum_{n=0}^{2} X^{(n)} (2x_i - 1)^n$$

where $X^{(n)}$ (n = 0–2) are adjustable parameters and x_i is the mole fraction of component i in the (i + j) mixture. These parameters were evaluated (14) by fitting eq. [1] to $X^E/x_i(1 - x_i)$ data by the least-squares method and are recorded along with the standard deviations, $\sigma(X^E)$ of $X^E(X = V \text{ or } H)$, defined by

$$[2] \qquad (X^E) = [\Sigma (X^E_{\text{expt}} - X^E_{\text{calcd.eq.[1]}})^2/(m - p)]^{0.5}$$

(where m is the number of data points and p is the number of adjustable parameters in eq. [1], in Tables 1 and 2.

Discussion

We are unaware of any V^E and H^E data with which to compare our results. V^E for MB(i) + A, +MA, and + DMA(j) mixtures are all positive and for an equimolar mixture vary in the order DMA > MA > A. On the other hand, while H^E data for MB(i) + A and + MA(j) mixtures are negative, those for the MB(i) + DMA(j) mixture are positive and for an equimolar mixture vary in the order A < MA < DMA.

Aniline and substituted anilines are known to be associated in the pure state (1, 2) through hydrogen bonding and

[1]Author to whom correspondence may be addressed.

Can. J. Chem. Downloaded from www.nrcresearchpress.com by 203.198.23.82 on 09/08/12
For personal use only.

Can. J. Chem. Downloaded from www.nrcresearchpress.com by 203.198.23.82 on 09/08/12
For personal use only.

TABLE 1. Measured molar excess volumes, V^E, data for various i + j mixtures as functions of mole fractions, x_i, of i at 308.15 K; also included are the various $V^{(n)}$ (n = 0–2) parameters and standard deviations $\sigma(V^E)$[a]

x_i	V^E (cm^3 mol^{-1})	x_i	V^E (cm^3 mol^{-1})
Methylene bromide (i) + aniline (j)			
0.0291	0.029	0.4916	0.324
0.0606	0.056	0.5691	0.321
0.1012	0.093	0.6106	0.316
0.1678	0.156	0.7219	0.264
0.2712	0.234	0.8675	0.151
0.3812	0.295	0.9201	0.093
0.4446	0.317	0.9582	0.053
$V^{(0)}$ = 1.3005; $V^{(1)}$ = 0.1510; $V^{(2)}$ = −0.2083; $\sigma(V^E)$ = 0.003			
Methylene bromide (i) + N-methyl aniline (j)			
0.0391	0.053	0.4801	0.424
0.0791	0.102	0.5426	0.426
0.1302	0.164	0.6212	0.407
0.1917	0.235	0.7346	0.344
0.2602	0.299	0.7901	0.293
0.3482	0.367	0.8829	0.181
0.4491	0.415	0.9329	0.111
$V^{(0)}$ = 1.694; $V^{(1)}$ = 0.2027; $V^{(2)}$ = 0.1602; $\sigma(V^E)$ = 0.004			
Methylene bromide (i) + N,N-dimethyl aniline (j)			
0.0416	0.057	0.5121	0.450
0.0625	0.088	0.5846	0.443
0.1182	0.158	0.6902	0.394
0.1976	0.254	0.7812	0.317
0.2702	0.325	0.8426	0.248
0.3639	0.399	0.8706	0.210
0.4692	0.442	0.9502	0.086
$V^{(0)}$ = 1.1701; $V^{(1)}$ = 0.2165; $V^{(2)}$ = −0.1706; $\sigma(V^E)$ = 0.005			

[a] $V^{(n)}$ (n = 0–2) and $\sigma(V^E)$ are in cm^3 mol^{-1}.

electron donor–acceptor interactions. The observed V^E and H^E data for MB (i) + A, + MA and + DMA(j) mixtures may then be explained if it be assumed that (i) aniline and substituted anilines are associated in the pure state through hydrogen bonding and electron donor–acceptor interaction, (*ii*) aniline and substituted anilines interact with the methylene bromide, and (*iii*) there is steric repulsion between substituted anilines and methylene bromide.

Since V^E for the binary mixture reflects the packing of the components of that mixture, V^E data for the MB(i) + A(j) mixture suggest that contributions due to factors (i) and (*iii*) far outweigh contributions due to factor (*ii*), so that the overall V^E for this mixture is positive. Further, as the measured H^E is due to the cumulative effects of (i), (*ii*), and (*iii*), the negative H^E values for the MB(i) + A(j) mixture suggest that the heat effect due to factor (*ii*) outweighs those due to (i) and (*iii*). The introduction of a CH_3 group in aniline, as in MA, would then increase electron density around the nitrogen atom, so the association in N-methyl molecules will be less than that in aniline molecules. The contribution to V^E and H^E due to factor (i) will then be greater in the case of MB(i) + MA(j) than in MB (i) + A(j) mixtures. In other words, while V^E for the MB(i) + MA(j) mixture should be more positive than that of the MB(i) + MA(j) mixture, H^E for the MB(i) + MA(j) mixture should be less negative than for the MB(i) + A(j) mixtures. The experimental V^E and H^E data for these mixtures lend credence to this viewpoint. Further, the presence of two methyl groups in aniline, as in DMA, would not allow DMA molecules to undergo a hydrogen-bonded interaction with MB, so that V^E and H^E data for the MB(i) + DMA(j) mixture should be more positive than those for MB(i) + A or MA(j) mixtures. This is indeed true.

If the addition of MB(i) to A, MA, and DMA(j) causes changes in the topology of i and or j, it must be reflected in the equilibrium thermodynamic properties of the (i) + (j) mixtures. It would, therefore, be worthwhile to analyse V^E data of MB(i) + A, + MA and + DMA(j) mixtures in terms of an approach (15) that employs the graph-theoretical concept of the third degree of the constituents of these (i + j) mixtures. According to this approach (15), V^E is given by

$$[3] \quad V^E = \alpha_{ij}\,[\{x_i\,({}^3\xi_i)_m + x_j({}^3\xi_j)_m\}^{-1} - \Sigma\, x_i/{}^3\xi_i]$$

where ${}^3\xi_i$ and $({}^3\xi_i)_m$ in eq. [3] denote, respectively, the values of component i in the pure state and in the mixture and are defined (16) by

$$[4] \quad {}^3\xi = \sum_{m\le n\le o\le p} (\delta^v_m \cdot \delta^v_n \cdot \delta^v_o \cdot \delta^v_p)^{-0.5}$$

where δ^v_m etc. have the same significance as explained elsewhere (16).

Since the degree of association of j is not known with certainty and as no theoretical method is available to evaluate $({}^3\xi_j)_m$ of j in the (i + j) mixtures, we regarded $({}^3\xi_i)_m$, $({}^3\xi_j)_m$, ${}^3\xi_i$, and ${}^3\xi_j$ as adjustable parameters and evaluated them by fitting experimental V^E data to eq. [3]. Only those $({}^3\xi_i)_m$ and ${}^3\xi_i$ values were retained that best reproduced the experimental V^E data, i.e., for which the variance to fit, ρ, defined by $\rho = \{\Sigma(V^E_{\text{exptl.}} - V^E_{\text{calcd.}})^2/(Q\text{-}P)\}^{0.5}$ (where $(Q\text{-}P)$ is the number of degrees of freedom) was minimum. Such $({}^3\xi_i)_m$, ${}^3\xi_i$ etc. values along with the V^E values (calculated using eq. [3]) at various x_i are recorded in Table 3.

A number of structures were then assumed for A, MA, and DMA, and their ${}^3\xi'_j$ values were determined from structural considerations. These ${}^3\xi'_j$ values were next compared with the corresponding ${}^3\xi_j$ values obtained for them via eq. [3] from V^E data; any structure or a combination of structures (for a component) that yielded a ${}^3\xi'$ value that compares favourably with its ${}^3\xi$ values was taken to be a good representation of the structure of that component. For the present (i + j) mixtures, we assumed that A, MA, and DMA exist as **1**–**2**, **3**–**4**, **5**–**5***a* entities. It was, however, assumed that in entities **2**, **4**, and **5**, δ^v (π) = 1 (16) (where the π-electron cloud of molecule is involved in specific interaction with another molecule). The δ^v values for the various vertices in the various entities are shown in Scheme 1.

The ${}^3\xi'_j$ values for the entities **1**–**5***a* were then calculated to be 1.361, 1.89, 1.256, 1.814, 2.10, and 1.181, respectively. Since the ${}^3\xi_j$ values of A, MA, and DMA (j) in the present (i + j) are 1.65, 1.728, and 1.88 (Table 3), they suggest that in these mixtures A, MA, and DMA exist, as an equilibrium mixture of monomer and dimer. Further, in MB(i) + A, + MA and + DMA(j) mixtures, it was assumed that these (i + j) mixtures may contain molecular entities **6**, **7**, and **8**, respectively (Scheme 2). In evaluating $({}^3\xi'_j)_m$ values for the molecular entities **6** and **7**, it was next assumed that only one C—Br edge of MB is involved in

TABLE 2. Measured molar excess enthalpies, H^E, data for various $i + j$ mixtures as functions of mole fractions, x_i, of i at 308.15 K; also included are the various $H^{(n)}$ (n = 0–2) parameters and standard deviations $\sigma(H^E)$[a]

x_i	H_E (J mol^{-1})	x_i	H^E (J mol^{-1})
Methylene bromide (i) + aniline (j)			
0.0478	− 52.8	0.4462	−430.2
0.0821	− 96.2	0.5129	−444.2
0.1401	−164.8	0.6006	−425.1
0.2121	−250.1	0.6612	−396.7
0.2402	−280.2	0.7401	−329.1
0.3168	−355.2	0.8491	−207.2
0.3907	−406.0	0.9205	−111.1
$H^{(0)}$ = −1769.15; $H^{(1)}$ = −159.41; $H^{(2)}$ = 546.9; $\sigma(H^E)$ = 4.4			
Methylene bromide (i) + N-methyl aniline (j)			
0.0618	− 52.0	0.5202	−380.1
0.1011	− 93.0	0.6161	−351.4
0.1621	−154.2	0.6802	−314.0
0.2412	−238.1	0.7241	−275.1
0.3391	−320.0	0.7828	−222.2
0.4126	−360.0	0.8410	−158.2
0.4907	−380.9	0.8928	−104.2
$H^{(0)}$ = −1520.8; $H^{(1)}$ = −40.0; $H^{(2)}$ = 760.0; $\sigma(H^E)$ = 4.4			
Methylene bromide (i) + N,N-dimethyl aniline (j)			
0.0578	33.1	0.5310	274.1
0.1212	79.8	0.6426	241.1
0.1826	125.1	0.6918	217.2
0.2612	182.8	0.7440	184.0
0.3627	243.2	0.7802	157.0
0.4428	267.6	0.8412	109.1
0.4982	274.2	0.9117	56.4
$H^{(0)}$ = 1099.3; $H^{(1)}$ = 14.45; $H^{(2)}$ = −608.7; $\sigma(H^E)$ = 3.2			

[a] $H^{(n)}$ (n = 0–2) and $\sigma(H^E)$ are in J mol^{-1}.

hydrogen-bond interaction with one hydrogen atom of the NH_2 group of A and MA, and the molecular entity **8** may be characterized by specific interaction between the vacant 3d level of the bromine atom of MB and the π-electron cloud of the aromatic ring of DMA. The $({}^3\xi_j')_m$ values for the molecular entities **6**, **7**, and **8** were then calculated to be 1.85, 1.77, and 1.414, respectively. Since the $({}^3\xi_j')_m$ values suggest that these mixtures contain the molecular entities **6**, **7**, and **8**, the presence of molecular entities **6** and **7** would then suggest that there must be changes in the C—Br vibration of MB and the N—H stretching vibration of A and MA. On the other hand, molecular entity **8** suggests that there must be a change in the ring vibration of DMA and the C—Br stretching of MB in the mixture.

We next analysed the infrared spectral data of pure i,j, and their equimolar mixtures. It was observed that while MB and A in the pure state show characteristic absorption at 620 cm^{-1} (C—Br stretch) (17) and 3400 cm^{-1} (N—H stretch) (17), the infrared spectrum of the equimolar mixture of MB(i) + A and + MA(j) shows characteristic bands at 610 and 605 cm^{-1} (C—Br stretch) and 3380 and 3385 cm^{-1} (N—H stretch), respectively. The infrared spectra of the MB(i) + A and + MA(j) mixtures clearly suggest that the addition of j to i does influence the C—Br vibration of MB and the N—H stretching vibration of A and MA and thus lends support to the presence of molecular entities **6** and **7** in MB(i) + A and + MA(j) mixtures. On the other hand, in the MB(i) + DMA(j) mixture, it was observed that DMA(j) in the pure state exhibits ring vibrations (17) at 1590, 1500, and 1430 cm^{-1}. The infrared spectrum of the MB(i) + DMA(j) mixture shows characteristic bands at 1582, 1490, 1422 cm^{-1} (ring vibration), and 602 cm^{-1} (C—Br stretch). The infrared spectrum of MB(i) + DMA(j) thus suggests that the addition of j in i influences the ring vibrations and C—Br stretching in the mixture and so points to the molecular entity in the mixture.

To understand the energetics of the various interactions involved in these binary mixtures, if A, MA, and DMA exist as an associated entity, then the present ($i + j$) binary mixture may be visualized (18) to involve (*i*) the establishment of unlike i–j contacts between i and j, (*ii*) this unlike contact formation between i and j would then cause depolymerization of j to yield free j monomers, and (*iii*) the monomers of j would then undergo a specific interaction with the bromine atom of MB to form the ij molecular entity. Molecular entities of the type i_2j, ij_2, and i_2j_2 may also be present in these mixtures containing ij molecular entities and the contributions made by other entities are very small compared to the H^E for these mixtures. This is also consistent with the information provided by the analysis of their V^E data in terms of eq. [3].

Consequently, if X_{ij} is the molar enthalpy interaction parameter of unlike i–j contact formation, then the change in enthalpy due to (*i*) would be given (19, 20) by

$$[5] \quad \Delta H_1 = x_i X_{ij} S_j$$

where S_j is the surface fraction of j involved in ($i - j$) contact and is defined (21, 22) by

$$[6] \quad S_j = x_j V_j / \Sigma x_i V_i$$

so that

$$[7] \quad \Delta H_1 = x_i x_j X_{ij} V_j / \Sigma x_i V_i$$

Further if X_{jj} and X_{12} are the molar enthalpy interaction parameters of $j - j$ and specific 1–2 interactions, respectively, then change in molar enthalpy due to processes (*ii*) and (*iii*) would be given (21) by

$$[8] \quad \Delta H_2 = x_i^2 x_j V_j X_{jj} / \Sigma x_i V_i$$

and

$$[9] \quad \Delta H_3 = x_i x_j^2 V_j X_{12} / \Sigma x_i V_i$$

The overall change in molar enthalpy due to processes (*i–iii*) would then be expressible (22) by

$$[10] \quad H^E = \sum_{i=1}^{3} \Delta H_i = [x_i x_j V_j / \Sigma x_i V_i] [X_{ij} + x_i X_{jj} + x_j X_{12}]$$

Since V_j/V_i has been taken equal to ${}^3\xi_i/{}^3\xi_j$ ($=Y$) then eq. [10] reduces to

$$[11] \quad H^E = [x_i x_j Y / (x_i + x_j Y)] (X_{ij} + x_i X_{jj} + x_j X_{12})$$

For MB(i) + A, + MA and + DMA(j) mixtures, it would, however, be more reasonable to assume that $X_{ij} = X_{jj} = X'_{jj}$ so that eq. [11] reduces to

$$[12] \quad H^E = [x_i x_j Y / (x_i + x_j Y)] [(1 + x_i) X'_{jj} + x_j X_{12}]$$

Equation [12] contains two adjustable parameters X'_{jj} and X_{12},

Can. J. Chem. Downloaded from www.nrcresearchpress.com by 203.198.23.82 on 09/08/12
For personal use only.

TABLE 3. Comparison of $X^E(X = V \text{ or } H)$ values (calculated from the appropriate equations (see text)) with their corresponding experimental values at 308.15 K for the various $(i + j)$ mixtures as functions of, x_i, mole fraction of i, alongwith various ${}^3\xi$ and X, etc., parameters[a]

Property	Mole fraction, x_i						
	0.1	0.2	0.3	0.6	0.7	0.8	0.9
Methylene bromide (i) + aniline (j)							
V(Exptl.)	0.095	0.182	0.254	0.317	0.278	0.210	0.115
V(Calcd.)	0.098	0.181	0.248	0.327	0.302	0.243	0.145
V(Sanchez)	−1.073	—	−1.113	—	−0.552	—	−0.082
H(Exptl.)	−117	−236	−340	−427	−367	−267	−139
H(Calcd.)	−131	−248	−343	−439	−395	−309	−178
H(Sanchez)	−709	—	−970	—	−552	—	−173
H(Chem)	−340	−728	−1092	−1522	−1354	−1028	−563
H(Chem)*	−415	−803	−1131	−1505	−1371	−1080	−626
${}^3\xi_i = ({}^3\xi_i)_m = 1.00$; ${}^3\xi_j = ({}^3\xi_j)_m = 1.65$; $\alpha_{ij} = -6.706$ cm^3 mol^{-1}							
$X_{12} = 309.4$; $X_{jj} = -1665.9$; $X^*_{12} = 1753.65$; $X^*_{jj} = -5896.6$							
Methylene bromide (i) + N-methyl aniline (j)							
V(Exptl.)	0.149	0.262	0.345	0.418	0.378	0.299	0.175
V(Calcd.)	0.126	0.234	0.322	0.431	0.399	0.324	0.195
V(Sanchez	−0.201	—	−1.175	—	−0.441	—	−0.133
H(Exptl.)	−90	−196	−291	−359	−297	−203	−96
H(Calcd.)	−146	−255	−311	−360	−311	−234	−131
H(Sanchez)	−441	—	−954	—	−652	—	−493
H(Chem)	−313	−687	−1043	−1454	−1277	−964	−520
H(Chem)*	−395	−771	−1033	−1467	−1336	−1053	−611
${}^3\xi_i = ({}^3\xi_i)_m = 1.0$; ${}^3\xi_j = ({}^3\xi_j)_m = 1.728$; $\alpha_{ij} = -7.5579$ cm^3 mol^{-1}							
$X_{12} = -416.26$; $X_{jj} = -1243.45$; $X^*_{12} = 2131.69$; $X^*_{jj} = -6024.65$							
Methylene bromide (i) + N,N-methyl aniline (j)							
V(Exptl.)	0.137	0.257	0.353	0.438	0.388	0.296	0.165
V(Calcd.)	0.129	0.247	0.335	0.458	0.428	0.352	0.213
V(Sanchez)	0.01	—	0.348	—	0.207	—	0.081
H(Exptl.)	91	165	221	271	245	191	111
H(Calcd.)	88	162	220	269	240	186	106
H(Sanchez)	240	—	224	—	150	—	76
${}^3\xi_i = ({}^3\xi_i)_m = 1.00$; ${}^3\xi_j = ({}^3\xi_j)_m = 1.88$; $\alpha_{ij} = -6.2606$ cm^3 mol^{-1}							
$X_{12} = -187.3$; $X_{jj} = 1118.45$							

[a]X and X^* etc. are in J mol^{-1} and V and H represent V^E (cm^3 mol^{-1}) and H^E (J mol^{-1}), respectively.

and these were calculated from the H^E data of the $(i + j)$ mixtures at two arbitrary compositions $x_i = 0.4$ and 0.5, which were subsequently employed to predict H^E data for the $(i + j)$ mixture at other values of x_i. Such H^E data along with various interaction parameters x_{jj} and X_{12} are recorded in Table 3 and are also compared with their corresponding experimental values.

Examination of Table 3 shows that H^E data calculated from eq. [12] for the $(i + j)$ mixtures compare reasonably well with their corresponding experimental values. This lends support to the assumption made in deriving eq. [12] and also to the validity of the assumption $V_j/V_i = {}^3\xi_i/{}^3\xi_j$.

Further examination of Table 3 reveals that the enthalpy interaction parameter X'_{jj} for A is more negative than that for MA, which is not true. The failure of X'_{jj} values to explain the boiling point of A and MA can be explained by the fact that in deriving eq. [12] it has been assumed that overall H^E is due to chemical interactions between the components of the $(i + j)$ mixtures. Since H^E is small for MB + A and + MA mixtures, it suggests that physical interactions play an important role in determining their H^E values. As

$$H^E = H^E_{phys} + H^E_{chem}$$

and if H^E for the reference system (23) MB(i) + cyclohexane (j) is taken to be H^E_{phys} for these systems, then the resulting H^E_{chem} for MB(i) + A and + MA(j) mixtures should be analysed in terms of eq. [12]. Such H^E_{chem} values at $x_i = 0.4$ and 0.5 were then employed to evaluate X^*_{jj} and X^*_{12} values, which were next employed to evaluate H^E_{chem} at other values of x_i. Such H^E_{chem} values along with interaction parameters X^*_{jj} and X^*_{12} are recorded in Table 3 as H(chem)* and also compared with their corresponding H^E_{chem} values.

Examination of Table 3 now reveals that H^E_{chem}* data[2] calculated from eq. [12] for MB + A and + MA mixtures compare reasonably well with their corresponding H^E_{chem} values and, further, the X^*_{jj} value for MA is more negative than A, which suggests that the boiling point of A must be less than that of MA. This is indeed true, which lends sup-

[2]H(chem)* values correspond to H^E values evaluated from eq. [12] utilizing X^*_{12} and X_{jj} data recorded in Table 3.

Can. J. Chem. Downloaded from www.nrcresearchpress.com by 203.198.23.82 on 09/08/12
For personal use only.

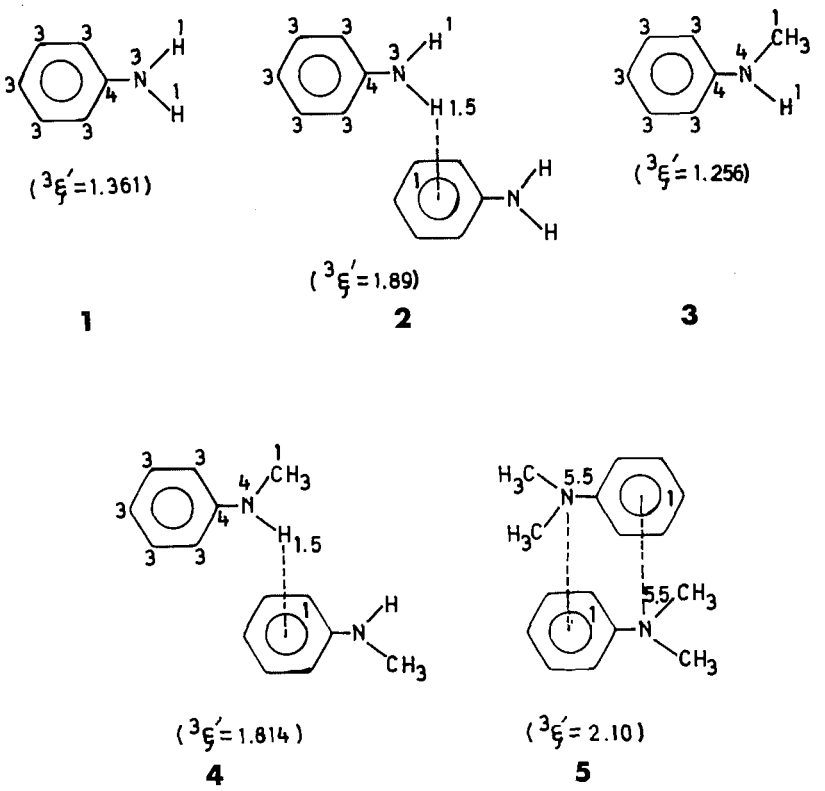

SCHEME 1

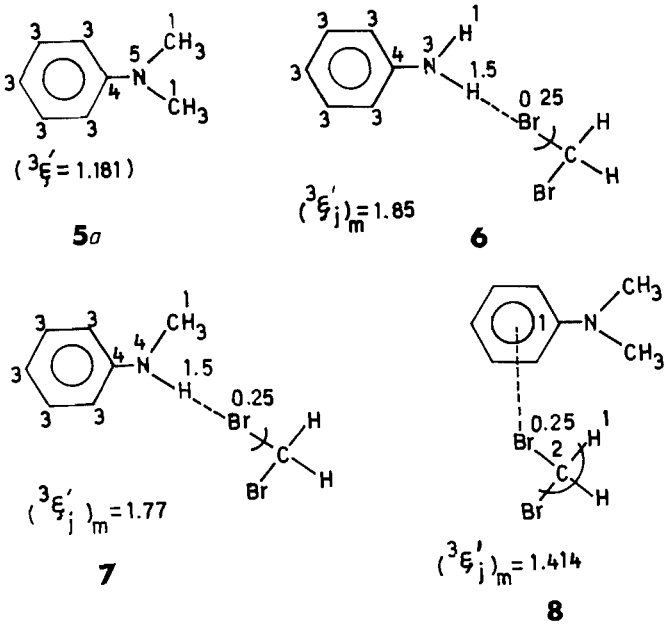

SCHEME 2

port to our assumption that H^{E}_{phys} plays an important role in the H^{E} data for MB(i) + A and + MA(j) mixtures.

V^{E} and H^{E} data for MB(i) + A, + MA and + DMA(j) mixtures were next analysed in terms of Sanchez and Lacombe theory in the manner explained earlier (24, 25). V^{E} and H^{E} values calculated according to this theory for the present (i + j) binary mixtures at x_i = 0.1, 0.3, 0.7, and 0.9 are recorded in Table 3 and are also compared with their corresponding experimental values. Examination of Table 3 has revealed that V^{E} and H^{E} values so calculated show poor agreement with the experimental values. This poor agreement between the calculated and experimental V^{E} and H^{E} for these (i + j) mixtures may be attributed to the failure of these mixtures to satisfy the equation of state of the mixture.

The present analysis thus has shown that the graph-theoretical approach reproduces well not only the V^{E} and H^{E} data of the present (i + j) mixtures but it can also be employed to understand the state of aggregation of the components and the energetics of molecular interaction between them, and that all the information is consistent with the general principles of organic chemistry.

Acknowledgement

S.M. expresses his thanks to the Council of Scientific and Industrial Research, New Delhi, for the award of a Research Associateship.

1. H. Kehiaian and K. Kehiaian. Trans. Faraday Soc. **62**, 838 (1966).
2. D. Phillippe, D. Guy, and H. Pieree. Ann. Sci. (Bruxelles), **82**, 91 (1968); Chem. Abstr. **69**, 100228, (1968).
3. L.J. Bellamy and R.L. Williams. Spectrochim. Acta, **9**, 341 (1957).
4. A. Kreglewski and R.C. Wilhoit. J. Phys. Chem. **79**, 449 (1975).
5. H. Wolff and D. Mathias. J. Phys. Chem. **77**, 2081 (1973).
6. A. Vogel. A text book of practical organic chemistry. 4th ed. English Language Book Society, London. 1978.
7. M. Chandriah Chowdhary and V.R. Krishnan. Aust. J. Chem. **20**, 2761 (1967).
8. P. Walden. Z. Phys. Chim. Leipzig, **65**, 129 (1909).
9. B.E. Trau. J. Chim. Phys. **32**, 501 (1935); **32**, 589 (1935).

Can. J. Chem. Downloaded from www.nrcresearchpress.com by 203.198.23.82 on 09/08/12
For personal use only.

10. A.V. Few and J.W. Smith. J. Chem. Soc. 753 (1949).
11. J. Timmermans. Physico-chemical constants of pure organic compounds. Elsevier, Amsterdam. 1950, p. 276.
12. P.P. Singh and S.P. Sharma. J. Chem. Eng. Data, **30**, 487 (1985).
13. H.P. Dahiya, P.P. Singh, and S. Dagar. Fluid Phase Equillb. **33**, 191 (1987).
14. J. Wisniak and A. Tamir. Mixing and excess thermodynamic properties. Elsevier, Amsterdam. 1978.
15. P.P. Singh, V.K. Sharma, and S.P. Sharma. Thermochim. Acta, **106**, 293 (1986).
16. P.P. Singh. Thermochim. Acta, **66**, 37 (1983).
17. C.N.R. Rao. Chemical application of infrared spectroscopy. Academic Press, London. 1963.
18. P.P. Singh. J. Chem. Soc. Faraday Trans. 1, **84**, 1807 (1988).
19. M.L. Huggins. J. Phys. Chem. **34**, 371 (1970).
20. M.L. Huggins. Polymer, **12**, 389 (1971).
21. P.P. Singh and M. Bhatia. J. Chem. Soc. Faraday Trans. 1, **85**, 3807 (1989).
22. D.H. Rouvary. RIC Rev. **4**, 173 (1971).
23. P.P. Singh, V.K. Sharma, S. Maken, and B. Singh. Thermochim. Acta. In press.
24. R.H. Lacombe and I.C. Sanchez. J. Phys. Chem. **80**, 2352 (1976).
25. R.H. Lacombe and I.C. Sanchez. J. Phys. Chem. **80**, 2568 (1976).

Can. J. Chem. Downloaded from www.nrcresearchpress.com by 203.198.23.82 on 09/08/12
For personal use only.

Molecular dynamics simulation of interhalogen compounds using two potential models 2. Liquid bromine trifluoride (BrF_3) — structure and thermodynamics[1]

VIVEK SAXENA
Department of Chemistry, University of Delhi, Delhi—110 007, India

Received September 16, 1992

VIVEK SAXENA. Can. J. Chem. **71**, 2189 (1993).

This paper reports on the molecular dynamics simulation results of liquid bromine trifluoride (BrF_3) at 299, 315, and 363 K. We have assumed that the molecules interact via Lennard–Jones 12–6 site–site pair potential and Lennard–Jones site–site + fractional charges over atomic sites. Lennard–Jones potential parameters of Singer et al. (Mol. Phys. **33**, 1757 (1977)) have been used for Br–Br, and F–F interactions and cross interaction terms are calculated using Lorentz–Berthelot mixing rules. Fractional charges are assigned to reproduce the experimentally determined gaseous-state molecular dipole moment. Various structural and thermodynamic properties for liquid state are reported and compared in detail with results from diffraction studies (Mittkin et al. J. Struct. Chem. **28**, 60 (1987)). Some mechanical properties such as mean-square force and torque, self-diffusion coefficient have also been calculated. The repulsive part of the proposed atom–atom pair potential is a good approximation since both molecular configurations are in good agreement with experimental results.

VIVEK SAXENA. Can. J. Chem. **71**, 2189 (1993).

On rapporte les résultats de simulations de la dynamique moléculaire du trifluorure de brome (BrF_3) à 299, 315 et 363 K. On a fait l'hypothèse que les molécules interagissent par le biais d'une paire de potentiel de Lennard–Jones à 12–6 site–site et de Lennard–Jones site–site + charges fractionnaires sur les sites atomiques. On a utilisé les paramètres du potentiel de Lennard–Jones rapportés par Singer et al. (Mol. Phys. **33**, 1757 (1977)) pour les interactions Br–Br et F–F et on a calculé les termes d'interactions croisées à l'aide des règles de mélange de Lorentz–Berthelot. On a obtenu les charges fractionnaires sous la forme de valeurs attribuées pour reproduire le moment dipolaire expérimental de la molécule dans son état gazeux. On rapporte diverses propriétés structurales et thermodynamiques de l'état liquide et l'on effectue une comparaison en profondeur avec les études de diffraction (Mittkin et al. J. Struct. Chem. **28**, 60 (1987)). On a aussi calculé quelques propriétés mécaniques comme la force et le moment de torsion quadratique moyen et le coefficient d'autodiffusion. La partie répulsive de la paire de potentiel atome–atome proposée est une bonne approximation puisque la configuration moléculaire de deux molécules est en bon accord avec les valeurs expérimentales.
[Traduit par la rédaction]

Can. J. Chem. Downloaded from www.nrcresearchpress.com by 203.198.23.82 on 09/08/12
For personal use only.

Introduction

As an extension of our work on interhalogen compounds (1), this article reports on the molecular dynamics (MD) simulation results of liquid bromine trifluoride (BrF_3). Simulations are carried out at three temperatures 299, 315, and 363 K using two potential models: (*i*) Lennard–Jones site–site pair potential and (*ii*) the first version slightly modified by including fractional charges over the atomic sites. The repulsive part of the atom–atom pair potential proposed by Singer et al. (2) has found to be good at predicting short range structure in the liquid state. Our structural properties are in good agreement with those from diffraction study and our two possible molecular configurations agree well with literature (3–7).

Chemical and structural information have been obtained from fluorine-19 nmr spectra of bromine trifluoride (4). Infrared studies (6) showed the presence of the following compounds in the liquid state:

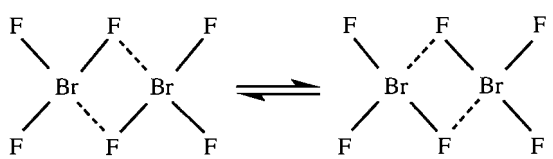

These structures provide a very simple and attractive mechanism for an exchange of non-equivalent fluorine atoms. The same observation applies to both chlorine trifluoride and bromine trifluoride. Probably, the dimer transient in the liquid state is stable in a rigid matrix (6).

The simulation averages for structural properties (radial distribution functions, closest contact distances, and possible molecular configurations for the two molecules), thermodynamic properties, and certain mechanical properties such as mean-square force, mean-square torque, and self-diffusion coefficients have been evaluated for the two models.

Method

Simulations have been carried out for microcanonical ensembles for liquid bromine trifluoride around temperatures 299, 315, and 363 K, yielding densities as given in Table 1. Molecular structure is assumed to be in a twisted "T" form for bromine trifluoride (Fig. 1), as confirmed by electron diffraction studies (8). Details in simulation and calculation of the properties have been described (1, 9). Lennard–Jones 12–6 site–site potential parameters used in the simulation are as follows: $\sigma_{F-F} = 2.83$ Å, $\epsilon_{F-F} = 58.8$ K, $\sigma_{Br-Br} = 3.54$ Å, and $\epsilon_{Br-Br} = 275.2$ K (2) and cross interaction terms σ_{ab} and ϵ_{ab} are obtained according to the Lorentz–Berthelot rule as:

$$\sigma_{ab} = \frac{\sigma_{aa} + \sigma_{bb}}{2} \quad \text{and} \quad \epsilon_{ab} = \sqrt{\epsilon_{aa}\,\epsilon_{bb}}$$

The second potential model is an improvement over the first; it included fractional charges at the atomic sites ($Q_F = -0.1264$ and $Q_{Br} = 0.3792$). These values are calculated to reproduce the molecular dipole moment ($\mu = 1.19$ D) (10). Charges are assigned to atoms while molecular electrical

[1]This paper is published without the benefit of the author's corrections.

TABLE 1. Simulation thermodynamic properties of liquid bromine trifluoride

Model	T (K)	ρ (g cm^{-3})	P/ρ (kT)	ν (kJ mol^{-1})
LJ	298.5 ± 10.7	2.803	5.265	−31.77 ± 6.27
LJ + FC	303.4 ± 10.6	2.803	4.591	−26.68 ± 6.50
LJ	315.0 ± 10.1	2.735	4.582	−28.15 ± 6.19
LJ + FC	319.7 ± 11.1	2.735	3.877	−22.55 ± 6.45
LJ	362.9 ± 11.2	2.635	4.027	−27.40 ± 6.97
LJ + FC	367.5 ± 11.9	2.635	3.456	−22.13 ± 6.82

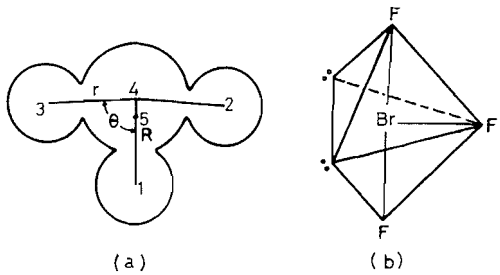

FIG. 1. Bromine trifluoride molecule: (*a*) sites 1, 2, and 3, fluorine; 4, bromine; 5, centre-of-mass. Internal parameters: R = 1.721 Å, r = 1.810 Å, and θ = 86° 12.6′; (*b*) orientation of three bond pairs and two lone pairs in the molecule.

TABLE 2. r_{max} and n_0 of the first peak in $g(r)$, simulation results of liquid bromine trifluoride using first potential model (Lennard–Jones 12–6 site–site pair potential) at three different temperatures

	298.5 K		315.0 K		362.9 K	
$g(r)^a$	r_{max} (Å)	n_0	r_{max} (Å)	n_0	r_{max} (Å)	n_0
5–5	4.5	13.0	4.5	12.9	4.6	12.9
1–1	3.0	1.8	3.0	1.5	3.0	1.6
1–2	2.9	1.7	3.0	1.6	3.0	1.7
1–4	3.8	4.8	4.0	4.9	4.1	4.3
2–2	3.0	1.9	3.0	1.9	3.0	2.0
2–4	3.8	6.2	4.1	7.6	4.1	5.7
4–4	4.7	13.0	4.6	12.9	4.8	13.0

[a]Numbers denote sites as in Fig. 1.

TABLE 3. r_{max} and n_0 of the first peak in $g(r)$, simulation results of liquid bromine trifluoride with the second potential model (Lennard–Jones potential + fractional charges) over sites at three different temperatures

	303.4 K		319.7 K		367.5 K	
$g(r)^a$	r_{max} (Å)	n_0	r_{max} (Å)	n_0	r_{max} (Å)	n_0
5–5	4.5	13.3	4.5	13.0	4.6	13.0
1–1	3.1	1.6	3.1	1.5	3.0	1.8
1–2	3.0	1.9	3.1	2.1	3.1	1.6
1–4	3.5	5.3	3.5	5.0	3.9	4.9
2–2	3.0	2.1	3.2	2.3	3.0	2.0
2–4	3.4	6.6	3.5	6.1	3.8	11.5
4–4	4.6	13.7	4.7	13.5	4.6	13.0

[a]Numbers denote sites as in Fig. 1.

neutrality is maintained. The molecular dipole moment μ and the fluorine charges q are related by

$$[1] \quad \mu = 2 \cdot q \cdot r \cdot \cos\theta + q \cdot R$$

where r and R are defined in Fig. 1. All calculations were carried out using the MDPOLY and MDMANY program (FORTRAN 77 coded) developed by Thompson and Ficham (9) for LJ and LJ + FC models, respectively. The electrostatic forces and energies in MDMANY are calculated by using the Ewald method (9).

Results and discussion

Site–site radial distribution functions (rdf's) for liquid bromine trifluoride are obtained by simultaneous analysis of molecular trajectories during simulation. Pair separations were then sorted in histograms each of width 0.01 nm. The rdf's describe the gross structural features of liquid bromine trifluoride at the three temperatures. Integration of the function $r^2g(r)$ up to the first minimum yields the coordination number n_0 of the first shell around a moiety (a molecule or a site). The first maximum represents the most probable distance r_{max} between the two moieties. Values for r_{max} and n_0 of the two models are listed in Tables 2 (LJ) and 3 (LJ + FC). Since there is no noticeable difference in short-range liquid structural properties (see r_{max} and n_0 values in Tables 2 and 3) we only list a few representative values. Including fractional charges in the first potential model only improves the attractive tail of the potential. Judging from the r_{max} and n_0 values in Tables 2 and 3, the centre-of-mass rdf's given for the two models in Fig. 2 did not seem to effect r and g(r) of the first peak of the various rdf's. It shows that the short range structure of the liquid depends on the repulsive part of the potential (11).

Molecular scattering of liquid bromine trifluoride by X-ray diffraction (5) at 298 K shows a sharp maximum at s = 1.55 Å^{-1}, which corresponds to a 4.54 Å mean molecular distance in the liquid state. Our simulation result from the center-of-mass yields r_{max} = 4.5 Å. Thus the potential seems to be well-behaved at short range in the liquid state. However, a mean molecular distance of 4.54 Å (5) is substantially smaller than that obtained by rigid rotator approximation (5.4 Å) for a molecular liquid corresponding to a density of 2.8040 g cm^{-3} at 298 K. Other studies such as infrared (6), and ^{19}F NMR (4) spectroscopy, X-ray diffraction (5), and high Trouton's constant (10), seem to indicate molecular association in the liquid state.

A radial distribution function calculated from the trajectories obtained from simulation results using both models gave 2.4, 2.9, and 3.4 Å to be the distances of closest ap-

Can. J. Chem. Downloaded from www.nrcresearchpress.com by 203.198.23.82 on 09/08/12
For personal use only.

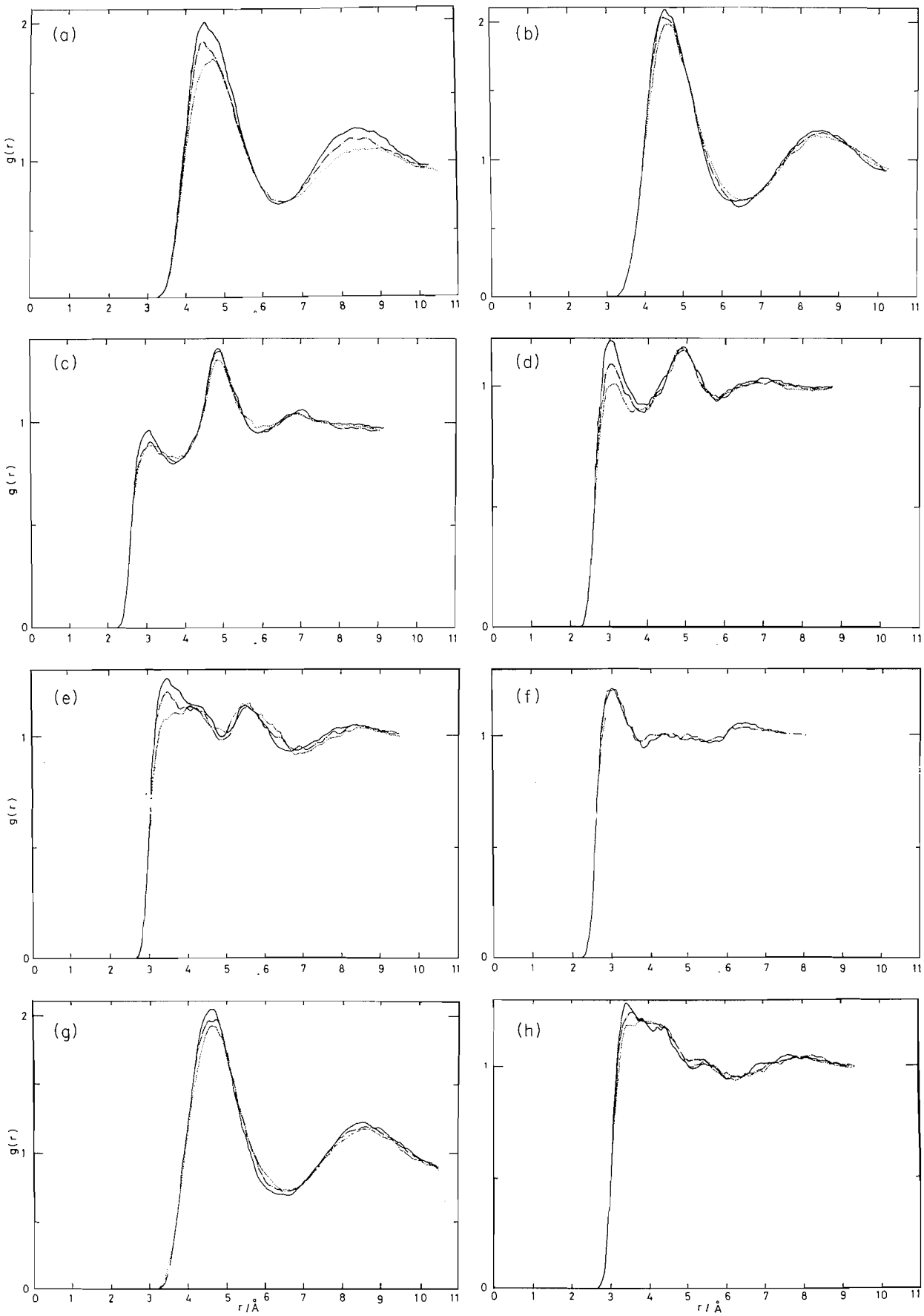

FIG. 2. Radial distribution functions: (——) 303 K, (–·–·–) 319 K (···) 367 K. (*a*) 5–5 for LJ model and (*b*) 5–5, (*c*) 1–1, (*d*) 1–2, (*e*) 1–4, (*f*) 2–2, (*g*) 2–4, and (*h*) 4–4 for LJ + FC model. The numbers denote the sites as marked in Fig. 1.

Can. J. Chem. Downloaded from www.nrcresearchpress.com by 203.198.23.82 on 09/08/12
For personal use only.

TABLE 4. The thermodynamic properties E, U, R, C_v, and ν for liquid bromine trifluoride for two potential models at 298, 323 and 360 K

Model	T (K)	E (kJ mol^{-1})	U (kJ mol^{-1})	Ratio	C_v (kJ mol^{-1})	ν (bar K^{-1})
LJ	298.5	−18.15 ± 0.00	−25.26 ± 0.27	0.99	26.14	17.57
LJ + FC	303.4	−20.02 ± 0.04	−27.59 ± 0.27	0.98	26.09	15.30
LJ	315.0	−16.94 ± 0.00	−24.80 ± 0.25	1.00	25.91	14.45
LJ + FC	319.7	−18.75 ± 0.08	−26.72 ± 0.29	1.00	26.06	14.37
LJ	362.9	−14.38 ± 0.01	−23.43 ± 0.28	1.00	25.83	13.02
LJ + FC	367.5	−15.98 ± 0.05	−25.15 ± 0.31	1.00	25.93	14.45

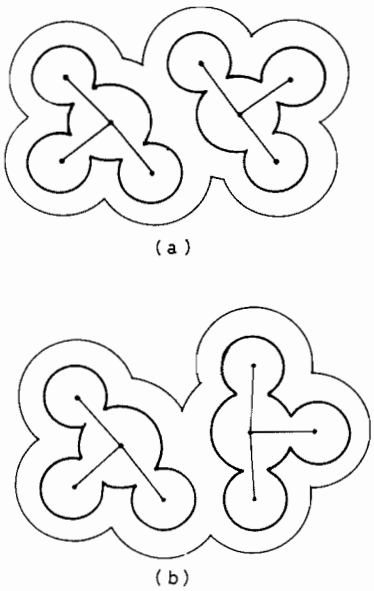

FIG. 3. Two probable dimer configurations derived from the closest approach distances for a pair of BrF_3 molecules at closest contact distances.

TABLE 5. Simulated mechanical properties of liquid bromine trifluoride

Model	T (K)	$\langle F \rangle$ (10^{-20} (J/m)^2)	$\langle \Gamma_i \rangle$ (10^{-40} J^2)	D (10^{-5} cm^2 s^{-1})
LJ	298.5	28.993	4.906(*XX*) 15.996(*YY*) 16.650(*ZZ*)	1.26
LJ + FC	303.4	30.157	12.970(*XX*) 12.960(*YY*) 13.030(*ZZ*)	1.40
LJ	315.0	29.351	5.137(*XX*) 16.287(*YY*) 16.441(*ZZ*)	1.75
LJ + FC	319.7	30.125	12.950(*XX*) 12.910(*YY*) 13.120(*ZZ*)	1.87
LJ	362.9	32.704	5.658(*XX*) 17.879(*YY*) 17.840(*ZZ*)	2.61
LJ + FC	367.5	33.566	14.080(*XX*) 14.160(*YY*) 14.520(*ZZ*)	2.91

proach for intermolecular F—F, Br—F, and Br—Br, respectively. They are in good agreement with results from X-ray diffraction study (5). The radial distribution function derived from X-ray diffraction study (5) shows a peak at 2.8 ± 0.1 Å. The intermolecular F–F, Br–F, and Br–Br distances derived from this peak correspond to 2.5 to 3.3 Å.

Since our short range structure parameters are in good agreement with spectral studies, the repulsive part of our proposed potential must be a good approximation. However, the heat of evaporation (−42.8 kJ mol^{-1} for liquid bromine trifluoride at boiling point (10)) is significantly different from the calculated configurational energy, i.e. −23.43 kJ mol^{-1} (LJ) and −25.15 kJ mol^{-1} (LJ + FC). Steinhauser and Neumann (12) proposed to remove this discrepancy by increasing the depth of the potential well (ϵ). They also suggested that the discrepancy did not affect the short range structure and dynamical properties. Weeks et al. (11) suggested that only the repulsive part in the pair potential was responsible for the short range structure of the liquid. Therefore, any improvement in the attractive portion would not appreciably change the liquid structure properties. It might be interesting to study the short range static and dynamic behaviour using our model.

Figure 3 shows our two dimer configurations at closest approach. The one in Fig. 3*a* matches well with that derived from an infrared spectral study of BrF_3 in argon matrix (6).

Table 1 lists simulation thermodynamic properties ρ, P/ρ, and ν for liquid bromine trifluoride. Table 4 lists the thermodynamic properties E, U, R, C_v, and ν at the three average temperatures 299, 315 and 363 K.

The mean-squared force and mean-squared torque are significant since they appear in short-time expansions of velocity, angular velocity correlation functions, and memory functions (13). They are also important in determining the quantum corrections to the free energy. They can be measured experimentally by infrared and Raman spectroscopy and neutron scattering. As far as we know, these values have not appeared in the literature. Table 5 lists our mean-squared force $\langle F^2 \rangle$ and mean-squared torque $\langle \Gamma_i^2 \rangle$ about axis i and self-diffusion coefficient D which is one sixth the slope of the MSD(t) line. An improvement in the potential model brings a net improvement in the mean-squared torque Γ_{XX}.

Can. J. Chem. Downloaded from www.nrcresearchpress.com by 203.198.23.82 on 09/08/12
For personal use only.

Acknowledgements

We thank Delhi University Computer Centre for generous CPU time and CSIR, New Delhi, for a research fellowship.

1. R.K. Wadi and V. Saxena. Can. J. Chem. **70**, 34 (1992).
2. K. Singer, A. Taylor, and J.V.L. Singer. Mol. Phys. **33**, 1757 (1977).
3. H.H. Classen, B. Weinstock, and S.G. Malm. J. Chem. Phys. **28**, 285 (1958).
4. E.L. Mutterties and W.D. Phillips. J. Chem. Phys. **79**, 322 (1957).
5. V.N. Mitt'kin, G.S. Yur'ev, S.V. Zemskov, and V.I. Kazakova. J. Struct. Chem. **28**, 60 (1987).
6. R.A. Frey, R.L. Redington, and A.L.K. Aljibury. J. Chem. Phys. **54**, 344 (1971).
7. V.F. Sukhoverkhov, I.V. Makshin, G.V. Romanov, and V.P. Spridonov. Novosibirsk, 58 (1981).
8. R.D. Burbank and F.N. Bensey. J. Chem. Phys. **21**, 609 (1953).
9. M.P. Allen and D.J. Tildesley. *In* Computer simulation of liquids. Clarenden Press, Oxford. 1987.
10. L. Stein. *In* Halogen chemistry. Vol. 1. *Edited by* V. Gutmann. Academic Press. 1967.
11. J.D. Weeks, D. Chandler, and H.C. Andersen. J. Chem. Phys. **54**, 5237 (1971).
12. O. Steinhauser and M. Neumann. **40**, 115 (1980).
13. J.P. Hensen and I.R. McDonald. Theory of simple liquids. Academic Press. 1976.

Can. J. Chem. Downloaded from www.nrcresearchpress.com by 203.198.23.82 on 09/08/12
For personal use only.

Synthesis of *O*-α-D-Rha*p*-(1 → 3)-*O*-α-D-Rha*p*-(1 → 2)-*O*-α-D-Rha*p*-(1 → 12)-oxydodecanoyl-bovine serum albumin

WEI ZOU, ASISH K. SEN, AND WALTER A. SZAREK[1]
Department of Chemistry, Queen's University, Kingston, ON K7L 3N6, Canada

AND

DAVID B. MACLEAN[1]
Department of Chemistry, McMaster University, Hamilton, ON L8S 4M1, Canada

Received May 11, 1993

WEI ZOU, ASISH K. SEN, WALTER A. SZAREK, and DAVID B. MACLEAN. Can. J. Chem. **71**, 2194 (1993).

The title compound (**19**), a conjugate of a trisaccharide based upon the repeating trisaccharide of α-D-rhamnose, which comprises the polysaccharide portion of "A-band" lipopolysaccharide from a mutant (AK1401) of *Pseudomonas aeruginosa*, strain PAO1, with bovine serum albumin (BSA) was synthesized starting with methyl α-D-mannopyranoside. Suitably protected D-rhamnose derivatives, namely, ethyl 3,4-di-*O*-benzyl-1-thio-α-D-rhamnopyranoside (**11**) and 3-*O*-acetyl-2,4-di-*O*-benzyl-α-D-rhamnopyranosyl chloride (**12**), were used as the glycosyl acceptor and donor, respectively, in the synthesis of disaccharide **13**. *O*-Deacetylation of **13** gave **14**, a glycosyl acceptor that reacted with **12** to yield the trisaccharide **15**. *N*-Iodosuccinimide – trifluoromethanesulfonic acid was used as an activator of the thioglycoside in the synthesis of **16** and **17** from **15**. Compound **16** was converted into the hydrazide **18** by treatment with hydrazine. The conjugation was achieved by coupling of the intermediate acyl azide derivative of **18** with BSA.

WEI ZOU, ASISH K. SEN, WALTER A. SZAREK et DAVID B. MACLEAN. Can. J. Chem. **71**, 2194 (1993).

Utilisant l'α-D-mannopyranoside de méthyle comme produit de départ, on a synthétisé le composé **19** mentionné dans le titre, un conjugué d'un trisaccharide basé sur l'homoséquence du trisaccharide de l'α-D-rhamnose qui comprend la portion polysaccharidique de la «bande-A» du lipopolysaccharide d'un mutant (AK1401) du *Pseudomonas aeruginosa*, souche PAO1, d'une albumine de sérum bovin (ASB). On a utilisé des dérivés D-rhamnose protégés d'une façon appropriée, soit les 3,4-di-*O*-benzyl-1-thio-α-D-rhamnopyranoside d'éthyle (**11**) et le chlorure de 3-*O*-acétyl-2,4-di-*O*-benzyl-α-D-rhamnopyranosyle (**12**) comme respectivement accepteur et donneur de glycosyle dans la synthèse du disaccharide **13**. La *O*-déacétylation de **13** conduit à **14**, un accepteur de glycosyle, qui par réaction avec **12**, fournit le trisaccharide **15**. On a utilisé la combinaison *N*-iodosuccinimide – acide trifluorométhanesulfonique comme activant du thioglycoside dans la synthèse des composés **16** et **17** à partir du composé **15**. Par traitement avec de l'hydrazine, on a transformé le composé **16** en son hydrazide **18**. On a réalisé la conjugaison en procédant au couplage du dérivé intermédiaire **18** avec le BSA.

[Traduit par la rédaction]

Introduction

During the past decade an increasing number of studies have demonstrated that carbohydrate–protein conjugates possess important seroreactivity (1–6); some of the conjugates were developed with the intention of preparing synthetic antigens and vaccines (1–6). *Pseudomonas aeruginosa* is an opportunistic pathogen that infects persons having compromised immune systems, such as cystic fibrosis patients (7). Vaccines currently used against pathogenic Gram-negative bacteria commonly consist of a mixture of O-antigens from several serotypes of the same species. "A-band" lipopolysaccharide (LPS) is often expressed in established colonies of *Pseudomonas aeruginosa* that do not express O-antigen; since the "A-band" LPS is conserved upon infection, and since it is a common antigen (8), vaccines based on this type of LPS might be more successful in preventing pulmonary infections of *P. aeruginosa* than the current vaccines based on O-antigens.

Recently we (9) reported the results of structural studies on the polysaccharide portion of "A-band" LPS from a mutant (AK1401) of *Pseudomonas aeruginosa* strain PAO1. The main structural feature is a repeating trisaccharide of α-D-rhamnose having the following structure: [→ 2)-*O*-α-D-Rha*p*-(1 → 3)-*O*-α-D-Rha*p*-(1 → 3)-*O*-α-D-Rha*p*-(1 →]$_n$; this structural assignment has been confirmed by further studies involving methylation analysis and Smith-degradation studies (10). As part of our program concerned with the synthesis of glycoconjugates for the investigation of their serological activity, with the intention of preparing synthetic vaccines based upon subunits of the structure that could be used for protection against *Pseudomonas* infections, it was planned to synthesize a trisaccharide based upon this trisaccharide repeating unit by a strategy that would permit the trisaccharide units to be joined readily to the extent of a nonasaccharide. It was also planned to make neoglycoproteins of the tri-, hexa-, and nona-saccharides.

Methods for the synthesis of glycoconjugates include diazo coupling, formation of isothiocyanates, amidation, amination, guanidination, and amidination (see ref. 6). Conjugates containing several types of spacer arms, such as a nine-carbon chain (11–14), and chains containing dioxa (15–17), amide (18), thioether (19–23), phenylthiourea (24), or *p*-*N*-acryloylphenyl (25) functional groups, have been prepared. Four-, seven-, twelve-, and fifteen-carbon spacer arms have also been employed (26). Here we describe the synthesis of a conjugate of the trisaccharide and bovine serum albumin (BSA) by using a 12-carbon spacer arm.

Results and discussion

Methyl 2,3-*O*-isopropylidene-α-D-rhamnopyranoside (**3**) was prepared from methyl 2,3-*O*-isopropylidene-α-D-mannopyranoside (**1**) in two steps (27) by treatment of **1** with

[1]Authors to whom correspondence may be addressed.

Can. J. Chem. Downloaded from www.nrcresearchpress.com by 203.198.23.82 on 09/08/12
For personal use only.

Can. J. Chem. Downloaded from www.nrcresearchpress.com by 203.198.23.82 on 09/08/12
For personal use only.

iodine–triphenylphosphine to give **2**, followed by catalytic hydrogenation of **2**. Benzylation of **3** with benzyl chloride – potassium hydroxide in dimethyl sulfoxide at room temperature gave **4** in good yield; the product, without further purification, was converted into **5** (28, 29) in 79% yield (from **3**) by treatment with 60% aqueous acetic acid at boiling temperature.

Benzylation of **5** to form methyl 2,4-di-*O*-benzyl-α-D-rhamnopyranoside (**6**) in 82% yield was performed in toluene at room temperature, in the presence of the phase-transfer catalyst, tetra-*n*-butylammonium iodide, and powdered potassium hydroxide. A selective benzylation of **5** to give **6** has been achieved also by a two-phase reaction in chloroform – aqueous sodium hydroxide using tetra-*n*-butylammonium bromide (28). In the present study, in addition to compound **6**, small amounts of methyl 3,4-di-*O*-benzyl-α-D-rhamnopyranoside (**7**) (ref. 30, for *L*-enantiomer, see refs. 31, 32) and another component having a higher R_f value, presumably methyl 2,3,4-tri-*O*-benzyl-α-D-rhamnopyranoside, were isolated also. Compound **7** could be prepared from **5** in large scale in 69% yield by reaction with (di-*n*-butyl) tin oxide, by way of its stannylene derivative (see refs. 33, 34), in toluene–benzene. Acetolysis of **6** or **7** with a 1.5% solution of sulfuric acid in acetic anhydride – acetic acid (5:2, v/v) at room temperature did not afford simply the corresponding acetate **8** (for L-enantiomer, see ref. 14) or **9** (32, 35), but resulted also in debenzylation. 1,2-Di-*O*-acetyl-3,4-di-*O*-benzyl-α-D-rhamnopyranose (**9**) could be obtained in 84% yield by hydrolysis of **7** in a 3% solution of sulfuric acid in water – acetic acid – acetone (1:1:1, v/v) at reflux temperature for 20 h, followed by acetylation with acetic anhydride – pyridine at room temperature for 4 h.

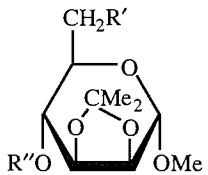

1 R′ = OH, R″ = H
2 R′ = I, R″ = H
3 R′ = H, R″ = H
4 R′ = H, R″ = Bn

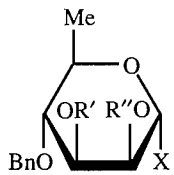

5 R′ = R″ = H, X = OMe
6 R′ = H, R″ = Bn, X = OMe
7 R′ = Bn, R″ = H, X = OMe
8 R′ = Ac, R″ = Bn, X = OAc
9 R′ = Bn, R″ = Ac, X = OAc
10 R′ = Bn, R″ = Ac, X = Cl
11 R′ = Bn, R″ = H, X = SEt
12 R′ = Ac, R″ = Bn, X = Cl

Ethyl thioglycosides have usually been synthesized by the reaction of a glycosyl acetate with thioethanol in the presence of a Lewis acid; however, in many cases the protecting groups are labile under these conditions. Although boron trifluoride etherate has been used (35) in the preparation of thioglycoside **11**, debenzylation has been observed (36) under such conditions. Consequently, in the present work glycosyl chloride **10**, which was prepared quantitatively by treatment of **9** with hydrogen chloride in acetic acid – dichloromethane at room temperature for 2 h, was treated with potassium thioethoxide in acetone at room temperature for 10–15 min to give **11** in 91% overall yield; no β isomer was isolated. Gated ^{13}C NMR measurements revealed $J_{H\text{-}1,C\text{-}1}$ = 166.48 Hz, a value in the range reported (37) for the α anomer of some *O*-glycosides of mannose derivatives. The other suitably protected, monosaccharide unit **12** was obtained from **6** in good yield by the same methods as those used in the preparation of **10** from **7**.

The reaction of the glycosyl acceptor **11** with the glycosyl donor **12** was performed in the presence of silver triflate and powdered 4 Å molecular sieves at −5 to −10°C to give the protected disaccharide **13** in 76% yield. The assignment of the configuration of the inter-glycosidic linkage was based on precedents in the literature (see, for example, refs. 37*a*, 37*b*, 38) for the synthesis of mannose-containing oligosaccharides under the same conditions. ^1H and ^{13}C NMR spectroscopy indicated the stereochemical integrity of **13**. *O*-Deacetylation of **13** with 0.5% sodium methoxide in methanol at room temperature for 4 h afforded quantitatively the glycosyl acceptor **14**, which was, in turn, glycosylated with the glycosyl donor **12**, again by use of silver triflate and powdered 4 Å molecular sieves, to give protected trisaccharide **15** as a syrup in 80% yield. ^1H NMR spectroscopy showed the presence of signals for three anomeric protons at δ 5.09 (H-1″), 5.19 (H-1′), and 5.21 (H-1); in the spectrum of **13** the signals for the two anomeric protons were observed at δ 5.14 (H-1′) and 5.25 (H-1).

The thioglycoside **15** was treated with methyl 12-hydroxydodecanoate using *N*-iodosuccinimide – trifluoromethanesulfonic acid as an activator (39, 40), to give the two diastereomers **16** and **17** (~1:1) in 68% yield. The ratio of **16** to **17** and the yield were not changed significantly by changing the reaction temperature from 0°C to room temperature. The trisaccharides **16** and **17** were separated by chromatography on silica gel. The ^1H NMR resonances of **16** and **17** were assigned on the basis of 2D ^1H-homonuclear chemical-shift correlated (^1H-COSY) experiments.

Attempted *O*-debenzylation of **16** by catalytic hydrogenolysis over 10% Pd–C in methanol was unsuccessful possibly because of the presence of a trace of sulfide derived from the thioglycoside precursor; however, the *O*-debenzylation was achieved in a binary solvent of 40% acetic acid in methanol at room temperature. The product was then converted into the hydrazide **18** in 62% yield by treatment overnight with hydrazine hydrate in ethanol; during the conversion process the 3″-Ac group was also removed. The ^1H and ^{13}C NMR spectral data, including data from ^1H-COSY experiments, and the MS(FAB) spectrum were consistent with the structure assigned for **18**. In the ^1H NMR spectrum of **18** in CD_3OD at 25°C the signal of the anomeric proton (H-1) at δ 4.71 was obscured by a protiated-solvent signal; signals for only two anomeric protons were observed (δ 4.85 and 4.99). When the temperature was raised to 30°C the signals of three anomeric protons were clearly observed at δ 4.77 (H-1), 4.91 (H-1′), and 5.04 (H-1″) (see Fig. 1).

The hydrazide **18** was converted into its acyl azide, which was conjugated to the carrier protein, bovine serum albumin, by the method described by Chatterjee et al. (13), to give the glycoconjugate **19**. The conjugate **19** could be purified by column chromatography on Bio-Gel P-30. The fractions were monitored for carbohydrate by the phenol – sulfuric acid colorimetric method (41); protein was assayed using bicinchoninic acid (Pierce BCA Protein Assay Reagent). The results in Fig. 2 indicated a successful conjugation. The glycoconjugate material was dialyzed, lyophilized, and stored at 4°C prior to serological analyses.

Preliminary tests have shown that both **18** and **19** possess binding reactivity to the "A-band"-specific monoclonal antibody, MAb N1F10 (see refs. 8, 42). The syntheses of

Can. J. Chem. Downloaded from www.nrcresearchpress.com by 203.198.23.82 on 09/08/12
For personal use only.

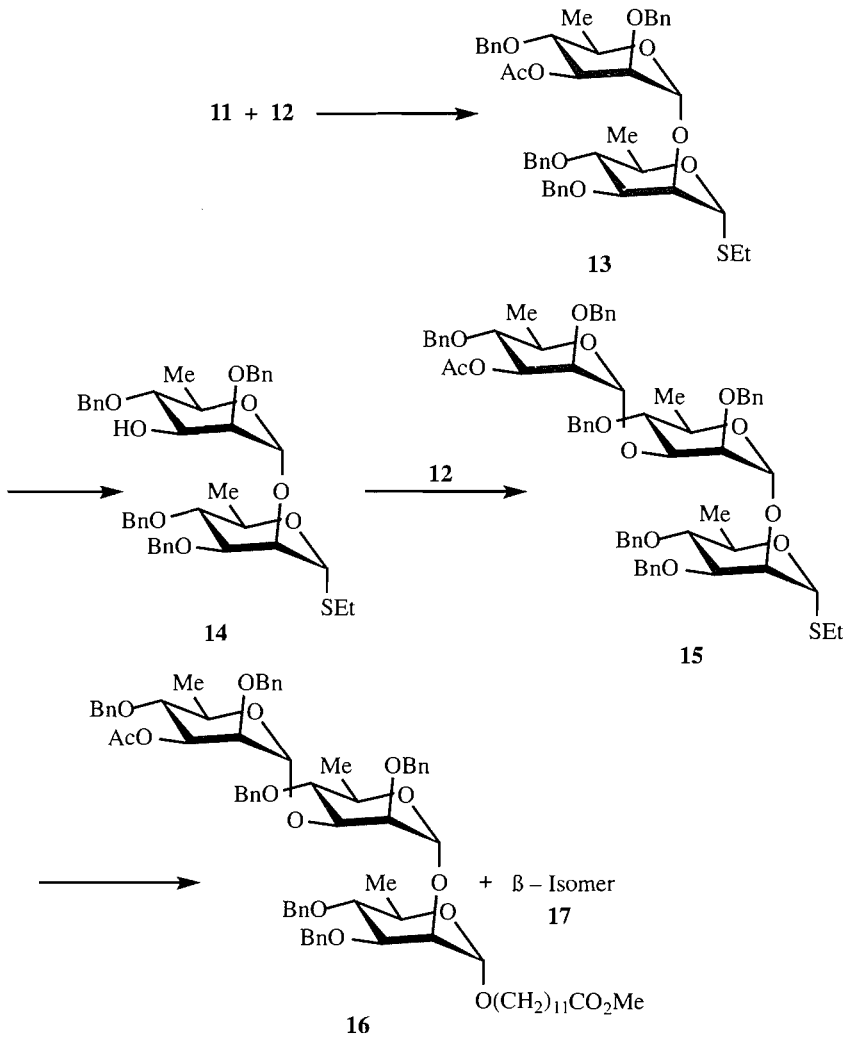

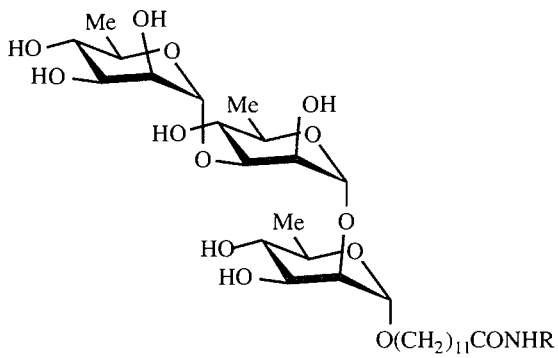

18 R = NH_2
19 R = BSA

hexa- and nona-saccharides and their conjugates should be achievable from **15** and **16** by the reactions described in this article.

Experimental

Melting points were determined on a Fisher–Johns apparatus and are uncorrected. Optical rotations were measured with a Perkin–Elmer model 241 automatic polarimeter for solutions in a 0.1-dm cell at room temperature. Nuclear magnetic resonance (^{1}H NMR and ^{13}C NMR) spectra were recorded on a Bruker AM-400 or Bruker AC-F200 spectrometer; chemical shifts (δ) are given in ppm downfield from the signal of Me_4Si. CI mass spectra were recorded on a VG Analytical ZAB-E mass spectrometer; the FAB mass spectrum was recorded on a VG Quattro mass spectrometer using *m*-nitrobenzyl alcohol as the matrix.

Thin-layer chromatography (TLC) was performed using glass precoated with E. Merck Silica Gel 60 F-254. The developed plates were dried and sprayed with a solution of cerium (IV) sulfate (1%) and molybdic acid (1.5%) in 10% aqueous sulfuric acid, and heated at 150°C. Column chromatography was performed using E. Merck 7734 Silica Gel 60 (70–230 mesh) as the solid phase. Solvents were evaporated under reduced pressure at <40°C.

Methyl 4-O-benzyl-α-D-rhamnopyranoside (5)

To a solution of **3** (27) (4.4 g, 20.1 mmol) in dimethyl sulfoxide (25 mL) were added powdered potassium hydroxide (4.0 g) and benzyl chloride (3.0 mL, 25.8 mmol) with stirring at room temperature, and the mixture was stirred for a further 4 h. Ice-water (50 mL) was then added and the solution was extracted with chloroform (3 × 50 mL). The combined organic solution was then washed with water (2 × 50 mL), dried over anhydrous sodium sulfate, and concentrated to give methyl 4-*O*-benzyl-2,3-*O*-isopropylidene-α-D-rhamnopyranoside (**4**) as an oil.

To the oil obtained above was added 60% aqueous acetic acid (50 mL) and the mixture was then stirred at 100°C for 1 h. Evaporation under reduced pressure gave a residue that crystallized in a short time after the addition of hexane (100 mL) to give a sample of **5** (4.31 g, 79.5% from **3**). The sample was recrystallized from ethyl acetate – hexane; mp 108–109°C, $[\alpha]_D$ +72.4 (*c* 1.56, $CHCl_3$) (lit. (28) mp 105°C, $[\alpha]_D$ +66.3 (*c* 5.3, $CHCl_3$); lit. (29) mp 105–107°C, $[\alpha]_D$ +72 (*c* 4, $CHCl_3$)); ^{1}H NMR (200 MHz, $CDCl_3$) δ: 1.35 (3H, d, $J_{5,6}$ = 6.2 Hz, 6-CH_3), 2.32 (2H, br, 2-OH and 3-OH),

Can. J. Chem. Downloaded from www.nrcresearchpress.com by 203.198.23.82 on 09/08/12
For personal use only.

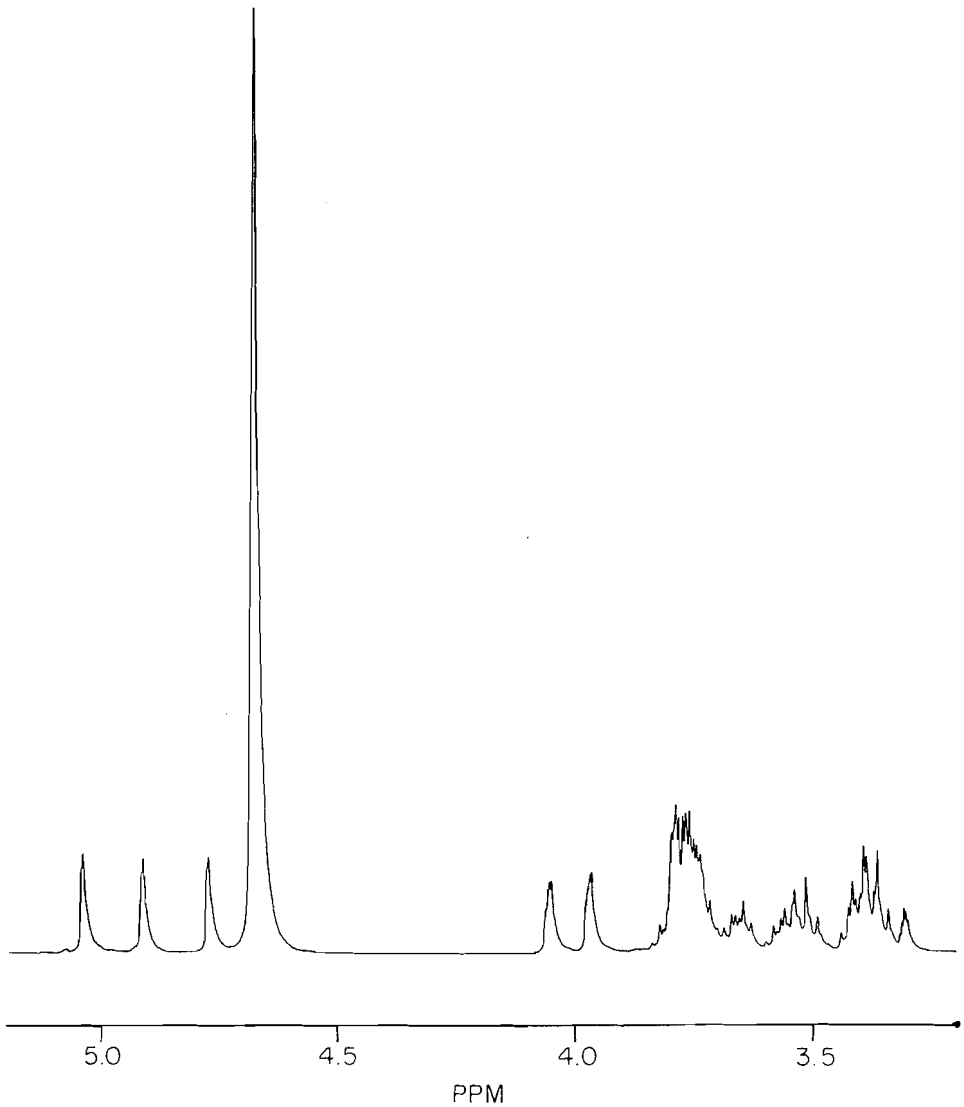

FIG. 1. Partial ^{1}H NMR spectrum of **18** at 400 MHz in CD_3OD at 30°C.

3.32 (1H, t, $J_{3,4} = J_{4,5} = 9.3$ Hz, H-4), 3.34 (3H, s, OMe), 3.71 (1H, dq, $J_{5,6} = 6.2$ Hz, $J_{4,5} = 9.3$ Hz, H-5), 3.84–3.91 (2H, m, H-2 and H-3), 4.65 (1H, br, H-1), 4.73 (2H, s, CH_2Ph), and 7.38 (5H, m, Ph). Anal. calcd. for $C_{14}H_{20}O_5$: C 62.67, H 7.52; found: C 62.46, H 7.34.

*Methyl 2,4-di-*O*-benzyl-α-*D*-rhamnopyranoside (6)*

To a solution of **5** (2.31 g, 8.62 mmol) in toluene (50 mL) were added tetra-*n*-butylammonium iodide (1.6 g, 4.3 mmol) and powdered potassium hydroxide (2.3 g), followed by benzyl bromide (1.47 g, 8.62 mmol). The mixture was stirred at room temperature for 4 h. Ice-cold water (50 mL) and ethyl acetate (50 mL) were added and the mixture was stirred for 10 h. The organic layer was then washed with water (2 × 50 mL), dried over anhydrous sodium sulfate, and evaporated to give a residue that was fractionated by column chromatography on silica gel (hexane – ethyl acetate (3:1, v/v)) to give compound **6** as an oil (2.52 g, 82%) and a small amount of **7**; ^{1}H NMR (200 MHz, $CDCl_3$) δ: 1.34 (3H, d, $J_{5,6} = 6.2$ Hz, 6-CH_3), 2.24 (1H, br, 3-OH), 3.33 (3H, s, OMe), 3.35 (1H, t, $J_{3,4} = J_{4,5} = 9.4$ Hz, H-4), 3.64 (1H, dq, $J_{4,5} = 9.4$ Hz, $J_{5,6} = 6.2$ Hz, H-5), 3.73 (1H, dd, $J_{1,2} = 1.4$ Hz, $J_{2,3} = 3.7$ Hz, H-2), 3.94 (1H, dd, $J_{2,3} = 3.7$ Hz, $J_{3,4} = 9.4$ Hz, H-3), 4.59 and 4.76 (2H, d and d, $J_{gem} = 11.9$ Hz, CH_2Ph), 4.72 (1H, br, H-1), 4.66 and 4.91 (2H, d and d, $J_{gem} = 11.1$ Hz, CH_2Ph), and 7.26–7.50 (10H, m, 2 Ph).

*Methyl 3,4-di-*O*-benzyl-α-*D*-rhamnopyranoside (7)*

To a solution of **5** (4.0 g, 14.93 mmol) in benzene–toluene (1:1, v/v, 200 mL) was added (di-*n*-butyl)tin oxide (4.1 g), and the mixture was heated at reflux temperature with azeotropic removal of water for 5 h. Benzene was removed by distillation, and tetra-*n*-butylammonium iodide (5.6 g, 15.16 mmol) and benzyl bromide (2.65 mL, 20.6 mmol) were added; the mixture was heated at reflux temperature for 3 h and then cooled to room temperature. Water (100 mL) and ethyl acetate (100 mL) were added and the organic layer was washed sequentially with an aqueous solution of sodium hydrogen carbonate and water. The organic solution was dried over anhydrous sodium sulfate and concentrated to a residue that was fractionated by column chromatography on silica gel (hexane – ethyl acetate (3:1, v/v)) to give compound **7** as an oil (3.67 g, 69%); ^{1}H NMR (200 MHz, $CDCl_3$) δ: 1.37 (3H, d, $J_{5,6} = 6.2$ Hz, 6-CH_3), 2.79 (1H, s, 2-OH), 3.37 (3H, s, OMe), 3.51 (1H, t, $J_{3,4} = J_{4,5} = 9.2$ Hz, H-4), 3.72 (1H, dq, $J_{5,6} = 6.2$ Hz, $J_{4,5} = 9.2$ Hz, H-5), 3.87 (1H, dd, $J_{3,4} = 9.2$ Hz, $J_{2,3} = 3.5$ Hz, H-3), 4.05 (1H, dd, $J_{1,2} = 1.5$ Hz, $J_{2,3} = 3.5$ Hz, H-2), 4.69 and 4.86 (2H, d and d, $J_{gem} = 11$ Hz, CH_2Ph), 4.72 (2H, s, CH_2Ph), 4.75 (1H, d, $J_{1,2} = 1.5$ Hz, H-1), and 7.25–7.45 (10H, m, 2 Ph).

*1,3-Di-*O*-acetyl-2,4-di-*O*-benzyl-α-*D*-rhamnopyranose (8)*

A solution of **6** (6.2 g, 17.32 mmol) in a 3% solution of sulfuric acid (80 mL) in acetic acid – water–acetone (1:1:1, v/v) was

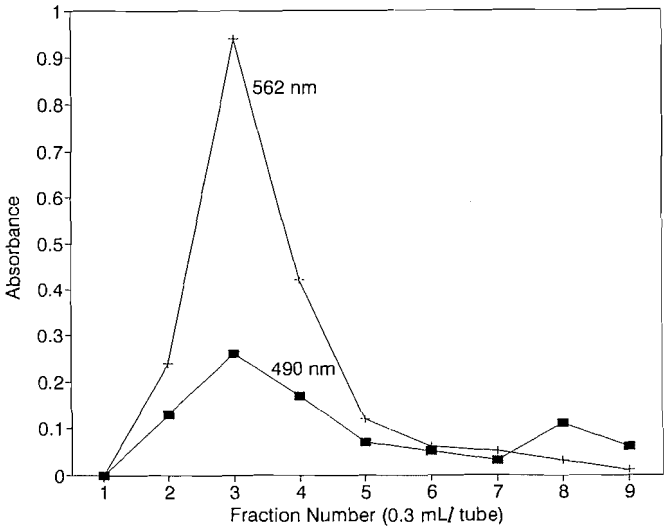

FIG. 2. Gel filtration chromatography of conjugate **19** on Bio-Gel P-30 (10 × 0.4 cm, water as eluant). Carbohydrate was assayed by the phenol – sulfuric acid colorimetric method at 490 nm (■); protein was assayed using bicinchoninic acid (Pierce BCA Protein Assay Reagent) at 562 nm (+).

heated at reflux temperature for 20 h. The solution was cooled to room temperature and extracted with chloroform (3 × 50 mL). The organic solution was washed sequentially with water (20 mL), an aqueous solution of sodium hydrogen carbonate (20 mL), and water (20 mL), dried over anhydrous sodium sulfate, and evaporated; the residue was treated with acetic anhydride – pyridine (1:1, v/v, 30 mL) at room temperature for 4 h. The mixture was poured into ice-water and extracted with ethyl acetate (4 × 25 mL). The solution was concentrated to a residue that was purified by column chromatography on silica gel (hexane – ethyl acetate (3:1, v/v)) to give compound **8** as a syrup (4.4 g, 60%), and another component (0.8 g) that appeared to be a mixture of α and β isomers; ^{1}H NMR (200 MHz, $CDCl_3$) δ: 1.37 (3H, d, $J_{5,6}$ = 6.2 Hz, 6-CH_3), 1.98 and 2.09 (3H each, s and s, 2 Ac), 3.72 (1H, t, $J_{3,4} = J_{4,5}$ = 9.2 Hz, H-4), 3.95–3.98 (2H, m, H-2 and H-5), 4.69–4.80 (4H, m, 2 CH_2Ph), 5.13 (1H, dd, $J_{2,3}$ = 2.9 Hz, $J_{3,4}$ = 9.2 Hz, H-3), 6.09 (1H, d, $J_{1,2}$ = 1.4 Hz, H-1), and 7.20–7.40 (10H, m, 2 Ph). Anal. calcd. for $C_{24}H_{28}O_7$: C 67.27, H 6.59; found: C 67.66, H, 6.70.

*1,2-Di-*O*-acetyl-3,4-di-*O*-benzyl-α-D-rhamnopyranose (**9**)*

Compound **7** (2.8 g, 7.82 mmol) was treated as described for the preparation of **8** from **6** to give **9** in crystalline form from hexane and a mixture of α and β isomers (total 2.85 g, 84%); mp 107°C, $[\alpha]_D$ +22.8 (*c* 1.36, $CHCl_3$) (lit. (35) mp 106–108°C, $[\alpha]_D$ +22.3 (*c* 0.73, $CHCl_3$); for *L*-enantiomer, lit. (32) mp 107–109°C, $[\alpha]_D$ −20 (*c* 1.1, CH_2Cl_2)); ^{1}H NMR (200 MHz, $CDCl_3$) δ: 1.33 (3H, d, $J_{5,6}$ = 6.2 Hz, 6-CH_3), 2.07 and 2.17 (3H each, s and s, 2 Ac), 3.47 (1H, t, $J_{3,4} = J_{4,5}$ = 9.5 Hz, H-4), 3.81 (1H, dq, $J_{5,4}$ = 9.5 Hz, $J_{5,6}$ = 6.2 Hz, H-5), 3.92 (1H, dd, $J_{3,4}$ = 9.5 Hz, $J_{2,3}$ = 3.4 Hz, H-3), 4.54 and 4.72 (2H, d and d, J_{gem} = 11.1 Hz, CH_2Ph), 4.62 and 4.92 (2H, d and d, J_{gem} = 10.7 Hz, CH_2Ph), 5.35 (1H, dd, $J_{1,2}$ = 2.0 Hz, $J_{2,3}$ = 3.4 Hz, H-2), 6.00 (1H, d, $J_{1,2}$ = 2.0 Hz, H-1), and 7.28–7.35 (10H, m, 2 Ph); ^{13}C NMR (50.32 MHz, $CDCl_3$) δ: 18.02 (C-6), 20.91 and 20.98 (2 CH_3C=O), 67.83 (C-5), 70.05, 71.94 (CH_2Ph), 75.63 (CH_2Ph), 77.63, 79.53, 91.17 (C-1), 127.88, 128.04, 128.12, 128.46, 137.76, and 138.24 (2 Ph), 168.53 and 170.04 (2 C=O). Anal. calcd. for $C_{24}H_{28}O_7$: C 67.27, H 6.59; found: C 67.41, H 6.56.

*2-O-Acetyl-3,4-di-O-benzyl-α-D-rhamnopyranosyl chloride (**10**)*

A solution of **9** (1.92 g, 4.5 mmol) in dichloromethane – acetic acid (1:1, v/v, 50 mL) was saturated with HCl(g) at 0°C for 4 h; TLC (hexane – ethyl acetate (3:1, v/v)) showed that the starting material had been completely converted into a product having a higher R_f value. Dichloromethane (50 mL) was added and the solution was washed sequentially with ice-water (twice), an aqueous solution of sodium hydrogen carbonate, and ice-water. The organic solution was dried over anhydrous sodium sulfate and concentrated to give compound **10** in quantitative yield.

*Ethyl 3,4-di-*O*-benzyl-1-thio-α-D-rhamnopyranoside (**11**)*

To a solution of potassium thioethoxide (0.5 g, 5 mmol) in acetone (10 mL) was added a solution of **10** (1.8 g, 4.4 mmol) in acetone (15 mL). The mixture was stirred at room temperature for 10 min; TLC (hexane – ethyl acetate (3:1, v/v)) showed that the reaction was complete. The mixture was diluted with chloroform (100 mL) and washed with water several times. The organic solution was then concentrated to a residue that was purified by chromatography on silica gel (hexane – ethyl acetate (3:1, v/v)) to give compound **11** as a syrup (1.6 g, 92%); $[\alpha]_D$ +150.6 (*c* 1.6, $CHCl_3$) (lit. (35) $[\alpha]_D$ +127 (*c* 0.56, $CHCl_3$)); ^{1}H NMR (200 MHz, $CDCl_3$) δ: 1.29 (3H, t, *J* = 7.4 Hz, SCH_2CH_3), 1.36 (3H, d, $J_{5,6}$ = 6.3 Hz, 6-CH_3), 2.58 (2H, m, SCH_2CH_3), 3.00 (1H, br, 2-OH), 3.55 (1H, t, $J_{3,4} = J_{4,5}$ = 9.2 Hz, H-4), 3.83 (1H, dd, $J_{2,3}$ = 3.3 Hz, $J_{3,4}$ = 9.2 Hz, H-3), 4.06–4.20 (2H, m, H-2 and H-5), 4.68 (2H, s, CH_2Ph), 4.61 and 4.92 (2H, d and d, J_{gem} = 11.0 Hz, CH_2Ph), 5.33 (1H, d, $J_{1,2}$ = 1.1 Hz, H-1), and 7.25–7.36 (10H, m, 2 Ph); ^{13}C NMR (50.32 MHz, $CDCl_3$) δ: 14.92 (SCH_2CH_3), 17.83 (C-6), 24.97 (SCH_2CH_3), 67.90 (C-5), 70.15, 72.10 (CH_2Ph), 75.34 (CH_2Ph), 80.30 (2 C's), 83.20 (C-1, $J_{C1,H1}$ = 166.48 Hz), 127.71, 127.93, 128.03, 128.38, 128.58, 138.07, and 138.46 (2 Ph). Anal. calcd. for $C_{22}H_{28}O_4S$: C 68.01, H 7.26, S 8.25; found: C 67.65, H 7.23, S 8.59.

*3-O-Acetyl-2,4-di-O-benzyl-α-D-rhamnopyranosyl chloride (**12**)*

Compound **12** was prepared from **8** by the procedure described for the preparation of **10**.

*Ethyl 2-O-(3'-O-acetyl-2',4'-di-O-benzyl-α-D-rhamnopyranosyl)-3,4-di-O-benzyl-1-thio-α-D-rhamnopyranoside (**13**)*

To a solution of **11** (1.0 g, 2.58 mmol) in dichloromethane (15 mL) were added powdered 4 Å molecular sieves (2 g) and silver triflate (1.3 g, 5.06 mmol). The mixture was stirred at −10°C under N_2. A solution of compound **12** (0.9 g, 2.22 mmol) in dichloromethane (12 mL) was slowly added and the mixture was stirred at −5 to −10°C for 30 min and then at room temperature for 5 h. The reaction mixture was diluted with dichloromethane (20 mL) and filtered through Celite. The filtrate was washed with an aqueous solution of sodium hydrogen carbonate and water, dried over anhydrous sodium sulfate, and concentrated to a residue. The residue was purified by column chromatography on silica gel (hexane – ethyl acetate (4:1, v/v)) to give compound **13** as a syrup (1.27 g, 76%); $[\alpha]_D$ +44 (*c* 1.67, $CHCl_3$); ^{1}H NMR (400 MHz, $CDCl_3$) δ: 1.34 (3H, t, *J* = 7.4 Hz, SCH_2CH_3), 1.36 (3H, d, $J_{5',6'}$ = 6.3 Hz, 6'-CH_3), 1.41 (3H, d, $J_{5,6}$ = 6.2 Hz, 6-CH_3), 2.03 (3H, s, 3'-Ac), 2.66 (2H, m, SCH_2CH_3), 3.59 (1H, t, $J_{3',4'} = J_{4',5'}$ = 9.4 Hz, H-4'), 3.69 (1H, t, $J_{3,4} = J_{4,5}$ = 9.4 Hz, H-4), 3.87 (1H, dd, $J_{3,4}$ = 9.4 Hz, $J_{2,3}$ = 2.9 Hz, H-3), 3.95–4.10 (3H, m, H-2', H-5, and H-5'), 4.19 (1H, m, H-2), 4.32–4.99 (8H, m, 8H, 4 CH_2Ph), 5.14 (1H, d, $J_{1',2'}$ = 1.8 Hz, H-1'), 5.25 (1H, d, $J_{1,2}$ = 1.3 Hz, H-1), 5.34 (1H, dd, $J_{2',3'}$ = 3.4 Hz, $J_{3',4'}$ = 9.4 Hz, H-3'), and 7.26–7.38 (20H, m, 4 Ph); ^{13}C NMR (50.32 MHz, $CDCl_3$) δ: 15.09 (SCH_2CH_3), 17.80 and 18.12 (C-6 and C-6'), 21.14 (CH_3C=O), 25.42 (SCH_2CH_3), 68.24 and 68.65 (C-5 and C-5'), 72.55 and 72.74 (2 CH_2Ph), 73.45, 74.94 and 75.44 (2 CH_2Ph), 76.03, 76.80, 79.33, 80.55, 80.68, 83.61 (C-1), 99.57 (C-1'), 127.75, 127.86, 128.00, 128.28, 128.44, 128.51, 138.53, and 138.72 (4 Ph), and 169.50 (C=O); MS (CI, NH_3): 774 $(M + NH_4)^+$, 684, 494. Anal. calcd. for $C_{44}H_{52}O_9S$: C 69.81, H 6.93, S 4.24; found: C 69.68, H 6.75, S 3.99.

*Ethyl 3,4-di-O-benzyl-2-O-(2',4'-di-O-benzyl-α-D-rhamnopyranosyl)-1-thio-α-D-rhamnopyranoside (**14**)*

A solution of compound **13** (0.49 g, 0.648 mmol) in 0.5% sodium methoxide – methanol (20 mL) was stirred at room temper-

Can. J. Chem. Downloaded from www.nrcresearchpress.com by 203.198.23.82 on 09/08/12
For personal use only.

Can. J. Chem. Downloaded from www.nrcresearchpress.com by 203.198.23.82 on 09/08/12
For personal use only.

ature for 4 h; TLC (hexane – ethyl acetate (4:1, v/v)) showed that the reaction was complete. Amberlite IR-120 (H^+ form) ion-exchange resin (5 mL) was added to the solution. The mixture was stirred for 5 min, filtered, and the filtrate was concentrated to give compound **14** in quantitative yield; ^{1}H NMR (200 MHz, $CDCl_3$) δ: 1.28 (3H, t, J = 7.4 Hz, SCH_2CH_3), 1.31 (3H, d, $J_{5',6'}$ = 6.2 Hz, 6′-CH_3), 1.36 (3H, d, $J_{5,6}$ = 6.2 Hz, 6-CH_3), 2.40 (1H, d, J = 8.0 Hz, 3′-OH), 2.60 (2H, m, SCH_2CH_3), 3.40 (1H, t, $J_{3',4'} = J_{4',5'}$ = 9.3 Hz, H-4′), 3.52 (1H, t, $J_{3,5} = J_{4,5}$ = 9.4 Hz, H-4), 3.85–3.94 (3H, m, H-3′, H-5, and H-5′), 4.04–4.14 (2H, m, H-2′ and H-3), 4.19 (1H, dd, $J_{1,2}$ = 1.1 Hz, $J_{2,3}$ = 2.8 Hz, H-2), 4.35 and 4.50 (2H, d and d, J_{gem} = 11.9 Hz, CH_2Ph), 4.61 and 4.75 (2H, d and d, J_{gem} = 10.9 Hz, CH_2Ph), 4.70 and 4.97 (4H, d and d, J_{gem} = 11.0 Hz, 2 CH_2Ph), 5.19 (1H, d, $J_{1',2'}$ = 1.2 Hz, H-1′), 5.25 (1H, d, $J_{1,2}$ = 1.1 Hz, H-1), and 7.25–7.35 (20H, m, 4 Ph).

Ethyl 2-O-{3′-O-(3″-O-acetyl-2″,4″-di-O-benzyl-α-D-rhamnopyranosyl)-2′,4′-di-O-benzyl-α-D-rhamnopyranosyl}-3,4-di-O-benzyl-1-thio-α-D-rhamnopyranoside (15)

To a solution of **14** (0.47 g, 0.648 mmol) in dichloromethane (8 mL) were added powdered 4 Å molecular sieves (2 g) and silver triflate (0.3 g). The mixture was cooled to −10°C under N_2, and a solution of compound **12** (0.28 g, 0.692 mmol) in dichloromethane (3 mL) was added slowly; the mixture was stirred at −5 to −10°C for 1 h and then at room temperature overnight. The reaction mixture was processed as described for the preparation of **13**. Compound **15** was obtained as a syrup (0.56 g, 80%); $[\alpha]_D$ +52.5 (*c* 2.12, $CHCl_3$); ^{1}H NMR (400 MHz, $CDCl_3$) δ: 1.22 (3H, d, $J_{5,6}$ = 6.2 Hz, 6-CH_3), 1.26 (3H, t, J = 7.4 Hz, SCH_2CH_3), 1.27 (3H, d, $J_{5',6'}$ = 6.2 Hz, 6′-CH_3), 1.29 (3H, d, $J_{5'',6''}$ = 6.2 Hz, 6″-CH_3), 1.95 (3H, s, 3″-Ac), 2.60 (2H, m, SCH_2CH_3), 3.44 (1H, t, $J_{3',4'} = J_{4',5'}$ = 9.4 Hz, H-4′), 3.62 (1H, t, $J_{3'',4''} = J_{4'',5''}$ = 9.4 Hz, H-4″), 3.66 (1H, t, $J_{3,4} = J_{4,5}$ = 9.4 Hz, H-4), 3.78–3.83 (3H, m, H-2′, H-3, and H-5), 3.87–3.89 (2H, m, H-2″ and 5″), 4.02 (1H, dq, $J_{5',6'}$ = 6.2 Hz, $J_{4',5'}$ = 9.4 Hz, H-5′), 4.12 (1H, dd, $J_{1,2}$ = 1.4 Hz, $J_{2,3}$ = 2.5 Hz, H-2), 4.19 (1H, d, J_{gem} = 12.0 Hz, one of CH_2Ph), 4.21 (1H, dd, $J_{2',3'}$ = 3.0 Hz, $J_{3',4'}$ = 9.4 Hz, H-3′), 4.39–4.88 (11H, m, 5.5 CH_2Ph), 5.09 (1H, d, $J_{1'',2''}$ = 1.4 Hz, H-1″), 5.19 (1H, d, $J_{1',2'}$ = 1.3 Hz, H-1′), 5.21 (1H, d, $J_{1,2}$ = 1.2 Hz, H-1), 5.32 (1H, dd, $J_{2'',3''}$ = 3.1 Hz, $J_{3'',4''}$ = 9.4 Hz, H-3″), and 7.2–7.4 (30H, m, 6 Ph); ^{13}C NMR (50.32 MHz, $CDCl_3$) δ: 15.07 (SCH_2CH_3), 18.02 (C-6, C-6′, and C-6″), 21.09 (CH_3C=O), 25.49 (SCH_2CH_3), 68.26, 68.50, and 69.03 (C-5, C-5′, and C-5″), 72.38, 72.76, 74.73, and 75.38 (6 CH_2Ph), 73.65, 76.59, 76.92, 77.06, 77.70, 79.12, 80.39, 80.70, 80.86; 83.72 (C-1), 99.38 (C-1′ and C-1″), 127.10, 127.52, 127.59, 127.67, 127.86, 127.99, 128.26, 128.35, 128.40, 128.48, 138.09, and 138.52 (6 Ph), and 170.00 (C=O); MS (CI, NH_3): 1100 $(M + NH_4)^+$, 1010, 820, 774, 712, 638. Anal. calcd. for $C_{64}H_{74}O_{13}S$: C 70.95, H 6.89, S 2.95; found: C 70.90, H 6.81, S 2.79.

11-(Methoxycarbonyl)undecyl 2-O-{3′-O-(3″-O-acetyl-2″,4″-di-O-benzyl-α-D-rhamnopyranosyl)-2′,4′-di-O-benzyl-α-D-rhamnopyranosyl}-3,4-di-O-benzyl-α-D-rhamnopyranoside (16)

To a solution of **15** (0.31 g, 0.287 mmol) and methyl 12-hydroxydodecanoate (0.1 g, 0.435 mmol) in dichloromethane (8 mL) were added powdered 4 Å molecular sieves (0.3 g) and *N*-iodosuccinimide (0.15 g, 0.667 mmol). Trifluoromethanesulfonic acid (20 μL) was added at 0°C under N_2 and the mixture was stirred at room temperature for 4 h. Triethylamine (0.2 mL) in dichloromethane (5 mL) was added to neutralize the solution. The reaction mixture was filtered and the filtrate was concentrated to a residue that was fractionated by column chromatography on silica gel (hexane – ethyl acetate (3:1, v/v)) to give compound **16** (66 mg), its β form **17** (73 mg), and their mixture (184 mg) (68% combined yield).

Compound 16: $[\alpha]_D$ +10 (*c* 1.54, $CHCl_3$); ^{1}H NMR (400 MHz, $CDCl_3$) δ: 1.22 (3H, d, $J_{5,6}$ = 6.2 Hz, 6-CH_3), 1.27–1.34 (20H, m, 2 6-CH_3 and $(CH_2)_7$), 1.54 (2H, m, CH_2CH_2C=O), 1.64 (2H, m, OCH_2CH_2), 1.95 (3H, s, 3″-Ac), 2.31 (2H, t, J = 7.6 Hz, CH_2C=O), 3.35 (1H, m, one of $OCH_2(CH_2)_7$), 3.40 (1H, t, $J_{3,4} = J_{4,5}$ = 9.4 Hz, H-4), 3.61 (1H, t, $J_{3'',4''} = J_{4'',5''}$ = 9.5 Hz, H-4″), 3.63 (1H, t, $J_{3',4'} = J_{4',5'}$ = 9.6 Hz, H-4′), 3.65 (1H, m, one of $OCH_2(CH_2)_7$), 3.66 (1H, m, H-5), 3.67 (3H, s, OMe), 3.75–3.82 (3H, m, H-2′, H-5′, and H-5″), 3.83–3.88 (2H, m, H-2″ and H-3), 4.05 (1H, dd, $J_{1,2}$ = 1.5 Hz, $J_{2,3}$ = 2.5 Hz, H-2), 4.19 (1H, dd, $J_{2',3'}$ = 2.9 Hz, $J_{3',4'}$ = 9.6 Hz, H-3′), 4.38 and 4.20 (2H, d and d, J_{gem} = 12.2 Hz, CH_2Ph), 4.50–4.90 (10H, m, 5 CH_2Ph), 4.71 (1H, d, $J_{1,2}$ = 1.5 Hz, H-1), 5.13 (1H, d, $J_{1',2'}$ = 1.4 Hz, H-1′), 5.18 (1H, d, $J_{1'',2''}$ = 1.3 Hz, H-1″), 5.30 (1H, dd, $J_{2'',3''}$ = 3.3 Hz, $J_{3'',4''}$ = 9.5 Hz, H-3″), and 7.15–7.40 (30H, m, 6 Ph); ^{13}C NMR (50.32 MHz, $CDCl_3$) δ: 18.01 (C-6, C-6′, and C-6″), 21.07 (CH_3C=O), 24.98, 26.17, 29.17, 29.26, 29.45, 29.56, and 34.13 ($(CH_2)_{10}$), 51.40 (OMe), 67.56 ($OCH_2(CH_2)_{10}$), 67.90, 68.21, and 68.83 (C-5, C-5′, and C-5″), 72.30, 72.42, 72.73, 74.70, and 75.42 (6 CH_2Ph), 73.63, 76.92, 77.39, 77.88, 79.11, 80.14, 80.61, 80.85; 98.94, 99.12, and 99.38 (C-1, C-1′,and C-1″), 127.03, 127.51, 127.58, 127.64, 127.74, 128.07, 128.24, 128.31, 128.40, 138.07, 138.11, 138.39, 138.57, and 138.72 (6 Ph), and 170.09 (C=O); MS (CI, NH_3): 1268 $(M + NH_4)^+$, 1178, 942, 820, 728, 638. Anal. calcd. for $C_{75}H_{94}O_{16}$: C 71.97, H 7.57; found: C 71.58, H 7.50.

Compound 17: $[\alpha]_D$ −16 (*c* 0.55, $CHCl_3$); ^{1}H NMR (400 MHz, $CDCl_3$) δ: 1.21 (3H, d, $J_{5'',6''}$ = 6.2 Hz, 6″-CH_3), 1.26 (17H, m, 6′-CH_3 and $(CH_2)_7$), 1.33 (3H, d, $J_{5,6}$ = 6.1 Hz, 6-CH_3), 1.61 (4H, m, OCH_2CH_2 and CH_2CH_2C=O), 1.92 (3H, s, 3″-Ac), 2.29 (2H, t, J = 7.5 Hz, CH_2C=O), 3.31 (1H, m, $J_{5,6}$ = 6.1 Hz, $J_{4,5}$ = 9.3 Hz, H-5), 3.40 (1H, m, one of OCH_2CH_2), 3.42 (1H, t, $J_{4,5} = J_{3,4}$ = 9.3 Hz, H-4), 3.51 (1H, dd, $J_{2,3}$ = 2.3 Hz, $J_{3,4}$ = 9.3 Hz, H-3), 3.59 (2H, t, $J_{3',4'} = J_{3'',4''} = J_{4',5'} = J_{4'',5''}$ = 9.5 Hz, H-4′ and H-4″), 3.66 (3H, s, OMe), 3.80–3.84 (3H, m, H-2′, H-2″, and H-5′), 3.91 (1H, m, one of OCH_2CH_2), 4.10 (1H, d, J_{gem} = 12.2 Hz, one of CH_2Ph), 4.19 (1H, d, $J_{2,3}$ = 2.3 Hz, H-2), 4.25 (1H, dd, $J_{2',3'}$ = 3.1 Hz, $J_{3',4'}$ = 9.5 Hz, H-3′), 4.31–4.36 (3H, m, H-1, H-5″, and one of CH_2Ph), 4.42–4.91 (10H, m, 5 CH_2Ph), 5.18 (1H, d, $J_{1'',2''}$ = 1.3 Hz, H-1″), 5.19 (1H, d, $J_{1',2'}$ = 1.3 Hz, H-1′), 5.29 (1H, dd, $J_{3'',4''}$ = 9.5 Hz, $J_{2'',3''}$ = 3.2 Hz, H-3″), and 7.18–7.35 (30H, m, 6 Ph); ^{13}C NMR (50.32 MHz, $CDCl_3$) δ: 17.85 (C-6), 18.02 (C-6′ and C-6″), 21.09 (CH_3 C=O), 25.00, 26.18, 29.17, 29.29, 29.44, 29.57, 29.79, and 34.14 ($(CH_2)_{10}$), 51.44 (OMe), 68.04, 69.98 ($OCH_2(CH_2)_{10}$), 71.76; 72.10, 72.60, 73.64, 74.37, and 74.65 (6 CH_2Ph), 72.68, 73.41, 77.04, 77.15, 77.79, 78.16, 79.14, 80.44, 80.87, 82.90; 98.23, 99.30, and 100.04 (C-1, C-1′, and C-1″), 126.69, 127.14, 127.33, 127.50, 127.61, 127.85, 127.96, 128.11, 128.23, 128.32, 128.48, 128.56, 137.91, 138.27, 138.63, and 139.23 (6 Ph), and 170.07 (C=O); MS (CI, NH_3): 1268 $(M + NH_4)^+$, 1178, 1038, 900, 712. Anal. calcd. for $C_{75}H_{94}O_{16}$: C 71.97, H 7.57; found: C 71.60, H 7.42.

11-Carbazoylundecyl O-α-D-rhamnopyranosyl-(1″ → 3′)-O-α-D-rhamnopyranosyl-(1′ → 2)-α-D-rhamnopyranoside (18)

A solution of **16** (0.24 g, 0.19 mmol) in 3:2 (v/v) methanol – acetic acid (10 mL) was subjected to a hydrogen pressure of 50 psig (1 psi = 6.9 kPa) in the presence of 10% Pd–C (0.2 g) at room temperature for 20 h; TLC (ethyl acetate) showed that the debenzylation was complete. The catalyst was removed by filtration and the filtrate was concentrated to a residue under vacuum. The residue was dissolved in 95% ethanol (5 mL) and the solution was treated with hydrazine (0.2 mL) for 16 h at room temperature. The solvent was evaporated and traces of hydrazine were removed by codistillation with ethanol; the residue was dried under vacuum. Purification on a column of Sephadex LH-20 (40 × 1 cm, methanol) gave **18** (80 mg, 62%); $[\alpha]_D$ +77.3 (*c* 0.44, MeOH); ^{1}H NMR (400 MHz, CD_3OD) δ: 1.18 (3H, d, $J_{5,6}$ = 6.1 Hz, 6-CH_3), 1.19 (3H, d, $J_{5',6'}$ = 6.2 Hz, 6′-CH_3), 1.22 (3H, d, $J_{5'',6''}$ = 6.2 Hz, 6″-CH_3), 1.26 (14H, br, $(CH_2)_7$), 1.53 (4H, m, OCH_2CH_2 and CH_2CH_2C=O), 2.09 (2H, t, J = 7.5 Hz, CH_2C=O), 3.28–3.38

(3H, m, H-4″, H-5, and one of OCH_2CH_2), 3.43–3.53 (2H, m, H-3 and H-4′), 3.60 (1H, m, H-5″), 3.68 (1H, m, one of OCH_2CH_2), 3.65–3.72 (3H, m, H-3″, H-4, and H-5′), 3.72–3.75 (2H, m, H-2 and H-3′), 3.92 (1H, dd, $J_{1'',2''}$ = 1.6 Hz, $J_{2'',3''}$ = 3.3 Hz, H-2″), 4.00 (1H, dd, $J_{1',2'}$ = 1.6 Hz, $J_{2',3'}$ = 2.9 Hz, H-2′), 4.77 (1H, d, $J_{1,2}$ = 1.6 Hz, H-1), 4.91 (1H, d, $J_{1',2'}$ = 1.6 Hz, H-1′), and 5.04 (1H, d, $J_{1'',2''}$ = 1.6 Hz, H-1″); ^{13}C NMR (100.61 MHz, CD_3OD) δ: 17.94, 17.99, and 18.15 (C-6, C-6′, and C-6″), 26.84, 27.30, 30.24, 30.40, 30.46, 30.55, 30.58, 30.65, and 35.00 ($(CH_2)_{10}$), 68.55 (OCH_2), 69.86, 70.13, and 70.51 (C-5, C-5′, and C-5″), 71.80, 72.14, 72.17, 73.23, 74.04, 74.29, 79.22, 80.16; 100.26, 103.88, and 103.95 (C-1, C-1′, and C-1″), and 175.37 ($CONHNH_2$); MS (FAB): 691 $(M + Na)^+$, 669 $(M + H)^+$, 523, 539, 377, 231. Anal. calcd. for $C_{30}H_{56}N_2O_{14}$: C 53.88, H 8.44, N 4.19; found: C 53.73, H 8.58, N 3.87.

*O-α-D-Rhamnopyranosyl-(1″ → 3′)-O-α-D-rhamnopyranosyl-(1′ → 2)-O-α-D-rhamnopyranosyl-(1 → 12)-oxydodecanoyl-BSA (**19**)*

To a stirred solution of **18** (8 mg) in dry *N,N*-dimethylformamide (0.2 mL) at −30°C was added 1.3 M HCl–1,4-dioxane (60 μL). *tert*-Butyl nitrite in *N,N*-dimethylformamide (1:10, w/v, 50 μL) was added, and the solution was stirred for 10 min at −30°C. The solution of the acyl azide (−30°C) was added dropwise to a solution of BSA (15 mg) in 0.1 M $Na_2B_4O_7$ at 0°C. The solution was stirred at 0°C for 4 h and dialyzed for 20 h against five changes of deionized water using a membrane that retains proteins of molecular weight 12 000 or greater. The water was removed by lyophilization to give **19** (18 mg).

Acknowledgements

The authors are grateful to the Canadian Cystic Fibrosis Foundation and the Natural Sciences and Engineering Research Council of Canada for financial support of this research in the form of grants to W.A.S. and D.B.M. They thank also John G. Allen of Queen's University for technical assistance, Thomas J. Hunter of Queen's University for recording the FAB mass spectrum, and Dr. J. S. Lam of the University of Guelph for the data from the binding studies.

1. H.J. Jennings. Adv. Carbohydr. Chem. Biochem. **41**, 155 (1983).
2. T. Feizi and R.A. Childs. Biochem. J. **245**, 1 (1987).
3. T. Feizi. Adv. Exp. Med. Biol. **228**, 317 (1988).
4. J.C. Paulson. Trends Biochem. Sci. **14**, 272 (1989).
5. S.J. Cryz, Jr., E. Fürer, and J.U. Que. Infect. Immun. **59**, 45 (1991).
6. A.C.P. Stowell and Y.C. Lee. Adv. Carbohydr. Chem. Biochem. **37**, 225 (1980).
7. J.R.W. Govan and S. Glass. Rev. Med. Microbiol. **1**, 19 (1990).
8. M.Y.C. Lam, E.J. McGroarty, A.M. Kropinski, L.A. MacDonald, S.S. Pedersen, N. Høiby, and J.S. Lam. J. Clin. Microbiol. **27**, 962 (1989).
9. T.L. Arsenault, D.W. Hughes, D.B. MacLean, W.A. Szarek, A. M.B. Kropinski, and J.S. Lam. Can. J. Chem. **69**, 1273 (1991).
10. T.L. Arsenault. Ph. D. Thesis, McMaster University. 1992; T.L. Arsenault, D.B. MacLean, W. Zou, and W.A. Szarek. Can. J. Chem. In press.
11. R.U. Lemieux, D.R. Bundle, and D.A. Baker. J. Am. Chem. Soc. **97**, 4076 (1975).
12. R.U. Lemieux, D.A. Baker, and D.R. Bundle. Can. J. Biochem. **55**, 507 (1977).
13. D. Chatterjee, S.-N. Cho, P.J. Brennan, and G.O. Aspinall. Carbohydr. Res. **156**, 39 (1986).
14. H. Paulsen and J.P. Lorentzen. Carbohydr. Res. **165**, 207 (1987).
15. P.-H. Amvam-Zollo and P. Sinaÿ. Carbohydr. Res. **150**, 199 (1986).
16. V. Fernandez-Santana, J.R. Marino-Albernas, V. Verez-Bencomo, and C.S. Perez-Martinez. J. Carbohydr. Chem. **8**, 531 (1989).
17. Z. Szurmai, L. Szabo, and A. Lipták. Acta Chim. Hung. **126**, 259 (1989).
18. H. Paulsen, J.C. Jacquinet, and W. Rust. Carbohydr. Res. **104**, 195 (1985).
19. R.T. Lee and Y.C. Lee. Carbohydr. Res. **37**, 193 (1974).
20. R.T. Lee and Y.C. Lee. Carbohydr. Res. **77**, 149 (1979).
21. R.T. Lee and Y.C. Lee. Carbohydr. Res. **101**, 49 (1982).
22. R.T. Lee and Y.C. Lee. Carbohydr. Res. **110**, 333 (1982).
23. J. Dahmén, T. Frejd, G. Grönberg, T. Lave, G. Magnusson, and G. Noori. Carbohydr. Res. **118**, 292 (1983).
24. C.R. McBroom, C.H. Samanen, and I.J. Goldstein. Methods Enzymol. **28**, 212 (1972).
25. R. Roy, F.D. Tropper, T. Morrison, and J. Boratynski. J. Chem. Soc. Chem. Commun. 536 (1991).
26. T. Sugawara, K. Irie, H. Iwasawa, T. Yoshikawa, S. Okuno, H.K. Watanabe, T. Kato, M. Shibukawa, and Y. Ito. Carbohydr. Res. **230**, 117 (1992).
27. D.R. Bundle, M. Gerken, and T. Peters. Carbohydr. Res. **174**, 239 (1988).
28. Y. Fang, F. Kong, and Q. Wang. J. Carbohydr. Chem. **6**, 169 (1987).
29. C.E. Ballou. J. Am. Chem. Soc. **79**, 984 (1957).
30. J.O. Kihlberg, D.A. Leigh, and D.R. Bundle. J. Org. Chem. **55**, 2860 (1990).
31. U.B. Maddali, A.K. Ray, and N. Roy. Carbohydr. Res. **208**, 59 (1990).
32. V. Pozsgay, J.-R. Brisson, and H.J. Jennings. Can. J. Chem. **65**, 2764 (1987).
33. S. David, A. Thieffry, and A. Veyrières. J. Chem. Soc. Perkin Trans. 1, **1**, 1796 (1981).
34. M.J. Eis and B. Ganem. Carbohydr. Res. **176**, 316 (1988).
35. J. Kihlberg, E. Eichler, and D.R. Bundle. Carbohydr. Res. **211**, 59 (1991).
36. H.G. Fletcher, Jr. and H.W. Diehl. Carbohydr. Res. **17**, 383 (1971).
37. (*a*) T. Ogawa and H. Yamamoto. Carbohydr. Res. **137**, 79 (1985); (*b*) K.K. Sadozai, Y. Ito, T. Nukada, T. Ogawa, and A. Kobata. Carbohydr. Res. **150**, 91 (1986); K. Bock, I. Lundt, and C. Pedersen. Tetrahedron Lett. 1037 (1973); K. Bock and C. Pedersen. J. Chem. Soc. Perkin II, 293 (1974); Acta Chem. Scand. B, **29**, 258 (1975).
38. K.K. Sadozai, T. Kitajima, Y. Nakahara, T. Ogawa, and A. Kobata. Carbohydr. Res. **152**, 173 (1986).
39. G.H. Veeneman, S.H. van Leeuwen, and J.H. van Boom. Tetrahedron Lett. 1331 (1990).
40. P. Konradsson, U.E. Udodong, and B. Fraser-Reid. Tetrahedron Lett. 4313 (1990).
41. J.E. Hodge and B.T. Hofreiter. Methods Carbohydr. Chem. **1**, 388 (1962).
42. J. Lightfoot and J.S. Lam. J. Bacteriol. **173**, 5624 (1991).

Can. J. Chem. Downloaded from www.nrcresearchpress.com by 203.198.23.82 on 09/08/12
For personal use only.

Indole alkaloids from "hairy roots" of *Rauwolfia serpentina*

HEIKE FALKENHAGEN AND JOACHIM STÖCKIGT[1]
Johannes Gutenberg-Universität Mainz, Institut für Pharmazie, Staudinger Weg 5, D(W)-55099 Mainz, Germany

INNA N. KUZOVKINA AND IRINA E. ALTERMAN
K.A. Timirjasev Institute of Plant Physiology, Russia, Academy of Science, Botanitcheskaya 35, Moscow 127276, Russia

AND

HEINZ KOLSHORN
Institute of Organic Chemistry, University of Mainz, Becherweg 18-22, 55099 Mainz, Germany

Received August 31, 1993

HEIKE FALKENHAGEN, JOACHIM STÖCKIGT, INNA N. KUZOVKINA, IRINA E. ALTERMAN, and HEINZ KOLSHORN. Can. J. Chem. **71**, 2201 (1993).

Three minor indole alkaloids have been isolated from "hairy roots" of *Rauwolfia serpentina* Benth.: 3-epi-α-yohimbine (**1**), 18β-hydroxy-3-epi-α-yohimbine (**2**), and 12-hydroxyajmaline (**3**). The latter compound (**3**) is a novel alkaloid. The alkaloid structures have been determined by spectroscopic data.

HEIKE FALKENHAGEN, JOACHIM STÖCKIGT, INNA KUZOVKINA, IRENE E. ALTERMAN et HEINZ KOLSHORN. Can. J. Chem. **71**, 2201 (1993).

On a isolé trois alcaloïdes de l'indole mineurs à partir des «racines poilues» du *Rauwolfia serpentina* Benth. : 3-épi-α-yohimbine (**1**), 18β-hydroxy-3-épi-α-yohimbine (**2**) et 12-hydroxy-ajmaline (**3**). Ce dernier composé (**3**) est un nouvel alcaloïde. On a déterminé les structures des alcaloïdes sur la base des données spectroscopiques.

[Traduit par la rédaction]

Can. J. Chem. Downloaded from www.nrcresearchpress.com by 203.198.23.82 on 09/08/12
For personal use only.

Introduction

In a recent paper we compared the alkaloid formation in cell suspension cultures with that of the "hairy roots" of the Indian medicinal plant *Rauwolfia serpentina* Benth. The results obtained clearly indicated that, in comparison with the normal *Rauwolfia* root bark used for the commercial extraction of alkaloids, both systems produced quite different alkaloids and that the amount of total alkaloids is lower in hairy roots than in the cell suspension (1).

The major alkaloids of the hairy roots were well-known *Rauwolfia* alkaloids but there were three minor compounds that could only be isolated from larger batches of roots. The isolation and structure elucidation of these alkaloids, one of them being a novel compound, is described in this paper.

Results and discussion

During the last few years we have successfully established an efficiently growing root culture of *Rauwolfia serpentina* by genetic transformation with the Ri plasmid A-4. The successful transformation could easily be demonstrated by determination of the opines agropine and mannopine. The *Agrobacterium* A-4 used produces agropine and also mannopine and both could be electrophoretically shown to be present in the hairy roots by the method of Petit et al. (2). As expected for a transformation with the Ri plasmid, the roots showed excellent growth characteristics with a doubling time of 5–7 days. The transformed roots allowed the accumulation of enough biomass for alkaloid extraction, even for alkaloids occurring only in trace amounts.

Alkaloid extraction and purification by flash and thin-layer chromatography (TLC) afforded three alkaloids, the structures of which could be determined by mass spectral data and detailed analyses of ^1H and ^{13}C NMR data.

Compound **1** revealed UV and MS data typical for an indole chromophore and a heteroyohimbine or yohimbine alkaloid, e.g., the fragmentation pattern of m/z 144, 156, 169, 184. The M^+ of **1** at 354 m/z pointed to a yohimbine structure (3). Acetylation of **1** gave a monoacetate the MS fragmentation of which was consistent with a yohimbine structure. Careful inspection of the ^1H and ^{13}C NMR data also suggested such an alkaloid, and comparison of the data of **1** with literature values (4) finally showed identity with data reported for 3-epi-α-yohimbine (5–8).

The component **2** showed the same UV data as **1** and a very similar CAS reaction, indicating that **2** could be of the same alkaloid group (yohimbine). The molecular ion of this compound was at M^+ 370 m/z, 16 amu higher than found for the alkaloid **1**. This observation coupled with the higher polarity of **2** on TLC and the formation of a diacetate (M^+ 454 m/z) was indicative of a hydroxyyohimbine structure. Because the characteristic MS fragments of the A-B-C ring system were not shifted towards higher values, the location of the additional OH group was expected in the D-E ring system and the following NMR data indicated clearly the position of the OH at C-18.

Comparing ^1H NMR data of **1** and **2**, the coupling pattern of H-17 is changed from a triplet of doublets (δ 3.85, J = 10.5, 10.5, 4.5 Hz) in **1** to a triplet in component **2** due to the equatorial hydroxyl group at C-18. In addition, H-18 at 3.5 ppm in **2** exhibits the same coupling as H-17 in **1**, indicating two axial and one equatorial hydrogens at neighbouring carbons C-17 and C-19. These findings are further confirmed by ^{13}C shifts of C-17, C-18, C-19 (δ 71.4, 74.0, 31.1) and carbons C-16 and C-20 (δ 51.4, 24.0), which ex-

[1]Author to whom correspondence may be addressed.

hibit non-steric upfield shifts of −2.4 and −1.6 ppm in comparison to corresponding carbons in 3-epi-α-yohimbine (**1**). The stereochemistry of ring connection in **2** is deduced from diagnostic ^{13}C shielding for C-3, C-6, C-14, and C-21 (δ 53.8, 16.6, 24.1, 49.2), indicating *cis* fusion of rings C/D and ring D/E (4).

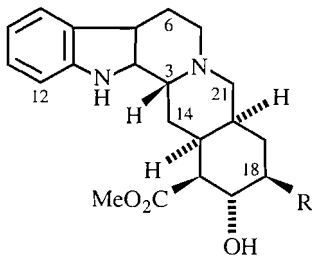

1:R = H; **2**:R = OH

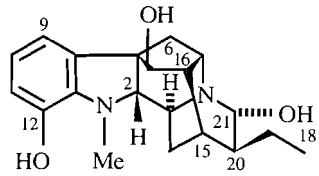

3

These data are consistent with the structure of 18β-hydroxy-3-epi-α-yohimbine (**2**), an alkaloid that has already been isolated (9, 10).

The third alkaloid was expected to be of the ajmaline type, because its reaction with CAS was slightly orange and the UV spectrum gave maximum absorption at 250 and 290 nm. However, all the major fragment ions in the mass spectrum were found to be 16 amu higher than in ajmaline. Conclusively, this alkaloid is a hydroxylated ajmaline with the OH group on the aromatic ring A represented by the fragment ion at 160 *m/z* instead of 144 *m/z*.

Inspection of the aromatic region of the ^1H NMR revealed two doublets (δ 7.5, 6.62) and one triplet (δ 6.58) with *ortho* coupling, which agrees with OH substitution at C-9 or C-12. In addition, the ^{13}C spectrum showed three signals for aromatic CH carbons (δ 119.8, 115.1, 114.9) and three quaternary carbons (δ 144.0, 140.8, 137.1). Analysis of ^1H and ^{13}C NMR data using known hydroxyl increments and NOE difference spectra clearly indicated that the OH group is located at C-12 of ajmaline. Further confirmation was deduced from the downfield shift for the N-CH_3 group, which showed an ^1H shift at δ 2.92 and a ^{13}C shift at δ 39.9, while ajmaline exhibits shifts at δ 2.64 and δ 34.3, indicating the proximity of the OH and NCH_3 groups in 12-hydroxyajmaline (**3**). The assignment of the remaining carbon atoms was established by 2-D HETCOR measurements and confirmed the final assignments made for ajmaline (11).

Experimental

Plant material

Hairy roots of *R. serpentina* were grown in liquid, hormone-free, B 5 medium on gyratory shakers (100 rpm) in 1000-mL Erlenmeyer flasks in the dark. The root material was harvested after 28 days of growth, freeze-dried, and stored at −25° C.

Chromatography

TLC was performed on 0.25 mm and 0.5 mm Silicagel 60 F_{254} plates (Merck, Darmstadt). Flash chromatography was carried out with silica gel 60 (230–400 mesh) from the same company. The following solvent systems were used: (a) $CHCl_3$–MeOH–NH_3 (4:1:0.01); (b) $CHCl_3$–MeOH–NH_3 (2.5:2.5:0.01); (c) MeOH–NH_3 (5:0.01); (d) EtOH–cyclohexane–diethylamine (4:4:1); (e) EtOAc–MeOH–H_2O–NH_3 (3.5:1:0.5:0.01); (f) EtOAc–EtOH–cyclohexane–NH_3 (2:2:0.5:0.01). Alkaloidal compounds on TLC were sprayed with ceric ammonium sulphate (CAS reaction).

Instrumentation

UV spectra in MeOH were recorded using a Perkin Elmer Lambda 2 photospectrometer. Mass spectra (EI) were obtained with a Finnigan MAT 44 S (quadrapole instrument) at 70 eV. The ^1H and ^{13}C NMR spectra were recorded using Bruker AM 400 and ARX 400 instruments.

Alkaloid isolation

The freeze-dried, powdered roots (30 g) were extracted twice with 500 mL MeOH by sonication for 60 min. The organic layer was filtered and evaporated, and the residue (1.5 g) was fractionated by flash chromatography with the solvent systems (a)–(c). Four major fractions were obtained containing ceric ammonium sulphate positive alkaloids. From these fractions the single alkaloids were isolated by TLC. Fraction 2 afforded 1.8 mg 12-hydroxyajmaline (**3**) exhibiting R_f values of 0.61 and 0.50 in solvent systems (d) and (f), respectively. From fractions 2 and 3 respectively, 3-epi-α-yohimbine (**1**) (2.5 mg) was isolated and purified in TLC solvents (a) and (b), R_f values 0.68 and 0.37, respectively. Fractions 3 and 4 gave 18β-hydroxy-3-epi-α-yohimbine (**2**) (1.9 mg) after purification with the solvent systems (a) and (b); R_f values were 0.4 and 0.31 respectively.

Spectroscopic data

3-Epi-α-yohimbine (1). UV λ_{max} (MeOH): 224, 282, 290 nm. ^{13}C NMR (100 MHz, $CDCl_3$) δ: 135.7 (C-13), 132.0 (C-2), 127.6 (C-8), 121.7 (C-11), 119.6 (C-10), 118.0 (C-9), 110.9 (C-12), 108.0 (C-7), 65.8 (C-17), 54.0 (C-3), 53.8 (C-16), 51.0 (C-5), 49.5 (C-21), 35.6 (C-20), 33.2 (C-18), 32.2 (C-15), 24.1 (C-19), 23.6 (C-14), 16.6 (C-6), 52.0 (OCH_3), 173.8 (CO). EI-MS *m/z* (rel. int.): 354 (M^+, 100), 353 (M^+ − H, 89), 339 (12), 295 (14), 223 (19), 197 (18), 184 (37), 170 (38), 169 (57), 156 (33), 144 (32).

18β-Hydroxy-3-epi-α-yohimbine (2). UV λ_{max} (MeOH):224, 282, 290 nm. ^{13}C NMR (100 Hz, $CDCl_3$) δ: 135.6 (C-13), 131.7 (C-2), 127.6 (C-8), 121.6 (C-11), 119.6 (C-10), 118.1 (C-9), 110.9 (C-12), 108.3 (C-7), 74.0 (C-18), 71.4 (C-17), 53.8 (C-3), 51.4 (C-16), 51.0 (C-5), 49.2 (C-21), 34.0 (C-20), 32.3 (C-15), 31.1 (C-19), 24.1 (C-14), 16.6 (C-6), 52.1 (OCH_3), 172.8 (CO). EI-MS *m/z* (rel. int.): 370 (M^+, 94), 369 (M^+ − H, 93), 353 (13), 352 (13), 293 (10), 237 (19), 224 (20), 221 (19), 197 (17), 182 (42), 169 (100), 156 (47), 144 (62), 129 (34); diacetate: *m/z* (rel. int.): 454 (M^+, 100), 412 (16), 411 (16), 394 (31), 393 (54), 351 (12), 335 (24), 221 (66), 197 (35), 184 (39), 170 (57), 169 (77), 156 (27), 144 (46), 129 (31).

12-Hydroxyajmaline (3). UV λ_{max} (MeOH): 250, 290 nm. ^1H NMR (400 MHz, DMSO-d_6, benzene-d_6) δ: 7.70 (1H, dd, J = 7.5, 1.5 Hz, H-9), 6.62 (1H, dd, J = 7.5, 1.5 Hz, H-11) 6.57 (1H, t, J = 7.5, H-10), 5.13 (1H, s, OH-17), 4.27 (1H, s, H-17), 4.15 (1H, s, H-21), 3.50 (1H, d, J = 9.5 Hz, H-3), 2.92 (4H, s, H-5, N-CH_3), 2.51 (1H, s, H-2), 2.15 (1H, m, H-15), 1.95 (1H, t, J = 6 Hz, H-16), 1.83 (1H, dd, J = 12.0, 5.0 Hz, H-6a), 1.76 (1H, d, J = 12 Hz, H-6b), 1.67 (1H, t, J = 12.0 Hz, H-14a), 1.55 (1H, dd, J = 12.0, 5.0 Hz, H-14b), 1.36 (2H, m, H-19), 1.33 (1H, m, H-20), 0.92 (3H, t, J = 7.5 Hz, H-18). ^{13}C NMR (100 MHz, DMSO-d_6) δ: 144 (C-13), 140.0 (C-8), 137.1 (C-12), 119.8 (C-10), 115.1 (C-9), 114.9 (C-11), 87.4 (C-21), 80.0 (C-2), 76.1 (C-17), 56.1 (C-7), 52.6 (C-5), 48.5 (C-20), 44.5 (C-16), 41.8 (C-3), 39.9 (N-CH_3), 35.3 (C-6), 31.1 (C-14), 28.3 (C-15), 25.2 (C-19), 12.2 (C-18). EI-MS *m/z* (rel. int.): 342 (M^+, 50), 327 (13), 312 (14), 215 (28), 199 (47), 198 (56), 182 (23), 173 (34), 162 (55), 160 (100), 147 (37); triacetate: *m/z* (rel. int.): 468 (M^+, 82), 426 (100), 411 (21), 384 (22), 369 (17), 341 (5), 323 (13), 240 (20), 198 (94), 183 (22), 173 (28), 160 (76), 147 (30).

Acknowledgments

Support by the Deutsche Forschungsgemeinschaft (Bonn – Bad Godesberg) and the Fonds der Chemischen Industrie (Frankfurt am Main) is gratefully acknowledged. We thank Prof. Dr. W.E. Court (Mold) for help in preparing the English version of this article.

Can. J. Chem. Downloaded from www.nrcresearchpress.com by 203.198.23.82 on 09/08/12
For personal use only.

1. H. Falkenhagen, I.N. Kuzovkina, I.E. Alterman, L.A. Nikolaeva, and J. Stöckigt. Nat. Prod. Lett. **3**, 107 (1993).
2. A. Petit, C. David, G.A. Dahl, J.G. Ellis, P. Guyon, F. Casse-Delbart, and J. Tempe. Mol. Gen. Genet. **190**, 204 (1983).
3. M. Hesse. *In* Progress in Mass Spectrometry, Indolalkaloide, Teil 1. *Edited by* H. Budzikiewicz. Verlag Chemie, Weinheim. 1974.
4. E. Wenkert, C.-J. Chang, H.P.S. Chawla, D.W. Cochran, E.W. Hagaman, J.C. King, and K. Orito. J. Am. Chem. Soc. **98**, 3645 (1976).
5. F.E. Bader, D.F. Dickel, R.A. Lucas, and E. Schlitter. Experientia, **10**, 298 (1954).
6. A. Hofmann. Helv. Chim. Acta, **37**, 314 (1954).
7. R. Goutarel, A. Hofmann, M.M. Janot, A. LeHir, and N. Neuss. Helv. Chim. Acta, **40**, 156 (1957).
8. L. Töke, K. Honty, L. Szabó, G. Blaskó, and C. Szántay. J. Org. Chem. **39**, 2496 (1973).
9. M.A. Amer and W.E. Court. Phytochemistry, **20**, 2569 (1981).
10. N.N. Sabri and W.E. Court. Phytochemistry, **17**, 2023 (1978).
11. B. Danieli, G. Palmisano, and G.S. Ricca. Tetrahedron Lett. **22**, 4007 (1981).

Can. J. Chem. Downloaded from www.nrcresearchpress.com by 203.198.23.82 on 09/08/12
For personal use only.